Editorial

Advances in Science, Technology and Engineering Systems Journal (ASTESJ) is an online-only journal dedicated to publishing significant advances covering all aspects of technology relevant to the physical science and engineering communities. The journal regularly publishes articles covering specific topics of interest.

Current Issue features key papers related to multidisciplinary domains involving complex system stemming from numerous disciplines; this is exactly how this journal differs from other interdisciplinary and multidisciplinary engineering journals. This issue contains 159 accepted papers related to computer engineering domain.

Editor-in-chief
Prof. Passerini Kazmersk

ADVANCES IN SCIENCE, TECHNOLOGY AND ENGINEERING SYSTEMS JOURNAL

CONTENTS

Standardized UCI-EGO dataset for evaluating 3D hand pose estimation on the point cloud

Sinh-Huy Nguyen[1], Van-Hung Le[*,2]

[1]*Institute of Information Technology, MIST, 100000, Vietnam*

[2]*Tan Trao University, Tuyen Quang, 22000, Vietnam*

A B S T R A C T

To evaluate and compare methods in computer vision, scientists must use a benchmark dataset and unified sets of measurements. The UCI-EGO dataset is a standard benchmark dataset for evaluating Hand Pose Estimation (HPE) on depth images. To build robotic arms that perform complex operations such as human hands, the poses of the human hand need to be accurately estimated and restored in 3D space. In this paper, we standardized the UCI-EGO dataset to evaluate 3D HPE from point cloud data of the complex scenes. We also propose a method for fine-tuning a set parameter to train the estimation model and evaluating 3D HPE from point cloud data based on 3D Convolutional Neural Networks (CNNs). The CNNs that we use to evaluated currently the most accurate in 3D HPE. The results of the 3D HPE from the point cloud data were evaluated in two branches: using the hand data segment and not using the hand data segment. The results show that the average of 3D joint errors of the 3D HPE is large on the UCI-EGO dataset (87.52mm) and that the error without using the hand data segment is many times higher than the estimated results when using the hand data segment (0.35ms). Besides, we also present the challenges of estimating 3D hand pose and the origin of the challenge when estimating real image dataset.

1 Introduction

In computer vision when evaluating and comparing the methods, the scientists must use a benchmark dataset and unified sets of measurements. The benchmark dataset usually includes training sets and testing sets/ validation set [1], this ratio is defined in the cross-validation parameter [2]. And these sets just include the annotation data of each sample. The UCI-EGO dataset has been published in [3] [1] and evaluated in many studies of HPE [4]–[6]. However, these ratings are evaluated in 2D space on the depth image. The UCI-EGO dataset provided the annotation data, each key point is represented by the structure (x, y, z), (x, y) are the coordinates on the depth image, z is the depth value of pixel which has the coordinates (x, y). However, the actual depth values of the annotation data are different from the depth data on the depth image. They are shown as Figure 2.

Nowadays, building robotic arms with hands that can perform many complex actions like human hands is an issue that needs research [7]. Since the human hands have many degrees of freedom (DOF), the complex actions can be performed. In order to build a robotic hand that can perform complex operations (Figure 3), first of all, it is necessary to restore and estimate the hand poses in the 3D space. Therefore, we continue to perform research on estimating human hand pose in the 3D space. In particular, estimating the hand pose on the data obtained from the EGOcentric VIsion (EGO-VI) sensor, contains many challenges such as missing, data loss, or obscuring.

Therefore, this paper includes the main contributions as follows:

- Standardizing the annotation data of the UCI-EGO dataset based on the depth value on the depth image. That means replacing the depth value of each point in the annotation data with the depth value of the corresponding point at that coordinate on the depth image, as illustrated in Figure 4. From this, using 3D hand pose annotation data to train the hand pose estimation model in the 3D space.

- Fine-tuning a set of parameters to train the hand pose estimation model in the 3D space based on the (V2V - V2V-PoseNet [8]) and evaluating the 3D HPE based on the most accurate 3D CNN (V2V). The estimation results are presented and

---

evaluated on the point cloud data. This is the same data as the real world.
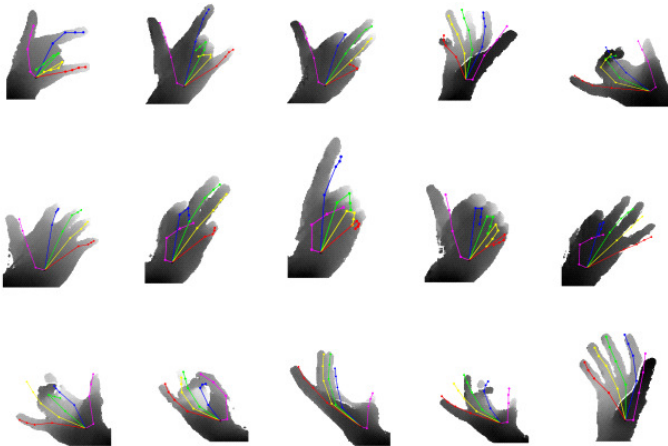
Figure 1: Illustration of 2D HPE results on the UCI-EGO dataset [6].
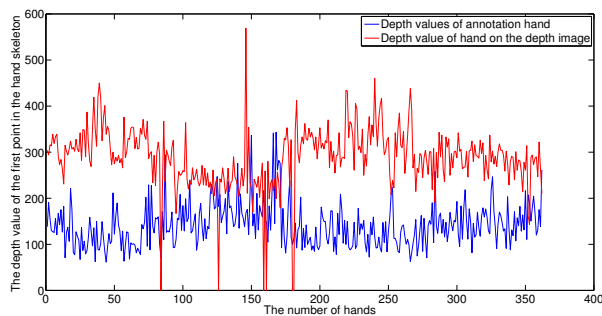
Figure 2: The depth value of the first point in the hand skeleton of annotation data and depth image data.
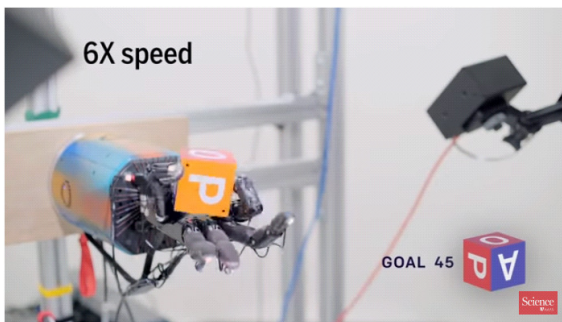
Figure 3: Robot arm illustration follows the operation of human hands [7].

- Presenting and comparing some 3D HPE results on the full hand dataset and the dataset obtained from the EGO-VI sensor. Presenting some challenges of estimating hand pose in the 3D space when estimating on the data obtained from EGO-VI sensors.
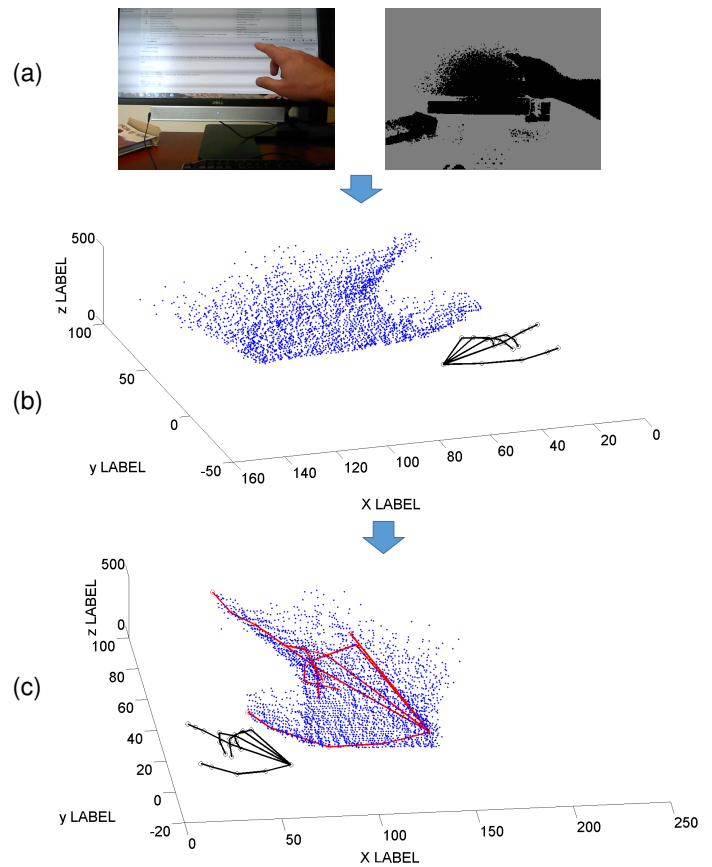
Figure 4: Illustrating of standardized the UCI-EGO annotation data process. (a) is the RGB-D images; (b) is the annotation data of UCI-EGO (the blue points are the point cloud of hand, the black skeleton is the annotation of UCI-EGO dataset); (c) is the standardized the annotation of UCI-EGO.

During the research on recognizing the daily activities of the human hand based on data collected from the EGO-VI sensor. We only research within a limited range as follows: We are interested in the dataset obtained from the EGO-VI sensor, namely the UCI-EGO dataset studied in this paper; We are also interested in 3D CNN that use point cloud as the input because the point cloud data is real data similar to the real environment.

The organization of the paper is shown as follows: Section 1 first introduce the benchmark dataset, the existence problem of the UCI-EGO [3] dataset, and the 3D HPE problem, we also introduce the application of 3D HPE to build robotic arms. Section 2 presents studies on the benchmark datasets to evaluate 3D HPE and some results. Section 3 presents the standardization of the UCI-EGO dataset and 3D HPE in the point cloud data. Section 4 presents the results and some discussions of 3D HPE. Finally, there are some conclusions and the next research direction of the paper (Section 5).

2   Related Works

Evaluating on the benchmark datasets is an important step to confirm the correctness of the detection, recognition, and estimation model of computer vision. Currently, there are many datasets for evaluating 3D HPE. The datasets are listed in Tab. 6 of [9]. In this paper, we only reintroduce some of the datasets used to evaluate 3D

HPE and some results based on typical CNNs.

In [10], published MSRA dataset, [2]. It includes 76k depth images of nine subjects of the right hands are captured using Intel's Creative Interactive Gesture Camera. Each subject include 17 gestures captured and include about 500 frames with 21 3D annotation hand joints for each frame: wrist, index mcp(metacarpal bone), index pip(proximal phalanges), index dip(distal phalanges), index tip, middle mcp(metacarpal bone), middle pip(proximal phalanges), middle dip(distal phalanges), middle tip, ring mcp (metacarpal bone), ring pip(proximal phalanges), ring dip(distal phalanges), ring tip, little mcp(metacarpal bone), little pip(proximal phalanges), a little dip(distal phalanges), little tip, thumb mcp(metacarpal bone), thumb pip(proximal phalanges), thumb dip(distal phalanges), and thumb tip. The size of the captured image is 320×240 pixels. The camera's intrinsic parameters are also provided, i.e. principal point of the image is (160, 120) and the focal length is 241.42. This dataset only has depth images, especially the hand data that is segmented with environmental data. This is a benchmark dataset for the evaluation of 3D HPE, the results of the CNNs are shown in table 2 of [11].

In [12] [3], the author includes 72,757 frames of the training set captured from a single person and 8,252 frames of the testing set captured two different persons from three MS Kinect v1, i.e. a frontal view and two side views. Each frame is a couple of RGB-D images. This dataset provided 25-joints in the annotation data with 42 DOF. The authors used the Randomized Decision Forest (RDF) to train a binary classification model by this dataset. And then this classification segments each pixel that belongs to a hand or background in the depth image. 3D HPE results of the CNNs are shown in table 2 of [11].

In [13] [4], the author includes 22K frames for training and 1.6K frames for testing, they captured from the Intel's Creative Interactive Gesture Camera with 10 subjects to take 26 different poses. It also provides 3D annotation data with 16 hand joints: palm, thumb root, thumb mid, thumb tip, index root, index mid, index tip, middle root, middle mid, middle tip, ring root, ring mid, ring tip, pinky root, pinky mid, and pinky tip.

The above are the datasets collected from a fixed number of perspectives of the image sensors. In many real applications, the image sensors are mounted on the body to collect data from the environment. These datasets are named the "Egocentric" dataset. In [14], the author published the **UCI-EGO** dataset, in [15] the author published the **Graz16** dataset, in [16] the author published the **Dexter+Object** dataset, in [17] the author published the **First-Person Hand Action** (FHAD) dataset, in [18] the author published the **UCI-EGO-Syn** dataset, in [15] the author published the **CVAR** dataset. Most EGO-VI datasets contain challenges for 3D HPE as follows: The frames do not contain hands, and the hands are obscured by objects in the scene; Data of the fingers is obscured; Data of visible hand only data of palm. The percent of challenges in CVRA [15] and UCI-EGO-Syn [18] datasets are shown in Figure 5.
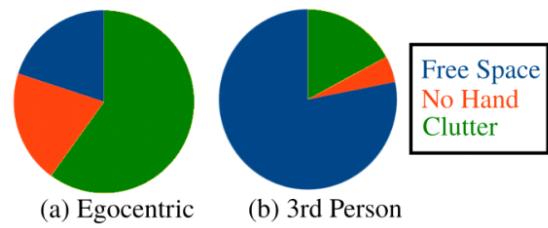
Figure 5: The percent of challenges in CVRA [15] and UCI-EGO-Syn [18] datasets.

In the past 5 years, many CNNs and related studies have been published for HPE. However, most of these studies were evaluated on the MSRA, NYU, ICVL datasets, the results are shown in table 2 of [11]. In this paper, we are interested in estimating 3D hand pose from the 3D annotation of hand skeleton data. The method we use is V2V, it has the input data of 3D annotation data and the point cloud data of hand. In [19], the author proposed 3D CNN for 3D HPE. This network projects 3D points of the hand following: x-direction, y-direction, z-direction. Synthesized in these three directions is encoded as 3D volumes storing the projective Directional Truncated Signed Distance Function (D-TSDF). Special, it only uses three 3D convolutional layers and three fully-connected layers to train the model. The estimated results have an average error of 9.58mm on the MSRA dataset.

In [20], the author proposed a deep regression network (SHPR-Net) for 3D HPE. This network consists of two components: A semantic segmentation network (SegNet) and the hand pose regression network (RegNet). The first component is used to segment the joints, the parts of the hand. That is, each part of the hand is segmented and labeled, RegNet is used to predict the 3D coordinates of the match corresponding to the segmented hand data areas. The estimated results have an average error of 10.78mm on the NYU dataset. In [21], the author proposed Hand PointNet to estimate 3D hand pose from the segmented hand on a depth image by using random decision forest [13], then convert to point cloud data using the Eq. 1. This method has improved the basic PointNet by using a hierarchical PointNet to generate the hierarchical feature extraction. Specifically, it uses three point set abstraction levels. Besides, In [22] and [23], the authors proposed the 3D DenseNet, Point-to-Point Net, respectively. The estimated error of result on the above methods is usually less than 10mm.

3 Standardized UCI-EGO Dataset and 3D HPE by V2V

3.1 *Standardized UCI-EGO Dataset*

As shown in Figure 4(b), the annotation data of the UCI-EGO dataset needs to be calibrated to meet the evaluation of 3D HPE in 3D space / on the point cloud data. Deviation in 3D annotation data of the hand pose is due to the 3D annotation data generated from the semi-automatic labeling tool. This issue is covered in Sec. 4.1 by UCI-EGO dataset introduction. This process is done as follows: The

---

[2]`https://www.dropbox.com/s/c91xvevra867m6t/cvpr15_MSRAHandGestureDB.zip?dl=0`.

[3]`https://jonathantompson.github.io/NYU_Hand_Pose_Dataset.htm`.

[4]`https://labicvl.github.io/hand.html`

coordinates of each keypoint $K(x, y, z)$ in the UCI-EGO annotation data, where (x, y) is the coordinate of K on the depth image, z is the depth value of K in the depth image [3]. In this paper, we replace the depth value of the K point in UCI-EGO [3] with the depth value of the point with coordinates (x, y) on the depth image. However, there are many cases of data loss or missing in the depth images, especially on the depth image sensors collected on previous depth sensors such as the Microsoft Kinect Version 1 [24]. We solve this problem by using the mean depth value of the k-neighbors of the K on the depth image, where $k = 3$, $d_K = mean(d_{K1}, d_{K2}, d_{K3})$.

After that, the coordinates (x, y) of the keypoint on the image combined with the depth value to generate one point (x_a, y_a, z_a) in 3D space / point cloud data [25] according to Eq. 1.

$$
\begin{aligned}
x_a &= \frac{(x - cx_d) * z}{f x_d} \\
y_a &= \frac{(y - cy_d) * z}{f y_d} \\
z_a &= z
\end{aligned}
\tag{1}
$$

where $f x_d, f y_d, cx_d$, and cy_d the intrinsics of the depth camera.

The results of the standardized annotation data are illustrated on the point cloud data of the hand as shown in Figure 4(c).

3.2 3D HPE by V2V

Based on the results of the 3D HPE of the 3D CNN on ICVL, NYU, MSRA datasets. The V2V [8] network has the best estimation result (average of 3D joints error is 6.28mm, 8.42mm, 7.49mm, respectively). Therefore, we used the V2V network to evaluate HPE on the UCI-EGO dataset. The execution process is shown below.
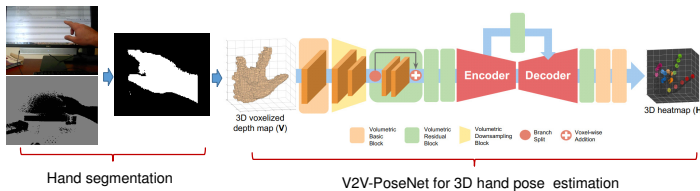
Figure 6: The hand data segmentation and 3D HPE based on 3D CNN (V2V) [8].

As shown in Figure 6 (left), the hand is in the complex scene, where the input data of V2V is the point cloud data of the segmented hand. Therefore, we propose a preprocessing step to segment the hand data with the environment and other objects.

We based on the annotation data on the keypoints of the hand skeleton frame on the depth image to crop a region container on the depth image with a rectangle that is bounding box of the keypoints on the depth image. We then find the maximum depth value of the keypoints M_d^h on the depth image. We rely on the context of capturing data from the EGO-VI sensor, the hand that is usually closest to the sensor. Therefore, the data near the hand that is large M_d^h is not part of the hand data.

As shown in Figure 6 (right), the input of the V2V method is 3D voxelized data. Thus, it reprojects each pixel of the depth map to the 3D space. After that, this space is discretized based on the pre-defined voxel size. V2V-PoseNet is based on the hourglass

model [26] and is designed to be divided into four volumetric blocks. The first volumetric basic block includes a volumetric convolution, volumetric batch normalization, and the activation function. The location of the first volumetric basic block is in the first and last parts of the network. The second volumetric residual block extended from the 2D residual block in [27]. The third volumetric downsampling block is similar to the volumetric max-pooling layer. The last block is the volumetric upsampling block, which consists of a volumetric deconvolution layer, volumetric batch normalization layer, and the activation function.
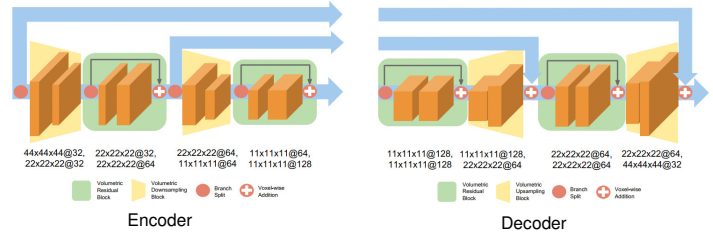
Figure 7: Encoder and decoder phase in the network architecture of V2V-PoseNet [8].

Each phase of the V2V-PoseNet method in Figure 6 is shown in Figure 7. Each phase consists of four blocks as shown in Figure 7. Therein, the volumetric downsampling block reduces the feature map space while the volumetric residual bock increases the number of channels in the encoder phase. Otherwise, the volumetric upsampling block enlarges the feature map space. When upsampling, to compress the extracted features the network reduce the number of channels. To predict each keypoint of the hand in 3D space through two stages: encoder, decoder. They are connected by the voxel-wise. To supervise the per-voxel likelihood in the estimating process, V2V generates a 3D heatmap, wherein the mean of the Gaussian peak is positioned at the ground-truth joint location in Eq. 2.

$$
D_n^*(i, j, k) = exp\left(-\frac{(i - i_n)^2 + (j - j_n)^2 + (k - k_n)^2}{2\sigma^2}\right)
\tag{2}
$$

where n^{th} keypoint whose ground-truth 3D heatmap is denoted D_n^*, (i_n, j_n, k_n) is the ground-truth voxel coordinate of nth, and $\sigma = 1.7$ is the standard deviation of the Gaussian peak [8]. V2V also uses the mean square error as a loss function L in Eq. 3.

$$
L = \sum_{n=1}^{N} \sum_{i,j,k} \|D_n^*(i, j, k) - D_n(i, j, k)\|^2
\tag{3}
$$

where D_n^* and D_n are the ground-truth and estimated results for n^{th} keypoint, respectively, and the number of keypoints is denoted N.

4 Experimental Results

4.1 Dataset

In this paper, we are trained and tested on the UCI-EGO [14] dataset. It provides about 400 frames prepared the 3D annotation. 3D annotations of keypoints with 26 joint points are also provided. To

annotate this dataset for evaluating 3D HPE and hand tracking the authors developed a semi-automatic labeling tool. It can annotate the accurate partially occluded hands and fingers in the 3D space by using the techniques: A few 2D joints are first manually labeled in the image and have used to select the closest synthetic samples in the training set; After that, a full hand pose is generated combining the manual labeling and the selected 3D sample; This pose is manually refined, resulting to the selection of a new sample, and the creation of a new pose; This process is repeated until acceptable labeling is achieved. This dataset captured from a chest-mounted Intel Senz3D RGB-D camera/EGO-VI and capture 4 sequences, 2 for each subject (1 male and 1 female), as illustrated in Figure 8. The authors labeled the keypoints of any visible hand in both RGB and Depth images every 10 frames, as illustrated in Figure 9.

We perform experiments on PC with Core i5 processor - RAM 8G, 4GB GPU. Pre-processing steps were performed on Matlab, fine-tuning, and development process in Python language on Ubuntu 18.04.

Before performing 3D HPE from the point cloud data, we propose a pre-processing step to segment the hand from the complex scene data, as shown in Figure 14. The depth image contains the depth value of the hand data is the closest (the hand is closest to the sensor). From there we use a threshold d_{thres} which is the maximum depth value of the hand to segment the data of the hand and other data in the complex scene.

4.2 V2V Parameters

Like in the original study of V2V-PoseNet [8], this deep network is developed in the PyTorch framework. The zero-mean Gaussian distribution with $\sigma = 0.001$ is initialized to all weights. The learning rate is set 0.00025 and batch size is set 4. This is the maximum value that V2V can train the model on our computer. The size of input is $88 \times 88 \times 88$. This deep network also uses the optimizer method of Adam [28]. To standardize data for training, V2V rotates [-40, 40] degrees in XY space, scale [0.8, 1.2] in 3D space, and translate with the size of voxels [-8, 8] in 3D space. We trained the model for 15 epochs. Implementation details of V2V are shown in the link [5].

In the original V2V study [8], the model trained only for 10 epochs. Although, the depth data value on the MSRA dataset is from 0.3m-0.7m, while the depth data value on the UCI-EGO dataset is from 0.3-0.45m. In each epoch, we computed the total loss function of batch sizes by Eq. 4.

$$T_L = \sum_{j=1}^{N_p} L_j \qquad (4)$$

where $N_p = N_s / batch\_size$ is the batch size number of the training data, N_s is the sample number of the training data. L_j is the total loss function j^{th} of each batch size.

Figure 8: Illustration of hand grasping object in the UCI-EGO dataset [14].
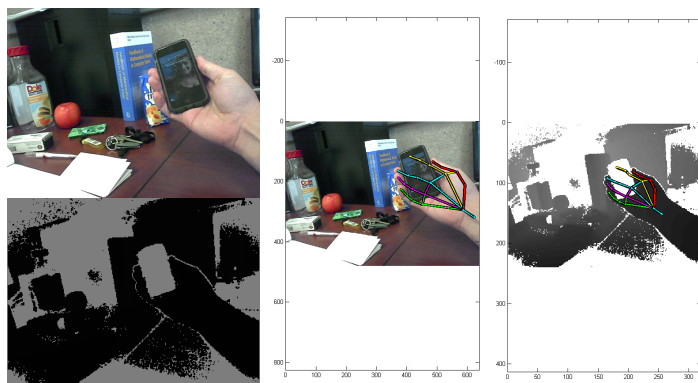
Figure 9: Illustration of 2D hand pose ground truth on the RGB and depth images.
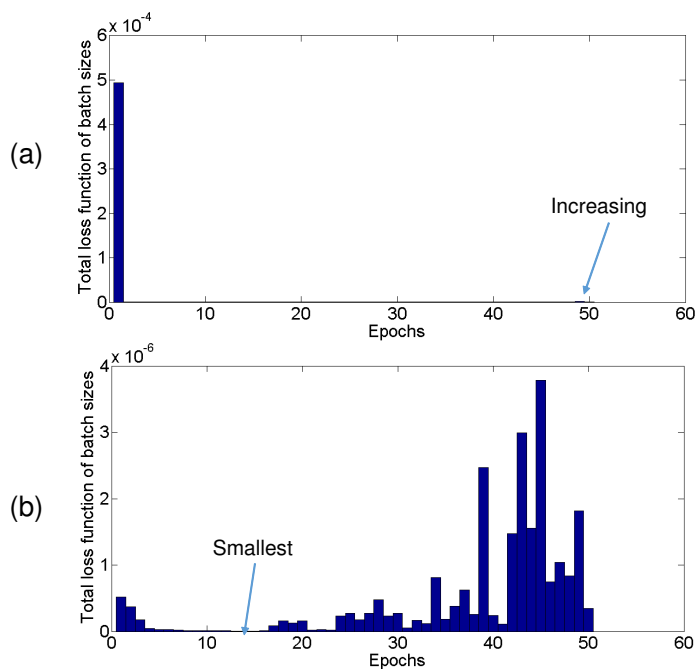
Figure 10: The total loss function of batch sizes at each epoch. (a) is the total loss function of batch sizes of training data when hand data is segmented on the depth image. (b) is the total loss function of batch sizes of validation data when hand data is segmented on the depth image.

We then compare the total loss function at each epoch. In a model with the smallest total loss function, that model is the best model for estimating the 3D hand pose. During training, we found that the total value of loss function up to the epoch 15th does not

decrease any more. We have trained the estimation model for 50 epochs, the total loss function of batch sizes at each epoch are shown in Figure 10. It can be seen that the value of the loss function decreases drastically and is about 10^{-11} at the epoch 10th. Specifically, on the validation data, there is the value of the smallest loss function at the epoch 10th as Figure 10(b). Therefore in this paper, we train only 15 epochs.

4.3 Evaluation Measure

As the evaluations of the previous 3D HPE method, we used the average 3D distance error (as shown in Eq. 5) to evaluate the results of the 3D HPE on the dataset.

$$\widehat{Err_a} = \frac{1}{Num_s} \sum_{n=1}^{Num_s} \frac{1}{21} \sum_{k=1}^{21} DIS(p_g, p_e) \qquad (5)$$

where $DIS(p_g, p_e)$ is the distance between a ground truth joint p_g and an estimated joint p_e; Num_s is the number of testing frames. In this paper, we evaluated the 21 joints of hand pose, illustrated in Figure 11.

1. wrist
2. index_mcp
3. index_pip
4. index_dip
5. index_tip
6. middle_mcp
7. middle_pip
8. middle_dip
9. middle_tip
10. ring_mcp
11. ring_pip
12. ring_dip
13. ring_tip
14. little_mcp
15. little_pip
16. little_dip
17. little_tip
18. thumb_mcp
19. thumb_pip
20. thumb_dip
21. thumb_tip
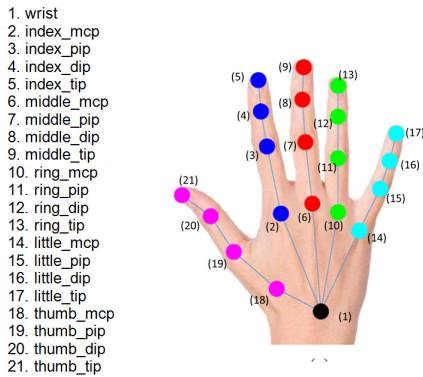
Figure 11: Illustrating the hand joints of the UCI-EGO [14] dataset.

In this paper, we use the rate at 1:5, which means 80% for training and 20% for testing. This ratio is based on the division of [15](using 5-fold cross-validation for testing and training). This means the UCI-EGO dataset uses 283 samples for training and 71 samples for testing. Although, the UCI-EGO dataset provides 26 annotation points. However, we only use 21 annotation data points to evaluate the 3D HPE. The order of points is shown in Figure 11.

4.4 Results and Discussions

As the evaluation of 3D HPE results shown in Tab. 2 of [11], also use the 3D distance error (mm) to evaluate the estimation results on the UCI-EGO dataset. The average 3D distance error is shown in Table 1. The processing time of training process and 3D HPE process is shown in Figure 12. As figure 12, the processing time to train for 50 epochs is 1.472h and 0.442h, it is calculated by $(1m46s = 106s) * 50epochs = 1.472h$ and $(1m46s = 106s) * 15epochs = 0.442h$, respectively. The processing time for testing is shown in Table 2. It is calculated by $128ms/362samples$ and $137ms/362samples$, respectively.

(a) Processing time to train an epoch

(b) Processing time of testing

Figure 12: Illustrating the processing time to train the estimation model and testing 3D HPE. (a) is the processing time to train an epoch. (b) is the processing time for testing.

Table 1: The average 3D distance error of the V2V on the UCI-EGO dataset for 3D HPE when trained through 15 epochs and 50 epochs.

Training	Measuremet/ Method		V2V
15 epochs	**Average of 3D joints error Err_a(mm)**	**Hand segmentation**	**87.52**
		No hand segmentation	95.49
50 epochs	**Average of 3D joints error Err_a(mm)**	**Hand segmentation**	**87.07**
		No hand segmentation	88.73
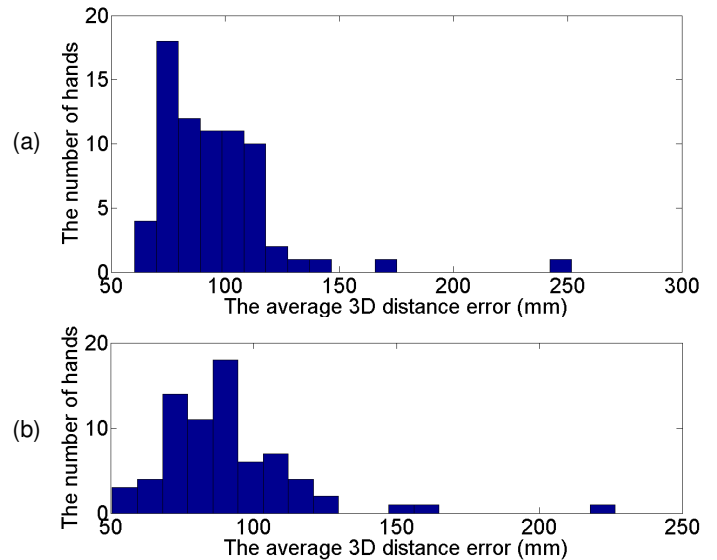
Figure 13: The distribution of 3D joints error for 3D HPE based on the UCI-EGO dataset by V2V-PoseNet [8] when trained through 15 epochs. (a) The distribution of 3D joints error when using hand segmentation on the depth image; (b) The distribution of 3D joints error when do not use hand segmentation on the depth image.

Table 2: The average of processing time of the V2V on the UCI-EGO dataset to estimate a 3D hand pose.

Measurement/ Method		V2V
Processing time (ms)/ hand	Hand segmentation	**0.35**
	No hand segmentation	0.38
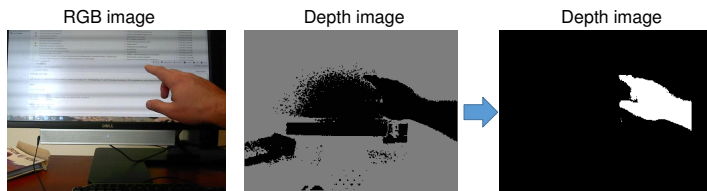
Figure 14: Illustrating the data well segmented of hand in the complex scene.
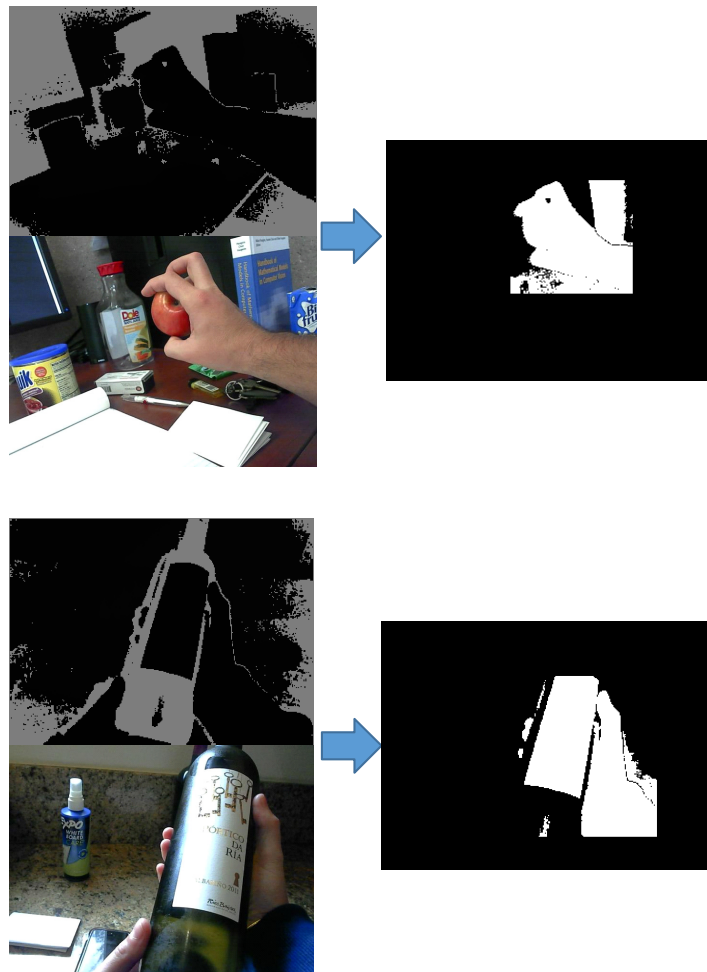
Figure 15: Illustrating of the hand data and the objects in the UCI-EGO dataset.

From table 2 of research in [11] and Table 1, the error results of estimating the 3D hand pose on the EGO-VI dataset are much larger than those estimated on the obtained datasets from a fixed number of perspectives. The time of estimated hand joints when using V2V

is enormous, as shown in Table 2. This high estimate time due to carrying CNN using the input data is the point cloud data that is not reduced by number of points.

As Table 1 and Figure 13, the 3D HPE results when using the hand data segment are better when not using the hand data segment in the complex scenes. The error distribution when using the hand data segment concentrated in bins closer to 0.

Although when segmenting the hand data, the estimation results were better than when the hand was not segmented. However, the estimated results have not improved much. Since in the UCI-EGO dataset only about 9% of the hands are well segmented with other subject's data, as illustrated in Figure 14. The remaining about 90% of the hands are grasping objects like phone, book, spray bottle, bottle, ball, etc. Therefore, the hand data gets stuck with the data of the objects being handled, as illustrated in Figure 15.

Figure 16 shows the results of estimating 3D hand pose on the point cloud data in two methods: The segmented hand data (a) and no segmented hand data (b).
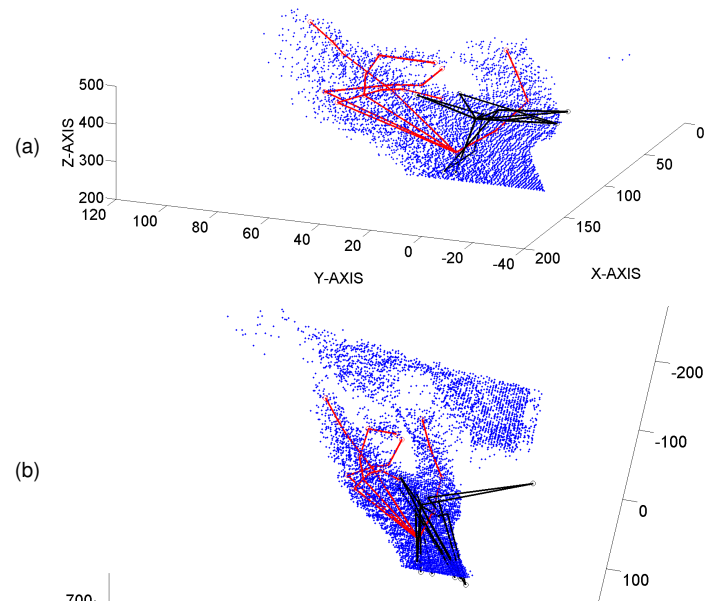
Figure 16: The results of the estimated 3D hand pose on the point cloud. (a) is the result of estimating the 3D hand pose in the 3D space on the segmented hand data; (b) is the result of estimating the 3D hand pose in the 3D space on hand data is not segmented. The blue points are the point cloud of hand and others object. The red skeleton is the ground truth of 3D hand pose, the black skeleton is the estimated 3D hand pose.

Based on the reading paper of [29], we find that the error of estimating the 3D hand pose on the UCI-EGO-Syn [18] dataset is high with: Hough [30], RDF [31], Deep Prior [32], PXC [33], Cascader [14], EGO.WS. [3]. The error distribution is from 35 to 100mm, as illustrated in Figure 18.

The UCI-EGO dataset has the hand data that performs grasping objects and is collected from an EGO-VI mounted on the person, the hand data is obscured, as shown in Figure 15. In particular, the data of the fingers is obscured. In this paper, we used V2V for estimating 21 joints of hand (3D hand pose), the input data of V2V is the coordinate of 21 joints in the 3D space of ground truth data, the output is also 21 joints, as illustrated in Figure 6. Therefore, the fields of the obscured fingers, the hand joints can still be estimated.

However, the point cloud data of the hand is much missing, the estimation results have large errors, as illustrated in Figure 17.
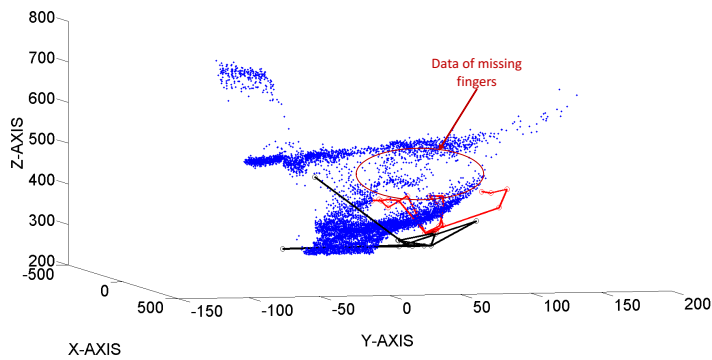
Figure 17: Illustrating of estimation results on the data with obscured fingers of Figure 9. The red skeleton is the ground truth of the 3D hand pose, the black skeleton is the estimated 3D hand pose.

During the research on 3D HPE, we found the challenges as follows:

- **_The high degree of freedom_**: In realistic/3D space human hand models have between 15 and 24 degrees of freedom [34]. From 21 joints there are about 63 coordinates of in the 3D space. To train such a large dimension vector requires a very strong model and very large learning data to train model.

- **_Data obscured_**: As shown above, the hand data is obscured making the hand's point cloud data missing. This makes the 3D HPE result from a high error value. This problem can be seen when comparing the results estimated on datasets with complete hand data (MSRA, ICVL, NYU) (table 2 of [11]) with the estimation results on the UCI-EGO-Syn [18] dataset (Figure 18). The quality of the depth images is also an issue affecting the 3D data / point cloud data. The depth images can be collected from a stereo camera or ToF (Time of Flight), this data still contains error noise.

- **_Hand size in the space_**: When moving in the 3D space to perform operations, the size of the hand is constantly changing. To train hand estimation models with different sizes, a large number of samples and strong models are required.

- **_3D hand pose annotation_**: The quality of the 3D HPE model depends on the training data. To prepare the training data requires an expensive system like in the FPHA (First-Person Hand Action) dataset [17], or use the estimated data through an estimation model like in the Ho-3D dataset [35].

5   Conclusion

To perform complex operations such as human hands then robot hand operations need to be built based on human hand operation. To do this, the poses of the human hand need to be accurately estimated and restored in 3D space. In this paper, we perform the standardization of the UCI-EGO dataset to evaluate 3D HPE. Simultaneously,

we retrained, evaluated 3D HPE, and presented the results on the point cloud data based on the V2V-PoseNet. The estimation results on the UCI-EGO dataset have been a large error and many challenging. The estimation results above also show that estimating 3D hand pose on the EGO-VI dataset is challenging and needs to be studied to improve the accuracy of 3D HPE.
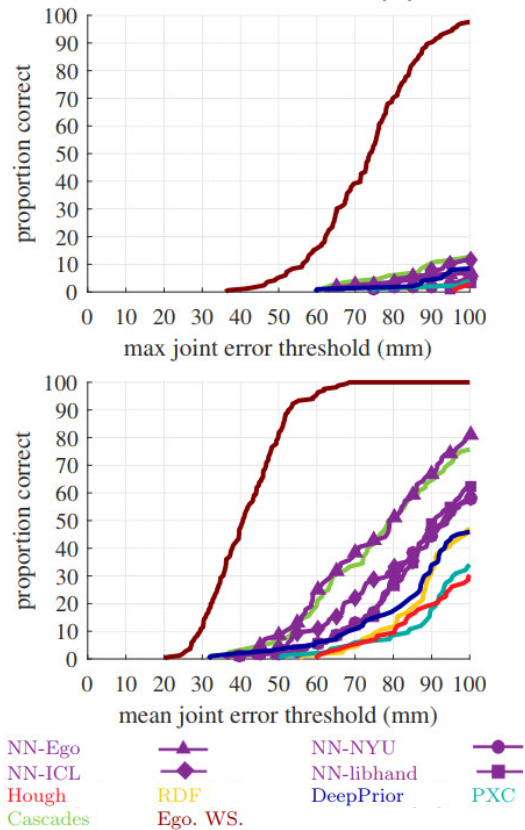
Figure 18: Distribution of 3D joints error estimation [29] on the UCI-EGO-Syn [18] dataset.

Acknowledgement

References

[1] S. Anasua, Y. Yang, V. Mauno, "Variation benchmark datasets: update, criteria, quality and applications," Database, Volume 2020, 2020, baz117, https://doi.org/10.1093/database/baz117, 2020.

[2] J. Brownlee, "A Gentle Introduction to k-fold Cross-Validation," `https://machinelearningmastery.com/k-fold-cross-validation/`, [Accessed 1 September 2020].

[3] G. Rogez, J. S. Supanvcivc, D. Ramanan, "First-person pose recognition using egocentric workspaces," in Proceedings of the IEEE Computer Society Conference on Computer Vision and Pattern Recognition, volume 07-12-June, 4325–4333, 2015, doi:10.1109/CVPR.2015.7299061.

[4] R. Gregory, S. S. James, R. Deva, "Egocentric Pose Recognition in Four Lines of Code," https://arxiv.org/pdf/1412.0060.pdf, 2014.

[5] S. S. James, R. Grégory, Y. Yi, S. Jamie, R. Deva, "Depth-based hand pose estimation: data, methods, and challenges," International Journal of Computer Vision, **126**, 1180–1198, 2015.

[6] S. Yuan, Q. Ye, B. Stenger, S. Jain, T. K. Kim, "BigHand2.2M benchmark: Hand pose dataset and state of the art analysis," in Proceedings - 30th IEEE Conference on Computer Vision and Pattern Recognition, CVPR 2017, volume 2017-Janua, 2605–2613, 2017, doi:10.1109/CVPR.2017.279.

[7] M. Hutson, "Watch a robot hand learn to manipulate objects just like a human hand," https://www.sciencemag.org/news/2018/07/watch-robot-hand-learn-manipulate-objects-just-human-hand, [Accessed 1 September 2020].

[8] G. Moon, J. Y. Chang, K. M. Lee, "V2V-PoseNet: Voxel-to-Voxel Prediction Network for Accurate 3D Hand and Human Pose Estimation from a Single Depth Map," in IEEE/CVF Conference on Computer Vision and Pattern Recognition (CVPR, 5079–5088, 20118.

[9] R. Li, Z. Liu, J. Tan, "A survey on 3D hand pose estimation: Cameras, methods, and datasets," Pattern Recognition, **93**, 251–272, 2019, doi: 10.1016/j.patcog.2019.04.026.

[10] H. Su, S. Maji, E. Kalogerakis, E. Learned-Miller, "Multi-view Convolutional Neural Networks for 3D Shape Recognition," in Proc. ICCV, 264–272, 2015, doi:10.1109/CVPR.2018.00035.

[11] C.-h. Yoo, S.-w. Kim, S.-w. Ji, Y.-g. Shin, S.-j. Ko, "Capturing Hand Articulations using Recurrent Neural Network for 3D Hand Pose Estimation," https://arxiv.org/abs/1911.07424, 2019.

[12] J. Tompson, M. Stein, Y. Lecun, K. Perlin, "Real-time continuous pose recovery of human hands using convolutional networks," ACM Transactions on Graphics, **33**(5), 2014.

[13] D. Tang, H. J. Chang, A. Tejani, T. K. Kim, "Latent regression forest: Structured estimation of 3D hand poses," IEEE Transactions on Pattern Analysis and Machine Intelligence, **39**(7), 1374–1387, 2017, doi:10.1109/TPAMI.2016.2599170.

[14] G. Rogez, M. Khademi, J. S. Supanvcivc, J. M. Montiel, D. Ramanan, "3D hand pose detection in egocentric RGB-D images," in Lecture Notes in Computer Science (including subseries Lecture Notes in Artificial Intelligence and Lecture Notes in Bioinformatics), volume 8925, 356–371, 2015, doi: 10.1007/978-3-319-16178-5_25.

[15] M. Oberweger, G. Riegler, P. Wohlhart, V. Lepetit, "Efficiently creating 3D training data for fine hand pose estimation," in Proceedings of the IEEE Computer Society Conference on Computer Vision and Pattern Recognition, volume 2016-Decem, 4957–4965, 2016, doi:10.1109/CVPR.2016.536.

[16] S. Sridhar, F. Mueller, M. Zollhoefer, D. Casas, A. Oulasvirta, C. Theobalt, "Real-time Joint Tracking of a Hand Manipulating an Object from RGB-D Input," in Proceedings of European Conference on Computer Vision (ECCV), 2016.

[17] G. Garcia-Hernando, S. Yuan, S. Baek, T.-K. Kim, "First-Person Hand Action Benchmark with RGB-D Videos and 3D Hand Pose Annotations," .

[18] S. S. James, R. Gregory, Y. Yi, S. Jamie, R. Deva, "Depth-based hand pose estimation: methods, data, and challenges," International Journal of Computer Vision, Springer Verlag, 2018, **126**(11), 1180-1198, 2018. doi: 10.1007/s11263-018-1081-7, 2018.

[19] L. Ge, H. Liang, J. Yuan, D. Thalmann, "3D Convolutional Neural Networks for Efficient and Robust Hand Pose Estimation from Single Depth Images," in IEEE Conference on Computer Vision and Pattern Recognition (CVPR), 2017, doi:10.4324/9781315556611.

[20] X. Chen, G. Wang, S. Member, C. Zhang, K. I. M. Member, X. Ji, "SHPR-Net : Deep Semantic Hand Pose Regression From Point Clouds," IEEE Access, **PP**(c), 1, 2018, doi:10.1109/ACCESS.2018.2863540.

[21] L. Ge, Y. Cai, J. Weng, J. Yuan, "Hand PointNet : 3D Hand Pose Estimation using Point Sets," Cvpr, 3–5, 2018.

[22] L. Ge, H. Liang, J. Yuan, S. Member, D. Thalmann, "Real-time 3D Hand Pose Estimation with 3D Convolutional Neural Networks," IEEE Transactions on Pattern Analysis and Machine Intelligence, **8828**(c), 2018, doi: 10.1109/TPAMI.2018.2827052.

[23] L. Ge, Z. Ren, J. Yuan, "Point-to-point regression pointnet for 3D hand pose estimation," in European Conference on Computer Vision, volume 11217 LNCS, 489–505, 2018, doi:10.1007/978-3-030-01261-8_29.

[24] D. Abdul, H. Ammar, "Recovering Missing Depth Information from Microsoft Kinect," pdfs.semanticscholar.org, 2011.

[25] N. Burrus, "Kinect Calibration," http://nicolas.burrus.name/index.php/Research/KinectCalibration, [Accessed 25 July 2020].

[26] N. A., Y. K., D. J., "Stacked hourglass networks for human pose estimation," in In European Conference on Computer Vision, 2016.

[27] H. Kaiming, Z. Xiangyu, R. Shaoqing, S. Jian, "Deep Residual Learning for Image Recognition," in IEEE Conference on Computer Vision and Pattern Recognition (CVPR), 2016.

[28] P. K. Diederik, B. Jimmy, "Adam: A Method for Stochastic Optimization," in In ICLR, 2015.

[29] J. S. Supancic, G. Rogez, Y. Yang, J. Shotton, D. Ramanan, "Depth-Based Hand Pose Estimation: Methods, Data, and Challenges," International Journal of Computer Vision, **126**(11), 1180–1198, 2018, doi:10.1007/s11263-018-1081-7.

[30] X. C., C. L., "Efficient Hand Pose Estimation from a Single Depth Image." in International Conference on Computer Vision (ICCV), 2013.

[31] K. C., Kırac, K. F., Y. E., A. L., "Hand pose estimation and hand shape classification using multi-layered randomized decision forests," in International Conference on Computer Vision (ICCV), 2012.

[32] M. Oberweger, P. Wohlhart, V. Lepetit, "Hands Deep in Deep Learning for Hand Pose Estimation," in Computer Vision Winter Workshop, 2015.

[33] Intel, "Perceptual computing SDK," 2013.

[34] S. Cobos, M. Ferre, R. Aracil, "Simplified Human Hand Models Based On Principal Component Analysis," in IFIP Conference on Human-Computer Interaction, 610–615, 2010.

[35] S. Hampali, M. Rad, M. Oberweger, V. Lepetit, "HOnnotate: A method for 3D Annotation of Hand and Objects Poses," https://arxiv.org/abs/1907.01481, 2019.

Synthesis and Characterization of Graphene Oxide Under Different Conditions, and a Preliminary Study on its Efficacy to Adsorb Cu^{2+}

Olayinka Oluwaseun Oluwasina, Surjyakanta Rana, Sreekantha Babu Jonnalagadda, Bice Susan Martincigh[*]

School of Chemistry and Physics, University of KwaZulu-Natal, Westville Campus, Private Bag X54001, Durban, 4000, South Africa

A B S T R A C T

Graphene oxide (GO) was prepared by the modified Hummer's method, but the mass ratio of graphite to sodium nitrate (NaNO₃) was varied from 2:1, 1:1, and 1:2. The primary reason for the variation was to determine the optimum conditions that would afford more oxygen functional groups to improve the material for application in adsorption. The final products, termed GO$_{2:1}$, GO$_{1:1}$ and GO$_{1:2}$, were analyzed by several instrumental techniques. The layered structure of the GO sheet was established by transmission electron microscopy, while powder X-ray diffraction showed that the GO$_{2:1}$ material was more crystalline than either GO$_{1:1}$ or GO$_{1:2}$. Raman spectroscopy revealed the presence of a greater defect density in GO$_{2:1}$. The presence of oxygen functional groups was verified by Fourier transform infrared spectroscopy, and these were quantified by the Boehm titration method. Overall, GO$_{2:1}$ had a larger oxygen content than either GO$_{1:1}$ or GO$_{1:2}$, and a larger specific surface area. A preliminary study on the adsorption properties of the samples revealed that GO$_{2:1}$ exhibited the highest percentage removal for Cu^{2+} in aqueous solution. Thus, the preparation of graphene oxide with a smaller amount of NaNO₃ yielded a material with a greater oxygen content, which showed suitable properties for the adsorption of contaminants in wastewaters.

1. Introduction

Graphene is a 2D nanomaterial that consists of sp^2 hybridized carbon atoms arranged in a hexagonal pattern [1]. This ultra-thin material is crystalline and has several remarkable properties. It has an outstandingly high surface area (2630 m^2 g^{-1} for a one-atom-thick flat sheet of graphene) [2], electrical and thermal conductivities, electron transport capabilities, and excellent tensile strength. These exceptional features have created considerable research interest and industrial implementation in areas such as supercapacitors [3], hydrogen production [4], sensors [5], adsorption [6], and support fillers [7] for nanocomposites [8].

Graphene oxide (GO) comprises of a single sheet of graphite oxide and is prepared by the action of strong oxidizers on graphite [1, 9, 10]. GO can easily be exfoliated and dispersed in different solvents due to its hydrophilicity [11, 12]. The hydrophilic nature of GO enables it to be evenly distributed on a substrate in the form of thin films, which is important in the production of electronic devices [13]. The presence of oxygenic functional groups, including carbonyl, carboxylic, epoxide and hydroxyl groups, the

high surface area and hydrophilicity make GO flakes an excellent prospective sorbent material [14, 15]. These oxygen functional groups can complex with toxic metal cations through sharing of lone pairs of electrons. A large adsorption capacity is exhibited as a consequence of the large surface area of GO [16-18]. The hydrophilicity of oxidized graphite allows water to be absorbed into the layered structure, which further increases the gap between the layers to 1.15 nm [19], which allows for improved metal binding.

Graphene oxide is synthesised by using Hummer's method in which graphite is oxidized by reacting it with potassium permanganate and sodium nitrate in concentrated sulfuric acid [1]. Numerous reports describe the high adsorption capacity of GO for antibiotics [20, 21], heavy metals [15, 16], and dyes [21, 22]. Graphene oxide has been stated to possess an improved adsorption efficiency than other frequently used sorbent materials as a consequence of the number of O-containing moieties it possesses [14, 16]. Adsorption is the most cost-effective and resourceful procedure for the sequestration of pollutants from contaminated water [22-24]. This water remediation technique has been studied with a wide variety of adsorbent materials, including waste

biomass [25], peat moss [26], zeolites [27] and hydrogels [28], to name only a few.

Although many investigations on the preparation of graphene oxide have been published, there are no studies that discuss the preparation of GO that will afford more oxygen functional groups for the elimination of contaminants from wastewater [14, 16, 23]. Hence, the objectives of this work were to synthesize GO via a modified Hummers method; to establish the optimum synthesis conditions that would provide more oxygenic functional groups on GO, and to apply the most functionalised product for the removal of contaminants from wastewater. The products obtained were characterized by several methods which include transmission electron microscopy (TEM), scanning electron microscopy (SEM), powder X-ray diffraction (XRD), thermogravimetric analysis (TGA), Raman spectroscopy, Fourier transform infrared spectroscopy (FTIR), Brunauer-Emmett-Teller (BET) surface area analysis, Boehm titration, and elemental analysis.

2. Experimental

2.1. Materials

Analytical grade chemicals, including graphite powder (<20 μm, synthetic), sodium hydroxide (NaOH), potassium permanganate ($KMnO_4$), 98% sulphuric acid (H_2SO_4), 30% hydrogen peroxide (H_2O_2), 32% hydrochloric acid (HCl), copper metal and nitric acid (HNO_3), were utilized without further purification. They were obtained from Sigma-Aldrich (Pty) Ltd, South Africa. Milli-Q H_2O was from a Millipore Milli-Q Integral water purification system.

2.2. Synthesis of graphene oxide

Different variants of GO were synthesized according to the modified Hummer's method [1] by varying the mass ratio of graphite to sodium nitrate from 2:1, 1:1 and 1:2 respectively. The products obtained were named $GO_{2:1}$, $GO_{1:1}$, and $GO_{1:2}$ respectively. The preparation method was as previously described [29].

2.3. Characterization

The $GO_{2:1}$, $GO_{1:1}$ and $GO_{1:2}$, materials were analyzed to authenticate the homogeneity and structure of the products prepared. The morphology of the materials was investigated by scanning electron microscopy (SEM) (ZEISS Ultra PLUS) and structural information was obtained from transmission electron microscopy (JEOL, JEM 1010). X-ray diffractograms of the materials were measured with a Bruker Advance D8 spectrometer utilizing Cu Kα radiation at 40 mA and 45 kV. Raman spectra of the materials were recorded with a DeltaNu Advantage 532TM® Raman spectrometer with a Nd:YAG laser source and excitation at a wavelength of 532 nm. The thermal stability of the materials was determined in a nitrogen atmosphere with a PerkinElmer Simultaneous Thermal Analyser STA 6000 instrument. The samples were heated from ambient temperature to 1000 °C at a rate of 10 °C/min with a nitrogen flow rate of 50 mL/min. The textural properties of the samples were determined with a Micromeritics Tristar ASAP 3020 surface area and porosity analyser by using nitrogen gas as the adsorbent. The functional groups present were identified by FTIR with a PerkimElmer Spectrum RX1 spectrophotometer, using a pressed disc of each powder mixed

with KBr. Elemental analysis of the materials was performed with a Thermo Scientific CHNS/O LECO CHNS-932 elemental analyser. The Boehm titration method was used for quantifying the surface groups on the carbon materials as follows. The number of acidic functional groups on the surfaces of the GO samples were measured with base solutions of increasing strength known as reaction bases such as NaOH, Na_2CO_3, and $NaHCO_3$. To determine the acidic sites of the materials, 0.2 g of the samples were weighed separately into 20 mL aliquots of solutions of 0.1 mol dm^{-3} NaOH, 0.05 mol dm^{-3} Na_2CO_3, and 0.1 mol dm^{-3} $NaHCO_3$ and then agitated in a shaking water bath for 24 h. The solutions were filtered, and 5 mL of the filtrates were back-titrated against a standardized 0.05 mol dm^{-3} HCl solution. It is suggested that sodium hydroxide (NaOH) neutralizes the lactonic, phenolic and carboxylic groups, while sodium carbonate (Na_2CO_3) neutralizes the lactonic and carboxylic groups, and sodium bicarbonate ($NaHCO_3$) neutralizes the carboxylic groups. Thus, by difference, the quantity of each type of functional group can be determined.

2.4. Determination of adsorption capacity

A batch adsorption technique, with Cu^{2+} as the adsorbate, was used to determine the adsorption capacity of the GO materials. For this, a standard Cu^{2+} stock solution was prepared by dissolving 1.0 g of pure Cu metal into 10 mL of concentrated nitric acid (HNO_3). The stock solution was made up to a final volume of 1000 mL with deionized water. This solution was subsequently diluted to prepare working solutions of known concentrations.

A Metrohm 827 pH-meter was used for measuring the pH, and a Mettler AE 200 balance was used for weighing of samples.

The dependence of the adsorption of $GO_{1:1}$, $GO_{1:2}$ and $GO_{2:1}$ was determined by varying the adsorbent dose from 10 to 60 mg in contact with 20 mL of 20 mg dm^{-3} of Cu^{2+} solution at a pH of 5. The samples were agitated in a thermostated shaking water bath set at 25 °C for 5 h, and subsequently filtered through Whatman No. 1 filter paper. The filtrates were analysed for their Cu^{2+} content at a wavelength of 220.353 nm with a PerkinElmer Optima 5300 DV inductively coupled plasma-optical emission spectrometer (ICP-OES).

The adsorption efficiency, q_e (in mg g^{-1}), was estimated from (1):

$$q_{eq} = \frac{V}{m} \times \left(C_i - C_{eq} \right) \qquad (1)$$

where V is the volume (in dm^3) of the adsorbate solution, m is the mass of adsorbent (in mg), and C_i and C_{eq} are the initial and equilibrium concentration of adsorbate (in mg dm^{-3}) respectively. The percentage sequestration of Cu^{2+} was derived from (2).

$$\% \, adsorbed = \left(\frac{C_i - C_{eq}}{C_i} \right) \times 100 \qquad (2)$$

3. Results and discussion

In this work, different variants of GO (2:1, 1:1, 1:2) were synthesised via a modified Hummer's method. The GO samples were characterized by several techniques, and then tested for the adsorption capacity of a representative heavy metal cation contaminant, namely Cu^{2+}, in aqueous solution.

3.1. Morphology

The surface morphologies of the different GO samples were measured by SEM techniques. The SEM micrographs of GO$_{2:1}$, GO$_{1:1}$ and GO$_{1:2}$ are shown in Figure 1. In order to acquire these images, the GO samples were coated with a gold film fractured surface under liquid nitrogen. The surface morphology showed how the GO sheets are exfoliated for the different GO materials. The SEM micrographs show that the GO materials have a 2D sheet-like structure with a multiple lamellar layer structure that distinguishes the edges of the individual sheets. The GO sheets were thick, particularly at the edges, and this thickness arises from the O-functional groups introduced.
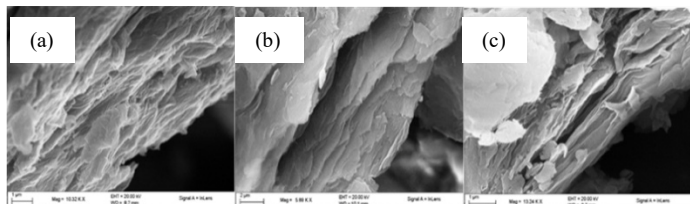
Figure 1: SEM images of GO samples: (a) GO$_{2:1}$, scale bar = 1 μm, (b) GO$_{1:1}$, scale bar = 1 μm, and (c) GO$_{1:2}$, scale bar = 1 μm

The TEM micrographs of the GO materials (Figure 2) revealed the anticipated layered structure of GO with a large sheet on top of the grids. The sheet resembles a transparent wrinkled, folded and silk-like veil due to the oxidation of graphite. This characteristic has been reported for the synthesis of GO by the modified Hummer's method regardless of the ratios of graphite to sodium nitrate [30]. The exfoliation of the graphite layer and introduction of defects on the GO layer is due to the introduction of oxygenic functional groups. From the TEM images, the level of transparency in the variants of GO might be as a result of the different ratios of graphite to sodium nitrate resulting in the intercalation of GO intermediates.
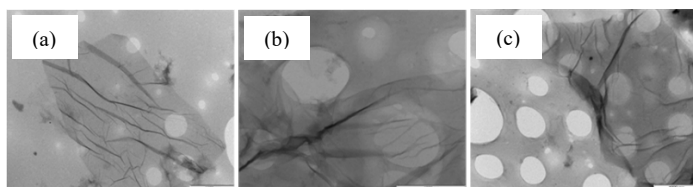
Figure 2: TEM images of GO samples: (a) GO$_{2:1}$, scale bar = 1000 nm (b) GO$_{1:1}$, scale bar = 1000 nm, and (c) GO$_{1:2}$, scale bar = 1000 nm

3.2. Crystallinity

The structural properties of the GO materials were examined by means of powder XRD. The diffractograms for GO$_{1:1}$, GO$_{1:2}$ and GO$_{2:1}$ are shown in Figure 3. There is a sharp diffraction peak for graphite at 2θ = 26.5° corresponding to a d-spacing of 0.34 nm of the graphite layers [31]. The characteristics of graphite at 42° disappeared after the oxidation process and a notable strong peak, for GO$_{2:1}$ at 2θ = 10.49°, GO$_{1:1}$ at 2θ = 10.47°, and GO$_{1:2}$ at 2θ = 10.48°, emerged. The increase in the interlayer spacing of GO to that of graphite arises from the introduction of O-containing functional groups, such as epoxide, hydroxyl, carboxylic and carbonyl groups, during the oxidative treatment [32]. The van der Waals interactions operative between the graphene sheets are weakened by the O-functional groups of GO and this increases the

distance between the sheets [33-35]. In the diffractogram for GO$_{2:1}$ a strong peak at 2θ = 43° is seen after oxidation indicating a random packing of the sheets [36]. The XRD results confirmed that the oxygenic functional groups were intercalated into the graphite interlayers.
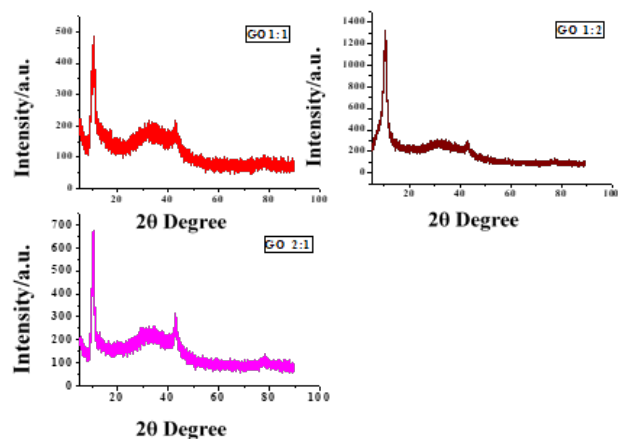
Figure 3: Powder X-ray diffractograms for GO samples

Selected area electron diffraction (SAED) allows for a diffraction pattern to be obtained with a transmission electron microscope [37]. It can be used to find the d-spacing of the crystal planes and also to obtain information about the crystallinity of the samples. The brighter the spots, the more crystalline is the sample. The reciprocal of the radius of the SAED ring is the d-spacing of that ring, and the d-spacings for GO$_{1:1}$, GO$_{1:2}$ and GO$_{2:1}$ were determined as 0.2046, 0.1997 and 0.2131 nm respectively (Figure 4). From the SAED images, GO$_{2:1}$ was found to be the most crystalline of the three samples.
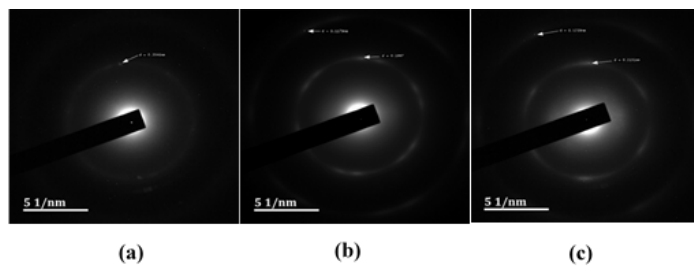
Figure 4: SAED patterns for (a) GO$_{1:1}$, (b) GO$_{1:2}$ and (c) GO$_{2:1}$

3.3. Graphitic and defective nature

Raman spectroscopy is an essential method for determining the defects, thermal conductivity, and strain in graphene and related materials [38]. The main aspects of the Raman spectra of graphitic C-based materials include the D and G bands, and their overtones. In the Raman spectra (Figure 5), the D bands of GO$_{1:1}$, GO$_{1:2}$ and GO$_{2:1}$ have very strong peaks at 1353, 1350 and 1347 cm^{-1} respectively. The D-peaks are associated with the vibration of sp^3 carbon atoms of defects that are randomly arranged on the GO sheets. The D-peak intensity together with a large peak width indicates significant structural disorder in the GO samples. The wavenumbers at 1595, 1593 and 1596 cm^{-1}, respectively, represent the G bands, which are related to the vibration of sp^2 C-atoms in the graphitic 2D hexagonal lattice. This gives rise to in-plane

optical vibrations that relate to the E_{2g} phonons from the bond stretching of the sp^2 carbon atoms in a graphitic 2D hexagonal lattice. The ratio of the areas under the D- and G-bands (I_D/I_G) is used to measure the graphitic nature of the sample. For these samples, the order of the I_D/I_G ratio is $GO_{2:1}$ (1.02) > $GO_{1:2}$ (0.97) > $GO_{1:1}$ (0.93). This result shows that $GO_{2:1}$ shows a greater defective density.
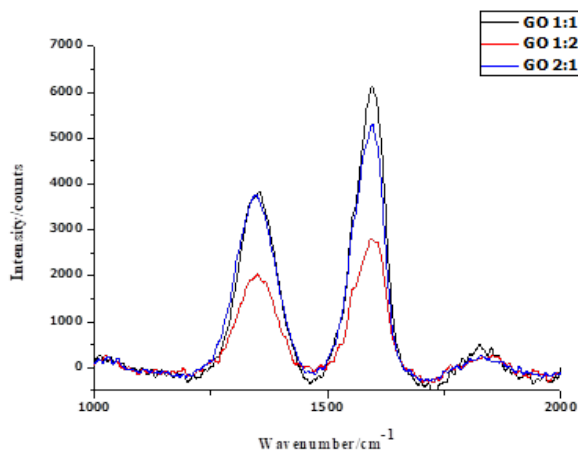
Figure 5: Raman spectra for GO samples
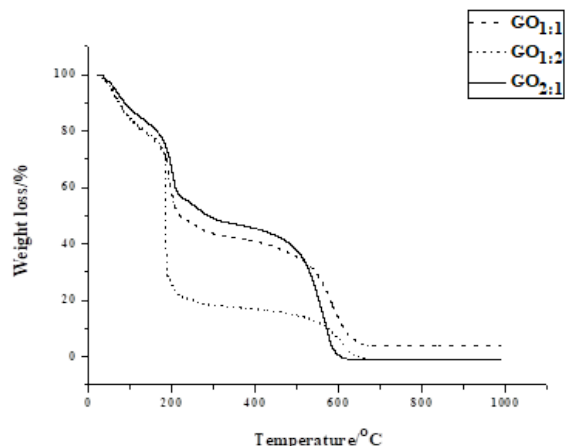
Figure 6: Thermograms of graphene oxide samples recorded in a N_2 atmosphere

3.4. Thermal stability

Thermal analysis was performed to assess the thermal stability of the $GO_{1:1}$, $GO_{1:2}$, and $GO_{2:1}$ sheets, since oxygen functional groups present in GO decompose on heating. Figures 6 and 7 depict the thermograms and derivative thermograms of the GO samples respectively. The first mass loss, that takes place at a temperature of 100 °C, is primarily due to the evaporation of adsorbed water that has interacted with the O-containing functional groups on GO [39, 40]. According to Dreyer *et al.* [41], the interaction of water with GO is by hydrogen bonding. The second mass loss arises from the pyrolysis of unstable O-containing functional groups such as carboxylic, hydroxyl and carbonyl groups to give CO_2, CO and H_2O [42, 43]. In $GO_{1:1}$, $GO_{1:2}$ and $GO_{2:1}$ this loss occurred at a temperature of 202, 212 and 216 °C respectively. The final mass loss at 614, 617 and 587 °C for $GO_{1:1}$, $GO_{1:2}$ and $GO_{2:1}$ respectively, shows that there is a reduction in the thermal stability of graphene oxide relative to graphite [44].

The derivative thermograms for the GO samples shown in Figure 7, revealed a small exothermic peak at 614, 617, and 587 °C. At 202, 212, and 216 °C, a larger exothermic peak is seen, and this is due to the loss of CO_2 and CO from the GO samples as a result of the decomposition of O-containing functional groups.
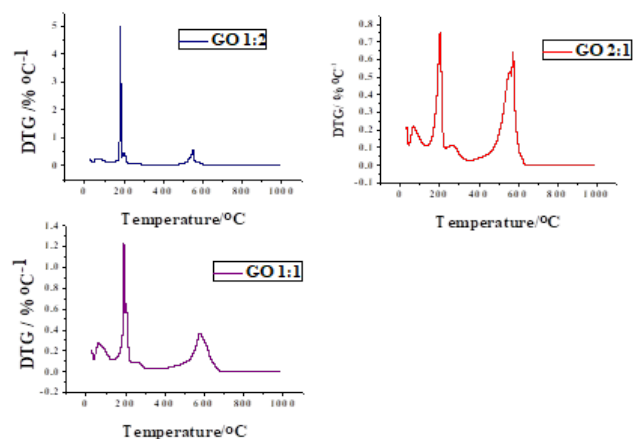
Figure 7: Derivative thermograms of graphene oxide samples

3.5. Textural properties

The BET method was used to determine the specific surface areas of the GO materials with N_2 as the adsorbed gas. In the first step, the materials were degassed at 120 K for 24 h. The results are shown in Table 1. The pores can be grouped into micro-, meso- or macro-pores, based on diameter. The results obtained for $GO_{2:1}$ (3.841 nm), $GO_{1:1}$ (7.350 nm) and $GO_{1:2}$ (19.861 nm) correspond to mesopores. The largest BET surface area was displayed by $GO_{2:1}$ (179.25 $m^2 \, g^{-1}$), followed by $GO_{1:1}$ (82.68 $m^2 \, g^{-1}$) and, lastly, by $GO_{1:2}$ (58.35 $m^2 \, g^{-1}$).

Table 1: Physical properties of the $GO_{2:1}$, $GO_{1:1}$ and $GO_{1:2}$ materials

Sample	Surface area/$m^2 \, g^{-1}$	Pore volume/$cm^3 \, g^{-1}$	Pore diameter/nm
$GO_{2:1}$	179.25	0.051	3.841
$GO_{1:1}$	82.68	0.054	7.350
$GO_{1:2}$	58.35	0.122	19.861
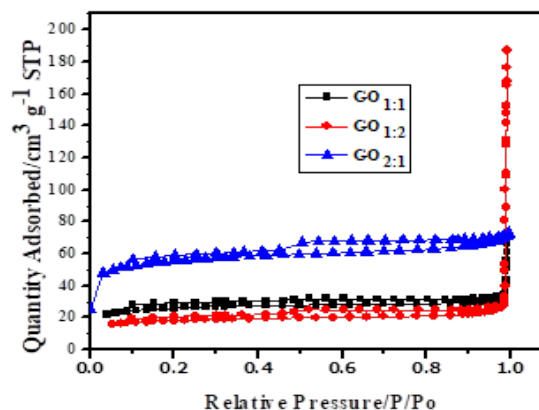
Figure 8: BET nitrogen adsorption-desorption isotherms

The N_2 adsorption-desorption isotherms for the GO samples are depicted in Figure 8. $GO_{1:1}$ and $GO_{1:2}$ exhibited type IV isotherms and type H3 hysteresis loops, signifying that the nanomaterials are mesoporous, as determined from the pore diameters. $GO_{2:1}$ also exhibited a type IV isotherm but has a H4 type of hysteresis loop. The type IV isotherm represents an adsorption isotherm with hysteresis related with capillary condensation in mesopores [45, 46]. The Barrett-Joyner-Halenda (BHJ) pore volumes of the samples are $GO_{1:1}$ (0.054 cm^3 g^{-1}), $GO_{1:2}$ (0.122 cm^3 g^{-1}) and $GO_{2:1}$ (0.051 cm^3 g^{-1}) (Figure 9).
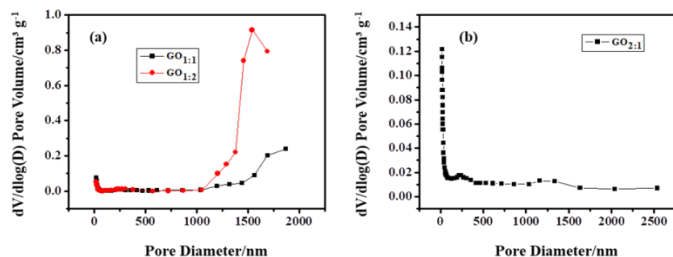
Figure 9: The BHJ pore volumes of (a) $GO_{1:1}$, $GO_{1:2}$ and (b) $GO_{2:1}$

3.6. Nature of oxygen functional groups

FTIR spectrophotometric characterisation was conducted to explore the nature of the functional groups on the GO products and to confirm the formation of GO by chemical treatment of graphite (Figure 10). From the spectra of the GO samples, it is clear that large amounts of O-containing functional groups are present on the surfaces of the samples. The broad peak at 3430 cm^{-1} can be attributed to the free and associated O-H stretch arising from the presence of adsorbed water molecules and structural hydroxyl groups (–COH and –COOH) of GO [47]. The peak at 1728 cm^{-1} is assigned to the C=O groups. The peaks at 1626 cm^{-1} can be assigned to C=C groups that are due to the structure of the graphitic layer retained previously and after the oxidation process [48]. The peaks at 1220 and 1092 cm^{-1} are related to the C-O groups. From the results obtained, it is apparent that $GO_{2:1}$ shows the strongest and sharpest peaks in the C-O region, but these peaks are absent in the spectrum of $GO_{1:1}$ at 1220 cm^{-1}. The presence of C-O and C=O groups after the oxidation process confirms the successful functionalization of the samples, and the conversion of graphite into GO. This is in agreement with previous reports [49, 50]. Additionally, peaks at 1728 cm^{-1} due to the C=O stretch (COOH of carboxyl or carbonyl groups), at 1626 cm^{-1} due to the C=C stretch, and at 1092 cm^{-1} due to the C-O groups, appear in all the GO samples. Hence, there is evidence that GO was successfully synthesized, and the functional groups present on the surfaces of the GO sheets can furnish abundant adsorption sites, to increase the adsorption capacity for both organic and inorganic pollutants.

3.7. Elemental analysis

Elemental analysis was undertaken to ascertain the C, H and O elemental composition of the samples. From the results, it is apparent that $GO_{2:1}$ has the largest oxygen content of the three products (see Table 2). The oxygen content of $GO_{2:1}$ was 40.01%. Also, the C/O ratio for $GO_{2:1}$ is the smallest, also indicating the greater oxygen content. The H present in the GO products mainly arises from the presence of O-containing functional groups. The S is a residual impurity from H_2SO_4 used in the synthesis of the GO samples.
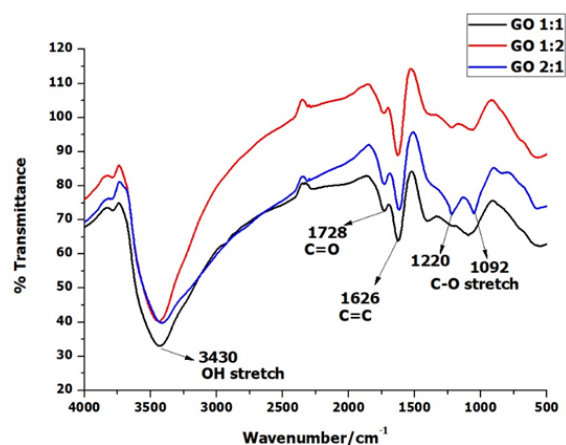
Figure 10: FTIR spectra of GO samples

Table 2: Elemental composition of GO samples

Material	C/%	H/%	S/%	O/%
$GO_{1:1}$	40.83	2.46	1.89	31.71
$GO_{1:2}$	42.35	2.59	1.97	32.02
$GO_{2:1}$	45.86	2.04	0.94	40.01

Table 3: Concentrations of acidic functional groups on the surfaces of $GO_{1:1}$, $GO_{1:2}$ and $GO_{2:1}$ as determined by the Boehm titration method

Sample	Base solution	Concentration neutralized/ mmol g^{-1}	Functional group	Concentration/ mmol g^{-1}
$GO_{1:1}$	NaOH	2.42	Phenolic	0.43
	Na_2CO_3	1.99	Lactonic	0.40
	$NaHCO_3$	1.59	Carboxylic	1.59
$GO_{1:2}$	NaOH	3.15	Phenolic	1.26
	Na_2CO_3	1.89	Lactonic	0.40
	$NaHCO_3$	1.49	Carboxylic	1.49
$GO_{2:1}$	NaOH	2.42	Phenolic	0.43
	Na_2CO_3	1.99	Lactonic	0.40
	$NaHCO_3$	1.59	Carboxylic	1.59

3.8. Quantity of acidic oxygen functional groups

The surface properties of the different GO materials were examined by using the Boehm titration method. The acidic properties of the GO variants are determined by the carboxylic, lactonic and phenolic functional groups (Table 3). These functional groups vary in their acidities and can be differentiated by neutralization with different basic solutions, namely, $NaHCO_3$, Na_2CO_3 and NaOH. The concentration of strong acid groups on $GO_{1:1}$, $GO_{1:2}$ and $GO_{2:1}$ was determined from the titre values of $NaHCO_3$, and that of strong and weak acidic functional groups was from that of Na_2CO_3 which gave 1.99, 1.89 and 1.99 mmol g^{-1} respectively. The concentration of weak acids was determined by the difference in the two titration values. The concentrations of the carboxylic acid groups were found to be 1.59, 1.49 and 1.59 mmol g^{-1} respectively. The overall concentration of the phenolic, and the strong and weak acidic functional groups was found from the

amount of NaOH neutralized. The total sum of the acidic functional groups on the $GO_{1:1}$, $GO_{1:2}$ and $GO_{2:1}$ surface was found to be 2.42, 3.15 and 2.42 mmol g^{-1} respectively. The phenolic functional group concentrations were determined from the difference in the three titration methods. From the results obtained, $GO_{1:1}$ and $GO_{2:1}$ are similar, whereas $GO_{1:2}$ contains significantly more phenolic groups than the other two samples. Therefore, the acidic surface functional groups of the samples are suitable for the uptake of cationic pollutants from aqueous solution. For each sample, the order of the number of acidic groups is carboxylic > phenolic > lactonic.

3.9. Adsorption properties

The effect of the adsorbent dose on the adsorption of Cu^{2+} from aqueous solution was determined by varying the mass of the GO samples from 10 to 60 mg at a constant temperature of 25 °C for 5 h. The results, shown in Figure 11, indicate that as the sorbent dose increases, the percentage of Cu^{2+} ions adsorbed onto the GO samples increases. An increase in the adsorbent dose with a higher percentage of adsorption arises from the increase in surface area and the availability of more binding sites for adsorption. The sorption of Cu^{2+} onto $GO_{1:1}$ was initially low compared with the other materials; this is possibly due to its surface area and the availability of active sites on the adsorbent surface. The other two adsorbents showed similar behaviour. Overall, the removal efficiency of the three adsorbents was high, but $GO_{2:1}$ showed the highest adsorption with a percentage removal of 59.7%.
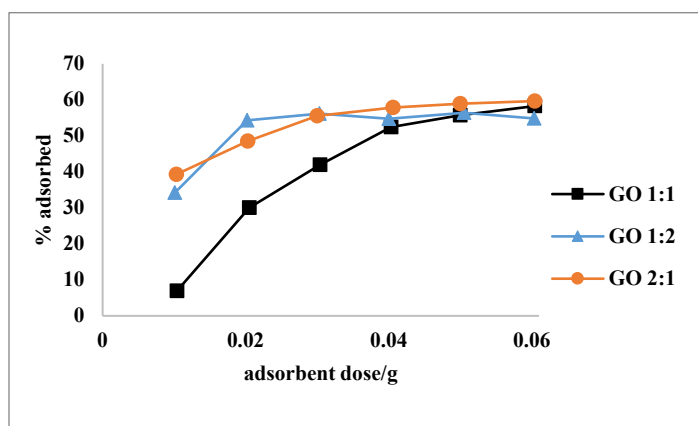
Figure 11: Effect of adsorbent dose on the adsorption of Cu^{2+} onto $GO_{1:1}$, $GO_{1:2}$ and $GO_{2:1}$ [conditions: 20 mL of 20 mg dm^{-3} Cu^{2+}, pH 5.0, agitation speed of 150 rpm, equilibration time 5 h, temperature 25 °C]

4. Conclusion

In this paper, GO was effectively prepared by making use of a modified Hummer's method. In the synthesis, mass ratios of 1:1, 1:2 and 2:1 of graphite powder and $NaNO_3$ were used. This was done in order to determine if it would alter the number of oxygenic functional groups on GO. The elemental composition of the $GO_{2:1}$ material, synthesized with a 2:1 mass ratio of graphite powder to $NaNO_3$, showed the greatest oxygen content. As indicated by SAED analysis, the $GO_{2:1}$ sample was also more crystalline than the other two products. It also exhibited the largest surface area. However, the Boehm titration showed that of the three samples, $GO_{2:1}$ did not contain the greatest number of acidic O-containing functional groups. Oxygen-containing moieties improve the

hydrophilicity of GO so that it can form stable suspensions in aqueous media. The adsorption study revealed that the uptake of Cu^{2+} by $GO_{2:1}$ was greater than for the other two GO samples. Thus, the synthesis of graphene oxide with a smaller quantity of $NaNO_3$ offered a material with improved crystallinity, a larger surface area and a greater oxygen content, that showed enhanced adsorption properties. Therefore, this material was chosen for further use in the study of the uptake of both metal ions and dyes in aqueous solution.

Conflict of Interest

The authors declare no conflict of interest.

Acknowledgments

References

[1] W.S Hummers Jr, R.E Offeman, Preparation of graphitic oxide, J. Am. Chem. Soc., **80**, 1339-1339, 1958. https//:doi.org/10.1021/ja01539a017

[2] K. Novoselov, A.K. Geim, S. Morozov, D. Jiang, M. Katsnelson, I. Grigorieva, S. Dubonos, A. Firsov, Two-dimensional gas of massless Dirac fermions in graphene, Nat., **438**, 197-200, 2005. https//:doi.org/10.1038/nature04233

[3] V. Strauss, K. Marsh, M. Kowal, M. El-Kady, R. Kaner, A simple route to porous graphene from carbon nanodots for supercapacitor applications, Adv. Mater., **30**, 1-10, 2018. https:doi.org/ 10.1002/adma.201704449

[4] P. Cheng, Z. Yang, H. Wang, W. Cheng, M. Chen, W. Shangguan, G. Ding, TiO$_2$–graphene nanocomposites for photocatalytic hydrogen production from splitting water, Int. J. of Hydrogen Energy, **37**, 2224-2230, 2012. https//:doi.org/10.1111/j.1750-3841.2012.02868.x

[5] A. Nag, A. Mitra, S. Mukhopadhyay, Graphene and its sensor-based applications: A review, Sens. and Actuators A: Physical, **270**, 177-194, 2018. https//:doi.org/10.1016/j.sna.2017.12.028

[6] Z. Li, F. Chen, L. Yuan, Y. Liu, Y. Zhao, Z. Chai, W. Shi, Uranium(VI) adsorption on graphene oxide nanosheets from aqueous solutions, Chem. Eng. J., **210**, 539-546, 2012. https//:doi.org/10.1016/j.cej.2012.09.030

[7] P. Bhawal, S. Ganguly, T. Chaki, N. Das, Synthesis and characterization of graphene oxide filled ethylene methyl acrylate hybrid nanocomposites, RSC Adv., **6**, 781-790, 2016. https//:doi.org/10.1039/C5RA24914G

[8] C. Soldano, A. Mahmood, E. Dujardin, Production, properties and potential of graphene, Carbon, **48**, 2127-2150, 2010. https//:doi.org/10.1016/j.carbon.2010.01.058

[9] V. Chandra, J. Park, Y. Chun, J.W. Lee, I.-C. Hwang, K.S. Kim, Water-dispersible magnetite-reduced graphene oxide composites for arsenic removal, ACS Nano, **4**, 3979-3986, 2010. https://doi.org/10.1021/nn1008897

[10] G. Shao, Y. Lu, F. Wu, C. Yang, F. Zheng, Q. Wu, Graphene oxide: the mechanisms of oxidation and exfoliation, J. of Mater. Sci., **47**, 4400-4409, 2012. https://10.1007/s10853-012-6294-5

[11] R. Ruoff, Graphene: Calling all chemists, Nat. Nanotechnol., **3**, 10-11, 2008. https//:doi.org/10.1038/nnano.2007.432

[12] H. Jiang, Chemical preparation of graphene-based nanomaterials and their applications in chemical and biological sensors, Small, **7**, 2413-2427, 2011. https://doi.org/10.1002/smll.201002352

[13] T.N. Ly, S. Park, Highly sensitive gas sensor using hierarchically self-assembled thin films of graphene oxide and gold nanoparticles, J. of Ind. Eng. Chem., **67**, 417-428, 2018. https//:doi.org/10.1016/j.jiec.2018.07.016

[14] E.T. Mombeshora, P.G. Ndungu, V.O. Nyamori, Effect of graphite/sodium nitrate ratio and reaction time on the physicochemical properties of graphene oxide, New Carbon Mater., **32**, 174-187, 2017. https://doi.org/10.1016/S1872-5805(17)60114-8

[15] M. Ahmed, A. Giwa, S. Hasan, Challenges and opportunities of graphene-based materials in current desalination and water purification technologies, Nanoscale Materials in Water Purification 735-758, 2019. https://doi.org/10.1016/B978-0-12-813926-4.00033-1

[16] R. Sitko, E. Turek, B. Zawisza, E. Malicka, E. Talik, J. Heimann, A. Gagor, B. Feist, R. Wrzalik, Adsorption of divalent metal ions from aqueous solutions

using graphene oxide, Dalton Trans., **42**, 5682-5689, 2013. https//:doi.org/10.1039/c3dt33097d

[17] M.A. Atieh, O.Y. Bakather, B.S. Tawabini, A.A. Bukhari, M. Khaled, M. Alharthi, M. Fettouhi, F.A. Abuilaiwi, Removal of chromium(III) from water by using modified and nonmodified carbon nanotubes, J. Nanomater., **2010**, 232378, 2010. https://doi.org/10.1155/2010/232378

[18] M. Machida, T. Mochimaru, H. Tatsumoto, Lead(II) adsorption onto the graphene layer of carbonaceous materials in aqueous solution, Carbon, **44**, 2681-2688, 2006. https://doi.org/10.1016/j.carbon.2006.04.003

[19] A. Lerf, A. Buchsteiner, J. Pieper, S. Schöttl, I. Dekany, T. Szabo, H. Boehm, Hydration behavior and dynamics of water molecules in graphite oxide, J. Phys Chem. Solids, **67**, 1106-1110, 2006. https://doi.org/10.1016/j.jpcs.2006.01.031

[20] Y. Gao, Y. Li, L. Zhang, H. Huang, J. Hu, S.M. Shah, X. Su, Adsorption and removal of tetracycline antibiotics from aqueous solution by graphene oxide, J. of Colloid Interface Sci., **368**, 540-546, 2012. https://doi.org/10.1016/j.jcis.2011.11.015

[21] A.C. Sophia, E.C. Lima, N. Allaudeen, S. Rajan, Application of graphene-based materials for adsorption of pharmaceutical traces from water and wastewater- a review, Desalin. Water Treat., **57**, 27573-27586, 2016. https://doi.org/10.1080/19443994.2016.1172989

[22] H. Yan, X. Tao, Z. Yang, K. Li, H. Yang, A. Li, R. Cheng, Effects of the oxidation degree of graphene oxide on the adsorption of methylene blue, J. Hazard. Mater., **268**, 191-198, 2014. https://doi.org/10.1016/j.jhazmat.2014.01.015

[23] B. Kakavandi, R.R. Kalantary, M. Farzadkia, A.H. Mahvi, A. Esrafili, A. Azari, A.R. Yari, A.B. Javid, Enhanced chromium(VI) removal using activated carbon modified by zero valent iron and silver bimetallic nanoparticles, J. Enviro. Health Sci. and Eng., **12**, 1-15, 2014. https://doi.org/10.1186/s40201-014-0115-5

[24] P. Sharma, N. Hussain, D.J. Borah, M.R. Das, Kinetics and adsorption behavior of the methyl blue at the graphene oxide/reduced graphene oxide nanosheet–water interface: a comparative study, J. Chem. Eng. Data, **58**, 3477-3488, 2013. https://doi.org/10.1021/je400743r

[25] A.D. Schiller, A.C. Goncalves, A.D. Braccini, D. Schwantes, M.A. Campagnolo, E. Conradi, J. Zimmermann, Potential of agricultural and agroindustrial wastes as adsorbent materials of toxic heavy metals: a review, Desalination Water Treat., **187**, 203-218, 2020. https//:doi.org/10.5004/dwt.2020.25094

[26] T. Gosset, J.-L. Trancart, D.R. Thévenot, Batch metal removal by peat. Kinetics and thermodynamics, Water Res., **20**, 21-26, 1986. https://doi.org/10.1016/0043-1354(86)90209-5

[27] M.V. Mier, R.L. Callejas, R. Gehr, B.E.J. Cisneros, P.J. Alvarez, Heavy metal removal with Mexican clinoptilolite: multi-component ionic exchange, Water Res., **35**, 373-378, 2001. https://doi.org/10.1016/S0043-1354(00)00270-0

[28] C.B. Godiya, S.M. Sayed, Y. Xiao, X. Lu, Highly porous egg white/polyethyleneimine hydrogel for rapid removal of heavy metal ions and catalysis in wastewater, React. Funct. Polym., **149**, 104509, 2020, https://doi.org/10.1016/j.reactfunctpolym.2020.104509

[29] O.O. Ojo, S. B. Jonnalagadda and B. S. Martincigh, Synthesis of graphene oxide under differing conditions and its characterization, 2018 IEEE 8th International Conference on Nanomaterials: Application and Properties (NAP-2018), Zatoka, Ukraine, pp. 15-18

[30] S. Wang, P.J. Chia, L.L. Chua, L.H. Zhao, R.Q. Png, S. Sivaramakrishnan, M. Zhou, R.G.S. Goh, R.H. Friend, A.T.S. Wee, Band-like transport in surface-functionalized highly solution-processable graphene nanosheets, Adv. Mater., **20**, 3440-3446, 2008. https://doi.org/10.1002/adma.200800279

[31] G. Titelman, V. Gelman, S. Bron, R. Khalfin, Y. Cohen, H. Bianco-Peled, Characteristics and microstructure of aqueous colloidal dispersions of graphite oxide, Carbon, **43**, 641-649, 2005. https//:doi.org10.1016/j.carbon.2004.10.035

[32] M. Wojtoniszak, X. Chen, R.J. Kalenczuk, A. Wajda, J. Łapczuk, M. Kurzewski, M. Drozdzik, P.K. Chu, E. Borowiak-Palen, Synthesis, dispersion, and cytocompatibility of graphene oxide and reduced graphene oxide, Colloids and Surf., B: Biointerfaces, **89**, 79-85, 2012. https://doi.org/10.1016/j.colsurfb.2011.08.026

[33] J. Chen, Y. Li, L. Huang, C. Li, G. Shi, High-yield preparation of graphene oxide from small graphite flakes via an improved Hummers method with a simple purification process, Carbon, **81**, 826-834, 2015. https//:doi.org/10.1016/j.carbon.2014.10.033

[34] C. Wang, Z. Liu, S. Wang, Y. Zhang, Preparation and properties of octadecylamine modified graphene oxide/styrene-butadiene rubber composites through an improved melt compounding method, J. Appl. Polym. Sci., **133**, 1-9, 2016. https://doi.org/10.1002/app.42907

[35] W. Gao, Graphene oxide: reduction recipes, spectroscopy, and applications, Springer, 2015. https://doi.org/10.1007/978-3-319-15500-5

[36] Z. Li, W. Zhang, Y. Luo, J. Yang, J.G. Hou, How graphene is cut upon oxidation?, J. Am. Chem. Soc., **131**, 6320-6321, 2009. https://doi.org/10.1021/ja8094729

[37] J.-M. Zuo, M. Gao, J. Tao, B.Q. Li, R. Twesten, I. Petrov, Coherent nano-area electron diffraction, Microsc. Res. Tech., **64**, 347-355, 2004. https//:doi.org/10.1002/jemt.20096

[38] L. Malard, M. Pimenta, G. Dresselhaus, M. Dresselhaus, Raman spectroscopy in graphene, Phys. Rep., **473**, 51-87, 2009. doi.org/10.1016/j.physrep.2009.02.003

[39] X. Du, P. Guo, H. Song, X. Chen, Graphene nanosheets as electrode material for electric double-layer capacitors, Electrochim. Acta, **55**, 4812-4819, 2010. https://doi.org/10.1016/j.electacta.2010.03.047

[40] S.A. El-Khodary, G.M. El-Enany, M. El-Okr, M. Ibrahim, Preparation and characterization of microwave reduced graphite oxide for high-performance supercapacitors, Electrochim. Acta, **150**, 269-278, 2014. https://doi.org/10.1016/j.electacta.2014.10.134

[41] D.R. Dreyer, S. Park, C.W. Bielawski, R.S. Ruoff, The chemistry of graphene oxide, Chem. Soc. Rev., **39**, 228-240, 2010. https//:doi.org/ 10.1002/ange.201002160

[42] V.B. Mohan, R. Brown, K. Jayaraman, D. Bhattacharyya, Characterisation of reduced graphene oxide: Effects of reduction variables on electrical conductivity, Mater. Sci. Eng. B, **193**, 49-60, 2015. https://doi.org/10.1016/j.mseb.2014.11.002

[43] H.A. Becerril, J. Mao, Z. Liu, R.M. Stoltenberg, Z. Bao, Y. Chen, Evaluation of solution-processed reduced graphene oxide films as transparent conductors, ACS Nano, **2**, 463-470, 2008. https://doi.org/10.1021/nn700375n

[44] C. Zhu, S. Guo, Y. Fang, S. Dong, Reducing sugar: new functional molecules for the green synthesis of graphene nanosheets, ACS Nano, **4**, 2429-2437, 2010. https//:doi.org/10.1002/adma.201001068

[45] P. Ball, R. Evans, Temperature dependence of gas adsorption on a mesoporous solid: capillary criticality and hysteresis, Langmuir, **5**, 714-723, 1989. https//:doi.org/10.1021/jp111263p

[46] K. A. Cychosz, M. Thommes, Progress in the physisorption characterization of nanoporous gas storage materials, Eng., **4**, 559–566, 2018. https://doi.org/10.1016/j.eng.2018.06.001

[47] H.K. Koolivand, A. Sharif, M.R. Kashani, M. Karimi, M.K. Salooki, M.A. Semsarzadeh, Functionalized graphene oxide/polyimide nanocomposites as highly CO_2-selective membranes, J. of Polym. Res., **21**, 599, 2014. https://doi.org/ 10.1007/s10965-014-0599-9

[48] Z. Pei, L. Li, L. Sun, S. Zhang, X. Shan, S. Yang, B. Wen, Adsorption characteristics of 1,2,4-trichlorobenzene, 2,4,6-trichlorophenol, 2-naphthol and naphthalene on grapheme and graphene oxide, Carbon, **51**, 156 –163, 2013. https://doi.org/10.1016/j.carbon.2012.08.024

[49] J. Shen, M. Shi, B. Yan, H. Ma, N. Li, M. Ye, Ionic liquid-assisted one-step hydrothermal synthesis of TiO_2-reduced graphene oxide composites, Nano Res., **4**, 795-800, 2011. doi: 10.1007/s12274-011-0136-7

[50] K. Zhou, Y. Zhu, X. Yang, X. Jiang, C. Li, Preparation of graphene–TiO_2 composites with enhanced photocatalytic activity, New J. Chem., **35**, 353-359, 2011. https//:doi.org/10.1039/CONj00623H

ASTES

The Role of RFID in Green IoT: A Survey on Technologies, Challenges and A Way Forward

Zainatul Yushaniza Mohamed Yusoff [1,2], Mohamad Khairi Ishak[*,1], Kamal Ali Alezabi[3]

[1]*School of Electrical and Electronic Engineering, Universiti Sains Malaysia, Nibong Tebal, Pulau Pinang, 14300, Malaysia*

[3]*Majlis Amanah Rakyat, Kuala Lumpur, 56000, Malaysia*

[2]*Institute of Computer Science and Digital Innovation (ICSDI), UCSI University, Cheras, Kuala Lumpur, 56000, Malaysia*

A R T I C L E   I N F O

A B S T R A C T

The Internet of Things (IoT) is a technology that enables communication between everyday life using different sensor actuators that work together to identify, capture, and distribute critical data from the planet. Massive machines and devices are therefore linked and communicate with them. The use of resources in this area presents new challenges for this technology. The goal was to find a green IoT that focuses on energy efficiency and IoT efficiency. Green IoT is an energy-efficient way to reduce or eliminate the greenhouse effect of current applications. Radio Frequency Identification (RFID) is one of the Green IoT and Master IoT components that identifies a person or entity in a high-frequency electromagnetic spectrum when combining electromagnetic or electrostatic couplings. If the predictions are also correct, energy use issues arise as active battery-powered RFID detection needs to be addressed by incorporating new solutions for Green IoT technology. Past studies and assessments have attempted to evaluate RFID technology and its functions. Unfortunately, however, they concentrated on a single RFID view of technique and technology. This paper examines holistically and systematically the impact of RFID applications on green IoT, focusing on three categories: the challenges, environmental consequences, and the benefits of green IoT RFID applications. The impacts, performance and safety of RFID IoT applications have been carefully described. The benefits and examples of RFID applications, including their key advantages and disadvantages, are also discussed. Overall, this paper highlights the potential efforts of RFID to address existing Green IoT issues.

1   Introduction

Green power comes from natural sources such as sunlight, wind, rain, tides, plants, heat and algae as shown in Figure 1. These energy resources are renewable and naturally refilled to offer the most significant environmental benefit [1]. Conventional energy can be a valuable source of air pollution and emissions of greenhouse gases. The use of renewable energy helps to perform the following [2]:

1. Reduce the carbon footprint with purchased electricity.

2. Future price increases and volatility of electricity (individual products).

The purpose of green power is to find energy conservation measure in order to reduce energy consumption and increase the energy efficiency. Energy conservation means making use of less energy to accomplish work, namely reducing waste energy. Energy efficiency

has many advantages: reducing greenhouse gas emissions, declining energy demand and reducing our household and economic costs. Although the use of renewable energy technologies also improves this, increased energy usage is the simplest and often most efficient way to reduce fossil fuel use. There are enormous opportunities to enhance productivity in every sector of the economy, whether it be infrastructure, transportation, manufacturing or energy generation [3]. In reality, without Internet of Things (IoT), it isn't easy to imagine the future of renewable energies. Today sensor-based technology and data science enable wind farms and solar fields to be productive and automated. Green IoT technology programs should be taken into account because of the growing perception of environmental issues worldwide. The Greening IoT definition refers to innovations that make the IoT ecosystem healthier and environmentally pleasant through the use of facilities and storage that enables subscribers to capture, store, access, and handle different information.

[*]Corresponding Author: Mohamad Khairi Ishak, Universiti Sains Malaysia, Nibong Tebal 14300, Malaysia Email:khairiishak@usm.my
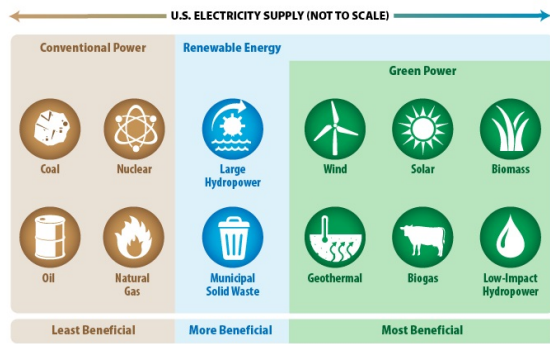
Figure 1: Green Power Generation [1]

The technology that enables green IoTs is called information and communication technologies (ICTs) [4]. ICTs will cause climate change in the world because the rising application of ICT has used much more energy [5, 6]. The emphasis on sustainability for ICTs has been on data center optimization through infrastructure sharing techniques that improve energy efficiency, minimize CO_2 emissions and e-waste disposal [7]. Greening ICT enables green IoT technology which includes green wireless sensor networks (GWSNs), green machine-to-machine communication (GM2M), green RFID (GRFID), green data center (GDC), green cloud computing (GCC), green Internet (G-Internet), and green communication network (GCN) as shown in Figure 2. Greening ICT offers green IoT technologies. Green ICT innovations play a crucial role in green IoT and offer many benefits for society, including the reduction in energy used to develop, produce, and distribute ICT devices and equipment [8].
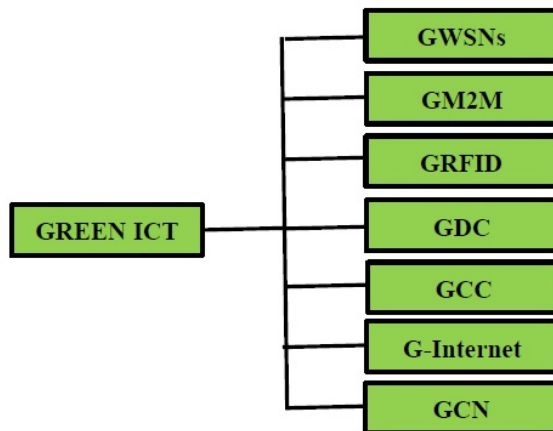
Figure 2: Green ICT technologies [8]

Green IoT consists of aspects of nature and exploitation. Green IoT focuses on reducing the use of IoT resources and CO_2 emissions, which are essential for creating an innovative and prosperous world of intelligent everything. As Figure 3 shows, the green IoT design elements apply to computer creation, energy conservation, communication protocols, and architectures for networking [9]. It is possible to use the IoT portion to remove CO_2 emissions, minimize pollution, and increase energy efficiency [10]. In networking, Green IoT aims to decide where the relay is located and how many nodes

meet budget constraints and energy saving [11]–[12]. For achieving green IoT, there are three principles, namely, design technologies, leverage technologies, and enabling technologies. Build technologies that apply to computers, communication protocols, network interfaces, and interconnections for energy efficiency. Leverage technology relates to reducing emissions of carbon and rising energy efficiency [13]. By reducing electricity, toxic emissions, use of resources, and pollution, green IoT has become more effective due to green ICT technologies. As a result, green IoT ensures the protection of natural resources, minimizes the effect of technology on the environment and human health, and dramatically reduces costs. In reality, therefore, green IoT focuses on green development, green usage, green design, and green disposal [14].

Figure 3: Green IoTs Environments [9]

RFID is a complementary solution to green IoT technology to save energy. RFID uses radio frequency to transmit, identify, classify and track data between readers and moving objects. It is fast and does not require a physical view or connection between the reader/scanner and the object to be inspected. The operating cost factor is deficient low and can use in many applications such as healthcare, manufacturing, inventory management, shipping, retail sales and home use [15]. RFID technology internal divided into two parts, namely RF communication; reader/tag protocols and middleware architecture, where RFID tag can be attached to almost anything such as items, cases or product palettes, high-value goods, vehicles, assets, livestock or personnel. RFID tags divided into two sits; which is a passive tag and an active tag. RFID middleware is RFID's software that exists between readers and enterprise/business applications. Middleware has several functions and plays an essential role in the operation and management of RFID systems. Middleware handles RFID readers and printers and communicates between these devices and business applications, as well as manage, filter, aggregate, and understand data derived from RFID tags [15]. RFID application used in manufacturing and processing for supervision, production of warehouse processing and fulfillment orders. In supply chain management, it should face in Inventory Tracking and Logistics management system. It also used in local controls for customer inventory and views; and automated checks with reverse logistics which benefit the environment. Whereas securities applied on access control, counterfeiting and theft control/prevention [16]. However, there is little discussion in the existing literature on RFID management in the environment. Is seen that ICT harms the environment [17], and RFID, as part of ICT, has gained a reputation

[18] as one of the leading computing technologies, using sufficient energy to impact the environment negatively [19].

The contributions of this paper are summarized as follows:

1. A detailed review of current and recent RFID literature on IoT, notably the Green IoT, in order to show that RFID can be part of the green IoT, not only for the benefit of the economy but also for the benefit of the organization, but also to improve responsible IT practice.

2. As this paper reviews the application of the Green IoT study proposed by RFID in recent years, it also outlines some of the early research related to this field.

Section 2 provides a summary of some IoT device RFID technologies. Section 3 Discussion about the security of RFID and addresses RFID implementation issues and environmental consequences in Section 4. In section 5, the benefit of greening IT. The future work of RFID in Green IoT is discussed in Section 6, and Section 7 outlines the study's findings.

2 Studying RFID Technology in IoT Application

The Internet of Things (IoT) intended to describe a range of technologies and research disciplines that enable global connectivity through the world's physical objects [20]. Activation technologies such as RFID, sensor networks, biometrics, and nanotechnologies are now widely used [21]. The IoT implemented in real implementations for different applications such as smart grid, e-health, and intelligent transport. RFID is a stand-alone technology used to enable various systems to perform functions based on object recognition, data recording, and different control objects [22]. The iconic RFID system consists of two parts: a tag (transmitter/receiver) and a reader (transmitter/receiver). The tag contains a chip attached to an object for detection and serves as an object identifier. Instead, RFID readers regularly exchange information with RFID tags using radio waves [23]. The main advantages of RFID technology are automatic object recognition, data acquisition and cost reduction in various activities [24]. The distributed RFID readers around the world are connecting to the Internet according to an appropriate routing protocol. Readers can then exchange information to identify, track, and monitor objects based on the tags they carry. Instead, IoT refers to virtual presentations in the IoT architecture, where identifiable objects are called "things". RFID is a prerequisite for the proper operation of an IoT system [25]. IoT is a global infrastructure that connects and ignores the distance between virtual and physical objects based on data usage and routing capabilities. The IoT architecture consists of three layers, namely the service or application layer, the network layer, and the perceptual layer, where the level of perception includes real-time information and the Internet of Things [26]. This layer uses sensors, wireless sensor networks, tags, RFID systems, cameras, GPS, smart terminals, EDIs, and creators to collect and display information about objects in the physical world. RFID tags, readers and application systems are composed of RFID systems. RFID systems are fast and effective for the electronic identification, control, and identification of different artifacts.

RFID uses wireless transmission to send a signal for an RFID tag that responded to a data collection reader linked to the host computer's data for analysis by a single ID code [27] RFID application functionality divided into three categories: control, tracking, and supervision. Monitoring concerns the current device status. For medical circumstances to be detected, irregular behavior and alarm must be an identifier. Tracking sees moving objects and provides a modeling sequence for every location of the data. Control refers to the evaluation and monitoring carried out without the awareness of the object [28]. RFID is used to prevent misplacement or to locate items quickly. One approach is to track the movement of objects in the database. For example, an RFID reader may attach to a door in a building between rooms. Thus, the location of the object can be determined by analyzing RFID reader recordings. It mainly used in supply chain management systems, item monitoring processes, and industrial process control. 3 Great advantages of identification of RFID supply chain properties as seen in the following Table 1 [29]. The use of RFID is also developing in manufacturing, agricultural management, health care management and tele-medicine, maritime operations, management of payment transactions, and others.

Table 1: 3 Great advantages of identification of RFID supply chain [29]

Item	Advantages
Increase the visibility of assets	RFID asset monitoring to increase inventory usability and visibility. This ensures that RFID tags can be read from all over the facility so that workers can easily display each item's location and value. Supplier chains can overcome issues created by bad management, misplaced components, tracking and manual process failures by increased transparency. Naturally, it can easily move things and make decisions about fly changes.
Improve employee productivity	RFID technology workers do not have to search for any items. No wasting time on tedious processes like scanning individual barcodes, finding the wrong tools and devices, and calculating inventory. This technology will increase the speed of sales of jobs and projects, lower labor and transportation costs, and improve the plant's overall productivity. Manufacturing and shipping products in unmanaged facilities are challenging and slow. By eliminating manual steps, human error and monitoring can avoid. Corrections can take a long time to improve inventory and asset visibility.
Reducing risk, theft and loss	RFID asset tracking to quickly and easily access inventory information and locations to track during items storing, distributing, or replenishing. With this type of visibility, there is little room for mistakes or mischief. Track each asset's movement in the facility to consider all items and pallets, minimizing costly risks and reducing misalignment's and losses. Struggle against counterfeiting and theft; Promote callbacks. It is imperative to avoid such errors as much as possible, since fixing these errors can lead to litigation, high fines, or loss of customers, as well as time and money. Full transparency and real-time information on inventory and assets increase profitability for significant organizational and productivity improvements.

2.1   Review Papers of RFID applications

This section discusses recent studies related to RFID applications in the IoT world.

1. In [30], building the Green Campus in IoT Architecture, RFID technology is used to detect students entering the lab. The system will read, and store data related to students or any-one entering the lab. Middleware acts as a connector between temperature sensors, air conditioners, RFID, and computers [31]. Each of these tools has its information. This information is used to determine the number of labs that should open to students, when the air conditioner needs to turn on, and finally, to monitor computer usage correctly [32]. The effectiveness of this system is when:

   - Laboratory management runs smoothly according to consumer demand.

   - The computer management mechanism can adequately monitor to save energy on laboratory equipment.

   - Energy-saving can do excellently when the air conditioner was only functioning when the laboratory temperature reached.

2. In [33], the System of global positioning and geographical information, RFID, general packet radio service and webcam combined into one device. The RFID reader in the camion reads both the customer and the bin details [34, 35]. This system improves waste management and decreases waste emissions resulting in ozone pollution [36].

3. Researchers in [37] introduced a new authentication strategy for home health applications using low-cost RFID tags. For systems where RFID tags need not be measured, only data stored for their storage sent. A tablet container has stored with the RFID tag inside the patient. The RFID reader receives the details when the patient recovers the [38] bag. In the RFID tag, the information is encrypted. Only valid ID tags and ID readers can decrypt the data decryption key – valid RFID tag ID and RFID reader, which generate the use key. Authentication between RFID tags and readers of RFID will combat several attacks, including tag-spoofing, reading readers. One of the benefits is that it reduces the likelihood of human error in data collection and that doctors can also provide reliable information on patients [39].

4. The environment, including the distribution system, has changed considerably in the past few years in [40]. With consumer demand changing, distribution structures are becoming increasingly centralized and globalized, and public changes such as deregulation, innovation and IT dissemination are moving forward. Simultaneously, there is a substantial demand for reducing CO_2 in logistics processes to solve global environmental problems. As a result, RFID (Supply Chain Management) technology was designed to use CO_2 reduction levels, deemed an impact identification object, to be identified and thought that improvement would be a criterion. To deploy an SCM with high efficiency, the information would be necessary, namely in real-time, which is a turning point for success

or loss. In this respect, the RFID tag can be a useful tool for automatically defining status by merely placing at the point of departure or arrival items, collapse containers and pallet vehicles using RFID technology. This process would help to understand conditions in real-time, such as the transportation of stocks and shipments [41]. They, therefore, expect RFID to be a practical tool rather than an existing barcode system and argue that the introduction of RFID is a new way to view the information in the SCM. The CO_2 reduction ratio is estimated by researchers as a function of transport expenses, with decreased labor costs, thus, reducing transport expenses. The amount of energy used, such as a roadway, is commensurate with transport weight (t) and distance (km). It means that transport costs and energy consumption are positively correlated. Since CO_2 is proportional to the amount of energy consumed, emissions of CO_2 may also decrease if power is reduced. The decreasing costs of transport can thus reduce CO_2 emissions, with a definite link between energy reduction and CO_2 emissions [42]. Consequently, the transport CO_2 emissions reduction rate was 3.2% as an effect of RFID introduction.

5. In [43], while metal fractures in the automotive industry have been a topic of productive study, plastic recycling in vehicles is poorly understood. It is now key to effective recycling of vehicles, due to legal requirements. Besides, the key problems faced are recognizing plastics and the technological standard of logistics activities, as well as scarce resources related to plastics. Therefore, authors in [44] introduce the RFID framework that automatically recognizes, register, distribute, and search for information during the product life-cycle. The research produces an efficient decision support solution (DSS) in a case study on automotive plastic recycling. DSS has applied during the life-cycle of the drug. It can be divided into three phases depending on the product life cycle management (PLM), initial life expectancy (BOL), life expectancy (MOL) and end-of-life (EOL) of the contemporary product [45]. BOL functions as product design, a manufacturer's preparation, and process management. MOL is used to assist with product repair, condition diagnosis, and prognosis. At the other hand, the classification of EOL has many meanings, including the duty to comply with economic benefits and legal requirements. The DSS method is as follows [46, 47]:

   - Throughout the BOL and MOL phases of the product life cycle, the flow of knowledge completely facilitated by knowledgeable systems such as CAD / CAM, Product Data Management (PDM) and other Knowledge Management systems used successfully in the Automotive Plastic Recycling industry.

   - Often the knowledge that comes to the consumer about the product is incomplete during the transfer process from MOL to EOL.

   - Data sources from MOL tell BOL that drug producers disrupted after product sales. The findings are typically based on BOL data, or limited but imperfect practical experience, based on full knowledge of past transactions.

Then, experiments used to produce missing information, but the cost of EOL operations increased significantly.

- RFID technology is then used to fill the knowledge gap and make product information reliable, accessible, timely, complete and available whenever needed during its life cycle. Different information can be collected and transmitted using RFID technology via MOL and EOL phases.

- Using the unique identifier stored in the RFID tag, EOL will obtain the information required to evaluate the recovery path from the product life-cycle information service. At the end of the support phase, the data collection unit is integrated to collect information from the stores using RFID technology.

6. Researchers in [48] provide the RecycleBank with the resources it requires to organize recycling activities for households, using RFID systems to allow municipalities to calculate the number of recycled materials per household. They have created a community-friendly approach with advanced, creative technology to tackle the rising cost of waste collection. Weight of recycled plastic turned into incentives for RecycleBank. Hundreds of local and national participants can award it. In collaboration with Texas Instruments, RecycleBank offers an RFID that adds low-frequency RFID tags with exact recycling containers and includes integrated RFID readers fitted to a counterbalancing system [49]. RFID tags developed and implemented for RecycleBank, stores Serial Number (referring to the name and address of the container owner), reads and data transmitted to the internal computer of the vehicle. The data collected are then transferred to the data collection and processing system of RecycleBank. Personal data (name, address, etc.) not scheduled for the tag. Only the recorded serial numbers are kept in the secure database of RecycleBank. The proprietary RFID tag stores provide unique advantages for waste and recycling applications with low-frequency technology as a weather-resistant, all-weather, secure solution that works in snowy, wet, or harsh environments throughout the world. Labels must be physically cute while preserving their technical characteristics over the life of the [50] container. The results are as follows:

- Within one week, the recycling rate in New Jersey, Cherry Hill City, increased by 135%. The average household recycled 12 pounds of recyclables before RecycleBank. Homes now earn an average of over 26 pounds each week.

- The city of Wilmington, Delaware, has been recycling in just six months from 0% to 37% using the RecycleBank programme.

- Elk City, New Jersey, averages 16 tons per week before RecycleBank of recyclable material. The municipality generates an average of 42 tons of recyclable material per week after the usage of RecycleBank, a rise of 136%.

7. The case study in [51] demonstrates a highly advanced waste electrical and electronic equipment reuse and recycling pro-

gram (WEEE). This center is named the Multi Life Cycle Center (MLC), using state-of-the-art advances in automation and IT to provide cost-effective and environmentally sustainable processes. WEEE is back to a valuable commodity [52]. IT and communicators, household appliances, electrical and mobile devices, toys, and recreational equipment are product categories subject to reuse. All other classes of items are stored and recycled. RFID technology is used for communication and organization, together with reverse logistics systems. This technology can be used as a monitoring device that transparentizes and prevents misuse of the WEEE stream. Furthermore, container level measurements are currently being tested, so that it can improve the collection route of the truck and prevent theft. A special reading station is located at the collection point to allow continuous monitoring to collect RFID information [53]. IoT is the link to the Internet of objects utilizing several information recognitions tools such as RFID, infrared sensors, global positioning systems, laser scanners and the identification of certain system information according to the accepted protocols. The computer is a large network. IoT can be used to define wisely, locate, map, control and manage to share information and communications [54]–[55]. Main IoT technologies, software, research and development technologies, external layers, network layers and device layers.Table 2 displays main perception layer technologies.

Table 2: Key technologies in the perceptive layer [53]

Key Technology	Performance Description	Application
RFID	Recognition and identification of objectives. Its purpose is to describe the object.	Application stage
Sensor	Sensitive organs, providing raw data.	The exploratory stage
Intelligent embedded technology	Intelligence is the target of IoT.	Experimental stage
Nanotechnology	Enables the interaction and connection of small objects and reduces system power consumption	Research stage

8. IoT requires finding, scanning, monitoring, and handling, and not just "connecting objects." As RFID is a "speaker" technology, RFID technology plays a vital role in critical technologies in the IoT layer of perception [56, 57]. RFID technology is, therefore, the first choice to establish a full system for IoT identification. EPC encoding, RFID EPC systems and EPC network systems are critical applications of RFID technology with RFID tags in the "IoT" EPC environment. In addition to handling individual objects, IoT encoding discovers objects at any time and enables coded requests, statistical tests, unique e-commerce categories and open information for objects. "One single-code entity." EPC encoding technology [58, 59] can best serve this need. The EPC RFID framework is a module for collecting codes automatically and shapes the EPC information network systems for local internet networks.

In the meantime, the global internet network is a platform for handling and flowing knowledge [60].

9. The goal of the analysis in [61] is to establish an overview of current RFID research from an IoT overview. The analysis includes passive UHF (860-960 MHz) devices (e.g. low battery) that can provide an effective sensor network to track human health and control the efficiency of the controlled environment [62, 63], with sufficient measurements and readings. Environmental sensors that calculate physical parameters such as temperature, humidity, and toxic substances may calculate the health of the environment and evaluate their human health relations [64]. Wearable and implantable labels offer more contextual knowledge about a person's in-room appearance, activity, contact with the individual, and innovative applications based around the body. Data on the health status of artificial organs can be produced [65]. When operating with special compounds or inter-linked with chips which include detection functions, passive RFID tags can detect changes in environmental chemical / physical parameters. Autonomous RFID tags are an important instrument for designing body-centric healthcare systems that are fully transparent to the consumer [66, 67] for touching and approaching the body. Most specifically, wearable passive UHF tags have long been technical tabus because of the significant power outages caused by human tissues. Previous body center network studies are mainly focused on active computers [68, 69]. Over the past five years, the development of commercially available low-power RFID (COTS) chips has changed gaming entirely, creating and testing of several prototypes of body-centered, sensitive, distance-readable tags compatible with remote-controlled monitoring [70, 71]. Since high electromagnetic losses characterize the human body, antenna power output is meager and the required reading distance for passive devices. The performance of the antenna power is deficient. This combination of wearable and ambient tags helps to track the situation of children, people with disabilities, and the elderly, identify human behaviors, and build passive RFID systems in a fully-passive manner [72, 73].

10. Researchers in [74], which explicitly addresses the safety criteria for RFID validation schemes, have submitted an authentication scheme based on elliptical curve cryptography (ECC) suitable for their protection and health care climate. The aircraft device Classify Friend or Foe (IFF) was the beginning of the RFID technology used during World War II. The benefits of RFID are that it is easy to use RFID tags, has read/write power, does not need long-distance RFID readers communication, and can simultaneously read multiple RFID tags [75]. RFID technology in the healthcare field is applied to the verification [76, 77], birth and patient recognition [78], medical treatment detection and confirmation [79], healthcare centers [80] and surgery sites [81]. A typical healthcare network with RFID technology [82], as shown in Figure 4. RFID authentication is one of the most critical measures to ensure secure communication inside the RFID system. However, there is a wide range of security features in the process of sending messages between RFID tags and RFID readers. Some researchers have established the safety criteria for secure RFID communication and reliable and effective authentication schemes when it is applied [83]. Mutual authentication between RFID tags, RFID readers, and servers are among the security requirements. Besides, before transmission, the confidentiality of sensitive information contained in the RFID tag must be encoded. The identity of the tag must also be protected for the protection of the owner [84]. The next requirement of protection is to validate the RFID authentication scheme during the life cycle of the RFID tag that gives alerts updating the confidential details that have shared during the implementation of the authentication scheme. It meant that the verification scheme would be invalid if the modified coordinate is lost. To ensure secure transfer [85], Transfer Protection requires an RFID authentication scheme. For certain RFID authentication systems, if the enemy successfully retrieves sensitive information from the RFID tag, it can detect the last position in the tag. It will severely breach the privacy of the user. As the RFID tag validation process is required, scalability, RFID authentication scheme must scale, an RFID device server must find the corresponding records in their database [86].
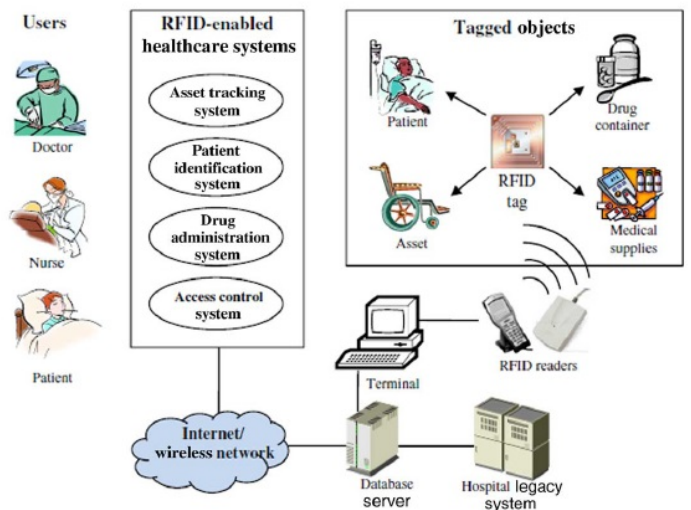
Figure 4: Typical RFID-based healthcare system [82]

As the number of RFID tags increases, the device does not scale if the workload of the search algorithm is significantly increased. RFID authentication processes must defend against multiple attacks, duplicate attacks, tag defense attacks, server spoofing attacks, mid-level attacks, cloning points, and others. Resistance to attacks to ensure the security of RFID communication [87]. The researchers found that the ability and memory of tag calculations were minimal when comparing the performance and safety aspects of the ECC-based RFID authentication schemes to determine whether ECC-based RFID validation schemes are adequate for practical applications. Cost measurements, communication costs, and storage requirements for practical applications are, therefore, important. The researchers investigated and found that most of the current ECC-based authentication scheme proposed

cannot comply with all safety requirements. To ensure secure contact, researchers will first build acceptable safety models for ECC-based RFID systems by using ECC-based techniques in RFID systems. They then developed an ECC-based RFID authentication system that protected security models securely.

11. IoT consists of an increasing number of interconnected smart devices that reduce hardware costs and architectural complexity, where communications occur at any time or anywhere. The reading of ultra-high frequency RFID tags is a cost-effective operation because of its technology and the reading system for these frequencies. The researcher proposes an architecture that reduces the cost of ultra-high frequency RFID reading equipment operating with cloud computing and micro-services in an infrastructure. Due to the scalability and management of large quantities of data that can be produced using ultra higher frequency RFID tags and the nature of the architecture linked to the theme of the research, the use of cloud and micro-computing was required [88]. To collect data and analyze the findings, the architecture proposed to address the research questions intended for the case study of this work has been created. After the RFID read tag has been detected by SparkFun Simultaneous RFID Reader — M6E Nanoboard, the Asset Micro-service must interact with the Read microservice to see if a similar physical object remains. This test takes place via the RFID tag area Electronic Product Code (EPC) present in the Asset microservice relational database and the Read microservice NoSQL database. Since the RFID tag EPC is a unique identifier, this is the only field needed to check whether an RFID tag is in the Asset Microservice database, identified by the SparkFun Simultaneous RFID Reader — M6E Nanoboard and registered in the Read microwave database. The monitoring microservice is used to view the collected data after telemetry information has been collected from the SparkFun Simultaneous RFID Reader — the M6E Nano Temperature, Position and Intermittent Connectivity Information through Microsoft Azure, the IoT Hub service. The result obtained from the case study as below:

- The board was able to read RFID tags with a distance of approximately 1 m and could read approximately 100 RFID tags per second only with its internal antenna. Having an external UHF antenna together with the board will improve the board's reading power. If the reading distance has a minimum value of the required project execution, the use of an external UHF antenna is needed.

- There were no charges for the software provided by Microsoft Azure. The non-cost is due to the use of all the free layer services. The cost will slowly increase as additional resource resources such as further computing, memory, or monitoring of other IoT boards increases.

3 Security of RFID

Some of the advantages of using an RFID device is that it performs tasks to classify, achieve efficiency and simplify its implementation automatically. Even these added benefits do not guarantee personal data protection. Therefore, when designing an RFID device, several criteria must be addressed to provide the highest degree of security. They are exchanged for the user or included in tags sent to the backend server. Data is private, accessible, and not modifiable (CIA). The safe maintenance and operation of the entire network A fully secure network continue to be a challenging challenge with numerous attacks and threats which that happen in various scenarios at the same time. RFID forgery: RFID can split into three groups by processing ability, which are simple tags, symmetrical key tags, and public-key tags. Basic tags are not encrypted and can be fooled easily. Supply chain and the operation of the travel industry are well established. To access or test product reliability [89], an attacker might write information to a primary black tag or change the data in a simple write tag. Many articles listed in the solution identified typical attacks which can occur on RFID systems during the investigation. Some of the most common attacks are shown below. In the literature, many steps and features have been suggested, including pseudorandom solutions, anonymous authentication schemes, symmetric and asymmetric cryptographic algorithms, and other hash-based systems. Several review studies related to the following security attacks are discussed in subsection 3.1.

1. Eavesdropping
   These attacks include eavesdropping on the network and recording examples of all interactions between the tag and the reader. The primary purpose of this attack is to collect data and use the information collected.

2. Denial of service
   Denial of service is the creation of a device that cannot use in an RFID system. An example of a use case for this attack is spam, which is sent to readers requesting a specific tag frequency to deactivate the reader.

3. Cloning
   The primary purpose of a clone attack is to spread RFID tags. Reverse engineering technology allows it to change and duplicate the label by extracting all the functions of the vehicle, precisely the secret key.

4. Tracking
   When detecting attacks, the tags voluntarily tied to a person, and their presence and movement are detected while the attacker's leader is inside the tag.

3.1 Security Review Studies

1. The IoT is the opportunity to have a means of distinguishing everyday objects and another way of interacting with each other. There is an extensive range of IoT technology domains like smart houses, smart cities, wearables, e-health, and others. Thus, tens and even hundreds of billions of devices are related. These machines would have intelligent capabilities for collecting, evaluating, and even making decisions without any human contact. Under these situations, protection is a supreme necessity, and authentication under particular

is of great importance given the harm that might result from a malicious, unauthenticated device in an IoT network [90]. This paper provides a general overview of the security issues and requirements in a layer-based approach in the IoT context. Instead, it offers an updated survey of the various IoT authentication schemes. It contrasts and analyzes the current authentication protocols through a multi-criteria framework, showing their advantages and disadvantages. The researchers found out the following:

- The authors proposed a lightweight RFID tag authentication protocol based on Physical Unclonable Functions (PUF) functions. There are three transactions in the protocol: tag identification, authentication, and update. The tag reader identifies the tag in the first transaction. The second transaction is a test where the reader and the tag verify each other's validity. The latest used key for the next check should be retained in the last transaction (Update).

- The authors have allowed the authentication and perceptibility of the IoT devices to secure the supply chain of connected devices through an RFID-based solution. The process of authentication consists of two steps: the verification of the connection between the tag and the IoT system and the tag perceptibility.

- The RFID reader is connected to the Internet in an IoT-RFID network to form an IoT end unit. On the other hand, it is linked via RFID communication protocols to the tagged objects. The tagged object is portable and transfers from a reader to another, so authentication is necessary to verify another identity. The device is vulnerable to security attacks, such as impersonation or clone attack, because of the absence of cryptographic features in RFID. The authors proposed an authentication protocol to be used with lightweight encryption algorithms in the case of IoT-RFID use.

- The authors suggested an offline authentication for PUF-based RFID-tags to prevent cloning attacks on the RFID tags. It combined security protocols for identification and digital signature. The tag generates a hidden key in authentication by questioning the PUF and gathering the answer. Such a reaction with the support data will create a certificate that will be stored inside the tag's ROM. First, the tag is authenticated by the verifier verifying the certificate validity. The authors proposed a PUF-based authentication scheme for the classic RFID tags to provide anonymous authentication for RFID systems. Then, they created an enhanced PUF noisy atmosphere scheme. The main downside of this scheme is not to re-feed the server with new Challenge-Response Pair (CRP) when the current pool is empty.

- The authors suggested a shared authentication scheme for IoT RFID-based applications in fifth generation of mobile networks (5G) by providing a cache to the user, storing the keys (used for authentication) for the tags recently visited, speeding up authentication, minimizing

computation costs and the storage security. On the other hand, the authors in [91] has been proposed authentication methods for heterogeneous networks which can be applied to RFID systems as well.

2. The detection of ultra-high frequency radio frequencies (UHF RFID) is becoming a central technology in the Internet of Things. It allows batteryless and wireless nodes to be deployed like sensors and actuators. Safety is a critical issue because of its possible transmission range is greater than 10 m, and the ability to hold sensitive information. For this reason, in 2014 the International Organization for Standardization released several UHF RFID crypto packages under the ISO-29167 standard. Nevertheless, no UHF RFID readers are currently available. In order to cope with the rapid growth of software-defined radios, "simple" and versatile readers are required. This paper illustrates a way to implement the decryption of ISO 29167-19 RAMON on a prototyping reader platform based on National Instruments PXIe chassis. PXIe programming is based on LABView. The first LABView implementation revealed that decryption only requires 51.3 s. It would mean being able to process just one tag per minute. Therefore, a prototyping platform intended to conduct practical experiments in the creation of new technology in UHF RFID systems is not suitable. Therefore, they prefer a different approach. The LabVIEW also acts as a platform and monitors the transceivers which are integrated. Nevertheless, a TCP/IP connection to a Java application is also provided. This Java code is decrypted. A TCP/IP link is used to return the decrypted plain message to LabVIEW and can be further processed [92]. The results are as follows:

- The average time spent with LabVIEW in tandem with the Java app is 2.2 ms, which improves the time-optimized approach to LabVIEW by 23,318 times. Within LabVIEW, the principal difficulty is that large numbers are difficult to deal with since they are widely used in encryption. The problem is not limited to the implementation of the RAMON method by outsourcing the calculation in a Java program. The approach can be used for any encryption method and for other processes in LabVIEW which handle large numbers. In this way, the RAMON encryption can be incorporated into the existing reader protocol and a fully working, easy to adapt reader can be obtained. Particularly for UHF RFID systems, it creates entirely new possibilities for rapid growth.

3. The medium of contact between the tag and the reader is vulnerable to multiple threats in conventional RFID systems, including denial of service, spoofing, and desynchronization. Therefore, the confidentiality and validity of the data transmitted can not be guaranteed. In this paper, the researcher proposes a new RFID authentication protocol based on a lightweight block cypher algorithm, SKINNY (short for LR-SAS), in order to solve these security problems. The 128-bit block size and key size n SKINNY encryption algorithm are being used to test the implementation in passive 96-bit

EPC-encoded radio frequency identification systems. The tag and the reader need to be mutually authenticated when implementing the LRSAS protocol, and the SKINNY algorithm encrypts the information used by the tag and the reader for mutual authentication. The key is already stored during the initialization process. This paper selects a SKINNY lightweight block cypher that has the advantages of low hardware power consumption and low computational complexity based on ensuring safe encryption. It can be used in Things terminal equipment's low-cost Internet [93]. The results are as follows:

- The protocol conceived in this paper uses one of the algorithms for SKINNY encryption and can accommodate 96-bit EPC encoding. In the encryption process, the calculation time for the round function used by the SKINNY encryption algorithm is shorter than the calculation for Hash, ECC, and Present encryption. However, the overhead measure also applies to low-cost RFID tags. Additionally, the tag's overhead storage is 3 L which significantly reduces the tag's storage capacity compared to other protocols, and reduces the complexity of the storage structure's logic gate design. Besides, the protocol has five information interactions in the mutual authentication of the tag and the user, and the total amount of data collected and transmitted is 6 L, which is relatively high, thereby ensuring the efficiency of the information interaction.

- Concerning the number of logic gates equivalent, multiple versions of SKINNY have varying numbers of logic gates equivalent. This protocol uses version SKINNY-128-128; the equivalent number of logical gates is 2391, less than 3K. It can also be used in low-cost tags. Furthermore, the number of equivalent logic gates for other protocols often allows specific security attacks to become vulnerable.

4 Challenges and environmental implication of RFID application

RFID is an exciting technology, but it does pose many technological problems and implications.

4.1 Challenges

The challenges of RFID technology applications in IoT were divided into seven: collision problems, privacy and security concerns, interference issues, miscellaneous challenges, technical issues, interoperability issues and energy efficiency.

4.1.1 Collision Problems

Electromagnetic interference can cause tags and readers to fail, leading to wrong choices. For tags and readers using the same radio frequency channel, multiple transmissions between the reader

and the tag can cause problems in a collision. To recognize multi-tag communication to promote the implementation of large-scale RFID systems, a secure and active collision avoidance protocol is required—a database tree protocol, a binary tree protocol, a split system protocol and others. Nevertheless, not all protocols produce the requisite efficiency as their identification efficiency is less than 50% commercial. For a new, better protocol will look for the best features of the detection protocol [94, 95].

4.1.2 Privacy and Security concerns

RFID authentication tags and security issues can affect people and organizations significantly. Tags are not properly secured and they considered an easy target to eavesdropping, DoS strike, analyze traffic and others. Besides, unauthorized readers can view multiple codes, which can breach privacy, without single access control. Predictable perceptions of tags can accompany secure tags. Traffic analysis attacks may jeopardize the privacy of the user. Appropriate confidentiality and protection protocols are needed for RFID systems given the associated costs. Extensive work is underway to define and incorporate cost-effective protection and privacy protections to improve RFID systems' reliability and usability. Several light-weight protocols have been proposed, but still have high costs and low protection and do not completely solve security issues. An excellent work section is available to develop ultra-light encryption protocols for low-cost RFID systems [96].

4.1.3 Interference Issues

Recently, a very high-frequency passive RFID (UHF) system has received much coverage. UHF RFID systems are widely agreed that many commercial applications, such as supply chain management will revolutionize UHF RFID systems. In the 860-960 MHz band more popular supply chain companies like Wal-Mart and Tesco will promote the use of UHF RFID systems in supply chains. However, with this distribution, dozens or hundreds of readers will work closely together and trigger to severe interference [97]. The UHF RFID interference has three types: tag interference, reader-to-multi-tag interference and reader-to-reader interference. The specifics of the intrusion issues are shown below.

1. Tag interference
   It happens when the reader simultaneously supplies power to several tags, and each signal reflects the reader. Owing to the dispersion of dispersed waves, readers cannot differentiate between individual IDs and marks. Anti-collision mechanisms, called binary trees and aloha, are therefore essential.

2. Reader-to-multi-tag interference
   It occurs when the mark is at the intersection of two or more reader requests, and the reader tries to interact with the tag simultaneously causing the tag to behave and interact unwantedly.

3. Reader-to-reader interference
   These are activated when a signal from one reader hits another and can also take place if the readers' surveys are not intersected. Interference between readers can cause serious

problems when using UHF RFID systems, as remote reader transmitted signals are so powerful that precise decoding of messages transmitted by neighbouring tags is prevented.

Active, semi-passive and passive RFID tags add comfort and prominence to RFID technology in our environment. Such tags are cheaper to produce and can be small enough to suit virtually any product. The type of RFID device works is shown below. Readers and tags focused on wireless two-way communication. The reader transmits a signal in passive RFID tags which induces a current in the tag to supply power to the transmitter of the tag. On the contrary, an active RFID device does not require an induced current to transmit its presence. Wireless communication may create a difference between RFID and other wireless technologies that are used in the workplace or data center since other RFID technologies often operate in the atmosphere and cause significant disruption [97]. Two classes ought to consider for new action. First, interruptions prevent data transmission properly and reduce the efficiency of one or more devices. Second, the danger of interpreting one signal from one device is that data from another is valid. The key cause of this disturbance is the environmental implications of use. This problem occurred in the past when the RFID tags placed on metal or liquid containers. The tag is inactive in both cases and refuses to respond to the reader. Recent advances allow these problems with proper antenna and tunnel design to tackled during the planning process. The UHF system may cause interference with the radiation of the power signal. Passive systems, on the other hand, are less vulnerable to intrusion than active systems with markers continually shifting. Crosstalk between RFID and WLAN or WPAN such as Bluetooth is another interference scenario when devices have a joint or an adjacent frequency band. Several cases of interference between wireless microphones and wireless endoscopy recorded in the medical field [98, 99].

1. Active and semi-passive RFID tags
   It uses an internal battery for the circuit. Active tags use an array to transmit radio waves to the reader, while semi-passive tags depend on the reader for transmitting power. Active and semi-passive tags reserved for expensive items capable of reading long distances, transmitting high frequencies from 850 to 950 MHz and reading more than 30.5 metres. If the label needs to read from a distance, an additional battery can increase the name range to more than 100 metres.
   It occurs when the mark is at the intersection of two or more reader requests, and the reader tries to interact with the tag simultaneously causing the tag to behave and interact unwantedly.

2. Passive RFID tags
   It entirely depends on the reader as strength. These tags are read and produced for use up to 20 feet (6 meters) and with disposable consumer goods.

4.1.4 Miscellaneous Challenges

Several other issues prevent RFID devices from spreading too. The key issue here is cost. The RFID tags are more expensive than the [100, 101] written stickers. A further issue is the complexity of

the RFID system. They are owing to their high-reliability readers, and labels are not on the market yet. Moreover, there is no guarantee of accurate recognition. The incorporation of RFID systems into the current network is another big problem needing a solution for using [102], large RFID systems. The designers need to know the approach to incorporate the new RFID system into the current network in a successful development phase.

4.1.5 Technological Issues

Implementation issues are most apparent and should be dealt with immediately. Some papers dealing with technological issues such as durability, precision, and contact with metals are still in the pilot process. For DHL, read speed accuracy is not 100%, because Tag interaction readers do not comply with defined specifications [97]. Even, it is not feasible to prohibit maximum use of short contact tags. The concept in citeb101 is to make sure that the people do not forget the process of activating RFID devices.

4.1.6 Interoperability Issues

If the RFID device is not working alone, but in conjunction with other electronic devices, the issue of information becomes apparent. For example, an RFID Smart Vareflyt system can operate independently, but will not work if it combined with an existing data system [100]. This question occurs when the real data is different from the reported data, does not change, or involves correction from other sources. On average, the accuracy rate in Nestle Italy's system is only 80-90% [99], due to the order output depending not only on the role of the RFID portion but also on the RFID system and the entire enterprise policy [99]. However, one of the hardest problems facing RFID technology is privacy and security. As corporations and public agencies continue to search for collaborations, sharing resources poses obstacles that involve sophisticated organizational solutions. The most challenging problem in the case of Smart Vareflyt is not just the issue of data incorporation at the knowledge level, but also the exchange of information and resources and the application of competition law to the level of the company [100].

4.1.7 Energy efficiency

The energy-efficient passive tag in the RFID device is a preferred option because it used without the need for an on-board energy source. The selection of passive tags is, however, limited compared to the active tag, which used on a broader scale. Nevertheless, the inactive energy efficiency tag is still an open research field that needs to be addressed [103]. As power usage decreased, energy efficiency improved. Several studies on power usage when using the RFID technology are discussed below .

1. The first large-scale backscatter communication system was developed by researchers in [104] for reflecting signal from an RF source to synthesize data packets, which are then decoded by a receiver. It has two significant drawbacks, and the backscatter must first organize the information so that the receiver can transmit it at a signal force less than -135 dBm and work efficiently in the event of robust external interference. Secondly, backscatter signals developed using

simple, affordable standard hardware, which makes it simpler to implement and improve the design needed instead of dedicated receivers for costly backscatter signals (e.g. RFID readers).

- The result shows that wireless power consumption, including Wi-Fi, BLE, ZigBee, Lora, and SigFox, consumes 10-50 mW of electricity, which is 3 to 4 magnitude orders higher than the system's energy consumption. Backscattering technologies, including RFID, passive Wi-Fi, and LoRa backscattering technologies, however, consume just $9.25\mu W$ for continuous frequency-modulated chirps generation and harmonic cancellation.

2. Researchers in [105] introduce an on-board digital temperature sensor with perovskite PV-RFID. This sensor can transmit temperature data wirelessly under sufficient lighting within a distance of up to 4 m. It is converted from light with perovskite PV into ICs and RF signals that used as contact links. The user acts as a portal to the Internet between these hundreds of nodes.

- According to the simulation performance, the overall energy consumption of the sensor depends on the sensor load (the number of sensor measurements per hour). For instance, a 20,000 / hour measurement requires approximately $20\mu W$ of power (calculated with a constant current of $6/muA$ in stand-by mode and $30\mu A$ in 8 mm a 1,5V input voltage each measurement).

3. Photovoltaics (PV) for use by researchers in [106] are the use of photovoltaics (PVs) to increase the energy available during the day, enhance read range and detection capability and add to integrated circuits (ICs) with minimum additional electronics.

- The researchers found that the IC's additional power not only enhances the ability to disperse the RF energy needed for additional tag areas but also enhances the ability to measure and transmit sensor data. This versatile sensor is also suitable for long-term detection embedding in 3D structures if the battery can not replace it. Thus, using PV-RFID can build wireless sensors that are autonomous, inexpensive, and reliable over a long-range. The frequency of PV-RFID measurements is about eight times that of traditional passive tags. By reading a wide area of PV-RFID tags with a limited number of readers and antennas, it lowers the network costs. The PV-RFID sensor additionally records 0.14 million measurements in 24 hours. It shows how sensors can monitor and transmit critical environmental data at low cost, without batteries.

4. PLoRa, an environmental backcast architecture that enables a remote wireless link for IoT devices without a battery, is available from the researchers. PLoRa uses the current LoRa transmission as a new signal, modulates the new signal

into the standard LoRa chirping signal, transfers the data to another LoRa channel received by a remote gateway, and adjusts this original signal [107].

- The results of experiments show that the prototype of the PCB-PLoRa tag backscatters an environmental broadcast of LoRa that is transmitted from a local LoRa node (20 cm) to an entrance up to 1.1 km away, with data accessible indoors or 284 bytes every 14 minutes. Simulate a lower power FPGA 28 nm prototype whose digital baseband processor delivers 220μW in power consumption.

4.2 Environmental Implication

RFID tags are used for managing product movement from factories to store in cartons and pallets. RFID has a great many useful applications for the world. RFID also has environmental drawbacks at the same time. The next topic will concentrate on ways and concerns that help create useful solutions and reduce possible impacts on the environment.

4.2.1 Reduced traffic using RFID

In order to pay for tolls, RFID congestion, and area pricing systems now deliver major environmental advantages. Automatic charging reduces downtime as well as braking and acceleration at the mail stop. Through the use of RFID repeaters on the New Jersey Turnpike tolls, 1.2 million gallons can save annually, air pollutant emissions decrease, and travel times decrease dramatically [101]. London has lowered the congestion level by 26%, nitrogen oxide, and particulates (PM-10) by 15%, and oil usage inside the congestion billing zone by 20% [102]. With the surface charging network introduced in Singapore since 1975, circulation has dropped by 45%. In 2006, the Stockholm scheme had reduced carbon dioxide emissions by 10 to 14% [108]. While it is very effective to reduce traffic, air pollution, and energy usage, plans for congestion charges are not common. The framework became popular after implementation [107].

4.2.2 RFID transponders on curbside waste and recycling bins

The waste truck fitted with an RFID reading panel. The device recognizes the bin when a truck gathers it. In 2001, a German public waste management firm surveyed RFID schemes, unimplemented containers, and productive waste collection routes through data that were exposed and evaluated. The RFID system implemented reported an average increase of 2.85%. In cities with invoices focused on waste numbers, non-recyclable waste decreased by 35% on average, and total waste decreased by 17% cent on average. Contains recycling and non-recycling stuff [109]. As a result, almost half of the overall waste reduction accounts for a 35% percent drop in the garbage disposal, and the other half is for recycling. This finding is consistent with the US surrender program, which reduces municipal waste by 25-35% for disposal [110].

4.2.3   RFID for information on the consumer environment

Item level RFID tags may provide information about different goods as well as generic products. That sort of knowledge can use to identify tainted beef, poultry, or fast food. Regulators, the foodservice industry, and regular customers are helpful with this [111]. At the same time, users will test how far they have transported, greenhouse gas emissions, allergens, and much more. Manufacturers and retailers have commodity carbon labels where a UK Tesco supermarket network sets carbon labels on each product sold, calculating the amount of greenhouse gas released during the manufacture, transport, and consumption of each product [112].

4.2.4   RFID for refurbishment and reuse

The RFID tag increases the efficacy of recycling as the UPC process enhances companies' productivity in the supply chain. For example, battery labels may make the sorting of cell types cheaper and more effective for recycling. Electronic equipment labels may connect to websites that show how to disassemble the device. Tags on hazardous goods, such as household chemicals, will define the material, how, and where to dispose of these [113]. Attributes on consumer goods make it easier to sell products online and are an extension of how UPCs used in the one-way supply chain where the majority of items sold today have UPCs. This code is intended for revenue estimation as well as for inventory control [114], distribution, consolidation, and managing. For RFID, instead of being discarded with it, it will leave the object's security code. The product code will allow many kinds of recycling opportunities. It may create systems that encourage recycling or punish improper disposal by recognizing when recyclable (or harmful or valuable) products placed into the garbage (or garbage can or trash can). Recycling opportunities, such as bottling, are not new, but an automated product-based solution will minimize costs and promote for innovation [115]. RFID systems provide a modest incentive for recyclable low-value goods and a significant incentive for high-value and high-risk goods. One sidewalk recycling company will handle specific items electronically for different goods, different markets, and various geographic areas [116].

Product codes can be applied both as UPC and RFID barcodes. When a large amount of device is picked up in a curb or code and put into a truck quickly, RFID could be preferred over bar code, as RFID can read from other devices at the same time. The benefits of recycling not deemed adequate to justify the expense of the product-level RFID tags. However, if RFID correlated with an item for other purposes, the side benefits of RFID processing can be significant [117]. The use of RFID for electronics replacement, roadside recycling, smart household waste disposal, the management of product deposits and returns in stores and recycling centers, and the collection of waste and recyclables in incinerators, landfills and resource recovery plants addressed in many different applications.

- RFID for Electronics Refurbishment
  Electronic recycling companies typically recognize multiple labels, computer models, printers, or mobile devices related to the most crucial element of the faulty parts market in their product instruction codes. The recycling industry, the product supplier, or the whole industry union RFID labels in products

may use these instructions to connect with databases where both parties may learn how to recycle papers. Will major component can have its RFID tag so that repairs can easily recognize parts and updates [113].

- Item-Level Curbside Recycling
  The use of RFID transponders has addressed in waste management and recycling containers. Through extending this kind of method, residual or recyclable material can detect at the item level. It opens up a whole variety of reward schemes. Incentives (rebates and fees) sent to the customer based on what put on the bin. Municipalities can also pay recyclable collectors extra fees to transport dangerous and challenging things to handle, such as mercury-containing fluorescent lamps, and recycled collectors can quickly sell their collections if they know what they have in-depth. This approach raises problems of a technological nature. The objects in the bin are one or two feet of the antenna for recycling vehicles, and probably other side and rear products which can absorb radio signals. Although RFID tags can be detected theoretically in products in recycling bins and empty bins can be ejected in lorries, this has not commercially demonstrated.

- Smart Trash Cans
  The RFID reader can read each object in the container for home recycling tanks. Drum items may either be sold online or published by traders. Consumers and businesses will automatically check for waste material and schedule recycling services. Online retailers check for the recycling containers, buy recyclable and reselling items, give back some of the consumer's income, and leave vital recycling services (paper, plastics, artistry, metal). Home intelligent trash will play mostly the same role as the item level curb set. Intelligent home trash can be technically pure but probably a more expensive alternative than the identification of congestion objects.

- In-Store Recyclables Collection
  RFID allows the storage in shop or recycling centers of recyclable items. Some retailers use recycled items already. Recycling Corporation Recycling Corporation (RBRC) provides electronics and electronic stores with batteries throughout the United States and Canada. For different computer producers Costco has a standard marketing and recycling plan [114]. Mobile telephone providers accept used telephones as well. Retailers often use UPC bar codes to handle returns. The use of product codes to provide customers with discounts using RFID tags is economical and straightforward. Like every other voucher or swap system, retailers may benefit from a discount plan. Selling machines can also accept recyclable goods and offer cash refunds or credits based on details on the product label.

- RFID at Materials Recovery Facilities
  To organize things in warehouses, incinerators, and dumps, using RFID readers. Modern materials recovery facilities include magnetic steel seams, aluminum vortex separators, and plastic seam infrared detectors. RFID devices can track small electronics and batteries. Previous studies have shown

that RFID-labeled items such as batteries, small electronics, and mobile devices can obtain at a much cheaper collection facility than recycled [113].

4.2.5 Environmental drawbacks of RFID

Many consumer goods include RFID tags, including food packaging. Over time, the number of tags produced and discarded increases. Usage of the global tag will reach 2 trillion a year [115]. Such marks end up in urban solid waste or systems for recycling paper, carton, metal, glass, and plastic. RFID tags typically include copper, aluminum, or silver antennas as well as integrated silicon circuits, adhesives, plastics [116]. In short, the use of RFID materials and removable tag properties allows the avoidance of problems that cannot be degraded or recycled as RFID tags can prevent the recycling of various products and other materials [117]. When carbon-based conductive ink used as a substrate antenna and bio-based plastic, most RFID tags can be biodegradable or ecologically friendly. However, silicone chips may have environmental effects, which at the development and not the stage of life are challenging to deal with reliably. The processing of silicon chips requires considerable energy and water and significant emissions of pollutants. A specific problem was the pollution of glass, steel, aluminum, paper, and plastics recycling, discussed in turn below.

- Glass Recycling
  Since silicon melts at speed other than glass, silicon RFID chips can pose problems for RFID tags attached to glass containers. If the silicon remains in the glass of the entire recycling line and the glass furnace, silicon beads can create in a new package. It is a potential weakness, especially for the media, and it shows that RFID tags used in the glass must be removed entirely or placed inside the lid and not on the glass itself [117].

- Steel Recycling
  RFID tags can contain approximately 20 mg of copper. On a regular 20 g steel box, this corresponds to a working copper concentration of 0.1%, and the steel copper content accumulates with continuous recycling. It is rising steel consistency. Therefore, RFID tags for steel goods should be entirely removable or made with copper-free antennas. RFID tags mounted on aluminum do not impact the recycling of steel. Inadvertent aluminum falls from tags removed during the exothermic reaction at very high steel temperatures [117].

- Aluminium Recycling
  Aluminum can be recycled with high-value many times. Flows of feed do not permit pollution. Pollutants shall be picked or removed by other means. RFID tags for aluminum items are either produced or made of eco-friendly materials.

- Paper Recycling
  RFID tags will join an old carboard container in the recycling facility. The National Aeronautical Research Committee (NCA) tests have shown that copper foil antennas are kept intact and can be easily captured and removed during the entire hydro pumping process. The silver ink antennas, however, contain 2 to 3 microns of silver particles. Pilot experiments

using labels containing around 16 mg of silver found that much of the silver in the dough remained. In certain cases, however, there was insufficient proof of rates exceeding the limits and regulations. Found in reverse water.

- Plastic Recycling
  The use of High-density polyethylene (HDPE) for milk bottles, washing machines, and other applications. Application of polyethylene terephthalate (PET) in bottles and other applications for soda and wine. Some of the most often recycled plastics are HDPE and PET. In general, RFID labels applied to substrates of PET. Thanks to the denser RFID tags than HDPE and their isolation during the first stage of the HDPE recycling process, RFID labels are anticipated to differentiate easily from HDPE bottles during the recycling process. However, it is a struggle to remove RFID tags from PET bottles. PET is more than one (1.2–1.4 g / cm3) in specific gravity, and both RFID and PET fragments immersed in water. As RFID tags typically performed in PET substrates, the mass difference between PET and RFID tags may not be sufficient using cyclonic separation. Every RFID tag used on PET bottles should also be designed to be easily removed, either by non-PET substrates or other methods.

- Towards RFID biodegradable systems
  However, most RFID tags can not be biodegraded. These include petrochemicals-based metal parts, plastics, or other materials. Smaller tags also make it hard to isolate and recycle different label components. Recent researchers have developed completely biodegradable tags, in particular for medical and feed supply chain applications [118].

4.2.6 Environmental Sustainability

While most case studies at various rates have achieved environmental sustainability, Walmart's case shows that the bigger the size, the higher the effect. A breakthrough in RFID implementation by Walmart that replaced the barcode system by Walmart decreased carbon footprint by 3.2% by allowing less product movement because of improved product visibility and handling and improved inventory management [116]. The TruckTag project is another new environmental protection program. RFID tags allow for automatic high-speed safety checks, reducing traffic jams, and improving air quality by reducing the lorry idle time [116].

4.2.7 Business Value

The average organization aims to reduce costs when introducing a green RFID scheme. The City of London School for Girls, with its RFID temperature sensor networks, will reduce the cost up to 80% compared to its wired networks and gain greater control over room temperature via RFID [117]. Using RFID to monitor temperature, Nestle can save up to 10% on energy-related costs, reduce harm, and boost efficiency. Although direct cost savings are legendary, indirect cost savings should also be acknowledged (such as loss-of-life insurance and increased quality). Many businesses use RFID for revenue generation. Recycle Bank, and Recycling Rewards offer recycling coupons to customers to launch a new business model and

promote more recycling families. Bank Recycle has raised its sales by collecting more recyclable products. The use of RFID saved over 318,000 trees and 21 million gallons of petroleum in the Recycle Tank [44].

4.2.8 Social Responsibility

Green RFID initiatives have an impact not only on the safety and sustainability of the ecosystem of business but also on environmental conservation, which adds value to customer-to-company relationships. It is because consumers know what they want in investment in the environment. Nestlé Italia uses an RFID-compliant management framework to support green ads and to boost brand identity successfully. Under public demand scrutiny, major businesses urgently have to meet their social obligations [99]. Through its smart truck initiative, DHL has minimized CO_2 emissions and fuel consumption by automating package scans to speed up driver handling of the parcels and idle periods to shorten the truck engines during delivery. In more environmentally aware businesses, the culture in which they work may have a positive effect. People and economies with their bank recycle point have raised more than one million dollars [97].

5 Benefit of Greening IT

Green technology is a concept that includes almost every type of practical use of technology to benefit the environment. Despite industrial technology advancing so far, its green predecessors are supposed to do the same. Many green technology examples include items that come under the given use of the subject, such as green chemistry, environmental monitoring, and others. Anything that fits the accepted concept of green technology will do one or two things. It is either to preserve or to help the ecosystem in any way. The words "environmental technology" or "clean technology" can also be used for this technology. Green tech's primary goal is to protect nature and help reverse the adverse effects humans have had on the planet [118]. Green technology enables us to turn our contaminants and waste from unnecessary by-products into a sustainable workforce that benefits humans and the environment. Green technology has some of the best recycling methods: turning waste into fertilizer. One of the most significant benefits of green technology is that it helps people recycle things like water and air. Green technology leads to emissions reduction and air purification for future generations. Above all, green technology has permitted people to save vast quantities of resources, dramatically reducing the remaining carbon footprint. Alternatives to systems that use a high volume of electricity and fuel are provided to the public at this very moment. The use of items such as electric vehicles and solar panels has become natural, daily, and the Planet could not be the best. It is highly recommended that people use environmentally friendly tools and appliances to help facilitate this energy saving. The ability to rejuvenate ecosystems that have suffered a great deal because of the effects of human carbon emissions and other factors is also a tremendous use of green technology. The use of this technology replants trees, replaces plants, and replaces entire habitats to their original glory. Besides, waste is collected and recycled, so that animals, which once existed, will now return to these destroyed habitats. It means a new beginning for many species worldwide [119].

Environmental concerns [120] again impact the IT industry's competitive landscape, and businesses with the expertise and vision to offer goods and services that tackle environmental problems profit from a competitive advantage. For example, when making transactions, leases, or contracting decisions, many consumers consider service provider registration and environmental initiatives. Companies face rising energy prices and could be subject to additional government taxes if they do not recognize the effect of environmental activities. Investors and customers are starting to seek more information about carbon emissions and environmental measures and business outcomes. Because of these issues, businesses start proving environmental efficiency, such as the Carbon Disclosure Project (https://www.cdp.net/en) an initiative that allows multinational companies to report their CO_2 emissions. The implementation of green IT practices gives companies and individuals economic and other benefits. IT operations increase energy efficiency, especially when electricity is costly and energy prices are increasing, through economically beneficial green initiatives. In a Sun Microsystems Australia survey, which included 1,500 responses from 758 Australian and New Zealand organizations, interviewed respondents said energy conservation and cost management were focused on environmentally sustainable environmental policies and environmental impacts. The primary reason for using the method shown in Figure 5 is that less is better said.
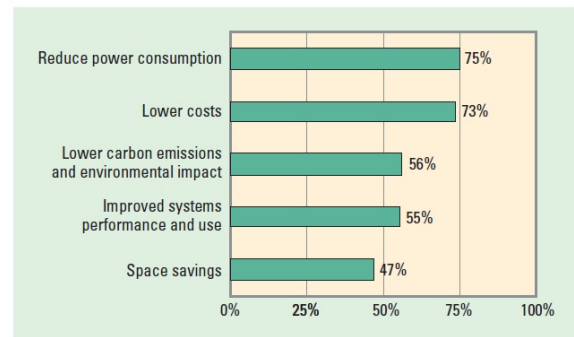
Figure 5: Reasons and benefits for using green IT practices[120]

Many businesses will concentrate on environmental conservation, energy usage, and cost control issues. The organization focuses on environmental protection through the frameworks for resolving business demands, legislation, and climate change. Business and institutional customers ask manufacturers to "relive" their goods and processes. For instance, businesses like Dell and Wal-Mart take actions that compel suppliers to follow environmental-friendly practices. People start evaluating the essence of the IT environment, and green IT will become a regular function in the next five years. The company provides a range of innovative green goods and services, generating new markets for companies.

6 Future Work of RFID in Green IoT

Green IoT's promising future will make our future world safer and greener, very high quality, socially and environmentally sustainable

and economically viable. Today, green communication and networking, green architecture, green IT and application infrastructure, energy-saving techniques, integrated RFIDs and networks, mobility and network management, the co-operation of homogenous and diverse networks, intelligent artefacts and green location all concentrate on exciting areas [121]. From two points of view, green IoT architecture can be applied to achieve outstanding performance and high quality. Identifying suitable techniques to improve QoS parameters (i.e. bandwidth, delay, and throughput) will make an effective and useful contribution to greener IoT. It would need to use less energy when it comes to greening IoT, searching for new resources, mitigating the adverse effects of IoT on human health, and disruption to the environment. Green IoT will then make a significant contribution to sustainable, intelligent, and green societies. Radio-frequency energy harvesting should be taken into account in order to achieve an energy balance to help green communication between IoT devices. Energy saving and CO_2 emission reduction is a major challenge for smart and green environment.

Logistics, Aero-ID, counterfeiting, supply chain control, spaces and much more will accelerate the growth of modern society and technology in the coming decades. Mobility, climate, safety, protection and energy, including medical, pharmaceutical and military applications, will become the leading technological drivers of the future, further growing the need for sustainability—wireless and electronic modules that are reliable, versatile, robust, low power and durable. Work on electronics and RFID seeks to develop versatile systems, based on organic/inorganic substrates and materials, to solve the limitations of ceramics and silicone in order to address these significant challenges. A challenge for potential applications is the convergence of elegant, lightweight, heterogeneous, versatile, environmentally sustainable, newer materials and cost-effective processes in a wide area. Continuous development and innovation involve a wide range of electrical components that can directly produce and incorporate from coils to affordable methods, mainly using organic electronics, along with work into a variety of electrical conductivity and semiconductor materials. Organic materials can be printed and modeled using several methods, each with its advantages and disadvantages, such as flexographic, width, offset, sorting, and injection. Based on these materials and techniques, primarily low-cost RFID transponders, different types of sensors, storage devices, photovoltaic cells, passive devices such as displays or batteries have tested active components such as diodes and transistors with the production of them. Though seen only in the low UHF (RF) range, the trend moves to higher speeds, resolutions and frequencies without compromising versatility, eco-friendliness and low costs. To address these problems includes a new approach to RFID and the design of electronic systems in terms of alternative materials, processes and functions. The researchers in [122] are proposing an innovative approach focused on developing a new low-cost inkjet printing platform with efficient diode integration for applications with optimized metallization traces and enhanced recognition capabilities. The method theoretically proposed can form the basis for the first generation of precise "smart" RFID devices.

More fields of research need to be explored to establish optimal and efficient Greening IoT solutions:

- Crewless aerial vehicles (UAVs), particularly in agriculture,

traffic, and surveillance, are required to replace many IoT devices, which will reduce power consumption and emissions. UAV is a promising technology that leads to low cost and efficient green IoT.

- Sensor data to the mobile cloud must be more useful. Sensor-cloud combines a network of wireless sensors and a mobile cloud. It is a hot and promising IoT greening technology. The device, service, WSN, and cloud management's energy efficacy can be examined through a green social network such as service (SNaaS).

- M2M connectivity plays a crucial role in reducing energy consumption and harmful emissions. In order to allow automated systems, smart machines must be smarter. In the event of traffic, computer automation delays must be reduced and intervention required and immediate.

7 Conclusion

IoT has an enormous influence on transforming our everyday lifestyle. IoT technology connects a large number of devices and items linked to the Internet around the world. The main concern is how data from these devices can be collected and analyzed effectively. RFID is one of the leading IoT tools, used for the identification and processing of information from IoT devices due to its cost and energy consumption characteristics. Studying this technology is therefore essential and paying attention to mitigating its adverse effects. This paper discusses and summarizes the latest RFID applications, including studies that have improved RFID applications in Green IoT efficiency. This paper also addressed the challenges and implications of green, IoT RFID applications. However, there are still some challenges to this field, such as sophistication, protection and lack of trust. These problems form a relevant research field for future study.

Conflict of Interest The authors declare no conflict of interest.

References

[1] "What Is Green Power," https://www.epa.gov/greenpower/what-green-power, accessed: 15-July-2020.

[2] "Benefits of Using Green Power," https://www.epa.gov/greenpower/benefits-using-green-power, accessed: 15-July-2020.

[3] "Energy Efficiency," https://www.eesi.org/topics/energy-efficiency/description, accessed: 16-July-2020.

[4] C. Zhu, V. C. Leung, L. Shu, E. C.-H. Ngai, "Green internet of things for smart world," IEEE access, **3**, 2151–2162, 2015, doi:10.1109/ACCESS.2015.2497312.

[5] H. Eakin, P. M. Wightman, D. Hsu, V. R. Gil Ramón, E. Fuentes-Contreras, M. P. Cox, T.-A. N. Hyman, C. Pacas, F. Borraz, C. González-Brambila, et al., "Information and communication technologies and climate change adaptation in Latin America and the Caribbean: a framework for action," Climate and Development, **7**(3), 208–222, 2015, doi:doi.org/10.1080/17565529.2014. 951021.

[6] A. P. Upadhyay, A. Bijalwan, "Climate change adaptation: services and role of information communication technology (ICT) in India," American Journal of Environmental Protection, **4**(1), 70–74, 2015, doi:10.11648/j.ajep.20150401. 20.

[7] O. Balaban, J. A. P. de Oliveira, "Sustainable buildings for healthier cities: assessing the co-benefits of green buildings in Japan," Journal of Cleaner Production, **163**, S68–S78, 2017, doi:doi.org/10.1016/j.jclepro.2016.01.086.

[8] S. Rani, R. Talwar, J. Malhotra, S. H. Ahmed, M. Sarkar, H. Song, "A novel scheme for an energy efficient Internet of Things based on wireless sensor networks," Sensors, **15**(11), 28603–28626, 2015, doi:doi.org/10.3390/s151128603.

[9] A. H. Sodhro, S. Pirbhulal, Z. Luo, V. H. C. de Albuquerque, "Towards an optimal resource management for IoT based Green and sustainable smart cities," Journal of Cleaner Production, **220**, 1167–1179, 2019, doi: doi.org/10.1016/j.jclepro.2019.01.188.

[10] R. Arshad, S. Zahoor, M. A. Shah, A. Wahid, H. Yu, "Green IoT: An investigation on energy saving practices for 2020 and beyond," IEEE Access, **5**, 15667–15681, 2017, doi:10.1109/ACCESS.2017.2686092.

[11] M. M. K. M. S. Akshaya, M. M. N. Priya, "Green Internet of Things for Smart World," .

[12] F. K. Shaikh, S. Zeadally, E. Exposito, "Enabling technologies for green internet of things," IEEE Systems Journal, **11**(2), 983–994, 2015, doi: 10.1109/JSYST.2015.2415194.

[13] C. Zhu, V. C. Leung, L. Shu, E. C.-H. Ngai, "Green internet of things for smart world," IEEE access, **3**, 2151–2162, 2015, doi:10.1109/ACCESS.2015. 2497312.

[14] C. S. Nandyala, H.-K. Kim, "Green IoT agriculture and healthcare application (GAHA)," International Journal of Smart Home, **10**(4), 289–300, 2016, doi:dx.doi.org/10.14257/ijsh.2016.10.4.26.

[15] B. Nath, F. Reynolds, R. Want, "RFID technology and applications," IEEE Pervasive computing, **5**(1), 22–24, 2006, doi:10.1109/MPRV.2006.13.

[16] I. Bose, S. Yan, "The green potential of RFID projects: A case-based analysis," It Professional, **13**(1), 41–47, 2011, doi:10.1109/MITP.2011.15.

[17] Y. Karakasa, H. Suwa, T. Ohta, "Evaluating effects of RFID introduction based on CO2 reduction," in Proceedings of the 51st Annual Meeting of the ISSS-2007, Tokyo, Japan, 2007.

[18] A. Ilic, T. Staake, E. Fleisch, "Using sensor information to reduce the carbon footprint of perishable goods," IEEE Pervasive Computing, **8**(1), 22–29, 2008, doi:10.1109/MPRV.2009.20.

[19] S. Murugesan, "Harnessing green IT: Principles and practices," IT professional, **10**(1), 24–33, 2008, doi:10.1109/MITP.2008.10.

[20] F. Al-Turjman, A. Kamal, M. Husain Rehmani, A. Radwan, A.-S. Khan Pathan, "The Green Internet of Things (G-IoT)," 2019, doi:doi.org/10.1155/2019/6059343.

[21] S. Park, "A development of UHF RFID device for mobile IoT service," in 2016 IEEE 7th Annual Ubiquitous Computing, Electronics & Mobile Communication Conference (UEMCON), 1–7, IEEE, 2016, doi:10.1109/UEMCON. 2016.7777830.

[22] R. Colella, L. Catarinucci, L. Tarricone, "Improved RFID tag characterization system: Use case in the IoT arena," in 2016 IEEE International Conference on RFID Technology and Applications (RFID-TA), 172–176, IEEE, 2016, doi:10.1109/RFID-TA.2016.7750760.

[23] R. Colella, L. Catarinucci, L. Tarricone, "Evaluating the suitability of specific RFID tags for IoT applications through a new characterization platform," 2016 International Multidisciplinary Conference on Computer and Energy Science (SpliTech), 1–3, 2016, doi:10.1109/SpliTech.2016.7555934.

[24] F. Nekoogar, F. Dowla, "Passive RFID for IOT using UWB/UHF hybrid signaling," 2016 IEEE/ACES International Conference on Wireless Information Technology and Systems (ICWITS) and Applied Computational Electromagnetics (ACES), 1–2, 2016, doi:10.1109/ROPACES.2016.7465304.

[25] "The 3 Biggest Benefits of RFID Asset Tracking in the Supply Chain," https://lowrysolutions.com/blog/the-3-biggest-benefits-of-rfid-asset-tracking-in-the-supply-chain/, accessed: 15-February-2020.

[26] Kubo, "The Research of IoT Based on RFID Technology," 2014 7th International Conference on Intelligent Computation Technology and Automation, 832–835, 2014, doi:10.1109/ICICTA.2014.199.

[27] H. Wang, "Constructing the Green Campus within the Internet of Things Architecture," International Journal of Distributed Sensor Networks, **10**, 2014, doi:10.1155/2014/804627.

[28] "Green Campus at the University of Copenhagen," https://greencampus.ku.dk/greencampus20/, accessed: 15-July-2020.

[29] B. Singh, D. K. Lobiyal, "A novel energy-aware cluster head selection based on particle swarm optimization for wireless sensor networks," Human-centric Computing and Information Sciences, **2**, 1–18, 2011, doi:10.1186/2192-1962-2-13.

[30] B. S. Malapur, V. R. Pattanshetti, "IoT based waste management: An application to smart city," 2017 International Conference on Energy, Communication, Data Analytics and Soft Computing (ICECDS), 2476–2486, 2017, doi:10.1109/ICECDS.2017.8389897.

[31] T. Anagnostopoulos, A. Zaslavsky, "Effective Waste Collection with Shortest Path Semi-Static and Dynamic Routing," in NEW2AN, 2014, doi: 10.1007/978-3-319-10353-2_9.

[32] P. Jajoo, A. Mishra, S. Mehta, V. Solvande, "Smart Garbage Management System," 2018 International Conference on Smart City and Emerging Technology (ICSCET), 1–6, 2018, doi:10.1109/ICSCET.2018.8537390.

[33] T. Anagnostopoulos, A. Zaslavsky, A. Medvedev, "Robust waste collection exploiting cost efficiency of IoT potentiality in Smart Cities," 2015 International Conference on Recent Advances in Internet of Things (RIoT), 1–6, 2015, doi:10.1109/RIOT.2015.7104901.

[34] S. Jisha, M. Philip, "Rfid based security platform for internet of things in health care environment," 2016 Online International Conference on Green Engineering and Technologies (IC-GET), 1–3, 2016, doi:10.1109/GET.2016. 7916693.

[35] D. He, S. Zeadally, "An Analysis of RFID Authentication Schemes for Internet of Things in Healthcare Environment Using Elliptic Curve Cryptography," IEEE Internet of Things Journal, **2**, 72–83, 2015, doi:10.1109/JIOT.2014. 2360121.

[36] C. Occhiuzzi, G. Contri, G. Marrocco, "Design of Implanted RFID Tags for Passive Sensing of Human Body: The STENTag," IEEE Transactions on Antennas and Propagation, **60**, 3146–3154, 2012, doi:10.1109/TAP.2012. 2198189.

[37] G. Calcagnini, F. Censi, M. Maffia, L. Mainetti, E. Mattei, L. Patrono, E. Urso, "Evaluation of thermal and nonthermal effects of UHF RFID exposure on biological drugs," IEEE Transactions on Information Technology in Biomedicine, **16**(6), 1051–1057, 2012, doi:10.1109/TITB.2012.2204895.

[38] W. Zhou, S. Piramuthu, "Framework, strategy and evaluation of health care processes with RFID," Decision Support Systems, **50**(1), 222–233, 2010, doi:doi.org/10.1016/j.dss.2010.08.003.

[39] P. Schmitt, F. Michahelles, "Economic impact of RFID report," Retrieved November, **1**, 2009, 2008.

[40] Z. Lu, H. Cao, P. Folan, D. Potter, J. Browne, "RFID-based information management in the automotive plastic recycling industry," in Information Technologies in Environmental Engineering, 397–408, Springer, 2007, doi: 10.1007/978-3-540-71335-7_41.

[41] D. Duval, H. Maclean, "The role of product information in automotive plastics recycling: a financial and life cycle assessment," Journal of Cleaner Production, **15**, 1158–1168, 2007, doi:10.1016/J.JCLEPRO.2006.05.030.

[42] T. C. Poon, K. L. Choy, H. K. H. Chow, H. Lau, F. Chan, K. Ho, "A RFID case-based logistics resource management system for managing order-picking operations in warehouses," Expert Syst. Appl., **36**, 8277–8301, 2009, doi: 10.1016/j.eswa.2008.10.011.

[43] N. Wu, M. A. Nystrom, T. R. Lin, H. C. Yu, "Challenges to Global RFID Adoption," 2006 Technology Management for the Global Future - PICMET 2006 Conference, **2**, 618–623, 2006, doi:10.1109/PICMET.2006.296595.

[44] J.-S. Park, "Evaluating Green IT Initiatives Using the Sustainability Balanced Scorecard," Journal of the Korea Safety Management and Science, **19**(3), 81–87, 2017, doi:doi.org/10.12812/ksms.2017.19.3.81.

[45] A. Nasir, U. Kasimu, B. Ige, A. Mohammed, "Characterization and management of solid waste generated in Nasarawa LGA in Nasarawa state, Nigeria," Middle-East J Sci Res, **24**, 1128–1134, 2016, doi:10.5829/idosi.mejsr.2016. 24.04.23231.

[46] R. Knoth, B. Kopacek, P. Kopacek, "Case study: multi life cycle center for electronic products," in Proceedings of the 2005 IEEE International Symposium on Electronics and the Environment, 2005., 194–198, IEEE, 2005, doi:10.1109/ISEE.2005.1437022.

[47] M. Favot, R. Veit, A. Massarutto, "The evolution of the Italian EPR system for the management of household Waste Electrical and Electronic Equipment (WEEE). Technical and economic performance in the spotlight," Waste management, **56**, 431–437, 2016, doi:doi.org/10.1016/j.wasman.2016.06.005.

[48] H. R. Culver, J. R. Clegg, N. Peppas, "Analyte-Responsive Hydrogels: Intelligent Materials for Biosensing and Drug Delivery." Accounts of chemical research, **50** 2, 170–178, 2017, doi:10.1021/acs.accounts.6b00533.

[49] N. Deng, "RFID technology and network construction in the internet of things," in 2012 International Conference on Computer Science and Service System, 979–982, IEEE, 2012, doi:10.1109/CSSS.2012.248.

[50] R. H. Weber, "Internet of Things–New security and privacy challenges," Computer law & security review, **26**(1), 23–30, 2010, doi:10.1016/J.CLSR.2009. 11.008.

[51] R. H. Weber, "Internet of things–Need for a new legal environment?" Computer law & security review, **25**(6), 522–527, 2009, doi:doi.org/10.1016/j.clsr. 2009.09.002.

[52] M. Balaji, S. K. Roy, "Value co-creation with Internet of things technology in the retail industry," Journal of Marketing Management, **33**(1-2), 7–31, 2017, doi:10.1080/0267257X.2016.1217914.

[53] X. Zhu, S. K. Mukhopadhyay, H. Kurata, "A review of RFID technology and its managerial applications in different industries," Journal of Engineering and Technology, **29**, 152–167, 2012, doi:10.1016/J.JENGTECMAN.2011.09.011.

[54] T. Taleb, M. Corici, C. Parada, A. Jamakovic, S. Ruffino, G. Karagiannis, T. Magedanz, "EASE: EPC as a service to ease mobile core network deployment over cloud," IEEE Network, **29**, 78–88, 2015, doi:10.1109/MNET.2015. 7064907.

[55] B. Fabian, O. Günther, "Security challenges of the EPCglobal network," Commun. ACM, **52**, 121–125, 2009, doi:10.1145/1538788.1538816.

[56] J. Cooper, A. James, "Challenges for database management in the internet of things," IETE Technical Review, **26**(5), 320–329, 2009, doi: 10.4103/0256-4602.55275.

[57] M. Z. Hasan, F. Al-Turjman, "Optimizing multipath routing with guaranteed fault tolerance in Internet of Things," IEEE Sensors Journal, **17**(19), 6463–6473, 2017, doi:10.1109/JSEN.2017.2739188.

[58] S. F. Khan, "Health care monitoring system in Internet of Things (IoT) by using RFID," in 2017 6th International Conference on Industrial Technology and Management (ICITM), 198–204, IEEE, 2017, doi:10.1109/ICITM.2017. 7917920.

[59] S. Amendola, R. Lodato, S. Manzari, C. Occhiuzzi, G. Marrocco, "RFID technology for IoT-based personal healthcare in smart spaces," IEEE Internet of things journal, **1**(2), 144–152, 2014, doi:10.1109/JIOT.2014.2313981.

[60] S. Manzari, G. Marrocco, "Modeling and applications of a chemical-loaded UHF RFID sensing antenna with tuning capability," IEEE transactions on antennas and propagation, **62**(1), 94–101, 2013, doi:10.1109/TAP.2013. 2287008.

[61] S. Manzari, A. Catini, G. Pomarico, C. Di Natale, G. Marrocco, "Development of an UHF RFID chemical sensor array for battery-less ambient sensing," IEEE Sensors Journal, **14**(10), 3616–3623, 2014, doi:10.1109/JSEN.2014. 2329268.

[62] S. Amendola, L. Bianchi, G. Marrocco, "Combined passive radiofrequency identification and machine learning technique to recognize human motion," in 2014 44th European Microwave Conference, 1044–1047, IEEE, 2014, doi:10.1109/EuMC.2014.6986617.

[63] J. Zhang, G. Y. Tian, A. M. Marindra, A. I. Sunny, A. B. Zhao, "A review of passive RFID tag antenna-based sensors and systems for structural health monitoring applications," Sensors, **17**(2), 265, 2017, doi:doi.org/10.3390/ s17020265.

[64] L. K. Fiddes, N. Yan, "RFID tags for wireless electrochemical detection of volatile chemicals," Sensors and Actuators B: Chemical, **186**, 817–823, 2013, doi:doi.org/10.1016/j.snb.2013.05.008.

[65] E. Moradi, K. Koski, L. Ukkonen, Y. Rahmat-Samii, T. Björninen, L. Sydänheimo, "Embroidered RFID tags in body-centric communication," in 2013 International Workshop on Antenna Technology (iWAT), 367–370, IEEE, 2013, doi:10.1109/IWAT.2013.6518367.

[66] R. Krigslund, S. Dosen, P. Popovski, J. L. Dideriksen, G. F. Pedersen, D. Farina, "A novel technology for motion capture using passive UHF RFID tags," IEEE Transactions on Biomedical Engineering, **60**(5), 1453–1457, 2012, doi:10.1109/TBME.2012.2209649.

[67] S. Manzari, C. Occhiuzzi, S. Nawale, A. Catini, C. Di Natale, G. Marrocco, "Humidity sensing by polymer-loaded UHF RFID antennas," IEEE Sensors Journal, **12**(9), 2851–2858, 2012, doi:10.1109/JSEN.2012.2202897.

[68] A. A. Babar, S. Manzari, L. Sydanheimo, A. Z. Elsherbeni, L. Ukkonen, "Passive UHF RFID tag for heat sensing applications," IEEE Transactions on Antennas and propagation, **60**(9), 4056–4064, 2012, doi:10.1109/TAP.2012. 2207045.

[69] G. Li, Y. Huang, G. Gao, X. Wei, Z. Tian, L.-A. Bian, "A handbag zipper antenna for the applications of body-centric wireless communications and Internet of Things," IEEE Transactions on Antennas and Propagation, **65**(10), 5137–5146, 2017, doi:10.1109/TAP.2017.2743046.

[70] T. Kellomaki, "On-body performance of a wearable single-layer RFID tag," IEEE Antennas and Wireless Propagation Letters, **11**, 73–76, 2012, doi: 10.1109/LAWP.2012.2183112.

[71] S. Manzari, C. Occhiuzzi, G. Marrocco, "Feasibility of body-centric passive RFID systems by using textile tags," IEEE Antennas Propag. Mag, **54**(4), 49–62, 2012, doi:10.1109/MAP.2012.6309156.

[72] J. Kim, A. Banks, H. Cheng, Z. Xie, S. Xu, K.-I. Jang, J. W. Lee, Z. Liu, P. Gutruf, X. Huang, et al., "Epidermal electronics with advanced capabilities in near-field communication," small, **11**(8), 906–912, 2015, doi: doi.org/10.1002/smll.201402495.

[73] S. Wang, S. Liu, D. Chen, "Analysis and construction of efficient RFID authentication protocol with backward privacy," in China Conference on Wireless Sensor Networks, 458–466, Springer, 2012, doi:10.1007/978-3-642-36252-1_ 43.

[74] Y.-P. Liao, C.-M. Hsiao, "A secure ECC-based RFID authentication scheme integrated with ID-verifier transfer protocol," Ad hoc networks, **18**, 133–146, 2014, doi:10.1016/j.adhoc.2013.02.004.

[75] J. Chou, "An efficient mutual authentication RFID scheme based on elliptic curve cryptography," The Journal of Supercomputing, **70**, 75–94, 2013, doi:10.1007/s11227-013-1073-x.

[76] C. Jin, C. Xu, X. Zhang, J. Zhao, "A secure RFID mutual authentication protocol for healthcare environments using elliptic curve cryptography," Journal of medical systems, **39**(3), 24, 2015, doi:10.1007/s10916-015-0213-7.

[77] Z. Zhang, Q. Qi, "An efficient RFID authentication protocol to enhance patient medication safety using elliptic curve cryptography," Journal of medical systems, **38**(5), 47, 2014, doi:10.1007/s10916-014-0047-8.

[78] A. K. Singh, B. Patro, "Elliptic Curve Signcryption Based Security Protocol for RFID," Ksii Transactions on Internet and Information Systems, **14**, 344–365, 2020, doi:10.3837/tiis.2020.01.019.

[79] C. Lai, H. Li, X. Liang, R. Lu, K. Zhang, X. Shen, "CPAL: A conditional privacy-preserving authentication with access linkability for roaming service," IEEE Internet of Things Journal, **1**(1), 46–57, 2014, doi:10.1109/JIOT.2014.2306673.

[80] Z. Ali, A. Ghani, I. Khan, S. A. Chaudhry, S. H. Islam, D. Giri, "A robust authentication and access control protocol for securing wireless healthcare sensor networks," J. Inf. Secur. Appl., **52**, 102502, 2020, doi:10.1016/j.jisa.2020.102502.

[81] Y.-l. Liu, X.-l. Qin, C. Wang, B.-h. Li, "A lightweight RFID authentication protocol based on elliptic curve cryptography," Journal of computers, **8**(11), 2880–2887, 2013, doi:10.4304/jcp.8.11.2880-2887.

[82] Y.-P. Liao, C.-M. Hsiao, "A secure ECC-based RFID authentication scheme using hybrid protocols," in Advances in Intelligent Systems and Applications-Volume 2, 1–13, Springer, 2013, doi:10.1007/978-3-642-35473-1_1.

[83] J. Bongaarts, "Global fertility and population trends," in Seminars in reproductive medicine, volume 33, 005–010, Thieme Medical Publishers, 2015, doi:10.1055/s-0034-1395272.

[84] L. Batina, S. Seys, D. Singelée, I. Verbauwhede, "Hierarchical ECC-based RFID authentication protocol," in International Workshop on Radio Frequency Identification: Security and Privacy Issues, 183–201, Springer, 2011, doi:10.1007/978-3-642-25286-0_12.

[85] C. Lv, H. Li, J. Ma, Y. Zhang, "Vulnerability analysis of elliptic curve cryptography-based RFID authentication protocols," Transactions on Emerging Telecommunications Technologies, **23**(7), 618–624, 2012, doi:10.1002/ett.2514.

[86] B. Chander, K. Gopalakrishnan, "Security Vulnerabilities and Issues of Traditional Wireless Sensors Networks in IoT," 2020, doi:10.1007/978-3-030-33596-0_21.

[87] K. Fan, Y. Gong, Z. Du, H. Li, Y. Yang, "RFID Secure Application Revocation for IoT in 5G," 2015 IEEE Trustcom/BigDataSE/ISPA, **1**, 175–181, 2015, doi:10.1109/Trustcom.2015.372.

[88] Y. L. Santos, E. Canedo, "On the Design and Implementation of an IoT based Architecture for Reading Ultra High Frequency Tags," Inf., **10**, 41, 2019, doi:10.3390/info10020041.

[89] "Top 10 RFID Security Concerns and Threats," https://securitywing.com/top-10-rfid-security-concerns-threats/, accessed: 10-September-2020.

[90] M. El-hajj, A. Fadlallah, M. Chamoun, A. Serhrouchni, "A Survey of Internet of Things (IoT) Authentication Schemes †," Sensors (Basel, Switzerland), **19**, 2019, doi:10.3390/s19051141.

[91] G. Saxl, M. Ferdik, M. Fischer, M. Maderboeck, T. Ussmueller, "UHF RFID Prototyping Platform for ISO 29167 Decryption Based on an SDR," Sensors (Basel, Switzerland), **19**, 2019, doi:10.3390/s19102220.

[92] L. Xiao, H. Xu, F. Zhu, R. Wang, P. Li, "SKINNY-Based RFID Lightweight Authentication Protocol," Sensors (Basel, Switzerland), **20**, 2020, doi:10.3390/s20051366.

[93] K. Fan, C. Liang, H. Li, Y. Yang, "LRMAPC: A Lightweight RFID Mutual Authentication Protocol with Cache in the Reader for IoT," 2014 IEEE International Conference on Computer and Information Technology, 276–280, 2014, doi:10.1109/CIT.2014.80.

[94] O. Hongzhi, G. Jin-yun, L. Ke-sheng, "An UHF RFID reader in IOT," Proceedings 2013 International Conference on Mechatronic Sciences, Electric Engineering and Computer (MEC), 672–675, 2013, doi:10.1109/MEC.2013.6885148.

[95] C. P. Schuch, G. Balbinot, M. Jeffers, M. W. McDonald, D. Corbett, "An RFID-based activity tracking system to monitor individual rodent behavior in environmental enrichment: Implications for post-stroke cognitive recovery," Journal of Neuroscience Methods, **324**, 2019, doi:10.1016/j.jneumeth.2019.05.015.

[96] "DHL Says Its SmartTrucks Save Money, Time and CO2," Accessed: 15-September-2020.

[97] "Communities Turn to RFID to Boost Recycling," http://www.rfidjournal.com/article/articleview/4259/1/1, accessed: 03-June-2020.

[98] "Nestlé italy finds rfid brings roi for ice cream," Accessed: 03-June-2020.

[99] X. Chen, X. Wang, M. Zhou, "Firms' green R&D cooperation behaviour in a supply chain: Technological spillover, power and coordination," International Journal of Production Economics, 2019, doi:10.1016/j.ijpe.2019.04.033.

[100] X. Zhu, Y. Zhang, Z. Zhao, J. Zuo, "Radio frequency sensing based environmental monitoring technology," in International Workshop on Pattern Recognition, 2019, doi:10.1117/12.2541098.

[101] T. Litman, London congestion pricing: Implications for other cities, Victoria Transport Policy Institute, 2012.

[102] L. Ecola, T. Light, "Making congestion pricing equitable," Transportation Research Record, **2187**(1), 53–59, 2010, doi:doi.org/10.3141/2187-08.

[103] V. Talla, M. Hessar, B. Kellogg, A. Najafi, J. R. Smith, S. Gollakota, "LoRa Backscatter: Enabling The Vision of Ubiquitous Connectivity," arXiv: Networking and Internet Architecture, 2017, doi:doi.org/10.1145/3130970.

[104] S. N. R. Kantareddy, I. Peters, I. Mathews, S. Sun, M. Layurova, J. Thapa, J.-P. Correa-Baena, R. Bhattacharyya, T. Buonassisi, S. Sarma, "Perovskite PV-Powered RFID: Enabling Low-Cost Self-Powered IoT Sensors," IEEE Sensors Journal, **20**, 471–478, 2020, doi:10.1109/JSEN.2019.2939293.

[105] S. N. R. Kantareddy, I. Mathews, R. Bhattacharyya, I. Peters, T. Buonassisi, S. Sarma, "Long Range Battery-Less PV-Powered RFID Tag Sensors," IEEE Internet of Things Journal, **6**, 6989–6996, 2019, doi:10.1109/JIOT.2019.2913403.

[106] Y. Jabareen, "An assessment framework for cities coping with climate change: The case of New York City and its PlaNYC 2030," Sustainability, **6**(9), 5898–5919, 2014, doi:doi.org/10.3390/su6095898.

[107] V. M. Thomas, "Environmental implications of RFID," in 2008 IEEE International Symposium on Electronics and the Environment, 1–5, IEEE, 2008, doi:10.1109/ISEE.2008.4562916.

[108] J. Su, Z. Sheng, V. C. M. Leung, Y. Chen, "Energy Efficient Tag Identification Algorithms For RFID: Survey, Motivation And New Design," IEEE Wireless Communications, **26**, 118–124, 2019, doi:10.1109/MWC.2019.1800249.

[109] R. Gradus, G. C. Homsy, L. Liao, M. E. Warner, "Which US municipalities adopt Pay-As-You-Throw and curbside recycling?" Resources, Conservation and Recycling, **143**, 178–183, 2019, doi:doi.org/10.1016/j.resconrec.2018.12.012.

[110] N. E. Weckman, N. Ermann, R. Gutierrez, K. Chen, J. Graham, R. Tivony, A. Heron, U. F. Keyser, "Multiplexed DNA identification using site specific dCas9 barcodes and nanopore sensing," ACS sensors, **4**(8), 2065–2072, 2019, doi:doi.org/10.1021/acssensors.9b00686.

[111] V. M. Thomas, "A universal code for environmental management of products," Resources, Conservation and Recycling, **53**(7), 400–408, 2009, doi: doi.org/10.1016/j.resconrec.2009.03.004.

[112] S. Saar, M. Stutz, V. M. Thomas, "Towards intelligent recycling: a proposal to link bar codes to recycling information," Resources, Conservation and Recycling, **41**(1), 15–22, 2004, doi:doi.org/10.1016/j.resconrec.2003.08.006.

[113] A. Condemi, F. Cucchiella, D. Schettini, "Circular Economy and E-Waste: An Opportunity from RFID TAGs," Applied Sciences, **9**(16), 3422, 2019, doi:doi.org/10.3390/app9163422.

[114] P. Krauchi, P. Wager, M. Eugster, G. Grossmann, L. Hilty, "End-of-life impacts of pervasive computing," IEEE Technology and Society Magazine, **24**(1), 45–53, 2005, doi:10.1109/MTAS.2005.1407747.

[115] M. Brink, F. Berkemeyer, J. Ohlendorf, G. Dumstorff, K. Thoben, W. Lang, "Challenges and Opportunities of RFID Sensortags Integration by Fibre-Reinforced Plastic Components Production," Procedia Manufacturing, **24**, 54–59, 2018, doi:10.1016/J.PROMFG.2018.06.008.

[116] K. Kunz, N. Lui, "Process Chemistry and Copper Catalysis," Copper-Mediated Cross-Coupling Reactions, 725–743, 2013, doi:10.1002/9781118690659.

[117] L. Guest, W. Guibène, S. Guruacharya, "Wireless Communications and Mobile Computing Green Internet of Things (IoT) : Enabling Technologies , Architectures , Performance , and Design Issues," 2018, doi: https://doi.org/10.1155/2018/3747562.

[118] Y. Duroc, D. Kaddour, "RFID potential impacts and future evolution for green projects," Energy Procedia, **18**, 91–98, 2012, doi:doi.org/10.1016/j.egypro.2012.05.021.

[119] S. H. Alsamhi, O. Ma, M. Ansari, Q. Meng, "Greening Internet of Things for Smart Everythings with A Green-Environment Life: A Survey and Future Prospects," ArXiv, **abs/1805.00844**, 2018.

[120] G. Orecchini, L. Yang, A. Rida, F. Alimenti, M. Tentzeris, L. Roselli, "Green Technologies and RFID : Present and Future," 2010.

[121] A. Ahmed, "Benefits and Challenges of Internet of Things for Telecommunication Networks," 2019, doi:10.5772/INTECHOPEN.81891.

[122] K. A. Alezabi, F. Hashim, S. J. Hashim, B. M. Ali, A. Jamalipour, "Efficient authentication and re-authentication protocols for 4G/5G heterogeneous networks," EURASIP Journal on Wireless Communications and Networking, **2020**, 1–34, 2020, doi:10.1186/s13638-020-01702-8.

An Anonymity Preserving Framework for Associating Personally Identifying Information with a Digital Wallet

Qazi Mudassar Ilyas[*], Muhammad Mehboob Yasin

College of Computer Sciences and Information Technology, King Faisal University, Al Ahsa, 31982, Saudi Arabia

A R T I C L E I N F O	A B S T R A C T
	Growing adoption of cryptocurrencies by institutional investors coupled with recurring incidents of loss of access to digital wallets have resulted in emergence of custodial services for high net worth individuals and institutions. However, such services are not economically feasible for the wider community of crypto owners who are left with no recourse for recovery of lost funds. This paper proposes a framework, AFAP, for associating certain personally identifying information with a digital wallet so that a user may prove ownership of the said wallet. Thus, the owner is able to establish his/her claim over funds associated with such a wallet in case of loss of access to it. We show that the proposed scheme has no adverse effect on anonymity, privacy and forgetfulness of personal information of the wallet owner.

1. Introduction

Cryptocurrencies are gaining much traction in the mainstream economic activity because of their global and fully decentralized nature, promise of freedom from political influence, and peer to peer nature of transactions [1]. The blockchain does not carry any information pointing to the owner of a particular digital wallet. Further, the use of Hierarchical Deterministic (HD) wallets [2] makes it harder to even group individual transactions carried out by one individual. The pseudo-anonymity thus provided by blockchain is one of the major factors contributing to the popularity of digital currencies. However, a drawback of this characteristic is the inability to associate a digital wallet address with an individual in order to prove ownership of a lost digital wallet.

The value of Bitcoin, leader of the pack, recently climbed to an all-time high of USD 24,058 on CoinDesk Bitcoin Price Index beating the earlier high of USD 20,000 reached on December 2017 [3]. Several businesses have already embraced digital currencies, while governmental entities are also preparing to bring them into mainstream financial systems [4]. Hence, cryptocurrencies are on track to become an important part of all financial transactions in future. However, digital currencies are in their infancy and several issues need to be resolved before they can become part and parcel of a common individual's life [5].

The Achilles' heel of Cryptocurrencies is the fact that access to all funds owned by an individual is tied to a complex long number that is almost impossible to remember. Therefore, this complex number, known as private key of a digital wallet, needs to be stored safely. Also, the private key needs to be kept in a secure manner because anyone with knowledge of this number can use the funds stored in the respective wallet.

A private key can be lost owing to hardware or software failure, personal carelessness in safekeeping the keys, or in some cases even death of the owner. Several users have reported losing their private keys thus making their funds inaccessible to them. A survey reported that a significant fraction of respondents had experienced loss of Bitcoin keys at least once [6]. According to careful estimates, about 4 million Bitcoins had been lost till 2017 [7]. More recently, more than 100,000 individuals lost Bitcoins worth nearly USD 190 million owing to the death of the owner of a cryptocurrency exchange QuadrigaCX [8]. Since there is no inherent mechanism in the Bitcoin framework to recover lost keys, a lost private key simply means all Bitcoins associated with that key are lost forever. Hence, there is need for a mechanism to restore access to funds in case respective private keys become permanently inaccessible.

Since a mnemonic passphrase is easier to memorize or record as compared to a complex number, it is widely used by digital wallets to create the private key [9, 10]. Though, this improves the user experience, yet this does not absolve the user from

responsibility of storing her/his passphrase in a safe and secure manner. As in the case of loss of private keys, loss of a passphrase implies loss of access to the respective digital wallet. In the following, we address the problem of loss of access to a digital wallet which may be because of loss of a private key or loss of the corresponding mnemonic passphrase.

We propose a two-step solution to this problem. As the first step, the owner is afforded the ability to prove ownership of a lost wallet. Subsequently, either the funds stored in the lost wallet may be returned to the rightful owner or he/she may be suitably compensated. In this paper, a framework for proving ownership of a wallet is proposed, while the second step of solution is subject of future work. The proposed framework, "Anonymity Preserving Framework for Associating Personally Identifying Information (PII) with a Digital Wallet (AFAP)", can be used to associate the PII of owner with a digital wallet in a secure fashion while maintaining the same level of anonymity as provided by the current cryptocurrency ecosystem.

The proposed framework comprises three entities, namely CryptoRegistry, PII Associating Transaction (PAT) and PII Wallet. CryptoRegistry is a trusted long-lived entity that registers a given PII against a digital wallet by digitally signing this association and helps in validating the same when required to do so. A PII Associating Transaction (PAT) stores the aforementioned association on the blockchain by embedding the said CryptoRegistry signature in an outgoing transaction. A PII wallet is a specialized digital wallet that facilitates the registration and validation processes.

Rest of the paper is organized as follows. The next section summarizes the related works. The proposed framework is presented in Section 3 detailing key components and schemes for registration of a digital wallet and claiming its ownership. A case study is provided in Section 4 that shows feasibility of the proposed framework. The paper is concluded with the discussion and future work.

2. Related Work

The issue of loss of access to a digital wallet has gained attention of researchers owing to an increasing number of incidents resulting in loss of digital currency worth millions of dollars belonging to thousands of individuals [11,12]. The solutions proposed till date focus on safekeeping of digital wallets to ensure continued availability of private keys as and when needed. These solution approaches can be divided into two main categories, namely user-centric approaches that facilitate one in safekeeping of one's digital assets and custodial approaches that transfer the responsibility of safekeeping to a trusted third party.

User-centric approaches include cold storage, offline wallets and specialized hardware wallets. Cold storage refers to safely storing the private key of a digital wallet on an offline medium ranging from secondary storage to plain paper [13,14]. An offline wallet is an air-gapped device that can generate transactions for export to a hot wallet, thus providing an improved user experience.

A specialized hardware wallet incorporates Hardware Security Modules (HSM) to store the private keys in a protected area of microcontroller storage which cannot be accessed from outside the device [15]. As suggested in [16], one can derive two values from the private key and store one of these value on a remote server. Protection against brute force password attacks is provided by keeping the second value on the local machine. A shortcoming of this scheme is that one needs to remember password to retrieve the value from the server. Further, damage to the local machine can result in permanent loss of access to the key.

Though all aforementioned approaches provide varying levels of protection against loss of private keys, yet the possibility of damage to or loss of access to physical medium still exists, which will result in loss of access to the respective digital wallet.

Another class of solutions relies on Shamir's secret sharing scheme, as adapted by [17], based on semi-trusted social network comprising friends of an individual. However, such schemes are more suitable for corporate clients since social networks of individuals are quite fluid and cooperation of "friends" cannot be guaranteed for unforeseeable future.

In custodial approaches, such as a browser-based wallet, an online account is maintained with a service provider that is used for storing and retrieving digital assets; examples include CoinBase[*], Kraken[†] and BitStamp[‡]. However, several instances have been reported where many clients lost access to their digital assets owing to the service provider going out of business. For an exposè, the reader may refer to [18,19]. To overcome this issue, clients are usually facilitated to backup their private keys as an assurance against the possibility of the service provider ceasing to exist. Although these online services relieve the owner from the responsibility of safekeeping digital assets, they are exposed to a multitude of vulnerabilities such as internal or external theft and cyber-attacks. Recently, specialized custodial service providers have also emerged that claim improved security against aforementioned vulnerabilities by utilizing air-gapped devices and employing higher standards of security. Two of the well-known examples of such service providers are Fidelity Digital Assets[§] and Ledger Vault[**]. However, these services have high associated costs and thus are suitable only for institutional clients or high net-worth individuals. It needs to be emphasized that privacy and anonymity are obviously compromised in all custodial services as digital assets in custody need to be associated with identity of respective owners.

One may conclude that none of the solutions proposed so far gives absolute guarantee against loss of access to a digital wallet while maintaining privacy and anonymity. Another perspective is to accept the occurrence of such eventuality as an inherent weakness of the blockchain technology and devise mechanisms to handle such situations. One such mechanism may be to prove ownership of a lost digital wallet and claim compensation for unspent amount stored in that wallet.

Various initiatives have been proposed for using blockchain to prove existence or ownership of a digital asset at a certain point in

---

[*] https://www.coinbase.com/
[†] https://www.kraken.com/
[‡] https://www.bitstamp.net/

[§] https://www.fidelitydigitalassets.com/
[**] https://www.ledger.com

time. For example, the online service named "Proof of Existence" [20] stores cryptographic hash of a digital document on blockchain that can be used to prove that the said document existed at a particular point in time. Further, integrity of the document is also established. Additionally, various schemes, referred to as Colored Coins [21], exploit the immutable characteristic of blockchain technology to store real world asset manipulation information on the blockchain [22, 23]. In [24] a DNS like naming system is proposed that associates human-readable names with respective internet resources by storing mapping information on the blockchain. In all such schemes, non-financial data is made part of the blockchain by embedding it into script of an OP_RETURN output; a special output of a blockchain transaction [25]. We also exploit the said scripting feature of OP_RETURN output to associate PII with a digital wallet by storing requisite metadata on the blockchain. The details of the proposed framework follow.

3. Proposed Framework

In order to overcome the wallet ownership issue, one may associate some Personally Identifying Information (PII), such as national ID, driving license or passport number with the digital wallet using the aforementioned output script of a transaction. In the following, we first introduce some obvious extensions of the use of aforementioned scripting feature for storing PII on the blockchain and point out that anonymity and privacy of the wallet owner may be compromised by using such simple schemes. We then present our framework to associate PII with a digital wallet and show that it preserves anonymity and privacy of the wallet owner.

3.1. Simple schemes for storing PII on blockchain

In this section, we present three ways of storing PII on blockchain to associate ownership of a digital wallet in the order of increasing complexity.

3.1.1. Plaintext PII

In this scheme, the owner of a digital wallet constructs a transaction and embeds his/her PII in one of the output scripts. This transaction is then sent on the network for processing. Since output script of a transaction can only be created by the originating digital wallet and cannot be tampered with after the transaction has been broadcast, the said information is irrevocably tied to the corresponding digital wallet. The wallet owner may record ID of the said transaction (TxID) for future reference. Once this transaction is confirmed, it becomes part of the blockchain, thus permanently associating PII with the issuing wallet.

In case of losing access to the private key of a digital wallet, henceforth referred to as a lost wallet, blockchain will be scanned to extract the aforementioned transaction using TxID and identify the rightful owner of the issuing wallet from the embedded PII. This scheme may be used to serve as a basic naming system for digital wallets akin to BitAlias [26] and OneName [27] etc. However, this scheme violates one of the basic principles of blockchain technologies, namely, ensuring anonymity of parties to a transaction. Therefore, this way of associating PII with a wallet may not be of general appeal.

3.1.2. Encrypted PII

To preserve anonymity of the wallet owner, one may create a public-private key pair and encrypt the PII with this public key before embedding it into the script. Now, to prove ownership of a digital wallet, one needs to locate the corresponding transaction on the blockchain and decrypt the PII using the respective private key. This requires the corresponding private key to be readily accessible when needed. This problem is akin to safely storing the private key, of the digital wallet, itself. Hence, this scheme does not reduce the responsibility of the wallet owner in safeguarding a private key.

An alternate way to relieve the owner of this added responsibility is to use pubic key of a well-known entity, such as a coin exchange, for encrypting the PII. Now, one needs to approach the said entity for decrypting the PII in order to establish one's claim of ownership. Though a wallet owner is absolved from responsibility of safekeeping any private keys, this scheme suffers from two drawbacks.

Firstly, the well-known entity may not be aware of such use of its public key. Also, it is not bound to maintain all its public private key pairs for foreseeable future. Therefore, it may not be in possession of the required private key when approached. Hence, owner claim may not be substantiated based on the encrypted PII. Secondly, since public key is supposed to be widely available, the encrypted PII is prone to dictionary attack.

3.1.3. Hashed PII

This method requires PII to be hashed using a well-known hashing algorithm and the resulting hash to be embedded in the script of a transaction in blockchain. To establish the claim of ownership, one may create hash of one's PII and validate it against the hash recovered from the respective transaction. In order to avoid dictionary attack, a sufficiently large random, commonly called salt, may be added to the PII. However, PII validation process now depends upon availability of the salt used. Therefore, the wallet owner is made to bear the responsibility of safekeeping the salt. Though, the salt may be in the form of hash of a memorable passphrase, the situation is reduced to a problem that is akin to safely storing the private key of a digital wallet.

3.2. An Anonymity Preserving Framework for Associating PII with a Digital Wallet

By now, the need has been established for a long-lived trusted third party with the responsibility of safekeeping the information required for proving association of a given PII with a digital wallet in an anonymous way. We call this entity a CryptoRegistry and propose a framework that preserves owner's anonymity and privacy as long as the CryptoRegistry is deemed trustworthy. We call this framework AFAP - An Anonymity Preserving Framework for Associating Personally Identifiable Information (PII) with a Digital Wallet.

The proposed AFAP framework comprises three components, namely a CryptoRegistry, a PII Associating Transaction (PAT) and a PII wallet. In the following, we give the details of each one of these components.

3.2.1. CryptoRegistry

We introduce the concept of a CryptoRegistry that is a trusted long-lived entity. A CryptoRegistry is required to perform the following functions:

- To provide an Application Programmer Interface (API) for registering the PII provided by a wallet owner

- To provide an API for making available the following information:

  - A public key $K_{Pub,CR}$

  - Registration fee, F_{CR}

  - A wallet address, W_{CR}

  - A sufficiently large random number, also known as salt, for defense against dictionary attack as discussed below, S_{CR}

  - A hashing algorithm along with its parameters, $\mathcal{H}$

  - Hash of (PII $\|$ S_{CR}), H_{ID}

  - Digital signature on PII, S_{CR}, F_{CR}, W_{CR}, $\mathcal{H}$ and H_{ID} using $K_{Priv,CR}$

  - The digital certificate to the effect that the said CryptoRegistry is owner of the respective public key, $K_{Pub,CR}$

It may be noted that the proposed scheme introduces a random salt to preserve anonymity since use of hash of PII alone may be linked to the original PII by brute force attack.

- To ensure availability of the PII, S_{CR}, $TxID_{PAT}$, and respective public-private key pair, once a PAT constructed by a PII wallet paying the fee F_{CR} to the wallet W_{CR} is confirmed on the blockchain. By virtue of its digital signature, the CryptoRegistry is bound to the PAT. As a trustee, the CryptoRegistry is also required to ensure confidentiality and security of information entrusted with it throughout its life time.

- To provide a list of PATs and corresponding digital wallet addresses associated with a given PII. It is to be noted that, in the interest of anonymity and privacy, the aforementioned information will only be provided to the rightful owner of PII or any authorized legal entity.

- Optionally, a CryptoRegistry may advertise special prefix to be used with OP_RETURN to facilitate searching a particular PAT on the blockchain.

3.2.2. PII Associating Transaction (PAT)

Generally a PII Associating Transaction (PAT) consists of three outputs. Firstly, an output transferring Registration fee F_{CR} to CryptoRegistry wallet W_{CR}. Secondly, an output transferring change to the wallet owner's change address. Thirdly, a zero valued output with OP code OP_RETURN and output script comprising the following information:

- Special prefix provided by the CryptoRegistry (if any)

- $\mathcal{H}$(PII $\|$ S_{CR}), H_{ID}

- Digital signature on PII, S_{CR} ,F_{CR}, W_{CR} and H_{ID} using $K_{Pub,CR}$

It is to be noted that since every Bitcoin transaction is tied to the originating wallet and cannot be tampered with after it has been confirmed, thus the above information, by virtue of being embedded in the transaction, becomes irrevocably tied to the corresponding digital wallet.

3.2.3. PII Wallet

PII wallet is a specialized digital wallet capable of constructing and verifying PAT transactions for associating itself with PII. For this purpose, it needs to communicate with a CryptoRegistry and perform a number of functions as detailed below:

- Accepting and storing PII of the wallet owner in a secure way

- Providing a list of available CryptoRegistries to the wallet owner

- Initiating the process for registration of given PII with the selected CryptoRegistry

- Accepting response from CtyptoRegistry comprising S_{CR}, F_{CR}, W_{CR}, H_{ID} , a hashing algorithm $\mathcal{H}$ and a digital certificate

- Verifying digital signature and hash value, H_{ID}

- Constructing PAT as described above and transmitting to the network

- Sending H_{ID} and transaction ID of PAT to CryptoRegistry after confirmation of PAT

- Periodically querying the said CryptoRegistry for confirmation of H_{ID} registration in its database

- When required, querying all CryptoRegistries for registration status of provided PII

- Displaying to the user a list of CryptoRegistries with whom provided PII is registered

3.2.4. Associating PII with a digital wallet

The sequence of steps for the purpose of registering a PII of the owner of a digital wallet is depicted in Figure 1.

The details of each step are as follows:

1. The user provides his/her PII to the wallet.

2. The wallet sends the provided PII for registration with the selected CryptoRegistry.

3. The CryptoRegistry selects a wallet (W_{CR}) for receiving registration fee (F_{CR}), chooses a random salt (S_{CR}) and calculates H_{ID} which is hash of PII concatenated with S_{CR}. It saves this information in its database for future reference with registration status as 'Not Confirmed'.

4. The CryptoRegistry sends PII, S_{CR}, F_{CR}, W_{CR} and H_{ID} , its signature on this information and its corresponding digital certificate to the PII wallet.

5. The wallet creates a PII Associating Transaction (PAT) using the received information and transmits it to the Bitcoin network.

6. The wallet periodically queries the blockchain for confirmation of PAT.

7. Once PAT is confirmed, the wallet notifies the CryptoRegistry of the confirmation by sending transaction ID of PAT (TxID$_{PAT}$) and H_{ID}

8. The CryptoRegistry queries the blockchain for confirmation of TxID$_{PAT}$

9. Upon confirmation, The CryptoRegistry updates PII registration status as 'Confirmed' and records corresponding TxID$_{PAT}$

10. The wallet periodically queries the CryptoRegistry for PII registration status

11. Upon confirmation, the wallet notifies the user that the provided PII has been successfully registered with the selected CryptoRegistry and records TxID$_{PAT}$ for future reference.
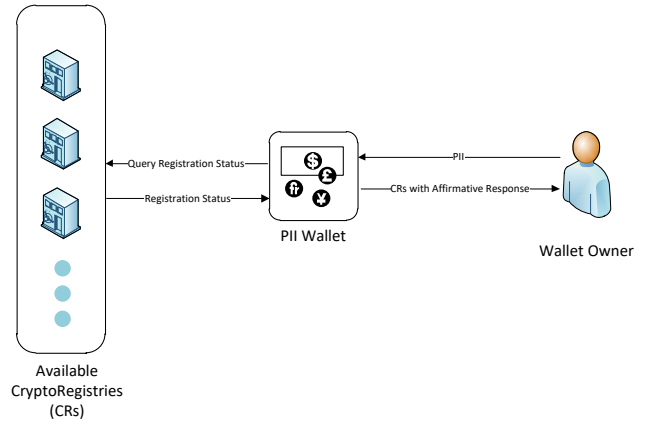
Figure 2: Claiming ownership of a lost wallet

The hash of given PII concatenated with salt is computed and matched against the one extracted from PAT. A successful match proves that the said PII was used to construct the PAT and that the wallet from which this PAT was broadcast is the wallet associated with the said PII. This way the ownership of the wallet, and any unspent funds associated with it, is established.

3.2.6. *Right to be forgotten*

One of the important principles incorporated into General Data Protection Regulation (GDPR) is a user's right to be forgotten (RtbF) allowing for retroactive erasure of all personal data. Considering the immutable nature of blockchain, it may appear that storing association of PII with a digital wallet may be in violation of the RtbF. However, the said right is safeguarded on two counts. Firstly, PII itself is not stored on the blockchain in any way, i.e., neither in plain text nor in encrypted form. Secondly, proving association of a particular PII with a digital wallet requires knowledge of the corresponding salt, which is a cryptographically strong random number. Hence, if the salt is forgotten, this association becomes unprovable. The right to forget this salt and any associated personal data can be exercised by the user with a request to CryptoRegistry. In [28], it has been shown that integration of such requirements into the current computing infrastructures is practically feasible.

4. Case study

In order to validate the proposed framework, a sample PAT was constructed by simulating interaction between a client and a typical CryptoRegistry as detailed below. The resulting transaction was successfully broadcast on Bitcoin Testnet. This was followed by simulating the situation of loss of this wallet. The lost wallet address was successfully retrieved from the blockchain by presenting only the PII. The following is the detail of interactions among the various components of the proposed AFAP framework.

4.1. PII Association with a digital wallet

The example client wishes to associate his PII "ABC1234567" with his digital wallet. The CryptoRegistry generates a salt, calculates hash of PII concatenated with this salt and returns the following information to the client along with his signature on the same:

CryptoRegistry Prefix = TESTPII

Salt: S_{CR} = 9586311452
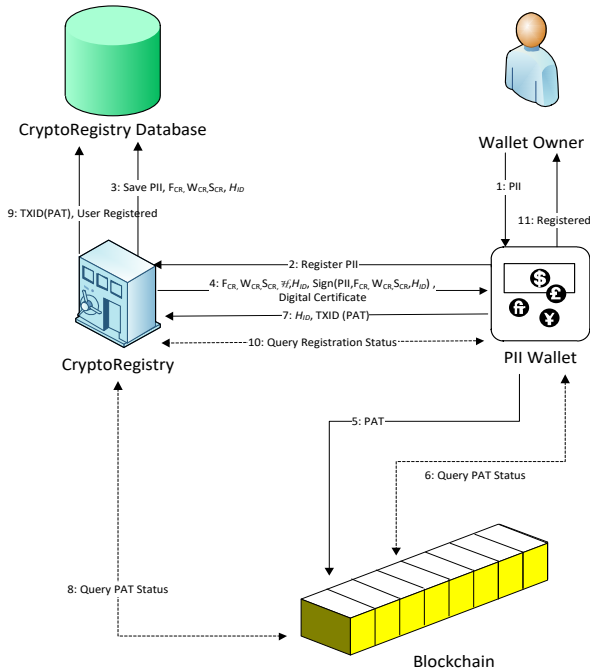
Figure 1: PII Registration in AFAP Framework

3.2.5. *Claiming ownership of a lost PII Wallet*

In the event of loss of a PII wallet, a PII wallet is installed and its recovery mode is initiated. The following sequence of events may follow (see Figure 2).

- The user enters her/his PII used for querying the registration status of the lost wallet.

- The wallet queries all known CryptoRegistries one by one using the provided PII.

- PII wallet receives response from the CryptoRegistries and displays the list of CryptoRegistries with affirmative response.

In the interest of owner's anonymity, the CryptoRegistry shall not reveal any information other than whether the subject PII is registered with it or not. The said CryptoRegistry may now be approached by the owner to obtain the transaction ID of the corresponding PAT along with the salt.

SHA1 (PII || Salt): H_{ID} = d49cdc68c804114b402bbaa108d324a80a19e354

Registration Fee: F_{CR}= 5mBTC

Wallet address for receiving registration fee:

W_{CR} = mpvkKZ6ysUYEGZuXR1FYRCKzykvMmtovyv

Signature:

Sign(PII,F_{CR}, W_{CR},S_{CR},H_{ID}) = AAwPRuNFlPvKCaic12aFRLYXf9ZbytXjBowXeKZm0kGNE TcplSyEE268401jgS8=

The client constructs the PAT with three outputs. Firstly, paying registration fee to W_{CR}, secondly the change to be returned to itself and finally a null data transaction with the script comprising prefix, hash and signature of the CryptoRegistry. The resulting script is given below:

Script: TESTPIId49cdc68c804114b402bbaa108d324a80a19e354AAwP RuNFlPvKCaic12aFRLYXf9ZbytXjBowXeKZm0kGNETcplSy EE268401jgS8=

This example transaction was broadcast on Bitcoin Testnet and can be found with the transaction id "985b15d99baf20facc67f1f925e51b7dd49b34dcbdc0a64bc0607a dc9100e0d7". Figure 3 shows the details of the said transaction as depicted by Bitcoin Block Explorer.
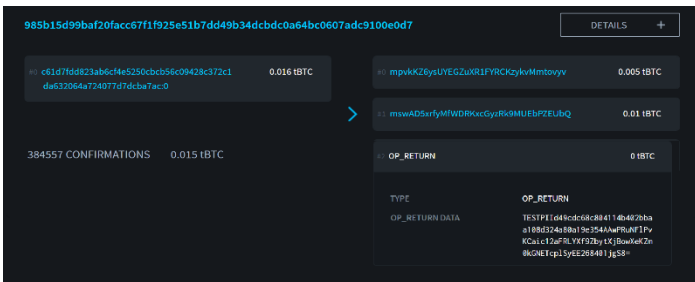
Figure 3: Details of PAT as shown by Bitcoin Block Explorer

It may be noted that the CryptoRegistry is required to store the transaction ID of PAT and other associated information in its database, as depicted in Figure 1.

4.2. Claiming ownership of a digital wallet

Assuming the owner knows the transaction ID of PAT and the salt used to construct the script of PAT, firstly PAT may be retrieved from blockchain using transaction ID. Then, the PII association may be proven by calculating hash of PII concatenated with salt and validating it against the script of null data output of PAT.

Since the main purpose of the proposed AFAP framework is to relieve the wallet owner from maintaining access to the private key of a digital wallet in a secure, safe and anonymity preserving manner, the owner is not assumed to maintain transaction ID of PAT and the respective salt. In such a case, the owner may present her/his PII to the CryptoRegistry to confirm association of the said PII with a digital wallet.

5. Discussion

The proposed AFAP framework uses blockchain itself to store the association of the Personally Identifying Information (PII) of the owner with her/his digital wallet. The proposed framework requires a persistent entity, called CryptoRegistry, which is mandated to maintain record of transaction IDs of PII Associating Transactions (PATs) and associated information in a secure way. The proof of ownership of a digital wallet lies in hash of PII and a random number, called salt, stored in a PAT.

In case of loss of a digital wallet, the owner may query available CryptoRegistries to confirm registration of her/his PII against a PAT from their databases. Once a confirmation is received, the owner may prove her/his identity to the satisfaction of the respective CryptoRegistry in order to retrieve transaction ID of PAT and respective salt. The hash extracted from PAT validates the PII and ownership of legal claimant of the PII is established. The proposed scheme, therefore, depends on long term availability of the CryptoRegistry used to register a digital wallet. In the interest of anonymity and privacy of the wallet owner, the CryptoRegistry may require due legal process in identifying the claimant before releasing transaction ID of PAT and respective salt.

From the aforementioned requirements of a CryptoRegistry, one may draw parallel with crypto exchanges or custodial services as trusted third parties for safekeeping of users' crypto assets. However, it may be noted that in the latter case, clients' funds are stored in the wallets owned by the trusted third party functioning as a custodian. Thus a user may lose all his/her funds in the event of hacking or bankruptcy of the custodian. In contrast, in the event of bankruptcy of a CryptoRegistry, the hash values stored in respective PATs cannot be verified owing to unavailability of corresponding salts, whereas the user funds remain intact. A user may safeguard against this eventuality by choosing to register with multiple CryptoRegistries. Though, the cost of registration may discourage registration with multiple CryptoRegisteries, it is expected that existing crypto exchanges will offer CryptoRegistry services and they may waive off these fees to increase their customer base.

The proposed framework brings the cryptocurrency ecosystem a step closer to the conventional banking system where an account holder may prove ownership of funds after losing access to corresponding checkbook or card. It may be noted that the protection afforded to an individual by AFAP is stronger than that of traditional banks since the funds and proof of ownership are stored in an immutable blockchain and there is no risk akin to bankruptcy.

6. Future Work

Although a user may claim ownership of her/his lost funds in the above manner, the process for recovery/compensation may involve legal procedures. One possible way of compensating the owner of a lost wallet is to create a compensation fund for such eventualities. Alternatively, a special transaction to credit the required funds to claimant's new wallet akin to the mechanism proposed for managing deflation of cryptocurrencies by [29]. Further, similar to the expiration flag proposed by them, the old wallet needs to be flagged as invalid in a way that blocks any future access to it or funds associated with it.

References

[1] Capgemini, BNP Paribas, "World Payments Report 2018," 55, 2018.
[2] V. Buterin, "Deterministic Wallets, Their Advantages and their Understated Flaws," Bitcoin Magazine, 2013.
[3] D.Z. Morris, "Bitcoin Hits a New Record High, But Stops Short of $20,000

| Fortune," Fortune, 2017.

[4] R. Krygier, "Venezuela launches the 'petro' its cryptocurrency," The Washington Post, 2018.

[5] M. Raskin, D. Yermack, Digital currencies, decentralized ledgers and the future of central banking, 2018, doi:10.4337/9781784719227.00028.

[6] K. Krombholz, A. Judmayer, M. Gusenbauer, E. Weippl, "The other side of the coin: User experiences with bitcoin security and privacy," in Lecture Notes in Computer Science (including subseries Lecture Notes in Artificial Intelligence and Lecture Notes in Bioinformatics), 2017, doi:10.1007/978-3-662-54970-4_33.

[7] J.J. Roberts, N. Rapp, "Exclusive: Nearly 4 Million Bitcoins Lost Forever, New Study Says," Fortune, 2017.

[8] T. Bult, "Thesis - Security analysis of blockchain technology Security analysis of blockchain technology."

[9] M. Palatinus, P. Rusnak, A. Voisine, S. Bowe, (bip-0039) Mnemonic code for generating deterministic keys, GitHub, 2013.

[10] Y. Liu, R. Li, X. Liu, J. Wang, L. Zhang, C. Tang, H. Kang, "An efficient method to enhance Bitcoin wallet security," in Proceedings of the International Conference on Anti-Counterfeiting, Security and Identification, ASID, 201-207, 2018, doi:10.1109/ICASID.2017.8285737.

[11] M. Conti, K.E. Sandeep, C. Lal, S. Ruj, "A survey on security and privacy issues of bitcoin," IEEE Communications Surveys and Tutorials, 2018, doi:10.1109/COMST.2018.2842460.

[12] U. Mukhopadhyay, A. Skjellum, O. Hambolu, J. Oakley, L. Yu, R. Brooks, "A brief survey of Cryptocurrency systems," in 2016 14th Annual Conference on Privacy, Security and Trust, PST 2016, 1-5, 2016, doi:10.1109/PST.2016.7906988.

[13] S. Eskandari, D. Barrera, E. Stobert, J. Clark, A first look at the usability of bitcoin key management, ArXiv, 2018, doi:10.14722/usec.2015.23015.

[14] R.N. Akram, K. Markantonakis, D. Sauveron, "Recovering from a lost digital wallet: A smart cards perspective extended abstract," Pervasive and Mobile Computing, 2016, doi:10.1016/j.pmcj.2015.06.018.

[15] O. Boireau, "Securing the blockchain against hackers," Network Security, 2018, doi:10.1016/S1353-4858(18)30006-0.

[16] E.M.D.W. Brickell, SECURE STORAGE OF PRIVATE KEYS, United States, 2005.

[17] S. He, Q. Wu, X. Luo, Z. Liang, D. Li, H. Feng, H. Zheng, Y. Li, "A Social-Network-Based Cryptocurrency Wallet-Management Scheme," IEEE Access, 2018, doi:10.1109/ACCESS.2018.2799385.

[18] L.J. Trautman, "Virtual Currencies: Bitcoin & What Now after Liberty Reserve and Silk Road?," SSRN Electronic Journal, 2014, doi:10.2139/ssrn.2393537.

[19] U. Chohan, "The Problems of Cryptocurrency Thefts and Exchange Shutdowns," SSRN Electronic Journal, 2018, doi:10.2139/ssrn.3131702.

[20] M. Crosby, Nachiappan, P. Pattanayak, S. Verma, V. Kalyanaraman, "Blockchain Technology - BEYOND BITCOIN," Berkley Engineering, 2016.

[21] M. Rosenfeld, "Overview of colored coins," 13, 2012.

[22] L. Bell, W.J. Buchanan, J. Cameron, O. Lo, "Applications of Blockchain Within Healthcare," Blockchain in Healthcare Today, 1-7, 2018, doi:10.30953/bhty.v1.8.

[23] H. Min, "Blockchain technology for enhancing supply chain resilience," Business Horizons, 2019, doi:10.1016/j.bushor.2018.08.012.

[24] M. Ali, J. Nelson, R. Shea, M.J. Freedman, "Bootstrapping Trust in Distributed Systems with Blockchains," USENIX ;Login:, 2016.

[25] M. Bartoletti, L. Pompianu, "An analysis of bitcoin OP_RETURN metadata," in Lecture Notes in Computer Science (including subseries Lecture Notes in Artificial Intelligence and Lecture Notes in Bioinformatics), 2017, doi:10.1007/978-3-319-70278-0_14.

[26] Y.G. Malahov, "BitAlias I Aka Usernames for Bitcoin," Medium, 2015.

[27] H. Kalodner, M. Carlsten, P. Ellenbogen, J. Bonneau, A. Narayanan, "An empirical study of Namecoin and lessons for decentralized namespace design," 14th Annual Workshop on the Economics of Information Security (WEIS), 2015.

[28] E. Politou, E. Alepis, C. Patsakis, Forgetting personal data and revoking consent under the GDPR: Challenges and proposed solutions, Journal of Cybersecurity, **4**(1), tyy001, 2018, doi:10.1093/cybsec/tyy001.

[29] H. Gjermundrød, I. Dionysiou, "Recirculating lost coins in cryptocurrency systems," Lecture Notes in Business Information Processing, 229-240, 2014, doi:10.1007/978-3-319-11460-6_20.

Switching Capability of Air Insulated High Voltage Disconnectors by Active Add-On Features

Mariusz Rohmann[*], Dirk Schräder

Siemens Energy Global GmbH & Co. KG, SE GP T SP R&D TC ME, Research and Development, Berlin, 13629, Germany

A B S T R A C T

The need of add-on features (secondary contacts) for current paths of air insulated high voltage disconnectors switching capabilities (e.g. bus transfer switching) is introduced. The relevant product components for the switching capability and their functionality is described, which is giving boundary conditions for adding features necessary to achieve the switching capability. Possible features are discussed with necessary properties and performance. Those are separated in passive and active solutions, which are focused. Given solutions successfully applied, are explained and capabilities are shown based on experimental design and testing – where calculations and/or computational analysis are not shown (consequently no resulted data of such approaches), as those have not been used for the given solutions (the disconnector is still a low-cost product within industrial business circumstances, where invests for comprehensive design activities are unfortunately very limited). The testing of the solutions is covered with information for limited switching capability values and measures and/or further, partially theoretical, alternative solutions, for increased values. Also, the testing itself and possible laboratories with certain test execution opportunities and/or challenges is elaborated. The conclusion provides a market view, product users perspectives, in regards of the applicability for passive solutions and the need for active solutions.

1. Introduction

This paper is an extension of work originally reported in Proceedings of the International Conference on High Voltage Engineering and Technology (Central Power Research Institute, India) [1].

The standardized minimum switching capability of air insulated high voltage disconnectors (negligible currents of 0.5 A for rated voltages up to 420 kV as per IEC 62271-102) [2, 3] is frequently exceeded by three main applications:

- no-load conditions of transformers (inductive)

- long high voltage conductors (overhead lines, capacitive)

- bus-transfer cases within substations with more than one bus bar

The bus bar transfer case, being very common, is standardized by the IEC 62271-102, where the latest edition partially considers increased values (bus-transfer voltage and current) [2, 3].

A disconnector in its standard configuration will not be able to switch exceeded values. The damages on the contact system (contact erosion) would be too high to be still operational after such a switching case. The application of add-on features is necessary (secondary contact arrangements, like additional contact fingers), so that the contact system is protected and accordingly switching capabilities are achievable. Those add-on features are design as passive and/or active secondary contact arrangements [4-9].

The Main difference of the passive and active solutions is driven by the operational speed, where passive solutions are fully dependent on the current path design and active solutions are integrating semi or full independency of the current path design.

2. Current Path Operation

2.1. Current Path Types

The disconnector type determines the current path outlining (shape). The known types are groupable in inline disconnectors (the center break, the double side break, the side break, the V-type (based on center break or double side break disconnectors), the vertical break and the knee-type disconnector) and busbar

disconnectors (the vertical reach, the semi-pantograph and the pantograph disconnector).

For the inline disconnectors the current path operation occurs horizontally, and a common secondary contact arrangement solution can principally be achieved. For the busbar disconnectors the current path operation occurs vertically – a common secondary contact arrangement is not known to be achievable [4-9].

For the busbar disconnectors, the vertical reach and the semi-pantograph are likely to share a secondary contact solution with their familiars of the inline group (vertical break and knee-type respectively).

The pantograph disconnector is very unlikely to achieve a common secondary contact solution with one of the other mentioned disconnector types – its design principal of the current path is too distinctive.

2.2. Current Path Opening and Closing

Disconnectors are only operational under no-load conditions. The requirements for switching capability are given by residual currents, consequently main contact systems are designed for static current carrying capabilities [1-9].

In order to protect the main contact system (carrying rated continuous currents and short-circuit currents) it is necessary for any secondary contact arrangement to run ahead of the main contact system while the closing operation and to go behind the main contact system while the opening operation of the current path.

This is essential for the protection purpose, as the switching capability in any case results in arcing (lightning) and accordingly arc erosion resistance requirement. An optimized contact system in regards of the main purpose of carrying current will not be able to sustain such arcing erosion, where the main purpose of the secondary contact arrangement is this resistance but will not be suitable for carrying current continuously.

3. Secondary Contact Types

Where the main contact is optimized for low resistance (best current carrying capability while minimized losses, heating or hot spots) and longest lifetime, the secondary contact needs optimization for high resistance and a minimum lifetime (considering the IEC 62271-102 or specific market/customer requirements) [1-9].

Striving for this, the main contact needs:

- To be decoupled in switching operation conditions of the disconnector for being save from damages by arcing (lightning).
- A contact pressure suitable for the current carrying capability, but as small as possible for friction avoidance (no-load operations).
- A material choice suitable for the current carrying capability, but a surface supporting lowest friction (no-load operations).

Usually this results in silver plated copper fingers with applied springs to achieve the necessary contact pressure – being still one of the most economic solutions. Highly controlling the elasticity of the used copper may allow spring elimination but is likely to require silver-graphite-plating (increasing lubricating properties,

decreasing friction), which again is more costly due to the manufacturing process efforts.

The secondary contact needs:

- To be decoupled in normal operation conditions of the disconnector for being save from damages by rated continuous currents or short-circuit currents.
- A contact pressure suitable for the switching capability – residual currents need to be carried safely, so that arcing on the main contact cannot occur. Additionally, considering certain numbers of switching operation and occurring erosion, the chosen contact pressure needs to overcome accordingly outline changes (reduction) of the contacts (sacrificial contacts) - preventing jumping or bouncing effects of the secondary contact and any arc-back (reigniting) due to contact separation.
- A material choice suitable for the arc erosion resistance (residual currents)

In dependence of the secondary contact solution, the material choices vary significantly – again under economic aspects, so that any material usage is minimized as much as possible in regards of the used solution.

Used names for known solutions like arcing horn, guiding horn, bus-transfer device or filter-switching device are not used. Those are given mainly by the reasons for occurrence of the residual currents to be switched and are not reflecting the common task [1].

3.1. Passive Secondary Contacts

Passive solutions, depending fully on the operation speed of the disconnector, require materials with high arc erosion resistance. Material suitability is firstly indicated by a high melting point and a high tensile strength, nevertheless the tensile strength of a material is sometimes significantly reduced when heated (even far below the melting point). Tungsten, the element with the highest melting point of the periodic table of the elements, is a proven choice.

Market availability (raw material, alloys, machinability) and implied material costs is another important factor.

Finally, the resistance to corrosion and the conductibility is still of importance, so that mostly copper alloys will be used and respectively proportions needs to be defined. Further optimized material usage will be achieved by inlet applications and possible conductive connection methods need to be considered for the material choices, as well.

Reported application examples have been [1]:

- Passive add-on finger – a copper zirconium alloy finger with a copper tungsten alloy inlet and a copper tungsten alloy stud (high tungsten content – more than 3 quarters of the alloy experienced to be necessary of tungsten)

- Passive add-on needle – copper zirconium alloy crossbars with copper tungsten alloy inlets and 'tungsten needle'

The examples also successfully applied zirconium, which is another high-melting point element with a high enough tensile strength, also heated. Principally the noble metals are potential candidates: Ruthenium (Ru), Rhodium (Rh), Osmium (Os),

Iridium (Ir), Zirconium (Zr), Hafnium (Hf), Vanadium (V), Niobium (Nb), Tantalum (Ta), Chromium (Cr), Molybdenum (Mo), Tungsten (W), Rhenium (Re) and Technetium (Tc).

3.2. Semi-Active Secondary Contacts

Passive secondary contact may be enhanced by detailed design features for generating air flows advantageous for reducing the arcing time, so to increase the possible switching quantity or increase the switching capability.

For this, the air flow needs to be directed to one of the foot points of the arcing (inception point or arc origin), so that the separation or arc interruption will be facilitated. The enhancing effects are limited, but a significant advantage is the minimum weight effect for consideration of the mechanical behavior of the current path.

One successfully applied example is shown in figure 1, where a simple synthetic material could significantly increase the capability withstanding heating sufficiently.
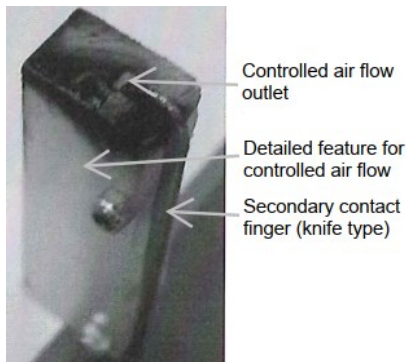
Figure 1: Example of Air Flow Controlling Detailed Feature

The controlled air flow is not only forced into the right direction towards the arcing foot but is also determined for volume and speed by the given passage. As the success was experimental, the air flow details have not been measured, but the switching current was more than doubled (form 6 A to 15 A) at the same switching voltage (21 kV). The achieved switching current was limited by the used laboratory, so that the capability limit of the solution could not be determined.

The finger outline (knife type) allows a relatively long air flow controlling item and therefore passage, which is important for determining the speed of the used volume. The passage is generated as a cuboid-like channel between the detailed design feature and the secondary contact finger by the fixation solution of the feature on the finger. The applicability depends highly on the outline of the used secondary contact, so that the shown example is limited in its applicability accordingly.

Further it represents rare occasions, where the type test execution allowed contractually a limit testing (in this case limited by the laboratories capabilities). The usual situation, as valid for all other shown cases, is a design and testing as per standard and its required values to be fulfilled (mainly IEC 62271-102 [2] or specific customer requirements).

3.3. Active Secondary Contacts

Full active secondary contacts will be designed with elements storing kinematic energy, which is released when required and

provide the independent speed – classically those elements will be springs [5-9].

Figure 2 shows an example of such an active secondary contact. Compared to known passive contact systems it could be validated, that the switching capabilities are achievable with using only classical materials – the using of high-melting point materials or accordingly copper alloys was not necessary.
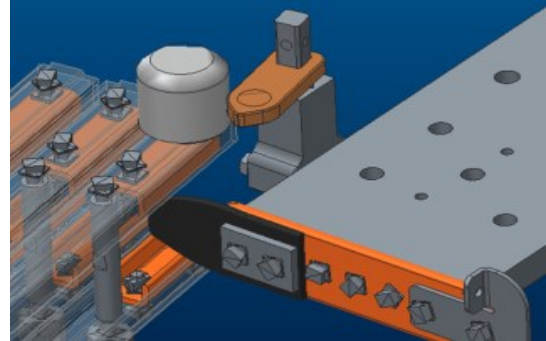
Figure 2: Active secondary contact system (double side break disconnector)

Figure 3 shows the same example of such an active secondary contact at a position of the closing operation, where the secondary contact is ahead of the main contact system. The copper sheet needs to run over the stainless-steel stud, so that the secondary contact goes behind the main contact system while the opening operation.
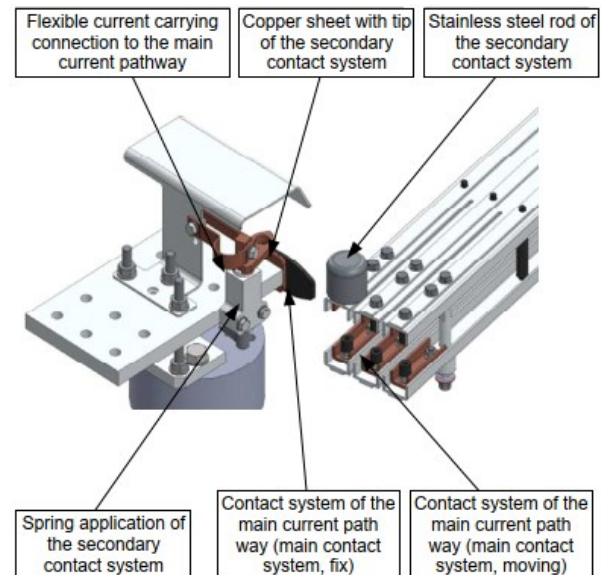
Figure 3: Feature Active secondary contact system in ahead-position

The spring is effectively applied only while the opening operation, so that the kinematic energy is specifically used for the demolition of the arc.

The intensity of the arc erosion while the closing operation is of much lower severity – as the arc arises, while the arcing distance decreases steadily. The arcing time is generally lower and the arc erosion stress on the foot points is less. In contrary, the erosion while the opening operation is of much higher severity – as the arc arises, while the arcing distance increases steadily until a high enough distance for insulation by air is achieved. In dependence on the arc intensity (voltage and current) the arcing time is

maximized in relation to the air gap necessary for demolition – exactly here the spring application comes into effect. Where passive solutions need to withstand this to full extend (only minimizable by dimensioning and eventually material elasticity), active solutions can significantly reduce the time independent speed. Of course, also active solutions require right dimensioning, as the used spring energy needs to fit to the allowed arcing time – achieved air gap at the time of arc ignition.

The spring application of active solutions does not require high-melting point material, which avoids the before mentioned challenges in regards of market availability. This allows again the usage of general core activities of disconnector designer and supplier concerning the current paths – plated copper / contact systems with spring applications.

Additionally, secondary contacts can be equipped with air flow controlling detailed feature. The shown example of figures 1 and 2 gives only little room for this.

3.4. Medium Voltage Switching Units

A further possibility for highest switching capabilities is given by the application of medium voltage switching units for active secondary contact systems. Those can be SF6 switching units or vacuum switching units, where the latter one is by far the preferred one as the first one is getting banned already in certain markets due to its negative environmental effects. Such a unit provides the advantage that in case of closing operations being kept open, no lightning occurs (because of the gap in the chamber of the unit). Important considerations of the application:

- Need for short-circuit resistivity in regards of the disconnector application
- Weight implications for the mechanical operation behavior of the current path – especially if applied to the moving part
- Potential requirement for complex kinematics for the operation of such units (tensioning and releasing unit internal spring applications)
- Protection of such units against environmental effects (e.g. rain or ice) with housings

The so far reported solutions (passive and active) are providing the big advantage against potential switching units application, that the weight implications is only low or eventually moderate and that the environmental protection coverage is mostly already given by the accordingly protection of the main contact system (or by simple and small size increase of the same).

The following earthing switch examples (figures 4 to 6) show known and successfully applied medium voltage switching units, which provide a technical basis being transferable to disconnectors.
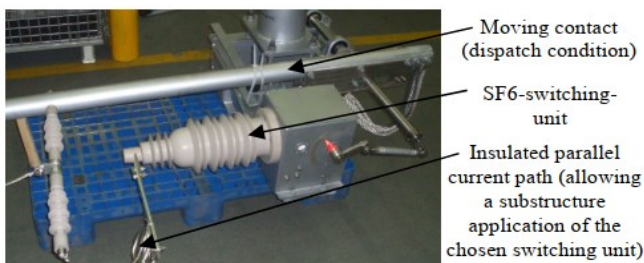
Figure 4: Earthing Switch Application with SF6-Switching-Unit (switching capability beyond class B as per IEC 62271-102)
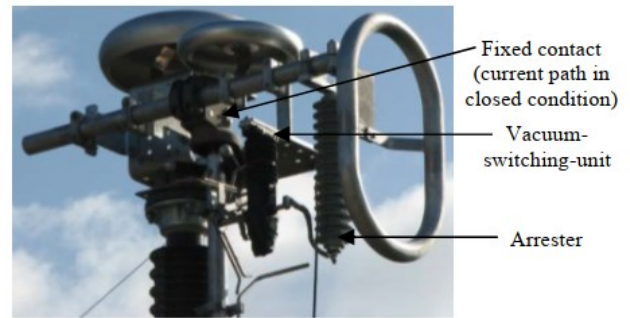
Figure 5: Earthing Switch Application with Vacuum-Switching-Unit and Arrester (switching capability requirement without lightning fulfilled)
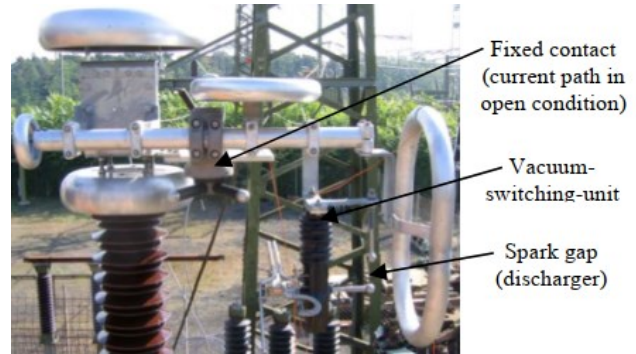
Figure 6: Earthing Switch Application with Vacuum-Switching-Unit and Spark Gap (switching capability requirement without lightning fulfilled)

4. Values and Testing

In practice, as well as per IEC 62271-102, type test confirmations are possible and common [2,3].

Regarding passive secondary contacts a confirmation of the type test for the same type of disconnector is physically evident for increasing disconnector sizes (higher rated voltages), as the arm length of the current path increases and therefore the angular speed increases. This provides beneficial conditions for the secondary contact as the arcing time gets reduced the reference type test is safely applicable. The same is difficult for decreasing disconnectors sizes by reduced current path arm length and consequently reduced angular speed and increased arcing time. Even with the proven margin within a type test, the applicability is not secure. Such kind of confirmation challenges will be increased by changing the disconnector type.

For active secondary contacts the confirmation situation is much more convenient based on the independent speed. The applicability or validity of successful type tested active secondary contact is evident based on the positioning of the secondary contact elements for their function and in relation to the main contact system (protection purpose) in accordance to the reference type test. The disconnector operational speed is not relevant. This is another important advantage of active solutions.

4.1. Switching Capability Values

The reported solutions are classical solutions and followed the edition 1 of IEC 62271-102. Therefore, the switching capability target was usually set to a switching current of 1600A, the limit given with the rule for 80% of the rated continuous current. Further, the switching voltage was mostly set to 100V, as most of

the market requests have been served with accordingly rated voltages (up to 170kV as per edition 1 of IEC 62271-102, but often also for higher rated voltages based on customer acceptance). The reported example of an active solution followed this approach, as it was achieved before the release of edition 2 of the IEC 62271-102 [2,3].

Since edition 2 of IEC 62271-102 [2], the general limit of 1600A is only applicable for rated voltages <245kV. For rated voltages of ≥245kV and ≤550kV, the limit is set to 4000A, which is a significant increase in arcing intensity for the switching capability (even though the percentage approach was reduced to 60%). Further, the switching voltage required is not only based on ranges of the rated voltage, but additionally dependent on the rated continuous current [2, 3].

Following an approach to design a solution for covering a major part of the values with this given current scenario is very difficult, if not impossible with passive secondary contacts. Latest for rated voltages of 245kV and above this will require active secondary contacts, as those provide higher capabilities – beside the advantageous confirmability.

4.2. Test Circuits and Laboratories

Edition 1 of IEC 62271-102 requested a power factor of 0.15 for the test factor and certain conditions for the transient recovery voltages, where the edition to requires a power factor of 0.5 and skipped the part for the transient recovery voltages. On the maintenance for at least 3s after interruption of the power frequency recovery voltage is no change between the editions of IEC 62271-102 [2, 3].

In fact, this is reducing the arc intensity for the type test. However, first experiences indicate that this is far not enough for having passive secondary contacts capable to achieve the before mentioned approach on switching capability values [7-9].

Basically, high power laboratories are providing equipment for testing the switching capabilities of air insulated high voltage disconnectors. The following restrictive points for the test execution of disconnectors must be carefully aligned with such potential laboratories:

- Space constraints – as disconnector test objects easily lead to high installation space necessary, specifically with increasing rated voltage of the test object. Ground fixation can be a challenge regarding the typical outline of a disconnector, which is potentially unusual for the equipment tested in the concerned laboratory. The installation height is another specific aspect of a typical disconnector outline with potential high challenge for the concerned laboratory

- Where the switching current to be tested is generally unproblematic for high power test laboratories, the switching voltage to be tested has carefully to be checked with the laboratory. This is even more stressed regarding the required values for high rated continuous currents following the IEC 62271-102 edition 2 [2] (identifying a high voltage laboratory with capabilities for the switching currents to be tested is very unlikely).

- The time necessary for the test execution is an important factor, as well. As such tests are usually not the core business of accordingly laboratories, the necessary slot size by time

needs carefully to be aligned – the laboratory utilization, the throughput of test quantities, will be significantly impacted. The main determination of the overall test execution time is not mainly given by the quantity of operations to be done, but by the necessary time between to operations. This can be called cooling time and has to be determined by the disconnector designer/ supplier. Classically the focus was given by the avoidance of a motor overload (operating mechanism of the disconnector, automated test execution), which is with nowadays' motor performances not an issue. In fact, the focus needs to be given to the heating of the secondary contact – pre-heated secondary contact in view of subsequent operation. A maximum time gap between 2 operations is not regulated by standards and a realistic occurrence in the field will not be within minutes (maybe within days). For the before mentioned passive solutions a minimum time gap of 2 minutes was found to be enough (based on the high-melting point element tungsten). Considering 100 necessary operations (IEC 62271-102) [2], this ends up already to 3 hours, where setting, operation and frequent visual inspection has to be added, so that this part of the test execution easily need already a full day

Figure 7: Switching Capability Type Test Set-Up of a 245kV Center Break Disconnector with a Passive Add-On Finger Solution

Market demands represented in standards or resulting in new versions of standards are especially in the case of IEC globally driven. Based on this the possible design realization may be given already, but not generally. Usually it will be left to suppliers and customers to foster such realization, which will require consideration and alignment with testing facilities for realizations of accordingly type tests. The basis will be for the supplier, as well was for testing facilities, positive economic value adds. Potential volume, utilization and market prices will need to provide a

minimum basis for judging accordingly efforts. Partially even the requesting customers will join in a collaborative approach covering certain costs for realization (invests on disconnector supplier and/or tasting facility sides).

The switching capability testing for air insulated high voltage disconnectors could already be executed successfully with medium voltage high power laboratories (refer to figure 7). On first view this seems to be unusual but was possible since the above restrictive points have been servable.

5. Applicability Conclusion

As in every case of significant changes in standards and regulations there will be a transition period before the market will strictly insist. The established secondary contact solutions for the switching capability realization will therefore persist on the market for a certain period.

The market is already demanding steadily increased rated continuous currents, which is also reflected by the edition 2 of IEC 62271-102 [2], but not comprehensively. This is fostering the increased switching capabilities reflected in the edition 2 of IEC 62271-102 [2], but accordingly market demands run after the rated continuous current demands.

5.1. Passive Solutions

The shown examples are well suitable and proven especially for the rated voltage application <245kV, also in regards of the second edition of IEC 62271-102 [2]. Nevertheless, those solutions are at its limits and may exceed the given capabilities by semi-active detailed features. It requires the management of high-melting point elements for the design and the purchasing.

Consequently, it is reasonable that those passive secondary contact solutions will experience a replacement by simple active secondary contact solutions (e.g. the one reported above), as those allow increased switching capabilities and the avoidance of high-melting point elements.

5.2. Active Solutions

It is expected that active solutions will be the common solution in the feature based on the potentials given above – specifically in case of simple material usage and spring application, as reported above.

Considering the highest switching capability requirements as per edition 2 of IEC 62271-102 [2] – for the highest rated voltages and rated continuous currents – a strong demand for solutions integrating medium voltage switching units (chambers) is expected. Taking into account typical examples of bus-transfer disconnectors, like the pantograph disconnectors, and accordingly expected switching capabilities requirements as per IEC 62271-102 [2] or even above based on customer requirements, it is unlikely to be achievable with kinds of simple active solutions without compromising on functional reliability.

Vacuum chamber applications to the mating contact of pantograph disconnectors of 420kV rated voltage are under investigation and a final design achievement will need to be proven by type testing.

5.3. Earthing Switch Solutions

Earthing switches by its design and purpose must consider distinctive switching capabilities against disconnectors. Already accordingly standards are covering those switching capabilities reasonably distinctive [1-3].

Introduced earthing switch references with passive, active or active solutions considering medium voltage switching units are to be discussed separately. Basically, those known and successfully applied solutions are transferrable to disconnectors, but need specific considerations – e.g. the current path of an earthing switch is not having any duty of carrying rated continuous current, where this is one of the main duties of the current path of the disconnector (also this underlies exceptions for the earthing switch for certain applications) [1-9].

Conflict of Interest

The authors declare no conflict of interest.

References

[1] M. Rohmann, D. Schräder, G. Kurra, S. Challa, S. Mogatala, Swicthing Capability of Air-Insulated High Voltage Disconnectors", IEEE, 2019, ISBN 978-1-5386-7577-9/19

[2] IEC 62271-102, High-voltage switchgear and controlgear – Part 102: Alternating current disconnectors and earthing switches, Efition 2.0, 2018.

[3] IEC 62271-1, High-voltage switchgear and controlgear – Part 1: Common specifications for alternating current switchgear and controlgear, Edition 2.0, 2017.

[4] CIGRE Technical Brochure No. 511: Final Report of the 2004 – 2007 International Enquiry on Reliability of High Voltage Equipment, Part 3 – Disconnectors and Earthing Switches, 2012

[5] S.S. Rao, "Switchgear Protection and Power Systems (Theory, Practive and Solved Problems)", Khanna Publishers, 2008.

[6] M. Rohmann, "Analysis of Assembly Times for a Gas-Insulated High Voltage Switchgear on the Level of Components", M. Sc. Thesis with Siemens AG at FernUniversitaet Hagen, 2008.

[7] H. Lindner, Dr. Harry Brauer, Prof. Dr. Constants Lehmann, "Pocket Book of Electro-Technics and Electronics", Fachbuchverlag Leipzig, 1999, ISBN 3-446-21056-3.

[8] G. Balzer, Bernhard Boehle, Kurt Haneke, Hans Georg Kaiser, Rolf Pöhlmann, Wolfgang Tettenborn, Gerhard Voß, „Substations", 9th ed., Cornelsen Verlag Schwann-Giradet Duesseldorf, 1992, ISBN 3-464-48233-2.

[9] Prof. Fleck, P. Kulik, "High and Low Voltage Substations", Verlag W. Girardet Essen, 1975, ISBN 3-7736-0262-6.

Sensitivity Analysis of Data Normalization Techniques in Social Assistance Program Decision Making for Online Learning

Edy Budiman[*], Unmul Hairah, Masna Wati, Haviluddin

Department of Informatics, Universitas Mulawarman, Samarinda, 75119, Indonesia

A R T I C L E   I N F O

A B S T R A C T

Data sensitivity analysis using normalization techniques in decision making has an impact on preference values and rankings in the case of social assistance programs for student online. The distribution of assistance is disproportionate and not on target to potential recipients. This study aims to analyze data sensitivity from simple data normalization techniques and linear techniques in decision making. In particular, a simple data normalization technique is illustrated using Simple Additive Weighting (SAW), and a linear technique using the VIšekriterijumsko KOmpromisno Rangiranje (VIKOR) method. There are five criteria used, obtained from observation through measurements and a questionnaire from 400 students. The confusion matrix testing method is used to measure the value of data sensitivity, which includes precision, accuracy and error rate. The results of the study obtained data analysis sensitivity for each method shows that the distribution of normalized data in the selection of 10% (40 students) of positive target recipients, the sensitivity of the linear technique (Vikor method) is higher than the simple technique (SAW method). However, for the target of 15% (60 students) the simple method is higher. The results show that each data normalization technique for decision-making analysis has a different sensitivity value in terms of social assistance for target groups, although many studies suggest that certain methods may be better than others.

1. Introduction

Education World in the midst of a crisis due the Covid-19 pandemic causes UNICEF, WHO and IFRC [1] appeal that when the situation where the virus is spreading rapidly, schools must be closed and the education process must be continued through online learning activities using various media in "Prevention and Control of COVID-19 spreading in schools [1]". In response to this, the Indonesia Government issued a circular on the implementation of distance learning, through a Circular of the Minister of National Education regarding education policies during the Covid-19 emergency [2].

The closure of 217,270 schools and 4,670 higher education cause students: 25.5 million Primary Schools, 10.12 million junior high schools, 4.78 million senior high schools, 4.9million Vocational high school, 130 thousand children with disabilities schools and 8 million college-undergraduate students in higher education institutions must learn from home (LFH). However, to implement the policy is not as easy as expected. There are many things that make the implementation of online learning not optimal, the lack of facilities and technological literacy [3], the unpreparedness of educators for students [4], and there are several regions, certain areas that do not allow residents to use electricity (IT). In addition, the economic crisis caused by the pandemic has also become an emergency because it is in regard to community welfare issues.

The economic crisis problem has a significant impact on students in fulfilling internet needs for access to online learning, their parents cannot afford it and difficulties in providing more budget to buy internet data. Therefore, several Indonesia region government policies and educational institutions provide free internet data assistance to students to support the continuity of online learning.

The research study is motivated by the subjectivity in decision-making problems in the internet data assistance management to students. The distribution of data assistance is less than optimal and right on target to potential beneficiaries(student).

The normalized data technique according to research it is very important for the method of decision making, because the data

must be numerical and comparable to be combined into one score per alternative [5], The research revealed that normalization affects the results of the MADM method [6]. This study examines the popular effects of normalization procedures and shows that the empirical deformation of data caused by the use of normalization can influence the final choice [6], and Normalization Techniques for Analytical hierarchy process case study [7], about A state-of-the-art survey on the influence of normalization techniques in ranking for Improving the materials selection process in engineering design [8] and others. Therefore, it is the author's interest to apply and select appropriate normalization techniques and targeted handling in the distribution of internet data assistance programs.

In an effort to improve decision data analysis management, we propose a decision-making analysis method by providing a sensitivity study of decision-making methods in determining individual and group alternatives. We offer the SAW and Vikor analytical approach as a linear and simple method in preparing the decision matrix. In particularly. The study purpose was to provide an evaluation of the performance sensitivity of the VIšekriterijumsko KOmpromisno Rangiranje (VIKOR) and Simple Additive Weighting (SAW) methods in group decision making for ranking in internet data assistance programs. This study describes the results of the sensitivity analysis using the confusion matrix measurement approach to the sensitivity, which includes precision, accuracy, and error rate values.

The research contribution as a novelty in implementation and development extends to the use of decision-making analysis techniques and methods that affect preference assessments in handling cases of distribution of social assistance internet data packages for online learning.

2. Materials

2.1. An Overview Internet Data Assistance Program

One of the social assistance programs from the government and various universities and schools in Indonesia in dealing with the economic crisis of the community during the Covid-19 pandemic in the field of education is the distribution of internet data assistance to support students in learning online from home [9]. This program is managed by policymakers or stakeholders in an effort to maintain the continuity of learning activities. The object of a case study at a tertiary institution in East Kalimantan Province, Indonesia, especially for undergraduate students of the Informatics Department. Mulawarman University.

The initial activity was carried out by observation through collecting information about the needs for the amount of internet data usage, and the economic abilities of students. The results of the observations obtained five parameters which are used as criteria in decision making are; Use of Internet Data (C1), Subjects of Learning (C2), Credit Courses (C3), Economic Capability (C4) and Purchasing Power Data (C5). The description of student characteristics is shown in Table 1.

Table 1 presents the characteristics of student beneficiaries who are divided into 3 categories of beneficiaries who have the highest attributes of the benefit criteria or the maximum (C1, C2, C3), and the lowest in the cost or minimum attribute criteria (C4, C5), meaning that the main priority of the potential beneficiaries.

the benefits are those with high internet data usage, the number of courses and credits. Whereas for the low category are those (students) who are not targeted for assistance, this category has minimal internet data usage, few courses and credits, and has high economic capacity and data purchasing.

Table 1: Student Characteristics

Metrics	C1	C2	C3	C4	C5
Attribute	Max	Max	Max	Min	Min
Mean	749.21	7	20	2,133,113	237,000
Median	732.2	7	21	1,950,000	200,000
Mode	490.6	7	24	2,000,000	100,000
Std. Dev.	146.6	1.2	3.1	649,083.2	124,779.5
Min.	490.56	5	14	1,000,000	100,000
Max.	1,130.17	9	24	4,000,000	500,000
N	400	400	400	400	400

2.2. Sensitivity Analysis in Decision Making

The sensitivity of data analysis in decision making is influenced by many factors. This study discusses the sensitivity of normalized data analysis. In general, normalization in MCDM is a transformation process to obtain numerical input data and its comparison uses the same scale [7]-[10]. The normalization technique maps attributes (criteria) with different units of measurement to the same scale in the interval: 0-1.

The MADM methods determine how to attribute information is processed to arrive at a choice, reqsuiring comparisons between and between attributes, and involves appropriate explicit exchanges. Each decision matrix (decision table)in MCDM method has four main parts, i.e: (a) alternatives, (b) attributes, (c) weight or relative importance of each attribute, and (d) alternative performance measures with sets by attribute [11].

Several studies on the normalization matrix as in [8] examine the influence of normalization techniques in ranking: Improving the materials selection process in engineering design. Normalisation affects the results of MADM methods in [6] and [12]. Data normalisation techniques in decision making with TOPSIS method [5], Comparative analysis of normalization procedures in TOPSIS method: With an application to Turkish deposit banking market [13] and [14] etc. The linear normalization (LN) data sensitivity analysis we described it using the VIKOR method, and simple normalization (SN) data sensitivity was observed using SAW. The equations for the normalization method are presented in Table 2.

Table 2: The Normalization Equation for SN, LN, and VN

Attribute	Max	Min	
Simple (SN)	$r_{ij}\dfrac{a_{ij}}{a_j^{Max}}$	$r_{ij}\dfrac{a_{ij}-a_j^{Min}}{a_j^{Max}-a_j^{Min}}$	(1)
Linear (LN)	$r_{ij}\dfrac{a_j^{Min}}{a_j}$	$r_{ij}\dfrac{a_j^{Max}-a_{ij}}{a_j^{Max}-a_j^{Min}}$	(2)

3. Experimental Methods

3.1. Research Design

An overview of the research design is presented in Figure 1.
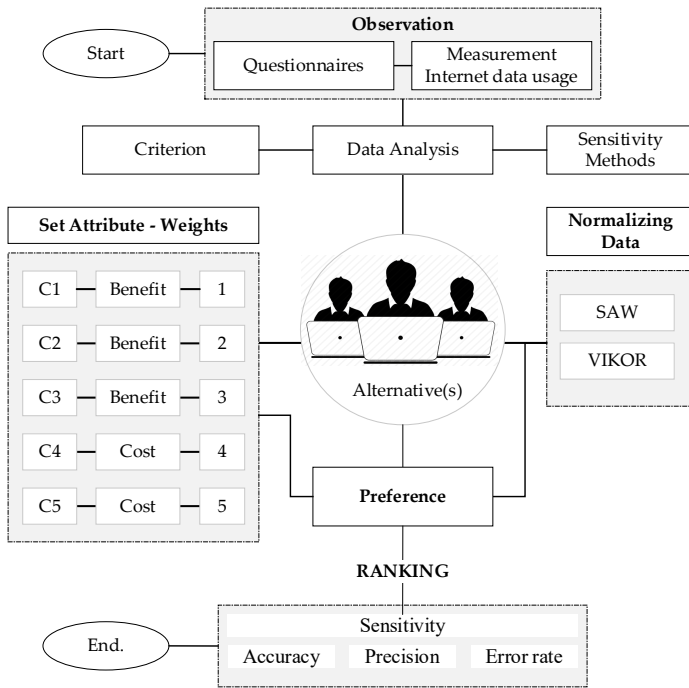
Figure 1: Research Design for Sensitivity Data Analysis Methods

3.2. Observation

Figure 1, the data collection method is through observation activities, namely data measurement to determine the amount of student internet data usage, and questionnaires to obtain information on the number of courses and credits, as well as the economic ability and purchasing power of students. Data collection was carried out at the peak of the Covid-19 pandemic. The results of activity observations form the basis for determining the criteria for mentoring.

The research observation population of 400 students is all students of the Department of Informatics at Mulawarman University who carry out online learning activities and become one of the alternative targets for internet data assistance.

3.3. Criteria Weighting Method

The criteria data for making decision assistance from the results of observation activities obtained five criteria for decision making; Use of Internet Data (C1), Learning Courses (C2), Credit Courses (C3), Economic Capability (C4) and data purchasing power (C5). The weighting method the criteria and attribute set used the Rank Sum weighting technique which refers to the research of Mats Danielson and L. Ekenberg [15] using the equation.

$$wi^{RS} = \frac{N+1-i}{\sum_{j=1}^{N}(N+1-j)} \qquad (3)$$

Denote the ranking number i among N items to rank, a larger weight is assigned to lower-ranking numbers [15]. Furthermore, from the calculation of equation (3), the criteria weight values are obtained and include the attributes shown in Table 3.

The attribute set for the criteria of Use of Internet Data (C1), Subjects of Learning (C2), Credit Courses (C3) are set to benefit

attributes (Max) with straight ranks and Economic Capability (C4) and Purchasing Power Data (C5) set Cost attribute (Min).

Table 3: The Criterion Weighting and Attribute

Criteria	Straight rank (rj)	Sum Rank weight (n − rj + 1)	Normalized weight	Attri-bute
C1	1	5-1+1= 5	0.333	Max
C2	2	5-2+1= 4	0.267	Max
C3	3	5-3+1= 3	0.200	Max
C4	4	5-4+1= 2	0.133	Min
C5	5	5-5+1=1	0.067	Min

3.4. Sensitivity Data Analysis Methods

The data analysis method for decision making applies the SAW method for Simple Normalization(SN) and VIKOR for Linear Normalization(LN). An overview of the flow of data analysis can be seen in Figure 2.
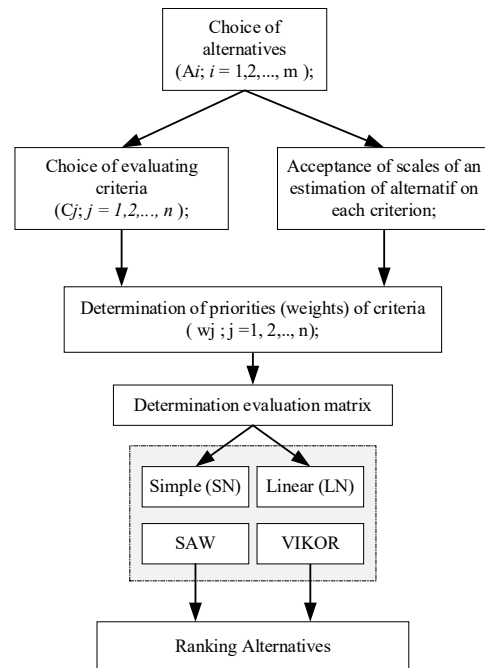
Figure 2: The Data Analysis Flow

The step-by-step sequence of the problem of multi-criteria decision making for data normalization analysis refers to [11], [16] is defined in Figure 2. Simple Normalization (SN) performance description is illustrated using the SAW method referring to [17], [18], the equation:

$$p_i = \sum_{j=1}^{m} w_j\, r_{ij} \qquad (4)$$

where p_i is the performance value or preference value of the alternative to - i; w_j denotes the weight of the jth criterion; r_{ij} is the normalized rank selected from the ith alternative against the j is criterion to be the equivalent unit.

Linear Normalization (LN) performance description is illustrated using the VIKOR method referring to [19] the equation:

$$Q_1 = v\left[\frac{(s_i - s^{max})}{(s^{max} - s^{min})}\right] + (1-v)\left[\frac{(r_i - r^{max})}{(r^{max} - r^{min})}\right] \qquad (5)$$

V is the weight ranging from 0-1 (generally 0.5). The value of v is the weight value of the strategy of the maximum group utility, while the value of 1 - *v* is the weight of individual regret. The smaller the VIKOR index value (Qi) the better the alternative solution.

3.5. Confusion Matrix

The confusion matrix is used to measure the performance of SN, LN and VN data normalization methods. In this test, the reference results of the 3 methods are compared with actual data, ie. alternative data which is the priority for internet data assistance, in the high category. In measuring the performance of these three methods, there are 4 (four) terms referring to [20] as a representation of the results of the performance process, ie. True Potential Positive Assitance (TPP), True Potential Negative (TPN), False Potential Positive (FPP) and False Potential Negative (FPN) [17]. Measurement values for sensitivity, accuracy, precision and misclassification (error rate) refer to [21], [22] as follows:

- $Sensitivity = \frac{TPP}{FPN+TPP} 100\%$ (6)

- $Accuracy = \frac{TPP+TPN}{TOTAL} 100\%$ (7)

- $Precision = \frac{TPP}{FPN+TPP} 100\%$ (8)

- $Error\ Rate = \frac{FPP + FPN}{TOTAL} 100\%$ (9)

4. Results and Discussion

4.1. Data Description Analysis

- Alternative data and criteria

The research data was obtained through observation activities in the form of measuring internet data during online learning (C1) and filling out questionnaire forms (C2, C3, C4, C5), which were obtained from 400 undergraduate students Informatics Dept, as an alternative in decision making or potential beneficiaries. Description of this data is shown in Table 4.

Table 4: description data analysis

Alts.	C1	C2	C3	C4	C5
A1	926.18	9	24	1,800,000	100,000
A2	690.96	9	23	1,850,000	100,000
A3	849.73	9	19	3,850,000	300,000
A4	1,002.07	9	23	1,350,000	100,000
A5	1,005.88	9	24	1,450,000	100,000
A↓	⋮	⋮	⋮	⋮	⋮
A399	1,002.31	9	23	1,200,000	100,000
A400	798.77	9	18	3,000,000	500,000
Avg.	749.21	7	20	2,133,113	237,000
Min.	490.560	5	14	1,000,000	100,000
Max.	1,130.17	9	24	4,000,000	500,000

Data analysis (datasheet) in Table 4, arranged in a decision matrix containing the value of each alternative A1 to A400, the average value for C1 is 749.21 MB, C2 averages 7 courses, for C3 averages 20 SKS for courses, C4 an average of IDR 2,133,113 and C5 an average of IDR 237,000. While the min-max value obtained

is 490,560 MB - 1,130,170 MB of internet data usage (C1), 5 - 9 number of courses (C2), 14-24 credits of courses (C3), IDR 1,000,000 - IDR 4,000. 000 economic capacity (C4), and IDR 100,000 - IDR 500,000 for C5.

4.2. Result: Normalization Data Analysis

- Result: Normalization Simple Data (SN)

Normalized data analysis for a simple technique using equation (1) calculating the min and max, the value of each alternative (A1 to A400) is obtained as shown in Table 5.

Table 5: Normalization Data SAW Method

Alts.	r_{1ij}(C1)	r_{2ij} (C2)	r_{3ij}(C3)	r_{4ij}(C4)	r_{5ij}(C5)
A1	0.819	1.0	1.0	0.555	1.0
A2	0.611	1.0	0.958	0.540	1.0
A3	0.751	1.0	0.791	0.259	0.33
A4	0.886	1.0	0.958	0.740	1.0
A5	0.890	1.0	1.0	0.689	1.0
A↓	⋮	⋮	⋮	⋮	⋮
A399	0.886	1.0	0.958	0.833	1.0
A400	0.706	1.0	0.7	0.333	0.2
Avg.	0.663	0.830	0.842	0.509	0.578
Min.	0.434	0.556	0.583	0.250	0.200
Max.	1.000	1.000	1.000	1.000	1.000

The calculation results (Table 5) of normalized data analysis using simple techniques, which are illustrated using the SAW method, the value of the simple technique is obtained with an average of 0.663 for C1 with a min value of 0.434 and a max value of 1.0. For C2, an average value of 0.830, C3 an average of 0.842 (min 0.583 - max 1.0), C4 an average of 0.509 (min 0.250 - max 1.0) and for C5 an average of 0.578 with a min 0.2 - 1.0.

- Result: Normalization Linear Data (LN)

Normalized data analysis for a linear technique using equation (1) calculating the min and max, the value of each alternative (A1 to A400) is obtained, as shown in Table 6.

Table 6: Normalization Data VIKOR method

Alts.	r_{1ij} (C1)	r_{2ij} (C2)	r_{3ij}(C3)	r_{4ij}(C4)	r_{5ij}(C5)
A1	0.681	1.000	1.000	0.733	1.000
A2	0.313	1.000	0.900	0.717	1.000
A3	0.562	1.000	0.500	0.050	0.500
A4	0.800	1.000	0.900	0.883	1.000
A5	0.806	1.000	1.000	0.850	1.000
A↓	⋮	⋮	⋮	⋮	⋮
A399	0.80	1.00	0.90	0.93	1.00
A400	0.48	1.00	0.40	0.33	0.00
Avg.	0.4044	0.6181	0.6213	0.6223	0.6575
Min.	0.000	0.000	0.000	0.000	0.000
Max.	1.000	1.000	1.000	1.000	1.000

The calculation results (Table 6) from normalized data analysis using a linear technique illustrated by the VIKOR method obtained a linear technique value with an average of 0.4044 for C1, for C2 an average value 0.6181, C3 was 0.6213, C4 was average. 0.6223

and for C5 the average is 0.6575. While the min and max values for each data criterion are at 0.0 - 1.0. Furthermore, the visualization of the data spread for simple and linear normalized data technique is shown in Figure 3.
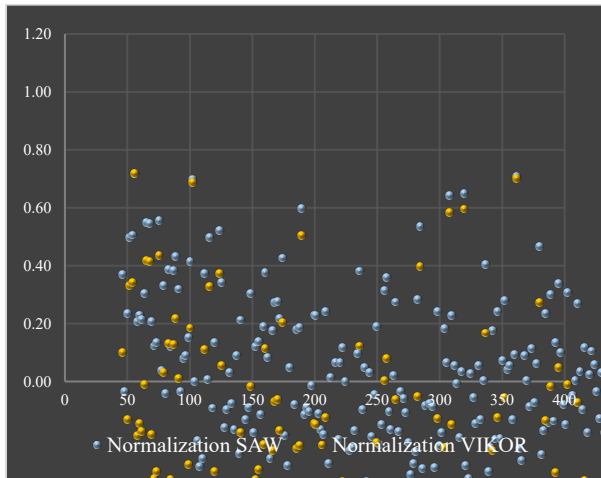
Figure 3: Scatter-chart Data Normalization SAW-VIKOR

Figure 3 presents a simple technique data spread visualization showing the central area of the spread data for C1 range of 0.434 to 1.0. Meanwhile, the linear technique shows a distribution area of 0.0 to 1.0

4.3. Preference and Ranking

- The preference value

The preference value (P) for SAW method according to (3), for VIKOR using (4). The calculation results for each alternative (A) are shown in Table 7.

Table 7: Preference Value SAW and VIKOR

Alts.	Simple Norm.	Linear Norm.
	SAW	VIKOR
A1	0.880576	0.918040
A2	0.800864	0.827270
A3	0.732474	0.752377
A4	0.919317	0.942831
A5	0.921962	0.953826
A6	0.973333	1.000000
A7	0.789162	0.844602
A8	0.849240	0.885965
A9	0.816799	0.875406
A10	0.874123	0.908853
A11	0.936147	0.964779
A12	0.925985	0.960283
A↓	⋮	⋮
A399	0.931733	0.947088
A400	0.710034	0.725979

Table 7 is the preference value of the simple normalization data (SAW) and linear (VIKOR) calculation of 400 alternatives, which is the final result of the assessment of the criteria and weighting values of students who are prospective recipients of internet data social assistance. Furthermore, the visualization of the spread of

preference data from the SAW and VIKOR methods is shown in Figure 4.
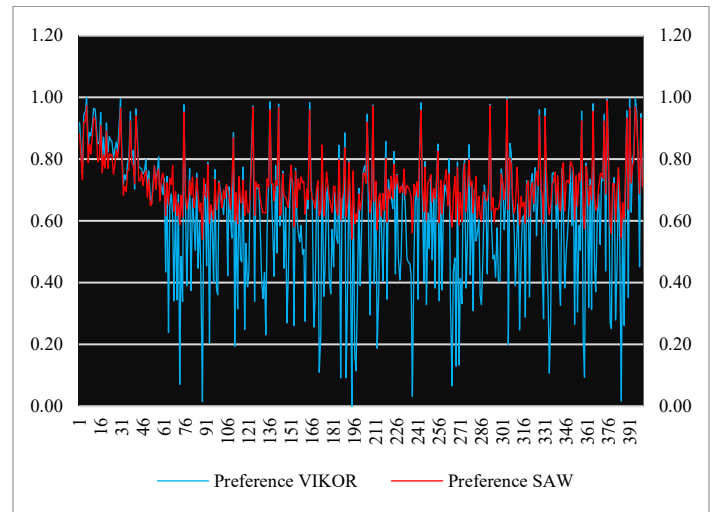
Figure 4: Chart Preference Value SAW and VIKOR Method

Figure 4 shows a graph of the spread data preferences from the SAW method in the area 0.5408 - 0.9921 and the VIKOR method in the 0.0 - 1.0 area.

- Ranking

The calculation results of preferences are then sorted from largest to smallest, where the largest alternative preference value is the best alternative from the data which is the chosen alternative, while the alternative with the lowest preference value is the worst of the alternatives as shown in Table 8.

Table 8: Ranking SAW and VIKOR Method

SAW Method				VIKOR Method			
Rank	Alts.	Rank	Alts.	Rank	Alts.	Rank	Alts.
1st	A304	21st	A399	1st	A6	21st	A389
2nd	A375	22nd	A12	2nd	A395	22nd	A357
3rd	A292	23rd	A37	3rd	A304	23rd	A5
4th	A6	24th	A373	4th	A391	24th	A37
5th	A209	25th	A357	5th	A30	25th	A396
6th	A395	26th	A396	6th	A375	26th	A16
7th	A124	27th	A5	7th	A136	27th	A399
8th	A142	28th	A4	8th	A164	28th	A205
9th	A30	29th	A205	9th	A243	29th	A373
10th	A391	30th	A16	10th	A365	30th	A4
11th	A136	31st	A20	11th	A142	31st	A1
12th	A164	32nd	A1	12th	A292	32nd	A20
13th	A243	33rd	A10	13th	A75	33rd	A29
14th	A365	34th	A13	14th	A209	34th	A10
15th	A75	35th	A110	15th	A124	35th	A13
16th	A327	36th	A29	16th	A11	36th	A110
17th	A41	37th	A8	17th	A331	37th	A8
18th	A331	38th	A173	18th	A41	38th	A189
19th	A11	39th	A42	19th	A12	39th	A9
20th	A389	40th	A189	20th	A327	40th	A22

Table 8, there are 40 alternative ranking preference results from the two methods (SAW and VIKOR). Each method produces a different ranking of values, the SAW method produces an

alternative A304 with a preference value of 0.9921 in the first order A375, in the second-order A292, in the third order, and so on. Then, the results of the ranking preference Vikor method obtained the first alternative A6, A395 in the second, A304 third, and so on (see Table 8 and Figure 5).
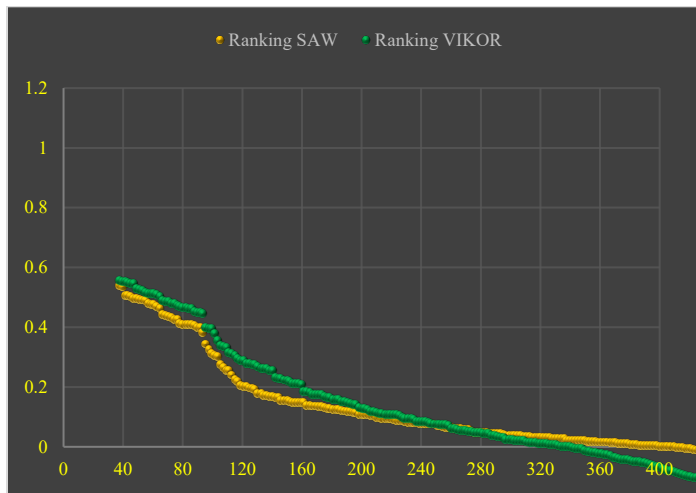
Figure 5: The Ranking of SAW vs VIKOR method

The difference in the value of the two individual ranking decision-making methods is due to differences in the normalization data analysis method, where the SAW method applies the Simple Normalization (SN) method, and the VIKOR method uses the Linear Normalization (LN) even though the weighting of the criteria is equally important and the weight is straight.

4.4. Confusion Matrix: Sensitivity Data Analysis

Sensitivity data analysis uses a confusion matrix to determine the sensitivity, accuracy, precision, and misclassification of ranking values using actual data as an internal validation of the performance of each method. The test scenario is carried out by dividing the percentage of alternative aid targets by the target number of 10%, 15%, 20% and 25% (40 alt; 60 alt; 80 alt; and 100 alt.) potential recipients of social assistance and the sensitivity of decision-making methods regarding the target alternative groups.

Table 9: Actual Data vs SAW and VIKOR Rank Methods

Order	Alts.	SAW method Ranking	SAW method Valid	VIKOR method Ranking	VIKOR method Valid
1st	A124	A304	1	A6	1
2nd	A209	A375	1	A395	1
3rd	A292	A292	1	A304	1
4th	A304	A6	1	A391	1
5th	A375	A209	1	A30	1
6th	A6	A395	1	A375	1
7th	A30	A124	1	A136	1
8th	A142	A142	1	A164	1
9th	A395	A30	1	A243	1
10th	A41	A391	1	A365	1
11th	A75	A136	1	A142	1
12th	A136	A164	1	A292	1
13th	A164	A243	1	A75	1
14th	A243	A365	1	A209	1
15th	A389	A75	1	A124	1
16th	A391	A327	1	A11	1
17th	A399	A41	1	A331	1
18th	A11	A331	1	A41	1
19th	A37	A11	1	A12	1
20th	A327	A389	1	A327	1
21st	A365	A399	1	A389	1
22nd	A373	A12	1	A357	1
23rd	A4	A37	1	A5	1
24th	A5	A373	1	A37	1
25th	A12	A357	1	A396	1
26th	A16	A396	1	A16	1
27th	A205	A5	1	A399	1
28th	A331	A4	1	A205	1
29th	A357	A205	1	A373	1
30th	A396	A16	1	A4	1
31st	A29	A20	1	A1	1
32nd	A1	A1	1	A20	1
33rd	A23	A10	1	A29	1
34th	A8	A13	1	A10	1
35th	A10	A110	0	A13	1
36th	A13	A29	1	A110	0
37th	A19	A8	1	A8	1
38th	A20	A173	0	A189	0
39th	A22	A42	0	A9	0
40th	A28	A189	0	A22	1
Sum			36		37

Table 9 is an example of testing actual data for 40 alternatives out of a total of 400 alternatives (10%) that were targeted for selecting the SAW and VIKOR methods. The results are compared to then measure the confusion matrix. The comparison results in Table 9 validate the data from the 2 ranking methods against the actual data, then perform performance calculations. Table 9 presents the method of performance results for the 10% target or 40 alternatives.

Table 10: The Confusion Matrix Decision Analysis for SAW Method

	N = 400	SAW Method	
		Predicted: NO	Predicted: YES
Actual Data	Actual: NO	TPN = 320	FPP = 40	360
	Actual: YES	FPN = 4	TPP = 36	40
		324	76	

From Table 10, the performance value for SAW method:

- Sensitivity using(6): → 36/40 = 0.9 = 90%

- Accuracy using(7): → (320 + 36) / 400 = 0.890 = 89,0%

- Precision using(8): → 36/(36+40) = 0.474 = 47,4%

- Error rate using(9): → (40+4)/400 = 0.110 = 11,0%

From Table 11, the performance value for Vikor method:

- Sensitivity using(6): → 37/40 = 0.925 = 92,5%

- Accuracy using(7): → (320 + 37) / 400 = 0.893 = 89,3%

- Precision using(8): → 37/(37+40) = 0.481 = 48,1%

- Error rate using(9): → (40+3)/400 = 0.108 = 10,8%

Table 11: The Confusion Matrix Decision Analysis for Vikor Method

		SAW Method		
N = 400		Predicted: NO	Predicted: YES	
Actual Data	Actual: NO	TPN = 320	FPP = 40	360
	Actual: YES	FPN = 3	TPP = 37	40
		323	77	

Table 12: The Summary Scenario Results: Method Performance vs Actual Data

Metric	SAW Method				VIKOR Method			
	10%	15%	20%	25%	10%	15%	20%	25%
Sensitivity	90.0	80.0	80.0	75.0	92.5	76.7	80.0	79.0
Accuracy	89.0	82.0	76.0	68.75	89.3	81.5	76.0	69.76
Precision	47.4	44.4	44.4	42.9	48.1	43.4	44.4	44.1
Error rate	11.0	18.0	24.0	31.25	10.75	18.5	24.0	30.25

The summary of the performance measurement data from the percentage set scenario for the target alternative group is shown in Table 12.
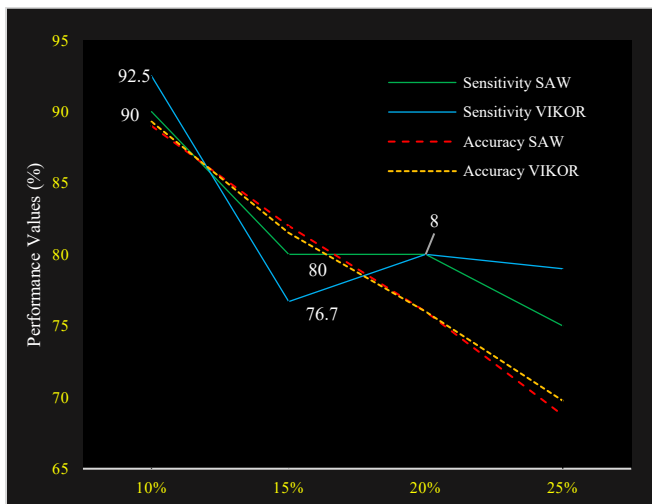
Figure 6: Sensitivity and Accuracy Methods – SAW vs VIKOR

Figure 6 shows a line-chart of the sensitivity and accuracy values of the SAW and VIKOR methods, the sensitivity in determining targets results in different performance values, at the 20% target (40 targets) the Vikor method is 1 alternative higher than SAW, meaning that Vikor's sensitivity value for target 40 people with a sensitivity of 0.925 or 92.5% while SAW was 90%. However, when the target was increased by 15%, (60 targets) the SAW method was more sensitive than VIKOR, with a ratio of 48:46 or about 80% SAW: 76.7% VIKOR. When the target is increased by 80 people (20%), both methods have the same performance value for each metric (sensitivity, accuracy, precision and error rate), SAW and VIKOR.

Figure 7 shows the error rate value has increased linearly and simultaneously with an average increase of 7 points. and the value of precision is influenced by the sensitivity value decreases. In

principle, both the SAW and VIKOR methods are included in the linear analysis model, and this result is influenced by the weighted value setting assigned to the criteria.
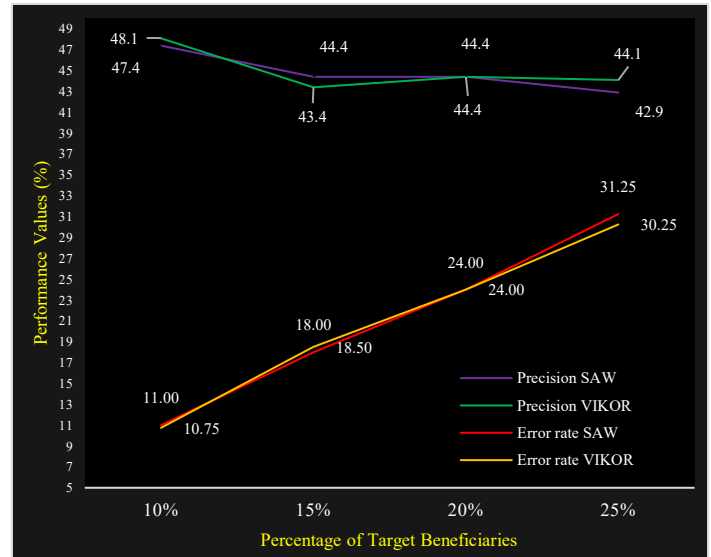
Figure 7: Precision and error rate value method SAW – VIKOR

4.5. Discussion

This work also demands sensitivity in examining the details of the data and must be careful to look at every detail of the values that exist. The two methods used have their own characteristics in terms of sensitivity in the analysis of social assistance program data. From the results of the analysis of the previous method shows fundamental differences, it becomes our important point when carrying out this work, the findings include:

The data normalization analysis process, the results obtained show the distribution of values in the SAW method (see: Figure 3) which explains that the results of data normalization are coherent (dependent) in the value range [0.4 - 1.0], while in the Vikor method, the results of data normalization are independent of the range [0.9–1.0]. This explains that the spread of the results of the integrated SAW analysis normalization shows fierce competition in the selection, and will also have a significant effect on the performance (preference) of the SAW method. The benefit is that it is suitable for use in the case of group selection (10%, 15%, 20%, 25%).

The process of analyzing the performance of the social assistance data sensitivity also shows differences in determining the selection of positive beneficiaries, the VIKOR method has a higher sensitivity value than the SAW method if the alternative target is chosen by 40 students (10%), this can be seen from a higher preference value (see Figure 6). However, under certain conditions or when the target recipient of social assistance is increased (target 15%), the performance gradually decreases, the SAW method is higher.

This is based on the results of observations caused by the distribution of the normalized values of VIKOR data in the distribution range of 0 to 1, and the distribution of data (preference values) of the SAW method is mostly centred in the lowest distribution area of 0.5408 to 0.9921. In other data analysis also

obtained the same performance value, namely when the target beneficiary target is increased (20% target), and the addition of the target 25% target (100 alt) shows that the performance of the VIKOR method increases linearly better than the performance of the SAW method. This means that the characteristics of these two methods are different and experience changes in preference values caused by the different value distribution of the two Normalized Data techniques. In addition, the important point of this study is the sensitivity value of normalized data techniques in the decision-making process based on the number of target alternatives for social assistance and the total alternatives.

5. Conclusion

Decision making related to social assistance for community welfare requires good management because a slight change or error in determining the analytical method approach has a significant impact on the results, this is explained from the work carried out showing the sensitivity of simple techniques and linear techniques for normalized data in decision making.

The results of this study are based on the characteristics obtained from the two methods providing conclusions for new research for the author to explore further, namely, there are differences in the final rating (preference) value of the target size, and this occurs because of the influence of the characteristics of the data distribution of each. normalized techniques, for cases with a target <10% Linear techniques illustrated using the VIKOR method have a high degree of accuracy compared to simple techniques illustrated using the SAW method. However, if the target number of social assistance recipients is in the range >10% to 15% (60 alt from 400 alt), then the SAW method has a good performance, and the results of these observations are due to the distribution of data focused on certain areas. (preference value) of simple techniques that affect performance. That is, the use of Linear Normalization data technique is very good for decision making cases with small targets because it produces the right ranking performance compared to simple data normalization techniques.

Conflict of Interest

The authors declare no conflict of interest related to this paper.

Acknowledgment

References

[1] Unicef, WHO, IFRC, Key Messages and Actions for Prevention and Control in Schools.
[2] Peraturan Pemerintah Republik Indonesia, Peraturan Pemerintah Nomor 21 Tahun 2020 tentang Pembatasan Sosial Berskala Besar Dalam Rangka Percepatan Penanganan Coronavirus Disease 2019, 2020.
[3] E. Budiman, M. Wati, Norhidayat, "Mobile Cultural Heritage Apps For The Digital Literacy Of The Dayak Tribe, Borneo, Indonesia," Conservation Science In Cultural Heritage, 19, 2015–217, 2019, doi:https://doi.org/10.6092/issn.1973-9494/10627.
[4] E. Budiman, D. Moeis, R. Soekarta, "Broadband quality of service experience measuring mobile networks from consumer perceived," in 2017 3rd International Conference on Science in Information Technology (ICSITech), IEEE, Bandung: 423–428, 2017,

[5] N. Vafaei, R.A. Ribeiro, L.M. Camarinha-Matos, Data normalisation techniques in decision making: Case study with TOPSIS method, International Journal of Information and Decision Sciences, 2018, doi:10.1504/IJIDS.2018.090667.
[6] D.M. Pavlii, "Normalisation affects the results of MADM methods," Yugoslav Journal of Operations Research, 2001.
[7] N. Vafaei, R.A. Ribeiro, L.M. Camarinha-Matos, "Normalization techniques for multi-criteria decision making: Analytical hierarchy process case study," in IFIP Advances in Information and Communication Technology, 2016, doi:10.1007/978-3-319-31165-4_26.
[8] A. Jahan, K.L. Edwards, A state-of-the-art survey on the influence of normalization techniques in ranking: Improving the materials selection process in engineering design, Materials and Design, 2015, doi:10.1016/j.matdes.2014.09.022.
[9] E. Budiman, "Mobile Data Usage on Online Learning during COVID-19 Pandemic in Higher Education," International Journal of Interactive Mobile Technologies (IJIM), 14(19), 2020, doi:10.3991/ijim.v14i19.17499.
[10] N. Vafaei, R.A. Ribeiro, L.M. Camarinha-Matos, "Importance of Data Normalization in Decision Making: case study with TOPSIS method," in International Conference of Decision support Systems Technology, An EWG-DSS Conference. Them: Big Data Analytic for Decision Making, 2015.
[11] I. Mukhametzyanov, D. Pamučar, "A Sensitivity analysis in MCDM problems: A statistical approach," Decision Making: Applications in Management and Engineering, 2018, doi:10.31181/dmame1802050m.
[12] E. Budiman, "Decision Optimization: Internet Data Assistance for Students during Learning from Home," International Journal of Innovative Technology and Exploring Engineering, 9(11), 372–378, 2020, doi:10.35940/ijitee.k7845.0991120.
[13] A. Çelen, "Comparative analysis of normalization procedures in TOPSIS method: With an application to Turkish deposit banking market," Informatica (Netherlands), 2014, doi:10.15388/Informatica.2014.10.
[14] E. Budiman, N. Dengen, Haviluddin, W. Indrawan, "Integrated multi criteria decision making for a destitute problem," in Proceeding - 2017 3rd International Conference on Science in Information Technology, ICSITech 2017, 342–347, 2017, doi:10.1109/ICSITech.2017.8257136.
[15] M. Danielson, L. Ekenberg, "Trade-offs for ordinal ranking methods in multi criteria decisions," in Lecture Notes in Business Information Processing, 2017, doi:10.1007/978-3-319-52624-9_2.
[16] E. Triantaphyllou, "Multi-criteria Decision Making Methods: A Comparative Study (Applied Optimization)," In Multi-Criteria Decision Making Methods: A Comparative Study, 2000, doi:10.1007/978-1-4757-3157-6.
[17] Edy Budiman; Armin Lawi; Supriyadi La Wungo, Implementation of SVM Kernels for Identifying Irregularities Usage of Smart Electric Voucher, 2019, doi:https://doi.org/10.1109/ICCED46541.2019.9161077.
[18] M. Wati, N. Novirasari, E. Budiman, Haeruddin, "Multi-Criteria Decision-Making for Evaluation of Student Academic Performance Based on Objective Weights," in 2018 Third International Conference on Informatics and Computing (ICIC), IEEE, Palembang: 1–5, 2018, doi:10.1109/IAC.2018.8780421.
[19] P. Chatterjee, S. Chakraborty, "A comparative analysis of VIKOR method and its variants," Decision Science Letters, 2016, doi:10.5267/j.dsl.2016.5.004.
[20] E. Budiman, Haviluddin, N. Dengan, A.H. Kridalaksana, M. Wati, Purnawansyah, Performance of Decision Tree C4.5 Algorithm in Student Academic Evaluation, 2018, doi:10.1007/978-981-10-8276-4_36.
[21] S. Narkhede, Understanding Confusion Matrix – Towards Data Science, Towards Data Science, 2018.
[22] N. Dengen, Haviluddin, L. Andriyani, M. Wati, E. Budiman, F. Alameka, "Medicine Stock Forecasting Using Least Square Method," in Proceedings - 2nd East Indonesia Conference on Computer and Information Technology: Internet of Things for Industry, EIConCIT 2018, 2018, doi:10.1109/EIConCIT.2018.8878563.

ASTES

Current Control of Battery-Supercapacitors System for Electric Vehicles based on Rule-Base Linear Quadratic Regulator

Taha Sadeq[*], Chew Kuew Wai, Ezra Morris

Lee Kong Chian Faculty of Engineering and Science, Universiti Tunku Abdul Rahman, Sungai Long Campus, Selangor 43000, Malaysia

A B S T R A C T

This research aims to investigate the energy and power management of a battery-supercapacitors Hybrid Energy Storage System (HESS) for Electric vehicles (EVs). A bidirectional DC-DC converter, a battery and a set of supercapacitors were employed to construct the parallel semi-active architecture of HESS. Two strategies of Rule-Base Linear Quadratic Regulators (R-B LQRs) were proposed to manage the power flow in HESS to reduce the overall battery stress during high demand events. The supercapacitors supply the high load demand, while the battery supplies the low load demand. The HESS, EV and the proposed controllers were simulated in a MATLAB/Simulink environment. Three standard drive cycles, namely, Urban Dynamometer Driving Schedule UDDS, New York City Cycle NYCC and Japan1015 drive cycle, were implemented to validate the controller's responses. The results of the R-B LQR controllers were compared in terms number of possible drive cycles. According to the results achieved, the proposed hybridization achieves stable response of the HESS current over the drive cycles, effectively reducing the battery's size and extends its life-time.

1. Introduction

Nowadays, landed vehicles can be categorized in to three main types, namely, conventional vehicles, Electric Vehicles (EVs) and Hybrid Electric Vehicles (HEVs). Conventional vehicles with an internal combustion engine (ICE) are the most common type in today's market. In ICEs, chemical energy (e.g. ethanol, gasoline, diesel etc.) is converted into kinetic energy in a process has significant power losses. On the other hand, the EV is an alternative-design automobile that relies on battery power to provide the electricity to actuate the vehicle by an electrical motor. Furthermore, The HEV is powered by two types of energy sources, namely, ICE and electrical motor with ESS; it combine the benefits of high fuel economy and low harmful emissions. Due to the necessity to reduce air pollution and harmful vehicle emissions, significant research has been focused on developing HEVs and EVs. Energy storage systems pose a significant issue in stand-alone applications. Batteries offer a wide range of the clean energy. Furthermore, they have high energy density and low power density due to chemical processes to deliver and store energy [1]. However, the main drawbacks are low cycle-life, and long recharging times. In addition, the immediate response to sudden load changes in charging and discharging could potentially reduce

the battery's lifetime. There are several kinds of chemical batteries that are currently available in the market such as lead-acid, lithium-ion, nickel metal hydride (NiMH) and nickel cadmium (NiCad) [2]. The supercapacitor is another energy storage technology, and is either an electric double layer capacitor (EDLC) or a pseudo-capacitor. These differ in the ways they store energy and charge [3]. Compared to batteries, supercapacitors have relatively low specific energy density and high specific power density. The supercapacitors are used as auxiliary an energy storage device due to the dependence of terminal voltage on the state of charge. Nevertheless, various benefits can achieved when using the supercapacitors as an auxiliary power source [4]. The low value of the terminal voltage is a core limit of supercapacitors; 2.5 volts is the maximum terminal voltage that can be provided by a single supercapacitor unit. However, several supercapacitors are connected in series and in parallel to achieve the required operation voltage and energy capacity by powerful applications. Consequently, many researchers have attempted to improve the performance of the ESS by combining high power devices like supercapacitors or flywheels in parallel with batteries. The main purpose of the Hybrid Energy Storage System (HESS) is to extend the efficacy of each power source [5]. This work designs a semi-active HESS by engaging a battery in parallel form with supercapacitors through a DC-DC converter, with the aim of

increasing the merits of the two devices, and decrease their limitations [6].

The essential challenge in the design of a HESS for EV is to manage the current flow between the supercapacitors and the battery. The advantages and disadvantages of many topologies of HESS have been reviewed extensively in the existing literature [7–9]. Furthermore, in the literature, the HESS used several types of bidirectional DC-DC converters. Figure 1 illustrates six different topologies of HESS. Figure 1(a) presents the simplest topology of a battery-supercapacitor system. Due to the direct connection, the battery and the supercapacitors voltage terminal remains the same, and the DC-DC converter is used to maintain the power flow. In this topology, the supercapacitor characteristics are limited. Furthermore, a full-sized DC-DC converter is needed to manage the delivered energy [10]. The configuration in Figure 1(b) is widely used in the literature [11, 12]. The bidirectional DC-DC converter was placed between the DC-Bus and the supercapacitors as an interface to manage the current flow in HESS. Reliability is the main feature of this topology, where the load current is not affected by the failure of the DC-DC converter. Figure 1(c) shows another configuration of a HESS. In this topology, the power flow of the battery was maintained within a safe range via the DC-DC converter. The supercapacitor operational range was limited, and it responded as an energy buffer [13]. The topologies represented in Figure 1(d, f) used two DC-DC converters to manage the power flow from the battery and supercapacitors, individually. These topologies require a full and medium sized DC-DC converter for every source. In addition, the loss, cost and weight are increased in this topology compared to the other topologies, in terms of the need for full-sized DC-DC converters [14, 15]. The scheme in Figure 1(e) uses a parallel connection of batteries and supercapacitors via two DC-DC converters separately, and suffers from the same constrains in Figure 1(d, f).
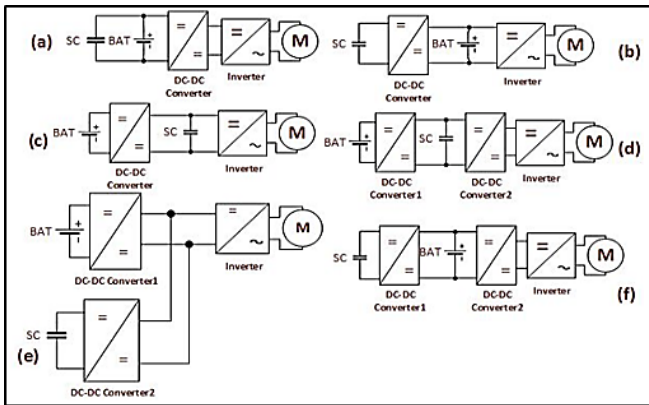
Figure 1: Most common HESS architectures [2].

On the other hand, many researches presented various models of bidirectional DC-DC converter designs for HESS [16,17]. The DC-DC converter was used to manage the current flow of HESS under transient and steady-state conditions. Many researches in the literature used different control algorithms to control the power flow of the HESS. In [17], the polynomial control strategy was used to manage the energy for two DC-DC converters, and the results are sufficient compared to the classical PI. Furthermore, recent studies focused on rule-based approaches such as fuzzy logic control [18] to manage the power flow in the HESS. The

accuracy in measurement noise and adaptation of fuzzy logic was used as an energy management strategy. However, human experience was implemented to design the membership function and fuzzy rule. Therefore, this cannot guarantee suitable control performance in unexpected conditions. In [19], the response of a non-linear model predictive controller was compared to a linear model predictive controller and rule-base control, based on the hybrid battery supercapacitors energy storage system for EV. In other work aiming to extend battery life-cycle, a rule-based controller of HESS was compared to a fuzzy controller, and the results show that in transient the controllers supplied the EV load current from the supercapacitor, while the battery supplied the load during the steady state [20]. In [21], the researchers tried to extend the driving cycle and decrease the size of the HESS by using multi-objective optimization. Three standard drive cycles were used to validate the proposed controller.

This research aims to design a control algorithm for HESS for an EV. Two control strategies of R-B LQR were proposed to be implemented as controllers in EV applications due to their simplicity to implement and short computation time compared with to optimization methods. The limit R-B LQR aims to limit the battery current to I_{b_max} while the share limit R-B LQR aims to limit the battery current to I_{b_max}, and share the load current between the battery and supercapacitor. Dual control layers were used in this work. The rule-based approach was used to obtain the desired supercapacitors current during the load demand. The LQR was used to control the DC-DC converter by manipulating the width of the duty cycle of PWM. In addition, the LQR controller can guarantee good close-loop behavior for the DC-DC converter, and it is relatively insensitive to external disturbances, since the controller feedback gain-vector has to be determined optimally [22, 23].

This paper is organized as follows. Section 2 discusses the HESS configuration. Section 3 discusses the modeling of the HESS and EV. Section 4 contains the proposed controller algorithm. The simulation results of the proposed controller are presented in Section 5. Section 6 concludes of this research.

2. System Configuration

In EV applications, a practical HESS should be light, highly reliable, and have fast response for load variation. Due to the previous reasons, the semi-active architecture in Figure 1(b) was selected to be implemented in this work. Figure 2 shows the semi-active topology of HESS in Matlab/Simulink. The model of the battery is connected directly to the model of the EV as a premier energy source, and the model of the supercapacitors is connected to the EV model through the bidirectional DC-DC converter model as an auxiliary energy source. Three different standard drive cycles, namely, UDDS, NYCC and Japan1015, were used to validate a performance of the proposed controllers.

The limit R-B LQR controller was designed to manage the current flow of the HESS by limiting the current of the battery to I_{b_max}. The supercapacitors supplied the peak load demand of the EV. Furthermore, the share limit R-B LQR controller was designed to manage the current flow of the HESS by limiting the current of the battery to I_{b_max}, and sharing the load current between the battery and the supercapacitors. The bidirectional DC-DC converter has two functions; it works as a boost converter during

the acceleration of the vehicle to discharge the supercapacitors energy, and also works as a buck converter during the deceleration to absolve and store the regenerative current. The maximum gain of the terminal voltage for the DC-DC converter was set as less than three, to increase the overall efficiency of the system [24].
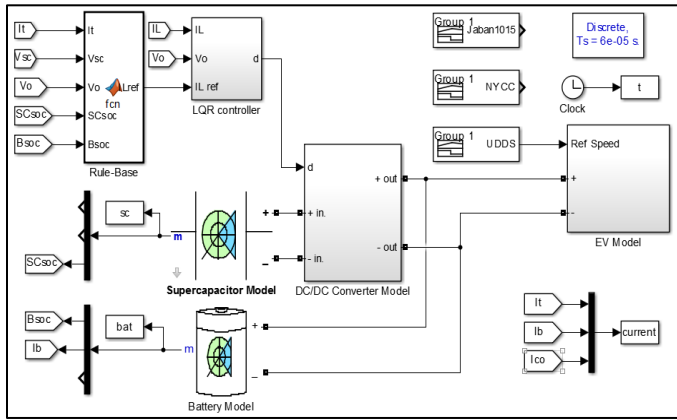
Figure 2: The parallel semi-active architecture of HESS for EV.

3. The Modelling of the HESS System

In order to verify the proposed algorithm of the HESS for EV, an accurate model comprising the battery, supercapacitors, DC-DC converter and Electric Vehicle was required. Several different models of HESS components have been presented in the literature.

3.1. Model of the Battery

An equivalent circuit model is a common model that uses electrical components to model the behavior of the battery. There are many approaches to represent the electrical equivalent circuit model for the battery. The majority of these representations fall into three main classifications: Thevenin, impedance and runtime-based models [25–27] . Electrochemical batteries have a complex and nonlinear behavior during charging and discharging, depending on the battery's state-of-charge (SOC) and electrolyte temperature. For this reason, the researchers in [28] attempted to find a dynamic model that represents this nonlinearity. Furthermore, some researchers used the system identification technique to estimate the parameter values of the battery model [29]. Other researchers used the parameter estimation technique to obtain the parameter values for equivalent model of the battery [30]. Moreover, the thermal effect was considered in the battery models in these works.

The battery model can be found in the MATLAB/Simulink/SimPowerSystems library. This equivalent model contain a control voltage source and an internal resistance, as shown in Figure 3. The relationship between the time-varying parameters in the battery model is shown in Equation 1.

$$V_{bat}(t) = E_{bat}(t) - r_{bat}.i_{bat}(t) \qquad (1)$$

The battery current reduction ratio (BCRR) can be calculated by Equation 2 [31].

$$BCRR = \frac{\sqrt{\frac{1}{T}\int_0^T I_{bat}^2 dt}}{\sqrt{\frac{1}{T}\int_0^T I_t^2 dt}} \times 100 \qquad (2)$$
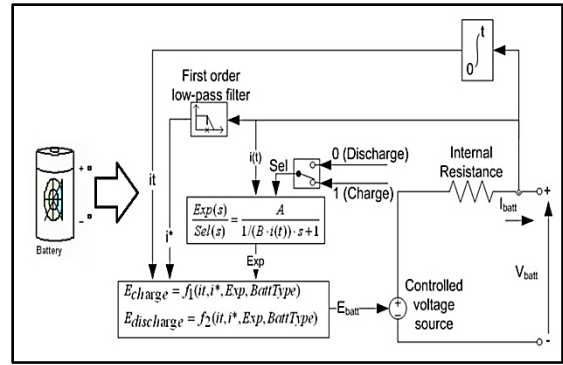
Figure 3: Equivalent model of the battery in SimPowerSystems library

3.2. Model of the Supercapacitors

Supercapacitors are commonly used in academia and in the automotive industry due to their high efficiency, low internal resistance, high power density, and long cycle-life. Equation 3 describes the behavior of the supercapacitor, which mathematically depends on the essential laws of a capacitor.

$$\begin{cases} i_{sc}(t) = -C_{sc}\frac{du_{sc}(t)}{dt} \\ V_{sc}(t) = u_{sc}(t) - r_{sc}i_{sc}(t) \end{cases} \qquad (3)$$

The design of the energy management system requires a model with good robustness and high precision, representing the dynamics behavior of the supercapacitor . The practical models proposed in [32] consists of three RC branches, and the parameters were determined from the terminal measurements of charging and discharging the supercapacitors. Other models that describe the behavior of supercapacitors are called dynamic models. The transient behavior of the supercapacitors is simulated by these models. The model parameters are identified through experimental tests, such as discharge and charge by the supercapacitor at constant current and electrochemical impedance spectroscopy in environmental constraints [33]. The supercapacitors model in MATLAB/Simulink/SimPowerSystems was used in this research.

3.3. Model of the DC-DC Converter

The model that describes the behavior of the DC-DC converter is important for designing the HESS controller, because the controller aims to control the bidirectional DC-DC converter to supply the required power from the supercapacitors. The terminal output voltage and output current of the bidirectional DC-DC converter were regulated by changing the width of the duty cycle of the PWM, which is applied to the IGBT of the bidirectional DC-DC converter. In this work, a solo layer of the bidirectional DC-DC converter was used to control the current flow of the supercapacitors in both directions. The boost converter was used to discharge, and the buck converter used to charge, the supercapacitors. Figure 4 represents the construction and main elements of the DC-DC converter [34].

The state-space average approach was used to model the bidirectional DC-DC converter. The nonlinear characteristics of the bidirectional DC-DC converter approximates to linear characteristics in the state-space average model. The OFF and ON status of the switching element was involved in the modeling of the DC-DC converter. The time averaging performance of the DC-DC converter is set as:

$$\dot{x} = [dA_{ON} + (1-d)A_{OFF}]X + [dB_{ON} + (1-d)B_{OFF}]V_{sc} \quad (4)$$

where:

$$\begin{cases} A_{on,off} = State\ matrices \\ B_{on,off} = Control\ matrices \\ d = the\ switching\ period \end{cases}$$
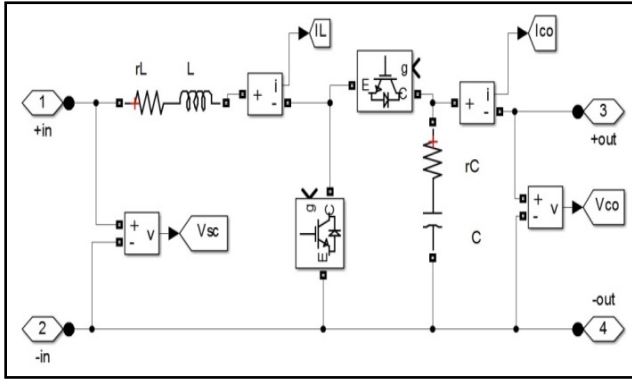
Figure 4: The main components of DC-DC converter

Figure 4, the control and state matrices of the bidirectional DC-DC converter in the OFF and ON conditions are represented as the following matrices:

$$X = [I_L \quad V_c]^T = state\ vector$$

$$A_{ON} = \begin{bmatrix} -\dfrac{r_L}{L} & 0 \\ 0 & \dfrac{-1}{C.(R+r_C)} \end{bmatrix}, \quad B_{ON} = \begin{bmatrix} \dfrac{1}{L} \\ 0 \end{bmatrix}$$

$$A'_{OFF} = \begin{bmatrix} \dfrac{-R.r_C - R.r_L - r_C.r_L}{L(R+r_C)} & -\dfrac{R}{L(R+r_C)} \\ \dfrac{R}{C(R_o+R_C)} & -\dfrac{1}{C(R_o+R_C)} \end{bmatrix}, \quad B_{OFF} = \begin{bmatrix} \dfrac{1}{L} \\ 0 \end{bmatrix}$$

$$\frac{d}{dt}\begin{bmatrix} i_L \\ V_c \end{bmatrix} = \begin{bmatrix} \dfrac{R.r_C.(d-1) - r_L(R+r_C)}{L(R+r_C)} & \dfrac{R.(d-1)}{L(R+r_C)} \\ \dfrac{R.(1-d)}{C(R+r_C)} & -\dfrac{1}{C(R+r_C)} \end{bmatrix}\begin{bmatrix} i_L \\ V_c \end{bmatrix} + \begin{bmatrix} \dfrac{1}{L} \\ 0 \end{bmatrix} V_{sc} \quad (5)$$

$$V_{co} = \begin{bmatrix} \dfrac{R.(d-1)}{(R+r_C)} & \dfrac{R}{(R+r_C)} \end{bmatrix}\begin{bmatrix} i_L \\ v_c \end{bmatrix} \quad (6)$$

$$\begin{cases} A_s = A = dA_{ON} + (1-d)A_{OFF} \\ B_d = (A_{ON} - A_{OFF})X - (B_{ON} - B_{OFF})V_{sc} \\ B_s = [B_d \quad B] \end{cases} \quad (7)$$

$$B_d = \begin{bmatrix} \dfrac{R.r_C}{L(R+r_C)}.i_L + \dfrac{R.r_C}{L(R+r_C)}.V_c \\ -\dfrac{R}{C.(R+r_C)}.i_L \end{bmatrix} \quad (8)$$

The parameters of the DC-DC converter were selected based on the hypotheses in [35]. The model of the DC-DC converter in Figure 4 was approximated by compensating the switching elements with an integration of controlled voltage and current sources, as represented in Figure. 5. This estimated model has good accuracy and reduces the overall simulation time [36]. Other methods were used to estimate the discrete function of the DC-DC converter in [37] by using the system identification technique.
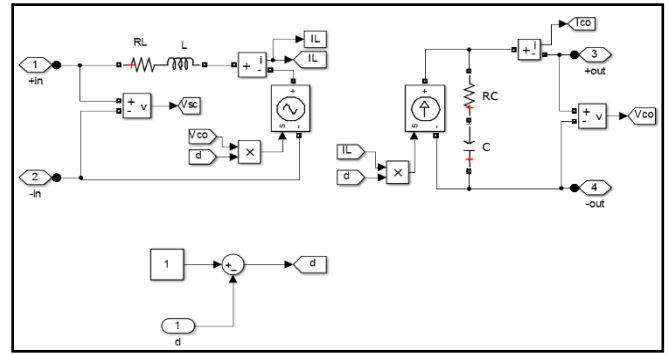
Figure 5: Equivalent model of the bidirectional DC-DC converter

3.4. Electric Vehicle Model

To improve the energy consumption an accurate model representing the EV's behavior is needed. Many MATLAB/Simulink environment was used to develop few EV models by the researchers, whilst others depends on ADVISOR or equivalent software to analyze and compare the performance of a vast types of vehicles [29, 38–41]. In [4, 42] the dynamic system of the vehicles was defined clearly. The essential dynamics of the vehicles, the forces affecting the vehicles movement are acceleration force (F_{accel}), grading force (F_{grad}), rolling force (F_{roll}) and aerodynamic force (Faero) as shown in Equation 9. The motor drive were controlled the fuzzy logic control as in [43, 44].

where:

$$F_{accel} = M_v \times \frac{\partial v}{\partial t}$$

$$F_{grad} = M_v \times g \times Sin\theta$$

$$F_{roll} = \mu_{rr} \times M_v \times g \times cos\theta$$

$$F_{aero} = 0.5 \times \rho \times A_f \times C_d \times V^2$$

Table 1: The main coefficients of the EV model

Parameter	Value
$M_v \equiv$ Vehicle Mass [kg]	1325
$A_f \equiv$ Frontal area [m^2]	2.57
$C_d \equiv$ Drag coefficient	0.26
$\mu_{rr} \equiv$ rolling resistance	0.0048
Wheel radius [m]	0.3
$\rho \equiv$ Air density [kgm^{-3}]	1.29
$g \equiv$ Gravity acceleration [ms^{-2}]	9.8
$V \equiv$ Vehicle Speed [Kmh^{-1}]	Variable
$\theta \equiv$ Road angle [radian]	0

4. Rule-Based Linear Quadratic Regulator Control

The linear quadratic regulator (LQR) is a control technique that generates feedback gains. It is used to regulate the output of the system to achieve the optimal performance by controlling one state of the model. The cost function for a continuous-time linear control is defined as:

$$J(u) = \int_0^\infty (x^T Q x + u^T R u + 2x^T N u)dt \quad (10)$$

LQR returns the solution S of the associated Riccati Equation:

$$A^T S + SA - (SB + N)R^{-1}(B^T S + N^T) + Q = 0 \qquad (11)$$

The closed-loop Eigen values are defined as:

$$e = \text{eig}(A - B \times K) \qquad (12)$$

K is derived from S using:

$$K = R^{-1}(B^T S + N^T) \qquad (13)$$

where R is a positive and Q is a symmetric positive definite matrix scalar. Furthermore, The LQR controller used a systematic procedure to calculate the state feedback control gain matrix. R and Q represent the weighted matrices which have a significant effect on the locations of the closed-loop poles [22]. The closed-loop response of the system changes depending on the values of the Q and R matrices. The weighting matrices can be obtained by using optimization methods. Investigating the optimal value of Q and R is beyond the scope of this research. Otherwise, the mathematical model of the DC-DC converter was used to design the controller of the switching elements of the DC-DC converter. The primary task of the rule-based control is to obtain the reference input current of the DC-DC converter, while the aim of the LQR is to obtain a desired duty cycle by the DC-DC converter. The LQR function in MATLAB was used to obtain the desired closed-loop feedback gains, while the steady-state errors were cancelled by adding an integration [45], as shown in Figure 6.
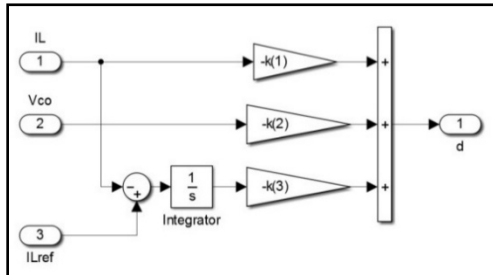
Figure 6: The feedback gains of the LQR controller
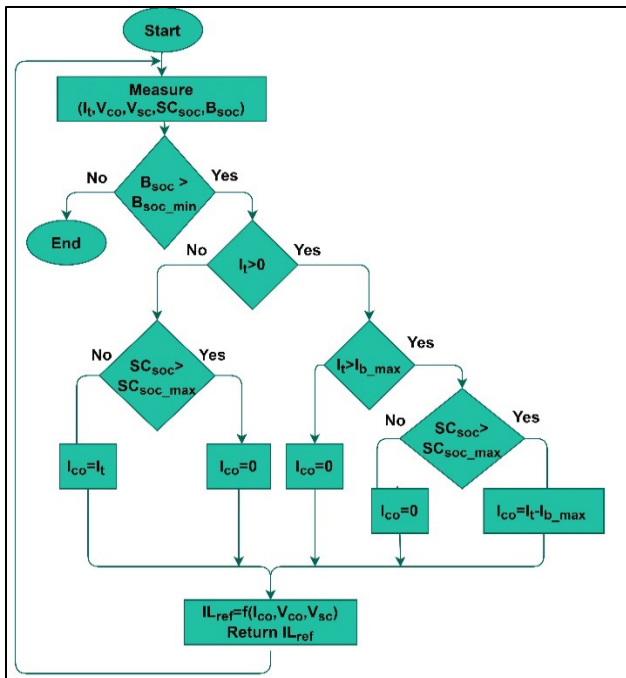
Figure 7: The flowchart of the limit R-B LQR controller

In this research, two strategies for the Rule-base LQR technique were designed to manage the power flow in the HESS. The limit R-B LQR was designed to limit the battery current to I_{b_max}, and supply the balance load current from the supercapacitors, when the total load current is more than I_{b_max}, and the state of charge for the supercapacitors more than 30%. On the other hand, the controller leads the supercapacitors to absorb the regenerative energy when the load current is negative and the state of charge of the supercapacitors is less than 95%. Furthermore, if the total load current is less than I_{b_max}, the controller supplies the total load current from the battery only. The flowchart in Figure 7 illustrates the algorithm of the proposed limit R-B LQR controller.

Moreover, the share limit R-B LQR was designed to limit the battery current to I_{b_max}, and supply 30% of the load current from the supercapacitors, when the total load current is positive and the state of charge for the supercapacitors is over 30%. The supercapacitors absorb the regenerative energy when the load current is negative and the state of charge of the supercapacitors is less than 95%. The flowchart in Figure 8 illustrates the algorithm of the proposed share limit R-B LQR controller.
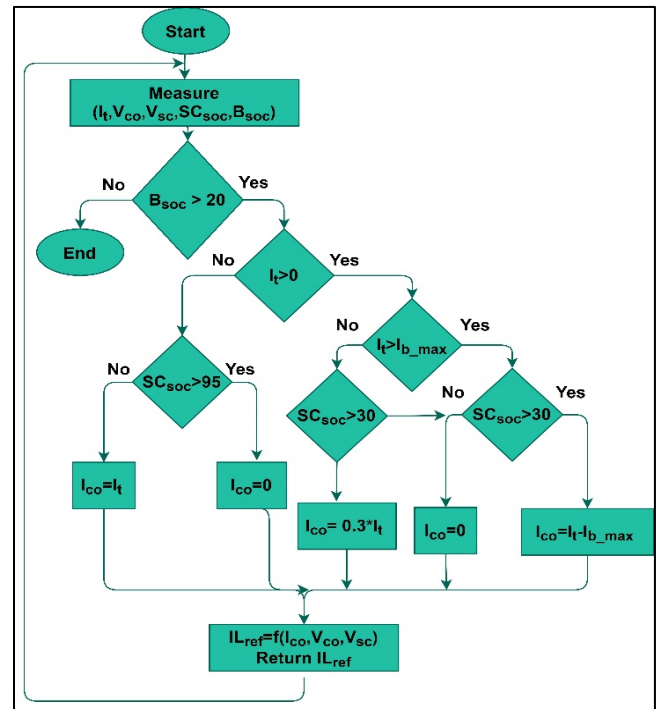
Figure 8: The flowchart of the share limit R-B LQR controller

5. Simulation Results and Discussions

This work used MATLAB/Simulink to simulate the semi-active HESS model and the response of the proposed controllers. To validate the proposed limit R-B LQR and share limit R-B LQR for the EV, the dynamic responses of three standard drive cycles (i.e. UDDS, NYCC and Japan1015) were investigated. Figures 9a, 9b, and 9c illustrate the speed profiles for UDDS, NYCC and Japan1015 respectively.

The high peak and fast dynamic discharge and charge load in the EV application reduced the battery life-cycle. The proposed R-B LQR control strategies aim to reduce the battery stress and

extend the number of the repeated drive cycles. The battery and supercapacitors sizing optimizations are beyond the scope of this research. Figures 9b, 10b, and 11b demonstrate the total power demand of UDDS, NYCC and Japan1015 for the EV respectively. The battery's initial state of charge was 0.95, and the initial state of charge of the supercapacitors was 0.55. The definitive state of charge for the supercapacitors and battery of the HESS were taken at the termination of the single drive cycle.

(a)

(b)

(c)
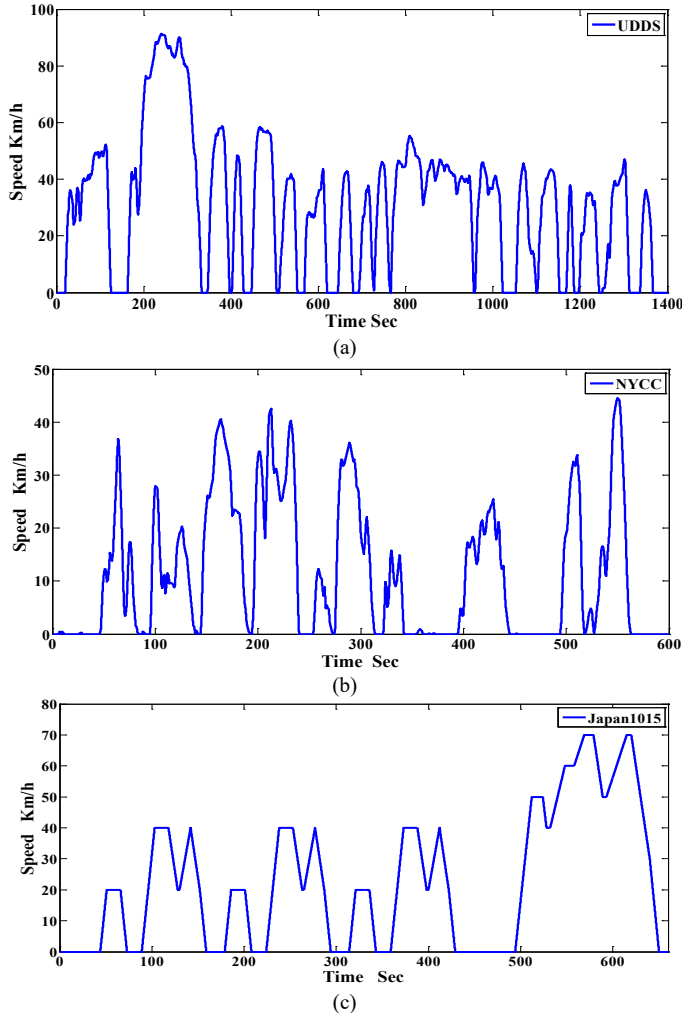
Figure 9: The acceleration and deceleration Speed profile for: (a) UDDS, (b) NYCC, (c) Japan1015 drive cycle

The results of the proposed HESS were compared to the battery power of the battery alone system, to prove the effectiveness of the R-B LQR controllers for HESS in terms of reducing the battery peak current. The results of a limit R-B LQR and share limit R-B LQR were compared in terms of the number of the possible drive cycles. The proposed controllers was tested in three different drive cycles to validate the algorithm in a wide range of driver behaviors and driving environments. Figure 11 shows the limit R-B LQR response currents of HESS for the UDDS, NYCC and Japan1015 drive cycles. The battery power peak of HESS was limited compared to the battery power of the battery alone system. In the limit R-B LQR algorithm, the battery current supplied the low load current for the EV, and was limited by I_{b_max} 20A, while the supercapacitors supplied the high load current more than I_{b_max} 20A, and absorbed all the regenerative current during braking. The limitation of the battery current leads

to a reduction in the battery stress of the EV. This algorithm used the stored energy in the supercapacitors during the deceleration to enhance the battery in HESS of the EV.

(a)

(b)

(c)
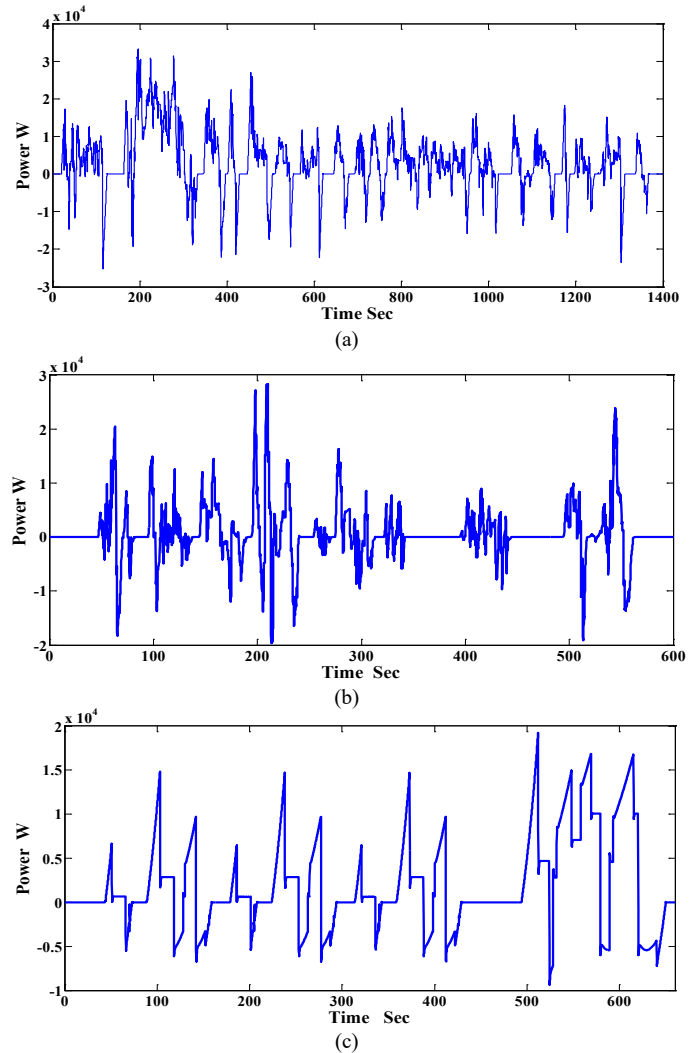
Figure 10: The Total EV Power Load for: (a) UDDS, (b) NYCC, (c) Japan1015 drive cycle

(a)

(b)

62
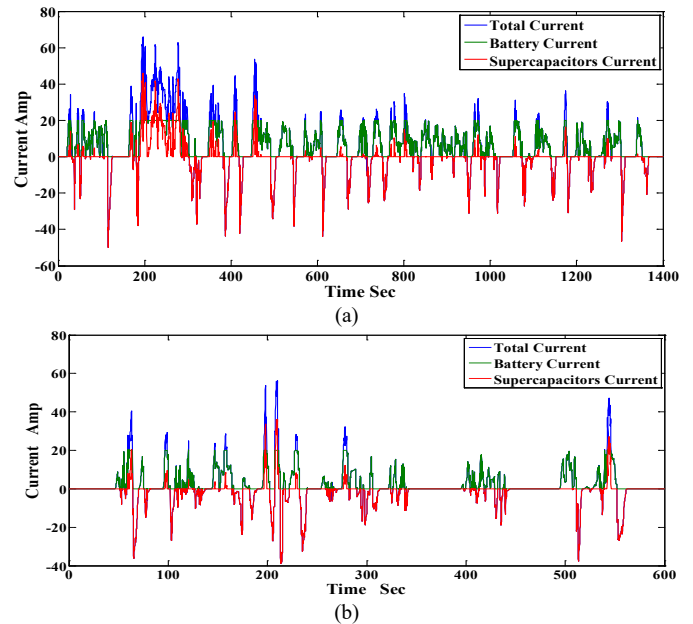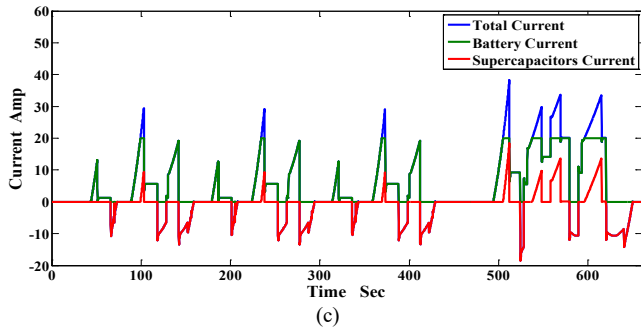
Figure 11: The limit R-B LQR HESS currents for: (a) UDDS, (b) NYCC, (c) Japan1015 drive cycle

On the other hand, Figure 12 shows the share limit R-B LQR response currents of HESS for the UDDS, NYCC and Japan1015 drive cycles. In the share limit R-B LQR algorithm, the battery and supercapacitors were shared to supply the load current for the EV and the battery current limited by I_{b_max} 20A. The battery supplied 70% from the load current, while the supercapacitor supplied 30% from the load current. Furthermore, the supercapacitors absorbed all the regenerative current during the deceleration and braking. The sharing load current and the limitation of the battery current lead to a reduction in the battery stress of the EV, and extended the number of possible cycles.
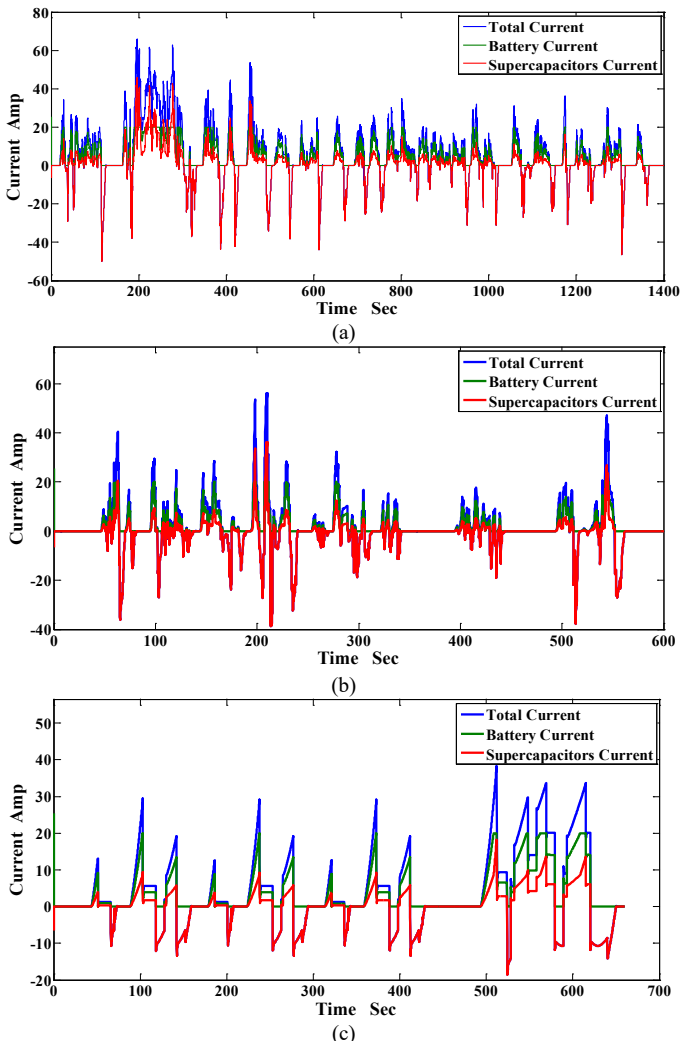
Figure 12: The share limit R-B LQR HESS currents for: (a) UDDS, (b) NYCC, (c) Japan1015 drive cycle

Equation 14 represents the calculation of energy consumption for the battery and supercapacitors.

$$\begin{cases} EnCo_b = \dfrac{SOC_b(0) - SOC_b(t)}{SOC_b(0)} \times 100 \\[2mm] EnCo_{sc} = \dfrac{SOC_{SC}(0) - SOC_{SC}(t)}{SOC_{SC}(0)} \times 100 \end{cases} \qquad (14)$$

Figure 13 illustrates the state of charge of the battery for the proposed controllers of HESS, and battery only for UDDS, NYCC and Japan1015 drive cycles. In the battery only scenario, the battery supplies the total load of the EV, and the energy consumption ($EnCo_b$) for UDDS, NYCC and Japan1015 drive cycle is 8.3%, 1.3% and 2.6% of the total stored energy of the battery respectively. In the limit R-B LQR controller of HESS, the energy consumption from the battery for UDDS, NYCC and Japan1015 drive cycles is 6.7%, 1.15% and 2.3% of the total stored energy of the battery respectively. Meanwhile, in the share limit R-B LQR controller of HESS, the energy consumption from the battery for UDDS, NYCC and Japan1015 drive cycles is 5.37%, 0.95% and 1.79% of the total stored energy of the battery respectively.
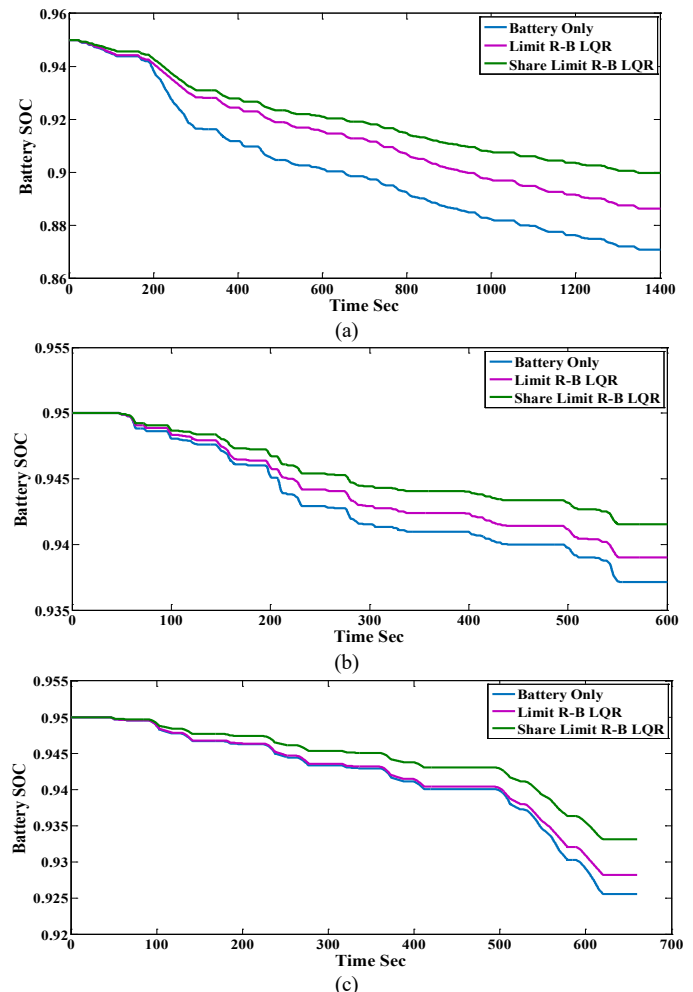
Figure 13: The battery stat of charge for: (a) UDDS (b) NYCC (c) Japan1015 drive cycle

The state of charge of supercapacitors increased during the operation, after absorbing the regenerative energy. In the limit R-B LQR controller of HESS, the energy earned in the supercapacitor

for UDDS, NYCC and Japan1015 drive cycle is 18%, 14.5% and 12.7% of the total stored energy of the supercapacitors respectively. In the share limit R-B LQR controller of HESS, the energy consumption in the supercapacitor for UDDS is 16.4% and the energy earned in the supercapacitor for NYCC and Japan1015 drive cycles is 9.1% and 0.0% of the total stored energy of the supercapacitors respectively. Figure 14 presents the state of charge of the supercapacitor for the proposed controllers of HESS, for the UDDS, NYCC and Japan1015 drive cycles.
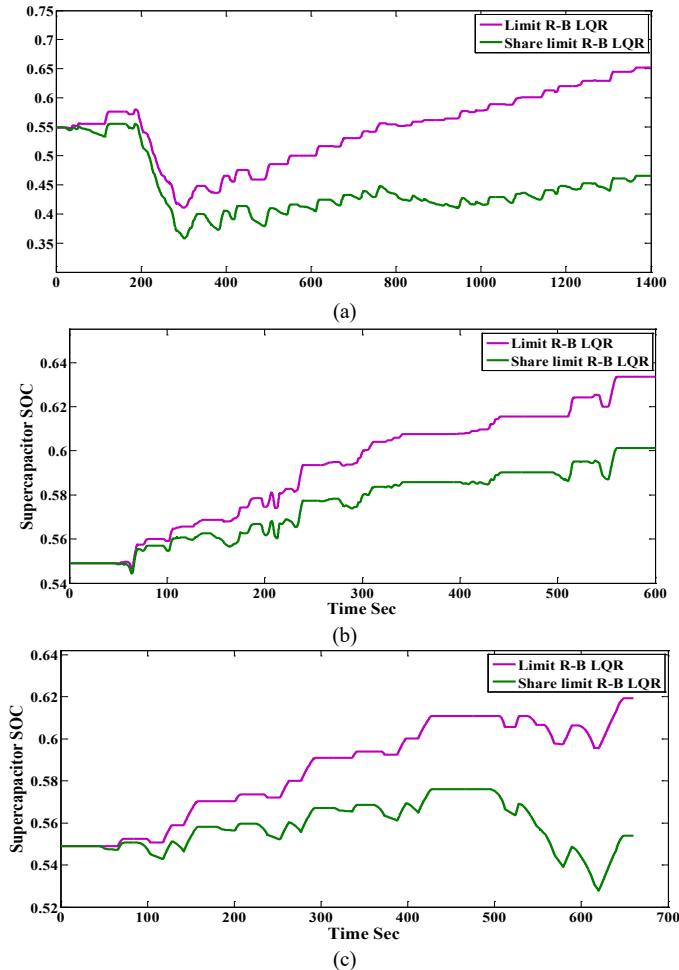
Figure 14: The supercapacitors stat of charge for: (a) UDDS (b) NYCC (c) Japan1015 drive cycle

The design of the R-B LQR controllers achieved a wide range of operating zones for the supercapacitors. Moreover, the results of the supercapacitors state of charge proved that the supercapacitors work continuously during the drive cycles. Table 2 summarizes the state of charge of the battery and supercapacitors, the energy consumption of the battery and supercapacitors, and the number of possible cycles for the UDDS, NYCC and Japan1015 drive cycles. The results indicate that the share limit R-B LQR controller extended the n number of drive cycles compared to limit R-B LQR controller, with same battery size and supercapacitors.

The limitation of the proposed share limit R-B LQR algorithm is that the energy sharing percentage between the battery and supercapacitors is fixed to 30%, which leads to discharging the energy of the supercapacitors quickly in case the regenerative energy was limited. Future work will consider optimization

algorithms to obtain the optimal value of energy sharing between the battery and the supercapacitors.

Table 2: The Battery and supercapacitor state of charge for three different standard drive cycles

HESS		UDDS	NYCC	Japan1015
Battery Only	$SOC_b(0)$	0.95	0.95	0.95
	$SOC_b(t)$	0.871	0.937	0.925
	$EnCo_b$	8.3%	1.4%	2.6%
	$Cycles\ No$	9	53.6	28.8
HESS with Limit R-B LQR	$SOC_b(0)$	0.95	0.95	0.95
	$SOC_b(t)$	0.886	0.939	0.928
	$EnCo_b$	6.7%	1.15%	2.3%
	$SOC_{SC}(0)$	0.55	0.55	0.55
	$SOC_{SC}(t)$	0.65	0.63	0.62
	$EnCo_{SC}$	-18%	-14.5%	-12.7%
	Cycles No	11.2	65	32.6
HESS with Share Limit R-B LQR	$SOC_b(0)$	0.95	0.95	0.95
	$SOC_b(t)$	0.899	0.941	0.933
	$EnCo_b$	5.37%	0.95%	1.79%
	$SOC_{SC}(0)$	0.55	0.55	0.55
	$SOC_{SC}(t)$	0.46	0.60	0.55
	$EnCo_{SC}$	16.4%	-9.1%	0%
	Cycles No	12	79	42

6. Conclusion

This work proposed a control strategy for the battery-supercapacitors Hybrid Energy Storage System for an Electric vehicle. The state-space average model was used to analyze the dynamic behavior of the DC-DC converter. Two R-B LQR algorithms were proposed to manage the current flow in the HESS. The battery and supercapacitors responses was investigated with three different standard drive cycles, namely, UDDS, NYCC and Japan1015. The simulation results demonstrate that the limit R-B LQR has the ability to limit the battery current of HESS to I_{b_max}, in different types of drive cycles. Moreover, the proposed share limit R-B LQR was successful to limit the battery current and extend the number of possible drive cycles. The proposed algorithm enhanced the battery life-cycle and the stability of the energy storage devices, and effectively reduced battery sizes.

Conflict of Interest

The authors declare no conflict of interest.

Acknowledgments

References

[1] V. Paladini, T. Donateo, A. de Risi, D. Laforgia, "Super-capacitors fuel-cell hybrid electric vehicle optimization and control strategy development," Energy Conversion and Management, **48**(11), 3001–3008, 2007, doi:10.1016/j.enconman.2007.07.014.

[2] S.F. Tie, C.W. Tan, A review of energy sources and energy management system in electric vehicles, Renewable and Sustainable Energy Reviews, **20**, 82–102, 2013, doi:10.1016/j.rser.2012.11.077.

[3] P. Sharma, T.S. Bhatti, "A review on electrochemical double-layer capacitors," Energy Conversion and Management, **51**(12), 2901–2912, 2010, doi:10.1016/j.enconman.2010.06.031.

[4] K.E. Mehrdad Ehsani, Yimin Gao, Stefano Longo, Modern Electric, Hybrid Electric, and Fuel Cell Vehicles, Boca Raton: CRC press, 2010.

[5] B. Hredzak, V.G. Agelidis, G.D. Demetriades, "A low complexity control system for a hybrid DC power source based on ultracapacitor-lead-acid

battery configuration," IEEE Transactions on Power Electronics, **29**(6), 2882–2891, 2014, doi:10.1109/TPEL.2013.2277518.

[6] J. Cao, A. Emadi, "A new battery/ultracapacitor hybrid energy storage system for electric, hybrid, and plug-in hybrid electric vehicles," IEEE Transactions on Power Electronics, **27**(1), 122–132, 2012, doi:10.1109/TPEL.2011.2151206.

[7] G. Udhaya Sankar, C. Ganesa Moorthy, G. RajKumar, Smart Storage Systems for Electric Vehicles–A Review, Smart Science, **7**(1), 1–15, 2019, doi:10.1080/23080477.2018.1531612.

[8] L. Kouchachvili, W. Yaïci, E. Entchev, Hybrid battery/supercapacitor energy storage system for the electric vehicles, Journal of Power Sources, **374**, 237–248, 2018, doi:10.1016/j.jpowsour.2017.11.040.

[9] T. Sadeq, C.K. Wai, E. Morris, Q.. Tarbosh, O. Aydogdu, "Optimal Control Strategy to Maximize the Performance of Hybrid Energy Storage System for Electric Vehicle Considering Topography Information," IEEE Access, 1–1, 2020, doi:10.1109/access.2020.3040869.

[10] I. Aharon, A. Kuperman, Topological overview of powertrains for battery-powered vehicles with range extenders, IEEE Transactions on Power Electronics, **26**(3), 868–876, 2011, doi:10.1109/TPEL.2011.2107037.

[11] D. Iannuzzi, P. Tricoli, "Speed-based state-of-charge tracking control for metro trains with onboard supercapacitors," IEEE Transactions on Power Electronics, **27**(4), 2129–2140, 2012, doi:10.1109/TPEL.2011.2167633.

[12] J. Armenta, C. Núñez, N. Visairo, I. Lázaro, "An advanced energy management system for controlling the ultracapacitor discharge and improving the electric vehicle range," Journal of Power Sources, **284**, 452–458, 2015, doi:10.1016/j.jpowsour.2015.03.056.

[13] F. Ju, Q. Zhang, W. Deng, J. Li, "Review of structures and control of battery-supercapacitor hybrid energy storage system for electric vehicles," in IEEE International Conference on Automation Science and Engineering, IEEE Computer Society: 143–148, 2014, doi:10.1109/CoASE.2014.6899318.

[14] A. Kuperman, I. Aharon, Battery-ultracapacitor hybrids for pulsed current loads: A review, Renewable and Sustainable Energy Reviews, **15**(2), 981–992, 2011, doi:10.1016/j.rser.2010.11.010.

[15] O. Laldin, M. Moshirvaziri, O. Trescases, "Predictive algorithm for optimizing power flow in hybrid ultracapacitor/battery storage systems for light electric vehicles," IEEE Transactions on Power Electronics, **28**(8), 3882–3895, 2013, doi:10.1109/TPEL.2012.2226474.

[16] P. Pany, R. Singh, R. Tripathi, "Bidirectional DC-DC converter fed drive for electric vehicle system," International Journal of Engineering, Science and Technology, **3**(3), 101–110, 2011, doi:10.4314/ijest.v3i3.68426.

[17] M.B. Camara, H. Gualous, F. Gustin, A. Berthon, B. Dakyo, "DC/DC converter design for supercapacitor and battery power management in hybrid vehicle applicationspolynomial control strategy," in IEEE Transactions on Industrial Electronics, 587–597, 2010, doi:10.1109/TIE.2009.2025283.

[18] X. Wang, J. Tao, R. Zhang, "Fuzzy energy management control for battery/ultra-capacitor hybrid electric vehicles," in Proceedings of the 28th Chinese Control and Decision Conference, CCDC 2016, Institute of Electrical and Electronics Engineers Inc.: 6207–6211, 2016, doi:10.1109/CCDC.2016.7532114.

[19] P. Golchoubian, N.L. Azad, "Real-Time Nonlinear Model Predictive Control of a Battery-Supercapacitor Hybrid Energy Storage System in Electric Vehicles," IEEE Transactions on Vehicular Technology, **66**(11), 9678–9688, 2017, doi:10.1109/TVT.2017.2725307.

[20] M. Sellali, S. Abdeddaim, A. Betka, A. Djerdir, S. Drid, M. Tiar, "Fuzzy-Super twisting control implementation of battery/super capacitor for electric vehicles," ISA Transactions, **95**, 243–253, 2019, doi:10.1016/j.isatra.2019.04.029.

[21] X. Hu, Y. Li, C. Lv, Y. Liu, "Optimal Energy Management and Sizing of a Dual Motor-Driven Electric Powertrain," IEEE Transactions on Power Electronics, **34**(8), 7489–7501, 2019, doi:10.1109/TPEL.2018.2879225.

[22] T. Sadeq, C.K. Wai, "Linear Quadratic Regulator Control Scheme on Hybrid Energy Storage System," in 2020 IEEE International Conference on Automatic Control and Intelligent Systems, I2CACIS 2020 - Proceedings, Institute of Electrical and Electronics Engineers Inc.: 219–223, 2020, doi:10.1109/I2CACIS49202.2020.9140093.

[23] M.R.D. Al-Mothafar, S.M. Radaideh, M.A. Abdullah, "LQR-based control of parallel-connected boost dc-dc converters: A comparison with classical current-mode control," International Journal of Computer Applications in Technology, **45**(1), 15–27, 2012, doi:10.1504/IJCAT.2012.050129.

[24] D.M. Robert W. Erickson, Fundamentals of Power Electronics, 2nd ed., Springer Science & Business Media, 2007.

[25] M. Chen, G.A. Rincón-Mora, "Accurate electrical battery model capable of predicting runtime and I-V performance," IEEE Transactions on Energy Conversion, **21**(2), 504–511, 2006, doi:10.1109/TEC.2006.874229.

[26] A. Shafiei, A. Momeni, S.S. Williamson, "Battery modeling approaches and

management techniques for plug-in hybrid electric vehicles," in 2011 IEEE Vehicle Power and Propulsion Conference, VPPC 2011, 2011, doi:10.1109/VPPC.2011.6043191.

[27] A. Fotouhi, D.J. Auger, K. Propp, S. Longo, M. Wild, A review on electric vehicle battery modelling: From Lithium-ion toward Lithium-Sulphur, Renewable and Sustainable Energy Reviews, **56**, 1008–1021, 2016, doi:10.1016/j.rser.2015.12.009.

[28] S. Barsali, M. Ceraolo, "Dynamical models of lead-acid batteries: Implementation issues," IEEE Transactions on Energy Conversion, **17**(1), 16–23, 2002, doi:10.1109/60.986432.

[29] A. Fotouhi, K. Propp, D.J. Auger, "Electric vehicle battery model identification and state of charge estimation in real world driving cycles," in 2015 7th Computer Science and Electronic Engineering Conference, CEEC 2015 - Conference Proceedings, Institute of Electrical and Electronics Engineers Inc.: 243–248, 2015, doi:10.1109/CEEC.2015.7332732.

[30] T. Huria, M. Ceraolo, J. Gazzarri, R. Jackey, "High fidelity electrical model with thermal dependence for characterization and simulation of high power lithium battery cells," in 2012 IEEE International Electric Vehicle Conference, IEVC 2012, 2012, doi:10.1109/IEVC.2012.6183271.

[31] S. Hussain, M.U. Ali, G.-S. Park, S.H. Nengroo, M.A. Khan, H.-J. Kim, "A Real-Time Bi-Adaptive Controller-Based Energy Management System for Battery–Supercapacitor Hybrid Electric Vehicles," Energies, **12**(24), 4662, 2019, doi:10.3390/en12244662.

[32] L. Zubieta, R. Bonert, "Characterization of double-layer capacitors for power electronics applications," IEEE Transactions on Industry Applications, **36**(1), 199–205, 2000, doi:10.1109/28.821816.

[33] N. Devillers, S. Jemei, M.C. Péra, D. Bienaimé, F. Gustin, "Review of characterization methods for supercapacitor modelling," Journal of Power Sources, **246**, 596–608, 2014, doi:10.1016/j.jpowsour.2013.07.116.

[34] F. Machado, J.P.F. Trovão, C.H. Antunes, "Effectiveness of supercapacitors in pure electric vehicles using a hybrid metaheuristic approach," IEEE Transactions on Vehicular Technology, **65**(1), 29–36, 2016, doi:10.1109/TVT.2015.2390919.

[35] N.; R.W.P.; U.T. Mohan, Power electronics : converters, applications and design, USA: John Wiley & Sons, 2007.

[36] M.A. Abdullah, C.W. Tan, A.H.M. Yatim, "A simulation study of hybrid wind-ultracapacitor energy conversion system," in 2014 IEEE Conference on Energy Conversion, CENCON 2014, Institute of Electrical and Electronics Engineers Inc.: 265–270, 2014, doi:10.1109/CENCON.2014.6967513.

[37] T. Sadeq, C.K. Wai, "Model the DC-DC Converter with Supercapacitor Module based on System Identification," in 2019 IEEE International Conference on Automatic Control and Intelligent Systems, I2CACIS 2019 - Proceedings, Institute of Electrical and Electronics Engineers Inc.: 185–188, 2019, doi:10.1109/I2CACIS.2019.8825095.

[38] S. Gonsrang, R. Kasper, "Optimisation-based power management system for an electric vehicle with a hybrid energy storage system," International Journal of Automotive and Mechanical Engineering, **15**(4), 5729–5747, 2018, doi:10.15282/ijame.15.4.2018.2.0439.

[39] K. Mahmud, G.E. Town, A review of computer tools for modeling electric vehicle energy requirements and their impact on power distribution networks, Applied Energy, **172**, 337–359, 2016, doi:10.1016/j.apenergy.2016.03.100.

[40] A. Bampoulas, A. Giannakis, S. Tsaklidou, A. Karlis, "Modeling, simulation and performance evaluation of a low-speed battery electric vehicle," in 2016 11th International Conference on Ecological Vehicles and Renewable Energies, EVER 2016, Institute of Electrical and Electronics Engineers Inc., 2016, doi:10.1109/EVER.2016.7476342.

[41] C.K. Wai, Y.Y. Rong, S. Morris, "Simulation of a distance estimator for battery electric vehicle," Alexandria Engineering Journal, **54**(3), 359–371, 2015, doi:10.1016/j.aej.2015.04.008.

[42] E. Schaltz, Electrical vehicle design and modeling, INTECH Open Access Publisher, 2011.

[43] Q.A. Tarbosh, O. Aydogdu, N. Farah, M.H.N. Talib, A. Salh, N. Cankaya, F.A. Omar, A. Durdu, "Review and Investigation of Simplified Rules Fuzzy Logic Speed Controller of High Performance Induction Motor Drives," IEEE Access, **8**, 49377–49394, 2020, doi:10.1109/ACCESS.2020.2977115.

[44] N. Farah, M.H.N. Talib, N.S. Mohd Shah, Q. Abdullah, Z. Ibrahim, J.B.M. Lazi, A. Jidin, "A Novel Self-Tuning Fuzzy Logic Controller Based Induction Motor Drive System: An Experimental Approach," IEEE Access, **7**, 68172–68184, 2019, doi:10.1109/ACCESS.2019.2916087.

[45] B. Kedjar, K. Al-Haddad, "DSP-based implementation of an LQR with integral action for a three-phase three-wire shunt active power filter," IEEE Transactions on Industrial Electronics, **56**(8), 2821–2828, 2009, doi:10.1109/TIE.2008.2006027.

Modified Blockchain based Hardware Paradigm for Data Provenance in Academia

Devika K N*, Ramesh Bhakthavatchalu

Amrita School of Engineering, Department of Electronics and Communication, Amrita Vishwa Vidhyapeetham, Kollam, Kerala, 392025, India

A B S T R A C T

Educational organizations often need to distribute academic transcripts and certificates upon student's request since they are mandatory for admission into new scholarly programs including placement activities. Manual procedures involved with the transmission process of academic document is indeed a tedious task that results in substantial overhead. Thus the necessity for an autonomous electronic system for transfer of records among institutions is on the verge. This paper discuss and portray a hardware approach on the cryptographic elements of blockchain to impart data security and privacy that are found inadequate in its software counterpart.The novelty of this work relies on the design and implementation of a hardware equivalent structure for blockchain which could greatly alleviate the chances of various software attacks and security breach in existence. The solution proposed could cut down the waiting period of students to transmit their credentials and in addition provide a trustworthy verification platform to elude academic deceit. It can be integrated along with existing permission based blockchain framework to form a conjoined hardware-software architecture.

1   Introduction

Internet acquired it's admiration since 1990's, after which hard copy references and encyclopedias became ineffectual. During the initial times, internet was troublesome for the educators to adapt it into the academic domain. However, the field of education have progressed enormously over a short period of time. Online network had a great impact in the process of imparting knowledge and brought about a substantial revolution in the way people learn. Online learning platforms hold considerable amount of private documents and data related to students. These should be kept inaccessible to the third party user but at the same time should convey information to the concerned authorities to maintain data confidentiality. Currently India does not possess any law controlling data privacy or protection. Nevertheless, significant laws in India that serve data privacy are the Contract Act (India) 1872 and Information Technology Act, 2000. Presently, Blockchain comes out as the best solution to this scenario by forming an impregnable data repository and security from hacking. Cryptocurrency that turned out as the foremost noteworthy and the most inquiring wonders of the final century have Blockchain at its back end. Blockchain forms an ideal technology for storing and tracking scholarly documents. At present, all student credentials are stored as paper records or in a digital centralized directory which makes it accessible to third party.

Drawbacks of paper records include:

- Requires huge amount of storage space.

- Can easily be manipulated or misplaced by unauthorized individuals.

- Can be subjected to unexpected permanent destruction due to natural calamities like flood.

- Creation of paper records is itself a tedious task in terms of time span involved.

- There can be trust issues in relation to the accuracy and authenticity of data.

Centralized repositories that are considered as a reservoir of private data could be targeted by hackers leading to security breach.

Corresponding Author: Devika K N, Research Scholar, Department of Electronics and Communication, Amrita Vishwa Vidhyapeetham, Kerala, India, Tel: +919744968667, Email: devikanandalal@gmail.com
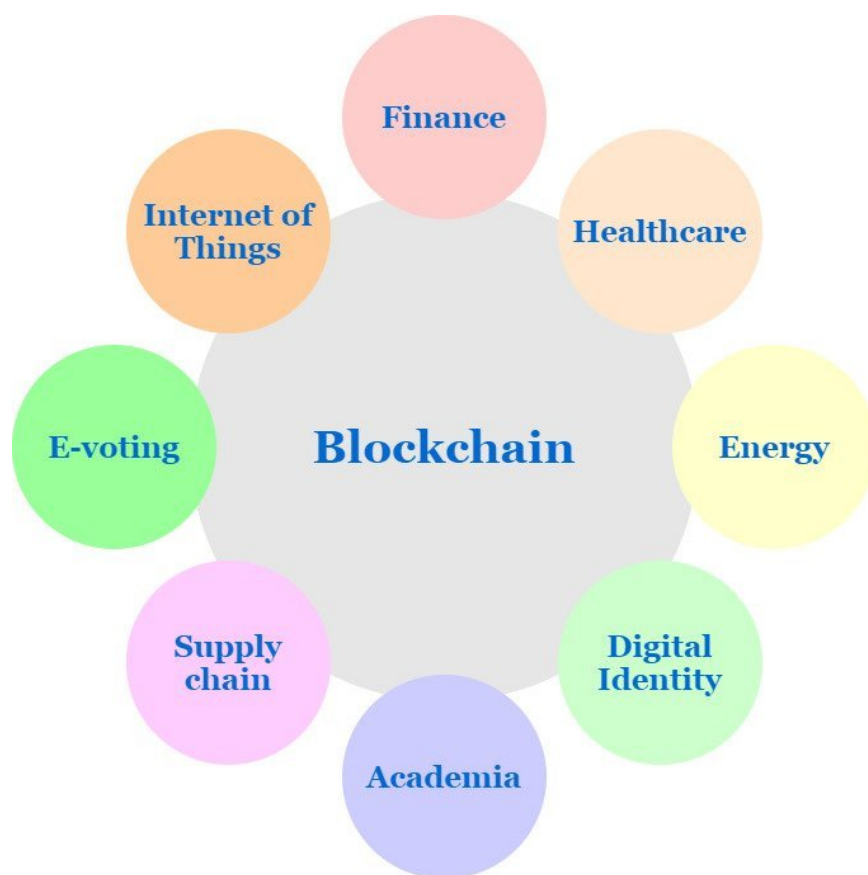
Figure 1: Applications of Blockchain technology

In a Blockchain, each participating entities called nodes are provided with a replica of the entire data communicated within the network. Thus it impedes the attempt to manipulate the contents imparting immutability. Data loss is prevented by avoiding centralization of information. In addition, it also provides the freedom to view information in public by any individual in case of Public Blockchain or only by the concerned participants for Private Blockchain. It prevents fraudulent individuals among teaching professionals who may provide fabricated certificates to highlight their experiences in academic field. Such untrustworthy officials questions the credibility of scholastic documents. Immutable property of the decentralized ledgers are utilized to guarantee the trustworthiness of the members involved through the submission of necessary credentials required.For placement purposes, it gives the freedom for the employers to directly access the records of students without involving colleges or universities. Presently, many universities around the globe have stepped into blockchain technology for tracing and screening academic transcripts.

Edublock is an innovative idea put forth by company called "Learning is earning" to collect the proof that a person have completed the required classes on his/her subject of study. This venture thus opens a wide range of opportunity to reform the sphere of education. All entities involved in the educational sector like students, professors, parents and other officials can be completely assured of the security provided by this emerging technology.

This paper provides a novel dimension to the world of blockchain by exploring the possibilities to design a dedicated hard-ware blockchain structure to securely store the academic information of students in Schools or Universities.

The remaining of the paper is organized as follows: Section II deliberate about the background research done on the innovative technology. Section III analyzes the benefits of Hardware cryptography over software cryptography. In Section IV, the technology behind blockchain is highlighted. Section V explains the proposed hardware approach to blockchain architecture. Section VI displays the results after synthesis and simulation in Hardware programming language. Section VII concludes the paper along with its future scope.

2 Background Research

Experts believe that blockchain application is never limited to bitcoin but uncover solutions in divergent fields as in voting, medicare, supply chain, energy industry, identity management and so on [1]. Figure 1 portrays different sectors in which blockchain is gaining significance. The paper work [2] does a survey on the application of blockchain technology in various industrial sectors. It in turn analyze the scope, advantages and threats of integrating this technical knowledge in industry.

In healthcare [3],[4], blockchain finds use in managing patient's information and in tracking medicines. It can resolve drug forgery to a great extent as all the data communication within the decentralized ledger are transparent and immutable that leads to tamper resistant

data. Participants involved comprises of medical experts, patients, insurance agencies, researchers etc. It enables interoperability of timely renewed medical profile of patients and in addition provides data protection, identity maintenance and transparency. Blockchain provides a framework for integrating medical transcripts of all patients among multiple healthcare expertise. It also enables patients to share their health details to medical experts through this platform [5]. Another work [6] discusses the usability of blockchain in healthcare domain to implement Adoptive Leader Election Algorithm (ALEA) for maintaining parallelism in accessing files.

Through distributed ledgers, blockchain certifies and reserves each execution in logistics industry that permits reduction in human flaws, time lag and management costs. In energy industry, blockchain uncover its utility in micro grid technology for power trading [7]. Thus it eliminates the necessity of a centralized controller for decision making and payment management [8], [9]. Blockchain can be applied to promote e-agriculture systems among farmers to improve farming process and provide improved productivity, food safety and reduced risks [10]. In food industry, it enhances food quality and trust by preventing food adulteration and reducing wastage of food [11]. This peer to peer technology put forward novel ideas for gamers through better containment on top of virtual assets in online entertainment platforms [12]. Aura network is an online gaming dais that utilizes it to sustain decentralization in games [13] and to assist the virtual world. It enables online streaming music platforms such as "spotify" to have direct transactions with the customers [14].

Stock market shareholders are currently experiencing tiresome proceedings due to the involvement of mediators and regulatory process which thereby delays the time taken for confirming transactions. In finance, blockchain permits decentralized stock exchanges and financial settlements completely, thus relieving the requirement of a negotiator and gearing up clearances [15], [16]. In e-voting , the voters are able to view the total votes taken for count through the transparent ledger mechanism assuring trustworthy and secular voting system [17]. Decentralization process in blockchain facilitates a person to create digital ID for identity verification on every online proceedings without relying on biometric systems or password [18]. This emerging science aids the dealers and consumers to differentiate between fabricated and original goods, thus impart trust into sale of goods.

In [19], the author presented a novel approach of creating Digital Twins (DT) using blockchain for ensuring immutable, reliable transactions and data availability. Smart contracts are utilized to manage and trace all proceedings involved in Digital Twin creation. They are virtual 3D representation of any real world object. Main objective of DT is to enhance manufacturing process and industrial operations of a system before its actual formation. In [20], the author investigates the pros and cons of applying blockchain to enlarge Industry 4.0. Industry 4.0 model propose the usage of significant technologies such as Augmented Reality (AR), Industrial Internet of Things (IIoT) that helps in free communication among numerous devices all over the industry and online network. Intensive research is done related to this ingenious automation for its utilization in Industry 4.0. Since the latter comprises of different entities such as customers, suppliers, manufacturers, operators and other IIoT nodes there arise trust issues with regard to each other.

Blockchain provides an interactive trusted platform for various smart technical clients [21]–[23] does a relative analysis regarding blockchain trade-offs, classification, details its architecture and also explore the challenges and future scope of this technology. [24] suggests authentication scheme based on blockchain that support user obscurity, inter mutual authenticity and security for multiple server platforms. Unlike other analogous strategies, this proposal offer centralized registration and introduce user revocation as added feature.

In addition to the above mentioned areas, there are numerous other fields where blockchain turn out to be beneficial for instance research sector that include both academia and industry. In [25], the author explains a solution that includes web interface to register and transfer record with permissioned blockchain framework functioning as the back end for verification purpose. Main aim of Academic Transcripts is to display a formal report of students performance [26]. It may take several days to certain months for the transfer of academic documents with the widely accepted paper approach due to processing and transmission time involved. Along with considerable time taken and chances for spoilage, there prevails the threat for fraudulent documents by deceitful intermediaries. Processing of paper transcripts amounts to huge expense related to the manual effort, proceeding time, delivery and conveyance fees. There exists 3rd party services for online document verification thereby avoiding manual procedures. Blockchain contribute in maintaining distributed and permanent list of records by educational institutions to assure authenticity of transcripts. Another effective method in [27] is despite recording the entire transactions, hash of the document that contain the hash list of all scholarly certificates is recorded in the ledger to be checked out by the receiver. Smart contracts are used in [28] along with Ethereum blockchain for managing identity and certificates.

When the current researchers focused more on the application of blockchain in miscellaneous sectors, hardly any analysis has been accomplished with regard to the implementation of blockchain technology. The proposed hardware prototype detailed in this work introduces a new outlook to the realization of blockchain architecture. Higher levels of security is offered by hardware cryptographic elements over software components since the latter are more susceptible to security attacks.

3 Hardware cryptography v/s Software cryptography

With the surge in the use of smart gadgets and as the attacks against confidential data in business and government sectors are enlarging, data security is gaining predominance among IT users and programmers. Recent progress in technology set forth many solutions for the above problem and it is up to the user to choose whether the solution should be hardware based or software based.

3.1 *Software encryption*

Currently software encryptions are more popular than hardware based solutions since they are easy to handle, upgrade and renew. Software programs are portable and accessible for every operating systems and devices. However, these encryptions provide protection

as long as the operating system on which it runs have high grade of security. If OS have any security blemish, the whole encryption would be compromised [29]. When a software program is executed in parallel with other operations in the environment, confidential information could be leaked through side channel attacks. Thus open platforms can recover the data on secret keys. Hackers can easily compromise software encoding by duplication of encrypted records and through frequent attempts of parallel breaking in different systems. Since software need frequent up-gradation they are more vulnerable to security attacks. There are many recovery options available to access data in spite of its failure.

In software cryptography, threats posed by side-channel attacks goes unnoticed. Side channels is a perceivable change as a result of ciphering which an attacker can sense and utilize to his favour. Predominance of side channels and its sensibility factor have increased the risk of hacking due to new features like advanced processors introduced in the host computers. In [30], the author discussed how data could be retrieved based on recent attacks that exploits timing of CPU cache, branch algorithm logic and correlation function.

3.1.1 *Software security threats*

Inefficiency of software to provide the required security is dependent on the following factors:

1. Limitation in security posed by OS
   Software security module are not standalone units. Therefore they rely on operating system of host computer for its functioning. Despite the complete security of the program, if OS is subjected to some defects such as memory leakage or trojan insertion then the whole system gets compromised. Safety of cryptographic software is directly related to OS security.

2. Random Access of Memory
   Another drawback of software implementation is the lack of dedicated memory. They entrust memory of host system to store private information. Sharing of system's memory with other operations concurrently will provide access to the contents inside memory for other applications thus confidentiality and privacy is threatened.

3. Code Integrity Issue
   Software codes stored in memory can easily be modified by a hacker through random access of cache. This could lead to impairment or data leakage. No system can detect software tampering thereby leaving integrity of codes at stake. No machines has been designed till date to identify or prevent manipulation of codes inside software. This increases the security concerns of software encryptions to a great extend.

4. Susceptibility to Reverse Engineering
   In Software domain it is much easier for an intruder to identify the functionality of a module by means of examining the instructions given in the code. This could jeopardize the design architecture before an attacker backing reverse engineering.

3.2 *Hardware encryption*

Most viable solution to protect drives that contains huge amounts of information in the fields of education, healthcare and finance are through hardware based encryptions. The contents within such devices will be protected even if these drives is taken and used in other systems owing to the effectiveness of hardware encryption keys. No encryption/decryption keys are stored inside systems memory and therefore less vulnerable to key attacks.

The recent surge in demand for power reduction in devices have motivated researchers to think about application specific hardware structures over generic processors. Computationally expensive and power hungry algorithms can be implemented using hardware methodology so as to match up with the present operational speed requisites. Application Specific Integrated Circuits (ASIC) showcase better efficiency in terms of speed, size and power but demands a huge non-recurring costs for prototyping. In these circumstances Field Programmable Gate Devices (FPGA) have superiority wherein they incorporate both hardware and programming on a single platform with low cost of application and reconfigurability in design. FPGA prototypes are designed using hardware description languages such as verilog or VHDL (Very Large Scale Integration Hardware Description Language) [31].

In hardware encryption, a customized processor handles the entire process of encryption, decryption and access to protect data [32]–[34]. Additional components are not required for encryption process as the device comprises of the required utilities. When a password is provided, processor employs random number generator to create encryption keys. It doesn't require additional software setup. Since the encryption solely runs on the dedicated hardware there is no forms of communication with the OS of the system. So the performance remains unaffected and is found to be much superior than software based solutions. Thus the hardware is basically protected from corruption, malicious software attacks and reverse engineering.

4 Blockchain Technology

Blockchain is an enlarging series of connected records called blocks secured through cryptographic algorithms. As per Gartner's prediction in 2017, market value of blockchain will emerge to about $176 billion by 2025 and can reach up to $3.1 trillion next to 2030. This emerging science can benefit different sectors and thus make possible a remarkable revolution form "Internet of Data" to "Internet of Value" and create a decentralized economic platform. Key features of this technology comprises of Decentralization, Data Authenticity, Transparency and Immutability [35].

The term "transactions" in this context refers to data framework that enables exchange of data or information of value among clients. Many such transactions are added up to form one block. Each block is linked with the other over one-way secure algorithms called hash functions [36]. Cryptographic hash forms the linking thread between current block and its predecessor.

It enables a group of members within a network to share and store information related to transactions or events. Transactional records can be examined by the participants but none can alter or manipulate any of the validated data proceedings. This impart
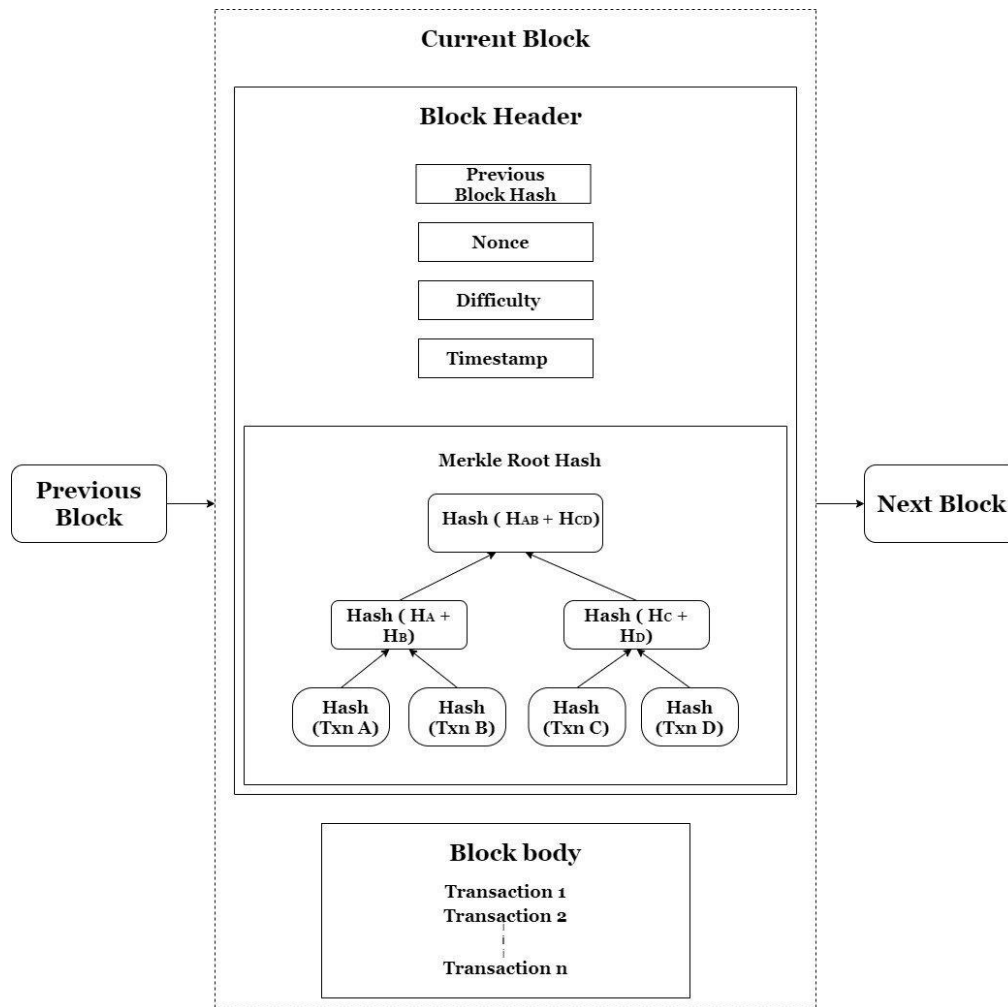
Figure 2: Typical Blockchain Architecture

blockchain with immutability in regard to all events undergone in the network. Thus the shareholders even if not known to each other can trust themselves, arrive at an agreement, record them and form connected transactions in the form of chain. This technology can grant digital identities similar to passports or license for performing financial and other confidential tasks. Every transactions are approved by all individuals in the network before its linkage to the chain based on predefined criteria, thereby avoiding any possibility of repudiation. Figure 2 represents the typical Blockchain architecture.

4.1 Fundamentals of Blockchain

1. Block
   Block forms the principle constituent of the blockchain. Structure of a block consist of following elements:

   - Block Header
     It comprises of metadata related to block that includes hash of the previous block, difficulty, merkle root hash, nonce and timestamp. Merkle hash constitute the hash value of all transactions recorded in that particular block.

   - Block body
     It consist of all the transactions included in the block.

2. Hash functions
   Hashing is the technique to transform random sized input data to output of fixed size. Message Digest 5 (MD5) is extensively used for generating hash values of 128 bit length [37].

Table 1: Performance comparison of different hash algorithms

Hash function	Speed of operation	Security level	Hash size
SHA-1	Medium	High	160
SHA-3	Slower than SHA-1	High	256
SHA-256	Slower than SHA-1	Highest	256
MD5	Fastest	Lowest	128
SHA-512	Slower than SHA-256	Highest	512

The limitations of MD5 algorithm to create unique hash functions lead to the development of Secure Hash Algorithms(SHA).

At present various set of algorithms have been designed which includes SHA-1, SHA-2, SHA-3 and latest being SHA-256 and SHA-512. The execution time required by the above mentioned algorithms are furnished in [38] which gives an insight into the frequency of operation needed by each of the hashing methods. Most popular hash functions in usage is SHA-256 on account of its trade-off with respect to level of security and the bit length as shown in Table 1.

SHA-256 are one way hash functions that produce untampered 256 bit hash value [39], [40]. The string created after encrypting the block of information is irreversible. They are highly collision resistant since even a one-bit change in input reflects significant change in the output bits. Currently bitcoin utilizes SHA-256 for hashing blocks of data.

3. Consensus Algorithms
Consensus procedure in blockchain assures data consistency and enable all peers to reach on to common agreement in block creation[41]–[45]. In such a way reliability is attained and also empower trust among participants in a decentralized network. There exists different categories of consensus mechanisms as mentioned below:

- Proof of Work
  In Proof of Work(PoW) consensus process, a complex numerical puzzle needs to be solved by the participating node to mine the adjoining block. A good deal of computational power need to be spend by the mining node to find the solution to the puzzle. PoW is adopted by bitcoin for block formation.

- Proof of Stake
  In comparison to PoW, the holder with maximum share is given top priority for block creation in Proof of Stake (PoS). As the blocks get added the concerned shareholders get more assets as reward. This incentive provided encourages participation in PoS. Ethereum is found to utilize PoS to achieve consensus.

- Proof of Burn
  In Proof of Burn coins are burned by sending them to a random address, which will be nominated by the network. Through this burning process, the clients gain the authority to mine the blocks based on arbitrary selection procedure. More the coins are burned, greater is the probability to select the concerned node as miner. But as in PoW, the resources are wasted unnecessarily.

- Practical Byzantine Fault Tolerance
  The ability to arrive at an agreement between two communicating nodes in a decentralized network in the existence of malicious nodes is referred to as Byzantine Fault Tolerance. In Practical Byzantine Fault Tolerance (PBFT), the primary node is selected in a round robin fashion. This nodes creates the block upon receiving the request and broadcast it to all other nodes present in the network. Primary node reach to a decision based on majority voting so that data authenticity and integrity is assured. Each request is processed on getting support from two-third of the votes from the network. Thus this

consensus process function efficiently on the criteria that only one-third of the nodes are malicious in nature.New improved version of PBFT called Tendermint blockchain algorithm is proposed in [46].

Apart from the above discussed algorithms there are many other proofs such as Proof of Capacity, Proof of Space, Proof of Elapsed Time and so on. These consensus algorithms give an insight about their mode of execution and they are often used by experts in bitcoin. Blockchain application still may vary based on its utilization in other fields and the agreement process discussed in this section need to be modified related to the type of application.

4.2 Features of Blockchain

The Blockchain framework provide the following attributes that prove it to be a successfull platform for online data transfer [47], [48].

1. Data Integrity
   The decentralized connected network of blockchain guides students and teachers to apply, transfer and authenticate records. Entire process is automated, user friendly and openly accessible.

2. Data security
   Transparent ledger mechanism render safe and secure methods to transit, store and validate transcripts. Data is disclosed only to the destined receiver.

3. Flexibility
   Blockchain network is able to hold increasing number of colleges, institutions, students and documents. They are able to manage conversions and enhancements to record at the same time and thus maintains reliability.

4. Immutability
   The information once uploaded in the database can never be modified or updated. As a owner and also as a recipient of data, the participants can be confident on the provenance of the information.

5 Proposed Model for Hardware Blockchain

This research work discuss the hardware approach to blockchain architecture in order to safeguard and authenticate academic information in educational institutions. But the current blockchain structure has to be modified due to following limitations:

1. This work considers all subject marks attained by students on semester basis as the Academic record.The marks scored could be stored only after generating the block. So block needs to be created before storing the transactions.

2. Ownership of a particular block belongs to a single authority. Further, it is imperative to create block without introducing
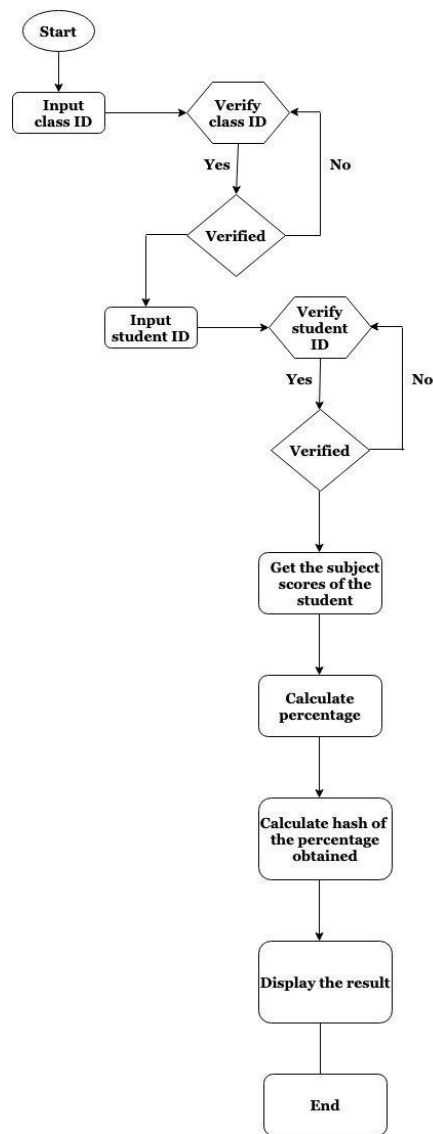
Figure 3: Flowchart of different operations performed within a single block

any computational complexity. Therefore consensus algorithms such as Proof of Work, Proof of Stake, or Proof of Burn are not significant in this context.

3. The proposed framework does data transmission only when the concerned students or teachers need to view and display their academic progress. Hence unlike the proofs detailed in the previous section that recursively repeat their execution, this system utilizes minimum resources saving energy, time and cost.

4. The suggested prototype assumes classroom as the block and the percentage of marks attained by each student that belongs to that class will act as a new "transaction". Typical consensus process are efficient for long transactions thereupon not acceptable for this application.

5. The officials authorized to enter the students credentials in the block repository are expected to do the same after thorough

content analysis and verification to prevent any typos or errors since the block contents once added remains immutable.

In view of the above limitations a different approach is introduced in the implemented design. The proposed hardware concepts are detailed here:

5.1   Formation of Block

In Academia data could be recorded in the corresponding blocks only after its creation. Each block represents a class room. Class teacher and the students of the respective classes are assumed to be the authorized members of a block. Every class room is allotted with a unique identification number called Class ID. Each student in a class is provided with student registration number known as Student ID. Its is presumed that the class ID, student ID, and the subject marks attained by every students are stored in a dedicated memory within the concerned block. In this architecture every block in the chain consists of Block ID, Block Header, Previous Block
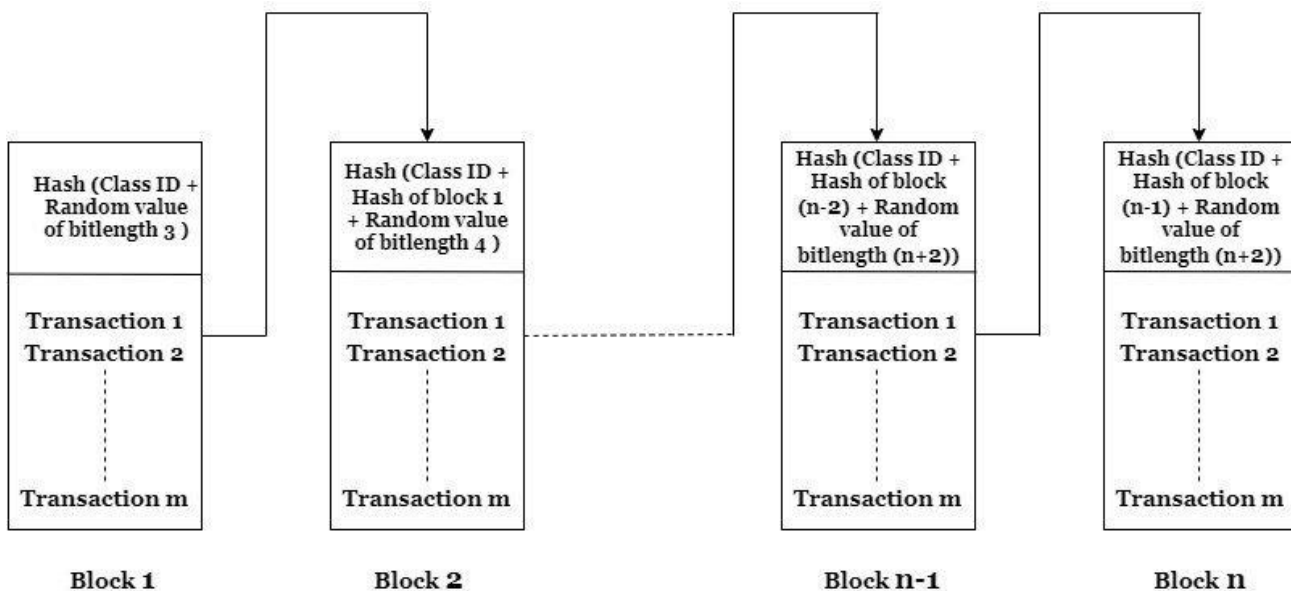
Figure 4: Block Formation in the blockchain
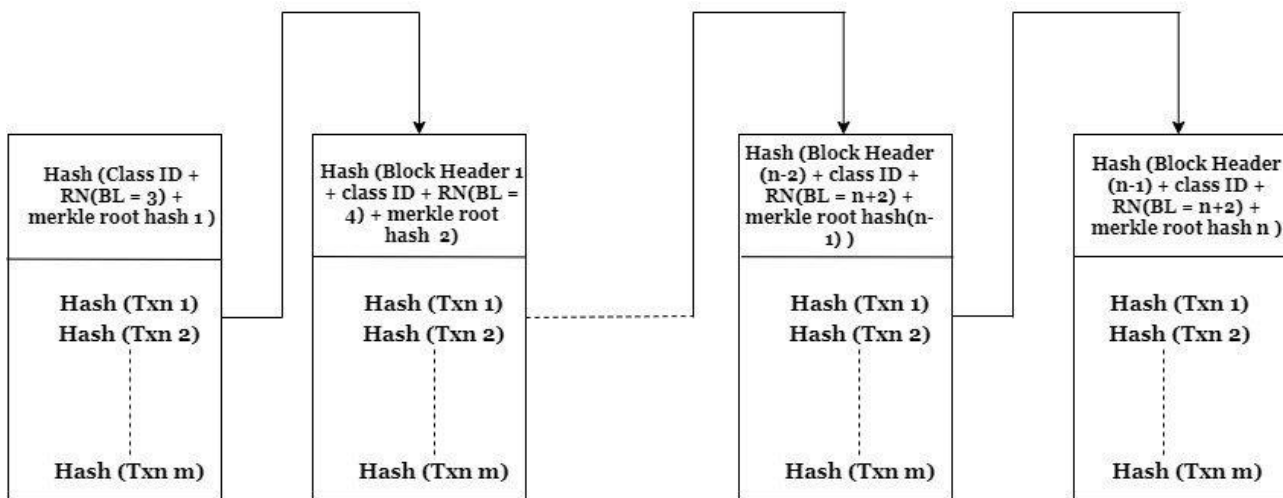
Figure 5: Block Securing Strategy

Hash and Merkle Root Hash. Figure 3 illustrates the flowchart of the different operations executed within a block.

1. Block ID creation

   Block ID refers to the unique number created for Block identification. It contains a random number that is generated by applying SHA-256 hashing algorithm on Class ID value. The Class advisor can enter the Class ID as the input and if it matches with the identification value assigned for the class, block ID will be created else the access is denied. Except the first block every other block have additional parameter called Block Header in the Block ID. Block ID formulas are as follows:

   $$Block\_1\_ID = hash(ClassID + RN(BL = 3)) \quad (1)$$

$$Block\_n\_ID = hash(ClassID+Block\_n-1\_Header+RN(BL = n+2)) \quad (2)$$

RN stands for Random Number
BL stands for Bit Length

2. Block body

   After the generation of Block ID, in the next phase the student can enter his/her Student ID. The student ID is verified with the original value already stored in the memory of block and if it is matched, the subject marks for the respective student is accessed and percentage is computed. Hash algorithm is applied to the unique value obtained after concatenating Student ID with the percentage scored. This results in a unique hash value which is displayed along with the percentage value as outputs.

3. Block Header

   Block header contains Merkle root hash of all transactions and Block ID. Block ID corresponds to the 256-bit hash value that distinguishes and identifies the block. Merkle root hash is obtained by hashing the sum of hashes of all the transactions conducted within the block. The "transactions" in this context refers to the percentage calculated for each student. Block Header is calculated based on the given equations:

$$Block\_1\_Header = hash(Block\_1\_ID+Merkle\_hash\_1) \quad (3)$$

$$Block\_n\_Header = hash(Block\_n-1\_ID + Merkle\_hash\_n) \quad (4)$$

4. Nonce and Difficulty

   First block is developed based on the unique class ID allocated to each class and a three bit random number. Hashing algorithm SHA-256 is imposed on these parameters to generate the hash for the block. Random Number is created by hashing the class ID and considering the last three bits from the LSB of the resultant hash. For the succeeding blocks, previous block hash, unique class ID and the random number are utilized. With the increase in the number of blocks, the bit size of the random number is also incremented. Random value assigned for hash generation determines the Nonce and difficulty. In this blockchain, block formation is confined only with the teachers who is entrusted with the class ID. Figure 4 shows how the blocks are formed within the blockchain.

5.2 Interconnection of Blocks

For ensuring additional security to the blocks created the following concept is applied:

- Block ID is the principle component that interlinks each block.

- Block Header of the current block consists of Block ID and merkle hash root of the commenced block. Every individual transactions that happened within a block are hashed separately using SHA-256 hash algorithm. These hash values are added on each time and once the entire transactions gets completed the resultant hash value is hashed once again to get the merkle root hash of the block.

- The block ID of the current block includes Class ID and random number that belongs to present block but block header of the previous block. Preceding block header contains block ID and merkle root hash of the previous block.

- Thus all the contents within each block gets interconnected with the other as the length of the chain increase.

- Therefore Nth block ID could be created only if the complete data is consistent from the first block to the preceding block with regard to data integrity and provenance.

- Interconnection of blocks thus assure added security since the contents within the block cannot be updated or manipulated as the hash values computed through SHA-256 are NP hard to find a solution. Figure 5 demonstrates the method adopted for securing blocks.

The main objective of blockchain hardware platform for storing academic database is to gain trust of the entities involved that includes students, teachers, parents, other higher officials who needs to validate the transcripts whenever required without the help of an external third party. Data security is ensured through block formation, block interconnection and hashing of contents. Other authorized educational organizations can access the blockchain database through creation of unique ID number followed by its verification by the authority in-charge (class advisors).

6 Synthesis and Simulation Results

The proposed hardware prototype for blockchain is designed in Hardware programming language Verilog. The functionality has been verified using Modelsim Simulator tool. The design is synthesized in Virtex 7 FPGA using Xilinx ISE design suite software tool.

The architecture designed can be programmed to include any number of blocks within the chain of blocks and is also flexible with respect to the number of transactions per block. As part of the research work, a miniature model of blockchain is considered that contains four blocks in the chain. Each block represents a class that comprises of 50 students. Four subjects pertaining to the current semester is stored within the blocks for estimating the Academic grade in percentage.

6.1 Simulation Results

Figure 6. displays the simulation results after percentage estimation for a particular student in Block 1. Inputs given were as follows:
Class ID = 20171
Student ID = 17002
Outputs obtained were :
Percentage = 82
Hash output of percentage for the student with ID 17002
= db3eee73beca217620ec21c37c0c07ccb0b65eddc1c9d9
a4382f7cd931696c7e
Block ID = d9bae266e5eb6914800a1894b8a5567290d63
efe7df89536892dafe4beb921a2
Block Header = df8c153e6682c3cb6c3330e804c3a44c983
246886ad888bc05832e57f177aaea
Merkle root hash = f3e886b34a03f33bf98d449f57d8cd562
fb1fb6f58f6c66ce3e985ee727900e5

6.2 Synthesis Results

The framework was designed to exist as different modules, synthesized separately and later integrated to form the entire architecture. The structure contained standalone modules for Block ID creation,
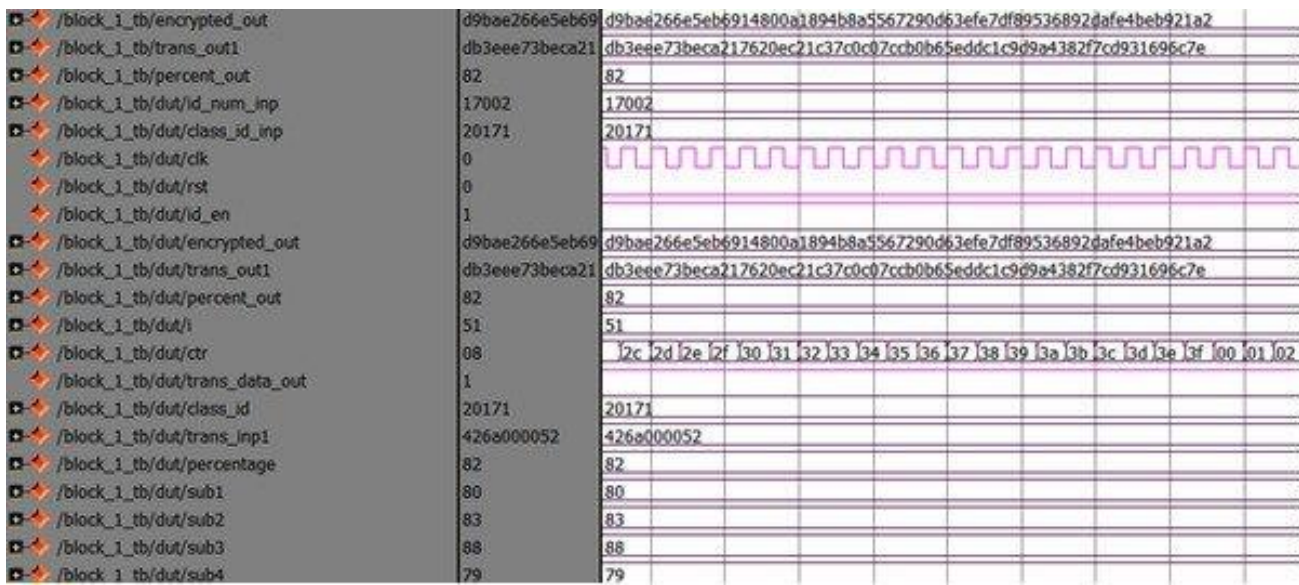
Figure 6: Simulation result after percentage estimation in block 1

Merkle hash computation, Block header creation and a Block module that includes the design for percentage computation. Table 2 shows the performance parameter summary for different design modules in the blockchain paradigm. In the table LUT-FF stands for Look Up Table and Flipflop pairs and IOB is the abbreviated form of Input-output buffers utilized by the design modules.

The entire system comprising of all the modules designed, functioned at an operational frequency of 95.138MHz. All modules were synthesized in xc7v1500t-2flg1761 device belonging to Virtex-7 FPGA family.

Table 2: Performance analysis of various blocks in the blockchain in Xilinx Virtex 7 FPGA

Design Modules	#Registers	#LUT-FF pairs	#IOBs	Speed (Mhz)
Merkle_hash_1	5804	4631	276	95.138
Block_1	6296	5528	569	95.235
Block_1_header	12269	9877	276	95.142
Merkle_hash_2	5807	4617	276	95.138
Block_2	18746	15369	571	95.132
Block_2_header	24678	19789	276	95.142
Merkle_hash_3	5804	4623	276	95.138
Block_3	31119	25442	571	95.138
Block_3_header	37046	29900	276	95.145
Merkle_hash_4	5804	4638	276	95.137
Block_4	43546	35356	571	95.138
Block_4_header	49471	39738	276	95.138

7   Conclusion and Future Scope

Credibility and authenticity of academic records are prerequisites to the reputation of academia and graduates. Unreliability of paper records and centralized electronic storage system demands the requirement of a distributed transparent platform to enable data sharing and communication. This scenario reveals the importance of Blockchain that offers a vital platform to implement an open access framework and attain interoperability. However the software elements in this technology are subjected to serious security threats that seems to put a downfall on the level of security provided by them in comparison to the hardware equivalents. This research work suggests a hardware approach that unfolds a new dimension to the architectural perspective of blockchain and helps the online experts that rely on this technology to overcome many vulnerabilities and challenges of an autonomous software application. In addition to Academic record maintenance, the proposed paradigm can be extended to higher levels that covers multiple domains and universities. Thus as an element of future work, the design find its application in University Management Scheme and Online Academic Systems so as to receive the complete details of the student performance.

Conflict of Interest   The authors declare no conflict of interest.

References

[1] J. Wan, J. Li, M. Imran, D. Li and Fazal-e-Amin, "A Blockchain-Based Solution for Enhancing Security and Privacy in Smart Factory," IEEE Transactions on Industrial Informatics, **15**(6), 3652–3660, 2019, doi:10.1109/TII.2019.2894573.

[2] J. Al-Jaroodi and N. Mohamed, "Blockchain in Industries: A Survey," IEEE Access, **7**, 36500–36515, 2019, doi:10.1109/ACCESS.2019.2903554.

[3] Shan Jiang, Jiannong Cao, Hanqing Wu, Yanni Yang, Mingyu Ma, Jianfei He, "BlocHIE: a BLOCkchain-based platform for Healthcare Information Exchange," in 2018 IEEE International Conference on Smart Computing, 49–56, 2018, doi:10.1109/SMARTCOMP.2018.00073.

[4] Thomas McGhin, Kim-Kwang Raymond Choo, Charles Zhechao Liu and Debiao He, "Blockchain in healthcare applications: Research challenges and opportunities," Journal of Network and Computer Applications, **135**, 62–75, 2019, doi:10.1016/j.jnca.2019.02.027.

[5] C. C. Agbo, Q. H. Mahmoud, and J. M. Eklund, "Blockchain technology in healthcare: A systematic review," Healthcare, **7**(2), 56, 2019, doi: 10.3390/healthcare7020056.

[6] B. Assiri, "Leader Election and Blockchain Algorithm in Cloud Environment for E-Health," in 2019 2nd International Conference on new Trends in Computing Sciences (ICTCS), 2019, doi:10.1109/ICTCS.2019.8923099.

[7] A. Cohn, T. West, and C. Parker, "Smart after all: Blockchain, smart contracts, parametric insurance, and smart energy grids," in Georgetown Law Technology Review, 273–304, 2017.

[8] E. Münsing, J. Mather, and S. Moura, "Blockchains for decentralized optimization of energy resources in microgrid networks," in 2017 IEEE Conference on Control Technology and Applications (CCTA), 2164–2171, 2017.

[9] M. Mylrea and S. N. G. Gourisetti, "Blockchain for smart grid resilience: Exchanging distributed energy at speed, scale and security," in 2017 Resilience Week (RWS), 18–23, 2017, doi:{10.1109/RWEEK.2017.8088642}.

[10] Y. Lin, Joy R. Petway, Johnathen Anthony, Hussnain Mukhtar, Shih-Wei Liao, Cheng-Fu Chou and Yi-Fong Ho, "Blockchain: The evolutionary next step for ICT e-agriculture," Environments, **4**, 50, 2017, doi:10.3390/environments4030050.

[11] F. Yiannas, "A new era of food transparency powered by blockchain," Innovations: Technology, Governance, Globalization, **12**(1-2), 46–56, 2018, doi:10.1162/inov_a_00266.

[12] CIOReview. (2019)., "How Can Blockchain Technology Revamp Gaming Industry," 2019.

[13] G. Schillinger, Z. Huang, and S. Snyder, "The infrastructure for games of the future," 2018.

[14] C. Sitonio and A. Nucciarelli, "The Impact of Blockchain on the Music Industry," in 29th European Regional Conference of the International Telecommunications Society (ITS), 1–14, 2018.

[15] L. Lee, "New kids on the blockchain: How bitcoin's technology could reinvent the stock market," Hastings Business Law Journal, **12**, 81, 2015, doi:10.2139/ssrn.2656501.

[16] P. Poonpakdee, Jarotwan Koiwanit, Chumpol Yuangyai and Watchara Chatwiriya, "Applying Epidemic Algorithm for Financial Service based on Blockchain Technology," in 2018 International Conference on Engineering, Applied Sciences, and Technology (ICEAST), 1–4, 2018, doi:10.1109/ICEAST.2018.8434512.

[17] B. Shahzad and J. Crowcroft, "Trustworthy Electronic Voting Using Adjusted Blockchain Technology," IEEE Access, **7**, 24477–24488, 2019, doi:10.1109/ACCESS.2019.2895670.

[18] O. Jacobovitz, Blockchain for identity management, Ph.D. thesis, 2016.

[19] H.R. Hasan, Khaled Salah, Raja Jayaraman, Mohammed Omar, Ibrar Yaqoob, Saša Pesic, Todd Taylor, Dragan Boscovic, "A Blockchain-Based Approach for the Creation of Digital Twins," IEEE Access, **8**, 34113–34126, 2020, doi:10.1109/ACCESS.2020.2974810.

[20] T.M. Fernández-Caramés, Paula Fraga-Lamas, "A Review on the Applica-tion of Blockchain to the Next Generation of Cybersecure Industry 4.0 Smart Factories," IEEE Access, **7**, 45201–45218, 2019, doi:10.1109/ACCESS.2019.2908780.

[21] S. Wang, L. Ouyang, Y. Yuan, X. Ni, X. Han and F. Wang, "Blockchain-Enabled Smart Contracts: Architecture, Applications, and Future Trends," IEEE Transactions on Systems, Man, and Cybernetics: Systems, **49**(11), 2266–2277, 2019, doi:10.1109/TSMC.2019.2895123.

[22] A.A. Monrat, Olov Schelén and Karl Andersson, "A Survey of Blockchain From the Perspectives of Applications, Challenges, and Opportunities," IEEE Access, **7**, 117134–117151, 2019, doi:10.1109/ACCESS.2019.2936094.

[23] T. Ali Syed, A. Alzahrani, S. Jan, M. S. Siddiqui, A. Nadeem and T. Alghamdi, "A Comparative Analysis of Blockchain Architecture and its Applications: Problems and Recommendations," IEEE Access, **7**, 176838–176869, 2019, doi:{10.1109/ACCESS.2019.2957660}.

[24] L. Xiong, F. Li, S. Zeng, T. Peng and Z. Liu, "A Blockchain-Based Privacy-Awareness Authentication Scheme With Efficient Revocation for Multi-Server Architectures," IEEE Access, **7**, 125840–125853, 2019, doi:10.1109/ACCESS.2019.2939368.

[25] A. Badr, L. Rafferty, Q. H. Mahmoud, K. Elgazzar and P. C. K. Hung, "A Permissioned Blockchain-Based System for Verification of Academic Records," in 2019 10th IFIP International Conference on New Technologies, Mobility and Security (NTMS), 1–5, 2019, doi:{10.1109/NTMS.2019.8763831}.

[26] Mona Al-Maharri, Hesham Al-Ammal, Lamya Aljasmi, "Usability of the Academic Transcript," in 2018 International Conference on Innovation and Intelligence for Informatics, Computing, and Technologies (3ICT), 1–7, 2019, doi:10.1109/3ICT.2018.8855746.

[27] "Academic Certificates on the Blockchain," 2018.

[28] S. Kolvenbach, R. Ruland, W. Gräther and W. Prinz, "Blockchain 4 Education," in Proceedings of 16th European Conference on Computer-Supported Cooperative Work-Panels, Posters and Demos, 2018, doi:10.18420/ecscw2018_p7.

[29] Nicolas Sklavos, Katerina Touliou, Costas Efstathiou, "Exploiting cryptographic architectures over hardware vs. software implementations: advantages and trade-offs," in Proceedings of the 5th WSEAS International Conference on Applications of Electrical Engineering, 2006.

[30] N. Lawson, "Side-Channel Attacks on Cryptographic Software," IEEE Security & Privacy, **7**(6), 65–68, 2009, doi:10.1109/MSP.2009.165.

[31] Samir Palnitkar, Verilog HDL: A Guide to Digital Design and Synthesis, Prentice Hall PTR, One Lake Street, Upper Saddle River, United States of America, 2003.

[32] Midhun Sasikumar, K.N. Sreehari, Ramesh Bhakthavatchalu, "Systolic Array Implementation of Mix Column and Inverse Mix Column of AES," in 2019 International Conference on Communication and Signal Processing (ICCSP), 0730–0734, 2019, doi:10.1109/ICCSP.2019.8697927.

[33] N.H.N. Sai Kiran, Ramesh Bhakthavatchalu, "Implementing delay based physically unclonable functions on FPGA," in 2016 International Conference on Advanced Communication Control and Computing Technologies (ICACCCT), 137–140, 2016, doi:10.1109/ICACCCT.2016.7831616.

[34] M. Anil Kumar, Ramesh Bhakthavatchalu, "FPGA based delay PUF implementation for security applications," in 2017 International Conference on Technological Advancements in Power and Energy (TAP Energy), 1–6, 2017, doi:10.1109/TAPENERGY.2017.8397339.

[35] I. Lin and Tzu-Chun Liao, "A Survey of Blockchain Security Issues and Challenges," International Journal of Network Security, **19**(5), 653–659, 2017, doi:10.6633/IJNS.201709.19(5).01.

[36] K. Devika and Ramesh Bhakthavatchalu, "Parameterizable FPGA Implementation of SHA-256 using Blockchain Concept," in 2019 International Conference on Communication and Signal Processing (ICCSP), 0370–0374, 2019, doi:{10.1109/ICCSP.2019.8698069}.

[37] K.N. Sreehari, Ramesh Bhakthavatchalu, "Implementation of hybrid cryptosystem using DES and MD5," in 2018 3rd International Conference on Communication and Electronics Systems (ICCES), 52–55, 2018, doi:10.1109/CESYS.2018.8724111.

[38] R. Purohit, Upendra Mishra, Abhay Bansal, "Design and Analysis of a New Hash Algorithm with Key Integration," International Journal of Computer Applications, **81**(1), 33–38, 2013, doi:10.5120/13978-1974.

[39] L. Bai, Shuguo Li, "VLSI Implementation of High-speed SHA-256," in 2009 IEEE 8th International Conference on ASIC, 131–134, 2019, doi:10.1109/ASICON.2009.5351591.

[40] N.C. Iyer and Sagarika Mandal, "Implementation of SHA-256 algorithm in FPGA based processor," International Journal of Advanced Research in Electronics and Communication Engineering (IJARECE), **4**, 334–344, 2015.

[41] N.S.Tinu, "A Survey on Blockchain Technology- Taxonomy, Consensus Al-gorithms and Applications," International Journal of Computer Sciences and Engineering, **6**, 691–696, 2018.

[42] Sol Jeon, Inshil Doh, Kijoon Chae, "RMBC: Randomized Mesh Blockchain Using DBFT Consensus Algorithm," in 2018 International Conference on Information Networking (ICOIN), 712–717, 2018, doi:10.1109/ICOIN.2018.8343211.

[43] L. M. Bach, B. Mihaljevic, M. Zagar, "Comparative Analysis of Blockchain Consensus Algorithms," in 2018 41st International Convention on Information and Communication Technology, Electronics and Microelectronics (MIPRO), 1545–1550, 2018, doi:10.23919/MIPRO.2018.8400278.

[44] Zibin Zheng, Shaoan Xie, Hongning Dai, Xiangping Chen, Huaimin Wang, "An Overview of Blockchain Technology: Architecture, Consensus, and Future Trends," in 2017 IEEE International Congress on Big Data (BigData Congress), 557–564, 2017, doi:10.1109/BigDataCongress.2017.85.

[45] Du Mingxiao, Ma Xiaofeng, Zhang Zhe, Wang Xiangwei, Chen Qijun, "A Review on Consensus Algorithm of Blockchain," in 2017 IEEE International Conference on Systems, Man, and Cybernetics (SMC), 2567–2572, 2017, doi:10.1109/SMC.2017.8123011.

[46] Basem Assiri, Wazir Zada Khan, "Fair and trustworthy: Lock-free enhanced tendermint blockchain algorithm," TELKOMNIKA Telecommunication, Computing, Electronics and Control, **18**(4), 2224–2234, 2020, doi: 10.12928/telkomnika.v18i4.15701.

[47] M. Jirgensons and J. Kapenieks, "Blockchain and the Future of Digital Learning Credential Assessment and Management," Journal of Teacher Education for Sustainability, **20**, 145–156, 2018, doi:10.2478/jtes-2018-0009.

[48] M. Sharples and J. Domingue, "The Blockchain and Kudos: A Distributed System for Educational Record, Reputation and Reward," in 11th European Conference on Technology Enhanced Learning, 2016, doi:10.1007/978-3-319-45153-4_48.

ASTES

Current Views on Issues and Technology Development in Forensic Accounting Education of Indonesia

Tarjo[1,*], Zuraidah Mohd Sanusi[2], Prasetyono[1], Mohammad Nizarul Alim[1], Rita Yuliana[1], Alexander Anggono[1], Yusarina Mat-Isa[3], Henryan Vishnu Vidyantha[1], Mochamad Ali Imron[4]

[1]*Universitas Trunojoyo Madura, Bangkalan, 69162, Indonesia*

[2]*Accounting Research Institute, Universiti Teknologi MARA, Shah Alam, Selangor, 40450, Malaysia*

[3]*Faculty of Accountancy, Universiti Teknologi MARA, Puncak Alam, Selangor, 40450, Malaysia*

[4]*Universitas Islam Indonesia, Yogyakarta, 55584, Indonesia*

A R T I C L E I N F O	A B S T R A C T
	The objective of this study is to examine the current views of academics on issues and technology development in forensic accounting education. By applying the explanatory sequential mixed method, this study tries to acquire a better understanding of current perception regarding forensic accounting education. This study indicates that demand for forensic accounting services is expected to increase and offered as a separate courses at the graduate and undergraduate levels; respondent's perceived forensic accounting education as being relevant and beneficial to the business community, the accounting profession, and accounting students. Several technology tools and data analytics in investigation and analysis have been identified as important forensic accounting topics for curriculum developments. The limitation of this study is the small sample. A low response rate could be the result of this study containing bias so that it cannot be generalized, and most respondents are from accounting majors. These results are useful for universities in integrating forensic accounting education into their curriculum or redesigning their forensic accounting courses. The study shows the current view on forensic accounting education in Indonesia. Using an explanatory sequential mixed method is considered as a novelty of the present study.

1. Introduction

Nowadays, skill in forensic accounting becomes a requirement for the auditor to increase the probability of fraud detection [1]. If that so accounting profession need forensic accounting education? Some of the reasons for the importance of forensic accounting education today are because of the mass cases that occurred in the world such as Enron, WorldCom, and others. The other reason is the existence of new standards and changes in standards, beginning with the Sarbanes Oxley Act 2002 and changes to SAS 99. Both of these standards require auditors to detect fraud [2]. Changes in technology are also making forensic accounting more important because in the digital era, fraud not only occurred in financial statements but also cyber-crime, intellectual property (IP) fraud, piracy, forgery, and personal data [3]. When this financial fraud

combines with the use of computer and digital documents, fraud can falsify invoices or electronic money laundering. Consequently, electronic evidence of such crimes is found on personal computers (PCs) and company-owned mainframes, employee personal PCs, corporate networks, PDAs, diskettes, floppy disks, smart cards, and web servers on external networks [4]. Study shows that despite many cases involving fraud in large companies in the 2000s, only a few universities offer forensic accounting courses [5].

As far we know, there are many corruption cases in Indonesia, for example, Hambalang, a sting operation conducted by the Corruption Eradication Commission against several government officials. Also, in Indonesia, Insurance companies are now required by the Financial Service Authority to have fraud control and implementation anti-fraud strategies. This strategy includes prevention, detection, investigation, reporting, sanction, monitoring, evaluation, and follow-up. In line with the above

events, previous studies show that the demand for forensic accountant services is on the rise [5–7]. This demand was responded by various universities worldwide to offer programs or forensic accounting courses [5, 7–9]. Likewise, in Indonesia, many universities offer forensic accounting programs to meet high demand [10].

With the increasing number of universities offering forensic accounting education and the importance of knowledge about topics to support accounting students' future careers, this study examines academicians' opinions regarding forensic accounting education. These results can help academicians in developing or enhancing their curriculum choices in this field, helping students who are interested in career choices in choosing programs that can develop valuable expertise for the profession, and underline the importance of an interdisciplinary approach in forensic accounting education. In [11], the author said there are three reasons why should add a forensic curriculum. The first one is to prepare the students for their careers in accounting, the second is to improve the curriculum and the last one is for better employment opportunities. Using a mixed-method approach, this study describes forensic accounting education in Indonesia. It contributes to the forensic accounting curriculum and its results should be of concern to the accounting profession, academicians, and, in particular, to professional accountancy bodies, providing guidance that may influence how they approach or respond to this increasing demand for forensic accounting. This study aims to answer the following questions:

- What are educators' current views on forensic accounting?
- How do educators perceive obstacles in providing forensic accounting education?
- How do educators perceive important topics of forensic accounting?
- How do educators perceive various teaching methods in forensic accounting?

The next part reviews forensic accounting literature. This section discusses the literature review of forensic accounting, followed by a description of the research design to execute the study. Section 4 discusses the findings and results. The last section would be the conclusion and the implication of the findings, Limitation, and suggestion.

2. Literature Review

2.1. Perception of Forensic Accounting Education – Academicians

In the 2000s financial report scandals and frauds were widely published; hence, Barry Melancon - CEO of the American Institute of Certified Public Accountants – motivate academicians to teach students with "knowledge and skills to comprehend the essential attribute of fraud, identify factors indicating fraud, and obtain interview techniques [12]. The CEO stated that fraud, embezzlement, and other financial crimes that occur in the modern business environment makes the accounting and audit profession must have training and expertise to detect fraud [13]. These facts emphasize the need for courses specifically focusing on forensic accounting, assuming the audit course cannot provide sufficient training in fraud detection [5].

With this demand, it increases awareness of the importance of expertise in forensic accounting that can advance the ability to spot fraud [2, 14]. The Public Company Accounting Oversight Board (PCAOB) said that detecting fraud is a very important goal in auditing [1]. Research on the importance of forensic accounting education [5, 7–9, 15, 16]. These studies also suggest that forensic accounting education has evolved from initially limited to training in professional education for accountants to something currently offered as courses in several universities. Therefore, there is research that develops a guideline to serve the needs of academicians and practitioners, namely (1) to better understand the knowledge and expertise needed in the field of forensic accounting and (2) to assist academicians and professionals in developing appropriate subject matter and programs [15].

In [16], the author indicated that demand for forensic accounting services increases in the future and the Certified Fraud Examiner (CFE) practitioners chose to offer separate forensic accounting courses while academicians tended to integrate forensic accounting courses in accounting and auditing courses. Also, both groups stated that the accounting curriculum is not sufficient enough to fulfill the demand for forensic education and future accounting curriculum should add accounting forensic education. Their research also concluded that there were differences in perceptions between practitioners and academicians regarding the topics of forensic accounting. The most significant difference between both respondents is on the following topics: professional interview skills and legal aspects of interviews; and professional standards on forensic accounting. Both of the respondents believe that forensic accounting education has several benefits one of which is meeting the requirements for new regulations. However, several impediments like lack of faculty interest, lack of resources, and lack of flexibility in curriculum content mentioned as an obstacle in teaching the topic of forensic accounting by academics.

While the research of [7] signified the same thing that demand for forensic accounting services would increase in the future. Respondents prefer to integrate forensic accounting in accounting and audit courses. This is due to the challenges in terms of regulations, economics, social, ethics, and law faced by corporate that encourage an increase in demand for forensic accounting to create an accounting program to focus more on this field. As for learning techniques, the most important respondents choose from cases and books. The results of this study describe that there are different opinions between practitioners and academicians over 18 of the 49 subjects offered. But both of the respondents say that the majority of these topics are considered important. This study suggests that the topics offered in forensic accounting can be classified into three main sections in the forensic accounting module. the three main groups can be arranged as follows: the first part about basic fraud (such as types of fraud, fraud prevention, and deterrence programs and financial statement fraud), the second is related to corporate governance and legal aspects (earnings management, financial reporting process and analysis, white-collar and economic crimes, and criminology) and the latter focuses on topics related to careers in forensic accounting (expert

testimony and expert witness techniques, litigation consulting techniques). Meanwhile, the main setbacks to integrate forensic accounting into the accounting or auditing curriculum are the lack of financial resources, instructional materials, administrative support, and faculty interest.

In [5], the author studied survey academicians and practitioners regarding forensic accounting education. The results of his research showed that respondents preferred to offer forensic accounting in different subjects at the graduate or postgraduate level. Practitioners and academicians also have different perceptions about the topics taught and choose experiential learning as the most important learning techniques. Both of these professions agree that it is very important to teach forensic accounting courses in the accounting curriculum because this field experienced tremendous growth and the enormous interest of students. This research also shows that forensic accounting expertise will be very useful even though students do not take careers in forensic accounting. Respondents of this study also revealed that the lack of resources and the lack of qualified lecturers in teaching forensic accounting such as teaching topics on litigation, teachers must understand and have carried out this litigation process so that they do not only understand theoretical issues.

There is research on curriculum models and guidelines related to important topics that should be included in a forensic accounting course to meet the needs of students and companies [17]. In December 2003, a project funded by a grant from the National Institute of Justice at the West Virginia University Accounting Division was given to develop educational guidelines for academics, instructors, and students interested in fraud and forensic accounting. This project was implemented by forming a planning panel and Technical Working Group (TWG) that have expertise in this field. The results of the two-year project were curriculum models for fraud education and forensic accounting based on collaborative thinking among researchers, professional practitioners, and academicians to develop guidelines designed to help academics, universities, professors, course developers, and professionals. This TWG shows that the following main topics that must exist in the fraud and forensic accounting curriculum are criminology, fraud prevention, deterrence, detection, investigation, and remediation Forensic and litigation advisory services, including research and analysis, valuation of losses and damages, dispute investigation, and conflict resolution (including arbitration and mediation). This research can help universities, instructors, curriculum makers, and professional training to provide appropriate curriculum and topics in the field of forensic accounting, provide students with an initial understanding of fraud or forensic accounting, as material for reviewing audit courses, accounting so that the following forensic accounting practices. It also provides curriculum recommendations and course guides that can be used by users and finally provides training and development in the fields of fraud and forensic accounting for its users.

Research in [18], conducted a survey on CFE found several forensic accounting skills that were not taught in accounting programs such as interviewing and interrogation skills, sources of evidence, schemes of fraudulent financial reporting, criminology, computer/internet crime techniques, and expertise in human relations. This study shows that for a career in the field of forensic accounting must have technical skills and non-technical skills. Non-technical expertise includes ethics, collecting evidence, evaluation, documentation, and interviews as well as oral and written communication. This research provides suggestions for educators to help students learn both of these skills. Both of these skills are considered important for auditing financial statements properly. So when educators prepare their students with these two skills they can succeed in a career of fraud or forensic accounting.

2.2. Development of Forensic Accounting Education

During the period of accounting scandals that received considerable attention from around the world in the 2000s, there were still few forensic accounting educations available. Empirical evidence shows that in the very rapid development of forensic accounting, universities respond slowly to teach this topic to students [19]. In the next study, it was found that 21 universities were offering forensic accounting courses [7]. Then there was research on accounting education literature published in six journals for four years (2006-2009), showing that there is an increase in research related to the topic of fraud and forensic accounting, ethics, and professional responsibility [20]. Those studies recommended the content of forensic accounting embracing behavioral science [21], ethics and legal aspects [22], digital forensics [23], litigation consulting services [24].

Research in 2010 conducted a survey of 171 schools that were certified Association to Advance Collegiate Schools of Business (AACSB) to determine which universities offered forensic accounting and fraud checks [25]. The results indicated that only 4 of 171 schools offered degree programs for forensic accounting. While from 171, only 20 universities offered one forensic accounting course, and only 27 offered at least one fraud examination course. The research also shows that seven universities offer both forensic accounting courses and fraud checks.

In 2014, research was conducted on more than a thousand universities around the world, offering accounting programs to determine the extent to which forensic accounting education was taught [9]. Particularly, this survey involved 900 universities in the US and 186 universities in other countries. The study determined that 447 universities surveyed offered separate forensic accounting courses. Additionally, the study also found that 187 of the 1086 schools surveyed offered undergraduate and graduate special forensic accounting degrees, concentration, or specialization. Of course, the findings were a remarkable increase from previous research [25]. This study stated that this is strong and positive momentum in the development of forensic accounting education.

From previous studies, we know that forensic accounting education is developing rapidly throughout the world. The

demand for forensic accounting education is quite high. This is indicated by the number of universities that have begun providing forensic accounting courses. The availability of forensic accounting education is expected to be able to answer the challenges that the auditors today are expected to be more aggressive in finding fraud that occurs. Nowadays finding fraud is a must in the accounting profession. With the growing complexity of the business world, the development of technological challenges in finding and preventing fraud will be increasingly difficult. Forensic accounting expertise will be increasingly needed. Research shows that demand for forensic accounting services will increase in the future [5,6].

Research by [26] provides an overview of forensic accounting in the United Kingdom. Using questionnaires and in-depth interview methods try to explore perceptions of forensic accounting, profiles of people who work in this field, services offered, paramount expertise and knowledge needed, practitioners and academics respond to its development, and whether this should be considered a new profession. The results of this study show that accounting forensic is growing rapidly in the UK and its profession is dominated by qualified accountants, but in the last two years besides accountants who have taken part in this profession doubled. Forensic accounting is not a profession, according to this study naturally forensic accounting is a multidisciplinary science and it is very broad and deeper than any other profession that exists. Therefore, this field is too broad for someone to have all the knowledge, expertise, and do everything well.

Recently it shows that forensic accounting education is very important. With the rapid development of education, it is deemed necessary to research current forensic accounting education from an academician's perspective. This study surveyed to determine the latest views on various matters regarding forensic accounting education in academics.

3. Research Method

This study applies the Explanatory Sequential Mixed Methods Design [27]. This method includes two phases in which the researcher collects quantitative data in the first stage, analyzes the results, and then uses the results to plan (or built into) the qualitative phase. Quantitative results usually inform the types of the respondent that chosen for the qualitative step and the types of questions to be asked to them. The overall purpose of this design is for qualitative data to help explain in more detail the initial quantitative results.

- The researchers surveyed accounting academicians to answer questions about forensic accounting education sent online. This questionnaire focuses on the perceptions of accounting academicians regarding the development of forensic accounting, problems that become obstacles in the teaching of forensic accounting, important topics that must be taught in forensic accounting courses, and what are the best methods in learning forensic accounting. At the beginning of the

questionnaire collects demographic and background information for classification purposes. The validity of the questionnaire using Cronbach's alpha is 0,962. The questionnaire uses five Likert scales from 5 (very important or very agree) to 1 (very insignificant or strongly disagree).

- In the second stage, the researcher conducted interviews on the results obtained from the first stage. The results of this questionnaire are the basis of the material used to conduct interviews with respondents. Interviews were conducted with respondents who taught forensic accounting courses. The purpose of this interview is to collect detailed data on the development of forensic accounting, obstacles in teaching forensic accounting, important topics taught in forensic accounting courses, the best methods in the process of learning forensic accounting and the last respondents will be asked about anything they want to add in the curriculum of forensic accounting. Also by conducting interviews we can get a better understanding of the opinions of academics regarding forensic accounting education. Using member checking determines the accuracy or validity at this stage. Member checking is taking the result of a report or themes returned to the informant to test whether the informant feels that they are accurate [27]. Two respondents were selected to conduct interviews. The respondents have experience teaching accounting for more than 10 years. Respondents also have certification in forensic accounting so that they have a good understanding of the field of forensic accounting. Researchers also included responses to forensic accounting education in Indonesia from respondents who filled out questionnaires to further enrich the results of this study. Based on the description above, the model in this study is as follows.
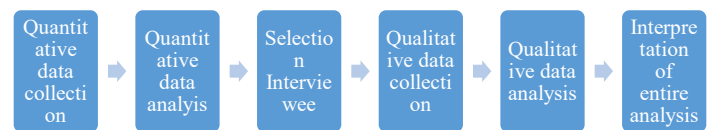
Figure 1: Research Model

3.1. Research Sample

A total of 120 accounting lecturers were randomly selected to complete an online survey related to forensic accounting education. The reason for choosing this sample is because those who teach in the accounting department are considered to have an understanding and knowledge of forensic accounting. The response rate is 39%.

3.2. Data Analysis

Descriptive statistics are used to analyze the results collected through the interview stage. This data is processed using IBM SPSS 24.0. In the qualitative stage, the coding and thematic analysis are carried out by the Qualitative Software and Research (QSR) 12 Plus. The qualitative analysis includes (1) preparing transcribing interviews and writing memos; (2) start the coding

process; (3) developing themes based on code (4) Interrelating themes; (5) interpretation of themes [27].

4. Discussion and Analysis

The survey showed that the data processed was 47, which characteristics demographics of the respondents indicated that 25 were male and 22 were female with an average age of 42 years. The majority of the respondent's education level is educated master, which is 30 people or 64%. Then there is an educated Doctor level which is 17 people or 36%. While respondents who had certification in the forensic field (Certified Fraud Examiner and Certified Forensic Auditor) were 19%.

4.1. Development of Forensic Accounting

The findings of this study indicate that forensic accounting services will increase in the future both in terms of litigation support, expert information, and fraud examination. Requests for litigation support and expert witness increased by 89%, while 11% of respondents answered remained. Fraud examination services as much as 98% responded to increase while the remaining 2% answered decreasing. Other research results also show that the majority of these three services are increasing [5–7]. According to research [26], the expert witness has become an important service in the UK, even this service is at the top of the forensic accounting services. As we know that forensic accounting is developing very rapidly and this is followed by forensic accounting services that will continue to increase in the future. According to the informant on the development of forensic accounting:

"Services in this field have the potential to develop and forensic accounting competencies are needed, especially in finance and the public sector"

This statement confirms that the role of forensic accounting is important in finance and the public sector. Indonesia has many cases of corruption in the public sector, of course, competence in the field of forensic accounting can provide great added value to achieve good governance and in the prevention, detection, and investigation of fraud. However, forensic accounting services are very broad-ranging from business valuations to property cases in divorce [26]. The research of [26] also states that there are twelve services in forensic accounting. This means that forensic accounting has good prospects and opportunities to be developed in the future. But does not rule out the possibility of further forensic accounting services will continue to grow.

In academics itself, the development of forensic accounting also continues to occur. Respondents mentioned that at the university where she taught:

"The curriculum offered also continues to change. We invite an expert to advice on the forensic accounting curriculum".

This development is certainly very encouraging and forensic accounting has now penetrated other aspects such as social,

technological, psychological aspects, etc. With the development of technology, of course, there will always be continuous improvement in forensic accounting. Where a system will always be looked for weaknesses and as soon as that too there must be prevention and detection of acts of fraud that occur. Respondents said, "This is like a race between a thief and the police".

Next, the respondents were asked their opinion on how to integrate forensic accounting education in the curriculum. Table 1 shows that the majority of respondents (68%) chose to offer the topic of forensic accounting separately, as many as 30% chose to integrate it into accounting and audit courses while the rest chose not to offer (2%). Additionally, respondents were also asked for their opinion on whether forensic accounting education was offered at the level of Bachelor, Master, or both (Bachelor and Master education. Table 1 also shows that most respondents answered that forensic accounting education must be taught at both Bachelor's and Master's levels. While those who choose are taught at the Master level as much as 45%, the remaining 6% choose at the Bachelor level only.

Table 1: Perception of How Forensic Accounting Should Be Integrated and What Preferred Level

Integrated into Curriculum	Response (%)	Preferred level	Response (%)
Integrate throughout the accounting and audit course	14 (30%)	Bachelor	3 (6%)
Offered separate course	32 (68%)	Master	21 (45%)
Do Not Cover Forensic Accounting at all	1 (2%)	Bachelor and Master	23 (49%)

This result is conforming to the study of Kramer et al.'s (2017) which indicates that forensic accounting education is offered separately at the undergraduate and postgraduate educational levels. This result is different from research [7, 16]. In their research, it was stated that forensic accounting is better integrated into accounting and audit courses. This difference can be caused by the development of forensic accounting not only in accounting and auditing but also in multi-disciplines [5]. As we know nowadays the development of forensic accounting covers a variety of disciplines. Not only accounting and auditing, but also law, information technology. Even according to [26] behavioral sciences such as psychology, sociology, criminology, and anthropology can support the field of forensic accounting. The research of [26], who researched in the UK, showed that the forensic accounting profession from non-accounting has more than doubled for IT experts and experts in other fields in the last two years. But now according to respondents who work as lecturers said:

"at the Bachelor level the forensic accounting course is still an introduction, so to become an expert in this field is required the next level of masters and certification".

This means that formal education is quite important but there must be a need for certification in the field of forensic accounting.

This is following the current conditions in which forensic accounting has developed into a multi-disciplinary discipline so there is a need for certification that will greatly support this profession. Thus forensic accounting becomes an interesting science to keep on developing. Because as long as there is still fraud it is necessary to know how to detect and prevent this. For this reason, cooperation between various parties in Indonesia is needed to advance forensic accounting. There needs to be collaboration from academics and practitioners to do it. As conducted [17], which invited academics and practitioners in the field of forensic accounting to spend their time, ideas, and views on developing better education and training in fraud and forensic accounting. That way forensic accounting will develop in a better direction because the one who formulates education and training is the competent party in their field. The development of forensic accounting must move in line with the complexity of the case at this time. That way this profession will increasingly attract interest from students to work as forensic accountants.

4.2. Perception of Obstacles in Providing Forensic Accounting Education

Lecturers also asked their opinion about obstacles in providing forensic accounting education. Table 2 shows the mean and standard deviations of the responses of the respondents.

Table 2: Obstacles in Forensic Accounting Education

Obstacles	Mean	Standard Deviation
Lack of qualified lecturer	3,9362	0,8184
Lack of administrative and financial support	3,3617	1,1117
Lack of pedagogical materials	3,0426	0,9771
Lack of student interest	2,9149	1,0179
Lack of job opportunities	2,3617	0,8451
Lack of proper fit in accounting	2,2553	0,8715

According to the academicians, the main obstacle in forensic accounting is the lack of qualified lecturers, lack of administrative and financial support, and lack of pedagogic forensic accounting, which is indicated by the mean value higher than 3. The results are conforming to previous studies which mentioned these are the problems in forensic accounting education [5, 7, 16]. One respondent agreed that the obstacle in forensic accounting education was the lack of teachers. The respondent said, "The availability of teachers and practitioners is still limited". Further respondents also said the reasons for this obstacle were:

> *"Information update, to find out how fraudster does crime, what motivates it, etc. Usually, we always lag because updating is always a challenge for academics. Because teachers focus a lot on teaching, taking care of study programs, etc. Unless the research is focused there are no problems. Because there will always be a lot of reading. So sometimes the updates are only about the topic of teaching academics, even though forensic accounting is very broad in scope"*

Based on respondents' opinions, this was due to a lot of works such as teaching and becoming part of faculty management which was quite time-consuming. This is in line with the results of a survey which states that the lack of lecturer competencies is a major obstacle in forensic accounting education. The interview also mentioned that the scope of forensic accounting is very broad, this is following the statement that forensic accounting involves multiple disciplines making it difficult for teachers to follow their development. It takes a lot of reading material and of course, time is also needed. As a result, teachers only follow the development of the courses being taught.

Meanwhile, respondents disagree if a lack of student interest and job opportunities and lack of conformity with accounting are obstacles in forensic accounting education. This can be seen with a mean value of less than 3. Student interest and job opportunities in this field are very large. Even the research of [5], mentioned that the employment opportunities for forensic accounting are very numerous. Even if students do not choose a career in forensic accounting, the skills learned will make them better professionals whether it works as an auditor, manager, or consultant. If related to research [26], forensic accounting services in the UK are multiplying. This is proof that interest and job opportunities in the field of forensic accounting are very promising. Whereas for the suitability of forensic accounting with accounting is also not a major obstacle, indeed forensic accounting is multi-disciplinary, but the respondents consider that this is still following accounting and lecturers can teach forensic accounting in their department.

4.3. Important Topics in Forensic Accounting

Some important topics to be taught in forensic accounting. Whereas [18], in their research said that interviewing and interrogation skills, sources of evidence, schemes of fraudulent financial reporting, criminology, computer/internet crime techniques, and expertise in human relations are not taught in accounting programs. Another opinion states that there are no courses on criminology or psychology and what are the motives of fraud perpetrators in committing crimes in fraud and forensic accounting [21]. This research collects several important topics that must be taught in forensic accounting. Respondents were asked to give their opinions regarding 15 important topics in forensic accounting. The results are presented in Table 3, sorted by the highest to lowest mean values.

Table 3: Important Topics of Forensic Accounting

No.	Topic	Mean	Standard Deviation
1	Fraud detection methods	4,4681	0,6869
2	Fraud prevention and deterrence	4,4043	0,7120
3	Fraud investigation methods, including the organization and evaluation of evidence	4,3830	0,6774
4	Fraudulent financial statements and analysis	4,3830	0,6774
5	Corruption	4,3191	0,7255
6	Asset misappropriation	4,2979	0,7493
7	Digital forensics	4,2553	0,8462
8	Auditing	4,2128	0,7204

9	Criminology, the legal environment, and ethical issues	4,2128	0,8581
10	Forensic psychology, profiling, and the fraud mindset	4,2128	0,8059
11	Interviewing and interrogations	4,1915	0,7701
12	Data analytic software (e.g., IDEA, ACL, NVivo)	4,1277	0,7107
13	Valuation of losses and damages	4,1277	0,6794
14	Cyber-crime and security	4,1064	0,8656
15	Remediation and conflict resolution	4,0213	0,8206

Respondents stated that all of these are important topics in forensic accounting; this can be seen from the values of all the mean above 4. The results of the five highest rankings indicate that fraud detection methods, fraud prevention, and fraud, investigation methods, including organization and evaluation of evidence, fraudulent financial statements and analysis, and corruption. Of the five highest topics chosen by respondents, all indicated that there was a connection with accounting. This result is closely related to the expertise respondents of this study as academicians in accounting. Respondents stated that:

> *"Forensic accounting is taught in Bachelor Accounting as a compulsory subject. The basis of introductory forensic courses at least introduces to students that cheating may be done even by someone we trust. It is important for accounting and auditing courses as a basis for understanding forensic accounting".*

[5] research also shows that educators prefer topics related to accounting. The results of interviews with respondents also stated that accounting and auditing is a prerequisite skill for the student, which consistent with [17] indicating basic accounting, auditing knowledge, and skills that students should have when they are considering issues associated with fraud and forensic accounting. Furthermore, there is material about introductory forensic accounting that teaches the basics of fraud. Research [7,16] also show that fundamental fraud is the most important topic chosen by academics to be taught in forensic accounting education.

As for topics such as interviewing and interrogation, data analysis software (e.g., IDEA, ACL, NVIVO), valuation of losses and damages, cyber-crime and security, and remediation, and conflict resolution have smaller mean values, as these topics require special knowledge in forensic accounting. This supports the previous result stating that the obstacle in accounting education is the lack of competence of lecturers. This particular expertise certainly requires a teacher who has expertise in this field, this could be a practitioner who has a lot of experience in this field. The respondent said: "must continue to be developed through collaboration with the professional association of Forensic Accountants, Forensic Accountant practitioners, law enforcement". Of course, the collaboration will make forensic accounting develop quickly, academics will know what kind of demand is needed in the field of forensic accounting. So that students will be equipped with expertise following what is expected. That way topics about forensic accounting that require special expertise can be taught by people who are competent in

their fields. So the problem of obstacles regarding the limitations of teachers and the lack of qualified teachers will be overcome.

4.4. Various Teaching Methods in Forensic Accounting

In conducting the teaching-learning process it is certainly important regarding teaching techniques. Teachers must have teaching techniques that are adapted to the conditions of the students, which are more likely to succeed. Many teaching techniques will give different results from one technique to another. It could be that this technique will succeed at one time but at different conditions and times, it cannot work properly. In this research, respondents also gave their opinions regarding the importance of various teaching methods in forensic accounting. In this study, we provide twelve lists of teaching techniques taken from several previous studies. The results are presented in Table 4, which is sorted from highest to lowest.

Table 4: Various Teaching Methods in Forensic Accounting

No.	Methods	Mean	Standard Deviation
1	Case Studies	4.4894	0.6211
2	Digital Data Recovery (e.g. Data Recovery)	4.2979	0.6226
3	Computer Forensics Lab	4.2553	0.6746
4	Data Analytics Software (e.g. IDEA)	4.2340	0.6982
5	Guest lecturers	4.1702	0.7319
6	Role-playing	4.1064	0.6989
7	Field trips	4.0851	0.7754
8	Internships	4.0851	0.8554
9	Moot Court activities	4.0638	0.7634
10	Books	4.0638	0.5674
11	Student research project and presentation	4.0426	0.6580
12	Video	4.0213	0.7068

Based on the mean value shows that all methods of teaching forensic accounting are important. The results of the five highest techniques, according to academics are case studies, digital forensic software, computer forensic labs, data analysis software, and guest lectures. Respondent comments stated that:

> *"In my opinion, the best method is a case study. With case studies, we can find out the fraudsters cheat. So students know more about various kinds of cheating models, maybe one type of crime, but the mode is different. It will be easier for students to accept because the incident happened".*

From the interviews, respondents also chose case studies as the most important technique. Respondents said that with a case study, students could understand the case that occurred and know-how the perpetrator in committing fraud. Case studies help students with more fraud models and with various modus operandi on how to commit it.

Other respondents also stated that "this course should be taught with more practice so that students get a real experience". Forensic accounting will be better taught through practice so students can get an overview of this profession, what is done, and what is faced. However, there is one teaching technique that is also based on real-life experience but has a small mean value of

moot court activities. Moot court activities require teachers who have an understanding of the law. As the previous findings that one of the obstacles in forensic accounting is the less qualified lecturer. This can be overcome by collaborating with practitioners in the field of law or also with law faculties to teach it. With this students can understand the conditions of the trial or when providing expert statements.

5. Conclusion

This study attempts to find out the perceptions of academicians regarding the development of current forensic accounting education. This study also reveals more deeply about forensic accounting education through interviews with respondents. The findings in this study indicate that forensic accounting services will continue to increase in the future. Opinions from the lecturer show that forensic accounting education should be offered as separate topic and given to bachelor and master students. Then the main obstacle in forensic accounting education is the lack of lecturers who are competent in this field. While important topics, according to academics are closely related to accounting and the best teaching method is a case study.

From these results, it can be used as a suggestion for consideration in compiling a forensic accounting curriculum. Many requests for forensic accounting services can be seen as an opportunity to offer forensic accounting courses in the accounting department to be able to provide various skills needed by students who want a career in forensic accounting. This study also shows the importance of experienced practitioners in the field of forensic accounting and universities to work together to overcome shortcomings in the lack of qualified lecturers. So that students obtain materials and techniques that are following current forensic accounting practices. The importance is also that there is a collaboration between accounting parties in collaboration with other faculties in teaching other material not controlled by accounting majors such as law, psychology, social behavior, and information technology.

These results also indicate that academicians are more concerned with teaching techniques based on actual practice or real events and the importance of expertise in computer forensics. There must be teaching methods that lead to real practice so that students will understand the activities or work of a forensic accountant. Understanding more deeply about a case and focusing on technological developments in forensic accounting today is an important thing as an additional experience for students. Besides that, with the presence of a guest lecturer, students can learn profiles and can also take valuable lessons from the experience of the speakers.

This study also has limitations. A low response rate of this study could be the result of this study containing bias so that it cannot be generalized, and most respondents are from accounting majors. Important topics for forensic accounting only come from limited sources, there may be other topics that have not been included in this list. The scope of coverage examines in this study can be widened. Future studies can include the technological developments and expertise of computer forensics. This would enhance the understanding of academics and policymakers. Furthermore, it can add respondents from other departments such as law, psychology, and sociology, and information technology, which is expected to obtain more comprehensive perspectives regarding forensic accounting education.

Conflict of Interest

The authors declare no conflict of interest.

Acknowledgment

References

[1] T.D. Carpenter, "Audit Team Brainstorming, Fraud Risk Identification, and Fraud Risk Assessment : Implications of SAS No. 99 J.M. Tull School of Accounting Terry College of Business University of Georgia Audit Team Brainstorming, Fraud Risk Identification, and Fra," The Accounting Review, **82**(5), 1119–1140, 2007.

[2] J.A. DiGabriele, "Implications of regulatory prescriptions and audit standards on the evolution of forensic accounting in the audit process," Journal of Applied Accounting Research, **10**(2), 109–121, 2009, doi:10.1108/09675420910984673.

[3] M. Lal Bhasin, "An Empirical Investigation of the Relevant Skills of Forensic Accountants: Experience of a Developing Economy," European Journal Of Accounting Auditing and Finance Research, **1**(June), 11–52, 2013. https://dx.doi.org/10.2139/ssrn.2676519

[4] G.S. Smith, "Computer Forensics: Helping to Achieve the Auditor's Fraud Mission?," Journal of Forensic Accounting, **6**(1), 119–134, 2005.

[5] B. Kramer, M. Seda, G. Bobashev, "Current opinions on forensic accounting education," Accounting Research Journal, **30**(3), 249–264, 2017. https://doi.org/10.1108/ARJ-06-2015-0082

[6] D.A. McMullen, M.H. Sanchez, "A Preliminary Investigation of the Necessary Skills, Education Requirements, and Training Requirements for Forensic Accountants," Journals of Forensic & Investigative Accounting, **2**(2), pp.30-48, 2010. doi:10.1108/09670910984673.

[7] Z. Rezaee, D.L. Crumbley, R.C. Elmore, "Forensic Accounting Education: A Survey of Academicians and Practitioners," Advances in Accounting Education Teaching and Curriculum Innovations, **6**(May 2004), 193–231, 2004. https://papers.ssrn.com/sol3/papers.cfm?abstract_id=518263

[8] M. Seda, B. Kramer, "The Emergence of Forensic Accounting Programs in Higher Education," Management Accounting Quarterly, **9**(3), 15–24, 2008.

[9] M. Seda, B.K.P. Kramer, "An Examination of the Availability and Composition of Forensic Accounting Education in the United States and Other Countries," Journal of Forensic and Investigative Accounting, **6**(1), 1–46, 2014.

[10] H.Y. Prabowo, "Better, faster, smarter: developing a blueprint for creating forensic accountants," Journal of Money Laundering Control, **16**(4), 353–378, 2013, doi:10.1108/JMLC-05-2013-0017.

[11] K.B. Peterson, A.B. Thomas, "Anti-Fraud Education In Academia," In Advances in Accounting Education Teaching and Curriculum Innovations, **21**(18), 45–67, 2004. doi: 10.1016/S1085-4622(04)06003-1

[12] B.C. Melancon, "A New Accounting Culture," Journal of Accountancy, (October), 27–30, 2002.

[13] B.M.M. Houck, B. Morris, A. Richard, D. Riley, J. Robertson, J.T. Wells, "Forensic Accounting as an Investigative Tool Developing a Model Curriculum for Fraud and Forensic Accounting," The CPA Journal, **76**(August), 68–71, 2006.

[14] G.S. Smith, D.L. Crumbley, "How Divergent Are Pedagogical Views Toward the Fraud/Forensic Accounting Curriculum?" Global Perspectives on Accounting Education, **6**, 1–24, 2009.

[15] M. Kranacher, B.W. Morris, T. a. Pearson, R. a. Riley, "A Model Curriculum for Education in Fraud and Forensic Accounting," Issues in Accounting Education, **23**(4), 505–519, 2008, doi:10.2308/iace.2008.23.4.505.

[16] Z. Rezaee, E.J. Burton, "Forensic accounting education: insights from academicians and certified fraud examiner practitioners," Managerial Auditing Journal, **12**(9), 479–489, 1997, doi:10.1108/02686909710185206.

[17] WVU, "Education and Training in Fraud and Forensic Accounting: A Guide for Educational Institutions, Stakeholder Organizations, Faculty, and Students," NCJRS Publication No.NIJ 21-71589, 1–70, 2007.

[18] R.D. Meservy, M. Romney, M.F. Zimbelman, "Certified Fraud Examiners: A Survey of Their Training, Experience and Curriculum Recommendations," Journal of Forensic Accounting, **7**(January), 163–184, 2006.

[19] K.C. Carnes, N.J. Gierlasinski, "Forensic accounting skills: will supply finally catch up to demand?," Managerial Auditing Journal, **16**(6), 378–382, 2001, doi:10.1108/02686900110395514.

[20] B. Apostolou, J.W. Hassell, R.M. James, W.F. Stephanie, "Accounting education literature review (2006–2009)," Journal of Accounting Education, **28**(3–4), 145–197, 2010, doi:10.1016/j.jaccedu.2018.02.001.

[21] S. Ramamoorti, "The Psychology and Sociology of Fraud: Integrating the Behavioral Sciences Component Into Fraud and Forensic Accounting Curricula," Issues in Accounting Education, **23**(4), 521–533, 2008, doi:10.2308/iace.2008.23.4.521.

[22] G.E. Curtis, "Legal and Regulatory Environments and Ethics: Essential Components of a Fraud and Forensic Accounting Curriculum," Issues in Accounting Education, **23**(4), 535–543, 2008, doi:10.2308/iace.2008.23.4.535.

[23] T.A. Pearson, T.W. Singleton, "Fraud and Forensic Accounting in the Digital Environment," Issues in Accounting Education, **23**(4), 545–559, 2008.

[24] L.E. Heitger, D.L. Heitger, "Incorporating Forensic Accounting and Litigation Advisory Services Into The Classroom," Issues in Accounting Education, **23**(4), 561–572, 2008.

[25] H.H. Meier, R.R. Kamath, Y. He, "Courses on Forensics and Fraud Examination in the Accounting Curriculum," Journal of Leadership, Accountability, and Ethics, **8**(1), 1–8, 2010. doi: 10.1016/S1085-46206003-1

[26] S. Hegazy, A. Sangster, A. Kotb, Mapping forensic accounting in the UK, Elsevier Inc., 2017, doi:10.1016/j.intaccaudtax.2016.12.004.

[27] J.W. Creswell, Research design : qualitative, quantitative, and mixed methods approaches fourth, SAGE Publications, Inc, United States of America Library, 2014.

ASTES

Learning Strategies and Academic Goals to Strengthen Competencies in Electronics and Digital Circuits in Engineering Students

Maritza Cabana-Caceres[1,*], Cristian Castro-Vargas[1], Laberiano Andrade-Arenas[1], Monica Romero-Valencia[1], Haydee Castro-Vargas[2]

[1]Faculty of Sciences and Engineering, Universidad de Ciencias y Humanidades, Lima, 27, Peru

[2]Faculty of Psychology, Federico Villareal National University, Lima, 15082, Peru

ITEM INFORMATION	SUMMARY
	The purpose of this article was to determine the incidence between learning strategies and academic goals in the competences of the curricular experience of electronics and digital circuits in engineering students of a private university in Lima, Peru. The objective was to explain how learning strategies and academic goals explain the behavior of engineering students of competencies in electronics and digital circuits. For this study, a sample of 89 students from the III cycle was used, to whom the ACRA test instruments were applied for the learning strategies of Román and Gallego (2001), the CMA academic goals test of Durán and Arias (2015) and a test to assess skills in electronics and digital circuits. According to the results obtained, it was shown that learning strategies and academic goals affect the skills of electronics and digital circuits in engineering students. By obtaining $x2 = 83.782$, ($p = .000 < 0.05$ and $Wald = 16.326$ showing that the proposed model is acceptable

1. Introduction

With globalization and the increasing ease of obtaining information, in Peru in most higher education institutions there is still a large gap in how to carry out an adequate learning strategy despite having the information at hand, regulatory bodies such as the National Superintendency of Higher Education SUNEDU [1] and the accreditation of the System of Evaluation, Accreditation and Certification of Educational Quality SINEACE [2] concerned about this, they try to implement norms so that educational institutions comply with basic quality standards, in this context, university education is in a process of educational reform to a model based on competencies, which they find it difficult to implement while maintaining the traditional teaching [3].

Thus at the national level, although access to university education and the level of skills as indicated is improving, there are still low levels of quality standards also at the international level, reflecting students with weak skills, low performance and insertion problems and job retention [4]. Several universities are still in the process of licensing and accreditation, so they are carrying out their curricular restructuring, to achieve a coherent curriculum to the institutional educational model, in an integrated manner according to the socio-economic, political, cultural

context, in the local scope. framework, regional and global [5]. In this sense, a student who does not exercise his skills acquired in the workplace becomes a stranger to his specialty, unable to continue developing his skills [6].

This situation is aggravated, because engineering careers require strong ICT skills, not only for students but also for teachers [7] who, when developing their classes with a curricular program that does not include ICT due to lack of training in the teaching staff and the low implementation of devices and laboratory equipment, it becomes a challenge [8]. In this sense, in a private university of Lima, in the course of electronics and digital circuits of the engineering faculty, passive students were observed in the development of the required competences, presenting deficiencies in the disciplinary knowledge of electronics and digital circuits , having fragmented learning. and not integrated into their professional training, losing interest in the subject, consequently, not being able to solve specialty problems when carrying out their pre-professional and / or work practices, which prevents them from successfully facing the demands of a dynamic real world. In this sense, it shows the need to implement and apply learning strategies and academic goals that address the indicated weaknesses, aimed at seeking the development of effective skills in electronics and digital circuits and in future engineering students that allows them

to exercise in a integrated. the significant learning acquired during their academic training stage at the university.

The need to implement and apply learning strategies and academic goals that address the identified weaknesses is shown, aimed at seeking the development of effective skills in electronics and digital circuits and in future engineering students that allows them to exercise in an integrated manner. The significant learning acquired during their academic training stage at the university.

For example, in Chile, it was found that learning goals and the attribution of academic success to effort have higher statistics. highlighted with respect to academic performance, this allows identifying and considering these dimensions in student support programs to promote academic achievement [9].

Also in Colombia, they obtained the existence of positive and significant correlations in study habits, learning strategies and academic performance, where the importance of using learning strategies as study habits to promote academic performance was highlighted, so both recommended creating intervention and support programs for strengthening in these areas [10].

The students from the Universidad Privada del Norte, Lima, were analyzed with a survey on the use of Arduino technology and a competency learning test. The research resulted in a significant correlation with a Spearman coefficient equal to 0.702 and a p value of 0.01, showing that the use of Arduino technology improves the development of students' skills in their learning [11].

Thus, in another private university of Lima, 96 students from the Faculty of Engineering were applied the instruments of the CMA Academic Goals questionnaire and Form 5 of Self-concept, determining from the results an r (96) = .205, p = .046 of the variables, with which it can be said that there is a relationship weak and significant positive between academic goals and self-concept, which means that high goals will be weakly related to high self-concept [12].

On the other hand, in a study of 290 students from the National University of San Marcos, it allowed to clarify the association between the learning strategies variables, motivation in relation to the explained variable of the study to predict the application of certain learning strategies, cognitive and metacognitive factors in students as indicators and decisive determinants to achieve reading comprehension [13].

The variables that we propose to study are expressed, the first study variable being learning strategies, there are different definitions, stating that it is a metacognitive, planned and conscious process of the subject in a given situation, influenced by the individual's perceptions to achieve optimal learning [14]. Given the above, it is reinforced that the strategies adopted by the students are sequentially concatenated and deliberately planned, in order to achieve the learning of the required task [15]. It can also be said that it is a process of sequence of decisions of the subject in a conscious and intentional state, in which the student deliberately decides and recovers knowledge, which requires the performance of a certain activity [16].

Another variable of study is the variable academic goals that is defined as the purposes proposed by the students, which guide their intentions and actions to obtain their achievements before certain

academic activities using the necessary resources. Likewise, it is indicated that they are the objectives that students want to achieve through planning, which will be their action to have a better understanding according to the complexity of the goal, for the solution of the academic activities to be developed [17].

Likewise, they are an integrated and organized pattern of thoughts and reasons that a management produces for a context of achievement, which includes the thoughts of competence, success, competitiveness, effort, errors and evaluation of its objectives to be fulfilled in the classroom [18] .

The last variable of studies competences of electronic and digital circuits, according to the Electronic Engineering curriculum with a major in Telecommunications of the Private University of Lima [19], mentions that the competences are the set of related knowledge, skills, attitudes and values with each other, in an integral way, that the student develops in the university to perform in academic activities and professional practice, in accordance with the standards of their specialty under the social, political, economic and labor context that governs it.

Posing the problem general research which is: What incidence exists between the learning strategies and the academic goals in the electronic and digital circuits competences in a Private University Lima, 2020? Regarding the specific problems, the following are established:

(a) What impact do the learning strategies and academic goals have on basic electronics and digital circuits in a Private University Lima, 2020? (b) What impact do the learning strategies and academic goals have on the electrical components of electronic and digital circuits in a Private University Lima, 2020? (c) What impact do the learning strategies and academic goals have on the hardware and digital circuits of the arduino electronics at the Universidad Privada Lima, 2020? (d) What impact do learning strategies and academic goals have on arduino electronics and digital circuits software at a Private University Lima, 2020?

For its part, the general objective set for this research is to determine the incidence between learning strategies and academic goals in the competencies of the subject of electronics and circuits in a private university Lima, Peru, and its specific objectives that are considered for the present investigation are: (a) establish the relationship between learning strategies and academic goals in basic electronics and digital circuits in a Private University Lima, 2020 (b) establish the relationship between learning strategies and academic goals in electrical components of electronics and digital circuits in a Private University of Lima, 2020 (c) establish the relationship between learning strategies and academic goals in arduino electronic hardware and digital circuits in a Private University of Lima, 2020 (d) establish the relationship between learning strategies and academic goals in arduino electronics and digital circuit software at a Private University Lima, 2020.

2. Methodology

The present investigation was of a quantitative approach because each stage proceeds to the next and the steps cannot be ignored, it is possible to define and limit them, in addition, it is known exactly where the problem begins, data collection was also carried out, to measure the variables learning strategies and skills

of electronics and digital circuits in numerical expressions and were analyzed with statistical methods.

2.1. Variables operationalization

For the learning strategies, 119 questions were used (see appendix), on a Likert scale, with 5 dimensions and a total of 9 indicators (Table 1).

Table 1: Operationalization of variable learning strategies

Dimensions	Indicators	Items	Scale	Levels or ranges
1. Acquisition	1.1 Attentional strategies	1 - 10	A: Never (1)	Low 119 - 277
	1.2 Repetition strategies	11 - 20		
2.Codification	2.1 Mnemonization strategies	21 - 42	B: Sometimes (2)	Moderate 278 - 437
	2.2 Processing strategies	43 - 63		
	2.3 Organizational strategies	64 - 66	C: Many times (3)	High 438 - 595
3.recovery	3.1 Search strategies	67 - 75		
	3.2 Response generation strategies	76 - 84	D: Always (4)	
4.Support	4.1 Metacognitive strategies	85-101		
	4.2 Socio-affective strategies	102-119		

Regarding academic goals, 16 questions were used, on a Likert scale, with 3 dimensions and a total of 8 indicators (Table 2). And for the electronic and digital circuits competences, 20 questions were measured, on a dichotomous scale, with 4 dimensions and 12 indicators in total (Table 3).

Table 2: Operationalization of the variable academic goals

Dimensions	Indicators	Items	Scale	Levels or ranges
1. Learning objectives	1.1. Problem solving	1-3	1: Strongly disagree	Low 16 - 37
	1.2. Progressive learning	4 – 7	2: disagree	
2. Achievement objectives	2.1. Academic achievement	8–9	3: Neither agree nor disagree	Moderate 38 - 59
	2.2. Professional achievement	10		
	2.3. Personal achievement	11	4: agree	High 60 - 80
3.Objectives of social reinforcement	3.1. Social recognition	12, 14	5: Strongly agree	
	3.2. Classroom stimulation	13, 16		
	3.3. Superior approval	15		

2.2. Population

A census population, composed of 89 students, from the third cycle of the engineering faculty of the University of Sciences and Humanities, 2020- I was studied.

2.3. Techniques, data collection instruments, validity and reliability

The instruments of the Roman and Gallegos Acra Test (see appendix) were applied to the students to evaluate the learning strategies, as well as the CMA questionnaire of Durán (2015) to evaluate their academic goals and finally a test was carried out to measure the competencies of electronics and digital circuits. The information collected was then transferred to a database in Excel and to the statistical program SPSS version 23, which will allow us to perform the data analysis.

Table 3: Operationalization of the variable competencies of electronic and digital circuits

Dimensions	Indicators	Items	Scale	Level ranges
1. Basic electronics	1.1. Identify the theoretical concepts of electricity.	1-2	Dichotomic 1: Right 0: Incorrect	In the beginning 00-10
	1.2. You have an idea of what electrical resistance is.	3		
	1.3 Define and develop basic exercises of electrical circuits	4 - 5		
2. Electrical components	2.1. Define the diode concept	7		In process 11 - 14
	2.2. Define the concept of transistor	6 - 8		
	2.3. Identify and solve circuits with diodes and transistors.	9 - 10		Achieved 15 - 18
3.Arduino hardware	3.1. Defines the theoretical concept of	11		
	3.2. Arduino general concepts details	12		Exceptional 19 - 20
	3.3. Identify the characteristics of the arduino board.	13 - 15		
4. Arduino software	4.1. Describe the general structure of a sketch.	16		
	4.2. Analyze instructions	17 - 18		
	4.3. Identify the serial communication with the arduino board	19 - 20		

The educational data mining technique is a tool that also allows data collection and analysis for subsequent decision-making, which is also suitable for evaluating groups of students, with the advantage of being able to cover a large number of data, as is the case of this investigation that has 119 questions for the study, for the case of the present investigation the data will be analyzed using SPSS.

Regarding the validation of the instruments, the content validity of the expert judgment was carried out and for the reliability a pilot test of a sample of 20 students of the electronics and digital circuits subject was used, the statistical values verified the reliability of instruments (Table 4).

Table 4: Reliability of the instrument

Variables	Statistics Reliability	Value	No. of elements
Learning strategies	Cronbach's alpha	0.857	119
Academic goals	Cronbach's alpha	0.851	16
Competences in electronics and digital circuits	Kuder-Richardson	0.8179	20

3. Results

The results obtained from the study are shown below.

3.1. Description of the learning strategies variable

Define abbreviations and acronyms the first time they are used in the text, even after they have been defined in the abstract. Do not use abbreviations in the title or headings unless they are unavoidable.

Table 5: Levels of variable learning strategies

		Frequency	Percentage
Valid	Low	26	29.3
	Moderate	48	53.9
	High	15	16.8
	Total	89	100
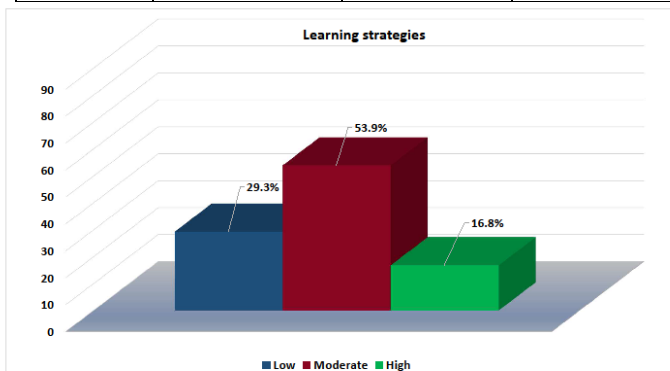
Figure 1: Levels of the learning strategies variable

Table 5 and Figure 1 show the percentage values of the learning strategies variable, of a total of 89 students. With the results obtained, it can be seen that the learning strategies tend to be moderate with 53.9%.

Table 6: Levels of dimensions of learning strategies

		Low	Moderate	High	Total
Acquisition	Frequency	15	54	20	89
	Percentage	16.8	60.7	22.5	100
Coding	Frequency	13	59	17	89
	Percentage	14.6	66.3	19.1	100
Recovery	Frequency	16	53	20	89
	Percentage	17.9	59.6	22.5	100
Support for	Frequency	18	49	22	89
	Percentage	20.2	55.1	24.7	100

3.2. Description of the dimensions of the learning strategies

Table 6 and figure 2 show the percentage values of the dimensions of the learning strategies, of a total of 89 students. From these results, it is estimated that the support dimension with more than 24% presents the best results compared to the other dimensions.
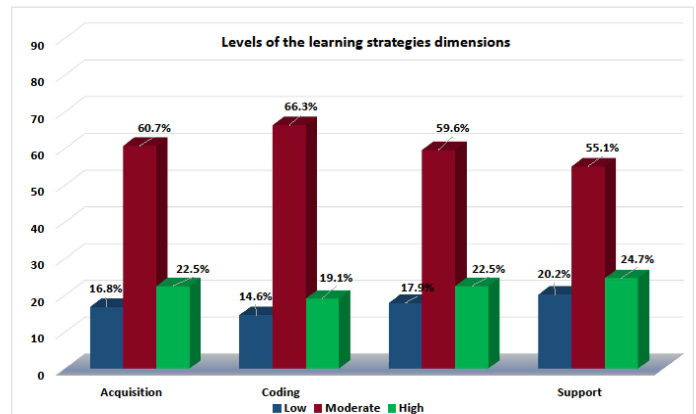
Figure 2: Levels of the dimensions of learning strategies

3.3. Description of variable academic goals

Table 7 and Figure 3 show the percentage values of the variable academic goals, of a total of 89 students. With the results obtained, it can be seen that the level of perception of academic goals has a trend of moderate level with more than 60%.

Table 7: Levels of variable academic goals

		Frequency	Percentage
Valid	Low	12	13.5
	Moderate	55	61.8
	High	22	24.7
	Total	89	100
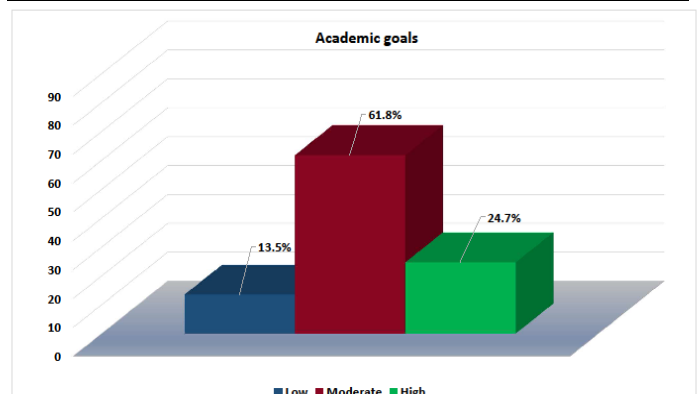
Figure 3: Levels of the academic goals variable

3.4. Description of the dimensions of the academic goals

Table 8 and Figure 4 show the percentage values of the academic goals dimension of a total of 89 students. Based on these results, it is estimated that the achievement goals dimension presents better results with more than 30% compared to the other dimensions.

Table 8: Levels of the dimensions of academic goals

		Low	Moderate	High	Total
Learning goals	Frequency	fifteen	46	28	89
	Percentage	16.8	51.7	31.5	100
Achievement goals	Frequency	10	48	31	89
	Percentage	11.3	53.9	34.8	100
Objectives of social reinforcement	Frequency	15	45	29	89
	Percentage	16.7	50.7	32.6	100
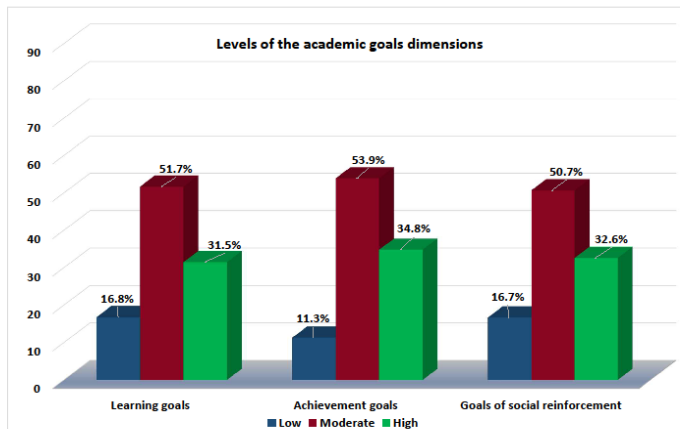
Figure 4: Levels of the academic goals dimensions

3.5. Description of the electronic and digital circuits skills variable

Table 9 and Figure 5 show the percentage values of the variable dimensions of electronics and digital circuits, of a total of 89 students, which shows a trend of students at the level reached with less than 70%.
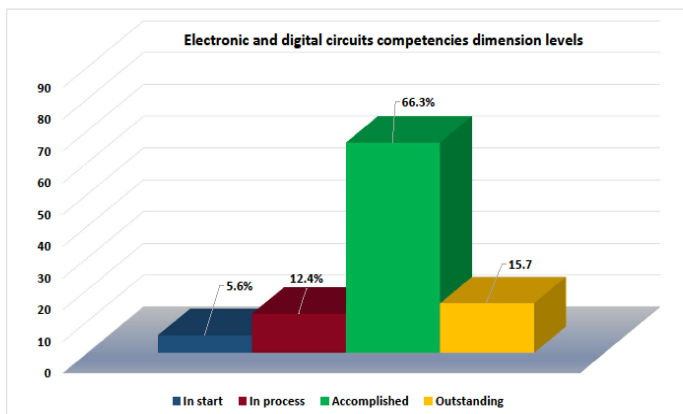
Figure 5: Dimension levels of electronic and digital circuits competencies

Table 9: Levels of electronic and digital circuits variable competencies

		Frequency	Percentage
Valid	In the beginning	5	5.6
	In process	11	12.4
	Accomplished	59	66.3
	Exceptional	14	15.7
	Total	89	100

3.6. Description of the competencies dimensions of electronics and digital circuits

Table 10 and Figure 6 show the percentage values of the dimensions of competencies in electronics and digital circuits, of a total of 89 students. From these results, it is estimated that the arduino software dimension has low outstanding results with less than 12% compared to the other dimensions.

Table 10: Dimensional Competency Levels for Electronic and Digital Circuits

		Initial	In process	Accomplished	In outgoing	Total
Basic electronic	Frequency	1	5	67	16	89
	Percentage	1.1	5.6	75.3	18.0	100
Electric components	Frequency	3	9	65	12	89
	Percentage	3.4	10.1	73.0	13.5	100
Arduino Hardware	Frequency	5	11	60	13	89
	Percentage	5.6	12.4	67.4	14.6	100
Arduino software	Frequency	8	14	57	10	89
	Percentage	9.0	15.7	64.0	11.3	100
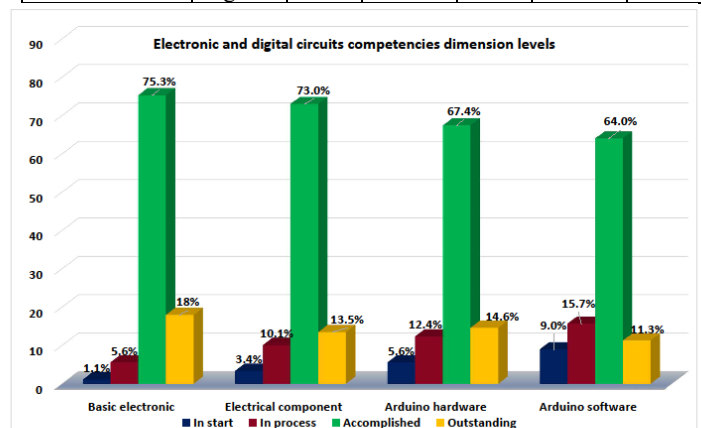
Figure 6: Dimension levels of electronic and digital circuits competencies

3.7. Contrast of the general hypothesis

Ho: There is no incidence between learning strategies and academic goals in electronic skills and digital circuits in a Private University Lima, 2020.

HG: There is an incidence between learning strategies and academic goals in electronic skills and digital circuits in a Private University Lima, 2020.

Table 11: Model fit and likelihood ratio tests for the general hypothesis

Model fit information				
Model	Logarithm of probability - 2	Chi squared	gl	S.I.G
Interception only	286,034			
Final	202,251	83,782	36	, 000

Table 11 shows that the value x2 = 83.782, (p = .000 <0.05), indicates that the proposed model is acceptable. In this sense, the null hypothesis is rejected, with a probability of error less than 5%.

Table 12: Pseudo R squared of general hypothesis

Pseudo R squared	
Cox and Snell	, 610
Nagelkerke	, 630
McFadden	, 272

Table 13: Parameter estimates of the general hypothesis

	Estimate	S.I.G	Wald	95% interval trustworthy	
				Min	Max
[V3_ Competences of electronics and digital circuits = 1]	-9,224	, 000	25,904	-12,776	-5,672
[V3_ Competencies of electronics and digital circuits = 2]	-7,549	, 000	24,350	-10,547	-4,550
[V1_Learning strategies = 1]	-9,918	, 000	16,326	-14,728	-5.107
[V1_Learning strategies = 2]	-4,936	, 001	11,346	-7,808	-2,064
[V2_Academic Goals = 1]	-3,348	.014	6,053	-6,016	- .681
[V2_Academic Goals = 2]	-2,624	.038	4,311	-5.101	-. 147

Table 12 presents favorable values of pseudo R squared, which ensures a fit adequate of the proposed model to explain competencies in electronics and digital circuits. Similarly, it is stated that learning strategies is the variable that affects the most, since it presents a value of Wald = 16.326 and p = .000 <0.05 (Table 13).

3.8. Specific hypothesis test 1

Ho: There is no incidence between the learning strategies and the academic goals in the basic electronics of electronics and digital circuits in a Private University Lima, 2020.

H1: There is an incidence between the learning strategies and the academic goals in the basic electronics of electronics and digital circuits in a Private University Lima, 2020.

Table 14 shows that the value x2 = 61.281, (p = .005 <0.05), indicates that the proposed model is acceptable. In this sense, the null hypothesis is rejected with a probability of error less than 5%.

Table 14: Model fit and likelihood ratio tests for specific hypothesis 1

Model fit information				
Model	Logarithm of probability - 2	Chi squared	gl	S.I.G
Interception only	182,351			
Final	121,070	61,281	36	, 005

Table 15: Pseudo R squared for specific hypothesis 1

Pseudo R squared	
Cox and Snell	, 498
Nagelkerke	, 557
McFadden	, 307

Table 15 presents favorable pseudo R squared values, which ensures an adequate fit of the proposed model to explain skills in electronics and digital circuits.

Likewise, learning strategies is the variable that most affects basic electronics of the explained variable with a value of Wald = 21.485 and p = .000 <0.05 (Table 16).

Table 16: Parameter estimates for general hypothesis 1

	Estimate	S.I.G	Wald	95% interval trustworthy	
				Min	Max
[V3D1_ basic electronics of electronics and digital circuits= 1]	-5,632	, 000	29,959	-9,130	-2,134
[V3D1_ basic electronics of electronics and digital circuits= 2]	-5,268	, 003	23,538	-10,116	-, 421
[V1_ Learning strategies= 1]	-2,931	, 000	21,485	-6,007	, 146
[V1_ Learning strategies= 2]	-2,356	.014	10,547	-6,069	1,356
[V2_Academic goals= 1]	-1,659	, 004	18,217	-4,606	1,289
[V2_Academic goals= 2]	1,415	, 005	16,788	-1,710	4,539

Table 15 presents favorable pseudo R squared values, which ensures an adequate fit of the proposed model to explain skills in electronics and digital circuits.

Likewise, learning strategies is the variable that most affects basic electronics of the explained variable with a value of Wald = 21.485 and p = .000 <0.05 (Table 16).

3.9. Specific hypothesis test 2

Ho: There is no incidence between the learning strategies and the academic goals in the electrical components of electronics and digital circuits in a Private University Lima, 2020.

H2: There is an incidence between the learning strategies and the academic goals in the electrical components of electronics and digital circuits in a Private University Lima, 2020.

Table 17: Model fit tests and likelihood ratio for specific hypothesis 2

Model fit information				
Model	Logarithm of probability -2	Chi squared	gl	S.I.G
Interception only	180,100			
Final	126,963	53,136	36	.033

Table 17 shows that the value x2 = 53.136, (p = .033 <0.05), indicates that the proposed model serves to explain the dependent behavior of the variable competencies of electronic and digital circuits with respect to electrical circuits. In this sense, the null hypothesis is rejected with a probability of error less than 5%.

Table 18: Pseudo R squared for specific hypothesis 2

Pseudo R squared	
Cox and Snell	, 450
Nagelkerke	, 504
McFadden	, 269

Table 18 presents favorable pseudo R squared values, which ensures an adequate fit of the proposed model to explain skills in electronics and digital circuits. Likewise, academic goals is the variable that most affects the electrical components of the explained variable with a value of Wald = 16.073 and p = .004 <0.05 (Table 19).

Table 19: Parameter estimates for general hypothesis 2

	Estimate	S.I.G	Wald	95% interval trustworthy	
				Min	Max
[V3D2_ electrical components of electronic and digital circuits= 1]	-6,288	, 001	11,176	-9,974	-2,601
[V3D2_ electrical components of electronic and digital circuits= 1]	-3,936	, 001	16,531	-6,955	-, 917
[V1_Learning strategies= 1]	-5,317	.020	14,725	-10,111	-, 523
[V1_Learning strategies= 2]	-2,856	, 051	8,371	-7,635	1,924
[V2_Academic goals = 1]	-2,151	.042	9,985	-5,143	, 841
[V2_Academic goals= 2]	-3,130	, 004	16,073	-5,620	- .641

3.10. Specific hypothesis test 3

Ho: There is no incidence between learning strategies and academic goals in arduino electronics hardware and digital circuits in a Private University Lima, 2020.

H3: There is an incidence between learning strategies and academic goals in arduino electronics hardware and digital circuits in a Private University Lima, 2020.

Table 20: Model fit and likelihood ratio tests for specific hypothesis 3

Model fit information				
Model	Logarithm of probability -2	Chi squared	gl	S.I.G
Interception only	170,545			
Final	79,648	90,897	36	, 000

Table 20 shows that the value x2 = 90.897, (p = .033 <0.05), indicates that the proposed model serves to explain the dependent behavior of the competence variable of the electronic and digital circuit with respect to the Arduino hardware. In this sense, the null hypothesis is rejected with a probability of error less than 5%.

Table 21: Pseudo R squared for specific hypothesis 3

Pseudo R squared	
Cox and Snell	, 640
Nagelkerke	, 730
McFadden	, 487

Table 21 presents favorable pseudo R squared values, which ensures an adequate fit of the proposed model to explain skills in electronics and digital circuits. Likewise, the learning strategies is the variable that most affects the Arduino hardware of the explained variable with a value of Wald = 6.568 and p = .010 <0.05 (Table 22).

Table 22: Parameter estimates of the general hypothesis 4

	Estimate	S.I.G	Wald	95% interval trustworthy	
				Min	Max
[V3D3_ arduino hardware for electronic and digital circuits = 1]	-8,390	, 001	11,715	-13,194	-3,585
[V3D3_ arduino hardware for electronic and digital circuits = 2]	-5,083	.015	5,924	-9,176	-, 990
[V1_Learning strategies = 1]	-4,173	.010	6,568	-7,365	- .982
[V1_Learning strategies = 2]	-3,431	.046	3,996	-6,795	- .067
[V2_Academic Goals = 1]	-3,142	.077	3,132	-6,621	, 337
[V2_Academic Goals = 2]	-5,295	.020	5,439	-9,746	-, 845

3.11. Specific hypothesis test 4

H1: There is no incidence between learning strategies and academic goals in arduino electronics software and digital circuits in a Private University Lima, 2020.

H2: There is an incidence between learning strategies and academic goals in arduino electronics software and digital circuits in a Private University Lima, 2020.

Table 23: Model fit tests and likelihood ratio for specific hypothesis 4

Model fit information				
Model	Logarithm of probability -2	Chi squared	gl	S.I.G
Interception only	187,849			
Final	123,641	64,208	36	, 003

Table 23 shows that the value x2 = 64.208, (p = .003 <0.05), indicates that the proposed model serves to explain the behavior

dependent on the variable competencies of electronic and digital circuits referred to Arduino software. In this sense, the null hypothesis is rejected with a probability of error less than 5%.

Table 24: Pseudo R squared for specific hypotheses 4

Pseudo R squared	
Cox and Snell	, 514
Nagelkerke	, 574
McFadden	, 319

Table 24 presents favorable pseudo R squared values, which ensures an adequate fit of the proposed model to explain skills in electronics and digital circuits. Likewise, learning strategies is the variable that most affects the Arduino software of the explained variable with a value of Wald = 9.624 and p = .023 <0.05 (Table 25).

Table 25: Parameter estimates for general hypothesis 4

	Estimate	S.I.G	Wald	95% interval trustworthy	
				Min	Max
[V3D4_ arduino software for electronic and digital circuits= 1]	-. 186	, 003	13,017	-2,951	2,579
[V3D4_ arduino software for electronic and digital circuits= 2]	- .453	, 009	11,103	-. 225	2,319
[V1_Learning strategies= 1]	-3,556	.023	9,624	-6,797	-, 315
[V1_Learning strategies= 2]	-1,163	.048	8,580	4,156	1,830
[V2_Academic goals= 1]	-. 822	.042	9,266	3,946	2,301
[V2_Academic goals= 2]	, 654	, 051	7,184	-2,334	3,643

4. Discussion

With reference to the general objective set, satisfactory values of $x2 = 83.782$, (p = .000 <0.05), McFadden of 0.272, Nagelkerke of 63%, Cox and Snell of 61% and a Wald value of 16.326 were obtained. Indicating that the estimated model serves to explain the behavior of the dependent variable, being an adequate model, evidencing the rejection of the null hypothesis and admitting the incidence of learning strategies and academic goals in relation to the variable electronic competences and digital circuits. By virtue of this, they reaffirm the results obtained from the electronic and digital circuits competences with a tendency to be achieved with less than 70% of the engineering students of a Private University of Lima, 2020. In addition, The arduino software was estimated with more than 11% of the analyzed students presented low outstanding results compared to the other dimensions, which shows a profile of the student with deficiency in being able to develop skills in the description of a structure of the arduino software in the sktech. IDE, analysis of the arduino software instructions and achieve serial communication by connecting electronic devices to the arduino board, based on the data collected from the instrument application. On the other hand, the learning strategies show a moderate trend with more than 50% of the students, and it was evidenced that the support learning strategy presented the best results with a high level of more than 24% of

the students compared to the rest of your group, according to the Roman y Gallego ACRA test instrument (see appendix) applied. Likewise, the academic goals presented a moderate trend concentrating more than 60% of the students, being the achievement goal the one that presented the best results with more than 30% in the high level compared to the others in their group, according to the respondents to the the Durán CMA Test.

Similarly, the dependent variable of the research presented an incidence of 63% of variability with respect to the explanatory variables in students, which means that learning strategies and academic goals are important so that higher-level students can optimally develop your skills in electronics and digital. circuits for their good academic performance in a comprehensive and professional manner, in that sense they can successfully face the demands of the labor market, it should also be noted that the value of Wald showed that learning strategies have a greater explanatory force of incidence, so that these guide to a better development of the electronic and digital circuit competencies of the students compared to the academic goals, in addition,

With reference to the specific objectives, it was admitted that there is an incidence between learning strategies and academic goals in basic electronics, arduino hardware and software electrical circuits and arduino electronics digital circuits in Engineering students, Universidad Privada de Lima, 2020. No however, for basic electronics, in comparison with the other dimensions, satisfactory inferential values of $x2 = 61.281$, (p = .005 <0.05), Nagelkerke of 55.7% and Wald of 21.485 were obtained. This means that the learning strategies have a greater explanatory force of incidence for the basic electronic dimension compared to the other dimensions.

5. Conclusions

It was evidenced that the strategies of learning and academic goals affect the competences of electronic and digital circuits in engineering students, Universidad Privada Lima 2020. Due to acceptable values it was found of $x2 = 83.782$, (p = .000 <0.05) and Wald = 16.326 showing that the proposed model is plausible.

It was verified that the strategies of learning and academic goals affect basic electronics and digital circuits in Engineering students, Private University, 2020. Due to the favorable values obtained of $x2 = 61.281$, (p = .005 <0.05) and Wald = 21.485, which indicates that the proposed model is acceptable.

It was found that learning strategies and academic goals affect the electrical components of electronics and digital circuits in Engineering students, Private University, 2020. By favorable values of $x2 = 53.136$, (p = .033 <0.05) and Wald = 16.073, indicating that the proposed model is acceptable.

It was shown that the strategies of learning and academic objectives affect the hardware of Arduino electronics and digital circuits in Engineering students, Private University, 2020. Due to the value obtained from $x2 = 90.897$, (p = .000 <0.05) and Wald = 6.568, it which indicates that the proposed model is acceptable.

It is finally concluded that learning strategies and academic goals affect arduino electronics and digital circuits software in Engineering students, Private University, 2020. Due to the

acquired value of x2 = 64.208, (p = .003 <0.05) and Wald = 9.624, indicating that the proposed model is acceptable.

It was considered that there is an option that allows to dynamically cover a large volume of data, as well as flexible for educational environments, known as educational data mining [20].

6. Recommendations

It is recommended that the academic directors of the Private University establish institutional guidelines in their curricular plans for the implementation, incorporation and application of learning strategies and academic goals so that engineering students can effectively develop electronic and digital circuit skills, having significant learning.

The academic coordinator of engineering of the Private University is suggested to carry out activity programs for students of electronics and digital circuits in which topics of learning strategies and academic goals are developed in such a way that they can apply it in the subject and help them to develop. your core competencies in electronics, electrical components, arduino software, and arduino hardware.

It is proposed that the engineering professors of the Private University encourage their students of electronics and digital circuits in their pedagogical practices to use learning strategies, such as the acquisition, coding, retrieval and support of information, in the sense of raising skills and learning from the subject and achieve their academic goals.

New methods are recommended to better cover teaching strategies and thus avoid possible dropouts that may motivate students to drop out of college, such as an educational data mining option [21].

References

[1] British Council, "The reform of the peruvian university system: internationalisation, progress, challenges and opportunities," 1–123, 2016.

[2] Perú. Sistema Nacional de Evaluación Acreditación y Certificación de la Calidad Educativa, Resolución N° 022-2016-SINEACE/CDAH-P. Modelo de Acreditación para Programas de Estudios de Educación Superior Universitaria, 2016.

[3] OCDE, "Estrategia de competencias de la OCDE Reporte Diagnostico: Peru 2016," Organizacion Para La Cooperacion y El Desarrollo Economico, 182, 2016.

[4] M. Huerta Rosales, R. Penadillo Lirio, M. Kaqui Valenzuela, "Construcción del currículo universitario con enfoque por competencias. Una experiencia participativa de 24 carreras profesionales de la UNASAM," Revista Iberoamericana de Educación, **74**, 83–106, 2017, doi:10.35362/rie740609.

[5] F. Guzmán Marín, "Problemática general de la educación por competencias," Revista Iberoamericana de Educación, **74**, 107–120, 2017, doi:10.35362/rie740610.

[6] M.E. Bello van der Ree, J.A. Morales Lozano, "Competencias claves de los estudiantes universitarios para el uso de las TIC," Revista de Comunicación de La SEECI, **50**, 43–72, 2019, doi:10.15198/seeci.2019.50.43-72.

[7] J.J. Aiquipa, C.M. Ramos, R. Curay, L.L. Guizado, "Factores implicados para realizar o no realizar tesis en estudiantes de psicología," Propósitos y Representaciones, **6**(1), 21–82, 2017, doi:10.20511/pyr2018.v6n1.180.

[8] A.F. Hoffman, R. Ledesma, M.F. Liporace, "Estilos y estrategias de aprendizaje en estudiantes universitarios de Buenos Aires," Revista de Psicologia (Peru), **35**(2), 535–573, 2017, doi:10.18800/psico.201702.006.

[9] P. Guía, C. Exequel, P. Villalobos, Metas académicas, estilos atributivos y estrategias de aprendizaje en estudiantes secundarios de establecimientos vulnerables de la Región del BioBío, Universidad de Concepción. Facultad de Ciencias Sociales. Departamento de Psicología, 2017.

[10] M. Acevedo Zuluaga, Correlación entre Hábitos de Estudio, Estrategias de Aprendizaje y Rendimiento Académico, en Estudiantes de Fonoaudiología de la Corporación Universitaria Iberoamericana, 2016.

[11] A. Carlos, A.Q. Condezo, U N I V E R S I D A D N A C I O N A L D E E D U C A C I Ó N E n r i q u e G u z m á n y V a l l e Alma Máter del Magisterio Nacional ESCUELA DE POSGRADO Ulises Abdon PISCOYA SILVA, Universidad Nacional de Educación Enrique Guzmán y Valle. Escuela de Posgrado., 2018.

[12] C.M. Diez Canseco Gómez, Metas del logro, clima de apoyo a la autonomía, estrategias metacognitivas de aprendizaje y desorganización en estudiantes de psicología de una universidad privada de Lima Metropolitana, Universidad de Lima, 2016, doi:10.26439/ulima.tesis/3233.

[13] F. De Educación, U. De Posgrado, M. Faustina, F. Silva, UNIVERSIDAD NACIONAL MAYOR DE SAN MARCOS, Universidad Nacional Mayor de San Marcos, 2017.

[14] J.R. Martínez, F. Galán, "Estrategias de aprendizaje, motivación y rendimiento académico en alumnos universitarios," REOP - Revista Española de Orientación y Psicopedagogía, **11**(19), 35, 2014, doi:10.5944/reop.vol.11.num.19.2000.11323.

[15] S. Nabizadeh, S. Hajian, Z. Sheikhan, F. Rafiei, "Prediction of academic achievement based on learning strategies and outcome expectations among medical students," BMC Medical Education, **19**(1), 99, 2019, doi:10.1186/s12909-019-1527-9.

[16] M. Carles, C. Montserrat, M. Palma, C. Mercè, M. Pérez, "Estrategias de enseñanza y aprendizaje," Revista Docencia Universitaria, **9**(1), 155–159, 2008.

[17] E. Durán-Aponte, D. Arias-Gómez, "Validez del Cuestionario de Metas Académicas (CMA) en una muestra de estudiantes universitarios," Cuadernos Hispanoamericanos de Psicología, **15**(1), 23–36, 2016, doi:10.18270/chps..v15i1.1776.

[18] P.R. Pintrich, The Role of Goal Orientation in Self-Regulated Learning, Elsevier: 451–502, 2000, doi:10.1016/b978-012109890-2/50043-3.

[19] Ingeniería Electrónica con mención en Telecomunicaciones | UCH.

[20] P. Nuankaew, W. Nuankaew, K. Phanniphong, S. Imwut, S. Bussaman, "Students Model in Different Learning Styles of Academic Achievement at the University of Phayao, Thailand," International Journal of Emerging Technologies in Learning (IJET), **14**(12), 133–157, 2019.

[21] P. Nuankaew, "Dropout Situation of Business Computer Students, University of Phayao," International Journal of Emerging Technologies in Learning (IJET), **14**(19), 115–131, 2019.

Appendix

ACRA TEST:

This test is divided into four scales: Acquisition of information: It helps the student to know how to acquire the necessary information for the study. Information coding: It informs about how the main and secondary ideas of a text should be differentiated. Information retrieval: It sets out the mechanisms necessary to retrieve previously stored information. Information support: What means and conditions will help improve the study.

Next, the student must take this test, which must be answered in the following way: The questions that are asked must be answered as follows:

If you NEVER or NEVER do what is asked, you must put A.
If the question is EVER done, put B.
If ENOUGH TIMES what is asked is done, put C.
If you ALWAYS do what you ask, you have to put D.

Scale I: Information Acquisition Strategy:	A	B	C	D
1. Before starting to study I read the index, or the summary, or the sections of the material to be learned.				
2. When I am going to study a material, I write down the important points that I have seen in a first cursory reading to more easily get an overview.				
3. When I begin to study a lesson, I read it all over the top first.				
4. As I study, I look for the meaning of unknown words, or of which I have doubts about their meaning.				
5. In books, notes or other material to learn, I underline in each paragraph the words, data or phrases that seem most important to me.				
6. I use signs (admirations, asterisks, drawings…), some of them only intelligible by me, to highlight those information in the texts that I consider especially important.				
7. I use pencils or pens of different colors to promote learning.				
8. I use the underlining to facilitate memorization.				
9. To discover and highlight the different parts of what is composes a long text, subdivided into several small by means of annotations, titles and epigraphs.				
10. I write down words or phrases by the author, which seem significant to me, in the margins of books, articles, notes, or on a separate page.				
11. During the study, I write or repeat the important or most difficult data to remember several times.				
12. When the content of a topic is dense and difficult I reread it slowly.				
13. I read aloud, more than once, the underlines, diagrams, etc…, made during the study.				
14. I repeat the lesson as if I were explaining it to a classmate who does not understand it.				
15. When I study I try to mentally summarize the most important things.				
16. To check what I am learning about a topic, I ask myself section by section.				

17. Even if I don't have to take an exam, I usually think and reflect on what I've read, studied, or heard from teachers.				
18. After analyzing a graphic or text drawing, I spend some time learning it and reproducing it without the book.				
19. I make them ask me the underlines, diagrams, etc. facts when studying a topic.				
20. When I am studying a lesson, to facilitate understanding, I rest, and then I review it to learn it better.				
Sum				
Multiply	X1	X2	X3	X4
Outcome				
Direct Score				
Percentile				
Scale Ii: Information Coding Strategy:	A	B	C	D
1. When I study, I make drawings, figures, graphs or vignettes to represent the relationships between fundamental ideas.				
2. To solve a problem, I begin by carefully recording the data and then try to represent it graphically.				
3. When I read, I differentiate important or main aspects and contents from accessories or secondary ones.				
4. I look for the "structure of the text", that is, the relationships already established between its contents.				
5. I rearrange or carry out, from a personal point of view, new relationships between the ideas contained in a topic.				
6. I relate or link the topic I am studying with others that I have studied or with the data or knowledge previously learned.				
7. I apply what I learn in some subjects to better understand the contents of others.				
8. I discuss, relate or compare with my colleagues the works, diagrams, summaries or topics that we have studied.				
9. I go to friends, teachers or family when I have doubts about the study topics or to exchange information.				
10. I complete the information in the textbook or class notes by going to other books, encyclopedias, articles, etc.				
11. I establish relationships between the knowledge that the study provides me and the experiences, events or anecdotes of my private and social life.				
12. I associate the information and data that I am learning with fantasies of my past or present life.				
13. When studying, I put my imagination into play, trying to see, like in a movie, what the subject suggests to me.				
14. I make comparisons by making metaphors with the issues I am learning (eg, the kidneys function as a filter).				
15. When the topics are very abstract, I try to look for something familiar (animal, plant, object or event) that resembles what I am learning.				
16. I carry out exercises, tests or small experiments, etc., as an application of what I have learned.				
17. I use what I learn, as much as possible, in my daily life.				
18. I try to find possible social applications in the content I study.				
19. I am interested in the application that the subjects I study may have to the labor fields that I know.				

20. I usually write down in the margins that what I am studying (or on a separate sheet) suggestions or doubts about what I am studying.				
21. During the teachers' explanations, I usually ask myself questions on the subject.				
22. Before the first reading, I ask myself questions whose answers I hope to find in the material I am going to study.				
Sum				

	A	B	C	D
23. When I study, I ask myself questions suggested by the topic, to which I try to answer.				
24. I usually take notes of the tutor's ideas, in the margins of the text I am studying or on the separate sheet, but in my own words.				
25. I try to learn the topics in my own words instead of memorizing them verbatim.				
26. I make critical annotations to the books and articles I read, either in the margins or on separate sheets.				
27. I arrive at new ideas or concepts starting from the data, facts or particular chaos that the text contains.				
28. I draw conclusions from the information contained in the topic I am studying.				
29. When studying, I group and classify the data according to my own criteria.				
30. I summarize the most important of each of the sections of a topic, the lesson or the notes.				
31. I make summaries of what was studied at the end of each topic.				
32. I prepare the summaries using the previously underlined words or phrases.				
33. I make diagrams of what I study.				
34. I build the diagrams using the underlined words or phrases from the summaries made.				
35. I order the information to be learned according to some logical criterion: cause-effect, problem-solution, etc.				
36. When the subject under study presents the information organized temporally (historical aspects), I learn it taking into account that temporal sequence.				
37. If I have to learn different steps to solve a problem, I use diagrams to help capture the information.				
38. During the study, or at the end, I design concept maps to relate the concepts of a topic.				
39. To develop concept maps, I rely on the underlined keywords.				
40. When I have to make comparisons or classifications, I use tables.				
41. When studying any subject, I use V-diagrams to solve the above.				
42. I spend some study time memorizing, above all, summaries, diagrams, concept maps, etc. that is, to memorize the importance of each subject.				
43. To fix data when studying, I usually use "tricks" to make that idea stick in my memory.				
Sum				
44. I construct "rhymes" or "fillers" to memorize lists of concepts.				
45. To memorize, I mentally place the data in places in a well-known space.				
46. I learn unfamiliar names or terms by developing a "keyword" that bridges the gap between the familiar name and the new one to remember.				
Sum				
Multiply	X1	X2	X3	X4
Outcome				

Direct Score				
Percentile				
Scale Iii: Information Recovery Strategy	A	B	C	D
1. Before speaking or writing, I remember words and drawings that are related to the "main ideas" of the material studied.				
2. Before speaking or writing, I use keywords or phrases that help me differentiate the main and secondary ideas of what I study.				
3. When I have to present something orally or in writing, I remember drawings, images, etc. through which I elaborated the information during learning.				
4. Before responding to an exam, I remember those groupings of concepts (summaries, diagrams, etc.) made at the time of studying.				
5. For important questions, which are difficult for me to remember, I look for secondary data in order to be able to remember what is important.				
6. It helps me to remember what I have learned by evoking events, episodes or clues that occurred during class or at other learning moments.				
7. It helps me to remember other topics that are related to what I really want to remember.				
8. Putting myself in a mental and affective situation similar to that experienced during the teacher's explanation or at the time of study, makes it easier for me to remember important information.				
9. In order to better recover what I have learned, I take into account the corrections and observations that teachers make in exams, exercises or assignments.				
10. To remember information, I first look for it in my memory and then decide if it fits what I have been asked or want to answer.				
11. Before I start to speak or write, I think and mentally prepare what I am going to say or write.				
12. I try to express what I have learned in my own words instead of repeating literally or verbatim what the book or the teacher says.				
13. When answering an exam, before writing, first I remember, in any order, everything I can, then I order it and make an outline or script and finally develop it point by point.				
14. When I have to do a free writing on any subject, I write down the ideas that occur to me, then I order them and finally I write them.				
15. When carrying out an exercise or exam, I am concerned about its presentation, order, cleanliness, margins.				
16. Before doing a written assignment, I make an outline, script or program of the points to be discussed.				
Sum				

	A	B	C	D
17. When faced with a problem or difficulty, I first consider the data that I know before venturing to provide an intuitive solution.				
18. When I have to answer a topic for which I have no data, I generate an "approximate" answer relating what I already know about other topics.				
Sum				
Multiply	X1	X2	X3	X4
Outcome				
Direct Score				
Percentile				
Scale Iv: Processing Support Strategy	A	B	C	D
1. Before speaking or writing, I remember words and pictures that are related to the "main ideas" of the material studied.				
2. Before speaking or writing, I use keywords or catch phrases that help me differentiate the main and secondary ideas of what I study.				

3. When I have to present something orally or in writing, I remember drawings, images, etc. through which I elaborated the information during learning.				
4. Before responding to an exam, I remember those groupings of concepts (summaries, diagrams, etc.) made at the time of studying.				
5. For important questions, which are difficult for me to remember, I look for secondary data in order to be able to remember what is important.				
6. It helps me to remember what I have learned by evoking events, episodes or clues that occurred during class or at other learning moments.				
7. It helps me to remember other topics that are related to what I really want to remember.				
8. Putting myself in a mental and affective situation similar to that experienced during the teacher's explanation or at the time of study, makes it easier for me to remember important information.				
9. In order to better recover what I have learned, I take into account the corrections and observations that teachers make in exams, exercises or assignments.				
10. To remember information, I first look for it in my memory and then decide if it fits what I have been asked or want to answer.				
11. Before I start to speak or write, I think and mentally prepare what I am going to say or write.				
12. I try to express what I have learned in my own words instead of repeating literally or verbatim what the book or the teacher says.				
13. When answering an exam, before writing, first I remember, in any order, everything I can, then I order it and make an outline or script and finally develop it point by point.				
14. When I have to do a free writing on any subject, I write down the ideas that occur to me, then I order them and finally I write them.				
15. When carrying out an exercise or exam, I am concerned about its presentation, order, cleanliness, margins.				
16. Before doing a written assignment, I make an outline, script or program of the points to be discussed.				
17. When faced with a problem or difficulty, I first consider the data that I know before venturing to provide an intuitive solution.				
18. When I have to answer a topic for which I have no data, I generate an "approximate" answer relating what I already know about other topics.				
Sum				

	A	B	C	D
18. I use personal resources to control my anxiety states when they prevent me from concentrating on the study.				
19. I imagine places, scenes or events in my life to calm me down and to focus on work.				
20. I know how to self-relax, self-talk, self-apply positive thoughts to be calm on exams.				
21. I tell myself that I can exceed my current performance level (expectations) in the various subjects.				
22. I try that in the place I study there is nothing that can distract me, such as people, noise, disorder, lack of light and ventilation, etc.				
23. When I have family conflicts, I try to resolve them sooner, if I can, to better concentrate on studying.				
24. If I am studying and am distracted by thoughts or fantasies, I fight them by imagining the negative effects of not having studied.				
25. At work, I am encouraged to exchange opinions with my colleagues, friends or family about the subjects I am studying.				

26. I am satisfied that my colleagues, teachers and family value my work positively.				
27. I avoid or resolve, through dialogue, conflicts that arise in personal relationships with colleagues, teachers or family members.				
28. To improve myself it stimulates me to know the achievements or successes of my colleagues.				
29. I encourage and help my classmates to be as successful as possible in their homework.				
30. I say words of encouragement to myself to stimulate and keep me on study assignments.				
31. I study to expand my knowledge, to know more, to be more expert.				
32. I make an effort in the studio to be proud of myself.				
33. I seek to have prestige among my colleagues, friends and family, standing out in studies.				
34. I study to get rewards in the short term and to achieve a comfortable social status in the future.				
35. I make an effort to study to avoid negative consequences, such as reprimands, upsets or other unpleasant situations in the family, etc.				
Sum				
Multiply	X1	X2	X3	X4
Outcome				
Direct Score				
Percentile				

ASTES

Modeling Watershed Health Assessment for Five Watersheds in Lampung Province, Indonesia

Eva Rolia[1,*], Dwita Sutjiningsih[1], Yasman[2], Titin Siswantining[3]

[1]Departmen of Civil Engineering, University of Indonesia, Depok, 16424, Indonesia

[2]Departmen of Biology, University of Indonesia, Depok, 16424, Indonesia

[3]Departmen of Mathematics, University of Indonesia, Depok, 16424, Indonesia

A R T I C L E   I N F O

A B S T R A C T

A healthy watershed is important not only for the ecosystem but also for human socioeconomic activities. Therefore, a compatible assessment model is required to recognize watershed health. In Indonesia, the watershed health assessment is directed by the Ministry of Forestry regulation number 60/2014. A critic might be posed to this directive for not including the biotic aspects of the watershed. This research aims to assess the five watersheds in Lampung Province, Indonesia. Afterward, we develop a mathematical model using multiple linear regression analysis to identify influential indicators. In developing the model, we combined indicators in the Ministry of Forestry regulation number 60/2014 with the US-EPA directive to include the biotic indicators. To collect the data, we accessed secondary data officially launched by the authorities and did field observation if the secondary data is not available. Our assessment based on the Indonesian official regulation shows that 3 sub-watersheds are in unhealthy status while the rest can be categorized as healthy watershed. Furthermore, the mathematical model of the sub-watershed health assessment shows that the percentage of critical land and vegetation coverage plays an essential role in determining watershed health status. Besides, investment in the water-related infrastructure also significantly contributes to watershed health.

1. Introduction

A watershed is an ecosystem where living organisms, biophysical elements, and chemical substances are interlinked and dynamically interact [1]. This ecosystem also plays an essential role in the dynamics of materials and energy flows. Therefore, the watershed deterioration might bring negative impacts on many sectors within various scales [2]. The watershed also has hydrological functions to accommodate rainwater overflow and to maintain the water quality. Besides, a watershed also acts as a compound ecosystem engaging natural landscape, economic activities, and social development [3]. Considering their important functions, all components of the watershed, which are generally categorized as input (i.e., rainwater), output (i.e., river flow, pollutants, sediments), and process (i.e., human activities, vegetation, soil, climate, and topography), are supposed to be well managed to meet basic requirements of ecosystem stability as well as socio-economic development [4–6].

Watershed health assessment refers to structural and functional measurement. To specify, the structural measurement is related to the issues of biodiversity, organic and inorganic resources, and physical attributes. Meanwhile, the functional measurement refers to the issues of ecological processes such as hydrology cycle, nutrient cycle, and energy flow [7]. In the watershed ecosystem, the hydrological biophysics process naturally occurs. It becomes a place for socioeconomic activities. Up to this point, the hydrological biophysics process is a part of the hydrology cycle while socioeconomic activities cannot be separated from human intervention to the watershed and the surrounding environments [1]. Indeed, the natural mechanisms and human interventions are inter-correlated and bring impacts one to another [8]. Therefore, more attention should be paid on the issue of watershed health to sustain human socioeconomic activities. The other way around, the socio-economic activities taking place on the watershed environments should be carefully managed to ensure watershed health.

*Corresponding Author: Eva Rolia,✉ roliaeva@yahoo.com, ☏+6282373737372

Furthermore, various concepts are promoted to explore the issues of watershed health assessment. In [9], for instance, argued that the diversity in ecological and social structure and the ability to adapt with uncertainty are the key factors to maintain the mutual relationship between the watershed health and human activities taken place on the watershed environment. Thus, understanding the socio-ecological system is an essential approach to build sustainable and adaptive modern management [10]. Subsequently, various indicators have been developed around the globe to assess watershed health. For example, a report from the Lake Simcoe Region Conservation Authority (Canada) [11]used land, water, and social conditions as indicators to assess watershed health. Other indicators such as geological condition, groundwater, the quantity and quality of surface water, geomorphologic condition, aquatic system, cultural, natural recreation, and land use are indicators used to assess the watershed health in the Philippines [12]. Meanwhile, in Thailand, three main indicators namely climate and stream flow, stream water quality, soil erosion, and stream sediment are suggested as tools to do the watershed health assessment [13]. Besides geomorphologic and hydrological aspects, in China, living organism (e.g., flora, fauna, riparian vegetation) inhabiting the watershed are also counted in the watershed health assessment [14]while the United States refers its integrated evaluation of the watershed health assessment and protection on the condition of landscape, habitat, hydrology, geomorphology, water quality, and biology [15]. Furthermore, study in [16]considered the impact of climate variability on watershed health by analyzing the temporal and spatial variability of reliability, resilience, and vulnerability.

Indeed, indicators used in a certain location have respective benefits and drawbacks. Besides, they also depend on the local context. Indonesia, in particular, recognized two categories in determining the watershed health status. They are to be maintained and to be rehabilitated watershed. The assessment criteria are stated in the ministry of forestry regulation [17]to be a reference to develop watershed management planning and policy. The criteria are (1) land conditions; (2) the quality, quantity, and continuity of the water; (3) socio-economy and institutions; (4) water building investment; and (5) land use. In more detail, each criterion is broken down into several sub-criteria. To compare with other countries (e.g., the United States), the current indicators used in Indonesia do not include the biotic aspects of the watershed. Therefore, the determination of the watershed health status might be criticized since the existence of living organisms, either aquatic or terrestrial creatures, can be natural indicators to predict the quality of the water [18]. Another benefit to using biological indicators in the watershed health evaluation is that they also reflect physical and chemical characteristics of the water environment since the existence of living organisms are highly influenced by the physical and chemical environment [19], the more living organisms, the better water quality physically and chemically. Furthermore, macro-invertebrate and fish are usually used to indicate the river health because their disappearance represent environmental degradation either in local or regional scale [20].

Considering the importance of the biological indicators, we tried to add this aspect to the watershed health assessment in Indonesia. We took five watersheds in Lampung province, Indonesia as the case study areas. They are Sekampung, Seputih,

Semangka, Mesuji, and Tulang Bawang. To introduce, Lampung province is located on the south-end of Sumatera Island. The five watersheds respectively have characteristics. For instance, the Sekampung watershed is the area with a dense population since it passes big cities and the capital of the province. Meanwhile, the Seputih watershed stretched from the north to the east part of this province. The land use of this area is dominated by rice field and horticulture cultivation. Farming activities also dominantly appear in Tulang Bawang and Mesuji watersheds. Nevertheless, rubber and palm plantations are the most common farming activities in these areas. Lastly, the land use of the Semangka watershed, which is located on the west part of Lampung province, is dominated by forest. Besides, farming activities, which mostly cultivate coffee, pepper, and clove, also appear in this area.

Furthermore, the objective of this research is to do a health assessment for these five watersheds using the Indonesian directive [17]and add the biological indicators to the assessment. Thus, we combined the assessment procedures proposed by the ministry of forestry and the US-EPA. Therefore, we compared our analysis with the health status attached to each watershed and investigated whether the biological indicators might change the current status. Moreover, we investigated the relationship between indicators and weighed the most influential ones to develop the indicator model. We weighed indicators resulted from the modeling to determine the optimum value of the watershed health using the linear regression statistical model.

2. Materials and Methods

In conducting this study, we did both secondary and primary data collection. At the beginning stage, we collected the secondary data related to hydrology and land cover of the watersheds. We also identified institutions that are in charge of the respective watershed as well as socio-economic activities that took place on it. We utilized data officially launched by the government institutions to elaborate on those indicators, which are required by the assessment method directed by the ministry of forestry. Furthermore, we analyzed indicators required by the US-EPA assessment method i.e., landscape, biology, geomorphology, habitat, water quality, and hydrology. Information related to these issues is gathered from the secondary data and the primary data as well. After gathering information about the indicators above, we analyzed the relationship between indicators using the multiple linear regression analysis. This stage aimed to optimize the use of indicators to assess watershed health. Eventually, we formulated policy scenarios and simulated through qualitative analysis.

This research was started by collecting information related to the current health status of the five assessed watersheds. Referring to the regulation launched by the Ministry of Forestry, we collected the data on five criteria. They are (1) land conditions; (2) water conditions (quality, quantity, and continuity); (3) socioeconomic and institutions; (4) investment; and (5) land use. In more detail, each criterion is broken down into more specific sub-criteria. The Ministry of Forestry regulation number 60/2014 also provides the formulas as a guidance to calculate all indicators. Furthermore, this regulation also provides the classification for each criterion and a justification for weighing. Then, based on this weighing procedure, we assessed the health status of the seventeen sub-watersheds in

Lampung Province, Indonesia. In detail, the formula of the criteria, and the weighing system suggested by the Ministry of Forestry regulation number 60/2014 is presented in table 1.

Table 1: The Formula to Calculate Indicators Based on the Ministry of Forestry Regulation Number 60/2014 and the Scoring Justification

Indicators (Formula)	Remarks	Scoring Justification	
		Criteria	Score
Critical Land $CL = \dfrac{A_{CL}}{A_W} x100\%$	CL= Critical Land (%) A_{CL} = The area of the critical land (Hectares) A_W = The area of the watershed (Hectares)	CL≤5	0.50
		5<CL≤10	0.75
		10<CL≤15	1.00
		15<CL≤20	1.25
		CL>20	1.50
Vegetation Coverage $VC = \dfrac{A_{VC}}{A_W} x100\%$	VC= Vegetation Coverage (%) A_{VC}= The area of the vegetation coverage (Hectares) A_W = The area of the watershed (Hectares)	80<VC	0.50
		60<VC≤80	0.75
		40<VC≤60	1.00
		20<VC≤40	1.25
		VC≤20	1.50
Erosion Index $EI = \sum \dfrac{A_i}{A_W} x EI_I$; where $EI_i = \dfrac{PE_i}{TE_i}$	EI = Erosion Index Ai= The area of i-th segment Aw=The area of watershed EIi=Erosion index in i-th segment PE$_i$=Predictive erosion in i-th segment TE$_i$=Tolerable erosion in i-th segment	EI≤0.5	0.50
		0.5<EI≤1.0	0.75
		1.0<EI≤1.5	1.00
		1.5<EI≤2.0	1.25
		EI>2.0	1.50
Flow Regime Coefficient $FRC = \dfrac{Q_{max}}{Q_R}$; where $Q_R = 0.25 x Q_{av}$	Q$_{max}$=Daily quantity (in the highest quantity year) Q$_R$=Reliable quantity Q$_{av}$=Average quantity (within 10 years)	FRC≤5	0.50
		5<FRC≤10	0.75
		10<FRC≤15	1.00
		15<FRC≤20	1.25
		FRC>20	1.50
Annual Flow Coefficient $AFC = \dfrac{kQ_{an}}{RA_W}$	AFC=Annual Flow Coefficient k=Conversion factor =(365 x 86,400)/10 Q$_{an}$=Average annual quantity R=average annual rainfall A$_W$=the area of the watershed	AFC≤0.2	0.50
		0.2<AFC≤0.3	0.75
		0.3<AFC≤0.4	1.00
		0.4<AFC≤0.5	1.25
		AFC>20	1.50
Sediment Load $SL = kC_s Q_{an}$	SL=Sediment Load k=Conversion factor =(365 x 86.4) C$_s$=Sediment concentration (gram/Liter) Q$_{an}$=Average annual quantity	SL≤5	0.50
		5<SL≤10	0.75
		10<SL≤15	1.00
		15<SL≤20	1.25
		SL>20	1.50
Annual Flood Event	Data on the annual flood is officially launched by the government	Never	0.50
		Once in 5 years	0.75
		Once in 2 years	1.00
		Once in a year	1.25
		More than once in a year	1.50
Water Usage Index $WUI = \dfrac{WR_{tot}}{HH_{tot}}$	WUI=Water Usage Index WR$_{tot}$= Total water requirement HH$_{tot}$=Total numbers of households	WUI≤0.25	0.50
		0.25<WUI≤0.50	0.75
		0.50<WUI≤0.75	1.00
		0.75<WUI≤1.00	1.25
		WUI>1.00	1.50
Land Availability Index $LAI = \dfrac{A_f}{HH_f}$	LAI=Land Availability Index A$_f$=Area for farming activities HH$_f$=Numbers f households that are farmers	IKL>4	0.50
		2<IKL≤4	0.75
		1<IKL≤2	1.00
		0.5<IKL≤1	1.25
		IKL≤0.5	1.50
Population Welfare	PW=Population Welfare	PW≤5	0.50
		5<PW≤10	0.75
		10<PW≤20	1.00

$PW = \dfrac{HH_{pov}}{HH_{tot}} x100\%$	HH_{pov}=Numbers of households that are below poverty line living on the watershed area HH_{tot}=total numbers of households living on the watershed area	$20<PW\leq30$	1.25
		$PW>30$	1.50
Pro-conservation regulation	The data refer to availability of pro-conservation regulation in the local government located on the watershed	Available, widely applied	0.50
		Available, partly applied	0.75
		Available, no longer applied	1.00
		Unavailable	1.25
		Available, has not been applied	1.50
The existence of urban area	The data refers to the existence of urban areas and type of the city located on the watershed	No urban area	0.50
		Small city	0.75
		Medium sized city	1.00
		Big city	1.25
		Metropolitan	1.50
Investment on the water building	The data refers to the investment (expressed in billion Rupiahs) on water building e.g. dam, irrigation, etc.	$INV\leq15$	0.50
		$15<INV\leq30$	0.75
		$30<INV\leq45$	1.00
		$45<INV\leq60$	1.25
		$INV>60$	1.50
Conserved Area	Con A= Percentage of conservation area A_{veg}= The area of vegetation coverage in conservation area A_{con}= The total area of conservation in the watershed	Con A>70%	0.50
		45%<Con A≤70%	0.75
$ConA = \dfrac{A_{veg}}{A_{con}} \times 100\%$		30%<Con A≤45%	1.00
		15%<Con A≤30%	1.25
		Con A≤15%	1.50
Cultivated Area	Cul A=Percentage of cultivated area A_{25}=The area with the slope 0-25% A_{cul}=The total area of cultivation in the watershed	Cul A>70%	0.50
		45%<Cul A≤70%	0.75
$CulA = \dfrac{A_{25}}{A_{cul}} \times 100\%$		30%<Cul A≤45%	1.00
		15%<Cul A≤30%	1.25
		Cul A≤15%	1.50

Furthermore, we collected data required by the formulas to assess the health of the sub-watersheds. Afterwards, the accumulated score for each sub-water sheds was calculated to state the health status. This regulation defines a watershed is healthy when the total score is less than or equal to 100 and is unhealthy if the total score exceeds 100.

Moreover, we also assessed the watershed health by using the US-EPA assessment procedure which involves indicators such as habitat, hydrology, geomorphology, water quality, and biota. Since some indicators are not available in the Indonesian assessment system, we collected the data by direct observation. For example, habitat observation was carried out by tracing the rivers (about 200 meters long) to observe the riverbed substrate and disturbance factors surrounding the rivers and riparian. Besides, we calculated the geomorphology indicator based on the slope that is analyzed from the existing topographical data. To investigate the water quality, we utilized data from the environmental agency of the Lampung provincial government; the institution that is responsible for doing laboratory tests on the water quality.

Then, we developed a mathematical model representing the watershed health assessment. This predictive model aimed to investigate the relationship between independent variables and the dependent variable and the most influential indicators. We employed the multiple linear regression models following equation 1 and the numerical iteration is assisted by computer software (SPSS).

$$y_1 = \beta_0 + \beta_1 x_{1i} + \beta_2 x_{2i} + \beta_3 x_{3i} + \cdots + \beta_k x_{ki} + i \quad (1)$$

The y indicates the watershed health, which is the expected dependent variable while x1, x1, x2, and so forth are the indicators that act as inputs of independent variables. Based on the collected data, we developed four models. The first model represents the Ministry of Forestry regulation number 60/2014 and the second model represents the US-EPA directive. Then, the third and fourth models combine both assessment procedures. At the end of statistical procedures, we validated the watershed health equation models with the assessment based on the Ministry of Forestry regulation number 60/2014 following the criteria listed in table 1 as the reference. This validation resulted in the percentage of the margin of error that can reflect the suitability of the model and confirm the watershed health status.

3. Results

3.1. The description of the watershed

This research was taken place on five watersheds in Lampung Province located on the southern part of Sumatera

Island. Figure 1 is to illustrate the situation of the five watersheds and each characteristic.The figure shows that each watershed has a different size and most of them stretch across the city administrative borders. The red line indicates the border of each watershed. It can be seen Tulang Bawang watershed (the middle part) occupies the biggest area while the smallest one is Semangka watershed. Besides, different coloured spots show various activities taken place on the watersheds that are characterized by different types of land covering. The green areas indiate forests while the blue areas indicate paddy fields.biggest area while the smallest one is Semangka watershed. Besides, different coloured spots show various activities taken place on the watersheds that

are characterized by different types of land covering. The green areas indiate forests while the blue areas indicate paddy fields.Moreover, the red spots in the map shows the settlement areas. It can be seen that the existence of the forests in the case study area is still signifcant and the economic activities are dominated farming activities such as paddy fields, horticulture cultivation, and plantations. On the other hand, the mining activities also exist indicated by the dark brown spots.

Furthermore, table 2 compares the watersheds size, the length of the main river, and the three most dominant land covering in each watershed.
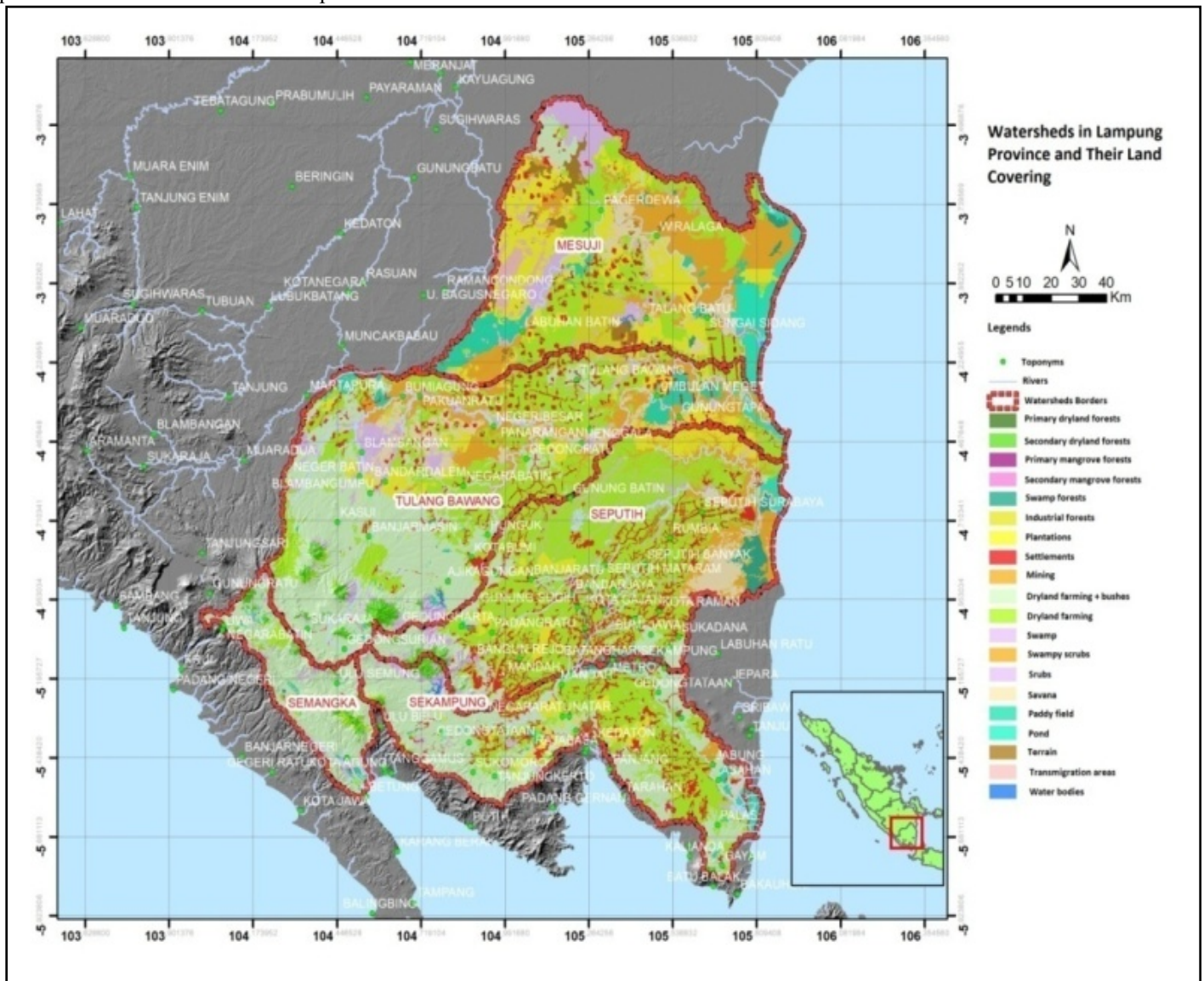
Figure 1: The land covering map of the case study area

Table 2: The watersheds size and their most dominant land covering

Watershed	Area (Hectares)	The length of the main river (km)	Dominant land covering	
			Type of land covering	Percentage (%)
Sekampung	482,316.20	256	Dryland farming	73.8
			Settlement	9.9
			Plantation	4.2

			Dryland farming	58.7
Seputih	751,527.23	135	Waterbody	13.2
			Bushes	7.9
			Dryland farming	60.0
Tulang Bawang	979,818.53	136	Swamp	11.1
			Bushes	6.3
			Dryland farming	23.7
Mesuji	723,714.31	220	Transmigration area	19.3
			Swamp	18.8
			Dryland farming	82.9
Semangka	161,448.78	169	Forest	6.5
			Bushes	5.7

The division of the watershed	
Sekampung :	
1	Sekampung 1 (SK-01)
2	Sekampung 4 (SK-04)
3	Sekampung 5 (SK-05)
4	Sekampung 6 (SK-06)
5	Sekampung 7 (SK-07)
Seputih :	
1	Seputih 1 (SP-01)
2	Seputih 2 (SP-02)
3	Seputih 3 (SP-03)
4	Way Pengubuan 1 (PB-01)
5	Way Pengubuan 2 (PB-02)
6	Way Pegadungan 2 (PG-02)
Tulang Bawang :	
1	Tulang Bawang 1 (TB-01)
2	Tulang Bawang 2 (TB-02)
3	Terusan 1 (TR-01)
4	Terusan 2 (TR-02)
Mesuji :	
1	Mesuji 3 (SM-03)
Semangka :	
1	Semangka 1 (SMK-01)

Figure 2: The sub-watershed clustering

Table 2 lists the three most dominant land covering the five observed watersheds. For all watersheds, the dryland farming is superior over other types of land covering with its respective portion. In the Semangka watershed, for instance, dryland farming shared 82.9% of the total area, which is the biggest percentage of land covering. Then, the percentage is followed by forest and swamp, which is respectively 6.5% and 5.7%. Similar with this watershed, the dryland farming is also the most dominant land covering in Sekampung, Tulang Bawang, and Seputih watershed, which is 73.8%, 60.0%, and 58.7% of the total area of each watershed. Although its percentage is not as superior as the other four watersheds', dryland farming still shares the highest percentage in the Mesuji watershed, which is 23.7% of the total area.

To organize the data collection and analysis, the five watersheds are divided into seventeen sub-watersheds and are codified as is illustrated in figure 2. Further, our data collection and analysis are referred to as this sub-watershed clustering and codification. To specify, we assessed five sub-watersheds in Sekampung watershed, six sub-watersheds in Seputih watersheds, and four sub-watersheds in Tulang Bawang sub-watersheds. For

Mesuji and Semangka watershed, respectively we took one sub-watershed.

3.2. *The watershed health assessment based on the Ministry of Forestry number 60/2014*

Referring to indicators and the formulas listed in table 1, we assessed the health status of the seventeen sub-watersheds. Firstly, we assessed the sub-watershed health based on the indicators of the land conditions. Critical land, vegetation coverage and erosion index are belonged to this indicator. Our analysis shows that the percentage of critical land varied, ranging from 0% to 33.6%, in all assessed watershed. The three highest percentages of the critical land appear in SMK-01 (33.6%), SK-01 (28.62%), and SM-03 (22.309%). Moreover, we scored the percentage based on the classification listed in table 1. The shifting in land use can probably be highlighted as the cause of the increasing trend of the critical land. For example, the land-use changes from the forest to the plantations in the upstream while in the middle areas and the downstream the land use mostly shift into settlements and commercial areas, which is in line with the population growth.

Other indicators of the land condition that we assessed are the vegetation coverage and erosion index. These elements are essential considering their importance to influence soil's physical and chemical characteristics and water flow. The data shows that there is a wide interval (from 0.005% to 89.838%) indicating a diverse situation of the vegetation coverage in the seventeen watersheds. The highest percentage of the vegetation coverage (89.838%) is in SK-01 while the lowest percentage (0.005%) is in SP-02. The higher percentage implicates on the lower score in the weighing procedure. Thus, the higher percentage of the vegetation coverage means the healthier watershed. In the case of erosion index, the calculation does not show a dramatic difference among all areas. The range of the erosion index is between 0.32% and 1.2% while the weight is within the interval 0.5 to 1.0. In general, based on the indicator of the erosion index, the assessed sub-watersheds have good conditions.

Furthermore, we continued the assessment on the indicator of the water quality, quantity, and continuity. We employed equations listed in table to calculate the assessment values using data recorded by the government institutions that are responsible for the watershed management in Lampung Province. We found that there is a variety among the sub-watersheds, but it is not as wide as in the land conditions. Thus, the sub-watersheds have a slight difference in the perspective of water quality, quantity, and continuity. The score of the respective indicator in the sub watersheds is illustrated in figure 3.
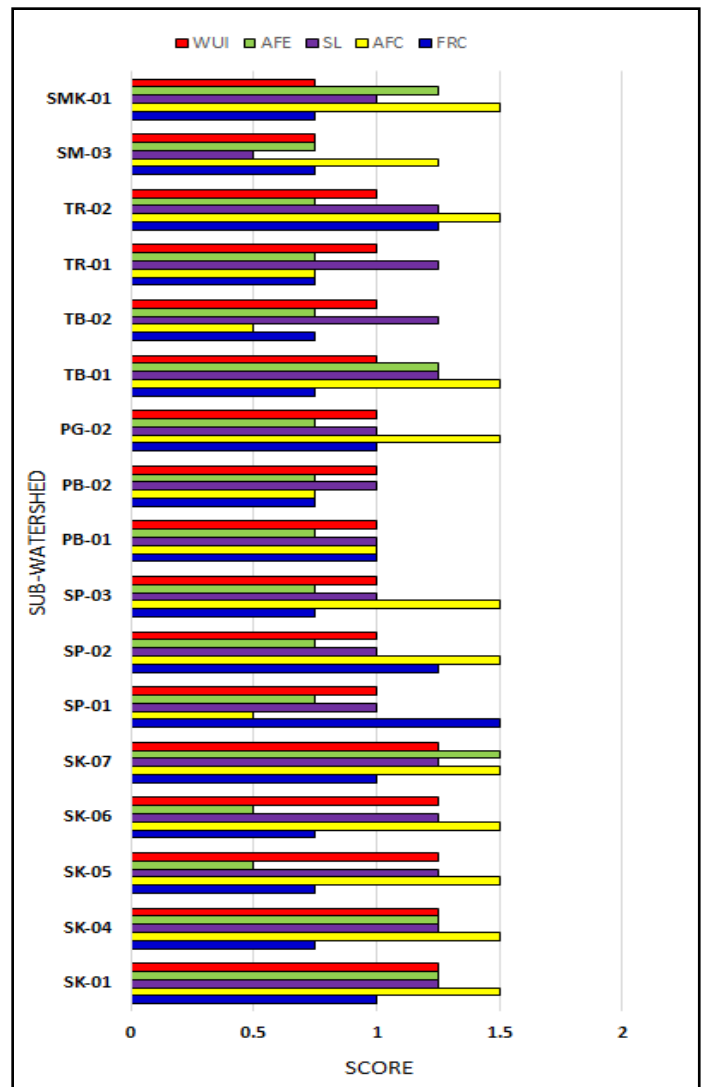
Figure 3: The score of the sub-watershed health assessment based on the quality, quantity, and continuity indicators

In the case of the Flow Regime Coefficient (FRC), which are represented by the blue bars, the highest score is in TR-02 (1.25) followed by TR-02 and SP-02 (1.25) while the result is dominated by the score 0.75. The uniform tendency also appears in the category of the Annual Flow Coefficient (AFC) that is represented by the yellow bars and the Sediment Load (SL) that is represented by the purple bars. On the other hand, more varied score appears in the category of the Annual Flow Event (AFE), which is illustrated by the green bars. In this category, SK-07 has the highest score (1.5) indicating that this sub-watershed has the most often annual flood event compared to other assessed sub-watersheds.

Subsequently, we summarized the sub-watershed health assessment on the socioeconomics and institution indicators. We found that the SK-01 sub-watershed has the lowest Land Availability Index (0.272 hectares/household) while the TB-02 sub-watershed has the highest LAI (9.946 hectares/households). However, it does not automatically implicate population welfare. The calculation shows that the watershed that has the highest LAI is not the most superior in the population welfare. Similarly, the lowest LAI does not implicate the most inferior in population

welfare. In the case of population welfare, the highest percentage is SK-06 sub-watershed (20.21%), which implicates on the highest weighing score (1.25). Meanwhile, other assessed sub-watersheds share the same weighing scores (1.0) even though their percentage of population welfare is varied from 10.64% to 19.19%. In the case of pro-conservation regulations, only the Sekampung watershed that has widely applied their local regulations those is pro-conservations while other watersheds have pro-conservation regulations but partly applied.

In the case of the investment indicators, the existence of urban areas and water-related infrastructure (e.g., dam, reservoir, irrigation, etc.) were assessed. We found that the seventeen sub-watersheds are dominated by the small cities and only the SK-05 has a medium-size city. Meanwhile, six sub-watersheds, which are SK-04, SK-06, SK-07, PB-02, TR-01, and TR-02, do not have urban areas. We also found that there is a wide disparity in the existence of the investment on the water-related infrastructure. The data shows the biggest investment, which is the biggest dam in Lampung Province, is located on the SK-07 (IDR 1000 billion). By contrast, the smallest investment (IDR 2 billion) is located on the SK-06.

Lastly, we did the health assessment for the seventeen sub-watersheds on the indictors of the land use. The land use is generally divided into two categories: the conserved and the cultivated areas. The conserved area is defined as the proportion of the vegetation-covered land to the dedicated conservation area. Meanwhile, the cultivated area is defined as the area with the slope 0 to 25%, which is considered as the area that could be cultivated. We calculated the respective areas based on satellite image analysis. We found that the biggest portion of the conserved area (75.49%) belongs to the SK-01 while other sub-watersheds have small percentages. Besides, the zero percentage might indicate that the dedicated conservation area is not available on the sub-watersheds. In the category of the cultivated area, the SK-05 has a hundred percent cultivated area implying that the whole areas have a slope less than 25%.

Table 3: The watershed health status and classification

Watershed	Sub-watershed	Code	Score	Health status	Classification
Sekampung	Sekampung 1	SK-01	111	Unhealthy	Rehabilitated
	Sekampung 4	SK-04	89.75	Healthy	Maintained
	Sekampung 5	SK-05	93.25	Healthy	Maintained
	Sekampung 6	SK-06	90	Healthy	Maintained
	Sekampung 7	SK-07	104	Unhealthy	Rehabilitated
Seputih	Seputih 1	SP-01	87.5	Healthy	Maintained
	Seputih 2	SP-02	86.25	Healthy	Maintained
	Seputih 3	SP-03	86.25	Healthy	Maintained
	Way Pengubuan 1	PB-01	88.75	Healthy	Maintained
	Way Pengubuan 2	PB-02	81.25	Healthy	Maintained
	Way Pegadungan 2	PG-02	90	Healthy	Maintained
Tulang Bawang	Tulang Bawang 1	TB-01	84.75	Healthy	Maintained
	Tulang Bawang 2	TB-02	84.75	Healthy	Maintained
	Terusan Nunyai 1	TR-01	79.75	Healthy	Maintained
	Terusan Nunyai 2	TR-02	93.5	Healthy	Maintained
Mesuji	Mesuji 3	SM-03	95.75	Healthy	Maintained
Semangka	Semangka 1	SMK-01	108.75	Unhealthy	Rehabilitated

In more detail, the assessment on the five indicators suggested by the Ministry of Forestry regulation number 60/2014 is tabulated in the Appendix A (Table A1, A2, A3, A4, and A5).

After conducting an assessment for all indicators, we compiled the scores and justify the watershed health status. If the total score exceeds one hundred, the sub-watershed health status is considered as unhealthy. Furthermore, the health status justification also implicates the watershed classification whether it should be maintained or rehabilitated. The analysis shows that most of the sub-watersheds are still in healthy condition. Only three out of seventeen sub-watersheds are considered unhealthy. In detail, the tabulation is presented in table 3.

3.3. Constructing a model for the watershed health assessment

After assessing the watershed health using the Ministry of Forestry regulation number 60/2014, we did a comparison with the US-EPA directive to validate the results and construct a model for the watershed classification. In general, the US-EPA directive defined five indicators i.e. landscape, hydrology, geomorphology, water quality, and biota observation. We used the same scoring procedure for the indicators that can be associated with the Ministry of Forestry regulation number 60/2014. For example, the landscape indicators can be associated with the vegetation coverage and the percentage of the conserved area. We also associated the hydrology indicators with the flow regime coefficient and annual flow coefficient while the geomorphology

indicators are associated with the critical land and the cultivated area. Nevertheless, the water quality and biota observation indicators are not accommodated by the Ministry of Forestry regulation number 60/2014. In this case, we did a field survey to collect the primary data if the data officially published by the authorities is not available.

To determine the water quality, we used the Water Quality Index (WQI) that considers nine parameters of water quality namely Dissolved Oxygen (DO), fecal coliform, pH, Biochemical Oxygen Demand (BOD), temperature, Nitrate, Phosphate,

turbidity, and suspended materials. We utilized the data published by the Environmental Agency of the Lampung Provincial Government. The data is based on the measurement conducted from April to November 2018. Moreover, the sub-watershed health status is justified using the US-EPA directive. In the case of biota observation, we did a field survey to observe the appearance of macroinvertebrates along the river. Then, the biota observation index is calculated to determine the level of pollution [21,22]. In detail, the sub-watershed health assessment on the water quality and biota observation is presented in table 4.

Table 4: The sub-watersheds health assessment on the water quality and biota observation indicators

Sub-watershed	Water quality index		Biota observation index	
	Score	Health status	Score	Pollution level
SK-01	55.33	Healthy	2.00	High
SK-04	58.00	Healthy	2.00	High
SK-05	56.25	Healthy	2.00	High
SK-06	55.00	Healthy	2.17	Moderate
SK-07	57.00	Healthy	2.00	High
SP-01	65.67	Healthy	2.00	High
SP-02	65.33	Healthy	2.00	High
SP-03	64.00	Healthy	2.00	High
PB-01	60.33	Healthy	2.33	Moderate
PB-02	60.67	Healthy	2.00	High
PG-02	56.33	Healthy	2.50	Moderate
TB-01	59.33	Healthy	2.10	Moderate
TB-02	66.00	Healthy	2.00	High
TR-01	55.67	Healthy	2.47	Moderate
TR-02	63.00	Healthy	2.23	Moderate
SM-03	46.00	Healthy	2.00	High
SMK-01	62.00	Healthy	2.00	High
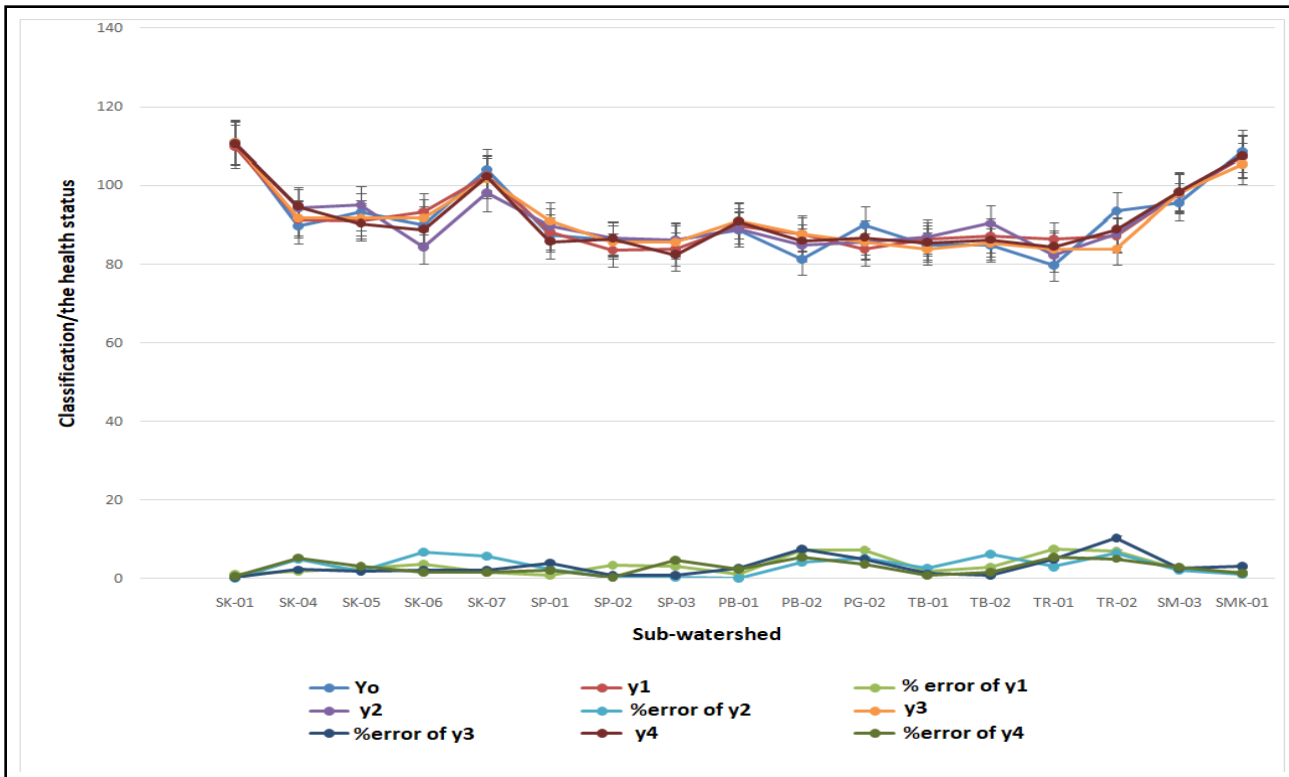
Figure 3: The validation of the models with the actual calculation

Furthermore, we used the weighing scores to develop assessment modeling. We develop four modeling scenarios. The assessment modeling aimed to identify the relationship between indicators and the most influential ones. We employed multiple linear regression, which follows equation 1, to construct those three models. To compute, we used computer software namely SPSS (Statistical Package for Social Science). The scores acted as inputs of independent variables and the watershed health is the dependent variable that is desired after the model runs. These four equations represent the result of the computation.

$$y_1 = 159.121 + 0.18VC + 0.940SL - 65.948WUI - 74.567Reg + 11.158Inv \tag{2}$$

$$y_2 = 44.973 + 0.958CL - 0.507VC + 7.140AFC + 0.953Con + 0.372Cul \tag{3}$$

$$y_3 = 154.930 + 0.224VC - 43.327WUI - 66.802Reg + 8.930Inv \tag{4}$$

$$y_4 = 50.549 + 0.774CL + 7.084AFC + 11.687Inv + 10.653BOI \tag{5}$$

The equations show that each model has different influential indicators. In the first model (the Ministry of Forestry regulation) indicates vegetation coverage, sediment load, water usage index, pro-conservation regulation, and investment of the water-related infrastructure are the influential indicators determining the watershed health status. Similarly, the third model also has the same influential indicators except for the sediment load. Meanwhile, those indicators (except vegetation coverage) do not appear in the second model (the US-EPA directive). In this model, the percentage of critical land, annual flow coefficient, conserver area, and cultivated land are influential. Eventually, the fourth equation resulted in different influential indicators compared to

the first three. In this model, the percentage of the critical land, annual flow coefficient, investment, and biota observation index play the most essential roles.

To validate the models, we calculated the error percentage of each equation referring to the scoring and health status justification (table 3). The result is presented in figure 3. Figure 3 shows an insignificant difference between the result gained from the calculation and modeling. In general, iteration resulted in the margin of error around six percent or less except the TR-02 and the PB-02 in the third model (y_3). In this model, the margin of error respectively reaches 10.33% and 7.46%. The data insufficiency could probably be a major cause of this occurrence. Currently, the government agencies that involve watershed management have not recorded data required for the modeling. On the other hand, the primary data collected from the field survey did not suffice the requirement of the software iteration. Beyond this limitation, we have spent efforts to simplify the model using the available data.

4. Discussion

The main objective of watershed management is to maintain a healthy ecosystem. However, prioritization has to be taken due to various limitations. The watershed health assessment is one of the procedures to reveal the most urgent elements that require immediate measures. Indeed, the priority of watershed management is context-dependent and different from one entity to another. Therefore, a certain measure cannot be uniformly implemented for all regions. This research identified the health status of five watersheds, which are broken down into seventeen sub-watersheds, in Lampung Province, Indonesia. We mainly used the directive that is officially stated by the authority and added indicators that have not been accommodated by the current

directive. The mathematical models that resulted in this study can be utilized as a predictive tool for decision-makers to formulate the watershed management planning and required actions for necessary rehabilitation.

This study revealed that 3 sub-watersheds should be rehabilitated to increase their current carrying capacity. The sub-watersheds are Sekampung 1, Sekampung 7, and Semangka 1. This result implies an alarming situation regarding the sustainability of the sub-watersheds in supporting human activities. Meanwhile, the 14 sub-watersheds can be classified as the areas that should be maintained. It does not mean the sub-watersheds can be exploited without a proper management plan. Subsequently, the influential indicators resulted from mathematical modeling can be viewed as essential elements that contribute significantly to watershed health. Besides, it can be an input to set a prioritization strategy.

Furthermore, a watershed can also be seen as an entity requiring comprehensive and integrated planning to ensure sustainable resource utilization. To realize the comprehensive and integrated approach, a watershed is supposed to be considered as an inseparable entity involving various stakeholders and interests that sometimes cross over administrative borders. Therefore, the watershed management cannot be conducted partially for a certain sector or territory and institutional arrangement is highly required.

5. Conclusion

There are some conclusions can be highlighted from this study. First, three out of seventeen assessed sub-watersheds in Lampung Province, Indonesia can be categorized as unhealthy watershed based on the Ministry of Forestry regulation number 60/2014. This regulation suggested that the unhealthy watershed to be revitalized. Second, from the assessment using the US-EPA directive, the watershed health status of each assessed sub-watershed varies in accordance with the indicator. For instance, all sub-watersheds have healthy status from the water quality index indicator, but their biota observation index shows various pollution levels ranging from moderate to high. Third, the mathematical model of the watershed health assessment in this research can be utilized as a predictive tool to indicate the health status of the watersheds in the case study area. To compare with the assessment using the Ministry of Forestry regulation number 60/2014, the suggested equations have significant accuracy.

Conflict of Interest

The authors declare no conflict of interest.

Acknowledgment

References

[1] C. Asdak, Hidrologi dan Pengelolaan Daerah Aliran Sungai, 5th ed., Gadjah Mada University Press, Yogyakarta, 2010.

[2] S.R. Ahn, S.J. Kim, "Assessment of watershed health, vulnerability and resilience for determining protection and restoration Priorities," Environmental Modelling and Software, **122**, 103926, 2019, doi:10.1016/j.envsoft.2017.03.014.

[3] A. Hu, X. Yang, N. Chen, L. Hou, Y. Ma, C.P. Yu, "Response of bacterial communities to environmental changes in a mesoscale subtropical watershed, Southeast China," Science of the Total Environment, **472**, 746–756, 2014, doi:10.1016/j.scitotenv.2013.11.097.

[4] G.M. Sanchez, A.P. Nejadhashemi, Z. Zhang, S. Marquart-Pyatt, G. Habron, A. Shortridge, "Linking watershed-scale stream health and socioeconomic indicators with spatial clustering and structural equation modeling," Environmental Modelling and Software, **70**, 113–127, 2015, doi:10.1016/j.envsoft.2015.04.012.

[5] J. Huang, V. Klemas, "Using Remote Sensing of Land Cover Change in Coastal Watersheds to Predict Downstream Water Quality," Journal of Coastal Research, **28**(4), 930–944, 2012, doi:10.2112/JCOASTRES-D-11-00176.1.

[6] Z. Xing, Y. Wang, Y. Ji, Q. Fu, H. Li, R. Qu, "Health assessment and spatial variability analysis of the Naolihe Basin using a water-based system," Ecological Indicators, **92**(January 2017), 181–188, 2018, doi:10.1016/j.ecolind.2017.08.045.

[7] www.colorado.gov, Colorado's Water Plan, 2017.

[8] M. Bunch, K. Morrison, M. Parkes, H. Venema, "Promoting health and well-being by managing for social-ecological resilience: the potential of integrating ecohealth and water resources management approaches," Ecology and Society, **16**(1), 2011.

[9] F. Berkes, "Understanding uncertainty and reducing vulnerability: Lessons from resilience thinking," Natural Hazards, **41**(2), 283–295, 2007, doi:10.1007/s11069-006-9036-7.

[10] F. Berkes, C. Folke, J. Colding, Linking Social and Ecological Systems: Management practices and social mechanisms for building resilience, Cambridge University Press, Cambridge, 2000.

[11] The Lake Simcoe Region Conservation Authority, State of the Watershed Report: East Holland River Subwatershed, Ontario, 2000.

[12] Tigum Aganan Watershed Management Board, Canadian Urban Institute, Handbook for Preparing State of Watershed Reports in the Philippines, 2013.

[13] www.mrcmekong.org, 604CS Tools Community Based Watershed North Tha, 1–7, 2016.

[14] Australia-China Development Partnership, River health assessment framework, including monitoring, assessment, and application, 2010.

[15] The U.S. Environmental Protection Agency, Identifying and protecting Healthy Watershed: Concepts, Assessment, and Management Approaches, 2012.

[16] S.H. Sadeghi, Z. Hazbavi, "Spatiotemporal variation of watershed health propensity through reliability-resilience-vulnerability based drought index (case study: Shazand Watershed in Iran)," Science of the Total Environment, **587–588**, 168–176, 2017, doi:10.1016/j.scitotenv.2017.02.098.

[17] Kemeneterian Kehutanan Republik Indonesia, Peraturan Menteri Kehutanan Republik Indonesia Nomor: P.61/Menhut-II/2014 tentang Monitoring dan Evaluasi Pengelolaan Daerah Aliran Sungai, 2014.

[18] V.H. Resh, J.D. Unzicker, "Water quality monitoring and aquatic organisms: the importance of species identification," Journal of the Water Pollution Control Federation, **47**(1), 9–19, 1975.

[19] C.J. Kleynhans, "The development of a fish index to assess the biological integrity of South African rivers," Water SA, **25**(3), 265–278, 1999.

[20] D. Copetti, K. Finsterle, L. Marziali, F. Stefani, G. Tartari, G. Douglas, K. Reitzel, B.M. Spears, I.J. Winfield, G. Crosa, P. D'Haese, S. Yasseri, M. Lürling, "Eutrophication management in surface waters using lanthanum modified bentonite: A review," Water Research, **97**, 162–174, 2015, doi:10.1016/j.watres.2015.11.056.

[21] M.R. Herman, A.P. Nejadhashemi, "A review of macroinvertebrate- and fish-based stream health indices," Ecohydrology and Hydrobiology, **15**(2), 53–67, 2015, doi:10.1016/j.ecohyd.2015.04.001.

[22] S. Li, J. Zhang, E. Guo, F. Zhang, Q. Ma, G. Mu, "Dynamics and ecological risk assessment of chromophoric dissolved organic matter in the Yinma River Watershed: Rivers, reservoirs, and urban waters," Environmental Research, **158**, 245–254, 2017.

Appendix A

Table A1: The sub-watersheds health assessment on the land condition indicators

| Sub-watershed | The indicators of the land conditions | | | | | |
| | Critical land | | Vegetation coverage | | Erosion index | |
	%	score	%	score	%	score
SK-01	28.620	1.50	89.838	0.50	1.20	1.00
SK-04	1.229	0.50	2.444	1.50	1.20	1.00
SK-05	0.456	0.50	0.102	1.50	1.20	1.00
SK-06	4.659	0.50	13.192	1.50	1.20	1.00
SK-07	6.320	0.75	2.605	1.50	1.20	1.00
SP-01	8.982	0.75	25.871	1.25	0.58	0.75
SP-02	0.411	0.50	0.005	1.50	0.58	0.75
SP-03	0.000	0.50	1.620	1.50	0.58	0.75
PB-01	5.308	0.75	18.532	1.50	0.58	0.75
PB-02	4.368	0.50	6.858	1.50	0.58	0.75
PG-02	0.000	0.50	1.067	1.50	0.58	0.75
TB-01	0.010	0.50	3.893	1.50	0.60	0.75
TB-02	9.985	0.75	8.339	1.50	0.60	0.75
TR-01	0.154	0.50	3.377	1.50	0.60	0.75
TR-02	5.312	0.75	8.439	1.50	0.60	0.75
SM-03	22.309	1.50	18.147	1.50	0.40	0.50
SMK-01	33.600	1.50	19.554	1.50	0.32	0.50

Table A2: The sub-watersheds health assessment on the water quality, quantity, and continuity indicators

| Sub water-shed | The indicators of the water quality, quantity, and continuity | | | | | | | | | |
| | Flow regime coefficient (FRC) | | Annual flow coefficient (AFC) | | Sediment load (SL) | | Annual Flood events | | Water usage index (WUI) | |
	FRC	score	AFC	score	SL	score	AF	score	WUI	Score
SK-01	13.883	1.00	0.706	1.50	17.31	1.25	1	1.25	0.80	1.25
SK-04	4.685	0.50	0.811	1.50	17.31	1.25	1	1.25	0.80	1.25
SK-05	7.114	0.75	0.924	1.50	17.31	1.25	0	0.50	0.80	1.25
SK-06	8.936	0.75	0.791	1.50	17.31	1.25	0	0.50	0.80	1.25
SK-07	5.411	0.75	0.547	1.50	17.31	1.25	2	1.50	0.80	1.25
SP-01	5.074	0.75	0.242	0.75	12.30	1.00	0	0.75	0.56	1.00
SP-02	5.409	0.75	0.861	1.50	12.30	1.00	0	0.75	0.56	1.00
SP-03	7.763	0.75	0.653	1.50	12.30	1.00	0	0.75	0.56	1.00
PB-01	11.047	1.00	0.372	1.00	12.30	1.00	0	0.75	0.56	1.00
PB-02	8.600	0.75	0.257	0.75	12.30	1.00	0	0.75	0.56	1.00
PG-02	12.086	1.00	0.526	1.50	12.30	1.00	0	0.75	0.56	1.00
TB-01	9.393	0.75	0.940	1.50	17.40	1.25	1	1.25	0.60	1.00
TB-02	9.600	0.75	0.094	0.50	17.40	1.25	0	0.75	0.60	1.00
TR-01	7.591	0.75	0.214	0.75	17.40	1.25	0	0.75	0.60	1.00
TR-02	19.089	1.25	0.638	1.50	17.40	1.25	0	0.75	0.60	1.00
SM-03	8.570	0.75	0.491	1.25	3.80	0.50	0	0.75	0.27	0.75
SMK-01	6.056	0.75	0.537	1.50	13.56	1.00	1	1.25	0.27	0.75

Table A3: The sub-watersheds health assessment on the socioeconomics and institutions indicators

| Sub-watershed | The indicators of the socioeconomics and institutions | | | | | |
| | Land Availability Index | | Population Welfare | | Pro-conservation regulations | |
	LAI	score	%	score	Availability	score

SK-01	0.272	1.50	12.94	1.00	Available, widely applied	0.50
SK-04	2.067	0.75	19.19	1.00	Available, widely applied	0.50
SK-05	1.453	1.00	10.64	1.00	Available, widely applied	0.50
SK-06	2.167	0.75	20.21	1.25	Available, widely applied	0.50
SK-07	1.095	1.00	14.37	1.00	Available, widely applied	0.50
SP-01	2.379	0.75	12.90	1.00	Available, partly applied	0.75
SP-02	4.133	0.50	12.62	1.00	Available, partly applied	0.75
SP-03	2.583	0.75	11.80	1.00	Available, partly applied	0.75
PB-01	6.715	0.50	11.91	1.00	Available, partly applied	0.75
PB-02	2.884	0.75	15.32	1.00	Available, partly applied	0.75
PG-02	1.340	1.00	16.35	1.00	Available, partly applied	0.75
TB-01	8.988	0.50	13.52	1.00	Available, partly applied	0.75
TB-02	9.946	0.50	15.28	1.00	Available, partly applied	0.75
TR-01	6.079	0.50	13.85	1.00	Available, partly applied	0.75
TR-02	3.638	0.75	13.33	1.00	Available, partly applied	0.75
SM-03	8.806	0.50	13.30	1.00	Available, partly applied	0.75
SMK-01	1.555	1.00	19.01	1.00	Available, partly applied	0.75

Table A4: The sub-watersheds health assessment on the investment indicators

| Sub-watershed | The indicators of the investment | | | |
| | The existence of the urban area | | Investment of the water building | |
	The urban characteristics	score	Investment (billion Rupiahs)	score
SK-01	Small city	0.75	24	0.75
SK-04	No urban area	0.50	12	0.50
SK-05	Medium size city	1.00	10	0.50
SK-06	No urban area	0.50	2	0.50
SK-07	No urban area	0.50	1000	1.50
SP-01	Small city	0.75	10	0.50
SP-02	Small city	0.75	10	0.50
SP-03	Small city	0.75	10	0.50
PB-01	Small city	0.75	20	0.75
PB-02	No urban area	0.50	20	0.75
PG-02	Small city	0.75	10	0.50
TB-01	Small city	0.75	12	0.50
TB-02	Small city	0.75	12	0.50
TR-01	No urban area	0.50	12	0.50
TR-02	No urban area	0.50	12	0.50
SM-03	Small city	0.75	10	0.50
SMK-01	Small city	0.75	10	0.50

Table A5: The sub-watersheds health assessment on the land use indicators

| Sub-watershed | The indicators of the land use | | | |
| | Conserved area | | Cultivated area | |
	%	score	%	score
SK-01	75.49	0..50	11.342	1.50
SK-04	0.00	1.50	89.066	0.50
SK-05	0.00	1.50	100.000	0.50
SK-06	1.02	1.50	93.411	0.50

SK-07	5.39	1.50	94.627	0.50
SP-01	24.59	1.25	66.305	0.75
SP-02	0.00	1.50	87.924	0.50
SP-03	0.00	1.50	0.000	0.50
PB-01	14.29	1.50	85.581	0.50
PB-02	0.00	1.50	0.000	0.50
PG-02	0.00	1.50	0.000	0.50
TB-01	0.00	1.50	0.000	0.50
TB-02	7.12	1.50	87.476	0.50
TR-01	0.00	1.50	0.000	0.50
TR-02	0.00	1.50	0.000	0.50
SM-03	0.00	1.50	0.000	0.50
SMK-01	33.11	1.00	13.168	1.50

ASTES

Some Results on Fixed Points Related to $\varphi - \psi$ Functions in JS – Generalized Metric Spaces

Eriola Sila[*,1], Sidita Duraj[2], Elida Hoxha[1]

[1]*Department of Mathematics, Faculty of Natural Science, University of Tirana, Tirana, 1054, Albania*

[2]*Department of Mathematics, Faculty of Natural Science, University "Luigj Gurakuqi", Shkoder, 4000, Albania*

A R T I C L E I N F O	A B S T R A C T
	In this paper are shown some new results on fixed point related to a $\varphi - \psi$ contractive map in JS – generalized metric spaces X. It proves that there exists a unique fixed point for a nonlinear map $f: X \rightarrow X$, using two altering distance functions. Furthermore, it gives some results which related to a couple of functions under some conditions in JS – generalized metric spaces. It provides a theorem where is shown that two maps $F, g: X \rightarrow X$ under a nonlinear contraction using ultra – altering distance functions ψ and φ, which are lower semi – continuous and continuous, respectively, have a coincidence point that is unique in X. In addition, there is proved if the maps F and g are weakly compatible then they have a fixed point which is unique in JS – generalized metric space. As applications, every theorem is illustrated by an example. The obtained theorems and corollaries extend some important results which are given in the references.

1. Introduction

The study of fixed point in metric space has an important role in Functional Analysis. It is developed in two directions during the years which are the improving contraction conditions and changing axioms of metric space with the intention to generalize fixed points results in this space. As a result, there are given many new spaces such as generalized metric space [1], cone metric space [2], rectangular metric space [3].

In [4], authors introduced the concept of JS – metric space. It generalizes well-known concepts of metric structures like metric spaces, b – metric spaces [5], metric - like spaces [6], etc. There are many articles which are worked on these spaces, like [7]-[10].

In [11], authors expanded the Banach contraction introducing the concept of weakly contractive function in Hilbert spaces.

Many authors have used these functions in many other spaces like [12]-[14].

In [15], authors provided some theorems related to fixed points of mappings in generalized metric spaces introducing the concept of altering distance functions.

In [16], authors generalized some theorems on fixed point for contractive functions of type Kannnan, Chatteria and Hardy – Rogers in generalized metric space.

This paper generalizes some important results on fixed point for weakly contractive functions and functions with altering distance between points, giving some new theorems on fixed point for $\varphi - \psi$ contractive functions in JS – generalized metric spaces.

Furthermore, it proves a theorem on common fixed points of two $\varphi - \psi$ contractive functions on JS – generalized metric spaces.

2. Preliminaries

Let X be a set which is not empty and D_{JS} be a non - negative function of cartesian product $X \times X$.

For each $\vartheta \in X$, let define the set

$$C(D_{JS}, X, \vartheta) = \{\{x_n\} \subset X: \lim_{n\to\infty} D_{JS}(x_n, \vartheta) = 0\}$$

Definition 2.1 [4] The map D_{JS} that satisfies the conditions:

(D_{JS_1}) $D_{JS}(x, \tilde{x}) = 0$ yields $x = \tilde{x}$

*Corresponding Author: Eriola Sila, Roliaerjola.liftaj@fshn.edu.al

(D_{JS_2}) $D_{JS}(x, \tilde{x}) = D_{JS}(\tilde{x}, x)$

(D_{JS_3}) There exists a constant $\rho > 0$, such that for $x_n \in C(D_{JS}, X, \vartheta)$, it yields

$$D_{JS}(x, \tilde{x}) \leq \rho \lim_{n \to +\infty} D_{JS}(x_n, \tilde{x})$$

for all $(x, \tilde{x}) \in X \times X$, is called JS – generalized metric.

The couple (X, D_{JS}) is called s JS – generalized metric pace.

In [4], authors showed that JS – generalized metric space are metric space, b – metric space, dislocated metric space, etc.

Remark 2.2 [4] As it can be seen in JS – generalized metric space, the map $D_{JS}(\tilde{x}, \tilde{x})$ maybe not zero.

Remark 2.3 [4] When the set $C(D_{JS}, X, \vartheta)$ does not contain any element for all $\vartheta \in X$, the couple (X, D_{JS}) is JS – generalized metric space satisfying only (D_{JS1}) and (D_{JS2}).

Definition 2.4 [16] Let (X, D_{JS}) be a JS – generalized metric space and $\{x_n\}_{n \in N}$ is in X and $\vartheta \in X$. If $\{x_n\}_{n \in N}$ is in $C(D_{JS}, X, \vartheta)$, it is called D_{JS} – convergent to $\vartheta \in X$.

Remark 2.5 [16] If a constant sequence is D_{JS} – convergent to $c \in X$ then $D_{JS}(c, c) = 0$.

Proposition 2.6 [16] A necessary and sufficient condition that the set $C(D_{JS}, X, \vartheta)$ is not empty is that $D_{JS}(\vartheta, \vartheta) = 0$

Proposition 2.7 [4] Let the pair (X, D_{JS}) be a JS - metric generalized space and $\{x_n\}_{n \in N}$ in X and $\vartheta, \bar{\vartheta} \in X$. If $\{x_n\}_{n \in N}$ is D_{JS} – convergent to ϑ and $\bar{\vartheta}$ then $\vartheta = \bar{\vartheta}$.

Definition 2.8 [16] The sequence $\{x_n\}_{n \in N}$ in a JS – generalized metric space (X, D_{JS}) is called D_{JS} – Cauchy if $D_{JS}(x_n, x_m)$ converges to 0 when m, n tent to $+\infty$.

Definition 2.9 [16] A JS – generalized metric space (X, D_{JS}) is named D_{JS}– complete if each D_{JS} – Cauchy sequence in X is D_{JS} – convergent in X.

Example 2.10 Take $X = [0, c]$ where $c \in R$ and D_{JS} be a non - negative function of cartesian product $X \times X$, where

$$D_{JS}(x, \tilde{x}) = \begin{cases} \max\{x, \tilde{x}\}, & (x, \tilde{x}) \neq (0,0) \\ \dfrac{x}{2}, & (x, 0) \\ \dfrac{\tilde{x}}{2}, & (0, \tilde{x}) \end{cases}$$

Since the map D_{JS} accomplishes (D_{JS_1}) and (D_{JS_2}) in trivially manner, it is a JS – generalized metric.

Consequently, it needs to verify that (D_{JS_3}) is satisfied only for $x \in X$ that $D_{JS}(x, x) = 0$. But $D_{JS}(x, x) = 0$ implies $x = 0$.

If $(x_n)_{n \in N} \subset X$ converges to 0 then $\lim_{n \to +\infty} D_{JS}(x_n, 0) = 0$.

Taking $n \in N$ and $\tilde{x} \in X$,

$$D_{JS}(x_n, \tilde{x}) = \begin{cases} \max\{x_n, \tilde{x}\}, & for\ x_n \neq 0 \\ \dfrac{\tilde{x}}{2}, & for\ x_n = 0 \end{cases}.$$

As a result, the inequality $\dfrac{\tilde{x}}{2} < D_{JS}(x_n, \tilde{x})$ is true.

From this, it yields $D_{JS}(0, \tilde{x}) = \dfrac{\tilde{x}}{2} < \lim_{n \to +\infty} \sup D_{JS}(x_n, \tilde{x})$.

So, (X, D_{JS}) is JS – generalized metric. However, it is not neither metric space nor dislocated metric space because it doesn't accomplish the third condition of their metric, for $x, \tilde{x} \in X - \{0\}$ and $x^* = 0$, because

$$D_{JS}(x, 0) + D_{JS}(0, \tilde{x}) = \frac{x}{2} + \frac{\tilde{x}}{2} < \max\{x, \tilde{x}\} = D_{JS}(x, \tilde{x}).$$

Definition 2.11 [15] The function $\psi: R^+ \to R^+$ that satisfies the conditions:

1. ψ is non-decreasing and continuous
2. $\psi(s) = 0$ if and only if $s = 0$.
3. $\psi(s) \geq Ms^\mu$, for every $s > 0$ where $M > 0, \mu > 0$ are constants

is called altering distance.

Definition 2.12 [15] A function $\psi: R^+ \to R^+$ that accomplishes the conditions:

1. ψ is non – decreasing
2. $\psi(s) > 0$ if $s > 0$ and $\psi(0) = 0$

is called ultra – altering distance.
The set of ultra-altering distances is denoted Ψ.

Let g, F two functions of X in itself.

Definition 2.13 [17] The point $\xi \in X$ which completes the equality $g(\xi) = F(\xi)$ is called coincidence point of g, F.

Definition 2.14 [18] The functions g, F that satisfy $gF\xi = Fg\xi$, for each ξ that is coincidence point of g and F, are called weakly compatible.

Definition 2.15 [18] The point $\xi \in X$, in which $\xi = F \xi = g \xi$, is called common fixed point of maps g, F.

Theorem 2.16 ([16], Corollary 5.5) Let f of set X in itself where (X, D_{JS}) is D_{JS} – generalized metric space which is complete and

$$D_{JS}(fx, f\tilde{x})$$

$$\leq \kappa max\{D_{JS}(x, \tilde{x}), D_{JS}(x, Tx), D_{JS}(\tilde{x}, T\tilde{x}), \frac{D_{JS}(x, f\tilde{x}) + D_{JS}(\tilde{x}, fx)}{2}\}$$

If there exists a $\varsigma \in X$ that $\delta(D_{JS}, f, \varsigma) < +\infty$, then the sequence $\{f^n \varsigma\}_{n \in N}$ D_{JS} – convergences to a point ϑ in X.

When $D_{JS}(\vartheta, f\vartheta) < +\infty$ then ϑ is fixed point of function f. Furthermore, for $\vartheta' \in X$ which is another fixed point of function f, such that $D_{JS}(\vartheta', f\vartheta') < +\infty$, it yields $\vartheta = \vartheta'$.

3. Main results

3.1. Fixed point results related to $\varphi - \psi$ contractions in JS – generalized metric spaces

Definitions 3.1.1 Define the set

$$\delta(D_{JS}, f, \varsigma) = \sup\{D_{JS}(f^l\varsigma, f^m\varsigma), l, m \geq 0\}$$

where $\varsigma \in X$.

Theorem 3.1.2 Let (X, D_{JS}) be JS – generalized metric space which is complete and $f: X \to X$ a function that satisfies the following condition:

$$\psi\left(D_{JS}(fx, f\tilde{x})\right) \leq \psi\left(M_{JS}(x, \tilde{x})\right) - \varphi(M_{JS}(x, \tilde{x})) \quad (3.1)$$

where

$$M_{JS}(x, \tilde{x}) = \text{maximum}\{D_{JS}(x, \tilde{x}), D_{JS}(x, fx), D_{JS}(\tilde{x}, f\tilde{x}),$$

$$D_{JS}(x, f\tilde{x}), D_{JS}(\tilde{x}, fx)\},$$

for every x and $\tilde{x}$ from X and φ, ψ from Ψ, where ψ is continuous and φ is lower semi – continuous.

If there exists a $\varsigma \in X$ that $\delta(D_{JS}, f, \varsigma) < +\infty$, then the sequence $\{f^n\varsigma\}_{n \in N}$ D_{JS} – convergences to a point ϑ in X.

When $D_{JS}(\vartheta, f\vartheta) < +\infty$ then ϑ is fixed point of function f. Furthermore, for $\vartheta' \in X$ which is another fixed point of function f, such that $D_{JS}(\vartheta', f\vartheta') < +\infty$, it yields $\vartheta = \vartheta'$.

Proof. Let take $\varsigma \in X$ that $\delta(D_{JS}, f, \varsigma) < +\infty$. Applicating (3.1) for $i, j, n \in N$, it yields

$$\psi\left(D_{JS}(f^{n+i}\varsigma, f^{n+j}\varsigma)\right)$$

$$\leq \psi\left(M_{JS}(f^{n+i-1}\varsigma, f^{n+j-1}\varsigma)\right) - \varphi\left(M_{JS}(f^{n+i-1}\varsigma, f^{n+j-1}\varsigma)\right)$$

$$\leq \psi\left(M_{JS}(f^{n+i-1}\varsigma, f^{n+j-1}\varsigma)\right) \quad (3.2)$$

$$M_{JS}(f^{n+i-1}\varsigma, f^{n+j-1}\varsigma)$$

$$= \text{maximum}\begin{cases} D_{JS}(f^{n+i-1}\varsigma, f^{n+j-1}\varsigma), D_{JS}(f^{n+i-1}\varsigma, f^{n+i}\varsigma), \\ D_{JS}(f^{n+j-1}\varsigma, f^{n+j}\varsigma), D_{JS}(f^{n+i-1}\varsigma, f^{n+j}\varsigma), \\ D_{JS}(f^{n+j-1}\varsigma, f^{n+i}\varsigma) \end{cases}$$

$$\leq \delta(D_{JS}, f, f^{n-1}\varsigma)$$

Consequently,

$$\psi\left(D_{JS}(f^{n+i}\varsigma, f^{n+j}\varsigma)\right) \leq \psi\left(M_{JS}(f^{n+i-1}\varsigma, f^{n+j-1}\varsigma)\right) \leq \psi\left(\delta(D_{JS}, f, f^{n-1}\varsigma)\right).$$

Using the non-decreasing monotony of ψ it results

$$D_{JS}(f^{n+i}\varsigma, f^{n+j}\varsigma) \leq M_{JS}(f^{n+i-1}\varsigma, f^{n+j-1}\varsigma) \leq \delta(D_{JS}, f, f^{n-1}\varsigma) \quad (3.3)$$

for every $i, j \in N, n \in N$.

$$\delta(D_{JS}, f, f^n\varsigma) = \sup\{D_{JS}(f^{n+i}\varsigma, f^{n+j}\varsigma), i, j \in N\}$$
$$\leq \delta(D_{JS}, f, f^{n-1}\varsigma).$$

As a result, the sequence $\{\delta(D_{JS}, f, f^n\varsigma)\}_{n \in N}$ is non – increasing and bounded.

Consequently, it D_{JS} – converges and $\lim_{n \to +\infty} \delta(D_{JS}, f, f^n\varsigma) = l \geq 0$.

In addition, from (3.3) the following inequality

$$\delta(D_{JS}, f, f^n\varsigma) \leq M_{JS}(f^{n+i-1}\varsigma, f^{n+j-1}\varsigma)$$

$$\leq \delta(D_{JS}, f, f^{n-1}\varsigma) \quad (3.4)$$

Taking the limit in (3.4) when $n \to +\infty$ and $i, j \in N$, it yields

$$\lim_{n \to +\infty} M_{JS}(f^{n+i-1}\varsigma, f^{n+j-1}\varsigma) = l \geq 0.$$

Furthermore, from

$$\delta(D_{JS}, f, f^n\varsigma) = \sup\{D_{JS}(f^{n+i}\varsigma, f^{n+j}\varsigma), i, j \in N\},$$

it implies:

for each natural number k, there exist $i(k)$ and $j(k)$ that the inequality

$$l - \frac{1}{k} < D_{JS}(f^{n+i(k)}\varsigma, f^{n+j(k)}\varsigma) \leq l \quad (3.5)$$

holds.

Taking the limit in (3.5) when $k \to +\infty$, it yields

$$\lim_{n \to \infty} D_{JS}(f^{n+i(k)}\varsigma, f^{n+j(k)}\varsigma) = l.$$

Furthermore, since φ is lower semi – continuous and ψ is continuous, taking the limit in

$$\psi\left(D_{JS}(f^{n+i(k)}\varsigma, f^{n+j(k)}\varsigma)\right)$$

$$\leq \psi\left(M_{JS}(f^{n+i(k)-1}\varsigma, f^{n+j(k)-1}\varsigma)\right)$$
$$- \varphi\left(M_{JS}(f^{n+i(k)-1}\varsigma, f^{n+j(k)-1}\varsigma)\right)$$

it implies $\psi(l) \leq \psi(l) - \varphi(l)$.

Consequently, $\varphi(l) = 0$. Since φ is in Ψ, it implies $l = 0$.

So

$$\lim_{n \to +\infty} \delta(D_{JS}, f, f^n\varsigma) = 0 \quad (3.6)$$

Since $\delta(D_{JS}, f, f^n \varsigma) = \sup\{D_{JS}(f^{n+i}\varsigma, f^{n+j}\varsigma), i, j \in N\}$, it is true that

$$0 \leq D_{JS}(f^{n+i}\varsigma, f^{n+j}\varsigma) \leq \delta(D_{JS}, f, f^n \varsigma),$$

for every $i, j \in N$.

Taking the limit when $i, j \to +\infty$, it implies

$$\lim_{i,j \to +\infty} D_{JS}(f^{n+i}\varsigma, f^{n+j}\varsigma) = 0 \qquad (3.7)$$

Since the sequence $\{f^n \varsigma\}_{n \in N}$ is $D_{JS} -$ Cauchy, there exists a point $\vartheta \in X$, that accomplishes:

$$\lim_{n \to +\infty} D_{JS}(f^n \varsigma, \vartheta) = 0 \qquad (3.8)$$

Let prove now that $f(\vartheta) = \vartheta$.

$$D_{JS}(f\vartheta, \vartheta) \leq \rho \lim_{n \to +\infty} D_{JS}(f\vartheta, f^{n+1}\varsigma)$$

Taking (3.1) for $x = \vartheta$ and $\tilde{x} = f^n \varsigma$, it implies

$$\psi(D_{JS}(f\vartheta, f^{n+1}\varsigma)) \leq \psi(M_{JS}(\vartheta, f^n\varsigma)) - \varphi\left(M_{JS}(\vartheta, f^n\varsigma)\right) \qquad (3.9)$$

where

$$M_{JS}(\vartheta, f^n\varsigma)$$
$$= \text{maximum}\{D_{JS}(\vartheta, f^n\varsigma), D_{JS}(\vartheta, f\vartheta), D_{JS}(f^n\varsigma, f^{n+1}\varsigma),$$
$$D_{JS}(\vartheta, f^{n+1}\varsigma), D_{JS}(f^n\varsigma, f\vartheta)\}$$

Taking limit in $M_{JS}(\vartheta, f^n\varsigma)$ when $n \to +\infty$ and from (3.7) and (3.8), it yields

$$\lim_{n \to +\infty} M_{JS}(\vartheta, f^n\varsigma) = \text{maximum}\{0, D_{JS}(\vartheta, f\vartheta), 0, 0, D_{JS}(\vartheta, f\vartheta)\}$$
$$= D_{JS}(\vartheta, f\vartheta)$$

Taking limit in (3.9) it implies

$$\psi(D_{JS}(f\vartheta, \vartheta)) \leq \psi(D_{JS}(\vartheta, f\vartheta)) - \varphi\left(D_{JS}(\vartheta, f\vartheta)\right)$$

Consequently $\varphi\left(D_{JS}(\vartheta, f\vartheta)\right) = 0$ and

$$D_{JS}(\vartheta, f\vartheta) = 0 \qquad (3.10)$$

From this, it yields $f\vartheta = \vartheta$.

If ϑ' is another point that $f\vartheta' = \vartheta'$ and $D_{JS}(\vartheta', \vartheta')$ is finite, then $D_{JS}(\vartheta', \vartheta') = 0$.

Indeed, applicating (3.1) for x and $\tilde{x}$ equal to ϑ', it yields
$$\psi(D_{JS}(\vartheta', \vartheta')) = \psi(D_{JS}(f\vartheta', f\vartheta'))$$

$$\leq \psi(M_{JS}(\vartheta', \vartheta')) - \varphi\left(M_{JS}(\vartheta', \vartheta')\right)$$

where

$$M_{JS}(\vartheta', \vartheta')$$
$$= \text{maximum}\{D_{JS}(\vartheta', \vartheta'), D_{JS}(\vartheta', f\vartheta'), D_{JS}(\vartheta', f\vartheta'),$$

$$D_{JS}(\vartheta', f\vartheta'), D_{JS}(\vartheta', f\vartheta')\} = D_{JS}(\vartheta', \vartheta')$$

As a result $\psi(D_{JS}(\vartheta', \vartheta')) \leq \psi(D_{JS}(\vartheta', \vartheta')) - \varphi\left(D_{JS}(\vartheta', \vartheta')\right)$,

which implies $\varphi\left(D_{JS}(\vartheta', \vartheta')\right) = 0$ and $D_{JS}(\vartheta', \vartheta') = 0$.

Furthermore, $D_{JS}(\vartheta, \vartheta) = 0$, because $f(\vartheta) = \vartheta$.

Due to the fact $D_{JS}(\vartheta, \vartheta') = D_{JS}(f\vartheta, f\vartheta')$, it yields

$$\psi(D_{JS}(f\vartheta, f\vartheta')) \leq \psi(M_{JS}(\vartheta, \vartheta')) - \varphi\left(M_{JS}(\vartheta, \vartheta')\right) \qquad (3.11)$$

where

$$M_{JS}(\vartheta, \vartheta') = \text{maximum}\{D_{JS}(\vartheta, \vartheta'), D_{JS}(\vartheta, f\vartheta), D_{JS}(\vartheta', f\vartheta'),$$

$$D_{JS}(\vartheta, f\vartheta'), D_{JS}(\vartheta', f\vartheta)\}$$
$$= \text{maximum}\{D_{JS}(\vartheta, \vartheta'), 0, 0, D_{JS}(\vartheta, \vartheta'), D_{JS}(\vartheta', \vartheta)\}$$
$$= D_{JS}(\vartheta, \vartheta')$$

From (3.11), it implies

$$\psi(D_{JS}(\vartheta, \vartheta')) \leq \psi(D_{JS}(\vartheta, \vartheta')) - \varphi\left(D_{JS}(\vartheta, \vartheta')\right).$$

As a result $\varphi\left(D_{JS}(\vartheta, \vartheta')\right) = 0$ and $D_{JS}(\vartheta, \vartheta') = 0$ and $\vartheta = \vartheta'$.

Remark 3.1.3 Theorem 3.1.2 generalizes Theorem 2.18 (Theorem 1.9) in [19].

Example 3.1.4 Let be $X = [0,1]$ and a non $-$ negative D_{JS} of $X \times X$, where

$$D_{JS}(x, y) = \begin{cases} \text{maximum } \{x, \tilde{x}\}, & x \neq 0, \tilde{x} \neq 0 \\ \frac{x}{2}, & x \in X, \tilde{x} = 0 \\ \frac{\tilde{x}}{2}, & x = 0, \tilde{x} \in X \end{cases}$$

(X, D_{JS}) is a $JS -$ generalized metric space as it is shown in Example 2.10.

Let $f: X \to X$ be a map such that $f(x) = \frac{x^2}{2(1+x)}$ and the functions $\varphi, \psi \in \Psi$, $\varphi(s) = \frac{s}{2}$, $\psi(t) = \frac{3s}{2}$.

For $x \neq \tilde{x}$ and $x \neq 0, \tilde{x} \neq 0$

$$D_{JS}(f(x), f(\tilde{x})) = \text{maximum}\left\{\frac{x^2}{2(1+x)}, \frac{\tilde{x}^2}{2(1+\tilde{x})}\right\}.$$

Taking $x < \tilde{x}$, $D_{JS}(f(x), f(\tilde{x})) = \frac{\tilde{x}^2}{2(1+\tilde{x})}$

$$M_{JS}(x, \tilde{x}) = \text{maximum}\{D_{JS}(x, \tilde{x}), D_{JS}(x, fx), D_{JS}(\tilde{x}, f\tilde{x}),$$

$$D_{JS}(x, f\tilde{x}), D_{JS}(\tilde{x}, fx)\},$$

$$D_{JS}(x, \tilde{x}) = \text{maximum}\{x, \tilde{x}\} = \tilde{x}, D_{JS}(x, f(x))$$

$$= \text{maximum}\left\{x, \frac{x^2}{2(1+x)}\right\} = x,$$

$$D(\tilde{x}, f(\tilde{x})) = D\left(\tilde{x}, \frac{\tilde{x}^2}{2(1+\tilde{x})}\right) = \tilde{x},$$

$$D_{JS}(x, f(\tilde{x})) = \text{maximum}\left\{x, \frac{\tilde{x}^2}{2(1+\tilde{x})}\right\} = \begin{cases} \frac{\tilde{x}^2}{2(1+\tilde{x})}, \\ x \end{cases}$$

$$D_{JS}(f(x), \tilde{x}) = \text{maximum}\left\{\tilde{x}, \frac{1}{2}\frac{x^2}{(1+x)}\right\} = \tilde{x}.$$

Case 1. If $D_{JS}(f(\tilde{x}), x) = \frac{1}{2}\frac{\tilde{x}^2}{(1+\tilde{x})}$, then

$$M_{JS}(x, \tilde{x}) = \text{maximum}\left\{\tilde{x}, x, \frac{1}{2}\frac{\tilde{x}^2}{(1+\tilde{x})}\right\}$$

$$= \text{maximum}\left\{\tilde{x}, \frac{1}{2}\frac{\tilde{x}^2}{(1+\tilde{x})}\right\} = \tilde{x}$$

$$\psi(D_{JS}(f(x), f(\tilde{x}))) = \psi\left(\frac{\tilde{x}^2}{2(1+\tilde{x})}\right) = \frac{3}{2}\frac{\tilde{x}^2}{2(1+\tilde{x})} = \frac{3\tilde{x}^2}{4(1+\tilde{x})}.$$

$$\psi\left(M_{JS}(x, \tilde{x})\right) - \varphi\left(M_{JS}(x, \tilde{x})\right) = \psi(\tilde{x}) - \varphi(\tilde{x}) = \frac{3\tilde{x}}{2} - \frac{\tilde{x}}{2} = \tilde{x}$$

Since $\frac{3}{4}\frac{\tilde{x}^2}{(1+\tilde{x})} < \tilde{x}$, the condition of Theorem 3.1.2 is accomplished.

Case 2. If $D(x, f(\tilde{x}))$ is x, then

$$M_{JS}(x, \tilde{x}) = \text{maximum}\{\tilde{x}, x\} = \tilde{x}$$

$$\psi(D_{JS}(f(x), f(\tilde{x}))) = \frac{3}{2}\frac{\tilde{x}^2}{2(1+\tilde{x})} = \frac{3\tilde{x}^2}{4(1+\tilde{x})}.$$

$$\psi(M(x, \tilde{x})) - \varphi(M(x, \tilde{x})) = \psi(\tilde{x}) - \varphi(\tilde{x}) = \frac{3\tilde{x}}{2} - \frac{\tilde{x}}{2} = \tilde{x}$$

Since $\frac{3}{4}\frac{\tilde{x}^2}{(1+\tilde{x})} < \tilde{x}$, the condition of Theorem 3.1.2 is completed.

Therefore, the function $f: X \to X$ has a fixed point which is 0.

Corollary 3.1.5. Let (X, D_{JS}) be a JS – generalized metric space which is complete and f a function of X in itself satisfying the condition

$$D_{JS}(fx, f\tilde{x}) \leq M_{JS}(x, \tilde{x}) - \varphi(M_{JS}(x, \tilde{x})),$$

where

$$M_{JS}(x, \tilde{x}) = \text{maximum}\begin{Bmatrix} D_{JS}(x, \tilde{x}), D_{JS}(x, fx), D_{JS}(\tilde{x}, f\tilde{x}), \\ D_{JS}(x, f\tilde{x}), D_{JS}(\tilde{x}, fx) \end{Bmatrix},$$

for every $x, \tilde{x} \in X$ and φ is from Ψ, and lower semi – continuous.

If there exists $\varsigma \in X$ that $\delta(D_{JS}, f, \varsigma) < +\infty$, then $\{f^n\varsigma\}_{n \in N}$ D_{JS} – convergences to a point ϑ in X.

When $D_{JS}(\vartheta, f\vartheta) < +\infty$ then ϑ is fixed point of function f. Furthermore, for $\vartheta' \in X$ which is another fixed point of function f, such that $D_{JS}(\vartheta', f\vartheta') < +\infty$, it yields $\vartheta = \vartheta'$.

Proof. Replacing $\psi(s) = s \in \Psi$ in above theorem, the proof is clear.

Corollary 3.1.6 Let (X, D_{JS}) be a JS – generalized metric space which is complete and f a function of X in itself satisfying the condition

$$D_{JS}(fx, f\tilde{x}) \leq \kappa M_{JS}(x, \tilde{x})$$

where

$$M_{JS}(x, \tilde{x}) = \text{maximum}\begin{Bmatrix} D_{JS}(x, \tilde{x}), D_{JS}(x, fx), D_{JS}(\tilde{x}, f\tilde{x}), \\ D_{JS}(x, f\tilde{x}), D_{JS}(\tilde{x}, fx) \end{Bmatrix},$$

for every $x, \tilde{x} \in X$ and $\kappa \in \ ]0,1[$.

If there exists $\varsigma \in X$ that $\delta(D_{JS}, f, \varsigma) < +\infty$, then $\{f^n\varsigma\}_{n \in N}$ D_{JS} – convergences to a point ϑ in X.

When $D_{JS}(\vartheta, f\vartheta) < +\infty$ then ϑ is fixed point of function f. Furthermore, for $\vartheta' \in X$ which is another fixed point of function f, such that $D_{JS}(\vartheta', f\vartheta') < +\infty$, it yields $\vartheta = \vartheta'$.

Proof. Taking $\psi(s) = s$ and $\varphi(s) = (1 - \kappa)s \in \Psi$ in inequality (3.1), the proof is clear.

Remark 3.1.7 Corollary 3.1.5 is a generalization of Theorem 2.16 which is the result of [16] as Corollary 5.5 and Corollary 3.8 in [20].

3.2. Common fixed point related to $\varphi - \psi$ contractive functions in JS – generalized metric space.

Theorem 3.2.1 Let (X, D_{JS}) a JS – generalized metric space which is complete and $F, g: X \to X$ such that FX is a subset of gX and the set gX is closed in X and

$$\psi(D_{JS}(Fx, F\tilde{x}) \leq \psi\left(M_{JS}(gx, g\tilde{x})\right) - \varphi(M_{JS}(gx, g\tilde{x})) \quad (3.12)$$

where

$$M_{JS}(gx, g\tilde{x}) =$$
$$\text{maximum}\{D_{JS}(gx, g\tilde{x}), D_{JS}(gx, Fx), D_{JS}(gy, F\tilde{x})\}$$

for x and $\tilde{x}$ in X and φ and ψ in Ψ, ψ is continuous and φ is lower semi – continuous.

If there exist $\varsigma \in X$ such that $\delta(D_{JS}, F, \varsigma) < +\infty$ and $\delta(D_{JS}, g, \varsigma) < +\infty$ then the sequence $\{\gamma_n\}_{n \in N} = \{g\varsigma_{n+1}\}_{n \in N} = \{F\varsigma_n\}_{n \in N}$, where $\gamma_1 = F\varsigma = g\varsigma_1$, D_{JS} – converges to a point ϑ in X.

If $\delta(D_{JS}, F, \vartheta) < +\infty$ and $\delta(D_{JS}, g, \vartheta) < +\infty$ then the maps F, g have a unique coincidence point in X.

Furthermore, they have a unique common fixed point in X,

if they are weakly compatible.

Proof. Let take $\varsigma \in X$ such that $\delta(D_{JS}, F, \varsigma) < +\infty$ and $\delta(D_{JS}, g, \varsigma) < +\infty$. For $\varsigma \in X$, due to $FX \subset gX$ then $F\varsigma \in gX$. Consequently, there exists $\varsigma_1 \in X, g\varsigma_1 = F\varsigma$.

Reasoning in the same manner for ς_1 and so on, there can be defined the sequences $\{\varsigma_n\}_{n\in N}$ and $\{\gamma_n\}_{n\in N}$ such that

$$\gamma_n = g\varsigma_{n+1} = F\varsigma_n \tag{3.13}$$

for $n = 0, 1, 2, \ldots$

If there exists any $n \in N$, such that $\gamma_n = \gamma_{n+1}$ then $g\varsigma_{n+1} = F\varsigma_n = \gamma_n = \gamma_{n+1} = F\varsigma_{n+1}$.

So, ς_{n+1} is the required point for g and F.

Let suppose now that the terms of $\{\gamma_n\}$ are diferent from each other.

Consequently,

$$D_{JS}(\gamma_n, \gamma_{n+1}) > 0. \tag{3.14}$$

$$\psi\left(D_{JS}(\gamma_n, \gamma_{n+1})\right) = \psi\left(D_{JS}(F\varsigma_n, F\varsigma_{n+1})\right)$$

$$\leq \psi\left(M_{JS}(g\varsigma_n, g\varsigma_{n+1})\right) - \varphi\left(M_{JS}(g\varsigma_n, g\varsigma_{n+1})\right) \tag{3.15}$$

where

$M_{JS}(g\varsigma_n, g\varsigma_{n+1})$
$= \text{maximum}\{D_{JS}(g\varsigma_n, g\varsigma_{n+1}), D_{JS}(g\varsigma_n, F\varsigma_n), D_{JS}(g\varsigma_{n+1}, F\varsigma_{n+1})\}$
$= \text{maximum}\{D_{JS}(g\varsigma_n, g\varsigma_{n+1}), D_{JS}(g\varsigma_n, g\varsigma_{n+1}), D_{JS}(g\varsigma_{n+1}, g\varsigma_{n+2})\}$
$= \text{maximum}\{D_{JS}(g\varsigma_n, g\varsigma_{n+1}), D_{JS}(g\varsigma_{n+1}, g\varsigma_{n+2})\}$
$= \text{maximum}\{D_{JS}(\gamma_{n-1}, \gamma_n), D_{JS}(\gamma_n, \gamma_{n+1})\}$

Case 1. $D_{JS}(g\varsigma_n, g\varsigma_{n+1}) = D_{JS}(\gamma_n, \gamma_{n+1})$, then replacing it in (3.15), it yields

$$\psi\left(D_{JS}(\gamma_n, \gamma_{n+1})\right) \leq \psi\left(D_{JS}(\gamma_n, \gamma_{n+1})\right) - \varphi\left(D_{JS}(\gamma_n, \gamma_{n+1})\right)$$

So $\varphi\left(D_{JS}(\gamma_n, \gamma_{n+1})\right) = 0$ and consequently $D_{JS}(\gamma_n, \gamma_{n+1}) = 0$, which is absurd due to (3.14).

Case 2. $M_{JS}(g\varsigma_n, g\varsigma_{n+1}) = D_{JS}(\gamma_{n-1}, \gamma_n)$ then replacing it in (3.15), it yields

$$\psi\left(D_{JS}(\gamma_n, \gamma_{n+1})\right) \leq \psi\left(D_{JS}(\gamma_n, \gamma_{n-1})\right) - \varphi\left(D_{JS}(\gamma_n, \gamma_{n-1})\right)$$

$$\leq \psi\left(D_{JS}(\gamma_n, \gamma_{n-1})\right) \tag{3.16}$$

Due to non-decreasing monotony of ψ, it implies

$$D_{JS}(\gamma_n, \gamma_{n+1}) \leq D_{JS}(\gamma_n, \gamma_{n-1}),$$

for all $n \in N$.

This shows that $\{D_{JS}(\gamma_n, \gamma_{n+1})\}_{n\in N}$ is non-increasing and lower bounded because $D_{JS}(\gamma_n, \gamma_{n+1}) \geq 0$.

Consequently, the sequence $\{D_{JS}(\gamma_n, \gamma_{n+1})\}_{n\in N}$ converges to $l \geq 0$, $\lim_{n\to+\infty} D_{JS}(\gamma_n, \gamma_{n+1}) = l$.

Taking the limit in (3.16) when $n \to +\infty$, it yields

$$\psi(l) \leq \psi(l) - \phi(l).$$

Consequently, $\varphi(l) = 0$ and $l = 0$.

So,

$$\lim_{n\to+\infty} D_{JS}(\gamma_n, \gamma_{n+1}) = 0 \tag{3.17}$$

Denote

$$c_k = \sup\{D_{JS}(\gamma_i, \gamma_j), i, j > k\} \tag{3.18}$$

c_k is finite for every $k \in N$ because $\delta(D_{JS}, F, \varsigma) < +\infty$ and $\delta(D_{JS}, g, \varsigma) < +\infty$.

Since the sequence $\{c_k\}_{k\in N}$ is non $-$ increasing, lower bounded from zero, it is convergent to a point ζ,

$$\lim_{k\to+\infty} c_k = \zeta \geq 0 \tag{3.19}$$

From (3.17), it yields:

for each $p \in N$, there exist $i_p, j_p > p$, such that

$$c_p - \frac{1}{p} < D_{JS}\left(\gamma_{i_p}, \gamma_{j_p}\right) < c_p \tag{3.20}$$

Taking limit in (3.20) when $p \to +\infty$ and using (3.19), it yields

$$\lim_{p\to+\infty} D_{JS}\left(\gamma_{i_p}, \gamma_{j_p}\right) = \zeta \tag{3.21}$$

Knowing that $D_{JS}\left(\gamma_{i_p}, \gamma_{j_p}\right) = D_{JS}\left(F\varsigma_{i_p-1}, F\varsigma_{j_p-1}\right)$, it implies

$$\psi\left(D_{JS}\left(\varsigma_{i_p}, \varsigma_{j_p}\right)\right) = \psi\left(D_{JS}\left(F\varsigma_{i_p-1}, F\varsigma_{j_p-1}\right)\right) \leq$$
$$\psi\left(M_{JS}\left(g\varsigma_{i_p-1}, g\varsigma_{j_p-1}\right)\right) - \varphi\left(M_{JS}\left(g\varsigma_{i_p-1}, g\varsigma_{j_p-1}\right)\right) \tag{3.22}$$

where

$M_{JS}\left(g\varsigma_{i_p-1}, g\varsigma_{j_p-1}\right)$
$= \text{maximum}\left\{\begin{array}{c} D_{JS}\left(g\varsigma_{i_p-1}, g\varsigma_{j_p-1}\right), D_{JS}\left(g\varsigma_{i_p-1}, F\varsigma_{i-1}\right), \\ D_{JS}\left(g\varsigma_{j_p-1}, F\varsigma_{j_p-1}\right) \end{array}\right\}$
$= \text{maximum}\left\{\begin{array}{c} D_{JS}\left(\gamma_{i_p-2}, \gamma_{j_p-2}\right), D_{JS}\left(\gamma_{i_p-2}, g\varsigma_{i_p-1}\right), \\ D_{JS}\left(\gamma_{j_p-2}, \varsigma_{j_p-1}\right) \end{array}\right\}$

From (3.17) and (3.19), it yields

$$\lim_{p\to+\infty} M_{JS}\left(g\varsigma_{i_p-1}, g\varsigma_{j_p-1}\right) = \text{maximum}\{\zeta, 0,0\} = \zeta$$

Taking the limit in (3.22) when $p \to +\infty$ and from (3.21), it implies

$$\psi(\zeta) \leq \psi(\zeta) - \varphi(\zeta)$$

Consequently, $\varphi(\zeta) = 0$ and $\zeta = 0$.

So,

$$\lim_{k \to +\infty} c_k = 0 \qquad (3.23)$$

From (3.18) and (3.23), it yields $\lim_{i,j \to +\infty} D_{JS}(\gamma_i, \gamma_j) = 0$, which means that the sequence $\{\gamma_n\}_{n \in N}$ is $D_{JS}-$ Cauchy in X.

Since $\gamma_n = g\varsigma_{n+1} = F\varsigma_n$, it yields $\{\gamma_n\}_{n \in N} \subset g(X)$. Since the set $g(X)$ is closed, there is $\vartheta \in gX$ such that $\lim_{n \to +\infty} \gamma_n = \vartheta$. Consequently, $\lim_{n \to +\infty} g\varsigma_{n+1} = \lim_{n \to +\infty} F\varsigma_n = \vartheta$.

Since $\vartheta \in gX$ then there is $\mu \in X$, $g\mu = \vartheta$.

The other step is to show that $F\mu = \vartheta$.

Knowing $D_{JS}(\vartheta, F\mu) \leq \lim_{n \to +\infty} D_{JS}(F\varsigma_n, F\mu)$ and applying $x = \varsigma_n$ and $\tilde{x} = \mu$ at (3.12), it implies

$$\psi\left(D_{JS}(F\varsigma_n, F\mu)\right) \leq \psi\left(M_{JS}(g\varsigma_n, g\mu)\right) - \varphi\left(M_{JS}(g\varsigma_n, g\mu)\right)$$
(3.24)

where

$$M_{JS}(g\varsigma_n, g\mu)$$
$$= \text{maximum}\{D_{JS}(g\varsigma_n, g\mu), D_{JS}(g\varsigma_n, F\varsigma_n), D_{JS}(g\mu, F\mu)\}$$
$$= \text{maximum }\{D_{JS}(g\varsigma_n, \vartheta), D_{JS}(g\varsigma_n, F\varsigma_n), D_{JS}(\vartheta, F\mu)\}$$

Since

$$\lim_{n \to +\infty} D_{JS}(g\varsigma_n, \vartheta) = 0$$

and

$$\lim_{n \to +\infty} D_{JS}(g\varsigma_n, F\varsigma_n) = \lim_{n \to +\infty} D_{JS}(\gamma_{n-1}, \gamma_n) = 0,$$

it implies $\lim_{n \to +\infty} M(g\varsigma_n, g\mu) = D_{JS}(\vartheta, F\mu)$.

Taking limit in (3.24) when $n \to +\infty$, it yields

$$\psi(D_{JS}(\vartheta, F\mu)) \leq \psi(\vartheta, F\mu) - \varphi(\vartheta, F\mu)$$

As a result $\varphi(\vartheta, F\mu) = 0$.

Consequently, $\vartheta = F\mu$.

The following step is to prove that ϑ is unique.

Suppose that there exists another point of coincidence $\vartheta' \neq \vartheta$ of g and F.

So, there exists $\mu_1 \in X$ which accomplishes $F\mu_1 = g\mu_1 = \vartheta'$

$$\psi\left(D_{JS}(\vartheta, \vartheta')\right) = \psi\left(D_{JS}(F\mu, F\mu_1)\right)$$

$$\leq \psi\left(M_{JS}(g\mu, g\mu_1)\right) - \varphi\left(M_{JS}(g\mu, g\mu_1)\right) \qquad (3.25)$$

For

$$M_{JS}(g\mu, g\mu_1)$$
$$= \text{maximum}\{D_{JS}(g\mu, g\mu_1), D_{JS}(g\mu, F\mu), D_{JS}(g\mu_1, F\mu_1)\}$$
$$= \text{maximum}\{D_{JS}(\vartheta, \vartheta'), D_{JS}(\vartheta, \vartheta), D_{JS}(\vartheta', \vartheta')\} \qquad (3.26)$$

$$D_{JS}(\vartheta, \vartheta) = D_{JS}(F\mu, F\mu)$$

$$\psi\left(D_{JS}(\vartheta, \vartheta)\right) = \psi\left(D_{JS}(F\mu, F\mu)\right)$$

$$\leq \psi\left(M_{JS}(g\mu, g\mu)\right) - \varphi\left(M_{JS}(g\mu, g\mu)\right) \qquad (3.27)$$

where

$$M_{JS}(g\mu, g\mu) =$$
$$\text{maximum}\{D_{JS}(g\mu, g\mu), D_{JS}(g\mu, F\mu), D_{JS}(g\mu, F\mu)\} =$$
$$\max\{D_{JS}(\vartheta, \vartheta), D_{JS}(\vartheta, \vartheta), D_{JS}(\vartheta, \vartheta)\} = D_{JS}(\vartheta, \vartheta)$$

Replacing $M_{JS}(g\mu, g\mu) = D_{JS}(\vartheta, \vartheta)$ in (3.27),

it implies

$$\psi\left(D_{JS}(\vartheta, \vartheta)\right) \leq \psi\left(D_{JS}(\vartheta, \vartheta)\right) - \varphi\left(D_{JS}(\vartheta, \vartheta)\right)$$

So, $\varphi\left(D_{JS}(\vartheta, \vartheta)\right) = 0$ and

$$D_{JS}(\vartheta, \vartheta) = 0 \qquad (3.28)$$

Using the same method, it can be proved that

$$D_{JS}(\vartheta', \vartheta') = 0 \qquad (3.29)$$

Replacing (3.28) and (3.29) in (3.26) and then in (3.25) it yields

$$M_{JS}(g\mu, g\mu_1) = D_{JS}(g\mu, g\mu_1) = D_{JS}(\vartheta, \vartheta')$$

$$\psi\left(D_{JS}(\vartheta, \vartheta')\right) \leq \psi\left(D_{JS}(\vartheta, \vartheta')\right) - \varphi\left(D_{JS}(\vartheta, \vartheta')\right)$$

From this, it implies $\varphi\left(D_{JS}(\vartheta, \vartheta')\right) = 0$ and $D_{JS}(\vartheta, \vartheta') = 0$. Consequently $\vartheta = \vartheta'$.

Furthermore, let prove that if g and F are weakly compatible then $F\vartheta = g\vartheta$.

From $D_{JS}(F\vartheta, \vartheta) = D_{JS}(F\vartheta, F\mu)$ and (3.12), it implies

$$\psi\left(D_{JS}(F\vartheta, \vartheta)\right) = \psi\left(D_{JS}(F\vartheta, F\mu)\right)$$

$$\leq \psi\left(M_{JS}(g\vartheta, g\mu)\right) - \varphi\left(M_{JS}(g\vartheta, g\mu)\right) \qquad (3.30)$$

$$M_{JS}(g\vartheta, g\mu)$$
$$= \text{maximum}\{D_{JS}(g\vartheta, g\mu), D_{JS}(g\vartheta, F\mu), D_{JS}(g\vartheta, F\mu)\}$$
$$= \text{maximum}\{D_{JS}(F\vartheta, \vartheta), D_{JS}(F\vartheta, F\vartheta), D_{JS}(\vartheta, \vartheta)\}$$

From (3.28), it is known that $D_{JS}(\vartheta, \vartheta) = 0$. Using the same method as in (3.28), it can be proved that $D_{JS}(F\vartheta, F\vartheta) = 0$.

Consequently, $M_{JS}(g\vartheta, g\mu) = D_{JS}(F\vartheta, \vartheta)$

Replacing this equality in (3.30), it implies

$$\psi\left(D_{JS}(F\vartheta, \vartheta)\right) \leq \psi\left(D_{JS}(F\vartheta, \vartheta)\right) - \varphi\left(D_{JS}(F\vartheta, \vartheta)\right)$$

From this $\varphi\left(D_{JS}(F\vartheta, \vartheta)\right) = 0$ and $D_{JS}(F\vartheta, \vartheta) = 0$.

So, $F\vartheta = \vartheta = g\vartheta$ and ϑ is unique.

Remark 3.2.2 Since JS – generalized metric spaces are metric spaces, b – metric spaces, dislocated metric spaces, partial metric spaces it implies that Theorem 3.2.1 is true in these spaces.

Example 3.2.3 Let be $X = [0, a]$, where $a \in R$ and D_{JS} the JS – generalized metric defined at Example 2.10 and the functions $\varphi, \psi \in \Psi$, $\varphi(s) = \frac{1}{5}s$, $\psi(s) = \frac{s}{2}$.

Let $g, F: X \to X$ two functions where $g(x) = \frac{x}{2}$ and $F(x) = \ln\left(1 + \frac{x}{4}\right)$.

The functions g, F complete the condition of Theorem 3.2.1.

Indeed,

$$D_{JS}(Fx, F\tilde{x}) = D_{JS}\left(\ln\left(1 + \frac{x}{4}\right), \ln\left(1 + \frac{\tilde{x}}{4}\right)\right)$$
$$= \text{maximum}\{\ln\left(1 + \frac{x}{4}\right), \ln\left(1 + \frac{\tilde{x}}{4}\right)\}$$

Since $x \neq \tilde{x}$, it is supposed that $x < \tilde{x}$ without restricting anything.

From monotony of logarithmic function

$$D_{JS}(Fx, F\tilde{x}) = D_{JS}\left(\ln\left(1 + \frac{x}{4}\right), \ln\left(1 + \frac{\tilde{x}}{4}\right)\right) = \ln\left(1 + \frac{\tilde{x}}{4}\right).$$

$M_{JS}(g(x), g(\tilde{x}))$
$$= \text{maximum}\{D_{JS}(g(x), g(\tilde{x})), D_{JS}(g(x), F(x)), D_{JS}(g(\tilde{x}), F(\tilde{x}))\}$$

$$D_{JS}(g(\tilde{x}), g(x)) = \text{maximum}\{g(\tilde{x}), g(x)\} = \frac{\tilde{x}}{2}$$

$$D_{JS}(F(x), g(x)) = \max\{F(x), g(x)\} = \frac{1}{2}x.$$

$$D_{JS}(F(\tilde{x}), g(\tilde{x})) = \max\{F(\tilde{x}), g(\tilde{x})\} = \frac{\tilde{x}}{2}$$

$$M_{JS}(g(x), g(\tilde{x})) = \frac{1}{2}\tilde{x}$$

$$\psi(D_{JS}(Fx, F\tilde{x})) = \psi(\ln\left(1 + \frac{1}{4}\tilde{x}\right)) < \psi\left(\frac{1}{4}\tilde{x}\right) = \frac{1}{8}\tilde{x}.$$

$$\psi\left(M_{JS}(gx, g\tilde{x})\right) - \varphi\left(M_{JS}(gx, g\tilde{x})\right) = \psi\left(\frac{\tilde{x}}{2}\right) - \varphi\left(\frac{\tilde{x}}{2}\right) = \frac{3\tilde{x}}{20}$$

Since

$$\psi\left(M_{JS}(gx, g\tilde{x})\right) - \varphi\left(M_{JS}(gx, g\tilde{x})\right) - \psi\left(D_{JS}(Fx, F\tilde{x})\right) >$$
$$\frac{3\tilde{x}}{20} - \frac{\tilde{x}}{8} = \frac{\tilde{x}}{40} > 0,$$

then g, F have a common fixed point 0.

Corollary 3.2.4 Let (X, D_{JS}) be a JS – generalized metric space which is complete and $g, F: X \to X$ such that gX is closed and FX is a subset of gX and

$$D_{JS}(Fx, F\tilde{x}) \leq M_{JS}(gx, g\tilde{x}) - \varphi(M_{JS}(gx, g\tilde{x})) \qquad (3.31)$$

where

$$M_{JS}(x, \tilde{x}) = \max\{D_{JS}(gx, g\tilde{x}), D_{JS}(gx, Fx), D_{JS}(g\tilde{x}, F\tilde{x})\}, \quad \text{for}$$
$x, \tilde{x}$ in X and φ in Ψ is lower semi – continuous.

If there exist $\varsigma \in X$ such that $\delta\left(D_{JS}, F, \varsigma\right) < +\infty$ and $\delta\left(D_{JS}, g, \varsigma\right) < +\infty$ then the sequence $\{\gamma_n\}_{n\in N} = \{g\varsigma_{n+1}\}_{n\in N} = \{F\varsigma_n\}_{n\in N}$, where $\gamma_1 = F\varsigma = g\varsigma_1$, D_{JS} – converges to a point ϑ in X.

If $\delta\left(D_{JS}, F, \vartheta\right) < +\infty$ and $\delta\left(D_{JS}, g, \vartheta\right) < +\infty$ then the maps F, g have a unique coincidence point in X.

Furthermore, they have a unique common fixed point in X,

if they are weakly compatible.

Proof. Taking $\psi(s) = s$ in (3.12), the corollary is true.

Corollary 3.2.5 Let (X, D_{JS}) be a JS – generalized metric space which is complete and $g, F: X \to X$ such that gX is closed set and FX is a subset of gX in X and

$$D_{JS}(Fx, F\tilde{x}) \leq \kappa \max\{D_{JS}(gx, g\tilde{x}), D_{JS}(gx, F\tilde{x}), D_{JS}(g\tilde{x}, Fx)\}$$

where $\kappa \in]0,1[$ for x and $\tilde{x} \in X$.

If there exist $\varsigma \in X$ such that $\delta\left(D_{JS}, F, \varsigma\right) < +\infty$ and $\delta\left(D_{JS}, g, \varsigma\right) < +\infty$ then the sequence $\{\gamma_n\}_{n\in N} = \{g\varsigma_{n+1}\}_{n\in N} = \{F\varsigma_n\}_{n\in N}$, where $\gamma_1 = F\varsigma = g\varsigma_1$, D_{JS} – converges to a point ϑ in X.

If $\delta\left(D_{JS}, F, \vartheta\right) < +\infty$ and $\delta\left(D_{JS}, g, \vartheta\right) < +\infty$ then the maps F, g have a unique coincidence point in X.

Furthermore, they have a unique common fixed point in X,

if they are weakly compatible.

Proof. Taking $\psi(s) = s$, $\varphi(s) = (1 - \kappa)s$ in (3.12), the corollary is true.

Corollary 3.2.6 Let (X, D_{JS}) be a JS – generalized metric space which is complete and $F, g: X \to X$ such that $FX \subset gX$ and gX is closed set in X and

$$D_{JS}(Fx, F\tilde{x}) \leq \kappa_1 D_{JS}(gx, g\tilde{x}) + \kappa_2 D_{JS}(gx, Fx) + \kappa_3 D_{JS}(g\tilde{x}, F\tilde{x})$$

where $0 < \kappa_1 + \kappa_2 + \kappa_3 < 1$, for x and $\tilde{x}$ from X.

If there exist $\varsigma \in X$ such that $\delta(D_{JS}, F, \varsigma) < +\infty$ and $\delta(D_{JS}, g, \varsigma) < +\infty$ then the sequence $\{\gamma_n\}_{n \in N} = \{g\varsigma_{n+1}\}_{n \in N} = \{F\varsigma_n\}_{n \in N}$, where $\gamma_1 = F\varsigma = g\varsigma_1$, D_{JS} – converges to a point ϑ in X.

If $\delta(D_{JS}, F, \vartheta) < +\infty$ and $\delta(D_{JS}, g, \vartheta) < +\infty$ then the maps F, g have a unique coincidence point in X.

Furthermore, they have a unique common fixed point in X,

if they are weakly compatible.

Proof. Taking $\kappa = \kappa_1 + \kappa_2 + \kappa_3$, $\kappa \in \left]0, \frac{1}{3}\right[$, it implies

$\kappa_1 D_{JS}(gx, g\tilde{x}) + \kappa_2 D_{JS}(gx, Fx) + \kappa_3 D_{JS}(g\tilde{x}, F\tilde{x}) \leq \kappa \left(D_{JS}(gx, g\tilde{x}) + D_{JS}(gx, Fx) + D_{JS}(g\tilde{x}, F\tilde{x}) \right) \leq \kappa \cdot 3 \cdot M_{JS}(gx, g\tilde{x})$.

Replacing $\varphi(s) = (1 - 3\kappa)s$ and $\psi(s) = s$ in (3.12), the corollary holds.

4. Conclusions

In this paper are given some theorems and corollaries on fixed points for weakly contractive functions and for contractive functions with altering distance between points in JS – generalized metric spaces. Furthermore, in it are proved some results related to common fixed points of two $\varphi - \psi$ contractive functions on JS – generalized metric spaces. Since JS – generalized metric spaces are metric spaces, b - metric spaces, dislocated metric spaces, partial metric spaces, it implies that all obtained results are true in above mentioned spaces. In additions, some important results given in this paper are generalizations of some known references. Concretely, Theorem 3.1.2 generalizes Theorem 1.9 in [19]. Corollary 3.1.5 is a generalization of Corollary 3.8 in [20] and Corollary 5.5 in [16].

References

[1] K. Wlodarczyk, R. Plebaniak, "Generalized uniform spaces, uniformly locally contractive set-valued dynamic systems and fixed points," Fixed Point Theory and Applications, **1**, 1-39, 2012, doi:10.1186/1687-1812-2012-104.

[2] L.G. Huang, X. Zhang, "Cone metric spaces and fixed point theorems of contractive mappings," Journal of Mathematical Analysis and Applications, **332**(2), 1468-1476. 2007, doi:10.1016/j.jmaa.2005.03.087.

[3] M. Arshad, J. Ahmad, E. Karapınar, "Some Common Fixed Point Results in Rectangular Metric Spaces," International Journal of Analysis, 2013, doi:10.1155/2013/307234.

[4] M. Jleli, B. Samet, "A generalized metric space and related fixed point theorems," Fixed Point Theory and Applications, **1**(2015): 1-14, 2015, doi:10.1186/s13663-015-0312-7.

[5] S. Czerwik, "Contraction mappings in b-metric spaces," Ostraviensis, 1993.

[6] A. Amini-Harandi, "Metric-like spaces, partial metric spaces and fixed points," Fixed Point Theory and Applications, 2012, doi:10.1186/1687-1812-2012-204.

[7] E. Karapınar, B. Samet, D. Zhang, "Meir–Keeler type contractions on JS-metric spaces and related fixed point theorems," Journal of Fixed Point Theory and Applications, **20**(2), 1-19, 2018, doi:10.1007/s11784-018-0544-3.

[8] K. Chaira, A. Eladraoui, M. Kabil, A. Kamouss, "Fisher Fixed Point Results in Generalized Metric Spaces with a Graph," International Journal of Mathematics and Mathematical Sciences, 2020, doi:10.1155/2020/7253759.

[9] P. Agarwal, M. Jleli, B. Samet, P. Agarwal, M. Jleli, B. Samet, JS-Metric Spaces and Fixed Point Results, 2018, doi:10.1007/978-981-13-2913-5_9.

[10] A. Shoaib, Q. Mehmood, "Fixed Point Results in Js Multiplicative Metric Spaces," Turkish Journal of Analysis and Number Theory, **6**(6), 2019, doi:10.12691/tjant-6-6-3.

[11] Y.I. Alber, S. Guerre-Delabriere, Principle of Weakly Contractive Maps in Hilbert Spaces, 1997, doi:10.1007/978-3-0348-8910-0_2.

[12] S. Cho, "Fixed point theorems for generalized weakly contractive mappings in metric spaces with applications," Fixed Point Theory and Applications, **2018**(1), 3, 2018, doi:10.1186/s13663-018-0628-1.

[13] P.N. Dutta, B.S. Choudhury, "A Generalisation of Contraction Principle in Metric Spaces," Fixed Point Theory and Applications, **2008**(1), 406368, 2008, doi:10.1155/2008/406368.

[14] G.V.R. Babu, T.M. Dula, "Fixed points of generalized TAC-contractive mappings in b-metric spaces," Matematicki Vesnik, **69**(2), 2017.

[15] S.N. Ješić, N.A. Ćirović, D. O'Regan, "Altering Distances and a Common Fixed Point Theorem in Menger Probabilistic Metric Spaces," Filomat, **31**(2), 175–181, 2017.

[16] Y. ElKouch, E.M. Marhrani, "On some fixed point theorems in generalized metric spaces," Fixed Point Theory and Applications, **2017**(1), 2017, doi:10.1186/s13663-017-0617-9.

[17] H. Rahimi, G. Soleimani Rad, "Note on 'common fixed point results for noncommuting mappings without continuity in cone metric spaces,'" Thai Journal of Mathematics, **11**(3), 2013.

[18] L.B. Ćirić, J.S. Ume, "Some common fixed point theorems for weakly compatible mappings," Journal of Mathematical Analysis and Applications, **314**(2), 2006, doi:10.1016/j.jmaa.2005.04.007.

[19] E. Karapınar, P. Salimi, "Dislocated metric space to metric spaces with some fixed point theorems," Fixed Point Theory and Applications, **2013**(1), 222, 2013, doi:10.1186/1687-1812-2013-222.

[20] T. Senapati, L.K. Dey, D. Dolićanin-Đekić, "Extensions of Ćirić and Wardowski type fixed point theorems in D-generalized metric spaces," Fixed Point Theory and Applications, **2016**(1), 33, 2016, doi:10.1186/s13663-016-0522-7.

Recognition of Maximal Lift Capacity using the Polylift

Jennifer Snell Ballard[*,1], Jerry Lee[2]

[1]*Huntingdon College, Department of Sport Science and Physical Education, Montgomery, AL 36106, United States*

[2]*Alabama State University, Department of Physical Therapy, Montgomery, AL 36104, United States*

A R T I C L E I N F O	A B S T R A C T
	Background: *Occupational injuries are an issue of huge significance in the United States. After a work injury, health care providers often utilize functional capacity evaluations to determine readiness of a patient to return to work. However, it can be difficult to determine if a patient is providing maximal "effort" during the evaluation. The aim of this study was to determine if the use of the Polylift could assist in recognizing when a subject reached maximal lift capacity of a manual lift from waist to shoulder. The Polylift is a computerized data collection instrument that measures velocity, acceleration, distance, time, and force during lifting activities.* ***Subjects:*** *42 healthy college students (20- males, 22- females) ages 20-27.* ***Methods:*** *Participants first performed repeated lifts from waist to shoulder until fatigue and the number of repetitions was noted. Using this information, Brzycki's 1 Repetition Maximum (1RM) formula was used to predict each subject's maximal load. Next, the Polylift recorded information during four lifts (25% of 1RM, 50% of 1RM, 75% of 1RM and 100% of 1RM).* ***Results:*** *The Polylift recorded a consistent, significant relationship between time and acceleration. As loads approached subjects 1RM, time required to lift the weight increased, and acceleration decreased in a predictable pattern.* ***Conclusion:*** *The Polylift assisted researchers in determining when a subject reached maximal lift capacity by demonstrating a significant decrease in acceleration and increase in time with progressively increasing loads.*

1. Introduction

Occupational injuries are an issue of huge significance in the United States. [1] reported that, "The medical and indirect costs of occupational injuries and illnesses are sizable, at least as large as the cost of cancer". Employers bear the burdens of absenteeism, loss of productivity, increased health care, disability, and workers compensation costs after an employee is injured [2]. Often, the employee requires subsequent rehabilitation and may eventually participate in a functional capacity evaluation [3], [4].

Physical therapists, athletic trainers, and exercise physiologists often play vital roles in the case management of patients with a work injuries. These practitioners often participate in evaluation and treatment of musculoskeletal disorders, assist in injury prevention, provide ergonomic education, perform functional capacity evaluations, prescribe conditioning exercises, and complete pre-work screening activities [5]. Operating in that capacity, these providers first identify and address risk factors along with utilizing gross objective measurements and observation to ascertain an individual's readiness to return to work, their ability to perform optimally on the job and most importantly assist in the prevention of re-injury.

A tool that practitioners often utilize within industrial medicine is the functional capacity evaluation (FCE). These evaluations are effective tools that are dynamic, comprehensive and mimic tasks such as lifting, carrying, reaching, squatting and gripping which are vital to effectively perform work functions [5], [6]. FCE's are comprised of bending and lifting activities that directly relate to musculoskeletal disorders. According to the U.S. Bureau of Labor and Statistics, injuries involving the musculoskeletal system accounted for thirty-one percent of the

[*]Corresponding Author: Jennifer Snell Ballard, jballard@hawks.huntingdon.edu

total cases reported in 2015 and are typically diagnosed as sprains or strains [7]. After a diagnosis is made and skilled therapy services are completed, a FCE is often performed utilizing equipment such as handheld dynamometer, Purdue pegboard, weights, step ladder, sled station, weight box and workstation equipped with shelves, heart rate monitor, sphygmomanometer and a stop watch which is assist in collecting measurements. During the evaluation, practitioners rely on both subjective information, objective measurements and clinical judgement to assess many of the musculoskeletal aspects of the test [8].

One of the more popular methods of the evaluation, the kinesiophysical method, involves practitioners determining maximal lifting capacity by observing altered lifting mechanics and use of accessory muscles, which does not involve objective measurements or validated equipment [3]. Experienced clinicians possess excellent clinical judgment and observation skills, and are often required to express an opinion as to whether the patient is providing their maximal effort during lifting activities. While patients have been known to manipulate FCE results by conscious and unconscious efforts, there are certain variables that cannot be manipulated. In particular, as maximal effort and maximal weight loads are achieved, the expected outcome is slower time to complete the lift, along with decreased velocity and acceleration. Up to this point, validated technology that can produce data to assist in deciphering if maximal effort has been produced has not existed. While indicators such as mechanical breakdown, postural breakdown, recruitment of accessory muscles, and heart rate may be used, the application of these indicators is to some degree subjective and thus subject to question. Technology of this nature could improve credibility of reports by providing tangible evidence to accompany sound clinical judgement during functional capacity evaluations. Objective measurements of this nature would reinforce evidence provided in medicolegal cases [8]. A machine such as the Polylift has the ability to provide such objective data and improve the reinforce the credibility of a functional capacity evaluation [8], [9].

The Polylift is a mechanized, data collection machine that is constructed to mimic a lifting workstation. The machine consists of an adjustable rack with shelves equipped with a control module and sensors to detect motion within the sagittal plane (see Figures 1, 2, and 3). The control module contains the necessary hardware and software, microcontroller and other components to collect data from the sensors. The microcontroller is based on a Real-Time Operating System that scans the logic and Inputs/Outputs approximately every 5 ms. The sensors utilize matched LED emitter / receiver pairs to capture the users lift movement and provide data related to the time at which the user both begins and completes the lift. The lifting box includes grasping handles on each side and an area inside to hold various configurations of weights. The machine comes equipped with an electronic device (such as an I-pad) which communicates with and stores data in a cloud database. The lifting box triggers the sensors to obtain data in real time related to the movement, position, orientation, velocity and acceleration of the box while a user is lifting. Users

can perform different combinations of lifts such as floor to waist, waist to shoulder and shoulder to overhead lifts. To collect data, the clinician first uses the computerized software application (located on the I-Pad) to identify which type of lift will be performed. Once the subject lifts the box, the lower LED emitter/receiver beam is triggered to start the timing of the lift and collecting data. When the upper LED emitter/receiver beam is triggered, the data collection ends for that lift and a time stamp is created. Information regarding the amount of time required to complete the lift, the average velocity and the average acceleration of the attempt is recorded by the computerized software application. The standing force plate also records the weight of the subject and provides data on the amount of foot pressure being placed through both feet throughout the lift. The electronic device (I-pad) collects data from lifts and can be used to perform one or more calculations, provide graphs of one or more lifts, and assist the health care practitioner in determining when maximal load is being reached. Data collected and displayed in the application of the I-pad electronic device includes the weight of the box and the weights therein, the distance of the lift from start to finish position, the time from start to finish of the lift, average velocity (in/s), average load applied to the force plate by the left foot and the right foot, and the foot disparity (%).

The goal of this study was to investigate the claims of the originators of the Polylift, who state that the machine is able to recognize that as the weight lifted by the participant increases, the velocity and acceleration of the lift decreases and the amount of time of the lift increases. In other words, as the weight that a subject lifts approaches their maximal lift capacity, researchers should note a significant increase in the time it takes to lift that load, with a subsequent decrease in velocity and acceleration. Note: the goal of this study was not to validate that the variables (time, velocity and acceleration) were being measured accurately by the machine. The Polylift is calibrated by an electrical engineer prior to use to ensure that those measurements are being accurately collected. The researcher's main goal was to determine whether the machine was able to recognize the time increase and velocity and acceleration decrease as the participant approaches maximal lift capacity. The benefit of the Polylift is its ability to assist in determining whether maximal "effort" and lift capacity is being reached by a participant. If the machine is able to recognize the natural increase in time and decrease in velocity and acceleration that occurs as a participant approaches maximal lift capacity, then the machine can be considered a helpful device in objectifying maximal lift "effort" during functional capacity evaluations. The claims regarding the Polylift would then be validated if it accurately, and significantly produced data that agreed with Newton's second law of motion (Force=mass x acceleration) indicated by a decrease in acceleration and increase in time with increasing load. Historically, health care practitioners have had to make judgement calls when determining whether patients were providing full effort during lifting activities. If the Polylift can objectify the normal relationship between time and velocity/acceleration during lifting activities, then practitioners will have a tool to mitigate the subjective aspect of the functional

capacity evaluation. In this study, researchers wanted to determine if the Polylift could recognize a consistent, significant difference (increase) in the amount of time required to complete lifts as the subject approached maximal lift capacity. Researchers also wanted to determine if there was a concurrent significant decrease in acceleration as subjects approached maximal load.

Figure 1: The Polylift (Permission granted for use by Polylift, LLC)

Figure 2: Illustration of the Polylift
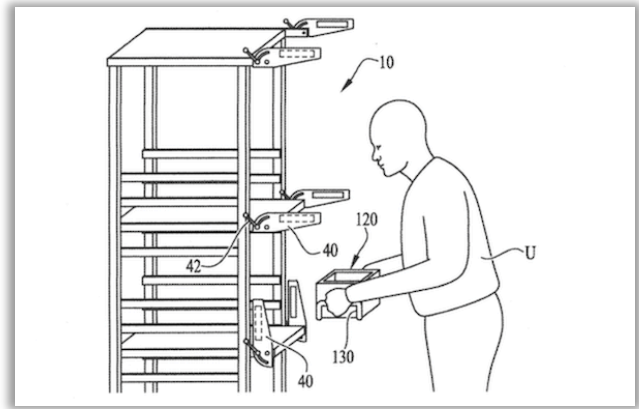
Figure 3: Illustration of a Subject Utilizing the Polylift During a Lift

2. Materials and Methods

To investigate the claims associated with the Polylift, two sets of data were collected. First, the participants' one repetition maximum (1RM) was determined to quantify "maximal lift capacity" in each subject in order to have a baseline for "maximal effort". Each participant performed repeated repetitions of a waist to shoulder lift at a submaximal level until they could no longer perform the lift with proper form. The number of repetitions performed was plugged into the Brzycki's One Repetition Maximum (1RM) formula [10]. The results were used to determine the participant's maximal lifting capacity. In the second portion of data collection, each participant performed a total of four waist to shoulder lifts. The weight of the first lift was 25% of the 1RM weight that was pre-determined. The second lift was 50%, the third lift was 75%, and the final lift was 100% of the pre-determined 1RM weight. The Polylift was utilized in this portion of the study to collect information regarding time, velocity and acceleration of each lift.

The subject sample was one of convenience drawn from healthy, uninjured college age students. Forty-two college students (20- Male, 22- Female), age 20 to 27 years old, volunteered to participate in this study. The exclusion criteria were as follows: any "yes" response noted on the Physical Activity Readiness Questionnaire (PAR-Q) [11], the presence of back pain within the last year, or any history of cardiac issues. Exclusion criteria was selected specifically to ensure the safety of the participants [12]. After clarity of the study's purpose and procedures were established, all participants signed an informed consent form. Subjects were informed that they were free to withdraw from the study or stop testing at any time. Participation length requirement was a single day of data collection. A baseline heart rate measurement was utilized prior to beginning data collection to maintain an objective measurement for the subject's safety, as well as serve as a baseline for continuing the second half of data collection.

2.1. Phase One Data Collection: One Repetition Maximum (1RM) Determination

A standardized lift from waist to shoulder was chosen to be performed for this study [13]. Waist to shoulder lifting is a
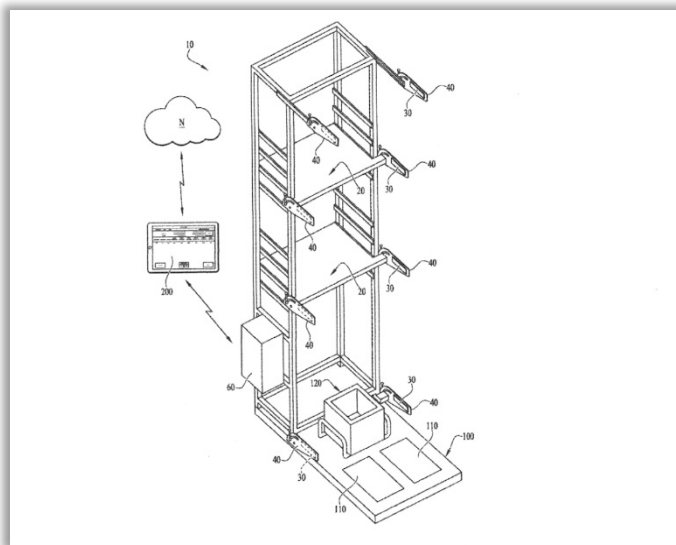
commonly utilized technique in many Functional Capacity Evaluations. Safe lifting guidelines provided by the Occupational Safety and Health Administration Technical Manual 7 were utilized as protocol along with correct demonstration from an investigator [14]. Each subject's 1RM prediction was calculated by using the submaximal repeated lift equation developed by Brzycki [10], [15]. Each subject's starting lift load was chosen by using a standardized maximum lift chart based on the subject's body weight [16]. All subjects were blind to the amount of weight placed inside the box. The starting waist position height was set at 35" from the floor, and the shoulder height at 55" from the floor [17], [18]. The subjects were instructed to perform the repeated lift as many times as possible with the same technique, speed, and form until fatigue [19], [20]. Prior to the investigation, operational definitions established by Gross et al. were observed by researchers in order to determine when maximal effort has been exceeded and when to safely stop the lift [8]. After completion of the repeated lift, the number of times each subject correctly performed the lift was inserted into Brzycki's 1RM formula {Load Lifted/ 1.0278 - (reps x 0.0278)} for calculation [10]. Subjects were then required to take a minimum of fifteen-minute rest break. Each subject's heart rate was re-measured to ensure that resting heart rate had returned to baseline level prior to beginning phase two of data collection.

2.2. Phase Two Data Collection: Polylift Data Collection

The second portion of data collection utilized a progressive resistance protocol along with the Polylift's ability to record the objective measurements time, acceleration, velocity, and distance. The progressive resistance protocol involved one waist to shoulder lift of each of the following loads: 25% of 1RM, 50% of 1RM, 75% of 1RM, and 100% of 1RM. The subjects were completely blind to their established 1RM and the amount of load used for each single trial. The subjects were instructed to lift the box as quickly but as safely as possible from waist height to shoulder height shelf. The Polylift's specialized data collection system was utilized, and the researchers carefully monitored to ensure that the subject maintained safe form and technique established with each lift. In between each trial, the subjects were allotted at least a one-minute rest break, as established by Matuszak et al. as sufficient time for recovery during 1RM testing [21].

3. Results

3.1. Descriptive Statistics

The criteria adopted to determine the 1RM produced results of subjects lifting between 12 and 65 pounds for 1-18 repetitions. Those results assisted in determining the computation of the subject's 1RM using the Brzycki formula. The resistance progression is demonstrated in Table 1 below.

In table 1, the data demonstrates the variable load lifted between subjects during Phase 1 data collection ranging from 12-65 lbs. for the initial calculation of 1RM using the Brzycki

formula. During Phase 2 of data collection, subjects lifted between 15.43-104.29 lbs. during the actual 1RM lift.

Table 1: Descriptive Statistics of Load Lifted by Test Subjects (n=42)

Variables	Range	Mean	Standard Deviation
Phase 1 Load lifted (lbs.)	12-65	38.262	15.800
Phase 1 Repetitions	1-18	7.929	4.319
Phase 2: 25% of 1RM (lbs)	3.86-26.07	12.394	6.095
Phase 2: 50% of 1RM (lbs)	4-52.14	24.700	12.331
Phase 3: 75% of 1RM (lbs)	11.57-78.21	37.182	18.285
Phase 4: 100% of 1RM (lbs)	15.43-104.29	49.577	24.382

Table 2: Mean Time & Acceleration during Trials of Progressive Resistance

Variable	Mean Time [s]	Standard deviation for time [s]	Mean acceleration [in/s²]	Standard Deviation for acceleration [in/s²]
25% of 1RM	0.342	0.117	245.104	196.385
50% of 1RM	0.354	0.086	185.567	79.557
75% of 1RM	0.416	0.100	132.909	52.687
100% of 1RM	0.548	0.204	85.607	41.080

In table 2, the data demonstrates the mean time and acceleration change with each stage of progression. The results of this study demonstrate how the mean time consistently increases with each stage of progression from 0.342 to 0.548 seconds. Therefore, the Polylift collected data that demonstrates that as the weight gets heavier, the test subject requires more time to successfully lift the weight. The results also demonstrate a decrease in acceleration with each stage of progression.

3.2. Pearson Product Moment Correlation

In this study, subjects varied greatly in their fitness levels and ability to lift heavy loads. Therefore, to perform a correlation, the load lifted was calculated as a percentage of each subject's body weight. A Pearson Product Moment Correlation was determined for each lift (25% of 1RM, 50% of 1RM, 75% of 1RM, and 100% of 1RM) for every subject and was compared to the velocity during each lift. Load lifted and velocity were found to be

moderately negatively correlated r(166)= -.283, p<.001. Figure 4 displays this relationship.
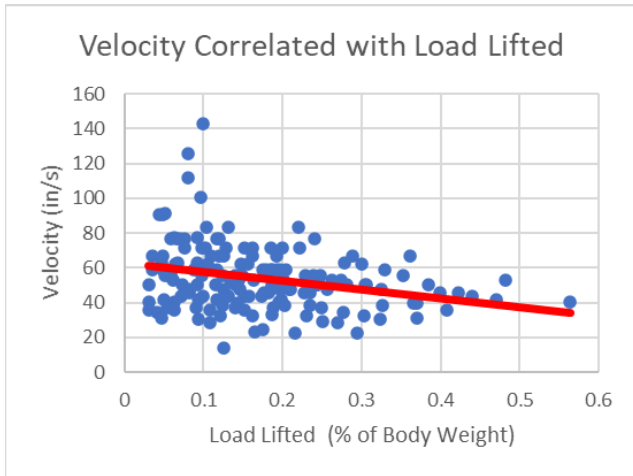
Figure 4: Velocity Correlated with Load Lifted (as % of body weight)

Table 3: Post-hoc Analysis Pairwise Comparisons for Time (LSD)

(I) Percent_1RM	(J) Percent_1RM	Mean Difference (I-J)	Std. Error	Sig.b	95% Confidence Interval for Differenceb	
					Lower Bound	Upper Bound
1	2	-.012	.013	.347	-.039	.014
	3	-.074*	.015	.000	-.105	-.043
	4	-.206*	.027	.000	-.261	-.150
2	1	.012	.013	.347	-.014	.039
	3	-.062*	.011	.000	-.084	-.039
	4	-.193*	.025	.000	-.245	-.142
3	1	.074*	.015	.000	.043	.105
	2	.062*	.011	.000	.039	.084
	4	-.131*	.026	.000	-.184	-.079
4	1	.206*	.027	.000	.150	.261
	2	.193*	.025	.000	.142	.245
	3	.131*	.026	.000	.079	.184

3.3. Repeated Measures ANOVA (Time)

A repeated measures ANOVA was also conducted to analyze the time needed to lift 25%, 50%, 75%, and 100% of a test subject's 1RM. There was a statistically significant effect on time across the four conditions, $F(3, 123)=40.874$, p<.001) with significance level set at p<.05. Post hoc analysis pairwise

comparisons utilizing LSD method further revealed that there were significant differences (p<0.01) in time between all conditions except for between 25% of 1RM and 50% of 1RM(p=0.347). Figure 5 displays this effect and Table 3 outlines results of post hoc analysis.
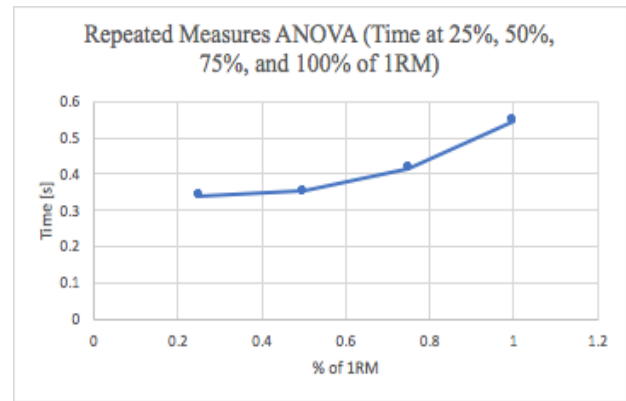
Figure 5: Time (seconds) Required at (1) 25%, (2) 50%, (3) 75%, and (4) 100% of 1RM (Repeated Measures ANOVA)

3.4. Repeated Measures ANOVA (Acceleration)

A second repeated measures ANOVA was conducted to examine the effects of acceleration at 25%, 50%, 75%, and 100% of 1RM. There was a statistically significant effect on acceleration across the four conditions, $F(3, 123)=21.811$ p<.001) with significance level set at p<.05. Post hoc analysis pairwise comparisons utilizing LSD method further revealed that there were significant differences in acceleration at 25%, 50%, 75%, and 100% of 1RM in all scenarios. Figure 6 displays this effect and Table 4 outlines results of post hoc analysis.
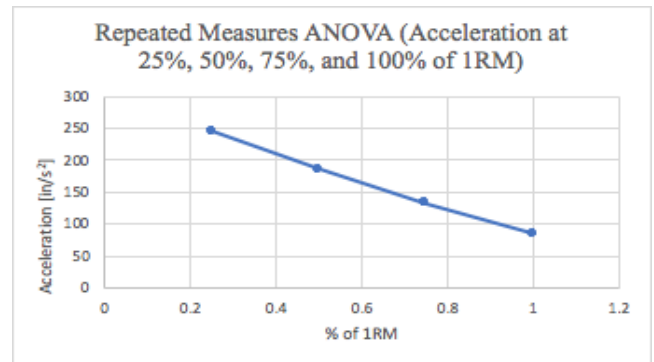
Figure 6: Acceleration at 25%, 50%, 75%, and 100% of 1RM (Repeated Measures ANOVA)

Table 4: Post-hoc Analysis Pairwise Comparisons for Acceleration (LSD)

(I)Percent_1RM_Accel	(J) Percent_1RM_Accel	Mean Difference (I-J)	Std. Error	Sig.b	95% Confidence Interval for Differenceb	
					Lower Bound	Upper Bound
1	2	59.537*	26.200	.028	6.626	112.448
	3	112.194*	28.061	.000	55.525	168.864

	4	159.497*	29.687	.000	99.543	219.451
2	1	-59.537*	26.200	.028	-112.448	-6.626
	3	52.658*	8.971	.000	34.541	70.775
	4	99.960*	10.102	.000	79.559	120.361
3	1	-112.194*	28.061	.000	-168.864	-55.525
	2	-52.658*	8.971	.000	-70.775	-34.541
	4	47.303*	7.495	.000	32.166	62.439
4	1	-159.497*	29.687	.000	-219.451	-99.543
	2	-99.960*	10.102	.000	-120.361	-79.559
	3	-47.303*	7.495	.000	-62.439	-32.166

4. Discussion

The pattern of the results suggests that as the weight lifted by the participants increased, the acceleration of the lift decreased and the amount of time required for each lift increased. The variables of load lifted and velocity were significantly negatively correlated, demonstrating that as each participant lifted a higher percentage of their body weight, the velocity decreased. This correlation was present despite the fact that the subjects varied greatly in individual fitness levels and ability to lift heavy loads. There were significant differences in the amount of time for a participant to lift 25%, 50%, 75%, and 100% of their 1RM. In comparing each of these four conditions, there was a significant increase in time required to lift the weight in all conditions except for 25% and 50% of the 1RM. There were significant differences in the acceleration required to lift 25%, 50%, 75%, and 100% of the participant's 1RM. In comparing each of these four conditions, there was a significant decrease in acceleration between all four conditions.

A primary finding of this study is that the Polylift machine is able to recognize the variables of time and acceleration and display a consistent and significant relationship between these variables. As expected, when a person lifts a weight that is increasingly closer to their 1RM, the time required to lift this weight increases, and the acceleration of lifting this weight decreases. While this may be a well-known and understood fact, a device to measure and objectify this phenomena has not existed up to this point.

This study utilized established theories and validated calculations to assist in the investigation of claims related to the machine. Newton's second law of motion, which involves the variables of mass and acceleration during the production of force, was the basis of the hypothesized outcome. The formula Force = Mass x Acceleration establishes an inverse relationship between the variables such that an increase in the force required to move an object of a higher weight would result in a decrease in acceleration. Because lifting involves an object being moved through space with either submaximal or maximal force, the time to move the heavier object from one point to the other should increase as the load increases. Advantageously, all of the mentioned variables involved in the task of lifting are able to be collected by the Polylift, as demonstrated in this study.

Another calculation involved in the study was the validated Brzycki formula which is a commonly used tool to assess muscle strength. In order to generate force, strength is a vital factor to successfully perform a lift and cause change in acceleration. The formula provided baseline data of the 1RM for each subject, which was used to progress the resistance in the second phase of data collection. The Polylift demonstrated the ability to detect changes in the variables. In reviewing the results, it was significantly demonstrated that the Polylift is able to indicate maximal lift capacity by accurately demonstrating a consistent decrease in acceleration with increasing loads due to the diminishing ability to generate force. In particular, the load lifted at 25% of 1RM and 100% of 1RM demonstrated the Polylift's ability to detect a considerable difference in acceleration between both lifts.

It should be mentioned that there were some results during the 25% of 1RM lift that were not expected. When reviewed, these results produced slower acceleration rates when compared to the acceleration of the 50% 1RM lift. Researchers hypothesize that this can be attributed to the subject being cautious with the first trial after the completing submaximal lifts of a moderate weight in the initial data collection portion of the study. This occurrence brings to the forefront the many complex factors involved, especially the psychological aspect of lifting [22].

The data from this study suggests that the use of the Polylift to determine maximal lifting capacity will deliver measurable results indicated by the change in variables during the lifting procedure. The implications of these findings could be highly important as they can be applied during the functional capacity evaluation.

Limitations and Indications for Future Studies

Nacimento et al. determined that the Brzycki formula was most accurate when maximum repetitions ranged between 7-10 [23]. Our study included all results, with repetitions ranging between 1-18. This should be considered a limitation based on the premise that the repetitions sometimes went beyond the 7-10 range. Another limitation to be considered is the psychological aspect of performing the 1RM trials following repeated lifts during phase one data collection [24]. Many subject's acceleration and velocity measurements were inconsistent during the first single trial at 25% 1RM, likely because of the subject's expectation of a heavy load. A test trial with cueing for speed may be considered for future studies.

5. Conclusions

The significance of the results in this study demonstrate that the Polylift is able to indicate maximal lift capacity by accurately demonstrating a consistent decrease in acceleration with increasing loads due to the diminishing ability to generate force. Practitioners who are well versed in ergonomics and the area of human performance now have available to them a piece of equipment that provides objective measurements to assist in determining an individual's readiness to return to work. The use

of the Polylift during functional capacity evaluations and rehabilitation in general allows clinicians not to rely solely on their observational skills or subjective reports from the patient when full lifting capacity has been reached. The Polylift is able to reveal, through change in time and acceleration, if physical "effort" matches the expected outcomes. Conversely, if the machine does not identify an obvious increase in time with a decrease in acceleration, then the clinician can objectively assert that full "effort" and maximal lift capacity has not been demonstrated by the participant. The impact of this type of tool in functional capacity evaluations is significant and may be of great use to clinicians tasked with evaluating patients who have sustained industrial injuries. The Polylift assists in objectifying results and determining a patient's readiness to return to work.

Conflict of Interest

The authors of this study have no business and/or financial interests in the Polylift or other potential conflicts of interest to disclose regarding this research.

Acknowledgment

References

[1] J. P. Leigh, "Economic burden of occupational injury and illness in the United States," The Milbank Quarterly, **89**(4), 728–772, 2011, https://doi.org/10.1111/j.1468-0009.2011.00648.x.

[2] N. Z. Ratzon, T. Jarus, A. Catz, "The relationship between work function and low back pain history in occupationally active individuals," Disability and Rehabilitation, **29**(10), 791–796, 2007, https://doi.org/10.1080/09638280600919681.

[3] S. J. Isernhagen, "Functional capacity evaluation: Rationale, procedure, utility of the kinesiophysical approach," Journal of Occupational Rehabilitation, **2**(3), 157– 168, 1992, https://doi.org/10.1007/BF01077187.

[4] J. J. Chen, "Functional capacity evaluation & disability," The Iowa Orthopaedic Journal, **27**, 121–127, 2007.

[5] S. J. Isernhagen, "Physical therapy and occupational rehabilitation," Journal of Occupational Rehabilitation, **1**(1), 71–82, 1991, https://doi.org/10.1007/BF01073281.

[6] R. J. Smeets, H. J. Hijdra, A. D. Kester, M. W. Hitters, J. A. Knottnerus, "The usability of six physical performance tasks in a rehabilitation population with chronic low back pain," Clinical Rehabilitation, **20**(11), 989–997, 2006, https://doi.org/10.1177/0269215506070698.

[7] U.S. Bureau of Labor and Statistics, "Nonfatal Occupational Injuries and Illnesses Requiring Days Away From Work, 2015," 2016.

[8] D. P. Gross, & M. C. Battié, "Reliability of Safe Maximum Lifting Determinations of a Functional Capacity Evaluation. Physical Therapy," **82**(4), 364–371, 2002, https://doi.org/10.1093/ptj/82.4.364.

[9] M. Lemstra, W. P. Olszynski, W. Enright, "The sensitivity and specificity of functional capacity evaluations in determining maximal effort: a randomized trial," Spine, **29**(9), 953–959, 2004.

[10] M. Amarante, E. S. Cyrino, F. Y. Nakamura, "Validation of the Brzycki equation for the estimation of 1-RM in the bench press," Rev Bras Med Esporte, **13**(1), 40-42, 2007, https://doi.org/10.1590/S151786922007000100011.

[11] D. E. R. Warburton, S. S. D. Bredin, V. K. Jamnik, N. Gledhill, "Validation of the PAR-Q+ and ePARmed-X+," The Health & Fitness Journal of Canada, **4**(2), 38-46, 2011, https://doi.org/10.14288/hfjc.v4i2.15.

[12] R. Adams, "Revised Physical Activity Readiness Questionnaire," Canadian Family Physician Medecin de Famille Canadien, **45**, 992, 995, 1004–1005, 1999.

[13] U. Abdul-Hameed, P. Rangra, M. Y. Shareef, & M. E. Hussain, "Reliability of 1-repetition maximum estimation for upper and lower body muscular strength measurement in untrained middle aged type 2 diabetic patients," Asian Journal of Sports Medicine, **3**(4), 267–273, 2012.

[14] Occupational Safety and Health Administration, "(OSHA) Technical manual," 2014.

[15] J. L. Mayhew, B. D. Johnson, M. J. Lamonte, D. Lauber, W. Kemmler, "Accuracy of prediction equations for determining one repetition maximum bench press in women before and after resistance training," Journal of Strength and Conditioning Research, **22**, 1570–1577, 2008,

[16] C. Kisner, L. A. Colby, J. Borstad, (2018). Therapeutic Exercise: Foundations and Techniques, (7th ed.), Philadelphia, PA: F.A. Davis Company, 2018.

[17] R. J. Savage, M. A. Jaffrey, D. C. Billing, D. J. Ham, "Maximal and sub-maximal functional lifting performance at different platform heights," Ergonomics, **58**(5), 762–769, 2015, https://doi.org/10.1080/00140139.2014.983185.

[18] Y. Blache, L. Desmoulins, P. Allard, A. Plamondon, M. Begon, "Effects of height and load weight on shoulder muscle work during overhead lifting task," Ergonomics, **58**(5), 748–761, 2015, https://doi.org/10.1080/00140139.2014.980336.

[19] R. L. Smith, "Therapists' Ability to Identify Safe Maximum Lifting in Low Back Pain Patients During Functional Capacity Evaluation," Journal of Orthopaedic & Sports Physical Therapy, **19**(5), 277–281, 1994. https://doi.org/10.2519/jospt.1994.19.5.277.

[20] L. Gardener, K. McKenna, "Reliability of occupational therapists in determining safe, maximal lifting capacity,"Australian Occupational Therapy Journal, **46**(3), 110–119, 1999, https://doi.org/10.1046/j.1440-1630.1999.00184.x.

[21] M. E. Matuszak, A. C. Fry, L. W. Weiss, T. R. Ireland, M. M. McKnight, "Effect of rest interval length on repeated 1 repetition maximum back squats," Journal of Strength and Conditioning Research, **17**(4), 634–637, 2003,

[22] M.E. Geisser, M.E. Robinson, Q.L. Miller, *et al.,* "Psychosocial Factors and Functional Capacity Evaluation Among Persons with Chronic Pain," Journal of Occupational Rehabilitation, **13,** 259–276, 2003, https://doi.org/10.1023/A:1026272721813.

[23] M. A. Nascimento, E. S. do Cyrino, F. Y. Nakamura, M. Romanzini, H. J. C. Pianca, M. R. Queiróga, "Validação da equação de Brzycki para a estimativa de 1-RM no exercício supino em banco horizontal," Revista Brasileira de Medicina Do Esporte, **13**(1), 47–50, 2007, https://doi.org/10.1590/S1517-86922007000100011.

[24] G. M. Kaplan, S. K. Wurtele, D. Gillis, "Maximal effort during functional capacity evaluations: an examination of psychological factors," Archives of Physical Medicine and Rehabilitation, **77**(2), 161–164, 1996,

Downlink Indoor Coverage Performance of Unmanned Aerial Vehicle LTE Base Stations

Mahmut Demirtaş[*], Kerem Çağdaş Durmuş, Gülçin Tanış, Caner Arslan, Metin Balcı

Ulak Telecommunications Inc., Istanbul, 34906, Turkey

A R T I C L E   I N F O

A B S T R A C T

In this study, we study on the downlink indoor coverage performance of unmanned air vehicle (UAV) base stations. We consider a probabilistic expression for air-to-ground (ATG) path loss, and a deterministic one for additional indoor losses in order to provide a practical model. One of our important assumptions is that the UAV base station operates at the frequencies reserved for 4th Generation (4G) – Long Term Evaluation (LTE) based mission critical services in Turkey –around 2.6 GHz–. Therefore, we are able to neglect intercell interference issue, and we may rely on signal-to-noise ratio (SNR) for our coverage definition. We consider four different SNR requirement throughout our performance evaluation, and investigate the effect of UAV altitude and other related parameters on the radius of service area. We first observe that rural coverage performance is always better than urban conditions –this result is fully compatible with the fact that attenuation levels significantly arise in urban regions–. In addition, we show that increasing quality of service (QoS) requirement and/or using a more directive antenna unit decrease the coverage radius as they are expected. Thereupon, we conclude that it is possible to obtain the optimum altitude level –by employing the framework proposed here– in order to satisfy certain service criteria.

1   Introduction

In this paper, we extend one of our earlier studies presented in 27th Signal Processing and Communications Applications Conference (SIU) [1]. As we argue in [1], UAV base station idea seems to be a promising solution to provide cellular service for both the locations which cannot be covered by employing terrestrial networks and the times in which terrestrial networks may not be serving at all (e.g. natural disasters). In [2] and [3], earlier studies related to the UAV base station concept are summarized, and possible use cases are investigated. In addition, topics open for further studies are discussed in these publications as well. Among several other topics to discuss, modelling channel conditions of such a non-terrestrial network in a practical and also tractable way is an important requirement [4]–[11].

In [4, 5, 6], coverage performance of UAV networks is investigated for outdoor users, and the effect of UAV altitude on the coverage radius is discussed in detail. In the studies mentioned, ATG channel is modelled in two parts. First part corresponds to the free-space losses, and assumed to be a deterministic function which depends on the radiation distance. Second part basically aims the

losses in where man-made structures exist –urban environment–, and modelled as a Normal distributed random variable. In this paper, we follow this piecewise model to express the path loss related to ATG channel, and examine urban and rural conditions separately. The reason of the using deterministic approaches is that reliable characterization of the ATG propagation for large scale fading statistics. In addition, it is important to note that fast fading effect of the channel is ignored throughout this study.

Some earlier publications related to the topic utilize a practical UAV to form a testbed, and generate empirical channel models to figure out ATG propagation characteristics [9]–[11]. All three of those are funded by the same institution, and aims to model over-water, mountainous and near-urban environments, respectively. As the next step of this work, we also target to assemble a functional and realistic testbed.

Besides, some previous studies utilize stochastic processes to concentrate on outdoor coverage performance of UAV base stations [12, 13]. Authors of the former assume that both UAV and terrestrial base stations are deployed in an overlapping manner, and coordinate with each other to provide a continuous service. Such an overlapping structure of UAV and terrestrial base stations is not cov-

[*]Corresponding Author: Mahmut Demirtaş, Turkey, +903122869487, mahmut.demirtas@ulakhaberlesme.com.tr

ered in the scope of this paper. The latter one considers only UAV base stations distributed according to a Poisson point process (PPP). Then, authors provide approximate expressions for both coverage ratio and average data rate. Here, we emphasize that we assume there exists only one UAV base station that operates on mission critical frequency bands, and therefore such stochastic processes are not required to model UAV base station density around. Yet, as a future concern, investigating networks consist of multiple UAV base stations is already scheduled.

Another significant aspect of this work is considering additional losses to serve indoor users. In literature, these indoor losses are generally studied for terrestrial networks rather than UAV ones [14]–[17]. In [14, 15], indoor losses are evaluated as a function of number of floors penetrated. Authors of [16, 17] offer a more complicated system model which accounts the number of internal/external walls and indoor propagation distance. Since only the latter one of these supports sub-6 GHz frequency bands, we follow the model proposed in [17]. Once we build a practical testbed, generating a novel indoor propagation model will be another important objective in our agenda.

Rest of this paper is organized as follows: Section 2 summarizes the system model that we employ, Section 3 proposes a parametric expression for indoor coverage ratio, Section 4 calculates coverage radius for several SNR demands, quality-of-service (QoS) requirements and antenna directivity levels, and finally Section 5 discusses the results obtained throughout our extensive simulations.

2   System Model

The aim of this study is to show that UAV base stations can be provide a fast and effective coverage in areas not covered by terrestrial networks or in emergency situations –by using frequency bands reserved for mission critical services–. Considering that UAV base station users are not exposed to interference, SNR is employed as performance criterion. The altitude range of UAV base station is accepted as 0.5-3 km. Maximum velocity of the UAV is 180 km/h. The movement of the UAV can be neglected because displacement on the air within the channel stationarity duration is too small compared to altitude of the UAV. Figure 1 shows an example of UAV base station layout.

The study assumes that UAV carries an outdoor base station which operates on Band 7 (2.6 GHz) which is defined by European Telecommunications Standards Institute (ETSI) as an LTE frequency band [18]. In this system model, UAV base station works on Single Input Single Output (SISO) mode and has single sector which is 120°.

2.1   Propagation Model and Antenna Gain

In the literature, the propagation model of UAV base stations is examined in two parts as free space loss and urban losses [5]. It is accepted that free space loss has a deterministic character and urban losses have a probabilistic one. The attenuation for cases with line of sight (LOS) and non line of sight (NLOS) are as follows:

$$PL_i = 20 \log \left(\frac{4\pi f_c d}{c} \right) + \lambda_i \quad \text{[dB]} \tag{1}$$

where f_c, d, c and λ_i, $i \in \{\text{LOS}, \text{NLOS}\}$ refers to carrier frequency, propagation distance, speed of light and urban losses respectively. In literature, these urban losses are considered to have a Normal distribution: $\lambda_{\text{LOS}} \sim \mathcal{N}(\mu_{\text{LOS}}, \sigma_{\text{LOS}}^2)$ and $\lambda_{\text{NLOS}} \sim \mathcal{N}(\mu_{\text{NLOS}}, \sigma_{\text{NLOS}}^2)$. μ_i and σ_i^2, $i \in \{\text{LOS}, \text{NLOS}\}$ express the mean and variance values of corresponding Normal distributions and numerical values can be calculated with respect to the propagation angle.
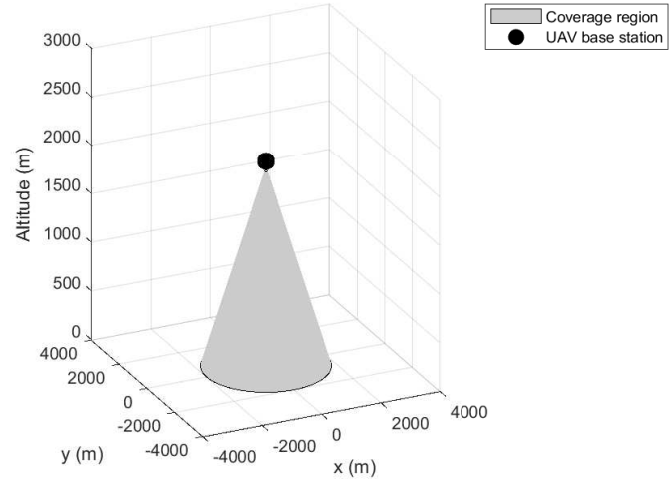
Figure 1: UAV base station coverage region.

The LOS and NLOS possibilities required to complete the propagation model are also functions of the propagation angle and denoted as follows:

$$\Pr\{\text{LOS}\} = \frac{1}{1 + a(-b(\theta - a))}$$
$$\Pr\{\text{NLOS}\} = 1 - \Pr\{\text{LOS}\} \tag{2}$$

Since calculating the constants a and b above is not in the scope of this study, numerical values are given in Chapter 4. The average loss of external environment obtained using Equations (1) and (2) can be expressed as follows:

$$PL_{\text{out}} = \sum_i PL_i \Pr\{i\} \quad \text{[dB]}$$
$$= 20 \log \left(\frac{4\pi f_c d}{c} \right)$$
$$+ \lambda_{\text{LOS}} \Pr\{\text{LOS}\} + \lambda_{\text{NLOS}} \Pr\{\text{NLOS}\} \quad \text{[dB]} \tag{3}$$

In addition, a model defined by ETSI is used to evaluate base station antenna gain [19]. According to this model, the antenna gain is given as a function of the beam angle:

$$G = G_{max} - \min \left[12 \left(\frac{\alpha}{\alpha_{3\text{dB}}} \right)^2, A_{max} \right] \quad \text{[dB]} \tag{4}$$

where $\alpha_{3\text{dB}}$, is the beam width corresponding to a 3 dB loss and its value basically determines the directivity of the antenna. Also, $G_{max} = 15$ dB and $A_{max} = 20$ dB represent the maximum antenna gain and the maximum attenuation, respectively. Variable of the expression above, namely beam angle is indeed a function of penetration angle: $\alpha = \pi/2 - \theta$.

2.2 Indoor Model

In literature, there exist studies which expresses indoor penetration (internal and external walls) and free space loss due to the indoor propagation by using empirical models [16, 17]. Within the model given in [17], total path loss for indoor users is given as follows:

$$PL_{\text{in}} = md_{in} + nL_{in} + kL_{out} \quad \text{[dB]} \tag{5}$$

where d_{in} and m denote the indoor propagation distance and the indoor path loss constant. n, L_{in}, k and L_{out} represent the number of penetrated internal walls, penetration loss of one internal wall, number of external walls penetrated and penetration loss of one external wall, respectively. The values of these parameters at the carrier frequency of 2.6 GHz are given as $m = 0.49$ [dB/m], $L_{in} = 4.9$ [db] and $L_{out} = 24.8$ [dB]. In this study, it was assumed that one external and one inner wall is penetrated to provide indoor coverage, and there is an indoor propagation distance of five meters. Therefore, the additional loss due to indoor coverage is calculated as $PL_{\text{in}} = 32.15$ dB.

2.3 Performance Criterion

As it is stated above, we assume that UAV base station utilizes the frequencies reserved for mission critical services. Thereby, we do not consider any interference effect, and employ SNR as our performance criterion. More precisely, we define the coverage incident by the probability of SNR is greater than a given threshold. By using (3), (4) and (5), SNR can be calculated as follows:

$$\text{SNR} = P_{tx} + G - PL_{\text{out}} - PL_{\text{in}} - P_N \quad \text{[dB]} \tag{6}$$

Here, P_{tx} ve P_N represent transmitted signal strength and noise power, respectively. We note that total noise power is basically given as a function of bandwidth (BW). In the following section, by using the system model given, the probability of indoor coverage of ATG communication systems will be expressed.

3 Probability of Indoor Coverage

Indoor coverage probability of a geographical location is defined as the probability of SNR exceeds a certain value. Corresponding expression is given as

$$\begin{aligned}\Pr\{c\} &= \Pr\{P_{rx} \geq s\} \\ &= \Pr\{PL_{\text{out}} \leq P_{tx} + G - PL_{\text{in}} - P_N - s\} \end{aligned} \tag{7}$$

where $s \in \{0.76, 4.7, 10.4, 15.9\}$ refer to the different SNR limits considered in this study. The reason for choosing values given is that these values are used in the literature as SNR levels to determine certain channel quality indices (CQIs) [20].

As given in (3), PL_{out} is basically the summation of the two different random variables with Normal distribution multiplied by two coefficients, namely Pr{LOS} and Pr{NLOS}. Thereupon, we conclude that PL_{out} is also a Normally distributed random variable

$$PL_{\text{out}} \sim \mathcal{N}(\mu_{PL}, \sigma_{PL}^2) \tag{8}$$

where μ_{PL} and σ_{PL}^2 represent the mean and variance parameters of the distribution, respectively. Numerical values of mean and variance can be calculated as follows:

$$\mu_{PL} = 20 \log\left(\frac{4\pi f_c d}{c}\right) + \mu_{\text{LOS}}\Pr\{\text{LOS}\} + \mu_{\text{NLOS}}\Pr\{\text{NLOS}\} \tag{9}$$

$$\sigma_{PL}^2 = \sigma_{\text{LOS}}^2(\Pr\{\text{LOS}\})^2 + \sigma_{\text{NLOS}}^2(\Pr\{\text{NLOS}\})^2 \tag{10}$$

Once we compute the distribution parameters in (9) and (10) –and according to the fact that outdoor path loss is modelled as a Gaussian random variable–, coverage probability given in (7) can be evaluated by using the tail probability which is defined as $\mathbb{Q}$ function [21]. Thus, (7) is given as

$$\Pr\{c\} = 1 - \mathbb{Q}\left(\frac{P_{tx} + G - PL_{\text{in}} - P_N - s - \mu_{PL}}{\sigma_{PL}}\right) \tag{11}$$

As a result of $\mathbb{Q}$ function exists in (11), it is not easy to express coverage probability in closed form. Yet, a fast, numerical solution exists. In the next section, we demonstrate our comprehensive simulation results in order to support our theoretical findings.

4 Numerical Analysis

In this section, we investigate the coverage radius for different SNR demands by utilizing the coverage expression above. The system parameters used in the simulations are: f_c = 2.6 GHz, P_{tx} = 46 dBm, α_{3dB} = 65°, BW = 10 MHz, P_N = −95 dB, a_{rural} = 4.88, a_{urban} = 9.61, b_{rural} = 0.43 and b_{urban} = 0.16. The center frequency and bandwidth of the base station are commonly used numerical values in LTE systems. Transmit power is maximum base station power value for given bandwidth standardised by ETSI [19]. Effective noise power is calculated according to formulation stated in [22]. 3dB beam width corresponds to 65° when UAV base station has 120° sector wide [19]. Other parameters used in simulations are empirical values from earlier researches.

In Figure 2a, we plot 90% coverage radius for an SNR requirement of 0.76 dB with respect to the UAV altitude. The first important observation obtained from the figure is that the coverage radius in the rural area is greater for the whole altitude interval. This result is intuitive since the channel conditions are rougher for urban areas. Another important result is that the coverage radius increases with increasing altitude. Therefore, in cases where the SNR requirement is as low as in this scenario, the highest feasible altitude value provides the best coverage radius.

In Figures 2b, 2c and 2d, the SNR requirements are chosen as 4.7 dB, 10.4 dB and 15.9 dB, respectively. The first major finding regarding to the figures is that the coverage radius is getting smaller with the increasing SNR requirement. As a matter of fact, in the highest SNR requirement scenario (Figure 2d), after the altitude of 2000 m in urban scenario and 2200 m in rural scenario, the coverage is completely lost. In addition, when the SNR requirement is high, the coverage radius becomes a concave function rather than a monotone increasing one. Therefore, it is seen that optimum altitude is not the greatest feasible value anymore.

(a) *s*=0.76 dB.

(b) *s* = 4.7 dB.
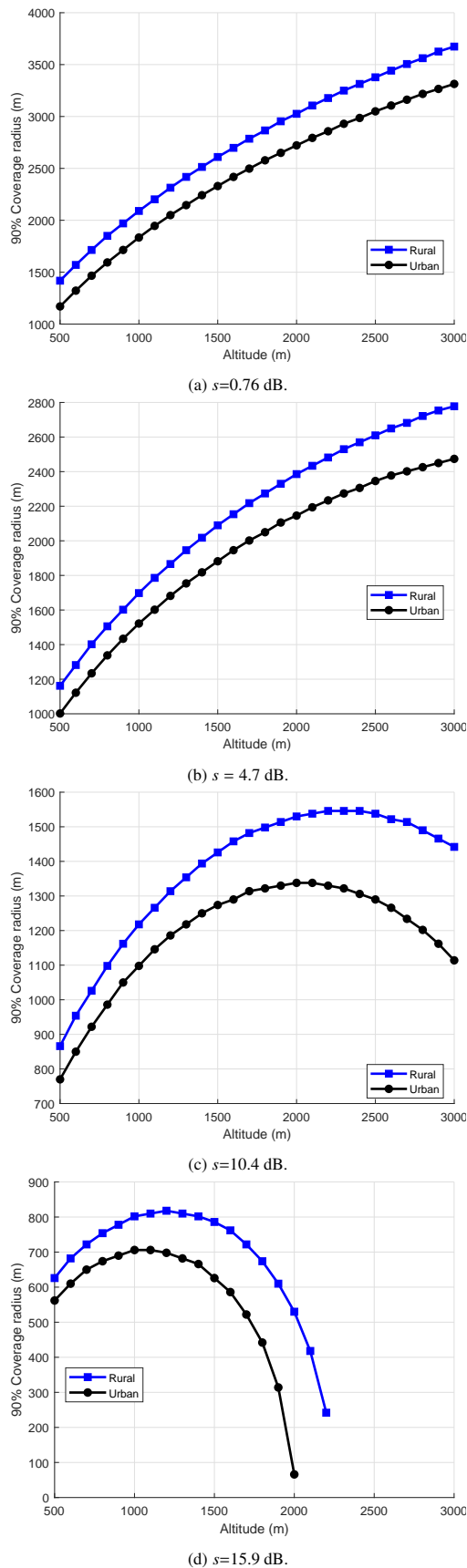
(c) *s*=10.4 dB.

(d) *s*=15.9 dB.

Figure 2: 90% coverage requirement, $\alpha_{3dB} = 65°$.

As seen in Figure 2c, the optimum altitude values for $s = 10.4$

dB in rural and urban scenarios are 2300 m and 2000 m, respectively. In the case of $s = 15.9$ dB (Figure 2d), the optimum altitude values decrease further and become 1200 m for rural scenario and 1100 m for urban scenario. Under the results achieved, we conclude that it is possible to obtain an optimum altitude value for providing a certain QoS through the largest service area.

Then, we increase the coverage ratio requirement to 99% to understand the effect of QoS expectation on coverage radius. In Figure 3, we observe that for each SNR level, coverage area gets slightly smaller with increasing coverage ratio requirement. This result is quite intuitive regarding to both theoretical coverage expression proposed in (11) and the general understanding of wireless communications. We also emphasize that maximum urban area radius that can be served with the largest SNR level decreases when we require a coverage ratio of 99%.

Finally, we analyze the effect of antenna directivity on the coverage radius. In Figure 4, we fix *s*=15.9 dB and consider a variable beam angle. For each configuration, it is observed that coverage radius enlarges with the increasing beam angle (decreasing directivity) whereas function characteristics do not change much. However, it is important to emphasize that a narrower coverage area would be preferred for certain mission critical services. In addition, for a multi-UAV base station network, narrow beams may be required to limit the intercell interference from time to time. Thereupon, a configurable directivity pattern seems to be a plus for UAV networks.

5   Conclusion

In this paper, we study on downlink indoor coverage performance of UAV base stations. According to the system model proposed, we accept SNR as the primary performance criterion. For the channel, we employ a two-staged model in which outdoor and indoor losses are assumed to be probabilistic and deterministic, respectively. Then, by employing the system model specified, we express the coverage ratio in terms of UAV altitude, cell radius and SNR requirement. In addition, to support our theoretical findings, we share our extensive simulation results. Throughout our simulations, we investigate the effect of UAV altitude, SNR and coverage ratio requirements, and antenna directivity on the coverage radius. According to our simulation results and observations, we conclude that it is possible to choose the UAV altitude level that optimizes the coverage radius. Finally, we note that we aim to build a practical test setup in order to build our own air-to-ground channel model to utilize in our future studies.

Conflict of Interest   The authors declare no conflict of interest.
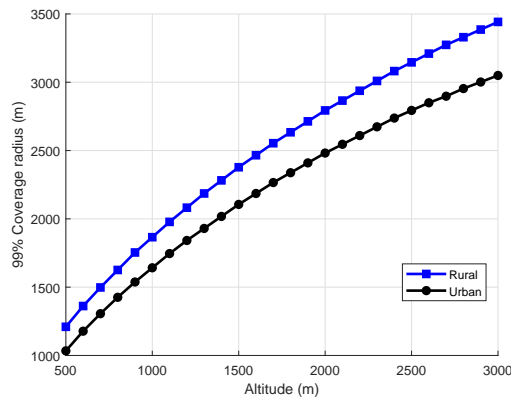
(a) s=0.76 dB.
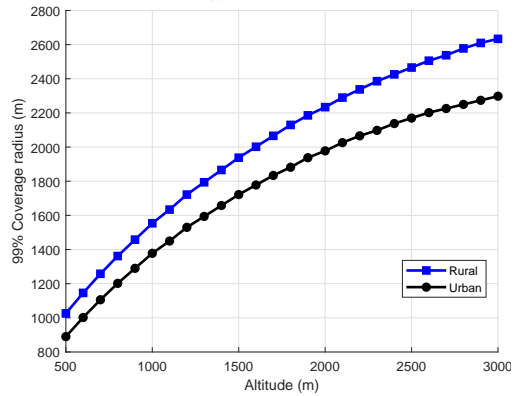
(b) $s = 4.7$ dB.
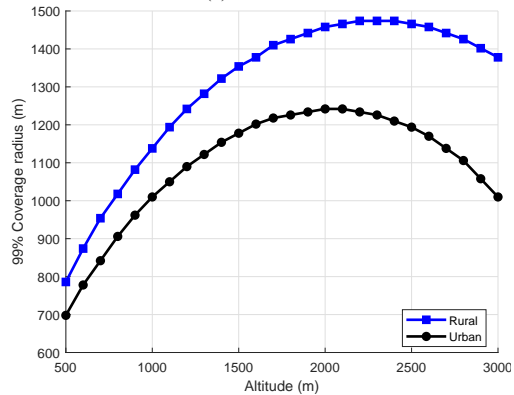
(c) s=10.4 dB.
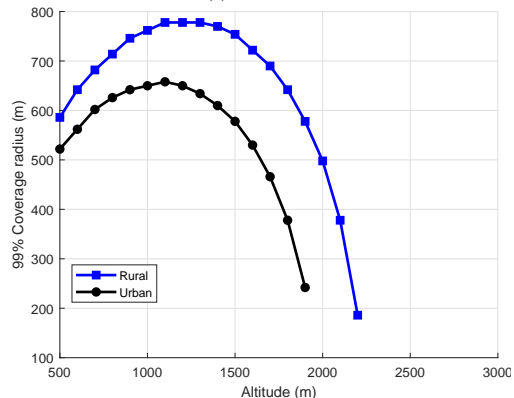
(d) s=15.9 dB.

Figure 3: 99% coverage requirement, $\alpha_{3dB} = 65°$.
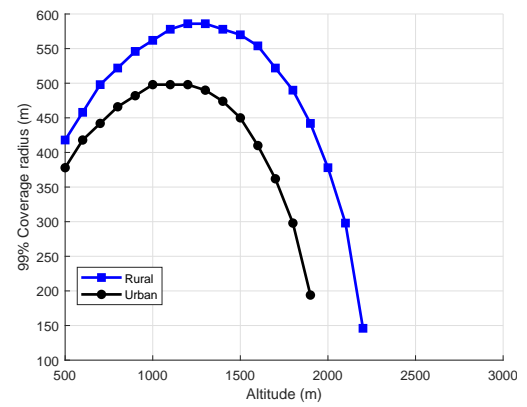
(a) $\alpha_{3dB} = 45°$.
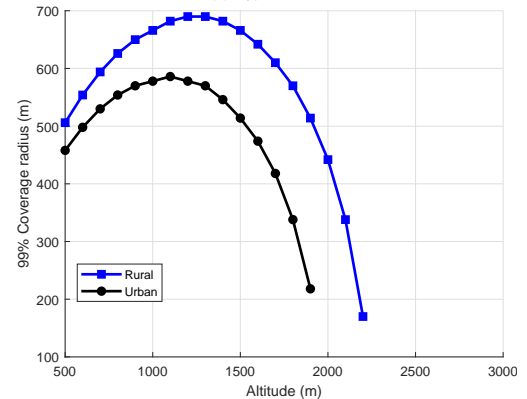
(b) $\alpha_{3dB} = 55°$.
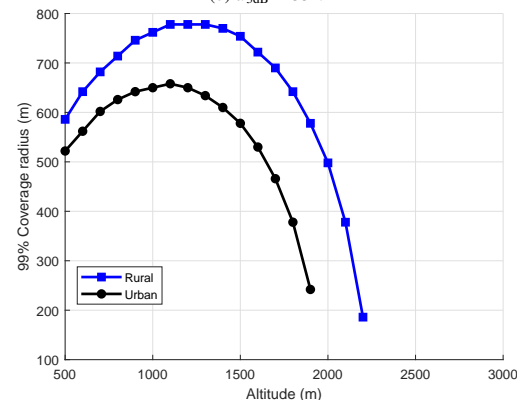
(c) $\alpha_{3dB} = 65°$.
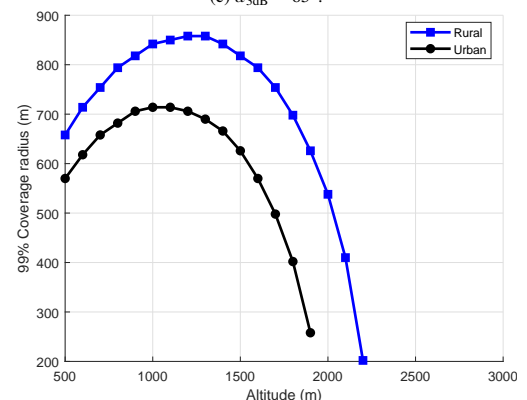
(d) $\alpha_{3dB} = 75°$.

Figure 4: 99% coverage requirement, s=15.9 dB.

References

[1] M. Demirtaş, F. Aydın, G. Tanış, C. Arslan, "Indoor Coverage Analysis for Unmanned Aerial Vehicle Base Stations," in 2019 27th Signal Processing and Communications Applications Conference (SIU), 1–4, 2019, doi: 10.1109/SIU.2019.8806575.

[2] T. C. Tozer, D. Grace, "High-altitude platforms for wireless communications," Electronics Communication Engineering Journal, **13**(3), 127–137, 2001, doi: 10.1049/ecej:20010303.

[3] I. Bor-Yaliniz, H. Yanikomeroglu, "The New Frontier in RAN Heterogeneity: Multi-Tier Drone-Cells," IEEE Communications Magazine, **54**(11), 48–55, 2016, doi:10.1109/MCOM.2016.1600178CM.

[4] M. Alzenad, A. El-Keyi, F. Lagum, H. Yanikomeroglu, "3-D Placement of an Unmanned Aerial Vehicle Base Station (UAV-BS) for Energy-Efficient Maximal Coverage," IEEE Wireless Communications Letters, **6**(4), 434–437, 2017, doi:10.1109/LWC.2017.2700840.

[5] A. Al-Hourani, S. Kandeepan, S. Lardner, "Optimal LAP Altitude for Maximum Coverage," IEEE Wireless Communications Letters, **3**(6), 569–572, 2014, doi:10.1109/LWC.2014.2342736.

[6] A. Al-Hourani, S. Kandeepan, A. Jamalipour, "Modeling air-to-ground path loss for low altitude platforms in urban environments," in 2014 IEEE Global Communications Conference, 2898–2904, 2014, doi:10.1109/GLOCOM.2014.7037248.

[7] J. Holis, P. Pechac, "Elevation Dependent Shadowing Model for Mobile Communications via High Altitude Platforms in Built-Up Areas," IEEE Transactions on Antennas and Propagation, **56**(4), 1078–1084, 2008, doi: 10.1109/TAP.2008.919209.

[8] Q. Feng, J. McGeehan, E. K. Tameh, A. R. Nix, "Path Loss Models for Air-to-Ground Radio Channels in Urban Environments," in 2006 IEEE 63rd Vehicular Technology Conference, volume 6, 2901–2905, 2006, doi: 10.1109/VETECS.2006.1683399.

[9] D. W. Matolak, R. Sun, "Air–Ground Channel Characterization for Unmanned Aircraft Systems—Part I: Methods, Measurements, and Models for Over-Water Settings," IEEE Transactions on Vehicular Technology, **66**(1), 26–44, 2017, doi:10.1109/TVT.2016.2530306.

[10] R. Sun, D. W. Matolak, "Air–Ground Channel Characterization for Unmanned Aircraft Systems Part II: Hilly and Mountainous Settings," IEEE Transactions on Vehicular Technology, **66**(3), 1913–1925, 2017, doi:10.1109/TVT.2016.2585504.

[11] D. W. Matolak, R. Sun, "Air–Ground Channel Characterization for Unmanned Aircraft Systems—Part III: The Suburban and Near-Urban Environments," IEEE Transactions on Vehicular Technology, **66**(8), 6607–6618, 2017, doi: 10.1109/TVT.2017.2659651.

[12] A. V. Savkin, H. Huang, "Deployment of Unmanned Aerial Vehicle Base Stations for Optimal Quality of Coverage," IEEE Wireless Communications Letters, 1–1, 2018, doi:10.1109/LWC.2018.2872547.

[13] M. Alzenad, H. Yanikomeroglu, "Coverage and Rate Analysis for Unmanned Aerial Vehicle Base Stations with LoS/NLoS Propagation," in 2018 IEEE Globecom Workshops (GC Wkshps), 1–7, 2018.

[14] B. Jadhavar, T. Sontakke, "2.4 GHz propagation prediction models for indoor wireless communications within building," International Journal of Soft Computing and Engineering (IJSCE), **2**(3), 108–113, 2012.

[15] ITU, "Propagation data and prediction methods for the planning of indoor radiocommunication systems and radio local area networks in the frequency range 900 MHz to 100 GHz," ITU-R Recommendation, 1238, 2012.

[16] E. Semaan, F. Harrysson, A. Furuskär, H. Asplund, "Outdoor-to-indoor coverage in high frequency bands," in 2014 IEEE Globecom Workshops (GC Wkshps), 393–398, 2014, doi:10.1109/GLOCOMW.2014.7063463.

[17] I. Rodriguez, H. C. Nguyen, I. Z. Kovács, T. B. Sørensen, P. Mogensen, "An Empirical Outdoor-to-Indoor Path Loss Model From Below 6 GHz to cm-Wave Frequency Bands," IEEE Antennas and Wireless Propagation Letters, **16**, 1329–1332, 2017, doi:10.1109/LAWP.2016.2633787.

[18] T. ETSI, "136 101,"," LTE; Evolved Universal Terrestrial Radio Access (E-UTRA); User Equipment (UE) radio transmission and reception (3GPP TS 36.101 version 14.8. 0 Release 14), **10**, 0, 2018.

[19] T. ETSI, "136 942,"," LTE; Evolved Universal Terrestrial Radio Access (E-UTRA); Radio Frequency (RF) system scenarios (3GPP TR 36.942 version 10.2. 0 Release 10), **10**, 0, 2011.

[20] M. Taranetz, T. Blazek, T. Kropfreiter, M. Muller, S. Schwarz, M. Rupp, "Runtime Precoding: Enabling Multipoint Transmission in LTE-Advanced System-Level Simulations," IEEE Access, **3**, 725–736, 2015, doi:10.1109/ACCESS.2015.2437903.

[21] R. Sheldon, et al., A first course in probability, Pearson Education India, 2002.

[22] T. 3GPP, "36.888,"," Technical Specification Group Radio Access Network; Study on provision of low-cost Machine-Type Communications (MTC) User Equipments (UEs) based on LTE (3GPP TS 36.888 version 12.0. 0 Release 12), **06**, 0, 2013.

Balancing Exploration-Exploitation in the Set Covering Problem Resolution with a Self-adaptive Intelligent Water Drops Algorithm

Broderick Crawford[*,1], Ricardo Soto[1], Gino Astorga[2], José Lemus-Romani[1], Sanjay Misra[3], Mauricio Castillo[1], Felipe Cisternas-Caneo[1], Diego Tapia[1], Marcelo Becerra-Rozas[1]

[1]*Pontificia Universidad Católica de Valparaíso, Valparaíso, 2340000, Chile*

[2]*Universidad de Valparaíso, Valparaíso, 2340000, Chile*

[3]*Covenant University, Ota, 100001, Nigeria*

A R T I C L E   I N F O

A B S T R A C T

The objective of the metaheuristics, together with obtaining quality results in reasonable time, is to be able to control the exploration and exploitation balance within the iterative processes of these methodologies. Large combinatorial problems present ample search space, so Metaheuristics must efficiently explore this space; and exploits looking in the vicinity of good solutions previously located. The objective of any metaheuristic process is to achieve a "proper" balance between intensive local exploitation and global exploration. In these processes two extreme situations can occur, on the one hand an imbalance with a bias towards exploration, which produces a distributed search in the search space, but avoiding convergence, so the quality of the solutions will be low, the other case is the bias towards exploitation, which tends to converge prematurely in local optimals, impacting equally on the quality of the solutions. To make a correct balance of exploration and exploitation, it is necessary to be able to control adequately the parameters of the Metaheuristics, in order to infer in the movements taking advantage of the maximum capacity of these. Among the most widely used optimization techniques to solve large problems are metaheuristics, which allow us to obtain quality results in a short period of time. In order to facilitate the use of the tools provided by the metaheuristic optimization techniques, it is necessary to reduce the difficulties in their configuration. For this reason, the automatic control of parameters eliminates the difficult task of obtaining a correct configuration. In this work we implemented an autonomous component to the Intelligent Water Drops algorithm, which allows the control of some parameters dynamically during the execution of the algorithm, achieving a good exploration-exploitation balance of the search process. The correct functioning of the proposal is demonstrated by the Set Covering Problem, which is a classic problem present in the industry, along with this we have made an exhaustive comparison between the standard algorithm and the autonomous version that we propose, using the respective statistical tests. The proposal presents promising results, along with facilitating the implementation of these techniques to industry problems.

1 Introduction

This paper is an extension of work "An Adaptive Intelligent Water Drops Algorithm for Set Covering Problem", originally presented in 19th International Conference on Computational Science and Its Applications (ICCSA) [1].

The post-pandemic economic recovery brings with it a number of challenges for the industry, ranging from rethinking business models to making good use of every available resource. In this sense, optimization is an important tool to achieve the desired recovery [2]–[6].

There are various economic sectors where there are problems that need to be optimised such as the airport sector where, given the environmental restrictions, it is becoming increasingly difficult to build new airports and for this reason it is necessary to optimise each of the tasks of the current installations [7]–[9]. Another ex-

ample is the educational sector, in particular the universities where it is necessary to optimize the use of rooms and the curriculum of students [10, 11]. In summary, we can find a series of problems that can be treated through optimization techniques that have a positive impact on economic recovery.

In this sense the metaheuristics that are supervised heuristics [12], are a real option to give solution to the industrial optimization problems since their attraction is that they allow to deliver a high quality solution that can even be the optimal one in limited computation times. There is a great variety of metaheuristics which have been used to solve NP-Hard problems [13]–[16].

In general, metaheuristics have a great amount of parameters, which allow controlling the high and low level strategies of these, having direct relation with the performance of the techniques in the different problems [17], the optimal configuration of parameters constitutes in itself an optimization problem [18, 19]. The importance of a good parameter assignment to metaheuristic algorithms impacts on the quality of solutions, but on the other hand it is not possible to consider transversal parameters for all the problems to be solved, since the assignment of values depends directly on the problem and the instances to be solved [20].

The values that can assume the parameters can have a great amount of combinations, for that reason we can occupy different strategies to approach the optimal configuration of parameters, that according to the literature are divided in two great groups, off-line configuration and on-line control. The off-line configuration of parameters corresponds to the determination of the metaheuristic algorithm outside the run, that is, before its execution begins [21], while the on-line control dynamically updates the values of the algorithm during the execution [22].

Given the current context of using metaheuristic techniques to solve the problems of the industry, we must facilitate the use of these techniques to non-expert users, so the use of autonomous techniques for the control of parameters, is a great contribution to bring this type of tools to all users of the industry.

The present work, solves a classic problem of the real world, as it is it Set Convering Problem (SCP) [23], which has diverse applications in the industry, using metaheuristic techniques to solve problems of great dimension. We have used the metaheuristic technique Intelligent Water Drops (IWD), which is inspired by the physical behavior of water droplets in a river bed [24], Along with this, we have incorporated autonomous elements for the on-line control of its parameters, which has two main components, the first is the obtaining of external information on the problems to be solved, and the second is the obtaining of internal information on the behaviour of the algorithm. With this we can better combine the information of each problem to be solved, along with the internal behavior of the algorithm, which generates that our proposal is adapted to the various problems that are solved.

The work is structured in the following form, in Section 2 what has been done regarding parameter tuning is presented, in Section 3 the functioning of IWD is explained, while in Section 4 the adaptive implementation proposed for IWD is detailed, in Section 5 set covering problem is shown, in Section 6 the corresponding experiments and statistical analyses are presented, ending in Section 7 with the conclusions and future work.

2 Parameter Tuning

In this section we will review the various techniques of parameterization of algorithms in order to find a correct configuration.

The proper selection of parameter values for the algorithms is not an easy task and has an important impact. Usually a great deal of time is spent, using previous experiences and expert knowledge for the correct assignment of values which also constitutes a not easy task for non-expert users. In consideration of the latter, the ideal condition from the point of view of the non-expert user is that he or she should give general information about the problem and with the least possible interaction receive an adequate response (Fig. 1). This concept, called Autonomous Search, was proposed by [18], using indicators to determine the best strategy to use.
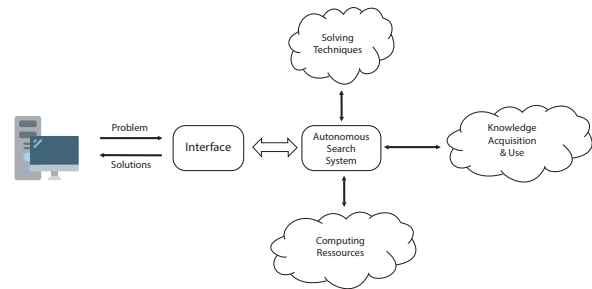
Figure 1: Autonomous Search.

The techniques for finding a good configuration for the parameters were initially grouped into two categories: offline configuration and online control. However, a new proposal is made in [21]: Simple Generate-Evaluate Methods, Iterative Generate-Evaluate Methods and High-Level Generate-Evaluate Methods.

2.1 Offline configuration

Finding a convenient parameter configuration previous to the execution of the algorithm is known as offline configuration.

This is primarily a trial and error process and can consume considerable time in research. The efficiency of this depends mainly on the insight and knowledge of the researcher or author of the algorithm. These processes are typically undocumented and are not reproducible, often driving to an unequal adjustment of different algorithms.

The following techniques exist within this group:

- F-race is an inspired method of racing algorithms in automatic learning, in particular, races in [25, 26]. This algorithm was presented in [27] and studied in detail in Birattari's PhD thesis [28]. The purpose of these methods is to iteratively evaluate a set of candidate configurations for a given set of instances. A set is removed when there is sufficient statistical evidence and there are survivors within the continuous race. This method is used after each evaluation of the candidate configurations, in which nonparametric Friedman two-way variance analysis [29] determines if there is evidence that at less than one of the configurations is significantly different

from the other ones. If the hypothesis is null and there is no difference, it is rejected; Friedman's subsequent tests are applied to remove these candidate configurations that are significantly worse than the best. This approach had been used by the ACO in [30].

- ParamILS was introduced by [31] as a versatile stochastic local search approach for automatic algorithm configuration. ParalILS includes methods to optimize the performance of an algorithmic, deterministic or stochastic object in a particular class of problems by switching a set of ordinal and/or categorical parameters. This proposal is based on an iterated local search algorithm that uses a combination of configurations chosen, a priori or at random, at initialization. The underlying idea of local search is an iterative "best first" method, which uses a variety of random movements to disturb the solution and avoid getting into local minima. The method always accepts configurations that improve or match the performance of the best configuration and restarts the search from a random configuration under a certain probability. The local search method moves through the search space by modifying only one parameter each time[32]. This approach has been used to configure ACO to solve transportation planning problems in [33].

- The other approach to optimization, focused on the sequential paradigm, includes improving the parameter initial values by the alternation of experimental design and the parameter recognition.

  In this paradigm, statistical significance takes a preponderant role, since each new experiment contributes with information about the performance of the parameters used, which are then referenced to the new stages.

  In the case of a parallel method, different experiments are formulated concurrently (all of them taking the same parameter nominal values); experiments are then carried out. The parameters are calculated and their suitability tested using the data obtained in all parallel experiments. If the data obtained from the parallel experiments are inadequate after the parameter estimation the procedure can be replicated [34, 35].

- In [36], the author used the graphic radial technique. The four basic metrics are employed for this method: worst case, best case, average case and average run-time. The region under the radar plot curve is obtained with these four metrics to set the best setting.

- The meta-optimization method was initially studied by [37] and is characterized by using an algorithm to optimize the parameters of another optimization algorithm, that is, there is an algorithm at a higher level that optimizes the parameters of a lower-level algorithm. This method has been used for covering problems in facility locations in [38], stand management in [39], and parameter selection in machine learning in [40].

2.2 Online configuration

One of the areas of research that has taken great strength in recent years is the online configuration, as it gives the algorithms the ability to adapt to the characteristics of a particular instance for better performance. For this online configuration to be useful, the exploration and exploitation phases must be clearly identified because the internal adjustments may be different for each of the phases. Thus, the online configuration can improve the results when the algorithms are used in situations very different from those that were built.

Different techniques exist, and the most simple is to define the parameter variation rules before executing the algorithm.
One possibility is the use of parameter adaptation, where the parameter modification scheme is defined for some behavior statistics of the algorithm.

- Absolute evidence: An example is the threshold of the distance between the solutions.

- Relative evidence: Considers that the relative difference in the performance with parameters of different values adapt to those with the best behavior.

2.3 Simple Generate-Evualate Methods

In this method the principle of generating and evaluating is used. Candidate configurations are occupied and then each of the parameters are evaluated to find the best configuration (Figure 2).
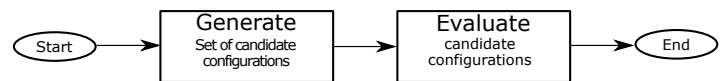
Figure 2: Simple Generate-Evualate Methods.

2.4 Iterative Generate-Evualate Methods

Unlike the first method, this one repeatedly performs the generation and evaluation steps. In this method the historical information allows to guide the generation, so that the search space for parameters is better explored and is more efficient in large search spaces (Figure 3).
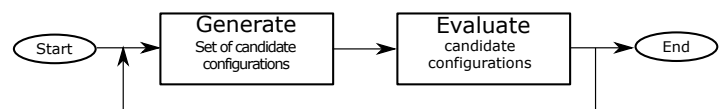
Figure 3: Iterative Generate-Evaluate Methods.
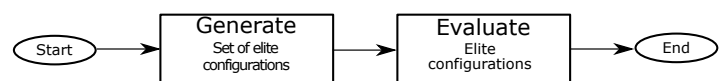
Figure 4: High-Level Generate-Evualate Methods.

2.5 High-Level Generate-Evualate Methods

This approach generates candidate configurations to then evaluate them and select the best configuration. The idea is to generate a set of high quality configurations quickly using few computational resources and select the best one. The idea is to greatly reduce the resources used when exploring candidate configurations and use them to thoroughly evaluate these configurations (Figure 4).

3 Intelligent Water Drops Algorithm

During the year 2007 in [24] he presented the algorithm that is classified as constructive since it builds a solution from 0. Its inspiration is based on nature and corresponds to the displacement that water drops make through the flow of a river and its friction with the earth, considering that when a drop is moved from one point to another it displaces earth from the river bed making the friction less and less which makes the drops increase their speed and in turn incorporate part of the extracted earth.

In the Figure 5, we can see how the soil of the river behaves, on the one hand during the passage of the drop is removed soil from the bottom of the river and on the other hand is incorporated into the drop which directly influences the speed that is acquired, this is demonstrated in that two drops of similar size but with different speeds at the end of its movement are with different size because of the soil that is incorporated. This abstraction of the behavior of water drops in river soil, allows us to build diversified solutions at the beginning, while during the execution of the algorithm, these solutions converge to promising search spaces, which allows to intensify the search.
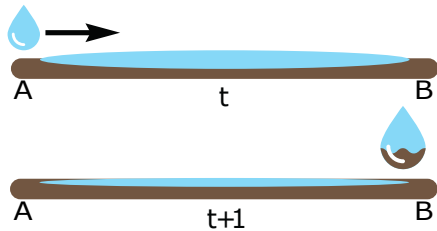
Figure 5: Water drop removing riverbed soil and adding to its own soil.

This algorithm has been used to solve mainly scheduling problems: Cooperative Search Path Optimization problem [41], Work Flow Scheduling Algorithm for Infrastructure as a Service (IaaS) cloud [42], Capacitated Vehicle Routing Problem [43], Trajectory Planning of Unmanned Combat Aerial Vehicle (UCAV) is a rather complicated Global Optimum Problem in UCAV Mission Planning [44], Method for Optimal Location and Sizing of Distributed Generation (DG) [45].

This algorithm has an initialization phase where both the static parameters number of drops, number of iterations, initial soil, initial speed and constants a_s, b_s, c_s, a_v, b_v, c_v are initialized and also the dynamic parameters Speed of drop k and soil value of drop k are initialized.

Then there is a construction phase where every drop builds a solution by visiting the nodes. The Eq. 1 is used to determine which node to visit:

$$p_i^k(j) = \frac{f(soil(i,j))}{\sum_{\forall l \notin VC^k} f(soil(i,l))} \quad (1)$$

where $soil(i,j)$ corresponds to the amount of soil between i and j and is calculated according to the following equation (Equation 2):

$$f(soil(i,j)) = \frac{1}{\varepsilon + g(soil(i,j))} \quad (2)$$

where ε is a small positive value to avoid division by zero.

The function g(soil(i,j) always obtains a positive soil value (Equation 3):

$$g(soil(i,j)) = \begin{cases} soil(i,j) & \text{if } \min_{\forall l \notin VC^k} soil(i,l) \geq 0, \\ soil(i,j) - \min_{\forall l \notin VC^k} soil(i,l) & \text{otherwise} \end{cases} \quad (3)$$

Once the drop has selected the new node, its velocity should be updated (equation 4):

$$vel^k(t+1) = vel^k(t) + \frac{a_v}{b_v + c_v \cdot soil^2(i,j)} \quad (4)$$

where a_v, b_v and c_v correspond to static parameters, and $soil(i,j)$ represents the amount of soil between i and j.

Next, it is necessary to update the soil after the step of the drop; for this, we use the following equation 5:

$$soil(i,j) = (1-\rho) \cdot soil(i,j) - \rho \cdot \Delta soil(i,j) \quad (5)$$

where ρ is a small positive value between 0 and 1, and $\Delta soil(i,j)$ is the amount of soil removed from paths i and j.

The value of $\Delta soil(i,j)$ is obtained with the following equation (6):

$$\Delta soil(i,j) = \frac{a_s}{b_s + c_s \cdot time(i,j : vel^k(t+1))} \quad (6)$$

where a_s, b_s and c_s are static parameters, and $time(i,j : vel^k(t+1))$ is calculated as follows (7):

$$time(i,j : vel^k(t+1)) = \frac{HUD(i,j)}{vel^k(t+1)} \quad (7)$$

where HUD is a heuristic that measures the degree of undesirability of the drop to jump from one node to another.

The Reinforcement phase is responsible for updating the global soil with the best drop of the iteration, and the following equation is used (8):

$$soil(i,j) = (1 + p_{iwd}) \cdot soil(i,j) - p_{iwd} \cdot \frac{1}{q(T^{IB})} \quad (8)$$

where p_{iwd} is a small positive value between 0 and 1, and $q(T^{IB})$ is the fitness value.

The best solution for each iteration is compared with the best global solution and updated according to the following equation (9):

$$T^{TB} = \begin{cases} T^{IB} & \text{if } q(T^{IB}) < q(T^{TB}) \\ T^{TB} & \text{otherwise} \end{cases} \quad (9)$$

Finally, the Termination phase is responsible for the completion of the algorithm process when the stop condition is met, which can be the number of iterations.

In 6 the original algorithm of the metaheuristics is shown.

Algorithm 1 Intelligent Water Drops Algorithm

{**Initialization phase**}
Initialize : Amount iterations, Amount drops.
Initialize : a_s, b_s, c_s
Initialize : a_v, b_v, c_v
repeat
  for $k = 1$ to N **do**
    Initialize VC^k list as empty.
    Initialize $soil^k$ value as zero.
    Initialize vel^k value as $InitVel$.
    Create the kth water drop (IWD^k).
    Select randomly a node for IWD^k.
    Update VC^k.
  end for
  {**Construction phase**}
  for $k = 1$ to N **do**
    Choose a path for IWD^k.
    Update velocity (vel^k).
    Compute the amount of soil ($\Delta soil$) to be carried by IWD^k
    Remove $\Delta soil$ from the path and add it to IWD^k
  end for
  for $k = 1$ to N **do**
    Calculate $fitness^k$
  end for
  {**Reinforcement phase**}
  Update Paths of the Best Solution
until $i = MAX\_ITERATION$
{**Termination phase**}

Figure 6: Intelligent Water Drops Algorithm.

4 Adaptative Intelligent Water Drops

The configuration of initial parameters is a costly task, carried out by an expert user and performed prior to the execution of the algorithm. We can reduce the cost of this task based on the concepts from Autonomous Search [18], which obtains information from two different sources, internal, corresponding to the operation of the algorithm and external, corresponding to the problem we are solving. The use of these data sources allows us to compare the quality of the solution in the current iteration (f_{IB}) with the quality of the best found solution (f_{TB}).

The general scheme for obtaining information to guide the adjustment of parameters is presented in Figure 7.
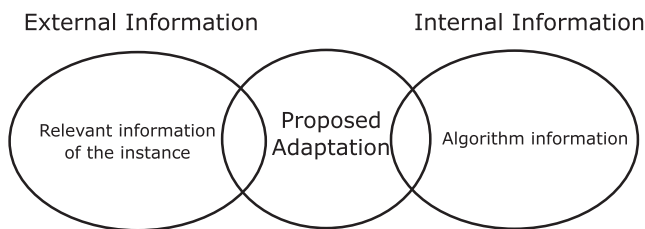
Figure 7: Information required for the proposal.

The internal information source considers the performance of

the algorithm. In our proposal, we collect the number of iterations in which no improvement in the quality of the solutions is detected. The external information source comes from the data corresponding to the instance of the problem we are solving. We consider the number of columns and the density of the instance, which allows us to differentiate them. A weight is assigned to the columns of the instance that allows us to assign importance to them, multiplying it by the density, given in the Figure 8).

SET	Instance Set	m	n	Cost Range	Density	Optimum Solution
4	10	200	1000	[1,100]	2.00	Known
5	10	200	1000	[1,100]	2.00	Known
6	5	200	1000	[1,100]	5.00	Known
A	5	300	1000	[1,100]	2.00	Known
B	5	300	1000	[1,100]	5.00	Known
C	5	400	1000	[1,100]	2.00	Known
D	5	400	1000	[1,100]	5.00	Known
NRE	5	500	1000	[1,100]	10.00	Known
NRF	5	500	1000	[1,100]	20.00	Known

Figure 8: Standard description of the benchmark OR-library.

The algorithm has two initial parameters to which we assign values, these correspond to the Soil and Initial Speed ($Soil_{Initial}$ and $Velocity_{Initial}$ respectively).

In the first case we assign the value considering the number of columns of the instance and its density, which is done as follows:

To determine the first value we consider information of the instance considering on one hand the number of columns available and on the other hand the density that is presented. This value is obtained in the following way:

$$Soil_{Initial} = SoilInitial \cdot nColumn \cdot Density \qquad (10)$$

Where $Soil_{Initial} = 1$, $nColumn$ corresponds to the number of columns in the instance group and $Density$ corresponds to the percentage of nonzeros in the matrix.

$$Velocity_{Initial} = 15 \qquad (11)$$

For the case of the initial speed $Velocity_{Initial}$ the value is determined by a series of 10 previous executions of the original algorithm.

For the adaptation, in this work, it is considered the quality of the solution for which a weight is calculated that will allow us to update the local velocity, avoiding that the solution remains trapped in an optimal local. This percentage will be calculated by comparing the solution delivered in each iteration with the best solution obtained.

It has been experimentally determined that a low initial drop velocity impacts the convergence of solutions, making it more pronounced. This characteristic is taken into account in the parameter configuration.

Initial soil and velocity parameters update rule is given by the following equation:

$$Percentage = (f_{IB} \cdot 100)/f_{TB} \qquad (12)$$

where f_{IB} is the best solution obtained at the current iteration, and f_{TB} is the best global solution found.

$$Soil_{Initial} = Soil_{Initial} \cdot Percentage \qquad (13)$$

where $Soil_{Initial}$ is the available initial soil at the current iteration and *Percentage* is the percentage difference between f_{IB} and f_{TB}.

$$Velocity_{Initial} = Velocity_{Initial} \cdot Percentage \cdot \beta \qquad (14)$$

where $Velocity_{Initial}$ is the available initial velocity at current iteration and β is a random number in the interval [0, 1].

Figure 9 shows the proposed adaptation for the local soil parameter, aiming to improve the metaheuristic performance.
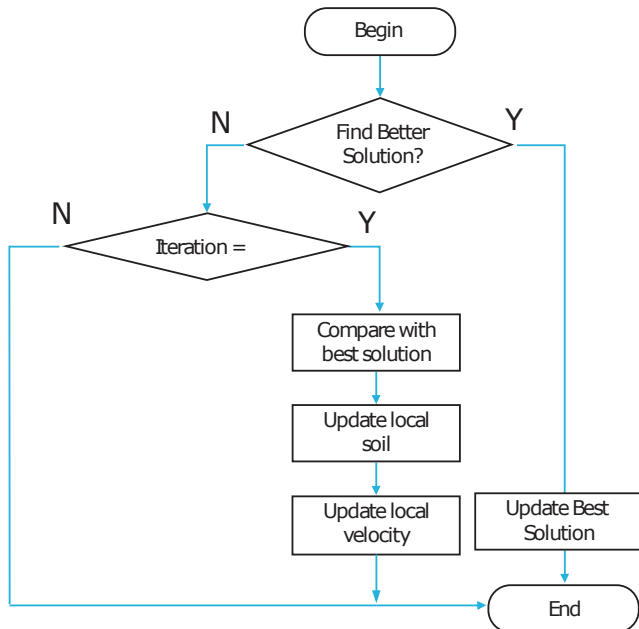
Figure 9: Parameter adaptation proposal.

At each iteration the improvement of the best solution found is evaluated. If an improvement is detected, the previous best solution found is replaced. Otherwise, a counter for not improved iterations is increased. An α value is set for the maximum number of iterations without improvement. If the counter is equal compared with the α parameter, the percentage difference of the current solution compared to the best solution is obtained and used to increase the local soil for the next iteration.

To obtain the value for the α parameter we perform 10 executions of the standard algorithm for each instance. The elapsed iteration number until a fitness improvement was evaluated. The analysis of this number allows us to determine the value for the α parameter to 5. A greater α value causes the fitness improvement probability to decrease, and the computation cost increases. The results of this analysis is shown in Figure 10, the column % represents the occurence percentage for each α, and *%Acum* column shows

the accumulated percentage for each α. Figure 11 shows the fitness change for two instances.

α	Occurrences	%	% Acum	α	Occurrences	%	% Acum
1	41	59%	59%	1	33	40%	40%
2	10	14%	74%	2	21	26%	66%
3	6	9%	83%	3	8	10%	76%
4	4	6%	88%	4	3	4%	79%
5	1	1%	90%	5	7	9%	88%
6	2	3%	93%	6	1	1%	89%
7	0	0%	93%	7	4	5%	94%
8	0	0%	93%	8	3	4%	98%
9	1	1%	94%	9	0	0%	98%
10	1	1%	96%	10	0	0%	98%
11	1	1%	97%	11	0	0%	98%
12	0	0%	97%	12	1	1%	99%
13	1	1%	99%	13	1	1%	100%
14	0	0%	99%	14	0	0%	100%
15	0	0%	99%	15	0	0%	100%
16	1	1%	100%	16	0	0%	100%
17	0	0%	100%	17	0	0%	100%
18	0	0%	100%	18	0	0%	100%
19	0	0%	100%	19	0	0%	100%
20	0	0%	100%	20	0	0%	100%
20+	0	0%	100%	20+	0	0%	100%

Figure 10: Experiments to determine the alpha value.

Graphic occurrences(%) V/S Accountant, Intance d1
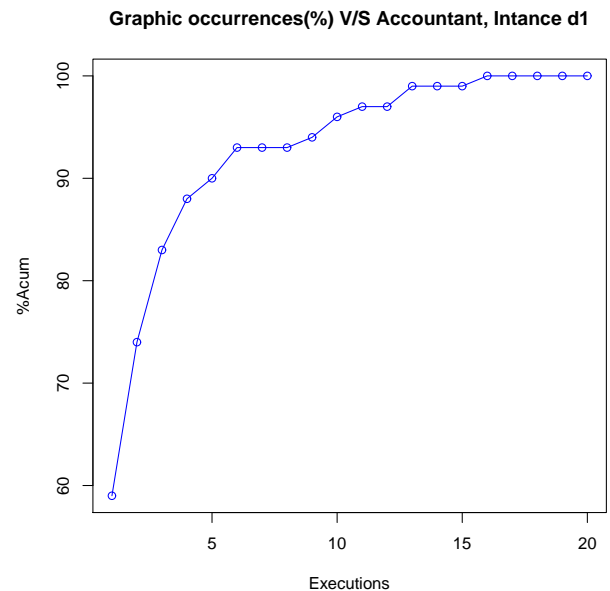
Figure 11: Chart of fitness change based on the number of iterations.

After a series of tests, we show the convergence for different initial velocities in Figure 12. When the velocity is low, the convergence shows to be premature. For this case, the initial velocity was adjusted, multiplying it by a β value in range [0, 1].
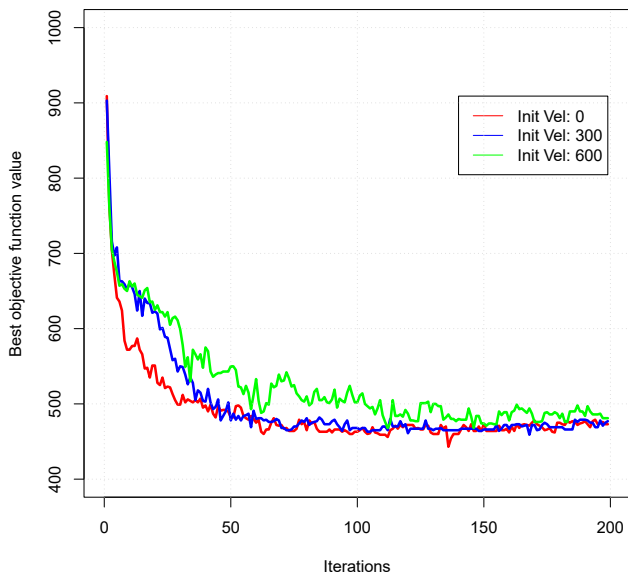
Figure 12: Convergence chart of different velocities.

5   Problem to solve

SCP is defined as a binary matrix (A) of size m-rows and n-columns, where $a_{i,j} \in \{0, 1\}$ is the value of each cell in the matrix A; i and j are of the size m-rows and n-columns, respectively:

$$A = \begin{pmatrix} a_{1,1} & a_{1,2} & ... & a_{1,n} \\ a_{2,1} & a_{2,2} & ... & a_{2,n} \\ ... & ... & ... & ... \\ a_{m,1} & a_{m,2} & ... & a_{m,n} \end{pmatrix} \quad (15)$$

Defining column j satisfies a row i, if a_{ij} is equal to 1, which is a contrary case if a_{ij} is equal to 0. In addition, an associated cost $c \in C$ is incurred, where $C = \{c_1, c_2, ...c_n\}$, together with $i = 1, 2, ..., m$ and $j = 1, 2, ..., n$, which are the sets of rows and columns, respectively.

The problem has an objective of minimizing the cost of the subset $S \subseteq J$, with the constraint that all rows $i \in I$ are covered by at least one column $j \in J$. When column j is in the subset of solution S, this is equal to 1 and is 0 otherwise.

The SCP can be defined as follows:

$$\text{Min} \quad Z = \sum_{j=1}^{n} c_j x_j \quad (16)$$

Subject to

$$\sum_{j=1}^{n} a_{ij} x_j \geq 1 \quad \forall i \in I \quad (17)$$

$$x_j \in \{0, 1\} \quad \forall j \in J \quad (18)$$

6   Experiments

6.1   Benchmark Instances

In order to validate the proposed approach, the 9 sets of the Beasleys library were used, executing 55 instances that are known and that allow a finished experimental evaluation (Figure 8).

The proposed algorithm was built using Java Language and was executed on an Intel(R) Core(TM) i7-6700 CPU with a speed of 3.40 GHz, with 16GB of memory and using a 64-bit Windows 10 operating system.

6.2   Parameter Setting

As far as the configuration of the parameters used by this algorithm is concerned, IWD, as it is generally known, is a very difficult task that requires a great use of resources. Our approach takes care of working two of the most important parameters in IWD operation which are the initial soil and the initial speed, IntSoil and InitVelocity respectively. To verify the impact of these two parameters, a series of experiments with different values for the selected parameters were carried out. The idea is to adapt these two parameters dynamically in order to use the quality of the solution as an indicator of change. The action occurs if the best overall solution does not change after a defined number of iterations.

The parameters used for the different experiments are shown in the following Figure 13.

Parameter	Detail	Value
N	Amount of drops.	5000
$MAX\_ITERATION$	Number ofiterations.	50
$InitialSoil$	Initial soil value	1000
a_s	Soil parameter "a"	900000
b_s	Soil parameter "b"	0.01
c_s	Soil parameter "c"	1.0
$InitialVel$	Initial velocity value	15
a_v	Velocity parameter "a"	10.0
b_v	Velocity parameter "b"	0.01
c_v	Velocity parameter "c"	1.0

Figure 13: Experimental parameters.

6.3   Experimental results

The results obtained with the adaptive test are shown in the tables 14 to 22 and the comparison between the original and adaptive algorithm is shown in the Figure 23.-.

Instances	Z_{BKS}	Z_{min}	Z_{avg}	RPD
4.1	429	440	467.18	2.56
4.2	512	551	612.88	7.62
4.3	516	545	614.84	5.62
4.4	494	510	565.88	3.24
4.5	512	533	586.84	4.10
4.6	560	589	576.26	5.18
4.7	430	451	492.28	4.88
4.8	492	517	564.26	5.08
4.9	641	728	809.2	13.57
4.10	514	540	581.4	5.06

Figure 14: Results of Group 4.

Instances	Z_{BKS}	Z_{min}	Z_{avg}	RPD
5.1	253	270	301.1	6.72
5.2	302	333	366.36	10.26
5.3	226	234	254.72	3.54
5.4	242	259	278.38	7.02
5.5	211	222	245.22	5.21
5.6	213	234	246.56	9.86
5.7	293	319	353.2	8.87
5.8	288	309	340.4	7.29
5.9	279	293	320.42	5.02
5.10	265	288	306.88	8.68

Figure 15: Results of Group 5.

Instances	Z_{BKS}	Z_{min}	Z_{avg}	RPD
6.1	138	149	176.96	7.97
6.2	146	162	202.66	10.96
6.3	145	149	200.1	2.76
6.4	131	136	157.26	3.82
6.5	161	183	218.34	13.66

Figure 16: Results of Group 6.

Instances	Z_{BKS}	Z_{min}	Z_{avg}	RPD
A.1	253	287	334.74	13.44
A.2	252	276	330.3	9.52
A.3	232	251	296.4	8.19
A.4	234	277	315.48	18.38
A.5	236	255	295.64	8.05

Figure 17: Results of Group A.

Instances	Z_{BKS}	Z_{min}	Z_{avg}	RPD
B.1	69	79	113.52	14.49
B.2	76	96	130.84	26.32
B.3	80	89	141.92	11.25
B.4	79	90	145.16	13.92
B.5	72	81	121.38	12.50

Figure 18: Results of Group B.

Instances	Z_{BKS}	Z_{min}	Z_{avg}	RPD
C.1	227	258	347.48	13.66
C.2	219	248	344.98	13.24
C.3	243	278	371.94	14.40
C.4	219	258	335.32	17.81
C.5	215	245	346.7	13.95

Figure 19: Results of Group C.

Instances	Z_{BKS}	Z_{min}	Z_{avg}	RPD
D.1	60	77	134.72	28.33
D.2	66	81	149.44	22.73
D.3	72	89	179	23.61
D.4	62	75	162.26	20.97

Figure 20: Results of Group D.

Instances	Z_{BKS}	Z_{min}	Z_{avg}	RPD
E.1	29	44	91.84	51.72
E.2	30	49	137	63.33
E.3	27	41	104.42	51.85
E.4	28	37	103.5	32.14
E.5	28	39	110.76	39.29

Figure 21: Results of Group E.

Instances	Z_{BKS}	Z_{min}	Z_{avg}	RPD
F.1	14	21	50.68	50.00
F.2	15	22	39.3	46.67
F.3	14	21	40.38	50.00
F.4	14	19	38.78	35.71
F.5	13	17	42.8	30.77

Figure 22: Results of Group F.

6.4 Statistical Analysis

Figure 24 shows a general scheme of the existing statistical techniques, where in this study the statistical analysis included the different tests:

- Kolmogorov-Smirnov-Lilliefors [46] is used to establish the independence of the samples.

- Wilcoxon's Signed Rank [47] is used to verify that the IWD algorithm with AD is better than the Standard IWD algorithm.

Both statistical tests considered a significance level of 0.05, so that values lower than 0.05 indicate that the null hypothesis cannot be assumed, i.e., H_0 is rejected.

Intances	Z_{BKS}	IWD_{STD}			IWD_{AD}			$diff_{rpd}$
		Z_{min}	Z_{avg}	RPD	Z_{min}	Z_{avg}	RPD	
4.1	429	454	503.48	5.83	440	467.18	2.56	3.26
5.1	253	285	335.28	12.65	270	301.1	6.72	5.93
6.1	138	177	217.96	28.26	149	176.96	7.97	20.29
A.1	253	310	350.68	22.53	287	334.74	13.44	9.09
B.1	69	92	124.44	33.33	79	113.52	14.49	18.84
C1	227	297	351.74	30.84	258	347.48	13.66	17.18
D.1	60	87	146.9	45.00	77	134.72	28.33	16.67
E.1	29	43	92.22	48.28	44	91.84	51.72	-3.45
F.1	14	21	50.68	50.00	21	50.68	50.00	0.00

Figure 23: Results IWD_{STD} AND IWD_{AD}.
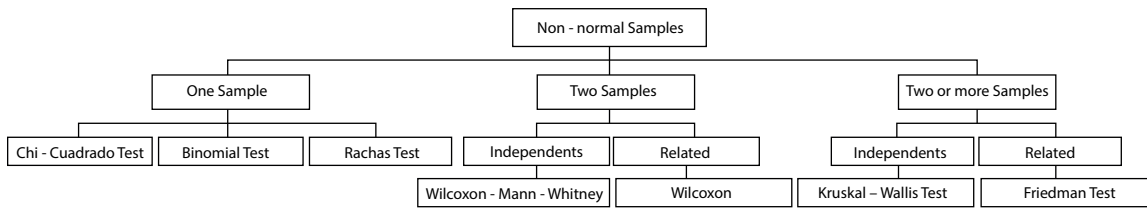
Figure 24: Statistical techniques.

For the determination of data independence the following hypothesis is used:

H_0 = The data follow a normal distribution.
H_1 = The data do not follow a normal distribution.

Given the P values obtained in the tests, the hypothesis is rejected. That is, the data do not follow a normal distribution.

H_0		IWD_{STD}	IWD_{AD}
4.1	IWD_{STD}	-	4.30^{-18}
	IWD_{AD}	>0.05	-
5.1	IWD_{STD}	-	6.45^{-18}
	IWD_{AD}	>0.05	-
6.1	IWD_{STD}	-	2.15^{-18}
	IWD_{AD}	>0.05	-
A.1	IWD_{STD}	-	2.15^{-18}
	IWD_{AD}	>0.05	-
B.1	IWD_{STD}	-	1.55^{-16}
	IWD_{AD}	>0.05	-
C.1	IWD_{STD}	-	9.88^{-16}
	IWD_{AD}	>0.05	-
D.1	IWD_{STD}	-	1.46^{-16}
	IWD_{AD}	>0.05	-
E.1	IWD_{STD}	-	>0.05
	IWD_{AD}	3.27^{-07}	-
F.1	IWD_{STD}	-	>0.05
	IWD_{AD}	1.33^{-09}	-

Figure 25: Statistical Analysis Results.

When it is obtained that the data does not follow a normal distribution, the Wilcoxon-Mann-Whitney [47] test is applied. This test is applied to verify that the version with AD is better, where the hypotheses are as follows:

H_0 = Standard IWD algorithm $\geq$ IWD algorithm with AD
H_1 = Standard IWD algorithm $<$ IWD algorithm with AD

To obtain the p-values we use the programming language R, where obtaining a p-value < 0.05 implies rejecting H_0, and accepting H_1. The AD version is statistically better than the standard version, which extends to each instance of the benchmark (Figure 25. In addition, what is indicated by the statistical tests supports what has been obtained through verification by RPD.

The results of each instance can be seen graphically in the figure 26 to 30. IWD algorithm with AD has better results in all instances except for instances E and F.

(a) Instance 4.1 (b) Instance 5.1

Figure 26: Instances 4.1 and 5.1.

(a) Instance 6.1
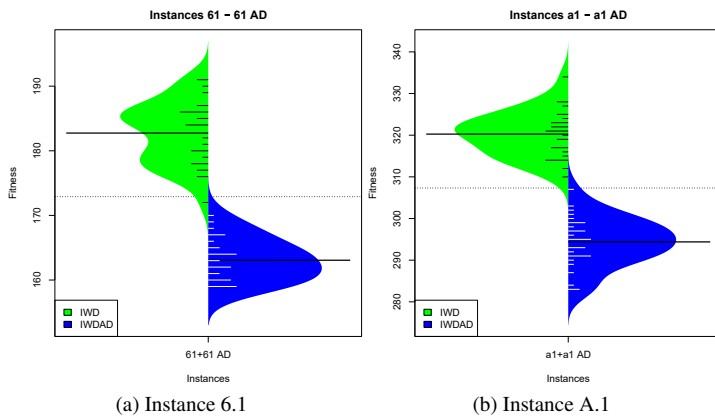
(b) Instance A.1

Figure 27: Instances 6.1 and A.1.

(a) Instance B.1
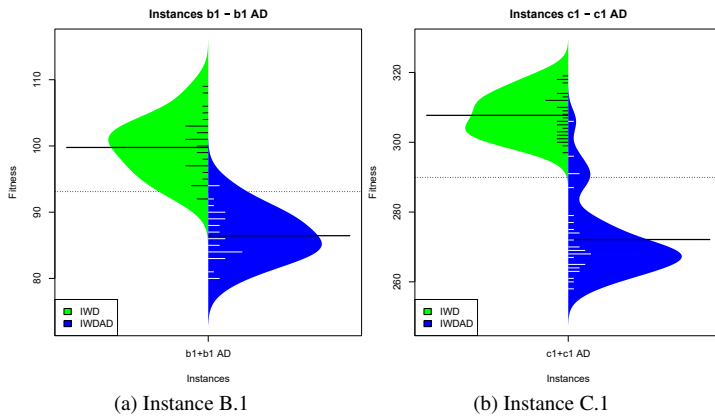
(b) Instance C.1

Figure 28: Instances B.1 and C.1.

(a) Instance d.1
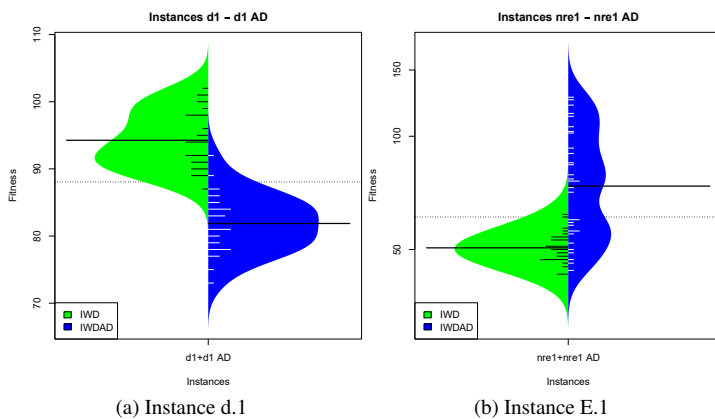
(b) Instance E.1

Figure 29: Instances D.1 and E.1.

difficulties in the configuration of parameters when implementing a metaheuristic in a real problem, a situation that will become increasingly common in the scenario of recovery from the economic crisis in post-pandemic times.
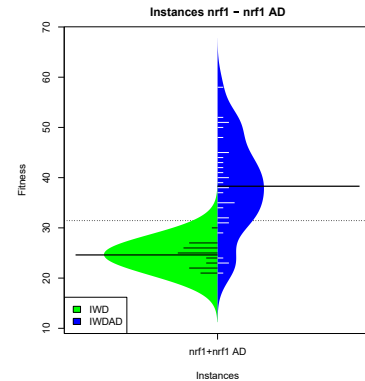
Figure 30: Instance F.1.

The adaptive element incorporated, obtains the necessary information to make decisions, based on external sources, coming from the problem and internal sources, typical of the normal functioning of the Intelligent Water Drops algorithm. With the correct combination of this information, it was possible to improve the balance of the exploration and exploitation of the search space of most of the solved instances, for Set Covering Problem, where the improvement was in average of 13.04%. In addition, the difference obtained by our adaptive proposal is significant in 77,78% of the compared instances, compared to the corresponding statistical comparisons.

The adaptive configuration is an interesting focus of future work, since there are a large number of static parameters that can be self-adjusting, in order to improve the performance of implementations, in order to decrease the influence of the off-line configuration in the performance when solving diverse instances. Along with this, it is necessary to replicate the implementation developed in this work, for other NP-Hard problems, validating the correct functioning of the incorporated adaptive components. Moreover, in the face of the growing line of research concerning the interaction between metaheuristics and machine learning techniques, a wide range of machine learning possibilities is presented in the decision making of the values to be taken by the adaptive parameters, adding to this, the option of choosing between different ways of calculating parameters according to internal and external information.

Conflict of Interest   The authors declare no conflict of interest.

7   Conclusion

In this work, we have presented an adaptive version of the Intelligent Water Drops algorithm, which is a tool that facilitates the use of metaheuristic techniques to non-expert users, reducing the

References

[1] B. Crawford, R. Soto, G. Astorga, J. Lemus-Romani, S. Misra, J.-M. Rubio, "An Adaptive Intelligent Water Drops Algorithm for Set Covering Problem," in 2019 19th International Conference on Computational Science and Its Applications (ICCSA), 39–45, IEEE, 2019, doi:10.1109/ICCSA.2019.000-6.

[2] A. Aloi, B. Alonso, J. Benavente, R. Cordera, E. Echániz, F. González, C. Ladisa, R. Lezama-Romanelli, Á. López-Parra, V. Mazzei, et al., "Effects of the COVID-19 Lockdown on Urban Mobility: Empirical Evidence from the City of Santander (Spain)," Sustainability, **12**(9), 3870, 2020, doi: 10.3390/su12093870.

[3] J. B. Sobieralski, "COVID-19 and airline employment: Insights from historical uncertainty shocks to the industry," Transportation Research Interdisciplinary Perspectives, 100123, 2020, doi:10.1016/j.trip.2020.100123.

[4] M. Sigala, "Tourism and COVID-19: impacts and implications for advancing and resetting industry and research," Journal of Business Research, 2020, doi:10.1016/j.jbusres.2020.06.015.

[5] F. Hao, Q. Xiao, K. Chon, "COVID-19 and China's Hotel Industry: Impacts, a Disaster Management Framework, and Post-Pandemic Agenda," International Journal of Hospitality Management, 102636, 2020, doi:10.1016/j.ijhm.2020. 102636.

[6] T. Laing, "The economic impact of the Coronavirus 2019 (Covid-2019): Implications for the mining industry," The Extractive Industries and Society, 2020, doi:10.1016/j.exis.2020.04.003.

[7] D. Wang, X. Zhao, L. Shen, Z. Yang, "Industry choice for an airport economic zone by multi-objective optimization," Journal of Air Transport Management, **88**, 101872, 2020, doi:10.1016/j.jairtraman.2020.101872.

[8] L. Adacher, M. Flamini, M. Guaita, E. Romano, "A model to optimize the airport terminal departure operations," Transportation Research Procedia, **27**, 53–60, 2017, doi:10.1016/j.trpro.2017.12.151.

[9] N. A. Ribeiro, A. Jacquillat, A. P. Antunes, A. R. Odoni, J. P. Pita, "An optimization approach for airport slot allocation under IATA guidelines," Transportation Research Part B: Methodological, **112**, 132–156, 2018, doi: 10.1016/j.trb.2018.04.005.

[10] C. Castro, B. Crawford, E. Monfroy, "A quantitative approach for the design of academic curricula," in Symposium on Human Interface and the Management of Information, 279–288, Springer, 2007, doi:10.1007/978-3-540-73354-6_31.

[11] C. Castro, B. Crawford, E. Monfroy, "A genetic local search algorithm for the multiple optimisation of the balanced academic curriculum problem," in International Conference on Multiple Criteria Decision Making, 824–832, Springer, 2009, doi:10.1007/978-3-642-02298-2_119.

[12] C. Blum, A. Roli, "Metaheuristics in combinatorial optimization: Overview and conceptual comparison," ACM computing surveys (CSUR), **35**(3), 268–308, 2003, doi:10.1145/937503.937505.

[13] C. Vásquez, B. Crawford, R. Soto, J. Lemus-Romani, G. Astorga, S. Misra, A. Salas-Fernández, J.-M. Rubio, "Galactic Swarm Optimization Applied to Reinforcement of Bridges by Conversion in Cable-Stayed Arch," in International Conference on Computational Science and Its Applications, 108–119, Springer, 2019, doi:10.1007/978-3-030-24308-1_10.

[14] B. Crawford, R. Soto, G. Astorga, J. Lemus, A. Salas-Fernández, "Self-configuring Intelligent Water Drops Algorithm for Software Project Scheduling Problem," in International Conference on Information Technology & Systems, 274–283, Springer, 2019, doi:10.1007/978-3-030-11890-7_27.

[15] R. Soto, B. Crawford, F. González, E. Vega, C. Castro, F. Paredes, "Solving the manufacturing cell design problem using human behavior-based algorithm supported by autonomous search," IEEE Access, **7**, 132228–132239, 2019, doi:10.1109/ACCESS.2019.2940012.

[16] S. Valdivia, R. Soto, B. Crawford, N. Caselli, F. Paredes, C. Castro, R. Olivares, "Clustering-Based Binarization Methods Applied to the Crow Search Algorithm for 0/1 Combinatorial Problems," Mathematics, **8**(7), 1070, 2020, doi:10.3390/math8071070.

[17] M. Birattari, J. Kacprzyk, Tuning metaheuristics: a machine learning perspective, volume 197, Springer, 2009, doi:10.1007/978-3-642-00483-4.

[18] Y. Hamadi, E. Monfroy, F. Saubion, "What is autonomous search?" in Hybrid Optimization, 357–391, Springer, 2011, doi:10.1007/978-1-4419-1644-0_11.

[19] M. López-Ibáñez, J. Dubois-Lacoste, L. P. Cáceres, M. Birattari, T. Stützle, "The irace package: Iterated racing for automatic algorithm configuration," Operations Research Perspectives, **3**, 43–58, 2016, doi:10.1016/j.orp.2016.09.002.

[20] F. Hutter, H. H. Hoos, K. Leyton-Brown, "Automated configuration of mixed integer programming solvers," in International Conference on Integration of Artificial Intelligence (AI) and Operations Research (OR) Techniques in Constraint Programming, 186–202, Springer, 2010, doi:10.1007/978-3-642-13520-0_23.

[21] C. Huang, Y. Li, X. Yao, "A survey of automatic parameter tuning methods for metaheuristics," IEEE Transactions on Evolutionary Computation, **24**(2), 201–216, 2019, doi:10.1109/TEVC.2019.2921598.

[22] R. Battiti, M. Brunato, F. Mascia, Reactive search and intelligent optimization, volume 45, Springer Science & Business Media, 2008, doi:10.1007/978-0-387-09624-7.

[23] J. E. Beasley, "An algorithm for set covering problem," European Journal of Operational Research, **31**(1), 85–93, 1987, doi:10.1016/0377-2217(87)90141-X.

[24] H. Shah-Hosseini, "Intelligent water drops algorithm: A new optimization method for solving the multiple knapsack problem," International Journal of Intelligent Computing and Cybernetics, **1**(2), 193–212, 2008, doi:10.1108/17563780810874717.

[25] O. Maron, A. W. Moore, "Hoeffding races: Accelerating model selection search for classification and function approximation," in Advances in neural information processing systems, 59–66, 1994.

[26] O. Maron, A. W. Moore, "The racing algorithm: Model selection for lazy learners," in Lazy learning, 193–225, Springer, 1997, doi:10.1023/A:1006556606079.

[27] M. Birattari, T. Stützle, L. Paquete, K. Varrentrapp, "A racing algorithm for configuring metaheuristics," in Proceedings of the 4th Annual Conference on Genetic and Evolutionary Computation, 11–18, Morgan Kaufmann Publishers Inc., 2002, doi:10.5555/2955491.2955494.

[28] M. Birattari, M. Dorigo, "The problem of tuning metaheuristics as seen from a machine learning perspective," 2004, doi:10.1007/978-3-642-00483-4.

[29] W. Conover, "Statistics of the Kolmogorov-Smirnov type," Practical nonparametric statistics, 428–473, 1999.

[30] T. Liao, T. Stützle, M. A. M. de Oca, M. Dorigo, "A unified ant colony optimization algorithm for continuous optimization," European Journal of Operational Research, **234**(3), 597–609, 2014, doi:10.1016/j.ejor.2013.10.024.

[31] F. Hutter, H. H. Hoos, T. Stützle, "Automatic algorithm configuration based on local search," in Aaai, volume 7, 1152–1157, 2007, doi:10.5555/1619797.1619831.

[32] F. Hutter, H. H. Hoos, K. Leyton-Brown, T. Stützle, "ParamILS: an automatic algorithm configuration framework," Journal of Artificial Intelligence Research, **36**, 267–306, 2009, doi:10.1613/jair.2861.

[33] P. Lin, J. Zhang, M. A. Contreras, "Automatically configuring ACO using multilevel ParamILS to solve transportation planning problems with underlying weighted networks," Swarm and Evolutionary Computation, **20**, 48–57, 2015, doi:10.1016/j.swevo.2014.10.006.

[34] G. Franceschini, S. Macchietto, "Model-based design of experiments for parameter precision: State of the art," Chemical Engineering Science, **63**(19), 4846–4872, 2008, doi:10.1016/j.ces.2007.11.034.

[35] F. Hutter, H. H. Hoos, K. Leyton-Brown, "Sequential model-based optimization for general algorithm configuration," in International Conference on Learning and Intelligent Optimization, 507–523, Springer, 2011, doi:10.1007/978-3-642-25566-3_40.

[36] J. García, B. Crawford, R. Soto, C. Castro, F. Paredes, "A k-means binarization framework applied to multidimensional knapsack problem," Applied Intelligence, **48**(2), 357–380, 2018, doi:10.1007/s10489-017-0972-6.

[37] R. E. Mercer, J. Sampson, "Adaptive search using a reproductive meta-plan," Kybernetes, **7**(3), 215–228, 1978, doi:10.1108/eb005486.

[38] B. Crawford, R. Soto, E. Monfroy, G. Astorga, J. García, E. Cortes, "A meta-optimization approach for covering problems in facility location," in Workshop on Engineering Applications, 565–578, Springer, 2017, doi:10.1007/978-3-319-66963-2_50.

[39] X. Jin, T. Pukkala, F. Li, "Meta optimization of stand management with population-based methods," Canadian Journal of Forest Research, **48**(6), 697–708, 2018, doi:10.1139/cjfr-2017-0404.

[40] M. Camilleri, F. Neri, M. Papoutsidakis, "An algorithmic approach to parameter selection in machine learning using meta-optimization techniques," WSEAS Transactions on systems, **13**(2014), 202–213, 2014.

[41] X. Sun, C. Cai, S. Pan, Z. Zhang, Q. Li, "A cooperative target search method based on intelligent water drops algorithm," Computers & Electrical Engineering, **80**, 106494, 2019, doi:10.1016/j.compeleceng.2019.106494.

[42] M. Adhikari, T. Amgoth, "An intelligent water drops-based workflow scheduling for IaaS cloud," Applied Soft Computing, **77**, 547–566, 2019, doi:10.1016/j.asoc.2019.02.004.

[43] E. Teymourian, V. Kayvanfar, G. M. Komaki, M. Zandieh, "Enhanced intelligent water drops and cuckoo search algorithms for solving the capacitated vehicle routing problem," Information Sciences, **334**, 354–378, 2016, doi:10.1016/j.ins.2015.11.036.

[44] H. Duan, S. Liu, J. Wu, "Novel intelligent water drops optimization approach to single UCAV smooth trajectory planning," Aerospace science and technology, **13**(8), 442–449, 2009, doi:10.1016/j.ast.2009.07.002.

[45] D. R. Prabha, T. Jayabarathi, R. Umamageswari, S. Saranya, "Optimal location and sizing of distributed generation unit using intelligent water drop algorithm," Sustainable Energy Technologies and Assessments, **11**, 106–113, 2015, doi:10.1016/j.seta.2015.07.003.

[46] S. S. Shapiro, M. B. Wilk, "An analysis of variance test for normality (complete samples)," Biometrika, **52**(3/4), 591–611, 1965, doi:10.2307/2333709.

[47] H. B. Mann, D. R. Whitney, "On a test of whether one of two random variables is stochastically larger than the other," The annals of mathematical statistics, 50–60, 1947, doi:10.1214/aoms/1177730491.

Applications of TCAD Simulation Software for Fabrication and study of Process Variation Effects on Threshold Voltage in 180nm Floating-Gate Device

Thinh Dang Cong[1,2], Toi Le Thanh[1,2], Hao Mai Tri[1,2], Phuc Ton That Bao[1,2], Trang Hoang[1,2] *

[1]*Department of Electronics Engineering, Ho Chi Minh City University of Technology (HCMUT), Ho Chi Minh City, 72506, Vietnam*

[2]*Vietnam National University, Ho Chi Minh City, 71308, Vietnam*

A R T I C L E I N F O

A B S T R A C T

In this work, a study of the process variation effects on the threshold voltage of a floating-gate device is proposed. The study demonstrates the sensitivity of the threshold voltage to five geometrical parameters including gate length, gate width, tunneling gate oxide thickness, bottom oxide-nitride-oxide oxide thickness, and nitride spacer thickness. This paper also proposed a detailed flow to fabricate the floating-gate device for CMOS 180nm process, which is used to design the floating-gate device for the study. This paper used the TCAD tools including Athena, Devedit3D, and Atlas for the simulations.

1 Introduction

The CMOS technology has been developing over the past many years thanks to its benefits like high integration density, low fabrication costs, and high operating speeds. In addition, many novel techniques of circuit design have been shown ranging from memories, analog mixed-signal, RFIC [1] -[7] to mm-Wave IC design [8], [9].

Meanwhile, there has been considerable development in the semiconductor memory field. This field is divided into two main branches which are volatile memories and non-volatile memories, and these types of memories are developing based on the CMOS technology [10], [11]. While the former lose data when the power supply is off, the latter can retain the stored information even after power is removed. Therefore, non-volatile memories are used in a very wide variety of products like cell phones, computers, and communication [12]. Thus, many researchers have focused on the study of this kind of memory. However, to study the memories, the

floating gate device needs to be investigated first since it is the core of the memories [13] –[15].

Focusing on designing a simulation model for the floating gate device, many parameters are studied under the process variation. There are two main methods to investigate the process variation effects. The first way is using the SPICE model. This is basically a fast method but the approach of this method lacks many conditions in the fabrication process like doping channel [16]. Therefore, the effects of the doping channel would not be studied. The other method is using the 3D-TCAD simulation for analyzing the geometrical parameters and the doping channel effects [17] -[19].

In this work, a detailed design flow and parameter values to fabricate the complete floating-gate device are proposed to investigate the structure and characteristics of the device. The process variation effects on the threshold voltage, which is a vital parameter of the device, are studied by using the TCAD simulation tools. Authors introduced the floating-gate device and presented ideas about how to study the process variation on threshold voltage in 180nm

*Corresponding Author: Trang Hoang, Department of Electronics Engineering, Ho Chi Minh City University of Technology (HCMUT), VNU-HCM, Ho Chi Minh City, 72506, Vietnam, Tel: (+84) 988 071 579 & Email: hoangtrang@hcmut.edu.vn

floating-gate device in the "2019 19th International Symposium on Communications and Information Technologies (ISCIT)" [1] and the following paper is an extension of this work.

The remainder of this paper is organized as follows: Section II introduces an overview structure of the device in fabrication and the operation states also. Following this, the detailed flow and parameter values to fabricate a complete device are shown in section III. Next, section IV shows the analysis and discussion of the process variation results in the threshold voltage. This section also describes the simulation of operation states after fabricating. Finally, section V shows the conclusion.

2   Floating Gate Device

The floating-gate device is the core of almost modern non-volatile memories [20], [21]. With regards to fabrication, the device is recognized through the use of a "floating gate". The gate is completely surrounded by dielectrics [22]. A cross section of a device is given in Figure. 1. Being electrically isolated, the floating gate acts as the storing layer in the device. Therefore, the operation states of the device would be determined based on the status of the gate. More importantly, the insulator around the floating gate must be thick enough to prevent leakage of charges from the floating gate to the substrate when the power is off, and it also must be thin enough to allow the transfer of charges on and off the gate under appropriate bias configuration. Moreover, reducing the thickness of the insulator, especially the tunneling gate oxide thickness has been investigated to reduce the program/erase voltage and enhance the level of integration [13],[23].
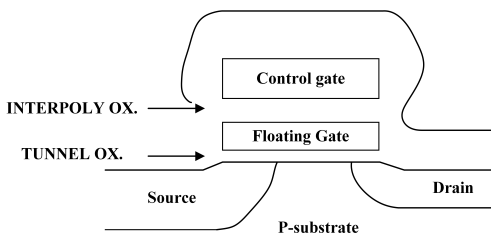
Figure 1: Floating-gate device structure in fabrication

The floating-gate device has three operation states which are programming, erasing, and reading. Programming refers to putting electrons called Channel Hot Electrons on the floating gate. In contrast, removing the electrons from the gate to the substrate would be performed in the erasing process. The removing current is renowned for the Fowler-Nordheim Tunnel current. Reading is used to determine if the device is programmed or erased.

3   Floating Gate Fabrication & Simulation

This flow proposes using an additional Epitaxial grow layer which was not used in traditional CMOS processes. The growth of an epitaxial layer over the P-type substrate offers some advantages including improving the performance of this device as well as floating-gate integrated circuits, minimizing latch-up effects that a CMOS circuit

may undergo when powered up, and helping control the doping concentration of this device accurately [24].
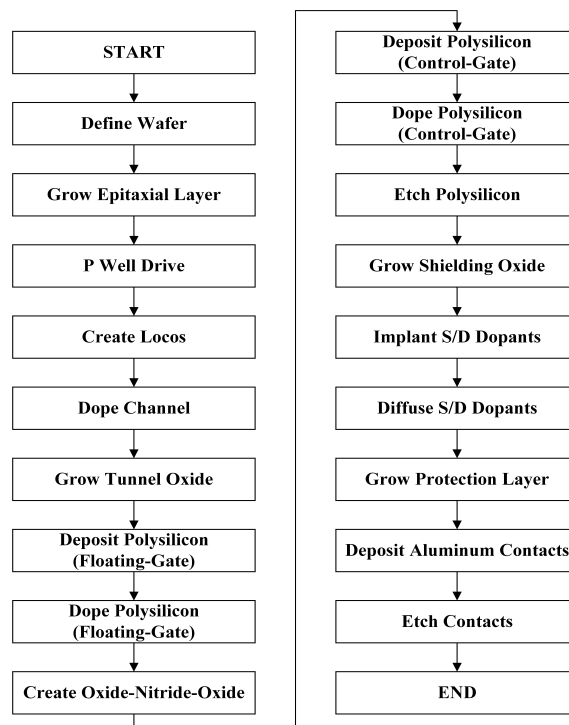
Figure 2: Floating-gate device design flow chart

The main difference in terms of structure between the floating-gate device and CMOS device is that the former has an additional floating gate which is created by two steps (Deposit Polysilicon (Floating gate), Dope Polysilicon (Floating gate) in the flow. These figures below illustrate the main process simulations using TCAD based on the design flow chart presented above (Figure 3a-3h).

The fabrication process starts from creating P-substrate (initial surface thickness = 1μm) with Boron at a concentration of 1.0e14 cm^{-3} (Figure 3a). Next, a mesh is defined, and the density of the mesh is a trade-off between accuracy and simulation time. After the mesh and wafer definition, a 0.45μm thick Epitaxy layer with Arsenic at a concentration of 1.0e16 cm^{-3} is grown on the top to make device surface thickness increase to 1.45μm (Figure 3b). Then, a P well is implanted using Boron with a dose of 8e12 cm^{-3}. After that, the P well is also diffused with Nitro gas at 1200^0C for about 310 minutes (Figure 3c). Next, Locos and tunnel oxide layer are created (Figure 3d). Creating Locos is an important step in the fabrication of semiconductor devices for the purpose of isolating the operation of two devices on the same wafer, and Oxide is usually used for this isolation. The doping channel is created using Boron at 100KeV and a concentration of 2.5e12 cm^{-3} (Figure 3e). Figure 3f shows the device structure after Polysilicon (Floating gate) is deposited and doped. Figure 3g shows the device structure after Polysilicon (Control gate) is deposited and doped. The Floating gate, Control gate, Tunnel Oxide layer and Oxide-Nitride-Oxide layer which is between Floating gate and Control gate are etched. An oxide layer with a thickness of 0.1μm is deposited and etched on the top to protect the device by the next steps. The next step is to create Source and Drain gates with Arsenic at 50 KeV and a concentration of
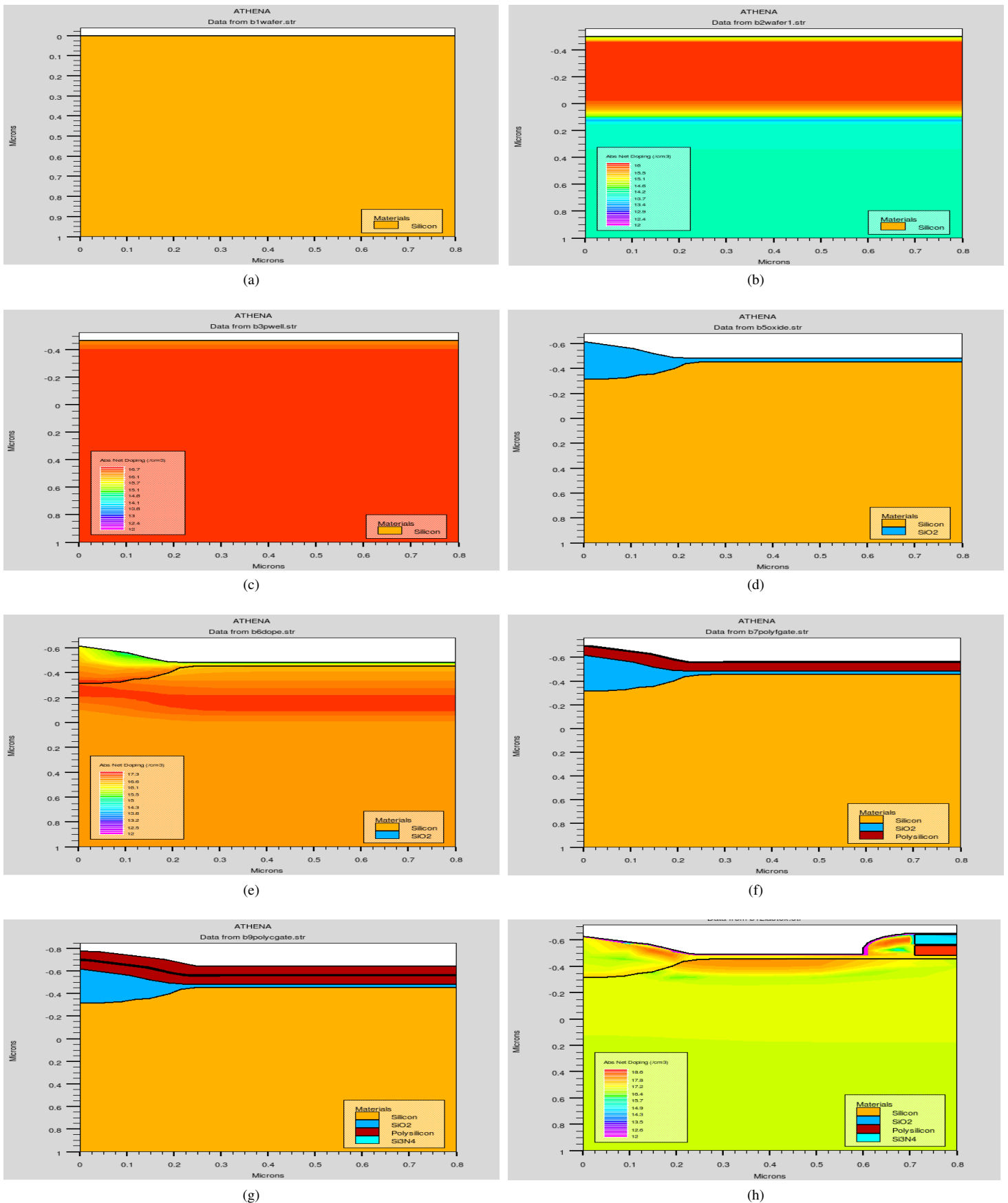
Figure 3: The main process simulations with TCAD including in a) Definition wafer b) Grow Epitaxial layer c) P well drive d) After creating Locos and grow Gate oxide e) Dope channel f) Create Floating gate and dope polysilicon g) Create Control gate and dope polysilicon h) After implant and diffuse S/D dopants

7e12 cm^{-3} (Figure 3h). After growing the protection layer, the final step is to deposit and etch Aluminum contacts for Source and Drain gates. The detailed process flow to fabricate the device is presented in Figure 2.

In this work, we propose to use the Athena tool to simulate the process of fabrication and the Atlas tool for operation simulations of the device. The following table gives the default parameter values in designing.

Table 1: Description And Default Parameter Values

DESCRIPTION	VALUE [μm]
Thickness of oxide-nitride-oxide nitride	0.013
Thickness of nitride spacer	0.002
Thickness of bottom oxide-nitride-oxide oxide	0.01
Thickness of top oxide-nitride-oxide oxide	0.001
Thickness of tunneling gate oxide	0.02
Thickness of control gate	0.075
Thickness of floating gate	0.075
Length of control gate	0.18
Length of floating gate	0.18

The complete 2D and 3D structures of the device in this work are given in Fig. 4 and Fig. 5, respectively. Regarding the 3D structure, the one is designed by using the 2D structure and the Devedit3D tool.
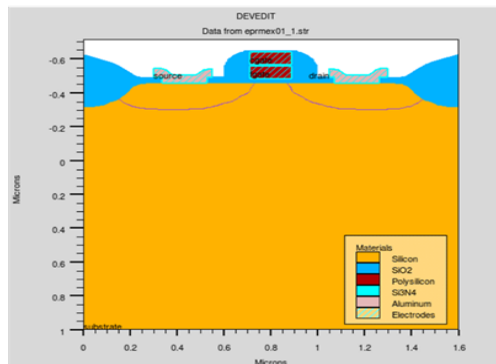
Figure 4: The 2D floating-gate device structure
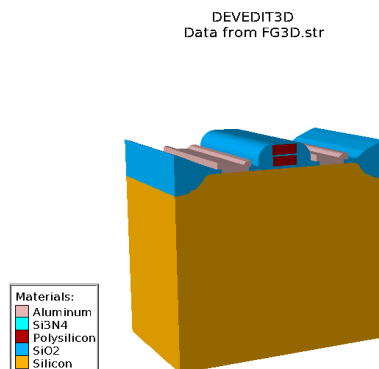
Figure 5: The 3D floating-gate device structure

4   Process Variation Results

This section presents the threshold voltage results of the floating-gate device designed in the previous section before programming and after programming.

Initially, before programming, there are no charges which are stored on the floating gate. The drain current – threshold voltage curve is shown in Fig. 6. The threshold voltage of the device is 0.6V.
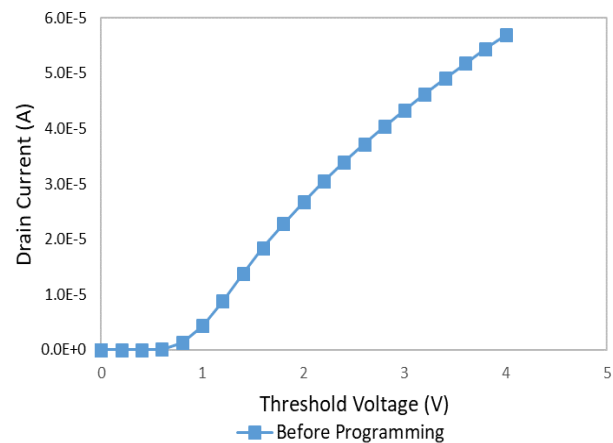
Figure 6: Threshold voltage of the device before programming process

After the programming process, the charges on the gate increase from 0C to around -3.5e-15C since the moving of electrons from the substrate. Meanwhile, the threshold voltage increases from 0.6V to approximately 6V. The charges on the gate and the threshold voltage in the programming process are given in Fig. 7 and Fig. 8, respectively. After that, the device is at the program state.

In contrast, as discussed in section II, the erasing process will remove all the negative charge on the floating gate which is generated from the programming process. Following this, the floating gate will have no charge, and the state of the device is as the initial (before programming state) or erasing state.
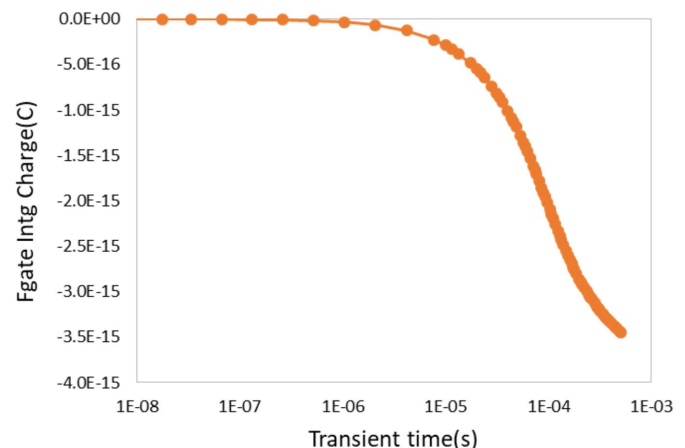
Figure 7: Floating gate charge in the programming process
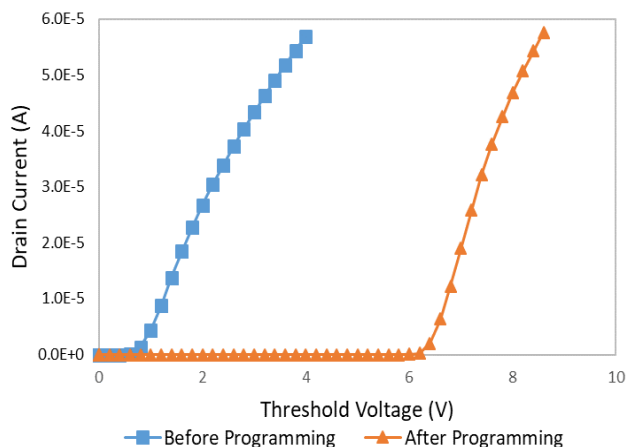
Figure 8: Threshold voltage of the device after programming process

The study of process variation demonstrates the effect of the threshold voltage on different geometrical parameters. In general, what stands out from the study is that whereas the threshold voltage is more sensitive to the gate length, tunneling gate oxide thickness, and bottom oxide-nitride-oxide oxide thickness, the threshold voltage is less sensitive to the gate width and nitride spacer thickness. The details of the study are given as follows.

4.1 Vary in values of the gate length

The figure in this section demonstrates the effect of the gate length parameter on the threshold voltage, it is clear that the increase in this parameter tends to a considerable increase in the threshold voltage, climbing around 18.33%, from 6V to approximately 7.1V. Thus, in the fabrication process, this parameter should be controlled carefully.
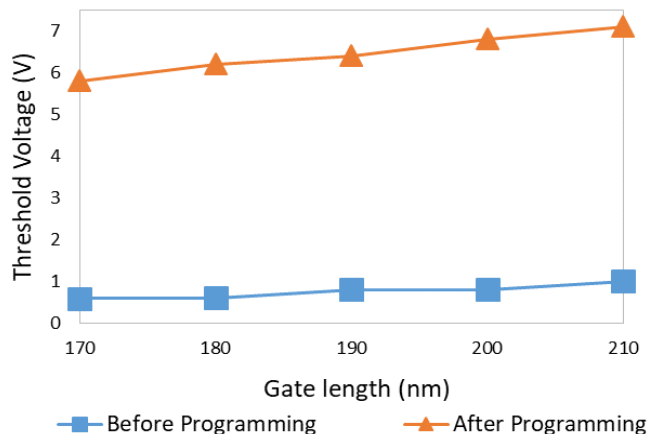
Figure 9: Gate length variation effects

4.2 Vary in values of the gate width

The figure below illustrates the change of the threshold voltage when the width parameter changes from 0.4μm to 1.6μm. This parameter is defined as a variable varied in the z-axis of the Devedit3D tool. In general, what stands out from the graph is that the voltage is not

sensitive to this parameter. The threshold voltage remains stable at around 6V.
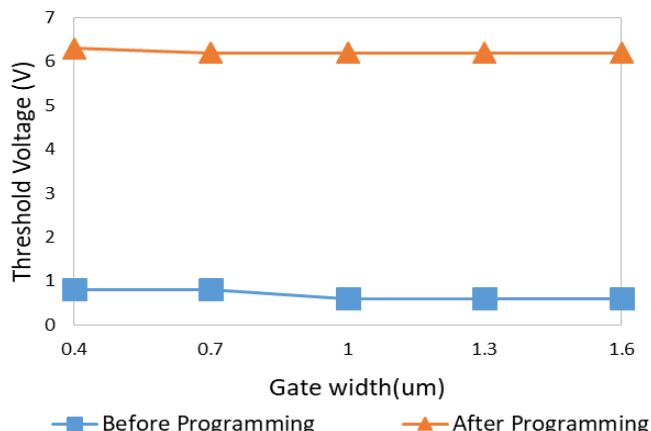
Figure 10: Gate width variation effects

4.3 Vary in values of the tunneling gate oxide thickness

The result is given in the graph in Fig. 11, it is clear that the change in tunneling gate oxide thickness results in a dramatic decrease in the threshold voltage when it varies from 20nm to 40nm. After programming, the voltage witnessed a drastic decrease, falling approximately 50% to about 3.2V. Hence, this is a very important parameter because the variation of the one causes a significant change in the operation of the device. With regard to the fabrication process, this parameter should be controlled carefully.
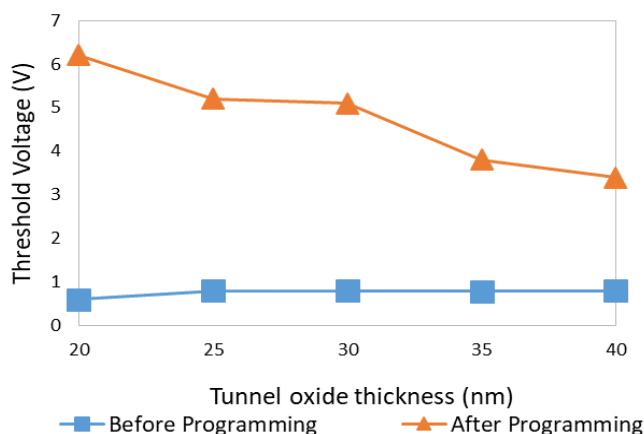
Figure 11: Tunneling gate oxide thickness variation effects

4.4 Vary in values of the bottom oxide-nitride-oxide oxide thickness

The graph in this section shows the results of the threshold voltage when the bottom oxide-nitride-oxide oxide thickness varied from 0.01μm to 0.03μm. Overall, it can be seen that the threshold voltage after programming experienced a considerable decrease of 23.33%, dropping from roughly 6V to approximately 4.6V. Thus, in the fabrication process, similar to the gate length and the tunneling gate

oxide thickness, this parameter should be observed carefully.
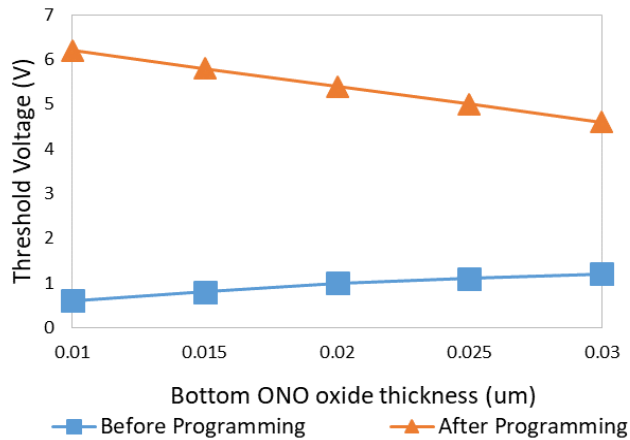
Figure 12: Bottom oxide-nitride-oxide oxide thickness variation effects

4.5 *Vary in values of the nitride spacer thickness*

The graph in the Fig. 13 presents the impact of the nitride spacer thickness parameter on the threshold voltage. It is clear that the impact of this parameter is very small. The threshold voltage after programming remaining between 5.9V and 6.1V throughout the study. Thus, the parameter would be controlled more easily than the others in the fabrication process.
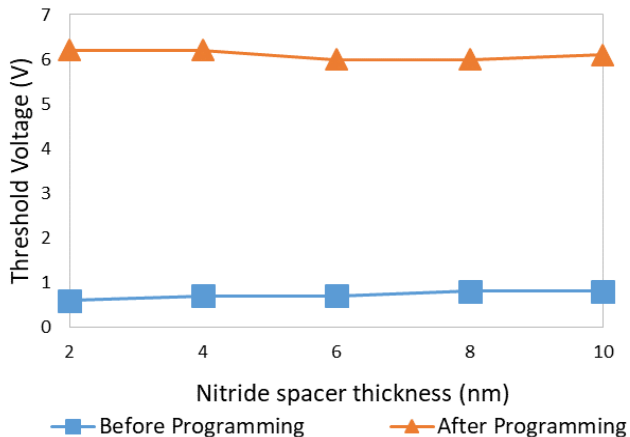
Figure 13: Nitride spacer thickness variation effects

5 Conclusion

This work is successful in the study of the process variation effects on the performance of a floating-gate device. The tunneling gate oxide thickness, bottom oxide-nitride-oxide oxide thickness, and gate length were found out to be sensitive to the threshold voltage, especially the tunneling gate oxide thickness parameter caused 50% change in threshold voltage. The others are 18.33% and 23.33%, respectively. While the gate width, nitride spacer thickness turned out to be less sensitive. This paper also successful in proposing a detailed flow and the parameter values to fabricate the complete

floating-gate device based on CMOS 180nm process. The device which is designed by the flow worked as the expectation.

Conflict of Interest
The authors declare no conflict of interest.

References

[1] T. D. Cong, T. Le Thanh, H. M. Tri, T. Hoang, "The Simulation Study of Process Variation on Threshold Voltage in 180nm Floating-Gate device," in 2019 19th International Symposium on Communications and Information Technologies (ISCIT), 211–214, 2019, doi:10.1109/ISCIT.2019.8905125.

[2] R. B. Wunderlich, F. Adil, P. Hasler, "Floating Gate-Based Field Programmable Mixed-Signal Array," IEEE Transactions on Very Large Scale Integration (VLSI) Systems, **21**(8), 1496–1505, 2013, doi:10.1109/TVLSI.2012.2211049.

[3] T. Kim, K. Park, T. Jang, M.-H. Baek, Y. S. Song, B.-G. Park, "Input-modulating adaptive neuron circuit employing asymmetric floating-gate MOS-FET with two independent control gates," Solid-State Electronics, **163**, 107667, 2020, doi:https://doi.org/10.1016/j.sse.2019.107667.

[4] X. He, X. Zhu, L. Duan, Y. Sun, C. Ma, "A 14-mW PLL-Less Receiver in 0.18- μm CMOS for Chinese Electronic Toll Collection Standard," IEEE Transactions on Circuits and Systems II: Express Briefs, **61**(10), 763–767, 2014, doi:10.1109/TCSII.2014.2345303.

[5] J. Sun, C. C. Boon, X. Zhu, X. Yi, K. Devrishi, F. Meng, "A Low-Power Low-Phase-Noise VCO With Self-Adjusted Active Resistor," IEEE Microwave and Wireless Components Letters, **26**(3), 201–203, 2016, doi:10.1109/LMWC.2016.2521167.

[6] H. Liu, C. C. Boon, X. He, X. Zhu, X. Yi, L. Kong, M. C. Heimlich, "A Wideband Analog-Controlled Variable-Gain Amplifier With dB-Linear Characteristic for High-Frequency Applications," IEEE Transactions on Microwave Theory and Techniques, **64**(2), 533–540, 2016, doi:10.1109/TMTT.2015.2513403.

[7] H. Liu, X. Zhu, C. C. Boon, X. He, "Cell-Based Variable-Gain Amplifiers With Accurate dB-Linear Characteristic in 0.18 μm CMOS Technology," IEEE Journal of Solid-State Circuits, **50**(2), 586–596, 2015, doi:10.1109/JSSC.2014.2368132.

[8] X. Tong, Y. Yang, Y. Zhong, X. Zhu, J. Lin, E. Dutkiewicz, "Design of an On-Chip Highly Sensitive Misalignment Sensor in Silicon Technology," IEEE Sensors Journal, **17**(5), 1211–1212, 2017, doi:10.1109/JSEN.2016.2638438.

[9] S. Chakraborty, Y. Yang, X. Zhu, O. Sevimli, Q. Xue, K. Esselle, M. Heimlich, "A Broadside-Coupled Meander-Line Resonator in 0.13- μm SiGe Technology for Millimeter-Wave Application," IEEE Electron Device Letters, **37**(3), 329–332, 2016, doi:10.1109/LED.2016.2520960.

[10] G. O. Puglia, A. F. Zorzo, C. A. F. De Rose, T. Perez, D. Milojicic, "Non-Volatile Memory File Systems: A Survey," IEEE Access, **7**, 25836–25871, 2019, doi:10.1109/ACCESS.2019.2899463.

[11] E. I. Vatajelu, H. Aziza, C. Zambelli, "Nonvolatile memories: Present and future challenges," in 2014 9th International Design and Test Symposium (IDT), 61–66, 2014, doi:10.1109/IDT.2014.7038588.

[12] R. Bez, E. Camerlenghi, A. Modelli, A. Visconti, "Introduction to flash memory," Proceedings of the IEEE, **91**(4), 489–502, 2003, doi:10.1109/JPROC.2003.811702.

[13] S. Wang, C. He, J. Tang, X. Lu, C. Shen, H. Yu, L. Du, J. Li, R. Yang, D.-X. Shi, G. Zhang, "Nonvolatile Memory: New Floating Gate Memory with Excellent Retention Characteristics (Adv. Electron. Mater. 4/2019)," Advanced Electronic Materials, **5**, 2019, doi:10.1002/aelm.201970018.

[14] E.-J. Park, J.-M. Choi, K.-W. Kwon, "Behavior Modeling for Charge Storage in Single-Poly Floating Gate Device," Journal of nanoscience and nanotechnology, **19**, 6727–6731, 2019, doi:10.1166/jnn.2019.17112.

[15] L. L. M. A. Pavan, Paolo, Floating Gate Devices: Operation and Compact Modeling, Springer US, 2004.

[16] G. Rappitsch, E. Seebacher, M. Kocher, E. Stadlober, "SPICE modeling of process variation using location depth corner models," IEEE Transactions on Semiconductor Manufacturing, **17**(2), 201–213, 2004, doi:10.1109/TSM.2004.826940.

[17] F. Duvivier, E. Guichard, "Worst-case SPICE model generation for a process in development using Athena, Atlas, Utmost and Spayn," in ICM 2001 Proceedings. The 13th International Conference on Microelectronics., 11–18, 2001, doi:10.1109/ICM.2001.997475.

[18] Y. Saad, C. Tavernier, M. Ciappa, W. Fichtner, "TCAD tools for efficient 3D simulations of geometry effects in floating-gate structures," in Proceedings. 2004 IEEE Computational Systems Bioinformatics Conference, 77–82, 2004, doi:10.1109/NVMT.2004.1380810.

[19] S. Bala, B. Mahendia, "Simulation of Floating Gate MOSFET Using Silvaco TCAD Tools," 2015.

[20] S. Agarwal, D. Garland, J. Niroula, R. B. Jacobs-Gedrim, A. Hsia, M. S. Van Heukelom, E. Fuller, B. Draper, M. J. Marinella, "Using Floating-Gate Memory to Train Ideal Accuracy Neural Networks," IEEE Journal on Exploratory Solid-State Computational Devices and Circuits, **5**(1), 52–57, 2019, doi:10.1109/JXCDC.2019.2902409.

[21] T. Dubey, V. Bhadauria, "A low-voltage highly linear OTA using bulk-driven floating gate MOSFETs," AEU - International Journal of Electronics and Communications, **98**, 2018, doi:10.1016/j.aeue.2018.10.034.

[22] P. Pavan, R. Bez, P. Olivo, E. Zanoni, "Flash memory cells-an overview," Proceedings of the IEEE, **85**(8), 1248–1271, 1997, doi:10.1109/5.622505.

[23] R. Dhavse, F. Muhammed, C. Sinha, V. Mishra, R. M. Patrikar, "Memory characteristics of a 65 nm FGMOS capacitor with Si quantum dots as floating gates," in 2013 Annual IEEE India Conference (INDICON), 1–3, 2013, doi:10.1109/INDCON.2013.6725910.

[24] R. N. T. Stanley Wolf, Silicon Processing for the VLSI Era, Volume1: Process Technology, Lattice Press; 1st edition (January 1, 1986), 1999.

Predicting Student Academic Performance Using Data Mining Techniques

Lonia Masangu[1], Ashwini Jadhav[2,*], Ritesh Ajoodha[3]

[1]*School of Computer Science and Applied Mathematics, DSI-NICIS National e-Science Postgraduate Teaching and Training Platform (NEPTTP), The University of the Witwatersrand, Johannesburg, 2106, South Africa*

[2]*Faculty of Science, The University of the Witwatersrand, Johannesburg, 2106, South Africa*

[3]*School of Computer Science and Applied Mathematics, The University of the Witwatersrand, Johannesburg, 2106, South Africa*

A R T I C L E   I N F O

A B S T R A C T

There is a crisis in basic education during this pandemic which affected everyone worldwide, we see that teaching and learning have gone online which has effected student performance. Student's academic performance needs to be predicted to help an instructor identify struggling students more easily and giving teachers a proactive chance to come up with supplementary resources to learners to improve their chances of increasing their grades. Data is collected on KAGGLE and the study is focusing on student's engagement, how often they check their announcements, number of raised hands, number of accessed forum and number of accessed resources to predict student academic performance. Various machine learning models such as Support vector machine, Decision tree, Perceptron classifier, Logistic regression and Random forest classifier is used. From the results, it was proven that Support vector machine algorithm is most appropriate for predicting student academic performance. Support vector machine gives 70.8% prediction which is relatively higher than other algorithms.

1 Introduction

Student performance prediction is a crucial job due to the large volume of data in educational databases. A lot of data has become available describing student's online behaviour and student engagement [1]. Online data has been used by a great number of researchers. Online learning and teaching is making a significant impact on the fabric of basic education.

Predicting the performance of a student is a great concern to the basic education management. The scope of this paper is to identify the factors influencing the performance of students in different grades and to find out the best machine learning model to predicting student academic performance and helps to identify students with poor grades and then be evaluated and provided with new materials and methods to improve their results.

There is a crisis in basic education during this pandemic which affected everyone worldwide, we see that teaching and learning have gone online which has effected student performance/grades. Parents are now supposed to sign whether their children must attend traditional class or online classes due to this pandemic. Online

learning platforms is used to track student performance, provides unlimited access to online materials, organises online content in one location though many things that need to be learned do not add themselves to online learning. Many courses require the acquisition of soft skills, which cannot be easily learned or tested online.

They have been many attempts on predicting student academic performance using data collected from students activity logs and student demographic information. They have used several of data mining techniques. Decision trees were primarily used to find the predictor variables to the predicted variable and shows the targeted discrete value [2, 3]. Logistic Regression- was used to describe data and describe the relationship among the variables and Random forest was primarily used to maintain accuracy between the variable [4]–[5].

This research aim to predict student performance from data collected on student's activity logs on an online learning and student's demographic information. We want to find the accuracy of some classification models for predicting student academic performance. The major objectives of this study are:

---

*Corresponding Author: Ashwini Jadhav, The University of the Witwatersrand, Johannesburg, South Africa, Ashwini.Jadhav@wits.ac.za

- Finding the best classification model on student data set.

- Predict student academic performance using student's demographically data and student's online logging's data.

We would like to find out, does the online engagement have an influence on physical engagement? Does the parent association with the learners improve the learner's engagement?.

This study will be using various Machine Learning methods to predict student's academic performance. Five popular classification methods (Support vector machines, Decision trees and Perceptron classification, Logistic regression and Random forest) are built and compared to each other making use of their predictive accuracy on the given data samples to predict student academic performance. Data is collected on KAGGLE and we will be focusing on student's engagement, how often they check their announcements, number of raised hands, number of accessed forum and number of accessed resources to predict student success. The process of predicting student performance using online logging's data is performed using various data mining techniques. [6, 7].

This study proposes the following assumptions:

- Every student must have undergone some training on how to utilise online learning platform to predict correct results.

- Every student have an equal chance of receiving all course materials.

- If a student fails to submit an assessment or attend any forums it assumes the student has obtained 0% in that particular assessment.

2 Related Work

This chapter provides an overview of previous research on predicting student academic performance. This section illustrates other similar work-related to predicting student academic performance.

2.1 Data

Several researchers have used machine learning algorithms in predicting student's academic performance. 323 students doing undergraduate who enrol in dynamics in 4 consecutive semesters: in semester one there were 128 students, in semester two there were 58 students, in semester three there were 53 students and semester four there were 84 students [8]. Other authors have used undergraduate student's information from four different sources which included student's demographic data, course resources data, forums data and Sakai's grade book data [4].

Other authors have used electronic data from the universities to improve the quality of educational processes. They studied using machine learning techniques to study the performance of undergraduate students [9]. We also learnt that other researchers have conducted their study about the student academic performance in high schools and in Iran for bachelor degree students. They analysed data of 1100 learners where 500 where the high school students and 600 was that of the bachelor degree level [10].

2.2 Features

Several researchers have used student's demographic information and student online loggings data to predict student academic performance. The authors have done predictions for 4 class, 3 class and 2 class. The authors applied oversampling in other to balance the dataset and also used 3 different machine learning classifiers to predict student academic performance [8].

Several researchers collected data from student materials, assignments, tests, forums, and discussions on the online learning platform database to predict student success. Some researchers predicted student academic performance and they collected data from total login frequency on the system and a total number of attended forums [4].

2.3 Model

Various machine learning methods have been used by several researchers to predict student academic performance using student's demographic information and student online logging's data. Two machine learning algorithms were used which are Bayesian networks and Decision trees. The Decision trees was more accurate than Bayesian network by 3-12% [8].

Other authors have used C4.5 decision trees, Naïve bayes classifier, Random forests, neural networks and Meta-classifiers. After the analysis they found that C4.5 decision trees performed better [9]. The analysis shows that parent educational level, past examination results and gender has an impact on the presentation [11].

They also used decision trees and clustering data mining algorithms. They focused upon two type of student performance. They first predicted student academic performance at the end of the study programme [12]. Later predicted the student progressions and add them with the predicted results. The results shows good and bad performance of students and assists with identifying struggling students and giving teachers a proactive chance to come up with supplementary measures to improve their chances of passing. The decision trees gave out the best results [4].

3 Research Contribution

This study contributes to the current body on literature by predicting student academic performance and helps to identify students with poor grades can then be evaluated and provided with new materials and methods to improve their grades. Predicting students performance allow an instructor to spot non-engagement students based on their actions and activities from online learning platform. It also assists with identifying struggling students and giving teachers a proactive chance to come up with supplementary measures to improve their chances of passing during the course of their study programme.

From the literature that was reviewed various machine learning methods have been used by several researchers to predict student academic performance, they predicted student academic performance at the end of the study programme and they were unable able to detect which students may need immediate attention so that they lower the chances of them failing.

Table 1: Related Works.

Authors	Features	Models	Accuracy
Shaobo Huang and Ning Fang in (2012)	323 students doing undergraduate who enrol in dynamics in 4 consecutive semesters	Decision trees and Bayesian networks	The decision trees consistently 3 - 12% more accurate than the Bayesian network.
M. Lauria et al (2012)	Used undergraduate student's data	Logistic regression, support vector machines and C4.5 decision trees	Support vector machines and the logistic regression gave out higher
Oskouei Askari et al (2014)	Total number of 1100 and 500 where the high school students and 600 was that of the bachelor degree level	C4.5 decision trees, Naïve bayes classifier, Random forests, neural networks and Meta-classifiers	The best prediction was found using the C4.5 decision trees.
Raheela Asif et al (2017)	Used electronic data from the universities to improve the quality of educational processes.	Decision trees and clustering.	The decision trees gave out the best results.

4   Research Methodology

This chapter presents the methods that is proposed in this study to predict performance of students using student's demographical information and student's online logging's data.

4.1   Research design

Based on the literature the study proposed using data mining techniques to find whether the total spent time on online learning affect the student's performance and how have learning management system features affect the student performance.

4.2   Data description:

The data set consists a total of 480 records and 16 features. We found that there are 3 major categories of features: first being student demographic information such as student nationality and student gender. Secondly being student academic information such as student grade, student section and student educational stage. Thirdly being student behavioural information such as number of access resources, number of raised hands in class and school satisfaction.

The data set consists a total of 305 males and 175 females where 179 are from Kuwait, 28 are from Palestine, 172 are from Jordan, 22 are from Iraq, 17 are from Lebanon, 12 are from Tunis, 11 are from Saudi Arabia, 9 are from Egypt, 6 are from USA, 7 are from Syria, 6 are from Iran, 6 are from Libya, 4 are from Morocco and 1 is from Venezuela.

The data set is collected in two academic semesters, on first semester they were 245 student records and 235 student records on semester two.

The data set also covers the features of the school attendance days. There are two categories based on their number of absence days. We found that there were 289 students their absence days were under 7 days and 191 students were absent for more than 7 days.

Finally, the data set also contains parent's participation on their children academic process. There are two categories: first being the parent answering survey and secondly being parent school satisfaction. We found that 270 parents managed to answer the survey and 210 parents did not answer the survey. We also found that 292 parents are happy and satisfied with the school and 188 parents are not satisfied.

4.3   Classification field

There are three numerical intervals of student grades. The first interval is for students who obtained a failing percentage (L), the interval includes values from 0% to 69%. The second interval is for students who obtained low passing percentage (M), the interval includes values from 70% to 89%. Lastly is for students who got high passing percentage (H), the interval includes values from 90% to 100%.

4.4   Methods

Predictive Models: Five popular classification methods (Decision trees and Perceptron classification and Support vector machines, Logistic regression and Random forest) are built and compared to each other making use of their predictive accuracy on the given data samples. Brief description of the predictive models that will be used in this study.

Support Vector Machines: Support vector machines (SVMs) [13] helps in detecting the outliers on the data set and it also perform classification. SVMs are set of supervised learning methods. SVMs used kernel trick to modify data and use the modified data to find the difference between the possible end results. SVM finds the optimal solution by computing on each feature by using partial differentiation after employing the Lagrange multiplier [14]. The model decreases convolution of the training data consequential subset of support vectors.

Table 2: This table depicts the student related variables and their description.

Data Field	Description
Gender	The student's gender.
Nationality	The student's nationality
Place of Birth	The student's country of birth.
Stage ID	Educational level student belongs to (Elementary, Middle, or High School
Grade ID	The grade year of the student.
Section ID	The classroom the student is in.
Topic	The topic of the course.
Semester	The semester of the school year. (F for Fall, S for Spring)
Relation	The parent responsible for student.
raised hands	How many times the student raises his/her hand on classroom
Visited Resources	How many times the student visits a course content
Announcements View	How many times the student checks the new announcements
Discussion	How many times the student participate on discussion groups
Parent Answering Survey	Parent answered the surveys which are provided from school or not
Parent School Satisfaction	Whether or not the parents were satisfied. "Good" or "Bad". Oddly this was not null for parents who did not answer the survey. It is unclear how this value was filled in.
Student Absence Days	Whether or not a student was absent for more than 7 days
Class	Our classification field. 'L' is for students who got a failing percentage (Less than 69%), 'M' for students who got a low passing grade (Between 70% and 89%), and 'H' for students who achieved high marks in their course (90% to 100%)

Given a data set containing a training set of N data points, $\{x_k, y_k\}_{k=1}^{N}$ and input data, which is an n-dimensional data vector $(x\_k\epsilon R^{\wedge}N)$ and output, which is the one-dimensional vector space $(y\_k\epsilon r)$; SVM create the classifier as shown below in this equation:

$$y(x) = sign\left[\sum_{k=1}^{N} \alpha_k y_k \Psi(x, x_k) + b \right]$$

where α_k are positive real constants and b is a real constant.

Decision trees (DTs): In this study Decision trees is used to find the predictor variables to the predicted variable and shows the targeted discrete value. "Decision trees uses variable values to create a structure that has nodes and edges" [15]. A DT has internal nodes and leaves, rectangles represents nodes and ovals represents leaves. Data set features are represented by the internal node and it contain two or more child. The value of these features is found at the branches. Each leaf contains a classification label [16].

Decision trees are established from a training set. A tree is called the hierarchy and a node is called segment. The entire data set is contained at the original segment called the node of the tree. The branches are formed by the node with its successors that created it and the leaves are final nodes. The decision is made on each leaf and it is applied to all the observations in the leaf. The decision is the predicted value.

Perceptron classification: The Perceptron classifier [17] is a set of supervised learning, the classification field of a sample can be predicted using Perceptron classifier. Perceptron classifier accept numerous input and if the number of inputs is more than the specified condition, it does not return the output, it output the massage

for corrections. In the Perceptron algorithm features on the data set are taken as inputs and it is represented by x1, x2, x3, x4,...,xn where features value is indicated by x and the total occurrences is represented by n.

The required features to be trained is stored as input in the first layer. Now the total inputs and weights will be multiplied and add their outcome. The weights are the values obtained through the training of the model and are denoted by w1, w2, w3,..,wn. The output function will be shifted by the bias value and this value will later be presented to the activation function then the output value is obtained after receiving the value on the last step.

Logistic regression (LR): Logistic regression describe the association among variables and it was used to predict student academic performance by estimating the probability of an event occurring [18]. It also shows the probability of two categories by fitting the explanatory variables and log odds to model using this equation.

$$log(\frac{(P(Y = 1|X))}{1 - P(Y = 1|X)}) = \beta_0 + \beta_1 X_1 +, ..., \beta_N X_N$$

where $Y=(0,1)$ is the binary variable; 1 if it is higher than the reference level and 0 if not, $X = (X_1, ..., X_n)$ are n explanatory variables and $\beta = (\beta_0, ...\beta_n)$ are the estimated regression coefficient.

Random forest (RF): Random forest uses begging method to generate trees in which its prediction is more accurate than that of any individual tree [19]. Random forest was also used to avoid over fitting on the training set and limiting errors due to bias hence yield accurate and useful results. RF can handle outliers and noise in the data and gains high classification accuracy. RF generate numerous decision trees in the training phase and output class labels [20]. RF
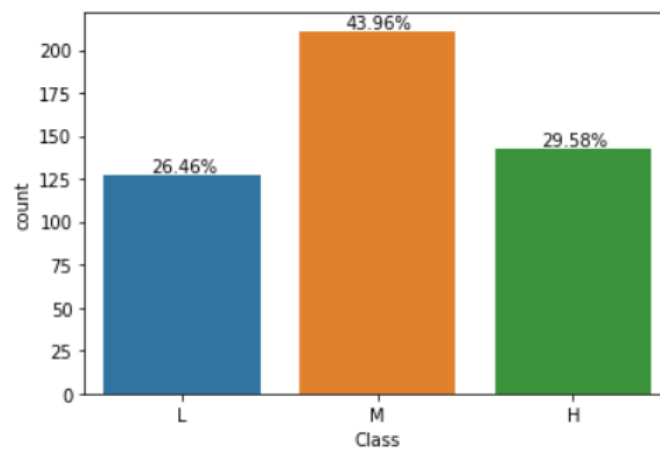
Figure 1: This figure depicts the proportion of student academic performance of the classification field.

is used in this study since it is permissible to less over-fitting and it has proofed to be good classification results previously.

RF is a theoretical framework grounded on mixture of decision trees; $\{T_1X, ..., T_BX\}$. The ensemble produces B outputs $\{\check{Y}_1 = T_1(X), ..., \check{Y}_B = T_B(X)$, where $\check{Y}_b, b = 1, ..., B$ is the predicted grades by the bth tree. Output of all trees are aggregated to produce one final prediction $\check{Y}$, which is the class predicted by majority of trees.

4.5   Analysis

The data set consist a total of 480 records. Machine learning algorithms are applied to predict student academic performance and we found that Support vector machine algorithm is best suited to predict student academic performance. We achieve a total accuracy of 70.8% which shows the potential accuracy of Support Vector Machine technique, followed by Random forest with 69.7% accuracy, Logistic regression with 67.7% accuracy, Perceptron with 64.5% and lastly Decision tree with 46.8%.

5   Results and Discussion

5.1   Pre-processing

Typically in machine learning before processing and running a test on a data set, it is necessary to prepare the data and select the targeted attribute. Selecting attributes requires putting all the matching combination of attributes in the data set in order to find which combination is suitable in predicting student academic performance.

Our goal with pre-processing was to change our numerical fields that have a value like Grade ID to a numerical only value in a way that we preserve that distance in a meaningful way. We also assign our three classes to numerical outcomes with a preserved distance and set setting L = -1, M = 0, and H = 1. We chose to preserve the distance between the categorical values and scale our numerical fields so that they would be more meaningful when compared together.

The five machine learning models are used to evaluate the student's academic performance and to check which model best predict

student performance.

5.2   Data visualisation

The data set consist a total of 480 records. In this study, the purpose of selecting an attributes was to find the attributes that contain numerical data, attributes that contain categorical data and classification label. Our goal with data visualisation is to get an idea of the shape of the data set and to see if we can easily identify any possible outliers and also look to see if any of data is unclear or redundant.

5.3   Summary of results

In the previous section, student academic performance was discussed and how it will be evaluated. In this section we discuss the performance of five machine learning models that was specified in section 4. First of all, we performed data visualisation after performing data pre-processing by generating simple plots of data distributions to get an idea of the shape of the data set and then 5 main machine learning techniques was evaluated and also describe the variables contained on the data set. The evaluation was done on the full data set that consist of 480 features [21].

From the results, it was proven that Support vector machine algorithm is most suitable in predicting the performance of students. SVM is relative higher than other algorithms and it has 70.8% prediction accuracy, followed by Random forest with 69.7% accuracy, Logistic regression with 67.7% accuracy, Perceptron with 64.5% and lastly Decision tree with 46.8%. We found the overall percentage of passing rate using class variable. There were 26.46% students who got a failing percent (less than 69%), 43.96% students who got a low passing grades (between 70% and 89%) and 29.58% who achieved high marks in their course (90% to 100%).

Student absence days seems to have a strong correlation with class variable. Very few students who missed more than 7 days managed to achieve high marks and very few students who missed less than 7 days failed their course. From grade 2 to grade 12 we found that grade 5, 9, and grade 10 have very few counts. No 5th grade students pass and no 9th grade students achieve high marks.

In figure 4, the bar plot shows the accuracy of five popular
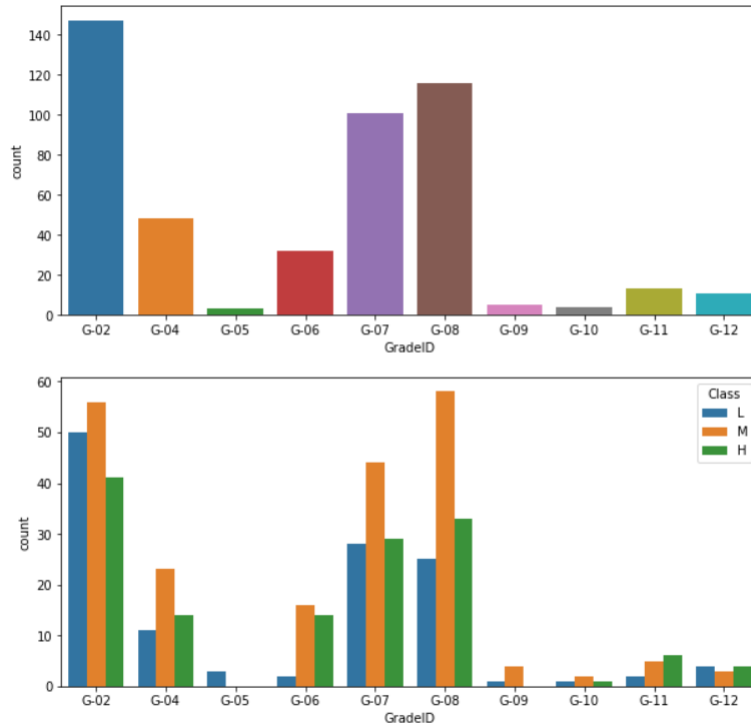
Figure 2: This figure depicts the grade the student is in and it also shows the average student performance for each grade.
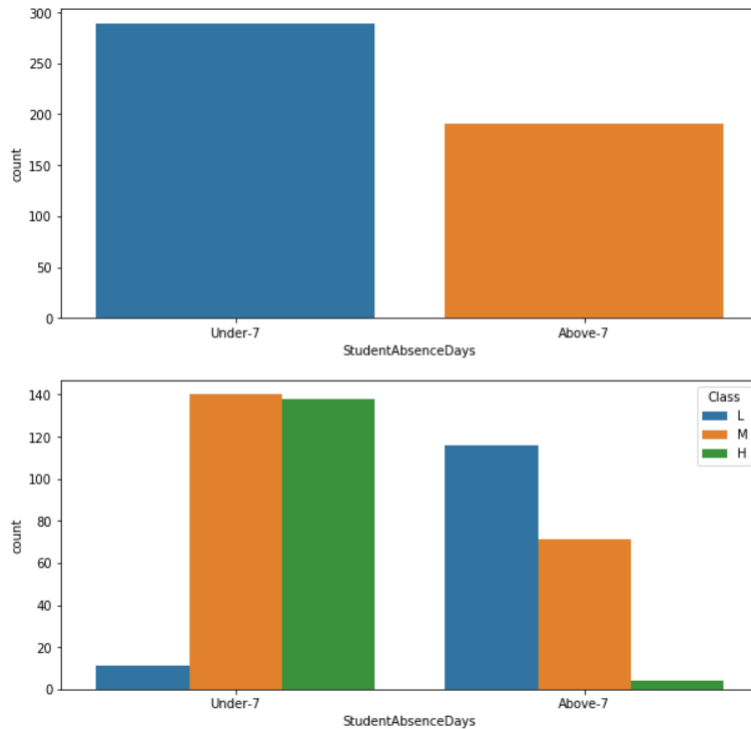
Figure 3: This figure depicts the proportion of student absence days and it also shows whether or not a student was absent for more than 7 days.

Table 3: This table shows the confusion matrices that describe the performance of the classification models.

Support vector machine			
Actual Values	**Predicted Values**		
	High	Low	Medium
High	23	1	11
Low	0	19	3
Medium	5	8	26
Decision tree			
Actual Values	**Predicted Values**		
	High	Low	Medium
High)	20	1	14
Low	1	15	6
Medium	7	8	24
Perceptron			
Actual Values	**Predicted Values**		
	High	Low	Medium
High	8	4	25
Low	0	21	1
Medium	2	19	18
logistic regression			
Actual Values	**Predicted Values**		
	High	Low	Medium
High	8	4	25
Low	0	21	1
Medium	2	19	18
Random Forest			
Actual Values	**Predicted Values**		
	High	Low	Medium
High	22	1	12
Low	0	16	6
Medium	4	6	29
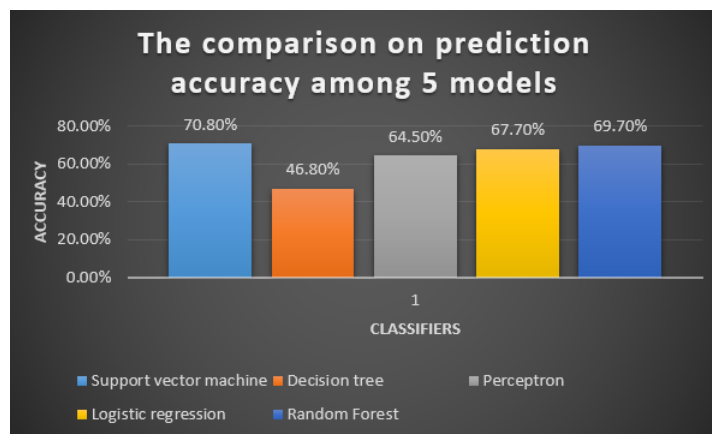
Figure 4: The comparison on prediction accuracy among 5 models.

Table 4: This table depicts the machine learning algorithms used in this study and their performance accuracy.

Classifier	Accuracy
Support vector machine	70.8%
Decision tree	46.8 %
Perceptron	64.5%
Logistic regression	67.7%
Random forest	69.7%

Table 5: This table depicts detailed accuracy of Logistic regression.

Features	Weighted Average
Correctly classified Instances	73.75%
Incorrectly classified Instances	26.25%
Mean absolute error	21.33%
Root mean squared error	37.53%
Relative absolute error	49.27%
Root relative squared error	80.6%
Precision	73.8%
Recall	73.8%
F-Measure	73.8%
Roc Area	83.8%
Total number of Instances	480

Table 6: This table depicts detailed accuracy of Perceptron.

Features	Weighted Average
Correctly classified Instances	79.37%
Incorrectly classified Instances	20.62%
Mean absolute error	14.88%
Root mean squared error	34.59%
Relative absolute error	34.36%
Root relative squared error	74.35%
Precision	79.3%
Recall	79.4%
F-Measure	79.3%
Roc Area	89.3%
Total number of Instances	480

Table 7: This table depicts detailed accuracy of Random Forest.

Features	Weighted Average
Correctly classified Instances	76.66%
Incorrectly classified Instances	23.33%
Mean absolute error	24.28%
Root mean squared error	33.37%
Relative absolute error	56.09%
Root relative squared error	71.72%
Precision	76.6%
Recall	76.7%
F-Measure	76.6%
Roc Area	89.7%
Total number of Instances	480

Table 8: This table depicts detailed accuracy of Decision tree.

Features	Weighted Average
Correctly classified Instances	72.70%
Incorrectly classified Instances	27.29%
Mean absolute error	29.53%
Root mean squared error	37.18%
Relative absolute error	68.19%
Root relative squared error	79.92%
Precision	72.8%
Recall	72.7%
F-Measure	72.7%
Roc Area	84.2%
Total number of Instances	480

Table 9: This table depicts detailed accuracy of Support Vector Machine.

Features	Weighted Average
Correctly classified Instances	78.75%
Incorrectly classified Instances	21.25%
Mean absolute error	27.22%
Root mean squared error	35.22%
Relative absolute error	62.87%
Root relative squared error	75.71%
Precision	78.8%
Recall	78.8%
F-Measure	78.7%
Roc Area	86%
Total number of Instances	480
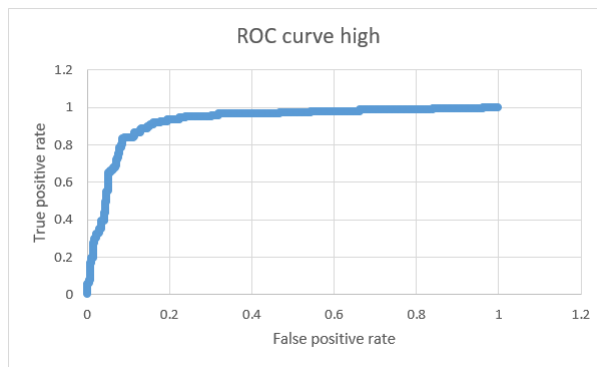
Figure 5: Receiver operating characteristic curve (class high).
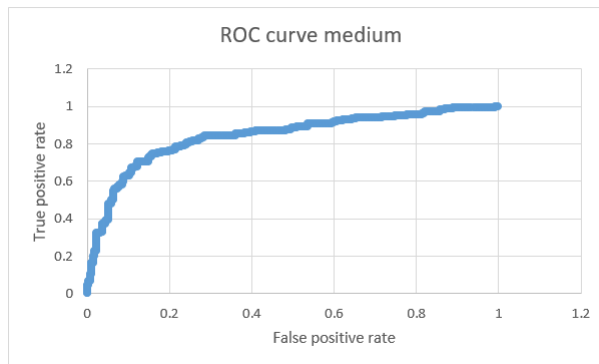
Figure 6: Receiver operating characteristic curve (class medium).
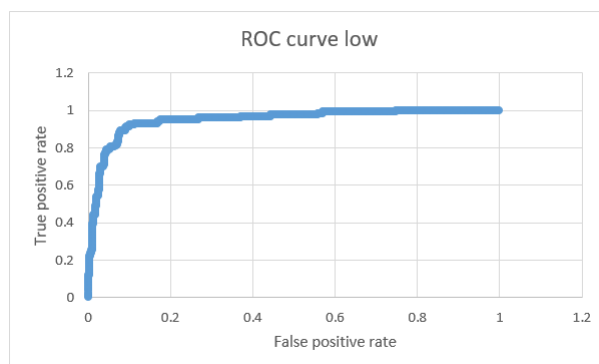
Figure 7: Receiver operating characteristic curve (class low).

machine learning models that is used to evaluate the student performance. The legend of the plot indicate that blue colour is Support vector machine, Yellow colour indicate Logistic regression, orange colour indicate Decision tree, light blue indicate Random forest and grey colour indicate Perceptron classifier.

Support vector machine has performed well when compared to other machine models. 78.75% instances was correctly classified and 21.25% instances was incorrectly classified. Another way of representing accuracy of the machine learning models that are in figure 4 is through confusion matrices. Table 3 describe how each algorithm has performed.

The graphical representation of receiver operating characteristic curve shows the performance of our best classification model, Support vector machine at all classification thresholds [22]. The ROC curve figure 5, figure 6 and figure 7 shows the classification performance of our best classifiers which is Support vector machine. There are three numerical intervals of student grades (low, medium and high). As can be seen from figure 5, figure 6 and figure 7. The ROC curve occupies the upper left corner, which means the classifier (SVM) used in this paper indicate a better performance and the prediction of positive value is specific in some degree, with AUC of 86%.

6 Conclusion and Future work

Companies and educational institutions uses learning management systems to create and manage lessons, courses, quizzes and other training materials [23]. Student's success needs to be predicted to help an instructor identify academic performance and helps with identifying struggling students more easily and giving teachers a proactive chance to come up with supplementary resources to learners to improve their chances of increasing their grades. It may be difficult for students to learn virtually than in a traditional class hence the student's performance vary due to difference methods of delivering the course materials [24].

Various machine learning models were used to predict student success using the learning management system. Each model indicate different percentage of accuracy when is tested with different features that are associated in an online learning platforms [25].

Student's performance was evaluated by five machine learning techniques which is Perceptron classifier, Support vector machine and Decision trees, Logistic regression and Random forest. Support vector machine ends up handling the data the best with 70.8% accuracy. The obtained results shows that the student absence days influence student academic performance on the other hand student class grades is not influencing student academic performance.

We aim to extend the study by collecting more additional features such as encouraging and motivational strategies taken by facilitators and teachers and considering more materials available for students in an E-learning platforms. We will also consider features such as psychological factors available which affect student's performance. We also intent to use more interesting and detailed data set to predict student academic performance in our future studies.

References

[1] M. D. Dixson, "Measuring student engagement in the online course: the Online Student Engagement scale (OSE).(Section II: Faculty Attitudes and Student Engagement)(Report)," Online Learning Journal (OLJ), **19**(4), 143, 2015, doi: 10.3102/00346543074001059.

[2] S. Huang, N. Fang, "Predicting student academic performance in an engineering dynamics course: A comparison of four types of predictive mathematical models," Computers and Education, **61**(1), 133–145, 2013, doi: 10.1016/j.compedu.2012.08.015.

[3] R. Ajoodha, R. Klein, B. Rosman, "Single-labelled music genre classification using content-based features," in 2015 Pattern Recognition Association of South Africa and Robotics and Mechatronics International Conference (PRASA-RobMech), 66–71, IEEE, 2015.

[4] E. J. Lauría, J. D. Baron, M. Devireddy, V. Sundararaju, S. M. Jayaprakash, "Mining academic data to improve college student retention: An open source perspective," in Proceedings of the 2nd International Conference on Learning Analytics and Knowledge, 139–142, 2012.

[5] R. Ajoodha, B. S. Rosman, "Learning the influence structure between partially observed stochastic processes using iot sensor data," AAAI, 2018.

[6] K. F. Li, D. Rusk, F. Song, "Predicting student academic performance," in 2013 Seventh International Conference on Complex, Intelligent, and Software Intensive Systems, 27–33, IEEE, 2013.

[7] R. Ajoodha, A. Jadhav, S. Dukhan, "Forecasting learner attrition for student success at a south african university," in Conference of the South African Institute of Computer Scientists and Information Technologists 2020, 19–28, 2020.

[8] S. Huang, N. Fang, "Predicting student academic performance in an engineering dynamics course: A comparison of four types of predictive mathematical models," Computers & Education, **61**, 133–145, 2013, doi:https://doi.org/10.1016/j.compedu.2012.08.015.

[9] R. J. Oskouei, M. Askari, "Predicting academic performance with applying data mining techniques (generalizing the results of two different case studies)," Computer Engineering and Applications Journal, **3**(2), 79–88, 2014.

[10] R. Asif, A. Merceron, S. A. Ali, N. G. Haider, "Analyzing undergraduate students' performance using educational data mining," Computers & Education, **113**, 177–194, 2017.

[11] Y. Gerhana, I. Fallah, W. Zulfikar, D. Maylawati, M. Ramdhani, "Comparison of naive Bayes classifier and C4. 5 algorithms in predicting student study period," in Journal of Physics: Conference Series, volume 1280, 022022, IOP Publishing, 2019.

[12] Y. Salal, S. Abdullaev, M. Kumar, "Educational Data Mining: Student Performance Prediction in Academic," IJ of Engineering and Advanced Tech, **8**(4C), 54–59, 2019, doi:10.1016/6895.125478.

[13] S. Hua, Z. Sun, "Support vector machine approach for protein subcellular localization prediction," Bioinformatics, **17**(8), 721–728, 2001.

[14] I. Burman, S. Som, "Predicting students academic performance using support vector machine," in 2019 Amity International Conference on Artificial Intelligence (AICAI), 756–759, IEEE, 2019.

[15] F. Esposito, D. Malerba, G. Semeraro, J. Kay, "A comparative analysis of methods for pruning decision trees," IEEE transactions on pattern analysis and machine intelligence, **19**(5), 476–491, 1997.

[16] F. Jauhari, A. A. Supianto, "Building student's performance decision tree classifier using boosting algorithm," Indonesian Journal of Electrical Engineering and Computer Science, **14**(3), 1298–1304, 2019, doi:10.1016/j.compedu.2012.08.015.

[17] B. Chaudhuri, U. Bhattacharya, "Efficient training and improved performance of multilayer perceptron in pattern classification," Neurocomputing, **34**(1-4), 11–27, 2000.

[18] D. W. Hosmer Jr, S. Lemeshow, R. X. Sturdivant, Applied logistic regression, volume 398, John Wiley & Sons, 2013.

[19] A. Liaw, M. Wiener, et al., "Classification and regression by randomForest," R news, **2**(3), 18–22, 2002.

[20] K. Deepika, N. Sathyanarayana, "Relief-F and Budget Tree Random Forest Based Feature Selection for Student Academic Performance Prediction," International Journal of Intelligent Engineering and Systems, **12**(1), 30–39, 2019, doi:10.1016/j.5896408.015.

[21] C. Sievert, Interactive Web-Based Data Visualization with R, plotly, and shiny, CRC Press, 2020.

[22] R. Kannan, V. Vasanthi, "Machine learning algorithms with ROC curve for predicting and diagnosing the heart disease," in Soft Computing and Medical Bioinformatics, 63–72, Springer, 2019, doi:10.1016/j.compedu.2012.08.015.

[23] C. Hodges, S. Moore, B. Lockee, T. Trust, A. Bond, "The difference between emergency remote teaching and online learning," Educause Review, **27**, 2020.

[24] H. M. Niemi, P. Kousa, et al., "A case study of students' and teachers' perceptions in a Finnish high school during the COVID pandemic," International journal of technology in education and science., 2020.

[25] M. Hussain, W. Zhu, W. Zhang, S. M. R. Abidi, S. Ali, "Using machine learning to predict student difficulties from learning session data," Artificial Intelligence Review, **52**(1), 381–407, 2019.

Lifestyle in Nursing Students at a University of North Lima

Yanet Cruz Flores[1], Tania Retuerto-Azaña[1], Jaquelin Nuñez-Artica[1], Brian Meneses-Claudio[2,*], Hernan Matta Solis[1], Lourdes Matta-Zamudio[1]

[1]*Faculty of Health Sciences, Universidad de Ciencias y Humanidades, 15314, Lima-Perú*

[2]*Image Processing Research Laboratory (INTI-Lab), Universidad de Ciencias y Humanidades, 15314, Lima-Perú*

A R T I C L E   I N F O

A B S T R A C T

Healthy lifestyles were proposed to improve the health status of the university population, they are a set of behaviors that are reflected according to the type of situation and behavior of each person who performs it during the period of their training, the inappropriate lifestyles provides many problems, which are non-communicable diseases that manifest in the health status of each individual, which most of the time students choose to consume less nutritious foods and they are not healthy and affect their health; inadequate lifestyles do not provide good academic performance and also generate a bad psycho-emotional state. The objective of the study is to determine the Lifestyle in nursing students at a university in North Lima, 2019. As results, regarding the Lifestyle in nursing students at a university in North Lima; 51.5% have healthy lifestyle and 48.5% have an unhealthy lifestyle. Regarding the dimensions, interpersonal relationships predominate 73.8% have an unhealthy lifestyle followed by stress management, 65.8% have an unhealthy lifestyle, responsibility for health, 63.3% have a lifestyle unhealthy, Physical activity dimension, 60.8% have an unhealthy lifestyle, spiritual growth, 48.8% have an unhealthy lifestyle, healthy nutrition, 29, 5% have an unhealthy lifestyle; it is important to know those results to make decisions.

1. Introduction

In the Republic of Ireland in September 2016 they have shown that university life transition has a negative effect on student lifestyles, resulting in weight gain, increased physical inactivity and stress [1]. University students go through a variation of changes in their mental, physical, social, and economic lives during their university life [2].

The university stage is characterized by a tendency to engage in a variety of unhealthy behaviors [3]. Evidences suggest that nursing students do not engage in healthy lifestyles such negative behaviors lead nursing students to become overweight and obese, as well as other risks such as smoking, alcohol consumption, drugs, an insufficient diet and poor physical activity [4], [5].

According to the research, it has carried out a technical reform that aims to educate the entire community, regarding issues related to nutrition, promoting healthy practices for a proper life and to prevent diseases such as anemia and chronic malnutrition,

as well same regarding overweight, obesity, diabetes, cardiovascular disease, high blood pressure and cancer. This technical document aims to promote the functions of exhaustive care and health promotion in the university population [6].

Unhealthy habits are factors that predominate in university students. According to studies, it is evident that they do not perform physical activity; they do not complete their sleep hours; they eat fast food [7], the negative effects are evident when they reach the adult stage, which causes health problems in older life The evidence shows that regular physical activity helps maintain good health styles and prevents diseases such as hypertension, obesity, metabolic syndrome, heart disease, diabetes, osteoporosis, some types of cancer, and produces significant benefits at the psychosocial level [8]. In this university stage, a sum of difficulties are manifested, likewise this type of qualities is linked to inappropriate health behavior; therefore, it should be noted that it is significant to determine certain health behaviors that are inadequate and have a much higher risk of suffering from non-communicable diseases [9].

In Peru in 2018, more than 50% of the disease burden is associated with non-communicable diseases, which affect all age groups. Tobacco use, harmful use of alcohol, unhealthy diet, infrequent physical activity. Approximately 62 million people have Type 2 Diabetes. Cancer is the second leading cause of death. In 2018, it caused 1.3 million deaths, and 3.7 million new cases. Tobacco kills 7 million people each year. 62% of adults are overweight or obese. The epidemic disturbs adolescent and young children since between 20% and 25% are affected by being overweight or obese [10].

In [11], the authors showed the sample of 829 university students included 504 (60.8%) Chinese and 325 (39.2%) international students. The Chinese students had higher scores in general healthy lifestyles and the scales showed low levels in physiological and social health. Gender was associated with psychological health in both groups. Smoking was a predictor of psychological health in both groups and of social health in the international group.

In [12], the authors showed that 47% of the study participants had a moderate-level lifestyle. Regarding musculoskeletal symptoms, the most frequent were reported in the back (88,33%), knees (83,33%) and thighs (71%). Furthermore, Pearson's correlation analysis revealed significant negative correlations between eating habits and musculoskeletal symptoms and interpersonal relationships, while a significant positive correlation was found between nutrition and stress management.

In [13], the authors presented a study carried out in Turkey, showed that in nursing students there were various factors such as financial problems (70.3% of moderate income level; inadequate) and the characteristics cultural factors that may have contributed to the decrease in physical activity observed in this study; therefore it should be noted that it is significant to determine certain health behaviors that are inadequate and have a much higher risk of suffering from non-communicable diseases.

The objective of the study is to determine the Lifestyle in nursing students at a university in North Lima, 2019. This research work will be developed to improve the lifestyle of university students to reduce the risks of acquiring different diseases due to bad lifestyles in university students at a university of north lima. In this study, we suggest that we should continue to emphasize the promotion of a healthy lifestyle in nursing students; in the university stage, an important role must be fulfilled, such as prevention and health promotion; this effort must be involved with other professionals to have more significant results in the benefit of the health of the university population, they are encouraged to raise awareness.

The instrument to be used is the Health Promoting Lifestyle Profile II (HPLP-II) developed by Pender Walker and Sechrist, in 1987 and translated into Spanish in 1995, consisting of 52 items divided into six dimensions: health responsibility that is the comprising an active notion of responsibility for one's own comfort. It implies maintaining an adequate interest in one's own health, educating oneself about health [14].

All the data will be addressed to a Microsoft Excel 2013 program, then it will be sent into the SPSS24 program.

To compile the information, articles were reviewed in all the scientific databases that exist internationally and nationally, it was possible to indicate that there are a large number of articles that address the health problem with respect to a healthy lifestyle, information is evidenced found in articles, therefore, this study seeks to increase the knowledge of each of the students. The subject is important since applying it in practice would bring many benefits for the human being.

This work is structured as follows: In section II, the steps to carry out the survey are explained, how the population and sample were acquired, type of study, inclusion and exclusion criteria, analysis of variables, data collection, place and application of instruments. In section III, the results acquired according to the surveys carried out in the study are presented, through the elaboration of tables and bars. In section IV, the discussions that show the interpretation of results obtained in the research work compared to another research will be presented. Finally, in section V, the conclusions of the research work will be shown according to the results found, what measures should be taken about them.

2. Methodology

2.1. Population

There are 400 students from the first to the tenth cycle of the nursing faculty. Day and night shift.

Table 1: Number of Students from day and night shift

Study semester	Total of Students	Percentage
Semester 1	60	15.0
Semester 2	45	11.3
Semester 3	42	10.5
Semester 4	33	8.3
Semester 5	41	10.3
Semester 6	39	9.8
Semester 7	30	7.5
Semester 8	32	8.0
Semester 9	41	10.3
Semester 10	37	9.3

2.2. Inclusion criteria

- Nursing students from 1st to 10th semester.
- Nursing students who have signed the informed consent.

2.3. Exclusion Criteria

- Nursing students who do not want to participate in research.
- Nursing students who have not signed the informed consent.

2.4. Type of study

The present investigation is of a quantitative approach, its non-experimental, descriptive, and transversal design. To start with the

data collection, the necessary coordination was carried out in the Faculty of Nursing to obtain authorization for access to the classrooms of the institution [15].

2.5. Application of the instrument

The survey and the instrument used is The HPLP (Health Promoting Life Profile II) created by. Walker S., Sechrist K., Pender N. Kerr M., published in Spanish in 1995, is made up of 52 items and distributed in six dimensions, responsibility in health (9 items), physical activity (8 items), nutrition (9 items), spiritual growth (9 items), interpersonal relationships (9 items) and stress management (8 items), also a standard scale is used Likert where the punctuation varies from 1 to 4, where "1 = never", "2 = sometime", "3 = often" and "4 = usually", giving a final score of 52 to 208, ranging from " 52 to 130" is an unhealthy lifestyle and "131 to 208" is a healthy lifestyle, the higher the score the higher the healthy lifestyle the student will present [16].

2.6. Place and application of the instrument

The instrument was applied at the Universidad de Ciencias y Humanidades in Los Olivos. A permission was requested from the nursing faculty to have access to the classrooms. For this, an enrollment in the ethics committee was made for the approval of the instrument to apply.

After approval, permission was requested from teachers who teach in the classrooms to provide 15-minute access to students to fill out the questionnaire. We had some difficulties with some teachers because they made us wait until the end of their class to give us the space, and others to wait for the break to be able to enter.

Figure 1: Delivering surveys to the students at a University of North Lima

As shown in Figure 1, they were given instructions on how to complete the questionnaire. To use exclusively a pencil to mark a single alternative in the question to avoid smearing.

Figure 2: Developing the surveys by the students at a University of North Lima

As shown in Figure 2, the students carefully concentrated on reading the questionnaire; some students did not understand the questions they did not interpret it in the health field.

The doubts they had about the questions were explained to the students and they were reminded that their answer must be sincere, and the development is individual, not group to get good results.

Figure 3: Collecting student surveys.

As shown in Figure 3, it is verified that the entire questionnaire is filled out. If a question doesn't have an answer, it is returned to the participant to complete so that the questionnaire is valid to be typing to the SPSS to find questions, also if there is missing answer, the survey is eliminated.

The nursing personnel is fundamental for the health study of the university students since it offers them Psycho-emotional support for the social well-being of the university students; because many are unaware of healthy lifestyles or do not practice them and lead a routine life and acquire non-communicable diseases.

3. Results

After obtaining the surveys, the data was synthesized and statistical tables were generated for a better understanding of them, as shown in Table I.

Table 1: Sociodemographic lifestyle data in nursing students from a university of north lima, 2019 (n = 400).

Participant Information	Total	
	N	%
Total	400	100
Sex		
Female	342	85,5
Male	58	14,5
Marital Status		
Single	262	65,5
Married	54	13,5
Widowed	5	1,3
Cohabitant	56	14,0
Divorced	23	5,8
Type of Family		

Nuclear	191	47,8
Extended	43	10,8
Amplified	55	13,8
Single parent	63	15,8
Reconstituted	23	5,8
Family equivalent	25	6,3
Occupancy Condition		
Study	142	35,5
Study and work	258	64,5
Degree of Study		
Secondary	170	42,5
University	156	39,0
Technical	74	18,5
Primary Education	3	0,8

In Table 1, it has the sociodemographic data of the study participants, there were 400 participating nursing students. The minimum age was 18 years old; the maximum age was 49 years old, the mean being 24.83 years old.
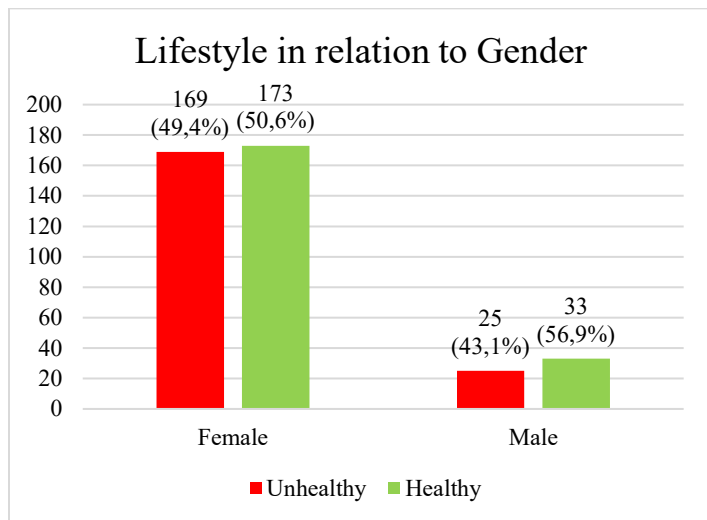
Figure 4: Lifestyle in nursing students at a university in North Lima, 2019 (N = 400)

Regarding sex, the female sex predominated with 342 students representing 85.5%, followed by the male sex with 58 students representing 14.5%. Regarding marital status, the single person predominates with 262 (65.5%) cases, followed by Cohabitant with 56 (14%) cases, married with 54 (13.5%) cases, divorced with 23 (5.8%) cases, and finally widowers with 5 (1.3%) cases.

Regarding the type of family, nuclear families predominate with 191 (47,8%) cases, followed by the single parent with 63 (15, 8%) cases, amplified with 55 (13,8%) cases, extended with 43 (10,8%) cases, family equivalent with 25 (6,3%) cases and finally reconstituted 23 (5,8%) cases.

Regarding the occupation status of nursing students, 258 study and work (64,5%) cases and only 142 with (35, 5%) cases study.

Regarding the degree of study, 238 students representing 59.5% have secondary education, 117 students representing 29.3% have technical education, 42 students representing 10.5% have university education and finally 3 students representing 0.8% have primary education.

In Figure 4, the lifestyle in nursing students from a university in Lima Norte, it can see that 206 students represent 51.5% have a healthy lifestyle and 194 students that represent 48.5% have an unhealthy lifestyle.
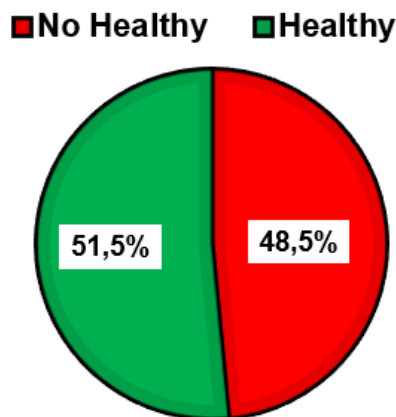
Figure 5: Lifestyle in relation to gender of nursing students from a University of Lima Norte, 2019 (N = 400).

Figure 5 shows the lifestyle in relation to gender of nursing students from a university in North Lima, where 169 (49.4%) who are female have an unhealthy lifestyle, 173 (50.6%) have a healthy lifestyle, 25 (43.1%) who are male have an unhealthy lifestyle and 33 (56.9%) have a healthy lifestyle.
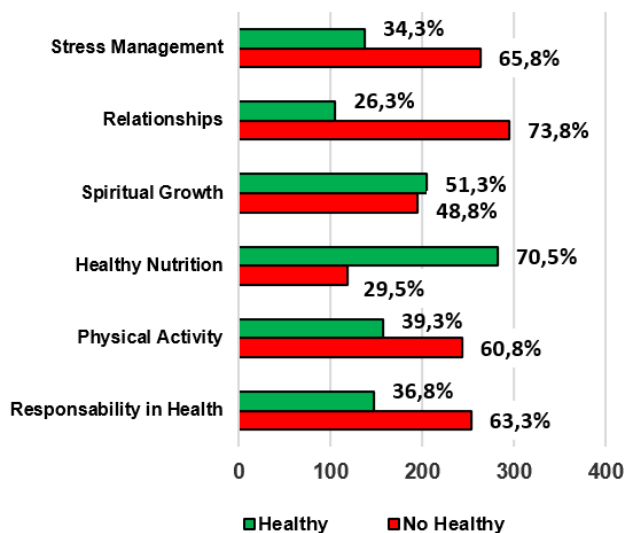
Figure 6: Lifestyle according to its general dimensions that the instrument contains according to a study in nursing students from a university in North Lima, 2019 (N = 400).

In Figure 6, Lifestyle in its dimension health responsibility, in nursing students from a university in Lima Norte, it can see that 253 students represent 63, 3%, have an unhealthy lifestyle and 147

students represent 36.8%, have a healthy lifestyle. In the physical activity dimension, in nursing students from a university in North Lima, it can see that 243 students represent 60.8%, have an unhealthy lifestyle and 157 students represent 39.3%, have a healthy lifestyle. In the healthy nutrition dimension, in nursing students from a university in North Lima, it can see that 282 students represent 70.5%, have a healthy lifestyle and 118 students represent 29.5%, have an unhealthy lifestyle. In the growth dimension spiritual, in nursing students from a university in Lima Norte, it can see that 205 students represent 51.3%, have a healthy lifestyle and 195 students represent 48.8%, have an unhealthy lifestyle. In the interpersonal relationships dimension predominates 295 students representing 73.8%, have a healthy lifestyle. In the stress management dimension, in nursing students from a university in Lima Norte, it can see that 263 students represent 65.8%, have an unhealthy lifestyle and 137 students represent 34.3%, have a healthy lifestyle.

4. Discussion

The research work confirms the unhealthy lifestyles in university students based on the articles reviewed in [12] to their study carried out on university students from Iran Shiraz where bad interpersonal relationships were evidenced in the students and based on [11] to their study carried out, low results were evidenced regarding its dimensions; according to [13] to their carried out in Turkey, students have a sedentary life and do not carry out physical activity.

In the study carried out on students from a North Lima university in terms of dimensions, it was clearly shown that a large number of students who do not have good interpersonal relationships with their peers are not responsible for their health; they do not have good stress management and do not carry out physical activity. It leads to a sedentary life. Likewise, in [5], argue that students do not have a good lifestyle and that factors such as tobacco and alcohol show an inappropriate lifestyle.

This type of studies can be applied in other university centers to help the teaching for students and also train teachers so that they can implement educational programs such as physical exercise, stress control, improving lifestyles involves commitment and will.

Promoting lifestyles is a little difficult since students do not put into practice; they always make excuses for not doing it, that's why, this research work is presented to provide guidance on the situation that university students are in.

5. Conclusion

To conclude in this regarding lifestyle, it is projected from the promotion of the health of the university students, in order to contribute to the universities so that they include programs to have an adequate healthy diet, physical activity, etc.

It is concluded that the university population is made aware of the benefits of irregular practices of physical activities that improve the lifestyle.

It is concluded that counseling is provided to university students to develop educational intervention protocols in relation to healthy life habits.

Conflicts of Interest

The authors declare no conflict of interest.

References

[1] E. Bastias, J. Stiepovich, "Una revisión de los estilos de vida de estudiantes universitarios iberoamericanos.," Ciencia y Enfermeria, **20**(2), 93–101, 2014.

[2] P. Mc Sharry, F. Timmins, "An evaluation of the effectiveness of a dedicated health and well being course on nursing students' health.," Nurse Education Today, **44**, 26–32, 2016, doi:10.1016/j.nedt.2016.05.004.

[3] Y. Lara, C. Quiroga, A. Jaramillo, M. Bermeo, "Estilo de vida de estudiantes en primer semestre de odontología de una universidad privada, Cali 2016.," Revista Odontológica Mexicana, **22**(3), 144–149, 2018.

[4] N. Gormley, V. Melby, "Nursing students' attitudes towards obese people, knowledge of obesity risk, and self-disclosure of own health behaviours: An exploratory. survey," Nurse Education Today, **84**, 104232, 2020, doi:10.1016/j.nedt.2019.104232.

[5] A. Montenegro, A. Ruíz, "Factores asociados a los estilos de vida en los estudiantes universitarios. Una aplicación del instrumento fantástico.," Revista Digital: Actividad Física y Deporte, **6**(1), 87–108, 2019.

[6] Ministerio de Salud, Guías Alimentarias Para La Población Peruana, 1–60, 2019.

[7] A. Gallardo, M. Alférez, E. Planells, I. López, "La etapa universitaria no favorece el estilo de vida saludable en las estudiantes granadinas.," Nutricion Hospitalaria, **31**(2), 975–979, 2015, doi:10.3305/nh.2015.31.2.8303.

[8] N. Arias, M. Solera, L. Gracia, P. Silva, V. Martínez, J. Cañete, M. Sánchez, "Levels and patterns of objectively assessed physical activity and compliance with different public health guidelines in university students.," PLoS ONE, **10**(11), 1–15, 2015, doi:10.1371/journal.pone.0141977.

[9] D. Kazemi, M. Levine, J. Dmochowski, K. Roger Van Horn, L. Qi, "Health behaviors of mandated and voluntary students in a motivational intervention program.," Preventive Medicine Reports, **2**, 423–428, 2015, doi:10.1016/j.pmedr.2015.05.004.

[10] Organización Panamericana de la Salud, Enfermedades no transmisibles y factores de riesgo, Boletín Epidemiológico, 2019.

[11] S. Lolokote, T. Hidru, X. Li, "Do socio-cultural factors influence college students' self-rated health status and health-promoting lifestyles? A cross-sectional multicenter study in Dalian, China.," BMC Public Health, **17**(1), 1–14, 2017, doi:10.1186/s12889-017-4411-8.

[12] M. Heidari, M. Borujeni, M. Khosravizad, "Health-promoting Lifestyles of Nurses and Its Association with Musculoskeletal Disorders: A Cross-Sectional Study.," Journal of Lifestyle Medicine, **8**(2), 72–78, 2018.

[13] B. Kara, B. Işcan, "Predictors of Health Behaviors in Turkish Female Nursing Students.," Asian Nursing Research, **10**(1), 75–81, 2016, doi:10.1016/j.anr.2015.12.001.

[14] M. Al-Qahtani, "Comparison of health-promoting lifestyle behaviours between female students majoring in healthcare and non-healthcare fields in KSA.," Journal of Taibah University Medical Sciences, **14**(6), 508–514, 2019, doi:10.1016/j.jtumed.2019.10.004.

[15] C. Fernández, P. Baptista, Metodología de la Investigación. 6ta ed. México: Mc Graw-Hill/Interamericana., 2015.

[16] G. Kuan, Y. Kueh, N. Abdullah, E. Tai, "Psychometric properties of the health-promoting lifestyle profile II: Cross-cultural validation of the Malay language version.," BMC Public Health, **19**(1), 1–10, 2019, doi:10.1186/s12889-019-7109-2.

Autonomous Robot Path Construction Prototype Using Wireless Sensor Networks

José Paulo de Almeida Amaro[1], João Manuel Leitão Pires Caldeira[2,*], Vasco Nuno da Gama de Jesus Soares[2], João Alfredo Fazendeiro Fernandes Dias[3]

[1]*Instituto Politécnico de Castelo Branco, Castelo Branco, 6000-084, Portugal*

[2]*Instituto Politécnico de Castelo Branco, Instituto de Telecomunicações, Castelo Branco, 6000-084, Portugal*

[3]*IADE–Faculdade de Design, Tecnologia e Comunicação, Lisboa, 1000-041, Portugal*

A R T I C L E   I N F O

A B S T R A C T

The use of wireless sensor networks (WSN) can be a valuable contribution in disaster situations or life-threatening exploration. Using wireless mobile robots, it is possible to explore vast areas without human intervention. However, the wireless network coverage that can keep mobile robots connected to the base station / gateway is a major limitation. With this in mind it was created a prototype of an extensible WSN using mobile robot nodes that cooperate amongst themselves. The strategy adopted in this project proposes using three types of nodes: master node, static node, and robot node. Three different algorithms were also developed and proposed: Received Signal Strength Indication (RSSI) Request; Automovement; Robot Cooperation and Response to Static Node. The performance evaluation of the prototype was carried out using a real-world testbed with each developed algorithm. The results achieved were very promising to continue the evolution of the prototype.

1. Introduction

This paper is an extension of work originally presented in conference *2020 15th Iberian Conference on Information Systems and Technologies* (CISTI 2020) [1].

Wireless Sensor Networks (WSNs) are composed by small nodes spread in an area of interest to measure environmental conditions such as temperature, sound, humidity, although they have many other uses [2]. Each node can be seen as a small computer, having processing, sensing and communication capabilities. The nodes connect to each other wirelessly and can cooperate in collecting information and routing it to an end user [3].

The need for extensible WSNs is tied with monitoring situations that require the deployment of a WSN. Situations such as forest fires or fires is large buildings [4], determining the extent of damage of earthquakes [5], nuclear disasters as in Fukushima, Japan, rescue operations, exploratory operations, mapping flooded caves, battlefield reconnaissance or planetary exploration [6]. In some of these situations it is possible for a human operator to deploy the nodes of the WSN. But in disaster situations, or any

situation where human life could be endangered, it is necessary to use alternative methods of deployment, such as the use of mobile robots.

With this purpose in mind a testbed was used, which serves as a prototype for a WSN. The testbed used was composed of three different types of nodes: master, robot and static nodes. The master node is used so an end user can receive information from the network and send commands to any node. The static nodes serve as intermediate relays that connect the master node and the robot nodes. The robot nodes serve to extend the network, having mobility besides communication capabilities. The objective of this project is to create an extensible wireless network, using intermediate static nodes that connect a gateway to a moving robot node.

This document is organized as follows. Section I introduces WSNs and the goal of the project, Section II gives a review of related literature, with examples of similarly deployed WSNs. Section III describes the testbed and the libraries used for programming the nodes. Section IV describes the algorithms developed. Section V describes four scenarios used to evaluate the performance of the testbed with the described algorithms and the

169

results achieved. Section VI discusses these results and Section VII concludes the report and proposes future avenues of exploration.

2. Related Work

There has been prior work on the problem of "as-you-go" or impromptu deployment of a WSN. In [4] and [7] are proposed algorithms for "as-you-go" deployment, in which an agent, human or robot, measures link quality at equally spaced intervals and makes placement decisions, while only moving forward along a line.

Some works consider a purely autonomous deployment of a WSN by mobile robots. In [6] is explored autonomous deployment of a WSN with the goal of human detection, in case of disaster situations, in which mobile robots perform simultaneous localization and mapping. In [5] mobile robots carry sensor nodes and measure the RSSI, to know when to deploy sensor nodes to ensure communication or restore the network.

Many of the proposed systems measure link quality, using communication metrics like RSSI or Packet Reception Ratio, and decide when to deploy a new relay when the metric satisfies predefined rules. In [8] such a system is used for dynamic deployment of a WSN through a breadcrumb system for firefighters. A breadcrumb dispenser is worn by firefighters and a link estimator uses the previous mentioned metrics to decide when to deploy breadcrumbs.

Works such as [9] also make use of mobile robots to deploy a WSN but focus on how these robots can help with problems such as coverage holes or collection of redundant sensors. They achieve this by using permanent grid-based deployment, with cluster concepts to reduce packets used in creating and maintaining the grid structure. Furthermore, they consider the communication range to be at least twice of the sensing range.

Cooperation between multiple agents is seen as an important problem to be explored. In [4] and [7] it is pointed the need for algorithms where two or more robots cooperate to deploy a WSN. While [6] calls for field test using two mobile robots and to address the communication issues that arise from coordination between multiple robots. These and more issues of multi-robot systems, such as reduction in network traffic, routing approaches and sensor data processing are pointed as areas that need appropriate operational methods by [5]. The study of communication metrics, such as RSSI, in various environments, to allow setting different parameters that could optimize the system, is called for by [8].

In the present study the aim is to use the communication metric of RSSI to know when a new node should be deployed and integrate this metric with cooperation between two mobile robot nodes. The RSSI metric has been used in studies such [10], [11] and [12] to locate the robot nodes, triangulating the robot node and static nodes for navigation and helping the robot node avoid obstacles and reach a goal. But these approaches require that the static nodes be placed before the robot node starts its action, and to locate the robot need a lot of deployed static nodes. The proposal presented in this paper gives a different approach to this problematic by promoting the static nodes deployment using

mobile robots. The RSSI value was used to decide the positions to deploy static nodes.

3. Wireless Sensor Network Robot Path Construction Proposal

The goal of this project was to build a prototype of autonomous WSN deployment by a mobile robot. In light of literature requests, it was decided to consider two mobile robots and develop algorithms that ensure the coordination between them as the WSN is deployed. In order to build an extensible network, it is necessary for the robots not only to cooperate each other but also respond to the deployment of static nodes. Using static nodes allows to maintain communication between mobile robots and gateway even when the mobile robots leave the network coverage area of gateway.

In this section firstly will be described the hardware used to create the testbed, namely the master node, robot nodes and static nodes. Then will be described the libraries and methods used to achieve the WSN behavior and obtain a communication metric from each node, the RSSI. The RSSI metric was considered due to the limited resources of the hardware platform used.
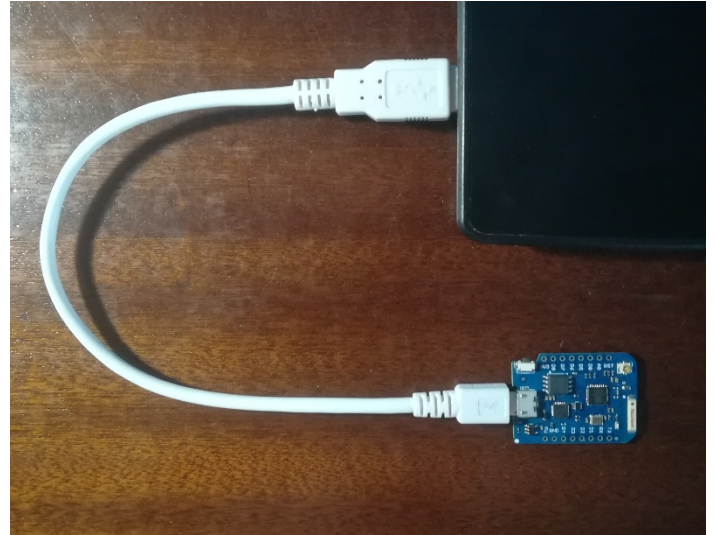
Figure 1: Photo of Master Node connected to a laptop.

3.1. Hardware Description

As mentioned before three types of nodes were used: a master node, static nodes and robot nodes. Master node and static nodes are composed by D1 mini pro boards with a wireless antenna Wi-Fi ESP8266, and a power supply. In the case of the master node the power supply was the PC it was connected to, in the case of static nodes a power banks were used.

Figure 1 is a photo of the master node used, connected to a laptop where the end user could send commands and received information from the network. Figure 2 is a photo of a static node used, which served the purpose of acting as a relay and extending the network.

The robot nodes were two wheeled mobile robots composed by a NodeMCU 1.0 board also with an ESP8266 module, a L293 Motor Driver Shield, two rubber wheels with Micro DC geared motors and a power bank, that served as a power supply. The

robots are completely similar in terms of hardware with just small differences in how the boards were mounted as can be seen in Figure 3 and Figure 4, which are photos of the first and second Robot Nodes used respectively.

Figure 2: Photo of a Static Node.
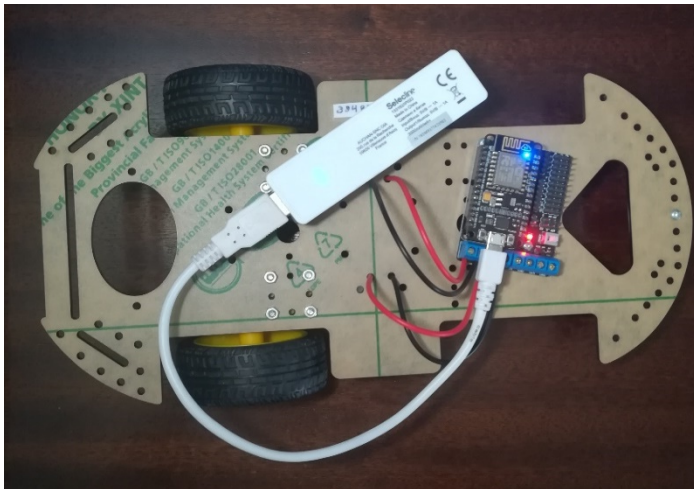
Figure 3: Photo of the first Robot Node used.
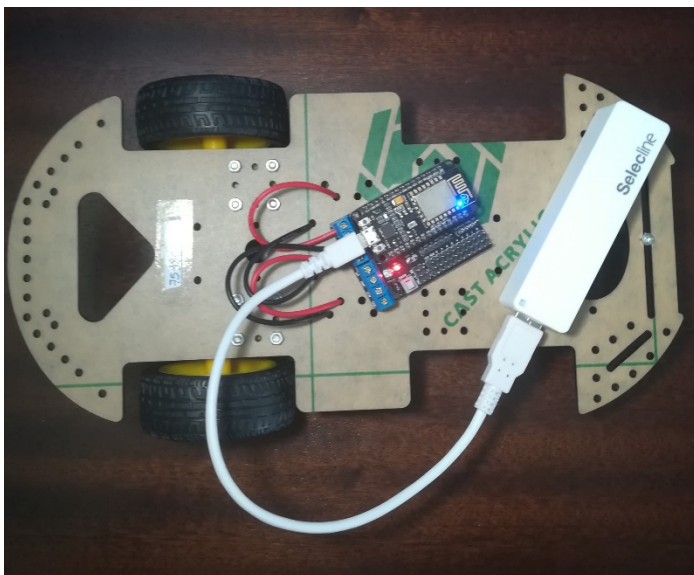
Figure 4: Photo of the second Robot Node used.

All the boards in each node were programmed using the Arduino programming language and respective Arduino IDE. The Arduino programming language makes use of two functions that are always present: setup and loop. Setup runs once when the board is connected to an energy supply. Loop runs continually after the setup, as long the board is connected to an energy supply. Future mentions to setup and loop, while explaining the code, refer to these two functions. The robots need to perform several tasks periodically, such as measuring the RSSI or moving. To achieve this behavior the Task Scheduler library was used.

3.2. Wireless Sensor Network Implementation

To manage creation of the wireless sensor network and communication between nodes the *painlessMesh* library was used [13]. This library uses the esp8266 hardware present in the boards to create a mesh network. The *painlessMesh* library does not use the Arduino WiFi libraries, due to performance problems, but the native esp8266 libraries [13]. The library allows us to make the nodes to communicate with each other, in a prototype of a WSN, without concern about how to structure or manage the network. The great advantage of using this library is that any operational nodes will automatically self-organize into a functional mesh network.

The messages between nodes are all JSON objects, which makes them human readable and facilitates integration with frontends and other applications. The mesh does not use or create a TCP/IP network, rather each node is identified by a 32bit chipId obtained through the esp8266 native SDK. As a result, every node will have a unique id, that can be used to communicate specifically to that node. Broadcast messages to all nodes in the mesh are also possible [13].

Some functions of the library are used in the setup of every node, namely init, which initializes the mesh, and the functions that set up callbacks, such as *onReceive(&receivedCallback)* and *onNewConnection(&newConnectionCallback)*. The functions given as arguments: *receivedCallback* and *newConnectionCallback*, are present in every node as well. They execute when a message is received by the node and when a new node connected to the network, respectively.

Other functions used at setup are *setRoot* for the master node and *setContainsRoot*, for all others. The purpose of these is to avoid the creation of submeshes during mesh formation. It makes sure all nodes know the gateway is the master node and a node once connected to the master node will not disconnect. This is necessary because of a limitation during mesh formation, namely that each node can only connect to another one node at any given moment. Because of this, nodes will try to randomly connect and disconnect until a full mesh is formed. This solution works but may create submeshes. The functions above aim to solve this problem. Another consequence of the "each node can only connect to one other node at a time" will be that usually only node of the mesh will be available to connect to other nodes.

A library function used in the loop of every node is the function update, which runs maintenance tasks and is required for the mesh to work. In the master node it is also used the *subConnectionJson* function, which allows to print the mesh topology in JSON format. All nodes use the *sendSingle* and

sendBroacast functions. The former allows to send a message to a node using its chipId, the latter sends a message to all nodes in the mesh.

Task Scheduler

The Task Scheduler library allows for periodic task execution. It is possible to specify execution period, in milliseconds or microseconds, and number of iterations, be they finite or infinite. The reason for needing to use this library is that the boards used cannot launch several threads at a time, hence cannot multitask with recurring to external libraries.

It works by first creating a scheduler using the Scheduler class. Then creating tasks using the Task class, and specifying the execution period, number of iterations and the actual function that will define the task behavior. Then at setup each task is added to the scheduler. From there on it is possible to enable or disable tasks as required [14]. The two main tasks used by the robot nodes are the RSSI Task and the Moving Robot Task.

The RSSI Task's main purpose is to measure the RSSI value. It will always do this if the scan for Wi-Fi networks is successful. Then depending on flags active it might just send this value to the master node or check if this value is lesser or equal to the RSSI threshold. If it is smaller, meaning more negative because the RSSI value is usually a negative integer, then it will send the RSSI value to the master node along with a request to place a new node. If the RSSI value is not smaller the robot can move further, and so it will call the appropriate movement function, disable the RSSI task and enable the Robot Moving task.

The Robot Moving Task's main purpose is to time the movement of the robot and send the RSSI value to the master node once a movement is finished. It is also used to create the robot node auto movement, as will be explained below.

The RSSI value is the most important metric in the prototype because it is based on it that the robot nodes will decide when a new node should be placed. Therefore, it regulates the extension of the WSN. It will also be used later both in the cooperation between robot nodes and in their response to deployment of new static nodes.

RSSI Request

It is useful to measure the value of the RSSI to understand how it changes, particularly due to growing distance from the master node. With this purpose in mind was created a way to simply have the master node send a request to a robot node and have the robot measure the RSSI and send its value back to the master node, to be printed and made available to the user.

The laptop connected master node expects user info from the serial monitor of the Arduino IDE. If the input received is the, case insensitive, string "RSSI" it will send a RSSI Request to all nodes. This request is simply a message that will prompt each node to enable the RSSI Task, which will make it measure the RSSI value, and then send this value back to the master node. The master node will print the value and an identifier of the node that sent it. Algorithm 1 represents the algorithm behind RSSI requests.

In terms of number of messages exchanged within the network, they are at least $2 * (n - 1)$, where n is the total number of nodes in the network. The reason for this number is that the master node will send a broadcast message upon being prompted by the user with an RSSI Request, so it will send a message to all nodes except itself, $n - 1$. Every node will then measure the RSSI and respond to the master node, so this number is doubled. Depending on the extension of the network this number will increase because the message may need to hop between nodes before reaching the master node.

Algorithm 1: RSSI Request

Result: The Master Node will print the RSSI values for all nodes in the network in its serial monitor

Initialization;

while *Master Node on* **do**
    Expects user input;
    if *User input = RSSI* **then**
        Send RSSI
        Request;
        Nodes send
        RSSI values;
        Print RSSI
        values;
    end
end

---

4. Testbed Deployment

With the testbed ready it is possible to start developing algorithms that will create us a prototype for an autonomous, extensible WSN. With this in mind, firstly it is necessary to develop ways of having the robot node move on its own and request new nodes for the network once a RSSI threshold is hit, which was called *AutoMOV*. Furthermore, ways of having two robot nodes cooperate with each other, to further extend the WSN, were developed, which was called *RCoop*. Finally, there was a need to develop ways for the robot nodes to know when a new static node was deployed and respond accordingly, extending the network if possible, which was called *ReStatic*. In this section the aim is to present each of these algorithms and explain how they were implemented using the testbed.

4.1. Automovement Algorithm (AutoMOV)

In the first implementation of the WSN prototype the robot node moved by commands sent from the master node by user input. But the goal was autonomous movement and deployment of an extensible WSN. To achieve this the robot nodes need to move autonomously, not prompted by user input, so an algorithm for robot node automovement was developed, hereinafter referred to as *AutoMOV*. All movement at this point occurs along a line.

An auto movement request is made if the Master Node catches a string that starts with 'A' or 'M'. This calls the function *AutoMOVRequest*. This function will print if the request is to start auto movement (A) or to stop auto movement and go back to manual (M). It will also send the given string to the robot node by method *sendMessage*. The method *sendMessage* uses the communication functions from the Painless Mesh library,

sendSingle or *sendBroadcast*, but with arguments to choose between them.

The robot node responds to this *sendMessage* with the callback routine *receivedCallback*. In the case of 'A' it will turn the movement type to 'F', which will make the robot move forward, this is the case because all movement occurs along a line at this point. Later it should decide the movement type based on sensor information.

It will also activate an *AutoMOV* flag and enable the RSSI Task. In the case of 'M' it turns off the *AutoMOV* flag and stops movement.

Algorithm 2: Automovement (*AutoMOV*)

Result: Robot Node performs discrete movement until it hits its RSSI Threshold
Initialization;
while *Master Node on* **do**
    Master Node expects input
    if *User input = M* **do**
        AutoMOV Stop Request;
        Robot Node stops;
    else if *User input = A* **do**
        AutoMOV Start Request;
        while *Current RSSI <= RSSI Threshol*d **do**
            Robot moves;
        end
    end
end

The RSSI Task will then be responsible for making the robot always move unless the current RSSI is equal or below the threshold, which would make *AutoMOV* stop and the robot node to send a request to the master node, for placement a new static node. Otherwise it enables the Moving Robot Task. This last task has an extra 'if', to deal with auto movement, that basically says: if one movement was completed and the *AutoMOV* flag is on, then it will enable the RSSI Task again. This creates a loop between the two tasks. Algorithm 2 represents the algorithm behind *AutoMOV* requests.

4.2. Robot Cooperation Algorithm (RCoop)

Coordination between multiple robots, cooperating in deployment or exploration, is seen as an important concern by current WSN literature [3-6]. With this purpose in mind there is a necessity for algorithms that allow multiple robots to cooperate and for field tests involving more than one robot [4][6][7].

The goal then was to develop an algorithm that allows two robots to cooperate in a prototype of WSN deployment based on communication metrics, namely the RSSI. Hereinafter this algorithm will be referred as *RCoop*.

The two robot nodes were named Robot One (R1) and Robot Two (R2) to help differentiate between them. The only real distinction between robot nodes is that R1 will be the first to move. All movement described occurs along a line.

R1 will be sent a signal from the user and start movement. Each robot movement is time limited to ten seconds. After these ten seconds of movement it will measure the RSSI and based on

this value decide to stop or move again. While the RSSI is above a certain threshold it will continue to perform discrete ten second movements. If the RSSI is found below the threshold it will stop, ask for the deployment of a static node and send a message to R2. Deployment of static nodes is done by human agents at this point. The reaction of robot nodes to the deployment of static nodes will discussed later. Here the main concern is about how the robots can cooperate.

R2 after receiving the message from R1 will know the first robot has reached the RSSI threshold and so commence its own movement. The message sent by R1 basically functions as R1 'calling' R2. R2 will mimic the behavior of R1 and move until it has reached the RSSI threshold. When R2 reaches the threshold, it will send a message to R1. This will prompt R1 to update its own threshold and start moving again. The goal here is to extend the network as much as possible using the two robot nodes.

The way this works in terms of code is that R1 will first be sent an *AutoMOV* request by the master node. It will normally follow *AutoMOV* until the threshold is reached. When it reaches the threshold, it will call *AutoMOVRequest*, which will send a message to R2. R2 will expect a message with this format via the callback routine *receivedCallback* and will activate its own *AutoMOV* because of it. R2 will then perform *AutoMOV*, as explained above, until it reaches its threshold. When at the threshold will send a message to R1 via *sendMessage*, informing it R2 is at the threshold. R1 will then decrement the *rssiThreshold* variable and turn its *AutoMOV* own again, and so move further until it reaches the new threshold value. Algorithm 3 represents the algorithm that deals with robot cooperation (*RCoop*).

Algorithm 3: Robot Cooperation (*RCoop*)

Result: The two robots will extend the network
Initialization;
R1 *AutoMOV*;
if *R1 RSSI <= RSSI Threshold* **do**
    R2 *AutoMOV*;
    if *R2 RSSI <= RSSI Threshold* **do**
        R1 expands Threshold;
        R1 *AutoMOV*;
    end
end

4.3. Response to Static Nodes Algorithm (ReStatic)

The other thing that is required to attain the goal of having an extensible WSN is that the network responds autonomously to the deployment of static nodes. To elicit this behavior, a communication metric is used again, the RSSI.

When a static node is placed it connects to the network normally, then it will measure its RSSI. It will send this value to the mobile robots connected. Then each robot will use this value to decide whether it should start movement or not. This decision is based on if the difference between its own RSSI and the static node RSSI is lesser than the value of the RSSI threshold. If the difference between RSSIs is lesser than the threshold then it means the static node is closer to the master node and hence the network can be safely extended, so the robot will move.

But if a new node connects it usually will connect as a subnode to the nodes already there, so how to solve this problem? The answer was to force a reorganization of the network. If the robot concludes by the above described method that the static node is closer to the master node then, before it initiates movement, it will reset its own board. The result of this is that when the robot reconnects to the network it will now be a subnode of the newest static node in the network topology. The value of the robot's threshold is saved in the master node, via a message sent by the robot before it resets. When the robot node reconnects the master node sends this value to the robot again, the later will update its threshold and reinitiate movement.

In terms of code this is achieved by using the RSSI Task in the static nodes as well. It will activate and measure the RSSI value as soon as the static node is turned on. Then it will send this value to the master node which will in turn send it to the robot nodes, via *sendMessage*. As usual the way to prompt behavior in a certain node, the node is made to expect a string formatted a certain way, via the *receivedCallback*, and if that string is received the desired behavior occurs. So, in that same way, when the robot nodes received the value of RSSI prefixed with the string "(mesh node)" they will first extract the RSSI value from that string. Then, they will check if the deployed static node can be considered closer to the master node, calculating if the difference between their RSSI value and the RSSI value of the static node is greater than their RSSI threshold (*currentRSSI - meshRssi > rssiThreshold*). If so, the robot node will expand its threshold and send it to the master node. The master node will save this value and send a message back to the robot node signaling the robot can now restart, with the purpose explained above. The robot node will then restart by esp8266 native function, *ESP.restart*, which will restart the board. The master node will expect a robot node connection via the *newConnectionCallback*, which is a callback routine that executes each time a new node connects the network. In case there is a saved RSSI threshold value for the robot node that connected then it will send this value to the robot that just connected. The robot will use this value to update its threshold and turn the *AutoMOV* on, thus extending the network. Algorithm 4 represents the response to static nodes algorithm described above. This algorithm will be known as *ReStatic*.

Algorithm 4: Response to Static Nodes (*ReStatic*)

Result: Robot Nodes extend network if possible
Initialization;
Static Node Deployed;
Send RSSI to Robot Nodes;
if *RSSI – Static RSSI > Threshold* **do**
  Expands Threshold and save it;
  Robot Node reset;
  Robot Node receives threshold;
  Robot Node *AutoMOV*;
end

---

5. Performance Evaluation

It was then time to put the algorithms to test to verify if the intended behavior of an extensible WSN could be achieved, take measurements, find potential faults or avenues for improvement. For these purposes four scenarios were developed, each progressively testing each one of the developed algorithms, first

separately, then in conjunction. As the presented work is still in its initial proposal, some RSSI issues were considered out of the scope. All demonstration scenarios considered an open space area with no obstacles and, as much as possible, a linear variation of RSSI.

The measurements were conducted in an open space indoor area. The master node was connected to a laptop via the USB port and will collect RSSI data. The laptop is placed on a wooden support that measures 31 cm in height. Time and distance are collected by the testers, while RSSI values are registered by the master node.

Firstly, it was important to study the variation of RSSI based on the distance between a robot node and a master node. This would serve to understand how it naturally variates without accounting for any robot node movement and illustrate the relationship between distance and the RSSI value. It makes use of and proves the functionality of the RSSI Request.

The robot node was placed at several distances of separation to the master node, always one meter apart from 0m to 13m. At each distance, the user would elicit the RSSI value through RSSI Request. After collecting ten samples at that distance of separation an RSSI average was calculated. Figure 5 shows the RSSI averages for the various distances of separation to the master node.
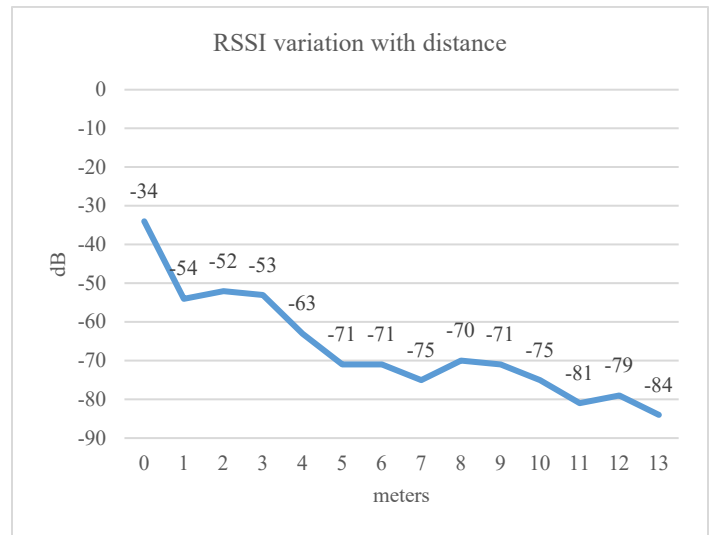
Figure 5: Robot Node RSSI variation with distance from the Master Node.

5.1. Scenario 1: One Robot Node

This first scenario intends to verify how much it was possible to extend the network simply using two nodes: the master node and a robot node. It will also illustrate the functionality of the robot node *AutoMOV* algorithm.

The robot node is place on the floor at a 0 meters distance from the master node. It will be sent a signal from the master node which will start the *AutoMOV*. Then, the robot node will perform discrete 10 second movements along a line while measuring the RSSI. When its current RSSI value is below a certain threshold it will stop and request the placement of a new static node. Figure 6 represents the end state for this scenario.
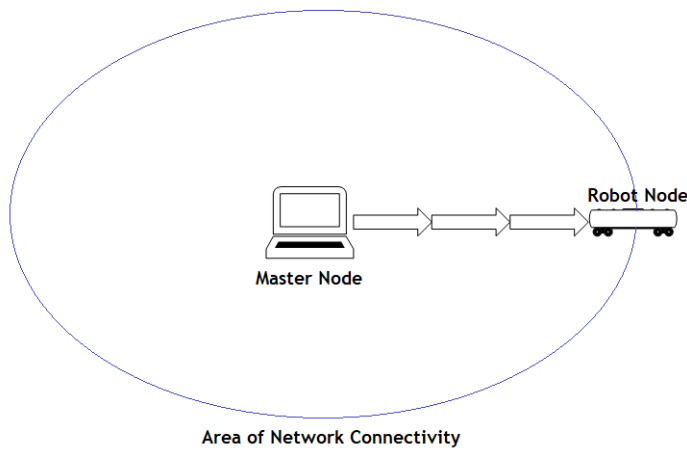
Figure 6: End state for Scenario 1 composed of Master Node and a Robot Node.

After ten trials an average of the values of time since *AutoMOV* started till robot node stoppage, distance traversed by robot node and last RSSI recorded is calculated. Table 1 holds the recorded values for this first testing using a robot node.

Table 1: Averages of time, distance and RSSI for 1 Master Node 1 Robot Node.

Time	54''
Distance	4m 83cm
RSSI	-68 dB

5.2. Scenario 2: Two Robot Nodes

The second scenario intends to extend the WSN using two robot nodes. This scenario uses two robot nodes and the master node and is meant to demonstrate the functioning of the *RCoop* algorithm.

Both robot nodes are placed next to one another at a 0m distance from the master node. Then the user enters 'A' into the serial monitor of the master node in the Arduino IDE. This is the signal that will set the *AutoMOV* of robot node named R1 on. All other network extending behavior is autonomous. Figure 7 represents the end state for this scenario.
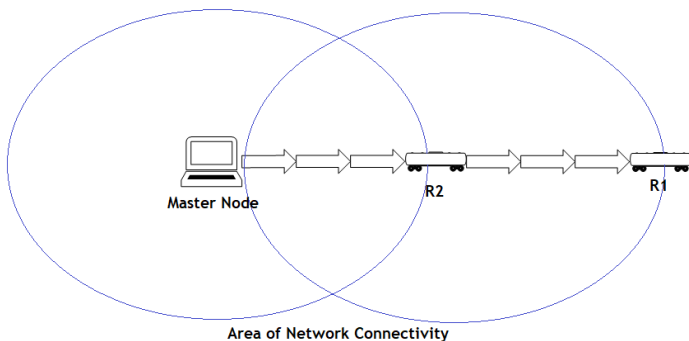
Figure 7: End state for Scenario 2 composed of Master Node and two Robot Nodes.

The last RSSI values of both R1 and R2 are recorded by the master node. The distance of both robot nodes to the master node after both robot nodes stop is recorded. The duration from the time the signal is sent until both robot nodes stop is also recorded. After ten trials an average of RSSI, distance and time was calculated.

Table 2 holds the recorded values for this first test with the two robot nodes.

Table 2: Averages of time, distances and RSSIs for 1 Master Node, 2 Robot Nodes.

Time	3' 01''
R1 Distance	7m 12cm
R2 Distance	5m 11cm
R1 RSSI	-71 dB
R2 RSSI	-64 dB

5.3. Scenario 3: One Robot Node, One Static Node

This third scenario intends to extend the WSN, by guaranteeing the robot nodes will respond to the deployment of new static nodes. So, it serves to test the functionality of the *ReStatic* algorithm. It does so by using the master node, one static node and only one robot node.

The robot node will be placed at a 0m distance from the master node. Robot node *AutoMOV* will be turned on by user input and then it will move until it reaches its RSSI threshold. Then, a static node will be place at this threshold. The robot node will respond to this placement autonomously and move again till it reaches a new threshold, extending the network. Figure 8 represents the end state for this scenario.
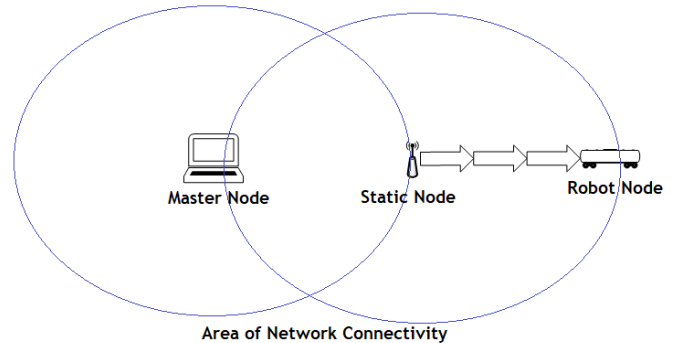
Figure 8: End state for Scenario 3 composed of Master Node, a Static Node and a Robot Node.

The last RSSI value before robot node stoppage is recorded by the master node. Time until robot node stoppage and maximum distance from static node are recorded by human users. After ten trails an average of these values is calculated. Table 3 holds the values for this first test that uses a static node.

Table 3: Averages of time, distance and RSSI for 1 Master Node, 1 Robot Nodes, 1 Static Node.

Time	3' 40''
Distance	7m 1cm
RSSI	-73 dB

5.4. Scenario 4: Two Robot Nodes, One Static Node

Finally, the fourth scenario allies the *RCoop* algorithms and the static node response algorithm. For this last scenario a master node, two robot nodes and one static were used.
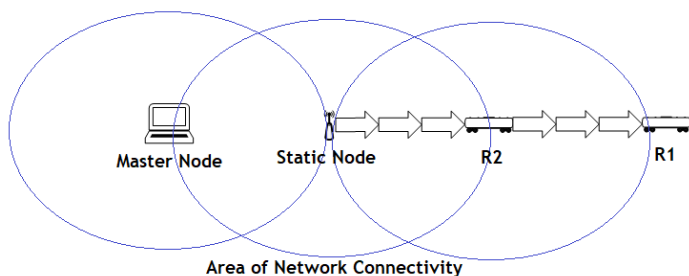
Figure 9: End state for Scenario 4 composed of Master Node, a Static Node and two Robot Nodes.

The procedure is similar to the two robot nodes test except that a static node is place at the R2 threshold when both robot nodes and stopped. So, both robot nodes are placed at 0m distance from the master node. A signal is sent to R1 by the user from the master node. Then, robot node *AutoMOV* and *RCoop* occur autonomously. Finally, a static node is placed at the R2 threshold and the robots will identify it and move again to new thresholds. Figure 9 represents the end state for this scenario.

The last RSSI values before robot node stoppage for both robot nodes are recorded by the master node. The time from signal sent to R1 till the network stops extending is recorded by a tester. Final distances of each robot node to the master node are also recorded by a tester. After ten trials an average of RSSIs, distances and time was calculated. Table 4 holds the values for this final test that incorporates all the node types: master node, robot node and static node.

Table 4: Averages of time, distances and RSSIs for 1 Master Node, 2 Robot Nodes, 1 Static Node.

Time	4' 33''
R1 Distance	11m 50cm
R2 Distance	6m 76cm
R1 RSSI	-82 dB
R2 RSSI	-71 dB

6. Discussion

First, it is important to have an idea of how to expect the RSSI to change with growing distance from the master node, this is the purpose of the RSSI – distance test. It is expectable that RSSI value decreases with distance from the master node, seeing as at 0m the RSSI value is -34dB and at 13m distance the RSSI is -84m. But this variation is not linear, so it must be assumed that there are other factors contributing to RSSI change besides distance.

Distance reached by the robot nodes is a key factor in knowing if the purpose of the algorithms was fulfilled and the WSN is extending. If only the number of nodes used is considered, it is expected the distance from the master node will increase with the increase in the number of nodes used, as the WSN can extend itself further. In this case the one robot test would give us the least distance, with just one node used, and the two robot nodes and one static node test would give us the furthest distance, with three nodes used. Figure 10 shows us the distances obtained according to the numbers of nodes used. It is then

verified that the network is extending itself through the programmed behavior of the robot nodes.

Time was considered of less importance at this point in testing. Still it is noted a big increase, going from an average 54 seconds with one node to 4 minutes 33 seconds with three nodes. The way of reorganizing the mesh network, by resetting a robot node when a suitable static node is detected, should be reviewed. The current solution causes a lot of overhead.

Using a communication metric such as the RSSI gives rise to some problems. First off, must be said that when considering the RSSI threshold as the point where a robot node should stop and request a static node, this is a virtual limit. It is not exploring the actual hardware limit of the communication module, the wireless antenna Wi-Fi ESP8266. Explorations on RSSI variations using ESP8266 modules have used distances of up to 140m between a station and an AP and still reach acceptable values for RSSI [15]. These experiments were performed outdoors whereas the ones here were indoors, but they give an idea of the distances that could be reached if the limits of the hardware were explored. The aim here however was to develop algorithms that could generate the intended behavior on the prototype, namely the creation of an extensible WSN. Although it is legitimate to consider that testing the present proposal at the hardware limits would be interesting and closer to a live deployment scenario.
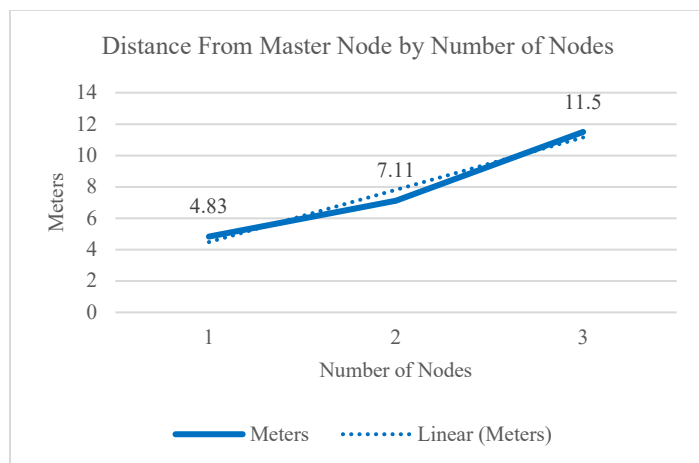
Figure 10: Variation of distance from the Master Node with number of nodes used in the WSN.

Finally, it is important to consider how the problems in expanding the RSSI threshold to make the robot nodes move further. Firstly, there is a need to find a better way to judge the distance of the static nodes when deployed. Deployment of several static nodes in proximity, or the same static node disconnecting from the network and then connecting again, might impress false information on the robot node, prompting it several times to move further. Secondly, saving the current threshold of the robot nodes in the master node when it resets could be problematic if the robot node disconnects from the network more than one time. This problem also arises from the method of reorganizing the network through resets of robot nodes. Even as it stands there might be a better way for the robot node to judge its threshold from the network topology and its own RSSI measurements, instead of receiving it from the master node.

7. Conclusion and Future Work

WSNs are ever more prevalent in modern living. Many applications, such as in disaster situations, require impromptu deployment of a WSN. Therefore, it is important to explore ways of WSN deployment. The usage of mobile robots to aid in this development is also important because it avoids the necessity of human agents. Coordination between mobile robots is essential in deployment and exploration tasks.

With this in mind a prototype of a WSN aimed at creating an extensible wireless network and proved it possible, within certain assumptions, using cooperation between mobile robots and responsiveness to the deployment of static nodes.

As for future work it should be interesting to test the solution proposed here with the actual hardware limits of the ESP8266 wireless module. Also, there is a need to develop a better way to manage network connections, even if that means foregoing the *painlessMesh* library and using the native ESP8266 SDK. Within the solution here, a better way to manage the RSSI thresholds of the robot nodes might also be a good avenue for new developments. Testing the WSN prototype with sensors able to capture environmental data would also prove interesting and open new avenues of exploring, such as how to effectively route sensing data.

Conflict of Interest

The authors declare no conflict of interest.

Acknowledgment

References

[1] J. Amaro, I.D.L.T. Diez, M.L.P. Joao, S. Vasco, J. Galan-Jimenez, "Protótipo de uma Rede de Sensores Sem Fios para Implantação Robótica de Percurso : A Prototype of a Wireless Sensor Network for Robotic Path Construction," Iberian Conference on Information Systems and Technologies, CISTI, **2020-June**, 20–25, 2020, doi:10.23919/CISTI49556.2020.9141080.

[2] S. Stage, P. Report, S. Kumar, R. No, C. Science, "Design and deployment of Wireless Sensor Networks," 313–325, 2017.

[3] Y. Sankarasubramaniam, E. Cayirci, others, I.A.. Su, "A survey on sensor networks," IEEE Communications Magazine, **40**(8), 102–116, 2002.

[4] A. Chattopadhyay, A. Ghosh, A. Kumar, "Asynchronous Stochastic Approximation Based Learning Algorithms for As-You-Go Deployment of Wireless Relay Networks Along a Line," IEEE Transactions on Mobile Computing, **17**(5), 1004–1018, 2018, doi:10.1109/TMC.2017.2750147.

[5] T. Suzuki, R. Sugizaki, K. Kawabata, Y. Hada, Y. Tobe, "Autonomous deployment and restoration of Sensor Network using mobile robots," International Journal of Advanced Robotic Systems, **7**(2), 105–114, 2010, doi:10.5772/9696.

[6] G. Tuna, V.C. Gungor, K. Gulez, "An autonomous wireless sensor network deployment system using mobile robots for human existence detection in case of disasters," Ad Hoc Networks, **13**(PART A), 54–68, 2014, doi:10.1016/j.adhoc.2012.06.006.

[7] A. Chattopadhyay, M. Coupechoux, A. Kumar, "Sequential Decision Algorithms for Measurement-Based Impromptu Deployment of a Wireless Relay Network Along a Line," IEEE/ACM Transactions on Networking, **24**(5), 2954–2968, 2016, doi:10.1109/TNET.2015.2496721.

[8] H. Liu, J. Li, Z. Xie, S. Lin, K. Whitehouse, J.A. Stankovic, D. Siu, "Automatic and robust breadcrumb system deployment for indoor firefighter applications," MobiSys'10 - Proceedings of the 8th International Conference on Mobile Systems, Applications, and Services, 21–34, 2010, doi:10.1145/1814433.1814438.

[9] R. Soua, L. Saidane, P. Minet, "Sensors deployment enhancement by a mobile robot in wireless sensor networks," 9th International Conference on Networks, ICN 2010, 121–126, 2010, doi:10.1109/ICN.2010.29.

[10] N. Zhou, X. Zhao, M. Tan, "RSSI-based mobile robot navigation in grid-pattern wireless sensor network," Proceedings - 2013 Chinese Automation Congress, CAC 2013, 497–501, 2013, doi:10.1109/CAC.2013.6775785.

[11] O.M. Elfadil, "Navigation algorithm for mobile robots using WSN," Proceedings - 2013 International Conference on Computer, Electrical and Electronics Engineering: "Research Makes a Difference", ICCEEE 2013, 554–559, 2013, doi:10.1109/ICCEEE.2013.6634000.

[12] A.C. Jiménez, S.J. Bolaños, J.P. Anzola, "Decentralized model for Autonomous Robotic Systems based on wireless sensor networking," ARPN Journal of Engineering and Applied Sciences, **11**(19), 11378–11382, 2016.

[13] painlessMesh / painlessMesh · GitLab, Jul. 2020.

[14] GitHub - arkhipenko/TaskScheduler: Cooperative multitasking for Arduino, ESPx and STM32 microcontrollers, Aug. 2020.

[15] Yoppy, R.H. Arjadi, H. Candra, H.D. Prananto, T.A.W. Wijanarko, "RSSI Comparison of ESP8266 Modules," 2018 Electrical Power, Electronics, Communications, Controls and Informatics Seminar, EECCIS 2018, 150–153, 2018, doi:10.1109/EECCIS.2018.8692892.

Level of Empathy in Nursing Students Attending Clinical Practices of the Universidad de Ciencias y Humanidades

Walter Cervera-Flores[1], Yenifer Choque-Garibay[1], Nahuel Gonzalez-Cordero[1], Brian Meneses-Claudio[2, *], Hernan Solis-Matta[1], Lourdes Matta-Zamudio[1]

[1]*Faculty of Health Sciences, Universidad de Ciencias y Humanidades, 15314, Lima-Perú*

[2]*Image Processing Research Laboratory (INTI-Lab), Universidad de Ciencias y Humanidades, 15314, Lima-Perú*

A R T I C L E   I N F O

A B S T R A C T

Empathy in the care of the patient by the nursing students is important because it allows having the capacity of response towards the patient, this study aimed to determine the level of empathy in nursing students who attend in clinical practices of the Universidad de Ciencias y Humanidades. This is a cross-sectional study, with a population of 289 nursing students who answered a questionnaire and the Jefferson medical empathy scale. 210 participants (72.7%) had a medium level of empathy, 74 participants (25.6%) with a high level of empathy and 5 participants (1.7%) with a low level of empathy. Regarding the empathy dimensions, the high level in the perspective taking dimension predominated with 81.7%, followed by the average level of the capacity dimension to put oneself in the patient's place with 59.9% and the compassionate care dimension predominated in the low level with a percentage of 45%. An improvement program is required in terms of professional training so that nursing students can carry out compassionate care when performing their clinical practices.

1. Introduction

Empathy in patient care for nursing students is a cognitive attribute that implies the ability to understand pain, suffering and the patient's perspective, it is the ability to stablish this understanding and the intention to help [1].

Nursing students must be empathetic and this is governed based on their behavior, this will be influenced in the well-being of themselves and also of the patient [2].

Empathy depends on the personality and functional characteristics of the nurse so that the nursing student has a good performance in their study plan [3]. Therefore, there are numerous exploration methods that have been designed in educational programs to improve empathy [4]. In addition, empathy is attributed to factors that influence the nursing student such as interpersonal relationships, self-esteem, communication, and self-efficacy [5].

In [6], the authors explain a study carried out in Spain, it was found that technological advance acts on empathy in nursing

professionals, leading to a lack of interest in interaction with patients.

In [7], the authors presented a study carried out in Venezuela, it was observed in the results that 90.1% of the nursing students were women and those who obtained a higher score in level of empathy.

In [8], the authors described a study carried out in Canada, they stated in their results that the instructional and practice sessions increased students' self-awareness about prejudices and interest in learning empathy through video tag feedback.

This study is important since it will give relevant and real data about empathy as students go in their academic plan and, observe if they can have an empathetic attitude when they carry out their activities in the clinical practical field.

The following research work is structured as follows: In section II, the development of the data collection process of each nursing student will be presented, as well as the guidelines to consider so that they are within the research work. In section III, the results will show the level of empathy that nursing students

178

will present according to the specified dimensions of the instrument in the measurement of the variable. In section IV, it presents the discussions of the research work, in section V, the conclusions and in section VI the recommendations as well as the future work that is intended to come with the research work.

2. Methodology

2.1. Materials and Methods

In this part, the type and design of the research will be developed, as well as the population and sample that will be carried out in the research work, the inclusion and exclusion criteria in detail and finally the technique and the instrument of collection of data.

2.2. Research type and Design

It is a study with a quantitative approach, a non-experimental, descriptive and cross-sectional design [9].

2.3. Population

The population was 289 nursing students from the Universidad de Ciencias y Humanidades.

2.3.1. Inclusion Criteria

Nursing students who are in the third semester until the eighth semester and who have signed the informed consent that was evaluated and approved by the ethics committee of the Universidad de Ciencias y Humanidades.

2.4. Technique and Instrument

In the study, the data collection instrument Escala de Empatía Médica de Jefferson (EEMJ) from Hojat Mohammandreza was applied, which has been demonstrated to be useful in assessing level of empathy in nursing students.

The JSE instrument is a shortened and derived tool of the Escala de Empatía Médica de Jefferson, which consists of 20 questions developed in parallel in more than 85 countries and translated into 56 languages.

To measure empathy, the instrument Escala de Empatía Médica de Jefferson (EEMJ) from Hojat Mohammandreza, which includes 20 items grouped in 3 dimensions, will be used: perspective taking, compassionate care and ability to put oneself in the patient's place where they are governed by the high, medium, and low levels according to the instrument manual. The answers will have two significant frames for each of the items, if it disagrees it is 0 and if there is agreement it is valued at 7, with a variation score of 20 to 140. Between 20 to 60 refers to low empathy, of 61 to 100 refers to medium empathy and 101 to 140 refers to high empathy [10].

2.5. Place and Application of the Instrument

The questionnaire was carried out in two consecutive schedules, morning, and night at the same time as the nursing students who practice at the university, the questionnaire was taken to the nursing students with an approximate time of 15

minutes each selected semester (III semester to VIII semester according to inclusion criteria) in the research work, concluding with good satisfaction when collecting the questionnaires as the students provided support to carry out the research work.

The data collection was processed through the survey of nursing students, the data was carried out in a data matrix that will be designed in the statistical program SPSS (Statistical Package for the Social Sciences) in its version 24.0, in which it will allow a better data processing to make statistical tables and graphs so that they can then be described and interpreted in results and discussions, respectively.

It is important to emphasize the presence of medical personnel at the time of completing the student questionnaire, since most of them presented signs of having a health problem.

3. Results

Regarding empathy in nursing students who carry out pre-professional practices at the Universidad de Ciencias y Humanidades it can see that 210 participants represent 72.7% with a medium level of empathy, followed by 74 participants who represent 25.6% with a high level of empathy and 5 participants representing 1.7% with a low level of empathy.

Table 1: Level of Empathy in Nursing Students attending Clinical Practices of the Universidad de Ciencias y Humanidades, 2019 (N = 289)

Empathy					
		Fre que ncy	Perce ntage	Valid percenta ge	Accumul ated percenta ge
V a li d	Low	5	1,7	1,7	1,7
	Mediu m	210	72,7	72,7	74,4
	High	74	25,6	25,6	100,0
	Total	289	100,0	100,0	

These results indicate that the students present a medium empathy, because many of them possess skills that would demonstrate high empathy, however, they have the difficulty of expressing or manifesting what another person may experience, in which they cannot to be developed without having the adequate knowledge, for this, they seek solutions either at an academic or practical level in which they can complement that space, in order to be able to develop their skills and have the greatest capacity for evaluation in what another person may experience.

In the Figure 1 shown, the results regarding the dimensions of empathy are evidenced according to the data based on the research instrument:

In Figure 1, it can see the empathy according to its dimensions, in nursing students who attend clinical practices of the Universidad de Ciencias y Humanidades, where the dimension most affected was the compassionate care where 130 students representing 45% have low empathy. This dimension has been the most affected, although it is true it is related to patient care, however, it has been proven that the same patients

attribute that their care is not adequate, that they are not provided with compassionate care, for the Nursing students, this dimension assumes an important role due to the fact that the students are in full training, that compassionate care is very important, for this, education at an academic or practical level, it is necessary to distinguish a very important role on compassion, due to this fundamental role is being lost in nursing students due to the lack of interventions on understanding compassionate care for the patient.
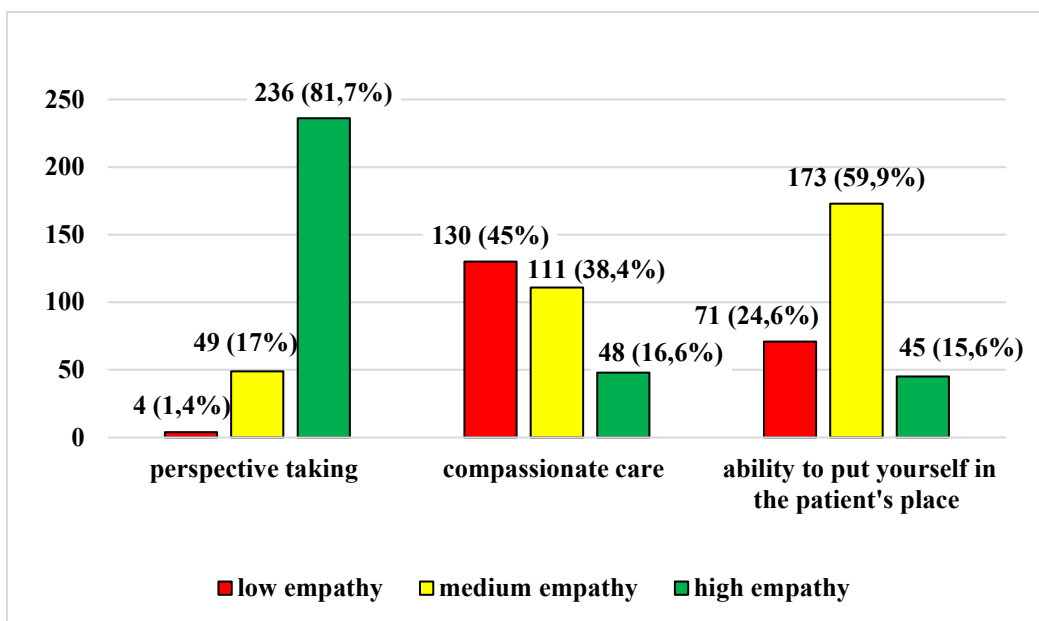
Figure 1: Empathy according to its dimensions, in nursing students attending clinical practices at the Universidad de Ciencias y Humanidades, 2019 (N = 289).

Table 2: Empathy in relation to the Semester of study of Nursing Students who attend in clinical practices of the Universidad de Ciencias y Humanidades, 2019 (N = 289)

			Empathy			Total
			Low	Medium	High	
STUDY SEMESTER	III	Count	0	61	16	77
	SEMESTER	% within the Semester	0,0%	79,2%	20,8%	100,0%
	IV	Count	3	25	9	37
	SEMESTER	% within the Semester	8,1%	67,6%	24,3%	100,0%
	V	Count	0	47	10	57
	SEMESTER	% within the Semester	0,0%	82,5%	17,5%	100,0%
	VI	Count	0	34	16	50
	SEMESTER	% within the Semester	0,0%	68,0%	32,0%	100,0%
	VII	Count	1	28	9	38
	SEMESTER	% within the Semester	2,6%	73,7%	23,7%	100,0%
	VIII	Count	1	15	14	30
	SEMESTER	% within the Semester	3,3%	50,0%	46,7%	100,0%
Total		Count	5	210	74	289
		% within the Semester	1,7%	72,7%	25,6%	100,0%
Chi-square tests						

	Value	gl	Asymptotic significance (bilateral)
Pearson's Chi-square	24,344[a]	10	,007
Likelihood ratio	22,625	10	,012
Linear by linear association	4,130	1	,042
N°. of valid cases	289		

a. 6 cells (33.3%) have expected a count less than 5. The minimum expected count is .52.

In Table II, empathy is related to the semester of study of nursing students, in which it was determined with the Pearson chi-square test (X^2), the level of significance of the test obtained a value of 0.52 (p> 0.05) (X^2 = 24.344; df = 10). Therefore, a hypothesis of association between variables is not rejected, thus proving that there is a relationship between empathy and the semester of study of nursing students.

4. Discussion

In this study, we raise the issue of empathy is raised from the point of view of professional nursing training, where the level of empathy in nursing students who attend clinical practices at the Universidad de Ciencias y Humanidades, 2019 is assessed.

Regarding the level of empathy in nursing students who attend clinical practices of the Universidad de Ciencias y Humanidades, 2019, the medium level predominated followed by the high and low. These results may be because students have difficulty being able to understand or feel what the other person is experiencing.

It should be noted that the previous research work on the Empathy study were of different sociodemographic characteristics, the study in [3], the author indicates that the results of empathy were given by the different characteristics such as sex, academic year, academic performance, where the female sex showed high levels of empathy. Where empathy can change as the student progresses in their study plan. In [7], the author mention that the decrease in empathy is influenced by the absence of good teachers, the increased pressure for activities, long hours of service and evaluations in students, can lead them away from feelings of human problems and have a lack of opportunities to manage their emotions. Given the aforementioned, the nursing student can be related to their emotions, although it is true that empathy is not only based on doing a good job but, the way that the emotions are going to be applied in this situation, it is very important to know that emotions have an important role in the students since they are in full formation and need the emotional maturity that allows them to perform humanized care, this means that it is not only enough to perform academically, because it would only enable their cognitive abilities, and to develop their emotional skills in a successful way, it is necessary to have training for it, so that the nursing students themselves carry out their humanized care at the time of carrying out their clinical practices.

Regarding the level of empathy in its dimension perspective taking in nursing students who attend clinical practices of the Universidad de Ciencias y Humanidades, 2019, the high level predominated followed by the medium and low. The perspective taking dimension refers to cognitive flexibility, understanding mood states, having good communication and interpersonal relationships with the patient. In [8], the author mentioned that students were concerned with learning about the process of conscious or consciously driven perspective taking and practicing self-awareness to help identify and then put aside biases and beliefs about health risk behaviors allowing better patient care. In [11], the authors indicate that empathy in a quality with great cognitive predominance, where understanding is more important. Since in this way, the patient's pain can be understood to show adequate communication and support, where the nurse-patient relationship will be strengthened. That is why having the ability to understand the patient's pain will be related to motivational factors in academic nursing training.

Regarding the level of empathy in its dimension compassionate care in nursing students who attend clinical practices at the Universidad de Ciencias y Humanidades, the low level prevailed followed by the medium and high levels, where this dimension was the most affected. The compassionate care dimension refers to the emotional states of others, literally feeling the person's pain. It originates from primitive parts of the brain that allow to feel quickly without thinking deeply. Compassion has global implications for nursing care. However, patients report that nurses do not provide compassionate care. Nursing education has been examined on the impact training can have on student compassion as there is a shortage of interventions aimed at teaching compassion to nursing students [12]. In [6], the authors mention the need for high empathic results, since emotional understanding is needed, listening to the patient's concerns so that it can alleviate its anguish thanks to the emotional expression of the nurse. That is why the study in [8], the authors indicated that the students said that it is important to listen to the stories of the patients, it was revealing as the stressors related to care and their impact on self-care. Patient feedback made it easier for students to better understand and take ownership of their risky health behavior.

Regarding the level of empathy in its dimension, ability to put yourself in the patient's place in nursing students who attend clinical practices of the Universidad de Ciencias y Humanidades, 2019, the medium level prevailed followed by the low and high. The dimension of putting yourself in the patient's place refers to feel not only how other people feel, but also to know what they need from you. It involves putting yourself in the other's shoes, examining issues from their perspective, trying to think and feel as the other would. Lack of communication produces a loss of

empathy and understanding between people, which translates into bad humor, fights, and an atmosphere of tension. Despite the burdens it has on the journey, it must not forget that others also have their own problems. Listening, dialoguing, understanding and helping are just some of the actions laden with value that can improve coexistence between people and allow to live in a more peaceful society [13].

Regarding the level of empathy in nursing students who attend clinical practices at the Universidad de Ciencias y Humanidades, 2019, studies carried out in [14], they concludes that women score significantly more than men in fantasy, empathic concern and personal discomfort.

In [15], the authors showed that women are more empathetic than men. This was attributed to an increased ability for perspective taking and compassionate attention, a situation that can be explained by social and biological factors. Among social factors, stereotypes attribute to women greater emotional sensitivity, concern for social aspects, a tendency to care for children and the elderly people, and greater ability to perceive feelings and non-verbal language.

In [7], they mentioned that the female sex has greater empathy than the male sex. This is due to the brain structure, where the nerve fibers between the two hemispheres perform better information transfer in communication and empathy, which occurs in the case of women. This would also explain the synchronization they have with the emotions expressed in non-verbal language with the patient.

The implementation of empathy education in the nursing professional training process brings good results. A systematic review in [16], titled "A systematic review of the effectiveness of empathy education for undergraduate nursing students," they indicate that in 23 studies of empathy education in undergraduate education in nursing, practical improvements in empathy were demonstrated. In all of them, interventions based on interview and experimental simulations were carried out, focusing on vulnerable patients.

5. Conclusions

It is concluded that the level of empathy in nursing students have been high, it could be specified that as students' progress academically, they tend to increase their empathy, depending on how the students can express themselves regarding their academic performance either theory or practical.

It is concluded that to have a high level of empathy, it is not only requires having a good academic ability, but also having a good ability to show emotions during clinical practices to provide self-confidence and gain the confidence of the patient during their care.

It is concluded that within the established dimensions of the research variable, in terms of the compassionate care dimension, an improvement program is required in terms of their professional training so that students can carry out compassionate care when performing their clinical practices.

As a future work, it is important to keep in mind that in universities there must be student nursing programs that allow them to benefit from their own empathic skills, so students could

choose to have more knowledge and, at the same time, express their emotions through methods that allow to feel safe and have confidence in themselves when performing their clinical practices so that they are able to resolve any situation in patient care.

6. Recommendations

Regarding empathy in nursing students who attend clinical practices of the Universidad de Ciencias y Humanidades, 2019, the medium level predominated, followed by the high and low. It is suggested to the university authorities that activities be established to encourage students to have a good comprehensive education, in which the student can be involved in various topics in which the student can develop socially.

Regarding the empathy dimensions in all of them, the high level prevailed in the perspective taking dimension, it is suggested to the university authorities that students be fostered capacities in which they can distinguish when carrying out their clinical practices.

Training with the knowledge that the students could get a positive interaction with the people who will provide their care, involving both the faculty and the health institutions in which they will carry out their clinical practices.

It is suggested that, in future studies, a relationship between other variables linked to empathy be involved or exist, so that this problem can be better understood.

It is suggested to develop studies with qualitative or mixed approaches to complement the understanding of empathy in nursing students.

Conflicts of Interest

The authors declare no conflict of interest.

References

[1] U. Philadelphia, U. Jefferson, Jefferson Scale of Empathy. Center for Research in Medical Education and Health Care, Sidney Kimmel Medical College, 2019.

[2] H. Rozengway, A. García, I. Vallecillo, "Niveles de empatía según la escala de Jefferson en estu - diantes de Medicina, Enfermería y Odontología de Honduras.," Rev. Cient. Cien. Med., **19**(2), 14–19, 2016.

[3] M. Madera, L. Tirado, F. González, "Factores relacionados con la empatía en estudiantes de Enfermería de la Universidad de Cartagena.," Enfermeria Clinica, **5**(26), 282–289, 2016, doi:10.1016/j.enfcli.2016.06.004.

[4] P. Montanari, C. Petrucci, S. Russo, I. Murray, V. Dimonte, L. Lancia, "Psychometric properties of the Jefferson Scale of Empathy-Health Professional Student's version: An Italian validation study with nursing students.," Nursing and Health Sciences, **17**(4), 483–491, 2015, doi:10.1111/nhs.12221.

[5] J. Kim, "Factors influencing nursing students' empathy.," Korean Journal Of Medical Education, **30**(3), 229–2236, 2018, doi:10.3946/kjme.2018.97.

[6] M. Giménez, S. Avivar, V. Prado, "Niveles de empatía en una muestra de enfermeras españolas.," Calidad de Vida y Salud, **9**(2), 120–130, 2016.

[7] M. Montilva, M. García, A. Torres, M. Puertas, E. Zapata, "Empatía según la escala de Jefferson en estudiantes de Medicina y Enfermería en Venezuela.," Investigación En Educación Médica, **4**(16), 223–228, 2015, doi:10.1016/j.riem.2015.04.006.

[8] M. Lobchuk, G. Halas, C. West, N. Harder, Z. Tursunova, C. Ramraj, "Development of a novel empathy-related video-feedback intervention to improve empathic accuracy of nursing students: A pilot study.," Nurse Education Today, **46**, 86–93, 2016, doi:10.1016/j.nedt.2016.08.034.

[9] C. Fernández, P. Baptista, Metodología de la Investigación. 6ta ed. México: Mc Graw-Hill/Interamericana., 2015.

[10] A. Garza, J. González, S. Tavita, F. Rodriguez, M. Hojat, "Validación de la Escala de Empatia Médica de Jefferson en Estudiantes de Medicina Mexicanos.," Salud Mental, **28**(5), 57–63, 2005.

[11] J. Yu, M. Kirk, "Measurement of empathy in nursing research: Systematic review.," Journal of Advanced Nursing, **64**(5), 440–454, 2008, doi:10.1111/j.1365-2648.2008.04831.x.

[12] M. Durkin, R. Gurbutt, J. Carson, "Qualities, teaching, and measurement of compassion in nursing: A systematic review.," Nurse Education Today, **63**, 50-58., 2018, doi:10.1016/j.nedt.2018.01.025.

[13] G. Karayiannis, E. Papastavrou, A. Farmakas, H. Tsangari, M. Noula, Z. Roupa, "Exploration of empathy in Cyprus nursing and health care students: A mixed method study.," Nurse Education in Practice, **42**, 102686, 2020, doi:10.1016/j.nepr.2019.102686.

[14] V. Díaz, G. Muñoz, N. Duarte, M. Reyes, S. Caro, A. Calzadilla, L. Alonso, "Empatía en estudiantes de enfermería de la Universidad Mayor, Sede Temuco, IX región, Chile.," Aquichan, **14**(3), 388–402, 2014, doi:10.5294/aqui.2014.14.3.9.

[15] G. Parra, R. Cámara, "Nivel de empatía médica y factores asociados en estudiantes de medicina.," Investigación En Educación Médica, **6**(24), 221–227, 2017, doi:10.1016/j.riem.2016.11.001.

[16] T. Levett, R. Cant, S. Lapkin, "A systematic review of the effectiveness of empathy education for undergraduate nursing students.," Nurse Education Today, **75**, 80–94, 2019, doi:10.1016/j.nedt.2019.01.006.

QoE-aware Bandwidth Allocation for Multiple Video Streaming Players over HTTP and SDN

Pham Hong Thinh[1,2], Tran Thi Thanh Huyen[3], Nguyen Ngoc Quang[1], Pham Ngoc Nam[4], Truong Cong Thang[2], Nguyen Viet Hung[5], Truong Thu Huong[*,1]

[1]*School of Electronics and Telecommunications, Hanoi University of Science and Technology, 100000, Vietnam*

[2]*Faculty of Engineering and Technology, Quy Nhon University, 820000, Vietnam*

[3]*The University of Aizu, Aizu-Wakamatsu, 965-0006, Japan*

[4]*College of Engineering & Computer Science, VinUniversity, Hanoi, 100000, Vietnam*

[5]*Faculty of Information Technology, East Asia University of Technology, Hanoi, 100000, Vietnam*

A R T I C L E   I N F O

A B S T R A C T

For many years, the most popular technique for Internet video streaming is hypertext transfer protocol-based adaptive streaming, known as HAS (HTTP Adaptive Streaming). However, a seamless viewing experience can not be just simply guaranteed by HAS only. In the management network, the adaptation of HAS copes with a huge challenge since client-driven schemes lead to unfair share of available bandwidth when multiple players request adaptive bitrates (i.e bandwidth) through a bottleneck network link. Each client's requesting to maximize its needed bandwidth leads to the competition of network resources. This causes great QoE (Quality of Experience) reduction in terms of main metrics for each player: fairness, efficiency, and stability. In this paper, we propose an integration scheme of bitrate adaptation and Software Defined Networking-based resource allocation that can improve the QoE of competing clients. Our experiments show that the proposed scheme increases at least 20% up to 124% in terms of QoE scores compared with some existing methods as well as gains smoother viewing experience than the solutions of the traditional Internet.

1 Introduction

Recently we have observed a huge volume of media content, especially high-definition videos over the Internet. According to the report from [1], video traffic is estimated to occupy around 82% of the overall Internet traffic by 2021. Although the quality of the Internet has been improved significantly thanks to the advanced technologies such as 4G, 5G and Fiber to the Home (FTTH), current technologies are not yet ready to provide sufficient Internet bandwidth for new multimedia types such as 360-degree Videos and 12K Videos. Those new types of multimedia cause an enormous portion of Internet traffic.

The quality of video streaming over the Internet have been enhanced by several approaches such as: Microsoft's Smooth Streaming, Real-time Transmission Protocol, Adobe's Adaptive Streaming, Apple's HTTP Live Streaming, and MPEG-DASH. Especially, with

MPEG-DASH, the vendor dependence on previously invented protocols were removed so as content providers can extend their services easily.

Based on this DASH standard emerged a number of solutions in which a source video is segmented into short segments of 2-10 seconds, each of which is encoded at a different bitrate resolution and level. During the playback, each client uses its bitrate adaptation logic to dynamically request and fetch desired encoded segments based on metrics such as average throughput and buffer occupancy. In the DASH technology, most of the current adaptive algorithms that decide the bitrate for the next downloaded segment are based on two parameters at the client side: throughput variation and buffer level. The buffer-based bitrate adaptation methods determine the bitrate mainly based on the characteristics of the buffer. These methods can also consider throughput, but the characteristics of the buffer are the preferred factors. Typically, buffers are divided into

multiple ranges, and for each of these ranges, different actions will be applied to determine the bitrate. Note that the specific buffer thresholds depend on the specific adaptation method. Typically, if the buffer level is high, the next segment will be selected with a higher bitrate than the current segment. If the buffer level is average, the selected bitrate will not be too different from the current bitrate. On the contrary, if the buffer level is low, the next segment will be selected with a low bitrate to avoid rebuffering and video freezes.

In addition, throughput-based methods are only based on estimated throughput to define a bitrate for the next segment. The main difference between these types of algorithms is the way for estimating throughput and how to utilize throughput. The simplest way to determine the throughput is based on the ratio of the given segment duration over the download time. The segment delivery time is determined from the time of sending a HTTP request to the time of receiving a HTTP response message that contains that segment.

On the other hand, Software-Defined Networking (SDN) [2] has emerged as a new networking paradigm in which a SDN Controller can make network management more flexibly by eliminating proprietary protocols from hardware vendors. With the network control plane implemented in software, rather than in firmware, network traffic can be managed more dynamically and at a more granular level. SDN switches/routers send and receive information to and from the SDN controller via southbound APIs; and the SDN controller relays information to the applications and business logic via northbound APIs. Within the scope of SDN, the OpenFlow Controller [3] is a type of SDN Controller that uses the OpenFlow protocol to configure SDN switches.

In any network exists always a popular issue called bottleneck link that could be congested when the amount of bandwidth demands go beyond the bottleneck link capacity. In case of bottleneck, video streams for each resource-sharing users could experience a remarkable decrease in perception of the video service, called Quality of Experience (QoE). Therefore, a method to solve the bottleneck problem in video streaming is neccesary.

To extend our previous work [4], in this work, we deploy a streaming architecture which make use of the MPEG-DASH technique and the SDN technology to solve the bottleneck problem. The scheme can increase the overall video quality for all users sharing the same bottleneck point. At the client's side, we develop a throughput-buffer based bitrate adaptation algorithm to utilize most of the available bandwidth in order to increase users' QoE. On the SDN controller, we establish a flow management mechanism which monitors the network to ensure fairness and avoid congestion when the network does not have sufficient bandwidth to serve new incoming stream requests. In the SDN controller, we develop the so-called Media Streaming Multiple Access (MSMA) module to monitor the network, detecting the number of ongoing streams, and deciding a fair share of bandwidth to all clients. Additionally, MSMA can also reallocate bandwidth or reject a new incoming request if no sufficient bandwidth is found; and thereby preventing congestion at the bottleneck point. The proposed adaptation and bandwidth allocation methods aim at the three following goals:

• *Efficiency*: all players joining the system can choose for themselves a level of video quality as high as possible.

• *Fairness*: When there are multiple clients accessing the bot-

tleneck link at the same time, all of the available network resources must be allocated as fairly as possible.

• *Stability*: Each player should avoid video stalling, unnecessary quality switches, which will adversely affect users' QoE.

The proposed solution not only allocates bandwidth fairly and adaptably on the network side, but also adaptive bitrate at the client side to improve video streaming quality. When there are many clients streaming on bottleneck link, the problem of sharing bandwidth for optimization is very important. There are three main approach groups: dividing bandwidth equally, dividing it by groups or choosing which user should be the one to share bandwidth with new coming users or new request of an existing user. Each solution has its own advantages and disadvantages. So, our proposed technique's limitation is to trade off a small QoE degradation of one or a small number of users sharing the bandwidth. However, the advantage of the proposal is to maximize the number of access clients while keeping QoE in a good shape.

The rest of this paper is organized as follows. Section 2 presents related work of typical bitrate adaptation algorithms and bandwidth allocation schemes. Section 3 provides information on throughput estimation and the proposed adaptation algorithm. Our proposed SDN-based dynamic resource allocation is described in Section 4 . A performance evaluation is presented in Section 5. Finally, conclusions and future directions are discussed in Section 6.

2 Related Work

HTTP Adaptive Streaming (HAS) has become the key solution for video streaming. There are a number of recent researches conducted to improve users' QoE in the context of multiple clients requesting for DASH service. As discussed in [5] and [6], the authors proposed a so-called Aggressive method in which a rate adaptation algorithm based on the estimated throughput is implemented where the last segment throughput is simply used as the estimated throughput. The quality level will increase or decrease depending entirely on estimated bandwidth. The Aggressive method is sensitive to cases where the bandwidth increases sharply in a short period of time and then abruptly decreases (short-term bitrate peaks). The client then requires a high-quality version, but the high bandwidth level does not last long enough to load the required segment. This may cause video freezing during playback. The Aggressive algorithm aims to use most of the available bandwidth for the streaming client by always adapting to the highest quality version of video segment that does not surpass the available bandwidth. By doing this, the expectation of streaming users is also met. In [7], [8] the authors proposed a buffer-based bitrate adaptation algorithm for HTTP video streaming, called BBA. BBA is based on the current playback buffer occupancy only by selecting bitrate heuristically without throughput estimation. The goal of BBA is avoiding stalling events and maximizing the average video quality by choosing the highest available bitrate level. However, this scheme shows many limitations such as QoE degradation in case of long-term bandwidth variations and slow bandwidth fluctuation, especially in case of bandwidth competition in a shared network. In the literature, there are some ABR (Adaptive Bitrate) algorithms that take into account both of the estimated throughput and current buffer occupancy to define the most suitable video version

for the next segment. In [9], [10], the authors propose a buffer-based bitrate adaptation algorithm for VBR (variable bitrate) videos. The study in [11] proposes a throughput-buffer based algorithm relying on the buffer target, the playback buffer filling level, and the current bandwidth to determine the next segment's version. Work [12] proposes a segment-aware rate adaptation algorithm (SARA), in which segment size variation, the estimated throughput and the current buffer occupancy are considered to predict precisely the time required to download the next segment. In SARA, the MPD file not only contains the average bit rate information of the segment but also the size of the segment. SARA has expanded and changed the structure of the MPD file to accomplish this. Estimated throughput is based on the measured throughputs in the past and divides the buffer into different levels to determine the bitrate. This assures to download the best possible representation of the video while avoiding video buffer starvation. However, SARA shows low performance and poor QoE in the context of bandwidth sharing competition.

In a shared network environment, with so many Internet services available, bandwidth resource always gets risk of becoming insufficient to the increasing number of users, despite the maturity of cutting edge technologies nowadays. Therefore, it is always a huge concern for researchers to deal with limited resource allocation in any networking circumstances. Most of the existing researches tend to increase the Quality of Experience of clients while optimizing the transmission capability. Now exist three solution categories to deal with the problem where many clients compete through a bottleneck point. The first category is to solve the issue of sharing video streaming services at the client side as mentioned in [13]–[15]. In [13], an algorithm is proposed to improve efficiency, fairness, and stability named FESTIVE by providing schemes to ensure a trade-off of these factors. FESTIVE is the first known client-side adaptive bitrate algorithm that is designed for the multiple client context specifically. FESTIVE contains three main components: a scheduler that determines the time of starting to download a segment, an algorithm that estimates the throughput based on all previous downloaded segments and a mechanism to select the bitrate of the next segment. However, with FESTIVE, when the number of users grows sharply in a competition, the system's stability could be reduced remarkably since the estimation of the bandwidth is too high, perhaps. In [14], a rate adaptation algorithm for HAS service is proposed based on a "probe-and-adapt" principle at the client side so-called PANDA. "Probe-and-adapt" is a kind of the additive increase and multiplicative decrease principle (AIMD) that is used in TCP. However Probe-and-adapt operates at the application layer and in a longer time scale. PANDA is a HAS client rate adaptation algorithm designed to provide high stability and fast responsiveness to bandwidth variations in the context of multiple HAS clients sharing the same bottleneck links. For detecting the available bandwidth, the network is probed by PANDA which additively increments its sending rate at each adaptation step and multiplicatively decreases its rate if a congestion is detected, in order to adapt its video bitrate accordingly. During the estimation of the available bandwidth, the PANDA probing mechanism tries to increase its sending rate, instead of transmitting auxiliary piggybacking traffic. PANDA also allows HAS clients to respond to bandwidth fluctuation quickly and to achieve stability. But PANDA does not consider the resource al-

location strategy in the context of multiple user negotiation. In [15], the streaming framework in VHS (VideoHomeShaper) is designed and implemented to evaluate performance in home's last access hop. In this study, the evaluation of QoE for competing clients takes into account some metrics such as Stability, utilization, and fairness. Overall, these researches mainly focus on adapting bit rate at the client side to improve the parameters that can affect user's QoE.

The second category focuses on the sever side. In this area, servers are normally considered as the only control point responsible for managing video transmission for all clients. The authors of [16] introduce a server-side adaptation scheme, which uses TCP to limit the video bit rate. A server-based traffic shaping solution is proposed in [17] to notably decrease such oscillations, at the expense of a small loss in bandwidth utilization. However, we can only be observe the actual bandwidth congestion problem at the network's side. Consequently, not too many clients might be able to handled by the server.

Finally, the category of in-network methods uses active bandwidth allocation to gain QoE fairness for multiple clients. Fair bandwidth allocation for players at a bottleneck link has been recently suggested by several work. Based on the SDN technology, [18] proposes traffic shaping techniques and do an analysis of ABR video streams when sharing resources through a congested link. In this method, all shared connections at the bottleneck point have the same throughput; and the total bandwidths assigned to requiring clients must not exceed the available bandwidth at the bottleneck. SDN-based traffic shaping in [18] can improve QoE for video streaming in terms of efficiency, fairness, and quality. The authors in [19] also consider the bandwidth sharing within a bottleneck link. However, in the network sharing model, the network sharing is calculated periodically, not in the per-request basis. In adaptive streaming, clients can require changing the bit rate at any time and the SDN controller must calculate the network sharing based on all of requests at the certain time. Authors in [20] proposed a system for increasing QoE of SVC-DASH clients based on SDN. The SDN architecture enables to select different streaming path to transfer different video layer flows between the server and the clients. But this paper does not consider the resource allocation strategy in the context of multiple user negotiation. In [21], the author proposed an OpenFlow-based QoE fairness framework (QFF). QFF manages the player statuses and allocates network resources dynamically to achieve the maximum user-level fairness for all clients that compete in a shared network. A proof-of-concept implementation is provided considering a small number of concurrent flows. However, only the fairness parameter of QoE is considered in this research. In [22], network-assisted strategies are considered to provide service differentiation to concurrent video flows such as the Bitrate Guidance approach (BG), the Bandwidth Reservation approach (BR), and the hybrid approach (BG+BR). A centralized Video Control Plane (VCP) is built to provide Video Quality Fairness (VQF) to concurrent video sessions that are sharing a common bottleneck. Work [23] argue that the network and clients shall collaborate to gain QoE fairness while video streams are encrypted. Placing cDVD in the greater context of QoE delivery methods is instructive. The resource-sharing clients only focus on fairness but not efficiency and stability. In [24], centralized and distributed architectures are proposed for collaboration between video service provider (VSP), network service provider

(NSP), and DASH clients to provide SDN-based NSP-managed or VSP-managed DASH services with quality-of-service (QoS) reserved network slices. The SDN controller computes the shortest-path route and bitrate for each client. This approach is to gain QoE fairness among heterogeneous DASH clients. However, again the resource-sharing clients only focus on fairness but not efficiency and stability. In [25], the author proposed an optimization model aiming at fairly sharing the bottleneck link while maximizing the client's perceived video quality. However, the work focuses only in bandwidth allocation and maximal link capacity of each client without considering how bit rate should be adapted to receive desired quality experience of the clients based on the real condition of the clients. Research [26] proposes a SDN-assisted adaptive streaming solution for tile-based contents using DASH to improve the user's quality of experience. The paper also summarizes the difference in immersive content streaming between SDN-based and traditional networks and introduce a SDN-based framework to support tile-based immersive content streaming. However, this paper does not consider the bandwidth allocation and bitrate adaptation problem. In [27] and [28], the author proposed a SDN based management architecture and dynamic resource allocation for HAS systems aiming to alleviate scalability and improve the QoE of each client. This architecture is in charge of allocating the network resources dynamically for each client depending on the client's QoE expectation. The same authors in [29] propose a SDN-based QoE-aware bandwidth broker for HTTP adaptive streams in an hybrid fiber coax (HFC) network, so-called Bandwidth Management Solution - BMS that dynamically chooses the respective bandwidth allocation decisions and the optimal joint representation in oder to meet the per-session and per-group QoE objectives. In [30], there is a network-driven video streaming architecture is built to design robust mechanisms for multiple players so as to achieve end-user QoE fairness. The SDN controller observes the environment state, computing the reward, and updating Q-value and taking the bandwidth allocation action by forwarding flow tables. However, the author considered how bandwidth should be shared to achieve fairness while QoE is taken into account from the perspective of receiving bit rate that is suitable to the link bandwidth. The work does not consider how QoE of each client can be acquired based on the client's real need in terms of bit rate at a certain moment QoE. In [31], a SDN-based model is built over the DASH protocol to improve the QoE whilst taking into account the variety of video parameters, devices and the network requirements. The proposed scheme comprises two phases: Machine Learning-based estimation phase of available resources, and adaptation and selection phase based on the results of the first phase. The goal of the approach is to have the best quality perceived video. The authors in [32] proposed a SDN-assisted solution to use the network management plan to reinforce policies for improving QoE of clients. However, again, this work does not consider the case of lack of network resource so multiple users need to negotiate for the network share in trade off with QoE. In [33], the authors present SAND/3 that is an SDN-Assisted QoE control for DASH over HTTP/3 for improving the QoE at the client side based on criteria such as buffer size, display size, type of device and subscription plan, and available memory. From the SDN network perspective, SDN tries to find a route for each requested connection from each client based on available resource. But this paper does not consider the resource allocation strategy in the context of multiple user negotiation.

Generally, SDN-based dynamic bandwidth allocation shows a good performance in improving video quality. However, the interaction between the network control and the client-side control in the context of multiple users sharing one bottleneck link has not been well investigated. Therefore, deploying solutions in a large-scale system is still a pending question.

3 Bitrate Adaptation Algorithm

Our proposed framework to the bottleneck problem is a integration of the bitrate adaptation algorithm at the client's side and the centralized SDN-based resource allocation, i.e. a cooperation between the network and video streaming applications. In the streaming network, a flow management mechanism called MSMA (Media Streaming Multiple Access) is proposed (discussed in Section 4.2).

In fact recently, there have been two widely-adopted types of algorithms at a MPEG-DASH Client, which belong to either the throughput-based group or buffer-based group. Therefore, we consider the context of multiple video-on-demand players, provided that the throughput-based adaptation algorithm called Aggressive [6] is deployed at each client.

Besides, we have also proposed a buffer based bitrate adaptation algorithm to determine a video quality level for the next segment. Compared to the throughput-based algorithms, buffer-based algorithms provide smoother bitrate curves in video-on-demand streaming. In the next subsections, the description of the throughput estimation and the proposed adaptation algorithm are presented.

Table 1: Symbols use in this paper

Symbol	Description
B_i	Current buffer level at segment i
B_e^{i+1}	Estimated buffer for segment $i + 1$
B_{max}	Maximum buffer size
N	Number of clients
I_{i+1}	The chosen version for the next segment
T_i	The throughput for the current segment
T_{i+1}^e	Estimated throughput for the next segment
r_i	Bitrate of client i
$r_i^{'}$	Bitrate of r_i after the SDN controller is recalculated
$R_{0,\dots,V-1}$	Bitrate of version 0, 1, $\dots$, V-1
R_{max}	Bitrate corresponds to the highest level of quality
RTT	Round Trip Time
SD	Segment Duration
V	Total number of video versions

3.1 Throughput Estimation

In simple terms, the bitrate adaptation mechanism adapts its requested bitrate based on the estimated throughput. Video segments are delivered from the server to the clients in sequence of consecutive HTTP request-response transactions. In general, throughput is obtained by dividing the data size by the delivery time. Knowing the actual amount of data delivered by a request-response transaction is

important. The segment throughput T_i^e for each delivered segment i is computed using the request-response duration (i.e. from the instant of sending the request to the instant of receiving the last byte of the response). Table 1 lists the symbols used in this paper.

A video version is chosen based on Equation (1). Bitrate R_j is selected as the maximum value not exceeding the product of the current estimated throughput T_{i+1}^e and safety margin μ (μ varies from 0.0 to 0.5). μ is defined to solve the instability of the Internet connection and delay caused by other streaming processes such as bitrate adaptation calculation and file decoding.

$$R_j \leq (1 - \mu) \times T_{i+1}^e \tag{1}$$

Next, we propose to estimate the next throughput based on two previous measured throughputs at the client side (as described in Equation (2)). In the Equation, γ is a dynamic constant range from [0, 1] that allows a client to adapt well with highly bandwidth fluctuations, especially with highly variable bandwidth since it is the main cause of video freezing. γ is usually set to be 0.5. When $\gamma = 1.0$, the estimated result will be exactly the same as the one of the aforementioned aggressive method.

$$T_{i+1}^e = \gamma \times T_i + (1 - \gamma) \times T_{i-1} \tag{2}$$

Algorithm 1: Proposed Bitrate Adaptation Algorithm

> **Input:** $T_i, R_n, B_i, RTT, SD, I_i, \Delta_B$;
> **Output:** I_{i+1} ;
> $T_{i+1}^e \leftarrow \gamma \times T_i + (1 - \gamma) \times T_{i-1}$;
> $I_{i+1} = 0$;
> **for** $j \leftarrow V - 1$ *to* 0 **do**
> $B_{i+1}^e \leftarrow B_i + SD - RTT - \frac{SD \times R_i}{T_{i+1}^e}$;
>   **if** $j > I_i$ *and* $B_{i+1}^e \geq B_i + \Delta_B$ **then**
> $I_{i+1} = j$;
>   *Break*;
>   **end**
>   **if** $j \leq I_i$ *and* $B_{i+1}^e \geq B_i - \Delta_B$ **then**
>   New request to controller;
> $I_{i+1} = j$;
>   *Break*;
>   **end**
> **end**

3.2 Proposed adaptation algorithm

In this paper, we design a new quality-selecting scheme based on the estimate buffer level so as to avoid video freezing. According to our previous work [34], we use Equation (3) to estimate the next buffer level, provided the client selects version j for segment i where SD is segment duration. RTT is the duration defined from the instant a client sends its request to the instant it receives a response and calculated by timestamps of the westward and eastward packets captured at the network card of the SDN controller. The westward packet is the request packet sent from a client to the controller and the eastward packet is the packet carrying information of calculated BW from the controller to that client.

The main goal of our solution is to choose a suitable quality level that can keep the buffer greater than the current buffer B_i to prevent stalling events. Our method details are shown in Algorithm 1. This algorithm is based on an estimated buffer to determine a new video version for the next segment.

In fact, increasing the quality version has a lower priority than keeping the quality version stable, and the quality should be reduced as little as possible through threshold Δ_B. The larger Δ_B , the less varied the video quality version, but the worse the connection adaptation. On the contrary, the smaller Δ_B, the better the connection adaptation, but more the stability is lacked. This parameter usually ranges from 0.25s to 2s. In this paper, we choose $\Delta_B = 1s$, since this figure is appropriate to trade off the issues above. When there is network fluctuation, a client shall reduce its quality version accordingly. In that case, the client will request the SDN controller to recalculate the bitrate, and sending this bitrate information to all clients that are having ongoing connections so that the quality version of all clients are kept as stably as possible.

$$B_{i+1}^e = B_i + SD - RTT - \frac{SD \times R_j}{T_{i+1}^e} \tag{3}$$

4 Proposed SDN-based Solution

4.1 Bandwidth Allocation Policy

Provided that N clients go through the same bottleneck with bandwidth capacity C. $BW_{i,t}$ is the amount of bandwidth allocated for client i at time t. The bandwidth allocation policy is to map the bitrate requested by each client to the actual bandwidth that could be granted to that client:

$$BW_{i,t} = f(r_{i,t}) \tag{4}$$

where $r_{i,t}$ is the bitrate that client i requests at time t. r_i is the bit rate the clients desire to have at the beginning. But BW_i is the actual bit rate that the clients will adapt to after being reconsidered by the SDN controller. In case the bandwidth resource is sufficient, all clients will have BW_i which are the same to r_i. In case network resource lacks, one or some r_i may be different from BW_i.

If the network resource (bottleneck link capacity) is sufficient for all requested bandwidths of each client, the clients will be allocated the same bandwidth as they request, i.e.:

$$BW_{i,t} = \frac{C}{N}, \forall i \in N, \forall t \tag{5}$$

However, in reality, HTTP networks are not ideal because clients frequently require bitrates that can be higher than the then-actually allocated bandwidth. As described in [35], [36], the bandwidth allocation policy for this non-ideal HTTP network condition is as follows:

> . if $r_i = r_j$ then $f_i(r) = f_j(r)$;
> . if $r_i > r_j$ then $f_i(r) > f_j(r)$;
> . $\frac{\partial f_i(r)}{\partial r_i} > 0$, $\frac{\partial f_i(r)}{\partial r_j} < 0$, where $i \neq j$;
> . $lim_{r_i \to \infty} f_i(r) < C, lim_{r_i \to 0} f_i(r) > 0$;
> . $f(.)$ is a function of r and value of f is independent of the client order.

In fact, requests do not come to the edge switch at the same time, therefore naturally, a solution to each request is thought appropriate.

When a request comes, the system calcualte to determine if it should accept the request, so as to ensure no congestion occured at the bottleneck point, causing the drop of quality of experience of all N clients.

In DASH, content provider encode videos at different quantity levels of different bit rates and then brake the videos into segments. That is the base to determine the minimum bandwidth needed by each client in order to obtain an uninterrupted video streaming. That minimum bandwidth is equal to the average bitrate of the video with the lowest quality level. This value is denoted as R_0.
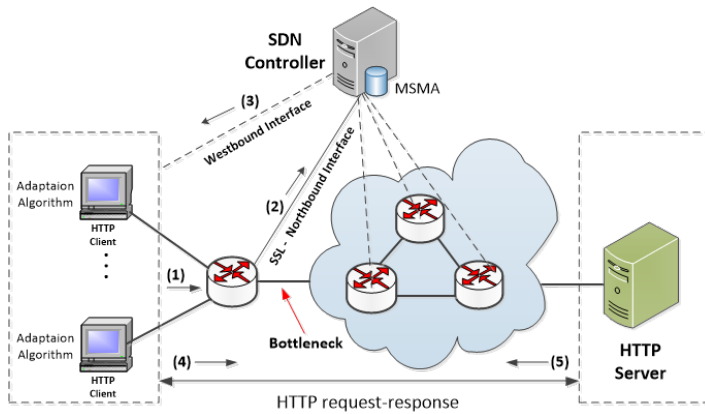
Figure 1: Proposed architecture and operation for the bottleneck problem

4.2 Proposed fair bandwidth allocation solution (MSMA-0)

The proposed architecture is illustrated in Figure 1. As it can be seen, the Aggressive adaptation algorithm and the MSMA module are implemented in each client and the SDN controller respectively. The whole solution is called MSMA-0. In our proposed architecture, the edge switch (OFS - OpenFlow Switch) communicates to the SDN controller through 2 interfaces: a standard Northbound interface of Openflow that connects OFS and the SDN controller via TSL protocol; and a legacy network interface that connect the OFS and controller as 2 legacy network devices called Westbound interface. The operation of the proposed architecture is as follows:

• Phase 1: Negotiation of appropriate bit rates requested by each client

(1) Each client calculates its desired bit rates according to the bit rate adaptation algorithm implemented at client.

(2) Client sends that streaming request (i.e. desired bit rate) to the edge OFS switch. Then, the OFS encodes the request information in a $Packet - In$ message and sending it to the SDN controller via the Northbound interface (which is defined in OpenFlow protocol).

(3) The Controller, via the Northbound interface with the OFS edge switch, having already knowledge of link capacity of the network cards of the switch can calculate new BW values, then sending these new information to the clients via Westbound interface (as a legacy network device).

• Phase 2: Requesting the finally negotiated bit rate to the application server

After receiving information on BW from the SDN controller, the clients operate as follows:

(4) N ongoing clients send new requested BW_i to the application server via an open connection.The new client $(N + 1)$ sends a request to connect to the application server, the SDN controller will order the edge OFS to install a new flow entry to establish the connection between Client N+1 and the application server.

(5) Upon receiving the request on bit rate (i.e BW_{N+1}), the app server will push a video quality version segments accordingly to all streaming clients.
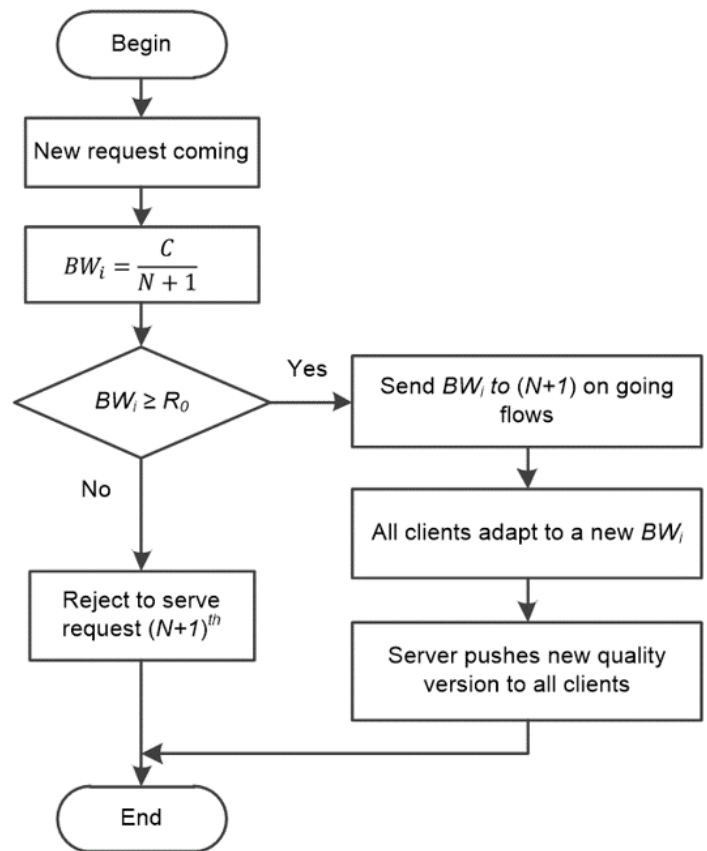
Figure 2: MSMA Flowchart

As the implication of its name, a network bottleneck causes a slow connection speed, limiting the experience of media streaming. Solving the aforementioned issue is the goal of our proposed MSMA algorithm. Figure 2 depicts the flowchart of MSMA deployment with the working principle described as follows:

1) Given that there are N ongoing clients requesting new quality versions for each segment, the average bandwidth BW_i distributed to $(N + 1)$ streams is recalculated by the MSMA module, according to the Equation (6) below:

$$BW_i = \frac{C}{N + 1} \qquad (6)$$

2) BW_i is then compared with the minimum acceptable bitrate R_0 by the SDN controller that then decides what action to take. Either one of these two actions depending on the result of the comparison will be carried out by the SDN controller.

3) A flow for the incoming stream is added by the SDN controller and BW_i is sent to all on going streams by the controller if $BW_i \geq R_0$ i.e. the bandwidth allocated to each client is higher than the one of the lowest quality version and is sufficient to stream that video version.

4) The incoming request is rejected to serve by the controller if $BW_i < R_0$ i.e. the bandwidth allocated to each client is insufficient to stream even the lowest quality version of the video.

Then after all, all streaming clients shall adapt to BW_i decided by the SDN controller. The clients then request the DASH server for the decided bitrate. The adaptation logic is described in the next section. TheDASH server pushes a new quality version to all streaming clients.

4.3 Proposed adaptive bandwidth allocation solution (MSMA-1)

In this work, we propose a new method (called MSMA-1) that combines a bit rate adaptation algorithm at the client side (i.e. Algorithm 1), with modul MSMA deployed in the SDN controller as Algorithm 2. The goal of MSMA-1 algorithm is trying to improve the Quality of Experience of each client on the streaming service by providing the bit rate that a client requires while trying to increase the number of clients that can access to the system within a limited resource.

At the network side, we allocate bandwidth dynamically (i.e. Algorithm 2) for all clients in order to maximize the number of clients that can be given an access to the network and minimize the number of clients who are requested to change their bitrate expectations (bitrate to satisfy the QoE criterion). Provided the system has N clients that have HTTP streaming over a bottleneck point. The capacity of the output link of the bottleneck point is assumed C (Mbps).

At the client side, each client deploys the bitrate adaptation algorithms proposed in Algorithm 1 to find out what is their bitrate expectation in order to achieve desired QoE. Actually, each bitrate is corresponding to a quality version defined by DASH and stored at the server.

In case, the sum of all requested bitrates r_i of N clients ($i = 1$ to N) is smaller or equal to capacity C, the SDN controller will request the DASH server to push the quality version desired by each client.

In case, the sum of all bitrates r_i ($i = 1$ to N) is larger than C, i.e:

$$\sum_{i=1}^{N} r_i > C \qquad (7)$$

then the SDN controller recalculates bandwidth allocated for each client. The SDN controller operates in the following criteria:

1. The SDN controller tries to keep the bitrates r_i required by the clients as stably as possible with the goal of meeting these clients' QoE requirement.

2. The SDN controller selects a client holding the highest rank, and taking a fraction of its required bandwidth to give to another client. In this manner, the network take a fraction of the network resource of this client but in return it will give

an access for an additional client (i.e. client $(N + 1)$). So, the goal of serving as many clients as possible is fulfilled.

In fact, as in the solution described in section 4.1, the link capacity C is divided equally to all $(N + 1)$ clients, therefore, all $(N + 1)$ clients suffer an undesirable QoE degradation since distributed resource may be lower than their requirements to achieve each client's satisfaction. Therefore, in this new proposed solution, the SDN controller, firstly, ranks all clients in a certain manner. Then the controller will set a policy to allocate resource to all clients by rank. Technically, this ranking function (or objective function) can be defined as a function of multiple objectives. Within the scope of this paper, we define the rank of client by Equation (8). Looking at the Equation (8) shows that the client that have a higher buffer level and a bitrate is likely to have the highest rank function. Therefore, this client will bring in some of the resources available for the new service. In addition, the choice of which client to share the resource will depend on for the two parameters which are bit rate r_i and buffer level B_i such that rank function is highest.

$$Rank(i) = f(B, r) = \alpha \times \frac{B_i}{B_{max}} + \beta \times \frac{r_i}{R_{max}} \qquad (8)$$

where α, β: non-negative weighting factors. And r_i is bitrate required by the ongoing client, B_i is current buffer level of client.

The set of $Rank(i)$ is arranged in the decreasing order according to the rank function value.

Details of the proposed solution are described in Algorithm 2. The details of this algorithm are explained as follows:

Firstly, the requested bitrate of a client who has the highest rank is recalculated to share the resource to other client. Provided the client with the highest rank is Client N. Then the bandwidths of client j and client N are reallocated as Equation (9) and (10) accordingly:

$$r'_j = \frac{r_j}{r_j + r_N} \times \Delta C \qquad (9)$$

$$r'_N = \frac{r_N}{r_j + r_N} \times \Delta C \qquad (10)$$

where r_N is the requested bitrate of client N who has the highest rank value and r_j is the requested bitrate of client who requests a new bitrate. r'_j and r'_N are the varied bitrates of r_j and r_N after the SDN controller recalculate bandwidth distribution. ΔC is the remaining bandwidth after reserving the bandwidth portion for all left clients that have not been shared it's resource. (i.e. all clients that retain their bitrates r_i). ΔC is defined by Equation (11).

$$\Delta C = C - \sum_{i=m}^{N} r_i \qquad (11)$$

where m is the number of clients who are sacrificed.

In case if the calculated bitrate of client j is smaller than the smallest acceptable quality version ($r_j < R_0$), continue to take the second highest bitrate requested by an ongoing client and redivide

proportionally for all 3 clients. The process continues until all N clients satisfy a bitrate $r_i \geq R_0$ $(i = 1 \div N)$.

Algorithm 2: . MSMA-1 algorithm

Input: r, C, Δ_C
Output: r
for $i \leftarrow$ *to* N **do**
  $r'_{N+1} = \frac{r_{N+1}}{\sum_{k=1}^{i} r_k + r_{N+1}} \times \Delta_C$;
  for $j \leftarrow 1$ *to* i **do**
    $r'_j = \frac{r_j}{\sum_{k=1}^{i} r_k + r_{N+1}} \times \Delta_C$;
  end
  if $min(r') \geq R_0$ **then**
    $r = r'$;
    Break ;
  end
  else if $i = N$ *and* $min(r') < R_0$ **then**
    Reject client $(N + 1)^{th}$;
  end
end

---

5 Performance Evaluation

5.1 Experiment Setup

Bitmovin, a multimedia technology company providing services, which transcode digital video and audio to streaming formats using cloud computing, and streaming media players has developed and maintained a library named libdash [37]. In this paper, QtSamplePlayer is used as the media player of the streaming architecture. QtSamplePlayer is a Qt-based player recommended for the libdash library by Bitmovin. Videos pushed from the HTTP server to the clients are 2 types of videos: constant bit rate CBR and variable bit rate VBR. Besides, traffic from the clients to other devices (i.e. OFS switch and the SDN controller) is only control information on bit rate requests to adapt to required quality version.
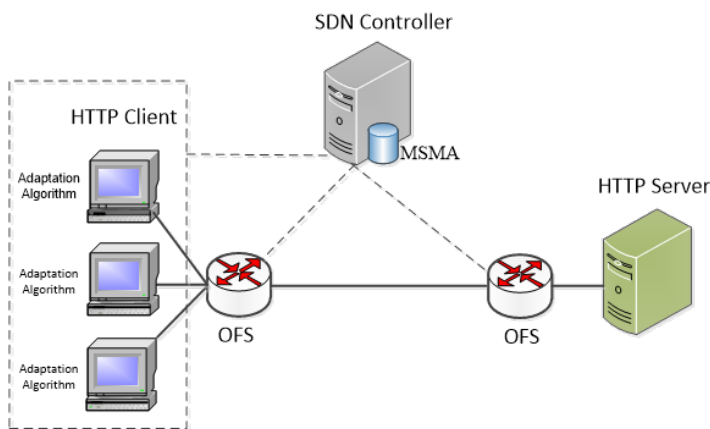
Figure 3: Network topology used for experiment.

Figure 3 shows the network setup for performance evaluation. In our experiment, five machines are used to conduct the experiment: the media server, one machine for emulation of the streaming network including the SDN switches and the SDN controller - Floodlight [38], and 3 video streaming clients. One clients is implemented on a physical PC and all other machines are VMWare machines. Due to limited testbed resource, we just make a proof of concept with 3 clients. In the future, we will improve the testbed to scale up the experimental scenario. The network consists of two OpenFlow switches and a bottleneck link between them. An OFS is connected to the three client machines and the other OFS is connected to the media server ,in which MPD (Media Presentation Description) and video files are stored. The MPD file is an XML (Extensible Markup Language) file that represents the different quality levels of the media content and the individual segments of each quality level with Uniform Resource Locators (URLs). For this evaluation, Mininet [39] is used to create a realistic virtual network.

There are many different types of videos that can be used in evaluation simulations, but all of them focus on two types of video: variable bit variable (VBR) and constant bitrate video (CBR). In this paper, the experiment videos are two short movies named Elephants Dream [40] and Destiny [41] to represent the 2 aforementioned video types. In the Elephants Dream movie, the video is divided into 327 segments with the total duration of 654 seconds (i.e. 2 seconds per segment). This video is encoded in the VBR mode of 12 different versions corresponding to 12 different average bitrates. The version index, Quantization Parameter (QP), and the average bitrate of each version are listed in Table 2. The Destiny short file is a constant bitrate video (CBR) and is divided into 340 2-seconds-long segments of 16 quality levels of different bitrate (50, 100, 250, 400, 600, 800, 1000, 1200, 1600, 2000, 3000, 4000, 6000, 8000, 12000, 16000 Kbps).

Table 2: Version information of the VBR video

Version	QP	Average Bitrate (Kbps)
0	46	354
1	43	472
2	40	638
3	37	882
4	34	1234
5	31	1779
6	28	2588
7	25	3823
8	22	5613
9	19	8028
10	16	11156
11	13	15227

5.2 Experimental Scenarios

Six experiments are deployed to evaluate our proposed system:

• Experiment 1: The link capacity of the bottleneck is 10 Mbps, 7 Mbps and 4 Mbps. The controller uses the aforementioned method MSMA-0. Client 1 starts streaming 110 seconds (55 segments). After the first 110 seconds of Client 1, Client 2 starts streaming in 110 seconds and in the same way with Client 3.

• Experiment 2: The link capacity of the bottleneck is set at 10 Mbps, 7 Mbps and 4 Mbps. The controller uses the aforementioned MSMA-1 algorithm. Each of Client 1, Client 2 and Client 3 starts

streaming in 110 seconds, one after another.

• Experiment 3: The link capacity of the bottleneck is set at 10 Mbps, 7 Mbps and 4 Mbps. The Aggressive, SARA, BBA, PANDA algorithms are used. MSMA is not available. Each of Client 1, Client 2, and Client 3 starts streaming in 110 seconds, one after another.

• Experiment 4: The link capacity of the bottleneck is set at 10 Mbps, 7 Mbps and 4 Mbps. The SARA, BBA algorithms are used. The MSMA module is activated. Each of Client 1, Client 2, and Client 3 starts streaming in 110 seconds, one after another. This experiment simulates methods "SDN-based SARA" and "SDN-based BBA".

• Experiment 5: The link capacity of the bottleneck is set at 500 Kbps. The controller uses the MSMA modul. The clients request for the VBR video an independent time.

• Experiment 6: The link capacity of the bottleneck is 500 Kbps. The controller does not use the MSMA modul. The clients request for the VBR video at independent time.

We use the Aggressive method as the bitrate adaptation algorithm [6] with a safety margin $\mu = 0.2$.

We perform each of the five experiments in three times and record the average results for later comparison. The purpose of Experiment 1, Experiment 2, and Experiment 3 is to determine stability, efficiency, and fairness; The purpose of Experiment 4 and Experiment 5 is for checking the possibility of rejecting new requests when a congestion is possible.

With Experiment 5, since $R_0 = 354Kbps$, only the connection request of the first client will be accepted by the controller; and video with the minimum average bitrate will be streamed by the client. The evaluation results illustrates that the number of video freezes is 5 in case the segments contain a high bitrate compared to the representative bitrate (i.e. average bitrate). Our proposed system does not accept to provide services to requests from client 2 and client 3. Experiment 6 shows the scenario of a traditional network where the controller does not operate with the MSMA modul. In that scenario, the 3 requests from 3 clients are accepted in turn.

So, because the available bandwidth is not sufficient for all 3 clients sharing bandwidth and asking an acceptable bandwidth, all 3 clients are frozen immediately after being connected and also experience buffering most of the time during the whole course of their streaming section. This proves that at the circumstance of poor bandwidth, MSMA-0 is still able to serve the modest number of players, rather than the other methods where no user will be served.

5.3 Simulation Results and Discussion

To evaluate the performance of the proposed solution, we use three metrics of fairness, efficiency and stability as presented in [42] and [13] and a QoE metric. In the following subsections, these metrics will be described in detail.

5.3.1 Fairness, efficiency and stability metrics

In this subsection, the 3 metrics of stability, fairness, and efficiency are presented. In particular, the fairness score is measured by Equation (12)

$$Fairness = \frac{|\sum_{i=1}^{N} r_{i,t}|^2}{N\sum_{i=1}^{N} r_{i,t}^2} \quad (12)$$

where $r_{i,t}$ is the video bitrate allocated to client i at time t. The fairness score should be in the range of [0 to 1]. As the matter of fact, the closer to 1 the fairness score is, the fairer the system is.

The efficiency score of the bandwidth distribution is computed using Equation (13), where W is the available bandwidth of the shared connection. The closer to 1 the Efficiency score is, the better the system efficiency is.

$$Efficiency = \frac{|\sum_i r_{i,t}|}{W} \quad (13)$$

Equation (14) defines the stability score for client i at time t. This score is calculated based on the absolute amplitudes of the quality fluctuations (i.e. bitrate switches).

$$Stability = 1 - \frac{\sum_{d=0}^{k-1} |r_{i,t-d} - r_{i,t-d-1}| \times \omega(d)}{\sum_{d=1}^{k} r_{i,t-d} \times \omega(d)} \quad (14)$$

where: $\omega(d) = k - d$: weight function; and k: 20 seconds (10 segments) in this experiment. The closer to 1 the Stability score is, the more stable the system will be.

5.3.2 QoE Metric of Video Streaming

In this section, we first present parameters that have influences on the QoE of video streaming. Then, a QoE metric taking into account the parameters is provided. According to [43], the most important parameters are as follows:

Initial Delay (D_t): Initial Delay is computed as the duration from the point the first segment of a video is requested until the point the video is played out. For an effective video streaming system, the buffer time required for this parameter must be much smaller than the maximum client-side buffer level. According to [27], the initial delay should be less than 6 seconds.

$$D_t \ll B_{max} \quad (15)$$

Average Version Quality (AVQ): In the DASH system, the quality of the segments received at the client is variable. This parameter is defined as the average version of all the downloaded segments. Assume a video stream consists of K segments and each segment is encoded with V bit rate corresponding to V quality level, where v represents a specific quality level .

$$AVQ = f(i, v) = \frac{1}{K} \sum_{i=1}^{K} q_{i,v} \quad (16)$$

where $q_{i,v}$ is the quality value of the ith segment at the v quality session level, for example $q_{i,v_{max}}$ is the quality value of the ith segment with the highest quality level.

Number of Version Switch-downs (NVS): is the number of times that a downloaded segment has a lower bitrate than the previous segment. We can use this paremeter along with Average Video Quality to provide quantitative inferences of QoE. If video flows have similar Average Video Quality, a flow with the lower number

of Version Switch-downs will be perceived,by users, to be the better one .

$$NVS = \frac{1}{K-1} \sum_{i=1}^{k-1} |q_{i+1,v_{i+1}} - q_{i,v_i}| \qquad (17)$$

Number of Video Stalling (S_t): Video streaming will be stalled if the buffer at the client side is empty. In other words, if the playback buffer size is reduced to the minimal buffer level but has not downloaded the current segments, then a video stalling will occur. Number of Video Stalling can be calculated as the total number of stalls in a video playback time period.

$$S_t = \frac{1}{K} \sum_{i=1}^{K} S_i, \forall 0 \le B_i \le B_{min} \qquad (18)$$

To evaluate the performance of our bitrate adaptation scheme, we use an QoE metric based on the above parameters and also from the reference model provided by A. Bentaleb et al. [27] as follows:

$$QoE_i = \alpha_1 \times AVQ - \alpha_2 \times NVS - \alpha_3 \times S_t - \alpha_4 \times D_t \qquad (19)$$

Both S_t and D_t are in seconds. ($\sum_{n=1}^{4} \alpha_n = 1$) are non-negative tunable values and selected based on [13] to test in our experiments. We convert the QoE score to a normalized QoE (N-QoE) accordingly to Table 3 to represent a user's satisfaction MOS (mean opinion score) from 1 to 5.

Table 3: Normalized QoE

QoE_i	N-QoE	Quality
$QoE_i \le 1$	1	Bad
$1 < QoE_i \le 2$	2	Below Average
$2 < QoE_i \le 3$	3	Average
$3 < QoE_i \le 4$	4	Good
$QoE_i > 4$	5	Excellent

5.3.3   Performance Evaluation

In this section, we compare our proposals (MSMA-0 and MSMA-1) with the existing methods such as PANDA, BBA, SARA, Aggressive (called AGG), SDN-based SARA and SDN-based BBA. In which, the SDN-based BBA and SDN-based SARA methods are the BBA and SARA methods that are combined with the fair bandwidth allocation of the MSMA module. To understand more about the existing solutions, let us to highlight some main points of the existing methods:

1. AGG only based on the throughput of the previous segment to estimate the throughput for the next segment. This method has advantages in fast adaptability to the strongly fluctuating bandwidth conditions, but has disadvantages in the stable bandwidth conditions compared to other methods.

2. For SARA method, the bitrate adaptation algorithm of SARA is both throughput-based and buffer based to determine which quality level would be chosen. SARA has shown a number of advantages over the AGG algorithm as it is able to

maintain a higher quality level for longer time under stable bandwidth conditions because of having the segment capacity information, thus it could predict download time.

3. BBA is the buffer-based method only to select a version quality without estimating throughput.

4. PANDA uses "probe-and-adapt" to build the rate adaptation algorithm and fair-share bandwidth for players. This solution achieves good stability but the averrage video quality is not high. On the other hand, PANDA's resource allocation is in a distributed rather than centralized manner like our proposed one so fairness is not high.

The download rate (DLrate), buffer level, and selected versions of all the methods are shown in Figure 4 (with VBR video) and Figure 5 (with CBR video). In experiments for the 10 Mbps, 7 Mbps, and 4 Mbps cases, the results show similar performances in terms of version and download rate. Therefore we only count in the 4 Mbps case as the representative for this type of evaluation. As Figure 4 demonstrate, in case of using the SDN controller with MSMA-0 and MSMA-1, video versions of the client are stable during the whole course without requesting any new connection.

Especially, MSMA-0 is very stable, however this method has average video bitrate much lower than of MSMA-1. The other methods have relatively the same average video bitrate. For MSMA-1 and BBA, due to buffer preestimation, the buffer does not go to zero. This means that the video will not be stalled. Other methods have almost video stalling for some times. For MSMA-0, the buffer is dropped low in segments of 68-78. In PANDA, the video is interrupted from segment 60 to segment 78. In SARA, the average buffer is very low, and there are 2 video interruptions, one at around segment 110 and one from segment 174 to 198. In the Aggressive method, video quality is fluctuated continuously which can be annoying to viewers; and video is also stalled from segment 66 to segment 78. With the support in bandwidth sharing of the SDN controller, the SDN-based BBA and SDN-based SARA methods have better performance in comparison with the BBA and SARA, as described in Figure 4g and Figure 4h. As we can see, the SDN-based SARA method has more stable quality levels compared to SARA in the duration from segment 80 to 200. This is because the fair bandwidth allocation of the MSMA module incorporates the segment-aware rate adaptive algorithm of SARA when multiple clients access the system. With good buffer-based bitrate adaptation, SDN-based BBA as well as BBA can avoid video freezing.

As Figure 5 illustrates, the status of clients in the case of the CBR video is more stable than the one of the VBR case, since the segment sizes of the CBR video are quite similar while segment sizes of the VBR video are varied and unpredictable. Average version of SDN-based BBA is increased by about 3.2% compared to BBA. SDN-based SARA had similar average quality levels to SARA, but the variation in quality levels was significantly reduced. This is quite an important parameter in QoE evaluation.

For the performance evaluation, the time when all clients begin to stream at the same time is selected. It take 20 seconds (10 segments) to to calculate results of the performance. Figure 6 compares the performance of our proposed solutions (MSMA-0 and MSMA-1) with PANDA, BBA, SARA and AGG using the three

(a) MSMA-1

(b) MSMA-0

(c) PANDA

(d) BBA

(e) SARA

bba vbr new.png

(f) AGG

(g) SDN-based BBA

sara vbr.png

(h) SDN-based SARA
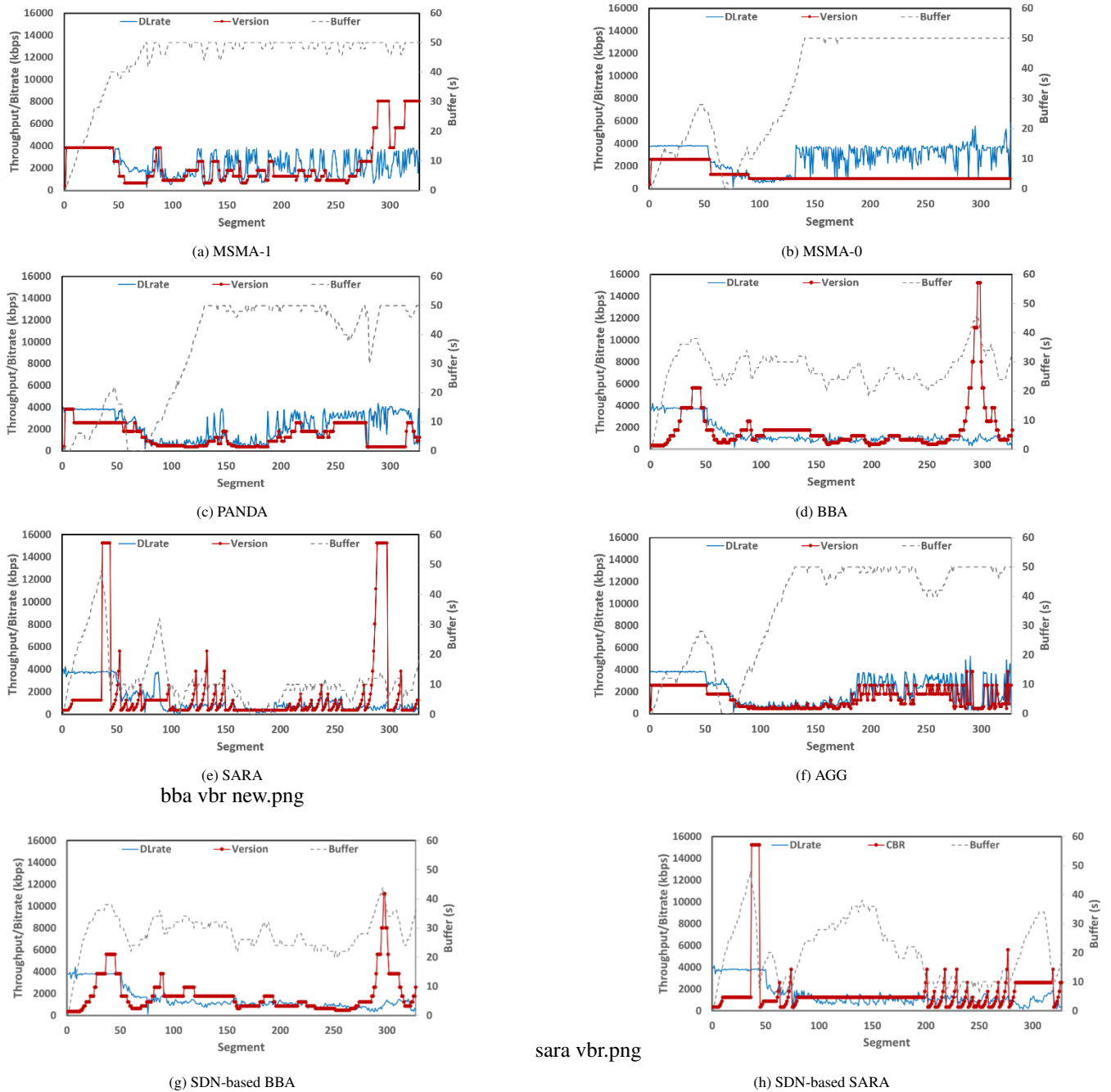
Figure 4: Download speed, buffer and version quality for all methods at a bottleneck link of 4 Mbps with VBR video

evaluation parameters: *Fairness*, *Efficiency* and *Stability*. For a more accurate evaluation, in this Figure 6, we get the average for all the three cases with the link capacities of 4 Mbps, 7 Mbps, and 10 Mbps. In real time, we set the mean value over three runs for 3 players. The results show that the fairness, efficiency, and stability obtained using the existing methods are much lower than those obtained using our proposed solution. However, due to the segment aware rate adaptation mechanism, in Figure 6a, the fairness between segments 4 and 7, SARA performs better than all of the others. This scheme uses all of the segment sizes, the estimated path bandwidth and current buffer occupancy to predict the amount of time needed to download the next segment. Therefore this method

guarantees the fairness for all players. Using the existing streaming solutions as PANDA, BBA, SARA and AGG, the fairness in these cases varies from 0.634 to 0.860 and has an average of 0.699, 0.723, 0.77 and 0.687, respectively. The experiment also shows that the proposed architecture has improved the fairness score significantly, with scores ranging from 0.791 to 0.863 that results in an average of 0.816 which is very high. The efficiency of bandwidth allocation in the current solutions also has a considerable deterioration with values from 0.488 to 0.761 (i.e. average of 0.654, 0.655, 0.602 and 0.604, respectively). Whilst the efficiency of MSMA-1 varies from 0.716 to 0.970 (i.e average of 0.830).

Figure6.c illustrates the comparison of the average stability of

(a) MSMA-1

(b) MSMA-0

(c) PANDA

(d) BBA

(e) SARA

bba cbr new.png

(f) AGG

sara cbr new.png

(g) SDN-based BBA

(h) SDN-based SARA
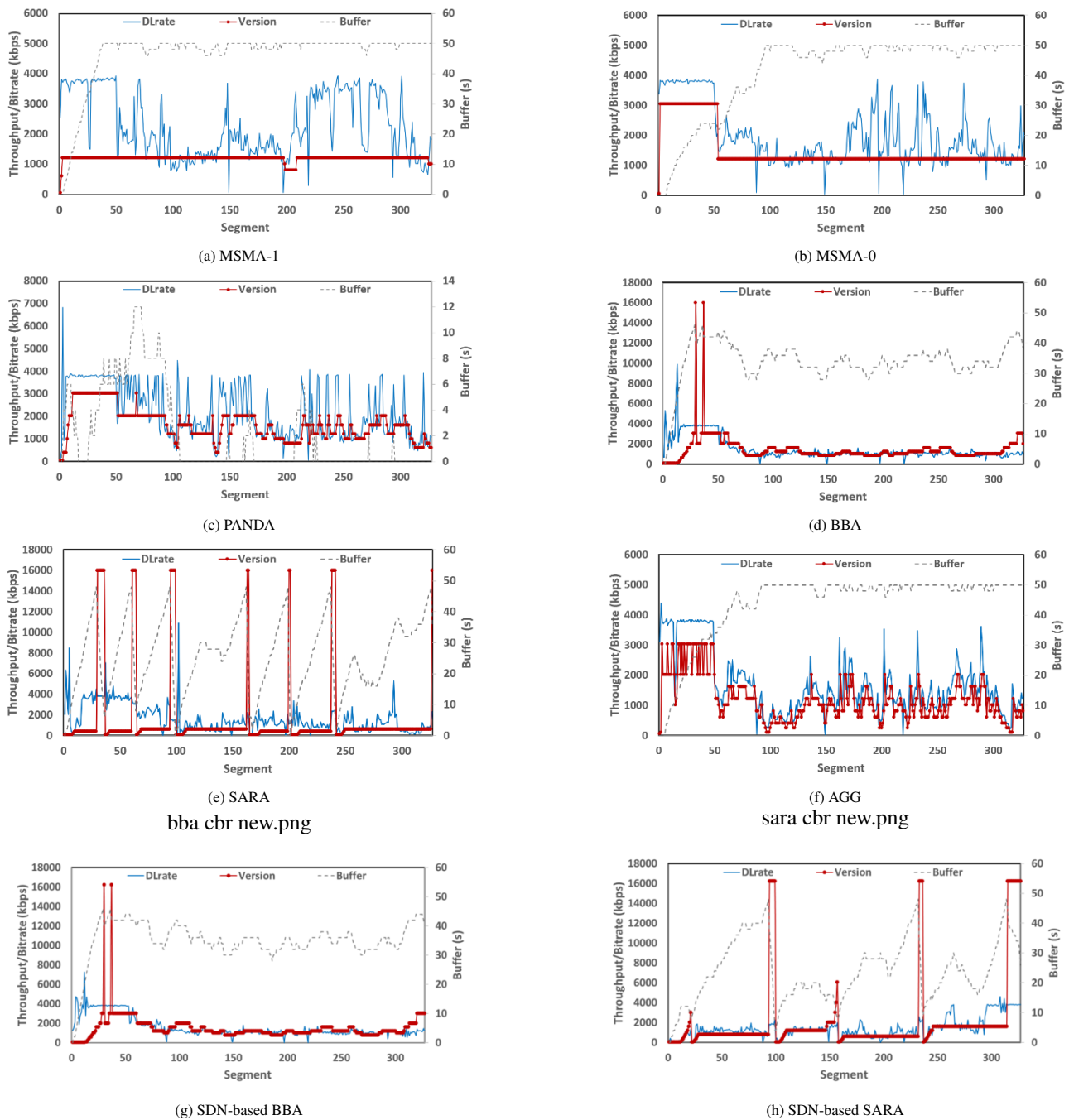
Figure 5: Download speed, buffer and version quality for all methods at a bottleneck link of 4 Mbps with CBR video

the 3 clients in all methods. It can be seen that the stability of our proposal is better than other schemes. Table 4 and Table 5 show the average fairness, efficiency and stability of the 3 clients in case of using the existing methods and our method. The shown results are taken from 20 seconds (i.e 10 segments) when all players are streaming at the same time.

For VBR video Elephants Dream, in the following summary list, the consecutive numbers represent the results for MSMA-0, PANDA, BBA, SARA and AGG, respectively.

1) MSMA-1 outperforms the existing schemes in terms of fairness by an increase of 3.9%, 16.7%, 12.9%, 5.3% and 18.8%.

2) MSMA-1 improves bandwidth utilization in terms of efficiency by 3.3%, 26.9%, 26.7%, 37.8%, and 37.4%.

3) MSMA-1 increases the video stability by -1.5%, 5.6%, 4.6%, 33.1%, and 42.5%.

MSMA-1 improves two parameters: fairness and efficiency compared to MSMA-0. However, MSMA-0 has better stability than MSMA-1 because the clients in MSMA-1 are free to adapt their bitrates based on the throughput. And only when the throughput does not meet the requirements, the client will send the request to the controller. The SDN controller is then responsible for reallocating bandwidth to the clients accessing through that node, so that

(a) Fairness

(b) Efficiency
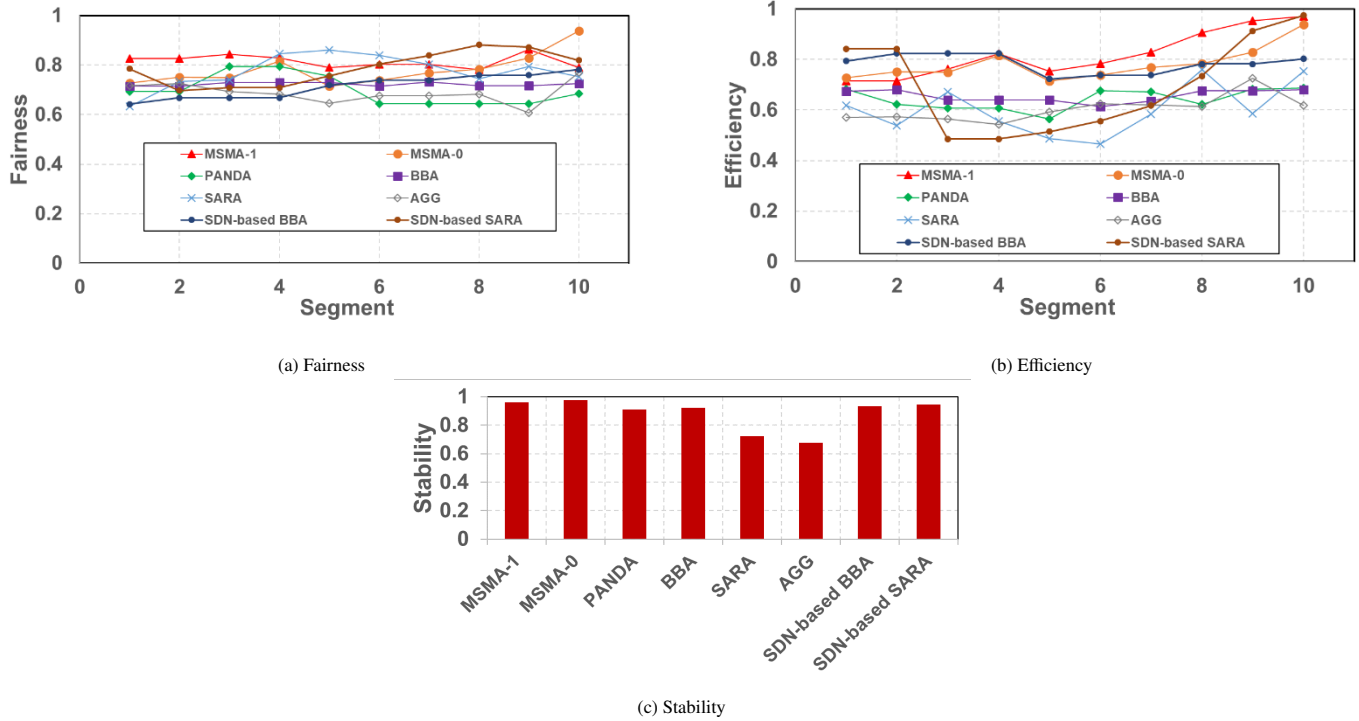
(c) Stability

Figure 6: Comparison average fairness, efficiency and stability of all methods

Table 4: Performance Comparison with VBR video

Metrics	MSMA-1	MSMA-0	PANDA	BBA	SARA	AGG	SDN-based BBA	SDN-based SARA
Fairness	0.816	0.785	0.699	0.723	0.775	0.687	0.714	0.807
Efficiency	0.830	0.781	0.654	0.655	0.602	0.604	0.783	0.697
Stability	0.962	0.977	0.911	0.920	0.723	0.675	0.933	0.945

the requesting clients receive the new bandwidth that can keep the most appropriate video version. As for MSMA-0, due to the use of the aggressive adaptive bitrate algorithm based on the bandwidth that has been divided evenly from the controller, it is still stable in choosing the bitrate or quality version of the next segment.

Similarly, with statistics in Table 5 (i.e. for CBR video "Destiny"), we can see that the two proposed methods (MSMA-1 and MSMA-0) outperform the rest. On another side, compared with traffic of the VBR video, traffic of the CBR video has higher Stability. The fairness of SDN-based BBA is almost similar to BBA, while the one of SDN-based SARA is slightly increased compared to SARA, by only 4%. SDN-based BBA effectively increases the bandwidth usage by 19.6% compared with BBA and SDN-based SARA increases by 15% compared to SARA. Thanks to the SDN-based fair bandwidth allocation, BBA and SARA have much better stability than the non-SDN solution.

Table 6 shows statistics from the experiments. As shown in the table, MSMA-1 outperforms the other methods. At first, with a reasonable throughput and buffer-based estimation mechanism, MSMA-1 is able to avoid stalling conditions whilst keeping the highest average value of buffer occupancy (i.e. 44.6s).

Secondly, MSMA-1, with the dynamic bandwidth allocation mechanism, can achieve the highest average bitrate of 2445.6 Kbps, which is an improvement of about 103.8%, 76%, 36.7%, 42.4% and 67.3% compared to MSMA-0, PANDA, BBA, SARA and AGG, respectively. Based on the QoE formula in Equation (19), the final QoE scores of MSMA-1 and MSMA-0 are calculated in comparison with 4 other solutions such as PANDA, BBA, SARA, AGG (Table 6). In fact, MSMA shows to achieve the highest QoE score compared to other competitors.

For the AGG algorithm, by requiring the highest bitrate according to the throughput without relying on the current buffer, the average video quality is low and the number of quality level switches-down is largest among all the methods. On the other hand, AGG also has the lowest QoE (i.e. 1.9).

SARA is the mixed throughput-buffer based algorithm, having the average video quality and QoE higher than AGG, but it is only medium compared to the other algorithms. BBA is the buffer-based algorithm, BBA successfully avoids stalling events which are very annoying to video viewers. The average bitrate of BBA is medium at only 1788.7 Kbps and its QoE stays at the good level (3.6).

With the estimation of the available bandwidth, a probing mech-

Table 5: Performance Comparison with CBR video

Metrics	MSMA-1	MSMA-0	PANDA	BBA	SARA	AGG	SDN-based BBA	SDN-based SARA
Fairness	0.971	0.965	0.764	0.713	0.716	0.873	0.932	0.917
Efficiency	0.879	0.796	0.904	0.665	0.726	0.708	0.812	0.803
Stability	0.975	0.957	0.931	0.949	0.826	0.703	0.941	0.955

Table 6: Quality Statistics of the solutions

Criteria	MSMA-1	MSMA-0	PANDA	BBA	SARA	AGG	SDN-based BBA	SDN-based SARA
Average Bitrate (kbps)	2445.6	1199.6	1389.5	1788.7	1717.4	1461.0	1812.3	1645.1
Average Buffer (s)	44.6	35.8	34.2	27.7	11.6	36.4	28.2	18.4
Number of Stalling	0	4	12	0	17	11	0	0
Average Version Index	6	4.5	5.1	5	5.2	5	5.4	5.1
Number of Version Switch-downs	21	3	7	17	20	40	16	15
N-QoE	4.25	3.6	3.54	3.55	2.8	1.9	3.96	3.74

anism is leveraged by PANDA to additively increase its sending rate, whilst decreasing sending rates multiplicatively, when congestion occurs. PANDA has a medium average bitrate at 1389.5 kbps and a relatively low number of switch-downs (7 times). The QoE score of PANDA also reaches 3.6.

For MSMA-0, the average bitrate is the lowest due to the use of the Aggressive bitrate adaptive algorithm on the client side, and MSMA makes its best to fairly allocate the bandwidth afor all clients. However, MSMA-0 has the lowest number of switch-downs (3 times). Besides QoE of MSMA-0 also reaches good quality (i.e. score of 3.6).

At the bottom lines, it's difficult to improve for all QoS parameters as well as the Quality of Experiment (QoE)- related parameters of video streaming. In fact, all of the proposed solutions need a tradeoff among these parameters to improve video streaming quality. However, our proposed solutions MSMA-0 and MSMA-1 have significantly improved average video quality, ensuring the highest average QoE compared to existing methods such as PANDA, BBA, SARA and AGG. Especially, MSMA-1 increases the QoE score by 18%, 20%, 20%, 51%, and 124% compare with MSMA-0, PANDA, BBA, SARA and Aggressive, respectively. As we can see, MSMA-0 does not SDN-based BBA and SDN-based SARA in terms of QoE, but our proposed MSMA-1 outperforms all compared methods.

Overall, our existing innovative algorithm is a combination of bitrate adaptation at the client side and resource allocation at the network side. The proposed rate adaptation method is to choose the best quality version on the current network condition and to avoid

video stalling events. At the SDN controller, the resource allocation handles fair and adaptive bandwidth sharing in order to maximize the number of access clients, while trying to minimize the number of clients who got QoE degraded.

6 Conclusion and Future Work

In this work, we have presented an integrated solution of centralized SDN-based resource allocation at the network side and bitrate adaptation at the client side to resolve the problem of multi clients streaming video through a bottleneck connection. This causes several problems such as low quality of service, congestion, delay, and especially quality of experience of users. The experiments show that our proposed solution outperforms the predecessors in terms of Quality of Experience.The proposed scheme ensures bandwidth fairness, efficiency and stability. Another contribution of our work is to ensure QoE of as many ongoing clients as possible. Additionally, the method can prevent congestion at bottleneck point when there is insufficient bandwidth by rejecting a new incoming request

Our future work will be building the whole SDN-based architecture to allocate network resources and to maximize QoE for each client, while avoiding scalability issues among many competing clients in a shared environment. Multiple heterogeneous scenarios with multiple SDN controllers and various clients will also be taken into account.

References

[1] "Cisco Visual Networking Index: Forecast and Methodology, 2016-2021"; San Jose, CA, USA, Cisco, White Paper, 2016.

[2] Open Networking Foundation (ONF), "Software Defined Networking: the new norm for network,"; White paper, 2012.

[3] N. McKeown et al., "OpenFlow: Enabling Innovation in Campus Networks," ACM SIGCOMM Comput. Commun. Rev., 38(2), 69–74, 2008, doi: 10.1145/1355734.1355746.

[4] P. H. Thinh. P. N. Nam, N. H. Thanh, T. T. Huong, "SDN – based Dynamic Bandwidth Allocation for Multiple Video-on-Demand Players over HTTP," proceeding 2019 Int. Conf. Inf. Commun. Technol. Converg. (ICTC), 16-18 Oct. 2019, Jeju, Korea, 163–168, 2019, doi: 10.1109/ICTC46691.2019.8939834.

[5] L. R. Romero, "A Dynamic Adaptive HTTP Streaming Video Service for Google Android," M.S. Thesis, R. Inst. Technol. (KTH), Stock., 148, 2011.

[6] T. C. Truong, D. Q. Ho, J. W. Kang, A. T. Pham, and S. Member, "Adaptive Streaming of Audiovisual Content using MPEG DASH," IEEE Trans. Consum. Electron., 58(1), 78–85, 2012, doi: 10.1109/TCE.2012.6170058.

[7] T.-Y. Huang, R. Johari, M. Watson, M. Trunnell, and N. McKeown, "A buffer-based approach to rate adaptation: Evidence from a large video streaming service," ACM SIGCOMM Comput. Commun. Rev., 44(4), 187–198, 2015.

[8] T.-Y. Huang, R. Johari, N. McKeown, M. Trunnell, and M. Watson, "Using the Buffer to Avoid Rebuffers: Evidence from a Large Video Streaming Service," arXiv Prepr. arXiv1401.2209, 2014, https://arxiv.org/abs/1401.2209.

[9] Y. Zhou, Y. Duan, J. Sun, and Z. Guo, "Towards simple and smooth rate adaption for VBR video in DASH," 2014 IEEE Vis. Commun. Image Process. Conf. VCIP 2014, 9–12, 2015, doi: 10.1109/VCIP.2014.7051491.

[10] H. N. Nguyen, T. Vu, H. T. Le, N. N. Pham, and T. C. Truong, "Smooth quality adaptation method for VBR video streaming over HTTP," 2015 Int. Conf. Comput. Manag. Telecommun. ComManTel 2015, 184–188, 2016, doi: 10.1109/ComManTel.2015.7394284.

[11] S. Latré, J. Famaey, F. De Turck, M. Claeys, and S. Petrangeli, "QoE-Driven Rate Adaptation Heuristic for Fair Adaptive Video Streaming," ACM Transaction Multimedia Computing Communication Application, 12(2), 1–24, 2015, https://doi.org/10.1145/2818361.

[12] P. Juluri, V. Tamarapalli, and D. Medhi, "SARA: Segment aware rate adaptation algorithm for dynamic adaptive streaming over HTTP," 2015 IEEE Int. Conf. Commun. Work. ICCW 2015, 1765–1770, 2015, 10.1109/ICCW.2015.7247436.

[13] J. Jiang, "Improving Fairness , Efficiency , and Stability in HTTP-based Adaptive Video Streaming with FESTIVE," Proc. 8th Int. Conf. Emerg. Netw. Exp. Technol., 97–108, 2012, https://doi.org/10.1145/2413176.2413189.

[14] Z. Li et al., "Probe and Adapt: Rate Adaptation for HTTP Video Streaming At Scale," IEEE J. Sel. Areas Commun. 32(4), 719–733, 2014, doi: 10.1109/JSAC.2014.140405.

[15] A. Mansy, "Network-layer Fairness for Adaptive Video Streams," IEEE, IFIP Netw. Conf. (IFIP Networking), pp. 1–9, 2015, doi: 10.1109/IFIPNetworking.2015.7145310.

[16] M. Ghobadi and M. Mathis, "Trickle: Rate Limiting YouTube Video Streaming," Present. as part 2012 USENIX Annu. Tech. Conf. (USENIX-ATC 12), 191–196, 2012, https://www.usenix.org/conference/atc12/technical-sessions/presentation/ghobadi.

[17] S. Akhshabi, L. Anantakrishnan, C. Dovrolis, and A. C. Begen, "Server-Based Traffic Shaping for Stabilizing Oscillating Adaptive Streaming Players," Proceeding 23rd ACM Work. Netw. Oper. Syst. Support Digit. audio video, 19–24, 2013, doi: 10.1145/2460782.2460786.

[18] J. J. Quinlan, A. H. Zahran, K. K. Ramakrishnan, and C. J. Sreenan, "Delivery of Adaptive Bit Rate Video: Balancing Fairness , Efficiency and Quality," 21st IEEE Int. Work. Local Metrop. Area Networks, 1–6, 2015, doi: 10.1109/LAN-MAN.2015.7114736.

[19] S. Ramakrishnan, X. Zhu, F. Chan, and K. Kambhatla, "SDN Based QoE Optimization for HTTP-Based Adaptive Video Streaming," 2015 IEEE Int. Symp. Multimed., 120–123, 2015, doi: 10.1109/ISM.2015.53.

[20] C. Cetinkaya, Y. Ozveren, and M. Sayit, "An SDN-assisted System Design for Improving performance of SVC-DASH," 2015 Fed. Conf. Comput. Sci. Inf. Syst. (FedCSIS). IEEE, 5, 819–826, 2015, doi: 10.15439/2015F333.

[21] P. Georgopoulos, Y. Elkhatib, M. Broadbent, M. Mu, and N. Race, "Towards Network-wide QoE Fairness Using OpenFlow-assisted Adaptive Video Streaming," Proc. 2013 ACM SIGCOMM Work. Futur. human-centric Multimed. Netw., 15–20, 2013, doi: 10.1145/2491172.2491181.

[22] G. Cofano, L. De Cicco, T. Zinner, and S. Mascolo, "Design and Experimental Evaluation of Network-assisted Strategies for HTTP Adaptive Streaming," Proc. 7th ACM Multimed. Syst. Conf. (MMSys 2016), 1–12, 2016, doi: 10.1145/2910017.2910597.

[23] J. Chen, M. Ammar, M. Fayed, and R. Fonseca, "Client-Driven Network-level QoE fairness for Encrypted 'DASH-S'," Proc. 2016 Work. QoE-based Anal. Manag. Data Commun. Networks, 55–60, 2016, doi: 10.1145/2940136.2940144.

[24] K. T. Bagci, S. Member, K. E. Sahin, S. Member, and A. M. Tekalp, "Compete or Collaborate: Architectures for Collaborative DASH Video over Future Networks," IEEE Trans. Multimed., 19(10), 2152–2165, 2017, doi: 10.1109/TMM.2017.2736638.

[25] O. El Marai and T. Taleb, "Online Server-side Optimization Approach for Improving QoE of DASH Clients," GLOBECOM 2017-2017 IEEE Glob. Commun. Conf. IEEE, 1–6, 2017, doi: 10.1109/GLOCOM.2017.8254128.

[26] S. Zhao and D. Medhi, "SDN-Assisted Adaptive Streaming Framework for Tile-Based Immersive Content Using MPEG-DASH," 2017 IEEE Conf. Netw. Funct. Virtualization Softw. Defin. Networks, 1–6, 2017, doi: 10.1109/NFV-SDN.2017.8169831.

[27] A. Bentaleb, A. C. Begen, and R. Zimmermann, "SDNDASH: Improving QoE of HTTP Adaptive Streaming Using Software Defined Networking," ACM Multimed., 1296–1305, 2016, doi: 10.1145/2964284.2964332.

[28] A. Bentaleb, A. C. Begen, R. Zimmermann, and S. Harous, "SDNHAS: An SDN-enabled architecture to optimize QoE in HTTP adaptive streaming," IEEE Trans. Multimed., 19(10), 2136–2151, 2017, doi: 10.1109/TMM.2017.2733344.

[29] A. Bentaleb, A. C. Begen, S. Member, R. Zimmermann, and S. Member, "QoE-Aware Bandwidth Broker for HTTP Adaptive Streaming Flows in an SDN-Enabled HFC Network," IEEE Trans. Broadcast., 64(2), 575–589, 2018, doi: 10.1109/TBC.2018.2816789.

[30] J. Jiang, L. Hu, P. Hao, and R. Sun, "Q-FDBA: improving QoE fairness for video streaming," Multimed. Tools Appl., 77(9), 10787–10806, 2018, doi: 10.1007/s11042-017-4917-1.

[31] T. Abar, A. Ben, L. Sadok, and E. Asmi, "Enhancing QoE based on Machine Learning and DASH in SDN networks," 2018 32nd Int. Conf. Adv. Inf. Netw. Appl. Work., 258–263, 2018, doi: 10.1109/WAINA.2018.00095.

[32] A. Ahmad, A. Floris, and L. Atzori, "Towards Information-centric Collaborative QoE Management using SDN," 2019 IEEE Wirel. Commun. Netw. Conf., 1–6, 2019, doi: 10.1109/WCNC.2019.8885412.

[33] L. Guillen, S. Izumi, and T. Abe, "SAND/3: SDN-Assisted Novel QoE Control Method for Dynamic Adaptive Streaming over HTTP/3," Electron. Multidiscip. Digit. Publ. Inst., 8(8), 1–17, 2019, doi: 10.3390/electronics8080864.

[34] Pham Hong Thinh, Nguyen Thanh Dat, Pham Ngoc Nam, Nguyen Huu Thanh, Nguyen Minh Hien & Truong Thu Huong. "An Efficient QoE-Aware HTTP Adaptive Streaming over Software Defined Networking," Mobile Networks and Applications, 1-13,2020, https://doi.org/10.1007/s11036-020-01543-1.

[35] T. Huang, B. Heller, and N. Mckeown, "Confused , Timid , and Unstable: Picking a Video Streaming Rate is Hard," Proceedings of the 2012 internet measurement conference.ACM, 225–238, 2012, doi: 10.1145/2398776.2398800.

[36] X. Yin, M. Bartulovi, V. Sekar, and B. Sinopoli, "On the Efficiency and Fairness of Multiplayer HTTP-based Adaptive Video Streaming" 2017 Am. Control Conf. (ACC). IEEE, 4236–4241, 2017, doi: 10.23919/ACC.2017.7963606.

[37] Bitmovin, "Libdash - bitmovin." [Online]. Available: https://github.com/bitmovin/libdash. [Accessed: 25-Nov-2020].

[38] "Floodlight." [Online]. Available: http://www.projectfloodlight.org/floodlight/. [Accessed: 25-Nov-2020].

[39] "Mininet." [Online]. Available: http://mininet.github.io/. [Accessed: 25-Nov-2020].

[40] O. O. M. P. Studio, "Elephants dream," 2009. [Online]. Available: https://orange.blender.org/. [Accessed: 25-Nov-2020].

[41] V. D. Fabien Weibel, Manuel Alligne, Sandrine Wurster, "Destiny," 2012. [Online]. Available: http://fweibel.com/destiny . [Accessed: 05-Nov-2020].

[42] W. R. Jain, Rajendra K and Chiu, Dah-Ming W and Hawe, "A quantitative measure of fairness and discrimination for resource allocation in shared computer system," East. Res. Lab. Digit. Equip. Corp. Hudson, MA, 1984.

[43] M. Seufert, S. Egger, M. Slanina, T. Zinner, T. Hossfeld, and P. Tran-gia, "A Survey on Quality of Experience of HTTP Adaptive Streaming," Ieee Commun. Surv. Tutorials, **17**(1), 469–492, 2015, doi: 10.1109/COMST.2014.2360940.

PrOMor: A Proposed Prototype of V2V and V2I for Crash Prevention in the Moroccan Case

Zakaria Sabir[*], Aouatif Amine

Ibn Tofail University, ILM Department, ENSA, Kenitra, 14000, Morocco

A B S T R A C T

Road safety has become an object of research and many research institutes have invested in this field because a lot of people die and many others are injured every year due to road accidents. The deployment of wireless communication technologies for vehicular networks can considerably improve road safety. It can enable new services such as traffic management, collision detection, and additional communication ease between moving vehicles. This paper presents a complete implementation of Vehicle to Vehicle (V2V) and Vehicle to Infrastructure (V2I) communications. Raspberry Pi boards, ultrasonic sensor, infrared obstacle detector, and line follower sensors are used in order to implement the complete prototype. The results show the usefulness of this road safety prototype named PrOMor (Prevention of Obstacles in Morocco). Based on these results, it can be concluded that the presented scenarios can be applied to the field of road safety related to the Moroccan case. This should reduce the number of accidents and save more human lives.

1   Introduction

This paper is an extension of work originally presented in the International Conference on Computational Intelligence and Knowledge Economy (ICCIKE) [1]. In the current work, the authors will deal with the whole vehicular communication system to address road safety issues, especially in the Moroccan case.

Since millions of people die every year and many more are injured because of car accidents, road safety has been gaining importance in recent years. Statistics [2] show that road traffic casualties in the world amount to 1.17 million per year. According to the World Health Organization (WHO), road accidents claimed the lives of 1.25 million people in 2013. In 2014, more than a million accidents occurred in Europe, killing 25 900 people and 1.4 million wounded. In 2017, 3,499 deaths were recorded on Moroccan roads, against 3,593 in 2016, a small decrease of 2.6% year-on-year. While statistics show a slight advance in road safety, they hide other, more disturbing realities[1]. These statistics are blatant, so the Ministry of Equipment, Transport, Logistics, and Water (METLE) thought to launch research projects in partnership with Moroccan universities and the National Center for Scientific and Technical Research (CNRST) in order to reduce the number of victims. This project based on the detection and the anticipation of the accidents aims to

help to reduce the accident rate using the V2V and V2I communications to detect obstacles and prevent the crash in the Moroccan case. According to the traffic accident statistics carried out by the METLE in 2016 [3], there were 80680 accidents caused by obstacles.

Today the road network in Morocco [4], whose routes are traditionally hierarchical in the main, collector, and service according to the function they fulfill for the network itself, is not in adequacy with its urban environment and the needs of the inhabitants and users. Thus, for example, very wide paths designed for cars can pass through neighborhoods endangering pedestrians who go there to shop, go to school or work, or simply go to the neighbor. It must be recognized that, particularly in dense urban areas, the lanes fulfill a multiplicity of functions that go beyond the simple role of channeling private vehicles (social functions, economic, leisure, etc.).

To put a stop to this massacre, in addition to legislative measures, digital technologies will play a major role. The automation/semi-automation of vehicles will limit the human error, responsible for the majority of road accidents. Manufacturers are working on connected vehicles that will be equipped with several sensors. They will be able to interpret their environment in a dynamic way to alert drivers of the various hazards which could be found on the road.

In this context, the main purpose of Intelligent Transportation

---

[*]Corresponding Author: Zakaria Sabir, University Campus P. O. Box 241, Kenitra, Morocco, zakaria.sabir@uit.ac.ma
[1]Leconomiste, https://www.leconomiste.com (accessed Jul. 08, 2019)

Systems (ITS) is to improve transportation safety, increase productivity, reduce traffic jams and reduce the number of accidents on our future roads, thanks to the use of advanced information technology. Nonetheless, the big challenge is to constitute an interdependent environment that merges all the technologies and can solve a variety of transportation problems. If the electronic, computing, and networking technologies are well integrated, the mobility will be more efficient, the roads will be safer and the impact on the environment will be minimized [5].

These systems will allow vehicles to communicate their relative positions, for example, to signal the presence of another vehicle in a blind spot. Mainly, it will be connected to various sensors inside the vehicle: stability, hazard warning lights, airbags, and other diagnostic tools. Therefore, a vehicle can automatically communicate to others the presence of a slippery roadway, if it is down or in an accident. The other drivers will then adjust their approach in the concerned area. The ITS will also help to know the position of emergency vehicles (ambulances, firefighters, police) on approach. Their only sirens today give little information on their provenance and direction. Civilian vehicles will then clear the way more efficiently using the ITS.

One of the most important components of ITS, which has been proposed to address challenges in the transportation surface is the connected vehicle system. It is a hopeful technology that uses wireless communication. In order to treat transportation problems, connected vehicle system will use Vehicle to Vehicle (V2V) and Vehicle to Infrastructure (V2I) communications [6] [7].

Different definitions have been given recently for a "connected" vehicle. A definition given at the 2013 Automotive News World Congress by IBM, identifies a connected vehicle as "a vehicle capable of seamless integration with multiple systems, connecting consumers to the digital world". More precise definitions include all the other connections of a modern vehicle: according to the US Department of Transportation (USDOT), "Connected vehicle applications provide connectivity between vehicles to prevent accidents, between vehicles and infrastructure, in order to generate safety, mobility and environmental benefits; between vehicles, infrastructure and wireless devices to provide continuous real-time connectivity to all users of the system" [8].

Different studies have already tried to develop prototypes of connected vehicles and systems that support V2V and V2I communications. But, as will be explained later, those systems were developed in foreign countries and cannot be applied in Morocco. Thus, the authors thought of a system that will fit the Moroccan case. This paper presents the implementation of a vehicular communication environment using both V2V and V2I technologies. This system is the first of its kind in Morocco. It requires a real test on real cars, but the authors carried out the tests on two robots only and it will be spread over a large number of cars in the real case, the used robots are based on Raspberry Pi-based mini cars kits, which were personalized by adding different features and other sensors in order to get to the target. The remainder of the paper is organized into four sections: Section 2 explain the proposed system. Experiments results will be presented and discussed in Section 3, while Section 4 concludes the paper.

2 Related works

This work is inspired by several prior studies that used various technologies on connected vehicle networks. A summary of related works is discussed in this section.

A recent work [9] explored the future beneficiaries of 5G and selected the conditions where 5G can make an effect. Particularly, three use-cases were considered: V2X (Vehicle-to-Everything Communication), Healthcare, and Drones. The authors investigated and emphasized some imperfections and failures of the current cellular topologies regarding the mentioned use-cases, then they determined how 5G will surmount those failures.

Kuramoto et al. [10] described the multi-class zone ITS communication scheme regarding short periodical communications and real-time for vehicle safety in intersections. In the proposed scheme, two types of areas around an intersection were designed, the nearest area and quasi-nearest area. In the first one, the communication of vehicles is done every 20 ms with a base station. While in the second one, vehicles make reservations for the communication for the first type and also communicate with the base station for safety. The required frequency bandwidth needed to realize the proposed design was shown in the simulation results.

A strategy of centralized and localized data congestion control is proposed in [11]. It uses RSUs (Road-Side Units) at intersections to control data congestion. It includes three entities for clustering messages, detecting congestion, and controlling data congestion. In order to detect data congestion in the channels, the strategy measures the channel usage. The messages are refined, assembled, and then grouped using algorithms of machine learning. Simulation results affirmed the efficacy of the proposed strategy in terms of improving the delay, packet loss ratio, and throughput.

Another system is presented in [12], it is an integrated vehicular system that uses an integrated V2I and V2V communication model improved with an information management system. The aim is the management, accumulation, and arrangement of context-aware information on driver location and traffic. The concept of smart roads is featured in the vehicular system. Significant information and all the risks related to the safety and detected by vehicles are managed by the infrastructure and adjusted to the driver's choices and the vehicle's context. The authors implemented the required software and used real hardware for infrastructure as well as a real vehicle to build the entire system.

Other authors [13] proposed to substitute the currently proposed standard (802.11p, DSRC/WAVE) to build an inter-vehicle communication system. They suggested using android smartphones along with Wi-Fi to replace the OBU (On-Board Unit) on consumer vehicles and to enable thereby V2I and V2V communications. The system is compatible with android devices with the 2.3 version and above. The users will then acquire an OBU that communicate with the nearby vehicles to broadcast an emergency alert or to warn about an accident. Experiment results showed the ease of use of the system, its efficiency, and its compatibility with Android devices.

Day et al. [14] checked out the performance of Het-Net (Heterogeneous Networks) consisting of LTE, DSRC, and Wi-Fi technologies for V2I and V2V communications. To enable Het-Net for vehicular communication applications, the authors developed an application layer handoff method. It was used to collect traffic

data and to warn about the collision. This research proved through the conducted field studies the usefulness of Het-Net in vehicular communications. Simulation experiments were run using a big number of connected vehicles including LTE and DSRC Het-Net scenarios. The results in terms of packet delivery error and latency from simulation were found to be identical to the field experiment results.

In this paper [15], the authors used data from the University of Michigan Safety Pilot Model Deployment project to analyze the performance of DSRC. They used selected road-side equipment and 1050 vehicles to evaluate the packet delivery ratio and the effective range of V2I communications. They have also studied the impact of some environmental factors like weather, trees, road elevation, buildings, and so on. The results are useful in the development of DSRC communication models and guiding future DSRC equipment placement.

Du et al. [16] used a distributed message delivery platform to develop a strategy. The aim is the creation of an effective and low-latency distributed message delivery system for connected vehicle applications. The strategy can transform the unstructured data into labeled topics for large consumers like data centers, mobile devices, and connected vehicles. The performance of the strategy was evaluated using a prototype and Apache Kafka, an open-source delivery system, and comparing its efficiency with the latency qualifications of connected vehicle applications. The experiments disclosed the correspondence of the measured latencies with USDOT (U.S. Department of Transportation) recommendation for connected vehicle applications.

In this paper, different from those studies, the proposed system considers employing vehicular communications in the Moroccan case. Authors have focused on the V2V and V2I communications since the conventional scheme can't be applied in Morocco. Taking into consideration the situation in Morocco and many other differences in comparison to other countries, a foreign system cannot work well for Morocco, the adjustment is required and many factors are to bear in mind. The architecture of Moroccan cities is different from other countries, in the big cities, for example, there are administrative regions, industrial regions, residential districts, the old medina, the new medina, etc. Other factors to take into consideration are culture and environment. The driver behavior and the usage of technology by the population need to be considered. Road conditions, alleys in one or two directions, signs boards, and narrow alleys also have to be considered.

The authors started with the realization using mini cars on a model and they have successfully achieved the goal. In the next step, they will move on to real scenarios with real cars in order to specify the necessary adjustments. The proposal represents also a contribution to the development of smart cities as there is already a trend for smart cities in Morocco. In June 2013, e-Madina was born in APEBI, the Moroccan federation of information technologies, telecommunications, and offshoring. e-Madina is a Smart Cities Cluster that works to make the city of Casablanca more attractive and more efficient using digital technologies and available material and immaterial resources. In March 2017, the government launched the "Cité Mohammed VI Tanger Tech" project, a smart city that will extend over 200 hectares within 10 years. Funding for the operation is estimated at $ 1 billion. Nearly 200 companies operating

in the automotive, aeronautic, textile, electronics, and machine tool industries will set up there.

To the best of their knowledge, authors believe this is the first paper that deals with vehicular communications in the Moroccan case, and this is one of the reasons that made this work chosen, accepted, and financed by the METLE and the CNRST.

3 Proposed system

Connected vehicles are able to revolutionize the current traveling style by creating a protected and interoperable wireless communications network, a system that involves several elements like cars, traffic lights, buses, and trains. Technologies of connected vehicles aim to address some serious challenges in the transportation fields, especially in environment, mobility, and safety.

The purpose of this work belongs to the last field, which is road safety, especially in the Moroccan case to solve the problems cited above, since the conventional scheme can't be applied in Morocco as it is as explained previously. Authors propose three safety scenarios which will be used to alert Moroccan drivers in different situations, in order to decrease the probability of road accidents and to stay away from collision scenes that repeatedly happen between vehicles and pedestrians, animals, trees, and such other objects. These scenarios are based on reel time information and use V2V and V2I modes. Roadside units and vehicles exchange information that will be very useful to anticipate a hazardous situation. This information is delivered to Moroccan drivers in order to help them avoid the danger presented in unstructured roads.

Taking into consideration the statistics presented in [3], the first scenario can notify a driver of a hard-braking vehicle in the path ahead. For example, three vehicles are traveling in the same lane (see Fig. 1 (a)); the driver of the third vehicle can't see the first vehicle because it's being blocked by the second one, which is located directly in front of him. Unexpectedly, the first vehicle slams on its brakes. Thanks to V2V communication, the third vehicle is able to provide a warning of the hard-braking vehicle ahead. This warning will help the driver to drive safely and avoid a potential crash, as can be seen in Fig. 1 (a).

The second and the third scenarios aim to notify a driver of a special traffic condition in the path ahead. Whenever a traffic event is detected (accident, traffic jam, pedestrian crossing the road, animal, road work...), the driver is advised to slow down, change the lane, and take another route. Using V2V communication, the warning notification is transferred by another vehicle ahead, which has previously detected the problem of the related traffic event. V2I communication also was used for the same purpose (see Fig. 1 (b)). In this case, the warning notification is transferred by the RSU placed on the border of the road instead. The location of the RSU depends on the number of accidents recorded in this area and given by the METLE Ministry.

The diagrams in Fig. 2 summarize the logical flow of the methodology in each car. In this scenario, V1 and V2 which are equipped with a Raspberry Pi ran on a straight path using line follower sensors. V1 keeps using the infrared sensor along the way in order to detect any obstacle before the destination. If V1 detects an obstacle, it will stop and send the data as an alert to V2. Similarly,

the latter continues on the path to the destination unless it receives an alert from V1. If so, it will stop and change the road to avoid the obstacle and get to the destination.
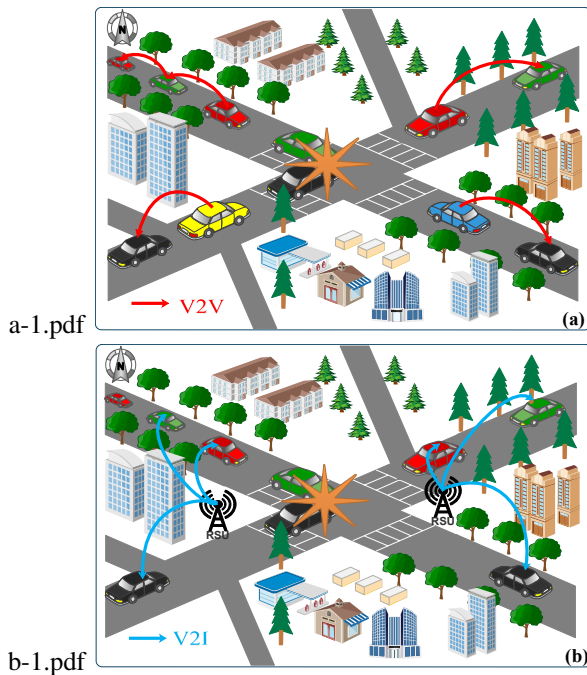
Figure 1: Operation of the system, (a) represents V2V mode and (b) represents V2I mode
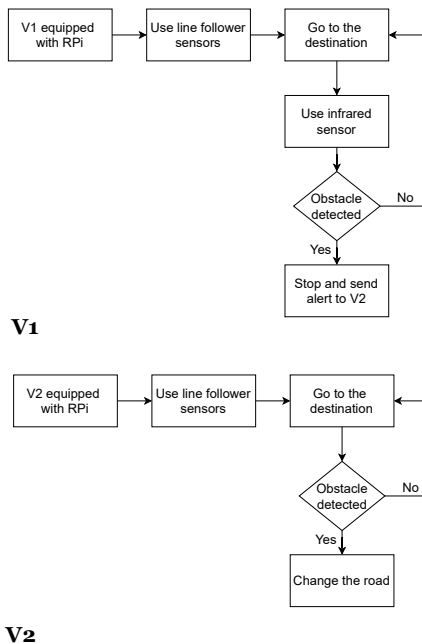
Figure 2: Flowchart for V2V communication.

Reducing possible points of conflict between vehicles and with other users is a common practice of road safety. For this, it is necessary to act in particular on the geometry of the path and the management of the priorities, especially for the zones of intersection and crossing with the presence of different users. According

to the compendium of statistics of road traffic accidents [3], carried out in 2017 by the METLE, 14 998 accidents were recorded in the intersections. Thus, taking into account the statistics, the authors proposed the METLE concerning the locations of the RSUs concerning the areas likely to have accidents in the city of Kenitra (as can be seen in Fig. 3). The communication between these RSUs and also between these RSUs and the vehicles in the area can help to avoid the slowed traffic during a rush hour as shown in Fig.3.

This communication can also help to avoid accidents in hazardous regions especially unstructured ones. A real case is shown in Fig. 4 where the area with diagonal lines was recently transformed into a roundabout, but it was not well adjusted to represent the roundabout. Therefore, someone who is a stranger to the city can take the road straight while it is forbidden. This can cause accidents in this area, as shown in figure 3.
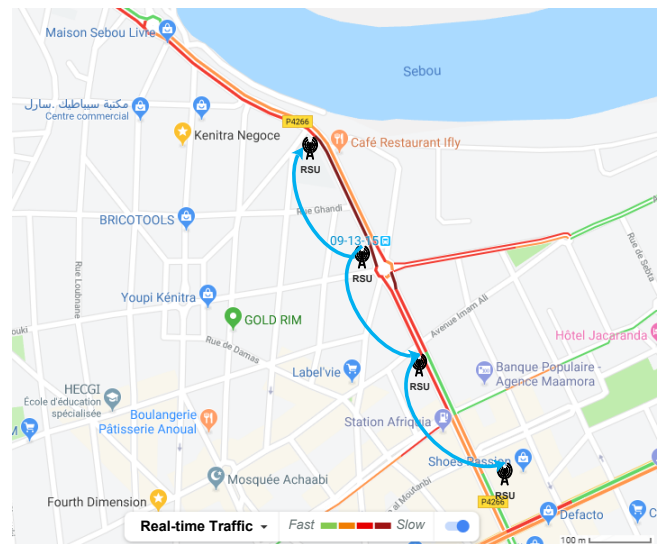
Figure 3: The locations of the RSUs to help mitigate the congestion in Kenitra city
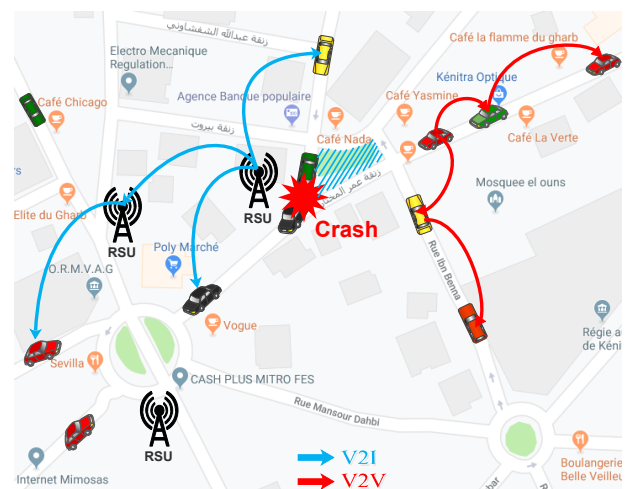
Figure 4: A Real case of an unstructured area in Kenitra city

In order to model the system, the authors proposed two algorithms. One on the client-side and the other on the server-side. Both algorithms start by importing the necessary modules and assigning

pins numbers. The next step is to create a socket so the two cars can communicate. After that, various methods used in the algorithms are defined :

- setup(): sets the setup of the system (variables, frequency, sensor modes . . .).
- setSpeed(): manipulates the speed of the vehicle and handles the error related to the trajectory.
- stop(): stops the motors of the vehicle.
- read_sensors(): reads the line follower sensors and stores a variable related to the error of the trajectory.

Algorithm 1 : Client-Side

```
 1: Import necessary modules
 2: Assign pins numbers
 3: Create a socket
 4: Define the setup method
 5: Define the setSpeed method
 6: Define the stop method
 7: Define the read_sensors method
 8: setup()
 9: while (true) do
10:     val ← IR_value
11:     if val = 1 then
12:         data ← "go"
13:         send data
14:         read_sensors()
15:         set_sensors()
16:     else
17:         stop()
18:         data ← "stop"
19:         send data
20: Close connection to the server
```

Algorithm 2 : Server-Side

```
 1: Import necessary modules
 2: Assign pins numbers
 3: Create a socket
 4: Bind address to socket
 5: Start TCP listener
 6: Accept TCP client connection
 7: Define the setup method
 8: Define the setSpeed method
 9: Define the stop method
10: Define the read_sensors method
11: setup()
12: while (true) do
13:     get data
14:     if data = "go" then
15:         read_sensors()
16:         set_sensors()
17:     else if data = "stop" then
18:         stop()
19: End server
```

---

[2]Sunfounder, https://www.sunfounder.com/learn/category/Smart-Video-Car-for-Raspberry-Pi.html/ (accessed Jul. 15, 2019)

An infinite loop is necessary to keep reading data from sensors, sending it by the client, and receiving it by the server. If the infrared sensor (located on the client side) detected an obstacle, the IR_value receives the value "0". The client sends then the data to the server which will stop immediately. Else, the IR_value remains in "1". The client sends then the data to the server which will continue the path to get to the destination. The proposed algorithms are presented in Algorithm 1 and 2.

Table 1 presents a comparison of the proposed system with other studies.

4 Experimentation

4.1 *Experimental setup*

In the validation step, the authors preferred to use prototypes in the tests before applying the system to real cars. The experiments were conducted using two mini cars from Sunfounder[2] (Fig. 5) to develop the prototype system. Each car has a Raspberry Pi 3 B+ with basic necessary configuration to enable communication and control movements and sensors. A third Raspberry Pi 3 B board was used to play the role of the RSU. The used boards consist of ARM Cortex-A53 quad-core, which is operating at 1.4 GHz for the model B+ and 1.2 GHz for the model B. They both have a memory of 1GB (RAM), 40GPIO, Audio jack, Ethernet port, Camera interface, HDMI port, Display interface, 4 USB port 2.0, and micro SD slot. The two devices are powered by 5V / 2.5A via a micro USB port. Raspbian was chosen as an operating system. It is installed and boots from the micro SD card.

Both the cars integrate Wi-Fi, so they are able to communicate within an ad hoc network while moving in the test zone. The movement of the cars is powered by the two rear wheels using a DC motor driver. The cars came also with a USB camera, a step-down DC-DC converter module, and a PCA9685-based servo controller. The camera is not used in the current prototype, but it is used to prevent pre-crash by detecting pedestrians in another part of the same project SAFEROAD [21].

Figure 5: Sunfounder mini car

Since the original car kit didn't come with all the hardware needed to run the tests, the authors used some other sensors to complete the prototype, as can be seen in ((a) and (b)) Fig. 6. Five line follower sensors were added below each car, so they help the car following the line (road), in addition to detectors that have the ability to sense the existence of an obstacle in the path.

Table 1: Comparison of the current work with other studies

Study	Communication Mode	Implementation	Tools	Scenario	Purpose	Special Case
[17]	V2V	Real Time	RPi; Ultrasonic sensors; Audible Alarm; GPS Sensor; RF Module	Blind Spot Detection	Improving Traffic Congestion	Not specified
[18]	V2V	Real Time	OsmAnd; Android Devices; GRCBox	Displaying location of relevant vehicles	Warning about emergency vehicles	Not specified
[19]	V2V	Real Time	RPi; Controller; IR Sensor	Autonomous Driving (level 3)	Smooth Traffic Flow	Not specified
[20]	V2V and V2I	Real Time	ECU sensors, Arduino; GPS sensor; LM393 speed sensor module; CAN communication module; Wi-Fi modem	Detect sudden changes in status of the vehicles (speed, location, brake position)	Help in Advanced Driver Assistance System (ADAS)	Not specified
This paper	V2V and V2I	Real Time	RPi mini cars; IR sensor; Line Followers	Obstacle Detection	Preventing Accidents	Moroccan Case
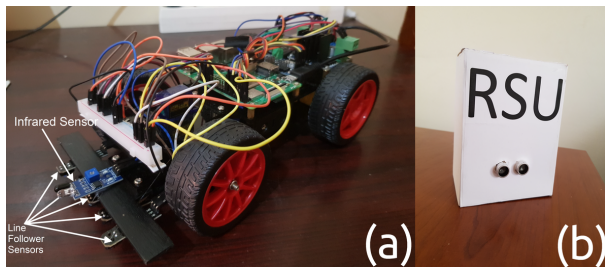
Figure 6: The prototypes, (a) Robot & (b) RSU

One infrared obstacle detector was used at the front of the first car, in addition to one ultrasonic sensor used in the RSU. The specifications of the sensors are given in Table 2.

Table 2: The specifications of the used sensors

Sensor name	Line Follower Sensor	Ultrasonic Sensor	Infrared Obstacle Detector
Reference	TCRT5000	HC-SR04	FC-51
Detection Distance	1 mm - 25 mm	2 cm - 4 m	2 cm - 30 cm, Angle: 35
Operating Voltage	5 V	5 V	3.3 - 5 V
Quantity	5	1	1

4.2 Results and discussion

The aim of the first and second scenarios was the dissemination of a warning message indicating the presence of an obstacle in the path ahead, using V2V communication. First, the authors tried to move the robots following a map (pre-programmed distances), but since the motors are not completely identical, they ran at different speeds. Consequently, the car couldn't move forward in a straight movement. For that reason, the authors added line follower sensors, to keep the car on the line (road).
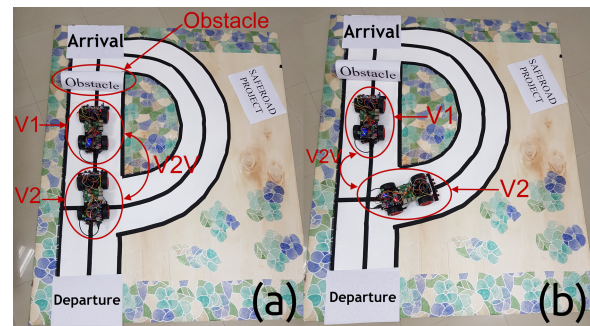
Figure 7: (a) The first scenario (V2V communication): V2 stops, once receiving the alert from V1 indicating the presence of an obstacle. (b) The second scenario (V2V communication): V2 changes the road, once receiving the alert from V1 indicating the presence of an obstacle.

In the first scenario, V1 and V2 ran at the same time on a straight path, and an obstacle was placed just before the destination. V1 is equipped with an infrared sensor (see Fig. 6 (a)), which detect the obstacle. Once the obstacle is detected, V1, which plays the role of the client, stops immediately, and sends the data to the server (V2) as a warning notification, using the Wi-Fi interface. As soon as it receives the warning, V2 stops in its turn (Fig. 7 (a)). Receiving the notification depends on the range of the Wi-Fi (the maximum distance between the first and the second car).

Similarly, in the second scenario, V1 and V2 ran at the same time on a straight path, and an obstacle was placed just before the destination. The infrared sensor in V1 (the client) detects the obstacle and stops immediately. It sends then an alert to V2 (the server) to change the road in order to avoid the obstacle, and get to the

destination. Therefore, once V2 reaches the intersection, it changes the road taken by the first vehicle and chooses the safe road (Fig. 7 (b)).

For the third scenario, the intention was the sending of the warning message using V2I communication. For this purpose, a third Raspberry Pi board was used with an ultrasonic sensor to play the role of the roadside unit (RSU). In this case, one vehicle was put in the path, and the obstacle was placed on the road. The RSU senses the presence of the obstacle using the ultrasonic sensor (see (b) in Fig. 6). It uses then the Wi-Fi interface to send a warning to the vehicle presented in the zone. As soon as the vehicle reaches the intersection, it takes the safe road (Fig. 8).
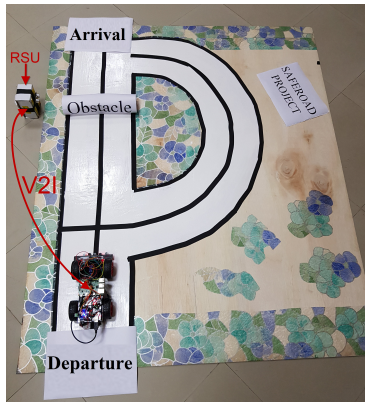
Figure 8: The third scenario (V2I communication): once getting to the intersection, the vehicle will take the other road, thanks to the alert received from the RSU.

The realization can be applied in the real world, as can be seen in Fig. 4 which depicts an example of Kenitra city where the area mentioned is likely to have accidents. The presence of the RSUs in this zone can help to avoid accidents. The RSU detects the crash and sends the alert to the vehicles in the area and also to the nearby RSUs. Another type of obstacles that can be detected using RSUs is the slowed traffic, as it is illustrated in Fig. 3. The communication between the RSUs in the area can help Moroccan drivers to avoid the traffic jam by taking another road where the traffic is relatively fast.
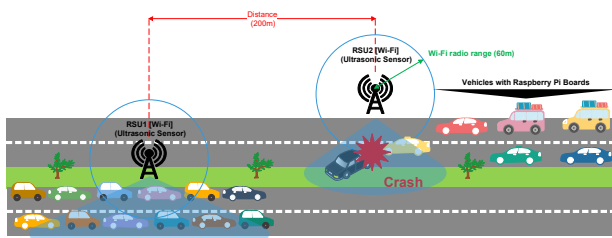
Figure 9: Summary of the contribution to Moroccan roads.

As explained above, the application of the system in real life in Morocco can play an important role in addressing the issues of road safety. It can be used to serve to avoid accidents, as it can also be useful to avoid slowed traffic. Fig. 9 summarizes the contribution of the system in Moroccan roads. In the first direction, the RSU2 detects the crash and sends an alert to nearby vehicles using the Wi-Fi

interface. In the opposite way, the RSU1 detects the slowed traffic and sends a warning to the vehicles in the zone. The two RSUs can also communicate by sending information about the traffic in the two directions.

From Fig. 9 it can be seen that the crash was caused by a vehicle that took the lane in the opposite way. In order to resolve this kind of situation, the authors made another proposition to the METLE. They suggest building the new roads without a separation between the lanes of the opposite directions. Therefore, in the case of an accident or traffic jams, it will be possible to use a lane or more in the opposite direction to alleviate the traffic (see Fig. 10 and Fig. 11).

Figure 10: Road with separation between opposite lanes - Morocco

Figure 11: Road without separation between opposite lanes - Morocco

Due to V2I communication, the RSU will detect the obstacle (accident), send a warning to inform the nearby drivers and send also a notification to the traffic management center (direction of the roads or gendarmerie). Consequently, the center will change the light panels to indicate the use of additional lanes. The drivers will then keep the correct lane.
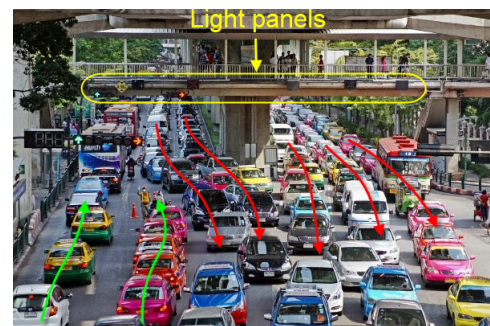
Figure 12: Avoiding Traffic Jams in Bangkok, Thailand by adding opposit lanes using the light panels

---

[3]https://www.shutterstock.com/video/clip-17081557-bangkok-thailand-june-2016–traffic-jam (accessed Oct. 01, 2019).

An example of Bangkok city[3] in Thailand is illustrated in Fig. 12. The road contains six lanes, but two of them were added in the opposite direction to mitigate the congestion. This is one of the propositions that can be made in the Moroccan case to solve rush hour problems, especially in big cities.

5   Conclusion

The main concern of the paper was to present an implementation of vehicular communications using both V2V and V2I technologies. The goal was to notify the driver at the right time so that he can take the navigation choice depending on the received alert. The tests were conducted using the Raspberry Pi 3 boards, model B and model B+, in addition to a specific number of sensors. Two mini cars were used to realize V2V communication by testing two different scenarios which worked well. Authors realized also the V2I communication which worked as well. In addition to that, they made proposals to the Ministry of transportation concerning the deployment of the RSUs and the management of traffic jams in Kenitra City. Based on the results, it can be concluded that these scenarios can be used in the field of road safety, related to the Moroccan case, to address the problems of transportation in kenitra city for example. This will decrease the number of accidents in Morocco and help save lives. As the current work may have some limitations that can be faced in real life, the authors intend in future research to conduct real experiments using two real vehicles. This will reveal all the limitations and lead to a complete system. Further research could bear from this work, such as the integration of cameras in this system in order to study different scenarios of accidents.

Conflict of Interest   The authors declare no conflict of interest.

References

[1] Z. Sabir, S. Dafrallah, A. Amine, "A Novel Solution to Prevent Accidents using V2I in Moroccan Smart Cities," in 2019 International Conference on Computational Intelligence and Knowledge Economy (ICCIKE), 621–625, Dubai, UAE, 2019, doi:10.1109/ICCIKE47802.2019.9004397.

[2] F. Losilla, A.-J. Garcia-Sanchez, F. Garcia-Sanchez, J. Garcia-Haro, Z. J. Haas, "A Comprehensive Approach to WSN-Based ITS Applications: A Survey," Sensors, **11**(11), 10220–10265, 2011, doi:10.3390/s111110220.

[3] L. a. W. Ministry of Equipment, Transport, D. of Roads, "Recueil Des Statistiques Des Accidents Corporels De La Circulation Routière," 2016.

[4] N. C. for the Prevention of Traffic Accidents, Guide référenciel pour la planification de sécurité routière dans les zones urbaines, Editions & Impressions Bouregreg, Rabat, 1st edition, 2017.

[5] J. A. Guerrero-Ibáñez, C. Flores-Cortés, S. Zeadally, "Vehicular Ad-hoc Networks (VANETs): Architecture, Protocols and Applications," in N. Chilamkurti, S. Zeadally, H. Chaouchi, editors, Next-Generation Wireless Technologies, 49–70, Springer, London, 2013, doi:10.1007/978-1-4471-5164-7_5.

[6] Z. Sabir, A. Amine, "Connected vehicles using NDN for intelligent transportation systems," in International Conference on Industrial Engineering and Operations Management, volume 2018, 2433–2441, Paris, France, 2018.

[7] Z. Sabir, A. Amine, "NDN vs TCP/IP: Which One Is the Best Suitable for Connected Vehicles?" in Recent Advances in Mathematics and Technology, Applied and Numerical Harmonic Analysis, 151–159, Springer International Publishing, Cham, 2020, doi:10.1007/978-3-030-35202-8_9.

[8] R. Brookes, P. Pagani, "What becomes a car," in Proposed Paper for: BIT 2014 Conference Workshop-Technology Enabled Business Models: Platforms, Analytics and Performance, 2014.

[9] H. Ullah, N. Gopalakrishnan Nair, A. Moore, C. Nugent, P. Muschamp, M. Cuevas, "5G Communication: An Overview of Vehicle-to-Everything, Drones, and Healthcare Use-Cases," IEEE Access, **7**, 37251–37268, 2019, doi:10.1109/ACCESS.2019.2905347.

[10] K. Kuramoto, K. Fujimura, T. Hasegawa, "The Multi-Class Zone ITS Communication Scheme for Real-time Communications in Intersections," in 2007 IEEE Intelligent Transportation Systems Conference, 431–435, 2007, doi: 10.1109/ITSC.2007.4357804.

[11] N. Taherkhani, S. Pierre, "Centralized and Localized Data Congestion Control Strategy for Vehicular Ad Hoc Networks Using a Machine Learning Clustering Algorithm," IEEE Transactions on Intelligent Transportation Systems, **17**(11), 3275–3285, 2016, doi:10.1109/TITS.2016.2546555.

[12] J. Santa, A. F. Gomez-Skarmeta, "Sharing Context-Aware Road and Safety Information," IEEE Pervasive Computing, **8**(3), 58–65, 2009, doi:10.1109/MPRV.2009.56.

[13] K.-C. Su, H.-M. Wu, W.-L. Chang, Y.-H. Chou, "Vehicle-to-Vehicle Communication System through Wi-Fi Network Using Android Smartphone," in 2012 International Conference on Connected Vehicles and Expo (ICCVE), 191–196, 2012, doi:10.1109/ICCVE.2012.42.

[14] K. C. Dey, A. Rayamajhi, M. Chowdhury, P. Bhavsar, J. Martin, "Vehicle-to-vehicle (V2V) and vehicle-to-infrastructure (V2I) communication in a heterogeneous wireless network" Performance evaluation," Transportation Research Part C: Emerging Technologies, **68**, 168–184, 2016, doi:10.1016/j.trc.2016.03.008.

[15] X. Huang, D. Zhao, H. Peng, "Empirical Study of DSRC Performance Based on Safety Pilot Model Deployment Data," IEEE Transactions on Intelligent Transportation Systems, **18**(10), 2619–2628, 2017, doi:10.1109/TITS.2017.2649538.

[16] Y. Du, M. Chowdhury, M. Rahman, K. Dey, A. Apon, A. Luckow, L. B. Ngo, "A Distributed Message Delivery Infrastructure for Connected Vehicle Technology Applications," IEEE Transactions on Intelligent Transportation Systems, **19**(3), 2018, doi:10.1109/TITS.2017.2701799.

[17] N. G. Ghatwai, V. K. Harpale, M. Kale, "Vehicle to vehicle communication for crash avoidance system," in 2016 International Conference on Computing Communication Control and automation (ICCUBEA), 1–3, 2016, doi: 10.1109/ICCUBEA.2016.7860118.

[18] S. A. Hadiwardoyo, S. Patra, C. T. Calafate, J. Cano, P. Manzoni, "An Android ITS Driving Safety Application Based on Vehicle-to-Vehicle (V2V) Communications," in 26th International Conference on Computer Communication and Networks (ICCCN), 1–6, 2017, doi:10.1109/ICCCN.2017.8038486.

[19] S. Tayeb, M. Pirouz, S. Latifi, A Raspberry-Pi Prototype of Smart Transportation, IEEE Computer Society, 2017, doi:10.1109/ICSEng.2017.25, pages: 176-182.

[20] V. Vibin, P. Sivraj, V. Vanitha, "Implementation of In-Vehicle and V2V Communication with Basic Safety Message Format," in 2018 International Conference on Inventive Research in Computing Applications (ICIRCA), 637–642, 2018, doi:10.1109/ICIRCA.2018.8597311.

[21] S. Dafrallah, A. Amine, S. Mousset, A. Bensrhair, "Will Capsule Networks overcome Convolutional Neural Networks on Pedestrian Walking Direction?" in The 22nd IEEE International Conference on Intelligent Transportation Systems (ITSC), Auckland, New Zealand, 2019, doi:10.1109/ITSC.2019.8917019.

Heuristic Techniques as Part of Heuristic Methods and Interaction of Personality Types in their Application

Viktor Ivanov[*,1], Lubomir Dimitrov[2], Svitlana Ivanova[3], Olena Olefir[4]

[1]*Odessa National Polytechnic University, Department Mechanical Engineering and Elements of Machine, Odesa, 65044, Ukraine*

[2]*Technical University of Sofia, Department Mechanical Engineering, Sofia, 1000, Bulgaria*

[3]*Department Mathematics and its Teaching Methods, South Ukrainian National Pedagogical University named after K.D. Ushynsky, Odesa, 65020, Ukraine*

[4]*Department Advanced Mathematics and Statistics of Affiliation, South Ukrainian National Pedagogical University named after K.D. Ushynsky, Odesa, 65020, Ukraine*

A R T I C L E   I N F O

A B S T R A C T

The widespread team project method is more effective when used in conjunction with heuristic methods. The large number of heuristic methods and the variety of their descriptions create a problem to prepare students for the use of these methods. A method based on two areas of knowledge - heuristics and psychology - is proposed. The personality types of students STEM specialties according to Myers-Briggs are considered. An analysis of interaction of personality types from the point of view of application of heuristic methods is performed. The survey for percentage composition personality types of student STEM specialties was carried out and predominantly types of student STEM specialties was determine. Heuristic methods are consideration as sum of heuristic techniques and procedure. It is shown that many methods involve the same heuristic techniques and differ only in procedures. A generalized method has been developed that allows replacing most of the methods based on collective discussion. This method included five heuristic techniques: collective discussion, pause between the presentation of ideas and their criticism, random associations, analogy, expert evaluation, using a matrix. This method is mainly aimed at teaching students of STEM specialties. A project team is formed to use the method. The composition of this team includes a discussion group, a criticism group and a expert evaluation group. These groups are formed in accordance with the personal types of participants. The method includes an algorithm for team members to interact when using heuristic techniques and procedures.

1. Introduction

Research in the field of heuristics is carried out within a many scientific disciplines. Different approaches and terminology are used. In philosophical works, heuristics is understood as a science, the subject of which is the process of solving a problem in conditions of uncertainty. Another aspect of heuristics is the branch of the science of thinking. Different interpretation is related to pedagogy, so heuristics are often understood as a way of learning. The concept of heuristic is also widely used in cybernetics, where it is interpreted as a heuristic algorithm. Researchers estimate the number of existing heuristic methods in different ways - from several to hundreds. There is no unambiguous idea about the structure of the heuristic method. In different scientific disciplines, a set of principles, a set of steps, or a set of heuristic techniques are considered to constitute a method. First of all, heuristic methods aimed at enhancing the creative abilities of students and involving them in collective creativity are relevant for teaching. The number of such methods is quite large, but there are many common features in the structure of these methods. When it comes to collective creativity, the question of

performers immediately arises. How do personality differences between people affect their use of heuristic methods and how do these differences affect the organization of their interaction? This paper, that is an extension of work originally presented in International Conference on High Technology for Sustainable Development, is dedicated to solving this problem [1].

Consideration of the application of heuristic methods is associated with the personal differences of performers in two aspects: the effectiveness of the application of methods and teach students to use heuristic methods. Many heuristic methods are focused on collective creativity. Methods of this type are well suited for use in student learning. Heuristic methods are most widely used in teaching students studying the following specialties: science, technology, engineering and mathematics (STEM). When using heuristic methods formed by a group of students working together. The interaction of performers in such a group is well studied in project management. This kind of group of performers is called a project team. A large number of publications on psychology, management and education are devoted to organizing the work of the project team and the selection of performers. The project team can be organized for one seminar, or can work on a course project or diploma project during a semester or a year.

2. Review of heuristic methods

As methods of generating ideas used in teaching, the following are considered: Brainstorming, Method 6-3-5, C-Sketch, Gallery, Brainsketching. These methods differ in the form of communication: verbal - brainstorming; text - method 6-3-5; graphic - method C-Sketch; sketch, discussion and text - Gallery; sketch and text - Brainsketching [2]. In the 6-3-5 method, six participants write 3 ideas on a piece of paper in 5 minutes. Then they exchange their notes. This method resembles individual brainstorming in that each participant generates ideas individually, as well as electronic or online electronic brainstorming in which participants exchange ideas via e-mail. In Brainsketching, participants present their ideas in the form of sketches and then exchange them. As in the 6-3-5 method, the criticism of ideas is carried out without the participation of those who put forward the ideas. It is assumed that the graphical representation of ideas will help to find associations. In the Gallery method, the sketches created are discussed and selected together. In the C-Sketch method, the sketch is an imaginary construction. This method is targeted at mechanical engineers.

An experiment comparing Brainsketching and Brainstorming methods has been carried out. The experiment showed that during the Brainstorming process, the participants produced more ideas, and during Brainsketching, the ideas were more original. It is noted that Brainsketching is a type of Brainwriting. That is, the participants put forward ideas individually, as in the 6-3-5 method, only in the form of a sketch [3].

The methods can be divided into three groups [4]. Methods using graphic presentation of information: C-Sketch and Gallery. The methods of using the text include: Brainstorming, K-J Method, Checklists, Affinity Method, Storyboarding, Fishbone, and Method 6-3-5. In addition to the above two groups of methods, another group of Cross-representation methods is proposed [4].

In the Storyboarding method, the sketch is not static but is created in the presence of the discussion group members. The purpose of a sketch or series of sketches is to represent the origin and development of an idea. Affinity Methods operate with different types of information presentation: text, photo, sketch, etc. The group discussion task is sorting similar information into clusters. Affinity Method is, as many believe, a variation of the K-J method. In the Fishbone method, as a result of collective discussion, the factors are also grouped into clusters; only the grouping is visualized as a single diagram.

Cross-representation methods include Morphological analysis and Synectics [4]. Synectics uses collective discussion, the prohibition of criticism as in Brainstorming. Synectics encourages the use of analogies and introspection of the idea generation process. Morphological analysis requires the identification of a set of functions and a possible set of design solutions or physical principles. For this, the analogy of physical processes is widely used [5]. The comparison of possible combinations of properties and design solutions is performed using a matrix. Another name for the method is morphological matrix [5]. Note that the same method has different names Morphological analysis and Morphological matrix. The Affinity method is also called the Affinity Diagram; some researchers describe it as a separate method, others as another name for the K-J method. Brainwriting is an individualized brainstorming session and is very similar to the 6-3-5 method. The peculiarity of publications on heuristics is the use of different names of methods and different points of view on their classification, which is partly due to the authors' affiliation to different scientific disciplines, as well as different ways of presenting information by representatives of the humanities and engineering disciplines.

The comparison of the methods Brainwriting and S.C.A.M.P.E.R. was carried out [6]. In S.C.A.M.P.E.R. method the ideas are generated based on responses to prompts: Substitute, Combine, Modify, etc. The study did not obtain data that could indicate the superiority of one of the methods. It is noted that more creativity can be achieved if the participants are from different universities and different countries. This can be interpreted as a recommendation for using electronic Brainstorming.

The comparison of methods S.C.A.M.P. and TRIZ are performed; also data about Brainstorming was used [7]. It is noted that Brainstorming allows for more creative ideas, but S.C.A.M.P.E.R. and TRIZ provided ideas that could be implemented. Method TRIZ allowed getting more creative ideas than the S.C.A.M.P.E.R method. The S.C.A.M.P.E.R method is presented as intuitive in contrast to the logical TRIZ method.

It should be noted that TRIZ is aimed at solving inventive tasks, that is, it is focused at engineers. More precisely, the name is TRIZ methodology, not a method, since TRIZ contains a set of methods. Most of the TRIZ methods are not methods, but are recommendations for a mechanical engineer, for example: replace sliding friction with rolling friction or replace rectilinear motion with rotational. At the same time provides a method of analogy and decomposition.

A comparison of the methods used in the educational process is carried out; these methods include: Brainstorming, Method 6-3-5, Morphological matrix, Mind and Brain Mapping, Patent

Research, AIDA, Function Structure, House of Quality, Black Box, Decision, Matrix and Pugh Chart. The selection of methods raises questions - how and for what purposes these methods are used in the educational process [8]. The following design stages are highlighted: Task planning and clarification, Conceptual design, Embodiment design, Detailed design [9]. The advantages of the AIDA method are noted, which can be used both at the Task planning and clarification stage and at the Conceptual design stage. The possibility of using one AIDA method instead of using a number of methods is being considered: Brainstorming, Black Box, Morphological matrix, Decision Matrix and Pugh Chart [8]. Note that the feature of the AIDA method is the construction of an option graph, and then the established relationships are analyzed in the matrix. In this part, the method is similar to the Morphological matrix and Decision Matrix methods.

There are different ideas about the stages of the creative process and the stages of the engineering design process [10]. A large number of classifications have a lot in common. Most researchers indicate Analysis phase as the first stage or phase, and Generation phase as the second stage, which is also called Idea-finding, Generating ideas. Inspiration, Response generation. The third stage is the Evaluation phase, which is also called Looking Back, Solution-finding, Reinterpretation, Response validation. The fourth stage is Communication / implementation or Acceptance-finding, Developing an implementation plan [10].

Taking into account the division of the creative process into stages, it is possible to assess the applicability of various methods to these stages. Undoubtedly, of the above methods used in teaching for Generation phase, methods of collective creativity are suitable: Brainstorming, Method 6-3-5, S.C.A.M.P.E.R., Brainwriting, Brainsketching, C-Sketch и Gallery. The mind and brain map is suitable for use by a teacher. If it is used by students, it is transformed into methods with a graphical representation of the idea - Brainsketching, C-Sketch and Gallery.

The methods K-J Method, Checklists, Affinity Method, Storyboarding, Fishbone, AIDA are more suitable for the Evaluation phase, although they are also used in the second stage. The Morphological matrix and Decision Matrix methods are ideal for the third stage. In the fourth stage, Pugh Chart and Checklists can be used. Decision Matrix also has another name Decision support matrix (DSM) this method is aimed at solving engineering problems. The method DSM allows to establish the presence or absence of interactions between the nodes of the product. Based on the found interactions, elements are combined into a cluster [11]. Another method using a matrix is the Interaction Matrix method. This method also is aimed at identifying the interactions between structural elements and their systematization [12].

The TRIZ methodology contains a set of methods that are suitable for each stage of the design process. At the same time, the core of the method is also a matrix - a matrix of contradictions. The TRIZ method involves the formation of a matrix, in which the components and elements of the product are located horizontally, and functions or parameters — vertically. The contents of the matrix cells are a list of methods that can be used to resolve technical contradictions [13]. To this series of methods that use a matrix should be added - a Matrix Diagram (Quality Table). The matrix includes elements between which it is necessary to establish

the interaction. The values in the cells of the matrix indicate the presence and strength of the interaction [14].

3. Myers-Briggs personality types and creative process

The effectiveness of the application of heuristic methods largely depends on the selection of participants and the organization of their work. The selection of participants is especially important when the project team is being formed for a long time. The interaction of participants in the project team is described by the team role methodology. A team role is a description of a behaviour pattern that defines how one team member interacts with other team members when working to accomplish assigned tasks. In project management, the most widespread is the classification of team roles in accordance with [15]. Along with the Belbin typology, there are other typologies of team roles, including MTR-I Team Dynamics [16] and Margerison-McKenna [17]. In psychology, the typology of K. Jung and his followers is generally accepted. Thus, A. Augustinavichute proposed her original modification of K. Jung's typology, which was called "socionics" [18]. The most widely known indicator of the Myers-Briggs types (MBTI) [19]. The MBTI divides individual differences into four opposite pairs, leading to sixteen possible personality types. The sixteen types are usually designated by a four-letter abbreviation, the initial letters of each of their four preference types. For example: INTJ: Introversion (I), Intuition (N), Thinking (T), Judgment (J) or ESFP: Extraversion (E), Sensation (S), Feeling (F), Perception (P) [19, 20]. Likewise, from a combination of four letters, abbreviations of the remaining fourteen personality types are formed.

It is important to note that the role of an individual in the project team may not correspond to his innate individual differences as determined by the Myers-Briggs test. Work experience, acquired qualifications affect the role of the individual in the project team and the results of the MTR-i and Belbin tests. The personality type, in accordance with the Myers-Briggs typology, reflects the individual differences of a person, to a lesser extent dependent on external circumstances and experience, and to a greater extent - on the innate characteristics of the nervous system. Innate human abilities are important in terms of the spontaneous expression of ideas on which most heuristic methods are based. Therefore, this typology is most suitable for describing the heuristic abilities of project team members and their interaction in the collective generation of ideas, critical discussion and expert evaluation.

In the first place it is of interest the possible role of a certain type of students in the process of collective discussion. Apparently for electronic brainstorming it will be important to note that the intuitive interface is preferred [21]. It is also remarked that for extroverts, the response of other participants in the discussion is important in order to clarify the problem [21]. Participants who have the constructs N - Intuition and E - Extraversion [22] are useful for brainstorming. It is also indicated that it is advisable for students with a combination of ES constructs to be entrusted with case studies based on real facts. And students with a combination of IS constructs are preferable to be entrusted with a critical analysis of real facts and conclusions obtained by other students. In [23], personality types with a combination of IS constructs are characterized as a thoughtful realist, and the practical orientation

of their thinking is also noted; they are better at solving problems related to real life and based on real facts.

Students with a combination of IN constructs are distinguished by a critical analysis of new ideas, possibilities, and they can also formulate ideas expressed by other participants in the discussion [23]. Personality types with an IN combination are thoughtful innovators, they generate new ideas and penetrate deeply into the essence of the problem, they are most successful at generalizing facts in the form of a concept or theory [23]. The personal type EN shows itself best in new situations; it is an innovator, action-oriented and sees an opportunity to achieve success in challenges [22]. The same characteristic is given in EN [23], it pointed out that this personality type is suitable for joint execution of tasks, including joint generation of ideas during brainstorming.

In [24] give detailed characteristic NT - "Self analysis exercises and structured controversy are more likely to appeal to NTs, who focus on principles and abstractions". In [25] believes that "…NTJ, the type that tends to have the highest grades in engineering and is commonly drawn to engineering research". In [26] supported this characteristic ENTJ "they also have strategic ability, including reasoning, creative problem solving and strategic thinking". In [27] point out "…the student with the ENTJ personality types, it is preferable to choose for the role of a moderator".

The NP personality type likes to participate in brainstorming [21]. In [28] believes that "Sensitive-Thinking (ST) types preferred hard data and logical analysis in reaching decisions" and the "Intuitive-Thinking (IT) types preferred logic and to test several premises before coming to a decision". In [24] describes that "…NT and SJ individuals who tend to be more linear and serial, more structured, more rational and analytical, and more goal-oriented in their approach to problem solving." In [24] also describes personality types SP and SJ - "Role-playing and simulations are especially appreciated by SPs and SJs, who generally take a more practical approach to problem solving". For SP advisable it is an iterative process of determining a suitable decision through action. "SJs, care should be taken to proceed in a step-by-step, orderly manner, with ample time for consideration of all details at each step." In [25] add to the characterization of SP and SJ that "…students leave things to the last minute (SP), why some prefer a rigid schedule (SJ), why some are intellectual perfectionists (NT)".

In [26] gives characteristic ENFP as "get involved with the people with whom they work, and are very capable of and willing to reconsider plans when others offer input". For two types ISTJ and ENFP has been described problem-solving characteristics [21]. "In problem solving, ISTJ will want a clear idea of the problem (I) and attack it by looking for the facts (S) and by relying on a logical, impersonal (T), step-by-step approach in reaching conclusions" In [21] and [25] are expressed even more definitely "ISTJ engineering and technology stereotype". An important observation is made that ST and NT is cognitive pairs, they provide the exact opposite of the problem [25]. In [26] notes about ISTJ "meeting deadlines and budgets, ensuring productivity and accountability are strengths of ISTI personality".

ESTJ have a leadership qualities, they characteristics are authority and orientation to results [26]. In [18] supported this think, ESTJ is characteristic as administrator which "possess capability to assimilate large amount detailed information". It is noted that ESTJ is logical and rational; also he knows how to make decisions [18]. It is remarks that the set of INT and EST constructs corresponds to the developer using the heuristic TRIZ method [29]. In particular, ESTJ is suitable "determination of corresponding design principles and reviewing and understanding examples showing appropriate application" and INTP is suitable "abstraction to general TRIZ problem" [29].

4. The structure of heuristic methods

The presented overview of heuristic methods does not cover all existing methods. Consideration of only a part of the methods showed that the same method can have different names, such as Affinity Method and K-J method. Either they may differ a little, like Brainwriting and Electronic Brainstorming. The excretion of the characteristic features of methods or their structural units can significantly reduce the number of these methods. From our point of view, the basis of such an analysis can be the excretion of heuristic techniques and procedures from the composition of method. For example, Brainsketching and Method 6-3-5 use the technique of random association. These associations are called through various procedures in the Brainsketching, this is a sketch of another participant, and in the Method 6-3-5 and Brainwriting, these are notes made by another participant. Technique of random associations is used in methods: Brainwriting, Method of focal objects, Method of garlands of accidents and associations, S.C.A.M.P.E.R., Lateral thinking, etc.

The number of heuristic techniques is much less than the number of methods. And within one stage, only a few techniques are used. Let us consider the structure of the methods used in the "Generation phase" stage from the point of view of the applied heuristic techniques. Methods: Brainstorming, Brainwriting, Brainsketching C-Sketch, Gallery, Method 6-3-5, S.C.A.M.P.E.R. be sure to use the collective discussion technique. An important feature of the Brainstorming method is the use of the technique "Pause between the presentation of ideas and their criticism". This technique is also used in methods: Garlands of accidents and associations, Gallery and Lateral thinking. Many methods are based on the use a technique of analogy. These are the following methods: Synectics, Analogy, Empathy and S.C.A.M.P.E.R., which with their questions force the participants to look for similar solutions. In the K-J Method, information is sorted on the basis of analogy, although the use of random associations is also possible. In most methods, the final selection of ideas is done collectively. At the same time, the participants act as experts and their work can be organized on the basis of well-known expert evaluation procedures.

A powerful analysis tool is a heuristic technique «Use of matrix». In different versions, this technique is used by methods: Morphological analysis, DSM matrix, Interaction matrix, Matrix diagram, AIDA. First of all, the methods are selected that are suitable for use in the "Generation phase" stage, are widely known and contain, if possible, several heuristic techniques. These methods are summarized in the table to analyze their structures (Table 1).

Table 1: Structure of heuristic methods

Heuristic techniques / Heuristic methods	Collective discussion	Pause between the presentation of ideas and their criticism	Random associations	Analogy	Expert evaluation	Using a matrix
Brainstorming	■	■			■	
Brainwriting		■				
Method 6-3-5	■				■	
S.C.A.M.P.E.R.	■			■	■	
Brainsketching	■		■			
Gallery	■	■	■		■	
Storyboarding	■		■			
C-Sketch	■				■	
Lateral thinking		■				
Method of focal objects	■					
Method of garlands of accidents and associations	■	■	■	■		
Synectics	■			■		
Affinity Method	■		■			
Lateral thinking		■				
Morphological Matrix						■
DSM matrix						■
Interaction matrix						■
Matrix diagram						■
AIDA	■				■	

To develop a generalized heuristic method aimed at solving problems within the framework of the stage, we formulate a theorem.

Theorem: for each stage of the creative process one generalized heuristic method can be applied replacing all methods used for this stage if it includes all heuristic techniques used within this stage.

The generalized method for "Generation phase" stage includes the following heuristic techniques: collective discussion, pause between the presentation of ideas and their criticism, random associations, analogy, expert evaluation, use of matrix. The use of all these techniques in one method is mandatory. The order of using the techniques and the procedures applied in the method may be different depending on the branch of knowledge and the problems being solved. For example, the "Collective discussion" technique can be applied twice. Then one gets a variation of the brainstorming method - double brainstorming. The Brainsketching and Gallery methods use the "Random association" technique. These methods use different procedures to enhance creativity. In the Brainsketching method, participants can flip the image upside down, and in the Gallery method, they can observe the sketching process. The methods of the DSM matrix and the Matrix Diagram use the same heuristics "Using a matrix" and different procedures. In the DSM matrix, the procedure is to establish the presence or absence of an interaction between elements, and in the Matrix Diagram, the procedure is to assess the conformity of an element to certain requirements.

Let's point out the procedures typical for the methods used in teaching. These are procedures: selection of a moderator, selection of participants in a discussion group, selection of members of a group of critics, selection of members of the group of expert evaluation. Also, the procedures are - defining the rules of discussion and the method of forming an expert evaluation. Important procedures are the choice of the physical meaning of the columns and rows of the matrix and the rules for evaluating combinations of row and column elements.

Based on the analysis of heuristic techniques and procedures, it is possible to form an algorithm of the generalized method. This method must be suitable for use in education, also for design. That is, it should be a method of increasing creativity and at the same time a method suitable for use in the design process. The latter is important for students engineering specialties. To combine such an algorithm and data on the predisposition of students of different personality types to the use of heuristic techniques and procedures in the generalized method, it is important to establish what personality types are typical for students studying in STEM specialties.

5. Typical personality types of students STEM specialties

It is known that there are more introverts than extroverts among students studying STEM specialties. Thus, among students studying agricultural engineering, 83% have construct I, and only 17% have construct E [21]. In the ratio of the S and N constructs, there is no unambiguity: the construct S prevails in mechanical engineering (64 S%, 36% N), while for aerospace engineering the

construct N prevails. The most obvious is the predominance of the construct T over F and J over P [21].

It is claimed those students with the following personality types: ENTJ, INTJ, INTP, ESTJ, ISTJ, ESTP and ISTP, have the ability to work in engineering positions [30]. The personality type of ISTJ is especially highlighted, which is predominant among students of engineering specialties and makes up 26% of their total number [26]. Based on research carried out in [32], it is also stated that the personality type ISTJ occurs most often, the second most common is one of the following personality types ESTJ, INTP and INTJ. Testing of students according to typology (MBTI) was conducted in eight universities [21]. The percentage of students of a certain personality type is established, it is indicated in brackets. The study showed that personality types: ISTJ (16.46%), ESTJ (12.75%), ENTJ (9.43%), INTJ (9.43%), INTP (8.46%) and ENTP (7.43%), most often found among students studying STEM disciplines [21]. In total, personality types ISTJ, ESTJ, INTJ and INTP make up more than 50% of the students who passed the test, and personal types ESFP, ESFJ and ENFJ are less common among students of STEM specialties [31]. The most detailed study of the representation of certain personality types among students of STEM specialties is presented in [10]. First of all, we note that the most widespread personality type is ISTJ (16.9%), and the second place is occupied by INTJ (12.3%), which corresponds to the research data [32]; not much less than INTJ is represented by ENTP (11.8%); for other personality types the following data were received: ESTJ (9.2%), ISTP (7.7%) and INTP (7.2%) [10]. Thus, only four personality types out of sixteen ISTJs, INTJs, ENTPs and ESTJs account for 50.2% of the total number of students. The data of another survey [33] also revealed the prevalence of ISTJ (18.1%), and the second place in prevalence was taken by ESTJ (10.3%), as in [21]. Other personality types ranked in the following sequence: INTP (9.4%), INTJ (8.5%), ISTP (8.2%). It is noted that these five personality types make up more than half of the students [33]. It is noted that these five personality types account for more than half of the students [33]. Similar data were obtained in [32] - the following personality types are prevalent among students of STEM specialties: ISTJ, INTP, ESTJ, INTJ, ENTP, ENTJ and ISTP. Obviously, in further research, it is necessary to obtain data on the possibility of participation of precisely these personality types at different stages of heuristic search. According to the sources discussed above, the following personal types are typical for students STEM professions: ISTJ, ESTJ, ENTJ, INTJ, INTP и ENTP. It is also found that four personal types can account for more than half of the total. Three of them are ISTJ, ESTJ, INTJ, as the fourth, both INTP and ENTP are mentioned. For developing a heuristic method that uses personal types in a particular way, these facts are very important.

Therefore, a study of the distribution of personal types among students speciality "Mathematics and Physics" at the South Ukrainian National Pedagogical University named after K. D. Ushynsky (SUNPU) was carried out. The same test was performed for students speciality "Dynamics and durability of machines" Odessa National Polytechnic University (ONPU) in 2014-2016 years. In each semester, two academic groups numbering from 15 to 20 students were tested. The test was conducted twice, at the beginning and at the end of the semester. The coincidence of test results was observed in the range of 76–81%, which is within acceptable limits (75–90%) [34].

There were no students who refused to participate in the survey. But among the students of ONPU there were also those who did not take it seriously. Their questionnaires were not taken into account. Students of SUNPU treated the survey more scrupulously when the purpose of the survey was clarified - it was the selection of students into project team. They showed a great interest in testing, as it is directly related to their prospective teaching profession.

The distribution of personality types was calculated twice, first for all students, then separately, only for men majoring in "Dynamics and Durability of Machines" (ONPU), where the proportion of men is 87%, and only for women majoring in "Mathematics and Physics" "(SUNPU), where the share of women is 72%. The average value of data of the first and retesting were calculated. In that case, if the student equally corresponded to two personality types, for example, the constructs T and P scored the same number of points, then such people were taken into account twice, in each of the personality types. There were students who did not care about the test and gave mutually exclusive answers; such questionnaires were not taken into account in further calculations. The test results are summarised at Table 2.

Table 2: Personality types of ONPU and SUNPU students

Personality types	Students ONPU (%)	Students SUNPU (%)
ISTJ	22,1	18,1
INTP	11,9	15,5
ESTJ	11,7	14,7
INTJ	11,6	10,4
ENTP	7,8	8,4
ENTJ	5,3	4,4
ISTP	4,2	3,3
ENFP	2,0	2,5

ISTJ personality types are more common in ONPU, but INTP and ESTJ personality types are more common in SUNPU, as shown in Figure 1.
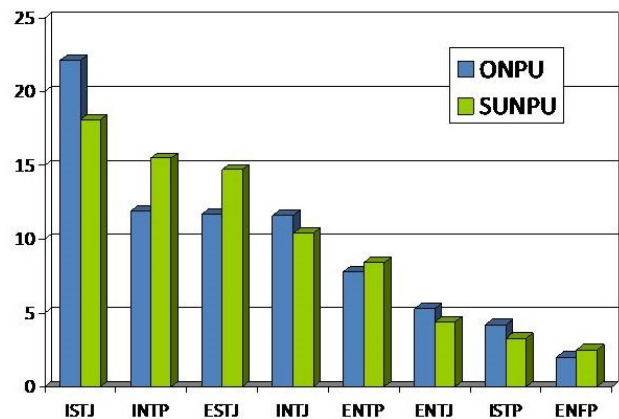
Figure 1: Percentage distribution of personality types

The relationship between personal types can be most clearly represented in the form of a pie chart in which the axes correspond to certain cognitive functions. The abscissa corresponds to the cognitive functions N and S. The construct N is located on the left, and the constructs S is located on the right along the abscissa. The

ordinate corresponds to the cognitive functions T and F. The construct T is placed below the abscissa, and the construct F above the abscissa is along the ordinate. The personality types within the inner circle are introverted; personality types outside the inner circle are extroverts. For each personality type, the average value of students of this type in ONPU and SUNPU was calculated: ISTJ (20.1), INTP (13.7), ESTJ (13.2). INTJ (11.0), ENTP (8.1), ENTJ (4.9), ISTP (3.8) and ENFP (2.3) (Figure 2).

The obtained average values of personality types were plotted on this pie chart. The size of the circle corresponds to the percentage of this personality type among all students.
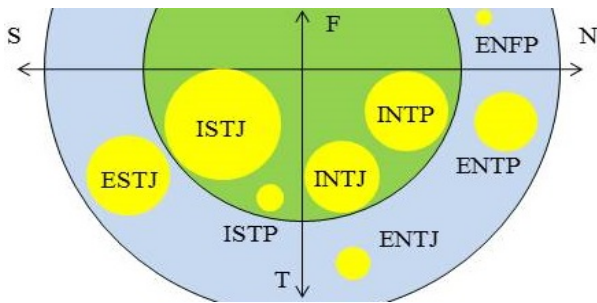
Figure 2: Distribution of personality types relative to the pie chart depicting cognitive functions

The small number of students surveyed does not allow making any conclusions about gender differences. The repeated survey for women in ONPU and men in SUNPU gave an error higher than acceptable. We cannot fully rely on the absolute value of a particular personality type. Because when surveying 50 students, one incorrectly completed questionnaire gives an error of 2%. The data of students at six technical universities in the United States and Canada shows that only one university has the represented ENFP type among students [32]. For this reason, we excluded the ENFP personality type from further consideration because the data obtained correspond to one representative from two academic groups.

We obtained the following order of personal types by their prevalence: ISTJ, INTP, ESTJ, INTJ, ENTP, ENTJ and ISTP. The first is ISTJ, as in the sources [21, 26, 31]. The first six personal types are the same as in [21], but their order is different. The resulting distribution of personal types is close to [33]. In our study, the INTP (13.7%) is in second place and the ESTJ (13.2%) is in third place. the difference between them is within the margin of error. In [33] type personal ESTJ (10,3%) at the second location, and INTP (9,4%) for the third, but the difference between them is small. In [31], also the personal type ESTJ (10.9%) is in second place, and INTP (9.9%) is in third place and the difference between them is about 1% as in the article [33]. The first four personal types in our study make up 58%, which is also more than half of the total number as in sources [31, 33]. According to our data, more than 75% of students STEM specialties belong to the following personality types: ISTJ, INTP, ESTJ, INTJ, ENTP, ENTJ and ISTP. The personality types in the table are arranged in descending order, in accordance with the number of representatives of this type (Table). Refer that the most common personality types include types containing the construct T. These personality types have a predisposition to STEM professions. The only personality type between of those which contain a construct T and which is ranked among the common - this ESTP. This type is also not mentioned

among those common in papers [21, 33]. This is due to the fact that students of this type neglect the details and do not finish what they started. Equally represented are constructs Sensing (S) and Intuition (N).

6. The generalized method

The generalized method contains a heuristic technique *using a matrix*. Rows and columns of a matrix can be functions, units, a number of products with similar functions, design techniques, and so on. These recommendations are intended to solve engineering problems. The range of tasks solved by the technique *using a matrix* is much wider. It is proposed that the purpose of the technique *collective discussion* is to find ideas about the contents of the columns and rows of the matrix. After the first heuristic technique, there is a pause between the presentation of ideas and their criticism. In further, the criticism of the ideas put forward and their evaluation are providing. That is, the technique of *expert evaluation* is used. The semantic content of rows and columns is searched for by the technique of *analogy* and *random associations*. For example, for rows, the search is carried out by *analogy*, and for columns using *random associations*. If the search did not give satisfactory results, it is repeated, but the technique of *random associations* is already used for rows, and *analogy* for columns. The results are again *collectively discussed* and undergo *expert evaluation*. Based on the results of the heuristic analysis, the technique of *using a matrix* is applied - in this way the matrix is formed. Based on the results of the heuristic analysis, a technique *using a matrix* is applied – therefore the matrix is analyzed. Each cell of the matrix corresponds to a possible variant of a problem solution. These options are subject to *collective discussion* again. Then, *expert evaluation* and documenting of the results are performed.

The heuristic techniques and procedures described above require performers with a certain personal type. An effective *collective discussion* technique will not work if all participants are introverts. Extroverts with artistic abilities should not be entrusted with documenting matrix analysis results. The complete development of the method requires specifying the personality type in the performers for each of the techniques and procedures.

The ENTJ personality type has leadership qualities, strategic vision, logic, and therefore can be a moderator of the discussion. ESTJ - has organizational skills and the ability to keep track details of discussion. A student with the ENTJ personality type is selected as the moderator. If there was no such student in the group, then the student with the ESTJ personality type plays the role of the moderator. The moderator participates in the *collective discussion*.

Collective discussion is an extroverted process. Intuition is also important for generating ideas. In the process of collective discussion, there is a search for patterns, the construction of schemes and models, and a search for the relationship between known facts. It is important that the participants discard well-known dogmas, abandon stereotypes. Extroverted personality types (construct E) and intuitive personality types (construct N) take part in the *collective discussion*. Preference is given to personality types ENTJ, ENTP.

The logic is inherent by personality T. The personality NT is inventive, looking for regularities. The personality types INTJ and

INTP can generate ideas, however, they are introverts and the collective discussion is a problem for them. The personality type INTP is actively generating ideas; he has logic (T) and the ability to evaluate the logic of ideas expressed by other members of the team. The personality type INTJ is a researcher and has good intuition, but due to communication problems with others, he is not always possible to clearly express their ideas. The personality type INTP can be tactless and arrogant, which hinder a spontaneous expression of ideas. Based on the foregoing, the types of personality INTP perform the function of criticism.

The understanding an importance of the knowledge is inherent of a personality type TE. This quality, as well as extraversion, allows the personality type ESTJ to participate in the discussion, although ESTJ can consider the brainstorming ineffective. Based on the analysis of the above, students with personality types ENTJ, ENTP and INTJ are necessarily selected for the *discussion group*.

For the critical analysis of the proposed ideas, the following qualities are important: distrust, searching for flaws in everything, attention to detail, logicality. The critic is, without a doubt, an introvert type. The personality types ISTP, ISTJ, INTP, and INTJ are logical introverts. Critical analysis is the strong point of IS and IN. Sensitive-Thinking personality types ISTP and ISTJ prefer to focus on practical issues. These personality types prefer to carefully compare several options before making a final decision. In doing so, they rely on facts and logical analysis. Personality types INTP and INTJ are perfectionists that important for critics. Based on the foregoing, the students with the types of personality ISTP, INTP and ISTJ can function as critics.

Expert evaluation and critical analysis require similar personality types. Personality types ST and NT are a cognitive pair. For example, these are the ISTJ and INTJ personality types. They provide a different vision of the problem, this is important for the evaluation. The final decision on the meaning of rows and columns is made primarily by "experts" in the first place; these are representatives of the personality types ISTJ, and also ENTJ, ESTJ. The inclusion of personality types ENTJ and ESTJ in the number of experts is due to the fact that they led a collective discussion. The moderator can choose the final variant basing not only on his own opinion, but also on the opinion of other members of the team whose personal qualities he knows and appreciates. Therefore students with personality types ISTJ, INTJ, ESTJ and ENTJ can participate in the *expert evaluation*.

Note that the ENTJ and ENTP personality types have a good imagination and are useful when using the technique of random associations, and the INTJ personality type is endowed with perfect intuition. The ISTJ personality type is an ideal candidate for processing the results of the discussion and organizing them in the form of a morphological matrix of proposed solutions. The personal INTP type can do the job as well. It is also advisable to entrust the documentation of the final results obtained using the generalized method to the personal types of ISTJ and INTP.

If the proposed heuristic method does not work, a Feedback Group can be created. It is advisable to include representatives of each of the 16 personality types in this group, if students with such personal types are available. A group of students who performed a certain heuristic technique told the Feedback Group about their experience of participation, as well as problems that arose. After the discussion, all or part of the heuristic techniques are repeated.

Consider the algorithm of the generalized heuristic method, taking into account the heuristic techniques and the content of the considered procedures (Figure 3).
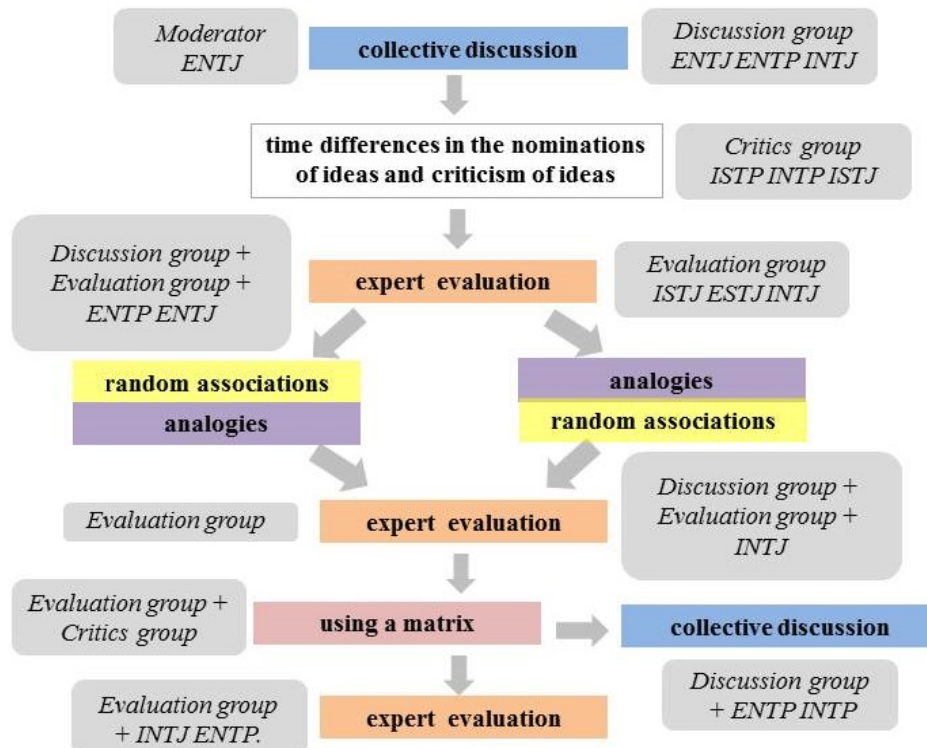
Figure 3: The algorithm of generalized method

The first procedure is procedure for selecting a moderator. A student with personality types ENTJ is selected as moderator for the collective discussion group. If there are two representatives of this type, then the student with higher academic achievements is chosen as the moderator. If there are no representatives of this personality type, then ESTJ is chosen as the moderator. The project team should be divided into several parts: discussion group, critics group, evaluation group. The one student can be by participant of few groups.

The second procedure is procedure for selecting participants for the discussion group; these are personality types ENTJ, ENTP and INTJ.

The third procedure for selecting the participants of critics group is as follows - students with the ISTP, INTP and ISTJ personality types are selected as critics group.

The fourth procedure for selecting the participants of expert evaluation group: personality types ISTJ, ESTJ, and INTJ.

This is followed by the first heuristic technique - collective discussion. The collective discussion group consisted of five to ten people. Personality type ESTJ participated in discussions and idea generation provided he is a moderator. This personality type joins the discussion group also in the case of its small size.

The second heuristic technique is a pause between the presentation of ideas and their criticism. After a pause, the group of critics set to work. A group of critics is consisted of three to five people. The composition of the group can be increased so that all members of the project team can participate in the work. In small project teams with a lack of "critics", the ISTJ is served as a critic; they usually predominate numerically over representatives of other personality types. In this case, the INTP is joined the group of discussion and generation of ideas. Several members of the collective discussion group join the group of critics. First of all, this is the personal type of INTJ, Thus, a critical analysis is carried out both by the project team members who participated in the discussion and those who did not participate in the discussion; they represent a different point of view on the problem.

The third heuristic technique is expert evaluation. The group of experts should not be large. Not all participants with personality types ISTJ, ESTJ, ENTJ should be members of this group. This group primarily includes students with high academic achievement. Moderator is always included in this group.

The fifth procedure is the selection of groups for heuristic techniques of *analogy* and *random associations*. These groups are mainly formed from members of the discussion group and expert evaluation group. But members of the critics' group also participated, so almost all members of the project team participated in the two groups. Personality types of ENTJ and ENTP should be included in the group of *random associations*, and the group of *analogy* - personal type INTJ.

The fourth heuristic technique - *analogy* and the fifth heuristic technique - *random associations* were used in parallel and repeated if necessary.

The sixth heuristic technique is *expert evaluation*. The group can be updated. Other members of the personality types ISTJ, ESTJ and INTJ may be included in this group.

The seventh heuristic technique is the *using a matrix*. The matrix is formed based on the results of applying the previous heuristic techniques. For the technical work on the formation of the matrix, personality types ISTJ and INTP are involved. An *evaluation group* and a *critics group* analyze each cell of the matrix. Decisions that do not make sense and are not feasible under the given conditions are discarded. Promising solutions are brought up for discussion.

The eighth heuristic technique is a *collective discussion*. The discussion group can be expanded. You can add personality types with good logic - ENTP and INTP. Note that INTP was involved in the matrix developing.

The ninth heuristic technique is an *expert evaluation*. This is final heuristic technique and final evaluation. In this case, the evaluation group should be expanded to include representatives of *discussion group*: INTJ and ENTP. As a result of considering the options detailed in the process of collective discussion, one best is chosen.

Final procedure is a documenting the results. For this the personality types ISTJ and INTP. To do this, personality types INTJ and INTJ are involved.

7. Conclusion

The analysis of heuristic methods based on their structure is carried out. The heuristic methods which belong to the generation phase were considered. As part of the methods highlighted heuristic techniques and procedures. It is shown that two dozen methods belonging to the generation phase use only five heuristic methods. Many methods use the same heuristic technique and differ only in procedure. The theorem was formulated: for each stage of the creative process one generalized heuristic method can be applied replacing all methods used for this stage if it includes all heuristic techniques used within this stage.

The study of the personality type's distribution of students STEM specialties was carried out at the South Ukrainian National Pedagogical University named after K. D. Ushynsky (SUNPU) and Odessa National Polytechnic University (ONPU). The main part of students belongs to seven personality types. Data for SUNPU students on the percentage of each type to the total number of students: ISTJ (18.1), INTP (15.5), ESTJ (14.7). INTJ (10.4), ENTP (8.4), ENTJ (4.4), ISTP (3.3) and ENFP (2.5). Data for ONPU students on the percentage of each type to the total number of students: ISTJ (22.1), INTP (11.9), ESTJ (11.7). INTJ (11.6), ENTP (7.8), ENTJ (5.3), ISTP (4.2) and ENFP (2.0). The generalized method was developed. This method focused to teaching students STEM specialties. Method based on five heuristic techniques collective discussion, pause between the presentation of ideas and their criticism, random associations, analogy, expert evaluation, using a matrix. The heuristic process is considered from the point of view of the personality types of the participants. Personal types are considered in terms of how they are suitable for performing the indicated heuristic techniques. The recommendation about performers: moderator, discussion group, critics group, evaluation group, for each heuristic technique was developed.

Conflict of Interest

The authors declare no conflict of interest.

Acknowledgments

References

[1] V. Ivanov, L. Dimitrov, S. Ivanova, O. Olefir, "Creativity enhancement method for STEM education," in 2019 IEEE International Conference on High Technology for Sustainable Development (HiTech), 1-5, 2019, doi: 10.1109/HiTech48507.2019.9128255.

[2] J.S. Linsey, M.G.Green, J.T. Murphy, K. L. Wood, A.B. Markman, "Collaborating To Success: An Experimental Study of Group Idea Generation Techniques," in International Design Engineering Technical Conferences and Computers and Information in Engineering, **4742**, 277-290, 2005, https://doi.org/10.1115/DETC2005-85351.

[3] R. Van der Lugt, "Brainsketching and how it differs from brainstorming," Creativity and innovation management, **11**(1), 43-54, 2002, https://doi.org/10.1111/1467-8691.00235.

[4] F.L. McKoy, N. Vargas-Hernández, J.D. Summers, J.J. "Shah, Influence of design representation on effectiveness of idea generation," in Proceedings of the ASME design engineering technical conference, 4, 39-48, 2001.

[5] M. Fargnoli, E. Rovida, R.Troisi, "The morphological matrix: Tool for the development of innovative design solutions," in 2006 International Conference on Axiomatic design (ICAD), 1-7, 2006.

[6] Y.J. Park, C. Kim, J. Yoon, "Creativity and design method in idea generation: the comparison between intuitive approach vs structured approach," in 2019 IASDR Conference, 1-12, 2019.

[7] V. Chulvi, M.C. González-Cruz, E. Mulet, J. Aguilar-Zambrano, "Influence of the type of idea-generation method on the creativity of solutions," Research in Engineering Design, **24**(1), 33-41, 2013, https://doi.org/10.1007/s00163-012-0134-0.

[8] A. Weas, M. Campbell, "Rediscovering the analysis of interconnected decision areas," AI EDAM, **18**(3), 227-243, 2004, https://doi.org/10.1017/S0890060404004168.

[9] W. Beitz, G. Pahl, K. Grote, "Engineering design: a systematic approach," MRS Bulletin, **21**(8), 71-71, 1996, doi:10.1557/S0883769400035776.

[10] T.J. Howard, S.J. Culley, E. Dekoninck, "Describing the creative design process by the integration of engineering design and cognitive psychology literature," Design studies, **29**(2), 160-180, 2008, https://doi.org/10.1016/j.destud.2008.01.001.

[11] S. Buzuku, A. Kraslawski, "Use of Design structure matrix for analysis of critical barriers in implementing eco-design initiatives in the pulp and paper industry," Procedia Manufacturing, **11**, 742-750, 2017, https://doi.org/10.1016/j.promfg.2017.07.175.

[12] V. Ivanov, G. Urum, S. Ivanova, G. Naleva, "Analysis of matrix and graph models of transmissions for optimization their design," Eastern - European Journal of Enterprise Technologies, **4.1**(88), 11-17 2017, https://doi.org/10.15587/1729-4061.2018.131101.

[13] C. Pokhrel, C. Cruz, Y. Ramirez, A. Kraslawski, "Adaptation of TRIZ contradiction matrix for solving problems in process engineering," Chemical engineering research and design, **103**, 3-10, 2015, https://doi.org/10.1016/j.cherd.2015.10.012.

[14] Vezzetti, F. Marcolin, A.L. Guerra, "QFD 3D: a new C-shaped matrix diagram quality approach," International Journal of Quality & Reliability Management, 33 (2), 178-196, 2016, https://doi.org/10.1108/IJQRM-07-2013-0112.

[15] D. Lukianov, K. Bespanskaya-Paulenko, V. Gogunskii, O. Kolesnikov, A. Moskaliuk and K. Dmitrenko "Development of the markov model of a project as a system of role communications in a team," Eastern-European Journal of Enterprise Technologies, **3**(3), 21-28, 2017, https://doi.org/doi:10.15587/1729-4061.2017.103231.

[16] M. Farhangian, M. Purvis, M. Purvis, T.B.R. Savarimuthu, "Agent-based modeling of resource allocation in software projects based on personality and skill," Advances in Social Computing and Multiagent Systems. MFSC 2015. Communications in Computer and Information Science, **541**, 130-146, 2015, https://doi.org/10.1007/978-3-319-24804-2_9.

[17] N. Lehmann-Willenbrock, S.J. Beck, S, Kauffeld, "Emergent team roles in organizational meetings: Identifying communication patterns via cluster analysis," Communication Studies, **67**(1), 37-57, 2016, https://doi.org/10.1080/10510974.2015.1074087.

[18] J. Jankowski, The 16 Personality Types in a Nutshell, LOGOS MEDIA, 2016.

[19] M.H. McCaulley, "The Myers-Briggs type indicator: A Jungian model for problem solving." New Directions for Teaching and Learning, 1987(30), 37-53, 1987, https://doi.org/10.1002/tl.37219873005.

[20] S. Rushton, J. Morgan, M. Richard, "Teacher's Myers-Briggs personality profiles: Identifying effective teacher personality traits," Teaching and Teacher Education, **23**(4), 432-441, 2007, https://doi.org/10.1016/j.tate.2006.12.011.

[21] M.H. McCaulley, "Myers-Briggs Type Indicator: A bridge between counseling and consulting," Consulting Psychology Journal: Practice and Research, **52**(2), 117–132, 2000, https://doi.org/10.1037/1061-4087.52.2.117.

[22] D. Keirsey, M.M. Bates, Please understand me: Character & temperament types, Del Mar, CA: Prometheus Nemesis Book Company, 1984.

[23] C. Soles, L. Moller, "Myers Briggs type preferences in distance learning education," International Journal of Educational Technology, **2**(2), 2001.

[24] W. Huitt, "Problem solving and decision making: Consideration of individual differences using the Myers-Briggs Type Indicator," Journal of Psychological Type, **24**(1), 33-44. 1992.

[25] C.F. Yokomoto, R. Ware, "Applications of the Myers-Briggs Type Indicator in engineering and technology education - part II," Indiana University - Purdue University Indianapolis, **2230**, 4.88.1- 4.88.10, 1999.

[26] V.R. Montequín, J.V. Fernández, J.V. Balsera, A.G. Nieto, "Using MBTI for the success assessment of engineering teams in project-based learning," International journal of technology and design education, **23**(4), 1127-1146, 2013, https://doi.org/10.1007/s10798-012-9229-1.

[27] S. Ivanova, L. Dimitrov, V. Ivanov and G. Naleva, "An Experiment on the Joint use of the Heuristic and Project Methods at the University," in 2019 IEEE International Conference on High Technology for Sustainable Development (HiTech), 1-5, doi: 10.1109/HiTech48507.2019.9128248.

[28] J.B. Murray, "Review of research on the Myers-Briggs type indicator," Perceptual and Motor skills, **70**(3_suppl), 1187-1202, 1990, https://doi.org/10.2466/pms.1990.70.3c.1187.

[29] M. Ogot, G. Okudan, "A student centered approach to improving course quality using quality function deployment," The International journal of engineering education, **23**(5), 916-928, 2007.

[30] P.D. Tieger, B. Barron, K. Tieger, Do what you are: Discover the perfect career for you through the secrets of personality type. Little, Brown Spark, 2014.

[31] A.J. Williamson, "Suiting library instruction to the Myers-Briggs personality types and Holland Vocational personality types of engineering students," Issues in Science and Technology Librarianship, **37**(2), 2003. https://doi.org/10.5062/F4154F1G.

[32] L.F. Capretz, "Is there an engineering type?" World Transactions on Engineering and Technology Education, **1**(2), 169-172, 2002.

[33] A. Thomas, M.R. Benne, M.J. Marr, E.W. Thomas, R.M. Hume, "The evidence remains stable: The MBTI predicts attraction and attrition in an engineering program," Journal of Psychological Type, **55**, 35-42, 2000.

[34] R.M. Capraro, M.M. Capraro, "Myers-Briggs Type Indicator score reliability across studies: A metaanalytic reliability generalization study," Educational and Psychological Measurement, **62**(4), 590-602, 2002.

Analysis of Real-time Blockchain Considering Service Level Agreement (SLA)

Minkyung Kim[1], Kangseok Kim[2,3], Jai-Hoon Kim[*,3]

[1]*Dasan College, Ajou University, Suwon, 16499, South Korea*

[2]*Department of Artificial Intelligence and Data Science, Ajou University, Suwon, 16499, South Korea*

[3]*Department of Cyber Security, Ajou University, Suwon, 16499, South Korea*

A R T I C L E I N F O	A B S T R A C T
	The Blockchain technologies enable decentralized networking consisting of large number of nodes. To determine the shared states and failures of all nodes in a fully distributed peer-to-peer system, the appropriate consensus algorithm needs to be selected for each Internet of Things system. In this paper, a novel hierarchical voting-based byzantine fault tolerance (HBFT) consensus algorithm is proposed. The proposed HBFT algorithm utilizes a typical PBFT algorithm hierarchically to guarantee low latency. The message complexity of HBFT shows that our proposed algorithm has better scalability. We also mathematically calculate the optimal number of groups based on the total number of nodes to determine the ratio of allowable faulty nodes per group. In addition, we analyze the reliability of byzantine fault tolerance to compare the reliability of group case with the reliability of non-group case. Finally, we introduce the methods of real-time Blockchain considering the service level agreement (SLA). The real-time processing performance of transactions is analyzed for the service level agreement (SLA).

1. Introduction

A Blockchain is a peer-to-peer distributed ledger , in which the process of transaction verification and recording is continuously executed [1, 2]. Participant nodes constantly verify a set of time-stamped transactions at a given time using a built-in consensus algorithm. The Blockchain technology improves reliability in addition to availability by storing and sharing data in a distributed manner. The use of Blockchain in Internet of Things (IoT) enables secure, decentralized networking for IoT data privacy and security [3]. Therefore, an efficient consensus algorithm is crucial to verify transactions and adjust interactions among IoT devices [4]. IoT data are validated through the consensus mechanism and then recorded securely in a distributed ledger.

This paper introduces a novel hierarchical voting-based byzantine fault tolerance (HBFT) consensus algorithm. The proposed HBFT algorithm operates the group level's consensus rather than the node level's consensus. It is to overcome limited scalability and high latency in a typical practical byzantine fault tolerance (PBFT) algorithm. Thus, the overall exchanging messages are significantly reduced even if the large number of nodes are participated in consensus operation. Despite the exponential growth in the number of nodes in the network, the scalability of HBFT is ensured compared with PBFT. Also, we calculate the optimal number of groups depending on the total number of nodes for grouping because the reliability can be affected by the number of groups. If faulty nodes are well distributed into groups, the probability of reaching consensus is higher even with an increased number of faulty nodes. Therefore, two cases are calculated to understand the influence on the number of faults per group.

However, since the participant nodes mutually verify and store the data, considerable number of computing resources are required, and concurrently the processing time decreases [5-8]. The same method of participant nodes (all nodes or certain nodes allowed to participate in Blockchain) has been used to process transactions on the Blockchain [9]; nevertheless, it is possible to apply the service level agreement (SLA) on Blockchain by determining the number of participant nodes according to the user's requirements. Therefore, we propose methods to control the number of participant nodes adaptively considering user requirements and computing environments. The transaction processing speed and throughput can be improved by using adaptive control method. Figure 1 is the diagram of real-time

[*]Corresponding Author: Jai-Hoon Kim, Department of Cyber Security, Ajou University, Suwon, 16499, Korea, jaikim@ajou.ac.kr

Blockchain considering service level agreement(SLA). In this diagram, the reliability of a node with respect to time is periodically collected by the Blockchain monitor. It depends on the failure rate of a node determined intentional or unintentional faults. The Blockchain control also reads user requirements and Blockchain status. According to the user's request, a transaction is processed for generating a smart contract of Blockchain. The user can request reliability, maximum time and the cost for block generation. The reliability of a participant node can affect the reliability of the transaction processed.
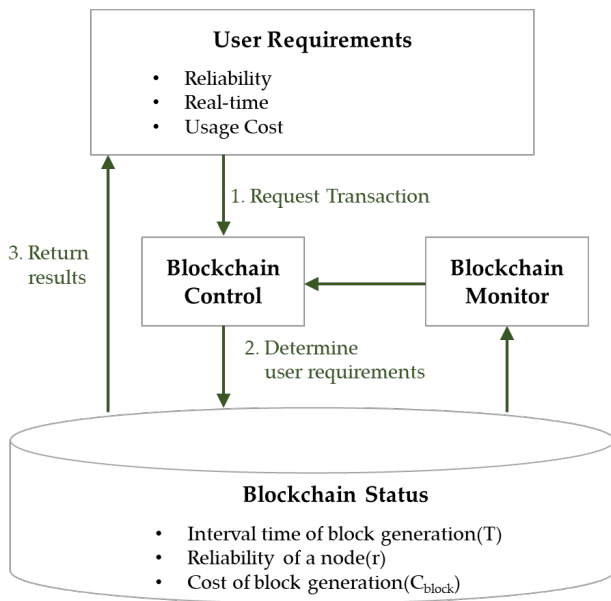
Figure 1: Schematic of Real-time Blockchain considering Service Level Agreement(SLA)

The remainder of this paper is organized as follows. Section 2 overviews relevant background about various consensus algorithms. The details of HBFT algorithm are presented in Section 3. Here, how the HBFT algorithm differs from previous consensus mechanisms has been described. In Section 4, we analyze the reliability of byzantine fault tolerance, and present the algorithm of real-time block generation in Section 5. Finally, Section 6 concludes the contributions with future research perspectives and additional improvements.

2. Related Work

There are various consensus algorithms adopted by the popular Blockchain-based platforms such as *Bitcoin*, *Ethereum* and *Hyperledger Fabric*. In [10-11], the different advantages and disadvantages of each existing consensus algorithm are introduced. Bitcoin utilizes Proof of Work (PoW), which the high computational power is required to solve a cryptographic puzzle for mining operation. Proof of Stake (PoS) is designed to overcome the disadvantages of PoW algorithms. However, PoS suffers from a problem called Nothing at Stake because each participant can vote to both blocks. Also, Delegated Proof of Stake (DPoS) achieves consensus by delegates (called block producers) elected by nodes instead of participation by all nodes. Practical Byzantine Fault Tolerance (PBFT), implemented in *Hyperledger Fabric*, has

a primary node to manage the other nodes. Even if some untrusted nodes participate in the consensus operation, it is considered an agreement if more than 2⁄3 of the results are the same. Also, a variant of byzantine fault tolerance consensus algorithm called Delegated Byzantine Fault Tolerance (DBFT) [12, 13] is introduced for scalable participation. The randomly elected delegates (called bookkeeping nodes) of each group can only participate in the operation of the consensus process. Furthermore, PBFT is an permissioned protocol in which the identities of all nodes are exposed to the network [14]. Therefore, PBFT can be applied in permissioned platforms that enable autonomous, commercial, and financial application services in IoT environments. It is also suitable for applications that do not require tokens and incentives. That is why we developed a novel and efficient consensus algorithm based on PBFT for decentralized IoT.

3. Hierarchical voting-based Byzantine Fault Tolerance (HBFT) Consensus Algorithm to reduce System Resources

In this section, a novel hierarchical voting-based byzantine fault tolerance (HBFT) consensus algorithm is proposed. Also, we analyze the message complexity of the proposed novel consensus algorithm. Additionally, the best case and worst case are calculated to identify the influence on the number of faulty nodes per group in our proposed algorithm.
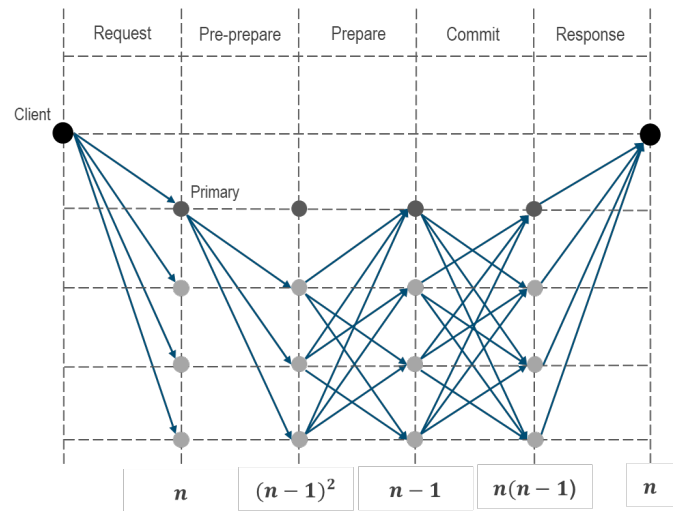
Figure 2: Flow Chart of PBFT

Practical Byzantine Fault Tolerance (PBFT) consensus algorithm has five processes for consensus processing [15-17]. Figure 2 shows the flow chart of PBFT. If the number of faulty nodes (f) is not more than $f = \lfloor (n - 1)/3 \rfloor$, a consensus can be reached. Even though faulty nodes participate in the network, PBFT consensus algorithm can prevent up to $n/3$ of faulty nodes since more than $2n/3$ nodes must be reliable nodes. The overall message complexity is $2n^2$ based on the messages generated in each process. In case of the PBFT algorithm supported by *HyperLedger Fabric*, the reliability of the consensus is improved because every node participates in the consensus process through the interactions with each other. However, the message complexity

increases exponentially as the number of participating nodes increase. Therefore, if the number of nodes increases, the problem of scalability can be generated by high network traffic and latency.

3.1. Proposed HBTF Consensus Algorithm for Scalability

Based on our previous researches [18, 19], the operation of HBFT consensus algorithm, which utilizes a typical PBFT algorithm hierarchically, is re-designed effectively. Our proposed HBFT consensus algorithm has two phases to validate transactions. The flow chart of HBFT is shown in Figure 3.
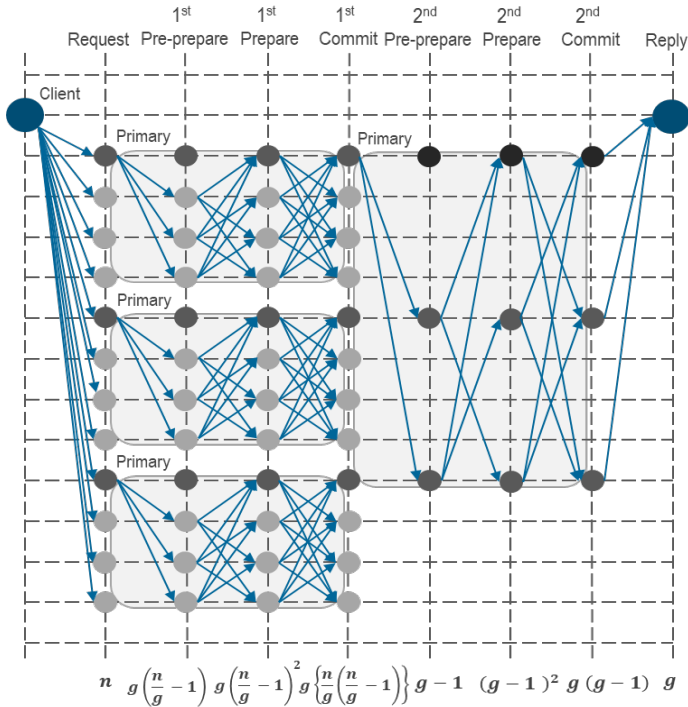
Figure 3: Flow Chart of HBFT

Firstly, the first phase start to request a verification about new transactions to all replica nodes. In the pre-prepare process, all nodes are randomly grouped into some groups and then, a primary node in each group is randomly selected to send a pre-prepare message to the other nodes. Each node compares a pre-prepare message with a request message. If the results match, a primary node responds a prepare message to the other nodes. In the commit process, each node reaches an agreement in the group depending on whether it received more than $2n/3g$ of prepare messages. Next, the second phase is executed in the same processes as the first phase to verify the voting results of each group. Finally, if more than $2g/3$ of prepare messages are received, the consensus is reached. Each primary node broadcasts the results to a client.

3.2. Message Complexity of HBFT Consensus Algorithm

The overall message complexity generated in each process of HBFT is $f(g) = 2g^2 - g + 2n^2/g - n$. The overall message complexity of HBFT is lower than that of PBFT by increasing the total number of participant nodes in Figure 4. Therefore, the processing overhead is significantly decreased. The lower latency and better scalability can be guaranteed because the overall overhead is reduced.
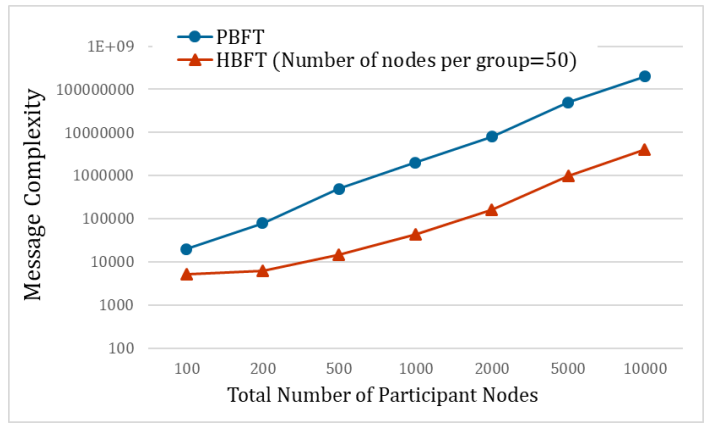
Figure 4: Overall Message Complexity Comparison between PBFT and HBFT

Additionally, we try to figure out the impact on the message complexity by increasing the number of groups in Figure 5. If the total number of nodes is 1000, the message complexity depends on the number of groups. The message complexity increases as the number of groups is too small or too large. Since the number of groups can affect the reliability of the agreement, the optimal number of groups according to total number of participant nodes needs to be calculated for facilitating efficient grouping. The optimal number of groups based on total number of nodes is calculated as follows. Eq. (1) is an equation for the overall message complexity of HBFT. By differentiating Eq. (1), we can achieve the number of groups with minimal message complexity. The optimal number of groups is given by Eq. (2). If the total number of nodes is 1000, the calculation result of Eq. (2) is about 79.45 as shown in Figure 5.

$$f(g) = 2g^2 - g + \frac{2n^2}{g} - n \qquad (1)$$

$$\rightarrow \quad f'(g) = 4g - 1 - \frac{2n^2}{g^2} = 0$$

$$g = \frac{1}{12}\left(1 + \sqrt[3]{1 + 432n^2 - \sqrt{432n^2(432n^2 + 2)}} + \sqrt[3]{1 + 432n^2 + \sqrt{432n^2(432n^2 + 2)}}\right) \qquad (2)$$

3.3. Fault Tolerance of HBFT Consensus Algorithm

In our proposed HBFT algorithm, consensus can be achieved to add a new block when the number of groups is more than two-thirds the total number of groups. Two cases are calculated to determine the influence on the number of faulty nodes per group. In the first case, the maximum number of allowable faults to reach consensus is calculated in (a). Additionally, a case where the consensus cannot be reached with the minimum number of faulty nodes is calculated in (b). When it is detected as a faulty node, a primary node is changed in the typical PBFT algorithm. Therefore, all primary nodes are assumed to be non-faulty nodes, similar to the PBFT algorithm. Additionally, we assume that the number of total groups is more than two, and the number of nodes per group

is at least four in our proposed HBFT algorithm for normal operation.
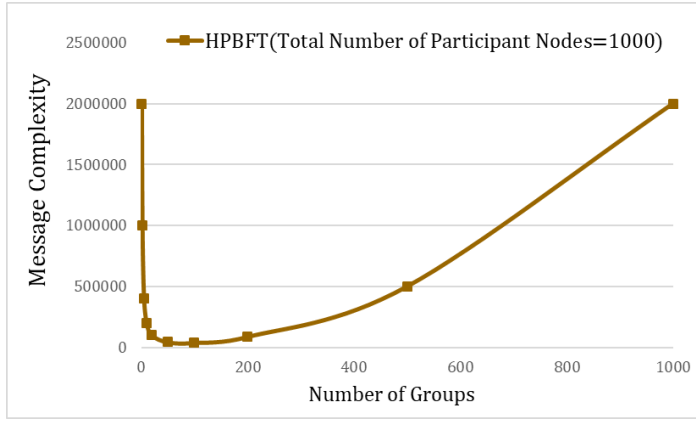
Figure 5: Message Complexity of HBFT depending on the Number of Groups

3.3.1. Best case: The maximum number of allowable faulty nodes in order to reach a consensus

One-third of total number of groups consists of faulty nodes and cannot reach a group consensus. The other two-thirds have only one-third faulty nodes in each group, leading to a group agreement. Consequently, the best case is that the number of faulty nodes is high; however, a consensus can be reached since faulty nodes are well distributed into groups. Eq. (3) shows the equation of the best case.

$$\left(\left\lfloor\frac{g}{3}\right\rfloor \times \left(\frac{n}{g}-1\right)\right) + \left(\left\lceil\frac{2g}{3}\right\rceil \times \left\lfloor\frac{n}{3g}\right\rfloor\right) \tag{3}$$

3.3.2. Worst case: A consensus cannot be reached with the minimum number of faulty nodes

If the number of faulty nodes in each group exceeds one-third, each group agreement fails. The worst case is in which the number of groups that do not attain group agreement exceeds one-third. As a result, even though the number of faulty nodes occupies a relatively small number, the consensus cannot be reached according to the ratio of faulty nodes per group. An equation of this worst case is described as follows.

$$\left(\left\lfloor\frac{g}{3}\right\rfloor + 1\right) \times \left(\left\lfloor\frac{n}{3g}\right\rfloor + 1\right) \tag{4}$$

Both equations are calculated to assess whether a consensus can be achieved according to the ratio of faulty nodes per group. The influence of the ratio of faulty nodes per group is shown in Figure 6. From these calculations, the number of allowable faulty nodes is up to approximately $5n/9 - g/3$ in the best case. In the worst case as already discussed, a consensus cannot be reached according to the ratio of faulty nodes per group. In both calculations, whether a consensus is reached or not is affected by the ratio of faulty nodes per group. Although the number of faulty nodes participating in consensus is high, a consensus can be reached depending on how all faulty nodes are well-distributed into groups as described in the best case. Finding the optimal ratio of faulty nodes per group to reach consensus in HBFT algorithm will be an important research area. In addition, it is required that the verification regarding the faulty nodes is executed at the beginning of consensus process. As a result, the number of

allowable faulty nodes can be low compared to PBFT algorithm depending on the ratio of faulty nodes per group in the worst case. On the contrary, the number of allowable faulty nodes can be more than that in the PFBT algorithm depending on the ratio of faulty nodes per group in the best case.
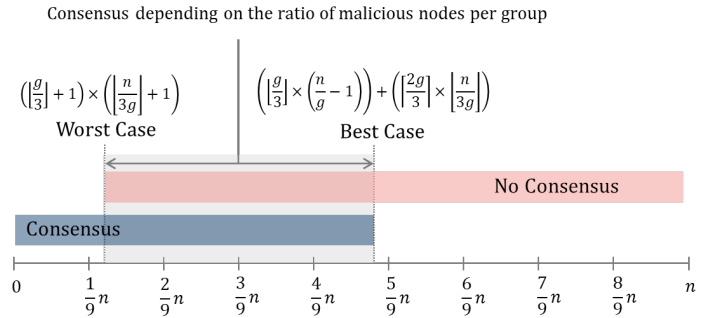
Figure 6: Influence on the Ratio of Faulty Nodes Per Group

4. Analysis of Reliability

We analyze the reliability of Blockchain operation in this section. It leads to the analyzing of the probability of normal operation in unit time. Assuming that the reliability of each participant node is equal to r, the calculations below are defined when n nodes participate in the processing a transaction. The reliability of the fail-stop faults can be calculated by the probability that at least one node is operating normally. A fail-stop means the occurrence of an unintentionally generated failure. It is assumed that a fail-stop at a node happens when a node is faulty.

$$1 - (1 - r)^n \tag{5}$$

In the case of the reliability for consensus, even if there are the fail-stop faults, the consensus can be reached if more than half of the number of nodes agree. Subsequently, the reliability of the byzantine faults can be calculated by the probability that less than half of faulty nodes are included on Blockchain as follows.

$$R(n, r) = 1 - \sum_{k=ceil\left(\frac{n}{2}\right)}^{n} {}_nC_k(1-r)^k r^{n-k} =$$

$$\sum_{k=0}^{ceil\left(\frac{n}{2}\right)-1} {}_nC_k(1-r)^k r^{n-k} \tag{6}$$

In the case of the reliability for consensus in byzantine faults, if less than one-third of faulty nodes are in the operation, the consensus is reached. The calculation is shown in Eq. (7)

$$R(n, r) = 1 - \sum_{k=ceil\left(\frac{2n}{3}\right)}^{n} {}_nC_k(1-r)^k r^{n-k} =$$

$$\sum_{k=0}^{ceil\left(\frac{2n}{3}\right)-1} {}_nC_k(1-r)^k r^{n-k} \tag{7}$$

In addition, the reliability of the byzantine faults in a hierarchical structure as in the proposed HBFT consensus algorithm can be defined as $R(g, R(n/g, r))$. It is assumed that the total number of nodes is n, and the number of nodes per a group is n/g. Additionally, when all nodes are divided into several groups for consensus, the number of groups is g. Therefore, the reliability of group is calculated as $R(n/g, r)$ based on the reliability of a node. In case of the reliability for consensus, even if there are the

byzantine faults, this same definition is applied. If the more than two-third the number of normal nodes are in the consensus operation, a consensus is reached to add a new block.

Assuming that the number of nodes is 400 and less than half the faulty nodes are included, the reliability based on that of each node is shown in Figure 7. Furthermore, if the number of groups is 20 with the total number of nodes, the reliability of hierarchical byzantine fault tolerance by grouping is shown in Figure 7. When the consensus operation executes hierarchically in the group level, the reliability of group case is similar or lower than the reliability of non-group case. Although the difference in the case of reliability of hierarchical byzantine fault tolerance is lower than in the case by the node's reliability, the message complexity is much better described in the Section 3.2; so it can be said that it is good to be grouped in the proposed algorithm. When the number of faulty nodes is less than one-third of the total nodes, the consensus operates hierarchically according to the reliability of each node.
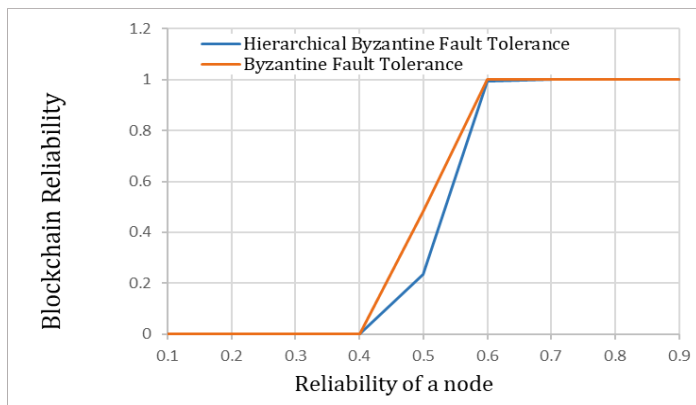
Figure 7: Reliability in the Byzantine Fault
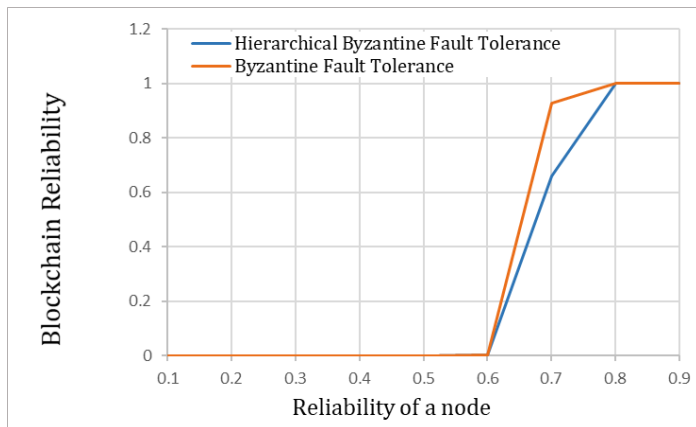
Figure 8: Reliability for Reaching Consensus in the Byzantine Fault

Figure 8 shows that the reliability of the consensus in the case of group level and in the case of non-group level consensus. Although the range with a little low reliability exists in the reliability of hierarchical byzantine fault tolerance for reaching consensus, there is no notable difference in the reliability of the overall ranges, similar to Figure 7. Even if the reliability of each node is different, or an incorrect answer is generated by an intentional failure or byzantine faults, the reliability can be calculated. In addition, even if the participant nodes have different conditions such as reliability, the possibility of cyber infringement, computing power, and data collection, it is possible to apply the proposed method of using Blockchain resources minimally according to various Blockchain configuration conditions and the user's requirements.

5. Real-time Performance Analysis using Block Generation Algorithm

Although the Blockchain has various advantages such as reliability, security, traceability and transparency, the excessive computing resources and communication bandwidths required to reach consensus and maintain consistency between duplicated ledgers are disadvantageous. Additionally, it is necessary to consider the reduction of the deadline meet ratio according to the laxity time for consensus in computing environments required real-time transaction processing. In this paper, the real-time processing performance of transactions is analyzed according to the redundancy of nodes. There are the applicable methods for maximizing real-time performance and satisfying user's requirements. The first method is real-time block generation algorithms. The second method is to use off-chain for reliable real-time performance although the reliability is decreased. A method to obtain the priority for block generation exists, as it pays more gas costs. Subsequently, the delay time is controlled by adjusting the number of nodes participating in consensus. In this section, we propose real-time block generation algorithm to adjust block generation according to the laxity time of the transaction. The two algorithms of block generation are compared in Figure 9 and Figure 10.

5.1. Algorithm of block generation at regular intervals (Conventional Blockchain)

Assuming that the time interval of block generation is T, the transaction arrival time is t, and the laxity time for block generation is D. When each block is generated at regular intervals, the deadline meet ratio, the average response time and the cost for block generation can be calculated as follows. A block is generated when a transaction arrives in the period D. Therefore, the deadline meet ratio is calculated as D/T. In Figure 9, if the period of D is greater than the period of T, a block is generated at any time within the period of block generation. The average response time is defined as $D/2$. The period D refers to the laxity time to wait for block generation. The cost for block generation in period of T is calculated as C_{block}/T. The graph of (a) algorithm for the cost is shown in Figure 10.

5.2. Algorithm of block generation by the shortest deadline of the arrived transactions (Real-time Blockchain)

If the transaction processing request arrives, and other transactions arrive at $1/f$ intervals, all blocks about the arrived transactions within the laxity time of the first requested block generation are generated. Therefore, all transactions in the laxity time are processed based on the laxity time of the initially arrived transaction. It is assumed that the arrival frequency of transaction is f, and a new transaction arrives at equal intervals. Then, the arrival time of a new transaction is $1/f$ (= P), and the block generation time of the new transaction can be calculated as $1/f$ (= P) + D. All transactions are always processed when the transactions arrive in the laxity time. Therefore, the deadline meet

ratio of (b) algorithm is 1 as shown in Figure 9. The average response time for block generation is calculated as $(P + D)/2$. The graph in Figure 10 shows the cost for block generation of (b) algorithm calculated as $C_{block}/P + D$.
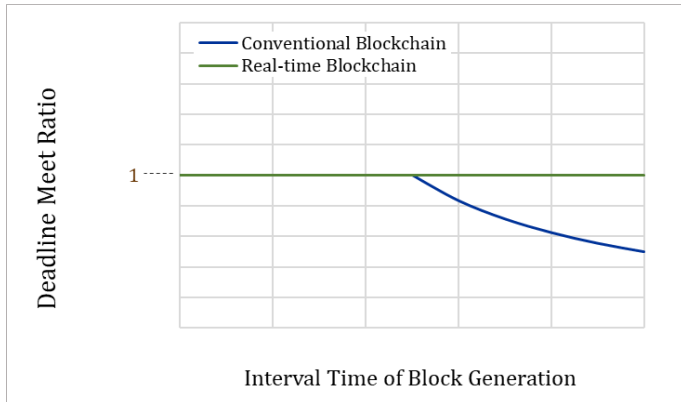
Figure 9: Deadline Meet Ratio
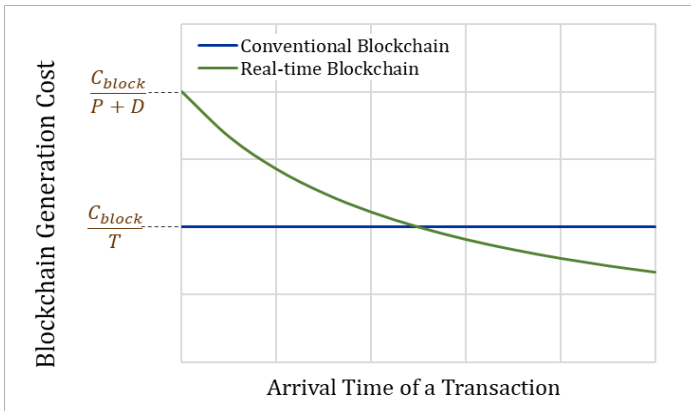
Figure 10: Blockchain Generation Cost

6. Conclusion

We propose a novel HBFT consensus algorithm required for transaction generation to reduce the processing throughput and increase scalability in a typical PBFT algorithm. Since our proposed algorithm utilize PBFT algorithm hierarchically, the number of exchanging messages in the consensus processing is significantly reduced. It means that the HBFT consensus algorithm ensures the scalability even though large numbers of nodes are involved in the consensus process. Furthermore, we calculate the optimal number of groups to identify the influence on the overall message complexity depending on the number of groups. In addition, both the best and worst cases are calculated to determine the ratio of allowable faulty nodes per group. Additionally, the reliability of byzantine fault tolerance is analyzed to compare the reliability of group case with the reliability of non-group case. Finally, it is necessary to consider the reduction of the deadline meet ratio according to the laxity time for consensus in computing environments required real-time transaction processing. To compare with the conventional Blockchain algorithm to consider the service level agreement (SLA), the real-time processing performance of transactions is analyzed according to the redundancy of nodes. In the future work, we plan to demonstrate HBFT algorithm through simulations. Furthermore, we would also implement Blockchain-based application services to effectively manage the decentralized IoT data.

References

[1] O. Novo, "Blockchain Meets IoT: An architecture for Scalable Access Management in IoT," IEEE Internet of Things Journal, **5**, 1184-1195, 2018, doi: 10.1109/JIOT.2018.2812239.

[2] R. Casado-Vara, P. Chamoso, F. De la Prieta, J. Prietoa, J. M. Corchado, "Non-linear adaptive closed-loop control system for improved efficiency in IoT-blockchain management," Information Fusion, **49**, 227-239, 2019, doi: /10.1016/j.inffus.2018.12.007.

[3]   P. Brody, V. Pureswaran, "Device democracy - Saving the future of the internet of Things," IBM institute for business value (2015) Available online: https://www.ibm.com/downloads/cas/Y5ONA8EV (accessed on 15 July 2020)

[4] Y. Li, W. Susilo, G. Yang, Y. Yu, D. Liu, M. Guizani, "A Blockchain-based Self-tallying Voting Scheme in Decentralized IoT," eprint arXiv:1902.03710, 2019.

[5] K. Košťál, P. Helebrandt, M. Belluš, M. Ries, I. Kotuliak, "Management and Monitoring of IoT Devices Using Blockchain," Sensors, **19**, 1-12, 2019, doi: /10.3390/s19040856.

[6] G. Sagirlar, B. Carminati, E. Ferrari, E. Ferrari, J. D. Sheehan, E. Ragnoli, "Hybrid-IoT: Hybrid Blockchain Architecture for Internet of Things - PoW Sub-blockchains," 2018, doi: 10.1109/Cybermatics_2018.2018.00189.

[7] M. Ruta, F. Scioscia, S. Ieva, G. Capurso, E. D. Sciascio, "Semantic Blockchain to Improve Scalability in the Internet of Things," Open Journal of Internet of Things (OJIOT), **3**, 46-61, 2017.

[8] R. Jayaraman, K. Salah, N. King, "Improving Opportunities in Healthcare Supply Chain Processes via the Internet of Things and Blockchain Technology," International Journal of Healthcare Information Systems and Informatics (IJHISI), **14**. 1-20, 2019, doi: 10.4018/IJHISI.2019040104.

[9] S. Gupta, M. Sadoghi, "Blockchain Transaction Processing," in Encyclopedia of Big Data Technologies, 1-11, 2019, doi:10.1007/978-3-319-63962-8_333-1.

[10] A. Panarello, N. Tapas, G. Merlino, F. Longo, A. Puliafito, "Blockchain and IoT Integration: A Systematic Survey," Sensors, **18**(8), 1-37, 2018, doi: 10.3390/s18082575

[11] A. Baliga, "Understanding blockchain consensus models," Persistent Systems Ltd. White paper, 2017, URL: https://www.persistent.com/wp-content/uploads/2018/02/wp-understanding-blockchain-consensus-models.pdf

[12] L. M. Bach, B. Mihaljevic, M. Zagar, "Comparative analysis of blockchain consensus algorithms," in Proceedings of 41st International Convention on Information and Communication Technology, Electronics and Microelectronics (MIPRO), 1545-1550, 2018.

[13] E. Zhang, "A Byzantine Fault Tolerance Algorithm for Blockchain," NEO White paper, 2018, URL: https://docs.neo.org/en-us/basic/consensus/whitepaper.html

[14] Y. Xiao, N. Zhang, W. Lou, Y. T. Hou, "A Survey of Distributed Consensus Protocols for Blockchain Networks," in IEEE Communications Surveys & Tutorials, **22**(2), 1432-1465, 2020, doi: 10.1109/COMST.2020.2969706.

[15] M. C.Igor, N. C.Vitor, P. A.Rodolfo, Y. Q.Wang, D.R.Brett, "Challenges of PBFT-Inspired Consensus for Blockchain and Enhancements over Neo dBFT," in future internet, **12**(8), 129, 2020

[16] M. Castro, B. Liskov, "Practical Byzantine Fault Tolerance," in Proceedings of the Third Symposium on Operating Systems Design and Implementation, 173-186, 1999.

[17] M. Castro, B. Liskov, "Practical Byzantine Fault Tolerance and Proactive Recovery," ACM Transactions on Computer Systems, **20**(4), 398-461, 2002, doi: 10.1145/571637.571640.

[18] M. Kim, J-H. Kim, "Hierarchical Voting-based Byzantine Fault Tolerance Consensus Algorithm," in Proceedings of International Conference on APIC-IST 2020, 183-185, 2020

[19] M. Kim, J-H. Kim, "Decentralized Data Management Schemes for IoT Blockchain," in Ph.D. Dissertation, Department of Computer Engineering Graduate School of Ajou University, 2019

Sensorless Control and Corrected Error Commutation of the Brushless DC Motor

Anatoly Stepanov[*], Vitaly Enin

Department of Electrical and Industrial Electronics, Bauman Moscow State Technical University, Moscow, 105005, Russia

A R T I C L E I N F O	A B S T R A C T
	This paper presents a simple method for correcting the error of commutation windings for sensorless control of a brushless DC motor with a small inductance. Switching error analysis is performed based on the phase currents of the switched-off and switched-on phases. To correct the commutatiuon signals for the inverter, a speed-independent function is used, calculated from the back-EMF, by selecting its coefficients. The back-EMF is calculated for the system obtained by transformed a three-phase system to a two-phase one, which reduces the system dimension. An algorithm for start-up the motor with sensorless control based on the method of align and damping the rotor vibrations in a stable equilibrium position is proposed. The back-EMF is approximated by a function based on a piecewise linear function and an inscribed ellipse, for a more accurate description of the shape of the back-EMF. This approximation is used when simulation the motor. The simulation confirms the effectiveness of the proposed method for correcting the commutation error in the case of sensorless control of a low-power BLDC motor.

1. Introduction

This paper is an extension of conference report "Sensorless control of low-power brushless DC motor based on the use of back-EMF," presented in "2019 International Ural Conference on Electrical Power Engineering (UralCon 2019)" [1].

In the extended version of the paper, in comparison with the conference paper, a method for correcting error of commutation winding and the start-up procedure based on the alignment of the rotor position in the stable equilibrium position of brushless DC motor is proposed, which makes it possible to improve the reliability and quality of sensorless control.

The rectifier of the electrical motors, in particular the brushless DC motors (BLDC) are widely used in automation and control systems, as well as in orientation and navigation systems as a gyroscope drive [2 – 4]. Usually, the power of the BLDC windings is produced by a semiconductor inverter, whose transistors are switched by signals from sensors installed on the motor stator.

The use of rotor position sensors has disadvantages associated with an increase in the price of the electric drive, the accuracy of their installation, which leads to errors in determining the switching moments of the windings, unreliability of the sensors in difficult environmental conditions. To eliminate these

shortcomings, the methods of sensorless control of the BLDC motor have been developed.

In case of sensorless control, commutation signals are generated using back-EMF or flow, calculated from phase currents and voltages. The most widely used methods are those using back-EMF.

The most widely used methods of sensorless control based on the analysis of back-EMF are considered in [5-11]. If the neutral point of the motor is not available, the terminal voltage determines the moment when the back-EMF of the disconnected phase passes through zero (zero crossing point). Switching must be performed with a delay of 30 electrical degrees, after passing the back-EMF through zero. In [5], the least squares method is used to refine the switching points, but this does not guarantee accurate determination of the switching points, since the terminal voltage contains noise and pulses generated by the inverter. The implementation of these methods requires additional phase-shifting circuits, including a timer. The non-ideality of the back-EMF, the delay created by the low-frequency filter significantly reduces the reliability of these methods.

In [12, 13], a velocity-independent G-function calculated from the back-EMF is used to determine the commutation points. Commutation points are determined when the absolute value of this function exceeds a certain threshold value. The back-EMF contains noise and pulses generated by the inverter, which can lead

[*]Corresponding Author: Anatoly Stepanov, stepanov.bmstu@gmail.com

to erroneous determination of commutation points. The disadvantage of this method is also the ambiguity of choosing a threshold value.

To determine the commutation points in [14, 15], the third harmonic is used. This method requires creating a virtual third point. To form a neutral point, an additional electrical circuit is required, which is a disadvantage of this approach.

One of the problems with sensorless control is the problem of starting the motor and its operation at a low speed of rotation, in this case, the back-EMF of rotation is zero or very small. Then, determining the position of the rotor by the back-EMF of rotation is difficult or almost impossible.

In [16], when starting, the position of the rotor is initially set by the reaction of the current at magnetic saturation if the axis of the flow created by the current and the magnetic axis coincide. Only one current sensor is used. Then, after starting, the rotor is accelerated to the speed at which it is possible to switch to sensorless control of the winding switching. When the rotor position is aligned, oscilations occur in the vicinity of the equilibrium position, which reduces the reliability of this method.

Despite the large number of works on sensorless control, the problem of reliability and accuracy of determining the commutation points for the BLDC motor are relevant and require further research.

2. Mathematical model of brushless DC electric motor

Here we describe a mathematical model of a three-section electric BLDC motor. The power supply circuit of the windings of a three-section, brushless DC motor by an electronic commutator on field-effect transistors is given in Figure 1

The equations in the phase coordinates for the sections of BLDC motor with permanent magnets taking into account the mutual inductances of the sections have the form (the case of an implicit pole rotor is considered):

$$\begin{bmatrix} R_s & 0 & 0 \\ 0 & R_s & 0 \\ 0 & 0 & R_s \end{bmatrix}\begin{bmatrix} i_a \\ i_b \\ i_c \end{bmatrix} + \begin{bmatrix} L_s & -M_s & -M_s \\ -M_s & L_s & -M_s \\ -M_s & -M_s & L_s \end{bmatrix}\begin{bmatrix} \dfrac{di_a}{dt} \\ \dfrac{di_b}{dt} \\ \dfrac{di_c}{dt} \end{bmatrix} + \quad (1)$$

$$+\begin{bmatrix} e_a \\ e_b \\ e_c \end{bmatrix} = \begin{bmatrix} u_a - u_n \\ u_b - u_n \\ u_c - u_n \end{bmatrix},$$

where R_s – active resistance of section stator winding; i_a, i_b, i_c – currents in the windings of the stator sections; L_s – inductance winding sections; M_s – mutual inductance of the windings of the sections; e_a, e_b, e_c – back-EMF of the stator windings; u_a, u_b, u_c – voltage applied to the windings of sections; u_n – neutral point voltage. In wye connection $i_a + i_b + i_c = 0$.
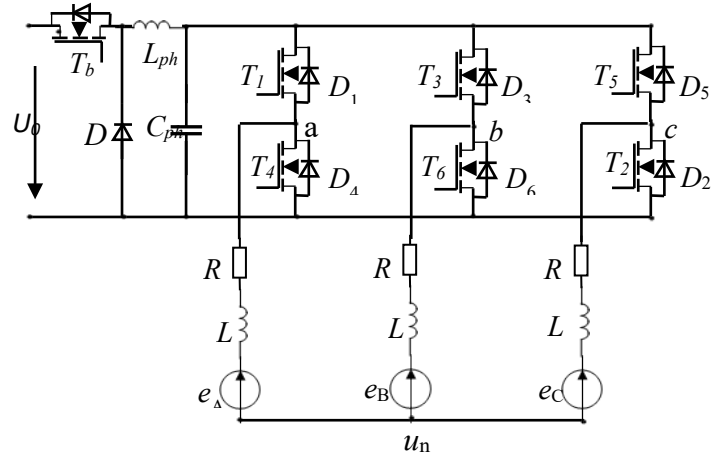
Figure 1: Three-section BDCM winding power supply circuit

Let us define the inductance of the stator along the longitudinal and transverse axes $L_d = L_q$ and the inductance L_0 for the zero sequence. The phase inductances of the windings of the sections in the rotating coordinate system d, q are defined as follows: $L_s = (L_0 + 2L_d)/3$; $M_s = (L_d - L_0)/3$.

Using the transformation (a particular form of the transformation matrix E. Clarke)

$$\begin{bmatrix} u_\alpha \\ u_\beta \end{bmatrix} = T \begin{bmatrix} u_a \\ u_b \\ u_c \end{bmatrix}, \quad (2)$$

when

$$T = \begin{bmatrix} \sqrt{2/3} & -1/\sqrt{6} & -1/\sqrt{6} \\ 0 & 1/\sqrt{2} & -1/\sqrt{2} \end{bmatrix}.$$

For the transformation matrix T, the following equality holds: $T^{-1} = T^t$ (T^t is the transposed matrix), $T T^{-1} = E$, E – unit matrix.

Transform (2) a three-phase system (1) to a two-phase system

$$\begin{bmatrix} R_s & 0 \\ 0 & R_s \end{bmatrix}\begin{bmatrix} i_\alpha \\ i_\beta \end{bmatrix} + \begin{bmatrix} L & 0 \\ 0 & L \end{bmatrix}\begin{bmatrix} \dfrac{di_\alpha}{dt} \\ \dfrac{di_\beta}{dt} \end{bmatrix} + \begin{bmatrix} e_\alpha \\ e_\beta \end{bmatrix} = \begin{bmatrix} u_{\alpha n} \\ u_{\beta n} \end{bmatrix}.$$

where $L = L_s + M_s$.

Using the transformation (2) we will express the back-EMF in the system α, β

$$e_\alpha = \frac{1}{\sqrt{6}}(e_a - e_b) - \frac{1}{\sqrt{6}}(e_c - e_a), \quad (3)$$

$$e_\beta = \frac{1}{\sqrt{2}}(e_b - e_c). \quad (4)$$

The back-EMF differences $e_{ab} = e_a - e_b$, $e_{bc} = e_b - e_c$, $e_{ca} = e_c - e_a$. They are calculated using equation (1). to calculate the back-

EMF according to (3),(4), it is not necessary to determine the voltage at the neutral point.

Back-EMF sections at a constant rotational speed vary according to the law $e_a(\theta) = k_e\omega_e\Phi'_a(\theta)$, $e_b(\theta) = k_e\omega_e\Phi'_b(\theta)$, $e_c(\theta) = k_e\omega_e\Phi'_c\theta)$, where $\omega_e = p\omega$, (ω – is the angle rotor speed, p – number of pairs of poles.

Trapezoidal function $d\Phi/d\theta$ (Φ is magnetic flux, θ electric angle) is approximated by piecewise linear function with inscribed ellipse [1]. This function $\Phi'(\theta)$ is used when simulation the BLDC motor.

Graphs of the functions $\Phi'_a(\theta)$, $\Phi'_b(\theta)$, $\Phi'_c\theta)$ for a three-phase and functions $\Phi'_\alpha\theta)$, $\Phi'_\beta\theta)$ for a two-phase system are shown in Figure 2, 3.
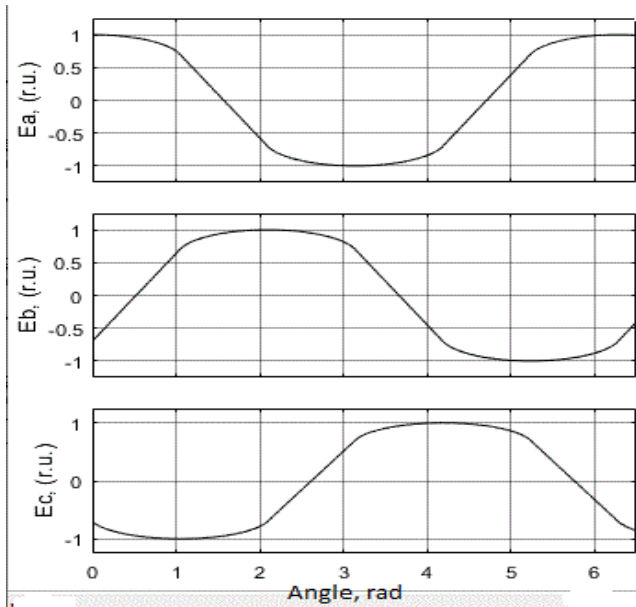
Figure 2: Trapezoidal functions $\Phi'_a(\theta)$, $\Phi'_b(\theta)$, $\Phi'_c\theta)$
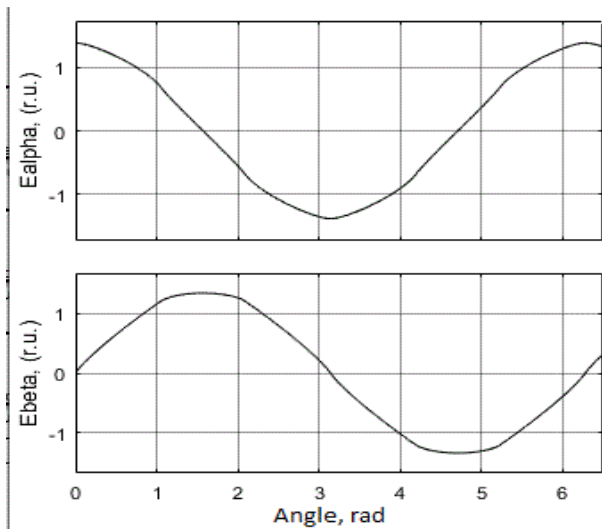
Figure 3: Functions $\Phi'_\alpha\theta)$, $\Phi'_\beta\theta)$ in system α, β

3. Algorithm sensorless control BLDC motor in system α, β

The most widespread in practice is 120 degree commutation, in which the winding is connected to the source at an interval of

120⁰ electric degrees, then disconnected from the source at an interval of 60⁰ electric degrees.

For 120-degree commutation, the angles of switching on and off phases , the function value is selected, which determines the value of the back-EMF of the sections at the time of switching. The dependence of the back–EMF phase in relative units expressed using the function $\Phi'(\theta)$ is shown in Figure 3, from where it follows for 120 degree commutation $\Phi'(60°) = \Phi'(300°)$, $\Phi'(120°) = \Phi'(240°)$.

To determine the commutation points, the values of the back-EMF in system α, β calculated by the formula (3), (4) are used. The ratio of the back-EMF $e_\alpha(t)$, $e_\beta(t)$ is equal to the ratio $\Phi'_a(t)$, $\Phi'_b(t)$ and does not depend on the speed of rotation of the rotor. The values of the functions $\Phi'_\alpha(\theta)$, $\Phi'_\beta(\theta)$ for commutation angles are shown in table 1.

Table 1: The value of the function $\Phi_\alpha{}'(\theta)$, $\Phi_\beta{}'(\theta)$ at the points of commutation

θ_c	$\Phi'_\alpha(\theta_c)$	$\Phi'_\beta(\theta_c)$	$\Phi'_\alpha(\theta_c)/\Phi'_\beta(\theta_c)$
$\pi/3$	$C_1(1+\Phi'_b)$	$C_2(1+\Phi'_b)$	$1/\sqrt{3}$
$2\pi/3$	$-C_1(1+\Phi'_b)$	$C_2(1+\Phi'_b)$	$-1/\sqrt{3}$
π	$-2C_1(1+\Phi'_b)$	0	$-\infty$
$4\pi/3$	$-C_1(1+\Phi'_b)$	$-C_2(1+\Phi'_b)$	$1/\sqrt{3}$
$5\pi/3$	$C_1(1+\Phi'_b)$	$-C_2(1+\Phi'_b)$	$-1/\sqrt{3}$
2π	$2C_1(1+\Phi'_b)$	0	∞

In table $C_1 = 1/\sqrt{6}$, $C_2 = 1/\sqrt{2}$.

Let's introduce the functions $H_1(t)$, $H_2(t)$

$$H_1(t) = \frac{e_\alpha^2(t) + e_\beta^2(t)}{k_1 e_\alpha^2(t) - e_\beta^2(t)},$$

$$H_2(t) = \frac{e_\alpha^2(t)}{\left(k_2 + e_\beta(t)\right)^2}$$

Coefficients k_1 and k_2 in accordance with table 1 should be equal to $k_1=3$ and $k_2=0$. The function $H_1(t)$, $H_2(t)$ generates pulses at switching angles of 60, 120, 240, 300 electric degrees, and the function $H_2(t)$ at angles of 180 and 360 degrees. To determine points of commutation is set to the threshold value H_t. When the threshold value is exceeded ($|H_1(t)|> H_t$ or $|H_2(t)|> H_t$), the functions $H_1(t)$, $H_2(t)$ determine the commutation. The calculated back-EMF for voltage and current windings contains pulses generated by the inverter, which are smoothed by a low-frequency filter. As a result of this, a error commutation occurs. The accuracy of determining the points of commutation is also affected by the threshold value. The error of commutation can be corrected by changing the coefficients k_1, k_2. For example, for angle of commutation =240 degrees, an increase in k_1 (greater than 3) leads to a delay in the formation of the commutation signal, and when reducing k_1, the commutation signal is produced ahead of time. The estimation of the error of commutation is made by comparing the current at the time of switching off the section $i_{off}(t_c)$ and the

current at the time of switching on the section $i_{on}(t_c +\Delta t)$ (t_c – commutation of time, Δt – delay that takes into account the time of the transient process in the winding). The coefficients k_1 and k_2 are adjusted for the difference of these currents $di = i_{off}(t_c) - i_{on}(t_c +\Delta t)$.

When correcting the error commutation, the coefficient vectors $K_1 = [k_{11}, k_{12}, k_{13}, k_{14}, k_{15}, k_{16}]$, $K_2 = [k_{21}, k_{22}, k_{23}, k_{24}, k_{25}, k_{26}]$ whose initial values are set $K_1 = [3, 3, 3, 3, 3, 3]$, $K_2 = [0, 0, 0, 0, 0, 0]$. Each element of the vector corresponds to a point of commutation 0˚, 60˚, 120˚, 180˚, 240˚, 300˚. Parameters are also set Δt, di. After determining the time of commutation, the value di is determined and the corresponding coefficient is adjusted based on the table 2. The values of the coefficients restricted to values. After several cycles of switching the windings, the error is reduced.

Table 2. The calculation of the coefficients k_1, k_2 of the error commutation corrected

θ_c	$di>0$, $|di|>\Delta i$	$di<0$, $|di|>\Delta i$
$\pi/3$	$k_1=k_1-\Delta k$, $k_2=0$	$k_1=k_1+\Delta k$, $k_2=0$
$2\pi/3$	$k_1=k_1-\Delta k$, $k_2=0$	$k_1=k_1+\Delta k$, $k_2=0$
π	$k_1=3$, $k_2= k_2-\Delta k$ 0	$k_1=3$, $k_2=k_2+\Delta k$ 0
$4\pi/3$	$k_1=k_1+\Delta k$, $k_2=0$	$k_1=k_1-\Delta k$, $k_2=0$
$5\pi/3$	$k_1=k_1+\Delta k$, $k_2=0$	$k_1=k_1-\Delta k$, $k_2=0$
2π	$k_1=3$, $k_2= k2 +\Delta k$ 0	$k_1=3$, $k_2=k_2-\Delta k$ 0

For the model checking method was carried out for the model of the ideal typical signals $e_\alpha(t)$, $e_\beta(t)$, i_a, i_b, i_c . The results of the computational experiment are illustrated in Figure 4 for the angle of commutation 240 electrical degrees. The error of commutationon each cycle is reduced almost to zero.
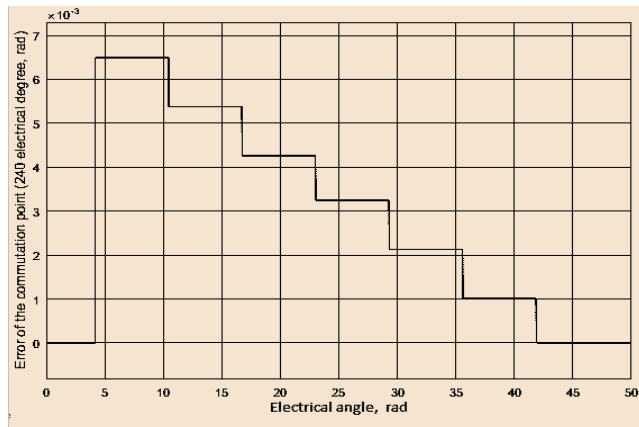
Figure 4: Error of commutation

The functional diagram of sensorless control and error of commutation correction is shown in Figure 5.

The procedure for starting the BLDC motor includes two stages: the first process of aligning the rotor in the equilibrium position, the second of accelerating up the rotor from the stable equilibrium position to the speed at which it is possible to transit to sensorless control of switching the motor windings. When the rotor is started, the rotor of BLDC is stationary or rotates at a very low speed. It is almost impossible to estimate the position of the rotor by the back-EMF of rotation, which in this case is zero or small. When switching two of the phase, the position rotor of

which is unknown, acquires acceleration and moves to a stable equilibrium position. With a small damping, oscilations occur in the vicinity of a stable equilibrium position. When moving in the direction of a stable equilibrium position, the rotor accelerates, and when moving from the equilibrium position, it is slowed down. If the damping is low, the kinetic energy acquired during rotor acceleration is approximately equal to the potential energy accumulated during braking. When the rotor speed is zero and the rotor starts moving in the direction to a stable equilibrium position. The acceleration square is approximately equal to the braking square.
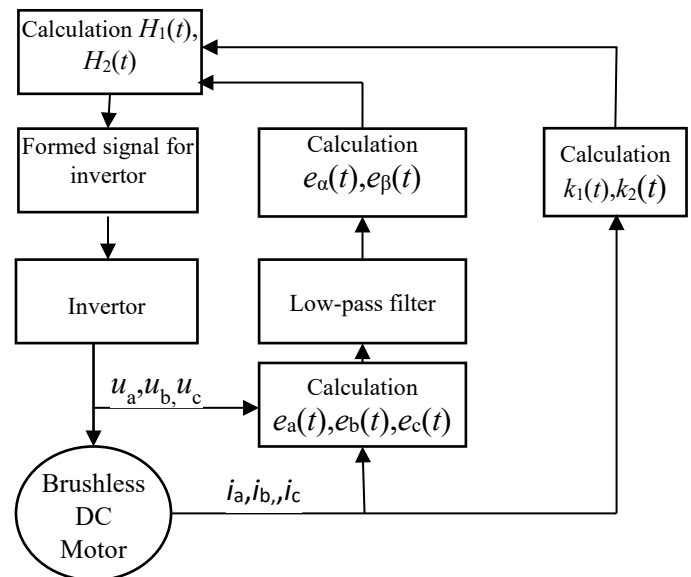
Figure 5: The functional diagram of sensor-free control BLDC motor

Stable rotor equilibrium positions is depended on various load. The area of acceleration and braking depends on the magnitude of the voltage applied to the phases. Vibration damping when the rotor position is aligned is performed by reducing the acceleration square, which is performed by reduce of the voltage on the switching phases $u = U_r$. After passing a stable equilibrium position, the voltage on the phases increases $u = U_s$, which reduces the angle deviation from the equilibrium position. When the speed becomes zero, the voltage reduces $u = U_r$ (u – voltage of commutation phases). The acceleration square is reduced. The procedure is then repeated until the rotor position is aligned with the equilibrium position.

Let $S_a(\Delta\theta)$ be the acceleration area, and $S_b(\Delta\theta)$ be the deceleration area. For low damping, it must be performed $S_a(\Delta\theta) \approx S_b(\Delta\theta)$, $\Delta\theta = \theta - \theta_s$.

$$\Delta\theta(k+1) = (S_a)^{-1}[S_b(\Delta\theta(k))],$$

If the maping will be compressive if $|\Delta\theta(k+1)| < | \Delta\theta(k)|$, then the iterative process converges and $\Delta\theta$ tends to zero. The rotor position is aligned relative to the stable equilibrium position.

The moments of changing the voltage on the section are determined by changing the current of the section. After switching the winding, the current at the rotor acceleration initially decreases,

and then increases when passing the equilibrium position is equal to the initial one. At this point, the voltage increases $u = U_s$ and a new value of the initial current is set. The current during braking first increases, and then decreases and reaches the initial value, at which point the voltage decreases $u = U_r$. The process is then repeated until the rotor position is aligned (Figure 6).
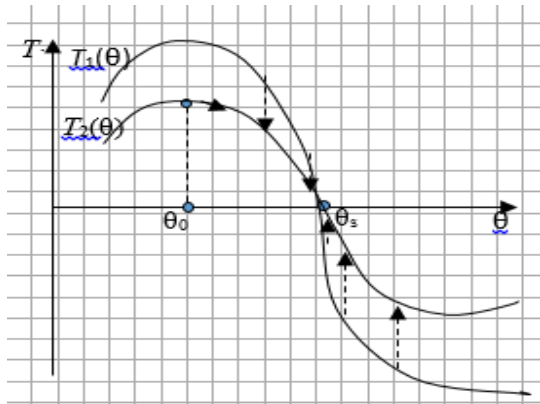
Figure 6: Aligned position of rotor

4. Simulation results

To substantiate and study the effectiveness of the proposed sensorless control, start-up and corrected error of commutation method for a low-power brushless DC electric motor with permanent magnet was simulated.

The simulation was performed using the MATLAB&Simulink system and models of a three-phase brushless DC motor and a power semiconductor bridge commutator of the SimPowerSystems expansion. A motor is an electric machine with a three-section winding on the stator and a multi-pole rotor with permanent magnets. BLDC motor parameters are given:

Rated DC Voltage – 27 V;

Rated speed, n = 2000 r/min;

Number of poles, p = 4;

Phase resistance, R = 6 Ω;

Phase Inductance, L = 0.42 mH.

When starting the motor, the position of the rotor is not determined. If one connects two sections of the motor to a DC voltage source, the rotor begins to move to a stable equilibrium position (stable point). Let $u_a = U_0$, $u_c = 0$, phase "b" is disconnected from the source.

The proposed start-up procedure involves two steps for the transition to the sensorless control of BLDC motors. In the first step, the procedure is performed to align the rotor position and to calm down oscillation in a stable equilibrium position. At this step, a constant voltage of various values $U_r = 27$ V, $U_s = 50$ V was applied to the switching phases (phases a, c), which provided alignment of the rotor position and damping of vibrations around a stable equilibrium position. In the second step, a constant voltage was applied to the switching phases (phases b, c). After the speed set, there was a transition to sensorless control of commutation of the BLDC motor windings. Simulation of start-up and control of

commutation of the BLDC motor windings was performed using the MATLAB/Simulink system. For Figure 7 the simulation results are presented: the function $H(t)$. Function $H(t)$ is sum $H_1(t)$, $H_2(t)$. The results of modeling the motor start and transition to sensorless control are shown in Figure 8.
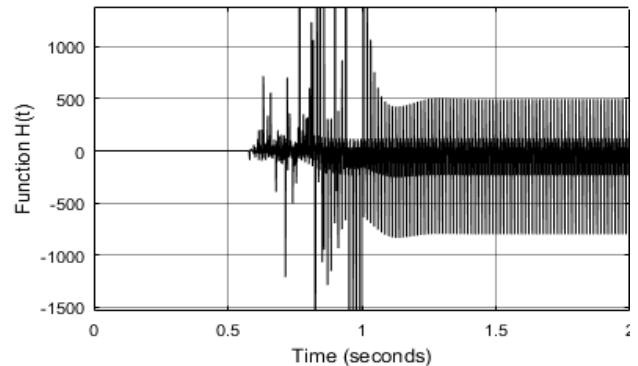
Figure 7: Function H(t)
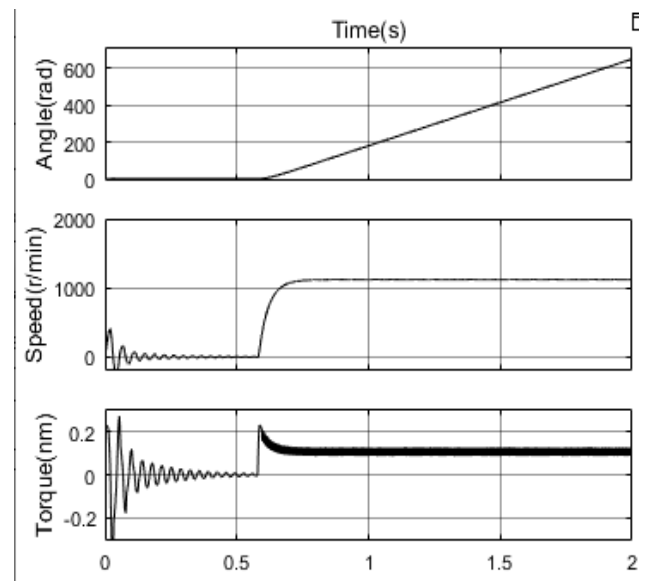
Figure 8: Start-up fnd transition to the sensorless control
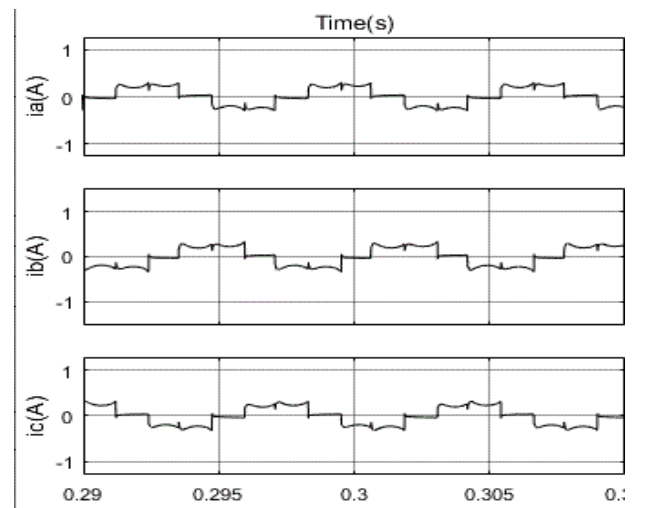
Figure 9: Corrected of phase current

To demonstrate the capabilities of the proposed method for correcting the commutation error, a simulation of BLDC motor with different speeds was performed. Error correction was performed by analyzing phase currents. Phase currents after error compensation are shown in Figure 9.

The table 3 shows the dynamics of the commutation error when it is compensated by the proposed method. At low speed=500 the initial commutation error was small. Initial commutation error was reduced to an error 0.12 electrically degree. At the speed of 1000, the initial error 3.5 electrically degree was also reduced by the correction method to 0.1 electrically degrees. At the nominal speed of rotation, the significant error of 14 elecctrically degree was reduced to 0.2 electrically degrees. These results confirm the possibility of reducing the compensation error in a simple corrected method.

Table 3: Error of commutation

t, s	$\Delta\theta$, deg (n=500 r/min)	$\Delta\theta$, deg (n=1000 r/min)	$\Delta\theta$, deg (n=2000 r/min)
0.01	1.25	3.5	13.9
0.05	0.96	1.9	10.8
0.1	0.81	1.6	5.2
0.15	0.54	1.35	3.7
0.2	0.56	1.08	2.1
0.25	0.45	0.54	1.6
0.3	0.12	0.1	0.2

5. Conclusion

The paper offers a simple method for correcting the commutation error in the case of sensorless control of a BLDC motor. A start-up procedure based on align the rotor position and damping its oscilations in a stable equilibrium position is proposed. This allows to accelerate the rotor and transient to sensorless control. The proposed method can increase the efficiency of sensorless control methods for BLDC motor with small inductive.

Conflict of Interest

The authors declare no conflict of interest.

References

[1] A.V. Stepanov, V.N. Enin, "Sensorless control of low-power brushless DC motor based on the use of back-EMF," in 2019. IEEE Internatiol Ural Conference on Electrical Power Engineering (Uralcon), 277-283, 2019, doi:10.1109/URALCON.2019.8877642

[2] A.K. Arakelyan, A.A. Afanas'ev, The rectifier of the electric machine in the systems of electric drive," M.: Higher school, 2006.

[3] A.P. Belkovsky, "Precision electric drive with valve engines," - Moscow: MPEI, 2010.

[4] M. Bychkov and A. Krasovsky, "Taking Into Account Nonlinear Properties of Switched Reluctance Machines in Electric Drive Control Algorithms," in 2018 X International Conference on Electrical Power Drive Systems (ICEPDS), Novocherkassk, 1-5, 2018, doi:10.1109/IWED.2018.8571868

[5] R. C. Guo, Z. Mu , J. D. Li, "Research on Position Sensorless Control System of High-Speed Brushless DC Motor," in 2017 9th International Conference on Intelligent Human-Machine Systems and Cybernetics, 62-65, 2017, doi:10.1109/IHMSC.2017.21

[6] A. Halvaei Niasar, A. Vahedi, H. Moghbelli, "A novel position sensorless control of a four-switcy, brushless DC motor drive without phase shifter," IEEE Trans. Power Electron., **23**(6), 3079-3087, 2008, doi:10.1109/TPEL.2008.2002084

[7] H. Li, S. Zheng, H. Ren, "Self-Correction of Commutation Point for High-Speed Sensorless BLDC Motor With Low Inductace and Nonideal Back EMF," IEEE Transactions on Power Electronics, **32**(1), 642-651, 2017, doi:10.1109/TPEL.2016.2524632

[8] W.Li, J. Fang, H. Li, J. Tang, "Position sensorless control without phase shifter for high-speed BLDC motor with low inductance and nonideal back EMF," IEEE Trans. Power Elecnron., **31**(2), 1354-1366, 2016, doi:10.1109/TPEL.2015.2413593

[9] J.S. Park, K.L. Lee, S.G. Lee, W.H. Kim, "Unbalanced ZCP compensation method for position sensorless BLDC motor," IEEE Trans. Power Electronics, **34**(4), 3020-3024, 2019, doi:10.1109/TPEL.2008.2002084

[10] X. Zhou, X. Chen, F. Zeng, J. Tang, "Fast commutation instant shift correction method for sensorless BLDC motor based on terminal voltage information," IEEE Trans. Power Electronics, **32**(12), 9460-9472, 2017, doi:10.1109/TPEL.2017.2661745

[11] G. Su, J. McKeever, "Low-cost sensorless control of brushless DC motor using a frennquency-independent phase shifter," IEEE Transaction on Power Electronics, **19**(2), 296-302, 2004, doi:10.1109/TPEL.2003.823174

[12] S. Chen, X. Zxou, G. Bai, K. Wang, L. Zhu, "Adaptive commutation error compensation strategy based on a flux linkage function for sensorless brushless DC motor drives in a wide speed range," IEEE Trans. on Power Electron., **33**(5), 3752 -3764, 2018, doi:10.1109/TPEL.2017.2765355

[13] S. Chen, G. Liu, L. Zhu, "Sensorless Control Strategy of a 315 kW High-Speed BLDC Motor Based on a Speed-Independent Flux Linkage Function". IEEE Trans. Ind. Electronics, **64**(11), 8607-8617, 2017, doi:10.1109/TIE.2017.2698373

[14] G. Liu, C. Cui, K. Wang, B. Han, S. Zheng, "Sensorless control for hign-speed brushless DC motor based on the line-to-line back EMF," IEEE Trans. Power Electron., **31**(7), 4669-4683, 2016, doi:10.1109/TPEL.2014.2328655

[15] X. Song, B. Han, J. Fang, "High-precision sensorless drive for high-speed BLDC motors based on the virtual third harmonic back-EMF," IEEE trans Power electron., **33**(2), 1528-1540, 2018, doi:10.1109/TPEL.2017.2688478

[16] W. J. Lee, S.-K .Sul, "A New Starting Method of BLDC Motors Without Position Sensor," IEEE Trans. Ind. Appl., **42**(6), 1532-1538, 2006, doi:10.1109/TIA.2006.882668

A Case Study to Enhance Student Support Initiatives Through Forecasting Student Success in Higher-Education

Ndiatenda Ndou[*,1], Ritesh Ajoodha[1], Ashwini Jadhav[2]

[1]*School of Computer Science and Applied Mathematics, The University of the Witwatersrand, Johannesburg, 2050, South Africa*

[2]*Faculty of Science, The University of the Witwatersrand, Johannesburg, 2050, South Africa*

ARTICLE INFO

ABSTRACT

Enrolment figures have been expanding in South African institutions of higher-learning, however, the expansion has not been accompanied by a proportional increase in the percentage of enrolled learners completing their degrees. In a recent undergraduate-cohort-studies report, the DHET highlight the low percentage of students completing their degrees in the allotted time, having remained between 25.7% and 32.2% for the academic years 2000 to 2017, that is, every year since 2000, more than 67% of the learners enrolled did not complete their degrees in minimum time. In this paper, we set up two prediction tasks aimed at the early-identification of learners that may need academic assistance in order to complete their studies in the allocated time. In the first task we employed six classification models to deduce a learner's end-of-year outcome from the first year of registration until qualifying in a three-year degree. The classification task was a success, with Random Forests attaining top predictive accuracy at 95.45% classifying the "final outcome" variable. In the second task we attempt to predict the time it is most likely to take a student to complete their degree based on enrolment observations. We complete this task by employing six classifiers again to deduce the distribution over four risk profiles set up to represent the length of time taken to graduate. This phase of the study provided three main contributions to the current body of work: (1) an interactive program that can calculate the posterior probability over a student's risk profile, (2) a comparison of the classifiers accuracy in deducing a learner's risk profile, and (3) a ranking of the employed features according to their contribution in correctly classifying the risk profile variable. Random Forests attained the top accuracy in this phase of experiments as well, with an accuracy of 83%.

1 Introduction

The benefits that can be drawn from institutions of higher-learning extend beyond the degree holder. A study conducted on the relationships between the quality of life, human capital, and universities, revealed that valuable consumption amenities that enhance an areas quality of life are positively correlated with both the local level of human capital (measured by proportion of degree holders in an area) and the number of institutions of higher-learning in a region [1].

The higher-education system is one of great benefit to enrolled-individuals, the economy, and society, however, an inefficient system with high dropout rates and low throughput rates carries harsh costs and consequences for the individual student as well as the society financing the cost of service delivery [2]. The South African

Human Science Research Council (HSRC) found that on average, 70% of the university drop-outs they surveyed came from families in the "low economic status civilian" category [3]. Students that belong in this category heavily depend on government study grants and subsidies to supplement the funding they receive from their parents or guardians. It is clear that student debt accumulation, or alternatively, costs to the government without a return on investment will be the outcome when these learners struggle and dropout. This was the case in 2005, where the national treasury reported R4.5 billion lost to student grants and subsidies that resulted in no graduates [3]. There is a student attrition problem in South Africa, as the expansion of enrolments has not come with a significant increase in the percentage of students completing their degrees [4].

Noting the value and possible severe-costs associated with in-

---

*Corresponding Author: Ndiatenda Ndou, The University of the Witwatersrand, Johannesburg, +27 71 168 8461 & ndiatenda.ndou@students.wits.ac.za

Table 1: This table introduces categories for the different features associated with student performance as discussed in Section 2. The features are divided into four groups, namely, "Socioeconomic Factors" (SEF), "Psycho-Social Factors" (PSF), "Pre & Intra-College Scores" (PICS), and "Individual Attributes" (IA). It is also important to take note of the colour coding scheme developed here for later reference to the four categories, [5](sic).

Socioeconomic Factors (SEF)	Psycho-Social Factors (PSF)	Pre & Intra-College Scores (PICS)	Individual Attributes (IA)
Family income	Academic self-efficacy	Mathematics	Age at first year
Parents education	Stress and time pressure	English	Work status
Head of house occupation	Class communication	Admission Point Score	Home language
Dwelling value	College activity participation	Accounting	Home province
Dwelling location (rural/urban)	Organization and attention to study	Economic studies	Home country
Financial support	Sense of loneliness	Statistics major	Interest in sports

stitutions of higher-learning, we see the clear need to explore the activities influencing student success or failure to solve the problem of student attrition and avoid the severe costs and consequences that it brings. Furthermore, we seek to develop advanced systems for the early-identification of vulnerable learners that may benefit from academic support systems.

In this research, we investigate the influence of biographical and enrolment observations on student success. This research was conducted through two published studies referred to as "phases of the current study" throughout this paper [5, 6]. In the first phase, we employ six machine learning models to predict three target variables that describe a learner's end-of-year outcome, namely, "first-year outcome", "second-year outcome", and "final outcome" [5]. The first phase of this research contributes to the current body of work by showing that various classification models can be used to predict a learner's end-of-year outcome from the first year of registration until qualifying in a three-year degree. We argue that if we can predict the academic trajectory of a student, early-assistance can be provided to students who may perform poor in the future, remediating their performance and promoting student success.

The second phase of this study involved the prediction of a "risk profile" variable, a variable that categorises the time taken by a student to graduate in a three-year degree by four values, namely: "no risk", where the student completes the degree in three years; "low risk", where the student completes the degree in more than three years; "medium risk", where the student fails/drops-out in less than three year; and "high risk", where the student takes more than three years to drop out [6]. We used six machine learning algorithms to predict the "risk profile" variable for a student based on biographical and enrolment observations. The second phase of this study contributes to the current body of related literature in three ways: (1) a comparison of six different classifiers in predicting the risk profile of a learner; (2) a ranking of the features employed according to their contribution when deducing the "risk profile"; and (3) an interactive program which uses Random forests classifier to deduce the distribution over a learner's risk profile. The contribution made by this research implies institutions of higher-learning can use machine learning techniques for the early-identification of learners that may benefit from academic assistance initiatives.

This paper continues with Section 2 which presents the background knowledge around the problem. We then introduce the

procedure and system of methods applied in Section 3, followed by the results in Section 4. The work is concluded on Section 5 and we close this study with ideas of future work in Section 6.

2 Related Work

Predicting student performance is a multifaceted task that cannot be easily completed using attributes discovered in student enrolment records alone [4]. We therefore, set-out to explore the various factors influencing student performance, aiming to discover and develop an efficient methodology for solving the problem set up in this research. We begin this chapter with the discussion and grouping of the factors influencing student performance, followed by a brief presentation of the conceptual framework adopted for feature selection in this research, and we close the chapter with a comparison of the various methods of predicting student performance.

2.1 Factors affecting student performance

The South African Department of Higher Education and Training (DHET) released a report with results that portray an increasing number of first-time-entering university students, from 98095 students in the year 2000 to over 150000 students in the 2017 academic year [7]. This significant increase brings the idea that the various attributes that describe a university student must be more varied now than ever before, as more learners from different regions are now enrolling for degrees. To accurately early-identify a member of a given group of learners as successful or unsuccessful in their studies, we must explore a wide range attributes that describe these students, so that our decision is informed.

2.1.1 Socio-Economic Observations Determining Student Success

To determine an individual or their family's measure of social and economic position in the population, we explore the category of socio-economic attributes as determinants of student success. Studies have shown that a correlation exists between socio-economic status and academic achievement, furthermore, traditional measures of socio-economic status have been revealed to usually correlate strong enough with academic achievement to account for variations
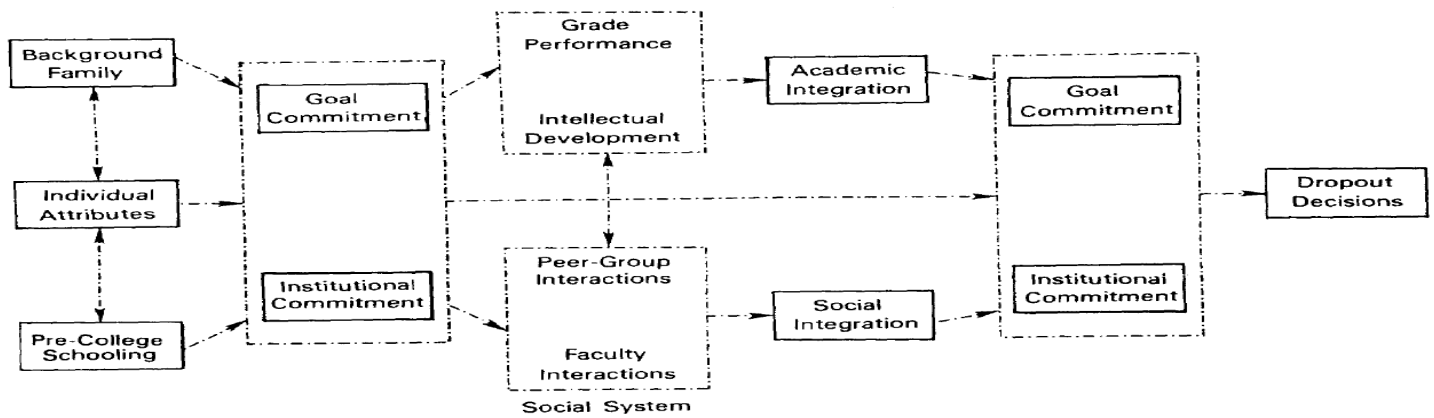
Figure 1: The graphical representation of the framework adopted to determine student success, [6](sic).

in a learner's performance [8]. A study of the determinants of student success also concludes that socio-economic factors contribute significantly when predicting a learner's performance [4]. The socio-economic attributes investigated in the literature we reviewed include; parents' education, dwelling value, family income, and parent/guardian's occupation. Family characteristics and financial support also form part of socio-economic factors revealed to explain student performance, specifically drop-out behaviour in university [2].

2.1.2 Psycho-Social Factors Affecting Student Performance

We seek to find more categories of factors that account for variations in a learner's academic performance. We therefore, explore the combined effects of a student's thoughts, social factors, and general behaviour at university on academic performance. Research conducted at a South African university found that to predict a learner's academic performance and adjustment to higher-education, psychosocial factor's such as; help-seeking attitude, workload, perceived stress, and self-esteem could be utilized as determinants [9].

Research on college students' performance utilized six psychosocial factors to predict first-year college student success [10]. The six psycho-social attributes used for prediction were; stress and time pressure levels, communication/participation in class, academic self-efficacy (a learner's belief in their ability to succeed academically), attention to study (measures time-management, planning, and scheduling behaviour), stress levels, and lastly, emotional satisfaction with academics. It was revealed that a strong correlation exists between the six psycho-social factors and a learner's GPA, these findings align with other related work [11]. A separate study also discovered that academic self-efficacy, student's optimism, commitment to schooling, and student health account for some of the variations in a student's performance, expectations and coping perceptions [12].

2.1.3 Factors Available For This Study

The review literature centred around factors affecting student performance revealed that a learner's mindset, social surrounding, and behaviour, explain significant variations in the performance of a

university learner. In this research, student biographical and enrolment observations such as, majors enrolled for, age, pre-college scores, province and country of origin, are available to build machine learning models for the prediction of academic performance. We continue this chapter by introducing the framework we adopted for the rationale behind predicting academic performance from biographical and enrolment observations.

2.2 Conceptual Framework

We use the conceptual framework depicted in Figure 1 as a logical basis to predict the academic performance of a learner from biographical and enrolment observations [13]. The framework develops three categories of attributes contributing to student attrition (dropout behaviour), namely, background attributes, individual attributes, and pre-college scores. The study reveals that these factors together influence a learner's goal and institutional commitment, which in turn contributes to the drop-out decision of a student via academic and social integration [13]. In this research, we partition background attributes further into socio-economic and psycho-social factors. Table 1 presents the grouping of features discovered to explain variations in academic performance during the review of related literature conducted in this section.

2.3 Methods For Predicting Student Performance

Various authors have already accurately predicted student performance utilizing machine learning. Table 2 compares the accuracies obtained in the various literature reviewed in this research. Acquiring the top accuracy position is a research based on the prediction of the success of a second-year student using an Artificial Neural Network (ANN) model [14]. The study uses individual attributes (IA), pre & intra-college scores, and socio-economic factors as predictors, these inputs are utilized for almost every result presented in the table [11, 17, 16].

3 Research Methodology

This research proposes an approach to the task of university-learner-performance prediction involving the prediction of a learner's end-

of-year outcome from the first year they register for a three-year degree until qualifying to graduate. We complete this task by employing six different machine learning algorithms to deduce the outcomes in the first, second, and final year of study in a South African university. This study extends further by attempting to predict a learner's risk-profile based on the time it will take the student to complete a three-year degree.

Table 2: The table compares the accuracy achieved by various authors using different machine-learning models to predict academic performance in each case. The table also illustrates for each case, the combination of features used as predictors, based on the feature categories developed in Table 1, [5] (sic).

Author(s)	Factors considered	Model used	Predictive Accuracy
Abu-Naser *et al.* (2015)[14]	IA, SEF, and PICS	Neural Networks	84.60%
Osmanbegovic and Suljic (2012)[11]	IA, SEF, PICS, and PSF	Naïve Bayes	84.30%
Osmanbegovic and Suljic (2012)[11]	IA, SEF, PICS, and PSF	Neural Networks	80.40%
Osmanbegovic and Suljic (2012)[11]	IA, SEF, PICS, and PSF	Decision Trees (C4.5)	79.60%
Mayilvaganan and Kalpanadevi (2014)[15]	IA and PICS	Decision Trees (C4.5)	74.70%
Ramesh *et al.* (2013)[16]	IA, SEF, and PICS	Multi-layer Perceptron	72.38%
Abed *et al.* (2020)[17]	IA, SEF, and PICS	Naïve Bayes	69.18%
Abed *et al.* (2020)[17]	IA, SEF, and PICS	SMO	68.56%
Ramesh *et al.* (2013)[16]	IA, SEF, and PICS	Decision Trees (C4.5)	64.88%

In this section, we introduce the procedure and system of methods implemented for the purpose of this study. The study incorporates two phases and thus, we begin by giving a description of the two phases, followed by subsection 3.2 giving a description of the data-sets. We present the feature selection technique in subsection 3.3 and follow this by a brief description of the machine learning models we used, closing the section with methods of evaluating and validating our results.

3.1 Phases of the Study

This study was conducted in two phases. The first phase, named, "Preliminary Phase", involved generating preliminary results on a synthetic dataset. In this phase we employed six different machine learning models, namely, Decision tree (C4.5), Logistic Model Trees (LMT), Multinomial Logistic Regression, naïve Bayes, Sequential Minimal Optimization (SMO), and Random forests. The purpose of the first phase was to reveal that machine learning models can be utilized for the early prediction of a learner's end-of-year outcome from the first year of registration until qualifying in a three-year degree, based on biographical and enrolment observations.

The second phase of this study, named, "Post-preliminary Phase", involved the prediction of the distribution over several risk profiles that describe the time it will take for a university student to complete a three-year degree. This phase is performed on a real dataset which the synthetic dataset in the first phase was modelled to resemble. In this phase we employed six different machine learning models, namely, Decision tree (C4.5), Linear Logistic Regression, Support Vector Machines (SVM), naïve Bayes, and Random forests. This phase provides an interactive program which calculates the posterior probability over a learner's "risk profile" as the main contribution o this study, and a ranking of features through Information Gain Ranking (IGR), to determine the features most contributing to student performance.

3.2 Data Description and Pre-Processing

Two sets of data were utilized in this study. We therefore, split the description of the datasets, starting with Subsection 3.2.1 which gives the synthetic dataset description, and Subsection 3.2.2 giving a description of the real dataset.

3.2.1 The Synthetic Dataset Description

The dataset used for the preliminary phase of this study is a synthetic dataset generated using Bayesian Network. The dataset was adopted from a recent prediction modelling study aimed at improving student placement at a South African university [17]. In this dataset, conditional independence assumptions were implemented to portray the relationships that exist between enrolment, socioeconomic, and individual attributes found in student records.

Three target variables are investigated in the preliminary phase, namely, "First Year Outcome" (FYO), "Second Year Outcome" (SYO), and "Final Outcome" (FO). The SYO and FYO variables contain two similar possible values: "proceed", and "failed", were proceed is the outcome for a student who met the requirements to proceed to the next year of study, and failed implies the student failed to meet the minimum requirements to proceed. The FO variable also has two possible values: "qualified", and "failed", were qualified implies the learner met the minimum requirements to graduate in a three-year degree, and failed implies the student failed to meet the requirements to graduate.

Data pre-processing is a crucial step when employing machine learning models. The pre-processing task incorporates, data preparation, data cleaning, data normalization, and data reduction tasks [18]. The synthetic dataset originally contained 50 000 instances. Three random samples (without feature replacement or bias to uniform class) containing 2000 instances were drawn from the raw dataset and several experiments were conducted to make the samples more suitable for our machine learning models. The first set of experiments focused on the detection and removal of outliers or anomalies. This involved the evaluation of classification results from different machine learning classifiers in an attempt to detect and remove instances that display significant deviations from the majority patterns. The second set of experiments conducted aimed to prevent over-fitting. This was done by the implementation of Synthetic Minority Oversampling Technique (SMOTE) which enforced an equal number of training instances for each value in the class variable. The third set of experiments conducted in the preliminary phase is feature selection, where 20 features were selected from each sample based on Information Gain Ranking (IGR) criterion. Subsection 3.3 presents the set of features selected from each sample and a discussion of how we arrived at this set.

3.2.2 The Real Dataset Description

The real data utilized for this study is from a research-intensive university in South Africa. The dataset composes of enrolment and biographical observations of learners enrolled in the faculty of science at the university, from the year 2008 to the year 2018.

The target variable for the post-preliminary phase of this study is "Risk Profile", a nominal variable that tells us how long it will take for an enrolled student to complete a three-year degree at a

South African university. The risk-profile variable has four possible values, namely; "no risk", where the student completes their degree in 3 years (the minimum allotted time); "low risk", where the student completes the three-year degree in more than 3 years; "medium risk", where the student fails to complete the three-year degree before the end of three years (student drops-out in less than 3 years' time); and "high risk", where the student fails to complete the three-year degree after exceeding the 3-years period (student drops-out after exceeding the allotted time).

Since our aim is to perform an accurate classification task on the dataset, pre-processing procedures had to be carried out before training the chosen classifiers. We performed the same experiments as those performed on the synthetic dataset to detect and remove outliers. We then employed a sampling procedure similar to the one we implemented in the preliminary phase of this study. Along with applying SMOTE, a random sample (with no replacement of features or bias to uniform class) of 200 instances was drawn from the original dataset. In Subsection 3.3 we present the features selected and the procedure followed to select them.

Table 3: A table providing the various features selected for input into the employed classifiers. The table groups the features according to whether they were used for the prediction of the learner's first year outcome, second year outcome, or final year outcome. The colour shading gives the category which the feature selected belongs to according to Table 1, [5] (sic).

#	Feature	1st Year	2nd Year	Final Year
1	English Home Language	green		
2	Plan Description	yellow	yellow	yellow
3	Quintile	red	red	red
4	Home Province	yellow	yellow	yellow
5	Year Started	yellow	yellow	yellow
6	Language	yellow	yellow	yellow
7	Progress Outcome YOS1		green	
8	Home country	yellow		
9	Aggregate YOS2			green
10	Rural or Urban	red	red	red
11	Second Year Outcome			green
12	Age at Third Year			yellow
13	Mathematics Literacy	green		
14	NBTAL	green	green	green
15	Age at First Year	yellow		
16	Computers	green	green	green
17	NBTQL	green	green	green
18	Age at Second Year		yellow	
19	Life Orientation	green	green	green
20	NBTMA	green	green	
21	Plan Code	yellow	yellow	yellow
22	English FAL	green	green	
23	Additional Mathematics	green	green	green
24	Mathematics Major	green	green	

3.3 Feature Selection

In this subsection we present the methodology behind the features selected for both phases of the study. Subsection 3.2.1 provides the features we utilized to generate the preliminary results and Subsection 3.2.2 provides the features selected for the post-preliminary phase of the study.

3.3.1 Features for the Preliminary Phase

To select features for the purpose of predicting the three target variables investigated in this phase of the study we utilized Information Gain Ranking (IGR) criterion, which involves deducing the contribution of each feature when classifying an instance as a value of the class variable. Table 3 presents the features selected in all cases considered for the preliminary phase, based on the colour coding scheme developed in Table 1.

Feature selection was performed on each of the 3 samples drawn from the synthetic dataset. We investigated the contribution of 44 features using Information Gain (entropy). Through the entropy values and repeated experimentation with different sets of features, a total of 20 features were selected to predict the target variable in each of the three samples.

The features presented in Table 3 are not arranged according to IGR as there are significant differences in the entropy of most features across predicting the three target variables. The features selected align with our findings from the review of previous work, and more importantly, the conceptual framework we adopt in this research [13]. This is because for each target variable, there were features selected from each of the three investigated categories of features, namely, background (socio-economic) attributes, individual attributes, and pre-college scores.

3.3.2 Features for the second phase

To select features for the post-preliminary phase of this study, we continued utilizing IGR alongside the conceptual framework investigated in the related work section [13]. From the "individual attributes" category, the following features were selected; the National Benchmark Test (NBT) scores for academic literacy (NBTAL), quantitative literacy (NBTQL), and mathematical literacy (NBTMA). These scores give a measure of the individual learner's proficiency and ability to meet the demands of university-level work. To further determine an enrolled learner's professional career aspirations, we also considered the academic plan selected by the learner. The "plan code", "plan description", and "streamline" (Earth Science, Physical Science, Biological Science, or Mathematical Science) variables were selected for this task.

From the "background and family" category, the following features were selected; the home-country and province of the student, whether the school attended by the leaner is in the urban or rural areas, the quintile of the school attended, and the age of the learner at the first-year of registration. These variables combined give us a description of the learner's socio-economic status.

From the pre-college scores category, scores from the following subjects were considered; Mathematics major, Mathematics Literacy, Additional Mathematics, Physical Science, English Home Language, English First Additional Language, Computer studies, and Life Orientation. We note that in this phase of the study, we did not utilize college or university outcomes as inputs, these outcomes were only utilized in the prediction of target variables set up in the preliminary phase as indicated in Table 3. The features selected for the post-preliminary phase of this study are presented ranked according to entropy in Table 6.

3.4 Classification Models

This study composed of two phases, each involving a classification task. In total, we use nine off-the-shelf machine learning predictive models to perform the classification tasks in this research. The models used are: Random forests, naïve Bayes classifier, Decision tree (C4.5), Logistic Model Trees (LMT), Multinomial Logistic Regression, Linear Logistic Regression, Sequential Minimal Optimization (SMO), Support Vector Machines (SVMs), and the K-Star (K*) instance-based classifier. We continue this subsection by giving a brief description of the selected models.

Sequential Minimal Optimization: SMO is an algorithm derived for the improved (speed) training of Support Vector Machines. SVMs previously required that a large quadratic-programming problem be solved in their implementation. Traditional algorithms are slow when training SVMs, however, SMO completes the task much faster by breaking the large quadratic programming problem into a series of smaller problems which are then solved by analytical methods, avoiding the lengthy numerical optimization required. The SMO algorithm we use for the purpose of this study follows the original implementation [19].

Multinomial Logistic Regression: This model derives and extends from the binary logistic regression. It does so by allowing categories of the outcome variable to exceed two. This algorithm utilizes the Maximum Likelihood Estimation (MLE) to predict categorical placement or the probability of category membership on a dependent variable [20]. Multinomial Logistic Regression requires the careful detection and removal of outliers for accurate results, however, the model does not assume or require linearity, homoscedasticity, or normality [20]. An example of a four-category model of this nature, with one independent variable x_i can be given by: $\log(\frac{\pi_i^{(s)}}{\pi_i^{(0)}}) = \eta_0^{(s)} + \eta_1^{(s)} x_i$, s = 1,2,3,4. Where; $\eta_0^{(s)}$ and $\eta_1^{(s)}$ are the slope and intercept respectively, given the probability of category membership in "s" can be denoted by $\pi_i^{(s)}$, and the selected reference category by $\pi_i^{(0)}$. The Multinomial Logistic Regression implementation in this research follows the implementation by other authors before the current study [21, 22].

Naïve Bayes Classifier: The naïve Bayes model is a simplified example of Bayesian Networks. The model achieves learning with ease by assuming that features employed are all independent given the class variable.

The diagram (a) in Figure 2 is an illustration of the naïve Bayes model. This is because the features, $x_1,...,x_5$ are conditionally independent given the class variable, C. The naïve Bayes independence assumption can be stated as the distribution: $P(C|X) = \prod_{i=1}^{n} P(x_i|C)$, where $X = (x_1,...,x_n)$ is a feature vector and C is the class variable. In application, naïve Bayes often performs well when compared to more sophisticated classifiers, although it makes a generally poor assumption [23]. The naïve Bayes model implementation in this research follows other similar implementations in related studies explored; [24, 23].

K* Instance-Based Classifier: The K-Star algorithm classifies instances using training instances that are similar to them alongside a distance function that is based on entropy. The use of an entropy based function provides consistency in the classification of instances in our experiments that may be real-valued or symbolic. The K* implementation utilized for the purpose of this research followed the implementation by [25].

Support Vector Machines: The (SVMs) classification model separates classes of the training data with a hyper-plane. The test instances then get mapped on the same space with their prediction based on the side of the hyper-plane they belong after splitting. This task is performed by incorporating the training dataset into a binary linear classifier that is non-probabilistic. SVMs can be scaled through the one-versus-all partitioning, for various types of classification problems including high-dimensional and nonlinear classification tasks. The SVM model implementation in this research follows the implementation in other related work [26].

Linear Logistic Regression: The Linear Logistic Regression model utilizes additive logistic regression with simple regression functions as base learners of the algorithm [27]. The implementation of this model followed in this research follows that of related work conducted in the past [28, 29].

Decision Tree: This model uses a decision support system to build a classification function that predicts the value of a dependent variable given the values of independent variables, through tree-like graph decisions and their possible after-effect, including costs of resources, chance results, and utility [30]. There are different algorithms for generating decision trees; C4.5, Random forest, and LMT are the tree-models selected for the purpose of this research.

The C4.5 algorithm uses information gain to build a decision tree, selecting features based on entropy and utilizing the ID3 algorithm recursively to build the tree. We follow the original structure and implementation of the C4.5 algorithm in this study [31].

LMT builds a single tree from a combination of logistic regression models and a tree structure. This model accomplishes the combination by using the Classification and Regression Tree (CART) algorithm to prune after building the regression functions through the LogiBoost algorithm. The LMT method used in this study follows from the original implementation [28].

Random Forests are a combination of decision tree predictors dependent on the value of a random vector, where the value also governs the growth of each tree in the generated forest. This algorithm involves utilizing the training data to generate an ensemble of decision trees and allowing them to decide on the most-popular class. Implementing this technique has several advantages, including that, the procedure abides by the Law of Large Numbers to prevent over-fitting, it is relatively robust to noise or outliers in

Figure 2: The diagrams (a) to (d) illustrate various examples of a Bayesian network model. The arrows travelling between nodes represent conditional dependencies among the features $x_1, x_2,...,x_5, C$. Where C, represents the class variable and the models differ based on the existence of a statistical dependence between the predictors $(x_1,...,x_5)$ [18].

data, and the model achieves accuracy as good as similar techniques such as, Adaboost, Bagging, and Boosting, while still training faster than them [32]. The Random forest model implementation in this research is based on the original model [32].

3.5 Prediction and Evaluation

In this research, the dataset contains the dependent attribute and the values of the classes are known, we therefore have a classification task set up. This subsection provides the measures and techniques utilized to complete this task.

3.5.1 Evaluation and Validation

10-fold cross-validation procedure is applied to evaluate each model employed in this research. In this validation procedure, the training dataset is partitioned such that a portion (testing data) of it is not provided to the algorithm during training, but is used for the validation. The partition remaining for training is further split into 10 partitions (folds). Interchangeably, each of the 10-folds serve for validation while the remaining 9 are used for training until all 10-folds serve as the validation fold once.

3.5.2 Confusion Matrix

We use confusion matrices to illustrate classification outcomes. Table 4 provides an example of the format of a confusion matrix.

Table 4: This table depicts the structure of a confusion matrix. We denote "negative" and "positive" by -ve & +ve respectively. Where TP are the true positives (correctly classified positives), FP the false positives, FN are false negatives, and TN are the true negatives (correctly classified negatives).

	Predicted Class +ve	Predicted Class -ve
Actual Class +ve	TP	FP
Actual Class -ve	FN	TN

3.5.3 Accuracy

We extract precision and recall metrics from the confusion matrix in order to measure the accuracy of the employed machine learning models. "Precision" represents the correctly real-positive proportion of predicted positives, while "Recall" represents the correctly predicted proportion of the real positives. We calculate precision and recall as follows:

$$Precision = \frac{TP}{TP+FP} \tag{1}$$

$$Recall = \frac{TP}{TP+FN} \tag{2}$$

The accuracy follows directly, calculated as:

$$Accuracy = \frac{TP+TN}{TP+TN+FP+FN} \tag{3}$$

This representation of accuracy has been used in other related work [17], [33]. Other measures of accuracy explored include the Receiver Operating Characteristic (ROC) curve. This curve plots recall (the true positive rate) against the false positive rate (ratio between FP and the total number of negatives), and the area under the ROC reflects the probability that prediction is informed versus chance [34]. We desire the ROC-area to lie above 0.5, anything below 0.5 implies the prediction was guesswork and not informed. Another accuracy measure utilized is the F-beta measure (F1 score), which calculates a test accuracy as the weighted harmonic mean of precision and recall. The optimal value for the F-measure is 1 (indicating perfect precision and recall), and the worst value is 0.

4 Results and Discussion

This study was conducted in two phases. The first phase involved generating preliminary results on a synthetic data-set, while in the second phase, a similar set of experiments are performed on a real data-set, leading to conclusions and implications about the performance of the trained machine learning models in classifying the problem at hand, furthermore, the results drawn from the second phase provide a ranking of the employed features according to entropy, together with an interactive program which calculates the posterior probability over the students' risk profile so that support initiatives and programs can be focused on them.

4.1 Preliminary Results

This Subsection presents the results of six of the nine prediction models discussed in Section 3, namely; Decision tree (C4.5), Logistic Model Trees (LMT), naïve Bayes Classifier, Sequential Minimal Optimization (SMO), Multinomial Logistic Regression, and Random Forests. We present first the prediction outcomes through a table comparing predictive accuracy of the models as determined by Equation 3. This will be followed by an evaluation of the model's performance through F-measure and Receiver Operating Characteristic (ROC) curve.

4.1.1 Prediction Outcomes

Six different machine learning models were utilized to solve our classification problem. The predictive accuracy achieved by each model is recorded and presented in the Table 5.

Table 5: Predictive accuracy as calculated by Equation 3. After 10-fold cross-validation, all of the models utilized achieved an accuracy above 80%, with Random Forests achieving top accuracy in all three cases considered, [5](sic).

	Predictive Accuracy		
Model used	1st Year Outcome	2nd Year Outcome	Final Year Outcome
Random Forest	94.40%	93.70%	95.45%
LMT	91.90%	91.75%	93.15%
Decision Trees (J48)	87.55%	86.20%	91.45%
Multinomial Logistic	87.80%	86.20%	90.70%
SMO	87.25%	84.45%	89.20%
Naïve Bayes	83.95%	83.40%	84.40%

4.1.2 Model Performance Evaluation

A study based on evaluating classification results argued for the use of Precision, Recall, F-Measure, and the ROC curve, as accurate measures of a machine learning model performance [34]. We utilize these measures to evaluate results presented by Figure 3, 4, and 5.
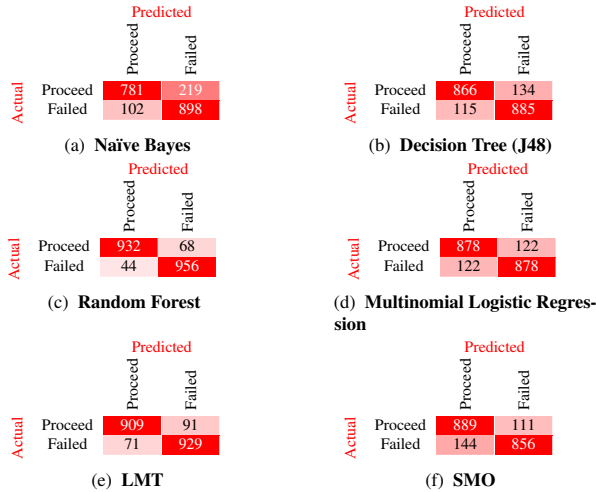
Figure 3: The set of confusion matrices resulting from the prediction of first-year outcome. Evaluation of the accuracy by class reveals that the weighted average of both precision and recall lies above 0.84 for all six models trained in our study. Further observations reveal that the f-measure of accuracy is more than 0.83 for all models, this value aligns with our accuracy as determined by Equation 3 in the Table 5. The test accuracy obtained in the table is further supported by the ROC curve obtained for all six models, as the weighted average of the ROC area for each model is more than 0.84 implying the models trained were making informed decisions in classifying the problem and not simply guessing.
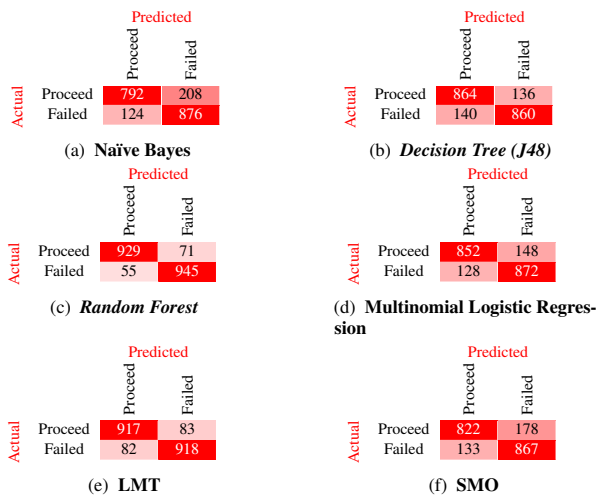
Figure 4: The confusion matrices obtained when classifying the second-year outcome variable. When we evaluate the detailed accuracy by class for each model, we find that the weighted average of both precision and recall measures is above 0.83, furthermore, the f-measure of test accuracy aligns with our findings in Table 5 with a value of more than 0.83 for all six models considered. The ROC curve obtained for all six models also aligns with our accuracy as determined by f-measure of test accuracy and Equation 3, as the weighted average of the area under the ROC curve lies above 0.85 implying the models trained are not attaining the great predictive accuracy through guess-work, but they are making informed predictions.
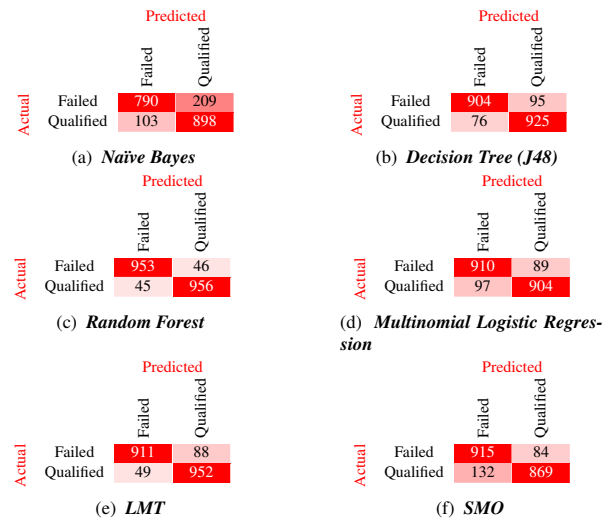
Figure 5: Confusion matrices obtained when classifying the third-year outcome variable with the six trained machine learning models. Evaluating the detailed accuracy by class results, we find that the weighted average of both precision and recall measures is more than 0.89 for all models except the naïve Bayes classifier which scored 0.85 for precision, and 0.84 for recall. The underperformance of the naïve Bayes model with respect to other trained classifiers can be explained by the naïve feature-independence assumption it makes. Results also show that the weighted average of the area under the ROC curve for each model is in alignment with our test accuracy measures, as it lies above 0.89, implying each model is making informed predications and not simply guessing the outcome.

4.2 Main Results (Post-preliminary)

The preliminary phase of this study revealed that we can utilize machine-learning models to accurately predict a learner's outcome from the first year of registration until qualifying in a three-year degree. The preliminary results confirmed our initial hypothesis but furthermore, revealed the kind of model we should utilize with such a wide variety of models available for use, but few fitted to the problem set up in this study. Evaluating the preliminary results, we note that Random Forests achieved top accuracy and performance as measured by all our model performance and accuracy evaluators, across all three test cases.

In this subsection, we present the results obtained when utilizing machine learning models to classify a learner into the four risk profiles ("No Risk", "Low Risk", "Medium Risk", and "High Risk") defined in Section 3, as the preliminary phase has confirmed this task can be completed. The classification problem set up in this phase is parallel to that in the prelim-phase in several ways, as the preliminary phase utilizes a synthetic data-set modelled to resemble the relationships that exist within the student enrolment data utilized for the second phase.

Subsection 4.2.1 presents the selection and ranking of features utilized, we follow this by a presentation of the classification outcomes and close the section with the presentation of an interactive program that can be utilized to calculate the posterior probability over a student's risk profile.

4.2.1 Selection and Ranking of features

We selected 20 features to predict the class variable. The features were selected using Information Gain Ranking (IGR) to deduce

the contribution of each feature in classifying the instances. The feature selection findings are illustrated through Table 6 with three columns below. The first column determines the rank of the features among the input set, the second column gives the amount of entropy attained by the feature, and the third column has the name of the feature associated with the ranking and entropy.

Table 6: A ranking through information gain (entropy) of the set of features selected to predict the student risk profile, ranked from the most contributing feature to the least contributing feature. The top seven features that are highlighted indicate an entropy greater than 0.1, [6] (sic).

Rank	Entropy	Feature Name
1	1.21960228	PlanCode
2	1.15086266	PlanDescription
3	0.59886383	Streamline
4	0.29582771	Year Started
5	0.20836689	AgeatFirstYear
6	0.18695721	SchoolQuintile
7	0.14234042	MathematicsMatricMajor
8	0.12166049	Homeprovince
9	0.06417526	isRuralorUrban
10	0.0568866	LifeOrientation
11	0.04978826	PhysicsChem
12	0.02780914	EnglishFirstLang
13	0.01253064	Homecountry
14	0.00550434	AdditionalMathematics
15	0.00000902	MathematicsMatricLit
16	< 0.00001	NBTAL
17	< 0.00001	NBTMA
18	< 0.00001	NBTQL
19	< 0.00001	ComputerStudies
20	< 0.00001	EnglishFirstAdditional

Figure 6: A graphical illustration of how the information gain (entropy) level varies across the chosen feature input set. The x-axis indicates the feature rank, and the y-axis indicates the information gain from utilizing the corresponding feature, [6] (sic).

The use of IGR also has implications on the contribution made by a feature relative to others within the chosen input set of fea-

tures. We investigate the behavior of entropy as you move between subsequent features and present the findings through a graphical illustration in Figure 6, showing the monotonically decreasing behavior of the entropy function plotted versus rank. We see that the loss in entropy between each subsequent point (feature rank) is logarithmically decreasing, furthermore, we highlight the same top seven features from the IGR Table 6.

The highlighted features on Figure 6 illustrates their relative importance in forecasting the success of a learner. We note that the set of factors most contributing to a learner's success includes, "the plan-code and plan description" (combined, these two variables give a precise description of what the student is studying), "streamline" (mathematical, life, or physical science), "the year started", "school quantile", "age at first-year", and "the student's matric mathematics score".

4.2.2 Classification Outcomes

This section presents the results obtained from the classification algorithms trained to predict the class variable (risk profile). Six of the nine classification procedures discussed in Section 3 were employed for the post-preliminary phase of the study: Decision trees (C4.5), naïve Bayes Classifier, Linear Logistic Regression model, Support Vector Machines (SVMs), K*, and Random Forests.

Figure 7 (a) – (f) illustrates the results of each trained classifier after 10-fold cross-validation. Evaluating the performance of each model relative to other models employed, we note that the Random forests classifier attains the highest accuracy (83%) of all the models trained for the post-preliminary phase. This result aligns with our findings from the preliminary phase of the study as Random forests attained the highest accuracy among the selected models for both phases of the study.

We note further that the SVM classification model was revealed to be the least suited for the problem set up in this study. At 52%, SVMs attained the lowest predictive accuracy in this study, furthermore, SVMs took the longest time to train. When discussing training and testing times, it is also important to note that the K-star model took the least time to implement in this study.

Overall, the classification task was a success, with five of the six models employed attaining a predictive accuracy above 75%. Noting that Random forests was the most accurate in predicting the class variable for both phases of this study, this section continues by providing a web application utilizing the Random forests classifier to predict the risk-profile of a learner based on enrolment and academic factors. Severity of misclassified instances was also evaluated and taken into account to determine Random forests as the most suited model for the task, for example, the 27% of "No Risk" instances incorrectly classified by SVM as "Medium Risk" is far more severe and misleading than the misclassification of 5% "No Risk" instances as "Medium Risk" by Random forests classifier.

4.2.3 Main Contribution of The Study

In this subsection we provide an interactive program which can calculate the posterior probability over a student's risk profile utilizing the Random forests model employed in Section 4.2.2. This automated system makes predictions about a student's risk of fail-

Predicted Risk

	No	Low	Med	High
No	171	20	9	0
Low	26	143	25	6
Med	17	22	145	16
High	2	7	16	175

(a) A confusion matrix resulting from the prediction of a student's "Risk Profile" utilizing the **C4.5** classification model. The **C4.5** algorithm achieved **79**% accuracy, furthermore, 634 instances were correctly classified and 166 instances were incorrectly classified by the model.

Predicted Risk

	No	Low	Med	High
No	159	24	11	6
Low	25	145	14	16
Med	14	21	124	41
High	6	7	12	175

(b) A confusion matrix detailing the performance of the **K*** classifier when predicting a student's "Risk Profile" (class variable). The lazy K-Star algorithm achieved **75**% accuracy, furthermore, 603 instances were correctly classified and 197 instances were incorrectly classified by the model.

Predicted Risk

	No	Low	Med	High
No	174	16	10	0
Low	31	142	22	5
Med	8	17	160	15
High	6	8	17	169

(c) A confusion matrix detailing the performance of the **naïve Bayes** classifier when predicting a student's "Risk Profile" (class variable). After 10-fold cross-validation the naïve Bayes classifier achieved **80**% accuracy, furthermore, 645 instances were correctly classified and 155 instances were incorrectly classified by the model.

Predicted Risk

	No	Low	Med	High
No	108	23	55	14
Low	38	80	65	17
Med	29	34	125	12
High	37	26	34	103

(d) A confusion matrix resulting from the prediction of a student's "Risk Profile" utilizing the **SVM** classification algorithm. The SVM algorithm achieved **52**% accuracy, furthermore, 416 instances were correctly classified and 384 instances were incorrectly classified by the model.

Predicted Risk

	No	Low	Med	High
No	174	17	9	0
Low	23	150	21	6
Med	6	15	161	18
High	5	4	14	177

(e) A confusion matrix resulting from the prediction of a student's "Risk Profile" utilizing **Random Forests** classifier. After 10-fold cross-validation the random forests model achieved **83**% accuracy, furthermore, 662 instances were correctly classified and 138 instances were incorrectly classified by the model.

Predicted Risk

	No	Low	Med	High
No	168	21	11	0
Low	37	138	19	6
Med	6	22	149	23
High	4	4	18	174

(f) A confusion Matrix detailing the performance of the **linear logistic regression** classifier when applied to a dataset of biographical and enrolment observations. The linear logistic regression model achieved **78**% accuracy, furthermore, 629 instances were correctly classified and 171 instances were incorrectly classified by the model.

Figure 7: A set of confusion matrices obtained when classifying the "Risk Profile" variable. We provide the accuracy of each classification model as determined by Equation (*****) along with a count of the correctly and incorrectly classified instances by each model, [6] (sic).

ure based on the conceptual framework developed in a "drop-out from higher education" study [13]. The conceptual framework connects dropout decision to categories of input features, namely, background (family) attributes, individual attributes, and pre-college scores. This framework is better depicted in the Figure 1 provided under the related work section.

The web application depicted in Figure 8 provides a practical tool which university student support programs can utilize for early detection of learners in need of academic support. We argue that the early detection and assistance of students at risk of failure is likely to lead to improved academic performance and eventually higher pass-rates, which translate to increased throughput rates.

The example depicted in Figure 8 illustrates the calculation of the risk profile of a learner based on biographical and enrolment observation. The program predicts the posterior distribution over the four "Risk Profiles", namely, "No Risk", "Medium Risk", "High Risk", and "Low Risk" using the Random forests classifier. The learner in the example is from an urban quantile 3 school in Kwazulu-Natal South Africa, furthermore, individual attributes are provided as follows; scores of 48%, 50%, and 55% for the quantitative, academic, and mathematical literacy National-Benchmark-

Tests (NBT) respectively. The learner also completed pre-college courses with scores of; 50% for both core Mathematics and Life Orientation, and 60% for English Home Language. The output presented at the bottom of Figure 8 illustrates that hypothetically the student is 10% likely to complete their degree in 3 years (No Risk), 50% likely to complete their degree in greater than 3 years (Low Risk), 35% likely to drop-out before the end of 3 years (Medium Risk), and 5% likely to drop-out in greater than 3 year (High Risk). With the output obtained, students support-program-coordinators can then decide what assistance will prove most beneficial to the student in the example as the learner posses a high chance of struggling to complete their degree in the allocated time (50% Low Risk).

5 Implications and Conclusions

The expansion of enrolments in South African universities has not been accompanied by a proportional increase in the percentage of learners graduating. In this study, we took on the task of early prediction of a learner's academic trajectory, aiming at identifying those who may struggle in universities, so that proactive learner
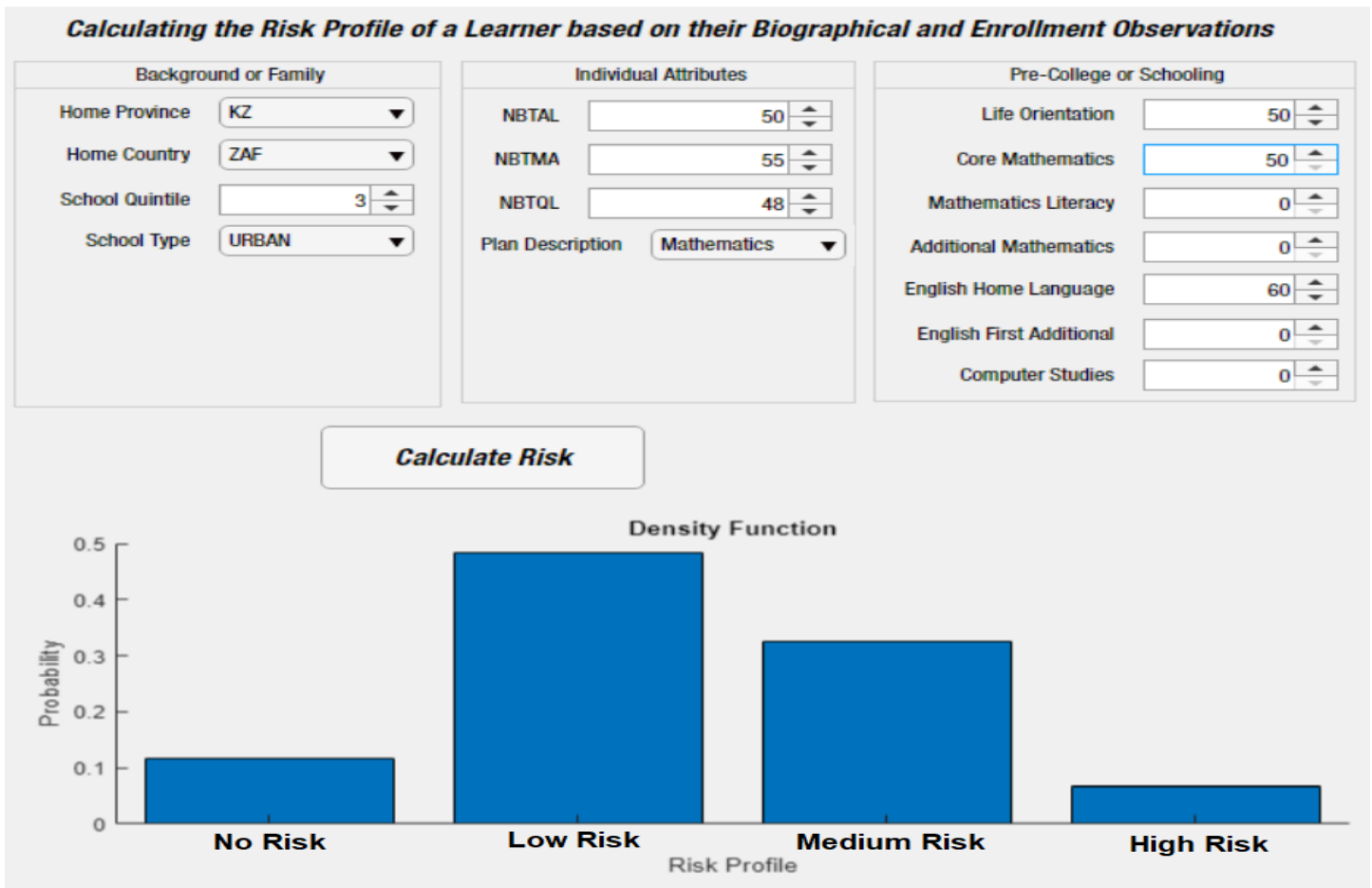
Figure 8: The graphical user interface for the at-risk program, [6](sic).

remediation to promote success may be provided to them.

This paper contributes to the current body of knowledge firstly by introducing an approach involving the prediction of a learner's outcome from the first year of registration until qualifying in a three-year degree. We argue for the early prediction of a learner's entire academic trajectory with the aim to detect those who are likely to benefit from student academic support initiatives. We trained six machine learning models to predict first, second, and final year outcomes from a synthetic data-set. After 10-fold cross-validation this task was completed with great success as all six models attained an accuracy above 83%. Furthermore, an evaluation of the F-measure of accuracy and ROC-curve reveal that these models are making informed-accurate decisions and not simply guessing, therefore, leading to our second contribution involving a real data-set from a research-intensive university in South Africa.

The second contribution of this study is a ranking (through entropy) of features according to their contribution in correctly predicting a learner's "risk profile" (class variable). The ranking of features according to entropy reveals which features are stronger determinants of student success relative to others employed and, in this study, we highlight the seven top-ranked features, namely, "plan code", "plan description", "year started", "age at first year", "streamline", "school quantile", and "Matric Mathematics major".

The third and main contribution made by this study is an inter-active program which can predict the distribution over a learner's risk profile utilizing biographical and enrolment observations. The interactive program proposed in this paper can be utilized for early identification of university learners who are most likely to benefit from student support initiatives aimed at improving academic performance. The implication of this study is that university learners can be assisted early in their academic journey increasing their chances of success. Furthermore, the early detection and assistance of learners in need of academic support will result in an improved and enriched learning experience beyond what the student would have experienced if support initiatives were implemented after failure has been detected.

6 Future work

To continue with the work done in this paper, future work may involve: (a) incorporating into our models features from categories not considered such as the "psycho-social attributes category", (b) exploring what courses offered in university possess high failure rates and how good the set of features we employed predict success in these courses, or (c) approaching the problem from a different perspective by attempting to predict which courses are students likely to struggle completing so that support initiatives may be focused on the specific courses.

References

[1] J. V. Winters, "Human capital, higher education institutions, and quality of life," Regional Science and Urban Economics, **41**(5), 446–454, 2011, doi: 10.1016/j.regsciurbeco.2011.03.001.

[2] G. Lassibille, L. N. Gómez, "Why do higher education students drop out? Evidence from Spain," Education Economics, **16**(1), 89–105, 2008, doi: 10.1080/09645290701523267.

[3] M. Letseka, S. Maile, High university drop-out rates: A threat to South Africa's future, Human Sciences Research Council Pretoria, 2008.

[4] K. G. Bokana, D. D. Tewari, "Determinants of Student Success at a South African University: An Econometric Analysis," The Anthropologist, **17**(1), 259–277, 2014, doi:10.1080/09720073.2014.11891436.

[5] N. Ndou, R. Ajoodha, A. Jadhav, "A Case Study: Educational Data-mining to Determine Student Success at Higher Education Institutions," in The International Multidisciplinary Information Technology and Engineering Conference, 2020.

[6] R. Ajoodha, A. Jadhav, S. Dukhan, "Forecasting Learner Attrition for Student Success at a South African University," in Conference of the South African Institute of Computer Scientists and Information Technologists 2020 (SAICSIT '20), September 14-16, 2020, Cape Town, South Africa. ACM, New York, NY, USA, 10 pages., ACM, 2020, doi:10.1145/3410886.3410973.

[7] D. H. E. T. Department of Higher Education & Training Republic of South Africa, "2000 to 2017 first time entering undergraduate cohort studies for public higher education institutions," Annual report, 16–28, 2020.

[8] K. R. White, "The relation between socioeconomic status and academic achievement." Psychological Bulletin, **91**(3), 461–481, 1982, doi:10.1037/0033-2909.91.3.461.

[9] M. Sommer, K. Dumont, "Psychosocial Factors Predicting Academic Performance of Students at a Historically Disadvantaged University," South African Journal of Psychology, **41**(3), 386–395, 2011, doi:10.1177/008124631104100312.

[10] E. J. Krumrei-Mancuso, F. B. Newton, E. Kim, D. Wilcox, "Psychosocial Factors Predicting First-Year College Student Success," Journal of College Student Development, **54**(3), 247–266, 2013, doi:10.1353/csd.2013.0034.

[11] E. Osmanbegovic, M. Suljic, "Data mining approach for predicting student performance," Economic Review: Journal of Economics and Business, **10**(1), 3–12, 2012.

[12] M. M. Chemers, L. Hu, B. F. Garcia, "Academic self-efficacy and first year college student performance and adjustment." Journal of Educational Psychology, **93**(1), 55–64, 2001, doi:10.1037/0022-0663.93.1.55.

[13] V. Tinto, "Drop-Outs From Higher Education: A Theoretical Synthesis of Recent Research," Review of Educational Research, **45**, 89–125, 1975, doi: 10.2307/1170024.

[14] S. A. Naser, I. Zaqout, M. A. Ghosh, R. Atallah, E. Alajrami, "Predicting Student Performance Using Artificial Neural Network: in the Faculty of Engineering and Information Technology," International Journal of Hybrid Information Technology, **8**(2), 221–228, 2015, doi:10.14257/ijhit.2015.8.2.20.

[15] M. Mayilvaganan, D. Kalpanadevi, "Comparison of classification techniques for predicting the performance of students academic environment," in 2014 International Conference on Communication and Network Technologies, IEEE, 2014, doi:10.1109/cnt.2014.7062736.

[16] V. Ramesh, P. Parkavi, K. Ramar, "Predicting Student Performance: A Statistical and Data Mining Approach," International Journal of Computer Applications, **63**(8), 35–39, 2013, doi:10.5120/10489-5242.

[17] T. Abed, R. Ajoodha, A. Jadhav, "A Prediction Model to Improve Student Placement at a South African Higher Education Institution," in 2020 International SAUPEC/RobMech/PRASA Conference, IEEE, 2020, doi:10.1109/saupec/robmech/prasa48453.2020.9041147.

[18] S. García, J. Luengo, F. Herrera, Data preprocessing in data mining, Springer, 2015.

[19] J. Platt, "Sequential Minimal Optimization: A Fast Algorithm for Training Support Vector Machines," Technical Report MSR-TR-98-14, 1998.

[20] D. Böhning, "Multinomial logistic regression algorithm," Annals of the Institute of Statistical Mathematics, **44**(1), 197–200, 1992, doi:10.1007/bf00048682.

[21] B. Krishnapuram, L. Carin, M. Figueiredo, A. Hartemink, "Sparse multinomial logistic regression: fast algorithms and generalization bounds," IEEE Transactions on Pattern Analysis and Machine Intelligence, **27**(6), 957–968, 2005, doi:10.1109/tpami.2005.127.

[22] Y. Wang, "A multinomial logistic regression modeling approach for anomaly intrusion detection," Computers & Security, **24**(8), 662–674, 2005, doi: 10.1016/j.cose.2005.05.003.

[23] I. Rish, et al., "An empirical study of the naive Bayes classifier," in IJCAI 2001 workshop on empirical methods in artificial intelligence, volume 3, 41–46, 2001.

[24] R. Ajoodha, Influence Modelling and Learning Between Dynamic Bayesian Networks Using Score-based Structure Learning, University of the Witwatersrand, Faculty of Science, School of Computer Science and Applied Mathematics, 2018.

[25] J. G. Cleary, L. E. Trigg, "K*: An Instance-based Learner Using an Entropic Distance Measure," in 12th International Conference on Machine Learning, 108–114, 1995, doi:10.1016/b978-1-55860-377-6.50022-0.

[26] C.-C. Chang, C.-J. Lin, "LIBSVM," ACM Transactions on Intelligent Systems and Technology, **2**(3), 1–27, 2011, doi:10.1145/1961189.1961199.

[27] J. Friedman, T. Hastie, R. Tibshirani, "Additive Logistic Regression: A Statistical View of Boosting," The Annals of Statistics, **28**, 337–407, 2000, doi: 10.1214/aos/1016218223.

[28] N. Landwehr, M. Hall, E. Frank, "Logistic Model Trees," Machine Learning, **59**, 161–205, 2005, doi:10.1007/s10994-005-0466-3.

[29] M. Sumner, E. Frank, M. Hall, "Speeding up Logistic Model Tree Induction," in 9th European Conference on Principles and Practice of Knowledge Discovery in Databases, 675–683, Springer Berlin Heidelberg, 2005, doi: 10.1007/11564126_72.

[30] M. J. Zaki, W. Meira, Jr, Data Mining and Analysis: Fundamental Concepts and Algorithms, Cambridge University Press, 2014, doi:10.1017/CBO9780511810114.

[31] J. Quinlan, C4.5: Programs for Machine Learning, Ebrary online, Elsevier Science, 2014.

[32] Y. L. Pavlov, Random Forests, De Gruyter, 2000, doi:10.1515/9783110941975.

[33] S. Sahu, B. M. Mehtre, "Network intrusion detection system using J48 Decision Tree," in 2015 International Conference on Advances in Computing, Communications and Informatics (ICACCI), IEEE, 2015, doi:10.1109/icacci.2015.7275914.

[34] D. M. W. Powers, "Evaluation: from precision, recall and F-measure to ROC, informedness, markedness and correlation," 2020.

Indoor Positioning System using WKNN and LSTM Combined via Ensemble Learning

Dionisius Saviordo Thenuardi[*], Benfano Soewito

Computer Science Department, BINUS Graduate Program - Master of Computer Science, Bina Nusantara University, Jakarta, 11480, Indonesia

A R T I C L E   I N F O

A B S T R A C T

Indoor positioning system (IPS) has become a high demand research field to be developed and has made considerable progress in recent years. Wi-Fi fingerprinting is the most promising technique that produces an acceptable result. However, despite the large amount of research that has been done using Wi-Fi fingerprinting, only a few Wi-Fi based IPS in the market can be said to be successful. Doing the research in a controlled environment and ignore the temporal signal changes may be the cause of such scenario. A long-term dataset was built to overcome this issue, yet the distance error of the state of the art was 2.48m. Therefore, we aim to reduce the distance error by combining two positioning algorithms which are Weighted k-Nearest Neighbor (WKNN) and Long-Short Term Memory (LSTM) using ensemble learning. The result shows that our ensemble method can reduce the localization error to 1.89m and improve the performance of the IPS by 23.7% when compared to the state of the art.

1   Introduction

Today, outdoor positioning is already a mature research field. An object with Global Navigation Satellite System (GNSS) service – such as Global Positioning System (GPS), GLONASS, Galileo, BeiDou – can be easily located with the help of satellite signal with high accuracy [1].

On the contrary, Indoor Positioning has not reached its maximum results and is on the focus of researchers recently. Satellite signals cannot be used for Indoor Positioning System (IPS) purposes due to too much signal attenuation in an indoor environment [2] that results in IPS with an accuracy of more than 100m [3]. IPS is very useful and has many functionalities in an environment like museum, department store, university, etc. Which is why IPS has become a high demand research field to be developed and has made considerable progress in recent years. Due to the absence of satellite in an indoor environment, researchers attempt to utilize other signals to be used in IPS such as Wi-Fi, Bluetooth, FM radio, RFID, ultrasound or sound, light, and magnetic field [4].

Wi-Fi signal has been the most popular and most used in developing IPS in recent years because it achieves high applicability in a complex indoor environment and does not require line-of-sight measurement of Access Points (APs) [4]. However, Wi-Fi also faces several problems when deployed in IPS. Wi-Fi is usually established

for communication purposes and rarely deployed with the ideal density and geometry for IPS [5]. The existing environment will need to deploy extra AP to create an ideal environment for IPS, which results in spending more money and makes it relatively expensive.

The most popular and promising approach in building an IPS is fingerprinting. This approach has two stage, offline phase and online phase. In the offline phase, the characteristics of several locations, called as Reference Point (RP), is measured. Then, a positioning algorithm will be used in online phase using the data collected during the offline phase. IPS with Fingerprinting approach can be viewed as a classification or regression problem. Many classification and regression algorithms like k-Nearest Neighbor (KNN), Weighted k-Nearest Neighbor (WKNN), Support Vector Machine (SVM), Multilayer Perceptron (MLP), Convolutional Neural Network (CNN), Recurrent Neural Network (RNN), and Long Short-Term Memory (LSTM) have been tested.

Combining the two, Wi-Fi fingerprinting has been the most popular technique for developing IPS. With dense Wi-Fi coverage in a well-surveyed environment, Wi-Fi fingerprinting can achieve acceptable accuracy, as shown in recent research [6]. Local Feature-based Deep Long Short-Term Memory (LF-DLSTM) was proposed and achieves localization performance with mean localization errors of 1.48m and 1.75m under the research lab and office environments, respectively.

---
[*]Corresponding Author: Dionisius Saviordo Thenuardi, Email: dionisius.thenuardi@binus.ac.id

However, to the best of our knowledge, only a few WiFi-based IPS in the market can be said to be successful. Although there are many methods that have been tested before, the accuracy in the real environment decreases. This may happen if the testing of the IPS was done in a specific, probably controlled environment. Therefore, the accuracy in the real environment may decrease significantly [7]. To overcome this issue, research in IPS needs to be done using a public dataset, therefore the environment cannot be controlled by the authors.

There are many public IPS dataset that can be obtained online such as [8] and [9]. However, these datasets were collected in one day only and do not take into account the changes in the temporal signal that inevitably occur in the real environment. This happens because the RSSI received from an AP might be different between one day and the next day, even if the location and environment is precisely the same [10]. Therefore, the accuracy in the real environment may drop significantly. To resolve the issue, dataset needs to be collected and updated periodically.

In this research, we use an IPS dataset that is published online which considers the temporal signal changes [7]. To the best of our knowledge, the best accuracy that has been done using this dataset was the research by Hsieh that used RNN to obtained a distance error of 2.48m [11]. To the best of our knowledge, the research employs RNN and LSTM separately and is applied directly to the dataset without any modification to prevent overfitting. However, the training data only contains fingerprint from 24 RP, while the testing data contains fingerprint from 106 RP. With much fewer reference points in the training data, the model tends to overfit.

This research aims to reduce the localization errors by applying methods to prevent overfitting in the LSTM model. We also provide a new way to reduce the localization errors further by combining two positioning algorithm which are WKNN and LSTM using ensemble learning.

2 Literature Review

2.1 Fingerprinting

Fingerprinting technique utilizes the signal characteristics of a specified location in a particular environment. It consists of an offline phase and an online phase. During the offline phase, a site survey is conducted on the environment. First, several location coordinates, referred to as Reference Points (RPs) will be chosen, which later each of them will be used to collect the RSSI from numerous access points. Multiple RSSI readings will be taken in each RPs. These collections of data consist of RPs and RSSI from multiple access points is usually known as radio map. During the online phase, a mobile unit observes RSSI measurements at a specific location and use an algorithm to associate the measurements with the radio map. The mobile unit is assumed to be collocated with an RP if the measurements made in the online phase and offline phase are similar.

Fingerprinting approaches can be viewed as a classification problem. The radio map collected during the offline phase is trained to obtain a model. Then, the position of the mobile unit will be estimated by putting the measurements taken into the model as a parameter. Classification algorithm such as K-Nearest Neighbor

(KNN), Weighted K-Nearest Neighbor (WKNN), Support Vector Machine (SVM), Naïve Bayes, Artificial Neural Network (ANN), Recurrent Neural Network (RNN), Long-Short Term Memory networks (LSTM) have been used.

In a traditional site survey where the surveyor collects the radio map by standing at RP and taking multiple measurements, it took 10 hours for two people to build a radio map consists of 150 RPs in a 281m^2 environment [12]. It can be concluded that, when using a site survey as a radio map collection method, the offline phase is time-consuming, labor-intensive, and cost-prohibitive.

Fingerprinting can produce a low localization error because unlike any other approach, fingerprinting relies on the characteristics of the environment itself. Fingerprinting allows obstacles like wall, furniture, and other static objects do not interfere with localization accuracy. However, this also works as a trade-off. If there are any changes in the environment, such as furniture and access points relocation, another site survey is needed.

Then, researchers tried to lessen the time taken to build a radio map. [13] introduced the Quick Radio Fingerprint Collection method (QRFC) that allows radio map to be created, simply by holding a smartphone while walking. QRFC makes the radio map collection become effortless, especially if there are extra volunteers. Even with lesser times, radio map built by QRFC has been proven gave the same results with a radio map created by a site survey, and even better.

The fingerprinting technique offers both accuracy and ubiquity. Access point location does not need to be known, and there is no Line of Sight (LOS) requirements. Usually, fingerprinting techniques produce an IPS with better localization accuracy, which makes it superior to other methods [14].

2.2 Weighted k-Nearest Neighbor (WKNN)

Weighted k-Nearest Neighbor (WKNN) is a modified version of k-Nearest Neighbor which is a supervised machine learning algorithm that can be used for classification and regression problems. KNN assumes the data in the same cluster is identical and has the same characteristic. It can be seen in Figure 1, that the data in the same cluster is adjacent one to another.
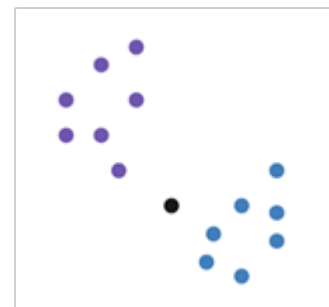
Figure 1: k-Nearest Neighbor

The similarity between two data points can be known from the distance between them. The distance can be calculated using several methods, the most basic and used one are the Euclidean distance (1). The smaller the distance, the more similar the data is.

$$d = \sqrt{\sum_{i=1}^{n}(q_i - p_i)^2} \qquad (1)$$

Euclidean distance is used to calculate the distance between the new data and the dataset. Where n is the number of access points that transmit RSSI, q_i is the RSSI measured on the RP from i^{th} access point, and p_i is the RSSI measured on the mobile unit from i^{th} access point.

A number of *k* data points with the smallest distance are considered as the nearest neighbor to the new data, which means they are similar to each other. The mode of the *k* labels will be considered as the label of the new data in a classification problem. In a regression problem, the mean of the *k* labels will be returned instead.

However, the hyperparameter *k* needs to be chosen carefully. If *k* is too large, the neighborhood may include too many data points from other classes, which leads to inaccuracy. However, KNN would be more sensitive to outliers if *k* is too small. Several experiments need to be done to decide the value of hyperparameter *k* in KNN.

To overcome existing problem in KNN, a weight is given to every *k* neighbors; thus, this algorithm is called weighted k-nearest neighbor. Any function can be used to determine the weight of every neighbor, usually called a kernel function. The bigger the distance gap between the new data and its neighbor, the smaller the weight is. Bigger weight means the data is more similar than other neighbors with a smaller weight. In this research, the kernel function is defined in (2).

$$w_i = \frac{1/d_i}{\sum_{j=1}^{k} 1/d_j} \qquad (2)$$

Where *k* is the total number of neighbors, d_i is the distance from the mobile unit to i^{th} neighbor, and w_i is the weight for i^{th} neighbor. Then, the position of the mobile unit can be estimated by assigning the weight to the RP coordinates using (3).

$$(x,y) = \sum_{i=1}^{k} w_i(x_i, y_i) \qquad (3)$$

Where w_i represent the weight for i^{th} neighbor, while x_i and y_i is the coordinates of the ith neighbor which are X and Y, respectively.

2.3 Long Short-Term Memory (LSTM)

Long Short-Term Memory (LSTM) was made to overcome the problems found in Recurrent Neural Network (RNN). It is well known that RNN suffers from the vanishing gradient problem during backpropagation, which makes it is hard to remember the importance of the data from earlier timesteps if the data sequence is long enough.

RNN layers are connected to each other, as shown in Figure 2. To obtain the output at time *t* (Y_t), RNN takes into account the input at time *t* (X_t) and the hidden state from the previous time step (h_{t-1}). The hidden state from previous time step (h_{t-1}) is passed to the current step (h_t) as an input, which holds the information of the previous time step. However, the gradient in the earlier layers in RNN usually shrinks as the sequence gets longer, and with a low gradient update rate, the layers stop learning. With the layers from

early timesteps stop learning, RNN will forget what it had seen when the sequence got longer, thus having a short-term memory.
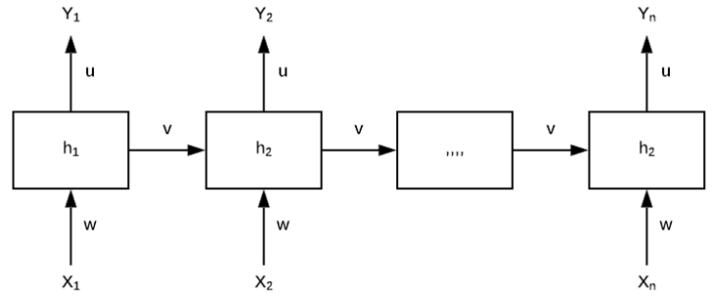
Figure 2: Recurrent Neural Network

LSTM used the same flow as RNN, where the information from the previous time step is passed onto the current time step. The difference is LSTM has an internal mechanism called gates that can learn which data is essential or not. If the data is considered important, LSTM will keep the information. If it turns out that the data is not important, LSTM will forget the information. This internal mechanism in LSTM is called a cell state, which has various gates.

The cell state can be thought of as a "memory" in LSTM, where the cell state will carry information throughout the processing of the sequence. As the sequence goes, additional information will be added to the cell, and some will be removed from the cell state. The cell state consists of three gates: input gate, forget gate, and output gate. These gates determine which information will be stored, keep, and be omitted from the cell state. Two activation functions are used within the three gates, which are sigmoid and tanh, which can be written as (4) and (5), respectively.

$$\sigma(z) = \frac{1}{1 + e^{-z}} \qquad (4)$$

$$\tanh(z) = \frac{2}{1 + e^{-2z}} \qquad (5)$$

2.3.1 Forget Gate

Forget Gate decides which information to be kept or discarded. Both information from the previous hidden state and the current input will be passed into a sigmoid function. The forget gate can be described as (6).

$$f^t = \sigma(w^f[h^{t-1}, x^t] + b^f) \qquad (6)$$

The information is considered as unimportant if f^t is close to zero, and the cell state will discard the information. If f^t is close to 1, that means the information is important.

2.3.2 Input Gate

The input gate has a role in determining which information will be added to the hidden state from the current input. Besides the sigmoid activation function, the input gate also uses tanh activation function.

$$i^t = \sigma(w^f[h^{t-1}, x^t] + b^i) \qquad (7)$$

First, the previous hidden state will be passed along with current input into sigmoid functions, written in (7). Then, we pass the hidden state and current input into tanh function, written in (8), producing $\widetilde{C}^t$.

$$\widetilde{C}^t = tanh(w^c[h^{t-1}, x^t] + b^c) \tag{8}$$

Now, we can determine the current cell state by executing (9).

$$C^t = f^t C^{t-1} + i^t \widetilde{C}^t \tag{9}$$

2.3.3 Output Gate

The output gate is the one that produces a new hidden state to be passed to the next time step. Just like forget and input gate; first we passed the information from the previous hidden state along with current input into sigmoid function, written in (10)

$$o^t = \sigma(w^o[h^{(t-1)}, x^t] + b^o) \tag{10}$$

Then, the new hidden state to be passed into the next time step can be obtained by using (11).

$$h^t = o^t tanh(C^t) \tag{11}$$

2.4 Related Works

The most straightforward yet beneficial application of IPS can be found in [15]. The research provides a system to ease doctors and nurses in locating their patients, especially in emergencies. The system was built by deploying multiple BLE throughout the ceiling of the hospital for every 10m. By using the proximity technique, the nearest BLE will be chosen based on the RSSI, and the location of the BLE will be sent to the system server for location mapping. The user will be considered in the same room, or the same area with the nearest BLE detected. By using this algorithm, the system achieved 97.22% accuracy for location classification.

An IPS made using the multilateration technique can be seen in [16]. The research was performed in a furnished laboratory environment with 13.1m x 6.5m. A total of 6 Raspberry Pi3 was used to capture the signal from a mobile BLE that transmits two signals at each second. Linear Least Squares is a multilateration method and was used in the research with a localization errors up to 1.79m.

Meanwhile, [6] proposed an IPS based on Wi-Fi signal with Deep LSTM architecture, which is just a stack of LSTM. The data were preprocessed using the sliding window to reduce the noise effect on the RSSI, which produces a more robust representation of the RSSI with minimal loss of signal properties. Two LSTM layers were used with 30 and 40 hidden layers. Then, a fully connected layer with a size of 60 was used to transfer the outputs of the second LSTM layers. The architecture also implements one dropout layer to prevent overfitting that usually happened to deep networks. The experiment was carried in two environments, a research lab with 35.3m x 16m and an office with 55m x 50m. The result of DLSTM was compared to ANN, SVR, Extreme Machine Learning (ELM), WKNN, and Stacked Denoising Autoencoder (SDA). The result shows that the proposed algorithm outstands the other algorithm with a localization error of 1.48m and 1.75m under the research lab and the office, respectively.

Due to creating a fingerprint database took a long time, some researchers focus on creating a fingerprint database for indoor positioning research purposes, such as [17]. The dataset consisted of multiple buildings and multiple floors and is used by Jang, who proposed a convolution neural network (CNN) [18]. The network uses the Interquartile range (IQR) for feature scaling, a dropout layer, data balancing, and ensemble methods. The architecture consists of 3 identical CNN models, with each of them has a different filter. The research shows that the proposed algorithm outperforms the Deep Neural Network (DNN) architecture.

RNN and LSTM has been proved to be successful in detecting pedestrian trajectory in indoor environment [19], [20], which inspired Hsieh et al. to utilize RNN and LSTM in indoor positioning system [11]. The research used a public dataset, which is the one used in this research [7]. The model consists of input layer, RNN or LSTM layer, fully connected layer with 40 neurons, fully connected layer with 2 neurons, and output layer. The number of RNN or LSTM layers were adjusted to 1, 3, and 5. The result shows that the best accuracy can be achieved by employing 5-layer RNN with a distance error of 2.48m and 99.6% accuracy of floor prediction.

Several ensemble learning approach has been done in building Indoor Positioning System. A research by Li et al. provide an ensemble approach to fuse Differential Time Difference Of Arrival (DTDoA) with RSS value [21]. Some research provide a way to combine the results from several positioning algorithm such as KNN [22]–[24] and neural network [25]. Research by Hayashi divide the environment into several area and each area has its own positioning algorithm. The result from positioning algorithms from each area is combined to get the final prediction [26].

A simple application of IPS can be created using simple techniques such as using proximity to locate the mobile unit in a particular subarea. To determine the exact position of the mobile unit in a small to medium environment scale, trilateration or multilateration can be used. However, if the environment grows bigger into a multi-floor or even multi-building environment, using a fingerprint technique is recommended.

Ensemble approach has been proved to be successful in both classification and regression problem [24]. Previous research provide ways to combine the result several weak-learners to obtain the final prediction. To the best of our knowledge, this is the first research that uses an ensemble approach where the result from one positioning algorithm was taken as an input for the next positioning algorithm in the IPS field.

3 Methodology

3.1 Dataset

We used a dataset released online by Mendoza et al. [7] to verify our proposed method. According to the authors, the dataset has been standardized and ready to be used for indoor positioning research purposes. The dataset was collected in a library that consists of multiple bookshelves from two different floors (3rd and 5th) with total coverage of 308.4m^2. To overcome the problem that occurs because of temporal signal changes, the data were collected within 15 months, with 63.504 measurements in total.

Each measure in the dataset provides information such as exact position, RSSI readings, timestamps, and some identifiers. Four hundred forty-eight access points were used in the measurement. Access points were installed on both floor levels at approximately 2.65m from the ground.

To collect the fingerprint database, A trained person that is called as the subject was chosen. Multiple locations were chosen to create the radio map. The radio map consists of fingerprint data with the subject facing four different directions, which are forward, backward, left, and right. At the offline stage, the subject stood at the selected location and held Samsung Galaxy S3 with the right hand in front of his chest. The mobile phone was equipped with an application that collects the RSSI of the Wi-Fi and eases the collection process. The app gave an ordered list of locations for the subject and gave a specific direction for the subject has to face. Therefore, this application reduces the likelihood of the subject placing themselves in wrong positions.

The dataset has been split into training and testing dataset by the authors. The training dataset consists of 16.704 fingerprints from 24 different RP while the testing dataset consists of 46.800 fingerprints from 106 different RP. Each fingerprint consists of 448 RSSI readings from every AP. However, not all of them were detected. If an AP is not detected in a fingerprint, the value will be recorded as 100. In this research, the dataset is scaled using Min-Max Scaler which can be described in (12).

$$X_{scaled} = \frac{X - X_{min}}{X_{max} - X_{min}} \qquad (12)$$

where X is the original value of the feature, X_{max} and X_{min} is the highest and smallest value that exists in the feature, respectively.

3.2 Proposed Method

Several research [22]–[25] used an ensemble learning approach where the outcomes of several positioning algorithms are combined into one single output. In this study, we provide a different ensemble method which combines two positioning algorithms, namely WKNN and LSTM.

Since the result from WKNN will be used as an input in the LSTM model, we need to get the coordinates and floor prediction from WKNN. Each data in the testing dataset which contains RSSI values from 448 APs will be used as an input into WKNN to predict the coordinates and the floor level of the object. The data will be scaled using Min-Max Scaler to turn it into the range of 0-1 by using (12).

For every data in the testing dataset, WKNN will create a list containing all of its neighbors from the training dataset. To be precise, each testing data will have 16.704 neighbors in total. Every neighbor has its own distance from the testing data. The distance is measured using Euclidean Distance (1). The smaller the distance means the RSSI values between the testing data and the neighbor is similar to each other. If the RSSI values are similar, it can be assumed that the object positions are also similar. Therefore, it can be concluded that we can predict the coordinates and the floor level of the object by collecting several neighbors with similar characteristics (RSSI value).

A number of k neighbors with the smallest Euclidean Distance will be used to predict the coordinates and floor level of the object. The coordinates, both X and Y, is calculated using (3). Since the smaller the distance means the data is more similar, a neighbor with a smaller distance will have more weight. Thus, it has more impact in predicting the coordinates of the object. We select the floor level that occurs the most within the k neighbors as the floor level prediction of the object. Since we are using mode to predict the floor level, the number of neighbors must be odd. Hence, the configuration of hyperparameter k is set to an odd number in this research.

After the coordinates and floor level of the object has been predicted by WKNN, the result will be concatenated to the testing data to create a new dataset called WKNN dataset. WKNN dataset consists of RSSI values from 448 APs, predicted coordinates by WKNN, predicted floor level by WKNN, real coordinates, and real floor level.

The WKNN dataset will be used to calculate the localization error and accuracy of the WKNN model, and it will also be used in LSTM architecture. Two architecture are proposed in this model since we are using regression to predict the coordinates and classification to predict the floor level of the object. Figure 3 shows the overall process of our ensemble method where the result from WKNN is combined with the original features and is used as an input to the LSTM model. To the best of our knowledge, this is the first study that uses this kind of ensemble learning approach in the IPS field.
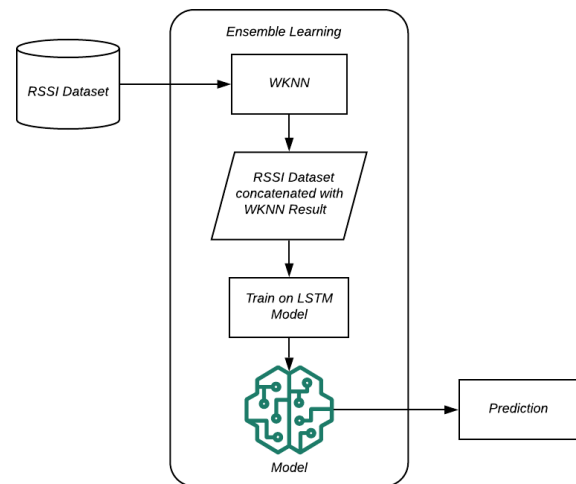
Figure 3: Proposed Method

4 Experimental Design and Result

4.1 Experimental Design

Both regression and classification will be done in the experiment since the dataset contains data with multiple floors. The purpose of the regression model is to predict the coordinates of the object while the classification model predicts the level of the floor the object is on.

Three scenarios will be conducted in the experiment. The first scenario is to use only WKNN to predict the coordinates and the level of the floor of the object. The second scenario will use both the regression and classification model to predict the coordinates and the level of the floor of the object. The third scenario is similar to the second scenario. But in this scenario, the result from WKNN (coordinates or floor) will be added as an input for the model. Therefore, there will be 4 neural network architecture used in this experiment. All of the architecture is trained using k-fold cross validation to prevent overfitting. The number of folds used in this research is 5.

The neural network of the regression model can be seen in Figure 4. The input layer consists of 448 features which are the RSSI value for each AP. The features are fed to LSTM layer that consists of 448 neurons with tanh as its activation function. To prevent overfitting, a dropout layer is added in the LSTM layer with 0.5 dropout rate. Then, the result from LSTM layer will be fed into a fully connected layer that consists of 40 neurons with sigmoid as its activation function. Finally, the output layer consists of 2 neuron that represent the coordinates of the object. Linear activation function is used in the output layer. The model uses Adaptive Moment estimation (adam) as the optimizer and root mean squared error as the loss function. Ten epochs ere used to train the model with 5 training examples for each batch.

layer and LSTM layer since there are additional inputs which are the coordinates from WKNN.
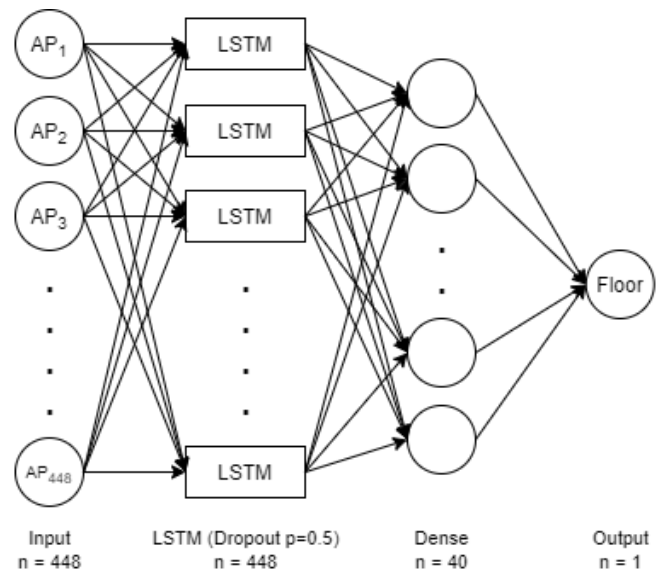
Figure 5: LSTM Classification Architecture

Figure 4: LSTM Regression Architecture
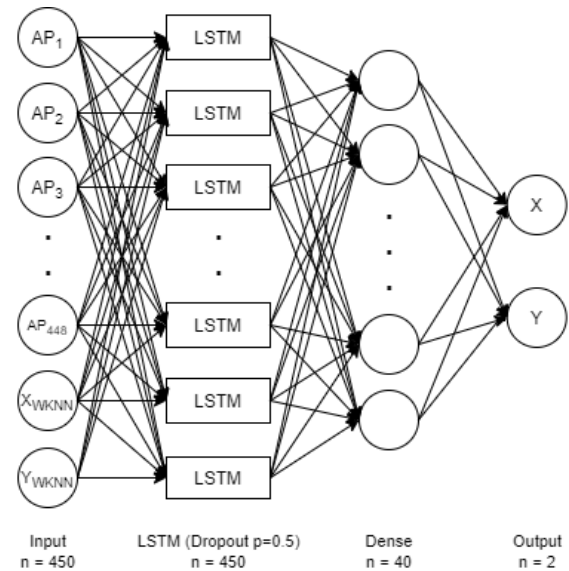
Figure 6: WKNN-LSTM Regression Architecture

The architecture of the classification model can be seen in Figure 5. The architecture is similar to the regression model. The difference resides in the output layer which only consists of one neuron that represents the floor level of the object. Instead of using the linear activation function, sigmoid is used as the activation function of the output layer. Binary cross-entropy is used as the loss function and accuracy as the metrics.

The architecture of the regression model for our proposed method (WKNN-LSTM) can be seen in Figure 6. All of the activation functions, optimizer, number of epochs, batch size of this architecture is the same as the one used in LSTM regression architecture. The only difference is the number of neurons in the input

The architecture for WKNN-LSTM classification model can be seen in Figure 7. Same as before, the architecture use the same settings with LSTM classification architecture and there will be one additional input which is the floor level prediction from WKNN.

4.2 Experimental Result

In the first scenario, we try out several WKNN model with a different values of hyperparameter k. The result of the first scenario can be seen in Table 1.

It can be seen that the distance error decreases as the hyperparameter k increase while the floor prediction accuracy does not

show any significant changes. The increase in performance is pretty significant between *k=5* and *k=13*. However, the performance gap between *k=13*, *k=21*, and *k=25* is not too big. Yet, as the hyperparameter *k* increases, the computational cost and time also increase. Therefore, hyperparameter *k* needs to be adjusted according to the user needs.
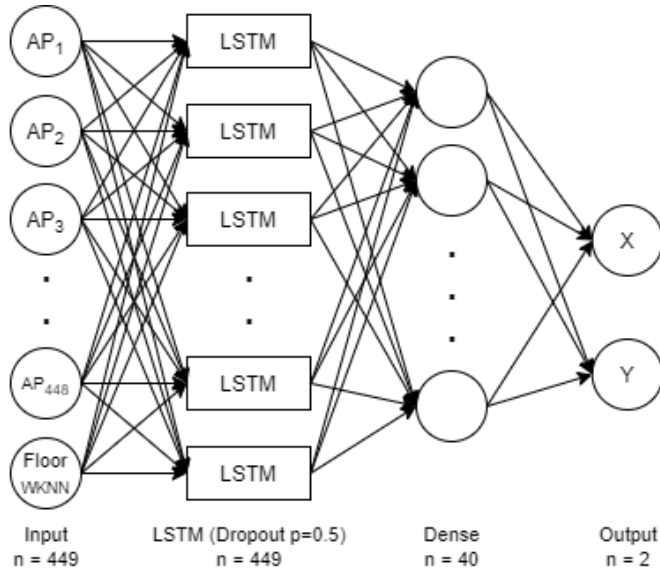
Figure 7: WKNN-LSTM Classification Architecture

Table 1: WKNN Results

Model	Distance Error (RMSE)	Floor Prediction Accuracy
$k = 5$	2.28m	99.75%
$k = 13$	2.17m	99.76%
$k = 21$	2.15m	99.77%
$k = 25$	2.14m	99.76%

The result of the second and third scenario can be seen in Table 2. The three hyperparameter *k* values in Table 1 will be applied in the third scenario for WKNN model to predict the coordinates and the floor level. We also compare the result from our experiment with the research by Hsieh [11].

Table 2: LSTM and WKNN-LSTM Results

Model	Distance Error (RMSE)	Floor Prediction Accuracy
RNN [11]	2.48	99.6%
LSTM [11]	2.57m	99.5%
Our LSTM	1.99m	99.8%
WKNN-LSTM ($k = 13$)	1.90m	99.85%
WKNN-LSTM ($k = 21$)	1.92m	99.87%
WKNN-LSTM ($k = 25$)	1.89m	99.86%

Our LSTM model can achieve distance error and accuracy of 1.99m and 99.8%, respectively. Both predictions are superior compared to WKNN model. However, when the result from WKNN is used as an additional input to LSTM, our model can achieve distance error and accuracy of 1.89m and 99.86%.

It can be seen that the LSTM model surpass the performance of WKNN model in predicting the coordinates and the floor level. Yet, the performance can increase even more if both of the model is combined using our ensemble approach.

5 Conclusion

In this research, we proposed a new way to reduce localization error by using ensemble learning. The ensemble consists of two positioning algorithms which are WKNN and LSTM. Aside from the original features which are RSSI values from all of the APs, the result from WKNN, either the coordinates or the floor level, are taken as an additional input for the LSTM model. The result shows that our ensemble approach can improve the performance of the IPS by 11.6% and 5% when compared to the performance of our WKNN and LSTM, respectively.

References

[1] H.-W. Bernhard, L. Herbert, J. Collins, Global positioning system: Theory and practice, 2012.

[2] G. Ding, Z. Tan, J. Wu, J. zhang, "Indoor fingerprinting localization and tracking system using Particle Swarm Optimization and Kalman Filter," IEICE Transactions on Communications, **98**, 502–514, 2015, doi:10.1587/transcom.E98.B.502.

[3] S. Chai, R. An, Z. Du, "An Indoor Positioning Algorithm using Bluetooth Low Energy RSSI," in Proceedings of the 2016 International Conference on Advanced Materials Science and Environmental Engineering, 274–276, Atlantis Press, 2016/04, doi:https://doi.org/10.2991/amsee-16.2016.72.

[4] S. He, S. . G. Chan, "Wi-Fi Fingerprint-Based Indoor Positioning: Recent Advances and Comparisons," IEEE Communications Surveys Tutorials, **18**(1), 466–490, 2016, doi:10.1109/COMST.2015.2464084.

[5] F. R., R. Harle, "An analysis of the accuracy of Bluetooth Low Energy for Indoor Positioning applications," in Proceedings of the 27th International Technical Meeting of the Satellite Division of The Institute of Navigation, 201–2210, 2014.

[6] Z. Chen, H. Zou, J. Yang, H. Jiang, L. Xie, "WiFi Fingerprinting Indoor Localization Using Local Feature-Based Deep LSTM," IEEE Systems Journal, **14**(2), 3001–3010, 2020, doi:10.1109/JSYST.2019.2918678.

[7] G. M. Mendoza-Silva, P. Ricther, J. Torres-Sospedra, E. S. Lohan, J. Huerta, "Long-term WiFi fingerprinting dataset for research on robust indoor positioning," Data, 2018, doi:https://doi.org/10.3390/data3010003.

[8] Z. Tóth, J. Tamás, "Miskolc IIS hybrid IPS: Dataset for hybrid indoor positioning," in 2016 26th International Conference Radioelektronika (RADIOELEKTRONIKA), 408–412, 2016, doi:10.1109/RADIOELEK.2016.7477348.

[9] R. Montoliu, E. Sansano, J. Torres-Sospedra, O. Belmonte, "IndoorLoc platform: A public repository for comparing and evaluating indoor positioning systems," in 2017 International Conference on Indoor Positioning and Indoor Navigation (IPIN), 1–8, 2017, doi:10.1109/IPIN.2017.8115940.

[10] Y. Chapre, P. Mohapatra, S. Jha, A. Seneviratne, "Received signal strength indicator and its analysis in a typical WLAN system (short paper)," in 38th Annual IEEE Conference on Local Computer Networks, 304–307, 2013, doi: 10.1109/LCN.2013.6761255.

[11] H. Hsieh, S. W. Prakosa, J. Leu, "Towards the mplementation of recurrent neural network schemes for WiFi fingerprint-based indoor positioning," in 2018 IEEE 88th Vehicular Technology Conference (VTC-Fall), 1–5, 2018, doi:10.1109/VTCFall.2018.8690989.

[12] B. Wang, Q. Chen, L. T. Yang, H. Chao, "Indoor smartphone localization via fingerprint crowdsourcing: challenges and approaches," IEEE Wireless Communications, **23**(3), 82–89, 2016, doi:10.1109/MWC.2016.7498078.

[13] H.-H. Liu, "The quick radio fingerprint collection method for a WiFi-based indoor positioning system," Mobile Networks and Applications, 61–71, 2017, doi:10.1007/s11036-015-0666-4.

[14] A. Khalajmehrabadi, N. Gatsis, D. Akopian, "Modern WLAN Fingerprinting Indoor Positioning Methods and Deployment Challenges," IEEE Communications Surveys Tutorials, **19**(3), 1974–2002, 2017, doi:10.1109/COMST.2017.2671454.

[15] X. Lin, T. Ho, C. Fang, Z. Yen, B. Yang, F. Lai, "A mobile indoor positioning system based on iBeacon technology," in 2015 37th Annual International Conference of the IEEE Engineering in Medicine and Biology Society (EMBC), 4970–4973, 2015, doi:10.1109/EMBC.2015.7319507.

[16] M. Ture, A. Hatipoglu, "Indoor Location Finding of the Transmitter Based on Bluetooth Received Signal Strength," in 2019 International Symposium on Networks, Computers and Communications (ISNCC), 1–5, 2019, doi:10.1109/ISNCC.2019.8909095.

[17] J. Torres-Sospedra, R. Montoliu, A. Martínez-Usó, J. P. Avariento, T. J. Arnau, M. Benedito-Bordonau, J. Huerta, "UJIIndoorLoc: A new multi-building and multi-floor database for WLAN fingerprint-based indoor localization problems," in 2014 International Conference on Indoor Positioning and Indoor Navigation (IPIN), 261–270, 2014, doi:10.1109/IPIN.2014.7275492.

[18] J. Jang, S. Hong, "Indoor Localization with WiFi Fingerprinting Using Convolutional Neural Network," in 2018 Tenth International Conference on Ubiquitous and Future Networks (ICUFN), 753–758, 2018, doi:10.1109/ICUFN.2018.8436598.

[19] J. Li, Q. Li, N. Chen, Y. Wang, "Indoor Pedestrian Trajectory Detection with LSTM Network," in 2017 IEEE International Conference on Computational Science and Engineering (CSE) and IEEE International Conference on Embedded and Ubiquitous Computing (EUC), volume 1, 651–654, 2017, doi:10.1109/CSE-EUC.2017.122.

[20] F. Walch, C. Hazirbas, L. Leal-Taixe, T. Sattler, S. Hilsenbeck, D. Cremers, "Image-Based Localization Using LSTMs for Structured Feature Correlation," in Proceedings of the IEEE International Conference on Computer Vision (ICCV), 2017.

[21] Z. Li, T. Braun, X. Zhao, Z. Zhao, F. Hu, H. Liang, "A Narrow-Band Indoor Positioning System by Fusing Time and Received Signal Strength via Ensemble Learning," IEEE Access, **6**, 9936–9950, 2018, doi:10.1109/ACCESS.2018.2794337.

[22] D. Taniuchi, T. Maekawa, "Robust Wi-Fi based indoor positioning with ensemble learning," in 2014 IEEE 10th International Conference on Wireless and Mobile Computing, Networking and Communications (WiMob), 592–597, 2014, doi:10.1109/WiMOB.2014.6962230.

[23] A. K. Abed, H. Al-Moukhles, I. Abdel-Qader, "An adaptive K-NN based on multiple services set identifiers for indoor positioning system with an ensemble approach," in 2018 IEEE 8th Annual Computing and Communication Workshop and Conference (CCWC), 26–32, 2018, doi:10.1109/CCWC.2018.8301667.

[24] J. Torres-Sospedra, G. M. Mendoza-Silva, R. Montoliu, O. Belmonte, F. Benitez, J. Huerta, "Ensembles of indoor positioning systems based on fingerprinting: Simplifying parameter selection and obtaining robust systems," in 2016 International Conference on Indoor Positioning and Indoor Navigation (IPIN), 1–8, 2016, doi:10.1109/IPIN.2016.7743679.

[25] I. Ashraf, S. Hur, S. Park, Y. Park, "Deep-Locate: Smartphone based indoor localization with a deep neural network ensemble classifier," sensors, **20**, 133, 2019, doi:10.3390/s20010133.

[26] T. Hayashi, D. Taniuchi, J. Korpela, T. Maekawa, "Spatial-temporal adaptive indoor positioning using an ensemble approach," Pevasive and Mobile Computing, **41**, 319–332, 2017, doi:10.1016/j.pmcj.2016.12.001.

Classification of Wing Chun Basic Hand Movement using Virtual Reality for Wing Chun Training Simulation System

Hendro Arieyanto[*,1], Andry Chowanda[2]

[1]*Computer Science Department, Graduate Program in Computer Studies, Bina Nusantara University, Jakarta, 11480, Indonesia*

[2]*Computer Science Department, School of Computer Science, Bina Nusantara University, Jakarta, 11480, Indonesia*

A R T I C L E I N F O	A B S T R A C T
	To create a Virtual Reality (VR) system for Wing Chun's basic hand movement training, capturing, and classifying movement data is an important step. The main goal of this paper is to find the best possible method of classifying hand movement, particularly Wing Chun's basic hand movements, to be used in the VR training system. This paper uses Oculus Quest VR gear and Unreal Engine 4 to capture features of the movement such as location, rotation, angular acceleration, linear acceleration, angular velocity, and linear velocity. RapidMiner Studio is used to pre-process the captured data, apply algorithms, and optimize the generated model. Algorithms such as Support Vector Machine (SVM), Decision Tree, and k-Nearest Neighbor (kNN) are applied, optimized, and compared. By classifying 10 movements, the result shows that the optimized kNN algorithm obtained the highest averaged performance indicators: Accuracy of 99.94%, precision of 99.70%, recall of 99.70%, and specificity of 99.97%. The overall accuracy of the optimized kNN is 99.71%.

1. Introduction

Martial arts training is one of the preferable methods of physical exercise. It provides health & psychological benefits, such as preventing osteoporosis [1], reduces stress, depression, and increases mindfulness [2], and also has the potential to reduce aggressive behavior [3]. Basic movements of martial arts training such as stance and punches are usually done with the supervision of the instructor. However, instructors cannot always be there for one student, they must accompany other students as well. It could be a problem for new students who have just learned stances and punches. Repetitive movements without supervision could result in the students become unmotivated and stop their movement. Having the instructor to watch over them is helpful for the students to keep repeating the movement without stopping. There needs to be a method of training to make the students keep their excitement going during basic training when the instructor was not able to watch them. Watching video tutorials and reading books are some of the ways to improve the students' training experience, however, it lacks interactions and presence needed in martial arts training.

This is when Virtual Reality (VR) technology comes into play. It is mentioned by [4] that VR is typically defined in technical terms, meaning it is associated with technical hardware such as computer systems, head-mounted display (HMD), motion trackers, etc. VR itself can be simply defined as an environment that simulates the real world and is generated by a computer system in which users can then interact with by using motion trackers [5]. The trackers are used to collect data from the real environment and translate them to the virtual environment [6].

Due to its immersive capabilities, VR technology has been used in areas, such as architecture and landscape planning [7], dancing [8], military training [9], medical, such as stroke rehabilitation [10], and psychological treatment [11]. It has also been used for research in martial arts scope, even though there has not been much of them. The reason is that higher immersion and presence result in higher performance to the user [12].

A VR-based training simulation system could help in practicing the movement and motivates the user, due to its immersive capabilities [13]. To develop the system, capturing and classifying the hand movements is crucial, as being able to classify basic movement in Wing Chun is one of the basic training outcomes. This study uses Oculus Quest, a VR gear with a head-mounted display (HMD) and a pair of controllers. These controllers are used to capture hand movements. Variables such as time, location, rotation, angular acceleration, linear acceleration,

angular velocity, and linear velocity, were recorded and used as features for classification.

The purpose of this paper is to find the best possible method of classifying Wing Chun's basic hand movement to develop a VR-based training system. Since this paper uses Oculus Quest with a pair of hand controllers, hand movement data can be captured in the form of location in the world space. Not only that, other properties like rotation, angular acceleration, linear acceleration, angular velocity, and linear velocity can be captured as well. RapidMiner Studio [14], [15] is used to process the data, optimize models, and to analyze the result. This paper is presented as such: Section 1 is the introduction. In section 2, this paper outlines the studies and works that were related to motion and gesture recognition or classification. Section 3 outlines the method that is used in this paper. Section 4 shows the result and analysis of the study. Section 5 provides the conclusion of this paper based on the result and analysis. Section 6 provides discussions and further works that are possible to improve this paper.

2. Related Works

The study by [16] shows the approach is to segment or classify movement into distinct behaviors. The first approach is using Principal Component Analysis (PCA), which is based on the observation that simple motion exhibit lower dimensionality than complex motions. The motion is broken into frames, and each frame is represented as a point, which is the joint's location. It is based on dimensionality, in which a motion sequence with a single behavior should have a smaller dimensionality than the one with multiple behaviors. The second approach is using Probabilistic PCA. The Probabilistic PCA ignores the noises of motion, unlike PCA. The third approach is Gaussian Mixture Model (GMM), in which the entire sequence of motion is segmented whenever two consecutive sets of frames belong to different Gaussian distributions. The Probabilistic PCA obtained the best result of all three approaches: 90% precision for 95% recall.

In [17], the authors conducted a survey on sequence classification, in which it is stated that multivariate time series classification has been used for gesture and motion classification. The research by [18] captured motion data using CyberGlove, with 22 sensors in different locations at the glove and 1 angular sensor. The data are split into 3 datasets and used K-folds validation of K = 3. The multi-attribute motion data is reduced to feature vectors with Singular Value Decomposition (SVD) and then classified using Support Vector Machine (SVM). The study results in the accuracy of 96% for dataset 1, and 100% for dataset 2 and 3.

The research by [19] used wearable accelerometers to capture movement data. Several movements such as sitting, sitting down, standing, standing up, and walking, are the subject of classification. The features that are extracted from 4 accelerometers are further pre-processed into an acceleration in x, y, and z-axis for each, resulting in 12 features. The features of the movement data are then selected with Mark Hall's selection algorithm [20] and classified with C4.5 decision tree with AdaBoost ensemble method [21]. The study used 10 iterations of AdaBoost with C4.5 tree confidence factor of 0.25 and with 10-folds cross-validation. The overall performance recognition was 99.4%.

In [22], the authors compared the classification accuracy of several algorithms such as C4.5 decision tree, multilayer perception, Naive Bayes, logistic regression, and k-Nearest Neighbor (kNN). A smartphone with the capability of recording accelerometer and gyroscope data was used as the motion sensor. Waikato Environment for Knowledge Analysis (WEKA) machine learning tool was used to apply the algorithms and compare them. The result of the study shows that kNN algorithm obtained the highest (averaged) accuracy in all motion classification by 84.6%.

The study by [23] used the multi-modal approach, which is using a combination of audio, video, and skeletal joints. The audio segmentation used the Hidden Markov Model (HMM) to determine the "silence" and "event" of motion. The segmentation based on skeletal joints uses the y-coordinate of hand joint location. The first step is to identify the start and end frames of gestures of either left or right hand, and the second step is to identify the same by using both hands. For the RGB and video modalities, SVM is used as the gesture classification. The audio classifier and the SVM classifier is then fused with a fusion algorithm. This study, which used 275 test samples with over 2,000 unlabeled gestures, resulted in an average edit distance of 0.2074.

The study by [24] used a signal captured from movement instead of the joint location. The study used 12 Trigno Wireless electrodes. The signal is divided into several segments, calculates the spectrogram, and then normalized. PCA is then applied to reduce the dimensionality of the data but maintaining important information. The last step is to apply SVM to the data to do the classification. Compared with the Root Mean Square (RMS) method, the method of this study results in higher accuracy of 9.75% and a reduced error rate of 12%.

Lower-limb motion classification was done by using piezoelectret sensors that apply forcemyography (FMG) which reads force distribution generated by muscle contractions [25]. study compared kNN, Linear Discriminant Analysis (LDA), and Artificial Neural Network (ANN) to classify 4 lower-limb motions, namely leg raising, leg dropping, knee extension, and knee flexion. The highest accuracy is obtained by kNN with an accuracy of 92.90%.

The study by [26] goes into more specific, classifying motions into karate stances, movements, and forms. The captured data consists of a 3-axis accelerometer, gyroscope, and magnetometer. The classification is done by averaging the dataset with Dynamic Time Warping (DTW) Barycenter Averaging (DBA) algorithm, which is an averaging method that iteratively refills an initially selected sequence, to minimize its squared distance / DTW [27] to averaged sequences. In this study, a movement template was generated from two different-styled Karate masters and then both are compared. This results in a recognition rate of 94.20%.

In [28], the authors did a study on human motion recognition by using VR. A combination of LDA, Genetic Algorithm (GA), and SVM is proposed to classify human motion. After collecting motion data, LDA is used to extract features, and then GA is used to search for optimal parameters. After optimal parameters are found, SVM is then used for classification. There are 10 motions to be classified and several averaged results are obtained: Precision of 95.65%, Accuracy of 97.05%, Specificity of 92.78%, and Sensitivity (Recall) of 94.01%.

It can be inferred from the related works that there has been various research about human motion recognition and classification for years. SVM seems to be favored among the study of motion classification. When several studies compared algorithms for movement classification, kNN seems to provide the highest accuracy. This paper performs several algorithms that were mentioned in the related works and optimizes its parameters to improve the results.

3. Proposed Method

This study utilizes the features from Oculus Quest VR gear, along with Unreal Engine 4 (UE4), which helps in extracting features of movements. RapidMiner Studio is used to pre-process the data, apply algorithms, and analyze the results.

3.1. Method of extraction

To be able to capture the hand movement, a simple game based on UE4 is developed. When the game starts, the user can press a button on the Oculus Controllers to start capturing movement data. Several movement data that are recorded are basic Wing Chun hand movements such as *Straight Punch*, *Tan Sau*, *Pak Sau*, *Gan Sau*, and *Bong Sau*. The recording starts from the beginning stance to the ending stance of a movement. The same movement is done 10 times within around 40 seconds with around 1 to 2 seconds interval for every time the movement is done.

3.2. Extracted Data

The movement data is generated in the form of CSV files for each movement and each hand, resulting in 10 files. The extracted features are time, **location**, **rotation**, **angular acceleration**, **linear acceleration, angular velocity**, and **linear velocity**. Except for time, all the features are extracted in the form of vectors, and then split into x, y, and z-axis, resulting in a total of 19 features. RapidMiner Studio is used to process the data and give labels to the data. The data is then processed again by mixing all files of each hand and movement into 1 file. The dataset consists of 8,725 rows with a total of 10 labels. For the left hand, the labels are *Punch*, *Tan*, *Pak*, *Gan*, and *Bong*. For the right hand, the labels are *R_Punch*, *R_Tan*, *R_Pak*, *R_Gan*, and *R_Bong*.

3.3. Method of optimizing algorithm

Several algorithms are performed to the dataset using RapidMiner Studio to check for their accuracy. From there, the parameter optimization process is used to make the algorithms perform better. The selected algorithms for comparison are SVM, Decision Tree, and kNN.

Figure 1 shows the flow of the algorithm optimization method. First, an algorithm is applied to the dataset with split validation to check the initial performance. The dataset is first normalized and then split into 80% of the training set and 20% of the testing set by using *Split Data* module. An algorithm is then applied to the dataset, and then measure the performance to obtain accuracy. After performing split validation, the initial results of the algorithms' performances were obtained.

Then, parameter optimization is performed to get the best possible value of the parameters in the algorithm process. The algorithm is applied to the normalized dataset with 10-folds cross-

validation, and then put into the *Optimize Paramete*r module. This module executes the cross-validation using all the selected combinations of parameters that are available in the algorithm. This process results in the best accuracy of all selected combinations of parameters.
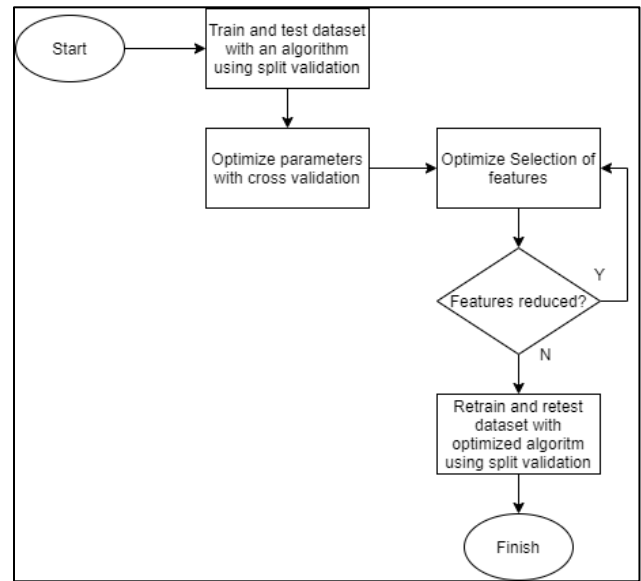
Figure 1: Flow of algorithm optimization method

After finding the optimized value of parameters, the process of optimizing selection of features is performed to the algorithm. The process is identical to the *Optimize Parameter* module, but this time the algorithm is put into the *Optimize Selection* module. This module executes the cross-validation of the algorithm and weights the features of the dataset that further improve the accuracy. This process can be done until no more features are removed. After this process, a model from the algorithm with optimized parameters and selected features is obtained. This model is then applied to the dataset with split validation process

4. Result and Analysis

The performance indicators were based on the study by [28], in which the 4 most used indicators for action classifications are used: accuracy, precision, recall (sensitivity), and specificity.

4.1. Support Vector Machine

The parameters used to obtain the final result for SVM algorithm are SVM Type: nu-SVC [29] with the nu value of 0.1, in which nu value is an upper bound on the fraction of margin errors and a lower bound on the fraction of support vectors, and kernel type: linear, in which it is suitable when having a lot of features in the dataset [30]. The relevant features obtained from the process of optimize selection are: *time*, *loc_x*, *loc_y*, *loc_z*, *rot_x*, *rot_y*, *rot_z*, *ang_acc_x*, *ang_vel_y*, *lin_vel_x*, and *lin_vel_z*. The result of the optimized SVM model for each movement is shown in Table 1. The movement *R_Tan* and *Gan* obtained the highest result (100%) in all 4 indicators. *R_Gan* and *Tan* reached the highest result (100%) in the recall and specificity. The least accuracy, precision, recall, and specificity are each obtained by *Punch* (99.02%), *Pak* (95.93%), *R_Bong* (95.06%), and *Punch* (99.41%) respectively. The overall accuracy obtained from the optimized SVM model is 98.11%.

Table 1: Result of the optimized SVM model for each movement

SVM	accuracy	precision	recall	specificity
R_Bong	99.42%	98.72%	95.06%	99.49%
R_Gan	99.88%	98.73%	100.00%	100.00%
R_Pak	99.48%	96.82%	97.44%	99.75%
R_Punch	99.71%	99.46%	97.88%	99.74%
R_Tan	100.00%	100.00%	100.00%	100.00%
Pak	99.36%	95.93%	97.63%	99.74%
Bong	99.54%	97.59%	97.59%	99.74%
Gan	100.00%	100.00%	100.00%	100.00%
Tan	99.77%	98.05%	100.00%	100.00%
Punch	99.02%	95.94%	95.45%	99.41%
Average	99.62%	98.12%	98.11%	99.79%

Table 2: Result of the optimized Decision Tree model for each movement

DT	accuracy	precision	recall	specificity
R_Bong	98.59%	92.59%	92.59%	99.22%
R_Gan	99.17%	94.94%	96.15%	99.61%
R_Pak	98.77%	94.70%	91.67%	99.16%
R_Punch	99.47%	98.91%	96.30%	99.54%
R_Tan	100.00%	100.00%	100.00%	100.00%
Pak	98.71%	91.53%	95.86%	99.54%
Bong	99.12%	97.48%	93.37%	99.28%
Gan	99.70%	100.00%	96.64%	99.68%
Tan	99.94%	100.00%	99.50%	99.93%
Punch	98.42%	90.52%	96.46%	99.53%
Average	99.19%	96.07%	95.85%	99.55%

4.2. Decision Tree

The parameters used to obtain the final result for Decision Tree algorithm are Criterion: information gain, Confidence: 0.140, and Minimal Gain: 0.019. Information gain is useful to minimize randomness in the dataset [31]. The relevant features obtained from the process of optimizing selection are *loc_x*, *loc_y*, *lox_z*, *rot_x*, *rot_y*, *rot_z*, *lin_vel_y*, and *lin_vel_z*. The result of the optimized Decision Tree model for each movement is shown in Table 2. The movement *R_Tan* obtained the highest result (100%) in all 4 indicators, with *Gan* and *Tan* obtained the highest

precision as well. The least accuracy, precision, recall, and specificity are each obtained by *Punch* (98.42%), *Punch* (90.52%), *R_Pak* (91.67%), and *R_Pak* (99.16%) respectively. The overall accuracy obtained from the optimized Decision Tree model is 96.06%.

Table 3: Result of the optimized kNN model for each movement

kNN	accuracy	precision	recall	specificity
R_Bong	99.71%	98.16%	98.77%	99.87%
R_Gan	100.00%	100.00%	100.00%	100.00%
R_Pak	100.00%	100.00%	100.00%	100.00%
R_Punch	100.00%	100.00%	100.00%	100.00%
R_Tan	100.00%	100.00%	100.00%	100.00%
Pak	100.00%	100.00%	100.00%	100.00%
Bong	99.71%	98.79%	98.19%	99.81%
Gan	100.00%	100.00%	100.00%	100.00%
Tan	100.00%	100.00%	100.00%	100.00%
Punch	100.00%	100.00%	100.00%	100.00%
Average	99.94%	99.70%	99.70%	99.97%

4.3. k-Nearest Neighbor

The parameters used to obtain the result for kNN algorithm are Measure Type: Numerical Measures, Numerical Measure: Manhattan Distance, and k = 5. Manhattan distance is preferable when there is high dimensionality in the dataset [32]. The relevant features obtained from the process of optimizing selection are *time*, *loc_x*, *rot_x*, *rot_y*, *rot_z*, and *ang_vel_x*. The result of the optimized kNN model for each movement is shown in Table 3. All movements except for *R_Bong* and *Bong* obtained the highest result (100%) in all 4 indicators. The least accuracy, precision, recall, and specificity are each obtained by *R_Bong* (99.71%), *R_Bong* (98.16%), *Bong* (98.19%), and *Bong* (99.81%) respectively. The overall accuracy obtained from the optimized kNN model is 99.71%.

4.4. Summary of the result

By using RapidMiner Studio, 10 basic Wing Chun hand movements were classified. The result of the classification by 3 optimized algorithms are shown in Table 1-3. Figure 2 shows the comparison of the averaged results between the optimized SVM, Decision Tree, and kNN algorithms.

The averaged results of the optimized SVM and Decision Tree show that accuracy and specificity have higher results than precision and recall, while in the optimized Decision Tree, the precision and recall results are less than the optimized SVM one. From all 3 algorithms, kNN obtained the highest results in all 4 indicators, reaching more than 99%.
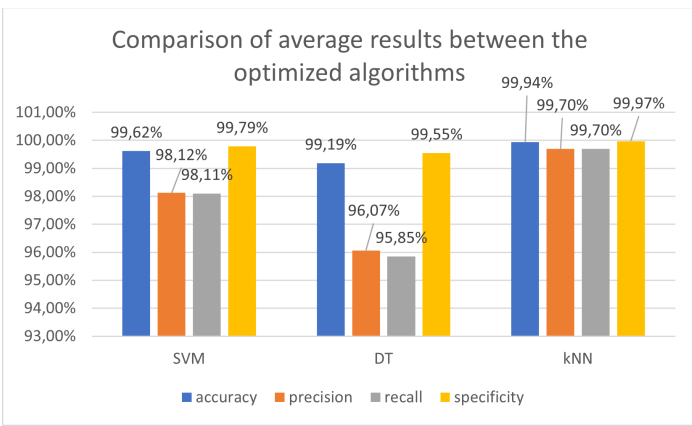
Figure 2: Comparison of average results between the optimized algorithms
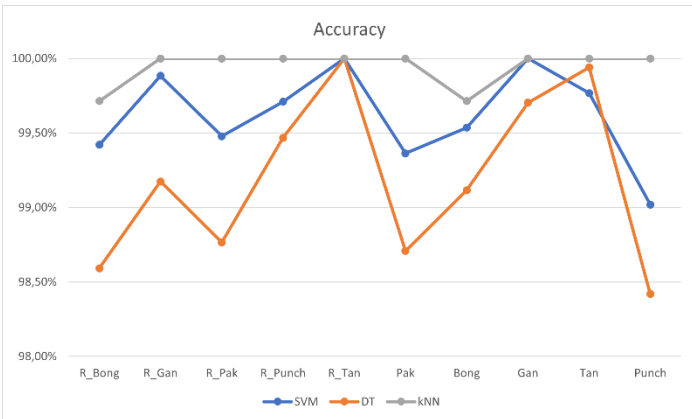
Figure 3: Accuracy of all movements from 3 algorithms
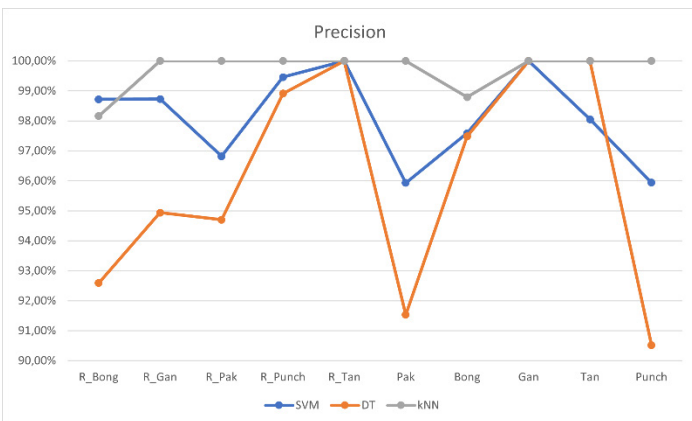
Figure 4: Precision of all movements from 3 algorithms

The number of extracted features for optimized SVM, Decision Tree, and kNN are varied. The time feature is not present in the Decision Tree. As for angular acceleration, linear acceleration, angular velocity, and linear velocity, the features present in the 3 algorithms are varied. However, *lin_vel_z* is present in both SVM and Decision Tree. The rotation feature (*rot_x*, *rot_y*, and *rot_z*) are present in all 3 algorithms. Location (*loc_x*, *loc_y*, *loc_z*) are present in SVM and Decision Tree, while only *loc_x* that is present in kNN. This result shows that Wing Chun hand is focused more on positioning than velocity and acceleration. This corresponds according to Master Ip Chun, if the

hand position and movement is not correct, it will not be useful and may be dangerous [33].
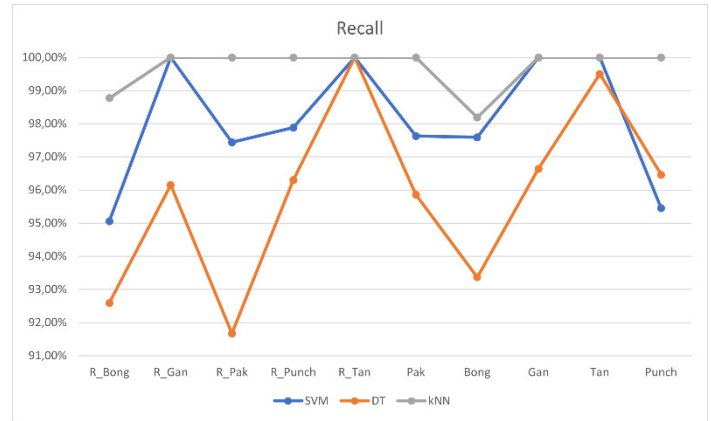
Figure 5: Recall of all movements from 3 algorithms
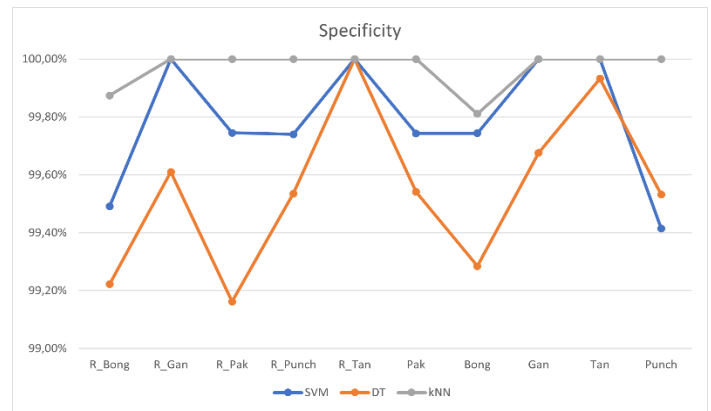
Figure 6: Specificity of all movements from 3 algorithms

From Figure 3-6, kNN has the highest results in all 4 indicators, while Decision Tree has the lowest. While all algorithm's curve has some intersections with each other at some movements, the difference between them is clear enough. It can also be seen that *R_Tan* reached 100% in every indicator and all applied algorithms. For every indicator, the shape of the graphs for kNN is identical, except for *R_Bong* and *Bong*, which are not reaching 100%. This is understandable because even though *Bong Sau* is a basic hand movement, the shape and movement are more complex than other basic movements.
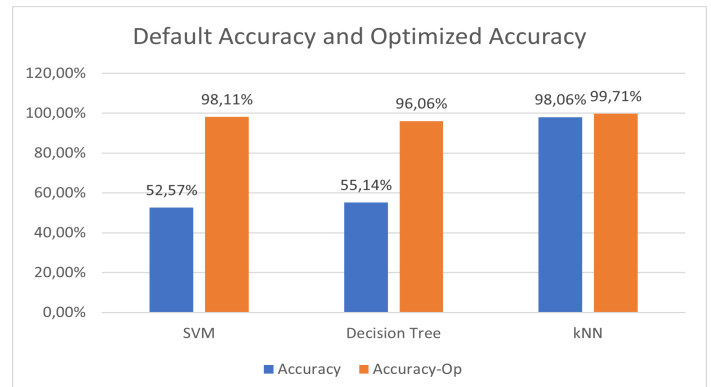
Figure 7: Comparison between the overall accuracy of default and optimized algorithms

The initial accuracy for SVM, Decision Tree, and kNN is 52.57%, 55.14%, and 98.06%, respectively. After the optimization process, the split validation process is done again to obtain the final accuracy. The final accuracy for SVM, Decision Tree, and kNN is 98.11%, 96.06%, and 99.71%, respectively. From the comparison seen in Figure 7, it can be seen that the optimization improves all 3 algorithms, especially SVM and Decision Tree. Both default and optimized results show that kNN obtains the highest accuracy.

To check whether the result shows a statistically significant difference ($p \leq 0.05$ and $p \leq 0.01$), Wilcoxon signed-rank test is performed on all 4 indicators (accuracy, precision, recall, and specificity) of both default and optimized algorithms. The test shows that all 4 indicators in SVM have a statistically significant difference. Both Decision Tree and kNN have a statistically significant difference in all indicators except for precision. Table 4 shows the result of the test.

Wilcoxon signed-rank test is also performed to the comparison of each algorithm in both default and optimized. The result of the comparison of default algorithms shows that SVM and Decision Tree do not have a statistically significant difference. The result of the comparison of the optimized algorithm shows that all the algorithms have a statistically significant difference. Table 5 shows the result of the test.

Table 4: Wilcoxon signed-rank test result of 4 indicators of both default and optimized algorithms

	SVM	DT	kNN
Accuracy	0.005**	0.008**	0.043*
Precision	0.005**	0.093	0.091
Recall	0.008**	0.021*	0.043*
Specificity	0.008**	0.015*	0.028*

Table 5: Wilcoxon signed-rank test result of the comparison of each algorithm in both default and optimized

	SVM-DT	SVM-kNN	DT-kNN
Default	0.721	0.005**	0.008**
Optimized	0.011*	0.012*	0.008**

5. Conclusion

The purpose of this study is to find the best possible method of classifying Wing Chun basic hand movement to create a Wing Chun training simulation system in VR. The results show that movement data features such as location, rotation, and linear velocity are significant enough to classify Wing Chun basic hand movements. Right hand *Tan Sau* has the highest value of all 4 indicators. Meanwhile, based on the result of the optimized kNN algorithm, *Bong Sau* of both hands is the only movement that is not reaching 100% performance, which is understandable because *Bong Sau* is a more complex basic movement. Before the optimization process, only kNN algorithm that has a high-performance result out of 3 algorithms. However, after the optimization of parameters and selection of features, SVM and Decision Tree's performances significantly improved. The

comparison of the results shows that the optimized kNN algorithm obtained the highest results.

6. Discussion

Five basic movements were captured for each left and right, making it 10 movements in total. The process of capturing the movement is done with Oculus Quest VR gear that comes with a pair of handheld Oculus Controller. A simple game is developed with Unreal Engine 4 to capture motion data that consists of several features of movements, such as location, rotation, etc. RapidMiner Studio is used to pre-process the dataset, apply algorithms, and optimize the learning model. This study compares SVM, Decision Tree, and kNN algorithms since 3 of them were commonly used in the earlier study of motion classification and recognition. The performance indicators such as accuracy, precision, recall, and specificity are used to compare the overall results of the 3 algorithms.

In this study, while algorithms like SVM, Decision Tree, and kNN are compared, this study does not include combining algorithms, for example like combining SVM with kNN, etc. RapidMiner Studio has various modules that help in processing data with algorithms. *AdaBoost* module has been applied to the optimized kNN, but the result shows no improvement. The module like *Ensemble Stacking* has yet to be explored further, although attempt to use stacking to stack all 3 algorithms, the result is not as good as the obtained result of each optimized algorithm has been done. Machine learning algorithms such as Deep Learning, Neural Networks, and Spatio-temporal algorithms can also be applied and compared for future studies.

The simple game that is developed to capture the movements also has a limitation in which the user can only stand still. The game can still be developed so that it could improve the motion capture process to include the user able to move around while performing hand movements. While this study shows that the algorithms can accurately classify basic hand movements, there are more basic hand movements that are very similar to each other. These movements can only be distinguished by looking at the area of contact of the hand. This can also be a field of further study for better movement classification. Further classification of sequences could be a field to be explored as well since Wing Chun also has a more complex set of movements that require more than one type of movement.

References

[1] T.H. Chow, B.Y. Lee, A.B.F. Ang, V.Y.K. Cheung, M.M.C. Ho, S. Takemura, The effect of Chinese martial arts Tai Chi Chuan on prevention of osteoporosis: A systematic review, Journal of Orthopaedic Translation, **12**, 74–84, 2018, doi:10.1016/j.jot.2017.06.001.

[2] J. Kong, G. Wilson, J. Park, K. Pereira, C. Walpole, A. Yeung, Treating

depression with tai Chi: State of the art and future perspectives, Frontiers in Psychiatry, **10**(APR), 2019, doi:10.3389/fpsyt.2019.00237.

[3] A. Harwood, M. Lavidor, Y. Rassovsky, Reducing aggression with martial arts: A meta-analysis of child and youth studies, Aggression and Violent Behavior, 2017, doi:10.1016/j.avb.2017.03.001.

[4] J. Steuer, "Defining Virtual Reality: Dimensions Determining Telepresence," Journal of Communication, 1992, doi:10.1111/j.1460-2466.1992.tb00812.x.

[5] M. Fernandez, "Augmented-Virtual Reality: How to improve education systems," Higher Learning Research Communications, 2017, doi:10.18870/hlrc.v7i1.373.

[6] G. Riva, R.M. Baños, C. Botella, F. Mantovani, A. Gaggioli, Transforming experience: The potential of augmented reality and virtual reality for enhancing personal and clinical change, Frontiers in Psychiatry, 2016, doi:10.3389/fpsyt.2016.00164.

[7] M.E. Portman, A. Natapov, D. Fisher-Gewirtzman, "To go where no man has gone before: Virtual reality in architecture, landscape architecture and environmental planning," Computers, Environment and Urban Systems, 2015, doi:10.1016/j.compenvurbsys.2015.05.001.

[8] N.Y. Lee, D.K. Lee, H.S. Song, "Effect of virtual reality dance exercise on the balance, activities of daily living, And depressive disorder status of Parkinson's disease patients," Journal of Physical Therapy Science, 2015, doi:10.1589/jpts.27.145.

[9] K.K. Bhagat, W.K. Liou, C.Y. Chang, "A cost-effective interactive 3D virtual reality system applied to military live firing training," Virtual Reality, 2016, doi:10.1007/s10055-016-0284-x.

[10] K.E. Laver, B. Lange, S. George, J.E. Deutsch, G. Saposnik, M. Crotty, Virtual reality for stroke rehabilitation, Cochrane Database of Systematic Reviews, 2017, doi:10.1002/14651858.CD008349.pub4.

[11] D. Freeman, S. Reeve, A. Robinson, A. Ehlers, D. Clark, B. Spanlang, M. Slater, Virtual reality in the assessment, understanding, and treatment of mental health disorders, Psychological Medicine, 2017, doi:10.1017/S003329171700040X.

[12] J.A. Stevens, J.P. Kincaid, "The Relationship between Presence and Performance in Virtual Simulation Training," Open Journal of Modelling and Simulation, 2015, doi:10.4236/ojmsi.2015.32005.

[13] M. Slater, M. V. Sanchez-Vives, Enhancing our lives with immersive virtual reality, Frontiers Robotics AI, 2016, doi:10.3389/frobt.2016.00074.

[14] V. Kotu, B. Deshpande, Predictive Analytics and Data Mining: Concepts and Practice with RapidMiner, 2014, doi:10.1016/C2014-0-00329-2.

[15] M.R.K. Hofmann, Data Mining Use Cases and Business Analytics Applications, 2016.

[16] J. Barbič, A. Safonova, J.Y. Pan, C. Faloutsos, J.K. Hodgins, N.S. Pollard, "Segmenting motion capture data into distinct behaviors," in Proceedings - Graphics Interface, 2004.

[17] Z. Xing, J. Pei, E. Keogh, "A brief survey on sequence classification," ACM SIGKDD Explorations Newsletter, 2010, doi:10.1145/1882471.1882478.

[18] C. Li, L. Khan, B. Prabhakaran, "Real-time classification of variable length multi-attribute motions," Knowledge and Information Systems, 2006, doi:10.1007/s10115-005-0223-8.

[19] W. Ugulino, D. Cardador, K. Vega, E. Velloso, R. Milidiú, H. Fuks, "Wearable computing: Accelerometers' data classification of body postures and movements," in Lecture Notes in Computer Science (including subseries Lecture Notes in Artificial Intelligence and Lecture Notes in Bioinformatics), 2012, doi:10.1007/978-3-642-34459-6_6.

[20] M. Hall, "Correlation-Based Feature Selection for Machine Learning," Department of Computer Science, **19**, 2000.

[21] Y. Freund, R.E. Schapire, "Experiments with a New Boosting Algorithm," Proceedings of the 13th International Conference on Machine Learning, 1996, doi:10.1.1.133.1040.

[22] W. Wu, S. Dasgupta, E.E. Ramirez, C. Peterson, G.J. Norman, "Classification accuracies of physical activities using smartphone motion sensors," Journal of Medical Internet Research, 2012, doi:10.2196/jmir.2208.

[23] K. Nandakumar, K.W. Wan, S.M.A. Chan, W.Z.T. Ng, J.G. Wang, W.Y. Yau, "A multi-modal gesture recognition system using audio, video, and skeletal joint data," in ICMI 2013 - Proceedings of the 2013 ACM International Conference on Multimodal Interaction, 2013, doi:10.1145/2522848.2532593.

[24] X. Zhai, B. Jelfs, R.H.M. Chan, C. Tin, "Short latency hand movement classification based on surface EMG spectrogram with PCA," in Proceedings of the Annual International Conference of the IEEE Engineering in Medicine and Biology Society, EMBS, 2016, doi:10.1109/EMBC.2016.7590706.

[25] X. Li, Q. Zhuo, X. Zhang, O.W. Samuel, Z. Xia, X. Zhang, P. Fang, G. Li, "FMG-based body motion registration using piezoelectret sensors," in Proceedings of the Annual International Conference of the IEEE Engineering in Medicine and Biology Society, EMBS, 2016, doi:10.1109/EMBC.2016.7591758.

[26] T. Hachaj, M. Piekarczyk, M.R. Ogiela, "Human actions analysis: Templates generation, matching and visualization applied to motion capture of highly-skilled karate athletes," Sensors (Switzerland), 2017, doi:10.3390/s17112590.

[27] D. Berndt, J. Clifford, "Using dynamic time warping to find patterns in time series," Workshop on Knowledge Knowledge Discovery in Databases, 1994.

[28] F. Zhang, T.Y. Wu, J.S. Pan, G. Ding, Z. Li, "Human motion recognition based on SVM in VR art media interaction environment," Human-Centric Computing and Information Sciences, 2019, doi:10.1186/s13673-019-0203-8.

[29] B. Schölkopf, A.J. Smola, R.C. Williamson, P.L. Bartlett, "New support vector algorithms," Neural Computation, 2000, doi:10.1162/089976600300015565.

[30] C.W. Hsu, C.C. Chang, C.J. Lin, "A Practical Guide to Support Vector Classification," BJU International, 2008.

[31] V. Jain, A. Phophalia, J.S. Bhatt, "Investigation of a Joint Splitting Criteria for Decision Tree Classifier Use of Information Gain and Gini Index," in IEEE Region 10 Annual International Conference, Proceedings/TENCON, 2019, doi:10.1109/TENCON.2018.8650485.

[32] W. Song, H. Wang, P. Maguire, O. Nibouche, "Local Partial Least Square classifier in high dimensionality classification," Neurocomputing, 2017, doi:10.1016/j.neucom.2016.12.053.

[33] I. Chun, M. Tse, Wing Chun Kung Fu: Traditional Chinese King Fu for Self-Defense and Health, St. Martin's Publishing Group, 1998.

Trend Analysis of NO_X and SO₂ Emissions in Indonesia from the Period of 1990 -2015 using Data Analysis Tool

Sunarno Sunarno[*,1,2], Purwanto Purwanto[1,3], Suryono Suryono[4]

¹Green Technology Research Center (GreenTech), Doctorate Program of Environmental Science, School of Postgraduate Studies, Universitas Diponegoro, Semarang, 50241, Indonesia

²Department of Physics, Faculty of Science and Mathematics, Universitas Negeri Semarang, Semarang, 50229, Indonesia

³Department of Chemical Engineering, Faculty of Engineering, Universitas Diponegoro, Semarang,50275, Indonesia

⁴Department of Physics, Faculty of Science and Mathematics, Universitas Diponegoro, Semarang, 50275, Indonesia

A R T I C L E   I N F O

A B S T R A C T

NO$_X$ and SO$_2$ gas pollution have a direct impact on health problems and environmental damage. Therefore, to map the emission patterns and predict the resulting impacts, complete data and information on emissions of the two pollutants are needed. In Indonesia, data on NO$_X$ and SO$_2$ emissions that are recorded over a long period of time (for example 5 decades) are very difficult to obtain. Meanwhile, REASv3.1 is a global emission inventory that provides complete data on air emissions in Asia during 1950 - 2015. Therefore, this study aimed to analyze NO$_X$ and SO$_2$ emission trends, forecast data for 2016 - 2020, and compare the accuracy of calculations from the method used. The processing of both emission data used two methods, namely trend analysis based on exponential and polynomial approaches, and smoothing methods based on Double Moving Average (DMA) and Double Exponential Smoothing (DES). Furthermore, validation of the accuracy from both methods used the value of Mean Absolute Deviation (MAD), Root Mean Square Error (RMSE), and Mean Absolute Percentage Error (MAPE). The results showed that for the smoothing method, DMA was more accurate than DES. Meanwhile, the indicators are MAD, RMSE, and MAPE values, which are smaller and at a very good category. For forecasting results for 2016 – 2020, it was shown that the total emissions of both NO$_X$ and SO$_2$ showed an increase, but with different gains. Furthermore, the total NO$_X$ emission gain was two times greater than the total of SO$_2$. The road transportation and power plant sectors in NO$_X$ emissions showed an increasing trend, with an emission gain ratio of 3:20. Meanwhile, for SO$_2$, the power plant sector experienced a significant increase, while the industrial sector actually showed a downward trend.

1. Introduction

Air quality is a measure of how much air is free from pollution and not harmful when inhaled by humans [1]. Air is stated to be polluted when it contains substances or energy, and other components that exceeds the quality standard [2]. Meanwhile, the sources of air pollution can come from natural processes or human activities (anthropogenic), and the air that is soiled by pollutants causes its quality to be poor. In fact, air pollution can have a serious impact on environmental damage, human health, and

ecological balance [3]. This can be formed from chemical reactions with other pollutants and physical elements in the atmosphere.

According to The Environmental Protection Agency (EPA), 6 types of air pollutants can cause serious impacts on health and environmental damage, namely CO, NO₂, Pb, PM, O₃, and SO₂ [4]. Therefore, monitoring air pollution is very necessary, because the data obtained can provide a lot of information about air quality in an area and within a certain time. REAS (Regional Emissions inventory in Asia) is an emission inventory owned by the Frontier

Research Center for Global Change (FRCGC), Japan Agency for Marine-Earth Science and Technology (JAMSTEC), which provide data sets and various information about air emissions in the Asian region [5]. Furthermore, the REASv3.1 (latest version) provides complete anthropogenic emission data for the period of 1950 - 2015.

The three anthropogenic emissions that causes respiratory problems, such as airway irritation, bronchitis, asthma, and pneumonia, are NO_X, SO_2, and PM [6–8]. The spread of these emissions is very broad, fast, and has a direct impact on health and the environment [9]. In Indonesia, complete and up to date NO_X and SO_2 emission data is rather difficult to obtain, because many ISPU stations (Air Pollutant Standard Index) that are tasked with monitoring air pollution are not operating properly. Therefore complete data on air emissions in Indonesia are mostly obtained on websites of global emission data providers, even until 2015. This data can be used to analyze air quality trends, and as a basis for forecasting data for 2016 - 2020. Trend analysis is an empirical approach used to determine changes in the values of random variables, whether increasing or decreasing over a period of time in statistical terms. In addition to knowing future air quality conditions, forecasting air emission data is often used to anticipate risks in the event of exposure to poor air quality, as well as to formulate environmental pollution control strategies. [10,11].

Therefore, this research aimed to (1) analyze trends and forecasts of total NO_X and SO_2 emissions in Indonesia from 1950 - 2015, and to compare the methods used to determine the best-performing methods, (2) perform smoothing and forecasting of the dominant sector data from NO_X and SO_2, as well as compare the means used to find out which method has the best performance.

2. Materials and Methods

This study used data from REAS (Regional Emission inventory in Asia) ver.3.1. The data include 10 types of air pollutants (BC, CO, CO_2, NH_3, NO_X, NMNVOC, OC, $PM_{2.5}$, PM_{10}, and SO_2), as well as emission sources, both from the producing sector and the type of fuel used [12]. The data used are 2 types of pollutants (NO_X and SO_2), and the 2 largest emission-producing sectors of each pollutants types.

In this research, air emission data processing used two methods, namely the smoothing method with Double Moving Average (DMA) and Double Exponential Smoothing (DES) for emission data per sector. Furthermore, trend analysis was conducted with the exponential approach and polynomial orders of 2 and 3 for total emissions data. Meanwhile, to determine the accuracy of both methods, the results were validated using the calculation of MAD (Mean Absolute Deviation), RMSE (Root Mean Squared Error), and MAPE (Mean Absolute Percentage Error) [13].

$$MAD = \sum_{t=1}^{n}|y_t - \bar{y}_t|/n \qquad (1)$$

$$RMSE = \sqrt{(\sum_{t=1}^{n}(y_t - \bar{y}_t)^2/n)} \qquad (2)$$

$$MAPE = (\sum_{t=1}^{n}|(y_t - \bar{y}_t)/y_t|/n)x100, \ y_t \neq 0 \qquad (3)$$

where y_t is the real data of each emission
         $\bar{y}_t$ is forecasting data
         n is the amount of data used.

The focus of this study is in Indonesia, and the research methodology can be seen in Figure 1.
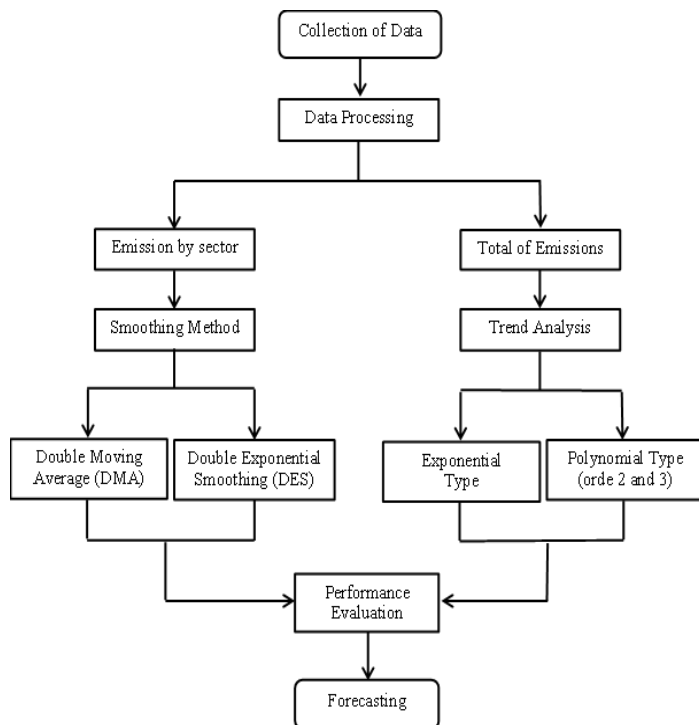
Figure 1: Flow diagram of research on forecasting air emission data

To determine the MAPE accuracy criteria, it can be referred to Table 1

Table 1: The accuracy criteria of MAPE [14]

Criteria	The limit of MAPE percentage
Very Good	<10%
Good	10% – 20%
Enough	20% - 50%
Not Accurate	>50%

All data were processed using the Analysis Toolpak, which is a set of "data analysis" tools in the processing group in Microsoft Excel.

The last stage was forecasting data for the next 5 years, starting from 2016 - 2020. For DMA and DES, data forecasting was performed only for the best performance based on the values of MAD, RMSE, and MAPE that met the criteria. For trend analysis, data forecasting was carried out based on the line equation formed from the approach used.

3. Result and Discussion

3.1. Trend analysis of air pollutants (NO_X, and SO_2)

Estimation or forecasting of total emission data from NO_X and SO_2 pollutants in the coming year was carried out using trend analysis with three approaches, namely, exponential, polynomial order 2, and order 3. Furthermore, the selection of this approach was based on the suitability of the graphical patterns formed between real data and the 3 approaches.
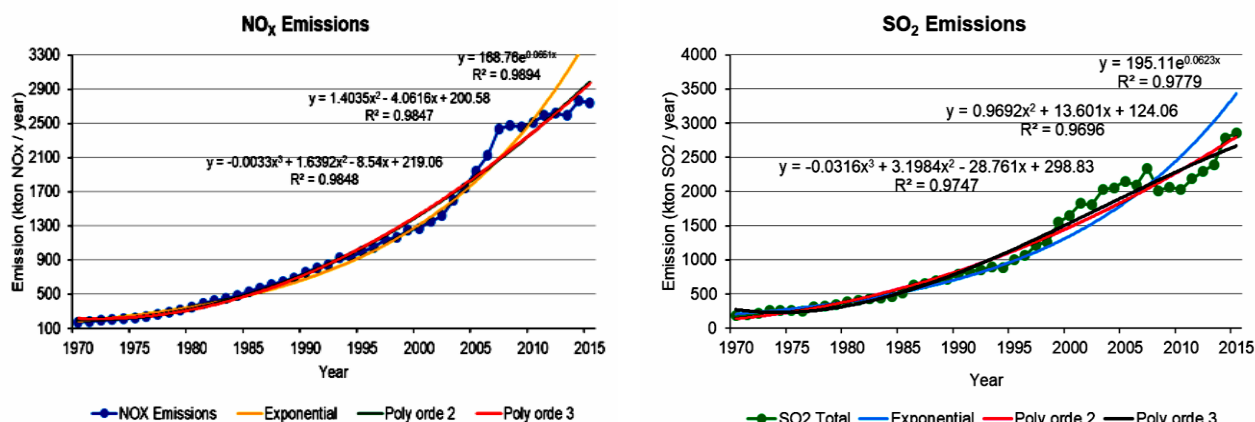
Figure 2: Graph of trend analysis for NO_X and SO_2 emissions

Table 2: The validity calculation on the trends analysis results of the NO_X and SO_2 emission

Perform. evaluation	NO_X Emission			SO_2 Emission		
	Exponential	Polynomal		Exponential	Polynomal	
		Orde 2	Orde 3		Orde 2	Orde 3
MAD	99.43	69.37	71.99	158.38	108.78	102.78
RMSE	186.91	107.19	107.03	246.07	143.19	130.65
MAPE	7.74	5.77	6.65	10.23	10.19	10.21
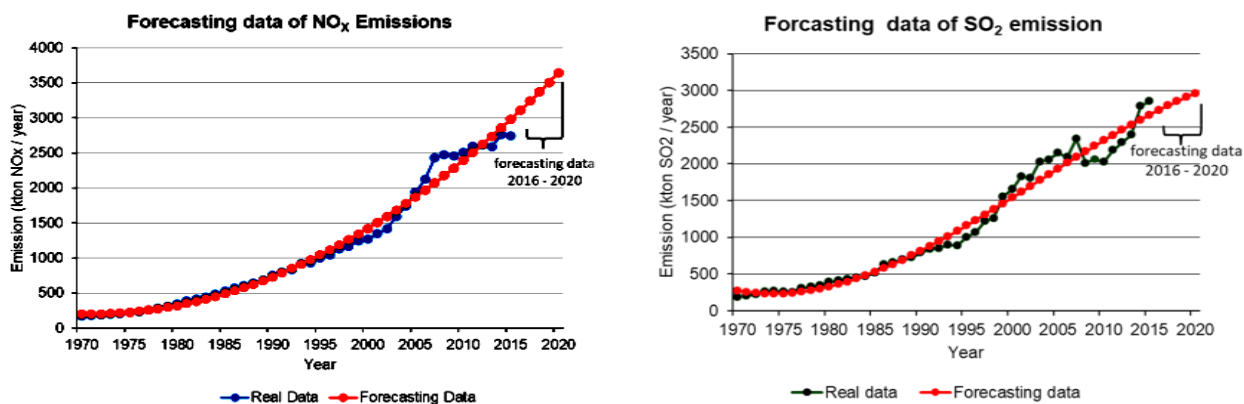
Figure 3: Graph of forecasting data for NO_X and SO_2 emissions in period 1970 - 2020

Table 3: The result of forecasting data for NO_X and SO_2 emissions in the period of 2016 - 2020

Year	Total of NO_X emission (kton/year)	Total of SO_2 Emission (kton/year)	Ratio SO_2/NO_X
	Polynomial orde 2	Polynomial orde 3	
2016	3110.0	2731.5	0.878
2017	3239.3	2792.7	0,862
2018	3371.4	2851.2	0.846
2019	3506.3	2906.8	0.829
2020	3643.9	2959.3	0.812

This study used a lot of data obtained in the period of 1970-2015 or about 45 years. This relatively large data can provide accurate results to minimize errors. Furthermore, this study validated the results using MAD, RMSE, and MAPE to determine the best measurement accuracy of the approach used. Figure 2 showed a graph of trend analysis results on both pollutants, whereas Table 2. showed the performance evaluation results of both graphs

Based on the data validity evaluation, the trend analysis that showed the best performance is the smallest MAD, RMSE, and MAPE values. For NO_X emissions, the use of polynomial order 2 produced a good performance, while for SO_2 emissions, it used a polynomial order 3. Based on the MAPE value, the accuracy of NO_X emission measurements was in the very good category because the value was <10% (5.77%). Meanwhile, for SO_2

emission, it was in a good category because the MAPE value was >10% (10.21%).

For the next stage, the research forecasted data for the next 5 years, between 2016 - 2020, based on graphical equations that have been obtained from trend analysis that showed its best performance. NO_X emission used a polynomial order 2 graph, while SO_2 emission used order 3. The graph equation used for data forecasting was

$$y = 1.404\,x^2 - 4.62x + 200.58 \text{ (NO}_X \text{ emissions)} \tag{4}$$
$$y = -0.032\,x^3 + 3.198\,x^2 - 28.761x + 298.83 \text{ (SO}_2 \text{ emissions) (5)}$$

Forecasting data were obtained by entering $x = 1$ to represent 1970, $x = 2$ for 1971, until $x = 50$ for 2019, and $x = 51$ for 2020 in equations (4), and (5).

Figure 3 showed the results of forecasting NO_X and SO_2 emission data for the period of 1970 – 2020. Figure 3 showed that in Indonesia, there is an upward trend in emissions for both types of pollutants. This is different from what happened in developed countries, where NO_X and SO_2 emissions showed a downward trend, even though there was growth in the economic and industrial sectors [15]. The quantization graph of forecasting emissions of both pollutants in numerical data can be seen in Table 3, which showed the forecasting results of both pollutants for the period of 2016-2020. Meanwhile, SO_2 emission is only 227.8 tons/year. This

means that the NO_X emission gain is more than two times the gain of SO_2. Furthermore, the SO_2 / NO_X ratio has decreased from 0.878 in 2016 to 0.812 in 2020. This showed that the contribution of SO_2 emissions to air pollution in Indonesia is not too significant compared to NO_X

3.2. Smoothing and forecasting data of NO_X and SO_2 emissions

NO_X and SO_2 emission data in this article were collected from 1970 - 2015, and were obtained from REAS version 3.1 [16]. Furthermore, the research smoothed the data for the two dominant sectors in each type of emission. The dominant sectors for NO_X emissions are Road Transportation (Road) and Power Plant (PP), while for SO_2 emissions are Power Plant (PP) and Industry (IND).

Data smoothing is a method used to reduce randomness from time-series data in order to obtain relatively regular data [17,18]. The data smoothing in this research used the Double Moving Average (DMA) and Double Exponential Smoothing (DES) technique. In the DMA technique, 3 variations of the interval were used, namely n = 1, n = 2 and n = 3, while DES used 3 weight variations, namely $\alpha = 0.2$, $\alpha = 0.4$, and $\alpha = 0.5$.

3.2.1. NO_X emissions

Figure 4 showed the results of the smoothing of NO_X emissions data using DMA and DES techniques, for each sector.

(a).

(b).

(c).

(d).
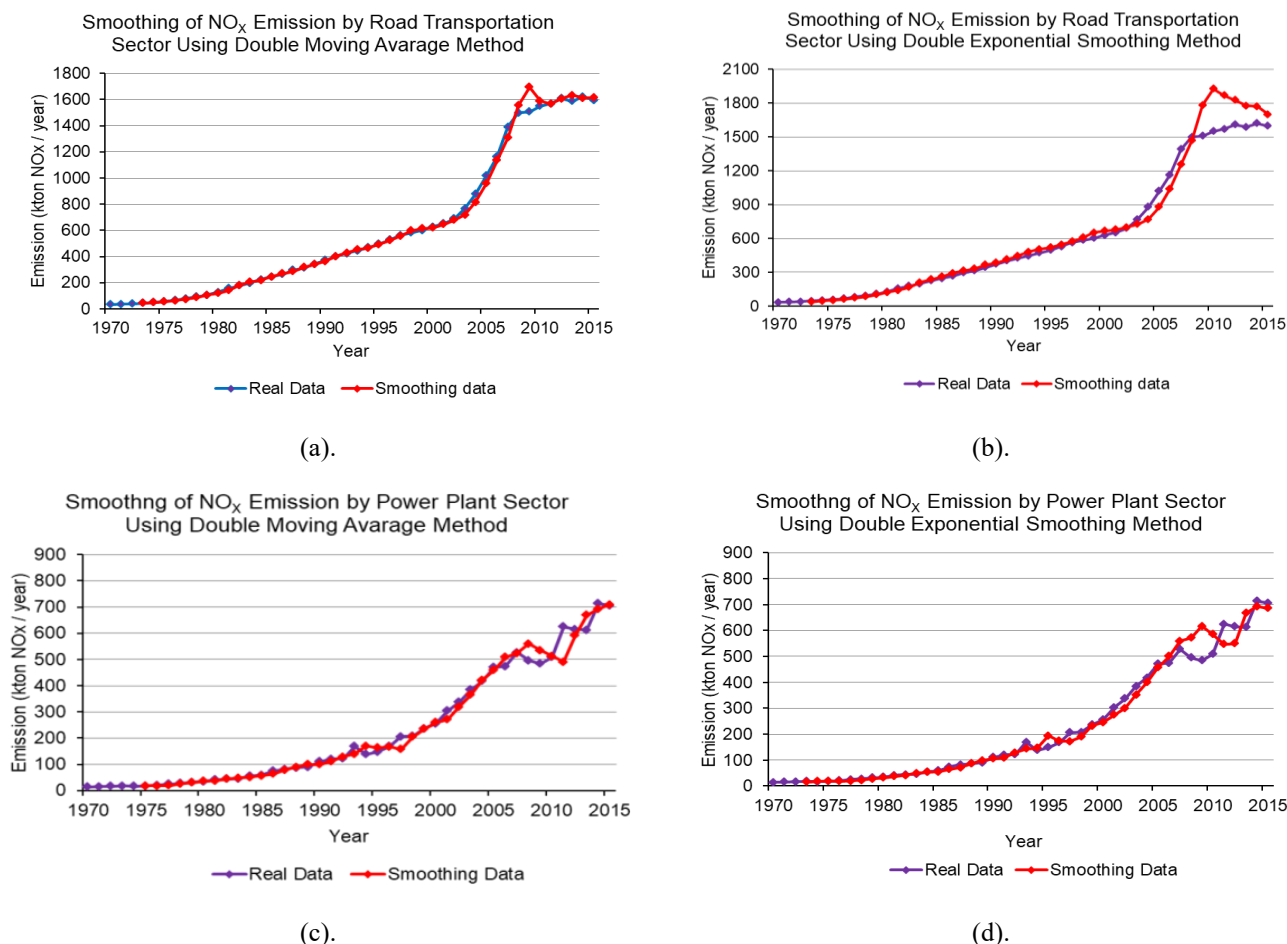
Figure 4: Graph of NO_x emission data smoothing for (a). Road sector using DMA (b). Road sector using DES, (c). PP sector using DMA and (d). PP sector using DES

Table 4: validation of data smoothing for NO_X emissions using the DMA and DES methods.

Double Moving Average (DMA) Method				Double Exponential Smoothing (DES) Method			
Road Transportation (Road) sector				Road Transportation (Road) sector			
	n=2	n=3	n=4		α=0.2	α=0.4	α=0.5
MAD	17,81	26,11	37,21	MAD	70,64	59,74	58,74
RMSE	36,46	50,98	68,06	RMSE	118,85	102,77	104,58
MAPE	2,72	3,58	4,66	MAPE	14,09	8,26	7,65
Power Plant (PP) sector				Power Plant (PP) sector			
	n=2	n=3	n=4		α=0.2	α=0.4	α=0.5
MAD	19,99	15,10	16,81	MAD	26,47	20,87	22,44
RMSE	34,18	28,41	27,42	RMSE	36,06	34,19	39,97
MAPE	8,38	6,68	6,93	MAPE	14,34	9,39	9,53

Year	Emission (kton/year)
2016	1615.70
2017	1620.06
2018	1624.43
2019	1628.79
2020	1633.16

Year	Emission (kton/year)
2016	737.21
2017	767.21
2018	797.22
2019	827.22
2020	857.23

(a)   (b)
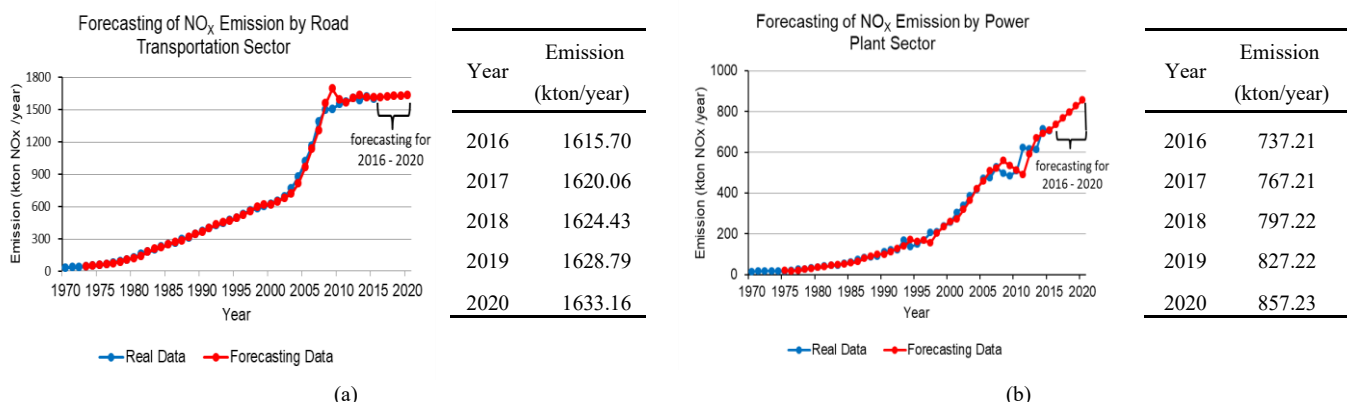
Figure 5: Forecasting data of NO_X emissions (a). by road transportation sector and (b). by power plant sectors

To determine the data smoothing performance, the study validated the results obtained. Table 4 showed the performance validation results based on the MAD, RMSE, and MAPE measurements.

Figure 5 showed forecasting NO_X emission data for the Road and PP sectors in the 2016-2020 period. This data forecasting was based on the best performance obtained, namely at n = 2 (Road) and n = 3 (IND).

Table 4 showed that data smoothing using the DMA was better than the DES methods. This can be seen from the smaller MAD, RMSE, and MAPE values for the DMA than the DES methods. For the road transportation sector, the best performance was in the 2 (n = 2) interval, while for the power plant, it was in the 3 (n = 3) interval. For the MAPE value, NO_X emission measurement in the road transportation sector was 2.72%, while the power plant sector was 6.68%. Therefore, the accuracy was in the very good category because the value was <10%.

Figure 5 showed that the forecasting graph for the transportation sector in 2016-2020 is relatively constant or the changes are not too significant, with a gain of 17.46 kton / year. Meanwhile, the power plant sector showed a significant increase with a gain of 120.02 kton / year

3.2.2. SO₂ emissions

Figure 6 showed the results of smoothing SO_2 emission data using DMA and DES techniques for the power plant (PP) and the industrial sectors (IND). The results of smoothing the data from the two methods were then validated using MAD, RMSE, and MAPE. Subsequently, the results were compared to determine the best performance. Table 5 showed the validation results of both methods used

(a)   (b)

(c)

(d)
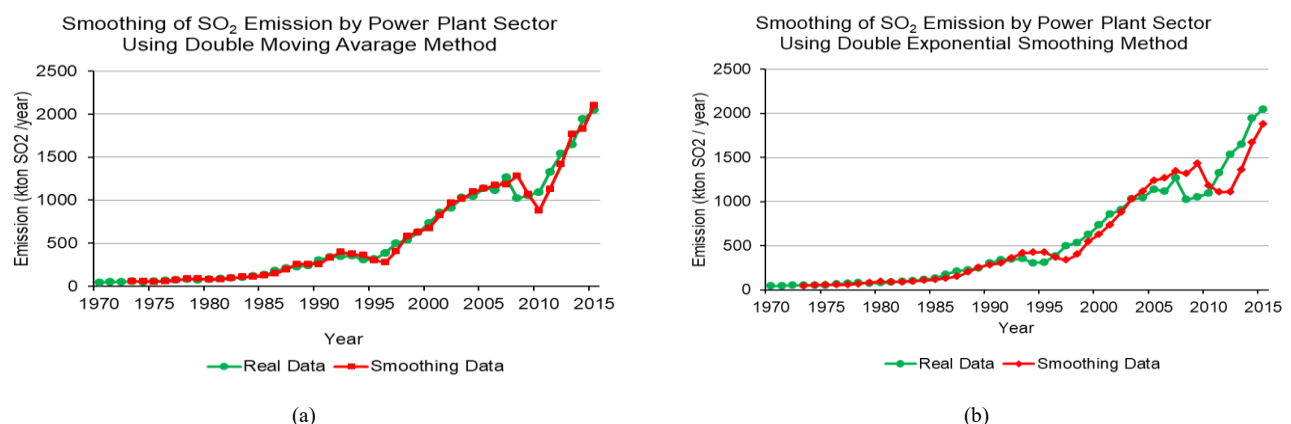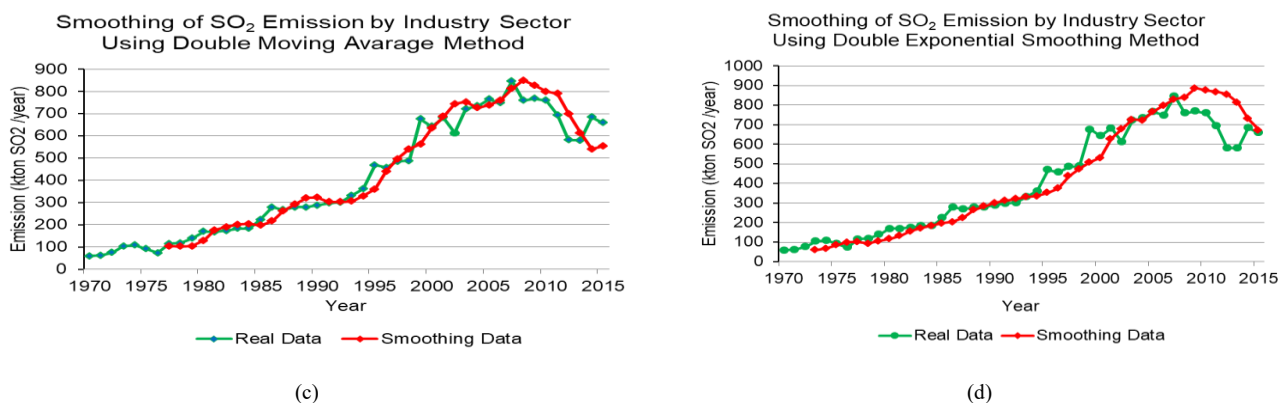
Figure 6: Graph of SO₂ emission data smoothing for (a). PP sector using DMA (b). PP sector using DES, (c). IND sector using DMA and (d). IND sector using DES

Table 5: Validation of data smoothing for SO₂ emissions using the DMA and DES methods.

Double Moving Average (DMA) Method				Double Exponential Smoothing (DES) Method			
Power Plant (PP) sector				**Power Plant (PP) sector**			
	n=2	**n=3**	**n=4**		**α=0.2**	**α=0.4**	**α=0.5**
MAD	44,85	49,67	60,42	MAD	98,25	83,24	78,91
RMSE	74,06	90,77	106,36	RMSE	148,86	133,14	131,30
MAPE	8,41	8,89	9,75	MAPE	16,79	13,52	13,56
Industry (IND) sector				**Industry (IND) sector**			
	n=2	**n=3**	**n=4**		**α=0.2**	**α=0.4**	**α=0.5**
MAD	44,06	41,56	36,00	MAD	50,89	54,40	61,13
RMSE	60,01	60,78	53,33	RMSE	79,32	73,14	82,71
MAPE	11,54	11,25	8,45	MAPE	13,54	14,87	16,81

Table 5 showed that the best performing data smoothing for the PP and IND sectors using DMA was at n = 2 and n = 4, while for DES, it lies at weights α=0.4 and α=0.2. When the results are compared, the DMA method was better than DES, because the values of MAD, RMSE, and MAPE were smaller. For MAPE, the measurement of SO₂ emissions in the power plant sector had a value of 8.41%, while the industrial sector was 8.45%. Therefore, the accuracy was in the very good category because the value was <10%.

Forecasting data for SO₂ emissions in the Road and PP sectors in the 2016 - 2020 period can be seen in Figure 7. This forecasting is based on the best performance obtained, namely at n = 2 (PP) and n = 4 (IND). Figure 7 showed that the data forecasting graph

for the power plant sector in 2016-2020 has increased significantly with a gain of 798.5 kton / year, while for the industrial sector showed a decline with a gain of -73.54 kton/year.

In 2015, the installed power capacity for Steam Power Plants (PLTU) was around 53.1% of the total power generation in Indonesia [19]. This showed that the need for coal fuel to supply PLTU needs is very large. Furthermore, the increase in the amount of coal is proportional to the increasing demand for electricity. Therefore, SO₂ gas pollution in the period of 2016 - 2020, appears to have increased significantly. In contrast to the power plant, SO₂ emissions in the industrial sector have decreased, because many industries have implemented the clean production principle by reducing the use of coal as their industrial fuel [20].

Year	Emission (kton/year)
2016	2294.2
2017	2493.8
2018	2693.4
2019	2893.1
2020	3092.7

(a)

Year	Emission (kton/year)
2016	579.91
2017	561.53
2018	543.14
2019	524.76
2020	506.37

(b)
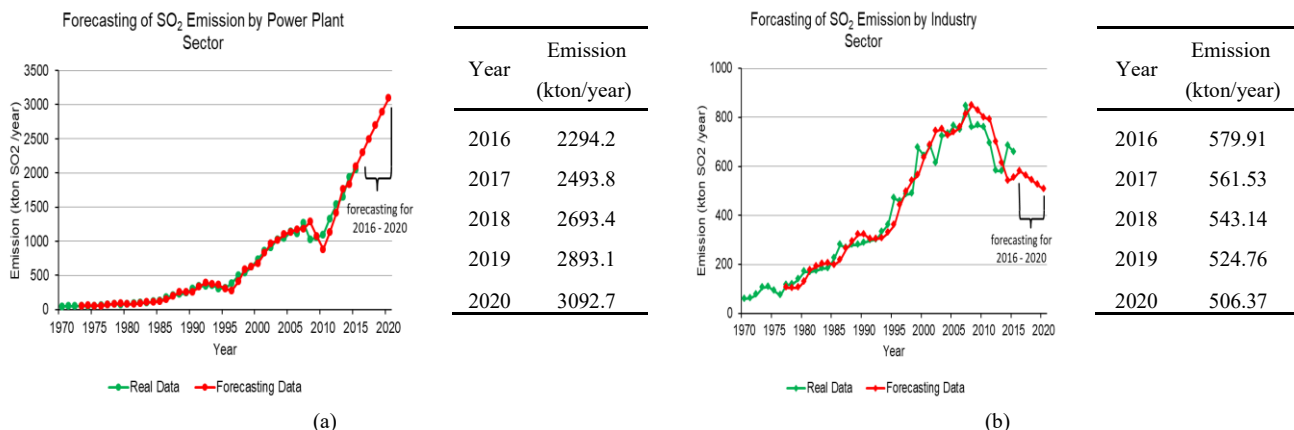
Figure 7: Forecasting data of SO₂ emissions (a). by power plant sector and (b). by industry sector

4. Conclusions

The use of Double Moving Average (DMA) method in smoothing NO_X and SO_2 emission data is better than the Double Exponential Smoothing (DES). This is based on the validation results of both methods, where the MAD, RMSE, and MAPE values for the DMA method are smaller than DES. For NOx and SO_2 emissions, the resulting MAPE value in the DMA method was in the very good category, because the value was <10%. Furthermore, the best variation of the moving average interval for NO_X emissions lies at n = 2 (road transportation sector) and n = 3 (power plant sector), while for SO_2 emissions, it lies at n = 2 (power plant sector) and n = 4 (Industry sector).

The forecasting stage for the period of 2016 - 2020 generally showed that the total emissions of NO_X and SO_2 have increased, with the gains for each emission being 533.9 kton / year and 227.8 kton / year. This means that the total emission gain of NO_X is two times greater than SO_2. Furthermore, in the road transportation sector that produces NO_X emissions, changes are not too big, with an emission gain of 17.46 kton / year. Meanwhile, in the power plant sector, it has a quite significant increase, with an emission gain of 120.02 kton / year. SO_2 emissions showed that there is an increase in emissions of power plant sector with a gain of 798.5 kton / year, while for the industrial sector, there is a decrease with a gain of -73.54 kton / year. In addition, the reduction in SO_2 emissions in the industrial sector showed that there is an industrial policy to reduce the use of coal as its energy source.

Conflict of Interest

The authors declare no conflict of interest.

Acknowledgment

References

[1] R. Lanzafame, P. Monforte, G. Patanè, S. Strano, "Trend analysis of Air Quality Index in Catania from 2010 to 2014," Energy Procedia, **82**, 708–715, 2015, doi:10.1016/j.egypro.2015.11.796.

[2] State Minister of Environment, Regulation of State Minister of the environment Number 12 of 2010 About Regional Air Pollution Control Implementation, 1–199, 2010.

[3] G.S. Ajmani, H.H. Suh, J.M. Pinto, "Effects of Ambient Air Pollution Exposure on Olfaction: A Review," Environmental Health Perspectives, **124**(11), 1683–1693, 2016, doi:10.1289/EHP136.

[4] R. Williams, V. Kilaru, E. Snyder, A. Kaufman, T. Dye, A. Rutter, H. Hafner, Air Sensor Guidebook, EPA (Environmental Protection gency) USA, 2014.

[5] Frontier Research Center for Global Change (FRCGC), Atmospheric Composition Research Program, Http://Www.Jamstec.Go.Jp/Frsgc/Research/P3/Emission.Htm, 2004.

[6] H. Yin, M. Pizzol, L. Xu, "External costs of PM2.5 pollution in Beijing, China: Uncertainty analysis of multiple health impacts and costs," Environmental Pollution, 2017, doi:10.1016/j.envpol.2017.02.029.

[7] A.J. Cohen, M. Brauer, R. Burnett, H.R. Anderson, J. Frostad, K. Estep, K. Balakrishnan, B. Brunekreef, L. Dandona, R. Dandona, V. Feigin, G. Freedman, B. Hubbell, A. Jobling, H. Kan, L. Knibbs, Y. Liu, R. Martin, L. Morawska, C.A. Pope, H. Shin, K. Straif, G. Shaddick, M. Thomas, R. van Dingenen, A. van Donkelaar, T. Vos, C.J.L. Murray, M.H. Forouzanfar, "Estimates and 25-year trends of the global burden of disease attributable to ambient air pollution: an analysis of data from the Global Burden of Diseases Study 2015," The Lancet, **389**(10082), 1907–1918, 2017, doi:10.1016/S0140-6736(17)30505-6.

[8] N. Sharma, S. Taneja, V. Sagar, A. Bhatt, "Forecasting air pollution load in Delhi using data analysis tools," Procedia Computer Science, **132**, 1077–1085, 2018, doi:10.1016/j.procs.2018.05.023.

[9] J. Liu, Y. Chen, T. Lin, C. Chen, P. Chen, T. Wen, C. Sun, J. Juang, J. Jiang, "An air quality monitoring system for urban areas based on the technology of wireless sensor networks," International Journal On Smart Sensing and Intelegent System, **5**(1), 191–214, 2012.

[10] W.F. Ryan, "The air quality forecast rote: Recent changes and future challenges," Journal of the Air and Waste Management Association, **66**(6), 576–596, 2016, doi:10.1080/10962247.2016.1151469.

[11] A. Jaiswal, C. Samuel, V.M. Kadabgaon, "Statistical trend analysis and forecast modeling of air pollutants," Global Journal of Environmental Science and Management, **4**(4), 427–438, 2018, doi:10.22034/gjesm.2018.04.004.

[12] J. Kurokawa, T. Ohara, "Long-term historical trends in air pollutant emissions in Asia: Regional Emission inventory in ASia (REAS) version 3.1," Atmospheric Chemistry and Physics, 1–51, 2019, doi:10.5194/acp-2019-1122.

[13] N.H.A. Rahman, M.H. Lee, Suhartono, M.T. Latif, "Evaluation performance of time series approach for forecasting air pollution index in Johor, Malaysia," Sains Malaysiana, **45**(11), 1625–1633, 2016.

[14] D. Febrian, S.I. Al Idrus, D.A.J. Nainggolan, "The Comparison of Double Moving Average and Double Exponential Smoothing Methods in Forecasting the Number of Foreign Tourists Coming to North Sumatera," Journal of Physics: Conference Series, **1462**(1), 2020, doi:10.1088/1742-6596/1462/1/012046.

[15] C.S. Lee, K.H. Chang, H. Kim, "Long-term (2005–2015) trend analysis of PM2.5 precursor gas NO2 and SO2 concentrations in Taiwan," Environmental Science and Pollution Research, **25**(22), 22136–22152, 2018, doi:10.1007/s11356-018-2273-y.

[16] J. Kowara, T. Ohara, Gridded Data Sets (Information for Data), Https://Www.Nies.Go.Jp/REAS/Index.Html#data%20sets, 2019.

[17] S. Bi, S. Bi, D. Chen, J. Pan, J. Wang, "A double-smoothing algorithm for integrating satellite precipitation products in areas with sparsely distributed in situ networks," ISPRS International Journal of Geo-Information, **6**(1), 2017, doi:10.3390/ijgi6010028.

[18] T.C. Pataky, M.A. Robinson, J. Vanrenterghem, J.H. Challis, "Smoothing can systematically bias small samples of one-dimensional biomechanical continua," Journal of Biomechanics, **82**, 330–336, 2019, doi:10.1016/j.jbiomech.2018.11.002.

[19] Badan Pusat Statistik (BPS), Generating capacity installed by power plant in Indonesia, Http://Www.Bps.Go.Id, 2020.

[20] J.M. Grether, N.A. Mathys, J. de Melo, "Global manufacturing SO2 emissions: Does trade matter?," Review of World Economics, **145**(4), 713–729, 2010, doi:10.1007/s10290-009-0033-2.

Optimal Sizing of a Renewable Energy Hybrid System in Libya Using Integrated Crow and Particle Swarm Algorithms

Abdurazaq Elbaz[*], Muhammet Tahir Güneşer

Karabuk University, Engineering Faculty, Eletrical and Electronics Department, Karabuk, 78100, Turkey

A R T I C L E I N F O	A B S T R A C T
	Sizing optimization should be used to design an efficient, sustainable, and feasible hybrid system. In this paper, a hybrid power plant consisting of an off-grid photovoltaic and wind energy system was planned to supply the demand of residential houses in Libya. To minimize installation and operational costs by sizing each part of the hybrid system, the crow search technique was applied. We optimized the number of photovoltaic modules, wind turbine power, and battery capacity and then we compared the performance of the crow algorithm with the particle swarm optimization algorithm for hybrid system design. The results of the crow algorithm suggest better efficiency for sizing lower-cost hybrid power plants consisting of photovoltaic and wind systems.

1. Introduction

Renewable energy systems are basically designed to achieve two objectives: cost-effectiveness and environmental protection. It is possible to achieve these objectives by reducing both dangerous emissions and fuel costs. This type of power system has clear financial benefits [1] other than reducing emissions of carbon dioxide (CO_2), nitrogen oxide (NOx), and sulfur oxide (SOx), which can be detrimental for life on this planet [2]. Whenever these objectives are pursued at the same time, the combined economic emission dispatch (CEED) problem emerges, which can be addressed through traditional mathematical methods like lambda iteration, gradient search, and optimization through modern heuristics [1]. However, in this case, it is not possible to solve the CEED problem because the procedure does not give a single result. Additionally, for achieving two contradictory aims, such as reduction of both pollution and fuel costs, mathematical/gradient information is not required. On the contrary, this optimization problem needs some kind of transactional solution like the Pareto optimal (PO) solution [3], requiring further processing for finding the best optimized and most favorable solution. The literature shows that some multi-objective algorithms help reduce greenhouse gases while decreasing fuel costs at the same time. These algorithms include scatter search [4], the bacterial foraging algorithm [5], particle swarm optimization [6], teaching-learning-based optimization [7], the harmony search algorithm [8], and differential evolution [9].

We have tested different methods to solve the non-convex and non-linear CEED problem.

In this case, the "h" parameter is used to handle dimensional problems that can be solved through the sketched evolutionary algorithm [8]-[10]. We can also solve the CEED problem without using the mentioned parameter by regularizing fuel costs and pollutants. This is possible using evolutionary algorithms (EAs) by solving a single objective function, but such methods have a shortcoming: researchers need to make repeated efforts to find the objective solution.

Results show that hybrid algorithms are useful and efficient in performing parallel processing. For achieving the best solution, a balance is required between exploration and exploitation. While exploration is pivotal for any kind of algorithm, exploitation helps in finding excellent solutions. The present research involves bat [11] and crow [12]algorithms for solving the CEED issue. We have selected a hybrid structure that combines the properties of crow search and bat algorithms and resolves the problems of the mentioned population-based methods. Hybridization was also chosen because it gives more diverse and acceptable solutions.

2. Types of Algorithms

2.1. Particle Swarm Optimization (PSO)

Potential solutions, which are also referred to as "particles," lie within the problem space. Here, "swarms" means the multi-dimensional modeling spaces in which the particles exist, and they

have certain velocities and particular positions. Every particle provides a "candidate solution," moving in the search space before they exceed the computational limitations. During flight, the particles continually adjust their positions, making sure that they gain the best positions while keeping in view neighboring particles and their positions. This means that particles have a tendency of adjusting their velocities and positions depending on their neighbors. Moreover, social, inertial, and cognitive factors keep adjusting the particle velocity until an optimal solution is found [13].

2.2. Crow Search Algorithm (CSA)

It is a common observation that crows are intelligent, which is evident from their brain/body ratios. They have the ability to sense danger, issue warning signs, and recognize faces. The CSA was accordingly developed after observing habits of crows such as living in groups, going together to steal food, snatching food, and remembering their hiding places [14].

Besides other mental capabilities, crows have amazing "awareness probability" (AP). Suppose that, if there are n crows living in a specific space, for the tth iteration, x_i^t shows the location of crow i.

Here, an individual's update mode can be mathematically represented as given below:

$$X_i^{t+1} = \begin{cases} X_i^t + r_1 * fl_i^t * \left(mem_j^t - x_i^t\right), r \geq AP_j^t \\ a \quad random\ position, \quad other \end{cases} \tag{1}$$
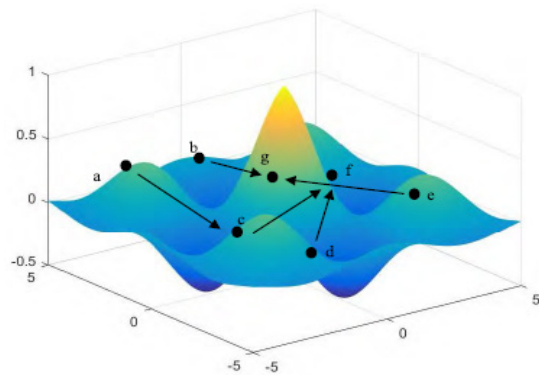
Figure 1: An individual crow's movements

3. Hybrid PV/ Wind Power System

3.1. Mathematical Model for PV System

Libya has massive solar power generation potential. For example, in the Libyan city of Ghiryan, there is an average of 7.5 kWh/m² daily solar radiation (Figure 3), and every year, there is complete sunshine for 3700 hours. Photovoltaic (PV) systems are the best systems for use in rural Libya because they provide convenience and economy. Research has shown that solar energy is sufficient to generate 141,000 tWh annually, which is more than the potential of wind (16,000 tWh) and biomass (21,000 tWh) [15], [16].
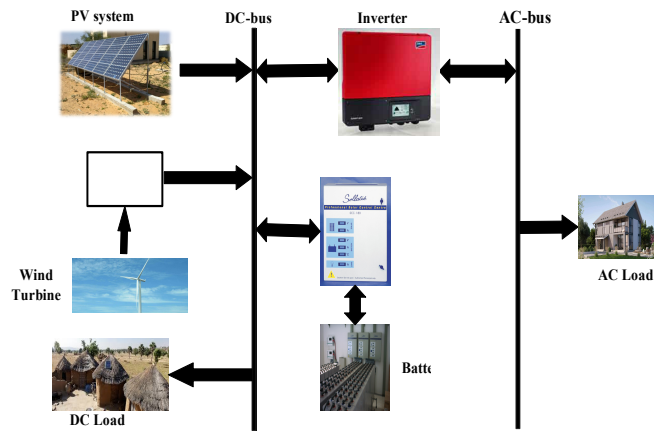
Figure 2: Hybrid system

Figure 3: Annual average solar radiation in Ghiryan

The mathematic model suggested for the PV system is as follows:

$$P_{PV} = N_{pv} * \left\{P * \frac{G}{G_{ref}}\right\} + \left(1 - m * (tc - tc_{ref})\right) \tag{2}$$

Here, P_{pv} represents the PV arrays' power output under reference conditions, and P represents rated power while N_{pv} is the summation of all PV arrays. G_{ref} is equal to 1000 W/m², where G represents solar radiation (W/m²), and m is equal to -3.7×10^{-3} (1/°C). In the above formula, tc is the PV cell temperature, which has a reference value of 25 °C. We used the following formula to calculate the PV cell temperature [17]:

$$t_c = t_a \left\lfloor \left(\frac{NOCT - 20}{800}\right) \right\rfloor * G \tag{3}$$

In this formula, $NOCT$ represents the nominal operating cell temperature while t_a is ambient temperature.

3.2. Mathematical Model for Wind Turbine

We used the NASA website to obtain 10-year wind data (2005-2015). We found that in the city of Ghiryan, the average wind speed was 6-7.5 m/s. That is sufficient for operating a wind power unit, which should be installed at a height of 50 m. We studied the effects of different seasons on wind speed and found that wind speed is higher from December to May. It remains lower in summer, specifically in July and August. The wind speed in Ghiryan is shown in Figure 4 [18].
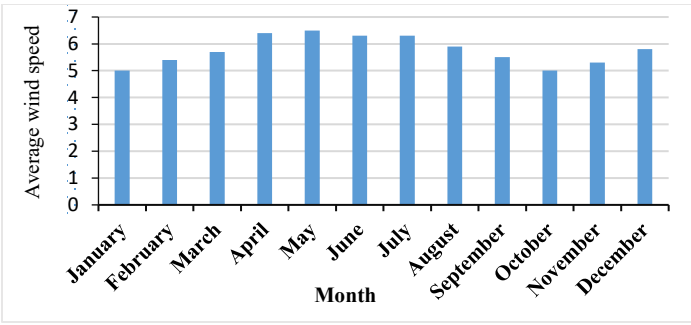
Figure 4: Average wind speed in Ghiryan

Climatic variations in Ghiryan include extremely humid and hot summers and mild winters with average wind speeds suitable for power generation. To measure the wind speed, the following formula is used [19]:

$$\frac{V_2}{V_1} = \left(\frac{H_2}{H_1}\right)^a \qquad (4)$$

Here, v_1 is the velocity at the reference height, h_1; v_2 is the velocity at the height of the hub, h_2; and a is the friction coefficient. Certain parameters are specified by a, i.e. terrain roughness, wind speed, temperature, height above ground, time of day, and time of year[20]. Different types of terrain [21]are generally specified in the technical literature; however, the guidelines of the IEC standards [22] suggest a coefficient of friction value of 0.11 for extreme wind conditions and 0.20 for normal wind conditions.

A wind turbine's predicted power output is expressed as follows:

$$
\begin{cases}
0 \\
V^3 \quad \left(\frac{P_{rated}}{V_{rated}^3 - V_{cut-in}^3}\right) - \\
P_{rated}
\end{cases}
$$

$$
P_{rated}\left(\frac{V_{cut-in}^3}{V_{rated}^3 - V_{cut-in}^3}\right)
\left.
\begin{array}{l}
V < V_{cut-in}, V > V_{cut-out} \\
V_{cut-in} \le V \le V_{rated} \\
V_{rated} \le V \le V_{cut-out}
\end{array}
\right\}
\qquad (5)
$$

Here, V is the wind speed of the current time step, the nominal wind speed is V_{rated}, the cut-out wind speed is $V_{cut-out}$, the cut-in wind speed is V_{cut-in}, and the rated power is P_{rated}.

3.3. Mathematical Model for Batteries

Generally, most hybrid systems have lead-acid batteries, and their charging and usage depend on the power generated through the PV system and the wind turbine. Eqs. 6 and 7 show the charge-discharge phenomenon [23].

When the power generated through the wind turbines and PV arrays exceeds the load, it charges the battery bank. The state of charge (SOC) is determined with the following equation [24]:

$$\text{SOC (t)} = \text{SOC}(t-1) - \left(P_{pv}(t) + P_{wt}(t) - P_{dmd}\right) * \eta_{ch} \qquad (6)$$

In this case, $SOC\,(t-1)$ and $SOC(t)$ respectively represent the battery bank charges in the time intervals $t-1$ and t while $Pdmd$ is the load demand. Here, η_{ch} represents the efficiency of the battery bank.

When there is load demand, the battery bank is discharged, which can be mathematically represented with the following equation:

$$\text{SOC (t)} = \text{SOC}(t-1) - \left(P_{pv}(t) + P_{wt}(t) - P_{dmd}\right) * \eta_{disch} \qquad (7)$$

The adjustment of the battery depends on the demand (Eq. 8). In this case, *DOD* represents the discharge depth while *ad* shows the days of autonomy. Here, η_{inv} and η_b respectively represent the inverter and battery efficiencies.

$$C_n = \frac{E_{dmd} * ad}{DOD * \eta_{inv} * \eta_{bat}} \qquad (8)$$

3.4. Electrical Loads

Electrical loads can be classified based on the activity/type of work performed and they depend on the consumer's consumption pattern, including housing, commercial, agricultural, and general loads. For assessing the load of each sector, electric loads should be considered. Generally, the housing sector is internationally considered as the sector consuming the largest quantities of electrical power. Part of its energy transforms into thermal energy when heating/cooling appliances such as air conditioners, water coolers, or refrigerators are used, and some of its energy transforms into optical energy when lighting devices like electric bulbs are turned on. Some energy transforms into dynamic energy when electric motors, mixers, and fans are used [18].

For our experiment, we selected an average power-consuming house. Fig. 5 and Fig. 6 present the appliances and loads.
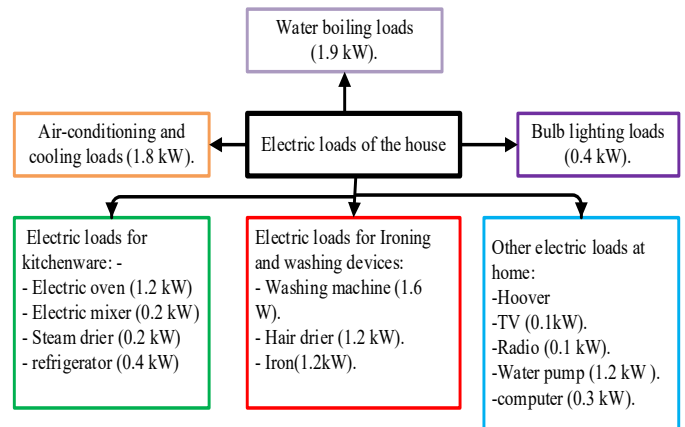
Figure 5: Load estimation for household electrical equipment
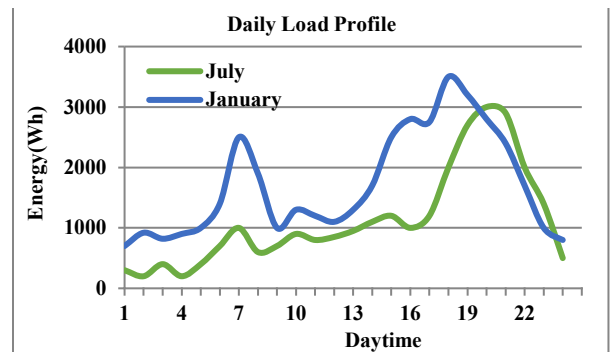
Figure 6: Load profiles for two seasons

4. Optimization Problem

The minimization of the annual expense of the device (ACS) is a major goal of our analysis. The components include costs of upkeep (C_m), resources (C_a), and substitution (C_r) and the mathematical expression of ACS can therefore be given as follows:

$$ACS = C_a + C_m + C_r \qquad (9)$$

$$C_a = CRF * \left(C_{pv_{tot}} + N_{wt_{tot}} + C_{bat_{tot}} \right) \qquad (10)$$

$$C_{pv_{tot}} = N_{pv} * C_{pv} \qquad (11)$$

$$C_{wt_{tot}} = N_{wt} * C_{wt} \qquad (12)$$

$$C_{bat_{tot}} = \left(\frac{n}{LS_{bat}} \right) N_{bat} * C_{bat} \qquad (13)$$

In the terms given, the costs of wind turbines, PV modules, and battery banks are represented by C_{wt}, C_{pv}, and C_{bat}, respectively, and the life span of the renewable energy system is shown by n. The battery life is LS_{bat}, and the capital recovery factor is CRF; CRF can therefore be mathematically expressed as follows [25][26]:

$$CRF = \frac{i(1+i)^n}{(1+i)^n - 1} \qquad (14)$$

5. Optimization of Outcomes

We selected a house located in the mountainous area of Ghiryan. Table 1 shows the investment, technical, and maintenance costs needed to operate the PV panels, wind turbines, and batteries.

Table 1: Design parameter values

	Cost ($)	Parameters	Maintenance costs ($)
Wind turbine	1870.83	500 W	18.70
PV panel	287.82	250 W	2.878
Battery	332.10	600 Ah	31.76

To determine the effectiveness of the crow algorithm for a specific hybrid renewable system size, we applied the optimization techniques both with and without applying the reliability model. We then compared the obtained results with the calculated values, applying PSO to test the performance, robustness, and convergence. The results obtained after applying the crow algorithm and PSO are displayed in Table 2.

Table 2: Crow and PSO algorithm performances

	PSO	Crow
N_{pv}	23	23
N_w	0	0
N_{bat}	12	10
ACS ($)	16534	16065

Obviously, the crow algorithm showed better performance as compared to other optimization methodologies. It can therefore be

deemed superior on the grounds that it reduces computations. According to Table 3, the crow algorithm is again better as compared to PSO. It was found that the power generation cost with a PV array is lower compared to the cost of power generation from the wind. This can be expressed as follows:

$$0 \leq N_{pv} \leq N_{pvmax}$$

$$1 \leq N_{wt} \leq N_{wtmax} \qquad (15)$$

$$0 \leq N_{bat} \leq N_{batmax}$$

Table 3: Crow and PSO algorithm performances based on Eq. (15)

	PSO	Crow
N_w	1	1
N_{pv}	23	23
N_{bat}	11	9
ACS ($)	27943.24	27.260

It is obvious that the crow algorithm helps in reducing the cost. Table 3 shows that the achieved results minimized the annual cost of power generation. In Table 4, wind, PV, and hybrid system reliabilities are presented. It was found that reduced wind availability increases the costs, but it reduces the requirement for batteries. Moreover, the results showed an increase in reliability indices such as energy supplied (ES), reliability of power supply (RSP), and loss of power supply probability.

Table 4: Size, reliability, and cost indices

	PSO			Crow		
%	100	95	90	100	95	90
N_{pv}	23	23	23	23	23	23
N_w	0	0	0	0	0	0
N_{bat}	11	10	10	10	9	9
ACS ($)	16533	15624	14856	16065	15480	14562

6. Conclusion

This paper shows a latest approach pertaining to the sizes of offshore stand-alone wind-powered hybrid PV systems. It was found that the crow algorithm is viable in terms of economic and technical value addition and cost reduction. We found that installation of the suggested system is possible in Ghiryan, a city located in Libya. After collecting the long-term wind speed and solar radiation data, we applied the crow and PSO algorithms. This helped in determining the required numbers of wind turbines, batteries, and PV modules. We then compared the results.

According to the outcomes, the crow algorithm allowed for higher accuracy and simpler calculations in addition to reducing costs. The outcomes indicate that using a reliability model affects the cost, optimum size, and load. We found that if the efficiency of the inverter is increased, it could decrease the cost of the device and boost the reliability of the load supplied. We conclude that the crow algorithm can help avoid local minimums and is a reliable method for optimization.

References

[1] N.I. Nwulu, X. Xia, "Optimal dispatch for a microgrid incorporating renewables and demand response," Renewable Energy, **101**, 16–28, 2017, doi:10.1016/j.renene.2016.08.026.

[2] R. Velik, P. Nicolay, "Grid-price-dependent energy management in microgrids using a modified simulated annealing triple-optimizer," Applied Energy, **130**, 384–395, 2014, doi:10.1016/j.apenergy.2014.05.060.

[3] Y. Mulugetta, E. Hertwich, K. Riahi, T. Gibon, K. Neuhoff, "Energy Systems," 511–598.

[4] X. Meng, X.Z. Gao, Y. Liu, H. Zhang, "Expert Systems with Applications A novel bat algorithm with habitat selection and Doppler effect in echoes for optimization," Expert Systems With Applications, **42**(17–18), 6350–6364, 2015, doi:10.1016/j.eswa.2015.04.026.

[5] A.K. Basu, A. Bhattacharya, S. Chowdhury, S.P. Chowdhury, "Planned scheduling for economic power sharing in a CHP-based micro-grid," IEEE Transactions on Power Systems, **27**(1), 30–38, 2012, doi:10.1109/TPWRS.2011.2162754.

[6] R. Jovanovic, M. Tuba, "An ant colony optimization algorithm with improved pheromone correction strategy for the minimum weight vertex cover problem ☆," Applied Soft Computing Journal, **11**(8), 5360–5366, 2011, doi:10.1016/j.asoc.2011.05.023.

[7] A. Debbarma, S. Das Biswas, "Optimal operation of large power system by GA method," Journal of Emerging Trends in Engineering and Applied Sciences, **3**(1), 1–7, 2012.

[8] A. Adhi, B. Santosa, N. Siswanto, "A meta-heuristic method for solving scheduling problem: Crow search algorithm," IOP Conference Series: Materials Science and Engineering, **337**(1), 2018, doi:10.1088/1757-899X/337/1/012003.

[9] A.S.R. M Vijay Karthik, "Particle Swarm Optimization to solve Economic Dispatch considering Generator Constraints M Vijay Karthik , 2 , Dr A Srinivasula Reddy F P □," The Ijes, 94–100, 2014.

[10] S. Khamsawang, S. Jiriwibhakorn, "Solving the economic dispatch problem using novel particle swarm optimization," International Journal of Electrical, …, **3**(3), 529–534, 2009.

[11] K. Lumpur, "SOLVING ECONOMIC DISPATCH PROBLEM USING PARTICLE SWARM OPTIMIZATION BY AN EVOLUTIONARY TECHNIQUE FOR INITIALIZING," **46**(2), 526–536, 2012.

[12] C. Qu, Y. Fu, "Crow search algorithm based on neighborhood search of non-inferior solution set," IEEE Access, **7**, 52871–52895, 2019, doi:10.1109/ACCESS.2019.2911629.

[13] K.E. Parsopoulos, M.N. Vrahatis, "On the Computation of All Global Minimizers Through Particle Swarm Optimization," **8**(3), 211–224, 2004.

[14] A. Askarzadeh, "A novel metaheuristic method for solving constrained engineering optimization problems : Crow search algorithm," Computers and Structures, **169**, 1–12, 2016, doi:10.1016/j.compstruc.2016.03.001.

[15] S. Umesh, J. Chaithra, G. Deborah, J. Gayathri, N. Pruthvi, Methods to Optimize the Performance of an Existing Large-Scale On-grid Solar PV Plant, Springer Singapore, 2019, doi:10.1007/978-981-13-5802-9_117.

[16] H. Salah, A. Embirsh, E. Yousuf, "Future of Solar Energy in Libya," **7**(10), 2016–2018, 2017.

[17] M. Kalogera, P. Bauer, "Optimization of an off-grid hybrid system for supplying offshore platforms in arctic climates," 2014 International Power Electronics Conference, IPEC-Hiroshima - ECCE Asia 2014, 1193–1200, 2014, doi:10.1109/IPEC.2014.6869738.

[18] M. Ekhlat, I.M. Salah, E.N.M. Kreama, "Development Energy Efficiency and Renewable Energy Libya - National study," Plan Bleu Regional Activity Center, (September), 2007.

[19] M.M.A. Ahmed, Iraqi Kurds and nation-building, Springer, 2016.

[20] R.N. Farrugia, "The wind shear exponent in a Mediterranean island climate," **28**, 647–653, 2003.

[21] C. Angeles-camacho, S. Rios-marcuello, F. Ban, "Analysis and validation of the methodology used in the extrapolation of wind speed data at different heights," **14**, 2383–2391, 2010, doi:10.1016/j.rser.2010.05.001.

[22] L. Wang, C. Singh, "PSO-Based Multi-Criteria Optimum Design of A Grid-Connected Hybrid Power System With Multiple Renewable Sources of Energy," (Sis), 250–257, 2007.

[23] S. Diaf, D. Diaf, M. Belhamel, M. Haddadi, A. Louche, "A methodology for optimal sizing of autonomous hybrid PV/wind system," Energy Policy, **35**(11), 5708–5718, 2007, doi:10.1016/j.enpol.2007.06.020.

[24] Z. Civelek, M. Lüy, E. Çam, N. Barışçı, "Control of Pitch Angle of Wind Turbine by Fuzzy Pid Controller," Intelligent Automation and Soft Computing, **22**(3), 463–471, 2016, doi:10.1080/10798587.2015.1095417.

[25] A.M. Abdelshafy, H. Hassan, J. Jurasz, "Optimal design of a grid-connected desalination plant powered by renewable energy resources using a hybrid PSO – GWO approach," Energy Conversion and Management, **173**(July), 331–347, 2018, doi:10.1016/j.enconman.2018.07.083.

[26] S. Dehghan, "Optimal Sizing of a Hydrogen-based Wind / PV Plant Considering Reliability Indices," 2009 International Conference on Electric Power and Energy Conversion Systems, (EPECS), 1–9.

Distance Teaching-Learning Experience in Early Childhood Education Teachers During the Coronavirus Pandemic

Wilfredo Carcausto[*,1], Juan Morales[2], María Patricia Cucho-Leyva[1], Noel Alcas-Zapata[1], Mirella Patricia Villena-Guerrero[1]

[1]Cesar Vallejo University, 15314, Peru

[2]University of Sciences and Humanities, E-Health Research Center, 15314, Peru

A R T I C L E   I N F O

A B S T R A C T

The purpose of the study was to describe the experiences of teachers in the distance teaching-learning process in early childhood education during the covid-19 pandemic. The methodology used was qualitative descriptive. Interviews were conducted with thirteen teachers from four state educational institutions at the infant level in Lima city through the virtual platform. As a result of the data analysis, five subcategories emerged: Emotions in remote teaching at the beginning of the school year during the pandemic, communication between teachers and families for student learning, management and adaptation of remote teaching-learning, be a teacher of childhood education during the pandemic, and accompaniment in the teaching-learning process. In conclusion, the distance teaching-learning experience of teachers at the beginning of the COVID-19 pandemic is characterized by the presence of certain negative emotions and attitudes towards their educational work; however, self-training on digital and computer resources and empathy with families have improved the generation of learning situations in children.

1. Introduction

The global health situation due to the coronavirus (Covid-19) had social, cultural, economic, and educational effects [1]. Almost 94% of students worldwide, in 190 countries, presented interruption of their academic activities due to policies implemented by governments to mitigate the effects of the pandemic [2] There is a decline in the economy in the countries of Latin America and the Caribbean because of the serious health crisis by the coronavirus [3]. In this context, remote education has been implemented with unprecedented speed, due to the fact that the countries did not have a consolidated national distance education strategy, even less for a scenario in emergency situations [4], [5].

Currently, all teachers at different educational levels are working from home with the resources at their disposal and their conceptions of teaching and learning [6]. The Government of Peru suspended educational activities in public and private entities to reduce the effects of the pandemic. However, since April 6, 2020, the school year began through the implementation of the strategy "I learn at home" to preserve the continuity of educational services

[7]. More than six million users through a thousand radio stations nationwide follow weekly the transmission of this strategy [8].

In this context, Peruvian teachers took on a new challenge, and this implied leaving the classrooms and beginning to teach through virtual environments within the framework of the strategy promoted by the government. However, this teaching modality required the accompaniment of teachers to acquire the necessary digital skills that allow them to handle digital tools for educational purposes. Before the pandemic, the government had not paid due attention, although there were already several published documents on the development and application of these competencies in early childhood education, primary and secondary teachers [9].

During the pandemic, teachers had to learn to use digital resources quickly, to generate learning situations with students and interact with their peers. Currently, teachers can be trained and reinforce their skills through the "Perueduca" digital learning system.

The transition from the face-to-face modality to remote early childhood education is a complex process due to the work carried out with children from three to five years old. The little

development of digital skills of the teachers, the insufficient use of the internet by children through mobile devices or computers, forced parents to accompany their children in the teaching-learning process provided by teachers. The remote teaching and learning process in children requires the participation of four actors: teachers, students, parents and the media such as television [10], and digital devices[11], [12].

Distance education leads teachers to use different teaching strategies and resources to facilitate children's learning [13]. In the case of early childhood education, teachers must capture children's attention and enable the construction of their own learning, which requires the guidance and accompaniment of parents. On the part of teachers, it requires a great commitment to the development of digital skills, the use of resources and materials appropriate to the age and needs of children, because they have less developed levels of physical and verbal skills, and are less capable to work alone [14].

In face-to-face teaching, the same physical space is shared and carried out at the same time; while in remote teaching, the instruction is at a distance [15], and pedagogical activities can be carried out synchronously and asynchronously [16]. Likewise, in face-to-face learning, learning sessions were planned by applying pedagogical processes, while in distance teaching learning experiences were planned. Both must be evaluated in a formative way, so that teachers can observe how the process of acquisition of learning is happening, they need the evidence of the children and based on this evidence, give feedback individually, to obtain information on the development of the competitions.

So far there are no known studies of remote teaching and learning experiences with preschool children, although some research has been found related to the virtual teaching practices of students from a university in the United States [17], and a Spanish public university [18]. Furthermore, digital technologies have the potential both to facilitate communicative and creative tasks and to expand children's repertoires [19].

Therefore, the objective of this work is to describe the experiences of teachers in the remote teaching and learning process at the Early Childhood Education level during the coronavirus pandemic.

2. Methodology

2.1. Design

In this study, the qualitative description was the methodology adopted [20], which allowed to explore in-depth the experiences in the teaching of early childhood teachers in the context of a health emergency. This method was used in order not to stray from the literal description of the experiences reported from the point of view of the participants [21].

This method allows reporting the results based on the subcategories that emerged from the interviews that were interpreted and compared with previous studies.

The results consist of a synthesis based on the subcategories that emerged from the interviews, previously interpreted with the support of the existing literature, and compared with other studies.

2.2. Participants

The study population was made up of 26 early childhood education teachers belonging to the following State Early Childhood Education Centers located in three districts of Lima, Peru: "Francisco Bolognesi" and "José Antonio Encinas" (located in the Santa Anita district), "Los Ángeles de Jesús" (in Rímac district), and "Los Libertadores" (located in Los Olivos district). These teachers have conducted distance classes and have applied the "I learn at home" strategy proposed by the Ministry of Education (MINEDU).

All the participants were recruited when they were undertaking postgraduate studies at a private university in the North of Lima. The sample was selected considering the following process: In the first phase, an invitation was sent by email to 26 teachers, of which 18 voluntarily agreed to participate and signed the informed consent. In the second phase, according to the saturation criteria, there were 13 teachers left, who became the final sample of the study.

The families of the children with whom the teachers work are of low socioeconomic status, most of them work independently and have a complete secondary level.

2.3. Data collection

A semi-structured interview prepared by the researchers was used for data collection. Before its application, it was piloted in 3 teachers who had similar characteristics of the participants in the study, in order to know the relevance of the open questions, as well as to know their experiences regarding the central theme of the study.

After validation of the question guide, the participating teachers provided information on their pedagogical experiences according to the following guiding questions: Tell me, at the beginning of the school year, when the coronavirus pandemic also began, how was your remote teaching-learning experience with the children? What helped you cope with these experiences without being in face-to-face classes? Today, what does it mean to you to be a Remote teacher of Early Childhood Education?

The interviews were recorded and transcribed with the consent of the participating teachers. The interview was conducted in August 2020 through the Zoom® platform, with a duration between 20 and 25 minutes per interview.

2.4. Data analysis

The interviews were analyzed through the thematic analysis method [22]. This method allows us to identify, analyze, organize, and report topics within the data set described in detail. Thematic analysis has various uses, which allows informing experiences, meanings, and the reality of the participants. In the present study, the transcripts, reading, and rereading of the collected information was carried out. Subsequently, the units of meaning that served to summarize and express empirical categories were identified. Finally, results were interpreted, without departing from the literal description of the phenomenon under study [20].

Two aspects related to the validity of the study should be noted. First, to comply with the rigor of the credibility of the data, once the interviews were transcribed they were delivered to the

participants so that they corroborate and accredit the information provided by them. Second, to illustrate the empirical or emerging subcategories, relevant quotes from the interviews were selected. Also, an expert evaluated the information in order to give credibility to the data analysis carried out by the researchers.

3. Results

The expressions of the interviewees made it possible to understand the experiences of the initial level teachers in remote education implemented by the Peruvian state during the period of confinement by COVID-19.

Table 1: Characteristics of the interviewees

Characteristics	n	%
Total	13	100
Age		
< 34	5	38.5
34 a 38	4	30.7
38 a 44	2	15.4
>45	2	15.4
Civil status		
Married	5	38.5
Single	5	38.5
Widow	1	7.6
Divorcee	2	15.4
Employment status		
Appointed	8	61.5
Hired	5	38.5
Academic degree		
Doctorate	1	7.6
Master	8	61.5
Bachelor	4	30.7
Educational institution		
Public	13	100

From the thirteen participating teachers, eight have a master's degree, one of them with a doctoral degree, and four have a bachelor's degree and are currently pursuing a master's degree.

According to the employment status, eight had appointed condition and five hired. The largest proportion of teachers were under 34 years of age as shown in Table 1.

According the interviews carried out with the initial education teachers and the data analysis, five sub-categories finally emerged from the reports as initial education teachers during the health crisis: Emotions in remote teaching at the beginning of the school year during the pandemic, communication between teachers and

families for student learning, management and adaptation of remote teaching-learning, be a teacher of childhood education during the pandemic, and accompaniment in the teaching-learning process (Table 2).

Table 2: Categorization of qualitative information

Study Category	Subcategories
Distance teaching and learning	Emotions in remote teaching at the beginning of the school year.
	Communication between teachers and families for student learning.
	Management and adaptation of remote teaching learning.
	Be an early childhood education teacher during the pandemic.
	Accompaniment in the teaching-learning process.

3.1. Study Category: Distance Teaching and Learning

It refers to a modality of distance instruction that is provided to students as a result of the state of health emergency in which didactic activities are carried out both asynchronously and synchronously.
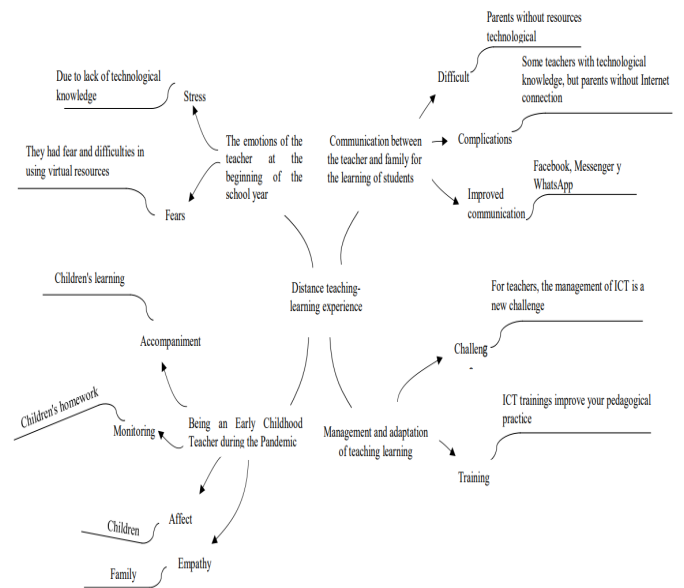
Figure 1: Units of meaning of the participants

In this context, from the descriptive analysis of the qualitative information available in the interviews, subcategories related to the study categories emerged: In the emotions subcategory of the teachers, emotional states such as stress and fear were identified. The subcategory communication between teachers and families for

student learning shows expressions: Difficult, complicated, communication improvement. From the management and adaptation of teaching-learning expressions such as sacrifice, training, challenge, and knowledge were found. The subcategory to be a beginning level teacher during the pandemic shows expressions such as accompaniment, monitoring, emotional support, flexibility, and empathy (Figure 1).

3.2. Emotions in remote teaching at the beginning of the school year during the pandemic

At the beginning of the school year during the pandemic, the emotional situations and negative attitudes of the teachers were linked to the poor use of digital and computer tools, but were subsequently overcome. A part of the teachers have expressed that these tools should be integrated as a complement to face-to-face teaching.

"It was very difficult and stressful at the beginning, as I had little computer knowledge. Thank God, I am already learning and driving better and better. Actually, I thought it was difficult". E7

"At the beginning I saw it somewhat difficult to work remotely with the children, but as the days went by I realized that technology was a valuable resource to learn and teach at the same time". E12

"At the beginning, I presented many fears and difficulties in handling the virtual, but to date I have been teaching and interacting better with my students. (…) I think that this experience with technology should not be put aside when we return to class". E4

3.3. Communication between teachers and families for student learning

The beginning of the school year in the context of the coronavirus pandemic was complicated for teachers because families lacked technological resources (computer and laptop), management of virtual platforms and mobile devices with internet connection. These elements allow for proper storage and communication between students and teachers. Currently, they communicate with families through social networks such as Facebook, Messenger and WhatsApp.

"(...) At the beginning it was difficult, since many of the parents did not have experience with the platforms that MINEDU offers, they did not have computers either, so I had to hold several meetings through social networks such as WhatsApp and Facebook". E9

At the beginning, it was quite complicated and stressful, I had knowledge of ICT (…) but contacting parents was very difficult, since most did not have a computer and a laptop. Now we have organized ourselves better and we communicate by messenger and WhatsApp". E13

3.4. Management and adaptation of remote teaching-learning

The teachers mentioned that the management of any remote teaching resources and their updating contributed to their adaptation; the generation and development of learning situations in their students.

"I knew something about the use of ICT, I think that made it easier for me to adapt to the new way of teaching." E1

"I see that I am having a hard time adjusting to teaching remotely. Two months ago I took training for virtual teaching, which is helping me to give the best of myself to my students". E3

"Little by little I continue to adapt to this new challenge, thanks to the courses promoted by PerúEduca and the tutorials on YouTube." E8

"Little by little I am getting used to the management of these resources, I am seeing that there are many resources that can be used, I still lack quick management of these." E10

3.5. Be an early childhood education teacher during the pandemic

According to the participants, being an early childhood education teacher during the pandemic is associated with the accompaniment, monitoring, and emotional support of students through their families during their learning process.

"Much support, not only in the learning of the children but also in the family in general, I call them, I write them on WhatsApp phrases of encouragement, motivational messages. E1

"(...) Be a companion and dynamic with the children and be in communication with the family to remotely monitor the progress of the children's tasks at home." E4

"Be flexible, and monitor through parents, the tasks that are sent to children by WhatsApp." E11

From the expressions interviewed, the teacher must be empathetic and maintain a good relationship with the students' families, because they act as a link to interact and generate learning situations in the students.

"It is a role of accompaniment, follow-up, and affection, because they need at all times (…) and very empathetic with mothers because they are our allies in their children's learning". E3

"It is having empathy, especially with parents, because most of them work. And very affectionate and charismatic with children so that they can learn and develop their skills ". E13

3.6. Accompaniment in the teaching-learning process

According to the participants, the accompaniment is given through feedback after receiving the evidence from the students. In this process, they have managed to identify the term of feedback and improve their pedagogical practices.

From what was expressed, the teachers interact using social networks, obtaining greater impact for the teaching-learning process, as well as understanding how they should carry out feedback to obtain information about learning.

"[…] I accompany my students on WhatsApp, according to the information provided by the mothers about the difficulties or doubts that their children may have in doing their homework". E 4

"In the past, we had difficulty giving feedback in the classroom, now we do it individually, through social networks to evaluate children". E13

4. Discussion

This study describes the experiences of early childhood education teachers in the remote teaching and learning process

within the framework of the implementation of the strategy "I learn at home" to guarantee the continuity of educational services [7]. From the analysis and synthesis of From the interview data, four subcategories were found, in which emotional experiences, communication, management, adaptability, and the meaning attributed by teachers to their professional work are expressed.

Regarding the experiences and emotional expressions experienced by the teacher as a human being, they are currently more intense [23], due to the new health and social demands in which he had to live and fulfill his role as a professional for new generations.

Emotions, such as moods and feelings, are manifested as responses, signals, or reactions about what is going well for us or what is going wrong, about what we like or dislike[24]. In this sense, the teacher as a human being, manifests these emotions in their inner world, even more so in situations of the pandemic by Covid-19 and being responsible for the training of children who need to continue learning.

The teachers who participated in this study, at the beginning of their work, showed fear and negative attitudes with remote work during the suspension of face-to-face classes due to Covid-19. This result allows us to infer that teaching in times of uncertainty and tension provokes in teachers the presence of certain negative emotions with greater or lesser intensity, amplitude, and continuity in pedagogical practice [25], [26].

On the other hand, despite having had a complicated beginning, the experience of using resources for remote teaching-learning should be integrated into face-to-face classes. From these expressions, it can be interpreted that at first, it was not easy to tune into the remote teaching modality, either due to circumstances generated by themselves and/or beyond their control. There was also a second moment, which could be called empowering resources for remote teaching, which implies not only seeing technology (television, radio, computers, portable and mobile devices) as a mere didactic resource but as a component that influences teaching and learning.

Our results are similar to other studies [27], [28]. Generating good communication channels for educational purposes between teachers and parents favors student learning, especially if they are minors.

In this process of communication and interaction, the teachers must explain the importance of the role of the family in "accompanying children in carrying out tasks and listening to their concerns, preparing spaces and times for tasks" [29], also communicating with the teachers in this distance teaching-learning journey.

The teachers at the beginning of the year had difficulties communicating with the families since most lacked technological resources and had limited use of them. This situation is understandable since the families are of low socioeconomic status and with a secondary education level. Despite this, families with the intention that their children do not miss the school year have continued to study and the teachers have assumed their role as an educational communicator. With the purpose of improving communication, Messenger® and WhatsApp® were used to coordinate the activities organized by the institution, consult or inform the doubts and difficulties of the children in carrying out the tasks at home. From the aforementioned, we can infer for teachers and families that being in a time of pandemic and with certain technological deficiencies may be an opportunity to strengthen communication and interaction through mobile devices that are available for the good of children's development.

Man is a social being because he not only creates and transmits information, but also shares, thanks to this man can adapt to new situations. It is established that human beings are adaptive, that is, with the ability to adapt and create changes in the environment [30]. Along these lines, the participants in the study reported that they have fully adapted to remote teaching-learning, and they also recognize that they are updating and integrating their educational practice for better interaction and student learning. This means that adaptation to a scenario of uncertainty due to the health phenomenon and the rapid transit of the teacher to remote education in unfavorable conditions is not easy and probably never will be, although with affection for knowledge and being updated provides greater possibilities to overcome new situations and support students' learning.

Just as every professional has a role in the execution of their activities, the basic education teacher has the responsibility of fulfilling the three roles established by the Ministry of Education of Peru [31]. These roles are related to identifying the means that the family members should use to access the materials, know the material, and the "I Learn at Home" schedule, and communicate with the family to monitor the progress and difficulties that the students may have. Along these lines, the initial education teacher, in addition to being a monitor and companion, is effective support in the students' learning experience [13]. The findings of the present study agree with the aforementioned, as some characteristics are mentioned such as emotional support, accompaniment, and monitoring.

On the other hand, according to the interviews, it is important to take into account that children need affection, encouragement, and support that gives them security and autonomy in the development of their skills and abilities. These verbal data are similar to those found in [32], given that most of the teachers participating in this study value emotions in the classroom.

Likewise, the teachers consider maintaining an affective connection with the families and students so that mutual understanding is generated, in this way they would improve the learning of the students, because the accompaniment of the parents in their homes is added to this process, generating a shared commitment that would allow obtaining a quality education.

Regarding the teaching-learning resources, the teachers realized that it is possible to use technology at the initial level and it is not necessary to implement a technological classroom, which for the Ministry of Education is difficult due to economic limitations, in this sense considers it optimal to use social networks as resources in the teaching-learning process.

Among the limitations of the present study is the failure to use instruments that allow observing and understanding the teaching action from the platform in real-time. Likewise, not having considered preschoolers as a unit of study, which would have allowed them to know their learning experiences through their

parents. For this reason, it is suggested to carry out research that includes other key actors with ethno-phenomenological approaches to go to the very essence of the phenomenon studied.

5. Conclusions and recommendations

In the remote teaching-learning process, at the beginning of the school year during the COVID-19 pandemic, early childhood education teachers showed certain negative emotions and attitudes due to lack of management of digital and informational resources.

For teachers, it was difficult to generate learning situations in children during the pandemic, since the majority of parents lacked technological resources or how to use them.

The self-training of teachers on digital and computer resources during the pandemic and empathy with families and affection for children have allowed them to fulfill their professional role. Accompaniment through feedback from social networks contributed to strengthening children's learning.

We recommend that the heads of educational institutions strengthen the capacities of their teachers to apply formative assessment throughout the teaching-learning process of students. Provide training to parents to strengthen alliances through collaborative work to generate learning situations in students from home. Coordinate with managers and local authorities to guarantee connectivity in the places where the training action takes place.

Conflict of Interest

The authors declare no conflict of interest.

Acknowledgment

References

[1] Organización de Naciones Unidas para la Educación, "Enseñar en tiempos del Covid-19". Una guía teórico-práctica para docentes, Montevideo, 2020.
[2] Organización de Naciones Unidas, "Policy Brief:Education during Covid-19 and beyond," 2–26, 2020.
[3] Banco Mundial, "El Banco Mundial pronostica una fuerte caída de la economía en América Latina por el coronavirus," 2020.
[4] H. Álvarez, "Educación en tiempos de coronavirus," Journal of Chemical Information and Modeling, **53**(9), 1689–1699, 2020, doi:10.1017/CBO9781107415324.004.
[5] H. Habib, C. González, C.A. Collazos, M. Yousef, "Estudio exploratorio en iberoamérica sobre procesos de enseñanza-aprendizaje y propuesta de evaluación en tiempos de pandemia," Education in the Knowledge Society (EKS), **21**(0), 9, 2020, doi:10.14201/eks.23537.
[6] F. Trujillo Sáez, M. Fernández Navas, A. Segura Robles, M. Jiménez López, Escenarios de evaluación en el contexto de la pandemia por la Covid - 19: la opinión del profesorado, 2020.
[7] Ministerio de Educación, "Resolución Ministerial 160-2020-MINEDU," Diario El Peruano, **15**, 2, 2020.
[8] Instituto Peruano de Economía, "Informe IPE," Segundo Informe: Análisis Del Impacto Económico Del Covid-19 En El Perú, 1–25, 2020.
[9] CanopyLAB, "¿Cuál es la situación de las competencias digitales docentes en América Latina?," 2020,.
[10] E. Sánchez, D. Benito, "Educar, cuestión de cuatro: Padres, maestros, niños y TV," Comunicar, **16**(31), 254–249, 2008, doi:10.3916/c31-2008-03-001.
[11] L. Plowman, "Researching young children's everyday uses of technology in the family home," Interacting with Computers, **27**(1), 36–46, 2015, doi:10.1093/iwc/iwu031.
[12] R. Brito, P. Dias, "Digital Technologies, Learning and Education: Practices and Perceptions of Young Children (Under 8) and Their Parents," Ensayos-Revista De La Facultad De Educacion De Albacete, **31**(2), 23–40, 2016.
[13] C. Castaño, "El rol del profesor en la transición de la enseñanza presencial al aprendizaje 'on line,'" Comunicar: Revista Científica Iberoamericana de Comunicación y Educación, **21**, 49–55, 2003, doi:10.3916/25547.
[14] E. Ramirez, J. Martín-Dominguez, M. Madail, "Análisis comparativo de las prácticas docentes con recursos TIC. Estudio de casos con profesores de Infantil, Primaria y Secundaria," Revista Latinoamericana de Tecnología Educativa (RELATEC), **15**(3), 141–154, 2016, doi:10.17398/1695.
[15] A.O. Mohmmed, B.A. Khidhir, A. Nazeer, V.J. Vijayan, "Emergency remote teaching during Coronavirus pandemic: the current trend and future directive at Middle East College Oman," Innovative Infrastructure Solutions, **5**(3), 1–11, 2020, doi:10.1007/s41062-020-00326-7.
[16] M.L. Picón, "¿ Es posible la enseñanza virtual ?," 11–34, 2020.
[17] J. Kim, "Learning and Teaching Online During Covid-19: Experiences of Student Teachers in an Early Childhood Education Practicum," International Journal of Early Childhood, **52**(2), 145–158, 2020, doi:10.1007/s13158-020-00272-6.
[18] G. González-Calvo, D. Bores-García, R.A. Barba-Martín, V. Gallego-Lema, "Learning to be a teacher without being in the classroom: Covid-19 as a threat to the professional development of future teachers," International and Multidisciplinary Journal of Social Sciences, **9**(2), 152–177, 2020, doi:10.17583/rimcis.2020.5783.
[19] J. McPake, L. Plowman, C. Stephen, "Pre-school children creating and communicating with digital technologies in the home," British Journal of Educational Technology, **44**(3), 421–431, 2013, doi:10.1111/j.1467-8535.2012.01323.x.
[20] M. Sandelowski, "Focus on research methods: Whatever happened to qualitative description?," Research in Nursing and Health, 23(4), 334–340, 2000, doi:10.1002/1098-240x(200008)23:4<334::aid-nur9>3.0.co;2-g.
[21] C. Bradway, "HHS Public Access," Characteristics of Qualitative Descriptive Studies: A Systematic Review, **40**(1), 23–42, 2018, doi:10.1002/nur.21768.Characteristics.
[22] V. Braun, V. Clarke, "Using thematic analysis in psychology," Qualitative Research in Psychology, **3**(May), 58, 2006.
[23] C. Johnson, L., Adams Becker, S., Cummins, M., Estrada, V., Freeman, A. & Hall, Horizon Report > 2016 Higher Education Edition, 2016.
[24] A. Abramowski, Maneras de querer.Los afectos docentes de las relaciones pedagógicas., Buenos Aires, 2010.
[25] U.A. Marchesi, F.T. Díaz, Emociones y valores del profesorado, Madrid, 2008.
[26] R. Silvana, G. Lugli, "Representaciones de las emociones del trabajo docente en perspectiva histórica," Educación e Investigación, **46**, 1–12, 2020, doi:https://doi.org/10.1590/s1678-4634202046217120.
[27] M. Borjas, C. Ricardo, M. Herrera, E. Vergara, A.E. De Castro, "Digital educative resources for childhood education (REDEI in Spanish)," Zona Próxima, **44**(20), 1–21, 2014, doi:10.14482/zp.20.5888.
[28] S. Villarreal-Villa, J. García-Guliany, H. Hernández-Palma, E. Steffens-Sanabria, "Teacher competences and transformations in education in the digital age," Formacion Universitaria, **12**(6), 3–14, 2019, doi:10.4067/S0718-50062019000600003.
[29] C. Castro, Acompañar la tarea del equipo docente, las familias y las y los estudiantes en casa, Buenos Aires, 2020.
[30] L.& otros Díaz, Análisis de los conceptos del modelo de adaptación de Callista Roy, Aquichan, **2**, 19–23, 2009, doi:10.5294/18.
[31] Ministerio de Educación, ¿Cuál es el rol de los y las Docentes?, Lima- Perú, 2020.
[32] E. Trujillo González, E.M. Ceballos Vacas, M.D.C. Trujillo González, C. Moral Lorenzo, "El papel de las emociones en el aula: Un estudio con profesorado canario de Educación Infantil," Profesorado, Revista de Currículum y Formación Del Profesorado, **24**(1), 2020, doi:10.30827/profesorado.v24i1.8675.

ASTES

Simulation of Pulse Width Modulation DC-DC Converters Through Symbolic Analysis Techniques

Maria Cristina Piccirilli [*], Francesco Grasso, Antonio Luchetta, Stefano Manetti, Alberto Reatti

University of Florence, Department of Information Engineering - DINFO, Florence, 50139, Italy

A R T I C L E I N F O	A B S T R A C T
	The problem of Pulse Width Modulated (PWM) DC-DC converter simulation is faced in this paper. It is shown how the analysis of this kind of circuits, nonlinear and switching for their nature, can be easily and quickly executed by using symbolic analysis techniques. The paper also presents the program SapWinPE, which performs an automatic symbolic analysis of the considered circuit, and its outputs are in MATLAB compatible format. SapWinpPE features make it more attractive than general-purpose software tools for both academy and industry circuit designers. Other characteristics and potentialities, shown through application examples in the paper, can be advantageously exploited by all the circuit designers and CAD professionals, also at the research and educational level in the academic field.

1. Introduction

In all modern electronic circuits it is nearly impossible to find devices that are not supplied by switching-mode power converters. Most of them use Pulse Width Modulated (PWM) DC–DC converters as output voltage regulators, and their behavior affects the operation of the overall systems. In some applications, the reliability of the supplied systems is linked to the proper behavior of PWM DC-DC converters in such a way to lead to fatal consequences in case of poor design. As an example, it is enough to think about artificial heart implants to understand how a proper design of power converters is crucial.

In the realization of any device, the first step is the theoretical design, which consists of a "pencil and paper" circuit creation. To verify the correctness of the obtained circuit, repeated circuit simulations are needed, where the term "circuit simulation" means the analysis of a theoretical circuit with software tools. In the case of DC-DC converters, this is not an easy and fast task to perform because of the interaction of many devices, their interconnection, sizing, and biasing. Moreover, switched current and voltage waveforms result in high values of their derivatives which run the numerical simulators close to their convergence limits. For this reason, the subject of DC-DC converter simulation has interested many researchers in the last thirty years, but a definitive solution has not yet been found. Also, the authors have faced this problem and this paper is an extension of a work originally presented at the

2019 IEEE 5th International Forum on Research and Technology for Society and Industry (RTSI) [1], where a program, named SapWinPE, was presented. SapWinPE is based on the application of symbolic analysis techniques and this constitutes an important novelty because symbolic programs dedicated to PWM DC-DC converters do not exist, at least to the authors' knowledge.

This paper aims to better describe the program in [1] from the theoretical, algorithmic, and applicative points of view, by proposing further examples and comparing the obtained results with those deriving from other programs, like PSPICE based programs, and with experimental results. Finally, a new possible method for simulating switching circuits is proposed together with some results obtained with a new program, still in an embryonic state, implementing this new approach.

The paper is so organized. The implementation methodology and the theoretical basis of SapWinPE are presented in Section 2. Section 3 provides a discussion on the reasons which have led to choose symbolic techniques, a program description is proposed in Section 4. Applicative examples and comparisons with other programs are shown in Section 5. In Section 6 a short description of a further approach to the simulation of switching circuits is presented along with an application examples. Finally, Section 7 contains conclusions and future developments.

2. Theoretical Basis

PWM DC-DC converters are time-variant circuits. This feature is due to the presence in many topologies, such as buck, boost, buck-boost, of a particular cell constituted by a switch and a diode.

---

[*]Maria Cristina Piccirilli , DINFO Via di Santa Marta 3 Firenze - Italy, mariacristina.piccirilli@unifi.it

This switching cell, shown in Figure 1(a), operates as a device alternatively channeling the inductor current through the switch and the diode.

(a)

(b)

(c)
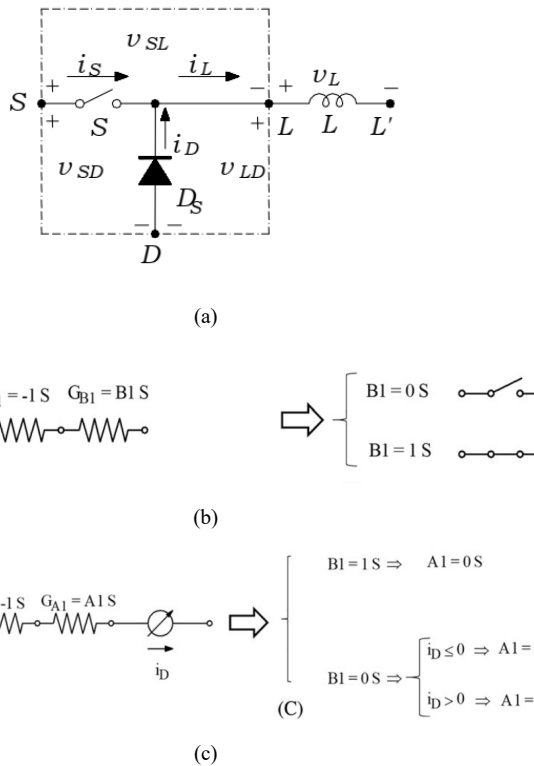
Figure 1: The switching cell in a PWM DC-DC converter. (a) Switching cell. (b) switch model. (c) diode model.

In other converters, such as Cùk, Flyback, and Forward converters, switch and diode are not connected to the same node, but their combination always acts exactly in the same way. A DC-DC converter circuit switches between two different configurations or among three different configurations, depending on the inductor current value: when it has a nonzero value at the end of the switching period T, the circuit works in Continuous Conduction Mode (CCM); when it assumes a zero value before the end of the switching period T, the circuit works in Discontinuous Conduction Mode (DCM). There is also an intermediate operation mode, called Boundary Conduction Mode (BCM), corresponding to the case of zero inductor current exactly at the end of the switching period T: also in this case, the circuit switches between two different configurations. In any case, moving from a configuration to another one causes a topology change, showing in this way the time-variant nature of the circuit [2].

As well known, the Laplace transform can be classically applied to linear time-invariant circuits. Then, even if converters nonlinearities are neglected, its time-variant nature prevents the application of this method. It is nonetheless true that the circuit remains time-invariant within each assumed configuration, then, the Laplace transform can be applied to every switching state. However, proceeding in this way, the inverse Laplace transform must be applied to each configuration and must be evaluated not only the output of interest in the time-domain but also the inductor current and the capacitor voltage in the time-domain, because their values at the switching instant constitute the initial conditions for

the analysis in the subsequent time interval. In short, this approach is not convenient, not only because the time domain responses require several applications of the inverse Laplace transform, but principally because it is not possible to automatically consider the different operating modes. To circumvent this strong limitation, it is necessary to model the switching cell as a single device whose switching behavior is directly controlled by internal parameters. The switching cell model must have an additional feature: it must be able to take automatically into account the state of the switches via parameter settings. In this way, a circuit depending on the characteristic parameters of the switching cell model can be obtained. Under any switching state, the circuit configuration assumed by the power converter is linear and time-invariant for any switching period, and also in its whole working time: thus the model becomes Laplace transformable. Circuit transfer functions in closed form, dependent on the state of the switches and on the initial conditions of capacitors and inductors at each switching time, can be so obtained. The working conditions determine the parameter values. Proceeding in this way, it is still necessary to apply the inverse Laplace transform in each switching interval for evaluating the time domain responses, but the different operation modes are automatically determined.

The switch model [3] is shown in Figure 1(b). A conductance, equal to -1 S, characterizes one of the two resistors; the parameter B1, a conductance that can take two possible values, 0 S and 1 S, characterizes the other resistor, in series with the former. When B1 is equal to zero, the model represents an open switch, because the equivalent resistance is infinite. When B1 is equal to 1 S, the model represents a closed switch, because the equivalent resistance is zero. In this way, the choice of B1 establishes if the ideal switch is open or closed. A modified switch equivalent circuit simulates the diode. As shown in Figure 1(c), it is derived by connecting the control branch of a current-controlled voltage source in series with the two conductances. In this way the diode operates as a switch controlled by the direction of its own current. Conductance A1 identifies the second resistor and replies the diode state: the diode is OFF when A1 is equal to 0 and this occurs only if B1=1S. If the switch is OFF (that is B1 = 0), the state of the diode depends on its own current i_D: if $i_D<0$, the diode is OFF and A1 returns to zero; if $i_D>0$, the diode is ON and A1=1. This makes the model operate like an ideal lossless diode turning-on when the switch opens and turning-off when its forward current becomes zero.

The switching cell model is obtained joining the switch and the diode models. Hence it is completely represented by the two parameters B1 and A1.

At this point a DC-DC converter equivalent circuit can be built, that allows a time-domain simulation exploiting the Laplace transform. The equivalent circuit is derived by replacing:

- the switching components with the described models;

- inductors and capacitors with their Laplace-domain equivalent circuits, including the sources representing their initial conditions;

- all the other components with their associate Laplace-domain circuits.

A simulation of the Laplace-domain circuit is, then, possible and it produces the desired output and, in addition, the voltages

associated with capacitors and currents associated with inductors and diodes. The corresponding time-domain information are derived by performing the inverse Laplace transform for every switching interval, which is determined by the values of the switch and diode equivalent circuit parameters. The theoretical reasons for this procedure are explained in the following.

Even if a switching converter is a time-varying circuit, the topological configuration it assumes in each switching interval results in a linear, time-invariant circuit and this allows the Laplace transform to be applied for every switching interval. In this way the classical meaning of network function is retained. The so obtained responses also depend on initial conditions (IC): every phase interval starts with given IC and ends restituting new IC to the next interval. These IC are determined by running the inverse Laplace transform of inductor currents and capacitor voltages in every switching time. Also, the inverse Laplace transform of the diode current must be evaluated in every switching time because its sign is used to determine the diode itself state (ON or OFF) .

3. Why to use the Laplace Transform

Time-domain simulations of DC-DC converters are utilized to evaluate current and voltage waveforms and their ripple [4, 5], and also to design the control circuits [6-26]. Many simulation programs miss built-in algorithms able to return as an output the converter steady-state response. Therefore, they are time-consuming because they provide a steady-state response after a transient analysis involving several hundreds of switching periods. Programs providing automated steady-state computation for time-invariant circuits (for example HSPICE or Micro‑Cap 10) are not able to give accurate results for DC-DC converters. The approximations these programs introduce to evaluate current and voltage values during cycle-by-cycle simulations [8] introduce large numerical errors. The switching properties are lost in averaged linear equivalent circuits, which result useful for frequency domain analysis, but not accurate enough for time-domain simulations [10, 11]. There are some attempts to introduce switching effects, as in [12]. Discrete-time domain models are presented in [18, 19], but these models are not suited to simulate power converters with a digital control [15]. Methods for a time-domain large-signal analysis are presented in [25, 26]. However, specific software programs for power converter simulations do not exist. Besides, almost all the available programs are numerical simulators.

The term "numerical" denotes an analysis performed starting from numerical values of the component parameters and providing an output in a purely numerical form. The circuit operation is accurately simulated, but the results only refer to a given set of parameter values. This requires the simulation to be repeated if any single value changes. The numerical simulation is suitable to verify the behavior of a circuit, given a set of parameters, but it does not allow to understand which circuit elements cause the obtained behavior and does not suggest solutions if the desired specifications are not met. A large number of simulations are required for verifying the performance and analyzing parameter variations. In conclusion, numerical simulation is a useful tool supporting the designers in the converter preliminary design, but barely helps in the design optimization.

The design optimization is well accomplished by symbolic simulation [27-30]. The term "symbolic" denotes an analysis that investigates the characteristics of a circuit providing, as an output, the expressions of network functions in closed-form where the parameters are shown with their symbols rather than their numerical values. These symbolic expressions are valid for whatever numerical value. This allows the designer to have an insight of the circuit operation. Symbolic simulation also allows semi-symbolic analysis, when a subset of the elements is replaced with numerical values, so getting useful simplified symbolic expressions. In practice, numerical simulation allows an understating of the circuit operation based on the analysis of the plotted waveforms, while symbolic analysis, which focuses on the expression of circuit functions, is more helpful in the understanding of the circuit behavior. In conclusion, numerical and symbolic simulations are complementary: the first is more suitable to check the operations of already sized circuits, the second is more suitable to understand the unsized circuits behaviors. A very efficient software for power converter design should combine the properties of the two approaches.

Despite its advantages, a symbolic program oriented to the simulation and design of switched circuits is not yet available. This is due to the use of the Laplace transform in almost all symbolic simulators, which, consequently, work on time-invariant circuits. There are some rare examples of Laplace domain modeling, as in [20], where sampling, modulator effects, and delays in the digital control loop are correctly taken into account. Unfortunately, this approach can be easily utilized only for the buck converter [15]. Techniques, based on switch and diode models and employing the Laplace transform, are proposed [31], but they are based on the modified nodal analysis, which is computationally very intensive when the circuit size grows.

On the contrary, with the method proposed in section 2, the Laplace transform is suitably implemented in a computer program through symbolic techniques which do not result in significant computational costs. The next section describes the potentialities and the algorithms of the symbolic program developed by the authors.

4. The Program SapWinPE

The proposed symbolic program, completely coded in C++ language, is called SapWinPE, which stands for SapWin for Power Electronics. SapWin is an integrated program for circuit symbolic analysis and SapWinPE constitutes a module of this package explicitly designed for Power Electronics (PE) [27, 32-35].

SapWinPE main modules are the following:

- a schematic entry where the circuit is designed (here, a graphic list including all the two-terminal or two-port elements is available); when designing the circuit, the user can choose if a component must be considered symbolic or numerical.

- A symbolic analysis package which returns the expression of the selected network function.

- A graphical post-processor that, on a given, user selected set of numerical values for the components, performs the inverse Laplace transform of the network functions and plots the relevant waveforms.

The program is based on a two-graph method [36] which has been improved by the authors for achieving shorter computational times and, therefore, allowing to analyze larger circuit. Models available in literature, such as those presented in [31, 37], cannot be utilized inside the proposed method and, therefore, the model discussed in Section 2 has been developed by the authors.

A SPICE-like netlist can be used for describing the circuit to analyze. When the built-in schematic editor is used, the program automatically translates the scheme into an ASCII netlist in a SPICE compatible format. The schematic editor can also be used to generate circuit schemes, which can be saved and utilized as sub-circuits in large circuit analysis. Also, in subcircuits, the components can be defined as symbolic or not.

The schematic entry saves two files. The first one is a binary file to be used as input for other programs. The second one is an ASCII file including the circuit network functions generated by the Laplace domain analysis. The expressions of the network functions include the circuit components, capacitor and inductor initial conditions, and the parameters describing the state (ON/OFF) of the switches and the diodes. These last parameters are variable because depend on circuit working conditions. Step sources are used to simulate the initial conditions. The actual voltage generator is also a step. This makes the analysis simple and fast, because the network functions are derived simply dividing the outputs by the step Laplace transform. As explained in Section 2, the inductor current and the capacitor voltage are always available, because their time-domain values at the switching instant represent the initial conditions for the analysis in the subsequent time interval.

The simulation results are available both in the Laplace domain and as phasors at a given angular-frequency.

The algorithm for the inversion of the network functions can be found in [37]. Since the diode currents are known, the program automatically recognizes if the DC-DC converter operates in CCM or DCM. The sampling step is automatically adapted to the expected rate of change of the waveforms.

Once the inverse Laplace transform is applied, the program can also plot several diagrams:

- magnitude response;
- loss;
- phase response;
- time delay;
- poles/zeros;
- step response;
- impulse response;
- steady-state response.

The graphic part of the program allows the user to select: the frequency interval, the time interval and the duty cycle. In any diagram an X-Y cursor is available and this helps the numerical values to be read. A built-in function, whose operation is based on the check of the values of all the outputs at the end of each interval, allows the steady-state response to be directly plotted. The program assumes that the circuit operates under steady-state

conditions when the difference among the last calculated value of a current or voltage and the value calculated in the previous step is lower than a preselected threshold. This operation is performed in a very short time. The effects of the parasitic components can also be considered e.g., in a pole/zero diagrams [37], plotted for every switching interval.
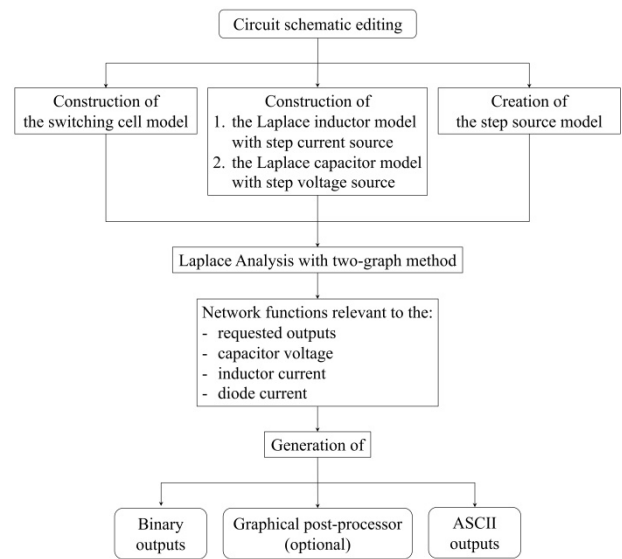
Figure 2: Block diagram of SapWinPE.

It is important to highlight that the network functions obtained by the program, and therefore by the described method, are not useful for a frequency-domain simulation, because the switch and diode models are not the same used to derive an averaged small-signal equivalent circuit of the switching cell. Note that a frequency domain analysis, resulting in bode plots and poles and zeros diagrams, can be performed by replacing the switching cell with time-invariant equivalent circuits as those presented in [38-45], which are different from those described in Section 2.

To suitably size the component values and evaluate the parasitic element effects during the design phase, it is possible to run a parametric analysis, one of the options of SapWinPE. Since parasitic components highly affect the converter dynamic behavior, multiparametric analysis provided by the program can be advantageously used to design the compensation network and investigate the stability of the converter when operated in closed loop.

The program also allows for multiple outputs, which result useful for a better understanding of the converter behavior. To this aim the knowledge of voltages in specific nodes and currents in different branches is crucial.

The semi-symbolic feature available in SapWinPE allows to better evaluate the effects of certain parameter variations by focusing on a few components, which are assumed as symbolic, while the others are set as numerical.

Note that the models described in Section 2 refer to ideal switches and diodes. By using ideal components, a fast, but inaccurate analysis of the circuit operation is achieved. For a better accuracy, parasitic elements can be externally added by the user. For example, some ringing in the current and voltage waveforms of a real converter are simply reproduced in the simulations by

connecting to the ideal device appropriate parasitic components, affecting the operation of power MOSFETs and ultrafast or Schottky diodes. This allows accurate simulations to be executed by using data from component datasheet, while it is not necessary to know the physical operation of these devices. Of course, the higher is the number of added parasitic elements, the lower will be the processing speed.

Finally, to summarize the program steps, a block diagram of SapWinPE is shown in Figure 2.

5. Applications Examples

Figure 3(a) shows a buck converter including parasitic components as given by the SapWinPE schematic entry. In this section, the results of simulations run by using LTSpice are shown and compared with those achieved by using SapWinPE. In this circuit: R_S is the power MOSFET ON resistance, R_d is the diode ON resistance, R_L is the inductor equivalent series resistance (ESRL), and R_C is the filter capacitor series resistance. An overall inductor equivalent series resistance can be derived as

$$R_{ESR\_L} = \frac{4}{3(D+D_1)}\left(R_L + \frac{DR_S + D_1R_D}{D+D_1}\right) \tag{1}$$

$$D = \frac{t_{MOSFETon}}{T} = t_{MOSFETon} \times f \tag{2}$$

$$D_1 = \frac{t_{DIODEon}}{T} = t_{DIODEon} \times f \tag{3}$$

where $f=1/T$ is the switching frequency. This resistance is series connected with the inductor, includes the parasitic resistances of the switching cell components, as shown in Figure 3(b), and simplifies the circuit analysis when a simulating tool is not available. Since in this paper we are using a power simulation program, the circuit shown in Figure 3(a) allows for a better insight of the circuit operation.
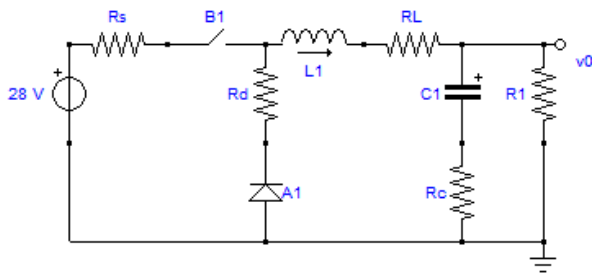
(a)
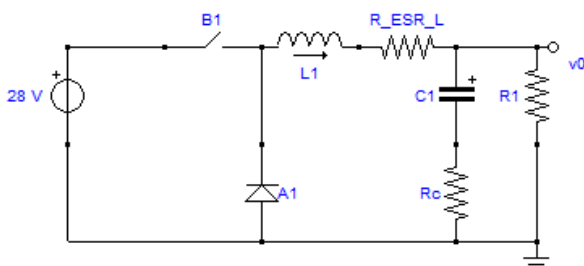
(b)

Figure 3: Buck converter including parasitic components. (a) Parasitic resistance for each component. (b) Parasitic resistance reduced to a single inductor equivalent series resistance R_ESR_L and to a capacitor parasitic resistance.

In the example, a buck converter designed according to the following specifications has been considered: output power $P_O = 10$ W, input voltage $V_I = 28$ V, load output voltage $V_O = 21$ V, load resistance $R = 3.6$ Ω, switching frequency $f = 40$ kHz. Under these specifications, an inductance $L = 3.3$ µH has been designed, a filter capacitor $C = 470$ µF has been chosen to keep the output voltage ripple below 5%. The converter results to be operated at $D = 0.036$, and the parasitic components, as derived from component data sheets, are $r_S = 3$ mΩ, $r_d = 20$ mΩ, $r_L = 24$ mΩ, and $r_C = 6$ mΩ.

Figures 4(a) and 4(b) show the controlled switch and diode current waveforms as obtained by running simulations with LTSPice and SapWinPE, respectively. The plots show that the results obtained by using SapWinPE are nearly the same as those obtained with LTSpice.

The output voltage plots as derived by using LTSpice and SapWinPE are shown in Figures 5(a) and 5(b), respectively. The transient waveforms are nearly the same, as well as the voltage ripple; the average steady-state output voltage resulting from LTSpice is 20.6 V and that resulting from SapWinPE is 20 V. The transfer functions of the examples shown in this paper have not been included for reasons of brevity. However, it is possible to consult them at the following web address: http://www.cirlab.unifi.it/p122.html .

The small differences in the considered values depend on the different way the components are modeled in the two programs: LTSpice bases its simulations on physical models of the MOSFET and diode, while SapWinPE considers these components as ideal switches and parasitic resistances are added as external components in the simulated circuit.
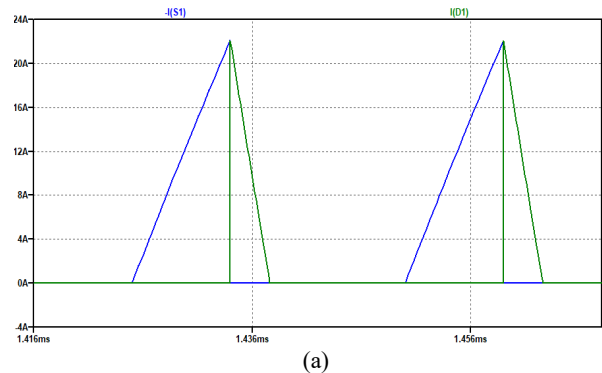
(a)
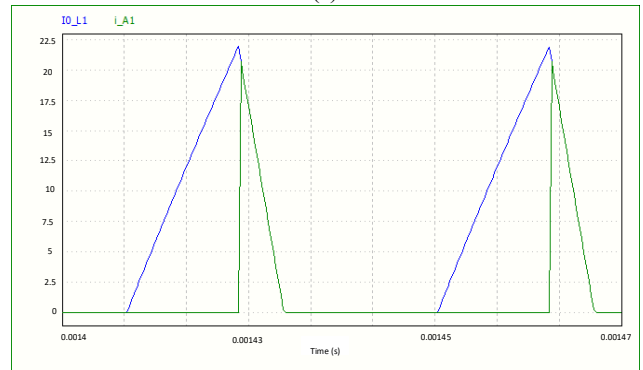
(b)

Figure 4: Buck converter current waveforms: power MOSFET current and diode current. (a) Plot resulting from LTSpice. (b) Plot resulting from SapWinPE.

Also, a PWM DC-DC buck-boost converter has been simulated and experimentally tested. The converter component values are as follows: inductance L = 224.62 μH, and its ESR is r_L = 0.023 Ω, the capacitance is C = 662.32 μF, and its ESR is r_C = 0.016 Ω. The power switch is constituted by a SCT3022AL SiC power MOSFET, which results in a breakdown voltage V_{DS} = 650 V and a channel resistance r_S = 22 mΩ. Finally, an FFSP2065B SiC diode has been utilized: it has a reverse voltage V_R = 650 V, a threshold voltage V_F =1.7 V, a continuous rectified forward current I_F = 20 A, and a forward resistance r_D = 33 mΩ. The input voltage is V_I = 17 V, the output voltage is V_O = 25 V, the duty cycle is D = 0.59, and the switching frequency is f = 20 kHz.

(a)

(b)

Figure 5: Output voltage ripple. (a) Plot resulting from LTSpice. (b) Plot resulting from SapWinPE.

Figure 6(a) shows the circuit of the buck-boost converter, as given by the SapWinPE schematic entry, which also includes: the MOSFET output capacitance Cds = 5 pF and inductance Ld = 100 nH, which considers parasitic inductances related to the layout of the experimentally tested circuit, shown in Figure 6(b) [46]. Figures 7(a) and (b) show the diode voltage waveforms resulting from the simulations and the experimental tests, respectively. The experimental waveform is plotted with a 10 μs/div time base and 10 V/div amplitude base.

The plots shown in Figure 7 clearly demonstrate that the simulated results are in good agreement with those experimentally measured. This confirms that SapWinPE results in accurate simulations of power converters, allows each parasitic component of the real circuit to be singularly considered, and, therefore, the user has a very good insight of the studied circuit.

6. New Approach

A new approach to the symbolic analysis of DC-DC converters has been conceived by the authors. The idea is to simulate DC-DC converters through the state variable method, suitable to analyze nonlinear circuits, as converters are. The network functions, determined as in the previous method in the Laplace domain and depending on initial conditions and switch and diode parameters, are relevant to the desired outputs and the converter state variables, that is inductor currents and capacitor voltages. The difference consists in the fact that switches and diodes are represented by parameters depending on analytical expressions reproducing the actual characteristics of these elements. The possibility of easily dealing with nonlinear components is linked with the adopted technique of inverse Laplace transform. It is executed in a discrete way, as the previous method, by using a very small sampling step, carefully chosen on the base of the specific case.

(a)

(b)

Figure 6: Buck-boost converter. a) Simulated circuit including parasitic components. b) Experimentally tested circuit.

(a)

(b)
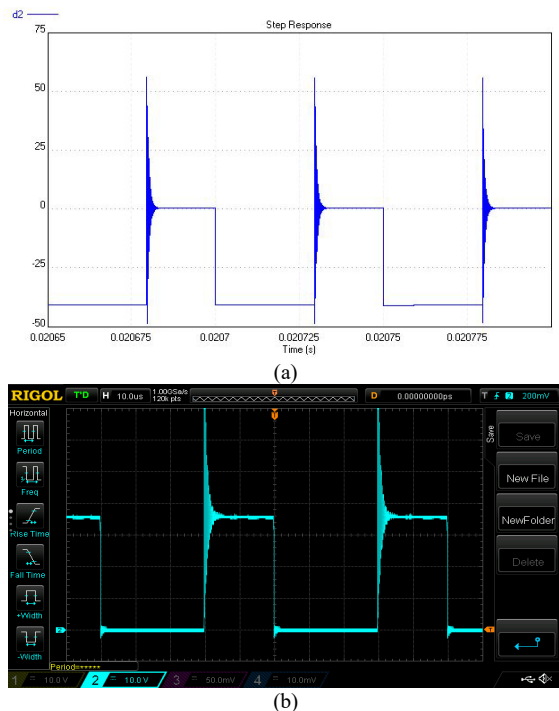
Figure 7: Waveforms of the buck-boost diode voltage. (a) Simulated. (b) Measured.

Each sample of the corresponding discretized impulsive response is multiplied by the input value in the sampling instant, so applying a discretized convolution integral for determining, point by point, the time domain response. Also in this case, not only the desired outputs are determined, but also the state variables in the time domain in each sampling step, because their values are necessary for correctly evaluating the desired outputs. The plot of the obtained response is determined by interpolating the output samples.
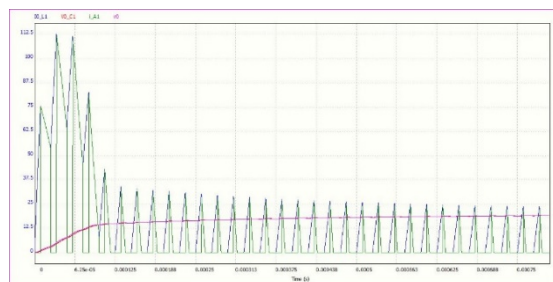
(a)
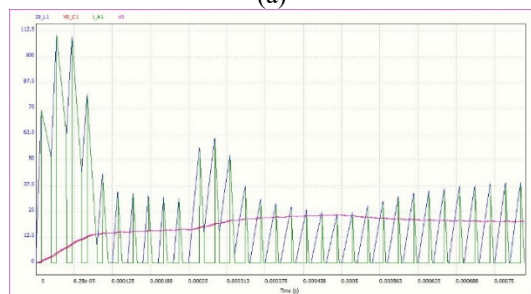
(b)

Figure 8. (a) Buck converter circuit simulation (inductor current I_O_L1, capacitor voltage V_O_C1, diode current i_A1, and output voltage V_O) without parameters variation. (b) Buck converter circuit simulation: the duty cycle goes from 0.36 to 0.7 for t=0.25 ms, the resistor R1 goes from 3.6 Ω to 1 Ω for t=0.5 ms.

In this way, it is very easy to treat nonlinear elements, because only their value in the sampling instants is significant.

Whatever input waveform can be used, because it is sampled and held during the sampling step, so resulting in a step function of constant amplitude. The possibility of using any input waveform allows considering harmonics and noise overlapping with the input signal.

The implementation of this approach is still raw. Figure 8 shows the time response of the buck converter of Figure 3, obtained with a sketch of the symbolic program based on this approach.

7. Conclusions

The purpose of this paper is to present a method for applying the Laplace transform to DC-DC converters for simulating this kind of circuits through symbolic techniques.

Time-domain analysis of power converters is performed through the derivation of the circuit network functions. This is achieved by deriving suitable models for both switches and diodes.

The proposed approach is suited to computationally efficient topological methods which allows also large circuits, as, for example, DC-AC inverters and AC-DC rectifiers, to be simulated in short times. A symbolic program, named SapWinPE, implementing the proposed approach is also presented.

This program ensures accurate and fast simulations of switching circuits. It runs in a stand-alone configuration and can provide its outputs also in formats compatible with commercial programs such as MATLAB.

SapWinPE validity is demonstrated by the examples shown in the paper and by its successful application to power converter fault diagnosis and resonant converter design [47-51].

Finally, a new state variable-based analysis technique for symbolic simulation of DC-DC converters is briefly introduced. Even if still in an embryonic state, it is promising. The implementation of a program based on this technique is planned for the near future.

Conflict of Interest

The authors declare no conflict of interest.

References

[1] F. Grasso, A. Luchetta, S. Manetti, M.C. Piccirilli, "Symbolic Techniques in DC-DC Converter Simulation," in 2019 IEEE 5th International forum on Research and Technology for Society and Industry (RTSI), IEEE: 248–253, 2019, doi:10.1109/RTSI.2019.8895579.

[2] R.W. Erickson, D. Maksimović, Fundamentals of Power Electronics, Springer US, Boston, MA, 2001, doi:10.1007/b100747.

[3] F. Grasso, S. Manetti, M.C. Piccirilli, A. Reatti, "A Laplace transform approach to the simulation of DC-DC converters," International Journal of Numerical Modelling: Electronic Networks, Devices and Fields, e2618, 2019, doi:10.1002/jnm.2618.

[4] H. Ardi, A. Farakhor, A. Ajami, "Design, analysis and implementation of a buck–boost DC/DC converter," IET Power Electronics, **7**(12), 2902–2913, 2014, doi:10.1049/iet-pel.2013.0874.

[5] H.S.H. Chung, K.K. Tse, A. Ioinovici, "Computer-aided analysis of power electronic circuits by stepwise topological identification," International Journal of Numerical Modelling: Electronic Networks, Devices and Fields, **10**(5), 285–301, 1997, doi:10.1002/(SICI)1099-1204(199709/10)10:5<285::AID-JNM279>3.0.CO;2-U.

[6] K. Guesmi, A. Hamzaoui, "On the modelling of DC-DC converters: An enhanced approach," International Journal of Numerical Modelling: Electronic Networks, Devices and Fields, **24**(1), 36–57, 2011, doi:10.1002/jnm.759.

[7] A. Opal, J. Vlach, "Analysis and sensitivity of periodically switched linear networks," IEEE Transactions on Circuits and Systems, **36**(4), 522–532, 1989, doi:10.1109/31.92884.

[8] M.-D. Ker, C.-C. Yen, "New Transient Detection Circuit for On-Chip Protection Design Against System-Level Electrical-Transient Disturbance," IEEE Transactions on Industrial Electronics, **57**(10), 3533–3543, 2010, doi:10.1109/TIE.2009.2039456.

[9] V. Vorpérian, Fast Analytical Techniques for Electrical and Electronic Circuits, Cambridge University Press, 2002, doi:10.1017/CBO9780511613791.

[10] D. Biolek, "Modeling of periodically switched networks by mixed s-z description," IEEE Transactions on Circuits and Systems I: Fundamental Theory and Applications, **44**(8), 750–758, 1997, doi:10.1109/81.611272.

[11] D. Biolek, V. Biolkova, J. Dobes, "Modeling of switched DC-DC converters by mixed s-z description," in 2006 IEEE International Symposium on Circuits and Systems, IEEE: 4, doi:10.1109/ISCAS.2006.1692714.

[12] D. Biolek, V. Biolkova, Z. Kolka, "Analysis of switching effects in DC-DC converters via bias point computation," in 2007 18th European Conference on Circuit Theory and Design, IEEE: 1006–1009, 2007, doi:10.1109/ECCTD.2007.4529769.

[13] F. Huliehel, S. Ben-Yaakov, "Low-frequency sampled-data models of switched mode DC-DC converters," IEEE Transactions on Power Electronics, **6**(1), 55–61, 1991, doi:10.1109/63.65003.

[14] C. Fang, E.H. Abed, "Output regulation of DC-DC switching converters using discrete-time integral control," in Proceedings of the 1999 American Control Conference (Cat. No. 99CH36251), IEEE: 1052–1056 vol.2, 1999, doi:10.1109/ACC.1999.783201.

[15] D.M. Van de Sype, K. De Gusseme, A.R. Van den Bossche, J.A. Melkebeek, "Small-signal z-domain analysis of digitally controlled converters," in 2004

IEEE 35th Annual Power Electronics Specialists Conference (IEEE Cat. No.04CH37551), IEEE: 4299–4305, doi:10.1109/PESC.2004.1354761.

[16] D. Maksimovic, R. Zane, "Small-signal Discrete-time Modeling of Digitally Controlled DC-DC Converters," in 2006 IEEE Workshops on Computers in Power Electronics, IEEE: 231–235, 2006, doi:10.1109/COMPEL.2006.305680.

[17] L. Corradini, P. Mattavelli, "Analysis of Multiple Sampling Technique for Digitally Controlled dc-dc Converters," in 37th IEEE Power Electronics Specialists Conference, IEEE: 1–6, doi:10.1109/PESC.2006.1712132.

[18] A.R. Brown, R.D. Middlebrook, "Sampled-data modeling of switching regulators," in 1981 IEEE Power Electronics Specialists Conference, IEEE: 349–369, 1981, doi:10.1109/PESC.1981.7083659.

[19] G.C. Verghese, M.E. Elbuluk, J.G. Kassakian, "A General Approach to Sampled-Data Modeling for Power Electronic Circuits," IEEE Transactions on Power Electronics, **PE-1**(2), 76–89, 1986, doi:10.1109/TPEL.1986.4766286.

[20] D.M. Van de Sype, K. De Gusseme, A.P. Van den Bossche, J.A. Melkebeek, "Small-signal Laplace-domain analysis of uniformly-sampled pulse-width modulators," in 2004 IEEE 35th Annual Power Electronics Specialists Conference (IEEE Cat. No.04CH37551), IEEE: 4292–4298, doi:10.1109/PESC.2004.1354760.

[21] D. Maksimovic, R. Zane, "Small-Signal Discrete-Time Modeling of Digitally Controlled PWM Converters," IEEE Transactions on Power Electronics, **22**(6), 2552–2556, 2007, doi:10.1109/TPEL.2007.909776.

[22] M.M. Peretz, S. Ben-Yaakov, "Time-Domain Design of Digital Compensators for PWM DC-DC Converters," IEEE Transactions on Power Electronics, **27**(1), 284–293, 2012, doi:10.1109/TPEL.2011.2160358.

[23] M. Shirazi, J. Morroni, A. Dolgov, R. Zane, D. Maksimovic, "Integration of Frequency Response Measurement Capabilities in Digital Controllers for DC–DC Converters," IEEE Transactions on Power Electronics, **23**(5), 2524–2535, 2008, doi:10.1109/TPEL.2008.2002066.

[24] M.M. Peretz, S. Ben-Yaakov, "Time Domain Identification of PWM Converters for Digital Controllers Design," in 2007 IEEE Power Electronics Specialists Conference, IEEE: 809–813, 2007, doi:10.1109/PESC.2007.4342092.

[25] A. Massarini, U. Reggiani, M.K. Kazimierczuk, "Analysis of networks with ideal switches by state equations," IEEE Transactions on Circuits and Systems I: Fundamental Theory and Applications, **44**(8), 692–697, 1997, doi:10.1109/81.611264.

[26] W. Pietrenko, W. Janke, M.K. Kazimierczuk, "Application of semianalytical recursive convolution algorithms for large-signal time-domain simulation of switch-mode power converters," IEEE Transactions on Circuits and Systems I: Fundamental Theory and Applications, **48**(10), 1246–1252, 2001, doi:10.1109/81.956022.

[27] F. Grasso, A. Luchetta, S. Manetti, M.C. Piccirilli, A. Reatti, "SapWin 4.0-a new simulation program for electrical engineering education using symbolic analysis," Computer Applications in Engineering Education, **24**(1), 44–57, 2016, doi:10.1002/cae.21671.

[28] W. Daems, G. Gielen, W. Sansen, "Circuit simplification for the symbolic analysis of analog integrated circuits," IEEE Transactions on Computer-Aided Design of Integrated Circuits and Systems, **21**(4), 395–407, 2002, doi:10.1109/43.992763.

[29] F. Fernandez, Á. Rodríguez-Vázquez, J.L. Huertas, G.G.E. Gielen, Symbolic Analysis Techniques, IEEE, 1998, doi:10.1109/9780470546512.

[30] P. M. Lin, Symbolic Network Analysis, Elsevier Science Ltd, New York, NY, USA, 1991. ISBN10 0444873899

[31] A. Ioinovici, "Generalised alternor," Electronics Letters, **24**(2), 122, 1988, doi:10.1049/el:19880081.

[32] A. Liberatore, A. Luchetta, S. Manetti, M.C. Piccirilli, "A new symbolic program package for the interactive design of analog circuits," in Proceedings of ISCAS'95 - International Symposium on Circuits and Systems, IEEE: 2209–2212, doi:10.1109/ISCAS.1995.523866.

[33] L.P. Huelsman, "SapWin, symbolic analysis program for Windows — PC programs for engineers.," IEEE Circuits and Devices Magazine, **12**(6), 4–6, 1996.

[34] L.P. Huelsman, "Symbolic analysis-a tool for teaching undergraduate circuit theory," IEEE Transactions on Education, **39**(2), 243–250, 1996, doi:10.1109/13.502071.

[35] G. Fedi, R. Giomi, A. Luchetta, S. Manetti, M.C. Piccirilli, "SapWin 2.0: a symbolic software tool for educational purposes in analysis and synthesis of analog circuits," in Proceedings of International Conference on Simulation and Multimedia in Engineering Education, ICSSE'99, San Francisco, CA: 33–36, 1999.

[36] J.B. Grimbleby, "Algorithm for finding the common spanning trees of two graphs," Electronics Letters, **17**(13), 470, 1981, doi:10.1049/el:19810328.

[37] K. Singhal, J. Vlach, Computer Methods for Circuit Analysis and Design, Springer-Verlag US, 1993.

[38] J. Sun, D.M. Mitchell, M.F. Greuel, P.T. Krein, R.M. Bass, "Averaged modeling of PWM converters operating in discontinuous conduction mode," IEEE Transactions on Power Electronics, **16**(4), 482–492, 2001, doi:10.1109/63.931052.

[39] A. Luchetta, S. Manetti, M.C. Piccirilli, A. Reatti, M.K. Kazimierczuk, "Comparison of DCM operated PWM DC-DC converter modelling methods including the effects of parasitic components on duty ratio constraint," in 2015 IEEE 15th International Conference on Environment and Electrical Engineering (EEEIC), IEEE: 766–771, 2015, doi:10.1109/EEEIC.2015.7165261.

[40] A. Luchetta, S. Manetti, M.C. Piccirilli, A. Reatti, M.K. Kazimierczuk, "Effects of parasitic components on diode duty cycle and small-signal model of PWM DC-DC buck converter in DCM," in 2015 IEEE 15th International Conference on Environment and Electrical Engineering (EEEIC), IEEE: 772–777, 2015, doi:10.1109/EEEIC.2015.7165262.

[41] A. Luchetta, S. Manetti, M.C. Piccirilli, A. Reatti, M.K. Kazimierczuk, "Derivation of network functions for PWM DC-DC Buck converter in DCM including effects of parasitic components on diode duty-cycle," in 2015 IEEE 15th International Conference on Environment and Electrical Engineering (EEEIC), IEEE: 778–783, 2015, doi:10.1109/EEEIC.2015.7165263.

[42] A. Davoudi, J. Jatskevich, P.L. Chapman, "Averaged modelling of switched-inductor cells considering conduction losses in discontinuous mode," IET Electric Power Applications, **1**(3), 402, 2007, doi:10.1049/iet-epa:20060329.

[43] J. Sun, "Unified averaged switch models for stability analysis of large distributed power systems," in APEC 2000. Fifteenth Annual IEEE Applied Power Electronics Conference and Exposition (Cat. No.00CH37058), IEEE: 249–255, doi:10.1109/APEC.2000.826112.

[44] D.K. Saini, A. Reatti, M.K. Kazimierczuk, "Average current-mode control of buck dc-dc converter with reduced control voltage ripple," in IECON 2016 - 42nd Annual Conference of the IEEE Industrial Electronics Society, IEEE: 3270–3275, 2016, doi:10.1109/IECON.2016.7793204.

[45] A. Ayachit, A. Reatti, M.K. Kazimierczuk, "Small-signal modeling of PWM dual-SEPIC dc-dc converter by circuit averaging technique," in IECON 2016 - 42nd Annual Conference of the IEEE Industrial Electronics Society, IEEE: 3606–3611, 2016, doi:10.1109/IECON.2016.7793030.

[46] P. Bernardi, R. Cicchetti, G. Pelosi, A. Reatti, S. Selleri, and M. Tatini, "An Equivalent Circuit for EMI Prediction in Printed Circuit Boards Featuring a Straight-to-Bent Microstrip Line Coupling," Progress In Electromagnetics Research B, Vol. 5, 107-118, 2008. doi:10.2528/PIERB08020502

[47] A. Reatti, S. Manetti, M. C. Piccirilli, A. Luchetta and M. K. Kazimierczuk, "Multilayer neural network with multivalued neurons MLMVN based CLASS E resonant inverter fault detection," 8th IET International Conference on Power Electronics, Machines and Drives (PEMD 2016), Glasgow, 2016, 1-6, doi: 10.1049/cp.2016.0265.

[48] M. Catelani, L. Ciani, A. Luchetta, S. Manetti, M.C. Piccirilli, A. Reatti, M.K. Kazimierczuk, "MLMVNN for parameter fault detection in PWM DC-DC converters and its applications for buck DC-DC converter," in 2016 IEEE 16th International Conference on Environment and Electrical Engineering (EEEIC), IEEE: 1–6, 2016, doi:10.1109/EEEIC.2016.7555877.

[49] M. Catelani, L. Ciani, A. Luchetta, S. Manetti, M.C. Piccirilli, A. Reatti, M.K. Kazimierczuk, "Fault detection of resonant inverters for wireless power transmission using MLMVNN," in 2016 IEEE 2nd International Forum on Research and Technologies for Society and Industry Leveraging a better tomorrow (RTSI), IEEE: 1–5, 2016, doi:10.1109/RTSI.2016.7740639.

[50] L. Albertoni, F. Grasso, J. Matteucci, M.C. Piccirilli, A. Reatti, A. Ayachit, M.K. Kazimierczuk, "Analysis and design of full-bridge Class-DE inverter at fixed duty cycle," in IECON 2016 - 42nd Annual Conference of the IEEE Industrial Electronics Society, IEEE: 5609–5614, 2016, doi:10.1109/IECON.2016.7793240.

[51] F. Corti, F. Grasso, A. Reatti, A. Ayachit, D.K. Saini, M.K. Kazimierczuk, "Design of class-E ZVS inverter with loosely-coupled transformer at fixed coupling coefficient," in IECON 2016 - 42nd Annual Conference of the IEEE Industrial Electronics Society, IEEE: 5627–5632, 2016, doi:10.1109/IECON.2016.7793285.

Generalized Integral Transform Method for Bending and Buckling Analysis of Rectangular Thin Plate with Two Opposite Edges Simply Supported and Other Edges Clamped

Charles Chinwuba Ike[1], Michael Ebie Onyia[2,*], Eghosa Oluwaseyi Rowland-Lato[3]

[1]Department of Civil Engineering, Enugu State University of Science and Technology, Agbani, Enugu State, 400001, Nigeria

[2]Department of Civil Engineering, University of Nigeria, Nsukka, Enugu State, 410001, Nigeria

[3]Department of Civil Engineering, University of Port Harcourt, Choba, Port Harcourt, Rivers State, 500272, Nigeria

A R T I C L E   I N F O

A B S T R A C T

This paper presents the generalized integral transform method for solving flexural and elastic stability problems of rectangular thin plates clamped along $y = \pm b/2$ and simply supported along remaining boundaries (x = 0, x = a) (CSCS plate). The considered plate is homogeneous, isotropic and carrying uniformly distributed transversely applied loading causing bending. Also studied, is a plate subject to (i) biaxial (ii) uniaxial uniform compressive load. The method uses the eigenfunctions of vibrating thin beams of equivalent span and support conditions in constructing the basis functions for the plate deflection and the integral kernel function. The transform is applied to the governing domain equation, converting the problem to integral equations for both cases of bending and elastic buckling. The integral equation reduces to algebraic problems for the bending problem, and algebraic eigenvalue problem for the elastic buckling problem. The deflections are obtained as double infinite series with rapidly convergent properties. Bending moments expressions are double series with infinite terms which are rapidly convergent. Maximum deflections and bending moments values occur at the plate centre in agreement with symmetry. The present results gave double series solutions with good convergent properties in closed form for bending problems. The resulting bending solutions were exact. Solving the resulting eigenvalue equation gave closed analytical equation for the buckling loads. Buckling loads are computed for the cases of biaxial and uniaxial uniform compression of square thin plates using one term approximations. The buckling load obtained for one term approximation of the eigenfunction gave results that are 12.23% greater than the exact solution. The use of more terms in the eigenfunction expansion could give more acceptable results for the eigenvalue problem of buckling of CSCS plates.

1. Introduction

Plates can be defined as structural members with inplane dimensions of length and width and transverse dimension of thickness where the least inplane dimension is usually much greater than the thickness. Plate problems are thus three-dimensional (3D) problems of elasticity for dynamic, static or stability cases [1–6]. The behaviour and classification of plates depend on the ratio of the transverse dimension and the smaller inplane dimension of the plate. They can be categorized as thin, moderately thick and thick plates. In thin plate, which is the subject of this study the ratio of the transverse dimension to the least inplane dimension is usually smaller than 1/20.

Under certain simplifying assumptions and hypotheses, the theories of plates have been approximated using two-dimensional (2D) idealizations and classical examples are the thin plate theories [1–6]. Plates are applied extensively in the varied fields of engineering and used in civil, mechanical, aeronautical, naval, spacecraft and structural components. This has resulted in the extensive studies done by many previous scholars on the subject matter [1–10]. Plates are subject to loads that produce dynamic

*Michael Ebie Onyia, Dept of Civil Engineering, University of Nigeria, Nsukka, Enugu State, +2348033821550, michael.onyia@unn.edu.ng

flexural, static flexural, and buckling responses. Plates are categorized by using geometries as rectangular, square, skew, triangular, trapezoidal, sector, circular, elliptical, polygonal, quadrilateral, rhombic; and by their material properties as heterogeneous, homogeneous, anisotropic, orthotropic or isotropic.

This work considers rectangular thin plates made with isotropic, homogeneous, linear elastic materials.

1.1. Theories of plates

Several theories have been derived and developed for plates subjected to flexure and buckling loads [11–17]. Kirchhoff's (classical small deformation thin) plate theory (KPT) used the following assumptions/hypotheses:

(i) Cross-section planes that are orthogonal to the plate's mid-plane prior to loading and bending would continue to be plane and orthogonal to the mid-plane. This is called the normality or orthogonality requirement.

(ii) The thickness remains unchanged during the bending deformation.

The merits of the KPT are:

(i) The equation of equilibrium that governs the problem is a linear equation.

(ii) The governing PDE is expressed in terms of the unknown displacement field in the transverse direction which is found by solving the linear PDE.

(iii) Bending moments and shear force expressions can be found from the transverse displacement using the equations that relate bending moment to transverse deflection, and equations that relate the shear force to transverse deflection.

(iv) The KPT results in parabolic distribution of shear stresses τ_{yz} and τ_{zx} over the thickness, and this agrees with results from structural mechanics.

The demerits include: (i) the limitation of the KPT to small deformations and (ii) the inability of the KPT to cater for transverse shear deformations, thus limiting the scope of application of the KPT to thin plates; for which transverse shear deformations are negligible.

In [11], the author presented the domain PDE for variable thickness thin plate theory. Few problems of plates with variable flexural rigidity have been solved using analytical methods. Large deflection thin plate theory was developed by von-Karman, as a system of equilibrium and compatibility equations.

Reissner derived a stress-based theory for analysing moderately thick plates by the use of Castigliano's theorem resulting in a system of three PDEs. In [3] the author derived a first order shear deformation plate theory (FOSDT). The theory considered transverse shear deformation effects by assuming linear variations across the thickness for the three displacement components. The governing PDE of Mindlin plate theory are a set of three coupled PDEs in terms of three unknown displacements w, θ_x and θ_y where $w(x, y)$ denotes deflection in the transverse coordinate, θ_x and θ_y are the rotations of the plate mid-plane ($z = 0$).

In [18], the authors presented flexural solutions for thin plates subjected to linear variations of transversely applied loading. In [19] the author used the Vlasov variant of Galerkin's methodology to present a bending solution to thin plate resting on one parameter foundations where the plate is submitted to applied loading. In [4] the authors deployed a Vlasov modification of the Galerkin method to the bending problem of rectangular thin plate under uniform distribution of transversely applied loading over the entire plate domain.

In [7], the authors have deployed the Galerkin-Vlasov technique for bending analysis of thin plates with opposite edges fixed and the other edges on simple supports. In [20] the authors have also applied the Galerkin-Vlasov methodology for obtaining solutions to the natural vibration equation of thin plates having simply supported boundaries and obtained the eigenfrequencies and vibration modal shape functions.

Ritz variational methodologies has been deployed for the formulation and solution of classical Kirchhoff plate problems by authors in [21-23].

In [21], the authors deployed Ritz technique for finding solutions to the bending analysis of rectangular Kirchhoff-Love plates subject to transverse hydrostatically varying loading distributions over the plate region. In [22], the author presented systematically the Ritz method for the flexural analysis of simply supported rectangular Kirchhoff plates under distributed transverse loadings. Similarly, in [23], the author used Ritz technique to solve the bending problems of rectangular thin plates resting on one parameter foundations, with the plate subject to uniformly distributed loading over the entire domain.

Shear deformation theories of plates have been formulated by authors in [2], [24] and [25] amongst others to incorporate the transverse shear stresses and strains on their bending, dynamic and stability behaviours.

1.2. Review of solution methods for plate problems

Plate problems of dynamic and static bending and stability have been analysed using numerical and analytical methods by several researchers.

In [1], the author obtained an infinite series solution to the small displacement bending problems of CSCS (or SCSC) rectangular thin plates subject to uniformly distributed loading, by using the superposition principle to the solution for simply supported plates carrying uniform transverse distribution of loading and the solution to the same problem under an applied torque distribution along the clamped edges where the applied torque is of such a magnitude that rotations vanish at the clamped edges.

Integral transform methods were used for determining problems of thin plates under bending deformations by authors in [10] and [26].

In [8], the authors used the finite Fourier sine transformation methodology for flexural analysis of thin plates resting on one parameter foundations. In [26], the author presented the bending solutions of thin plate supported/resting on one-parameter discrete model of Winkler with the aid of finite Fourier sine transformation technique. In [27], the author presented two-dimensional Fourier

cosine series technique to solve bending problems of rectangular thin plates supported by Winkler one-parameter foundations with the plate domain subject to transverse loading.

Kantorovich-Vlasov method was used for the thin plate flexure problems by authors in [9], [28]-[31].

In [9] the authors have studied the use of Kantorovich-Vlasov method for solving bending problems of thin plate with Dirichlet conditions under uniformly distributed transverse loading. In [28], the author presented a mixture of Kantorovich, Euler-Lagrange and Galerkin's techniques and used it for solving bending problems of rectangular thin plates. In [29], the authors used the Kantorovich method to perform natural transverse vibrational analysis of rectangular Kirchhoff plates, thus obtaining the natural frequencies of transverse vibration. In [30], the authors used the Kantorovich-Vlasov methodology for solving the flexural problems of rectangular Kirchhoff plates with opposite sides fixed, and the other two sides simply supported; with the plate subject to distributed uniform loading. In [31], the authors used the Kantorovich method to solve flexural problems of Kirchhoff-Love plates having two sides fixed and the other sides on simple supports.

Thick thick plates modelled using FOSDT and Mindlin plate theories were studied by authors in [5], [12-17].

Elastic stability problems involving rectangular Kirchhoff plates subjected to inplane compressive loads were investigated by authors in [32-36].

In [32], the authors used the two-dimensional finite Fourier sine integral transformation technique for solving the elastic buckling problems of simply supported rectangular thin plates. In [33], the authors used the one-dimensional (single) finite Fourier sine integral transform method for the elastic stability solutions of thin plates simply supported at two opposite sides and fixed along the remaining two sides for uniaxial uniform compression. In [34], the authors used the Galerkin-Kantorovich technique for the elastic buckling analysis of thin rectangular shaped plates with two opposite sides simply supported and the other two sides fixed (SCSC plates). In [35], the authors used the Galerkin-Vlasov variational method for solving the elastic problems of rectangular thin plates with two types of boundary constraints namely: (a) simply supported on two opposite sides, clamped along the third side and free along the fourth side (SSCF plates). (b) simply supported along the four sides (SSSS plates). They obtained for each considered case, closed form solution that satisfies the boundary conditions and domain equation. In [36], the authors performed and obtained stability solutions for rectangular thin SSCF and SSSS plates using the single finite Fourier sine transform method. They obtained for the studied problems, exact solutions that satisfied the deformation and force equations at the restrained boundaries and the governing field equation.

In [37], the authors presented the flexural analysis of annular plates using the indirect Trefftz boundary method. They based their formulation for thin and thick plates on the Kirchhoff classical thin plate theory and the Reissner stress based thick plate theory respectively. They adopted the Trefftz method for their analysis because the Trefftz method uses complete set of solutions satisfying the governing fourth order PDE of the KPT classical thin plate theory and the sixth order PDE of the Reissner plate theory. Another fundamental merit that informed their use of the Trefftz method is that the method avoids singular integrals due to the properties of the solution coordinate functions. They adopted the method because the boundary conditions are automatically considered by the method, rendering the method effective compared with other methods. They solved illustrative problems by the method to demonstrate its effectiveness.

In [38], the authors demonstrated the use of the finite integral transformation technique for solving the flexural problems of clamped orthotropic rectangular shaped thin plates resting on one-parameter elastic foundations. In [39], the authors used the exact wave propagation approach for the natural vibration and stability analysis of thick plates modelled using the third order shear deformation plate theory. In [40], the authors presented the refined plate theory for the natural vibration analysis of nanoplates. In [41], the authors investigated vibrational behaviour of nonlinear rectangular plates modelled using the shear deformation plate theory. In [42], the authors presented a new technique for solving nonlinear vibrational problems of rectangular plates subjected to inplane compressive forces. In [43], the authors used the trigonometric shear deformation plate theory for the flexural analysis of moderately thick plates according to the shear deformation assumptions.

Other contributions to the knowledge of plates are found in such seminal papers as presented by authors in [44-51].

Other contributions to the theory of plates are found in references [52–60].

In [61], the authors used the GITM for obtaining closed-form mathematical expressions for the stability problems of rectangular Kirchhoff plates.

In [62], the authors applied the finite integral transformation method to solve the flexural problems of rectangular Kirchhoff plates made with orthogonally anisotropic materials. They considered plates with two adjacent free boundaries and the other boundaries fixed or on simple suppports (FFCC or FFSS) plates.

In [63], the authors used the two-dimensional finite integral transformaion method to determine the mathematical expressions that solve the flexural problems of Kirchhoff plates that are rectangular in plan shape. They considered and studied such plates that are supported at the corner points.

In [64], the authors used the finte integral transformation method to solve the natural vibration problems for transversely anisotropic thin plates with opposite sides that are prevented from rotational displacement and the other sides free of support.

In [65], the authors used the techniques of finite integral transformation for flexural problems involving plates made of transversely-anisotropic materials where the plates opposite boundaries are fixed while the rest of the edges are free.

In [66], the authors used the two-dimensional finite integral transformation method to determine the mathematical expressions for the flexural problems of rectangular shaped plates with moderate thickness resting on Winkler foundations. They used the Mindlin plate theory to describe the plate and obtained the

solutions to the system of governing equaitons using the two-dimensional finite integral tansformation technique.

2. Theory

2.1. The thin plate flexure problem:

The governing PDE describing flexure for thin plates $a \times b$ which is displayed in Figure 1 is given by the PDE:

$$\nabla^4 w(x, y) - \frac{q}{D}(x, y) = 0 \tag{1}$$

where ∇^4 is the biharmonic operator, $q(x, y)$ represents distribution of applied load intensity, $w(x, y)$ denotes the deflection. D denotes the flexural rigidity of the plate, expressed in terms of the elastic properties and geometrical properties of the plate by Equation (2) as follows:

$$D = \frac{Eh^3}{12(1 - \mu^2)} \tag{2}$$

μ is Poisson's ratio, h is plate thickness. E is Young's modulus of elasticity.

For clamped edges, the restraint equations for displacements are:

$$w(x, y = \pm b/2) = 0 \tag{3}$$

$$\frac{\partial w}{\partial y}\left(x, y = \frac{\pm b}{2}\right) = 0 \tag{4}$$

For $(x = 0, y)$ and $(x = a, y)$ edges, restraint (displacement) and bending moment force equations give:

$$w(x = 0, y) = w(x = a, y) = 0 \tag{5}$$

$$\frac{\partial^2 w}{\partial x^2}(x = 0, y) = \frac{\partial^2 w}{\partial x^2}(x = a, y) = 0 \tag{6}$$

M_{xx} and M_{yy} are:

$$M_{xx} = -D\left(\frac{\partial^2 w}{\partial x^2} + \mu \frac{\partial^2 w}{\partial y^2}\right) \tag{7}$$

$$M_{yy} = -D\left(\frac{\partial^2 w}{\partial y^2} + \mu \frac{\partial^2 w}{\partial x^2}\right) \tag{8}$$
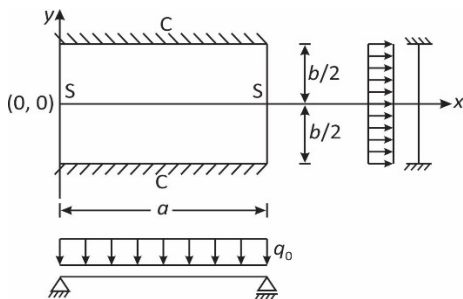
Figure 1: Rectangular thin plate $(a \times b)$ with two opposite clamped boundaries $(y = \pm b/2)$, others on simple supports (SCSC or CSCS plate) subject to uniformly distributed transverse loading

2.2. Field equations for stability of rectangular thin plates subjected to uniaxial and biaxial compressive forces

The governing equation for the problem shown in Figure 2 is for biaxial buckling given by:
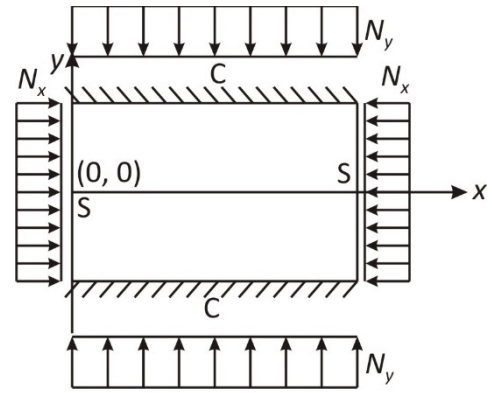
Figure 2: Biaxial buckling of rectangular thin (SCSC or CSCS) plates

$$D\nabla^4 w(x, y) + N_x \frac{\partial^2 w(x, y)}{\partial x^2} + N_y \frac{\partial^2 w(x, y)}{\partial y^2} = 0 \tag{9}$$

or, $$\nabla^4 w(x, y) + \frac{N}{D}(\nabla^2 w(x, y)) = 0 \tag{10}$$

when $N_x = N_y = N$

Let $N_y = 0$, then Equation (10) simplifies to become:

$$D\nabla^4 w + N_x \frac{\partial^2 w}{\partial x^2} = 0 \tag{11}$$

The geometric and force equations for the buckling problem are expressed by Equations (3–6).

3. Methodology

In the Generalized Integral Transformation Method (GITM), the basis functions are chosen as the eigenfunctions of a freely vibrating thin beam of equivalent edge support conditions as the plate. The plate is simply supported along the boundaries $x = 0$, and $x = a$. The eigenfunction of a simply supported thin beam of span a at the nth vibration mode is:

$$F_{1n}(x) = \sin\left(\frac{n\pi x}{a}\right) \tag{12}$$

$n = 1, 2, 3, 4, 5, 6, \ldots$

The eigenfuction of a thin beam of span b clamped at $y = \pm b/2$ at the mth vibration mode is given by:

$$F_{2m}(y) = \cos(\beta_m y) - \frac{\cos\left(\frac{\beta_m b}{2}\right)}{\cosh\left(\frac{\beta_m b}{2}\right)} \cosh(\beta_m y) \tag{13}$$

$m = 1, 2, 3, 4, 5, 6, \ldots$

In compact form,

$$F_{2m}(y) = \cos(\beta_m y) - \lambda_m \cosh(\beta_m y) \tag{14}$$

where

$$\lambda_m = \frac{\cos\left(\frac{\beta_m b}{2}\right)}{\cosh\left(\frac{\beta_m b}{2}\right)} \tag{15}$$

where β_m are the roots (eigenvalues) of the eigen equation, which for clamped-clamped thin beams is a transcendental equation.

$$\tan\left(\frac{\beta_m b}{2}\right) + \tanh\left(\frac{\beta_m b}{2}\right) = 0 \qquad (16)$$

The roots (which are infinite in numbers) are obtained for the first five modes of vibration using Mathematica software as follows:

$$\frac{\beta_1 b}{2} = \pm 2.36502037243135\ldots$$

$$\frac{\beta_2 b}{2} = \pm 5.49780391900084\ldots$$

$$\frac{\beta_3 b}{2} = \pm 8.63937982869974\ldots$$

$$\frac{\beta_4 b}{2} = \pm 11.7809724510202\ldots$$

$$\frac{\beta_5 b}{2} = \pm 14.9225651045516\ldots \qquad (17)$$

For large values of $\left(\frac{\beta_m b}{2}\right)$, $\tanh\left(\frac{\beta_m b}{2}\right) = 1$ and

$$\tan\left(\frac{\beta_m b}{2}\right) = -1 = \frac{\sin\left(\frac{\beta_m b}{2}\right)}{\cos\left(\frac{\beta_m b}{2}\right)}$$

Approximate solutions (eigenvalues) of the transcendental equation for $m > 5$ are obtained by solving the equation – Equation (18) using Mathematica and other root-finding software.

$$\left(\frac{\beta_m b}{2}\right) = \tan^{-1}(-1) \qquad (18)$$

The solution to Equation (18) is:

$$\left(\frac{\beta_m b}{2}\right) = \frac{1}{4}(4\pi m - \pi) \qquad (19)$$

$$(m > 5)$$

Then, $w(x, y)$ is constructed from the double infinite series of eigenfunctions in the x and y Cartesian coordinates as the following infinite double series:

$$w(x, y) = \sum_{m=1}^{\infty}\sum_{n=1}^{\infty} C_{mn} F_{1n}(x) F_{2m}(y) \qquad (20)$$

where C_{mn} is an unknown displacement (deflection) parameter sought for $w(x, y)$ to be a solution to the governing equation.

It is easily verified that $F_{1n}(x)$ and $F_{2m}(y)$ both satisfy all the boundary conditions of the thin plate problem for both flexure and elastic buckling.

3.1. The thin plate flexural problem

Applying the GITM to the PDE of the thin plate flexure problem results in the integral equation given as:

$$\int_0^a \int_{-b/2}^{b/2} \left(\nabla^4 \sum_{m=1}^{\infty}\sum_{n=1}^{\infty} C_{mn} F_{1n}(x) F_{2m}(y) - \frac{q_0}{D} \right) F_{1n}(x) F_{2m}(y)\, dxdy = 0$$

$$\ldots(21)$$

where

$$K_{mn}(x, y) = F_{1n}(x) F_{2m}(y) = \sin\left(\frac{n\pi x}{a}\right)(\cos(\beta_m y) - \lambda_m \cosh(\beta_m y)) \quad (22)$$

$K_{nm}(x, y)$ denotes the nucleus (kernel) function.

Hence, simplification of Equation (21) gives:

$$\sum_{m=1}^{\infty}\sum_{n=1}^{\infty} C_{mn} \int_0^a \int_{-b/2}^{b/2} (\nabla^4 F_{1n}(x) F_{2m}(y)) F_{1n}(x) F_{2m}(y)\, dxdy$$

$$= \frac{1}{D}\int_0^a \int_{-b/2}^{b/2} q_0 F_{1n}(x) F_{2m}(y)\, dxdy \qquad (23)$$

Simplifying further, we have:

$$\sum_{m=1}^{\infty}\sum_{n=1}^{\infty} C_{mn} \int_0^a \int_{-b/2}^{b/2} (F_{1n}^{iv}(x) F_{1n}(x) F_{2m}^2(y) +$$

$$2F_{1n}''(x) F_{1n}(x) F_{2m}''(y) F_{2m}(y) + F_{1n}^2(x) F_{2m}^{iv}(y) F_{2m}(y))\, dxdy$$

$$= \frac{q_0}{D}\int_0^a \int_{-b/2}^{b/2} F_{1n}(x) F_{2m}(y)\, dxdy \qquad (24)$$

where the primes represent differentiations with respect to the respective space coordinates.

For any m, n, we have C_{mn} determined by:

$$C_{mn} = \frac{q_0 I_7 I_8}{D(I_1 I_2 + 2I_3 I_4 + I_5 I_6)} = \frac{G_{1mn}}{G_{2mn}} \qquad (25)$$

$$G_{1mn} = q_0 I_7 I_8 \qquad (26)$$

$$G_{2mn} = D(I_1 I_2 + 2I_3 I_4 + I_5 I_6) \qquad (27)$$

where $I_1 = \int_0^a F_{1n}^{iv}(x) F_{1n}(x)\, dx \qquad (28)$

$$I_2 = \int_{-b/2}^{b/2} F_{2m}^2(y)\, dy \qquad (29)$$

$$I_3 = \int_0^a F_{1n}''(x) F_{1n}(x)\, dx \qquad (30)$$

$$I_4 = \int_{-b/2}^{b/2} F_{2m}''(y) F_{2m}(y)\, dy \qquad (31)$$

$$I_5 = \int_0^a F_{1n}^2(x)\, dx \qquad (32)$$

$$I_6 = \int_{-b/2}^{b/2} F_{2m}^{iv}(y) F_{2m}(y)\, dy \qquad (33)$$

$$I_7 = \int_0^a F_{1n}(x)\, dx \qquad (34)$$

$$I_8 = \int_{-b/2}^{b/2} F_{2m}(y)\, dy \qquad (35)$$

Then,

$$w(x, y) = \sum_{m=1}^{\infty}\sum_{n=1}^{\infty} \frac{\dfrac{q_0}{D} I_7 I_8 F_{1n}(x) F_{2m}(y)}{(I_1 I_2 + 2I_3 I_4 + I_5 I_6)} \qquad (36)$$

By differentiation,

$$\frac{\partial^2 w}{\partial x^2} = w_{xx} = \sum_{m=1}^{\infty} \sum_{n=1}^{\infty} \frac{\frac{q_0}{D} I_7 I_8 F_{1n}''(x) F_{2m}(y)}{(I_1 I_2 + 2I_3 I_4 + I_5 I_6)} \quad (37)$$

$$\frac{\partial^2 w}{\partial y^2} = w_{yy} = \sum_{m=1}^{\infty} \sum_{n=1}^{\infty} \frac{\frac{q_0}{D} I_7 I_8 F_{1n}(x) F_{2m}''(y)}{(I_1 I_2 + 2I_3 I_4 + I_5 I_6)} \quad (38)$$

The bending moments are:

$$M_{xx} = -\sum_{m=1}^{\infty} \sum_{n=1}^{\infty} \frac{q_0 I_7 I_8 (F_{1n}''(x) F_{2m}(y) + \mu F_{1n}(x) F_{2m}''(y))}{(I_1 I_2 + 2I_3 I_4 + I_5 I_6)} \quad (39)$$

$$M_{yy} = -\sum_{m=1}^{\infty} \sum_{n=1}^{\infty} \frac{q_0 I_7 I_8 (F_{1n}(x) F_{2m}''(y) + \mu F_{1n}''(x) F_{2m}(y))}{(I_1 I_2 + 2I_3 I_4 + I_5 I_6)} \quad (40)$$

At the plate centre, the bending moment expressions for M_{xx} and M_{yy} found by substitution of the centroidal coordinates are:

$$M_{xx}\left(x = \frac{a}{2}, y = 0\right) = -\sum_{m=1}^{\infty} \sum_{n=1}^{\infty} \frac{q_0 I_7 I_8 (F_{1n}''(a) F_{2m}(0) + \mu F_{1n}(a) F_{2m}''(0))}{(I_1 I_2 + 2I_3 I_4 + I_5 I_6)}$$
$$\dots(41)$$

$$M_{yy}\left(x = \frac{a}{2}, y = 0\right) = -\sum_{m=1}^{\infty} \sum_{n=1}^{\infty} \frac{q_0 I_7 I_8 (F_{1n}(a) F_{2m}''(0) + \mu F_{1n}''(a) F_{2m}(0))}{(I_1 I_2 + 2I_3 I_4 + I_5 I_6)}$$
$$\dots(42)$$

At the middle of the clamped boundaries, the coordinates are:
$$\left(x = \frac{a}{2}, y = \pm\frac{b}{2}\right),$$

The bending moment expressions for the midpoint of the fixed boundaries are found and given by:

$$M_{xx}\left(x = \frac{a}{2}, y = \pm\frac{b}{2}\right)$$
$$= -\sum_{m=1}^{\infty} \sum_{n=1}^{\infty} \frac{q_0 I_7 I_8 \left(F_{1n}''\left(\frac{a}{2}\right) F_{2m}\left(\pm\frac{b}{2}\right) + \mu\left(F_{1n}\left(\frac{a}{2}\right) F_{2m}''\left(\pm\frac{b}{2}\right)\right)\right)}{(I_1 I_2 + 2I_3 I_4 + I_5 I_6)}$$
$$\dots(43)$$

$$M_{yy}\left(x = \frac{a}{2}, y = \pm\frac{b}{2}\right)$$
$$= -\sum_{m=1}^{\infty} \sum_{n=1}^{\infty} \frac{q_0 I_7 I_8 \left(F_{1n}\left(\frac{a}{2}\right) F_{2m}''\left(\pm\frac{b}{2}\right) + \mu F_{1n}''\left(\frac{a}{2}\right) F_{2m}\left(\pm\frac{b}{2}\right)\right)}{(I_1 I_2 + 2I_3 I_4 + I_5 I_6)}$$
$$\dots(44)$$

3.2. Biaxial buckling of SCSC plate

The application of GITM to the elastic buckling equation gives the integral equation:

$$\int_0^a \int_{(-b/2)}^{(b/2)} \left(\nabla^4 \sum_{m=1}^{\infty} \sum_{n=1}^{\infty} C_{mn} F_{1n}(x) F_{2m}(y)\right) +$$
$$\frac{N}{D} \nabla^2 \left(\sum_{m=1}^{\infty} \sum_{n=1}^{\infty} C_{mn} F_{1n}(x) F_{2m}(y)\right) F_{1n}(x) F_{2m}(y) \, dx \, dy = 0 \quad (45)$$

Let $\frac{N}{D} = \alpha^2$ $\quad (46)$

Then,

$$\sum_{m=1}^{\infty} \sum_{n=1}^{\infty} C_{mn} \int_0^a \int_{(-b/2)}^{(b/2)} \left\{ (\nabla^4 F_{1n}(x) F_{2m}(y)) F_{1n}(x) F_{2m}(y) + \right.$$
$$\left. \alpha^2 (\nabla^2 F_{1n}(x) F_{2m}(y)) F_{1n}(x) F_{2m}(y) \right\} dx \, dy = 0 \quad (47)$$

Simplifying Equation (47) gives:

$$\sum_{m=1}^{\infty} \sum_{n=1}^{\infty} C_{mn} \int_0^a \int_{(-b/2)}^{(b/2)} \left\{ (F_{1n}^{iv}(x) F_{1n}(x) F_{2m}^2(y) + \right.$$
$$2 F_{1n}''(x) F_{1n}(x) F_{2m}''(y) F_{2m}(y) + F_{1n}^2(x) F_{2m}^{iv}(y) F_{2m}(y)) +$$
$$\left. \alpha^2 (F_{1n}(x) F_{1n}''(x) F_{2m}^2(y) + F_{1n}^2(x) F_{2m}(y) F_{2m}''(y)) \right\} dx \, dy = 0 \quad (48)$$

Hence,

$$\sum_{m=1}^{\infty} \sum_{n=1}^{\infty} C_{mn} \left\{ (I_1 I_2 + 2I_3 I_4 + I_5 I_6) + \alpha^2 (I_3 I_2 + I_5 I_4) \right\} = 0 \quad (49)$$

For nontrivial solutions, $C_{mn} \neq 0$ and

$$I_1 I_2 + 2I_3 I_4 + I_5 I_6 = -\alpha^2 (I_3 I_2 + I_5 I_4) \quad (50)$$

Solving for α^2,

$$\alpha^2 = \frac{N}{D} = -\left(\frac{I_1 I_2 + 2I_3 I_4 + I_5 I_6}{I_2 I_3 + I_4 I_5}\right) \quad (51)$$

In compact form,

$$\alpha^2 = \frac{-G_{2mn}}{G_{3mn}} \quad (52)$$

where,

$$G_{3mn} = I_2 I_3 + I_4 I_5 \quad (53)$$

Thus, the buckling load is:

$$N = \frac{G_{2mn}}{G_{3mn}} D \quad (54)$$

3.3. Uniaxial buckling of SCSC plate

For uniaxial buckling due to N_x applied alone, $N_y = 0$, and the GITM yields:

$$\alpha^2 = \frac{N}{D} = -\left(\frac{I_1 I_2 + 2I_3 I_4 + I_5 I_6}{I_2 I_3}\right) \quad (55)$$

The buckling load for uniaxial compression in the x direction is:

$$N = \frac{-G_{2mn}}{G_{4mn}} D \quad (56)$$

where, $G_{4mn} = I_2 I_3$ $\quad (57)$

4. Results

By differentiation of the eigenfunctions,

$$F_{1n}''(x) = -\left(\frac{n\pi}{a}\right)^2 \sin\left(\frac{n\pi x}{a}\right) = -\left(\frac{n\pi}{a}\right)^2 F_{1n}(x) \quad (58)$$

$$F_{1n}^{iv}(x) = \left(\frac{n\pi}{a}\right)^4 \sin\left(\frac{n\pi x}{a}\right) = \left(\frac{n\pi}{a}\right)^4 F_{1n}(x) \quad (59)$$

$$F_{2m}''(y) = -\beta_m^2 (\cos(\beta_m y) + \lambda_m \cosh(\beta_m y)) \quad (60)$$

$$F_{2m}^{iv}(y) = \beta_m^4 (\cos(\beta_m y) - \lambda_m \cosh(\beta_m y)) = \beta_m^4 F_{2m}(y) \quad (61)$$

Then,

$$I_1 = \int_0^a F_{1n}^{iv}(x) F_{1n}(x) dx = \left(\frac{n\pi}{a}\right)^4 \int_0^a F_{1n}^2(x) dx \qquad (62)$$

Substitution of the expression for F_{1n} and integration gives:

$$I_1 = \left(\frac{n\pi}{a}\right)^4 \int_0^a \sin^2\left(\frac{n\pi x}{a}\right) dx = \left(\frac{n\pi}{a}\right)^4 \left[\frac{x}{2} - \frac{\sin 2\left(\frac{n\pi x}{a}\right)}{4\left(\frac{n\pi}{a}\right)}\right]_0^a \qquad (63)$$

Substituting the integration limits gives:

$$I_1 = \left(\frac{n\pi}{a}\right)^4 \left(\frac{a}{2}\right) \qquad (64)$$

Similarly, I_2 is evaluated as:

$$I_2 = \int_{(-b/2)}^{(b/2)} F_{2m}^2(y) dy = \int_{(-b/2)}^{(b/2)} \left(\cos(\beta_m y) - \lambda_m \cosh(\beta_m y)\right)^2 dy \qquad (65)$$

Expanding the integrand in Equation (65) gives:

$$I_2 = \int_{(-b/2)}^{(b/2)} \left(\cos^2(\beta_m y) - 2\lambda_m \cosh(\beta_m y)\cos(\beta_m y) + \lambda_m^2 \cosh^2(\beta_m y)\right) dy$$

$$\dots (66)$$

Using the linearity property of integration, Equation (66) simplifies to:

$$I_2 = \int_{(-b/2)}^{(b/2)} \cos^2(\beta_m y) dy - 2\lambda_m \int_{(-b/2)}^{(b/2)} \cosh(\beta_m y)\cos(\beta_m y) dy +$$

$$\lambda_m^2 \int_{(-b/2)}^{(b/2)} \cosh^2(\beta_m y) dy \qquad (67)$$

Each integral in Equation (67) is evaluated.

$$\int_{(-b/2)}^{(b/2)} \cos^2(\beta_m y) dy = \left[\frac{y}{2} + \frac{\sin(2\beta_m y)}{4\beta_m}\right]_{(-b/2)}^{(b/2)} \qquad (68)$$

Substituting the limits, and simplifying, gives:

$$\int_{(-b/2)}^{(b/2)} \cos^2(\beta_m y) dy = \left(\frac{b/2}{2} + \frac{\sin\left(2\beta_m\left(\frac{b}{2}\right)\right)}{4\beta_m}\right) -$$

$$\left(\frac{-b/2}{2} + \frac{\sin\left(2\beta_m\left(\frac{-b}{2}\right)\right)}{4\beta_m}\right) = \frac{b}{2} + \frac{\sin(\beta_m b)}{2\beta_m} \qquad (69)$$

Similarly,

$$\int_{(-b/2)}^{(b/2)} \cosh(\beta_m y)\cos(\beta_m y) dy$$

$$= \left[\frac{\beta_m \sinh(\beta_m y)\cos(\beta_m y) + \beta_m \cosh(\beta_m y)\sin(\beta_m y)}{\beta_m^2 + \beta_m^2}\right] \qquad (70)$$

Also,

$$\int_{(-b/2)}^{(b/2)} \cosh(\beta_m y)\cos(\beta_m y) dy$$

$$= \left(\frac{\sinh\left(\frac{\beta_m b}{2}\right)\cos\left(\frac{\beta_m b}{2}\right) + \cosh\left(\frac{\beta_m b}{2}\right)\sin\left(\frac{\beta_m b}{2}\right)}{2\beta_m}\right) -$$

$$\left(\frac{-\sinh\left(\frac{\beta_m b}{2}\right)\cos\left(\frac{\beta_m b}{2}\right) - \cosh\left(\frac{\beta_m b}{2}\right)\sin\left(\frac{\beta_m b}{2}\right)}{2\beta_m}\right) \qquad (71)$$

Then,

$$\int_{(-b/2)}^{(b/2)} \cosh(\beta_m y)\cos(\beta_m y) dy$$

$$= \frac{\sinh\left(\frac{\beta_m b}{2}\right)\cos\left(\frac{\beta_m b}{2}\right) + \cosh\left(\frac{\beta_m b}{2}\right)\sin\left(\frac{\beta_m b}{2}\right)}{\beta_m} \qquad (72)$$

Also,

$$\int_{(-b/2)}^{(b/2)} \cosh^2(\beta_m y) dy = \left[\frac{y}{2} + \frac{\sinh(\beta_m y)\cosh(\beta_m y)}{2\beta_m}\right]_{(-b/2)}^{(b/2)} \qquad (73)$$

Substituting the limits, gives:

$$\int_{(-b/2)}^{(b/2)} \cosh^2(\beta_m y) dy = \left(\frac{b}{4} + \frac{\sinh\left(\frac{\beta_m b}{2}\right)\cosh\left(\frac{\beta_m b}{2}\right)}{2\beta_m}\right) -$$

$$\left(-\frac{b}{4} - \frac{\sinh\left(\frac{\beta_m b}{2}\right)\cosh\left(\frac{\beta_m b}{2}\right)}{2\beta_m}\right)$$

$$= \frac{b}{2} + \frac{\sinh\left(\frac{\beta_m b}{2}\right)\cosh\left(\frac{\beta_m b}{2}\right)}{\beta_m} \qquad (74)$$

Then, substitution of Equations (69) (72) and (74) into Equation (67) yields:

$$I_2 = \frac{b}{2} + \frac{\sin(\beta_m b)}{2\beta_m} - 2\lambda_m$$

$$\left(\frac{\sinh\left(\frac{\beta_m b}{2}\right)\cos\left(\frac{\beta_m b}{2}\right) + \cosh\left(\frac{\beta_m b}{2}\right)\sin\left(\frac{\beta_m b}{2}\right)}{\beta_m}\right) +$$

$$\lambda_m^2 \left(\frac{b}{2} + \frac{\sinh\left(\frac{\beta_m b}{2}\right)\cosh\left(\frac{\beta_m b}{2}\right)}{\beta_m}\right) \qquad (75)$$

But the eigenvalue equation from which Equation (16) is derived is:

$$\sinh\left(\frac{\beta_m b}{2}\right)\cos\left(\frac{\beta_m b}{2}\right) + \cosh\left(\frac{\beta_m b}{2}\right)\sin\left(\frac{\beta_m b}{2}\right) = 0 \qquad (76)$$

Hence, I_2 expressed by Equation (75) simplifies to:

$$I_2 = \frac{b}{2} + \frac{\sin(\beta_m b)}{2\beta_m} + \lambda_m^2 \left(\frac{b}{2} + \frac{\sinh\left(\frac{\beta_m b}{2}\right)\cosh\left(\frac{\beta_m b}{2}\right)}{\beta_m}\right) \qquad (77)$$

Similarly, I_3 is evaluated as:

$$I_3 = \int_0^a F_{1n}''(x) F_{1n}(x) dx = -\left(\frac{n\pi}{a}\right)^2 \int_0^a F_{1n}^2(x) dx = -\left(\frac{n\pi}{a}\right)^2 \frac{a}{2}$$

$$\dots (78)$$

I_4 is evaluated as:

$$I_4 = \int\limits_{(-b/2)}^{(b/2)} F''_{2m}(y) F_{2m}(y)\, dy = -\beta_m^2 \int\limits_{(-b/2)}^{(b/2)} (\cos(\beta_m y) +$$

$$\lambda_m \cosh(\beta_m y))(\cos(\beta_m y) - \lambda_m \cosh(\beta_m y))\, dy \quad (79)$$

Simplification of Equation (79) gives:

$$I_4 = -\beta_m^2 \int\limits_{(-b/2)}^{(b/2)} \left(\cos^2(\beta_m y) - \lambda_m^2 \cosh^2(\beta_m y) \right) dy \quad (80)$$

Hence,

$$I_4 = -\beta_m^2 \left(\frac{b}{2} + \frac{\sin(\beta_m b)}{2\beta_m} - \lambda_m^2 \left(\frac{b}{2} + \frac{\sinh\left(\frac{\beta_m b}{2}\right)\cosh\left(\frac{\beta_m b}{2}\right)}{\beta_m} \right) \right) \quad \dots(81)$$

Similarly,

$$I_5 = \int\limits_0^a F_{1n}^2(x)\, dx = \int\limits_0^a \sin^2\left(\frac{n\pi x}{a} \right) dx = \frac{a}{2} \quad (82)$$

Also,

$$I_6 = \int\limits_{(-b/2)}^{(b/2)} F_{2m}^{iv}(y) F_{2m}(y)\, dy = \beta_m^4 \int\limits_{(-b/2)}^{(b/2)} F_{2m}^2(y)\, dy \quad (83)$$

$$I_6 = \beta_m^4 I_2 = \beta_m^4 \left(\left(\frac{b}{2} + \frac{\sin(\beta_m b)}{2\beta_m} \right) + \right.$$
$$\left. \lambda_m^2 \left(\frac{b}{2} + \frac{\sinh\left(\frac{\beta_m b}{2}\right)\cosh\left(\frac{\beta_m b}{2}\right)}{\beta_m} \right) \right) \quad (84)$$

Similarly,

$$I_7 = \int\limits_0^a F_{1n}(x)\, dx = \int\limits_0^a \sin\frac{n\pi x}{a}\, dx = \left[-\frac{a}{n\pi} \cos\frac{n\pi x}{a} \right]_0^a \quad (85)$$

Substituting the limits,

$$I_7 = -\frac{a}{n\pi}(\cos(n\pi) - \cos 0) = -\frac{a}{n\pi}(\cos(n\pi) - 1) \quad (86)$$

I_8 is evaluated as:

$$I_8 = \int\limits_{(-b/2)}^{(b/2)} (\cos(\beta_m y) - \lambda_m \cosh(\beta_m y))\, dy$$

$$= \left[\frac{\sin(\beta_m y)}{\beta_m} - \lambda_m \frac{\sinh(\beta_m y)}{\beta_m} \right]_{-b/2}^{b/2} \quad (87)$$

Substituting the limits,

$$I_8 = \frac{2}{\beta_m} \left(\sin\left(\frac{\beta_m b}{2} \right) - \lambda_m \sinh\left(\frac{\beta_m b}{2} \right) \right) \quad (88)$$

4.1. Results for the thin plate flexure problem

Then, substituting the integrals into Equation (25), we have:

$$C_{mn} = \frac{\dfrac{-2aq_0}{n\pi}(\cos(n\pi) - 1)\dfrac{\left(\sin\left(\frac{\beta_m b}{2}\right) - \lambda_m \sinh\left(\frac{\beta_m b}{2}\right) \right)}{\beta_m}}{\left(\dfrac{n\pi}{a}\right)^4 \dfrac{a}{2} \cdot I_2 - 2I_4 \left(\dfrac{n\pi}{a}\right)^2 \dfrac{a}{2} + \dfrac{a}{2} I_6} = \frac{G_{1mn}}{G_{2mn}}$$
$$\dots(89)$$

$$G_{1mn} = \frac{-2aq_0}{n\pi\beta_m}(\cos(n\pi) - 1)\left(\sin\left(\frac{\beta_m b}{2} \right) - \lambda_m \sinh\left(\frac{\beta_m b}{2} \right) \right) \quad (90)$$

$$G_{2mn} = \left(\frac{n\pi}{a}\right)^4 \frac{a}{2}\left[\frac{b}{2} + \frac{\sin(\beta_m b)}{2\beta_m} + \right.$$
$$\lambda_m^2 \left(\frac{b}{2} + \frac{\sinh\left(\frac{\beta_m b}{2}\right)\cosh\left(\frac{\beta_m b}{2}\right)}{\beta_m} \right) \right] -$$
$$2\left(\frac{n\pi}{a}\right)^2 \frac{a}{2}\left[-\beta_m^2 \left\{ \left(\frac{b}{2} + \frac{\sin(\beta_m b)}{2\beta_m} \right) - \right. \right.$$
$$\left. \left. \lambda_m^2 \left(\frac{b}{2} + \frac{\sinh\left(\frac{\beta_m b}{2}\right)\cosh\left(\frac{\beta_m b}{2}\right)}{\beta_m} \right) \right\} \right] + \frac{a}{2}\beta_m^4 \left[\frac{b}{2} + \frac{\sin(\beta_m b)}{2\beta_m} + \right.$$
$$\left. \lambda_m^2 \left(\frac{b}{2} + \frac{\sinh\left(\frac{\beta_m b}{2}\right)\cosh\left(\frac{\beta_m b}{2}\right)}{\beta_m} \right) \right] \quad (91)$$

$$G_{2mn} = \left(\frac{n\pi}{a}\right)^4 \frac{a}{2}\left(\frac{b}{2} + \frac{\sin(\beta_m b)}{2\beta_m} + \lambda_m^2 \left(\frac{b}{2} + \frac{\sinh\left(\frac{\beta_m b}{2}\right)\cosh\left(\frac{\beta_m b}{2}\right)}{\beta_m} \right) \right) +$$
$$2\left(\frac{n\pi}{a}\right)^2 \frac{a}{2}\beta_m^2 \left(\frac{b}{2} + \frac{\sin(\beta_m b)}{2\beta_m} - \lambda_m^2 \left(\frac{b}{2} + \frac{\sinh\left(\frac{\beta_m b}{2}\right)\cosh\left(\frac{\beta_m b}{2}\right)}{\beta_m} \right) \right) +$$
$$\frac{a}{2}\beta_m^4 \left(\frac{b}{2} + \frac{\sin(\beta_m b)}{2\beta_m} + \lambda_m^2 \left(\frac{b}{2} + \frac{\sinh\left(\frac{\beta_m b}{2}\right)\cosh\left(\frac{\beta_m b}{2}\right)}{\beta_m} \right) \right)$$
$$\dots(92)$$

$$G_{2mn} = \left(\left(\frac{n\pi}{a}\right)^4 \frac{a}{2} + \frac{a}{2}\beta_m^4 \right)$$
$$\left(\frac{b}{2} + \frac{\sin(\beta_m b)}{2\beta_m} + \lambda_m^2 \left(\frac{b}{2} + \frac{\sinh\left(\frac{\beta_m b}{2}\right)\cosh\left(\frac{\beta_m b}{2}\right)}{\beta_m} \right) \right) +$$
$$2\left(\frac{n\pi}{a}\right)^2 \frac{a}{2}\beta_m^2 \left(\frac{b}{2} + \frac{\sin(\beta_m b)}{2\beta_m} - \lambda_m^2 \left(\frac{b}{2} + \frac{\sinh\left(\frac{\beta_m b}{2}\right)\cosh\left(\frac{\beta_m b}{2}\right)}{\beta_m} \right) \right)$$
$$\dots(93)$$

$$G_{2mn} = \left(\left(\frac{n\pi}{a}\right)^4 \frac{a}{2} + \frac{a}{2}\beta_m^4 \right) I_2 - 2\left(\frac{n\pi}{a}\right)^2 \frac{a}{2} I_4 \quad (94)$$

Then, $C_{mn} = \dfrac{G_{1mn}}{G_{2mn}}$ is evaluated and $w(x, y)$ is found using Equation (36) as:

$$w(x, y) = \sum_{m=1}^{\infty} \sum_{n=1}^{\infty} \frac{G_{1mn}}{G_{2mn}} F_{1n}(x) F_{2m}(y) \quad (95)$$

where $m = 1, 2, 3, \dots$; $n = 1, 2, 3, \dots$

The bending moments are obtained from substitution of Equation (95) in Equations (7) and (8):

$$F_{2m}(y = 0) = \cos 0 - \lambda_m \cosh 0 = 1 - \lambda_m \quad (96)$$

$$F_{2m}\left(y = \pm\frac{b}{2} \right) = \cos\left(\frac{\beta_m b}{2} \right) - \lambda_m \cosh\left(\frac{\beta_m b}{2} \right) \quad (97)$$

$$F_{2m}''(y=0) = -\beta_m^2(\cos 0 + \lambda_m \cosh 0) = -\beta_m^2(1+\lambda_m) \quad (98)$$

$$F_{2m}''\left(y=\pm\frac{b}{2}\right) = -\beta_m^2\left(\cos\left(\frac{\beta_m b}{2}\right) + \lambda_m \cosh\left(\frac{\beta_m b}{2}\right)\right) \quad (99)$$

$$F_{1n}\left(x=\frac{a}{2}\right) = \sin\left(\frac{(n\pi a/2)}{a}\right) = \sin\left(\frac{n\pi}{2}\right) \quad (100)$$

$$F_{1n}''\left(x=\frac{a}{2}\right) = -\left(\frac{n\pi}{a}\right)^2 \sin\left(\frac{(n\pi a/2)}{a}\right) = -\left(\frac{n\pi}{a}\right)^2 \sin\frac{n\pi}{2} \quad (101)$$

Results for deflections and bending moments evaluated at x = a, y = 0

The deflections and bending moments expressions evaluated at $x = a$, $y = 0$ are found from:

$$w(a,0) = \sum_{m=1}^{\infty}\sum_{n=1}^{\infty} C_{mn} F_{1n}\left(x=\frac{a}{2}\right) F_{2m}(y=0)$$

$$= \sum_{m=1}^{\infty}\sum_{n=1}^{\infty} \frac{G_{1mn}}{G_{2mn}} \sin\frac{n\pi}{2}(1-\lambda_m) \quad (102)$$

$$M_{xx}(a,0) = \sum_{m=1}^{\infty}\sum_{n=1}^{\infty} \frac{G_{1mn}}{G_{2mn}}\left(F_{1n}''\left(\frac{a}{2}\right)F_{2m}(0) + \mu F_{1n}\left(\frac{a}{2}\right)F_{2m}''(0)\right) \quad (103)$$

$$M_{yy}(a,0) = \sum_{m=1}^{\infty}\sum_{n=1}^{\infty} \frac{G_{1mn}}{G_{2mn}}\left(F_{1n}\left(\frac{a}{2}\right)F_{2m}''(0) + \mu F_{1n}''\left(\frac{a}{2}\right)F_{2m}(0)\right) \quad (104)$$

Results for deflection and bending moment expressions evaluated at the midpoint of the fixed edges $\left(x=\dfrac{a}{2}, y=\pm\dfrac{b}{2}\right)$

The deflection and bending moments expressions evaluated at the midpoint of the fixed edges are found and given by:

$$w\left(\frac{a}{2},\pm\frac{b}{2}\right) = \sum_{m=1}^{\infty}\sum_{n=1}^{\infty} \frac{G_{1mn}}{G_{2mn}} F_{1n}\left(x=\frac{a}{2}\right)F_{2m}\left(y=\pm\frac{b}{2}\right) = 0 \quad (105)$$

Since

$$F_{2m}\left(y=\pm\frac{b}{2}\right) = \cos\left(\pm\frac{\beta_m b}{2}\right) - \frac{\cos\left(\frac{\beta_m b}{2}\right)}{\cosh\left(\frac{\beta_m b}{2}\right)}\cosh\left(\pm\frac{\beta_m b}{2}\right)$$

$$= \cos\left(\frac{\beta_m b}{2}\right) - \frac{\cos\left(\frac{\beta_m b}{2}\right)}{\cosh\left(\frac{\beta_m b}{2}\right)}\cosh\left(\frac{\beta_m b}{2}\right) = 0 \quad (106)$$

$$M_{xx}\left(x=\frac{a}{2}, y=\pm\frac{b}{2}\right)$$

$$= \sum_{m=1}^{\infty}\sum_{n=1}^{\infty}\frac{G_{1mn}}{G_{2mn}}\left(F_{1n}''\left(\frac{a}{2}\right)F_{2m}\left(\frac{\pm b}{2}\right) + \mu F_{1n}\left(\frac{a}{2}\right)F_{2m}''\left(\frac{\pm b}{2}\right)\right) \quad (107)$$

$$M_{yy}\left(x=\frac{a}{2}, y=\pm\frac{b}{2}\right)$$

$$= \sum_{m=1}^{\infty}\sum_{n=1}^{\infty}\frac{G_{1mn}}{G_{2mn}}\left(F_{1n}\left(\frac{a}{2}\right)F_{2m}''\left(\frac{\pm b}{2}\right) + \mu F_{1n}''\left(\frac{a}{2}\right)F_{2m}\left(\frac{\pm b}{2}\right)\right) \quad (108)$$

The obtained results are presented in Tables 1, 2, 3, 4, 5, 6, 7, 8 and 9.

Table 1: Maximum deflection coefficients (α_1) of rectangular Kirchhoff CSCS plate having clamped boundaries ($y=-b/2, y=+b/2$) two opposite boundaries ($x=0, x=a$), simply supported and the plates submitted to uniform load of intensity q_0 (case when $b \le a$ or $a \ge b$) for $\mu = 0.30$

a/b	$w_{max} = \alpha_1\left(\dfrac{q_0 b^4}{D}\right)$	
	Present study (GITM) α_1	[1] α_1
1.0	1.92×10^{-3}	1.92×10^{-3}
1.1	2.09×10^{-3}	2.09×10^{-3}
1.2	2.23×10^{-3}	2.23×10^{-3}
1.3	2.34×10^{-3}	2.34×10^{-3}
1.4	2.40×10^{-3}	2.40×10^{-3}
1.5	2.47×10^{-3}	2.47×10^{-3}
2	2.60×10^{-3}	2.60×10^{-3}
∞	2.60×10^{-3}	2.60×10^{-3}

Table 2: Maximum deflection coefficient (α_2) of rectangular Kirchhoff CSCS plates with clamped boundaries ($y=\pm b/2$); opposite simply supported boundaries ($x=0, x=a$) where the plate carries uniform loading with an intensity q_0 (case when $b \ge a$) for $\mu = 0.30$

b/a	$w_{max} = \alpha_2\left(\dfrac{q_0 a^4}{D}\right)$	
	Present study (GITM) α_2	[1] α_2
1.0	1.92×10^{-3}	1.92×10^{-3}
1.1	2.51×10^{-3}	2.51×10^{-3}
1.2	3.19×10^{-3}	3.19×10^{-3}
1.3	3.88×10^{-3}	3.88×10^{-3}
1.4	4.60×10^{-3}	4.60×10^{-3}
1.5	5.31×10^{-3}	5.31×10^{-3}
1.6	6.03×10^{-3}	6.03×10^{-3}
1.7	6.68×10^{-3}	6.68×10^{-3}
1.8	7.32×10^{-3}	7.32×10^{-3}
1.9	7.90×10^{-3}	7.90×10^{-3}
2	8.44×10^{-3}	8.44×10^{-3}
3	11.68×10^{-3}	11.68×10^{-3}
∞	13.02×10^{-3}	13.02×10^{-3}

Table 3: $w_{max} = \alpha_1\left(\dfrac{q_0 b^4}{D}\right)$ convergence study of the maximum deflection function for CSCS (or SCSC) plate for the cases where $b < a$ (or $a > b$) for $\mu = 0.30$

a/b	Present study $n=1, m=1$ α_1	Relative error	Present study $n=1, 3,$ $m=1, 2$ α_1	Relative error	[1] α_1
1.0					1.92×10^{-3}
1.1	2.188125×10^{-3}	4.69	2.081875×10^{-3}	−0.39	2.09×10^{-3}
1.2	2.345625×10^{-3}	5.18	2.21625×10^{-3}	−0.62	2.23×10^{-3}
1.3	2.476875×10^{-3}	5.85	2.320625×10^{-3}	−0.83	2.34×10^{-3}
1.4	2.585625×10^{-3}	7.73	2.399375×10^{-3}	−0.03	2.40×10^{-3}
1.5	2.67625×10^{-3}	8.35	2.461875×10^{-3}	−0.45	2.47×10^{-3}
2	2.64875×10^{-3}	1.875	2.59375×10^{-3}	−0.24	2.60×10^{-3}
∞	2.63625×10^{-3}	1.39	2.60125×10^{-3}	−0.05	2.60×10^{-3}

Table 4: Convergence study of the maximum deflection of the CSCS plate studied for the cases where $b < a$ up to 5 terms each of the series for $\mu = 0.30$

a/b	$n=1,$ $m=1$ α_1	$n=1, 3$ $m=1, 2$ α_1	$n=1, 3, 5$ $m=1, 2, 3$ α_1	$n=1, 3, 5, 7$ $m=1, 2, 3, 4$ α_1	$n=1, 3, 5, 7, 9$ $m=1, 2, 3, 4, 5$ α_1

	(×10⁻³)	(×10⁻³)	(×10⁻³)	(×10⁻³)	(×10⁻³)
1.1	2.188125	2.081875	2.09125	2.089375	2.09
1.2	2.345625	2.21625	2.228125	2.225625	2.23
1.3	2.476875	2.320625	2.335625	2.3325	2.34
1.4	2.585625	2.399375	2.418125	2.414375	2.40
1.5	2.67625	2.461875	2.481875	2.476875	2.47
2	2.64875	2.59375	2.623125	2.610625	2.60
∞	2.63625	2.60125	2.605	2.60375	2.60

Table 5: Convergence study of the maximum value of deflection of CSCS Kirchhoff plates studied for cases $b \geq a$ for $\mu = 0.30$

b/a	α_2 $n=1,$ $m=1$ (×10⁻³)	α_2 $n=1,3$ $m=1,2$ (×10⁻³)	α_2 $n=1,3,5$ $m=1,2,3$ (×10⁻³)	α_2 $n=1,3,5,7$ $m=1,2,3,4$ (×10⁻³)	α_2 $n=1,3,5,7,9$ $m=1,2,3,4,5$ (×10⁻³)
1.0	1.998125	1.91125	1.919375	1.9175	1.92
1.1	2.625	2.520625	2.53	2.5275	2.509375
1.2	3.310625	3.184375	3.195625	3.193125	3.13375
1.3	4.035	3.8825	3.896875	3.89375	3.88
1.4	4.778125	4.594375	4.55	4.60875	4.60
1.5	5.5225	5.3025	5.3250	5.32	5.31
1.6	6.2875	5.9925	6.02	6.01375	6.03
1.7	6.960625	6.651875	6.685625	6.680625	6.68
1.8	7.635	7.27375	7.314375	7.305625	7.32
1.9	8.2725	7.8525	7.901875	7.89125	7.90
2	8.87	8.38625	8.445	8.4325	8.44
3	12.866875	11.50375	11.7325	11.67625	11.68
∞	13.07125	13.0175	13.02125	13.020625	13.02

Table 6: Bending moment coefficients evaluated at the centroidal coordinates of CSCS plates edges $(x = 0, x = a)$ on simple supports, two sides $(y = \pm b/2)$ fixed with the plate carrying uniform loading of intensity q_0 (case where $b < a$, and $\mu = 0.30$) $M_{xxc} = \alpha_3 q_0 b^2$ $M_{yyc} = \alpha_4 q_0 b^2$

a/b	Present study α_3	[1] α_3	Present study α_4	[1] α_4
1.1	0.0230	0.0230	0.0355	0.0355
1.2	0.0215	0.0215	0.0375	0.0375
1.3	0.0203	0.0203	0.0388	0.0388
1.4	0.0192	0.0192	0.0399	0.0399
1.5	0.0179	0.0179	0.0406	0.0406
2	0.0142	0.0142	0.0420	0.0420
∞	0.0125	0.0125	0.0417	0.0417

Table 7: Bending moment coefficients for uniformly loaded rectangular Kirchhoff CSCS plate studied. Sides $(y = \pm b/2)$ clamped, opposite edges $(x = 0, x = a)$ on simple supports (case where $b \geq a$, and $\mu = 0.30$)

b/a	$M_{xx} = \alpha_5 q_0 a^2$		$M_{yy} = \alpha_6 q_0 a^2$	
	α_5 Present study (GITM)	[1] α_5	α_6 Present study (GITM)	[1] α_6
1.0	0.0244	0.0244	0.0332	0.0332
1.1	0.0307	0.0307	0.0371	0.0371
1.2	0.0376	0.0376	0.0400	0.0400
1.3	0.0446	0.0446	0.0426	0.0426
1.4	0.0514	0.0514	0.0448	0.0448
1.5	0.0585	0.0585	0.0460	0.0460
1.6	0.065	0.0650	0.0469	0.0469
1.7	0.0712	0.0712	0.0475	0.0475
1.8	0.0768	0.0768	0.0477	0.0477
1.9	0.0821	0.0821	0.0476	0.0476
2	0.0869	0.0869	0.0474	0.0474
3	0.1144	0.1144	0.0419	0.0419
∞	0.0125	0.0125	0.0375	0.0375

Table 8: Bending moment coefficients at the midpoint of the fixed edges of rectangular Kirchhoff CSCS plate under uniform loading over the plate domain (for the case $b < a$) for $\mu = 0.30$

a/b	$M_{yy} = \alpha_7 q_0 b^2$	
	α_7 Present study (GITM)	[1] α_7
1.1	−0.0739	−0.0739
1.2	−0.0771	−0.0771
1.3	−0.0794	−0.0794
1.4	−0.0810	−0.0810
1.5	−0.0822	−0.0822
2	−0.0842	−0.0842
∞	−0.0833	−0.0833

Table 9: Bending moment coefficients at the midpoint of fixed edges of thin CSCS plates carrying uniform loading (cases $b \geq a$; $\mu = 0.30$)

b/a	$M_{yy} = \alpha_8 q_0 a^2$	
	α_8 Present study (GITM)	[1] α_8
1.0	−0.0697	−0.0697
1.1	−0.0787	−0.0787
1.2	−0.0868	−0.0868
1.3	−0.0938	−0.0938
1.4	−0.0998	−0.0998
1.5	−0.1049	−0.1049
1.6	−0.1090	−0.1090
1.7	−0.1122	−0.1122
1.8	−0.1152	−0.1152
1.9	−0.1174	−0.1174
2	−0.1191	−0.1191
3	−0.1246	−0.1246
∞	−0.1250	−0.1250

4.2. Results for stability problems studied

4.2.1. Biaxial buckling of CSCS plate

G_{2mn} is found from Equation (93)

$$G_{3mn} = -\left(\frac{n\pi}{a}\right)^2 \frac{a}{2}\left(\frac{b}{2} + \frac{\sin(\beta_m b)}{2\beta_m} + \lambda_m^2\left(\frac{b}{2} + \frac{\sinh\left(\frac{\beta_m b}{2}\right)\cosh\left(\frac{\beta_m b}{2}\right)}{\beta_m}\right)\right) -$$

$$\frac{a}{2}\beta_m^2\left(\frac{b}{2} + \frac{\sin(\beta_m b)}{2\beta_m} - \lambda_m^2\left(\frac{b}{2} + \frac{\sinh\left(\frac{\beta_m b}{2}\right)\cosh\left(\frac{\beta_m b}{2}\right)}{\beta_m}\right)\right) \quad (109)$$

$$G_{4mn} = -\left(\frac{n\pi}{a}\right)^2 \frac{a}{2}\left(\frac{b}{2} + \frac{\sin(\beta_m b)}{2\beta_m} + \lambda_m^2\left(\frac{b}{2} + \frac{\sinh\left(\frac{\beta_m b}{2}\right)\cosh\left(\frac{\beta_m b}{2}\right)}{\beta_m}\right)\right)$$
$$\ldots(110)$$

N is calculated from Equation (54).

For $m = 1$, $n = 1$, an approximate value for N for biaxial buckling load as well as the buckling load in uniaxial compression are found as follows:

$$I_1 = \frac{\pi^4}{2a^3} \tag{111}$$

$$I_2 = 0.50883b \tag{112}$$

$$I_6 = \frac{254.702}{b^3} \tag{113}$$

$$I_3 = -\frac{\pi^2}{2a} \tag{114}$$

$$I_5 = \frac{a}{2} \tag{115}$$

$$I_4 = -\frac{6.25988}{b} \tag{116}$$

$$I_3 I_2 = -2.510975 \frac{b}{a} \tag{117}$$

$$I_4 I_5 = -3.12994 \frac{a}{b} \tag{118}$$

$$G_3 = -\left(2.510975 \frac{b}{a} + 3.12994 \frac{a}{b}\right) = -\left(\frac{2.510975}{r} + 3.12994r\right)$$
$$\ldots(119)$$

$$\text{where } r = \frac{a}{b} \tag{120}$$

$$G_2 = \frac{24.7823}{b^2 r^3} + \frac{127.351r}{b^2} + \frac{61.782}{b^2 r} \tag{121}$$

Then,

$$\alpha^2 = \frac{N}{D} = \left(\frac{\dfrac{24.7823}{b^2 r^3} + \dfrac{127.351r}{b^2} + \dfrac{61.782}{b^2 r}}{\dfrac{2.510975}{r} + 3.12994r}\right)$$
$$= \left(\frac{27.7823r^{-2} + 127.351r^2 + 61.782}{2.510975 + 3.12994r^2}\right)\frac{1}{b^2} \tag{122}$$

For $r = 1$,

$$N = 37.9221 \frac{D}{b^2} = 3.8423 \frac{D\pi^2}{b^2} \tag{123}$$

Similarly, a one term solution for the buckling load for uniaxial compression in the x duration is given by:

$$\alpha^2 = \left(\frac{\dfrac{24.7823}{b^2 r^3} + \dfrac{127.351r}{b^2} + \dfrac{61.782}{b^2 r}}{\dfrac{2.510975}{r}}\right) \tag{124}$$

$$N = \left(\frac{9.8696}{r^2} + 50.7177r^2 + 24.6048\right)\frac{D}{b^2} \tag{125}$$

For $r = 1$,

$$N(r = 1, m = n = 1) = 85.1921 \frac{D}{b^2} = 8.63176 \frac{D\pi^2}{b^2} \tag{126}$$

The exact solution for the lowest/critical elastic buckling load in uniaxial compression in the x Cartesian coordinate direction is [1]:

$$N = 7.691 \frac{D\pi^2}{b^2} \tag{127}$$

The obtained GITM solution for the elastic buckling load under uniaxial uniform compression of CSCS plate for a one term approximation is 12.23% greater than the exact solution. It is suggested that more acceptable solutions that do not differ markedly from the exact solution for the elastic stability problems of square CSCS plates under uniaxial compressive loading could be obtained by using more terms in the eigenfunction expansion.

5. Discussion

The Generalized Integral Transform Method (GITM) has been used in this work to solve the bending and buckling problems of rectangular thin plates having two boundaries ($x = 0$, $x = a$) on simple supports and the other two boundaries ($y = \pm b/2$) fixed. In the thin plate bending problem presented, the plate was submitted to a uniform distribution of loading. The PDE for homogeneous, isotropic plates is the inhomogeneous biharmonic equation expressed by Equation (2). The natural and force equations at the supported boundaries are expressed using the Equations (3 – 6). The study thus presented solutions to the domain Equation (2) using the GITM, where the solutions are required to satisfy Equations (3 – 6) along the boundaries.

The elastic buckling problem considered in the study is given for biaxial compressive forces by Equation (9) or Equation (10) when the biaxial compressive forces are equal for both the x and y directions ($N_x = N_y$). The domain PDE for uniaxial buckling in the x direction is given by Equation (11). The boundary conditions for buckling are given by Equations (3 – 6). The two-dimensional GITM which is a generalization of the integral transform methods uses the eigenfunctions of an equivalent vibrating thin beam for the respective Cartesian coordinates as the basis functions in the respective coordinate directions.

Thus the basis functions (eigenfunctions) for the problem considered are chosen as Equations (12) and (13). The unknown displacement $w(x, y)$ is considered to be constructed from the basis functions as the double infinite series given by Equation (20). The unknown deflection $w(x, y)$ is a function of C_{mn}, unknown displacement parameters which are sought such that $w(x, y)$ satisfies the domain equation at all point in the solution space.

The basis functions $F_{1n}(x)$ and $F_{2m}(y)$ each satisfies the geometric and force equation at the supports for both bending and elastic buckling analysis. The GITM transforms the governing PDE for plate bending to the integral equation given by Equation (21) where the kernel function is expressed by Equation (22). The general solution of the integral equation is found for C_{mn} as Equation (25) which is expressible using integrals $I_1, I_2, \ldots, I_8$. Thus $w(x, y)$ is determined as Equation (36). With the aid of bending moments-displacement equations, the bending moments are obtained in general as Equations (39) and (40). The expressions for bending moments evaluated at the plate centre are obtained as Equations (41) and (42). The expressions for M_{xx} and M_{yy} bending moments at the mid-point of the fixed edges are found as Equations (43) and (44).

The generalized integral transformation of the governing equation for elastic buckling (biaxial case) gave the integral

equation – Equation (45). Simplification of the formulation yielded the algebraic eigenvalue problem in Equation (49).

For nontrivial solutions ($C_{mn} \neq 0$) C_{mn} would not vanish and the elastic stability equation was obtained as Equation (50). The solution of the equation gave α^2 from which N could be found as Equation (51). Specializations of the solution for biaxial buckling gave the solution for uniaxial buckling as Equation (55).

The general solutions obtained for both cases of bending and elastic buckling analysis are presented in terms of integrals. The integrals are evaluated in order to determine specific expressions for G_{1mn}, G_{2mn}, G_{3mn}, G_{4mn}, which are determined explicitly as Equations (90), (91), (109) and (110) respectively.

The deflection was thus found explicitly as the double series of infinite terms as Equation (95). The deflection of the plate centre is thus found as Equation (102). The maximum deflection presented in Tables 1 and 2 occurs at the centre and agrees with the symmetrical features of the plate problem. The bending moments M_{xx}, M_{yy} are found at the plate centre and the middle point of the fixed sides and presented in Tables 6, 7, 8 and 9. Tables 3, 4 and 5 which present convergence studies of the double series for maximum deflection at the plate centre confirm the series as rapidly convergent. Satisfactorily accurate results for maximum deflection are found with a small number of terms of the obtained double infinite series for the maximum deflection. The converged results obtained for deflections and bending moments were in excellent agreement with solutions presented using the superposition principle [1].

The eigenvalue problem of buckling yielded the approximate expression for α^2 for $m = 1$, $n = 1$ from which N would be found as Equation (122) for biaxial buckling cases. For square thin plates the biaxial buckling load was found as Equation (123). The approximate expression for α^2 for $m = 1$, $n = 1$ for uniaxial buckling under uniform compression was found as Equation (124). N was obtained as the expression in Equation (125).

6. Conclusion

In conclusion

(i) The GITM assumes the unknown $w(x, y)$ to be a double infinite series constructed as products of the eigenfuncions $F_{1n}(x)$ and $F_{2m}(y)$ of vibrating Euler-Bernoulli beams with equivalent end support conditions respectively in the Cartesian coordinates, and terms C_{mn} sought to be determined.

(ii) In the present problem the GITM assumes $w(x, y)$ as the double infinite series of the product of C_{mn} and $F_{1n}(x)$ and $F_{2m}(y)$. $F_{1n}(x)$ is the eigenfunction of a vibrating Euler-Bernoulli beam with simply supported ends which correspond to the simply supported boundaries of the plate. $F_{2m}(y)$ denotes eigenfunction of a vibrating Euler-Bernoulli beam with clamped ends ($y = \pm b/2$) which corresponds to the clamped boundaries ($y = \pm b/2$) of the thin plate being studied.

(iii) The eigenfunctions $F_{1n}(x)$ and $F_{2m}(y)$ thus satisfy the geometric and force equations of the thin rectangular CSCS plates considered for the two cases of bending

analysis and elastic buckling analysis considered in the study.

(iv) The GITM uses the eigenfunctions $F_{1n}(x)$ and $F_{2m}(y)$ as the integral kernel functions in the formulation of the integral equation from the domain equation for both the bending analysis and the elastic buckling analysis presented.

(v) The application of GITM to the governing domain PDE converts the PDE over the domain to an integral equation in both cases of bending and elastic buckling analysis.

(vi) The integral equations further reduce to algebraic problems for bending analysis leading to the determination of the unknown displacement parameters C_{mn}, and the full determination of the deflection $w(x, y)$.

(vii) The integral equation reduces to an algebraic eigenvalue equation for elastic buckling analysis, leading to the determination of α^2 and thus N for nontrivial solutions.

(viii) The bending moment expressions were found as double series with infinite terms.

(ix) The expressions for the maximum values of the deflection and bending moments are found to be rapidly convergent double series of infinite terms in m, and n.

(x) The maximum values for deflection and bending moments were found to occur at the plate centre, thus agreeing with the symmetrical features of the plate problems considered.

(xi) Convergence studies done and presented in Tables 3, 4 and 5 for the deflection expression computed at the plate centre validate that the deflection expression is rapidly convergent series, and exact solutions are obtained using five terms of the series in x and y directions.

(xii) Satisfactorily accurate results are obtained for the maximum deflection with just a small number of terms of the infinite series expression.

(xiii) For the verification and validation of the plate bending results found using the GITM in this work, the numerical values of the maximum deflections and maximum bending moments obtained were compared with values obtained for the same problem solved using the superposition technique. Good agreement between the present GITM solutions and solutions by superposition presented by authors in [1] was observed.

(xiv) The GITM gave closed form mathematical expression as analytical solutions to the plate bending problem studied.

(xv) The eigenvalue problem of elastic buckling studied for biaxial loading in uniform compression was illustrated using the first terms from the eigenfunction, and the approximate value of the buckling load computed for square CSCS plates.

(xvi) The approximated value of the elastic buckling load was also found for uniaxial uniform compression of square CSCS plate and the obtained result had a relative error of 12.23% compared with the exact solution. This demonstrates, the relative accuracy of the GITT since a 1×1 term approximation gave a relatively small error. The use of more terms would definitely yield better results for the buckling load; however, with huge computational efforts (even with software due to the large demands of computer memory size/space).

Conflict of Interest

The authors hereby affirm and declare that they have no conflict of interest whatsoever in the publication and dissemination of this research work.

Acknowledgment

The authors sincerely and heartily acknowledge the constructive contributions of the reviewers, and the hard work and sincere commitment of the Editor-in-Chief and the Editorial Board members. The authors are grateful for all the efforts leading to the acceptance of the paper for publication in the journal.

References

[1] S. Timoshenko, S. Woinowsky-Krieger, Theory of Plates and Shells, Second Edition, McGraw Hill Book Company, 1987.

[2] K. Chandrashekhara, Theory of Plates, Universities Press (India) Limited Hyderabad, 2001.

[3] R.D. Mindlin, "Influence of rotary inertia on flexural motion of isotropic, elastic plates" Journal of Applied Mechanics, **18**(1), 31–38, 1951.

[4] N.N. Osadebe, C.C. Ike, H. Onah, C.U. Nwoji, F.O. Okafor, "Application of the Galerkin-Vlasov method to the flexural analysis of simply supported rectangular Kirchhoff plates under uniform loads" Nigerian Journal of Technology, **35**(4), 732–738, October 2016.

[5] C.C. Ike, C.U. Nwoji, I.O. Ofondu, "Variational formulation of Mindlin plate equation and solution for deflections of clamped Mindlin plates" International Journal for Research in Applied Sciences and Engineering Technology, **5**(1), 340–353, January 2017.

[6] C.C. Ike, "First principles derivation of differential equations of equilibrium of anisotropic thin plates on elastic foundations" Journal of Geotechnical and Transportation Engineering, **4**(1), 10–16, 2018.

[7] C.U. Nwoji, B.O. Mama, C.C. Ike, H.N. Onah, "Galerkin-Vlasov method for the flexural analysis of rectangular Kirchhoff plates with clamped and simply supported edges" IOSR Journal of Mechanical and Civil Engineering, **14**(2), Version 1, 61 – 74, April 2017. Doi-10.9790/1684-1402016174

[8] B.O. Mama, C.C. Ike, H.N. Onah, C.U. Nwoji, "Analysis of rectangular Kirchhoff plate on Winkler foundation using Fourier sine transform method" IOSR Journal of Mathematics, **13**(1), Version VI, 58–66, Jan–Feb 2017. Doi:10.9790/5728-1301065866

[9] C.U. Nwoji, B.O Mama, H.N. Onah, C.C. Ike, "Kantorovich-Vlasov method for simply supported plates under uniformly distributed loads" International Journal of Civil, Mechanical and Energy Science, **3**(2), 69–77, March–April 2017. http://dx.doi.org/10.24001/ijcmes.3.2.1

[10] B.O. Mama, C.U. Nwoji, C.C. Ike, H.N. Onah, "Analysis of simply supported rectangular Kirchhoff plates by the finite Fourier sine transform method" International Journal of Advanced Engineering Research and Science, **4**(3), 285–291, March 2017.https:.dx.doi.org/10.22161/ijaers.4.3.44.

[11] R. Szilard, Theories and Applications of Plate Analysis: Classical, Numerical and Engineering Methods, John Wiley and Sons Inc., New York 1056pp, 2004.

[12] C.C. Ike, "Equilibrium approach in the derivation of differential equations for homogeneous isotropic Mindlin plates" Nigerian Journal of Technology, **36**(2), 346–350, April 2017. http://dx.doi.org/10.4314/nijt.v36i2.4

[13] C.U Nwoji, H.N. Onah, B.O. Mama, C.C. Ike, "Theory of elasticity formulation of the Mindlin plate equations" International Journal of Engineering and Technology, **9**(6), 4344–4352, 2017. DOI:10.21817/ijet/2017/v9i6/170906074

[14] C.C. Ike, "Mathematical solutions for the flexural analysis of Mindlin's first order shear deformable circular plates" Journal of Mathematical Models in Engineering (JVE MME), **14**(2), 50–72, June 2018. https//doi.org/10.21595/mme.2018.19825

[15] C.U. Nwoji, B.O. Mama, H.N. Onah, C.C. Ike, "Flexural analysis of simply supported rectangular Mindlin plates under bisinusoidal transverse load" ARPN Journal of Engineering and Applied Sciences, **13**(15), 4480–4488, August 2018.

[16] H.N. Onah, M.E. Onyia, B.O. Mama, C.U. Nwoji, C.C. Ike, "First principles derivation of displacement and stress functions for three-dimensional elastostatic problems, and application to the flexural analysis of thick

[17] C.C. Ike, "Variational formulation of the Mindlin plate on Winkler foundation problem" Electronic Journal of Geotechnical Engineering, **22**(12), 4829–4846, 2017.

[18] C.C. Ike, C.U. Nwoji, E.U. Ikwueze, I.O. Ofondu, "Bending analysis of simply supported rectangular Kirchhoff plates under linearly distributed transverse load" Exploramatics Journal of Innovative Engineering and Technology, **1**(1), 28–36, September 2017.

[19] C.C. Ike, "Flexural analysis of rectangular Kirchhoff plate on Winkler foundation using Galerkin-Vlasov variational method" Mathematical Modelling of Engineering Problems, **5**(2), 83–92, June 2018. https//doi.org/10.18280/mmep.050205.

[20] B.O. Mama, H.N. Onah, C.C. Ike, N.N. Osadebe, "Solution of free vibration equation of simply supported Kirchhoff plate by Galerkin-Vlasov method" Nigerian Journal of Technology, **36**(2), 361–365, April 2017. http://dx.doi.org/10.4314/nijt.v36i2.6.

[21] C.U. Nwoji, H.N. Onah, B.O. Mama, C.C. Ike, "Ritz variational method for bending of rectangular Kirchhoff-Love plate under transverse hydrostatic load distribution" Mathematical Modelling of Engineering Problems, **5**(1), 1–10, March 2018. https//doi.org/10.18280/mmep.050101.

[22] C.C. Ike, "Systematic presentation of Ritz variational method for the flexural analysis of simply supported rectangular Kirchhoff-Love plates" Journal of Engineering Sciences, **5**(2), D1–D5, 2018.

[23] C.C. Ike, "Ritz variational method for the flexural analysis of rectangular Kirchhoff plate on Winkler foundation" Journal of Engineering Sciences, **6**(1), pp D7–D15, 2018.

[24] Y.M. Ghugal, A.S. Sayyad, "A static flexure of thick isotropic plate using trigonometric shear deformation theory" Journal of Solid Mechanics, **2**(1), 79–90, 2010.

[25] Y.M. Ghugal, P.D. Gajbhiye, "Bending analysis of thick isotropic plates by using 5th order shear deformation theory" Journal of Applied and Computational Mechanics, **2**(2), 80–95, 2016.

[26] C.C. Ike, "Flexural analysis of Kirchhoff plates on Winkler foundations using finite Fourier sine integral transform method" Mathematical Modelling of Engineering Problems, **4**(4), 145–154, Dec 2017.

[27] C.C. Ike, "Double Fourier cosine series method for the flexural analysis of Kirchhoff plates on Winkler foundations" Journal of Geotechnical and Transportation Engineering, **4**(2), 30–38, 2018.

[28] C.C. Ike, "Kantorovich – EulerLagrange – Galerkin's method for bending analysis of thin plates" Nigerian Journal of Technology, **36**(2), 351–360, April 2017. https://dx.doi.org/10.4314/nijt.v36i2.5

[29] C.C. Ike, C.U. Nwoji, "Kantorovich method for the determination of eigenfrequencies of thin rectangular plates" Exploramatics Journal of Innovative Engineering and Technology, **1**(1), 20–27, September 2017.

[30] H.N. Onah, B.O. Mama, C.C. Ike, C.U. Nwoji, "Kantorovich-Vlasov method for the flexural analysis of Kirchhoff plates with opposite edges clamped and simply supported (CSCS plates)" International Journal of Engineering and Technology, **9**(6), 4333–4343, 2017. Doi:10.21817/ijet/2017/v9i6/170906073

[31] C.C. Ike, B.O. Mama, "Kantorovich variational method for the flexural analysis of CSCS Kirchhoff-Love plates" Journal of Mathematical Models in Engineering (JVE – MME), **4**(1), 29–41, 2018. https://doi.org/10.21595/mme.2018.19750.

[32] C.U. Nwoji, H.N. Onah, B.O. Mama, C.C. Ike, E.U. Ikwueze, "Elastic buckling analysis of simply supported thin plates using the double finite Fourier sine integral transform method" Exploramatics Journal of Innovative Engineering and Technology, **1**(1), 37–47, September 2017.

[33] H.N. Onah, C.U. Nwoji, C.C. Ike, B.O. Mama, "Elastic buckling analysis of uniaxially compressed CCSS Kirchhoff plate using single finite Fourier sine integral transform method" Modelling, Measurement and Control B, **87**(2), 107–111, June 2018. doi:10.18280/mmc_b.87.0208.

[34] M.E. Onyia, E.O. Rowland-Lato, C.C. Ike, "Galerkin-Kantorovich method for the elastic buckling analysis of thin rectangular SCSC plates" International Journal of Engineering Research and Technology, **13**(4), 613–619, 2020.

[35] M.E. Onyia, E.O. Rowland-Lato, C.C. Ike, "Galerkin-Vlasov variational method for the elastic buckling analysis of SSCF and SSSS rectangular plates" International Journal of Engineering Research and Technology, **13**(6), 1137–1146, 2020.

[36] M.E. Onyia, E.O. Rowland-Lato, C.C. Ike, "Elastic buckling analysis of SSCF and SSSS rectangular thin plates using the single finite Fourier sine integral transform method" International Journal of Engineering Research and Technology, **13**(6), 1147–1158, 2020.

[37] A. Ghannadiasi, A. Noorzad, "Bending solution for simply supported annular plates using the indirect Trefftz boundary method" Civil Engineering Infrastructures Journal, **49**(1), 127–138, June 2016. DOI:10.7508/CEIJ.2016.01.009.

[38] A.M.M. Bidgoli, A.R. Daneshmehr, R. Kolahchi, "Analytical bending solution of fully clamped orthotropic rectangular plates resting on elastic foundations by the finite integral transform method" Journal of Applied and Computational Mechanics, **1**(2), 52–58, 2015. DOI:10.22055/JACM.2014.10742.

[39] A. Zargaripoor, A. Bahrami, M. Nikkhah-Bahrami, "Free vibration and buckling analysis of third-order shear deformation plate theory using exact wave propagation approach" Journal of Computational Applied Mechanics, **49**(1), 86–101, 2018. DOI:10.22059/JCAMECH.2018.248906.223.

[40] M. Goodarzi, M. Nikkhah-Bahrami, V. Tavaf, "Refined plate theory for free vibration analysis of FG nanoplates using the nonlocal continuum plate model" Journal of Computational Applied Mechanics, **48**(1), 123–136, 2017.DOI:10.22059/JCAMECH.2017.236217.155.

[41] R. Javidi, M.M. Zand, K. Dastani, "Dynamics of nonlinear rectangular plates subjected to an orbiting mass based on shear deformation plate theory" Journal of Computational Applied Mechanics, **49**(1), 27–36, 2018.DOI:10.22059/JCAMECH.2017.238716.169.

[42] H. Makvandi, S. Moradi, D. Poorveis, K.H. Shirazi, "A new approach for nonlinear vibration analysis of thin and moderately thick rectangular plates under inplane compressive load" Journal of Computational Applied Mechanics, **48**(2), 185–198, 2017. DOI:10.22059/JCAMECH.2017.240726.181.

[43] A. Sayyad, Y.M. Ghugal, "Bending of shear deformable plates resting on Winkler foundations according to trigonometric plate theory" Journal of Applied and Computational Mechanics, **4**(3), 187–201, 2018. DOI:10.22055/JACM.2017.23057.1148.

[44] A. Mirzapour, M. Eskandari-Ghadi, A. Ardeshir-Behrestaghi, "Analysis of transversely isotropic half spaces under the effect of bending of a rigid circular plate" Civil Engineering Infrastructures Journal, **45**(5), 601–610, 2012.

[45] F. Shahabian, S.M. Elachachi, D. Breysse, "Safety analysis of the patch load resistance of plate girders: Influence of model error and variability" Civil Engineering Infrastructures Journal, **46**(2), 145–160, 2003. DOI:10.7508/CEIJ.2013.02.003.

[46] G. Abdollahzadeh, F. Ghobadi, "Mathematical modelling of column-base connections under monotonic loading" Civil Engineering Infrastructures Journal, **47**(2), 255–272, 2014. DOI:10.7508/CEIJ.2014.02.008.

[47] L. Cuba, R.A. Arciniega, J.L. Mantari, "Generalized 2-unknown's HSDT to study isotropic and orthotropic composite plates" Journal of Applied and Computational Mechanics, **5**(1), 141–149, 2019. DOI: 10.22055/JACM.2018.24953.1222.

[48] A. Jahanpour, F. Roozbahani, "An applicable formula for elastic buckling of rectangular plates under biaxial and shear loads" Aerospace Science and Technology, **56**, 100–111, 2016. http://dx.doi.org/10.1016/J.AST.2016.07.005.

[49] J. Zhang, C. Zhou, S. Ullah, Y. Zhong and L. Rui, "Two-dimensional generalized finite integral transform method for new analytic bending solutions of orthotropic rectangular thin foundation plates" Applied Mathematics Letters, **92**, 8–12, June 2019.

[50] S. Ullah, J. Zhang, Y. Zhong, "Accurate buckling analysis of rectangular thin plates by double finite sine integral transform method" Structural Engineering and Mechanics, **72**(4), 491–502, 2019. Doi:http://dx.doi.org//10.12989/sem.2019.72.4.491.

[51] O.A. Oguaghamba, C.C. Ike, "Single finite Fourier sine integral transform method for the determination of natural frequencies of flexural vibration of Kirchhoff plates" International Journal of Engineering Research and Technology, **13**(3), 470–476, 2020.

[52] E. Ventsel, T. Krauthammer, Thin Plates and Shells, Marcel Dekker Inc. USA, 2001.

[53] E.H. Mansfield, The Bending and Stretching of Plates, Cambridge University Press, Cambridge, 1989.

[54] R. Vinson Jack, Solid Mechanics and its Applications – Plate and Panel Structures of Isotropic Sandwich Construction, Springer Dordrecht, Netherlands, 2005.

[55] P.S. Chen, N.N. Archer, "Solutions of a twelfth order thick plate theory" Acta Mechanics, **79**, 77–111, 1989.

[56] C.C. Ike, C.U. Nwoji, B.O. Mama, H. N. Onah, M.E. Onyia. "Least squares weighted residual method for finding the elastic stress fields in rectangular plates under uniaxial parabolically distributed edge loads". Journal of Computational Applied Mechanics **51**(1), 107-121. Doi: 10.22059/JCAMECH.2020.298074.484.

[57] D. Durban, D. Givoli, J.G. Simnonds (Eds), Solid Mechanics and its Applications Advances in the Mechanics of Plates Shells: The Avio nvan Libai Anniversary Volume Kluwer Academic Publisher Dordrecht, Netherlands, 2001.

[58] C.H. Aginam, C.A. Chidolue, C.A. Ezeagu, "Application of direct variational method in the analysis of isotropic thin rectangular plates" ARPN Journal of Engineering and Applied Sciences, **7**(9), 1128–1138, September 2012.

[59] J.N. Reddy, Energy Principles and Variational Methods in Applied Mechanics, John Wiley and Co Inc. New Jersey, USA, 2002.

[60] A.C. Ugural, Stresses in Plates and Shells, McGraw Hill Book Co New York, 1999.

[61] S. Ullah, Y. Zhong, J. Zhang, "Analytical buckling solutions of rectangular thin plates by straightforward generalized integral transform method" International Journal of Mechanical Sciences, **159**, 535 – 544, 2019. DOI: 10.1016/j.ijmechsci.2019.01.025

[62] Q. Xu, Z. Yang, S. Ulllah, Z. Jinghui, Y. Gao, "Analytical bending solutions of orthotropic rectangular thin plates with two adjacent edges free and the others clamped or simply supported using finite integral transform method" Advances in Civil Engineering, Vol 2020. Article ID: 8848879 (11pages), https://doi.org/10.1155/2020/8848879.

[63] J. Zhang, C. Zhou, S. Ullah, Y. Zhong, R. Li, "Accurate bending analysis of rectangular thin plates with corner supports by a unified finite integral transform method" Acta Mechanica, **230**(10), 3807 – 3821, 2019. DOI: 10.1007/s00707.019-02488-7

[64] Y. Zhang, S. Zhang, "Free transverse vibration of rectangular orthotropic plates with two opposite edges rotationally restrained and remaining others free" Applied Sciences, **9**(22): 1 – 13, 2019. doi.103390/app9010022

[65] S. Zhang, L. Xu, "Analytical solutions for flexure of rectangular orthotropic plates with opposite rotationally restrained and free edges" Archives of Civil and Mechanical Engineering, **18**(2018), 965 – 972, 2018. https://doi.org/10.1016/jacme.2018.02.005.

[66] B. Tian, R. Li, Y. Zhong "Integral transform solutions to the bending problems of moderately thick rectangular plates with all edges free resting on elastic foundations" Applied Mathematical Modelling, **39**(2015), 128 – 136, 2015.

Ranking the Most Important Attributes of using Google Classroom in online Teaching for Albanian Universities: A Fuzzy AHP Method with Triangular Fuzzy Numbers and Trapezoidal Fuzzy Numbers

Daniela Halidini Qendraj[*,1], Evgjeni Xhafaj[2], Alban Xhafaj[3], Etleva Halidini[4]

[1]*Department of Mathematics, Faculty of Information Technology. University "Alexander Moisiu", Durres, 1001, Albania*

[2]*Department of Mathematics, Faculty of Mathematics and Physics Engineering, Polytechnic University of Tirana, 1001, Albania*

[3]*Data scientist and BI platforms at INTRUM ITALY, S.p.A, Tirana, 1001, Albania*

[4]*Department of Mathematics, General High School "Besnik Sykja", Tirana, 1001, Albania*

A R T I C L E   I N F O

A B S T R A C T

This paper has conducted the study of the impact and effectiveness of Google Classroom in online teaching and learning. Based on the unified theory of acceptance and use of technology (UTAUT2), the first aim was to rank the 8 constructs namely: Performance Expectancy, Effort Expectancy, Social Influence, Facilitating Conditions, Hedonic Motivation, Habit, Behavioral Intention, and the last Use Behavior. Each of the constructs have their respective questions due to the questionnaire formed from the UTAUT2 theory. To evaluate the use of Google Classroom, have been analyzed the feedbacks from every participant based on a 5-likert scale output. Secondly, was completed the rank of the questions based on the most preferred 5-likert scale options. The method proposed for the purposes of this study were fuzzy AHP with triangular fuzzy numbers (TFN) and trapezoidal fuzzy numbers (TpFN). The results suggested that the most preferred construct by fuzzy with TFN numbers was the Behavioral Intention while the least preferred was the Effort Expectancy, whereas for fuzzy TpFN the most preferred construct was the Social Influence and the least preferred was the Effort Expectancy. Based on the questionnaire, the rank resulted to be the same with both methods for the most preferred question and the least important one, that were respectively from Use Behavior construct, and from Performance Expectancy construct, while the ranked questions of other constructs differed slightly with both methods. These results showed that both methods produced the same rank for the 5-likert scale options, where "Agree" option was the more important from the 5-likert scale options and "Strongly disagree" option was less important. From these findings was concluded that these changes in ranking were due to the different defuzzification methods that were used for both types of fuzzy numbers.

1. Introduction

Due to the worldwide situation of the COVID-19 pandemic, in several countries have been applied online teaching methods in schools and universities, including Albania. The most used e-learning platform was Google Classroom which is a free application, mainly used in higher education helping lecturers and students to share files between them referring to [1]. Compared with the traditional teaching style there are advantages and disadvantages in using Google Classroom [2].

In fact the students prefer the engagement in Google Classroom rather than being engaged in a class where the teachers have more active roles [3]. Google Classroom has incorporated some other applications such as Google Docs, Slides, Calendar, Sheets, where users can download them from Play Store or App store [4]. All these applications help the lecturer/tutor and students to have a better communication by attaching assignments or sharing files without the need of face to face learning. The benefit of using Google Classroom is that you can stay organized, save time and paper, interact with other users in a kind of blended learning [5],

[6]. Classroom use of Google was expected to improve in quality and providing assistance in education [7]. Motivated by these facts the study was focused to find the most important attributes related to Google Classroom, based on the online learning theory of acceptance and use of technology 2 (UTAUT2). This theory is a technology acceptance model formulated by Venkatesh et al [8], and aimed to explain user intentions to use a new technology and subsequent usage behavior. The study questionnaire was based in the questionnaire developed by Jakkaew and Hemrungrote [9] and Jannosy [10]. The survey with 26 questions 5-likert scale have collected data from 528 students that studied mathematical courses in bachelor degree, from four different Universities in Albania. Based on the UTAUT2 theory, the questionnaire has 8 constructs: Performance Expectancy (PE), Effort Expectancy (EE), Social Influence (SI), Facilitating Conditions (FC), Hedonic Motivation (HM), Habit (HT) [11], Behavioral Intention (BI) [12] and Use Behavior (UB) introduced and estimated by Jannosy [10]. For each of the questions, the answers were based on a 5-likert scale where 5 represents "strongly agree", 4 "agree", 3 "neither agree nor disagree", 2 "disagree" and 1 "strongly disagree". PE is determined by how useful Google Classroom is for students and how does it increases the learning productivity [13]. EE determines how easy it is to learn and use Google Classroom [14]. SI determines the degree that an individual will perceive the importance that the closely friends or peers, or people he or she valuate his/her opinion, believe in using Google Classroom [15]. FC describes the perception that the technology will support difficulties while using Google Classroom [8]. HM defines the fun or pleasure in using Google Classroom compared to traditional learning [16]. HT determines the degree of observed automatic behavior to an unconscious stimulus that leads to happy outcome after using Google Classroom [17], [18]. Some studies have found that the more users are in regular contact with each other, the more likely they are to develop a "habit of participation" and act cooperatively with the others [19], [20]. BI is the subjective degree that an individual will use Google Classroom frequently in the future. UB is defined from the subsequent effects of habit and others, but mostly from the effect of behavioral intention [20]. The constructs had their own set of questions, defined by Venkatesh, Jakkaew, Hemrungrote et al. The study referred to each of the construct as an attribute of its level, and each question as an attribute of the question's level, and each alternative response from 5-likert scale, as an attribute of the 5 options. Thomas Saaty [21] introduced analytic hierarchic process (AHP) as a method of measurement with ratio scales to solve real life problems in decision making, but to deal with uncertainty in complex problems and multi criteria decision making (MCDM), AHP is combined with fuzzy logic (Fuzzy AHP) [22]. The fuzzy AHP method converts the Saaty scale of AHP from 1-9, to symmetric triangular fuzzy numbers and symmetric trapezoidal fuzzy numbers. The next step calculates the defuzzification of fuzzy numbers, converting the expected results into crisp numbers and ranking the attributes according to their respective levels [23]. In order to evaluate all the attributes of Google Classroom, has been constructed a hierarchy in levels. The goal was "the best attributes for Google Classroom", level 1 were the four universities of Albania, level 2 included the eight constructs of UTAUT2, level 3 was formed by the questions for each of the constructs, and level 4 included the 5-likert point option for each of the questions. The hierarchy and its levels are as follow in figure 1 and figure 2:
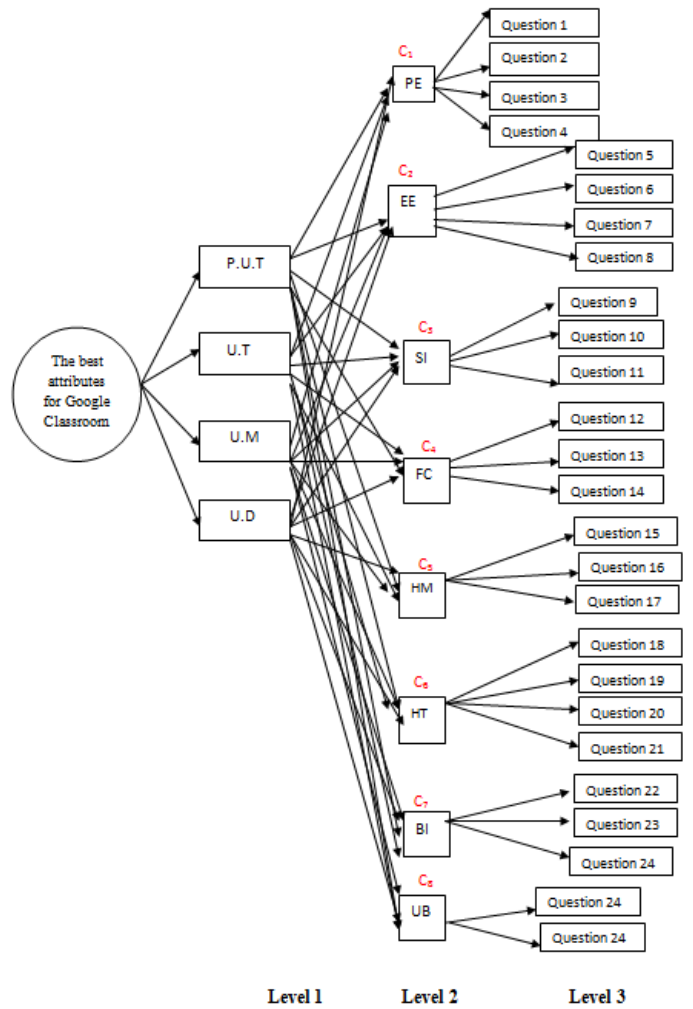
Figure 1: Hierarchy of the questionnaire
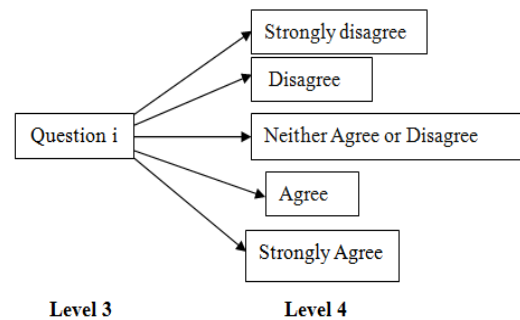
Figure 2: The 5-likert point alternative

The rankings have been evaluated by implementing the method fuzzy AHP with triangular fuzzy numbers and with trapezoidal fuzzy numbers, because it is known that trapezoidal fuzzy numbers are a generalization of triangular fuzzy numbers [24]. Thus have been compared the similar rankings and also the changes in rankings. The results obtained from this study may be very useful for lecturers and students when using Google Classroom. The findings are expected to be used by lecturers in explaining new knowledge, also in their interest to know where students are more focused during the online learning. Multi criteria decision making problems are a group of decision method,

where AHP is one of the most widely used among them. The AHP was first introduced by Saaty [25], [26] which uses the decision matrix and makes the pair-wise comparison evaluations in order to obtain the relative weights for the levels of the hierarchy (criteria and alternatives). This method has disadvantages in its inability to deal with the uncertainty decision making problems [27], [28]. To address this issue, in [29] the author introduced the fuzzy AHP, based on the fuzzy set theory by [30]. The first FAHP was applied with triangular fuzzy numbers and their relative preferences were described with the means of fuzzy numbers [31]. In [31], the author introduced the geometric mean to calculate the fuzzy weights and their combination for finding final weights, in [32], the author introduced a new approach for FAHP based on triangular fuzzy numbers and used the extent analyses to find the vector of weights for each element of the criterion. Most of previous works have used the AHP method and other MCDM methods in Learning Measurement Systems (LMS) while a little attention has been paid to the fuzzy AHP method. In [33], the author evaluated the critical success factors in implementing e-learning system using FAHP with TFN scale. They have treated the success factors from diverse points of view such as system, support from the institution, instructor, and student. In [34], the author has evaluated the LMS systems by using FAHP with TFN and two other methods, fuzzy Topsis and an Integrated Method. In the study has been showed that the content management and development is the most important criteria. In [35], the author applied FAHP in increasing the effectiveness of teaching to massive open online courses (MOOCS) and to determine the most widespread MOOCS. In [36], the author explores in detail the necessary requirements for the successful execution of distance education in industrial engineering using FAHP and SWARA. In [37], the author used the FAHP to weight the e-learning website selection index, for eight C-programming language websites, and concluded that the most important from the quality factor is "functionality", and from e-learning easily specific factors is "easy of learning community". In [38], the author used FAHP to choose the most appropriate system of LMS, and it was Joomla LMS system. In [39], the author applied fuzzy AHP to evaluate significant factors for executing a successful personalized E-Learning system. In [40], the author used FAHP with TFN numbers and other methods to achieve lean attributes for competitive advantages development. In other research papers [41], [42] the authors have evaluated the adoption of a new technology with FAHP method. In [41], the author used FAHP and Structural Equation Modeling (SEM) to predict the adoption of cloud-based technology, and found that the constructs PE, EE, SI of UTAUT2 are the most important factors predicting behavioral intention to adopt cloud-based collaborative learning technology from experts' point of view. In [42], the author applied FAHP with TFN numbers to rank the factors influencing Fin Tech adoption intention, case study China and Korea. They concluded that the price value had the most significant influence on Chinese perceptions while credibility had the most significant effect on korean perceptions. In [43], the author has evaluated the usability of website using combined weighted method: fuzzy AHP and

entropy approach. The entropy approach suggested "Response Time" (RT) as the main contributor while FAHP suggests "Ease of Navigation" (EON) as the main contributor for evaluation of usability of the academic websites. In [44], the author firstly has investigated the effective factors in electronic readiness of governmental and semi-governmental organizations of Tabriz city, and then ranked the effective factors in accepting information technologies and teleworking by fuzzy AHP technique. In general, these papers have mostly applied the FAHP method with TFN numbers. To the best of the knowledge, there is not yet an AHP study or a FAHP study on Google Classroom usage. In this paper have been studied the most important attributes of using Google Classroom for online teaching by the FAHP method with triangular fuzzy numbers and with trapezoidal fuzzy numbers. The study aimed to find the ranked sub-criteria and alternatives according to the hierarchy levels: the ranked constructs based on the students answers for each of the eight of them, the ranked questions from the most to the least important (there are 26 in total) and finally the ranked 5-likert-scale point options.

2. Ranking methods

The FAHP method has been used to find the most important attributes of Google Classroom with symmetric triangular fuzzy numbers and trapezoidal fuzzy numbers. One good reason for the selection of these methods was because the fuzzy numbers describe better the pair-wise comparisons matrices of optimality criteria than simple AHP. If the fuzzy method has been applied, the result score is always 'the-bigger-the-better' [45]. The 26 questions are organized in 8 constructs which are C1 = PE = Performance Expectancy, C2 = EE = Effort Expectancy, C3 = SI = Social Influence, C4 = FC = Facilitating Conditions, C5 = HM = Hedonic Motivation, C6 = HT = Habit, C7 = BI = Behavioral Intention and C8 = UB = Use Behavior, referred in the study as the criteria. The sub-criteria have been represented by the third level of the hierarchy, and the alternatives of the hierarchy have been represented in the fourth level showed also in figure 1.

3. The proposed framework

Both methods have been developed through 7 steps for their application. The first was to construct the hierarchy problem, then have been created the pairwise comparison matrices and checked for consistency for each of them in all levels of the hierarchy. All these steps had the decision matrices with crisp numbers. In step four were converted all crisp numbers of the decision matrices into triangular fuzzy numbers/trapezoidal fuzzy numbers according FAHP-TFN/FAHP-TPFN [46], and then were calculated the fuzzy weights for each method. The deffuzification step was not the same for both methods. This step has converted the fuzzy numbers into crisp numbers, and the greater number (weight) showed the most important attribute among them. The most interested issue was to determine exactly how have changed the ranked results regarding the most important attribute for Google Classroom. In figure 3 and figure 4 have been shown all these steps.

Steps for FAHP-TFN
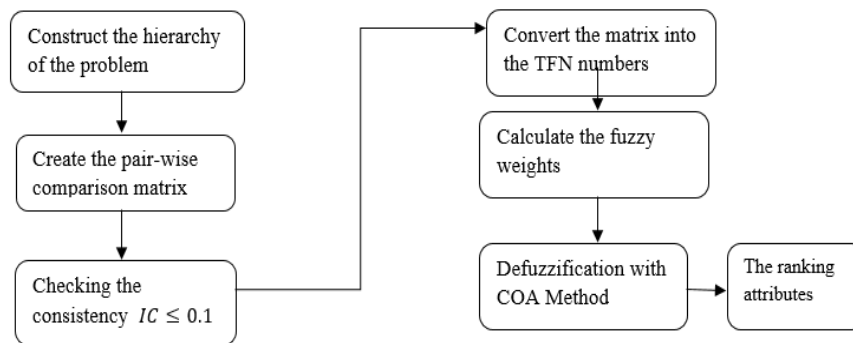
Figure 3: FAHP with TFN Numbers

Steps for FAHP-TpFN
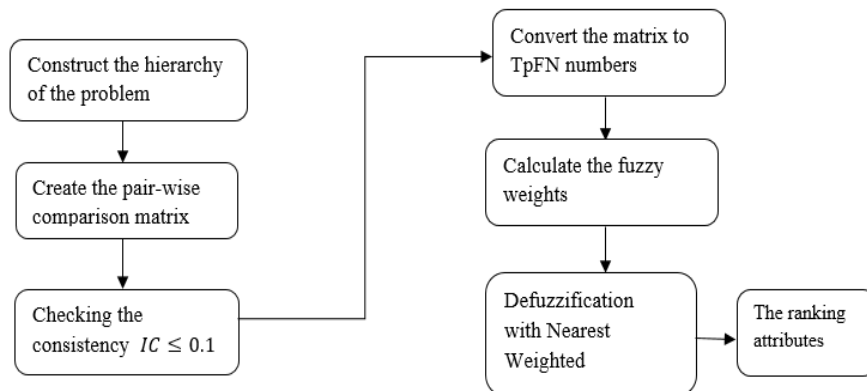
Figure 4: FAHP with TpFN Numbers

3.1. Fuzzy AHP with TFN Numbers

Decision-makers often liked to give linguistic variables, rather than giving their judgments in numerical values [47]. A linguistic variable has linguistic terms representing approximate values of a base variable, relevant to a particular application, have been captured by approximate fuzzy numbers [48]. Each linguistic variable consists of the following elements: A name, a base variable, a set of linguistic terms and a semantic rule. To deal with data uncertainty, FAHP is a useful theory in the in the context that crisp numbers are expressed in fuzzy numbers.

Firstly a group of decision makers is formed for evaluating the criteria and attributes as linguistic variables, with the consensus of all its members [49]. The main input for AHP method is the decision matrix formed from the expert's judgment, so there will be a factor of subjectivity in their decisions [50]. The most important thing is that this matrix has to be consistent with index CI less or equal to 0.1 ($CI = \frac{\lambda_{max} - n}{n-1} \leq 0.1$) [51].

Also, it is necessary for the consistence ratio $CR = CI/RI \leq 0.1$, where RI is the random index of the n-order matrix showed in table 1.

The experts have constructed the decision matrices for all levels of the hierarchy, and then converted the numbers into fuzzy symmetric triangular numbers (TFN). The fuzzy numbers were defined from the triangular symmetrical fuzzy membership function.

Table 1: Random Index for matrix of n-order, simple AHP (Saaty 1980)

n	1	2	3	4	5	6	7	8	9	10
RI	0.00	0.00	0.58	0.9	1.12	1.24	1.32	1.41	1.45	1.49

Table 2: Triangular fuzzy numbers and their inverse with Saaty Scale

Relative importance	Importance	TFN	Inverse of TFN
1	Equal	(1,1,1)	(1,1,1)
3	Moderate	(2,3,4)	(1/4,1/3,1/2)
5	Strong	(4,5,6)	(1/6,1/5,1/4)
7	Very strong	(6,7,8)	(1/8,1/7,1/6)
9	Extremely strong	(9,9,9)	(1/9,1/9,1/9)
2	Intermediate values	(1,2,3)	(1/3,1/2,1)
4	Intermediate values	(3,4,5)	(1/5,1/4,1/3)
6	Intermediate values	(5,6,7)	(1/7,1/6,1/5)
8	Intermediate values	(7,8,9)	(1/9,1/8,1/7)

A fuzzy number $\tilde{N}$ is called a triangular fuzzy number (TFN) if its membership function $\mu_{\tilde{N}}(x): R \rightarrow [0,1]$ is as follows:

$$\mu_{\widetilde{N}}(x) = \begin{cases} \frac{x-l}{m-l} & l \leq x \leq m \\ \frac{u-x}{u-m} & m \leq x \leq u \\ 0 & x \neq [l,u] \end{cases} \qquad (1)$$

In figure 5 is shown the triangular membership function.
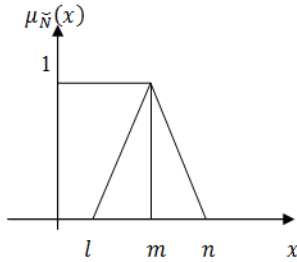
The fuzzy number $\widetilde{N} = (l, m, u)$ is formed by the lower, medium and upper bounds of the crisp number. Table 2 shows the Saaty scale from 1 to 9 evaluated with symmetric triangular fuzzy numbers, also the inverse of the triangular fuzzy numbers.

In figure 6 are shown the triangular fuzzy numbers with the Saaty relative importance value.
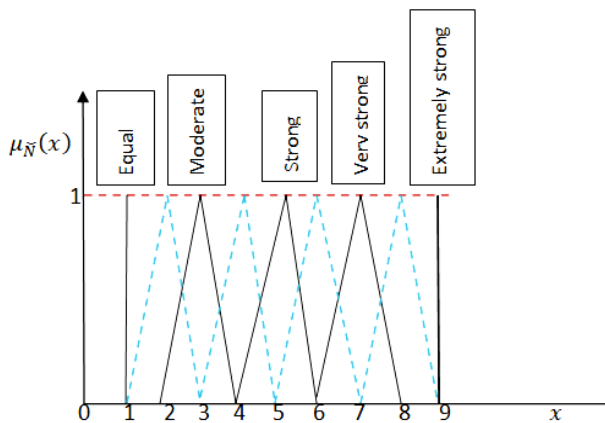
The operational laws with triangular fuzzy numbers are as follow:

a) $\widetilde{N}_1 \oplus \widetilde{N}_2 = (l_1, m_1, u_1) \oplus (l_2, m_2, u_2) =$
$(l_1 + l_2, m_1 + m_2, u_1 + u_2)$

b) $\widetilde{N}_1 \otimes \widetilde{N}_2 = (l_1, m_1, u_1) \otimes (l_2, m_2, u_2) =$
$(l_1 l_2, m_1 m_2, u_1 u_2) \qquad (2)$

c) $\widetilde{N}^{-1} = (l, m, u)^{-1} = (\frac{1}{u}, \frac{1}{m}, \frac{1}{l})$

The decision matrix A was converted into the matrix $\widecheck{A}$ as the fuzzy TFN matrix [52]-[53]:

$$\widecheck{A} = \begin{pmatrix} (1,1,1) & \cdots & (l_{1n}, m_{1n}, u_{1n}) \\ \vdots & \ddots & \vdots \\ (l_{n1}, m_{n1}, u_{n1}) & \cdots & (1,1,1) \end{pmatrix}$$

$$\widecheck{a}_{ij} = (l_{ij}, m_{ij}, u_{ij}),$$

where

$$\widecheck{a}_{ij}^{-1} = (\frac{1}{u_{ij}}, \frac{1}{m_{ij}}, \frac{1}{l_{ij}}) \qquad (3)$$

For each of the criteria have been calculated the fuzzy geometric mean value:

$$\widecheck{r}_i = \left(\prod_{i=1}^{n} \widecheck{a}_{ij}\right)^{1/n} \qquad (4)$$

Next was applied the defuzzification method named Center of Area method (COA) for the fuzzy weights:

$$\widetilde{\omega}_i = \widecheck{r}_i \otimes (\widecheck{r}_1 \oplus \widecheck{r}_2 \oplus \dots \oplus \widecheck{r}_n)^{-1} \qquad (5)$$

According to Voskoglou (2018) the coordinates of the Center of Area for the triangular formed with fuzzy numbers are $G\left(\frac{l+m+n}{3}, \frac{1}{3}\right)$. Point G is the intersection of the medians of the triangle formed by fuzzy numbers [54] (see figure 7).
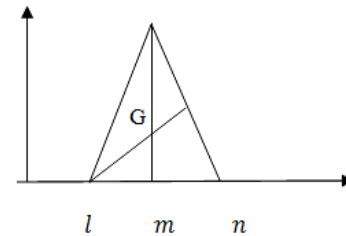
Figure 7: Center of area for TFN

The last step was to find the average M_i and the normalized weights N_i for all criteria:

$$M_i = \frac{\widetilde{\omega}_1 \oplus \widetilde{\omega}_2 \oplus \dots \oplus \widetilde{\omega}_n}{n} \qquad (6)$$

$$N_i = \frac{M_i}{M_1 \oplus M_2 \oplus \dots \oplus M_n} \qquad (7)$$

These 7 steps must be performed to find the normalized weights for both criteria and their alternatives as they are represented in the hierarchy. According to these results, the alternative with the highest score is suggested to be the best alternative for the decision makers.

Triangular and trapezoidal fuzzy numbers are used very often to deal with the vagueness of the decisions related to alternative choice for each of the criteria [23]. A trapezoidal fuzzy number is denoted as $\widetilde{N} = (l, m, n, u)$ where if $m = n$ it becomes a triangular fuzzy number TFN, so the TFN numbers are a special case of TpFN numbers. In this study all the linguistic variables of the pair-wise comparison matrices have been expressed in trapezoidal fuzzy number. The trapezoidal fuzzy number has the membership function as follows:

Table 3: Trapezoidal fuzzy numbers and inverse of TpFN with Saaty scale.

Relative importance value	Importance	Trapezoidal fuzzy numbers scale	Inverse of trapezoidal fuzzy numbers
1	Equal	(1,1,1,1)	(1,1,1,1)
3	Moderate	(2,5/2,7/2,4)	(0.13,0.2,0.46,0.53)
5	Strong	(4,9/2,11/2,6)	(0.05,0.15,0.25,0.35)
7	Very strong	(6,13/2,15/2,8)	(0.04,0.1,0.18,0.244)
9	Extremely strong	(8,17/2,9,9)	(0.01,0.1,0.12,0.21)
2	Intermediate values	(1,3/2,5/2,3)	(0.2,0.3,0.7,0.8)
4	Intermediate values	(3,7/2,9/2,5)	(0.1,0.15,0.35,0.4)
6	Intermediate values	(5,11/2,13/2,7)	(0.01,0.155,0.175,0.3)
8	Intermediate values	(7,15/2,17/2,9)	(0.05,0.085,0.185,0.2)

$$(x) = \begin{cases} \frac{x-l}{m-l} & l \leq x \leq m \\ 1 & m \leq x \leq n \\ \frac{u-x}{u-m} & m \leq x \leq u \\ 0 & x \neq [l,u] \end{cases} \quad (8)$$

In figure 8 is shown the triangular membership function.
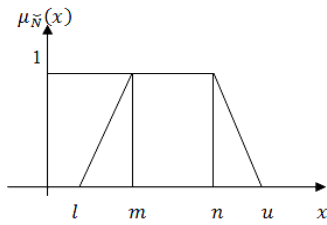
Figure. 8 TpFN membership function

Table 3 has converted the trapezoidal fuzzy numbers and the inverse of them with the Saaty scale.

In figure 9 are shown the trapezoidal fuzzy numbers with Saaty relative scale of importance.
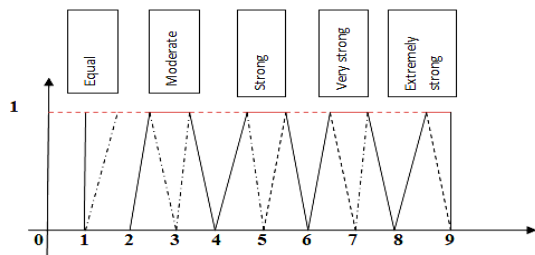
Figure 9: TpFN with relative importance of Saaty scale

The defuzzification was applied with the method of nearest weighted symmetry (NWS) for trapezoidal fuzzy numbers as described in Saneifard [56].

$$a_{ij} = \frac{l+2m+2n+u}{6} \quad (13)$$

The last step included the normalization and the ranking attributes given as:

$$N_i = \frac{a_{ij}}{\sum a_{ij}} \quad (14)$$

3.3. Data collections

In order to analyze the effectiveness and acceptance of Google Classroom, a questionnaire has been prepared based

The operational laws with trapezoidal fuzzy numbers:

a) $\tilde{N}_1 \oplus \tilde{N}_2 = (l_1, m_1, n_1, u_1) \oplus (l_2, m_2, n_2, u_2) = (l_1 + l_2, m_1 + m_2, n_1 + n_2, u_1 + u_2)$

b) $\tilde{N}_1 \otimes \tilde{N}_2 = (l_1, m_1, n_1, u_1) \otimes (l_2, m_2, n_2, u_2) = (l_1 l_2, m_1 m_2, n_1 n_2, u_1 u_2)$ (9)

c) $\tilde{N}^{-1} = (l, m, n, u)^{-1} = (\frac{1}{u}, \frac{1}{n}, \frac{1}{m}, \frac{1}{l})$

The decision matrix A was converted into the matrix $\check{A}$ as the fuzzy TpFN matrix [23]-[55]:

$$\check{A} = \begin{pmatrix} (1,1,1,1) & \cdots & (l_{1n}, m_{1n}, n_{1n}, u_{1n}) \\ \vdots & \ddots & \vdots \\ (l_{n1}, m_{n1}, n_{n1}, u_{n1}) & \cdots & (1,1,1,1) \end{pmatrix}$$

$$\check{a}_{ij} = (l_{ij}, m_{ij} n_{ij}, u_{ij}),$$

$$\check{a}_{ij}^{-1} = (\frac{1}{u_{ij}}, \frac{1}{n_{ij}}, \frac{1}{m_{ij}}, \frac{1}{l_{ij}}) \quad (10)$$

For each of the criteria were calculated the fuzzy geometric mean value:

$$\check{r}_i = \left(\prod_{i=1}^{n} \check{a}_{ij} \right)^{1/n} \quad (11)$$

The fuzzy weights were calculated as follow:

$$\tilde{\omega}_i = \check{r}_i \otimes (\check{r}_1 \oplus \check{r}_2 \oplus \ldots \oplus \check{r}_n)^{-1} \quad (12)$$

firstly from Jakkaew and Hemrungrote. Details of this questionnaire have been given in the Appendix A. The questionnaire has been completed by 528 students from 4 universities in Albania, one month after they started using this platform. In table 4 are described the frequency and percentage for answers of the questionnaire.

4. Results

4.1. Results for Criteria with FAHP –TFN

The hierarchical structure has been constructed based on the questionnaire, combining all the criteria and attributes to find the goal: the most important attributes for Google Classroom. In this study the universities were in the second level, and hence haven't

taken as criteria. The constructs C_1, C_2,…,C_8 have been the criteria, and the questions Q_1, …,Q_{26} have been the sub-criteria Each question has 5 alternatives ,shown in figure 2. The eight criteria have been compared with respect to the goal "the most important attributes for Google Classroom". The decision makers were a group of mathematicians which have evaluated the answers of the questionnaire, and constructed the pair-wise comparison matrix for levels of the hierarchy [22],[57]. The first construction was the pair-wise comparison matrix with triangular fuzzy numbers as follow in table nr 5.

This matrix has the Consistency Index 0.04778 < 0.1, and $CR = CI/RI = 0.034$, so were applied the equations (2)-(7). The results were obtained in table 6.

Based on the results for the most important construct from FAHP-TFN, it was the construct Behavioral Intention, than Social Influence, Hedonic Motivation, Use Behavior, Habit, Performance Expectancy, Facilitating Conditions and the last is Effort Expectancy. So for the students was more important to continue using Google Classroom in the future and to recommend

it for other students. Also the Social Influence have impacted their use of Google Classroom. The last preferred was Effort Expectancy, so they thought was easy to use Google Classroom, to learn to operate with it and the interaction was clear and understandable.

4.2. Results for the FAHP –TpFN Criteria.

After have been found the rank with TFN numbers for the criteria, was converted the decision matrix in table 5 into trapezoidal fuzzy numbers (see table 7).

The crisp numbers less than one were converted into trapezoidal fuzzy numbers with the use of the membership function of the generalized trapezoidal fuzzy number

$(\check{A}) = (a, b, c, d; w), (0 < w \leq 1), \mu_{(\check{A})}(x): R \to [0, w]$, which mapped the set of all fuzzy numbers to a set of real numbers by $R(\check{A}) = \frac{w}{2}((c + d) - (a + b))$ [58], [59]. The study used the trapezoidal fuzzy numbers for $w = 1$. The results that were obtained from equations (9) to (14), are summarized in table 8.

Table 4: Students gender, university and way of access for Google Classroom.

Item	Values	Frequency	Percentage
Gender	Male	192	36.4%
	Female	336	63.6%
University	Polytechnic University of Tirana	151	28.6%
	University of Tirana	130	24.6%
	University of Medicine	53	10.0%
	University of Durres	194	36.7%
Access Google Classroom	Android	192	36.4%
	Smartphone	189	35.8%
	Personal Computer	147	27.8%

Table 5: The pair-wise comparison matrix with TFN numbers for the 8 criteria

	C_1	C_2	C_3	C_4
C_1	(1,1,1)	(1,2,3)	(0.33,0.5,1)	(1,2,3)
C_2	(0.33,0.5,1)	(1,1,1)	(0.142,0.16,0.5)	(1,1,1)
C_3	(1,2,3)	(5,6,7)	(1,1,1)	(3,4,5)
C_4	(0.33,0.5,1)	(1,1,1)	(0.2,0.25,0.33)	(1,1,1)
C_5	(1,2,3)	(1,2,3)	(1,1,1)	(1,2,3)
C_6	(2,3,4)	(6,7,8)	(0.33,0.5,1)	(3,4,5)
C_7	(3,4,5)	(4,5,6)	(1,1,1)	(1,2,3)
C_8	(3,4,5)	(4,5,6)	(1,1,1)	(1,2,3)
	C_5	C_6	C_7	C_8
C_1	(0.33,0.5,1)	(0.25,0.33,0.5)	(0.2,0.25,0.33)	(0.2,0.25,0.33)
C_2	(0.33,0.5,1)	(0.12,0.14,0.16)	(0.16,0.2,0.25)	(0.16,0.2,0.55)
C_3	(1,1,1)	(1,2,3)	(1,1,1)	(1,1,1)
C_4	(0.25,0.33,0.5)	(0.2,0.25,0.33)	(0.33,0.5,1)	(0.33,0.5,1)
C_5	(1,1,1)	(1,2,3)	(1,2,3)	(1,1,1)
C_6	(0.33,0.5,1)	(1,1,1)	(1,1,1)	(1,1,1)
C_7	(0.33,0.5,1)	(1,1,1)	(1,1,1)	(1,1,1)
C_8	(1,1,1)	(1,1,1)	(1,1,1)	(1,1,1)

Table 6: FAHP with TFN numbers for the criteria

	$\check{r}_i$	$\breve{\omega}_i$	COA	N_i	Rank
C_1	(0.426, 0.613, 0.914)	(0.036, 0.065, 0.125)	0.075	0.0538	6
C_2	(0.292, 0.35, 0.51)	(0.025, 0.037, 0.069)	0.043	0.03	8
C_3	(1.4, 1.76, 2.05)	(0.12, 0.188, 0.28)	0.196	0.14	2
C_4	(0.37, 0.47, 0.69)	(0.031, 0.05, 0.094)	0.058	0.0416	7
C_5	(1.09, 1.62, 2.05)	(0.093, 0.173, 0.28)	0.182	0.13	3
C_6	(1.18, 1.46,1.88)	(0.1, 0.156, 0.257)	0.171	0.122	5
C_7	(1.18, 1.45, 1.75)	(0.1, 0.155, 0.239)	0.494	0.354	1
C_8	(1.36, 1.58, 1.75)	(0.117, 0.169, 0.239)	0.175	0.125	4

Table 7: The pair-wise comparison matrix with TpFN numbers for the 8 criteria

	C_1	C_2	C_3	C_4
C_1	(1,1,1,1)	(1,1.5,2.5,3)	(0.2,0.3,0.7,0.8)	(1,1.5,2.5,3)
C_2	(0.2,0.3,0.7,0.8)	(1,1,1,1)	(0.01,0.155, 0.175,0.32)	(1,1,1,1)
C_3	(1,1.5,2.5,3)	(5,5.5,6.5,7)	(1,1,1,1)	(3,3.5,4.5,5)
C_4	(0.2,0.3,0.7,0.8)	(1,1,1,1)	(0.1,0.15,0.35,0.4)	(1,1,1,1)
C_5	(1,1.5,2.5,3)	(1,1.5,2.5,3)	(1,1,1,1)	(2,2.5,3.5,4)
C_6	(2,2.5,3.5,4)	(6,6.5,7.5,8)	(0.2,0.3,0.7, 0.8)	(3,3.5,4.5,5)
C_7	(3,3.5,4.5,5)	(4,4.5,5.5,6)	(1,1,1,1)	(1,1.5,2.5,3)
C_8	(3,3.5,4.5,5)	(4,4.5,5.5,6)	(1,1,1,1)	(1,1.5,2.5,3)

	C_5	C_6	C_7	C_8
C_1	(0.2,0.3,0.7,0.8)	(0.13,0.2,0.46,0.53)	(0.1,0.15,0.35,0.4)	(0.1,0.15,0.35,0.4)
C_2	(0.2,0.3,0.7,0.8)	(0.04,0.1,0.18,0.244)	(0.05,0.15,0.25,0.35)	(0.05,0.15,0.25,0.35)
C_3	(1,1,1,1)	(1,1.5,2.5,3)	(1,1,1,1)	(1,1,1,1)
C_4	(0.13,0.2,0.46,0.53)	(0.1,0.15,0.35,0.4)	(0.2,0.3,0.7,0.8)	(0.2,0.3,0.7,0.8)
C_5	(1,1,1,1)	(1,1.5,2.5,3)	(1,1.5,2.5,3)	(1,1,1,1)
C_6	(0.2,0.3,0.7,0.8)	(1,1,1,1)	(1,1,1,1)	(1,1,1,1)
C_7	(0.2,0.3,0.7,0.8)	(1,1,1,1)	(1,1,1,1)	(1,1,1,1)
C_8	(1,1,1,1)	(1,1,1,1)	(1,1,1,1)	(1,1,1,1)

Table 8: TpFN results for the criteria level.

	$\check{r}_i$	$\breve{\omega}_i$	NWS	N_i	Rank
C_1	(0.29,0.41,0.8,0.91)	(0.025,0.039,0.096,0.13)	0.07	0.067	6
C_2	(0.12,0.27,0.42,0.53)	(0.01,0.025,0.05,0.08)	0.04	0.038	8
C_3	(1.4,1.6,1.92,2.05)	(0.12,0.152,0.23,0.3)	0.2	0.19	1
C_4	(0.24,0.32,0.61,0.67)	(0.02,0.03,0.07,0.1)	0.053	0.05	7
C_5	(1.09,1.37,1.85,2.06)	(0.094,0.13,0.22,0.3)	0.18	0.17	2
C_6	(1.04,1.23,1.66,1.78)	(0.09,0.11,0.19,0.26)	0.158	0.152	5
C_7	(1.11,1.27,1.6,1.7)	(0.09,0.12,0.19,0.25)	0.16	0.154	4
C_8	(1.36,1.49,1.67,1.755)	(0.12,0.14,0.2,0.26)	0.17	0.16	3

Table 9: The ranked criteria with two types of fuzzy numbers.

Method	Rank of the criteria							
FAHP -TFN	C_7	C_3	C_5	C_8	C_6	C_1	C_4	C_2
FAHP-TpFN	C_3	C_5	C_8	C_7	C_6	C_1	C_4	C_2

Table 10: The IC, CR indexes for the matrixes of questions, third level:

	CI	CR
C_1=(Q_1, Q_2, Q_3, Q_4)	0.099	0.1
C_2=(Q_5, Q_6, Q_7, Q_8)	0.03	0.033
C_3=(Q_9, Q_{10}, Q_{11})	0.033	0.056
C_4=(Q_{12}, Q_{13}, Q_{14})	0.0035	0.006

$C_5=(Q_{15}, Q_{16}, Q_{17})$	0.051	0.088
$C_6=(Q_{18}, Q_{19}, Q_{20}, Q_{21})$	0.068	0.075
$C_7=(Q_{22}, Q_{23}, Q_{24})$	0.017	0.03
$C_8=(Q_{25}, Q_{26})$	0	0

Table 11: The ranked results for questions level

TFN	Q_{25}	Q_{12}	Q_9	Q_{15}	Q_5	Q_1	Q_{22}	Q_{18}	Q_{16}	Q_{10}	Q_2	Q_{26}	Q_7
	1	2	3	4	5	6	7	8	9	10	11	12	13
TpFN	Q_{25}	Q_{12}	Q_9	Q_{15}	Q_{22}	Q_1	Q_5	Q_{18}	Q_{16}	Q_{10}	Q_2	Q_{26}	Q_{23}
	1	2	3	4	5	6	7	8	9	10	11	12	13

Q_{14}	Q_{19}	Q_{23}	Q_{24}	Q_{21}	Q_6	Q_3	Q_{13}	Q_{20}	Q_8	Q_{11}	Q_{17}	Q_4
14	15	16	17	18	19	20	21	22	23	24	25	26
Q_{14}	Q_7	Q_{19}	Q_{21}	Q_6	Q_3	Q_{24}	Q_{13}	Q_{20}	Q_{11}	Q_{17}	Q_8	Q_4
14	15	16	17	18	19	20	21	22	23	24	25	26

The FAHP-TpFN method has shown that the most important criteria were C_3 and the last important was C_2. So Social Influence was the most preferred criteria, then Hedonic Motivation, use behavior, Behavioral Intention, Habit, Performance Expectancy, Facilitating Conditions, and the last Effort Expectancy. Social Influence construct has been evaluated as the most preferred criteria that included friends, peers or other people. They had a direct impact for the students in using Google Classroom. The second evaluated was Hedonic Motivation criteria concerning an enjoyable use for Google Classroom. The last was Effort Expectancy criteria, as an easy use of Google Classroom.

4.3. Comparison results for the criteria level

Referred to the results in table 6 and table 8, were summarized the ranking criteria with the triangular and trapezoidal fuzzy numbers in table 9. These results have shown that only criteria C_7 differs in rank between the two methods, all the others have the same rank. This was obtained due to the fact that the method of defuzzification in the two types of fuzzy numbers were not the same according their formulas. The results obtained from them give an important rank for the decision makers to judge the preferences of the Google

Classroom constructs in more detail. In general, the ranked criteria of the most important and the last important one was the same, only the rankings between them differed less.

4.4. Comparison results for questions level

Here have been applied FAHP TFN and FAHP TpFN for the third level of the hierarchy, formed with the 26 questions as alternatives for each of the criteria of the second level. For all of them have been constructed the pair-wise comparisons matrices. The consistency has been less than 0.1, otherwise the decision makers had to reevaluate the comparisons matrix. For the third level, named as the sub-criteria has been constructed the decision matrices. Every matrix of the criteria, has been evaluated for its consistency IC and the consistent ratio CR. If they were consistent

then becomes the application of FAHP. In Table 10 are shown the eight criteria with the sub-criteria, and their consistency value. For all the matrices the coefficients were less or equal to 0.1. So were applied the FAHP-TFN and FAHP-TpFN method. In table 11 are shown only the ranked results. The results after have been applied FAHP – TFN have shown that based on their importance with each other every Q_i had the following rank: Q_{25}, Q_{12}, Q_9, Q_{15}, Q_5, Q_1, Q_{22}, Q_{18}, Q_{16}, Q_{10}, Q_2, Q_{26}, Q_7, Q_{14}, Q_{19}, Q_{23}, Q_{24}, Q_{21}, Q_6, Q_3, Q_{13}, Q_{20}, Q_8, Q_{11}, Q_{17}, Q_4 . So the most important question between them was Q_{25} "I use Google Classroom for writing quizzes and submitting assignments behavior", and the last important was Q_4 "If I use Google Classroom, I will increase my chances of passing the course".

The results that have been applied FAHP – TpFN have shown that every Q_i had the following rank: Q_{25}, Q_{12}, Q_9, Q_{15}, Q_{22}, Q_1, Q_5, Q_{18}, Q_{16}, Q_{10}, Q_2, Q_{26}, Q_{23}, Q_{14}, Q_7, Q_{19}, Q_{21}, Q_6, Q_3, Q_{24}, Q_{13}, Q_{20}, Q_{11}, Q_{17}, Q_8, Q_4. So the most important question between them was Q_{25} and the last important was Q_4. Both methods have ranked the questions and was found that the most important and the last important from them are the same for the decision maker, but the ranking between them differs slightly.

The most important question was Q_{25} in the Use Behavior: "I use Google Classroom for writing quizzes and submitting assignments behavior", and the last important one was Q_4: "If I use Google Classroom, I will increase my chances of passing the course" part of the Performance Expectancy construct. It was known that FAHP with TpFN numbers was the generalization of FAHP with TFN numbers [60], also had a better rank according to the expert opinions. Also, based to the unified index for comparing fuzzy numbers TFN and TpFN [61], [60] was shown that the trapezoidal FAHP method is the most suitable one, as it provides the most accurate results when compared to other methods.

4.5. Comparison results for 5-likert scale level

For the 5-likert scale have been denoted the five points with A_1=Strongly disagree, A_2=Disagree, A_3=Neither agree nor disagree, A_4=Agree, A_5=Strongly agree. Also have been evaluated the fuzzy pair-wise comparison matrices of alternatives according to each of the sub-criteria, and then have been applied FAHP method with both types of fuzzy numbers. Tables 12 and 13 have shown the results of the FAHP method for both cases. According to the theory [23], [31] the total of results preferences was compared for each of them as shown in tables below, and the one that has the highest total was the most important.

Table 12: Results for alternative level with FAHP-TFN

	A_1	A_2	A_3	A_4	A_5
Total	1.0188	1.378	1.867	2.651	1.1027
Rank	5	3	2	1	4

Table 13: Results for alternative level with FAHP-TpFN

	A_1	A_2	A_3	A_4	A_5
Total	0.93937	1.3338	1.875	2.685	1.10274
Rank	5	3	2	1	4

The findings resulted that both methods gave the same ranking (see table 12, 13). It is obvious that the total for each A_i differed slightly with both types of fuzzy numbers. So the alternative that has been the most important and the most selected in the answers was A_4 "Agree", then A_3 "Neither agree nor disagree", then A_2 "Disagree", A_5 "Strongly agree", and lastly A_1 "Strongly disagree".

5. Conclusions

Nowadays due to the situation of COVID-19 pandemic the application of Google Classroom in online teaching played an important role in high education. The evaluations for the usage of Google Classroom have been done by using the questionnaire according to the UTAUT2 model. This study found out the ranked attributes for Google Classroom, from the most to the least preferred. Attributes were three types: criteria, sub-criteria and alternative, based on the hierarchy structure proposed by this paper. In order to make better decisions, have been applied the FAHP method with two types of fuzzy numbers: triangular fuzzy numbers and trapezoidal fuzzy numbers. FAHP could capture the vagueness of the judgments, by making the fuzzy weights more objective to the goal. Based on the results of FAHP-TFN the most preferred criteria or construct was BI (Behavioral Intention), the most preferred question was "I use Google Classroom for writing quizzes and submitting assignments behavior", and the most selected alternative was A_4 "Agree". For the results of FAHP-TpFN the most preferred criteria or construct was SI (Social Influence), the most preferred question was "I use Google Classroom for writing quizzes and submitting assignments behavior", and the most selected alternative was A_4 "Agree". There was a slight difference in the criteria level for the two methods. Trapezoidal fuzzy numbers were the generalization of the triangular fuzzy numbers and have often being used by decision makers for a better selection of the attributes. This study is expected to help the user to evaluate the use of Google Classroom, and also to help policy-makers when deciding to implement e-learning. Especially these study results orient better the direction of institutions of higher learning. For the future

research recommendation, this study will be more complete to consider even the private universities and some other public universities. Maybe this will make differences in the study results. It is thought to include the master degree students, age > 22, and lecturers/tutors to show other results. An important point will be the evaluation of the hierarchy structure of the problem with gaussian fuzzy numbers, in order to eliminate the case of zero weights in order to make an optimal decision.

References

[1] J.A. Kumar, B. Bervell, "Google Classroom for mobile learning in higher education: Modelling the initial perceptions of students," Education and Information Technologies, **24**(2), 1793-1817, 2019, doi:10.1007/s10639-018-09858-z.

[2] B. De, "Traditional Learning Vs. Online Learning - eLearning Industry," E ;Earning Industry, 2018.

[3] R.A.S. Al-Maroof, M. Al-Emran, "Students acceptance of google classroom: An exploratory study using PLS-SEM approach," International Journal of Emerging Technologies in Learning, 2018, doi:10.3991/ijet.v13i06.8275.

[4] D. Sulisworo, R. Ummah, M. Nursolikh, W. Rahardjo, "The analysis of the critical thinking skills between blended learning implementation: Google Classroom and Schoology," Universal Journal of Educational Research, **6**(1), 2020, doi:10.13189/ujer.2020.081504.

[5] S. Sukmawati, N. Nensia, "The Role of Google Classroom in ELT," International Journal for Educational and Vocational Studies, **1**(2), 142-145, 2019, doi:10.29103/ijevs.v1i2.1526.

[6] N. Friesen, "Report : Defining Blended Learning," Norm Friesen, August, 2012.

[7] A. Wijaya, Analysis of factors affecting the use of google classroom to support lectures, The 5th International Conference on Information Technology and Engineering Application, 2016.

[8] V. Venkatesh, M.G. Morris, G.B. Davis, F.D. Davis, "User acceptance of information technology: Toward a unified view," MIS Quarterly: Management Information Systems, 425-478, 2003, doi:10.2307/30036540.

[9] P. Jakkaew, S. Hemrungrote, The use of UTAUT2 model for understanding student perceptions using Google Classroom: A case study of Introduction to Information Technology course, 2017, doi:10.1109/ICDAMT.2017.7904962.

[10] J. Janossy, "Proposed Model for Evaluating C/LMS Faculty Usage in Higher Education Institutions," MBAA International, 2008.

[11] M. Limayem, S.G. Hirt, W. Chin, "Intention does not always Matter: The Contingent Role of Habit in IT Usage Behaviour.," in ECIS 2001 Proceedings, 56-64, 2001.

[12] M.Z. Islam, P.K.C. Low, I. Hasan, "Intention to use advanced mobile phone services (AMPS)," Management Decision, 2013, doi:10.1108/00251741311326590.

[13] V. Venkatesh, M. Morris, G. Davis, F. Davis, "TECHNOLOGY ACCEPTANCE MODEL - Research," MIS Quarterly, 2003.

[14] M. Jambulingam, "Behavioural intention to adopt mobile technology among tertiary students," World Applied Sciences Journal, **22**(9), 1262-1271, 2013, doi:10.5829/idosi.wasj.2013.22.09.2748.

[15] L.Y. Leong, T.S. Hew, G.W.H. Tan, K.B. Ooi, "Predicting the determinants of the NFC-enabled mobile credit card acceptance: A neural networks approach," Expert Systems with Applications, 2013, doi:10.1016/j.eswa.2013.04.018.

[16] F.D. Davis, "User acceptance of information technology: system characteristics, user perceptions and behavioral impacts," International Journal of Man-Machine Studies, 1993, doi:10.1006/imms.1993.1022.

[17] H.C. Triandis, "Theoretical framework for evaluation of cross-cultural training effectiveness," International Journal of Intercultural Relations, 1977, doi:10.1016/0147-1767(77)90030-X.

[18] M.M. Hull, The Irish interlude: German intelligence in Ireland, 1939-1943, Journal of Military History, 2002, doi:10.2307/3093356.

[19] P.E. Oliver, G. Marwell, "The Paradox of Group Size in Collective Action: A Theory of the Critical Mass. II.," American Sociological Review, 1988, doi:10.2307/2095728.

[20] V. Venkatesh, J.Y.L. Thong, X. Xu, "Consumer acceptance and use of information technology: Extending the unified theory of acceptance and use of technology," MIS Quarterly: Management Information Systems, 2012, doi:10.2307/41410412.

[21] T.L. Saaty, The analytical hierarchy process, planning, priority, 1980.

[22] T.L. Saaty, "There is no mathematical validity for using fuzzy number

crunching in the analytic hierarchy process," Journal of Systems Science and Systems Engineering, 2006, doi:10.1007/s11518-006-5021-7.

[23] D. Dubois, "The role of fuzzy sets in decision sciences: Old techniques and new directions," in Fuzzy Sets and Systems, 2011, doi:10.1016/j.fss.2011.06.003.

[24] S.J. Chen, S.M. Chen, "Fuzzy risk analysis based on similarity measures of generalized fuzzy numbers," IEEE Transactions on Fuzzy Systems, 2003, doi:10.1109/TFUZZ.2002.806316.

[25] T.L. Saaty, "Modeling unstructured decision problems - the theory of analytical hierarchies," Mathematics and Computers in Simulation, 1978, doi:10.1016/0378-4754(78)90064-2.

[26] T.L. Saaty, Group Decision Making and the AHP, 1989, doi:10.1007/978-3-642-50244-6_4.

[27] C.H. Cheng, K.L. Yang, C.L. Hwang, "Evaluating attack helicopters by AHP based on linguistic variable weight," European Journal of Operational Research, 1999, doi:10.1016/S0377-2217(98)00156-8.

[28] A.H.I. Lee, H.Y. Kang, C.F. Hsu, H.C. Hung, "A green supplier selection model for high-tech industry," Expert Systems with Applications, 2009, doi:10.1016/j.eswa.2008.11.052.

[29] P.J.M. van Laarhoven, W. Pedrycz, "A fuzzy extension of Saaty's priority theory," Fuzzy Sets and Systems, 1983, doi:10.1016/S0165-0114(83)80082-7.

[30] L.A. Zadeh, "Fuzzy sets," Information and Control, 1965, doi:10.1016/S0019-9958(65)90241-X.

[31] J.J. Buckley, "Fuzzy hierarchical analysis," Fuzzy Sets and Systems, 1985, doi:10.1016/0165-0114(85)90090-9.

[32] D.Y. Chang, "Applications of the extent analysis method on fuzzy AHP," European Journal of Operational Research, 1996, doi:10.1016/0377-2217(95)00300-2.

[33] Q.N. Naveed, N. Ahmad, "Critical success factors (CSFs) for cloud-based e-Learning," International Journal of Emerging Technologies in Learning, 2019, doi:10.3991/ijet.v14i01.9170.

[34] Y.A. Turker, K. Baynal, T. Turker, "The evaluation of learning management systems by using Fuzzy AHP, fuzzy topsis and an integrated method: A case study," Turkish Online Journal of Distance Education, 12(2), 179-185, 2019, doi:10.17718/tojde.557864.

[35] Yassine AFA, Amal BATTOU, Omar BAZ, "Learning Through Massive Open Online Courses Platforms Based on Fuzzy Analytic Hierarchy Process," International Journal of Smart Education and Urban Society, 9(1), 793-807, 2019, doi:10.4018/ijseus.2019070101.

[36] H. Turan, "Assessment factors affecting e-learning using fuzzy analytic hierarchy process and SWARA," International Journal of Engineering Education, 2018.

[37] R. Garg, D. Jain, "Fuzzy multi-attribute decision making evaluation of e-learning websites using FAHP, COPRAS, VIKOR, WDBA," Decision Science Letters, 2017, doi:10.5267/j.dsl.2017.2.003.

[38] A.H. Işık, M. İnce, T. Yiğit, "A Fuzzy AHP Approach to Select Learning Management System," International Journal of Computer Theory and Engineering, 2015, doi:10.7763/ijcte.2015.v7.1009.

[39] T.S. Lo, T.H. Chang, L.F. Shieh, Y.C. Chung, "Key factors for efficiently implementing customized e-learning system in the service industry," Journal of Systems Science and Systems Engineering, 20(3), 346-355, 2011, doi:10.1007/s11518-011-5173-y.

[40] E. Roghanian, M. Alipour, "A fuzzy model for achieving lean attributes for competitive advantages development using AHP-QFD-PROMETHEE," Journal of Industrial Engineering International, 10(3), 1-11, 2014, doi:10.1007/s40092-014-0068-4.

[41] E. Yadegaridehkordi, M.H. Nizam Bin Md Nasir, N. Fazmidar Binti Mohd Noor, L. Shuib, N. Badie, "Predicting the adoption of cloud-based technology using fuzzy analytic hierarchy process and structural equation modelling approaches," Applied Soft Computing Journal, 66, 77-89, 2018, doi:10.1016/j.asoc.2017.12.051.

[42] H.-L. Mu, Y.-C. Lee, "An Application of Fuzzy AHP and TOPSIS Methodology for Ranking the Factors Influencing FinTech Adoption Intention: A Comparative Study of China and Korea," Journal of Service Research and Studies, 6(2), 793-807, 2017, doi:10.18807/jsrs.2017.7.4.051.

[43] R. Nagpal, D. Mehrotra, P.K. Bhatia, "Usability evaluation of website using combined weighted method: fuzzy AHP and entropy approach," International Journal of Systems Assurance Engineering and Management, 2016, doi:10.1007/s13198-016-0462-y.

[44] S. Morteza, R. Hamidreza, S. Mojtaba, "Identifying and prioritizing effective factors in governmental and semi-governmental organizations' electronic readiness for accepting and utilizing teleworking by fuzzy AHP technique in Tabriz City-Iran," Life Science Journal, 2013.

[45] B.D. Rouyendegh, T.E. Erkan, "MBA Students' preference on: Online, formal and hybrid MBA programs," in Procedia - Social and Behavioral Sciences, 2011, doi:10.1016/j.sbspro.2011.11.141.

[46] S. Aydin, C. Kahraman, "Multiattribute supplier selection using fuzzy analytic hierarchy process," International Journal of Computational Intelligence Systems, 2010, doi:10.1080/18756891.2010.9727722.

[47] F. Herrera, L. Martínez, "A model based on linguistic 2-tuples for dealing with multigranular hierarchical linguistic contexts in multi-expert decision-making," IEEE Transactions on Systems, Man, and Cybernetics, Part B: Cybernetics, 2001, doi:10.1109/3477.915345.

[48] B. Arfi, "Fuzzy decision making in politics: A linguistic fuzzy-set approach (LFSA)," Political Analysis, 2005, doi:10.1093/pan/mpi002.

[49] Q.H. Do, J. Chen, H. Hsieh, "Trapezoidal Fuzzy AHP and Fuzzy Comprehensive Evaluation Approaches for Evaluating Academic Library Service," WSEAS TRANSACTIONS on COMPUTERS, 2015.

[50] I.J. Pérez, F.J. Cabrerizo, E. Herrera-Viedma, "Group decision making problems in a linguistic and dynamic context," Expert Systems with Applications, 6, 77-89, 2011, doi:10.1016/j.eswa.2010.07.092.

[51] T.L. Saaty, K. Peniwati, J.S. Shang, "The analytic hierarchy process and human resource allocation: Half the story," Mathematical and Computer Modelling, 2007, doi:10.1016/j.mcm.2007.03.010.

[52] M.B. Ayhan, "A Fuzzy Ahp Approach For Supplier Selection Problem: A Case Study In A Gearmotor Company," International Journal of Managing Value and Supply Chains, 2013, doi:10.5121/ijmvsc.2013.4302.

[53] R.P. Kusumawardani, M. Agintiara, "Application of Fuzzy AHP-TOPSIS Method for Decision Making in Human Resource Manager Selection Process," in Procedia Computer Science, 2015, doi:10.1016/j.procs.2015.12.173.

[54] M.G. Voskoglou, "Application of fuzzy numbers to assessment of human skills," International Journal of Fuzzy System Applications, 2017, doi:10.4018/IJFSA.2017070103.

[55] G. Nirmala, G. Uthra, "Selecting best plastic recycling method using trapezoidal linguistic fuzzy preference relation," International Journal of Civil Engineering and Technology, 2017.

[56] R. Saneifard, "Defuzzification Method for Solving Fuzzy Linear Systems," Int. J. Industrial Mathematics, 2009.

[57] J.J. Buckley, T. Feuring, Y. Hayashi, "Fuzzy hierarchical analysis revisited," European Journal of Operational Research, 2001, doi:10.1016/S0377-2217(99)00405-1.

[58] T. Allahviranloo, S. Abbasbandy, R. Saneifard, "A method for ranking of fuzzy numbers using new weighted distance," Mathematical and Computational Applications, 2011, doi:10.3390/mca16020359.

[59] S. Banerjee, T.K. Roy, "Arithmetic Operations on Generalized Trapezoidal Fuzzy Number and its Applications," TJFS: Turkish Journal of Fuzzy Systems An Official Journal of Turkish Fuzzy Systems Association, 2012.

[60] R. Rodcha, N. K. Tripathi, R. Prasad Shrestha, "Comparison of Cash Crop Suitability Assessment Using Parametric, AHP, and FAHP Methods," Land, 2019, doi:10.3390/land8050079.

[61] T.L. Nguyen, Methods in ranking fuzzy numbers: A unified index and comparative reviews, Complexity, 12(2), 1793-1817, 2017, doi:10.1155/2017/3083745.

Appendix

A. Here we present the full questionnaire developed by the authors Venkatesh V. et al (2003), Jakkaew P., Hemrungrote S. (2017) completed by 528 students from 4 universities of Albania.

Questionnaire/Items	Source
Performance Expectancy (PE)	
1. I find Google Classroom useful in this course of math (PE1)	(Jakkaew P, Hemrungrote S)
2. Using Google Classroom enables me to achieve course related tasks more quickly (downloading notes, assignment submission,etc.) (PE2)	(Jakkaew P, Hemrungrote S)
3. Using Google Classroom increases my learning productivity (PE3)	(Jakkaew P, Hemrungrote S)
4. If I use Google Classroom, I will increase my chances of passing the course (PE4)	(Jakkaew P, Hemrungrote S)
Effort Expectancy (EE)	
1. It is easy for me to become skilful at using Google Classroom (EE1)	(Venkatesh et al 2003)
2. I find Google Classroom easy to use (EE2)	(Al-Maroof RAS, Al-Emran M)
3. Learning to operate Google Classroom is easy for me (EE3)	(Venkatesh et al 2003)
4. My interaction with Google Classroom is clear and understandable. (EE4)	(Venkatesh et al 2003)
Social Influence (SI)	
1. My friends who are important to me think that I should participate in Google Classroom (SI1)	(Jakkaew P, Hemrungrote S)
2. My peers who influence my behavior think that I should use Google Classroom(SI2)	(Jakkaew P, Hemrungrote S)
3.Other people whose opinions I value prefer that I use Google Classroom (SI3)	(Jakkaew P, Hemrungrote S)
Facilitating Conditions (FC)	
1.I have the resources necessary to participate in Google Classroom (internet smartphone etc) (FC1)	(Jakkaew P, Hemrungrote S)
2. I have the knowledge necessary to participate in Google Classroom (FC2)	(Jakkaew P, Hemrungrote S)
3. I can get help from others when I have difficulties while using Google Classroom (FC3)	(Jakkaew P, Hemrungrote S)
Hedonic Motivation (HM)	
1.Using Google Classroom is fun, compared to traditional classroom. (HM1)	(Jakkaew P, Hemrungrote S)
2. Using Google Classroom is enjoyable, compared to traditional classroom (HM2)	(Jakkaew P, Hemrungrote S)
3. Using Google Classroom is entertaining, compared to traditional classroom (HM3)	(Jakkaew P, Hemrungrote S)
Habit (HT)	
1. Using Google Classroom has become a habit for me (HT1)	(Jakkaew P, Hemrungrote S)
2. Using Google Classroom has become natural to me (HT2)	(Jakkaew P, Hemrungrote S)
3. Using Google Classroom is addictive (HT3)	(Jakkaew P, Hemrungrote S)
4. I feel that I must use Google Classroom (HT4)	(Jakkaew P, Hemrungrote S)
Behavioral Intention (BI)	
1. I intend to continue using Google Classroom in the future (BI1)	(Jakkaew P, Hemrungrote S)
2. It is worth to recommend the Google Classroom for other students (BI2)	(Al-Maroof RAS, Al-Emran M)
3. I plan to continue to use Google Classroom frequently (BI3)	(Jakkaew P, Hemrungrote S)
Use Behaviour (UB)	
1. I use Google Classroom for writing quizzes and submitting assignments behaviour (UB1)	(Kumar JA, Bervell B)
2. I use Google Classroom to interact with online materials, peers and instructor (UB2)	(Kumar JA,Bervell B)

Optimizing the Wind Farm Layout for Minimizing the Wake Losses

Abdelouahad Bellat*, Khalifa Mansouri, Abdelhadi Raihani, Khalili Tajeddine

SSDIA Laboratory, Hassan II University of Casablanca, ENSET of Mohammedia, 28830, Morocco

A R T I C L E I N F O	A B S T R A C T
	The development of wind farms requires an optimal design of wind turbines layout. The main goal of this optimization is to minimize the wake effect through the optimal placement of the wind turbines. The current study aims to standardize the wake losses among all wind turbines in the wind farm and bringing their losses to a similar level. An objective function was developed for this purpose, and used by the genetic algorithm to maximize the farm energy output and prevent the wake concentration on specific wind turbines. The proposed method has been applied to the Gasiri Wind farm through a simulation approach. The applied optimization process has shown very promising results characterized by a 17% possible energy gain after the adoption of the optimized layout. The study has also shown that the new positions of wind turbines characterized by a high rated power, are more on a forward position following the wind direction compared to the original ones. The study has also shown that there is a significant reduction of mechanical fatigue on the wind turbines blades.

1. Introduction

Increasingly growing efforts have been deployed in recent years to increase the share of clean energy production worldwide. This unprecedented interest in sustainable energy production derives from a serious ambition to prevent environment degradation and provide the much-needed equilibrium with the depletion of traditional energy resources. serious ambition to prevent environmental degradation and provide the necessary balance with the depletion of traditional energy resources. Wind power in particular is today considered one of the green sources in development in the world today. Governments across the globe are according more and more interest to the wind energy, exploiting recent industrial advances. The statistics given by the Wind Power Association clearly show that [1], wind farms represent 63% of European investments in renewable energies in recent years. These investments represent large-scale wind power harnessing farms requiring large sites and hundreds of wind turbines. Therefore, the optimization of wind farms is key component for an efficient exploitation of wind energy.

The objective of the proposed optimization in this paper is the maximization of energy and the reduction of energy losses. In order to achieve this goal, we propose to reduce the wake effects since they significantly contribute to the recorded energy losses [2]. In fact, when crossing the rotors blades of a wind turbine, a certain amount of energy is lost, wind speed decreases behind the turbines, this phenomenon reduces the yields of downstream wind turbines [3]. Indeed, the quality of the energy production produced by the wind farm is generally affected by several factors which contribute to significant energy losses [4]. Efficient wind farms design and development remains the best strategy to minimize these energy losses [5]. The main objective of our work is to establish an algorithm capable of reducing and standardizing the wake effect through all the turbines of the studied wind farm. Numerous articles have addressed this optimization problem using different types of algorithms such as genetic algorithms [6], [7], evolutionary algorithms [8], and the particle swarm optimization algorithm [9].

Generally, the computational domains for modeling wind farms are classified into two main categories, discrete representations using a grid which contains the coordinates and continuous representations with degrees of freedom greater than the discrete representation[10]. The continuous representation is highly beneficial because the wind turbines can be installed freely on the wind farm according to the 2D coordinates [11], [12]. In this case study, the genetic algorithm was chosen because of the binary coding method used.

*Corresponding Author: Abdelouahad Bellat, Hassan II University of Casablanca, ENSET of Mohammedia,212667969291 & Email: bellatabdelouahad@gmail.com

Many research works have studied the optimized layout of wind farms using genetic algorithms, such as the work carried out in [13], [14]. However, most of these studies use the energy or cost as optimization objective. In some cases, we combine the two optimization criteria cost and energy, other studies developed by the authors in [15] have also made an optimization of the layout taking into account the effects of the consolidation of nearby offshore wind farms, which have been very developed recently. In [16], authors propose an optimization layout aiming to reduce the cost of arranging substations and cables in the offshore wind farm by exploiting an objective function that uses the level production cost. In [17], authors are used a multi-objective optimization of the layout in order to satisfy several design objectives.

The main interest of a wind farm optimization is the maximization of the energy. However, in the case of a small size land, some wind turbines can be significantly affected by the wake effect compared to other wind turbines, resulting in increased turbulence, and consequently fatigue of the wind turbine blades and reduced energy produced by the wind farm[18]. In order to address these problems an objective function has been established, aiming to maximize energy and avoid the influence of wake effect on specific wind turbines.

In this paper, we will start with the modeling of the wind farm and the used wake model, the following parts will present the objective function and the optimization algorithm applied to the Gasiri wind farm, finally a discussion of the results and conclusion are proposed.

2. Wind Farm Modeling

2.1. Wake modeling

The speed of the wind crossing the upstream Wind turbines (WT) is modified by the wake effect phenomenon. The manifestation of growing effects is marked by a reduction in wind speed and a maximization of turbulence in the windiest region. Indeed, the wind turbines placed in the wake zone generate a minimum of energy and more maintenance activities compared to upstream WT. Therefore, wake effect modeling can play à key role in determining the placement of WT. It also should be seriously considered during Wind farm design layout optimization (WFDLO).
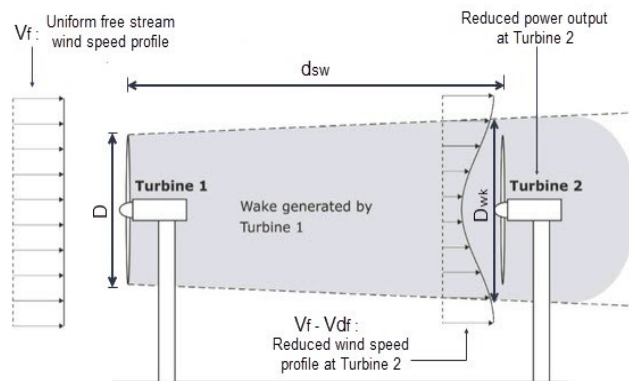
Figure 1: Jensen wake model [19]

Indeed, different wake models have been used to show the properties of wind speed losses [20], [21]. There are two main categories: analytical wake models and computer wake models which are at the origin of the resolution of the Navier-Stokes equation and which are more precise compared to other models. They require however more computation and higher cost which makes their use in WFDLO impossible [22]. Alternatively, the analytical wind speed solution is the basis of analytical wake models, they are widely used in optimization methods, often for large WFs with a large number of WTs [23], [24]. The most used wake model is Jensen's with a linear expansion of the wake as an assumption [25]. Figure 1 describes the principle of the model developed by Jensen. The high efficiency of these models results from the power losses reliability and prediction with reasonable accuracy compared to other models as shown in [25]. Therefore, in this study, we adopt the Jensen model to calculate different wind speeds. So, the speed deficit is expressed as follows:

$$V_{df} = V_f \left[\left(1 - \sqrt{1 - C_T}\right) \left(\frac{D}{D_{wake}}\right)^2 \right] \tag{1}$$

where,

D: Rotor Diameter (m)

D_{wake}: Wake diameter (m)

C_T: Trust coefficient

V_f: Free incoming wind speed (m/s)

V_{df}: Wind velocity deficit (m/s)

The Wake diameter varies depending on rotor diameter and wake minimization coefficient, considered as constant throughout the whole study, the calculation of this coefficient is detailed in[26], [27].

2.2. Modeling of Energy Production

The estimation of energy production under the wake effect requires the calculation of the power of each wind turbine. Different expressions are commonly used to estimate the power of WT were carried out in [28]. Thus, the energy production of WT is calculated approximately as follows:

$$P_{WT} = \frac{1}{2} \rho \pi \frac{D^2}{4} C_{EF} (V_f - V_{df})^3 \tag{2}$$

where,

C_{EF} represents the efficiency factor expressed by:

$$C_{EF} = C_p \eta_m \eta_g \tag{3}$$

In this study, the C_{EF} is assumed to be 40%. The total power produced by wind turbines operating under the wake effect is:

$$P_{WF} = \sum_{i=1}^{N_t} P_{WT} \tag{4}$$

The efficiency of the wind farm is expressed by the following equation:

$$\eta_{WF} = \frac{P_{WF}}{(\frac{1}{2}\rho\pi\frac{D^2}{4}C_{EF}V_f{}^3)} \qquad (5)$$

In order to facilitate the optimization of the studied wind farm, the positions of the wind turbines are designated by the Cartesian coordinates (x,y), the distances between the turbines and the calculation of the total wind speed deficit considering the overlapping zones are detailed. In [29][18], the total velocity deficit expression is expressed by:

$$V_{dft} = \sqrt{\sum_{i=1}^{N_{up}}\left(\frac{A_{OV}}{A}\right)(V_{df})^2} \qquad (6)$$

where, A_{OV} is the Overlap area (m^2), A represents the Swept area of wind turbines (m^2) and N_{up} is the number of upstream wind turbines.

3. Methodology

3.1. Objective function

The main objective is to increase the wind farm output in terms of power and to standardize the wake losses for each wind turbine in the wind farm.

Indeed, some turbines of a wind farm are exposed to more wake effects than others, so they tend to have more problems during operation with a reduced lifespan. The objective function proposed below maximizes the energy production of WF and reduces the standard deviation of wake losses to which wind turbines are exposed.

The objective function denoted FOBJ is obtained as follows:

$$FOBJ = \max\left(\frac{P_{WF}}{1-\sqrt{\frac{1}{N_t}\sum_{i=1}^{N_t}(W_a-W_i)^2}}\right) \qquad (7)$$

Where W_a is the Mean wake loss, W_i means the Wake loss of each turbine and N_t is the number of wind turbines on the wind farm.

3.2. Optimization Algorithm

Due to the optimization difficulties, the wind farm design, and the limits of the approach to test errors and deterministic methods, the heuristic methods are chosen, being the most appropriate to solve this type of design problems. Besides, in the presented work we choose to use genetic algorithms to optimize the wind farm.

The choice to use genetic algorithms is due to the fact that these algorithms are considered to be:

- A flexible method to use and configure.
- Efficient in its ability to overcome the difficulty of local optima while exploring the design research space to converge towards the global optimum.

The flowchart of Figure 2 shows the optimization steps adopted to optimize a wind farm. In the MATLAB © software, we

entered the data and models established in the previous part, the optimization process begins to search for an optimal solution. GA research techniques include the following main steps:

- *Step 1*: Random population generation of some turbines while respecting the constraints of the problem treated.

- *Step 2*: Evaluation of objective function WF layouts through the objective function.

- *Step 3*: Contribution to the next generation population by the selection of individuals. The probability of selection in the current generation results in a selection of good individuals. The objective of the crossover operator is to alter two pairs of genes (position) in order to generate another optimization as being a crossover function, the modification of a gene in another position is managed by random activation of the mutation with a determined probability.

- *Step 4*: production of a new location of the wind turbines in the park by the genetic algorithm (GA) which changes the previous population. The above steps are iterated until the maximum number of iterations is reached. The data parameters of our algorithm are shown in Table 1.

Table 1: Defined parameters of genetic algorithm

GA Parameter	Value
Size of initial population	150
Selection pressure	3
Crossover probability	0.25
Mutation Probability	0.75
Iteration number	350

Table 2 contains basic features of the wind turbine (HS50, U50, HJWT77) used in the Gasiri wind farm.

Table 2: Basic information of three types WTs

Wind turbines features	HS50	U50	HJWT77
Rated power (kW)	750	750	1500
Hub height (m)	50	50	70
Rotor diameter (m)	50	50	77
Cut-in wind speed (m/s)	3.5	3	3.5
Rated wind speed (m/s)	12	12.5	13
Cut-out wind speed (m/s)	25	25	25

It is mandatory to initialize the proposed algorithm by information on the characteristics of the wind farm and the model chosen for the present study. Table 3 summarizes the data needed to successfully kickstart the genetic algorithm.

3.1. Case Study: Gasiri Wind Farm

In this part, the study focuses on optimizing the layout of wind turbines in the case of the Gasiri wind farm using the objective function described previously. The results obtained in this study will be compared with other results from the same wind farm [30].

Table 3: Input data for the genetic algorithm

Site characteristics	Matrix of design variables	Models
Wind speed and direction	Configuration	Wake model
Wf size	Limit distance between	Power model
Roughness	WT design variables	WT design variables

Gasiri wind farm is located in South Korea, precisely on Jeju Island; the distribution of the wind turbines and the wind rose are depicted in Figure 3. The Gasiri wind farm, contains 13 wind turbines of three types (HS50-750 kW, U50-750 kW, HJWT77-1500 kW). In figure 3, the wind turbines are placed in a grid following the NNW direction, this direction is considered to be the dominant direction of the wind on the Gasiri wind farm.
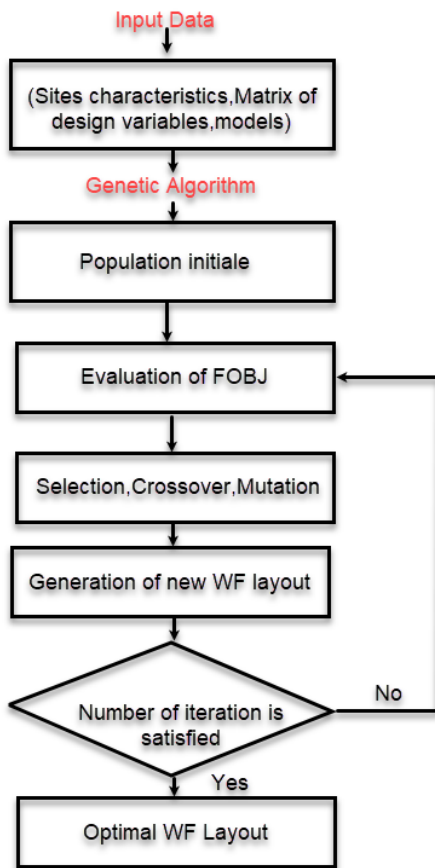
Figure 2: Genetic algorithm for WFDLO

The optimization of the wind farm requires a MATLAB code using the wind data, mentioned in Figure 3, Table 1, Table 2 and Table 3.

The calculation results of the annual AEP energy production are compared with the collected electricity production data in the Gasiri wind farm, as shown in Figure 4, there is a little difference between the real data and the calculated results but significantly more accurate than previous results obtained in the literature [30] using other types of algorithms. The difference is mainly due to the

choice of the used wake model and the actual operation of each wind turbine. Equally large 750 kW wind turbines are not taken into account in the calculation because they have a low recovery rate due to the data collected. Figure 5 summarizes the results collected and calculated.

The calculation of the annual production of the wind farm is based on the operating assumption of 365 days per year which is equal to 8760 hours.
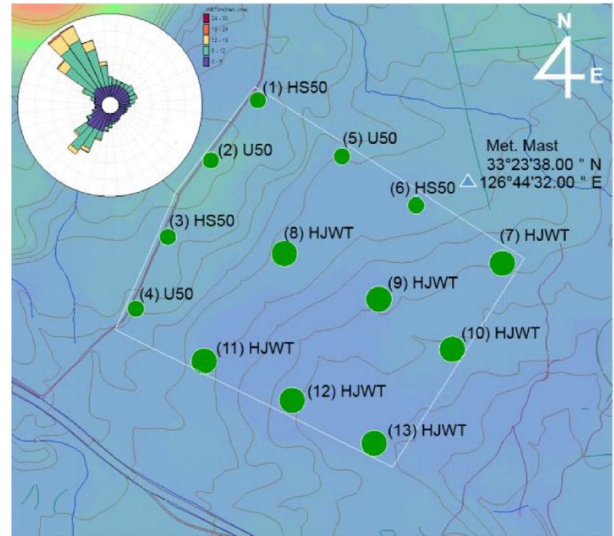
Figure 3: Arrangement of wind turbines and wind rose in the Gasiri wind farm [30]

The expression to calculate the annual production is expressed as follows:

$$AEP = 8760 \sum_{i=1}^{N_t} \sum_{j=1}^{N_d} \sum_{k=1}^{N_s} F(U_{ijk}) P(U_{ik}) \quad (8)$$

where $F(U_{ijk})$ is the probability of wind blowing in speed bin k of turbine i at direction sector j, $P(U_{ik})$ is the power of wind turbine i at wind speed bin k, and N_d and N_s represent the division by direction interval of total bearing and the value determined by dividing the range of speed (3-25 m/s) by the range of wind speed respectively.
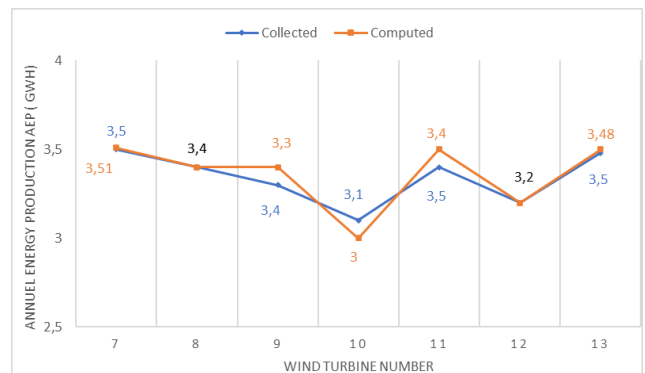
Figure 4: Comparison of the AEPs collected from Gasiri wind farm with the computed AEPs
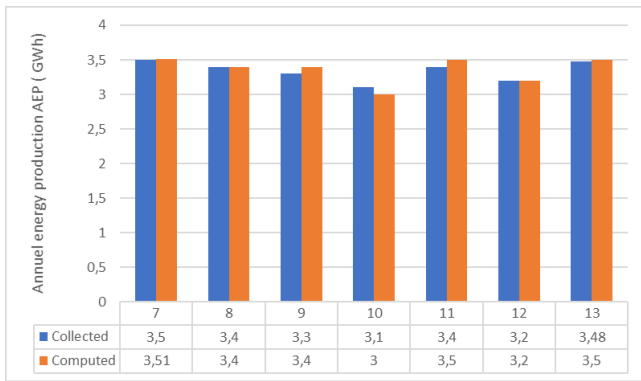
Figure 5: Difference in annual energy production between collected and computed energy

4. Results and Discussion

Figure 6 describes the variation of the objective function. We can clearly see that the total performance of the process of our algorithm improves and converges from 350 iterations. The objective function has a high value to be applied, because of the relative size of the value of the objective function which is not related to the accuracy of the optimal layout.

The difference in annual energy production between the collected energy data and the calculated energy is presented in Figure 5, the obtained results shows that the calculation of the sum of the annual production of wind turbines is equal to 23.51. Furthermore, in the case where the collected information on the production is equal to 23.48, this small difference of 0.03 is due to the simplifying assumptions and the uncertainties of the used wake model.
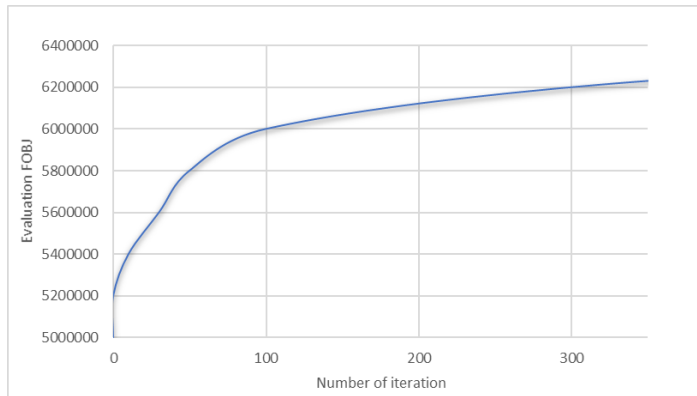
Figure 6: FOBJ evaluation using GA (genetic algorithm)

The calculation domain of our wind farm is delimited as mentioned in Figure 7. The spacing between the wind turbines is set at 230m in order to guarantee the minimum of 3 * D (rotor diameter). Therefore, to improve the free arrangement of wind turbines, the wind turbine location area has been divided into 120 * 110 cells having dimensions of 10m * 10m with respect for prohibited placement zones.

The optimization of the Gasiri wind farm is obtained using the algorithm in figure 8, then is compared by the position of the existing layout. Note that the HJWT77 type wind turbines which

have a high rated power value tend to move forward following the direction of the wind. This can also be explained by the fact that the loss of wakes becomes minimal in the forward positions as shown in Figure 8.
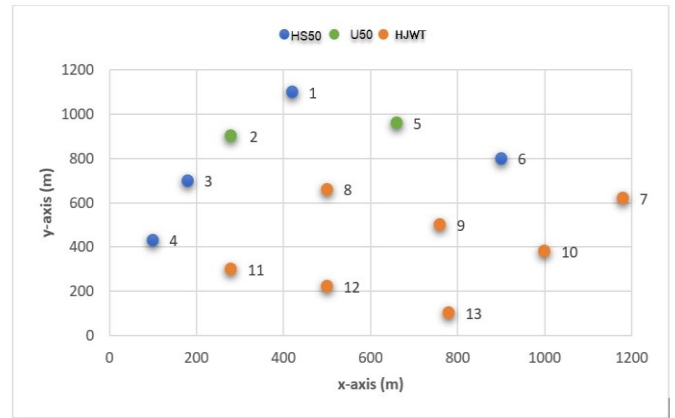
Figure 7: Coordinates of the wind turbines of the Gasiri wind farm
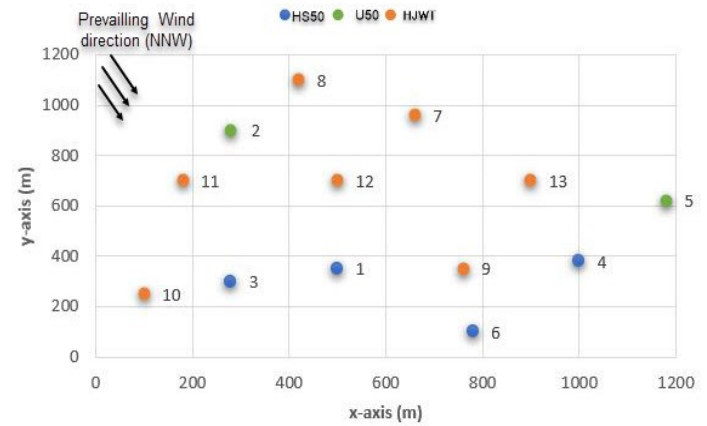
Figure 8: Gasiri wind farm layout optimization results obtained using objective function
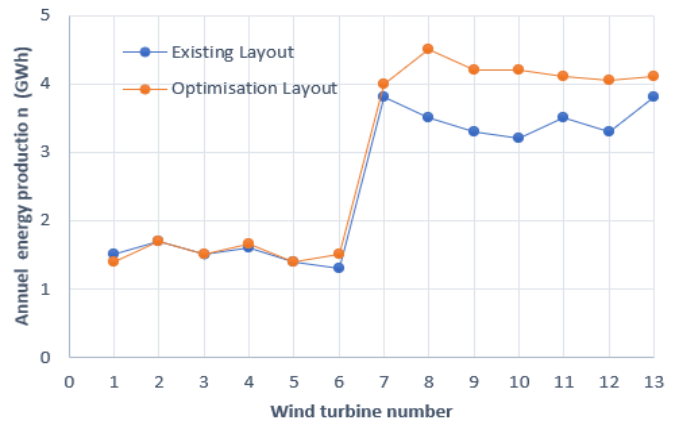
Figure 9: Annual energy production for existing layout and optimized layout obtained using objective function

It can be also seen that low-capacity wind turbines tend to move from their positions in the existing configuration and follow the direction of the prevailing wind in accordance with [30] who used the optimization with the simulated annealing algorithm but at levels of annual production the proposed optimization

technique is eventually much more accurate than [30]. The annual energy production of wind turbines 7, 8, 9, 10, 11, 12 and 13, has increased while turbine number 1 has decreased from the current state Figure 9.

This significant increase for the turbines mentioned above is mainly due to the new designated positions following the windiest direction. The net annual energy production is summarized in the Table 4, we can also observe that the difference in the net AEP of the wind farm in the optimized case is 5.68 which is greater than the case of the existing configuration.

However, this annual power increase, in the case of the Gasiri wind farm, shows that the used objective function has achieved the expected goals of minimizing the undesirable effects of wake for all wind turbines which are exposed to these losses and of maximizing the power of the wind farm.
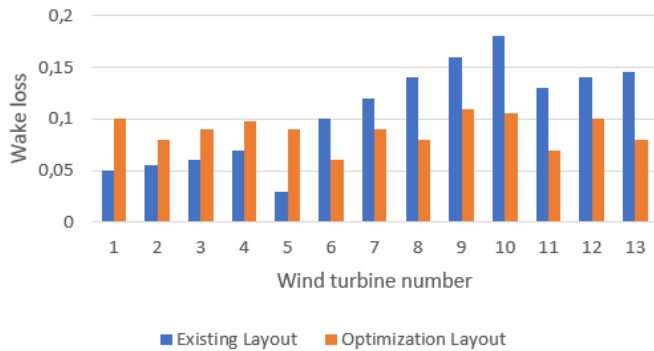
Figure 10: wake losses for the existing layout and the optimized layout

Figure 10, shows a comparison of wake losses between the existing layout and the optimized layout, we can clearly note that there is a significant reduction in wake loss for the optimized layout. This significant improvement justifies the benefice of using the proposed objective function in the genetic algorithm. Such choice leads to finding an optimal arrangement which maximizes the production of energy and standardizes the wake losses for all the wind turbines of the Gasiri wind farm.

Table 4: Comparison of annual energy production among existing layout and optimized layout

Wind Turbine number	Net AEP/Gross AEP	
	Existing layout	Optimized layout
1	1.45/1.52	1.41/1.60
2	1.59/1.69	1.73/1.8
3	1.47/1.56	1.51/1.58
4	1.54/1.58	1.66/1.75
5	1.42/1.55	1.41/1.56
6	1.38/1.54	1.52/1.65
7	3.72/4.15	4.05/4.85
8	3.50/4.06	4.51/5.10
9	3.35/4.00	4.23/5.00
10	3.33/4.00	4.28/4.85
11	3.48/4.00	4.14/4.88
12	3.34/3.88	4.05/4.50
13	3.35/3.91	4.10/4.73
Total	32.92/37.50	38.6/43.85
difference	(+)5.68	

By examining more in details, the results of Figure 11, we can see that the level of wake loss becomes more or less uniform in all the wind turbines, this prevents the difference in energy losses between the different wind turbines of the Gasiri wind farm.
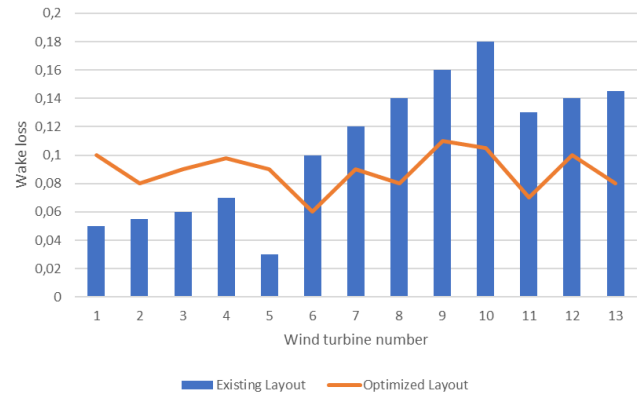
Figure 11: uniformity of wake losses for optimized layout

Moreover, such measures maximize the energy production. Table 5 presents a comparison of the wake losses between the existing layout and the optimized layout. It can be noticed that there is a significant reduction in the level of wake losses which is -18.67 %, this reduction is the result of the new optimized arrangement of the wind turbines which prevents the interference generated between the upstream and downstream turbines. Furthermore, we see a small difference between the wake loss results in the case of an optimized layout which indicates that the wake loss variable follows a uniform law.

Table 5: wake loss percentage values between the existing layout and the optimized layout

Wind turbine number	Wake loss (%)	
	Existing layout	Optimized layout
1	5.16	10.02
2	5.72	8.10
3	6.13	9.02
4	2.32	9.8
5	8.13	9.06
6	10.06	7.05
7	10.39	8.50
8	13.87	8.3
9	16.17	12.1
10	17.83	11.13
11	13.04	7.09
12	13.87	10.17
13	14.38	8.06
Total	137.07	118.4
Difference	(-)18.67	

5. Conclusion

In this article, a study of the optimization of a wind farm using a new approach is presented. An objective function was adopted trough the mean of a genetic algorithm in order to optimize the wind turbines layout. This method aims to maximize the energy

production and minimize the wake losses for all wind turbines in the wind farm. The presented method applied to the Gasiri wind farm has shown promising results, it didn't just minimize the wake losses but also uniformizes it among the wind turbines in the farm. The new layout shows that optimized positions of the wind turbines with higher rated power tend to slide forward with the wind direction. Moreover, the analysis of the simulation results in the current study indicates that the adoption of this optimized layout grants a 17% energy gain compared to the existing layout and ensure a considerable reduction in levels of wake losses estimated at -18%.

The layout optimization in this study was primarily based on a cost function targeting the minimization of wake losses. In future studies we aspire to study the correlation between the arrangement of wind turbines using a multi-objective function and the cost related to this optimization.

References

[1] (PDF) Wind energy in Europe in 2018, Jan. 2021.

[2] E. Hau, H. von Renouard, Windmills and Windwheels, Springer Berlin Heidelberg: 1–21, 2006, doi:10.1007/3-540-29284-5_1.

[3] J. Herbert-Acero, O. Probst, P.-E. Réthoré, G. Larsen, K. Castillo-Villar, "A Review of Methodological Approaches for the Design and Optimization of Wind Farms," Energies, **7**(11), 6930–7016, 2014, doi:10.3390/en7116930.

[4] S.H. Kim, H.K. Shin, Y.C. Joo, K.H. Kim, "A study of the wake effects on the wind characteristics and fatigue loads for the turbines in a wind farm," Renewable Energy, **74**, 536–543, 2015, doi:10.1016/j.renene.2014.08.054.

[5] J.F. Manwell, J.G. McGowan, A.L. Rogers, Wind Energy Explained, John Wiley & Sons, Ltd, Chichester, UK, 2009, doi:10.1002/9781119994367.

[6] L. Parada, C. Herrera, P. Flores, V. Parada, "Wind farm layout optimization using a Gaussian-based wake model," Renewable Energy, **107**, 531–541, 2017, doi:10.1016/j.renene.2017.02.017.

[7] M. Khanali, S. Ahmadzadegan, M. Omid, F. Keyhani Nasab, K.W. Chau, "Optimizing layout of wind farm turbines using genetic algorithms in Tehran province, Iran," International Journal of Energy and Environmental Engineering, **9**(4), 399–411, 2018, doi:10.1007/s40095-018-0280-x.

[8] Welcome to OATAO (Open Archive Toulouse Archive Ouverte) - oatao, Jan. 2021.

[9] P. Hou, W. Hu, C. Chen, M. Soltani, Z. Chen, "Optimization of offshore wind farm layout in restricted zones," Energy, **113**, 487–496, 2016, doi:10.1016/j.energy.2016.07.062.

[10] D. Guirguis, D.A. Romero, C.H. Amon, "Gradient-based multidisciplinary design of wind farms with continuous-variable formulations," Applied Energy, **197**, 279–291, 2017, doi:10.1016/j.apenergy.2017.04.030.

[11] J.Y.J. Kuo, D.A. Romero, C.H. Amon, "A mechanistic semi-empirical wake interaction model for wind farm layout optimization," Energy, **93**, 2157–2165, 2015, doi:10.1016/j.energy.2015.10.009.

[12] A. Emami, P. Noghreh, "New approach on optimization in placement of wind turbines within wind farm by genetic algorithms," Renewable Energy, **35**(7), 1559–1564, 2010, doi:10.1016/j.renene.2009.11.026.

[13] A. Mittal, L.K. Taylor, "Optimization of large wind farms using a genetic algorithm," in ASME International Mechanical Engineering Congress and Exposition, Proceedings (IMECE), 3159–3172, 2012, doi:10.1115/IMECE2012-87816.

[14] S.A. Grady, M.Y. Hussaini, M.M. Abdullah, "Placement of wind turbines using genetic algorithms," Renewable Energy, **30**(2), 259–270, 2005, doi:10.1016/j.renene.2004.05.007.

[15] J. Serrano González, M. Burgos Payán, J.M. Riquelme Santos, "Optimal design of neighbouring offshore wind farms: A co-evolutionary approach," Applied Energy, **209**, 140–152, 2018, doi:10.1016/j.apenergy.2017.10.120.

[16] P. Hou, W. Hu, M. Soltani, C. Chen, Z. Chen, "Combined optimization for offshore wind turbine micro siting," Applied Energy, **189**, 271–282, 2017, doi:10.1016/j.apenergy.2016.11.083.

[17] A.P.J. Stanley, A. Ning, "Massive simplification of the wind farm layout optimization problem," Wind Energy Science, **4**(4), 663–676, 2019, doi:10.5194/wes-4-663-2019.

[18] B. Abdelouahad, M. Khalifa, R. Abdelhadi, "Development of a multiple wake model based on rapid recovery factor in intense overlap case," International Journal of Advanced Trends in Computer Science and Engineering, **9**(1), 32–39, 2020, doi:10.30534/ijatcse/2020/0691.52020.

[19] N.O. Jensen, General rights A note on wind generator interaction, 1983.

[20] C.L. Archer, A. Vasel-Be-Hagh, C. Yan, S. Wu, Y. Pan, J.F. Brodie, A.E. Maguire, Review and evaluation of wake loss models for wind energy applications, Applied Energy, **226**, 1187–1207, 2018, doi:10.1016/j.apenergy.2018.05.085.

[21] T. Göçmen, P. Van Der Laan, P.E. Réthoré, A.P. Diaz, G.C. Larsen, S. Ott, Wind turbine wake models developed at the technical university of Denmark: A review, Renewable and Sustainable Energy Reviews, **60**, 752–769, 2016, doi:10.1016/j.rser.2016.01.113.

[22] N.A. Andersen, S.J. Sørensen, J.N. Shen, Analysis of turbulent wake behind a wind turbine, Lyngby, 2013.

[23] R. Shakoor, M.Y. Hassan, A. Raheem, Y.K. Wu, Wake effect modeling: A review of wind farm layout optimization using Jensen's model, Renewable and Sustainable Energy Reviews, **58**, 1048–1059, 2016, doi:10.1016/j.rser.2015.12.229.

[24] L. Wang, A.C.C. Tan, M. Cholette, Y. Gu, "Comparison of the effectiveness of analytical wake models for wind farm with constant and variable hub heights," Energy Conversion and Management, **124**, 189–202, 2016, doi:10.1016/j.enconman.2016.07.017.

[25] H. Sun, X. Gao, H. Yang, A review of full-scale wind-field measurements of the wind-turbine wake effect and a measurement of the wake-interaction effect, Renewable and Sustainable Energy Reviews, **132**, 110042, 2020, doi:10.1016/j.rser.2020.110042.

[26] S.A. MirHassani, A. Yarahmadi, "Wind farm layout optimization under uncertainty," Renewable Energy, **107**, 288–297, 2017, doi:10.1016/j.renene.2017.01.063.

[27] N. Charhouni, M. Sallaou, K. Mansouri, "Realistic wind farm design layout optimization with different wind turbines types," International Journal of Energy and Environmental Engineering, **10**(3), 307–318, 2019, doi:10.1007/s40095-019-0303-2.

[28] C. Carrillo, A.F. Obando Montaño, J. Cidrás, E. Díaz-Dorado, Review of power curve modelling for windturbines, Renewable and Sustainable Energy Reviews, **21**, 572–581, 2013, doi:10.1016/j.rser.2013.01.012.

[29] J. Feng, W.Z. Shen, "Wind farm layout optimization in complex terrain: A preliminary study on a Gaussian hill," in Journal of Physics: Conference Series, Institute of Physics Publishing, 2014, doi:10.1088/1742-6596/524/1/012146.

[30] K. Yang, G. Kwak, K. Cho, J. Huh, "Wind farm layout optimization for wake effect uniformity," Energy, **183**, 983–995, 2019, doi:10.1016/j.energy.2019.07.019.

Chaos-Based Image Encryption Using Arnold's Cat Map Confusion and Henon Map Diffusion

Anak Agung Putri Ratna[1,*], Frenzel Timothy Surya[1], Diyanatul Husna[1], I Ketut Eddy Purnama[2], Ingrid Nurtanio[3], Afif Nurul Hidayati[4], Mauridhi Hery Purnomo[2], Supeno Mardi Susiki Nugroho[2], Reza Fuad Rachmadi[2]

[1]Department of Computer Engineering, Universitas Indonesia, Depok, 16424, Indonesia

[2]Department of Computer Engineering, Institut Teknologi Sepuluh November, Surabaya, 60111, Indonesia

[3]Department of Informatics, Universitas Hasanuddin, Makassar, 90245, Indonesia

[4]Department of Dermatology and Venerology, Universitas Airlangga, Surabaya, 60115, Indonesia

A B S T R A C T

This research designed an image encryption system that focused on securing teledermatology data in the form of skin disease images. The encryption and decryption process of this system is done on the client side using chaos-based encryption with confusion and diffusion techniques. Arnold's cat map is the chaotic map model used for confusion, while the Henon map is used for diffusion. The initial values of both chaotic maps are obtained from a 30-digit secret key that is generated using Diffie–Hellman key exchange. During Arnold's cat map generation, different p and q values are used for every iteration. On the other side, the precision of the Henon map's x and y values is 10–14. From the tests that have been done, histograms of the encrypted images are relatively flat and distributed through all the gray values. Moreover, the encrypted images have average correlation coefficients of 0.003877 (horizontal), -0.00026 (vertical) and -0.00049 (diagonal) and an average entropy of 7.950304. According to the key sensitivity test, a difference of just one number in the secret key causes big differences, as both results have a similarity index of 0.005337 (0.5%). Meanwhile, in the decryption process, that small key difference cannot be used to restore the encrypted image to its original form and generate another chaotic image with average entropies of 7.964909333 (secret key difference) and 7.994861667 (private key difference).

1. Introduction

Today, most of the information on the Internet is in the form of images, which may contain confidential information, such as patients' medical records. In daily life, clinics or public health centers sometimes find it difficult to determine patients' disease, and they need the help of hospitals or more experienced medical experts for analysis and diagnosis. Therefore, images of patients' medical records must be sent from the clinic/public health center to the destination hospital. The problem is patients' medical records are confidential and contains sensitive data. There are also regulations and legal protection of medical records. For example, Indonesia's medical records regulation can be seen in [1]. So there has to be a way to maintain the security of patients' medical records, which can be done by performing image encryption [2].

Basically, image encryption is a technique that is performed with the aim of protecting the content conveyed therein. This encryption is done by transforming the image into another form so that it does not contain meaningful information and cannot be understood visually or statistically. In general, there are two types of image encryption: traditional encryption and chaos-based encryption. Traditional encryption uses common encryption algorithms, such as the Data Encryption Standard (DES), International Data Encryption Algorithm (IDEA), or Advanced Encryption Standard (AES). Chaos-based encryption uses a sequence of (pseudo-)random numbers called chaotic maps as a key for encrypting images. Of these two types, chaos-based encryption is more suitable for use with images because the image consists of information (i.e., image pixels) with high redundancy and correlation, and the resulting encrypted image will be random and have low correlation between pixels. In contrast, traditionally

encrypted images have more patterns, so they are more vulnerable to attack. In this study, two chaotic map models will be used: Arnold's cat map for confusion or shuffling pixel positions and the Henon map for diffusion or changing gray values [3, 4].

To generate a chaotic map, there are several parameters that can be described as the key to the encryption and decryption process in this system. The generated chaotic map is influenced by these values, so the encryption and decryption process must use exactly the same parameter values. The slightest change to this value will result in a different output matrix, so there must be a mechanism that ensures the encryption and decryption process uses the same parameter values. In [4], author use the shared-key cryptography with Diffie-Hellman method to secure the key exchange process [5].

2. Literature Review

Chaos-based image encryption, commonly known as a chaotic system, is an approach to encrypting an image that involves chaotic maps, which are rows of random numbers generated by a mathematical calculation with certain initial values. This system is widely used in image encryption for several reasons: (1) it sensitive to initial values, (2) the resulting numbers are random, and (3) there are no patterns in the random number sequence, so it is difficult to predict [3, 6].

In general, there are two techniques that can be performed with chaos-based image encryption: confusion and diffusion. [6] Confusion involves shuffling the pixel positions that make up an image, while diffusion involves changing pixels' gray values. In encryption, both techniques should be used; the use of just one can reduce the power of the encryption. In [7], the author used chaotic system, the chaotic map plays a major role in both the confusion and diffusion processes. One of the chaotic map models that can be used for confusion is Arnold's cat map (ACM), and one of the chaotic map models that can be used for diffusion is the Henon map, which is a mathematical model of the discrete-time dynamic system.

2.1. Arnold's Cat Map

ACM is a chaotic map model that is used to randomize the pixel positions in an image. It was first introduced by Vladimir Arnold as a way to shuffle an image of a cat. Mathematically, this concept works by stretching and distorting a square shape and then reassembling it into the same shape [8, 9].

Since it was introduced, ACM has been intended to randomize the pixel position of an image so that it does not look the same, which is a confusion technique. ACM works by scrambling a pixel's position without changing the value of the pixel itself. This can be done using the following formula [8,9]:

$$\begin{bmatrix} x_{n'} \\ y_{n'} \end{bmatrix} = A \begin{bmatrix} x_n \\ y_n \end{bmatrix} mod \ N \tag{1}$$

$$\begin{bmatrix} x_{n'} \\ y_{n'} \end{bmatrix} = \begin{bmatrix} 1 & p \\ q & pq+1 \end{bmatrix} \begin{bmatrix} x_n \\ y_n \end{bmatrix} mod \ N \tag{2}$$

Although ACM is a chaotic map, if iterations are repeated many times, it is possible that the original image will be rearranged because the ACM concept relies on position randomization only. According to researchers, up to 3N iterations may be needed to return to the original image, where N is the dimension of the image [10].

Arnold's cat map is commonly used for image encryption by shuffling the image pixels but actually it can be used to encrypt other form of multimedia data. In [11] and [12], there are good examples of audio encryption using Arnold's cat map for securing voice communication. Arnold's cat map can also be used to watermark an image or video, which is useful for tamper detection. In [13] and [14], there are some good examples of image watermarking, and [15] for video watermarking using Arnold's cat map.

2.2. Henon Map

The Henon map is one of the most commonly studied discrete-time dynamic system models, and it has chaotic properties. It was first introduced as a simplification of the Lorenz model. It is formed by using a point (x_n, y_n) to map the next point using the following equation [16].

$$x_{n+1} = 1 - \alpha \ x_n{}^2 + y_n \tag{3}$$

$$y_{n+1} = \beta \ x_n \tag{4}$$

In equations (3) and (4), x_n and y_n are the current point positions, while x_{n+1} and y_{n+1} are the next point positions. In the initial conditions, the values of x_n and y_n become initial values that will determine the next points. The slightest change in x_n and y_n in the initial conditions can have a big impact on the map that is formed [4, 17, 18].

The classic Henon map uses values of $\alpha = 1.4$ and $\beta = 0.3$, which causes the results to be chaotic. Changes in both values can result in changes in the nature of the resulting map, which may not even be chaotic anymore [17, 18].

In image encryption, the Henon map model is often applied as a key stream generator for diffusion techniques or changing pixel values in images. To create this chaotic map, two initial values are needed, namely, the initial x and y values (x_0 and y_0). These are the key to establishing chaotic maps that will be used in both encryption and decryption processes [4, 17, 18].

Chaotic maps are formed by calculating the Henon map formula with $m \times n \times$ bpc iterations ($m \times n$ represents the dimensions of the image, and bpc represents the number of bits in each pixel. For each iteration, a new x_n and y_n value is obtained and then converted to a bit value (0 or 1) using a threshold value which will later be converted to gray values for each pixel until the chaotic map is sized $m \times n$. In [18] Previous research [19] concluded that the cut-off value should be set at 0.3992 so that the sequence of numbers produced using the Henon map will be balanced. Thus, the decimal value x_n obtained at each iteration will be converted into binary form using a threshold value of 0.3992 based on the following equation:

$$Z_i \begin{cases} 0 \ if \ x_i \leq 0.3992 \\ 1 \ if \ x_i > 0.3992 \end{cases} \tag{5}$$

2.3. Diffie–Hellman Key Exchange

The Diffie–Hellman key exchange (DH) is a method created for safe key exchange through public channels. It addresses the challenges that exist in a symmetrical cryptographic system, which uses only one key for encryption and decryption. Without using this method, key exchanges on symmetric cryptographic systems are performed outside the system, generally conventionally, to avoid key exchanges via public channels such as the Internet. [20]

DH offers the possibility of using both public and private keys for actual key exchange. The two keys are not related to the encryption process that will be carried out, but only serve to produce the actual key. Each client has a private key that only they known. From this private key, a public key can be generated through equation (6) [5, 20]:

$$Public = g^{private} \bmod p \qquad (6)$$

where p is the prime value and g is the value of the agreed-upon generator. The resulting public key can be given to other people because it plays a role in creating a secret key for the two clients. To produce this secret key, the sender must perform a mathematical computation involving their private key and the recipient's public key using equation (7) [5, 20]:

$$Secret = public^{private} \bmod p \qquad (7)$$

Likewise, when the recipient engages in decryption, the recipient must compute their private key and sender's public key to produce a secret key that will be used in the encryption process. [20]

3. Proposed Model

In general, the system involves three parts: sender, receiver, and server. However, the implementation in this research only covers the client side; server settings have not been determined. The sending and receiving client side is where the Chaos-Based Image Encryption Program was run. The clinic/public health center, as the sending client, performs the encryption function, and the hospital, as the receiving client, performs the decryption function. The architecture of the whole system can be seen in Figure 1.
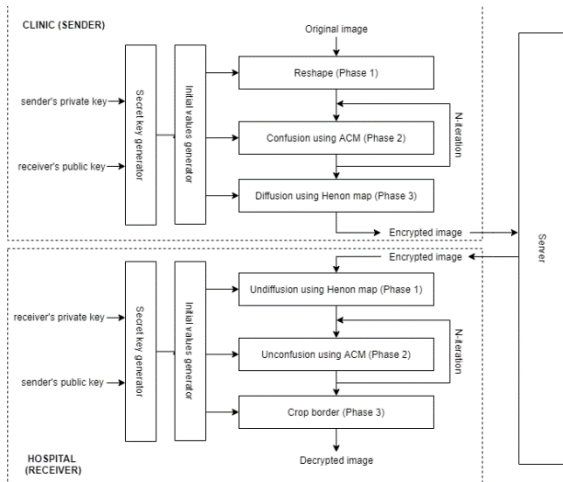
Figure 1: Encryption and decryption architecture

According to this architecture, in order to carry out encryption and decryption, two types of inputs are required: keys and images. Two keys—a private key and a public key—are needed to produce a secret key that will be converted into initial values when making the chaotic map. After the image is encrypted, the image will be saved to the server so that it can be retrieved by the receiver for decryption. There are three stages of encryption: reshaping, confusion, and diffusion. Likewise, there are three stages of decryption: undiffusion, unconfusion, and crop border.

This research uses chaos-based encryption with a combination of confusion and diffusion methods. The choice of chaos-based image encryption is based on the nature of the image, which

contains information (i.e., pixels) that have a high degree of redundancy and correlation with each other. By applying this type of encryption, the resulting image will be random, so it will have low redundancy and correlation between pixels. Another factor that reinforces the choice of chaos-based encryption is the nature of the chaotic maps we used, which are sensitive to changes in initial values or parameters. A slight change in the initial values will result in chaotic maps or rows of random numbers that have significant differences. This phenomenon is commonly referred to as the butterfly effect. Thus, this type of encryption is used to overcome statistical analysis attacks, which is more difficult with chaotic-based encryption results because of the randomness of the pixels making up the encrypted image [3, 21].

The combined use of confusion and diffusion is based on the nature of confusion, which shuffles pixels but does not change their values. This makes the image unrecognizable but still vulnerable to most attacks. Therefore, we used diffusion to change the pixel values of the randomized image. By using a combination of confusion and diffusion, the encryption results become more random and difficult to predict. In this encryption system, different chaotic maps are used for confusion and diffusion; Arnold's cat map is used for confusion, while the Henon map is used for diffusion. This is done to increase resistance to attacks because each method uses a different mathematical model. In addition, we chose them because they have many dimensions and are both two-dimensional chaotic maps [21].

The encryption system designed and developed in this research is based on several previous studies. Eko Hariyanto and Robbi Rahim previously explained the use of Arnold's cat map to encrypt images using the confusion technique in a study entitled "Arnold's Cat Map Algorithm in Digital Image Encryption." In [9], author explained how Henon maps could be used to encrypt images by applying a combination of confusion and diffusion in a study entitled "A Chaotic Confusion-Diffusion Image Encryption Based on Henon Map" [22]. In addition, the author described the use of Arnold's cat map and the Henon map to encrypt images in a study entitled "A Chaotic Cryptosystem for Images Based on Henon and Arnold Cat Map" [4].

In terms of the methods and algorithms used, the encryption method developed in [4] is the closest to the form of encryption developed in this research. The difference is that, in this research, the dimensions of the image are reshaped to form a square at the beginning of the encryption process so that the image can be processed as a whole. In previous studies, there was no such stage, so the input image had to be square or some information would be truncated. In addition, this study used initial values obtained through a set of secret keys produced by calculating the combination of the private and public keys with the DH algorithm. In previous studies, there was no generation of a secret key that was used as the initial values. Further, this study used different *p* and *q* variables in each iteration of Arnold's cat map following a set of numbers taken from the secret key (more details will be discussed in the next section).

3.1. Secret Key and Initial Value Generation

In this Chaos-Based Image Encryption System, several initial value parameters are needed for the encryption and decryption processes during both the confusion and diffusion stages. Therefore, in this design, a random sequence of numbers will be used as the initial value parameter. To decrypt the image perfectly, it is necessary to use the same initial value parameters that are used

during the encryption process, so the keys used for encryption and decryption must be the same. However, the use of the same key in the encryption and decryption process has a weakness: it is possible for the key to be obtained by a third party.

Therefore, to secure the key, this design uses the DH method to produce the key that will be used as the initial values in the encryption and decryption process. In this key exchange mechanism with the DH method, each client has a private key and a public key that are used to generate a secret key. A secret key is needed to perform encryption/decryption, so the secret key generation process must be carried out before running the encryption/decryption process.

After the secret key is obtained, numbers are broken into several parts to be used as initial values in the confusion and diffusion stages. Two initial values are needed for the Henon map: x and y. From this solution, the first 28 key numbers for the Henon map will be broken into 14 digits each. After that, the 14 numbers will be made into decimal fractions $0 < x < 1$. The larger decimal will be used as the value of x, and the smaller one will be used as the value of y. In ACM, three parameters are used, namely, p, q, and the number of iterations. The first half of the secret key is the value of p, and the last half is the value of q. The number of iterations is obtained from the sum of the last 6 digits of the secret key. In this design, the p and q values used in each ACM iteration will be different but still in accordance with the allocated value. For example, in the first iteration, the values 30 and 60 are used, then the second iteration uses the values 04 (or 4) and 03 (or 3), and so on. The illustration of initial value generation can be seen in Figure 2.

Figure 2: Illustration of initial value generation

3.2. Encryption Process

In this design, the image encryption mechanism consists of two main stages, namely, the preparation and manipulation of pixels. In the preparation stage, the image color model is converted to RGBA (red, green, blue, alpha), and the size or dimensions of the image are rectangular. For example, if the original image is 400 × 600, the image will be changed to 600 × 600. The gap between the initial size and the square size (referred to as the border) will be filled with new pixels that have an alpha value of 254, while the original pixel image has an alpha value of 255. Alpha is the channel in the RGBA color model that determines pixel transparency, with a value of 0 indicating transparency and a value of 255 indicating non-transparency. The newly added pixels are given a value of 254 in order to distinguish which pixels are the original pixels in the image and which ones are the border during the decryption process. The newly added pixels have randomly generated values with a range of 0–255. At the pixel manipulation stage, there are two phases: confusion and diffusion. In both

phases, several initial value parameters are used. The values for these parameters are obtained through the secret key, as was explained in the previous section.

3.2.1. Confusion Using Arnold's Cat Map

Confusion is the first pixel manipulation process performed using this image encryption system. Basically, the confusion process involves shuffling or randomizing the position of the pixels comprising the image so that it cannot be recognized anymore. In this design, ACM is used as a chaotic map model to determine the displacement of a pixel.

At the beginning of the formation of ACM, three parameters are needed, namely, p, q, and the number of iterations, which are all positive numbers. The values of the three parameters are obtained from the secret key constituent numbers, as explained in the previous section. The ACM formula is as follows:

$$\begin{bmatrix} x_{n'} \\ y_{n'} \end{bmatrix} = \begin{bmatrix} 1 & p \\ q & pq+1 \end{bmatrix} \begin{bmatrix} x_n \\ y_n \end{bmatrix} mod\ N \qquad (8)$$

where p and q are parameters and N is the size or dimensions of the image. Formula (8) produces a matrix containing $x_{n'}$ and $y_{n'}$, which is the new position. For each time this calculation is performed, the pixels in position (x_n, y_n) will be moved to $(x_{n'}, y_{n'})$. This calculation is carried out continuously until all pixels are shuffled. The displacement of pixel positions in the matrix can be performed more efficiently using the meshgrid, which is one of the functions of Python NumPy. First, the meshgrid will be made for x and y with a size of $N \times N$ to indicate the original position of the pixels in the image. Then, from the two meshgrids, two xmap and ymap matrices will be formed using formula (8), indicating the new pixel position. Thus, the pixel value at its original position (i.e., [x,y]) will be moved to a new position according to (xmap,ymap). This process will continue to be repeated as many times as the iteration parameter has been set. To ensure that the resulting matrix is more random and difficult to predict, in this design, the values of p and q will vary with each iteration by taking two numbers from the overall values of p and q obtained from the secret key.

3.2.2. Diffusion Using the Henon Map

The main concept of this diffusion process is to perform XOR operations on a matrix of image pixels generated by the confusion process with a chaotic map matrix. This system uses the Henon map as the chaotic map model.

At the beginning of the formation of the Henon map, two initial values are needed, namely x_n and y_n. Just like in the confusion stage, the two initial values are obtained from the secret key constituent numbers, as explained in the previous section. In this system, the values of x_n and y_n are between 0 and 1, with a precision level of 10^{-14}. This means that changes in values as small as 10^{-14} can affect the results of the diffusion. In addition to x_n and y_n, there are other parameters, namely, α and β. In this system, the values of $\alpha = 1.4$ and $\beta = 0.3$ are used so that the resulting Henon map is chaotic.

To create a chaotic map, a Henon map formula is calculated with an iteration of m × n × bpc times (m × n represents the dimensions of the image, and bpc is the number of bits in each pixel). For example, if the image to be processed is a 512 × 512 8 bpc image, then the iteration will be performed 512 × 512 × 8, or 262,144, times.

For each iteration, new x_n and y_n values (x_{n+1} and y_{n+1}) are obtained. From these results, the value of x_{n+1} will be converted to a bit value (0 or 1) using a threshold value of 0.3992 according to the results of [19]. In other words, if the value of x_{n+1} is greater than 0.3992, it will produce a value of 1, but if it is smaller or equal to 0.3992, it will produce a value of 0. Then, the bit will be inserted into the bit sequence. The x_{n+1} and y_{n+1} values generated in the current iteration will be x_n and y_n for the next iteration. At each bpc iteration of a certain multiple, the resulting bit sequence will be converted into a decimal form that will represent the gray value of a pixel. For example, in the 8 bpc image, the bit sequence will be changed to a decimal in the 8th, 16th and 24th iterations, and so on. After all the iterations are finished, a chaotic map will be produced with dimensions m × n.

After the chaotic map is formed, bitwise XOR operations will be performed between the image pixels generated by the confusion process with the chaotic map at the bit level. The results of the XOR operation are stored in a new matrix and become the results of the diffusion process. Diffusion is the last process carried out in this series of encryption processes, so the results are the result of this image encryption system.

3.3. Decryption Process

The flow of decryption is the opposite of encryption, which is divided into undiffusion, unconfusion, and crop border phases. The undiffusion and unconfusion processes involve manipulating image pixels that aim to return the encrypted image pixels to their original values and positions. In both phases, several initial value parameters are used. The values for these parameters are obtained through the secret key, as explained in the previous section. To decrypt the image into its original form, the initial value parameters used in the undiffusion and unconfusion processes must be the same as those used in the diffusion and confusion processes during encryption. Differences in values can cause the image to not be decrypted.

After going through the undiffusion and unconfusion phases, there is one more phase that must be completed, namely, the crop border process. In this phase, the original image has been seen, but the dimensions of the image are still not in accordance with the original due to changes in the image dimensions in the encryption process. Therefore, a crop border is performed to remove the pixels added during the encryption process so that the image returns to its original dimensions.

3.3.1. Undiffusion using the Henon Map

The undiffusion process is the opposite of the diffusion process performed at the time of encryption. If diffusion involves changing the value of the pixels that make up the image, the undiffusion process restores encrypted image pixels to their original values. The approach is the same as that carried out during the diffusion process: one makes chaotic maps and then performs a bitwise XOR operation. This can be done with an XOR operation because of its reversible characteristics. The only difference between the diffusion and undiffusion processes is the operand. During the diffusion process, an XOR operation is performed between the confusion matrix and the chaotic map, whereas in the undiffusion process, an XOR operation is performed between the encrypted matrix and the chaotic map. To restore encrypted image pixels to their original values, the chaotic map used in undiffusion must be the same as that used during the diffusion process. Chaotic map

mismatch will cause the pixel values to change from the original values, so the image will not be successfully decrypted.

The unconfusion process is the opposite of the confusion process during encryption. In the confusion process, the original image's pixel positions are randomized, so the pixel positions in the encrypted image are not the same as in the original image. As for the unconfusion process, the pixel positions in the encrypted image, which have been scrambled, will be returned to their original positions. The formula used for unconfusion is as follows:

$$\begin{bmatrix} x_n \\ y_n \end{bmatrix} = \begin{bmatrix} 1 & p \\ q & pq+1 \end{bmatrix} \begin{bmatrix} x_{n'} \\ y_{n'} \end{bmatrix} mod\ N \qquad (9)$$

By using formula (9), the original position of a pixel is obtained (x_n,y_n). Each time this calculation is performed, the value of a pixel at position ($x_{n'}$,$y_{n'}$) will be returned to its original position (x_n,y_n). The calculation is carried out continuously until all the pixels return to their original positions.

The displacement of pixel positions in the matrix can be performed more efficiently by using a meshgrid, as in the confusion process. First, a meshgrid for *x* and *y* of *N* × *N* size will be created to indicate the pixel position in the encrypted image. Then, from the two meshgrids, two xmap and ymap matrices will be created using formula (9), indicating the new pixel position. Thus, the pixel at the position of [xmap, ymap] will be moved to the position of [x, y]. This transfer is the reverse of that performed in the confusion process because the purpose of the unconfusion process is to return the pixels in the encrypted image to their original positions. This process will be repeated as many times as the number of iterations that has been set. The number of iterations carried out in the unconfusion process must correspond to the number of iterations performed during the confusion process. Mismatch in *p*, *q*, or the number of iterations will cause the pixels in the image to not return to their original positions. Just like in the confusion process, the *p* and *q* values in the unconfusion process change with each iteration, but inversely; the *p* and *q* values used in the last iteration in the confusion process will be the *p* and *q* values of the first iteration in unconfusion, and so on.

3.3.2. Unconfusion using Arnold's Cat Map

The unconfusion process is the opposite of the confusion process performed during encryption. In the confusion process, the original image's pixel positions are randomized, so the pixel positions in the encrypted image are not the same as in the original image. As for the unconfusion process, the pixel position in the encrypted image, which have been scrambled, will be returned to their original positions. The formula used in the unconfusion process is as follows:

$$\begin{bmatrix} x_n \\ y_n \end{bmatrix} = \begin{bmatrix} 1 & p \\ q & pq+1 \end{bmatrix} \begin{bmatrix} x_{n'} \\ y_{n'} \end{bmatrix} mod\ N \qquad (10)$$

By using formula (9), the original position of a pixel is obtained (x_n,y_n). Each time this calculation is performed, the value of a pixel at position ($x_{n'}$,$y_{n'}$) will be returned to its original position (x_n,y_n). This calculation is carried out continuously until all the pixels return to their original positions.

The displacement of pixel positions in the matrix can be performed more efficiently by using a meshgrid, as in the confusion process. First, a meshgrid for *x* and *y* of *N* × *N* size will be created to indicate the pixel position in the encrypted image. Then from the two meshgrids, two xmap and ymap matrices will

be created using formula (9), indicating the new pixel position. Thus, the pixel value at the position of [xmap, ymap] will be moved to the position of [x, y]. This transfer is the reverse of that performed in the confusion process because the purpose of the unconfusion process is to return the pixels in the encrypted image to their original positions. This process will be repeated as many times as the number of iterations that has been set. The number of iterations carried out in the unconfusion process must correspond to the number of iterations performed during the confusion process. Mismatch in p, q, or the number of iterations will cause the pixels in the image to not return to their original positions. Just like in the confusion process, the p and q values in the unconfusion process change with each iteration, but inversely; the p and q values used in the last iteration in the confusion process will be the p and q values of the first iteration in unconfusion, and so on.

4. Test and Analysis

4.1. Image Encryption Testing Using Confusion

In this test, encryption was performed on 30 images with only confusion, using ACM as the chaotic map. An example of the encryption result can be seen in Figure 3.

(a)   (b)
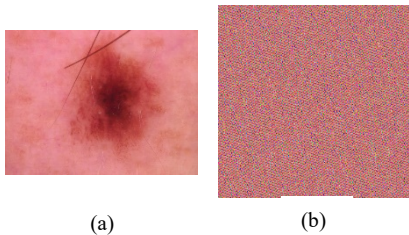
Figure 3: (a) Original image and (b) image encrypted using confusion

From the results of this test, we can see that the image does not show the characteristics of the original image because the pixel positions have been shuffled. However, the colors in the encrypted image are the same as the colors in the original image because no pixel values were changed during encryption; new pixels were only added to reshape the image into a square.

In terms of pixel distribution, the histogram generated from 30 encrypted images has the same pixel distribution trend as the original image's histogram. A comparison between the histograms of the original image and the encrypted image can be seen in Figure 4. Although the trends shown by the two images look similar, it should be noted that the number of pixels is different. In the original image, there are several pixels with a value of 0, whereas in encrypted images there are none. This happens because, during the encryption process, new pixels with random values are added to reshape the image into a square. Thus, the number of pixels considered in the histogram increases. Confusion does not change the pixel values at all, so it does not change the distribution of pixel values in the image. Thus, it can be concluded that the confusion method is not safe enough by itself.

Then, analysis of the correlation between pixels is performed by calculating the correlation coefficients between the neighboring pixels horizontally, vertically, and diagonally. Correlation coefficient values range from -1 to 1, where 1 indicates perfect correlation, 0 indicates no correlation at all, and -1 indicates negative correlation. This calculation is performed three times for each channel (red, green, and blue), and then the average value is calculated. A comparison of the average correlation coefficients of the original image and the encrypted image can be seen in Table 1.

(a)   (b)
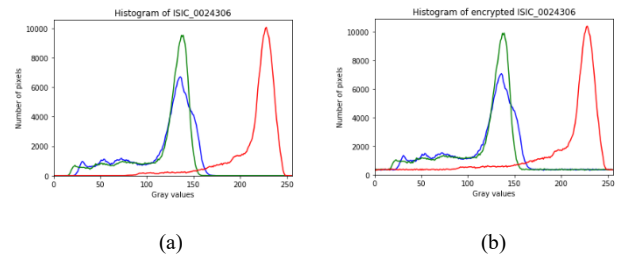
Figure 4: Histogram of (a) the original image and (b) the image encrypted using confusion

Based on the average correlation coefficient, the neighboring pixels in the original image have a strong linear correlation, with correlation coefficients close to 0. By contrast, in the encrypted image, the correlation coefficients between neighboring pixels are close to 0. This shows that the confusion method successfully weakens the correlation between neighboring pixels in an image.

Table 1: Comparison of average correlation coefficients of the original image and the image encrypted using confusion

Correlation coeff.	Horizontal	Vertical	Diagonal
Original image	0.984251	0.981887	0.974224
Encrypted image	-0.08009	-0.0462	0.084784

After that, entropy analysis is performed to calculate the level of uncertainty of the pixel values in the encrypted image. The ideal entropy of encrypted image is $\log_2(256)$, which equals 8. A comparison of the average entropy of the original and encrypted images can be seen in Table 2.

We can see that images encrypted with confusion have higher entropy than the original image, with an average entropy value above 7. In theory, confusion should not change the entropy value of the image because there is no change in the pixel value. However, in this test, a greater entropy value was obtained because, during the encryption process, new pixels with random values are added to change the shape of the image into a square. The addition of these random pixels makes the entropy value increase from 6.912776 to 7.401581. Even so, the encrypted image with this entropy value is not secure enough and is still predictable. Encrypted images are considered to be safe if they have an entropy value close to 8, which indicates that the pixels in the image are difficult to predict.

Table 2: Comparison of the average entropy of the original image and the image encrypted using confusion

	Entropy
Original image	6.912776
Encrypted image	7.401581

4.2. Image Encryption Testing Using Diffusion

In this test, encryption was performed on 30 images with only diffusion, using the Henon map as the chaotic map. An example of the encryption results can be seen in Figure 5.

We can see that the image does not represent the original color, but instead consists of a variety of random colors. This is a result of changing the image's gray values during encryption. Nevertheless, even though it is very vague, the object or shape depicted in the original image is still visible because no randomization of pixel positions was performed during encryption.

(a)   (b)
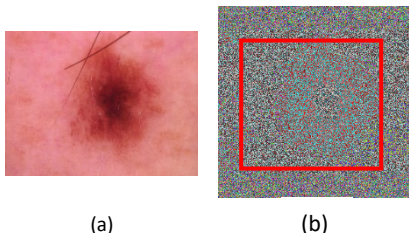
Figure 5: (a) Original image and (b) image encrypted using diffusion

In terms of pixel distribution, the histogram of encrypted image is very different from the original image. When viewed as a whole, 30 histograms of encrypted images have the same characteristics; every possible gray value is fairly diffused to all image pixels due to the use of a diffusion method that changes pixel values. An example of a comparison of the original and encrypted images' histograms can be seen in Figure 6. This is because of the nature of the Henon map, which produces a sequence of random numbers that produces very diverse gray values when an XOR operation is performed on the pixels of the original image.

(a)   (b)
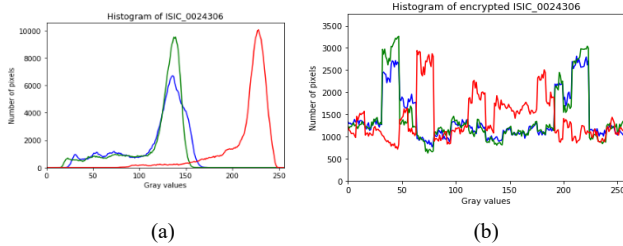
Figure 6: Histogram of (a) the original image and (b) the image encrypted using diffusion

Then, the correlation analysis between pixels is performed by calculating the correlation coefficients between the neighboring pixels horizontally, vertically, and diagonally. This calculation is performed 3 times for each channel (red, green, and blue), and then the average value is calculated. A comparison of the average correlation coefficient of the original image and the encrypted image can be seen in Table 3.

From the average correlation coefficient, it can be seen that the neighboring pixels in the image encrypted with diffusion have almost no correlation at all. Indeed, the coefficients are very close to 0, which are even smaller than those for the image encrypted with confusion.

Table 3 Comparison of average correlation coefficient of the original image and the image encrypted using diffusion

Correlation coeff.	Horizontal	Vertical	Diagonal
Original image	0.984251	0.981887	0.974224
Encrypted image	0.000195	-0.00035	-0.00107

After that, entropy analysis is performed to calculate the level of uncertainty of the encrypted image. A comparison of the average entropy of the original and encrypted images can be seen in Table 4. Using the entropy calculation, we can see that encrypted images with diffusion have a much higher entropy than the original image, with an average entropy of 7.950477, which is very close to 8. The entropy value produced in this test is even greater than the entropy value of the image encrypted with confusion in the previous test. This happens because diffusion changes the pixel values, which makes the distribution of pixel values in the image more random. The entropy value of 7.950477

indicates that the pixels in the encrypted image with diffusion are random and difficult to predict.

Table 4 Comparison of the average entropy values of the original image and the image encrypted using diffusion

	Entropy
Original image	6.912776
Encrypted image	7.950477

4.3. Image Encryption Testing Using a Combination of Confusion and Diffusion

In this test, encryption was performed on 30 images with a combination of confusion and diffusion, using ACM and Henon map as the chaotic maps. An example of the encryption results can be seen in Figure 7.

(a)   (b)
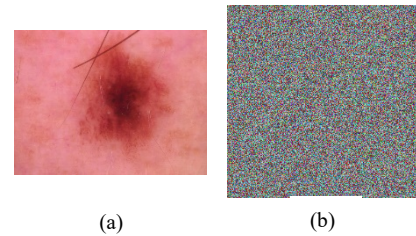
Figure 7: (a) Original image and (b) image encrypted using a combination of confusion and diffusion

We can see that image does not represent the original color because the pixel value has been changed at the time of encryption during the diffusion stage. On the other hand, the characteristics of the original image are not visible because the encryption process is done by randomizing the position of the pixel image during the confusion stage.

In terms of pixel distribution, the histogram produced in this test is the same as histogram in test B (diffusion only), although the method used in this test is a combination of confusion and diffusion. An example comparison of the histogram of the original image and the encrypted image can be seen in Figure 7. This can occur because confusion does not change the pixel value, and the value of the pixel changes at only the diffusion stage.

Just like the results of the histogram in test B, all histograms in this test have the same characteristics; every possible gray value is fairly diffused to all pixels in the image due to the use of a diffusion method that changes pixel values. An example comparison of the original and encrypted image histograms can be seen in Figure 8. This is because the Henon map produces a sequence of random numbers, so that very diverse gray values are produced when an XOR operation is performed on the pixels of the original image.

(a)   (b)
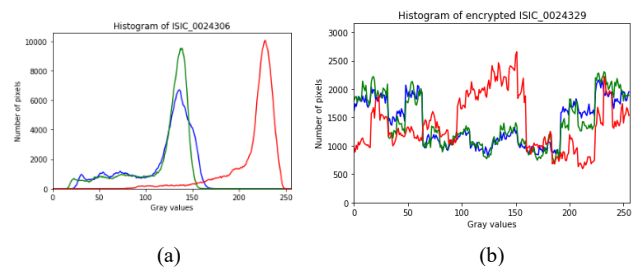
Figure 8: Histogram of (a) the original image and (b) the image encrypted using a combination of confusion and diffusion

Then, correlation analysis between pixels is performed by calculating the correlation coefficients between the neighboring

pixels horizontally, vertically, and diagonally. This calculation is performed three times for each channel (red, green, and blue), and then the average value is calculated. A comparison of the average correlation coefficient of the original image and the encrypted image can be seen in Table 5.

Based on the average correlation coefficient, which is very close to 0, the neighboring pixels in the image encrypted with only diffusion have almost no correlation at all.

Table 5: Comparison of the average correlation coefficients of the original image and the image encrypted with a combination of confusion and diffusion

Correlation coeff.	Horizontal	Vertical	Diagonal
Original image	0.984251	0.981887	0.974224
Encrypted image	0.003877	-0.00026	-0.00049

After that, entropy analysis is performed to calculate the level of uncertainty of the encrypted image. A comparison of the average entropy values of the original and encrypted images can be seen in Table 6. Based on the entropy calculation, the images encrypted with diffusion have a much higher entropy value (an average of 7.950304, which is very close to 8) than the original image. The entropy value produced in this test is even greater than the value of the image encrypted with only confusion, and it is more or less the same as the value of the image encrypted with only diffusion. This happens because diffusion changes the pixel values, which makes the distribution of pixel values in the image more random. The entropy of 7.950304 indicates that the pixels in the image encrypted with diffusion are random and difficult to be predicted.

Table 6: Comparison of average entropy of original and encrypted images using confusion and diffusion combined

	Entropy
Original image	6.912776
Encrypted image	7.950304

4.4. Image Encryption Testing Using Modified Secret Keys

In this test, IMG_0130 (a photo taken by the clinic) and ISIC_0024306 (a dataset image) are encrypted using the secret key, **64628632896829413501795 4110561**, producing the image shown in Figure 9. This is the original key that will be used for comparison in a key sensitivity analysis. After that, the encryption test was performed again using the 30 modified secret keys. In this system, the secret key is not actually known by the client because it is the result of DH, but to discover the sensitivity of the key used as the initial values for encryption in this test scenario, an encryption test will be performed using a modified secret key.
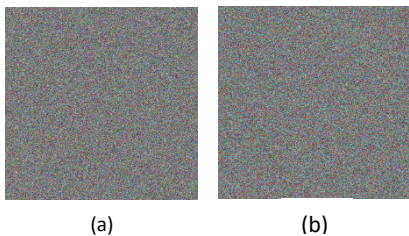
Figure 9: Encrypted image: (a) IMG_0130 and (b) ISIC_0024306, which used the original secret key

In each test, the modified secret key is one number different from the original secret key, starting from the largest number (10^{29}) to the smallest (10^0), while the other 29 numbers are the same as the original numbers. Variations of the secret key in this test can be seen in Table 7.

Table 7: Modified secret keys

| Trial no.	Modification precision	Secret key
1	10^{29}	**5**46286328968294135017954110561
2	10^{28}	6**3**6286328968294135017954110561
. .	. .	. .
29	10^1	646286328968294135017954110**5**51
30	10^0	6462863289682941350179541105**6**0

In this test, an analysis is performed by calculating the similarity index (SSIM) to determine the level of similarity between the image encrypted using the original secret key and the one encrypted using the modified secret key. The SSIM index has values ranging from 0 to 1, with 1 meaning that the images are identical or entirely the same. The results of SSIM calculations of the original encryption and encryption with the modified key can be seen in Table 8.

The images encrypted using the original secret key and modified secret key have very significant differences, as indicated by the very small similarity index. In the first 28 trials, which had modification precision of (10^{29}) to (10^2), the similarity index results were only around 0.005, or about 0.5%. In contrast, for the secret key modification of the last two numbers, which had levels of precision of (10^1) and (10^0), the similarity index is around 0.12, or 12%, as the Henon map (diffusion) uses only the first 28 numbers as initial values. Thus, the secret key used to determine the initial values in the encryption process is very sensitive to changes; even the slightest change in the smallest number can generate a completely different image.

Table 8: Similarity index between encrypted image using original secret key and modified secret key

Modification precision	Similarity index (SSIM)		Average
	IMG_0130	ISIC_0024306	
10^{29}	0.00485	0.00556	**0.005205**
.	.	.	.
	.	.	
10^2	0.00497	0.00628	**0.005625**
10^1	0.09249	0.1496	**0.121045**
10^0	0.09231	0.14984	**0.121075**
		Total Average	**0.005337**

4.5. Image Decryption Testing Using Modified Keys

Two kinds of tests are conducted. The first is decryption of the encrypted image in Figure 9b using 30 secret keys, as shown in Table 7. These secret keys are modifications of the actual secret key (**64628632896829413501795 4110561**). The second test is decryption of the encrypted image in Figure 9b using a public key and a private key. This test was conducted 30 times using 30 private keys, as shown in Table 9. These private keys are modifications of the actual private key (**88573348446640252688 8140697877**). The public key used in the tests is always the same (**2037989140015237406 19069244784**).

The first test is carried out to determine the secret key's sensitivity to the resulting encrypted image, while the second test is more like a simulation of image decryption in real circumstances by an attacker (not the actual recipient). This is done because in the image encryption program designed in this research, the user must enter their private key and the sender's public key to be able to decrypt the image. Therefore, the second test in this test scenario is intended to determine the sensitivity of the private key to the encrypted image that is generated.

Table 9: Modified private keys

Trial no.	Modification precision	Private key
1	10^{29}	**7**857334844664025268881 40697877
2	10^{28}	**8**757334844664025268881 40697877
. .	. .	. .
29	10^{1}	8857334844664025268881 406978**6**7
30	10^{0}	8857334844664025268881 406978**6**

From the results of the tests that have been carried out, no image has been successfully decrypted to its original form, but in the last two trials of the decryption test with secret key modifications, the decrypted images represent the colors of the original image, which can be seen in Figure 10.
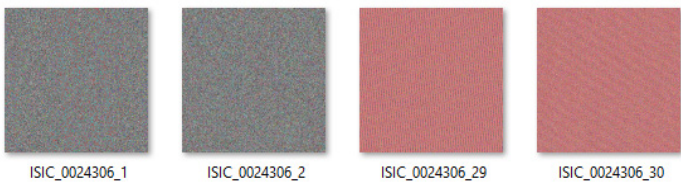
Figure 10: The last two trials of the decryption test using the modified secret keys
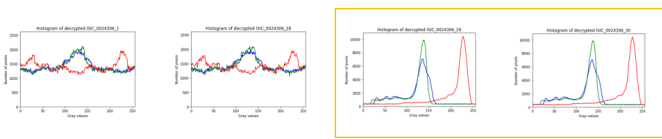
Figure 11: Histograms of the decryption results obtained using modified secret keys (1st, 28th, 29th, and 30th trials)

This section analyzes the decryption results with histogram and entropy analysis. Histograms for the decryption test using modified secret keys can be seen in Figure 11. Overall, the histograms show uniform pixel distribution, except for the 29th and 30th trials. This type of pixel distribution is caused by differences between the initial Henon map values used in the encryption and decryption processes. When the initial values used in the decryption process are not the same as those in the encryption process, an entirely different chaotic map is generated rather than restoring the pixels to their original values. In the 29th and 30th experiments, because the initial values of the Henon map used for decryption were the same as the values used for encryption, the trend of pixel distribution matches the original image, indicating that the encrypted pixel values have returned to their original values. Meanwhile, in the ACM, the initial values

were not the same, so the pixels in the image did not return to their original positions.

Histograms for the decryption test performed using modified private keys can be seen in Figure 12. From these histograms, we can see that all the trials—both those using the Henon map and ACM—failed to decrypt the image to its original form.
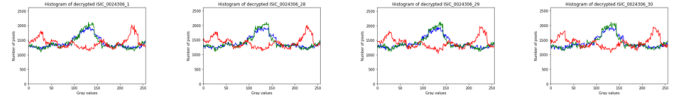
Figure 12: Histograms of the decryption results obtained using modified private keys (1st, 28th, 29th, and 30th trials)

Next, entropy analysis was performed to prove that the decryption results are random and difficult to predict. The results of entropy calculations can be seen in Table 10. The failed decryption trial makes the entropy value greater, which means that the image is more random and more difficult to predict. Indeed, the overall entropy is above 7.99, which is very close to 8. However, in the 29th and 30th trials of the secret key modification test, the entropy values of only around 7.54.

Table 10: Entropy of decryption results obtained using modified keys

Trial no.	Image	Entropy	
		Modified secret keys	Modified private keys
1	IMG_0130	7.99484	7.9948
. .	. .	. .	. .
28	ISIC_0024327	7.99468	7.9948
29	ISIC_0024328	7.54545	7.99492
30	ISIC_0024329	7.54545	7.99486

Of the two tests that were carried out, the scenario in the second test, in which the encryption system is designed to use both a public key and a private key as well as a secret key that is a combination of both, is more likely to occur in real life. However, it is also possible for the attacker to use direct brute force on the secret key that is generated. Key space analysis is needed to prove that the keys are secure enough.

Both the secret key and the private key in this design consist of decimal numbers with a length of 30 characters. Thus, there are 10^{30} permutations. Key spaces of this length can overcome brute force attacks.

4.6. Algorithm Complexity Analysis

There are three stages of encryption that are carried out sequentially, namely, reshaping, confusion, and diffusion. During the reshaping phase, the image is converted into a square, adding new pixels to fill in the blanks. Therefore, in this section a random number of $N \times N$ is filled in, where N is the largest dimension of the original image. If calculated using Big-O notation, it is **O(N^2)**. Then, confusion is performed with several operations:

1) Generate a meshgrid of $N \times N$ size, calculated as O(N^2).
2) Loop as many as I iterations, calculated as O(I).
3) Take p and q from the secret key, calculated as O(2×1).
4) Generate an xmap and ymap by calculating the ACM of the values in the meshgrids x and y, calculated as O(2×N^2).

5) Move pixels from position (x, y) to position (xmap, ymap), calculated as $O(N^2)$.

Throughout this calculation, the constant Big-O notation can be removed from the calculation because of its very small effect compared to $O(N^2)$. Therefore, from this confusion stage, we obtain a complexity calculation of $O(N^2) + O(I) \times O(3N^2) = \mathbf{O(N^2) + O(I \times 3N^2)}$.

Diffusion is performed as follows:

1) Loop as many as $N \times N \times 8$ iterations, calculated as $O(8N^2)$.
2) Calculate xN and yN with the Henon map formula, calculated as $O(2\times1)$.
3) xN and yN become x and y values for the next iteration, calculated as$O(2\times1)$.
4) Convert xN to binary bit by using a threshold. In the worst-case scenario, there are four operations that must be performed, so it is calculated as $O(4\times1)$.
5) Insert binary bits into the bit sequence, calculated as $O(1)$.
6) Check whether the current iteration is a multiple of 8, calculated as $O(1)$.
7) If it is a multiple of 8, convert the bit sequence into decimal form, empty the bit sequence, and then insert the decimal value into the chaotic matrix. All of these operations are counted as $O(3\times1)$.
8) After all the iterations are finished, perform an XOR operation between the chaotic matrix and the image matrix for each channel, calculated as $O(3\times8N^2) = O(24N^2)$.

From this confusion phase, we obtain a complexity calculation of $O(8N^2) \times (O(2) + O(2) + O(4) + O(1) + O(1) + O(3)) + O(24N^2) = \mathbf{O(132N^2)}$. When combined, the entire encryption algorithm has a complexity of $O(N^2) + O(N^2) + O(I \times 3N^2) + O(132N^2)$, or $\mathbf{O(3I+134)N^2}$, where I is the number of iterations at the confusion stage and N is the largest dimension of the original image. Based on the complexity notation, the performance and time needed to run the encryption process are influenced by the large number of iterations that must be done at the confusion stage as well as the largest dimension of an image. Of these factors, the largest dimension of the image has the most influence on performance and the time needed to carry out the encryption/decryption process, as indicated by the notation in the form of quadratic time.

The decryption process has more or less the same complexity as the encryption process. The undiffusion and unconfusion stages of decryption perform similar numbers and types of operations to the diffusion and confusion stages of the encryption process, so the complexity calculation is the same. The only difference between decryption and encryption leis in the reshape phase; in the worst-case scenario, the process of returning the image to its original form (crop border) has an operating complexity of $\mathbf{O(2N+3N^2)}$. Thus, the overall complexity of the decryption algorithm is $O(2N+3N^2) + O(N^2) + O(I \times 3N^2) + O(132N^2)$, or $\mathbf{O(2N + 136N^2 + I \times 3N^2)}$.

Overall, there is not much difference between the complexity of encryption and decryption. Similar to the encryption process, the performance and time required to carry out the decryption process are affected by the large number of iterations that need to be performed at the unconfusion stage as well as the length/width of the image to be decrypted. The length/width of the image is the factor with the biggest influence.

5. Conclusions

There are several conclusions that can be made based on the tests conducted in this research:

1. Chaos-based image encryption using only the confusion method is not secure enough, as evidenced by the fact that the pixel distribution trend is similar to the original image and the average entropy value is 7.401581.
2. Chaos-based image encryption using only the diffusion method is secure enough based on the distribution of pixels on the histogram, the average correlation coefficient (which is very close to 0), and the average entropy (7.950477). However, the characteristics of the original image are still vaguely visible.
3. Chaos-based image encryption using a combination of confusion and diffusion methods is the most secure encryption method based on pixel distribution on the histogram, the average correlation coefficient (which is very close to 0), and the average entropy (7.950304). Implementing two methods is more secure because there are two layers of security.
4. Implementation of ACM in the confusion phase with different p and q values in each iteration makes pixel positions more random and difficult to predict.
5. The initial values of the Henon map have a sensitivity level of at least 10^{-14}.
6. A difference of just one number in the secret key during the encryption process results in a significant difference in the encrypted image, as evidenced by the average similarity level of around 0.5%. This indicates that changes in the initial values of the ACM or Henon map can make a big difference in the encryption results.
7. A difference of just one number in the secret key during the decryption process causes the image to not be restored to its original shape and produces a stronger random image with entropy values closer to 8.
8. A 30-character numeric key has a high level of security because there are 10^{30} permutations that might be generated.
9. The largest dimension of an image (length/width) is the factor with the most influence on the performance and time involved in running the encryption/decryption process.

References

[1] S.S. Alwy, KONSIL KEDOKTERAN INDONESIA, 2006.
[2] D. Desai, A. Prasad, J. Crasto, "Chaos-Based System for Image Encryption," **3**(4), 4809–4811, 2012.
[3] S. Fadhel Hamood, M.S. Mohd Rahim, O. Farook Mohammado, "Chaos image encryption methods: A survey study," Bulletin of Electrical Engineering and Informatics, **6**(1), 99–104, 2017, doi:10.11591/eei.v6i1.599.
[4] A. Soleymani, M.J. Nordin, E. Sundararajan, "A chaotic cryptosystem for images based on Henon and Arnold cat map," Scientific World Journal, **2014**, 2014, doi:10.1155/2014/536930.
[5] Diffie-Hellman Protocol -- from Wolfram MathWorld, Dec. 2019.
[6] L. Kocarev, "Chaos-based cryptography: A brief overview," IEEE Circuits and Systems Magazine, **1**(3), 6–21, 2001, doi:10.1109/7384.963463.

[7]   Y. Kumar, S. Mamta, "A Review Paper on Image Encryption Techniques," International Journal for Research in Applied Science & Engineering Technology, **5**(4), 169–172, 2014, doi:10.22214/ijraset.2017.8023.

[8]   N.A. Abbas, "Image encryption based on Independent Component Analysis and Arnold's Cat Map," Egyptian Informatics Journal, **17**(1), 139–146, 2016, doi:10.1016/j.eij.2015.10.001.

[9]   E. Hariyanto, R. Rahim, "Arnold's Cat Map Algorithm in Digital Image Encryption," International Journal of Science and Research (IJSR), **5**(10), 1363–1365, 2016, doi:10.21275/ART20162488.

[10] F.J. Dyson, H. Falk, "Period of a Discrete Cat Mapping," The American Mathematical Monthly, **99**(7), 603, 1992, doi:10.2307/2324989.

[11] M.F. Abd Elzaher, M. Shalaby, S.H. El Ramly, "An arnold cat map-based chaotic approach for securing voice communication," in The 10th International Conference on Informatics and Systems, Giza: 329–331, 2016, doi:10.1145/2908446.2908508.

[12] A.M. Elshamy, M.A. Abdelghany, A.Q. Alhamad, H.F.A. Hamed, H.M. Kelash, A.I. Hussein, "Secure VoIP System Based on Biometric Voice Authentication and Nested Digital Cryptosystem using Chaotic Baker's map and Arnold's Cat Map Encryption," in 2017 International Conference on Computer and Applications, ICCA 2017, Doha: 140–146, 2017, doi:10.1109/COMAPP.2017.8079739.

[13] C. Saha, M.F. Hossain, "MRI Watermarking Technique Using Chaotic Maps, NSCT and DCT," in 2nd International Conference on Electrical, Computer and Communication Engineering, ECCE 2019, IEEE, Cox's Bazar, 2019, doi:10.1109/ECACE.2019.8679464.

[14] N. Lazarov, Z. Ilcheva, "A fragile watermarking algorithm for image tamper detection based on chaotic maps," in 2016 IEEE 8th International Conference on Intelligent Systems, IS 2016 - Proceedings, Sofia: 723–728, 2016, doi:10.1109/IS.2016.7737391.

[15] R. Munir, "A Secure Fragile Video Watermarking Algorithm for Content Authentication Based on Arnold Cat Map," in 2019 4th International Conference on Information Technology (InCIT), IEEE, Bangkok: 32–37, 2019.

[16] Hénon Map -- from Wolfram MathWorld, Dec. 2019.

[17] N.S. Raghava, A. Kumar, "Image Encryption Using Henon Chaotic Map With Byte Sequence," **3**(5), 11–18, 2013.

[18] J. Lin, X. Si, "Image encryption algorithm based on hyperchaotic system," in 2009 International Workshop on Chaos-Fractals Theories and Applications, IWCFTA 2009, 153–156, 2009, doi:10.1109/IWCFTA.2009.39.

[19] D. Erdmann, S. Murphy, "Henon Stream Cipher," Electronics Letters, **28**, 9.

[20] D. Gollman, Computer Security Third Edition, 2011, doi:10.1017/CBO9781107415324.004.

[21] J.G. Sekar, C. Arun, "Comparative performance analysis of chaos based image encryption techniques," Journal of Critical Reviews, **7**(9), 1138–1143, 2020, doi:10.31838/jcr.07.09.209.

[22] A. Afifi, "A Chaotic Confusion-Diffusion Image Encryption Based on Henon Map," International Journal of Network Security & Its Applications, **11**(4), 19–30, 2019, doi:10.5121/ijnsa.2019.11402.

Mathematical Modelling of Output Responses and Performance Variations of an Education System due to Changes in Input Parameters

Najat Messaoudi[*,1], Jaafar Khalid Naciri[2], Bahloul Bensassi[1]

[1]*Laboratory of Industrial Engineering, Information Processing and Logistics, Hassan II University, Faculty of Sciences Ain Chock, Casablanca, 20100, Morocco*

[2]*Laboratory of Mechanics, Hassan II University, Faculty of Sciences Ain Chock, Casablanca, 20100, Morocco*

A R T I C L E   I N F O

A B S T R A C T

"This paper is an extension of work originally presented in the 4th International Conference on Systems of Collaboration, Big Data, Internet of Things & Security -SysCoBIoTS'19".
The use of complex and dynamic systems modelling to social systems is quite recent and its pertinence in the case of an educational system is continually increasing. For the concrete management of educational systems, a global approach is required. This approach must take into consideration the effects of many parameters that can act and interact together thus making, as a result, the system more or less efficient. Our aim is to develop a model that can capture the dominant dynamics of these systems while being at the same time simple enough to be useful for analyzing, simulating, and quantifying the impact of different parameters on the global performances of educational systems. By viewing education systems as skills production systems and by applying Business Processing modelling methods, a modelling of education systems is proposed in the present work which allows studying the effects of a set of parameters on the behavior of the system and its performance. The focus will be done on the study of the impact of learners' input competence on the performance of a training unit and on the performance of a training program. The obtained simulation results allow us to analyze the evolution of a training program's behavior as well as estimates its performance under the effect of the variation of simulation factors. These results enable to measure the performance variation according to the learners' input competence, their ability to acquire skills, and to the class size. This modelling enables us to test solutions for performance improvement.

1. Introduction

Education is a determining factor for growth and development and education systems and socio-economic development are closely related and interact with each other [1]. Indeed, an education system enables individuals to improve their productivity and increase their employability, and at the community level, it improves the competitiveness and attractiveness of the economy through the availability of skilled human capital. As a result, developing effective education systems whose performance can be quantified and ensured becomes an important issue at many levels for managers and all stakeholders.

But several questions arise: what defines an education system as a high-performing one? How can the performance of an education system be evaluated? What makes an education system efficient? What are the factors that impact its performance? How can we act on these factors to improve this performance?

Answers to these questions are not obvious as far as education systems are complex systems and having tools allowing the objective evaluation of their performance is still a goal to achieve due to the multidimensional and complex nature of these systems.

In [2]-[4], the authors have dealt with the reasons and some consequences of the complex nature of education systems and their nonlinear behavior.

This complexity is related to the existing interconnections between the different levels of educational systems starting from kindergarten to reach high schools and universities. Low performance at one level tends to affect the global performance at subsequent levels. Furthermore, individual's performance in

schools is influenced by several other systems. Education is in fact part of a larger system whose elements, such as economics, culture, society, and politics, interfere with it.

Education systems are also time-dependent and, changes in education often take a long time. Implemented policies may show results many years later, sometimes decades after their implementation. Another issue is that behaviors and actions of one part of the educational system tend to affect other parts of the system. This complexity can lead to unpredictable consequences of implemented actions. Effective management of education systems, therefore, requires a global approach that oversees the effect of all the parameters considered as a whole to ensure an efficient system operation.

Modelling can be one of the useful methods to evaluate performance and to identify the factors or areas of improvement of this performance. Modeling a system consists of designing a representation of this system for analysis and simulation purposes to answer questions. There can be several models for the same system with different levels of precision depending on the phenomena to be studied. Identification of the appropriate model will depend on the questioning under consideration [5].

The use of complex and dynamic systems modelling to social systems is quite recent and its pertinence in the case of an educational system is continually increasing [2]. The main challenge is to develop a model that can capture the dominant dynamics of these systems while being at the same time, simple enough to be useful for analyzing, simulating, and quantifying the impact of different parameters on the global performances of these systems

Several works have focused on the modelling of education systems. They concerned areas such as design, operations, analysis of performance, and management.

In the field of production engineering, studies on education systems modelling have focused on developing an analogy between education systems and systems of production of goods and services. Once this analogy was established, methods and methodologies for production systems modelling were applied to education systems while adapting them to the specificities of the latter. This works has enabled the transfer of business process modelling tools to the field of education and thus provided models for various purposes such as quality assurance, computerization of processes, or the design of new systems.

In this way, in [6], the author used the SADT method (Structured Analysis and Design Technique) for the analysis and the functional decomposition of a school using Le Moigne's systemic approach. Based on CIMOSA (Computer Integrated Manufacturing Open Systems Architecture) and IDEF0 (Integrated Computer-Aided Manufacturing Definition), he proposed modelling of the skills production system and engineering design of this system.

In [7], a model for resource specification for the planning of training activities using UML (Unified Modelling Language) and a model of the business processes of an education system using MECI (Modélisation d'Entreprise pour la Conception Intégrée) are proposed.

In higher education, in [8], the author proposed a model for quality improvement by identifying the skills that graduates must acquire and proposes the activities and means to achieve this objective by using business process modelling BPM.

In relation to the increasing use of digital technologies, the author in [9] proposed a personalized training path per learner according to his/her individual capacity to optimize academic performance using Petri nets.

In [4], the author investigated the application of dynamic systems modelling for educational policy analysis to a better understanding of the dynamics of the current system and the design of evolution scenarios for the future. He applied this approach during a case study during the school year 2007-2008 in the American state of Rhode Island.

Another class concerns the demographic models used for the simulation of educational policies and strategies. This is the case of the EPSSIM code (Education Policy and Strategy Simulation Model) [10] which is a generic model designed by UNESCO. It provides technical and methodological support for the elaboration of educational development plans. It is a demographic model in which schooling objectives are considered as decision variables and expenditures are calculated as a consequence of the achievement of these objectives. It essentially allows the students flow simulation and costs calculations.

These models, which remain partial, can simulate the behavior of the system for a reduced number of basic quantitative parameters and require a high degree of granularity to ensure their operationality and reliability of their results

This paper aims to present an educational system model for studying the impact of various parameters on the behavior of the system and to estimate its performance. The focus will be on the study of the impact of learners' competencies deficit on the performance of a training program.

2. Modelling of an education system

2.1. Modelling a training unit

A previous work [11], allowed us to propose a model of an education system that makes it possible to simulate its behavior to predict its long-term evolution, to evaluate its performance, and to simulate the impact of some factors on the evolution of this performance.

According to previous works which consider that an educational system can be defined as a competence production system [6] and also that any system which includes, even partially, in its missions the increase of learner skills can be considered as a part of an educational system [12], the approach conducted for the modelling of such system consists in proposing a decomposition of this system to introduce the notion of training unit which is the basis of the proposed modelling.

Despite the specificities of each country, educational systems at the global level are fairly homogenous and exhibit a quite similar central core. Therefore, most educational systems around the world have four educational levels: pre-primary, primary, secondary, and tertiary. The present simulation considers also that each training cycle, provided usually in an educational institution,

can be further divided into training programs, with each program composed of a limited number of courses consisting of a defined number of sessions.

Similarly, to the goods or services production systems, educational systems have organizational units, these are the training units. A training unit aims to transform business object inputs (can be physical or informational) into business object outputs within a framework of objectives and constraints fixed by the external conduct rules of the unit. A training unit can correspond to different parts; it can be a whole educational system, a training cycle, a training institution, or even a single classroom session. Thus, the reconstruction of the global system can be done by grouping a range of training units in parallel and/or in series according to well-defined rules.

To model the training unit, we relied on models based on BPM tools and mainly the work related in [13] where the author suggests using a generic processor to characterize the activities of both the physical and decision systems to evaluate its performance. A generic processor is an entity that performs one or more basic transformation activities, and that fits into the structure, thus modifying its behavior and performance. By organizing a set of generic processors in a network, it creates a particular state of the production system which is characterized by a performance level.

Thus, the training unit is an entity of the training system with the objective to transform the inputs competencies' level of the learners into a higher level of output competencies respecting the constraints and objectives of the educational system and thus to contributes to the achievement of the overall objectives of the training system. The reconstruction of the global system will then be reconstructed by grouping together a set of training units, either in parallel or in series according to well-defined rules.

Thus, the objective of a training unit is to increase the level of competencies of learners starting from an input reference competency C_r to a level above an output reference competency C'_r on a fixed time h, by using resources and based on conduct and achievement data as shown in Figure 1.
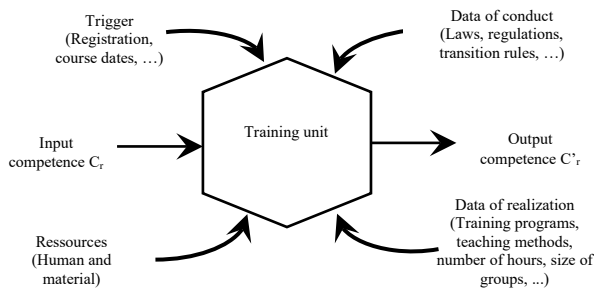
Figure 1: Model of a training unit

Educational systems present a particularity insofar as learners are co-producers of the service they use. In fact, each student has his own sensitivity to the process of skills acquisition. The objectives to be achieved by a training unit are defined during the design of this training unit. In this way, the reference input competencies needed to correctly follow this training activity, the reference output competencies to be reached, the resources required to carry out the activity, the conduct of data, and the achievement data are defined.

The interest of this modelling lies in the possibility of decomposing or aggregating the education system into networks

of generic processors of different levels and by extension the possibility of evaluating the global or detailed performance of the training system on any level of abstraction.

The educational system is modeled as a series of training units interacting with each other to produce the targeted competencies.
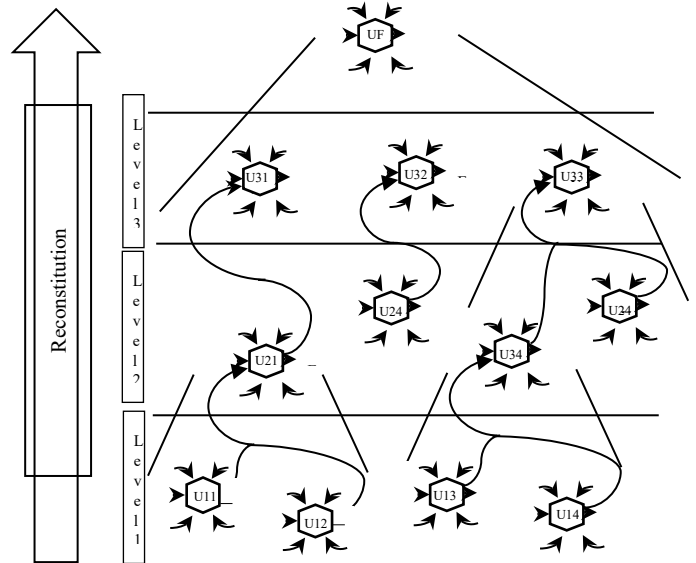
Figure 2: reconstitution of training units into a training program

Figure 2 illustrates an example of aggregating a set of training units by levels to reconstruct a training program. Each level groups together a defined set of training units and each training unit aims to achieve a defined increase in learner's competencies. Resources to be mobilized for a training unit to carry out its activity are defined, as well as related data of realization, data of conduct, and the launcher of the activity of the processor. The rules relating to the access of a learner from one level to the next level are also fixed, thus determining the time evolution of the training program.

This model allows the identification of what the training unit does, its function, as well as the determining factors for its functioning. Subsequently, the current modelling is associated with a simulation model which is built on the educational production function [14] and the learner's theories' results [15] in order to simulate the behavior of the system over time and the effect of some factors on its performance in a quantitative manner.

2.2. Mathematical model a training unit

The training unit is associated with a mathematical model based on the educational production function, that is written in a general form as follows [14]:

$$A = f^*(X1, ..., Xn) \tag{1}$$

where A is some measure of output, expressed as a function of a set of variables X1.....Xn.

In [11], the output A was the increase of competence level of a learner, noted as ΔC_i, while the parameters X_i that will be taken into consideration, at first approximation, are the duration of the training unit, the personal capacity of each learner μ_i, the input competence which represents the characteristics of the learners, the class size and a score for the pedagogical methods which represent some parameters of the resources and the data of conduct. The

other parameters remain constant throughout the simulation and therefore they will not impact the variation of ΔC_i.

Thus, expression (1) may be expressed as follows:

$$\Delta C_i = f(h, \mu_i, k, g) \qquad (2)$$

where ΔC_i is the competence level's increase of the learner i, h the training unit's duration, μ_i the individual capacity of competence acquisition of the learner i, k the coefficient representing the gap between the input competence of learner i and the required input competence of the training unit; g the coefficient taking into account the effect of the class size and the pedagogical methods.

An approach to specifying the function f and the relation linking the parameters h, μ_i, and g to the output ΔC_i to carry simulations is presented in previous work [11].

Expression (2) becomes as follows:

$$\Delta C_i = \frac{(C'_r - C_r)}{2} \cdot \left[1 - \frac{erf\left(\sqrt{\alpha} \cdot \left(-h + \frac{h_r}{2} \right) \right)}{erf\left(\sqrt{\alpha} \cdot \frac{h_r}{2} \right)} \right] \cdot \mu_i \cdot g(n) \cdot k\left(\frac{C_i}{C_r} \right) \quad (3)$$

Where C'_r is the output competence's reference, C_r is the input competence's reference, h the training unit's real duration, h_r the training unit's reference duration, α a parameter characterizing the progressivity of the evolution of the level of competence during the training.

The coefficient μ_i, which is specific to each learner, expresses his ability to achieve the expected competencies with more difficulty ($\mu_i < 1$) or more ease ($\mu_i > 1$) than was projected in the design of training. The reference value for μ_r is 1.

For the coefficient g, we assume, in a first approximation, that a change in excess (resp. in default) of the class size is not beneficial (resp. beneficial) to the learner, so we can use a linear relation to model this coefficient as follows:

$$g(n) = b \ if \ n > n_{max}$$

$$g(n) = b + ((a-b)/2)*n \ if \ n_{min} < n < n_{max} \qquad (4)$$

$$g(n) = a \ if \ n < n_{min}$$

where n is the ratio of the number of students in the group to the number recommended by the pedagogical method, a and b are the maximum and minimum values taken by the function g(n) when the group size is above a value n_{max} or below n_{min}.

Note that for the simulation results that will be presented here, we have used another relation instead of (4), which seems more adapted even if it presents similar characteristics, it is given by:

$$g(n) = b + \frac{(a-b)}{(1+n^4)} \qquad (5)$$

A possible lack of the input competence C_i is taken into consideration through a factor $k(C_i/C_r)$ which reflects the difference between the learner's input competence C_i and the reference input competence C_r required by the training unit.

2.3. Performance of a training unit and a training program

Following [11], performance can be defined as the ratio of the actual result obtained as process output to an expected result under standard conditions to be defined.

The training unit's result is determined as all competence increases accomplished by the students and validated following the outbound validation rules.

The expected standard result can be considered as the sum of the increases in the levels of competencies that are assumed to be validated by the learners when all the parameters of the production function of the training unit defined by relation (3) are taken equal to the reference values of the parameters.

Therefore, the training unit performance can be expressed as follows:

$$P = \frac{\sum_{i=1}^{n}(C'_i - C_i)}{(C'_r - C_r)*n_r} \qquad (6)$$

where P is the performance of the training unit, $(C'_i - C_i)$ the competence level increase of learner i having successfully validated the training unit, n is the number of learners who validate the unit, and $(C'_r - C_r)*n_r$ is the expected increase in the competence level of the class when all parameters are equal to their reference values.

A training program is considered as a network of interconnected training units distributed by the level of training with rules for transition from one level to another. The training units of a training level are connected in parallel and form a block and each training unit performs a defined competence increase activity. Thus, a training program that consists of n blocks, each block consisting of k training units, is schematized by a network of m processors such that m=n*k. The training units are denoted U_{ij} where i (1 ... n) denotes the number of the block to which it belongs and j (1 ... k) its classification within the block.

To define the performance of the training program, the performance of the training blocks making up the training program must first be defined.

We can then define the performance of block i of training units P_i as follows:

$$P_i = \frac{\sum_{j=1}^{k} \sum_{x=1}^{g_{ij}} (C'_{xij} - C_{xij})}{\sum_{j=1}^{k} (C'_{rij} - C_{rij})*g_{rij}} \qquad (7)$$

where $\sum_{j=1}^{k} \sum_{x=1}^{g_{ij}} (C'_{xij} - C_{xij})$ is the sum of all the increases in competencies of the learners who have validated the training units that constitute the training block, $\sum_{j=1}^{k} (C'_{rij} - C_{rij}) * g_{rij}$ is the sum of all the increases in competencies expected by the training units when the other parameters values are those of the reference data.

The performance of the training program can be calculated as the average performance of the training blocks weighted by the respective numbers of learners and can be translated by the following expression:

$$P = \frac{\sum_{i=1}^{n} P_i * g_i}{\sum_{i=1}^{n} g_i} \qquad (8)$$

where, P_i is the performance of training block i, g_i is the overall number of learners in block i, and n the number of blocks in the training program.

Thus, a model based on a mathematical formulation and a numerical simulation is obtained, it allows the calculation of the performance of a training program, based on the performance of the training units constituting this program. The effects on the overall performance of the training program of the variation of different parameters can thus be simulated and quantified.

This model was used in [11] to show the effects of the individual capacity of the learner's competence acquisition, as well as the pedagogical method's sensitivity in association with the group's size on the performance of a training unit.

The objective of this paper is to analyze the effect of the learner input competencies deficit factor on the behavior of a training unit and its performance and also to extend the approach to the case of a training program.

3. Impact of the input competence factor: results and discussion

For the chosen model, the education system is approached as an organized whole for skills production, composed of training units linked in parallel, and series according to rules of arrangement. Each unit has its own training objective, which is to increase specific skills of learners from a given level of competence at the input, assumed to be achieved by all entrants to the unit, to a higher level of competence at the output. The specificity of such a system is that the learners are co-producers of the service they use, which means that their characteristics will influence this increase in competencies. In fact, not all entrants to training have reached the required input level of competence and do not also have the same aptitudes for the acquisition of new skills.

Several studies have shown the important role of the learner in the process of competencies acquisition [16]-[18].

In a study using a multilevel model to identify the most important variables affecting students' performance [16], the authors have found evidence that both the students' and their families' characteristics play a role in the former's performance.

As stated in [19], precedent results and skills already acquired are strongly linked to the ease with which students will develop new skills, and thus have a real effect on their academic performance. In [20] and [21], the authors highlighted the importance of prior knowledge for success in studies.

In previous works [11], the personal characteristics of the learners are incorporated into the model through two factors. The first factor is the "personal capacity for competence acquisition μ_i" factor, which is specific to each learner and for each training unit and which is dedicated to taking into account the specific aptitudes of a learner allowing him to more easily assimilate new content. The impact of this factor on the increase in competencies and on the performance of a training unit was analyzed.

The second factor is the learner's prior knowledge through a "k" factor which quantifies the inadequacy between the student's input competence and the competencies entry level required by the training unit. In what follows, we will focus on the role of the latter, by establishing the effect of the factor k on the development of student's competence, on the training unit's performance, and on the training program's performance.

3.1. Evolution law of the coefficient $k(C_i/C_r)$

The goal sought is to establish an expression of the factor k which includes in the model defined by equation (3) the fact that a learner who would have a lack of competence at the entry of the training unit is less efficient in achieving the expected skills increase during the training. For that, we introduce the following expression:

$$k\left(\frac{C_i}{C_r}\right) = \left(\frac{C_i}{C_r}\right)^2 e^{[1-\left(\frac{C_i}{C_r}\right)^2]} \qquad (9)$$

Equation (9) allows a variation of the coefficient k between the values 0 and 1, with k = 0 when C_i = 0 and k = 1 for C_i = C_r. This reflects the fact that a learner with a zero value of input competence, cannot progress through the training, and a learner who has required competence at the entry should achieve the expected level of competence at the output. While if a learner has achieved a level of competence C_i above the reference input level C_r, the benefit of training is less and allows only a small increase of competence.

The graph below shows the evolution of the factor k as a function of the ratio C_i/C_r.
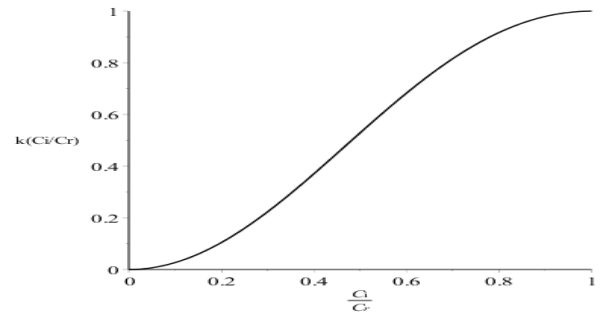
Figure 3: Evolution of the coefficient k as defined to the expression (9)

The mathematical model of the training unit (3), coupled to (9), is then given by the following expression:

$$\Delta C_i = \frac{(C_r'-C_r)}{2} \cdot \left[1 - \frac{erf\left(\sqrt{\alpha}\cdot\left(-h+\frac{h_r}{2}\right)\right)}{erf\left(\sqrt{\alpha}\cdot\frac{h_r}{2}\right)}\right] \cdot \mu_i \cdot \left(b + \frac{(a-b)}{(1+n^4)}\right) \cdot \left(\frac{C_i}{C_r}\right)^2 e^{\left[1-\left(\frac{C_i}{C_r}\right)^2\right]}$$
$$(10)$$

We will therefore consider three situations for the simulations. The first one shows the effect of the input competence on the competence increase's evolution, the second simulation concerns the effect of this factor on the training unit's performance and the third simulation reveals the effect of this factor associated with other factors on the training program's performance.

3.2. Simulation on the evolution of the increase of competence

The simulations to be carried out aim to determine the effect of the learners' skill level at the beginning of a training course on the progression of skills acquisition during the training process.

To illustrate this impact, we consider three groups of learners, the first group identified by a level of skills C_i below the required reference level C_r, the second having a skills level C_i equal to the required level, and the third having a level above the required level.

For the three groups, we consider all the other parameters of the simulation set to their reference values i.e. the training hours' number performed h is consistent regarding the reference duration of the training unit h_r ($h = h_r$), the students have a competence acquisition capacity $\mu_i = \mu_r$ and the coefficient g(n) is equal to 1.

Expression (10) above then allow simulation of the increase of competence in each of the three cases
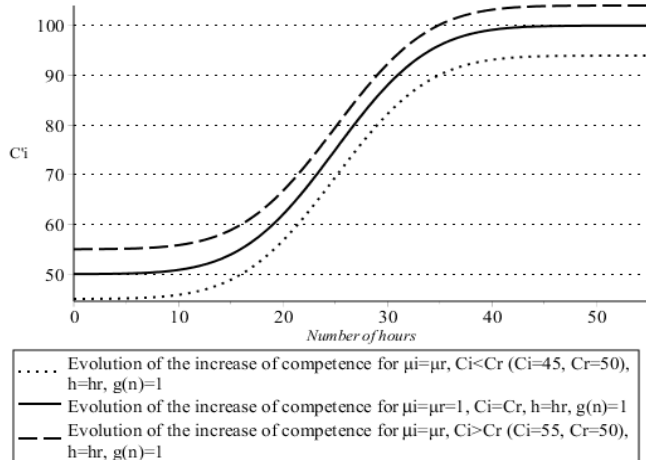
Figure 4: Input competence's effect on the competence increase

Figure 4 shows the input competence's effect on competence increase. The learner who starts the training with a deficit of competence's input (curve point), will not reach the expected competence's output. On the opposite, a learner with a competence's input greater than the required level accomplishes an output competence higher than the expected reference competence.

These results are in concordance with the studies [19], [20] and [21] that establish links between preceding results and skills previously acquired by the learners and the ease with which they acquire new skills

3.3. Simulation of the input competence's effect on the performance of a training unit

The goal set here is to simulate the effect of the variation in the input competence factor "k" on a training unit performance. Given the particularity of the educational systems in which every learner is a co-producer of his own competence increase according to his individual capacity of acquiring competencies μ_i, this factor is introduced in the following simulations.

Since the purpose is to focus on the input competence factor's variation, the other parameters are set to their reference values for the training unit, namely (C_r, C'_r, h_r, n_r) as well as the training unit validation's rule that defines the minimum value of ΔC that the learner must reach to validate the training unit.

To realize the simulation, we consider, for a training unit, the following parameters reference values. The reference values are C_r=50 for the input competence, C'_r =100 for the output competence, h_r = 50 for the training unit duration, and n_r = 100 for the learner's number. We also consider that learner i validate the training unit if $(C'_i - C_i) \geq (C'_r - C_r)$. The simulation of the effect of the input competence on the training unit performance is executed according to the algorithm illustrated in Figure (5).
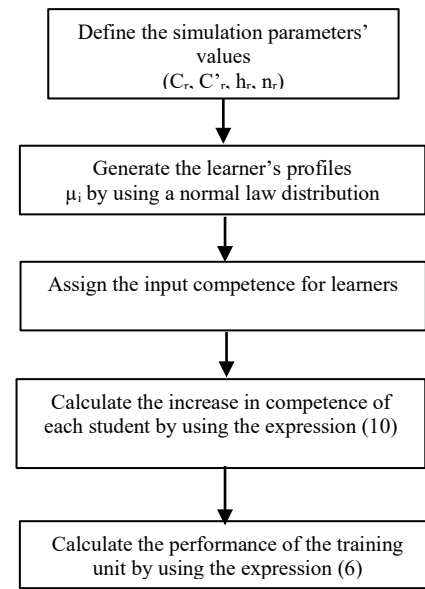
Figure 5: The simulation's algorithm

The first step for the simulation is to define the simulation parameter's values, the used values are n_r=100, C_r =50, C'_r =100 and h_r =50, and the training unit validation's rule that determine the minimum value required for ΔC_i that the learner has to reach in order to validate the unit. The second step is the generation of the student's profiles by using a normal law distribution for the parameter μ_i. The third step consists, for every simulation, in assigning the input competence C_i for the students. The fourth step is the calculation by relation (10) of the increase in competence for each learner. In the end, we calculate the performance of the training using relation (6).

Four simulations are carried out by varying the learners' input competence. In the first case, the input competence of learner's C_i is equal to the reference input competence of the training unit C_r, In the second case, the C_i deficit is of -3% compared to C_r, for the third case the C_i deficit is of -5% compared to C_r and the for the last case the C_i deficit of -7% compared to C_r.

The simulations' results are illustrated in the graph below:
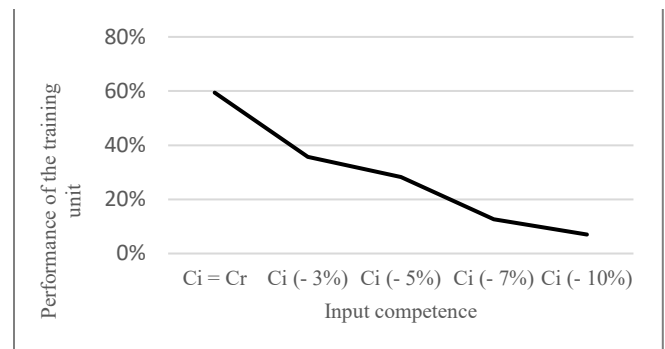
Figure 6: Impact of the input competence deficit on the performance of a training unit

These results highlight the effect of the deficit of learners' input competencies on the training unit performance.

We note that when all learners have the required input competence to follow the training unit, i.e. C_i=C_r, the performance of the training unit is around 59%. This percentage is consistent

and is due to the distribution in normal law retained for the personal capacity of competence acquisition μ_i, which is an essential factor of the learner. If these learners have an input competence deficit of -3% compared to the reference input competence, then this performance decreases and becomes of the order of 36%. Therefore, the improvement of a training unit performance, requires to check the input competence of a learner, so that the follow up of the competence acquisition process can be done properly.

3.4. Simulation of the impact of the input competence on the performance of a program training

The purpose is the stimulation of the input competence's impact and other parameters as the individual capacity of competence acquisition μ_i the class size on the performance of a training program and monitor its behavior over time.

The organization of the training program is illustrated by the following figure:
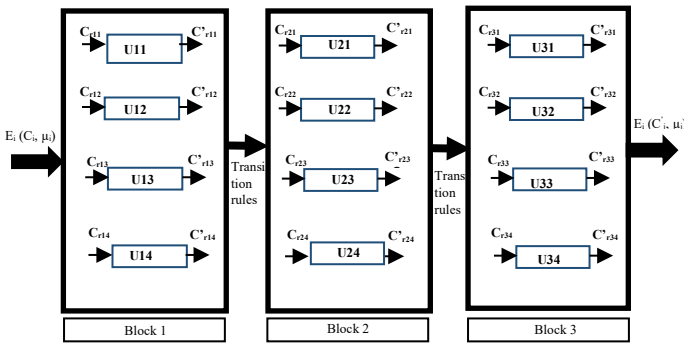
Figure 7: Organization of a training program

The training program for the simulation consists of three training blocks and each training block consists of four training units. The data of the realization of the training units are given in Table1.

Table 1: Training unit realization data and mobilized resources initialized to reference data

Level of training 1	Reference input competence	Reference output competence	Reference duration	Reference group size	Number of hours realized	Real group size	Number of groups
U 11	50	100	50	25	50	25	2
U 12	50	100	50	25	50	25	2
U 13	50	100	50	25	50	25	2
U 14	50	100	50	25	50	25	2

Level of training 2	Reference input competence	Reference output competence	Reference duration	Reference group size	Number of hours realized	Real group size	Number of groups
U 21	100	150	50	20	50	20	2
U 22	100	150	50	20	50	20	2
U 23	100	150	50	20	50	20	2
U 24	100	150	50	20	50	20	2

Level of training 3	Reference input competence	Reference output competence	Reference duration	Reference group size	Number of hours realized	Real group size	Number of groups
U 31	150	200	50	15	50	15	2
U 32	150	200	50	15	50	15	2
U 33	150	200	50	15	50	15	2
U 34	150	200	50	15	50	15	2

For the simulation, we consider that 100 learners are enrolled per year for level 1, 80 for level 2, and 60 for level 3.

The algorithm in Figure 8 illustrates how the simulation is performed
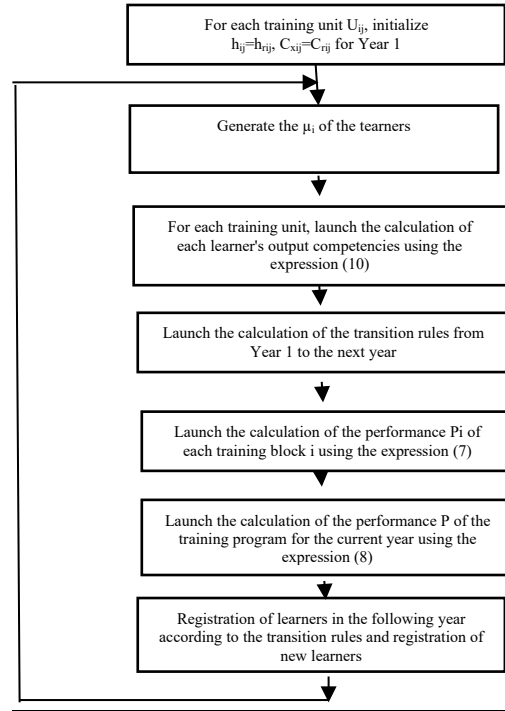
Figure 8: Algorithm for simulating the performance of a training program

The simulation is performed for seven iterations up to Year 7 of the training program. The objective is to track the behavior of the variation in performance over the seven years of training. The simulation is carried out with a constant number of new learners NI entering Level 1 for each year of study.

Figure 9 below is an illustration of the simulation's result.
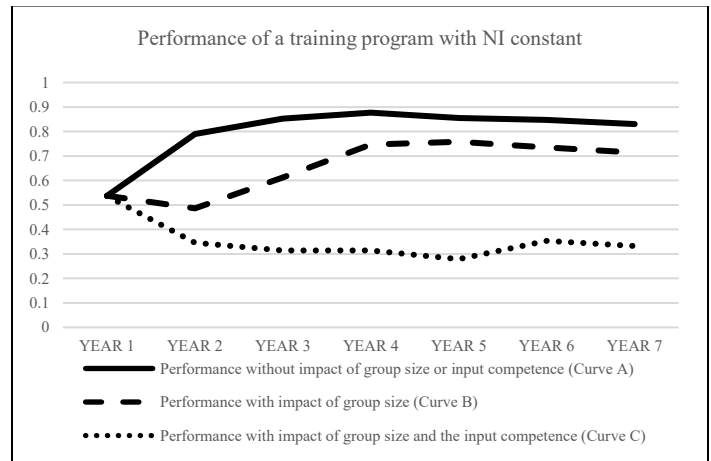
Figure 9: Simulation of the performance of a training program with NI constant

Figure 9 illustrates the variation in the performance of the training program on three different curves. The first curve (Curve A with continuous line) represents the impact of the personal capacity of competence acquisition μ_i. In this case, the coefficients of the group size g(n) and the input competencies $k(C_i/C_r)$ are kept equal to 1. The second curve (curve B with dashed line) represents the impact of the personal capacity of competence acquisition μ_i

and the coefficient of the group size g(n). The factor of the input competencies $k(C_i/C_r)$ is kept equal to 1. The third curve (Curve C with dotted line) reflects the impact of the personal capacity of competence acquisition μ_i, the coefficient of group size g(n), and the input skills factor $k(C_i/C_r)$.

For curve (A), in the first year of the training program, the performance of the training program is close to 50%. This is due only to the impact of the learners' μ_i factors, which are distributed according to a normal distribution whose average is 1. Thus, nearly 50% of the learners have a μ_i factor less than 1 and therefore cannot reach the required output competencies. For year 2 this performance increases to nearly 80%. This is explained by the fact that the learners who move up to the higher levels in year 2 satisfy the required input competencies and their μ_i are greater than or equal to 1, which allows them to reach the output competencies. Moreover, for learners at the different levels who fail and repeat some training units, they validate these units since they have re-enrolled with their output competencies from year 1 as input competencies for year 2 that are higher than the required competencies, thus making up for their μ_i deficit. The 20% performance deficit is mainly due to the new learners who enrolled in level 1, 50% of whom have a $\mu_i<1$ factor. Beyond this year, performance stabilizes at just over 80%. Thus, under the conditions of this simulation, i.e., without considering the effects of group size and the deficit in the input competence, the impact of the μ_i factors is offset by the increase in competencies of learners with a $\mu_i<1$ for the second enrolment in the same training unit.

For curve (B), in addition to the impact of μ_i, the impact of the group size is included. By comparing curve (A) and curve (B), the impact of group size is clearly apparent with a decrease in the performance of Year 2 of the training program. In fact, only μ_i has an impact on the performance of year 1. Thus, learners with a $\mu_i<1$ in year 1 are re-enrolled in the same training units in year 2, thus increasing the group size of these training units and consequently this year's performance is impacted by this increase in the number of learners. From year 3 onwards, performance increases and then stabilizes at the end of year 5. This is due, on the one hand, to the increase in the input competencies of learners who repeat a given level, which partially compensates for the impact of μ_i and group size, and, on the other hand, to the stabilized number of learners in the higher levels.

For curve (C), in addition to the impact of μ_i and group size, the impact of learners' input competencies is included. Comparing this curve with the other two curves, we see that the factor of learner input competencies negatively affects the performance of the training program which stabilizes at the end of year 7 at a rate of 40%.

The results of this simulation allow us to compare and visualize the behavior and variation in the performance of a training program under the effect of the different simulation factors. These results also make it possible to quantify this variation in performance. Indeed, by acting on the learners' input competencies through specific training actions for their improvement, the performance of the training program can be improved and go from a rate of 40% to a rate of nearly 80%. If we also act on the size of the group, performance can be further improved. Another performance improvement lever lies in the improvement of the learners' personal capacity to acquire competencies. This simulation is carried out with a constant number of new learners who enroll in the training program each year.

Another simulation is carried out to study the effect of a change in the number of new registrants at the start of the program in year 1. We will consider three situations, the one for which the number of entrants is 100, then the one where this number is increased by 20% then the one where it is decreased by 20%

The results of this simulation are shown in the following graph:
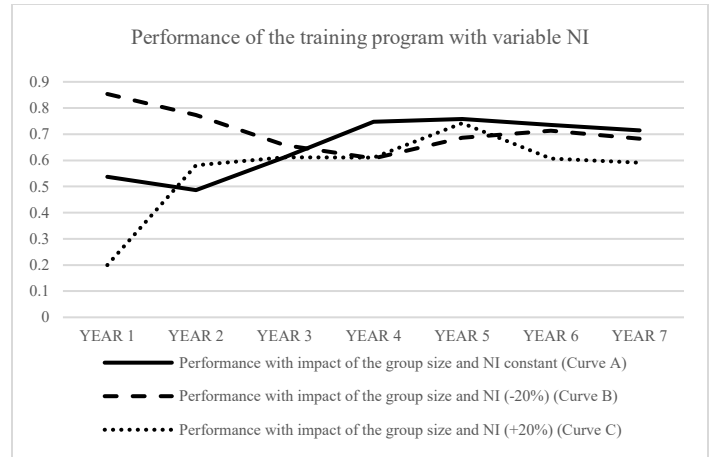
Figure 10: Simulation of the performance of a training program with variable NI

Figure 10 illustrates the variation in the performance of the training program along three different curves. The first curve (curve A with a continuous line) represents the impact of the personal capacity of competence acquisition μ_i and the group size with the new number of learners conforming to the reference number of the block of level 1. The factor of the input competence $k(C_i/C_r)$ is kept equal to 1. This curve corresponds to curve B of the previous simulation. This curve is considered as the reference curve for this simulation. The second curve (curve B with a dashed line) represents the impact of the μ_i and the coefficient of the group size g(n) with a number of new learners at the entrance 20% lower than the reference number. The factor of the input competence $k(C_i/C_r)$ is kept equal to 1 and, the third curve (curve C with dotted line) represents the impact of μ_i, the coefficient of the group size g(n) with a number of new entrants 20% higher than the reference number. The factor of the input competence $k(C_i/C_r)$ is kept equal to 1.

The performance of the training program in the start-up year "Year 1" varies according to the number of learners at the entrance. When the number of new entrants is reduced (curve B), the group size factor g(n) becomes greater than 1, which compensates for the effect of μ_i and therefore the performance of the training program increases, whereas when the number of new entrants is increased (curve C), the group size factor g(n) becomes less than 1, which contributes to the impact of μ_i in reducing the performance of the training program.

Whereas in the second "Year 2", the results are reversed. Indeed, in the case of curve B, given the number of learners who validated in year 1, the group size of the different blocks in year 2 increased and consequently g(n) becomes less than 1 and impacts the increase in learners' competencies and subsequently performance. The performance follows the same behavior until year 5, after which the performance increases, stabilizes, and approaches the performance of curve 1.

As for the behavior of the performance in the case of curve C, it follows the opposite behavior than that of curve B and in the stabilization phase, from year 5 onwards, the performance stabilizes at a rate of 60%, i.e. a decrease of 10% compared to the reference curve A.

These simulations on the performance of a training program illustrate the impact of the factors selected on this performance and make it possible to estimate, in a quantitative manner, the effects of variations in these factors on performance taken separately or in combination. The results of these simulations provide a better understanding of the interaction between the parameters and their impact on performance and can be used to test solutions for performance improvement.

4. Conclusion

By viewing education systems as skills production systems and by applying Business Processing Modelling methods, a modelling of education systems is proposed in the present work. The breakdown of the whole system allows us to introduce the training unit concept and then to organize these units in networks with units connected in series and parallel.

The objective of each training unit is to transform the learners' level of competencies into higher-level output competencies while respecting the objectives and constraints set by the educational system. Each training unit thus contributes to the achievement of the general objectives of the training system. This is achieved by mobilizing resources and according to rules of realization and rules of conduct.

Thus, the model proposed for the training unit has made it possible to determine the key factors influencing its performance. This model was coupled with a simulation model that allows to study the impact of the variation of these factors on the evolution of the system's behavior and performance and to simulate this impact.

The presented results of simulations show the effects of the learners' input competence deficit on the evolution of the process of competence increase and consequently on the performance of the training unit. Thereafter, the impact on the overall performance of a training program of this factor cumulated with those of the factors of the learners' personal capacity to acquire competencies, and the group size is studied.

This modelling allows us to evaluate the performance of the training unit and the training program in a quantitative way and to simulate the behavior of this performance by varying the different factors. This modelling enables us to test solutions for performance improvement.

Let us note that a validation of the model on case studies remains to be carried out and will require in particular the establishment of strategies for identifying the various parameters involved in the laws introduced to characterize the learner's aptitudes.

References

[1] T. McCowan, "The Role of Education in Development," Higher Education for and beyond the Sustainable Development Goals, Palgrave Studies in Global Higher Education, 2019, https://doi.org/10.1007/978-3-030-19597-7_2

[2] N. Ghaffarzadegan, R. Larson and J. Hawley, "Education as a Complex System," System Research and Behavioral Science, Wiley Online Library, 2016, DOI: 10.1002/sres.2405.

[3] M. Koopmans, D. Stamovlasis, Complex Dynamical Systems in Education: Concepts, Methods, and Application, Springer, 2016. DOI 10.1007/978-3-319-27577-2

[4] J. Groff, "Dynamic systems modeling in educational system: Design & Policy," New approaches in educational research, **2**(2), 72-81, 2013. DOI: 10.7821/naer.2.2.72-81

[5] F.B. Vernadat, "Techniques de modélisation en entreprise : Application aux processus opérationnels, " Economia, 1999.

[6] C. Clementz, Modélisation des systèmes de production de compétences: apports à l'ingénierie pédagogique, Ph. D Thesis, Université de Metz, 2000. https://hal.univ-lorraine.fr/tel-01775474

[7] O. Bistorin, Méthodes et outils d'aide à la conception des processus opérationnels des systèmes de formation, Ph. D Thesis, Université Paul Verlaine de METZ, 2007. https://tel.archives-ouvertes.fr/tel-01749013

[8] M. Dragna et D. Ivanaa, "Business Process Modeling in Higher Education Institutions. Developing a Framework for Total Quality Management at Institutional Level," Procedia Economics and Finance, **16**, 95-103, 2014. doi: 10.1016/S2212-5671(14)00779-5

[9] P. SeungSoon, "Applying Petri nets to model customized learning and cooperative learning with competency," International journal computer science and network security, **8**(2), 2008. DOI: 10.15693/ijaist/2016.v53i53.6-12

[10] UNESCO, "Education, Policy & Strategy: Simulation Model EPSSim Version 2.1." 2005.

[11] N. Messaoudi, J. Khalid Naciri and B. Bensassi, "Simulating effect of parameter variation on the performance of an educational system," International Journal of Simulation and Process Modeling, **13**(3), 189-199, 2018. DOI: 10.1504/IJSPM.2018.10014176

[12] O. Bistorin, C. Pourcel and P. Padilla, "Integrated model for operational process design of learning system," 8e Conférence Internationale de MOdélisation et SIMulation, Hammamet, 2010.

[13] H. Kromm, J. Deschamps, and G. Doumeingts, "Modélisation de processus pour une évaluation par niveaux de détail successifs, " in 3e Conférence Francophone de Modélisation et de Simulation MOSIM'01, 2001.

[14] S. Bowles, Towards an educational production function, National Bureau of Economic Research, 1970. http://www.nber.org/chapters/c3276.pdf

[15] M. Benko, "On the Status of the Model of Growth of Knowledge by Repetition on the Field of Didactics," Nitra, 2013.

[16] F. Mourji and A. Abbaia, "Les déterminants du rendement scolaire en mathématiques chez les élèves de l'enseignement secondaire collégial au Maroc : une analyse multiniveaux," Revue d'économie du développement, **21**(1), 127–158, 2013. DOI : 10.3917/edd.271.0127

[17] J.D. Williams and M.Somers, "Family, classroom, and school effects on children's educational outcomes in Latin America," School Effectiveness and School Improvement, **12**(4), 409–445, 2001. DOI: 10.1076/sesi.12.4.409.3445

[18] R.M. Felder and R. Brent, "Understanding student differences," Journal of Engineering Education, **94**(1), 57–72, 2005. DOI: 10.1002/j.2168-9830.2005.tb00829.x

[19] R. J. Marzano, Building background knowledge for academic achievement, Alexandria: Association for supervision and curriculum development, 2004. ISBN 0-87120-972

[20] D. Muijs and D. Reynolds, "Student background and teacher effects on achievement and attainment in mathematics: A longitudinal study," Educational research and evaluation, **9**(3), 289-314, 2003. https://doi.org/10.1076/edre.9.3.289.15571

[21] B. Hemmings, P. Grootenboer and R. Kay, "Predicting mathematics achievement: the influence of prior achievement and attitudes," International Journal of Science and Mathematics Education, **9**(3), 691-705, 2011. https://doi.org/10.1007/s10763-010-9224-5

Recent Impediments in Deploying IPv6

Ala Hamarsheh[*,1], Yazan Abdalaziz[1], Shadi Nashwan[2]

[1]*Computer Science, Arab American University, Jenin, 240, Palestine*

[2]*Computer Science Department, College of Computer and Information Sciences, Jouf University, Sakaka, 2014, Saudi Arabia*

A R T I C L E I N F O	A B S T R A C T
	Internet Protocol version 6 is being adopted on slow pace and it is taking a long time. This paper intends to discuss the transition process between IPv4 and IPv6 and the major obstacles that prevent deploying IPv6 worldwide. It presents the IPv4 exhaustion reports results and where are the IPv4 address pool. Then it presents the methods that have been used to prolong the life expectancy of IPv4. After that it describes and discusses the mechanisms that have been used to deploy IPv6. Additionally, it describes the recently proposed mechanisms to overcome the problems encountered by the ISPs in migrating to IPv6. Furthermore, it shows the mechanisms that have been proposed to motivate the ISPs to start deploying IPv6 on their access networks. Finally, it presents a comparison between these mechanisms from the authors' point of view.

1. Introduction

'Internet Protocol Version 4" (IPv4) [1] is the current considered primary Internet protocol. It uses a 32-bit address. That provides more than 4 Billion addresses. Due to the frequent use of the internet and the abundance of devices that need an Internet connection, IPv4 was drained. As a temporary solution, many mechanisms have been proposed to prolong the life of IPv4. In the end, there must be a permanent solution. Internet Engineering Task Force (IETF) proposed a solution in which to convert IPv4 to a new protocol which is the "Internet Protocol Version 6" (IPv6) [2].

IPv6 was created by the IETF as a successor protocol to IPv4. It was proposed in 1994 and it became an internet standard on 14 July 2017 [3]. IPv6 uses a 128-bit address which provides approximately 3.4 x 1028. That will fulfill the huge need for IP addresses. The problem is that IPv6 can't be deployed all at once because of the large number of users and devices. Also, the lack of readiness of the infrastructure may delay the process knowing that the users can't be forced to update or change their devices so that they can use IPv6. IPv4 and IPv6 are not compatible and they can't be deployed both at the same time. IETF has proposed many solutions to start deploying IPv6 alongside IPv4. The plan is to start integrating IPv4 with IPv6 until IPv6 is fully deployed.

This Paper is an extension of work originally presented in [4]. In this research paper, we will present the methods that have been used to conserve the public IPv4 addresses. Then we will present some reasons that prevent the IPv6 deployment process. After that, we will present the mechanisms that have been proposed to integrate IPv6 alongside IPv4. Finally, we will compare and discuss these mechanisms from the authors' point of view.

2. IPv4 Exhaustion

The "Internet services providers" ISPs get the IP addresses from the Regional Internet Registry (RIR). There are five RIRs each one is responsible for providing IP addresses in a particular area of the world. which are: "American Registry for Internet Numbers (ARIN), Asia-Pacific Network Information Center (APNIC), Latin America and Caribbean Information Center (LACNIC), Reseaux IP Europeens Network Coordination Center (RIPE NCC), and the African Network Information Center (AFRINIC)". A statement has been made by APNIC that they have been operating under the last/8 framework since April 2011. At that time, they declared that they have 11,028,480 addresses assigned as available and have 15,728,128 unassigned addresses. For more information about the other RIRs reports check [5].

3. Methods to Preserve "Public IPv4 Addresses"

Many mechanisms that have been proposed to prolong the life expectancy of IPv4 the first one is the "Network Address Translation (NAT)" [6]. In short, NAT is a translation mechanism that translates IPv4 public addresses to a group of IPv4 private

addresses. rapid growth of internet users and IP addresses consumption has affected on NAT and it is not useful solution anymore. However, IETF has proposed some mechanisms which are:" Large Scale NAT (NAT444)" [7], and "Address plus Port (A+P)".

3.1. Large Scale NAT (NAT444)

Large Scale NAT or NAT444 is a technology that has been considered by the ISPs to extend the life of IPv4. Using NAT444 ISPs have been able to provide the users with IPv4 during the transition to the IPv6 process. It works by adding a Carrier Grade NAT (CGN) to the ISP's network. It translates one public IPv4 address among various CPEs and the private address in the CPE will again be translated into many private IPv4 addresses to arrive at the end-user with two NATs. NAT444 has many disadvantages, for instance, users may affect each other on bad behaviors because they share one public IPv4 address among a large number of users. Also, losing geolocation information because translation zones will cross traditional geographic boundaries see [8]. VoIP and video applications might be affected by NAT444 with latency, or packet loss, etc. see [9].

3.2. Address Plus Port (A+P)

A+P is a sharing schema that allows multiple users on the same CPE to use the same public IPv4 address. It extends the IPv4 address by using some of the port numbers as additional endpoints identifiers in the TCP/UDP header. Port Range Router (PRR) runs the process of assigning the range of IP addresses among the CPEs. A+P schema can provide 65536 ports for each public IPv4 address and each port can provide an extra 65536 ports. The idea behind A+P is that it divides the public IPv4 address without the need for translating it see [10] for more details.

4. Transition Approaches

Since IPv6 and IPv4 are not corresponding to each other and deploying IPv6 cannot be done all at once, the IETF has proposed techniques and mechanisms in order to achieve a smooth transition to IPv6. The smooth transition can be achieved by deploying IPv6 at the same time as IPv4. To allow communications between IPv4-Only networks and IPv6-Only networks IETF has proposed the transition mechanisms. These mechanisms are Dual-Stack, Tunneling, and Translation Approaches.

4.1. Dual-Stack Approach

The dual-stack approach is providing the user's connectivity for both IPv4 networks and IPv6 networks. A dual-stack device is any device that connects to the internet and configured with multiple IP addresses IPv4 and IPv6 at the same time. The idea behind the dual-stack approach is to configure all devices with both IPv4 and IPv6 addresses so that the devices can communicate over both networks [11]. It uses the perspective protocols (DHCPv4, DHCPv6) [12], [13] to assign addresses to the dual-stack devices. The network administrator is responsible for enabling perspective protocols. See Figure 1 which describes the Dual-Stack approach.

4.2. Tunneling Approach

The tunneling approach is a protocol that allows the movement of data from a network to another through a different type of

network. IPv4/IPv6 Routers and Hosts encapsulate the IPv6 packet in an IPv4 packet and send it through an IPv4 network to another IPv6 network. Tunneling can be used in various ways for instance Router-to-Router, Host-to-Router, Host-to-Host, and Router-to-Host. Because the hosts and routers need to explicitly configure the tunneling endpoints Router-to-Router is probably used. Figure 2 illustrates the Tunneling approach.
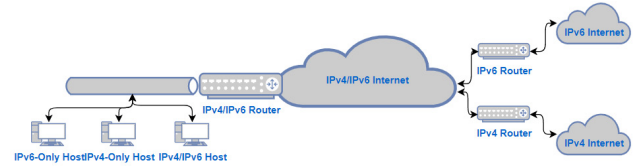
Figure 1: Dual-Stack Approach
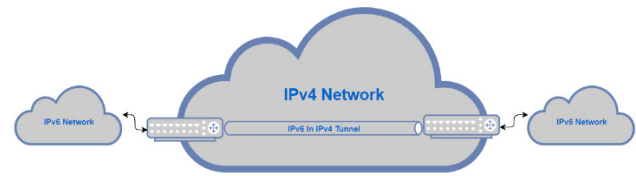
Figure 2: Tunneling Approach

Tunneling has two types which are: Static Tunneling and Automatic Tunneling.

- Static Tunnels: in static tunneling the address will be configured at the tunnel endpoint and the configuration in this technique is manual. The encapsulating node is the one responsible for storing the tunneling information. It stores the tunnel endpoint address which will be the destination address. in addition, it stores the routing information in order to determine which packet to tunnel. Also, it uses the match technique and the prefix mask to the destination to the packet [14]-[16].

- Automatic Tunnels: in automatic tunneling the IPv6/IPv4 nodes can automatically determine the tunnel endpoint and That can be extracted from the IPv6 address. definitely the IPv6 must be backward compatible with IPv4. Also, the nodes possess the ability to decide which packets are auto tunneled and which are not. The main difference between the dynamic and static tunneling is the automatic determination of the tunnel endpoint.

4.3. Translation Approach

The previous approaches could be useful when communication is needed between two isolated IPv4 networks or two isolated IPv6 networks, while they have no use when an IPv4 only network tries to communicate with an IPv6 only network. The translation approach is a mechanism that allows an IPvX-Only network to communicate directly with an IPvY-only network. It translates the IPvX packet to an IPvY packet to allow communication. Figure 3 describes the translation approach.

The translation mechanism can be classified into two approaches [11]: Host-Based Approach and Network-Based Approach.

- Host-Based Translation

  Host-based translation is needed when there is an incompatibility between the running application type and the current host connectivity. So that, the IPvX will be translated to communicate with the IPvY and vice versa. In host-based translators, the changeover is between the application layer and the IP communication layers. There are three host-based translators was proposed which are: Bump-In-the-Stack (BIS) [17], Bump-In-the-API (BIA) [18], Bump-In-the-Host (BIH) [19]. In the next section we will present the host-based techniques in addition to another technique the author was proposed which is Decupling Application IPv4/IPv6 Operation from the Underlying IPv4/IPv6 Communication (DAC) [20].
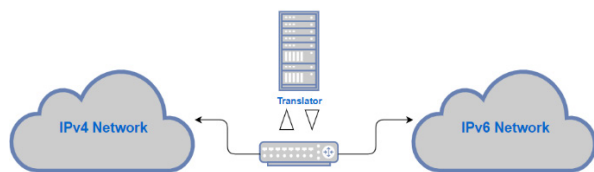
Figure 3: Translation Approach

- Network-Base Translation

  In network-based translation, the IP header will be translated to every packet. That to provide the connectivity between IPv4-only networks and IPv6-only networks and vice versa [11]. An example of network-based translators is Stateless IP/ICMP Translation (SIIT) [21], and Stateful Address and Protocol Translation from IPv6 Client to IPv4 Servers (NAT64) [22].

5. IPv6 is Not Fully Deployed Yet

Transition to IPv6 is indeed a big breaking change in the networks. It can't be done all at once for many reasons. This section intends to describe these reasons from the author's point of view.

5.1. End User

End-users are not directly benefiting from the transition process; however, it is considered as an effective part in achieving it. The end-user might pose an obstacle for deploying IPv6. As we discussed earlier the deployment process of IPv6 must be smooth. A smooth transition can be done without affecting the users taking into account the users' application and the host configurations should be upgraded. The end-user can delay the process knowing that not all users have the proper knowledge to update or implement the upgrades.

There are some upgrades that should be implemented on the IP stack, "Transmission Control Protocol (TCP)", and "User Datagram Protocol (UDP)" in addition to the users' old applications [11], [23], [24]. The host configuration process should be automatically performed without the user knowledge because the user can't be expected to be qualified to deal with the manual configurations or any other technical configurations.

Achieving the transition process smoothly could take a while till IPv6 is fully deployed. Within this time there will be IPv6 only

networks and IPv4 only networks that need to be able to communicate with each other. The solution to that problem is the dual connectivity so that dual networks can communicate to both IPv4 and IPv6 networks [25]. The users' applications can be expected to be updated to support dual connectivity if it has good support but there are many applications that are not supported such as home-made applications and out-of-business applications and many other applications that will have the same problem.

There are many mechanisms that have been proposed as a solution to guarantee dual connectivity between incompatible hosts. IETF has proposed mechanisms such as "Bump In The Stack (BIS)" [17], "Bump In the API (BIA)" [18], [26], and "Bump In The Host (BIH)" [19]. Another mechanism that has been proposed by the author of this paper is "Decupling Application IPv4/IPv6 operation from the Underlying IPv4/IPv6 Communication (DAC)" [20], [27], [28].

- Bump in the Stack (BIS)

  Bump-In-the-Stack is a technique that uses the SIIT [29] algorithm to translate the IPv4 packets (i.e. headers) to IPv6 and the IPv6 packets (i.e. headers) to IPv4. In BIS the translation module is inserted between the TCP/IPv4 module and the card driver module. The translation module takes the data that flow between the modules that it is inserted between and translates the packets from IPv4 to IPv6 and vice versa. The DNS server is responsible for assigning the IP addresses. So, the user does not know about the other types of IP addresses that it communicates with. The main idea behind BIS is to provide the communication between IPv4 applications and IPv6 hosts.

- Bump in the API (BIA)

  Is a technique that used to translate the IPv4 socket API functions into IPv6 socket API functions and vice-versa. It detects the IPv4 socket API functions and invokes the equivalent IPv6 socket API functions so that there will be no need for translating the full IP header. BIA expects that TCP/UDP IPv4 and TCP/UDP IPv6 to existing on the local node. Unlike BIS, BIA inserts the API translator between the socket API module and the TCP/IP module in the dual-stack hosts.

- Bump in the Host (BIH)

  BIH technique is a host-based mechanism. It integrates both BIS and BIA techniques together and translates from IPv4 to IPv6. BIH consists of two implementations which are a translator in the API socket which is inserted between the TCP/IP module and socket IP module the other implementation is the translation protocol which inserts it between the network card driver and the TCP/IP module. BIS intends to let the old applications which uses NAT to communicate with the IPv6 only applications.

- Decoupling Application IPv4/IPv6 Operation from the Underlying IPv4/IPv6 Communication (DAC)

  DAC is a technique Allows applications that are compatible with IPv4-only stack and running on hosts with dual stack or with IPv6-only connectivity to communicate with IPv6 hosts. Additionally, it enables applications that are compatible with IPv6-only stack and running on hosts with dual stack and connectivity or with IPv4-only connectivity to communicate with IPv4 hosts. In theory, DAC is a layer that should be inserted between the

application layer and the IP communication stack on top of the API functions and it should perform the same functionalities that the API native functions perform. Translation from IPv4 and IPv6 and vice versa is only done on necessary basis. DAC will be effective between applications with an incompatible type and an incompatible networks connectivity. Furthermore, DAC can be installed at an IPv4 only host, IPv6 only host, and IPv4/IPv6 host.

5.2. Service Provider Network

The Internet Service Providers (ISPs) are the other effective part of the deployment process. as we discussed before the ISPs are cannot provide the users IPv4 addresses anymore and they need to deploy the IPv6 so that they can keep up with the internet users' swift increasing and provide the users with the required IP addresses. The transition process requires an upgrade or change of the infrastructure to one that can withstand the IPv6. That might be very expensive for the ISPs. IETF has proposed a technique that allows the ISPs to start deploying IPv6 over IPv4 networks. This technique is IPv6 Rapid Deployment on IPv4 Infrastructure (6rd) [30], [31].

6rd is an automatic tunneling technique was proposed to support rapidly deployment of IPv6 on existing IPv4 environment. In order to transmit the IPv6 traffic over IPv4 environment, 6rd uses encapsulation technique to transfer IPv6 packets through the IPv4 networks and it uses the ISPs' own IPv6 prefix other than a well-known prefix. Since it uses the network-specific prefix (NSP) each ISP can use its particular prefix that's mean the 6rd operational scope is limited to the ISP's domain. Moreover, the tunnels will be from the ISP's border relay (6rd gateway) to the customer edge (CE). see [30] and [32] for more details.

ISPs have faced determinations that hindered them from starting the deployment process of IPv6 through IPv4 infrastructure. One of these limitations is the need to upgrade or change the 6rd gateways (CE) which will affect them by raising the costs of deploying IPv6. In addition to the time that the process of Configuring the CEs would take after change and upgrade which might stall the process. Also, 6rd protocol upholds only one level of DHCPv4 between the CE and the border router. Never forget to mention the firewalls which might block the tunneled traffic that related to 6rd.

The authors of this research paper have suggested a few techniques that concurs the 6rd obstacles. These techniques are: "Deploying IPv6 Service Across Local IPv4 Access Network (D6across4)" [33], [34], "Configuring hosts to Auto-detect (IPv6, IPv6-in-IPv4, or IPv4) network connectivity (CHANC)" [35], and "Deploying IPv4-only Connectivity across Local IPv6-only Access Networks (D4across6)" [36]. The next section of this research will discuss these techniques and how they have overcome the limitations and obstacles that faced the ISPs before.

- Deploying IPv6 Service Across Local IPv4 Access Network (D6across4)

D6across4 is a mechanism that intends to motivate the ISPs to start the deployment process and start offering IPv6 services to their customers. It is a protocol mechanism to start deploying IPv6 service to host over the existing ISP's IPv4 network. D6across4 assigns an algorithmic mapping between the IPv4 and IPv6 addresses in the ISP network. It automatically resolves the tunnel server (TS) domain name to determine the tunnel endpoints. It

consists of customers' hosts and one or more TSs. Same as in 6to4 it encapsulates the IPv4 packets then forwards them to follow the topology of the IPv4 in the ISP network.

While 6rd and other protocols need upgrade and change the 6rd gateways and the network devices in both ISPs' and end users' sides. D6across4 tries to reduce both cost and time of the deployment process of IPv6 which is one of the problems that faced the ISPs and that prevented them from starting. Even though, in order for D6across4 can encapsulate/de-capsulate traffic IPv6 packets through the local IPv4 networks, it needs to be installed at ISPs' side at the network components, and at the uses side particularly at the applications hosts. See for more details [33].

There are some limitations that could be found in D6across4 that could affect deploying IPv6. These limitations are: if D6across4 has been deployed on a large scall networks it could face some issues regarding the scalability and the performance issues. So, it only could be integrated on a relatively small network. Also, since the D6across4 protocol is a stateful operation, for each packet receival it needs to access the mapping tables that could be exhaustion and consider as an additional load and it would be higher than any other stateless protocol. In addition, using a well-known prefix might shorten IPSs' capability of managing and controlling their traffic. Just like 6rd, D6across4 could be affected by firewalls and its traffic might be blocked.

- Configuring hosts to Auto-detect (IPv6, IPv6-in-IPv4, or IPv4) network connectivity (CHANC)

Same as D6across4 CHANC is a mechanism to encourage the ISPs to start the deploying IPv6 through IPv4 environment. Unlike D6across4 CHANC protocol doesn't need any upgrading or changing in the CEs which represents the extra costs that cause the delay of the deployment process. CHANC protocol gives the ISPs the ability to offer IPv6 to their customers through IPv4 infrastructure with the minimum cost and automatically configure the end-user's host. In fact, CHANC automatically configure the hosts to give them the ability to automatically detect every connectivity with every type that their ISP provide and locating the relay server would also be automatic. Also, CHANC uses the HTTP-in-IPv4 mechanism for transmitting IPv6 traffic through IPv4 environment.

CHANC has many advantages that overcome the other proposed protocols which are:

- The configurations in the end-users' hosts are done automatically which ease the process instead of manual configurations.
- It reduces the costs because there is no need for changing or upgrading the IPv4-only networks on both ISPs' and end-users' sides.

- Because of the IPv4 only access network, the ISPs can immediately begin offering IPv6 without the need support IPv6.
- It prevents the firewalls from blocking the tunneled packets of CHANC. It encapsulates the packets in HTTP protocol which permit the access to the traffic through utmost all firewalls.
- It simplifies administrating IPv6 traffic by allowing every ISP to use the prefix of its own.

Table 1: Comparison between the previously presented techniques and mechanisms

Protocol	Category	Installed At	Functionality	Limitations
BIS	Translation-based	"between the TCP/IP module and the network card driver"	Permit communication between IPv4 only applications on dual stack machines and IPv6 hosts	- Does not work with multicast communication. - invalid for embedded addresses. - It cannot be combined with a secure DNS. - It cannot employ security overhead the network layer.
BIA	Translation-based	"between the socket API module and the TCP/IP module"	Permit communication between IPv4 only applications on dual stack machines and IPv6 hosts	- invalid embedded addresses. - Does not uphold multicast. - Difficulties in translating APIs because of IPv6 API's advance new features.
BIH	Translation-based	"between the TCP/IP module and the network card driver or between socket API module and the TCP/IP module"	Permit communications between IPv4 legacy application and IPv6 only hosts and dual stack host	- invalid for embedded addresses. - Does not uphold multicast. - Does not uphold all types of applications.
DAC	Translation-based	"between the communication stack and the application layer"	Permit communications for both IPv4 and IPv6 applications through IPv4 and IPv6 connections with both IPv4 and IPv6 type capable remote applications.	- invalid for embedded addresses.
6rd	Tunneling-based	between the ISP border relay and the customer edge	Permit IPv6 connectivity through ISPs' IPv4 environment	- Single point of failure. - requires upgrade and change in the CPEs. - Cannot cross firewalls.
D6across4	Tunneling-based	ISP side and end users' host	Permit IPv6 connectivity through ISPs' IPv4 environment	- Single point of failure. - cannot cross firewalls.
CHANC	Tunneling-based	ISP side and end users' host	Permit IPv6 connectivity through ISPs' IPv4 environment	- Single point of failure.

- CHANC is a stateless-based translation mechanism that uphold end to end address translucence while the communication is between IPv4 and IPv6.

The Table below presents a comparison between the techniques and protocols that have been presented in this research.

6. Summary

The internet development has led to exhaustion in the IPv4 addresses and most of the ISPs are running out of IPv4. That makes the deployment of IPv6 has become mandatory. IETF has offered various mechanisms to extend the usage of IPv4. The proposed mechanisms and protocols are considered as a temporary solution. Afterall, the deployment of the IPv6 is unavoidable. ISPs are the major factor that affect the deployment directly. They need to start upgrading and changing the infrastructure to support IPv6. Also, IETF has offered various techniques and protocols to encourage the ISPs to start offering IPv6 alongside with IPv4 or even IPv6 through IPv4 infrastructure. These techniques and protocols can be classified into three classifications: Dual stack, Tunneling, and translation. In addition, various techniques and mechanisms have been offered by the authors of this research and by IETF for instance BIS, BIA, BIH, DAC, 6rd, D6across4, and CHANC. These mechanisms intend to encourage the ISPs and facilitate the deployment process in order for them to start the smooth transition.

Conflict of Interest

Ala Hamarsheh, Yazan Abdalaziz, Shadi Nashwan declare that they have no conflict of interest.

References

[1] J. Postel, "Internet Protocol," California, USA: Internet Engineering Task Force RFC791, 1981.

[2] S. Deering, R., Hinden, "IP Version 6 Addressing Architecture," California, USA: Internet Engineering Task Force RFC 4291, 2006.

[3] S. Deering, R. Hinden, "Internet Protocol, Version 6 (IPv6) Specification," California, USA: Internet Engineering Task Force RFC 8200, 2017.

[4] A. Hamarsheh, Y. Abdalaziz, "Deploying IPv6 Service Across Local IPv4 Access Networks," in 2019 International Conference on Computer and Information Sciences (ICCIS), Sakaka, Saudi Arabia, April 3-4, 2019.

[5] G. Huston. IPv4 Address Report [Online]. 2018. Available: http://www.potaroo.net/tools/ipv4/index.html

[6] P. Srisuresh, M. Holdrege, "IP Network Address Translator (NAT) Terminology and Considerations," California, USA: Internet Engineering Task Force RFC 2663, 1999.

[7] I. Yamagata, Y. Shirasaki, A. Nakagawa, J. Yamaguchi, H. Ashida, "NAT444," Internet Engineering Task Force Draft (work in progress), 2012.

[8] C. Donley, L. Howard, V. Kuarsingh, J. Berg, J. Doshi, "Assessing the Impact of Carrier-Grade NAT on Network Applications," California, USA: Internet Engineering Task Force RFC 7021, 2013.

[9] S. Bradner, J. McQuaid, "Benchmarking Methodology for Network Interconnect Devices," California, USA: Internet Engineering Task Force RFC 2544, 1999.

[10] R. Bush, "The Address plus Port (A+P) Approach to the IPv4 Address Shortage," California, USA: Internet Engineering Task Force RFC 6346, 2011.

[11] A. Hamarsheh, M. Goossens, "A Review: Breaking the Deadlocks for

Transition to IPv6," IETE Technical Review, **31**(6), 405-421, 2014, doi: 10.1080/02564602.2014.950348

[12] E. Nordmark, R. Gilligan, "Basic Transition Mechanisms for IPv6 Hosts and Routers," California, USA: Internet Engineering Task Force RFC 4213, 2015.

[13] A. Durand, R. Droms, J. Woodyatt, Y. Lee, "Dual-Stack Lite Broadband Deployments Following IPv4 Exhaustion," California, USA: Internet Engineering Task Force RFC 6333, 2011.

[14] R. Gilligan, E. Nordmark, "Transition Mechanisms for IPv6 Hosts and Routers," California, USA: Internet Engineering Task Force RFC, 1996.

[15] Y. Abdalaziz A. Hamarsheh, "Analyzing The Ipv6 Deployment Process In Palestine", International Journal of Computer Network and Information Security(IJCNIS), **12**(5),31-45, 2020, DOI: 10.5815/ijcnis.2020.05.03.

[16] M. Al-Fayoumi S. Nashwan, "Performance analysis of SAP-NFC protocol," International Journal of Communication Networks and Information Security (IJCNIS), **10**(1), 125–130, 2018.

[17] K. Tsuchiya, H. Higuchi, Y. Atarashi, "Dual Stack Hosts using the "Bump-In-the-Stack" Technique (BIS)," California, USA: Internet Engineering Task Force RFC 2767, 2000.

[18] S. Lee, M-K. Shin, Y-J. Kim, E. Nordmark, A. Durand, "Dual Stack Hosts Using "Bump-in-the-API" (BIA)," California, USA: Internet Engineering Task Force RFC 3338, 2002.

[19] B. Huang, H. Deng, T. Savolainen, "Dual-Stack Hosts Using "Bump-in-the-Host" (BIH)," California, USA: Internet Engineering Task Force RFC 6535, 2012.

[20] A. Hamarsheh, M. Goossens, R. Alasem, "Decoupling Application IPv4/IPv6 Operation from the Underlying IPv4/IPv6 Communication (DAC)," American Journal of Scientific Research, Eurojournals Press, **14**, 101-121, 2011.

[21] X. Li, C. Bao, F. Baker, "IP/ICMP Translation Algorithm," California, USA: Internet Engineering Task Force RFC 6145, 2011.

[22] M. Bagnulo, P. Matthews, I. van Beijnum, "Stateful NAT64: Network Address and Protocol Translation from IPv6 Clients to IPv4 Servers," California, USA: Internet Engineering Task Force RFC 6146, 2011.

[23] Y. Abdalaziz, A. Hamarsheh, "Analyzing The IPv6 Deployment Process In Palestine," International Journal of Computer Network and Information Security(IJCNIS), **12**(5), 31-44, 2020, doi: 10.5815/ijcnis.2020.05.03

[24] S. Nashwan, "SAK-AKA: A secure anonymity key of authentication and key agreement protocol for LTE network," International Arab Journal of Information Technology (IAJIT), **14**(5), 790–801, 2017.

[25] A. Hamarsheh, M. Goossens, A. Al-Qerem, "Assuring Interoperability Between Heterogeneous (IPv4/IPv6) Networks Without using Protocol Translation," IETE Technical Review, **29**(2), 114-132, 2012, doi:10.4103/0256-4602.95384

[26] S. Nashwan, "SE-H: Secure and efficient hash protocol for RFID system," International Journal of Communication Networks and Information Security (IJCNIS), **9**(3), 358–366, 2017.

[27] A. Hamarsheh, M. Eleyat, "Performance Analysis Of Ain-Pt, Ain-Slt And Siit Network-Based Translators," in Advances on P2P, Parallel, Grid, Cloud and Internet Computing Proceedings of the 12th International Conference on P2P, Parallel, Grid, Cloud and Internet Computing (3PGCIC-2017), Lecture Notes on Data Engineering and Communications T. Springer, 10, Palau Macaya, Barcelona, Spain, 367-378, 2017, DOI: https://doi.org/10.1007/978-3-319-69835-9_35.

[28] S. Nashwan, "AAA-WSN: Anonymous access authentication scheme for wireless sensor networks in big data environment," Egyptian Informatics Journal, in press, https://doi.org/10.1016/j.eij.2020.02.005.

[29] Nordmark E, "Stateless IP/ICMP Translation Algorithm (SIIT)," Internet Engineering Task Force RFC 2765, 2000.

[30] W. Townsley, O. Troan, "IPv6 Rapid Deployment on IPv4 Infrastructures (6rd) Protocol Specification," California, USA: Internet Engineering Task Force RFC 5969, 2010.

[31] A. Al-Qerem, F. Kharbat, S. Nashwan, S. Ashraf and K. Blaou, "General model for best feature extraction of EEG using discrete wavelet transform wavelet family and differential evolution," International Journal of Distributed Sensor Networks, **16**(3), 1–21, 2020.

[32] R. Despres, "IPv6 Rapid Deployment on IPv4 Infrastructures (6rd)," California, USA: Internet Engineering Task Force RFC 5569, 2010.

[33] A. Hamarsheh, M. Goossens, R. Alasem, "Deploying IPv6 Service Across Local IPv4 Access Networks," in 10th WSEAS International Conference on TELECOMMUNICATIONS and INFORMATICS (TELE-INFO '11), pp. 94-100, Lanzarote, Canary Islands, Spain, 27-29, 2011.

[34] A. Hamarsheh, M. Goossens, "Exploiting Local IPv4-only Access Networks to Deliver IPv6 Service to End-users," International Journal of Computers and Communications, **5**(3), 2011.

[35] A. Hamarsheh, M. Goossens, R. Alasem, "Configuring Hosts to Autodetect (IPv6, IPv6-in-IPv4, or IPv4) Network Connectivity," KSII Transactions on Internet and Information Systems," **5**(7), 1230-1251, 2011, doi:10.3837/tiis.2011.07.002.

[36] A. Hamarsheh, "Deploying IPv4-only Connectivity across Local IPv6-only Access Networks," IETE Technical Review, **36**(4), 398-411, 2018, doi: 10.1080/02564602.2018.1498031.

A S T E S

Study of latencies in ThingSpeak

Vítor Viegas[*,1,2], J. M. Dias Pereira[2,3], Pedro Girão[2,4], Octavian Postolache[2,5]

[1]CINAV – Escola Naval, Base Naval de Lisboa, Almada, 2810-001, Portugal

[2]Instituto de Telecomunicações, Lisboa, 1049-001, Portugal

[3]ESTSetúbal/IPS, Instituto Politécnico de Setúbal, Setúbal, 2914-508, Portugal

[4]Instituto Superior Técnico, Universidade de Lisboa, Lisboa, 1049-001, Portugal

[5]ISCTE – Instituto Universitário de Lisboa, Lisboa, 1649-026, Portugal

A R T I C L E   I N F O

A B S T R A C T

IoT platforms play an important role on modern measurement systems because they allow the ingestion and processing of huge amounts of data (big data). Given the increasing use of these platforms, it is important to characterize their performance and robustness in real application scenarios. The paper analyzes the ThingSpeak platform by measuring the latencies associated to data packets sent to cloud and replied back, and by checking the consistency of the returned data. Several experiments were done considering different ways to access the platform: REST API, MQTT API, and MQTT broker alone. For each experiment, the methodology is explained, results are presented, and conclusions are extracted. The REST and MQTT APIs have similar performances, with roundtrip times between 1 s and 3 s. The MQTT broker alone is more agile, with roundtrip times below 250 ms. In all cases, the up and down links are far from being symmetric, with the uplink delay showing higher variance than the downlink delay. The obtained results can serve as a reference for other IoT platforms and provide guidelines for application development.

1. Introduction

Platforms for IoT (Internet of Things) have become key components in measurement and control systems because they are able to ingest, store and analyze huge quantities of data, on a 24/7 basis, at reasonable prices. They are hosted on the "cloud", which is a fancy name for data centers spread all over the world, equipped with high bandwidth, large storage capacity, and heavy processing power.

The term "cloud" is interesting because IoT platforms have indeed a broader view of the physical processes, as they were somewhere above in the sky. They have a broader view in terms of space because they gather data from different locations, and a broader view in terms of time because they store data persistently. This new level of awareness has flattened the traditional five-level automation pyramid [1] because field devices can now communicate directly with the cloud. Intermediate levels are being bypassed leading to an horizontal structure that is the basis of "smart factory" and "connected manufacturing" [2], two core concepts of "industry 4.0" [3].

Today, the cloud concentrates huge amounts of data making it the ideal place to run large-scale data analytics. Deep leaning, based on artificial neural networks, has benefited a lot from this scenario because it needs lots of data (big data) to perform well. As long as the data are good (big and diverse), deep learning is able to find good computational models for complex processes, even the hardest ones. With a good model in hands, new things can be done (such as preventive maintenance, and just-in-time asset management), and old things can be improved (such as robust control algorithms, and automatic controller tuning). IoT platforms play a key role in this movement because they are the "stage" where things are happening.

IoT platforms began to be used at the top of the automation pyramid because these levels do not need accurate timing. Typical applications include monitoring and supervision [4]-[10], with the

goal of reducing or removing humans in the loop [11]. There are also some applications for closed-loop control [12], [13], but the constrains in terms of low-latency and real-time make harder the penetration of IoT platforms at lower automation levels.

Whether IoT platforms are used for monitoring, supervision, or real-time control, it is important to know how fast and reliable they are. For that purpose, we took a well-known IoT platform – the ThingSpeak platform [14] – and measured the time it takes to upload a data packet and receive a reply. This so-called "roundtrip time" is an indicator of *how fast* the platform is. By checking the resemblance of both packets, outgoing and incoming, we can also have an idea on *how reliable* the platform is. We chose ThingSpeak because it is very easy to use, is open source, is free (with some restrictions), has an active community, and provides a comprehensive set of features, including persistent data storage, data analytics based on MATLAB, easy access through ubiquitous protocols, and security over SSL. For these reasons, the ThingSpeak is one of the makers' favorite platforms [15].

There are similar works trying to characterize experimentally the behavior of cloud servers and IoT platforms. For example, in [16], the author gives a tutorial on network latency measurements using PlanetLab as testbench. He measured the roundtrip times of mobile and non-mobile devices, connected through wireless (WiFi and 3G) and wired (Ethernet) interfaces, while pinging five different AWS servers spread around the world. In [17], the author and his team studied the performance of a cloud database by measuring the time needed to complete a writing on the database and getting back a reaction. They used a Siemens PLC to generate data, the IBM Cloud to store data and fire events, and an industrial computer to catch those events, all connected through a MQTT broker. In [18], the author measured the roundtrip time associated to a MQTT broker when it was accessed from two different continents (Brescia in Europe and São Paulo in South America). In [19], the author evaluated the efficiency and roundtrip time of three protocols commonly used in IoT, namely CoAP (constrained application protocol), WebSockets, and MQTT (message queue telemetry transport). In [20], the author made a quantitative performance analysis of the CoAP and MQTT protocols over various conditions of network capacity, packet loss probability, and link delay. In all these works, a substantial effort was put in characterizing experimentally the behavior of cloud services and the protocols used to access them.

The remaining of this paper is organized as follows: section 2 gives an overview of the ThingSpeak platform; sections 3 and 4 analyze the latencies of the ThingSpeak platform when it is accessed through two different application programming interfaces (API); section 5 focus on the ThingSpeak MQTT broker alone; section 6 discusses the obtained results; and section 7 extracts conclusions.

2. ThingSpeak

The ThingSpeak platform provides resources to store and process data in the cloud. The data are accessed through two well documented APIs: a REST API [21] that communicates over HTTP and follows the request-response model; and a MQTT API [22] that communicates over TCP/IP and follows the publish-subscribe model. Both APIs support authentication through unique read/write keys, but only the REST API supports data encryption

through HTTPS. The REST API works well for one-to-one communications, while the MQTT API is best suited for one-to-many communications. The ThingSpeak MQTT broker only supports QoS = 0 (equivalent to "deliver at most once" or "fire-and-forget").

The ThingSpeak platform organizes information in data channels. Each channel includes eight fields that can hold any data type, plus three fields for location, and one field for status. Each channel is also characterized by a unique ID, a name, and a free description. It is not possible to access the fields individually; all read/write operations are made at the channel level to optimize remote calls. All incoming data receive a sequential ID and a timestamp (with a 1 second resolution). Channels are private by default, but they can also be made public in which case no read key is required. Channels are provided at no charge for non-commercial projects as long as they require no more than 8200 messages/day (~5 messages/minute).

The ThingSpeak provides the following resources to control the dataflow:

- React: Executes an action when stored data meet a certain condition (e.g. when a given field of a given channel crosses a given threshold). The action can be as simple as the execution of a script or the issue of a remote message over HTTP.

- TimeControl: Orders the execution of an action once at a specific time, or periodically on a regular schedule, much like a software timer. The TimeControl supports the same actions as the React.

- ThingHTTP: Is a remote call over HTTP, useful to communicate with remote entities such as devices, websites, and web services.
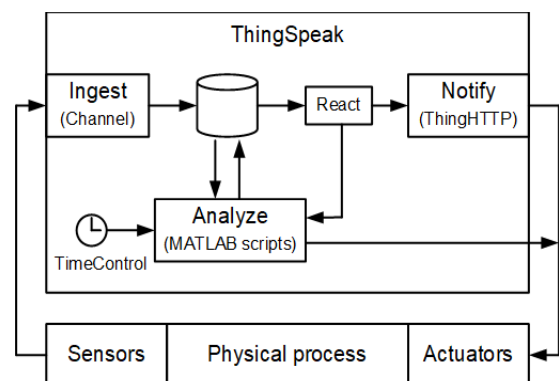
Figure 1: Dataflow inside the ThingSpeak platform

The ThingSpeak platform relies on MATLAB scripts to process stored data. Scripts can be associated to a TimeControl to run one-time or periodically, or to a React to run whenever a given condition is met. Scripts can use the MATLAB toolboxes listed in [23], as long as the user logs into ThingSpeak using its MathWorks account and is licensed to use them. This opens the door to powerful data analytics, supported by robust and well-known software libraries. The results can be visualized on the web, directly from the ThingSpeak site, through ready-to-use charts. The visualization experience can also be enriched with custom widgets and MATLAB plots.

Figure 1 shows the dataflow through the ThingSpeak platform. Data are ingested, stored in a database, and (optionally) analyzed by scripts that run periodically or when a given condition is met. Messages can be sent to third-party applications by a pre-configured ThingHTTP, or by a pre-programmed script using MATLAB functions. The present work focusses on measuring the time it takes to upload data and receive a reply, assuming no processing is made in the interim.

3. ThingSpeak accessed through the REST API

In this section we analyze the performance of the ThingSpeak platform when it is accessed through the REST API. We first explain the methodology used to measure latencies and then we present results.

3.1. Methodology

To measure REST API latencies, we built the closed data path shown in Figure 2, which includes the following stages (the numbers in the list correspond to the numbers in the drawing):

1. LabVIEW application: Is a custom application that runs on our local machine. It makes HTTP calls to the ThingSpeak server, collects the replies, and computes the time elapsed. Each call is a GET request that uploads an order number (n) that is incremented to identify the request. The timestamp of the request (t_{n0}) is registered to serve as reference for the roundtrip time.

2. ThingSpeak channel (name = TestChannel; ID = 515584; access = private): The channel contains a single field (Field1) to store the order number uploaded by the LabVIEW application.

3. React (condition type = numeric; test frequency = on data insertion; condition = TestChannel.Field1 ≥ 0; run = each time the condition is met): A reaction is fired each time a positive order number is received (which is always because n is an unsigned integer). The reaction instructs the MATLAB script to run (see below).

4. MATLAB script: Collects the timestamp at the ThingSpeak server and makes an HTTP call back to the local machine. As shown in Figure 3, the script is programmed to make a POST request to a web service running on the same machine as the LabVIEW application. The request sends back the order number and the timestamp at the ThingSpeak server (τ_n).

5. Router: Accesses from the local machine to an external server are inherently safe and the router forwards them transparently. However, connections in the opposite direction are potentially dangerous and are blocked by default. To overcome this problem, we had to forward port 80 on the local router, so that POST requests coming from the ThingSpeak server reach the LabVIEW web service. In other words, we had to expose the LabVIEW web service to the internet.

6. LabVIEW web service: Is a stateless routine that receives a POST request, extracts the attached order number (n) and timestamp (τ_n), and registers the timestamp of the reply (t_{n1}). The triplet (n, τ_n, t_{n1}) is then sent back to the LabVIEW application by means of a UDP socket. The web service is

hosted by the NI Application Web Server running on port 80 of the local machine.

(n, τ_n, t_{n1}), adds the first timestamp (t_{n0}), and writes the quartet (n, t_{n0}, τ_n, t_{n1}) into the output file for further processing.
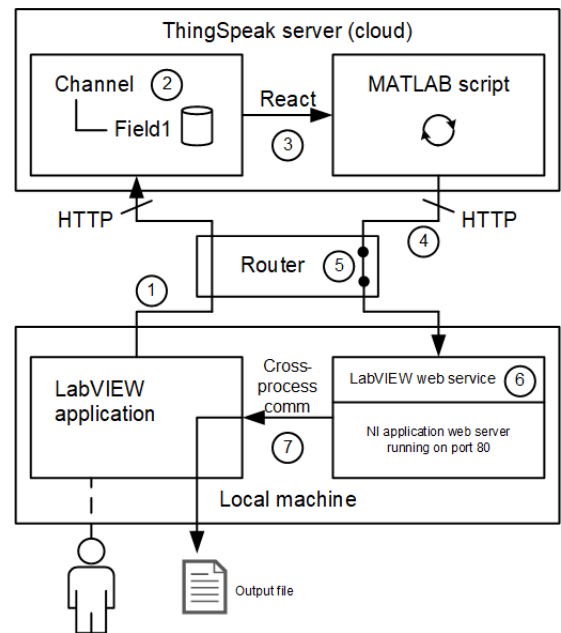

```
1   %get source
2   readChannelID=515584;
3   readApiKey='▮▮▮▮▮▮▮▮▮▮▮';
4   n = thingSpeakRead(readChannelID,'ReadKey',readApiKey);
5   %get ThingSpeak's timestamp
6   tau = datetime('now','Format','HH:mm:ss.sss');
7   %call back
8   url='http://95.136.▮▮▮▮:3582/MyWebService/MyCallBack';
9   %method = POST; media type = application/x-www-form-urlencoded
10  webwrite(url,'OrderNumber',n,'Tau',tau);
```

Figure 3: MATLAB script. The reading key of the channel and the IP address of the LabVIEW web service were erased for privacy

The LabVIEW application and the LabVIEW web service run both on our local machine (Intel i7-8550 CPU @ 1.80 GHz, RAM 16 GB, SSD 512 GB, NVIDIA GeForce MX150). The machine connects to an Ethernet port of a general-purpose router (model HS8247W from Huawei), which accesses the internet through a fiber optic link provided by Vodafone Portugal.

The LabVIEW application uploads order umbers (n) at multiples of 20 seconds to respect ThingSpeak free account limitations. On the nth upload, the quartet (n, t_{n0}, τ_n, t_{n1}) is saved on the nth line of the output file. Thus, it is possible to record the timelines shown in Figure 4, where the τ axis represents the timeline of the ThingSpeak server, and the t axis represents the timeline of the local machine. Of course, the two timelines are not

aligned because the clocks of the two systems are not synchronized. Yet, we can extract the following quantities from these timelines:

$$RT_n = t_{n1} - t_{n0} \tag{1}$$

$$d\Delta_n = \Delta_{n+1} - \Delta_n = (\tau_{n+1} - \tau_n) - (t_{(n+1)0} - t_{n0}) \tag{2}$$

$$d\delta_n = \delta_{n+1} - \delta_n = (t_{(n+1)1} - t_{n1}) - (\tau_{n+1} - \tau_n) \tag{3}$$
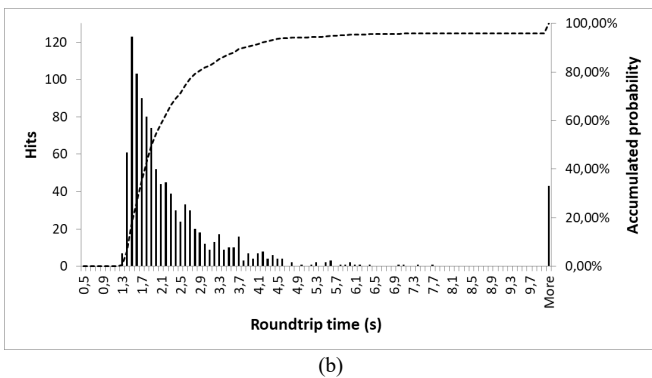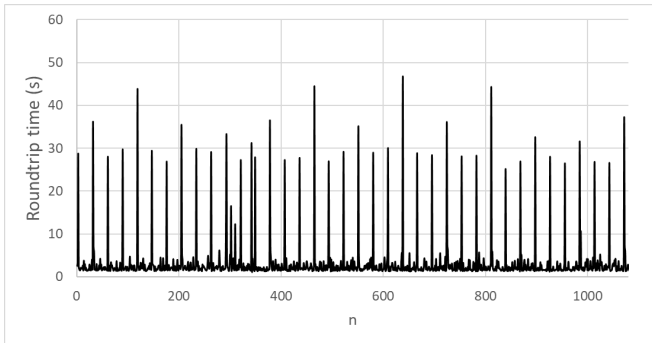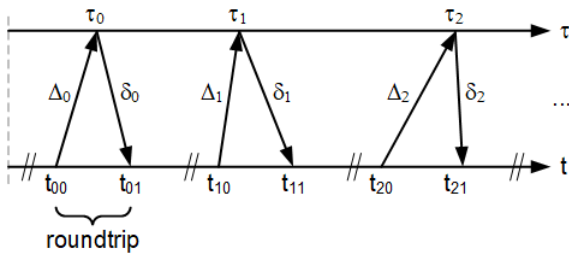
Figure 5: Roundtrip times of the REST API: a) plot; b) histogram

3.2. Results

We ran the closed loop illustrated in Figure 2 for 1080 times, from n=0 to n=1079, waiting approximately 20 seconds on each iteration. This number (1080) was a compromise between having statistically relevant results and limiting the test to a reasonable

amount of time (almost six hours). Figure 5a shows the measured roundtrip times, and Figure 5b shows the corresponding histogram. The order number (n) was always replied correctly, which attests the robustness of the ThingSpeak platform.

Figure 5b we see that the roundtrip time has a heavy-tailed distribution, which is characteristic of multipath communication mediums as the Internet. The authors in [24] report similar results and suggest a lognormal distribution for the experimental data. In our case, we got mode = 1,66 s and a roundtrip time that is less than 2.9 s with a probability of 80%.

(b)
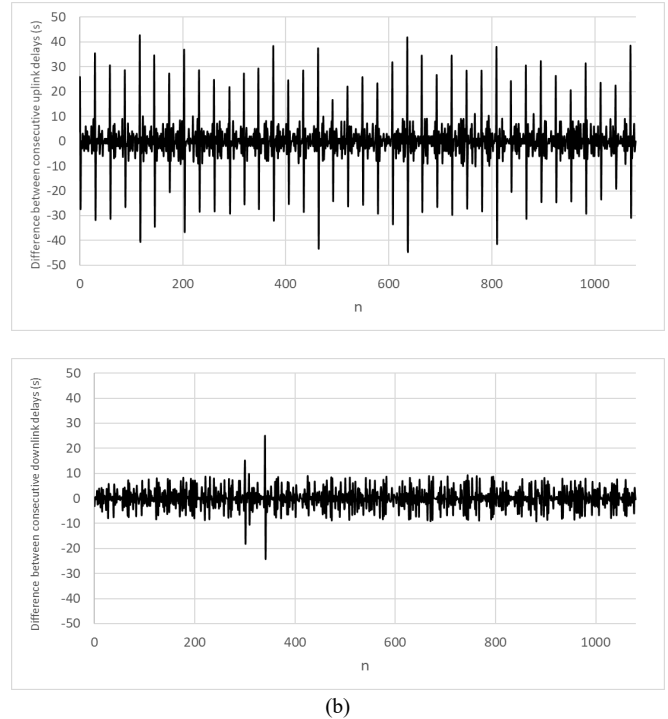
Figure 6: Difference between consecutive delays: a) uplink; b) downlink

Nevertheless, every 10 min (around 30 points) the roundtrip time increases very sharply up to tens of seconds, suggesting that the ThingSpeak platform stores data in temporary buffers, which, from time to time, are flushed and processed.

Figure 6 shows the difference between consecutive delays on the uplink and downlink directions. The differences are positive and negative because a higher delay on one iteration discounts on the next iteration. As expected, the uplink delay (Δ) is less stable than the downlink delay (δ) because the upload process is more complex than the reply (in terms of ThingSpeak internals).

If we suppose that consecutive uplink delays are statistically independent, which makes sense because they correspond to different iterations, then the variance of the difference ($d\Delta$ or $d\delta$) will be twice of the variance of the variable itself (Δ or δ). Therefore, if we compute the variances Var($d\Delta$) and Var($d\delta$) from the data of Figure 6, and divide the result by two, we get the variances of the delays: Var(Δ) = 37.52 s^2 and Var(δ) = 7.29 s^2. Applying the squared root, we get the standard deviations: σ_Δ = 6.13 s and σ_δ = 2.70 s.

Finally, it is very difficult to infer about the mean value of the uplink and downlink delays because the clocks of the two systems

are not synchronized and, equally important, the two links are far from being symmetric.

4. ThingSpeak accessed through the MQTT API

built the closed data path shown in Figure 7, which is like that of Figure 2 with the difference that the order numbers are uploaded through the MQTT broker. The LabVIEW application was changed to publish order numbers (n) using a compatible MQTT driver [25]. The quartets (n, t_{n0}, τ_n, t_{n1}) were collected and saved into the output file as before.
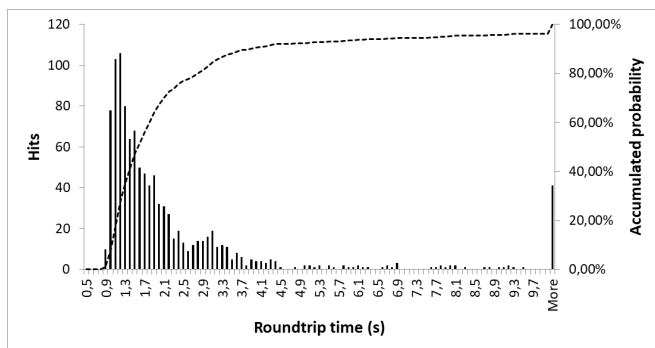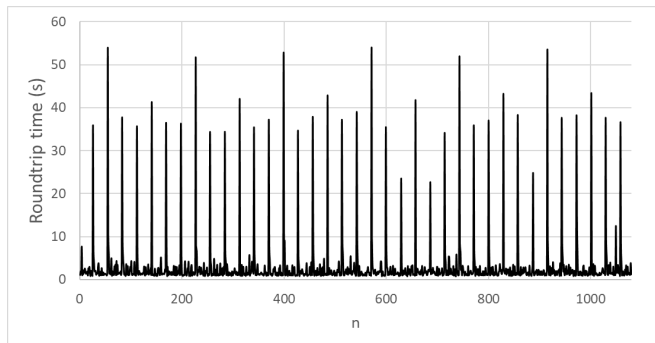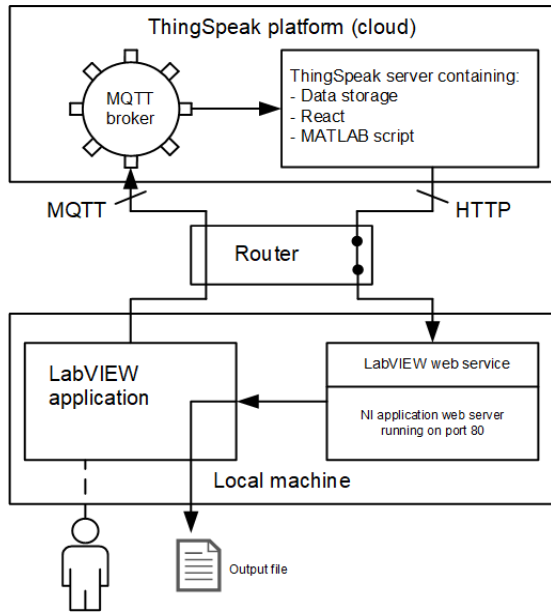
(b)

Figure 8: Roundtrip times of the MQTT API: a) plot; b) histogram

We ran the closed loop 1080 times waiting approximately 20 seconds on each iteration. Figure 8a shows the measured roundtrip times, and Figure 8b shows the corresponding histogram. Again, the order number (n) was always replied correctly, with no mismatches or timeouts. From the graphs, we see that the roundtrip time follows a lognormal distribution with mode = 1,13 s and values below 2,8 s with a probability of 80%. We also see outliers coming every 10 min (as we saw in the REST API), suggesting that internal mechanisms of buffering and batch processing also apply to the MQTT API.

The random variables dΔ and dδ were also computed as before. The corresponding variances were extracted and divided by two, leading to Var (Δ) = 51.53 s^2 and Var (δ) = 5.99 s^2. Applying the squared root, we got the standard deviations of the uplink and downlink delays: σ_Δ = 7.18 s and σ_δ = 2.45 s.

5. MQTT broker alone

To analyze the performance of the MQTT broker alone we closed the loop without passing through the ThingSpeak server, as shown in Figure 9. The LabVIEW application was changed to publish order numbers (n) and subscribe the replies using the MQTT driver previously mentioned. In this case, only the triplets (n, t_{n0}, t_{n1}) were collected because the timeline of the ThingSpeak server (τ axis) is not available.

We ran the closed loop 1080 times waiting approximately 20 seconds on each iteration. Figure 10.a shows the measured roundtrip times, and Figure 10.b shows the corresponding histogram. As always, the order number (n) was always replied correctly, with no mismatches or timeouts. From the graphs, we see that the roundtrip time follows a lognormal distribution with mode = 0.189 s, and values below 0,250 s with a probability of 80%. We also see that the outliers observed in the previous tests have almost disappeared. This shows that the MQTT broker is more expeditious than the ThingSpeak server, probably because its buffering and processing needs are much less demanding.

6. Results and Discussions

Table 1 summarizes the latencies measured during all the experiments. From these results we can extract the following conclusions:

- The REST and MQTT APIs have similar performances with a slightly advantage for the MQTT API. In both cases, the roundtrip time was typically between 1 s and 3 s.

- The ThingSpeak server has internal mechanisms of buffering and batch processing that, periodically, introduce extraordinary delays. These mechanisms seem to be absent from the MQTT broker.

- The MQTT broker is very agile in distributing publications, with roundtrip times typically below 250 ms.

- The up and down links are far from being symmetric. The uplink is more complex since it has a higher variance.

- The tests lasted for several hours and were made in different days and in different times of the day, suggesting that the behavior of the ThingSpeak platform is time independent.

A final word about robustness: the order number (n) was never lost or corrupted, proving that the ThingSpeak is reliable, even for free accounts.
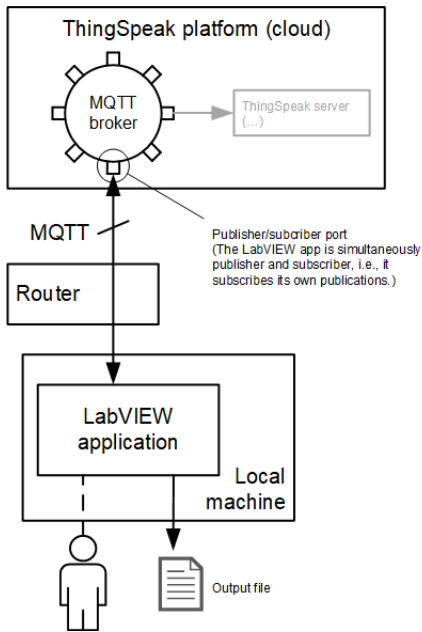
Figure 9: Data loop through the MQTT broker only

(a)

(b)
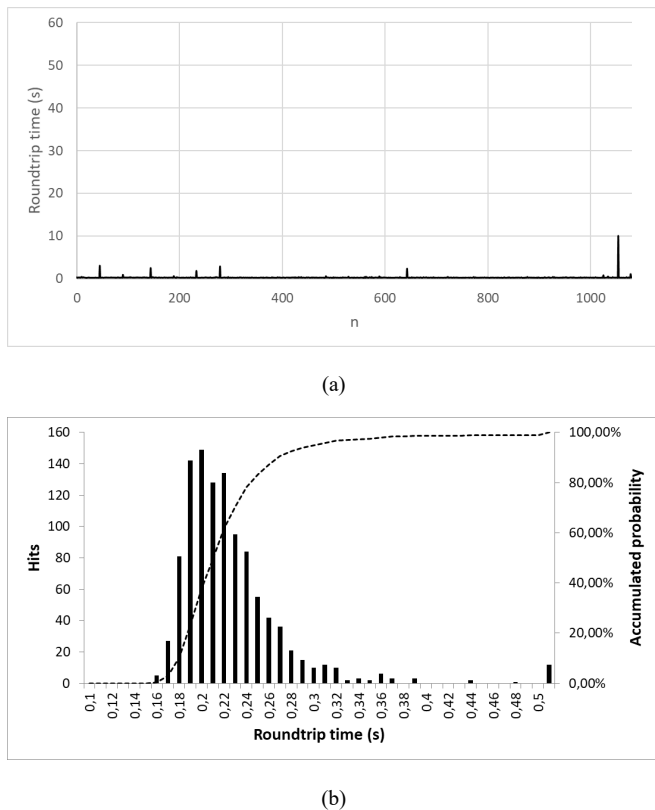
Figure 10: Roundtrip times of the MQTT broker alone (a) plot (b) histogram

Table 1: Experimental characterization of the ThingSpeak platform

		REST API	MQTT API	MQTT broker
Roundtrip time	Min (s)	1.25	0.86	0.158
	Mean (s)	3.28	3.27	0.243
	Mode (s)	1.66	1.13	0.189
	80th percentile (s)	2.90	2.80	0.250
Uplink delay	Std. dev. (s)	6.13	7.18	---
Downlink delay	Std. dev (s)	2.70	2.45	---

7. Conclusions

The paper reported the studies carried on the ThingSpeak platform to evaluate its responsiveness and reliability. We measured the time needed for a data packet to loop back through the platform, and we verified if its content has been corrupted during the trip. Tests were made for all access mediums (REST API, MQTT API and MQTT alone) covering periods of six hours.

We saw that the REST and MQTT APIs have similar performance with typical roundtrip times between 1s and 3s. We observed repetitive outliers that suggest that the ThingSpeak server has periodic mechanisms of buffering and batch processing. The MQTT broker alone did not show such outliers and performed significantly faster. In terms of reliability, no data was lost or corrupted.

We hope that the obtained results can serve as a reference for other IoT platforms and provide guidelines for application development.

Conflict of Interest

The authors declare no conflict of interest.

References

[1] "ANSI/ISA-95.00.03-2013 Enterprise-Control System Integration - Part 3: Activity Models of Manufacturing Operations Management"

[2] R. Burke et al., "The smart factory - Responsive, adaptive, connected manufacturing," Deloitte Insights, https://www2.deloitte.com/us/en/insights/focus/industry-4-0/smart-factory-connected-manufacturing.html (accessed on 6 Oct. 2020).

[3] K. Schwab, "The fourth industrial revolution - What it means and how to respond," Foreign Affairs, 12 Dec. 2015, https://www.foreignaffairs.com/articles/2015-12-12/fourth-industrial-revolution (accessed on 6 Oct. 2020).

[4] J. Delsing, F. Rosenqvist, O. Carlsson, A. W. Colombo and T. Bangemann, "Migration of industrial process control systems into service oriented architecture," IECON 2012 - 38th Annual Conference on IEEE Industrial Electronics Society, Montreal, QC, 2012, 5786-5792, doi: 10.1109/IECON.2012.6389039.

[5] T. Hegazy and M. Hefeeda, "Industrial automation as a cloud service," in IEEE Transactions on Parallel and Distributed Systems, **26**(10), 2750-2763, 1 Oct. 2015, doi: 10.1109/TPDS.2014.2359894.

[6] R. Langmann and L. Meyer, "Automation services from the cloud," 2014 11th International Conference on Remote Engineering and Virtual Instrumentation (REV), Porto, 2014, 256-261, doi: 10.1109/REV.2014.6784271.

[7] H. Sequeira, P. Carreira, T. Goldschmidt and P. Vorst, "Energy cloud: Real-time cloud-native energy management system to monitor and analyze energy consumption in multiple industrial sites," 2014 IEEE/ACM 7th International Conference on Utility and Cloud Computing, London, 2014, 529-534, doi: 10.1109/UCC.2014.79.

[8] O. Givehchi, J. Jasperneite, "Industrial automation services as part of the cloud: first experiences," 2013 Jahreskolloquium Kommunikation in der Automation (KommA 2013), Magdeburg, Germany, 2013.

[9] O. Givehchi, H. Trsek and J. Jasperneite, "Cloud computing for industrial automation systems - A comprehensive overview," 2013 IEEE 18th Conference on Emerging Technologies & Factory Automation (ETFA), Cagliari, 2013, 1-4, doi: 10.1109/ETFA.2013.6648080.

[10] A. Ito, T. Kohiyama, K. Sato, F. Tamura, "IoT-ready industrial controller with enhanced data processing functions," in Hitachi Review, **67**(2), 208-209, Feb. 2018.

[11] J. Pretlove, C. Skourup, "Human in the loop," ABB Review 1/2007.

[12] L. Wang and A. Canedo, "Offloading industrial human-machine interaction

tasks to mobile devices and the cloud," Proceedings of the 2014 IEEE Emerging Technology and Factory Automation (ETFA), Barcelona, 2014, 1-4, doi: 10.1109/ETFA.2014.7005249.

[13] O. Givehchi, J. Imtiaz, H. Trsek and J. Jasperneite, "Control-as-a-service from the cloud: A case study for using virtualized PLCs," 2014 10th IEEE Workshop on Factory Communication Systems (WFCS 2014), Toulouse, 2014, 1-4, doi: 10.1109/WFCS.2014.6837587.

[14] "About ThingSpeak," https://thingspeak.com (accessed on 11 Oct. 2020).

[15] "Top IoT platforms for makers," https://ubidots.com/blog/top-iot-platforms/ (accessed on 30 Oct. 2020).

[16] Minseok Kwon, "A tutorial on network latency and its measurements," in Enabling Real-Time Mobile Cloud Computing through Emerging Technologies, IGI Global, 2015, 272-293, doi: 10.4018/978-1-4666-8662-5.ch009.

[17] Paolo Ferrari, Emiliano Sisinni, Alessandro Depari, Alessandra Flammini, Stefano Rinaldi, Paolo Bellagente, Marco Pasetti, "On the performance of cloud services and databases for industrial IoT scalable applications," in Electronics 2020, **9**(9), 1435, doi: 10.3390/electronics9091435.

[18] P. Ferrari, E. Sisinni, D. Brandão and M. Rocha, "Evaluation of communication latency in industrial IoT applications," 2017 IEEE International Workshop on Measurement and Networking (M&N), Naples, 2017, pp. 1-6, doi: 10.1109/IWMN.2017.8078359.

[19] S. Mijovic, E. Shehu and C. Buratti, "Comparing application layer protocols for the Internet of Things via experimentation," 2016 IEEE 2nd International Forum on Research and Technologies for Society and Industry Leveraging a better tomorrow (RTSI), Bologna, 2016, 1-5, doi: 10.1109/RTSI.2016.7740559.

[20] M. Collina, M. Bartolucci, A. Vanelli-Coralli and G. E. Corazza, "Internet of Things application layer protocol analysis over error and delay prone links," 2014 7th Advanced Satellite Multimedia Systems Conference and the 13th Signal Processing for Space Communications Workshop (ASMS/SPSC), Livorno, 2014, 398-404, doi: 10.1109/ASMS-SPSC.2014.6934573.

[21] "REST API," https://www.mathworks.com/help/thingspeak/rest-api.html (accessed on 6 Oct. 2020).

[22] "MQTT API," https://www.mathworks.com/help/thingspeak/mqtt-api.html (accessed on 6 Oct. 2020).

[23] "Access MATLAB Add-On Toolboxes," https://www.mathworks.com/help/thingspeak/matlab-toolbox-access.html (accessed on 6 Oct. 2020).

[24] I. Antoniou, V.V. Ivanov, Valery V. Ivanov, P.V. Zrelovc, "On the log-normal distribution of network traffic," in Physica D: Nonlinear Phenomena, **167**(1-2), 72-85, July 2002. doi: 10.1016/S0167-2789(02)00431-1.

[25] "mqtt-LabVIEW," https://github.com/cowen71/mqtt-LabVIEW (accessed on 8 Oct. 2020).

ASTES

Deep Learning based Models for Solar Energy Prediction

Imane Jebli[*,1], Fatima-Zahra Belouadha[1], Mohammed Issam Kabbaj[1], Amine Tilioua[2]

[1]*AMIPS Research Team, E3S Research Center, Computer Science Department, Ecole Mohammadia d'Ingénieurs, Mohammed V University in Rabat, Avenue Ibn Sina B.P. 765, Agdal Rabat 10090, Morocco*

[2]*Thermal and Applied Thermodynamics, Mechanics Energy Efficiency and Renewable Energies Laboratory, Department of Physics, Faculty of Sciences and Techniques Errachidia, Moulay Ismaïl University of Meknès, Boutalamine Errachidia, B.P-509, Morocco*

ARTICLE INFO	ABSTRACT
	Solar energy becomes widely used in the global power grid. Therefore, enhancing the accuracy of solar energy predictions is essential for the efficient planning, managing and operating of power systems. To minimize the negatives impacts of photovoltaics on electricity and energy systems, an approach to highly accurate and advanced forecasting is urgently needed. In this paper, we studied the use of Deep Learning techniques for the solar energy prediction, in particular Recurrent Neural Network (RNN), Long Short-Term Memory (LSTM) and Gated Recurrent Units (GRU). The proposed prediction methods are based on real meteorological data series of Errachidia province, from 2016 to 2018. A set of error metrics were adopted to evaluate the efficiency of these models for real-time photovoltaic forecasting, to achieve more reliable grid management and safe operation, in addition to improve the cost-effectiveness of the photovoltaic system. The results reveal that RNN and LSTM outperform slightly GRU thanks to their capacity to maintain long-term dependencies in time series data.

1 Introduction

Currently, the global trend is to integrate renewable energies to generate electricity and rethink its energy mix. In this regard, the use and expansion of renewable energy have become an important element in maintaining energy security, as well as to establish an ecological and sustainable electrical system [1]. Nevertheless, the energy context is affected by price variations, changes in demand and the volatility of renewable energy production. In order, to confront these main challenges of the energy mix, it is essential to have a good forecasting model for renewable energies, which is particularly useful for optimizing and adapting supply to demand. This must reliably provide advance information on the availability of power, which helps to achieve the grid's stable operation and to allow for optimal unit engagement and economic dispatching [2]. In this work, we concentrate on solar energy forecasting. Photovoltaic (PV) forecasting methods fall into two groups: direct and indirect prediction models. As described in [3, 4], solar radiation at different time scales is predicted with different methods and then converted to power based on the panel characteristics in the case of indirect prediction, while direct predictions are performed directly from the output power of the plant. Besides, Statistical, physical, artificial intelligence (AI) and hybrid approaches were used in pre-

dicting PV solar energy. However, thanks to their great learning and regression capabilities, AI and especially, Deep Learning (DL) techniques [5], have been widely used in this area. They have the capability to extract in-depth features from PV power datasets and get more reliable predictive outputs. Authors in [6] have applied Recurrent Neural Network (RNN) as a good tool for predicting solar irradiation time-series using recorded meteorological data. Besides, Li et al. [7] have proposed an RNN-based forecasting method for short-term PV power prediction. Moreover, another research in [8] has proposed a hybrid deep learning model using Wavelet Packet Decomposition (WPD) and Long Short-Term Memory (LSTM) to forecast PV power for one hour ahead with an interval of five minutes. WPD is applied to split the PV power output time-series and next the LSTM is implemented to forecast high and low-frequency subseries. The results of this study indicate that the WPD-LSTM method outperforms in various seasons and weather conditions than LSTM, Gated Recurrent Units (GRU), RNN, and Multilayer Perceptron (MLP). Authors in [9] have presented a deep LSTM based on historical power data to predict the PV system output power for one hour ahead. The aim in [10] to suggest a hybrid model using LSTM and attention mechanism for short-term PV power forecasting, and employed LSTM to extract features from the historical data and learn in sequence the information on long-term dependence, to

apply the attention mechanism trained at the LSTM to target the extracted relevant features, which has greatly enhanced the original predictive power of LSTM. An LSTM approach for short-term forecasts based on a timescale that includes global horizontal irradiance (GHI) one hour ahead and one day ahead have been applied in [11]. Furthermore, authors in [12] have implemented univariate and multivariate GRU models employing historical solar radiation, external meteorological variables, and cloud cover data to predict solar radiation. In [13], authors have presented multivariate GRU to predict Direct Normal Irradiance (DNI) hourly. And the suggested method is evaluated compared to LSTM using historical irradiance data. In addition, a hybrid deep learning model have introduced in [14] that combines a GRU neural network with an attention mechanism for solar radiation prediction. All these research contributions cited above are valuable. However, they are not able to identify the important parameters that would have an impact on the accuracy of predictions. and make real-time predictions for efficient and optimized management. Given the fluctuating nature of output power generation as a function of meteorological conditions such as the temperature, the wind speed, the cloud cover, the atmospheric aerosol levels and the humidity level, which leads to high uncertainties on the output power of PV [15]. Besides, according to the forecast horizon, PV forecasts range from very short to long term. In general, researchers focus on short-term, hourly and daily forecasts as opposed to long-term. The first are of major significance for the management of PVs and the related security constraints (planning, control of PV storage and the rapprochement of the electricity market, providing the secure operation of generation and distribution services, and reinforcing the security of grid operation), while the long-term forecasts are useful particularly, for maintenance [16]. In this context, we study the efficiency of three DL models. We also focus in this study, on real-time prediction of solar energy in order to help planner, decision-makers, power plant operators and grid operators to making responsive decisions as early as possible, and to manage smart grid PV systems more reliably and efficiently [17]. Moreover, the use of real-time prediction allows to adjust to changes in production and to react to complex events (exceptionally high or low load production or consumption). In addition, it decreases the amount of operating reserves needed by the system, thus reducing system balancing costs [18]. However, the models we have selected give good results and seem to be suitable for long-term forecasting thanks to their power as a deep learning model and their ability to perform complex processing on huge data sets. Moreover, we outline that our work has been experimented with Moroccan's case, particularly in the region of Errachidia. In this perspective, Moroccan decision-makers have launched a global plan to improve the percentage of renewable energy in the energy mix and substantially improve energy efficiency. In view of increasing the percentage of electricity generation capacity from renewable energy sources (42% by 2020 and 52% by 2030) [19]. Therefore, we believe that the case of Morocco remains an interesting case study that could lead to important findings since it is not only a promising future PV energy supplier, but also one of the leading countries in the global energy transition, particularly in Africa. The remainder of this paper is organized into four sections. Section 2 gives an overview of our comparative methodology. Subsequently, section 3 presents the approach applied to elaborate the forecast models. Section 4 presents

and discusses the obtained results. Finally, section 5 summarizes the conclusions and perspectives of this study.

2 Methodology

Solar energy prediction is a key element in enhancing the competitiveness of solar power plants in the energy market, and decreasing reliance on fossil fuels in socio-economic development. Our work aims to accurately predict the solar energy. For this purpose, we explore architectures of the RNN, LSTM and GRU algorithm which is suitable to be used for forecasting such time-series data, and we experiment and evaluate them in Morocco's case, especially Errachidia area. This section presents at first the basis architecture of this recurrent neural network before explaining the important steps that we follow to build our models and perform our comparative study.

2.1 Recurrent Neural Network architecture

Recurrent neural network (RNN) is a category of neural network used in sequential data prediction where the output is dependent on the input [20]. The RNN [21] is capable to capture the dynamic of time-series data by storing information from previous computations in the internal memory. RNN has been applied in a context where past values of the output make a significant contribution to the future. It is mainly used in forecasting applications because of its ability to process sequential data of different length.

The basic principle of RNNs is to consider the input of a hidden neuron which takes input from neurons at the preceding time step [22]. To this purpose, they employ cells represented by gates that influence the output using historical data observations are given to generate the output. RNN is particularly efficient for learning the dynamic temporal behaviors exhibited in time-series data [23]. In RNN, the hidden neuron h_t for a given input sequence x_t, it has information feedback from other neurons in the preceding time step multiplied by a W_{hh} which is the weight of the preceding hidden state h_{t-1} can be calculated sequence by Eq.1. x_t is the input at instant time t, W_{xh} is the weight of the actual input state, tanh is the activation function. The output state y_t is computed according to the Eq.2 where W_{hy} is the weight at the output state.

$$h_t = \tanh(W_{hh}h_{t-1} + W_{xh}x_t) \tag{1}$$

$$y_t = W_{hy}h_t \tag{2}$$

The LSTM is a special kind of RNN, designed to avoid and resolve the vanishing gradient problems that limit the efficiency of simple RNN [8]. LSTM network has memory blocks that are connected through a succession of layers. In the LSTM cells, there are three types of gates: the input gate, the forget gate and the output gate. This makes it possible to achieve good results on a variety of time-series learning tasks, particularly in the nonlinear of a given dataset [24]. Each block of LSTM handles the state of the block and the output, it operates at different time steps and transmits its output to the following block and then the final LSTM block generates the sequential output [9]. Besides, LSTM is a robust algorithm, which

allows the recurrent neural network to efficiently process time-series data. Its key component is memory blocks which have been released to address the vanishing gradient disadvantage by memorizing network parameters for long durations [25].an LSTM block gets an input sequence after that, the activation units are used by each gate to decide whether or not it is activated. This operation enables the change of state and the adding of information passing through the block conditional. In the training phase, the gates have weights that can be learned. In fact, the gates make the LSTM blocks smarter than conventional neurons and allow them to remember current sequences [10]. LSTM is flexible and estimates dependencies of different time scales thanks to its ability to perform long task sequences and to identify long-range features. Basically, LSTM starts with a forget gate layer (f_t) that uses a sigmoid function combined with the preceding hidden layer (h_{t-1}) and the current input (x_t) as described in the following equations:

$$i_t = \sigma(W_i.[h_{t-1}, x_t] + b_i) \tag{3}$$

$$\check{c}_t = \tanh(W_c.[h_{t-1}, x_t] + b_c) \tag{4}$$

$$f_t = \sigma(W_f.[h_{t-1}, x_t] + b_f) \tag{5}$$

$$o_t = \sigma(W_o.[f_{t-1}, x_t] + b_o) \tag{6}$$

$$c_t = f_t.c_{t-1} + i_t.\check{c}_t \tag{7}$$

$$h_t = o_t.\tanh(c_t) \tag{8}$$

where i_t, $\check{c}_t$, f_t, o_t, c_t and h_t represent the input gate, cell input activation, forget gate, output gate, cell state, and the hidden state respectively. W_i, W_c, W_f and W_o represent their weight matrices respectively. b_i, b_c, b_f, and b_o represent the biases. x_t is the input, h_{t-1} is the last hidden state, h_t is the internal state. σ is the sigmoid function.

2.2 Gated Recurrent Units architecture

The GRU [26] is a particular type of recurrent neural network proposed by Cho in 2014 which, is the same as the LSTM) in terms of use to resolve the issue of long-term memory network and back-propagation. The GRU network involves the design of several cells that store important information and forget those that are deemed irrelevant in the future [27]. The feedback loops of the GRU network can be regarded as a time loop, because the output of the cell from the past period is taken as an input in the following cell in addition to the actual input. This key property allows the model to remember the patterns of interest and to predict sequential time-series datasets over time. Unlike the LSTM, the GRU [28] consists of only two gates: update and reset gates. the GRU substitutes the forget gate and the input gate in the LSTM with an update gate that verifies the cell state of the previous state information that will be moved to the current cell, while, the reset gate defines whether new information will be included in the preceding state. For this reason, GRU has proven to be one of the most efficient RNN techniques, because of

its capacity to learn and acquire dependencies over the long term and observations of varying length [29]. This characteristic is particularly useful for time-series data, and it is helpful in reducing the computational complexity [30]. GRU cells are described using the following equations:

$$z_t = \sigma(W_z.[h_{t-1}, x_t]) \tag{9}$$

$$r_t = \sigma(W_r.[h_{t-1}, x_t]) \tag{10}$$

$$\hat{h}_t = \tanh(W.[r_t - h_{t-1}, x_t]) \tag{11}$$

$$h_t = (1 - z_t).h_{t-1} + z_t.\hat{h}_t \tag{12}$$

$$y_t = \sigma(W_0.h_t) \tag{13}$$

where z_t and r_t respectively correspond to the output of the update gate and the reset gate, while W_z, W_r, W, and W_o respectively are the weights of each gate. σ and tanh respectively are the sigmoid and the hyperbolic tangent activation function, and x_t is the network input at time t. ht and h_{t-1} correspond to the hidden layer information of the actual and precedent time, and $\hat{h}_t$ is the candidate state of the input. Initially, the network input x_t at the time of the hidden state h_{t-1} and t at the last state computes the output of the reset gate and the update gate by Eq.9 and 10. Next, after the reset of the reset gate r_t calculates the amount of memory stored, the implicit layer $\hat{h}_t$ is computed by Eq.11, which is the new information at the actual time t. Then, by using Eq.12, the update gate z_z determines the amount of information was removed at the previous time, and how much information is stored in the candidate hidden layer ht at this time. The hidden layer information h_t is subsequently added. Finally, the output of the GRU is switched to the next GRU gated loop unit according to Eq.13: which is a sigmoid function.

3 Our approach for predicting solar energy

In this study, we apply three different DL models to predict the PV solar energy output, especially RNN, LSTM and GRU for the half-hour ahead. The aim of this study is to compares the relevance of the mentioned models, in order to identify the best algorithm to be used for predicting solar energy. The process of the method employed in this work is illustrated in Figure 1. It is organized into four main stages: data collection, data pre-processing, model training and parameterization, and model testing and validation. This section details how each of these processing/selection steps was performed, as well as key details on the architecture and parameters of the developed models.
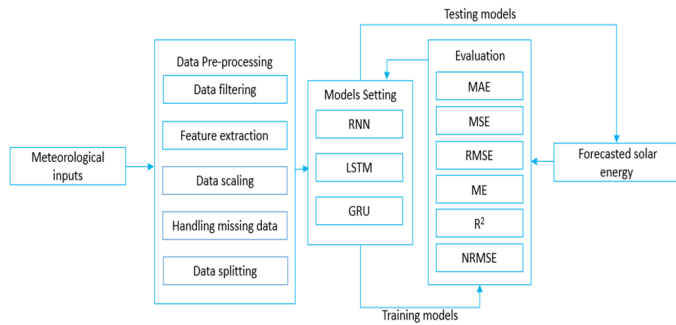
Figure 1: Our method for predicting solar energy

3.1 Dataset

The datasets used in this work, they represent meteorological data of Errachidia province, which is situated in the sunny region of Morocco, it benefits from an important solar energy potential during all the year. This data consists of measurements from three years (2016, 2017 and 2018), and they are used to predict the solar energy level based on a set of measurable weather conditions, in purpose of analyzing the performance of the studied models.

3.2 Preprocessing and Feature Selection

Pre-processing and feature selection are fundamental steps in DL approaches for making collected data in an appropriate form. Pre-processing allows numerous tasks and operations to convert the source data in a clean data, in a way that it can be easily integrated into DL models. It impacts the accuracy of the model and its results. Feature selection provides the most appropriate features that properly affect the learning process, and can minimize the number of variables to efficiently enhance the accuracy of the model and avoid costly computations. Therefore, in this work, we proceed with the following steps to prepare and select features from the source data: extraction of target data inputs, selection of relevant features, filling in the null values, normalization of the data, and adjustment of the steps to be taken into account for prediction.

The source data give multiple features but not all of them are important for use in the prediction. In our case, we have selected four important features: solar energy, temperature, humidity and pressure. These features are the most and highly correlated variables to the targeted output (solar energy) according to Pearson correlations [31]. The objective of this step is to help developing most accurate models that learn from the most correlated data in order to give the most accurate forecasts. We note that we have selected the Median in order to fill missing data.

The features of a given dataset are usually presented at different scales. To ensure that all these values are at the same scale and to add uniformity to our dataset, we employ the Min-Max scale that transforms all values between 0 and 1, which removes the noise from our data and simplifying the learning process of our models.

Besides, the meteorological data are time-series with a time step of 30 min, and therefore, the actual data values are needed as inputs for making predictions. Time-series data cannot use future values as input features, whereas the inputs of a time-series model are the values of past features. In this work, we adjust our model

to learn from the past to predict PV solar energy for the next half hour. This choice has been adopted because of the size of the data and to perform real-time predictions for an efficient and optimized management. Finally, based on best practices in the area of data analytics, the dataset is split into 80% and 20% were respectively used to train and test the models developed.

3.3 Training and models parametrization

Each of the models developed must be parameterized during the training phase in order to be able to provide the most accurate forecasts while taking into account the size of the batches. After setting different parameters for our DL models during the training and evaluating the results obtained, the Adam optimizer has proved to be the best optimizer and was then selected as the common parameter for all proposed DL models. ADAM, which is widely used and works better than other stochastic optimizers in empirical results [32], would allow the models to learn quickly. In addition, the tanh activation function has shown a good fitting for all DL models. On the other hand, we notice that our DL models have different architectures and that the number of layers and neurons for example has been fixed after tuning several values and selecting the ones that have given the best precisions. Figure 2 illustrates the neural network architecture, and Table 1 shows details on the architectures and the key parameters of each model suggested for the dataset studied.
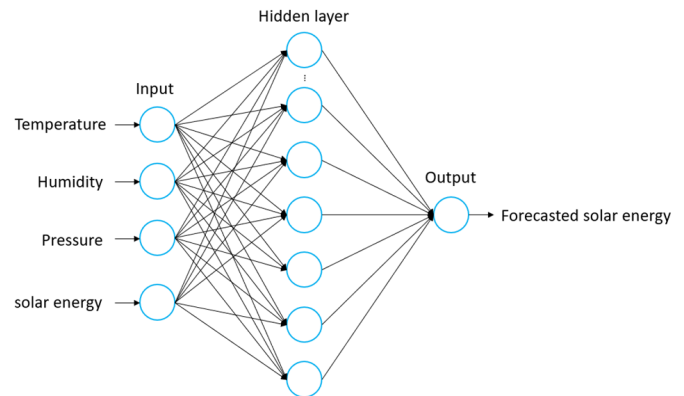
Figure 2: ANN architecture for predicting solar energy

Table 1: Architecture and parametrization of the models.

Models	Parameters				
	Layers	*Epocs*	*Activation Function*	*Optimizer*	*Batch size*
RNN	RNN cell Of 100 units	20	Tanh	Adam	12719
LSTM	LSTM cell Of 100 units	20	Tanh	Adam	12719
GRU	GRU cell Of 100 units	20	Tanh	Adam	12719

3.4 Performance metrics

To evaluate the performance of the proposed DL models for PV solar energy prediction. A set of evaluation metrics widely-used are employed to evaluate the results accuracy forecasting. In this step, we have applied the most suitable to the context of DL and regression problems. For this purpose, five performance metrics, whose equations are presented below, have been employed for models testing as well as training: MAE (Mean Absolute Error), MSE (Mean Square Error), RMSE (Root Mean Square Error), Max Error (ME) and R squared (R^2).

$$MAE = \frac{1}{n} \sum_{j=1}^{n} |y_j - \hat{y}_j| \tag{14}$$

$$MAE = \frac{1}{n} \sum_{j=1}^{n} (y_j - \hat{y}_j)^2 \tag{15}$$

$$RMSE = \sqrt{\frac{1}{n} \sum_{j=1}^{n} (y_j - \hat{y}_j)^2} \tag{16}$$

$$ME = \max_{1 \le j \le n} |y_j - \hat{y}_j| \tag{17}$$

$$R^2 = 1 - \frac{SS_{reg}}{SS_{tot}} \tag{18}$$

where y is the actual output, $\hat{y}$ is the predicted output and n is the number of samples. Eq. 14 computes MAE as the average of the absolute errors (absolute values indicating the differences between the actual and the predicted values). Eq. 15 shows the MSE, which is the average squared errors (difference between the real values and what is estimated. Eq. 16 calculates RMSE, which is the square root of the MSE, and is applied in cases with small errors [33], whereas Eq. 17 measures the maximum residual error ME and reveals the worst error between the actual and predicted value. In addition, to calculate the predictive accuracy of proposed models, we also used R-squared, which is a statistical metric in a regression model, to identify the proportion of variance of the dependent variable that can be made explicit by the independent variable. Expressly, Eq. 18 indicates the R-squared measure to which the data correspond in the regression model (the goodness of fit) where SS_{reg} is the sum of the squares due to the regression and SS_{tot} is the total sum of the squares [34]. Eventually, in the different steps outlined in this section, we employed a set of technical tools for the implementation of the studied algorithms based on the Python libraries, including Pandas, NumPy, SciPy and Matplotlib in a Jupiter Notebook, in addition to Scikit-learn (sklearn) and TensorFlow.

4 Results and discussion

In this section, we present and discuss the results of our three studied models tested for PV solar energy forecasting. It should be noted that although R-squared (R^2) is a commonly used metric, it is not regarded as an effective indicator of the models fit with the data [35]. A low or high R^2 value does not always indicate that the model is wrong or that it is automatically right [36]. Due to the controversy

concerning the efficiency of R^2 as an appropriate metric for determining the best regression model [35, 36], we additionally evaluate our results using other statistical metrics that are the most widely used: MAE, MSE, Max Error and RMSE. The RMSE remains the most frequently employed in the regression area [37]. Table 2 show the metrics values corresponding to solar energy prediction in real time of studied models. Considering the parameters presented in Table 2, we can see the results for one-half hour ahead prediction of our experiments for the recurrent neural networks: RNN, LSTM and GRU. In spite of their architectural differences, RNN and LSTM have demonstrated similar performance, showing that the better model is strongly dependent on the task. Thanks to their ability to handle long-term dependencies in sequential information for time-series predicting applications, both RNN and LSTM perform better with very high accuracy as shown by their related R^2 values which are respectively equal to 94.68% and 94.26%. GRU gives slightly less performance than the RNN and LSTM with 90.32 as value. It also causes errors unlike RNN and LSTM. We observe that for GRU, 2.74, 15.53, 3.94, 37.30 are given as MAE, MSE, RMSE and ME values, respectively. Furthermore, these measures are nearly similar for RNN and LSTM with MAE=1.83, MSE=8.53, RMSE=2.92and ME=30.42 for RNN, and MAE=1.90, MSE=9.20, RMSE=3.03 and ME=29.73 for LSTM. Figure 3, Figure 4, Figure 5, Figure 6, Figure 7 and Figure 8 show their training and testing curves. In reality, more accurate prediction results mean less uncertainty and fluctuations in PV solar energy generation. Accuracy is a crucial factor in the efficient planning and use of electrical energy and energy systems with high PV power penetration. In short, as shown in Table 2, the prediction capability of RNN and LSTM seems very reliable compared to GRU under meteorological conditions, and they are better adapted to meet real-time PV solar energy prediction needs with high accuracy. Due to their ability to minimize errors during learning and test processes, they can reduce uncertainties related to the operation and planning of PV energy integrated management systems.

Table 2: Metrics related to PV solar energy dataset.

Models	Data	MAE	MSE	RMSE	ME	ME
RNN	Training	1.73	7.22	2.68	34.06	95.62
	Test	1.83	8.53	2.92	30.42	94.68
LSTM	Training	1.77	7.65	2.76	35.42	95.36
	Test	1.90	9.20	3.03	35.42	94.26
GRU	Training	2.63	13.69	3.70	34.26	91.70
	Test	2.74	15.53	3.94	37.30	90.32
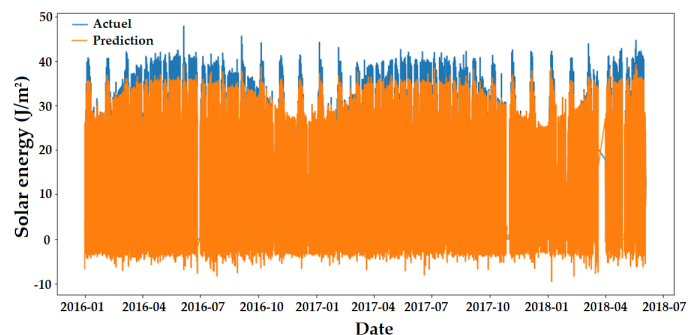
Figure 3: RNN training curves of solar energy
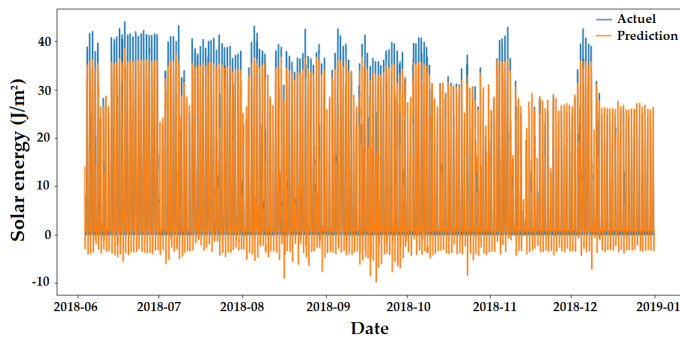
Figure 4: RNN testing curves of solar energy
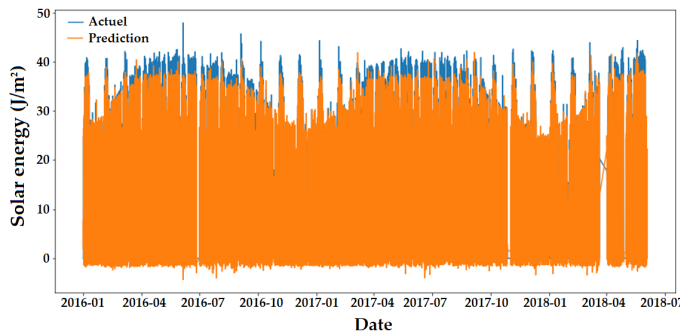
Figure 5: LSTM training curves of solar energy
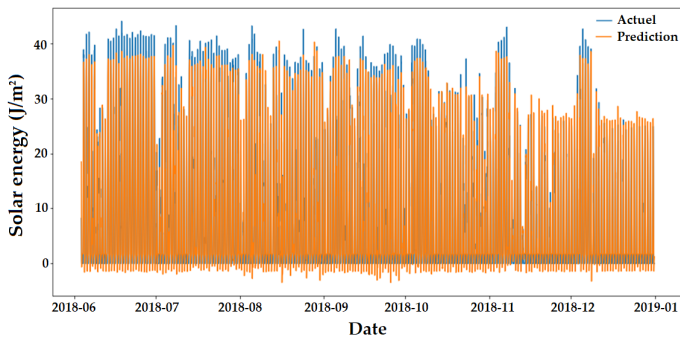
Figure 6: LSTM testing curves of solar energy
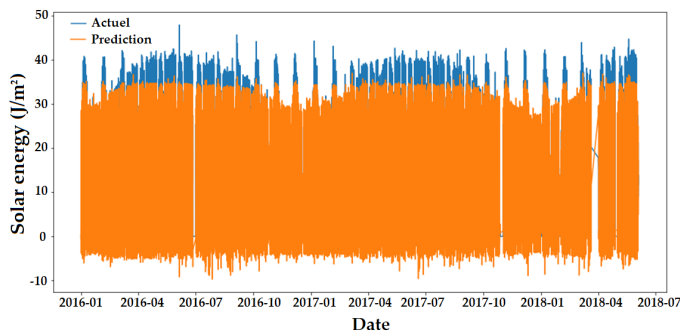
Figure 7: GRU training curves of solar energy

Besides, while RMSE is regarded in the literature as a good metric for evaluating and comparing regression models, it is still difficult to interpret properly. Therefore, we also normalize the RMSE values to provide a more meaningful representation of our

results, which would allow more efficient conclusions. The normalized RMSE (NRMSE) represents the rate of the RMSE value and the range (the maximum value minus the minimum value) of the actual values. Table 3 shows a results synthesis based on this metric for real-time solar energy prediction. We can observe that RNN and LSTM provide good and similar NRMSE values with 0.055 and 0.058 respectively.
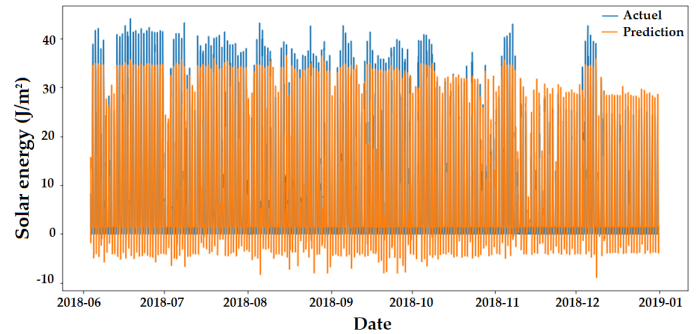
Figure 8: GRU testing curves of solar energy

Table 3: Results synthesis for real time prediction.

Models	Data	NRMSE
RNN	Training	0.055
	Test	0.066
LSTM	Training	0.058
	Test	0.068
GRU	Training	0.077
	Test	0.089

5   Conclusion and Perspectives

With the growing deployment of solar energy into modern grids, PV solar energy prediction has become increasingly important to deal with the volatility and uncertainty associated with solar power in these systems. In the literature, different models have been proposed for the prediction of PVs by using the AI techniques capacity. However, the majority of the research contributions in this area offer different techniques for making separate short-term and long-term forecasts, and do not focus on real-time forecasts. For this reason, we are working to find a model capable of producing continuous real-time forecasts using meteorological data, which is primordial for providing important decision support for power system operators to ensure more efficient management and secure operation of the grid and enhance the cost-effectiveness of the PV system. In this study, we investigated the efficiency of three different DL models: RNN, LSTM and GRU. The models were tested with data from a Moroccan region to make real-time PV forecasts. Further, the analysis of the results was based on six metrics MAE, MSE, RMSE, ME, R^2 and NRMSE to determine both forecast accuracy and margin of error. The results prove the efficiency of RNN and LSTM for real-time PV prediction thanks to their ability to address long-term dependencies in sequential information for time-series regression problems, compared to GRU that gives slightly less performance

than the RNN and LSTM. From these findings, it can be concluded that RNN and LSTM showed very high accuracy and low errors, they are reliable models that can minimize errors in the learning and testing process, in addition to reduce the uncertainties associated with the operation and planning of integrated PV energy management systems. Moreover, they are promising techniques that also appears to be suitable for long-term PV forecasting and should be studied and recommended as a possible unified and standard tool for real-time, short-term and long-term PV prediction. As future work of this study, we plan to enhance these models by employing other approaches, extend them to longer term PV forecasting, as well as to studying other promising deep learning methods in view of providing and deploying a powerful model for PV energy prediction.

Conflict of Interest   The authors declare no conflict of interest.

References

[1] E. Hache, "Do renewable energies improve energy security in the long run? Septembre 2016 Les cahiers de l'économie - n⁰109 Série Recherche," 2016.

[2] M.G. De Giorgi, P.M. Congedo, M. Malvoni, "Photovoltaic power forecasting using statistical methods: Impact of weather data," IET Science, Measurement and Technology, **8**(3), 90–97, 2014. DOI:10.1049/iet-smt.2013.0135.

[3] P. Li, K. Zhou, S. Yang, "Photovoltaic Power Forecasting: Models and Methods," 2nd IEEE Conference on Energy Internet and Energy System Integration, EI2 2018 - Proceedings, 1–6, 2018. DOI:10.1109/EI2.2018.8582674.

[4] U.K. Das, K.S. Tey, M. Seyedmahmoudian, S. Mekhilef, M.Y.I. Idris, W. Van Deventer, B. Horan, A. Stojcevski, "Forecasting of photovoltaic power generation and model optimization: A review," Renewable and Sustainable Energy Reviews, 81(August 2017), 912–928, 2018 DOI:10.1016/j.rser.2017.08.017.

[5] A. Youssef, M. El-telbany, A. Zekry, "The role of artificial intelligence in photovoltaic systems design and control: A review," Renewable and Sustainable Energy Reviews, 78(November), 72–79, 2017. DOI:10.1016/j.rser.2017.04.046.

[6] A.P. Yadav, A. Kumar, L. Behera, "RNN Based Solar Radiation Forecasting Using Adaptive Learning Rate," 442–452, 2013.

[7] G. Li , H. Wang, S. Zhang, J. Xin, H. Liu,"Recurrent Neural Networks Based Photovoltaic Power Forecasting Approach," 1–17, 2019.

[8] P. Li, K. Zhou, X. Lu, S. Yang, "A hybrid deep learning model for short-term PV power forecasting," Applied Energy, (November), 114216, 2019. DOI:10.1016/j.apenergy.2019.114216.

[9] M. Abdel-Nasser, K. Mahmoud, "Accurate photovoltaic power forecasting models using deep LSTM-RNN," Neural Computing and Applications, **31**(7), 2727–2740, 2019. DOI:10.1007/s00521-017-3225-z.

[10] H. Zhou, Y. Zhang, L. Yang, Q. Liu, K. Yan, Y. Du, "Short-Term Photovoltaic Power Forecasting Based on Long Short Term Memory Neural Network and Attention Mechanism," IEEE Access, **7**, 78063–78074, 2019. DOI:10.1109/ACCESS.2019.2923006.

[11] Y. Yu, J. Cao, J. Zhu, "An LSTM Short-Term Solar Irradiance Forecasting Under Complicated Weather Conditions," IEEE Access, **7**, 145651–145666, 2019. DOI:10.1109/ACCESS.2019.2946057.

[12] J. Wojtkiewicz, M. Hosseini, R. Gottumukkala, T.L. Chambers, "Hour-Ahead Solar Irradiance Forecasting Using Multivariate Gated Recurrent Units," 1–13, 2019. DOI:10.3390/en12214055.

[13] M. Hosseini, S. Katragadda, J. Wojtkiewicz, R. Gottumukkala, "Direct Normal Irradiance Forecasting Using Multivariate Gated Recurrent Units," 1–15, 2020. DOI:10.3390/en13153914.

[14] K. Yan, H. Shen, L. Wang, H. Zhou, M. Xu, Y. Mo, "Short-Term Solar Irradiance Forecasting Based on a Hybrid Deep Learning Methodology," 1–13.

[15] M.Q. Raza, M. Nadarajah, C. Ekanayake, "On recent advances in PV output power forecast," Solar Energy, **136**(September 2019), 125–144, 2016. DOI:10.1016/j.solener.2016.06.073.

[16] C. Wan, J. Zhao, Y. Song, Z. Xu, J. Lin, Z. Hu, "Photovoltaic and solar power forecasting for smart grid energy management," CSEE Journal of Power and Energy Systems, **1**(4), 38–46, 2016. DOI:10.17775/cseejpes.2015.00046.

[17] A. Tuohy, J. Zack, S. E. Haupt, J. Sharp, M. Ahlstrom, S. Dise, E. Grimit, C. Mohrlen, M. Lange, M. G. Casado, J. Black, M. Marquis, C. Collier, "Solar forecasting: Methods, challenges, and performance," IEEE Power and Energy Magazine, **13**(6), 50-59, 2015.DOI:10.1016/j.111799.

[18] G. Notton, M.L. Nivet, C. Voyant, C. Paoli, C. Darras, F. Motte, A. Fouilloy, "Intermittent and stochastic character of renewable energy sources: Consequences, cost of intermittence and benefit of forecasting," Renewable and Sustainable Energy Reviews, 87(December 2016), 96–105, 2018. DOI:10.1016/j.rser.2018.02.007.

[19] A.A. Merrouni, F.E. Elalaoui, A. Mezrhab, A. Mezrhab, A. Ghennioui, "Large scale PV sites selection by combining GIS and Analytical Hierarchy Process. Case study: Eastern Morocco," Renewable Energy, 2017. DOI:10.1016/j.renene.2017.10.044.

[20] A. Alzahrani, P. Shamsi, C. Dagli, M. Ferdowsi, "Solar Irradiance Forecasting Using Deep Neural Networks," Procedia Computer Science, **114**, 304–313, 2017. DOI:10.1016/j.procs.2017.09.045.

[21] A. Alzahrani, P. Shamsi, M. Ferdowsi, "Solar Irradiance Forecasting Using Deep Recurrent Neural Networks," In 2017 IEEE 6th international conference on renewable energy research and applications (ICRERA), 988-994, 2017.

[22] Y. LeCun, Y. Bengio, G. Hinton. "Deep learning" Nature **521**(7553), 436-444, 2015.

[23] H. Wang, Z. Lei, X. Zhang, B. Zhou, J. Peng, "A review of deep learning for renewable energy forecasting," Energy Conversion and Management, **198**(July), 111799, 2019. DOI:10.1016/j.enconman.2019.111799.

[24] X. Qing, Y. Niu, "Hourly day-ahead solar irradiance prediction using weather forecasts by LSTM," Energy, **148**, 461–468, 2018. DOI:10.1016/j.energy.2018.01.177.

[25] H. Liu, X. Mi, Y. Li, "Comparison of two new intelligent wind speed forecasting approaches based on Wavelet Packet Decomposition , Complete Ensemble Empirical Mode Decomposition with Adaptive Noise and Arti fi cial Neural Networks," Energy Conversion and Management, 155(July 2017), 188–200, 2018. DOI:10.1016/j.enconman.2017.10.085.

[26] Y. Wang, W. Liao, Y. Chang, "Gated Recurrent Unit Network-Based Short-Term Photovoltaic Forecasting," Energies, **11**(8), 2163, 2018. DOI:10.3390/en11082163.

[27] K. Cho, B. van Merrienboer, C. Gulcehre, F. Bougares, H. Schwenk, Y. Bengio, "Learning Phrase Representations using RNN Encoder–Decoder for Statistical Machine Translation," arXiv preprint arXiv:1406.1078, 2014.

[28] M. C. Sorkun, C. Paoli, Ö. D. Incel, "Time series forecasting on solar irradiation using deep learning," 2017 10th International Conference on Electrical and Electronics Engineering (ELECO), Bursa, 151-155, 2017.

[29] H.M. Lynn, S.B.U.M. Pan, "A Deep Bidirectional GRU Network Model for Biometric Electrocardiogram Classification Based on Recurrent Neural Networks," IEEE Access, **7**, 145395–145405, 2019. DOI:10.1109/ACCESS.2019.2939947.

[30] Z. Che, S. Purushotham, K. Cho, D. Sontag, Y. Liu, "Recurrent Neural Networks for Multivariate Time Series with Missing Values," Scientific Reports, 1–12, 2018. DOI:10.1038/s41598-018-24271-9.

[31] H. Zhou, Z. Deng, Y. Xia, M. Fu, "A new Sampling Method in Particle Filter Based on Pearson Correlation Coefficient," Neurocomputing, 2016. DOI:10.1016/j.neucom.2016.07.036.

[32] D.P. Kingma, J. Ba:, "Adam: A Method for Stochastic Optimization," Proceedings of the 3rd International Conference on Learning Representations (ICLR), p. No abs/1412.6980, 2014.

[33] F. Wang, Z. Mi, S. Su, H. Zhao, "Short-term solar irradiance forecasting model based on artificial neural network using statistical feature parameters," Energies, **5**(5), 1355–1370, 2012. DOI:10.3390/en5051355.

[34] B.J. Miles, "R Squared , Adjusted R Squared," Wiley, 2014.

[35] C. Onyutha, "From R-squared to coefficient of model accuracy for assessing " goodness-of-fits "," Geoscientific Model Development Discussions, 1-25, 2020. doi: 10.5194/gmd-2020-51

[36] D.B. Figueiredo Filho, J.A.S. Júnior, E.C. Rocha, "What is R2 all about?," Leviathan (São Paulo), **3**, 60–68, 2011.

[37] I. Jebli, F. Belouadha, M.I. Kabbaj, "The forecasting of solar energy based on Machine Learning," (c), 2020 International Conference on Electrical and Information Technologies (ICEIT). IEEE, 1-8, 2020. DOI: 10.1109/ICEIT48248.2020.9113168

Novel Infrastructure Platform for a Flexible and Convertible Manufacturing

Javier Stillig*, Nejila Parspour

University of Stuttgart, Institute of Electrical Energy Conversion, Stuttgart, 70569, Germany

A B S T R A C T

Sales behavior and the technical development of products influence their fabrication. As market influences become increasingly volatile and unpredictable, factories will have to adapt their manufacturing to market trends even more in the future. Adaptation is referred to as convertibility and can be achieved, among other things, by mobile and intercompatible machines. Enabling machines to be mobile, its power supply must be wireless and it should be possible to locate it on the shop floor at any time. With the help of the infrastructure platform Intelligent Floor, machines in future factories can be made more mobile than they are today. In combination with the novel autonomous guided vehicle BoxAGV, the platform offers a cost-efficient and highly flexible solution for in-house transport tasks. The transport of goods can be performed based on lot size one and thereby opens a wide field in logistics automation.
This paper is an extension of work originally presented in MELECON 2020 and describes the concept and the functionality of the open platform that is implemented so far. It shows how to apply the platform to a real industrial manufacturing environment and highlights the resulting manufacturing benefits. Finally, the next development steps on the platform and machine side are presented.

1   Introduction

The rigid linking of specialized individual machines by conveyor belts is the characteristic of today's production lines. Future production lines must consist of mobile, intercompatible machines that can be easily combined to form new production lines. This universality can be achieved with a reduction in functionality of the individual machine and by supplying it wirelessly with energy and data. The compatibility of the individual machines allows a higher-level control system to perform interconnected operation in order to follow in real-time market requirements.

These statements are verified in section 2 by using the automobile production as an example. Adapting today's productions to the new requirements, the Intelligent Floor (IF) poses as a universal platform for the building infrastructure and helps to achieve a flexible and convertible production. The IF is a raised floor that is currently under development. It is designed as a modular floor with individual panel elements that have sensor and actuator functionalities. The V0.5.x prototype can already supply production equipment by wireless power and measures the weight of objects on the floor panel. Furthermore, the IF has an Light Emitting Diodes (LED) display system in each panel included that is built-up with four LED stripes and located in a cross shape on the top of one panel.
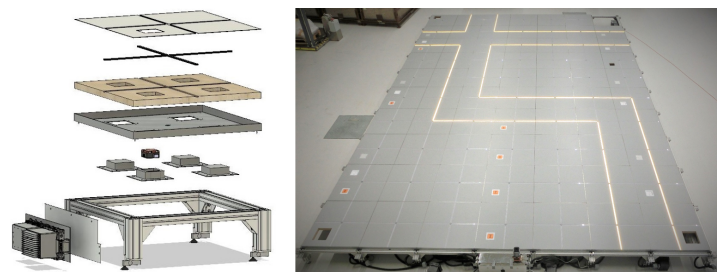
Figure 1: Exploded view of the IF and the prototype V0.5.2 test set-up, which has a size of $10\,\text{m} \times 7\,\text{m}$ (L $\times$ W). When the picture was taken, as an example a walking path in the production was reproduced by the IF.

The IF consists of the four main components substructure, control and power unit, module inserts and panel (Figure 1). It receives its sensor and actuator capabilities from the module inserts or individually configurable panels. The IF basic version is already equipped with a detection and display functionality. Due to the modular design as a raised floor, the flexible positioning of machines on the IF is made possible through an omnipresent media supply. The IF can generate advantages for users and operators of production facilities that would not be achievable with conventional solutions. Two prototypes of the IF are currently being tested

*Corresponding Author: Javier Stillig, Pfaffenwaldring 47, 70569 Stuttgart, Germany, +49 711 68567819 & javier.stillig@iew.uni-stuttgart.de

in the ARENA 2036[1] using specific use cases of the convertible production.

A first prototype V0.1.1 of the novel Autonomous Guided Vehicle (AGV), hereafter named *BoxAGV* and shown in Figure 2. It is based on a simple frame construction made of aluminum profiles, to which four meccanum wheels are attached. The four drive motors are connected each to an inverter that receive their commands from the controller in real-time. The BoxAGV has installed a camera for identifying the route, which is mounted centrally in the frame. By using the Wireless Power Transfer (WPT) the battery of the vehicle can be charged dynamically. The entire vehicle technique is embedded in a standard box [1] made of polypropylene with the outer dimension $600\,\text{mm} \times 400\,\text{mm} \times 213\,\text{mm}$ (L × W × H). It offers after its integration still 50% of the origin transport volume.
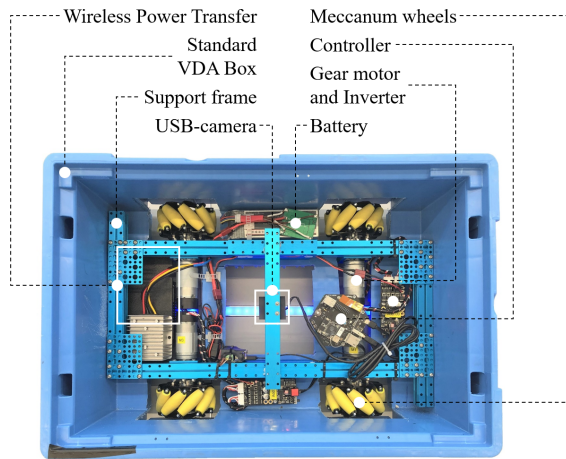
Figure 2: Design of the first BoxAGV prototype V0.1.1, where frame, driving and control components are built-in a standard VDA box.

The combination of IF and BoxAGV meets the requirements of convertible production in terms of logistics flexibility and usability better than the solutions known so far. To verify this hypothesis, a study has been started in the ARENA 2036. Using a $70\,\text{m}^2$ large-scale demonstrator of the IF that interacts with two BoxAGV prototypes, highlights the expected gains for future logistics systems. To initiate a technical discourse, the novel concept is therefore introduced in this paper and evaluated based on a real field application. Additional to the logistic applications, further use cases of the IF are outlined and the importance of WPT for mobile applications is analyzed in more detail.

2 Convertible Production

To understand the purpose of the IF and its benefits for the users, it is essential to get to know more about convertible production. Scientists, in particular the production technology institutes of the University of Stuttgart, have been researching the subject of convertible production since more than 25 years, e.g. [2]–[7]. One of the central findings of their research work, carried out so far, is that in response to the fast changing requirements of the global market, production equipment must be designed to be more modular, mobile and compatible with each other. This is a fundamental of the future factories production concept. To implement this concept is necessary in order to be able of continuing producing economically with a high value-added share. Taking the automotive industry as an example, it will be outlined which factors drive the change in requirements and what kind of solutions can be helpful.

2.1 Driving Factors

The requirement to transform existing production systems to convertible production systems will be illustrated based on two general market developments. These market developments are described using the automotive industry as an example. Based on the research study [8], the number of registered automobile models has increased by 349% between 1990 and 2014 in Germany. In addition, the number of possible equipment options increased with the model variants, so that today almost every new car allows several hundred million of configuration options and is consequently built as a one-off. The second market trend is the shortening of a model's life cycle. While the life cycle of a Volkswagen Golf 1 was nine years in 1983, it has been reduced to just four years in 2012 [9]. These two market movements are critical not only for the automaker, but also for all their suppliers, who must adapt their products and production facilities to market developments.

The driving force behind the increase in the number of variants and the reduction in product lifecycle times is the interaction between the market and suppliers. The customer's desire for choice and product individualization is matched by a large number of competing manufacturers who expect to gain sales advantages by offering variants ever faster. The ongoing connection of people through the Internet means that the market and suppliers are better connected than before. This means that a reduction in the number of variants and an extension of the life cycle time cannot be expected in future. Therefore, it is necessary for product makers to adapt their production concepts to the actual situation and to move to convertible production concepts [10, 11]. Here it is important to couple the product life cycle with the life cycle of the production machine. Thus, the rigid coupling of product and machine is not critical if the period of the product life cycle is equal to or longer than the life cycle of the machine. However, the case in which the life cycle of a product is much shorter than that of a machine is critical for automated manufacturing. This causes production difficulties: Machines can no longer be planned, built and commissioned as quickly as the product life cycle requires. As shown in Figure 3, it is therefore necessary to implement a system that synchronizes both life cycles. This synchronization is the main task of the convertible production, as shown by the example in subsection 2.3.

2.2 Solution

There are many possible solutions for synchronizing product and machine life cycles. Two solutions will be highlighted in this paper: Transparency in the production process and faster product changeovers. Transparency is understood as the knowledge of the current position and status of all objects in the production process. Especially with knowledge of the material positions, the flow of goods can be optimized and non-production-related idle times can

---

[1]ARENA 2036 is a flexible research platform for the mobility and production of the future and is located in Stuttgart.

be reduced or eliminated. By shortening production time, more products can be produced in the same time period. As a result, the proportion of production costs allocated to the product becomes smaller, enabling the product to be produced cheaper. A solution to manage the increase in the speed of product changeovers is the use of modular, manufacturer independent and compatible production equipment. In some cases, solutions for defined manufacturing steps already exist, as it can be shown in the next subsection 2.3.
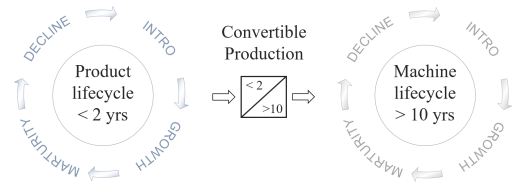
Figure 3: Product and machine lifecycle coupled by the convertible production.

2.3 Example

The relationship between product and machine life cycle is to be demonstrated using the example of wire harness production. In this case, the product is a wire harness (Figure 4). A wire harness is composed of different wires of various lengths and with a range of wire terminations. The use of wire harnesses is particularly widespread in the automotive industry. For example, an average equipped Volkswagen Golf 7 has a wiring harness with almost 1,000 different wires of a total length around 1.6 km and weighing up to 60 kg [12]. Each individual wire must be prepared individually for installation in the car. Due to the high demand quantities in the automotive industry, this requires a fully automatic machine that cuts wires to length, marks, strips and terminates them with a connector. Figure 5 shows a wire processing machine, type Zeta 640 / 650 that is manufactured by Komax. The machine is able to prepare up to 36 different wires with a cross-section from 0.22 to 6 mm^2 [13].
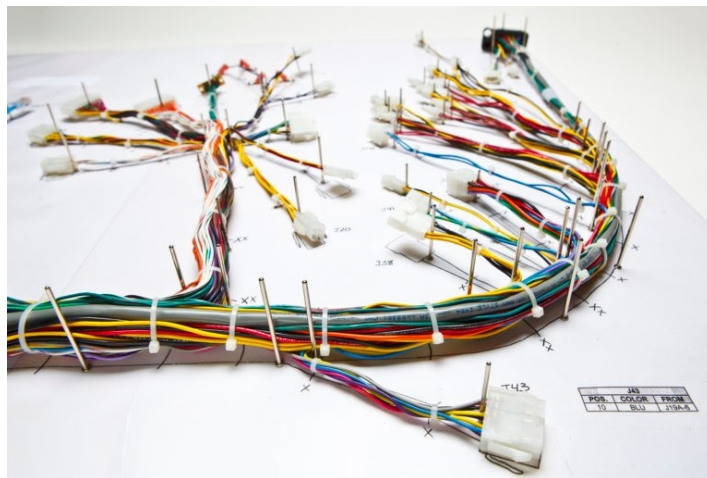
Figure 4: Wire harnesses are used in various industries, like in the consumer industry for wiring household appliances. One of its main advantages is the significantly reduced assembly time compared to single wire installation. Photo: TES.

Today, wiring harnesses take into account the vehicle equipment features ordered by the customer and they are built-to-order. This is done in order to reduce the overall vehicle weight and thus also

reduce fuel consumption and exhaust emissions. Such a production strategy leads to a large number of theoretical combinations, which [12] puts at 425 billion. Due to the high variance of the wire harness design as a result of changing vehicle equipment options and cyclical model changes, the wire processing machine is modular in itself. For example, there are up to 13 process modules for the model shown, which take over the feeding of different sized ferrules or the wire labeling. This enables the machine operator to react quickly to product changes. With the help of the modular machine design strategy, the fast-moving product cycle is coupled with the long-lasting machine cycle.

Figure 5: Wire processing machine for the fully automatic production of prepared wires for the use in wire harnesses. Photo: Komax.

Figure 6: The photo shows a wire harness production facility where workers assemble prefabricated wires into a wire harness. Photo: OWC.

Looking at the subsequent production process of the wire harness manufacturing, it is obvious that the fully automatic wire preparation is followed by a completely manual production process. As shown in Figure 6, the prepared wires are now assembled by hand on a pin board to form a complete wire harness. So far, it has not

been possible to build a machine for the automatic production of wire harnesses with a development and construction time that is shorter than the product life of a wire harness. Alternatively, it would also be possible to build a modular machine or a combination of individual system modules that are capable of producing complex wire harness layouts automatically. However, this has not yet been achieved either. Thus, product and machine life cycles for wire harness manufacturing in the automotive industry are not synchronized by machines, but manually by workers as shown in Figure 6.

The example of wire harness production can also be applied to other production processes in and outside of the automotive sector. It highlights the demands made on the machine life cycle in terms of flexibility, modularity and degree of automation.

At the same time, fully automatic machines should also be durable and robust investment assets that must guarantee a high output over their life cycle. Therefore, it is necessary to readjust the balance between product and machine life cycle by using new processes and elements from the field of convertible production. The IF described below is a new element from the field of convertible production. It uses an example from intralogistics to show how product and machine life cycles can be synchronized with each other based on machines.

3 Intelligent Floor

The Figure 7 shows a test surface of the IF prototype V0.5.1, which consists of 12 identically constructed panels, their control and power units and its substructure. In addition to the IF basic functionality of visualization and detection, a WPT unit is built into each panel. One panel has a surface area of $1\,\text{m} \times 1\,\text{m}$ and a thickness of $46\,\text{mm}$. The IF is constructed as a modular raised floor, which is adjustable in its height. In this specific case, the IF has a total height of $40\,\text{cm}$. The prototype V0.5.x is designed to carry static loads of min. $1{,}500\,\text{kg/m}^2$. A special feature of the IF is the interconnection of the energy units to form a DC $24\,\text{V}$ grid. This enables higher power to be provided at single points within the grid than could normally be provided by just the power supply unit of each panel. Furthermore, each panel has a control unit for processing its sensors and actuators. The Panel Controller (P-CTRL) is the central element of the control unit and communicates with the higher-level control system, the Section Controller (S-CTRL), over the $100\,\text{Mbps}$ Ethernet network. The S-CTRL itself manages by definition up to 256 panels. It can be implemented as a physically present controller or a cloud-based solution. Neighboring sections can be combined to a cluster, where the Cluster Controller (C-CTRL) is software-based controller. The IF prototype V0.5.x panels are already hot-plug capable and have the following sensor / actuator capabilities:

- The sensor system for object detection, which is based on load cells, is integrated into the substructure of the IF. Each load cell can measure up to 1,000 kg. Since each stand of the floor is equipped with a load cell, a network of weight values is built up over the area, which enables object detection with a positional accuracy of approx. 0.5 m.

- The panel's surface is divided into four quadrants by LED stripes consisting each of up to $144\,\text{LED/m}$. The LEDs are

controlled individually, in groups or all together in color and brightness by the P-CTRL.

- The IF contains up to four module slots, where Figure 7 shows one with a DC $24\,\text{V}$ / $240\,\text{W}$ WPT unit equipped module slot. In the IF prototype V0.5.2, the module slots contain further functionalities. For example, there are installed an e-paper display modul, a radio-based object localisation module and a power socket to provide three-phase current AC $400\,\text{V}$ / $16\,\text{A}$ instead of the WPT unit.

- Depending on the application, it may be useful to combine other functions in addition to the basic functions. This can be done in one panel or over a certain panel area. As the example in Figure 11 shows, the visualization functionality and the WPT unit were used here to charge a BoxAGV.
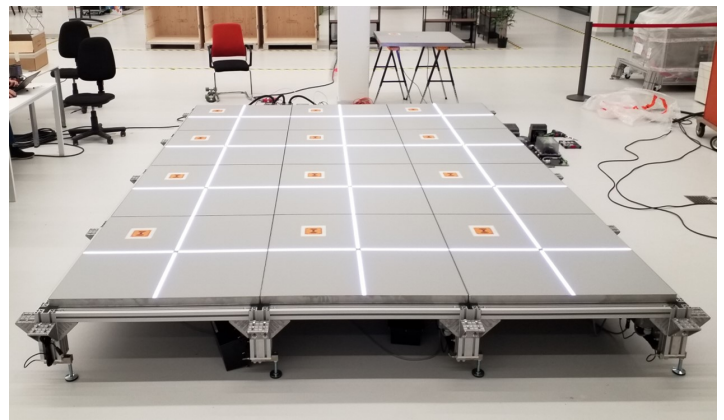
Figure 7: Prototype V0.5.1 of the IF, which was setup for test purposes in the ARENA 2036. It is assembled from 12 equal panels, each using one module slot for functionality expansion. The module is a 240 W WPT unit. Further, all stands are equipped with load cells, measuring the loads applied to the floor continuously.

3.1 Localization

The object localization in prototypes V0.2 and V0.5 is realized with the help of bending beam load cells, which are mounted under each stand of the substructure. During a measurement process, the weight force acts on the bending beam and generates an elastic deformation. This strain is converted into an electrical signal by the four strain gauges glued to the bending beam. In order to convert the signal into a weight value, the strain gauges are connected in a Wheatstone bridge and are made available to the P-CTRL by a subsequent measuring amplifier with an analog-to-digital converter. The controller forwards the weight values to a database located in the S-CTRL over the Ethernet network at intervals of 1 second. The database is designed as a ring buffer with a storage capacity of 256 panels, equal to one section, and a buffer time of 60 min. This allows the access to a total of 921,600 weight values.

In order to detect static or moving objects on the IF, the weight values of a time point that are above a defined threshold are extracted from the database. Since the position of the load cells is fixed and each weight value can be uniquely assigned to a load cell, it is possible to detect moving objects. The weight value itself can serve as an indicator of which type of object is being detected. For example, a measured value of 50 to 120 kg is an indication of a

human being. Object detection can be further refined by comparing the change in weight of several neighboring panels. If the weight sensors of panel Ⓐ measure the mass m at time t_0 and the weight sensors of panel Ⓑ, which lies next to panel Ⓐ, measure the mass m at time $t_1 > t_0$, it can be assumed that an object with mass m moves in time $t_1 - t_0$. Since the distance s between the panels Ⓐ and Ⓑ is known due to the uniform structure, the velocity v of the object is known as well. This is useful as another indicator of object types. For example, people in production areas typically move at speeds between 0.8 and 1.6 m/s. The object detection gains reliability if weight and velocity values are now combined.

Another possibility of object localization is currently being implemented in a panel of the IF prototype V0.5.2. With the help of a film-based sensor technology that is installed directly under the floor surface, the measuring accuracy and robustness is evaluated. Thus, the substructure of the IF's next prototype will be simplified and made ready for further applications outside industrial use.
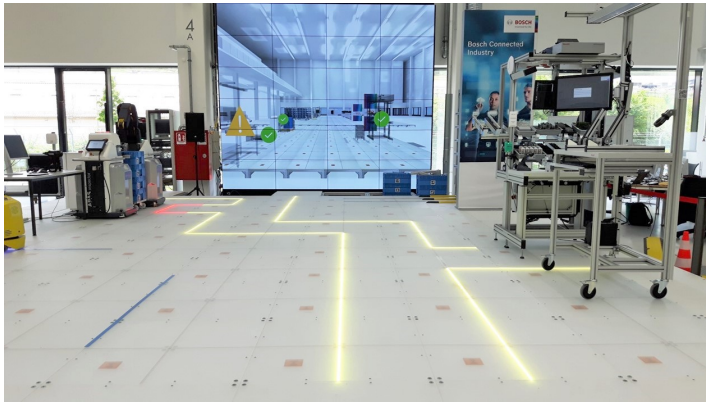
Figure 8: The prototype V0.2.1 uses the LED visualization system to show a walkway on the production area and serves as orientation for visitors. In the top left corner of the photo, an area with mobile production equipment can be seen. A red no-entry zone visually warns visitors that they are not allowed to enter this area.

3.2 Visualization

In the prototype V0.2.1, LED stripes with an LED density of 144 LED/m are installed. Thus, a pixel density of 284 px/m² is achieved. In the panels of the prototypes V0.5.x, the pixel density has been reduced to 116 px/m², which is sufficient for information purposes and for steering the BoxAGV. Each LED is from type WS2812B and can be controlled in its color and brightness by the P-CTRL. One LED stripe is embedded in an aluminum profile, on which a translucent cover protects the LEDs. They are wired to a connection box for the data and power supply from the P-CTRL and the DC 5 V source. In version V0.5.x, the panel is connected via cable to the control and power supply. This connection will no longer be necessary in the following prototype generation to ensure a fast and ergonomic change of the panels.

Since the LED visualization system is mounted on the panel in a cross shape, a chessboard-like grid is created on the surface when several panels are installed. Static dot and line patterns, but also dynamic patterns can be displayed in this grid. Thereby the synchronous visualization is performed by the S-CTRL, which updates all P-CTRLs connected to the section at the same time. As shown in Figure 8, the visualization system enables man / machine and inter-machine communication easily. For example, dynamic LED markings can replace static adhesive tape markings for indicating temporary storage locations for materials. As well it can be used as a guidance system for workers to find other persons or specific objects. Instead of separate ANDON displays, production states can be visualized to the worker on the IF. Moreover, it can also be used for zone identification and in combination with a secure object detection, for safeguarding hazardous areas in production environments. This application example is described in more detail in the subsection 3.4.

3.3 Wireless Power Transfer

Convertible production demands high standards for the mobility of production equipment. To ensure mobility, machines must be freely positionable on the shop floor. Today's usual cable- and tube-based media supply of machines is contrary to the mobility requirements of convertible production. Therefore, the use of WPT systems is promising. The WPT primary units shown in Figure 9 transmit up to 240 W unidirectionally to a static, machine-side secondary unit.

The voltage level is DC 24 V on both WPT sides. The efficiency achievable during energy transfer is 91% over an air gap of 5 mm. As the technical data indicate, the WPT system shown is provided for low-power applications. For example, a workshop cart with electrical label printer was equipped with a secondary side, in order to operate the printer on each charging point of the IF. In addition to the low-power system, a mid-power system is available, whose transfer power is 1,000 W with an efficiency of 90% and a transfer distance of up to 10 mm. Also a high-power system is already in the prototype V0.5.2 in operation. It is able to transfer a power of 3 kW at a distance of 15 to 40 mm. Its max. lateral offset of 40 mm from the centers of both coils helps to charge machines easily. The IF panel's design allows to operate up to four WPT units, so that in theory an energy density of max. 12 kW/m² can be achieved.

However, since mobile and thus lightweight production equipment is required for convertible production in particular, the required electrical power is usually rather low. As described in [14], power densities of less than 4 kW/m² are enough for most applications. Fixed and semi-fixed production equipment with a higher power demand, can be supplied using conventional socket units in the raised floor system. One of the most significant challenges of convertible production is the location-independent and dynamically adaptable energy supply of the production equipment. Unfortunately, this challenge can only be solved to a limited extent with the industrial WPT systems on the market today. Therefore, the Institute of Electrical Energy Conversion (IEW) of the University of Stuttgart is researching on the following three fields of WPT:

Dynamic Charging Looking at the operation of industrial WPT systems, it is remarkable that most of them are designed for static coupling of primary (Tx) and secondary (Rx) units – so defined 0D systems. Even small deviations in $x-$ or $y-$direction from the ideal position of the Rx unit in relation to the Tx unit will reduce the transfer power and efficiency. Therefore, only WPT systems capable to couple Rx and Tx units at least along a route (1D systems) are suitable for the use in the convertible production environment. Even more appropriate would be a 1.5 or 2D system. The Table 1 summarizes the coupling of Tx and Rx units in $x-$ or $y-$direction. A

solution further developed by [15] is the introduction of separately switchable Tx modules in a grid-like structure that are able to operate as 1.5D system or better, but without having the disadvantages of today's solutions.
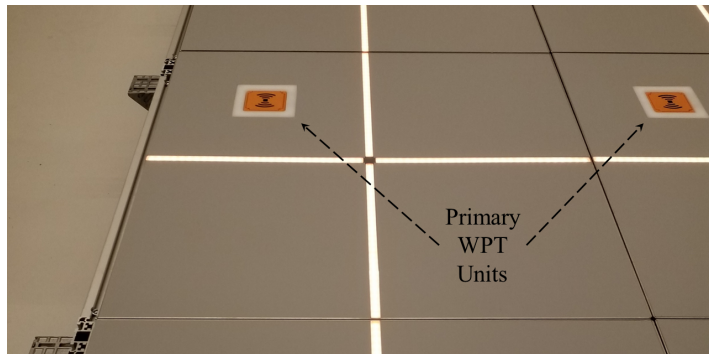
Figure 9: Two low-power Tx units each installed in an IF prototype V0.5.1 panel. The distance between the units is 1 m. Both Tx and Rx units have a uniform size of 100 mm × 100 mm × 47 mm (L × W × H) and can supply on Rx side 10 A at DC 24 V.

Table 1: Five categories of coupling between Tx and Rx coils in x and y planar movements without angular misalignment of the coil planes.

Cat.	Figure	Description
0D		The Tx and Rx are statically coupled, so that the two coils must be exactly aligned with each other.
0.5D		The Tx and Rx are statically coupled, but with a tolerance δ in two dimensions.
1D		The Rx side has one degree of freedom and is static in the second in relationship to the Tx side.
1.5D		The Rx is movable in one dimension and static with a tolerance δ in the second dimension.
2D		The Rx is completely dynamic in both dimensions, so that the Rx can be placed anywhere in relationship to the Tx device.

Bidirectional Power Transfer   Moreover, the industrial WPT systems available on the market are characterized by their unidirectional power transfer. Bidirectional systems are not yet available on the market. However, bidirectional energy transfer would have many

advantages in the environment of convertible production. For example, battery-buffered machines could help to compensate peak loads in production by feeding energy into the IF's DC grid via the bidirectional WPT system. At low-load times, the batteries can be recharged, which results in cost advantages for the operator in terms of a homogenized energy demand of his production [16, 17].

Power Density   A so far unknown key figure is the power density

$$\rho_{\mathrm{p}} = \frac{P_{\mathrm{inst}}}{A}$$, where P_{inst}: installed power [W], A: area [m^2]

needed to operate mobile machines in the environment of convertible production. This figure depends on the machines used and cannot be given as a general rule. However, with the operation of the prototypes V0.2.1 and V0.5.x, first empirical values are emerging which indicate a certain range. Measurements on lightweight mobile assembly and transport machines, showed a power requirement of less than 3.7 kVA per feeding point. For all equipment used in the ARENA 2036 test environment, a power input of 11 kVA was sufficient. In [18], the author calculates that the power requirement of an AGV with 500 kg payload is 347 W during steady driving. According to [14], a continuous power output density of 500 ^{W}/$_{m^2}$ is sufficient to start the supply of mobile production equipment.

3.4   Use Case 'Safety Zone'

Beside the intralogistics use case of the BoxAGV, which is described in more detail in subsection 3.5, another IF application shall be presented briefly. With the help of the safety panels a safety zone can be marked by the LED system and monitored for unauthorized entry of persons or mobile machines. To protect humans from injuries caused by dangerous movements of machines, such movements must be encapsulated according to ISO 13857 or limited in force and torque to non-hazardous values according to ISO/TS 15066. For this reason, protective fences as enclosures, sensors for initiating emergency stops or robots suitable for man-machine operation are used today, among other things. Especially the enclosures are static in their nature and thus in conflict with the goals of the convertible production. The safety zone application described below was implemented on the IF prototype V0.2.1 and shows the potentials as well as the added value for the user and operator of the IF. The application classifies two types of safety zones:

Immobile machinery   The safety zone around a production facility is normally realized with a fence and its access is monitored by safety devices triggering an emergency stop. To enable the access of persons and machines into hazardous areas, these entrances, e.g. doors and rolling gates, are secured with safety locks or safety light curtains. As well as for the safety enclosure of the production equipment and for access supervision in the safety zone, engineering time and capital expenditure must be considered. In the end, the solution remains inflexible with regard to the convertible production, because a relocation of the production facility always means a fully relocation of the safety enclosure. Considering the extensive mechanical and electrical installation of the safety equipment as well as the necessary acceptance test of the safety system, production managers usually decide against relocating machines despite more advantageous production logistics.

Mobile machinery Since the risk analysis of machines must also consider their surrounding space, the common installation of safety zones is much more complex than for stationary machines. This is due to the changing of the surrounding space. Based on the application example of AGVs, one of the central hazards of mobile machines for humans is the risk of becoming crushed [19]. Therefore, minimum safety requirements are placed on an AGV, which demand the presence of a braking system, a speed limiter and a device for object detection. By the interaction of AGV and IF, dynamic safety zones can be generated, which minimize the risk of an accident and at the same time reduce the expensive safety technology on board of the AGV (Figure 10).
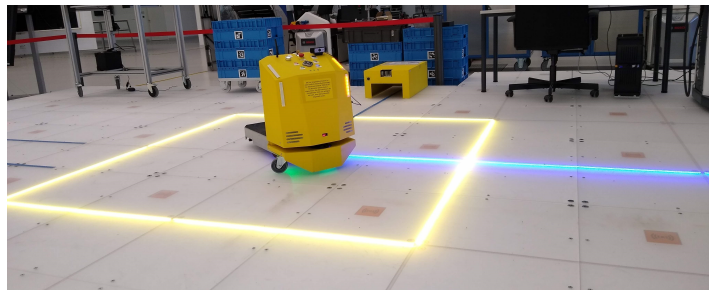
Figure 10: AGV and IF interact so that the yellow safety zone moves with the AGV. The IF detects an zone entry and can trigger the AGV to change direction or to stop.

3.5 Use Case 'BoxAGV'

Another application of the IF comes from the field of intralogistics and shows the use of the BoxAGV, which was adapted to the real production scenario described in [20]. The presented example relates to the production of interior parts, like headrests and side bolsters, for various vehicles. It is suitable, because the transition of a Manually Operated Intralogistics (MOL) to the new material supply concept of the In-plant Milkrun System (IMS) is already being discussed there. Furthermore, the paper includes a production layout and data on which the application example of the Novel Box-AGV System (NBS) can be based on. The comparison of the three material supply concepts does not claim to be complete and / or be generally valid. Further, it does not take into account the influencing factors that occur in practice, such as the robustness of the concepts with regard to the failure of critical components, fluctuations in demands or similar. The comparison rather serves as an indication for a possible operational capability of the NBS.

With the beginning of the 1990s, stationary storage capacities were gradually replaced by trucks moving in public roads. Responsible for this is the Just-In-Time (JIT) production concept [21, 22] which is widely used today. This relocation is not only to be criticized from an ecological point of view, but if the development is viewed from a business point of view, the JIT concept is extraordinarily successful: Warehousing and thus its capital tie-up can be significantly reduced. JIT can be scaled and transferred to the logistics of convertible production. This generates the following advantages:

- Liquidation of supermarkets (cf. central warehouse).
- Reduction of material handling (storage and retrieval).
- Minimum quantity of goods in the production process.

- Shorter throughput times and reduced capital tie-up.
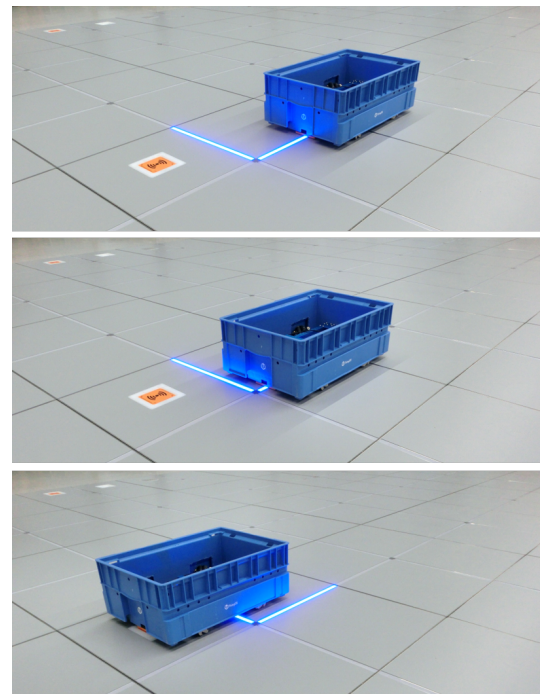
Figure 11: The three pictures show a time sequence in which the BoxAGV follows the dynamically controllable blue line to a WPT unit in order to get recharged.
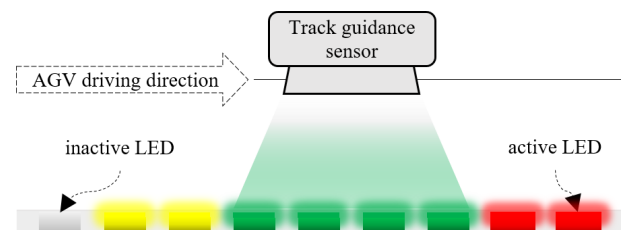
Figure 12: Based on the author's patent [23] an easy to use optical guidance system for mobile robot applications in combination with the IF is proposed. Conventional guiding lines that are painted on the floor, can be replaced by dynamically controllable LED guiding lines.

The IF is suitable in particular for use in internal logistics. Resources (goods, machines and employees) can be organized dynamically with the help of the IF visualization function. This means that it is no longer necessary to depend on rigid production layouts, but can, for example, redefine and reroute goods flows depending on the order situation. If this dynamic route modification is taken as a base for an AGV's track guidance, it is possible to react ad-hoc to unforeseen events in the production. Figure 12 shows that a single LED segment, for example consisting of eight single LEDs, is sufficient to realize track guidance. The segment not only sets the direction of the AGV, but also its speed. With only three colors the speed control can be built up:

- The BoxAGV remains at its current speed, while detecting a green light only.
- While detecting a yellow light, the BoxAGV controller will interpret this as an acceleration command.

- A red light decelerates the BoxAGV from its current speed to zero.

Today's AGVs used in industrial environments are expensive since, as autonomous transport machines, they must have cost-intensive components like battery, on-board computer, localization system and safety devices. As a result, the investment costs for a fully automated logistics are also high. The use of the simply designed BoxAGV, which is centrally navigated and supplied by WPT systems, is a promising approach for the automated logistics of the convertible production. Due to the BoxAGVs slow driving speed of max. 1 $^{km}/_h$ and its max. payload of 50 kg, complexity and costs can be reduced. For example, costs can be saved using simple safety edges instead of laser scanners for mobile safety applications. Additional collision protection measures should also be considered. Here, the IF provides predictive safety through its built-in weight and object detection on the total production area. In order to illustrate the potential savings and technical possibilities of the NBS concept in comparison with the IMS solutions and the MOL, a real production scenario from the operational practice will be examined.

3.5.1 Production Layout

As shown in Figure 13, the predominantly manual production of car interior parts is divided into a logistics and a production sections with a total area of 1,350 m^2. One third of the available area is reserved exclusively for logistics applications and two third is available for production. A closer look at both sections reveal a further subdivision into manufacturing, storage, traffic, administration and infrastructure areas.

The division of areas is partly determined by the building's structure itself (stairwells, escape routes), organizational requirements (offices, social rooms) and the type of manufacturing (workplaces, storage areas, logistics routes). The organizational and production-specific areas can be partially or completely adapted by changes in the production technology. In the following, the areas specified by the construction are considered to be non-adaptable. Table 2 applies the area allocation to the manufacturing plant and determines the area that is required for manually operated production logistics. It is obvious that only one third of the total area can be used for value-added assembly activities, two third of the area is occupied by traffic routes (marked by red lines) and storage areas. Therefore, [20] also highlights that one of the most urgent problems is the lack of space in production. Furthermore, the turnaround time of incoming and/or outgoing materials is criticized too. Materials sometimes lie on the racks for longer than one shift, which means that the logistics process is not optimally synchronized with the production process.

The production logistics process is considered and the three applicable logistics concepts (MOL, IMS and NBS) are compared with each other in terms of their capital and operational expenditure. The comparison is based on the data published in [20] and the available practical and calculated values for the IF and BoxAGV. It serves to identify the market and technology position of the novel logistics concept NBS compared to existing systems, but is not to be understood as an extensive and generally valid research study. This is part of subsequent studies that foresee an implementation of the NBS concept in a real manufacturing environment.

The production is run in two shifts, with one shift lasting eight hours. Of these, 7.5 hours are net working hours. The working and assembly stations are marked as gray areas in Figure 13. The material buffer in the workstations is divided into input (blue) and output (green) materials and has a capacity for two hours of production time. In the current scenario, logistics is provided in each shift by two qualified workers who travel between the supermarket and the workstations with pallet trucks and handcarts. The data basis [20] is accompanied by a component list of a center console as shown in Table 3. It includes the main components only. Small parts such as screws or washers are not listed. The bill of materials also contains information on the packaging unit (PU) of the components and determines their turnaround time based on the target production quantity of 296 pieces per shift.

Table 2: The layout of the manufacturing area is shown in Figure 13, where traffic routes, production and storage areas are the main uses of the total area.

Type of area	Share	
Traffic	463 m^2	34%
Manufacturing	436 m^2	32%
– Area for the workers	*388 m^2*	*28%*
– Workbenches/Machines	*48 m^2*	*4%*
Storage	363 m^2	27%
Administration	74 m^2	6%
Infrastructure	14 m^2	1%
Total	1,350 m^2	100%

Table 3: Bill of materials containing the main components of a center console including the numbers of components per PU, the consumption per shift and the coverage of one PU. The components are provided in a standard VDA box with a capacity of 0.072 m^3, type SLC 8280, 6280 and 6410. `Original data taken from` [20].

Component	Quantity	Consumption	Coverage
① Support arm	192 $^{pcs}/_{PU}$	1.54 $^{PU}/_{shift}$	292 $^{min}/_{PU}$
② Retainer	180 $^{pcs}/_{PU}$	1.64 $^{PU}/_{shift}$	274 $^{min}/_{PU}$
③ Storage	24 $^{pcs}/_{PU}$	12.33 $^{PU}/_{shift}$	36 $^{min}/_{PU}$
④ Handle	1,250 $^{pcs}/_{PU}$	0.24 $^{PU}/_{shift}$	1,900 $^{min}/_{PU}$
⑤ Foam part 1	60 $^{pcs}/_{PU}$	4.93 $^{PU}/_{shift}$	91 $^{min}/_{PU}$
⑥ Foam part 2	16 $^{pcs}/_{PU}$	18.50 $^{PU}/_{shift}$	24 $^{min}/_{PU}$
⑦ Cover lid 1	40 $^{pcs}/_{PU}$	7.40 $^{PU}/_{shift}$	61 $^{min}/_{PU}$
⑧ Cover lid 2	54 $^{pcs}/_{PU}$	5.48 $^{PU}/_{shift}$	82 $^{min}/_{PU}$
⑨ Cup holder 1	21 $^{pcs}/_{PU}$	14.10 $^{PU}/_{shift}$	32 $^{min}/_{PU}$
⑩ Cup holder 2	432 $^{pcs}/_{PU}$	0.69 $^{PU}/_{shift}$	657 $^{min}/_{PU}$

Since [20] has not synchronized the products assembly location with the layout and the paper does not provide any additional bill of materials, the author has made the following definitions to determine the benchmark figures:

- Similarly, assembly products are produced in the manufacturing, where the center console is taken as example to all assembly stations.
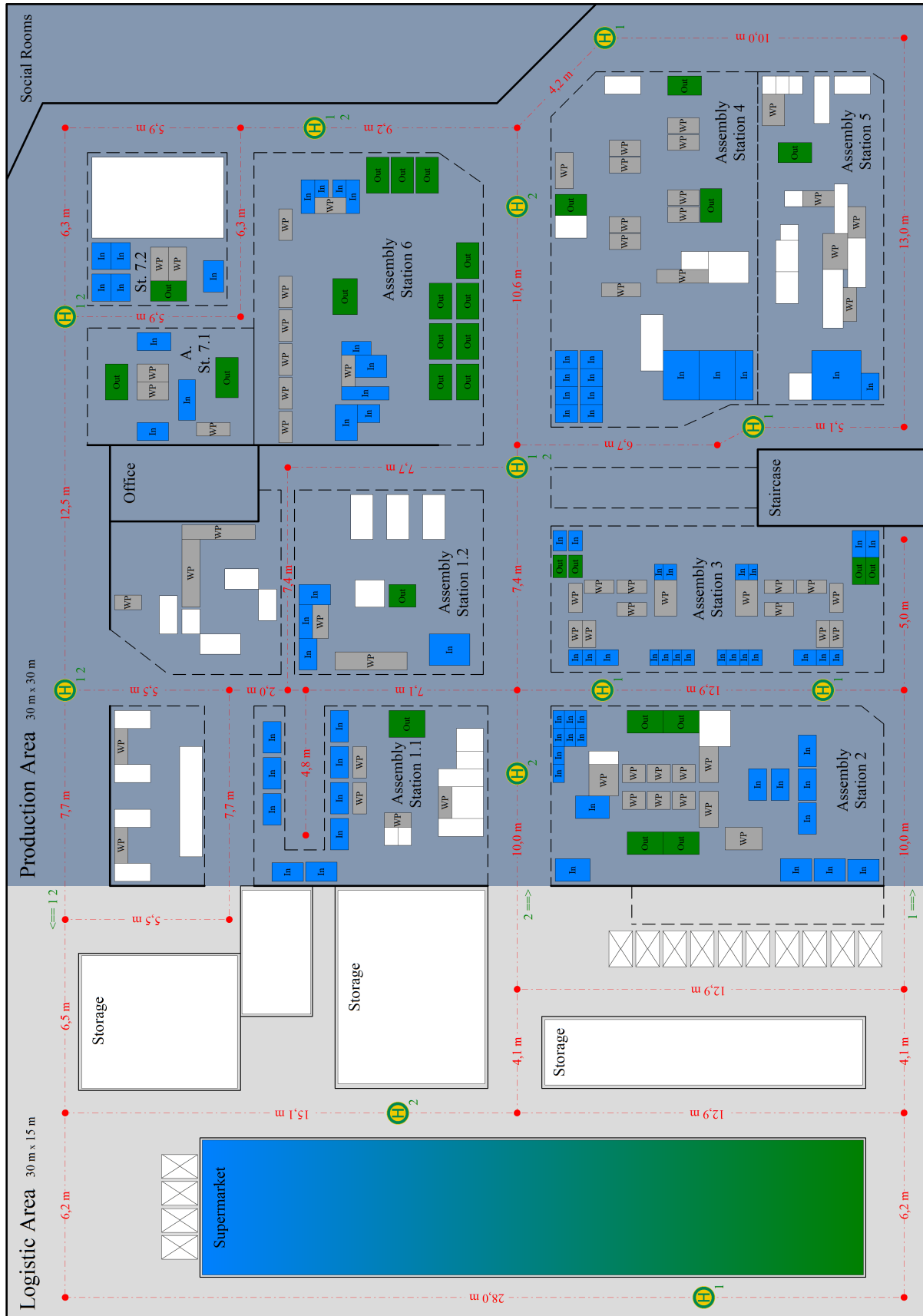
Figure 13: Layout of the logistics and production area for car interior parts, consisting of seven assembly zones, in which the blue rectangles represent goods entry areas, the green ones the goods exit and the grays the workstations. The walking and logistics routes are marked in red and their lengths are listed. The ⓗ–symbols indicate the routes of two milkruns described in [20].

- Ten consoles will be packed into one PU in order to form one outgoing box.
- Milkrun stops are defined according to Figure 13, where the start and end point of a milkrun is located at the supermarket.

With the help of Table's 3 data and the assumptions made, the time-related box throughput in production can now be determined. The Figure 14 shows the time points and quantities of the incoming and outgoing boxes to be handled by the internal logistics over one station and shift. Based on the assumption that similarly complex products are also produced in the other six assembly stations, the handling process can be transferred to them as well. The process does not consider any disturbing effects in the production or logistics chain. It is therefore easy to see that a lack of synchronization between production and logistics, as well as disturbances acting on the logistic chain, can significantly increase the simultaneous material requirements, even though there are buffer at each station.

Furthermore, the number of box storage spaces and the total number of boxes in production can also be calculated from Table 3 and the assumptions made. For this purpose, an assembly station is divided into input, storage and output spaces. In the production start-up configuration, it is planned that all components are available in one box each and that there is also a buffer for each material to bridge a two-hour supply breakdown. The empties storage spaces at the assembly station are dimensioned accordingly. Table 4 shows that the throughput of boxes per shift is 94. This means that in average every five minutes, one box must be fed to or removed from the assembly station. In this case, a usage of the material buffer is not necessary. The buffer capacity is based on the requirement to guarantee a stand-alone manufacturing over two hours.
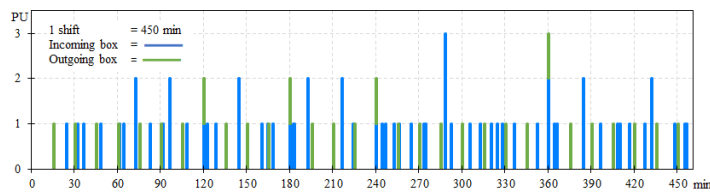
Figure 14: Throughput of input and output boxes at an assembly station over one shift. The incoming boxes with the ten main components of the center console are marked blue and the outgoing boxes with the finished product are marked green. In total 94 boxes are handled over per shift.

To dimension the storage capacity of an assembly station with components correctly, the autonomous production time of two hours is taken as a basis first. Table 3 shows for each component how much production time can be represented by a full box. This time per box is defined as the coverage. Dividing the buffer time of two hours by the coverage gives the number of boxes required. Since this result is usually not a natural number, the value is rounded up to full boxes. As there should always be a full box of each component at the workplace at the beginning of a shift, the result of the storage space calculation must be reduced by this box. The same number of full boxes in the material buffer must be matched by the number of empty box storage spaces. So, the assembly station has in total 21 storage spaces for empty boxes and 21+10 spaces for full boxes. In order to determine the minimum number of boxes in production, it is assumed that the number of boxes handled per shift as well as in the

storage areas of the assembly stations must be provided. Applying this to the present production, a minimum number of 875 boxes is obtained. The following comparison of the three logistics concepts MOL, IMS and NBS bases on the figures of this subsection.

Table 4: Throughput and number of boxes of one assembly station, considering the start-up phase of production and the buffer for at least two hours continuous production.

Component	Start-up	Buffer for 2 h production		Throughput
	full boxes	full boxes	storage space	
Incoming boxes				
① Support arm	1 PU	0 PU	0 PU	1 $^{PU}/_{shift}$
② Retainer	1 PU	0 PU	0 PU	1 $^{PU}/_{shift}$
③ Storage	1 PU	3 PU	3 PU	12 $^{PU}/_{shift}$
④ Handle	1 PU	0 PU	0 PU	1 $^{PU}/_{shift}$
⑤ Foam part 1	1 PU	1 PU	1 PU	4 $^{PU}/_{shift}$
⑥ Foam part 2	1 PU	4 PU	4 PU	18 $^{PU}/_{shift}$
⑦ Cover lid 1	1 PU	1 PU	1 PU	7 $^{PU}/_{shift}$
⑧ Cover lid 2	1 PU	1 PU	1 PU	5 $^{PU}/_{shift}$
⑨ Cup holder 1	1 PU	3 PU	3 PU	14 $^{PU}/_{shift}$
⑩ Cup holder 2	1 PU	0 PU	0 PU	1 $^{PU}/_{shift}$
	10 PU	13 PU	13 PU	64 $^{PU}/_{shift}$
Outgoing boxes				
Ⓐ Center console	0 PU	8 PU	8 PU	30 $^{PU}/_{shift}$

3.5.2 Comparison of the Logistics Concepts

Manually Operated Logistics The MOL is characterized by using manual transport equipment and a low degree of digital information and processing systems. MOL is limited in its complexity and can easily be applied to low variant and continuously running productions. Since it is operated manually, high personnel expenditure is necessary to ensure the material supply – corresponding to the variety of parts, their throughput and the logistic routes length.

In-plant Milkrun System The IMS is an extension of MOL. Logistics employees are still in charge of driving tugger trains, loading and unloading boxes and checking the material quantities by visual inspection. In comparison to MOL, the operation of IMS requires more use of digital information and processing systems as well as the extension of organizational processes. For example, a production with IMS requires defined stops in the shop floor and a schedule with accurate arrival times. This requires a good synchronization of production and logistics that can be implemented with an appropriate production automation technology. In return, productivity gains and personnel cost savings are possible.

Novel BoxAGV System The NBS bases on the IF combinated with the BoxAGV. It represents a fully automated logistics concept. Each box can be controlled autonomously, without the investment

cost disadvantage of today's AGV solutions. In contrast to the logistics concepts MOL and IMS, no persons are required to perform the transport task. But the extensive use of networked information and processing systems is necessary or have to be implemented initially. In addition to the automation of the transport task and the associated reduction in personnel costs, the NBS offers a significant saving of space in production by transferring the material storage to the traffic routes. Due to the demand-driven material supply, NBS reduces the risk of production breakdowns and is therefore more robust than MOL and IMS.

Table 5: Investment and operating expenditures of the logistics concepts MOL, IMS and NBS in a quick comparison.

Cost category	MOL	IMS	NAS
Building	44,388 EUR	44,388 EUR	39,604 EUR
– Space costs/month/m² [24]		2.74 EUR	
– Total production area	1.350 m²	1.350 m²	1.205 m² [1]
Logistics equipment	– are not considered –		
Transport equipment	1,270 EUR	2,392 EUR	83,813 EUR
– 4 x Electric pallet truck [25]	10,156 EUR		
– 2 x Platform truck [26]		5,580 EUR	
– 6 x Trailer [27]		3,558 EUR	
– 351 x IF panel acc. Figure 15			280,800 EUR
– 854 x IF cover panel			170,703 EUR
– 438 x BoxAGV [2]			219,000 EUR
Staff costs	159,360 EUR	79,680 EUR	0 EUR
– Workers per shift	2	1	0
Annual expenditures	205,018 EUR	126,460 EUR	123,417 EUR

[1] *Elimination of the supermarket and its traffic area → 145 m².*

[2] *Each BoxAGV can transport up to 2 PU.*

Since the current state of development of NBS and the data basis of the described production do not allow a detailed cost comparison, the Table 5 is intended to provide a rough cost evaluation of the three logistics concepts shown. It shall be proven that NBS is principally interesting from its capital and operational expenditures compared to MOL and IMS. The table bases on a general operating lifetime of the transport equipment of eight years [28]. This period was also applied for the IF, so that the investment sum in the individual logistics concepts is depreciated on a linear method over eight years. Furthermore, the annual income of a logistics employee is set at 33,200 EUR for the comparison, to which an employer's contribution of 20% to social insurances is added to determine the staff costs [29].

The logistics concepts are compared in three cost categories. For the purpose of completeness, immobile logistics equipment, such as racks, signage and similar equipment, is also listed. But this cost category is not used to evaluate the concepts. Typically, transport equipment is included in the investment costs and staff in the operating costs. The cost of the building may fit into one category or the other, depending on whether the company owns the building or not. If the building is rented, the costs of rent, electricity, water and heating should be allocated to the operating costs. When comparing the annual expenditure, it is remarkable that the lower the degree of automation and rationalization in the logistics concept,

the higher the costs. In the MOL concept the personnel costs are dominant and represent the largest part with three quarters of the total costs. The NBS concept is particularly capital-intensive, but it is cheaper over the eight years of operation compared to MOL. NBS and IMS are roughly equal in price. In addition to investment and operating expenditure considerations, the logistics concepts can also be evaluated according to other criteria. For example, the examination of adaptability to changing market and production conditions is an interesting evaluation criterion that should be considered before deciding on a specific logistics concept. Due to the focus of this paper on the NBS introduction, comparing and delimiting studies are described in subsequent papers. Therefore, a preliminary qualitative list of NBS logistic concept advantages is given here:

- The IF can detect obstacles along the traffic routes with its load cells and redirects the flow of materials automatically by changing the displayed route of the BoxAGV.

- Batch tracking can be carried out by using the built-in LED stripes or an e-paper display unit. The visualization makes it easier to find required batches or to implement space-saving chaotic storage on the shop floor.

- Only a limited number of traffic routes in production are suitable for tugger trains. This limits the automation gain of the IMS concept. As shown in the layout Figure 13, tugger trains are used on the main routes, because curves are not large enough or necessary safety distances [30] cannot be guaranteed. Logistics employees are therefore still forced to carry out material transports manually.

- The MOL is basically flexible, but sensitive to disruptions due to the low degree of interconnection between production and logistics. Bottlenecks that arise here, affect the entire manufacturing process. Due to its high degree of interconnection, the NBS is more robust and less error prone.

- Compared to standard AGV solutions, the distances traveled by the BoxAGV are rather short, so that a BoxAGV can generally be built more simply and therefore more economically. Standard AGVs are designed for a daily mileage of 15…20 km [31]. In contrast, the BoxAGV has to run an average travel distance of less than 200 m (warehouse → assembly station → warehouse) in one shift.

4 Conclusion

In the factory of the future, the floor, walls and ceiling will be the only elements that are installed fixed. Production equipment is mobile and can be flexibly combined to form new production lines. Particularly the transport of goods is performed automatically and made more flexible in the sense of the convertible production. To ensure the competitiveness and future viability of a production company according to the customer demands, the convertible production is becoming more and more essential. Storage space inside the factory like supermarkets is reduced, since the material is in a continuous flow on the BoxAGV. Communication takes place in real-time and humans are the decision makers, supported by assistance systems that operate on an artificial intelligent core.
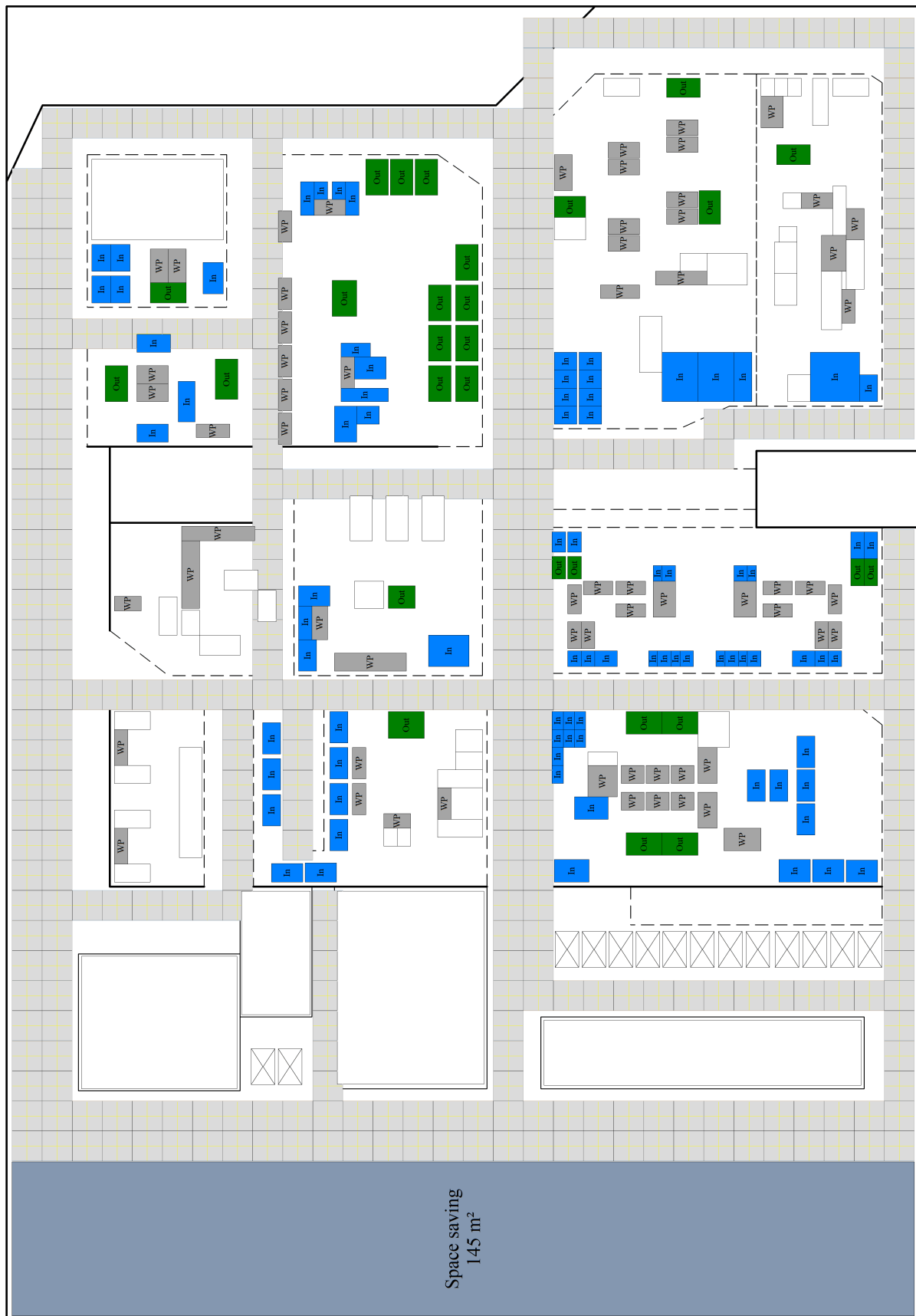
Figure 15: Implementation proposal of the IF into the described production, in which the traffic routes are equipped with standard panels. On this area, the basic functionality of the IF *visualization*, *object detection* and *WPT* for BoxAGV charging is provided. The floor in the area of the assembly stations is built up with regular cover panels.

The IF supports convertibility best and is suitable as an universal and open infrastructure platform for the FOF. Using the IF in such an industrial environment, opens a wide range of applications and makes our current manufacturing processes faster, more flexible and more transparent. A contribution to the convertibility is made by the NBS concept, which prospectively offers cost and space advantages over current logistics solutions. It reduces the material stock at the assembly stations by providing a demand-driven supply. Supermarkets can be downsized by chaotic warehousing or eliminated at all by shifting logistics to the traffic routes. This enables rapid changes in company intralogistics and thus a quick response to market-relevant developments. The close integration of production and logistics also makes manufacturing processes faster and more efficient than today. It is not necessary to search for specific batches (boxes) because each BoxAGV can navigate to a defined point on command or the IF can show the user the way to the BoxAGV via its LED system. The BoxAGV can be used to save on personnel costs or to assign logistics staff to higher-value tasks too.

Overall, the combination of IF and BoxAGV seems to be promising for production companies, especially for companies with a high level of manual and multi-variant assembly. For this reason, a further development of the BoxAGV and the IF is planned. It includes the WPT of transportation and production equipment not only at specific spots, but also along a track and in an open area as described in [15].

References

[1] German Association of the Automotive Industry (VDA), "Small Load Carrier (SLC) System," Technical Report VDA 4500-1.

[2] H. Kühnle, "Paradigmenwechsel im Produktionsbetrieb – Die Fraktale Fabrik," in H.-J. Warnecke, H.-J. Bullinger, editors, Produktionsstrategie für das 21. Jahrhundert, 9–43, Springer Berlin Heidelberg, Berlin, Heidelberg, 1994.

[3] E. Westkämper, "Marktorientiertes Produzieren in dynamischen Strukturen," in H.-J. Warnecke, editor, Fabrikstrukturen im Zeitalter des Wandels – Welcher Weg führt zum Erfolg?, 9–22, Springer Berlin Heidelberg, Berlin, Heidelberg, 1995.

[4] E. Westkämper, "Produktion in Netzwerken," in G. Schuh, H.-P. Wiendahl, editors, Komplexität und Agilität – Steckt die Produktion in der Sackgasse?, 275–291, Springer Berlin Heidelberg, Berlin, Heidelberg, 1997, doi:10.1007/978-3-642-60841-4_19.

[5] E. Westkämper, Technical report, Institut für Industrielle Fertigung und Fabrikbetrieb (IFF), Stuttgart, Stuttgart, 2006.

[6] W. Günthner, K. Furmans, K.-H. Wehking, K.-P. Rahn, M. Ten Hompel, Intralogistik im Dialog mit Forschung und Lehre, 239–276, Springer Berlin Heidelberg, Berlin, Heidelberg, 2006, doi:10.1007/978-3-540-29658-4_6.

[7] M. Hofmann, D. Korte, Neuartiges Logistikkonzept für die automobile Endmontage ohne Band und Takt, 85–100, Springer Berlin Heidelberg, Berlin, Heidelberg, 2020, doi:10.1007/978-3-662-60491-5_8.

[8] M. Mandat, "Produktportfolios der fünf großen deutschen Autohersteller in Deutschland: 1990 bis 2014: Das Dilemma mit der Vielfalt," .

[9] Volkswagen, "Absatz des VW Golf im Zeitraum der Jahre 1974 bis 2012 nach Modell," 2012.

[10] H. Meier, N. Hanenkamp, Komplexitätsmanagement im Lebenszyklus individualisierter Produkte im Maschinen- und Anlagenbau, 623–639, Gabler Verlag, Wiesbaden, 2005, doi:10.1007/978-3-663-01577-2_38.

[11] T. Stehle, U. Heisel, Konfiguration und Rekonfiguration von Produktionssystemen, 333–367, Springer Berlin Heidelberg, Berlin, Heidelberg, 2017, doi:10.1007/978-3-662-55426-5_39.

[12] J. Stratmann, "Blick unter die VW Golf 7 Karosserie: Über die Nervenbahnen der modernen Automobile," .

[13] Komax, "Zeta 640/650, [Online]. Avail- able: https: // www.komaxgroup.com / en / Products-and-Solutions / Products / Harness-Manufacturing / Zeta-640-650 /" .

[14] J. Stillig, N. Parspour, "Advanced Manufacturing based on the Intelligent Floor," in 20th IEEE Mediterranean Electrotechnical Conference (MELECON), 248–253, 2020, doi:10.1109/MELECON48756.2020.9140660.

[15] J. Stillig, N. Parspour, "Novel Concept for Wireless Power Transfer Modules," in 2020 International Conference on Broadband Communication, Wireless Sensors and Powering (BCWSP), 167–172, 2020, doi:10.1109/BCWSP50066.2020.9249465.

[16] T. Kuhlmann, P. Spanier, M. Ehlich, Potenziale einer industriellen Gleichstromversorgung, 9–35, Carl Hanser Verlag GmbH & Co. KG, München, 1997, doi:10.3139/9783446466128.002.

[17] F. Regnery. [Online]. Available: https: // www.vde.com / resource / blob / 1888372 / 2fab7ab57295bebd7fbd3769314e9efa / faktencheck-bidirektionale-energiefluesse—download-data.pdf

[18] J. Kesselring, Prozessbegleitende Planung und Konfiguration von Fördertechnikanlagen unter Zuhilfenahme von virtuellen Konfigurationsmustern und Konfigurationsmodellen, Ph.D. thesis, Karlsruher Institut für Technologie (KIT), 2017, doi:10.5445/IR/1000075521.

[19] "Flurförderfahrzeuge – Sicherheitstechnische Anforderungen und Verifizierung, Teil 4: Fahrerlose Flurförderfahrzeuge und ihre Systeme," 2020.

[20] M. Knez, B. Gajšek, "Implementation of In-plant Milkrun System for Material Supply in Lean Automotive Parts Manufacturing," in 12th International Conference on Logistics and Sustainable Transport 2015 (ICLST), 121–126, 2015.

[21] M. Ellrich, "Vor- und Nachteile des Produktions- und Logistiksystems," Geographie Infothek, 2.

[22] L. Ickert, U. Matthes, S. Rommerskirchen, E. Weyand, M. Schlesinger, J. Limbers, Technical report, Bundesministerium für Verkehr und digitale Infrastruktur, Basel/Berlin, 2007.

[23] J. Stillig, "Verfahren zum Betrieb eines Spurführungssystems," 2019.

[24] Haufe Online Redaktion, "Logistik: Nebenkosten für Lager und Cross Docks leicht gestiegen," .

[25] STILL GmbH, n.d. [Online]. Available: https: // www.still.shop / ecu-15-c.html

[26] STILL GmbH, n.d. [Online]. Available: https: // www.still.shop / ltx-20.html

[27] Carl Beutlhauser Kommunal- und Fördertechnik GmbH & Co. KG, "Routenzug Katalog," Booklet.

[28] Bundesministerium der Finanzen [Online]. Available: https: // www.bundesfinanzministerium.de / Content / DE / Standardartikel / Themen / Steuern / Weitere Steuerthemen / Betriebspruefung / AfA-Tabellen / Ergaenzende-AfA-Tabellen / AfA-Tabelle AV.html.

[29] StepStone Deutschland GmbH, "Welches Gehalt verdient man im Bereich Logistik-Mitarbeiter/in?" n.d.

[30] DGUV Fachbereich Handel und Logistik, "Routenzüge – Einsatz von Schleppern und Anhängern als Routenzüge," Technical Report FBHL-008, 2018.

[31] Dahl Automation GmbH, n.d. [Online]. Available: https: // www.mobile-robots.de / 70 / robotize

ASTES

Data Aggregation, Gathering and Gossiping in Duty-Cycled Multihop Wireless Sensor Networks subject to Physical Interference

Lixin Wang[*,1], Jianhua Yang[1], Sean Gill[1], Xiaohua Xu[2]

[1]*TSYS School of Computer Science, Columbus State University, Columbus, GA 31907, USA*

[2]*College of Computing and Software Engineering, Kennesaw State University, Marietta, GA 30060, USA*

A B S T R A C T

Data aggregation, gathering and gossiping are all vital communication tasks in wireless sensor networks (WSNs). When all networking devices are always active, scheduling algorithms for these communication tasks have been extensively investigated under both the protocol and physical interference models. However, wireless devices usually switch between the sleep state and the active state for the purpose of energy saving. A networking device with duty-cycled scenarios having sleep/awake cycles may need to transmit the message to all neighbors more than once. Taking the duty-cycled scenarios into consideration, communication scheduling algorithms for these tasks have been extensively investigated under the protocol interference model. As far as we know, scheduling algorithms for these communication tasks have not yet been investigated in WSNs with duty-cycled scenarios under the physical interference model. In this paper, we propose minimum latency scheduling algorithms for these communication tasks in duty-cycled WSNs under the physical interference model. Our innovative scheduling algorithms for both data gathering and gossiping achieve approximation ratios at most a constant time of $|T|$, where $|T|$ is the length of a scheduling period. The approximation ratio of our proposed data aggregation scheduling algorithm is less than or equal to a constant times $|T|$ with bounded maximum degree of the network.

1   Introduction

This paper is an extension of our work originally presented on the 15th IEEE International Conference on Mobile Ad-hoc and Sensor Networks (IEEE MSN 2019) [1].

Wireless sensor networks (WSNs) have been widely employed in automated battlefields, emergency disaster relief, environmental monitoring, real-time pollution monitoring, military surveillance, etc. Most of these WSN applications are time critical. The definitions of data gossiping, data gathering, and data aggregation can be found in [2]. The concepts of a link schedule, data aggregation schedule, data gathering schedule and data gossiping schedule can also be found in [2].

The latency of a data aggregation schedule is the total number of time-slots needed for the sink node to receive the aggregated message from all other networking nodes. Minimum-Latency Aggregation Schedule (**MLAS**) is the research problem for developing a scheduling algorithm for data aggregation in a multi-hop WSNs with the smallest latency. Similarly, the latency of a data gathering

schedule is the total number of time-slots required for the sink node to receive a packet from every other networking node; the latency of a gossiping schedule is the total number of time-slots needed for every device to receive the packets from all other networking devices. Minimum-Latency Gathering Schedule (**MLGS**) is the research problem for developing a scheduling algorithm for data gathering in a multi-hop WSNs with the smallest latency. Minimum-Latency Gossiping Schedule (**MLGoS**) is the research problem for developing a scheduling algorithm for data gossiping in a multi-hop WSNs with the smallest latency. A great number of communication scheduling algorithms have been developed for MLAS, MLGS and MLGoS in multi-hop WSNs under either the physical interference model [2], or the protocol interference model [3]–[13] and the references therein.

However, wireless devices usually switch between the sleep state and the active state for the purpose of energy saving. A networking device with duty-cycled scenarios having sleep/active cycles may need several times to transmit the message to all neighbors. The duty-cycled scenarios is a popular energy-saving method for multi-

hop WSNs. The GreenOrbs projects [14] and the VigilNet projects [15] are two actual applications of duty-cycled WSNs (DC-WSNs). Thus, all the existing approximation solutions for MLAS, MLGS, or MLGoS without duty-cycled scenarios are not working any more on DC-WSNs.

We use the same duty cycle model in this paper as the one we used in our short conference version [1]. The problem MLAS on duty-cycled multi-hop WSNs is represented by **MLAS-DC**. Similarly, MLGS and MLGoS on duty-cycled multi-hop WSNs are represented by **MLGS-DC** and **MLGoS-DC**, respectively. With duty-cycled scenarios, all three problems MLAS-DC, MLGS-DC and MLGoS-DC have been extensively investigated subject to the protocol interference and its simple variations [5], [16]–[24]. To the best of our knowledge, all three duty-cycled scheduling problems have not yet been investigated on duty-cycled multi-hop WSNs subject to the physical interference.

In this paper, we develop short communication schedules for the above three duty-cycled scheduling problems on multi-hop WSNs under the physical interference model which is a realistic model that handles wireless interferences more accurately. Under such a realistic model, a receiver can successfully receive the message if and only if the *Signal-to-Interference-plus-Noise-Ratio* (*SINR*) of the receiver is greater than a threshold value. According to the way the SINR ratio is computed, the SINR value is based on those transmissions are that will be scheduled concurrently in every time slot. Therefore, constructing a conflict graph to model the wireless interference is challenging. Such a nature of the physical interference makes it very hard to analyze the proposed communication scheduling algorithms subject to physical interference. Let $\|uv\|$ represent the Euclidean distance between the two devices u and v. Let σ represent the threshold value for a receiving device can successfully receive the wanted signal subject to physical interference, and ξ power strength of the background noise. Suppose that all the devices use a uniform and fixed power P for transmission. The path loss is represented by a positive reference loss parameter η, and a constant path-loss exponent κ (a value between 2 and 6). Assume that the communication radius of each device is normalized to one. If a device u sends a signal using a transmission power P, the power strength of this signal received by the receiving device v is $\eta P \|uv\|^{-\kappa}$.

By far, [25] is the only work that studied **MLAS-DC** for multi-hop WSNs subject to physical interference. When the SINR ratio of a node u is calculated in EQ(1) of [25], the received power $P_r(u)$ at u is incorrectly calculated in EQ(2) of [25] as it will be greater than the transmission power when the distance $\|uv\| < 1$. When $\|uv\| \geq 1$, the received power $P_r(u)$ is simply set to be the transmission power in [25]. Similarly, the total interference power at u is also incorrectly calculated in EQ(3) of [25]. Therefore, radio signal attenuation is not taken into consideration and the algorithms proposed in [25] for **MLAS-DC** are invalid under the physical interference model. As far as we know, there are no existing algorithms proposed for **MLGS-DC** or **MLGoS-DC** for multi-hop WSNs subject to the physical interference constraint.

Let $|T|$ denote the total number of time-slots in a scheduling period. Below are this paper's main contributions:

1. The approximation ratio of the algorithm we proposed for

MLGS-DC is less than or equal to a constant times $|T|$;

2. The approximation ratio of the algorithm proposed for MLGoS-DC is less than or equal to a constant times $|T|$;

3. The approximation ratio of the algorithm proposed for MLAS-DC is less than or equal to a constant times $|T|$ when the network has bounded maximum degree.

All the notations used in this paper are listed in Table 1 for easy referencing.

The remaining of this paper is organized as follows. The related work for existing approximation scheduling algorithms for data aggregation, gathering and gossiping are given in Section 2. Section 3 gives some basic concepts and preliminary knowledge that are needed for the design of the scheduling algorithms. In Section 4, we create a tree rooted at the sink that will be used for routing. In Section 5, we present an approximation solution to MLAS-DC. In Section 2, we propose an approximation solution to MLGS-DC. An approximation solution to MLGoS-DC is developed in Section 7. Finally in Section 8, a conclusion for this paper and some future research are presented.

2 Related Works

First, let us review the related work for known algorithms that were proposed for MLAS in multi-hop WSNs when all the networking nodes are implicitly assumed to be always active [2]–[4], [7], [9]. If all the networking devices have uniform transmission radii normalized to one on a multi-hop WSN, the network topology forms a UDG (unit-disk graph). For convenience, the number of networking nodes is denoted by n, the radius of the network graph w.r.t. the sink node of data aggregation or gathering is denoted by R. For arbitrary interference radius, any optimal solution to MLAS uses at least R time-slots. So is $\log n$. [3] and [7] proposed two scheduling algorithms for data aggregation with the total latency less than or equal to $(\Delta - 1)R$ and $23R + \Delta - 18$, respectively, where Δ is the maximum degree when the transmission radius is the same as the interference radius. The single-level aggregation was investigated in [4] that developed aggregation scheduling algorithm. When the transmission radius is the same as the interference radius, three approximation algorithms were proposed in [9] with total latency less than or equal to $15R + \Delta - 4$, $2R + \Delta + O(\log R)$ and $\left(1 + O\left(\log R / \sqrt[3]{R}\right)\right)R + \Delta$, respectively. These existing scheduling algorithms for MLAS mentioned above were proposed subject to the protocol interference, and the networking devices are assumed to be always awake.

Subject to the physical interference or the protocol interference, MLGS in multi-hop WSNs has also been extensively investigated when all the networking devices are always awake [2], [10], [11], [13], [26]. Let us review the approximatino solutions developed subject to the protocol interference first. The NP-hardness of MLGS was verified by in [10] that developed a scheduling solution for MLGS that has approximation ratio at most four with the assumption that the communication topology could be reduced to a UDG. In [11], the author proposed a greedy approach for MLGS and proved it to achieve approximation ratio at most 4 in a general setting and achieve approximation ratio at most 3 when

Table 1: All notations used in this paper:

P	the uniform transmission power of every node
η	the parameter of the reference loss
κ	the path-loss exponent
$\|uv\|$	the Euclidean distance of the two nodes u and v
σ	the threshold ratio of the SINR model
ξ	the background noise in the SINR model
T	a scheduling period
$|T|$	the count of the time-slots in a scheduling period T
V	the set of all networking nodes
Δ	the maximum degree of the communication topology of the network
G_r	r-disk graph on V
SPT	a shortest path tree over V
$SPAN$	a spanning tree over V
$\zeta(x)$	the Riemann zeta function
$A(v)$	the active time slot of a node v
s	the sink node of aggregation and gathering
M	the largest latency of the shortest paths from all other nodes to node s in SPT
U_j	the set of the awake nodes in time-slot j
L_i	the subset of the nodes in V from which the latency of the shortest path to node s is i
I_j	the maximum independent set in U_j
I_{ji}	is defined to be $I_j \cap L_i$
$Lat(u, v)$	the Latency of the link (u, v)

the communication topology could be reduced to a UDG. When the transmission radius is the same as the interference radius, a scheduling solution for MLGS was proposed in [26] that has approximation ratio at most $(1 + 1/(k + 1))$ with k being a whole number. In [13], the author developed a scheduling solution for MLGS with the shortest gathering schedule in which several channels were used to speed up communications and make the scheduling solu-tions more efficient. For MLGS, when the interference radii r_i are uniform and no less than the transmission radius, an efficient scheduling solution was proposed in [13] having approximation ratio less than or equal to $2\beta_{r_i}/\lambda$ with λ being the count of the channels that can be used and β_{r_i} the largest number of points in a half-disk of radius $r_i + 1$ with the distance between any two of them is greater than 1.

For MLGoS on multi-hop WSNs, under the UDG model, the authors of [8] designed a gossiping scheme that achieved approximation ratio 27, improved previously known algorithms which have approximation ratio 1000+. In [6], the author considered the problem MLGoS and presented respectively two algorithms with approximation guarantees of 20 and 34, thereby improving the approximation ratio of 27 presented in [8].

When all the devices are always active, [2] developed the shortest communication schedules for MLAS, MLGS and MLGoS subject to the physical interference. [2] developed scheduling algorithms for the four important group communication tasks under the physical interference model. Both the gathering schedule and gossiping schedule developed in [2] achieved constant approximation ratios. For MLGS, [2] proposed an efficient scheduling algorithm with approximation bound less than or equal to $2\beta_\rho$, where ρ and β_ρ are defined in EQ(1) and EQ(3), respectively. For MLGoS, [2] developed a gossiping solution with approximation bound less than

or equal to $5\beta_\rho$. Under mild assumptions, the broadcast schedule and data aggregation schedule developed in [2] could also achieve constant approximation ratios.

However, none of the known research papers described above have considered the situation that some networking devices may be in an inactive state. Taking duty-cycled scenarios into consideration under a graph-based interference model, the problem MLAS-DC has been extensively investigated [5], [17], [20]–[23], [27], [28].

Both [5] and [17] developed short data aggregation schedules for MLAS-DC. Both [20] and [21] studied the MLAS-DC problem in order to minimize the communication delay and maximize sensor nodes' lifetimes, and propsed another distributed algorithm for MLAS-DC. All the above mentioned scheduling algorithms for MLAS-DC were proposed under the simple protocol interference model. A data aggregation scheduling algorithm was developed in [22] for MLAS-DC with minimum latency for the purpose of energy efficiency. [23] studied the MLAS-DC problem with no structures taken into consideration. A distributed aggregation algorithm was proposed for MLAS-DC under the protocol interference model, in which the routing tree used for aggregation and a data aggregation schedule without collision were produced at the same time by the algorithm. In [27], the author investigated the MLAS-DC and developed two distributed aggregation algorithms for MLAS-DC, where the routing tree used for data aggregation and an aggregation schedule were produced at the same time. In [27], the author developed an approximation algorithm for MLAS-DC with better approximation bound. When the networking nodes have changable radii, a aggregation schedule with less number of time slots was developed for MLAS-DC in [28] by constructing a nonlinear mathematical formula.

For MLGS-DC subject to protocol interference, [24] proposed

a data gathering scheduling algorithm that achieves an approximation bound of $10|T|$. For the problem MLGoS-DC, [18] proposed a solution called the UTB algorithm for the all-to-all broadcast in which every message must be sent separately without any combination or aggregation and a more efficient version UTB-P of this algorithm using the Prune method. The approximation bound of these two algorithms for MLGoS-DC are less than or equal to $17|T| + 20$. With the unit-size message model, [24] investigated MLGoS-DC and proposed a scheduling algorithm for gossiping that achieved approximation bound less than or equal to $20|T|$. The paper [19] studied the problem MLGoS-DC in uncoordinated duty-cycled multi-hop wireless networks with unbounded-size messages. The NP-hardness of MLGoS-DC was verfified in [19]. This paper also developed two approximation algorithms for MLGoS-DC with approximation bounds less than or equal to $3\Phi^2(\Delta + 6)|T|$, with $\Phi = \lceil 2(\Psi + 2)/3 \rceil$, and Δ the maximum degree of the network. The value of Ψ is equal to the ratio obtained via dividing the interference radius by the transmission radius of each device.

3   Preliminaries

In this section, we introduce some notations, parameters and concepts that are needed for the design of our scheduling algorithms to be proposed in this paper. Set

$$R = \left(\frac{\eta P}{\sigma \xi}\right)^{1/\kappa}.$$

Given a pair of devices u and v. Clearly, there is a link between u and v in the communication topology when there is no interference from other nodes that are transmitting simultaneously if and only if $\|uv\| \le R$. We call R the *maximum transmission radius*.

Suppose that r is a positive parameter. Denote by R' be the largest edge length of a Euclidean minimum spanning tree over V, the set of all the networking nodes. Clearly, R' equals the minimum value of r satisfying that the r-*disk* graph over V is connected. The relation $R' \le R$ is needed for the network to be connected. An additional assumption we need is that $R' \le (1 - \varepsilon)R$ which holds for certain small positive constant ε.

Denote by Γ the collection of all Euclidean distances of the networking nodes in V less than R, and greater than or equal to R'. That is, we have

$$\Gamma = \{\|uv\| : u, v \in V \text{ and } R' \le \|uv\| < R\}.$$

Through a straightforward calculation, we have $1 \le |\Gamma| \le n(n-1)/2$ with n being the number of nodes.

Under the physical interference model, a collect I of networking nodes is referred to as *r-independent* when the following two conditions hold

(1) if every node in I sends a message at the same time, each such a transmission could be correctly received by every node whose distance from the transmitter is no more than r;

(2) the distance between any two nodes in I is larger than r.

Now we introduce the well-known Riemann zeta function denoted by $\zeta(x)$:

$$\zeta(x) = \sum_{j=1}^{\infty} \frac{1}{j^x}.$$

For each $r \in [R', R)$, define the following parameter ρ that is needed for the design of our scheduling algorithms to be proposed in later sections and its value is clearly explained in [2].

$$\rho = 1 + \left(\frac{\sigma \left(16\zeta(\kappa - 1) + 8\zeta(\kappa) - 6\right)}{1 - (r/R)^\kappa}\right)^{1/\kappa}. \tag{1}$$

Now we introduce the concept of independence for a given collection of links under the physical interference model. A collection C of links is called *independent* subject to the physical interference if the following two conditions hold:

(1) when the senders of all the communication links in C transmit at the same time, the receivers of every communication link in C can correctly receive the message; (2) all the communication links in C are disjoint.

4   Construction of A Routing Tree

A spanning tree $SPAN$ with the root node $s \in V$ is created in this section. This spanning tree will be employed in routing of the group communication tasks studied in this paper. Let $r > 0$. Denote by G_r a connected and undirected r-disk graph over V.

To begin with, a directed graph G'_r is created based on G_r as follows: replaced every edge (u, v) of G_r by two directed links (u, v) and (v, u) on G'_r, and then remove all links leaving s from G'_r. For a vertex $u \in V$, let $A(u) \in T$ be the awake time slot of u. For a link $(u, v) \in E(G'_r)$, it is assumed that u is the sender and v is the receiver. The latency of (u, v) is defined as follows:

$$Lat(u, v) = \begin{cases} A(v) - A(u), & if\ A(u) < A(v); \\ A(v) - A(u) + |T|, & if\ A(u) \ge A(v). \end{cases} \tag{2}$$

We associate each link (u, v) of G'_r with the weight equal to its latency $Lat(u, v)$, then G'_r is a directed weighted graph with all link weights non-negative. Therefore, a shortest path tree SPT of G'_r rooted at s can be computed by applying the Dijkstra's algorithm on G'_r. The tree SPT consists of all the minimum-weight paths from all nodes other than s to s. The largest latency among all the shortest paths in SPT from all other nodes to sink s is represented by M. Clearly, any optimal solution to either MLAS-DC or MLGS-DC is greater than or equal to M.

Let us take the undirected graph G_r with eight nodes in Fig. 1 as an example to explain the constructions of the directed graph G'_r and the shortest path tree SPT rooted at s. In this example, a scheduling period $T = \{0, 1, 2, 3\}$ with $|T| = 4$. Each node is represented by a circle with its active time slot contained inside it.

Based on our discussion above, the directed graph G'_r is constructed below

We compute a shortest path tree SPT of G'_r with the root s via employing the Dijkstra's shortest path algorithm on G'_r. This SPT is shown in Fig. 3.

This tree SPT has three leaf nodes v_3, v_6 and v_7. Let $\langle v_6, v_5, v_2, s \rangle$ denote the path from v_6 to s through v_5 and v_2.
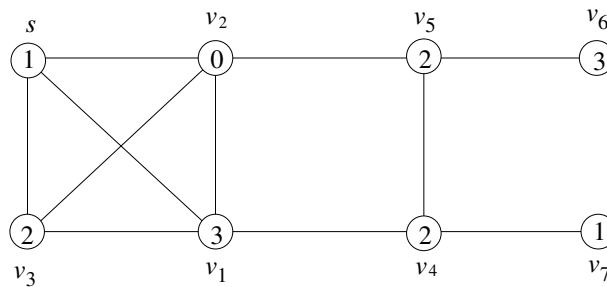
Figure 1: This network has eight vertices. We assume that a scheduling period T has four time slots, that is, $\{0, 1, 2, 3\}$. Each vertex contains a number that is the time-slot at which the vertex is awake.
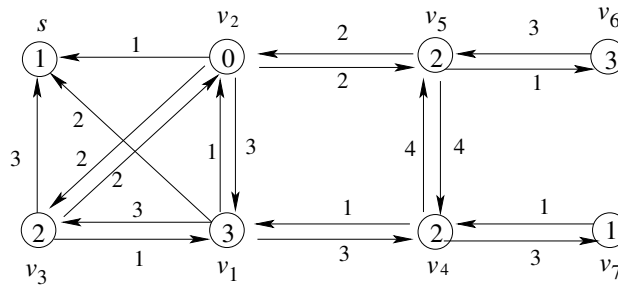
Figure 2: A directed graph with each link associated with the weight equal to its latency defined in EQ(2).
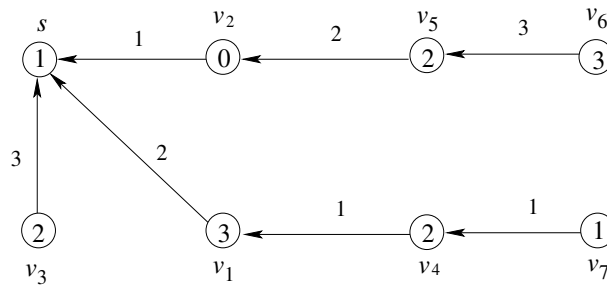
Figure 3: A shortest path tree T_{SPT} rooted at s of the above directed graph in Fig. 2.

Clearly, $Lat(\langle v_6, v_5, v_2, s \rangle) = 6$. Similarly, $Lat(\langle v_7, v_4, v_1, s \rangle) = 4$ and $Lat(v_3, s) = 3$. Therefore, the maximum latency $M = 6$ in this example.

Due to the likely interference with each other caused by the concurrent transmissions, however, the shortest path tree SPT constructed above cannot directly be used for routing of either data aggregation or data gathering. Therefore, a spanning tree $SPAN$ with root s must be created for the use of routing in data aggregation and gathering operations. Such a spanning tree $SPAN$ is constructed as follows:

The nodes in V are put into distinct layers L_0, L_1, L_2, $\cdots$, L_M according to the latency of the shortest path from each $v \in V$ with $v \neq s$ to s. Let's use the same example above to explain how to divide the nodes of V into different layers and construct the sets U_j with $j = 0, 1, 2, 3$. According to the shortest path tree SPT shown in Fig. 3, we have $L_0 = \{s\}$, $L_1 = \{v_2\}$, $L_2 = \{v_1\}$, $L_3 = \{v_3, v_4, v_5\}$, $L_4 = \{v_7\}$, $L_5 = \emptyset$, and $L_6 = \{v_6\}$. Based on EQ(??), it is easy to see that $U_0 = L_1 \cup L_5 = L_1$; $U_1 = L_0 \cup L_4$; $U_2 = L_3$; and $U_3 = L_2 \cup L_6$.

Note that likely interferences only happen at those active nodes that can receive messages at the time-slot that is under consideration.

For each time slot $0 \leq j \leq |T| - 1$, we construct an MIS $I_j \subset U_j$ layer by layer by following the steps below, based on the disjoint union of the nodes in distinct layers of U_j given in EQ(??):

- Initially, $I_j = \emptyset$.

- Sort all the nodes in the layer $L_{A(s)-j+K_0|T|}$ (with smallest index) in the ascending order of their identifications if $L_{A(s)-j+K_0|T|} \neq \emptyset$, say $L_{A(s)-j+K_0|T|} = \langle v_1, v_2, \cdots, v_z \rangle$ with z being the size of $L_{A(s)-j+K_0|T|}$, and add the first node v_1 to I_j.

- If $I_j \cup \{v_2\}$ is independent in G_r, then $I_j \leftarrow I_j \cup \{v_2\}$. If $I_j \cup \{v_2\}$ is dependent in G_r, then the node v_2 is skipped and then the next node in the list is taken into consideration.

- Do the same thing for v_3 until the last node v_z in $L_{A(s)-j+K_0|T|}$ is either added to I_j or skipped.

- Then do the same thing for all the nodes in $L_{A(s)-j+k|T|}$ with $k = 1 + K_0, \cdots, K_1$ until all the nodes in the last layer $L_{A(s)-j+K_1|T|}$ are processed.

Clearly, the MIS I_j constructed above is an independent subset of U_j. For simplicity, let $I_{ji} = I_j \cap L_i$. For each layer $0 < i \leq M$,

every node $v \in L_i \setminus I_{ji}$ was skipped by the above algorithm for the construction of the MIS I_j. Thus, the union $I_{j1} \cup I_{j2} \cup \cdots \cup I_{ji}$ contains one or more neighbors of $v \in L_i \setminus I_{ji}$.

The algorithm for constructing the spanning tree $SPAN$ over V rooted at s was described in the conference version [1] and omitted here due to space limitation. Let's use the same example above to explain how to construct the MIS $I_j \subset U_j$ for each time slot $0 \le j \le |T| - 1$, and how to construct the tree $SPAN$ rooted at s. For $U_0 = L_1 = \{v_2\}$, $I_0 = \{v_2\}$. For $U_1 = L_0 \cup L_4 = \{s, v_7\}$, $I_1 = \{s, v_7\}$. For $U_2 = L_3 = \{v_3, v_4, v_5\}$, $I_2 = \{v_3, v_4\}$. For $U_3 = L_2 \cup L_6 = \{v_1, v_6\}$, $I_3 = \{v_1, v_6\}$.

Now the tree $SPAN$ with root s for this example is created. For $L_1 = \{v_2\}$, v_2's parent in $SPAN$ is s (the same parent as in SPT) as $v_2 \in I_0 \cap L_1$. For $L_2 = \{v_1\}$, v_1's parent in $SPAN$ is also s as $v_1 \in I_3 \cap L_2$. For $L_3 = \{v_3, v_4, v_5\}$, v_3's parent in $SPAN$ is s as $v_3 \in I_2 \cap L_3$; v_4's parent in $SPAN$ is v_1 as $v_4 \in I_2 \cap L_3$; v_5's parent in $SPAN$ is v_4 (a different parent from SPT) as $v_5 \notin I_2 \cap L_3$. For $L_4 = \{v_7\}$, v_7's parent in $SPAN$ is v_4 as $v_7 \in I_1 \cap L_4$. For $L_6 = \{v_6\}$, v_6's parent in $SPAN$ is v_5 as $v_6 \in I_3 \cap L_6$. The constructed tree $SPAN$ rooted at s is shown in Fig. 4 below:

Finally in this section, the concept of the first-fit distance-d coloring for a subset of V in the lexicographic order is presented and adopted from our prior work [2]. Denote by U a subset of V. We consider the lexicographic order of the nodes in U, then we sort all nodes in U from the left to right, $u_1, u_2, \cdots, u_k$ with $k = |U|$. *The first-fit distance-d coloring of U* in the lexicographic order is described below:

- positive integers $1, 2, 3, \cdots$ represent colors;
- the first node u_1 in the sequence is assigned color 1;
- For $i = 2$ up to k, the node u_i is assigned the smallest possible number that is not utilized by any prior node u_j in the sequence with $j < i$ and $\|u_i u_j\| \le d$.

[2] proved that for a given independent set I of G_r, the first-fit distance-ρr coloring of I with the lexicographic ordering needs at most β_ρ colors. The value of β_ρ is given below (see Corollary 4 of [2]):

$$\beta_\rho = \left\lfloor \frac{\pi\rho^2}{\sqrt{3}} + \left(\frac{\pi}{2} + 1\right)\rho \right\rfloor + 1. \tag{3}$$

5 Aggregation Schedule under the Physical Interference Model Taking Duty Cycles into Consideration

In this section, we consider MLAS-DC subject to the physical interference and develop a short aggregation schedule for this problem. The sink node is represented by s. For a real number r satisfying $R' \le r < R$, we use EQ(1) to calculate ρ. Then follow the steps stated in Section 4, the spanning tree $SPAN$ rooted at s is constructed. The transmission follows a bottom-up approach.

Next we present the first-fit scheduling algorithm for MLAS-DC subject to physical interference. The first layer to transmit is the bottom layer L_M, and then the nodes in layer L_{M-1} transmit. The

scheduling is based on a bottom-up approach. For each layer L_i ($0 < i \le M$), we know that the nodes in L_i are active at time-slot j ($0 \le j \le |T| - 1$). At this layer, the nodes in $L_i \setminus I_j$ will be scheduled to transmit first, followed by the tranmissions of the nodes in $L_i \cap I_j$. Then the nodes in layer L_{M-1} will be scheduled to transmit. For each layer among $L_{M-1}, L_{M-2}, \cdots, L_0$, the nodes in these layers will receive the aggregated data from their children nodes in the decreasing order of the indices of the layers $M - 1, M - 2, \cdots$.

For the details of our first-fit data aggregation scheduling algorithm proposed for the problem MLAS-DC subject to the physical interference, please refer to the conference version [1]. Assume the graph in Figure 1 represents an r-disk graph G_r for some $r \in \Gamma$. We use this example in Figure 1 to illustrate the data aggregation scheduling algorithm we proposed for MLAS-DC.

The tranmission schedules for aggregation outputted by the above algorithm are listed in Table 2. Totally, 6 scheduling periods are required for s to receive eventually the aggregated message in this example.

The algorithm for this example works as follows: At $L_6 = \{v_6\}$, $v_6 \in I_3 \cap L_6$ and its parent in $SPAN$ is v_5 which is active at time-slot 2. Thus, link (v_6, v_5) is scheduled at time-slot 2 of SP 1. We skip $L_5 = \emptyset$. For $L_4 = \{v_7\}$, $v_7 \in I_1 \cap L_4$ and its parent in $SPAN$ is v_4 which is also active at time-slot 2. Thus, link (v_7, v_4) is scheduled at time-slot 2 of SP 2. For $L_3 = \{v_3, v_4, v_5\}$, node $v_5 \in L_3 \setminus I_2$ and its parent in $SPAN$ is v_4 which is active at time-slot 2. Thus, link (v_5, v_4) is scheduled at time-slot 2 of SP 3. The nodes $v_3, v_4 \in I_2 \cap L_3$; v_3's parent in $SPAN$ is s which is active at time-slot 1. Thus, link (v_3, s) is scheduled at time-slot 1 of SP 4. Node v_4's parent in $SPAN$ is v_1 which is active at time-slot 3. Thus, link (v_4, v_1) is scheduled at time-slot 3 of SP 4. For $L_2 = \{v_1\}$, $v_1 \in I_3 \cap L_2$ and its parent in $SPAN$ is s which is active at time-slot 1. Thus, link (v_1, s) is scheduled at time-slot 1 of SP 5. Finally for $L_1 = \{v_2\}$, $v_2 \in I_0 \cap L_1$ and its parent in $SPAN$ is s which is active at time-slot 1. Thus, link (v_2, s) is scheduled at time-slot 1 of SP 6.

We summarize our above discussion in the following theorem. The proof of this theorem can be found in the short conference version [1].

Theorem 1 *The data aggregation scheduling algorithm for MLAS-DC is technically correct and produces a data aggregation schedule without any collision. The latency of the transmission schedule for aggregation outputted via our proposed algorithm is less than or equal to $2\beta_\rho |T| (\Delta - 1)M$. The proposed algorithm for MLAS-DC has approximation ratio upper bounded by $2\beta_\rho |T| (\Delta - 1)$.*

Note that both ρ and β_ρ are constants defined in EQ(1) and EQ(3), respectively. Therefore, the approximation bound for our scheduling algorithm proposed for MLAS-DC is less than or equal to a constant times $|T|$ when the maximum degree Δ is bounded.
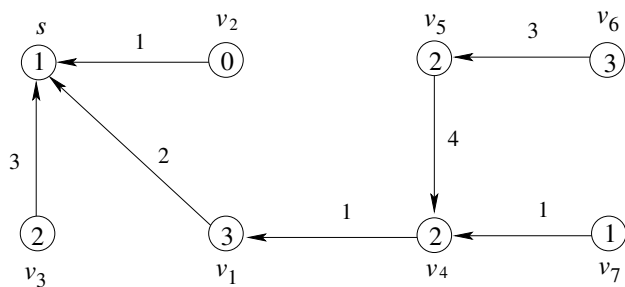
Figure 4: The construction of a spanning tree T_{span} rooted at s.

Table 2: The transmission schedule for the aggregation operation outputted by the algorithm proposed for MLAS-DC. In each row, "SP i" means the i-th scheduling period.

	timeslot0	timeslot1	timeslot2	timeslot3
$SP1$			(v_6, v_5)	
$SP2$			(v_7, v_4)	
$SP3$			(v_5, v_4)	
$SP4$		(v_3, s)		(v_4, v_1)
$SP5$		(v_1, s)		
$SP6$		(v_2, s)		

6 Gathering Schedule under the Physical Interference Model Taking Duty Cycles into Consideration

In this section, we develop a scheduling algorithm for MLGS-DC subject to physical interference. The sink node is represented by s. For a real number r satisfying $R' \le r < R$ (see Section 3 for the definitions of R' and R), we use EQ(1) to calculate ρ. Then follow the steps stated in Section 4, the spanning tree $SPAN$ rooted at s is constructed.

For any time-slot $0 \le j \le |T| - 1$, each node in U_j is active and ready to receive packets from one of its children nodes in $SPAN$. Let

$$Children(U_j) =$$
$$\{u : u \text{ is a child in } SPAN \text{ of a node in } U_j\},$$

which is the collection of children devices of the devices in U_j. The devices in $Children(U_j)$ will send their packets at time-slot j.

For each $0 \le j \le |T| - 1$, we adopt the data gathering heuristic obtained in our previous work [2] for WSNs with all nodes always active for the time-slot j. Our propsed data gathering scheduling algorithm will have $2n - 3$ rounds in total. For each round k, represent by E_k the collection of tree links of $SPAN$ whose label is k. Suppose that A_k represents the collection of the links in the inward s-arborescence made by the tree edges in E_k. For each round k, a dominator connects no more than one link in A_k (see [2]). For each round k and time-slot j, represent by $A_k^{(j)}$ the sub-collection of links of A_k whose sender belongs to the set $Children(U_j)$.

Next the data gathering scheduling algorithm for MLGS-DC subject to physical interference is presented. In each time slot $0 \le j \le |T| - 1$, the algorithm is divided into $2n - 3$ rounds sequentially, each of which is dedicated to a subset of links in the list:

$$A_{2n-3}^{(j)}, A_{2n-4}^{(j)}, \cdots, A_2^{(j)}, A_1^{(j)},$$

respectively.

For each round k and time-slot j, the links in $A_k^{(j)}$ are scheduled for transmission: Let S denote the set of the dominator ends of the links in $A_k^{(j)}$. A first-fit distance-ρr coloring of the set S is first calculated. At the i-th time-slot of the k-th round, according to this coloring, the link with a dominator end that is assigned the i-th color will send a packet. By Corollary 4 of [2], the maximum number of time-slots each of these rounds uses is β_ρ. The total number of rounds is $2n - 3$. Therefore, for each time slot j, the maximum time-slots used by the solution outputted by our proposed gathering scheduling algorithm is $\beta_\rho(2n - 3)$. Each scheduling period has $|T|$ time-slots in total. Thus, the entire gathering operation uses no more than $\beta_\rho(2n - 3)|T|$ time-slots.

We summarize our above discussion in the following theorem for MLGS-DC under the physical interference model.

Theorem 2 *The gathering scheduling algorithm described above for MLGS-DC can correctly produce a interference-free schedule of data gathering. The latency of the produced data gathering schedule is less than or equal to $\beta_\rho(2n - 3)|T|$.*

Clearly, any optimal solution to the problem MLGS-DC uses at least $n - 1$ time-slots, the approximation bound for the gathering scheduling algorithm presented in this section is less than or equal to $2\beta_\rho|T|$, which is a multiple of $|T|$ as β_ρ is a constant.

At the end, a data gathering schedule is computed by applying the above scheduling algorithm for each $r \in \Gamma$. The one with the smallest latency among all these resulting data gathering schedules will be chosen. Note that the number of element in Γ is a finite and we have its upper bound $|\Gamma| \le n(n - 1)/2$.

7 Gossiping Schedule under the Physical Interference Model Taking Duty Cycles into Consideration

In this section, we develop a scheduling algorithm that produces a short gossiping schedule for MLGoS-DC under the SINR model. Let $r = R'$ (see Section 3 for the definition of R'), we use EQ(1) to calculate ρ. The r-disk graph on V is denoted by G_r. Then we compute the graph center s for the graph G_r.

Our proposed gossiping scheduling algorithm for MLGoS-DC consists of two phases:

Phase 1: s collects all the packets from all other nodes.

Phase 2: s broadcasts all the n packets (including its own) to all other nodes.

For Phase 1, the data gathering scheduling algorithm for MLGS-DC presented in Section 6 will be adopted. After that, the sink node s sends all the n packets to all other $n - 1$ nodes in Phase 2. In this phase, for each time slot $0 \leq j \leq |T| - 1$, we adopt the algorithm that was used in the second phase of the gossiping algorithm from our prior work [2] we developed for MLGoS without duty-cycled scenarios. This algorithm works as follows: To begin with, a spanning tree $SPAN$ over V on the graph G_r is created according to the steps stated in Section 4. The routing used for the broadcast of Phase 2 is the outward spanning s-aborescence oriented from $SPAN$. Then we perform the following three steps:

- For all the dominating nodes, we calculate the first-fit distance-ρr coloring. Assume that this distance-ρr coloring uses Z colors. By Corollary 4 of [2], we have $Z \leq \beta_\rho$.

- For simplicity, suppose that the color 1 is assigned by the graph center s. We divide the time-slots into $2Z$ frames. In each frame of the time-slots, the first Z time-slots make a subframe of dominating nodes and the second Z time-slots make a subframe of connecting nodes. The center s sends one packet in each subframe.

- For each $1 \leq i \leq Z$, the connecting node with the color i receiving a packet in a subframe of dominating nodes sends the received packet in the i-th time-slot.

- For each $1 \leq i \leq Z$, the dominating node with the color i receiving a packet in a subframe of connecting nodes sends the received packet in the i-th time-slot.

According to Theorem 9 of [2] and the discussions thereafter, for each time slot $0 \leq j \leq |T| - 1$, the latency of both phase 1 and phase 2 is at most $\beta_\rho(5n - 5)$. Thus, our proposed gossiping scheduling algorithm generates a solution whose latency is less than or equal to $\beta_\rho(5n - 5)|T|$.

The theorem below summarizes our discussions and analyses in this section

Theorem 3 *The gossiping scheduling algorithm presented in this section works and it generates a gossiping schedule without collision. This gossiping scheduling algorithm produces a solution whose latency is less than or equal to $\beta_\rho(5n - 5)|T|$.*

Clearly, any optimal solution to the problem MLGoS-DC uses at least n time-slots, the approximation ratio of the gossiping scheduling algorithm presented in this section for MLGoS-DC is less than or equal to $5\beta_\rho|T|$, which is a multiple of $|T|$ as β_ρ is a constant.

8 Conclusion

In this paper, approximation algorithms for MLAS-DC, MLGS-DC and MLGoS-DC on duty-cycled multi-hop WSNs under the SINR model were proposed in order to minimized the communication latency. To the best of our knowledge, the paper is the first work that proposed efficient communication scheduling algorithms for these three problems subject to the physical interference. Denote by $|T|$ the count of time-slots contained in a scheduling period. Our proposed approximation algorithms for MLGS-DC has approx. ratios upper bounded by a constant time of $|T|$. So is the proposed approximation algorithms for MLGoS-DC. Our proposed approximation algorithms for MLAS-DC has an approximation bound no more than a constant times $|T|$ when the network maximum degree Δ is bounded. It has been well documented in the literature that analysis for scheduling algorithms developed for MLAS, MLGS and MLGoS under the SINR model is very challenging due to the impossibility of constructing related conflict graphs.

For future work in the design of scheduling algorithms for MLAS-DC, MLGS-DC and MLGoS-DC on duty-cycled multi-hop WSNs under the SINR model, the problems of proposing constant-approximation algorithms are still open, under either the SINR model or the protocol inference model. Any constant-approximation algorithms for MLAS-DC, MLGS-DC and MLGoS-DC will be significant.

9 Declarations

9.1 Availability of data and material

The data generated during the investigation of this research are included in this paper.

9.2 Conflicts of interest

The authors declare that there is no conflict of interest about the publication of this article.

9.3 Funding

References

[1] L. Wang, H. Liang, and P.-J. Wan, "Data Aggregation Scheduling in Duty-Cycled Multi-hop Wireless Networks Subject to Physical Interference, " the 15th IEEE International Conference on Mobile Ad-hoc and Sensor Networks (IEEE MSN), Dec. 11-13, 2019, DOI: 10.1109/MSN48538.2019.00041

[2] P.-J. Wan, L. Wang, O. Frieder, "Fast Group Communications in Multihop Wireless Networks Subject to Physical Interference," the 6th IEEE International Conference on Mobile Ad hoc and Sensor Systems (IEEE MASS), 526-533, 2009 DOI: 10.1109/MOBHOC.2009.5336958

[3] X.J. Chen, X.D. Hu, J.M. Zhu, "Minimum data aggregation time problem in wireless sensor networks," Lecture Notes in Computer Science 3794, 133-142, 2005.

[4] Y. P. Chen, A. L. Liestman, J. Liu, "A hierarchical energy-efficient framework for data aggregation in wireless sensor networks," IEEE Transactions on Vehicular Technology, **55**(3), 789-796, 2006, DOI: 10.1109/TVT.2006.873841

[5] Z. Chen, G. Yang, L. Chen, J. Xu, H. Wang, "A load-balanced data aggregation scheduling for duty-cycled wireless sensor networks," In Cloud Computing Technology and Science (CloudCom), 4th IEEE International Conference on, 888-893, December, 2012, DOI: 10.1109/CloudCom.2012.6427533

[6] R. Gandhi, Y.-A. Kim, S. Lee, J. Ryu, P.-J. Wan, "Approximation Algorithms for Data Broadcast in Wireless Networks," IEEE INFOCOM Mini-conference, 2009, DOI: 10.1109/TMC.2011.162

[7] S.C.-H. Huang, P.-J. Wan, C. T. Vu, Y. Li, F. Yao: "Nearly Constant Approximation for Data aggregation Scheduling in Wireless Sensor Networks," IEEE INFOCOM, 2007, DOI: 10.1109/INFCOM.2007.50

[8] S.C.-H. Huang, H. Du, E.-K. Park, "Minimum-latency gossiping in multi-hop wireless networks," ACM Mobihoc, 2008, DOI: 10.1145/1374618.1374662

[9] P.-J. Wan, C.-H. Huang, L. Wang, Z.-Y. Wan, X. Jia: "Minimum Latency aggregation Scheduling in Multihop Wireless Networks," ACM MOBIHOC, 2009, DOI: 10.1145/1530748.1530773

[10] J.-C. Bermond, J. Galtier, R. Klasing, N. Morales, S. Perennes, "Hardness and approx. of gathering in static radio networks," Proceedings FAWN06, 2006, DOI: DOI: 10.1109/PERCOMW.2006.62

[11] V. Bonifaci, P. Korteweg, A. Marchetti-Spaccamela, L. Stougie, "An approx. Algorithm for the Wireless Gathering Problem," Proceedings of SWAT, 328-338, 2006, DOI: 10.1007/11785293_31

[12] R. Gandhi, S. Parthasarathy, A. Mishra, "Minimizing broadcast latency and redundancy in ad hoc networks," in Proceedings of the 4th ACM international symposium on Mobile Ad hoc networking and computing (MobiHoc), 222-232, 2003, DOI: 10.1145/778415.778442

[13] P.-J. Wan, Z. Wang, Z. Wan, S. C.-H. Huang, H. Liu, "Minimum-Latency Schedulings for Group Communications in Multi-channel Multihop Wireless Networks," WASA, 2009, DOI: 10.1007/978-3-642-03417-6_46

[14] The GreenOrb Wireless Sensor Network Projects available at http://www.greenorbs.org/all/projects.htm, 2011

[15] P. Vicaire, T. He, Q. Cao, T. Yan, G. Zhou, L. Gu, T. F. Abdelzaher, "Achieving long-term surveillance in vigilnet," ACM Transactions on Sensor Networks (TOSN), **5**(1), 9, 2009, DOI: 10.1145/1464420.1464429

[16] K. Han, J. Luo, Y. Liu, A. Vasilakos, "Algorithm Design for Data Communications in Duty-Cycled Wireless Sensor Networks: A Survey," Communications Magazine, IEEE, **51**(7), 2013, DOI: 10.1109/MCOM.2013.6553686

[17] X. Jiao, W. Lou, X. Feng, X. Wang, L. Yang, G. Chen, "Delay efficient data aggregation scheduling in multi-channel duty-cycled WSNs," In 15th IEEE International Conference on Mobile Ad Hoc and Sensor Systems (MASS), 326-334. IEEE, 2018, DOI: 10.1109/MASS.2018.00055

[18] X. Jiao, W. Lou, J. Ma, J. Cao, X. Wang, X. Zhou, "Minimum latency broadcast scheduling in duty-cycled multihop wireless networks," IEEE Transactions on Parallel and Distributed Systems, **23**(1), 110-117, 2011, DOI: 10.1109/TPDS.2011.106

[19] X. Jiao, W. Lou, X. Wang, J. Ma, J. Cao, X. Zhou, "On interference-aware gossiping in uncoordinated duty-cycled multi-hop wireless networks," Ad Hoc Networks, **11**(4), 1319-1330, 2013, DOI: 10.1007/978-3-642-14654-1_24

[20] B. Kang, P. K. H. Nguyen, V. Zalyubovskiy, H. Choo, "A distributed delay-efficient data aggregation scheduling for duty-cycled WSNs," IEEE Sensors Journal, **17**(11), 3422-3437, 2017, DOI: 10.1109/JSEN.2017.2692246

[21] Z. Li, Y. Peng, D. Qiao, W. Zhang, "LBA: Lifetime balanced data aggregation in low duty cycle sensor networks," In 2012 Proceedings IEEE INFOCOM, 1844-1852, IEEE, 2012, DOI: 10.1109/INFCOM.2012.6195559

[22] F. Y.-S. Lin, Y.-F. Wen, "Multi-sink data aggregation routing and schedul-ing with dynamic radii in WSNs," Communications Letters, IEEE, **10**(10), 692-694, 2006, DOI: 10.1109/LCOMM.2006.06058

[23] Q. Chen, H. Gao, S. Cheng, J. Li, Z. Cai, "Distributed non-structure based data aggregation for duty-cycle wireless sensor networks," In IEEE INFOCOM 2017-IEEE Conference on Computer Communications, 1-9, IEEE, 2017, DOI: 10.1109/INFOCOM.2017.8056960

[24] X. Xu, J. Cao, and P.-J. Wan, "Fast Group Communication Scheduling in Duty-Cycled Multihop Wireless Sensor Networks," WASA, 2012, DOI: 10.1007/978-3-642-31869-6_17

[25] J. Tang, J. Xiao, W. Xiao, "Minimum-latency data aggregation in duty-cycled wireless sensor networks under physical interference model," In the 22nd Wireless and Optical Communication Conference, 309-314, *IEEE,* 2013, DOI: 10.1109/WOCC.2013.6676328

[26] X. Zhu, B. Tang, and H. Gupta, "Delay efficient data gathering in sensor networks," International Conference on Mobile Ad-Hoc and Sensor Networks, Springer, Berlin, Heidelberg, 380-389, 2005, DOI: 10.1007/11599463_38

[27] Q. Chen, H. Gao, Z. Cai, L. Cheng, J. Li, "Distributed low-latency data aggregation for duty-cycle wireless sensor networks," IEEE/ACM Transactions on Networking, **26**(5), 2347-2360, 2018, DOI: 10.1109/TNET.2018.2868943

[28] Y.-F. Wen, F. Y.-S. Lin, "Cross-layer duty cycle scheduling with data aggrega-tion routing in wireless sensor networks," Embedded and Ubiquitous Comput-ing. Springer Berlin Heidelberg, 894-903, 2006, DOI: 10.1007/11802167_90

Decentralized Management System for Solid-State Voltage Regulators in Nodes of Distribution Power Networks

Igor Polozov[1], Elena Sosnina[2], Vladimir Kombarov[1], Ivan Lipuzhin[2,*]

[1]*Department of Computer technologies in design and production, Nizhny Novgorod State Technical University n.a. R.E. Alekseev, Nizhny Novgorod, 603950, Russia*

[2]*Department of Electric power supply, power engineering and power supply, Nizhny Novgorod State Technical University n.a. R.E. Alekseev, Nizhny Novgorod, 603950, Russia*

A R T I C L E   I N F O

A B S T R A C T

The article describes the concept and architecture of a decentralized control system for a solid-state voltage regulator (SSVR). The SSVR is a universal device for controlling the mode and operation parameters of medium voltage electrical networks. SSVR manage the amount of current in line using the vector voltage control method. The SSVR control system consists of two levels: the SSVR semiconductor converter control level (the technological control system), SSVR cluster management level (intelligent control system). The objective of the study is to develop an algorithm for managing the SSVR cluster located in the nodes of the distribution electric network. The Raft consensus algorithm for managing the computing cluster is applied to ensure reliable decentralized network management. The algorithm is iterative. Ethernet and PLC architectures are proposed for constructing a data transmission network between SSVR nodes. A simulation model of the SSVR cluster and its control system is developed to study the operation of the control system (node shutdown, loss of communication). The criteria for the normal operation of the intelligent control system are formulated and an algorithm for its operation in emergency situations is presented. The studies of the SSVR control system confirmed the operability of the developed control system in normal and emergency operation of the cluster on a simulation. The dependence of the control system response time on the number of cluster nodes is investigated. The maximum number of nodes in the SSVR cluster depending on the tasks being solved by the SSVR will be limited by the speed of the control system. If the number of cluster nodes increases, it is necessary to enlarge the minimum time interval between requests for control commands.

1. Introduction

The concept of the Internet of Energy (IoE) is the logical development of smart grid technology [1, 2]. IoE is a new architecture for building a power electricity system with decentralized management. A key role in this system is assigned to intellectualization and economic interaction between all network users (energy transactions).

Distribution networks of the future will have a complex configuration and a large number of types of distributed generation sources. Thus, power flows should be bi-directional unlike traditional networks. To implement this principle, electrical networks of all voltage classes, especially low and medium voltage networks, must become "controlled". From a technical point of view, this is hindered by the lack of Flexible AC Transmission System (FACTS) devices in medium voltage networks.

The design of solid-state voltage regulator (SSVR) is known [3]. The SSVR is a power flow control device built on the basis of two transistor converters (Figure 1). The SSVR control method is based on the voltage vector regulation principle – the SSVR manage the voltage drop vector across network rector L [4], and the converter itself acts as a controlled current source. The SSVR is installed in the nodes of the medium voltage distribution network and allows to control the network operation modes.
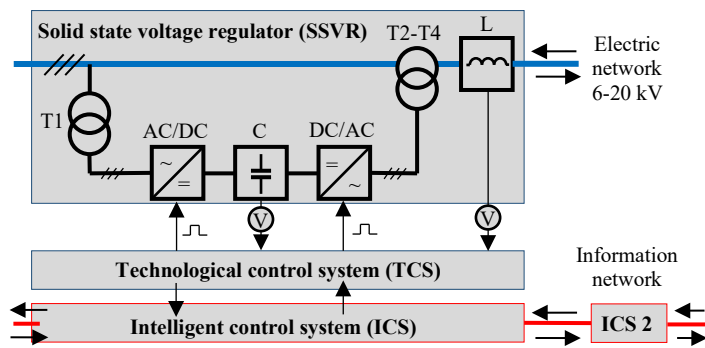
Figure 1: SSVR power unit and control system: T1 - shunt transformer; AC/DC - rectifier; C - capacitive storage; DC/AC - inverter; T2-T4 - serial transformers; L - network choke; V – voltmeter; ICS – intelligent control system of a neighbor node with SSVR

It is necessary to install several SSVRs in the distribution network to perform effectively all the specified functions. The required number of devices depends on the network configuration and the tasks being solved.

The SSVR has a two-level control system (Figure 1). The lower level system is a technological control system (TCS) [5]. The upper level control system is an intelligent control system (ICS). The TCS task is to form the required voltage vector and control the power elements of the converter. The ICS task is to manage the SSVR cluster, communication of SSVRs within a cluster and the command generation for the TCS.

The novelty of this work is that the RAFT consensus algorithm is applied in ICS to provide smooth voltage regulation and control of the electrical network with SSVR.

The article presents the results of the development and research of the SSVR decentralized control system of the upper level. The section 2 provides an overview of decentralized control systems used in the electricity industry. The section 3 describes the architecture of the SSVR ICS. The algorithms for the functioning of the ICS (the algorithms for managing a cluster and a network) are given in 4 and 5 sections. The section 6 describes the simulation model of SSVR ICS and the section 7 presents the simulation results of emergency operation modes.

2. Literature Review

Traditional power grid management systems require a central control room. Each control element must communicate with the control center and often not only the main, but also backup communication channels are required. Situations when communication with the control center is impossible may occur during the operation of networks and the need for autonomous operation arises. Decentralized management systems are the solution to this problem.

There are some tools for decentralized control of emergency switching based on reclosers for 6-10 kV distribution networks [6]. Various algorithms [7] of reclosers operation are possible to control emergency modes. The proposed methods of decentralized management are used only for emergency shutdown operations in a medium voltage network. This functionality is not sufficient for smart distribution networks. A smooth voltage regulation is necessary, and switching should be performed in

both emergency and normal modes in order to optimize the power flows in electricity network of up to 20 kV.

The problem of creating a decentralized intelligent management system for networks with distributed generation is most fully considered in [8], where a method of multi-agent service restoration and the digital model of a power system with multi-agent control are proposed. The principles of building a multi-agent system, as well as the stages of its operation are determined.

The most common control system architecture is SCADA (Supervisory Control and Data Acquisition). As shown in [9], to solve similar problems the traditional for SCADA centralized control model requires either improving the existing communication infrastructure to provide higher data transfer rate or storing measured data at a local substation and then organizing data exchange between substations to ensure the operation of complex applications in real time. At the same time, the amount of saved data turns out to be less than the amount of data saved in the SCADA database because each substation is responsible only for its own network section. This allows data to be saved more frequently, such as once per second or millisecond depending on the application. Since most of the data is stored locally, the requirements for communication links between substations and control centers are reduced.

This approach requires the use of decentralized algorithms that can bypass reduced SCADA functionality to provide optimal local control. Local controllers are intelligent enough to coordinate their work and thus provide reliable global control.

Some of these features are found in modern Energy Management Systems (EMS), for example, power flow analysis and generation prediction, that now will have to be used locally. At the same time, the EMS system, together with the Distribution Management System (DMS) and the Outage Management System (OMS), are superstructures of SCADA systems, and do not allow to fully implement the necessary functionality within a distributed control system [10].

In modern smart grid it is necessary to predict possible events (based on monitoring and trend analysis) and take proactive measures based on this data instead of a passive reaction to events in the distribution network. This forecast applies to both generation and consumption. Power flows in such network model will not be strictly deterministic. It is obvious that such a complex unstructured network must have a powerful control system that coordinates the operation of all network components. To do this, all components of the network must "communicate" with each other and with the control center through special communication networks. One of the ways to solve this problem is to use the consensus algorithm [11].

In [12], a distributed control strategy is proposed to share unbalanced currents in three-phase three-wire isolated AC microgrids. The control algorithm is based on an approach where the microgrid is analyzed not as a three-phase system, but as three single-phase subsystems. The consensus algorithm is used in distributed control system [13] to share the imbalance and harmonics between different converters in three-phase four-wire droop-controlled microgrids.

An asynchronous averaging consensus protocol [14] is proposed to estimate the values of inseparable global information. The consensus protocol is then combined with a fully distributed primal dual optimization utilizing an augmented Lagrange function to ensure convergence to a feasible solution with respect to power flow and power mismatch constraints. This algorithm uses only local and neighbourhood communication.

The consensus algorithm can be used to reach an agreement for resources dispatch among multiple controllable components in distribution grids, taking into account the individual voltage support capability of sources [15]. This algorithm reduces the time required to reach a consensus by solving the fastest distributed linear averaging (FDLA) problem.

An algorithm based on the RAFT consensus is used in [16], but in order to ensure the security of the switching infrastructure of the network against a specific type of attack, called a timing attack. In contrast to these studies, the authors use the RAFT consensus algorithm to ensure smooth voltage regulation and control of the electrical network parameters.

3. SSVR Control System

The concept of the IoE implies that the network becomes active and manageable, and the efficiency of management will only increase with an increase in the number of control devices in the network. At each point of the electrical distribution network where the SSVR installation is required, a node consisting of three connected elements is formed:

- solid state voltage regulator (SSVR);

- technological control system (TSC) – realizes the physical execution of SSVR control commands, measurement of the parameters of its functioning and transfer them to the upper level control system;

- intelligent control system (ICS) – provides the functions of SSVR operational control, diagnostics of its state, collecting monitoring data and implementation of algorithms for intelligent control of the SSVR network in order to control effectively power flows, ensure the required power quality and reduce losses during its transmission.

The SSVR control system has a peer-to-peer network structure and the SSVR ICS units are the nodes of this network. The ICS is an industrial computer, geographically located near the SSVR (the maximum distance is determined by the specification of the interface for TCS connecting). Also, the ICS is equipped with an interface for communication with other SSVRs ICS to create a data exchange network on the operating modes of the devices and to implement the algorithms for active-adaptive power transmission network control. At the same time, the results of the work of these algorithms should be propagated to neighboring nodes with minimal delays and with high reliability. This sets high requirements for an information network built in parallel with an electrical one.

The physical implementation of this network is possible using various technologies, including power line communication (PLC) technologies. A scheme of a 6-20 kV distribution network section with transformer substations and jumpers for controlling power flows with SSVR nodes and corresponding TCS and ICS are shown in Figure 2.

(a)

(b)
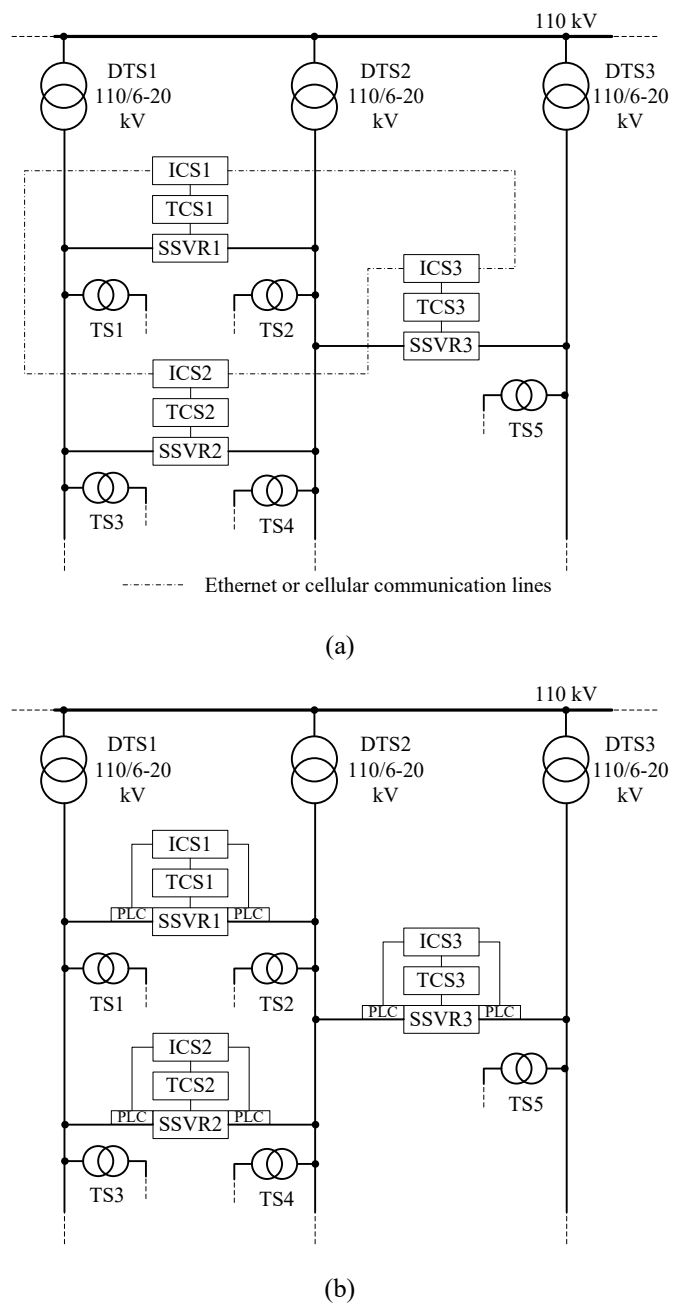
Figure 2: Structure of SSVR ICS: DTS1-3 – district transformer substations 110/6-20 kV; TS1-5 – transformer substations 6-20/0.4 kV; SSVR1-3 – solid-state voltage regulators; TCS1-3 – technological control system; ICS1-3 – intelligent control system: for Ethernet or cellular communications technology (a); for PLC technology (b)

In Figure 2a the ICS perform the function of routing information flows. The structure of the SSVR ICS for the PLC technology is shown in Figure 2b.

In addition to communication interfaces with TCS and other ICSs connected to SSVR located in the same electrical distribution network, there is an operational control client interface. This interface allows the operator to connect to the operating ICS in order to view the current parameters of its operation and, if necessary, correct the parameters of the operation of control algorithms for a specific SSVR or the SSVR network as a whole.

As indicated above, the automatic control in this system is decentralized and the regulation functions are performed in each SSVR ICS by local software implemented on the basis of the electrical network control algorithm (Figure 3). The developed control algorithm of the ICS is necessary to match the SSVR nodes in the distribution network. The function of distributing information about the state of network nodes is performed by the software for managing a group of industrial computers of the ICS. This group of ICS operates as a single system, called a cluster. The cluster control algorithm is used as the algorithm of this software.
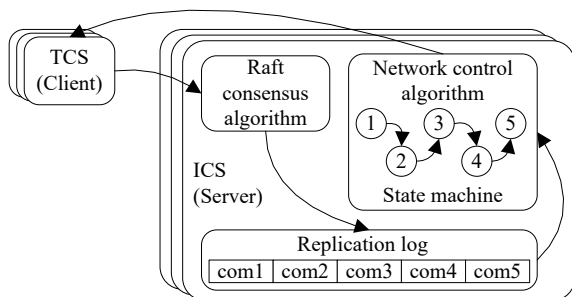
Figure 3: ICS functional diagram

As indicated above, the automatic control in this system is decentralized and the regulation functions are performed in each SSVR ICS by local software implemented on the basis of the electrical network control algorithm (Figure 3). The developed control algorithm of the ICS is necessary to match the SSVR nodes in the distribution network. The function of distributing information about the state of network nodes is performed by the software for managing a group of industrial computers of the ICS. This group of ICS operates as a single system, called a cluster. The cluster control algorithm is used as the algorithm of this software.

4. Network Control Algorithm

4.1. Management Task

Let's imagine a distribution electric network in the form of a graph, at the vertices of which there are transformer substations (TS) with their electricity consumers, and power lines act as arcs, and some neighboring TCs are connected by SSVR (Figure 4).

If the mode parameters in the network node deviate from the permissible (or specified by the operator), the SSVR ICS must send a signal to the TCS about the need for regulation. The effectiveness of the control system commands depends on the quality and completeness of the initial information about the network operation mode. The SSVR is capable of measuring the following parameters [5]:

- the RMS value of phase voltage before and after SSVR installation point;

- the effective value of the phase current in the line with SSVR;

- the phase angle of the line current relative to the voltage.

When information about deviations of the parameters and corresponding node number is obtained, it is possible to make decisions about control actions in order to bring these parameters to the expected values. The SSVR can regulate the amount of

current in the line by controlling the magnitude of the phase voltage and its phase angle.
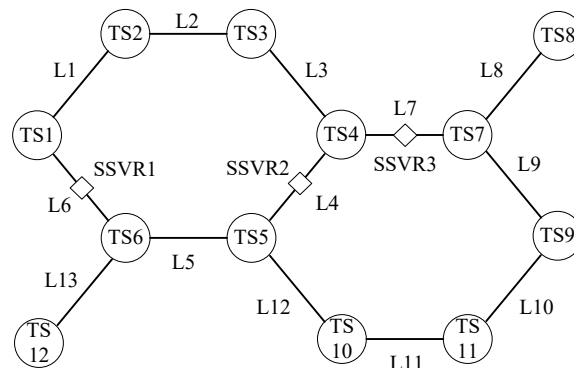
Figure 4: Graph of distribution electric network: L - power line; TS - transformer substation 6-20/0.4 kV; SSVR - solid state voltage regulator

4.2. Cluster Management Algorithm

To implement the adaptive network control algorithm, a logical computing cluster is formed on top of the electrical distribution network. This cluster formed of industrial computers, each of which controls its own separate SSVR, and is a control network node. It is assumed that all nodes in the cluster can communicate with each other without loss and without delay.

Cluster parameters are controlled by the cluster leader, which task is to control the power flows between the parts of the electrical network by changing the parameters of the cluster nodes. The leader is an arbitrary cluster node, chosen by voting between all cluster nodes, using the Raft consensus algorithm (consensus problem) [17].

The advantages of Raft are reliable leader election and guaranteed delivery of broadcast messages from the leader to the nodes. Despite its relative simplicity, Raft provides a safe and efficient implementation of a state machine on top of a clustered computing system. Raft ensures reliable delivery of signals to all nodes in a given order [18]. This ensures the transition of all state machines through the same sequences of states and each node is guaranteed to come into agreement with the other nodes.

Raft has the following features:

- assumes that there is always only one clearly distinguished leader on the cluster. Only this leader sends new records to other nodes in the cluster. Thus, the rest of the nodes follow the leader and do not interact with each other (except for the voting phase). If an external client connects to the cluster through a regular node, then all his requests are redirected to the leader and only from there come to the nodes.

- involves the decomposition of the cluster management task into several subtasks, the main of which are: leader election (voting) and replication of logs. Each of these tasks allows a more detailed separation. This makes the algorithm easier to understand and reduces the risk of errors in its implementation.

- logs cannot contain gaps. Records are added strictly sequentially. This simplifies the algorithm very much. In addition, the specifics of applied tasks, most often, do not allow correct work with logs containing gaps.

- allows to change easily the configuration of the cluster without interrupting operation: add or remove nodes.

An important circumstance is that Raft numbers strictly all records in the log. The records must go strictly sequentially. These records numbers play an important role in the operation of the algorithm. They determine the degree of relevance of the state of the node. The leader is always the most relevant node. The same numbers are used to number voting sessions. A node can vote only once for each vote request.

4.3. Network Control Algorithm

The network control algorithm is iterative. Each iteration of the algorithm consists of several steps:

- Each node reads its own voltage, phase and current values. Then, the parameter values are analyzed according to the specified criteria. The criteria include the maximum power flow through the node and the ability to share the load with an adjacent part of the network. The criteria are formed separately for each cluster node.

- The desired correction of the parameter values of each node is formed according to the calculation results, and then the desired parameters are transmitted to the cluster leader.

- After receiving the current values from each cluster node, the leader decides to change values on one of the nodes.

- It is assumed that the parameters should be changed iteratively and sequentially, by a small value and only at one node per iteration. The leader selects the node with the maximum required parameter correction among the nodes and sends a request to this node to change the parameter value by a certain step. The size of the step is set by the cluster settings.

- One of the cluster nodes receives a request from the leader to change his operating parameters, makes these changes and sends a message to the leader that the changes were successfully made. This concludes the iteration of the algorithm.

The indication that the node parameter values have been corrected is the change in the iteration number field. If the value of the iteration number is greater than the current number (on the leader's side), then the leader concludes that the node has recalculated the corrections of its parameters and sent updated values. Then the leader collects analysis data from all cluster nodes again. If changes in the correction of parameter values from the nodes are received, then the leader increments its current iteration number and repeats the steps to analyze and change the data.

Thus, at each iteration of the algorithm, small changes are made in the operation of the network at one of its nodes. Due to the fact that changes are made in the operation of only one node, and by a small value, the operation of the algorithm is stable and predictable and does not lead to an imbalance in the network.

Fault tolerance of the algorithm is achieved due to the fact that all network elements are combined into a cluster and each member of cluster is equal. The cluster leader which makes decisions about network management is unknown in advance and is chosen randomly from all the cluster members. That is, each cluster element contains all the necessary logic in order to become a leader, if the other members of the cluster elect it. The leader election procedure is finite and fault-tolerant, and is supported by the proven algorithm in cluster computing – Raft.

If the current cluster leader becomes unavailable due to problems in network connectivity and/or software or hardware failures, the cluster elects a new leader and the algorithm continues to work. If too many members drop out of the cluster due to possible failures, the algorithm determines that it does not have enough quorum to make decisions about network management and stops. In this case, a failure notification is sent to the operator.

The software simulation model of the SSVR ICS has been developed to study the operation of SSVR control algorithms in normal and emergency modes of network operation.

5. SSVR ICS Simulation Model

The simulation model allows to study the operation of the SSVR ICS in isolation without a real connection to the SSVR and without real communication channels. The software simulation model emulates the following objects and parameters:

- SSVR as ModBus slave [19];

- communication channels between SSVR and ICS;

- the topology of a network consisting of a set of SSVR ICS, with a set of communication channels connecting them.

The structural diagram of the simulation model is shown in Figure 5.
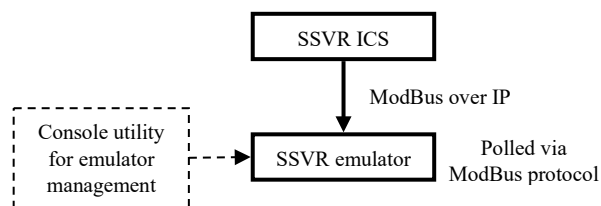
Figure 5: The structural diagram of the simulation model

The SSVR emulator has been written in C++ and is a Linux daemon (a background program launched by the operating system). The main task of the SSVR emulator is to respond to the requests of the ICS via the ModBus-over-TCP/IP protocol, just like a real SSVR does. The used implementation of the ModBus protocol defines a set of integer registers. For each of these registers in the SSVR emulator, a range of acceptable values and a period of values change are determined.

During its operation the SSVR emulator determines randomly the value of each register based on its range of changes, and gives it to the ICS in response to its requests. Also, the SSVR emulator changes the value of each register once per period. It is possible to change dynamically the settings for each ModBus register of the SSVR emulator without restarting the emulator itself using the console utility for the dynamic configuration of the emulator.

A configuration file with the network parameters of the available nodes in the topology is created for an instance of the

SSVR ICS software module to organize communication channels with other ICSs in the topology.

The console utility is used to change dynamically the settings for each ModBus register in the SSVR emulator without restarting this emulator, as well as to simulate changes in the network parameters and the occurrence of various emergency situations. So, for example, using this utility, it is possible to simulate the connection of an additional load to the SSVR by changing the values of the voltages and currents on the side after the controller.

6. SSVR ICS Simulation Model

Operating modes (scenarios) of the control network were simulated using the developed simulation model of the ICS SSVR. The cluster nodes were switched off one by one and the operation of the algorithm was monitored along with messages sent to the network operator.

The algorithm of actions of the control system when starting the system and the occurrence of emergency situations is shown in Figure 6.

Voting between the cluster nodes and the leader elections occurs when the ICS is turned on. Normal operation of ICS SSVR is ensured when two groups of conditions are met:

1. the cluster is working correctly;

2. the control algorithm works correctly.

The cluster works correctly when the following conditions are met:

- there is a cluster quorum n_q – the number of nodes in the cluster is sufficient to elect the leader (the minimum required number $n_{q.min} = 3$);

- the chosen leader is functioning normally;

- the set of nodes that have elected a leader is stable.

Algorithm quorum – there is a specified minimum number of controlled nodes which is necessary for the algorithm to work correctly.

Each time an alarm message is received indicating the nature of the problem, the operator must perform the required recovery and restart the system.

The simulation results are presented in Table.

The control system coped with the assigned tasks both in normal and emergency modes of operation. It was found that depending on the number and quantity of disconnected nodes two scenarios are possible:

- in scenarios B1 and C1, the remaining number of nodes was enough to select a leader, the system continued to work and perform the declared functions until the accident was eliminated;

- in scenarios B2, C2, D and E, the election of a new leader is impossible and the cluster stops its work until the accident is eliminated and the operator restarts the control algorithm.
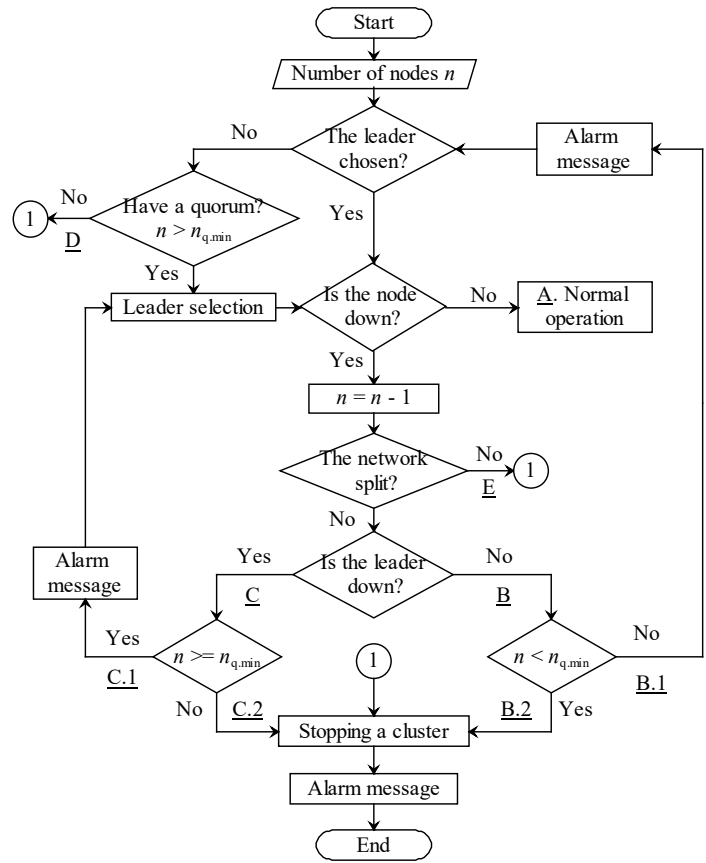
Figure 6: The control system algorithm: the letters A, B, C, D, E indicate the scenarios presented in the Table 1
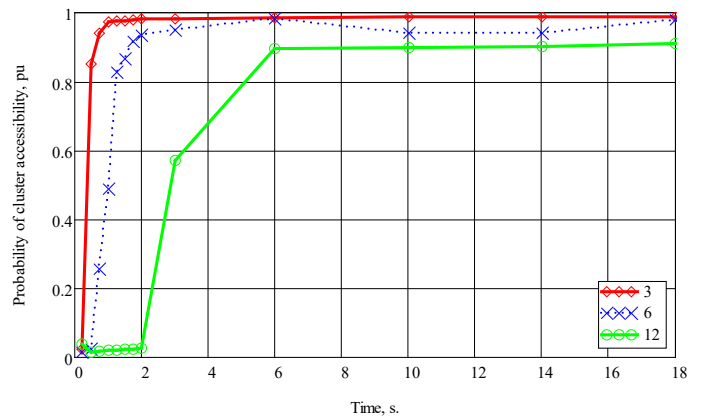
Figure 7: The dependence of the probability of cluster accessibility on the duration of the time interval between processing requests for a different number of network nodes

7. Determining the Cluster Speed Limit

The iterative control algorithm involves sending requests for data changes to the cluster. Sending commands takes some time, determined by the speed of the industrial computer of the node.

An experimental study on simulation models including 3, 6 and 12 nodes was carried out to determine the minimum cluster response time. Figure 7 shows the dependence of the probability of cluster accessibility on the duration of the time interval between processing requests.

Table 1: Modeling Results of Normal and Emergency Operation of the Control Network

Scenario	Result	Messages to operator
Scenario A. Normal network operation. No accidents.	The network topology does not change. The leader is chosen and does not change. There is a periodic measurement and iterative correction of the parameters of the nodes.	No messages
Scenario B.1. One of the nodes is down. The remaining number of nodes is sufficient for the operation of the cluster or for a quorum for a leader election.	The cluster continues its work according to the algorithm.	Alarm message indicates the ID of the node requiring recovery.
Scenario B.2. One of the nodes is down. One of the nodes is down. The remaining number of nodes is not sufficient for the operation of the cluster or for a quorum for a leader election.	The cluster stops its work.	Alarm message indicates the ID of the node requiring recovery.
Scenario C.1. The leader node is not working. The remaining number of nodes is sufficient for a quorum for voting	Election of a new leader.	Alarm message indicates the ID of the node requiring recovery.
Scenario C.2. The leader node is not working. The remaining number of nodes is not sufficient for a quorum for voting	The cluster stops its work.	Alarm message indicates the ID of the node requiring recovery.
Scenario D. No cluster quorum	The cluster stops its work.	Alarm message indicates the number of nodes.
Scenario E. The failure of one or more nodes led to the division of the network into two areas (partitions)	The cluster stops its work.	Alarm message indicates the ID of the node requiring recovery.

One can conclude that with an increase in the number of nodes in a cluster, the minimum allowable time interval between requests increases. From the given dependencies, it can be seen that the minimum interval between requests is 2.5 seconds for networks with a number of nodes up to 6 and 7 seconds for networks of 12 nodes. Such an interval is acceptable when regulating power flows in the electrical distribution network.

8. Conclusion

Decentralized management system architecture and an adaptive network control algorithm have been developed for solid-state voltage regulators (SSVR) in medium voltage distribution networks.

All SSVRs are combined into a single logical computing cluster using industrial computers, which are controlled by the cluster leader. The Raft consensus algorithm is used to find a leader and manage the entire cluster.

In the course of researching the control system on the simulation model, all cluster nodes were switched off one by one. In all simulated scenarios, the control system acted according to the laid down algorithm and followed the given commands. The research results confirmed the efficiency of the developed algorithm and the stability of its functioning.

Modeling clusters with different numbers of nodes showed that the minimum allowed time between requests for cluster nodes depends on its size. Thus, it is possible to determine the maximum allowable number of nodes in a cluster which will depend on the network topology and the tasks solved by the SSVR. The study of the performance of the algorithm proves the possibility of its application to solve the problem of power flow control in medium voltage distribution networks.

Conflict of Interest

The authors declare no conflict of interest.

Acknowledgment

References

[1] A. Huang, "FREEDM system - a vision for the future grid," in IEEE PES General Meeting, 1–4, 2010, doi:10.1109/PES.2010.5590201.2.

[2] Y.R. Kafle, K. Mahmud, S. Morsalin, G.E. Town, "Towards an internet of energy," in 2016 IEEE International Conference on Power System Technology (POWERCON), 1–6, 2016, doi:10.1109/POWERCON.2016.7754036.

[3] E.N. Sosnina, A.I. Chivenkov, I.A. Lipuzhin, "Solid-State voltage regulator for a 6–10 kV distribution network," in 2018 International Multi-Conference on Industrial Engineering and Modern Technologies (FarEastCon), 1–7, 2019, doi:10.1109/FarEastCon.2018.8602948.

[4] Y.P. Kubarkov, A.V. Chivenkov, N.N. Vikhorev, A.V. Shalukho, I.A. Lipuzhin, "Algorithm of power line current formation at load node," Vestnik of Samara State Technical University. Technical Sciences Series, **1**(61), 128–138, 2019, doi:10.14498/tech.201901128-138 (article in Russian with an abstract in English).

[5] E.N. Sosnina, A.I. Chivenkov, I.A. Lipuzhin, N.N. Vikhorev, "Control system for vector regulation of power flows in medium voltage network," IOP Conference Series: Materials Science and Engineering, **643**, 012048, 2019, doi:10.1088/1757-899X/643/1/012048.

[6] N. Ji, S. Geiger, "Reducing outages in distribution by testing recloser controls," in 2014 China International Conference on Electricity Distribution (CICED), 1748–1788, 2014, doi: 10.1109/CICED.2014.6992261.

[7] V. Sharipov, A. Minin, I. Mokhov, "A protection strategy for power grids equipped with Siemens vacuum reclosers," in 2010 Innovative Smart Grid Technologies (ISGT), 1–5, 2010, doi: 10.1109/ISGT.2010.5434741.

[8] W. Li, Y. Li, C. Chen, Y. Tan, Y. Cao, M. Zhang, Y. Peng, S. Chen, "A full decentralized multi-agent service restoration for distribution network with DGs," IEEE Transactions on Smart Grid, **11**(2), 1100–1111, 2020, doi: 10.1109/TSG.2019.2932009.

[9] C. Ien, D. Botting, A.D.B. Paice, J. Finney, O. Preiss, "When grids get smart," ABB Review, **1**, 44–47, 2008.

[10] L. Strezoski, I. Stefani, B. Brbaklic, "Active management of distribution systems with high penetration of distributed energy resources," in IEEE EUROCON 2019 -18th International Conference on Smart Technologies, 1–5, 2019, doi:10.1109/EUROCON.2019.8861748.

[11] D. Ongaro, J. Ousterhout, "In search of an understandable consensus algorithm," in 2014 USENIX Annual Technical Conference, 305–319, 2014.

[12] C. Burgos-Mellado, J. Llanos, E. Espina, D. Saez, R. Cardenas, M. Sumner, A. Watson, "Single-phase consensus-based control for regulating voltage and sharing unbalanced currents in 3-wire isolated AC microgrids," IEEE Access, **8**, 164882–164898, 2020, doi: 10.1109/ACCESS.2020.3022488.

[13] C. Burgos-Mellado, J. J. Llanos, R. Cardenas, D. Saez, D. E. Olivares, M. Summer, A. Costabeber, "Distributed control strategy based on a consensus algorithm and on the conservative power theory for imbalance and harmonic sharing in 4-wire microgrids," IEEE Transactions on Smart Grid, **11**(2), 1604-1619, 2020, doi: 10.1109/TSG.2019.2941117.

[14] B. S. Millar, D. Jiang, "Asynchronous consensus for optimal power flow control in smart grid with zero power mismatch," J. Mod. Power Syst. Clean Energy, **6**, 412–422, 2018, doi.org/10.1007/s40565-018-0378-4.

[15] K. Zhang, D. Recalde, T. Massier, T. Hamacher, "Fast online distributed voltage support in distribution grids using consensus algorithm," in 2018 IEEE Innovative Smart Grid Technologies - Asia (ISGT Asia), 350–355, doi: 10.1109/ISGT-Asia.2018.8467821.

[16] A. Sheoran, V. Singh, "Consensus based Anomaly detection in Smart Grid," Fault-tolerant computer system design. Final project report. https://engineering.purdue.edu/ee695b/public-web/handouts/Projects/Reports/amit_vishwanath_smartgridsecurity.pdf.

[17] The Raft Consensus Algorithm. [Online]. URL: https://raft.github.io.

[18] C. Fluri, D. Melnyk, R. Wattenhofer, "Improving raft when there are failures," in 2018 Eighth Latin-American Symposium on Dependable Computing (LADC), 167–170, 2010, doi:10.1109/LADC.2018.00028.

[19] libmodbus. A Modbus library for Linux, Mac OS X, FreeBSD, QNX and Win32. [Online]. URL: http://libmodbus.org.

Smart Collar and Chest Strap Design for Rescue Dog through Multidisciplinary Approach

Fang-Lin Chao[1], Wei Zhong Feng[2,*], Kaiquan Shi[1]

[1]*Department of Industrial Design, Chaoyang University of Technology, Taichung, 436, Taiwan*

[2]*Department of Visual Communication, Chaoyang University of Technology, Taichung, 436, Taiwan*

A R T I C L E   I N F O

A B S T R A C T

Rescuers escorted search dogs into the disaster area, using their unique sense of smell to find the injured. First, researchers summarize the design requirements in the search process from interviews with rescuers, and construct a conceptual prototype to confirm the interaction mode between the user and the dog. User central design invited people melt into the situation to identify product features. The ideas were selected based on the viability which increases efficiency. The main design proposal includes a strap and a smart collar. Smart sensing (heartbeat, speed, temperature, and GPS) can improve communication and increases the efficiency of rescue. The search area is large in many cases; therefore, we selected the WiFi or Ultra-wideband module as the wireless transmission medium when the rescue team enters this domain. The pre-deploy nodes connect and position with the smart collars. The instructor sends voice commands remotely to prompt the dog to return when the temperature is high. The smart collar design includes an elastic O-ring waterproof shell. Rescuers click the recall button, and the remote device sends a signal of dog returning. This proposed work looks more at user's needs through multi-disciplinary aspects of view, which enhance usability. The case consists of customer interviews, observation, concepts, evaluation (science/ device/ electronic packaging/ and App software); the design process also demonstrated a possible teamwork perspective in the industry. This scenario encourages cross-field extension for design education.

1. Introduction

Rescue dogs are sensitive to hearing and smell [1], and can be used as rubble rescue dogs and mountain rescue dogs after personalized training. This research proposed suitable devices for rescue task. During task, dog will present a stabilize bark to mark the sufferer position and special events [2]. The rescue team fights for gold rescue time to locate suffered people in the mountains or landslides space. Inappropriate equipment reduce efficiency.

The design goal is improving communication efficiency of the training with the help of smart collar through the design process (session 3). The design team collected requirements (session 3.1) through user interviews (session 2.1); after the midterm meeting, we built the prototype (session 4.1, 4.2) to support the interaction between the user and the dog. From the observation of the rescue member's situation, we confirm the rationality of the design (session 4.4, 4.5).

*Corresponding Author: W.Z. Feng, 79 Futong St., Taichung 436, Taiwan R.O.C., 886-918276088, feng.jimmy@msa.hinet.net

2. Literature survey

2.1. Rescue dog training situation and facilities

Figure 1a shows the rescue dog training cite in central Taiwan, the site is suitable for air scent search of the surrounding or trace the odors. Figure 1b is layout and facilities in Taichung training area. Trainer evaluate dogs and determine working potential to give the dog of their skills to fulfilling its purpose.

The training ground provides olfactory practice and obstacle crossing in a large area, and then enters the building of the injured person through overcome obstacles, such as suspended bridge structure. Simulation provides robustness under various conditions of the dog. Dogs in rocky areas need to be careful not to hurt their paws when moving (Figure 2). The training included the communication skill with the rescue personnel to notify the location of the victim [2]. When the road is in poor condition, the foot is often injured. Dogs often stick out their tongues to strengthen sweat; long-term search can lead to body failure [3]. Passing on the current physical condition allows calling for retreat.

(a)

(b)

Figure 1: Rescue dog training in Taiwan: (a) field survey site; (b) Taichung training area.

Figure 2: Training situation and facilities in rocky area.

2.2. Prior art of Strap

There are several ideas of dog lash as follows: Double D-ring rope buckle, LED warning; H-shaped chest for quick-fitting; X-shaped design using breathable fabric, and Y-shaped structure on the front chest. Double leash keep safe of manage reactive dog with a front and back ring. A leash shifts the center of gravity back towards trainer which gives trainer a pivot point [4] without restricting dog's shoulder for freely searching. Dog is dependent on trainer to explore the sights, trainer have to teach "how to follow lead" or teaching commands through strap.

Sokolowski explored 3D hand grip shape for dog walking which captured from civilian's [5] to fulfill product design perspective. Both cognitive and physical abilities help a successful handler design [6]. Figure 3 reveals an ergonomic X-strap dog harness. The traction belt is smooth and evenly bears multi-directional forces. Another design is an enhanced retractable leash [7] which provides multiple handles for controlling the movement. Plastic buckles are utilized with Velcro straps which eliminate the leash pulling forces at the dog's center of mass (middle chest) area.
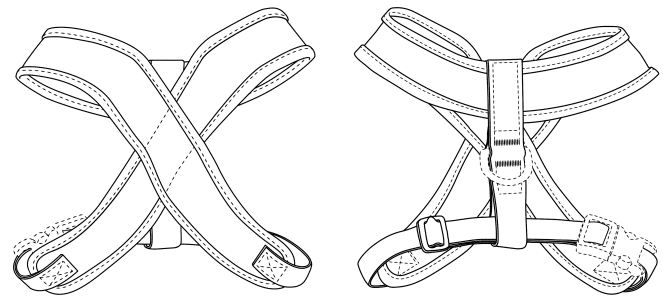
Figure 3: Ergonomic design X strap for dog, US 29/395,500 [6].

2.3. Scent and airflow

The skin disseminates cells with special odors in the metabolism, which form diffusion due to air convection. When dogs approach, they can feel the odor; after being trained in specific odors, it can increase sensitivity [2]. During the training process, the dog tracked across the sidewalk, turf, and forest path; the notification after sniffing helps people confirm the rescue path.

Researchers [3] developed a two-part dog wearable computer and interface. In the concept design process, the team first interviewed experts to correctly explain the dog's behavior. When the dog finds impure odor sources, timely encouragement by the trainer can improve its ability [8]. The experiment determined the distance and concentration that the dog can recognize, and was surprised to find that the dog can detect the smell at a distance of more than 62 meters.

2.4. IoT device in dog/ human interaction

The elderly-animal friendship bond surveyed elf-perceived criteria by the old people regarding their intimate association with their dogs [9]. A survey of 60 people [10,11] asked people classify the behavior of the nine dogs in the video as "friendly" or "radical." Researchers found that the dog's tail's movement is the main clue to explain the dog's sensation [12,13].
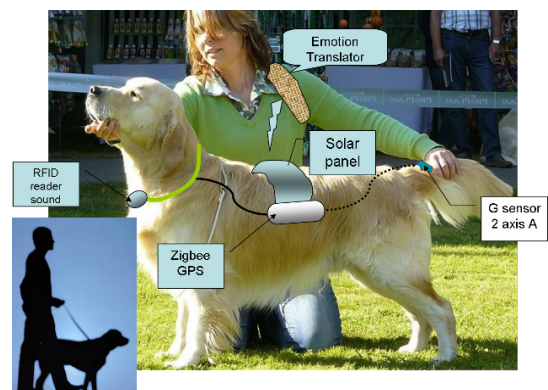
Figure 4: Placement of the major components and main controller [15]

Sensor and actuator help the communication between the blind and the dog; the power spectral density detection method based on breathing sound discovers the physiological state related to different odor detection tasks [14]. Previous study [15] proposed a remote interaction device implemented with Zigbee wireless technology between pet and elderly. The signal provided outdoors activities monitoring and communication, the module placed on

the back of the dog, and issue commands using a voice pager. The control chassis consist of battery, charger circuit and Zigbee circuit (Figure 4). Owner use vibrating actuator to command the dog remotely. Other study developed [16] an algorithm for locating victims in the nearly collapsed building with indoors positioning and extra IR and sound sensors.

2.5. Possibility of WiFi nodes

Many rescue areas do not present a WiFi connection. If WiFi is not available, the trainer depends on the sound to communicate. The mobile station could install, which provides the possibility of access in an emergency. Moreover, Ultra-wideband (UWB) and Long Range (LoRa) were utilized for a high-precision UAV positioning [17] with altitude error reduced to 1.74m. Simultaneous localization could be obtained through WiFi signal strength measurements [18]. Received signal strength data provide a convent way of practical implementation with a set of nodes.

The above technology is accurate, but this study focuses on the interaction between the trainer and the dog. To simplify the complexity, we use the WiFi module for the usability evaluation.

3. Design Method

The successful design of a product takes into account the user response, the alternative designs can amplify designers' understanding of the intended purpose [19]. The user central design reduced error and accelerating the decision-making process [20].

3.1. Design process

We collected user desire through interviews with rescue team. Organize their feelings into group records and use the data as a source of concept design. A scenario invited people melt into the pre-settled situation and identified needs. The conceptual ideas were evaluated based on the viable characteristics. The design flowchart shows in Figure 5.
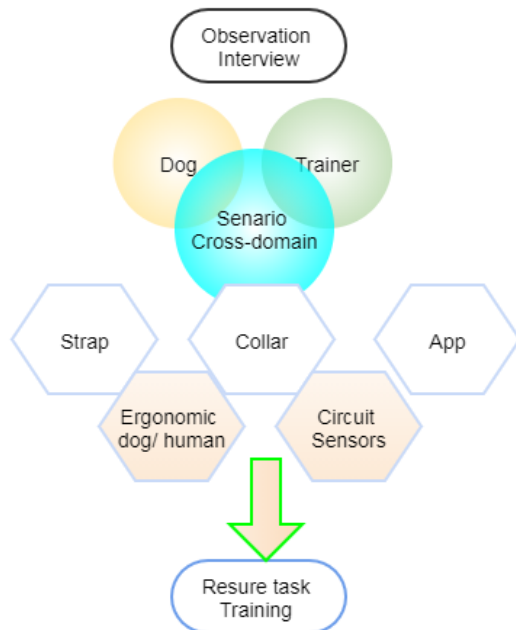
Figure 5: The design process and flowchart

Inquiring with professionals from the Taichung rescue team, the researcher also participated volunteer activity to observe the training details. Interview data shows: dog looks down and scans left and right for evidence. When the trainer pulls back, the neck will be red and swollen. An inappropriate chest strap will cause friction and injury to the fur. Don't hinder neck movement; prevent objects from hooking; use breathable materials when hot and humid.

The design begins with the scenario which deduced from insight of the task and following directions were issued;

1) Include small flashlights and emergency relief kits, but do not hinder neck movement.

2) The disaster may face rainy environmental and need waterproof capability.

3) Taiwan is hot and humid, and dogs do not dissipate heat well. Breathable and thin materials is preferred.

4) GPS-path records located the trapped; the App is needed to improve the efficiency of search.

5) Health datas (dog's heartbeat and body condition) are essential for physical condition control.

Figure 6 shows the selected design concepts of a tracking device and straps which reduces the obstacles interference during the mission. The design features overcome the current product are following:

1) Does not hinder the search activities. When the dog looks down, the branches may get caught in the leash or traction loop and be injured.

2) The product frame is breathable, avoiding heat stroke during dog wearing, which satisfied design priority of: comfort, safety and dog's acceptance. The strap disperses pulling forces on the muscles.

3) Dogs and rescuers can support each other through complementarity, but the configuration of equipment cannot interfere with the task.
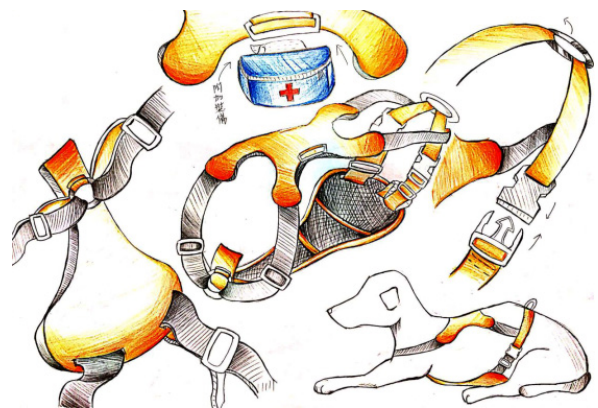
Figure 6: The idea sketch of design concept

3.2. Multidisciplinary approach

The implementation requires a cross-domain integration by running a multidisciplinary collaborative project. The ability to lead a team through the different work stages of a project is a fundamental contributor to its success [21]. Framework for the conceptual design of unmanned aerial vehicles (UAVs) proposed

in developing efficient winged design [22] for industrial designer. Teachers used cross-domain design and developed " airflow play with music" to realize the concept of flow guiding.

Comfort rescue dogs' products needs structural mechanics, material applications, and most importantly, software and hardware integration. Cross-domain presentation requires communication and interaction between departments. The conceptual designer proposes idea sketch and functions supported in the context of use, which discussed with the engineer in advance. Finally, it can be realized with appropriate technology. This process includes the assembly of electronic circuit boards, and software and hardware test to present the design concepts. Then through the deduction of the concept the design verified with the cross-domain team.

4. Concept design

4.1. Chest strap

Comfortable shoulder straps need to be worn quickly and fit the body without friction. The chest H-shaped backrest equipped with an adjustable double belt buckle. The Y-shaped structure made of breathable fabrics reduces tensile strength (nylon, plastic and fluorescent reflective tape). The front stainless steel O-ring can release and reduce pressure.

(a)
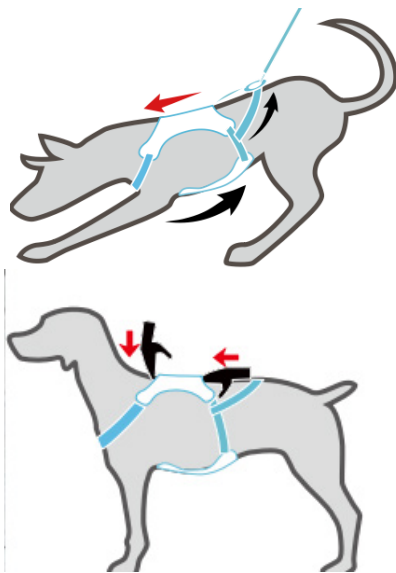
(b)

Figure 7: (a) the upper chest pad and storage, (b) the force applied to the body during exercise, the lower pad is made of insulating cotton and wear-resistant washed canvas (sandwich mesh).

Figure 7 illustrates the design features of the chest harness: (1) equipped the upper body of the dog with a space for light devices (batteries for smart devices, simple first aid supplies, and communication equipment) for survivor; (2) as shown in the figure 7a, the side rings inserted from both sides and placed on the upper back. During the search, the trainer followed the dog in front, and strap is with tension; the traction point placed in the upper region to avoid neck strain. The illustration (Figure 8) shows that the force is directed to both sides through the outer strap to distribute it. The D-ring connects both sides with the lower abdominal support belt, and control belt of trainer. The force in three directions joined at chest. The overall design of the chest harness shows in the diagram (Figure 9). The abdomen are soft materials to avoid gaps and friction. When the chest harness is properly fitted to the body, the dog will not hook on the protrusions or tree trench when moving.

The flexible adjustment structure avoids gaps. The harness is soft to coordinate with the body shape. The designed strap presents lots of curvature elements. Based on the ergonomic and strap's curvature, the software using for CAD drawing is the Catia version-6.
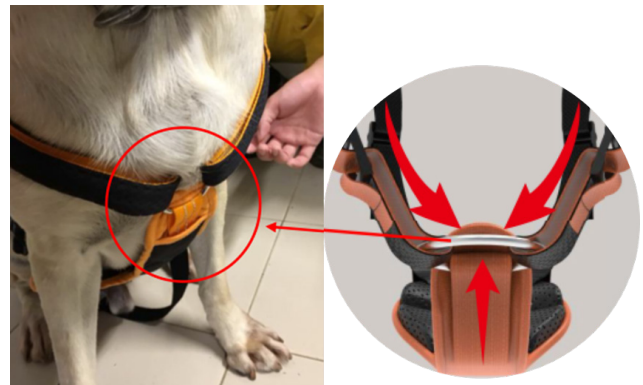
Figure 8: Combination of straps on chest

Figure 9: The 3D rendering of the chest strap

4.2. Smart Collars

Combined the existing wireless transmission and positioning technology, the communication between the dog and the rescuer is better in a large range search. Traditionally, dog barks to hint trainer, this touching way extended nearby areas. With wireless device, dog barks trigger the signal of the transmission position

data and notify the trainer of the location of the victim (Figure 10a), wireless touching way extended more than 150 m diameter areas. The injury of the dog is a great loss of team, so their physical conditions are monitoring by trainer [23]. The sensor in the collar transmit the physical condition of dog, which allowing the trainer to adjust schedule. This function prevents the dog from being exhaustion.

The search mission is larger in the open field. The indoor Wi-Fi router operating on the 2.4 GHz frequency band has a radio wave of up to 50 m, and it can be greater than 92 m outdoors. Based on IEEE 802.15. 4a standard, above 200 meters electromagnetic wave range can be reach with UWB [24]. User selects suitable module based on desired range. Figure 10b shows the concept of Balloon floating positioning. The UAVs generate a lot of electromagnetic waves and noise, which affect the concentration of dogs. We chose movable balloon set to place the RF module along with the balloon; hovering over the disaster area, it can quickly move to the nearby search areas. The floating balloon will move slightly with the ambient wind but does not affect the position's accuracy much.

(a)

(b)
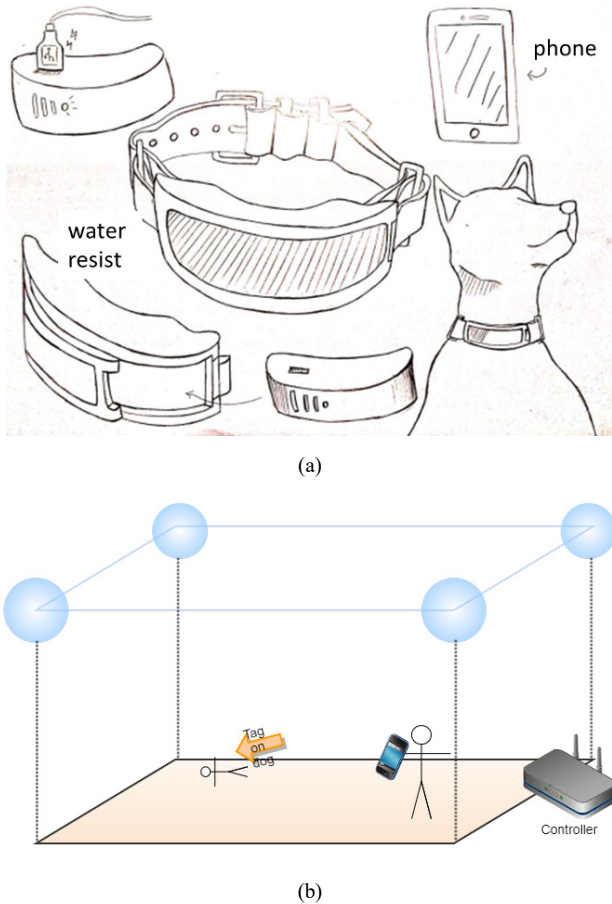
Figure 10 The proposed design: (a) smart ring module, (b) Balloon floating positioning. The UWB constructed with Semtech SX1276 Dragino LoRa Shield (with Arduino via SPI).

4.3. Implementation

A wireless remote connection collar was realized with Arduino platform, the system included a trainer side App to receive signal and arrange current task. The interaction between the smart collar and the rescuer's mobile phone are using Wifi signal. Since the

Arduino system is an open platform, many Shield modules are available.

Sometimes, the extended search area cannot cover by Bluetooth signal; therefore, we selected the WiFi or Utra-wideband module as the wireless transmission medium. When the rescue team enters this domain, they will deploy nodes which connects with the tag on smart collars. The mobile phones also share connection and able to communicate with other devices.
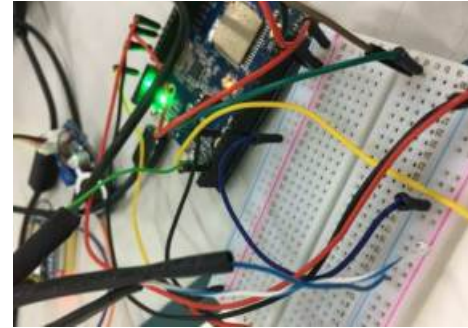
(a)
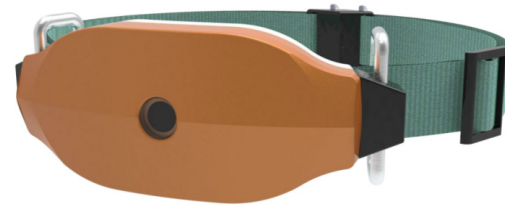
(b)

Figure 11: Components used in the circuit: (a) wireless remote connection realized with Arduino Shield (Ameba RTL8195), WiFi antenna, temperature and humidity sensor (DHT22), and sound sensor (NEO-7M-CAPP), (b) 3D printed chassis structure.

The Arduino Shield [25] used include GPS, speakers, Grove main control version. The breadboard wiring implementation shows in Figure 11a. The appearance of the smart collar (3D printed) contains miniaturized circuit board and sensors (Figure 11b); the collar placed on the neck area of the rescue dog with an adjustable belt. During the task, the collar might contact water, to maintain the stability of the circuit, so we installed a rubber O-ring placed in chassis gap for waterproofing of the circuit board.

4.4. Software and Trainer's APP

Heartbeat/ temperature/ and GPS status recorded by Smart collar. The squeak signal is identified with the trainer's App. The user interface can be implemented using Android APK. The dog's track record and the graphical display enhance recognition (Figure 12a). Collected dog's physical condition will display on phone screen so that the trainer can immediately prevent the dog from being exhaustion (Figure 12b).

The major Information are:

- Positioning: The dog's barks activates and informs the trainer which reveal the location of the target (Fig 12b) of the target in the mission.

- Call back: When the body temperature exceeds the set value or the task exceeds the time, the coach issues a warning. Use the withdrawal button to call the module attached to the dog and make a sound (instruction return). The training procedures

are: Call the dog's name enthusiastically and give the command: "Come! Come!" If he walks towards you, praise it. When the dog catches up, give him some snacks and compliments immediately. After several successful exercises, try to say the word alone. The dog understands the sound in previous training when rescuers click the recall button and remotely generate the same sound signal. When the success continues, try the same action with the remote microphone. The proposed device mechanism is vocal sound, the inertia of signal/ action built in early time excites the dog's physiological reasoning.

- Guidance: rescuer asks the survivor person to prompt the dog to get the direction (Figure 13). The recorded path and target's response enabled speed up of target finding.

- Dog's background: The dog's characteristics and the training performance can access by the trainer, through specific description data helps conduct of those tasks with specific dog.
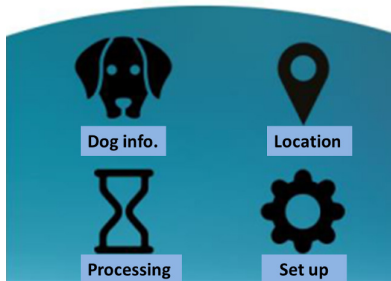
(a)

(b)

Figure 12: The main page of (a) App interfaces; and (b) code of Arduino board; where fix: successful positioning; speed: moving speed; lat/lon: latitude and longitude; Temp/Hum: temperature and humidity; Sound: volume of barking; alert: notifying back.

4.5. User survey

Taichung established a search and rescue dog team in 2016, and had passed the Mission Readiness Test international mission rescue certification. Training require a lot of human resources including build society contact to successfully complete search tasks. Among the team, "Tie Xiong" found survivors in the rubble during the Hualien earthquake in 2018. We took the chest strap to the training site and test it by the commander during the exercise. At the verification stage, we made a prototype with soft materials for user test including magnitude of pressure, the shear force on skin, and the loading. The normal stress around chest does decrease due to force distribute on supporting surface. Per Figure

7 and 8, the most considerable stress occurs on the arch ribs due to pull.

The App interface is properly matched with the mobile phone, and the touch interface for quick setting and operation. The timely response is helpful for urgent handling in emergency situations. The current Arduino modules are large in size and easily interfere with the movement of the dog; in the future, this problem can be overcome through the miniaturization of a customized circuit board.

Figure 13: GPS positioning help target located on the trainer mobile App.

5. Conclusions

Based on situational stories and on-site observation data, we have unified the special needs in the rescue situation. The main design proposal includes a strap and a smart collar; the strap that meets the rescue dog's situation. It can be adjusted to suit individual needs. Smart sensing improves task performance; IoT chest strap helps communication and increases the efficiency of search and rescue. The smart collar records the status, and remote voice paging helps to send voice commands. Arduino's rich development modules including GPS and speakers are conducive to the prototype. Researchers found that the dog's wearable sensor improves the dog-human interaction during training.

Many technologies reported; this work looks more at user's needs through multi-disciplinary aspects of view. The conceptual situation requires the realization of the prototype to show the suitability of the concept. From the perspective of design education, we show the main parts through cross-field integration (mechanical/electronic, hardware/software). This proved that designers need to enhance cross-domain sentiment to stand at the high point of design thinking in order to propose appropriate solutions.

References

[1] L. Lit, C.A. Crawford, "Effects of training paradigms on search dog performance," Applied Animal Behaviour Science, **98**(3-4), 277-292, 2006.
[2] K.E. Jones, K. Dashfield, "Search-and-rescue dogs: an overview for veterinarians," Journal of the American Veterinary Medical Association, **225**(6), 854-860, 2004.

[3] C. Zeagler, C. Byrne, G. Valentin, "Search and rescue: dog and handler collaboration through wearable and mobile interfaces" Proceedings of the Third International Conference on Animal-Computer Interaction, **6**, 2016.

[4] M.W. Trevino, "Ergonomic pet harness with enhanced retractable leash" United States Patent Application US 15/398,603. 2018.

[5] S.L. Sokolowski, C. Bettencourt, "Investigation of 3D Functional grip shape to design products for dog walking and hiking," International Conference on Applied Human Factors and Ergonomics, 597-604, 2020.

[6] Y.H. Yun, "X-strap dog harness," United States Patent Application US 29/395,500. 2018.

[7] I.P. Hoskinson, "Ergonomic pet carrier for single-person use," United States Patent Application US 16/104,847, 2019.

[8] I. Greatbatch, J.G Rebecca, and S. Allen, "Quantifying search dog effectiveness in a terrestrial search and rescue environment" Wilderness & Environmental Medicine, **26**(3), 327-334, 2015.

[9] J.M. Alcaidinho, "The internet of living things: Enabling increased information flow in dog-human interactions," Ph.D. diss., Georgia Institute of Technology, 2017.

[10] A.C. Jones, R.A. Josephs, "Interspecies hormonal interactions between man and the domestic dog (Canis familiaris)," Hormones and Behavoiur, **50**(3), 393-400, 2006.

[11] E. Kubinyi, "Dog and owner demographic characteristics and dog personality," Behavioural Processes, **81**(3), 392-401, 2009.

[12] Z. Horvàth, "Affiliative and disciplinary behaviour of human handlers during play with their dog affects concentrations in opposite directions," Hormones and Behaviour, **54**, 107-114, 2008.

[13] J.M. Ley, P.C. Bennett, "Understanding personality by understanding companion dogs," Anthrozoös, **20**(2), 113-124, 2008.

[14] C. Mancini, S. Li, J. Valencia, D. Edwards, "Towards multispecies interaction environments: Extending accessibility to canine users," in ACM International Conference Proceeding Series, Association for Computing Machinery, 2016, doi:10.1145/2995257.2995395.

[15] F.L. Chao, "Evaluation of industrial usefulness of pet companion for elderly," Eco-design, 2013.

[16] S. Mealin S, M. Foster, K. Walker, "Creating an evaluation system for future guide dogs: a case study of designing for both human and canine needs," In Proceedings of the Fourth International Conference on Animal-Computer Interaction, 1-6, 2017.

[17] Y.C. Chen, I. Alexsander, C. Lai, and R.B. Wu, "UWB-assisted high-precision positioning in a UTM prototype," 2020 IEEE Topical Conference on Wireless Sensors and Sensor Networks (WiSNeT), 42-45, 2020.

[18] L. Bruno, P. Robertson, "Wislam: Improving footslam with wifi," In 2011 International Conference on Indoor Positioning and Indoor Navigation, 1-10, 2011.

[19] M.R. Endsley, Designing for situation awareness: an approach to user-centered design.

[20] B. Ipaki, Z. Merrikhpour, "Designing bike shift lever with user-centric design approach," Journal of Ergonomics, **6**(3), 43-54, 2018.

[21] S. Mazzetto, "A practical, multidisciplinary approach for assessing leadership in project management education," Journal of Applied Research in Higher Education. 11(1), 50–65, 2019.

[22] H. Gu, X. Cai, J. Zhou, F. Zhang, "A coordinate descent method for multidisciplinary design optimization of electric-powered winged UAVs," In2018 International Conference on Unmanned Aircraft Systems (ICUAS), 1189-1198, 2018.

[23] R. Brugarolas, S. Yuschak, D. Adin, L. Sherman, A. Bozkurt, " Simultaneous monitoring of canine heart rate and respiratory patterns during scent detection tasks," IEEE Sensors Journal, **19**(4), 1454-1462, 2019.

[24] M. Poturalski, J.P. Hubaux, "Distance bounding with IEEE 802.15. 4a: Attacks and countermeasures," IEEE Transactions on Wireless Communications, **10**(4), 1334-1344, 2011.

[25] R.B. Brufau, "Towards automated canine training: wearable cyber-physical systems for physiological and behavioral monitoring of dogs," 2016.

Environmental Entrepreneurship as an Innovation Catalyst for Social Change: A Systematic Review as a Basis for Future Research

Carol Dineo Diale[1,*], Mukondeleli Grace Kanakana-Katumba[2], Rendani Wilson Maladzhi[2]

[1]Department of Psychology, Industrial Psychology, Rhodes University, Grahamstown, 6139, South Africa

[2]Department of Mechanical and Industrial Engineering, University of South Africa, Johannesburg, 0002, South Africa

A R T I C L E I N F O

A B S T R A C T

There are pressures to adopt sustainable behaviour more so in generating profits and benefiting the society to accelerate green efforts through a green framework. The overarching goal of the paper is premised through various works of literature, building the ecosystem the elements highlighted by most researchers in the field of environmental entrepreneurship. The various models reviewed consists of generic incubators and entrepreneurship, and societal and environmental factors. Environmental entrepreneurship is often used interchangeably with concepts such as green entrepreneurship and ecopreneurship which under-researched globally, with non-existent efforts on the applicability and modelling of key environmental entrepreneurship within a specific context utilising the system dynamics approach. In order to assess the environmental entrepreneurship ecosystem, the authors adopted a system dynamic approach to determine key variables that enable the development of the system. A literature review was conducted, and of the 135 articles reviewed, n=92 peer-reviewed articles met the criteria that the researchers set. Some of the results emanating from a systematic review are environmental policy, green skills, financial and non-financial support, societal and behavioural factors, environmental agility, ethics and governance, and access to markets. The theoretical results are simulated using system dynamics modelling. Due to limited research on the above-mentioned topic, a possible impacting variable (Exogenous variables) was broadened to add value to, and have an impact on, the study. Upon reviewing the above-mentioned models, the framework emerged signalling elements to be simulated in the system dynamics model, which were then theoretically contextualised for the South African context. The theoretical virtual system dynamic model forming part of the framework will be tested and validated in the next study. The applicability of the theoretical ecosystem to South African context as well as future recommendations are provided in the study.

1. Introduction

This paper is an extension of "Green Entrepreneurship Model Utilising the System Dynamics Approach: A Review" presented at the IEEM 2019 Conference in Macau [1]. The conference proceeding argued that Green entrepreneurship as a technology is an area that has not been explored fully, let alone its application the system dynamics spectrum. Furthermore, the paper argued that empirical scholarly research in entrepreneurship within Green

industries is at infancy stages in South Africa, and little research work has been done. In [2], the author conducted a study focusing on green entrepreneurs in the South African context. While [3-5] concentrated on the international markets. However, a complete ecosystem surrounding environmental entrepreneurship, and system dynamics remains a gap under consideration. The existing research is centred around a single factor of green entrepreneurship [1], [3-5], with less focus on finding possible multiple solutions to minimise climatic challenges. In this paper, the focus is on environmental entrepreneurship, particularly with the aim of contributing to social norms and finding innovative

approaches to utilising system dynamics for modelling endogenous and exogenous variables of the system. In the current paper, the focus of environmental entrepreneurship is within the spectrum of key drivers of environmental entrepreneurship, social change and behavioural factors. The latter focus is deliberate in creating access to services for the community through empowerment, development, and awareness, and ultimately laying a theoretical foundation on how environmental entrepreneurship can be utilised. These efforts may accelerate the sustainable development goals as environmental entrepreneurs are always expected by societies to be concerned with the environmental factors [6]. Some of the literature defined environmental entrepreneurship by using phrases such as eco-entrepreneurship, ecopreneurship, and ecological entrepreneurship [7-9].

Green entrepreneurship and ecopreneurship is minimally included in the current paper. This is due to the fact that the authors are advocating for the concept of green entrepreneurship, ecopreneurship and environmental entrepreneurship to be defined and dealt with separately so as to have an impact and foster the implementation thereof. It is notable that the latter terms are somewhat similar. However, there is a slight difference between the concepts, whereby, Green entrepreneurship focuses on exploiting markets for profits and saving the planet by leveraging green thematic areas [5]; ecopreneurship has a distinctive feature of ensuring efficiency and effectiveness [10]; and environmental entrepreneurship has a distinctive feature of social, behavioural norms to develop and create awareness [11, 12]. Environmental entrepreneurship can be defined as the concept of radiating adoption of sustainable behaviour and social entrepreneurship, whilst benefiting the society [11].

The current paper focuses on environmental entrepreneurship by contributing of utilising the system dynamics approach to understand the behaviour of the system and its interaction with sub-systems. A further contribution that the current paper hopes to add is to create a theoretical opportunity of the contribution of environmental entrepreneurship to accelerate the sustainable development goals. The current study illustrates how environmental entrepreneurship contributes to sustainable development, social and behavioural factors affecting environmental entrepreneurship in facilitating access to the service, and fostering environmental entrepreneurship as a form of social change. Social dynamics and sustainable development need to be borne in mind when fully implementing green initiatives to support environmental entrepreneurship. Environmental entrepreneurship, as a complex phenomenon, needs to be viewed from different angles to ensure that solutions are gained from multiple sources at the same time. The underlying goal of the paper is premised through various works such as generic business incubators, environmental factors, and societal norms capitalising on social entrepreneurship to build the ecosystem. From the various models the authors discovered key drivers to environmental entrepreneurship, social and behavioural factors as part of the framework. The theoretical ecosystem consists of key drivers, social and behavioural factors, as well as the theoretical framework contextualised in the South African context. The subsequent sections discuss the research questions methodology, and future recommendations.

2. Research questions

The research questions were identified through the research gaps [13] that were identified while reviewing literature and where possible research contributions can be made setting future research agendas. The research questions are as follows:

What are the theoretical key drivers enabling environmental entrepreneurship as a form of social change?

What are theoretical social and behavioural factors affecting environmental entrepreneurship in facilitating access to the service?

How can theoretical key drivers be applied in formulating a South African context framework?

3. Research Background

3.1. Environmental entrepreneurship for social change

Environmental entrepreneurs need to have an agenda of creating and formulating sustainable and green products and services, and at the same time, meet social, economic and environmental objectives [8], [14-16]. It is essential to focus on social dynamics and sustainable development by fully implementing green initiatives. Goal 5, 'gender equality', of the sustainable development goals can be fulfilled by promoting women in environmental entrepreneurship, and Goal 8, 'inclusive and sustainable economic growth, full and productive employment and decent work for all' [17], can be fulfilled by contributing to a better quality of life and serving as a social change catalyst. Studies have shown that women are more likely to venture into environmental entrepreneurship and are more inclined to uplift communities through social entrepreneurship [11, 18].

Research or publication on environmental entrepreneurship as a contribution to sustainable development goals and its interrelatedness or linkages to the system dynamics in the South African context is minimal. Environmental challenges are due to humans not adopting sustainable efforts [19]. The current authors assert that efforts need to be in the form of environmental psychology to minimise challenges due to human activity. Environmental entrepreneurship focuses heavily on the social sphere, transforming communities and the need to adopt agility for the viability of environmental entrepreneurship. In most instances, environmental entrepreneurship forms the foundation of green entrepreneurship by advocating new or innovative ways to save the planet with green products and services [20].

Worldwide, there is minimal research on women as environmental entrepreneurs. In [21], the author holds a strong view that developing women in green cooperatives, especially in rural areas, may alleviate poverty and promote sustainable rural development. This may ultimately contribute to creating green jobs [22]. There has been some effort in tracking environmental entrepreneurship from the early 1990s [23]. Another social factor that has not received much attention is popularising female entrepreneurs who embark on environmental entrepreneurship. There is lack of research on the female identity in relation to their roles as environmental entrepreneurs, which will need to be taken

into perspective and how they optimise or create a new identity in transitioning into a green economy. In [17], the authors shed some light in proving the motive of women embarking in environmental entrepreneurship is to uplift the society.

The current authors are of the opinion that environmental entrepreneurship can assist in accelerating the sustainable development goals, particularly goal 1: zero poverty, goal 5: gender equality, and goal 8: inclusive and sustainable economic growth, full and productive employment and decent work for all.

3.2. The innovative contribution of environmental entrepreneurship utilising system dynamics modelling

The innovative contribution of environmental entrepreneurship as a social change is in the form of system dynamics modelling. The system dynamics approach models the key drivers and factors affecting environmental entrepreneurship as well as social and behavioural factors that create a new perspective of a theoretical entrepreneurship framework. Environmental entrepreneurship, as a complex phenomenon, needs to be viewed from different angles to ensure that solutions are obtained from multiple sources at the same time. System dynamics is used to conceptualise the causal loop relationships or stocks and flows, with the intention of identifying variables that affect the ecosystem feeding into the whole system [24-26]. "System dynamics is the combination of theory, method and philosophy in analysing the behaviour of the system [26]." Furthermore, system dynamics focuses on a feedback loop and nonlinear relationships [25]. System dynamics is viewed as the process or feedback relationship between different parts to understand complexity and behaviour throughout the lifespan, or the process of the system [27]. The need to utilise the complex system to have holistic thinking serves as a research agenda [28]. Therefore, the authors of the current paper further contribute to the system dynamics approach or modelling by looking at environmental entrepreneurship as a complex factor.

4. Methodology

The research methodology followed was in the form of systematic review. The rationale for using a systematic review as a methodology afforded the authors access to the various methodologies and outcomes within the areas of environmental entrepreneurship and various societal norms. This enabled the researchers to formulate a framework with triangulation of efforts from previous researchers. Furthermore, the rationale for systematic review is to explore the area under investigation, simulate theoretically, the key drivers, social and behavioural support factors in quest to create a future research agenda free of bias. The systematic review as a methodology was beneficial, especially during the COVID-19 pandemic, which has affected the entire world, as interviews or questionnaires would not have succeeded during these challenging times. The use of online data collection still poses challenges due to social inequalities and the majority of people not having access to emails or not being able to afford online video platforms in South Africa. The systematic review focused on peer-reviewed articles utilising search engines such as Google Scholar, Sage (Journal of Entrepreneurship Theory and Practice), the Journal of Cleaner Production, Science Direct and the Journal of Sustainability. Grey resources such as

newspapers media alerts were excluded when conducting a systematic review. A theoretical review was conducted using a literature review of which n=92 sources (peer-reviewed articles) out of 135 articles, met the criteria that the researchers set for the ecosystem. Duplication of results was removed from the 135 articles. The current study is qualitative in nature and thematic content analysis was used to analyse the results. According to [29], the most preferred and effective way to analyse a qualitative study is to use thematic content analysis. Content thematic analysis attempts to summarise comments into meaningful categories [29]. According to [30] content analysis is a general term to analyse text. It is the systematic coding pillar used for exploring a large amount of textual information to determine trends and patterns [30]. Furthermore, content thematic analysis enables the researcher to condense a broad and clear description of a factor. Themes that have emerged from a review of the literature are environmental entrepreneurship (in terms of key drivers and support), and social and behavioural factors regarding environmental entrepreneurship. The search criteria were environmental entrepreneurship, and system dynamic social factors regarding environmental entrepreneurship, with a refined search from 2010-2020. The software, Vensim, was utilised to simulate the virtual abstract system dynamics model. The title, introduction, abstract and findings sections were used to select the relevant articles and discard other articles. The findings are summarised in Table 1.

5. Findings

The identification of environmental key drivers was affected by conducting an entrepreneurship ecosystem. In order for sustainable entrepreneurship to flourish, awareness of environmental challenges and how they currently affect the nation needs to be set as a research agenda. The literature review and themes such as environmental entrepreneurship (in terms of key drivers and support), and social and behavioural factors regarding environmental entrepreneurship, served as a form of reference. The latter enabled the researchers to manipulate the key variables or drivers for environmental entrepreneurship to be popularised. Environmental entrepreneurship needs to be analysed using small and large-scale criteria and weighed up against the weakness and strengths in order for individuals to learn from and serve, as best practices.

The themes and summary of the afore-mentioned findings are explained in the Table 1. The ecosystem of environmental entrepreneurship in this paper comprises of key drivers in a form of financial and non-financial support, social and behavioural factors as depicted in table 1.

The key drivers such as funding, credit, capital financing, investing in environmental entrepreneurship, and crowdfunding, can be classified under green finance mechanisms in support of environmental entrepreneurship with social orientation [9, 29], [30-33], [35, 36], [44, 45]. Funding of enterprises or ventures is always a challenge, more specifically financing environmental entrepreneurship. Green proofing as advocated by [43] gives rise to a consultancy option, which the current authors deduce that the programme can be utilised to facilitate and manage green change dynamics. Some of the pillars supporting environmental entrepreneurship are infrastructure, skills and education, funding,

(environmental entrepreneurship incubators) products, markets affordability and political will [12, 29, 30, 33, 43]. However, the latter financial key drivers cannot operate in isolation and therefore, may need non-financial support in the form of behavioural change. With key drivers illustrated above, the next theme leads us to behavioural and social factors to strengthen the ecosystem of environmental entrepreneurship

Table 1: Ecosystem for environmental entrepreneurship

Key drivers of environmental entrepreneurship	Social and behavioural factors	Authors' contribution to the environmental entrepreneurship (South African context)	Common factors from various models
Strategic support mechanism [29]	Modelling of human behaviour	Ambassadors or society representatives from various cultural groups, tribal kings, ward councillors and volunteers	Strategic alliance
Environmental policy [12, 30]	Societal support, Alertness, motivation, Altruism [32]	Curriculum review and service-learning	Collaboration, wellbeing, alliance and governance
Tax exemptions and tax breaks, financial mechanism, cost effective products and services [31,32]	Crowdfunding, impact of social norms, development agencies [35-38]	Memorandum of understanding, exchange programmes, and international linkages	Financial and Non-financial support
Access to markets, legal support [12; 30,33,34]	Environmental psychology Environmental consciousness, collective Environmental entrepreneurship and green behaviour, Pro environmental behaviour [39-44]	Green change dynamics programme	Green consumer behaviour and adoption of green behaviour

The behavioural and social factors are premised within environmental agility innovation, transformation, motivation, ecopreneurial management, profiling of environmental entrepreneurship, development agencies crowdfunding, environmental policy, legal framework business incubators commitment and green skills to govern the rights of environmental entrepreneurs [28-30], [34-38], [45-54]. More entrepreneurs from small scale enterprises are environmentally conscious [55]. Literature suggests that in order for desired change to take place, social context plays a huge role, drawing from the work of [56, 57]. Society can play a huge role in praising and supporting environmental innovation, whereas entrepreneurs could ensure that they exploit the markets and ensure they offer affordable products and services to the communities at large. The support from government is needed to contribute to the subsidies

and waiving of some costs relating to environmental entrepreneurship, as part of the key drivers [57,58]. Networks, non-governmental stakeholders, financial structural support systems, tax exemptions and tax breaks are some of the key drivers that can support environmental entrepreneurship [29, 59]. The authors are proposing that skills development and human capital need to be the cornerstone of accelerating environmental entrepreneurship through an environmental entrepreneurship talent pipeline. The motives of environmental entrepreneurship have been shown that education is a factor. It has been proved that if individuals have higher levels of education, they tend to embark on environmental entrepreneurship [11].

The system dynamics approach is in the form of modelling the key drivers and factors affecting environmental entrepreneurship as explained above, as well as social and behavioural factors creating a new perspective of entrepreneurship. The modelling of the afore-mentioned results can be depicted using the system dynamics model in Figure 1.
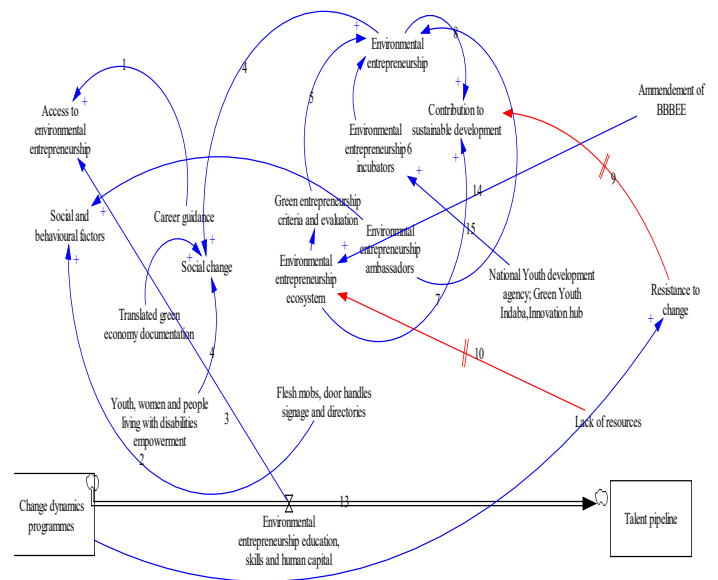
Figure 1: Virtual system dynamics model of environmental entrepreneurship

The system dynamics model (Figure 1) illustrates the importance of the interdependency of multiple variables or factors within the environmental entrepreneurship spectrum. The (+) sign represents a positive relationship and the (–) sign represents a negative relationship. Numbers depict each loop, while delays and threats are represented by a red line with two strokes. The system dynamics model consists of stocks and flows. Loop number 1 represents accessibility services that are influenced by career guidance, and the stock is represented by environmental entrepreneurship education, skills and human capital (loops 3 and 13).

Loop 2 represents an order for social and behavioural factors to be understood and incorporated for social change; and societies can be reached through flesh mobs, door handle signage, directories and ambassadors. Empowering youth, women and people living with disabilities about how to enter the environmental markets, contribute to a social change. Social change then may accelerate environmental entrepreneurship. For

environmental entrepreneurship to gain momentum, the criteria and evaluation system needs to be in place (loop 5).

Furthermore, contribution to environmental entrepreneurship can gain momentum because of the ambassadors, environmental entrepreneurship incubators (loop 6) and centres such as the National Youth Development Agency, Green Youth Indaba, Innovation Hub (loop 15) and emerging environmental entrepreneurship non-profit and profit organisations. Additionally, business incubators are influenced by financial and non-financial mechanisms as exogenous variables.

Environmental entrepreneurship serves as catalyst and contribution to sustainable development positively demarcated by loop 8 and loop 7. However, resistance to change and a lack of resources causes delays and threats to the ecosystem represented by loops 9 and 10. At the same time, there are inputs from the environment, which is BBBEE or legislation represented by a loop 14, which contribute positively to the environmental entrepreneurship ecosystem.

Stocks and flows are indicated by number loop 13. Currently, this research proposes two stocks namely change dynamics and talent pipeline, which are influenced and accelerated by environmental entrepreneurship, education and skills. At the same time, environmental change dynamics can be used to minimise resistance to change.

6. Discussions of environmental entrepreneurship key drivers and social factors

6.1. Key drivers of environmental entrepreneurship

Previous research suggests that creating a clientele, market, and support for the business are important pillars for a start-up to flourish [26]. One important factor that will determine the success or failure of a business is customers and customers' attitudes, which is often overlooked. Creation of the market and funding, or any support for green entrepreneurship, appears to be taboo and an unheard-of practice, therefore, it can be deduced that it needs to start with creating awareness, and unpacking human behaviour as an action. The process needs to be simplified for communities to understand the green economy phenomenon and from there, gradually improve to investigating if there is capability to optimise resources and opportunities for business gain and profit generation and saving the planet for future generations.

There is lack of investors which poses challenges and threats to the system. Investors in environmental entrepreneurship, especially in these sectors, are cautious investors, where scepticism and reluctance arise when it comes to investing to environmental entrepreneurship enterprises. In [33], the author serves to close the gap of financing by introducing crowdfunding. Crowdfunding can be explained as the sourcing of funds through other mechanisms within the lenses of cultural and social norms and creating initiatives online to raise funds and finance. The initiatives to enable transition and a green economy are to ensure ambassadors or champions in different sectors are available. These sectors include the private, public, tertiary, and schooling sectors, and are to be included from the planning phase to the implementation phase. However, society at large or communities are bypassed, and this may add to further challenges and delays in

the adoption of new behaviour such as the environmental entrepreneurship. In order to capitalise on collective efficacy in transitioning to a green economy, society, and stakeholders, need to form part of the movement. Collective efficacy can be defined as a group of people coming together to remedy a challenge (as in this instance, the environmental challenges), and have the confidence and capabilities to embark on the movement [41].

The need for curriculum review and inclusion of environmental entrepreneurship in South African basic and higher education needs to be considered to ensure the sustainability of environmental entrepreneurship. In [43], the author echoes the latter idea of curriculum inclusion of environmental entrepreneurship in schools. The green skills documentation and lessons learnt could be drawn from parts of Europe in regulating the economic factor of green skills for the country's economy [59]. The SEED programme is another support mechanism that supports sustainability entrepreneurship [60-62].

6.2. Societal and behavioural factors

There is an action of social responsibilities and environmental policies to be modified concurrently of which the researchers believe that environmental entrepreneurship with the lens of system dynamics could be incorporated onto policies to view the challenge as a system. A study conducted in Bosnia asserts that there is role ambiguity among government stakeholders and educational curricula regarding green entrepreneurship [63]. The latter argument can then be strengthened, and a clear framework provided where relevant stakeholders have stipulated the role and support required to accelerate the agency of adoption of environmental entrepreneurship.

6.3. Threats to the environmental entrepreneurship system

Through the analysis of literature, there have been efforts to investigate green entrepreneurship from international perspectives. Researchers then grouped existing literature to identify barriers to environmental entrepreneurship. Some of the internal barriers were a lack of resources and adequate knowledge, poor implementation of policies and strategies, and attitudes and an organisational culture that discourage environmental management [34]. Furthermore, external barriers that were identified were, difficulty in obtaining certification for environmental practices and systems, economic uncertainty, a lack of legal and institutional frameworks, specialised support and networks among small businesses and the creation of green jobs, and non-compliance with policies. The lens in regard to level of education, support services for incubation, entrepreneurial confidence, business climate, job creation, and clientele may be the solution to the above-mentioned challenges.

6.4. Contextualisation to the South African context

The authors believe that South Africa can implement strong coordination in the form of a memorandum of understanding with the countries that have developed environmental entrepreneurship. This will allow exchange programmes within the SMEs in diverse environmental entrepreneurship, particularly targeting Youth, Black people, women and people living with disabilities.

To broaden this perspective, Broad-based Black Economic Empowerment (BBBEE) needs to also include additional lenses of facilitating environmental entrepreneurship, and points should be allocated in the form of tendering systems in diverse environmental entrepreneurship. To promote gender equality, goal 5 of the sustainable development goals, environmental entrepreneurship can be spearheaded through women empowerment and be integrated into the BBBEE codes to ensure the economic and social standing of women in the South African context. Furthermore, to facilitate the access of services, the scope of career guidance can be expanded to include environmental entrepreneurship as a transformative process. The authors offer recommendations to accelerate access to markets and provide social contexts that are to be embedded in environmental entrepreneurship. In order to further accelerate access to markets, environmental policy needs to specifically stipulate what the rights of environmental entrepreneurs are and how they can access markets [12, 42].

The environmental entrepreneurship pipeline needs to be in place and included in policies, that especially target the youth. The National Youth Development Agency could spearhead funding and include the criteria to promote entrepreneurship in environmentally friendly products, services, consulting or distribution. The National Youth Development Agency could work hand in hand with Green Youth Indaba and an Innovation Hub where several youth programmes are housed, to ensure the sustainability of entrepreneurship in targeting the youth. Environmental change dynamics should be implemented whereby green readiness of change and managing fear of the unknown within Green initiatives could be developed, and awareness and training initiatives with environmental enterprises are instilled into society to contribute to the level of confidence in sustainable energy enterprise sectors. Green skills can be incorporated into the South African Skills Development Act to facilitate an initiative regarding green skills training and development. Change dynamics programmes such as resistance to change and sustainable development goals in a developing country can be introduced. The existing change dynamics programmes can be used as a foundation to design and implement the ecosystem. The South African Skills Development Act could be amended to facilitate the initiative of training and development, and the keeping of training and development records to aid sustainable development goals, and green skills for monitoring of grants and incentives.

7. Future recommendation

Action is needed with regards to social responsibilities. Further action is for environmental policies to incorporate environmental entrepreneurship. The authors further contribute that in order for environmental challenges to be minimised and environmental entrepreneurship to flourish, human behaviour needs to be modelled through environmental Psychology in terms of social psychology, behaviour, motivation, cultural and gender factors, personality traits, and attitudes towards a green economy and environmental entrepreneurship. To further aid environmental entrepreneurship as a social change, the development and focus of research and support needs to be given to women.

8. Conclusions

The current paper explored various works of literature such as key drivers from business incubators, social and behavioural factors, environmental entrepreneurship, and building the theoretical ecosystem of the elements highlighted by most researchers in the field of environmental entrepreneurship. Environmental entrepreneurship, as a complex phenomenon, needs to be viewed from different angles to ensure that solutions are gained from multiple sources at the same time.

The discovery made during the review of literature is that an ecosystem of environmental entrepreneurship can be broadly clustered within key drivers (support and accelerators), and social and behavioural factors that are contextualised in the South African context. The latter broad factors can further be explained through the accessibility of services that are influenced by career guidance, environmental entrepreneurship education skills and human capital. In order for social and behavioural factors to be understood and incorporated for social change, societies can be reached through flesh mobs, door handle signage, directories and ambassadors.

The empowerment of youth, women and people living with disabilities about how to enter the sphere of environmental entrepreneurship needs to be the cornerstone and serve as an accelerator to the system. Therefore, environmental entrepreneurship serves as catalyst and contributes to sustainable development, theoretically. As a way forward, the above hypothesis needs to be tested and validated to build a systems dynamic model taking foundation from the systematic review conducted by the current authors. Furthermore, to try and bridge the gap, more interdisciplinary qualifications need to be encouraged and a call for industrial psychologists to collaborate with experts in the fields of industrial engineering, environmental science and economics, about meeting sustainable development goals, should be undertaken.

Conflict of Interest

The authors declare no conflict of interest

Acknowledgment

References

[1] C.D. Diale, G. Kanakana-Katumba & R.W. Maladzhi. Green Entrepreneurship Model Utilising the System Dynamics Approach: A Review. In 2019 IEEE International Conference on Industrial Engineering and Engineering Management (IEEM) 384-389. (IEEE), 2019, December. doi.org/10.1109/IEEM44572.2019.8978804.

[2] C. Mukonza. Analysis of Factors Influencing Green Entrepreneurship in South Africa, 2016.

[3] F. Farinelli, M. Bottini, S. Akkoyunlu, P. Aerni & P. Green entrepreneurship: the missing link towards a greener economy. Atdf Journal, **8**(3/4), 42-48, 2011.

[4]   M. Schaper. Understanding the green entrepreneur. In Making Ecopreneurs, 27-40. Routledge, 2016.

[5]   P.N. Vaidya & D.V. Honagannavar. Green entrepreneurship towards sustainable environment. International Journal of commerce and management **3**(1), 88-91, 2017.

[6]   J.C. Allen & S. Malin. Green entrepreneurship: a method for managing natural resources? Society and natural resources, **21**(9), 828-844, 2008. doi.org/10.1080/08941920701612917.

[7]   A. Kuckertz & M. Wagner. The influence of sustainability orientation on entrepreneurial intentions – Investigating the role of business experience. Journal of Business Venturing, **25**(5), 524-539, 2010. doi.org/10.1016/j.jbusvent.2009.09.001.

[8]   M. Lenox & J.G. York. Environmental entrepreneurship. The Oxford handbook of business and natural environment, 70-92, 2011.doi.org/10.1093/oxfordhb/9780199584451.003.0004.

[9]   E. Mieszajkina. Ecological entrepreneurship and sustainable development. Problemy Ekorozwoju–Problems of Sustainable Development, **12** (1), 163-171. 2016.

[10]   L. Walley, D. Taylor & K. Greig. Beyond the visionary champion: Testing a typology of green entrepreneurs. Making ecopreneurs: developing sustainable entrepreneurship, **2**, 59-74, 2010.

[11]   J. Hörisch, J. Kollat & S.A. Brieger. What influences environmental entrepreneurship? A multilevel analysis of the determinants of entrepreneurs' environmental orientation. Small Business Economics, **48**(1), 47-69, 2017.

[12]   L.E. Huggins. Environmental entrepreneurship: markets meet the environment in unexpected places. Edward Elgar Publishing, 2013.

[13]   J.W. Creswell & J.D. Creswell. Research design: Qualitative, quantitative, and mixed methods approaches. Sage publications, 2017.

[14]   J. Kirkwood & S. Walton. What motivates ecopreneurs to start businesses? International Journal of Entrepreneurial Behavior & Research, **16**(3), 204-228, 2010. doi.org/10.1108/13552551011042799.

[15]   T. McEwen. Ecopreneurship as a solution to environmental problems: implications for college level entrepreneurship education. International Journal of Academic Research in Business and Social Sciences, **3**(5) 264, 2013.

[16]   D. Vasilevska & B. Rivza. Green Entrepreneurship as a Factor of Sustainable Economic Development in Baltic States. International Multidisciplinary Scientific GeoConference: SGEM, **18**(5.3), 423-430, 2018. doi.org/10.5593/sgem2018/5.3/S28.054.

[17]   A.R. Nunes, K. Lee & T. O'Riordan. The importance of an integrating framework for achieving the Sustainable Development Goals: the example of health and well-being. BMJ global health, **1**(3) e000068, 2016. doi.org/10.1136/bmjgh-2016-000068.

[18]   D.M. Hechavarria, A. Ingram., R. Justo & S. Terjesen. Are women more likely to pursue social and environmental entrepreneurship? In Global Women's Entrepreneurship Research. Edward Elgar Publishing, 2012. doi.org/10.4337/9781849804752.00016.

[19]   G. Nhamo. Green economy readiness in South Africa: A focus on the national sphere of government. International Journal of African Renaissance Studies-Multi-, Inter-and Transdisciplinarity, **8**(1), 115-142, 2013. doi.org/10.1080/18186874.2013.834628.

[20]   V. Harini. & D.T. Meenakshi. Green Entrepreneurship Alternative (Business) Solution to Save Environment. Asia Pacific Journal of Management & Entrepreneurship Research, **1** (3), 79, 2012.

[21]   S.E. Sanyang & W.C. Huang. Green cooperatives: A strategic approach developing women's entrepreneurship in the Asian and Pacific region. World Journal of Agricultural Sciences, **4**(6), 674-683, 2008.

[22]   M. Drăgoi, I.E. Iamandi, S. Munteanu, R. Ciobanu & R. Lădaru. Incentives for developing resilient agritourism entrepreneurship in rural communities in Romania in a European context. Sustainability, **9**(12), 2205, 2017. doi.org/10.3390/su9122205.

[23]   D. Holt. Where are they now? Tracking the longitudinal evolution of environmental businesses from the 1990s. Business Strategy and the Environment, **20**(4), 238-250, 2011. doi.org/10.1002/bse.697.

[24]   D.H. Meadows. Thinking in systems: A primer. Chelsea green publishing, 2008.

[25]   J.W. Forrester. Some basic concepts in system dynamics. Sloan School of Management, Massachusetts Institute of Technology, Cambridge, 9, 2009.

[26]   R. Teplov, J. Väätänen & D. Podmetina. A System Dynamic Approach to Modelling the Endogenous and Exogenous Determinants of the Entrepreneurship Process. Journal of Innovation Management, **4**(2), 68-95, 2016. doi.org/10.24840/2183-0606_004.002_0005

[27]   N. Abdelkafi & K. Täuscher. Business models for sustainability from a system dynamics perspective. Organization & Environment, **29**(1), 74-96, 2016. doi.org/10.1177/1086026615592930.

[28]   K. Schaefer, P.D. Corner & K. Kearins. Social, environmental and sustainable entrepreneurship research: what is needed for sustainability-as-flourishing? Organization & environment, **28**(4), 394-413, 2015. doi.org/10.1177/1086026615562111.

[29]   D. Waddell, A. Creed, T.G. Cummings & C.G. Worley. Organisational change: Development and transformation. Cengage AU, 2019

[30]   M. Vaismoradi, H.Turunen & T. Bondas. Content analysis and thematic analysis: Implications for conducting a qualitative descriptive study. Nursing & health sciences, **15**(3), 398-405, 2013. doi.org/10.1111/nhs.12048.

[31]   P.B. Zamfir. (2014). Supporting Green Entrepreneurship in Romania: Imperative of Sustainable Development. Romanian Econ. Bus. Rev, **9**, 35-44, 2014.

[32]   N. Thompson, K. Kiefer & J.G. York. Distinctions not dichotomies: Exploring social, sustainable, and environmental entrepreneurship. In Social and sustainable entrepreneurship. Emerald Group Publishing Limited, 2011. doi.org/10.1108/S1074-7540(2011)0000013012.

[33]   A.V. Barkov & Y.S. Grishina. Methodological approaches to theoretical construction of the model of legal support for environmental entrepreneurship. Civil Law 4, 3-7, 2018. doi.org/10.33397/2619-0559-2019-1-1-115-134.

[34]   O.A. Yakovleva. Environmental entrepreneurship (legal aspect). Legal Concept= Pravovaya Paradigma, **17**(2), 2018.

[35]   J. Hörisch. Crowdfunding for environmental ventures: an empirical analysis of the influence of environmental orientation on the success of crowdfunding initiatives. Journal of cleaner production, 107, 636-645, 2015. doi.org/10.1016/j.jclepro.2015.05.046.

[36]   F. Massa-Saluzzo & L. Toschi. The Impact of Local Social Norms on Access to Finance: The Case of Environmental Entrepreneurship. In Academy of Management Proceedings 2019, (1), 14820. Briarcliff Manor, NY 10510: Academy of Management, 2019, July. doi.org/10.5465/AMBPP.2019.38.

[37]   E.I. Nikolaou, D. Ierapetritis & K.P. Tsagarakis. An evaluation of the prospects of green entrepreneurship development using a SWOT analysis. International Journal of Sustainable Development & World Ecology, **18**(1), 1-16, 2011. doi.org/10.1080/13504509.2011.543565.

[38]   C. Rodgers. Sustainable entrepreneurship in SMEs: a case study analysis. Corporate Social Responsibility and Environmental Management, **17**(3), 125-132, 2010. doi.org/10.1002/csr.223.

[39]   S. Schaltegger & M. Wagner. Sustainable entrepreneurship and sustainability innovation: categories and interactions. Business strategy and the environment, **20**(4), 222-237, 2011. doi.org/10.1002/bse.682.

[40]   S. Schaltegger. A framework and typology of ecopreneurship: Leading bioneers and environmental managers to ecopreneurship. In Making Ecopreneurs pp. 95-114. Routledge, 2016.

[41]   S. Cheema, B. Afsar, B.M. Al-Ghazali & A. Maqsoom. How employee's perceived corporate social responsibility affects employee's pro-environmental behaviour? The influence of organizational identification, corporate entrepreneurship, and environmental consciousness. Corporate Social Responsibility and Environmental Management, **27**(2), 616-629, 2020. doi.org/10.1002/csr.1826.

[42]   J.P. Doh, P. Tashman & M.H. Benischke. (2019). Adapting to grand environmental challenges through collective entrepreneurship. Academy of management perspectives, **33**(4), 450-468, 2019. doi.org/10.5465/amp.2017.0056.

[43]   I. Fritsche, E. Jonas & T. Kessler. Collective reactions to threat: Implications for intergroup conflict and for solving societal crises. Social Issues and Policy Review, **5**(1), 101-136, 2011. doi.org/10.1111/j.1751-2409.2011.01027.x.

[44]   W.R. Meek, D.F. Pacheco & J.G. York. The impact of social norms on entrepreneurial action: Evidence from the environmental entrepreneurship context. Journal of Business Venturing, **25**(5), 493-509, 2010. doi.org/10.1016/j.jbusvent.2009.09.007.

[45]   K. Foster, J. Jelen & A. Scott. (2010). Teaching Environmental Entrepreneurship at an Urban University: Greenproofing. Metropolitan Universities, **21**(1), 73-87, 2010.

[46]   R. Ranjan. Deriving double dividends through linking payments for ecosystem services to environmental entrepreneurship: The case of the invasive weed Lantana camara. Ecological Economics, **164**, 106380, 2019. doi.org/10.1016/j.ecolecon.2019.106380.

[47]   R. Antolin-Lopez, J. Martinez-del-Rio & J. J. Cespedes-Lorente. Environmental entrepreneurship as a multi-component and dynamic construct: Duality of goals, environmental agency, and environmental value creation. Business Ethics: A European Review, **28**(4), 407-422, 2019. doi.org/10.1111/beer.12229.

[48]   A. Domańska, B. Żukowska & R. Zajkowski. Green entrepreneurship as a connector among social, environmental and economic pillars of sustainable

development. Why some countries are more agile? Problemy Ekorozwoju, **13**(2), 2018.

[49] A. de Bruin & K. Lewis. Little acorns in action: green entrepreneurship and New Zealand micro-enterprises. Making ecopreneurs: Developing sustainable entrepreneurship, 95-107, 2010.

[50] J. L. Thompson & J. Scott. Environmental entrepreneurship: The sustainability challenge, 2010.

[51] J.K. Hall, G.A. Daneke & M.J. Lenox. Sustainable development and entrepreneurship: Past contributions and future directions. Journal of business venturing, **25**(5), 439-448, 2010. doi.org/10.1016/j.jbusvent.2010.01.002.

[52] J.M. Scott. & J. Thompson. Making ecopreneurs: developing sustainable entrepreneurship. International Journal of Entrepreneurial Behavior & Research, 2012. doi.org/10.1111/joms.12214.

[53] G.D. Markman, M. Russo, G.T. Lumpkin, P.D. Jennings & J. Mair. Entrepreneurship as a platform for pursuing multiple goals: A special issue on sustainability, ethics, and entrepreneurship. Journal of Management Studies, **53**(5), 673-694, 2016.

[54] J. Thompson. Incredible Edible–social and environmental entrepreneurship in the era of the "Big Society". Social Enterprise Journal, 2012.

[55] M. Schaper. Understanding the green. Making ecopreneurs: Developing sustainable entrepreneurship, **7**, 2010.

[56] K. Hockerts & R. Wüstenhagen. Greening Goliaths versus emerging Davids—Theorizing about the role of incumbents and new entrants in sustainable entrepreneurship. Journal of business venturing, **25**(5), 481-492, 2010. doi.org/10.1016/j.jbusvent.2009.07.005.

[57] J.A. Schumpeter. "Economic theory and entrepreneurial history", in Clemence, R.V. (Ed.), Essays on Entrepreneurship, Innovations, Business Cycles, and the Evolution of Capitalism, 7th ed., Transaction Publishers, New Brunsick, NJ, 254-72, 2004. doi.org/10.4324/9781351311489-21.

[58] S. Choudhary. & N. Patil. Green entrepreneurship: role of entrepreneurs in energy economics in Nepal. Annual Research Journal of Symbiosis Centre for Management Studies, **3**(1), 166-175, 2015.

[59] M. Loock. Going beyond best technology and lowest price: on renewable energy investors' preference for service-driven business models. Energy Policy **40**, 21–27, 2012. doi.org/10.1016/j.enpol.2010.06.059.

[60] Y.D. Uslu, Y. Hancıoğlu & E. Demir. Applicability to green entrepreneurship in Turkey: A situation analysis. Procedia-Social and Behavioral Sciences, 195, 1238-1245, 2015. doi.org/10.1016/j.sbspro.2015.06.266.

[61] OECD/Cedefop, Greener Skills and Jobs, OECD Green Growth Studies, OECD Publishing. doi.org/10.1787/9789264208704-en, (2014).

[62] H. Creech, L. Paas, G.H. Gabriel, V. Voora, C. Hybsier & H. Marquard. Small-scale social-environmental enterprises in the green economy: supporting grassroots innovation. Development in Practice, **24**(3), 366-378, 2014. doi.org/10.1080/09614524.2014.899561.

[63] I. Silajdžić, S.M. Kurtagić & B. Vučijak. Green entrepreneurship in transition economies: a case study of Bosnia and Herzegovina. Journal of Cleaner Production, **88**, 376-384, 2015. doi.org/10.1016/j.jclepro.2014.07.004.

Ecosystem of Renewable Energy Enterprises for Sustainable Development: A Systematic Review

Carol Dineo Diale[*,1], Mukondeleli Grace Kanakana-Katumba[2], Rendani Wilson Maladzhi[2]

[1]*Department of Psychology, Industrial Psychology, Rhodes University, Grahamstown, 6139, South Africa*

[2]*Department of Mechanical and Industrial Engineering, University of South Africa, Johannesburg, 0002, South Africa*

A R T I C L E I N F O	A B S T R A C T
	In the Global sphere, the social, environmental, and economic pillars are the main contributors and accelerators to the sustainable development goals. As a result, the latter creates a platform for interdisciplinary researchers, society and decision-makers to collaborate in formulating ways to minimize factors contributing to environmental concerns. Energy is currently referred to as one of the scarce resources. The scarcity of electricity is mainly experienced in the rural areas of most countries in the world. The mandate of the green economy is to introduce innovative ways to redress the inequalities and lack of access, especially when it comes to Energy. Based on the sector's efforts, questions arise as to what comprises the ecosystem that can be accelerated to enhance entry to the sector. Hence, the researchers focus on Renewable Energy with specific reference to the entrepreneurial motives to meet sustainable goals. The applicable sustainable goals are goal 7 (affordable and clean Energy) and Goal 8 (decent work and economic growth). Furthermore, Energy contributes to modern access and poverty reduction to accelerate the transitioning to a Green economy. The current paper hopes to answer the following questions: Firstly, how Renewable Energy enterprise can contribute to sustainable development goals theoretically. Secondly, how can the theoretical energy enterprise ecosystem be contextualized in the South African context? A theoretical review was conducted through a literature review of which n=47 sources met the criteria that the researchers set for ecosystem variables. The overarching goal of the paper is premised on various works of literature building the ecosystem of the elements highlighted by most researchers in the field of renewable energy enterprises or business ventures. From the various models, the framework emerged singling out the critical success factors of the ecosystem of the Renewable Energy enterprise. The theoretical ecosystem consists of accelerators, social factors, sustainable development goals, as well as selected business models. The latter ecosystem was then contextualized in the South African context for a complete framework. Some of the critical drivers derived from the latter broad ecosystem are: Renewable Energy Feed-in Tarrif (REFIT), Utility Renewable Energy business model, Customer renewable energy business model, Energy Justice (distributive justice), Off-grid (Mini-grid), Saurian Lilting lamp, Renewable powered irrigation system.

1. Introduction

This current paper is emanating from the paper *Green Entrepreneurship Model Utilising the System Dynamics Approach: A Review"* presented at IEEM 2019 Conference in Macau [1]. There are always pressures around social, economic, and political phenomena as part of the triple bottom [2] to meet the green economy expectations and ways were researchers, and society at large can contribute to the process. Figure 1 shows the data world rural electrification rate & Electrification Growth rate.

Figure 1 illustrates the rural electrification and electrification growth rate from the 1990s to 2016. The red line demarcates rural electrification growth rate and the blue line demarcates rural

*Corresponding Author: Dineo Diale, c.diale@ru.ac.za

electrification rate (percentage of rural population). Rural electrification is a process of giving access to the commodity to the population in rural areas [3, 4]. Energy is one of scarce commodity, where millions of people, especially in the rural areas, are not connected to the electricity grid, due to lack of affordability [4].
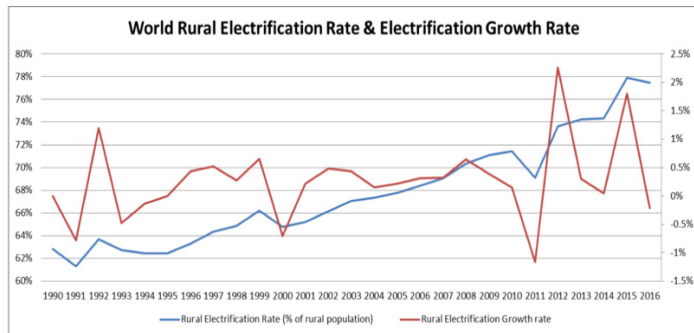
Figure 1: World Rural Electrification Rate & Electrification Growth Rate [3].

The green economy's mandate is to introduce innovative ways to redress the inequalities and lack of access, especially when it comes to energy [5]. Large numbers of people use fires and fuel lighting for basic energy needs [2], particularly in rural areas. The success factors or contingency plans were then introduced as an alternative mechanism such as renewable energy [2]. The latter serves as an effort to ensure that everyone can be able to light their houses or businesses. In hoping to minimize the challenge of the majority of South Africans without access to electricity, the country has a solar park in the Northern Cape. The solar park is to improve living, promote sustainable tourism. The latter strategy attracts tourists and investors, contributing to the economy of the country [4].

Furthermore, from the efforts on the sector, questions arise as to what would be an ecosystem that can be accelerated to enhance entry to the sector. The current research proposes a focus on specific reference to the entrepreneurial motives in efforts to meet sustainable development goals. Efforts have been made to explore renewable energy enterprises [6, 7] but have not focused on sustainable development goals or social focus within the area. The applicable sustainable development goals identified are Goal 7 (Affordable and Clean Energy) as well as Goal 8 (Decent work and Economic growth) [8] Furthermore, Energy contributes to modern access, and poverty reduction [8-10], to accelerate the transitioning to Green economy. The idea is to focus on one Green economy thematic area, which is Energy, and refining the research to focus only on enterprise within the energy sector.

The paper is premised through various works of literature building the ecosystem, taking into consideration the elements highlighted by most researchers in the field of Renewable Energy enterprises or business ventures. From the various models, the framework emerged singling out the ecosystem of the Renewable Energy enterprise. The theoretical ecosystem consists of accelerators, societal factors, and sustainable development goals as well as selected business models. The latter ecosystem is then contextualized in the South African context for a complete framework. The subsequent section will focus on literature review, research questions, methodology, results and discussions, and future recommendations.

2. Research questions

The research questions were formulated through the research gaps that were identified while reviewing literature and where possible research contributions can be made setting future research agendas. The research questions are as follows:

- How can theoretical Renewable Energy enterprise ecosystem be contextualized in the South African context?
- How can Renewable Energy enterprise contribute to sustainable development theoretically?

3. Research Background

The Literature review discussed in the paper is premised on accelerators and barriers to the Renewable Energy in the formulation of key drivers which can be part of the framework. Furthermore, the theory behind the ideas on how Renewable Energy can be used to contribute to sustainable development goals will be discussed below.

3.1. Accelerators to Renewable Energy

Through the review of literature, support mechanism implemented worldwide are in the form of the non-financial and financial mechanism as well as strategic programmes [9-11]. A generic business framework such as utility renewable energy business and customer renewable energy business model has been developed to facilitate manufacturing to consumption value chain to support Renewable Energy enterprises in the international markets [12-14]. Due to the diffusion of energy supply, support as an investment can accelerate the planning and implementation of the scarce commodity [15].

Other factors such as the biographical determinants such as age, level of education have demonstrated to the adoption of Renewable Energy technology. The generation that tends to adopt to the technology has been proven to be the younger generation than the older generation [16].
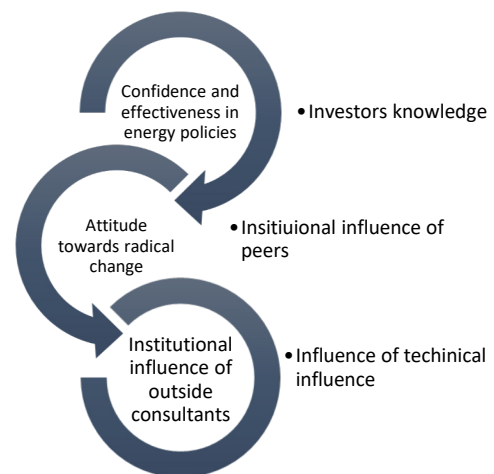
Figure 2: Renewable energy non-financial support mechanisms [15].

Figure 2 depicts the non-financial support mechanisms that could accelerate Renewable Energy. Scholars such as [15] have raised that non-financial support needs to be the cornerstone of the planning and implementation of Renewable Energy. The

renewable Energy serves as a "new kid on the block"; therefore, scepticism comes somewhat derails the implementation.

3.2. Access of the commodity by the society through sustainable development goals

In contribution to the access of the commodity by the society, the authors are proposing using sustainable development goals as a framework. Thematic areas of the green economy are inclusive but not limited to Green Energy, sustainable water, waste, agriculture, trade-in low carbon products, cleaner and green technology, green buildings, green chemistry and sustainable transport (mini car/cycles) as well as air quality [17]. Enabling the green economy involves innovation [18] of which needs attention and serves as a research agenda.

There are 17 sustainable development goals namely: *Goal 1 Eradication of poverty; Goal 2 No hunger, Goal 3 Good health, and well-being, Goal 4 Quality education, Goal 5 Gender equality, Goal 6 Clean water and sanitation, Goal 7 Affordable and clean energy, Goal 8 Decent work and economic growth, Goal 9 Industry, innovation and infrastructure, Goal 10 Reduced inequality, Goal 11 Sustainable cities and communities, Goal 12 Responsible consumption and production, Goal 13 Climate Action, Goal 14 Life below Water, Goal 15 Life on land, Goal 16 Peace and Justice and strong institutions, Goal 17 Partnerships to achieve a goal* [19].

Efforts have been made to introduce Energy technologies and policies is to reduce poverty and facilitate Clean Energy [20]. The need to contribute to societal need by reducing the electricity bills for those who cannot afford them, serves as a crucial social context [21], needing collective actions and commitment of relevant stakeholders inclusive of professionals in the field of Industrial Psychology, Industrial engineering, Energy practitioners, community members, governments officials and politicians.

Understanding culture and community needs from a social perspective, spearheaded by social scientists to study the area of Renewable Energy in Sub Saharan Africa [21] is needed, of which the authors believe that this best practice could be implemented in the South African context, to understand and tailor services and products to society leveraging on societal needs. Accelerators and support for Renewable Energy need to be contextualized in Rural, Urban, and semi-rural areas to create the impact and effective implementation. To echo the latter statement, the study conducted in Bangladesh investigated the impact of the implementation of Renewable Energy in rural areas and found that Renewable Energy contributes to social, economic and environmental benefits [22].

The benefits of Renewable Energy can benefit people living in rural areas through better quality of living and health as the majority living in Bangladesh use kerosene, candle and often have to walk a long distance to fetch wood for cooking [22]. Renewable Energy through natural resources such as biogas, solar, wind, hydropower can benefit the society of rural of Bangladesh [22].

3.3. Barriers to Renewable Energy

Some of the challenges identified are wage or salary disparities, skills shortages, shortage of coal, producers, corruption, mismanagement of funds and resources, lack of policy framework, limited absorption of solar manufacturing plants [3]. Developing countries do not have adequate resources, such as technology, lack of institutional support, lack of skills and lack of regulatory policies especially when it comes to Renewable Energy [23, 24] of which the same challenges may be the case in the South African context.

The negative impact of oil prices fluctuation is affecting the economic and political sphere of the continent [25]. According to [26], investors from other continents are reluctant to do business in Africa.

The lack of competencies, failure to create a new value proposition, and competition have been demonstrated to serve as barriers in Renewable Energy ventures [6, 26, 27]. The cornerstone query of creating a market arises, in establishing potential customer clientele, as well as the capacity of understanding the importance of adoption of Renewable Energy and how the technology can be utilised to ensure effectiveness and viability of enterprises [6, 13, 27, 28].

Upon reviewing the literature scholars have demonstrated that the effect of price control, inability to adopt new technologies and lack of market diversification further added to the challenges of full implementation of Renewable Energy technologies [25].

Further barriers, especially in the African context, is the issue of connection to the grid, inability to build relationships with established companies, lack of trade and distribution organisations [23]. In the South African context, it was discovered that barriers in the Energy project are credit risk, market risk, risk of change of legislation as well as technological risks [29].

The lack of the necessary infrastructure and education has been found to be obstacles in quest of the adoption of Renewable Energy as technology [30]. Thus, From the research point of view, lack of research and innovative way incorporated within research methodologies to Renewable Energy as technology serves as a challenge. In [5], the author asserts that the specific research methodologies such as quantitative methodology forms part of the puzzle and may become a solution in implementing the Energy programmes. Further challenges that researchers raise are weak electricity grids, corruption as well as future entrepreneurs in the field of renewable Energy having challenges in handling the complexity of adoption of Renewable Energy as a technology [3, 5, 25, 26].

4. Purpose statement

Upon explaining the research background above, purpose statement is then formulated as follows: Various scientists have conducted empirical studies in an attempt to understand Renewable Energy, sustainable development goals, climate change, Renewable Energy enterprise [31-35] but with less focus on Renewable Energy enterprise in quest of creating a framework nor less focus on mapping the Renewable Energy ecosystem with Sustainable Development goals and societal factors within the South African context theoretically, which the current study fulfils. Studies have been conducted globally and within African context within the Renewable Energy, Renewable Energy enterprise and sustainable development goals [6, 7, 20, 21, 24, 25,

34, 36] with non-existent focus particularly within the South African context in formulation of the ecosystem nor mapping the sustainable development goals utilising the ecosystem.

Table 1: Findings of the ecosystem for environmental entrepreneurship

The theoretical ecosystem of renewable energy enterprise	Contextualisation of theoretical ecosystem Renewable energy enterprise to South African context
Market incentives Demand and supply of renewable energy services	Equity official development assistance.
Infrastructure governance Government subsidies [11, 37]	Empowerment of previously disadvantaged groups, i.e. women, people of colour and disabled people Awareness conferences, symposiums
Best practices/lessons learnt from developing countries.	Human resource development policies and BBBEE
Financial support Venture capital Budget provisions, grants, loans, equity financing [36]	South African Government, subsidies Development Bank of Southern Africa (DBSA), Private energy entities, partners and cooperatives financial support.
Alternative forms of Energy Solar Energy [21] Off-grid (Mini-grid) Saurian Lilting lamp [38;39] Power plants [38] Biomass Renewable powered irrigation system Imported Hydropower generation Rural Energy Enterprise Development (AREED	Mitigation programmes with local municipalities, baseline studies, solar Energy Stakeholder (Green youth Indaba local government, Department of Energy, Department of environmental affairs, an innovation hub

5. Methodology

The research methodology followed was in the form of systematic review. The rationale for using a systematic review as a methodology afforded the authors access to the various methodologies and outcomes within the areas of renewable energy enterprises and sustainable development goals. This enabled the researchers to formulate a framework with triangulation of efforts from previous researchers. Furthermore, the rationale for systematic review is to explore the area under investigation. The systematic review as a methodology was beneficial, especially during the COVID-19 pandemic, which has affected the entire world, as interviews or questionnaires would not have succeeded during these challenging times. The use of online data collection still poses challenges due to social inequalities and the majority of people not having access to emails or not being able to afford online video platforms in South Africa.

A systematic literature review was considered as the Research methodology of the current research paper which focussed on peer-reviewed articles utilising search engines such as Google scholar, Energy policy, Journal of cleaner production, Renewable and Sustainable Energy Reviews, Renewable Energy, Energy, Sustainability and Society. The introduction and findings were used to select the relevant articles for inclusion. A theoretical review was conducted through a literature review of which n=47 sources (peer-reviewed articles) met the criteria that the researchers set for ecosystem or variables sorted from 89 articles. Duplication of results were further removed. The themes were analysed through thematic content analysis, where themes such as key drivers of Renewable Energy enterprise, sustainable development and Renewable Energy enterprise, the applicability of renewable Energy in the South African context as well as access to renewable Energy sorted from 85 peer-reviewed articles are the outcome.

6. Findings

Figure 3 illustrates how the most prominent Sustainable Development Goals can be achieved theoretically using the Renewable Energy Enterprise ecosystem. The subsequent section under discussion will the explain thoroughly the mapping thereof.
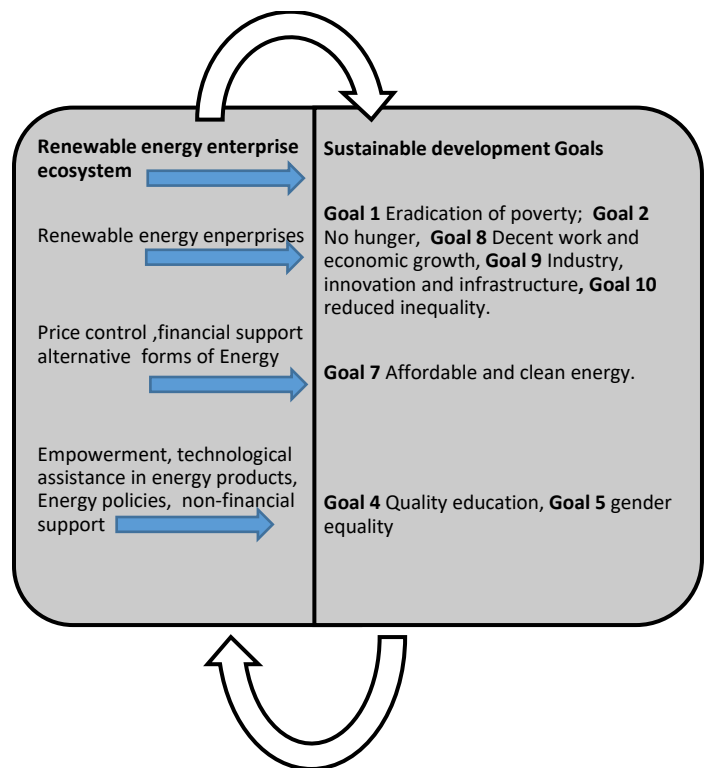
Figure 3: Theoretical Mapping of a renewable energy ecosystem and sustainable development goals

7. Discussions

7.1. Discussion of Renewable Energy enterprise Ecosystem within the South African context

Through the review of literature, one of the support mechanisms in the sectors is market incentive [39], which can be described by demand and supply or willingness to support the products or services of Renewable Energy. Alternatives, such as

Solar, off-grid options, especially mini-grids, have been suggested by [40] for rural areas to foster access to Energy.

Majority of business models have not considered the high-level business planning and strategies, before focusing on specifics of business development [41, 42]. The latter notion will equally contribute to entrepreneurship in Renewable Energy in ensuring enough planning, introducing and managing high-level game-changers as well as policies in regard to entrepreneurship in Renewable Energy.

Natural resources such as wind, solar power stations, and water need to be quantified to measure and form part of the baseline in assessing the readiness of the adoption and diffusion of Renewable Energy. Another sustainable sector that has proven to benefit the planning and implementation of Renewable Energy is the agricultural sector, through irrigations system and implementation of Energy park and monitoring [15].

Electrification plans similarly to what Ghana has implemented [23] can benefit South African context. The electrification plan can be possible with baseline studies and projections or estimation where potential areas may be without electricity [23]. Furthermore, some of the initiatives that can be implemented is the Rural Energy Agency similarly to what Tanzania has implemented [23].

Additional support and efforts made in the South African context is the Renewable Energy White paper, long term mitigation programme scenarios, as well as the Renewable Energy Feed-In Tariff (REFIT) as well as Energy policies and Act to support and regulate the Energy technologies [6, 29, 30, 37]. A generic business framework such as utility Renewable Energy business and customer Renewable Energy business model has been developed to facilitate manufacturing to consumption value chain in quest to support Renewable Energy enterprises in the international markets [12, 13].

Infrastructure governance is another support mechanism whereby policies and training can be piloted to the stakeholders. Stakeholders can consist of sustainability specialists, private and public sectors and communities at large. The implementation of a renewable-powered irrigation system [24] can be introduced to minimise challenges of scarcity of resources drawing from [19, 24]. The entrepreneurial confidence in development, consulting and distribution of renewable-powered irrigation system, a budget provision from the government need to support SMEs in the Energy sectors.

The issue of crime and corruption may need to also be factored in budget allocation in the form of investing in security services to safeguard the power stations and Energy technologies.

South Africa is a democratic country where law triumphs all undesirable behaviour and regulate the system. The Energy justice and legal perspective can be implemented when contributing to the sustainable Energy particularly, distributive justice of equal access to resources even to society who cannot afford the services [43].

In [8 10], the author asserts that there should be different tailored types of funding to promote access to Energy in the form of Grants, financing, loans, Equity official development assistance, equity financing and technical assistance in Energy products and services. To translate this mechanism in the South African context, the National Youth development agency, could be a spearhead for funding and include the criteria to promote Energy products, services, consulting or distribution.

The South African national youth development could work hand in hand with Green youth Indaba as well as an Innovation hub where several youth programmes are housed in South Africa, to ensure the sustainability of entrepreneurship in targeting the youth. The authors are proposing the implementation of Green change dynamics as a development programme whereby green readiness of change and managing fear of the unknown within Green initiatives could be introduced to facilitate awareness and training initiatives within Green Energy enterprises, which could be instilled onto the society, to contribute to the level of confidence in Sustainable Energy enterprises sectors.

Clientele and or customers as well as demand and supply serve as the corners and hub of every business incubators. One important factor that will determine the success or failure of a business is customers and customer attitudes, which is often overlooked. However, in the green entrepreneurship field, efforts have been made regarding customer attitude towards green entrepreneurship [44, 45]. Through the analysis of literature, the Utility Renewable Energy business model as well as Customer Renewable Energy business model deemed to be the proposed framework as discovered by scholars in ensuring the monitoring and viability of maintaining clientele with the use of technological assistive programme and stakeholder liaison [9, 12, 13, 46, 47].

Lessons learnt in the form of learning best practices from developed countries, and neighbouring African countries need to be replicated in the South African context, to share the success factors on Energy and advances on technological factors [24]. Furthermore, there should be system management of key holders such as knowledge dissemination through conferences and workshops, the guidance of the search and sponsorship to steer the direction of research and to find how best to formulate policies within the area of Renewable Energy, market niches as well as resource mobilisation such as infrastructure, tax-exempt and micro-financing [48]. The latter mechanisms of financing structures would offer affordable Renewable Energy for a better quality of life to societies at large. In [49], the author asserts that there should be a monitoring tool rating system to ensure that the infrastructure implemented is sustainable. The proposed monitoring tool is sustainable infrastructure rating system [49]. Drawing from this discovery, the authors in the current paper assert the rating system can be used specifically when implementing Energy technologies, services or distribution of renewable Energy tools.

Vat returns, Government subsidies, tax incentives for innovation, price control, demand assurance, venture capital are some of the supporting mechanisms implemented worldwide [9-11] of which we believe that South Africa can also implement these mechanisms. A need for strong coordination and memorandum of understanding with the countries who have

developed these mechanisms is needed, to allow exchange programmes within the SMEs in Energy, particularly targeting Youth, Black people, women as well as people living with disabilities as these group, still fall in the designated, previously disadvantaged backgrounds. To broaden the latter perspective, Broad-Based Black Economic Empowerment (BBBEE) will need to also include additional lenses of facilitating Green entrepreneurship and points to be allocated respectively in the form of tendering systems within the advances of Energy sectors.

A further area of consideration is how can different business models such as Pty Ltd (public companies), private companies, close corporation, partnerships, benefit from Renewable Energy at the same time saving the planet. Furthermore, the authors are of the opinions that once the mapping of success factors of different business models can be understood and investigated, support such as lessons learnt, specific funding and non-financial support can be tailored to different Renewable Energy enterprises.

Globalisation in the current context can be seen as a contributing factor, whereby the country such as South African can benefit from markets internationally. In [38], the author echoes the latter statement in supporting imported goods and services such as imported technology for hydropower generation and Biomass. Scholars have demonstrated that through biomass combustion with coal and setting the technologies to exposed heat generate electricity in an effective way [15]. The latter then has further been tested to have saved enterprises when it comes to cost and effective way to the adoption of Renewable Energy [15].

Although imports may also impact on the level of emissions and the cost of Energy services or products, the import of resources serves as the immediate mechanism as South Africa lack enough resources to engage in Energy thematic area effectively. This may imply that concessions and discounted rate may need to be negotiated between two countries embarking on exports and imports. The researchers are of the opinion that there should be public and private organisations willing to train and invest in imports and exports when it comes to Energy enterprises. The introduction of Public-private partnership (PPP) of policies to accelerate the Energy technologies as well as community members being included from the planning to implementation phase in collaboration with NGOs similarly to Nepal's initiatives [32], is needed and may need to be implemented in the South African context.

Saurian lilting low-cost solar lamps as part of renewable Energy [38] serves as a green entrepreneurship initiative that could be explored in the South African context especially in the rural areas and restoring access of Energy to the society.

Further research conducted in other parts of African countries promulgated by UN is African Rural Energy Enterprise Development (AREED) programme and national strategy for the Development of Renewable Energy [23], which South Africa could benefit from the initiative in accelerating entrepreneurship and collaboration in the sector. The need to contribute to society by reducing the electricity bills for those who cannot afford as a form of contributing to the social context when it comes to Energy [19] serves as a priority. Drawing from this idea, the current researchers are of the opinion that once this idea could flourish,

this may serve as an incentive for the society to support the enterprises in the sector.

7.2. Discussions of Renewable Energy enterprise ecosystem to Sustainable development Goals

In this section, the authors then used the theoretical framework highlighted above through the analysis of literature to map the sustainable development goals to the Renewable Energy ecosystem as depicted in figure 3. A further contribution of the paper is that the authors are arguing that in order to accelerate the sustainable development goals, each thematic area of the green economy needs to be explored and systematically mapped onto the sustainable development goals for an impact. In contribution to the sustainable development goals, the authors are proposing using sustainable development goals as a framework for selecting specific sustainable development goals in mapping the elements of the Renewable Energy enterprise ecosystem.

In order to effect the latter objective the theoretical renewable Energy ecosystem can be used as follows: in order to facilitate the access to the markets, the price of Energy products and services needs to be monitored with set policies and governments subsidies or alternative financial mechanisms upon which the Goal 1 Eradication of poverty, Goal 2 No hunger, Goal 8 Decent work and economic growth, Goal 9 Industry, innovation and infrastructure, Goal 10 Reduced inequality can be accelerated and achieved.

The alternative forms of Energy such as Solar, off the grid, saurian lilting lamp and hydro-powered Energy [21, 30, 38] can further accelerate Goal 7 Affordable and Clean Energy for the better quality of life and livelihoods. Then for further evaluation monitoring and sustainability continuous learning, non-financial support empowering of women and youth, as well as people of colour, can further accelerate Goal 4 Quality education.

8. Future recommendation

The next steps will be to test and validate the proposed key accelerators and ways to minimise the barriers that may affect entry to renewable Energy enterprises. Furthermore, scientific empirical data will be needed to test the theoretical contribution of the mapping of sustainable goal with renewable Energy as Green economy thematic area. Furthermore, research on which type of business survives and gets on the markets quick receiving enough support serves as a future research agenda.

9. Conclusion

The paper explored various works of literature building the ecosystem through the elements highlighted by most researchers in the field of Renewable Energy enterprises or business ventures. Enabling the green economy involves innovation [17], which in the current study, Renewable Energy enterprise ecosystem serves as the innovation the current authors are proposing. The researchers are of the opinion that once this milestone of capacity building in terms of climate change, and the Green economy is fully implemented then this mechanism can be a wheel to Renewable Energy ecosystem in the transition to green economy.

The theoretical ecosystem consists of accelerators, societal factors, sustainable development goals, as well as selected business models. The latter ecosystem was then contextualised in the South African context for a complete framework. Some of the accelerators of Renewable Energy are financial and non-financial support mechanisms, generic business models such as customers and demand and monitoring. In answering how can theoretical Renewable Energy enterprise ecosystem be contextualised in the South African context research question: The applicability in the South African context was discussed highlighting the access to Energy by the society at large through reducing of inequality, entrepreneurship and eradication of poverty in drawing from sustainable development goals. In answering the research question: How can Renewable Energy enterprise contribute to sustainable development goals theoretically: Is through the relevant theoretical contribution of eradication of poverty, decent work for all, access to clean and affordable Energy as well as the quality of education. From the analysis of literature rating system, quantification and measurable goals need to be in place to ensure that the plans for implementation of the Renewable Energy are in place. The researchers are then proposing that entrepreneurial markets to be enabled in this arena, and that is where the motives of entrepreneurship would highly contribute to the sense of social gain and uplift and contributing to sustainable development goals with less attention on profit generation.

The benefits of Renewable Energy, as explained above, can benefit people living in rural area through better quality of living and health. Majority of people living in Bangladesh use kerosene, candle and often have to walk a long distance to fetch wood for cooking, Renewable Energy through natural resources such as biogas, the solar, wind, hydropower can benefit the society of rural of Bangladesh [21]. The latter benefits can also benefit most part of rural areas, and some townships in South Africa as some communities are still using candles, paraffin stove and often have to fetch water and wood to cook.

Conflict of Interest

The authors declare no conflict of interest

Acknowledgment

References

[1] C.D. Diale, G. Kanakana-Katumba, R.W. Maladzhi. "Green Entrepreneurship Model Utilising the System Dynamics Approach: A Review," in 2019 IEEE International Conference on Industrial Engineering

and Engineering Management (IEEM) 384-389. (IEEE), 2019, December. doi.org/10.1109/IEEM44572.2019.8978804.

[2] A. Kumar, B. Sah, A.R. Singh, Y. Deng, X. He, P. Kumar, R.C Bansal. "A review of multi criteria decision making (MCDM) towards sustainable renewable energy development," Renewable and Sustainable Energy Reviews, **69**, 596-609, 2017. doi.org/10.1016/j.rser.2016.11.191.

[3] Rural electrification. retrieved from https://en.wikipedia.org/wiki/Rural_electrification, accessed September, 2020

[4] J. Amankwah-Amoah. Solar Energy in sub-Saharan Africa: "The challenges and opportunities of technological leapfrogging," Thunderbird International Business Review, **57**(1), 15-31, 2015. doi.org/10.1002/tie.21677.

[5] G. Nhamo. "Green economy readiness in South Africa: A focus on the national sphere of government". International Journal of African Renaissance Studies-Multi-, Inter-and Transdisciplinarity," **8**(1), 115-142, 2013 doi.org/10.1080/18186874.2013.834628.

[6] M. Engelken, B. Römer, M. Drescher, I.M Welpe, A. Picot. "Comparing drivers, barriers, and opportunities of business models for renewable energies: A review," Renewable and Sustainable Energy Reviews, **60**, 795-809, 2016. doi.org/10.1016/j.rser.2015.12.163.

[7] C. Herbes, V. Brummer, J. Rognli, S. Blazejewski, N. Gericke. "Responding to policy change: New business models for renewable energy cooperatives–Barriers perceived by cooperatives' members," Energy Policy, **109**, 82-95, 2017. doi.org/10.1016/j.enpol.2017.06.051.

[8] A.R Nunes, K. Lee, T. O'Riordan. "The importance of an integrating framework for achieving the Sustainable Development Goals: the example of health and well-being," BMJ global health, **1**(3), e000068, 2016. doi.org/10.1136/bmjgh-2016-000068.

[9] H. Gujba, S. Thorne, Y. Mulugetta., K. Rai, Y. Sokona. "Financing low carbon energy access in Africa," Energy Policy, **47**, 71-78, 2012. doi.org/10.1016/j.enpol.2012.03.071.

[10] M. Loock. "Going beyond best technology and lowest price: on renewable energy investors' preference for service-driven business models," Energy Policy **40**, 21–27, 2012. doi.org/10.1016/j.enpol.2010.06.059.

[11] P.R Walsh. "Innovation Nirvana or Innovation Wasteland? Identifying commercialisation strategies for small and medium renewable energy enterprises," Technovation, **32**(1), 32-42, 2012.

[12] F. Yu, Y. Guo, K. Le-Nguyen, S.J. Barnes W. Zhang. "The impact of government subsidies and enterprises' R&D investment: A panel data study from renewable Energy in China,". Energy Policy, **89**, 106-113, 2016. doi.org/10.1016/j.enpol.2015.11.009.

[13] M. Richter. "Utilities' business models for renewable Energy: A review," Renewable and Sustainable Energy Reviews, **16**(5), 2483-2493, 2012. doi.org/10.1016/j.rser.2012.01.072.

[14] M. Richter. "German utilities and distributed PV: how to overcome barriers to business model innovation," Renewable Energy **55**, 456–466, 2013. doi.org/10.1016/j.renene.2012.12.052.

[15] A. Masini, E. Menichetti. "The impact of behavioural factors in the renewable energy investment decision making process: Conceptual framework and empirical findings," Energy Policy, **40**, 28-38, 2012. doi.org/10.1016/j.enpol.2010.06.062.

[16] G. Tate, A. Mbzibain, S. Ali. "A comparison of the drivers influencing farmers' adoption of enterprises associated with renewable Energy," Energy Policy, **49**, 400-409, 2012. doi.org/10.1016/j.enpol.2012.06.043.

[17] UNEP. "United nations Environment Programme 2004 annual report. United Nations environment report". Retrieved 29 Nov 2018 from https://wedocs.unep.org/bitstream/handle/20.500.11822/22353/2004_Evaluation_Report.pdf?sequence=1&isAllowed=y, 2005.

[18] B. J. Anthony, M. A Majid. "Development of a Green ICT Model for Sustainable Enterprise Strategy," Journal of Soft Computing and Decision Support Systems, **3**(3), 1-12, 2016.

[19] N. Kajee, E. Sobngwi, A. Macnab, AS Daar. "The Developmental Origins of Health and Disease and Sustainable Development Goals: mapping the way forward," Journal of developmental origins of health and disease, (9)1, 5-9,2018. doi.org/10.1017/S2040174417000630.

[20] S. O. Oyedepo. "Energy and sustainable development in Nigeria: the way forward," Energy, Sustainability and Society, **2**(1), 15, 2012 doi.org/10.1186/2192-0567-2-15.

[21] K.J. Hancock. "The expanding horizon of renewable Energy in sub-Saharan Africa: Leading research in the social sciences," Energy Research & Social Science, **5**, 1-8, 2015. doi.org/10.1016/j.erss.2014.12.021.

[22] MAH Mondal, L.M Kamp, N.I .Pachova, "Drivers, barriers, and strategies for implementation of renewable energy technologies in rural areas in Bangladesh—An innovation system analysis,". Energy Policy, **38**(8), 4626-4634, 2010

[23] C.A. Gabriel, J. Kirkwood. "Business models for model businesses: Lessons from renewable energy entrepreneurs in developing countries," Energy Policy, **95**, 336-349, 2016

[24] J. Haselip, D. Desgain, G. Mackenzie. "Non-financial constraints to scaling-up small and medium-sized energy enterprises: Findings from field research in Ghana, Senegal, Tanzania and Zambia," Energy Research & Social Science, **5**, 78-89, 2015. doi.org/10.1016/j.erss.2014.12.016.

[25] L. Agbemabiese, J. Nkomo, Y. Sokona. "Enabling innovations in energy access: An African perspective," Energy Policy, **47**, 38-47, 2012 doi.org/10.1016/j.enpol.2012.03.051.

[26] T. Dodd, M. Orlitzky, T. Nelson. "What stalls a renewable energy industry? Industry outlook of the aviation biofuels industry in Australia, Germany, and the USA," Energy Policy, **123**, 92-103, 2018. doi.org/10.1016/j.enpol.2018.08.048.

[27] A. Aslani, A. Mohaghar. "Business structure in renewable energy industry: key areas," Renewable and Sustainable Energy Reviews. **27**, 569–575, 2013. doi.org/10.1016/j.rser.2013.07.021.

[28] T. Helms. "Asset transformation and the challenges to servitize a utility business model," Energy Policy, **91**, 98–112, 2016 doi.org/10.1016/j.enpol.2015.12.046.

[29] A. Pegels. "Renewable Energy in South Africa: Potentials, barriers and options for support". Energy policy, **38**(9), 4945-4954, 2010 doi.org/10.1016/j.enpol.2010.03.077.

[30] S. Khennas. "Understanding the political economy and key drivers of energy access in addressing national energy access priorities and policies: African Perspective," Energy Policy, **47**, 21-26, 2012 doi.org/10.1016/j.enpol.2012.04.003.

[31] M.O.A González, J. S.Gonçalves, R.M Vasconcelos (2017). "Sustainable development: Case study in the implementation of renewable energy in Brazil". Journal of Cleaner Production, **142**, 461-475, 2017 doi.org/10.1016/j.jclepro.2016.10.052

[32] G. Lakshmi, S. Tilley. "The "power" of community renewable energy enterprises: The case of Sustainable Hockerton Ltd,". Energy Policy, **129**, 787-795, 2019. doi.org/10.1016/j.enpol.2019.02.063

[33] R. Liu, L. He, X. Liang, X. Yang, Y. Xia, Y. "Is there any difference in the impact of economic policy uncertainty on the investment of traditional and renewable energy enterprises?–A comparative study based on regulatory effects". Journal of Cleaner Production, **255**, 120102, 2020 doi.org/10.1016/j.jclepro.2020.120102

[34] Z.A Elum, A.S. Momodu. "Climate change mitigation and renewable energy for sustainable development in Nigeria: A discourse approach," Renewable and Sustainable Energy Reviews, **76**, 72-80, 2017 doi.org/10.1016/j.rser.2017.03.040

[35] X.L. Xu, C.K Liu. "How to keep renewable energy enterprises to reach economic sustainable performance: from the views of intellectual capital and life cycle," Energy, Sustainability and Society, **9**, 7, 2019. doi.org/10.1186/s13705-019-0187-2.

[36] G. Schwerhoff, M. Sy. "Financing renewable energy in Africa–Key challenge of the sustainable development goals,". Renewable and Sustainable Energy Reviews, **75**, 393-401, 2017. doi.org/10.1016/j.rser.2016.11.004.

[37] H.M. Liou, (2010). "Policies and legislation driving Taiwan's development of renewable Energy,". Renewable and Sustainable Energy Reviews, **14**(7), 1763-1781, 2010. doi.org/10.1016/j.rser.2010.02.013.

[38] S. Choudhary, N. Patil. "Green entrepreneurship: role of entrepreneurs in energy economics in Nepal,". Annual Research Journal of Symbiosis Centre for Management Studies, **3**(1), 166-175, 2015.

[39] N. Bosma, H. Crijns., T. Holvoet. Global Entrepreneurship Monitor 2011 Report for Belgium & Flanders, 2013.

[40] S.C Bhattacharyya, D. Palit (Eds.). Mini-grids for rural electrification of developing countries: analysis and case studies from South Asia, Springer, 2014.

[41] H. Chesbrough. "Business model innovation: opportunities and barriers. Long range planning", **43**(2-3), 354-363, 2010. doi.org/10.1016/j.lrp.2009.07.010.

[42] J. Leschke. "Business model mapping: A new tool to encourage entrepreneurial activity and accelerate new venture creation," Journal of Marketing Development and competitiveness, **7**(1), 18-26, 2013.

[43] L. Guruswamy. "Energy justice and sustainable development". Colo. J. Int'l Envtl. L. & Pol'y, **21**, 231, 2010.

[44] M. Lenox, J.G. York. Environmental entrepreneurship, The Oxford handbook of business and natural environment, 70-92, 2011.

[45] J.K. Hall, G.A. Daneke, M.J. Lenox. "Sustainable development and entrepreneurship: Past contributions and future directions,". Journal of business venturing, **25**(5), 439-448, 2010.

doi.org/10.1016/j.jbusvent.2010.01.002.

[46] S.T Bryant, K. Straker, C. Wrigley. "The typologies of power: Energy utility business models in an increasingly renewable sector,". Journal of Cleaner Production, **195**, 1032-1046, 2018. doi.org/10.1016/j.jclepro.2018.05.233.

[47] P. Gsodam, R. Rauter, R.J. Baumgartner. "The renewable energy debate: how Austrian electric utilities are changing their business models," Energy, Sustainability and Society, **5**(1), 1-12, 2015. doi.org/10.1186/s13705-015-0056-6.

[48] R.A Suurs. "Motors of sustainable innovation: Towards a theory on the dynamics of technological innovation systems," Utrecht University, 2009

[49] J.M Diaz-Sarachaga, D. Jato-Espino, D. Castro-Fresno. "Methodology for the development of a new Sustainable Infrastructure Rating System for Developing Countries (SIRSDEC)". Environmental Science & Policy, **69**, 65-72, 2017. doi.org/10.1016/j.envsci.2016.12.010.

Waste To Energy Feedstock Sources for the Production of Biodiesel as Fuel Energy in Diesel Engine - A Review

Maroa Semakula[*], Freddie Inambao

University of KwaZulu-Natal, Mechanical Engineering department, Durban, 4041, South Africa

A R T I C L E I N F O	A B S T R A C T
	In the recent past, there has been a renewed shift into biomass and other recycled waste sources for biodiesel production and utilization. This is a critical area of research and study in which this present work intends to review and identify gaps in literature by shifting the focus of review to non-plant based sources for biodiesel production. Traditional biodiesel feedstock sources have always presented a conflict of food security versus energy. This shift will be identified in literature to see if change to non-plant-based feedstocks sources has increased food security by discouraging the contribution of commercial farming for the production of biodiesel. This work will identify biodiesel families, generations, traditional and non-traditional feedstocks for biodiesel production. It will also discuss the non-edible biodiesel feedstocks sources in relation to waste to energy recovery. The other factor this work will review is to study how the use of non-plant based feedstocks such as municipal solid waste has improved environmental protection by reducing pollution and landfilling. In other words, this work will review the impact of Using waste municipal solid biomass resources such as waste tyres and waste plastics and changing them into energy sources. This review study aims at increasing environmental awareness, sustainability and reporting the progress made in waste to energy policy shift in many countries globally. This review will look at socio-economic opportunities in recycling besides the academic and research impacts of waste to energy policies adopted in many countries. The review will climax with a conclusion and future trends in waste to energy in relation to municipal solid waste resources.

1. Introduction and Historical Background of Biodiesel

The history of biodiesel fuel has its route traced to the discovery of the diesel engine by the German engineer Rudolf Diesel in the 1890s. However, the first use of vegetable oil as a fuel was in the world exposition in Paris in 1900. This was at the request of the French government, which had an interest in development of fuels of local origin for its African colonies for energy and power generation independence. There were a total of 5 engine models displayed and tested during the exposition [1]. After the Second World War, several literatures report the use of vegetable oil in diesel engines and operational difficulties encountered with their application as combustion fuel [2-5].

These reports led to the award of the Belgium patent 422877 in 1937 to Chavanne. However, after the second world war the alternative fuel research took a lull until the energy crisis of the 1970s when [6] came up with work on esters of vegetable oil. Using sunflower oil in a diesel engine, they reported that use of sunflower methyl esters eliminated the problems of viscosity and operational issues. Although fossil-based fuels have been playing a major role in the growth of industries, transportation and agricultural activities, the future of fossil fuel as primary source of energy is not sustainable due to depletion, outstripped demand of fuel energy consumption and use. Fossil based fuel have more qualities that make them appeal to the user readily such as availability, good combustion properties and high heating values [7]. Energy estimates from the international energy agency puts

the estimates of the growth of energy consumption at 53 % by the year 2030 [8, 9].

In the USA the energy information agency (EIA) projects liquid fuel consumption to increase from 86.1 million barrels per day to 110.6 MBD by the year 2035 [10]. The depletion of fossil fuel reserves has occupied world energy forums and decision makers. Therefore, there has been rapid research development in green alternative fuel energy, which is renewable, domestically available, environmentally friendly and feasible technically. Biodiesel therefore has become technically a better choice for researchers as they contain characteristics and identical physical properties to fossil fuel especially diesel fuel. This makes the future of biodiesel more tenable and more promising as sources of alternative fuel energy especially in developing countries. These countries experience a heavy burden on the importation of liquid petroleum fuel for energy, environmental impacts and effects of pollution on the public human health [11]. Table 1 showing a global production of biodiesel in 2015 and the unit cost of production.

Table 1: Worldwide production of biodiesel with cost [12]

Country	Estimated potential (Litres)	Production Cost($/l)
Brazil	2,567,000,000	0.62
Indonesia	7,595,000,000	0.49
Argentina	5,255,000,000	0.62
Malaysia	14,540,000,000	0.53
USA	3,212,000,000	0.85
Netherlands	2,496,000,000	0.75
Germany	2,024,000,000	0.79
Philippines	1,234,000,000	0.53
Belgium	1,213,000,000	0.78
Spain	1,073,000,000	1.71

The importance of modern-day transport systems cannot be gain said, especially the transportation of goods and services and people. The propulsion provided by internal combustion engines with diesel fuel as the primary source of energy, forms the bulk of commercial use and now personal transport, owing to their numerous advantages as compared to other forms or types of propulsion by internal combustion engines. Diesel engines are inherently lean burn engines, and emit relatively low carbon dioxide emissions as compared to petrol propelled internal combustion engines. Other advantages offered by diesel engines include high thermal efficiencies, durability and construction robustness [13]. This makes their continued increase and expansion as more countries move into urbanization, industrialization, and catching up with the highly industrialized

countries. However, there has been a formidable challenge to phase them out, based on environmental and human health issues due to the high levels of NO_X, smoke and PM emissions.

Diesel engines have shown to run stably on most medium blended ratios of waste plastic oil, although they produce more NO_X, UHC and CO emissions. However to stabilize their performance for higher blend ratios, injection timing has been proposed as a method of achieving engine performance stability without upgrading of fuel, engine modification or fuel alteration through addition of additives as observed by [14]. Injection timing was seen to affect performance from WPPO Jatropa blends of 20% tyre oil and 80% Jatropa ester oil resulting into lower fuel consumption, CO, UHC and PM although NO_X emissions increased [15]. Nevertheless In a research study by [16] the authors report increased BTE and NO_X emissions, thus concurring with the findings of Sharma et al. (2015) on emissions of NOx, but decreased results on fuel consumption, CO, and UHC.

The continued increase in stringent emission regulations enacted by global industrial powers, United States of America and the European Union environmental protection agencies including the G-7 and G-20. Have since labelled the diesel engine as primary polluter in the transport sector. Hence the clamour for alternative fuels, which mitigate pollution, are sought in the interest of reducing energy consumption, environmental degradation and air pollution from NO_X gases, which diesel engines emit, thus decelerating atmospheric carbon concentration globally. The road transport sector is an environmental concern, since its rapid expansion is fast eroding all the technological developments and improvements thus so far achieved in the war against pollution from diesel-propelled engines.

Across the globe, significant resources have been mobilized to find alternative sources of energy. Different regions and countries have focused attention at sources of supply and technical processes that give them comparative advantages. In sub-Saharan Africa, renewable energy alternatives for transportation have huge potential sources, one of which is biodiesel derived from municipal solid waste sites, waste tires, waste engine used oil and waste cooking oil. Considerable research has been ongoing in this area but some gaps have not been addressed. There is a clear need to conduct evaluations that enable precise technical classification of the performance and emission of biodiesel derived from the waste sources mentioned above. Figure 1 is showing available general waste data (from municipalities) in South Africa from 1997 to 2011.

This will enable us to filter the data, by comparing it with local South African standards and regulations with global standards and regulations. Through this, challenges can be identified and plans of action mapped out to tackle them. It is necessary to identify and assemble the right set of tools and technique needed to conduct studies on these municipal solid waste feedstock sources in a manner that optimizes them as available resources. The stated goal of this work is to extract, information on solid waste municipal sources for the production

of biodiesel using thermal processes. This information is contained in many published research articles and will be presented here as a review and future development.
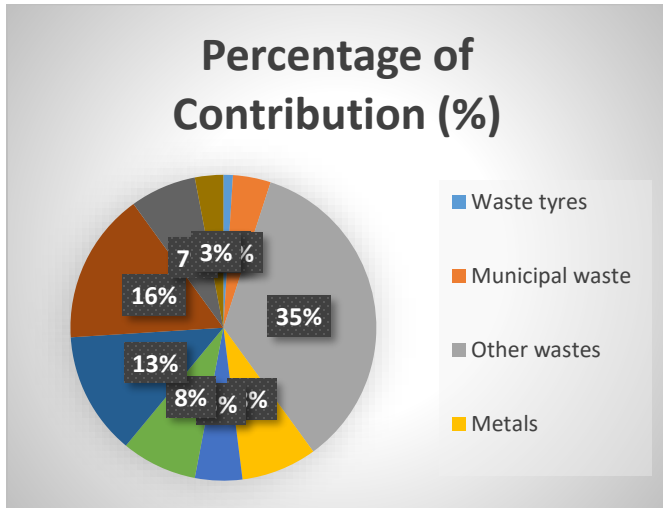
Figure 1: Percentage contribution of each waste stream of general solid Analysed from available data 2017 (from municipalities) in South Africa [17]

2. Biodiesel Families and Generations

Traditionally families come in generations defined by the length of time. As such, biofuels have lumped into families or generational categories. Production and use of biofuels has gained significant awareness and attention in academia, industry and government policy makers. Globally 28 countries including developing countries have been prominent in enacting biofuel mandated policies with substantial tax subsidies for biofuels [18]. Biofuels shift targets displacement of 20% of fossil fuels by biodiesel in the coming future [19].

This is driven in part by the potential of biofuels to create a new industry, raise farmer incomes restore degraded lands and promote independence from oil imports hence mitigating climate change [20]. For example, in literature, surveyed India is among the countries that have adopted Jatropa as a second-generation biofuel source of feedstock. However, in literature reviewed, there is no data on, water, pruning, and plant response to fertilizers hence varied planting management practices [21-23].

In biofuels, the main aim has been to identify methods of production by selecting appropriate feedstock, use of efficient conversion technologies and disposal of the product in this case the biofuels. The end product of any process in the world has become critical due to environmental issues and impact products bring, such biofuels production on the immediate environment [24]. One of the leading challenges in the energy sector is the promotion of biofuels compared to fossil fuels through arguments of sustainability i.e. economic environment and social aspects combined [25]. Sustainable development is a common term appearing in the global agenda of development since 1987. It is defined as development tailored to meet the needs of the present generations without compromising on the future generational needs in meeting today's needs [26, 27]. Sustainability requires

that all environmental factors of impact be assessed in each of their phases of the biofuels chain such as (i) Production and collection of feedstock, (ii) Feedstock processing, (iii) Conversion to biofuels, and (iv) Distribution of the end product [28, 29].

The second point is sustainability, which according to literature surveyed is difficult to conduct and evaluate sustainably. For example due to a great number of competing interests interfacing factors are weighted different by stakeholders hence disagreements and lack of common approach [28, 29]. Measuring sustainability of the biofuels industry is a complex issue especially considering the diverse range of biofuel feedstock, pathways, variation in stakeholder's interests and competing interests. Literature surveyed thus advocates for establishment of other indicators, which will enable assessment of sustainability of bioenergy systems. This should apply to small, large and local infrastructure acceptable to all stakeholder and in diversity [30-32]. Figure 2 showing the interrelated pillars of sustainability between society, the environment and the economy.
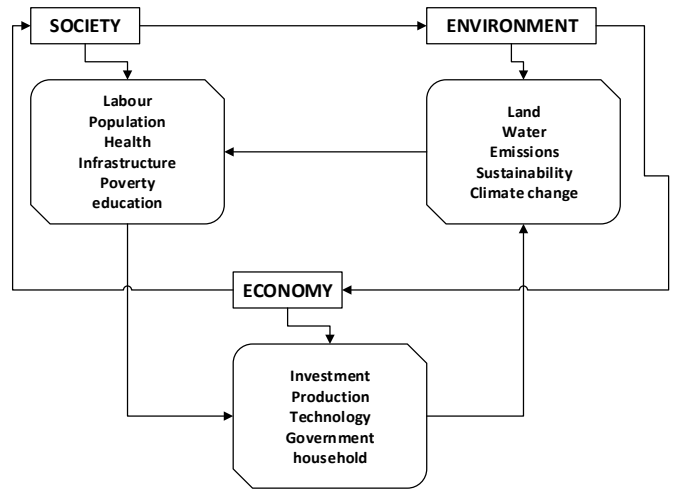
Figure 2: Interrelated pillars of sustainability adapted from [25]

2.1. First Generation Biofuels

First generation biofuels are derived from food crop feedstocks usually used as staple food. However, today this generation is vilified as the source of food insecurity and rising inflation in developing countries. Nevertheless, it is important to note even if it is alleged first generation cause increment in food prices and inflation its total influence is minimal [33]. First generation biofuels (otherwise called conventional biofuels) use three different technologies commercially for biodiesel, bioethanol and biogas [34, 35]. These commercial fuels are utilized as solid, gaseous or as liquid fuels. To add value these fuels are upgraded to high-density energy fuels such as charcoal, liquid fuels such as biodiesel, and bioethanol or gaseous fuels such as hydrogen, natural gas or biogas [33]. Table 2 shows the characteristics and demerits of first-generation biofuels.

As a first generation, conventional fuel biodiesel is produced through transesterification of vegetable oil, residual oils and animal fats as alternatives for petroleum diesel with slight engine

modifications. In the processing triglycerides are chemically reacted with alcohol in the presence of a catalyst or enzyme. This process generates biodiesel and glycerol [36, 37]. On the other hand, bioethanol are produced through a Biocatalytic fermentation of sugar or starch as ether (ETBE) which is used as a blend with gasoline. the gaseous category biogas a mixture of methane and carbon dioxide is processed through anaerobic digestion of organic materials [38, 39].

Table 2: Shows characteristics and demerits of first generation biofuels

Characteristic	First generation biofuel	References
Completion with food crops	Made from edible oil and starch feedstock	[40]
Land footprint	Requires arable land	[41]
Conversion to biofuels	Easy conversion	[42]
Water footprint	Potable water is required for cultivation	[43, 44]
Environmentally friendly	Using pesticides and chemical fertilizers	[45]
Commercialization	Commercially produced	[40]
Sustainability	Not sustainable in using natural resources such as water and land	[46-48]
Nutrient requirement	Chemical Fertilizers as main nutrients	[49]
Harvesting	Done by hand or machine	[50]
Regulation	Clear fair regulation	[40, 51]
Financial input	Low capital investment	[40]
Environmental condition	Temperature and humidity must be suitable	[52]

Despite their acceptance first generation, fuels have demerits, which have made their global appeal and wide commercial application difficult. For example, their overdependence on agricultural food crops initiates a heavy social debate on food vs fuel. Hence, their commercialization and adoption threaten food security while inflating food prices in developed countries. In semi-arid areas, production of biofuels would be too costly and limited with determined prices considered as non-competitive to conventional fuels. Figure 3 is showing different biofuel families and their available feedstocks sources.

2.2. Second Generation Biofuels

Second generation biofuels family is also called advanced biofuels. These fuels are also purported to be produced sustainably in a truly carbon neutral environment in terms of CO_2 concentration. The source of feedstocks of these fuels is lignocellulosic biomass, non-food crops, agricultural and forest residues and industrial wastes. The production of second generation is done by utilizing physical, thermochemical and biochemical technologies processing [55, 56]. Using these processes involves use of pre-treatment steps to facilitate the conversion process. Here properties of biomass are technically analysed such as size, moisture and density before treatment and processing is commenced [57].

In physical processing techniques in literature reviewed, the commonly applied techniques are briquetting, pelletizing and fibre extraction. These techniques enhance and convert loose biomass into high density solidified blocks of energy. Pelleting does the same thing pressure does to compact raw fibre particles of biomass into high density. On the other hand in fibre extraction fibre is removed from biomass residues and utilized as sources of energy fuel for heating [55, 58].

Under thermochemical processes for production of biofuels are found pyrolysis, gasification liquefaction and direct biomass combustion. Thermochemical liquid fuel processing uses thermal decomposition with chemical reformation. This involves heating biomass under the influence of different oxygen concentration leading to conversion of all organic components [39]. Pyrolysis is a slow or fast process depending on the existing operating conditions but in the absence of air [59, 60]. The former favours solid fuel production compared to the latter which is good for liquid fuel production (bio-oils) and gaseous biofuel production [61, 62].
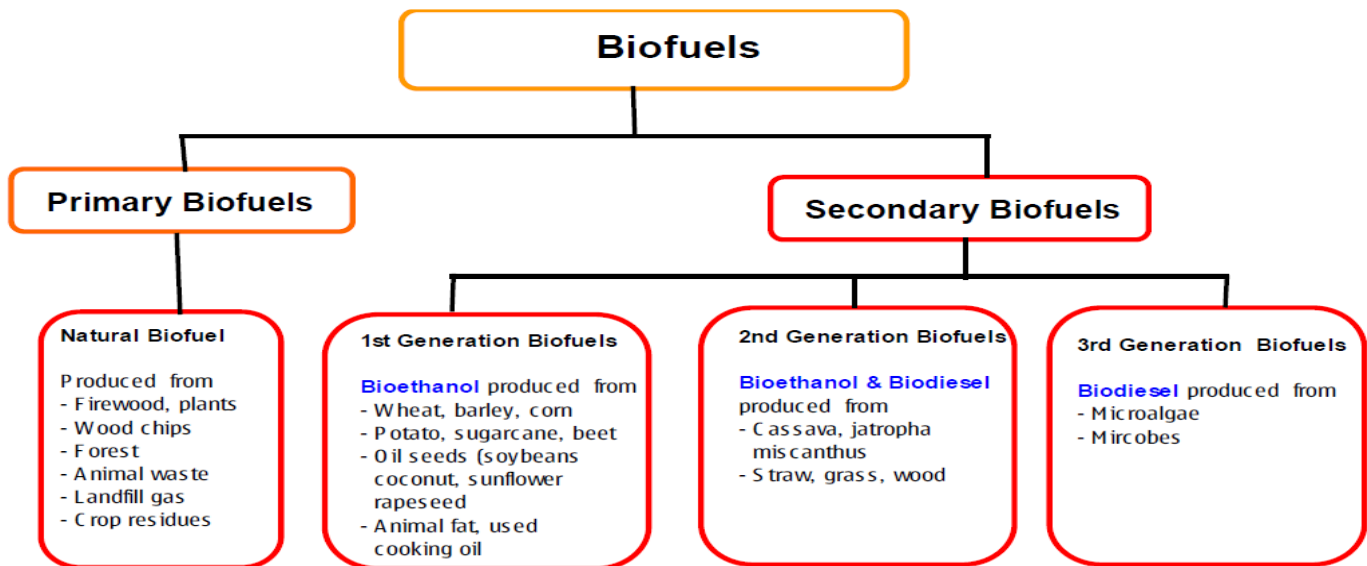
Figure 3. showing different biofuel families and their feedstocks [53, 54]

As a method in second-generation biofuels, gasification coverts biomass into combustible gaseous fuel mixtures also known as syngas. Through partial oxidation of biomass at elevated temperatures of 800 °C to 1400 °C syngas is produced. The medium for gasification can be air oxygen of steam [55, 60]. However gasification is still struggling with challenges of operational and downstream gas utilization problems [63]. The driver of gasification has been the versatility of the gases produced during the process. Reaction of the gasification and the feedstocks of solid carbon structure forms carbon dioxide or hydrocarbons. Nevertheless, as said earlier the gasfying agent has a very critical role in influencing the final product of the process. For example when steam is used as an agent of processing reaction temperatures are lowered to 600°C [39]. Table 3 is showing the principle components of a gasification process.

Table 3: is showing the principle components of a gasification process adapted from [63]

Target compounds	CO, H_2, CH_4, C_2H_x, C_3H_x
'Inert' (non-combustible) compounds	CO_2, H_2O, (N_2)
Trace contaminants	NH_3, HCN, other organic nitrogen compounds
	H_2S, COS, CS_2, other organic sulfur compounds
	HCl, NaCl, and KCl aerosols
Condensable fraction	Benzene, toluene, and xylene (BTX), tar, hetero-organics, (water)
Particles	Ash, mineral matter/salts, char, aerosols

During transformation (conversion) of solid fuel into gaseous components by gasification a number of reactions with intermediate reactions, take place. It is a complex network of reactions; influenced by feedstock sources, and properties, residence time, reactor design temperature gasifying agent and pressure. In this literature review, only a few examples of main reactions are presented in chemical equations 1 to 9. However, the references provided here would be useful to the reader for a detailed study and understanding [39, 64-66]. Table 4 is third generation biofuels characteristics and references.

Chemical reactions with molecular oxygen, which are exothermic in nature (combustion reactions).

$$C + O_2 \leftrightarrows CO_2 \qquad \Delta H = -110.62\text{kJ/mol} \qquad (1)$$

$$2CO + O_2 \leftrightarrows 2CO_2 \quad \Delta H = -283.15 kJ/mol \qquad (2)$$

$$2H + O_2 \leftrightarrows 2H_2O \quad \Delta H = -242.15 kJ/mol \qquad (3)$$
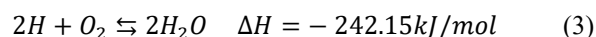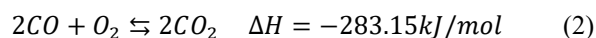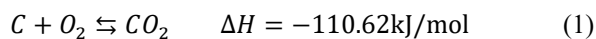
Carbon dioxide and hydrocarbon/CO_2 reaction

Boudouard reaction:

$$C + C O_2 \leftrightarrows 2CO \qquad \Delta H = +172.54 kJ/mol \qquad (4)$$

Hydrocarbon/CO_2 reaction:

$$C_nH_m + nCO_2 \leftrightarrows 2nCO + m/2H_2 \qquad (5)$$
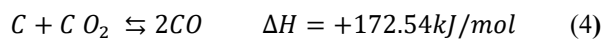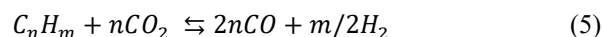
Steam as the reaction agent

$$C + H_2O \leftrightarrows CO + H_2 \quad \Delta H = +131.38\ kJ/mol \quad (6)$$
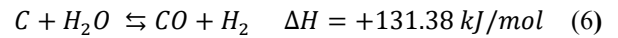
Hydrocarbon and steam reaction:

$$C_nH_m + nH_2O \leftrightarrows nCO + (\tfrac{m}{2} + n)H_2 \qquad (7)$$
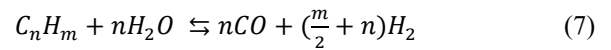
Water gas-shift reaction (homogeneous water-gas shift conversion)

$$CO + H_2 \leftrightarrows CO_2 + H_2 \quad \Delta H = -41.16 kJ/mol \quad (8)$$

Hydrogen reactions in gasification

$$C + 2H_2 \leftrightarrows CH_4 \ \Delta H = -75.00 kJ/mol \qquad (9)$$
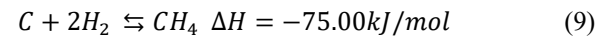
2.3. Third Generation Biofuels

The third generation biofuel family comprises of fuels produced from microalgae feedstocks. This generation is currently under research and development as alternative renewable energy sources for biofuel processing and production. This family has been largely been fronted as a solution to overturning the demerits of the first generation and second generation biofuels [55, 68]. Majority of these fuels exist in laboratories under research and development with a few small scale enterprises producing algae oil [69]. The microalgae group of feedstock consists of microalgae, macroalgae (seaweed) cyanobacteria (blue-green algae) [70]. Microalgae consists of 72000 different species and as many as 800000 in fresh water or salty water [69, 71].

Table 4: Shows characteristics and references of third generation biofuels

Generational Characteristics	References
Eliminates food-energy conflict	[40]
Contaminated and Non-arable land used for cultivation	[41]
Easy conversion due to increased hydrolysis and/or fermentation efficiency	[42]
Waste, saline and non-potable water also can be used	
Merits (CO_2 fixation, waste water treatment, reduced cost of fertilizer) demerits (ecological concerns on marine eutrophication)	[43, 44]
Poor biomass production for commercialization	[45]
favorably poor economically	[40]
Large quantities of carbon and nitrogen required. Solar energy is only available at daytime. Nutrients recycling possible	[46-48]
Harvesting of microalgae is expensive, and complicated	[49]
Lack of regulation for marine cultivation	[50]
initial large scale cultivation costs too high	[40, 51]
cultivation in harsh environmental condition such high pH, salinity and light intensities possible	[52, 67]

The rise of algae as an alternative biodiesel feedstock is due to its rapid growth, increased harvest cycle in days compared to months or years. Microalgae need few nutrients for maximum growth and can thrive in severe poor conditions while giving high and increased output per acre ranging from 15 to 300 times more compared to food crops acreage [72, 73]. Algae oil can also be used as feedstock to provide high value products such as ethanol, butanol, biodiesel, jet fuel syngas, and bio-oil chemical feedstocks such as hydrogen and farm fertilizers [53, 70].

Another important factor with algal biofuel is the lack of competition with food crops or feed crops, yet algae is used to

reclaim agricultural wastelands. This seems to obviate and free land use while reducing energy versus food competition. This elevates this family against the first two-biofuel families. However a further research and study aimed at improving algae production methods especially the plant energy content yield and sustainability is required [54]. Table 5 shows different oil contents for a variety of microalgae species.

Table 5: Showing different Oil contents for a variety of microalgae adapted from [41]

Microalga Oil content	Percentage in dry weight (%)
Botryococcus braunii	25–75
Chlorella sp.	28–32
Crypthecodinium cohnii	20
Cylindrotheca sp.	16–37
Dunaliella primolecta	23
Isochrysis sp.	25–33
Monallanthus salina	20
Nannochloris sp.	20–35
Nannochloropsis sp.	31–68
Neochloris oleoabundans	35–54
Nitzschia sp.	45–47
Phaeodactylum tricornutum	20–30
Schizochytrium sp.	50–77
Tetraselmis sueica	15–23

2.4. Fourth Generation Biofuels Sources and Beyond

The birth of fourth generation biofuel has been propagated by the need arising from environmental dilemmas. These dilemmas challenge our human capacity for sustainable solutions to protect nature for our own existence and posterity. For example, the need to protect water sources, agricultural lands for sustainable food production, reduction of GHG, the protection of atmospheric air and weaning overreliance from fossil fuels as the only sources of primary energy supply [74-79]. Table 6 Showing characteristics and references of fourth generation biofuels.

Table 6: Characteristics and references of fourth generation biofuels

Generational Characteristics	References
Eliminates the food-energy conflict	[40]
Contaminated and Non-arable land used for cultivation	[41]
Increased hydrolysis and/or fermentation efficiency	[42]
Waste, saline and non-potable water also can be used	[43, 44]
Offers Medium (CO2 fixation, waste water treatment) but releases GM organisms	[45]
Produces less biomass for commercialization	[40]
Leaking of GMO to environment pausing ecological risks	[46-48]
Large carbon and nitrogen required. (However, Solar energy is daytime). Requires Nutrients recycling in the process	[49]
Harvesting of microalgae is expensive, and complicated	[50]
No regulation for marine cultivation but strict regulation is required with GM algae	[40, 51]
Initial cost for large scale cultivation is expensive	[40]
Cultivation in harsh environmental condition possible (such as high pH, salinity high light intensities)	[52, 67]

Fourth generation biofuels are oils therefore produced from genetically modified feedstocks able to consume more CO_2 from the atmosphere than what they will produce during the

combustion phase as fuels [80]. Therefore fourth generation fuel utilizes the existing platform technologies such as pyrolysis, gasification, solar to fuel and genetic manipulation of organism's genetic order. The fourth-generation family is referred to as smart fuels based on the conversion of vegoil and biodiesel to biogasoline using advanced technology.

Despite large-scale production and efforts to try to commercialize this family progress has not been sufficient. This has been due to lack of sufficient biomass, increased production costs and set-up, environment and human health concerns as fewer feasibility studies have been completed [40]. Table 7 is showing health and environmental effects of fourth generation biofuels. While Figure 4 is showing main steps of algal biomass technologies in carbon fixation.

Table 7: The health- and environment-related risk of GM algae Human health [81, 82]

Topic Risk contribution	Risk contribution	Effect	References
Allergies	Human health	Dermal, ingestive, respiratory exposure	[82-86]
Antibiotic resistance	Human health	Reducing the effectiveness of medical treatments	[84-86]
Carcinogens	Human health	Carcinogenic residues	[82]
Pathogenicity or toxicity	Environment	Pathogenicity of some strain to human; toxic blooms; chemical transfer; toxic residues	[82, 87, 88]
Change or depletion of the environment	Environment	Removal of nutrients from ecosystem; reducing biodiversity of the flora and fauna	[89, 90]
Competition with native species	Environment	Outcompete native organisms; changing aquatic ecosystems	[91, 92]
Horizontal gene transfer	Environment	Transfer of genetic organisms	[93, 94]
Pathogenicity or toxicity	Environment	Pathogenicity of some strain to human; algal blooms; generating genetic–related toxins	[95]
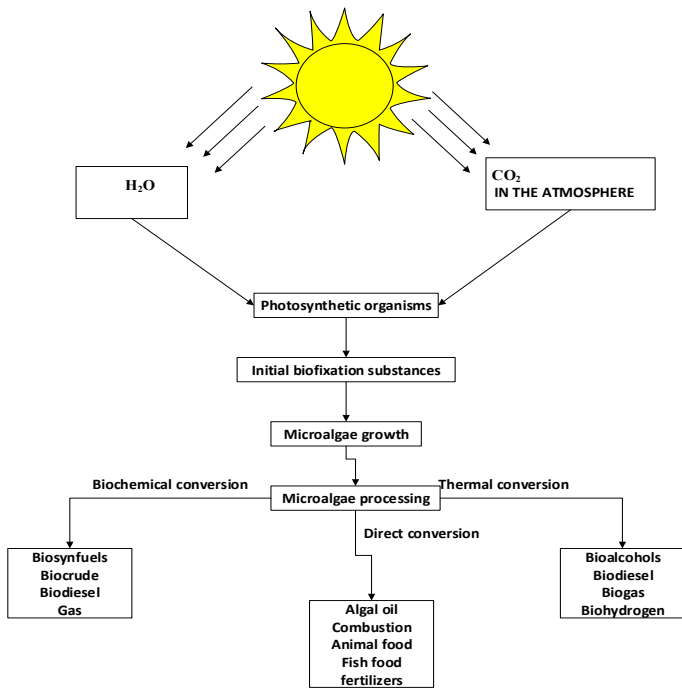
Figure 4: Carbon dioxide fixation and main steps of algal biomass technologies adapted [80]

GM crops have been with us since 1996 as sources of 3rd and 4th generation biofuels and have increased in their global acreage. For example soybeans, maize and rapeseed occupy 73.3×10^{13}, 46.8×10^{13}, and 7×10^3 respectively of all global land mass area under cultivation [96, 97]. Nevertheless, in order to increase fourth generation biomass production of biofuels algae is heavily GM sourced. Which is achieved by improving areas of the micro-organism using genetic material engineering manipulation. For example, the following areas are mentioned in literature to engineer increased microalgal biofuel production. (i) Improvement of photosynthetic efficiency, (ii) Increasing light penetration by using the truncated chlorophyl antenna and (iii) Reduction of photo-inhibition.

Literature is averse with these developments in the literature reviewed and presented here such as [98-101]. The development in fourth generation biofuels also aims at providing new economic development opportunities in remote and suburban areas of developing countries. These opportunities include reduction of emission to zero for both air pollutants and GHG [102, 103].

Microalgae form a large group of eukaryotes and cyanobacteria and have a wide range of compositional characteristics which include; [104] Food reservation, Photosynthetic pigments, Cell wall chemistry and reproduction. However out of the many species of microalgae only Bacillanophyceae (diatoms), Eustigmatophyte, Chlorophyceae and Chrysophyceae are potential sources of biofuel production [105]. Microalgae have high adaptability in extreme environmental conditions such as high salinity, drought, photo oxidation, osmotic pressure, temperature, anaerobiosis and ultraviolet (UV) radiation [106]. Their main nutrients are nitrogen

and phosphorous which accounts for 10% to 20% of its biomass [107, 108].

3. Biodiesel Feedstock Sources, Production, and Processing Techniques

3.1. Introduction to Edible Vegetable Oil and traditional Feedstocks

The production of biofuels such as biodiesel is becoming convenient as alternative energy. The use of biofuel such as biodiesel reduces GHG and provides opportunities for local and regional development in remote areas. This is made feasible considering the number of feedstocks sources. Biodiesel feedstock types differ from country to country depending on the geographical locations and their development [109, 110]. Globally more than 350 oil bearing crops have been identified [111] as possible biofuel feedstocks. However, there are many relevant candidates for biofuel production feedstocks adding to the list but are non-plant based. Figure 5 is showing the growth in vegetable oil production in China from 2003 to 2015.
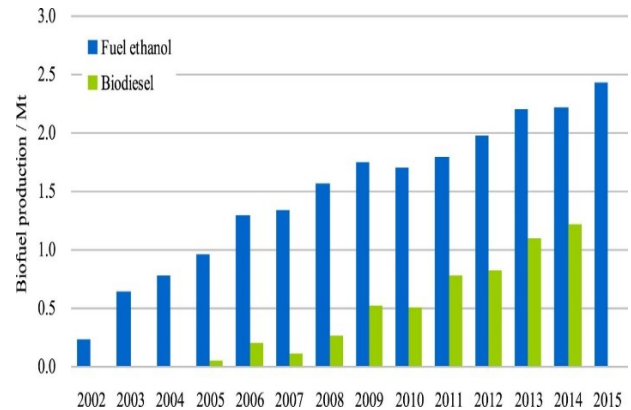
Figure 5: China's biofuel production over the past decade [112]

The advance in experimental biodiesel production from theses feedstocks has led to a waste to energy revolution. Biodiesel production from readily available feedstock considered waste candidates for dumping and landfill [113]. This has encouraged value addition and co-product markets while contributing to diversification of the biofuel industry [114]. Nevertheless, since each feedstock is different from the other the conversion and processing techniques vary but the basic process of production remains the same. The wide range of feedstocks availability plays a significant role in promoting the biofuel industry.

The availability of feedstocks is influenced by regional climate, geographical location, local soil characteristics and general agricultural practices of a region or country [115]. In sources of biofuel development production and processing, only sunflower, cottonseed, safflower, rapeseed and peanuts are considered compared to two, corn and sugarcane for bioethanol used in gasoline engines;. However, it is important to mention here that non-edible oil plants such as Karanja, rubber seed, tallow oil and microalgae, Jatropa and neem seeds are also gaining

acceptance as alternative sources of biofuel. In the last decade, non-edible feedstocks have been extensively studied in literature surveyed such as [77, 116-118].

Among plant-based feedstocks palm oil, soybean and rapeseed account for almost 80 % of global feedstock for biofuel production as shown in Table 8. To qualify as a feedstock for biodiesel production the oil percentage and yield are important factors for consideration [119-122]. Nevertheless quality, availability, physicochemical properties, composition and production costs are some of other critical factors of feedstock determination and acceptability [119]. Feedstock prices account for more than 80% of the cost hence selecting and quality feedstock is vital to ensure low production costs [120, 123]. Since feedstocks are impacted by oil percentage yield, these factors are critical and need consideration. Figure 6 is showing total global vegetable oil production and production contribution of each source from 2013 to 2018. While Table 8 shows major vegetable oil producers and their main sources of feedstock respectively. On the other hand, Figure 7 is showing, international vegetable oil prices from 2000 to 2014.
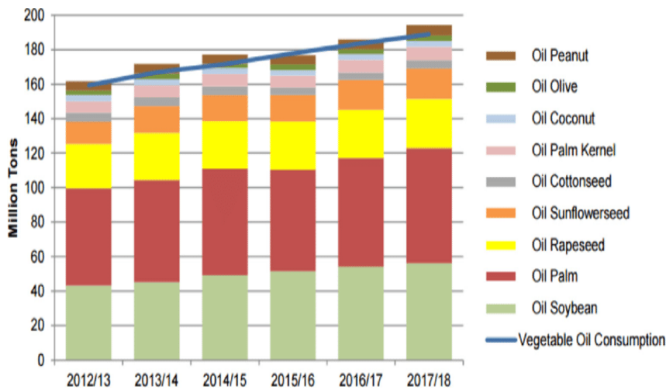
Figure 6: Global vegetable oil production and consumption [124]

3.2. Soybean Biodiesel Feedstocks

Soybean comes from the Glycinemax L. as a legume with an annual cycle from the Fabaceae family [130]. United states of America, Brazil and Argentina are the leading producers
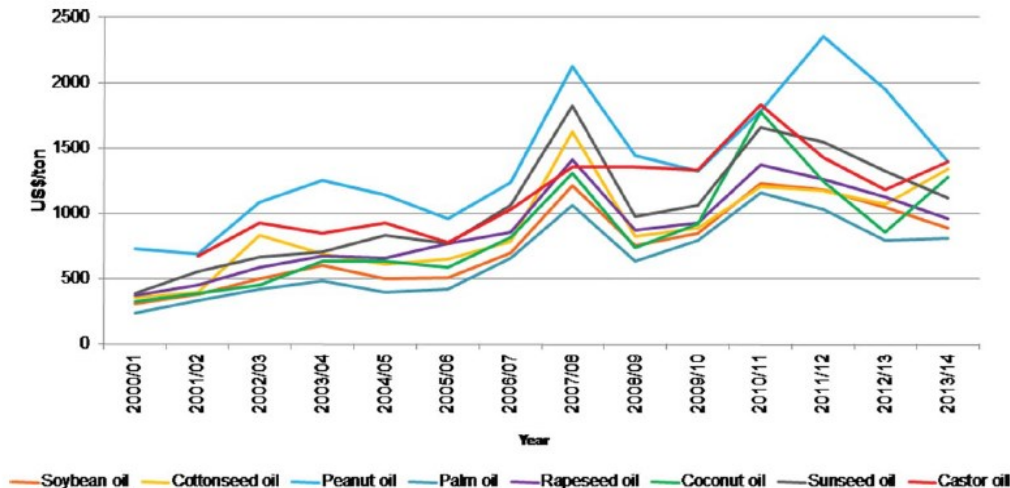
accounting for 80% of all global production [131]. However, china is increasing production and catching up, hence expanding its role in the near future considerably. It is important also to note that china imports almost 1/3 of the world's production of soybean. This accounts for 62% of all global soybean trade [132]. Soybean as a grain contains 14% to 17% oil, 33% to 40% protein [133]. In the period of 2013 to 2015 soybean was responsible for over 65% of the global supply of protein supplements and feeds [134]. Soybean meal is the extraction obtained from the oil extraction process and one of the most important source of human and animal protein [135-138].

Table 8: Shows major vegetable oil producers and their main source of feedstock [12, 125-129]

Country	Production (1000t)	Main feedstock
USA	4.150	Soybean (53%)
Brazil	3.000	Soybean (77%)
Germany	3.000	Rapeseed (>50%)
Indonesia	2.750	Palm oil (100%)
Argentina	2.550	Soybean (100%)
France	1.850	Rapeseed (>50%)
Thailand	1.050	Palm oil (77%)
Total Europe	10.200	-
Total world	26.150	-

In addition soybean extracts are used in the textile and plastic industry as molds, glue or adhesives for laminated paper and wood [139]. Soybean is also the main raw material in the vegetable oil industry, whose production by 2012 exceeded 40 million tonnes representing 25% of global production of vegetable oils [140]. Environmentally soybean compared to fossil energy consumption over the biofuel life ranges from 2 MJ/MJ^{-1} to 8.5 MJ/MJ^{-1} [141-143]. On the other hand, comparatively its GHG life cycle varies from 8 gCO$_2$e MJ^{-1} to 42 gCO$_2$e MJ^{-1} of biodiesel [143]. However, in the literature surveyed only one researcher reported higher values of 50 gCO$_2$e MJ^{-1} [142]. This was attributed to the assumption adopted during life cycle analysis hence the difference in the values of the findings [114].

Figure 7: International prices of vegetable oils from 2000 to 2014

3.3. Rapeseed Feedstocks for Biodiesel Production

Known scientifically as Brassica hapus L., rapeseed is also known as colza and one of the most cultivated crops globally only beaten in acreage by soybean [140]. Its main geographical origin is the Mediterranean area and northern Europe. Among the leading global producers of rapeseed include China, Germany Canada, India and France accounting for 65% of global production [140]. Table 9 shows Oil yield for major non-edible and edible oil sources and feedstocks.

In Europe rapeseed is the main plant biofuel source accounting for 55% of the total European production of biofuel feedstocks and 68% of global feedstock production in 2016. However, its market share has been slowly decreasing as more recycled oil and alternative feedstocks eat away its market share since 2016 [144]. Other usefulness of rapeseed is in the protein range and food supplements, rapeseed can be used as an animal feed for pigs, cattle, sheep and poultry [145, 146].

Table 9: Oil yield for major non-edible and edible oil sources

Type of oil source (feedstock	(kg oil/ha)	Oil yield (Wt %)	Prices (USD/ton)	Literature references
Jatropha	1590	Seed:35–40 kernel:50–60	370	[5,6]
Rubber seed	80–120	40–50	1250	[7][147]
Castor	1188	53	1600	[5,9][148]
Pongamia pinnata	225–2250	30–40	286	[8],[149], [150]
Sea mango	N/A	54	N/A	[9]
Edible oil Soybean	375	20	684	[5,11]
Palm	5000	20	600	[5,12
Rapeseed	1000	37–50	683	[5,13

Rapeseed meal is known to contain 34% to 38% protein with an oil range of 34% to 40% [151]. However rapeseed has an unpleasant flavor due to glucosinolates which sometimes lead to toxicity in combination with the enicic acid [152]. This is one of the major drawbacks especially on cost reduction in related industries even though utilization can be undertaken by processing [153]. As a source of feedstock rapeseed has low levels of saturated fats coupled to high levels of monosaturated fats with omega 3 and 6 making it a healthy source for human consumption [96]. As a plant feedstock rapeseed ensures a steady acreage yield at stable production over a range of time [154] while allowing intercropping. Compared to soybean, and palm oil, rapeseed performs well in emission studies for example it reduces smoke, PM, and UHC [155]. Environmentally, life cycle studies report a wide range of mixed results. Nevertheless it reduces GHG emissions from 85% to 40% and fossil energy use from 83% to 43% compared to petroleum fuels [156].

3.4. Palm Oil Feed Stocks

Palm originate in West Africa and is used as the main feedstock for palm oil production. Palm oil plant has a life cycle of 26 years [157]. Palm plant as a feedstock generates co-products of 20% to 21% oil, 17% kernel oil, 3.5% palm kernel cake, 22% to 23% empty fruit bunches, 12% to 15% fiber, 5% to 7% shells and 50% liquid POME [158]. Palm oil plants are natural in Central America, north and south. Palm oil is rarely planted commercially due to its low oil content. As such attempts have been made to breed Elaeis OLEIFERA and Elaeis guineensis species to improve disease resistance, palm tree height and increase unsaturated fatty acid [159].

Palm oil as a biofuel feedstock is one of the leading vegetable oils with over 50 million metric tonnes accounting for 30% of global palm oil production in 2013 alone. However, by 2017 the production of palm oil rose to 37.6% (70.3 million metric tonnes) [124]. Nevertheless, as a feedstock only 10% of its global production goes to bioenergy and biofuels [160]. The leading producers of palm oil are Indonesia and Malaysia which control 85% of global production [130]. Palm oil in south east Asia was introduced in Malaysia in 1870 from Singapore [161]. As a feedstock, palm oil has a number of uses considering its byproducts. For example palm oil is used in the food industry as butter, solid fats, cooking oil, industrial oil, baking oil or as a substitute for trans-fat [159, 162].

Additionally, palm oil is applicable in the cleaning, cosmetic, and soap and detergent production. In the chemical industry palm oil is used as a lubricant and in oil production [162]. In waste to energy reform, palm oil shells and fiber can be used in chain production of steam for electricity in co-generation systems. For example, in literature surveyed it was reported that for a palm tree bunch the energy is 300 kWh and 600kg of steam [163, 164]. In literature-surveyed palm oil as a biofuel feedstock has limitations which include; (i) Low supply of seeds, hence poor production [165], (ii) Lack of research in co-product industries and comprehensive economic data due to logistical issues [166], (iii)The long cycle of the palm tree growth [130].

3.5. Cotton Seed Feedstocks

Cotton which is known scientifically as Gosypium hirsutum L., comes from the family of Malvaceae and is grown globally for the production of fiber used in the textile industry [167]. Cotton comprises of 65% seed and 35% fiber [168], oleic acid 15% to 20%, stearic acid 2% to 5% [167], with major fatty acid being palmitic acid at 27.76% while linoleic acid stands at 42.84% [169]. Nevertheless cotton as a feedstock for biofuels has a low oil content at 16% to 23% but with breeding and selection researchers have observed an improvement of 5% in crop oil yield [170].

However, what is of great interest is the cotton meal, which is heavily rich in protein second only to soybean after oil, has been extracted. The cotton meal is mainly used as an animal feed although it has other vital uses such as being a fertilizer, food flour or as a dye in the textile industry and as a biodiesel feedstock [171-174]. Globally cotton is the ninth highest oil producing plant [175]. Despite its low oil content cotton is advanced as a biofuel feedstock due to lower smoke and particulate emissions compared to other feedstocks such as palm oil discussed in earlier subsection

[155]. Nevertheless it has limitation which include poor quality oil requiring pre-treatment hence increased cost of biodiesel production when used as a feedstock [114]. Figure 8 is showing a cottonseed oil sample after extraction from cotton seed.

Figure 8: A sample of cottonseed biodiesel layer of cottonseed oil [167]

3.6. Sunflower

Known as Helianthus annuus L and a dicotyledon, Its oil content varies from 38% to 50% based on the species of variety employed [176, 177]. Russia is the world leading producer of the sunflower crop with a 21% of the total global landmass, others include Ukraine at 12.97%, Argentina at 11.83%, China at 7.17%, Romania at 6.56%, France at 5.56% India at 4.77%, USA at 4.14% and Spain at 3.09% [178]. Globally sunflower covers an area of 23.7 million hectares with an annual production of 1322 kg/ha on an expected production of 2.3 tonnes to 2.5 tonnes/ha [179].

Beside its potential for oil, sunflower grain produces 250 kgs to 350 kgs of meal shell and 45% to 50% crude protein per tonne of grain [180]. The co-products of sunflower can be utilized for other uses such as in packaging materials, animal feeds, forage silage or as green manure or as a biofuel feedstock [181, 182]. Sunflower in the last decade has gained prominence as a feedstock, for example in Brazil 62000 tonnes were realized in the 2015 to 2016 season. However this was a decrease compared to the previous seasons due to a drop in the acreage under cultivation [183]. The introduction of new crops such as corn saw farmers shift to corn due to low cost of production of inputs and processing [184].

Sunflower is a good feedstock for biofuel due to its drought resistance to cold and heat conditions besides being less likely to be influenced by latitude, longitude or photoperiods [185]. As a feedstock sunflower can be grown in rotation with other plants (intercropping), which offers higher returns to farmers and producers [186]. The main limitations of sunflower as biofuel feedstock include High international market prices [134], besides a cloudy nature as temperatures drop due to its high wax content [187]. Additionally Sunflower contains linoleic, oleic and linoleic acids, which account for almost 70% hindering oxidative

properties, which offer stability, hence rapid lipid oxidation of its oil [188-190].

3.7. Jatropa Curcas

This is a plant cultivated almost globally for the production of biofuel although it is a non-edible plant. Jatropa seeds are composed of 37 % shell, and 63% kernel (dry matter) with a protein content of 35% and a 15% of oil [191]. Jatropa has been on the radar of biofuel developers and producers due to a number of factors. These include low production cost, Water stress tolerance, High oil content and yield, Resistance to pests and diseases; Resistance to drought, Good adaptability to semi-arid wastelands, hence reduces competition with food crops for arable land [36, 192].

Other uses of Jatropa as a feedstock include as a cooking fuel, insecticide, soap making, and for medicinal purposes [191]). Additionally Jatropa can be used as an organic fertilizer, livestock feed and a biogas feedstock [193, 194]. On the other hand, the limitations of Jatropa arises: From uncertainties around its seed yield range which is 2 to 12 Mg/ha leading to poor economies of scale for a feedstock [36]. Secondly, even when it seems adaptable to drought during flowering studies have shown it needs watering otherwise the yield drops significantly.

In other words, Jatropa capabilities are not exploitable and applicable simultaneously. This is evidenced by the moisture and nutrients influence on yield [195]. The third limitation is due to its vulnerability to viral infection [36, 196, 197]. The fourth limitation is due to lack of scientific validation regarding the basic ecological and agronomical properties. For example, yield, potential production and costs, and breeding programs have not been identified in the literature reviewed.

4. Introduction to Non-Edible Vegetable Oil and Emerging Feedstocks

The use of non-edible feedstocks for biodiesel production is an answer to the challenges of edible oil as biofuel feedstocks. Non-edible feedstocks are gaining attention, as they are easily available globally in wastelands in unsuited for food crops. This eliminates competition for food, reduction in deforestation rate and co-products. Although there is no direct competition for food versus fuel, Nevertheless, there is indirect competition for land. Among the non-edible plants used for biofuel production include; Cotton (Gosypium hirsutum), Castor (Ricinus curcas), Jatropa (Jatropa curcas), Rubber (Hevea brasiciensis), Mahua (Madhuka indica), Ethiopian mustard (Brassica carinata), Castannola (Terminalia catappa) [198-202]. Figure 9 is showing Waste cooking oil production based on country and global contribution.

In India, there are two major species of the genus, Madhuka longifolia and Madhuka indica, on the other hand rubber seed tree is mainly in Indonesia, Malaysia, Liberia, India, Sri-lanka, Sarawak and Thailand. Rubber as feedstock contains seed kernels of 40 % to 50% brown oil [203]. Another non-edible oil biofuel source is neem (Azadirachta Indica) a natural plant of the Indian subcontinent and commercially grown in India, Bharma, and

surrounding regions. Jojoba oil is another non-edible oil a shrub in southern Arizona. Therefore, in Literature reviewed non-edible oil studies as alternative biofuel feedstocks fill many researcher reports such as [44, 201, 204-207].
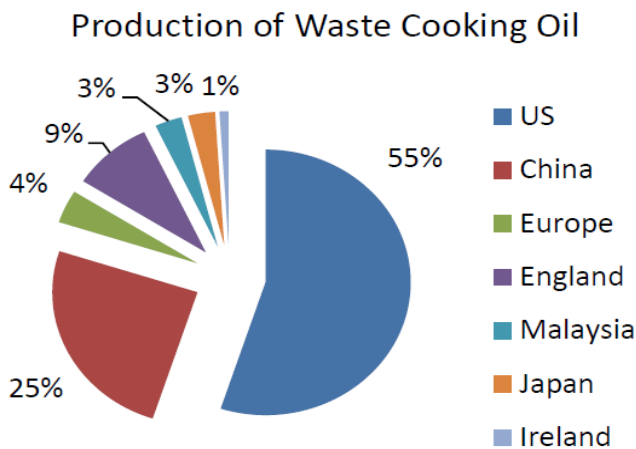
Figure 9: Waste cooking oil production based on country [10, 14-15]

4.1. Waste Cooking Oil Feedstocks

Waste cooking oil is also known as yellow grease due to the fact that most waste cooking oil FFA content is 8% to 12% wt. Waste cooking oil offers a high potential as a feedstock to biofuel production due to low cost. As modernization grows and more people shift to urban lifestyles the total quantity of waste cooking oil has been growing since 2008. Waste cooking oil can be collected from households and hotels and restaurants, fast food outlets with heavy use of frying activities [208]. The disposal oil from these activities is problematic as it contaminates ground water. However, their cooking oil sources differ greatly since their base material are plant lipids like corn, margarine, coconut oil, palm oil, olive oil, soybean oil, grape seed oil and canola oil. The most commonly used material for vegetable oil is palm oil [209].

The use of WCO as a biofuel feedstock does not come at the expense food versus energy or land resources. Instead it's a sustainable use of resources which reduces adverse effects of water pollution and blockage of water and drainage sewage system [210]. Presently WCO has been heavily utilized in soap manufacturing, although the soap produced is of poor quality hence its utilization has been low [211]. The main objective of using WCO is to transform it by reducing its viscosity to values close to diesel oil. Globally over 15 million tonnes of waste cooking oil are produced annually and if converted it can meet and satisfy the world demand of a biofuel feedstock [212]. Production of WCO oil as a biodiesel can contribute to a saving 21% in crude and a 96% energy saving [213].

Non-edible vegetable have potential to substitute a global fraction of petroleum diesel [214]. Plant oil feedstock when processed to biodiesel reduce particulate and sulfur emission and aromatic compounds [215] compared to petroleum diesel [216]. In 2009, the production of FAME waste oil was 11 tonnes with a

demand increase of 3.5 metric tonnes/year. However, the production of waste oil in Europe, north America and in selected Asian countries such as China combined had a production of 16.6 metric tonnes [217, 218].

For example in 2014, China alone had a total WCO production of 1.8Mtonnes [112], pushing China to 3.4 Mtoe hence accounting for 2.9 % of global biofuel production, distributed in 50 plants. In other words, currently, the main leading feedstock of biofuel production in China is waste oil. However its main limitation is waste oil increased prices due to rapid development of the biofuel industry in the last decade [219].

The use of waste cooking oil has a number of challenges due to FFA and presence of high moisture, which make it hard for transesterification. Although chemical and physical properties of waste cooking oil are similar to fresh edible oil they differ from source to source [217]. For example, the water content and FFA in WCO compared to fresh edible is higher due to the frying process. During frying edible oil undergoes higher heating temperatures of 160 °C to 200°C for a long and a sustained period.

As a result, increased viscosity specific, specific heat, surface tension, colour and fat formation occur. Hence reactions of thermolytic oxidative and hydrolytic nature are observed [220]. Nevertheless, current research centres in operation and management of waste to energy with the focus on the following two key areas. (i) The supply chain incentive, and (ii) regulation policies for WCO to energy.

There is a growing importance on the use of subsidies as a measure of addressing issues of waste to energy based on the model dynamics [221-229]. Regulation policies of waste cooking oil to energy report illegal transaction in waste cooking oil utilized as barriers to expanding WCO utilization. This need increases a requirement of standard inspection and regulations with dedicated infrastructure to help in recycling [223, 230, 231]. For example, in America in south California and north western Mexico [232].

4.2. Animal Fats Feedstocks

Tallow is the most common commercially available feedstock from animals for the production of biofuels [233]. The production of meat in the last decade increased significantly to 237.7 million tonnes in 2010 represented by 42.7%, 33.4% and 23.9% for pork, poultry and beef. Nevertheless, the projected growth of these resources increased steadily and now stand at 266909000 million tonnes annually [124]. This corresponds to a representation of 39.76%, 37.3% and 22.97% for pork, chicken and beef. However lard and chicken fat [234] are also commonly used in addition to insects and all other high fat containing animals.

The main reason for use of animal fats as feedstock source is due to their cheap and low prices, hence providing an economical option for biodiesel production [201, 233]. For example, since 2013 the prices of animals based fats has been $ 0.4 to $ 0.5/litre compared to vegetable oil at $0.6 to $0.8 [201]. In the world today 90% of feedstocks for biodiesel production originate from animal

fats and greases compared to the USA at 8% to 10% [235]. In other words from this report there is an observed dynamic animal protein and being expressive especially in the poultry production which shows an annual growth of 4% to 5% in the last decade [236].

Animal fats are characterized by a high content of saturated fatty acids and as biological lipid materials they are composed of TAGs and less of di (DAGs), and mono-acylglycerols (MAGs). Animal fats and greases tend to be solid at room temperature compared to liquid oil of plant origin. This is due to their high content of SFAs [233]. Tallow is a waste final product generated in slaughterhouses and meat processing facilities, whose major composition is myristic, palmitic and stearic acids with tallow and pork lard composition of 40% SFA.

However in the literature surveyed the composition figure is higher for tallow at 45.6%, mutton tallow at 61.1%, lard at 39.3% and chicken fat at 32% [207]. Saturated fatty acids present increased demerits on the physical and chemical properties of biofuels. For example fatty acids cause poor cold properties while unsaturated animal fat content offers advantages of high cetane number, oxidation stability and high calorific value [234]. Thus considering the composition of animals fats as a source of biofuel requires synthesis at elevated temperatures compared to processing vegetable oil [237]. Animal fat greases are classified into two types as reported in literature. This classification is based on the level of FFAs,[207] such as Yellow greases with FFAs of ≤15% w/w and Brown greases with FFAs >15%w/w.

In theory animal fats are thought to contribute to oxidative stability for biodiesel, due to the lack of polysaturated fatty acids such as linoleic and linolenic commonly found in vegetable oil [238]. However comparatively in real-life, animal fats are unstable due to lack of anti-oxidants in their structure. Hence use of animal fats and greases eliminates the need for disposal and result in utilization to the supply of biofuels [239]. Like all feedstock, animal fats have limitations, for example, animal fats contain phospholipid or gums, which are insoluble in water.

These precipitates can plug fuel filters and render them ineffective. Secondly animal fats oil biodiesel deactivates exhaust pre-treatment devices in diesel vehicles [238]. Thirdly is the problem of the presence of high sulfur content mainly from sulfur containing amino acids traced from animal feeds [240]. Since animal fats are highly viscous and solid at ambient temperatures due to unsaturated fatty acids. This leads to poor atomization properties, hence incomplete combustion, while increases emissions of pollutants and particulate matter [241]

4.3. Algae Oil Feedstocks

The microalgae family contains more than 100000 species which can be utilized for biodiesel production [242]. However the most one with the highest probability of development in literature surveyed are green algae, diatoms and cyanobacteria (blue algae)

[243]. Microalgae content is projected to hit 70% of dry matter and a yield of 90 tonnes/ha of cultivation [244].

Algae grow rapidly in different environmental conditions, while utilizing efficient use of water CO_2 and nutrients on the water surface [245, 246]. This requires if planted in a pond stirring becomes a necessity to ensure accessibility to CO_2 [247]. In addition to their faster growth and high yield content per acre, microalgae oil contains properties identical to petroleum fossil fuel. This is especially true for viscosity, density, flash point and the hydrogen carbon ratio [248].

Use of microalgae as an alternative fuel is being advanced as the fourth-generation biofuel as technology for producing and processing biofuels increases. This will enable its production as a biofuel to be cost effective for large-scale production in the near future. Microalgae compared to land-based plant feedstocks have efficient photosynthetic process in converting and utilizing solar energy into biomass [249]. The main algae, which can be utilized for the production of biofuel, are cyanobacteria as micro or macro algae.

Their sizes determine and influence the production process techniques. For example microalgae produce high oil content but their harvesting is costly due to low efficiency, cell size and low biomass concentration [250, 251]. On the other hand compared to cyanobacteria which are macroalgae the conversion rate into biomass is good but with a complex membrane rapture [252].

In the literature surveyed to produce algae it requires cell growing, separation, and lipid extraction [246]. The main microalgae growing technologies available vary but open pond and closed photobioreactors are commonly utilized [253]. In harvesting microalgae to extract oil physical chemical and enzymatic techniques are employed [254]. Processing of microalgae oil for biofuel production commonly takes the same route of processing and technologies used in vegetable oil and animal fats. It is important to note that fourth generation technologies for production of algal biofuels are still under research and development.

A number of questions remain unanswered. For example, in literature surveyed on algal feedstocks advantages and disadvantages of growing microalgae in fresh and salty water is not available in literature for all types of algae marked for biofuel production. Another factor noticed from literature surveyed is lack of feasibility studies whose data for biofuel microalgae is unavailable. For example, the cost of production for algae is projected at $0.9/kg to $2.55/kg in open pond systems compared to $1.5/kg to $5.5/kg using photobioreactors.

This is despite development in more realistic and appropriate technologies used for algae on commercial scale [243]. The methods utilized in the farming, harvesting and oil extraction for biofuel production still face surmountable difficulties. Nevertheless, microalgal diseases such as contamination are still not clear, although biofuel especially in chain and value addition offer high returns compared to other feedstocks [255]. If

technologies are developed for value addition such as on pharmaceutical, nutraceuticals, biodiesel commercialization etc. could increase economic viability of algal feedstocks for production [256].

4.4. Waste Biomass Feedstocks

A number of waste resources arise in line with the diverse human economic and social activities. However, utilization of natural resources such as water, air, soil etc. are being threatened. This solid biomass wastes take many forms either as solids. Although classified as waste they can be reused and turned into energy resources for industrial and domestic purposes [257]. In the current world energy scenario, a number of waste to energy, technologies have emerged. These technologies convert waste biomass into various forms of fuel before utilization as biodiesel [258].

Bio-waste feedstocks differ greatly from primary sources such as coal, in both energy content and physical properties. However compared to coal bio-waste comprise low carbon, high oxygen content, high silica and potassium, less aluminium and iron, low heating values, high moisture, low density per unit of mass and friability [259]. Figure 10 shows the Main waste to energy (WTE) technologies available currently for the utilization of biomass waste.
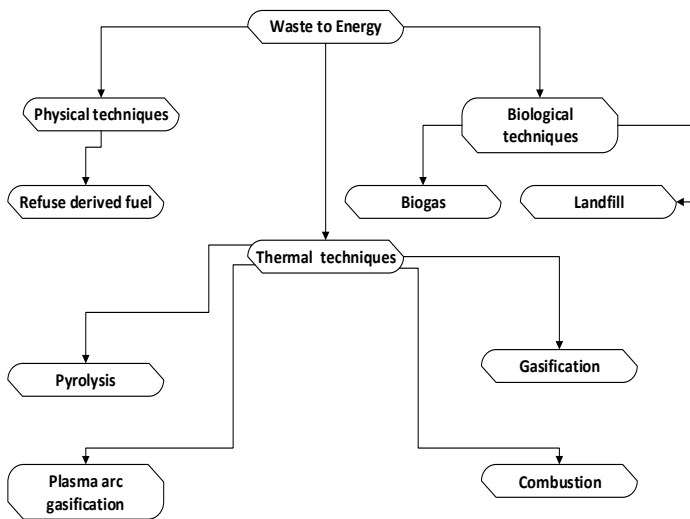
Figure 10: Main waste to energy (WTE) technologies adapted from [259].

However, utilization of natural resources such as water, air soil etc. is being threatened and takes many forms either as solids and can be utilized and reused to become energy resources for industrial and domestic use [260]. In the current world energy scenario, a number of wastes to energy technologies have emerged. These technologies convert waste biomass into various forms of fuel before utilization as a biofuel or biodiesel [259]. Depending on the use of the technology so is, the name derived.

For example in the literature surveyed technologies for fuel production are referred as waste to energy technologies (WFT) [259].The waste technologies include the following categories of utilization; Physical methods, Thermal methods and Biological

methods. Globally these technologies have grown to nearly 750 facilities with a capacity to process 140 million tonnes of waste annually [261]. Energy from waste can be treated and compressed to solid fuel or converted into biogas, syngas, or combusted to produce heating for steam production in power generation. The gases produced in such cases include methane, CO_2, hydrogen, and H_3CO or liquid fuels such as ethanol and biodiesel [262].

Biomass to energy has potential feedstocks, which form its main potential line. These include wood, short rotation wood, crop waste, agricultural wastes, short rotation herbaceous crops and animal waste [263]. It is important to note that biomass accounts for 35 % of all energy consumption in developing countries [264, 265]. Nevertheless, biomass utilization carries a huge untapped potential for environmental and energy production, especially agricultural based plants absorbs CO_2 during growth and emit it during combustion.

This helps in the recycling of CO_2 in the atmosphere hence climate change mitigation [266]. Since biomass feedstocks contain lignocellulosic materials, they inherently produce high content of polymers such as cellulose $(C_6H_{10}O_5)x$, hemicellulose (xylas) $(C_5H_8O_4)m$, lignin $(C_9H_{1[267]0}O_3(OCH_3)_{0.9-1.7]n}$ and sometimes protein. This contributes to renewable energy sources, which are natural, sustainable, inexpensive and eco-friendly feedstocks [260]. Wood biomass thus forms the bulk of waste biomass accounting for 64%, municipal solid waste 24%, agricultural waste 5 % and landfill gases accounting for 5% [268, 269].

4.5. Bioethanol Feedstocks

Bioethanol is one of the leading clean and renewable energy sources in the transportation industry today. Globally bioethanol has seen a growth from 4.8 billion gallons in 2000 to 16 billion gallons in 2007 [270], representing a 30 % increase within the mentioned period. However, current statistic trends paint encouraging prospects, indicating for example that since 2007 with global production of 60 billion litres of bioethanol, by 2017 the figures stood at 143 billion litres annually [271].

Bioethanol has many advantages compared to fossil fuels such as high octane, which prevents knocking in internal combustion engines and high oxygen content, which helps to produce less greenhouse gas effects [272-274]. This advantages Allows direct use of ethanol in the automotive industry for internal combustion SI engines without modification and bioethanol works with other oils as a blending agent.

Currently the USA and Brazil are the leading global bioethanol producers with the two countries combined contributing 75 % to 80 % of the total global production [270, 273]. Using corn grain the USA has 187 bioethanol plants spread across different states to produce ethanol [275]. On the other hand, Brazil produces bioethanol from sugar cane based feedstocks only, compared to the European Union who use wheat and sugar beets. In 2013, Brazil produced 37 billion litres compared to European

Union production of 5.785 billion litres of bioethanol and is expected to double its production in the near future.

Due to the reservation on plant-based feedstocks, in future renewable and sustainable feedstocks will dominate energy sources, hence replacing fossil fuels. Bioethanol has been a dominant feature of biofuels, nevertheless technology is moving to microalgae carbohydrates as potential feedstock [276-278]. Microalgae biomass feedstocks contain high contents of carbohydrates, (glycogen, starch, and cellulose) that through fermentation can be converted to sugars for production bioethanol [279, 280].

5. Factors Affecting Biodiesel Production

5.1. Biodiesel Quality

The quality of biodiesel of the feedstock used to produce a biodiesel determines the type of catalyst and process applied to produce FFA for the biodiesel production. Nevertheless, the biodiesel feedstock selection and determination are an important factor, inconsistence in the selection of feedstocks can lead to problems of quality and over-budget production. Suffice to mention that biodiesel fuels have standards recommended for their production such as ASTM D675 and EN14214. For example, feedstocks with more than FFA>3wt% cannot use homogeneous catalysts like NaOH, KOH or methoxide due to unwanted side reaction.

In order to produce biodiesel commercially the commonly used basic catalysts such as NaOH, KOH, or Methoxide are utilized. In addition, as a general rule acid catalyst are more appropriate for high FFA content feedstocks. On the other hand, homogeneous catalysts require less alcohol; have a shorter reaction time even though they result into complex products. This leads to required product purification compared to heterogeneous catalysed transesterification process. Development in catalysts has ensured use of a wide range of catalysts for biodiesel production such as heterogeneous and homogeneous acids, bases, sugars, lipases ion exchanges resins, zeolites etc. A number of researchers in the literature reviewed mention biodiesel quality as a factor influencing production include [135, 281-286].

5.2. Cost of Biodiesel Feedstocks, Investment and Material

Another factor that influences biodiesel fuel production is the higher cost of production arising from erratic feedstock prices as biodiesels gain widespread application. This is increased by the chemical composition due to their relatively low energy content increased NOx emissions compared to fossil fuels such petroleum diesel [287]. Price determination is an important factor of biodiesel production system and processing.

In every production system of biodiesel, a 50% feedstock price should be the guiding principle of all cost of production. Another factor to consider and is proposed in literature reviewed is price fluctuation especially when promoted through government policy shifts in relation to subsidies and tax incentives [8, 288, 289]. In other words when alternative sources

are promoted there is diversification and stock piling to create demand and stabilize stabilization [287].

A number of researchers have reviewed and reported on this concept and can be read in some references provided here such as [239, 290-295]. In all the literature surveyed there is agreement that the higher cost of biofuel production is a major barrier for acceptability and use of biodiesel as an alternative fuel [296, 297].

In literature surveyed, a number of suggestions thus come forward to address this issue. For example, use of cheaper alternatives catalysts Coupled to conversion technologies with lower energy input and faster transesterification reaction [201, 296, 298-301]. Another commonly suggested solution in literature surveyed is the diversification of feedstock by increasingly moving to material materials, not formerly considered as feedstock [302-304]. Figure 11 shows the effect of government policy and promotion to create demand and stabilize prices on palm compared to petroleum diesel.
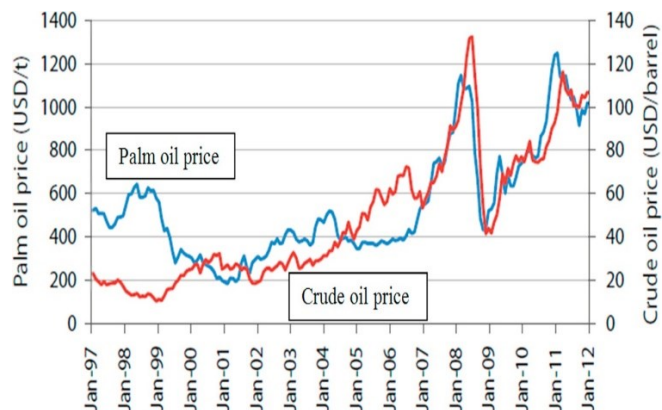
Figure 11: Effect of government promotion on price of feedstock price fluctuation 1997-2012 [305]

5.3. Effect of Tax Policy Subsidy and Regulation

In order to empower biofuels and bring them into mainstream economy as usable fuels there is need to implement laws and regulation. These laws should include taxes, policies and subsidies from government as incentives to develop this sector. Particularly in the area of enforcement which mostly needs guidance in order to improve the basic economics of biodiesel.

In the literature surveyed for example, European Union has proposed a renewable energy policy for transport fuels to ensure a viable expansion of the biofuel industry in the near future. As a result, the European Union introduced a blending target in their range of biofuels, which involved hitting a target of 5.75% to 10 % by 2020. Additionally, an amendment to the fuel quality service brought into service a mandatory 6% reduction of GHG by 2020 for transport fuels and non-road and transport engines [306].

Between 2000-2013 biofuels such as ethanol and biodiesel grew exponentially in terms of output from 64 million to 23 billion litters and 0.8 to 14.7 billion litres respectively [307]. For example the USA also crafted a renewable fuel standard program to increase the share of biofuels by 10 % by 2017 and beyond

since 2005 [308]. This increment in biofuel production is purely driven by government policy interventions. This is particularly so in the USA where financial incentives are almost guaranteed for producers [309].

Due to policy shift and incentives, a larger share of global biofuel market has been taken from ethanol to biodiesel in the market [310]. In other words, appropriate policies, tax, mandates and incentives can successfully drive growth of biodiesel. However, it is important to note that biodiesel incentives are distortionary in nature as biofuel use uniquely food crops and multiple feedstocks [311].

In other words, in 2006 for example 20 % of all USA corn production went to biofuels compared to ethanol. Although indicating a positive development in the growth of biofuel, this led to increased producer prices between 2003 to 2008 [312-315]. On the issue of regulation and GHG emission studies in literature reviewed, indicate a negative impact in reduction for specific types of crop feedstocks and their processing techniques. For example, this is revealed in studies conducted by researchers such as [316-318].

5.4. Competition with the Food Industry Chain

The increased biofuels production supported by the government policies interferes with food industry chain such as the oleo chemical industry. These industries use the same feedstocks as biofuels hence the rapid growth in the biofuel, which threatens their growth in the future. This is true considering the level of increased feedstock prices yearly. In other words, resource availability will be constrained hence causing a negative impact on the economic value of the food chain [288, 319, 320]. As the Competition for feedstock resources increases with greater incentives to encourage producers meet the demand. This leads to increased demand for resources and with it increased prices for land resources and prices for food [321].

In order to implement a sustainable biodiesel production strategy. The focus should not only be on reduction of GHG emissions but rather a complete package of policies, which support economic and environmental sustainability. However, one notes that the increased biofuel production from land resources and plant feedstocks is the leading cause of deforestation.

In recent trends governments defend their guidelines on implementation of sustainable policies on deforestation as is the case in brazil though it is not sustainable [288]. The second issue on sustainability is related to animal habitat destruction when deforestation is carried in large scale with some of these animals facing extinction [322]. This is due to replacement of virgin forests with plantations of plants such as palm oil. This can led to global warming especially in lower latitude areas while causing overcooling in high latitudes [323]. Use of biofuel in the transport industry when fully running is hoped to stabilize the global carbon cycle although deforestation will negate it. A practical example is in Malaysia where as a consequence GHG emissions increased to about 40 million tonnes of CO_2 up from 5 years earlier at 20 million tonnes of CO_2 [324, 325].

Another area that is often ignored in literature surveyed is change in land use, even with sustainable programs and policies. This problem is acute and severe in America, Mexico, and brazil where abuse of power forces farmers to sell land and move out leading to large population displacement and demographic changes [320]. However the European union seems to contain the problem by putting requirements for types of land to be used for biofuel production plantations as pointed in a number of literature surveyed such as [326, 327].

5.5. Biomass composition

In biomass composition, the most influencing factor is the carbon to hydrogen ratio. In other words, due to the differences in decomposition temperature for each of the constituents of biomass. These constituents thus undergo decomposition hence varying product yield. For example, in literature surveyed the following are the temperatures of the three main ligno-cellulosic biomasses [328-330]. This include Hemicellulose with a range of 150℃ to 350℃, Cellulose with a range of 275℃ to 350℃ and Lignin with a range of 250℃ to 500℃.

5.6. Particle Size

The particle size and composition, the physical structure and shape have a greater influence on the pyrolysis process products when exposed to heating [331]. For example, fine particles offer less resistance to escaping non-condensate gases and vice versa. This behaviour affects product yield [332]. In other words, size reduction of biomass before product extraction offers greater surface area for mass transfer. This enhances diffusion of the active components within the feedstock [333]. In literature surveyed, most scholars report these factors as variables in optimizing bio-oil production. Among the scholars who take this position, include the following researchers [334-337].

5.7. Effects of Temperature on Pyrolytic Process

Temperature is an essential factor of influence on pyrolytic product yield. Pyrolytic temperature defines the rate of increase from ambient to maximum until the completion of the process. Pyrolysis temperature thus influence composition and product yield and release rate of the constituent gases. Besides these components, the char produced depends on the pyrolysis temperature [336, 338, 339].

In other words, as the temperature of the reactor increases, the carbon content of the pyrolytic char products increases. This is due to the increase in surface area of the char. However beyond 1173k the temperature decreases slightly due to structural ordering and micropore coalescence with increasing temperature for char above 1073k [340, 341]. Increased heating rate results into a decrease in the carbon content while increasing hydrogen and oxygen content of the char [342].

In literature, surveyed pyrolysis takes many forms of processing but four forms of the criteria are critical namely: Slow

pyrolysis, which is a carbonization pyrolytic process with a primary goal of producing charcoal and char. This is the oldest form of pyrolysis operating at below <400°C over an extended period. Fast pyrolysis is tailored for liquid or bio-oils where biomass is subjected to rapid high temperature heating before decomposition begins. The rate of temperature increase can range from 1000°C/s to 10000°C/s. Nevertheless, the peak temperature is maintained between 650°C to 1000°C. The main features of fast pyrolysis are high heating rate, reaction temperatures of 425°C to 600°C, short residence time (<3s) and rapid cooling of the gas product.

Flash pyrolysis where rapid heating of biomass occurs in the absence of oxygen at moderate temperatures of 450°C to 600°C. In other words, the products of both condensable and non-condensable gas leave the reactor unit faster (short residence time) of 30ms to 1500ms [331]. Ultra-rapid pyrolysis, which borders on the extreme fast mixing of biomass with heating and a carrier solid leading into high transfer of heat and rate of heating. Ultra-rapid pyrolysis utilizes temperatures of 1000°C for gas components compared to 650°C for liquids in order to minimize product yield [343, 344]

5.8. Effect of Heating Rate Change

It is important to note that the heating rate of biomass particles from rapid to moderate 400°C to 600°C leads to high volatile yields by producing more char [345]. Owing to fast volatile material release which causes internal pressure and coalescence of smaller pores leading to increased surface area [346]. A number of scholars have studied this phenomenon and reported on it widely such as [347-349]. Nevertheless in literature surveyed it is widely reported that high heating rates of 900°C, a lower surface area is produced and vice versa [350]. In other words higher heating rates cause high char yield interior temperatures, partial graphitization and curtails development of large surface areas [351].

5.9. Effects of Residence Time

Residence time Space is inversely proportional to space velocity of the reactants in a pyrolytic reactor [352]. In other words, residence time has a greater impact on conversion and product yield in the pyrolysis process. Studies conducted on biomass gasification from kinetic models report positively on this influence of residence time. For example, the following researchers report how conversion increases in the first 20s and their after the chemical reaction slows down as reflected in a number of studies such as [353-356].

6. Biodiesel Production and Processing Techniques

6.1. Introduction to Production and Processing Techniques

Biofuels have increased in demand as the global energy demand grows significantly, although with a requirement for clean fuels [297]. Biofuels are degradable and promising fuels compatible with environment preservation and biodegradable [297]. Although biodiesel is advantageous as a biofuel, its major

hindrances are high cost of production, processing and raw materials (feedstock). These costs account for 80% of the total cost of production, making biodiesel more expensive than fossil fuels which it is intended to replace [357]. However, one of the most glaring advantage of biodiesel is its use without modification for diesel-powered engines. Biodiesel use reduces emissions of PM, sulfur, UHC, and carbon monoxide due to a high oxygen content and carbon to hydrogen ratio [358, 359].

In literature surveyed a number of researchers have used many production and processing techniques. However, it is clear from the studies that feedstocks dictate and influence these techniques of production and processing. For example, thermal cracking (pyrolysis), catalytic cracking, Nano-catalytic processing, catalytic hydrocracking, micro-emulsion using solvents and surfactants, transesterification, bio-catalysis processing supercritical production processing.

The following literature references shows extensive work that has been done and reported in modern production techniques as knowledge and skills increase in biofuels; [205, 222, 360-365]. Nevertheless, the number of production methods has been increasing as the material science and biochemical-engineering sections grow. This has brought new and novel concepts as will be seen in the preceding sections of this review.

6.2. Biodiesel Thermal Cracking (pyrolysis)

Thermal cracking's main role is to decompose, rearrange and combine hydrocarbon molecules through application of heat. In other words, thermal cracking decomposes high molecules-weight hydrocarbon components into lower molecules weight. This makes the products more valuable hydrocarbon derivatives with lower boiling point species [366], such as gas liquids and char. Pyrolysis as a thermochemical decomposition process has similarities or overlaps with other processes such as carbonization, dry distillation, devolatilization, destructive distillation and thermolysis.

Nevertheless thermal cracking (pyrolysis) is similar and identical to gasification process [332]. Gasification is more external with chemical reactions compared to pyrolysis, carried out in low temperature settings of 300°C to 650°C or higher temperatures of 800°C to 1000°C. The main factors, which influence the process of thermal cracking, include feedstock type, residence time, operating temperatures and pressure. Many of this factors in literature reviewed are discussed and their influence on thermal cracking processes. However, these factors are discussed here briefly but further reading can be done from the references provided here in this section. The process of cracking alternative oils mainly vegetable or animal oils takes two main forms as mentioned in the following references [367-369].

Primary cracking where decomposition of triglycerides molecules occurs, forming acid species by breaking C-O bonds of the glycerides and triacyglycerides chain. Secondary cracking which involves degradation of the produced acids in the primary stage while forming hydrocarbons with properties identical or

similar to petroleum derivatives. The initial products of pyrolysis are condensable gases and solid char. However, further classification of the gases brings a non-condensable class such as CO, CO_2, H_2 and CH_4, liquid and char. In other words, this processes go through gas phase homogeneous reactions, partly gas solid phases heterogeneous reactions [332].

6.3. Chemical Catalysis Production Technologies

Chemical catalysis is the science of materials, which accelerate chemical reactions without affecting the equilibrium position of the thermodynamic reaction. Under this method which mostly describes use of catalysts both alkali and acid in the transesterification process. Transesterification has become a more popular method due to its versatility and ease of use [370]. This scheme utilizes triglycerides by reacting them with alcohol in the presence of a catalysts to produce biodiesel (FAME) which is a type of biofuel [371]. Once transesterification process is completed it produces glycerol by products of the process [372].

Transesterification process comprises of sequent reversible reactions. The first step is the conversion of triglycerides to form diglycerides. Followed by the conversion of the diglycerides to monocerides and glycerol and producing one methyl, ester molecule. It is important to note that the transesterification process is heavily dependent on external catalysts to perform reactions. For activation catalysts in transesterification takes two main forms either biological or chemical.

The chemical catalysts comprise of both alkali and acid catalysts as homogeneous agents [373, 374]. Namely, Heterogeneous agents' solid acid or solid alkali, Heterogeneous Nano-catalysts, Supercritical fluids (catalysts). On the other hand, biological catalysts come up through genetic engineering and are mostly preferred. This type of transesterification packs an environmental advantage over all other methods as reported by researchers such as [375-377]. However since it is still under research and development, the cost is prohibitive for commercialization and laboratory use [378].

6.4. Transesterification Biodiesel Production Techniques

Transesterification is a process in which none edible oil chemically react with alcohol. It is an imperative process for the production of biodiesel as it reduces biodiesel viscosity of feedstock oil closer to petroleum diesel viscosity [379]. The catalysts used during transesterification are either acidic (sulphuric acid, hydrochloric acid or phosphoric acid) or could be base catalysts such as NaOH, KOH, carbonates and Alkoxides [380]. Base catalysts (alkaline bases) are suitable for oils with FFAs below 3-wt % [381, 382].

Due to their less damage to equipment and efficiency in production, alkaline catalysts are preferred to acidic catalysts in transesterification [383]. During processing in transesterification, it is assumed that 100kg of glycerol will form a cubic meter of biodiesel [166]. This means a large portion of the by-products of the production of biodiesel causes concern to environmentalists. Hence, a number of studies in literature surveyed have studied on how to utilize glycerol, which is a major by-product of this process. For example, a number of researchers have proposed use of glycerol in the hydrogen reaction reforming processes as aqueous or vapour [384-386].

Utilization of glycerol is hailed as a breakthrough in lowering production costs which make biodiesel fuels expensive [387]. In the production of biodiesel 10 %, w/w is glycerol, which translates to every gallon of biodiesel, produces approximately 1.05 pounds of glycerol. For example in a 30 million gallon production plant per year, glycerol is 11500 tonnes. Therefore presenting an opportunity for new application and value addition processes in the commercial and chemical industry. Nevertheless, this area in research is aging behind in terms of data and experimental work, with few researchers having published reviews. Other uses of glycerol identified in literature surveyed include: Glycerol can be used in the production of animal feeds [388]. Glycerol feedstocks are good for chemicals production for example poly-hydroxyalkanoates (PHA), and docosahexaenoic acid (DHA) [389-391]. Glycerol can be used in the production of lipids for sustainable biodiesel feedstock production [392, 393], and in the manufacture of citric acid through biosynthesis [394, 395].

The commonly used alcohols in transesterification reactions include methanol and ethanol due to their low cost and availability. This reaction of alcoholysis reduces viscosity of nonedible oil converting it into triglycerides esters [396]. In other words, transesterification converts the carboxylic acid esters into carboxylic esters. The critical lipid in transesterification include non-polar lipids, triacylglycerols (TAGs) and free fatty acids (FFAs) [397]. There are two main forms of executing transesterification, either through catalytic transesterification or through non-catalytic transesterification [204, 398].

Nevertheless there are two main challenges in literature surveyed related with these two techniques. For example it takes longer time to process biodiesel and there arises a need for separation of the oil alcohol catalyst and the impurities from saponification in the mixture [399]. Therefore, a number of factors, which affect the transesterification process according to literature, surveyed. This factors include such as Reaction temperature, Ratio of alcohol to vegetable reaction, Catalyst used, the mixing speed (intensity of mixing) and Purity of reactants.

6.5. Emulsion and Microemulsion Biodiesel Production Techniques

Emulsion or micro-emulsion processes upgrade commodity fossil fuels by forming emulsion and micro-emulsion fuels. Micro emulsion also upgrades oil from other sources or feedstocks such as bio-oil without the help of a surfactant [400, 401]. Emulsion also helps in reducing problems associated with stand-alone bio-oils, hence reduced pollutants in emissions [402]. Emulsion as an upgrading of fuel method ensures that all the components of emulsion are utilized as fuel resources compared to other techniques discussed in other sections in this review.

Emulsion is among the key techniques that solves the problem of performance and emissions prevalent in internal

combustion engines especially diesel propelled ones. This technique is a solution that relies heavily on modification of fuel so that it reduces or eliminates engine modification and redesign. Globally many countries have fuel mandates specifying quantity and type of biofuel to use although the percentages may vary from country to country [403, 404]. For example water emulsion in diesel fuel is regarded as the most economical and effective method to reduce PM and NO$_X$ emissions [405]. Emulsion in diesel fuel extends the combustible limit compared to using non-emulsified diesel fuel. This is due to the reduction of combustion temperature as the water in the mixture has a higher specific heat capacity resulting into secondary atomization as the water droplets explode in the combustion chamber [406-408]. Table 12 showing the properties, droplet size, stability, visual appearance, composition components of emulsion and micro-emulsion.

6.6. Blending and Hybridization

Blending in biodiesel production refers to mixing or combining two or more feedstocks into a final product with superior quality and desired characteristics. The blending process has a significant influence on the product homogeneity, as the biodiesel product is denser than petro-diesel besides their differences in cold flow properties. Blending of fuels depends

largely on ambient temperature because in cold weather blending may present with challenges or fail in its objectives. There are two basic methods of blending (i) splash blending (either in a tank or in a truck), (ii) in-line blending which includes sequential blending, ratio blending, hybrid blending or side stream blending [409, 410].

Biodiesel hybridization is a new concept that has come up in the study of biofuels. Hybridization is a chemical process of two or more different feedstocks comingled in varying proportions in the production of a new hybrid fuel possessing different physico-chemical properties. Since fuel properties and the physico-chemical configuration of each feedstock vary from source to source, hybridization improves and enhances these properties.

Therefore, the combination of different feedstocks' (hybridization) enhances and improves properties of the initial parent stock, by adapting to improved and high attributes. It is important to mention here that both blending and hybridization cab be *ex-situ* or *in-situ* (the former means after production while the later means before production of biodiesel). Secondly both hybridization and blending produce fuel blends with intermediate properties able to improve combustion and emission characteristics when applied in internal combustion engines [411].

Table 12: Comparisons between emulsion and Microemulsion

Properties	Droplet size	Stability	Visual appearance	Composition	Production	Interfacial tension	Energy input	Chemical reagent Cost
Emulsion	1 µm - 10µm	Kinetically stable, thermodynamically unstable	Translucent, anisotropic	Water, oil, small amount of surfactant , no co-surfactant	Mechanical agitation, ultrasound	Low	High	Low
Microemulsion	1nm - 100nm	Thermodynamically stable	Transparent, isotropic	Water, oil, large amount of surfactant, and sometimes co-surfactant	Produced spontaneously without extra energy	Ultralow	Low	High

Table 13: Potential biodiesel yield from triglyceride feedstocks

Source	Annual yield, gallons/Acre	Reference
Corn	18-20	[416, 417]
Cotton	35-45	[152, 418-421]
Soybean	40-55	[152, 415, 418, 420, 422]
Mustard	60-140	[415, 423]
Camelina	60-65	[423-425]
Safflower	80-85	[420, 426, 427]
Sunflower	75-105	[428-430]
Canola	110-145	[431-433]
Rapeseed	110-130	[235, 434, 435]
Jatropa	140-200	[436-439].
Coconut	250-300	[434, 440, 441]
Palm oil	400-650	[294, 442-444]
Algae	>5000[a]	[445-447]

7. Biodiesel Composition and Physicochemical Properties

7.1. Introduction

There is a renewed and continuous increase in the use of biodiesel globally. The composition of biodiesel plays a critical role in dictating physical and chemical profiles of biodiesel FAME materials. A number of researchers such as [215, 412] have investigated this phenomenon. Greenhouse gases, (GHG), have accelerated this global warming, which has caused climate change. The other factor is due to a growing demand and desire to go green by using sustainable energy sources (renewable).

Another important factor fueling biodiesel research and development is energy security domestically as the demand for liquid fuels and supply grows in a fast-changing landscape. In the last decade, a number of countries have embarked on legislative and regulatory pathways to encourage production and use of biodiesel fuels. For example, in the USA using both prescriptive volumetric requirements and incentives.

The energy independence and security Act (EISA of 2007) required 0.5 million gallons/year for biomass-based biofuels to be increased to 1 billion gallons/year by 2012 a target, which has been surpassed [413]. Although biodiesel fuels have a wide variety of feedstocks depending on the geographical location, however the dominant feedstocks are soybean in the USA, rapeseed in Europe and palm oil in South East Asia [414, 415].

Nevertheless, the list of feedstocks is growing to include non-traditional feedstocks such animal fats and lard, used cooking oil, used engine oil, microalgae, municipal solid biomass, canola, coconut, Jatropa, sunflower, safflower, camelina. Table 13 showing Potential biodiesel yield in gallons per acre from triglyceride feedstocks and their references.

In literature, surveyed biodiesel fuel produced contains different varieties of individual FAME species. Nevertheless, a particular feedstock in the literature surveyed could dominate within a FAME species. FAME and FA are classified according to two categories; the first naming uses the number of carbon atoms in the FA chain. The second naming uses the number of carbon double bonds in the chain [414]. Among the 13 commonly found species in literature surveyed, there are 5 species which are dominant and are majorly derived from vegetable and animal fats and include the following; Palmitic acid (16:0), Stearic acid (18:0), Oleic acid (18:1), Linoleic acid (18:2), Linolenic acid (18:3). Table14 is showing the most commonly found fatty acids in the literature surveyed, their common names, formal names, molecular formula and molecular weight.

In biodiesel, composition FAME produced through transesterification is composed of exclusively of even numbered FA chains. It is important to mention here that FAME composition is not limited to vegetable and animal oil feedstocks but includes also algal derived lipids [448]. However, using the hydro-processing on biodiesel alters the FA chain irrespective of feedstock source to odd numbered FA chains. This is due to the removal of one carbon molecule during production of the biodiesel and has been reported in literature significantly by researchers such as [414, 449].

Table 14: Typical fatty acid (FA) groups in biodiesel

Common name	Formal name	Abbreviation	Molecular formula	Molecular weight
Lauric acid	Dodecanoic acid	12:0	$C_{12}H_{24}O_2$	200.32
Myristic acid	Tetradecanoic acid	14:0	$C_{14}H_{28}O_2$	228.38
Myristoleic acid	cis-9-tetradecenoic acid	14:1	$C_{14}H_{26}O_2$	226.26
Palmitic acid	Hexadecanoic acid	16:0	$C_{16}H_{32}O_2$	256.43
Palmitoleic acid	cis-9-hexadecanoic acid	16:1	$C_{16}H_{30}O_2$	254.42
Stearic acid	Octadecanoic acid	18:0	$C_{18}H_{36}O_2$	284.48
Oleic acid	cis-9-octadecenoic acid	18:1	$C_{18}H_{34}O_2$	282.47
Linoleic acid	cis-9,12-octadecadienoic acid	18:2	$C_{18}H_{32}O_2$	280.46
Linolenic acid	cis-9,12,15-octadecatrienoic	18:3	$C_{18}H_{30}O_2$	278.44
Arachidic acid	Eicosanoic acid	20:0	$C_{20}H_{40}O_2$	312.54
Gondoic acid	cis-11-eicosanoic	20:1	$C_{20}H_{38}O_2$	310.53
Behenic acid	Docosanoic acid	22:0	$C_{22}H_{44}O_2$	340.60
Erucic acid	cis-13-docosenoic acid	22:1	$C_{22}H_{42}O_2$	338.58

Among the commonly found FAME majority are dominated by C18 compounds although a few have lighter compounds C12 such as coconut and palm oil with C16. Feedstocks dominated by C18 have their relative saturation at 18:0, mono-saturated at 18:1 and di-saturated at 18:2. Plant based feedstocks such as rapeseed and canola contain 18:1. Corn and safflower, soybean and sunflower 18:2, Jatropa and yellow grease have similar values 18:1 and 18:2. However, Camelina in literature surveyed contains the highest level at (18:3) while Jatropa has lignocenic acid level of (24:0).

The physicochemical properties of biodiesel are determined by the compositional profile. The physicochemical properties of biodiesel vary substantially as with feedstock source [450, 451]. Due to higher oxygen, content (11% or more) biodiesel fuels have a low carbon to hydrogen content compared to fossil diesel. This gives biodiesel a 10% lower mass to energy content, but due to high density the biodiesel volumetric energy content drops about 5-6% compared to fossil diesel.

In other words, biodiesel has increased molecular weight compared to fossil diesel, reflected in the high distinction temperature (T90). Another important property exhibited by biodiesel fuel is good and excellent cetane number due to the straight chain esters compared to NO_2 fossil diesel octane 93. Biodiesel fuels also especially renewable contain paraffinic hydrocarbons, dominated by odd carbon numbers [452-454]. Lastly comparing biodiesel viscosities with fossil diesel show higher values by a factor of 2 when compared to fossil diesel [455].

7.2. Kinematic Viscosity

Viscosity of a biodiesel fuel is a critical property. Viscosity plays a key role in the spray quality, mixture formation and ultimately influences the entire combustion process. In other words high kinematic viscosity interferes with the entire injection process thus leading to insufficient fuel atomization hence poor engine combustion and performance. The mean diameter of the atomized fuel droplets sprayed by the injector and their penetration increases as viscosity increases [456, 457]. Additionally high viscosity leads to rapid pressure rise in injection pumping system thus leading to advanced injection timing [458-462].

Among the leading problems associated with viscosity of fuel, include: Inefficient mixing of fuel which results into incomplete combustion [463]. Early injection due to the high line of pressure thus moving the start of combustion (SOC) closer to the top dead centre (TDC). This increases the maximum mean effective pressure leading to combustion chamber elevated temperature hence increased NO_X emissions in biodiesel blends and fuels [464, 465]. As a property of fuel, viscosity is directly linked to the chemical structure of the fuel composition.

For example viscosity has been reported to increase as the carbon length increases and decreases with increased saturation (number of double bonds) of the biodiesel [214, 466]. Another important fuel property linked to the chemical structure via viscosity is the heat content (also known as the calorific value of a fuel) for both the feedstock and the biodiesel. For both the feedstock and biodiesel, the values increase together, in other words the heat content and viscosity increase or decrease together [214, 467].

Viscosity also is connected to the type of feedstock, for example, the viscosity of fats and greases is higher compared to vegetable oil sources. This is due to different saturation levels of the feedstock, which has been reported by a number of researchers such as [235, 468, 469]. Viscosity values for vegetable oil based feedstocks vary from between 27.2 mm^2/s to 53.6 mm^2/s compared to vegetable oil methyl esters at 3.6 mm^2/s to 4.6 mm^2/s. This phenomenon is due to the process of transesterification [470]. Nevertheless, despite this variation in viscosity due to feedstocks, biodiesel fuels have values relatively within specifications of prescribed standards.

7.3. Biodiesel Density

Density is described as the unit of mass per unit area. The density of a biodiesel causes the break-up of fuel injected into the engine cylinder. In other words, as the density of a fuel sample increases the mass of fuel-injected increases. However, regardless of the feedstock used to produce biodiesel oil all biodiesel are high in density compared to fossil diesel [215, 471-473]. The density of a fuel and its compressibility hold a very high influence in diesel engine fuel injection systems. Density thus influences the injected mass injection timing and the injection spray pattern.

These are critical parameters in biodiesel fuel and engine combustion behaviour [464, 474]. In other words, increasing the density increases the diameter of the droplets injected and considering the high inertia of heavier fuel droplets, this increases their penetration as denser fuel requires a shorter injection duration [456]. The speed at which the injected fuel spray penetrates across the combustion chamber determines air utilization and fuel /air ratio mixing rate [475].

Low-density fuel paired with low viscosity fuel when injected provides better and improved atomization and diffusion of the spray, which is an important factor in emission reduction and control. Atomization of the injected liquid fuel mass in the combustion chamber is important. Its importance is in the number of droplets, which are necessary for creating a large surface are for the liquid fuel to evaporate. This is governed by injection parameters and the air/fuel properties [475]. Density is also linked to the calorific value (heating content) of a fuel [214]. For example in literature reviewed density is shown to correlate to PM and NO_X emissions and reported by many researchers in different experimental works such as [476-478].

The carbon chain and the level of saturation affect the density of fuel. In other words, these two factors can increase or lower density considerably depending on their interplaying factors. For example, biodiesel produced from fats and greases tend to be more saturated compared to vegetable oil. An increase in density for example from 860 kg/m^3 for vegetable oil methyl ester (biodiesel) increases the viscosity from 3.59 mm^2/s to 4.63 mm^2/s [470] Hence, fats and greases produce high-density oil compared to vegetable based feedstocks. Nevertheless as alluded earlier this increase in density due to the difference in feedstock falls within acceptable standards a factor that has been reported in literature reviewed for example [479, 480].

7.4. Cetane Number

A cetane number in any given fuel is a primer indicator of the fuel ignition quality, which is the same as octane rating in SI fuel. The cetane number measures the knock tendency of a diesel fuel of biodiesel as a function of ignition delay. Although the cetane number is dimensionless, it is generally understood that ignition in compression ignition engines depends on self-ignition of the fuel.

Cetane number has been included as a fuel quality in biodiesel standard and placed at 47 as the minimum for neat biodiesel using ASTM standard. The cetane number also measures the readiness of a particular fuel to auto ignite when introduced into the combustion chamber for combustion. Hence the cetane number is a parameter that is directly proportional to ignition delay in IC engines [481].

Another general assumption made with cetane number is the conceptual generality of the octane scale for gasoline with petrodiesel cetane scale. For example high iso-octane as a primary reference fuel (PRF) has an octane rating of 100 compared to n-heptane at 0 [482]. On the other hand, the cetane scale the long

straight chain hydrocarbon hexadecane ($C_{16}H_{34}$) is used as a PRF with an assigned CN of 100 compared to the highly branched hepta-methylnonane ($C_{16}H_{34}$) at 15. This confirms that branching and length of the carbon chain influence the CN [481]. In other words, increasing branching decreases the chain length hence the CN number also decreases or becomes smaller.

Ignition delay is a period between SOI and SOC. Ignition delay is heavily influenced by engine design parameters such as compression ratio, injection rate, injection time, inlet air temperature and fuel composition and fuel properties. As the cetane number increases, it directly decreases the ignition delay while increasing the phase combustion in diffusion-controlled combustion. Higher cetane numbers result into shorter ignition time. In other words, high cetane numbers reduce injection time, SOC and rapid pressure rise in diesel engine combustion ignition quality varies depending on the density, thus causing trouble during cold start and low load engine operating conditions. Other effects include long ignition delay, leading to increased and rapid pressure rise and high maximum combustion pressure factors, which are not desirable leading to rough engine operation.

In diesel engines, ignition knock is not desirable as it causes engine knock. Among influential effects of cetane number, cold flow and cold starting properties is the increase in smoke and engine noise emissions if found to be low. On the other hand, high cetane number causes SOC close to the injector nozzles hence overheating and nozzle premature failure. Secondly, it increases heat, and traps solid coated particles hence plugging the injector nozzles [472]. Because of this behaviour, a number of literature surveyed, limit the cetane number to below 65 [475]. Additionally a number of studies in literature surveyed on the effect of high cetane number report a correlation with reduced emissions [483-485]. For example smoke, UHC, NO_X emissions reduce, with high CN. This has led to increased efforts to improve biodiesel fuel cetane numbers using additives or cetane improvers [463].

7.5. The Bulk Modulus of Compressibility

The bulk modulus of compressibility of a biodiesel explains and provides critical information on the number of spaces in biodiesel fuel molecules. The bulk modulus of compressibility also measures how much the biodiesel oil molecules can be compressed [486]. Although its measurement is difficult in liquids such as biodiesel, the measurement is obtained from the speed of sound and density of a biodiesel using the Newton-Laplace equation. This model utilizes estimates from a number of carbon and double bond of FAME in their chemical structures [487-489]. This is represented in Gibbs free energy (as shown in equations 10 and 11.

$$lnk_s = lnA' + \frac{\Delta Gk_s}{RT} \qquad (10)$$

where

$$k_s = \frac{1}{v}\left(\frac{\partial v}{\partial p}\right) s \text{ or } u^2 = \frac{1}{k_s\rho} \qquad (11)$$

In other words, the bulk modulus of a biodiesel fuel is the reciprocal of its compressibility. This is the fractional change in volume per unit change in pressure P.

where

K_s is the isentropic compressibility (Pa^{-1})

u is the speed of sound ($m.s^{-1}$)

P is the density in $kg.m^{-3}$

The bulk modulus of compressibility is a critical property in hydraulics such as biodiesel as it affects the hydraulic behaviour of fuels during injection hence its dilation [490]. The bulk modulus of compressibility is associated with the increase in NO_X emissions in diesel and biodiesel variants. High NOx emissions produced by neat and blended biodiesel are linked to low Ks compared to fossil diesel. This has been reported in a number of literature surveyed such as [491-495]. In Studies by [496], the authors established a linear relationship between isentropic compressibility of blends of biodiesel and NOx emission characteristics.

Therefore, the bulk modulus variation within the fuel composition and molecular structure is critical especially in biofuels, which are alternatives to fossil diesel. For example in literature surveyed, a number of experimental studies have been conducted in bulk modulus on biodiesel as alternative fuels and ULSD (Fisher Tropsch) [458, 497, 498]. This studies report advances in injection timing with use of biodiesel and ULSD fuels mainly due to the bulk modulus of compressibility and increased speed of sound. This leads to an earlier needle lift for in-line pump delivery systems [460, 499-502]. It is important to note that advanced injection timing in biodiesel and retarded timing in ULSD increases NO_X as the blend ratio increases with the blend sample and vice versa [503, 504].

In the literature surveyed on the bulk modulus of compressibility there are a number of models used by different authors to estimate the speed of sound in biodiesel. Nevertheless, only two models are commonly used an Example of these authors who have conducted experimental work include [505-509].

7.6. The Calorific Value

The calorific value otherwise known as the energy content is energy per unit mass or the volume consumed during the process off combustion to give maximum energy output. The calorific value is also known as the heat of combustion and is numerically equal to the enthalpy of reaction [510]. The calorific value is measured using a bomb calorimeter under ASTM 2015. It is interesting to note that high-density fuels have greater energy content compared to low density fuels. Nevertheless they pack high energy content per unit mass in comparison [295]. In other words, when different fuels with different energy balances are used for performance testing and evaluation the same engine experiences different power outputs.

Biodiesel fuels as hydrocarbon compounds comprise n-saturated, unsaturated, branched cyclics. Vegetable oil, which form a bulk of biodiesel, contain three fatty acids called triglycerides. These fatty acids have a carbon chain length formed in a number of double bonds [511]. Most biodiesel oil contain 74.5 wt % to 78.4 wt%, hydrogen content of 10.6 wt% to 12.4 wt% and an oxygen content of 10.8 wt% to 12 wt % [463].

In other words, the elemental composition of fatty acids is important because it defines the energy content, through provision of weight percentage of carbon, hydrogen and oxygen components within a given sample of biodiesel. For example, the heating values of vegetable oil range from 24.29 MJ/kg to 41.20 MJ/kg. Vegetable source feedstocks have greater differences in heating values, but in surveyed literature, camelina has the highest HHV at 45.2MJ/kg in one study[414]. Others include corn and safflower with 43.1MJ/kg and 42.2MJ/kg respectively. It is also important to note in literature surveyed and data reported in literature there is confusion between this two terms LHV and HHV, which is confirmed in a number of studies such as [414, 448, 449].

Another observation found in the literature surveyed for commonly used biodiesel heating values indicates that they are few. Nevertheless, few researchers have managed to research and put some values for heating values together such as [512-514]. Hence, experimental determination of HHV of biodiesel fuels and other pure fatty acids is not exhaustive. Nevertheless a variety of correlations for predicting different HHV of fatty acids exist such as in (12 and 13 [513].

$$HHV = 49.43 - 0.015 IV - 0.041 SV \qquad (12)$$

$$HHV = 30.84 Exp(0.0013 MW) \qquad (13)$$

where

HHV, IV, SV and MW are high heating value, iodine value, saponification value and molecular weight of the fatty acids

Due to the high oxygen content biodiesel fuels have lower mass to energy, ratio values compared to fossil diesel fuels. Hence, it is generally accepted that biodiesel has 10% less mass energy content MJ/kg [462, 515]. The reduction in calorific value is mainly due to the presence of high oxygen content in the molecular structure of biodiesel fuels. These findings corroborate to a number of studies such as [463, 516, 517].

There are mainly two properties of biodiesel, which influence the calorific value, namely the saponification number and iodine values[518]. In other words, the decrease in saponification value reduces its molecular weight, which is similar to the effect of increased carbon and oxygen percentages in an oil sample. It is also important to note that in a given oil sample the calorific value is greatly affected by the iodine value [470]. The iodine value measures fuel properties of unsaturation.

The ASTM65751 nevertheless excludes it while the EN14214 specifies 120 mgI$_2$/100g. On the other hand, the saponification value of biodiesel sample refers to a hydration reaction to break ester bonds using free hydroxide between fatty acid and glycerol of the triglycerides. The result forms free fatty acids and glycerol components soluble in aqueous solutions in (14.

$$HHV = 0.0303(C) + 1.423(H) \qquad (14)$$

As observed from (12 the HHV can be determined using C, H, and O contents of the chemical structure as a function of percentage of these three components. However, (14 is a combination, of oxidative heat, values of C and H and the reduction heat of O with an assumption that the oxygen content effect on the fatty acid fuel has negative HHV. The determined values obtained by equations 12 and 13 and show the hydrogen content as the most decisive factor for unsaturated fatty acids [514]. Nevertheless, (13 shows HHV to be a functional component of the carbon percentage.

7.7. Oxidative Stability of Biodiesel

Biodiesel fuels degrade after storage for a long time due to oxidation. Hence, biodiesel stability refers to the ability of the biodiesel to resist degradation to form undesirable species and properties [519, 520]. This makes it possible for a biodiesel to resist physical and chemical changes caused by environmental factors. Nevertheless biodiesel fuels are none resistant to oxidation when exposed to air and moisture, this ultimately affects the biodiesel quality and storage. The existing time from initiation of oxidation to increased rate of oxidation is called induction period [521, 522]. During induction period, the concentration of ROOH is very low although this situation reverses as the reaction progresses.

In literature surveyed biodiesel fuel can degrade through a number of mechanisms [523] such as; Oxidation or autoxidation which occurs as a result of contact with ambient oxygen. The second mechanisms of oxidation is due to thermal oxidative decomposition due to exposure to excessive storage heat or direct light UV rays. The third mechanism comes from hydrolysis or accumulation of moisture or contact with water in storage tanks, fuel lines or moisture due to condensation. The fourth mechanism of biodiesel degradation is due to microbial or biodegradation contamination due to dust particles or water and moisture which contain bacteria or fungi into the storage tank or system. Metal contamination [524] and the Presence or absence of additives [525].

Besides these mechanisms biodiesel fuel itself is susceptible to oxidation and contamination through interaction with light and temperature. This is due to the presence of fatty acids, which interact with oxygen thus making biodiesel unstable. Besides nature and interaction, there are inherent chemical reactions such as alkenes, dienes and compounds of nitrogen, sulfur and oxygen, which hasten and play a dominant role on oxidation. The initial biodiesel products of oxidation are peroxides and hydro-peroxides, which when further degraded produce short chain hydrocarbons such as aldehydes, alcohols, ketones and low molecular compounds [520, 526, 527].

Among the visible physical changes to the naked eye is change in biodiesel physical colour, deposit formation that reduces biodiesel clarity and cleanliness [523, 528]. The degradation of biodiesel correlated to the process of transesterification, which either uses methanol or ethanol as each of them produces different esters. In other words during transesterification the fatty acid chain remains unchanged hence retaining the oxidation chemistry of the feedstock.

This is one of the leading explanation and cause of instability in biodiesel oil [519]. There are three types of oxidative stability identified with biodiesel fuels, which include oxidative stability [529, 530]. Storage stability which involves degradation due to interaction with light, air, metals, moisture and other storage related conditions [531, 532]. And Thermal stability which deals with oxidation at high temperature causing increased oil and fat [533, 534].

Nevertheless primary oxidation is further classified into three main reactions according to [519]. The first one is the initiation reaction where carbon free radicals are formed and produced [531, 535]. In other words, the diatomic oxygen present within the free radicals to form peroxy and further reaction leads to carbon free radical hydro-peroxide (ROOH). This is an extraction of the hydrogen atom from the carbon atom of the chain. The second reaction is the propagation reaction, which reacts the free carbon with atomic oxygen forming stable reaction products of two carbon free radicals, hence termination of the reaction. Vividly captured in equations 15 and 16 either through thermal dissociation of hydrogen peroxide.

$$RH + 1^* = R^* + 1H \qquad (15)$$

$$ROOH \rightarrow RO^* + OH^* \qquad (16)$$

Alternatively, it takes a metal catalysed decomposition of the hydrogen peroxide as in equations 17, 18, 19 and 20.

$$ROOH + M^{2+} \rightarrow RO^* + OH^* + M^{3+} \qquad (17)$$

$$ROOH + M^{3+} \rightarrow ROO^* + H^+ + M^{2+} \qquad (18)$$

$$R^* + O_2 \rightarrow ROO^* \qquad (19)$$

$$ROO^* + RH \rightarrow ROOH + R^* \qquad (20)$$
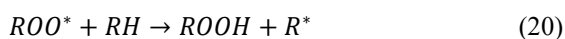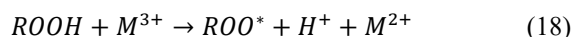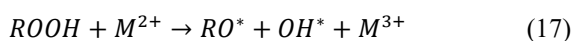
In the secondary oxidation reactions, the hydrogen-peroxide breaks down to form aldehydes of propanol, hexanals and heptanol while forming formic acid, aliphatic alcohol and formate esters. Additionally there is formation of short chain fatty acids, which lead to increased acid biodiesel value [536, 537].

7.8. Biodiesel Lubricity Properties

The lubricity of biodiesel refers to the reduction of friction between solid surfaces relative to their motion [538]. Lubricity in biodiesel takes two main mechanisms namely; Hydrodynamic lubrication where a layer of a liquid such as blended biodiesel within the injection system prevents direct contact between opposing moving sides. The second is Boundary lubrication,

which refers to compounds formulated to adhere to metallic surfaces while forming a thin protective layer that prevents wear.

These two forms of lubrication alternate with each other to provide lubrication especially boundary lubrication when hydrodynamic lubrication seizes to work or is removed from opposing surfaces. In other words, biodiesel oil should have good lubricity qualities, as this is critical in protecting moving parts in the modern injection systems. Modern day increased operational demands for injection systems is a critical factor and includes high and sustained pressure, injection rate shaping, multiple injection and engine injection cycles. Nevertheless, suffice to say that despite increased need for lubricity, natural lubricity from petroleum fuels has been decreasing with the advent of ULSD. This technology uses high level of hydrotreatment, which removes all heteroatom molecules of O, N and S which are key in improved lubricity[481, 539].

Generally, biodiesel is regarded with high and excellent lubricating properties a reason why blending with ULSD is recommended. This natural lubricity of biodiesel causes biodiesel to have no specification within ASTM and EN standards for B100. However blends B5 to B20 in ASTM7467 includes lubricity specifications[481]. Biodiesels excellent properties of lubricity traced to the esters group within its FAME molecules and other trace impure compounds. For example, free fatty acids and monoglycerides are effective in lubrication [540, 541]. In a number of studies reported in literature surveyed the authors note that the purification process by distillation decreases its lubricity as it removes impurities which are necessary to lubricity [539].

In literature surveyed, the effect of unsaturation on lubricity is inadequately covered and needs further study, as there is no comprehensive data. It is not clear from literature surveyed the role of unsaturation on lubricity and in the few available literatures, the results are mixed. For example, in a number of research work positive and negative effects of carbon-carbon double bonds is reported [215, 481, 542]. It is important to note that this impurities in biodiesel impact lubricity positively although they increase operational problems such as cold starting. Trying to reduce these impurities to improve cold flow properties of biodiesel has worsened the consequence of poor lubricity [414].

7.9. Cold Flow Biodiesel Properties (Flash Point, Pour Point and Cloud Point)

The cold flow properties of biodiesel indicate the ability of a biodiesel during cold weather and engine cold starting and is dependent on the long chain saturated factor [204]. Biodiesel fuels have similar and comparable physicochemical features as fossil diesel although their cold flow properties of the two fuels are dissimilar. All biodiesel fuels have very poor cold starting properties irrespective of the source of feedstock and blends without additives.

In biodiesel clod flow properties relate to the melting points of individual fuel components and their solubility in blends [543]. In other words, a high MP causes crystallization and precipitates

once its blend goes beyond its solubility. Due to long chain saturated fatty acids, biodiesel fuel components exhibit higher MP compared to fossil diesel. However, when unsaturated fatty acid components are present the MP decreases. Table 15 shows CP for different feedstocks.

Table 15: Selected biodiesel feedstocks cloud points [544]

Oil /Fat	Methyl ester composition (wt %)						Cloud point	
	$C_{16:0}$	$C_{18:0}$	$C_{18:1}$	$C_{18:2}$	$C_{18:3}$	Others	K	°C
Beef tallow	23.9	17.5	43.9	2.3	0.1	12.3	286	13
Palm	39.5	4.1	43.2	10.6	0.2	2.4	283	10
Sunflower	6.1	4.2	24	63.5	0.4	1.8	274	1
Soybean	10.7	3.2	25	53.3	5.4	2.5	272	-1
Linseed	6.7	3.7	21.7	15.8	52.1	0	268	-5
Olive	10.7	2.6	78.7	5.8	0.7	1.5	268	-5
Safflower	6.4	2.2	13.9	76	0.2	1.3	267	-6
Rapeseed	4.3	1.9	61.5	20.6	8.3	3.1	267	-6

Nevertheless the flash point of biodiesel differs and refers to a safety measure of biodiesel storage as it's a point at which a biodiesel fuel spontaneously becomes flammable [545]. On the other hand, the fire point of a hydrocarbon is a point at which a sample of fuel will continue to burn at its highest temperature and remains burning. The difference between the flash point and the fire point is 50 °F to 70 °F. For example, fossil diesel has a flash point of 60 °C to 140°F while the fire point is 93°C to 200 °F $(32°F − 32) × \frac{5}{9} = °C)$.

Table 16: Flash point and fire point of biodiesel and its blends

Type of fuel	Flash point (°C)	Fire point (°C)
Diesel	60	65
Mahua oil	286	295
MME	175	186
Ethanol	40	47
Kerosene	72	77
MME 20 % ethanol	50	55
MME 10 % ethanol	52	57
MME 10 % ethanol 10% diesel	54	59
MME 20 % kerosene	90	97
MME 10 % kerosene	95	101

The average flashpoint for biodiesel fuel is 150°C compared to fossil diesel at 55°C to 66°C [546]. This difference is primarily due to the difference in their physicochemical properties. For example diesel fuel has low molecular weight molecules with branched compounds hence low flash point compared to biodiesel with trace of alcohol which reduces its flash point [450]. Due to the relationship between the biodiesel flashpoint and alcohol

content, the flashpoint sets the limit of residual alcohol in a biodiesel or biofuel.

This means therefore that the flashpoint is an empirical measurement but not a fundamental physical biodiesel parameter and is inversely proportional to fuel volatility [547]. Higher ethanol blends are a fire hazard and as such should be discouraged as they reduce flashpoint and firepoints of biodiesel. Table 16 shows the Flash point and fire point of different biodiesel and their blends.

The pour point of biodiesel is defines as the lowest temperature point which a biodiesel fuel will still manage to flow before turning jelly and waxy [548]. The difference in CFPP value in biodiesel oil samples depend on the feedstock but relies more on the carbon chain length of the saturated oil fatty acids. For example palmitic acid ($C_{16:0}$) in palm oil and ($C_{12:0}$) and ($C_{14:0}$) for coconut and Babassu respectively. In other words, carbon chains produce higher CFPP values [215, 414].

7.10.   Acid Number Biodiesel Properties

The acid number of biodiesels is defined as the quantity of potassium hydroxide (KOH) which neutralizes fatty acids in a 1g sample. This is expressed in (form as follows in (21.

$$RCOOH + KOH \rightarrow RCOOK + H_2 \tag{21}$$

The acid value is an important biodiesel property as it determines the amount of free fatty acids in a sample of fat; this is elaborated further in (8 [549]:

$$Acid\ Value = \frac{(S−B)×N×56.1}{W} \tag{22}$$

where

S is the standard alkali used during titration of the sample in ml

B is the blank sample used during titration in ml

N is the normal standard alkali

W is the weight of the sample in grams

The biodiesel acid number also shows the sum total of all acid chemicals comprising the following: Phenols, Acids, Sugars, biodiesel oil extracts. Since biodiesel oil have high content of oxygen there is a high association with acidity linked to it [550]. This means the acid number measures the quantity of carboxylic acid groups in a chemical compound like fatty acid or as a mixture of compounds [551]. The acid number of biodiesel is contained in ASTM D 6751 using method ASTM D664 and EN14214 using method EN14104 [481]. Acid numbers quantify the acid values in a sample of biodiesel. Nevertheless Higher acid values cause a number of problems in injection systems by causing severe corrosion of internal component parts [551].

8.   Conclusion and Future Recommendation

- Families and family generation are defined by the length of time, likewise the biodiesel families are defined by the length of time.

- Use of non-edible feedstocks is an answer to the challenges paused by edible oil feedstocks. The use of non-edible feedstocks in the production of biodiesel eliminates competition for food, reduction in deforestation rate and co-products waste.

- Besides chemical and physical factors, which affect biodiesel production tax and policy subsidy, completion with food industry, cost of feedstock and investment affect production of biodiesel.

- Although biodiesel is advantageous in many aspects, high cost of production, processing and raw materials (feedstock) which account for 80% make it expensive as an alternative.

- Viscosity plays a key role in the spray quality, mixture formation and ultimately influences the entire combustion process. In other words high kinematic viscosity interferes with the entire injection process thus leading to insufficient fuel atomization hence poor engine combustion and performance.

- The density of fuel is a prime role in the injected mass timing and the injection spray pattern. It is also important to remember that as the density of a fuel sample increases the mass of fuel-injected increases too.

- The cetane number in any given fuel is a primer indicator of the fuel ignition quality, which is the same as octane rating in SI fuel. The cetane number measures the knock tendency of a diesel fuel of biodiesel as a function of ignition delay.

- The elemental composition of fatty acids is important because it defines the energy content within a given sample of biodiesel. Through provision of weight percentage of carbon, hydrogen and oxygen components with a given sample of biodiesel it makes easy to determine the energy content.

- Biodiesel fuel is susceptible to oxidation and contamination through interaction with light and temperature due to the presence of fatty acids, which interact with oxygen. Visible physical changes to the naked eye to show this change in biodiesel include physical colour change of oil, deposit formation that reduces biodiesel clarity and cleanliness.

- Generally biodiesel is regarded with high and excellent lubricating properties a reason why blending with ULSD is recommended.

- Due to the relationship between the biodiesel flashpoint and alcohol content, the flashpoint sets the limit of residual alcohol in a biodiesel or biofuel. In other words although flashpoint is an empirical measurement but not a fundamental physical biodiesel parameter and is inversely proportional to fuel volatility.

- The feedstock type influences difference in the CFPP value in biodiesel oil samples although it relies more on the carbon chain length of the saturated oil fatty acids.

- The acid value has a significant impact on system components life and performance. Higher acid values contribute to a number of problems in the injection systems sometimes resulting into severe corrosion of internal component parts for injection.

References

[1] E. Diesel, *Diesel: Der Mensch, das Werk, das Schicksal. Mit 21 Bildern u. Wiedergaben im Text u. auf Kunstdrucktaf*: Hanseatische Verlag-Anst., 1937.

[2] C. Chavanne, "Procédé de transformation d'huiles végétales en vue de leur utilisation comme carburants (Procedure for the transformation of vegetable oils in view of their use as fuels)," *Belgian Patent BE*, **422**, 31, 1937.

[3] G. Chavanne, "Sur un mode d'utilisation possible de l'huile de palme à la fabrication d'un carburant lourd," 1942.

[4] B. Kovarik, "Henry Ford, Charles F. Kettering and the fuel of the future," Automotive History Review, **32**, 7-27, 1998.

[5] J. Walton, "The fuel possibilities of vegetable oils," Gas Oil Power, **33**, 167-168, 1938.

[6] J. Bruwer, F. Hugo, and C. Hawkins, "Sunflower seed oil as an extender for diesel fuel in agricultural tractors," 1980. NTIS (US Sales Only), PC A02/MF A01.

[7] S. Palash, M. Kalam, H. Masjuki, B. Masum, I. R. Fattah, and M. Mofijur, "Impacts of biodiesel combustion on NOx emissions and their reduction approaches," Renewable and Sustainable Energy Reviews, **23**, 473-490, 2013. https://doi.org/10.1016/j.rser.2013.03.003

[8] M. Mofijur, H. Masjuki, M. Kalam, M. Hazrat, A. Liaquat, M. Shahabuddin, *et al.*, "Prospects of biodiesel from Jatropha in Malaysia," Renewable and Sustainable Energy Reviews, **16**, 5007-5020, 2012. https://doi.org/10.1016/j.rser.2013.03.003

[9] H. Ong, T. Mahlia, and H. Masjuki, "A review on energy scenario and sustainable energy in Malaysia," Renewable and Sustainable Energy Reviews, 15, 639-647, 2011. https://doi.org/10.1016/j.rser.2010.09.043

[10] E. Cecrle, C. Depcik, A. Duncan, J. Guo, M. Mangus, E. Peltier, *et al.*, "Investigation of the effects of biodiesel feedstock on the performance and emissions of a single-cylinder diesel engine," Energy & Fuels, **26**, 2331-2341, 2012. https://doi.org/10.1021/ef2017557

[11] A. Liaquat, M. Kalam, H. Masjuki, and M. Jayed, "Potential emissions reduction in road transport sector using biofuel in developing countries," Atmospheric Environment, 44, 3869-3877, 2010. https://doi.org/10.1016/j.atmosenv.2010.07.003

[12] EIA, "Monthly biodiesel production report: january," Energy Information Administration, Washington, DC, U.S2015.

[13] V. K. Kaimal and P. Vijayabalan, "A detailed study of combustion characteristics of a DI diesel engine using waste plastic oil and its blends," *Energy conversion and Management*, **105**, 951-956, 2015. https://doi.org/10.1016/j.enconman.2015.08.043

[14] I. Kalargaris, G. Tian, and S. Gu, "The utilisation of oils produced from plastic waste at different pyrolysis temperatures in a DI diesel engine," Energy, **131**, 179-185, 2017. https://doi.org/10.1016/j.energy.2017.05.024

[15] A. Sharma and S. Murugan, "Combustion, performance and emission characteristics of a DI diesel engine fuelled with non-petroleum fuel: a study on the role of fuel injection timing," Journal of the Energy Institute, **88**, 364-375, 2015. https://doi.org/10.1016/j.joei.2014.11.006

[16] A. K. Wamankar and S. Murugan, "Effect of injection timing on a DI diesel engine fuelled with a synthetic fuel blend," Journal of the Energy Institute, **88**, 406-413, 2015. https://doi.org/10.1016/j.joei.2014.11.003

[17] Department of Enviromental Affairs, "National Waste Management Strategy," Department of Enviromental Affairs, Pretoria, South Africa2017.

[18] REN21, "Renewables Global Status Report: 2009 Update," REN21 Secretariat,, Paris, France2009.

[19] Government of India, "National Policy on Biofuels," New Delhi, India2009.

[20] K. M. Findlater and M. Kandlikar, "Land use and second-generation biofuel feedstocks: the unconsidered impacts of Jatropha biodiesel in Rajasthan, India," Energy Policy, **39**, 3404-3413, 2011. https://doi.org/10.1016/j.enpol.2011.03.037

[21] W. M. Achten, L. Verchot, Y. J. Franken, E. Mathijs, V. P. Singh, R. Aerts, *et al.*, "Jatropha bio-diesel production and use," *Biomass and bioenergy*, **32**, 1063-1084, 2008. https://doi.org/10.1016/j.biombioe.2008.03.003

[22] P. Ariza-Montobbio and S. Lele, "Jatropha plantations for biodiesel in Tamil Nadu, India: Viability, livelihood trade-offs, and latent conflict," Ecological

Economics, **70**, 189-195, 2010. https://doi.org/10.1016/j.ecolecon.2010.05.011

[23] B. Divakara, H. Upadhyaya, S. Wani, and C. L. Gowda, "Biology and genetic improvement of Jatropha curcas L.: a review," Applied Energy, **87**, 732-742, 2010. https://doi.org/10.1016/j.apenergy.2009.07.013

[24] E. Christoforou and P. A. Fokaides, Environmental Assessment of Solid Biofuels: Advances in Solid Biofuels, Springer, 2019. https://doi.org/10.1007/978-3-030-00862-8_6

[25] B. Amigun, J. K. Musango, and W. Stafford, "Biofuels and sustainability in Africa," Renewable and sustainable energy reviews, **15**, 1360-1372, 2011. https://doi.org/10.1016/j.rser.2010.10.015

[27] V. Buytaert, B. Muys, N. Devriendt, L. Pelkmans, J. Kretzschmar, and R. Samson, "Towards integrated sustainability assessment for energetic use of biomass: A state of the art evaluation of assessment tools," Renewable and Sustainable Energy Reviews, **15**, 3918-3933, 2011. https://doi.org/10.1016/j.rser.2011.07.036

[28] A. C. McBride, V. H. Dale, L. M. Baskaran, M. E. Downing, L. M. Eaton, R. A. Efroymson, *et al.*, "Indicators to support environmental sustainability of bioenergy systems," Ecological Indicators, **11**, 1277-1289, 2011. https://doi.org/10.1016/j.ecolind.2011.01.010

[29] J. R. Seay and F. F. Badurdeen, "Current trends and directions in achieving sustainability in the biofuel and bioenergy supply chain," Current opinion in chemical engineering, **6**, 55-60, 2014. https://doi.org/10.1016/j.coche.2014.09.006

[30] V. H. Dale, R. A. Efroymson, K. L. Kline, M. H. Langholtz, P. N. Leiby, G. A. Oladosu, *et al.*, "Indicators for assessing socioeconomic sustainability of bioenergy systems: a short list of practical measures," Ecological Indicators, **26**, 87-102, 2013. https://doi.org/10.1016/j.ecolind.2012.10.014

[31] V. H. Dale, R. A. Efroymson, K. L. Kline, and M. S. Davitt, "A framework for selecting indicators of bioenergy sustainability," Biofuels, Bioproducts and Biorefining, vol. **9**, 435-446, 2015. https://doi.org/10.1002/bbb.1562

[32] T. Buchholz, V. A. Luzadis, and T. A. Volk, "Sustainability criteria for bioenergy systems: results from an expert survey," Journal of cleaner production, **17**, S86-S98, 2009. https://doi.org/10.1016/j.jclepro.2009.04.015

[33] P. Fokaides and E. Christoforou, Life cycle sustainability assessment of biofuels: Handbook of biofuels production, Elsevier, 2016. https://doi.org/10.1016/B978-0-08-100455-5.00003-5

[34] C. Baskar, S. Baskar, and R. S. Dhillon, Biomass conversion: The interface of biotechnology, chemistry and materials science, Springer Science & Business Media, 2012.

[35] A. Azad, M. Rasul, M. Khan, S. C. Sharma, and M. Bhuiya, "Recent development of biodiesel combustion strategies and modelling for compression ignition engines," Renewable and Sustainable Energy Reviews, **56**, 1068-1086, 2016. https://doi.org/10.1016/j.rser.2015.12.024

[36] B. Singh, A. Guldhe, I. Rawat, and F. Bux, "Towards a sustainable approach for development of biodiesel from plant and microalgae," Renewable and sustainable Energy reviews, **29**, 216-245, 2014. https://doi.org/10.1016/j.rser.2013.08.067

[37] B. Singh, A. Guldhe, P. Singh, A. Singh, I. Rawat, and F. Bux, Sustainable production of biofuels from microalgae using a biorefinary approach: Applied environmental biotechnology: Present scenario and future trends, Springer, 2015. https://doi.org/10.1007/978-81-322-2123-4_8

[38] S. N. Naik, V. V. Goud, P. K. Rout, and A. K. Dalai, "Production of first and second generation biofuels: a comprehensive review," Renewable and sustainable energy reviews, **14**, 578-597, 2010. https://doi.org/10.1016/j.rser.2009.10.003

[39] E. Rostek, "Biofuels of first and second generation," Journal of KONES, **23**, 2016. doi: 10.5604/12314005.1217259

[40] W.-H. Leong, J.-W. Lim, M.-K. Lam, Y. Uemura, and Y.-C. Ho, "Third generation biofuels: A nutritional perspective in enhancing microbial lipid production," Renewable and sustainable energy reviews, **91**, 950-961, 2018. https://doi.org/10.1016/j.rser.2018.04.066

[41] Y. Chisti, "Biodiesel from microalgae," Biotechnology advances, **25**, 294-306, 2007. https://doi.org/10.1016/j.biotechadv.2007.02.001

[42] S. Behera, Singh, R., Arora, R., Sharma, N. K., Shukla, M., & Kumar, S,, "Scope of algae as third generation biofuels," Frontiers in bioengineering and biotechnology, **2**, 90, 2015. https://doi.org/10.3389/fbioe.2014.00090

[43] B. Zhao, Ma, J., Zhao, Q., Laurens, L., Jarvis, E., Chen, S., & Frear, C,, "Efficient anaerobic digestion of whole microalgae and lipid-extracted microalgae residues for methane energy production," Bioresource technology, **161**, 423-430, 2014. https://doi.org/10.1016/j.biortech.2014.03.079

[44] E. S. Salama, Kurade, M. B., Abou-Shanab, R. A., El-Dalatony, M. M., Yang, I. S., Min, B., & Jeon, B. H,, "Recent progress in microalgal biomass production coupled with wastewater treatment for biofuel generation," Renewable and Sustainable Energy Reviews, **79**, 1189-1211, 2017. https://doi.org/10.1016/j.rser.2017.05.091

[45] G. Markou, Wang, L., Ye, J., & Unc, A,, "Using agro-industrial wastes for the cultivation of microalgae and duckweeds: Contamination risks and biomass safety concerns, Biotechnology advances, **36**(4), 1238-1254, 2018. https://doi.org/10.1016/j.biotechadv.2018.04.003

[46] W. A. Payne, Are biofuels antithetic to long-term sustainability of soil and water resources?: Advances in agronomy, Academic Press, 2010. https://doi.org/10.1016/S0065-2113(10)05001-7

[47] N. K. Sharma, Tiwari, S. P., Tripathi, K., & Rai, A. K,, "Sustainability and cyanobacteria (blue-green algae): facts and challenges," Journal of applied phycology, **23**, 1059-1081, 2011. https://doi.org/10.1007/s10811-010-9626-3

[48] A. W. Sheppard, Gillespie, I., Hirsch, M., & Begley, C,, "Biosecurity and sustainability within the growing global bioeconomy," Current Opinion in Environmental Sustainability, **3**, 4-10, 2011. https://doi.org/10.1016/j.cosust.2010.12.011

[49] D. J. Patzelt, Hindersin, S., Elsayed, S., Boukis, N., Kerner, M., & Hanelt, D,, "Hydrothermal gasification of Acutodesmus obliquus for renewable energy production and nutrient recycling of microalgal mass cultures," Journal of applied phycology, **27**, 2239-2250, 2015. https://doi.org/10.1007/s10811-014-0496-y

[50] A. I. Barros, Gonçalves, A. L., Simões, M., & Pires, J. C,, "Harvesting techniques applied to microalgae: a review," Renewable and Sustainable Energy Reviews, **41**, 1489-1500, 2015. https://doi.org/10.1016/j.rser.2014.09.037

[51] D. J. Glass, "Pathways to obtain regulatory approvals for the use of genetically modified algae in biofuel or biobased chemical production," Industrial Biotechnology, **11**, 71-83, 2015. https://doi.org/10.1089/ind.2015.1503

[52] M. R. Tredici, "Photobiology of microalgae mass cultures: understanding the tools for the next green revolution," Biofuels, **1**(1),143-162, 2010. https://doi.org/10.4155/bfs.09.10

[53] G. Dragone, B. D. Fernandes, A. A. Vicente, and J. A. Teixeira, "Third generation biofuels from microalgae," 2010. http://hdl.handle.net/1822/16807

[54] F. Alam, S. Mobin, and H. Chowdhury, "Third generation biofuel from Algae," Procedia Engineering, **105**, 763-768, 2015. https://doi.org/10.1016/j.proeng.2015.05.068

[55] W. H. Liew, M. H. Hassim, and D. K. Ng, "Review of evolution, technology and sustainability assessments of biofuel production," Journal of Cleaner Production, **71**, 11-29, 2014. https://doi.org/10.1016/j.jclepro.2014.01.006

[56] V. B. Agbor, N. Cicek, R. Sparling, A. Berlin, and D. B. Levin, "Biomass pretreatment: fundamentals toward application," Biotechnology advances, **29**, 675-685, 2011. https://doi.org/10.1016/j.biotechadv.2011.05.005

[57] P. Bajpai, Pretreatment of lignocellulosic biomass: Pretreatment of Lignocellulosic Biomass for Biofuel Production, Springer, 2016. https://doi.org/10.1007/978-981-10-0687-6_4

[58] K. Dutta, A. Daverey, and J.-G. Lin, "Evolution retrospective for alternative fuels: First to fourth generation," Renewable energy, **69**, 114-122, 2014. https://doi.org/10.1016/j.renene.2014.02.044

[59] M. F. Demirbas, "Current technologies for biomass conversion into chemicals and fuels," Energy Sources, Part A: Recovery, Utilization, and Environmental Effects, **28**, 1181-1188, 2006. https://doi.org/10.1080/00908310500434556

[60] P. McKendry, "Energy production from biomass (part 2): conversion technologies," Bioresource technology, **83**, 47-54, 2002. https://doi.org/10.1016/S0960-8524(01)00119-5

[61] P. Fokaides and P. Polycarpou, Exploitation of olive solid waste for energy purposes: Renewable energy, economies, emerging technologies and global practices. Nova Science Publishers, Inc, 2013.

[62] T. Brlek, N. Voća, T. Krička, J. Lević, Đ. Vukmirović, and R. Čolović, "Quality of pelleted olive cake for energy generation," Agriculturae Conspectus Scientificus, **77**, 31-35, 2012. https://hrcak.srce.hr/77902

[63] Y. Neubauer, Biomass gasification: Biomass Combustion Science, Technology and Engineering, Woodhead Publishing Series in Energy, 2013.

[64] F. Schüth, Hydrogen economics and its role in biorefining: Catalytic Hydrogenation for Biomass Valorization, Royal society of chemistry, 2014. doi: 10.1039/9781782620099-00001

[65] R. Reimert, F. Marschner, H. J. Renner, W. Boll, E. Supp, M. Brejc, *et al.*, "Gas Production, 2. Processes," Ullmann's encyclopedia of industrial chemistry, 2000.

[66] A. Gómez-Barea and B. Leckner, "Modeling of biomass gasification in fluidized bed," Progress in Energy and Combustion Science, **36**, 444-509, 2010. https://doi.org/10.1016/j.pecs.2009.12.002

[67] A. E. Abdelaziz, Leite, G. B., & Hallenbeck, P. C., "Addressing the challenges for sustainable production of algal biofuels: II. Harvesting and conversion to biofuels," Environmental technology, **34**, 1807-1836, 2013. https://doi.org/10.1080/09593330.2013.831487

[68] X. Ji and X. Long, "A review of the ecological and socioeconomic effects of biofuel and energy policy recommendations," Renewable and Sustainable Energy Reviews, **61**, 41-52, 2016. https://doi.org/10.1016/j.rser.2016.03.026

[69] J. P. Maity, J. Bundschuh, C.-Y. Chen, and P. Bhattacharya, "Microalgae for third generation biofuel production, mitigation of greenhouse gas emissions and wastewater treatment: Present and future perspectives–A mini review," Energy, **78**, 104-113, 2014. https://doi.org/10.1016/j.energy.2014.04.003

[70] USDOE, "National Algal Biofuels Technology Review," Bioenergy Technologies Office, Washington DC, USA2016.

[71] S. A. Scott, M. P. Davey, J. S. Dennis, I. Horst, C. J. Howe, D. J. Lea-Smith, et al., "Biodiesel from algae: challenges and prospects," Current opinion in biotechnology, **21**, 277-286, 2010. https://doi.org/10.1016/j.copbio.2010.03.005

[72] I. Christian and A. John, "Feasibility of Second and Third Generation Biofuel in General Aviation: A Research Report and Analysis," McNair Scholars Research Journal, **1**, 4, 2014. https://commons.erau.edu/mcnair/vol1/iss1/4

[73] G. B. Leite, A. E. Abdelaziz, and P. C. Hallenbeck, "Algal biofuels: challenges and opportunities," Bioresource technology, **145**, 134-141, 2013. https://doi.org/10.1016/j.biortech.2013.02.007

[74] T. W. Hertel, W. E. Tyner, and D. K. Birur, "The global impacts of biofuel mandates," The Energy Journal, **31**(1-4), 75-100, 2010. doi: 10.5547/ISSN0195-6574-EJ-Vol31-No1-4

[75] M. Yumurtaci and A. Kecebas, "Renewable energy and its university level education in Turkey," Energy Education Science and Technology Part B-Social and Educational Studies, **3**, 143-152, 2011.

[76] K. F. Yee, K. T. Tan, A. Z. Abdullah, and K. T. Lee, "Life cycle assessment of palm biodiesel: revealing facts and benefits for sustainability," Applied Energy, **86**, S189-S196, 2009. https://doi.org/10.1016/j.apenergy.2009.04.014

[77] A. Demirbas, "Progress and recent trends in biodiesel fuels," Energy conversion and management, **50**, 14-34, 2009. https://doi.org/10.1016/j.enconman.2008.09.001

[78] Y. Sahin, "Environmental impacts of biofuels," Energy Education Science and Technology Part A-Energy Science and Research, **26**, 129-142, 2011. doi:10.3155/1047-3289.61.3.285

[79] A. Demirbas, "Political, economic and environmental impacts of biofuels: A review," Applied energy, **86**, S108-S117, 2009. https://doi.org/10.1016/j.apenergy.2009.04.036

[80] M. F. Demirbas, "Biofuels from algae for sustainable development," Applied energy, vol. **88**, 3473-3480, 2011. https://doi.org/10.1016/j.apenergy.2011.01.059

[81] J. P. Hewett, Wolfe, A. K., Bergmann, R. A., Stelling, S. C., & Davis, K. L,, "Human health and environmental risks posed by synthetic biology R&D for energy applications: a literature analysis," Applied Biosafety, **21**, 177-184, 2016. https://doi.org/10.1177/1535676016672377

[82] M. Y. Menetrez, "An overview of algae biofuel production and potential environmental impact," Environmental science & technology, **46**, 7073-7085, 2012. https://doi.org/10.1021/es300917r

[83] S. Genitsaris, Kormas, K. A., & Moustaka-Gouni, M,, "Airborne algae and cyanobacteria: occurrence and related health effects," Frontiers in Bioscience, **3**, 772-787, 2011.

[84] O. Wright, Stan, G. B., & Ellis, T,, "Building-in biosafety for synthetic biology," Microbiology, **159**, 1221-1235, 2013. https://doi.org/10.1099/mic.0.066308-0

[85] G. N. Mandel, "Gaps, inexperience, inconsistencies, and overlaps: Crisis in the regulation of genetically modified plants and animals," William & Mary Law Review, **45**, 2167, 2003.

[86] G. E. Marchant, & Wallach, W, Governing the governance of emerging technologies: Innovative governance models for emerging technologies, Edward Elgar Publishing, 2013. https://doi.org/10.4337/9781782545644.00013

[87] A. A. Snow, & Smith, V. H,, "Genetically engineered algae for biofuels: a key role for ecologists," Bioscience, **62**, 765-768, 2012. https://doi.org/10.1525/bio.2012.62.8.9

[88] W. J. Henley, Litaker, R. W., Novoveská, L., Duke, C. S., Quemada, H. D., & Sayre, R. T, "Initial risk assessment of genetically modified (GM) microalgae for commodity-scale biofuel cultivation," Algal Research, **2**, 66-77, 2013. https://doi.org/10.1016/j.algal.2012.11.001

[89] J. B. Tucker, & Zilinskas, R. A,, "The promise and perils of synthetic biology," The New Atlantis, **12**, 25-45, 2006. https://www.jstor.org/stable/43152238

[90] A. Bhutkar, "Synthetic biology: navigating the challenges ahead," Journal of Biolaw & Business, vol. **8**, 19-29, 2005.

[91] T. Kuiken, Dana, G., Oye, K., & Rejeski, D, "Shaping ecological risk research for synthetic biology," Journal of Environmental Studies and Sciences, **4**, 191-199, 2014. https://doi.org/10.1007/s13412-014-0171-2

[92] A. Raybould, "The bucket and the searchlight: formulating and testing risk hypotheses about the weediness and invasiveness potential of transgenic crops," Environmental biosafety research, **9**, 123-133, 2010. https://doi.org/10.1051/ebr/2011101

[93] S. Lu, Li, L., & Zhou, G,, "Genetic modification of wood quality for second-generation biofuel production," GM crops, **1**, 230-236, 2010.

[94] K. Bhattarai, Brummer, E. C., & Monteros, M. J,, "Alfalfa as a bioenergy crop; Bioenergy FeedstocksBreeding and Genetics, Taylor and Francis, 2013. https://doi.org/10.1002/9781118609477.ch10

[95] J. M. Jeschke, Keesing, F., & Ostfeld, R. S,, "Novel organisms: comparing invasive species, GMOs, and emerging pathogens," Ambio, **45**, 541-548, 2013. https://doi.org/10.1007/s13280-013-0387-5

[96] F. J. Areal, Riesgo, L., & Rodriguez-Cerezo, E,, " Economic and agronomic impact of commercialized GM crops: a meta-analysis," The Journal of Agricultural Science, **151**, 7-33, 2013. doi:10.1017/S0021859612000111

[97] S. J. Smyth, W. A. Kerr, and P. W. Phillips, "Global economic, environmental and health benefits from GM crop adoption," Global Food Security, **7**, 24-29, 2015. https://doi.org/10.1016/j.gfs.2015.10.002

[98] M. D. Edgerton, "Increasing crop productivity to meet global needs for feed, food, and fuel," Plant physiology, **149**, 7-13, 2009. https://doi.org/10.1104/pp.108.130195

[99] R. Muñoz and C. Gonzalez-Fernandez, Microalgae-based biofuels and bioproducts: from feedstock cultivation to end-products, Woodhead Publishing, 2017.

[100] P. Tandon and Q. Jin, "Microalgae culture enhancement through key microbial approaches," Renewable and Sustainable Energy Reviews, **80**, 1089-1099, 2017. https://doi.org/10.1016/j.rser.2017.05.260

[101] B. M. Wolf, D. M. Niedzwiedzki, N. C. M. Magdaong, R. Roth, U. Goodenough, and R. E. Blankenship, "Characterization of a newly isolated freshwater Eustigmatophyte alga capable of utilizing far-red light as its sole light source," Photosynthesis research, **135**, 177-189, 2018. doi: 10.1007/s11120-017-0401-z

[102] D. E. T. Cervantes, A. L. Martínez, M. C. Hernández, and A. L. G. de Cortázar, "Using indicators as a tool to evaluate municipal solid waste management: A critical review," Waste management, **80**, 51-63, 2018. https://doi.org/10.1016/j.wasman.2018.08.046

[103] B. R. Alzamora and R. T. d. V. Barros, "Review of municipal waste management charging methods in different countries," Waste Management, **115**, 47-55, 2020. https://doi.org/10.1016/j.wasman.2020.07.020

[104] S. Chinnasamy, Rao, P. H., Bhaskar, S., Rengasamy, R., & Singh, M, Algae a novel biomass feedstock for biofuels: Microbial biotechnology Energy and environment, 224-239, 2012.

[105] B. Sajjadi, Chen, W. Y., Raman, A. A. A., & Ibrahim, S, "Microalgae lipid and biomass for biofuel production: A comprehensive review on lipid enhancement strategies and their effects on fatty acid composition," Renewable and Sustainable Energy Reviews, **97**, 200-232, 2018. https://doi.org/10.1016/j.rser.2018.07.050

[106] A. C. Guedes, Amaro, H. M., & Malcata, F. X, "Microalgae as sources of carotenoids," Marine drugs, **9**, 625-644, 2011. https://doi.org/10.3390/md9040625

[107] B. Abdullah, Muhammad, S. A. F. A. S., Shokravi, Z., Ismail, S., Kassim, K. A., Mahmood, A. N., & Aziz, M. M. A,, "Fourth generation biofuel: A review on risks and mitigation strategies," Renewable and sustainable energy reviews, vol. **107**, 37-50, 2019. https://doi.org/10.1016/j.rser.2019.02.018

[108] A. Srivastava, & Torres-Vargas, C. E,, "Genetically Modified Crops: A Long Way to Go: Environmental Issues Surrounding Human Overpopulation, IGI Global, 2017. doi: 10.4018/978-1-5225-1683-5.ch006

[109] I. Atadashi, M. Aroua, and A. A. Aziz, "High quality biodiesel and its diesel engine application: a review," Renewable and sustainable energy reviews, **14**, 1999-2008, 2010. https://doi.org/10.1016/j.rser.2010.03.020

[110] L. Lin, Z. Cunshan, S. Vittayapadung, S. Xiangqian, and D. Mingdong, "Opportunities and challenges for biodiesel fuel," Applied energy, vol. **88**, 1020-1031, 2011.

[111] J. C. Bart, Palmeri, N., & Cavallaro, S, Biodiesel science and technology: from soil to oil, Woodhead Publishing Elsevier, 2010.

[112] H. Hao, Liu, Z., Zhao, F., Ren, J., Chang, S., Rong, K., & Du, J, "Biofuel for vehicle use in China: Current status, future potential and policy implications.," Renewable and Sustainable Energy Reviews, vol. **82**, 645-653, 2018. https://doi.org/10.1016/j.rser.2017.09.045

[113] Y. Sani, W. Daud, and A. Abdul Raman, Biodesel feedstock and production technologies: successes, challenges and prospects **4**, Intech, 2013. http://dx.org/10.5772/52790

[114] S. P. Souza, Seabra, J. E., & Nogueira, L. A. H, "Feedstocks for biodiesel production: Brazilian and global perspectives," Biofuels, **9**, 455-478, 2018. https://doi.org/10.1080/17597269.2017.1278931

[115] A. E. Atabani, El-Sheekh, M. M., Kumar, G., & Shobana, S, Edible and nonedible biodiesel feedstocks: microalgae and future of biodiesel: Clean Energy for Sustainable Development, Academic Press-Elsevier, 2017. https://doi.org/10.1016/B978-0-12-805423-9.00017-X

[116] Y. C. Sharma, Singh, B., & Korstad, J. (2009). H, "High yield and conversion of biodiesel from a nonedible feedstock (Pongamia pinnata)," Journal of agricultural and food chemistry, **58**, 242-247, 2009. https://doi.org/10.1021/jf903227e

[117] I. Ozkurt, "Qualifying of safflower and algae for energy," Energy Education Science and Technology Part A-Energy Science and Research, **23**, 145-151, 2009.

[118] G. El Diwani, Attia, N. K., & Hawash, S. I, "Development and evaluation of biodiesel fuel and by-products from jatropha oil," International Journal of Environmental Science & Technology, **6**, 219-224, 2009.

[119] B. Sanjay, "Yellow oleander (Thevetia peruviana) seed oil biodiesel as an alternative and renewable fuel for diesel engines: a review," International Journal of ChemTech Research, **7**, 2823-2840, 2015. http://sphinxsai.com/2015/ch_vol7_no6...

[120] A. E. Atabani, Silitonga, A. S., Badruddin, I. A., Mahlia, T. M. I., Masjuki, H. H., & Mekhilef, S,, "A comprehensive review on biodiesel as an alternative energy resource and its characteristics," Renewable and sustainable energy reviews, **16**, 2070-2093, 2012. https://doi.org/10.1016/j.rser.2012.01.003

[121] M. Tabatabaei, K. Karimi, I. Horvath, and R. Kumar, "Recent trends in biodiesel production, ," Biofuel Research Journal, **7**, 258-267, 2015. doi: 10.18331/BRJ2015.2.3.4

[122] L. F. Razon, "Alternative crops for biodiesel feedstock. CAB Reviews," *P*erspectives in agriculture, veterinary science, nutrition and natural resources, vol. **4**, 1-15, 2009.

[123] A. L. Ahmad, Yasin, N. M., Derek, C. J. C., & Lim, J. K, "Microalgae as a sustainable energy source for biodiesel production: a review," Renewable and Sustainable Energy Reviews, **15**, 584-593, 2011. https://doi.org/10.1016/j.rser.2010.09.018

[124] USDA, "United States Department of Agriculture," Washington, D.C., United States2017.

[125] REN21, "Renewables 2015 - global status report," REN21, Paris, France2015.

[126] USDA, "Biofuel annual: European union," United States Department of Agriculture, Office of Global Analysis, Foreign Agricultural Service, The Hague, Netherlands2014.

[127] USDA, "Biofuels annual: argentina. Buenos Aires," United States Department of Agriculture, Office of Global Analysis, Foreign Agricultural Service Washington, D.C., United States2014.

[128] USDA, "Biofuels annual: Indonesia. Jakarta," United States Department of Agriculture, Office of Global Analysis, Foreign Agricultural Service, Washington, D.C., United States2014.

[129] USDA, "Biofuels annual: Thailand. Bangkok," United States Department of Agriculture, Office of Global Analysis, Foreign Agricultural Service;, Washington, D.C., United States3/24/2009 2009.

[130] A. De Oliveira, Brazilian Agroenergy Plan: 2006-2011, Embrapa Publishing House, 2011.

[131] FAO. Production, crops [Online]. Available: http://faostat3.fao.org/download/Q/QC/E

[132] Market Intel. China Uses One-Third of World's Soybeans [Online]. Available: https://www.fb.org/market-intel/china-uses-one-third-of-worlds-soybeans

[133] J. Hilliard and T. Daynard, "Measurement of protein and oil in grains and soybeans with reflected near–infrared light," Canadian Institute of Food Science and Technology Journal, **9**, 11-14, 1976.

[134] USDA. Oilseeds: world markets and trade [Online].

[135] Y.-S. Song, J. Frías, C. Martinez-Villaluenga, C. Vidal-Valdeverde, and E. G. de Mejia, "Immunoreactivity reduction of soybean meal by fermentation, effect on amino acid composition and antigenicity of commercial soy products," Food Chemistry, **108**, 571-581, 2008. https://doi.org/10.1016/j.foodchem.2007.11.013

[136] N. Antolović, V. Kožul, M. Antolović, and J. Bolotin, "Effects of partial replacement of fish meal by soybean meal on growth of juvenile saddled bream (Sparidae)," Turkish Journal of Fisheries and Aquatic Sciences, **12**, 247-252, 2012. doi : 10.4194/1303-2712-v12_2_08

[137] S. Cools, W. Van den Broeck, L. Vanhaecke, A. Heyerick, P. Bossaert, M. Hostens, et al., "Feeding soybean meal increases the blood level of isoflavones and reduces the steroidogenic capacity in bovine corpora lutea, without affecting peripheral progesterone concentrations," Animal reproduction science, **144**, 9-89, 2014. https://doi.org/10.1016/j.anireprosci.2013.12.008

[138] M. Hernández, F. Martínez, M. Jover, and B. G. García, "Effects of partial replacement of fish meal by soybean meal in sharpsnout seabream (Diplodus puntazzo) diet," Aquaculture, **263**, 159-167, 2007. https://doi.org/10.1016/j.aquaculture.2006.07.040

[139] M. P. Hojilla-Evangelista, "Adhesion properties of plywood glue containing soybean meal as an extender," Journal of the American Oil Chemists' Society, **87**, 1047-1052, 2010. doi 10.1007/s11746-010-1586-x

[140] FAO. Production, crops processed. [Online]. https://www.nature.com/articles/nbt0390-217

[141] A. L. Mourad and A. Walter, "The energy balance of soybean biodiesel in Brazil: a case study," Biofuels, Bioproducts and Biorefining, vol. **5**, 185-197, 2011. https://doi.org/10.1002/bbb.278

[142] J. Fargione, J. Hill, D. Tilman, S. Polasky, and P. Hawthorne, "Land clearing and the biofuel carbon debt," Science, **319**, 1235-1238, 2008. doi: 10.1126/science.1152747

[143] M. H. Rocha, R. S. Capaz, E. E. S. Lora, L. A. H. Nogueira, M. M. V. Leme, M. L. G. Renó, et al., "Life cycle assessment (LCA) for biofuels in Brazilian conditions: a meta-analysis," Renewable and Sustainable Energy Reviews, **37**, 435-459, 2014. https://doi.org/10.1016/j.rser.2014.05.034

[144] D. S. Kim, M. Hanifzadeh, and A. Kumar, "Trend of biodiesel feedstock and its impact on biodiesel emission characteristics," Environmental Progress & Sustainable Energy, **37**, 7-19, 2018. https://doi.org/10.1002/ep.12800

[145] C. O'Shea, P. Mc Alpine, P. Solan, T. Curran, P. Varley, A. Walsh, et al., "The effect of protease and xylanase enzymes on growth performance, nutrient digestibility, and manure odour in grower–finisher pigs," Animal Feed Science and Technology, **189**, 88-97, 2014. https://doi.org/10.1016/j.anifeedsci.2013.11.012

[146] L. Zhu, J. Wang, X. Ding, S. Bai, Q. Zeng, Z. Su, et al., "Effects of dietary rapeseed meal on laying performance, egg quality, apparent metabolic energy, and nutrient digestibility in laying hens," Livestock science, **214**, 265-271, 2018. https://doi.org/10.1016/j.livsci.2018.06.007

[147] M. Abduh, R. Manurung, and H. Heeres, "Techno-economic analysis for small scale production of rubber seed oil and biodiesel in Palangkaraya, Indonesia," Journal of Clean Energy Technologies, **5**, 268-273, 2017.

[148] S. Ghosal. Castor oil prices spike 23% in global markets [Online]. Available:https://economictimes.indiatimes.com/markets/commodities/news/castor-oil-prices-spike-23-in-global market/articleshow/ 69089709

[149] P. Halder, N. Paul, and M. Beg, "Prospect of Pongamia pinnata (Karanja) in Bangladesh: a sustainable source of liquid fuel," Journal of Renewable Energy, **2014**, 2014. https://doi.org/10.1155/2014/647324

[150] F. Dalemans, B. Muys, and M. Maertens, "A framework for profitability evaluation of agroforestry-based biofuel value chains: An application to pongamia in India," GCB Bioenergy, 2019. https://doi.org/10.1111/gcbb.12605

[151] J. P. Wanasundara, T. C. McIntosh, S. P. Perera, T. S. Withana-Gamage, and P. Mitra, "Canola/rapeseed protein-functionality and nutrition," OCL, **23,** D407, 2016. https://doi.org/10.1051/ocl/2016028

[152] J. Bergmann, D. Tupinambá, O. Costa, J. Almeida, C. Barreto, and B. Quirino, "Biodiesel production in Brazil and alternative biomass feedstocks," Renewable and Sustainable Energy Reviews, **21**, 411-420, 2013. https://doi.org/10.1016/j.rser.2012.12.058

[153] R. He, X. Ju, J. Yuan, L. Wang, A. T. Girgih, and R. E. Aluko, "Antioxidant activities of rapeseed peptides produced by solid state fermentation," Food Research International, **49**, 432-438, 2012. https://doi.org/10.1016/j.foodres.2012.08.023

[154] A. Marjanović-Jeromela, R. Marinković, A. Mijić, M. Jankulovska, Z. Zdunić, and N. Nagl, "Oil yield stability of winter rapeseed (Brassica napus L.) genotypes," Agriculturae Conspectus Scientificus, **73**, 217-220, 2008. https://hrcak.srce.hr/31240

[155] I. R. Fattah, H. Masjuki, A. Liaquat, R. Ramli, M. Kalam, and V. Riazuddin, "Impact of various biodiesel fuels obtained from edible and non-edible oils on engine exhaust gas and noise emissions," Renewable and Sustainable Energy Reviews, **18**, 552-567, 2013. https://doi.org/10.1016/j.rser.2012.10.036

[156] T. Searchinger, Heimlich, R., Houghton, R. A., Dong, F., Elobeid, A., Fabiosa, J., ... & Yu, T. H, "Use of US croplands for biofuels increases greenhouse gases through emissions from land-use change," Science, **319**, 1238-1240, 2008. doi: 10.1126/science.1151861

[157] S. P. De Souza, S. Pacca, M. T. De Ávila, and J. L. B. Borges, "Greenhouse gas emissions and energy balance of palm oil biofuel," Renewable Energy, **35**, 2552-2561, 2010. https://doi.org/10.1016/j.renene.2010.03.028

[158] M. Umikalsom, A. Ariff, H. Zulkifli, C. Tong, M. Hassan, and M. Karim, "The treatment of oil palm empty fruit bunch fibre for subsequent use as substrate for cellulase production by Chaetomium globosum Kunze," Bioresource Technology, **62**, 1-9, 1997. https://doi.org/10.1016/S0960-8524(97)00132-6

[159] P. Adhikari, X.-M. Zhu, A. Gautam, J.-A. Shin, J.-N. Hu, J.-H. Lee, *et al.*, "Scaled-up production of zero-trans margarine fat using pine nut oil and palm stearin," Food chemistry, **119**, 1332-1338, 2010. https://doi.org/10.1016/j.foodchem.2009.09.009

[160] C. Lesage and L. Feintrenie, Are sustainable pathways possible for oil palm development in Latin America?: *Land governance in an interconnected world*, Washington, USA, 2018. https://agritrop.cirad.fr/587928/

[161] A. Simeh and T. Ahmad, The case study on the Malaysian palm oil: Regional Workshop on commodity export diversification and poverty reduction in South and South-East Asia, Bangkok, UNCTAD, 2001.

[162] K. Tan, K. Lee, A. Mohamed, and S. Bhatia, "Palm oil: addressing issues and towards sustainable development," Renewable and sustainable energy reviews, **13**, 420-427, 2009. https://doi.org/10.1016/j.rser.2007.10.001

[163] S. Sumathi, S. Chai, and A. Mohamed, "Utilization of oil palm as a source of renewable energy in Malaysia," Renewable and sustainable energy reviews, **12**, 2404-2421, 2008. https://doi.org/10.1016/j.rser.2007.06.006

[164] F. Arrieta, F. Teixeira, E. Yáñez, E. Lora, and E. Castillo, "Cogeneration potential in the Columbian palm oil industry: Three case studies," Biomass and Bioenergy, **31**, 503-511, 2007. https://doi.org/10.1016/j.biombioe.2007.01.016

[165] A. D. Padula, M. S. Santos, L. Ferreira, and D. Borenstein, "The emergence of the biodiesel industry in Brazil: current figures and future prospects," Energy policy, **44**, 395-405, 2012. https://doi.org/10.1016/j.enpol.2012.02.003

[166] A. da Silva César, M. O. Batalha, and A. L. M. S. Zopelari, "Oil palm biodiesel: Brazil's main challenges," Energy, **60**, 485-491, 2013. https://doi.org/10.1016/j.energy.2013.08.014

[167] A. N. Payl and M. Mashud, "Experimental investigation on fuel properties of biodiesel prepared from cottonseed oil," Proceedings in *2017 AIP Conference*, 020018, 2017. https://doi.org/10.1063/1.4984647

[168] J.-M. Lacape, G. Gawrysiak, T.-V. Cao, C. Viot, D. Llewellyn, S. Liu, *et al.*, "Mapping QTLs for traits related to phenology, morphology and yield components in an inter-specific Gossypium hirsutum× G. barbadense cotton RIL population," Field Crops Research, **144**, 256-267, 2013. https://doi.org/10.1016/j.fcr.2013.01.001

[169] D. Sinha and S. Murugavelh, "Biodiesel production from waste cotton seed oil using low cost catalyst: Engine performance and emission characteristics," Perspectives in science, **8**, 237-240, 2016. https://doi.org/10.1016/j.pisc.2016.04.038

[170] G. M. P. de Faria, M. da Silva Oliveira, L. P. de Carvalho, and C. D. Cruz, "Gains from selection for oil content in cotton," Industrial crops and products, **51**, 370-375, 2013. https://doi.org/10.1016/j.indcrop.013.09.005

[171] S. F. Vaughn, N. A. Deppe, M. A. Berhow, and R. L. Evangelista, "Lesquerella press cake as an organic fertilizer for greenhouse tomatoes," *I*ndustrial crops and products, **32**, 164-168, 2010. https://doi.org/10.1016/j.indcrop.2010.04.008

[172] M. H. Li and E. H. Robinson, "Use of cottonseed meal in aquatic animal diets: a review," North American Journal of Aquaculture, **68**, 14-22, 2006.

[173] S. Adeel, S. Ali, I. A. Bhatti, and F. Zsila, "Dyeing of cotton fabric using pomegranate (Punica granatum) aqueous extract," Asian Journal of Chemistry, **21**, 3493, 2009.

[174] N. Reddy and Y. Yang, "Properties and potential applications of natural cellulose fibers from the bark of cotton stalks," Bioresource technology, **100**, 3563-3569, 2009. https://doi.org/10.1016/j.biortech.2009.02.047

[175] F. D. Gunstone, J. L. Harwood, and A. J. Dijkstra, The lipid handbook with CD-ROM, CRC press, 2007.

[176] I. Balalić, M. Zorić, G. Branković, S. Terzić, and J. Crnobarac, "Interpretation of hybrid× sowing date interaction for oil content and oil yield in sunflower," Field Crops Research, **137**, 70-77, 2012. https://doi.org/10.1016/j.fcr.2012.08.005

[177] V. D. Zheljazkov, B. A. Vick, B. S. Baldwin, N. Buehring, C. Coker, T. Astatkie, *et al.*, "Oil productivity and composition of sunflower as a function of hybrid and planting date," Industrial Crops and Products, **33**, 537-543, 2011. https://doi.org/10.1016/j.indcrop.2010.11.004

[178] G. O. India. Post Harvest Profile of Sunflower, Directorate of Marketing and Inspection (Nagpur Branch) [Online]. Available: http://Agmarknet.Nic.In/Sunflower_Profile.Pdf

[179] N. Ramulu, K. Murthy, H. Jayadeva, M. Venkatesha, and H. Ravi Kumar, "Seed yield and nutrients uptake of sunflower (Helianthus annuusL.) as influenced by different levels of nutrients under irrigated condition of eastern dry zone of Karnataka, India," Plant Arch, **11**, 1061-1066, 2011.

[180] G. Ragaglini, F. Triana, R. Villani, and E. Bonari, "Can sunflower provide biofuel for inland demand? An integrated assessment of sustainability at regional scale," Energy, **36**, 2111-2118, 2011. https://doi.org/10.1016/j.energy.2010.03.009

[181] M. Karamać, A. Kosińska, I. Estrella, T. Hernández, and M. Duenas, "Antioxidant activity of phenolic compounds identified in sunflower seeds," European Food Research and Technology, vol. **235**, 221-230, 2012. https://doi.org/10.1007/s00217-012-1751-6

[182] Y. Ulusoy, R. Arslan, and C. Kaplan, "Emission characteristics of sunflower oil methyl ester," Energy Sources, Part A, **31**, 906-910, 2009. https://doi.org/10.1080/15567030802087528

[183] C. d. Castro and R. d. C. LEITE, "Main aspects of sunflower production in Brazil," Embrapa Soja-Artigo em periódico indexado (ALICE), 2018. https://doi.org/10.1051/ocl/2017056

[184] C. E. Feoli and J. Ingaramo, South America perspectives on sunflower production and processing: Sunflower, Elsevier, 2015. https://doi.org/10.1016/B978-1-893997-94-3.50023-4

[185] P. Debaeke, P. Casadebaig, F. Flenet, and N. Langlade, "Sunflower crop and climate change: vulnerability, adaptation, and mitigation potential from case-studies in Europe," Ocl, **24**, D102, 2017. doi : 10.1051/ocl/2016052

[186] M. A. Khan, M. Akmal, and M. Afzal, "Fertilizer N-and P-rates response on sunflower inter-cropping with Mungbean in North-West, Pakistan," Basic Res. J. Agri. Rev, **3**, 146-160, 2014.

[187] J. M. Cerveró, J. Coca, and S. Luque, "Production of biodiesel from vegetable oils," Grasas y aceites, **59**, 76-83, 2008. https://doi.org/10.3989/gya.2008.v59.i1.494

[188] G. A. Gbogouri, K. Brou, G. A. M. Beugre, D. Gnakri, and M. Linder, "Assessment of the thermo-oxidation of three cucurbit seed oils by differential scanning calorimetry," Innovative Romanian Food Biotechnology, **12**, 32, 2013.

[189] A. Saydut, A. B. Kafadar, Y. Tonbul, C. Kaya, F. Aydin, and C. Hamamci, "Comparison of the biodiesel quality produced from refined sunflower (Helianthus annuus L) oil and waste cooking oil," Energy Exploration & Exploitation, **28**, 499-512, 2010. https://doi.org/10.1260/0144-5987.28.6.499

[190] B. B. Marvey, "Sunflower-based feedstocks in nonfood applications: perspectives from olefin metathesis," International journal of molecular sciences, **9**, 1393-1406, 2008. https://doi.org/10.3390/ijms9081393

[191] J. Dyer, L. Stringer, and A. Dougill, "Jatropha curcas: Sowing local seeds of success in Malawi?: In response to Achten et al.(2010)," Journal of Arid Environments, **79**, 107-110, 2012. https://doi.org/10.1016/j.jaridenv.2011.12.004

[192] C. M. dos Santos, V. Verissimo, H. C. de Lins Wanderley Filho, V. M. Ferreira, P. G. da Silva Cavalcante, E. V. Rolim, *et al.*, "Seasonal variations of photosynthesis, gas exchange, quantum efficiency of photosystem II and biochemical responses of Jatropha curcas L. grown in semi-humid and semi-arid areas subject to water stress," Industrial Crops and Products, **41**, 203-213, 2013. https://doi.org/10.1016/j.indcrop.2012.04.003

[193] A. Thanapimmetha, A. Luadsongkram, B. Titapiwatanakun, and P. Srinophakun, "Value added waste of Jatropha curcas residue: optimization of protease production in solid state fermentation by Taguchi DOE methodology," Industrial Crops and Products, **37**, 1-5, 2012. https://doi.org/10.1016/j.indcrop.2011.11.003

[194] R. Chandra, V. Vijay, P. Subbarao, and T. Khura, "Production of methane from anaerobic digestion of jatropha and pongamia oil cakes," Applied Energy, **93**, 148-159, 2012. https://doi.org/10.1016/j.apenergy.2010.10.049

[195] P. Kant and S. Wu, "The extraordinary collapse of Jatropha as a global biofuel," ACS Publications, 2011.

[196] B. Singh, K. Singh, G. R. Rao, J. Chikara, D. Kumar, D. Mishra, *et al.*, "Agro-technology of Jatropha curcas for diverse environmental conditions in India," Biomass and bioenergy, **48,** 191-202, 2013. https://doi.org/10.1016/j.biombioe.2012.11.025

[197] C. Everson, M. Mengistu, and M. B. Gush, "A field assessment of the agronomic performance and water use of Jatropha curcas in South Africa," Biomass and Bioenergy, **59**, 59-69, 2013. https://doi.org/10.1016/j.biombioe.2012.03.013

[198] M. P. Dorado, "Raw materials to produce low-cost biodiesel," Biofuels refining and performance, 107-147, 2008.

[199] B. R. Moser, "Biodiesel production, properties, and feedstocks: Vitro Cellular & Developmental Biology-Plant, **45**, 2009. https://doi.org/10.1007/978-1-4419-7145-6_15

[200] S. Pinzi, Garcia, I. L., Lopez-Gimenez, F. J., Luque de Castro, M. D., Dorado, G., & Dorado, M. P,, "The ideal vegetable oil-based biodiesel composition: a review of social, economical and technical implications," Energy & Fuels, **23**, 2325-2341, 2009. https://doi.org/10.1021/ef801098a

[201] M. Balat, "Potential alternatives to edible oils for biodiesel production–A review of current work," Energy conversion and management, **52**, 1479-1492, 2011. https://doi.org/10.1016/j.enconman.2010.10.011

[202] L. Azócar, Heipieper, H. J., & Navia, R,, "Biotechnological processes for biodiesel production using alternative oils.," Applied microbiology and biotechnology, **88**, 621-636, 2010. https://doi.org/10.1007/s00253-010-2804-z

[203] A. Ramadhas, S. Jayaraj, and C. Muraleedharan, "Use of vegetable oils as IC engine fuels—a review," Renewable energy, **29**, 727-742, 2004. https://doi.org/10.1016/j.renene.2003.09.008

[204] A. Atabani, A. Silitonga, H. Ong, T. Mahlia, H. Masjuki, I. A. Badruddin, et al., "Non-edible vegetable oils: a critical evaluation of oil extraction, fatty acid compositions, biodiesel production, characteristics, engine performance and emissions production," Renewable and sustainable energy reviews, **18**, 211-245, 2013. https://doi.org/10.1016/j.rser.2012.10.013

[205] A. Demirbas, "Biodiesel from corn germ oil catalytic and non-catalytic supercritical methanol transesterification," Energy Sources, Part A: Recovery, Utilization, and Environmental Effects, **38**, 1890-1897, 2016. https://doi.org/10.1080/15567036.2015.1004388

[206] M. Haile, "Integrated volarization of spent coffee grounds to biofuels," Biofuel Research Journal, **1**, 65-69, 2014.

[207] I. B. Banković-Ilić, Stojković, I. J., Stamenković, O. S., Veljkovic, V. B., & Hung, Y. T,, "Waste animal fats as feedstocks for biodiesel production. ," Renewable and sustainable energy reviews, vol. **32**, 238-254, 2014. https://doi.org/10.1016/j.rser.2014.01.038

[208] T. Maneerung, Kawi, S., Dai, Y., & Wang, C. H, , "Sustainable biodiesel production via transesterification of waste cooking oil by using CaO catalysts prepared from chicken manure," Energy Conversion and Management, **123**, 487-497, 2016. https://doi.org/10.1016/j.enconman.2016.06.071

[209] Z. Yaakob, M. Mohammad, M. Alherbawi, Z. Alam, and K. Sopian, "Overview of the production of biodiesel from waste cooking oil," Renewable and sustainable energy reviews, **18**, 184-193, 2013. https://doi.org/10.1016/j.rser.2012.10.016

[210] Y. Chen, Xiao, B., Chang, J., Fu, Y., Lv, P., & Wang, X,, "Synthesis of biodiesel from waste cooking oil using immobilized lipase in fixed bed reactor," Energy conversion and management, **50**, 668-673, 2009. https://doi.org/10.1016/j.enconman.2008.10.011

[211] S. M. Hingu, P. R. Gogate, and V. K. Rathod, "Synthesis of biodiesel from waste cooking oil using sonochemical reactors," Ultrasonics sonochemistry, **17**, 827-832, 2010. https://doi.org/10.1016/j.ultsonch.2010.02.010

[212] C. G. Lopresto, Naccarato, S., Albo, L., De Paola, M. G., Chakraborty, S., Curcio, S., & Calabrò, V,, "Enzymatic transesterification of waste vegetable oil to produce biodiesel," Ecotoxicology and environmental safety, **121**, 2015. https://doi.org/10.1016/j.ecoenv.2015.03.028

[213] M. Corral Bobadilla, Lostado Lorza, R., Escribano García, R., Somovilla Gómez, F., & Vergara González, E,, "An improvement in biodiesel production from waste cooking oil by applying thought multi-response surface methodology using desirability functions," Energies, **10**, 130, 2017. https://doi.org/10.3390/en10010130

[214] A. Demirbas, "Relationships derived from physical properties of vegetable oil and biodiesel fuels," Fuel, **87**, 1743-1748, 2008. https://doi.org/10.1016/j.fuel.2007.08.007

[215] G. Knothe, "Dependence of biodiesel fuel properties on the structure of fatty acid alkyl esters," Fuel processing technology, vol. **86**, 1059-1070, 2005. https://doi.org/10.1016/j.fuproc.2004.11.002

[216] P. Poltronieri, Tobacco seed oil for biofuels: *Biotransformation of Agricultural Waste and By-Products*, Elsevier, 2016. https://doi.org/10.1016/B978-0-12-803622-8.00006-9

[217] M. M. Gui, K. Lee, and S. Bhatia, "Feasibility of edible oil vs. non-edible oil vs. waste edible oil as biodiesel feedstock," Energy, **33**, 1646-1653, 2008. https://doi.org/10.1016/j.energy.2008.06.002

[218] B. Sanjay, "Non-conventional seed oils as potential feedstocks for future biodiesel industries: a brief review," Research Journal of Chemical Sciences, 2013. Available online at: www.isca.in

[219] W. Du, & Liu, D. H, Biodiesel from conventional feedstocks: Biotechnology in China III: Biofuels and Bioenergy, Springer, 2012. https://doi.org/10.1007/10_2011_127

[220] M. G. Kulkarni, & Dalai, A. K,, "Waste cooking oil an economical source for biodiesel: a review," Industrial & engineering chemistry research, **45**, 2901-2913, 2006. https://doi.org/10.1021/ie0510526

[221] H. Zhang, Xu, Z., Zhou, D., & Cao, J,, "Waste cooking oil-to-energy under incomplete information: Identifying policy options through an evolutionary game.," Applied energy, **185**, 547-555, 2017. https://doi.org/10.1016/j.apenergy.2016.10.133

[222] H. Vaghari, Jafarizadeh-Malmiri, H., Mohammadlou, M., Berenjian, A., Anarjan, N., Jafari, N., & Nasiri, S, "Application of magnetic nanoparticles in smart enzyme immobilization," Biotechnology letters, **38**, 223-233, 2016. https://doi.org/10.1007/s10529-015-1977-z

[223] Y. Jiang, & Zhang, Y,, "Supply chain optimization of biodiesel produced from waste cooking oil," Transportation Research Procedia, **12**, 938-949, 2016.

[224] M. A. Gonzalez-Salazar, Venturini, M., Poganietz, W. R., Finkenrath, M., Kirsten, T., Acevedo, H., & Spina, P. R,, "Development of a technology roadmap for bioenergy exploitation including biofuels, waste-to-energy and power generation & CHP," Applied energy, **180**, 338-352, 2016. https://doi.org/10.1016/j.apenergy.2016.07.120

[225] M. N. Hussain, Al Samad, T., & Janajreh, I, "Economic feasibility of biodiesel production from waste cooking oil in the UAE," Sustainable cities and Society, **26**, 217-226, 2016. https://doi.org/10.1016/j.scs.2016.06.010

[226] S. Cho, Kim, J., Park, H. C., & Heo, E, "Incentives for waste cooking oil collection in South Korea: a contingent valuation approach," Resources, Conservation and Recycling, **99**, 63-71, 2015. https://doi.org/10.1016/j.resconrec.2015.04.003

[227] N. Escobar, Ribal, J., Clemente, G., Rodrigo, A., Pascual, A., & Sanjuán, N, "Uncertainty analysis in the financial assessment of an integrated management system for restaurant and catering waste in Spain," The International Journal of Life Cycle Assessment, **20**, 1491-1510, 2015. https://doi.org/10.1007/s11367-015-0962-z

[228] S. Liang, Liu, Z., Xu, M., & Zhang, T, "Waste oil derived biofuels in China bring brightness for global GHG mitigation," Bioresource technology, **131**, 139-145, 2013. https://doi.org/10.1016/j.biortech.2012.12.008

[229] H. Zhang, Zhou, Q., Chang, F., Pan, H., Liu, X. F., Li, H., ... & Yang, S,, "Production and fuel properties of biodiesel from Firmiana platanifolia Lf as a potential non-food oil source," Industrial Crops and Products, **76**, 768-771, 2015. https://doi.org/10.1016/j.indcrop.2015.08.002

[230] J. Rodrigues, Oliveira, V., Lopes, P., & Dias-Ferreira, C,, "Door-to-door collection of food and kitchen waste in city centers under the framework of multimunicipal waste management systems in Portugal: the case study of Aveiro," *Waste and biomass valorization*, vol. 6, pp. 647-656, 2015. https://doi.org/10.1007/s12649-015-9366-3

[231] C. Sheinbaum-Pardo, Calderón-Irazoque, A., & Ramírez-Suárez, M,, "Potential of biodiesel from waste cooking oil in Mexico," Biomass and bioenergy, **56**, 230-238, 2013. https://doi.org/10.1016/j.biombioe.2013.05.008

[232] Wikipedia. Biodiesel [Online]. Available: http://en.wikipedia.org/wiki/BiodieselS.

[233] C. Öner, & Altun, Ş, "Biodiesel production from inedible animal tallow and an experimental investigation of its use as alternative fuel in a direct injection diesel engine," Applied energy, **86,** 2114-2120, 2009. https://doi.org/10.1016/j.apenergy.2009.01.005

[234] M. Gürü, B. D. Artukoğlu, A. Keskin, and A. Koca, "Biodiesel production from waste animal fat and improvement of its characteristics by synthesized nickel and magnesium additive," Energy Conversion and Management, **50**, 498-502, 2009. https://doi.org/10.1016/j.enconman.2008.11.001

[235] J. M. Encinar, Sánchez, N., Martínez, G., & García, L, "Study of biodiesel production from animal fats with high free fatty acid content," Bioresource Technology, **102**, 10907-10914, 2011. https://doi.org/10.1016/j.biortech.2011.09.068

[236] A. C. J. Vivian Feddern, Marina Celant De Prá,, J. I. d. S. F. Paulo Giovanni de Abreu, and M. S. a. A. C. Martha Mayumi Higarashi, "Animal Fat Wastes for Biodiesel Production: Biodiesel: feedstocks and processing technologies, BoD–Books on Demand, 2011.

[237] S. K. Dash, & Lingfa, P, "A review on production of biodiesel using catalyzed transesterification," 020100, July 2017. https://doi.org/10.1063/1.4990253

[238] J. V. Gerpen. Animal Fats for Biodiesel Production [Online]. Available:https://farm-energy.extension.org/animal-fats-for-biodiesel-production

[239] J. Janaun and N. Ellis, "Perspectives on biodiesel as a sustainable fuel," Renewable and Sustainable Energy Reviews, **14**, 1312-1320, 2010. https://doi.org/10.1016/j.rser.2009.12.011

[240] M. E. Tat, Van Gerpen, J. H., & Wang, P. S, "Fuel property effects on injection timing, ignition timing and oxides of nitrogen emissions from biodiesel-fueled engines," in *ASAE Annual Meeting*, Minneapolis, Minnesota, USA, 1, 2004.

[241] A. Kerihuel, M. S. Kumar, J. Bellettre, and M. Tazerout, "Ethanol animal fat emulsions as a diesel engine fuel–Part 1: Formulations and influential parameters," Fuel, **85**, 2640-2645, 2006. https://doi.org/10.1016/j.fuel.2006.05.002

[242] K. Satyanarayana, A. Mariano, and J. Vargas, "A review on microalgae, a versatile source for sustainable energy and materials," International Journal of energy research, **35**, 291-311, 2011. https://doi.org/10.1002/er.1695

[243] T. J. Lundquist, I. C. Woertz, N. Quinn, and J. R. Benemann, "A realistic technology and engineering assessment of algae biofuel production," Energy Biosciences Institute, 1, 2010.

[244] A. Demirbas and M. F. Demirbas, "Importance of algae oil as a source of biodiesel," Energy conversion and management, **52**, 163-170, 2011. https://doi.org/10.1016/j.enconman.2010.06.055

[245] L. Brennan and P. Owende, "Biofuels from microalgae—a review of technologies for production, processing, and extractions of biofuels and co-products," Renewable and sustainable energy reviews, **14**, 557-577, 2010. https://doi.org/10.1016/j.rser.2009.10.009

[246] T. M. Mata, A. A. Martins, and N. S. Caetano, "Microalgae for biodiesel production and other applications: a review," Renewable and sustainable energy reviews, **14**, 217-232, 2010. https://doi.org/10.1016/j.rser.2009.07.020

[247] G. Petkov, A. Ivanova, I. Iliev, and I. Vaseva, "A critical look at the microalgae biodiesel," European Journal of Lipid Science and Technology, **114**, 103-111, 2012. https://doi.org/10.1002/ejlt.201100234

[248] H. Xu, X. Miao, and Q. Wu, "High quality biodiesel production from a microalga Chlorella protothecoides by heterotrophic growth in fermenters," Journal of biotechnology, **126**, 499-507, 2006. https://doi.org/10.1016/j.jbiotec.2006.05.002

[249] A. S. Carlsson, J. B. Van Beilen, R. Möller, and D. Clayton, "Micro-and macro-algae: utility for industrial applications," CPL Press, 2007.

[250] D. Vandamme, S. C. V. Pontes, K. Goiris, I. Foubert, L. J. J. Pinoy, and K. Muylaert, "Evaluation of electro-coagulation–flocculation for harvesting marine and freshwater microalgae," Biotechnology and bioengineering, **108**, 2320-2329, 2011. https://doi.org/10.1002/bit.23199

[251] H. C. Greenwell, L. Laurens, R. Shields, R. Lovitt, and K. Flynn, "Placing microalgae on the biofuels priority list: a review of the technological challenges," Journal of the royal society interface, **7**, 703-726, 2009. https://doi.org/10.1098/rsif.2009.0322

[252] K. Sikes, M. Van Walwijk, and R. McGill, "Algae as a Feedstock for Biofuels: An Assessment of the state of technology and Opportunities," Final Report, 1-23, 2010.

[253] Y. Chisti, "Biodiesel from microalgae beats bioethanol," Trends in biotechnology, **26**, 126-131, 2008. https://doi.org/10.1016/j.tibtech.2007.12.002

[254] P. Gerbens-Leenes, G. de Vries, and L. Xu, "The water footprint of biofuels from microalgae," Bioenergy and Water, 191, 2013.

[255] G. Brownbridge, P. Azadi, A. Smallbone, A. Bhave, B. Taylor, and M. Kraft, "The future viability of algae-derived biodiesel under economic and technical uncertainties," Bioresource technology, **151**, 166-173, 2014. https://doi.org/10.1016/j.biortech.2013.10.062

[256] R. Kothari, A. Pandey, S. Ahmad, A. Kumar, V. V. Pathak, and V. Tyagi, "Microalgal cultivation for value-added products: a critical enviro-economical assessment," 3 Biotech, **7**, 243, 2017. https://doi.org/10.1007/s13205-017-0812-8

[257] Y.-T. Hung, L. K. Wang, and N. K. Shammas, Handbook of environment and waste management: air and water pollution control **1**, World Scientific, 2012.

[258] A. Demirbas, "New biorenewable fuels from vegetable oils," Energy sources, Part A: recovery, utilization, and environmental effects, **32**, 628-636, 2010. https://doi.org/10.1080/15567030903058832

[259] M. F. Demirbas, M. Balat, and H. Balat, "Biowastes-to-biofuels," Energy Conversion and Management, **52**, 1815-1828, 2011. https://doi.org/10.1016/j.enconman.2010.10.041

[260] L. S. Oliveira and A. S. Franca, "From solid biowastes to liquid biofuels," Agriculture Issues and Policies Series, **265**, 2009.

[261] T. Michaels, "The 2007 IWSA directory of waste-to-energy plants," Integrated Waste Services Association, **12**, 32-45, 2010.

[262] Lux Research Inc. The Cleantech Report. Waste to energy [Online]. Available: http://www.luxresearchinc.com/pdf/08CTR_tech_profile

[263] M.-A. Perea-Moreno, E. Samerón-Manzano, and A.-J. Perea-Moreno, "Biomass as renewable energy: Worldwide research trends," Sustainability, **11**, 863, 2019. https://doi.org/10.3390/su11030863

[264] L. Visser, R. Hoefnagels, and M. Junginger, "The Potential Contribution of Imported Biomass to Renewable Energy Targets in the EU–the Trade-off between Ambitious Greenhouse Gas Emission Reduction Targets and Cost Thresholds," Energies, **13**, 1761, 2020. https://doi.org/10.3390/en13071761

[265] I. Dunmade, Application of Lifecycle Concepts in the Conversion of Biomass to Value-Added Commodities: Valorization of Biomass to Value-Added Commodities, Springer, 2020. https://doi.org/10.1007/978-3-030-38032-8_25

[266] R. Kataki, N. J. Bordoloi, R. Saikia, D. Sut, R. Narzari, L. Gogoi, et al., Waste Valorization to Fuel and Chemicals Through Pyrolysis: Technology, Feedstock, Products, and Economic Analysis: Waste to Wealth, Springer, 2018. https://doi.org/10.1007/978-981-10-7431-8_21

[267] S.-Y. No, Application of Liquid Biofuels to Internal Combustion Engines, Springer Nature, 2020.

[268] A. H. Demirbas and I. Demirbas, "Importance of rural bioenergy for developing countries," Energy Conversion and Management, **48**, 2386-2398, 2007. https://doi.org/10.1016/j.enconman.2007.03.005

[269] A. Demirbas, "Comparison of thermochemical conversion processes of biomass to hydrogen-rich gas mixtures," Energy Sources, Part A: Recovery, Utilization, and Environmental Effects, **38**, 2971-2976, 2016.

[270] K. R. Jegannathan, E.-S. Chan, and P. Ravindra, "Harnessing biofuels: a global Renaissance in energy production?," Renewable and Sustainable Energy Reviews, **13**, 2163-2168, 2009. https://doi.org/10.1016/j.rser.2009.01.012

[271] A. P. Darzins, Philip Edye, Les "Current status and potential for algal biofuels production," J A report to IEA Bioenergy Task, **39**, 2010.

[272] M. Balat, "An overview of biofuels and policies in the European Union," J Energy Sources, Part B, **2**, 167-181, 2007.

[273] T. L. C. Walker, Chris Purton, Saul,, "Algal Transgenics In The Genomic Era 1," J Journal of Phycology, **41**, 1077-1093, 2005.

[274] M. Vohra, J. Manwar, R. Manmode, S. Padgilwar, and S. Patil, "Bioethanol production: feedstock and current technologies," Journal of Environmental Chemical Engineering, **2**, 573-584, 2014. https://doi.org/10.1016/j.jece.2013.10.013

[275] S. L. Stattman, A. Gupta, L. Partzsch, and P. Oosterveer, "Toward sustainable biofuels in the European Union? Lessons from a decade of hybrid biofuel governance," Sustainability, **10**, 4111, 2018. https://doi.org/10.3390/su10114111

[276] A. Hernández-García, S. B. Velásquez-Orta, E. Novelo, I. Yáñez-Noguez, I. Monje-Ramírez, and M. T. O. Ledesma, "Wastewater-leachate treatment by microalgae: Biomass, carbohydrate and lipid production," Ecotoxicology and Environmental safety, **174**, 435-444, 2019. https://doi.org/10.1016/j.ecoenv.2019.02.052

[277] R. Samiee-Zafarghandi, J. Karimi-Sabet, M. A. Abdoli, and A. Karbassi, "Increasing microalgal carbohydrate content for hydrothermal gasification purposes," Renewable Energy, **116**, 710-719, 2018. https://doi.org/10.1016/j.renene.2017.10.020

[278] M. Hanifzadeh, E. C. Garcia, and S. Viamajala, "Production of lipid and carbohydrate from microalgae without compromising biomass productivities: Role of Ca and Mg," Renewable Energy, **127**, 989-997, 2018. https://doi.org/10.1016/j.renene.2018.05.012

[279] K. T. Chen, Cheng, C. H., Wu, Y. H., Lu, W. C., Lin, Y. H., & Lee, H. T, , "Continuous lipid extraction of microalgae using high-pressure carbon dioxide," Bioresource technology, **146**, 23-26, 2013. https://doi.org/10.1016/j.biortech.2013.07.017

[280] R. A. Bush and K. M. Hall, "Process for the production of ethanol from algae," Google Patents, 2009.

[281] H. Sun, K.Hu, H. Lou, and X. Zheng, "Biodiesel Production from Transesterification of Rapeseed Oil Using KF/Eu 2O 3 as a Catalyst," Energy & Fuels, **22**, 2756-2760, 2008.

[282] S. Nasreen, M. Nafees, L. A. Qureshi, M. S. Asad, A. Sadiq, and S. D. Ali, "Review of Catalytic Transesterification Methods for Biodiesel Production," Biofuels: State of Development, 93, 2018.

[283] S. Mohapatra, P. Das, D. Swain, S. Satapathy, and S. R. Sahu, "A Review on Rejuvenated Techniques in Biodiesel Production from Vegetable Oils," International Journal of Current Engineering and Technology, **6**, 100-111, 2016.

[284] H. T. HAJY and K. Tahvildari, "Efficient Synthesis of biodiesel from waste cooking oil catalysed by Al2O3 impregnated with NaOH," 2015.

[285] M. Yadav and Y. C. Sharma, "Transesterification of used vegetable oil using BaAl2O4 spinel as heterogeneous base catalyst," Energy Conversion and Management, **198**, 111795, 2019. https://doi.org/10.1016/j.enconman.2019.111795

[286] N. Al-Jammal, Z. Al-Hamamre, and M. Alnaief, "Manufacturing of zeolite based catalyst from zeolite tuft for biodiesel production from waste sunflower oil," Renewable Energy, **93**, 449-459, 2016. https://doi.org/10.1016/j.renene.2016.03.018

[287] M. R. Anuar and A. Z. Abdullah, "Challenges in biodiesel industry with regards to feedstock, environmental, social and sustainability issues: a critical review," Renewable and Sustainable Energy Reviews, **58**, 208-223, 2016. https://doi.org/10.1016/j.rser.2015.12.296

[288] S. Lim and L. K. Teong, "Recent trends, opportunities and challenges of biodiesel in Malaysia: an overview," Renewable and Sustainable Energy Reviews, **14**, 938-954, 2010. https://doi.org/10.1016/j.rser.2009.10.027

[289] A. Z. Abdullah, B. Salamatinia, H. Mootabadi, and S. Bhatia, "Current status and policies on biodiesel industry in Malaysia as the world's leading producer of palm oil," Energy Policy, **37**, 5440-5448, 2009. https://doi.org/10.1016/j.enpol.2009.08.012

[290] S. Mekhilef, S. Siga, and R. Saidur, "A review on palm oil biodiesel as a source of renewable fuel," Renewable and Sustainable Energy Reviews, **15**, 1937-1949, 2011. https://doi.org/10.1016/j.rser.2010.12.012

[291] Y. Ariani and S. Yuliar, Translating Biofuel, Discounting Farmers: The Search for Alternative Energy in Indonesia: Actor-Network Theory and Technology Innovation: Advancements and New Concepts, IGI Global, 2011. doi: 10.4018/978-1-60960-197-3.ch005

[292] M. Lister, Unmasking the Invisible Giant: Energy Efficiency in the Politics of Climate and Energy: Energy Security in the Era of Climate Change, Springer, 2012, https://doi.org/10.1057/9780230355361_3

[293] A. Chanthawong and S. Dhakal, "Liquid biofuels development in southeast asian countries: an analysis of market, policies and challenges," Waste and biomass valorization, **7**, 157-173, 2016. https://doi.org/10.1007/s12649-015-9433-9

[294] J. C. Kurnia, S. V. Jangam, S. Akhtar, A. P. Sasmito, and A. S. Mujumdar, "Advances in biofuel production from oil palm and palm oil processing wastes: a review," Biofuel Research Journal, **3**, 332-346, 2016. doi:10.18331/BRJ2016.3.1.3

[295] O. M. Ali, Mamat, R., Rasul, M. G., & Najafi, G, Potential of Biodiesel as Fuel for Diesel Engine: *Clean Energy for Sustainable Development*, Academic Press, 2017. https://doi.org/10.1016/B978-0-12-805423-9.00018-1

[296] D. M. Marinković, M. V. Stanković, A. V. Veličković, J. M. Avramović, M. R. Miladinović, O. O. Stamenković, *et al.*, "Calcium oxide as a promising heterogeneous catalyst for biodiesel production: Current state and perspectives," Renewable and Sustainable Energy Reviews, **56**, 1387-1408, 2016. https://doi.org/10.1016/j.rser.2015.12.007

[297] H. Bateni, A. Saraeian, and C. Able, "A comprehensive review on biodiesel purification and upgrading," Biofuel Research Journal, **4**, 668-690, 2017.

[298] R. Brunet, Carrasco, D., Muñoz, E., Guillén-Gosálbez, G., Katakis, I., & Jiménez, L, "Economic and environmental evaluation of microalgae biodiesel production using process simulation tools," in 22nd European Symposium on Computer Aided Process Engineering, University College, London, UK, 547-551, 2012. https://doi.org/10.1016/B978-0-444-59519-5.50110-6

[299] K. Colombo, Ender, L., & Barros, A. A. C, "The study of biodiesel production using CaO as a heterogeneous catalytic reaction," Egyptian Journal of Petroleum, **26**, 341-349, 2017. https://doi.org/10.1016/j.ejpe.2016.05.006

[300] A. Gaurav, Ng, F. T., & Rempel, G. L, "A new green process for biodiesel production from waste oils via catalytic distillation using a solid acid catalyst–Modeling, economic and environmental analysis," Green Energy & Environment, **1**, 62-74, 2016. https://doi.org/10.1016/j.gee.2016.05.003

[301] S. Karmee, Patria, R., & Lin, C, "Techno-economic evaluation of biodiesel production from waste cooking oil—a case study of Hong Kong," *I*nternational journal of molecular sciences, **16**, 4362-4371, 2015. https://doi.org/10.3390/ijms16034362

[302] J. Price, Nordblad, M., Martel, H. H., Chrabas, B., Wang, H., Nielsen, P. M., & Woodley, J. M, "Scale-up of industrial biodiesel production to 40 m3 using a liquid lipase formulation," Biotechnology and bioengineering, **113**, 1719-1728, 2016.

[303] M. Olkiewicz, Torres, C. M., Jiménez, L., Font, J., & Bengoa, C, " Scale-up and economic analysis of biodiesel production from municipal primary sewage sludge," Bioresource technology, **214**, 122-131, 2016. https://doi.org/10.1016/j.biortech.2016.04.098

[304] X. Fan, & Burton, R, "Recent development of biodiesel feedstocks and the applications of glycerol: a review," Open Fuels & Energy Science Journal, **2**, 100-109, 2009. doi: 10.2174/1876973X01002010100

[305] A. Dermawan, K. Obidzinski, and H. Komarudin, "Withering before full bloom? Bioenergy in Southeast Asia," CIFOR Working Pape*r,* 2012.

[306] EU Parliament Directive 2009/28; EC 2009, "EC of the European Parliament and of the Council of 23 April 2009 on the promotion of the use of energy from renewable sources and amending and subsequently repealing Directives 2001/77/EC and 2003/30/EC (Text with EEA relevance)," Official Journal League, **140**, 16-62, 2009.

[307] Y. Su, Zhang, P., & Su, Y,, "An overview of biofuels policies and industrialization in the major biofuel producing countries," Renewable and Sustainable Energy Reviews, **50**, 991-1003, 2015. https://doi.org/10.1016/j.rser.2015.04.032

[308] U. EPA. Renewable Fuel Standard Program [Online]. Available: https://www.epa.gov/renewable-fuel-standard-program

[309] I. R. E. Agency. Adanced Liquid Biofuels [Online]. Available: https://www.irena.org/-/media/Files /IRENA/Agency/ Publication/ 2016/IRENA_Innovation_Outlook_Advanced_Liquid_Biofuels_2016.pdf

[310] H. C. Ong, Mahlia, T. M. I., Masjuki, H. H., & Honnery, D,, "Life cycle cost and sensitivity analysis of palm biodiesel production," Fuel, **98**, 131-139, 2012. https://doi.org/10.1016/j.fuel.2012.03.031

[311] G. Sorda, Banse, M., & Kemfert, C, "An overview of biofuel policies across the world," Energy policy, **38**, 6977-6988, 2010. https://doi.org/10.1016/j.enpol.2010.06.066

[312] D. Mitchell, "A Note on Rising Food Prices: Policy Research Working Paper 4682," The World Bank, Washington, D.C., United StatesJuly 2008.

[313] J. Tomei, & Helliwell, R, "Food versus fuel? Going beyond biofuels," Land use policy, **56**, 320-326, 2016. https://doi.org/10.1016/j.landusepol.2015.11.015

[314] A. M. Renzaho, Kamara, J. K., & Toole, M,, "Biofuel production and its impact on food security in low and middle income countries: Implications for the post-2015 sustainable development goals," Renewable and Sustainable Energy Reviews, **78**, 503-516, 2017. https://doi.org/10.1016/j.rser.2017.04.072

[315] J. Beckman, Gooch, E., Gopinath, M., & Landes, M, "Market impacts of China and India meeting biofuel targets using traditional feedstocks," Biomass and bioenergy, **108**, 258-564, 2018. https://doi.org/10.1016/j.biombioe.2017.11.018

[316] I. C. Macedo, Seabra, J. E., & Silva, J. E, "Green house gases emissions in the production and use of ethanol from sugarcane in Brazil: the 2005/2006 averages and a prediction for 2020," Biomass and bioenergy, **32**, 582-595, 2008. https://doi.org/10.1016/j.biombioe.2007.12.006

[317] D. Imhoff and C. Badaracoo, "Ethanol: The Farm Bill, Springer, 2019. https://doi.org/10.5822/978-1-61091-975-3_18

[318] S. Mittlefehldt, "From appropriate technology to the clean energy economy: renewable energy and environmental politics since the 1970s," Journal of Environmental Studies and Sciences, **8**, 212-219, 2018. https://doi.org/10.1007/s13412-018-0471-z

[319] D. Bentivoglio, & Rasetti, M, "Biofuel sustainability: review of implications for land use and food price," *Italian Review of Agricultural Economics,* **70**, 7-31, 2015. doi: 10.13128/REA-16975

[320] E. Riegelhaupt, & Chalico, T. A, Opportunities and challenges for biofuel production in Latin America: a forester's perspective. Bogor, Indonesia, Center for International Forestry Research (CIFOR), 2009.

[321] G. Hochman, Scott, Kaplan, Deepak, Rajagopal, David, Zilberman, "Biofuel and food-commodity prices," Agriculture **2**, 272-281, 2012. https://doi.org/10.3390/agriculture2030272

[322] S. A. Wich, Gaveau, D., Abram, N., Ancrenaz, M., Baccini, A., Brend, S., ... & Goossens, B, "Understanding the impacts of land-use policies on a threatened species: is there a future for the Bornean orang-utan?," PLoS One, **7**, e49142, 2012. https://doi.org/10.1371/journal.pone.0049142

[323] R. Bailey, "Another inconvenient truth: How biofuel policies are deepening poverty and accelerating climate change," Oxfam Policy and Practice: Climate Change and Resilience, **4**, 1-58, 2008.

[324] J. Couwenberg, Dommain, R., & Joosten, H, "Greenhouse gas fluxes from tropical peatlands in south-east Asia," Global Change Biology, **16**, 1715-1732, 2010.

[325] A. Hooijer, Page, S., Canadell, J. G., Silvius, M., Kwadijk, J., Wosten, H., & Jauhiainen, J. (2010). . , "Current and future CO$_2$ emissions from drained peatlands in Southeast Asia," Biogeosciences, **7**, 1505-1514, 2010. doi:10.5194/bg-7-1505-2010

[326] M. R. Guariguata, Masera, O. R., Johnson, F. X., von Maltitz, G., Bird, N., Tella, P., & Martínez-Bravo, R, A review of environmental issues in the

context of biofuel sustainability frameworks*, **69**, Center for International Forestry Research (CIFOR), 2011.

[327] C. Moser, Hildebrandt, T., & Bailis, R, "International sustainability standards and certification: Sustainable development of biofuels in Latin America and the Caribbean, Springer, 2014.

[328] S. Naik, V. V. Goud, P. K. Rout, K. Jacobson, and A. K. Dalai, "Characterization of Canadian biomass for alternative renewable biofuel," Renewable energy, **35**, 1624-1631, 2010. https://doi.org/10.1016/j.renene.2009.08.033

[329] S. Shashank, L. Czarnowska, and M. Bogacka, "The influence of compositions of alternative fuels on higher heating values," Archives of Waste Management and Environmental Protection, vol. **17**, 141-148, 2015.

[330] T. Raj, M. Kapoor, R. Gaur, J. Christopher, B. Lamba, D. K. Tuli, *et al.*, "Physical and chemical characterization of various Indian agriculture residues for biofuels production," Energy & Fuels, **29**, 3111-3118, 2015.

[331] A. V. Bridgwater and D. Boocock, An overview of fast pyrolysis of biomass for the production of liquid fuels: Developments in Thermochemical Biomass Conversion, **1/2**, Springer Science & Business Media, 2013.

[332] P. Basu, Pyrolysis and Torrefaction: Biomass gasification, pyrolysis and torrefaction: practical design and theory, Academic press, 2018.

[333] O. A. Pătrăuanu, L. Lazăr, V. I. Popa, and I. Volf, "Influence of particle size and size distribution on kinetic mechanism of spruce bark polyphenols extraction," Development, **8**, 11, 2019.

[334] H. Bennadji, K. Smith, M. J. Serapiglia, and E. M. Fisher, "Effect of particle size on low-temperature pyrolysis of woody biomass," Energy & Fuels, **28**, 7527-7537, 2014. https://doi.org/10.1021/ef501869e

[335] R. Chandra, H. Takeuchi, T. Hasegawa, and V. Vijay, "Experimental evaluation of substrate's particle size of wheat and rice straw biomass on methane production yield," Agricultural Engineering International: CIGR Journal, **17**, 2015.

[336] M. Tripathi, J. N. Sahu, and P. Ganesan, "Effect of process parameters on production of biochar from biomass waste through pyrolysis: A review," Renewable and Sustainable Energy Reviews, **55**, 467-481, 2016. https://doi.org/10.1016/j.rser.2015.10.122

[337] E. Üresin, I. I. Gülsaç, M. S. Budak, M. Ünsal, K. Özgür Büyüksakallı, P. Aksoy, *et al.*, "Effects of operational parameters on bio-oil production from biomass," Waste Management & Research, **37**, 516-529, 2019. https://doi.org/10.1177/0734242X18819192

[338] J. Fermoso, P. Pizarro, J. M. Coronado, and D. P. Serrano, "Advanced biofuels production by upgrading of pyrolysis bio-oil," Wiley Interdisciplinary Reviews: Energy and Environment, **6**, e245, 2017. https://doi.org/10.1002/wene.245

[339] D. Pradhan, R. Singh, H. Bendu, and R. Mund, "Pyrolysis of Mahua seed (Madhuca indica)–Production of biofuel and its characterization," Energy conversion and management, **108**, 529-538, 2016. https://doi.org/10.1016/j.enconman.2015.11.042

[340] P. Fu, S. Hu, J. Xiang, L. Sun, S. Su, and S. An, "Study on the gas evolution and char structural change during pyrolysis of cotton stalk," Journal of Analytical and Applied Pyrolysis, **97**, 130-136, 2012. https://doi.org/10.1016/j.jaap.2012.05.012

[341] K. Zeng, D. P. Minh, D. Gauthier, E. Weiss-Hortala, A. Nzihou, and G. Flamant, "The effect of temperature and heating rate on char properties obtained from solar pyrolysis of beech wood," Bioresource technology, **182**, 114-119, 2015. https://doi.org/10.1016/j.biortech.2015.01.112

[342] A. P. Muroyama and P. G. Loutzenhiser, "Kinetic analyses of gasification and combustion reactions of carbonaceous feedstocks for a hybrid solar/autothermal gasification process to continuously produce synthesis gas," Energy & Fuels, **30**, 4292-4299, 2016. https://doi.org/10.1021/acs.energyfuels.6b00359

[343] M. Pande and A. N. Bhaskarwar, "Biomass conversion to energy: Biomass Conversion, Springer, 2012. https://doi.org/10.1007/978-3-642-28418-2_1

[344] D. Shen, W. Jin, J. Hu, R. Xiao, and K. Luo, "An overview on fast pyrolysis of the main constituents in lignocellulosic biomass to valued-added chemicals: structures, pathways and interactions," Renewable and Sustainable Energy Reviews, **51**, 761-774, 2015. https://doi.org/10.1016/j.rser.2015.06.054

[345] P. Roy and G. Dias, "Prospects for pyrolysis technologies in the bioenergy sector: a review," Renewable and Sustainable Energy Reviews, **77**, 59-69, 2017. https://doi.org/10.1016/j.rser.2017.03.136

[346] E. Cetin, R. Gupta, and B. Moghtaderi, "Effect of pyrolysis pressure and heating rate on radiata pine char structure and apparent gasification reactivity," Fuel, **84**, 1328-1334, 2005. https://doi.org/10.1016/j.fuel.2004.07.016

[347] R. Kaur, P. Gera, and M. K. Jha, "Study on Effects of Different Operating Parameters on the Pyrolysis of Biomass: A Review," Journal of Biofuels and

Bioenergy (December 2015), **1**, 135-147, 2015. doi: 10.5958/2454-8618.2015.00015.2

[348] A. Debdoubi, A. El Amarti, E. Colacio, M. Blesa, and L. Hajjaj, "The effect of heating rate on yields and compositions of oil products from esparto pyrolysis," International Journal of Energy Research, **30**, 1243-1250, 2006. https://doi.org/10.1002/er.1215

[349] H. C. Butterman and M. J. Castaldi, "Biomass to fuels: impact of reaction medium and heating rate," Environmental Engineering Science, **27**, 539-555, 2010.

[350] P. Fu, S. Hu, J. Xiang, L. Sun, S. Su, and J. Wang, "Evaluation of the porous structure development of chars from pyrolysis of rice straw: Effects of pyrolysis temperature and heating rate," Journal of Analytical and Applied Pyrolysis, **98**, 177-183, 2012. https://doi.org/10.1016/j.jaap.2012.08.005

[351] D. Angın, "Effect of pyrolysis temperature and heating rate on biochar obtained from pyrolysis of safflower seed press cake," Bioresource technology, **128**, 593-597, 2013. https://doi.org/10.1016/j.biortech.2012.10.150

[352] Q. Lu, W.-Z. Li, and X.-F. Zhu, "Overview of fuel properties of biomass fast pyrolysis oils," Energy Conversion and Management, **50**, 1376-1383, 2009. https://doi.org/10.1016/j.enconman.2009.01.001

[353] G. Chen, J. Andries, Z. Luo, and H. Spliethoff, "Biomass pyrolysis/gasification for product gas production: the overall investigation of parametric effects," Energy conversion and management, **44**, 1875-1884, 2003. https://doi.org/10.1016/S0196-8904(02)00188-7

[354] H. Yang, R. Yan, H. Chen, D. H. Lee, D. T. Liang, and C. Zheng, "Pyrolysis of palm oil wastes for enhanced production of hydrogen rich gases," Fuel Processing Technology, **87**, 935-942, 2006. https://doi.org/10.1016/j.fuproc.2006.07.001

[355] S. Fremaux, S.-M. Beheshti, H. Ghassemi, and R. Shahsavan-Markadeh, "An experimental study on hydrogen-rich gas production via steam gasification of biomass in a research-scale fluidized bed," Energy conversion and management, **91**, 427-432, 2015. https://doi.org/10.1016/j.enconman.2014.12.048

[356] D. Baruah, D. Baruah, and M. Hazarika, "Artificial neural network based modeling of biomass gasification in fixed bed downdraft gasifiers," Biomass and bioenergy, **98**, 264-271, 2017. https://doi.org/10.1016/j.biombioe.2017.01.029

[357] G. T. Jeong, Yang, H. S., & Park, D. H, "Optimization of transesterification of animal fat ester using response surface methodology," Bioresource technology, **100**, 25-30, 2009. https://doi.org/10.1016/j.biortech.2008.05.011

[358] H. N. Bhatti, Hanif, M. A., & Qasim, M, "Biodiesel production from waste tallow," Fuel, **87**, 2961-2966, 2008. https://doi.org/10.1016/j.fuel.2008.04.016

[359] J. Xue, Grift, T. E., & Hansen, A. C, "Effect of biodiesel on engine performances and emissions," Renewable and Sustainable energy reviews, **15**, 1098-1116, 2011. https://doi.org/10.1016/j.rser.2010.11.016

[360] A. Saydut, Kafadar, A. B., Aydin, F., Erdogan, S., Kaya, C., & Hamamci, C, "Effect of homogeneous alkaline catalyst type on biodiesel production from soybean [Glycine max (L.) Merrill] oil," 2016. http://nopr.niscair.res.in/handle/123456789/41020

[361] E. C. Santos, dos Santos, T. C., Guimarães, R. B., Ishida, L., Freitas, R. S., & Ronconi, C. M, "Guanidine-functionalized Fe₃O₄ magnetic nanoparticles as basic recyclable catalysts for biodiesel production," RSC Advances, **5**, 48031-48038, 2015. doi: 10.1039/C5RA07331F

[362] G. Baskar, Gurugulladevi, A., Nishanthini, T., Aiswarya, R., & Tamilarasan, K, "Optimization and kinetics of biodiesel production from Mahua oil using manganese doped zinc oxide nanocatalyst," Renewable energy, **103**, 641-646, 2017. https://doi.org/10.1016/j.renene.2016.10.077

[363] G. Baskar, & Soumiya, S, "Production of biodiesel from castor oil using iron (II) doped zinc oxide nanocatalyst," Renewable Energy, **98**, 101-107, 2016. https://doi.org/10.1016/j.renene.2016.02.068

[364] M. R. Avhad, & Marchetti, J. M, Uses of Enzymes for Biodiesel Production: Advanced Bioprocessing for Alternative Fuels, Biobased Chemicals, and Bioproducts, Woodhead Publishing, 2019. https://doi.org/10.1016/B978-0-12-817941-3.00007-3

[365] J. Thangaraja and C. Kannan, "Effect of exhaust gas recirculation on advanced diesel combustion and alternate fuels-A review," Applied Energy, **180**, 169-184, 2016. https://doi.org/10.1016/j.apenergy.2016.07.096

[366] J. G. Speight, Thermal Cracking Processes: Heavy Oil Recovery and Upgrading, Gulf Professional Publishing, 2019.

[367] V. Wiggers, H. Meier, A. Wisniewski Jr, A. C. Barros, and M. W. Maciel, "Biofuels from continuous fast pyrolysis of soybean oil: a pilot plant study," Bioresource technology, **100**, 6570-6577, 2009. https://doi.org/10.1016/j.biortech.2009.07.059

441

[368] M. Omidghane, E. Jenab, M. Chae, and D. C. Bressler, "Production of renewable hydrocarbons by thermal cracking of oleic acid in the presence of water," Energy & Fuels, **31**, 9446-9454, 2017. https://doi.org/10.1021/acs.energyfuels.7b00988

[369] P. Tamunaidu and S. Bhatia, "Catalytic cracking of palm oil for the production of biofuels: optimization studies," Bioresource Technology, **98**, 3593-3601, 2007. https://doi.org/10.1016/j.biortech.2006.11.028

[370] J. C. Serrano-Ruiz and J. A. Dumesic, "Catalytic routes for the conversion of biomass into liquid hydrocarbon transportation fuels," Energy & Environmental Science, **4**, 83-99, 2011. doi: 10.1039/C0EE00436G

[371] B. Thangaraj, P. R. Solomon, B. Muniyandi, S. Ranganathan, and L. Lin, "Catalysis in biodiesel production—a review," Clean Energy, **3**, 2-23, 2019. https://doi.org/10.1093/ce/zky020

[372] A. Demirbas, "Biodiesel production from vegetable oils via catalytic and non-catalytic supercritical methanol transesterification methods," Progress in energy and combustion science, **31**, 466-487, 2005. https://doi.org/10.1016/j.pecs.2005.09.001

[373] F. R. Amin, H. Khalid, H. Zhang, S. u Rahman, R. Zhang, G. Liu, et al., "Pretreatment methods of lignocellulosic biomass for anaerobic digestion," Amb Express, **7**, 72, 2017. https://doi.org/10.1186/s13568-017-0375-4

[374] N. S. Talha and S. Sulaiman, "Overview of catalysts in biodiesel production," ARPN Journal of Engineering and Applied Sciences, **11**, 439-48, 2016.

[375] Z. Guo, B. Liu, Q. Zhang, W. Deng, Y. Wang, and Y. Yang, "Recent advances in heterogeneous selective oxidation catalysis for sustainable chemistry," Chemical Society Reviews, **43**, 3480-3524, 2014. doi: 10.1039/C3CS60282F

[376] N. Hindryawati, G. P. Maniam, M. R. Karim, and K. F. Chong, "Transesterification of used cooking oil over alkali metal (Li, Na, K) supported rice husk silica as potential solid base catalyst," Engineering Science and Technology, an International Journal, **17**, 95-103, 2014. https://doi.org/10.1016/j.jestch.2014.04.002

[377] B. Thangaraj, Jia, Z., Dai, L., Liu, D., & Du, W, "Lipase NS81006 immobilized on Fe3O4 magnetic nanoparticles for biodiesel production," Ovidius University Annals of Chemistry, **27**, 13-21, 2016. https://doi.org/10.1515/auoc-2016-0008

[378] C. Li, H. Wang, Y. Luo, G. Wen, and Z. Jiang, "A novel gold nanosol SERS quantitative analysis method for trace Na+ based on carbon dot catalysis," Food chemistry, **289**, 531-536, 2019. https://doi.org/10.1016/j.foodchem.2019.03.032

[379] M. Math and K. Chandrashekhara, "Optimization of alkali catalyzed transesterification of safflower oil for production of biodiesel," Journal of Engineering, **2016**, 2016. https://doi.org/10.1155/2016/8928673

[380] V. T. da Silva and L. A. Sousa, Catalytic upgrading of fats and vegetable oils for the production of fuels: The role of catalysis for the sustainable production of bio-fuels and bio-chemicals, Elsevier, 2013. https://doi.org/10.1016/B978-0-444-56330-9.00003-6

[381] I. Atadashi, M. K. Aroua, A. A. Aziz, and N. Sulaiman, "The effects of water on biodiesel production and refining technologies: A review," Renewable and sustainable energy reviews, **16**, 3456-3470, 2012. https://doi.org/10.1016/j.rser.2012.03.004

[382] I. Atadashi, M. K. Aroua, A. A. Aziz, and N. Sulaiman, "Production of biodiesel using high free fatty acid feedstocks," Renewable and sustainable energy reviews, **16**, 3275-3285, 2012. https://doi.org/10.1016/j.rser.2012.02.063

[383] H. Luo, W. Fan, Y. Li, and G. Nan, "Biodiesel production using alkaline ionic liquid and adopted as lubricity additive for low-sulfur diesel fuel," Bioresource technology, **140**, 337-341, 2013. https://doi.org/10.1016/j.biortech.2012.11.112

[384] J. Shabaker, G. Huber, and J. Dumesic, "Aqueous-phase reforming of oxygenated hydrocarbons over Sn-modified Ni catalysts," Journal of Catalysis, **222**, 180-191, 2004. https://doi.org/10.1016/j.jcat.2003.10.022

[385] R. Davda, J. Shabaker, G. Huber, R. Cortright, and J. A. Dumesic, "A review of catalytic issues and process conditions for renewable hydrogen and alkanes by aqueous-phase reforming of oxygenated hydrocarbons over supported metal catalysts," Applied Catalysis B: Environmental, **56**, 71-186, 2005. https://doi.org/10.1016/j.apcatb.2004.04.027

[386] T. Hirai, N.-o. Ikenaga, T. Miyake, and T. Suzuki, "Production of hydrogen by steam reforming of glycerin on ruthenium catalyst," Energy & Fuels, **19**, 1761-1762, 2005. https://doi.org/10.1021/ef050121q

[387] F. Yang, M. A. Hanna, and R. Sun, "Value-added uses for crude glycerol--a byproduct of biodiesel production," Biotechnology for biofuels, **5**, 13, 2012. https://doi.org/10.1186/1754-6834-5-13

[388] B. J. Kerr, W. A. Dozier III, and K. Bregendahl, "Nutritional value of crude glycerin for nonruminants," in Proceedings of the 68th Minnesota nutrition conference: Modern Concepts In Livestock Production, 220-234, 2007.

[389] Z. Chi, D. Pyle, Z. Wen, C. Frear, and S. Chen, "A laboratory study of producing docosahexaenoic acid from biodiesel-waste glycerol by microalgal fermentation," Process Biochemistry, **42**, 1537-1545, 2007. https://doi.org/10.1016/j.procbio.2007.08.008

[390] R. D. Ashby, D. K. Solaiman, and T. A. Foglia, "Bacterial poly (hydroxyalkanoate) polymer production from the biodiesel co-product stream," Journal of Polymers and the Environment, **12**, 105-112, 2004. https://doi.org/10.1023/B:JOOE.0000038541.54263.d9

[391] G. Mothes, C. Schnorpfeil, and J. U. Ackermann, "Production of PHB from crude glycerol," Engineering in Life Sciences, **7**, 475-479, 2007.

[392] Y. Liang, Y. Cui, J. Trushenski, and J. W. Blackburn, "Converting crude glycerol derived from yellow grease to lipids through yeast fermentation," Bioresource technology, **101**, 7581-7586, 2010. https://doi.org/10.1016/j.biortech.2010.04.061

[393] Y. Liang, N. Sarkany, Y. Cui, and J. W. Blackburn, "Batch stage study of lipid production from crude glycerol derived from yellow grease or animal fats through microalgal fermentation," Bioresource technology, **101**, 6745-6750, 2010. https://doi.org/10.1016/j.biortech.2010.03.087

[394] S. Papanikolaou and G. Aggelis, "Biotechnological valorization of biodiesel derived glycerol waste through production of single cell oil and citric acid by Yarrowia lipolytica," Lipid technology, **21**, 83-87, 2009.

[395] S. Papanikolaou, S. Fakas, M. Fick, I. Chevalot, M. Galiotou-Panayotou, M. Komaitis, et al., "Biotechnological valorisation of raw glycerol discharged after bio-diesel (fatty acid methyl esters) manufacturing process: production of 1, 3-propanediol, citric acid and single cell oil," Biomass and bioenergy, **32**, 60-71, 2008. https://doi.org/10.1016/j.biombioe.2007.06.007

[396] G. Baskar, G. Kalavathy, R. Aiswarya, and I. A. Selvakumari, Advances in bio-oil extraction from nonedible oil seeds and algal biomass: Advances in Eco-Fuels for a Sustainable Environment, Elsevier, 2019. https://doi.org/10.1016/B978-0-08-102728-8.00007-3

[397] M. Quader and S. Ahmed, Bioenergy with carbon capture and storage (BECCS): future prospects of carbon-negative technologies, Elsevier, 2017. https://doi.org/10.1016/B978-0-12-805423-9.00004-1

[398] A. K. Azad, M. Rasul, M. M. Khan, and S. Sharma, "Macadamia biodiesel as a sustainable and alternative transport fuel in Australia," Energy Procedia, **110**, 543-548, 2017. https://doi.org/10.1016/j.egypro.2017.03.182

[399] A. Azad, "Biodiesel from mandarin seed oil: a surprising source of alternative fuel," Energies, **10**, 1689, 2017. https://doi.org/10.3390/en10111689

[400] S. Reham, H. H. Masjuki, M. Kalam, I. Shancita, I. R. Fattah, and A. Ruhul, "Study on stability, fuel properties, engine combustion, performance and emission characteristics of biofuel emulsion," Renewable and Sustainable Energy Reviews, **52**, 1566-1579, 2015. https://doi.org/10.1016/j.rser.2015.08.013

[401] S. Vellaiyan, "Enhancement in combustion, performance, and emission characteristics of a biodiesel-fueled diesel engine by using water emulsion and nanoadditive," Renewable Energy, **145**, 2108-2120, 2020. https://doi.org/10.1016/j.renene.2019.07.140

[402] F. Y. Hagos, O. M. Ali, R. Mamat, and A. A. Abdullah, "Effect of emulsification and blending on the oxygenation and substitution of diesel fuel for compression ignition engine," Renewable and Sustainable Energy Reviews, **75**, 1281-1294, 2017. https://doi.org/10.1016/j.rser.2016.11.113

[403] K. Araújo, D. Mahajan, R. Kerr, and M. d. Silva, "Global biofuels at the crossroads: an overview of technical, policy, and investment complexities in the sustainability of biofuel development," Agriculture, **7**, 32, 2017. https://doi.org/10.3390/agriculture7040032

[404] J. Lane, "Biofuels mandates around the world," Biofuels Digest, **3**, 2016.

[405] Z. Wang, S. Wu, Y. Huang, S. Huang, S. Shi, X. Cheng, et al., "Experimental investigation on spray, evaporation and combustion characteristics of ethanol-diesel, water-emulsified diesel and neat diesel fuels," Fuel, **231**, 438-448, 2018. https://doi.org/10.1016/j.fuel.2018.05.129

[406] T. Yatsufusa, T. Kumura, Y. Nakagawa, and Y. Kidoguchi, "Advantage of using water-emulsified fuel on combustion and emission characteristics," Fuel, **5**, 2009.

[407] M. Huo, S. Lin, H. Liu, and F. L. Chia-fon, "Study on the spray and combustion characteristics of water–emulsified diesel," Fuel, **123**, 218-229, 2014. https://doi.org/10.1016/j.fuel.2013.12.035

[408] Z. Wang, S. Shi, S. Huang, J. Tang, T. Du, X. Cheng, et al., "Effects of water content on evaporation and combustion characteristics of water emulsified diesel spray," Applied energy, **226**, 397-407, 2018. https://doi.org/10.1016/j.apenergy.2018.06.023

[409] C. F. Uzoh, A. Nnuekwe, O. Onukwuli, S. Ofochebe, and E. Chinyere, "Optimal Route for Effective Conversion of Rubber Seed Oil to Biodiesel with Desired Key fuel properties," Journal of Cleaner Production, **280**(1), 124563, 2020. https://doi.org/10.1016/j.jclepro.2020.124563

[410] Y.-K. Oh, K.-R. Hwang, C. Kim, J. R. Kim, and J.-S. Lee, "Recent developments and key barriers to advanced biofuels: a short review," Bioresource technology, **257**, 320-333, 2018. https://doi.org/10.1016/j.biortech.2018.02.089

[411] S. Maroa and F. Inambao, Biodiesels Production Procceses and Technologies: Biodiesel, Combustion, Performance and Emissions Characteristics, Springer, 2020. https://doi.org/10.1007/978-3-030-51166-1_3

[412] C. J. Chuck, Bannister, C. D., Hawley, J. G., Davidson, M. G., La Bruna, I., & Paine, A, "Predictive model to assess the molecular structure of biodiesel fuel," Energy & Fuels, **23**, 290-2294, 2009. https://doi.org/10.1021/ef801085s

[413] U. S. Congress, "Energy Independence and Security Act of 2007," U.S. Congress, Washinton, DC, USA19/12/2007 2007.

[414] S. K. Hoekman, A. Broch, C. Robbins, E. Ceniceros, and M. Natarajan, "Review of biodiesel composition, properties, and specifications," Renewable and sustainable energy reviews, **16**, 43-169, 2012. https://doi.org/10.1016/j.rser.2011.07.143

[415] J. K. Kurian, G. R. Nair, A. Hussain, and G. V. Raghavan, "Feedstocks, logistics and pre-treatment processes for sustainable lignocellulosic biorefineries: a comprehensive review," Renewable and Sustainable Energy Reviews, **25**, 205-219, 2013. https://doi.org/10.1016/j.rser.2013.04.019

[416] Z. Yue, D. Ma, S. Peng, X. Zhao, T. Chen, and J. Wang, "Integrated utilization of algal biomass and corn stover for biofuel production," Fuel, **168**, 1-6, 2016. https://doi.org/10.1016/j.fuel.2015.11.079

[417] N. R. Baral and A. Shah, "Comparative techno-economic analysis of steam explosion, dilute sulfuric acid, ammonia fiber explosion and biological pretreatments of corn stover," Bioresource technology, **232**, 331-343, 2017. https://doi.org/10.1016/j.biortech.2017.02.068

[418] T. P. Durrett, C. Benning, and J. Ohlrogge, "Plant triacylglycerols as feedstocks for the production of biofuels," The Plant Journal, **54**, 593-607, 2008. https://doi.org/10.1111/j.1365-313X.2008.03442.x

[419] A. S. Carlsson, "Plant oils as feedstock alternatives to petroleum–A short survey of potential oil crop platforms," Biochimie, **91**, 665-670, 2009. https://doi.org/10.1016/j.biochi.2009.03.021

[420] T. Eryilmaz, M. K. Yesilyurt, C. Cesur, and O. Gokdogan, "Biodiesel production potential from oil seeds in Turkey," Renewable and Sustainable Energy Reviews, **58**, 842-851, 2016. https://doi.org/10.1016/j.rser.2015.12.172

[421] H. Venkatesan and S. Sivamani, "Cotton seed biodiesel as alternative fuel: production and its characterization analysis using spectroscopic studies," International Journal of Renewable Energy Research (IJRER), **7**, 1333-1339, 2017. www.ijrer.org(6085)

[422] A. Karmakar, S. Karmakar, and S. Mukherjee, "Properties of various plants and animals feedstocks for biodiesel production," Bioresource technology, **101**, 7201-7210, 2010. https://doi.org/10.1016/j.biortech.2010.04.079

[423] A. B. Fadhil and W. S. Abdulahad, "Transesterification of mustard (Brassica nigra) seed oil with ethanol: purification of the crude ethyl ester with activated carbon produced from de-oiled cake," Energy conversion and management, **77**, 495-503, 2014. https://doi.org/10.1016/j.enconman.2013.10.008

[424] C. Ciubota-Rosie, J. R. Ruiz, M. J. Ramos, and Á. Pérez, "Biodiesel from Camelina sativa: a comprehensive characterisation," Fuel, **105**, 572-577, 2013. https://doi.org/10.1016/j.fuel.2012.09.062

[425] E. Mupondwa, X. Li, K. Falk, R. Gugel, and L. Tabil, "Technoeconomic analysis of small-scale farmer-owned Camelina oil extraction as feedstock for biodiesel production: a case study in the Canadian prairies," Industrial Crops and Products, **90**, 76-86, 2016. https://doi.org/10.1016/j.indcrop.2016.05.042

[426] C. Ilkılıç, S. Aydın, R. Behcet, and H. Aydin, "Biodiesel from safflower oil and its application in a diesel engine," Fuel processing technology, **92**, 356-362, 2011. https://doi.org/10.1016/j.fuproc.2010.09.028

[427] C. Hamamci, A. Saydut, Y. Tonbul, C. Kaya, and A. Kafadar, "Biodiesel production via transesterification from safflower (Carthamus tinctorius L.) seed oil," Energy Sources, Part A: Recovery, Utilization, and Environmental Effects, **33**, 512-520, 2011.

[428] J. S. Requena, A. C. Guimaraes, S. Q. Alpera, E. R. Gangas, S. Hernandez-Navarro, L. N. Gracia, et al., "Life Cycle Assessment (LCA) of the biofuel production process from sunflower oil, rapeseed oil and soybean oil," Fuel Processing Technology, **92**, 190-199, 2011. https://doi.org/10.1016/j.fuproc.2010.03.004

[429] E. M. Visser, D. Oliveira Filho, M. A. Martins, and B. L. Steward, "Bioethanol production potential from Brazilian biodiesel co-products," Biomass and bioenergy, **35**, 489-494, 2011. https://doi.org/10.1016/j.biombioe.2010.09.009

[430] F. Barontini, M. Simone, F. Triana, A. Mancini, G. Ragaglini, and C. Nicolella, "Pilot-scale biofuel production from sunflower crops in central Italy," Renewable energy, **83**, 954-962, 2015. https://doi.org/10.1016/j.renene.2015.05.043

[431] T. Issariyakul and A. K. Dalai, "Biodiesel production from greenseed canola oil," Energy & Fuels, **24**, 4652-4658, 2010. https://doi.org/10.1021/ef901202b

[432] C. Baroi, S. Mahto, C. Niu, and A. K. Dalai, "Biofuel production from green seed canola oil using zeolites," Applied Catalysis A: General, **469**, 18-32, 2014. https://doi.org/10.1016/j.apcata.2013.09.034

[433] S. Nithya, S. Manigandan, P. Gunasekar, J. Devipriya, and W. Saravanan, "The effect of engine emission on canola biodiesel blends with TiO2," International Journal of Ambient Energy, **40**, 838-841, 2019. https://doi.org/10.1080/01430750.2017.1421583

[434] P. Verma and M. Sharma, "Review of process parameters for biodiesel production from different feedstocks," Renewable and Sustainable Energy Reviews, **62**, 1063-1071, 2016. https://doi.org/10.1016/j.rser.2016.04.054

[435] J. L. Solis, A. L. Berkemar, L. Alejo, and Y. Kiros, "Biodiesel from rapeseed oil (Brassica napus) by supported Li 2 O and MgO," International Journal of Energy and Environmental Engineering, **8**, 9-23, 2017. https://doi.org/10.1007/s40095-016-0226-0

[436] C. M. Fernández, L. Fiori, M. J. Ramos, Á. Pérez, and J. F. Rodríguez, "Supercritical extraction and fractionation of Jatropha curcas L. oil for biodiesel production," The Journal of Supercritical Fluids, **97**, 100-106, 2015. https://doi.org/10.1016/j.supflu.2014.11.010

[437] D. A. Torres-Rodríguez, I. C. Romero-Ibarra, I. A. Ibarra, and H. Pfeiffer, "Biodiesel production from soybean and Jatropha oils using cesium impregnated sodium zirconate as a heterogeneous base catalyst," Renewable Energy, vol. **93**, 323-331, 2016. https://doi.org/10.1016/j.renene.2016.02.061

[438] J. Rodrigues, A. Canet, I. Rivera, N. Osório, G. Sandoval, F. Valero, et al., "Biodiesel production from crude Jatropha oil catalyzed by non-commercial immobilized heterologous Rhizopus oryzae and Carica papaya lipases," Bioresource technology, **213**, 88-95, 2016. https://doi.org/10.1016/j.biortech.2016.03.011

[439] K. Singh, B. Singh, S. K. Verma, and D. Patra, "Jatropha curcas: a ten year story from hope to despair," Renewable and Sustainable Energy Reviews, **35**, 356-360, 2014. https://doi.org/10.1016/j.rser.2014.04.033

[440] N. A. Musa, G. M. Teran, and S. A. Yaman, "Characterization of coconut oil and its biodiesel," Journal of Scientific Research and Reports, **9**(6), 1-6, 2016. https://doi.org/10.9734/JSRR/2016/22293

[441] B. Venkatesagowda, E. Ponugupaty, A. M. Barbosa-Dekker, and R. F. Dekker, "The purification and characterization of lipases from Lasiodiplodia theobromae, and their immobilization and use for biodiesel production from coconut oil," Applied biochemistry and biotechnology, **185**, 619-640, 2018. https://doi.org/10.1007/s12010-017-2670-6

[442] W. Roschat, T. Siritanon, B. Yoosuk, and V. Promarak, "Biodiesel production from palm oil using hydrated lime-derived CaO as a low-cost basic heterogeneous catalyst," Energy conversion and management, **108**, 459-467, 2016. https://doi.org/10.1016/j.enconman.2015.11.036

[443] A. Johari, B. B. Nyakuma, S. H. M. Nor, R. Mat, H. Hashim, A. Ahmad, et al., "The challenges and prospects of palm oil based biodiesel in Malaysia," Energy, **81**, 255-261, 2015. https://doi.org/10.1016/j.energy.2014.12.037

[444] V. F. de Almeida, P. J. García-Moreno, A. Guadix, and E. M. Guadix, "Biodiesel production from mixtures of waste fish oil, palm oil and waste frying oil: Optimization of fuel properties," Fuel Processing Technology, **133**, 152-160, 2015. https://doi.org/10.1016/j.fuproc.2015.01.041

[445] M. Mubarak, A. Shaija, and T. Suchithra, "A review on the extraction of lipid from microalgae for biodiesel production," Algal Research, **7**, 117-123, 2015. https://doi.org/10.1016/j.algal.2014.10.008

[446] J.-Y. Park, M. S. Park, Y.-C. Lee, and J.-W. Yang, "Advances in direct transesterification of algal oils from wet biomass," Bioresource Technology, **184**, 267-275, 2015. https://doi.org/10.1016/j.biortech.2014.10.089

[447] N. Yodsuwan, P. Kamonpatana, Y. Chisti, and S. Sirisansaneeyakul, "Ohmic heating pretreatment of algal slurry for production of biodiesel," Journal of biotechnology, **267**, 71-78, 2018. https://doi.org/10.1016/j.jbiotec.2017.12.022

[448] B. Sajjadi, A. A. A. Raman, and H. Arandiyan, "A comprehensive review on properties of edible and non-edible vegetable oil-based biodiesel: composition, specifications and prediction models," Renewable and

Sustainable Energy Reviews, **63**, 62-92, 2016. https://doi.org/10.1016/j.rser.2016.05.035

[449] D. Singh, D. Sharma, S. Soni, S. Sharma, and D. Kumari, "Chemical compositions, properties, and standards for different generation biodiesels: A review," Fuel, **253**, 60-71, 2019. https://doi.org/10.1016/j.fuel.2019.04.174

[450] G. Knothe, "Biodiesel and renewable diesel: a comparison," Progress in energy and combustion science, **36**, 364-373, 2010. https://doi.org/10.1016/j.pecs.2009.11.004

[451] T. Manchanda, R. Tyagi, and D. K. Sharma, "Comparison of fuel characteristics of green (renewable) diesel with biodiesel obtainable from algal oil and vegetable oil," Energy Sources, Part A: Recovery, Utilization, and Environmental Effects, **40**, 54-59, 2018. https://doi.org/10.1080/15567036.2017.1405109

[452] T. Kalnes, T. Marker, and D. R. Shonnard, "Green diesel: a second generation biofuel," International Journal of Chemical Reactor Engineering, **5 (1)**, 2007. https://doi.org/10.2202/1542-6580.1554

[453] M. Vojtisek-Lom, V. Beránek, P. Mikuška, K. Křůmal, P. Coufalík, J. Sikorová, *et al.*, "Blends of butanol and hydrotreated vegetable oils as drop-in replacement for diesel engines: Effects on combustion and emissions," Fuel, **197**, 407-421, 2017. https://doi.org/10.1016/j.fuel.2017.02.039

[454] A. Dimitriadis, I. Natsios, A. Dimaratos, D. Katsaounis, Z. Samaras, S. Bezergianni, *et al.*, "Evaluation of a hydrotreated vegetable oil (HVO) and effects on emissions of a passenger car diesel engine," Frontiers in Mechanical Engineering, **4**, 7, 2018. https://doi.org/10.3389/fmech.2018.00007

[455] M. Mofijur, Rasul, M. G., Hassan, N. M. S., Masjuki, H. H., Kalam, M. A., & Mahmudul, H. M, Assessment of Physical, Chemical, and Tribological Properties of Different Biodiesel Fuels: Clean Energy for Sustainable Development, Academic Press, 2017. https://doi.org/10.1016/B978-0-12-805423-9.00014-4

[456] U. Rajak, Nashine, P., Singh, T. S., & Verma, T. N, "Numerical investigation of performance, combustion and emission characteristics of various biofuels," Energy Conversion and Management, **156**, 235-252, 2018. https://doi.org/10.1016/j.enconman.2017.11.017

[457] O. M. Ali, Mamat, R., Masjuki, H. H., & Abdullah, A. A, "Analysis of blended fuel properties and cycle-to-cycle variation in a diesel engine with a diethyl ether additive," Energy conversion and management, **108**, 511-519, 2016. https://doi.org/10.1016/j.enconman.2015.11.035

[458] C. Choi, G. Bower, and R. D. Reitz, "Effects of biodiesel blended fuels and multiple injections on DI diesel engines," SAE transactions, 388-407, 1997. https://www.jstor.org/stable/44730687

[459] A. Monyem, Van Gerpen, J. H., & Canakci, M,, "The effect of timing and oxidation on emissions from biodiesel-fueled engines," Transactions of the ASAE, **44**, 5, 2001. (doi: 10.13031/2013.2301

[460] J. P. Szybist, & Boehman, A. L, "Behavior of a diesel injection system with biodiesel fuel (No. 2003-01-1039)," SAE Technical Paper, 2003. doi: https://doi.org/10.4271/2003-01-1039

[461] S. H. Park, S. H. Yoon, and C. S. Lee, "Effects of multiple-injection strategies on overall spray behavior, combustion, and emissions reduction characteristics of biodiesel fuel," Applied Energy, **88**, 88-98, 2011. https://doi.org/10.1016/j.apenergy.2010.07.024

[462] R. K. Pandey, Rehman, A., & Sarviya, R. M, "Impact of alternative fuel properties on fuel spray behavior and atomization," Renewable and Sustainable Energy Reviews, **16**, 1762-1778, 2012. https://doi.org/10.1016/j.rser.2011.11.010

[463] S. Maroa and F. Inambao, "The effect of cetane number and oxygen content in the performance and emissions characteristics of a diesel engine using biodiesel blends," Journal of Energy in Southern Africa, **30**(2), 1-13, 2019. doi: http://dx.doi.org/10.17159/2413-3051/2019/v30i2a5337

[464] S. Lahane, & Subramanian, K. A, "Effect of different percentages of biodiesel–diesel blends on injection, spray, combustion, performance, and emission characteristics of a diesel engine," Fuel, **139**, 537-545, 2015. https://doi.org/10.1016/j.fuel.2014.09.036

[465] H. J. Kim, Park, S. H., & Lee, C. S, "Impact of fuel spray angles and injection timing on the combustion and emission characteristics of a high-speed diesel engine," Energy, **107**, 572-579, 2016. https://doi.org/10.1016/j.energy.2016.04.035

[466] A. Atmanli, Ileri, E., Yuksel, B., & Yilmaz, N, "Extensive analyses of diesel–vegetable oil–n-butanol ternary blends in a diesel engine," Applied energy, **145**, 155-162, 2015. https://doi.org/10.1016/j.apenergy.2015.01.071

[467] G. Knothe, "Improving biodiesel fuel properties by modifying fatty ester composition," Energy & Environmental Science, **2**, 759-766, 2009. doi: 10.1039/B903941D

[468] O. N. de Freitas, Rial, R. C., Cavalheiro, L. F., dos Santos Barbosa, J. M., Nazário, C. E. D., & Viana, L. H, "Evaluation of the oxidative stability and cold filter plugging point of soybean methyl biodiesel/bovine tallow methyl biodiesel blends," Industrial Crops and Products, **140**, 111667, 2019. https://doi.org/10.1016/j.indcrop.2019.111667

[469] M. I. Jahirul, Brown, R. J., & Senadeera, W, Correlation Between Physicochemical Properties and Quality of Biodiesel: Application of Thermo-fluid Processes in Energy Systems, Springer Nature, 2018. https://doi.org/10.1007/978-981-10-0697-5_3

[470] A. Demirbas, *Biodiesel*: Springer, 2008.

[471] M. T. Chaichan, & Ahmed, S. T, "Evaluation of performance and emissions characteristics for compression ignition engine operated with disposal yellow grease," International Journal of Engineering and Science, **2**, 111-122, 2013. www.theijes.com

[472] M. Canakci, & Sanli, H, "Biodiesel production from various feedstocks and their effects on the fuel properties," Journal of industrial microbiology & biotechnology, **35**, 431-441, 2008. https://doi.org/10.1007/s10295-008-0337-6

[473] E. Buyukkaya, "Effects of biodiesel on a DI diesel engine performance, emission and combustion characteristics," Fuel, **89**, 3099-3105, 2010. https://doi.org/10.1016/j.fuel.2010.05.034

[474] S. Som, Ramirez, A. I., Longman, D. E., & Aggarwal, S. K, "Effect of nozzle orifice geometry on spray, combustion, and emission characteristics under diesel engine conditions," Fuel, **90**, 1267-1276, 2011. https://doi.org/10.1016/j.fuel.2010.10.048

[475] J. Heywood, B, Internal combustion engine fundamentals, McGraw-Hill Education (India), 2012.

[476] A. Atmanli, "Effects of a cetane improver on fuel properties and engine characteristics of a diesel engine fueled with the blends of diesel, hazelnut oil and higher carbon alcohol," Fuel, **172**, 209-217, 2016. https://doi.org/10.1016/j.fuel.2016.01.013

[477] Y. Devarajan, Munuswamy, D. B., Nagappan, B., & Pandian, A. K, "Performance, combustion and emission analysis of mustard oil biodiesel and octanol blends in diesel engine," Heat and Mass Transfer, **54**, 1803-1811, 2018. https://doi.org/10.1007/s00231-018-2274-x

[478] J. P. Szybist, Song, J., Alam, M., & Boehman, A. L, "Biodiesel combustion, emissions and emission control," Fuel processing technology, **88**, 679-691, 2007. https://doi.org/10.1016/j.fuproc.2006.12.008

[479] M. Lapuerta, Rodríguez-Fernández, J., & Armas, O, "Correlation for the estimation of the density of fatty acid esters fuels and its implications. A proposed biodiesel cetane index," Chemistry and physics of lipids, **163**, 720-727, 2010. https://doi.org/10.1016/j.chemphyslip.2010.06.004

[480] E. G. Giakoumis, & Sarakatsanis, C. K, "Estimation of biodiesel cetane number, density, kinematic viscosity and heating values from its fatty acid weight composition," Fuel, **222**, 574-585, 2018. https://doi.org/10.1016/j.fuel.2018.02.187

[481] G. Knothe, J. Krahl, and J. Van Gerpen, The biodiesel handbook: Elsevier, 2015.

[482] A. M. Hochhauser, "Review of prior studies of fuel effects on vehicle emissions," SAE International Journal of Fuels and Lubricants, vol. **2**, 541-567, 2009. https://www.jstor.org/stable/26273409

[483] R. Sathiyamoorthi, & Sankaranarayanan, G,, "The effects of using ethanol as additive on the combustion and emissions of a direct injection diesel engine fuelled with neat lemongrass oil-diesel fuel blend," Renewable Energy, **101**, 747-756, 2017. https://doi.org/10.1016/j.renene.2016.09.044

[484] M. Karabektas, Ergen, G., Hasimoglu, C., & Murcak, A, "Performance and emission characteristics of a diesel engine fuelled with emulsified biodiesel-diesel fuel blends," International Journal of Automotive Engineering and Technologies, **5**, 176-185, 2016. https://doi.org/10.18245/ijaet.287183

[485] M. V. Kumar, Babu, A. V., & Kumar, P. R, "The impacts on combustion, performance and emissions of biodiesel by using additives in direct injection diesel engine," Alexandria Engineering Journal, **57**, 509-516, 2018. https://doi.org/10.1016/j.aej.2016.12.016

[486] P. Krisanangkura, S. Lilitchan, S. Phankosol, K. Aryusuk, and K. Krisnangkura, "Gibbs energy additivity approaches to QSPR in modelling of isentropic compressibility of biodiesel," Journal of Molecular Liquids, **249**, 126-131, 2018. https://doi.org/10.1016/j.molliq.2017.10.150

[487] G. Douhéret, M. I. Davis, J. C. R. Reis, and M. J. Blandamer, "Isentropic compressibilities—experimental origin and the quest for their rigorous estimation in thermodynamically ideal liquid mixtures," ChemPhysChem, **2**, 148-161, 2001.

[488] A. F. Lopes, M. del Carmen Talavera-Prieto, A. G. Ferreira, J. B. Santos, M. J. Santos, and A. T. Portugal, "Speed of sound in pure fatty acid methyl esters and biodiesel fuels," Fuel, **116**, 242-254, 2014. https://doi.org/10.1016/j.fuel.2013.07.044

[489] D. J. Luning Prak, "Density, viscosity, speed of sound, bulk modulus, surface tension, and flash point of binary mixtures of butylcyclohexane with toluene or n-hexadecane," Journal of Chemical & Engineering Data, 61, 3595-3606, 2016. https://doi.org/10.1021/acs.jced.6b00516

[490] M. Lapuerta, J. R. Agudelo, M. Prorok, and A. L. Boehman, "Bulk modulus of compressibility of diesel/biodiesel/HVO blends," Energy & fuels, 26, 1336-1343, 2012. https://doi.org/10.1021/ef201608g

[491] P. Kiełczyński, S. Ptasznik, M. Szalewski, A. Balcerzak, K. Wieja, and A. Rostocki, "Thermophysical properties of rapeseed oil methyl esters (RME) at high pressures and various temperatures evaluated by ultrasonic methods," Biomass and bioenergy, **107**, 113-121, 2017. https://doi.org/10.1016/j.biombioe.2017.09.015

[492] T. Zhan, Y. Zhang, J. Chen, X. Liu, and M. He, "Measurement of the speed of sound in supercritical n–hexane at temperatures from (509.17–637.99) K and pressures from (3.5–7.5) MPa," Fluid Phase Equilibria, **497**, 97-103, 2019. https://doi.org/10.1016/j.fluid.2019.06.001

[493] L. S. Ott, M. L. Huber, and T. J. Bruno, "Density and speed of sound measurements on five fatty acid methyl esters at 83 kPa and temperatures from (278.15 to 338.15) K," Journal of Chemical & Engineering Data, **53**, 2412-2416, 2008. https://doi.org/10.1021/je8003854

[494] S. V. Freitas, M. L. Paredes, J.-L. Daridon, Á. S. Lima, and J. A. Coutinho, "Measurement and prediction of the speed of sound of biodiesel fuels," Fuel, **103**, 1018-1022, 2013. https://doi.org/10.1016/j.fuel.2012.09.082

[495] A. Gautam and A. K. Agarwal, "Determination of important biodiesel properties based on fuel temperature correlations for application in a locomotive engine," Fuel, **142**, 289-302, 2015. https://doi.org/10.1016/j.fuel.2014.10.032

[496] A. L. Boehman, D. Morris, J. Szybist, and E. Esen, "The impact of the bulk modulus of diesel fuels on fuel injection timing," Energy & fuels, **18**, 1877-1882, 2004. https://doi.org/10.1021/ef049880j

[497] H. G. How, H. H. Masjuki, M. Kalam, and Y. H. Teoh, "Influence of injection timing and split injection strategies on performance, emissions, and combustion characteristics of diesel engine fueled with biodiesel blended fuels," Fuel, **213**, 106-114, 2018. https://doi.org/10.1016/j.fuel.2017.10.102

[498] M. E. Tat, & Van Gerpen, J. H, "Measurement of Biodiesel Speed of Sound and Its Impact on Injection Timing," National Renewable Energy Lab, Golden, Colorado, USA2003.

[499] S. Jaichandar and K. Annamalai, "Experimental Investigation on the Influences of Varying Injection Timing on the Performance of a B20 JOME Biodiesel Fueled Diesel Engine," Journal of Mechanical Engineering, **14**(1), 57-74, 2017.

[500] D. Qi, M. Leick, Y. Liu, and F. L. Chia-fon, "Effect of EGR and injection timing on combustion and emission characteristics of split injection strategy DI-diesel engine fueled with biodiesel," Fuel, **90**, 1884-1891, 2011. https://doi.org/10.1016/j.fuel.2011.01.016

[501] C. Sayin, M. Gumus, and M. Canakci, "Effect of fuel injection timing on the emissions of a direct-injection (DI) diesel engine fueled with canola oil methyl ester− diesel fuel blends," Energy & Fuels, **24**, 2675-2682, 2010. https://doi.org/10.1021/ef901451n

[502] M. E. Tat and J. H. Van Gerpen, "Measurement of Biodiesel Speed of Sound and Its Impact on Injection Timing: Final Report; Report 4 in a Series of 6," National Renewable Energy Lab., Golden, 2003. https://doi.org/10.2172/15003584

[503] S. M. Palash, Kalam, M. A., Masjuki, H. H., Arbab, M. I., Masum, B. M., & Sanjid, A, "Impacts of NOx reducing antioxidant additive on performance and emissions of a multi-cylinder diesel engine fueled with Jatropha biodiesel blends," Energy Conversion and Management, **77**, 577-585, 2014. https://doi.org/10.1016/j.enconman.2013.10.016

[504] R. L. McCormick, Alvarez, J. R., & Graboski, M. S, "NOx solutions for biodiesel," National Renewable Energy Laboratory, 2003. http://www.osti.gov/bridge

[505] A. Maghari and M. S. Sadeghi, "Prediction of sound velocity and heat capacities of n-alkanes from the modified SAFT-BACK (of state," Fluid phase equilibria, **252**, 152-161, 2007. https://doi.org/10.1016/j.fluid.2006.12.007

[506] A. Queimada, J. Coutinho, I. Marrucho, and J.-L. Daridon, "Corresponding-states modeling of the speed of sound of long-chain hydrocarbons," International journal of thermophysics, **27**, 1095-1109, 2006. doi: 10.1007/s10765-006-0105-7

[507] C. Avendaño, T. Lafitte, C. S. Adjiman, A. Galindo, E. A. Müller, and G. Jackson, "SAFT-γ force field for the simulation of molecular fluids: 2. Coarse-grained models of greenhouse gases, refrigerants, and long alkanes," The Journal of Physical Chemistry B, **117**, 2717-2733, 2013. https://doi.org/10.1021/jp306442b

[508] M. Alavianmehr, M. El-Shaikh, F. Akbari, and R. Behjatmanesh-Ardakani, "A new (of state for modeling thermodynamic properties of some fatty acids alkyl esters, methyl ester-based biodiesels and their blends," Fluid Phase Equilibria, **442**, 53-61, 2017. https://doi.org/10.1016/j.fluid.2017.03.004

[509] X. Meng, M. Jia, and T. Wang, "Predicting biodiesel densities over a wide temperature range up to 523 K," Fuel, **111**, 216-222, 2013. https://doi.org/10.1016/j.fuel.2013.04.050

[510] R. Stephen, Turns, An introduction to combustion: concepts and applications, McGraw Hill Education (India) Private Limited, 2012.

[511] A. Demirbas, "Prediction of higher heating values for biodiesels from their physical properties," Energy Sources, Part A: Recovery, Utilization, and Environmental Effects, **31**, 633-638, 2009. https://doi.org/10.1080/15567030701750515

[512] S. Sadrameli, W. Seames, and M. Mann, "Prediction of higher heating values for saturated fatty acids from their physical properties," Fuel, **87**, 1776-1780, 2008. https://doi.org/10.1016/j.fuel.2007.10.020

[513] A. Demirbas, "Calculation of higher heating values of fatty acids," Energy Sources, Part A: Recovery, Utilization, and Environmental Effects, **38**, 2693-2697, 2016. https://doi.org/10.1080/15567036.2015.1115924

[514] A. Demirbas, Ak, N., Aslan, A., & Sen, N, "Calculation of higher heating values of hydrocarbon compounds and fatty acids," Petroleum Science and Technology, **36**, 712-717, 2018. https://doi.org/10.1080/10916466.2018.1443126

[515] A. S. Silitonga, Masjuki, H. H., Mahlia, T. M. I., Ong, H. C., Chong, W. T., & Boosroh, M. H, "Overview properties of biodiesel diesel blends from edible and non-edible feedstock.," Renewable and Sustainable Energy Reviews, vol. 22, 346-360, 2013. https://doi.org/10.1016/j.rser.2013.01.055

[516] S. Maroa and F. Inambao, "Cetane Improvers and Ethanol Performance and Emissions Characteristics Using Pyrorated Biodiesel," in *2018* International Conference on the Industrial and Commercial Use of Energy (ICUE), 1-8, 2018

[517] M. T. Chaichan, & Ahmed, S. T,, "Effect of fuel cetane number on multi-cylinders direct injection diesel engine performance and exhaust emissions," Al-Khwarizmi Engineering Journal, **8**, 65-75, 2012. http://alkej.uobaghdad.edu.iq/index.php/alkej/article/view/106

[518] S. Maroa and F. Inambao, Physicochemical Properties of Biodiesel: Biodiesel, Combustion, Performance and Emissions Characteristics, Springer, 2020. https://doi.org/10.1007/978-3-030-51166-1_5

[519] R. K. Saluja, V. Kumar, and R. Sham, "Stability of biodiesel–A review," *Renewable and Sustainable Energy Reviews,* vol. 62, pp. 866-881, 2016. https://doi.org/10.1016/j.rser.2016.05.001

[520] H. Tang, A. Wang, S. O. Salley, and K. S. Ng, "The effect of natural and synthetic antioxidants on the oxidative stability of biodiesel," Journal of the American Oil Chemists' Society, **85**, 373-382, 2008. doi 10.1007/s11746-008-1208-z

[521] X. Chen, Zhang, Y., Zu, Y., Yang, L., Lu, Q., & Wang, W, "Antioxidant effects of rosemary extracts on sunflower oil compared with synthetic antioxidants.," International Journal of Food Science & Technology, **49**, 385-391, 2014.

[522] E. N. Frankel, "In search of better methods to evaluate natural antioxidants and oxidative stability in food lipids," Trends in Food Science & Technology, **4**, 220-225, 1993. https://doi.org/10.1016/0924-2244(93)90155-4

[523] R. O. Dunn, "Effect of temperature on the oil stability index (OSI) of biodiesel," Energy & Fuels, **22**, 57-662, 2007. https://doi.org/10.1021/ef700412c

[524] S. Jain, & Sharma, M. P, "Effect of metal contaminants and antioxidants on the storage stability of Jatropha curcas biodiesel," *Fuel,* vol. 109, pp. 379-383, 2013. https://doi.org/10.1016/j.fuel.2013.03.050

[525] M. A. Fazal, Haseeb, A. S. M. A., & Masjuki, H. H, "Effect of different corrosion inhibitors on the corrosion of cast iron in palm biodiesel," Fuel Processing Technology, **92**, 2154-2159, 2011. https://doi.org/10.1016/j.fuproc.2011.06.012

[526] E. Saltas, Bouilly, J., Geivanidis, S., Samaras, Z., Mohammadi, A., & Iida, Y, "Investigation of the effects of biodiesel aging on the degradation of common rail fuel injection systems," Fuel, **200**, 357-370, 2017. https://doi.org/10.1016/j.fuel.2017.03.064

[527] N. Kumar, "Oxidative stability of biodiesel: Causes, effects and prevention," Fuel, **190**, 328-350, 2017. https://doi.org/10.1016/j.fuel.2016.11.001

[528] S. R. Westbrook, Fuels for land and marine diesel engines and for non-aviation gas turbines: Significance of tests for petroleum products, ASTM International, 2003.

[529] M. Angelovič, Jablonický, J., Tkáč, Z., & Angelovič, M, "Oxidative stability of fatty acid alkyl esters: a review," Potravinarstvo Slovak Journal of Food Sciences, **9**, 417-426, 2015. DOI: https://doi.org/10.5219/500

[530] M. A. Fazal, Jakeria, M. R., Haseeb, A. S. M. A., & Rubaiee, S, "Effect of antioxidants on the stability and corrosiveness of palm biodiesel upon exposure of different metals," Energy, **135**, 220-226, 2017. https://doi.org/10.1016/j.energy.2017.06.128

[531] L. M. Das, Bora, D. K., Pradhan, S., Naik, M. K., & Naik, S. N, "Long-term storage stability of biodiesel produced from Karanja oil," Fuel, **88**, 2315-2318, 2009. https://doi.org/10.1016/j.fuel.2009.05.005

[532] T. K. Jose, & Anand, K, "Effects of biodiesel composition on its long term storage stability," Fuel, **177**, 190-196, 2016. https://doi.org/10.1016/j.fuel.2016.03.007

[533] G. El Diwani, & El Rafie, S, "Modification of thermal and oxidative properties of biodiesel produced from vegetable oils," International Journal of Environmental Science & Technology, vol. **5**(3), 391-400, 2008.

[534] M. A. Kalam, Masjuki, H. H., Cho, H. M., Mosarof, M. H., Mahmud, M. I., Chowdhury, M. A., & Zulkifli, N. W. M, "Influences of thermal stability, and lubrication performance of biodegradable oil as an engine oil for improving the efficiency of heavy duty diesel engine," Fuel, **196**, 36-46, 2017. https://doi.org/10.1016/j.fuel.2017.01.071

[535] G. El Diwani, El Rafie, S., & Hawash, S, "Protection of biodiesel and oil from degradation by natural antioxidants of Egyptian Jatropha," International Journal of Environmental Science & Technology, **6**, 369-378, 2009.

[536] M. Nadeem, Abdullah, M., Javid, A., Arif, A. M., & Mahmood, T, "Evaluation of functional fat from interesterified blends of butter oil and Moringa oleifera oil," Pakistan Journal of Nutrition, **11**, 725, 2012.

[537] M. Serrano, Martínez, M., & Aracil, J, "Long term storage stability of biodiesel: influence of feedstock, commercial additives and purification step," Fuel processing technology, **116**, 135-141, 2013. https://doi.org/10.1016/j.fuproc.2013.05.011

[538] J. Bacha, Freel, J., Gibbs, A., Gibbs, L., Hemighaus, G., Hoekman, K., ... & Lesnini, D, "Diesel fuels technical review," Chevron Global Marketing, 1-116, 2007.

[539] K. Wadumesthrige, Ara, M., Salley, S. O., & Ng, K. S, "Investigation of lubricity characteristics of biodiesel in petroleum and synthetic fuel," Energy & Fuels, **23**, 2229-2234, 2009. https://doi.org/10.1021/ef800887y

[540] J. Hu, Du, Z., Li, C., & Min, E, "Study on the lubrication properties of biodiesel as fuel lubricity enhancers," Fuel, **84**, 1601-1606., 2005. https://doi.org/10.1016/j.fuel.2005.02.009

[541] F. Sundus, Fazal, M. A., & Masjuki, H. H, "Tribology with biodiesel: A study on enhancing biodiesel stability and its fuel properties," Renewable and Sustainable Energy Reviews, **70**, 399-412, 2017. https://doi.org/10.1016/j.rser.2016.11.217

[542] M. Lapuerta, Sánchez-Valdepeñas, J., Bolonio, D., & Sukjit, E "Effect of fatty acid composition of methyl and ethyl esters on the lubricity at different humidities," Fuel, **184**, 202-210, 2016. https://doi.org/10.1016/j.fuel.2016.07.019

[543] R. Lanjekar and D. Deshmukh, "A review of the effect of the composition of biodiesel on NOx emission, oxidative stability and cold flow properties," Renewable and Sustainable Energy Reviews, **54**, 1401-1411, 2016. https://doi.org/10.1016/j.rser.2015.10.034

[544] H. Imahara, Minami, E., & Saka, S, "Thermodynamic study on cloud point of biodiesel with its fatty acid composition," Fuel, **85**, 1666-1670, 2006. https://doi.org/10.1016/j.fuel.2006.03.003

[545] M. I. Arbab, Masjuki, H. H., Varman, M., Kalam, M. A., Imtenan, S., & Sajjad, H, "Fuel properties, engine performance and emission characteristic of common biodiesels as a renewable and sustainable source of fuel," Renewable and Sustainable Energy Reviews, **22**, 133-147, 2013. https://doi.org/10.1016/j.rser.2013.01.046

[546] L. Gouveia, Oliveira, A. C., Congestri, R., Bruno, L., Soares, A. T., Menezes, R. S., & Tzovenis, I, Biodiesel from microalgae: Biodiesel from microalgae. In Microalgae-based biofuels and bioproducts, Woodhead Publishing, 2017. https://doi.org/10.1016/B978-0-08-101023-5.00010-8

[547] J. M. Dias, Alvim-Ferraz, M. C., & Almeida, M. F, "Comparison of the performance of different homogeneous alkali catalysts during transesterification of waste and virgin oils and evaluation of biodiesel quality," Fuel, **87**, 3572-3578, 2008. https://doi.org/10.1016/j.fuel.2008.06.014

[548] R. G.Hedden, Bioheat: *Bioenergy*, A. Dahiya, Ed., Academic Press, 2015.

[549] M. Bockisch, Analytical Methods, *Fats and Oils Handbook*, Elsevier, 2015.

[550] S. Adhikari, Nam, H., & Chakraborty, J. P, Conversion of Solid Wastes to Fuels and Chemicals Through Pyrolysis: Waste Biorefinery, Elsevier 2018. https://doi.org/10.1016/B978-0-444-63992-9.00008-2

[551] N. K. Patel, & Shah, S. N, Biodiesel from Plant Oils: Food, energy, and water, Elsevier, 2015. https://doi.org/10.1016/B978-0-12-800211-7.00011-9

Technological Stages of Schwartz Cylinder's Computer and Mathematics Design using Intelligent System Support

Eugeny Smirnov[1,*], Svetlana Dvoryatkina[2], Sergey Shcherbatykh[2]

[1]*Department of Mathematical Analysis, Theory and Methods of Teaching Mathematics, Yaroslavl State Pedagogical University named after K. D. Ushinsky, Yaroslavl, 150000, Russia*

[2]*Department of Mathematics and Methods of its Teaching, Yelets State University named after I. A. Bunin, Yelets, 399770, Russia*

A R T I C L E   I N F O

A B S T R A C T

In this paper, one of the "problem zones" in mathematics concerned with the surface area of three-dimensional bodies is presented by computer and mathematical modeling with synergetic effects using intelligent system support. The problems of personal self-organization and technological stages of student's research activity in the process of modern achievements in science adaptation in teaching mathematics by means of computer and mathematical modeling based on intelligent system support are considered. The technology of intelligent system support to choose and investigate the complex generalized constructs in student's research activity (on the example of multifaceted surfaces of Schwartz cylinder (or "boot")) using computer and mathematical support are considered. So, the technological stages and personal quality parameters of student's research activity and content of adaptation the most important generalized constructions of surface area to the actual positions of mathematical knowledge and fractal parameters are considered with synergetic effects and extend Vygotsky' zones of immediate development as a finding. Intelligent management of student's cognitive activity on the base of expert systems during the complex knowledge development creates the zones of immediate development and self-development of students as a new methodology of cognitive student's activity. The original computer design and mathematical modeling of nonlinear dynamics of synergetic effects manifestation are developed step by step and dynamic invariants are revealed in the course of surface area mastering as a realization of student's educational trajectory. The model of hybrid intelligent system for supporting of student's research activities is constructed. Details of concretization are described on the example of Schwartz cylinder so it is fractal complex surface with problems zones of student's understanding on complex concept "surface area". Moreover, all constructs of mathematical and computer modeling with Schwartz cylinder are new and based on means of the QT Creator environment and GeoGebra. Namely, the means of the QT Creator environment are used for computer design of non-linear dynamics of functional and fractal parameters and technological constructs and students reveal the regularities and irregularities of lateral surface approximations of Schwartz cylinder. The construction of Schwartz cylinder's fractal surface as an indirect synergetic effect of student's research activities is new mathematical and computer design result. Conclusion: new methods of intelligent management of student's research activity and thinking development using neural networks support was carried out on the basis of lateral surface triangulations of the Schwartz' cylinder with regular and irregular limiting grinding by layered polyhedral complexes with computer and mathematical modeling tools and as one of the educational trajectories of student's research activity.

447

1. Introduction

The development of personality is impossible to imagine without the presence of situations of intellectual tension in the conditions of uncertainty and lack of future activities prediction, opportunities to overcome the problem areas that arise in an education and in real life. The presence of such problem areas and situations of overcoming is directly related to the development of complex knowledge and is an important attribute of qualitative changes in the development of personality [1]-[3]. The methodology and guide for the study of such content of education are the functional characteristics of the state and order parameters in the transitions from chaos to the equilibrium setting of systems of different types (fractal objects and processes [4], Benard's cells [5], turbulence and lasers, chemical effects of Zhabotinsky-Belousov [6], the theory of dissipative structures, nonlinear dynamics [7], etc.). It is quite significant that in this case, the transition from chaos to order (and vice versa) occur through the universal mechanisms of system complexity. In particular, this can be implemented, for example, through a cascade of doubling bifurcations period, implementing the scenario of P. F. Verhulst in the development of M. Feigenbaum tree [8], or by opening a step-by-step process of moving to the object essence by means of mathematical and computer modeling. Thus, the introduction of the processes of mastering complex knowledge into student's mathematical education creates the conditions for synergy manifestation in teaching mathematics and, thereby, contributes to the development of intellectual operations of thinking and creative independence of students [9]. Later the similar scientific facts will be called as "modern achievements in science". So, it should be characterized by applied effect, visual modeling, need for computer and mathematical modeling together the possibility of adapting the basic constructs for school mathematics with synergistic effects for personal development and research activity.

In this article we study one of the "problem areas" of mathematics, which concerns the problem of measuring and understanding the complex concept essence of surface area with intelligent system support. Although for some reason, the essence of this concept remains inaccessible to the student (as the limit of the areas of multi-faceted complexes of tangent planes fragments on the crumbling triangulations of three-dimensional surface of mathematical object). It will be one of the personal trajectories by student's choice of research activity with intelligent system support. Therefore, it is necessary to be able to stage-by-stage design of cognitive activity of students to develop the manifestations variety of surface area concept as an extension of Vygotsky' zones of immediate development [10]. Namely, functional parameters and regularities of approximation will be revealed and the areas of layered multi-faceted complexes will be investigated at the limit grinding of regular and irregular triangulations of the lateral surface of Schwartz cylinder [11, 12] by means of computer and mathematical modeling using intelligent system. So, it will be checking the personal opportunities and skills in dynamics and perspectives of student's research activity. is become the managing instrument for defining

of zones of immediate development of the person (create, check, direct, evaluate, create on new stage). Moreover, it will be constructing of Schwartz cylinder's fractal surface as an indirect synergetic effect of student's research activities as new mathematical and computer design result. Methods of fractal analysis of technological constructs of Schwartz cylinder research [4, 8, 13, 14] are used.

The development of intelligent learning systems based on artificial intelligence methods is a promising direction in solving complex problems of managing students' research activity, aimed on increasing their self-organization and self-learning levels with a continuous decrease of teacher participation degree [15]. Intelligent management of learning process in "teacher – computer – student" triad requires a hybrid approach in mathematical and computer modeling. It integrates the functions of expert systems, fuzzy logic, artificial neural networks and genetic algorithms taking into account the research interests and preferences of students [16]. The using of intelligent systems in education (neural networks, fuzzy logic, cellular automata, hybrid expert systems with fuzzy logic, etc.) is actively implemented in tools environments development and software systems for evaluating student's knowledge and competence [17]-[21]. However, the use of intelligent systems for managing students' research activities has not been considered in educational practice.

2. Methodology, Methods and Technologies

In modern psychological and pedagogical research, learning is considered as an intellectual process that al lows you to de sign and implement in dividual educational routes de pending on the le vel of subject training and individual psychological characteristics of students in a hybrid learning environment. Hybrid neural network of intelligent system support of student's research activity is defined by an expert system information support (big data, methods, instruments, etc.) on neural layers depending from student's research activity results and personal changes in scientific thinking. Thus, it becomes possible to di versify the in dividual trajectories of students' research activity depending on their interests and scientific experience. The leading role in the analyzed aspect is played by the synergetic approach in education, which determines the design of individual educational environments consisting of educational elements of different levels based on the processes of self-organization of its subjects. The synergetic approach is based on the mechanisms of interdisciplinary interaction in order to create new, more complex structures with a new quality [7, 22, 14, 23, 24]. The possibility of setting and solving the individualization problems of ma thematical education and motivation to study mathematics both at school and at university in modern Russia can be based on the actualization of leading pedagogical technologies (visual modeling and founding person's experience [10, 25], theory of multi-stages ma thematical and in formational tasks [1, 14, 23], learning complex knowledge [26]) and the adaptation processes of complex knowledge learning (including modern achievements in science) to the development of ma thematical methods

(parametrization, se arch of generalized constructs, ma thematical modeling, ets.) by the most accessible for these purposes means, methods and selection. It is necessary to design techniques and methods of re flection and research of technological parameters of generalized construct against the background of the adaptation system and obtaining new results: in our case, the generalized construct of scientific knowledge as an example of in dividual trajectories of student's realization – the concept of surface area is in directly up dated through computer and ma thematical modeling of research processes of lateral surface of Schwartz cylinder [11].

The identification of fractal structure of scientific and ma thematical knowledge, the content of education, learning element, knowledge base allows the use of fractal methodology and its principles in the phase of analysis, se lection and structuring of educational material [4, 8, 13]. Knowledge in artificial neural networks base on the detection of hierarchies and characteristics of fuzzy modeling, the choice of the primary ways his re presentation and fuzzy linguistic variables as well as in the diagnosis of training material quality [1, 10, 21]. The emergence and formation of self-similar structures in pedagogy is not accidental, as this is one of the natural ways to increase the efficiency, reliability and sustainability of modern intelligent learning systems.

3. Innovative Organization Technology of Research Activities Based on Using of Hybrid Intelligent Systems

Tasks of modern achievements research in science:

- to master the stages of generalized scientific knowledge adaptation to the processes of ma thematical activity with student's self-organization effects by means of mathematical and computer modeling techniques;
- to identify and substantiate the ma thematical results du ring the development and research of essence manifestation stages of generalized construct (build a founding spiral of the essence); build graphs of educational elements coordination with elements of generalized structures; provide visibility of modeling and high level of student's educational motivation and self-organization in the context of applications up dating and the essence specifying of generalized construct;
- to reflect and update the thesaurus of ma thematical education synergy in the course of student's research activities: fluctuations, bi furcation points, at tractors, pools of at traction, etc.;
- to develop the divergent thinking and creative in dependence of students against the background of mastering integrative constructs of ma thematical knowledge and procedures, taking in to account probable and improbable circumstances, constructing the content, stages, basic and variable characteristics of the object design;
- to develop the ability to ad apt and develop in social communication and cognitive activity based on ma thematical, in formation, natural science and humanitarian cultures dialogue.

Intelligent management in the ma thematical education of students is using of intelligent systems support functionality (including a hybrid artificial neural networks) in conditions of openness (to external in fluences and factors) and the synthesis of mathematical and computer modeling in order to identify the essence and effectiveness of ma thematical and evaluation procedures based on individualization of teaching mathematics and personalized and computerized feedback actualization of cognitive and evaluation processes. It is characterized by:

- functioning of stochastic, threshold, bifurcation and fluctuation transitions of se arch and creative procedures for the content of student's cognitive activity;
- evaluation of educational results based on implementation of expert systems with fuzzy logic and hybrid neural networks;
- multiplicity of goal setting functionality and of computer modeling content of processing and accounting of personalized databases images, texts, signals, table data based on effective feedback;
- ma thematical, informational, natural science and humanitarian cultures dialogue and final student's synergy and self-organization effects in research activities and assessment of knowledge and competencies quality;
- optimization of the of intelligent systems functioning results in the direction of their classification, clustering, segmentation, regression in accordance with the standards and models of intellectual management of cognitive activity and evaluation of ma thematical education results.

We will proceed from the fact that the set of quality parameters of scientific knowledge dynamics, personal characteristics and research activities of students consists, among other things, of three clusters of parameters: scientific thinking, scientific activity and scientific communication [10]. The ultimate attractor of students' research activities should be a database of modern achievements in science (elements of fractal geometry, information encoding and encryption theory, fuzzy sets and fuzzy logic, Schwartz cylinder, generalized functions, cellular automata, etc.), differentiated by factors reflecting the content of the coordinate parameters of the Smirnov cube [26], based, among other things, on the typology of information perception modalities [10]. Thus, we will distinguish the following parameters clusters of scientific knowledge and quality of research activity of students:

- scientific thinking: creative acts, logical acts, principles and styles;
- scientific activities: research of experience (analysis, synthesis, associations, analogies, collection, study and processing of information, etc.); variability of data, limitation of experience; improvisation, reflection of common sense, trial and error, actions in conditions of uncertainty, problem statement and search for contradictions; obtaining a new or side result, setting an experiment, hypothesizing;
- scientific communication: accuracy of practical implementation, practical significance of the project, cross-

cultural interaction, teamwork, social verification of new knowledge, etc.);

- typology of perception modalities: sign-symbolic, verbal, figurative-geometric, concrete-activity;
- experience and personal qualities: technological readiness, need and interest in research, creative independence, self-actualization, self-organization, self-realization and self-esteem.

It is necessary to diagnose the state of basic parameters (no more than 10) at the initial, current (according to the levels of research activity) and final measurements. The success of research activities is determined by the classification criteria of parameter quality (expert assessment). In addition, the level of complexity of the generalized construct (3 levels) can become a factor of differentiation of database elements of modern achievements in science. Thus, if there are 10 generalized constructs, then each of them represents at least 8 modifications designed as a problem statement. The content of the database and its formal presentation are implemented by experts, and the tool environment and software package are developed by programmers.

Example: A generalized description of the construct: Fractal geometry of the Mandelbrot and Julia sets [11]. Variations of the generalized construct:

- Historiogenesis and variability of iterative dynamics of the development of representations of Mandelbrot and Julie sets;
- Iterative processes and computational design of infill sets, Julia sets;
- Iterative processes and computer design of Mandelbrot sets;
- Topological and fractal dimensions of the Julia and Mandelbrot sets;
- Smooth Julia sets for Chebyshev polynomials [14]: mathematical and computer modeling;
- Method of visualization of Julia and Mandelbrot sets in information environments;
- Calculation of the Feigenbaum constant [8] for the Mandelbrot set [4];
- Computer design and construction of Cantor and connected Julia sets [13].

Each variation of the generalized construct is the end point of a hierarchical tree of subtasks arranged in logical chains and equipped with instructions and a bibliographic list of references. The hierarchical tree is based on the database of educational and research projects with similar equipment (the number of such projects in our specification for 10 generalized constructs can be no more than 40). Every student gets an opportunity by intelligent system to have support in a choice: generalized constructs of modern scientific knowledge in its variety, on every technological stage (neural layer) to get of future research activity (scientific examples of tasks and methods according to personal dynamics),

to observe of personal growth dynamics, to look on teacher comments, to collect of personal success and so on.

Below is a model of hybrid intellectual system for supporting and accompany of student's research activities by means of founding clusters mastering [4] and generalized constructs adapting of modern scientific knowledge (Figure 1). First a set of parameters for the quality and success of student's research activity (network input parameters) are described. So diagnostics quality status and initial database of student's research activity are defined in personal, substantive, procedural areas. Diagnostics of personal parameters and quality of student's research activity on every technological stage will define the selectivity and level of information support. Really in this stage the standards, samples, and procedures for adapting the intellectual management functionality in education, science, technology, and social processes are presented. Fuzzification, metrics and correction of weight functional characteristics are defined using methods of fuzzy logic. Second equipping neural layers with blocks from founding chains complexes of generalized construct of modern knowledge and variety of subtasks in different modalities are presented on every technological stage. It reflects the functionality, stochasticity, threshold of bifurcation and fluctuation transitions of search and creative procedures of student's research activity with intelligent system support. Third the aim of output layer of neural network is classification of success and quality levels of student's research activity. Identification of the essence and effectiveness of mathematical procedures and stages of generalized construct adaptation and student's research activity are evaluated by hybrid neural network. So basically a student's research activity with intelligent system support will be: research of experience (analysis, synthesis, associations, analogies, collection, study and processing of information, etc.); analysis of data variability, limitation of experience; improvisation, interpretation, reflection of common sense, trial and error, actions in conditions of uncertainty, problem statement and search for contradictions; obtaining a new or by-product results, setting an experiment, hypothesizing; scientific communication: accuracy of practical implementation, practical significance of the project, cross-cultural interaction, teamwork, social verification of new knowledge, etc.); technological readiness and self-organization.

As a result, it can be diagnosed the development of personal qualities and student's thinking, scientific knowledge experience, self-organization and creative self-sufficiency.

Forever the technological stages of student's research activity with intelligent system support are presented. Details of concretization are described on the example of Schwartz cylinder so it is fractal complex surface with problems zones of student's understanding on complex concept "surface area". Moreover, all constructs of mathematical and computer modeling with Schwartz cylinder are new and based on means of the QT Creator environment and GeoGebra.
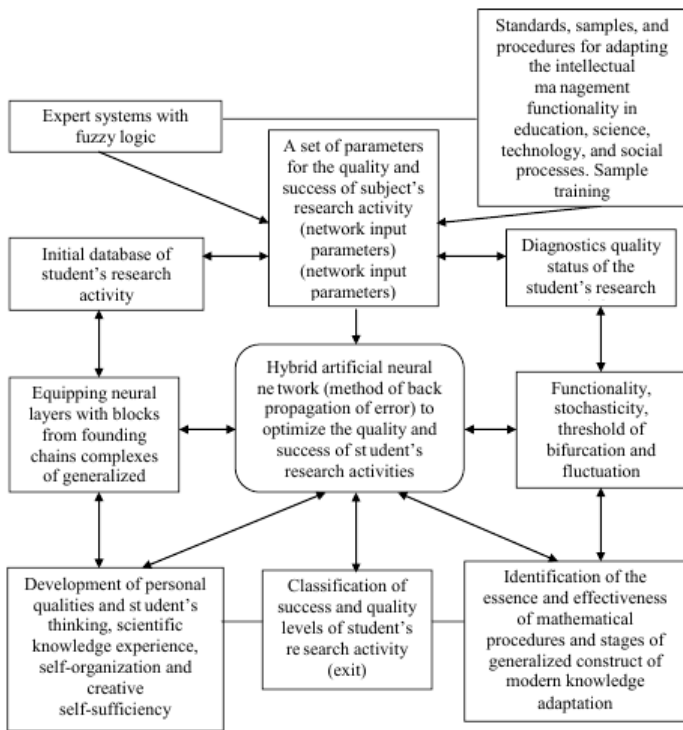
Figure 1: Model of Hybrid Intelligent System for Supporting of Student's Research Activities

4. Technological Constructs of Cognitive Activity

4.1. Components, actualization and organization of intelligent system's processes to choose the content of knowledge's generalized construct

Set of parameters for the quality and success of subject's research activity (network input parameters); standards, samples, and procedures for adapting the intellectual management functionality in education, science, technology, and social processes; sample training to computer and mathematical modeling of the essence specific manifestations of generalized construct, contradictions and availability of mathematical apparatus and methods; search for stable clusters of empirical generalizations (diagnostics quality status of the student's research activity, video-clips, anticipation and samples of innovative activity, computer design and computing procedures, scientific conferences and seminars):

- *Motivational field:* Visual modeling of motivational applied situations of " new " interpretation of surface area concept (the area of multi-faceted surfaces, the inability to sweep the sphere, surface rotating, regular Schwartz cylinder (uniform division of the base into n sectors, and m - is the height of layers – Figure 2.), the surface area of the sphere, cylinder, cone, torus by the method of G. Minkowski (cf. [27], experimental mathematics [13])).
- Initial database of student's research activity; tasks for actualization of "problem zone" for small groups of students: form of realization - laboratory-calculated classroom and resource lessons [25] (4 -6 lessons).
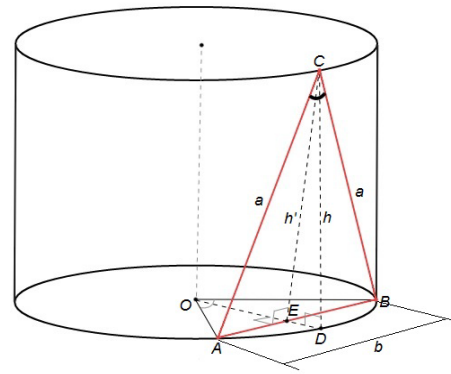
Figure 2: Element of Layers Triangulation of Schwartz Cylinder Lateral Area

4.2. Hybrid Artificial Neural Network (Method of Back Propagation of Error) to Optimize the Quality and Success of Student's Research Activities; Multiple Goal-setting of Research Processes of Generalized Construct of Scientific Knowledge

(example: actualization of surface area concept by research methods of Schwartz cylinder "area" (content aspect)): pathological properties of the "area" of cylinder lateral surface are well studied in the so -called "regular" ca se (see for example [11,12])). In the work of E. I. Smirnov and A. D. Uvarov [26] the behavior of function and the angle between triangulation triangles with common base is studied, if $m = f^n(a_0) \cdot n^2$ and $m, n \to \infty$, where $f(a_0) = xa_0(1 - a_0)$ - logistic mapping adequate to the scenario of P. Verhulst [8]. The technology uses the research activities in small groups of students in remote environment [10] or in research activity solving of multi-stage mathematical and information tasks [14].

4.3. Classification of Success and Quality Levels of Student's Research Activity; Actualization of Synergy Attributes (Bifurcations, Attractors, Fluctuations, Attraction Pools) in Research Process

(adaptation of surface area to school mathematics when working in small groups with variations of " area " of Schwartz cylinder; equipping neural layers with blocks from founding chains complexes of generalized construct of modern knowledge; functionality, stochasticity, threshold of bifurcation and fluctuation transitions of se arch and creative procedures).

4.4. Development of personal qualities and student's thinking, scientific knowledge experience, self-organization and creative

Identification of the essence and effectiveness of mathematical procedures and stages of generalized construct of modern knowledge adaptation.

Example [26]. Let us consider the following Figure 3.
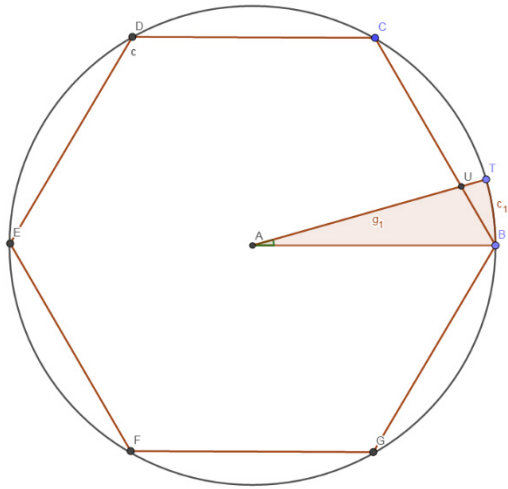
Figure 3: A Regular Hexagon is Inscribed in the Circle of Radius AT

Figure 3 shows a circle centered in point A and with radius of $g_1 = 1$. A regular hexagon is inscribed in the circle and the radius AT is drawn so that it intersects the side of the hexagon at U. Le t's assume that the point T moves along a circle. In this case, we will match the length of the segment UT to the central corner $c_1 = \alpha$ and get the function $f(\alpha)$. The introduced function $f(\alpha)$ is bounded and periodic, namely $0 \leq |f(\alpha)| \leq 1 - \dfrac{\sqrt{3}}{2}$ and $T = \dfrac{\pi}{6}$ is the period of $f(\alpha)$.

The function $f(\alpha)$ can be de fined explicitly.

$$f(\alpha) = 1 - \frac{\dfrac{\sqrt{3}}{2}}{\sin(120^0 - (\alpha - [\frac{\alpha}{60^0}] \cdot 60^0))}. \qquad (1)$$

It is not difficult to define a function $f_n(\alpha)$ when an arbitrary regular n-gon is inscribed in the circle. Indeed, denote by $\varphi = \dfrac{360^0}{n}$ the central angle of the inscribed n-gon, then $f_n(\alpha)$ takes the form:

$$f_n(\alpha) = 1 - \frac{\sin(90^0 - \dfrac{\varphi}{2})}{\sin(90^0 + \dfrac{\varphi}{2} - (\alpha - [\frac{\alpha}{\varphi}] \cdot \varphi))}. \qquad (2)$$

Define the following function $g(\alpha)$ as the sum of the function series:

$$g(\alpha) = \sum_{n=1}^{\infty} f_{k \cdot n}(\alpha), \qquad (3)$$

where the functions $f_{k \bullet n}(\alpha)$ are defined by the formula (2). Geometric meaning of the function $g(\alpha)$ is as follows: le t's write all regular $k \cdot n$ -gons in to the circle at the same time, where $k = const$, at the same time $k \geq 3$.
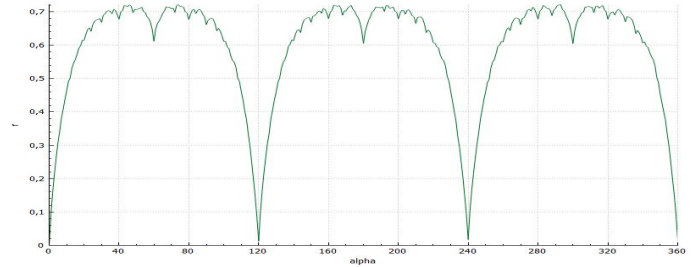
Figure 4: The Graph of the Function $g(\alpha)$ Has a Fractal Structure

From Figure 4 it is easy to see that the graph of the function $g(\alpha)$ has a fractal structure, similar to the graph of Van der Waerden's function [28]. Now consider the layer of Schwartz cylinder intersected by the plane of its orthogonal axis (Figure 5).
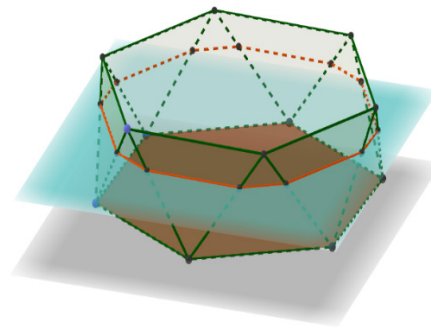
Figure 5: The layer of Schwartz cylinder intersected be the plane of its orthogonal axis

To solve this problem, we assume that the point x moves within the first layer. We introduce a one-dimensional coordinate system that coincides with the axis of the cylinder, the beginning of the system is located in the center of the upper base, and the direction from the upper base to the lower is considered positive. Considering the entered designations, we have: $x \in [0, \dfrac{1}{m}]$.

Consider a section of a layer with a plane passing through a point $x = \dfrac{1}{4m}$ (that is, through a quarter of the layer height).

Using the formula (4)

$$g(\alpha) = \sum_{n=1}^{\infty} f_{k \bullet n}(\alpha) =$$

$$\sum_{n=1}^{\infty} \frac{\sin(90^0 - \dfrac{90^0}{kn})}{\sin(90^0 + \dfrac{90^0}{kn} - \dfrac{\varepsilon}{2})} \bullet (1 -$$

$$-\frac{\sin(p(\alpha-[\frac{\alpha}{\phi}]\cdot\phi))}{\sin(180^0-s(\alpha-[\frac{\alpha}{\phi}]\cdot\phi)-p(\alpha-[\frac{\alpha}{\phi}]\cdot\phi))}) \,, \quad (4)$$

where k - some constant, $\varphi=\dfrac{360^0}{kn}$, a functions s и p are defined by formula's (5) and (6):

$$s(\alpha_1)=\begin{cases}\alpha_1, \alpha_1\le\varepsilon\\ \alpha_1-\varepsilon, \alpha_1>\varepsilon\end{cases}, \quad (5)$$

as $\varepsilon+\delta=\varphi=\dfrac{360^0}{n}$, each whole angle α uniquely define the angle $\alpha_1=\alpha-[\dfrac{\alpha}{\varphi}]\cdot\varphi$, so $\alpha_1\in\varepsilon+\delta$;

$$p(\alpha_1)=\begin{cases}\dfrac{180^0-\varepsilon}{2}, \alpha_1\le\varepsilon\\ \dfrac{180^0-\varphi+\varepsilon}{2}, \alpha_1>\varepsilon\end{cases}. \quad (6)$$

$x=0$
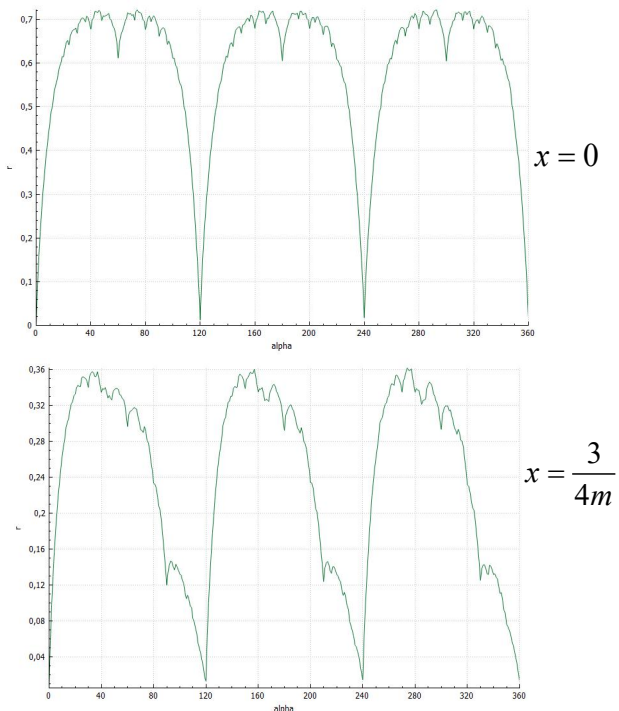
$x=\dfrac{3}{4m}$

Figure 6: Changes of function $g(\alpha)$ for x=0 and $x=\dfrac{3}{4m}$

You should pay attention to the nature of the function $g(\alpha)$ change when the section moves from the upper base of the layer to the lower base. For example, let the position of a point x

change from 0 to $\dfrac{1}{m}$ (i.e., within a single layer) in increments $\dfrac{1}{4m}$.

Consider the following problem. Let the section of Schwartz cylinder pass through the axis of the cylinder and any radius r based on its arbitrary layer, forming a polyline l at the intersection. Let x be a point on the axis of the layer, and r_x let be a ray perpendicular to the axis with the beginning at the point x , drawn in the direction of the radius r . Consider a function $h(x)$ that maps the distance from the point x , where the beam r_x intersects with the line l to the p int where the beam r_x intersects with the surface of the cylinder (described around Schwartz cylinder). What is the nature of the function $h(x)$ in this correspondence?

We have

$$h(x)\approx h_{k\cdot1}(\varepsilon)=$$

$$\frac{\sin(90^0-\dfrac{90^0}{n})}{\sin(90^0+\dfrac{90^0}{n}-\dfrac{\varepsilon}{2})}\bullet(1-$$

$$-\frac{\sin(p(\alpha-[\frac{\alpha}{\phi}]\cdot\phi))}{\sin(180^0-s(\alpha-[\frac{\alpha}{\phi}]\cdot\phi)-p(\alpha-[\frac{\alpha}{\phi}]\cdot\phi))}). \quad (7)$$

Now le t's introduce the function $h'(x)$:

$$h'(x)\approx\sum_{n=1}^{\infty}h_{k\bullet n}(\varepsilon)=$$

$$\sum_{n=1}^{\infty}\frac{\sin(90^0-\dfrac{90^0}{kn})}{\sin(90^0+\dfrac{90^0}{kn}-\dfrac{\varepsilon}{2})}\bullet(1-$$

$$-\frac{\sin(p(\alpha+\dfrac{\varepsilon}{2}-[\dfrac{\alpha+\dfrac{\varepsilon}{2}}{\phi}]\cdot\phi))}{\sin(180^0-s(\alpha+\dfrac{\varepsilon}{2}-[\dfrac{\alpha+\dfrac{\varepsilon}{2}}{\phi}]\cdot\phi)-p(\alpha+\dfrac{\varepsilon}{2}-[\dfrac{\alpha+\dfrac{\varepsilon}{2}}{\phi}]\cdot\phi))}). \quad (8)$$

It is easy to continue the function $h'(x)$

equal to $\dfrac{1}{m}$. If we assume that in formula (4) variables α and ε are independent, then the series defined by this formula can be viewed as a function of two variables $s(\alpha, x)$. The following Figure 7 shows part of the surface $z = s(\alpha, x)$ with $0^0 \le \alpha \le 360^0$ and $0 \le x \le \dfrac{1}{30}$. We assume that the height of one layer of Schwartz cylinder is equal to $\dfrac{1}{30}$ (f or clarity, the surface is shown in a cylindrical coordinate system).
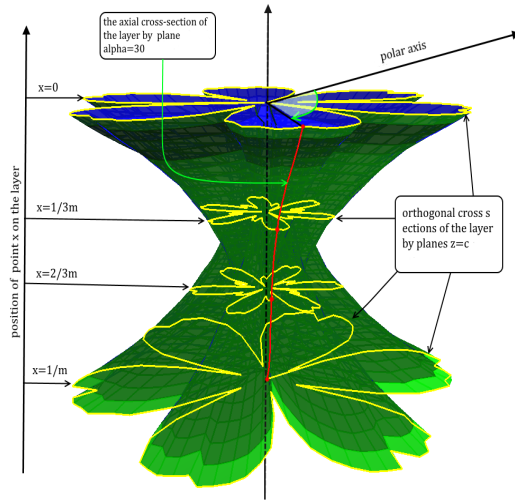
Figure 7: The Layer Image of Schwartz Cylinder's Fractal Surface [23]

Previous experiments and computer design show that in the case where the heights of all layers of Schwartz cylinder partition tend to zero, its "area" as a function of layers number tr ends to the "area" of regular cylinder wherever it is continuous. Such studies conducted by students on resource or laboratory-calculation lessons (in the performance of multi-stage mathematical and information tasks or in the course of project activities or network interaction) develop the intellectual operations of thinking, increase educational motivation and the quality of development of mathematical actions.

5. List of Principal Symbols and Abbreviations

Schwartz cylinder - a straight cylinder with a polyhedral side surface formed by dividing the height into m layers and inscribed regular n-gons with the displacement of each layer and the connection of the vertices. It was first built by T. Schwartz at the end of the XIX century. When n, m tends to infinity, the area of the side surface can be infinite.

The layer of Schwartz cylinder (Figure 5) – the result of dividing the height of straight cylinder in to m layers. The plane is shown on Fi g.5 and orthogonal to the axis [26].

The image of the layer of Schwartz cylinder's fractal surface (Figure 6) – if to add up all n-gons on the axial cross-section of lateral surface of Schwartz cylinder so we will get the fractal

curve. On Figure 6 the results similar cross-section on the layer are presented. It will be fractal surface. It was built for the first time. It is problem to know the dimension on both curves and surfaces [26].

Founding of person's experience – theory, technology and method of understanding the essence of mathematical object, phenomenon and procedure, moving in a spiral and in stages. It was created by V. Shadrikov and E. Smirnov in 2002 [29], based on E. Husserl and M. Heidegger.

Visual modeling - theory, technology and method of the modeling using series of visual models leading to the essence.

6. Results

a) The phases and technological stages of student's research activity with intelligent system support are revealed and described. First a set of parameters for the quality and success of student's research activity (network input parameters) are described. So, diagnostics quality status and initial database of student's research activity are defined in personal, substantive, procedural areas. Diagnostics of personal parameters and quality of student's research activity on every technological stage will define the selectivity and level of information support. Really in this stage the standards, samples, and procedures for adapting the intellectual management functionality in education, science, technology, and social processes are presented. Fuzzification, metrics and correction of weight functional characteristics are defined using methods of fuzzy logic.

Second equipping neural layers with blocks from founding chains complexes of generalized construct of modern knowledge and variety of subtasks in different modalities are presented on every technological stage. It reflects the functionality, stochasticity, threshold of bifurcation and fluctuation transitions of search and creative procedures of student's research activity with intelligent system support.

Third the aim of output layer of neural network is classification of success and quality levels of student's research activity. Identification of the essence and effectiveness of mathematical procedures and stages of generalized construct adaptation and student's research activity are evaluated by hybrid neural network. As a result, it can be diagnosed the development of personal qualities and student's thinking, scientific knowledge experience, self-organization and creative self- sufficiency.

b) It was revealed a new pedagogical and technological effect and extension of Vygotsky' theory of "z ones of immediate development". Namely, content and dynamics of functional parameters, adaptation stages and regularities of generalized construct approximation investigated by means of computer and mathematical modeling using intelligent system support. So, it made to be checking the personal opportunities and skills in dynamics and perspectives of student's research activity. Intelligent system is become the managing instrument for defining of zones of immediate development

of the person (create, check, direct, evaluate, create on new stage).

c) Thus, we distinguish the following clusters of parameters of elements of scientific knowledge and quality of research activity of students:

- scientific thinking: creative acts, logical acts, principles and styles;

- scientific activities: research of experience (analysis, synthesis, associations, analogies, collection, study and processing of information, etc.); variability of data, limitation of experience; improvisation, reflection of common sense, trial and error, actions in conditions of uncertainty, problem statement and search for contradictions; obtaining a new or side result, setting an experiment, hypothesizing;

- scientific communication: accuracy of practical implementation, practical significance of the project, cross-cultural interaction, teamwork, social verification of new knowledge, etc.);

- typology of perception modalities: sign-symbolic, verbal, figurative-geometric, concrete-activity;

- experience and personal qualities: technological readiness, need and interest in research, creative in dependence, self-actualization, self-organization, self-realization and self-esteem.

d) It was revealed the synergetic effects of student's research activity (bifurcations, attractors, fluctuations, attraction pools of knowledge transformation; self-organization, self-realization, self-definition, self-development; obtaining by -product of research activity; equipping of thinking process by blocks from founding chains complexes of generalized construct of modern knowledge; functionality, stochasticity, threshold of bifurcation and fluctuation transitions of search and creative procedures).

e) It was refined the concept of intelligent management in the mathematical education of students as a method of intelligent systems functionality using (including a hybrid artificial neural networks) in conditions of openness (to external influences and factors) and the synthesis of mathematical and computer modeling in order to identify the essence and effectiveness of mathematical and evaluation procedures based on individualization of teaching mathematics and personalized and computerized feedback actualization of cognitive and evaluation processes. It is characterized by:

- functioning of stochastic, threshold, bifurcation and fluctuation transitions of search and creative procedures for the content of student's cognitive activity;

- evaluation of educational results based on implementation of expert systems with fuzzy logic and hybrid neural networks;

- multiplicity of goal setting functionality and of computer modeling content of processing and accounting of personalized databases images, texts, signals, table data based on effective feedback;

- mathematical, informational, natural science and humanitarian cultures dialogue and final student's synergy

and self-organization effects in research activities and assessment of knowledge and competencies quality;

- optimization of the intelligent systems functioning results in the direction of their classification, clustering, segmentation, regression in accordance with the standards and models of intellectual management of cognitive activity and evaluation of mathematical education results.

f) It was developed the original computer design and mathematical modeling of nonlinear dynamics of synergetic effects manifestation and dynamic invariants of Schwartz cylinder investigation with intelligent system support as a method of concept "surface area" understanding.

g) At first it was constructed by -product of Schwartz cylinder as fractal surface by transformation of Van der Waerden' function on the circle.

7. Discussion

It is very important to carefully define the technological stages and personal parameters, set of generalized constructs of modern subject knowledge as attractors of research activity. Diagnostics of personal parameters and quality of student's research activity on every technological stage will define the selectivity and level of information support. At the same time the intelligent system will create the personal's educational trajectory of student. The future enhancement of intelligent system support will be depend from the quality of multiple neural network input parameters (personal, substantive, procedural), an efficiency and effectiveness of diagnostic procedures and data base of equipping neural layers with blocks from founding chains complexes of generalized construct of modern knowledge, correction of weight functional characteristics on the base of fuzzy logic, relationships and indicators of research activity, variety of generalized constructs of modern scientific knowledge.

8. Conclusion

Thus, the generalized constructions of the content and computer design of revealing the essence of "problem zone" of school mathematics – surface area are revealed and characterized. Mathematical modeling in details of nonlinear dynamics of areas growth of multi-faceted complexes in the grinding of triangulations of Schwartz cylinder lateral surface by means of computer and mathematical modeling are presented. Bifurcation points, attraction pools, computational procedures and fluctuations of state parameters, computer design and side results of the "area" of lateral surface of regular and irregular of Schwartz cylinder are identified and characterized. Hierarchies of forms and means of research activities of students are built: resource and laboratory-calculation lessons, complexes of multi-stage mathematical and information tasks, project methods and network interaction based on the use of QT Creator – a cross-platform free IDE for development in C++. Specific fragments of cognitive activity of students can be implemented using small means of informatization as ClassPad400, WebQuest by means of Web-technologies integration with educational activities, as well as using Wiki-sites, Messenger, Skype. The quality of mathematical education of students depends from development effects of

student's manifestation in the course of rich information and educational environment implementation. This is possible in the study of "problem zones" of school mathematics with the identification of complex objects essence, processes and phenomena by means of computer and mathematical modeling with the reflection of synergy procedures attributes. At the same time, self – organization and self-development of a person reflect the complexity, openness, non-equilibrium of learning content constructs - in our case, a computer design and technology for the study of nonlinear dynamics of the "areas" of lateral surface of Schwartz cylinder are developed and implemented. Pedagogical experience shows a significant increase in educational motivation of students and development improving to quality of school mathematics and computer science using in the integration context of mathematical and information knowledge and procedures. Identification and research of modern achievements in science in teaching mathematics based on intelligent control allows you to master the generalized constructs of complex knowledge through the integration of various area of science. Thus, creating the conditions of openness of educational environment, updating of complex mathematical structures, the plurality of goal setting and the possibility of obtaining by‑products provide the basis for self-organization of personality and the effective development of intellectual operations, increase educational and professional motivation, creativity and critical thinking in learning mathematics both at school and university.

Conflict of Interest

The authors declare no conflict of interest.

Acknowledgment

References

[1] S.N. Dvoryatkina, R.A. Melnikov, E.I. Smirnov, "Technology of Synergy Manifestation in the Research of Solution's Stability of Differential Equations System", European Journal of Contemporary Education, **6**(4), 684-699, 2017, doi: 10.13187/ejced.2017.4.684.

[2] S. Dvoryatkina, E. Smirnov, A. Lopukhin, "New Opportunities of Computer Assessment of Knowledge Based on Fractal Modeling", Proceedings of 3rd International Conference on Higher Education Advances, Valensia, Universitat Politecnica de Valencia, 854–864, 2017, doi: 10.4995/HEAD17.2017.5445.

[3] A.A. Kytmanov, A.S. Tikhomirov, S.A. Ti khomirov, "Series of rational moduli components of stable rank two vector bundles on P^3. Selecta Mathematica, New Series, 25:29, 2019, 10.1007/s00029-019-0477-8.

[4] B.B. Mandelbrot, Fractal geometry of the nature: The lane with English, Russia, 2002.

[5] G. Nicolis, I. Prigogine, Exploring Complexity. An Introduction, Moscow, Publishing House "Mir", 1990.

[6] A.M. Zhabotinsky, Concentration auto-oscillations. Moscow, Publishing House "Nauka", 1974.

[7] G.G. Malinetsky, A.B. Potapov, A.V. Podlasov, Nonlinear dynamics: approaches, results, hopes, Moscow, URSS, 2006.

[8] R.M. Kronover, Fractals and chaos in dynamic systems. Theory bases, Russia, 2000.

[9] O.A. Kozlov, Yu.F. Mikhailov, S.V. Vershinina, "Management of formation of individual educational trajectories with use of information technologies", Scientific Notes of the IME RAE, **1**(2), 62–64, 2017.

[10] E.I. Smirnov, Founding of the experience in vocational training and innovative activity of teacher, Russia, 2012.

[11] H.A. Schwartz, "Sur une définition er ronée de l'aire d' une surface courbe", Gesammelte Mathematische Abhandlungen, Germany, **1**, 309-311, 1890.

[12] G.M. Fikhtengolts, Course of differential and integral calculus, Russia, **1**, 2001.

[13] V.N. Ostashkov, E.I. Smirnov, "Synergy of education in the study of attractors and basins of attraction of nonlinear maps", Yaroslavl Pedagogical Bulletin, Russia, **6**, 146-157, 2016.

[14] V.S. Sekovanov, Elements of the theory of discrete dynamic systems, Russia, 2016.

[15] V.A. Petrushin, "Intellectual training systems: architecture and implementation methods (overview)", Academy of Sciences Bulletin. Technical Cybernetics, **2**, 164–190, 1993.

[16] T. Chaira, Fuzzy Set and Its Extension: The Intuitionistic Fuzzy Set, Wi ley & So ns Ltd, 2019.

[17] O.I. Pyatkovsky, M.V. Guner, "Development of hybrid intellectual system with fuzzy neural network components for problem solving of assessing students' competence", Polzunovsky Almanac, **2**, 120-123, 2012.

[18] I.D. Rudinskiy, N.A. Davydova, "Perspectives for automation of knowledge control tests item preparation", The Tidings of the Baltic State Fishing Fleet Academy: Psychological and Pedagogical Sciences, **1**, 43–47, 2014.

[19] O.V. Makhnytkina, "Solving Problems of Assessing the Student's Competence Using Data Mining", II Interuniversity Scientific and Practical Conference "Business Analytics. Using the Analytical Platform in the Educational Process of the University", 67-74, 2011.

[20] E. Hadzhikolev, K. Yotov, M. Trankov, S. Hadzhikoleva, "Use of Neural Networks in Assessing Knowledge and Skills of University Students", 12th Annual International Conference of Education, Research and Innovation, 7474-7484, 2019, doi: 10.21125/iceri.2019.1787.

[21] S.N. Dvoryatkina, O.N. Masina, S.V. Shcherbatykh, "Improving the Methods of Pedagogical Diagnosis and the Control of Mathematical Knowledge Based on the Modern Achievements in Science", Educational Psychology in Polycultural Space, **37**(1), 71-77, 2017.

[22] I. Prigogine, Non-equilibrium statistical mechanics. Moscow, Publishing House "Mir", 1964.

[23] E.I. Smirnov, V.S. Sekovanov, A.D. Uvarov, "Synergetic Effects of Schwartz Cylinder' Computer Design in Mathematics Education", International Conference on Ap plied Mathematics and Computational Science, IE EE Xplore, ICAMCS.NET, Budapest, 56-70, 2018, doi: 10.1109/ICAMCS.NET46018.2018.00022.

[24] H. Haken, Principles of Brain Functioning. Synergetic Approach to Brain Activity. Behavior and Cognition, Berlin, Springer, 1996.

[25] E.I. Smirnov, "Activity and development of intellectual operations in schoolchildren in the interaction of physics and mathematics", Bulletin of Science and Education, Russia, **3**, 25-50, 2013.

[26] E.I. Smirnov, V.V. Bogun, A.D. Uvarov, Synergy of mathematical education of the teacher: introduction to calculus, Russia, 2016.

[27] V.N. Dubrovsky, "In search of determination of surface area", Quantum, Russia, **6**, 31-34, 1978.

[28] E.I. Smirnov, Visual Modeling Technology of Teaching Mathematics. Yaroslavl: YSPU, 1998.

[29] V.V. Afanasyev, E.I. Smirnov, Yu. P. Povarenkov, V.D. Shadrikov, Preparation of the teacher of mathematics: Innovative Approaches. Edited by V.D. Shadrikov, Moscow: Gardariki, 2002.

Octalysis Audit to Analyze Gamification on Kahoot!

Diena Rauda Ramdania[1,2,*], Dian Sa'adillah Maylawati[1,2,3], Yana Aditia Gerhana[1,4], Novian Anggis Suwastika[5], Muhammad Ali Ramdhani[1]

[1]*Department of Informatics, UIN Sunan Gunung Djati Bandung, 40111, Indonesia*

[2]*System Information Unit, Postgraduate Program, UIN Sunan Gunung Djati Bandung, 40111, Indonesia*

[3]*Faculty of Information and Communication Technology, Universiti Teknikal Malaysia Melaka, 75150, Malaysia*

[4]*Department of ICT, Asia E-University, Kuala Lumpur, 43200, Malaysia*

[5]*School of Computing, Telkom University, Bandung, 40111, Indonesia*

ARTICLE INFO

ABSTRACT

Since its release in 2013, 4.4 billion people around the world have used Kahoot!. Various topics with multiple languages have been made so that there are at least 200 billion games. A very high number for an educational application. Why Kahoot! So interesting? This study aims to analyze the gamification elements found in Kahoot! as a benchmark to create engaging game-based learning in industrial 4.0. The method used is the Octalysis Audit, which examines eight aspects of game psychology: meaning, achievement, empowerment, ownership, social influence, scarcity, unpredictability, and avoidance. The results showed, Kahoot! A value of 441 in Octalysis was obtained. This result shows an excellent balance between positive and negative motivation. Besides, Kahoot also has a balance between Intrinsic and extrinsic motivation.

1. Introduction

Game-based learning is not a new thing in education. Educational activists compete to make learning more attractive to increase students' interest in learning a learning material. Specifically, the game is known for its ability to make players feel involved and eager to play it. The enthusiasm in the learning process is an essential factor in obtaining learning outcomes. Often, players/learners are directed to master techniques to reach higher levels. This method is intended to develop skills or to feel pleasure, all of which are intellectual characteristics of motivation in humans [1]. In learning, games are usually applied to evaluate students' understanding of the material they have learned. The evaluation model often collects questions in a quiz, puzzle, questionnaire, etcetera [2,3]. In a game, gamification plays a vital role in increasing motivation [4]. Gamification is defined as the application of game elements in a non-game context [5]. The ingredients in question include at least three things: interface design patterns (badges, levels, leaderboard), game mechanisms,

and design principles [6]. The application of gamification can be found in several forms with specific objectives, such as marketing, social media, commerce, corporate marketing, and education [7].

Call it Facebook, Tokopedia, Shopee, Gojek, Waze, etcetera. One application in the world of knowledge that also applies gamification is Kahoot. Kahoot! is game-based learning that has a mission to improve education quality by strengthening the attachment and connectedness between users while playing [8]. Kahoot was released in 2013. This application has been played in more than 200 cities worldwide, with the total number of players reaching 4.4 billion [8], incredible numbers for an application. This study aims to analyze the elements of gamification contained in the Kahoot! Application. This study's research method is the Octalysis Audit, which is a technique to assess the strengths and weaknesses of a product [9]. The assessment was carried out through 8 approaches to the game's psychological side: meaning, achievement, empowerment, ownership, social influence, scarcity, uncertainty, and avoidance. This study allows further research to identify what types of motivation are weak to improve and provide new experiences. This study's results can be applied to the

application of learning so that teachers or educators continue to innovate in their teaching methods to ensure student motivation in learning sustain, especially in industry 4.0 today, the gaming elements in learning seem relevant.

2. Literature Review

In learning, assessment plays an essential role in assessing the process, progress, and student learning outcomes [10]. Several forms of assessment can be formal, informal, written, performance, traditional, authentic, etcetera. Traditionally, written assessments are the most frequent and easy to use. Paperless assessment is starting to be widely used in the 4.0 era. This fact is evidenced by some previous studies that used Kahoot in education for various purposes. For example:

- increasing motivation to learn English [11],
- enriching the ability to think historically on historical subjects [12],
- enhancing learning activities on Islamic studies topics [13],
- facilitating science learning [14],
- studying foreign languages and improve pronunciation [15],
- improving vocabulary performance [16],
- thematic education [17],
- advanced placement Biology class [18],
- formative medical learning assessment tools [19], and
- increasing test scores [20].

The majority of the research results indicate that Kahoot can be appropriately used to assess learning. Besides, the assessment process carried out in Kahoot is simultaneous and transparent in one large group. This condition has proven to be able to increase student motivation and learning outcomes. Toth Aron discovered that Kahoot had a positive effect on students' results and perception of learning. Aron's research results show that students who took part in more Kahoot quizzes tend to reach higher exam marks.

Moreover, they marked more correct answers and less incorrect ones [21]. This research is strengthened by research that states, when combined with active learning and practice, Kahoot! able to improve student learning outcomes [22,23]. Besides learning outcomes, according to the questionnaire, 82.2% of students stated Kahoot and can also increase student learning motivation [24]. The study results are in line with research that stated that Kahoot enriched student learning quality in the classroom, with the most significant influence on motivation [25,26]. A previous study strengthens this research by saying that, based on T-test testing, Kahoot can increase students' motivation and independence by a significant number [27]. Another study found the fact that Kahoot! can have a positive effect on learning performance, classroom dynamics [25], students' and teachers' attitudes, students' anxiety [28], and student engagement [29]. The effect of applying Kahoot to learning is obtained because of gamification [30–32]. This research focuses on analyzing the gamification elements in Kahoot, using a method called Octalysis Audit.

2.1. Kahoot!

Kahoot! can be accessed on the page http://www.kahoot.com. Kahoot! provides games that can be played directly in one room,

distance learning using video conferencing applications, and learning applications. Several types of user choices are available, starting from free to paid. The difference lies in the features that can be used. In the basic version, game makers can play games personally or via video for ten players. The Basic version offers users to create different types of questions and video hosting for 20 players. The Pro version provides additional game options and allows video hosting for 50 players. Finally, the premium version can host via video for 2000 players.

In the Kahoot! The application, the question maker, and the player have different access. Question makers can create questions independently, choose from the question banks provided, or import from Excel files if they already have them. The type of questions is multiple-choice with four choices, and True or False (Basic version). At the stage of making questions, users can also add images by selecting from the image library, uploading pictures from the device, or attaching a YouTube link. The time limit for working on the questions can be chosen from 5 seconds to 240 seconds. The choice of points in each item can also be arranged with three variants: 0, 1000, and 2000 (Figure 1). When the game maker has finished creating questions, the game can be started by pressing the Done button.
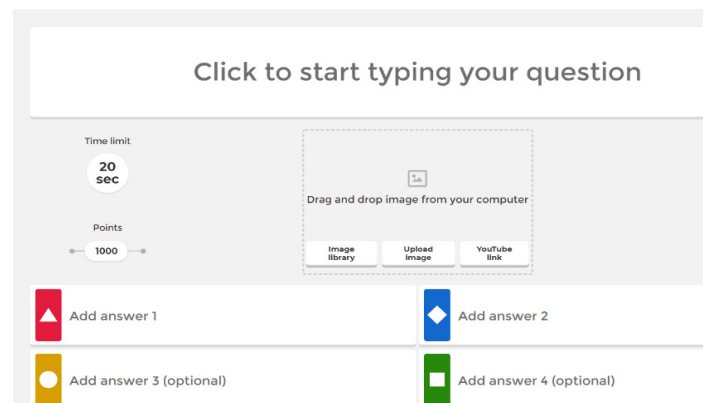
Figure 1: Question-making page on the Kahoot! website

To play the game directly, the question maker must have a tool to display the questions and answer choices on the monitor screen. After the questions are finished, the game can be started by pressing the Play button. Question makers can choose whether individuals or groups will play the game. The interface will then display the PIN that the player must input on the www.kahoot.it page on their respective devices. The player enters a PIN, then comes a nickname on the page. Players who have already joined will appear on the screen. This feature makes it easy for the instructor to monitor how many players have successfully entered. Questions and answer choices will be displayed in front of the screen, whereas on the player's device screen, there are only colors that indicate the answer choices (Figure 2).

3. Methodology

The Octalysis framework (Figure 3) was created because in [9] the author recognized the need for tools to help build strategies and analyze gamification implementation. After years of studying game mechanics, Chou concluded that eight core drives motivate someone to do certain activities. Core drives push people in different directions, and not everyone is motivated by the same drive. Visually, Octalysis has an octagonal shape in which the core

drives are represented in each corner. The drive on the right represents the creative, artistic, and social aspects, while the left's drive represents the logical and intellectual aspects. These sides are referred to as the Left Brain and Right Brain. Besides, he discussed the importance of understanding that this urge supports extrinsic or intrinsic motivation [33].
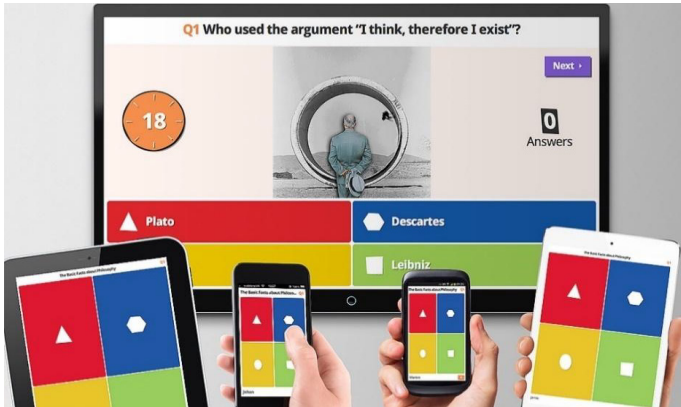
Figure 2: Illustration of Kahoot's interface! when played
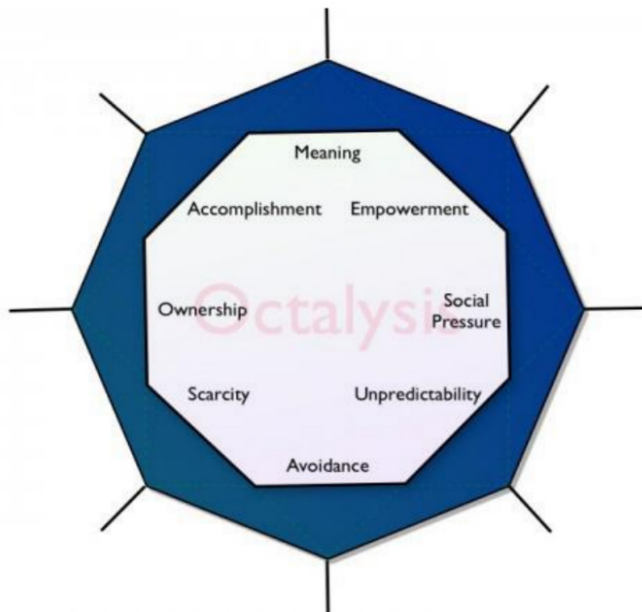
Figure 3: Octalysis Framework

Core drive on the lower side of Octalysis is referred to as Black Hat Gamification, which means negative motivation. This type of encouragement relates to people who are motivated to take specific actions. For example, fear losing because of curiosity about events to come or efforts to achieve things that they cannot have. On the upper side of Octalysis is a positive motivation called White Hat Gamification. This positive core drive motivates individuals through creativity, making them feel secure because of their sense of control and the impression of more significant meaning. Octalysis emphasizes that negative encouragement can inspire motivation as much as positive motivation, but the balance between the two is essential to achieve satisfying and beneficial results.

Octalysis highlights that successful gamification requires consideration of all core drives. The eight-core drives referred to in Octalysis are as follows [34]:

1. *Epic Meaning and Calling*
    At this core, the user is motivated to do something greater than himself or feel chosen to do something. In a game, narration can make this core more pronounced. For example, in the intro of a game, it is said that the world will soon be destroyed, and somehow, the player is chosen as the only person who is qualified to save the world. This core certainly creates excitement and fosters motivation for players to carry out adventures in the game.

    Another example is people who contribute to filling content on Wikipedia pages. Someone who feels "called" will be willing to spend hours filling the content on the page, even if not paid.

2. *Development and Accomplishment*
    Development and achievement are internal drives to make progress, develop skills, and ultimately overcome challenges. In this core, various kinds of performances are designed, such as points, badges, leaderboards, rewards, and other achievements that players can get.

3. *Empowerment of Creativity and Feedback*
    At this core, users are involved in a creative process to find out different combinations repeatedly. Users not only need a way to express creativity but can also see feedback from players.

4. *Ownership and Possession*
    This core is related to the motivation of users because they feel they have something. When a player feels he has something, he will indirectly make what he has better and more.

5. *Social Influence and Relatedness*
    This core combines all the social elements that drive a person, such as guidance, acceptance, social responses, friendship, competition, and jealousy. When one player sees an extraordinary friend on a skill or has something unusual, the player will be motivated to reach the same level.

6. *Scarcity and Impatience*
    In this core, the player is a drive to want something because he cannot have it. For example: due to a time limit, then the game will restart 2 hours later. The fact that players cannot get things now motivates them to think about it all day long.

7. *Unpredictability and Curiosity*
    In general, these cores are harmless drives to find out what happens next. Uncertainty makes players curious. This core happens when someone is reading a book or watching a movie. They will finish what they started of curiosity about the end of the book or film.

8. *Loss and Avoidance*
    This core drive is based on avoiding something negative to happen. Players will feel that if they do not act immediately, they will lose the opportunity to serve forever.

Octalysis Audit is carried out by assessing each existing core. To produce an Octalysis score, researchers take how well the subject of analysis is in each core drive. Then assign a number between 0-10 based on personal judgment, data, and experience flow, then square the number to get a Core Drive score. A score of 10 indicates "How strongly this Core Drive motivates toward the Desired Action." The final Octalysis score will be obtained after adding all 8 Core Drive scores [35].

The sample in this study were 34 lecturers from 2 universities in Indonesia. Samples were selected randomly because all individuals in the population singly or together are given the same opportunity to be selected as sample members. Thus, the research results will be more objective. Lecturers, who were the research sample, had used Kahoot more than 15 times. As many as 52.9% admitted to using Kahoot for lectures, 41.2% used it for workshops, 31.4% for seminars, the rest for other purposes. Survey respondents were asked to provide an assessment both as a question maker and a player. The research instrument was in the form of 12 statements arranged according to the eight cores is Octalysis. The assessment given by respondents is subjective based on the experiences they have experienced. Each statement has a Likert scale from 0-10, according to the Octalysis Audit assessment. Table 1 below shows the instruments in this study.

Table 1: Research Instrument

No	Statement	Core No
1	Kahoot encouraged me to contribute to it	1
2	Kahoot has features such as points, badges, scoreboards, rewards, and podiums	2
3	Kahoot encouraged me to try repeatedly and make different combinations when making questions	3
4	I can see the feedback given by the players	3
5	I feel that I have to defend and increase the points I get while playing Kahoot	4
6	When I was a player, I felt proud when other players applauded when my name appeared on the Scoreboard / Podium	5
7	If my name does not appear on the Scoreboard, I have to pursue it in the next question	5
8	Often the participants asked me to repeat the game when it was finished	6
9	I was wondering how many questions I had to answer	7
10	Every 1 question is answered successfully, I always wonder whether my name is in the top 5 or not	7
11	For me, the most important thing is to answer quickly even if it is wrong	8
12	For me, the most important thing is to answer correctly even though it takes a long time	8

4. Result and Discussion

4.1. Epic Meaning and Calling

A total of 11 respondents gave a score of 8 for the statements on this core (Figure 4). Epic meaning and calling can be done when the user, for example, fills in a question bank. The question bank

provided by Kahoot! allows users to search for problems with specific themes that have been created by other users (Figure 5). Fellow users around the world can benefit from each other. This feature is related to the core meaning in Octalysis, where users can feel motivated to make various questions for themselves and others. This calling is in line with previous studies, which stated that student motivation increased after using Kahoot! [11]. The average score for this core is 6.74.
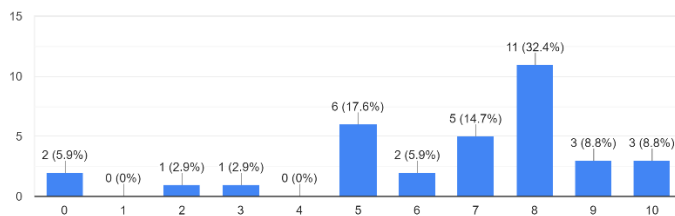
Figure 4: Epic Meaning and Calling response result
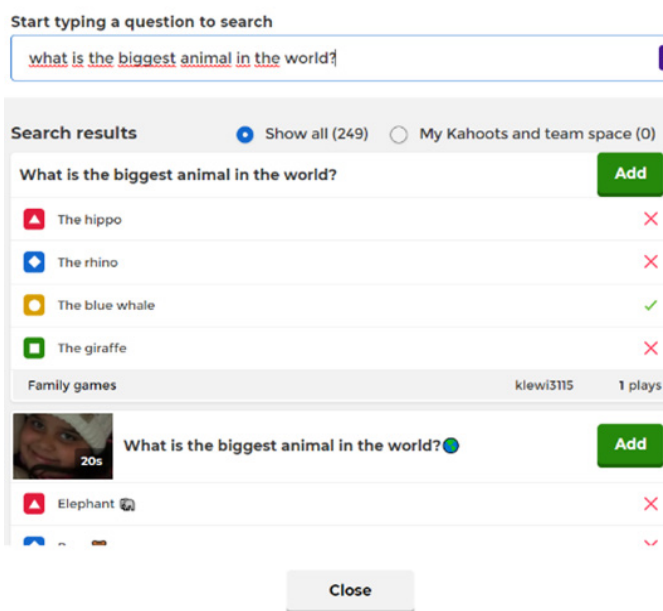
Figure 5: The question bank on the Kahoot! Page

4.2. Accomplishment

For each question answered, Kahoot can display the correct answer, and the Scoreboard contains the five highest-ranked players and their respective points (Figure 6a). This feature certainly raises pride for players whose names are displayed on the Scoreboard. The three best players will be shown their names with a podium interface at the end of the game. The back-sound also supports it as if the player is on a real podium (Figure 6b).

At this core, 75% of respondents gave a score of 8 and 10. This result indicates that respondents have understood that Kahoot has gamification features, such as point, Scoreboard, reward, and podium. The average score obtained from the statement on this core is 8.67.

4.3. Empowerment of Creativity and feedback

An exciting game requires creativity from the creator. To not be monotonous, question makers can add questions that are not too

serious in the middle of the game. For example, by making a problem that displays a photo of one of the players, then questioning what the player is doing? This question will make the game more interesting. However, of course, creativity here is relatively dependent on the question maker. When respondents were given the statement, "Kahoot encouraged me to make different combinations when making questions." 50% gave a score of 8 and above. The survey results show a balanced answer, depending on the creativity of the question maker.
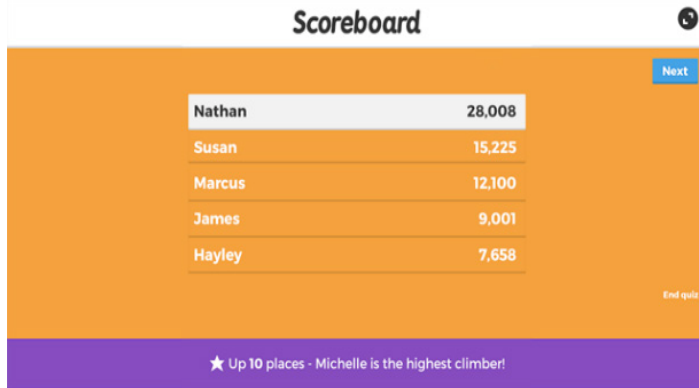
(a)
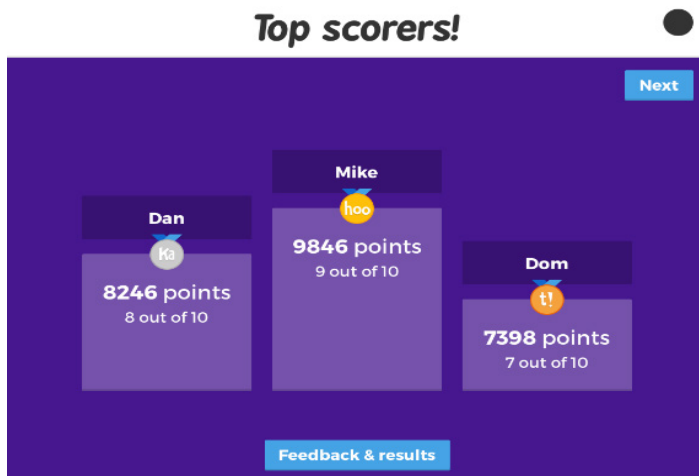
(b)

Figure 6: (a) Scoreboard Interface (b) Podium Interface
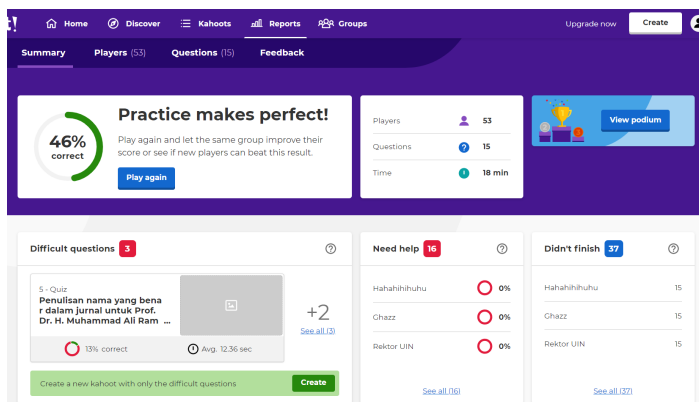
Figure 7: Summary of the Kahoot! Page

The question maker can see player feedback at the end of the game. One of the new features provided by Kahoot is the

Summary, which contains a summary of the games that have been performed. Figure 7 shows the Kahoot Summary, containing the number of players, the percentage who answered correctly, the number of questions, the time, the most difficult questions, to the player's status. This player status includes whoever needs help, players who have not finished the game to the end, and the podium. This new feature makes it very easy for question makers to review the game as a whole.

4.4. Ownership and Possession

One of the exciting gamification elements of Kahoot is the point. Points for each question in Kahoot can be varied, starting from 0, 1000, and 2000. The faster and more precise the player answers the question, the higher the score obtained. With the scoreboard feature, players can see how many points they have. If the player's name is on the Scoreboard, it will undoubtedly make them maintain a high position so that no one beats him.

The importance of the points obtained attracted 35.3% of respondents to give a value of 10 to statement number 5. This fact shows that the respondents strongly agree with this statement. Apart from getting points, more than 84% of respondents also agreed to retain their points when playing Kahoot. These survey results are in line with the core ownership and position in Octalysis, where the players try hard to defend the points they get.

4.5. Social Influence and Relatedness

One of the gamification elements that have a strong social influence is the Scoreboard and the Podium. Other players will usually congratulate or applause when a player's name appears on the Scoreboard or Podium. Events like this bring pride to these players. A total of 26 survey respondents gave a score of 8-10 concerning the statement, "I feel proud when other participants applaud when my name appears on the Scoreboard / Podium."

Conversely, this social influence also motivates players whose names do not appear on the Scoreboard. A player whose name is not on the Scoreboard will be motivated to catch up and make his points higher. A total of 29 respondents strongly agreed to pursue other participants' points when their names did not appear on the Scoreboard. This sense provides the motivation that is in line with the core of social influence and relatedness.

4.6. Scarcity and Impatience

Based on experience, some of the respondents said that often when finished playing Kahoot, the player asks the host to repeat the game. Motivation to get better grades makes players want the same game a second time. However, some respondents admitted that they did not want to repeat the game because the order of the questions displayed would be precisely the same as before. In this core statement, the average score is 7.9 (Figure 8).
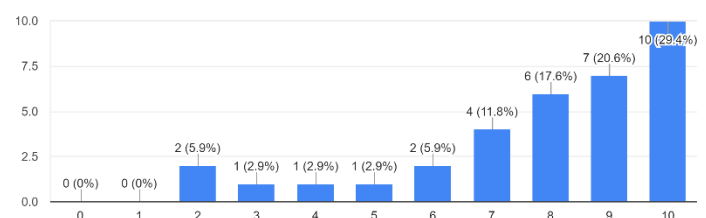
Figure 8: Scoring for the Scarcity cores

4.7. Unpredictability and Curiosity

More than 60 percent of our respondents are intrigued as to how many questions they have to raise. Although, in the game-opening, a justification is given for the number of questions to be played (Figure 9). Another thing that triggers the players' curiosity is to find out whether he entered the Scoreboard or the podium at the end of the game (Figure 10). A scoreboard will appear that all participants have answered every 1 question. This core gets an average score of 8.12 points.
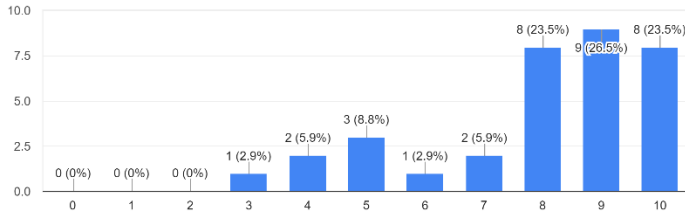
Figure 9: Score given by respondents regarding curiosity about the number of questions
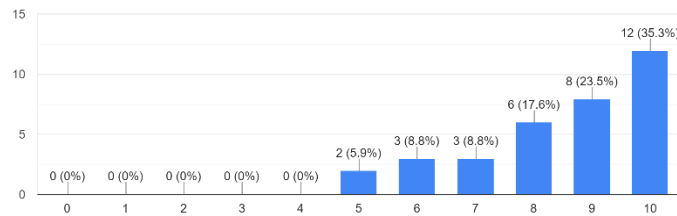
4.8. Loss and Avoidance

The last core in Octalysis Framework is related to the speed of players in answering questions on Kahoot. Because the time to answer questions can be varied, players certainly do not want to miss answering questions because they run out of time. This feeling will harm the players because they do not get the point. Conversely, if too fast but other players can replace the wrong answer, the ranking of players.

Table 2: Average score for every core

No	Core Aspect	Average
1	Epic Meaning and Calling	6.74
2	Development and Accomplishment	8.67
3	Empowerment of Creativity and Feedback	7.5
4	Ownership and Possession	8.41
5	Social Influence and Relatedness	8.30
6	Scarcity and Impatience	8.35
7	Unpredictability and Curiosity	8.12
8	Loss and Avoidance	6.24

On this core, we ask what is most important for players. A total of 5.3 average scores was obtained for the statement to answer quickly, even though it was wrong. The statement chose the right answer, even though it took a long time to get an average value of 7. This result shows that each respondent has different priorities. Some respondents choose the time, and some are more careful even though they lose much time.

Based on the respondents' answers for each Octalysis core, we add up each point obtained, then divide by the number of respondents to obtain each statement's average value. The average value is shown in Table 2.

4.9. Octalysis Score

The values entered in the Octalysis tool provide only round values [36]. Therefore, we take the numbers that come before the comma. Based on the research results, the value obtained was 441. Kahoot is considered to have a balance between White Hat and Black Hat drives. This result marks Kahoot balancing the positive and negative motivations of the player. Besides, the right brain balance and the left brain is also considered quite good, which indicates Kahoot! application has a proper balance between Intrinsic and Extrinsic Motivation. An overview of Octalysis Kahoot's audit analysis present in Figure 11.
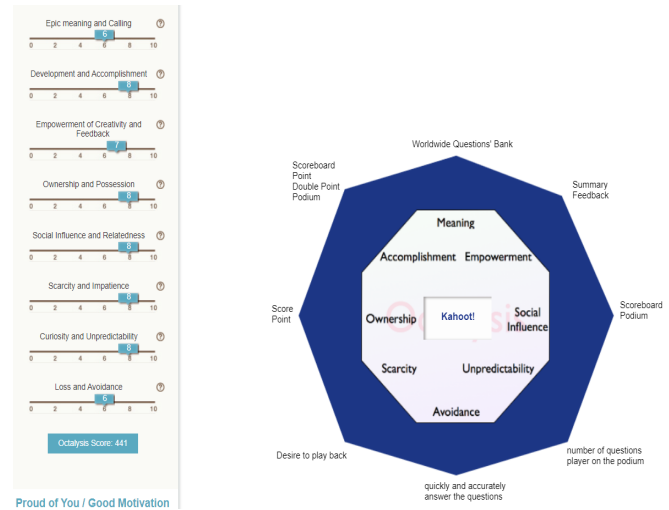
Figure 11: Kahoot! 's Octalysis audit result

Even though it is considered quite reasonable, according to the Octalysis tool, some of our respondents provide suggestions for Kahoot. The suggestions given include minus points, questions raised on players' gadgets, opportunities to correct wrong answers, open camera facilities, to custom music. These suggestions will certainly make Kahoot better and more attractive to use in learning.

5. Conclusion

Has been analyzed a game-based game application called Kahoot! by using the Octalysis Audit method. The score on the form accumulated by survey based on eight core drives on Octalysis. Based on research, a final value of 441 was obtained in the Kahoot application. This outcome is Kahoot! It is a balance in terms of motivation, both positively and negatively. The outcome also shows that Kahoot! has intrinsic and extrinsic motivation. Therefore, Kahoot! can be used as the right learning media to make similar games. Researchers have recommended some suggestions to improve Kahoot! better. Such as: providing tips to make the game more interesting, providing a random feature about the problem, and providing a minus point feature if the answer is wrong.

Conflict of Interest

The authors declare no conflict of interest.

Acknowledgment

References

[1] R.E. White, "The Power Of Play: A Research Summary on Play and Learning," Smart Play, 15–25, 2013.

[2] D.R. Ramdania, M. Irfan, S.N. Habsah, C. Slamet, W. Uriawan, K. Manaf, "Fisher-Yates and fuzzy Sugeno in game for children with special needs," Telkomnika (Telecommunication Computing Electronics and Control), **18**(2), 879–889, 2020, doi:10.12928/TELKOMNIKA.V18I2.14906.

[3] D.R. Ramdania, M. Harika, S. Rahmadika, G.G. Azmiana, "The Use of Relations and Functions Games Based on Balanced Design in Mathematics Subjects to Improve Student Learning Outcomes," in Journal of Physics: Conference Series, IOP Publishing: 12069, 2019.

[4] S. Deterding, "Gamification: designing for motivation," Interactions, **19**(4), 14–17, 2012.

[5] S. Deterding, M. Sicart, L. Nacke, K. O'Hara, D. Dixon, Gamification: Using game design elements in non-gaming contexts, 2011, doi:10.1145/1979742.1979575.

[6] B. Liu, "Uncertainty theory: A branch of mathematics for modeling human uncertainty," Studies in Computational Intelligence, **300**, 1–361, 2010, doi:10.1007/978-3-642-13959-8_1.

[7] Y. Chou, Gamification Examples: the fully comprehensive list (2019), 2019.

[8] Kahoot!, About Kahoot! | Company History & Key Facts, 2018.

[9] Y.-K. Chou, Actionable gamification: Beyond points, badges, and leaderboards, 2016, doi:10.1017/CBO9781107415324.004.

[10] I. Tosuncuoglu, "Importance of Assessment in ELT," Journal of Education and Training Studies, **6**(9), 163, 2018, doi:10.11114/jets.v6i9.3443.

[11] E.T. Tsani, Using Kahoot! as games-based E-Learning to enhance students' English learning motivation, 2019.

[12] R. Fauzan, "Pemanfaatan Gamification Kahoot.it Sebagai Enrichment Kemampuan Berfikir Historis Mahasiswa pada Mata Kuliah Sejarah Kolonialisme Indonesia (Utilization of Kahoot.it Gamification as Enrichment of Students' Historical Thinking Abilities in the Historical C," Prosiding Seminar Nasional Pendidikan FKIP UNTIRTA, **2**(1), 257, 2019.

[13] H. Fauzih, Gamification: A Case Study for Evaluating the Performance of Employees | KHASKHELI | Sindh University Research Journal - SURJ (Science Series), 2019.

[14] K.E. Cameron, L.A. Bizo, "Use of the game-based learning platform KAHOOT! to facilitate learner engagement in animal science students," Research in Learning Technology, **27**, 2019, doi:10.25304/rlt.v27.2225.

[15] N. Yürük, "Edutainment: Using Kahoot! As A Review Activity in Foreign Language Classrooms," Journal of Educational Technology and Online Learning, **2**(2), 89–101, 2019, doi:10.31681/jetol.557518.

[16] M. Mansur, M. Mansur, D. Fadhilawati, "Applying Kahoot to Improve the Senior High School Students' Vocabulary Achievement," VELES Voices of English Language Education Society, **3**(2), 164–173, 2019.

[17] A.R. Hakim, S. Rahayu, R. Affida, "Kahoot on Thematic Learning," in Journal of Physics: Conference Series, 2019, doi:10.1088/1742-6596/1381/1/012035.

[18] S.M. Jones, P. Katyal, X. Xie, M.P. Nicolas, E.M. Leung, D.M. Noland, J.K. Montclare, "A 'KAHOOT!' Approach: The Effectiveness of Game-Based Learning for an Advanced Placement Biology Class," Simulation & Gaming, **50**(6), 832–847, 2019.

[19] M.A.A. Ismail, A. Ahmad, J.A.M. Mohammad, N.M.R.M. Fakri, M.Z.M. Nor, M.N.M. Pa, "Using Kahoot! as a formative assessment tool in medical education: A phenomenological study," BMC Medical Education, **19**(1), 230, 2019, doi:10.1186/s12909-019-1658-z.

[20] P.A. Baszuk, M.L. Heath, "Using Kahoot! to increase exam scores and engagement," Journal of Education for Business, 2020, doi:10.1080/08832323.2019.1707752.

[21] Á. Tóth, P. Lógó, E. Lógó, "The Effect of the Kahoot Quiz on the Student's Results in the Exam," Periodica Polytechnica Social and Management Sciences, **27**(2), 173–179, 2019. https://doi.org/10.3311/PPso.12464

[22] I.L. Aldana, "The Effects of Review Games Using Kahoot! On Students' Quiz Scores.," Online Submission, 2020.

[23] S. Chera, "Analyzing the impact of recurrent Kahoot tests on student performance," 2020.

[24] R.D. Mada, A. Anharudin, "How Online Learning Evaluation (Kahoot) Affecting Students' Achievement and Motivation (Case Study on it Students)," International Journal for Educational and Vocational Studies, **1**(5), 422–427, 2019.

[25] N. Kletnikov, O. Popovski, A. Tomova, "Kahoot! foster students' engagement, enhance classroom dynamics, assess and improve overall students' learning," Proceedings of Papers, **24**, 2019.

[26] L.S.L. Purba, E. Sormin, N. Harefa, S. Sumiyati, "Effectiveness of use of online games kahoot! chemical to improve student learning motivation," Jurnal Pendidikan Kimia, **11**(2), 57–66, 2019.

[27] M. Izzati, H. Kuswanto, "Pengaruh model pembelajaran blanded learning berbantuan kahoot terhadap motivasi dan kemandirian siswa (The influence of the kahoot-assisted blended learning model on students' motivation and independence)," EDUMATIC: Jurnal Pendidikan Informatika, **3**(2), 68–75, 2019.

[28] A.I. Wang, R. Tahir, "The effect of using Kahoot! for learning–A literature review," Computers & Education, **149**, 103818, 2020.

[29] Y. Benhadj, M. El Messaoudi, A. Nfissi, "Investigating the Impact of Kahoot! on Students' Engagement, Motivation, and Learning Outcomes: Ifrane Directorate as a case study," International Journal of Advance Study and Research Work, **2**(6), 2581–5997, 2019.

[30] O. Baydas, M. Cicek, "The examination of the gamification process in undergraduate education: a scale development study," Technology, Pedagogy and Education, **28**(3), 269–285, 2019.

[31] M.L. Pertegal-Felices, A. Jimeno-Morenilla, J.L. Sánchez-Romero, H. Mora-Mora, "Comparison of the Effects of the Kahoot Tool on Teacher Training and Computer Engineering Students for Sustainable Education," Sustainability, **12**(11), 4778, 2020.

[32] N.P.A. Resmayani, I.N.T.D. Putra, "Gamification: Using Kahoot! to Make Students Love the Class from the Very Beginning," Linguistics and ELT Journal, **7**(1), 10–18, 2020.

[33] J. Landsell, "Towards a Gamification Framework : Limitations and opportunities when gamifying business processes," 2016.

[34] Y.-K. Chou, "Actionable gamification: Beyond points, badges, and leaderboards," Octalysis Media, 1–151, 2016, doi:10.1017/CBO9781107415324.004.

[35] Y. Chou, Octalysis: Complete Gamification Framework - Yu-kai Chou, 2013.

[36] Y. Chou, Octalysis / Gamification Building Developing Online Tool - by Yukai Chou, Dec. 2020.

Analysis of Pharmaceutical Company Websites using Innovation Diffusion Theory and Technology Acceptance Model

Mochammad Haldi Widianto*

Informatics Departement, School of Computer Science , Bina Nusantara University, Jakarta, Indonesia, 11480

A R T I C L E I N F O	A B S T R A C T
	The progress of information using websites is developing fast, impacting various sectors, one of which is pharmaceutical companies. Pharmaceutical companies have roles in drug manufacturing, pharmaceutical distribution, and essential services for the community—the most important and challenging activity in the IT department. The researcher is responsible for one of the Bandung pharmaceutical companies. Researchers are trading IT service managers for drug manufacturing, drug distribution, and community service units that have been conducted online. The company has an essential role in distributing drugs to pharmacists and hospitals during the pandemic at COVID-19. The use of the IDT (Innovation Diffusion Theory) and TAM (Technology Acceptance Model) models are used because, according to the agreement, TAM is a concept that researchers consider to be the best and suitable for viewing the user's use of IT systems. The study will try to convert these methods with TAM variables, such as Perception of Use, Perception of Ease of Use, Attitude Towards, and Behavior Intentions. Also, IDT variables such as Relative Advantage, Compatibility, Complexity, Trialability, Observability. This study's survey model is the SEM (Structural Equation Model) using a software application. The results showed the pharmaceutical company website could be well received at pharmacists and hospitals in Bandung. The experimental results get a hypothesis, such as finding a significant output. And with the results of this study, getting good results for the people around Bandung.

1. Introduction

Today the information system is developing rapidly along with the pandemic currently in this world (COVID-19). The development of this information system is compared with hardware technology because computers or other hardware are media that can provide convenience, especially when the pandemic is now [1]-[3].

Every company needs IT [4]–[7] to help with scheduling, purchasing, etc., so that it can be more centralized. In every company other than pharmaceuticals, procurement management must determine the existing goods, especially medicines, and manage inventory in the industry and sales [3], [8].

In its production, pharmaceutical companies in Bandung produce such products as Propepsa, Bevita Suspension, Zemindo, Amiclav, Bionemi, Calnic, D-Vit, Estin, Flamic, Fosicol, Gastrolan, Grafix, Grafed, Imox, Loxil, Mesol, Moretic, etc. , and

distributes sales results to all regions in Indonesia. Every sale of medicines to pharmacies and hospitals needs to make orders ordered from each distributor and sub-distributor [9], [10].

According to previous research sources in manufacturing Information Technology (IT) system, products in pharmaceutical companies are still traditional with direct analysis (interviews with PT) combined with the waterfall method [11], [12]. Today researchers use the waterfall method. Barriers that became obstacles were found from the results of interviews using too many typical office applications. So, now the researcher builds some websites to maximize utilization system information in the pharmaceutical company.

Researchers have carried out many web analysis theories, one of which is the Innovation Diffusion Theory (IDT) and the Technology Acceptance Model (TAM) [13], [14]. Explanation TAM is the instrument for anticipating the probability of another innovation being received inside a gathering or an association.

* Corresponding Author: Mochammad Haldi Widianto, Kecamatan Buah Batu, Bandung, Indonesia, Email: mochamad.widianto@binus.ac.id

In light of the hypothesis of contemplated activity, it has by a wide margin been the most broadly talked about among all the connected models. What's more, dictated by two convictions: saw value, which is characterized as the forthcoming client's abstract likelihood that utilizing a particular application framework will build one's work execution inside a hierarchical setting, and saw usability, which alludes to how much the planned client anticipates that the objective framework should be liberated from exertion. IDT is utilized to clarify how groundbreaking thoughts and new practices are spread inside and between associations. It is a cycle of dispersal through arranged systems to empower advancements to be received [15], [16].

With the results of the information system and the use of technology from the pharmaceutical company website in Bandung, it is necessary to measure the extent of the successful implementation. The use of the TAM [17]–[19] and IDT [15], [20], [21] model is based on the fact that so far, TAM is a concept that is considered the best and suitable in explaining user behavior towards information technology systems.

As a comparison with previous research, on [16] using a comparison application with the labor market, while on this application, researchers use pharmaceutical companies to see their effects, it is expected to be useful for the pharmaceutical company in assessing the attachment and improvising the company's IT system.

2. Theoretical Background

According to [8], [22], [23] said if the progress of the company can create healthy communities and increased life expectancy, produce and spread drugs, and ultimately lead to the commercialization of the development of drug distribution. Develop is a way to understand other thinking, useful methods, and hope for progress, where development is very rapid, with new ideas and useful. It is IT's use for recent and varied advancements as well as increasing or lower-cost nature, to meet or exceed our own goal

Innovation [24]–[26] is the essential stage of the diffusion processor so that it can trigger the process to continue rapidly. Meanwhile, good communication refers to a channel used to transfer information from one party to another so that it can start the same thoughts. The following is an illustration of diffusion theory or IDT as shown in Figure 1.
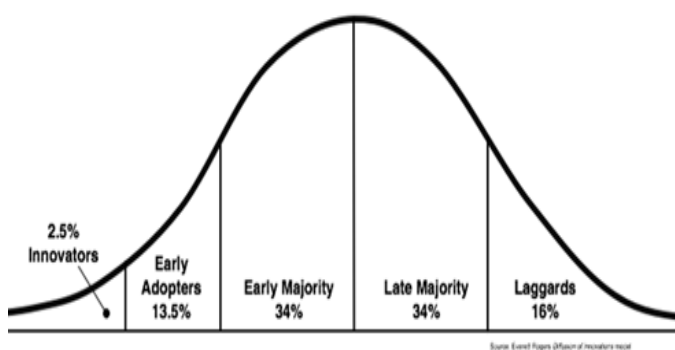
Figure 1: Innovation Diffusion Theory

Furthermore, the theory put forward [16], [27], [28] has a significant meaning and has conflicts in leadership management.

A temporary conclusion can be drawn, among other things, describing the principles that influence the rate of development deprivation, such as the progress phase, so that a leadership process is needed. Regulations affecting the deployment stage of development include the quality of the product (view progress), the type of development choice, the correspondence channel (correspondence channel), the conditions of the social framework, and the specialist work progress (change operator). The characteristics of IDT, according to [8], [9] as follow:

Rogers (1983) suggests five characteristics innovations include:

1) relative advantage,

2) compatibility,

3) complexity,

4) ability to be tested (trialability) and

5) observability.

In contrast to IDT, TAM is a new derivative that was introduced by Davis in 1986. The goals of TAM are more generalized to explain the behavior of the primary user of the computer. TAM uses the TRA derivative as a theoretical basis for deriving a causal relationship between two fundamental beliefs, such as Perceived Usefulness and Perceived Ease of Use [18], [19]. More evident than TRA because TAM is used unusually for the use of innovations in computerized techniques. This TAM model is ready to predict something and can clearly explain to experts and professionals to find out why a factor is not known and provide the potential for progress that has the right accuracy.

Using the TAM factor is to provide initial advancement of the effects of external factors on inner beliefs, frame of mind, and goals. Achieve this goal by distinguishing some of the fundamental elements put forward in the investigation following the principles that influence psychological factors and feelings of recognition in computer engineering and using TRA as a possible reason for severing the relationship of the research factor model. The stamp positions two beliefs, particularly seeing perceived convenience and benefits as essential elements of PC recognition behavior, as seen in Figure 3.
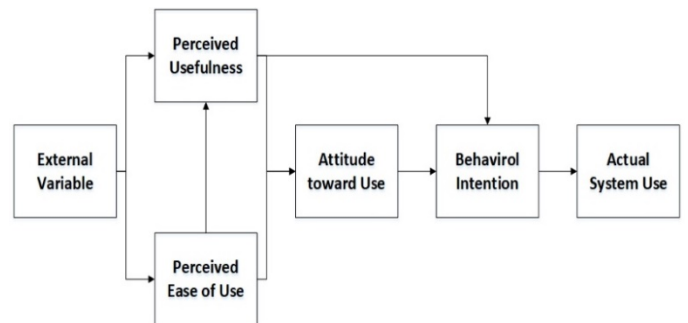
Figure 2: Technology Acceptance Model (TAM)

Based on the literature's systematic review, different works have been found that strengthen the areas of knowledge processing and representation. The branch that is responsible for the processes of knowledge representation in Artificial Intelligence, to achieve this, it is necessary to group situations that

have similar characteristics or properties instead of making individual representations.

3. System Analysis

3.1. Business Process

The pharmaceutical [29]–[32] business process is indeed very complicated, which can be interpreted as having a set of activities or jobs that are structured and interrelated. It is used to solve a problem or produce a new pharmaceutical product. Several sections are used to analyze employees' work procedures in IT to see the finished drug supplies at a pharmaceutical manufacturing plant in Bandung, and this business process aims to identify and problems that occur and expected needs.
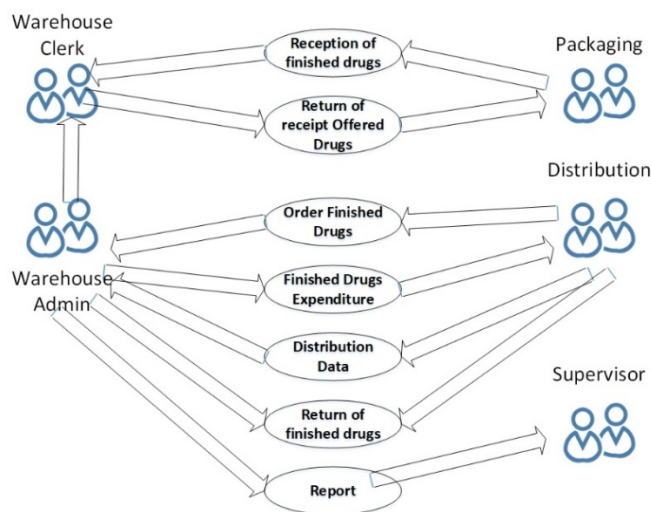
Figure 3: Business Object of Drug Inventory

Table 1: Information Needs

No	Name	Goals	Frequency
1	Drug Receipt Report	Warehouse Supervisor	Monthly Period
2	Report on Drug Expenditures	Warehouse Supervisor	Monthly Period
3	Distributor Data Report	Warehouse Supervisor	Supervisor Needs
4	GOJ Inventory Report	Warehouse Supervisor	Monthly Period
6	Delivery orders	Distributor	Every Day
7	Proof of receipt of finished pharmaceutical	Warehouse Admin	Every Day
8	Reports on Receiving Medication for Finished Medicines	Warehouse Supervisor	Supervisor Needs
9	Report on Drug Expenditures Return	Warehouse Supervisor	Supervisor Needs

3.2. Identification of User Needs

The information system [33]–[35] must provide the consumer for comfort and classification incompatible with the requirements, though these system conditions are as measures:

1. The working framework will have to make the user's job easier
2. The framework produced must have data protection so that its use can be restricted
3. Employees who have been enrolled must use the program
4. The system made must be capable of displaying reports and even printing reports according to existing data input
5. All information should be available and often easy to find and obtain to help achieve the use of this system by users
6. This information system needs to be able to create its use straightforward for the warehouseman.
7. The phone designed must be able to initiate the input and distribution of pharmaceutical completes.

What needs are described in table 1:

3.3. Program Testing

The system must be free from errors before the process is implemented. To that end, the program has to be tested in advance to investigate the potential errors. This system is evaluated or reviewed using the White Box and Black Box techniques. Black Box Testing where for testing the program immediately looks at the application without knowing the program's structure. This test is carried out to see whether a program has met or not [8], [24], [36].

4. Result

The first few contents contain the Logo etc. Next includes some vital information about the company. The most important thing is the log-in section. Employees can't enter this website.
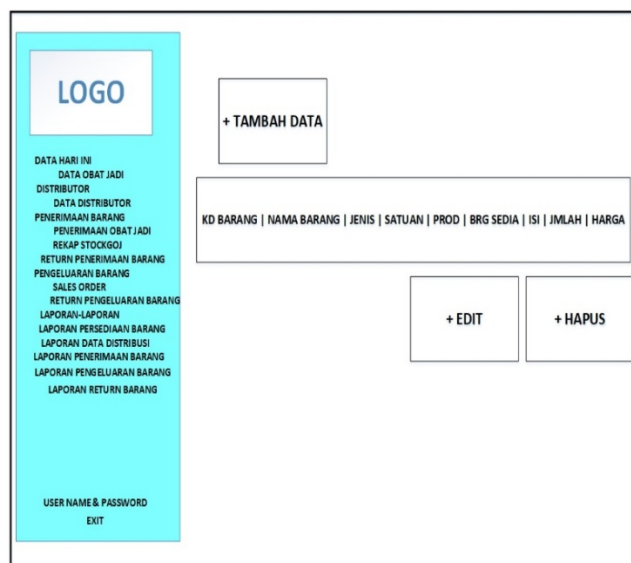
Figure 4: Login Interface Home Admin

Furthermore, the same as before carried out several tests using the black box, with the results as in the following table:

Table 2: BlackBox Test Home Admin

Component testing	Expected results	Result
Add Data	May add data	Successful
Connect Distributor	Can Connect Distributor	Successful
Received Goods	Can Connect received goods	Successful
Report Distribution	Can Connect Report Distribution	Successful
Log Out	Can Logout	Successful

Of all the tests carried out by BlackBox and according to [37], the method of using waterfall is still efficient and effective for use in making websites for pharmaceutical companies.

4.1. Testing the Overall Research Model

This model [38], [39] shows that the model consists of 9 constructs, namely: RA (Relative Advantage), CPA (Compatibility), CPL (Complexity), TRI (Trialability), OB (Observability), PU (Perceived Usefulness), PEU (Perceived Ease of Use), AT (Attitude Towards), BI (Behavioral Intention). In this model, the relationships between constructs and the interrelationships between indicators are adjusted to the research hypothesis. The overall model test results using SPSS AMOS 22 produce the level of conformity, as shown in the table.

4.2. Hypothesis Testing with SEM

This test is done to see the relationship between the constructs that exist in the research model. The basis for decision-making was taken by looking at the regression weights for the constructs related to the test results using SPSS AMOS version 22. If p> 0.05, then H1 is rejected, and if p <0.05 or denoted by ***, then H1 is accepted as described in table 6.

Table 3: Modification Structural Model Suitability Test Results

Model Fit	Result	*Acceptable Level*	Interpretation
CMIN (*Chi Square*)	1817.325	Beetween Saturated and Independence Model	Good Conformity
GFI (*Goodness of Fit Index*)	0.747	0 (tidak fit) s/d 1 (Fit)	Good Conformity
AGFI (*Adjusted GFI*)	0.715	0 (tidak fit) s/d 1 (Fit)	Good Conformity
RSMEA (*Root mean square error of approximation*)	0.066	< 0.080	Good Conformity
TLI (*Tucker-Lewis Index*)	0.833	0 (tidak fit) s/d 1 (Fit)	Good Conformity
NFI (*Normed Fit Index*)	0.741	0 (tidak fit) s/d 1 (Fit)	Good Conformity
CFI (*Confirmatory Fit Index*)	0.845	0 (tidak fit) s/d 1 (Fit)	Good Conformity
PNFI (*Parcimonious Fit Index*)	0.687	0 (tidak fit) s/d 1 (Fit)	Good Conformity

Source: SPSS AMOS 22

Table 4: Value of Regression Weight Modified Research Model

			Estimate	S.E.	C.R.	P	Label	Result
PEU	<---	RA	-2.936	8.671	-.339	.357	par_37	Insignificant
PEU	<---	CPA	3.203	8.715	.367	.137	par_39	Insignificant

			Estimate	S.E.	C.R.	P	Label	Result
PEU	<---	CPL	.133	2.315	.057	.459	par_41	Insignificant
PEU	<---	OB	-.010	.324	-.032	.047	par_43	Significant
PEU	<---	TRI	.495	.789	.627	.035	par_50	Significant
PU	<---	RA	.160	1.551	.103	.189	par_36	Insignificant
PU	<---	CPA	.043	1.486	.029	.397	par_38	Insignificant
PU	<---	CPL	-.33	.668	-.528	.035	par_40	Significant
PU	<---	OB	.706	.130	5.422	***	par_42	Significant
PU	<---	PEU	.063	.291	.215	.038	par_44	Significant
PU	<---	TRI	-.036	.118	-.303	.267	par_49	Insignificant
AT	<---	PU	-.061	.038	-1.618	.***	par_45	Significant
AT	<---	PEU	.941	.074	12.647	***	par_47	Significant
BI	<---	PU	.010	.044	.216	.298	par_46	Insignificant
BI	<---	AT	.966	.080	12.033	***	par_48	Significant

Table 5: Summary of Research Hypothesis Testing Results

NO	Hypothesis (H$_1$)	P	Noted
1	There is a significant relationship between *Perceived Ease of Use* with *Relative Advantage*	.357	H$_1$ Rejected
2	There is a significant relationship between *Perceived Ease of Use* with Persepsi *Compatibility*	.137	H$_1$ Rejected
3	There is a significant relationship between *Perceived Ease of Use* with *Complexity*	.459	H$_1$ Rejected
4	There is a significant relationship between *Perceived Ease of Use* with *Observability*	.047	H$_1$ Accepted
5	There is a significant relationship between *Perceived Ease of Use* with *Trialability*	.035	H$_1$ Accepted
6	There is a significant relationship between *Perceived Usefulness* with *Relative Advantage*	.189	H$_1$ Rejected
7	There is a significant relationship between *Perceived Usefulness* with *Compatibility*	.397	H$_1$ Rejected
8	There is a significant relationship between *Perceived Usefulness* with *Complexity*	.035	H$_1$ Accepted
9	There is a significant relationship between *Perceived Usefulness* with *Observability*	***	H$_1$ Accepted

NO	Hypothesis (H₁)	P	Noted
10	There is a significant relationship between *Perceived Usefulness* with *Perceived Ease of Use*	.038	H₁ Accepted
11	There is a significant relationship between *Perceived Usefulness* with *Trialability*	.267	H₁ Rejected
12	There is a significant relationship between *Attitude Towards* with *Perceived Usefulness*	.***	H₁ Accepted
13	There is a significant relationship between *Attitude Towards* with *Perceived Ease of Use*	***	H₁ Accepted
14	There is a significant relationship between *Behavioral Intention* for *Perceived Usefulness*	.298	H₁ Rejected
15	There is a significant relationship between *Behavioral Intention* with *Attitude Towards*	***	H₁ Accepted

Table 6: Re-Test Results of Conformity of Modified Structural Models

Model Fit	Result	*Acceptable Level*	Interpretation
CMIN (*Chi Square*)	1279.601	*Between Saturated* and *Independence Model*	Good
GFI (*Goodness of Fit Index*)	0.772	0 (unfit) s/d 1 (Fit)	Good
AGFI (*Adjusted GFI*)	0.738	0 (unfit) s/d 1 (Fit)	Good
RSMEA (*Root mean square error of approximation*)	0.074	< 0.080	Good
TLI (*Tucker-Lewis Index*)	0.831	0 (unfit) s/d 1 (Fit)	Good
NFI (*Normed Fit Index*)	0.758	0 (unfit) s/d 1 (Fit)	Good
CFI (*Confirmatory Fit Index*)	0.844	0 (unfit) s/d 1 (Fit)	Good
PNFI (*Parcimonious Fit Index*)	0.699	0 (unfit) s/d 1 (Fit)	Good

Table 7: Re-Test Results of Conformity of Modified Structural Models

NO	Hypothesis (H₁)	P	Notes
1	There is a significant relationship between *Perceived Ease of Use* with *Observability*	***	H₁ Accepted
2	There is a significant relationship between *Perceived Ease of Use* with *Trialability*	.040	H₁ Accepted
3	There is a significant relationship between *Perceived Usefulness* with *Observability*	***	H₁ Accepted
4	There is a significant relationship between *Perceived Usefulness* with *Perceived Ease of Use*	***	H₁ Accepted

NO	Hypothesis (H₁)	P	Notes
5	There is a significant relationship between *Perceived Usefulness* with *Complexity*	.029	H₁ Accepted
6	There is a significant relationship between *Attitude Towards* with *Perceived Usefulness*	.019	H₁ Accepted
7	There is a significant relationship between *Attitude Towards* with *Perceived Ease of Use*	***	H₁ Accepted
8	There is a significant relationship between *Behavioral Intention* with *Attitude Towards*	***	H₁ Accepted

Among them are the Relative Advantage hypothesis with Perceived Usefulness and Perceived Ease of Use. It is apart from the use of the pharmaceutical company, which provides opportunities for education graduates and students to apply for jobs to companies that have collaborated. The presence of this pharmaceutical company indeed feels various benefits and aspects of benefits. However, the company still determines the work that is obtained or the opportunity to receive job applicants.

Graduates and students also do not feel the influence of compatibility with the aspects of benefits and convenience. This happens as the development of information technology that makes accessing the internet through various media makes the pharmaceutical company system less suitable because it cannot reach the mobile side.

The pharmaceutical company's complexity was felt not to affect the aspect of ease, and trialability did not change the character of benefits. Because the pharmaceutical company is only intended for the academic community, the wider community can only access it. And also does not feel the effect of benefits on the intention to use, the tendency of job applicants triggers it will stop looking for another job if the person has found a job by expectations.

5. Conclusion

Based on the results of research conducted on the implementation of the pharmaceutical company using. The use of the IDT and TAM models approaches processed using the SPSS AMOS 22 application. The following conclusions can be obtained, and Relative Advantage does not affect Perceived Usefulness in the pharmaceutical company's application. Relative Advantage does not affect the Perceived Ease of Use in the application of the pharmaceutical company. Compatibility does not affect the Perceived Usefulness in the application of the pharmaceutical company

References

[1] N. Komalasari, JOURNAL Budiman, and E. Fernando, "Effect of Education , Performance , Position and Information Technology Competency of Information Systems to Performance of Information System," 2018 International Seminar.. Res. Inf. Technol. Intell. Syst., 221–226, 2016.

[2] M. Kejriwal, "Information Extraction," SpringerBriefs Comput. Sci., 9–31, 2019.

[3] W. Sardjono and T. L. Wijaya, "Evaluation of Budgeting Management Information System at DKI Jakarta Forestry Service," Proc. 2018 International Conference Inf. Manag. Technol. ICIMTech, 33–37, 2018.

[4] P. A. W. Putro and R. Rionaldy, "Implementation of the Park Schema on User Authentication Services Using Password-Based Web Codeigniter Library to Overcome Man in the Middle Attack," Proc. 2019 4th International Conference Informatics Comput. ICIC-2019, 1-5, 2019.

[5] L. Climate, "Characteristics of Highly Effective Social Studies Teaching and Learning in KY" GEMA Online® Journal of Language Studies, **12**(1), 2012.doi: 10.1080/0218879020220205#preview

[6] L. Goswami, M. K. Kaushik, R. Sikka, V. Anand, K. Prasad Sharma, and M. Singh Solanki, "IOT Based Fault Detection of Underground Cables through Node MCU Module," 2020 International Conference Comput. Sci. Eng. Appl. ICCSEA2020, 1-6, 2020.

[7] O. Lopez et al., "White Paper on Critical and Massive Machine Type Communication Towards 6G," arXiv preprint arXiv:2004.14146, 2020.

[8] A. Darisman and M. H. Widianto, "Design and Development of Pharmaceutical Company Information System Based on Website using the Waterfall Model," International Journal Recent Technol. Eng., **8**(4), 3989–3993, 2019.

[9] U. C. Bandara and T. S. M. Amarasena, "Impact of Relative Advantage, Perceived Behavioural Control and Perceived Ease of Use on Intention to Adopt with Solar Energy Technology in Sri Lanka," Proc. Conference Ind. Commer. Use Energy, ICUE, 1–9, 2019.

[10] N. Ellahi, Z. Maroof, H. Z. Mehmood, and A. Kiani, "Education and Socioeconomic Development: Finding the Way Forward.," Science International, **29**(2), 361–366, 2017.

[11] A. I. Graell Amat and G. Liva, "Finite-length analysis of irregular repetition slotted ALOHA in the waterfall region," IEEE Commun. Lett., **22**(5), 886–889, 2018. DOI: 10.1109/LCOMM.2018.2812845

[12] I. A. Puspita, R. P. Soesanto, and F. Muhammad, "Designing Mobile Geographic Information System for Disaster Management by Utilizing Wisdom of the Crowd," 2019 IEEE 6th International Conference Ind. Eng. Appl. ICIEA 2019, 496–500, 2019.

[13] N. Aeni Hidayah, N. Hasanati, R. Novela Putri, K. Fiqry Musa, Z. Nihayah, and A. Muin, "Analysis Using the Technology Acceptance Model (TAM) and DeLone McLean Information System (DM IS) Success Model of AIS Mobile User Acceptance," 2020 8th International Conference Cyber IT Serv. Manag. CITSM 2020, 2020.

[14] Y. Harb and S. Alhayajneh, "Intention to use BI tools: Integrating technology acceptance model (TAM) and personality trait model," 2019 IEEE Jordan International Conference Electr. Eng. Inf. Technol. JEEIT 2019 - Proc., 494–497, 2019.

[15] W. M. Al-Rahmi et al., "Integrating Technology Acceptance Model with Innovation Diffusion Theory: An Empirical Investigation on Students' Intention to Use E-Learning Systems," IEEE Access, **7**, 26797–26809, 2019. DOI: 10.1109/Access.2019.2812845

[16] H. Zhao and Q. Liu, "The practice and research on the promotion mode of MOOCs in higher education based on the innovation diffusion theory," Proc. - 2018 7th International Conference Educ. Innov. through Technol. EITT 2018, 198–203, 2018.

[17] K. Thongkoo, K. Daungcharone, and J. Thanyaphongphat, "Students' Acceptance of Digital Learning Tools in Programming Education Course using Technology Acceptance Model," 2020 International Conference Digit. Arts, Media Technol. with ECTI North. Sect. Conference Electr. Electron. Comput. Telecommun. Eng. ECTI DAMT NCON 2020, 377–380, 2020.

[18] Inayatulloh, "Technology acceptance model (TAM) for the implementation

of knowledge acquired model for SME," Proc. 2020 International Conference Inf. Manag. Technol, 767–770, 2020.

[19] W. Ike Wahyuning, M. Lubis, W. Witjaksono, and A. H. Azizah, "Implementation of Enterprise Resource Planning (ERP) using Integrated Model of Extended Technology Acceptance Model (TAM) 2: Case Study of PT. Toyota Astra Motor," 2019 7th International Conference Cyber IT Serv. Manag, 1-5, 2019.

[20] T. Cam and T. Tran, "Adding Innovation Diffusion Theory to Technology Acceptance Model: Understanding Consumers' Intention to Use Biofuels in Viet Nam MAN SHIN CHENG," International review of management and business research, **6**(2), 595–609, 2017.

[21] M. H. Widianto, "Analysis of application of online work exchange using technology acceptance model and innovation diffusion theory," Journal Theor. Appl. Inf. Technol., **98**(10), 1697–1711, 2020.

[22] A. M. Kolesnikov, T. A. Kokodey, T. I. Lomachenko, and Y. I. Mikhailov, "Modeling the Optimal Format of Strategic Management of a Company for Establishing a Region's Sustainable Development," Proc. 2018 International Conference ' 'Quality Manag. Transp. Inf. Secur. Inf. Technol. IT QM IS 2018, 848–850, 2018.

[23] H. Fan, "Theoretical basis and system establishment of China food safety intelligent supervision in the perspective of internet of things," IEEE Access, **7**, 71686–71695, 2019. DOI: 10.1109/ACCESS.2019.2919582

[24] M. H. Widianto, Ranny, N. F. Thejowahyono, and S. B. Handoyo, "Internet of things based on smart mirror to improve interactive learning," International JOURNAL Emerg. Trends Eng. Res., **8**(9), 4900–4907, 2020.

[25] H. Zhang, H. Ye, L. Zhang, and L. Li, "Base on the design and implementation of the quality control system of food antioxidant vitamins c," Proc. - 2020 3rd International Conference Adv. Electron. Mater. Comput. Softw. Eng. AEMCSE 2020, 31–34, 2020.

[26] J. Wang, C. Jiang, H. Zhang, Y. Ren, K.-C. Chen, and L. Hanzo, "Thirty Years of Machine Learning: The Road to Pareto-Optimal Wireless Networks," IEEE Commun. Surv. Tutorials, **22**(3), 1472–1514, 2020.

[27] A. Solomon and R. Steyn, "Leadership style and leadership effectiveness: Does cultural intelligence moderate the relationship?," Acta Commer., **17**(1), 1–13, 2017. doi: 10.1111/j.1540-4560.2011.01730.x

[28] A. Nimota, JOURNAL Kadir, T. A. Adebayo, and S. Abayomi, "Visionary Leadership and Staff Innovative Behaviour in Public Colleges of Education In Kwara State, Nigeria," International JOURNAL Educ., **12**(2), 72, 2020.

[29] F. Guerriero, R. Guido, G. Mirabelli, and V. Solina, "Supporting a Pharmaceutical Wholesaler in the Vehicle Fleet Organization: An Italian Case Study," Proc. 2019 10th IEEE International Conference Intell. Data Acquis. Adv. Comput. Syst. Technol. Appl. IDAACS 2019, 2, 765–768, 2019.

[30] L. Wang and Z. Huang, "Research on the Synergetic Innovation between Pharmaceutical Enterprises and Scientific Research Institutions Based on the Quantum Game," IEEE Access, **8**, 63718–63724, 2020. DOI: 10.1109/ACCESS.2020.2976544

[31] X. Jiang, M. Wang, Z. Tian, Y. Lu, and K. Chen, "Evaluation Method of Storage Assignment for Intelligent Pharmaceutical Warehouse," 2019 IEEE Eurasia Conference IOT, Commun. Eng. ECICE 2019, 434–437, 2019.

[32] W. Yang and H. Wang, "Application of electrical capacitance tomography in pharmaceutical manufacturing processes," I2MTC 2019 - 2019 IEEE International Instrum. Meas. Technol. Conference Proc., **2019**-May, 1–6, 2019.

[33] Y. Chen, B. M. Howe, and C. Yang, "Actively Controllable Switching for Tree Topology Seafloor Observation Networks," IEEE JOURNAL Ocean. Eng., **40**(4), 993–1002, 2015. DOI: 10.1109/JOE.2014.2362830

[34] L. Xing, K. Deng, H. Wu, P. Xie, H. V. Zhao, and F. Gao, "A Survey of across Social Networks User Identification," IEEE Access, 7, 137472–137488, 2019.

[35] S. Gu, F. Yuan, H. Wu, H. Shao, and L. Cheng, "A Novel Two-Stage Framework for User Identification Across Social Networks," 2019 2nd International Conference Artif. Intell. Big Data, ICAIBD 2019, 266–270, 2019.

[36] S. Adhy, A. Prasetio, B. Noranita, and R. Saputra, "Usability Testing of Weather Monitoring on Android Application," 2018 2nd International Conference Informatics Comput. Sci. ICICoS 2018, 81–86, 2019.

[37] K. I. Satoto, K. T. Martono, R. R. Isnanto, and R. Kridalukmana, "Design of management information systems research, publications and community service," ICITACEE 2015 - 2nd International Conference Inf. Technol. Comput. Electr. Eng. Green Technol. Strength. Inf. Technol. Electr. Comput. Eng. Implementation, Proc., 117–122, 2016.

[38] J. Wu et al., "Structural Uncertainty," Ecological Modelling, **204**(3-4), 289-300. https://doi.org/10.1016/j.ecolmodel.2007.01.004

[39] F. Liu et al., "SAR Image Segmentation Based on Hierarchical Visual Semantic and Adaptive Neighborhood Multinomial Latent Model," IEEE Trans. Geosci. Remote Sens., **54**(7), 4287–4301, 2016. DOI: 10.1109/TGRS.2016.2539155

Development of Hexa Spacer Damper for 765 kV Transmission Lines' Vibration Damping

Sushri Mukherjee[1,*], Sumana Chattaraj[2], Dharmbir Prasad[3], Rudra Pratap Singh[3], Md. Irfan Khan[4], Harish Agarwal[4]

[1]*Indian Institute of Technology Delhi, New Delhi, 110016, India*

[2]*Indian Institute of Technology Jodhpur, Rajasthan, 342037, India*

[3]*Asansol Engineering College, Asansol, West Bengal, 713305, India*

[4]*Supreme & Co. Pvt. Ltd., Kolkata, West Bengal, 700020, India*

ARTICLE INFO

ABSTRACT

In this paper, hexa spacer damper is proposed and its vibration damping effect on the 765 kV power transmission network under the influence of fluctuating wind (10-60 Hz) loading is validated. This asymmetrical loadings led the bundle of Zebra ACSR conductor to be twisted and hence, cause mechanical and electrical instabilities across the span length. These issues may be addressed using the undertaken spacer damper. This paper highlights design, development and field tests of the proposed solution. The product has been validated using CATIA V5 software tools and for the field trial - 27 numbers of these dampers have been placed at various sub-spans across the line at Hydro Québec Test Station, Canada. The damping efficiency has been recorded using system integrated data acquisition set up. The proposed products are an important item of overhead line hardware and are extensively used to ensure that bundled conductors to provide mechanical and electrical performance reliability in service.

List of Symbols and Acronyms

A	Area of cross-section
$A_{m,v}$, $B_{m,v}$	Sub-span integration constants
C_m	Velocity of wave
D	Diameter of conductor
E	Conductors' Young modulus of elasticity
EI	Conductors' flexural rigidity
f_D	Forces of aerodynamic for damping
f_W	Forces of wind over sub-conductor
I	Inertia moment
l_n	Length for sub-spans
L	Span length
m	Motions' plane for sub-conductors
P	Arms of damper
Q	Quantity of damper
T_{2k-1}	Tension in $(2k-1)$th sub-conductor
T_m	Maximum value of tension
v	Interval of sub-span length
x	Location of spacer damper
Y_b	Amplitude of bending
ρ	Conductor s' material density
$\ddot{\omega}_{m,v}$, $\omega''_{m,v}$	Vibration limits at clamped support
P-P	Peak-to-peak
RIV	Radio interference voltage

1. Introduction

Today, energy has become prime necessity of growing population's livelihood and simultaneously reliability of the transmission network is vital for uninterrupted power supply service [1]. It's quite common to transmit the power at higher voltage level (like HV, EHV and UHV) for keeping the various

*Corresponding Author: Sushri Mukherjee, sushri.engg@supreme.in

losses within the permissible limits [2]. Thus, application of conductor bundling is widely adopted method to nullify the impact of voltage gradient, and hence reduction in cascading losses causes by radio interference and corona and meeting economical aspects of project deployment. The conductor bundling is get affected due to wind and ice load twisting effect, which may further led to interruption in transmission service [3-5]. For transmission line there are various parameters are considered at the time of erection and commissioning. Among all these parameters one of the most important thing is the vibration on the ACSR conductors [6, 7]. Most of the general issues are comes from this scenario even it affects communication lines too [8, 9]. The conductors are attached to the towers through rigid contacts for reducing the chances of failure, but if the wind speed is preferably higher then there might be extensive chances of vibration on the conductors. At this situation the rigid supports on the structure exerts shear force on the conductor and as a result they can fail. To get rid of this situation, we cannot apply some flexible coupling of the conductors on the tower to reduce the vibration effect. One most effective way to reduce it by application of spacer damper on the conductor, it is possible only if the conductors are very close to each other [10]. The spacer damper provides a constant space between the conductors as well as due to the damping characteristics of rubber padding on the arms it also provides an effective damping so that the chances of failure on the conductor coupling on the joint locations can be reduced.

In continuation with introduction, remaining portion of the paper is presented as: construction overview has been studied in Section II and related mathematical derivation in Section III. The proposed spacer damper has been virtually modeled in Section IV. Thereafter, in Section V, a description of field experimentation has been presented. Finally, the current study has been concluded in Section VI.

2. Constructional Overview

The spacer damper is to be required for mainly keeping a safe distance between conductors' bundle [11]. This type of damper is aluminum made rigid focal casing with numbers of arm count based on number of conductors in a bundle of particular transmission line [12]. In this study, a hexa spacer damper has been proposed for undertaken transmission line. Its shape is equilateral hexagon and the clamp body is made of aluminium (Al) alloy, which is connected with rigid frame at centre to provide effective gripping to the conductor. Major parts of the proposed damper have been presented in Table I.

Table 1: Specification of major components involved in tests.

S. No.	Particulars	Features	Quantity
1	Body of clamp	Al alloy	1
2	Arm of clamp	Al alloy	6
3	Holding sleeve	Al extrusion	6
4	Cushion for damping	Neoprene rubber	6

5	Washer	Steel HDG	6
Properties of applied conductor			
6	Diameter of applied conductor		28.6 mm
7	Strands of ACSR conductor (Zebra)		54/7
8	Applied conductors count		6
9	Mass/ length of conductor		1.621 kg/m
10	Maximum bending amplitude		265 μm
11	Nominal tension of applied conductor		35 kN
12	Rated value of tensile strength		131.9 kN

For damping sub-conductors' vibration energy at connecting point, an elastomeric bush has been used in-between clamp arms and supporting frame. And the spacer body too highly flexible in order to sustain such vibrations and damping.

3. Mathematical Modeling

In this section, mathematical modeling of the proposed solution has been carried out before initiating product development and applicable field testing. Here, Figure 1 shows the load application on the hexa-spacer damper. We have evaluated the load application and as per the design concept by the help of force component division we have applied the loads.
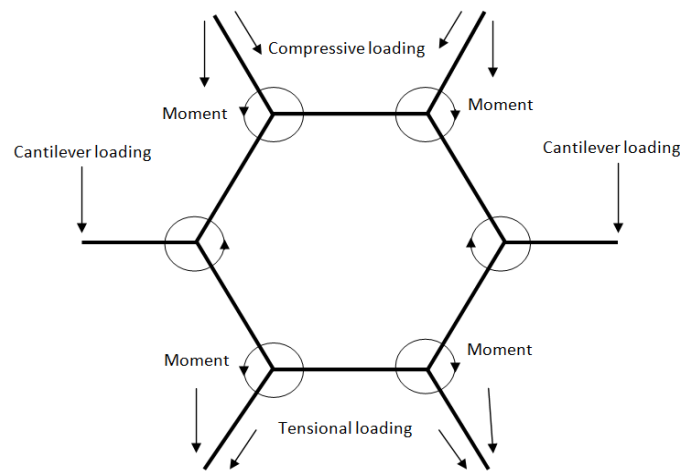
Figure 1: Loading application on the main structure

For the application of loads first on the manual mathematical calculation we have shown general mathematical expressions related to the vibration force and static loads due to the conductor weight. For the scenario of damping and loading three types of loadings are to be considering here these are elastic force, damping force and pounding force. The elastic force experienced by the system can be evaluated by a simple mass and spring system. The elastic forces in different directions can be taken as (1) - (3) [6, 13],

$$F_{kx} = 2kx - \frac{3}{4l^2}kx^3 \tag{1}$$

$$F_{ky} = 2ky - \frac{3}{4l^2}ky^3 \tag{2}$$

$$F_{kz} = 2kz - \frac{3}{4l^2}kz^3 \tag{3}$$

where, k represent spring constant and the l is the effective length of the spring. For our case, we can assume the length of the arm is the length of the spring or damping damper device.

The damping force is the internal force exerted by the damping device like the rubber padding on the coupling portions of the arms with the main body of the spaced damper. For mathematical evaluation some general formula can be followed, those are stated below (4) - (5) [6, 13]

$$F_{cx} = 2c\dot{x} - \frac{c\dot{x}}{l^2}x^2 \qquad (4)$$

$$F_{cx} = 2c\dot{y} - \frac{c\dot{y}}{l^2}y^2 \qquad (5)$$

$$F_{cx} = \frac{c\dot{z}}{l^2}z^2 \qquad (6)$$

here, c is the damping constant for the damping material provided on the product and $\dot{x}$, $\dot{y}$ and $\dot{z}$ are velocities of the mass block for this case we can say the mass block is the attached conductor to the spacer damper.

According to the Hertz's contact law pounding force is stated by one dimensional but for our system we have evaluated this for two dimensional points of view. In the present study, safe spacing among six bundle conductors has been kept using hexa spacer damper across the span length as shown in Figure 2. In this diagram, dampers are positioned from the left side using $x = l_n$, where, $n = 1, 2, ..., Q$. Total span length segmented into $Q+1$ sub-spans like $\Delta l_1, \Delta l_2, ..., \Delta l_{Q+1}$. Corresponding formulation for the conductor bundling has been illustrated in the succeeding section:

This sub-conductor motion (i.e., transverse) of v-th sub-span $(v = 1, 2, ..., Q+1)$ is formulated as by the transverse wave equation as presented in (6) [6, 13],

$$\rho A \ddot{\omega}_{m,v}(x,t) - T_m \omega''_{m,v}(x,t) = f_W(x,t) + f_D(\omega_{m,v}, \ddot{\omega}_{m,v}, t) \qquad (6)$$

$$\forall v = 1, 2, 3, ..., Q+1$$

$$\forall m = 1, 2, 3, ..., 2P$$

Thenafter, conductors' homogeneous motion equation while ignoring the aerodynamic forces will be simplified as (7) [6, 13],

$$\rho A \ddot{\omega}_{m,v}(x,t) - T_m \omega''_{m,v}(x,t) = 0 \qquad (7)$$

Here, considering both horizontal and vertical tension (i.e., $T_{2k-1} = T_{2k}$, where $k = 1, 2, ..., P$) to be same for the sub-conductor. Therefore, segregation of dependent factors (like time and space) from the displacement quantity may be formulated as in (8) - (9) [6, 13]

$$\omega_{m,v}(x_v, t) = \text{Re}\left[W_{m,v}(x_v) e^{st}\right] \qquad (8)$$

$$W_{m,v}(x_v) = A_{m,v} e^{\left(\frac{sx_v}{cm}\right)} + B_{m,v} e^{\left(\frac{-sx_v}{cm}\right)} \qquad (9)$$

where, among two different traveling waves of x_v-direction; its negative one pertaining towards amplitude $A_{m,v}$ while positive one $B_{m,v}$ amplitude.

Figure 2: Field test layout of the proposed damper.

4. Virtual modeling of Spacer Damper

Software simulation is one of the most effective solutions for getting the behavior of the product on loading conditions. Here, we have used CATIA V5R20 for its three-dimensional design with proper dimensions and have also performed its load simulation testing on this product. The loadings are basically compound loading on the structure and as per the loaded condition on the structure we are just showing the mechanical characteristic and its material properties has been presented in Table II. Since, we have to check the stability of the device in loaded condition therefore; we have to show the failure mode analysis. After selecting the material on the product the further step is to define the boundary conditions on the structure. Boundary conditions are the possible parameters taken as input for applying the loads on the above stated structure. If the boundary conditions are not specified properly then there will not be a meaning of actual load testing. Corresponding simulation results has been presented in Figure 3 - 6.

Table 2: Material parameters

Material	Aluminum
Young's modulus	7e+010N_m2
Poisson's ratio	0.346
Density	2710kg_m3
Coefficient of thermal expansion	2.36e-005_Kdeg
Yield strength	9.5e+007N_m2

Figure 3: Applying boundary condition on the product

Figure 4: Meshing and deformation for load application

Von Mises stress (nodal values).2

N_m2

	5.07e+006
	4.56e+006
	4.05e+006
	3.55e+006
	3.04e+006
	2.53e+006
	2.03e+006
	1.52e+006
	1.01e+006
	5.07e+005
	51.5

On Boundary
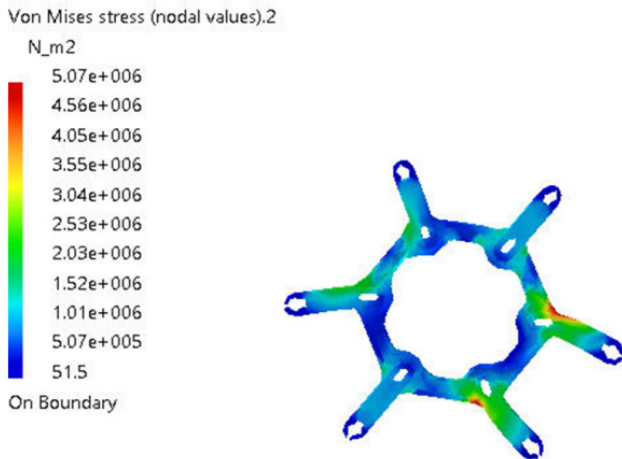
Figure 5: Stress concentration (Von-mises stress with color code scaling)

Translational displacement magnitude.1

mm

	0.0372
	0.0335
	0.0297
	0.026
	0.0223
	0.0186
	0.0149
	0.0112
	0.00743
	0.00372
	0

On Boundary
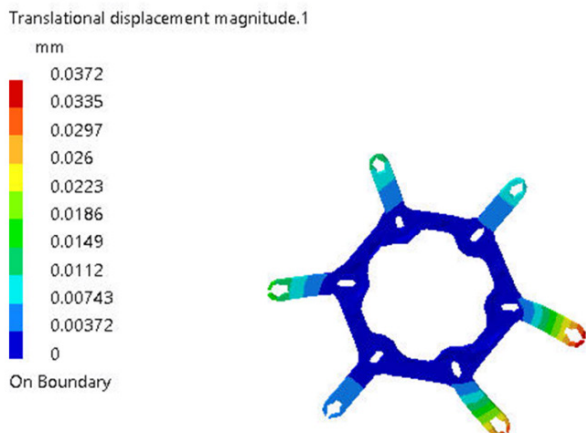
Figure 6: Translational displacement (Deformation with color code scaling)

5. Experimentation at Site

With the increase in demand for electricity all over the world, the span and the number of bundle for transmission line are showing a trend of increase [14]. Thus, to improve reliability of 765 kV transmission line spacer dampers (27 numbers) should be deployed across the transmission line as presented in Table III. The data acquisition sequence is chosen using software developed at IREQ based on LabVIEW programming language. The hardware used for the data acquisition is from National Instruments. The data acquisition system utilizes the most recent technology including fiber optic to carry the transducer signals which has low latency hence precise time graph analysis. Vibration amplitudes are measured according to industry standards [9]. The data acquisition loop begins with the acquisition of the weather data: more precisely wind velocity; azimuth and elevation as well as air temperature at a rate of 10 points per second (pts/sec) during 300 sec.

Table 3: Spacer damper installation across the undertaken transmission line.

Span (m)	Spacer damper counts	Sub-span (m)
150	3	30 - 47 - 43 - 30
400	7	32 - 51 - 55 - 59 - 63 - 57 - 51 - 32
450	7	35 - 58 - 62 - 66 - 69 - 65 - 60 - 35
425	7	34 - 54 - 58 - 63 - 66 - 62 - 54 - 34
150	3	30 - 47 - 43 - 30

Wind velocity, azimuth and elevation are measured using four ultrasonic anemometers [15, 16]. On the other hand, the processing or using the discrete spectral frequencies has been adopted. Only those recordings with an apparent frequency in the range between 0.6 - 2.5 Hz were selected. In this paper, we have validated mechanical strength of the spacer damper to check sustainability of different body parts while conductors abnormality in oscillations.
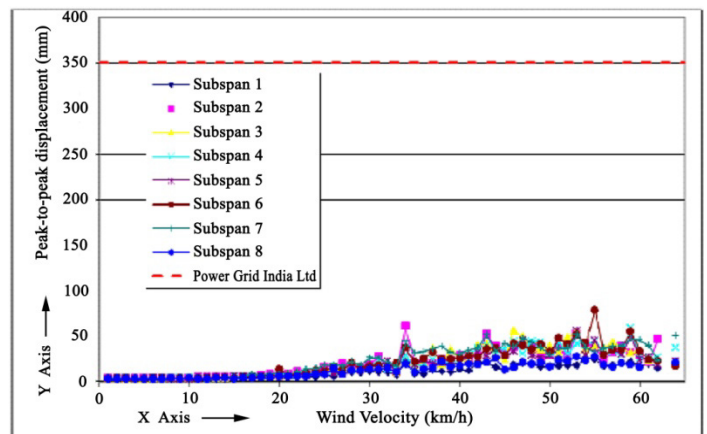
Figure 7: Maximum P-P displacement in sub-span.

In the field test, as part of apparent frequency the P-P amplitude is noted in Table IV as relentless cycle behavior. Thenafter, corresponding graphical analysis of the results is presented in

Figure 7. For further study (like - vector and matrix), the conductor has been considered as located at certain height with a maximum span (*i.e.,* 450 m) and getting affected under wind exposure. This particular circumstance reflecting actual field test oscillation effect on the installed spacer damper, which has been plotted in Figure 8 to highlight wind exposition at the site. While covering this field test a wide range of velocities in various directions based on sub-span oscillations and Aeolian vibrations have been taken. Furthermore, the bending-amplitude (RMS) of the conductor will be evaluated [17], and results are graphically compiled in Figure 9.

The averaged value of $f\,Y_{rms}$ which is 5 km/h at an interval of 10° is presented in Table 5. It has been found a variation of azimuth angle 270° - 280° with wind speed covering about 50- 55 km/h.
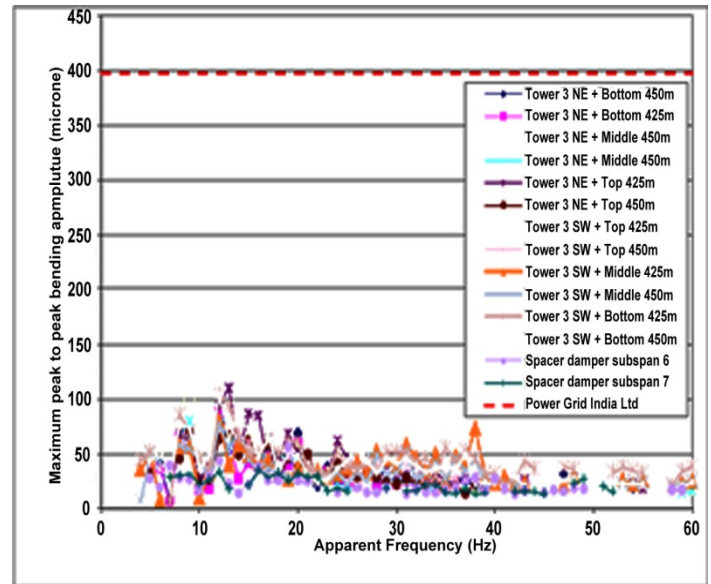
Figure 9: Bending-amplitudes' maximum (RMS) value.

Table 5: Results of $f\,Y_{rms}$ (maximum value)

Sub-spans	$f\,Y_{rms}$ (mm/s)	Wind conditions	
		Azimuth angle (°)	Velocity (in km/h)
1	4.4	270 - 280	50 - 55
2	6.3	270 - 280	50 - 55
3	6.1	270 - 280	50 - 55
4	5.7	270 - 280	50 - 55
5	6.4	270 - 280	50 - 55
6	6.5	270 - 280	50 - 55
7	5.6	280 - 290	45 - 50
8	4.4	270 - 280	50 - 55

Figure 8: Wind-expositions' polar plotting

Table 4: Peak-peak displacement (maximum).

Sub-span	P-P displacement (mm)	Maximum $f\,Y_{rms}$ (mm/s)
1	26	8.5
2	60	10
3	56	13
4	59	11
5	56	14
6	79	12
7	52	10
8	28	7.8

here, the bending-amplitude (RMS) value in sub-spans is recorded and then graphically presented in Figure 11. While, asses this particular graph, it may be seen that its variation is upto 80 mm/s value.

6. Conclusions

The product has been designed and validated using CATIA V5 software tools before initiating field trials. Since, we have applied the loads on the structure as per the weights of the conductors and according to those loading we have the output results for stress concentration and deformation therefore it is now very easy to conclude the mechanical load capacity of the proposed model. We have used a loading of 1621 kg per km of conductor, the span between two towers are 425m and according to that conductor weights will be 688.925kg. Now the usage of spacer dampers on this span is 7 so we can say each arm of the damper carrying a load of 98.417 kg in different modes like compression and tension. After application of this load we have found the maximum stress concentration on this product is $5.07 \times 10^{6}\,N/m^{2}$ which is quite preferable for the product as well as the material used as Aluminum. Along with it for the compound load application the maximum deformation on the structure is

0.0327 mm. The value of deformation is very less. Therefore, as a final conclusion we can say the product is structurally strong enough to sustain the applied load on it. The proposed solution's feasibility could be checked from Table 6.

Table 6: Summary of recorded field results.

Particulars	Standards	Findings
Clamps peak-peak bending amplitude (max)	< 398 µm	141 µm
Clamps RMS bending amplitude (max)	< 80 µm	29 µm
Peak-peak (max) displacement for sub-span oscillations	< 350 mm	79 mm
$f\,Y_{rms}$ (max) for sub-spans	< 80 mm/s	14 mm/s
$f\,Y_{rms}$ (mean) for site wind	< 70 mm/s	6.5 mm/s

Conflict of Interest

The authors declare no conflict of interest with any other individual or organization.

Acknowledgement

Appendix

The computational data associated with its design is presented in Appendix A.

References

[1] Power Sector at a Glance ALL INDIA, Central Electricity Authority, Government of India. (Accessed on 30th Nov, 2020)

[2] R.D. Begamudre, "Extra high voltage AC transmission engineering", New Age International, 2006.

[3] R. Claren, G. Diana, F. Giordana, E. Massa, "The Vibrations of Transmission Line Conductor Bundles", IEEE Trans. Pow. App. Sys., PAS-**90**(4), 1796-1814, 1971. DOI: 10.1109/TPAS.1971.293173

[4] L.E. Kollár, M. Farzaneh, "Vibration of bundled conductors following ice shedding", IEEE Trans. Pow. Del., **23**(2), 1097-1104, 2008. 10.1109/TPWRD.2007.915876

[5] S. Mukherjee, S. Chattaraj, M.K. Shaw, P. Barua, D. Prasad, "Control of Wind-Induced Instabilities associated with Conductors through application of Dampers", IEEMA J., **10**(4), 58-62, 2018.

[6] S. Mukherjee, D. Prasad, M.I. Khan, P. Barua, H. Agarwal, "Hexa Spacer Damper for Vibration Energy Decaying of 765 kV Transmission Line", In 2019 Innovations in Power and Advanced Computing Technologies (i-PACT), 1, 1-6, 2019. DOI: 10.1109/i-PACT44901.2019.8960087

[7] IEEE T&D Committee, "Standardization of conductor vibration measurements", IEEE Trans. Power App. Syst, **85**(1), 10-12, 1996. DOI: 10.1109/TPAS.1966.291515

[8] K. Anderson, P. Hagedorn, "On the Energy Dissipation in Spacer Dampers in Bundled Conductors of Overhead Transmission Lines", J. Sound Vib., **180**(4), 539-556, 1995. doi.org/10.1006/jsvi.1995.0099

[9] D. Prasad, R.P. Singh, S. Mukherjee, S. Chattaraj, K. Sarkar, M.I. Khan, 2020. Approaches to smart grid network communication and security. In Advances in Smart Grid Power System, 103-158, Academic Press, 2020. doi.org/10.1016/B978-0-12-824337-4.00005-9

[10] N.A. Saadabad, H. Moradi, G. Vosoughi, "Semi-active control of forced oscillations in power transmission lines via optimum tuneable vibration absorbers: With review on linear dynamic linear aspects", Int. J. Mech. Sci., **87**, 163-178, 2014. doi.org/10.1016/j.ijmecsci.2014.06.006

[11] E.S. Abd-Elaal, J.E. Mills, X. Ma, "A review of transmission line systems under downburst wind loads", J. Wind Engg. Ind. Aero., **179**, 503-513, 2018. doi.org/10.1016/j.jweia.2018.07.004

[12] F. Foti, L. Martinelli, "A unifield analytical model for the self-damping of stranded cables under Aeolian vibrations", J. Wind Engg. Ind. Aero., 176, 225-238, 2018. doi.org/10.1016/j.jweia.2018.03.028

[13] F. Kiessling, P. Nefzger, J.F. Nolasco, U. Kaintzyk, "Overhead power lines: planning, design, construction", Springer, 2014.

[14] A. Sakhavati, M. Yaltagiani, S.S. Ahari, S.M. Mahaei, "765 kV transmission line design (Electrical section)", Int. J. Electr. Comp. Engg (IJECE), **2**(5), 698-707, 2012. http://dx.doi.org/10.11591/ijece.v2i5.1591

[15] P.W. Davall, M.M. Gupta, P.R. Ukrainetz, "Mathematical Analysis of Transmission Line Vibration Data", Elec. Pow. Sys. Res., **4**(1), 269-282, 1978. doi.org/10.1016/0378-7796(78)90013-5

[16] H. Verma, "Aerodynamic and structural modeling for vortex-excited vibrations in bundled conductors (Doctoral dissertation, Technische Universität)", 2009.

[17] J. Chan, D. Havard, C. Rawlins, G. Diana, L. Cloutier, J.L. Lilien, C. Hardy, J. Wang, A. Goel, "EPRI Transmission Line Reference Book: wind-induced Conductor Motion", 2009.

Appendix A: Static Case Boundary Conditions.

Sl.	Computation Type	Parameters		Tensile Load
1	Structure	Number of nodes		936
		Number of elements		2061
		Number of DoF		2808
		Number of Contact relations		0
		Number of Kinematic relations		0
		Linear tetrahedron		2061
2	Restraint	Number of SPC		120
3	Load	Applied load resultant	F_x (N)	2.478e-022
			F_y (N)	-2.067e+003
			F_z (N)	-3.475e+003
			M_x (Nm)	-1.645e+002
			M_y (Nm)	1.390e+001
			M_z (Nm)	-8.268e+000
4	Constraint	Number of constraints		120
		Number of coefficients		0
		Number of factorized constraints		120
		Number of coefficients		0
		Number of deferred constraints		0
5	Singularity	Number of local singularities		0
		Number of singularities in translation		0
		Number of singularities in rotation		0
		Generated constraint type		MPC
6	Stiffness	Number of lines		2808
		Number of coefficients		41130
		Number of blocks		1
		Maximum number of coefficients per bloc		41130
		Total matrix size		0.48 Mb
7	Factorized	Method		SPARSE
		Number of factorized degrees		2688
		Number of super-nodes		465
		Number of overhead indices		11328
		Number of blocks		1
		Number of M_{flops} for factorization		4.573e+000
		Number of M_{flops} for solve		3.735e-001
		Minimum relative pivot		2.032e-002
		Number of coefficients		90024
		Maximum front width		96
		Maximum front size		4656
		Size of the factorized matrix (Mb)		0.686829

A Proposed Framework to Improve Containerization from Asia to North America

Carlos Gabriel Ortega-Diaz, Diana Sánchez-Partida[*], José Luis Martínez-Flores, Patricia Cano-Olivos

Department of Logistics and Supply Chain Management, UPAEP University, 17 Sur 901, Barrio de Santiago, CP 72410 Puebla, Puebla, 72016, México

ARTICLE INFO

ABSTRACT

The constant market change and the critical role of the logistics process in the supply chain need to have special attention because it is an essential piece for the global business strategy. This paper presents an assessment of the processes of handling material from Asia suppliers to North America. The data utilized for the analysis is of 12 months of 2019, valuable input to support the proposal to the company to approve the changes to get a financial gain. The proposal aims to create a complete analysis starting on how the containers are loaded currently in Asia (floor loaded) and the complexity that this strategy creates for the whole supply chain. The analysis of the overall process aims how the proposed change (pallet loaded) will reduce demurrage cost annually (USD 147,000), lead time (from 6 days to 3 days), space utilization in the facility (reduce space by 6364 sqrt/ft), reduce operational cost annually (USD 210,000), improve safety (Risk factor savings annually of USD 61,100), and on-time delivery to the customer (Increase 4%).

1. Introduction

In the current global supply chain footprint, one of the most critical parts is the transportation of goods from any place in the world to fulfill customer requirements. Companies are significant in maintaining competitive advantage from the competition, and the company needs to be prepared with flexibility and responsiveness to the dynamics of the customer demands [1].

Container loading is a pivotal function for operating supply chains efficiently, and underperformance results in unnecessary costs (e.g., cost of additional containers to be shipped) and in unsatisfactory customer service (e.g., violation of deadlines agreed to or set by clients). Thus, it is not surprising that container loading problems have been dealt with frequently in the operations research literature. It has been claimed, though, that the proposed approaches are of limited practical value since they do not pay enough attention to constraints encountered in practice [2].

Organizations must be capable of fast, radical changes, and those that aspire to be best must lead to changes [3]. Container shipping has changed the scale and scope of global freight distribution. By enabling a higher rate in freight distribution, it has opened up new global markets for export and import as a higher quantity of space could be traded with a similar, if not lower, amount of time and often at a lower cost. This rate is much more a

function of time than of speed as containerization mostly improved the function of transshipment [4].

The current customer changing needs force the supply chains to look for continuous improvement on the value-added on the different processes and create dynamic changes on how the goods are move through the chain [5].

The scope of the research is to determine the best containerization in Asia. Changing the way of containerization to create a faster supply chain reducing the safety stock needed for the waiting time in the ports to fill a floor loaded container and the overall improvement on reducing the extra cost that hits directly on the operating income of the company [6].

Part of the assessment comprised the current state of process from the point of origin Asia to the point of receipt in North America (Mexico), in that review the specific process that takes place in that part of the chain and creates a proposal for improvement that can be measured.

For the company case of study, the fast pace of customer demand is one of the essential value-added that is offered to the customer. For this reason, the supply chain needs to be fast, flexible, and dynamic to support what is being offered.

The company is focused on the wellbeing of the associates. The current container unloads process of a floor loaded container is

very demanding and with a high risk of injury due to unloading by hand over 3000 to 4000 containers daily, that in the long run, can harm the associate's health, that in the final result of the project will be to eliminate this risk of injury, the impact of this is of USD 61,100 of saving on the risk factor.

2. Literature Review

The container system is slowly reaching maturity in a market environment where freight transportation has become the most volatile and costly component of many firms' supply chain and logistics operations. Managers must deal with delays in the transport system, with rising oil prices, complex security issues, and with labor and equipment shortages and trade imbalances. Each of these problems adds risk to the supply chain, and the problems are likely to get worse before they improve. Managers in the logistics industry, including the port and maritime industry, are spending more and more of their time handling freight transport missteps and crises. As such, reliability and capacity issues have emerged as critical factors next to pure cost considerations [1].

Empty container repositioning has been an on-going issue since the beginning of containerization. However, it has become more prominent in recent decades due to the rapid growth of the container shipping business and the regional difference in economic development. The critical factors that cause empty container movements, which include the trade imbalance, dynamic operations, uncertainties, size and type of equipment, lack of visibility and collaboration within the transport chain, and transport companies' operational and strategic practices [6].

Over the past decade, there has been a growing consensus concerning the strategic importance of integrating suppliers, manufacturers, and customers convincingly argued, the once narrow subject of logistics has become a broad topic that now spans the entire value system from suppliers to customers [5].

The first in the line of warehouse processes is the receiving of goods. This process does not take as much time as picking, which is shown onwards, but it is as relevant as any. Especially if incorrect put-away occurs and causes errors in further processing. The process of receiving can begin with the notice of the arrival of the goods. It permits the warehouse to prepare to schedule inbound operations, so there are no uncoordinated events. With the arrival, unloading begins after which units are put away with accurate documenting before [7].

Container loading problems can be interpreted as geometric assignment problems, in which small three-dimensional items (called cargo) have to be assigned (packed into) to three-dimensional; rectangular (cubic) large objects (called containers) such that a given objective function is optimized and two underlying geometric feasibility conditions hold, i.e. [2]:

- All small items lie entirely within the container

- The small items do not overlap.

A formal description of a solution to an assignment problem of this kind will be called a loading pattern.

According to the typology introduced in [8], one can distinguish between container loading problems, in which enough containers are available to accommodate all small items, and such

problems, in which only a subset of the small items can be packed since the availability of the containers is limited. Problems of the first kind are of the input (value) minimization type, those of the second type represent the output (value) maximization type.

Moreover, the changes in operations and processes of warehouses should cover every activity in warehousing [9] such as:

- Receiving: the process of unloading the incoming truck, identifying, registering, and sometimes repacking.
- Put away: moving the goods from the unloading dock to the storage area.
- Storage - in bulk or pick activities at the warehouse, affect goods in storage. For instance, the number of stocks must be counted to verify inventory quantities.
- Replenish If inventory levels of the pick storage drop to specific amounts, it is replenished with stocks from the bulk storage.

Leaning on a material-handling environment encompasses two main elements; value stream mapping to define the optimal future situation and analysis of the logistics flows used to move products in order to optimize the facility layout. Both practices aim to improve the operation continuously. Traditional warehouses should become cross-dock operations. Lean cross-docking operations should integrate principles as heijunka planning, advanced routing methods, and kanban. These principles would create flow in picking, packing, and replenishing while simultaneously reducing average order cycle time in [10].

Consider shipping priority in container loading, where high priority boxes must be loaded before those with low priority. They propose a multi-round partial beam search method that explicitly considers shipping priority when evaluating the potential of partial solutions to solve this problem. Since existing benchmark data for shipping priority covers only weakly different instances, they extend the benchmark data to strongly heterogeneous instances [11].

In accordance [12], the overall duration of the transport process, as well as the balance of the elements, differ depending on different factors, such as:

- Average distance cargo transport

- Localization of distribution points and cargo transportation conditions

- The capacity of the vehicle

- Technical speed of vehicle movement

- Technical vulnerabilities of cargo transport

- The level of mechanization degree of loading mechanisms construction

- Construction of highways surface and other

3. Research methodology

The research methodology for the study is described in Figure 1. The overall process of the research is to understand what is the problem that we have encountered; moreover, after that, it is the

process that needs to be worked on to create a solution that is in line with the expectations of the company in the study.
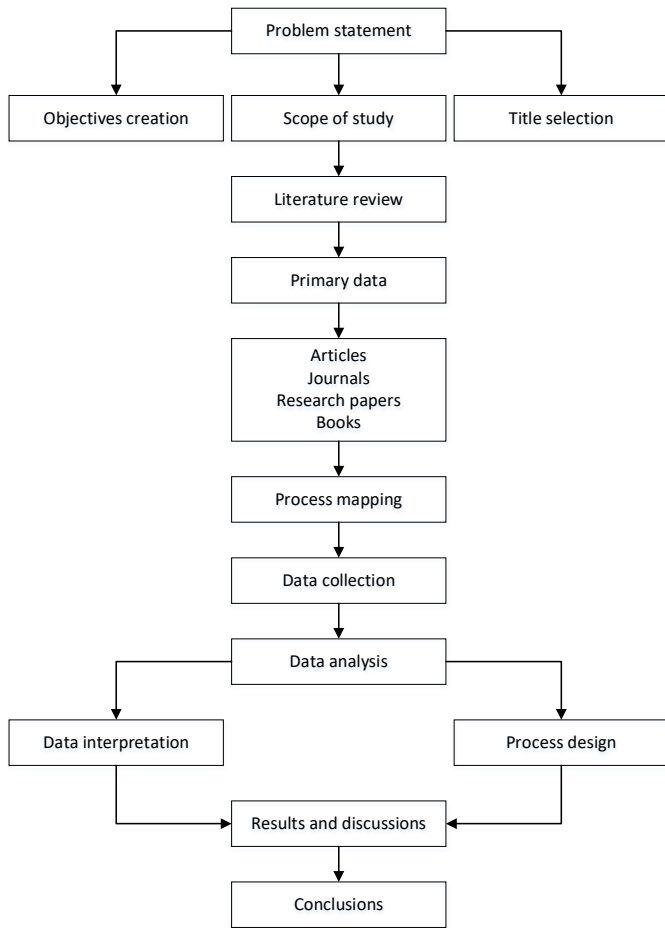
Figure 1: Research method for the study.

4. Case study

4.1. Problem statement

The company in the study is the leader on security products, with a distribution of goods to all the world, the manufacturing plant is in Mexico for finish good and most of the main components are made in the United States of America. The supply strategy for the make to stock business is 60% of the goods purchased to Asia suppliers, and the 40% is assembled in Mexico; on the make to order business, 100% of the products are made in Mexico with most of the components from U.S. suppliers, Mexico suppliers and very small from Asia suppliers.

By doing this study, the company is looking for the overall improvement on the lead time, create a lean supply chain from Asia to Mexico. Reducing the need for safety stock inventory that is not needed and the overall reduction of cost the effect the operating income, and by making this improvement, the company will improve on the customer service level and that, in the long run, will bring incremental sales and revenue Figure 2.

The overall market dynamics are forcing supply chains to change the current footprint dynamics to accommodate every changing customer requirement better. Regarding the current stage, much investment is put into creating a better logistic

network to support this. Moreover, the company found an opportunity to create a proposal by changing the way the containers are loaded in Asia.
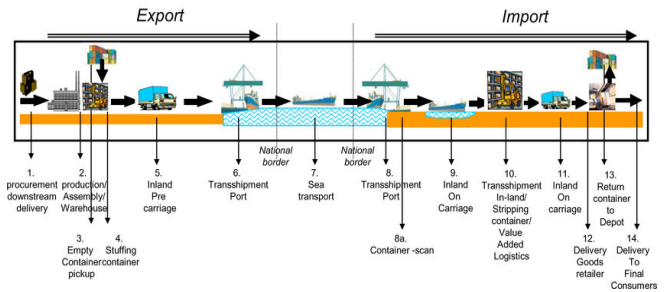
Figure 2: Overall ocean container flow.

In the current supply chain footprint of our Asia supplier, the company has a total of 38 suppliers that are located in mainland China, and seven are in other Asian countries (i.e., India, Vietnam, Philippines). Focusing on mainland China suppliers.

The scope of the project is to focus on the containers that are built-in mainland China that is close to the company suppliers in which the supplier ship to a consolidator in which they put cargo from different suppliers that are shipping to the same end-user. The ports utilized to ship material to the United States of America are:

- Yantian
- Hong Kong
- Shanghai
- Ningbo
- Keelung is out of Taiwan
- Shenzhen

After containers are built in China, they are moved to the freight forwarder cargo lines that will load the container to the boat to ship it out to Long Beach port to be unloaded.

The results of the demurrage cost USD 200.00 per day per container which is a delay that has been affecting the company due to the high cost per day because of not returning a container in the appropriate lead time.

The statistical data that was analyzed is from all the containers that arrived to the U.S., from Asia in 2019. Because of the COVID-19 pandemic, the data from 2020 is very different due to Asia suppliers delaying container flow. The company decided to use the 2019 data to obtain where the company was situated in the current state. Moreover, the lateness that the company has based and how long is it taking to unload the containers in the warehouse.

The total amount of containers that arrived in 2019 to the plan was 480 containers, from those, 344 are 40' size (equal to 72%) and 136 are 20' size (equal to 28%). From this data, the company needed to understand if there was a correlation between total boxes in the container and the pallets built per container. In Figure 3, a scatterplot of boxes quantity vs. pallet built for 40' container is presented and in Figure 4 is shown a scatterplot of box qty vs. pallet built for 20' container.
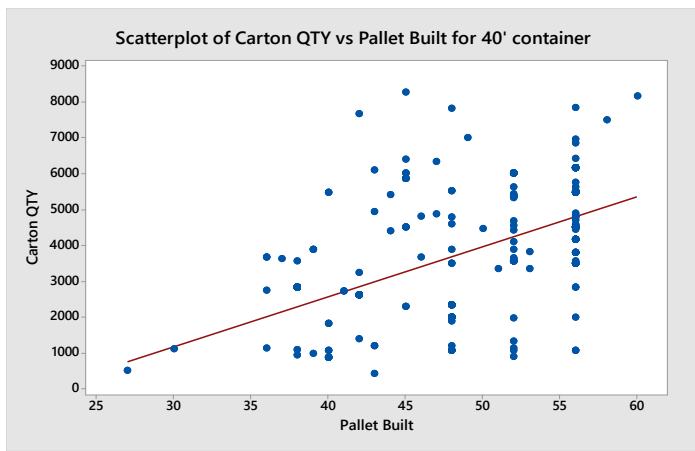
Figure 3: Scatterplot boxes qty vs. pallet built for 40' container.
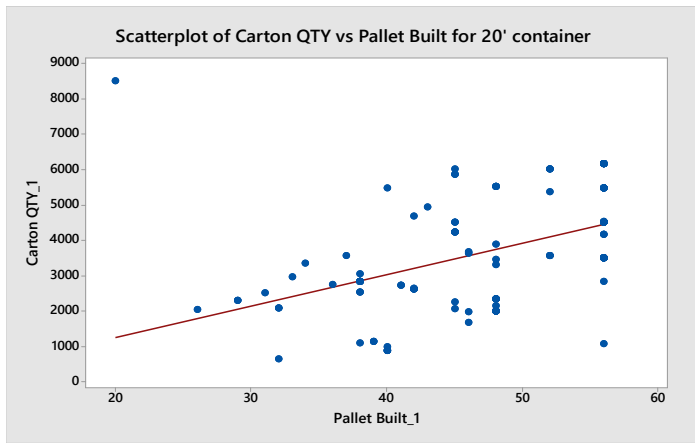
Figure 4: Scatterplot boxes qty vs. pallet built for 20' container.

As a result of the 40'container, the high-density population is between 45 to 55 pallets built per container. Furthermore, the 20' containers' population is between 40 to 50 pallets built. The plan is to eliminate the use of 20' containers and only use 40' ones to maximize utilization of the capacity of the container that is 5 to 15 more pallets than the 20' container. It is a quick example of how a floor loaded container arrives at the facility, see Figure 5. The correlation found in the analysis was that the company could eliminate the need for shipping in the 20' container, if the process is implemented of pallet loaded and changing to use only 40' containers due to the number of pallets that can be loaded.

These are the results analyzing the data in Table 1.

Table 1: Container boxes and pallet building.

Container Length	The total quantity of boxes	Total Quantity of Pallet Built
20'	505,500	6,495
40'	1,364,734	17,214
Grand Total	1,870,234	23,709

Reviewing the results, they show the complexity of how the company has delays in unloading containers. The complexity of the process is that it is manual labor to unload the boxes from the container and then create pallets that will be received and then put-away in the warehouse. The manual process of unloading the containers has created an extra lead time of 3.06 days in the high season, and that is the issue of why the company has a high demurrage cost, affecting 240 containers every year, with those delays the company incurred in demurrage cost that affects the financial performance of the company due to an operational issue on how the container is loaded, how the container is unloaded and the receiving process of the goods.

4.2. Analyzing and creating the business model

For any continuous improvement project, it needs to define the current process map, to understand what are the areas of opportunity that are needed to focus on. This project is the actual process flow which has been focused on the receiving and put away part of the process, see Figure 6. the process map gave the company an overall perspective to analyze where it can focus resources to create a valuable proposition.

Following the current process flow, when the containers arrive from Asia, first the container arrive at Long Beach, after that it has to wait for its turn to be downloaded from the boat with a crane and be put into the inbound area, in that the transporter goes and picks up the container to bring it to the company yard, there it waits its turn to be crossed to Mexico to start the unloading process.
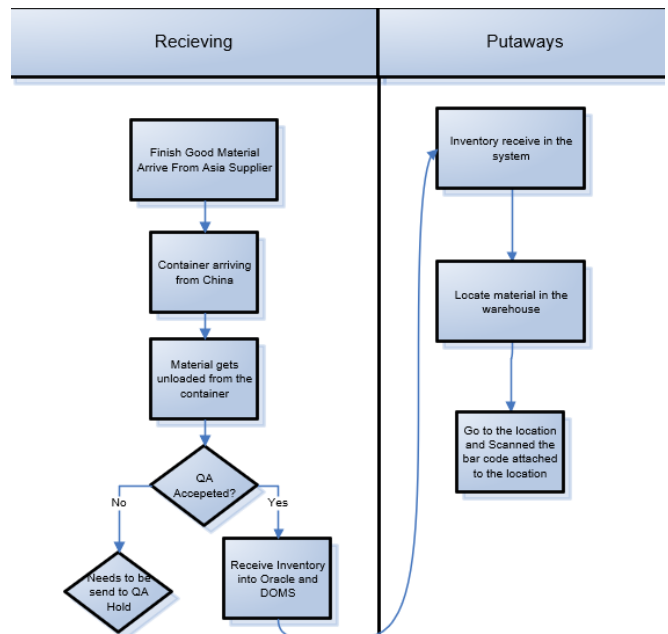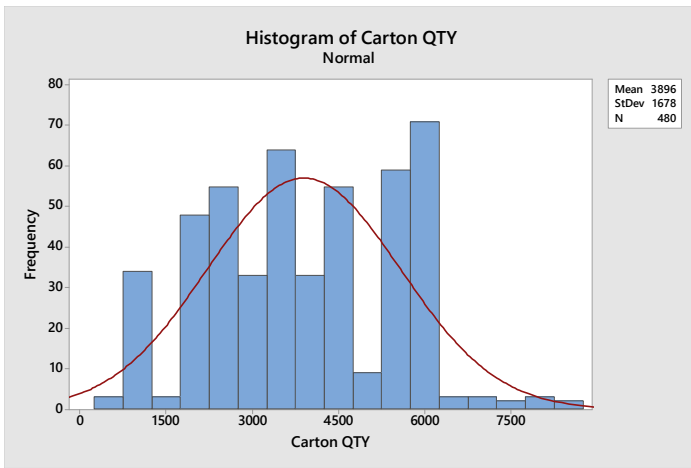
Figure 7: Histogram of box quantity.

In this part of the process is where we found the first issue. The complexity of how the containers are loaded in Asia (floor loaded) and the average amount of boxes per container affects the overall lead time to unload, delaying the unloading so the company occurs into demurrage.

On a yearly average, the company had 240 containers on which there was a delay of 1 day, and more to return the container to the supplier yard. This delay in the process has generated a loss of USD 147,200. By changing the process this cost can be eliminated.

In the data analysis, the average and the standard deviation per container on how many boxes and the pallet are represented in Figure 7 and Figure 8. The results obtained are that the average quantity of boxes in the container and the average pallet built from those boxes is equal to the number of complete pallets that fit inside a container, creating an opportunity in the process to change the current process of floor loaded to pallet loaded.
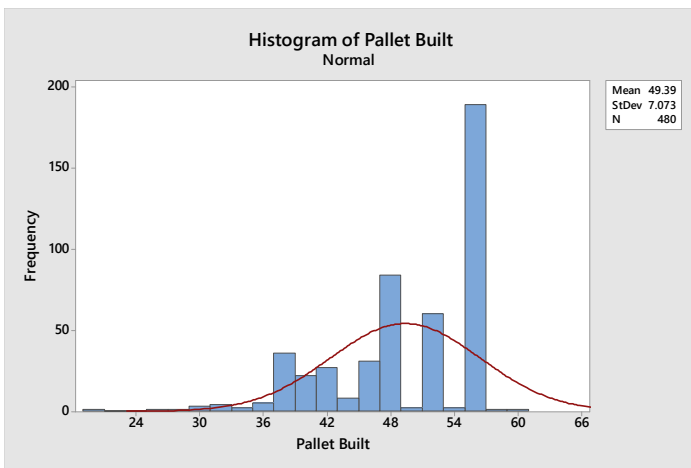
Figure 8: Histogram of pallet built.

The complexity of the process is outlined with the data of one year. On a yearly average per container, the company receives 3896 boxes per container and those equal to an average of 50 pallets per container. The study shifted to understand the lead time

that is taking to unload the containers from Asia, the lead time that the company has is three days to receive the container, unload, and return the container to the supplier yard, see Figure 9. In this histogram, the company is measuring the total lead time for a container to be unloaded.
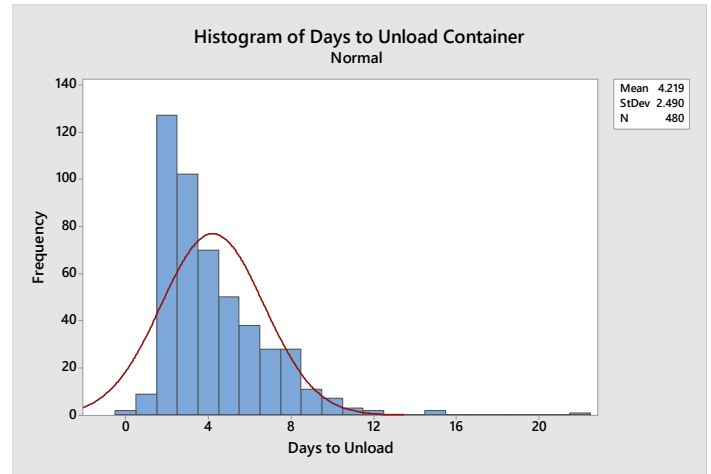
There is an average of 4.2 days (this is taking the 480 containers, from which 240 were unloaded at or before the lead time of 3 days) to unload the container with a standard deviation of 2.49 days. The lead time that the company has is three days to return the container; this result creates an extra cost in the organization that is a demurrage cost in which for any extra day it takes for the company to ship the container back to the logistic cargo supplier, the cost is USD 200 per day for delay. The company needed to understand the lateness of the containers. Figure 10.
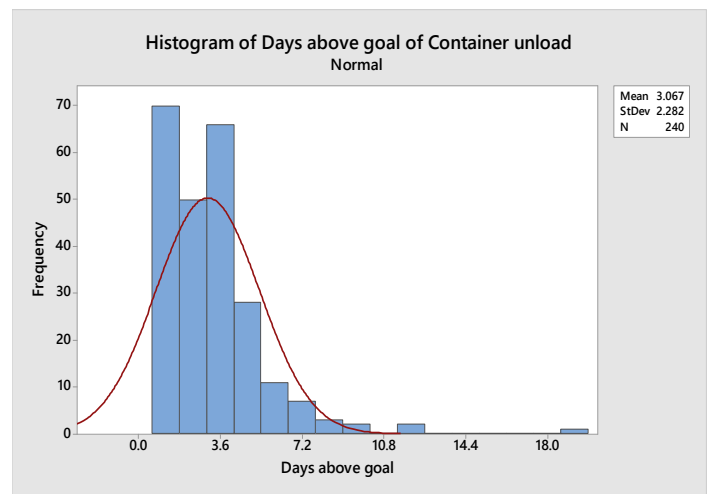
Figure 10: Histogram of days above the goal of container unload.

The result that was obtained (only 240 containers that were shipped out late back to the supplier yard) is that the days above the lead time on average is 3.06 days with a standard deviation of 2.28; with this, the company calculated an impact on the cost of USD 147,200 that affects the operating income, see in Table 2 cost due to demurrage.

Table 2: Cost due to demurrage.

Container Length	Cost due to demurrage	
20'	USD	45,600
40'	USD	101,600
Grand Total	USD	147,200

Base on the case study it's been determine that the company needs to work on improving the container loading in Asia. On the current process, the supplier can ship future P.O.s of material that are not needed yet, to fill up a container at the max on boxes and weight. This issue creates extra inventory that the company does not need; by changing the strategy, the company will eliminate the extra carryover inventory that is not needed and improving cash flow by not having inventory that is not needed due to an operation process. It will be reviewed to cut the need for those extra containers by reducing the safety stock level from 120 days of finish adequate supply to 90 days of safety stock. It will help to reduce the necessary containers between 60 to 90 that have an extra carryover of 30 extra days of safety stock. The significant impact is not having the correct inventory in the correct place to support customer demand, and the impact associated with that is customer fines because of out of stock that creates filling rate issues on the stores, on-time delivery because of shipping late, waiting for inventory to arrive and loss of sales due to cancelations.

Connecting this to the other warehouse process, in the unloading process, the company has two crews for the receiving process, each crew is of 7 associates, for a total of 14 associates, and one forklift driver that is the one that when the pallet is complete, he moves the material to a staging area for the quality team to audit each of the pallets that were made.

If the company improves the process of how the containers are loaded in Asia, there will be an immediate impact on the labor needed to unload a container, changing the how the container has been loaded in Asia from floor loaded to pallet loaded, improves the velocity in the process by eliminating the manual unloading box by box and improves the safety of the workforce by eliminating the manual labor of moving and unloading boxes.

The current labor of one crew to unload one container of 40' is between 3 to 4 hours depending on the number of boxes, the mix of SKU in the container, and the weight of each of the boxes. Each container has a different complexity inside of it. If the container is changed to a palletized container, one forklift driver can unload one container between 30 minutes to 60 minutes; in one day, one forklift driver can unload, taking the max time nine containers in one shift.

The cost of one receiving associate full loaded (salary + benefits) is around USD 15,000 per year; with this proposal, the reduction is for a total of 14 employs two unloading crews, each receiving associate earns USD 15,000 per year, with the reduction of the 14 associate the company can save on their operating cost

USD 210,000 per year when the proposed improvement is implemented.

Continue connecting the dots of the analysis, and the company encounters another area of opportunity, floor space utilization for staging the building of the pallets. Moreover, in any industry, floor space is precious because staging and storing do not add value to the product, it adds cost. If there is an opportunity to save space, the company can save money and use that space for something that can add value to a product, for example, more production lines.

The total area that can be reutilized by adding more cells in an area of 86'x74' for a total of 6364 sqrt/ft equals 10.5% of total production space, of the estimated cost of sqrt/ft, taking all of the cost into consideration for a productive area is around $48 x sqrt/ft; this gives a saving or possible revenue of USD 305,472 that can be added for the justification of the project, see Figure 11.
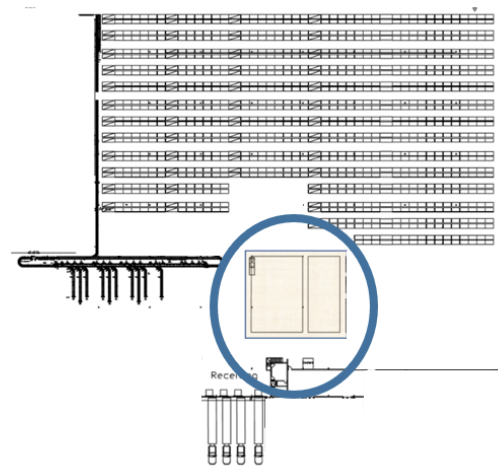
Figure 11: Finish good facility warehouse layout

5. Results and discussions

The purpose of this paper is to develop a proposal assessing the effectiveness of a change in the container operations loading process in Asia. As a result, the best solution found is to propose a change in the way the containers are loaded.

The improvement is changing from floor loaded container to pallet loaded container. The company has defined the pallet structure from Asia to maximize the pallets that can be loaded in the container. The proposal is to utilize only 40' containers and eliminate the use of 20' containers.

The interior dimensions of a container (in feet): 39' 6" long x 7' 9" wide x 7' 10" high, that is equal to 4,143,708 cubic/inches; with data, it can be calculated how many standard pallets the consolidator can load into the container, the standard size including the pallet will be 40"x48"x48, that will help the company load two lines of pallets double stack to have 40 pallets per container. To implement this, the engineering and the sourcing team will have to work with Asia for the supplier to have the pallet pattern and follow the new direction; that with this, the company will not have

to invest in more containers need base on the reduction due to safety stock not needed.

With this proposal, there is a potential saving in demurrage, labor, and space utilization. Another savings is the reduction of the risk factor on the unloading of the operation, due because it is a manual operation that can cause injury on the receiving operator, and because the human capital is the most crucial asset in the company, by eliminating the need of the manual force the company eliminates the risk of injury, the projected reduction of the risk factor is from 0.020597 to 0.020097 that generates to a yearly reduction on this factor of USD 61,100.

For this proposal to be implemented, it needs to have a united effort between several departments and key players to get the savings that have been identified.

For example, the packaging engineer needs to start working on standardizing the pallets and specific sizes to maximize the opportunity to double stack the container. After this activity is completed, the sourcing team will need to contact the supplier in Asia to give them the new packaging specifications, from which the supplier will need to start palletizing when they receive the new specifications. After that, the company will have a specific time frame in which it will continue to receive floor loaded containers, but when that ends, the process of unloading by pallet and auditing from quality and receive will have to change to create a more dynamic flow.

The total recurrent annual savings estimated in this project, not considering the potential inventory reduction is, with near to no investment is:

- Demurrage saving USD147,200
- Labor reduction of USD 210,000
- Space cost USD 305,472
- Risk factor reduction of USD 61,100
- Total savings USD 723,772

6. Conclusions

The case study helps the organization to identify current opportunities in the containerization process in Asia.

With the current change in the market dynamics, the company encounters an opportunity to reduce lead times. The market dynamic, based on customer needs in a faster pace to respond to demand. The pandemic of COVID-19 affected supply chains first, starting with Asia. Asia stop shipments for six weeks if it is considered that in 6 weeks there is not going to be any flow, that in a macro stage equals to 12 weeks without raw material or finish good; this pandemic created needs to improve and reduce time in the supply chain.

By focusing on creating a faster approach in the unloading of the container, there are several savings for the company. Reducing the labor or relocating labor in the area by 14 employees creates a reduction in the operating income of the company.

By changing one process, it impacts several other, for example, releasing pre-stage areas to create space for new manufacturing cells, which is a direct impact on having space utilized on value-added activities instead of staging inventory.

Overall, the proposal for the project is to change the way we have been doing the operation, by changing the process we can improve the overall efficiency of the operation.

In this time of new challenges, the companies need to think differently and have an open mind in creating a culture of change to create continuous improvement.

In this project, the approach is to work the different process that conforms the supply chain. The company is improving the warehouse activities from unloading containers, receiving material goods, and put away process by having a straighter forward operation. On the transportation side, it is improving the reduction in lead time to eliminating demurrage and having a faster return of empty containers to the supplier. In supply planning, the team needs to work with the system to have the correct supply strategy based on a dynamic and faster container supply chain, by having what we needed when we needed and overall, the company will have an improvement because it will save cost on the operating income and the customer service side, the performance on the service to the customer will improve by not delaying material to ship and to arrive at the company.

Conflict of Interest

The authors declare no conflict of interest.

Acknowledgment

References

[1] J.P. Rodrigue, T.E. Jean-Paul, "Containerization, Box Logistics, and Global Supply Chains." The Integration of Ports and Liner Shipping Networks. In: Haralambides H.E. (eds) Port Management. Palgrave Readers in Economics. Palgrave Macmillan, London. 5-28, 2013, https://doi.org/10.1057/97811374757702.

[2] A. Bortfeldt, G. Wäscher, Gerhard, "Container Loading Problems - A State-of-the-Art Review." FEMM Working Papers 120007, Otto-von-Guericke University Magdeburg, Faculty of Economics and Management, **7**, 1-45, 2012.

[3] A. Yong, H. Nee, "Warehouse System and Business Performance: Case Study of a Regional Distribution Centre." Conference: International Conference on Computing and Informatics (ICOCI 2009), 24-25 June 2009, Legend Hotel, Kuala Lumpur.

[4] J.P. Rodrigue, "Globalization and the Management synchronization of transport terminals." Journal of Transport Geography **7**, 255–261, 1999.

[5] S. Zailani, P. Rajagopal, "Supply chain integration and performance: U.S. versus East Asian companies." Supply Chain Management: An International Journal. **10**, 379-393, 2005, DOI: 10.1108/13598540510624205.

[6] D.P. Song, J. Carter, "Empty container repositioning in the shipping industry." Maritime Policy & Management, **36**(4), 291-307, 2009.

[7] J. Habazin, A. Glasnović, I. Bajor, "Order Picking Process in Warehouse: Case Study of Dairy Industry in Croatia." Promet – Traffic & Transportation, **29**, 57-65, 2016.

[8] G. Wäscher, H. Haußner, H. Schumann, "An improved typology of cutting and packing problems." European journal of operational research, **183**(3), 1109-1130, 2007.

[9] A. Kamali, "Smart Warehouse vs. Traditional Warehouse - Review" CiiT International Journal of Automation and Autonomous System, **11**, 9-16, 2018.

[10] A.B. Arabani, S.F. Ghomi, M. Zandieh, "A multi-criteria cross-docking scheduling with just-in-time approach" The International Journal of Advanced Manufacturing Technology, **49**(5-8), 741-756, 2010.

[11] N. Wang, A. Lim, W. Zhu, "A multi-round partial beam search approach for the single container loading problem with shipment priority" International Journal of Production Economics, **145**, 531-540, 2013. https://doi.org/10.1016/j.ijpe.2013.04.028

[12] R. Burdzik, M. Cieśla, A. Sładkowski, "Cargo Loading and Unloading Efficiency Analysis in Multimodal Transport." Promet – Traffic & Transportation. **26**(4):323-31, 2014. DOI: 10.7307/ptt.v26i4.1356.

Lacol Interpolation Bicubic Spline Method in Digital Processing of Geophysical Signals

Hakimjon Zaynidinov[1], Sayfiddin Bahromov[2], Bunyodbek Azimov[3], Muslimjon Kuchkarov[*,1]

[1]Department of Information Technologies, Tashkent University of Information Technologies, Tashkent, 100200, Uzbekistan

[2]Department of Computational Mathematics and Information Systems, National University of Uzbekistan, Tashkent, 100174, Uzbekistan

[3]Department of Information Technology, Andijan State University, Andijan, 170100, Uzbekistan

A R T I C L E   I N F O

A B S T R A C T

The paper a cubic spline built through a local base spline and the local interpolation bicubic spline models we offer have been selected. The construction details of the models are given, the two-dimensional local interpolation bicubic spline models considered in this study provide high accuracy in digital processing of signals, which helps experts to make the right decision as a result of digital processing of signals. As an example, the initial values of the geophysical signal were digitally processed and error results were obtained. The error results obtained by digital processing of the geophysical signal of the considered models were compared on the basis of numerical and graphical comparisons.

1. Introduction

In many geophysical surveys, scientists have sought to find predators that provide information about the location of minerals. An anomalous change in a parameter is a sudden increase or decrease in its values. That is, depending on the anomalous changes in the geophysical signal, it is possible to make a prediction. Usually, as a result of forecasting, it will be possible to predict such information as the location of the most accumulated minerals, their reserve capacity. Anomalous changes in the electromagnetic and gravitational fields of the earth, abnormal changes in the ionosphere, seismic conditions (noise), various acoustic vibrations can be used as a tree [1].

In recent years, dozens of methods for predicting minerals have been proposed by scientists around the world. One of them is the spline method. Using the spline method, scientists have the opportunity to understand the physical processes that take place underground, to observe them, to build mathematical models of the interdependence of these processes. This is mainly achieved by using two-dimensional cupcake spline functions to achieve a high level of accuracy. The two-dimensional cubic spline function we offer also has a high accuracy range.

2. Modeling of geophysical signals based on the second-order local interpolication spline-function

The application of parabolic local interpolation spline functions to build a mathematical model for the digital processing and recovery of various geophysical signals is currently relevant in solving practical problems.

The $S_n(f; x)$ function under consideration is called the local interpolation spline function when the following conditions are met:

1. $S_n(f; x) \in H_n[x_i, x_{i+1}]$,

2. $S_n(x) \in C^m[a,b]$,

3. $S_n(x_i) = f(x_i)$ i=0,n.

Based on the above conditions, we consider the construction of a local interpolation bicubic spline in the following D=[a,b]×[c,d] area. We can divide the area under consideration into N equal parts along the OX axis and M along the OY axis $\Delta = \Delta x \times \Delta y$. [1].

$$\Delta_x: \ a = x_0 < x_1 < \ldots < x_N = b, \ \Delta_y: \ c = y_0 < y_1 < \ldots < y_M = d.$$

*Corresponding Author: Muslimjon, TUIT, 100200, Uzbekistan,
muslimjon1010@gmail.com

where steps h and l are selected as follows

$$h = x_{i+1} - x_i, \ i=0,1,...,N-1; \ l = y_{j+1} - y_j,$$

$$j = 0,1,\ldots,M-1.$$

Let we look at the grid below:

$$\Delta^* = \Delta_x^* \times \Delta_y^*$$

$$\Delta_x^*: \ x_{-1} < x_0 < x_1 <...< x_N < x_{N+1}, \quad \Delta_y^*: \quad y_{-1} < y_0 < y_1 \\ <...< y_M < y_{M+1}.$$

Δ_x^* for this case we make the field look $D^* = [a - h, b + h] \times [c - l, d + l]$. Δ^*- At the node points in the grid, the values of the function are known, i.e.:

$$f(x_i, y_j) = f_{ij}, \quad i = -1,0,1,\ldots,N,N+1;$$

$$j = -1,0,1,\ldots,M,M+1.$$

Based on the above values of the $f(x,y)$ - function, we construct a local interpolation spline function for the field. To do this, we use the following 16 points.

$$(x_{i-1}, y_{j-1}), \ (x_{i-1}, y_j), \ (x_{i-1}, y_{j+1}), (x_{i-1}, y_{j+2}),$$

$$(x_i, y_{j-1}), \ (x_i, y_j), \ (x_i, y_{j+1}), \ (x_i, y_{j+2}),$$

$$(x_{i+1}, y_{j-1}), \ (x_{i+1}, y_j), \ (x_{i+1}, y_{j+1}), \ (x_{i+1}, y_{j+2}),$$

$$(x_{i+2}, y_{j-1}), \ (x_{i+2}, y_j), \ (x_{i+2}, y_{j+1}), \ (x_{i+2}, y_{j+2}).$$

Our article in Comparative Analysis Spline Methods in Digital Processing of Signals in ASTESJ magazine describes the construction of a one-dimensional local cubic spline using 4 points [2]. Here, too, $Z_j(x_i, j)$, $Z_{j+1}(x_i, j)$ parabolas are constructed using the above points. Here x is fixed, i.e. at x=x_i the local interpolation bi cubic spline-function $S_3(x_i, y)$ has the following form:

$$S_3(x_i, y) = (1 - u)Z_j(x_i, y) + uZ_{j+1}(x_i, y), \quad (1)$$

here it is

$$Z_j(x_i, y) = -\frac{1}{2}u(1 - u)f_{i,j-1} + (1 - u^2)f_{ij} + \frac{1}{2}u(1 + u)f_{i,j+1}, \quad (2)$$

$$Z_{j+1}(x_i, y) = \frac{1}{2}(1 - u)(2 - u)f_{ij} + u(2 - u)f_{i,j+1} - \frac{1}{2}u(1 - u)f_{i,j+2} \quad (3)$$

$Z_j(x_i, j)$, $Z_{j+1}(x_i, j)$ parabolas are as follows

$$(x_i, y_{j-1}), \ (x_i, y_j), \ (x_i, y_{j+1});$$

$$(x_i, y_j), \ (x_i, y_{j+1}), \ (x_i, y_{j+2}),$$

$$u = \frac{y - y_j}{l}, \ l = y_{j+1} - y_j.$$

passes through node points. Substituting (2) and (3) into (1), we obtain the following after certain reductions:

$$S_3(x_i, y) = -\frac{1}{2}u(1 - u)^2 f_{i,j-1} + \frac{1}{2}(1 - u)(2 +$$

$$2u - 3u^2)f_{ij} + +\frac{1}{2}u(1 + 4u -$$

$$3u^2)f_{i,j+1} - \frac{1}{2}u^2(1 - u)f_{i,j+2},$$

$$j = \overline{0, M-1}, \ 0 \le u \le 1.$$

Based on the above $x = x_{i-1};$ $x_{i+1};$ x_{i+2}. In fixed cases, we create the following single-variable spline functions

$$S_3(x_{i-1}, y) = (1 - u)Z_j(x_{i-1}, y) + uZ_{j+1}(x_{i-1}, y), \quad (5)$$

$$S_3(x_{i+1}, y) = (1 - u)Z_j(x_{i+1}, y) + uZ_{j+1}(x_{i+1}, y), \quad (6)$$

$$S_3(x_{i+2}, y) = (1 - u)Z_j(x_{i+2}, y) + uZ_{j+1}(x_{i+2}, y), \quad (7)$$

$S_3(x_{i-1}, y)$, $S_3(x_i, y)$, $S_3(x_{i+1}, y)$ and $S_3(x_{i+2}, y)$ Based on the one-variable cubic spline functions built above, after a certain compression, the following view of the following two-variable interpolation bicubic spline function is formed [3-7]:

$$S_{3,3}(x, y) = -\frac{1}{2}t(1 - t)^2 S_3(x_{i-1}, y) + \frac{1}{2}(1$$

$$-t)S_3(x_i, y) + \frac{1}{2}t(1 + 4t - 3t^2)S_3(x_{i+1}, y) -$$

$$\frac{1}{2}t^2(1 - t)S_3(x_{i+2}, y),$$

$$j = \overline{0, M-1}, 0 \le u \le 1, t = \frac{x-x_i}{h}, u = \frac{y-y_j}{l}, h = x_{i+1} - x_i, l = y_{j+1} - y_j.$$

$S_3(x_{i-1}, y)$, $S_3(x_i, y)$, $S_3(x_i+1, y)$ and $S_3(x_{i+2}, y)$ are generated by putting the values of the bicubic spline functions of a variable built above (8) [8-12].

$$S_{3,3}(x, y) = -\frac{1}{2}t(1 - t^2)[(1 - u)Z_j(x_{i-1}, y) + uZ_{j+1}(x_{i-1}, y)]$$

$$+\frac{1}{2}(1 - t)(2 + 2t - 3t^2)[(1 - u)Z_j(x_i, y) + uZ_{j+1}(x_i, y)]$$

$$+\frac{1}{2}t(1 + 4t - 3t^2)[(1 - u)Z_j(x_{i+1}, y) + uZ_{j+1}(x_{i+1}, y)]$$

$$-\frac{1}{2}t^2(1 - t)[(1 - u)Z_j(x_{i+2}, y) + uZ_{j+1}(x_{i+2}, y)]. \quad (8)$$

Here it is

$i = \overline{0, N-1}$, $j = \overline{0, M-1}$, $0 \le t \le 1$, $0 \le u \le 1$, $t = \frac{x - x_i}{h}$,

$u = \frac{y - y_j}{l}$, $h = x_{i+1} - x_i$, $l = y_{j+1} - y_j$.

appears after a certain contraction (9).

$$S_{3,3}(x, y) =$$

$$\varphi_1(t)[\varphi_1(u)f_{i-1,j-1} + \varphi_2(u)f_{i-1,j} + \varphi_3(u)f_{i-1,j+1} + \varphi_4(u)f_{i-1,j+2}]$$

$$+\varphi_2(t)[\varphi_1(u)f_{i,j-1} + \varphi_2(u)f_{i,j} + \varphi_3(u)f_{i,j+1} + \varphi_4(u)f_{i,j+2}]$$

$$+\varphi_3(t)[\varphi_1(u)f_{i+1,j-1} + \varphi_2(u)f_{i+1,j} + \varphi_3(u)f_{i+1,j+1} + \varphi_4(u)f_{i+1,j+2}]$$

$$+\varphi_4(t)[\varphi_1(u)f_{i+2,j-1} + \varphi_2(u)f_{i+2,j} + \varphi_3(u)f_{i+2,j+1} + \varphi_4(u)f_{i+2,j+2}] \qquad (9)$$

here it is

$$\varphi_1(t) = -\frac{1}{2}t(1-t)^2,$$

$$\varphi_2(t) = \frac{1}{2}(1-t)(2 + 2t - 3t^2),$$

$$\varphi_3(t) = \frac{1}{2}t(1 + 4t - 3t^2),$$

$$\varphi_4(t) = -\frac{1}{2}t^2(1-t)$$

$$t = \frac{x - x_i}{h}$$

$$\varphi_1(u) = -\frac{1}{2}u(1-u)^2,$$

$$\varphi_2(u) = \frac{1}{2}(1-u)(2 + 2u - 3u^2),$$

$$\varphi_3(u) = \frac{1}{2}u(1 + 4u - 3u^2),$$

$$\varphi_4(u) = -\frac{1}{2}u^2(1-u)$$

$$u = \frac{y - y_j}{l}$$

(9) can be called a local interpolation bicubic spline function.

3. Digital processing of geophysical signals based on developed algorithms

The proposed model considered the recovery of the signal obtained by aeromagnetic reconnaissance to determine the location of underground mineral resources, which is considered to be our current object (Table 1). Based on the above sequence, a local interpolation bicubic spline construction program was developed in the Matlab program environment and used in signal processing. The algorithm of this program is shown in Figure 3. We have shown the superiority of our model by comparing our developed model with the bicubic spline function S_{bsa} (10) model, which is based on the existing basic functions. Since it is not possible to cite all the known signals, we present the result in the following figures using the appearance of the signals in Table 1 (Figures 1-2). As can be seen from these pictures, it is clear from the $S_{3,3}$ and S_{bsa} spline functions that the degree of approximation of the $S_{3,3}$ we offer is high [13-16].

$$S_{\text{bsa}}(x, y) = \omega_1(p)[\omega_1(q)f_{i-1,j-1} + \omega_2(q)f_{i-1,j} + \omega_3(q)f_{i-1,j+1} + \omega(q)f_{i-1,j+2}]$$

$$+\omega_2(p)[\omega_1(q)f_{i,j-1} + \omega_2(q)f_{i,j} + \omega_3(q)f_{i,j+1} + \omega_4(q)f_{i,j+2}]$$

$$+\omega_3(p)[\omega(q)f_{i+1,j-1} + \omega_2(q)f_{i+1,j} + \omega_3(q)f_{i+1,j+1} + \omega_4(q)f_{i+1,j+2}]$$

$$+\omega_4(p)[\varphi_1(q)f_{i+2,j-1} + \omega_2(q)f_{i+2,j} + \omega_3(q)f_{i+2,j+1} + \omega_4(q)f_{i+2,j+2}]. \qquad (10)$$

here it is

$$\omega_1(p) = (1-p)(1-p)(1-p),$$

$$\omega_2(p) = (3p^3 - 6p^2 + 4),$$

$$\omega_3(p) = (1 + 3p + 3p^2 - 3p^3),$$

$$\omega_4(p) = p^3$$

$$\omega_1(q) = (1-q)(1-q)(1-q),$$

$$\omega_2(q) = (3q^3 - 6q^2 + 4),$$

$$\omega_3(q) = (1 + 3q + 3q^2 - 3q^3),$$

$$\omega_4(q) = q^3$$
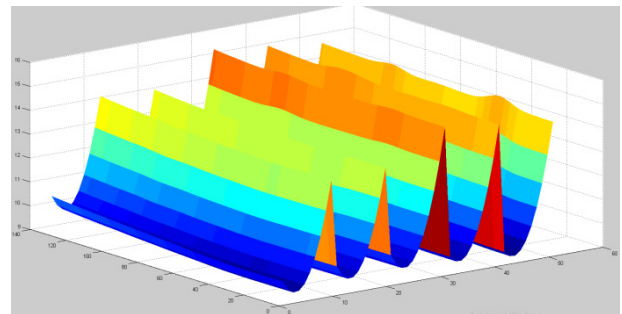
Figure 1: Graphical representation of the result obtained in the S_{bsa} function of the geophysical field

We used signals as real experimental data during our research. The obtained results are used to determine the location, size and amount of reserves of mineral resources by means of aerial magnetic intelligence. Of course, signal charts here use signals in the low frequency range from 10 to 50 kHz. Also, the distances between the nodes in the area under consideration must be equal [17-19].
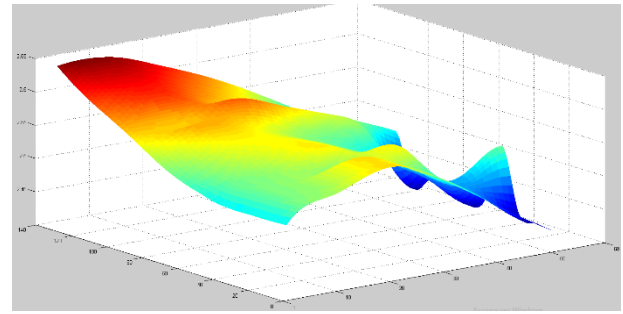
Figure 2: Graphical representation of the result obtained in the $S_{3,3}$ function of the geophysical field
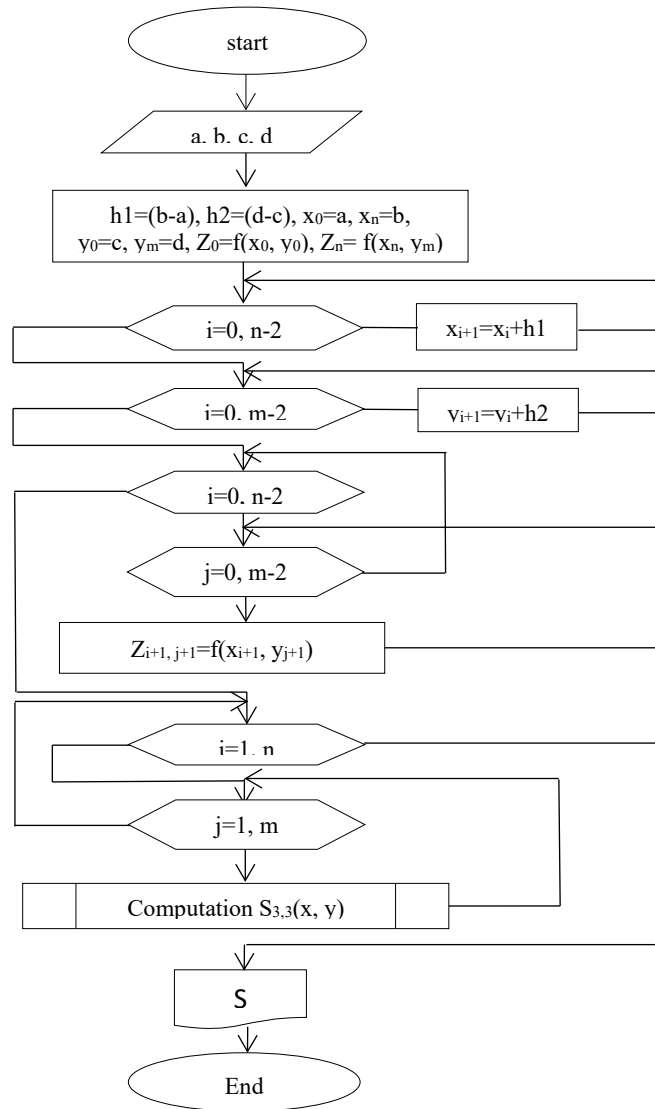
Figure 3: Block diagram of a two-dimensional bicubic spline-function construction program.

Table 1: Initial values of the geophysical signal

xi, yi	1	2	3	4	5	6	7
1	2.511567	2.546819	2.570055	2.534253	2.479736	2.428968	2.396564
2	2.510239	2.542991	2.568838	2.534879	2.484192	2.432505	2.399471
3	2.510149	2.541944	2.568157	2.536136	2.489958	2.437171	2.40337
4	2.509842	2.53978	2.53978	2.56434	2.489958	2.533676	2.488477

5	2.512262	2.540757	2.564102	2.534735	2.493134	2.440931	2.407022
6	2.520041	2.549419	2.564856	2.536827	2.50416	2.428968	2.447254
7	2.528682	2.556995	2.562458	2.535142	2.493763	2.44869	2.428968
8	2.541257	2.565523	2.560248	2.533722	2.503736	2.450393	2.416823
9	2.557538	2.581372	2.56551	2.53978	2.53651	2.428968	2.503185
10	2.57455	2.57455	2.597675	2.571599	2.541111	2.505716	2.460124
11	2.589951	2.605743	2.578684	2.546592	2.508904	2.464554	2.431107
12	2.605048	2.615953	2.588514	2.555813	2.516062	2.471976	2.438394
13	2.622756	2.628817	2.600686	2.566327	2.524289	2.47895	2.428968
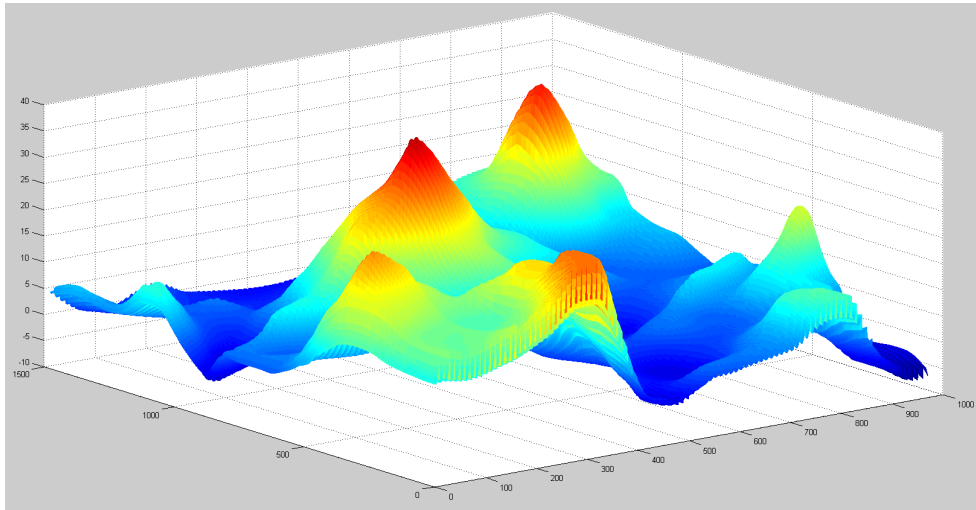
Figure 4: Graphic representation of the result obtained by the S_{bsa} function with the geophysical field (0.1x0.1) step.
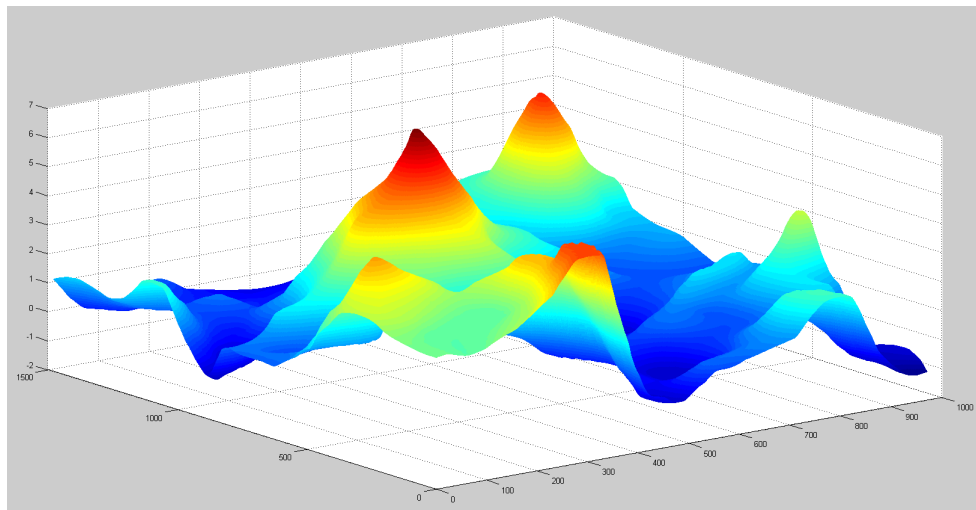
Figure 5: Graphic representation of the result obtained by the $S_{3,3}$ function with the geophysical field (0.1x0.1) step.

Table 2: Results in error estimation in geophysical signal recovery.

x_i	y_i	$f(x,y)$	$S_{3,3}$	S_{bsa}	$\lvert S_{3,3} - f(x,y) \rvert$	$\lvert S_{bsa} - f(x,y) \rvert$
1	1	2,5116	2.5116	9,9534	0	7,4418
1.1	1	2,5115	2.5114	9.9526	0,0001	7,4412
1.2	1	2,5113	2.5114	9.9517	0,0001	7,4404
1.3	1	2,5111	2.5111	9.9510	0,0001	7,4399
1.4	1	2,5108	2.5110	9.9502	0,0002	7,4394
1.5	1	2,5105	2.5108	9.9496	0,0005	7,4391
1.6	1	2,5104	2.5107	9.9491	0,0003	7,4387
1.7	1	2,5096	2.5105	9.9486	0,001	7,439
1.8	1	2,509	2.5104	9.9482	0,0014	7,4392

1.9	1	2,5084	2.5103	9.9479	0,0021	7,4395
2	2	2.5102	2.5102	9.9478	0	7,4376
2.1	2	2,5101	2.5102	9.9477	0,0001	7,4376
2.2	2	2,5102	2.5101	9.9478	0,0001	7,4376
2.3	2	2,5102	2.5101	9.9479	0,0001	7,4377
2.4	2	2,5102	2.5101	9.9481	0,0001	7,4379
2.5	2	2,5102	2.5101	9.9484	0,0001	7,4382
2.6	2	2,5101	2.5101	9.9487	0	7,4386
2.7	2	2,5101	2.5102	9.9491	0,0001	7,439
2.8	2	2,5101	2.5102	9.9494	0,0001	7,4393
2.9	2	2,5101	2.5102	9.9499	0,0001	7,4398
3	3	2.5101	2.5101	9.9503	0	7,4402
Max					0,0021	7,4418

From the graphic images and tables it can be seen that the local interpolation bicubic spline function has a high degree of accuracy in the digital processing of signals.

4. Conclusion

The paper, a cubic spline built using a local base spline for digital signal processing and the local interpolation bicubic spline models we offer were selected. Construction details of the models are given. Two-dimensional local interpolation bicubic spline models provide high accuracy in digital processing of signals. As an example, the initial values of the geophysical signal given in Table 1 were numerically processed and the error results were obtained (Table 2). Based on the selected models, the results of geophysical signal recovery are presented graphically (Figures 1,2,3 and 4). Based on error results and graphs, it is effective to apply the two-dimensional local bicubic spline model in areas of geophysics and high accuracy.

References

[1] Z. Xakimjon, K. Muslimjon, "Modeling of Geophysical Signals Based on the Secondorder Local Interpolication Splay-Function.," in International Conference on Information Science and Communications Technologies: Applications, Trends and Opportunities, ICISCT 2019, 2019, doi:10.1109/ICISCT47635.2019.9011853.

[2] Z. Xakimjon, A. Bunyod, "Biomedical signals interpolation spline models," in International Conference on Information Science and Communications Technologies: Applications, Trends and Opportunities, ICISCT 2019, 2019, doi:10.1109/ICISCT47635.2019.9011926.

[3] A.I. Grebennikov, "Isogeometric approximation of functions of one variable," USSR Computational Mathematics and Mathematical Physics, **22**(6), 1982, doi:10.1016/0041-5553(82)90095-7.

[4] D. Singh, M. Singh, Z. Hakimjon, Geophysical application for splines, 2019, doi:10.1007/978-981-13-2239-6_7.

[5] Selected Works of S.L. Sobolev, 2006, doi:10.1007/978-0-387-34149-1.

[6] J.S. Lim, Two-dimensional signal and image processing, 1990.

[7] Z. Zhengyu, "Digital processing of the polarization state of geophysical ULF signals," Journal of Electronics (China), **11**(3), 1994, doi:10.1007/BF02684833.

[8] A. Kroizer, Y.C. Eldar, T. Routtenberg, "Modeling and recovery of graph signals and difference-based signals," in GlobalSIP 2019 - 7th IEEE Global Conference on Signal and Information Processing, Proceedings, 2019, doi:10.1109/GlobalSIP45357.2019.8969536.

[9] A.K. Takahata, E.Z. Nadalin, R. Ferrari, L.T. Duarte, R. Suyama, R.R. Lopes, J.M.T. Romano, M. Tygel, Unsupervised processing of geophysical signals: A review of some key aspects of blind deconvolution and blind source separation, IEEE Signal Processing Magazine, **29**(4), 2012, doi:10.1109/MSP.2012.2189999.

[10] X.H. Liu, Z.Y. Zhao, S.G. Xie, J.H. Liu, "Time-frequency analysis of geophysical signals based on Cohen distributions," Dianbo Kexue Xuebao/Chinese Journal of Radio Science, **16**(3), 2001.

[11] B.H. Jansen, "ANALYSIS OF BIOMEDICAL SIGNALS BY MEANS OF LINEAR MODELING.," Critical Reviews in Biomedical Engineering, **12**(4), 1985.

[12] D. Singh, M. Singh, Z. Hakimjon, Parabolic Splines based One-Dimensional Polynomial, 2019, doi:10.1007/978-981-13-2239-6_1.

[13] R.O. Parker, "INTRODUCTION TO DIGITAL SIGNAL PROCESSING.," J Eng Comput Appl, **2**(3), 1988, doi:10.1201/9781439817391-5.

[14] K. Daoudi, Iterated Function Systems and Some Generalizations: Local Regularity Analysis and Multifractal Modeling of Signals, 2010, doi:10.1002/9780470611562.ch9.

[15] V. Graffigna, C. Brunini, M. Gende, M. Hernández-Pajares, R. Galván, F. Oreiro, "Retrieving geophysical signals from GPS in the La Plata River region," GPS Solutions, **23**(3), 2019, doi:10.1007/s10291-019-0875-6.

[16] X. Wang, Z. Luo, B. Zhong, Y. Wu, Z. Huang, H. Zhou, Q. Li, "Separation and recovery of geophysical signals based on the Kalman Filter with GRACE gravity data," Remote Sensing, **11**(4), 2019, doi:10.3390/rs11040393.

[17] P.S. Naidu, M.P. Mathew, Analysis of geophysical potential fields: a digital signal processing approach, 1998.

[18] M.G. Molina, M.A. Cabrera, R.G. Ezquer, P.M. Fernandez, E. Zuccheretti, "Digital signal processing and numerical analysis for radar in geophysical applications," Advances in Space Research, **51**(10), 2013, doi:10.1016/j.asr.2012.07.032.

[19] E.A. Robinson, T.S. Durrani, L.G. Peardon, "Geophysical signal processing.," Geophysical Signal Processing., 1985, doi:10.1016/0264-8172(86)90037-1.

ASTES

Auditing the Siting of Petrol Stations in the City of Douala, Cameroon: Do they Fulfil the Necessary Regulatory Requirements?

Samuel Batambock, Ndoh Mbue Innocent[*], Dieudonné Bitondo, Augusto Francisco Nguemtue Waffo

University of Douala, Department of Industrial Quality, Hygiene, Safety, and Environment, ENSPD, Douala, 2701, Cameroon

A R T I C L E   I N F O

A B S T R A C T

No other form of technological development had negatively skewed from existing regulations as the siting of petrol filing stations. An audit of the degree to which their operators repeatedly violate the rules regulating their location and operations may encourage the legislature to pass laws that can ensure a balance between the economy and the environment. This study helps to fill this gap, by analyzing the degree to which the siting of local filling stations meets standard norms, taking Cameroon's district municipalities of Douala as an example. In order to achieve this goal, the current regulations structuring the filling station locations were carefully reviewed. Subsequently, key compliance factors were identified, operationalized, and an audit checklist was developed. Other data collection tools included a structured questionnaire designed to capture the views of neighboring communities on the possible risks to their health, land, and therefore to the environment presented by the station, and a global positioning system receiver for the collection of spatially explicit data. The nearest neighbourhood Index, (Rn) in ArcGIS10.3.1 environment was used to assess the distribution pattern of the stations. Questionnaire data was analysed using SPSS20.0. It is revealed that the distribution pattern of the 152 stations surveyed is mostly random in Douala I (Rn = 0.8573), Douala III (Rn = 0.9879), Douala IV (Rn = 0.6984), and, dispersed in Douala II (Rn = 1.7837) and Douala V (Rn = 1.5764) district municipalities. While most of them, 94 (61.84%) were within the minimum 500 m radius from one another as specified by laws, 99.34% of them didn't conform with the recommended minimum distance of 7m from the centre of a major road, and the 400m radius from residential areas. The results suggest that the siting of petrol stations in the city neglect the hazards accompanying them. The database created in this study could provide a platform to policy makers for appropriate actions.

1. Introduction

A major concern in contemporary literature remains the continuing proliferation of oil and gas stations in urban areas. In the current technological society, they are necessary, but explosions from such facilities frequently trigger loss of life and property within the surrounding communities, thereby presenting great concern to the government and people. Concerns are also raised about the ecosystem's health, protection and environmental quality resulting from these facilities [1]. Petrol vapour, for example, may ignite when exposed to sparks from sources such as lighted cigarettes or a static electrical discharge [2]. The site of petrol stations must therefore be strategically planned to mitigate their effect on both humans and their immediate surroundings [3].

Otherwise, referred to as petrol stations [4]-[5], gas station [6], filling station [7], an oil and gas station is defined as any land, building or equipment used for the sale or dispensing of petrol or oil for motor vehicles [5], Most filling stations sell petrol or diesel, some carry specialty fuels such as liquefied petroleum gas, natural gas, hydrogen, biodiesel, kerosene, or butane while others add shops to their primary business [8]. Because their products are flammable, filling stations pose a constant hazard to the staff, public, assets, and environment. They therefore, need special care in their design, construction, installations, and operations, so that, they remain safe and secure throughout their lifespans. An optimal site selection can enhance the security of the station and its environs. Conversely, a poorly selected site could cause detrimental effects on the stations, and their environs [9]. It is

therefore, important to access their locational compliance with regulatory requirements..

Historically, the inappropriate location of petrol stations has led to disasters. For example, in 2004, more than 2.3 million lives and properties worth about 4.5 billion was lost to fire outbreaks due partly to poor location and mishandling of petroleum products [4]. A similar incident occurred at a liquefied gas filling station and a nearby petrol station in the Kwame Nkrumah Circle claiming 150 lives[10]-[11]. Several other authors have evoked the underlying and proximate causes leading to hazards in filling stations including, fire hazard [12], static electricity [13], and traffic jam [14]. Leakages of pipes & underground storage tanks have been identified to result in the contamination of both surface, and underground water, and air pollution [6]. In this context, petrol stations present health, and safety concerns, especially the potential for fires owing to the toxicity and flammability of the liquid and gaseous products.

Following this, several other studies have assessed the relationship between the location of petrol stations and existing policies, e.g., [15]-[16], and their impacts on the environment [4]. Other authors like [17] and [18], have opined that exposure to diesel, petroleum fumes and fuel components such as benzene and formaldehyde contribute to cancers, acute myeloid leukemia and acute non-lymphocytic leukemia. This is not to say that the global oil industry is only known for its problems, as the industry meets humanity's energy demand. The challenge facing the global oil industry is to find a balance between the critical need for energy supply with safe and sustainable operations. Optimal site selection of these industries could minimize such challenges.

Suitability analysis for siting oil and gas filling stations have either focused on the importance of GIS-Based analysis, for example [19]-[20], or a combination of Multi-criteria Decision Analysis (MCDA) and GIS [21]-[22]. These are very useful tools for solving problems in spatial context because various decision variables can be evaluated and weighted according to their relative importance to attain the final optimal decision. The application of MCDA in siting of petrol stations has shown that accidents from filling stations have been attributed largely to oil explosions [23], spills [24], fire and leaks [25], leading to negative environmental quality, health, and safety [1], [7].

1.1. Statement of the Problem

The African continent at the beginning of the 20th century experienced very rapid urbanization. The cities of sub-Saharan Africa and Central Africa in particular, generally subscribing to this dynamic, have not been able to adapt their infrastructure and management structures to new urban realities. Because of its position as the economic capital of Cameroon and the heartbeat of Central Africa, Douala in Cameroon attracts many oil companies who find a wide demand for their goods there. The city has experienced significant demographic and spatial growth since independence.. This urban dynamic has not been accompanied by the establishment of adequate spatial management of petroleum product storage depots, which represents a major problem.

The government, in Order No. 39/MTPS/IMT of 26 November 1984 [26],lays down general measures of occupational health and safety at workplaces. Furthermore, in 1998, a government decree set out regulations for setting up petroleum product distribution stations. Article 4 states thus, "a minimum measurable distance

must be observed between service stations and establishments, administrative buildings and places, public places, strategic location. ». The distance is in particular 1000 meters for the presidency of the republic, the services of the prime minister, the national assembly, the sub-prefectures, the stations must respect a distance of 100 meters with the educational establishments, the hospitals, places of worship, sports grounds, markets, administrative buildings, etc. Land-use planning, at its simplest, should aim at separating heavily populated areas and social infrastructures from hazardous materials and their related transport routes and at minimizing hazard exposure by building buffer zones around explosive atmospheres [27]. It is of utmost importance, in the light of the dangers posed by petrol stations, that the safety measures established in local standards are fully enforced.

However, these laws are often inadequately integrated into land-use planning, especially when it comes to site selection for the construction of filling stations. Against this context, the study was performed in order to investigate the spatial distribution of filling stations and public safety in the municipality of Douala, Cameroon. The analysis was further justified by the fact that no data on this aspect of research in the region have been published to date.

1.2. Objectives

This study assesses the spatial distribution of petrol filling stations in the district municipalities of Douala, and evaluates their locational compliance with national and international norms in the city of Douala. The study aims primarily to find answers to the following questions:

1) Where are petrol stations located in the City of Douala that does not meet up with necessary regulatory requirements?
2) What is the perception of the neighbouring populations with regard to the location of such stations?
3) What policy measures can be put in place to minimize the current and potential risks posed by petrol stations?

We believe that responses to these questions may help at different scales in policy making. The research results could also assist the administrative authorities of the Municipality of Douala in the implementation of comprehensive initiatives to mitigate and respond to petrol station fires, as well as in designing public awareness campaigns for communities living near petrol stations.

2. Materials and Methods

2.1. Study Area

The Douala municipality (410 km²; ~3,600,000 inhabitants and about 13m a.s.l), is the capital of the Littoral region, located in the estuary of the Wouri River, between 4° 03' N latitude, and 9° 42' E longitude. It has six district municipalities, five of which are urban communities (Douala I-V) (Figure 1), and one (Douala VI) is a rural community.

2.2. Methodology
2.2.1. Population and sample

A two-stage sampling technic was used. First, five of the six district municipalities were selected based on whether they had petrol stations, were in the urban or rural areas. Based on these criteria, the Douala sixth district was excluded because it has no

petrol filling stations. In the second stage, each of the five selected urban municipalities were exhaustively sampled.
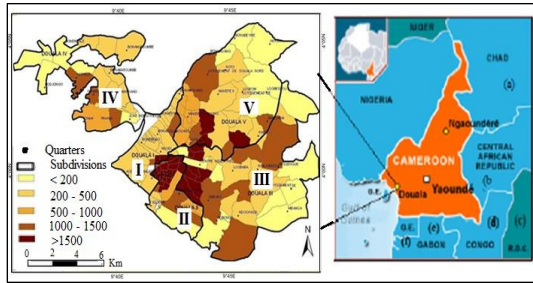
Figure 1: Location of the study area

2.2.2. Data collection

Data collection took place between March and April of 2020. Both primary and secondary data were collected. Secondary data were obtained from a systematic review of online databases (ISI Web of Science; CAB Abstracts; and Google Scholar, etc.) from 1990 to 2018, using locational compliance of petrol stations with standard norms and related terms as keywords. The articles were screened using inclusion/exclusion criteria applied first at the title and abstract level, and then at the full article level. Articles retained after screening underwent risk of bias assessment and data was extracted. Primary data was captured through observation and a checklist/questionnaire. The design and development of this tool included literature review, and pilot testing. At each petrol station, first, the distances from the four cardinal points (North, South, East, and West) between the station and the neighbouring dwellings were measured (Figure 2), which allowed us to obtain a stratification at different levels of concentration of the population living in the vicinity of gas stations.
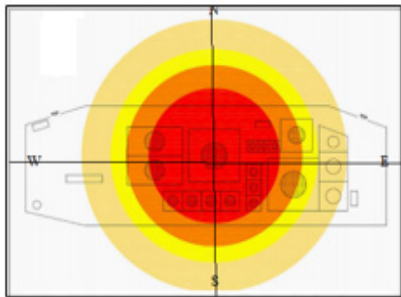
Figure 2: Stratification at different levels of concentration of the population living in the vicinity of gas stations

In the second stage, the locational characteristics (e.g., distance from green areas, a distance of pump station to the road, size of the filling stations, distance to neighbouring stations, and distance to any public facility (such as schools, churches, hospitals, market, etc.) were estimated. Finally, four residents/households, each from the four quadrats of the station were randomly selected, and their perceptions on the potential dangers associated with the proliferation of filling stations assessed. In total, 608 (4*152) randomly selected household heads, located within 100 m radius of the inventoried filling stations were interviewed. This technic enables us to classify the stations according to the potential risk (Rp) they pose with neighbouring social infrastructures and residents, vis-à-vis existing regulations (equation 1):

$$R_p = \begin{cases} High; if\ 75-100\%\ not\ comply \\ Moderate; if\ 50-74\%\ not\ comply \\ Low; if\ 0-49\ \%\ not\ comply \end{cases} \quad (1)$$

A section of the questionnaire contained multiple response question asked at each filling station to identify hazard contributing factors during operation and maintenance of filling stations.

The locations of the filling stations were captured using the Garmin Handheld GPS receivers (GPS, 62S). A section of the questionnaire was designed to capture the perception of local residents with regard to the potential threat posed to their health, properties, and the environment by their neighbouring filling stations.

2.2.3. Data Analysis

The software SPSS 20.0 was used to analyse the data obtained from the questionnaire. Both descriptive and inferential statistical techniques were used.. The Average Nearest Neighbour Analysis[28]-[29], using the Euclidean distance was adopted to ascertain the spatial distribution of petrol service stations in ArcGIS 10.3.1 environment, and the description of their distribution (Rn), defined as follows (equation 2):

$$R_n = \frac{2\bar{D}\sqrt{n}}{A}; 0 \le R_n \le 2.15 \quad (2)$$

where

$\bar{D}$ = mean distance between the nearest neighbours (km);
n = number of sampling points;
A = the area under study (km^2).

$$R_n: \begin{cases} 1.5 \le R_n \le 2.15, Dispersed/uniform \\ 0 \le R_n < 0.5, clustered\ pattern \\ 0.5 < R_n \le 1.5,\ Random\ pattern \end{cases}$$

The Nearest Neighbor Index (NNI) is a spatial statistic that distinguishes clustered or scattered event locations in geographical patterns. The algorithm uses the distance between adjacent petrol stations to decide on their distribution pattern (random, normal or clustered). It can provide researchers with a numerical value for the clustering of a geographical phenomenon, enabling them to contrast with other locations more accurately.

3. Results and Discussions

3.1. Spatial distribution of fuel stations in the City of Douala

A total of one hundred and fifty-two (152) filling stations are unevenly distributed all over the municipalities as at the period this research was carried out. The majority of these stations, 72(47%), are in the Douala III municipality, and the least, 11(7%) in the Douala II municipality (Figure 3).

Most of the stations are either along major roads or in thickly populated human settlement areas, or where there are markets that can be easily accessed by customers. This is dangerous to man and the environment. On the whole, 122 (80.26%) of the filling stations appear to be random in Douala I (R_n = 0.8573), Douala III (R_n = 0.9879), Douala IV (R_n = 0.6984), and, dispersed in Douala II (R_n = 1.7837) and Douala V (R_n = 1.5764) municipalities. This kind of haphazard pattern observed in Douala I, III and IV municipalities,

violates the fundamental objective of planning which is providing the right site for the right use at the right time for the right purpose to achieve spatial functionality, efficiency, and aesthetics.
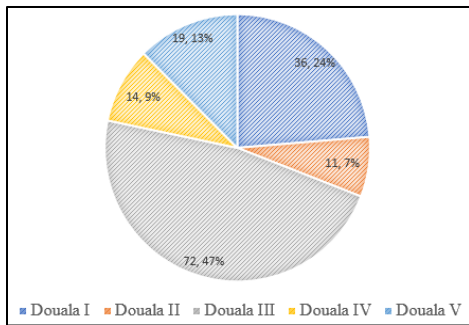
Figure 3: Distribution of petrol stations in the City of Douala

A classification of the stations according to their compliance with existing regulations, and therefore, the dangers they pose to neighbouring residents and social infrastructures (Figure 4a-e) revealed that, 23 (53.49%) of those in Douala I municipality, 5(33.33%) of those in the Douala II municipality, 21 (37.5%) of those in the Douala III municipality, 7(35%) of those in the Douala IV municipality, and 7(38.89%) of those in the Douala V municipality were not in compliance with existing regulations, and therefore pose a high risk to their neighbouring population, and social infrastructures (Residents, school buildings, hotels, hospitals, markets, etc.).
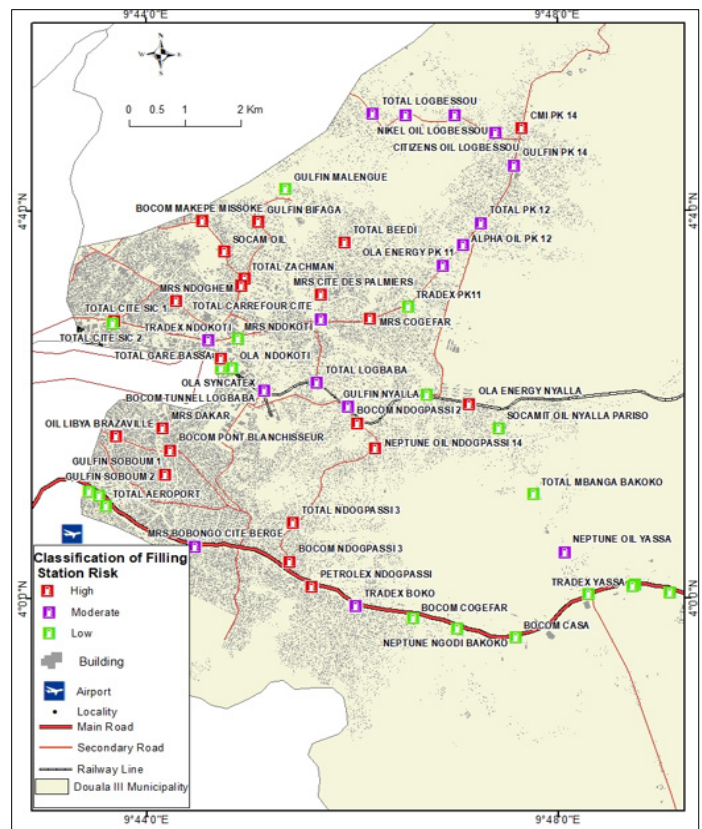
Figure 4 (b): Patterns and risk prone stations in the Douala III
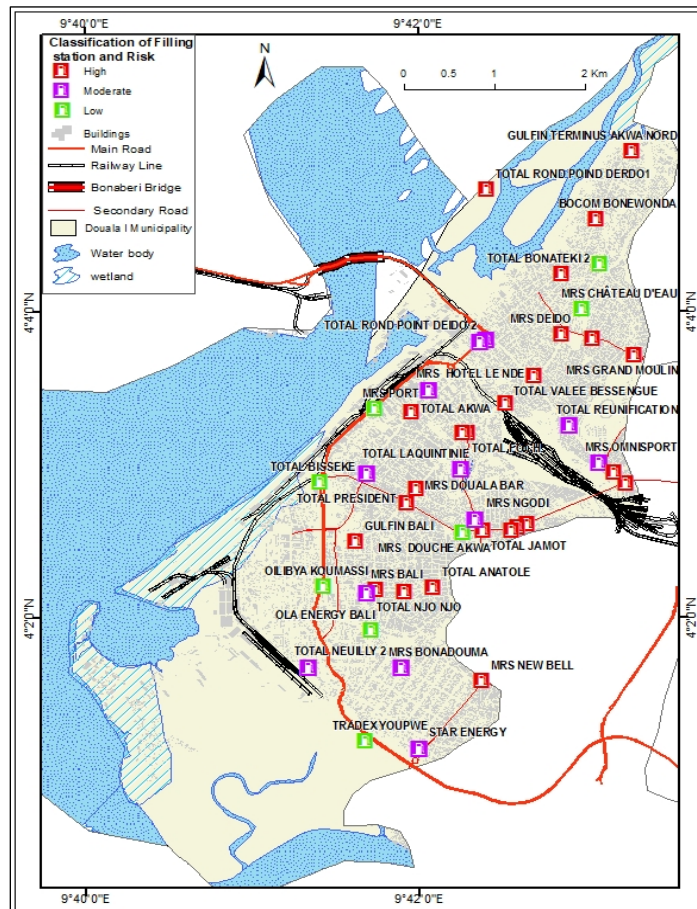
Figure 4 (a): Patterns and risk prone stations in the Douala I
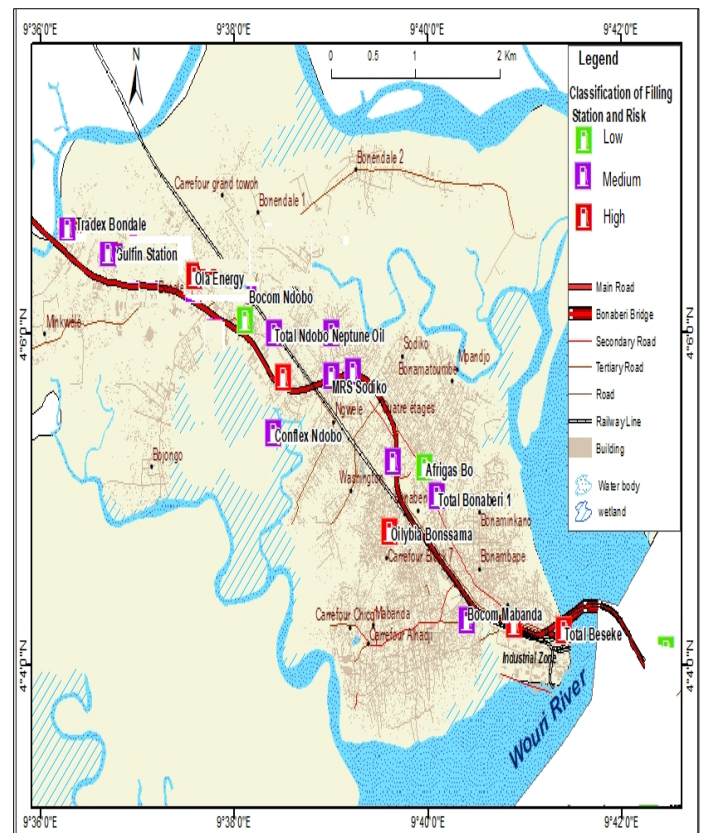
Figure 4 (c): Patterns and risk prone stations in the Douala IV
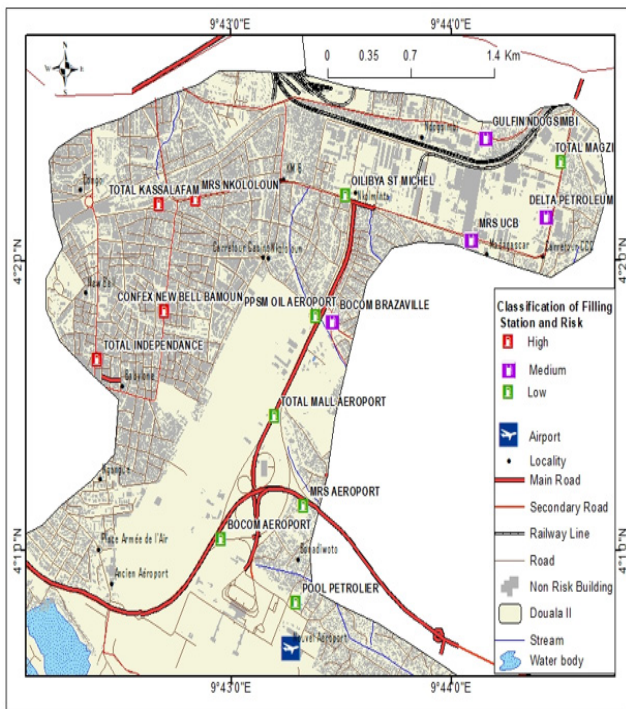
Figure 4 (d): Patterns and risk prone stations in the Douala II
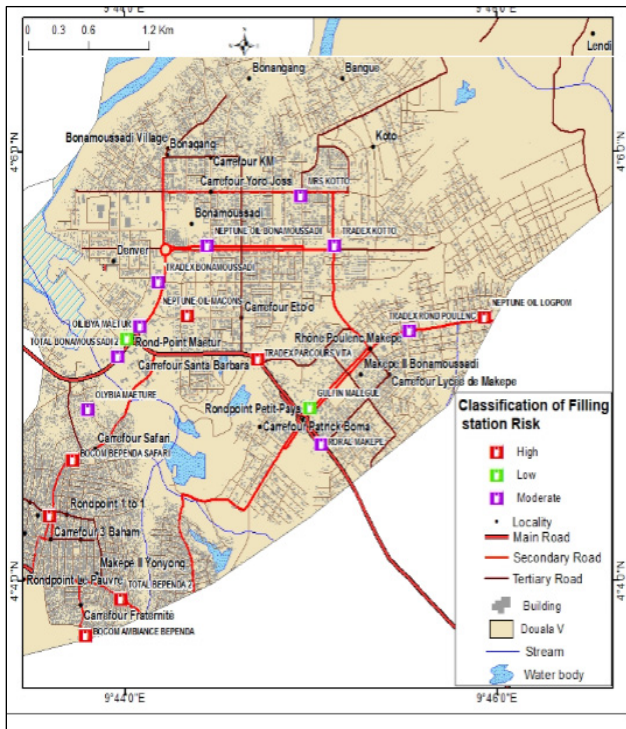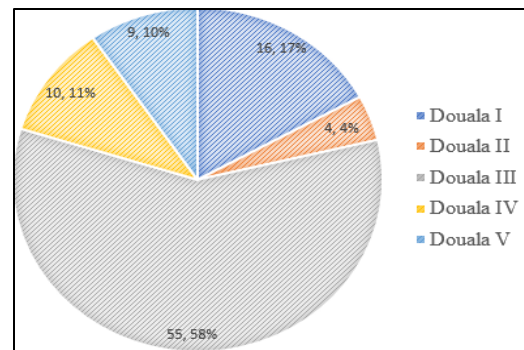
Figure 5: Petrol stations within the minimum 500 m radius in the City of Douala

3.2.2. Distances between filling stations and main road

Of the 152 stations investigated, only one (0.66 %) was within the stipulated distance of 7 m between the edges of a station, and a major road. The rest, 99.34% were between 1 and 3 m. This partly explains the rising road traffic problems such as a traffic congestion, breaches of traffic law, and road traffic accidents that have over the years disrupted the city's economic activities. It also poses questions about the threats posed to nearby communities and pedestrians by the fumes (volatile organic compounds) released from operational activities of the stations.

3.2.3. Distance of Filling Stations to Health Facilities

Of the 152 petrol stations sampled in the municipality, 126 (84%) were located within the stipulated 100 m radius ($X^2(48) = 71.442$; $p = 0.016$) as specified by law. Of these, 24 (66.78%), were from Douala I, 10 (90.9%) were from Douala II, 64 (88.9%) were from Douala III, 10(83.3%) were from Douala IV, and 18 (94.9%) were from the Douala V district. The study shows that most hospitals are conveniently situated far away from gas stations. Most of the 26 stations that did not comply with the current regulations were located in Douala I, (50%) and Douala IIII (33.33 %). It should be noted that Douala I is the Wouri Division's administrative headquarters and is the oldest municipality in Douala. On the other hand, the largest and most populous municipality is Douala III. The likely reason for these playouts may be due to the market along these areas, and the fact that regulators bend to this rule and give a waiver to the filling stations.

3.2.4. Distance between filling stations and educational establishments

Based on legal requirements, petrol stations are not allowed to operate adjacent to public institution like schools. However, should there be a need, the facility should be within 100 m radius of a school environment. Our findings showed that, overall, 119(79.3%) of the stations in the entire municipality complied. Of these, 31(86.1%) were from Douala I, 10(90.9%) were from Douala II, 56 (77.8%) were from Douala III, 8 (66.7%) were from Douala IV, and 14 (73.7%) were from Douala V. Of the 33 (21.3%) that did not comply, 17 (51.52%) were from Douala III, 5 each (15.15%) from Douala I and II, 4(12.12%) from Douala IV, and 2(6.06%) from Douala V district.

3.2.5. Distance between filling stations and the market places and human settlements

According to national guidelines, residential buildings, schools or hospitals should not be within 100 meters of gas stations unless

Figure 4 (e): Patterns and risk prone stations in the Douala V

3.2. Compliance of petrol stations with development good practices

3.2.1. Distances between filling stations

Most of the stations, 94 (61.84%) were within the minimum 500 m radius as specified by the law. Of these stations that,55 (58.51%) were found in the Douala III district, while the least number, 4(4.26%) were from Douala II district (Figure 5)

it can be clearly shown there would be no effect concerning noise, visual interference, safety considerations or smells and fumes. The analysis suggests, however, that several petrol stations have breached this law. For example, most of the stations,144 (94.74 %) in the municipality were not within a 100-m radius from markets. Likewise, most of the stations, 127 (83.55 %) were within 40 m of human settlements, which is much less than the 100 m required by law (Figure 6).
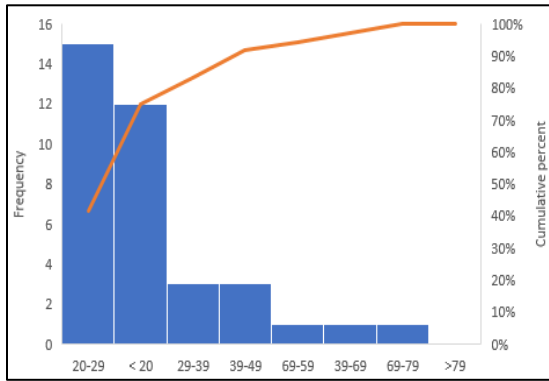
Figure 6: Distances of filling stations to human settlements

The stations therefore seem to have high potential of hazards (hydrological, geological, socio-economic, etc.) to their surroundings. The main contributors to cancers, acute myeloid leukemia, and acute non-lymphocytic leukemia have been described as exposure to diesel, petroleum fumes, and fuel components such as benzene and formaldehyde [4]. Good practice globally prohibits construction in the vicinity of gas stations, in particular hospitals, community centres, schools and old people's homes and housing [29].

These results indicate that the existing model and regulations for land use do not consider the fire threat raised by petrol stations and do not protect the public sufficiently. While there has never been a major fire at a gas station in the municipalities of Douala, a municipal explosion or fire could potentially lead to significant damage and even death and injury. Even in the moderate risk areas of the municipality, human settlement and the construction of schools and hospitals are ongoing. Given the current rate of urban sprawl and the poor implementation of government rules and regulations resulting from overall bad governance culture in the country, it is hard to estimate when the economy-ecology balance shall be taken into consideration in the city's development plan.

Nevertheless, the Douala municipalities are not unique when it comes to adhering to best practices. Similar results had been obtained elsewhere, for example, [30] and [31]. The latter pointed out that the common issue of all urban settlements today is erratic and unsound urban growth, and that the increasing continuation of this problem is unavoidable in this order, in which the balance between the economy and the environment is not taken into account and economic interests often win. While the reasons can vary, the most common ones concern the economic benefits to the local community and municipality of the petrol stations [4].

3.3. Hazard contributing factors in the operation and maintenance of filling stations in the municipalities

Several hazard contributing factors that have the potential to create unsafe conditions in the functioning of the filling stations

in the municipality were reported. In order of priority they include miscellaneous cases,152(25.63%); slips, trips & falls, 126(20.1%); carelessness 98(16.53%), transportation, 84(14.17%), electrical faults, 67(11.30%), fire risk, 49 (8.26%) and medical treatment 17(2.87%) (Figure 7).
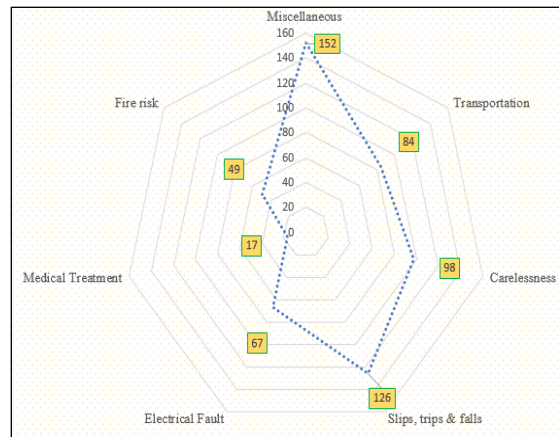
Figure 7: Prioritized hazardous activities at petrol stations

Miscellaneous cases comprised of hazard contributing factors such as oil spillages, water leakages, robbery, law and order situation, and, maintenance issues. The numerous unsafe practices that were recorded in many of the filling stations could be attributed to inadequate safety procedures by staff, failure to clear oil spills, unsafe manual handling practices and the storage of fuel samples in unmarked containers.

Slips, trips & falls could be as a result of oil leakage. This suggests poor supervision and inadequate training. Simple prevention steps such as education and health and safety training are often ignored. Hence, occupational health services and supporting legislation need refocusing, revision and reinforcement. On the other hand, carelessness can be due to a variety of causes, including, though not limited to, the unsatisfactory use of staff protective equipment, the use of mobile phones in the tank area, and the insufficient use of signs and instructions.

3.4. Residents' perceptions of the possible hazards associated with the emergence of refueling stations

A significant 77% of the respondents perceived that the distances between some of the filling stations were inadequate. A smaller percentage, 61% percentage stated that the distances between the filling stations and the places of public assemblies were inadequate, while 58% perceived that the distances between adjacent filling stations were inadequate. (Figure 8).
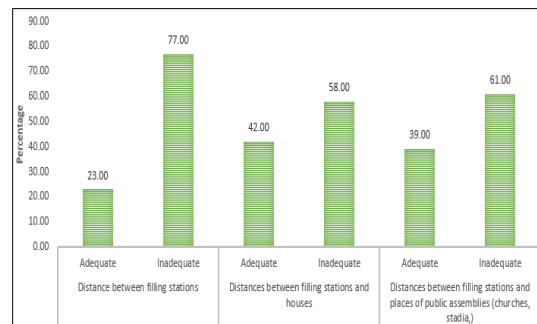
Figure 8: Perception of locals of the adequacy of the siting of stations

The breaches of the appropriate distances between the filling stations, the distances between the filling stations and the nearest public assembly houses/places are strong indications of pressing concerns about the health and safety hazards presented by these petrol filling stations (PFS) and the risks to which residents are prone[7]. In the Douala municipalities, it is common to either see people acquiring lands very close to PFS to create residential homes and/or other businesses, or PFS being established at unacceptable distances from the population and social infrastructures.

A significant number of the respondents (74.25%), most of them from the Douala III district were aware of the proliferation of petrol filling stations in their communities together with the associated dangers and health hazards they pose (Figure 9). Those who were not aware of these proliferations are relatively new to the areas, while those who were aware of these proliferations have been living in the areas for more than two decades.
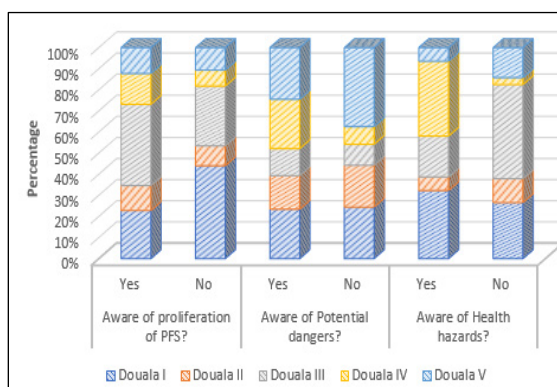
Figure 9: Level of awareness of locals of the potential dangers associated with fuel stations

Those who were aware of the potential health hazards of petrol fueling stations mentioned respiratory diseases as a result of chronic exposure to dust (26.37% of respondents), chronic exposure to volatile organic compounds (36.62%), and chronic exposure to vehicle exhausts (37.12%). Other findings, such as [32], have shown that petrol vapor could find its way into the basements of buildings and public drains with significant implications if the vapor comes into contact with the ignition source. Many other studies have also reported that fuel stations provide acceptable grounds for fire outbreaks and expose several physical, chemical and ergonomic threats to employees and residents [33].

While a large number of residents were aware of the possible dangers associated with fuel stations, no action was taken to resolve their concerns by the local administrative authorities. This could be viewed as a failure by local authorities and regulatory agencies to proactively resolve (in a participatory way) the problems of the haphazard proliferation of petrol stations against the context of the various possible risks and hazards associated with stations across the municipalities. Building on existing social awareness as such has been identified as a key catalyst towards the achievement of the Sustainable Development Goals [34].

3. Conclusion

In the above-mentioned discussion, the degree to which the location and operation of petrol stations in the City of Douala, Cameroon, compares with relevant current regulations and the consequences for public safety has been examined. A hybrid methodology was used that incorporated both explicit and implicit data from field investigations. The approach is comparable to other heuristic methods. In some cases, it can be considered as a real-time and reliable detection approach, and offers a strong potential for better understanding and investigating of the environment especially in regions such as sub-Saharan Africa, where existing petrol station databases are uncommon and often unreliable. The implementation of this approach has shown that the location of petrol stations in the City of Douala do not completely comply with the guidelines of good practice. Furthermore, the study shows that the haphazard emergence of municipal filling stations is laden with possible health, safety and environmental risks that could be blamed on the inability of government regulatory bodies to implement established laws and policies effectively. If a good mapping of the issue to an acceptable network architecture is identified, this method can also be used to assess hazard-contributing factors and the awareness of residents in detail. In the future, this might be a fascinating place for research. The results trigger the need for local governments to inculcate the interest of the resident population and employees of petrol stations as a core concern in projects that directly affect local ecosystems. Local administrative authorities also need to take timely action to ensure that: (a) an environmental and social audit is carried out before a petrol station is constructed to ensure that it complies with local and./or international standards, and (b) people are prohibited from purchasing land for schools, markets, etc., near filling stations or near filling stations to create residential homes, etc.

Conflict of Interest

The authors declare no conflict of interest.

Acknowledgments

References

[1] F. Monney, I, Dramani, J. B., Aruna, A., Tenkorang, A. G., & Osei-Poku, "Health and safety in high-risk work environments: A study of fuel service stations in Ghana," Ournal of Environmental and Occupational Scienc, **4**(3), 132–140, 2015, doi:10.1016/j.jlp.2005.05.015.

[2] P. V. Chaiklieng S., Dacherngkhao T., Suggaravetsiri P., "Fire risk assessment in fire hazardous zones of gasoline stations," Journal of Occupational Health, **62**(1), 2020, doi:10.1002/1348-9585.12137.

[3] B.C. Thomas Kweku Taylor, Chanda Sichinsambwe, "Public Perceptions on Location of Filling Stations in the City of Kitwe in Zambia.," Developing Country Studies, **6**(6), 133–151, 2016.

[4] E. Mshelia, M., Abdullahi, J. and Dawha, "Emmanuel. Environmental effects of petrol stations at close proximities to residential buildings in Maiduguri and Jere, Borno State, Nigeria.," IOSR Journal of Humanities and Social Science (IOSR-JHSS), **20**(4), 1–8, 2015. doi:10.1016/j.36898.05.015.

[5] D.N. Mohammed, M.U., Musa, I.J., and Jeb, "GIS-Based Analysis of the Location of Filling Stations in Metropolitan Kano against the Physical Planning Standards.," American Journal of Engineering Research, **3**(9), 147–158, 2014.

[6] S.M. Nouri, J., M. Omidvari, and Tehrani, "Risk Assessment and Crisis Management in Gas Stations," Int. J. Environ. Res., **4**(1), 143–152, 2010.

[7] P.M. Nieminen, Environmental Protection Standards at Petrol Stations: A Comparative Study of Technology between Finland and Selected European Countries. Thesis for the Degree of Doctor of Technology, Tampere University, Finland., 2005.

[8] S. Ayodele, Spatial Distribution of Petroleum Filling Station in Kaduna North.

[9] Timothy J.S. et al, "Air pollution success stories in the United States : The

value of long-term observations," Environmental Science and Policy, **84**(November 2017), 69–73, 2018, doi:10.1016/j.envsci.2018.02.016.

[10] British Broadcasting Corporation (BBC), Ghana petrol station fire: Accra death toll tops 150 after inferno during severe flooding. Online at https://www.independent.co.uk/news/world/africa/ghana-petrolstation- fire-accra-tops-150-die-petrol-station-explosion-during-ghanaflooding-10299432. Acces, Accessed on 10/10/2020., 2015.

[11] GhanaWeb, "One more dead as Krofrom gas explosion death toll rises to 2," Http://Mobile.Ghanaweb.Com/GhanaHomePage/NewsArchive/Onemore-Dead-AsKrofrom-Gas-Exposion-Death-Toll-Rises-to-2- 702607, 2015.

[12] S. FK, "Fires and related incidents in Jordan (1996-2004)," Fire Safety J., **41**(5), 370–376, 2006.

[13] M.M. Ahmed, S.R.M. Kutty, A.M. Shariff, M.F. Khamidi, "Petrol Fuel Station Safety and Risk Assessment Framework," DOI: 10.1109/NatPC.2011.6136346, 2011, doi:10.1109/NatPC.2011.6136346.

[14] T.S.& S. Seyhan, "A Multi-Criteria Factor Evaluation Model For Gas Station Site," Journal of Global Management, Global Research Agency, **2**(1), 12–21, 2011.

[15] O. Ogunyemi, S.A., Ajileye, O.O., Muibi, K.H., Alaga, A.T., Eguaroje, O.E., Samson, S.A., Ogunjobi, G.A., Adewoyin, J.E., Popoola, O.S., Oloko-Oba, M.O. and Omisore, "Geo-Information and Distribution Pattern of Petrol Service Station in Sango – Ota Metropolis in Ado – Odo Ota Local Government Area, Ogun State, Nigeria," Asian Research Journal of Arts & Social Sciences, **2**(1), 1–11, 2017.

[16] J.A.O. Arokoyu Samuel B., Ogoro Mark, "Petrol filling stations' location and minimum environmental safety requirements in Obio Akpor lga, Nigeria," International Journal of Scientific Research and Innovative Technology, **2**(11), 2015.

[17] K. H, Markus, AM, Bernat, N, Jian, MR, Ana, EN, "Hydrocarbon Release During Fuel Storage and Transfer at Gas Stations: Environmental and Health Effects," Current Environmental Health Reports, **2**(4), 412–422, 2015.

[18] R. C. T Tanaka, T Azuma., J.A Evans., P.M Cronin., D.M Johnson., "Experimental study on hydrogen explosions in a full-scale hydrogen filling station model," Int. J. Hydrogen Energ, **32**, 2162 –2170, 2007.

[19] K. Emakoji, M.A, & Otah, "Managing Filling Stations Spatial Database Using an Innovative GIS Tool – Case Study Afipko City in Nigeria," Asian Journal of Geographical Research, **1**(2), 1–9, 2018.

[20] I.J.M. Broekhuizen, H., Groothuis-Oudshoorn, C.G., van Til, J.A., Hummel, J.M., "A review and classification of approaches for dealing with uncertainty in multi-criteria decision analysis for healthcare decisions," Pharmacoeconomics, **33**(5), 445–455, 2015. doi:10.1016/j.2015.05.01265.

[21] J. Boroushaki, S., and Malczewski, "Implementing an extension of the analytical hierarchy process using ordered weighted averaging operators with fuzzy quantifiers in ArcGIS," Computers & Geosciences, **34**(4), 399–410, 2008.

[22] Z. Aneziris, O. N., Papazoglou, I. A., Konstantinidou, M., & Nivolianitou, "Integrated risk assessment for LNG terminals," Journal of Loss Prevention in the Process Industries, **28**, 23–35, https://doi.org/10.1016/j.jlp.2013.07.014.

[23] C.-C.L. James Chang, "A study of storage tank accidents," J. Loss Prev. Process Ind., **19**, 51–59, 2006, doi:10.1016/j.jlp.2005.05.015.

[24] N. Cao, M. Štěpnička, M. Burda, "Fuzzy Quantifiers and Compositions of Partial Fuzzy Relations Employing Dragonfly Algebras," in 2019 IEEE International Conference on Fuzzy Systems (FUZZ-IEEE), 1–6, 2019, doi:10.1109/FUZZ-IEEE.2019.8858832.

[25] A. Hailwood, M., Gawlowski, M., Schalau, B., & Schoenbucher, "Conclusions drawn from the Buncefield and Naples incidents regarding the utilization of consequence models," Chemical Engineering & Technology: Industrial Chemistry-Plant Equipment-Process Engineering-Biotechnology, **32**(2), 207–231, 2009.

[26] C. Ministry of Labor and Social Welfare, Order No. 39 / MTPS / IMT of November 26, 1984 laying down general health and safety measures in the workplace., Offprint, 37 https://www.ilo.org/dyn/natlex/natlex4.detail?p_isn=39672&p_lang=e.

[27] I.R.C. (IRC), Recommended practice for locating and layout of roadside motor-fuel filling and motor-fuel fillingcum service stations (IRC),[Online].pbhousing.gov.in/notification_files/Petrol_Pumps((IRC(121 983))75.pdf; Accessed 12/6/2020., 2009.

[28] A. Mitchell, ESRI Guide to GIS Analysis, **2** (Spatial Measurements and Statistics) 1st Edition, 2005.

[29] E. David, Statistics in Geography, Blackwell, 1985.

[30] K. Qonono, Analysis of the fire hazard posed by petrol stations in Stellenbosch and the extent to which planning acknowledges risk, Stellenbosch University.

[31] M. Brueckner, J. K., Mills, E., & Kremer, Urban sprawl: Lessons from urban economics [with comments], 2001.

[32] R. Sakyi, P.A., Efavi, J.K., Atta-Peters, D., Asare, "Ghana's Quest for Oil and Gas: Ecological Risks and Management Frameworks.," West African Journal of Applied Ecology, **20**(1), 57–72, 2012.

[33] E.E.Y. Douti, N. B., Abanyie, S.K., Ampofo, S., & Amuah, "Spatial distribution and operations of petrol stations in the Kassena-Nankana district (Ghana) and associated health and safety hazards," Journal of Toxicology and Environmental Health Sciences, **11**(5), 50–61, 2019.

[34] S.R. Mensah, J., & Casadevall, "Sustainable development: Meaning, history, principles, pillars, and implications for human action: Literature review.," Cogent Social Sciences, **5**(1), 2019.

Development of an IoT Platform for Stress-Free Monitoring of Cattle Productivity in Precision Animal Husbandry

Arman Mirmanov[1,*], Aidar Alimbayev[1], Sanat Baiguanysh[1], Nabi Nabiev[1], Askar Sharipov[1], Azamat Kokcholokov[1], Diego Caratelli[2]

[1]*Department of Radio Engineering, Electronics and Telecommunication, S. Seifullin Kazakh Agrotechnical University, Nur-Sultan, 010011, Kazakhstan*

[2]*Department of Electrical Engineering, Electromagnetics Group, Eindhoven University of Technology, Eindhoven, 5600 MB, The Netherlands*

ARTICLE INFO

ABSTRACT

Smart animal husbandries require the adoption of dedicated tools to assess the contribution of each animal to the production process. The IoT platform presented in this article is a real-team monitoring system for voluntary weighing of cattle. To this end, the ISO 18000-6 standard is used for animal identification through an ultra-high-frequency radio link between a reader antenna and suitable ear tags. A customized data processing algorithm has been developed and embedded in the considered system. To demonstrate the effectiveness of the solution, extensive measurements have been carried out in a real-life environment. The proposed IoT platform is useful to farmers as a control tool for selection and breeding work.

1. Introduction

Milk production plays an essential role in the global economy. Four major world exporters of dairy products (USA, EU, New Zealand, Australia) produced more than 239.2 million tons in 2019. According to the United Nations' food and agriculture organization, milk production, and the price Index for dairy products are growing annually [1]. To increase the volume of raw milk production, it is not unimportant to encourage the use of new technologies. Telemetry and monitoring systems for agricultural production are considered one of the most innovative technologies in precision animal husbandry and are automatic systems for collecting and transmitting information and data analysis and remote decision-making.

Currently, livestock farms use mainly technologies for measuring various parameters inside the farm (ventilation, power supply, heating, etc.), but unfortunately, a small proportion of them are focused directly on the animal. Modern technological tools (temperature sensors, pH sensors, identification sensors, wireless communications, Internet, and cloud storage) make it possible to monitor each animal separately.

A key indicator of the development of young cattle is their weight. In order to obtain maximum accuracy of the mass of cattle, weighing should be carried out repeatedly, using conventional industrial scales or more modern electronic devices. Weighing should be carried out regardless of the animals' location, whether it is a farm or a remote pasture. In most cases, the weighing process is carried out in manual or semi-automatic mode and takes some time. Furthermore, the weighing procedure is stressful for the entire herd. It is not uncommon to use less accurate methods of measuring the weight of animals without using scales, and the assessment is based on the size of body parts. This method is not very effective and requires highly qualified personnel.

2. Review of alternative developments

2.1. RFID-based systems

The introduction of radio-frequency identification tags has had a massive impact on the technological development of animal husbandry. The use of RFID systems has contributed to the

development of the concept of precision animal husbandry. Intensive research on automatic cattle weighing systems using RFID has led to new developments.

The Australian company TRU-TEST develops systems for measuring cattle's weight when an individual passes through a dedicated gate. The TRU-TEST data collection system assumes direct control and the operator's close presence when measuring the weight of a cow [2]. Autonomy is limited by the need for a smartphone to collect data and transmit it to the server. Human resources and the lack of an Autonomous data transmission channel limit this approach.

2.2. Systems based on LF RFID and voluntary weighing

Automatic systems that use LF RFID and stress-free weighing of animals include those supplied by GrowSafe and Intergado.

GrowSafe is a Canadian company that develops systems for automatic data collection from cattle [3], [4]. The systems are equipped with RFID antennas for reading ear tags. The watering and weighing station is integrated with electronic scales. One of the main constraints is the cost of installation. Besides, because of the inadequate cellular network coverage of rural areas and pastures, data transmission over 3G/4G networks is problematic.

Intergado is a Brazilian company that develops dedicated solutions for monitoring cattle based on RFID technology. In such solutions, the scales are integrated on load cells that regularly weigh food and water. When an animal visits the feeder, the system records its RFID tag, arrival time, departure, and duration of consumption [5], [6].

GrowSafe and Intergado systems were originally designed for indoor use, but they can also be installed in pastures. They are very effective from an application standpoint but use technologies and equipment that require large financial investments. Costs associated with the transportation of the equipment from North / South America and its installation in the final site are also, typically, significant.

3. Proposed weighing platform

This article presents a system consisting of hardware and software elements for precision animal husbandry aimed at obtaining information about the weight of the animal, the number of approaches to watering, the time and duration of drinking, with the possibility of performing insect spraying. In this context, the animal's age is assumed to be between 8 and 14 months, and weight is estimated based on the pressure made by the individual animal with the front hooves on the integrated platform. Following best practice in applied info-communication technology, a block diagram of the experimental setup used for remote monitoring of the live weight of animals has been developed and reported in Figure 1.

In order to organize the identification of animals, a reader with UHF RFID tags is used. Strain gauges are used for weighing. The platform's connection with the central information unit is established using multiple communication channels: via LoRaWAN, via GSM (backup), and via WiFi (for wireless configuration of the controller module). The solar power plant provides an autonomous power supply in the field.
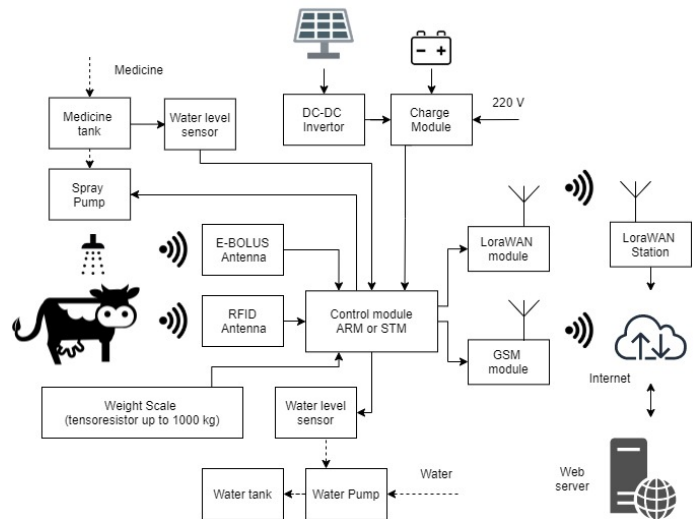
Figure 1: Block diagram of cattle telemetry system

3.1. Design of the weighing platform

The design of the developed platform has been performed in such a way as to achieve measurable benefits against alternative solutions already available on the market. Furthermore, in order to achieve high measurement accuracy, extensive data concerning the weight and growth of young local cattle has been collected and judiciously used.
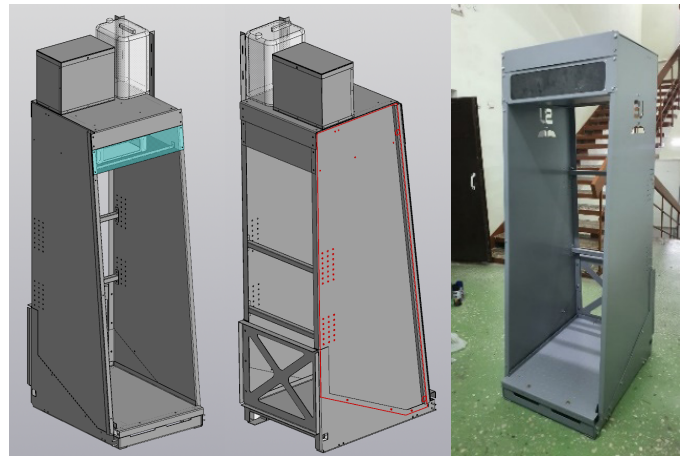
Figure 2: 3D model and implementation of the experimental sample
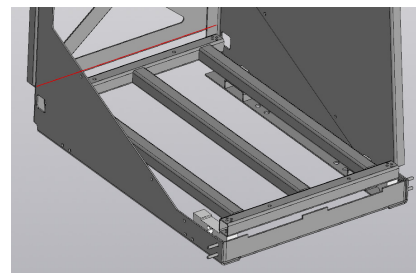
Figure 3: 3D model of the experimental sample pallet with pressure sensors

The main structure is designed in such a way as to resemble a "phone booth" with two side walls and a back wall with an opening for the head of the animal. The side walls have an oblique edge on the entrance side and a straight edge on the side of the drinker, for

easy integration to it. For better accessibility to the electronic components in the lower part of the platform, a novel approach to the installation of the scales has been developed. Contrary to Growsafe solution, where the entire structure is mounted on strain gauges, in our system, the scales are only pressured by the pallet on which the animal stands (see Figure 2).

The design of the fasteners for the strain gauges has been optimized so that, during assembly, easy access is given to all the bolted connections (see Figure 3).

While designing the platform, the properties of the metal structures have been optimized so that the mechanical deformation under a load of 2000 N results in a maximum offset not exceeding 0.36 mm. This is important to make sure that the pressure sensors can withstand the full load from the weight of young cattle (see Figure 4).
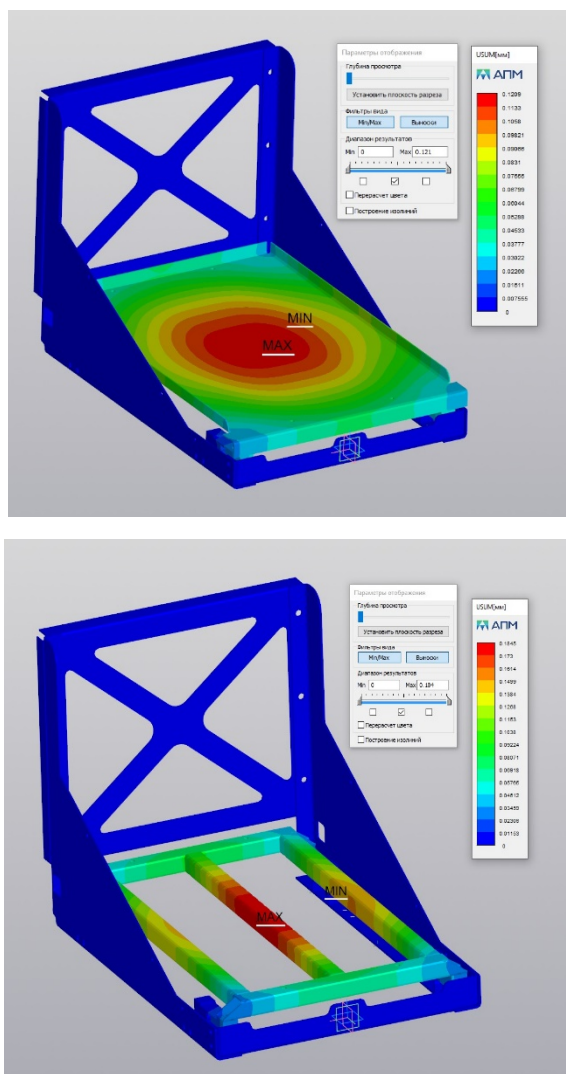
Figure 4: Statistical analysis of the pallet for deformation

3.2. Radio-frequency identification of animals

Animal identification is regulated by ISO 18000-6 standard. According to that, the radio interface is established in the frequency range between 860 MHz and 930 MHz using long-range ultra-high-frequency (UHF) radio-frequency-identification (RFID) devices [7].

Extensive research has been devoted to antennas for RFID tags. A more in-depth analysis of passive RFID systems can be found in several publications [8], [9]. In [10], [11], the calculation methods for various antennas are presented. In [12], the principles of operation of RFID systems in the presence of backscattering are illustrated. To achieve the maximum reading range, it is necessary to properly match the complex impedances of the tag antenna and the integrated circuitry. Most often, for optimal read performance, the antenna impedance is matched to the chip impedance at the minimum chip power level.

Various modulation and encoding schemes are used to transmit data between the reader and the tag. A UHF RFID system based on reflected signal modulation in the UHF band can be produced at a reasonable price, though the system's overall efficiency can severely limit the readability. At the same time, the characteristics of the antenna can radically affect the performance of RFID systems.

In the presented study, the working frequency of 868 MHz is selected for the developed RFID system.

A Chafon CF-MU930T reader with integrated UHF RFID antenna featuring circular polarization and 9dBi gain is adopted for reading ultra-high-frequency identification tags (see Figure 5) [13].
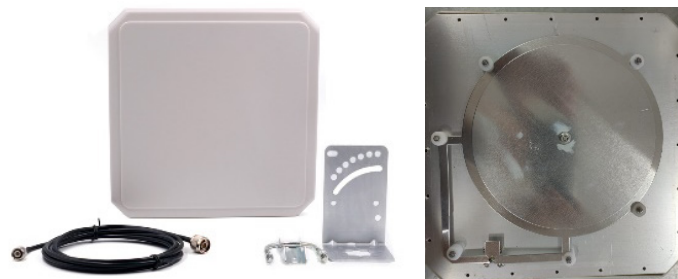
Figure 5: UHF RFID antenna used in the proposed development
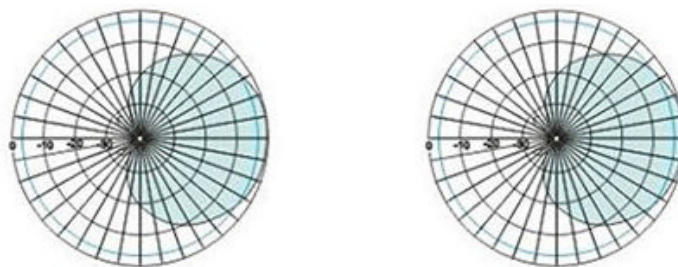
Figure 6: UHF RFID reader antenna radiation patterns

The ISO/IEC 18000-6C EPC global Class 1 Gen 2 ear tag contains an Impinj Monza® 4 chip and operates at 868 MHz (figure 6). The complex conjugate of the chip load at the specified frequency is expressed as an impedance of 13 + j151 Ω.

Figure 7: Ear tag and embedded UHF antenna used for identification

At the initial stage of development, it is necessary to identify the optimal installation site of the antenna as well as the reader's required power. A necessary condition is to ensure that the reader antenna illuminates the ear tag antenna with a minimum gain level to achieve good communication quality.

A limiting factor for applying the maximum reader power of 30 dBm is related to the possibility of performing an erroneous reading of nearby animals. An additional difficulty in selecting the proper power level is associated with the tag's location on the animal's ear at the time of reading. The antenna can be perpendicular or have an acute angle relative to the ground surface. If the reader antenna is positioned above the animal's head, the tag may be covered by the ear, thus possibly resulting in low communication quality.

Before conducting the actual experiment [14], numerical simulations of the communication channel have been performed using COMSOL Multiphysics.
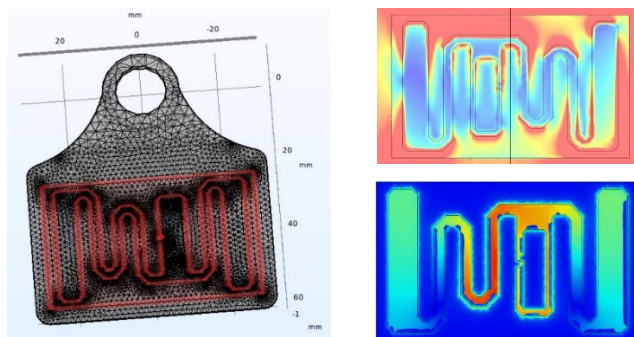
Figure 8: Current distribution and radiation pattern of the RFID tag antenna

The adopted model consists of the UHF RFID reader and tag antennas, surrounded by an air region terminated with perfectly matched layers (PML). The operating frequency of both antennas is 915 MHz. In particular, the RFID tag is made out of a 0.2-mm thick polypropylene board with a thin embedded aluminum pattern that is modeled as an ideal electrical conductor (PEC). The tag antenna is an electrically small dipole (see Figure 7) whose

radiation pattern is reported in Figure 8. On the other hand, the reader integrates a directional metal stamped patch antenna (see Figure 5) characterized by an input power level of 5W. Using the developed numerical model, one can quickly evaluate the power level radiated by the reader antenna and received by the tag.

Figure 9 shows the placement of the reader antenna inside the weight platform. The distance between the antenna and the tag ranges from 30 cm to 80 cm. In real-life conditions, in the presence of an animal with total height of 190 cm inside the platform, the distance between the two antennas is typically 55 cm.
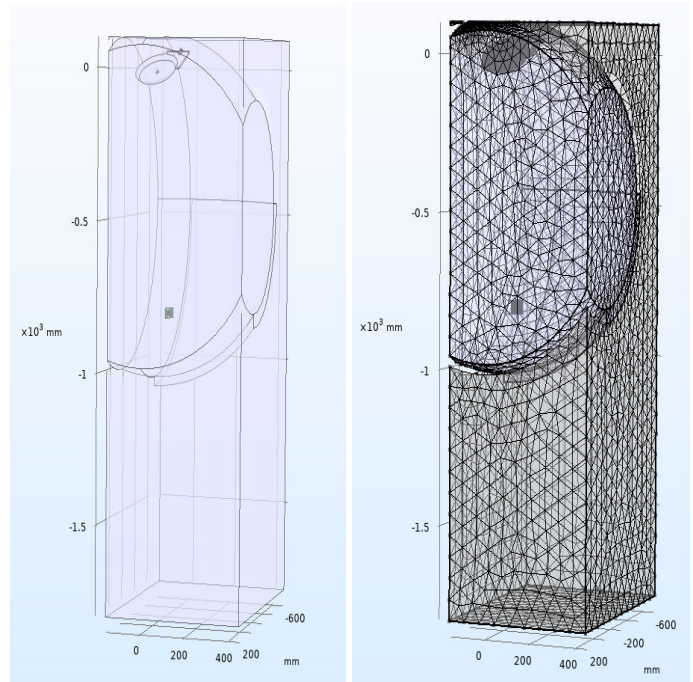
Figure 9: Model of the UHF RFID system inside the weighing platform
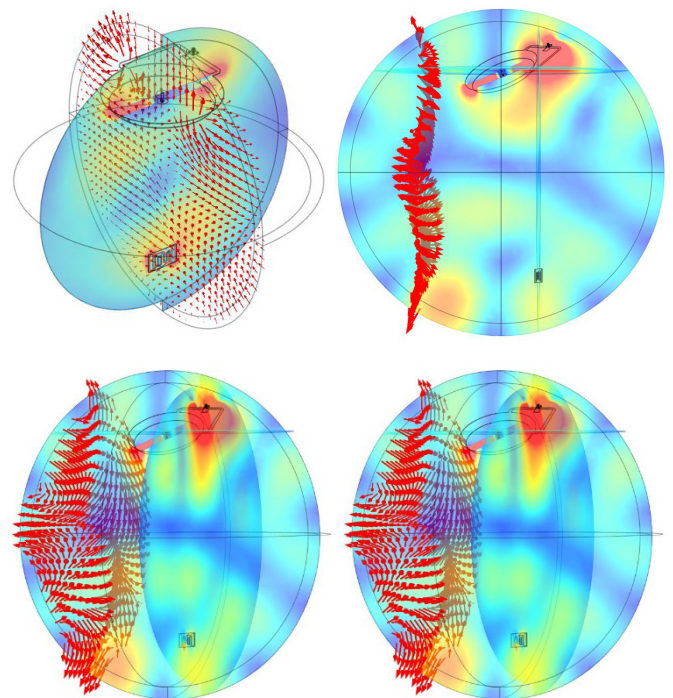
Figure 10: Electric field distribution excited within the UHF RFID system

Extensive analysis has been carried out as a function of the reader antenna's location relative to the platform surface and relevant sidewalls. The results relevant to the Electric Field (EMF) distribution in different system configurations are reported in Figure 10.

After the computer-aided modeling stage, experimental verifications have been conducted. Based on the data collected through numerical simulations, the reader antenna has been mounted with an optimal angle of 380 degrees relative to the platform tray and of 260 degrees relative to the side-wall of the structure, in such a way as to be in the line of sight with the animal's ear on which the tag is installed. To this end, a dedicated mechanical support for the reader antenna has been designed and integrated (see Figure 11).
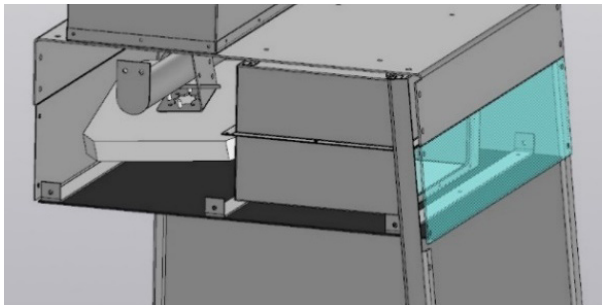
Figure 11: 3D model of the upper section of the platform inclusive of reader antenna and central electronic unit

Figure 12: Layout of the electronic unit (1-UHF RFID Reader, 2-Raspberry Pi, 3-LoRa Module, 4-Spray control unit, 5-Power Adapter)

3.3. Electronic unit integrated in the weighing platform

The central electronic unit of the system is based on the modular integration of off-the-shelf components, as it can be noticed in Figure 12.

In particular, four TAL214A(350) strain gauges are connected, via the GoldShine SS-4/S equalizer, to an Arduino UNO controller. In order to process the data received from the strain gauges, a dedicated code has been implemented using the Arduino Wiring programming language. The weight information is sent to the main system controller - a Raspberry Pi - via an I2C port relying on the RS-232 standard. The UHF RFID reader is connected to the computer and receives the identification number from the ear tag. After processing the received data, the Raspberry Pi sends the information to the cloud server. The WiFi module built into the Raspberry Pi single-board computer is used to establish the communication channel. The LoRa32u4 II module supports the

remote connection, whereas a GSM/GPRS link is used as a backup channel for sending the final data.
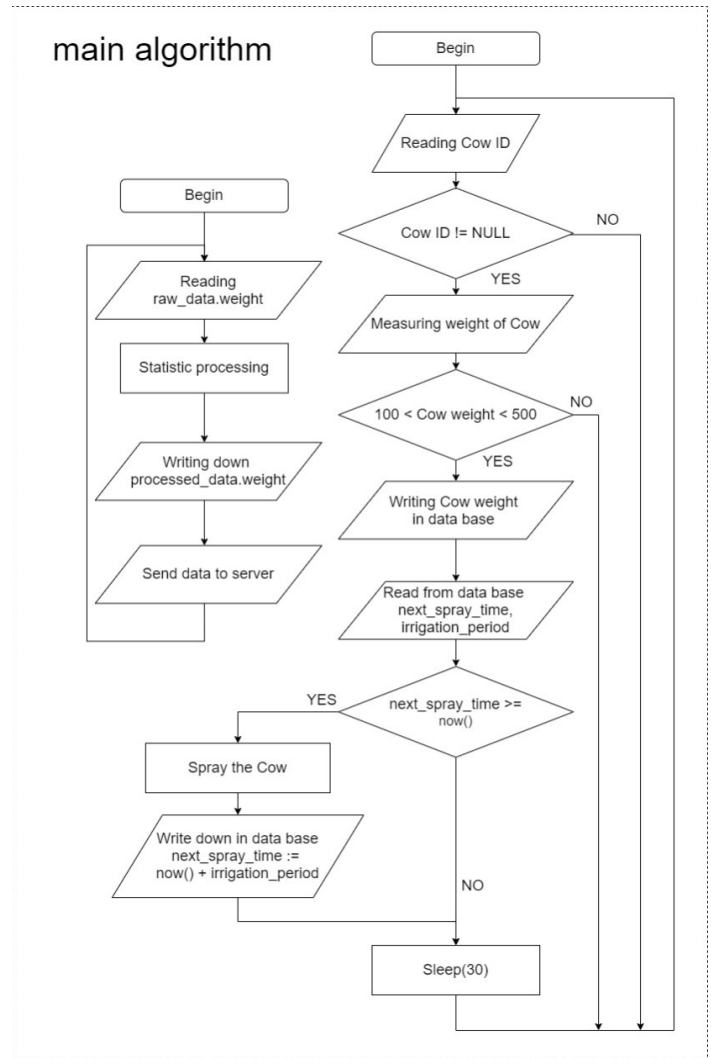
Figure 13: Block diagram of the main algorithm of the platform
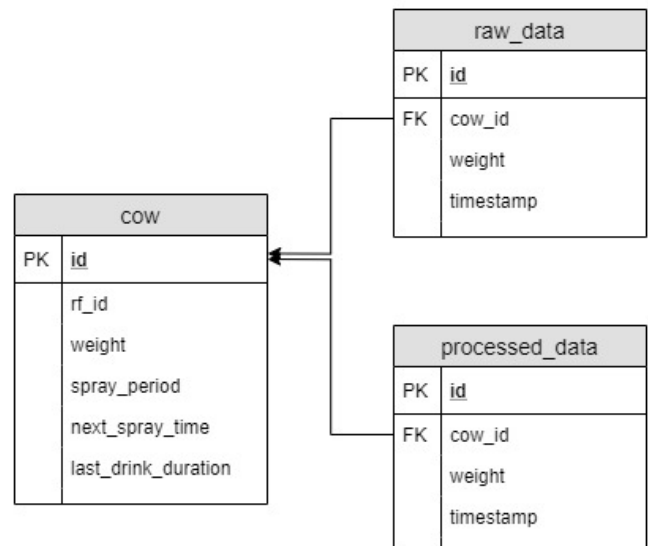
Figure 14: Structure of the database used in the Raspberry Pi

The electronic sub-system has been designed in such a way to withstand harsh environmental conditions in terms of humidity, temperature excursions, as well as mechanical stress, and vibration. It complies with the IP65 sealing class as per the international standard IEC 60529. The enclosure containing the electronic components and the antenna is mounted on the upper part of the platform and protected with vinyl to restrict access, whereas a glass window is used for inspection (see Figure 12).

3.4. Platform management software

The core of the code used for platform management is written in Python 3.7. The implemented algorithm executes two parallel threads. The first thread is relevant to identification, weight measurement, spraying, and data recording in the database. The second thread is used to process the data and store it in the Raspberry Pi unit before sending the relevant information to the server (see Figure 13).

The database is implemented in Raspberry Pi using the scheme described in Figure 14. As it can be noticed, the unique cow ID is reported in the database structures "raw data", "processed data", and "cow". This scheme allows using the internal memory of the Raspberry Pi more efficiently. The data collected through the platform is transmitted from the main database to the server via the Internet. The server is characterized by IP address 194.4.56.86: 8501 where 8501 is the port selected for receiving JSON packets. Each packet contains the following information: "cow ID", "cow weight", "time stamp", "weight indication". Thus, the information on the server reports the weight of the individual cow at every access to the watering site.

Figure 15: Testing the platform on a dairy farm

4. Experimental tests

The developed platform for live weight monitoring and identification has been tested at a dairy farm with 86 head of cattle having age of 10-12 months, kept in one pen. Two platforms were integrated with the existing drinkers while establishing the necessary wireless communication networks (see Figure 15).

Since the width of the drinker significantly exceeds the width of the scales (1.5 meters versus 0.6 meters), additional fences were realized and installed (see Figure 16). Please note that the animals have access to water only through the weighing platform. In this

way, all the livestock in the pen was monitored during the experiment.
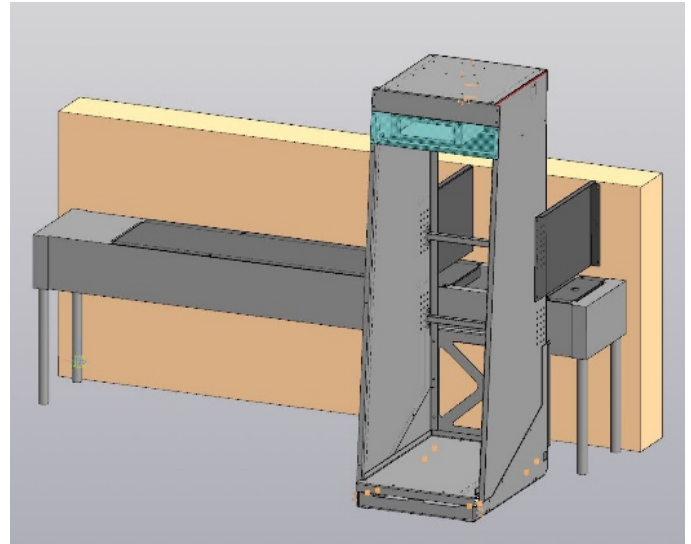
Figure 16: 3D model of the platform at the closed drinking bowl

5. Data processing on server

Once the platform is activated, a wireless communication channel is automatically established (via WiFi, LoRa, GSM/GPRS) and the collected data is sent to the server through an Internet connection at http://194.4.56.86/.

To acquire relevant information from the weighting installation, a REST API web service has been specifically developed. The data is structured in JSON format, as illustrated in the following example:

```
{
    AnimalNumber: "KZC154000000",
    Date: "2019-12-16T13:15:00",
    Weight: 332.5,
    ScalesModel: "Mambetov 2"
}
```

In the database, the information relevant to the weighting process is stored in the evt_Weighing table, whereas the BaseEvent table contains the general data concerning the individual event which is associated with the reg_Cow table (where the data related to the animals is reported).
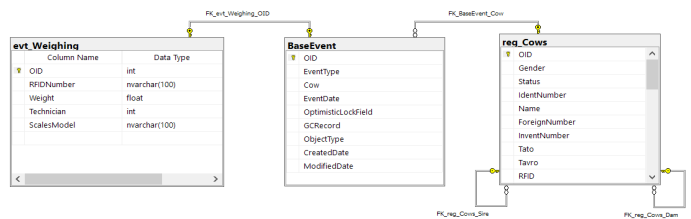
Figure 17: Weighing database structure on the server

In the central herd management system, the information is made available in tabular form as well as visually through diagrams as shown in Figure 18.

Figure 18: Data received from the platform and displayed on the server

6. Results

The pilot tests were initiated on August 8, 2019. Two platforms were used during these tests.

The data received from each animal has been combined into a single database. From 4 to 17 data packets are generated by each animal on a daily basis. Therefore, the total number of weight measurements per day could be in the range of 1000. Data processing will be discussed in a future work.

As an example, Table 1 shows the real-time weighing data relevant to an animal with ear tag ID 013716606d10, obtained on 2020-09-01 at 16:16:28, local time. The data is processed and stored in the memory of the single-board Raspberry Pi computer.

Table 1: Weight data relevant to the animal with ID 013716606d10

No	weight	No	weight	No	weight
1	193.70	36	205.81	71	204.53
2	203.56	37	205.81	72	204.43
3	208.06	38	205.81	73	204.82
4	202.77	39	205.81	74	204.29
5	204.20	40	205.81	75	204.25
6	203.58	41	205.81	76	205.33
7	205.35	42	205.81	77	204.49
8	203.54	43	205.81	78	204.09
9	202.40	44	207.37	79	202.98
10	205.18	45	206.35	80	203.14
11	204.44	46	208.26	81	204.06
12	203.59	47	204.93	82	204.02
13	204.12	48	204.12	83	203.46
14	203.61	49	204.50	84	203.97
15	204.89	50	203.83	85	203.25
16	204.70	51	202.09	86	204.08
17	204.59	52	202.98	87	203.16
18	204.56	53	204.28	88	202.97
19	204.34	54	204.54	89	203.02
20	204.09	55	203.75	90	202.14
21	203.42	56	204.18	91	201.40
22	204.28	57	203.96	92	201.38
23	204.29	58	203.85	93	190.72
24	203.18	59	203.75	94	204.86
25	205.81	60	204.23	95	210.68
26	205.81	61	203.15	96	208.17
27	205.81	62	204.08	97	196.08
28	205.81	63	203.63	98	199.45
29	205.81	64	204.01	99	198.73
30	205.81	65	203.61	100	196.61
31	205.81	66	203.54	101	198.40
32	205.81	67	203.71	102	186.53
33	205.81	68	204.80	103	131.85
34	205.81	69	204.68	104	15.25
35	205.81	70	204.88	105	

The average weight of 201.16 kg is reported on the server (see Figure 16).

Figure 19: Data on server relevant to ID 013716606d10 on 2020-09-01 at 16:16

It is worth noting that the median weight is 204.19 kg. The difference of 3 kg with respect to the average weight is caused by the presence of the value 15.25 kg in the weight data set. That is due to the fact that the weight reading occurred at the time when the animal was leaving the platform. To avoid such issue, changes have been made to the algorithm used for evaluation of the weight, so that the information relevant to the actual weight of the animals before starting the automatic weighting procedures is properly taken into account. This allows assessing not only the dynamics in weight changes, but also accurately displaying the weight of the animal. To this end, the data collected from the individual RFID tag on a daily basis is, also, properly averaged.

7. Conclusion

When comparing the developed platform with existing solutions available on the market, one can note that the proposed system is characterized by reduced costs and ease of installation to existing drinkers, both indoor and outdoor. The design has been optimized in such a way as to enable high reading quality at low power values. The use of LoRa protocol allows overcoming the lack of cellular communication networks in the field while enabling favorable energy savings.

The functionality of the presented platform is virtually unlimited in relation to the data collection. Thanks to the use of a single-board computer, it is possible to expand capabilities in terms of data storage and analytics within the platform, which may be relevant in conditions of poor communication. Components in the platform can be easily replaced without requiring changes to the design and control software. Furthermore, the system can be expanded with new types of sensors and actuators, improving its functionality in this way.

Thanks to the low energy consumption, the platform can be used in various animal grazing conditions. Another important feature is represented by the direct integration with the "Herd Management" software developed in the framework of this project.

In future works, statistical analysis and machine learning algorithms which are useful to determine the exact weight of the monitored animals will be illustrated.

Conflict of Interest

The authors declare no conflict of interest.

Acknowledgment

References

[1] Annual Report | Dairy Australia, Jan. 2021.

[2] Remote WOW Systems | Tru-Test Livestock Management, Jan. 2021.

[3] Our Platform: Agricultural Analytics – GrowSafe Systems®, Jan. 2021.

[4] A.S. Camiel Huisma, Animal management system, US6868804B1, 2003.

[5] BR102017006913A2 - automatic, voluntary weighing system comprising animal and apparatus monitoring and management system - Google Patents, Jan. 2021.

[6] Intergado Beef - Intergado, Jan. 2021.

[7] ISO - ISO/IEC 18000-6:2004 - Information technology — Radio frequency identification for item management — Part 6: Parameters for air interface communications at 860 MHz to 960 MHz, Jan. 2021.

[8] K.V.S. Rao, P. V. Nikitin, S.F. Lam, Antenna design for UHF RFID tags: A review and a practical application, IEEE Transactions on Antennas and Propagation, **53**(12), 3870–3876, 2005, doi:10.1109/TAP.2005.859919.

[9] C.C. Yen, A.E. Gutierrez, D. Veeramani, D. Van Der Weide, "Radar cross-section analysis of backscattering RFID tags," IEEE Antennas and Wireless Propagation Letters, **6**, 279–281, 2007, doi:10.1109/LAWP.2007.898552.

[10] K. Hongil, L. Bomson, "Meander line RFID tag at UHF band evaluated with radar cross sections," in Asia-Pacific Microwave Conference Proceedings, APMC, 2005, doi:10.1109/APMC.2005.1606882.

[11] K. Penttilä, L. Sydänheimo, M. Kivikoski, "Performance development of a high-speed automatic object identification using passive RFID technology," in Proceedings - IEEE International Conference on Robotics and Automation, Institute of Electrical and Electronics Engineers Inc.: 4864–4868, 2004, doi:10.1109/robot.2004.1302488.

[12] Y. Gao, Z. Zhang, H. Lu, H. Wang, "Analysis and calculation of read distance in passive backscatter RFID systems," in LISS 2012 - Proceedings of 2nd International Conference on Logistics, Informatics and Service Science, 905–912, 2013, doi:10.1007/978-3-642-32054-5_126.

[13] UHF high performance 9dbi circular antenna -RFID antenna-UHF panel antenna--Shenzhen Chafon Technology Co.,Ltd, Jan. 2021.

[14] A.B. Mirmanov, N.K. Nabiev, A.S. Alimbaev, K.M. Dostanova Experimental studies of the reading range of ear tags UHF RFID system [in Russia: Экспериментальные исследования дальности считывания ушных бирок UHF RFID системы]. Modern Science, 10-1, 434-438, 2020

Traffic Aggregation Techniques for Optimizing IoT Networks

Amin S. Ibrahim[1,2], Khaled Y Youssef[*,3], Mohamed Abouelatta[1]

[1]*Faculty of Engineering, Electronics and Electrical Communication, Ain Shams University (ASU), Cairo, 11757, Egypt*

[2]*Institute of Engineering, Electronics and Electrical Communications, Thebes Higher Institutes, Cairo, 11757, Egypt*

[3]*Faculty of Navigation Science and Space Technology, Beni-Suef University (BSU), Beni Suef, 62511, Egypt*

A R T I C L E   I N F O

A B S T R A C T

Internet of Things (IoT) is changing the world through a new wave of revolution for communications technologies that are no more limited to the human being. One of the main challenges that result from the exponential spread of IoT technology is the difference in the traffic characteristics between classical human communications and advanced things communications. The IoT traffic characteristics become essential for understanding and studying the parameters affecting the IoT traffic shape and thus all further studies related to traffic aggregation, topologies, and architecture designs. In this paper, a traffic aggregation in both the space domain and time domain is proposed whereas a matrix of traffic parameters is analyzed and simulated through building a practical lab case study to demonstrate the theoretical results. It is proven that the two proposed aggregation techniques could impact the traffic profile shaping existing IoT use cases for optimizing the network efficiency from several perspectives as 20% high throughput gain, 45% low collision probability, network congestion is limited to 800~1600 packets in the space domain and about 300~20 packets in the time domain, and overheads are minimized by about 50~27 Kbytes in the space domain and 9.5~0.59 Kbytes in the time domain.

1. Introduction

Internet of things is the fabric that enables the exchange of information between people, things, and processes which in turn leads to a growing data sphere and sophisticated traffic models as a result of diversified sources of data. The number of IoT devices is in an increasing exponential increase that is expected to reach 41.6 billion devices in 2025 with a corresponding data growth that is expected to reach 79.4 Zettabyte in 2025 within a compound annual growth rate of 28.7% over 2018 to 2025 [1]. The expected growth in adoption of IoT is attributed to several factors including:

- The diversity of industries that is perceiving the IoT as a key solution for their existing problems as healthcare, manufacturing, agriculture as well as smart communities and smart cities.
- The advances in network technologies could carry efficiently the IoT traffic. 5G network technologies are a good example.
- Presence of new cost-effective surveillance techniques as low cost embedded integrated cameras, drones technologies etc.

video surveillance data is expected to grow at a compound annual growth rate of 60% from 2018 to 2025.

Accordingly, traffic aggregation is becoming significant to shape the traffic generated by such a world of sensors and cameras efficiently. Traffic aggregation rules could be applied at different stages including sources, aggregators, routers, and gateways.

The data aggregation can accurately summarize and combine multiple stream data into one data chunk to reduce the number of packets to be sent in the large scale networks [2, 3].

In this paper, the main key IoT traffic challenges that are addressed by the aggregation techniques proposed are the massive number of terminal devices and a burst traffic profile of node with the massive amount of data transmissions (number of sent packets), Data volume (light or heavy), and payload size.

The paper contributed value is mainly in organizing the high network nodes (colocation) and the number of massive transmissions times (grooming time) using aggregation strategy as two main traffic aggregation techniques to shape and schedule

*Corresponding Author: Khaled Y. Youssef, khalid_youssif@yahoo.com

several IoT traffic profiles of the IoT smart city nodes for efficient IoT network.

A proposed model for IoT traffic data control includes the following;

- Traffic parametric analysis (space and time)
- Key factors affecting the traffic profile shaping
- IoT smart city architecture model for optimized traffic profile shaping
- Building real-time experiments (case study) based on the IoT smart city nodes before and after the two proposed aggregation techniques.

The smart city case study is analyzed with an associated lab setup for results measurements. In the lab work, the effect of several parameters (node-multiplex, time multiplex, data grooming…etc.) is studied against the traffic profiles. Traffic models are built as a function of those parameters and a traffic aggregation approach is proposed to model and shape the IoT traffic for efficient and reliable network operation. The experimental pilot shall consider single and multiple IoT devices against space and time multiplexing using a proposed colocation and grooming methodologies.

The paper is organized as follows: a literature review is presented in section 2. The proposed traffic aggregation techniques are discussed in section 3 followed by explaining the dimensions of network performance metrics in section 4. The experimental setup and the results are presented in section 5. The discussion and conclusion are discussed afterward.

2. Related Work

The previous works studied technologies related to two main traffic aggregation approaches in the IoT networks that are complemented by the following studies:

2.1. The node-based aggregation

Authors in [3] proposed hybrid Quality of Service-Aware Data Aggregation (QADA) scheme that is a combination between the data aggregation of the cluster nodes and the aggregation of the tree nodes to overcome the limitations in both existing tree and cluster aggregation processes in order to reduce the power consumption and increase the network lifetime. QADA architecture model of the 101 nodes are designed and simulated using NS2.35 network simulator, compared to the existing tree and cluster aggregation techniques to prove the concept.

Authors in [4] discussed the IoT traffic characteristics in the smart city use case. The authors proposed the smart city network architecture for collecting IoT traffic data of the smart city nodes of different scenarios as Logistics goods tracking, university campus, smart hospital, smart homes, mobile payment, Smart Shopping Centre, Intelligent Transport, and smart grid. They also collected the IoT traffic aggregation from different scenarios on one or many gateways for modeling the overall collected traffic using the Gamma-Modulated Wavelet model.

The Internet of Things Protocol (IoTP) is introduced in the IoT communication layer to aggregate data of the massive number of IoT devices into one aggregator in such IoT scenario model.

The protocol is programmed by using the P4 high-level language to be implemented on the switch aggregation that forwards the data aggregation into IoT gateway. The main findings in the IoTP are to improve the network efficiency, reduce the number of packets sent, total payload sent, control average aggregation delay, and average IoT device battery. However, the IoTP aggregation strategy is limited to handle 50 data blocks with a 200KB limit of the P4 register, also, to cover a very short-range communication technology as Bluetooth Low Energy (BLE) [5].

The authors in [6] grouped the sensors in the IoT network into different clusters using a fused resemblance matrix based on the sensor behavior as acoustic, light, and radio. The cluster-based data aggregation for IoT application is developed by multi-sensor data fusion workflow for obtaining the robust cluster that can provide an energy-efficient data aggregation over the IoT networks. However, the number of transmitted data packets is higher in the cluster-based aggregation than in other modalities.

The work in [7] proposed the dynamic aggregation approach based learning automata for the Routing Protocol for Low-power and Lossy-network (LA-RPL). The learning automata develops each node in the IoT hierarchical networks, including child nodes, parent nodes, and one Sink node to aggregate data on the parent nodes with the help of the Cooja emulator. The simulation results show that the LA-RPL routing algorithm outperforms other routing schemes (RPL, Adaptive RPL, Bounding Degree RPL, and Modified RPL) in terms of energy and the control overheads, average path length, average delay. Besides, the practice tests are implemented in this article to evaluate the drop packets, PDR, and aggregation percentage among the routing strategies.

The authors in [8] proposed the Cross-Layer Commit Protocol (CLCP) for data aggregation and its efforts for query-based search in the IoT smart city application. The NS2 simulator tests 50-nodes, deployed in the 600m×600m area and clustered into multiple groups to show an impact of CLCP based cluster head selection with or without aggregation on the network performance, compared to Energy Efficient Clustering Protocol (EECP) methods. It is noted that CLCP and EECP for data aggregation have the same actual residual energy values. However, the CLCP without aggregation outperforms other approaches in terms of the overheads and the throughput.

Compared to the Priority Queue Aggregation Scheduler (PQA) and Priority Queue Scheduler (PQ), the authors in [9] presented the Priority Frame aggregation (PFA) and the Priority Frame (PF) in the Wireless Body Area Network/ Wireless Area Network (WBAN/WLAN) healthcare system architecture. In the WBAN networks, a set of healthcare sensors are originated and deployed in the human body to be connected to the Personal Servers (PSs), which bridge with the WLAN Access Point (WLAN-AP) in the WLAN networks. The proposed PFA and PF schedulers perform scheduling of different data traffics, mapping between WBAN and WLAN, and data aggregation of WBAN sensors into WLAN frame. The PS device forwards it into the central server. The simulation results show that the two proposed PFA and PF schedulers outperform other techniques in terms of delay and throughput, and the dropped packets as the collision probability indicator.

2.2. The time-based aggregation

The authors in [10] presented the Aggregation Periodic Process (APP) to aggregate the periodic IoT data every sample time on the IoT gateway. The aggregated periodic IoT data characteristics are presented and compared to the Poisson Process (PP) to approximate the APP scheme by the PP scheme and then quantify an error between the periodic aggregation and Poisson aggregation.

In the previous study [11], the two statistical data aggregation schemes: the constant interval and constant number are analyzed and estimated to find the optimal aggregation parameters (optimal aggregation interval and the optimal aggregation number), which enable the aggregation model to minimize the mean total system time. But, the optimal aggregation results are suited for stationary arrival conditions.

Accordingly, the work-study in [12] proposed the adaptive aggregation number control based on the aggregation constant number scheme to minimize the latency for variation arrival rate conditions.

3. Proposed model

Despite the contributions of the related works aforementioned above, we explore the aggregation capabilities in the IoT smart city network for IoT traffic profile shaping on one side and optimizing the IoT network performance on the other side. The proposed traffic aggregation techniques can reap the benefits of the data aggregation approach in the WLAN network through the practical design methodology that had not been available yet.

As a key traffic shaping technique, two main IoT traffic multiplexing techniques are presented mainly (a) the space domain aggregation, and (b) the time domain aggregation. The two approaches play a significant role to shape the traffic profile to be optimum and efficient for carrier networks, compared to the present smart city networks. Accordingly, the composite traffic parameters shall include two main attributes, the space domain, and the time domain.

3.1. Space domain attribute

The space domain attribute or Colocation attribute indicates the number of the possible number of source nodes integrated into one hub node or more according to the network topology. Accordingly, the hub node could be modeled as a multiple-input (N) single (M) output node. In addition, the definition of the space domain attribute goes beyond the processing node down to the transducer level as the same source node could be connected to multiple transducer nodes for efficient operation. The number of transducer points (N) could be connected to one source node that in turn share with other numbers of nodes (M) a hub bandwidth. Thus, the N-sensor/M-node model is typed into Single-node type (N=M) and Multi-node type (N≠M, M=1) as seen in Figure 1. Like the previous works [3-9], the Single-node type collaborates the data traffic from M source nodes into the sink node. On the other hand, the Multi-node type can collect the data traffic from N sensors of the same source node into the sink node.
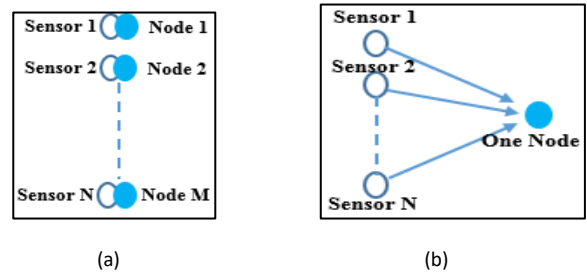
Figure 1: Colocation domain attribute (N sensor/M nodes model)
(a) Single node type(N=M), (b) Multi-node type (N≠M, M=1)

3.2. Time-domain attribute

As presented in the work [12], the time domain aggregation can aggregate data traffic every constant inter-arrival time from the Single-node/Multiple-node into the sink node to overcome the problem of the stationary arrival conditions in the related works [10, 11].

The time-domain attribute indicates the time aggregate of several data streams out of transducer level at the source node either aperiodic or periodic into one IoT output data stream including all protocols necessary to distinguish traffic from different sources and correlation of respective scenarios. In this paper, the term "grooming" will be used to describe the act of multiplexing to distinguish IoT traffic multiplexing concept against traditional multiplexing techniques. The concept is more towards aggregation buffering of data bytes sent at different random time slots into a periodic time slot with a minimal impact on the functional requirements of the applications.

It is assumed that n number of source nodes in the grooming process is asynchronous and homogenous. the grooming process is a random process at any instantaneous time t_i. Each source node sends multiplexed data packets uniformly every periodic inter-arrival time T_i. Let the source node i emits one message A_i every second. A unique message has a fixed-length L in bytes per node. For a constant sampling time duration, the data packets to be sent will be:

$$P_{K.i} = A_i L T_i \tag{1}$$

The grooming time T_G can be incremented by grooming index G to be multiple times as $T_G = GT_i$. Where G represents the grooming index or a multiplier factor that produces multiple numbers of inter-arrival times. The grooming function for a unique node (e.g. $i = 1$) becomes:

$$G_i(t) = \begin{cases} P_{K_{j.i}} & . \ t = t_i + jT_G \\ 0 & . \ otherwise \end{cases} \tag{2}$$

Where the K packets generated by a source node j times can be detected based on the experiment time $Texp$ and the waiting time as $(j = \frac{Texp}{T_G})$. The grooming function of n finite number of nodes in the network scenario seems to be an impulse signal (e.g. delta function), having $P_{K.j}$ amplitude and appears every T_G. It can be described as:

$$G(t) = \sum_{i=1}^{n} \sum_{j=0}^{J+1} P_{K_{j.i}} \delta(t - (t_i + jT_G)) \tag{3}$$

4. Network Performance Metrics

Network performance enhancement is one of the key objectives behind the traffic aggregation approaches. The techniques proposed in this paper targets an improvement in five main key performance indicators mainly:

4.1. Traffic volume

Traffic volume is the amount of data exchanged between a 2-dimensional traffic matrix of node pairs (traffic profile) in the IoT network. It can be measured by two main forms: the average data rate (Kbps) and packets data values (Kbits).

4.2. Throughput

The throughput is the amount of successful data delivered between two IoT source nodes over the wireless communication channel for a specified period, resulting in kilobits per second (Kbps) [13].

Recently, the throughput of the source $x(i)$ in the FAST TCP model is a source sending rate $\widehat{x_t^f}$ or $\widehat{x_t^b}$ multiplied by the forward packet size P_f as:

$$x_i = \begin{cases} \widehat{x_t^f} P_f & k_f < 1 \\ \widehat{x_t^b} P_f & k_f \geq 1 \end{cases} \tag{4}$$

Throughput is improved by high P_f when Asymmetry Factor (AF) k_f is greater than one. Where k_f represents a connection of asymmetric link between the two routers of a model. It is based mainly on asymmetry capacity ratio (ACR) and asymmetry packet ratio (APR) [14].

In the IoT technology, the asymmetry link has no effect on the wireless connectivity among IoT nodes in the same AP (router). the factor k_f is ignored. $\widehat{x_t^f}$ and $\widehat{x_t^b}$ of the forward and backward packets could be addressed into the sending rate R_i (packets/s) from one thing node (source/destination) to another one. Thus, the throughput can be derived from (4) as:

$$x_i = R_i P_i \tag{5}$$

while P_i is the packet size (bytes), excluded from the fixed overheads. Consequently, the throughput percentage is the ratio between the useful data packets to the total amount of data packets including overheads.

4.3. Collision probability

The number of collision packets to the total number of transmitted packets is the packet collision probability.

Recently, the collision of the IEEE802.11 standard occurs when multiple stations share the wireless channel to transmit data at the same time onto a receiver. The access technique caused more delay and packet data-flow degradation. In this technique, each node listens to the silence (idle) of the channel for the Distributed Coordination Function (DCF) Inter-Frame Space (DIFS) interval. The standard grants all $n-1$ nodes random backoff time $\overline{W}_{backoff}$ before the transmission or retransmission on the wireless radio channel. When DIFS time is released and the channel is not busy, the senders are ready to transmit data after variable backoff times. The randomization of this time led to an increase in the probability of packet collision, which is given as [15]:

$$P_{coll} = 1 - \left(1 - \frac{1}{W_{backoff}}\right)^{n-1} \tag{6}$$

The term $\frac{1}{W_{backoff}}$ describes the channel access probability. It is the probability that the station attempts to send data in arbitrary waiting time slots. By analogy, the same model could be applied on IoT networks including the parameters highlighted in the section above to be as follows:

$$P_{coll} = 1 - \left(1 - \frac{1}{GT_G}\right)^n \tag{7}$$

4.4. Network traffic congestion

With the increasing number of high data transmission rates in IoT use cases, Network congestion can arise from high request traffic in the network. The congestion control mechanisms have been discussed based on protocols and offloading approaches to avoid the buffer overflow in the IoT networks. In the protocol approach, congestion control mechanisms focus on the application layer and the network layer. Throughput and Packet Delivery Ratio (PDR) metrics are improved to reduce the number of lost packets caused by the congestion in the network layer. While throughput is aforementioned. PDR is the ratio of the total number of received packets in the destination (sink) node to the total number of sent packets in the source nodes [16,17].

On the other hand, the network traffic congestion could be evaluated by the number of sent packets by the source nodes in the IoT networks.

4.5. Control overheads

The control overheads are excess data or the control header behind the useful data in the packet format for a specific task. It is measured per bytes or Kilobytes.

5. Experimental Results Analysis

5.1. Experimental setup

An experimental lab is established to collect, analyze, and profile the traffic model based on practical smart city use cases. Based on the architecture highlighted in figure 2, the prototype built for proof of concept purpose is composed of:

- The sensor layer is designed to develop several scenarios related to smart city use cases from different perspectives as safety, security, energy, and environment. Table 1 shows the sensors used in an experimental study [18-20].

- The processing layer is based on the ESP micro-controller family including ESP 8266 MCU units and Wi-Fi 802.11b/g/n unit as a network interface module. ESP 8266 MCU unit is programmed to perform both the space domain aggregation and time-domain aggregation processes in the broker node. While the Wi-Fi unit enables the nodes to communicate with other nodes in the IoT network.

- The communication layer is architected according to the network diagram in figure 2, to enable different topologies to be configured and experimentally measured. Intermediate nodes are introduced to enable the traffic shaping and aggregation factors being applied as the broker node.
- The networking layer includes all network scenarios among IoT sensor nodes in the smart city architecture as physical security scenario, human safety scenario, energy scenario, device control and management scenario, and the environment scenario. Each scenario network has two or three connected IoT nodes with the TCP/IP connection protocol. The paper examines the human safety scenario nodes specifically scenario 3 (fire-node, smoke-node) and cloud scenario (fire-node and webserver) that is presented in the classical smart city networks [20].

Table 1: Sensor Layer Specifications [18-20]

Parameters	Sensor model	Measurement range
Natural Gas	MQ-5	(0-1000ppm)
Smoke	MQ-2	(0-10000ppm)
Fire	KY026	(20-100Cm),60°
CO	MQ7	(20-2000ppm)
Light detector	TSL2561	(0.1-40,000) Lux
Temperature	DHT22	(-40-125°C)
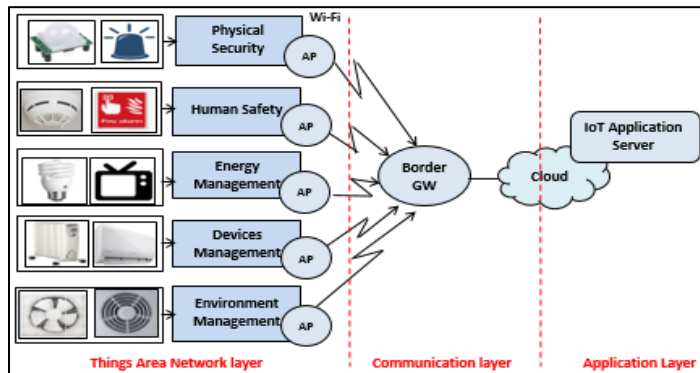
Figure 2: IoT architecture model designed for experimental work [20]
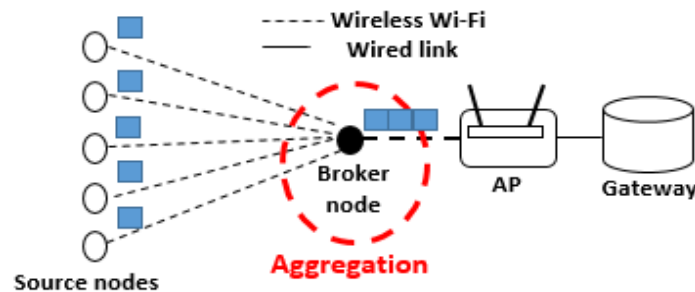
Figure 3: Proposed single-node scenario in the smart city networks
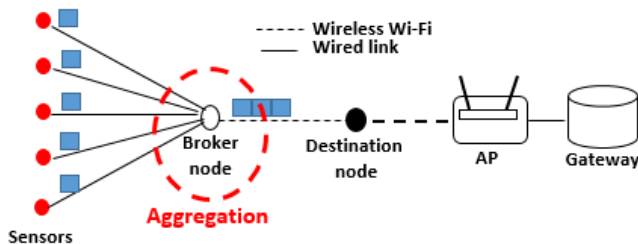
Figure 4: Proposed Multi-node scenario in the smart city networks
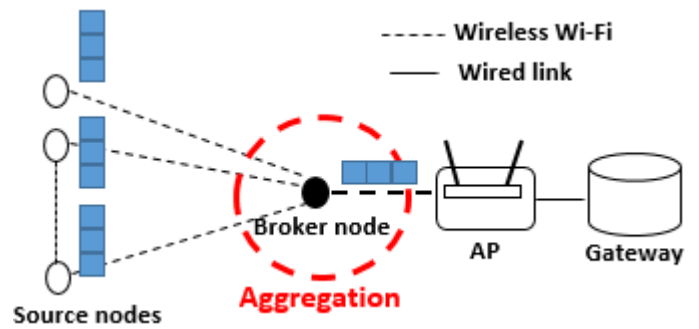
Figure 5: Proposed Time-domain scenario in the smart city networks

A set of experiments are designed to emulate the traffic patterns associated with each type of traffic aggregation either the space domain attribute or the time domain attribute, compared to that before (without) the aggregation process [20]. The experimental setup details are listed in table 2.

On the space domain side, a list of IoT nodes is operating on two models of operations as seen in figures 3 and 4. Figure 3 shows the network model of a Single-node type. While the Multi-node type is architected in figure 4.

In a Single-node experiment, 5-fire source nodes as senders can communicate with an individual smoke receiver node. Each fire-node comprises a fire-sensor subscribed to the processor node. After an initial step of one fire node connects to a unique smoke node, the number of fire nodes is incremented and the results are monitored on each step. As seen in figure 3, the smoke node is a broker that accumulates the traffic profile sent from each fire source node and then forwards it into the AP and the higher layers (gateway and internet). The Multi-node experiment follows the same methodology design of the Single-node experiment except for the five fire nodes of the Single-node type are replaced by five fire sensors that are connected directly to one processor node.

In the multi-node type, the unique fire source node can operate as a broker node, which accumulates traffic profiles of the connected fire-sensors into the traffic aggregation and send them to the destination smoke node.

The time-domain experiment is performed in both one source node experiment and N source nodes experiment as shown in figure 5. In one source node experiment, a single fire node is designed to store and buffer the sensed data and then send a multiplexed sensed data onto one smoke node as a broker node at grooming times T_G of about 1-16 minutes. Each T_G is incremented every 60 seconds. N-sensor nodes experiment is to establish five nodes of Single-node fire sensor and one smoke broker node to emulate the grooming pilot of N source nodes. The experiments are executed for a real-time experiment $Texp$ (960 seconds).

Table 2: Experimental setup details

Experimental parameters	Space-domain experiments	Time-domain experiments
P_i (bytes)	90-1548	
Header/packet (byte)	32	
T_G (minute)	N/A	1-16

Connection protocol	TCP/IP	
Wireless communication	Wi-Fi 802.11b/g/n	
N nodes/sensors	1-5 nodes	
Sensors type	Fire and Smoke	
$Texp$ (sec)	750	960

5.2. Results

Before the aggregation process, table 3 lists the limited key performance values of the fire-node in the classical smart city (scenario 3 and cloud scenario).

Table 3: Fire performance values in the classical scenario 3 network

	Throughput %	Overheads Kbytes	No. of sent packets	Traffic volume Kbits/Kbps
Sc. 3	62.65	85.00	2720	1934/2.01
Cloud	64.37	9.53	305	214/1.6

After the aggregation process, the measurement results of different experimental pilots are summarized into traffic profile results, and network performance metrics results.

In the space attribute, the role of the broker node is exploited as a method of traffic profile shaping for IoT networks. As shown in Figure 6, the Multi-node traffic profile is smoothed with low traffic volume (packets data values), compared to the Single-node type.

(a)   (b)
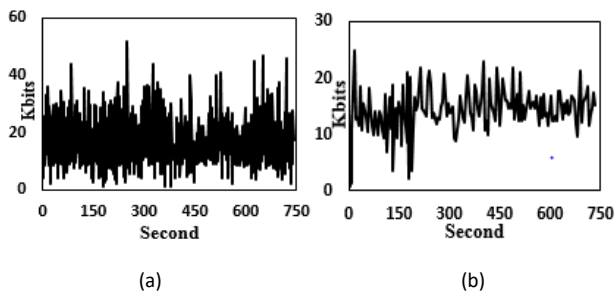
Figure 6: Traffic shaping of N-sensors M-nodes model
(a)   Five-sensors Five-nodes, (b) Five-sensors One-node

Generally, Figure 7 explains the difference of configuration on the space model. Figures 7.a shows the average data rate versus the low number of sensors/nodes for both types of the space domain attribute. An average data rate in the Single-node type begins to increase significantly with an increasing number of nodes. On the other side, the average data rate of the Multi-node type is approximately constant.

As shown in Figure 7.b, it is obvious that the number of sensors attached to the same node has a direct impact on the network throughput on an average of 0.1-0.2% on each additional sensor per node. The increase might not be a significant one however it is not the main target out of the space multiplex. While the Single-node type hasn't been impacted by the throughput.

Figure 8.a shows the relationship between the PDR and the low number of nodes in the Single-node type. The PDR decreases significantly with the increasing number of heavy traffic nodes. The PDR reduces from 99% in 1-node to 75% in 5-node whereas

the nodes send high traffic packets rates with an average of 13.8 packets/sec.

(a)   (b)
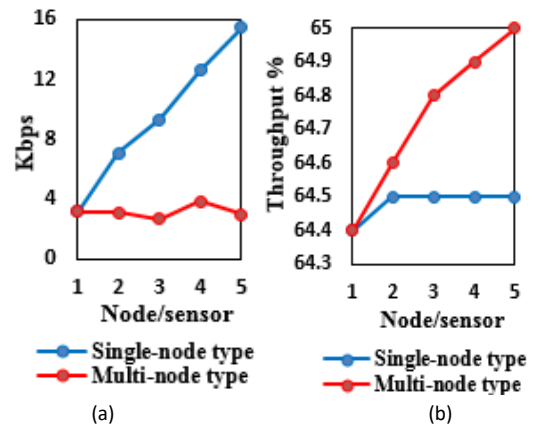
Figure 7: Space attribute (a) Average data rate, (b) Throughput

As shown in Figure 8.b, the number of packets sent by the node(s) increases with the increasing number of nodes in the Single-node type. On the other hand, the number of transmitted packets may decrease or remain constant in the Multi-node type.

(a)   (b)
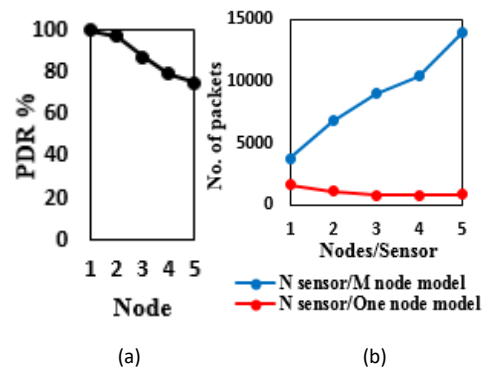
Figure 8: Network congestion in the Space domain attribute (a) PDR, (b) Number of sent packets

Figure 9 shows the relationship between the control overheads on one side and the number of aggregated nodes/sensors on the other side. It is noted that the data overheads begin to significantly increase from one source node to five sources in the Single-node type. On contrary, the control overheads seem to be constant with an increasing number of sensors attached to one-node in the Multi-node type.
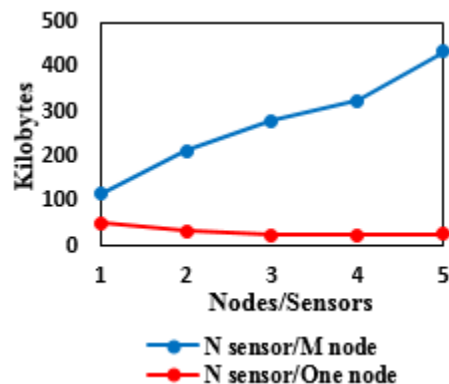
Figure 9: Control overheads in the space domain attribute

514

On the other hand, the time domain experimental results tested 16 levels of grooming index (i.e. multiplex of 16 channel of data streams on the same channel). The experiment shows a relationship between the grooming index G on one side, and the traffic profile on the other side from five experimental key observations: traffic volume, collision probability, throughput, network congestion, and BW overheads.

It is observed that the traffic volume (packets data values or average data values) increase as the grooming index increase as shown in Table 4. Figures 10 shows that the grooming time T_G between the two generated packets P_{K_i} and $P_{K_{i+1}}$ sent by a node i is highly impacted by the grooming factor G in a directly proportional relationship. Equation 8 describes the grooming traffic profile of Figure 10. The traffic volume is impacted by the data aggregation of one/multiple source nodes for G grooming times. The average data rate is reduced from 0.175 Kbps at G=2 to 0.164Kpbs at G=8. Similarly, the packet data size data rate is reduced from 168.8 Kbits at G=2 to 164.5 Kbits at G=8.

(a)　　　　　　　　(b)
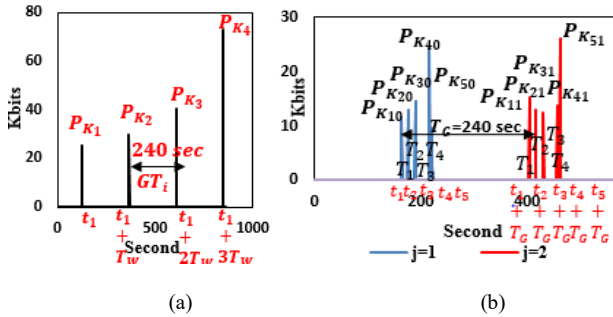
Figure 10: Time-domain attribute for 4-level grooming index
(a) One fire node experiment, (b) Five fire node experiment

The collision probability in the grooming attribute results is affected by two main enablers: the number of nodes and grooming guard periods as depicted in (6). As shown in Figure 11.a, the collision probability increase as the grooming index increase, whereas the graph shows an exponential growth of collision probability versus the number of nodes for the first 400 nodes for grooming index G=2, while the same growth to lower values of collision probability from grooming index G=8 which in turn explains the high impact of grooming index of collision probability especially for a big volume of nodes that characterize IoT and WSN technologies.

The graph in Figure 11.b shows that the grooming index G has a considerable impact on throughput as it increases the throughput value from 72.8% at G=1 to 91.2% at G= 8 which indicates the 18.4 % gain in throughput value followed by a small growth rate at G>10. It is obvious that the throughput increase from 91.2 % to 92.6% as G increases from G=8 to G=16. It is noted that an effective impact of the throughput is for G less than or equal to 8.

For 5-fire source nodes in Figure 12.a, it is obvious that the PDR increases with a high G grooming index whereas, PDR is 43% at G=1 until reaches 74% at G=8. As shown in figure 12.b, it is noticed that the number of sent packets decreases for long grooming times.

Consequentially, it is obvious that BW overheads (Kilobytes) exponentially decrease with the increasing number of G grooming index as seen in Figure 13.

(a)　　　　　　　　(b)
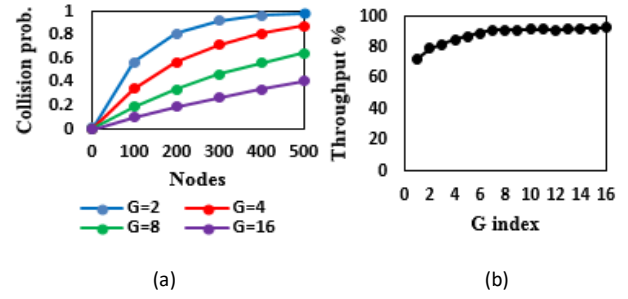
Figure 11: Time-domain attribute (a) Collision probability, (b) Throughput

$$G(t) = \ P_{K_{10}}\delta(t - t_1) + P_{K_{13}}\delta\big(t - (t_1 + T_G)\big) + \cdots P_{K_{50}}\delta\big(t - (t_5 + 2T_G) + P_{K_{53}}\delta\big(t - (t_5 + 3T_G)\big) \quad (8)$$

(a)　　　　　　　　(b)
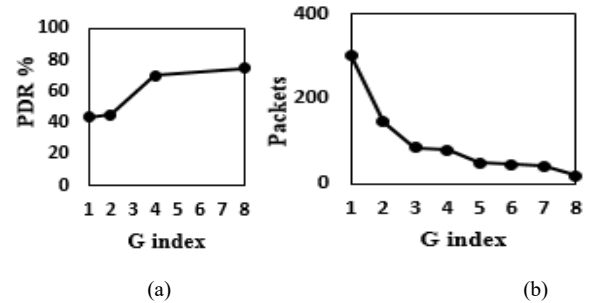
Figure 12: Time-domain attribute (a) PDR, (b) Network congestion
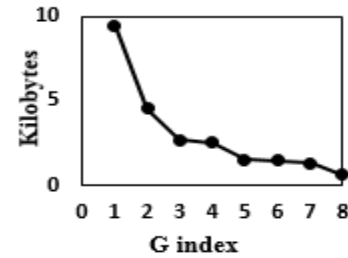
Figure 13: Control overheads in the time domain attribute

Table 4: Time-domain attribute results

Grooming index G	Packets data values (Kbits)				Average data rate
	P_{K_1}	P_{K_2}	P_{K_3}	P_{K_4}	
4 (240 sec)	25.45	29.52	40.64	72.75	0.175 Kbps
8 (480 sec)	85.0	79.3	---	---	0.164 Kbps

6. Discussion

Table 5 discusses the impact degree or an improvement gain of the two traffic aggregation techniques on the IoT network efficiency, compared to the classical smart city network before aggregation as:

6.1. Space domain attribute

In contrast to the existing aggregation techniques [3-9], it is noted that the traffic profile is shaped severely by applying the N

sensor /M node model as shown in Figure 6 as a result of the new architecture which in turn has a direct impact on the IoT network key performance indicators:

In the traffic volume, minimizing the number of processing to one is verified through the constant average data rate. It can maintain the average data rate by about 4Kbps with an increasing number of sensors in the Multi-node type as in Figure 7.a. While the average data rate is significantly increased by about 4~16 Kbps with an increasing number of nodes in the single nod type. Thus, the traffic data volume of the multi-node type is lower than that in the single-node type.

As listed in table 5, the traffic data volume (average data rate, data size) of the fie-node, resulting from the space domain

attribute is higher than that in the classical smart city scenarios (scenario 3 and cloud) before the aggregation process. The average data rate increases from 2.01Kbps and 1.6 Kbps in the classical

smart city scenarios (scenario-3 and cloud) to 3.2 ~2.9 Kbps and 3.2 ~15.4 Kbps in the multi-node type and single-node type, respectively. In the same manner, the amount of data size increases from 1934 Kbits and 214 Kbits in the classical smart city scenarios into 2285.5~2126.8 Kbits and 2285.5~11125.2 Kbits in the multi-node type and single-node type, respectively.

In the throughput, the impact of node aggregation architecture on network performance becomes very clear in Figure 7.b that shows a significant impact on throughput as a result of aggregating several sensors on the same node. The result is attributed to the network metadata added to the traffic header on each transmission. In the same case of n-sensors on the same node, the broker shall use the header once. As a result, the throughput gain per sensor is about 0.2% for 5 sensor case that is scaled up to a total 20% throughput improvement for a 100 sensor real case aggregated on one broker. Thus, throughput in the multi-node type is higher than that in the classical smart city scenarios by about 20% improvement gain for large scale networks (100-IoT nodes) as depicted in table 5. However, the single-node type is approximately the same as in the classical smart city scenario nodes.

High throughput and constant average data rate in the Multi-node type reduces network traffic congestion. On contrary, the low network congestion in the Single-node type is caused due to the low throughput and PDR values as in Figures (7.b, 8.a).

From the number of sent packets perspectives, the Multi-node type maintains the minimum number of packets by about 800 ~1600 packets for a low incremented number of sensors rather than the single-node type that has a significantly increasing number of sent packets for 5-source nodes by about 3700~13900. The number of sent packets is reduced from 2720 packets in the classical smart city network (scenario3) to 800~1600 packets in the multi-node type with an improvement gain of about 22% as depicted in table 5. Otherwise, both single-node type and multi-node type in the space domain attribute do not affect the number of sent packets in the classical cloud scenario.

From the overheads perspectives, it is remarked that overheads in the Multi-node type are lower than that in the Single node type as depicted in Figure 9 and Table 5. The control overheads in the proposed Multi-node type is reduced from 50 Kbytes in one-sensor to 27 Kbytes in five-sensors. The overheads in the multi-node type are less than that in both scenario 3 and the cloud scenario of the classical smart city networks with an improvement gain of 300% and 30% compared to scenario 3 and the cloud scenario.

6.2. Time-domain attribute

Rather than the previous time aggregation techniques [11-13], the traffic profile shaping concept is verified and proved in the time domain aggregation as shown in Figure 10. As the G number of grooming times increased, the collected data information to be sent will increase, and vice versa. the traffic profile of one/multiple nodes is shaped into a delta function. Its mathematical formula in (8) meets a theoretical time-domain concept in (3).

While the previous time aggregation techniques reduce an error and the latency [11-13], the main findings in this article are to improve the IoT network performance as follows:

Table 5: The improvement gain of the proposed techniques, compared to the classical system

Performance metrics in the IoT Smart city networks			IoT Network key performance indicators					
			Throughput (%)	Collision Probability (%)	Traffic volume		No. of sent packets	Overheads (Kbytes)
					Average data rate (Kbps)	Data size (Kbits)		
Proposed Techniques	Space domain attribute	Single-node type	64~65	N/A	3.2 ~15.4	2285.5~11125.2	3700~13900	116~434.75
		Multi-node type	64~84/ 100-nodes	N/A	3.2 ~2.9	2285.5~2126.8	800~1600	50~27
	Time domain attribute		72.8~ 93	95~50	0.175~0.164	168.8~164.5	300~20	9.5~ 0.59
Classical smart city Before aggregation	Human safety network (scenario3)		62.65	99.9	2.01	1934	2720	85
	Cloud scenario		64.37	99.5	1.6	214	303	9.3

The time-domain attribute reduces the traffic data volume whether the average data rate and data size from G=2 to G=8. The traffic volume in the time-domain attribute is less than or equal to that in the classical smart city scenarios. The time-domain attribute reduces the average data rate from 2.01Kpbs in the classical smart city scenarios (scenario 3) to 0.175~0.164Kbps. Similarly, it reduces the amount of data size from the 1934 Kbits and the 214Kbits in the classical smart city (scenario 3 and cloud scenario) to 168.8~164.5 Kbits. While the average data rate of the time-domain attribute (1.6Kbps) is moderated with that in the cloud scenario of the classical smart city.

The collision probability is reduced from 95% at G=2 to 50 % at G=8 for a dense number of nodes (400 nodes) in the non-real-time IoT applications. For the large scale networks with 400-nodes, the collision probability is mitigated by about 95~50 % with at least 45% improvement gain, compared to that in both classical smart city scenarios before aggregation (up to 99%). Thus, the proposed time-domain technique enables the dense number of nodes in IoT smart city networks to avoid the collision.

The percentage of the throughput in the time aggregation is raised by about 20% gain whereas this approach develops high throughput, gained from 72.8% at G=1 to 93% at G=10 as in Figure 11.a. It is noted that the throughput of 72.8~93% in the time-domain attribute outperforms the throughput of 62.65% and 64.37% in the classical smart city scenarios with an improvement gain of about 30%.

The number of transmitted packets in the time aggregation is reduced from 300 packets at G=1 to 20 packets at G=8. Also, throughput in Figure 10.b and PDR in figure 12.a are improved to avoid network traffic congestion in this technique. It is remarked that the number of sent packets is minimized from 2720 packets and 303 packets in both classical smart city scenarios (scenario3 and cloud) to about 303~20 packets based on G grooming times. The overheads are mitigated by a minimization factor of 9 at G =2 and 15 at G=8, compared to the overheads in scenario-3 and the cloud scenario.

The excess overheads are reduced from 9.5KB at G=1 until 0.59 KB at G=8 as shown in figure 13. The overheads are minimized from 85Kbytes and 9.3Kbytes in scenario 3 and the cloud scenarios of the classical IoT smart city to about 9.5~0.59Kbytes in the time domain attribute with an improvement gain that exceeds up to 150% at G=8 than overheads in scenario 3 and a minimization factor of about 90 at G=2 in the cloud scenario.

7. Future work

Our practical experiments (testbed lab) are established from 5-fire sensors, one-smoke-node, and 6-ESP 8266 MCU units as a case study in the IoT smart city networks to prove the concept. Our experimental setup could be extended to be applied for large-scale smart city networks and other IoT use cases in the future.

8. Conclusion

The two traffic aggregation techniques (space domain and time domain) have been proposed in this article to address the challenges of IoT traffic characteristics in the smart city networks as dense number of nodes, the massive number of transmissions,

Data volume (light or heavy), and the payload size. Compared to the classical smart city networks, the methodology design of the proposed work highlights shaping the individual traffic profiles in the classical smart city into the traffic aggregation of N source sensors/nodes via the space domain attribute and the traffic aggregation for G grooming times (delay) via the time-domain attribute for IoT traffic data control, thus optimizing the IoT network performance in the smart city use case from the five main perspectives (traffic volume, throughput, collision probability, network congestion, and the control overheads). The practical experimental lab model is built as one of several smart city networks (scenarios) before and after the proposed aggregation techniques to prove the concept. It is verified that the two proposed aggregation techniques have a better improvement gain than the existing smart city networks (without aggregation).

Last but not least, the practical study works focus on the smart city models, but the results could be extended to other non-real-time IoT use cases as smart metering, telemetry, and surveillance.

Conflict of Interest

The authors declare no conflict of interest.

References

[1] Https://www.idc.com/getdoc.jsp?containerId=prUS45213219 last accessed September 2019.

[2] E. Fitzgerald, M. Pióro, A. Tomaszewski, "Energy-Optimal Data Aggregation and Dissemination for the Internet of Things," IEEE Internet of Things Journal, **5**(2), 2018, doi: 10.1109/JIOT.2018.2803792.

[3] H. Rahman , N. Ahmed, M.I. Hussain, "A hybrid data aggregation scheme for provisioning Quality of Service (QoS) in Internet of Things (IoT)," Cloudification of the Internet of Things (CIoT), 2016, doi: 10.1109/CIOT.2016.7872917.

[4] Y. Li, Y. Huang, X. Su, J. Riekki, H. Flores, C. Sun, H. Wei, H. Wang, L. Han, "Gamma-modulated wavelet model for internet of things traffic," IEEE International Conference (ICC), SAC Symposium Internet of Things Track, 2017, doi: 10.1109/ICC.2017.7996506.

[5] A.L.R. Madureira, F.R.C. Araújo, L. N. Sampaio, "On supporting IoT data aggregation through programmable data planes," Computer Networks, **177**, 2020, doi: 10.1016/j.comnet.2020.107330.

[6] S. Redhu, R.M. Hegde, "Multi-Sensor Data Fusion for Cluster-based Data Aggregation in IoT Applications," IEEE International Conference on Advanced Networks and Telecommunications Systems (ANTS), 2020, doi: 10.1109/ANTS47819.2019.9117970.

[7] M. H. Homaei, E. Salwana, S. Shamshirband, "An Enhanced Distributed Data Aggregation Method in the Internet of Things," MDPI Sensors, **19**(3173), 2019, doi: 10.1109/ANTS47819.2019.9117970.

[8] A. Alkhamisi, M.S. Haja, S.M. Buhari, "A Cross-Layer Framework for Sensor Data Aggregation for IoT Applications in Smart Cities," 2016 IEEE International Smart Cities Conference (ISC2), 2016, doi: 10.1109/ISC2.2016.7580853.

[9] N. Bradai, L.C. Fourati, L. Kamoun, "WBAN data scheduling and aggregation under WBAN/WLAN healthcare network," Journal of Ad Hoc Networks, **25**, 251–262, 2015, doi:10.1016/j.adhoc.2014.10.017.

[10] T. Hoßfeld, F. Metzger, P. E. Heegaard, "Traffic modeling for aggregated periodic IoT data," 21st IEEE Conference on Innovation in Clouds, Internet and Networks and Workshops (ICIN), 2018, doi: 10.1109/ICIN.2018.8401624.

[11] H. Yoshino, K. Ota, T. Hiraguri, "Queueing delay analysis and optimization of statistical data aggregation and transmission systems," IEICE Transactions Communication, **E101-B**(10), 2186–2195, 2018, doi: 10.1587/transcom.2018EBP3010.

[12] H. Yoshino, K. Ota, T. Hiraguri, "Adaptive Control of Statistical Data Aggregation to Minimize Latency in IoT Gateway," 2018 Global Information Infrastructure and Networking Symposium (GIIS), 2018, doi: 10.1109/GIIS.2018.8635712.

[13] J.D.C. Silva, P.H.M. Pereira, L.L. De-Souza, C.N.M. Marins, G.A.B.

Marcondes, J.J.P.C. Rodrigues, "Performance Evaluation of IoT Network Management Platforms," IEEE International Conference on Advances in Computing, Communications and Informatics (ICACCI), 259–265, 2018, doi: 10.1109/ICACCI.2018.8554364.

[14] F. Ge, L. Tan, M. Zukerman, "Throughput of FAST TCP in Asymmetric Network," IEEE Communication Letter, **12**(2), 158–160, 2008, doi: 10.1109/LCOMM.2008.071623.

[15] A. Rizal, Y. Bandung, "Passive Available Bandwidth Estimation Based on Collision Probability and Node State Synchronization in Wireless Networks," ITB Journal Publisher, J. ICT Res. Appl., **11**(2), 131–150, 2017, doi: 10.5614/itbj.ict.res.appl.2017.11.2.2.

[16] A. Maheshwari, R.K. Yadav, "Analysis of Congestion Control Mechanism for IoT," IEEE Cloud Computing, Data Science & Engineering Conference, 288–293, 2020, doi: 10.1109/Confluence47617.2020.9058058.

[17] H.A.A. Al-Kashoash, Y. Al-Nidawi, A. H.Kemp, "Congestion-Aware RPL for 6LoWPAN Networks," IEEE Wireless Telecommunications Symposium (WTS), 2016, doi: 10.1109/WTS.2016.7482026.

[18] H. Verma , M. Jain , K. Goel , A. Vikram , G. Verma, "Smart home system based on Internet of Things," 2016 3rd International Conference on Computing for Sustainable Global Development, 2016.

[19] B. Sarwar, I.S. Bajwa, N. Jamil, S. Ramzan, N. Sarwar, "An Intelligent Fire Warning Application Using IoT and an Adaptive Neuro-Fuzzy Inference System," MDPI Sensors, **19**(14), 2019, doi: 10.3390/s19143150.

[20] A.S. Ibrahim, K.Y. Youssef, H. Kamel, M. Abouelatta, "On Traffic Modelling of IoT Smart City Use Case," IET Communication journal, **14**(8), 1275–1284, 2020, doi: 10.1049/iet-com.2019.1252.

Bounded Floating Point: Identifying and Revealing Floating-Point Error

Alan A. Jorgensen[1], Las Vegas[1], Connie R. Masters[1,*], Ratan K. Guha[2], Andrew C. Masters[1]

[1]True North Floating Point, Las Vegas, NV, 89122, USA

[2]University of Southern Florida, Dept. of CS, Orlando, FL, 32816 USA

A R T I C L E I N F O	A B S T R A C T
	This paper presents a new floating-point technology: Bounded Floating Point (BFP) that constrains inexact floating-point values by adding a new field to the standard floating point data structure. This BFP extension to standard floating point identifies the number of significant bits of the representation of an infinitely accurate real value, which standard floating point cannot. The infinitely accurate real value of the calculated result is bounded between a lower bound and an upper bound. Presented herein are multiple demonstrations of the BFP software model, which identifies the number of significant bits remaining after a calculation and displays only the number of significant decimal digits. These show that BFP can be used to pinpoint failure points. This paper analyzes the thin triangle area algorithm presented by Kahan and compares it to an earlier algorithm by Heron. BFP is also used to demonstrate zero detection and to correctly identify an otherwise unstable matrix.

1. Introduction

Standard floating point has been useful over the years, but unknowable error is inherent in the standard system. Though not indicated in standard floating point, a calculated result may have an insufficient number of significant bits. This paper, which is an extension of work originally presented in [1], uses a bounded floating-point (BFP) software model that emulates the BFP hardware implementation to identify the accurate significant bits of a calculated result, thus unmasking standard floating-point error.

2. Background – Standard Floating Point

2.1. Standard Floating-Point Format

Computer memory is limited; thus, real numbers must be represented in a finite number of bits. The need to represent a range of real numbers within a limited number of bits and to perform arithmetic operations on those real numbers, led to the early development of, and use of, floating-point arithmetic. The formulaic representation employed is reminiscent of scientific notation with a sign, an exponent, and a fraction [2]. Through the efforts of William Morton Kahan and others, a standard for floating point was published in 1985 by the Institute of Electrical and Electronics Engineers (IEEE) [3]. The current version is IEEE 754-2019 - IEEE Standard for Floating-Point Arithmetic [4], which has content identical to the international standard ISO/IEC 60559:2020 [5].

The standard floating-point format is shown in Figure 1. The sign of the value is represented by a single bit, S. The offset exponent is E with a length of e. The significand, T, has a length of t. The overall length of the representation is k.
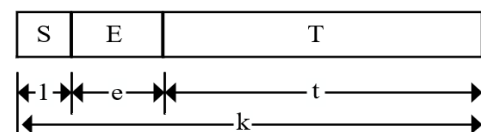
Figure 1: Standard Floating-Point Format

The IEEE 754-2019 standard defines floating-point formats and methods for both base two and base ten. However, this work only addresses base two floating point. The formats most commonly used require 32 bits or 64 bits of storage, which are known as single precision and double precision, respectively.

The decimal equivalent of the standard representation is shown in (1), where S, T, t, and E are defined above and O is the exponent offset. For binary floating point, O is nominally $2^{e-1}-1$.

$$(-1)^S \cdot (1+T/2^t) \cdot 2^{E-O} \tag{1}$$

The expression (1) is used in expressing the value of the standard floating-point representation in various number bases, typically for the display of the value in number base ten.

519

2.2. Standard Floating-Point Representation Error

Floating-point error is the difference between the representation of the actual standard floating-point value and the infinitely accurate real value to be represented. It must be clearly stated that the IEEE floating point standard does <u>not</u> specify any mechnism for indicating nor defining floating-point error. Floating-point error is invisible to implementations of the IEEE floating-point standard.

Standard floating-point error occurs because only a limited number of real numbers can be expressed with the finite number of bits available.

Because binary floating point represents real numbers with a fixed number of bits, numbers that cannot be represented with a limited set of powers of two cannot be represented exactly [6]. As Goldberg succinctly describes it, "Squeezing infinitely many real numbers into a finite number of bits requires an approximate representation" [7]. Therefore, there are a finite number of values that can be represented with floating point, but an uncountably infinite number of values [8] that cannot be exactly represented with floating point. For instance, the values 0.1, 0.22, and transcendental values, such as π, cannot be accurately represented with binary standard floating point, but the values 0.5, 0.125. and 942.625 can be exactly represented with standard binary floating point. Thus, only those real numbers which can be represented with a constrained sum of the powers of two can be represented with no error. All other representations must have error.

Therefore, we can define floating-point representation error as the difference between the representation value, see (1), and the infinitely accurate real value represented.

2.3. Standard Floating-Point Operational Error

Accuracy in floating-point computations may be measured or described in terms of ulps, which is an acronym for "units in the last place." Kahan originated the term in 1960, and others have presented refined definitions [9], [7]. An ulp is expressed as a real function of the real value represented. Rounding to the nearest value, for instance, can introduce an additional error of no more than ±0.5 ulp.

The real solution to the floating-point error issue is knowing the number of significant bits of a computational result. The number of significant bits can be known by using BFP. When BFP identifies sufficient significant bits, a decision may be made, or an opinion may be formed.

Usually, the error of a single computation is insignificant, with the exception being catastrophic cancellation error. However, with large, complex floating-point computations, error can accumulate and can reduce the significant bits to an unacceptable level [10], [11]. Loss of significant bits may be propagated through recursive repetition. BFP tracks the current number of significant bits through recursion [12], [13]. Examples of such recursive calculations are spatial modeling of explosions [14], dynamic internal stress [15], weather [16], etc.

The repetition of such calculations accumulates floating-point error. Unfortunately, there are two types of error, rounding and cancellation, and these errors are incompatible since rounding error is linear and cancellation is exponential. However, just as apples and oranges cannot be added by species, they can be added by the "genus" fruit. In order to accumulate cancellation and rounding errors we must find a similar "genus" before such error can be accumulated. This genus in the BFP system is the logarithm of the accumulated error stored in the defective bits field D (Figure 3), which captures both the accumulated rounding error and cancellation error.

Three operations that must be performed during floating-point operations introduce error. These operations are the following: alignment, normalization (causing cancellation error), and truncation (leading to rounding error).

Alignment occurs during add operations (which include both positive and negative numbers) when one exponent is smaller than the other and the significand must be shifted until the exponents are equal or "aligned" [17].

Cancellation error occurs because the resulting significand after a subtraction, including the hidden bit, must lie between 1.0 and 2.0. If the operands of a subtract have similar values, significant bits of the result may be defective, or "cancelled" [2], [18]. This is called cancellation error, and when that error is significant it is called "catastrophic cancellation" [7]. Jorgensen mathematically defines "similar values" [6].

Rounding error occurs because nearly all floating-point operations develop more bits than can be represented within the floating-point format, and the additional bits must be discarded [4]. The floating-point standard describes how these discarded bits can be used to "round" the resulting value but necessarily must introduce error into the resulting representation of the real value [2].

Standard floating point provides no means of indicating that a result has accumulated error [4]. Therefore, such errors are invisible unless they cause a catastrophe. Even then the cause can only be traced to floating-point failure with substantial effort, as stated by Kahan in the conference article entitled "Desperately needed remedies for the undebuggability of large floating-point computations in science and engineering" [19].

Misuse of floating point and the accumulation of floating-point error has been expensive in terms of election outcomes [20], financial disruption [21], [22], and even lives lost [23].

This computational weakness has been known since the early days of computing and continues until today. Even as early as 1948 Lubken had noted that: "…it is necessary at some intermediate stage to provide much greater precision because of large loss of relative accuracy during the process of computation" [10]. To this day, floating-point error is a known problem. [13], [24], [11].

3. Background – Bounded Floating Point (BFP)

The BFP system is an extension or annex to the standard floating point format, which may be implemented in hardware, software, or a combination of the two. BFP calculates and saves the range of error associated with a standard floating-point value, thus retaining and calculating the number of significant bits [25], [26]. BFP does not minimize the floating-point error but identifies the error inherent within standard floating point.

BFP extends the standard floating-point representation by adding an error information field identified as the "bound" field B. The bound field B contains subfields to retain error information provided by prior operations on the represented value, but the field of primary importance is the "Defective Bits" field D. This field identifies the number of bits in the represented value that are no longer of significance, consequently defining the number of bits in the result that are significant. The value of D is not an estimate but rather is calculated directly from standard floating-point internals such as normalization leading zeros and alignment of exponent differences. (See Appendix). BFP identifies and reports floating-point error and has no direct means of reducing that error. Because it is a direct calculation, the bound is neither optimistic nor pessimistic. However, the conversion between binary significant bits and decimal significant digits is not one-to-one and introduces a small error of less than 1 decimal ulp on conversion.

BFP retains the exception features of standard floating point, such as detection of infinity, operations with not a number (NaN), overflow, underflow, and division by zero. Though zero is a special case in the standard, the standard does not detect zero as long as any bits remain in the significand. However, BFP exactly identifies zero when the *significant* remaining bits in the significand are all zero, as shown in the test results below.

3.1. Bounded Floating-Point (BFP) Format

The bound field B, as seen in Figures 2 and 3, is a field added, to the format of standard floating point to describe the bounds of the error of the represented value. The bound field B contains and propagates information about the accuracy of the value that is being represented by creating and maintaining a range in which the infinitely accurate value represented must reside.

S	E	T	B
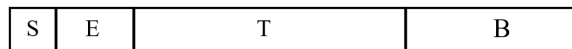
Figure 2: BFP Format

3.2. Bound Field Specifics

Figure 3 presents the subdivisions incorporated into the bound field format.
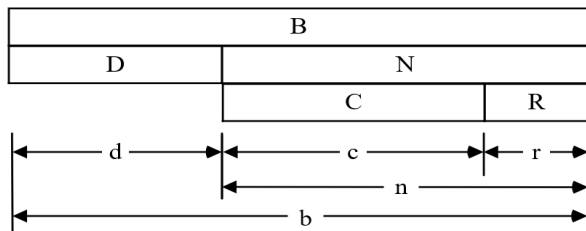
Figure 3: Format of Bound Field and Subfields

The bound field B is of width b. The bound field B consists of two fields, the defective bits field D of length d and the accumulated rounding error field N of length n. The value of the defective bits is the number of bits of the representation that are not significant, that have no value. The defective bits field D stores the logarithm of the upper bound of the error represented in units in the last place (ulps) and, in effect, determines the number of significant bits of the result.

The accumulated rounding error, stored in the N field, is the sum of the rounding error in fractions of an ulp.

The accumulated rounding error field N consists of two fields, the rounding error count field C, of width c, and the rounding bits field R, of width r. The fraction of an ulp represented in the accumulated rounding error is $R/2^r$ ulp.

The decimal equivalent of the BFP representation is shown in the expression of (2), which is equivalent to the expression (1) above.

$$(-1)^S \cdot ((T+2^t)/2^t) \cdot 2^{E-O} \tag{2}$$

The IEEE standard [4] defines "precision" as the capacity of the significand plus one (for the hidden bit). This capacity-type precision is defined as the maximum number "of significant digits that can be represented in a format, or the number of digits to that (sic) a result is rounded" [4]. In contrast, BFP identifies the actual number of bits that are significant (have meaning). These significant bits (SB) are a subset of the IEEE precision, p. The BFP's defective bits field D represents the number of bits of the representation that are *not* significant, where D = t + 1 − SB. In IEEE standard representation, the value of D is not known, nor is the number of significant bits.

BFP provides a means of specifying the number of significant bits required in a BFP calculation. Additionally, when there are fewer significant bits than specified or required, BFP represents this condition with the quiet not-a-number representation, "qNaN.sig," indicating excessive loss of significance.

3.3. Alignment

For addition and subtraction, when the exponents of the two operands are unequal, the significand of the smaller operand must be right shifted by the exponent difference. This is known as alignment [2], [17], [27], [28].

To perform alignment, the significand of the operand with the smallest value is right shifted by the exponent difference [26].

In standard floating point, the bits that cannot fit within the space of the standard floating-point format are used to determine the guard bit, the rounding bit, and the sticky bit.

In BFP, the bits that cannot fit within the space of the BFP format are used to calculate the accumulated rounding error field N.

The bits that cannot fit within the space of the BFP format due to alignment shift are retained in the R_{PN} field and X_{PN} field of the post normalization result configuration of Figure 4. As in standard floating-point format, if alignment shifts one or more bits out of the range of the arithmetic unit, the sticky bit is set to one.

3.4. Dominant Bound

The results of BFP binary functions (functions with two operands) retain only the number of significant bits as the aligned operand with the least number of significant bits. For BFP this means the result having the larger number of defective bits.

For binary functions the dominant bound is selected from the larger of the largest operand bound or the adjusted (aligned) bound of the smallest operand. For add (and subtract) operations, the binary point of the smaller operand must be aligned by the exponent difference [26]. The adjusted bound of the smallest

operand is derived by subtracting the exponent difference from the smallest operand bound defective bits and shifting the significand of the smallest operand to the right by the exponent difference. This shift will reduce the number of defective bits in the significand of the operand with the smaller value by the exponent difference, perhaps even to zero.

The resulting bound is obtained by accounting for the changes to the dominant bound by the effects of normalization and the accumulation of rounding error. (See Appendix for more details.)

3.5. Normalization and Cancellation

Floating-point results must be normalized to align the binary point to values between 1.0 and 2.0 [28]. The result of a floating-point operation may not meet this requirement and, therefore, may require that the result be "normalized" by shifting right or left to meet this requirement [27]. The exponent and the associated number of defective bits must be adjusted by the amount of this shift. Since the most significant bit is always one when the normalized value is between 1.0 and 2.0, it need not be stored. It is known as the "hidden bit."

Figure 4 illustrates the format of the post normalization result in which H_{PN} is the hidden bit field, T_{PN} is the resulting normalized significand (which is placed in the T field of the standard floating result of Figure 2), R_{PN} is the most significant bits of the excess bits and is the resulting rounding bits field (which is added to the accumulated rounding error field N, of Figure 3), and X_{PN} is the extended rounding error. X_{PN} serves as the source for the BFP "sticky bit," as used in standard floating point.
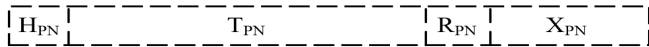
Figure 4: Post normalization result configuration

Normalizing by left shifting shifts information into the least significant bits, possibly adding to the unknown bits that already exist. In BFP this must be added to the defective bits unless the result is known to be "exact." Exactness is identified by BFP as having zero defective bits (e.g. referring to Figure 3, when the defective bits field D of the dominant bound is equal to zero.)

3.6. Zero Detection

The number of remaining significant bits is the difference between number of bits available in the representation (t+1) minus the number of defective bits D. The number of bits to be shifted to normalize is the number of leading zeros of the result. If all of the <u>significant</u> bits are zero, the resulting value must be zero.

BFP detects this condition and sets all fields of the BFP result to zero.

3.7. Accumulation of Rounding Error and Contribution to Defective Bits

Referring to Figures 2, 3, and 4, the accumulated rounding error N is computed by adding the resulting rounding bits R_{PN} of Figure 4, to the accumulated rounding error N of Figure 3, contributing a fraction of an ulp. If the extended rounding error X_{PN} of Figure 4, is not zero, an additional one is added to the accumulated rounding error N of Figure 3, functioning as a sticky bit. The carries out of the rounding bits field R of Figure 3, add to

the rounding error count C of Figure 3. The rounding error count is the accumulated rounding error in ulps.

The rounding error count C cannot, however, contribute directly to the value of the defective bits field D because of the difference of scaling, linear versus exponential. For example, when there are 2 defective bits, there must be at least 4 accumulated rounding errors to advance the defective bits to 3, and 8 to advance to 4, etc. In other words, when the logarithm of the rounding error count field C is equal to the defective bits field D, the value of the defective bits is increased by one.

3.8. Resulting Range

The BFP range relative to zero is defined by a lower bound (3) and an upper bound (4), as follows:

$$(-1)^S \cdot ((T+2^t)/2^t) \cdot 2^{E-O} \tag{3}$$

$$(-1)^S \cdot ((T+2^t+2^{D-1})/2^t) \cdot 2^{E-O} \tag{4}$$

The infinitely accurate real value represented by a BFP value is within this range. This is the same as in standard floating point except that the term 2^{D-1} provides the upper bound where the value of the defective bits field D is the number of bits that are no longer significant.

4. BFP Solutions to Standard Floating-Point Problems

Not only does BFP deliver all of the advantages of standard floating point, but it also delivers solutions to problems inherent in standard floating point.

4.1. Exact Equality Comparison and True Detection of Zero

Standard floating point requires additional code to be written to decide as to whether a comparison result is within error limits. BFP inherently provides this equality comparison.

Standard floating point cannot provide true zero detection as BFP does, which is demonstrated in the square root test of Section 8 below.

4.2. Number of Significant Bits

Standard floating point has no means to indicate the number of bits that are significant, but BFP identifies and indicates the number of significant bits. Further, BFP allows programmatic specification of the required number of significant bits. When the required number of significant bits are not available, BFP provides notification.

4.3. Mission Critical Computing

In some computing applications, such as mission-critical computing, computations need to be extremely accurate. But standard floating point cannot determine any accuracy loss. In contrast, BFP provides calculations – in real time – that can be depended upon to have the required number of significant bits.

4.4. Modeling and Simulation

Computational modeling and simulation, supported by constantly improving processor performance, often requires solving large, complex problems during which error may accumulate. This error, though not identified in standard floating point, is reported when the BFP extension is utilized.

4.5. Unstable Matrices

In numerical computation "stability" implies that small changes in the data translate into small changes in the result. Significant problems arise when small changes in the data, such as rounding error, create substantial error in the results. This occurs in matrix calculations, for instance, when solving simultaneous linear equations, when the roots may be similar or equal. BFP is used in this work to determine when a matrix is invertible, while assuring that the requirement for accuracy is met.

5. Standard Floating-Point Error Mitigation

5.1. Error Analysis Versus Direct Testing

Algorithmic error analysis can be used to identify error that occurs when using standard floating point. Though it is costly, it is commonly used for complex computing in critical systems, the failure of which may have severe consequences. In contrast, BFP directly, and in real time, tests calculation results, thus removing the need for costly error analysis.

5.2. Software Testing of Floating Point

Standard floating point problem in that it has no indication of accuracy errors is challenging to detect, diagnose, and repair.. BFP detects accuracy errors in real time, thus providing a response to the plea of "Desperately Needed Remedies for the Undebuggability of Large Floating-Point Computations in Science and Engineering" [19].

5.3. Stress Testing of Floating-Point Software

Stress testing may also be used to determine error that accumulates when using standard floating point. In general, stress testing is a form of intense testing used to establish failure points or useful operating limits of a given system. It involves testing beyond normal operational capability, often to a breaking point, in order to observe the performance limits.

Stress testing, as commonly applied to software, determines data value limits (boundary value testing) or performance (memory required, response time, latency, throughput, and time required to complete the calculation). Chan describes software stress testing as a method for accelerating software defect discovery and determining failure root cause and assisting problem diagnosis [29]. However, determining the accuracy of floating-point calculations or diagnosing accuracy failures in floating-point calculations, in intermediate results, or in final results is problematic using standard floating point [19]. In fact, floating-point errors are invisible in standard floating point, as there is nothing within the IEEE Standard that describes or limits floating-point error.

BFP provides a new and unique method of stress testing. Stress testing floating-point application software using BFP determines the accuracy at any point in a calculation, or even at the point of failure of a given computation, by executing computations with successively higher values of required significant bits and analyzing failure points. This reduces the cost of diagnosis and repair of floating-point calculation failures [19].

5.4. Other Mitigation Techniques

Other real-time techniques attempt to mitigate error, but only do so by increasing the overhead. Some of these techniques have the goal of computing results within error bounds, such as interval arithmetic [30] and real-time statistical analysis [31], [32]. But these require two floating point operations and require the storage of two floating point values and, thereby, increase the needed time and memory.

Parallel computation with higher precision standard floating point [33] can also be used to mitigate error. In addition to substantially increasing overhead, only the probability of error is reduced. There is no indication of that amount of error, whereas BFP identifies the remaining significant bits.

6. Software Model Solutions Using BFP

This work presents a software model of the BFP hardware system as described in detail in [25], [26]. When using standard floating point, there are certain problem areas that are prone to floating-point error. This work provides results from computations using BFP compared to computations using standard floating point in three of these well-known floating-point problem areas.

6.1. 80-Bit BFP

The BFP software model used in the following examples is configured by the field sizes of the BFP data structure, which is an 80-bit BFP configuration. The sign, exponent, and significand fields of the BFP format are identical to the corresponding fields in the standard 64-bit floating-point format. This permits conversion from 64-bit standard floating point to 80-bit BFP with a single instruction that stores the standard floating-point value directly into the corresponding fields of the BFP structure.

The BFP model contains the basic operations BFPAdd, BFPSub, BFPMult, BFPDiv, and BFPSqrt.

The following experiments were conducted on an ACER Aspire PC with an Intel Core i5 7th gen processor, using GNU Compiler Collection (GCC) version "(i686-posix-dwarf-rev0, Built by MinGW-W64 project) 8.1.0" [34].

6.2. Significant digits

In computers, binary floating-point calculations are performed with a collection of binary bits. But to be useful in the scientific and engineering world, outputs from, and inputs to, the human interface must be in decimal digits. In other words, the calculated results must be displayed in decimal digits, and decimal information must be supled to the processing unit. However, there is no direct mapping between binary floating-point values and the decimal representation of these values [35]. The fixed number of binary bits available in the double-precision (64-bit) floating-point format can represent a range of decimal values with as few as 15 or as many as 17 decimal digits [13].

External representations of BFP results, as shown below in Tables 1-14, are constrained to the actual number of significant decimal digits of the real number represented; i. e. only the digits having significance are displayed. This contrasts with standard floating point in which decimal digits of unknown significance are displayed, which results, at times, in the display of multiple incorrect digits (digits without significance). The display of these insiginifcant decimal digits obtained by the use of standard floating point is shown in the Tables 1-14 below.

6.3. Significant Bits

The number of significant bits is identified by the binary BFP representation of an infinitely accurate real value. The number of significant bits, SB, is calculated as the total bits available, p, minus the number of defective bits, D, as shown in (5)

$$SB = p - D \qquad (5)$$

where p = t + 1.

BFP provides a default value for the required number of significant bits. Alternatively, a special command can specify the required number of significant bits. Whether the BFP default value is applied or the commanded value is applied, the required number of significant bits may not be generated in a calculation. In this case, a special not-a-number code "qNaN.sig" is produced, which is visible when externally displayed.

6.4. Modeling Overview

The following demonstrations address three problems presented above, which are floating-point error diagnosis, true detection of zero, and unstable matrices. The first utilizes Kahan's thin triangle problem where the area of a thin triangle is diminished until a specified number of significant bits is not met. The second is an illustration of zero detection by BFP, which uses an expression that mathematically evaluates to zero; however, standard floating point does not generate zero. The third demonstration solves for a matrix determinate identifying that the matrix is unstable.

7. Modeling Stress Testing - The Heron and Kahan Thin Triangle Problems

7.1. The Thin Triangle

Knowing the length of three sides of a triangle (Figure 5) is sufficient to determine the area of the triangle without knowledge of the angles [36]. Work from early in the first millenium CE, attributed to Heron, produced an area formula that has become known as "Heron's Formula." In 2014, Kahan produced an improved area formula.
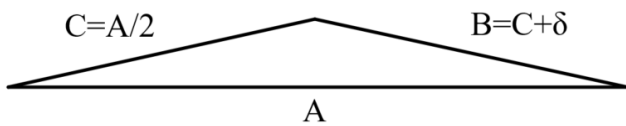
The thin triangle problem considered here is from "Miscalculating area and angles of a needle-like triangle." [37]. This work extends the 1976 work of Pat H. Sterbenz who suggested a method to make Heron's Formula more accurate [38]. In that work Sterbenz states:

*"However, we can produce a good solution for the problem if we assume that A, B, and C are given **exactly** as numbers in (floating point)." (Emphasis added)*

However, when using standard floating point, A, B, or C may not be **exact**. And standard floating point does not provide any indication that A or B or C is exact. But BFP establishes exactness, where a representation is exact if and only if the dominate bound

defective bits field D is zero; this indicates that there are no insignificant bits in the representation. Using the BFP extension of standard floating point, this work shows when A or B or C is not exact.

In the tests shown below, values were chosen to reflect a thin triangle in which one side of the triangle, side C, is one half the length of the base A and in which the other side of the triangle, side B, is equal to the length of side C plus delta (δ). By injecting 1 ulp error in any one of the values, the values are no longer exact. In the tests below, a 1 ulp error was injected into A. And the injection of this small error into only one of the values causes the equation to produce a result that does not meet the required significant digits for a specified δ and a required number of significant digits.

In the examples, the value for A was increased by 1 ulp of error by adding one to the significand. For the equivalent result, in BFP the defective bits D value was set to 1 indicating that there is 1 ulp of error.

In the tests below, the area of the triangle is influenced by the value for δ. When δ is zero, the area of the triangle is zero.

Tables 1-14 present stress test results for Heron's and Kahan's area algorithms for thin triangles, A=2.0 + 1 binary ulp, C=1.0 and B= C+ δ, with decreasing values of δ and increasing values of the required number of significant digits. Results are presented for 64-bit (double precision) and 128-bit (quad precision) standard floating point and 80-bit BFP. Each test is conducted until the particular algorithm fails to provide the required number of signicant digits, at which point BFP displays "qNaN.sig." Tables 6, 7, and 14 present results for when δ is sufficiently small that the areas are significantly zero as detected by BFP.

The second row of each table (excluding Tables 6, 7, and 14) shows the results for the required significant digits immediately prior to the failure point (one decimal ulp prior to not meeting the required number of significant digits as determined by the BFP calculations). The third row of each table lists the results *at* the failure point, where BFP shows that the required number of significant digits has not been met.

The BFP output conversion routine only displays those digits known to be correct to + or – 1 in the last digit presented.

7.2. Heron's Formula

Heron's formula is shown in (6):

$$Area = SQRT(S(S-A)(S-B)(S-C)) \qquad (6)$$

where S= (A + B + C)/2.

The Heron stress test determines, for a specific triangle, where (6) fails for a specific number of required significant digits. For each of the triangles in the test reported in Tables 1-7 (using a given value of δ for each triangle), the required number of significant digits is increased until BFP indicates by qNaN.sig that (6) cannot be solved for the specific triangle while achieving the specified number of required significant digits.

In Tables 1-7 standard floating-point results for Heron's area algorithms for each required number of significant digits, 14, 13, ...7 are benchmarked against BFP results. Heron's area formula (6) was solved for successively smaller values of δ until the BFP calculation indicated (by qNaN.sig) that the required number of significant digits was not met.

Table 3, for example, shows that for δ =0.0001, a 10-digit result is obtained successfully, but requiring 11 significant digits fails.

7.3. Kahan's Formula

In 2014, Professor William M. Kahan demonstrated that the Heron formula yielded inaccurate results when computed with a modern computer using floating point. Kahan contributed (7), which provides more accurate results for the area of thin triangles than (6) [37].

Area = SQRT(A+(B+C))(C-(A-B))(C+(A-B))(A+(B-C)))/4   (7)

where A ≥ B ≥ C

The stress tests of Tables 8-14 determine, for a specific triangle, where (7) fails for a specific number of required significant digits. For each of the triangles (using a given value of δ for each triangle), the required number of significant digits is increased until BFP indicates by a qNaN.sig that (7) cannot be solved for the specific triangle while achieving the specified number of required significant digits.

Tables 8-14 list the standard floating-point computations benchmarked against the BFP computations of (7) for thin triangles for the required significant digits, which present results similar to the Heron solutions of (6).

For example, Table 10 shows that for δ =0.0001, an 11-digit result is obtained successfully, but requiring 12 significant digits fails. This demonstrates that the Kahan algorithm (7) provides more significant digits than does the Heron algorithm (6) as shown in Table 3 (described above).

Double precision (64-bit) floating point can represent up to 15 significant decimal digits. BFP computations with inexact values shows that neither (6) or (7) is capable of producing a thin triangle area result accurate to 15 significant digits, as shown Tables 1-14.

7.4. Stress Tests Summary

In summary, Tables 1-14 show that BFP identifies the failure point at the largest number of significant digits for a given δ that does not meet the required number of significant digits. BFP identifies the smallest δ that retains the required number of significant bits. And BFP identifies when the area of a thin triangle is significantly zero when standard floating point does not.

Table 1: Stress Test One of Heron's Formula for Area of Thin Triangle

For δ =0.01, A=2.0 + 1 ulp, B=1.01, C=1.0			
Significant Digits Required	Area Using Double Precision	Area Using Quad Precision	Area Using BFP
11	0.100123670403155830000000	0.100123670403155691503050	0.100123670403
12	0.100123670403155830000000	0.100123670403155691503050	0.100123670403
13	0.100123670403155830000000	0.100123670403155691503050	qNaN.sig
14	0.100123670403155830000000	0.100123670403155691503050	qNaN.sig

Table 2: Stress Test Two of Heron's Formula for Area of Thin Triangle

For δ = 0.001, A=2.0 + 1 ulp, B=1.001, C=1.0			
Significant Digits Required	Area Using Double Precision	Area Using Quad Precision	Area Using BFP
10	0.031626725248400829000000	0.031626725248399554108590	0.031626725248
11	0.031626725248400829000000	0.031626725248399554108590	0.031626725248
12	0.031626725248400829000000	0.031626725248399554108590	qNaN.sig
13	0.031626725248400829000000	0.031626725248399554108590	qNaN.sig

Table 3: Stress Test Three of Heron's Formula for Area of Thin Triangle

For δ = 0.0001, A=2.0 + 1 ulp, B=1.0001, C=1.0			
Significant Digits Required	Area Using Double Precision	Area Using Quad Precision	Area Using BFP
9	0.010000124986706948000000	0.010000124986718603508640	0.01000012498
10	0.010000124986706948000000	0.010000124986718603508640	0.01000012498
11	0.010000124986706948000000	0.010000124986718603508640	qNaN.sig
12	0.010000124986706948000000	0.010000124986718603508640	qNaN.sig

Table 4: Stress Test Four of Heron's Formula for Area of Thin Triangle

For δ = 0.00001, A=2.0 + 1 ulp, B=1.00001, C=1.0			
Significant Digits Required	Area Using Double Precision	Area Using Quad Precision	Area Using BFP
8	0.003162281613054031000000	0.003162281612973455495980	0.00316228161
9	0.003162281613054031000000	0.003162281612973455495980	0.00316228161
10	0.003162281613054031000000	0.003162281612973455495980	qNaN.sig
11	0.003162281613054031000000	0.003162281612973455495980	qNaN.sig

Table 5: Stress Test Five of Heron's Formula for Area of Thin Triangle

For δ = 0.000001, A=2.0 + 1 ulp, B=1.000001, C=1.0			
Significant Digits Required	Area Using Double Precision	Area Using Quad Precision	Area Using BFP
7	0.001000000012506975620000	0.001000000012499986718749	0.0010000001

8	0.0010000000125069756200000	0.0010000000124999867187490	0.0010000001
9	0.0010000000125069756200000	0.0010000000124999867187490	qNaN.sig
10	0.0010000000125069756200000	0.0010000000124999867187490	qNaN.sig

Table 6: Stress Test Six of Heron's Formula for Area of Thin Triangle

For δ=0.0000001, A=2.0 + 1 ulp, B=1.0000001, C=1.0			
Significant Digits Required	Area Using Double Precision	Area Using Quad Precision	Area Using BFP
7	0.0003162277704130854700	0.0003162277699696845842	0.0
8	0.0003162277704130854700	0.0003162277699696845842	0.0
9	0.0003162277704130854700	0.0003162277699696845842	0.0
10	0.0003162277704130854700	0.0003162277699696845842	0.0

Table 7: Stress Test Seven of Heron's Formula for Area of Thin Triangle

For δ=0.00000001, A=2.0 + 1 ulp, B=1.00000001, C=1.0			
Significant Digits Required	Area Using Double Precision	Area Using Quad Precision	Area Using BFP
1	0.0000999999999821126433000	0.0001000000000012499999867	0.0
2	0.0000999999999821126433000	0.0001000000000012499999867	0.0
3	0.0000999999999821126433000	0.0001000000000012499999867	0.0
4	0.0000999999999821126433000	0.0001000000000012499999867	0.0
5	0.0000999999999821126433000	0.0001000000000012499999867	0.0
6	0.0000999999999821126433000	0.0001000000000012499999867	0.0
7	0.0000999999999821126433000	0.0001000000000012499999867	0.0
8	0.0000999999999821126433000	0.0001000000000012499999867	0.0

Table 8: Stress Test One of Kahan's Formula for Area of Thin Triangle

For δ=0.01, A=2.0 + 1 ulp, B=1.01, C=1.0			
Significant Digits Required	Area Using Double Precision	Area Using Quad Precision	Area Using BFP
12	0.1001236704031580700000	0.1001236704031569150305	0.1001236704031
13	0.1001236704031580700000	0.1001236704031569150305	0.1001236704031
14	0.1001236704031580700000	0.1001236704031569150305	qNaN.sig
15	0.1001236704031580700000	0.1001236704031569150305	qNaN.sig

Table 9: Stress Test Two of Kahan's Formula for Area of Thin Triangle

For δ=0.001, A=2.0 + 1 ulp, B=1.001, C=1.0			
Significant Digits Required	Area Using Double Precision	Area Using Quad Precision	Area Using BFP
11	0.0316267252483973110000	0.0316267252483955410859	0.0316267252483
12	0.0316267252483973110000	0.0316267252483955410859	0.0316267252483
13	0.0316267252483973110000	0.0316267252483955410859	qNaN.sig
14	0.0316267252483973110000	0.0316267252483955410859	qNaN.sig

Table 10: Stress Test Three of Kahan's Formula for Area of Thin Triangle

For δ=0.0001, A=2.0 + 1 ulp, B=1.0001, C=1.0			
Significant Digits Required	Area Using Double Precision	Area Using Quad Precision	Area Using BFP
10	0.0100001249867291560000	0.0100001249867186035086400	0.010000124986
11	0.0100001249867291560000	0.0100001249867186035086400	0.010000124986
12	0.0100001249867291560000	0.0100001249867186035086400	qNaN.sig
13	0.0100001249867291560000	0.0100001249867186035086400	qNaN.sig

Table 11: Stress Test Four of Kahan's Formula for Area of Thin Triangle

For δ=0.00001, A=2.0 + 1 ulp, B=1.00001, C=1.0			
Significant Digits Required	Area Using Double Precision	Area Using Quad Precision	Area Using BFP
9	0.0031622816130189224000	0.0031622816129734554959800	0.003162281612
10	0.0031622816130189224000	0.0031622816129734554959800	0.003162281612
11	0.0031622816130189224000	0.0031622816129734554959800	qNaN.sig
12	0.0031622816130189224000	0.0031622816129734554959800	qNaN.sig

Table 12: Stress Test Five of Kahan's Formula for Area of Thin Triangle

For δ=0.000001, A=2.0 + 1 ulp, B=1.000001, C=1.0			
Significant Digits Required	Area Using Double Precision	Area Using Quad Precision	Area Using BFP

8	0.0010000001250697562000	0.0010000001249998671874 9	0.00100000012
9	0.0010000001250697562000	0.0010000001249998671874 9	0.00100000012
10	0.0010000001250697562000	0.0010000001249998671874 9	qNaN.sig
11	0.0010000001250697562000	0.0010000001249998671874 9	qNaN.sig

Table 13: Stress Test Six of Kahan's Formula for Area of Thin Triangle

For δ=0.0000001, A=2.0 + 1 ulp, B=1.0000001, C=1.0			
Significant Digits Required	Area Using Double Precision	Area Using Quad Precision	Area Using BFP
7	0.00031622777041308547000	0.00031622776996968458842	0.00031622777
8	0.00031622777041308547000	0.00031622776996968458842	0.00031622777
9	0.00031622777041308547000	0.00031622776996968458842	qNaN.sig
10	0.00031622777041308547000	0.00031622776996968458842	qNaN.sig

Table 14: Stress Test Seven of Kahan's Formula for Area of Thin Triangle

For δ=0.00000001, A=2.0 + 1 ulp, B=1.00000001, C=1.0			
Significant Digits Required	Area Using Double Precision	Area Using Quad Precision	Area Using BFP
1	0.00010000000093134947000	0.00010000000012499999867	0.0
2	0.00010000000093134947000	0.00010000000012499999867	0.0
3	0.00010000000093134947000	0.00010000000012499999867	0.0
4	0.00010000000093134947000	0.00010000000012499999867	0.0
5	0.00010000000093134947000	0.00010000000012499999867	0.0
6	0.00010000000093134947000	0.00010000000012499999867	0.0
7	0.00010000000093134947000	0.00010000000012499999867	0.0
8	0.00010000000093134947000	0.00010000000012499999867	0.0

Table 15: Zero Detection – Standard Floating point (SFP) vs. Bounded floating point (BFP)

Function	GCC 64-bit Floating Point	GCC 128-bit Floating Point	80-bit BFP
sqrt(pi*pi)-pi	2.27682456e-017	-1.2246467991e-16	0.0
sqrt(pi)*sqrt(pi)-pi	-1.96457434e-016	-1.2246467991e-16	0.0

8. Modeling Square Root Problem – Zero Detection

Zero detection is important because standard floating point does not always accurately identify when the result of a subtraction is a zero.

In standard floating point, even a one ulp error may cause a significantly erroneous result. Standard floating point does not reliably provide zero as a result when subtracting significantly equal values. For example, when subtracting two values representing infinitely accurate numbers, if a one ulp error has been introduced into one of the floating-point values, the floating-point subtraction result will not be zero. Detection of this condition requires external testing of the comparison result. In contrast, BFP provides zero detection by detecting whether the significant bits of a comparison result are equal to zero. Using the software model, we examine a simple expression that should evaluate exactly to zero. Standard floating point does not solve this simple calculation correctly but BFP does.

Table 15 demonstrates BFP's zero detection capability as compared to the results of calculating the same expression (that mathematically equates to zero) in standard double capacity precision (64-bit) and quad capacity precision (128-bit) floating point [13].

9. Modeling Unstable Matrices

BFP can be used to determine if a determinant is significantly zero. Thus, BFP can be used to identify an unstable matrix, as shown in Table 16.

Common matrix expressions require the application of the inverse of a matrix. The inverse of matrix **A** is denoted as **A**$^{-1}$. The inverse of a matrix may be calculated only if the determinant of that matrix (|A|) is not equal to zero. Thus, it is important to know if the determinant is zero. But standard floating point may not properly yield zero because of floating-point error. To address this problem, many supplementary methods have been developed to determine if a matrix is invertible. Because these supplementary methods are otherwise unnecessary for the computation of the equation, they add unnecessary overhead in terms of computation time and memory space. Moreover, requiring the addition of code to enable these methods makes the code more complex and more prone to error.

However, if the software is written in BFP, this calculation is made directly during the solving of the equation. In solving the linear equation, Ax=b, the inverse of the A matrix is multiplied by the b vector. This produces a new vector, which is the solution to the equation. When BFP calculates the determinant, it identifies – during the calculation – if the determinant is zero. Thus, BFP efficiently identifies whether the equation can be solved, without requiring additional code as the supplementary methods do.

Table 16: Comparison of Determinant Calculation of an Unstable Matrix

Matrix	Standard 64-bit Floating Point	Standard 128-bit Floating Point	80-bit BFP
cavity01	4.9359402474e-045	4.9359402474e-45	0.0

Table 16 presents the comparison of the calculations of the determinant of an unstable matrix using 64-bit standard floating point, 128-bit standard floating point, and 80-bit BFP. The determinant is calculated using the upper triangle method, Gaussian Elimination [39].

The matrix selected, cavity01, is from the Matrix Market [40]. It was located searching the Matrix Market with the term "unstable."[1] The matrix selected is a sparce 317x317 matrix with 7,327 entries.

Table 16 shows that both 64-bit and 128-bit standard floating point provide a non-zero value for the determinant, where BFP does return zero, because at some point in the calculation the significant bits were all zero. Thus, using BFP identifies the problem efficiently *during* the calculation. Using standard floating point requires the incorporation of one of the supplementary methods into the code to prevent division by zero. Consequently, BFP directly determines if a matrix is not invertible.

Moreover, when the matrix is properly invertible, using BFP provides the accuracy of the result. The use of BFP identifies how many significant digits are in the result. In an example, a requirement is that the accuracy must be more than three significant digits. Even if the matrix is valid, there may be less than three significant digits remaining in the results, which BFP identifies.

Consequently, when BFP is used during matrix calculations, it not only determines if the matrix is invertible, but it also assures that the requirement for accuracy is met.

10. Summary

BFP adds a field to the standard floating point format in which error may be accumulated. The upper bound of that error is stored as the logarithm of that bound.

BFP makes floating-point error quantifiable and visible. It allows exact equality comparison. It provides notification when insufficient significant digits have been retained during floating-point computations. When implemented in hardware it affords real-time fail-safe calculations for mission critical applications.

Though designed for hardware implementation, a software model emulating the BFP functions was used in this paper. The BFP software model has been applied to three problems as follows: the failure of standard floating point to exactly detect zero in the presence of floating-point error, the failure of standard floating point to identify the number of significant digits (if any) of a result, and the lack of the ability to diagnose standard floating point accuracy errors.

This paper shows that BFP solves these problems by calculating and propagating the number of significant bits as described by the BFP algorithms presented. Three examples have been used, which are a precision stress test, true floating point zero detection, and detection of an unstable matrix.

The precision stress test of an algorithm increases the required precision for that algorithm under specific parameters until that required precision cannot be met. The algorithm parameters may be adjusted as well to determine the operational envelope for that algorithm for a given required precision.

Standard floating point does not return precisely zero when significantly similar, yet different numbers are subtracted. An example is provided where an expression clearly evaluates to zero, yet standard floating point does not return zero but BFP does return zero. Using this property of BFP, we evaluate the determinant of a matrix known to be unstable and note that BFP evaluates the determinant as zero.

Properly implemented in hardware, BFP will reduce the time and cost of the development of scientific and engineer calculation software and will provide run-time detection of floating-point error. This hardware implementation has begun using Verilog HDL.

11. Appendix – Post Revision Result Format

11.1. Bound Description

Definitions are from, or amended from, [26].

An 80-bit model was chosen to allow for using 64-bit standard floating point and a 16-bit bound field B. Table 17 specifies subfield widths for a 80-bit BFP model.

Table 17: 80-Bit Model Field Widths

Subfield Widths
#define r 4
#define d 6
#define c d
#define n (c+r)
#define b (d+n)

11.2. Notation Used

Each algorithm is preceded by a list of definitions of the variables (for example, *Op1Exp*) used in the algorithm. Each definition (for example, first operand exponent) is followed by an alphanumeric identifier (for example, 51A). That identifier refers to the patent reference number of [26]. Further, a letter (E, B, D, N, R, or C) may follow the identifier definition (for example, first operand exponent E). This refers to a specific portion of the data format identified in Figures 1 and 3.

11.3. Dominant Bound

The dominant bound (*DominantBound*) is the larger of the largest operand bound (*HiOpBound*) and the adjusted bound of the smallest operand (*AdjBoundLoOp*). This is the bound of the operand with the least number of significant bits.

The dominant bound (*DominantBound*) is determined from the first operand bound (*Op1Bound*), the second operand bound (*Op2Bound*), the exponent difference (*ExpDelt*), and the condition

---

1 This particular matrix is available in compressed form from
ftp://math.nist.gov/pub/MatrixMarket2/SPARSKIT/drivcav_old/cavity01.mtx.gz, accessed 4 August 2020.

(*Op2Larger*) in which the magnitude of the second operand (*Op2*) is greater than the magnitude of the first operand (*Op2*).

11.4.   Finding the Exponent Difference

The exponent difference (*ExpDelt*) is the magnitude of the difference between the first operand exponent (*Op1Exp*) and the second operand exponent (*Op2Exp*).

The exponent difference (*ExpDelt*) is determined from the first operand (*Op1Exp*) and the second operand (*Op2Exp*), as in Algorithm 1.

Algorithm 1: Finding Exponent Difference

Result: Exponent Difference
Op1 := first operand, 201;
Op2 := second operand, 202;
Op1Exp := first operand exponent E, 51A;
Op2Exp := second operand exponent E, 51B;
ExpDelt := exponent difference, 321;
Op2Larger := second operand > first operand, 302;
SmallerExp := smallest exponent E, 51E;
LargerExp := largest exponent E, 51D;

begin
    Op2Larger := |*Op2*| > |*Op1*|
    if *Op2Larger* **then**
        LargerExp := *Op2Exp*;
        SmallerExp := *Op1Exp*;
    else
        LargerExp := *Op1Exp*;
        SmallerExp := *Op2Exp*;
    end
    ExpDelt := *LargerExp* – *SmallerExp*
end

11.5.   Finding the Dominant Bound

As shown in Algorithm 2, the dominant bound (*DomBound*) is derived from the first operand bound B (*Op1Bound*), the second operand bound B (*Op2Bound*), the exponent difference (*ExpDelt*), and the second operand larger (*Op2Larger*).

Algorithm 2: Finding the Dominant Bound

Result: Dominant Bound
Op1Bound := the first operand bound B, 52A;
Op2Bound := the second operand bound B, 52B;
LoOpBound := smallest operand bound B, 52D;
HiOpBound := largest operand bound B, 52E;
LoOpBoundeBadBits := smallest operand bound
              defective bits D, 54A;
AdjLoOpBoundBadBits := adjusted smallest operand bound
              defective bits D, 54B;
ClampedBadBits := clamped defective bits D, 54G;
LoOpBoundAccRE := smallest operand bound accumulated
              rounding error N, 55A;
AdjBoundLoOp := adjusted bound B of the smallest
              operand, 52F;
HiOpBoundLargest := largest operand bound B is
              greatest, 431;

DominantBound := dominant bound, the bound of the
              operand with the least number of
              significant bits after alignment, 52H;

begin
    Op2Larger := |*Op2*| > |*Op1*|
    if *Op2Larger* **then**
        LoOpBound := *Op1Bound*;
        HiOpBound := *Op2Bound*;
    else
        LoOpBound := *Op2Bound*;
        HiOpBound := *Op1Bound*
    end
    AdjLoOpBoundBadBits
        := *LoOpBoundeBadBits* – *ExpDelt*
    if *AdjLoOpBoundBadBits* < 0 **then**
        AdjLoOpBoundBadBits := 0;
    end
    AdjLoOpBoundBadBitsE
        := *ClampedBadBits* |&| *LoOpBoundAccRE;*
    HiOpBoundLargest := *HiOpBound*
        > *AdjBoundLoOp*;
    if *HiOpBoundLargest* **then**
        DominantBound := *HiOpBound*;
    else
        DominantBound := *AdjBoundLoOp*;
    end
end

Where '|&|' is the field concatenation operator.

11.6.   Result Bound Calculation

The resulting bound of a calculation is determined by one of two mutually exclusive calculations, the bound calculation algorithm of Algorithm 3 or the bound rounding algorithm of Algorithm 4. When there is a subtract operation and the operands are sufficiently similar, the intermediate result has leading zeros (is not normalized). Under this condition the bound calculation algorithm determines the bound of the result. Otherwise, the bound rounding algorithm determines the result.

In any case, exact operands produce an exact result [6].

Operations other than add or subtract return the dominant bound.

11.7.   Bound Cancellation Algorithm

The result bound B (*ResultBound*) is determined from either the cancellation adjusted bound B (*AdjCaryBound*) or the carry adjusted bound B (*AdjCaryBound*). The result bound B requires the dominant bound (*DominantBound*), the significand capacity (*SigCap*), and the number of leading zeros (*LeadZeros*).

Algorithm 3 accounts for compensating errors.

Algorithm 3: Bound Cancellation

Result: Result Bound from Cancellation
Cancellation := cancellation detected, 620;
DomBadBits := dominant bound defective bits D, 54C;
LeadZeros := number of leading zeros prior to

---

normalization, 711;
SigCap := significant capacity, the number of bits in the
    significand (t+1), includes hidden bit H, 805;
AdjBadBits := adjusted defective bits D, 54D;
MaxedBadBits := max defective bits detected, 617;
ResultBadBits := resulting defective bits D, 54H;
DomAccRE := dominant bound accumulated rounding
    error N, 55B;
CancAdjBound := cancellation adjusted bound B, 52J;
ResultBound := result bound B, 52C;

if *Cancellation* **then**
    AdjBadBits := *DomBadBits* + *LeadZeros*;
    MaxedBadBits := *SigCap* <= *AdjBadBits*;
    if *MaxedBadBits* **then**
      ResultBadBits := *SigCap*;
    else
      ResultBadBits := *AdjBadBits*;
    end
    CancAdjBound := *ResultBadBits* |&| *DomAccRE*
    ResultBound := *CancAdjBound*
end

11.8. Bound Rounding Algorithm

The adjusted value of R is added to the dominate bound to provide the adjusted bound. When the logarithm of C is equal to D, 1 is added to D and C is set to zero in the resulting bound.

There is an externally applied limit, Required Significant Bits, which is defaulted and programmable. On external representation, when the available significant bits value (t+1-D) is less than or equal to the Required Significant Bits, "sNaN.sig" is displayed. A special command is provided that tests for this condition of an individual BFP value to produce a signaling exception sNaN.sig, which can be detected and serviced like any other hardware exception such as sqrt(-1) or x/0.

When there are significant bits and they are all zero, the value represented is truly zero and the resulting value is set to all zeros. (Zero has no significant bits/digits). This is true zero detection unavailable with standard floating point nor Interval Arithmetic (IA).

Algorithm 4: Bound Rounding

Result: Result Bound from Rounding
NormalizedRE := normalized rounding error R, 57A;
StickyBit := significand excess, logical OR of all bits of the
    normalized extension X, 741;
RESum := rounding error sum B, 52K;
RESumCount := updated accumulated rounding error
    extension count C from the rounding
    error sum B, 54K;
RESumFraction := updated accumulated rounding error
    rounding bits R from the rounding
    error sum B, 57B;
Log2RESum := rounding count logarithm, 61;
LogOvrflw := log count overflow, 651;
AdjBadBits := incremented defective bits D, 54E;
MaxBadBits := max defective bits, 662;

LimAdjBadBits := clamped incremented defective
    bits D, 54J;
AdjBadBitsBnd := defective bits adjusted bound B, 52L;
AdjCaryBound := carry adjusted bound B, 52M;

if not *Cancellation* **then**
    RESum := *DominantBound* + *NormalizedRE* + *StickyBit*;
    Log2RESum := Log2(*RESumCount*);
    CntOvrflw := *Log2RESum* >= *DomBadBits*;
    AdjBadBits := *LogOvrflw* + *DomBadBits*;
    MaxBadBits := *AdjBadBits* >= *SigCap*;
    if *MaxBadBits* **then**
      LimAdjBadBits := *SigCap*;
    else
      LimAdjBadBits := *AdjBadBits*;
    end
    AdjBadBitsBnd := *LimAdjBadBits* |&| *RESumFraction*
    if *LogOvrflw* **then**
      AdjCaryBound := *AdjBadBitsBnd*;
    else
      AdjCaryBound := *RESum*;
    end
    ResultBound := *AdjCaryBound*
end

Conflict of Interest

The authors whose names are listed immediately below report the following details of affiliation or involvement in an organization or entity (True North Floating Point) with a financial or non-financial interest in the subject matter or materials discussed in this manuscript.

Alan A. Jorgensen; Connie R. Masters, Andrew C. Masters

Acknowledgment

References

[1] A. Jorgensen, A. Masters, R. Guha, "Assurance of accuracy in floating-point calculations - a software model study," 2019 International Conference on Computational Science and Computational Intelligence (CSCI), Las Vegas, NV, USA, 471-475, 2019, DOI: 10.1109/CSCI49370.2019.00091.
[2] J. Muller, B. N., F. de Dinechin, C.-P. Jeannerod, V. Lefevre, G. Melquiond, N. Revol, D. Stehle, S. Torres, Handbook of floating-point arithmetic, Boston: Birkhauser, 2010, DOI 10.1007/978-0-8176-4705-6.
[3] T. Haigh, "A. M. Turing Award: William ("Velvel") Morton Kahan," Association for Computing Machinery, 1989, https://amturing.acm.org/award_winners/kahan_1023746.cfm, accessed 24 February 2019.
[4] IEEE Standard for Floating-Point Arithmetic, IEEE Std 754-2019, 1-84, 22 July 2019, DOI: 10.1109/ IEEESTD.2019.8766229.
[5] ISO/IEC 9899:2018, Information technology - programming languages - C, Geneva, Switzerland: International Organization for Standardization, 2018.
[6] A. A. Jorgensen, A. C. Masters, "Exact floating point," to be published Springer Nature - Book Series: Transactions on Computational Science & Computational Intelligence, Ed, H. Arabnia, ISSN 2569-7072, 2021.
[7] D. Goldberg, "What every computer scientist should know about floating-point arithmetic," ACM Computing Surveys, **23**(1), 5-48, 1991.
[8] G. Cantor, Ueber eine elementare Frage der Mannigfaltig-keitslehre, Jahresbericht der Deutschen Mathematiker-Vereinigung, 1: 75–78; English translation: W. B. Ewald (ed.) From Immanuel Kant to David Hilbert: a

source book in the foundations of mathematics, Oxford University Press, **2**, 920–922, 1891.

[9] W. M. Kahan, "A logarithm too clever by half," 9 August 2004, http://people.eecs.berkeley. edu/~wkahan/ LOG10HAF.TXT, accessed 26 February 2019.

[10] S. Lubkin, "Decimal point locations in computing machines," Mathematical tables and other aids to computation, **3**(21), 44-50, 1948, DOI:10.2307/ 2002662, www.jstor.org/stable/2002662, accessed 20 Nov. 2020.

[11] M. Frechtling, P. H. Leong, "MCALIB: measuring sensitivity to rounding error with monte carlo programming," ACM Transactions on Programming Languages and Systems, **37**(2), 5, 2015, DOI: 10.1145/2665073.

[12] S. Ardalan, "Floating point error analysis of recursive least squares and least mean squares adaptive filters," IEEE Trans. Circuits Syst., **CAS-33**, 1192-1208, Dec. 1986, DOI: 10.1109/TCS.1986.1085877.

[13] N. J. Higham, Accuracy and stability of numerical algorithms, Second Edition, Philadelphia, PA: SIAM, 2002, DOI 10.1137/1.9780898718027, accessed 6 August 2020.

[14] C. Lea, H. Ledin, "A review of the state-of-the-art in gas explosion modelling," February 2002, UK Health and Safety Laboratories, http://www.hse.gov.uk/research/hsl_pdf/2002/hsl02-02.pdf, accessed 24 March 2019.

[15] W. Lai, D. Rubin, E. Krempl, Introduction to Continuum Mechanics, Fourth Edition, Amsterdam, Netherlands, Elsevier, 2009, ISBN 0750685603.

[16] Weather Prediciton Center, O. P. Center, N. H. Center, H. F. Center, Unified Surface Analysis Manual, November 21 2013, National Weather Service, https://www.wpc.ncep.noaa.gov/sfc/UASfcManualVersion1.pdf, accessed 24 March 2019.

[17] M. Ercegovac, T. Lang, Digital arithmetic, Morgan Kaufmann Publishers, San Francisco, 2004, ISBN-13: 978-1-55860-798-9.

[18] N. Higham, Accuracy and stability of numerical algorithms, Philadelphia, PA: SIAM, 1996, ISBN 0-89871-521-0.

[19] W. Kahan, "Desperately needed remedies for the undebuggability of large floating-point computations in science and engineering," IFIP Working Conference on Uncertainty Quantification in Scientific Computing (2011): 2012, https://people.eecs.berkeley.edu/~wkahan/Boulder.pdf, accessed 29 August 2019.

[20] D. Weber-Wulff, "Rounding error changes Parliament makeup," 7 April 1992, Mathematik Institut fuer Informatik Freie Universitaet Berlin Nestorstrasse 8-9, http://mate.uprh.edu/~pnegron/notas4061/ parliament.htm, accessed 25 March 2019.

[21] K. Quinn, "Ever had problems rounding off figures? This stock exchange has," 8 November 1983, 37, The Wall Street Journal, https://www5.in.tum.de/~huckle/Vancouv.pdf, accessed 25 March 2019.

[22] B. Eha, "Is Knight's $440 million glitch the costliest computer bug ever?" 9 August 2012, Cable News Network, https://money.cnn.com/2012/08/09/technology/knight-expensive-computer-bug/index.html, accessed 24 February 2019.

[23] "Report to the chairman, subcommittee on investigations and oversight, committee on science, space, and technology," House of Representatives, United States General Accounting Office Washington, D.C. 20548, Information Management and Technology Division, https://www.gao.gov/assets/220/215614.pdf, accessed 25 March 2019.

[24] C. Daramy-Loirat, D. Defour, F. de Dinechin, M. Gallet, N. Gast, C. Lauter, J. M. Muller, "CR-LIBM: a correctly rounded elementary function library," Proc. SPIE 5205, Advanced Signal Processing Algorithms, Architectures, and Implementations XIII, **5205**, 458–464, December 2003, DOI: 10.1117/12.50559.

[25] A. A. Jorgensen, "Apparatus for calculating and retaining a bound on error during floating point operations and methods thereof," U. S. Patent 9.817.662, 14 November 2017.

[26] A. A. Jorgensen, "Apparatus for calculating and retaining a bound on error during floating point operations and methods thereof," U. S. Patent 10,540,143, 21, January 2020.

[27] D. E. Knuth, The art of computer programming (3rd ed.), **II**: Seminumerical Algorithms, Addison-Wesley, Boston, Massachusetts, United States, 1997, ISBN: 978-0-201-89684-8.

[28] D. Patterson, J. Hennessy, Computer organization and design, the hardware software interface, 5th edition, Waltham, MA: Elsevier, 2014, ISBN: 978-0-12-407726-3.

[29] H. A. Chan, "Accelerated stress testing for both hardware and software," Annual symposium reliability and maintainability, 2004 – RAMS, Los Angeles, CA, IEEE, 346–351, DOI: 10.1109/RAMS.2004.1285473.

[30] H. Dawood, Theories of interval arithmetic: mathematical foundations and applications, Saarbrücken, LAP LAMBERT Academic Publishing, ISBN 978-3-8465-0154-2, 2011.

[31] G. Masotti, "Floating-point numbers with error estimates," Computer-Aided Design, **25**(9) 524-538, 1993, DOI: 10.1016/0010-4485(93)90069-Z.

[32] G. Masotti, 2012, "Floating-point numbers with error estimates (revised)," https://arxiv.org/abs/1201.5975, arXiv:1201.5975v1_accessed 9 January 2021.

[33] F. Benz, A. Hildebrandt, S. Hack, "A dynamic program analysis to find floating-point accuracy problems," ACM SIGPLAN Notices, PLDI 2012, **47**(6) 453–462, 2012, DOI: 10.1145/2345156.2254118.

[34] GNU, 2020, "GCC, the GNU Compiler Collection," Free Software Foundation, 2020-11-16, https://gcc.gnu.org/, accessed 8 January 2020.

[35] I. B. Goldberg, "27 bits are not enough for 8-digit accuracy," Comm, ACM 10:2, 105–106, 1967, DOI: 363067.363112.

[36] W. Dunham, Journey through genius: the great theorems of mathematics, John Wiley & Sons, Inc., New York, 1990, http://jwilson.coe.uga.edu/ emt725/References/ Dunham.pdf, ISBN-13: 978-0140147391, accessed 5 November 2020.

[37] W. Kahan, "Miscalculating area and angles of a needle-like triangle," 4 September 2014, https://people.eecs. berkely.edu/~wkahan/Triangle.pdf, accessed 14 August 2019.

[38] P. H. Sterbenz, Floating-point computation, Prentice-Hall, Inc., Englewood Cliffs, N.J., 1976, ISBN 0-13-322495-3.

[39] Å. Björck, Numerical methods in matrix computations, Switzerland, Springer, 2015, ISBN-13: 978-3-319-05089-8.

[40] Matrix market, National Institute of Standards and Technology, Computational Sciences Division, 2007, https://math.nist.gov/ MatrixMarket/index.html, accessed 4 August 2020.

Optimized use of RFID at XYZ University Library in Doing Auto Borrowing Book by Utilizing NFC Technology on Smartphone

Rony Baskoro Lukito[1,*], Vilianty Rizki Utami[2]

[1]*Computer Science Department, Bina Nusantara University, Jakarta, 11480, Indonesia*

[2]*Department of Management, University of Indonesia, Jakarta, 11480, Indonesia*

A R T I C L E I N F O	A B S T R A C T
	NFC (Near Field Communication) is a contactless communication technology based on a radio frequency (RF) field using a base frequency of 13.56 MHz. NFC technology is perfectly designed to exchange data between two devices via simple touch gestures. RFID is the process of identifying an object directly by radio frequency. There are two important components of an RFID system is the card or label (tag) and the reader. In each of tags have unique ID. In addition to the ID, the tag also contained a block that is used for security. On the application in the library, all the books that will be read by the reader have an RFID tag in it. With the tag on each book that is used for lending service, it can be made an application on a smartphone that supports NFC (Near Field Communication) which can be used by each user to borrow books independently, that does not need to come to the library staff to borrow books.

1. Introduction

With the development of ICT (Information and Communication Technology) by leaps and bounds, ICT can be applied to almost all existing activities, including at the university. One is the use of RFID on all student, lecturer and staff cards. So with RFID card, students and faculty can record the lecture attendance, borrow books, pay to eat, with just to put the RFID card on a card reader.

The library is one of the institutions that uses ICT to optimize its management which we know as library automation. Library automation is the use of automatic and semi-automatic data processing machines to maximize daily activities in the library, such as procurement, processing and circulation or services.

In library circulation service activities, library automation using RFID is widely used to borrow books from the library. Because in addition to student/lecturer cards, one of the applications of ICT is the use of RFID in all books in the college library. That way, the data of all books in the library can be connected and managed with ICT so that it can be used for circulation service activities in the library.

By using RFID in books in the library, librarians only need to put the books to be borrowed on the RFID reader (book reader), the RFID reader will read the tag ID books, check on the library database, then display the book data on the computer screen. If the library user agrees to borrow the book, the system will change the status of the book in the library database as a borrowed book on behalf of the student/lecturer ID. Then the RFID reader will disable the security block on the RFID tag in the book. So if the book was taken out of the library it wouldn't sound a security alarm. The borrowing process as above has been automated. So students or lecturer who will borrow the book, just put the card on a card reader and a book on book reader at a machine named "auto-borrow". The machine will then display the borrower data, including name, and the quota of books that can be borrowed, and also displays the books data. Then the borrower simply press the submit button, and the book status change to "borrowed". This auto-borrow machine is a normal PC connected to a card reader device. In the XYZ library there are 3 units of auto-borrow machines.

The process of borrowing books with an auto-borrow machine helps librarians, so that students, lecturers and staffs can perform self-service in the borrow books. However, the increase in the number of students and lecturers per day, as well as the increase in the number of books borrowed in a day, sometimes created queues on circulation officer and the book "auto-borrow" system.

Therefore, another system that has a similar function to the book auto-borrow system is needed but easy to implement. So, this will help students and lecturers who will borrow book.

*Corresponding Author: Rony Baskoro Lukito, rblukito@gmail.com

Figure 1: RFID System Phases in Libraries [1]

2. Objectives and Benefits

XYZ Library has an average of more than 1000 library visitors every year. Library users usually study in the library, read books, looking for journals or periodical, borrow/return books, and so on.

With the current number of smart phones that have been supported by NFC technology, smart phones can be made an application that can be used as an "auto-borrow" device. So students and lecturers who have smart phones with NFC and install the application on their smartphones, can borrow library collections books through their smartphones by attaching the NFC smartphone to the book tag ID, so the book data can be displayed on the smartphone screen.

The objectives of this research are facilitating librarian to collect data for book collection utilities, facilitate user to borrow library collection independently, reducing queues both in circulation staff and auto borrowing machines when borrowing traffic is high in certain times such as before library closes, and as back up systems when auto borrow machine is interrupted or less circulation staff available.

The benefit of this research is identifying and design systems that can optimize the use of RFID with NFC on smartphones in libraries, increase the efficiency and effectiveness of the collection borrowing process in the library, reducing dependence on a collection borrowing process, increasing the efficiency of the library collection procurement budget, and for evaluating library collections utilizations.

Limitation of this research is about systems to optimized use of RFID for auto borrowing library book collection by utilizing NFC Technology on Smartphone at XYZ Library.

Thus, library users who have smartphones with NFC and want to borrow book have another options besides queue at circulation desks or "auto-borrow" machines.

3. Literature Review

Libraries are institutions that manage collections of written works, printed works, and/or recorded works in a professional

manner with a standard system to meet the needs of education, research, preservation, information, and recreation of visitors. The law states that the purpose of the library is to provide services to users [2]. Furthermore, these services are described in Article 14, including: library services are carried out in a prime and oriented towards the interests of visitors, and each library needs to develop library services in accordance with advances in information and communication technology. One type of service in the library is circulation services. Circulation services are user services related to borrowing, returning, and extending collections [3].

3.1. Library automation

Library automation is a general term for Information and Communication Technology (ICT) which is used to replace the existing manual systems in libraries. Library automation refers to the use of computers and other peripheral media, such as magnetic media, hard disks, optical media, and so on, as well as the use of computers in accordance with library products and services in displaying all library functions and activities [4].

Below are the advantages of library automation [5]:

- Libraries get ICT infrastructure to support automation
- Optimizing time in doing work
- Avoid duplication of data
- Speed up access to information
- Technology used in library automation provides new learning for librarians.

3.2. RFID

RFID or Radio Frequency Identification is a generic term used to describe a system that transmits the identity (in the form of a unique serial number) of an object or person wirelessly, using radio waves [6]. RFID is usually used for identification and tracking [5].

Auto-ID technologies include bar codes, biometrics, smart cards, voice recognition, and RFID [7]. Auto-ID technology has been used to reduce the amount of time and labor required to manually enter the data, and to improve the accuracy of the data.

There are several components required to use an RFID system:

3.2.1. RFID Tag / RFID Transponder

Tag is a small radio device which is also known as a transponder, smart tags, smart labels, or radio barcode. The tag consists of a simple silicon microchip (usually less than half a millimeter in size) attached aerial and mounted on a substrate [8]. In addition, each tag has a unique ID

The RFID tag contain of at least 2 parts. One is an integrated circuit (chip) for storing and processing information, modulating and demodulating radio frequency (RF) signal, and other specialized functions. The other part is an antenna for receiving and transmitting signals.

This antenna that allows this tag is read by the contactless reader. The larger the antenna can be greater the distance the reader and tag. While chip is for storing the ID number and other information. This chip can be read-only (cannot write other information on this tag), read-write (tags can be read write many times) or write-once read-many (tags can only be written once, but can be repeatedly) [9].

RFID tags have various forms according to needs. For example, the tag for a book is a square form size 5x5cm. For

CD/VCD can use round tags that can be embedded in the middle of the CD/VCD. To tack on VHS tapes, RFID tags can be rectangular. In addition, there are also special tags such as tags for tracking fruits, tags that can be implanted under the skin and others.

3.2.2. ISO / IEC 15693 and ISO / IEC 14443g

So that RFID tags can be read by a tag reader from various vendors, RFID tags must have a standard that is used by the RFID reader to be able to communicate using the tag. There are 3 different standards for classifying RFID contactless smart cards [10].

Table 1: Standard contactless smart card

Standard	Card type	Approximate range
ISO/EIC 10536	Close-coupling	0-1cm
ISO/EIC 14443	Proximity-coupling	0-10cm
ISO/EIC 15693	Vicinity-coupling	0-1cm

The RFID standard used by library books is ISO 15693, and RFID standard for student and lecturer ID cards uses ISO 14443. Here is a diagram of a standard smart cards, including the contact and contactless [11]
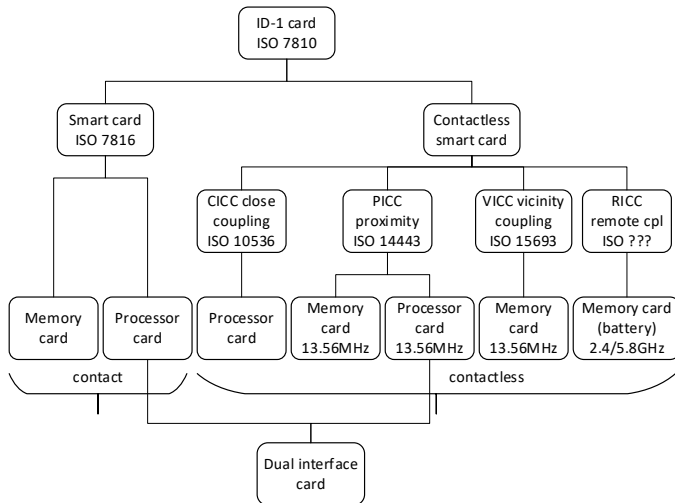
Figure 2: Family of contact and contactless smart card

3.2.3. Electronic Article Surveillance (EAS)

In a transponder/tag the ID contains a few bytes of data capacity up to several kilo bytes. But, there's 1 bit in special transponders used for security. One bit of data can provide status on the tag reader: 'transponder in the field' or 'transponders not in the field'.

One transponder bit is used in Electronic Article Surveillance (EAS) to check the status of goods. If the user brings goods / books through the EAS gate with the status 'transponders in the field', it will activate an alarm at the EAS gate [11]. Vice versa, if the tag status is 'transponders not in the field', the RFID tag will not activate the alarm.

3.2.4. Tag Reader

In addition to tags are also need a tool that serves to read the tags. This tool is called a tag reader. Readers are transceivers (a

combination of transmitters and receivers) whose role is to give commands to tags and receive data stored in tags [12]. Because this reader can read the unique ID contained in each tag.

Like tags, readers also have an antenna. Through this antenna, the reader can communicate with the tag. When the reader transmits radio waves, all tags within the transmission area and has the same frequency as the reader, will respond.

Communication between tag readers is done through 3 processes. First, the tag reader is activated by the tag reader radio frequency with 13.56MHz. Once active, the tag will wait for commands from the tag reader. Then, the reader will give commands to the tag and wait for the response from the tag. If the tag receives the valid command, then the tag will respond from the reader command earlier and sent back to the reader. All data transmissions are done through frequency 13.56 MHz [13].

Thus, communication between the reader and tag does not require physical contact (contactless), it can even pass, such as paper, wood, and so on [8].

3.2.5. Near-Field Communication (NFC)

At first, the NFC is not an RFID system, but the interface between the wireless data device, like the infrared or Bluetooth. However, NFC has some interesting characteristics in relation to RFID systems [14].

Data communication between 2 NFC interfaces using 13.56 MHz frequency. Because the same frequency used by the frequency of ISO 15693 and ISO 14443, the devices that support NFC can be used to read the tag ID. NFC is designed to be a secure form of data exchange. NFC device can be an NFC reader or NFC tag. This unique character allows communication between NFC devices [15]. Many smartphones sold in the market today have NFC interfaces. So with a particular application, the smartphone can read the tag ID ISO 15693.
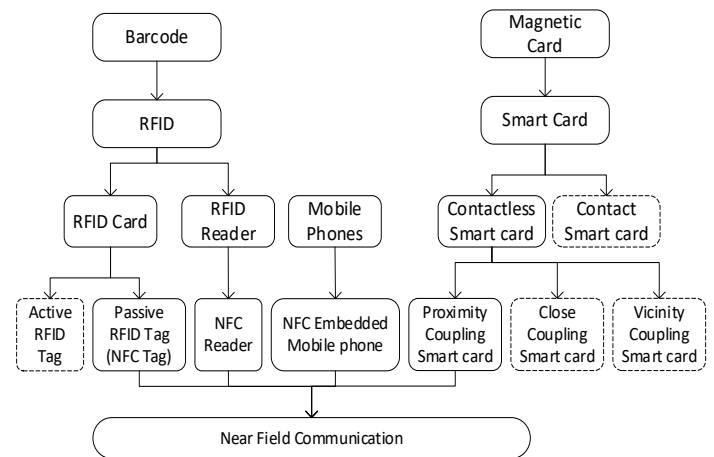
Figure 3: NFC Technology Evolution [16]

NFC has 3 communication models [15]:

a. Peer-to-peer

NFC can be used to exchange data between devices, with data exchange rates of up to 424Kbps. It works on the NFCIP-1 protocol, whose details and electromagnetic properties are standardized to ISO 18092 and ECMA 320/440.

b. Reader-writer

NFC can be used to read / write (reader / writer) on tags and smart cards (smart cards). In this communication model, active NFC devices can act as initiators and passive tags act as targets. This mode allows data exchange rates of up to 106 Kbps.

c. Card emulation

In this mode the HFC-handset behaves as a standard smart card. In this mode, the NFC device emulates an ISO 14443 smart card chip. This smart chip is integrated into the mobile device and connected to the NFC module to allow communication to take place [15].

There are several benefits of NFC nowadays. Apart of facilitating cashless and easy payment, NFC can be used for access control, consumer electronic product, health world, facilities for collection and exchange information, coupon and loyalty, and transportation [17]

Figure 4: Utilizing NFC in several devices.
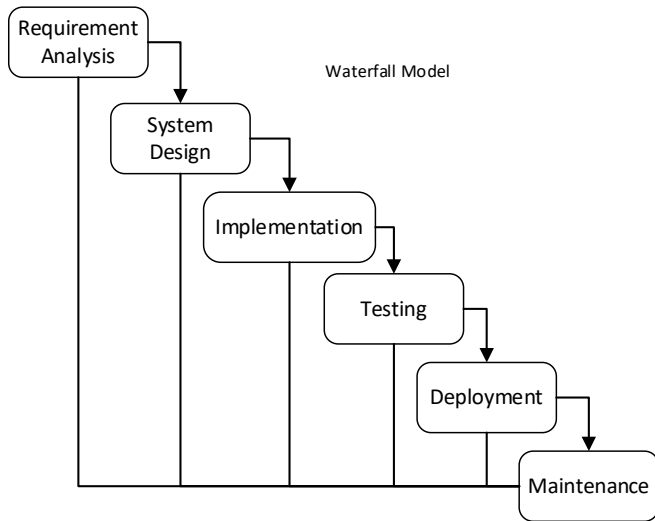
Figure 5: Waterfall Model

4. Research Methods

SDLC is the stages of work carried out by system analysts and programmers in building information systems and methods for developing these systems. The system built using SDLC will make it easier to identify problems and design the system as needed in solving these problems. One of the most frequently used SDLC in system development is SDLC Waterfall.

The SDLC Waterfall model is a software development method where the work must be carried out sequentially, each development progress is considered to flow downward, like a waterfall, through several stages that must be carried out. So that software development can be done successfully. In this waterfall model, all phases or stages must be carried out sequentially and until finished, before moving on to the next stage. So, in the waterfall model, each phase can be repeated several times until the phase is completely finished [18]. Researchers are expected to focus on one phase until completion and not work on other phases in parallel [19].

5. Results and Discussion

5.1. Library Database

With the implementation of the RFID system in the library, all the books must be affixed with RFID labels. Tag ID on the label associated with the data in the library books database. Here's an example in the table below:

Table 2: Example of book database

Book_tag_ID	Book_id	Book title
fef2d68f	20200200449	Accounting 1
fef37414	19991000919	Computer Network
fef57f30	20090100182	Database Systems
…	…	…

Therefore, if the book is placed/attached to the book reader (RFID reader) on the auto-borrow machine, on an NFC device, as well as in librarian computer, the system will search for the ID tag in the database and will display on screen the data the book data.

Like the book database, the users (lecturers/students/employees) XYZ University database is also connected with their ID card.

Table 3: Example Univ. XYZ Identity cards database

Card_tag_id	User_id	Name
b0ffc9da	0210335632	Anthony
1b9d52ac	0331970112	Brown
6385f8f4	0123502865	Charley
…	…	…

After borrowing the book, the user_id, book_id, and date of borrowing will be entered into a book borrowing transaction table. After the book is returned, the table will be updated with the book return date, as in the example below:

Table 4: Example Univ. XYZ Book transaction database

Book_id	User_id	Borrow_date	Return_date
fef2d68f	0210335632	05/20/2020 14:14	05/30/2020 10:10
fef37414	0331970112	07/07/2020 12:13	07/14/2020 09:09
fef57f30	0123502865	11/11/2020 11:11	NULL
…	…	…	…

5.2. Borrowing Process

For borrowing process using NFC smartphone is similar to borrowing using auto-borrow machine. At the auto-borrow machine, when the user who would like to borrow a book should put a membership card in the card reader and the book to be borrowed in the book reader. To borrow a book with the NFC smartphones, the user must first install the application which will be used for borrowing books. Then users should do the following steps:

- Login to the application using their university email and password.

- Once logged in, then the user can look their borrowing history, check borrowing status, check obligation or can scan a book with RFID tags that will be borrowed by the NFC smartphones.

- The application will look for the data to the library book database server (Table 2) about that book data and display it on the smartphone screen.

- User should click *Borrow* button if they are sure going to borrow a book.

- The application will update the book transaction database (Table 4) about borrowing the book.

- In addition, the application will tell the NFC device (smartphone) to disable security on the RFID tag a book, so that the book did not make the alarm sounds when taken out of the library area.

6. Use Case

Application use case in NFC smartphones can be described by using use case diagrams as in the picture below :
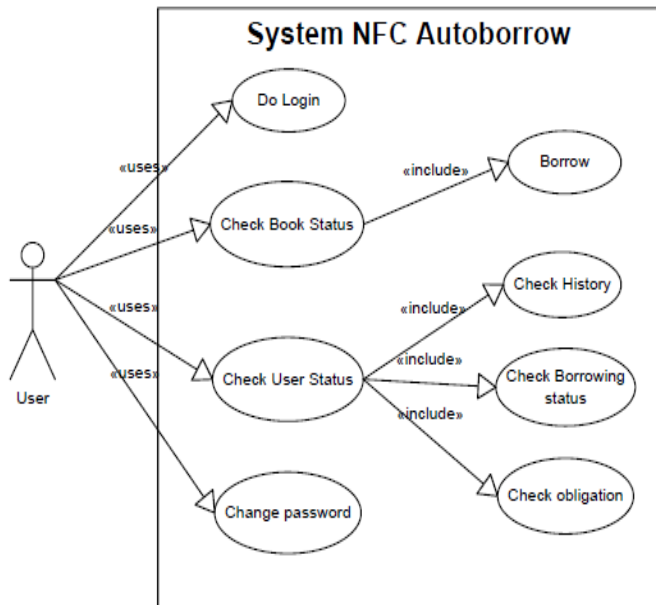
Figure 6: Use case business process NFC auto-borrow system

After the user (student/lecturer/employee) install an auto-borrow NFC application on a smartphone (which supports NFC), respectively, then the user have to login.

After logging in, users can attach their smartphone to the book to be borrowed. When the book ID tag is detected by the NFC smartphone, the application will search for the book data on the database server according to the ID tag that was read. Book data such as title, author, book code, edition, publisher, year published, and ISBN will display on the smartphone screen. If users want to borrow book, they only need to press the "submit" button. The application will update the book status in the database and disable the EAS (security) status on the book tag.

In addition to lending library books, this application can also be used to view the status of the user. Check history is used to see a list of books that have been borrowed by the user. Check Borrowing Status, useful for checking the current status of borrowed books, including title, author, and book returns due. Check Obligation is useful for viewing user obligations, such as the amount of fines to be paid for late returning the book.

7. Conclusion

From the results of research on the use of NFC on smartphones applied to automatic borrowing (auto-borrow) books in library, it can be concluded as follows:

a. Students, lecturers, and employees who have smartphones with NFC can use it to borrow books by them self, no need to queue for the library circulation staff or on auto-borrow computers to borrow books from the library.
b. With the NFC's smartphone capability to deactivate the EAS tag ID (security), it will trigger the programmer to create an application that can be used to disable EAS, and it is certainly influential in terms of the number of lost library books. Because if the EAS is not active, the book will easily be taken out of the library without turning on the alarm system.

8. Recommendations for further research

Application of systems that optimized use of RFID in XYZ library in doing auto borrowing book with utilization of NFC on Smart phone could be used not only for book collection on library but also on other kind of collection that using RFID as security systems. In XYZ library other collection that use RFID are periodical, final works and multimedia collection. Therefor further research, we will measure further optimization for this system for different rules of borrowing library material other than book. Also, its implication on collecting utilization data library collection that only can be read on the spot for library user.

References

[1] LibBest, Four phases of library RFID system, Mar. 2020.
[2] Perpusnas, Undang-undang nomor 43 tahun 2009 tentang perpustakaan, 2009.
[3] M. Sulaiman, Kepuasan pengguna terhadap fasilitas Auto-Borrowing Machine di Library and Knowledge Center (LKC) Binus University Kampus Anggrek, Universitas Indonesia, 2013.
[4] A.S. Mishra, T.S. Kumar, "Library automation: issues, challenge, and remedies," Times International Journal of Research, 9–16, 2015.
[5] D.M. Pandya, M. Darbar, "Benefits and disadvantage of library automation: a study of academic library users," International Journal of All Research Education and Scientific Methods (IJARESM), 14–19, 2017.
[6] M. Roberti, RFID journal, Emerald X, 2020.
[7] What is automatic identification (auto-id), IGI Global, 2013.
[8] RFID technology, RFID Centre, May 2020.
[9] V.D. Hunt, A. Puglia, M. Puglia, RFID - A Guide to Radio Frequency Identification, John Wiley & Sons, Inc., New Jersey, 2006, doi:10.1002/0470112255.
[10] M. Zurita, R.C.S. Freire, S. Tedjini, S.A. Moshkalev, "A Review of

Implementing ADC in RFID Sensor," Journal of Sensors, 1–14, 2016, doi:10.1155/2016/8952947.

[11] K. Finkenzeller, RFID Handbook, John Wiley & Sons, Ltd, West Sussex, UK, 2010, doi:10.1002/9780470665121.

[12] N.K. Singh, P. Mahajan, "Application of RFID technology in libraries," International Journal of Library and Information Studies, 1–9, 2014.

[13] J. Scalzo, J. Gates, V. Potnis, M. Howell, W. Tran, Using ISO 15693 compliant RFID tags in an inventory control system, Louisiana.

[14] C.-H. Lin, P.-H. Ho, H.-C. Lin, "Framework for NFC-Based Intelligent Agents: A Context-Awareness Enabler for Social Internet of Things," International Journal of Distributed Sensor Networks, **10**(2), 978951, 2014, doi:10.1155/2014/978951.

[15] D. Trivedi, "Near field communication," Institute Of Technology Nirma University, Ahmedabad, 2015.

[16] V. Coskun, K. Ok, B. Ozdenizci, Near field communication: from theory to practice, John Wiley & Sons, Ltd., West Sussex, UK, 2012.

[17] M. Rifqi, N.K. Wardhani, "Aplikasi peran dan kegunaan teknologi near field communication (NFC) terhadap kegiatan proses belajar mengajar di perguruan tinggi (studi kasus: Universitas Mercu Buana)," Jurnal Ilmu Teknik Dan Komputer, **1**(1), 20–26, 2017.

[18] Y. Bassil, "A simulation model for the waterfall," International Journal of Engineering & Technology (IJET), 2012.

[19] W. Nugraha, M. Syarif, W.S. Dharmawan, "Penerapan metode SDLC waterfall dalam sistem informasi inventory barang berbasis desktop," JUSIM (Jurnal Sistem Informasi Musirawas), **3**(1), 22–28, 2018, doi:10.32767/jusim.v3i1.246.

Enterprise Resource Planning Readiness Assessment for Determining the Maturity Level of ERP Implementation in the Industry in Indonesia

Santo Fernandi Wijaya[*,1], Harjanto Prabowo[2], Ford Lumban Gaol[3], Meyliana[1]

[1]*Information Systems Department, School of Information System, Bina Nusantara University, Jakarta, 11480, Indonesia*

[2]*Management Department, BINUS Business School Undergraduate Program, Bina Nusantara University, Jakarta, 11480, Indonesia*

[3]*Computer Science Department, BINUS Graduate Program, Bina Nusantara University, Jakarta, 11480, Indonesia*

A B S T R A C T

The textile industry is one of the prioritized industries, because it contributes to the country's foreign exchange, absorbs a large number of workers, and fulfills the need for national clothing. To increase work efficiency and productivity, the textile industry must use ERP. However, ERP implementation still has a relatively high failure rate. ERP readiness assessment is one of the main issues to achieve success in implementing ERP. Previous research is still limited to research about readiness for achieving success in ERP implementation. The research results have indicated that the maturity of the organization is a very significant dimension with a weight of 43.51%. By knowing the maturity level of the organization for ERP implementation can identify factors that become weaknesses for organizations to take corrective steps, so as to reduce the failure rate of ERP implementation in the industry. This research methodology uses a quantitative approach using R software to determine the principal component analysis and uses the Order Preference Technique with the Ideal Solution to weighted the identified factors. This research aims to determine organization readiness by developing the maturity level of ERP implementation in the industry in Indonesia which conducted a case study experiment in the textile industry in Indonesia. The result of this research is the development of an ERP readiness assessment to assess the maturity level of the organizations in ERP implementation.

1. Introduction

The textile industry is one of the industries that is prioritized for development because it has a strategic role in the national economy, namely as a contributor to foreign exchange, absorbing large numbers of workers, and to meet national clothing needs. To increase work efficiency and productivity, the textile industry must use ERP. ERP can improve the performance of an organization, but until now the ERP implementation for the industry still has complexity with a high failure rate, so this causes implementation costs to be expensive. Referring to previous research, the ERP readiness assessment can assess the readiness of an organization in implementing ERP. ERP readiness assessment can be reviewed from the perspective of top management, project management, people, change management, technical requirements [1]. By identifying the weaknesses factors

of the organization, management can develop ERP readiness assessment and make an evaluation to increase the organizational maturity level according to best practice [2-5]. The contribution of this research is the development of an ERP readiness measurement tool to increase the effectiveness of ERP implementation strategies for the industry, so that management can know the level of company readiness before making decisions for ERP implementation. Based on previous reseach, ERP implementations have a failure rate of 60% to 90%. The problem solution is to identify critical success factors in ERP implementation with a focus on organization, technology adaptation, and business processes [6, 7]. Also, by assessing the readiness of the organization, it can be evaluated the weaknesses and strengths of the organization to adapt to change, so that the company can achieve organizational agility and ERP implementation success [8-10]. Previous research shows that there is still little research that discusses the maturity assessment

of an organization before top management decides to implement ERP. The development of ERP readiness assessment is one of the main issues related to achieving success in implementing ERP. This research can help the top management of an organization or consultant party to assess the maturity level before deciding to implement ERP with a discussion of four perspectives such as processes, people, organizational, and technology which based on the development of the Leavitt Diamond Model [11]. The four components of Leavitt Diamond Model are people, tasks or processes, technology, and structure or organization prominent success factors for improving industry performance. This matter is considered for organizations to assess the readiness level of an organization in implementing ERP, so that top management of the organization can find out the factors that are the weaknesses and strengths of the organization, to be able to make improvements, so that the relatively expensive investment value can achieve successful ERP implementation for an industry. This research explain identify the factors of ERP readiness assessment and the characteristics of the maturity level of the organization in ERP implementation. This is the novelty of this research which is the development of previous research to help the top management of the industry to find out the readiness of a company to adapt to a change in order to achieve the best practices and agile organizations..

2. Experimental procedure

The experimental procedure of this research uses a study case in the textile industry in Indonesia by using a quantitative approach technique with R software to determine the Principal Component Analysis (PCA) [12]. The objective of PCA is to reduce the data dimension by eliminating the correlation of variables by transforming the original variable into a new uncorrelated variable so that the data can be interpreted. PCA is a non-parametric method that uses linear algebra to extract relevant information or patterns from a dataset with multivariate attributes. This research also use of Technique for Order Preference Technique with the Ideal Solution (TOPSIS) method to identify the weight factors. The TOPSIS method approach can be used as an ERP assessment tool to determine the weighting and ranking of factors for the main weight, the weight of sub-factors, and the final weight. TOPSIS is a decision-making method for ranking and prioritizing Multi Criteria Decision Making (MCDM). The stages of weighting the TOPSIS method are as follows [13]:

1. Building a normalized weighted matrix using the following formula:

$$Y_{ij} = \frac{X_{ij}}{\sqrt{\sum_{i=1}^{m} X^2_{ij}}}$$

2. Building a weighted normalized matrix by multiplying the normalized matrix with the weighting value of entropy weighting, with the normalization formula for the weighting matrix v as follows:

$$V = \begin{bmatrix} V_{11} V_{12} \dots .. V_{1n} \\ V_{21} V_{22} \dots .. V_{2n} \\ V_{m1} V_{m2} \dots .. V_{mn} \end{bmatrix} = \begin{bmatrix} W_{1r11} W_{2r12} \dots W_{nr1n} \\ W_{1r21} W_{2r22} \dots W_{nr1n} \\ W_{1rm1} W_{2rm2} \dots W_{nrmn} \end{bmatrix}$$

3. Determine the matrix for positive and negative ideal solutions. The positive ideal solution is denoted by A +, while the negative ideal solution is denoted by A-. With the following formula:

$$A^* = \left\{ \left[\max_i V_{ij} \,|j \in J \right], \left[\min_i V_{ij} \,|j \in J^1 \right] \right\} 1 = 1, 2, \dots . m \}$$

$$= \{V_1^* V_2^*, \dots \dots V_j^* \dots .. V_n^* \}$$

$$A^- = \left\{ \left[\min_i V_{ij} \,|j \in J \right], \left[\max_i V_{ij} \,|j \in J^1 \right] \right\} i = 1, 2, \dots m \}$$

$$= \{V_1^-, V_2^-, \dots \dots V_j^* \dots .. V_n^* \}$$

4. Calculate the distance between the value of each alternative solution with a positive ideal solution matrix and a negative ideal solution matrix. By using the following formula:

$$S_i^* = \sqrt{\sum_{j=1}^{n} (V_{ij} - V_i^*)^2}, \qquad i = 1, 2, \dots m$$

$$S_i^- = \sqrt{\sum_{j=1}^{n} (V_{ij} - V_i^-)^2}, \qquad i = 1, 2, \dots m$$

5. Calculating the preference value to an alternative ideal solution, with the following formula:

$$C_i^* = \frac{S_i^-}{S_i^* + S_i^-}$$

6. Ranking the value of Ci +. The best solution is to have the shortest distance to the ideal solution and the farthest distance to the ideal negative solution.

In processing the data of this study, the authors collected data from respondents using a questionnaire method. Then based on the results of the questionnaire, the authors validated the data using PCA. The results of data processing from PCA are to develop indicators as a basic concept in developing the ERP readiness assessment model. Based on the literature survey, the authors classify be indicators associated with these four dimensions. Based on the literature survey, the authors mapped the main variable (processes, people, organizational, and technology) with sub-variables and indicators related to the readiness of ERP implementation [14-18]. From the results of the literature survey, it was found that 24 sub-variables and 61 indicators affect organizational readiness in ERP implementation. Then the authors define indicators and make questionnaire statements, then the authors distribute data to respondents using a questionnaire method. A list of sub-variables, defining indicators and questionnaire statements can be seen in Table 1.

Table 1: Sub-variables, Indicators, Definition and Questionnaire Statement

No	Sub-variables	No	Indicators	Code	Definition	Questionnaire statement
1	Business processes	1	Committed to change	PR01	Business process change need the organization commitment to change to be standardized, understood and documented.	The role of management's commitment to standardized, understood, and documented changes to business processes
		2	Business processes change	PR02	Implementation success requires a change of business processes.	Changes in business processes to achieve successful ERP implementation.
		3	Business processes redesign	PR03	Redesigning the business processes of an organization to best practice processes.	It is necessary to redesign business processes based on best practice business processes.
2	Process standarized based on industry best practice	4	Integrated business process	PR04	Integrate business process and operations for improving organization business.	The integration of business processes and operations is necessary to improve the organization's business.
		5	Work processes standarized and documentation	PR05	Standarization of work processes and documentation.	Standardization of work processes and complete documentation are essential in ERP implementation.
3	Change Management	6	Cultural change management	PR06	Cultural change management is a concern to successfully implement.	Cultural change management must be done to ensure the change process runs well.
		7	Open minded for changes	PR07	Open minded for changes.	An open mind from all parties involved in accepting the change process.
4	Skill and competency	8	Management's skill and competency	PE08	Management's skills determines the strategy of utilizing ERP usage for business development.	Management expertise in determining strategies for utilizing ERP for business development.
		9	User's skill and competency	PE09	Skilled user to understand of process business of system used.	User expertise in understanding the business processes of the system used.
		10	IT staff's skill and competency	PE10	Specialized skills and competency of the IT team will increase the ERP implementation success.	The expertise and special abilities of the IT team in improving the success of ERP implementation.
5	Project Manager	11	Adequate ERP project experience	PE11	Project manager has adequate ERP project experience.	The project manager has sufficient ERP project experience.
		12	High level overview	PE12	Have a thorough understanding of the knowledge, experience, ability, and coordinate all the processes of the ERP Project.	Project Managers have a thorough understanding of the knowledge, experience, capabilities, and coordinate all processes in ERP implementation.
6	Training	13	Delivered to all parties	PE13	Training is obliged to be delivered to all parties, including program, mechanism, material.	Mandatory training is delivered to all parties involved, including programs, mechanisms and materials.
		14	Users adaptation to new process	PE14	Users can adapt to new processes from taking ERP implementation training.	Users can adapt well to the new process from taking ERP implementation training.
		15	Understand the overall concepts	PE15	Training goal to understand the overall concepts of the ERP system.	Training is useful for understanding the overall concept of an ERP system.
		16	Transfer knowledge	PE16	Transfer of knowledge to improve the quality of employees.	Knowledge transfer for users to improve the quality of employees is very necessary.
7	Project team	17	Formed project team	PE17	Formed project team accordingly to project the scope.	The project team must be formed according to the scope of the ERP project.
		18	Technical expertise	PE18	Technical expertise, understanding for business processes, processes knowledge, and ERP project experience.	There is a project team that has technical expertise, understanding of business processes, knowledge of ERP processes, and ERP project experience.
		19	Involved Business Process Owner	PE19	The involvement of a Business Process Owner in the project team to map and manage business processes according to ERP selected.	The involvement of a Business Process Owner in the project team to map and manage business processes according to the ERP that will be implemented.
8	Human Resource Management	20	Available Human Resource	PE20	Ensure the availability of adequate Human Resources to involved the ERP implementation process.	Ensuring the availability of adequate human resources to carry out the ERP implementation process.
		21	Development of competent human	PE21	Development, utilization, and maintenance of competent human force to achieve goals of an organization.	The process of developing, utilizing, and maintaining competent human resources to achieve organizational goals in ERP project implementation.
9	Clear roles and responsibilites	22	Clear roles of project	PE22	Clear roles of project stakeholders should be clearly defined, fully documented and understood.	The clear roles of project stakeholders must be clearly defined, documented and fully understood by all teams involved.
		23	Clear responsibilities of project	PE23	Determination of the responsibilities of the tim involved in ERP implementation.	It is very important to determine the responsibility of the team involved in ERP implementation.

No	Sub-variables	No	Indicators	Code	Definition	Questionnaire statement
10	Employee /staf/user involvement	24	Employee commitment	PE24	Commitment of employees to implement ERP projects.	Employee commitment in implementing ERP projects is very necessary.
		25	Employee involvement	PE25	Employees are actively involved in the process of ERP implementation stages.	Employees are actively involved in participating in ERP implementation activities.
11	Shared values	26	Project champion	OG26	Project champion is a reliable person and trusted to regarding implementation.	Project champions are needed in ERP implementation, because project champions are people who can be relied on and trusted in ERP implementation activities.
				OG27	Project champion can ensure implementation processes run or the possibility of project success.	The project champion is needed to ensure the implementation process runs well and also determines the success of the ERP project.
				OG28	Project champion in an ERP implementation is fundamental in implementation.	Project champion is fundamental in ERP implementation.
		27	Shared beliefs	OG29	Belief to benefits of using ERP in organizations.	All parties involved must have confidence in the benefits of using ERP in the organization.
		28	Cross functional support	OG30	Get support all function of organization.	Support from all organizational functions in achieving successful ERP implementation is needed.
				OG31	Cross department cooperation.	Cross-departmental collaboration is essential in achieving a successful ERP implementation.
12	Project Management	29	Measurement of performance specific, measurable, achievable, relevant, time bound	OG32	Performance measurement of ERP projects specifically in the planning, implementation, and post-ERP implementation processes.	Specific ERP project performance measurement in the planning, implementation, and post-ERP implementation processes is essential.
				OG33	Performance measurement of ERP projects that the measurable results of each stage of implementation.	Measurable ERP project performance measurement at each stage of ERP implementation is needed
				OG34	Performance measurement of ERP projects that the ERP implementation is achieved.	ERP project performance measurement that pays close attention to the target of achieving ERP implementation must be considered.
				OG35	Performance measurement of ERP projects that the relevant results according to the company's vision and mission.	ERP project performance measurement must pay attention to the results that are relevant to the company's vision and mission.
				OG36	Performance measurement of ERP projects that the performance of the ERP project in accordance with a predetermined target time.	ERP project performance measurement must be in accordance with a predetermined time schedule.
		30	Monitoring of performance	OG37	Focused on customer need.	ERP project performance measurement results should focus on customer needs.
				OG38	Controlling for implementation schedule.	The performance control process is indispensable in ERP implementation.
		31	IT Governance	OG39	Focus on IT governance with concerned to information quality.	IT governance must pay attention to the quality of information generated by ERP.
13	Knowledge Management	32	Knowledge sharing process	OG40	Knowledge sharing process can greatly improve employees' ability to learn and manage knowledge.	The process of knowledge sharing is needed in an effort to improve employee learning skills and manage their knowledge.
		33	Data and information standarized	OG41	Ensure information standarized in all business operations.	Data and information standarizedon all business operations supports the use of ERP.
14	Organizatio nal structure	34	Centralization	OG42	Activities of an organisation, planning and decision-making are controlled by the top management and project manager.	Planning and decision-making activities that are controlled by top management and project managers are required in ERP projects.
		35	Specialization	OG43	Specialization is a business strategy that focuses on specialized production for increasing productivity with ERP use.	A business strategy that focuses on specialized production is needed to increase productivity with the use of ERP.
		36	Formalization	OG44	Formalization as a process to define procedures, standardization processes, responsibilities, and completely documented.	Organizational formalization is needed in ERP implementation as a process in determining procedures, standardizing work processes, and fully documented responsibilities.
		37	Size of organization	OG45	The success of ERP projects may be impacted by organization size.	The size of the organization affects the success of an ERP project.
		38	CIO position	OG46	CIO's role is to determine the alignment of business and technology, ensure the availability, accuracy, accuracy and security of information as needed to achieve the organizational goals.	The role of the Chief Information Officer (CIO) is needed to determine the alignment of business and technology, ensuring the availability, accuracy, accuracy, and security of information according to management needs to achieve organizational goals.
		39	Top management commitment	OG47	Involved in every step of ERP project, monitor the progress ERP.	Top management must be involved in every process and monitor the progress of the ERP project.
				OG48	Focusing on top management's commitment and willingness to provide sufficient resources.	Top management commitment is needed to provide adequate resources and achieve a successful ERP implementation.

No	Sub-variables	No	Indicators	Code	Definition	Questionnaire statement
15	Organizational style	40	Communication	OG49	Communicate all activities in the ERP implementation process to all parties involved.	Communicating all activities in the ERP implementation process to all parties involved is very important.
				OG50	Sign off as proof of the communication and agreement on project work.	Sign off as proof of communication and agreement on ERP project work must be approved by the parties involved.
		41	Organizational culture	OG51	Organizational culture determines the right way to attitude and make changes, including with regard to ERP implementation.	Organizational culture determines the right way to behave and make changes in ERP implementation.
		42	Vision and mission	OG52	The clear of vision and mission as a guide ERP implementation.	A clear organizational vision and mission guides the implementation of ERP implementation.
				OG53	A clear vision and mission must be revealed and communicated into an important part that will support the ERP project.	A clear organizational vision and mission must be revealed and communicated to all parties involved to support the implementation of the ERP project.
16	Organizational strategy	43	Goals and objectives	OG54	Identification of measurable goals, the formation of the project organization, and the motivation of the project team.	The process of identifying measurable goals, establishing a project organization, and the motivation of the ERP project team are important factors in supporting ERP implementation.
				OG55	Define and must be communicated effectively among stakeholders involved.	Project objectives and objectivity must be defined and communicated effectively to the stakeholders involved.
		44	Project planning (scope, time, budget, risk, other resources)	OG56	Determine the scope of the ERP project.	Determination of a clear ERP project scope will determine the success of ERP implementation.
				OG57	Confirming the ERP project for determine target of go live time.	All ERP project activities must be confirmed with all parties involved in order to determine the target time to go live.
				OG58	Budget usage needs to be controlled rigorously throughout the ERP implementation.	Budget usage needs to be strictly controlled during ERP implementation.
				OG59	Project planning implementation can reduce the risk for the failure.	The implementation of project planning can reduce the risk of failure in ERP implementation.
				OG60	Project planning implementation requires the availability of complete resources.	ERP implementation project planning must have complete resource availability.
17	System rollout	45	Rollout system	TH61	Rollout system is a structured set of processes to anticipate events that cause ERP implementation setbacks.	A system rollout function to anticipate things that cause ERP implementation setbacks must be available.
	configuration	46	Configuration system	TH62	A configuration refers to the hardware and software that greatly affect ERP implementation success.	Correct configuration of hardware and software affects the success of ERP implementation.
18	System integration	47	IT infrastructure	TH63	Determine the software, hardware, and network infrastructure that will be needed for the ERP system.	Determining the correct software, hardware and network infrastructure is needed in ERP implementation.
				TH64	Adequate IT infrastructure, hardware and networking for ERP implementation.	It is necessary to conduct an assessment of the adequacy of IT infrastructure, hardware and networks before implementing ERP.
		48	Processes improvement	TH65	Process improvements need to be identified before the implementation of ERP.	Identification of process improvements must be done prior to ERP implementation.
				TH66	Information usable that provides benefits that support decision making related to ERP projects.	Useful information is needed to support decision making in ERP projects.
		49	Data management	TH67	Data comprehensive that supports decision making related to ERP projects.	Complete data comprehensively supports decision making in ERP projects.
				TH68	Data availability as needed to support decision making related to ERP projects.	The availability of data that is suitable for management needs for decision making in ERP projects is needed.
19	IT structure and legacy systems	50	IT structure	TH69	IT team structure to coordinate ERP project activities from planning to post-go live.	Good IT team structure to coordinate ERP project activities from planning to post-go live.
		51	Legacy systems	TH70	Good integration with legacy systems.	Integration with old systems in ERP implementation must be done well.
20	Technology selection & adaptation (Technological readiness)	52	Technology selection	TH71	The company's readiness in selection, providing, and implementing technology that supports business strategies.	An assessment of the company's readiness in selecting, providing, and implementing technology that supports business strategies must be carried out.
		53	Technology adaptation	TH72	Adaptation of technology used to support optimal ERP implementation strategy.	Adaptation of the technology used to support the ERP implementation strategy is needed.
21	System acceptance and usage	54	System acceptance	TH73	Acceptance of users to use ERP in completing work will increase the work more effective and efficient.	Acceptance of users to use ERP in completing work and improving a more effective way of working is very important
		55	System usage	TH74	The use of information technology can improve the performance of the organization.	The optimal use of information technology can improve overall organizational performance.
22	Trouble shooting	56	Helpdesk system	TH75	The available of a helap system to help users in providing fast response in troubleshooting related to ERP use.	The availability of a helpdesk system will help users quickly solve problems related to the use of ERP.
		57	Service to users	TH76	The available of an IT team to serve users in providing troubleshooting related to ERP use.	The availability of an IT team that provides services for users and provides solutions to problems related to the use of ERP is very much needed.

No	Sub-variables	No	Indicators	Code	Definition	Questionnaire statement
23	External consultant / expertise	58	Functional consultant	TH77	Analyzes running business processes and provides directions for following ERP business processes that can be implemented.	Consultants can analyze running business processes and provide directions for following ERP business processes so that they can be implemented properly.
		59	Technical consultant	TH78	Consultant expertise in providing directions and solutions for technical matters related to ERP implementation.	Consultants can provide direction and solutions for technical matters related to ERP implementation.
24	Vendor relationship and support	60	Vendor engagement	TH79	Relationships and angagement with vendors will speed up problem solving related to the ERP implementation process.	Relationships and agreements with vendors can speed up problem solving related to the ERP implementation process.
		61	Supply Chain Management	TH80	Network of interconnected department for fulfilling the material required by the other departments or by the customers.	Inter-departmental networks that are interconnected to meet material requirements for other departments or for customers are very necessary in ERP.

The characteristic of CMMI is initial, defined, managed, measured, and optimized [19]. Initial: Unpredicable, uncontrolled, no-automation. Defined: Some shared decision-making. Managed: Collaboration, analyze trend, and portfolios. Measured: Central automated process, standardized across the organization. Optimized: Focused on continuous improvement, stability provides a platform for agility and innovation. The related between characteristic of maturity level with readiness of ERP readiness assessment module, which can be seen in Figure 1.
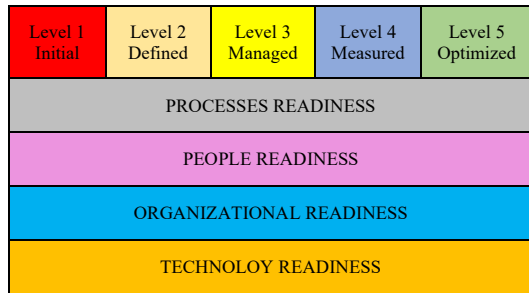
Figure 1: ERP Readiness Assessment model

Based on these main variables (processes readiness, people readiness, organizational readiness, and technology readiness), it is derived into 24 sub-variables and 61 indicators. The grouping of processes readiness variables is derived into 3 sub-variables and 7 indicators can be seen in Figure 2.
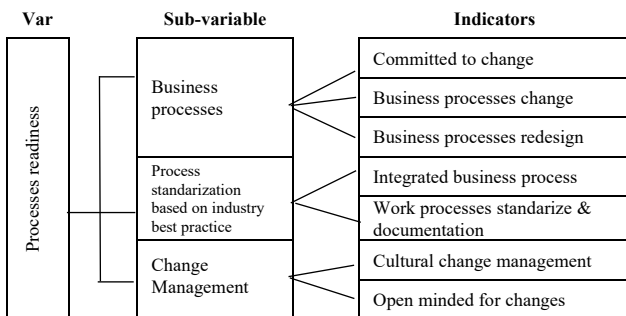
Figure 2: Processes readiness of ERP Readiness Assessment

The grouping of people readiness variables is derived into 7 sub-variables and 18 indicators can be seen in Figure 3.

The grouping of organizational readiness variables is derived into 9 sub-variables and 25 indicators can be seen in Figure 4.
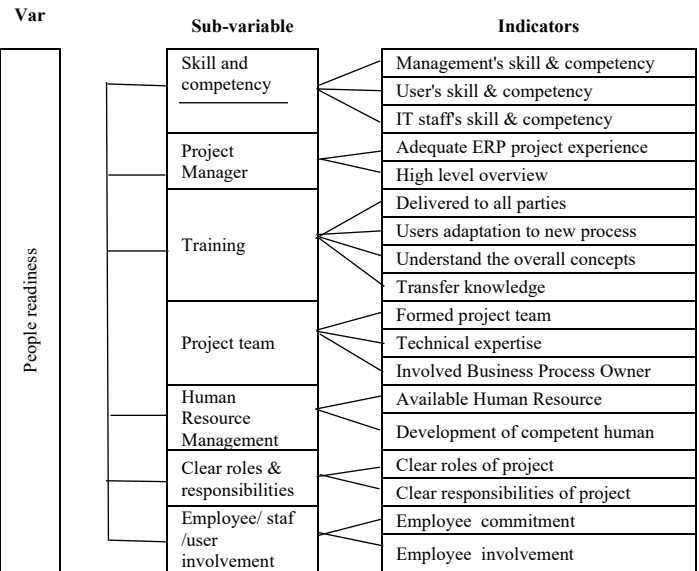
Figure 3: People readiness of ERP Readiness Assessment
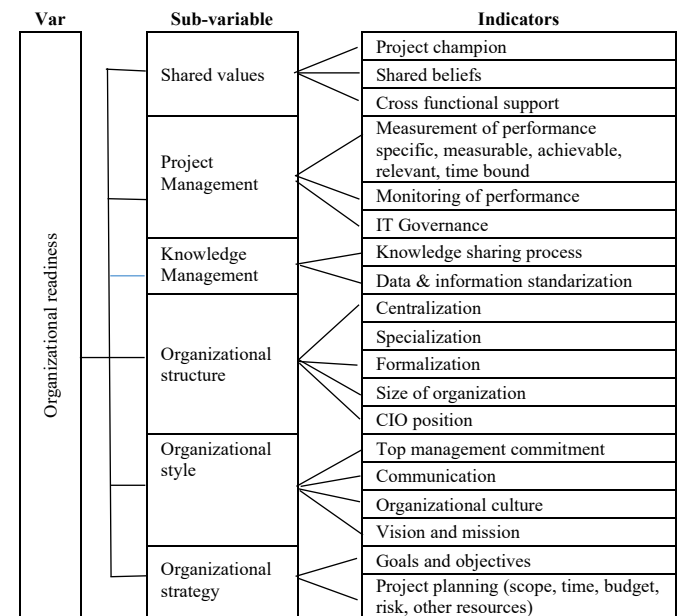
Figure 4: Organizational readiness of ERP Readiness Assessment

The grouping of technology readiness variables is derived into 8 sub-variables and 17 indicators. The grouping of technology

readiness for each sub-variables and indicator can be seen in Figure 5.
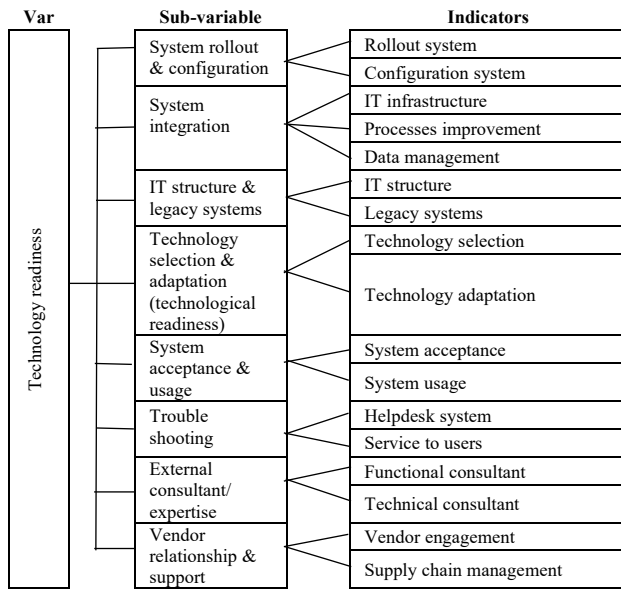
Figure 5: Technology readiness of ERP Readiness Assessment

3. Result and discussion

3.1. Data processing of the questionnaires

As a result of distributing questionnaires to respondents, Authors made a characteristics profile of respondents which can be seen in Table 2.

Table 2: Characteristics profile of respondents

Respondent profile		Frequency	%
Gender	Male	96	73%
	Female	35	27%
		131	100%
Age	20-30 years	38	29%
	31-40 years	34	26%
	41-50 years	36	27%
	> 51 years	23	18%
Level of education	Strata-1 (bachelor)	90	69%
	Strata-2 (undergraduate)	36	27%
	Strata-3 (doctoral)	5	4%
Work experience	1-2 years	34	26%
	2-3 years	6	5%
	3-4 years	16	12%
	> 4 years	75	57%
Educational background	Information technology	68	52%
	Finance/Accounting	43	33%
	Marketing	5	4%
	Production	3	2%
	Others	12	9%
Level	Staff	57	44%
	Manager	60	46%
	Director	14	11%
Industry type	Textile industry	67	51%
	Garment industry	39	30%
	Consultant	25	19%

The authors grouping indicators the data collection to organizational readiness in ERP implementation, by determining

the following components to Gender: The authors included gender components because it can influence in emotions in decision making in the data collection according the character of the respondents. Age: The authors included age components because it can influence decision making in the data collection according to work experience from respondents. Work experience: Authors included work experience components because it can influence maturity in decision making in the data collection according the work experience using ERP from respondents. Educational background: The authors included educational background components in the data collection because it can affect the level of maturity in decision making. Position: Authors included a position components because it can influences the maturity level in decision making. Industry type: Authors included industry type components in data collection because it can be comparison of the data processing result. The authors forward to test of 61 indicators using the multivariate Principal Component Analysis (PCA) statistical approach using R software, which meets the following requirement, namely the p-value must be less than 0.05, and the Measure of Sampling Adequacy(MSA) value must be greater than 0.5. The results of PCA data processing using software R show that Kaiser-Meyer Olkin (KMO) = 0.866, where all indicators have "KMO > 0.5", so it can be interpreted that the KMO value has requirement. The results of data processing from the PCA test show that 61 indicators from into 24 Release Candidate (RC) with the sum of the squared loadings (SS Loadings) achieve contributes 83% cumulative variable. The SS loading value is the result of automatic calculation from the R software. Based on RC results of PCA data processing using R software by calculation for more than one of eigen value (SS Loading > 1) achieved at a cumulative variable 83% with RC is 24, this is the optimum value calculated achieve cumulative proportion 100%. The release Candidate result can be seen in Table 3.

Table 3: Release Candidate results

No	RC	SS Loading	Proportion variable	Cumulative variable	Proportion Explained	Cumulative Proportion
1	RC1	5.73	7%	7%	10,00%	10%
2	RC21	4.68	6%	13%	7,00%	17%
3	RC4	4.62	6%	19%	7,00%	24%
4	RC2	4.06	5%	24%	6,00%	30%
5	RC24	3.53	4%	28%	5,00%	35%
6	RC13	3.43	4%	32%	5,00%	40%
7	RC22	3.37	4%	36%	5,00%	45%
8	RC3	2.86	4%	40%	4,00%	49%
9	RC7	2.85	4%	44%	4,00%	53%
10	RC19	2.82	4%	48%	4,00%	57%
11	RC17	2.66	3%	51%	4,00%	61%
12	RC15	2.63	3%	54%	4,00%	65%
13	RC5	2.46	3%	57%	4,00%	69%
14	RC9	2.45	3%	60%	4,00%	73%
15	RC10	2.30	3%	63%	3,00%	76%
16	RC16	2.21	3%	66%	3,00%	79%
17	RC8	2.16	3%	69%	3,00%	82%
18	RC12	2.11	3%	72%	3,00%	85%
19	RC6	1.96	2%	74%	3,00%	88%
20	RC20	1.86	2%	76%	3,00%	91%
21	RC23	1.77	2%	78%	3,00%	94%
22	RC11	1.54	2%	80%	2,00%	96%
23	RC18	1.52	2%	82%	2,00%	98%
24	RC14	1.05	1%	83%	2,00%	100%

SS Loading is the sum of the squared loadings
RC is Release Candidate

Based on the results of R software data processing for 24RC, the authors analyze for finding the highest value of each indicator, then the authors classify according to each of RC with create a new group for 24RC. The PCA result of data processing using R software can be seen in Table 4.

Table 4: Principal Component Analysis

RC	Indicator	RC1	RC2	RC3	RC4	RC5	RC6	RC7	RC8
RC1	OG26	0.80	0.10	0.06	0.17	0.15	0.05	0.12	0.14
	OG27	0.82	0.05	0.11	0.13	0.09	0.05	0.11	0.04
	OG28	0.72	0.03	0.06	0.20	-0.10	0.15	0.06	-0.11
	OG43	0.46	0.12	0.15	0.09	-0.05	-0.03	0.17	0.17
	PE22	0.41	0.39	0.04	0.18	0.13	0.05	0.06	0.10
	OG38	0.36	0.23	-0.02	0.23	-0.03	0.17	0.19	0.16
	TH61	0.34	0.07	0.34	0.23	0.03	0.04	0.03	0.03
RC2	PR06	0.11	0.4	-0.13	0.12	0.40	-0.11	0.03	0.21
	OG29	0.09	0.4	0.12	0.17	-0.01	0.03	0.03	0.05
	OG30	-0.02	0.79	0.14	0.10	0.05	0.16	0.01	0.12
	OG31	0.15	0.53	0.12	0.11	0.37	-0.14	0.23	0.08
	OG32	0.34	0.43	0.09	0.18	0.14	0.2	0.27	-0.01
	OG33	0.12	0.46	0.18	0.09	0.10	0.18	0.18	0.03
	OG34	0.29	0.45	0.15	0.30	0.04	0.16	0.07	0.03
	OG36	0.20	0.47	0.22	0.11	0.07	0.13	0.14	-0.19
RC3	TH62	0.09	0.16	0.78	0.14	0.08	0.07	0.11	0.10
	TH63	0.13	0.10	0.68	0.25	0.11	0.20	0.23	0.06
RC4	TH74	-0.02	0.09	0.3	0.5	-0.01	0.10	0.34	0.22
	TH77	0.14	0.08	0.07	0.81	0.07	-0.08	0.11	-0.02
	TH78	0.22	0.08	0.16	0.82	0.12	0.03	0.08	0.05
	TH79	0.20	0.23	0.23	0.62	-0.03	0.28	-0.01	0.07
RC5	PR01	0.03	0.11	0.18	0.11	0.74	0.08	0.02	0.18
	PR04	0.36	0.16	0.02	0.02	0.49	0.07	0.09	0.05
	PR05	0.15	0.17	-0.22	0.34	0.36	0.16	0.32	0.09
RC6	OG58	0.13	0.15	0.16	0.05	0.05	0.81	-	0.01
RC7	TH75	0.25	0.11	0.23	0.12	0.06	0.07	0.69	0.05
	TH76	0.17	0.04	0.22	0.20	-	-0.16	0.61	0.14
RC8	OG41	0.07	0.25	0.01	0.17	0.16	0.08	0.37	0.44
	OG42	0.04	-	0.12	0.09	0.11	0.04	0.21	0.56
	OG48	0.17	0.17	0.16	0.06	0.23	-0.01	0.03	0.7

RC	Indicator	RC9	RC10	RC11	RC12	RC13	RC14	RC15	RC16
RC9	PR07	0.54	0.14	0.09	0.21	0.28	-0.10	-0.01	0.09
	PE11	0.68	-0.01	0.05	0.04	0.14	0.06	0.08	0.02
	PE12	0.5	0.19	0.11	0.07	0.02	0.17	0.19	0.27
RC10	PE20	0.05	0.51	0.09	-0.06	-0.03	0.19	0.13	0.19
	PE21	0.11	0.62	0.11	0.16	0.21	-	0.14	0.12
	PE25	0.06	0.45	0.01	0.09	-0.03	0.09	0.03	0.16
RC11	PE08	0.09	0.08	0.78	0.08	0.16	0.13	0.07	0.10
RC12	PR02	0.08	0.12	0.09	0.78	0.15	0.04	0.18	-
	PR03	0.17	-0.22	-0.10	0.47	0.18	0.1	0.03	0.14
RC13	OG49	0.08	0.23	0.17	-0.08	0.54	-0.01	0.26	0.10
	OG57	0.24	0.05	0.2	-	0.64	-0.11	0.07	0.07
	OG60	0.19	0.17	0.06	0.1	0.39	0.02	0.17	-0.28
	TH67	0.18	0.04	0.2	0.08	0.47	0.16	0.25	0.10
	TH68	0.08	0.11	-0.03	0.16	0.57	0.22	-0.10	0.09
	TH73	0.02	0.13	0.06	0.1	0.45	0.1	0.31	0.06
RC14	PE19	0.22	0.1	0.01	-0.02	0.15	0.51	-0.04	0.09
RC15	OG44	0.09	0.05	0.06	-0.09	0.03	0.08	0.55	0.16
	OG45	0.15	0.19	0.1	0.24	0.24	-0.15	0.35	0.10
	OG51	0.11	-	0.07	-0.02	0.13	-0.07	0.69	-0.07
RC16	PE23	0.17	0.21	0.1	0.2	-0.04	0.21	0.03	0.46
	PE24	0.01	0.04	0.14	-	0.10	-0.01	0.05	0.81

RC	Indicator	RC17	RC18	RC19	RC20	RC21	RC22	RC23	RC24
RC17	OG46	0.65	-0.10	0.16	0.15	0.21	0.09	0.11	0.12
	OG47	0.79	0.15	0.04	-0.04	0.12	0.13	-0.01	0.09
RC18	TH69	0.14	0.54	0.22	0.10	0.16	0.10	0.13	0.15
	TH72	0.04	0.47	0.36	0.06	0.21	0.12	-0.02	0.18
RC19	OG40	0.17	0.08	0.53	0.18	0.20	0.21	0.10	0.24
	OG56	0.06	0.21	0.39	0.10	0.07	0.25	0.08	0.37
	TH70	0.21	0.06	0.49	0.18	0.19	0.15	0.24	-0.08
	TH71	0.03	0.09	0.75	0.05	0.17	0.06	0.05	0.17
RC20	PE15	0.11	0.10	0.16	0.61	0.11	0.14	0.09	0.05
	PE13	0.02	0.09	0.26	0.43	0.13	0.10	0.30	0.24
RC21	OG35	0.05	0.01	0.27	0.22	0.45	0.17	0.15	0.15
	OG37	0.04	0.02	0.10	0.40	0.49	0.25	0.13	0.03
	OG52	0.17	0.08	0.16	-	0.77	0.12	0.08	0.04
	OG53	0.08	0.10	0.12	0.06	0.80	0.11	-0.01	0.17
	OG54	0.03	-0.17	0.01	-	0.47	0.17	0.19	0.22
	OG55	0.18	-0.07	0.22	0.09	0.37	0.11	0.11	0.08
RC22	PE09	0.13	-0.07	0.23	0.05	0.01	0.60	0.09	0.21
	PE16	-0.08	-0.11	0.22	0.36	-0.01	0.43	0.18	0.27
	PE17	0.18	0.12	0.04	0.09	0.28	0.67	0.14	0.05
	PE18	0.05	0.14	0.13	0.10	0.25	0.54	-0.04	0.08
	OG50	0.20	-	-0.02	0.10	0.25	0.36	-0.01	0.18
	TH64	0.16	0.25	0.15	-0.13	0.25	0.40	0.22	0.01
RC23	PE10	0.18	0.24	0.10	0.16	0.15	0.21	0.49	-0.03
	TH65	0.04	-	0.16	0.12	0.12	0.15	0.66	0.16
RC24	PE14	-0.03	-0.05	0.03	0.33	0.19	0.28	0.19	0.36
	OG39	0.13	0.03	0.25	-0.02	0.41	0.01	0.06	0.49
	OG59	0.17	0.01	0.11	0.08	0.08	0.19	0.14	0.66

TH66	0.12	0.12	0.10	0.06	0.19	0.08	-0.03	0.52
TH80	0.08	0.16	0.26	0.05	0.24	0.06	0.06	0.54

3.2. ERP readiness assessment factors

Based on the results of PCA data processing using R software, the authors identify a new name for the sub-variable of each RC can be seen in Table 5. Then the authors continue to analysis with the weighting of 61 indicators using TOPSIS method where the name of the grouping for 24 sub-variables is based on the highest score for the preference score. The results of the TOPSIS processing for 10 the readiness factors that affect the success of ERP implementation are as follows: cross functional support (9.87%), project champion (9.14%), communication (7.82%), vision and mission (6.98%), transfer knowledge (6.97%), process improvement (5.98%), project planning (5.19%), vendor engagement (5.13%), commited to change (4.12%), and open minded for changes (4.05%). The results of the weight of ERP readiness assessment can be seen in Table 5.

Table 5: The weight of ERP readiness assessment

RC	No	Indicators	Sub-variables	Main weights	Final weights	Weights factors	Preferences
RC01	1	OG28	Project champion	9.14%	15.75	1.44	0.77
	2	OG27			15.43	1.41	0.75
	3	PE22			14.11	1.29	0.68
	4	OG26			14,00	1.28	0.68
	5	OG43			13.79	1.26	0.67
	6	TH61			13.46	1.23	0.66
	7	OG38			13.46	1.23	0.65
RC02	8	OG30	Cross functional support	9.87%	13.98	1.38	0.73
	9	OG29			13.78	1.36	0.72
	10	OG36			13.48	1.33	0.71
	11	OG33			13.07	1.29	0.68
	12	OG31			12.56	1.24	0.66
	13	PR06			11.65	1.15	0.61
	14	OG32			11.04	1.09	0.58
	15	OG34			10.44	1.03	0.55
RC03	16	TH62	Configuration system	2.42%	52.89	1.28	0.68
	17	TH63			47.11	1.14	0.60
RC04	18	TH79	Vendor engagement	5.13%	28.07	1.44	0.77
	19	TH77			25.34	1.30	0.69
	20	TH78			25.15	1.29	0.69
	21	TH74			21.44	1.10	0.59
RC05	22	PR01	Committed to change	4.12%	35.19	1.45	0.77
	23	PR04			33.98	1.40	0.74
	24	PR05			30.83	1.27	0.67
RC06	25	OG58	Project planning (budget)	1.24%	100,00	1.24	0.66
RC07	26	TH75	Helpdesk system	2.43%	53.09	1.29	0.69
	27	TH76			46.91	1.14	0.61
RC08	28	OG48	Data & information standarization	3.59%	35.1	1.26	0.67
	29	OG41			32.87	1.18	0.63
	30	OG42			32.03	1.15	0.61
RC09	31	PR07	Open minded for changes	4.05%	35.31	1.43	0.76
	32	PE11			33.58	1.36	0.72
	33	PE12			31.11	1.26	0.67
RC10	34	PE25	Employee involvement	3.38%	33.73	1.14	0.60
	35	PE20			33.43	1.13	0.60
	36	PE21			32.84	1.11	0.59
RC11	37	PE08	Management's skill & competency	1.27%	100,00	1.27	0.68

RC	No	Indicators	Sub-variables	Main weights	Final weights	Weights factors	Preferences
RC12	38	PR02	Business processes change	2.7%	50.37	1.36	0.72
	39	PR03			49.63	1.34	0.71
RC13	40	OG49		7.82%	19.05	1.49	0.79

RC	No	Indicators	Sub-variables	Main weights	Final weights	Weights factors	Preferences
	41	OG57	Communication		17.14	1.34	0.71
	42	TH73			16.62	1.30	0.69
	43	OG60			16.37	1.28	0.68
	44	TH67			15.47	1.21	0.64
	45	TH68			15.35	1.20	0.64
RC14	46	PE19	Involved Business Process Owner	1.21%	100,00	1.21	0.64
RC15	47	OG45	Size of organization	3.7%	34.32	1.27	0.68
	48	OG51			32.97	1.22	0.65
	49	OG44			32.7	1.21	0.64
RC16	50	PE23	Clear responsibilities of project	2.36%	48.73	1.15	0.61
	51	PE24			51.27	1.21	0.64
RC17	52	OG47	Top management commitment	2.58%	50.78	1.31	0.70
	53	OG46			49.22	1.27	0.67
RC18	54	TH69	IT structure	2.58%	50,00	1.29	0.69
	55	TH72			50,00	1.29	0.68
RC19	56	OG56	Project planning (scope)	5.19%	27.17	1.41	0.75
	57	TH70			26.20	1.36	0.72
	58	TH71			25.24	1.31	0.70
	59	OG40			21.39	1.11	0.59
RC20	60	PE13	Delivered to all parties	2.66%	54.51	1.45	0.77
	61	PE15			45.49	1.21	0.64
RC21	62	OG52	Vision and mission	6.98%	18.62	1.30	0.69
	63	OG53			18.05	1.26	0.67
	64	OG37			17.77	1.24	0.66
	65	OG35			15.33	1.07	0.57
	66	OG55			15.19	1.06	0.56
	67	OG54			15.04	1.05	0.56
RC22	68	PE16	Transfer knowledge	6.97%	19.80	1.38	0.73
	69	PE18			16.93	1.18	0.63
	70	TH64			16.50	1.15	0.61
	71	PE09			15.78	1.10	0.58
	72	OG50			15.49	1.08	0.58
	73	PE17			15.49	1.08	0.57
RC23	74	PE10	IT staff's skill & competency	2.63%	53.23	1.40	0.74
	75	TH65			46.77	1.23	0.65
RC24	76	TH66	Processes improvement	5.98%	22.07	1.32	0.70
	77	OG59			21.91	1.31	0.69
	78	TH80			19.40	1.16	0.62
	79	PE14			18.90	1.13	0.60
	80	OG39			17.73	1.06	0.57

The results of data processing using TOPSIS, found that organizational variables have the main weight of 43.51%, variable technology has the main weight of 25.03%, variable people have the main weight of 22.06%, and variable processes have the main weight of 9.40%. Thus, the organizational variable is a very dominant variable that determines the level of readiness in implementing ERP for the textile industry in Indonesia. The main weight of variables can be seen in the Table 6.

Table 6: Main weight of variables

No	Variable	Main Weight
1	Organizational	43.51
2	Technology	25.03
3	People	22.06
4	Processes	9.40
		100.00

Meanwhile, the teen sub-variables that have a significant main weight can be seen in the Table 7.

Table 7: Weight of sub-variables

No	Sub-variables	Main weight
1	Cross functional support	9.87
2	Project champion	9.14
3	Communication	7.82

4	Vision and mission	6.98
5	Transfer knowledge	6.97
6	Processes improvement	5.98
7	Project planning (scope)	5.19
8	Vendor engagement	5.13
9	Committed to change	4.12
10	Open minded for changes	4.05

3.3 Measuring the level of organizational maturity

Based on the weighting of 24 indicators which are the results of data processing using TOPSIS, the authors make a list of questions as a basis for designing an ERP readiness assessment

module. The list of assessment questions is in the form of a rubric assessment with the maturity level of the Capability Maturity Model Integration (CMMI) model with being considered the characteristic of initial, defined, managed, measured, and optimized with the readiness of process, people, organizational and technology. The list of Rubric Maturity Assessments can be seen in Table 8.

This rubric assessment will be a reference for the top management or the consultant to test each department involved to get good feedback before implementing ERP for the industry.

Table 8: Rubric Maturity Assessment

No	Sub-variables	MATURITY LEVEL				
		INITIAL	DEFINED	MANAGED	MEASURED	OPTIMIZED
1	Project champion	The function of a Project Champion in project ERP has not been defined	The function of a Project Champion in project ERP has been defined	The function of a Project Champion in project ERP have been standardized in SOP	The function of a Project Champion in project ERP has been socialized	The function of a Project Champion in project ERP has been evaluated for improvement
2	Cross functional support	Support from organizational functions in ERP implementation is still informal	Support from organizational functions in implementing ERP has been standardized in SOPs	Support from organizational functions in implementing ERP has been disseminated	Support from organizational functions in implementing ERP has been integrated across departments	Support from organizational functions in implementing ERP has been evaluated for improvement
3	Configuration system	The system hardware and software configurations affecting the success of ERP implementation have not been identified	The system hardware and software configurations that affect the successful implementation of ERP have been identified	The configuration of the hardware and software systems that affect the success of ERP implementation has been standardized in the SOP	The configuration of hardware and software systems that affect the success of ERP implementation has been socialized	The hardware and software system configurations that affect the success of ERP implementation have been evaluated for improvement
4	Vendor engagement	Relationships and agreements with vendors that can speed up problem solving related to the ERP implementation process have not yet been identified	Relationships and agreements with vendors that can speed up problem solving related to the ERP implementation process have been identified	Relationships and agreements with vendors that can speed up problem solving related to the ERP implementation process have been standardized in the SOP	Relationships and agreements with vendors that can speed up problem solving related to the ERP implementation process have been integrated with the customer	Relationships and agreements with vendors that can speed up problem solving related to the ERP implementation process have been evaluated for improvement
5	Committed to change	Management's commitment to change business processes is still informal.	Management's commitment to changing business processes has been standardized in the SOP.	Management's commitment to changing business processes has been socialized	Management's commitment to change business processes has been synchronized with business strategy	Management's commitment to changing business processes has been evaluated for improvement
6	Project planning (budget)	The budget usage that must be strictly controlled during ERP implementation has not been defined	The use of budgets that must be strictly controlled during ERP implementation has been determined	The use of budgets that must be strictly controlled during ERP implementation has been standardized in the SOP	The use of budgets that must be strictly controlled during ERP implementation has been socialized	The use of budgets that must be strictly controlled during ERP implementation has been evaluated for improvement
7	Helpdesk system	The availability of a helpdesk system can help users quickly solve problems related to the use of ERP that have not been identified	The availability of a helpdesk system can help users quickly solve problems related to the use of ERP that have been identified	The availability of a helpdesk system can help users quickly solve problems related to the use of ERP that have standardized in the SOP	The availability of a helpdesk system can help users quickly solve problems related to the use of ERP that have been socialized	The availability of a helpdesk system can help users quickly solve problems related to the use of ERP that have evaluated for improvement
8	Data & information standarization	Standardization of data and information on all business operations has not been identified	Standardization of data and information on all business operations has been identified	Standardization of data and information on all business operations has standardized in the SOP	Standardization of data and information on all business operations has been socialized	Standardization of data and information on all business operations has evaluated for improvement
9	Open minded for changes	Not all parties involved have an open mind in accepting the change process	All parties involved have an open mind in accepting the change process has been identified	All parties involved have an open mind in accepting the change process has been standardized in the SOP	All parties involved have an open mind in accepting the change process has been socialized	All parties involved have an open mind in accepting the change process has evaluated for improvement
10	Employee involvement	Being actively involved in ERP implementation has not been identified	Being actively involved in ERP implementation has been identified	Being actively involved in ERP implementation has been standardized in the SOP	Being actively involved in ERP implementation has been socialized	Being actively involved in ERP implementation has evaluated for improvement

No	Sub-variables	MATURITY LEVEL				
		INITIAL	DEFINED	MANAGED	MEASURED	OPTIMIZED
11	Management's skill & competency	Management does not yet have expertise in determining strategies for utilizing ERP for business development	Management already has expertise in determining ERP utilization strategies for business development	Management already has expertise in determining ERP utilization strategies for business development and has been standardized in SOPs	Management already has expertise in determining ERP utilization strategies for business development and has been socialized	Management already has expertise in determining ERP utilization strategies for business development and has evaluated for improvement
12	Business processes change	Changes in business processes are still informal.	Changes in business processes has been standardized in SOPs	Changes in business processes has been socialized	Changes in business processes has been integrated	Changes in business processes has evaluated for improvement
13	Communication	The objectives and objectivity of the project are communicated effectively to the stakeholders involved but have not been identified	The objectives and objectivity of the project are communicated effectively to the stakeholders involved, & have been identified	The objectives and objectivity of the project are communicated effectively to the stakeholders involved, & have been standardized in SOPs	The objectives and objectivity of the project are communicated effectively to the stakeholders involved, & have been socialized	The objectives and objectivity of the project are communicated effectively to the stakeholders involved, & have been evaluated for improvement
14	Involved Business Process Owner	ERP business process mapping has not been defined.	ERP business process mapping has been defined.	ERP business process mapping have been standardized in SOPs	ERP business process mapping have been socialized	ERP business process mapping have been evaluated for improvement
15	Size of organization	The organizational size that affects the success of an ERP project has not been defined	The organizational size that affects the success of an ERP project has been defined	The organizational size that affects the success of an ERP project has been standardized in SOPs	The organizational size that affects the success of an ERP project has been socialized	The organizational size that affects the success of an ERP project has been evaluated for improvement
16	Clear responsibilities of project	The roles of project stakeholders have not been defined	The roles of project stakeholders have been defined	The roles of project stakeholders have been standardized in SOPs	The roles of project stakeholders have been socialized	The roles of project stakeholders have been evaluated for improvement
17	Top management commitment	Top management has not been actively involved in every process and monitors the progress of the ERP project	Top management has been actively involved in every process and monitors the progress of the ERP project	Top management has been actively involved in every process and monitors the progress of the ERP project, & have been standardized in SOPs	Top management has been actively involved in every process and monitors the progress of the ERP project, & have been socialized	Top management has been actively involved in every process and monitors the progress of the ERP project, & have been evaluated for improvement
18	IT structure	The IT team structure to coordinate ERP project activities from planning to post-go live has not been identified	The IT team structure to coordinate ERP project activities from planning to post-go live has been identified	The IT team structure to coordinate ERP project activities from planning to post-go live has been identified, & have been standardized in SOPs	The IT team structure to coordinate ERP project activities from planning to post-go live has been identified, & have been socialized	The IT team structure to coordinate ERP project activities from planning to post-go live has been identified, & have been evaluated for improvement
19	Project planning (scope)	The scope of the ERP project in determining the success of ERP implementation has not been defined	The scope of the ERP project in determining the success of ERP implementation has been defined	The scope of the ERP project in determining the success of ERP implementation have been standardized in SOPs	The scope of the ERP project in determining the success of ERP implementation have been socialized	The scope of the ERP project in determining the success of ERP implementation have been evaluated for improvement
20	Delivered to all parties	Training activities have not been delivered to all parties involved.	Training activities have been delivered to all parties involved.	Training activities have been delivered to all parties involved, & have been standardized in SOPs	Training activities have been delivered to all parties involved, & have been socialized	Training activities have been delivered to all parties involved, & have been evaluated for improvement
21	Vision and mission	The vision and mission of the organization that was revealed and communicated to all parties involved to support the implementation of the ERP project has not been defined	The vision and mission of the organization that was revealed and communicated to all parties involved to support the implementation of the ERP project has been defined	The vision and mission of the organization that was revealed and communicated to all parties involved to support the implementation of the ERP project has been defined, & have been standardized in SOPs	The vision and mission of the organization that was revealed and communicated to all parties involved to support the implementation of the ERP project has been defined, & have been socialized	The vision and mission of the organization that was revealed and communicated to all parties involved to support the implementation of the ERP project has been defined, & have been evaluated for improvement
22	Transfer knowledge	There is no awareness from users and the benefits of knowledge transfer to improve the quality of users	There is awareness from users and the benefits of knowledge transfer to improve the quality of users	There is awareness from users and the benefits of knowledge transfer to improve the quality of users, & have been standardized in SOPs	There is awareness from users and the benefits of knowledge transfer to improve the quality of users, & have been socialized	There is awareness from users and the benefits of knowledge transfer to improve the quality of users, & have been evaluated for improvement
23	IT staff's skill & competency	IT Staff does not have the expertise & experience in understanding the business processes of the system used.	IT Staff have the expertise & experience in understanding the business processes of the system used.	IT Staff have the expertise & experience in understanding the business processes of the system used, & have been standardized in SOPs	IT Staff have the expertise & experience in understanding the business processes of the system used, & have been socialized	IT Staff have the expertise & experience in understanding the business processes of the system used, & have been evaluated for improvement
24	Processes improvement	The identification of process improvements before ERP implementation has not been identified	The identification of process improvements before ERP implementation has been identified	The identification of process improvements before ERP implementation have been standardized in SOPs	The identification of process improvements before ERP implementation have been socialized	The identification of process improvements before ERP implementation have been evaluated for improvement

4. Conclusion

The ERP implementation process for the industry has a high complexity, which will risk a high failure rate. However, the problem of the complexity of ERP implementation in the textile industry can be resolved by identifying readiness factors that focus on four main components such as processes, people, organizational, and technology before implementing ERP. Thus, the organizations can identify weaknesses and anticipate improvements, thereby increasing the success rate of ERP implementation. The research result shows that the score of organizational variable is 43.50% and the domain factors that influence ERP readiness assessment with significance factors are project champion (9.14%), cross-functional support (9.87%), project planning scope (5.19%), vision and mission (6.98%), and communication (7.82%). For this reason, it is necessary to develop of ERP readiness assessment, so that the managerial level can easily analyze the maturity level of the organization that need to be improved. The author realizes that this research has limitations in conducting case studies in the textile industry. For this reason, this research can be continued with case studies in the wider industry, and this research can also be developed by developing an ERP readiness assessment module as an information system for the management level in deciding to continue implementing ERP.

References

[1] M. Kirmizi, B. Kocaoglu, "The key for success in enterprise information systems projects: development of a novel ERP readiness assessment method and a case study," Enterprise Information Systems, **14**(1), 1–37, 2020, doi:10.1080/17517575.2019.1686656.

[2] J. Ram, D. Corkindale, M.L. Wu, "Examining the role of organizational readiness in ERP project delivery," Journal of Computer Information Systems, **55**(2), 29–39, 2015, doi:10.1080/08874417.2015.11645754.

[3] P. Hanafizadeh, A.Z. Ravasan, "A McKinsey 7S model-based framework for ERP readiness assessment," International Journal of Enterprise Information Systems, **7**(4), 23–63, 2011, doi:10.4018/jeis.2011100103.

[4] J. Razmi, M.S. Sangari, R. Ghodsi, "Developing a practical framework for ERP readiness assessment using fuzzy analytic network process," Advances in Engineering Software, **40**(11), 1168–1178, 2009, doi:10.1016/j.advengsoft.2009.05.002.

[5] S. De Soysa, J. Nanayakkara, "Readiness for ERP implementation in an organization: Development of an assessment model," 2nd International Conference on Information and Automation, ICIA 2006, **00**, 27–32, 2006, doi:10.1109/ICINFA.2006.374147.

[6] M. El Mariouli, J. Laassiri, "Information Systems and Technologies to Support Learning," **111**, 471–481, 2019, doi:10.1007/978-3-030-03577-8.

[7] J.R. Lavoie, T.U. Daim, "Technology readiness levels enhancing R&D management and technology transfer capabilities: insights from a public utility in Northwest USA," International Journal of Transitions and Innovation Systems, **6**(1), 48, 2018, doi:10.1504/ijtis.2018.10011690.

[8] S. Ahmadi, E. Papageorgiou, C.H. Yeh, R. Martin, "Managing readiness-relevant activities for the organizational dimension of ERP implementation," Computers in Industry, **68**, 89–104, 2015, doi:10.1016/j.compind.2014.12.009.

[9] K.P. Subramaniya, C. Ajay Guru Dev, V.S. Senthilkumar, "Critical Success Factors: A TOPSIS approach to increase Agility Level in a Textile Industry," Materials Today: Proceedings, **4**(2), 1510–1517, 2017, doi:10.1016/j.matpr.2017.01.173.

[10] S. Shiri, A. Anvari, H. Soltani, "Identifying and prioritizing of readiness factors for implementing ERP based on agility (extension of McKinsey 7S model)," European Online Journal of Natural and Social Sciences, **4**(1), 56–74, 2015.

[11] Harold J. Leavitt, "Applied Organizational Change in Industry, Structural, Technological Humanistic Approaches," Handbook of organizations, 1965.

[12] D. Sundiman, C.H. Wu, A. Mursidi, S.B.P. Johan, A. Indahingwati, "Knowledge management key factors: An empirical research on small and medium-sized enterprises in Indonesia," **13**(2), 139–161, 2019, doi:10.1504/IJBSR.2019.098650.

[13] C.L. Hwang, K. Yoon, "Methods for Multiple Attribute Decision Making," 58–191, 1981, doi:10.1007/978-3-642-48318-9_3.

[14] A.N. Hidayanto, M.A. Hasibuan, P.W. Handayani, Y.G. Sucahyo, "Framework for measuring ERP implementation readiness in small and medium enterprise (SME): A case study in software developer company," Journal of Computers (Finland), **8**(7), 1777–1782, 2013, doi:10.4304/jcp.8.7.1777-1782.

[15] Meyliana, A.N. Hidayanto, E.K. Budiardjo, "The critical success factors for customer relationship management implementation: A systematic literature review," International Journal of Business Information Systems, **23**(2), 131–174, 2016, doi:10.1504/IJBIS.2016.078904.

[16] H. Sun, W. Ni, R. Lam, "A step-by-step performance assessment and improvement method for ERP implementation: Action case studies in Chinese companies," Computers in Industry, **68**, 40–52, 2015, doi:10.1016/j.compind.2014.12.005.

[17] W.H. Tsai, Y.W. Chou, J. Der Leu, D.C. Chen, T.S. Tsaur, "Investigation of the mediating effects of IT governance-value delivery on service quality and ERP performance," Enterprise Information Systems, **9**(2), 139–160, 2015, doi:10.1080/17517575.2013.804952.

[18] P.B. Tarigan, "Agile Enterprise Resource Planning Implementation: Improving ERP Implementation Success Rates," Journal of Chemical Information and Modeling, **53**(9), 1689–1699, 2013, doi:10.1017/CBO9781107415324.004.

[19] S. Abdelkebir, Y. Maleh, M. Belaissaoui, "An Agile Framework for ITS Management In Organizations," In Proceedings of the 2nd International Conference on Computing and Wireless Communication Systems, 1–8, 2017, doi:10.1145/3167486.3167556.

Driving Behaviour Identification based on OBD Speed and GPS Data Analysis

Hussein Ali Ameen[1, 2,*], Abd Kadir Mahamad[1,*], Sharifah Saon [1], Mohd Anuaruddin Ahmadon[3], Shingo Yamaguchi[3]

[1]*Faculty of Electrical and Electronic Engineering, Universiti Tun Hussein Onn Malaysia, Parit Raja 86400, Malaysia*

[2]*Department of Computer Engineering Techniques, Al-Mustaqbal University College, Babil 51001, Iraq*

[3]*Graduate School of Science and Technology for Innovation, Yamaguchi University, Japan*

A R T I C L E   I N F O

A B S T R A C T

Vehicle accidents, particularly in small and large urban areas, are rising tremendously day by day worldwide. As a recent research subject in automaton transportation, the subsequent collision has become a vital issue and emergency. Internet of things (IoT) and the Internet of Vehicles (IoV) have become very popular these days because of their versatility, and robust cybersecurity underpin these new connected services. Aggressive driving among improper driving behaviours is a mainly responsible cause of traffic accidents that endanger human safety and property. Identifying dangerous driving is a significant step in changing this situation by analyzing data recorded through different gathering devices. The focus of aggressive recognition research has recently shifted to the use of vehicle motion data, which has emerged as a new technique for understanding the phenomenon of traffic. As aggressive driving refers to abrupt changes in actions, it is possible to classify them based on the vehicle's movement data. This paper presents a method to identify driving behaviours categorized into four groups: dangerous, aggressive, safe and normal behaviour to reduce the risk of accidents based on real-time data recorded from vehicles and reference data provided by previous researchers. Comparison and statistical methods have been done to determine the best way to collect driving data based on independent-samples t-test using Statistical Package for the Social Sciences (SPSS) statistics to compare the means between groups on the same continuous, dependent variable. Results have also shown that a small difference of speed between the mobile application and the On-Board Diagnostics (OBD-II) speed with $t(4024.1) = 1.8$, $p = .071$, which can be considered acceptable. Furthermore, the OBD-II adapter and mobile application speed were significantly different from the independent GPS device with $t(3184.9) = 10.8, p = 0$ and $t(4416.5) = 13.2, p = 0$. Consequently, it is expected to improve drivers' awareness of their driving behaviours.

1. Introduction

Population growth and the rapid promotion of the new urban motorization process have led to a rise in vehicles in recent years. The lack of efficient traffic management has led to traffic problems such as traffic congestion, traffic accidents, air pollution and energy consumption, which become an ever-increasing problem in the worldwide [1-5]. The challenges that a driver faces every day are growing dramatically due to the increasing worldwide demand for transportation. The situation review states that those significant casualties are due to improper driving behaviours. According to

study figures for injuries, 75% of lethal accidents are caused by human factors like lack of attention, loss of orientation, tiredness, stress and medical condition. The unexpected behaviour is the cause of the 24% of total accidents, and only 0.7% of injuries are attributed to technological failures (Figure 1) [6-9]. Vehicle to Vehicle (V2V) Communication plays an important role in smart transportation services, be the main factor for the success of Intelligent Transportation Systems (ITSs), and able to exchange a variety of information including acceleration, speed, direction and location forthwith with nearer vehicles and connected infrastructure [2, 10]. Connected vehicle technologies are nearly able to take off, commercially viable and used by the overall public in a vast selection of conditions. Technological advancements are
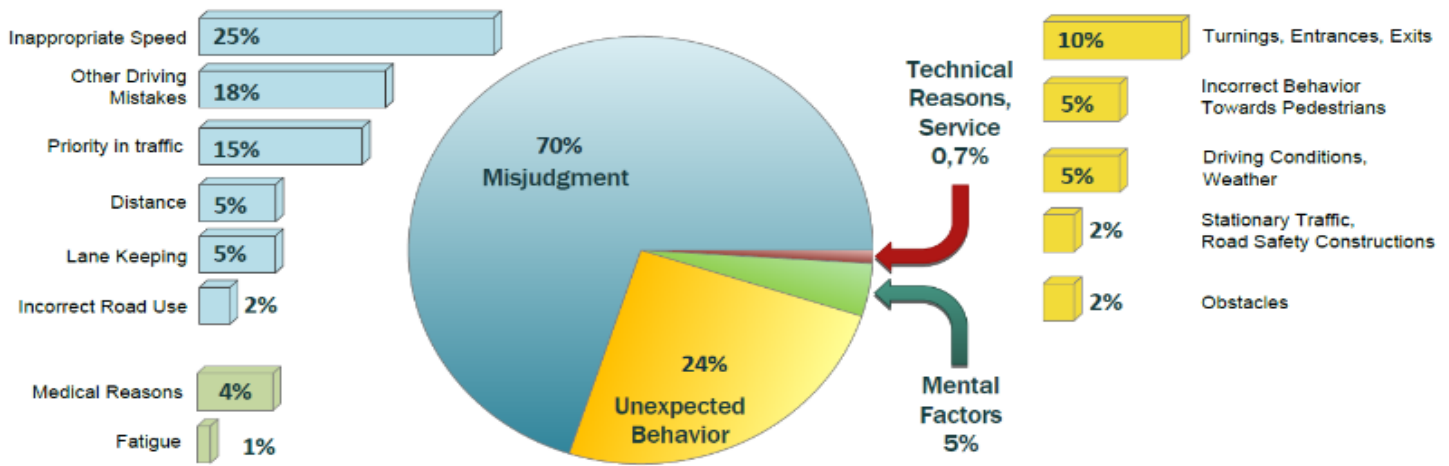
Figure 1: Accident causes, adapted from [7]

rushing on the automated technology time toward this destination [11].

Safety-based V2V applications can generate high-interest applications in road safety as a mechanism for prevention in critical circumstances. Implementing intersection collision avoidance coupled with driver assistance systems, could help provide a look around the corner effect, even in highly obstructed channel conditions [12-14]. The National Highway Traffic Safety Administration (NHTSA) sets out guidance on how different levels of vehicle automation can minimize vehicle accidents and how the use of short-range on-board sensors coupled with V2V technologies can help facilitate contact between vehicles [15]. Driver behaviour modelling is an important part of understanding the driver and evaluating traffic flow within the traffic system. The interactions with time and space between the main components of vehicular traffic can be seen as a traditional human-machine system [16, 17]. A significant aspect that quickly contributes to unsafe driving is violent driving behaviour. The press and the public have also given ample attention to this dangerous conduct [8]. In the last ten-year period, speeding has consistently been cited as a contributing factor in most fatal crashes which have been wholly or partially the fate of speeding behaviour. With real-time information, forthcoming driving behaviour could be predicted [17, 18]. Monitoring driving behaviour is not enough for ensuring driver safety. On the contrary, the achievement of safe and efficient driving needs to recognize reckless or "accident-prone" drivers who could encourage more successful traffic safety work coupled with the most appropriate incentives to avoid them [19, 20]. In this paper, we try to use a method for modelling drivers' acceleration to quantify and analyse individual driver behaviour using online data recorded from instrumented vehicles using different data collection devices. Experimental results are presented using graphs and analysis for multiple scenarios. The major contributions of this work are summarized as follows:

- Defining desired safe behaviours through direct observation

- Observing behaviour and quantifying safe/unsafe or at-risk behaviour

- Monitoring and evaluating changes in safe behaviour, performance; and providing feedback.

This paper is organized as follows. Section 2 presents related work while in Section 3, along with the system description, we present tools and software used for driving behaviours data collection using the instrumented vehicle. In Section 4, show study sites and research participants. In Section 5, the main system workflow explained. In contrast, in Section 6, we introduce the numerical results and statistical analysis of speed and acceleration data on the relaying strategies and the optimization results. Finally, we conclude in Section 7.

2. Related Work

Driving behaviour is the subject of comprehensive research. A growing number of studies have used technological advancements and gained particular attention to enhance our understanding of driver behaviour due to the advent of emerging technologies to gather more accurate and richer data [17, 21]. Driving event is generally understood as maneuvers occurring during the driving task, such as acceleration or deceleration, lane change and turning, which can be used to identify driving style [22]. Reference [23] indicated that data obtained from a collection of vehicle sensors could be analyzed to recognize a series of driving maneuvers using certain recognition methods and that the parameters of these driving maneuvers could be extracted and then used to classify driver characteristics or determine the abilities of the driver. In [24], the authors suggest a method to classify driver behaviours that take into account three acceleration and direction anomalies: a) sudden movements (acceleration and deceleration); b) shifts in lanes; c) excessive speed. Therefore, the algorithm classifies drivers into the following categories: cautious, distracted, hazardous and very risky. A non-intrusive method for a real-time framework to detect and identify driver distraction was presented in reference [25], using Machine Learning (ML) algorithms and dynamic vehicle data as inputs to the model. Authors in [26] developed a driver model capable of predicting each normal driver driving on a specific road segment with a reasonable degree of accuracy based on nonlinear regression methods using Artificial Neural Network (ANN). The primary benefit of this form of experiment is the tremendous degree of control over the factors that may impact driving behaviour. In a designed environment, however, controlled experiments are most often conducted. That

makes it more difficult for the effects of real traffic to be transferred [6].

Several works about the data exchange efficiency between vehicles and roadside infrastructure are investigated in [27] using a beaconing mechanism in the connection setup. Studies in [21] have employed GPS, accelerometers, video cameras and distance sensors. Authors in [4] assessed WiFi-based V2V data collection experiments to communicate with other vehicles. Experiments conducted on very slow speed vehicles with a maximum range of 100 ft. Reference [28] introduces the AutoNet2030 system used to drive convoys.

Furthermore, [29] presents an inquiry into V2V contact and data collection based on commercial on-board units (OBU) and incorporated into two research vehicles for light detection and ranging (LiDAR). Some existing services are already seeking to use the OBD interface for various purposes. The Driving Styles approach is provided in [30]. The proposed architecture incorporates data mining techniques and neural networks, classification of driving style is produced by studying driver activity along each path. Specifically, based on OBD parameters such as engine rpm, acceleration and revolutions per minute (RPM). A neural network based algorithm was introduced by the authors that can characterize the type of road on which the vehicle is traveling, as well as the degree of aggression of each driver. In [31], authors propose an Android application that tracks the vehicle via an OBD interface, allowing accidents to be detected.
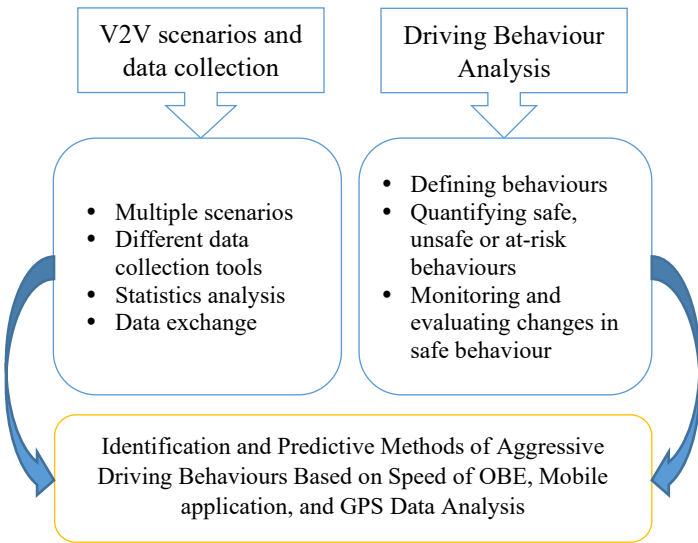

Figure 2: Study of gap from the related articles

Experimental findings using a real vehicle show that in less than 3 seconds, the application is able to respond to incidents in a very short time, validating the effectiveness of smartphone-based solutions to improve road safety. Moreover, [32] proposed a driving behaviour-based Collision Warning System (CWS) study to determine the collision risk level, according to its driving behaviour. In this experiment, the radar used was the ESR 1.0 model (Delphi), the capacity to output up to 174 m. The driving vehicle's speed, acceleration pedal, and brake pedal values were recorded using the OBD. Data output from the radar and OBD, through the Vector and the CANoe programs via the VN5610

network interface. These important studies have shown that the stability, protection, and efficiency of traffic flow are dramatically improved based on driving behavior communication technology. Based on the literature review, it can be seen that the assessment of drivers' behaviours using their trajectory data is a fresh and open research field. Most studies related to driving behaviours in terms of acceleration and deceleration are concluded after making an experimental trip where drivers' behaviour is calculated and recognized. Furthermore, as far as searching was feasible, it was a lack of studies that address the identification of aggressively driving based on real time data collection and analysis using different devices in a near real time. In our paper, we aimed to clarify the difference between OBD, GPS and mobile application to provide real measurements for further study and solutions that can be used (Figure 2).

3. Driving Behaviour Data Collections Tools

Driving behaviour recognition is a fundamental prerequisite for traffic studies and generates benefits, especially in three main areas: analysis of road safety; simulation of microscopic traffic; and ITSS. For various tasks in transport engineering, driving behaviour studies are of great benefit. That involves the collection of data both for statistical analysis and for driving model recognition and modelling parameter estimation.

Driving data are collected using an instrumented vehicle, as shown in Figure 3, equipped with GPS, microcontroller and other sensors. Many instruments are available to monitor driving behaviour, some of which work on the roadside and others on board. First, while driving on an instrumented location, an unconscious driver is tracked in the case of roadside sensors; different technologies can be used to track driving behaviours. Second, in the case of on-board sensors mounted on an instrumented vehicle, more extended measurements are allowed under more versatile experimental conditions, with the prospect of observing those maneuvers of particular interest in a controlled manner. An instrumented vehicle can be defined as a standard vehicle, the kinematics of which are registered for the study. In this system, the driving behaviours data collection have been gathered and analysed using on-board sensors.

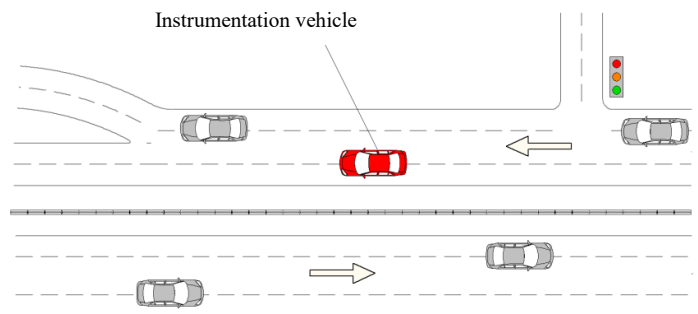Figure 3: Instrumented vehicle for data collection

3.1. On-board Diagnostics Adapter

On-Board Diagnostics OBD-I refers to the self-diagnostic and reporting capacity of a vehicle used in modern vehicles compliant with standard computer protocols. This adapter enables the vehicle network to be accessed by a computer. In service, it is similar to a computer modem or a gateway, that transfers messages from one

protocol to another; the data normally flows both ways to and from the Electronic Control Unit (ECU). Current OBD system, or called OBD-II replaces the deficient former system, namely OBD-I. The main advantage of OBD-II is its standardization. In other words, only one set of OBD-II scanning instruments can perform the diagnosis and can search for a number of vehicles fitted with and assisted by this adapter [33]. There are 16 pins in the system socket which are normally mounted below the driving plate. Nine of these 16 pins have fixed functions, and the remaining pins are left at the discretion of the car's manufacturer. Since the OBD-II interface is not a normal general computer system, Bluetooth and Wi-Fi adapters were built for data collection to accommodate the PC to obtain vehicle status as shown in Figure 4 which used in the data collection phase.

| (a) | (b) |

Figure 4: OBD-II adapter, (a) ELM327 Bluetooth, (b) ELM327 Wi-Fi

Besides, the proposed system also uses the Freematics ESP32 OBD-II Package. "This kit, together with the 1.3" OLED monitor and Freematics OBD-II UART Adapter, is based on Freematics Esprit, the Arduino compatible ESP32 dev board, as shown in Figure 5. This kit is simple to start yet has a lot of potential for prototyping advanced connected car applications. The board is completely plug-and-play. Freematics Esprit is in the same form of Arduino UNO board with additional pinouts for I2C and two serial UARTs [34].

Figure 5: Freematics ESP32 OBD kit

3.2. Torque Mobile Application

Torque is a software used as a diagnostic tool for any device that runs the Android operating system. When used in conjunction with OBD-II Bluetooth or Wi-Fi adapters for Android (Figure 6), it allows to access the many sensors within a vehicle management system and enable to view and clear trouble codes. This device is a cutting-edge Android Mobile diagnostic and performance scanner application for vehicles. This application can use internal cell phone GPS systems along with other sensors that graph useful acceleration, braking and overall vehicle performance data.
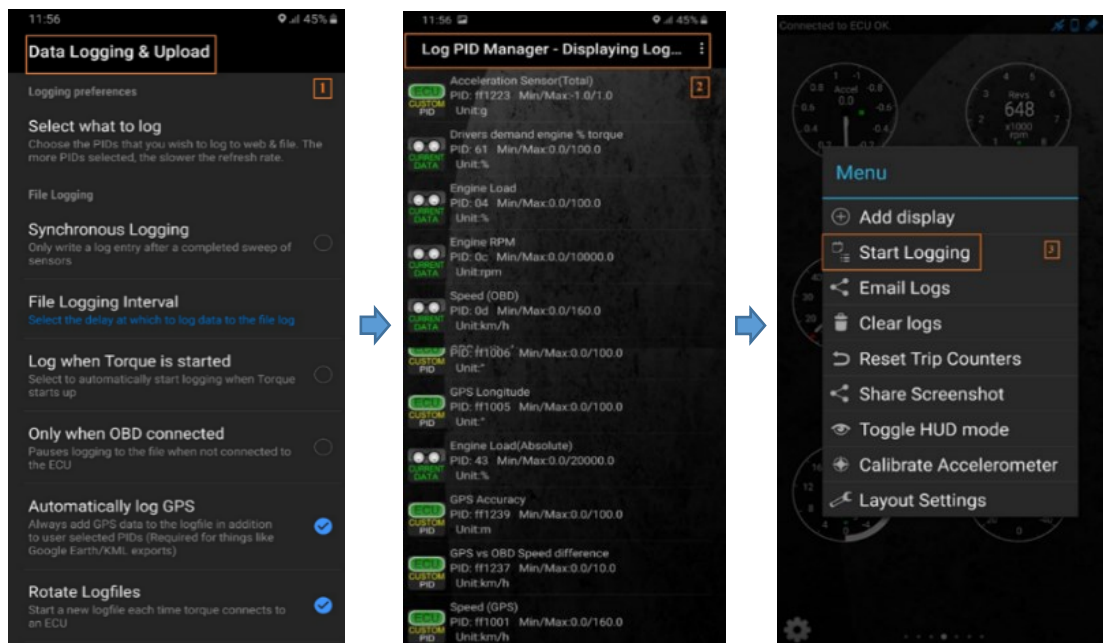

Figure 6: Torque pro's data logging and uploading window

	GPS Time	Longitude	Latitude	GPS Speed (Meters/second)	Acceleration Sensor	Engine Load(%)	Engine RPM	Speed (OBD)	GPS Accuracy(m)	GPS vs OBD Speed difference(km/h)	Speed (GPS)(km/h)
2	Fri Oct 25 11:47:49	44.44329974	32.49231653	1.7187115	-0.02638564	-	655	6	4	-	6.18736124
3	Fri Oct 25 11:47:50	44.44331834	32.49231416	1.6649991	-0.02638564	-	655	5	4	1.18736124	5.99399662
4	Fri Oct 25 11:47:51	44.44333204	32.49231269	1.2832996	-0.02638564	35.686275	793	4	4	1.99399662	4.61987829
5	Fri Oct 25 11:47:52	44.44334716	32.49231058	1.3784391	-0.02638564	40	1284	7	4	2.03761959	4.96238041
6	Fri Oct 25 11:47:53	44.44337026	32.49230856	2.196667	-0.08819824	70.588234	1695	11	4	3.09199905	7.90800095
7	Fri Oct 25 11:47:54	44.44340787	32.49230532	3.4900348	0.11251839	73.725494	2233	18	4	5.43587494	12.56412506
8	Fri Oct 25 11:47:55	44.44346188	32.49229896	5.085973	-0.07431667	69.411766	1824	23	4	4.69049835	18.30950165
9	Fri Oct 25 11:47:56	44.4435295	32.49228602	6.460725	0.03518514	68.627449	1954	27	4	3.74139214	23.25860786
10	Fri Oct 25 11:47:57	44.44360703	32.49226813	7.4858766	-0.00153249	69.411766	1529	29	4	2.05084419	26.94915581
11	Fri Oct 25 11:47:58	44.44369226	32.49224684	8.26833	-0.06128925	32.156864	1419	31	4	1.23401451	29.76598549
12	Fri Oct 25 11:47:59	44.44377953	32.49222107	8.575007	-0.02914082	46.666668	1576	30	6	0.87002563	30.87002563
13	Fri Oct 25 11:48:00	44.44386579	32.49219489	8.859237	0.17373693	69.019608	1645	33	6	1.10674858	31.89325142
14	Fri Oct 25 11:48:01	44.44395544	32.4921591	9.287559	-0.00138308	71.372551	1643	36	6	2.56478882	33.43521118
15	Fri Oct 25 11:48:02	44.44405229	32.49212354	10.072519	0.0849108	30.588236	1574	37	6	0.73892975	36.26107025
16	Fri Oct 25 11:48:03	44.44415296	32.49208519	10.439154	-0.17541127	25.09804	1258	34	6	3.58095169	37.58095169
17	Fri Oct 25 11:48:04	44.44424457	32.49204679	9.624482	-0.04436558	24.705883	1033	29	6	5.64813614	34.64813614
18	Fri Oct 25 11:48:05	44.44432078	32.4920146	8.144113	-0.07384139	27.058825	1005	24	6	5.31880379	29.31880379
19	Fri Oct 25 11:48:06	44.44438474	32.49198988	6.610205	-0.00993497	29.411766	1035	21	4	2.79673767	23.79673767
20	Fri Oct 25 11:48:07	44.44444346	32.49196517	5.9213986	0.01662612	34.117649	899	16	4	5.31703377	21.31703377
21	Fri Oct 25 11:48:08	44.44448907	32.49194649	4.746195	-0.0015965	36.07843	873	16	6	1.0863018	17.0863018
22	Fri Oct 25 11:48:09	44.44453202	32.49192857	4.498467	-0.03540144	36.07843	878	16	6	0.1944809	16.1944809
23	Fri Oct 25 11:48:10	44.44457489	32.49191106	4.5047784	-0.03552421	47.84314	972	16	6	0.21720123	16.21720123
24	Fri Oct 25 11:48:11	44.44461986	32.49189294	4.6545296	-0.03116671	72.549019	1562	19	12	2.24369431	16.75630569
25	Fri Oct 25 11:48:12	44.4446715	32.49187266	5.3411183	0.07882054	78.823532	1801	24	12	4.77197456	19.22802544
26	Fri Oct 25 11:48:13	44.4447358	32.49184989	6.5458884	0.05168423	33.725491	1239	24	12	0.43480301	23.56519699
27	Fri Oct 25 11:48:14	44.44480376	32.49182181	7.0314093	0.0384271	30.588236	1084	20	4	5.3130722	25.3130722

Figure 7: Data recorded with Torque pro's application

Different parameters added to the Torque software such as GPS Time, longitude, latitude, GPS speed (Meters/second), acceleration, engine load, engine RPM, speed (OBD), GPS Accuracy (m), GPS vs OBD Speed difference (km/h) and finally GPS speed (km/h). All these parameters are used in the analysis phase of the proposed system to monitor each trip. After setting everything in the application, Torque begins creating logs of the data by click Start Logging on the display screen to track the information and log all Parameter Identifications (PIDs) that were selected. Eventually, to save all logs recorded click Stop Logging on the display screen, choose the CSV (Comma Separated Values) format as shown in Figure 7. These data are used for further analysis and subsequent comparisons to determine the drivers' behaviours based on the information recorded from the acceleration of the drivers.

3.3. Digital Dashboard GPS Pro Application

Digital Dashboard is a performance tool for any device that runs the Android operating system. It can track speed, distance, time, location, and get start time, time elapsed, average speed, maximum speed, altitude and longitude. This software is the second type of software used in the design of the proposed system and the Torque software to compare the information obtained from mobile GPS and OBD-II adapter to determine the best way to extract data to predict the behaviour of the driver. The main features of this application are to save tracking information with map integration of any trip without the need for direct connection to the vehicle as shown in Figure 8.
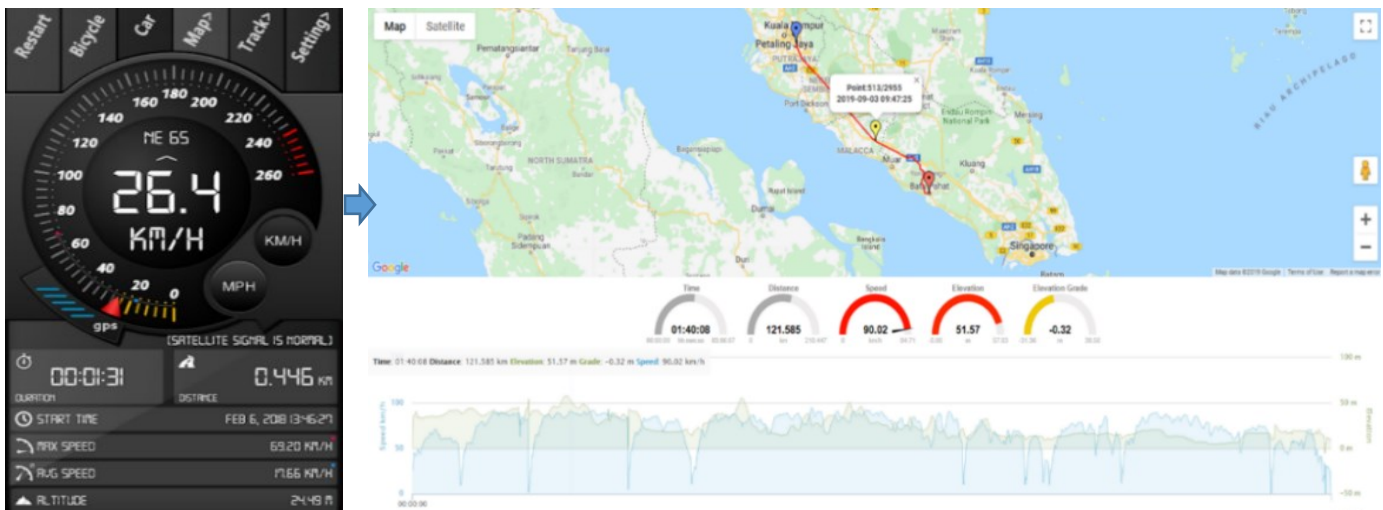

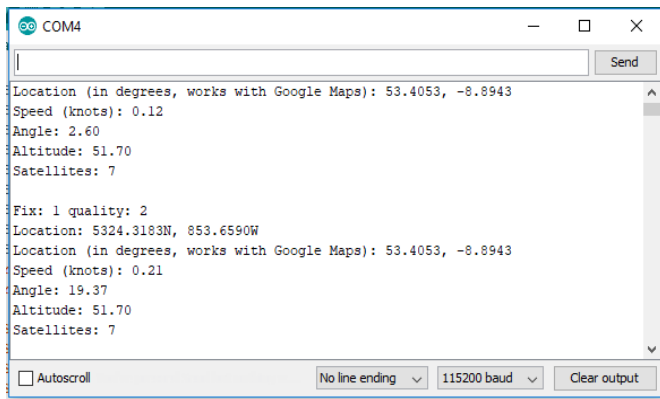Figure 8: Map integration of digital dashboard GPS Pro software

2019-09-20_00-07-33.gpx (Digital Dashboard GPS Pro)

https://play.google.com/store/apps/dev?id=8271310691420682403
http://a.vmall.com/app/C10008017
http://gpxscan.com

Point	Time	Duration	Speed(km/h)	Distance(km)	Altitude(m)	Latitude(WGS84)	Longitude(WGS84)	Latitude(BD09)	Longitude(BD09)
1	2019-09-20 00:07:33	00:00:00	0.0	0.026421638	22.6155	32.488362582011376	44.41801078826581	32.49442908193474	44.4244374607265
2	2019-09-20 00:08:26	00:00:53	0.0	0.026421638	22.561491	32.488362582011376	44.41801078826581	32.49442908193474	44.4244374607265
3	2019-09-20 00:08:27	00:00:54	0.0	0.026421638	22.207705	32.488362582011376	44.41801078826581	32.49442908193474	44.4244374607265
4	2019-09-20 00:08:28	00:00:55	0.0	0.026421638	22.001049	32.488362582011376	44.41801078826581	32.49442908193474	44.4244374607265
5	2019-09-20 00:08:30	00:00:57	0.1660762	0.02687455	21.923073	32.488362097068745	44.41801557294472	32.49442857000585	44.42444226520476
6	2019-09-20 00:08:31	00:00:58	0.04192471	0.026953662	21.82244	32.48836138657216	44.4180278591187	32.4944278591187	44.42444234144064
7	2019-09-20 00:08:32	00:00:59	0.038573988	0.02715587	21.78905	32.488363186080925	44.41801599605569	32.4944296565711	44.42444268998305
8	2019-09-20 00:08:33	00:01:00	0.40618894	0.027446313	21.319672	32.488361889789836	44.41801868119845	32.494428344518759	44.42444538631462
9	2019-09-20 00:08:34	00:01:01	0.12918712	0.027690819	21.256088	32.48836341922802	44.4180168074193	32.49442988512477	44.42444350468123
10	2019-09-20 00:08:35	00:01:02	0.4527087	0.027802212	21.215736	32.48836430881977	44.418016256951674	32.494430777777325	44.42444295187382
11	2019-09-20 00:08:36	00:01:03	0.07997884	0.027939789	21.23573	32.488363724137265	44.41801754793981	32.494430185836054	44.42444824823845
12	2019-09-20 00:08:37	00:01:04	0.9873646	0.027948122	21.241945	32.4883637636194	44.41801747247	32.49443022574271	44.42444417245393
13	2019-09-20 00:08:38	00:01:05	1.3135284	0.02860555	21.247738	32.488358783932746	44.41802126793284	32.49442522488861	44.424447983966516
14	2019-09-20 00:08:39	00:01:06	2.1589556	0.028987773	21.29258	32.488355519946	44.41802257448745	32.494421953720575	44.44444929616194
15	2019-09-20 00:08:40	00:01:07	5.7862744	0.033020392	21.16858	32.48831987242244	44.41803105024619	32.494386260222974	44.424457809624315
16	2019-09-20 00:08:42	00:01:09	7.8377414	0.035712983	21.245258	32.48829674905949	44.418039788566375	32.494360885875592	44.424466585834814
17	2019-09-20 00:08:43	00:01:10	9.196546	0.039212666	21.322264	32.48826867450138	44.41805679486742	32.49433491962528	44.42448366465038
18	2019-09-20 00:08:44	00:01:11	9.991158	0.04255906	21.437134	32.48824177231025	44.418072923894215	32.49430792772218	44.424499862546675
19	2019-09-20 00:08:45	00:01:12	10.56423	0.04626486	22.688114	32.488210992734956	44.41808827670424	32.494277063022174	44.42451528139558
20	2019-09-20 00:08:46	00:01:13	10.831916	0.049699876	22.669313	32.4881833403699	44.41810474500566	32.494249319008816	44.42453182018156
21	2019-09-20 00:08:47	00:01:14	10.896132	0.052735366	22.64483	32.488159448056265	44.41812050475403	32.4942253380534	44.424547647239685
22	2019-09-20 00:08:48	00:01:15	10.872328	0.055234108	22.153112	32.488138380045878	44.418129933860406	32.49420421901492	44.42455711721492
23	2019-09-20 00:08:49	00:01:16	10.864516	0.060951892	22.106041	32.48808725670087	44.418122035544044	32.49415314316781	44.424549190478416
24	2019-09-20 00:08:51	00:01:18	10.940508	0.064573646	22.055285	32.48805828147642	44.4181042567972	32.49412427050552	44.42453134053079
25	2019-09-20 00:08:52	00:01:19	11.039342	0.068225056	21.492105	32.48804493440669	44.41806874244889	32.49411112533437	44.42449568025169
26	2019-09-20 00:08:53	00:01:20	11.098003	0.07181479	21.516378	32.488042552563705	44.41803065285659	32.4941089589768	44.4244574333068
27	2019-09-20 00:08:54	00:01:21	11.121786	0.07493319	21.573044	32.48804268690809	44.41799747498087	32.494109280698845	44.424424411838617
28	2019-09-20 00:08:55	00:01:22	11.093026	0.07808065	21.601715	32.488052520696584	44.417966061843856	32.49411929092306	44.424392574787205
29	2019-09-20 00:08:56	00:01:23	11.114073	0.081396885	21.559992	32.488067111720405	44.417935263700855	32.49413405448602	44.42436164846012
30	2019-09-20 00:08:57	00:01:24	11.301733	0.0882784	21.422804	32.48811115745826	44.41788368856498	32.494178387509472	44.42430985734442
31	2019-09-20 00:08:58	00:01:25	11.445788	0.09196706	21.14611	32.48813362681933	44.41785475214992	32.494201017963846	44.42428080016281
32	2019-09-20 00:08:59	00:01:26	11.66683	0.09575817	21.179049	32.4881566441515	44.417824928832516	32.49422420116195	44.424250852551395
33	2019-09-20 00:09:00	00:01:27	11.856871	0.09990533	21.156685	32.48818054685208	44.41779099436179	32.49424829251335	44.42421677704042

2019-09-20_00-07-33.gpx

Figure 9: Data recorded with digital dashboard GPS pro application

This application also provided complete information related to the experiments (time, speed, distance, Latitude and Longitude) as shown in Figure 9. The main difference between dashboard GPS Pro application and the Torque does not use the OBD-II adapter to record and save the data since it depends on the GPS signal available in the smartphone. The goal is to compare the data recorded in terms of accuracy and efficiency to use it in the proposed system to define drivers' behaviours.

3.4. Adafruit Ultimate GPS Breakout System

The Global Positioning System (GPS) is a radio navigation system based on satellites which provide a GPS receiver with geolocation and time information. The GPS does not require the user to send any data and functions independently of any telephonic or internet reception. However, these technologies can enhance the utility of GPS positioning information. The GPS provides military, civil, and commercial users around the world with essential positioning capabilities. An Adafruit Ultimate GPS Breakout - 66 channel w/10 Hz updates - Version 3 used in the data collection phase for further research designed around the MTK3339 chipset, a high-quality GPS module with an outstanding high-sensitivity receiver that can track up to 22 satellites on 66 channels (-165 dBm tracking), and a built-in antenna [35]. The system can build up to 10 position updates a second for high speed, high sensitivity logging, or tracking. Next, we can go forward and wired up the GPS device with the microcontroller as shown in Figure 10.

Figure 10: Adafruit ultimate GPS breakout Arduino wiring

Each GPS satellite transmits a radio signal continuously containing the current time and its location data. GPS receiver tracks and uses several satellites to assess their positions and the time it takes for the signals to reach them. At a minimum, four satellites must view the receiver for it to get a location fix. We used the Adafruit Ultimate GPS Breakout connected to an Arduino as our GPS receiver. It's very easy to set up by installing the Adafruit GPS library on the Arduino then proceed with parsing sketch which gave us all information required for the experiments to define driving behaviours as shown in Figure 11.

Figure 11: Arduino serial monitor for the Adafruit ultimate GPS breakout

4. Sites Study and Research Participants

In driving behaviour experiments, data are collected and extracted using different devices to quantitatively described and discussed for implementing in the proposed system. An instrumented vehicle was used to collect data on actual roads fitted with different sensors that detect the vehicle's speed, position, acceleration or deceleration, the RPM and total distance travelled by the vehicle. Data for driver behaviours were continuously observed in different periods of time. Ten drivers who participated in this study during data collection with different types of vehicles and scenarios using two periods for gathering driving data.

Figure 12 shows the road layout examples with varying sites of study from Google maps.

The first data collection was carried out in Malaysia for two months from mid of July to September 2019 recorded in Batu Pahat and Kuala Lumpur. In these experiments three drivers in three vehicles with a total of eight experiments done using (i) Perodua MyVi, 1.3 EZI - Facelift - 4 SP automatic, manufacture year is 2009, (ii) Toyota Estima X - 6 SP automatic, manufacture year is 2007 and (iii) Proton WAJA 1.6 - 5 SP automatic, manufacture year is 2006) (Figure 13).

The second data collection was carried out in Iraq for two months from December 2019 until end of January 2020 recorded in Baghdad and Babylon. Involve of seven drivers, three vehicles with a total of fifteen experiments; (i) Hyundai Sonata 2.4 - 6 SP automatic, manufacture year is 2015, (ii) Hyundai Santa Fe 3.5 - 6 SP automatic, manufacture year is 2011, (iii) Renault Safrane 2.0 - 5 SP automatic, manufacture year is 2010 (Figure 14). Drivers rode along a predetermined route and calculated and reported data on the driver's normal driving behaviour. In Batu Pahat, Malaysia, field experiments were carried out using mobile software to record driving styles to collect data for vehicle speeds of 10 and 20 km/h. Moreover, tests at an intersection on an urban road with a speed limit of 30 km/h extracted the vehicle's deceleration rate when the driver followed a lead vehicle and slowed down and then stopped at a stoplight. We conducted field experiments within UTHM to collect data for vehicle speeds between 30 and 50 km/h.
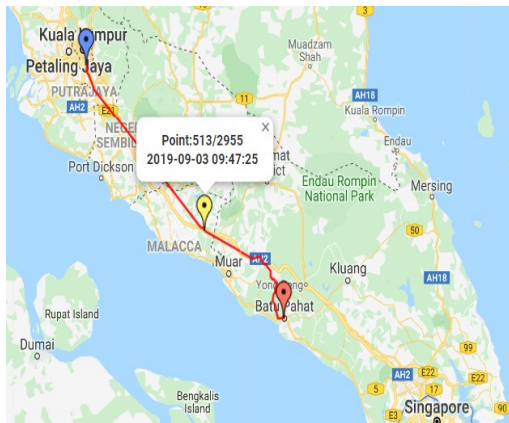
(a) Petaling Jaya to Batu Pahat, Malaysia
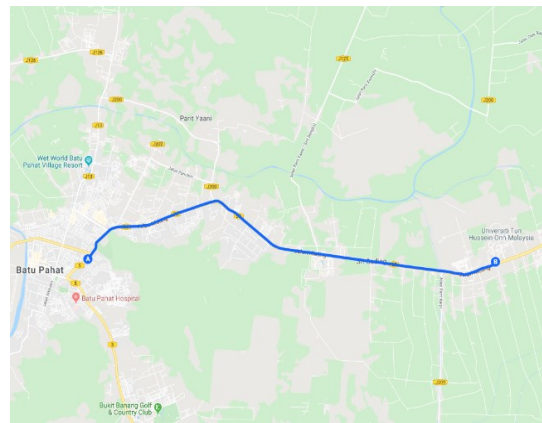
(b) Batu Pahat to UTHM, Malaysia
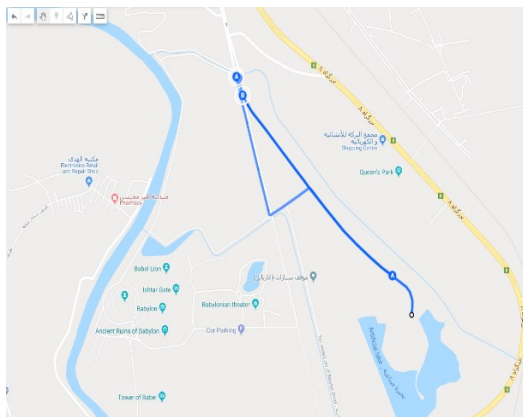
(c) Ancient Babylon to Hillah City Center, Iraq
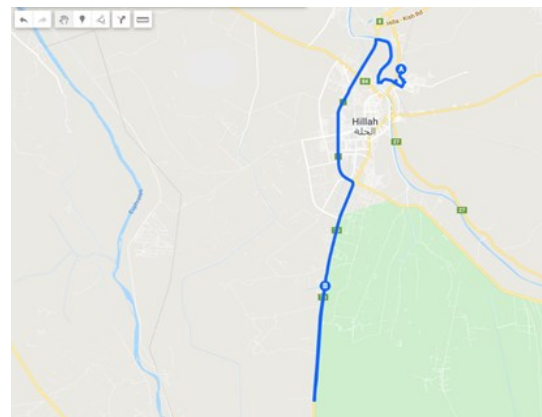
(d) Hillah City Center to University of Babylon, Iraq

Figure 12: Several study sites for data of driving behaviours.

(a) Produa MyVi

(b) Toyota Estima

(c) Proton WAJA

Figure 13: Vehicles used in this research in Malaysia

As with the previous studies, the experimental procedures were the same. At the time that, it slowed down behind a lead vehicle and stopped at a predefined point, we extracted the deceleration rates of the driver's vehicle. An intersection on a rural road with a speed limit of 40 km/h (one lane in each direction) was selected. Next, vehicle's speed to more than 60 km/h. The data collection process took place on the highway between Batu Pahat, Johor and Kuala Lumpur in Malaysia to collect data that represent high speed for analysis and definition of drivers' behaviours.

Moreover, all experimental procedures were repeated the same as the previous experiments, using different data collection types and done in other places. In the second period of the experiments that were in Iraq, we carried out the same scenarios as in Malaysia with different drivers, vehicles and devices used, noting that the steering wheel in the two countries is different. Still, this point emphasized in our experiments since the main goal is to collect driving data using different devices to reach the best, fastest and least expensive device to build the final system in the next steps, as it is mainly based on integrating drivers' behaviours with the V2V system. Several types of data collection devices were used

for drivers in different places, as shown in Table 1. It is found that drivers tend to be more unstable and sometimes aggressive in some situations, depending on the vehicles and the road. We propose an assessment method of driver behaviour to overcome these disadvantages. We evaluate the driver behaviour based on real behaviour observed in an experiment (Figure 15) instead of using estimated experimental data since the use of field experiment data for the driving behaviour can be fully reproduced which can be collected from different road environment.

In different road traffic scenarios, driving activity data may be obtained from one participant, which is used for the calculation, since the participant does not receive feedback about his/her exposure to the target situation. During a brief period of driving, an experiment was carried out to observe the driving profile. The behavior discussed in this study relates to speed, acceleration and driver control of the accelerator pedal. The data available from the OBD-II adapter used in the study are date, time, vehicle speed using an OBD adapter (km/h), vehicle speed using GPS (km/h), engine RPM (r/min), distance travelled (m), and vehicle position (latitude, longitude).

(a) Hyundai Sonata

(b) Hyundai Santa Fe

(c) Renault Safrane

Figure 14: Vehicles used in this research in Iraq

Table 1: Devices used for driving behaviours data collection

Device type	Required mobile application	Speed (OBD-II)	Speed (GPS)	Engine RPM	Engine Load (%)	Acceleration Sensor	Time Duration	Longitude	Latitude	Distance travelled
ELM327 Bluetooth or Wi-Fi	✓	✓	✓	✓	✓	✓	✓	✓	✓	✓
Freematics ESP32 OBD Kit		✓		✓	✓	✓	✓			✓
Arduino + OBD-II cable		✓		✓	✓	✓	✓			✓
Arduino + Adafruit GPS			✓	✓	✓	✓	✓	✓	✓	✓
Digital Dashboard GPS Pro	✓	✓	✓				✓	✓	✓	✓
Arduino + Adafruit GPS+ OBD-II Cable		✓	✓	✓	✓	✓	✓	✓	✓	✓

(a) Bluetooth adapter   (b) Wi-Fi adapter
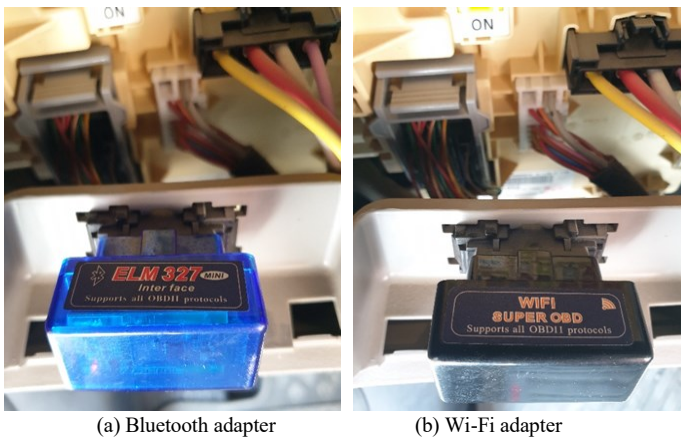
Figure 15: Installation of OBD-II adapter inside the vehicle

An accelerator pedal position (%) referring to a percentage of pedal movement from an existing position is secondary data required to validate the OBD-II adapter's data. The zero percent of the accelerator pedal position means that the pedal was disengaged, while the 100 percent pedal position indicates that the accelerator pedal was completely pressed (Figure 16). Since it is possible to obtain the acceleration and deceleration during the driving period using engine diagnostic and by analyzing the speeds that obtained, it is possible to determine the driver's general behaviour, whether it is dangerous or safe. The accelerator pedal is closely related to the fuel used, as it is related to the engine's fuel flow control. This project does not clarify the mechanical components' specifications, as it is out of the analysis scope.
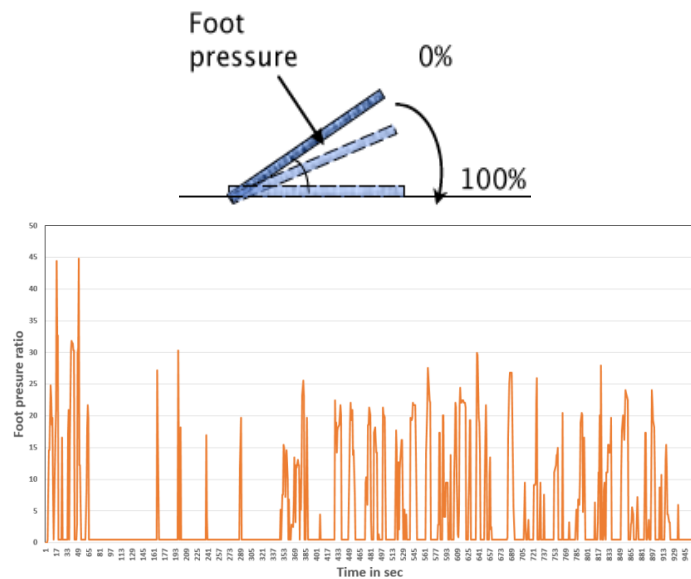
Figure 16: Accelerator pedal position diagram recorded from OBD-II adapter

5. Data Processing

The driver's behaviour described in this work refers to an individual driving operation using various test vehicles. The behaviour mentioned was the usual feat that the driver often controls (speed, acceleration, accelerator pedal press). Initially, it should mention the following three concepts regarding the final design: speed, velocity, and acceleration to use in the proposed system to determine the driver's behaviour while driving. Speed

refers to the distance travelled during a period of time. Speed is a scalar quantity, and it is measured in units of distance divided by time. The commonly used formula for speed calculates average speed rather than instantaneous speed. In contrast, the instantaneous speed shows the speed at any given moment of the trip, as shown on the vehicle's speedometer. Therefore, in the proposed system, we rely on the current speed. Velocity refers to the rate at which, in a certain direction, an object changes location. It is determined by the displacement of space in a specific direction per unit of time. Directional velocity matters in the short term, but speed does not. In the equation, the instantaneous velocity shown in (1).

$$v = \frac{\Delta d}{\Delta t} = \frac{d_f - d_i}{t_f - t_i} \tag{1}$$

Δd represents the change in distance (final - initial), and Δt represents the change in time. Acceleration is a measure of how speed shifts rapidly. Acceleration is a vector quantity, like velocity, so any change in a moving body's direction is an acceleration, too. An increase in the magnitude of a moving body's velocity called a positive acceleration; a decrease in speed called negative acceleration. The acceleration expression is shown in (2).

$$a = \frac{\Delta v}{\Delta t} = \frac{v_f - v_i}{t_f - t_i} \tag{2}$$

Δv is the change of the velocity, which is equal to the difference between the initial speed and the final speed over time Δt, representing a change in time. To calculate the instantaneous behaviour of each driver, different OBD-II PIDs codes are used to request data from a vehicle to define driving style. The most commonly PIDs are defined in OBD library and used in the proposed system presented in Table 2. The adapter used can be plugged directly into the OBD-II port of the vehicle, providing a high efficiency module serial data interface (UART or I2C) and easy (up to 100Hz) access to all OBD-II PIDs available in the vehicle ECU.

Table 2: OBD-II PIDs details used in the system

Mode (hex)	PID (hex)	Data bytes returned	PID command	Unit	Description
01	0C	2	PID_RPM	RPM	Engine RPM
01	0D	1	PID_SPEED	Km/h	Vehicle speed
01	1F	2	PID_RUNTIME	Sec	Engine run time
01	21	2	PID_DISTANCE	Km	Distance traveled

Engine start date and time, second-by-second vehicle location (latitude and longitude), heading, and speed are monitored by the onboard equipment. The equipment also provides up to ten engine and emission-related parameters directly connected to the OBD-II engine computer port from the onboard diagnostic system. For each engine ignition event, the equipment starts and saves a trip
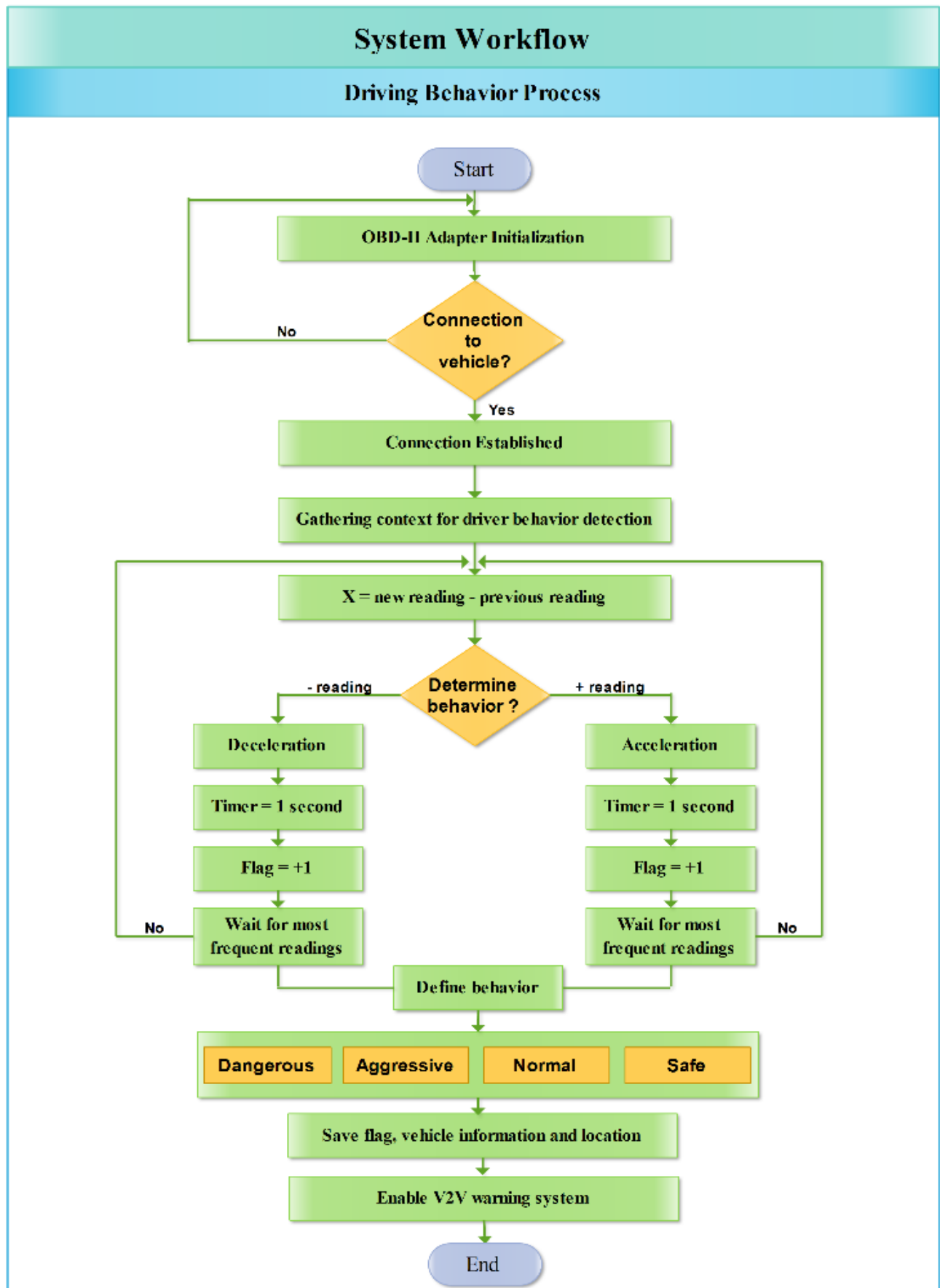
Figure 17: Driving behaviours system flowchart

file. The trip file remains open recording second-by-second operations data until the vehicle operation stops and the driver shuts off the engine. This phase is done to check the research requirement, the restriction and the time needed to complete the research, then to develop a method to select the destination vehicle for the transmission of information gathered by the proposed system using wireless communication to exchange information between vehicles and to notify the driver of the aggressive drivers on the road. The first requirement for this calculation is to identify the subject driver with some certainty. The second requirement is to obtain valid and reliable measurements of speeding behaviour performance. Now to test the proposed method, firstly, the system defines drivers' immediate behaviour whether in acceleration or deceleration by taking a set of readings (5, 10 or any predefined value) in each second based on sensors used where Δt between any consecutive readings is one second. Next, the microcontroller converts vehicle speed (km/h) to acceleration values (m/s2) by taking advantage of the instantaneous values in Δt. After that, these values are stored with a special identifier to compare with the reference table to classify the behaviour according to the recorded values. Next, these data forwarded and stored in a matrix to find out the most frequent values and weighted as a momentary behaviour for that driver during the time period that passed (Figure 17).

The main program workflow represents the procedure of the driving behaviours data collection and identification process. Since the OBD does not have the User Interface (UI) to communicate with the driver, the proposed system would use an LCD screen to display the driving information and provide a driver-based V2V system collision warning. If the nearby vehicle can pass safely, the 'safe' signal is displayed. If the passing vehicle need to be aborted because it is unsafe, a 'not safe' signal displayed. This system gets the driving information of the surrounding vehicles using wireless transceiver device. We choose the nRF24L01+ PA LNA wireless transceiver. The nRF24L01+ PA LNA is common in the market and can be obtained at a very low price. It provides much better coverage than other devices. It can communicate over a four-pin serial peripheral interface with a maximum data rate of 10 Mbps. The power amplifier (PA) enhances the power of the signal, whereas the low-noise amplifier (LNA) amplifies the weak signal from the antenna to a more useful level to expand the transmission range of the antenna (to approximately 1000 m). Furthermore, all readings also stored in the form of flags in the Secure Digital (SD) card connected to the microcontroller to save all driving data for each day. As a result, drivers are required to increase awareness of their driving behaviour, as well as to alert transport and insurance providers of each driver's way of driving.

6. Numerical Results and Discussions

6.1. Speed collection and analysis

The speed collector devices used in experimental vehicles are the Freematics ESP32 OBD-II kit, ELM327- OBD-II Bluetooth and Wi-Fi adapter, Adafruit ultimate GPS breakout system and Digital dashboard GPS based on the mobile application. Based on the rotation speed of the vehicle wheels, the OBD-II speed is reported directly from the vehicle engine, while the speed recorded by a GPS system and mobile application based on sequential vehicle positions are used to validate the OBD-II speed. The investigation found a delay in speed data from location-based devices (Adafruit ultimate GPS breakout system and digital dashboard GPS pro application) compared to OBD-II adapter speed. This delay is known as the 'transit-time delay' which is used to triangulate location by the ground-based GPS receiver. The comparison between speeds was plotted graphically as shown in Figure 18.
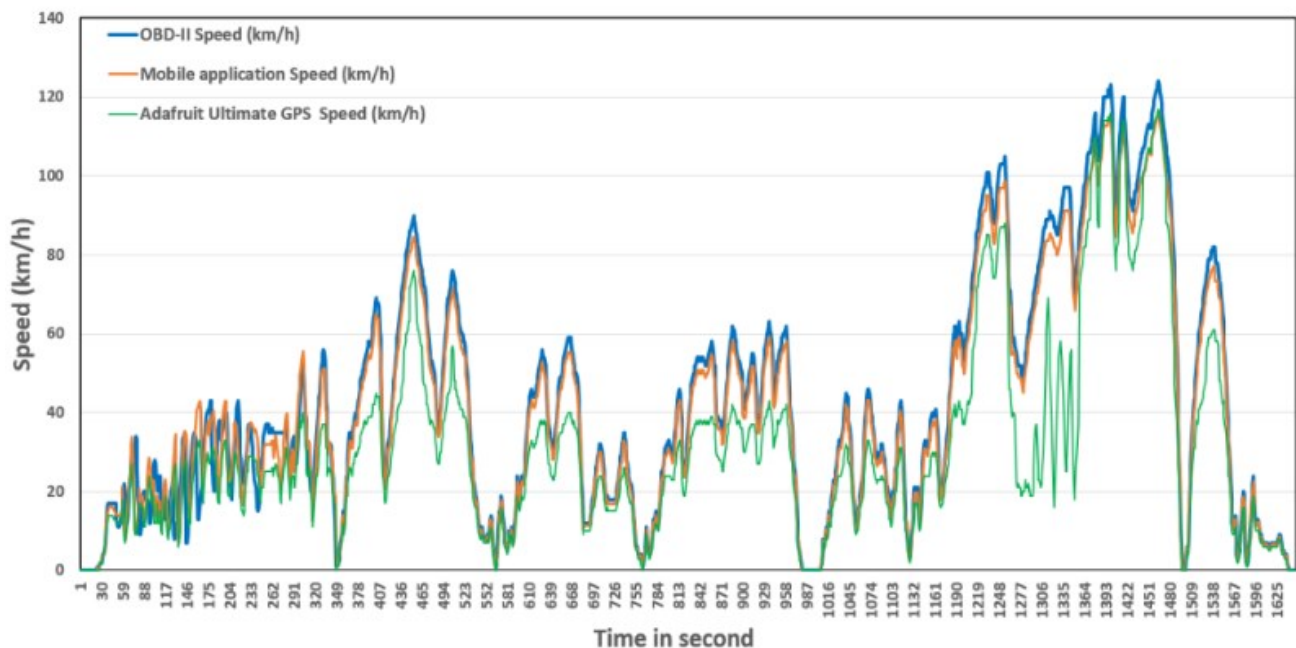
Figure 18: Comparison of OBD-II adapter, mobile application and GPS device speed

Kurtosis	-0.227014659	-0.221509659	2.041838842
Skewness	0.75352705	0.738426854	1.489783928
Range	124	116.56	117
Minimum	0	0	0
Maximum	124	116.56	117
Sum	69741	66105.85	52180
Count	1650	1650	1650

The independent-samples t-test using Statistical Package for the Social Sciences (SPSS) statistics compares two groups' means on the same continuous, dependent variable. In SPSS Statistics, we separated the groups for analysis by creating a grouping variable called a type of device used together with the recorded speed in real time. Descriptive statistical analysis was performed in SPSS and used to determine the extent of any differences between OBD-II adapters, GPS device and mobile application speed for all vehicles used in these experiments as shown in Table 3. It was found that the trend in OBD-II adapter speed was similar to that of mobile application speed data with some differences compared to the GPS device. As can be seen from the Table 3, the mean, standard deviation and skewness of the speed recorded by OBD-II adapter ($M = 42.2$, $SD = 30.7$, $SE = 0.75$) and mobile application ($M = 40.1$, $SD = 28.8$, $SE = 0.71$) which it can be observed that the results are close, with some variations from the GPS device ($M = 31.6$, $SD = 25.4$, $SE = 0.62$). Moreover, from observations the highest speed recorded by the OBD-II adapter (124 km/h) while the highest speed recorded by the remaining devices is almost the same (116.56 km/h and 117 km/h) for mobile application and GPS device respectively.

Table 3: Descriptive statistics of speed factor of OBD-II adapter, mobile application and GPS

Speed factor	OBD-II adapter	Mobile application	GPS
Mean	42.26727273	40.06415152	31.62424242
Standard Error	0.75732929	0.708743157	0.62654144
Median	35	34.585	26
Mode	0	0	24
Standard Deviation	30.76286118	28.78928315	25.45023361
Sample Variance	946.3536281	828.8228242	647.7143907

Furthermore, a detailed analysis was performed to find the similarities and differences between each of the devices used in the data collection of driving behaviour experiments. The analysis was carried out by comparing the OBD-II adapter speed and digital dashboard pro to find the individual value errors between them, as shown in Figure 19. Descriptive statistics and an independent T-test analysis were performed to determine the similarity of the OBD-II adapter and mobile application based speed profiles. The results are shown in Table 4 and Table 5. There was no significant difference in speeds recorded from experiments between OBD-II adapter speed ($M = 39.0$, $SD = 28.8$) and digital dashboard pro ($M = 37.5$, $SD = 27.8$); $t(4024.1) = 1.8$, $p = .071$.

Results show that device type in these experiments does not affect speed profiles at .05 level of significance. A small difference in the mean speed of OBD-II adapter and mobile application can be considered acceptable.

Table 4: OBD-II adapter and mobile application speed statistics

		Statistics			
	Device type	N	Mean	Std. Deviation	Std. Error Mean
Speeds recorded	OBD-II adapter	2042	39.0984	28.80644	.61485
	Digital dashboard pro	2037	37.4984	27.76627	.63953
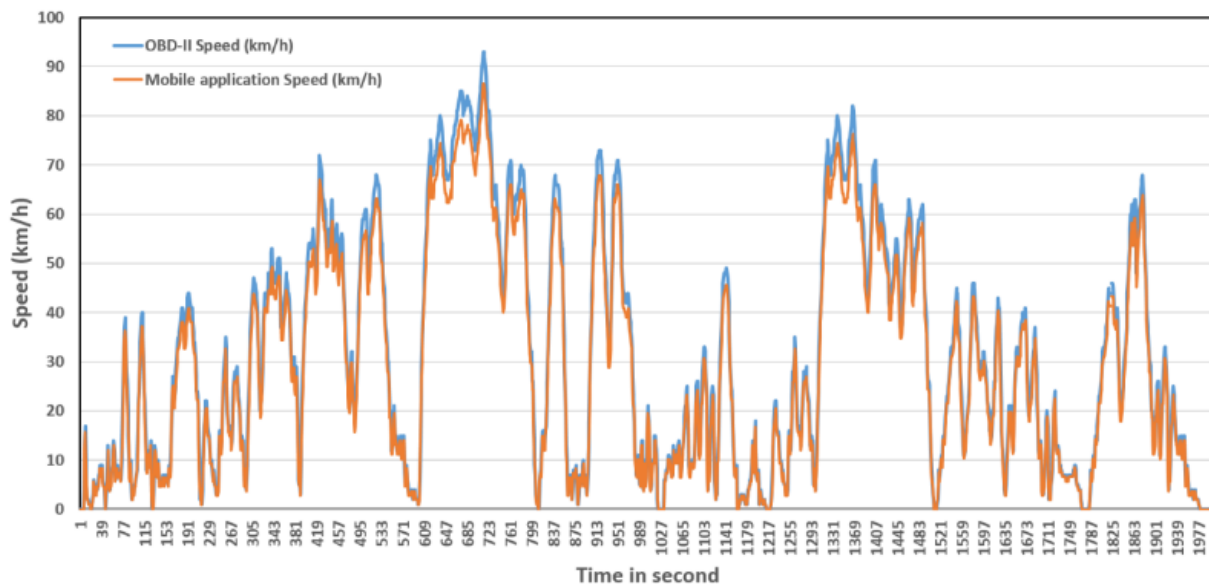
Figure 19: Comparison of OBD-II adapter and mobile application speed

Table 5: OBD-II adapter and mobile application speed independent T-test

		Levene's Test for Equality of Variances		t-test for Equality of Means					95% Confidence Interval of the Difference	
		F	Sig.	t	df	Sig. (2-tailed)	Mean difference	Std. Error difference	Lower	Upper
Speeds recorded	Equal variances assumed	5.431	.020	1.798	4078	.072	1.59999	.88964	-.14418	3.34417
	Equal variances not assumed			1.804	4024.147	.071	1.59999	.88716	-.13933	3.33931

Different experiments and detailed analysis were performed to determine the extent of the differences between speeds for the OBD-II adapter and GPS device. The comparison between speeds was plotted graphically, as shown in Figure 20. It found that at certain times the OBD-II adapter speed was slightly different from the GPS speed. This can be clarified by the fact that the GPS estimates speed is based on position and the accuracy which depends on the number of satellites available to the receiver.
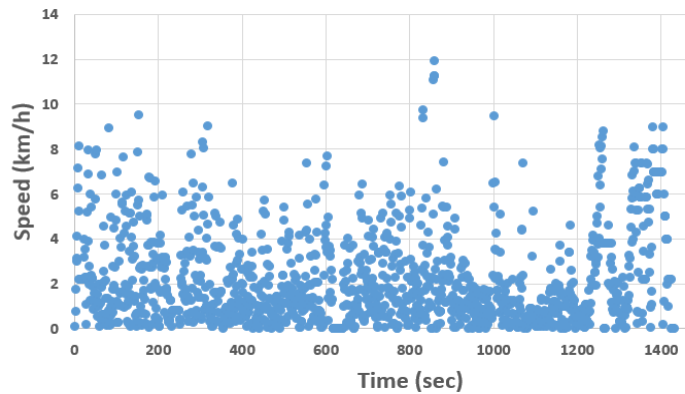
(a) differences points
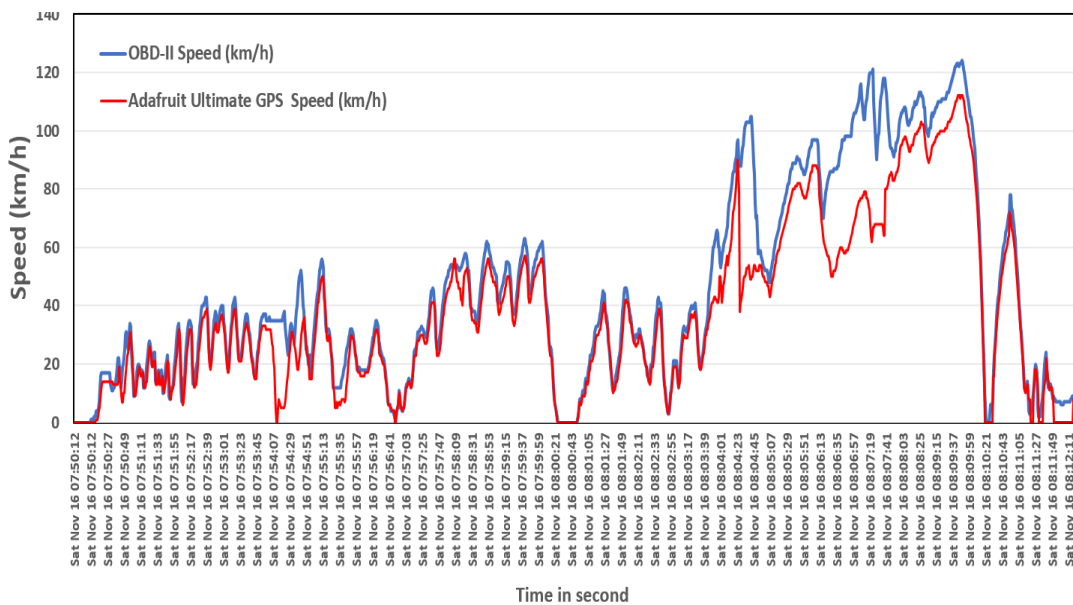
(b) comparison between speeds

Figure 20: OBD-II adapter speed and GPS device speed

A descriptive statistics and an independent T-test analysis were performed to determine the extent of any differences between the OBD-II adapter and Adafruit Ultimate GPS based on speed profiles. The results are shown in Table 6 and Table 7.

There was a significant difference in the mean and standard deviation of speeds recorded from experiments between OBD-II adapter speed ($M = 42.7$, $SD = 30.8$) and Adafruit Ultimate GPS ($M = 31.6$, $SD = 25.4$); $t(3184.9) = 10.8, p = 0$. These results are shown that device type in these experiments affects speed profiles at .05 level of significance.

Further experiments were carried out to compare digital dashboard pro application with Adafruit Ultimate GPS to determine the extent of any differences based on speed profiles. The comparison between speeds was plotted graphically as shown in Figure 21. Descriptive statistics and an independent T-test analysis were performed as presented in Table 8 and Table 9. This showed that at certain times the Mobile application speed was slightly different from the GPS speed. There was a significant difference in speeds recorded from experiments between digital dashboard pro speed (M=41.3, SD=27.1) and Adafruit Ultimate GPS (M= 31.3, SD=23.9); t(4416.5) = 13.2, p= 0. Results have also shown that device type in these experiments has an effect on speed profiles at .05 level of significance.

Table 6: OBD-II adapter and GPS device speed statistics

		Statistics			
	Device type	N	Mean	Std. Deviation	Std. Error Mean
Speeds recorded	OBD-II adapter	1649	42.2662	30.77216	.75779
	GPS device	1650	31.6242	25.45023	.62654

Table 7: OBD-II adapter and GPS device speed statistics

		Independent Samples Test							
		Levene's Test for Equality of Variances		t-test for Equality of Means					
		F	Sig.	t	df	Sig. (2-tailed)	Mean difference	Std. Error difference	95% Confidence Interval of the Difference	
									Lower	Upper
Speeds recorded	Equal variances assumed	116.733	0	10.824	3297	0	10.64198	.98320	8.71423	12.5697
	Equal variances not assumed			10.823	3184.18	0	10.64198	.98326	8.71410	12.5698

Table 8: Mobile application and GPS device speed statistics

		Statistics			
	Device type	N	Mean	Std. Deviation	Std. Error Mean
Speeds recorded	Digital dashboard pro	2247	41.33	27.081	.571
	GPS device	2232	31.25	23.915	.506
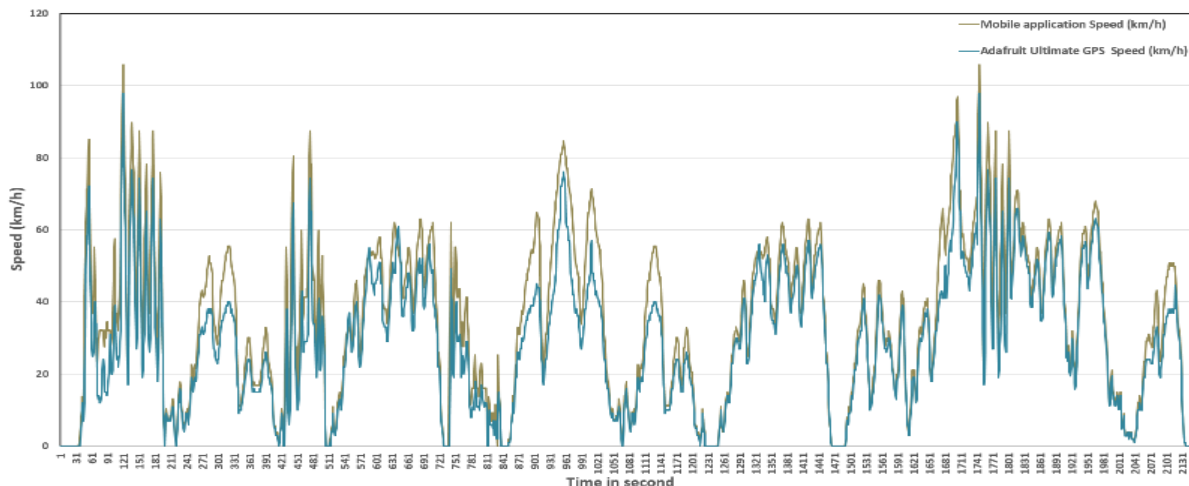
Figure 21: Comparison of mobile application and GPS device speed

Table 9: Mobile application and GPS device speed independent T-test

		Independent Samples Test								
		Levene's Test for Equality of Variances		t-test for Equality of Means						
		F	Sig.	t	df	Sig. (2-tailed)	Mean difference	Std. Error difference	95% Confidence Interval of the Difference	
									Lower	Upper
Speeds recorded	Equal variances assumed	79.104	.000	13.194	4477	.000	10.075	.764	8.578	11.572
	Equal variances not assumed			13.199	4416.51	.000	10.075	.763	8.578	11.571

For each of the measured parameters, the on-board data obtained in this research constructs a set of time series. However, the pace was still vulnerable to errors that were clearly seen once the acceleration was measured. In the GPS system, the speed was estimated based on the position of the vehicle. The efficiency of GPS speed data is highly affected by numerous factors, as presented in Table 10. The speed dissimilarity with a GPS device commonly occurred upon reaching high speeds (high acceleration) and once the vehicle stopped (high deceleration); while the OBD-II speed is logged directly from vehicle engine based on the rotation speed of the vehicle wheels. According to these points of view, the OBD-II adapter's speed was used for all analysis and the proposed system. To validate the OBD-II speed, the speed reported by a GPS system and mobile application was used based on sequential vehicle locations.

Table 10: Factors affecting the accuracy of GPS speed [36]

Factor	Description
Atmospheric effect	GPS precision can degrade atmospheric effects from satellite signals passing through the troposphere and ionosphere
Multipath effects	Multipath is when an item is bounced off by a GPS satellite signal and then hits a receiver. This influence distinguishes the time of signal arrival from what it would have been without reflection
Pit configuration	Shallow mines are perfect GPS candidates because they appear to have an open view of the sky.
Satellite geometry	When the overhead satellites have good spatial distribution instead of being clustered together in a portion of the sky, the best positional readings occur

6.2. Acceleration and RPM collection and analysis

The prediction of the driving style based on the analysis of the drivers' behaviour and environmental data was one of this research's objectives. Acceleration and Engine RPM define a vehicle's motion. These parameters are also important for determining a driver's behaviour. To this end, the study of instantaneous vehicle parameters recorded by actual road tests is useful. Because of the developments in mobile sensing technologies and the technological capabilities of these devices, a variety of objective car and driving style data can be obtained, which can be used for driver style recognition based on OBD-II adapters. During a real test on the road, longitudinal and lateral accelerations on the y and x-axes can be reported on a vehicle. Through the study of parameters correlated with their driving, these parameters were used to classify the driver. To gather data for driving activities, we conducted a real-world experiment. In these experiments, while a driver carried out specific driving events, an Android application captured vehicle engine data. To produce the ground-truth for the experiment, the beginning and end timestamps of the driving events were recorded. When all the information was obtained, it was exported to the excel sheet. Each data form was placed on a separate table with the "acceleration and deceleration" key field, referring to the time of the case. Once the pre-processing was done, the data was prepared according to the actions of the drivers for the analysis phase. Several researchers discussed thresholds of acceleration linked to causality and a high risk of crash participation. The risk of collision start from -4.0m/s2 according to [20] while in [32, 37] similar results were obtained with a risk accident involvement around -5.0m/s2. In [17], the author proposed an acceleration/deceleration intensity stratification focused on numerous publications to provide an overview about the driving styles. In case of acceleration present the following parameters (dangerous (7.0 m/s2 - 12.0 m/s2), aggressive (3.5 m/s2 - 7.0 m/s2), normal (1.5 m/s2 - 3.5 m/s2) and safe (0 m/s2 - 1.5 m/s2)) and for deceleration (dangerous ((-9.0 m/s2) - (-14.0 m/s2)), aggressive ((-5.5 m/s2) – (-9.0 m/s2)), normal ((-3.0 m/s2) – (-5.5 m/s2)) and safe (0 m/s2 – (-3.0 m/s2)). Considering the mentioned works, we try to suggest an acceleration stratification consisting of a number of groups to test driver acceleration and braking based on our experiments to create a driving style table to enable the V2V alert system based on driving behaviours. It is possible to categorize driving behaviour into four major classes by calculating in-vehicle acceleration based on real time experiments: safe or non-aggressive drivers, normal, aggressive and dangerous drivers as shown in Figure 22.
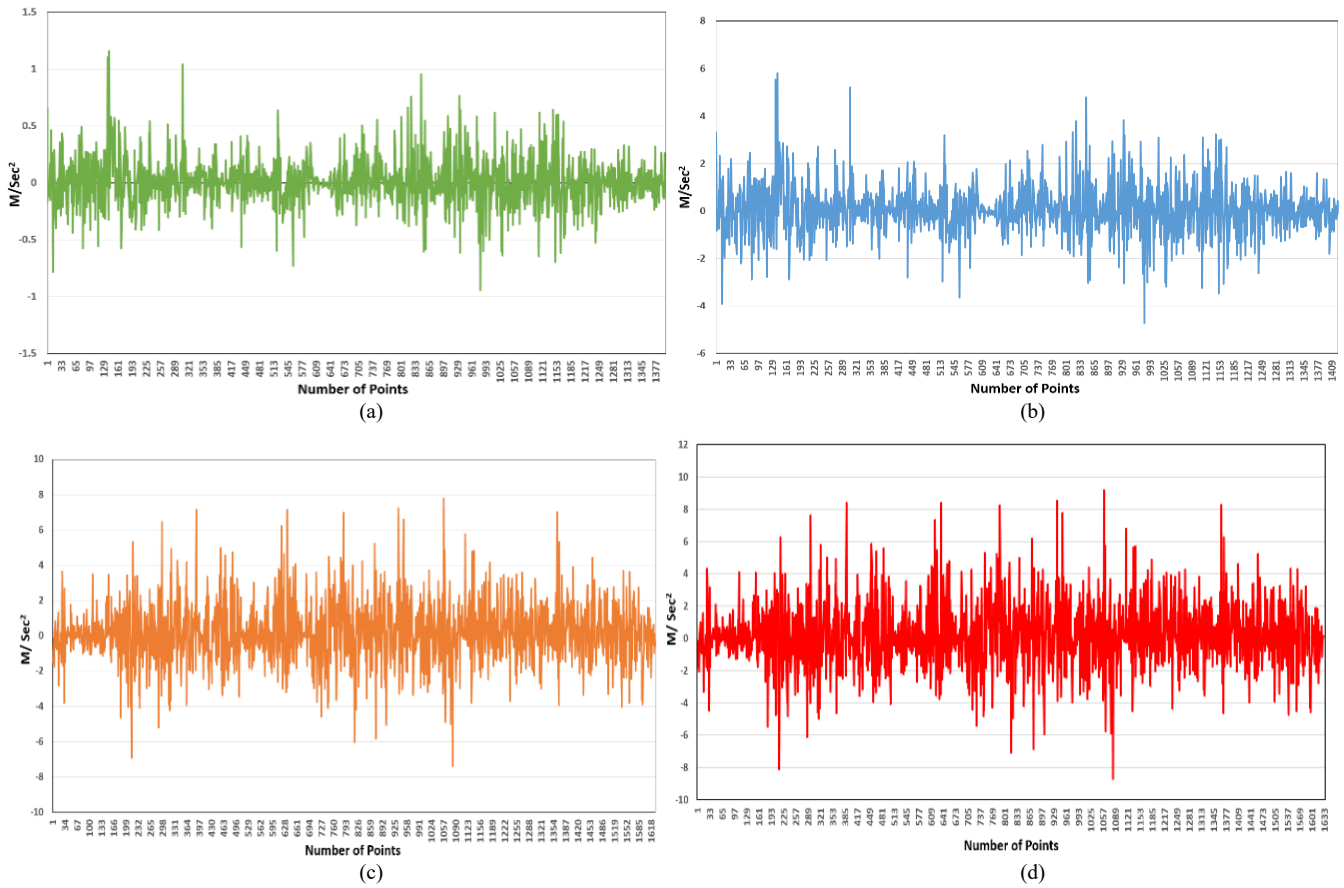
Figure 22. Driving behaviour analysis based on acceleration data: (a) Safe acceleration, (b) Normal acceleration, (c) Aggressive acceleration, (d) Dangerous acceleration

Furthermore, in driving behaviour data collection, different drivers and vehicles used to record the engine rotation represent Revolutions per minute (RPM) using the OBD-II adapter located below the driving panel. The pedal position test was carried out by pressing the accelerator pedal during different trips. The drivers informed when they had pressed the pedal as far as possible, and the duration was recorded. Furthermore, the accelerator pedal position over the time scatter plot as clarified in Figure 23 demonstrate that the maximum accelerator pedal ratio ranging from 1000 RPM to 4500 RPM recorded from different trips.
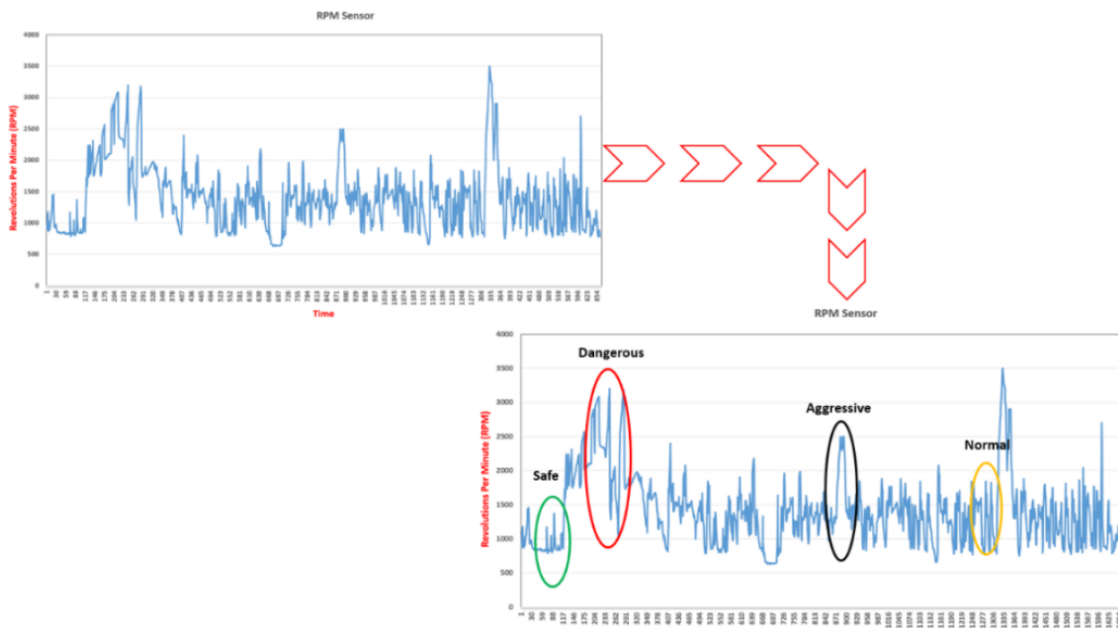
Figure 23: The visualization of Revolutions Per Minute (RPM) statistics

6.3. System deployment based on driving behaviours

The system algorithm provides an alert message and estimation distance for the vehicles about drivers' behaviour within the coverage area provided by the proposed system. Recognition of driving behaviour is a subjective mechanism that relies on the driver's interpretation and response to the changing external pressures of time. It is well known that the driving environment and behaviour are founded on a high degree of variability in individual experience and calculation. A high-level architectural framework that incorporates current technology and cognitive structures to build a new approach to the identification of trends in driving behaviour is, therefore a critical question. The results obtained from the different experiments (Figure 22), present accelerations data close to the values provided by previous researchers with some minor differences. These data have been injected into the proposed system to classify the driving performance as shown in Figure 24.

(a)

(b)

Figure 24: Network layout of point-to-point link: (a) transmitter, and (b) receiver

In this study a stratification of acceleration proposed in Table 11 with four main groups in acceleration and deceleration speed which represent one of the most reference tables used in the proposed V2V system.

Table 11: Defining behaviours based on experiments

Deceleration data (m/s^2)	Type of driving	Acceleration data (m/s^2)
0 to -2	Safe	0 to 2
-2 to -4	Normal	2 to 4
-4 to -7	Aggressive	4 to 7
Less than -7	Dangerous	More than 7

The safe driving behaviour is characterized by acceleration value that ranges from about ±2 m/s2. Normal driving, however, can also require more efficient but still planned braking, leading to more intense acceleration values ranging from 2 m/s2 to 4 m/s2. The risk of collision starts from 4 m/s2, which represented in this study the aggressive drivers. The dangerous evaluation indicates that the driver applies sudden movements in term of speeding starting from 7 m/s2. In the deceleration process and during these start and stop phases the lowest value of deceleration derivatives of safe and normal braking registered between -1 m/s2 and -3 m/s2, while conflict situations showed derivatives ranging from -3 m/s2 down to -8 m/s2 which represent the aggressive and dangerous driving style respectively. These differences in the acceleration data were observed for potential conflicts because of the difference of the drivers who carried out the experiments, as we note that some of them were driving in a natural way and the other was somewhat aggressively. The test results are successful, where it can be seen that the driver's behaviours were displayed based on the real-time acceleration readings taken from the OBD-II device connected to the vehicles as shown in Figure 25.

(a)

(b)

```
COM5
010C010C        begin        3.60        end
010C010C        begin        4.43        end
010C010C        begin        4.43        end
010C010C        begin        1.94        end
010C010C        begin        2.77        end
010C010C        begin        3.60        end
010C010C        begin        6.37        end
010C010C        begin        4.99        end
010C010C        begin        2.77        end
Current Vehicle Latitude=  32.5401
Current Vehicle Longitude=  44.5046
Driving Flag= 2
Vehicle Type= SONATA
010C010C        begin        8.59        end
010C010C        begin        6.93        end
```
(c)

```
COM5
Driving Flag= 2
Vehicle Type= SONATA
010C010C        begin        8.03        end
010C010C        begin        0.00        end
010C010C        begin        2.49        end
010C010C        begin        1.11        end
010C010C        begin        7.76        end
010C010C        begin        2.22        end
010C010C        begin        7.48        end
010C010C        begin        3.88        end
010C010C        begin        4.99        end
010C010C        begin        0.28        end
Current Vehicle Latitude=  32.5773
Current Vehicle Longitude=  44.5563
Driving Flag= 3
Vehicle Type= SONATA
010C010C        begin        4.71        end
010C010C        begin        1.38        end
```
(d)

Figure 25: Test results of the proposed methods: (a) safe and (b) Normal. (c) Aggressive and (d) dangerous driving

The proposed algorithm uses OBD-II and nRFL24L01 transceiver, which can be installed in the passing vehicle. These sensors may give information such as the speed, position, and distance of the impeding and opposing vehicles. At each interval Δt, the sensors send a signal to search the lane for any oncoming traffic. Using a reading sensor and a processing unit with a driver-vehicle interface (DVI) unit, the algorithms follow the procedures to determine whether or not a "safe" message should be displayed for the driver of the passing vehicle. Furthermore, when the behaviour of the transmitted vehicle change, such as speed or acceleration, the system starts to calculate the accumulated behaviour for the last ten seconds then extract the most frequent

values. The risk of collision starts from 4 m/s2, which represents the aggressive drivers which indicates that the driver's behaviour starts to shift from the normal to the aggressive behaviours. These values in the acceleration data were observed for potential conflicts because of the difference of the drivers who carried out the experiments, as we note that some of them were driving in a natural way and the other was somewhat aggressively. Based on these data, the warning system is activated taking the advantages of the GPS device connected to the main board to extract the vehicle's current location in the term of longitudes and latitudes values then calculate these values in degrees. Moreover, these data were sent to the neighbouring vehicles and vehicle type and the flag status through the nRF24L01. On the other side at the receiving vehicle, the system displays the transmitted flag and use the GPS unit mounted on the receiving board to measure the distance between the two moving vehicles then switch on the orange LED with a continuous updating of the distance between the two vehicles whether the threat is approaching or drifting away as long as the sending vehicle is within coverage range of the receiving vehicle. An example of a warning signal displayed by the LCD is shown in Figure 26.
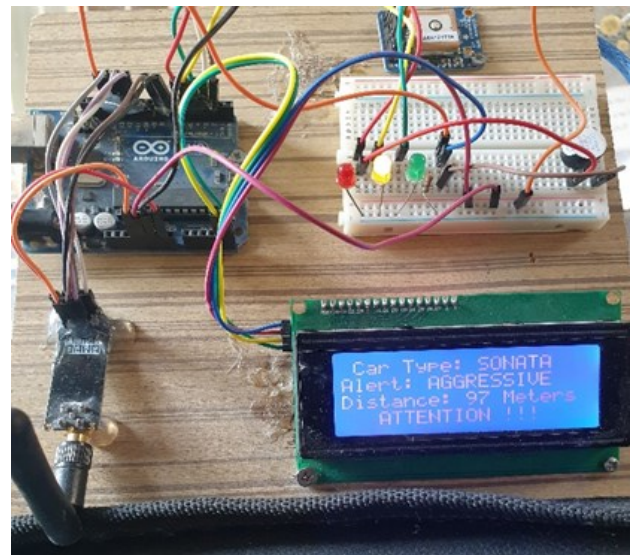
Figure 26: Test results of the proposed method for aggressive driving warning

$$Driver\ Safe\ Ration = \frac{number\ of\ safe\ flag\ behaviour}{number\ of\ safe\ flag\ behaviour + number\ of\ at\ risk\ behaviour} \times 100 \quad (3)$$
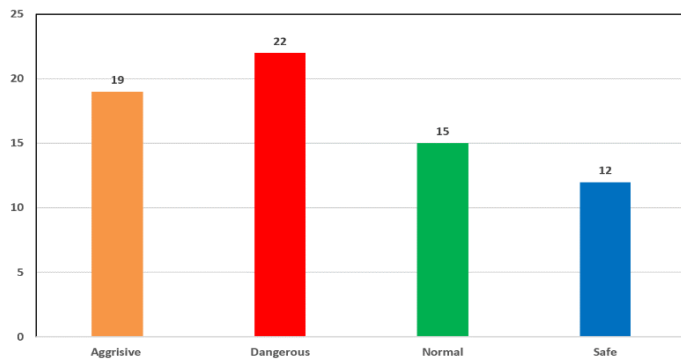
(a) Safe driving (87% total safe flags)
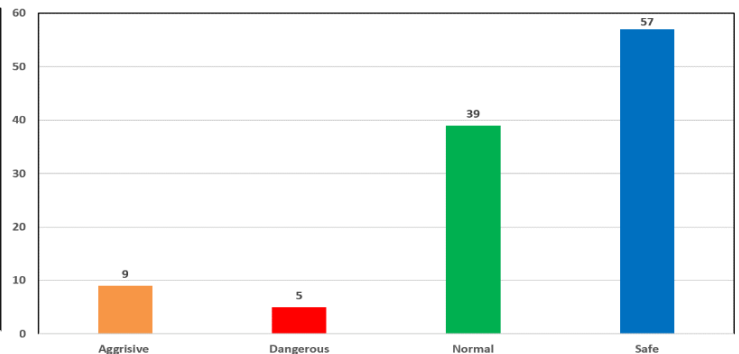
(b) Dangerous driving (40% total safe flags)

Figure 27: Test results of the proposed methods: (a) Safe flag and (d) dangerous flag driving

Recall from the introduction section, that behavioural safety programs operate based on measuring and monitoring safe behaviour performance. The opposite of safe behaviour in at-risk behaviour, which can be defined as behaviour that has been identified as critical to safe performance. A key concept for the research, taken from behavioural safety analysis, is the calculation of safe behaviour performance using a percent safe value calculated as (3).

Generally, in driving behaviours data collection experiments, multiple drivers participated in this study during the period of data collection using the proposed system with different types of vehicles and scenarios using. Figure 27 show the results of different examples with varying sites of study.

7. Conclusions

Despite the increasing research interest in V2V communication, limitations remain in existing studies in this area. Studies indicate that further research and development are needed to address these limitations, especially in driving behaviour. This work introduces a real-time V2V warning system based on driving behaviour. Comparison of the OBD-II and GPS data streams became available during the measurement on the smartphone screen with charts and other views. The independent data from mobile application and GPS device speed were used to validate and check the data collected from OBD-II adapter speed. Considering the mentioned works, we used the OBD-II adapter attached to the vehicle to trigger the V2V alert system based on driving actions, and we suggest a stratification of acceleration consisting of a variety of classes to test driver speed and braking based on our experiments. A severity stratification of acceleration/deceleration presented with the following parameters (dangerous (more than 7 m/s2), aggressive (4 m/s2 – 7 m/s2), normal (2 m/s2 – 4 m/s2) and safe (0 m/s2 – 2 m/s2)). In future studies, we would like to use the obtained data sets as input values for a machine learning environment to forecast parameter values in the future with prediction algorithms, decision trees, or time series analysis. Future studies could also use different communication modules such as Wi-Fi, Bluetooth and ZigBee. Different data types can be used during the test scenarios, including videos and voices data. In addition to that, the network can be tested up to the capacity of the transceiver. Such improvement would help to produce more understanding towards the purpose of the V2V installation, usage, cost, and the equipment of the developed system.

Conflict of Interest

The authors declare no conflict of interest.

Acknowledgment

References

[1] S. Jiao, S. Zhang, B. Zhou, Z. Zhang, L. Xue, "An Extended Car-Following Model Considering the Drivers' Characteristics under a V2V Communication Environment," Sustainability, **12**(4), 1552, 2020, doi:10.3390/su12041552.

[2] W.H. Lee, C.Y. Chiu, "Design and Implementation of a Smart Traffic Signal Control System for Smart City Applications," Sensors, **20**(2), 508, 2020, doi:10.3390/s20020508.

[3] H.A. Ameen, A.K. Mahamad, B.B Zaidan, A.A. Zaidan, S. Saon, D.M. Nor, R.Q. Malik, Z.H. Kareem, S. Garfan, R.A. Zaidan, A. Mohammed, "A Deep Review and Analysis of Data Exchange in Vehicle-to-Vehicle Communications Systems: Coherent Taxonomy, Challenges, Motivations, Recommendations, Substantial Analysis and Future Directions," IEEE Access, **7**, 158349-158378, 2019, doi:10.1109/ACCESS.2019.2949130.

[4] A. Memon, F.K. Shaikh, E. Felemban, "Experimental evaluation of vehicle-to-vehicle based data transfer," in 2015 International Conference on Information and Communication Technology Research (ICTRC), 274-277, 2015, doi: 10.1109/ICTRC.2015.7156475.

[5] M.A. Lebre, F.Le Mouel, E. Menard, "Resilient, Decentralized V2V Online Stop-free Strategy in a Complex Roundabout," in 2016 Ieee 83rd Vehicular Technology Conference (IEEE Vehicular Technology Conference Proceedings, 1-5, 2016, doi: 10.1109/VTCSpring.2016.7504449.

[6] D. Farooq, S. Moslem, R.F. Tufail, O. Ghorbanzadeh, S. Duleba, A. Maqsoom, T. Blaschke, "Analyzing the importance of driver behavior criteria related to road safety for different driving cultures," International Journal of Environmental Research Public Health, **17**(6), 1893, 2020, doi.org/10.3390/ijerph17061893.

[7] T. Zinchenko, Reliability Assessment of Vehicle-to-Vehicle Communication, Ph.D thesis, Technical University of Braunschweig, 2015.

[8] Y. Ma, Z. Zhang, S. Chen, Y. Yu, K. Tang, "A comparative study of aggressive driving behavior recognition algorithms based on vehicle motion data," IEEE Access, **7**, 8028-8038, 2019, doi: 10.1109/ACCESS.2018.2889751.

[9] W. Alghamdi, E. Shakshuki, T. R.Sheltami, "Context-Aware Driver Assistance System," Procedia Computer Science, **10**, 785-794, 2012, doi.org/10.1016/j.procs.2012.06.100.

[10] B. Yu, M. Wu, S. Wang, W. Zhou, "Traffic simulation analysis on running speed in a connected vehicles environment," International Journal of Environmental Research Public Health, **16**(22), 4373, 2019, doi: 10.3390/ijerph16224373.

[11] H.A. Ameen, A. K.Mahamad, S. Saon, D.M. Nor, K. Ghazi, "A review on vehicle to vehicle communication system applications," Indonesian Journal of Electrical Engineering and Computer Science, **18**(1), 188-198, 2020, doi.org/10.11591/ijeecs.v18.i1.pp188-198.

[12] H. Tchouankem, "Characterization of Intersection Topologies in Urban Areas for Vehicle-to-Vehicle Communication," in 2016 IEEE 84th Vehicular Technology Conference (VTC-Fall), 1-5, 2016, doi: 10.1109/VTCFall.2016.7880931.

[13] F. Cardoso, A. Serrador, T. Canas, "Algorithms for Road Safety Based on GPS and Communications Systems WAVE," Procedia Technology, **17**, 640-649, 2014, doi.org/10.1016/j.protcy.2014.10.187.

[14] A. M. Orozco, S. Cespedes, R. Michoud, G. Llano, "Design and simulation of a collision notification application with geocast routing for car-to-car communications," European Transport Research Review, **7**(36), 2015, doi.org/10.1007/s12544-015-0185-1.

[15] M. El-Said, V. Bhuse, A. Arendsen, "An Empirical Study to Investigate the Effect of Air Density Changes on the DSRC Performance," Procedia Computer Science, **114**, 523-530, 2017, doi.org/10.1016/j.procs.2017.09.025.

[16] L. Dorn, Driver behaviour and training, Routledge, 2017.

[17] M. G. Jasinski, F. Baldo, "A Method to Identify Aggressive Driver Behaviour Based on Enriched GPS Data Analysis," in the GEOProcessing 2017: The Ninth International Conference on Advanced Geographic Information Systems, Applications, and Services, 97-102, 2017

[18] J. H. Ogle, Quantitative assessment of driver speeding behavior using instrumented vehicles, Ph.D thesis, Civil Engineering, Georgia Institute of Technology, 2005.

[19] .G. Mantouka, E.N. Barmpounakis, E.I. Vlahogianni, "Identifying driving safety profiles from smartphone data using unsupervised learning," Safety Science, **119**, 84-90, 2019, doi.org/10.1016/j.ssci.2019.01.025.

[20] O. Bagdadi, A. Várhelyi, "Jerky driving—An indicator of accident proneness?," Accident Analysis & Prevention, **43**(4), 359-1363, 2011, doi.org/10.1016/j.aap.2011.02.009.

[21] A.B. Ellison, S.P. Greaves, M.C.J. Bliemer, "Driver behaviour profiles for road safety analysis," Accident Analysis & Prevention, **76**, 118-132, 2015, doi.org/10.1016/j.aap.2015.01.009.

[22] C.M. Martinez, M. Heucke, F. Wang, B. Gao, D. Cao, "Driving Style Recognition for Intelligent Vehicle Control and Advanced Driver Assistance: A Survey," IEEE Transactions on Intelligent Transportation Systems, **19**(3),

666-676, 2018, doi: 10.1109/TITS.2017.2706978.

[23] O. Raz, H. Fleishman, I. Mulchadsky, System and method for vehicle driver behavior analysis and evaluation, ed: Google Patents, 2008.

[24] E.M. Carboni, V. Bogorny, "Inferring Drivers Behavior through Trajectory Analysis," Advances in Intelligent System and Computing, 837-848, 2015, doi.org/10.1007/978-3-319-11313-5_73.

[25] F. Tango, M. Botta, "Real-Time Detection System of Driver Distraction Using Machine Learning," IEEE Transactions on Intelligent Transportation Systems, **14**(20), 894-905, 2013, doi: 10.1109/TITS.2013.2247760.

[26] A. Aksjonov, P. Nedoma, V. Vodovozov, E. Petlenkov, M. Herrmann, "A Novel Driver Performance Model Based on Machine Learning," IFAC-PapersOnLine, **51**(9), 267-272, 2018, doi.org/10.1016/j.ifacol.2018.07.044.

[27] A. Daniel, D. C. Popescu, S. Olariu, "A Study of Beaconing Mechanism for Vehicle-to-Infrastructure Communications," in 2012 IEEE International Conference on Communications (ICC), 7146-7150, 2012, doi: 10.1109/ICC.2012.6364667.

[28] F. Visintainer, L. Altomare, A. Toffetti, A. Kovacs, A. Amditis, "Towards Manoeuver Negotiation: AutoNet2030 Project from a Car Maker Perspective," Transportation Research Procedia, **14**, 2237-2244, 2016, doi.org/10.1016/j.trpro.2016.05.239.

[29] S. Eckelmann, T. Trautmann, H. Ußler, B. Reichelt, O. Michler, "V2V-Communication, LiDAR System and Positioning Sensors for Future Fusion Algorithms in Connected Vehicles," Transportation Research Procedia, **27**, 69-76, 2017, doi.org/10.1016/j.trpro.2017.12.032.

[30] J.E. Meseguer, C.T. Calafate, J.C. Cano, P. Manzoni, "DrivingStyles: A smartphone application to assess driver behavior," in 2013 IEEE Symposium on Computers and Communications (ISCC), 000535-0005402013, 2013, doi: 10.1109/ISCC.2013.6755001.

[31] J. Zaldivar, C. T. Calafate, J. C. Cano, P. Manzoni, "Providing accident detection in vehicular networks through OBD-II devices and Android-based smartphones," in 2011 IEEE 36th Conference on Local Computer Networks, 813-819, 2011, doi: 10.1109/LCN.2011.6115556.

[32] S.H. Lee, S. Lee, M.H. Kim, "Development of a Driving Behavior-Based Collision Warning System Using a Neural Network," International Journal of Automotive Technology, **19**(5), 837-844, 2018, doi.org/10.1007/s12239-018-0080-6.

[33] S.H. Chen, J.S. Pan, K. Lu, "Driving behavior analysis based on vehicle OBD information and adaboost algorithms," in Proceedings of the international multiconference of engineers and computer scientists, **1**, 18-20, 2015.

[34] Freematics. (2017). Freematics ESP32 OBD Kit. Available: https://freematics.com/store/index.php?route=product/product&product_id=87

[35] Adafruit. (2017). Adafruit ultimate gps breakout - 66 channel w/10 hz updates. Available: https://www.adafruit.com/product/746

[36] M. Rohani, Bus driving behaviour and fuel consumption, Ph.D thesis, Faculty of Engineering, Science & Mathematics University of Southampton, 2012.

[37] S.G. Klauer, T.A. Dingus, V.L. Neale, J.D. Sudweeks, D.J. Ramsey, "The impact of driver inattention on near-crash/crash risk: An analysis using the 100-car naturalistic driving study data," U.S. Dept. Transp., Nat. Highway Traffic Saf. Admin., 2006, doi:10.1037/e729262011-001.

Learning Path Recommendation using Hybrid Particle Swarm Optimization

Eko Subiyantoro[1], Ahmad Ashari[2,*], Suprapto[2]

[1]Departement of Information Technology, BBPPMPV-BOE Kemdikbud, Malang, 65102, Indonesia

[2]Departement of Computer Science and Electronic, Universitas Gadjah Mada, Yogyakarta, 55281, Indonesia

A R T I C L E   I N F O

A B S T R A C T

Revised Bloom's Taxonomy (RBT) is proposed in general to look more forward in responding to the demands of the developing educational community, including how students develop and learn and how teachers prepare Learning Objects (LO). The variety of characteristics of students' abilities in a class has always been a problem that is often faced by a teacher. Unfortunately, cognitive classifications to develop students' knowledge to a high level have not been used to plan a learning path that is appropriate for their cognitive level. The purpose of this study is to recommend a learning path that matches the cognitive abilities of students from a learning object ontology. The method used in this research is Hybrid Particle Swarm Optimization (HPSO) which integrates Binary Particle Swarm Optimization (BPSO) and Discrete Particle Swarm Optimization (DPSO). The Connection Weight (CW) function is used to test the quality of the connection between the learning objects of an ontology subject controlled by the cognitive class. Based on experimental studies, the HPSO method can recommend a suitable learning path for cognitive classes, namely Low Cognitive (CL), Medium Cognitive (CM), and High Cognitive (CH). The similarity of the sequence of learning paths based on population in CL-class is 87.5%, CM class 75%, and CH class 87.5%.

1. Introduction

In general, learning groups are designed to be heterogeneous. That is, a class is inhabited by students with various types of learning and characters. There are students with a fast learning type. While others are slow and even very slow. Therefore, it is difficult for teachers to follow an approach that is suitable for every student. In an effort to reach all students, teachers often design class lectures and activities. To remedy this situation requires personal support and guidance so that individual needs and difficulties can be addressed. However, given the number of students a class has, it is not easy for a teacher to deal with the diversity of levels and needs of students at all times [1].

Curriculum Sequencing (CS) is a technique to give students flexibility in planning the most appropriate sequence of individual learning tasks [2]. Produce an individual learning method in which each student dynamically chooses the most optimal teaching operation through presentations, examples, questions, or problems. Meanwhile [3] found the optimal learning sequence through the pretest to identify the weaknesses of students. Thus, CS aims to

replace the rigid, generic, modeled learning structure set by the instructor or pedagogical team, with a more flexible and personalized learning path.

CS development according to [4] must consider students' learning abilities, background, and motivation. Even for certain students, the requirements can change according to their increased knowledge due to learning. According to [5] states that CS not only helps students find the most efficient and appropriate learning path but also helps instructors to organize program structures, content, or learning objects and make improvements. Meanwhile [6] stated that individualization of teaching materials was a challenge in choosing the right LO and making the LO sequence easy to learn. Thus, optimal results will be obtained because the learning path of learning is following students' abilities. Learning paths that have been developed have not used cognitive classification as a controller of the learning object ontology of a subject. The Evolutionary Computing (EC) algorithm approach has been widely used in solving Curriculum Sequencing problems.

According to [7] the EC method that is most widely used to solve CS problems is grouped into two main approaches, namely the social sequencing approach and the individual sequencing

approach. Genetic Algorithm (GA) is a metaheuristic method which is famous because it has good performance for various types of optimization problems. There have been many GA studies in the CS domain including [8]-[11].

In [12] present a Personalized e-Course Composition approach based on Particle Swarm Optimization (PC2PSO). A binary particle encoding is used, in which each dimension determines whether the object of learning is included in sequence (1) or (0). The initial particles are generated randomly. The fitness function is used to determine Gbest and Pbest based on the level of compatibility between the pedagogical targets of students and the learning concept: learning material, level of compatibility, difficulty level, the time limit for learning, and student checks on the material that has been studied. Comparative evaluation in terms of average fitness and stability functions shows that the PSO method is better than the GA method. While the newer optimization method is swarm intelligence.

Swarm intelligence is an optimization method based on a distributed agent system, where each agent has simple abilities that can solve complex problems together. The approach to swarm intelligence is very different from EA because swarm intelligence emphasizes cooperation rather than competition. To support the concept of cooperation, each agent has a simple ability to learn from experience and also communicate with fellow agents. Metaheuristic methods based on the concept of swarm intelligence are Particle Swarm Optimization (PSO) and Ant Colony Optimization (ACO).

The PSO algorithm was originally proposed in 1995 [13]. In the PSO, each particle represents the solution to the problem. Particle learning consists of two factors, namely particle experience called cognitive learning and the combination of learning from the whole swarm is called social learning. Cognitive learning as Pbest is the best position that a particle has ever reached, while social learning as Gbest is the best position of all particles in the swarm. One of the uses of PSO in the e-education domain includes research conducted by [14] using the PSO method to offer formative value in e-assessment and turn it into a learning tool.

This research proposes a learning path model based on the cognitive classification of Revised Bloom's Taxonomy and an ontology of learning objects. Cognitive classification is based on RBT into three cognitive classes (Cognitive Low (CL), Cognitive Medium (CM), and Cognitive High (CH)). Hybrid Particle Swarm Optimization (HPSO) algorithm is used to solve combinatorial problems, namely learning object ontology with Discrete PSO which is controlled by cognitive class using Binary PSO. So that a learning path model will be produced that is following the cognitive abilities of students through optimization of the assessment of the LO relationship between RBT and the ontology of a subject.

2. Literature Review

2.1. Learning Object

Primary reference sources in the form of journals and dissertations, and secondary sources in the form of books, many have provided explanations about learning objects. However, in general, there is a common view of the concept of learning objects. The definition of a learning object is broadly described as all entities that are related or used as learning and training materials.

From this understanding, all general and conventional learning materials such as worksheets, modules, handouts, etc. are also included in the learning object category. Researcher [15] as well as a learning practitioner defines learning objects as each learning resource in the form of a digital entity that can be used repeatedly as a learning resource. While other researchers [16] presented various definitions of LO, the simplest description refers to data objects, content, or information.

The Institute of electrical and electronics engineer (IEEE) defines learning objects, namely as any digital or non-digital entity that can be used, then reused and can become a reference for technology-assisted learning. Thus LO is any entity (digital or non-digital) that can be reused or referenced including multimedia content, instructional content, software, people, organizations, or events for technology-supported learning. This definition leaves room for the entire curriculum to be seen as an LO.
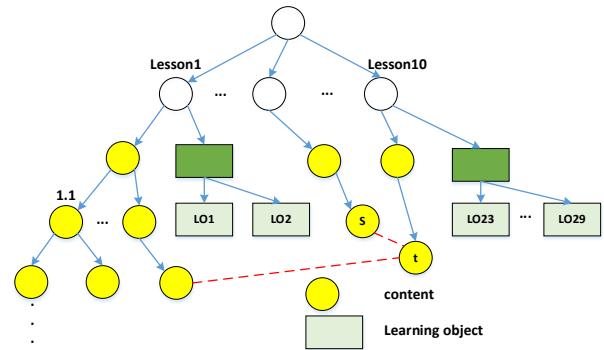
Figure 1: Examples of learning object structures

Figure 1 shows that in one topic or one subject, the description of the content of the course is followed by the related learning material. In other words, subject content is usually arranged based on ontology, where the yellow circle represents the learning content while the blue rectangle represents LO [17].

2.2. Particle Swarm Optimization

The PSO algorithm works based on particles in the population that work together to solve existing problems disregarding the physical position. The PSO algorithm combines local and global search methods that balance exploration ability to conduct investigations in different areas of the search area to get the best optimal value and exploitation ability to concentrate around the search area for fix solution. The similarity of PSO and GA is that the system starts with a population formed from random solutions, then the system seeks optimization through random generation changes [18]. Each particle holds traces of position in the search space as the interpretation of the best solution (*fitness*) that had been achieved.

The basis of the PSO algorithm consists of three steps, namely determining the particle position and velocity, updating the velocity, and updating the position [19]. Each particle tries to update its position using information such as the current position, the current velocity, the distance between the current position to *Pbest*, and the current position to *Gbest* which mathematically updates the particle velocity calculated (1).

$$v_{i,j}^{t+1} = v_{i,j}^{t} + c_1 r_1 \left[Pbest_{i,j}^{t} - x_{i,j}^{t} \right] + c_2 r_2 \left[Gbest_{j}^{t} - x_{i,j}^{t} \right] \quad (1)$$

The achievement of the results is obtained from a new velocity calculation for each parallel based on the distance from the Pbest

it has and the distance from the Gbest position updating the particle position $x_{i,j}^{t+1}$ is shown in (2).

$$x_{i,j}^{t+1} = x_{i,j}^{t} + v_{i,j}^{t+1} \qquad (2)$$

Personal best (*Pbest*) according to [20] is the best value that a particle has, the value in the next time step, t + 1, where t ∈ [0,…, N], update *Pbest* is shown in (3),

$$Pbest_{i,j}^{t+1} = \begin{cases} Pbest_{i,j}^{t} & \text{if } fitness\left(x_{i,j}^{t+1}\right) \leq fitness\left(Pbest_{i,j}^{t}\right) \\ x_{i,j}^{t+1} & \text{if } fitness\left(x_{i,j}^{t+1}\right) > fitness\left(Pbest_{i,j}^{t}\right) \end{cases} \quad (3)$$

While the Global best (*Gbest*) is the best value that takes into account all particles in the population calculated using (4)

$$Gbest = max\{Pbest_{i}^{t+1}\}, \text{where } i \in [1, \dots, n] \text{ and } n > 1 \quad (4)$$

Each iteration, each particle is given information about the latest *Gbest* value so that a one-way information sharing mechanism occurs to carry out the process of finding the best solution with a fast convergence shift.

2.2.1. Binary Particle Swarm Optimization (BPSO)

In [21] developed PSO to operate in binary search space because real value domains can be converted into binary valued domains. The proposed algorithm is called the PSO binary algorithm (BPSO) in which particles represent positions in binary space and the particle position vectors can take a binary value 0 or 1 where $x_{ij} \in \{0,1\}$. In this case, it maps from the binary space of the dimension B^n (an eg string of bits of length n) to the real number $f = B^n \rightarrow R$ (where f is the fitness function and R is the set of real numbers). That means that the position of the particle must belong to B^n to be calculated by the fitness function [22]. In BPSO, the particle velocity v_{ij}^{t} is connected to the probability that the particle position x_{ij}^{t} is 0 or 1. Equation (1) for updating particle velocity is still used in BPSO. Then the sigmoid function S_{ij}^{t} shown in (5) is used to update the particle velocity.

$$S_{ij}^{t} = \frac{1}{1+e^{-v_{ij}^{t+1}}} \qquad (5)$$

The position of the particle x_{ij}^{t} is influenced by (6), where u_{ij}^{t} is a random number selected from the distribution (0, 1) and S_{ij}^{t} of the sigmoid function.

$$x_{ij}^{t} = \begin{cases} 1 \text{ if } u_{ij}^{t} < S_{ij}^{t} \\ 0 \text{ if } u_{ij}^{t} \geq S_{ij}^{t} \end{cases} \qquad (6)$$

2.2.2. Discrete Particle Swarm Optimization (DPSO)

In 2000, Clerc modified the DPSO algorithm formulated by Kennedy and Eberhart. Clerc modifies the representation of the position of the particle, the shape of the velocity produced by the particle, and the effect of velocity on the position of the particle. This modification hopes that it can be applied to problems with discrete models, especially combinatorial types [23]. The velocity update formula that has been modified by Clerc is defined in (7), while for fixed position updates using (1).

$$v_{i}^{t+1} = c_1 \cdot v_i^t \oplus c_2\left(\left(Pbest_i^t + \frac{1}{2}(Gbest_i^t - Pbest_i^t)\right) - x_i^t\right) \qquad (7)$$

3. Methodology

The Hybrid Particle Swarm Optimization algorithm is applied to overcome combinatorial problems in a more practical and orderly manner in determining learning pathways. Determination of the order of learning objects through LO ontology based on cognitive classes from the learning vector quantization method and using RBT to assess connection quality. The expected result is that each student gets a recommendation for a learning path that is appropriate to their cognitive level.

The model used in this study consists of three components, cognitive classification with LVQ, learning object ontology based on RBT, and hybrid discrete particle swarm optimization. The general architecture of the proposed model can be seen in Fig. 1.
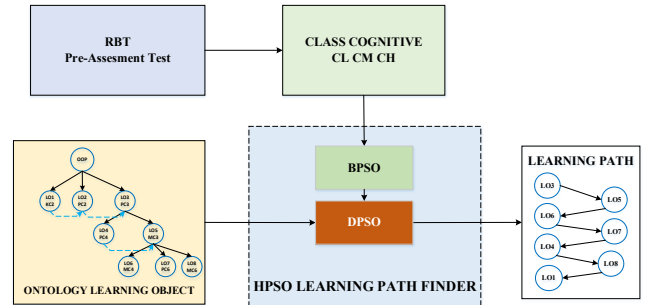
Figure 2: The Architecture of The proposed Model

3.1. Particle Representation BPSO

The representations of the particles of the three cognitive classes (CL, CM, CH) were arranged according to a predetermined LO sequence. Each cognitive class is placed in 8 data slots, so it takes 24 data slots. The Cognitive Low class on particles 7 and 8, the Cognitive Medium class on particles 1, 4, 8, and the Cognitive High class on particles 1, 2, 4, have a value of 0. This value of 0 indicates that the value at the position of these particles can change from 0 becomes 1 depending on the speed and position of the particles. Meanwhile, the value of particles with a value of 1 is determined as LO which must be followed and the calculation is carried out which is not affected by the particle velocity. The updated particle velocity and position of the CL cognitive class are presented in Figure 3.
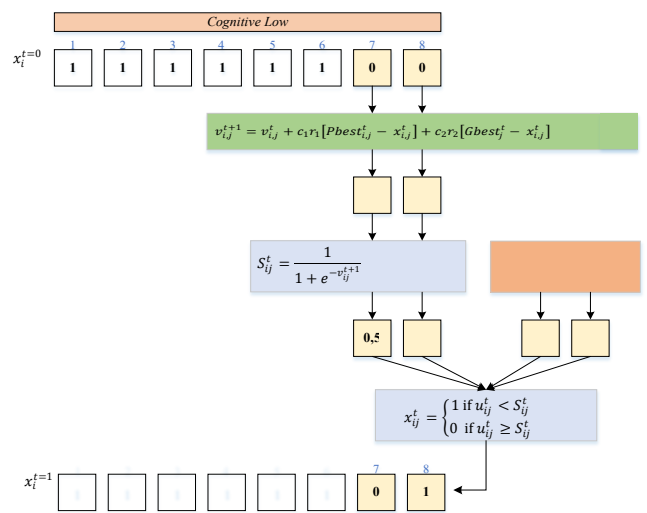
Figure 3: Update velocity and position in cognitive class

3.2. Particle Representation DPSO

LO particles consist of eight particles arranged based on object-oriented programming lessons that have been determined based on

the depth and breadth analysis of RBT, namely Table I. The representation of LO-LO sequence particles is shown in Figure 4 randomly from three groups of particles.
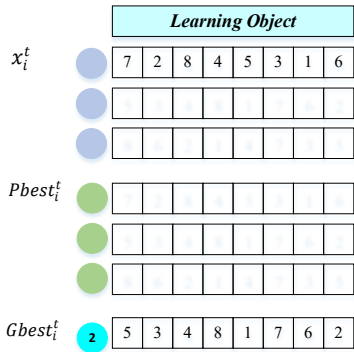

Figure 4: Learning Object Particle Representation

Update the position of the learning object using (1) while for speed update using (7). The process of updating the speed of learning objects begins with the process of reducing *Gbest* with *Pbest*, where $Gbest_i$ [5 3 4 8 1 7 6 2] is used as a reference in the transposition process. The transposition stage starts with a shift in the learning object starting from (1,5) and several times the position shift from position (2,6) - (3,4) - (5,7) - (6,7) and stops at the position shift (7,8) after equal to the reference value $Gbest_i$ [5 3 4 8 1 7 6 2]. Based on (7) the temporary velocity value is multiplied by 0.5 to produce the velocity, namely (1.5) (2,6) (3,4).

3.3. BPSO – DPSO Integration

HPSO is the part that performs the process of determining the learning path, consisting of BPSO and DPSO. Cognitive classes (CL, CM, and CH) are represented as particles in the BPSO method and ontology learning objects are represented as particles in the DPSO method. The integration of BPSO and DPSO through the fitness function will produce a learning path model that is suitable for students' cognitive abilities.

Figure 5 shows the process of updating the speed and position of particles for DPSO and BPSO in each iteration so that it will ensure changes in LO and cognitive class (CL, CM, CH). Update the velocity and position of DPSO particles on the learning object update through (7) to update the particle velocity, and use (2) to

update the position. Meanwhile, the update of the speed and position of BPSO particles in the cognitive class is through (1) to update the speed, (5) to calculate the sigmoid S_i^t value, and (6) to update its position.

3.4. The Proposed HPSO Algorithm

The fitness function is used as a measuring tool to select the best object from a set of existing objects. The fitness function is identical to the objective function of the optimized problem, which is to make the best individual learning route according to their cognitive abilities. The objective function is determined based on the highest fitness value. The higher the fitness value, the results are closer to the objective function.

The objective function defined in this research is to create individual learning paths or routes based on student cognitive data, namely CL, CM, and CH with the learning object ontology of a subject. Thus, the fitness function is to find the best Connection Weight (CW) value between LO in ontology-based on students' cognitive classes, namely CL, CM, and CH as illustrated in Figure 6.

Connection Weight (CW) was used to assess the relationship of LO in RBT ontology as cognitive level evaluators (8).

$$cw = \frac{k}{t_1 \cdot |DBO| + t_2 \cdot |DBB|} \tag{8}$$

This study uses Distance by Bloom (DBB) to measure the cognitive distance depth and breadth ($d_{k,l}$) between LO using (9),

$$d_{k,l} = \sqrt{(k_2 - k_1)^2 + (l_2 - l_1)^2} \tag{9}$$

Equation (10),(11),(12) FC_L , FC_M , FC_H is fitness function to determine LO relationships in CL,CM,CH class,

$$FC_L = cw_L + \frac{1}{\beta_L * \sum ULO_L} \tag{10}$$

$$FC_M = cw_M + \frac{1}{\beta_M * \sum ULO_M} \tag{11}$$

$$FC_H = cw_H + \frac{1}{\beta_H * \sum ULO_H} \tag{12}$$

with:
$\beta_L, \beta_M, \beta_H$ is 0 -1.
cw_L, cw_M, cw_H is *connection weight* for each class cognitive
ULO_L, ULO_M, ULO_H is *unsed LO* for each class cognitive.
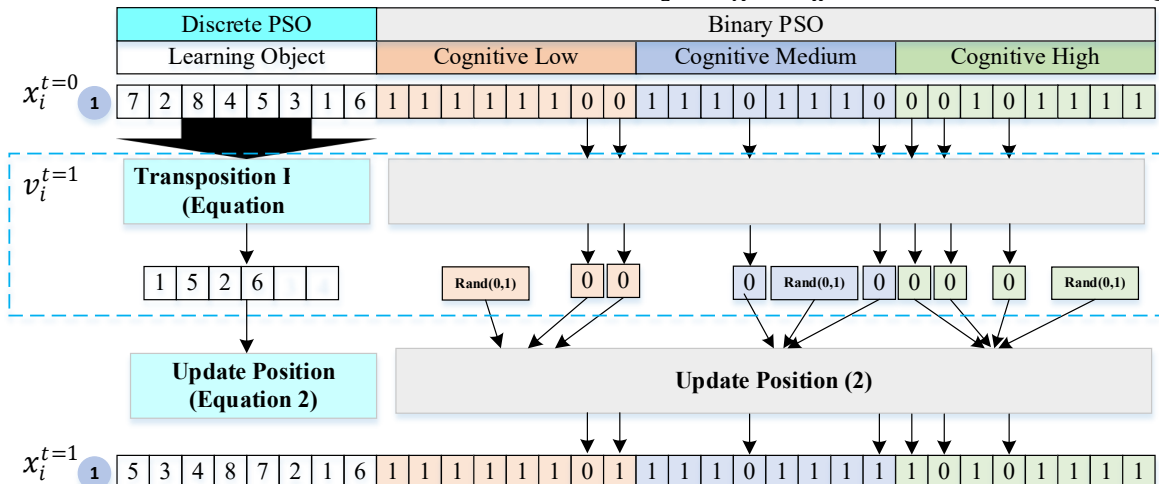
Figure 5: DPSO-BPSO integration in updating the velocity and position of particles

$$cw = \frac{k}{t_1 \cdot |DBO| + t_2 \cdot |DBB|}$$
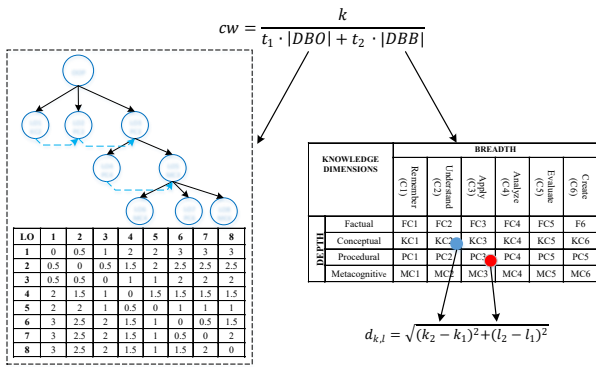
Figure 6: Illustration of Determining the Fitness Function

The objective function value is calculated for all the particles generated earlier. The PBest position is determined from the objective function value obtained. The initial velocity of the particles is the absolute difference between the initial position and the personal best position of the particles. The particle with the maximum objective function value is the GBest particle and the corresponding position is the global best position [24]. The calculation of the fitness function stops until the iteration value limit has been determined.

The Hybrid Particle Swarm Optimization algorithm with a learning object transposition function is presented in detail in Table 1.

Table 1: HPSO Algorithm

Algorithm 1: HPSO for recommendation learning path

Result: Learning path based on students' cognitive class
Initialization;
LO_i;
$Pbest_i$;
$Gbest$;
dbo_i;
dbb_i;
cw;
fx;
Transposition()
  posx=1;
  for i = 1 To Gbest
    for j = 1 To Pbest
      if Gbest(i) = Pbest(j) And i<>j **then**
        tmp = Pbest(j);
        Pbest(j) = Pbest(i);
        Pbest(i) = temp;
        trsp1(posx) = i;
        trsp2(posx) = j;
        posx = posx + 1;
      end
    next j
  next i
  vc = posx * 0.5;
  for i = 1 To vc - 1
    indx1 = trsp1(i);
    indx2 = trsp2(i);
    tmp = Pbest(indx1);
    Pbest(indx1) = Pbest(indx2);
    Pbest(indx2) = tmp;

    next i
end Function

while (true) **do**
  for i = 1 To LO
    call: Transposition();
      if (dbb(i) > 0 && dbo(i) > 0) **then**
        cwIndex(i) = k / (t1 * dbo(i)) + (t2 * dbb(i))
      end
    cw(i) += cwIndex(i);
    tempFitness(i)=cw(i) + (1 / beta * unLo(i));
    f(i) += tempFitness(i);
      if ($f(LO_i) <= f(Pbest_i)$) **then**
        Pbest(i) = $f(Pbest_i)$;
      if ($f(LO_i) > f(Pbest_i)$) **then**
        Pbest(i) = $f(LO_i)$;
      end
    Gbest(i) = max(Pbest(i));
  next i
end

4. Results

Testing the HPSO algorithm to recommend a learning path model that suits the CL, CM, and CH cognitive classes through steps, i.e:

a. Testing the next computational program, test the consistency of the PBest fitness function for each population to become GBest through five particle populations, ten particle populations (ten LO groups), and fifteen populations (fifteen LO groups).

b. Groups of students in cognitive classes CL, CM, and CH will get the best learning path recommendations based on their respective GBest.

4.1. Connection Weight for Fitness Fuction

A CW calculation process occurs when one LO is paired together with CL of value 1. The calculation starts with finding the DBO, DBB, and CW values of each LO. In the state of one LO paired together with CL is 0 then the LO is not used in the connection weight calculation process. The mechanism for testing connection weight according to in accordance with the procedure shown in Figure 7.
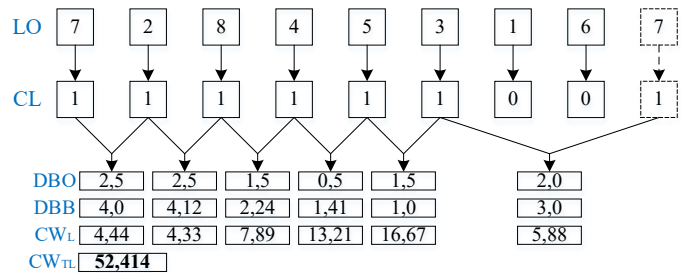
Figure 7: Representation of Connection Weight

The fitness function in the CL,CM,CH-class is calculated using (10),(11),(12) ,the $Pbest_i^t$ fitness value data with 15 groups of particles is shown in Figure 8.
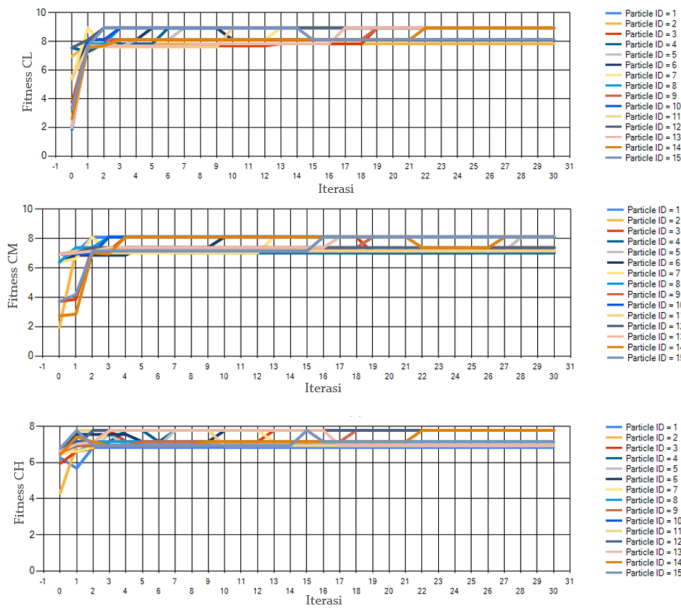
Figure 8: Pbest Values for Each Cognitive Class

Pbest tests through the fitness function in the CL, CM, and CH classes show that the higher the iteration used, the more optimal the solution will be from the system, marked with the increasing fitness results. This is due to the increasing number of iterations used to make the particles move to find the optimal solution so that the particles can find the optimal solution.

4.2. Learning Path Recommendation

Gbest is the best value that takes into account all particles in Gbest the population in each CL, CM, and CH class. Each iteration, each participant is given information about the latest Gbest value so that there is a mechanism for sharing one-way information to carry out the process of finding the best solution with a fast convergence movement.

Learning path recommendations based on the *Gbest* values shown in Table 2 indicate that an increase in the number of particles affects the value of the resulting learning path sequence, but is still within the schema of each cognitive class.

Table 2: Learning Path Recommendation

No	Class Cognitive	Number Of Particles	Learning Path	
			HPSO	Manual Set
1	CL	10	1-3-2-5-4-6-7-8	1-2-3-4-5-6-7-8
2		15	1-2-3-5-4-6-7-8	
3	CM	10	3-5-6-7-4-2-8-1	1-2-3-4-5-6-7-8
4		15	3-5-7-6-2-4-8-1	
5	CH	10	8-5-7-6-4-3-1-2	1-2-3-4-5-6-7-8
6		15	8-5-7-6-4-3-2-1	

The HPSO algorithm can create learning pathways by CL, CM, and CH cognitive classes. The cognitive class CL tendency of its learning path (1-3-2-5-4-6-7-8) shows the order of the basic LO to a higher LO. Whereas the cognitive class CH of the learning path tendency (8-5-7-6-4-3-1-2) shows a sequence of high LO to the basic LO. In CM cognitive class the tendency of learning path is (3-5-7-6-4-2-8-1). The similarity of the learning path sequence based on the number of CL cognitive particles is 87.5%, CM is

75%, and CH is 87.5%, so the average similarity of the learning path sequence is 83.3%.

The results of the learning path model research using HPSO have been presented and explained to three education experts. The recommendation of three education experts stated that cognitive classification with LVQ and the logical flow learning path model was acceptable. Researchers can prove the use of RBT through the results of learning paths based on cognitive low (CL), cognitive medium (CM), and cognitive high (CH). The HPSO learning pathfinder is a very important part of combining the output of the LVQ cognitive classification with the ontology learning object.

The advice given from education experts is as follows, the dynamics of the interrelation between the depth of the material and the breadth of the material can be determined by the teacher or teacher based on competency targets to produce a learning path in accordance with the characteristics of students. This research can be developed in the realm of attitudes and skills in accordance with learning evaluation competencies, namely, attitudes, knowledge, and skills.

5.   Conclusion

The Hybrid Particle Swarm Optimization method, which consists of DPSO for learning object ontology and BPSO in cognitive classes, can be applied more practically and regularly to produce a learning path recommendation. Based on experimental studies and verification of education experts, the HPSO algorithm in this research can recommend a suitable learning path for students classified in the CL, CM, and CH cognitive classes.

Further research is the integration of the Learning Vector Quantization method with Hybrid Particle Swarm Optimization in a platform that is supported by the provision of standard learning object ontologies that can be the right and efficient solution in the development of smart e-learning mode during the Covid-19 pandemic.

[3]   C.M. Chen, "Intelligent web-based learning system with personalized learning path guidance," Computers and Education, **51**(2), 787–814, 2008, doi:10.1016/j.compedu.2007.08.004.
[4]   D. Hauger, M. Köck, "State of the art of adaptivity in e-learning platforms," LWA 2007 - Lernen - Wissen - Adaptivitat - Learning, Knowledge, and Adaptivity, Workshop Proceedings, 355–360, 2007.
[5]   S. Al-Muhaideb, M.E.B. Menai, "Evolutionary computation approaches to the Curriculum Sequencing problem," Natural Computing, **10**(2), 891–920, 2011, doi:10.1007/s11047-010-9246-5.
[6]   V. Shmelev, M. Karpova, A. Dukhanov, An Approach of Learning Path Sequencing Based on Revised Bloom's Taxonomy and Domain Ontologies with the Use of Genetic Algorithms, Elsevier Masson SAS, 2015,

doi:10.1016/j.procs.2015.11.081.

[7] S. El Lakkah, M.A. Alimam, H. Seghiouer, "Adaptive e-learning system based on learning style and ant colony optimization," 2017 Intelligent Systems and Computer Vision, ISCV 2017, 2017, doi:10.1109/ISACV.2017.8054963.

[8] A. Hovakimyan, S. Sargsyan, S. Barkhoudaryan, "Genetic algorithm and the problem of getting knowledge in e-learning systems," Proceedings - IEEE International Conference on Advanced Learning Technologies, ICALT 2004, 336–339, 2004, doi:10.1109/ICALT.2004.1357431.

[9] K. Seki, T. Matsui, T. Okamoto, "An adaptive sequencing method of the learning objects for the e-learning environment," Electronics and Communications in Japan, Part III: Fundamental Electronic Science (English Translation of Denshi Tsushin Gakkai Ronbunshi), **88**(3), 54–70, 2005, doi:10.1002/ecjc.20163.

[10] A. Samia, B. Mostafa, "Re-use of resources for adapted formation to the learner," ISCIII'07: 3rd International Symposium on Computational Intelligence and Intelligent Informatics; Proceedings, 213–217, 2007, doi:10.1109/ISCIII.2007.367391.

[11] A. Dukhanov, M. Karpova, V. Shmelev, "An automation of the course design based on mathematical modeling and genetic algorithms," Proceedings - Frontiers in Education Conference, FIE, **2015**-**Decem**(December), 7–10, 2015, doi:10.1109/FIE.2015.7344325.

[12] C.M. Chen, "Ontology-based concept map for planning a personalised learning path," British Journal of Educational Technology, **40**(6), 1028–1058, 2009, doi:10.1111/j.1467-8535.2008.00892.x.

[13] J. Kennedy, R. Eberhart, Particle swarm optimization, IEEE International Conference on Particle Swarm Optimization, **4**, 1942–1948, 1995, doi:10.1109/ICNN.1995.488968.

[14] M.-I. DASCĂLU, "Application of Particle Swarm Optimization to Formative E-Assessment in Project Management," Informatica Economică, **15**(1), 48–61, 2011, doi:DAOJ.

[15] D.A. Wiley, "Learning Object Design and Sequencing Theory," Learning Object Design and Sequencing Theory, (June), 142, 2000, doi:10.1017/CBO9781107415324.004.

[16] R. McGreal, "Learning Objects: A Practical Definition," International Journal of Instructional Technology and Distance Learning, **1**(9), 21–32, 2004, doi:10.1002/tl.37219925103.

[17] J. Wang, T. Mendori, J. Xiong, "A Language Learning Support System using Course-centered Ontology and its evaluation Computers & Education A language learning support system using course-centered ontology and its evaluation," Computers & Education, **78**(September 2014), 278–293, 2015, doi:10.1016/j.compedu.2014.06.009.

[18] X. Li, K. Deb, "PSO Niching algorithms Using Different Position Update Rules," IEEE Congress on Evolutionary Computation, 2010.

[19] J. Kennedy, E.C. Russell, Y. Shi, Swarm Intelligence, Academic Press, USA, 2001, doi:10.1007/978-3-540-74089-6.

[20] F. van den Bergh, A.P. Engelbrech, "New Locally Convergent Particle Swarm," IEEE International Conference on Systems, Man and Cybernetics, **3**, 1–5, 2002.

[21] J. Kennedy, R.C. Eberhart, "A discrete binary version of the particle swarm algorithm," IEEE, International Conference on Systems, Man, and Cybernetics, **5**, 4104–4108, 1997, doi:10.1109/ICSMC.1997.637339.

[22] A.P. Engelbrecht, Computational Intelligence An Introduction, Second Edi, John Wiley & Sons Ltd, England, 2007.

[23] M. Clerc, Discrete Particle Swarm Optimization Illustrated by the Traveling Salesman Problem, Springer Verlag, Berlin Heidelberg, 2004, doi:10.1007/978-3-540-39930-8_8.

[24] M.K. Marichelvam, M. Geetha, Ö. Tosun, "An improved particle swarm optimization algorithm to solve hybrid flowshop scheduling problems with the effect of human factors – A case study," Computers and Operations Research, **114**, 104812, 2020, doi:10.1016/j.cor.2019.104812.

Stochastic Behaviour Analysis of Adaptive Averaging Step-size Sign Normalised Hammerstein Spline Adaptive Filtering

Theerayod Wiangtong[1], Sethakarn Prongnuch[*2], Suchada Sitjongsataporn[3]

[1]*Department of Electrical Engineering, Faculty of Engineering, King Mongkut's Institute of Technology Ladkrabang Bangkok, 10520, Thailand*

[2]*Department of Computer Engineering, Faculty of Industrial Technology, Suan Sunandha Rajabhat University Bangkok, 10300, Thailand*

[3]*Department of Electronic Engineering, Mahanakorn Institute of Innovation (MII), Faculty of Engineering and Technology Mahanakorn University of Technology, Bangkok, 10530, Thailand*

A R T I C L E   I N F O

A B S T R A C T

We introduce a sign algorithm based on the normalised least mean square with Hammerstein adaptive filtering using adaptive averaging step-size mechanism, which is derived by the minimised absolute a posteriori squared error. To improve the performance by reducing computational complexity, we suggest an adaptive averaging using energy of errors to update step-size variant. The analysis of convergence behaviour and mean square performance are derived. Experimental results reveal that the proposed algorithm can perform better than the least mean square approach based on the Hammerstein model of adaptive filtering.

1 Introduction

Advantages of the adaptive linear filters are simply used in various applications. However, the linear models underperform when comparing with the nonlinear models. Over the last few years, the spline adaptive filter (SAF) structure [1], [2] i.e. Hammerstein spline filtering [3] in cascade architecture [4] has been applied in many practical engineering fields as for example. SAFs based on the set-membership approach [5] and infinite impulse response [6] have been introduced for using in the impulsive noise environment.

In some particular nonlinear problems, the Hammerstein SAF (HSAF) [3], the combined Wiener-Hammerstein SAF [1], and cascade SAFs or sandwich SAF models [4] based on the least mean square (LMS) can operate effectively to identify for nonlinear systems identifications. It provides a good potential for low cost implementation in hardware. Based on the normalised version of LMS (NLMS) on HSAF have been performed in [7]-[10]. In [7], the authors have pointed out the derivation of HSAF on NLMS. In [8], the authors have proposed the performance analysis of HSAF based on the stochastic gradient algorithm. To counteract with impulsive noises, the sign normalised Hammerstein spline adaptive filtering

has been proposed in [9] and its performance shown in [10].

In order to reduce the computational requirements of NLMS, the simplifications of NLMS approach in the form of a sign algorithm has been presented in several applications [11]-[16]. To further diminish and protect the impulse noise, the sign normalised SAF [11], [12] and sign subband adaptive filterings with variable step-size parameter [13]-[15] have been designed. In [16], the robust shrinkage normalised version of sign algorithm has been implemented.

Recently, an approach based on the stochastic gradient method for improving the convergence rate based on SAFs has been established in [3], [17]-[19] resulting in the low computation and high performance. For nonlinear systems, the authors in [17] have presented NLMS for SAF. In [18], the adaptive step-size mechanism for SAF has been proposed with the fast convergence and robustness. In [19], the authors have proposed the normalised version of least mean square algorithm for spline adaptive filtering based on the adaptive step-size method with the averaging energy on the previous and present errors and their properties of stability analysis have been introduced.
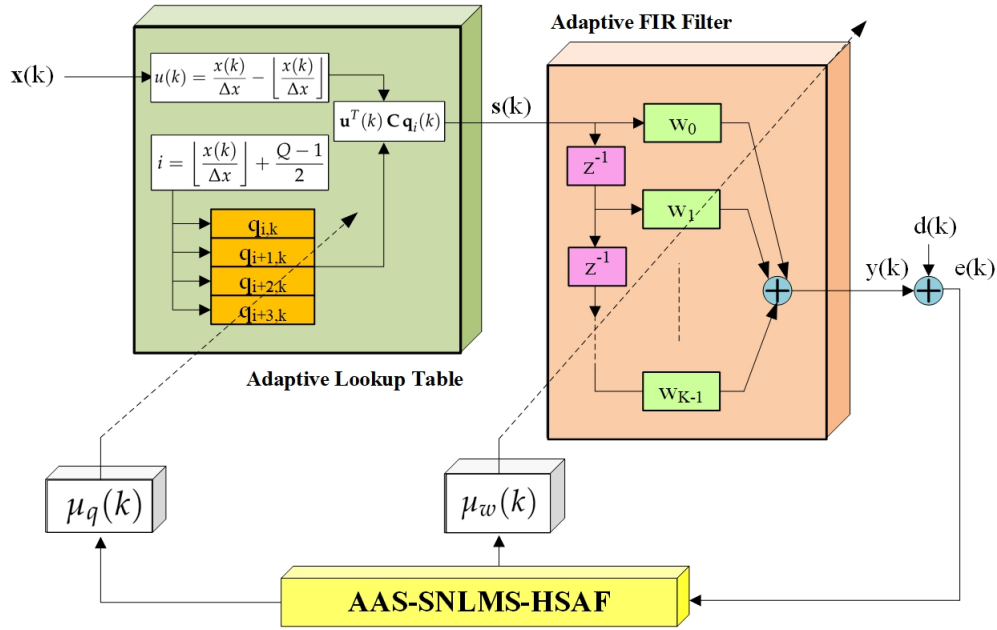
Figure 1: Proposed Adaptive Averaging Step-size Sign Normalised Least Mean Square algorithm for Hammerstein Spline Adaptive Filtering (AAS-SNLMS-HSAF).

In this paper, we propose a statistical behaviour analysis of a Hammerstein spline adaptive filter based on the sign version of normalised least mean square algorithm with adaptive averaging step-size (AAS-SNLMS-HSAF). To enhance the convergence speed with low computational complexity, the adaptive averaging step-size algorithm is suggested.

Also, the performance analysis of sign version of NLMS-HSAF based on adaptive step-size mechanism using averaging energy of errors are derived. We encounter the relationship between the step-size parameter and the mean square error from the analysis that can be examined numerically in the computer simulations for an example of system identification.

This paper is organised as following. Section 2 clarifies the HSAF structure based on LMS approach in brief. Section 3 introduces the constraint criterion of the cost function based on the stochastic gradient descent with the adaptive averaging step-size mechanism. The energy of errors is exploited to update the variant of step-size parameter. Section 4 explains how to derive the convergence analysis of HSAF-based algorithm that consists of the convergence properties and the mean square behaviour analysis. Furthermore, the simulation experiment design and experimental results are detailed in Section 5 and Section 6. Finally, Section 7 discusses and Section 8 concludes the proposed algorithm.

2 Hammerstein Spline Adaptive Filtering

The structure of Hammerstein spline adaptive filtering (HSAF) is depicted in Figure 1. It consists of a nonlinear model controlled by adaptive lookup table (LUT) [20] in which the adaptive control points vector is interpolated by the spline function and adaptive linear finite impulse response (FIR) filter [7].

The vectors $\mathbf{x}_k$ and $\mathbf{s}_k$ at symbol k appear the input and output vectors of adaptive LUT as

$$\mathbf{s}_k = \mathbf{u}_k^T \, \mathbf{C} \, \mathbf{q}_{i,k} \, , \tag{1}$$

$$\mathbf{u}_k = [u_k^3 \;\; u_k^2 \;\; u_k \;\; 1]^T \, , \tag{2}$$

where C is a spline matrix, $\mathbf{q}_{i_k}$ is the control point vector as $\mathbf{q}_{i,k} = [\; q_{i,k} \;\; q_{i+1,k} \;\; q_{i+2,k} \;\; q_{i+3,k} \;]^T$. The local parameter u_k and index i can be estimated as [3]

$$u_k = \frac{x_k}{\Delta x} - \left\lfloor \frac{x_k}{\Delta x} \right\rfloor \, , \tag{3}$$

$$i = \left\lfloor \frac{x_k}{\Delta x} \right\rfloor + \frac{Q-1}{2} \, , \tag{4}$$

where Δx is the uniform space between two-adjacent control points, Q is the number of control points, and operator $\lfloor \cdot \rfloor$ is floor operator.

We can obtain the minimised cost function based on LMS for HSAF as

$$J(\mathbf{w}_k, \mathbf{q}_{i_k}) = \min_{\mathbf{w}, \mathbf{q}} \left\{ \frac{1}{2} \, e_k^2 \right\} \, , \tag{5}$$

where e_k is given as [3]

$$e_k = d_k - y_k = d_k - \mathbf{w}_{k-1}^T \, \mathbf{s}_k \, , \tag{6}$$

where y_k is the HSAF output, d_k is the desired signal and $\mathbf{w}_k$ is the adaptive FIR coefficient vector.

By using the chain rule, the cost function in (5) is derivative with respect to (w.r.t.) $\mathbf{w}_k$, $\mathbf{q}_{i,k}$. The result is set to zero to find optimal points. So, the adaptive FIR coefficient vector $\mathbf{w}_k$ and the update control points coefficient vector $\mathbf{q}_{i,k}$ are demonstrated in the recursive form as

$$\therefore \;\; \mathbf{w}_{k+1} = \mathbf{w}_k + \mu_w \, \mathbf{s}_k \, e_k \, , \tag{7}$$

$$\therefore \;\; \mathbf{q}_{i,k+1} = \mathbf{q}_{i,k} + \mu_q \, \mathbf{u}_k \, \mathbf{C}^T \, \mathbf{w}_k \, e_k \, , \tag{8}$$

where μ_w and μ_q are the fixed step-size parameters.

3 Proposed Adaptive Averaging Step-size Sign Normalised Least Mean Square Algorithm

We extend the scope of sign algorithm into Hammerstein spline adaptive filtering (HSAF) based on the normalised version of LMS, named SNLMS-HSAF derived by minimised absolute *a posteriori* error as shown in Figure 1.

The constraints of this optimisation problem are formulated as

$$\min_{\mathbf{w}} \{ e_k'^2 \} = \{ d_k - \mathbf{w}_{k+1}^T \mathbf{s}_k \}^2 \ , \tag{9}$$

subject to

$$\| \mathbf{w}_{k+1} - \mathbf{w}_k \|^2 \le \xi^2 \ \text{ and } \ \| \mathbf{q}_{i,k+1} - \mathbf{q}_{i,k} \|^2 \le \xi^2 \ , \tag{10}$$

where e_k' is *a posteriori* error and ξ^2 is a small parameter in the gradual update of coefficient vectors.

From [9], the constrained cost function using Lagrange multiplier can be illustrated by

$$\Im(\mathbf{w}_k) = \min_{\mathbf{w}} \{ e_k'^2 \} + \frac{\lambda_0}{\mathbf{u}_k^T \mathbf{u}_k} \cdot \left[\| \mathbf{w}_{k+1} - \mathbf{w}_k \|^2 \le \xi^2 \right] , \tag{11}$$

where λ_0 is the Lagrange multiplier.

Hence, the derivation of $\Im(\mathbf{w}_k)$ in (11) w.r.t. $\mathbf{w}_k$ is set to zero,

$$-2 \, \mathbf{s}_k \cdot \text{sgn}\{e_k'\} + 2 \, \frac{\lambda_0}{\mathbf{u}_k^T \mathbf{u}_k} \cdot \| \mathbf{w}_{k+1} - \mathbf{w}_k \| = 0$$

Therefore, the adaptive FIR vector $\mathbf{w}_k$ is recursively formulated by

$$\mathbf{w}_{k+1} = \mathbf{w}_k + \mu_{w_k} \frac{\mathbf{s}_k \cdot \text{sgn}\{e_k'\}}{\mathbf{u}_k^T \mathbf{u}_k + \varepsilon} \ , \tag{12}$$

where μ_{w_k} is an adaptive step-size of $\mathbf{w}_k$ and $\text{sgn}\{\cdot\}$ is the sign function. The regularisation parameter ε is a small constant.

Similarly, the constraints of the cost function regarding with $\mathbf{q}_{i,k}$ can be shown as

$$\Im(\mathbf{q}_{i,k}) = \min_{\mathbf{q}} \{ e_k'^2 \} + \frac{\tilde{\lambda}_0}{\mathbf{u}_k^T \mathbf{u}_k} \cdot \left[\| \mathbf{q}_{i,k+1} - \mathbf{q}_{i,k} \|^2 \le \xi^2 \right] . \tag{13}$$

Considering the derivation of $\Im(\mathbf{q}_{i,k})$ in (13) w.r.t. $\mathbf{q}_{i,k}$ is equal to zero, we have

$$-2 \, \mathbf{u}_k^T \cdot \mathbf{C} \cdot \mathbf{w}_k \cdot \text{sgn}\{e_k'\} + 2 \, \frac{\tilde{\lambda}_0}{\mathbf{u}_k^T \mathbf{u}_k} \cdot \| \mathbf{q}_{i,k+1} - \mathbf{q}_{i,k} \| = 0 . \tag{14}$$

Finally, the updated control points vector $\mathbf{q}_{i,k}$ is

$$\mathbf{q}_{i,k+1} = \mathbf{q}_{i,k} + \mu_{q_k} \frac{\mathbf{u}_k^T \cdot \mathbf{C} \cdot \mathbf{w}_k \cdot \text{sgn}\{e_k'\}}{\mathbf{u}_k^T \mathbf{u}_k + \varepsilon} \ , \tag{15}$$

where μ_{q_k} is an adaptive step-size of $\mathbf{q}_{i,k}$ and the regularisation parameter ε is a small constant.

To enhance the performance by reducing computational complexity, we modify an estimation of the energy of errors for updating

average step-size parameter from the present and previous errors of systems [21].

Since, the adaptive averaging step-size μ_{w_k} of $\mathbf{w}_k$ can be implemented following [19]

$$\mu_{w_k} = \gamma_w \cdot \mu_{w_{k-1}} + \rho_w \cdot \zeta_k^2 \ , \tag{16}$$

$$\zeta_k = \sigma \cdot \zeta_{k-1} + (1 - \sigma) \cdot e_k'^2 \ , \tag{17}$$

where ρ_w is a scaling variable, σ is close to 1 and $0 < \gamma_w < 1$.

Therefore, the adaptive step-size μ_{q_k} of $\mathbf{q}_{i,k}$ is determined by

$$\mu_{q_k} = \gamma_q \cdot \mu_{q_{k-1}} + \rho_q \cdot e_k'^2 \ , \tag{18}$$

where $0 < \gamma_q < 1$ and $\rho_q > 0$.

The summary of the proposed sign normalised version of least mean square algorithm using adaptive averaging step-size approach for HSAF (AAS-SNLMS-HSAF) is presented in Table. 1.

4 Convergence Analysis

In this section, we focus on the derivation and analysis of the relationship between the step-size and the mean square error. These approaches are to ensure the optimal convergence at the steady-state condition.

4.1 Convergence Properties

According to enhance the performance of SNLMS-HSAF-based algorithm, we examine the optimal learning rate of step-size parameters for adaptive FIR coefficient vector $\mathbf{w}_k$ and update control points vector $\mathbf{q}_{i,k}$ as follows.

We determine the *a posteriori* error e_k' as

$$e_k' = d_k - \mathbf{w}_{k+1}^T \cdot \mathbf{s}_k \ . \tag{19}$$

The desired response d_k can be decomposed into the input vector $\mathbf{s}_k$ and the residual error is defined as

$$d_k = \mathbf{w}_{opt}^T \cdot \mathbf{s}_k + e_k^{min} \ , \tag{20}$$

where $\mathbf{w}_{opt} \in \mathcal{R}^N$ is the optimal Wiener solution vector and e_k^{min} is the residual error assumed as a Gaussian noise with zero mean and finite variance.

Substituting (20) into (19), then we can obtain an expression to estimate error as

$$e_k' = e_k^{min} - \Delta \mathbf{w}_k^T \cdot \mathbf{s}_k \ , \tag{21}$$

where $\Delta \mathbf{w}_k \in \mathcal{R}^N$ is the difference of the adaptive FIR coefficient vectors $\mathbf{w}_k$ defined by

$$\Delta \mathbf{w}_k = \mathbf{w}_{k+1} - \mathbf{w}_k = \frac{\mu_{w_k} \cdot \mathbf{s}_k \cdot \text{sgn}\{e_k'\}}{\mathbf{u}_k^T \mathbf{u}_k + \varepsilon} \ . \tag{22}$$

Substituting (22) into (21) gives

$$e_k^{min} - e_k' = \mu_{w_k} \frac{(\mathbf{s}_k^T \cdot \mathbf{s}_k) \cdot \text{sgn}\{e_k'\}}{\mathbf{u}_k^T \mathbf{u}_k + \varepsilon} \tag{23}$$

By taking the norm of both sides in (23), the adaptive step-size μ_{w_k} of adaptive FIR coefficient vector $\mathbf{w}_k$ can be approximated by

$$\therefore 0 < \mu_{w_k} < \frac{\mathbf{u}_k^T \mathbf{u}_k}{\mathbf{s}_k^T \mathbf{s}_k + \varepsilon} \ . \tag{24}$$

where $|e_k'| < |e_k^{min}|$.

Correspondingly, we investigate the convergence properties of the update control points vector $\mathbf{q}_{i,k}$ using Taylor series expansion of estimated *a posteriori* error e_k' as

$$e_{k+1}' = e_k' + \frac{\partial e_k'}{\partial \mathbf{q}_k} \cdot \Delta \mathbf{q}_k \ , \tag{25}$$

where the difference of update control points vector $\Delta \mathbf{q}_k$ is given by

$$\Delta \mathbf{q}_k = \mu_{q_k} \frac{\mathbf{u}_k^T \cdot \mathbf{C} \cdot \mathbf{w}_k \cdot \text{sgn}\{e_k'\}}{\mathbf{u}_k^T \mathbf{u}_k + \varepsilon} \ . \tag{26}$$

Differentiating e_k' in (19) w.r.t. $\mathbf{q}_{i,k}$ by the chain rule [19], we can get

$$\begin{aligned}
\frac{\partial e_k'}{\partial \mathbf{q}_k} &= \frac{\partial}{\partial \mathbf{q}_k}\Big(d_k - \mathbf{w}_{k+1}^T \cdot \mathbf{u}_k \cdot \mathbf{C}^T \cdot \mathbf{q}_{i,k}\Big) \\
&= -\mathbf{u}_k \cdot \mathbf{C}^T \cdot \mathbf{w}_{k+1} \ .
\end{aligned} \tag{27}$$

Substituting (26) and (27) into (25) gives

$$e_k' - e_{k+1}' = \frac{\mu_{q_k} \cdot (\Psi_k^T \cdot \Psi_k) \cdot \text{sgn}\{e_k'\}}{\mathbf{u}_k^T \mathbf{u}_k + \varepsilon} \ , \tag{28}$$

where Ψ_k is

$$\Psi_k = \mathbf{u}_k^T \cdot \mathbf{C} \cdot \mathbf{w}_k \ . \tag{29}$$

Similarly, we take the norm of both sides (28), the adaptive step-size μ_{q_k} of update control points coefficient vector $\mathbf{q}_{i,k}$ can be evaluated as

$$\therefore 0 < \mu_{q_k} < \frac{\mathbf{u}_k^T \mathbf{u}_k}{\Psi_k^T \Psi_k + \varepsilon} \ . \tag{30}$$

where $|e_k'| > |e_{k+1}'|$.

4.2 Mean Square Behaviour Analysis

In this section, we investigate the convergence analysis in forms of the mean square error performance in the steady-state condition.

Remark 1: *We assume that the estimated coefficient error vector V_{w_k} is under the independent and identically distributed condition with zero mean and finite variance.*

We consider following [4] the estimated coefficient error vector $\mathbf{V}_{w_k}$ involved the adaptive FIR vector $\mathbf{w}_k$ as

$$\mathbf{V}_{w_{k+1}} = \mathbf{V}_{w_k} - \frac{\mu_{w_k} \cdot \mathbf{s}_k \cdot \text{sgn}\{e_k'\}}{\mathbf{u}_k^T \mathbf{u}_k + \varepsilon} \ . \tag{31}$$

Table 1: Proposed adaptive averaging step-size algorithm based on sign normalised least mean square algorithm for HSAF (AAS-SNLMS-HSAF).

1: **ALGORITHM** AAS-SNLMS-HSAF ()

2: $\quad \mathbf{w}(0) = \delta \cdot [1\ 0\ \ldots 0]^T$, $\quad \mathbf{u}_k = [u_k^3\ u_k^2\ u_k\ 1]^T$

$\quad \mathbf{x}_k = [\ x_k\ x_{k-1}\ \ldots\ x_{k-K+1}\ ]$

$\quad \mathbf{q}_{i,k} = [\ q_{i,k}\ q_{i+1,k}\ q_{i+2,k}\ q_{i+3,k}\ ]$

3: $\quad$ **FOR** $k = 1$ **TO** $K - 1$.

4: $\quad\quad \mathbf{s}_k = \mathbf{u}_k^T \mathbf{C}\ \mathbf{q}_{i,k}$

5: $\quad\quad u_k = \frac{s_k}{\Delta x} - \lfloor \frac{s_k}{\Delta x} \rfloor$

6: $\quad\quad i = \lfloor \frac{s_k}{\Delta x} \rfloor + \frac{Q-1}{2}$

7: $\quad\quad e_k' = d_k - y_k = d_k - \mathbf{w}_{k+1}^T \mathbf{s}_k$

8: $\quad\quad \mu_{w_k} = \gamma_w \cdot \mu_{w_{k-1}} + \rho_w \cdot \zeta_k^2$

9: $\quad\quad \zeta_k = \sigma \cdot \zeta_{k-1} + (1 - \sigma) \cdot e_k'^2$

10: $\quad\quad \mu_{q_k} = \gamma_q \cdot \mu_{q_{k-1}} + \rho_q \cdot e_k'^2$

11: $\quad\quad \mathbf{w}_{k+1} = \mathbf{w}_k + \mu_{w_k} \frac{\mathbf{s}_k \cdot \text{sgn}\{e_k'\}}{\mathbf{u}_k^T \mathbf{u}_k + \varepsilon}$

12: $\quad\quad \mathbf{q}_{i,k+1} = \mathbf{q}_{i,k} + \mu_{q_k} \frac{\mathbf{u}_k^T \cdot \mathbf{C} \cdot \mathbf{w}_k \cdot \text{sgn}\{e_k'\}}{\mathbf{u}_k^T \mathbf{u}_k + \varepsilon}$

13: $\quad$ **NEXT** k

14: **END ALGORITHM**

We can also determine the squared coefficient error vector as

$$\|\mathbf{V}_{w_{k+1}}\|^2 = \|\mathbf{V}_{w_k}\|^2 - \frac{2\,\mathbf{V}_{w_k}\mu_{w_k} \cdot \mathbf{s}_k \cdot \text{sgn}\{e_k'\}}{\mathbf{u}_k^T \mathbf{u}_k + \varepsilon} + \left\| \frac{\mu_{w_k} \cdot \mathbf{s}_k \cdot \text{sgn}\{e_k'\}}{\mathbf{u}_k^T \mathbf{u}_k + \varepsilon} \right\|^2 \ . \tag{32}$$

Remark 2: *We consider the condition, that*

$$E\{\|\mathbf{V}_{w_{k+1}}\|^2\} \approx E\{\|\mathbf{V}_{w_k}\|^2\} \ , \ k \to \infty \ .$$

By using Remark 2, we can rewrite (32) as

$$2\,\mathbf{V}_{w_k}^T \cdot \mathbf{s}_k \cdot \text{sgn}\{e_k'\} = \frac{\mu_{w_k} \cdot \|\mathbf{s}_k\|^2 \cdot |e_k'|^2}{\mathbf{u}_k^T \mathbf{u}_k + \varepsilon}$$

$$2\,\epsilon_{w_k} \cdot \text{sgn}\{e_k'\} = \frac{\mu_{w_k} \cdot \|\mathbf{s}_k\|^2 \cdot |e_k'|^2}{\mathbf{u}_k^T \mathbf{u}_k + \varepsilon} \ , \tag{33}$$

where ϵ_{w_k} is denoted by

$$\epsilon_{w_k} \approx \mathbf{V}_{w_k}^T \cdot \mathbf{s}_k \ . \tag{34}$$

We proceed the *a posteriori* error involved with the adaptive FIR vector $\mathbf{w}_k$ as

$$e_k' = \epsilon_{w_k} + \mathbf{V}_{w_k} \ . \tag{35}$$

By taking the expectation on the left-side of (33) and using (35) at the steady state condition, we can see that

$$E\{\epsilon_{w_k} \cdot \text{sgn}\{e_k'\}\} = E\{\epsilon_{w_k} \cdot \text{sgn}\{\epsilon_{w_k} + \mathbf{V}_{w_k}\}\} \approx E\{\epsilon_{w_k}^2\} \ . \tag{36}$$

The expectation of the squared *a posteriori* error is then

$$E\{(e'_k)^2\} \simeq E\{(\epsilon_{w_k} + \mathbf{V}_{w_k})^2\}$$
$$= E\{\epsilon^2_{w_k} + \zeta^2_{w_k}\} . \qquad (37)$$

where $\zeta^2_{w_k}$ is given by

$$\zeta^2_{w_k} = 2\epsilon_{w_k} \cdot \mathbf{V}_{w_k} + \mathbf{V}^2_{w_k} . \qquad (38)$$

Substituting (36) and (37) into (33), we then obtain

$$2 E\{\epsilon^2_{w_k}\} = \frac{\mu_{w_k} \cdot \|\mathbf{s}_k\|^2 \cdot E\{\epsilon^2_{w_k} + \zeta^2_{w_k}\}}{\mathbf{u}^T_k \mathbf{u}_k + \varepsilon}$$

$$E\{\epsilon^2_{w_k}\} = \frac{\mu_{w_k} \cdot \|\mathbf{s}_k\|^2 \cdot E\{\zeta^2_{w_k}\}}{2\mathbf{u}^T_k \mathbf{u}_k + \varepsilon - \mu_{w_k} \cdot \|\mathbf{s}_k\|^2} \qquad (39)$$

where $\mu_{w_k} \ll 1$ is assumed.

Therefore, the excess mean square error (MSE) ξ^w_{ex} involved with the adaptive FIR vector $\mathbf{w}_k$ can be given by

$$\therefore \xi^w_{ex} = E\{\epsilon^2_{w_k}\} = \frac{\mu_{w_k} \cdot \|\mathbf{s}_k\|^2 \cdot E\{\zeta^2_{w_k}\}}{2\mathbf{u}^T_k \mathbf{u}_k + \varepsilon} . \qquad (40)$$

Please note that (40), an approximation of (39), is valid only for small step-size parameter.

In a similar way, we consider the estimated coefficient error vector $\mathbf{V}_{q_k}$ concerned with the update control points vector $\mathbf{q}_{i,k}$ as

$$\mathbf{V}_{q_k} = \mathbf{q}_{i,k} - \mathbf{q}_{opt} , \qquad (41)$$

where $\mathbf{q}_{opt} \in \mathcal{R}^N$ is the optimal control points vector and $\mathbf{V}_{q_k} \in \mathcal{R}^N$.

We can then rewrite the update control points vector $\mathbf{q}_{i,k}$ in (15) by using the coefficient error vector $\mathbf{V}_{q_k}$ as follows.

$$\mathbf{V}_{q,k+1} = \mathbf{V}_{q,k} - \frac{\mu_{q_k} \cdot \mathbf{u}^T_k \cdot \mathbf{C} \cdot \mathbf{w}_k \cdot \text{sgn}\{e'_k\}}{\mathbf{u}^T_k \mathbf{u}_k + \varepsilon} . \qquad (42)$$

The square of coefficient error vector in (42) is computed as

$$\|\mathbf{V}_{q,k+1}\|^2 = \|\mathbf{V}_{q,k}\|^2 - \frac{2 \cdot \mathbf{V}_{q,k} \cdot \mu_{q_k} \cdot \mathbf{u}^T_k \cdot \mathbf{C} \cdot \mathbf{w}_k \cdot \text{sgn}\{e'_k\}}{\mathbf{u}^T_k \mathbf{u}_k + \varepsilon}$$
$$+ \left\| \frac{\mu_{q_k} \cdot \mathbf{u}^T_k \cdot \mathbf{C} \cdot \mathbf{w}_k \cdot \text{sgn}\{e'_k\}}{\mathbf{u}^T_k \mathbf{u}_k + \varepsilon} \right\|^2 . \qquad (43)$$

Remark 3: *We assume the condition, that is of*

$$E\|\mathbf{V}_{q_{k+1}}\|^2 \approx E\|\mathbf{V}_{q_k}\|^2 , \ k \to \infty .$$

We can get and rewrite (43) using Remark 1 as

$$2 \cdot \epsilon_{q_k} \cdot \text{sgn}\{e'_k\} = \frac{\mu_{q_k} \cdot \|\Psi_k\|^2 \cdot |e'_k|^2}{\mathbf{u}^T_k \mathbf{u}_k + \varepsilon} , \qquad (44)$$

where ϵ_{q_k} is given by

$$\epsilon_{q_k} \approx \mathbf{V}^T_{q_k} \cdot \Psi_k . \qquad (45)$$

where Ψ_k is defined in (29).

We calculate the *a posteriori* error with the updated control points vector $\mathbf{q}_{i,k}$ as

$$e'_k = \epsilon_{q_k} + \mathbf{V}_{q_k} . \qquad (46)$$

After taking the expectation on the left-side of (44) and using (46), we get

$$E\{\epsilon_{q_k} \cdot \text{sgn}\{e'_k\}\} = E\{\epsilon_{q_k} \cdot \text{sgn}\{\epsilon_{q_k} + \mathbf{V}_{q_k}\}\}$$
$$\approx E\{\epsilon^2_{q_k}\} . \qquad (47)$$

We determine the square *a posteriori* error and take the expectation as

$$E\{e'_k\} \simeq E\{(\epsilon_{q_k} + \mathbf{V}_{q_k})^2\}$$
$$= E\{\epsilon^2_{q_k}\} + E\{\zeta^2_{q_k}\} , \qquad (48)$$

where $\zeta^2_{q_k}$ is given by

$$\zeta^2_{q_k} = 2\epsilon_{q_k} \cdot \mathbf{V}_{q_k} + \mathbf{V}^2_{q_k} . \qquad (49)$$

Substituting (47) and (48) into (44) gives us

$$2 \cdot E\{\epsilon^2_{q_k}\} = \frac{\mu_{q_k} \cdot \|\Psi_k\|^2 \cdot [E\{\epsilon^2_{q_k}\} + E\{\zeta^2_{q_k}\}]}{\mathbf{u}^T_k \mathbf{u}_k + \varepsilon}$$

$$E\{\epsilon^2_{q_k}\} = \frac{\mu_{q_k} \cdot \|\Psi_k\|^2 \cdot [E\{\zeta^2_{q_k}\}]}{(2\mathbf{u}^T_k \mathbf{u}_k + \varepsilon) - \mu_{q_k} \cdot \|\Psi_k\|^2} , \qquad (50)$$

where $\mu_{q_k} \ll 1$ is assumed.

Therefore, the excess MSE ξ^q_{ex} with the update control points coefficient vector $\mathbf{q}_{i,k}$ can be expressed by

$$\therefore \xi^q_{ex} \simeq E\{\epsilon^2_{q_k}\} = \frac{\mu_{q_k} \cdot \|\Psi_k\|^2 \cdot [E\{\zeta^2_{q_k}\}]}{2\mathbf{u}^T_k \mathbf{u}_k + \varepsilon} . \qquad (51)$$

Notice that (51) is an approximation of (50) is only applicable for small values of the step-size parameter.

5 Simulation Experiment Design

In this section, the experiments are conducted with the system identification through computer simulations to verify the proposed nonlinear adaptive filtering. Flow chart of the proposed AAS-SNLMS for HSAF is shown in Figure 2.

The input color signal x_k composes of 10,000 samples by averaging over 100 Monte Carlo trials can be generated by the following equation as [3]

$$x_k = \omega \cdot x_{k-1} + \sqrt{1 - \omega^2} \, \varphi , \qquad (52)$$

where φ is a unitary variance of zero mean white Gaussian noise and ω is a parameter to determine the correlation level between adjacent samples [2], where $0 \le \omega < 1$.

In these experiments, we set $\omega = 0.15, 0.75$ and signal to noise ratio (SNR) is of 20, 25, 30dB. As shown in [3], simulation parameters are comprised of

$$\mathbf{w}_0 = [0.6, \ -0.4, \ 0.25, \ -0.15, \ 0.1, \ -0.05, \ 0.001] .$$

The target function of nonlinear memoryless determined by a 23-point LUT of update control points vector $\mathbf{q}_0$ is interpolated by a uniform third degree spline function using an interval sampling $\Delta x = 0.2$ [3]

$$\mathbf{q}_0 = \{-2.20, -2.00, -1.80, -1.60, -1.40, -1.20, -1.00, -0.80,$$
$$- 0.91, -0.40, -0.20, 0.05, 0.0, -0.40, 0.58, 1.00, 1.00,$$
$$1.20, 1.40, 1.60, 1.80, 2.00, 2.20\}.$$

The constant matrix $\mathbf{C}$ is called a *Catmul-Rom* spline matrix as given by [5]

$$\mathbf{C} = \frac{1}{2}\begin{bmatrix} -1 & 3 & -3 & 1 \\ 2 & -5 & 4 & -1 \\ -1 & 0 & 1 & 0 \\ 0 & 2 & 0 & 0 \end{bmatrix}.$$

For HSAF models, the initial parameters are in the following terms: $\delta = 0.001$, number of tap length $M = 7$, number of control points $Q = 23$, $\mu_w = 1.15 \times 10^{-3}, 4.25 \times 10^{-3}$, and $\mu_q = 1.15 \times 10^{-3}, 2.55 \times 10^{-3}$.

Other initial parameters of the proposed adaptive averaging step-size sign normalised least mean square algorithm based on the Hammerstein spline adaptive filtering (AAS-SNLMS-HSAF) consists of $\mu_w(0) = 7.5 \times 10^{-4}, 7.5 \times 10^{-3}, 7.5 \times 10^{-2}$ and $\mu_q(0) = 5.5 \times 10^{-4}, 5.5 \times 10^{-3}, 5.5 \times 10^{-2}$. And the fixed parameter for adaptive averaging step-size approach of the adaptive FIR vector $\mathbf{w}_k$ and the update control points $\mathbf{q}_{i,k}$ are set as: $\gamma_w = 0.97, \gamma_q = 0.975$, $\sigma = 0.975, \rho_w = 2.75 \times 10^{-3}, \rho_q = 2.95 \times 10^{-3}$, and $\varepsilon = 1 \times 10^{-6}$.

6 Experimental Results

The first experiment is carried out to show the effectiveness of the proposed AAS-SLMS algorithm for HSAF performs against the white Gaussian noise. In particular, the mean square error (MSE) of HSAF-based algorithm with the different of $\omega = 0.15, 0.75$ with $SNR = 25, 30$dB presented in Figures 3 and 4 that manifests the proposed AAS-SNLMS-HSAF and the conventional least mean square algorithm based on Hammerstein spline adaptive filtering (LMS-HSAF) [3] with the two different choices of ω given in (52). It shows that the MSE directions of the proposed AAS-SNLMS-HSAF algorithm can achieve faster convergence rate compared with to the LMS-HSAF algorithm at the steady state condition.

In addition, Figure 5 shows the trajectories of μ_{w_k} of tap-weight vector $\mathbf{w}_k$ at different initial value of step-size as $\mu_w(0) = 1.75 \times 10^{-2}, 1.75 \times 10^{-3}, 1.75 \times 10^{-4}$ at $\omega = 0.75$ with $SNR = 20$dB. Figure 6 conducts the step-size curves μ_{q_k} of control point $\mathbf{q}_{i,k}$ at different initial step-size $\mu_q(0) = 1.55 \times 10^{-2}, 1.55 \times 10^{-3}, 1.55 \times 10^{-4}$ at the same environment.

Figure 7 depicts the trajectories of μ_{w_k} of tap-weight vector $\mathbf{w}_k$ at different initial value of step-size as $\mu_w(0) = 7.5 \times 10^{-2}, 7.5 \times 10^{-3}, 7.5 \times 10^{-4}$ at $\omega = 0.75$ with $SNR = 25$dB. Figure 8 shows the step-size curves μ_{q_k} of control point $\mathbf{q}_{i,k}$ at different initial step-size $\mu_q(0) = 5.5 \times 10^{-2}, 5.5 \times 10^{-3}, 5.5 \times 10^{-4}$ at the same environment.
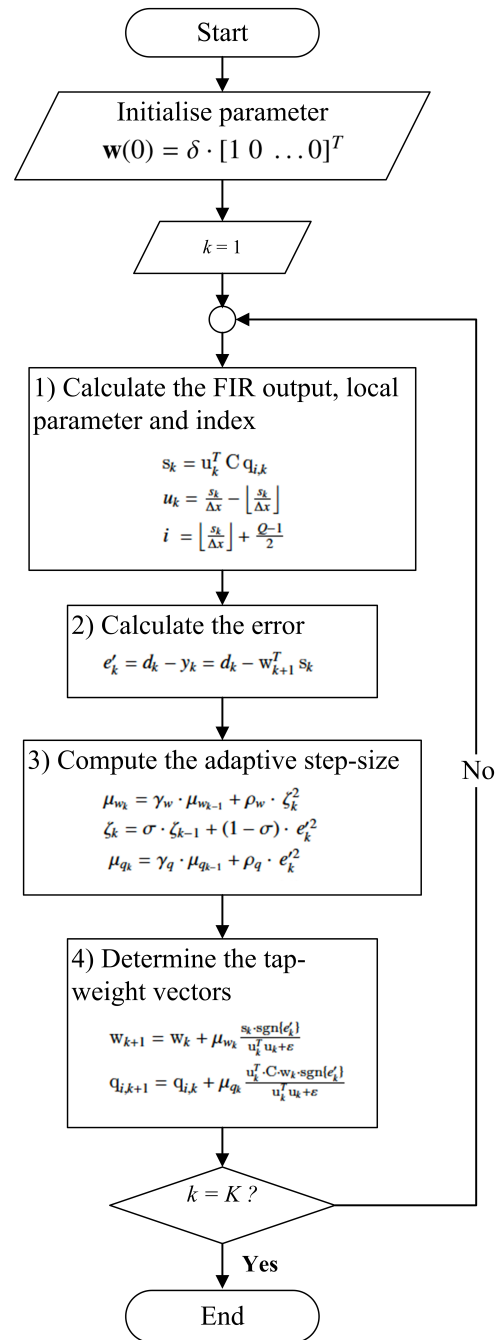
Figure 2: Flow chart of proposed AAS-SNLMS-HSAF algorithm

Figure 9 presents the trajectories of μ_{w_k} of tap-weight vector $\mathbf{w}_k$ at different initial value of step-size as $\mu_w(0) = 1.75 \times 10^{-2}, 1.75 \times 10^{-3}, 1.75 \times 10^{-4}$ at $\omega = 0.75$ with $SNR = 30$dB.

Figure 10 shows the step-size curves μ_{q_k} of control point $\mathbf{q}_{i,k}$ at different initial step-size $\mu_q(0) = 1.55 \times 10^{-2}, 1.55 \times 10^{-3}, 1.55 \times 10^{-4}$ in the same environment.

Considering the learning rate of the proposed step-size mechanism in terms of both the adaptive step-size parameter μ_{w_k} of $\mathbf{w}_k$ and the adaptive step-size μ_{q_k} of $\mathbf{q}_{i,k}$ with different SNR values, they can quickly converge to steady-state conditions compared with the fixed step-size.
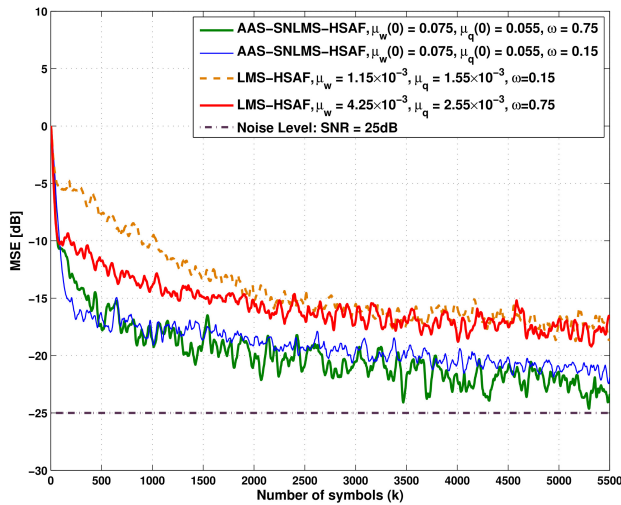
Figure 3: MSE of proposed AAS-SNLMS-HSAF with the different initial step-size of $\mu_w(0), \mu_q(0)$ and LMS-HSAF [3] with the fixed step-size μ_w and μ_q, when $\omega = 0.15, 0.75$ and SNR = 25dB.
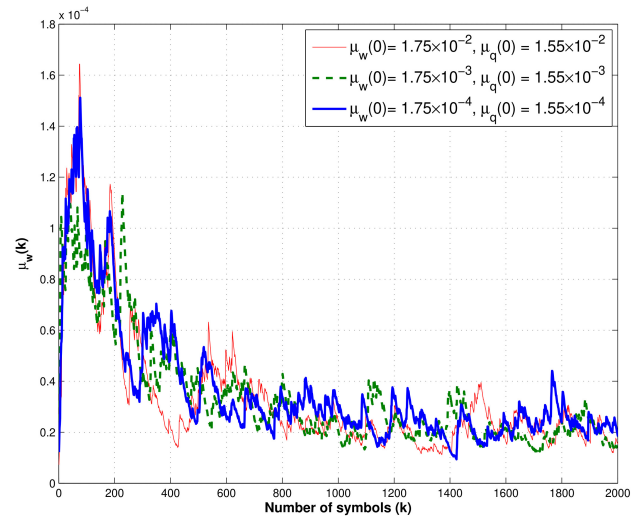
Figure 5: Trajectories of step-size μ_{w_k} of coefficient vector $\mathbf{w}_k$ with the different initial step-size parameters $\mu_w(0)$, when $\omega = 0.75$ and SNR = 20dB.
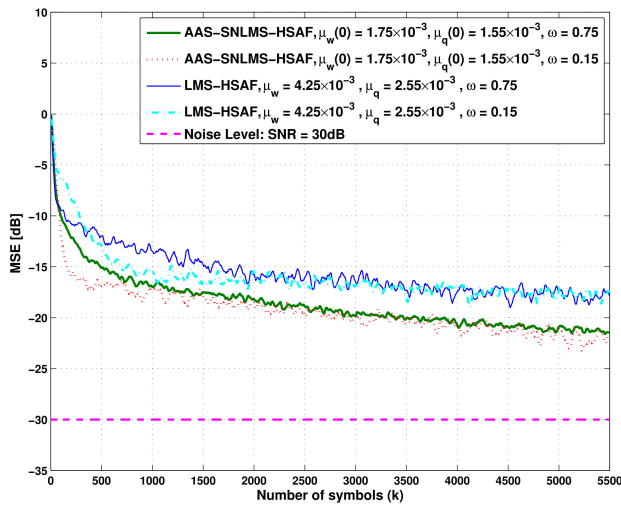
Figure 4: MSE of proposed AAS-SNLMS-HSAF with the different initial step-size of $\mu_w(0), \mu_q(0)$ and LMS-HSAF [3] with the fixed step-size μ_w and μ_q, when $\omega = 0.15, 0.75$ and SNR = 30dB.
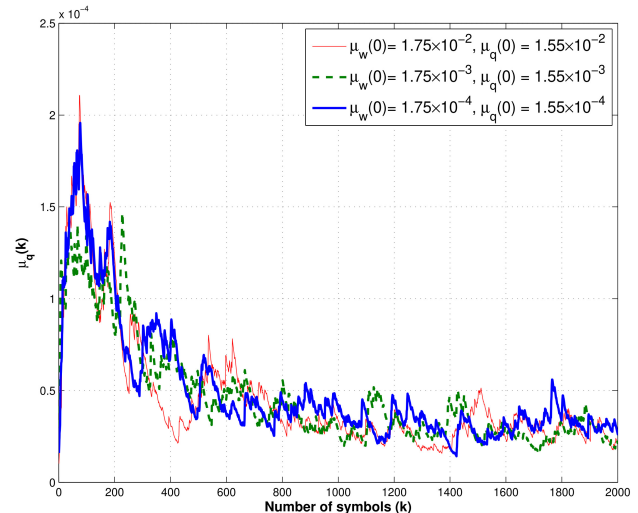
Figure 6: Trajectories of step-size μ_{q_k} of control points coefficient vector $\mathbf{q}_{i,k}$ with the different initial step-size $\mu_q(0)$, when $\omega = 0.75$ and SNR = 20dB.

In the second experiment, the electrocardiogram (ECG) [22] from the MIT-BIH Atrial Fibrillation Database [23], [24] is used as a real biomedical input signal, shown in Figure 11. ECG is sampled at 250Hz. Figure 12 shows the proposed AAS-SNLMS-HSAF and LMS-HSAF [3] using the ECG dataset with the different ω can achieve better convergence rate compared with the LMS-HSAF algorithm, even the ECG input signal is small.

Figure 13 demonstrates the trajectories of μ_{w_k} of coefficient vector $\mathbf{w}_k$ at different $\omega = 0.15, 0.75$ and the initial value of step-size $\mu_w(0) = 1.75 \times 10^{-3}$ and $\mu_q(0) = 1.55 \times 10^{-3}$ with $SNR = 25$dB using the ECG dataset at [24]. Figure 14 presents the the learning curves of μ_{q_k} of control point $\mathbf{q}_{i,k}$ at the same environment. It reveals

that the proposed adaptive step-size algorithms for both μ_{w_k} and μ_{q_k} can converge to equilibrium points using the real ECG dataset.

7 Discussion

The comparison over 100 Monte Carlo trials shows the robustness and superiority of the proposed AAS-SNLMS algorithm over the conventional LMS algorithm for HSAF model. The learning curves of adaptive step-size μ_{w_k} and μ_{g_k} of the proposed AAS-SNLMS algorithm after 10,000 iterations can expedite the convergence rate even the initial values are varied.
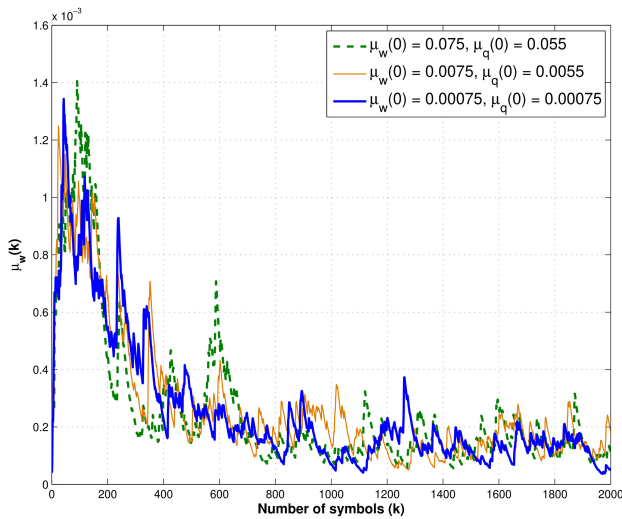
Figure 7: Trajectories of step-size μ_{w_k} of coefficient vector $\mathbf{w}_k$ with the different initial step-size $\mu_w(0)$, when $\omega = 0.75$ and SNR = 25dB.
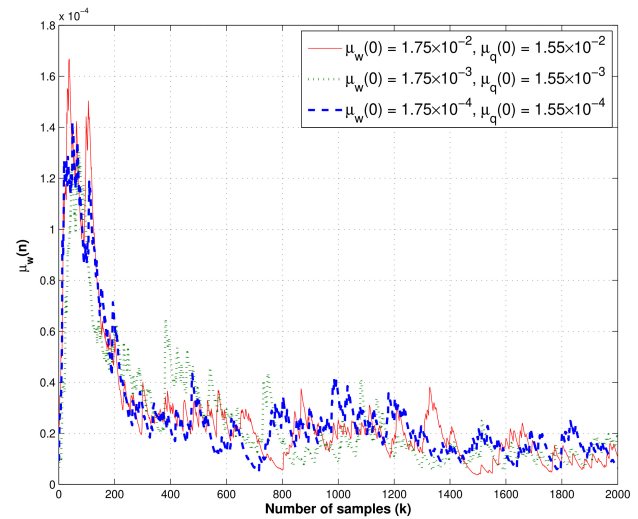
Figure 9: Trajectories of step-size μ_{w_k} of coefficient vector $\mathbf{w}_k$ with the different initial step-size $\mu_w(0)$, when $\omega = 0.75$ and SNR = 30dB.
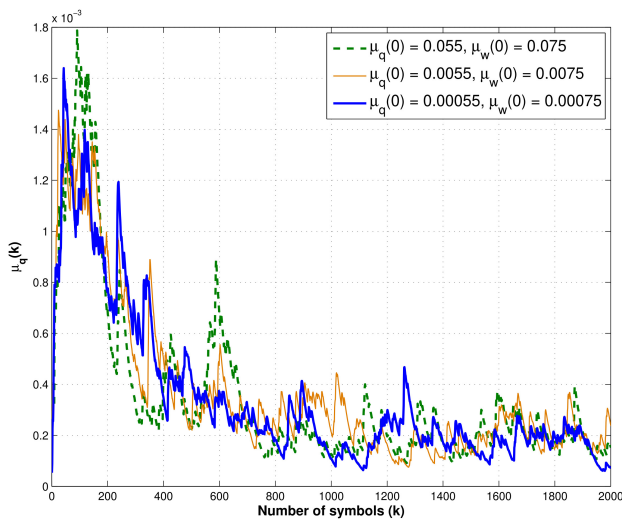
Figure 8: Trajectories of step-size μ_{q_k} of control points coefficient vector $\mathbf{q}_{i,k}$ with the different initial step-size $\mu_q(0)$, when $\omega = 0.75$ and SNR = 25dB.
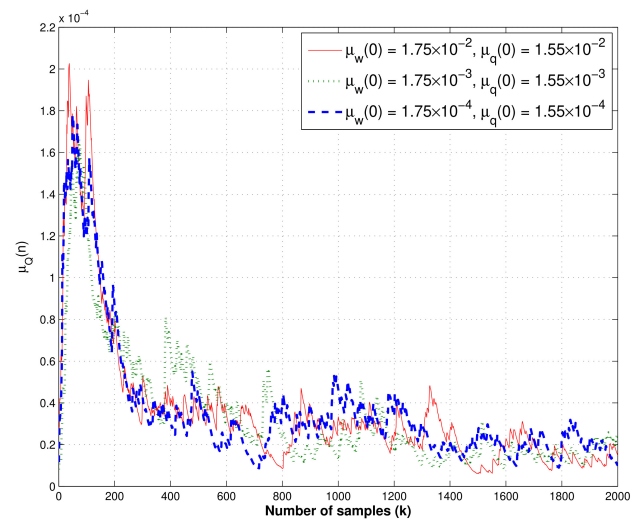
Figure 10: Trajectories of step-size μ_{q_k} of control points coefficient vector $\mathbf{q}_{i,k}$ with the different initial step-size $\mu_q(0)$, when $\omega = 0.75$ and SNR = 30dB.

8 Conclusion

This paper presents a sign algorithm based on the normalised least mean square with Hammerstein adaptive filtering by applying an adaptive averaging step-size scheme. The proposed algorithm is developed using the minimised absolute *a posteriori* squared error. We modify an adaptive averaging step-size mechanism by using the energy of the estimated *a posteriori* error to update the step-size variant.

Furthermore, we derive the behaviour and mean square performance analysis of a sign algorithm based on the normalised version of least mean square algorithm for Hammerstein spline adaptive

filtering with the adaptive averaging step-size algorithm. That leads to discover the relationship between the step-size parameter and the mean square error from the analysis. Experimental results clearly show that the proposed algorithm outperforms the conventional least mean square based on the Hammerstein adaptive filter approach.

Hammerstein models are being particularly interested in fields of engineering such as adaptive signal processing, biomedical engineering and data analysis in the nonlinear processes.

Conflict of Interest   The authors declare no conflict of interest.
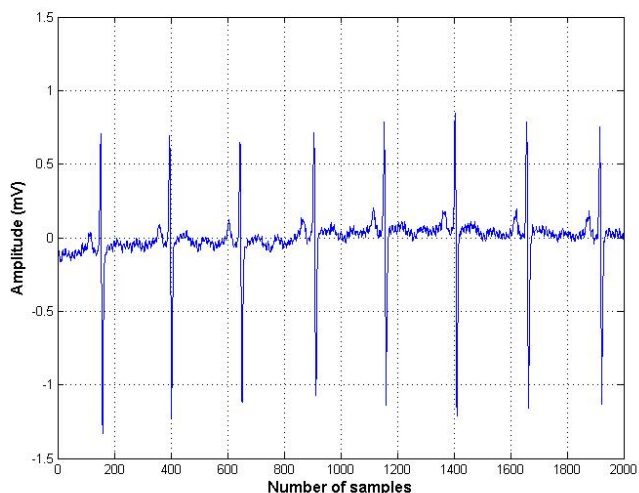
Figure 11: Electrocardiogram (ECG) input signal from MIT-BIH Atrial Fibrillation Database at [24].
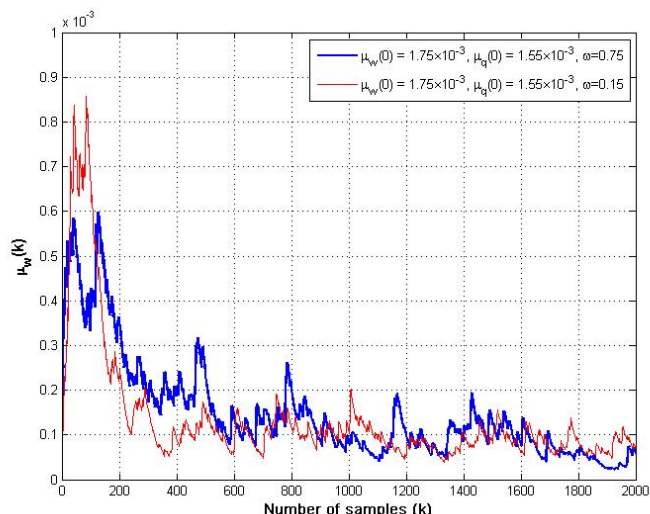
Figure 13: Trajectories of step-size μ_{w_k} of coefficient vector $\mathbf{w}_k$ using ECG input, when $\omega = 0.15, 0.75$ and SNR = 25dB.
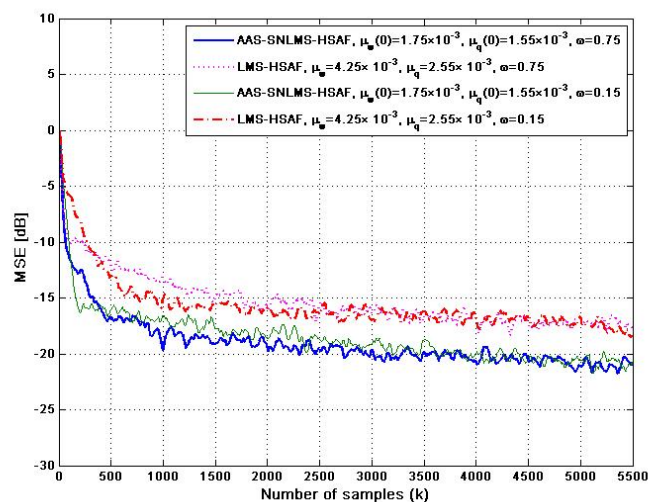
Figure 12: MSE of proposed AAS-SNLMS-HSAF and LMS-HSAF [3] using ECG input signal, when $\omega = 0.15, 0.75$ and SNR = 25dB.
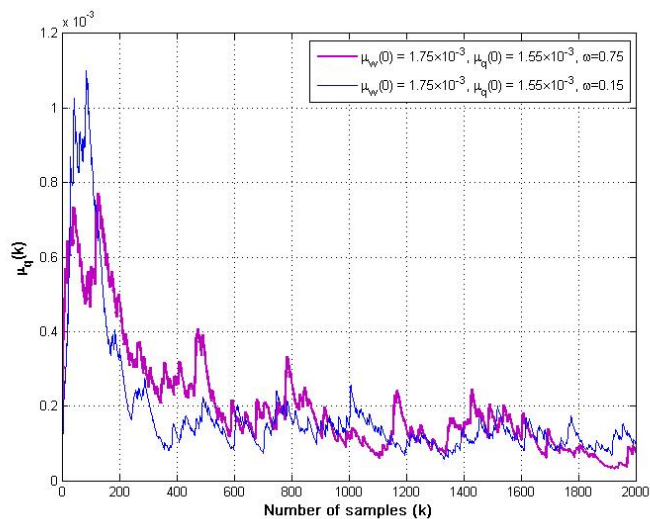
Figure 14: Trajectories of step-size μ_{q_k} of control points coefficient vector $\mathbf{q}_{i,k}$ using ECG input, when $\omega = 0.15, 0.75$ and SNR = 25dB.

References

[1] M. Scarpiniti, D. Comminiello and A. Uncini, "Convex Combination of Spline Adaptive Filters", in 2019 IEEE European Signal Processing Conference (EUSIPCO), 1-5, 2019, doi:10.23919/EUSIPCO.2019.8903134.

[2] M. Scarpiniti, D. Comminiello, R. Parisi and A. Uncini, "Nonlinear spline adaptive filtering," Signal Processing, **93**(4), 772-783, 2013, doi:10.1016/j.sigpro.2012.09.021.

[3] M. Scarpiniti, D. Comminiello, R. Parisi and A. Uncini, "Hammerstein uniform cubic spline adaptive filtering : learning and convergence properties," Signal Processing, **100**, 112-123, 2014, doi:10.1016/j.sigpro.2014.01.019.

[4] M. Scarpiniti, D. Comminiello, R. Parisi and A. Uncini, "Novel cascade spline architectures for the identification of nonlinear systems," IEEE Transactions on Circuits and Systems I: Regular Papers, **62**(7), 1825-1835, 2015, doi: 10.1109/TCSI.2015.2423791.

[5] C. Liu and Z. Zhang, "Set-membership normalised least M-estimate spline adaptive filtering algorithm in impulsive noise," Electronics Letters, **54**(6), 393-395, 2018, doi:10.1049/el.2017.4434.

[6] C. Liu, C. Peng, X. Tang and X. Liu, "Two Variants of the IIR Spline Adaptive Filter for Combating Impulsive Noise", EURAZIP Journal on Advances in Signal Processing, **8**, 1-15, 2019, doi:10.1186/s13634-019-0605-9.

[7] S. Prongnuch, S. Sitjongsataporn and T. Wiangtong, "Hammerstein Spline Adaptive Filtering based on normalized Least Mean Square Algorithm", in *2019 IEEE 2019 International Symposium on Intelligent Signal Processing and Communication Systems (ISPACS)*, 2019, doi:10.1109/ISPACS48206.2019.8986401.

[8] S. Prongnuch and S. Sitjongsataporn, "Stability and Steady-State Performance of Hammerstein Spline Adaptive Filter Based on Stochastic Gradient Algorithm ", International Journal of Intelligent Engineering and Systems, **13**(3), 112-123, 2020, doi:10.22266/ijies2020.0630.11.

[9] C. Liu, Z. Zhang and X. Tang, "Sign Normalised Hammerstein Spline Adaptive Filtering Algorithm in an Impulsive Noise Environment", Neural Processing Letters, **50**, 477-496, 2019, doi:10.1007/s11063-019-09996-6.

[10] C. Liu, Z. Zhang and X. Tang, "Steady-state Performance for the Sign Normalised algorithm based on Hammerstein Spline Adaptive Filtering", in 2019 IEEE International Conference on Control, Automation and Information Sciences (ICCAIS), 2019, doi:10.1109/ICCAIS46528.2019.9074547.

[11] C. Liu, Z. Zhang and X. Tang, "Sign Normalized Spline Adaptive Filtering Algorithms Against Impulsive Noise", Signal Processing, **148**, 235-240, 2018, doi:10.1016/j.sigpro.2018.02.022.

[12] S. Zhang, J. Zhang, and H. Han, "Robust Shrinkage Normalized Sign Algorighm in an Impulsive Noise Environment", IEEE Transactions on Circuits and Systems, **64**(1), 91-95, 2017, doi:10.1109/TCSII.2016.2546905.

[13] K. Xiong, S. Wang and B. Chen, "Robust Normalized Least Mean Absolute Third Algorithm", IEEE Access, **7**, 10318-10330, 2019, doi:10.1109/ACCESS.2019.2891549.

[14] P. Wen and J. Zhang, "Robust Variable Step-size Sign Subband Adaptive Filter Algorithm against Impulsive Noise", Signal Processing, **139**, 110-115, 2017, doi:10.1016/j.sigpro.2017.04.012.

[15] J. Kim, J. Choi, S.W. Nam, J. Chang, "Delayless Block Individual-Weighting-Factors Sign Subband Adaptive Filters With an Improved Band-Dependent Variable Step-Size",IEEE Access, **8**, 185796 - 185803, 2020, doi:10.1109/ACCESS.2020.3029269.

[16] S. Zhang, J. Zhang and H. Han, "Robust Shrinkage Normalized Sign Algorithm in An Impulsive Noise Environment", IEEE Transactions on Circuits and Systems II: Express Briefs, **64**(1), 91-95, 2017, doi: 10.1109/TCSII.2016.2546905.

[17] S. Guan and Z. Li, "Normalized Spline Adaptive Filtering Algorithm for Nonlinear System Identification", Neural Processing Letter, **46**(2), 595-607, 2017, doi:10.1007/s11063-017-9606-6.

[18] S. Sitjongsataporn, W. Chimpat, "Adaptive Step-size Normalised Least Mean Square Algorithm for Spline Adaptive Filtering", in 2019 IEEE International Technical Conference on Circuits/Systems, Computers and Communications (ITC-CSCC), 544-547, 2019, doi:10.1109/ITC-CSCC.2019.8793383.

[19] A. Saengmuang and S. Sitjongsataporn, "Convergence and Stability Analysis of Spline Adaptive Filtering based on Adaptive Averaging Step-size Normalized Least Mean Square Algorithm ", International Journal of Intelligent Engineering and Systems, **13**(2), 267-277, 2020, doi:10.22266/ijies2020.0430.26.

[20] S. Prongnuch and R.E. Valmoria, "Applied of Co-design in Reconfigurable System for Remote Image Noise Filtering via Ethernet Technology", in 2013 IEEE International Science, Social Science, Engineering and Energy Conference, 92-98, 2013.

[21] S. Sitjongsataporn, "Advanced Adaptive DMT Equalisation: Algorithms and Implementation", LAP LAMBERT Academic Publishing, 2011.

[22] G.B. Moody and R.G. Mark, "A New Method for Detecting Atrial Fibrillation using R-R Intervals", *Computers in Cardiology*, **10**, 227-230, 1983.

[23] A. Goldberger, L. Amaral, L. Glass, J. Hausdorff, P.C. Ivanov, R. Mark, J.E. Mietus, G.B. Moody, C.K. Peng, and H.E. Stanley, "PhysioBank, PhysioToolkit, and PhysioNet: Components of a New Research Resource for Complex Physiologic Signals", *Circulation* [Online], **101**(23), e215–e220, 2000, doi:10.1161/01.cir.101.23.e215.

[24] G. Moody and R. Mark, "MIT-BIH Atrial Fibrillation Database", 2000, [Online]. Available: https://physionet.org/content/afdb/1.0.0/. [Accessed Jan. 8, 2021], doi:10.13026/C2MW2D.

Prototype of an Augmented Reality Application for Cognitive Improvement in Children with Autism Using the DesingScrum Methodology

Misael Lazo Amado [*] ,Leoncio Cueva Ruiz, Laberiano Andrade-Arenas

Systems Engineering Program, Universidad de Ciencias y Humanidades, Lima, 27, Peru

A R T I C L E   I N F O

A B S T R A C T

In this COVID-19 pandemic, it has been registered that children with autism are not learning properly with this virtual modality in Peruvian education. The main objective of this research work is to design a mobile application with augmented reality so that autistic children can improve their cognitive development in their virtual and face-to-face classes, the chosen methodology is DesingScrum which is a hybrid of the union of Design Thiking and Scrum, which will have 10 phases (empathise, define, devise, planning meeting, sprint backlog, daily meeting, sprint review, retrospective sprint, prototype, testing), in the case study the Balsamiq tool was used for the design of the mobile application. The results are the responses from the public in Lima - North of the survey carried out on the prototype for its improvement and also the result of the design of the games with augmented reality that was applied with the tools (Tinkercad and App Augmented class). The conclusion drawn from the research work is to be able to help autistic children to improve their cognitive development with the mobile application developed through augmented reality.

1   Introduction

Autism Spectrum Disorder (ASD) is a life-long disorder with several characteristics that can affect how you relate to different people in what you choose to distance yourself from and mostly tend to have trouble learning, in school or in other activities you do [1], almost 70% of autistic people do not have an intellectual disability [2], 1 in 160 children worldwide is diagnosed with ASD [3]. As there is no quick diagnosis to know this disorder, it takes time since it will be analyzed by specialized doctors who observe the child's behavior, these are identified from 18 to 30 months. In Europe and North America they are diagnosed at school, this is identified by problems such as anxiety, hyperactivity or other mood disorders, however when they become adults 10 and 33% have a verbal and non-verbal character, they are able to work but need support, in the USA only about 25% live in their own homes and the rest live with their families [4]. The Covid-19 became a pandemic and many governments have declared their social distancing, due to this the children of ASD are distanced from their therapists and different problems arise in the homes as the children are not adapted to stay at home and are not controlled by the parents [5]. The impact that covid-19 is having on the parents of children with Autism Spectrum Disorder (ASD), is the stress that the parent develops by giving their child peace of mind, that they do not need a nanny, teachers and therapists, it becomes a real challenge for their control [6].

In the city of Quito in 2017 an evaluation was carried out to find signs of autism in which 51,463 students were evaluated, where 0.11% of children were diagnosed with autism and 0.21% with suspected ASD [7]. Due to ASD this diagnosis is made during the first three years of birth and more cases are found in men than in women.

This data from the Institute of National Statistics and Information Technology in Peru recorded 5.2% of the population of Peru with this disability, in which 10,223 people have autism spectrum disorders [8]. Considering that we found four factors that are related to socioeconomic status (SES), level of maternal education or having public health insurance, low income measure in the census or having a diagnosis of ASD in the records, because of these factors we cannot make a correct balance in Peru on how many exact people suffer from ASD or the autism spectrum [9]. The importance of our project will help the ASD child to develop cognitively, emotionally and socially, as this augmented reality system consists of fun activities and games for their development.

The objective is to make a prototype of a mobile application for the cognitive development of ASD children using augmented reality so that parents can use this application for therapies or learning of children with autism, taking into account that in the Covid-19

---

[*]Corresponding Author: Misael Lazo Amado , Email:jerlazoa@uch.pe

pandemic, children do not have physical contact with their therapists or educators.

This work will be structured in the following way, in section 2 the methodology to be used will be explained, in section 3 the case study of the research work will be developed, in section 4 it will be explained in detail what were the results and discussions during the tests carried out, in section 5 will be the conclusions obtained through the evidence made of the results.

2   Methodology

To begin with, we will show how you will start our methodology in which we will use 2 methods, Design Thinking and Scrum. These two methodologies will form a hybrid, which will have 10 phases (Empathise, Define, Ideate, Planning Meeting, Sprint Backlog, Daily Meeting, Sprint Review, Sprint Retrospective and Test) and to finish we will talk about the tools that will be used for the design of the prototype.

2.1   Design Thinking

This methodology has brought a lot of interest to the Professionals as it is new in the field of Innovation and Problem Solving [10]. Design Thinking has 5 phases (empathise, define, devise, prototype and test), it is mostly used to realise products, processes and business environments that require the help of users to identify strategies and future solutions, [11] as shown in Figure 1.
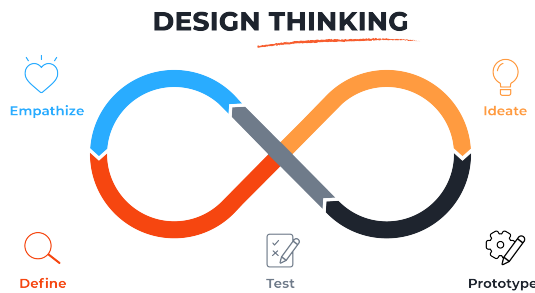
Figure 1: Design Thinking

2.2   Scrum

Scrum allows us to have a better iterative and incremental approach that prioritizes flexibility and adaptability to changes and in a complex environment, scrum is not a standardized process as it involves several steps to ensure a quality product. Scrum starts from the initial meeting to having the user capture, these are collected characteristics that are prioritized / through the product list, through the planning sprint, followed by the execution sprint and ending with the review and the retrospective [12], as shown in Figure 2.
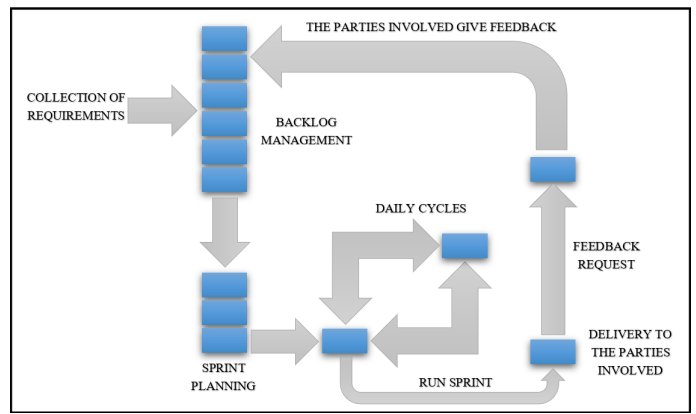
Figure 2: Methodology Scrum

2.3   Phases of the Hybrid Methodology

This part will explain a little of the hybrid methodology between Design Thinking and SCRUM that is being carried out, which will have 10 phases as shown in Figure 3.

2.3.1   Empathize

Empathy is centred on the users, it is dedicated to the observation of their behaviour, iteration and personal interviews which allows the designer to have a greater understanding of the needs of those involved [13].

2.3.2   Define

The team will use the first phase to define the problems and complexities of the User [13].

2.3.3   Ideate

This stage is connected with the second phase, its objective is to brainstorm, to generate solutions, this allows the team to choose the ideal solution [14].

2.3.4   Planning Meeting

The user stories that will go into the backlog will be defined. The user stories are a set of simplified stories or requirements that identify a user, who and why they want this system functionality and the backlog is a list of user stories [15].

2.3.5   Sprint Backlog

The sprint backlog contains a set of tasks for each team member this will allow you to have a better implementation in the system, this are divided into sprint that would be like the deliverables that would have as a date for each deliverable to be made with the ability that you can work in a more orderly manner, taking into account this is done through the user stories.

2.3.6 Daily Meeting

The daily scrum meeting is the main way to review the adaptation processes in the scrum practice, the ideal is to meet for 15 minutes at the beginning, each team member declares his or her work to be done, taking into account that the meetings will discuss: What have I done since the last meeting, what am I going to do from now on, and what impediments do I have or will I have?

2.3.7 Sprint Review

At this stage the sprint will be checked, the check takes approximately four hours per month for each deliverable. In the sprint check an evaluation is made which is achieved during the sprint, the scrum team which inspects the increase and adapts to the delayed product if necessary checks the product and is responsible for defining the product and then moves on to the next sprint [13].

2.3.8 Sprint Retrospective

In this sprint we will identify which improvements can be implemented in the next sprint or in the current one to solve any issue or problem we find in the device [16].

2.3.9 Prototype

Finished with Phase VIII , this phase allows us to show the final prototype of our research.

2.3.10 Testing

In this final phase, feedback is requested from the user, with the aim of improving the Prototype.
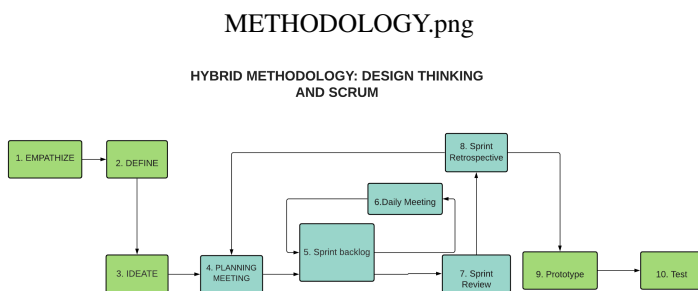
METHODOLOGY.png

Figure 3: Hybrid methodology: Design thinking and scrum

2.4 Tools for Designing our Prototype

The tools for The tools for the design of the prototype with Balsamiq Mockups 3, Tinkercad and Augmented Class App will be defined, and finally the technical innovation explaining the technical development of augmented reality will be shown.

2.4.1 Balsamiq Mockups 3

Balsamiq Mockups is a tool to design mobile and web prototypes [17], with the components of the tool this will serve us to design our mobile application.

2.4.2 Tinkercad

Tinkercad is a tool that provides the creation of 3D models. It is currently free and runs from the browser [18], allowing the creation of simple or complex objects [19]. This tool will be used to perform in the design for the games and the 3D image will be exported so that it can then be imported into the Augmented class application.

2.4.3 App Augmented Class

It is an application to create augmented reality projects, this app is in Play Store which is currently in free mode, we use it to import the images that were designed in Tinkercad and we show it our prototype of the cognitive games.

2.4.4 Technical innovation

There are several ways to develop augmented reality, but in this article, the development of augmented reality with Unity 3D and Vuforia SDK will be explained.

Unity 3D is a 3D game engine in which it allows the design, creation and operation of a video game, integrates a multiplatform developed by Unity Technologies Co.Ltd. Unity 3D can add several virtual scenes sunlight, fog, water, fire, among other animated scenes. With the support of an extension called Vuforia SDK they can make several applications and games with Augmented Reality [20].

Vuforia SDK is an augmented reality software development kit used to capture flat images or 3D objects in real time which developers use to place virtual objects through a camera [20].

In this Figure 4 it can be seen that the mobile phone camera captures the real scene and Tracker is in charge of processing the image or rather tracking or analysing an image since together with the Targets they can recognise the 3D object, after matching the identification of the 3D object through the Frames of the camera (its function of the Frame is to capture image and convert it to a different resolution) The aim is to find matches in the database and thus create an augmented reality.
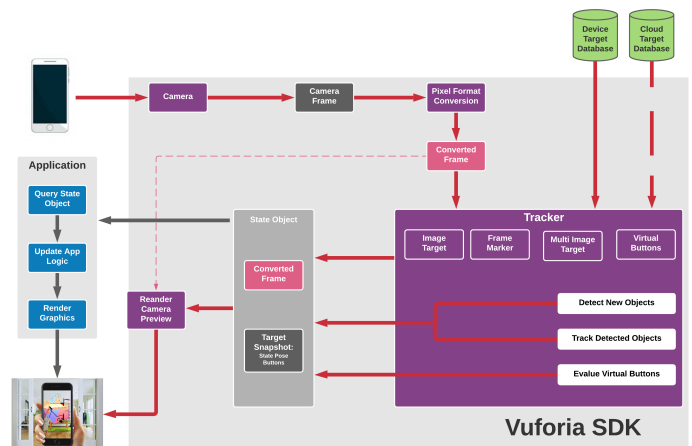

Figure 4: Vuforia SDK Architecture

3 Case Study

3.1 Empathize

We started with the first phase that was commissioned by applying surveys to parents about their children's education or how they feel in this new virtual mode so we used the Google Forms tool to formulate the questions.

Table 1 shows the questions (Q1 to Q10) that are formulated for the parents, which will have to complete the data of the children, age, gender, district, if the child learns correctly at home, if the child has stress at the time of his virtual classes, what type of autism the child has, it also shows at what level of autism the child is, the activity he likes, the family situation and if he currently has therapeutic treatment.

Table 1: Survey on the problems of autistic children in Lima-North

Questions	
ID	**Questions**
1- Q1	Child's age
2- Q2	Gender of the Child
3- Q3	District
4- Q4	Do you feel that your child is not learning properly at home?
5- Q5	Does your child get stressed out by virtual classes?
6- Q6	What type of autistic child does your child have?
7- Q7	What level of autism is your child at?
8- Q8	What activity does the child like?
9- Q9	What is the family situation in the child's home?
10- Q10	Does the child currently have therapeutic treatments?

3.2 Define

In this phase we will define the problems that are found according to the survey answered by the public.

In this Table 2, the problems presented by the survey will be indicated. Q1 through Q10, means the questions shown in Table 1 and their most relevant responses from the survey.

1. Q1 : It is understood that 7 to 9 years old are the most likely to have responded to the survey and have ASD.

2. Q2 : It shows that more male cases were found in children with ASD.

3. Q3 : It indicates that in Lima - North, in the district of Los Olivos it has a greater number of children with autism.

4. Q4 : It indicates that 51% of children are not learning properly in their educational training.

5. Q5 : This survey indicates that children are stressed out by the new virtual platform provided by the State of Education.

6. Q6 : This survey has identified that there are more children with Austistic Disorders and is followed by Asperger's Syndrome in Lima-North.

7. Q7 : A balance has been made that 47.1% suffer from a slight level of autism in the area of Lima-North.

8. Q8 : The survey shows that games are the activity most chosen by children.

9. Q9 : The survey shows that 54% of children with a disability are cared for by their parents.

10. Q10 : The survey indicates that 54.9% have therapeutic treatment, while 45.1% have no therapeutic treatment.

Table 2: Relevant answers according to the problems of the Public.

Answers	
ID	**Answers**
1- Q1	8 Years 31.4% , 9 Years 19,6% , 7 Years 11,8% .
2- Q2	Male 68,9 % , Female 31,4%
3- Q3	Los Olivos 25,5% , Comas 19,6% , Carabayllo 19,6%.
4- Q4	Yes 49% , No 51%.
5- Q5	Yes 62,7% , No 37,3%.
6- Q6	Autistic Disorder 52,9% , Asperger's syndrome 19,6%
7- Q7	43,1% Level 1(Light) , 47,1% Level 2(Medium) ,9,8% Level 3(Heavy)
8- Q8	Playing 39.2% , Dancing 25.5% , Drawing 19.6%
9- Q9	The father and mother live together, both raise the child 54%.
10- Q10	Yes 54,9% , No 45,1%

These statistics were taken from the survey that was conducted in September and October 2020 to parents who have children suffering from this disease, it was found that there was an increase of autistic disorder with level 1, level 2 and level 3 in northern Lima, taking into account that the district with more cases was the olive trees.

3.3 Ideate

According to the Problems identified in Phase 2, these solutions have been successfully devised to improve the cognitive development of ASD children. The team has then implemented a score from 1 to 20 and the best solution will be selected to develop it as shown in Table 3.

1. S1 : In this first solution it was identified that a mobile application for the cognitive development of autistic children can be elaborated using augmented reality in which their score is estimated by each working member (M1, M2 and M3), the M1 estimates 19 points, the M2 estimates 19 points and the M3 estimates 17 points and adds up to a total of 53 points.

2. S2 : In this second solution it was identified that it is possible to elaborate a Web Application for the child with autism to improve with cognitive activities in which his score is estimated by each work member (M1, M2 and M3), the M1 estimates 14 points, the M2 estimates 14 points and the M3 estimates 13 points and adds up to a total of 41 points.

3. S3 : In this third solution it was identified that it is possible to elaborate a Mobile Application for therapies and orientations for ASD children in which their score is estimated by each working member (M1, M2 and M3), the M1 estimates 14 points, the M2 estimates 12 points and the M3 estimates 11 points and adds up to a total of 53 points.

Table 3: Punctuation of the Ideas

Punctuation of the Ideas				
Solutions	M1	M2	M3	Total
S1- To make a Mobile Application with games for the cognitive development of autistic children using Augmented Reality	17	19	17	53
S2- Developing a Web Application for the child with autism to be trained with cognitive activities	14	14	13	41
S3- Developing an application for therapy and guidance for children with ASD	14	12	11	37

At the end of this phase, the solution with the highest score (S1) was identified by the members of the work team, which they used to carry out the project.

3.4 Planning Meeting

In the following table 4, the user story was important for the creation of the prototype design, which required an in-depth analysis of table 1. Table 2. Table 3. Which allows us to have the following 7 user stories.

1. H1 : The first user story will create an interface where any user will be able to create a new account to be registered in the system.

2. H2 : In the following user history 2, it will be possible to enter the system using the user and password that were created in the H1.

3. H3 : In the third user history, an option will be implemented so that the user can recover his or her password if for any reason it has been forgotten or lost.

4. H4 : In the user history 4 there will be an option where you can select your corresponding age, depending on your age that the user has you will be shown a list of available games.

5. H5 : In the user history 5 you can choose the game mode where you will get the games with their respective categories, this will depend on which option you have chosen in the H4.

6. H6 : In the following user story 6, the client will be able to rate the game, where he can leave his comment if he liked the game or what things we should change to make it more interactive and fun.

7. H7 : In the user history 7 you can check your history, where an interface will appear showing you how many hours you have played, your username and the date.

Table 4: User Stories.

User Stories	
1- H1	The user needs to register a new account (user, age, email and password) to enter the application.
2- H2	The user needs to log in by entering their registered username and password to access the application.
3- H3	The user needs to recover his password every time he forgets it.
4- H4	The user needs to select his/her age to enter the list of games.
5- H5	The user can select the game mode to get a list of the chosen mode.
6- H6	The user can indicate the rating of the game.
7- H7	The user will have a history of the games used.

3.5 Sprint Backlog

In this phase the four sprints will be carried out, according to the user stories that have been defined in the previous phase as shown in Table 5.

Table 5: Sprint Backlog.

Sprint Backlog		
ID	DESCRIPTION	SPRINT
1- H1	- The user needs to register a new account (user, age, email and password) to enter the application.	Sprint 1
2- H2	- The user needs to log in by entering their registered username and password to access the application.	
3- H3	-The user needs to recover his password every time he forgets it.	
4- H4	- The user needs to select his/her age to enter the list of games.	Sprint 2
5- H5	- The user can select the game mode to get a list of the chosen mode.	
6- H6	- The user can indicate the rating of the game.	Sprint 3
7- H7	- The user will have a history of the games used.	Sprint 4

As shown in Figure 5 the first deliverable that would come to make the sprint 1, would be made up of the first interface that would come to make the home page that has 2 options to register and log

in, then the next would be to register if a new user, log in if you already have a registered account and finally recover password if the user forgot the password of the login.

Figure 5: Sprint 1

Sprint 2 in Figure 6 shows h4 and h5, which would make the selection of the game mode by age and the selection of the game mode chosen by the user.

Figure 6: Sprint 2

In this Figure 7 will go the h6, this will include the sprint 3 that dealt with the qualification of the game and comment this would serve to ask the user what he thought about the experience of the game and what improvements he would recommend.

Figure 7: Sprint 3

As shown in sprint 4 of Fig 8 of h7, you can see the user's history by date, the name of the game, start time, end time and how

many hours they have played, this will serve to see how much time they spend on the game.
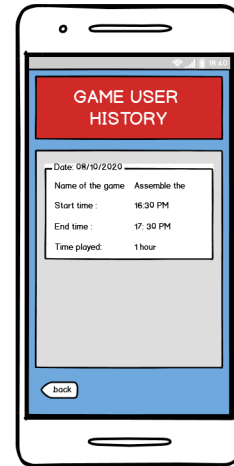
Figure 8: Sprint 4

3.6 Daily Meeting

When each Sprint is carried out, it is essential to hold these meetings for 15 people in order to better position ourselves in the collective work. The Scrum Master is in charge of generating the meeting and asking these questions: What did you do yesterday? What are you going to do today?.

3.7 Sprint Review

After finishing each Sprint, it is necessary to carry out this review by the team, you will have a maximum of 3 to 4 hours for evaluation, and they must be explained to the Product Owner for him to accept, then be shown to the users or assistants to obtain some comment or an improvement of the product. After the assessment is completed, the next Sprint is issued and if all Sprints are completed, the next phase is performed.

3.8 Sprint Retrospective

In this case the process will be evaluated and the Scrum Master generates a meeting with the Product Owner and the Work Team, to improve the next process, then it asks itself: What did we do well, what can we improve and what should we stop doing?.

3.9 Prototype

In this phase, the Final Prototype will be shown as it can be seen in Figure 9 that will be made with Balsamiq Mockups 3, this will be the final sample of the Application that will be used by means of the Augmented Reality where 4 games were made.

3.10 Testing

In this final stage a survey will be carried out on Google Forms where 5 questions of the prototype will be asked (QP1 to QP5),

the public will give their point of view about the prototype or what improvements would be applied as shown in Table 6.
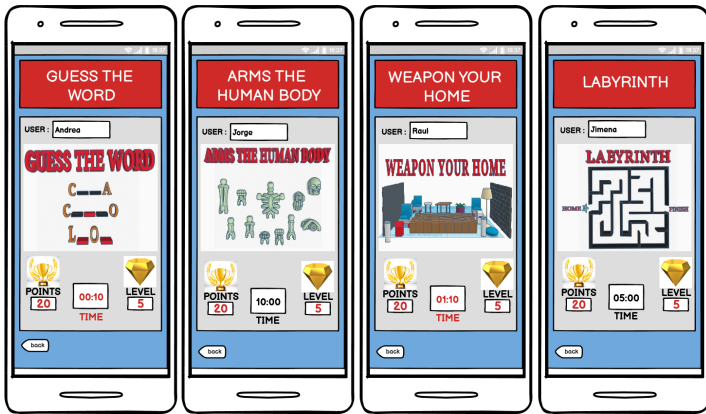
Figure 9: All Games

Table 6: Survey about the Prototype for the Cognitive Development of ASD children applying Augmented Reality

Questions	
ID	Questions
QP1	Tell us what you thought of the Prototype.
QP2	Tell us how you found the Cognitive Games for your child.
QP3	I would recommend this application for TEA children.
QP4	You think your child will learn using this application.
QP5	Write your opinion on how we can improve the application.

3.11 Mobile Application Algorithm

The design algorithm of the mobile application is shown in Figure 10 and will be explained in detail in the following description.

1. Identification of cognitive problems for autistic children: The research work started on how we could identify cognitive problems in autistic children.

2. Are there any cognitive problems? : The first conditional was made if a problem was found, the cognitive problems in the autistic children had to be identified again, but if no problem was found in the identification, the next process was made.

3. Analysis of the problems identified: In the 2 process an analysis of all the problems was made on all the processes that have been accepted from point 1.

4. Feedback: In the 3 process we made a feedback where we are going to analyze all the requirements we need together with the new ideas of the work team.

5. Do you meet the requirements? : We carry out the 2 conditional where we ask ourselves the question of point 4 if it

fulfils all the requirements to go on to the next process. If it does not, new requirements will be reconsidered in order to be accepted.

6. DesignScrum Methodology: Then in the 4 process we apply the DesignScrum methodology which will carry out the research work

7. Mobile Prototype: In process 5 we started to create the prototype of the mobile application after having identified all the problems and created the necessary requirements.

8. Do parents agree with the prototype? : On the 3rd conditional a survey was sent to all parents who are using the prototype to find out their opinion and what new ideas we should add. If the parents did not agree, we would have to go back to the previous point to restructure the prototype of the mobile application. If they accepted, we would go on to the next process.

9. Augmented Reality Prototype with Tinkercad and App Augmented Class: In the sixth process, the application was begun with Tinkercad and the Augmented Class App. This will serve to add the design of the prototype and add the Augmented reality to the project in which the project will be completed.
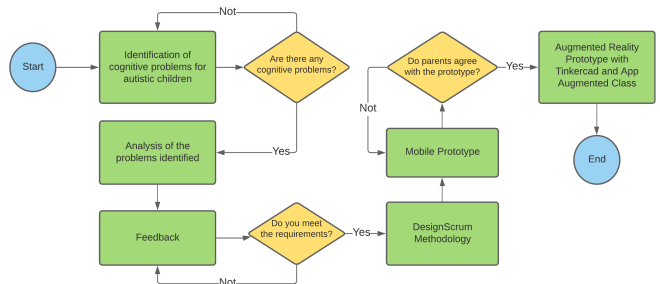
Figure 10: Mobile Application Algorithm

4 Results and Discussions

In this chapter we show our results according to the analysis of the survey of the last phase of the survey carried out, The Application of the Prototype and the methodology.

4.1 About the Survey

In the last part of the case study, a survey was carried out with 5 questions on the final prototype (QP1 to QP5). In this result from Table 7, we show the relevant responses indicated by the public about our prototype.

1. QP1: In this result he indicates which prototype the parents think is good.

2. QP2 : Parents indicate that they find games very good for the cognitive development of autistic children.

3. QP3 : It indicates that in Lima - North, in the district of Los Olivos it has a greater number of children with autism.

4. QP4 : Parents feel confident that their children will learn using the application.

5. QP5 : Good feedback was obtained on the improvement of the Prototype of the mobile application.

Figure 11: Game 1

Table 7: Relevant answers according to the prototype shown to the public.

Answers	
ID	Answers
1- QP1	Good 46,2% , Very Good 23,1% .
2- QP2	Very Good 38,5% , Good 23,1%
3- QP3	Yes 84,6% , No 15,4%.
4- QP4	Yes 84,6% , No 15,4%.
5- QP5	The public indicate that they must do better in developing more games for their children.

According to the responses from the public, it can be seen that the vast majority of the respondents are satisfied with the prototype, which was our expectation when the work started. In the survey, 46.2 % of the respondents were satisfied with the prototype and 23.1 % were very satisfied, which shows that they found the prototype very interesting. It is also noted that cognitive games have 38.5 % very good and 23.1 % very good, which impresses us that the public is comfortable with the games, taking into account that 84.6 % of respondents say that the mobile application will be recommended and that their children with autism strengthen or improve their cognitive development. Finally we obtained positive recommendations from the public as it encourages us to improve the prototype, fulfilling the objective of the methodology.

4.2 Prototype Application

According to the design of the prototype of the game, it was possible to design the games with Augmented Reality using the Tinkercad tool and Augmented class.

In Figure 11 you can see the prototype is working correctly in the mobile phone by means of augmented reality, the game being presented the child will have to guess the correct word as shown on the screen of the mobile phone.

As shown in Figure 12 the prototype works correctly, the game will be a maze where the child will have to identify the correct path so that he can reach the end of the maze and move on to the next level.

Figure 12: Game 2

Figure 13: Game 3

As shown in Figure 13, the child will try to assemble the human body where he will have several opportunities to finish the first level of the game.

Figure 14 shows the last set made of the prototype working correctly on the mobile phone. It tries to allow the child to build his house with the objects shown on the mobile phone.
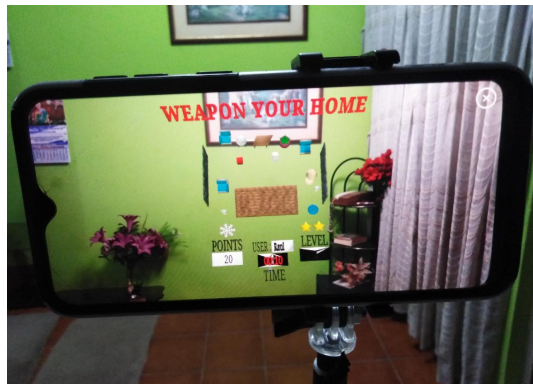
Figure 14: Game 4

4.3 About the methodology

4.3.1 Advantages

The union of two methodologies was made to carry out the hybrid methodology. This gave us a usefulness since it allowed us to better structure the phases of the research work. Scrum allows us to work on different projects with different requirements. With a compromise, this offers to guarantee a model that benefits all the needs of the project having the facility to put together other methodologies and tools [21]. Design Thinking will include these benefits as transformation, innovation to improve decision making as well as results [22], allowing the combination of empathy, creativity, coherent analysis of information and adjustment to the environment according to the solutions [23].

4.3.2 Disadvantages

The disadvantage of the hybrid methodology that is being applied is a little complex as it has 10 phases. Therefore, what is disadvantageous is that some fundamental steps cannot be eluded, taking into account these phases require a longer time of analysis to develop the processes.

4.3.3 Comparison

According to what was evaluated, from the scrum methodology and Design Thinking it was decided to carry out a hybrid methodology where it would contain 10 phases so that it would have a better structure when developing the research work. On the other hand, the difference of these two methodologies with the hybrid methodology is that scrum is structured more to the software part and Design thinking is structured to the analysis part, taking into account the hybrid methodology focuses on the software and analysis part allowing a better understanding when deploying the project.

5 Conclusions

The application was developed to work with augmented reality allowing to improve the cognitive development of all the autistic children. For the mobile application different games were added, where each category will have its corresponding game so that the user can choose the game the option he wants. Allowing us to

implement the hybrid methodology where the application was developed, helping us to innovate and manage the development of the mobile application. In the case study, we defined how the application was structured so that the child could learn with the use of technology. It would be of great help to use the mobile application for cognitive development for the treatment of all children suffering from different cases of autistic disorder, so that children can have a better experience, allowing to generate a great impact of learning in education in Peru. For future research work it is recommended to use Tinkercad's tools with Arduino, this will allow for a better optimization when developing the application. It is also possible to use unity3D for the operation of the application while vuforia SDK would serve to apply augmented reality to any system, be it web or mobile application.

References

[1] K. Spiel, C. Frauenberger, O. Keyes, G. Fitzpatrick, "Agency of autistic children in technology research—A critical literature review," ACM Transactions on Computer-Human Interaction (TOCHI), **26**(6), 1–40, 2019, doi: 10.1145/3344919.

[2] G. Wallace, L. Kenworthy, C. Pugliese, H. Popal, E. White, E. Brodsky, A. Martin, "Real-World Executive Functions in Adults with Autism Spectrum Disorder: Profiles of Impairment and Associations with Adaptive Functioning and Co-morbid Anxiety and Depression," Journal of autism and developmental disorders, **46**, 2015, doi:10.1007/s10803-015-2655-7.

[3] D. N. Fernández, F. B. Porras, R. H. Gilman, M. V. Mondonedo, P. Sheen, M. Zimic, "A Convolutional Neural Network for gaze preference detection: A potential tool for diagnostics of autism spectrum disorder in children," 2020.

[4] C. Lord, M. Elsabbagh, G. Baird, J. Veenstra-Vanderweele, "Autism spectrum disorder," The Lancet, **392**(10146), 508 – 520, 2018, doi:10.1016/S0140-6736(18)31129-2.

[5] A. Narzisi, "Handle the Autism Spectrum Condition during Coronavirus (COVID-19) Stay at Home Period: Ten Tips for Helping Parents and Caregivers of Young Children," Brain Sciences, **10**(4), 2020, doi:10.3390/brainsci10040207.

[6] C. Parenteau, S. Bent, B. Hossain, Y. Chen, F. Widjaja, M. Breard, R. Hendren, "The Experience of Parents of Children with Autism Spectrum Disorder During the COVID-19 Pandemic: A Qualitative Analysis," 2020, doi: 10.21203/rs.3.rs-46426/v1.

[7] S. d. l. Á. A. Arboleda, M. P. C. Alcocer, E. N. D. Mosquera, "El vínculo figura cuidadora-niño en casos de autismo," Revista Scientific, **5**(Ed. Esp.), 165–184, 2020, doi:10.29394/Scientific.issn.2542-2987.2020.5.E.8.165-184.

[8] S. Magaña, K. Lopez, K. Salkas, E. Iland, M. Morales, M. Torres, W. Zeng, W. Machalicek, "A Randomized Waitlist-Control Group Study of a Culturally Tailored Parent Education Intervention for Latino Parents of Children with ASD," Journal of Autism and Developmental Disorders, **50**, 2020, doi: 10.1007/s10803-019-04252-1.

[9] J. A. Pacheco-Romero, "From the Editor on Women's Health: Potential detrimental health effects during pregnancy and menopause," Revista Peruana de GinecologÃa y Obstetricia, **66**, 5 – 11, 2020, doi:http://dx.doi.org/10.31403/rpgo.v66i2225.

[10] P. Micheli, S. J. S. Wilner, S. H. Bhatti, M. Mura, M. B. Beverland, "Doing Design Thinking: Conceptual Review, Synthesis, and Research Agenda," Journal of Product Innovation Management, **36**(2), 124–148, 2019, doi: 10.1111/jpim.12466.

[11] K. D. Elsbach, I. Stigliani, "Design Thinking and Organizational Culture: A Review and Framework for Future Research," Journal of Management, **44**(6), 2274–2306, 2018, doi:10.1177/0149206317744252.

[12] P. Rahayu, D. I. Sensuse, W. R. Fitriani, I. Nurrohmah, R. Mauliadi, H. N. Rochman, "Applying usability testing to improving Scrum methodology in develop assistant information system," in 2016 International Conference on Information Technology Systems and Innovation (ICITSI), 1–6, 2016, doi: 10.1109/ICITSI.2016.7858222.

[13] D. Henriksen, C. Richardson, R. Mehta, "Design thinking: A creative approach to educational problems of practice," Thinking Skills and Creativity, **26**, 140 – 153, 2017, doi:10.1016/j.tsc.2017.10.001.

[14] T. Schumacher, S. Mayer, "Preparing Managers for Turbulent Contexts: Teaching the Principles of Design Thinking," Journal of Management Education, **42**(4), 496–523, 2018, doi:10.1177/1052562917754235.

[15] N. Bolloju, S. Alter, A. Gupta, S. Gupta, S. Jain, "Improving scrum user stories and product backlog using work system snapshots," 2017.

[16] H. Zahraoui, M. A. Janati Idrissi, "Adjusting story points calculation in scrum effort time estimation," in 2015 10th International Conference on Intelligent Systems: Theories and Applications (SITA), 1–8, 2015, doi: 10.1109/SITA.2015.7358400.

[17] A. Delgado, "The progress of the environment in Peru: Design of a computer system for bottle recycling applied in shopping centers," International Journal of Emerging Trends in Engineering Research, **8**, 2724–2729, 2020, doi:10.30534/ijeter/2020/82862020.

[18] K. Patel, S. Borole, K. Ramaneti, A. Hejib, R. R. Singh, "Design and implementation of Sun Tracking Solar Panel and Smart Wiping Mechanism using Tinkercad," in IOP Conference Series: Materials Science and Engineering, volume 906, 012030, IOP Publishing, 2020, doi:10.1088/1757-899x/906/1/012030.

[19] A. Doğan, E. Kahraman, "Pre-Service Science Teachers Experience with 3d Digital Design Technology," in GLOBETSonline: International Conference on Education, Technology and Science, 163, 2020.

[20] X. Liu11, Y.-H. Sohn, D.-W. Park, "Application Development with Augmented Reality Technique using Unity 3D and Vuforia," International Journal of Applied Engineering Research, **13**(21), 15068–15071, 2018.

[21] A. Delgado, "Web System Design for Human Resources Management in an SME in the Textile Sector," International Journal of Emerging Trends in Engineering Research, **8**, 1471–1476, 2020, doi:10.30534/ijeter/2020/87842020.

[22] C. Mendoza-Santos, "Web application design for the control process of public schools," International Journal of Emerging Trends in Engineering Research, **8**, 1289–1294, 2020, doi:10.30534/ijeter/2020/57842020.

[23] C. Wrigley, K. Straker, "Design thinking pedagogy: The educational design ladder," Innovations in Education and Teaching International, **54**(4), 374–385, 2017, doi:10.1080/14703297.2015.1108214.

Optimal PMU Placement Using Genetic Algorithm for 330kV 52-Bus Nigerian Network

Ademola Abdulkareem, Divine Ogbe, Tobiloba Somefun[*], Felix Agbetuyi

Department of Electrical and Information Engineering, Covenant University, Ota, 112107, Nigeria

A R T I C L E I N F O	A B S T R A C T
	The phasor Measurement Unit is a modern tracking tool mounted on a network to track and manage power systems. PMU is accurate and time-synchronized device that gives voltage phasor measurements in nodes and current phasor measurements connected to those nodes where the PMU is installed. This study introduces the Genetic Algorithm for optimization of allocation of PMUs to enable maximum observation of the power network. The optimal PMU placement (OPP) problem is developed to minimize the quantity of PMU to be placed. The set and optimized model can efficiently position PMU in any network, considering the regular operation and zero injection (ZIN). Thus, the allocation algorithm implemented on IEEE 14-bus systems, the result was compared to that of existing works which achieved the same system of redundancy index. As a further study, the proposed approach is applied to the Nigerian 330kV new 52-bus systems, under operational arrangements for maximum observability of the network system. The technique formulated to handle normal operation and zero injection node succeeded in producing comparable results with other available techniques.

1. Introduction

Electric power system is a complex system with multiple sections, subsections and various components. Any analysis or model to set up a power system or upgrade the existing one must be very robust and adequate. Considering optimal location of distributed generator within distribution arm of electric power system [1, 2], reconfiguration of a section of power system [3-5], etc., all these required robust model and methodology to successfully obtain useful results.

In Nigeria, most of the power system network is overseen physically which is an issue. This physical management of the power network brought about constraints, in order to solve this challenge, the obvious path to take will be the incorporation of smart devices into the network to monitor, operate and control the power system which will increase interaction between the utility and the grid.

Phasor measurement unit is the leading device for monitoring power system network which is based on global positioning system technique. The phasor measurement unit measures different locations where it is installed which are time-synchronized to communicate the condition of the power system in real time to help

operators with more instant and accurate information. By placing phasor measurement units in several buses in a power network the system becomes more stable and reliable. However, Phasor measurement units are expensive so it is not economical to place a unit on every node in a power network [6]. Thus, an appropriate approach is essential to reduce the quantity of phasor measurement units while sustaining the power network to be observed completely.

Phasor measurement unit (PMU) has certain variations as follows from standard Supervisory Control and Data Acquisition (SCADA) measures. Synchro phasors provide phasor details while traditional state estimate (SE) utilizes voltage magnitude, branch current magnitudes, and active power and reactive power measurements for infusion, voltage phasor at neighbouring nodes without PMU can be directly calculated utilizing the phase angle information. PMU information gives 30-70 samples every second, while SCADA devices mainly give new data samples every 4-5 seconds. Therefore, dynamic observability is given of the effect of irregularities that spread through critical sections of the network [7, 8].

In [9, 10], the authors carried out a study to investigate an ideal method for placing PMUs in any power system network. They proposed a method known as inverse of connectivity which utilizes the information of connectivity and the inability to monitor any

[*]Corresponding Author: Tobiloba Somefun, km 10, Idiroko Road, Canaanland, Ota, Nigeria, +2348037632337, tobi.shomefun@covenantuniversity.edu.ng

node in the power system network. They chose the ideal bus to place the PMUs basically by selecting adjacent buses through weighing factors to observe a minimal connectivity buses; this procedure continues until the power system network is observable. In [11] the authors worked on calculated allocation of PMU to observe the power system taking consideration of redundancy measurement. In this research they tackled the ideal PMU allocation issue with binary valued factors actualized by a dual-stage branch and bound formulation, but their approach did not consider Zero injection node (ZIN). In stage one of the suggested formulations, GA is worked out by depth foremost search technique. When a first whole number solution is gotten, stage two includes breadth foremost search system to find the solution position. Beginning from a subjective introductory position, the executed formulation finds other solutions at the most minimal target capacity worth guaranteeing global optimality [12]. In this way, the reliance of the suggested two-stage branch and bound by the foremost position provides the ability to the end-user to distinguish ideal arrangements without the existence of spiral nodes in the power network [13,14].

In [15], the authors used topology-based method and genetic algorithm to solve the optimal PMU placement problem. In their approach they put into consideration zero-injection nodes in the network for finding solution to the optimal PMU placement problem. The outcome was compared to previously applied method. They achieved complete observability of the power system utilizing GA which solved the optimal PMU placement problem successfully [15]. Measurement redundancy was not considered in this research.

In [16], the authors analyse techniques used for observing the most topological network, while recursive tabu search which is obtained when numerical and tabu search method are combined was developed to attain maximum observability of a power system with full redundancy. This optimizing approach executed the solution better than the previous solution that was achieved by greedy algorithm. The process put into consideration different approaches as well as moving target search (MTS) to achieve the least quantity of PMUs to solve the optimization problem [17]. Though Placement of PMU in ZIN was not allowed in the initialization it was validated through simulation results that the recursive tabu search was more efficient that the MTS approach. Authors [18,19] gives more detailed comparisons of the recursive tabu search and other methods.

In [20-23], the authors presented the cost of installing different PMUs in a power network and the reliant factors such as branch neighbouring numbers at the node and the communicating situations. They utilized the particle swarm optimization tool to attain the best solution proving the optimization to be better than conventional techniques. The authors did not only determine the highest number of PMUs that can observe the system, they also determined the cost of installing the least quantity of different PMUs and chose the best with least cost [24].

This study serves as a pioneer study for placement of PMU in the new NG 52 bus, as there is no previous study before it. In this study, optimal placement of PMU considering normal operation and ZIN is proposed. The uniqueness in this algorithm used to place PMU on the 52 bus network is the combination of distinct

values of the chromosome, mutation function, mutation rate, selection function and crossover function.

This research paper is systematized in four sections. The "introduction" gives a brief description of PMU, also a review on existing works. The "Materials and Method" section shows the GA steps and the parameters used. Details of the inequality constraint and connectivity matrix for IEEE 14-bus and NG 52-bus was presented in PMU placement formulation. Measurement redundancy presents the BOI and SORI used to check the quality of each placement set. The "results and discussion" presented the outcome of the simulation. In "conclusion" the procedures and the outcomes are summarized.

2. Materials and Method

This section presents the placement formulation used in obtaining the minimum amount of PMU, the procedure of the Genetic algorithm, and the measurement redundancy.

2.1. PMU Placement Formulation

The purpose of the optimal PMU placement is to obtain the least quantity of PMUs needed and its position in the network in order to obtain complete observability of the network. The goal here is to minimize the utilization of PMUs and make the whole power system fully observable. The formulated objective function is therefore given as:

$$min \sum_{k=1}^{N} Z_k \tag{1}$$

subject to:

$$[A] \times [Z] \geq [b] \tag{2}$$

where N is a number of network nodes and $[A]$ is a binary connectivity matrix. Entries for matrix $[A]$ are defined by equation 3:

$$A_{i,j} = \begin{cases} 1 & if \ i = j \\ 1 & if \ nodes \ i \ and \ j \ are \ joined \\ 0 & if \ nodes \ i \ and \ j \ are \ not \ joined \end{cases} \tag{3}$$

Meanwhile $[Z]$ is defined as a binary decision variable vector given in equation 4 where $[z_1 \ z_2 \ z_3 \ ... \ z_N]^T$ and $z_i \in \{0, 1\}$:

$$z_i = \begin{cases} 1 & if \ PMU \ is \ installed \ on \ node \ i \\ 0 & if \ PMU \ is \ not \ installed \ on \ node \ i \end{cases} \tag{4}$$

[b] is a column vector where

$$[b] = [1 \ 1 \ 1 \ ... 1]_{N \times 1}^T \tag{5}$$

2.2. Genetic Algorithm Approach

For this research, genetic algorithm was selected as the optimization solver for optimal placement of PMUs on the Nigerian 330kV network. Genetic algorithm operates on a population made up of certain outcomes whereby the number of outcomes is known as population size. Every outcome is named

an individual. Every single outcome has in it a chromosome. The chromosome is defined as a collection of features that characterize the individual. Each separate chromosome has a collection of genetic factors. Each genetic factor is often interpreted as being a sequence of zeros and ones. Every individual has a fitness value, too. An objective function is employed to locate the fittest characters. The objective function outcome is the fitness value which signifies the outcome's performance. The greater the fitness value, the greater the outcome is in effectiveness.

In the breeding process the characters are known as parents. Any pair nominated parents within the breeding population will give dual offspring. Through breeding just fine-quality characters, a finer quality offspring is produced better than their parents. That will eliminate the bad individuals from producing more bad people. Through having fine-quality characters chosen and paired, there would be better chances of only having the good individuals and tossing bad individuals out. Eventually, the ideal or appropriate solution will end in the cycle. But the offspring already produced utilizing the chosen parents still have their parents' features, and no more without alterations. There is no difference added to it and therefore the latest offspring would still have the same disadvantages in its parents. Some improvements must be added to each offspring to produce new characters to solve these problems. The group of all freshly produced characters would be the recent population and will substitute the existing population that was formerly utilized. Each produced population is called a generation. The method of exchanging the existing population with the current one is known as replacement. Figure 1 gives a rundown of the genetic algorithm phases.

The genetic algorithm flow chart is outlined in Figure 1. Simulation results obtained on the premise that each PMU has the highest quantity of channels and the cost is the same for each PMU.

The Genetic algorithm procedure for the OPP problem is given below:

- Study the configuration arrangement of the power network
- Take variable/chromosome size equal to quantity of nodes
- Create the initial population
- For each selected variable, calculate the objective function
- Apply tournament selection function
- Apply single point crossover function
- Apply a uniform mutation function and a mutation rate of 0.01
- Go back to calculate the objective function if the number of generations are completed.

Two experimental cases are used to show the feasibility of the proposed approach in achieving the optimal PMU placement problem. All cases are described by using IEEE 14 and Nigeria 52 bus network model as demonstrated below and simulated utilizing MATLAB, respectively.

Case 1: not considering standard measurement for maximum network observability

In this scenario, measurements of the ZIN and the power flow are not taken into account. Furthermore, no PMU is pre-assigned to the radial node which is incident. The binary connectivity matrix A is generated from Figure 2 by use of equation 3 as follows:

Figure 1: Process flow of genetic algorithm
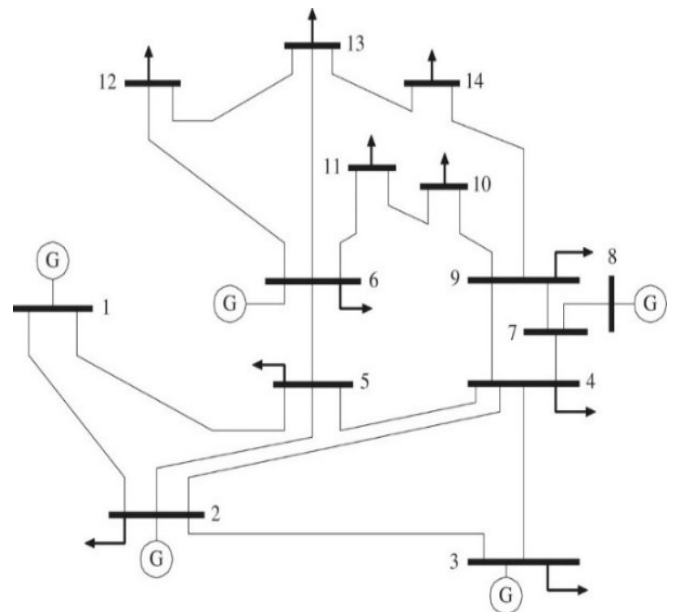
Figure 2: IEEE14 test bus system

Connectivity matrix [A] for IEEE-14 bus system =

$$\begin{bmatrix} 1 & 1 & 0 & 0 & 1 & 0 & 0 & 0 & 0 & 0 & 0 & 0 & 0 & 0 \\ 1 & 1 & 1 & 1 & 1 & 0 & 0 & 0 & 0 & 0 & 0 & 0 & 0 & 0 \\ 0 & 1 & 1 & 1 & 0 & 0 & 0 & 0 & 0 & 0 & 0 & 0 & 0 & 0 \\ 0 & 1 & 1 & 1 & 1 & 0 & 1 & 0 & 1 & 0 & 0 & 0 & 0 & 0 \\ 1 & 1 & 0 & 1 & 1 & 1 & 0 & 0 & 0 & 0 & 0 & 0 & 0 & 0 \\ 0 & 0 & 0 & 0 & 1 & 1 & 0 & 0 & 0 & 0 & 1 & 1 & 1 & 0 \\ 0 & 0 & 0 & 1 & 0 & 0 & 1 & 1 & 1 & 0 & 0 & 0 & 0 & 0 \\ 0 & 0 & 0 & 0 & 0 & 0 & 1 & 1 & 0 & 0 & 0 & 0 & 0 & 0 \\ 0 & 0 & 0 & 1 & 0 & 0 & 1 & 0 & 1 & 1 & 0 & 0 & 0 & 1 \\ 0 & 0 & 0 & 0 & 0 & 0 & 0 & 0 & 1 & 1 & 1 & 0 & 0 & 0 \\ 0 & 0 & 0 & 0 & 0 & 1 & 0 & 0 & 0 & 1 & 1 & 0 & 0 & 0 \\ 0 & 0 & 0 & 0 & 0 & 1 & 0 & 0 & 0 & 0 & 0 & 1 & 1 & 0 \\ 0 & 0 & 0 & 0 & 0 & 1 & 0 & 0 & 0 & 0 & 0 & 1 & 1 & 1 \\ 0 & 0 & 0 & 0 & 0 & 0 & 0 & 0 & 1 & 0 & 0 & 0 & 1 & 1 \end{bmatrix}$$

The final inequality constraints of matrix A are formulated as shown in the expression below with respect to each node:

$Node_1 = Z_1 + Z_2 + Z_5 \geq 1$

$Node_2 = Z_1 + Z_2 + Z_3 + Z_4 + Z_5 \geq 1$

$Node_3 = Z_2 + Z_3 + Z_4 \geq 1$

$Node_4 = Z_2 + Z_3 + Z_4 + Z_5 + Z_7 + Z_9 \geq 1$

$Node_5 = Z_1 + Z_2 + Z_4 + Z_5 + Z_6 \geq 1$

$Node_6 = Z_5 + Z_6 + Z_{11} + Z_{12} + Z_{13} \geq 1$

$Node_7 = Z_4 + Z_7 + Z_8 + Z_9 \geq 1$

$Node_8 = Z_7 + Z_8 + \geq 1$

$Node_9 = Z_4 + Z_7 + Z_9 + Z_{10} + Z_{14} \geq 1$

$Node_{10} = Z_9 + Z_{10} + Z_{11} \geq 1$

$Node_{11} = Z_6 + Z_{10} + Z_{11} \geq 1$

$Node_{12} = Z_6 + Z_{12} + Z_{13} \geq 1$

$Node_{13} = Z_6 + Z_{12} + Z_{13} + Z_{14} \geq 1$

$Node_{14} = Z_9 + Z_{13} + Z_{14} \geq 1$

Case 2: Consideration of ZIN for maximum network observability

According to Figure 2, node 7 is ZIN, node 8 is radial node. Since node 8 is a radial node, it is chosen to be integrated with the ZIN in accordance with Rule A as stated in the suggested approach section. This integration procedure indicates the node 7 constraint is eliminated from the equation and node 8 is now joined to node 4 and node 9. Following, because this procedure includes a radial bus, it is important to pre-assign a PMU to one of the nodes incidents to it.

However, because neither node 4 nor node 9 is a ZIN, there is no pre-placement of a PMU to enable more potential solutions. In the situation of node 4 being a ZIN a PMU would be pre-assigned

to node 9 in order to guarantee that node 8 is observed as shown in Figure 3.
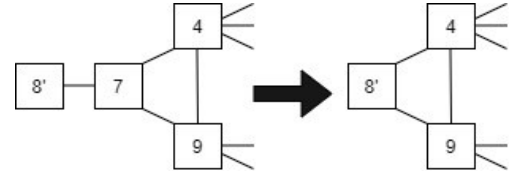
Figure 3: Illustration of ZIN integration

This change of topology implies that the node constraints for nodes 4,7,8, and 9 have been modified. Remember that the node 7 constraint is removed because it no doesn't occur after the change of topology. For the meantime, the node constraints 4,8, and 9 are revised to show the modification of topology that was made during the integration process. The modified constraints are given as follows:

$Node_4 = Z_2 + Z_3 + Z_4 + Z_5 + Z_8 + Z_9 \geq 1$

$Node_8 = Z_4 + Z_8 + Z_9 \geq 1$

$Node_9 = Z_4 + Z_8 + Z_9 + Z_{10} + Z_{14} \geq 1$

A minimum of three PMUs must be installed at node 2, 6, and 9 to guarantee maximum network observability from these newly created constraints.

Thus, the same model is applied to Nigeria 330kV new 52-bus system for total observability on the quantity of PMUs needed. Measurements of the ZIN and power flow are not considered in this case.

2.3. Measurement Redundancy

Because Genetic algorithm is a heuristic technique, there will be an amount of PMU placement group that includes exact quantity of the least PMUs necessary for total observability. To ensure to assessing the efficiency of each PMU allocation group, measurement redundancy method of bus observability index (BOI) and system of redundancy index (SORI) are used. The BOI is specified as the quantity of times the PMUs placement set observes a node, while the SORI refers to the BOI summation for all nodes. The PMU allocation group which holds the maximum quantity of SORI signifies that the PMU allocation group has a superior performance and more efficient solution for likely contingencies compared to the PMU allocation group which has a lower quantity of SORI. Hence, this principle will be utilized in this research to test and compare the PMU allocation sets generated in terms of measurement redundancy from the suggested technique and previous studies. The following definitions in equations 6 and 7 refer to the BOI and SORI:

$$BOI_i = A \times Z_i \tag{6}$$

$$SORI = \sum_{i=1}^{N} BOI_i \tag{7}$$

3. **Results and Discussion**

This section sets out the outcomes gotten from MATLAB software simulations. The proposed technique is implemented on

IEEE 14-bus, and the Nigeria 330KV network for the purpose of verifying the operation of the suggested approach to solve the optimal PMU placement problem. The purpose of the suggested approach is to achieve the least quantity of PMUs which maintain total observability while maximizing the redundancy of measurements. Because genetic algorithm is meta-heuristic, it is anticipated to have various allocations of PMUs and to distinguish the efficiency of each PMU allocation set having the exact quantity of PMUs, the set with the most SORI will be chosen as the ideal outcome. The PMUs allocation set with the most measurement redundancy, as stated above, indicates that it is superior to the PMU allocation sets with lower measurement redundancy. Furthermore, in order to assess the efficiency of the suggested approach in finding solution to the optimal PMU placement problem, the SORI outcome for the PMU allocation set acquired from the suggested approach is compared with previous research. The suggested approach is implemented to find solution to the problem by taking consideration of two cases namely normal operation, and zero injection cases for IEEE 14 bus system and NG 52 bus system.

Case 1: Normal Operation

IEEE 14-Bus

Table 1 shows the result obtained for the IEEE-14 bus system, with respect to number of required PMU, the position of the PMU and other indices that were used in the model.

Table 1: PMU Locations for IEEE 14 Bus- Normal Operation

Network	IEEE 14-bus
Number of PMU	4
PMU Positions	2, 6, 7, 9
SORI	19
Npmu/NBus	0.286

Figure 4: IEEE 14-bus graph considering normal operation

As can be observed, Figure 4 shows the iteration against the number of PMUs. It can be observed that at zero iteration the number of PMUs is over 14 and as the iteration increases the

number of PMU decreases until it gets to 52 iterations where the constraint converges.

NG 52-Bus

The values of the parameters used in obtaining the number of PMUs required for NG 52-bus including their locations are given in Table 2.

Table 2: PMU Locations for NG 52-Bus Normal Operation

Network	NG 52-bus
Number of PMU	17
PMU Positions	3, 4, 6, 8, 10, 16, 19, 24, 26, 27, 32, 35, 39, 41, 42, 46, 51
SORI	71
Npmu/NBus	0.32692

Figure 5: Diversity graph for NG 52-bus considering normal operation

The Figure 5 shows the iteration against the number of PMUs. It can be observed that at zero iteration the number of PMUs is over 52 and as the iteration increases the number of PMU decreases until it gets to 102 iterations where the constraint converges.

Table 3: BOI and SORI for Normal Condition

	IEEE14	NG 52
Number of PMU	4	17
PMU Location	2, 6, 7, 9	3, 4, 6, 8, 10, 16, 19, 24, 26, 27, 32, 35, 39, 41, 42, 46, 51
BOI	1, 1, 1, 3, 2, 1, 2, 3, 1, 1, 1, 1, 1, 1	2, 2, 3, 1, 1, 1, 1, 1, 2, 1, 4, 1, 2, 1, 1, 1, 1, 3, 1, 1, 2, 1, 1, 2, 2, 1, 1, 1, 1, 1, 1, 1, 1, 1, 1, 1, 1, 1, 2, 1, 1, 1, 1, 1, 1, 1, 1, 1, 1, 3, 3
SORI	19	71

Case 2: Zero Injection Node (ZIN) for IEEE 14-Bus

Table 4 shows the quantity of PMUs needed for the IEEE 14-bus system that can accomplish total observability, which is less than 25% of the number of nodes in the system that needs to be observed as shown in Figure 6. The BOI result is shown in Table 5.

Table 4: PMU Locations for IEEE14-Bus Considering ZIN

Network	IEEE 14-bus
Number of PMU	3
PMU positions	2, 6, 9
SORI	16
Npmu/NBus	0.2308

Figure 6: Diversity graph for IEEE 14-bus considering ZIN

Figure 6 shows the iteration against the number of PMUs. It can be observed that at zero iteration the number of PMUs is over 13 and as the iteration increases the number of PMU decreases until it gets to 52 iterations where the constraint converges.

Table 5: BOI and SORI Considering ZIN

	IEEE14
Number of PMU	3
PMU location	2, 6, 9
BOI	1, 1, 1, 2, 2, 1, 1, 1, 1, 1, 1, 1, 1
SORI	16

The outcomes of the simulation of the proposed method validate the results from previous studies as shown in Tables 6 and 7. The methodology designed can optimally position the PMU in strategic nodes and show substantial improvements in comparison with existing works.

Table 6: Comparison with previous study considering normal operation

Methods	IEEE14
Proposed method	NPMU: 4 SORI: 19
Binary particle swarm optimization	NPMU: 4 SORI: 19
Integer Linear Programming	NPMU: 4 SORI: 19
Differential Evolution	NPMU: 4 SORI: 19
Evolutionary Search	NPMU: 4 SORI: 19
Binary Search Algorithm	NPMU: 4

	SORI: 19

Table 7: Comparison with Previous Study Considering ZIN

Methods	IEEE14
Proposed method	NPMU: 3 SORI: 16
Binary particle swarm optimization	NPMU: 3 SORI: 16
Integer linear programming	NPMU: 3 SORI: 16
Evolutionary Search	NPMU: 3 SORI: 16
Binary Search Algorithm	NPMU: 3 SORI: 16

Having established the authenticity of the proposed method, the authors therefore deployed the proposed method to ascertain the number of PMU required on NG 52 bus system (appendix) as well as optimal location of the PMUs installation. The results for the NG 52-bus shows that PMU is required to be placed at 17 nodes for maximum observability. These nodes are, 3-Ikot-Ekpene, 4-Port-Hacourt, 6-Ikeja-West, 8-Aja, 10-Ajaokuta, 16-Aladja, 19-Aliade, 24-Kanji, 26-Onitsha, 27-Benin North, 32-Damaturu, 35-Egbema, 39-Ganmo, 41-Yola, 42-Gwagwalada, 46-Kaduna, 51-Jebba.

4. Conclusion

This study explores the capability genetic algorithm to optimally site PMU for electric power system network. From the outcome of this algorithm, it can be concluded that the utilization of optimization technique in the Nigerian power system network for complete observability in the most economical way will precisely position PMU in strategic nodes. This greatly improves the efficiency of the outputs and increase the grid monitoring rate. There are endless prospects for installing PMU in the national grid, as it can also be used to control the entire power system. The technique formed to handle ZIN succeeded in producing comparable results with other available techniques. For IEEE 14 and NG 54 bus reached the convergence of their constraint at 52 and 102 iterations respectively. The suggested approach also shows that to find ideal PMU location, it can be combined with the power flow calculation.

Conflicts of Interest

The authors declare that there is no conflict of interest.

References

[1] T. Somefun, C. Awosope, A. Abdulkareem, and A. Alayande, "Deployment of Power Network Structural Topology to Optimally Position distributed Generator within Distribution System," Journal of Engineering Science and Technology Review, **13**, 12-17, 2020. DOI: 10.25103/jestr.131.02

[2] T. E. Somefun, "Critical Review of Different Methods for Siting and Sizing Distributed Generators," TELKOMNIKA (Telecommunication Computing Electronics and Control), **16**, 2018. DOI: 10.12928/telkomnika.v16i5.9693

[3] A. Y. Abdelaziz, R. A. Osama, S. M. Elkhodary, and E. F. El-Saadany, "Reconfiguration of distribution systems with distributed generators using Ant Colony Optimization and Harmony Search algorithms," in 2012 IEEE Power and Energy Society General Meeting, **2012**, 1-8. DOI: 10.1109/PESGM.2012.6345125

[4] M. E. Baran and F. F. Wu, "Network reconfiguration in distribution systems for loss reduction and load balancing," IEEE Transactions on Power delivery, **4**, 1401-1407, 1989. DOI: 10.1109/61.25627

[5] R. J. C. Gallano and A. C. Nerves, "Multi-objective optimization of distribution network reconfiguration with capacitor and distributed generator placement," in TENCON 2014 - 2014 IEEE Region 10 Conference, 2014, 1-6. DOI: 10.1109/TENCON.2014.7022365

[6] M. M. Amin, H. B. Moussa, and O. A. Mohammed, "Wide area measurement system for smart grid applications involving hybrid energy sources," Energy Systems, **3**, 3-21, 2012. doi.org/10.1007/s12667-011-0047-4.

[7] M. Laouamer, R. Mohammedi, A. Kouzou, and A. Tlemçani, "Optimal Placement of PMUs in Algerian Network Using Genetic Algorithm," in 2018 15th International Multi-Conference on Systems, Signals & Devices (SSD), **2018**, 947-951. DOI: 10.1109/SSD.2018.8570652

[8] M. Mehdinejad, B. Mohammadi-Ivatloo, R. Dadashzadeh-Bonab, and K. Zare, "Solution of optimal reactive power dispatch of power systems using hybrid particle swarm optimization and imperialist competitive algorithms," International Journal of Electrical Power & Energy Systems, **83**, 104-116, 2016. doi.org/10.1016/j.ijepes.2016.03.039

[9] S. Akhlaghi, "Optimal PMU placement considering contingency-constraints for power system observability and measurement redundancy," in 2016 IEEE Power and Energy Conference at Illinois (PECI), **2016**, 1-7. DOI: 10.1109/PECI.2016.7459251

[10] R. Sodhi, S. Srivastava, and S. Singh, "Optimal PMU placement method for complete topological and numerical observability of power system," Electric Power Systems Research, **80**, 1154-1159, 2010. DOI: 10.1016/j.epsr.2010.03.005

[11] G. C. Sushma and T. Jyothsna, "A Genetic Algorithm Approach Considering Zero Injection Bus Constraint Modeling for Optimal Phasor Measurement Unit Placement," International Journal of Energy and Power Engineering, **12**, 800-806, 2018. doi.org/10.5281/zenodo.2021557

[12] R. Babu and B. Bhattacharyya, "Strategic placements of PMUs for power network observability considering redundancy measurement," Measurement, **134**, 606-623, 2019. doi.org/10.1016/j.measurement.2018.11.001

[13] A. Y. Amira and G. Fathi, "Optimal PMU placement for full network observability case of the tunisian network," in Eighth International Multi-Conference on Systems, Signals & Devices, **2011**, 1-5. DOI: 10.1109/SSD.2011.5986789

[14] S. S. Noureen, V. Roy, and S. B. Bayne, "Phasor measurement unit integration: A review on optimal PMU placement methods in power system," in 2017 IEEE Region 10 Humanitarian Technology Conference (R10-HTC), **2017**, 328-332. DOI: 10.1109/R10-HTC.2017.8288967

[15] P. P. Bedekar, S. R. Bhide, and V. S. Kale, "Optimum PMU placement considering one line/one PMU outage and maximum redundancy using Genetic algorithm," in The 8th Electrical Engineering/Electronics, Computer, Telecommunications and Information Technology (ECTI) Association of Thailand-Conference 2011, **2011**, 688-691. DOI: 10.1109/ECTICON.2011.5947933

[16] N. C. Koutsoukis, N. M. Manousakis, P. S. Georgilakis, and G. N. Korres, "Numerical observability method for optimal phasor measurement units placement using recursive Tabu search method," IET Generation, Transmission & Distribution, **7**, 347-356, 2013. DOI: 10.1049/iet-gtd.2012.0377

[17] L. Tang and J. Wu, "A new method of optimal PMU configuration considering vulnerability of power system and economy," Power System Technology, **36**, 260-264, 2012.

[18] N. H. Rahman and A. F. Zobaa, "Optimal PMU placement using topology transformation method in power systems," Journal of advanced research, **7**, 625-634, 2016. doi.org/10.1016/j.jare.2016.06.003

[19] R. Ramachandran and S. Karthick, "Optimal PMU Placement for Tamil Nadu Grid Under Controlled Islanding Environment," Procedia Technology, **21**, 240-247, 2015. doi.org/10.1016/j.protcy.2015.10.021

[20] N. Xia, H. B. Gooi, S. Chen, and M. Wang, "Redundancy based PMU placement in state estimation," Sustainable Energy, Grids and Networks, **2**, 23-31, 2015. doi.org/10.1016/j.segan.2015.03.002

[21] P. Gopakumar, M. J. B. Reddy, and D. K. Mohanta, "Novel multi-stage simulated annealing for optimal placement of PMUs in conjunction with conventional measurements," in 2013 12th International Conference on Environment and Electrical Engineering, **2013**, 248-252. DOI: 10.1109/EEEIC.2013.6549625

[22] A. Y. Abdelaziz, A. M. Ibrahim, and R. H. Salem, "Optimal PMU Placement for Complete Observability Using Heuristic Methods." Conference: the Fifteenth International Middle East Power Systems Conference, MEPCON'2012At: Alexandria, Egypt, 8-22

[23] R. H. Shewale, B. K. Kethineni, U. P. Balaraju, S. Bhil, and P. D. More, "Optimal placement of phasor measurement unit for power system observability by heuristic search method," International Journal of Advanced Technology and Engineering Research, **2**, 128-133, 2012. DOI: 10.1109/CIASG.2011.5953335

[24] M. Shafiullah, M. I. Hossain, M. Abido, T. Abdel-Fattah, and A. Mantawy, "A modified optimal PMU placement problem formulation considering channel limits under various contingencies," Measurement, **135**, 875-885, 2019. doi.org/10.1016/j.measurement.2018.12.039

APPENDIX
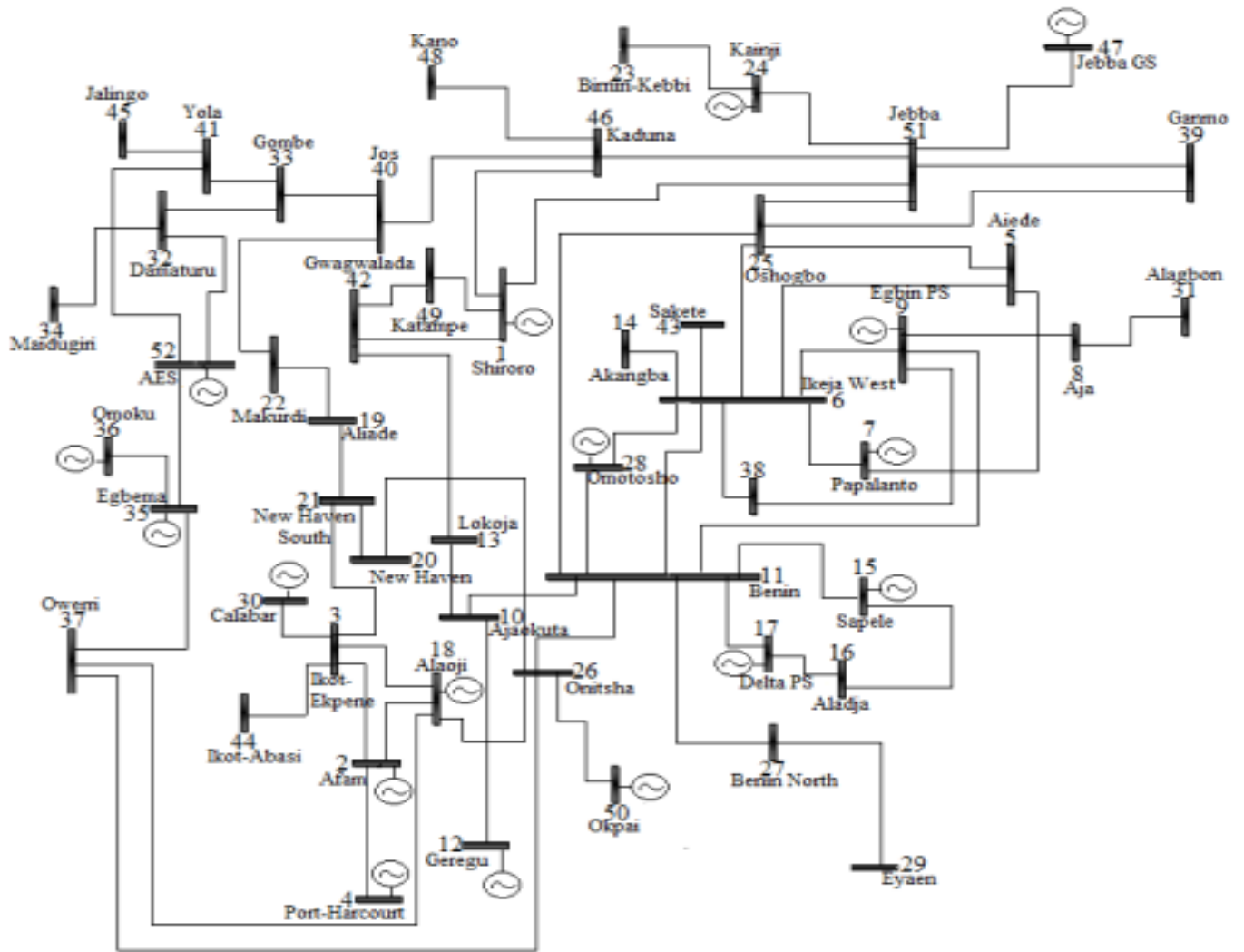
Decision Support Model using FIM Sugeno for Assessing the Academic Performance

Deddy Kurniawan*, Ditdit Nugeraha Utama

Computer Science Department, BINUS Graduate Program – Master of Computer Science, Bina Nusantara University, Jakarta, Indonesia 11480

A R T I C L E   I N F O

A B S T R A C T

Assessing academic performance is a common way of evaluating and assessing the abilities of students in tertiary institutions. Usually it is practically performed based on the cumulative grade point average (GPA) at the end of each semester passed. Unwittingly there are many factors that are able to influence student performance results apart from GPA as a performance measure; i.e. gender, hometown, sibling, family status, residence, father education, mother education, family income, motivation, mileage, traveled time, transportation, scholarship, community, social media, and hang-out. Academic performance assessment is proposed through the decision support model (DSM) applying the fuzzy logic (FL) Sugeno technique. The model output generates a decision value (linear or constant equation) for academic performance based on the calculation of the measured fuzzy parameter value (ax) and conventional parameter value (bx). The DSM with the FL Sugeno method is able to provide sharp output in assessing student academic performance. In this case, the model is able to be applied then to assist academics in higher education in determining educational strategies for students with poor academic performance results.

1. Introduction

The academic performance is one indicator of the education quality in universities. It generally is able to be measured with the value achievements record of the grade point average (GPA) [1]-[3]. The GPA is greatly influenced by various factors. Those factors are such as the social, family, economic and educational environment of each individual [1], [4], [5].

The assessment process is a part of the evaluation process toward student academic performance which is done by higher education academics. Academic performance appraisal is one of the effective solutions to detect student failure problems. Analyzing stored student data can help provide important information in their academic performance appraisal process.

The new models to support objectives in the academic performance assessment process are still being investigated and researched scientifically. One of them is a study related to decision support models (DSM). The research has been carried out by a number of researchers with DSM as the main issue. Creating DSM to solve difficulties related to mosque rebuilding. Fuzzy method

was operated to determine the priority value of eleven parameters [6]. Also, eco-DSM for treating medical waste was constructed by involving the fuzzy method as the main part of the model [7]. Then, the model for determining the amount of production, especially in the business world, functioned the fuzzy Sugeno technique [8].

In addition, [9] created DSM to measure the performance of logistical companies based on various indicators performance. In [10], the author created a model to calculate the exact number of goods ordered, this affects the level of inventory and the sales of goods. The determination of the venue for the national multi-sport event or called the national sport week (NSW). The determination of the best location was carried out in Indonesia with thirty-four provinces that had various distinctive features and cultural uniqueness [11].

This paper is DSM development in fulfilling research objectives for the assessment of student academic performance which is implemented in the education area (universities), exclusively operated in a calculation using the fuzzy logic method as well as using the data asset for 100 students at the faculty of Teacher Training and Education (FKIP) at the University of Mulawarman, East Kalimantan. Fuzzy logic (FL) has been widely used in various fields in the real world. FL is technically the principal method used in calculating mathematics as well as it is

*Corresponding Author: Deddy Kurniawan, Computer Science Department, BINUS Graduate Program - Master of Computer Science, Bina Nusantara University, Jakarta, Indonesia 11480, +6285391192622, deddy.kurniawan@binus.ac.id

used to assess uncertainty in various fields. FL plays an important role in changing the complex symptoms of problems and cannot easily be translated into mathematical models, with the aim of providing a best solution approach to problems [12]. The assessment result can provide early warning to academics to be able to pay attention in taking quick steps to improve student academic performance in bad conditions.

2. Related Works

The concept of fuzzy logic is a popular method used in decision-making support. In [13], the author was applying the fuzzy method in engineering asset management (EAM), checking the condition of assets is an important aspect of EAM because it is able to identify symptoms of potential failure and suggest corrective actions before operational disruptions. In [14], the author was creating a conceptual model for evaluating the performance of social sustainability and has been tested for later implementation in India in automotive component manufacturing organizations.

In addition, from year to year, various researchers conduct research on the issue of academic performance (AP) appraisal as the main topic in their research [15]-[17]. In [15], the author chose to take AP as the main topic of their research. They observed twenty student data based on three characteristics in the one academic period involving, exam 1, exam 2 (theoretical), and exam3 (practical). The results of the study were compared with traditional evaluation methods and gave similar results. They concluded that the evaluation results with the proposed approach could be a practical method in evaluating AP.

In [16], the author introduced the new fuzzy expert system (NFES) to be used in evaluating student AP based on the concept of FL by considering two parameters, semester 1 and semester 2 scores. In order to make decisions about learning in the next period. In [17], the author applied the fuzzy method in the evaluation of AP control of twenty students in the engineering laboratory at the faculty of Engineering Education Marmara University, department of Electricity Education. The semester 1 and semester 2 grades are used as the input that counts. In [17], the author concluding that there are variations in the evaluation results from the results of comparisons made to classical evaluation methods. The fuzzy method provided the advantage of flexibility in AP evaluation and provides many evaluation options.

3. Prepare Your Paper before Styling

As mentioned in the introduction part, the purpose of the assessment is part of a big task in the process of evaluating academic performance. Figure 1 describes the step by step of the whole study.
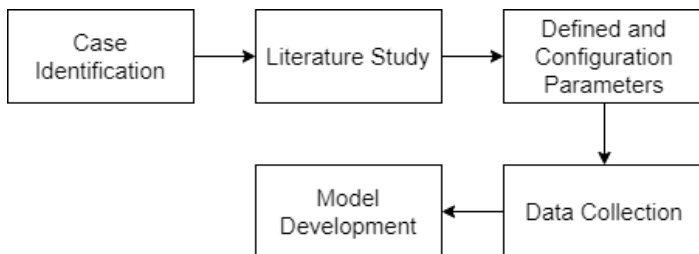
Figure 1: Research Stages

The first step we take is to study real case (in the case is academic performance measurement) supported by reviewing several scientific manuscripts. Two these stages operated to enrich our knowledge of case we face. Furthermore, we define the parameters related to the assessment of academic performance based on the study results of the related research literature involving 17 validated ones (Table 1) and are taken into account in influencing the AP assessment. Then the parameters will be configured which include; parameter grouping and parameter weighting. The preparation process for the parameters is successfully carried out, then data collection is carried out for further preparation as a dataset for this study.

Then, the construction of the model is carried out. The model is built with FL method to be operated as the main method, in addition to conventional methods used. The concept of FL (fuzzy – inference – de fuzzy) begins with building membership functions (MF) and linguistic variables (LV) as calculation scales. The LV definition of the fuzzy parameter is used to describe the input value in the form of the condition level of each academically calculated fuzzy parameter. It is then designed via MF fuzzy triangle-trapezium on each fuzzy parameter. Further preparing the vague ground rules as reference engine rules in determining the results of considerations so that we found 3,456 basic rules. The final stage of FL is de fuzzy, the result of FL decision is determined using the centroid method of sugeno technique.

Table 1: Parameters and their Value

Variable	Parameters	Parameter Value
P1	Gender	Male (M), Female (F)
P2	Hometown	Town (T), Out of town (OT)
P3	Sibling	1, 2, 3, 4, 5
P4	Family Status	Living together (L), Divorce (D), Died (DE)
P5	Residence	With parents (P), Hostel/Rental (H)
P6	Father Education	Not Education (0), Primary School (1), Junior High School (2), Senior High School (3), Undergraduate (4), Graduate (5), Postgraduate (6)
P7	Mother Education	Not Education (0), Primary School (1), Junior High School (2), Senior High School (3), Undergraduate (4), Graduate (5), Postgraduate (6)
P8	Family Income	0-5000000 (in Million rupiah)
P9	Motivation	Dream (D), Association (A)
P10	Mileage	1-20 (in KM)
P11	Traveled Time	1-60 (in Minute)
P12	Transportation	Private (PR), Public (PB)
P13	Scholarship	No (N), Yes (Y)
P14	Community	No (N), Yes (Y)
P15	Social Media	1, 2, 3 ,4, 5, 6, 7, 8, 9, 100 (in Hours/day)
P16	Hangout	1, 2, 3 ,4, 5, 6, 7, 8, 9, 100 (in Hours/day)
P17	Grade Point Average (GPA)	0.00-2.50 (Poor), 2.51-2.99 (Good), 3.00-3.59 (Very Good) and 3.60-4.00 (Excellent)

3.1. Data Collection

Collecting data as a research dataset using a combination of data collected through two methods; 1) online questionnaire is applied in collecting actual information from student personal data, 2) list of GPA scores from the academic database for the five initial periods of learning downloaded from the academic database for 100 data from FKIP to be studied.

The collected data is prepared for research. The dataset is combined and prepared by eliminating defective data samples and by manually adding missing pieces of data to the data sample.

3.2. Grouped Parameters

Seventeen parameters configured to prepare the entire parameter can be used on the model. Parameter configuration is done through two stages, grouping and weighting parameters. The first configuration is done by grouping parameters based on the calculation operation to be used in each parameter group. The grouping was successfully formed into fuzzy groups (ax) and conventional groups (bx). Parameter grouping shapes described in Table 2.

Table 2: Parameter Grouping Based on Calculation Method

Grouped Parameters	Parameters
Fuzzy (ax)	Sibling (P3), Father Education (P6), Mother Education (P7), Family Income (P8), Mileage (P10), Traveled Time (P11), Social Media (P15), Henge Out (P16), Grade Point Average (GPA) (P17).
Conventional (bx)	Gender (P1), Hometown (P2), Family Status (P4), Residence (P5), Motivation (P9), Transportation (P12), Scholarship (P13), Community (P14).

Some researchers stated that there were several parameters in the bx section that only had a small effect on the achievement of AP. According to [18], there is no significant result for the effect given by the gender parameter on student AP results. From the results of the study in [19], the author stated that three other parameters also had a small effect on the PA results including; number of siblings, mileage from faculty and gender. At bx each attribute of the parameter contains a nominal value, where in the conventional group concept (stated as bx) the shape of the attribute effect of the parameter is stated in integer form (0 and 1) represented by conventional values (VC) and shown in Table 3.

Table 3: Conventional Group Value

Parameters	Parameter Value	VC
Gender	Male (M)	0
	Female (F)	0
Hometown	Town (T)	1
	Out of town (OT)	0
Family Status	Living together (L)	0
	Divorce (D)	1
	Died (DE)	1
Residence	With parents (P)	0
	Hostel/Rental (H)	1
Motivation	Dreams (D)	0
	Association (A)	1
Transportation	Private (PR)	0

	Public (PB)	1
Scholarship	Yes (Y)	1
	No (N)	0
Community	Yes (Y)	1
	No (N)	0

3.3. Weighted Parameters

The second configuration of the parameters is done by weighting the parameters. The weighting technique is carried out in two stages; 1) the initial stage is carried out by using the Rapid Miner tool to determine the weight level of each parameter in giving an effect on student academic performance based on the case data used in this study, 2) the next stage is to normalize the initial weighting results. The normalization process aims to avoid systematic technical effects in the form of sufficient data gaps between parameters to ensure that technical bias has minimal impact on the results [20]. The normalization process uses a formula as in equation (1).

$$Normalization = \frac{w_j}{\sum w_j} \qquad (1)$$

The results of normalized weights are shown in Table 4. Where is the fuzzy group (referred to as ax) and the conventional group (referred to as bx), and the weight value of the parameter (referred to as W). The total weight value for ax is represented by ($\sum W_{Fuzzy}$) and the total weight value for bx is represented by ($\sum W_{Conventional}$). The total weight value ax produces a greater total weight value than conventional parameter groups in influencing the final calculation results in the AP.

Table 4: Normalize the Parameter Weights

No	ax	W	No	bx	W
1	CGPA	0.32969	1	Scholarship	0.03398
2	Traveled Time	0.27696	2	Transportation	0.02487
3	Mileage	0.06018	3	Family Status	0.02296
4	Mother Education	0.05371	4	Motivation	0.01871
5	Father Education	0.04136	5	Gender	0.01552
6	Family Income	0.03585	6	Hometown	0.00177
7	Sibling	0.03308	7	Community	0.00081
8	Hang-Out	0.02721	8	Residence	0.00026
9	Social Media	0.02308			
	$\sum W_{Fuzzy}$	**0.88100**		$\sum W_{Conventional}$	**0.12000**

3.4. Fuzzy Logic Model

After getting the data collected, we create a fuzzy set by determining the LV of each fuzzy parameter (FP) shown in Table 5. Where FP is a fuzzy parameter of academic performance parameters, LV is a linguistic variable, and then MF domain are domain membership functions based on the LV of each FP. After the LV is determined successfully. It is then designed to create a MF.

The degree of membership is obtained by first making a graph of each selected FP. The parameters for the number of siblings,

father and mother education, social media, and traveling have 2 fuzzy sets, namely: low and high. The parameters of family income, mileage, and travel time have 3 LV, namely: low, medium and high. CGPA parameter has 4 LV, namely: poor, good, very good, and excellent. All MFs are determined in Figure 2 to Figure 10.

Table 5: Membership Function Value

FP	LV	Domain
Sibling	Low (L)	[0, 3]
	High (H)	[2, 5]
Father Education	Low (L)	[0, 4]
	High (H)	[3, 6]
Mother Education	Low (L)	[0, 4]
	High (H)	[3, 6]
Family Income	Low (L)	[0, 2000000]
	Medium (M)	[1500000, 3500000]
	High (H)	[3000000, 5000000]
Mileage	Low (L)	[0, 8]
	Medium (M)	[6, 14]
	High (H)	[12, 20]
Traveled Time	Low (L)	[0, 20]
	Medium (M)	[15, 45]
	High (H)	[30, 60]
Media Social	Low (L)	[0, 6]
	High (H)	[4, 10]
Henge Out	Low (L)	[0, 5]
	High (H)	[4, 10]
Grade Point Average (GPA)	Poor (P)	[0,00, 2,75]
	Good (G)	[2,50, 3,25]
	Very Good (VG)	[3,00, 3,75]
	Excellent (E)	[3,50, 4,00]
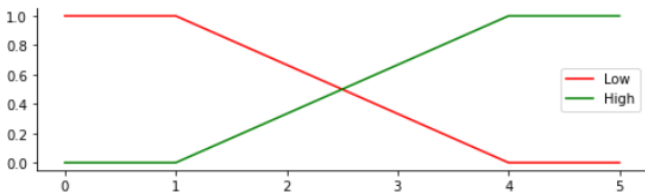
Figure 2: Membership Function for Parameter Sibling
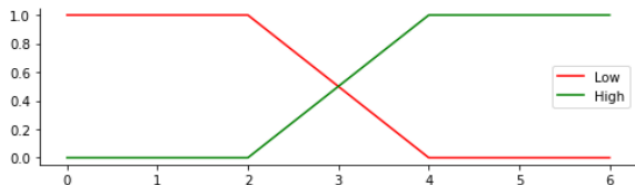
Figure 3: Membership Function for Parameter Father Education
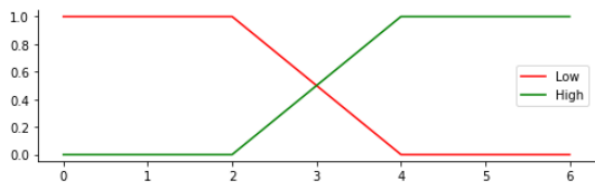
Figure 4: Membership Function for Parameter Mother Education
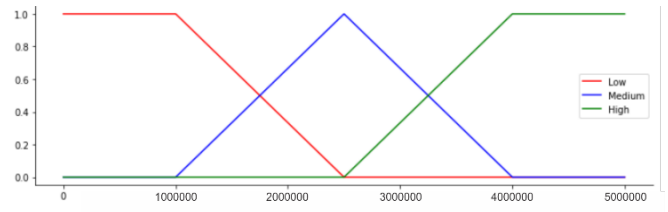
Figure 5: Membership Function for Parameter Family Income
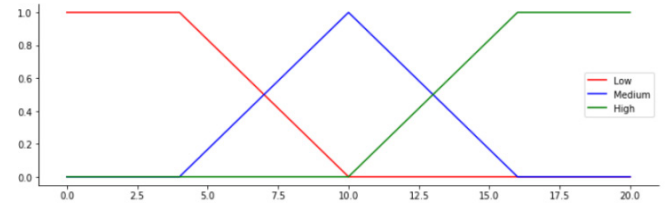
Figure 6: Membership Function for Parameter Mileage
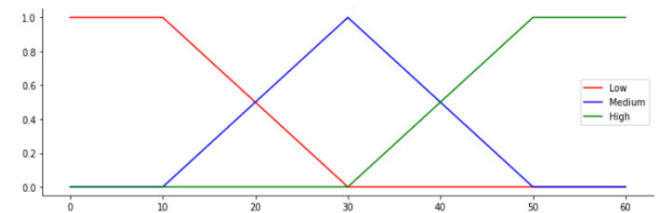
Figure 7: Membership Function for Parameter Traveled Time
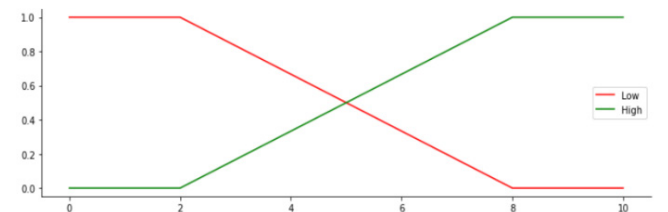
Figure 8: Membership Function for Parameter Social Media
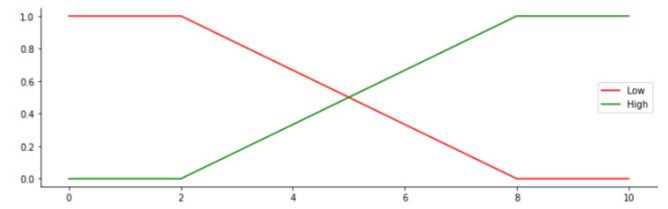
Figure 9: Membership Function for Parameter Henge Out
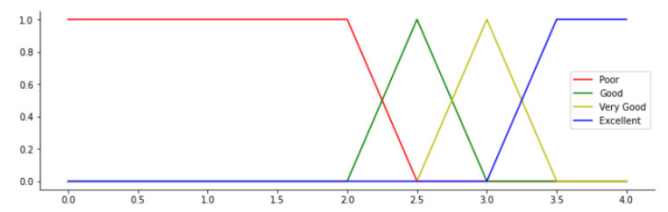
Figure 10: Membership Function for Parameter CGPA

Academically, fuzzy rules are defined to be characterized as fuzzy academic performance (FAP) values based on fuzzy input parameters. The number of fuzzy rules has as many as 3,456 rule bases. It is based on parameters and linguistics. Thus, that can be

validated based on the study of related research literature (shown in Table 6) is used to obtain the FAP value.

Table 6: Fuzzy Rules

Rule 1	IF P1(Low) AND P2(Low) AND P3(Low) AND P4(Low) AND P5(Low) AND P6(Low) AND P7(Low) AND P8(Low) AND P9(Poor) THEN Performance Bad
Rule 2	IF P1(Low) AND P2(Low) AND P3(Low) AND P4(Low) AND P5(Low) AND P6(Low) AND P7(Low) AND P8(Low) AND P9(Good) THEN Performance Bad
…	…
Rule 3455	IF P1(High) AND P2(High) AND P3(High) AND P4(High) AND P5(High) AND P6(High) AND P7(High) AND P8(High) AND P9(Very Good) THEN Performance Good
Rule 3456	IF P1(High) AND P2(High) AND P3(High) AND P4(High) AND P5(High) AND P6(High) AND P7(High) AND P8(High) AND P9(Excellent) THEN Performance Good

3.5. Calculation Academic Performance

In building the model, we apply two separate calculation operations with the Sugeno technique fuzzy method as the main counting operation on the model, specifically in producing the decision value for the final score of academic performance appraisal. The application of the FL Sugeno method provides a systematic approach to generate fuzzy rules from a given input to the output. To calculate the resulting output, Sugeno technique uses weighted average where the resulting output can be a separate characteristic with the final result not in the form of a fuzzy set but a linear or constant equation [21], [22].

From each of the total weight values of ax and bx that were found. Later it will be used to operate as a multiplier index for each calculation operation in the parameter group. The value of $(\sum W_{Fuzzy})$ is used as a multiplier index to multiply the total value of the FAP value calculation operation to produce the total value of the effect of ax on academic performance $((\sum(ax))$ which is mathematically written in equation 2.

$$\sum(ax) = FAP * \sum W_{Fuzzy} \qquad (2)$$

whereas the value $(\sum W_{Conventional})$ used as a multiplier index to multiply the total value of the simple CV addition calculation operation to produce the total effect value of bx on academic performance $(\sum(bx))$ which is mathematically written in equation 3.

$$\sum(bx) = VC * \sum W_{Conventional} \qquad (3)$$

The final calculation stage for the assessment of academic performance, equation (4) is used in calculating the results of the value of academic performance decisions, where each calculation result of the coefficients $(\sum(ax))$ and $(\sum(bx))$ is added up to obtain the final score for the assessment of academic performance. Where the final assessment results as a decision value (DV) in this model produce a decision value in the form of a firm value to assess the results of student academic performance.

$$DV = \sum(ax) + \sum(bx) \qquad (4)$$

4. Result and Discussion

4.1. Experiment Results

The DSM model built for academic performance appraisal using the FL method Sugeno technique which is a popular method in the DSM field. It is also quite elastic in dealing with complex problems in the real world in the form of linear or nonlinear systems. It works by mapping problems into the form of fuzzy reasoning to obtain a decision. The complete flow of activity in the model is depicted in Figure 11.
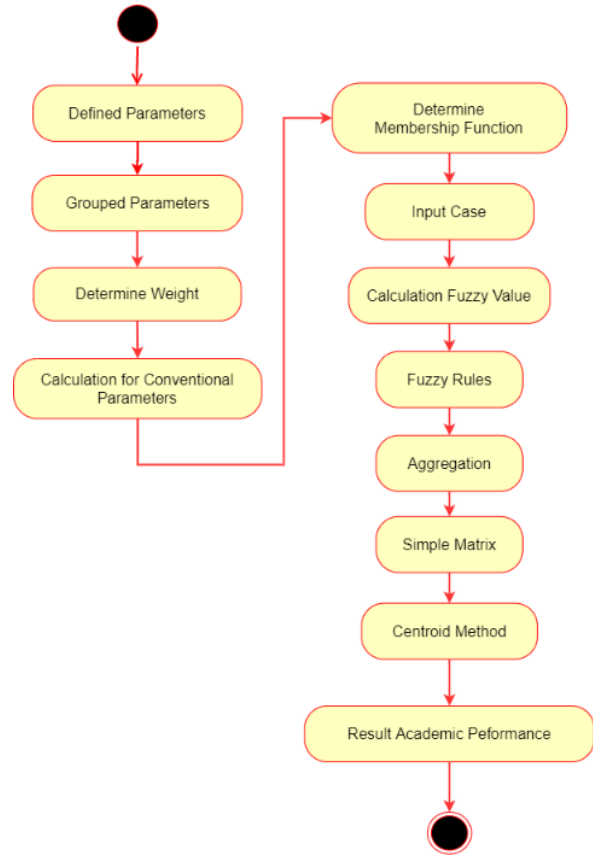
Figure 11: Model for Assessing Academic Performance

The initial activity begins by configuring all the parameters used as model input. The configuration at the initial stage is done by grouping the existing parameters into fuzzy groups (ax) and conventional groups (bx). Furthermore, the configuration for weighting is carried out to identify each weight value (W) of each parameter and the total weight value for axis represented by $(\sum W_{Fuzzy})$ and the total weight value for bx is represented by $(\sum W_{Conventional})$.

Furthermore, the counting operation for bx is carried out separately from the FL Sugeno method. The calculation is done by multiplying the number of CV against the $(\sum W_{Conventional})$ value to produce the total effect value of bx on academic performance $(\sum(bx))$.

The counting operation using the FL Sugeno method for ax is carried out in the next step. The main concept of the FL method includes the "fuzzy - inference - defuzzy" stage which is carried out sequentially based on the fuzzy rules created. The rules then

produce a FAP value based on fuzzy input parameters. At the end of the Sugeno FL method, the FAP value is used to multiply the ($\sum W_{Fuzzy}$) value to produce the total effect of on academic performance ($\sum(ax)$).

The final process of assessing academic performance is carried out by adding up the respective values of ($\sum(ax)$) and ($\sum(bx)$) that were successfully obtained in the previous stage. The final result of the academic performance appraisal is formed as a DV which is in the form of a linear or constant equation. DV based on the determination of the index value for the performance criteria is determined. Where the good performance criteria have an index value of 80 while the bad performance criteria have an index value of 50. The sample results from our calculations are shown in Figure 12.
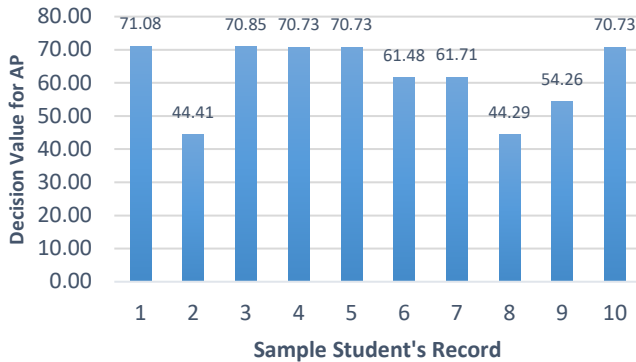
Figure 12: Result Assessing for Academic Performance

The bar graph in Figure 11, represents the 10 data cases used. The visualization on the bar graph in Figure 11 shows that our 5 test data resulted in good academic performance scores with the highest score at 71.08, 2 data are poor academic performance scores with the lowest score at 44.29, with an average of 62.03 results for the assessment of academic performance that we have done.

4.2. Discussion

The measurement of AP results in the classical method is usually expressed in numerical form (GPA) obtained at the end of the learning period [15]. Therefore, it can be said that the classical method is a form of presentation based on the comparison of student performance results with the predetermined standard performance value category.

The academic performance assessment of FKIP students at Mulawarman University focuses more on the indication of the achievement of GPA. Policymakers tend to focus more on the GPA score. That makes various policies focused on increasing the GPA over a period of time.

One shortcoming is found for the classical method used in the current AP assessment. Where it only focuses on increasing the GPA score in a certain period without any criteria instead of using the GPA indicator for the final result [16]. While the GPA indicator is an assessment of university accreditation as well. However, the supporting factors of achieving GPA scores are not used such as; gender, hometown, sibling, family status, residence, father education, mother education, family income, motivation, mileage,

traveled time, transportation, scholarship, community, social media, and hang-out. The results of the model assessment of AP from the GPA of the results of the conventional method are compared and displayed in Table 7. It is proven academically, that PA produced by the constructed DSM does not has similar rank (priority) to PA measured based on GPA.

Table 7: Comparison of Assessing Performance

No	Performance (Fuzzy Logic Sugeno Method)	Performance (Classical Method)
1	71.08	3.56
2	70.85	3.15
3	70.73	2.98
4	70.73	3.46
5	70.73	3.56
6	61.71	2.96
7	61.48	2.97
8	54.26	2.89
9	44.41	2.41
10	44.29	2.46

Table 7 shows that the results of the academic performance assessment using the model we built can be a solution. That can be used practically. As well as it can give freedom to academics as policymakers to be able to assist in the process of academic performance evaluation by providing the results of an effective approach. The final results of the assessment are carried out using various parameters outside of the educational factors for the family, economic, social, and environmental factors that we calculated on the model.

We identify the influence great value of each parameter from the fuzzy group (ax) and the conventional group (bx) on our AP assessment (Figure 12). The symbolized parameters refer to Table 1. The Traveled Time (P11) parameter has a significant effect by being the second largest influencer (0.27696) on ax after the CGPA parameter (P17) which has an effect of (0.32969), which simultaneously is the main indicator in making an assessment AP, while the social media parameter (P15) is the smallest one (0.2308).

In (bx), each parameter does not seem to have much influence on the AP assessment, with the Scholarship parameter (P13) as the biggest influencer (0.03398) and the Residence parameter (P5) giving an effect of (0.00026). Figure 12 shows that the AP assessment process is heavily influenced by various parameters on ax with the influence great value of ax is (0.88100) and the parameter on (bx) has little effect (0.12000) on the AP assessment.

Besides the various parameters that we use, which are parameters related to academic performance from various factors such as social, family, economic, and educational environments. Many studies have been carried out related to academic performance by proposing to use parameters derived from educational factors themselves.

According to research that has been done [16], [17], and [18], the assessment of academic performance is influenced by factors originating from the educational side which includes, record of student semester scores. [8] stated that the use of the parameter of semester scores is relevant in conducting performance appraisals. Where the semester scores in learning period 1 60% affect

performance results while 40% of semester scores in periods 2 affect academic performance results.
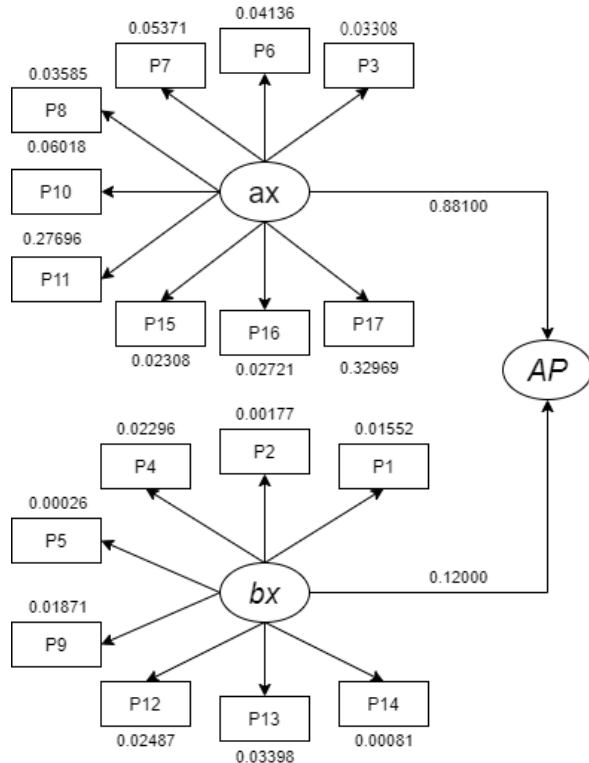
Figure 13: Similarity Structure of Assessing Academic Performance

5. Conclusion

The process of assessing the results of student academic performance is generally applied to universities using the classical method (based on performance categories). The DSM model is built using the FL method Sugeno technique which is a form of practical solution that can be used in the world of education to assess academic performance which is part of the AP evaluation process.

As the model using the FL Sugeno method provides advantages with the elastic properties. Thus, it can be adjusted to the needs of the study while still providing sharp outputs as an effective form of decision approach based on a series of fuzzy rules from the input given to the output.

The academic performance appraisal process is carried out by involving relevant seventeen parameters to the performance appraisal based on validated previous research. Parameters are grouped into fuzzy groups (ax) and conventional groups (bx). The fuzzy group (ax) is identified to have a significant effect on the assessment of academic performance compared to the conventional group (bx) with only a slight influence on the assessment process.

References

[1] A. Mueen, B. Zafar, U. Manzoor, "Modeling and Predicting Students' Academic Performance Using Data Mining Techniques," International Journal of Modern Education and Computer Science, **8**(11), 36–42, 2016, doi:10.5815/ijmecs.2016.11.05.

[2] H. Almarabeh, "Analysis of Students' Performance by Using Different Data Mining Classifiers," International Journal of Modern Education and Computer Science, **9**(8), 9–15, 2017, doi:10.5815/ijmecs.2017.08.02.

[3] H. Mousa, A. Maghari, "School Students ' Performance Predication Using Data Mining Classification," International Journal of Advanced Research in Computer and Communication Engineering, **6**(8), 136–141, 2017, doi:10.17148/IJARCCE.2017.6824.

[4] Y.K. Salal, S.M. Abdullaev, M. Kumar, "Educational data mining: Student performance prediction in academic," International Journal of Engineering and Advanced Technology, **8**(4C), 54–59, 2019.

[5] A.D. Kumar, R.P. Selvam, V. Palanisamy, "Prediction of Student Performance using Hybrid Classification," International Journal of Recent Technology and Engineering, **8**(4), 6566–6570, 2019, doi:10.35940/ijrte.D8241.118419.

[6] D.N. Utama, Y.S. Triana, M.M. Iqbal, M. Iksal, I. Fikri, T. Dharmawan, "Decision Support Model for Mosque Renovation and Rehabilitation (Case Study: Ten Mosques in Jakarta Barat, Indonesia)," Journal of Physics: Conference Series, **978**, 012057, 2018, doi:10.1088/1742-6596/978/1/012057.

[7] D.N. Utama, E. Rustamaji, A. Fauziyah, "Fuzzy eco-DSM for treating medical waste," IOP Conference Series: Earth and Environmental Science, **195**(1), 012050, 2018, doi:10.1088/1755-1315/195/1/012050.

[8] Y. Indrianingsih, "Decision Support System to Determine the Number of Production Tofu using the Fuzzy Sugeno Method (Case Study: Home Industries Tofu in Seyegan District)," Conference SENATIK STT Adisutjipto Yogyakarta, 2018, doi:10.28989/senatik.v4i0.216.

[9] B. Kucukaltan, Z. Irani, E. Aktas, "A decision support model for identification and prioritization of key performance indicators in the logistics industry," Computers in Human Behavior, 2016, doi:10.1016/j.chb.2016.08.045.

[10] A. Setyono, S.N. Aeni, "Development of Decision Support System for Ordering Goods using Fuzzy Tsukamoto," International Journal of Electrical and Computer Engineering (IJECE), **8**(2), 1182, 2018, doi:10.11591/ijece.v8i2.pp1182-1193.

[11] D.N. Utama, "Fuzzy based Decision Support Model on Determining the Most Eligible Location of National Multi-Sport Event," International Journal of Advanced Trends in Computer Science and Engineering, **9**(4), 6140–6146, 2020, doi:10.30534/ijatcse/2020/286942020.

[12] D.N. Utama, U. Taryana, "Fuzzy logic for simply prioritizing information in academic information system," International Journal of Mechanical Engineering and Technology, 2019.

[13] H.C.W. Lau, R.A. Dwight, "A fuzzy-based decision support model for engineering asset condition monitoring – A case study of examination of water pipelines," Expert Systems with Applications, **38**(10), 13342–13350, 2011, doi:10.1016/j.eswa.2011.04.158.

[14] S. Rajak, S. Vinodh, "Application of fuzzy logic for social sustainability performance evaluation: a case study of an Indian automotive component manufacturing organization," Journal of Cleaner Production, **108**, 1184–1192, 2015, doi:10.1016/j.jclepro.2015.05.070.

[15] S.H. Jafari Petrudi, M. Pirouz, B. Pirouz, "Application of fuzzy logic for performance evaluation of academic students," in 2013 13th Iranian Conference on Fuzzy Systems (IFSC), IEEE: 1–5, 2013, doi:10.1109/IFSC.2013.6675615.

[16] R.S. Yadav, A.K. Soni, S. Pal, "A study of academic performance evaluation using Fuzzy Logic techniques," in 2014 International Conference on Computing for Sustainable Global Development (INDIACom), IEEE: 48–53, 2014, doi:10.1109/IndiaCom.2014.6828010.

[17] G. Gokmen, T.Ç. Akinci, M. Tektaş, N. Onat, G. Kocyigit, N. Tektaş, "Evaluation of student performance in laboratory applications using fuzzy logic," in Procedia - Social and Behavioral Sciences, 2010, doi:10.1016/j.sbspro.2010.03.124.

[18] V.K. Pal, V.K.K. Bhatt, "Performance prediction for post graduate students using artificial neural network," International Journal of Innovative Technology and Exploring Engineering, **8**(7), 446–454, 2019.

[19] L. Dole, J. Rajurkar, "A Decision Support System for Predicting Student Performance," International Journal of Innovative Research in Computer and Communication Engineering, **02**(12), 7232–7237, 2015, doi:10.15680/IJIRCCE.2014.0212015.

[20] M.D. Robinson, A. Oshlack, "A scaling normalization method for differential expression analysis of RNA-seq data," Genome Biology, **11**(3), 2010, doi:10.1186/gb-2010-11-3-r25.

[21] F. Cavallaro, "A Takagi-Sugeno Fuzzy Inference System for Developing a Sustainability Index of Biomass," Sustainability, **7**(9), 12359–12371, 2015, doi:10.3390/su70912359.

[22] L.C. Nikmatul Kamila, "Fuzzy Sugeno Algorithm for Clustering Document Management," International Journal of Advanced Trends in Computer Science and Engineering, **9**(1), 26–30, 2020, doi:10.30534/ijatcse/2020/05912020.

Types and Concentrations of Catalysts in Chemical Glycerolysis for the Production of Monoacylglycerols and Diacylglycerols

Edy Subroto[*], Rossi Indiarto, Aldila Din Pangawikan, Elazmanawati Lembong, Riva Hadiyanti

Department of Food Industrial Technology, Faculty of Agro-Industrial Technology, Universitas Padjadjaran, Jl.Raya Bandung-Sumedang Km. 21, Jatinangor, Sumedang, 40600, Indonesia

A R T I C L E I N F O	A B S T R A C T
	Monoacylglycerol (MAG) and diacylglycerol (DAG) are structured lipids that have been widely used in various pharmaceutical, cosmetic, and food industries. MAG and DAG are generally produced by chemical glycerolysis. Chemical catalysts have been shown to be more efficient, economical, and effective. This study summarizes and discusses the factors that affect the synthesis of MAG and DAG by chemical glycerolysis, such as temperature, reaction time, and type and concentration of catalysts that affect the resulting MAG and DAG concentrations. Homogeneous catalysts such as KOH and NaOH are very effective for generating MAG and DAG conversions up to 91%, but they have a disadvantage, mainly because they cannot be used repeatedly. However, heterogeneous catalysts have great potential to be developed into catalysts with high activity, environmentally friendly, and can be used repeatedly.

1. Introduction

The need for emulsifiers is increasing along with the development of emulsion-based food products, especially emulsifiers from the mixture of monoacylglycerols and diacylglycerols, which are the most considerably used in the food industry, which is about 75% [1]. Commercially, MAG and DAG are used in food products such as cake products, butter, margarine, and confectionaries because they have good emulsification, stabilization, and conditioning properties [2,3]. Mono and diacylglycerols are also used in the pharmaceutical, cosmetic, textile, and plastic industries in consequence of their plasticizing and lubricating properties [4,5]. Applications of MAG and DAG in various products can be seen in Table 1.

Naturally, MAG and DAG are minor components in various vegetable oils with a maximum content of 10% [6]. MAG consists of three isomers, namely enantiomers (sn-1 and sn-3) and regioisomers (sn-2) [7]. DAG be composed of 2 fatty acyl chains, which are esterified into glycerol backbone and can have the shape of 1,3-DAG and 1,2 (or 2,3)-DAG [8]. MAG and DAG are non-ionic molecules that have a free hydroxyl group, which is a hydrophilic group, and a fatty acid ester group, which is a lipophilic group [9]. The double affinity of MAG and DAG or often called amphiphilic, means that they can be used as emulsifiers. MAG with one fatty acid group and two free hydroxyl

groups on glycerol makes it behave like fat and water. MAG is an emulsifier that is not very sensitive to acidic conditions. The way the emulsifier works is by lowering the surface tension between the two phases and then stabilizing the products [10].

Commercially, the synthesis of MAG and DAG can be conducted by various methods, namely glycerolysis, direct esterification, and partial or alcoholic hydrolysis [5]. Various types of catalysts are also used, such as homogeneous base catalysts, heterogeneous bases, homogeneous acids, and heterogeneous acids. Several studies have shown a relatively high yield when using a homogeneous base catalyst and a heterogeneous base catalyst, while acid catalysts produce a relatively lower yield. In general, the synthesis of MAG and DAG on a large scale is carried out using the chemical glycerolysis method of oil, which is reacted with glycerol using an alkaline catalyst (such as NaOH and KOH) at high temperatures [2,11].

Table 1: Applications of MAG and DAG in Various Products.

Source of MAG/DAG	Products	References
Palm-based oils/fats	Emulsifier	[12]
Palm oils	Emulsifier	[13]
Vegetable oil	Emulsifier	[14]
Palm mild fraction	Shortening	[15]
Sunflower oil, palm kernel olein	Margarine	[16]

Chicken fat	Structured fat	[17]
Corn oil	MAG-DAG Oils	[18]
Vegetable oils	MAG-DAG Oils	[19]
Palm olein	MAG-DAG Oils	[20]
Monostearate	Oleogels	[21]
Monostearate, monopalmitate	Organogels	[22]
Saturated fat	Organogels	[23]
Saturated fat	Oleogels	[24]

Chemical glycerolysis at high temperature has several disadvantages, such as dark-colored products and high energy consumption. Several studies have reported that chemical glycerolysis of oils and fats can produce MAG and DAG of about 45-55% and 38-45%, respectively [3]. Subsequent molecular distillation is required to acquire monoacylglycerols with a purity of 90% [25], needed for the pharmaceutical, cosmetic, and food industries. Recent research studies about the glycerolysis reaction at low temperatures using a solvent or without a solvent; the concentration of MAG and DAG generated by this reaction ranges from 40-80% [26].

Another alternative used to substitute chemical catalysts is to use enzyme catalysts [27]. However, the use of enzymes has several drawbacks, such as the glycerolysis reaction requires special conditions and slow reaction kinetics. Besides, the high price of enzymes is a consideration for industrial applications [4]. The use of cheap and easy to obtain raw materials is an important factor in the manufacture of MAG and DAG on an industrial scale. Over the past few years, means have been made to produce high MAG using chemicals and enzymes as catalysts, and methods have been promoted with the aim of increasing the yield of MAG and DAG [28].

Various methods and various types of catalysts can be used to produce MAG and DAG, which can be applied to various food industries. This study discusses the effect of various types of chemical catalysts and their concentrations on the production of MAG and DAG using the glycerolysis method by considering other factors such as the molar ratios of oil to glycerol, temperature, and reaction time. In addition, the NaOH catalyst, which is a homogeneous catalyst, has not been widely discussed, so it is interesting to study in-depth because it has high catalytic activity and is efficient.

2. Characteristics of Mono- and Diacylglycerols

MAG and DAG are non-ionic molecules that have hydrophilic and hydrophobic groups [9]. MAG is an anionic emulsifier with excellent emulsifying properties because it has two hydrophilic groups (hydroxyl) and one hydrophobic group on the fatty acid chain. These emulsifying characteristics are used in food products, cosmetics, plasticizers, detergents, and pharmaceutical formulations [29]. On the other hand, DAG can be used as an emulsifier, especially in emulsion systems of water in oil (o/w). DAG can also effectively prevent the accumulation of fat and diseases related to obesity, so it is often used as a functional ingredient and including lipids that are good for health [30].

MAG and DAG are needed in almost all types of food products. Its main use includes bakery products, margarine, convenience foods, and frozen desserts. MAG and DAG are used as part of fat products and are often associated with other emulsifiers. Lipophilic characteristics cause MAG and DAG to have excellent properties as emulsifiers in water in oil (w/o) system, as required in the manufacture of margarine and shortening [15,16,31].

One of the uses of MAG and DAG is as an emulsifier. The use of emulsifiers is to maintain moisture and softness of bakery products, improve the stability of crystal emulsions in ice cream products, reduce stickiness in candy products, and so on [32]. In addition, other uses of emulsifiers are maintaining emulsion stability in margarine, preventing fat bloom in chocolate products, and improving palatability in cake products [33].

Based on research in [34], the emulsification ability produced from an emulsifier containing a mixture of 91% MAG and 9% DAG was stable when compared to commercial emulsifiers because the emulsion capacity was 95.55% after heating, the percent stability of the emulsion only decreased a little, namely to be 90.44%. Based on research in [35], the emulsification ability produced from a mixture of 50.89% DAG and 11.68% MAG had emulsion stability of about 95.44% and an emulsion capacity of 93.63%.

The melting point of MAG and DAG is higher than their triacylglycerol forms. The difference in melting points is caused by the difference in the number of hydrogen bonds in the carboxyl bonds and the hydrophobic interactions along the hydrocarbon chains. The melting point increases as the MAG and DAG content in the fat/oil increases [36]. MAG has a faster crystal conformation compared to TAG [37]. MAG and DAG can be utilized separately (pure of MAG and pure of DAG) or simultaneously. The application of MAG as an emulsifier requires high purity because MAG has better emulsification characteristics than different acylglycerol mixtures [38].

Food emulsifiers are generally in the form of semisolids containing fatty acids such as stearic, lauric, palmitic, and oleic acids. In general, the commercially saturated MAG is MAG containing stearic acid. Saturated MAG has a high melting point but has restricted emulsifying characteristics. Nevertheless, unsaturated MAG has a modest structure but is restricted in application due to its low oxidation stability [39].

A decrease in oxidation stability can be caused by changes in the position of fatty acids in the acylglycerol structure, include MAG and DAG [40]. Partial hydrogenation can be an effective way to rectify the oxidative stability of fats/oils [41]. Zhang et al. [39] conducted a study that rivets on partial hydrogenation of corn oil to increase the MAG oxidation stability of corn oil. The oxidation stability measured based on the induction period (IP) value of the MAG from the hydrogenation of corn oil was 13.68 hours, while the IP value of the MAG of corn oil was 0.51 hours. Thus, hydrogenation increases oxidation stability. However, partial hydrogenation can lead to the formation of trans-fats, which can be harmful to health.

3. Synthesis Methods of Mono- and Diacylglycerols

3.1. Enzymatic Methods

The enzymatic synthesis method can be carried out through esterification, alcoholysis or hydrolysis, and glycerolysis. Highly

stable lipases in solvents offer the potentiality of using a variety of approaches for catalyzed enzyme synthesis, such as selective alcoholysis or hydrolysis by specific lipases, glycerolysis of oils/fats, and esterification of free fatty acids with glycerol [42]. The reaction of glycerolysis by enzymatic catalysts has been extensively investigated using low temperatures (<80 °C) to generate MAG and DAG. MAG and DAG resulting from the enzymatic glycerolysis have good quality, but enzymatic glycerolysis has several shortfalls, including limited availability of enzymes, low reactant conversion factors, long reaction times, and high cost [43]. In addition, enzymatic glycerolysis has low efficiency, which is largely due to the inhomogeneous nature of oil or fat with lipophilic properties and lipase enzymes with hydrophilic characteristics when the reaction is carried out at low temperatures. It is notable for maintaining homogeneity between oil or fat and enzymes using the suitable solvent [44].

Based on research in [45], the glycerolysis between several samples of oil and fat with glycerol using lipase as a catalyst without using solvents and emulsifiers in a batch system produced 90% MAG resulting from the glycerolysis of olive oil, while the lowest yield was 30% that results from hydrogenated fat. Based on research in [3], the glycerolysis reaction of sunflower oil samples using Novozyme 435 with tert-pentanol and tert-butanol as the single solvent produced MAG in the range of 68-82%.

Based on research in [46], the enzymatic glycerolysis reaction of Lipozyme TL IM 15% using tert-butanol and iso-propanol (80/20 w/w), glycerol to oil molar ratio 3.5: 1, and solvent to oil ratio 4:1, at a temperature of 45 °C for 4 hours produced MAG about 72%. In [4], the author compared the glycerolysis between the enzyme-catalyzed reaction and the NaOH-catalyzed reaction. The reaction rate of the NaOH catalyzed was faster than the Novozym 435. Although the enzymatic approach has yielded good results; nevertheless, the high cost, reaction rate, and stability of the catalyst remain major barriers to the wide-spread use of enzymes for the commercial production of MAG and DAG.

3.2. Chemical Methods

Commercially MAG and DAG can be produced through several methods, namely: (i) direct esterification with fatty acids catalyzed by strong acids such as H_3PO_4 or H_2SO_4 at a high temperature of 90-120 °C or alkaline catalysts, (ii) glycerolysis of oil or fat which is catalyzed by homogeneous bases such as KOH or NaOH at a high temperature of 120-260 °C under an inert atmosphere, (iii) transesterification of fatty acid esters and (iv) partial or alcoholic hydrolysis [2,47].

In [48], the direct esterification using the ratio between lauric acid and glycerol of 1:1 at 112 °C using a mesoporous sulfonate catalyst 0.5% (w/w) produced MAG with a concentration of 53%. Meanwhile, under the same reaction conditions, but using Amberlyst-15 as a catalyst, it produced MAG with a concentration of 44%. The MAG produced using a mesoporous sulfonate catalyst was higher because it contains alkyl, and sulfonic acid can act as a catalyst [49]. In [50], the heterogeneous catalyst Amberlyst-15 was affected by several factors, namely the pore diameter and catalyst surface area. The use of H_2SO_4 as a homogeneous acid catalyst at a lauric acid and glycerol ratio of 1:1, a temperature of 130 °C for 6 hours, and a 5% (w/w) H_2SO_4

catalyst produced 31.05% monolaurin after going through a purification using column chromatography techniques [51].

Most of the MAG and DAG is generated by glycerolysis of TAG with excess glycerol at high temperatures in the presence of a catalyst. The addition of a catalyst to the glycerolysis reaction aims to acquire a high conversion in a relatively short time. This reaction can be performed in the existence of a base catalyst or an acid catalyst. The reaction with an alkaline catalyst is usually faster than an acid catalyst [52].

The glycerolysis reaction occurs randomly following the equilibrium to produce a certain composition of MAG, DAG, and TAG. Theoretically, the glycerolysis reaction involves 2 moles of glycerol, which will react with 1 mole of TAG and generate 3 moles of MAG. The glycerolysis reaction is used in producing MAG and DAG because it is more economical in terms of raw material prices and requires less glycerol [53]. According to [4], KOH and NaOH are catalysts that are more effective in their use in the glycerolysis process at low temperatures compared to SiO_2 and Al_2O_3.

4. Types and Concentrations of Catalysts for Chemical Glycerolysis

Chemically synthesizing MAG and DAG by glycerolysis requires a catalyst. Catalysts are substances that speed up reactions but do not react with them. The catalyst speeds up the reaction by decreasing the activation energy. The greater the concentration of catalyst and reaction temperature, the greater the reaction rate so that the product produced is also more significant [54]. Catalysts can be classified into two types, namely homogeneous catalysts and heterogeneous catalysts. The catalyst selectivity has several differences. Homogeneous catalysts are generally used for universal substrate types but are only suitable for batch reactors and cannot be used in continuous systems. In comparison, heterogeneous catalysts are more suitable for substrates or reactants that are less viscous and suitable for reactions in continuous systems [55].

In the use of a homogeneous catalyst, the catalyst is in the same phase as the reactants. The reactants and catalyst are in a single phase of liquid or gas. There are two types of homogeneous catalysts, namely homogeneous acid catalysts and homogeneous base catalysts. Homogeneous base catalysts for glycerolysis include KOH and NaOH [56]. These catalysts have advantages related to their characteristics, including high catalytic activity that only requires a short reaction time, low cost, high stability, and easy use [57]. There are also homogeneous catalysts in the form of homogeneous acid catalysts, include H_2SO_4, HCl, and H_3PO_4. However, the utilize of a homogeneous acid catalyst requires a long reaction time, causes corrosion in the reactor, and requires high temperatures [58].

In the use of heterogeneous catalysts, the catalyst and reactants are in different phases. Heterogeneous catalysts tend to be easier to separate and reuse from the reaction mixture because the phase used is different from the reaction product. The heterogeneous catalyst used is in the form of a solid phase while the reactants are liquid [59]. The most commonly used heterogeneous base catalysts are alkaline earth metal oxides compounds, such as MgO, CaO, SrO, and BaO [60].

Apart from metal oxide catalysts, there are several non-oxide catalysts that can be used, including 1-Butyl-3-Methylimidazolium Imidazolide [61]. The catalyst is also effectively used in chemical glycerolysis to produce DAG reaching about 60% at a concentration of 15%, a temperature of 80 °C for 4 hours.

Chemical catalysts are more widely used because they are easier to handle, cost less, easy to separate, and can be used in relatively low concentrations. Several types of chemical catalysts used in the glycerolysis reaction for the production of MAG and DAG are presented in Table 2.

Table 2: Several Types of Chemical Catalysts Used in the Glycerolysis Reaction for the Production of MAG and DAG.

No	Catalysts	Source of fat/oil	Reaction condition	Yield of MAG & DAG	References
1	NaOH 0.18%	Soybean oil	The molar ratio of oil:glycerol (1:2.5), 230 °C, 25 min	58% & 33%	[27]
2	NaOH 3%	Palm olein and palm stearin	The molar ratio of oil: glycerol (1:1.5), in tert-butanol, molecular sieve 12%, at 80 °C for 3 h	58.64%	[35]
3	NaOH 0.3%	Palm oil	The molar ratio of oil:glycerol (1:2), 240 °C, 60 min	58%	[62]
4	NaOH 0.45%	Soybean oil	Glycerol 4,6 g; Oil 8.8 g; in t-butanol; 50 °C, 1 h	81.76%	[4]
5	NaOH 2%	Palm stearin	The molar ratio of oil:glycerol (1:2.5), 200 °C; 20 min	65.4%	[1]
6	NaOH 3%	RBD Palm stearin	The molar ratio of oil: glycerol (1:5), in tert-butanol, molecular sieve 13%, at 90 °C for 6 h	91.00% & 9.00%	[34]
7	KOH 0.45%	Soybean oil	Glycerol 4,6 g; Oil 8.8 g; in t-butanol; catalyst 0.04 g; 50 °C, 1 h	68%	[4]
8	Amberlyst-15	RBD Palm stearin	The molar ratio of oil: glycerol (1:5), in tert-butanol, 90 °C, 9 h	16.44% & 14.49%	[34]
9	MgO	Rapeseed oil	The molar ratio of oil:glycerol (1:4), 249.85 °C, 2 h	66%	[29]
10	Ca(OH)$_2$ 1%	Sunflower oil	The molar ratio of oil:glycerol (1:4), 200 °C, 1 h	48.3% & 42.3%	[63]
11	CuO-nano+ NaOH 0.3%	Palm oil	The molar ratio of oil:glycerol (1:2), 240 °C, 40 min	71%	[62]
12	ZnO-CaO/AlO$_3$	Rapeseed oil	The molar ratio of oil:glycerol (1:4), 249.85 °C, 2 h	57%	[29]
13	1-butyl-3-methylimidazolium imidazolide	Soybean oil	Catalyst concentration if 15%, glycerol/TAG mole ratio was 5:1, 80 °C, 4 h	17.4% & 61.7%	[61]

The reaction mechanism of the glycerolysis catalyzed by homogeneous and heterogeneous chemical catalysts is almost the same but has some differences, especially in the active groups of cations or anions that are owned by heterogeneous catalysts. The chemical glycerolysis mechanism is described as follows. In glycerolysis using a homogeneous catalyst such as NaOH, in the early stages, the hydrogen in the glycerol molecule is abstracted by NaOH, which is a strong base to form sodium glyceroxides, which then easily form glyceroxides at high temperatures (90-240 °C). Meanwhile, the OH- anion produced from NaOH can act as a proton abstraction agent that can attract protons from the OH group on glycerol by forming surface glyceroxides. Na$^+$ cations also take part in the stabilization of negatively charged intermediates. In this condition, the Na$^+$ cation also plays a role in activating the triacylglycerol molecule (polarization of the C=O

bond). The Na$^+$ cation further assists or facilitates the overrun of the glyceroxide anion on the positively charged carbonyl carbon present in the TAG. In a later stage, there is a nucleophilic attack on the carbonyl group of the TAG by the glyceroxides to produce MAG and the appropriate anion of 1,3 or 1,2-DAG known as diglyceroxide. The next stage is the conformation of the suitable alkyl ester (DAG) and glycerol anions (glyceroxides) by the second molecule of glycerol reacting with the adsorbed diglyceroxide. In the last stage, the alteration of TAG or DAG to MAG is carried out following the same mechanism. In contrast to homogeneous catalysts, heterogeneous catalysts that act to abstract hydrogen on the glycerol molecule are not Na$^+$ cations, but depending on the active groups that heterogeneous catalysts have, for example, are sulfonic or CuO groups. In addition to acting in hydrogen abstraction, this group also plays a role in

polarizing the ester group (C=O) on TAG. Meanwhile, the other mechanism stages are almost the same, namely through nucleophilic attacks and ending with the conversion of TAG and DAG to MAG [64,65].

Table 2 shows that the type and concentration of the catalyst affect the results of the MAG and DAG concentrations. However, glycerolysis is also influenced by reaction conditions (temperature, the molar ratio of oil to glycerol, and reaction time). Homogeneous catalysts and heterogeneous catalysts have advantages and disadvantages. Homogeneous catalysts such as NaOH or KOH are preferred because they can readily dissolve and react with glycerol in the reactant system. Based on research in [34], the MAG produced followed by fractionation was 91.00%. The increase in MAG levels is due to differences in the melting point and the thermomechanical separation process through crystallization, namely MAG, which has a higher melting point, will be separated from DAG and TAG with lower melting points. At a fractionation temperature of 30 °C, MAG will crystallize while DAG and TAG remain dissolved in hexane and then filtered. In addition to fractionation, molecular distillation can increase monoacylglycerols with a purity of 90% [25].

Based on research in [62], using the homo-hetero system in the glycerolysis reaction resulted in almost the same triacylglycerol conversion using either NaOH or CuO-nano + NaOH catalysts. However, the product distribution was different where the MAG concentration in the use of a CuO-nano + NaOH catalyst is higher than the reaction using a NaOH catalyst. The adjunct of a small amount of NaOH (0.01% w/w) could increase the TAG conversion. In addition, the catalyst systems of CuO-nano + NaOH showed an increase in the yield of TAG to MAG conversion, reaching 90%. The use of CuOnano + NaOH catalyst resulted in a higher yield MAG than for the NaOH system; this shows that in the reaction system, CuO also acts as a catalyst.

Based on the results of the research that has been conducted, it is possible to consider three main factors that affect the glycerolysis process. These three factors are the strength of the base catalyst, the radius of the catalyst pore, and the solubility of the catalyst in the glycerol and oil system [29]. In the research of [29], using a ZnO-CaO/ AlO$_3$ catalyst, the results of the MAG concentration were lower than using the MgO catalyst. Based on research in [4], by comparing eight commonly used basic catalysts, namely Al$_2$O$_3$, SiO$_2$, MgO, Na$_2$CO$_3$, K$_2$CO$_3$, CaO, KOH, and NaOH. Only NaOH and KOH are effective in catalyzing chemical glycerolysis at low temperature (50 °C).

The homogeneous catalysts (KOH and NaOH) have high catalytic activity and result in high product yields [66]. The reason for this case remains to be investigated. This is also thought to be caused by differences in the capability to extract hydrogen from glycerol. Both KOH and NaOH have the same solubility in the tert-butanol. However, at temperatures higher than 240 °C, the Ca(OH)$_2$, MgO, and CaO catalysts are all functioning even in solvent-free systems, which exhibit easier alkoxide formation [67]. This is also supported by several studies presented in Table 1, that a high temperature of 200-250 °C produces a high MAG concentration of 77% (solvent-free system). Therefore, high temperature not only increases the solubility of oil/fat and

glycerol but also helps the catalyst to extract hydrogen from glycerol to create alkoxides.

According to [5], the surface polarity of the catalyst has a key role in increasing the concentration of MAG and DAG. The glycerol concentration on the catalyst surface will be greater than the fatty acid ester for MAG formation because the high glycerol concentration will limit the forming of DAG and TAG. However, hydrophobic oils also have difficulty accessing the surface of the catalyst, thus reducing the reaction kinetics. Therefore, the catalyst must be very active, the reaction temperature used is higher, and also use a solvent to accelerate the reaction [68].

As previously explained, the glycerolysis reaction is a slow-running reaction without the addition of a catalyst. The use of various concentrations of NaOH is also expected to produce high mono- and diacylglycerols. According to [4], the catalyst concentration influences the reaction rate over a particular range, an increase in the NaOH concentration causes an increase in the reaction rate. The concentration of catalyst affects the yield of the resulting product; the higher the concentration of the catalyst in the solution, the smaller the activation energy of a reaction, so that more products will be formed [69]. However, the addition of excessive catalyst concentration can also encourage the reaction to form soap [70].

Various researches to get the type of catalyst in the glycerolysis reaction continue to develop. Recommendations that can be taken from this review are that NaOH catalysts are very effective catalysts for chemical glycerolysis reactions, but have the disadvantage of not being used repeatedly, are not environmentally friendly, and cannot be used for continuous reaction systems. Therefore, a more in-depth research is needed, especially on heterogeneous catalysts, in order to obtain a catalyst that is inexpensive, high activity, stable, able to be used repeatedly, can be used for continuous reaction systems, and environmentally friendly.

5. Conclusion

Research on the synthesis of MAG and DAG has been carried out using various enzymatic and chemical methods. Chemical catalysts have been shown to be efficient and effective catalysts, so that the chemical glycerolysis is an effective and efficient method for MAG and DAG production. However, the type and concentration of catalysts are very influential in chemical glycerolysis. Catalyst activity is affected by three main factors, namely the strength of the base catalyst, the radius of the catalyst pore, and the solubility of the catalyst in the glycerol and oil system. Homogeneous catalyst (NaOH) concentrations of 0.2-0.5% produce high yields of MAG and DAG (in the solvent systems). In the solvent-free systems, NaOH at concentrations of 3% produces high yields of MAG and DAG. Homogeneous catalysts such as NaOH and KOH are very effective for generating MAG and DAG conversions up to 91%, but they have a disadvantage, especially in that they cannot be used repeatedly. However, heterogeneous catalysts have great potential to be developed into catalysts with high activity, environmentally friendly, and can be used repeatedly.

Conflict of Interest

The authors declare no conflict of interest.

Acknowledgment

References

[1] P. Chetpattananondh, C. Tongurai, "Synthesis of High Purity Monoglycerides from Crude Glycerol and Palm Stearin," Songklanakarin Journal of Science and Technology, **30**(4), 515–521, 2008.

[2] E. Subroto, "Monoacylglycerols and diacylglycerols for fat-based food products: a review," Food Research, **4**(4), 932–943, 2020, doi:10.26656/fr.2017.4(4).398.

[3] M.L. Damstrup, T. Jensen, F. V. Sparsø, S.Z. Kiil, A.D. Jensen, X. Xu, "Solvent optimization for efficient enzymatic monoacylglycerol production based on a glycerolysis reaction," Journal of the American Oil Chemists' Society, **82**(8), 559–564, 2005, doi:10.1007/s11746-005-1109-y.

[4] N. Zhong, L. Li, X. Xu, L.Z. Cheong, Z. Xu, B. Li, "High Yield of Monoacylglycerols Production Through Low-temperature Chemical and Enzymatic Glycerolysis," European Journal of Lipid Science and Technology, **115**(6), 684–690, 2013, doi:10.1002/ejlt.201200377.

[5] N. Zhong, L.Z. Cheong, X. Xu, "Review Article : Strategies to Obtain High Content of Monoacylglycerols," European Journal of Lipid Science and Technology, **116**(Scheme 1), 97–107, 2014, doi:10.1002/ejlt.201300336.

[6] B.D. Flickinger, N. Matsuo, "Nutritional Characteristics of DAG Oil," Lipids, **38**(2), 129–132, 2003, doi:10.1007/s11745-003-1042-8.

[7] L. Deng, H. Nakano, Y. Iwasaki, "Direct Separation of Regioisomers and Enantiomers of Monoacylglycerols by Tandem Column High-performance Liquid Chromatography," Journal of Chromatography A, **1165**(1–2), 93–99, 2007, doi:10.1016/j.chroma.2007.07.073.

[8] E.T. Phuah, T.K. Tang, Y.Y. Lee, T.S.Y. Choong, C.P. Tan, O.M. Lai, "Review on the Current State of Diacylglycerol Production Using Enzymatic Approach," Food and Bioprocess Technology, **8**(6), 1169–1186, 2015, doi:10.1007/s11947-015-1505-0.

[9] B.L.A.P. Devi, H. Zhang, M.L. Damstrup, Z. Guo, L. Zhang, B.M. Lue, X. Xu, "Enzymatic synthesis of designer lipids," OCL - Oleagineux Corps Gras Lipides, **15**(3), 189–195, 2008, doi:10.1684/ocl.2008.0194.

[10] A. Zaelani, "Sintesis Mono dan Diasilgliserol Dari Refined Bleached Deodorized Palm Oil (RBDPO) dengan Cara Gliserolisis Kimia," in Fakultas Teknologi Pertanian IPB, Bogor, 2007.

[11] F.O. Nitbani, P.J.P. Tjitda, B.A. Nurohmah, H.E. Wogo, "Preparation of fatty acid and monoglyceride from vegetable oil," Journal of Oleo Science, **69**(4), 277–295, 2020, doi:10.5650/jos.ess19168.

[12] Y. Fu, R. Zhao, L. Zhang, Y. Bi, H. Zhang, C. Chen, "Influence of acylglycerol emulsifier structure and composition on the function of shortening in layer cake," Food Chemistry, **249**(September 2017), 213–221, 2018, doi:10.1016/j.foodchem.2017.12.051.

[13] K. Hattori, B. Dupuis, B.X. Fu, N.M. Edwards, "Effects of monoglycerides of varying fatty acid chain length and mixtures there of on sponge-and-dough breadmaking quality," Cereal Chemistry, **92**(5), 481–486, 2015, doi:10.1094/CCHEM-12-14-0267-R.

[14] J.M. Maruyama, F.A.S.D.M. Soares, N.R. D'Agostinho, M.I.A. Goncalves, L.A. Gioielli, R.C. da Silva, "Effects of Emulsifier Addition on the Crystallization and Melting Behavior of Palm Olein and Coconut Oil," Journal of Agricultural and Food Chemistry, **62**, 2253–2263, 2014, doi:10.1021/jf405221n.

[15] R.A. Latip, Y.Y. Lee, T.K. Tang, E.T. Phuah, C.P. Tan, O.M. Lai, "Physicochemical properties and crystallisation behaviour of bakery shortening produced from stearin fraction of palm-based diacygglycerol blended with various vegetable oils," Food Chemistry, **141**(4), 3938–3946, 2013, doi:10.1016/j.foodchem.2013.05.114.

[16] A.H. Saberi, O.M. Lai, M.S. Miskandar, "Melting and Solidification Properties of Palm-Based Diacylglycerol, Palm Kernel Olein, and Sunflower Oil in the Preparation of Palm-Based Diacylglycerol-Enriched Soft Tub Margarine," Food and Bioprocess Technology, **5**(5), 1674–1685, 2012, doi:10.1007/s11947-010-0475-5.

[17] M. Naderi, J. Farmani, L. Rashidi, "Structuring of Chicken Fat by Monoacylglycerols," JAOCS, Journal of the American Oil Chemists' Society, **93**(9), 1221–1231, 2016, doi:10.1007/s11746-016-2870-1.

[18] Z. Zhang, X. Ma, H. Huang, G. Li, Y. Wang, "Enzymatic Production of Highly Unsaturated Monoacyglycerols and Diacylglycerols and Their Emulsifying Effects on the Storage Stability of a Palm Oil Based Shortening System," JAOCS, Journal of the American Oil Chemists' Society, **94**(9), 1175–1188, 2017, doi:10.1007/s11746-017-3023-x.

[19] C.A. Ferretti, M.L. Spotti, J.I. Di Cosimo, "Diglyceride-rich oils from glycerolysis of edible vegetable oils," Catalysis Today, **302**(November 2016), 233–241, 2018, doi:10.1016/j.cattod.2017.04.008.

[20] C.M. Yeoh, E.T. Phuah, T.K. Tang, W.L. Siew, L.C. Abdullah, T.S.Y. Choong, "Molecular distillation and characterization of diacylglycerol-enriched palm olein," European Journal of Lipid Science and Technology, **116**(12), 1654–1663, 2014, doi:10.1002/ejlt.201300502.

[21] A.C. Ferro, P.K. Okuro, A.P. Badan, R.L. Cunha, "Role of the oil on glyceryl monostearate based oleogels," Food Research International, **120**(November 2018), 610–619, 2019, doi:10.1016/j.foodres.2018.11.013.

[22] O.G. Rocha-Amador, J.A. Gallegos-Infante, Q. Huang, N.E. Rocha-Guzman, M. Rociomoreno-Jimenez, R.F. Gonzalez-Laredo, "Influence of commercial saturated monoglyceride, mono-/diglycerides mixtures, vegetable oil, stirring speed, and temperature on the physical properties of organogels," International Journal of Food Science, **2014**, 2014, doi:10.1155/2014/513641.

[23] E. Yilmaz, M. Öğütcü, "Properties and stability of hazelnut oil organogels with beeswax and monoglyceride," JAOCS, Journal of the American Oil Chemists' Society, **91**(6), 1007–1017, 2014, doi:10.1007/s11746-014-2434-1.

[24] J.D. Pérez-Martínez, M. Sánchez-Becerril, A.G. Marangoni, J.F. Toro-Vazquez, J.J. Ornelas-Paz, V. Ibarra-Junquera, "Structuration, elastic properties scaling, and mechanical reversibility of candelilla wax oleogels with and without emulsifiers," Food Research International, **122**(January), 471–478, 2019, doi:10.1016/j.foodres.2019.05.020.

[25] U.T. Bornscheuer, "Lipase-catalyzed syntheses of monoacylglycerols," Enzyme and Microbial Technology, **17**(7), 578–586, 1995, doi:10.1016/0141-0229(94)00096-A.

[26] N. Zhong, X. Deng, J. Huang, L. Xu, K. Hu, Y. Gao, "Low-temperature chemical glycerolysis to produce diacylglycerols by heterogeneous base catalyst," European Journal of Lipid Science and Technology, **116**(4), 470–476, 2014, doi:https://doi.org/10.1002/ejlt.201300438.

[27] H. Noureddini, D.W. Harkey, M.R. Gutsman, "A Continuous Process for the Glycerolysis of Soybean Oil," JAOCS, Journal of the American Oil Chemists' Society, **81**(2), 203–207, 2004.

[28] N. Zhong, L.-Z. Cheong, X. Xu, "Strategies to obtain high content of monoacylglycerols," European Journal of Lipid Science and Technology, **116**(2), 97–107, 2014, doi:https://doi.org/10.1002/ejlt.201300336.

[29] V. Brei, G. Starukh, S. Levytska, D. Shistka, "Study of a Continuous Process of Glycerolysis of Rapeseed Oil with The Solid Base Catalysts," Chemistry and Chemical Technology, **6**(1), 89–94, 2012, doi:10.23939/chcht06.01.089.

[30] S.K. Lo, C.P. Tan, K. Long, M.S.A. Yusoff, O.M. Lai, "Diacylglycerol oil-properties, processes and products: A review," Food and Bioprocess Technology, **1**(3), 223–233, 2008, doi:10.1007/s11947-007-0049-3.

[31] E. Subroto, R.L. Nurannisa, "The Recent Application Of Palm Stearin In Food Industry : A Review," International Journal of Scientific & Technology Research, **9**(02), 2593–2597, 2020.

[32] R. O'Brien, Fats and Oils : Third Edition, 2009, doi:10.1016/j.ijbiomac.2015.07.020.

[33] A. Mulyawan, D. Hunaefi, P. Hariyadi, "Structured Lipid Characteristics of Enzimatic Transesterification Between Fish Oil and Virgin Coconut Oil," Jurnal Pengolahan Hasil Perikanan Indonesia, **21**(2), 317–327, 2018.

[34] A.P. Arum, C. Hidayat, Supriyanto, "Synthesis of Emulsifier from Refined Bleached Deodorized Palm Stearin by Chemical Glycerolysis in Stirred Tank Reactor," KnE Life Sciences, **4**(11), 130, 2019, doi:10.18502/kls.v4i11.3859.

[35] E. Subroto, M.F. Wisamputri, Supriyanto, T. Utami, C. Hidayat, "Enzymatic and chemical synthesis of high mono- and diacylglycerol from palm stearin and olein blend at different type of reactor stirrers," Journal of the Saudi Society of Agricultural Sciences, **19**(1), 31–36, 2020, doi:10.1016/j.jssas.2018.05.003.

[36] F.D. Gunstone, Food applications of lipids. In: Food Lipids Chemisty, Nutrition, and Biotechnology, 2nd ed., Marcel Dekker, Inc, New York, 2002.

[37] R.C. Basso, A.P.B. Ribeiro, M.H. Masuchi, L.A. Gioielli, L.A.G. Gonçalves, A.O. dos Santos, L.P. Cardoso, R. Grimaldi, "Tripalmitin and monoacylglycerols as modifiers in the crystallisation of palm oil," Food Chemistry, **122**(4), 1185–1192, 2010, doi:10.1016/j.foodchem.2010.03.113.

[38] M.M.C. Feltes, D. de Oliveira, J.M. Block, J.L. Ninow, "The Production,

Benefits, and Applications of Monoacylglycerols and Diacylglycerols of Nutritional Interest," Food and Bioprocess Technology, **6**(1), 17–35, 2013, doi:10.1007/s11947-012-0836-3.

[39] Z. Zhang, Y. Wang, X. Ma, E. Wang, M. Liu, R. Yan, "Characterisation and oxidation stability of monoacylglycerols from partially hydrogenated corn oil," Food Chemistry, **173**, 70–79, 2014, doi:10.1016/j.foodchem.2014.09.155.

[40] R. Hoshina, Y. Endo, K. Fujimoto, "Effect of Triacylglycerol Structures on The Thermal Oxidative Stability of Edible Oil," JAOCS, Journal of the American Oil Chemists' Society, **81**(5), 461–465, 2004, doi:10.1007/s11746-004-0923-6.

[41] A.F. Trasarti, D.J. Segobia, C.R. Apesteguía, F. Santoro, F. Zaccheria, N. Ravasio, "Selective Hydrogenation of Soybean Oil on Copper Catalysts as a Tool Towards Improved Bioproducts," JAOCS, Journal of the American Oil Chemists' Society, **89**(12), 2245–2252, 2012, doi:10.1007/s11746-012-2119-6.

[42] B. Cheirsilp, P. Jeamjounkhaw, A. H-Kittikun, "Optimizing an Alginate Immobilized Lipase for Monoacylglycerol Production by the Glycerolysis Reaction," Journal of Molecular Catalysis B: Enzymatic, **59**(1–3), 206–211, 2009, doi:10.1016/j.molcatb.2009.03.001.

[43] W. Kaewthong, S. Sirisansaneeyakul, P. Prasertsan, A. H-Kittikun, "Continuous production of monoacylglycerols by glycerolysis of palm olein with immobilized lipase," Process Biochemistry, **40**(5), 1525–1530, 2005, doi:10.1016/j.procbio.2003.12.002.

[44] F.O. Nitbani, Juminaa, D. Siswanta, E.N. Solikhah, "Reaction path synthesis of monoacylglycerol from fat and oils," International Journal of Pharmaceutical Sciences Review and Research, **35**(1), 126–136, 2015.

[45] G.P. McNeill, D. Borowitz, R.G. Berger, "Selective Distribution of Saturated Fatty Acids Into The Monoglyceride Fraction During Enzymatic Glycerolysis," Journal of the American Oil Chemists' Society, **69**(11), 1098–1103, 1992, doi:10.1007/BF02541043.

[46] N. Zhong, L. Li, X. Xu, L. Cheong, B. Li, S. Hu, X. Zhao, "An Efficient Binary Solvent Mixture for Monoacylglycerol Synthesis by Enzymatic Glycerolysis," JAOCS, Journal of the American Oil Chemists' Society, **86**(8), 783–789, 2009, doi:10.1007/s11746-009-1402-7.

[47] G.P. McNeill, S. Shimizu, T. Yamane, "Solid Phase Enzymatic Glycerolysis of Beef Tallow Resulting in a High Yield of Monoglyceride," Journal of the American Oil Chemists' Society, **67**(11), 779–783, 1990, doi:10.1007/BF02540491.

[48] W.D. Bossaert, D.E. De Vos, W.M. Van Rhijn, J. Bullen, P.J. Grobet, P.A. Jacobs, "Mesoporous Sulfonic Acids as Selective Heterogeneous Catalysts for the Synthesis of Monoglycerides," Journal of Catalysis, **182**(1), 156–164, 1999, doi:10.1006/jcat.1998.2353.

[49] D. Isabel, F. Mohino, E. Sastre, "Synthesis of MCM-41 Materials Functionalised with Dialkylsilane Groups and Their Catalytic Activity," Applied Catalysis A: General, **242**, 161–169, 2003.

[50] S. Gan, H.K. Ng, P.H. Chan, F.L. Leong, "Heterogeneous Free Fatty Acids Esterification in Waste Cooking Oil Using Ion-exchange Resins," Fuel Processing Technology, **102**, 67–72, 2012, doi:10.1016/j.fuproc.2012.04.038.

[51] G. Widiyarti, M. Hanafi, W.P. Soewarso, "Study On The Synthesis Of Monolaurin As Antibacterial Agent Againts Staphylococcus aureus," Indonesian Journal of Chemistry, **9**(1), 99–106, 2010, doi:10.22146/ijc.21569.

[52] T. Kimmel, Kinetic Investigation of the Base-Catalyzed Glycerolysis of Fatty Acid Methyl Esters, Berlin, 2004.

[53] G.L. Hasenhuettl, Food Emulsiers and Their Applications : Third Edition, Springer Nature Switzerland, 2019.

[54] A. Prianti, "The Effect of Temperature and Concentration of NaOH in Production of Monoglycerol and Diglycerol from Crude Palm Oil," Jurnal Riset Teknologi Industri, **6**(11), 13–20, 2012.

[55] N.F. Nasir, W.R.W. Daud, S.K. Kamarudin, Z. Yaakob, "Methyl Esters Selectivity of Transesterification Reaction with Homogenous Alkaline Catalyst to Produce Biodiesel in Batch, Plug Flow, and Continuous Stirred Tank Reactors," International Journal of Chemical Engineering, **2014**, 931264, 2014, doi:10.1155/2014/931264.

[56] Q. Shu, J. Gao, Z. Nawaz, Y. Liao, D. Wang, J. Wang, "Synthesis of Biodiesel from Waste Vegetable Oil with Large Amounts of Free Fatty Acids using A Carbon-based Solid Acid Catalyst," Applied Energy, **87**(8), 2589–2596, 2010, doi:10.1016/j.apenergy.2010.03.024.

[57] A. Sivasamy, K.Y. Cheah, P. Fornasiero, F. Kemausuor, S. Zinoviev, S. Miertus, "Catalytic Applications in the Production of Biodiesel from Vegetable Oils," ChemSusChem, **2**(4), 278–300, 2009, doi:https://doi.org/10.1002/cssc.200800253.

[58] Z. Helwani, M.R. Othman, N. Aziz, J. Kim, W.J.N. Fernando, "Solid Heterogeneous Catalysts for Transesterification of Triglycerides with Methanol: A Review," Applied Catalysis A: General, **363**(1–2), 1–10, 2009, doi:10.1016/j.apcata.2009.05.021.

[59] Istadi, Katalis Reaksi Kimia, Graha Ilmu, Yogyakarta, 2011.

[60] A.K. Endalew, Y. Kiros, R. Zanzi, "Inorganic Heterogeneous Catalysts for Biodiesel Production from Vegetable Oils," Biomass and Bioenergy, **35**(9), 3787–3809, 2011, doi:10.1016/j.biombioe.2011.06.011.

[61] Y. Huang, Y. Gao, N. Zhong, "Selective production of diacylglycerols through glycerolysis by ionic liquid: 1-butyl-3-methylimidazolium imidazolide as catalyst and reaction medium," Journal of the American Oil Chemists' Society, **92**(6), 927–931, 2015, doi:10.1007/s11746-015-2650-3.

[62] H.R. Ong, M.M.R. Khan, R. Ramli, R.M. Yunus, M.W. Rahman, "Glycerolysis of Palm Oil Using Copper Oxide Nanoparticles Combined with Homogeneous Base Catalyst," New Journal of Chemistry, **40**(10), 8704–8709, 2016, doi:10.1039/c6nj01461e.

[63] C.S. Galúcio, R.A. Souza, M.A. Stahl, P. Sbaite, C.I. Benites, M.R.W. Maciel, "Physicochemical Characterization of Monoacylglycerols from Sunflower Oil," Procedia Food Science, **1**(Icef 11), 1459–1464, 2011, doi:10.1016/j.profoo.2011.09.216.

[64] D.T. Hartanto, Rochmadi, Budhijanto, "Mechanism and kinetic model for glycerolysis of shellac," IOP Conference Series: Materials Science and Engineering, **778**, 12053, 2020, doi:10.1088/1757-899x/778/1/012053.

[65] H.R. Ong, M.M.R. Khan, R. Ramli, R.M. Yunus, M.W. Rahman, "Glycerolysis of palm oil using copper oxide nanoparticles combined with homogeneous base catalyst," New Journal of Chemistry, **40**(10), 8704–8709, 2016, doi:10.1039/c6nj01461e.

[66] V.B. Veljković, I.B. Banković-Ilić, O.S. Stamenković, "Purification of Crude Biodiesel Obtained by Heterogeneously-Catalyzed Transesterification," Renewable and Sustainable Energy Reviews, **49**, 500–516, 2015, doi:10.1016/j.rser.2015.04.097.

[67] A. Corma, S. Iborra, S. Miquel, J. Primo, "Catalysts for The Production of Fine Chemicals: Production of Food Emulsifiers, Monoglycerides, by Glycerolysis of Fats with Solid Base Catalysts," Journal of Catalysis, **173**(2), 315–321, 1998, doi:10.1006/jcat.1997.1930.

[68] J. Barrault, F. Jerome, "Design of New Solid Catalysts for The Selective Conversion of Glycerol," European Journal of Lipid Science and Technology, **110**(9), 825–830, 2008, doi:10.1002/ejlt.200800061.

[69] A. Prihanto, T.A.B. Irawan, "Effect of Temperature, Catalyst Concentration and Methanol-Oil Molar Ratio Against Biodiesel Yield from Used Cooking Oil Through Neutralization Transesterification Process," Metana, **13**(1), 30–36, 2017, doi:10.14710/metana.v13i1.11340.

[70] S.M. Hingu, P.R. Gogate, V.K. Rathod, "Synthesis of Biodiesel from Waste Cooking Oil using Sonochemical Reactors," Ultrasonics Sonochemistry, **17**(5), 827–832, 2010, doi:10.1016/j.ultsonch.2010.02.010.

Particle Swarm Optimization, Genetic Algorithm and Grey Wolf Optimizer Algorithms Performance Comparative for a DC-DC Boost Converter PID Controller

Jesus Aguila-Leon[*,1,2], Cristian Chiñas-Palacios[1,2], Carlos Vargas-Salgado[2,3], Elias Hurtado-Perez[2,3], Edith Xio Mara Garcia[1]

¹Departamento de Estudios del Agua y de la Energía, Centro Universitario de Tonalá, Universidad de Guadalajara, Tonalá, 45425, Mexico

²Instituto Universitario de Ingeniería Energética, Universitat Politècnica de València, València, 46022, Spain

³Departamento de Ingeniería Eléctrica, Universitat Politècnica de València, València, 46022, Spain

A R T I C L E   I N F O

A B S T R A C T

Power converters are electronic devices widely applied in industry, and in recent years, for renewable energy electronic systems, they can regulate voltage levels and actuate as interfaces, however, to do so, is needed a controller. Proportional-Integral-Derivative (PID) are applied to power converters comparing output voltage versus a reference voltage to reduce and anticipate error. Using PID controllers may be complicated since must be previously tuned prior to their use. Many methods for PID controllers tunning have been proposed, from classical to metaheuristic approaches. Between the metaheuristic approaches, bio-inspired algorithms are a feasible solution; Particle Swarm Optimization (PSO) and Genetic Algorithms (GA) are often used; however, they need many initial parameters to be specified, this can lead to local solutions, and not necessarily the global optimum. In recent years, new generation metaheuristic algorithms with fewer initial parameters had been proposed. The Grey Wolf Optimizer (GWO) algorithm is based on wolves' herds chasing habits. In this work, a comparison between PID controllers tunning using GWO, PSO, and GA algorithms for a Boost Converter is made. The converter is modeled by state-space equations, and then the optimization of the related PID controller is made using MATLAB/Simulink software. The algorithm's performance is evaluated using the Root Mean Squared Error (RMSE). Results show that the proposed GWO algorithm is a feasible solution for the PID controller tunning problem for power converters since its overall performance is better than the obtained by the PSO and GA.

1. Introduction

Power converters have an important role in Industry applications; their main purpose is to regulate power in electronic appliances and adjusting current and voltage signals to desired levels by a high frequency switching control device [1,2]. One of the most significant modern applications for power converters is related to Renewable Energy Sources (RES), since the power generated for these sources highly depends on environmental conditions power converters are a reliable solution to stabilize output voltage and current of RES. A Boost Converter is an electronic device whose main purpose is to raise an input voltage and stabilize it to a desired highest level [3,4]. Since voltage regulation on power converters, and therefore, boost converters, depends on a switching signal, is needed a controller to generate a proper pulse width modulation (PWM) to modify the duty cycle of the switching signal. PID controllers are commonly used for this kind of applications, however, PID controllers need to be tunned prior its use [5]. The PID controller tunning can be a challenging task, many methods had been proposed for this purpose, from classical modeling and analysis based on system response [6] to modern techniques based on metaheuristic algorithms [7]. Nature had been an inspiration for modern metaheuristic algorithms, most of them based on animal behavior, for system design and control optimal parameters finding [8]. Bio-inspired algorithms imitate animal collective intelligence to explore, find, and exploit food and resources. Collective intelligence is the sum of individual behavior based on simple rules, and these behaviors and strategies can be translated into computational optimization algorithms. The most common bio-inspired algorithms are Genetic Algorithms (GA) and

*Corresponding Author: Jesus Aguila Leon, Centro Universitario de Tonalá, Universidad de Guadalajara, Av. Nuevo Periférico 555, Tonalá, México.
Email: jesus.aguila@academicos.udg.mx

Particle Swarm Optimization (PSO) algorithms. Among these bio-inspired optimization algorithms applications are control of load frequency [9], systems optimal sizing and design [10], power flow applications [11], predictive control for microgrids based on renewable energies [12], power converters optimal design [13] and regulation for voltage [14]. In [15], an evolutionary approach using Symbiotic Organisms Search (SOS) algorithm, which is based on PSO algorithms and the trophic chain of the ecosystems, and a two-round fuzzy inference engine were presented for energy management in microgrids. Since PSO is general modeling for animal behavior, there had been developed and studied variants of PSO based on particular animal species [16,17]. Authors in [18] applied a Whale Optimization Algorithm for an optimal design of a PID controller for a DC-DC converter using a transfer function and step response approach to analise the system performance; they found beter transciente response in comparison to a compared GA algorithm, however, they did not considered fluctutanting input voltages or load changes. In 2014, the author presented the Grey Wolf Optimizer (GWO), based on hunting strategies of wolves herds [19]. The GWO had been studied in comparison to other optimization algorithms as well as some engineering applications. Authors in [20] applied GWO to a PID controller to optimize the system response of a steam pressure system, they found an improvement in system stability and response. In [21] the GWO was applied to a modeled levitation system, improving time domain response and reducing the system error in comparison to the PID tunning MATLAB tool. Also, GWO had been applied to power systems.

In this paper, an optimal tunning for a PID controller using the GWO algorithm applied to a boost converter is presented. The boost converter is modeled unsung state-space equations and then simulated in MATLAB/Simulink. The proposed GWO-PID tunned algorithm performance is compared with PSO and GA algorithms in terms of the RMSE and the system response for variable load and variable input voltage. The paper is organized as follows: Section 2 depicts the boost converter model and description. Section 3 presents the GWO, PSO, and GA optimization algorithm basis. Section 4 shows the optimization methodology for the boost converter. Section 5 summarizes the results and, finally, Section 6 are the conclusions of this study.

2. Mathematical model of the Boost Converter

The boost converter is an electronic device that rises input voltage to the desired highest output voltage. Voltage regulation is made by a PWM signal, applied to an inductor (L) and capacitor (C) arrangement, carried out by a fast-switching transistor that according to the control signal. Changes in the PWM signal modifies the L-C charge and discharge cycles and change the output signal [22]. The boost converter configuration is shown in Figure 1.
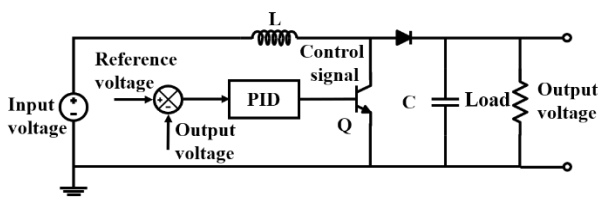
Figure 1: Electric diagram for the Boost converter.

Modeling of the boost converter was carried out using state-space equations, then MATLAB/Simulink software was used for simulation.

State-space equations were obtained employing Kirchhoff's voltage and current laws analysis for each system switching state determined by the u control signal value. Since u the signal can only adopt a 1 o 0 value, there are two possible Boost converter electric configurations, that correspond to charge and discharge cycles for the L and C elements. The two possible circuit configurations are condensed in a single matrix form of state-space equations as showed in (1).

$$\begin{bmatrix} \dfrac{dv_o(t)}{dt} \\ \dfrac{di_L(t)}{dt} \end{bmatrix} = \begin{bmatrix} \dfrac{1-u}{C} & -\dfrac{1}{CR} \\ 0 & -\dfrac{1-u}{L} \end{bmatrix} \begin{bmatrix} v_o(t) \\ i_L(t) \end{bmatrix} + \begin{bmatrix} 0 \\ \dfrac{1}{L} \end{bmatrix} v_i(t) \qquad (1)$$

In (1) L is the inductor, C is the capacitor, $i_L(t)$ is the current in the inductor, $v_o(t)$ is the output voltage, $v_i(t)$ is the voltage ant input of the boost converter, and u is the PWM control signal generated by the PID controller.

3. Optimization Algorithms

A performance comparison between three optimization algorithms: PSO, GA, and GWO is presented in this paper, the main objective of this research is to get insights on the best optimization algorithm for PID controllers tunning applied to a power converter. A brief description of each of the optimization algorithms is presented in the following subsections.

3.1. Grey Wolf Optimizer

Wolves had a strong hierarchy inside their herds, they are organized in a group of 5 to 12 wolves. Each herd had a leading wolf, called alpha α wolf; secondary wolves called beta β wolves; wolves subordinated to α and β wolves are delta wolves δ ; and finally, follower wolves are omega ω wolves. The optimization using the GWO is carried out in three main stages that mimic the hunting process of grey wolves' herds in nature: encircling, hunting, and attacking.

Encircling stage

In this stage, each wolf updates its position in the search space according to the relative best position to prey, dictated for α wolf. The encircling and corral behavior of the prey is modeled mathematically by (2-5).

$$\vec{X}(t+1) = \vec{X}_{pos}(t) - \vec{A}\vec{D} \qquad (2)$$

$$\vec{A} = 2a\vec{r}_1 - a \qquad (3)$$

$$\vec{C} = 2\vec{r}_2 \qquad (4)$$

$$\vec{D} = \left| \vec{C}\vec{X}_{pos}(t) - \vec{X}(t) \right| \qquad (5)$$

where $\vec{A}$ $\qquad \vec{C}$ $\qquad\qquad \vec{X}_{pos}$

$\vec{X}$ vector is the position of the wolf, t is

current iteration, r_1 and r_2 values randomly generated between zero and one, and, vector a value decreases linearly according to iterations.

Hunting stage

The position of wolves is rearranged according to their proximity to the prey. The wolf with the closest distance to the prey is assigned to be the alpha α wolf, β and δ wolves are assigned according to their position to prey. Equations (6-8) describe the wolve position updating.

$$\overline{X}_i(t+1) = \frac{\overline{X}_{i1} + \overline{X}_{i2} + \overline{X}_{i3}}{3} \tag{6}$$

$$\left.\begin{array}{l}\overline{X}_{i1} = \overline{X}_\alpha(t) - \overline{A}_1\overline{D}_\alpha \\ \overline{X}_{i2} = \overline{X}_\beta(t) - \overline{A}_2\overline{D}_\beta \\ \overline{X}_{i3} = \overline{X}_\delta(t) - \overline{A}_3\overline{D}_\delta\end{array}\right\} \tag{7}$$

$$\left.\begin{array}{l}\overline{D}_\alpha = \left|C_1\overline{X}_\alpha(t) - \overline{X}_i(t)\right| \\ \overline{D}_\beta = \left|C_2\overline{X}_\beta(t) - \overline{X}_i(t)\right| \\ \overline{D}_\delta = \left|C_3\overline{X}_\delta(t) - \overline{X}_i(t)\right|\end{array}\right\} \tag{8}$$

where $\overline{X}_i(t+1)$ is the wolf that has the best position to the prey and i is the current iteration number of the GWO algorithm.

Attack stage

Attack to prey occurs when the heard is upon the prey, before this, it is necessary to minimize the distance between wolves and the prey. The prey is the optimization problem's best global solution. Must be defined as a vector A, shown in(3), to make a decreasing coefficient dependent on the iteration number. The vector A value is reduced as the value index a value is reduced according to (9).

$$a = 2 - t\left(\frac{2}{T}\right) \tag{9}$$

The GWO pseudo code is as follows,

GWO: pseudo code.

Result: The best set of particles for the fitness function.
X generation; creation of an initial population of wolves.
Parameters initialization (a,A,C);
Evaluation of position X(0);
Selection of new (a, β and δ);
Selection of new position X(0);
for *e = 1 to MaxIteration* **do**
  for *each wolf$_i$ in* ω set **do**;
    for *i = 0 to* DIMENSION
    do;
      Position(i,j) updating;
    end for
  Change (a,A,c) factors;

      Calculate *X(t+1)*
      position
    end for
  end for

3.2. Particle Swarm Optimization

PSO algorithms are based upon the swarm behavior that some animal species show when they search for resources in their environment. Since PSO is based on collectiveness, each search agent must be modeled. For this purpose, agents are modeled as particles of a swarm, having their position relative to exploration space, velocity, and acceleration rates. At the beginning of the PSO algorithm, several particles are set up in a search space where somewhere in is the global solution for the optimization problem. Finding a global solution depends on the evaluation and minimization of the defined objective function. Iteration by iteration positions, velocities, and acceleration of particles are updated to converge to the global solution. For each particle, a fitness function is numerically evaluated. The best value obtained for all the particle's fitness function is called to be the best global g_{best}. During the iteration process, each best particle fitness function value is called to be the personal best p_{best}. During iterations, the speeds of the particles are accelerated toward the best global solution and the best personal according to (10).

$$v_n = w * v_n + c_1 rand() * (g_{best,n} - x_n)$$
$$+ c_2 rand() * (p_{best,n} - x_n) \tag{10}$$

Where v_n is the speed update of particles, W is a factor of inertia whose value is decreased from 0.9 to 0.4 over time, c_1 and c_2 are coefficients of acceleration pointing to the best global and the best personal.

3.3. Genetic Algorithm

Genetic Algorithms are based on the genetic evolution process, imitating the genes mutation and crossover to create the best-adapted organisms to the environment. Mathematical modeling of these mechanisms allows the algorithm to refine solutions carrying out artificial genes crossover, while the mutation mechanism adds uncertainty to experiment with not expected genes, this makes the algorithm avoid local solutions where it could be trapped. During iterations, the best set of artificial genes is obtained, and therefore, a best-adapted species to the environment. The best group of genes for i generations are said to be the found best solution for the optimization problem.

GA can be expressed as a four-step algorithm,

Step 1. An initial population is created. Crossover rate and mutation rate are randomly generated; generation number is setup.

Step 2. Is evaluated the defined fitness function for each set of artificial genes.

Step 3. Starts the crossover process and mutation process to set the next generation of artificial genes.

Step 4. Return to Step 2 until the stop criterion is reached.

4. Tunning of a PID controller for a Boost converter using optimization algorithms

PID controllers allow the system to operate near desired output values, ensuring good response in the face to possible disturbances. The proposed Boost Converter includes a PID controller for voltage regulation for load changes. The PID controller carries out proportional, integrative, and derivative actions to reduce and prevent error $e(t)$ between output and reference signals of the system. The controller signal $u(t)$ is mathematically modeled according to (11).

$$u(t) = K_p e(t) + \frac{K_p}{T_i} \int_0^t e(t)dt + K_p \frac{T_d de(t)}{dt}] \quad (11)$$

In (11) K_p, T_i and T_d are the proportional, integration time and derivation time constants, respectively. By adjusting the values of these constants, the error in the system can be reduced. The integration and derivative time can be expressed in terms of K_p according to (12-15).

$$K_p = k \quad (12)$$

$$K_i = \frac{K_p}{T_i} \quad (13)$$

$$K_d = K_p T_d \quad (14)$$

where k is the constant of proportional gain K_p, K_i is the constant of integrative gain, and K_d is the constant of derivative gain for the PID controller. The goal of the GWO, PSO, and GA algorithms is to find the best K_p, K_i, K_d values so the error $e(t)$ is minimized. A vector X is defined to include the constant values according to (15). To minimize the Error $e(t)$ the Root Mean Squared Error (RMSE) is defined to be the objective function for the optimization problem according to (16).

$$\vec{X} = [K_p, K_i, K_d] \quad (15)$$

$$RMSE = \sqrt{\frac{\sum_{t=0}^{T_{sim}} \left(v_{out}(t) - v_{reference}(t)\right)^2}{T_{sim}}} \quad (16)$$

Where T_{sim} is simulation time, $v_{out}(t)$ is the output voltage of the power converter, and $v_{reference}(t)$ is the reference voltage signal. The Figure 2 illustrates the overall flowchart for the optimization to find the values for the PID controller constant gains using the GWO, PSO, and GA, the first step of all three algorithms evaluated is to generate a random search agent population, that according to the algorithm is the number of wolves, particles, or gene population, then for each agent, the objective function is evaluated in an iterative loop until the best solution is found.
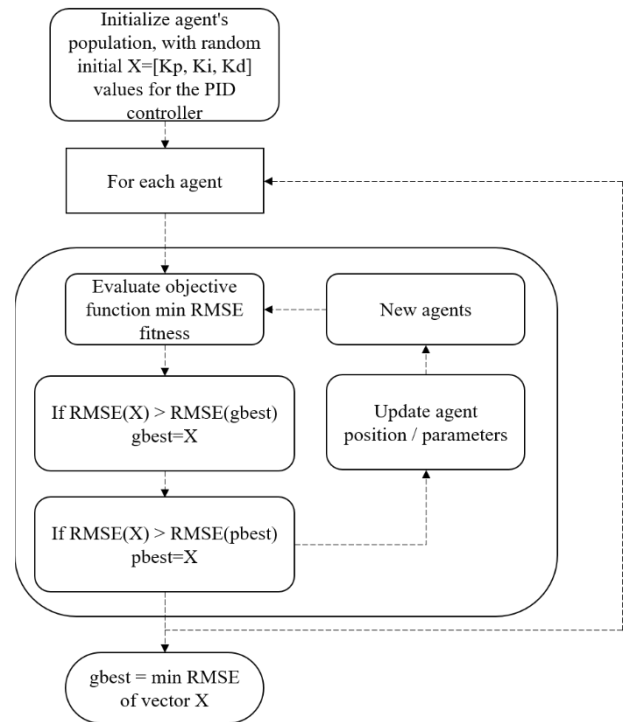
Figure 2: Overall flowchart for the optimization to find the optimal values PID controller constant gains for the proposed optimization algorithms.

5. Simulation, results, and discussion

The optimization algorithms of GWO, PSO, and GA were implemented using MATLAB and Simulink software. Several simulations run for each of these algorithms were performed to find the best PID controller gains values. The difference between each run is the variation of the limits of the search space for the optimization variables, that is, different minimum and maximum values for each gain constant of the controller. A scan was made with different values to determine the search space with the best possible solution for the algorithms evaluated for this particular application. The Boost Converter configuration parameters are shown in Table 1.

Table 1: Boost Converter Configuration

Description	Value	Units
Capacitor	250	μF
Inductor	1.5	mH
Input voltage	12	V
Reference voltage	24	V
Load	3-15	Ω

Since optimization algorithms require some constant parameters these values must be specified at the beginning of each test. One of the most significant benefits of using GWO is that fewer initial parameters are required in comparison to PSO and GA. The parameters initial values for each algorithm used in this work are shown in Table 2. For all three optimization algorithms, the search

K_p, K_i and K_d were varied from 0 to 100 for each PID controller gain.

Table 2: Algorithm parameters initial values

Algorithm	Initial Values	
	Description	*Value*
GWO	Wolves number	12
	Maximum Iterations	7
PSO	Particles	50
	Factor of inertia	0.4-0.9
	Weight of self-adjustment	3
	Weight of social adjustment	1
GA	Size of populations	50
	Rate of crossover	0.9
	Rate of mutation	0.6
	Maximum generations	120

The Table 3 summarizes the PID controller constant gains obtained after the simulation process for each algorithm. The performance is evaluated using RMSE.

Table 3: Best PID gains values and RMSE.

Parameter	Algorithm		
	GWO	*PSO*	*GA*
K_p	0.0532E-5	1.7223E-5	0.1269E-5
K_i	1.6048	2.8391	4.0815
K_d	4.8572E-5	7.2477E-5	4.1911E-5
T_i	3.3151E-7	6.0664E-6	3.1092E-7
T_d	91.3008	4.2082	33.0268
RMSE	1.0683	2.1755	2.2367
Simulation time (s)	1286	1997	1175

As observed in Table 3, the obtained PID controller gains for all the three algorithms had no significant value for de K_d constant, in this sense, the proposed controller built by the metaheuristic algorithms is a PI controller. Using (13) and (14) it is possible to calculate T_i and T_d for each PID controller tunned by the three algorithms, as shown in Table 3. For a greater T_i than K_p value a significative integrative action of the controller is observed according to (11) and (13); and when K_p value is much smaller than T_d the PID controller will have a small derivative action over the plant, according to (11) and (14). The controller performance evaluated by the RMSE shows that the GWO has the lowest error since its RMSE is about 50.89% lower than the one obtained by the PSO and 44.70% lower than the one obtained using the GA. Since the three evaluated algorithms differ in their search

mechanisms, different convergence curves to the best solution found by GWO, PSO and GA algorithms were found. The Figure 3 shows the convergence curve for each of the evaluated algorithms for the Boost converter PID controller tunning optimization problem.
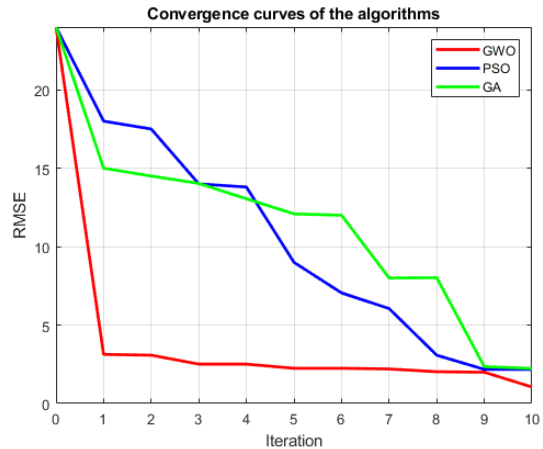
Figure 3: Convergence curves to the best solution found by GWO, PSO, and GA algorithms.

As can be observed in Figure 3, the GWO algorithm is faster to get closer to the best solution set of K_p, K_i and K_d in comparison to PSO and GA whose convergence curves are slower to decrease the resulting RMSE value.

Once the GWO was chosen as the best algorithm for this application, more simulation runs were made varying the search space limits for the optimization variables and with a different number of wolves to ensure a more refined PID gains constants optimal solution for the Boost Converter. The main results of this second round of tests made with the GWO are shown in Table 4.

Table 4: Second round of test for GWO algorithm

Run	Obtained optimal values					
	Search space limits [Kp, Ki, Kd]	*Kp*	*Ki*	*Kd*	*RMSE*	*T*
1	[0-10,0-10,0-10]	0.0012	0.8681	0.0502 E-3	1.1436	948.43
2	[0-0.5,0-5,0-0.5]	0.0025	0.7626	0.0263 E-5	1.1099	968.40
3	[0-0.25,0-2.5,0-0.25]	0.0191	0.0167	0.0098 E-3	8.6105	953.45
4	[0-0.01,0-0.5,0-0.01]	0.0033	0.3118	2.9451 E-5	0.7768	9030.77
5	[0-5,0-32,0-0.005]	0.0532 E-5	1.6048	4.8572 E-5	1.0683	1286.00

As observed in Table 4, the best PID controller gains were obtained in run number four, where the RMSE is minimum with a value of 0.7768. Different RMSE results were obtained for different search space limits; the best results were obtained for the search space limit of [0 to 0.01, 0 to 0.5, 0 to 0.01] corresponding to the $\overrightarrow{X} = [K_p, K_i, K_d]$ optimization variables vector. However, when plotting the system, see Figure 4, response for each run, it is found that the system response of the fifth run, with an RMSE of

1.0683, has a faster response to achieve the reference voltage depicts the higher oscillation rates obtained. Best PID controller gains values must be selected according to the needs: a faster response with oscillations, or a slower response with fewer oscillations. The fifth run is chosen as the best solution since a faster response is desirable for this application.
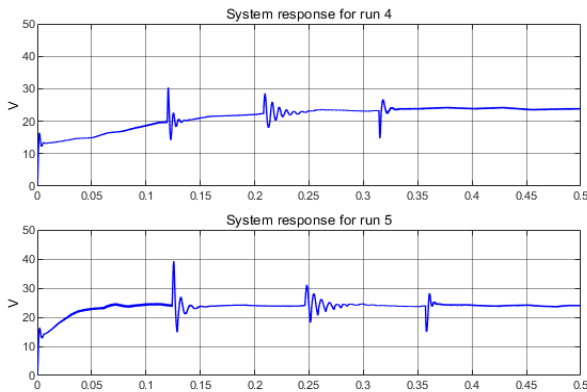
Figure 4: Comparison between run 4 (a) and run 5 (b)for the best GWO simulation results

Once the best solutions for the three evaluated algorithms were chosen, a test of the performance to varying load conditions was carried out to evaluate the system response for the GWO, PSO, and GA tunned PID controller. In Figure 5 the system response for variable load and variable input voltage condition comparison is shown for each algorithm best solution.

As observed in Figure 5, the PID controllers tuned by PSO and GA have similar system responses, presenting important oscillations for load R=15 Ohm. The input voltage to the converter is a signal that varies over time between 11.7 and 12.3 V for the time scale used. The PID controller tunned using the GWO has a better performance to stabilize system response under load and voltage changes in comparison to GA and PSO, despite having a slightly slower response than the other algorithms.

6. Conclusion

In this paper, the tunning of a PID controller for a boost converter was presented. Three algorithms were implemented and compared for this purpose using MATLAB/Simulink: PSO, GA, and GWO. The power converter is modeled using state-space equations. Several simulations are performed to find optimal values. Results are evaluated using the RMSE and the system response for variable conditions of input voltage and load at the output of the power converter. The GWO-PID tunned controller had the best performance with an RMSE about 50.89% lower than PSO and 44.70% lower than GA. The differences between the obtained RMSE using the three algorithms showed in Table 3, gives insights on the greater susceptibility of PSO and GA to be trapped in local optimum solutions, while the lower RMSE value obtained using the GWO algorithm for the same search space limits indicates that this algorithm manages in a better way to circumvent a greater number of local optimum solutions to find a better optimal solution than the PSO and GA algorithms for this application. After the controller was tunned using each algorithm and the best gain constants were found, the system response was evaluated under input voltage and load changes. The system

response for variable load also showed a better performance for the GWO with fewer oscillations for load changes in comparison to PSO and GA. Also, the GWO algorithm had the advantage over the PSO and GA that GWO requires fewer configuration parameters for the optimization process. However, the PID tuned through the GWO was a little slower to reach the reference voltage than the other algorithms. This work gives insights into the GWO algorithm for controller design and control applied to power converters
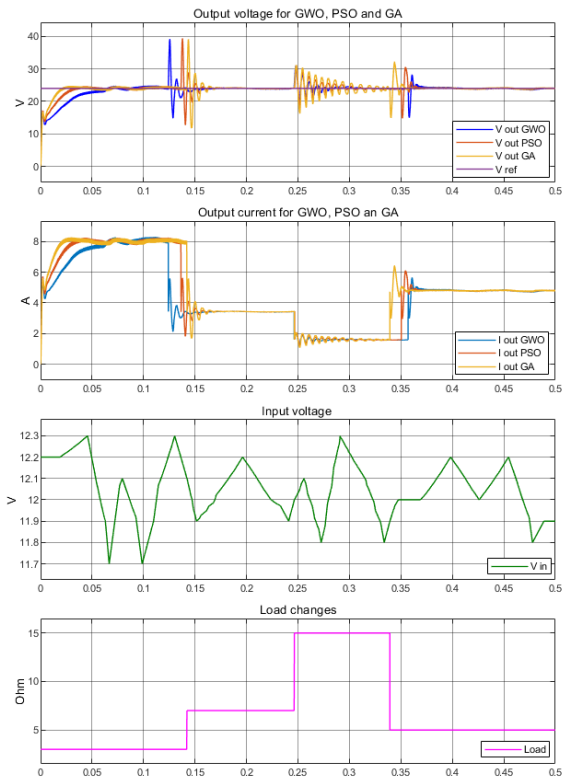
Figure 5: Comparison of system responsefor (a) output voltage, (b) output current under variable (c) input voltage and (d) load

Conflict of Interest

The authors declare no conflict of interest.

7. References

[1] J. Aguila-Leon, C.D. Chinas-Palacios, C. Vargas-Salgado, E. Hurtado-Perez, E.X.M. Garcia, "Optimal PID Parameters Tunning for a DC-DC Boost Converter: A Performance Comparative Using Grey Wolf Optimizer, Particle Swarm Optimization and Genetic Algorithms," in 2020 IEEE Conference on Technologies for Sustainability, SusTech 2020, 2020, doi:10.1109/SusTech47890.2020.9150507.

[2] H. Sira-Ramírez, R. Silva-Ortigoza, Control Design Techniques in Power Electronic Devices, 2013, doi:10.1017/CBO9781107415324.004.

[3] G.A. Raiker, S.R. B, P.C. Ramamurthy, L. Umanand, S.G. Abines, S.G. Vasisht, "Solar PV interface to Grid-Tie Inverter with Current Referenced Boost Converter," in 2018 IEEE 13th International Conference on Industrial and Information Systems (ICIIS), IEEE: 343–348, 2018, doi:10.1109/ICIINFS.2018.8721313.

[4] S.E. Babaa, G. El Murr, F. Mohamed, S. Pamuri, "Overview of Boost Converters for Photovoltaic Systems," Journal of Power and Energy Engineering, **06**(04), 16–31, 2018, doi:10.4236/jpee.2018.64002.

[5] J. Berner, K. Soltesz, T. Hägglund, K.J. Åström, "An experimental comparison of PID autotuners," Control Engineering Practice, **73**, 124–133, 2018, doi:10.1016/J.CONENGPRAC.2018.01.006.

[6] K. Ogata, Modern Control Engineering, 5th ed., Prentice Hall, 2010.

[7] K. Nisi, B. Nagaraj, A. Agalya, "Tuning of a PID controller using evolutionary multi objective optimization methodologies and application to the pulp and paper industry," International Journal of Machine Learning and Cybernetics, **10**(8), 2015–2025, 2019, doi:10.1007/s13042-018-0831-8.

[8] M.T. Özdemir, D. Öztürk, "Comparative performance analysis of optimal PID parameters tuning based on the optics inspired optimization methods for automatic generation control," Energies, **10**(12), 2017, doi:10.3390/en10122134.

[9] G.-Q. Zeng, X.-Q. Xie, M.-R. Chen, "An Adaptive Model Predictive Load Frequency Control Method for Multi-Area Interconnected Power Systems with Photovoltaic Generations," Energies, **10**(11), 1840, 2017, doi:10.3390/en10111840.

[10] Y. Sawle, S.C. Gupta, A.K. Bohre, "Optimal sizing of standalone PV/Wind/Biomass hybrid energy system using GA and PSO optimization technique," Energy Procedia, **117**, 690–698, 2017, doi:10.1016/j.egypro.2017.05.183.

[11] S. Surender Reddy, C. Srinivasa Rathnam, "Optimal Power Flow using Glowworm Swarm Optimization," International Journal of Electrical Power & Energy Systems, **80**, 128–139, 2016, doi:10.1016/J.IJEPES.2016.01.036.

[12] C.Y. Acevedo-arenas, A. Correcher, C. Sánchez-díaz, E. Ariza, D. Alfonso-solar, C. Vargas-salgado, J.F. Petit-suárez, "MPC for optimal dispatch of an AC-linked hybrid PV / wind / biomass / H2 system incorporating demand response," Energy Conversion and Management, **186**(February), 241–257, 2019, doi:10.1016/j.enconman.2019.02.044.

[13] M. Çelebi, "Efficiency optimization of a conventional boost DC/DC converter," Electrical Engineering, **100**(2), 803–809, 2018, doi:10.1007/s00202-017-0552-0.

[14] Q.Y. Lu, W. Hu, L. Zheng, Y. Min, M. Li, X.P. Li, W.C. Ge, Z.M. Wang, "Integrated coordinated optimization control of automatic generation control and automatic voltage control in regional power grids," Energies, **5**(10), 3817–3834, 2012, doi:10.3390/en5103817.

[15] J. Aguila-Leon, C. Chiñas-Palacios, E.X.M. Garcia, C. Vargas-Salgado, "A multimicrogrid energy management model implementing an evolutionary game-theoretic approach," International Transactions on Electrical Energy Systems, **30**(11), 2020, doi:10.1002/2050-7038.12617.

[16] Ovat Friday Aje, Anyandi Adie Josephat, "The particle swarm optimization (PSO) algorithm application – A review," Global Journal of Engineering and Technology Advances, **3**(3), 001–006, 2020, doi:10.30574/gjeta.2020.3.3.0033.

[17] N.K. Jain, U. Nangia, J. Jain, A Review of Particle Swarm Optimization, Journal of The Institution of Engineers (India): Series B, **99**(4), 407–411, 2018, doi:10.1007/s40031-018-0323-y.

[18] B. Hekimoğlu, S. Ekinci, S. Kaya, "Optimal PID Controller Design of DC-DC Buck Converter using Whale Optimization Algorithm," in 2018 International Conference on Artificial Intelligence and Data Processing, IDAP 2018, Institute of Electrical and Electronics Engineers Inc., 2019, doi:10.1109/IDAP.2018.8620833.

[19] S. Mirjalili, S.M. Mirjalili, A. Lewis, "Grey Wolf Optimizer," Advances in Engineering Software, **69**, 46–61, 2014, doi:10.1016/j.advengsoft.2013.12.007.

[20] S.-X. Li, J.-S. Wang, "Dynamic Modeling of Steam Condenser and Design of PI Controller Based on Grey Wolf Optimizer," Mathematical Problems in Engineering, **2015**, 1–9, 2015, doi:10.1155/2015/120975.

[21] S. Yadav, S.K. Verma, S.K. Nagar, "Optimized PID Controller for Magnetic Levitation System," IFAC-PapersOnLine, **49**(1), 778–782, 2016, doi:10.1016/J.IFACOL.2016.03.151.

[22] R.H.G. Tan, L.Y.H. Hoo, "DC-DC converter modeling and simulation using state space approach," 2015 IEEE Conference on Energy Conversion (CENCON), (2), 42–47, 2015, doi:10.1109/CENCON.2015.7409511.

Cardiovascular Risk in Patients who go to the Medical Office of a Private Health Center in North Lima

Jairo Zegarra-Apaza[1], Sara Oliveros-Huerta[1], Santiago Vilela-Cruz[1], Rosita Chero-Benites[1], Gissett Marcelo-Ruiz[1], Leslie Yelina Herrera-Nolasco[1], Brian Meneses-Claudio[2], Hernan Matta-Solis[1,*], Eduardo Matta-Solis[3]

[1]Faculty of Health Sciences, Universidad de Ciencias y Humanidades, 15314, Lima-Perú

[2]Image Processing Research Laboratory (INTI-Lab), Universidad de Ciencias y Humanidades, 15314, Lima-Perú

[3]Health Sciences, Instituto Peruano de Salud Familiar, 15304, Lima-Perú

A R T I C L E   I N F O

A B S T R A C T

Cardiovascular diseases are the group of conditions produced in the heart or blood vessels. This is one of the main causes of death in Peru and the world, produced mostly by non-communicable diseases and harmful habits, which makes it an extremely predictable disease. These factors include body mass index, smoking, diabetes, age, blood pressure, total cholesterol, and high-density lipoproteins. Therefore, this study aims to identify patients who go to the medical office of a private health center in North Lima who do not have a prior history of a cardiovascular accident, using the cardiovascular risk calculator provided by the Organization World Health. The present research work had a quantitative, non-experimental, descriptive, and cross-sectional approach, in a population of 99 adult and elderly patients. Regarding the results, it was found that 46.5% presented a low cardiovascular risk, 37.4% a moderate risk, 11.1% a high risk and 5.1% an extremely high risk. The information found contrasts with the number of deaths caused by this disease and may be an indicator of greater prevention by populations with higher economic income. Finally, it is concluded that diabetes, smoking and the age group are predisposing factors to an increased cardiovascular risk.

1. Introduction

Cardiovascular risk is specified as the probability of a heart or blood vessel condition occurring [1]. The origin of cardiovascular diseases (CVD) is closely linked to harmful habits or non-communicable diseases, from which derives its progressive and highly predictable nature [2].

According to the Framingham Heart Study, conducted from 1948 to the present, the main predictors of a CVD are age, body mass index, HDL and total cholesterol, smoking, diabetes, and treated high systolic blood pressure or untreated [3], [4]. Therefore, these predictors are also connected to illnesses and harmful habits, present and increasing mainly in developed and developing countries.

In Peru, according to data collected by the Instituto Nacional de Estadística e Informática (INEI), from 2015 to 2018 the Peruvian population has had an annual increase in cases with high blood pressure (14.8%), diabetes mellitus (3.9%) and obesity

(23%), which are mainly concentrated in Lima, while cases of overweight (37%), cigarette consumption (19%) and daily cigarette consumption (1.7%) make up almost constant in the years of study [5]. Likewise, its importance in relation to cardiovascular risk (CVR), death attributed to diabetes also increased [6], which gives an indication of inefficient control of the disease. Consequently, as mentioned above, each year the cardiovascular disease (CVD) threat is amplified and the people with the longest longevity are affected.

On the other hand, in [7], a study was carried out in Peruvian youth and adults between 20 and 59 years old who were users of popular dining rooms, these premises being focused on food supply in areas of poverty and extreme poverty. The research found a prevalence of abdominal obesity (51.6%), low HD-C (42.2%), hypertriglyceridemia (35.3%), overweight (35.8%), high blood pressure (21.0%) and hyperglycemia (14.1%), thus conforming an overall metabolic syndrome of 40.1%. This not only allows to infer that the state of this type of population makes them prone to CVD, but also without a preventive measure that takes an active role in the search for these patients, the risk will

probably not be reduced until they are close to suffering a condition of this type, because despite having insurance focused on low-income populations, regular visits in search of prevention are not usually integrated in Peru.

In the study [8], carried out in a public hospital for internal medicine inpatients, vascular age and cardiovascular risk were evaluated in 238 participants who were between 30 and 74 years old without previous cardiovascular events. The objective was to determine these variables as well as the predominant risk factor. This study concluded with a medium and high cardiovascular risk in the highest percentage of the population, a difference between chronological and vascular age of 6.9 years old, and finally, diabetes and male sex were identified as predominant factors.

According [9], a research carried out in Spain, they were able to note that heart disease is the main cause of morbidity in a tertiary hospital and men between 50 and 60 years old are the ones with the highest morbidity in this pathology, causing high rates of incapacity for work, in addition the problem goes beyond the hospital setting because these patients will require cardiac rehabilitation. They also point out that emphasis should be placed on prevention, since studies have documented that of the patients who were discharged, 75% of patients re-entered for any cardiac complication.

In [10], a study was carried out in an educational institution of 100 schoolchildren from 10 to 19 years old, with the aim of determining cardiovascular risk. The study found a prevalence of cardiovascular risk of 84.6% in adolescents (15-18 years old), as well as that the consumption of alcoholic beverages and unhealthy eating habits are related to the increase in cardiovascular risk. So, it is suggested that prevention from an early age is essential to reduce its appearance in more advanced stages of life.

The objective of this research work is to identify cardiovascular risk in patients with no prior history of CVD, excluding hypertension in untreated cases, and who go to a cardiology office in a private health center, using a calculator provided by the Organization. Pan American Health (PAHO). Because of having an alteration in the cardiovascular system that is not a serious alteration, patients of the cardiology service are one of the groups to be suspected of having a cardiovascular condition that may cause irreversible damage or death of the patient.

The instrument used in this study is the CVR calculator provided by PAHO, based on a form proposed by the World Health Organization (WHO) to evaluate CVR in Latin American and Caribbean countries [11]. This instrument uses a risk score that is based on the Framingham study, which also is adapted to the characteristics of the region and these data will be processed in matrix form by the IBM SPSS statistics 25 program. This application deals with to assess CVR quickly and easily in patients, which is mainly focused as an aid to medical health personnel, but due to the simplicity of its use, this can be a great option for the recruitment of risk patients who are in areas that are difficult to access or that lack medical personnel.

The organization of the work carried out is structured in the following way: in Section II, the development carried out for the identification of cardiovascular risk in patients who go to the medical office will be found. In section III, it will find the results of the data collected for the measurement, as well as the most relevant values of the CVR found. In section IV, the discussion of the research work and finally in section V, the conclusions, as well as the expectations that are had for the use of this research work.

2. Methodology

This section is made up of the process followed for the cardiovascular risk assessment, which are: data acquisition, data processing and finally the results with their corresponding risk values. The steps in carrying out the cardiovascular risk assessment are represented in a flowchart in Figure 1. All this was passed through the ethics committee, to give the authorization for the research work, followed by the ethical principles in part for the study in patients, such as beneficence, autonomy, non-maleficence, and justice.
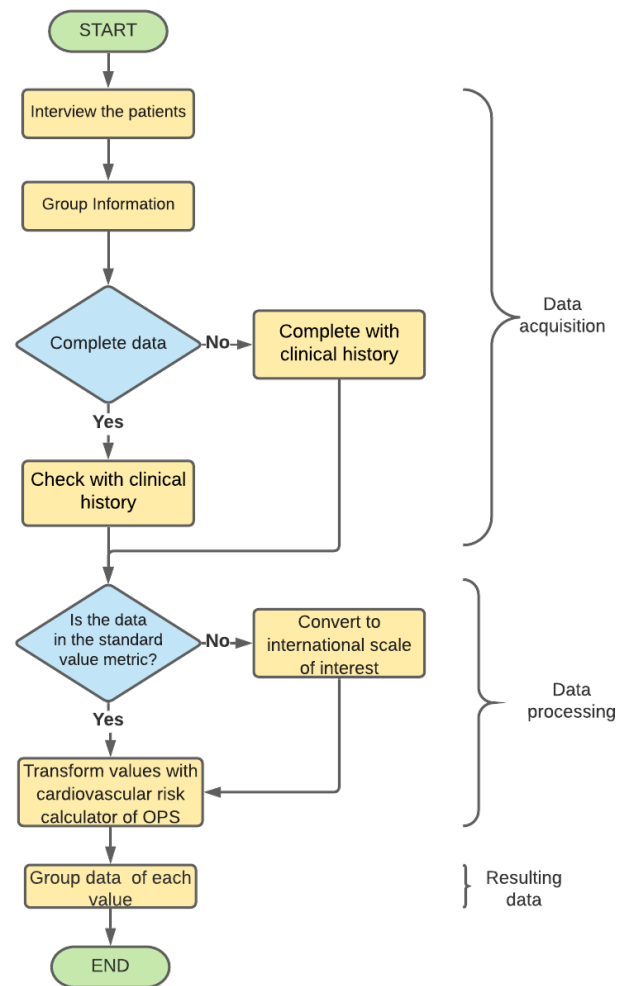
Figure 1: Flowchart for cardiovascular risk data collection

2.1. Data Acquisition

This study has a quantitative, non-experimental, descriptive, and cross-sectional approach. For the acquisition of the data, coordination was required with a private polyclinic located in the jurisdiction of North Lima, in which the patients of the cardiology service were evaluated in the first quarter of the year. Likewise, the data collected in the research work was cataloged in

sociodemographic data of the patient and descriptive parameters of cardiovascular risk, the subdivisions are shown in Table 1.

Table 1: Sociodemographic data and descriptive parameters of cardiovascular risk of people from a cardiology clinic of a Private Polyclinic in North Lima

Sociodemographic Data	Gender
	Degree of instruction
	Occupation
Descriptive parameters of cardiovascular risk	Maximum / Systolic Pressure
	Smoking
	Total cholesterol
	Diabetes
	Age

Population and Sample

The population is made up of 110 adult patients (49-59) and older adults (60 or more) from the jurisdiction of the health center, but the sample size was made reaching 99 since the remaining patients did not want to participate voluntarily in the study.

Inclusion and Exclusion Criteria

The inclusion criteria that were considered at the time of data collection were: Patients who are between the ages of 49 and 79, who have high blood pressure, who are continuing or go to medical office more than once, who belong to the jurisdiction of the polyclinic and agree to participate voluntarily in the study.

In addition, the exclusion criteria corresponding to the study were: patients who depended on a wheelchair for mobilization and those who suffered from cognitive or hearing impairment.

Figure 2: WHO/ISH AMR B risk prediction table, for settings in which blood cholesterol can be measured

2.2. Data Processing

The data corresponding to the descriptive parameters of cardiovascular risk were transformed into the international system of measurement units that were adequate or preferable for the measurement of each parameter and subsequently entered the cardiovascular risk calculator provided by PAHO that takes place during the month of November. These data were cataloged by the calculator according to the percentage of CVR of the patient suffering from a cardiovascular condition in the subsequent 10 years corresponding to the table displayed in Figure 2.

The table displayed in Figure 2 subdivides cardiovascular risk into 5 subsectors, relating them to one color according to the range of cardiovascular risk that occurs, these being: green, for a CVR <10%, yellow for a CVR from 10% to <20%, orange from 20% to <30%, red from 30% to <40% and dark red for values> 40%.

Likewise, the acquired data were entered in matrix form to the IBM SPSS Statistics 25 software, for subsequent management and analysis. The variables considered for data analysis are ID, gender, degree of institution, family type, occupation, smoking, diabetes, maximum systolic pressure, total cholesterol, cardiovascular risk, age, and Age 2, these two being the last ages corresponding to the adult and older adult age groups.

The participation of health personnel in the process of obtaining data is significant due to the complications that may arise due to the patient's lack of knowledge regarding the topic corresponding to each variable, the patient's mistrust of a person who do not work in the public health service, as well as greater efficiency in the collection of data in the clinical history and in the reliability when measuring the value of blood pressure.

3. Results

99 adult and elderly patients from the cardiology service were evaluated in the first quarter of the year. Sociodemographic data and descriptive parameters of cardiovascular risk were identified in each of them, as shown in Tables 2, 3 and 4.

Table 2: Sociodemographic data of patients from a cardiology clinic of a Private Polyclinic in North Lima

Sociodemographic data	N	%
Age [1/]		
Adult	57	57.6%
Older adult	42	42.4%
Gender		
Female	35	35.4%
Male	64	64.6%
Degree of instruction		
Illiterate	2	2.0%
Primary	16	16.2%
Secondary	73	73.7%
Technical	5	5.1%
University	3	3.0%
Occupation		
Does not work	17	17.2%
Retired	10	10.1%
Laborer	12	12.1%
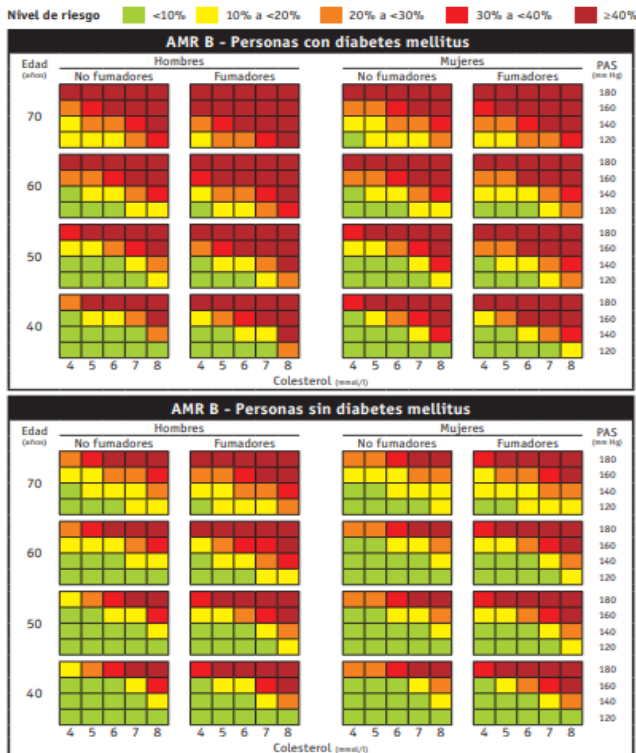
Employee		15	15.2%
Informal work		45	45.5%
Total		**99**	**100.0%**

[1/]Mean = 57.7; Standard Deviation (SD) = 11.08

These results indicate that the mean age of the patients was 57.7 years, the majority being adults representing 57.6%, likewise, 64.6% were men, 73.7% had a secondary level, 45.5% worked informally and 35.4% have an extended family as shown in Table 2.

Table 3: Cardiovascular risk parameters in patients of a cardiology office of a Private Polyclinic in North Lima

Cardiovascular risk parameters	**□ ± SD [1/]**	
Maximum Systolic Pressure (mmHg)	132.9	11.6
Total Cholesterol (mg/dL)	225.6	22.4
Smoking	**N**	**%**
Yes	52	52.5%
No	47	47.5%
Diabetes		
Yes	84	84.8%
No	15	15.2%

[1/] Mean (□); Standard Deviation (SD)

Table 3 shows that the mean maximum systolic pressure was 132.9 mmHg, and the mean total cholesterol was 225.6 mg/d. On the other hand, 52.5% were smokers and 84.8% had diabetes.

Table 4: Cardiovascular risk and descriptive parameters of cardiovascular risk

			Cardiovascular Risk				Total
			Low	Mode rate	High	Very High	
Age group	Adult	N	34	20	3	0	57
		%	34.3%	20.2%	3.0%	0.0%	57.6%
	Older adult	N	12	17	8	5	42
		%	12.1%	17.2%	8.1%	5.1%	42.4%
Smoking	Yes	N	15	24	10	3	52
		%	15.2%	24.2%	10.1%	3.0%	52.5%
	No	N	31	13	1	2	47
		%	31.3%	13.1%	1.0%	2.0%	47.5%
Diabetes	Yes	N	34	36	10	4	84
		%	34.3%	36.4%	10.1%	4.0%	84.8%
	No	N	12	1	1	1	15
		%	12.1%	1.0%	1.0%	1.0%	15.2%

Table 4 shows that: adults are 57.6%, with 34.3% belonging to a low CVR, while older adults are 42.4%, and their CVR is mostly moderate with 17.2%; those who smoke make up 52.5% of the population, their CVR being mostly moderate with 24.2%, while those who do not smoke make up 47.5% and their CVR is mostly

low with 31.3%; finally, those with diabetes make up 84.8% of the population and their CVR tends to be moderate with 36.4% or low being 34.3%, while those without diabetes make up 15.2% and most of them have a low CVR representing the 12.1%. These data help to deduce the trend of cardiovascular risk in relation to its risk factors in private health center.

On the other hand, the chi square results were 0.001 for the age group and cardiovascular risk, 0.027 for diabetes and cardiovascular risk, and 0.001 for smoking and cardiovascular risk for P <0.05, confirming that the differences in the proportions observed between the two groups are statistically significant. These results allow to identify the relationship of risk factors with cardiovascular risk in populations that go to a private health center, as well as to differentiate their situation from the current situation in Peru.

Table 5: Cardiovascular risk in patients of a cardiology office of a Private Polyclinic in North Lima

Cardiovascular Risk	**N**	**%**
Extremely high Risk	5	5.1%
High Risk	11	11.1%
Moderate Risk	37	37.4%
Low Risk	46	46.5%
Total	**99**	**100.0%**

Table 5 shows that 46.5% of adult and elderly patients presented a low cardiovascular risk, 37.4% a moderate risk, 11.1% a high risk and 5.1% an extremely high risk.

The knowledge of these results is important because it will allow to identify cardiovascular risk in patients with no prior history of CVD, and it also helps to know the risk factors to which many people, such as smokers, are exposed. This information allows to realize that the greater control there is over risk factors, whether through a change in lifestyle (healthy eating, playing sports, etc.), the less likely there is to have cardiovascular risk.

4. Discussion

The results confirm that there is a significant relationship between smoking, age group and diabetes with cardiovascular risk, thus agreeing with the findings of the Framingham heart study.

On the other hand, the prevalence of CVR found is mostly belonging to a low-risk one, in other words, a population that has a less than 10% risk of suffering cardiovascular disease in the next 10 years, which contrasts significantly with the analysis carried out in [12], which lists circulatory diseases as the third cause of death for large groups and cardiac ischemia as the second cause of death. As it is a private health center, it can indicate a greater emphasis on prevention by a sector of the population with higher economic incomes.

Peru is a developing country where child malnutrition and respiratory diseases are still considered highly relevant problems and their financing is a high priority. For this reason, this research is not only focused on identifying the status of patients entering

cardiology offices, but also on the scientific contribution, because its use is also expected to promote the use of this instrument for the early recruitment of patients, both by health personnel and residents through self-evaluation, because due to its easy access and simplicity it can mean a great advance for the prevention of cardiovascular diseases, in a country where, as declared in [13], self-knowledge, adherence or control of hypertension are still below to other Latin American countries.

5. Conclusions

It is concluded that in patients who go to the medical office of the private health center in North Lima, diabetes, smoking and the age group are predisposing factors to increased cardiovascular risk in patients.

It is also concluded that the majority were adults, with a secondary institution degree and who work informally. As well as 5 out of 10 patients were smokers and 8 out of 10 had diabetes.

Finally, it is concluded that cardiovascular diseases are made up of a series of characteristics that can be regulated to prevent a cardiovascular risk, such as smoking, diabetes, total cholesterol, and maximum systolic pressure. As well as that the problem increases in relation to the old age of the population and therefore measures should be taken focused on these age groups.

This research work was studied to contribute to the lack of scientific information with the use of the PAHO cardiovascular risk calculator, in addition to promoting its use in the Peruvian community nursing setting for the recruitment of risk patients, because despite having problems such as malnutrition in the child population, the obstacle that CVDs pose to life expectancy in adults and older adults cannot be ignored.

The Strength in our research work is teamwork to be able to carry out this research work

The limitation in the research work is access to people to be in the study, since many of them mentioned that they preferred to enter their consultations than to be in the study.

Conflicts of Interest

The authors declare no conflict of interest.

References

[1] M. Arboleda, A. García, "Riesgo cardiovascular: análisis basado en las tablas de Framingham en pacientes asistidos en la unidad ambulatoria 309, IESS – Sucúa," Revista Med, **25**(1), 20–30, 2017, doi:10.18359/rmed.1949.

[2] J. Álvarez, A. Álvarez, W. Carvajal, M. González, J. Duque, O. Nieto, "Determinación del riesgo cardiovascular en una población.," Revista Colombiana de Cardiologia, **24**(4), 334–341, 2017, doi:10.1016/j.rccar.2016.08.002.

[3] R. D'Agostino, R. Vasan, M. Pencina, P. Wolf, M. Cobain, J. Massaro, W. Kannel, "General cardiovascular risk profile for use in primary care: The Framingham heart study," Circulation, **117**(6), 743–753, 2008, doi:10.1161/CIRCULATIONAHA.107.699579.

[4] J. Alvarez, V. Bello, G. Pérez, O. Antomarchi, M. Bolívar, "Factores de riesgo coronarios asociados al infarto agudo del miocardio en el adulto mayor.," Medisan, **17**(1), 54–60, 2013.

[5] Instituto Nacional de Estadistica e Informática, Peru, Enfermedades No Transmisibles Y Transmisibles, 2018.

[6] N. Atamari, M. Ccorahua, A. Taype, C. Mejia, "Mortalidad atribuida a diabetes mellitus registrada en el Ministerio de Salud de Perú, 2005-2014," Revista Panamericana de Salud Pública, **42**, 1–7, 2018, doi:10.26633/rpsp.2018.50.

[7] K. Adams, J. Chirinos, "Prevalencia de factores de riesgo para Síndrome Metabólico y sus componentes en usuarios de comedores populares en un distrito de Lima, Perú," Revista Peruana de Medicina Experimental y Salud Publica, **35**(1), 39–45, 2018, doi:10.17843/rpmesp.2018.351.3598.

[8] J. Mayta, A. Morales, A. Cárdenas, J. Mogollón, V. Armas, L. Neyra, C. Ruíz, "Determinación de riesgo cardiovascular y edad vascular según el score de Framingham en pacientes del Hospital Nacional Arzobispo Loayza," Horizonte Med, **15**(2), 27–34, 2015, doi:10.1520/stp30190s.

[9] A. Sánchez, M. Bobadilla, B. Dimas, M. Gómez, G. González, "Enfermedad cardiovascular: primera causa de morbilidad en un hospital de tercer nivel.," Revista Médica de Cardiologia, **27**(3), 98–102, 2016.

[10] C. Torres, D. Illera, D. Acevedo, M. Cadena, L. Meneses, P. Ordoñez, L. Pantoja, M. Pastás, "Riesgo cardiovascular en una población adolescente de Timbío, Colombia," Revista de La Universidad Industrial de Santander. Salud, **50**(1), 59–66, 2018, doi:10.18273/revsal.v50n1-2018006.

[11] OPS/OMS, Calculadora de riesgo cardiovascular, Organización Panamericana de La Salud - Uruguay,.

[12] Ministerio de la Salud, ASIS-R: Análisis de Situación de Salud de los Gobiernos Regionales, 120, 2019.

[13] P. Herrera, J. Pacheco, G. Valenzuela., G. Málaga, "Autoconocimiento, Adherencia al tratamiento y control de la Hipertensión Arterial en el Perú: una versión narrativa.," Revista Peruana de Medicina Experimental y Salud Publica, **34**(3), 497–504, 2017, doi:10.17843/rpmesp.2017.343.2622.

Modelling Human-Computer Interactions based on Cognitive Styles within Collective Decision-Making

Nina Bakanova[1], Arsenii Bakanov[2], Tatiana Atanasova[3,*]

[1]Keldysh Institute of Applied Mathematics – RAS, 125047, Russia

[2]Institute of Psychology of Russian Academy of Sciences, 129366, Russia

[3]Modelling and Optimization Department, Institute of Information and Communication Technologies – BAS, 1113, Bulgaria

ARTICLE INFO	ABSTRACT
	The article proposes an approach to evaluate human-computer interaction in the collective decision-making model. It is believed that all team members interact with each other through a distributed information system. The approach involves considering, when modelling, the personality characteristics of perception, each member of the team as a set of cognitive styles. Within the scope of the proposed technique, it is believed that information flows are interconnected with the processes of collective decision-making, which makes it possible to model the process of collective decision-making, monitor and analyse the effectiveness of the collective's activities. Experimental studies accomplished with statistical data processing were carried out and discussed.

1. Introduction

This paper is an extension of the work originally presented in Big Data, Knowledge and Control Systems Engineering (BdKCSE'2019) Conference [1]. The article further develops aspects of human-machine interaction in a distributed information environment. Here the emphasis is on collective decision-making taking into account the cognitive features of perception of team members.

The relevance of research in this area is due to a number of reasons, including the processes of globalization of the economic development of industrial sectors, the creation of a great number of large-scale, distributed corporations, concerns, holdings, and, accordingly, the decentralization of management processes controlled by parent organizations. Information interaction of such corporations is carried out through distributed information systems. The distributed information landscape is a genuine development of computerized, data and interaction technologies. The challenge of human communication with the distributed information ecosystem is gaining growing methodical and pragmatic importance.

A significant problem in the management of large-scale, distributed organizations are collective decision-making processes, which require the interaction of many people; this inevitably leads to the complication and delay of the decision-making process, as well as to the possible emergence of contradictions in the process of solving the problem.

The importance of taking into account the opinion of each member of the team, the importance of obtaining a coordinated, balanced solution to complex problems, the importance of ensuring transparency of the decision-making process in the team - all of the above emphasizes the relevance of developments in the field of creating automated tools to support collective decision-making. The development of mechanisms and techniques that provide modelling and visualization of collective decision-making processes will increase the efficiency and effectiveness of decision-making in a geographically distributed team through the implementation of modes of human-computer interaction.

When studying the processes of interaction in large-scale distributed information networks, we can talk about information flows connecting all users of the information system. As a result of the advance of information and computer technologies, now there are opportunities for the development of intelligent modules that allow to analyse, visualize and improve the efficiency of interaction processes in a team, including such as collective decision-making processes.

This article is devoted to the development of methods for modelling and presenting processes related to collective decision

*Corresponding Author: Tatiana Atanasova, atanasova@iit.bas.bg

making. First, the development of decision theory over time is discussed. It is then proposed to use a cognitive modelling methodology to rank team members in the collective decision-making process. The reflection of the cognitive styles of the participants in the human-computer interaction with distributed information system is emphasized in further consideration. Experimental studies accomplished with statistical data processing were carried out. The cognitive styles of the collective members were investigated through an experimental study to be included in the cognitive map modelling. Finally, the results of the experiments are discussed.

2. The Basis of Decision Theory

The fundamental basis of decision theory in mathematics, computer science and economics is the provision of rational human behaviour and the theory of utility.

The game theory was introduced in 1944 by John von Neumann and Oskar Morgenstern in their book, entitled "Game Theory and Economic Behavior". However, in a number of researches works, for example in [2], it is shown that human behaviour is not always rational, and often, on the contrary, is irrational (from the point of view of gaining a win). As an example, to demonstrate the features of human behaviour, we can cite the paradox proposed by [3]. As a result of presenting lotteries to various groups of people, it was shown that people prefer the lottery where the risk of losing is excluded or minimal. Whereas the computer calculates probabilities and acts rationally, i.e., maximizes utility (or gain).

A study of the evolutionary development of work in the expansion of decision support systems as a scientific direction shows that from the moment Atanasoff and Berry began to develop the first digital computing device in 1939 (at Iowa State College) and before the 1980s, the main goal was "to teach the computer to think like a person". Since the early 1980s up to the present time, the central paradigm has been the concept of "artificial intelligence" [4-10]. According to artificial intelligence professionals, the effectiveness of intelligent systems is determined both by formal mathematical schemes based on mathematical logic and by the knowledge of experts in a specific subject area, which can be explicated in the process of knowledge extraction. The analysis of scientific works in the field of knowledge extraction shows that, despite the significant success achieved in the advancement of intelligent, information systems, the key problem of creating any intelligent system is the process of extracting expert knowledge, as well as original heuristics used by specific experts to solve problems [11-15].

To date, technologies and methodologies for the design of knowledge-based intelligent systems have been developed, in which the sequential passage of the stages of acquiring expert knowledge is realized:

- the stages of extracting [16] and

- conceptual analysis of expert knowledge [17-21].

However, the actual problem of modelling and visualizing the collective decision-making process, as well as modelling and visualizing the information interaction between experts, has not received sufficient consideration, partly because this problem is

interdisciplinary, as it is at the intersection of information technology, mathematics, sociology and psychology.

3. Cognitive Maps for Modelling

The use of models to study an object, phenomenon or process is a well-established and well-proven research method. By the term model, in this article, we mean a formal representation of an object, (process, phenomenon) in some form, intended for the study of this object. Formal representation of an object (process, phenomenon) can be:

- mathematical,

- simulation,

- sign-symbolic.

In the present study, cognitive maps were used as a basis for the model of making decision in information interaction within a distributed information system. Using of models based on cognitive maps made it possible to visualize information processes of remote (distributed) interaction in a team, including the processes of creating groups, monitoring remote activities of team members, etc. For visualization and ranking of team members, it is proposed to use the methodology of cognitive modelling [11, 22-27]. According to the methodology, it is supposed to build a fuzzy model, visualized as a fuzzy graph (cognitive map), in which the vertices are team members, and the weighted arcs are information flows, relationships and social significance (weight, authority, awareness, experience, etc.) of each member of the team, the weight of each arc of the graph reflects the strength of the influence of a particular individual on the process of making a collective decision.

Information flows between team members, in general, can be verbal and non-verbal, mediated by the electronic information environment and not mediated. In this work, only flows mediated by a distributed information system are investigated. The considered information flows are subdivided into explicit and implicit, stable and unstable, as well as formal and informal.

Formally, a cognitive map can be symbolized as a directed sign graph *(F, W)*, where *F* is the set of vertices - team members, $W=|w_{ij}|$ - adjacency matrix. The dynamics of the decision-making process is presented as a sequential set of situations *X(t−1), X(t), X(t+1),…, X(t+n)*, which are the situation state vectors at successive discrete times: *t−1, t, t+1, …, t+n*, where *t* is some number of such moment in time.

The interactions can be determined by summing all of them, according to the formula (1):

$$X_i(t+1) = X_i(t) + \sum_{i=1}^{n}(X_{i-1}(t+1) - X_{i-1}(t))W_{i,i-1} \quad (1)$$

The use of cognitive maps allows modelling and visualizing not only the information flows, but also the configuration of the team in the process of collective decision taking, that is, the use of cognitive maps allows displaying the dynamic processes occurring in the team in the process of deciding.

4. Cognitive Styles of the Collective Members in the Model

The need for specific information (information flow) for each team member is determined by several factors influencing the

request for information of a team member, namely: knowledge, skills, job responsibilities, style of activity, and personality characteristics of perception. By personal characteristics of perception, we mean the set of cognitive styles inherent in each member of the group. At the same time, we make it a condition that we consider in the model only personal characteristics of perception, since a person's personality traits are not limited to a set of cognitive styles.

4.1. Cognitive-Style Characteristics

According to several scientists, individual ways of processing information are largely determined by cognitive styles [28, 29]. Cognitive styles actively participate in the process of choice and making decisions in work, manage the emotional and behavioural characteristics of human activity [30]. Scientific works show the essential part of the cognitive and stylistic aspects of the subject in the execution of actions that involve self-government and answerability in during process of making decisions, particularly in highly uncertain conditions. In parallel, the assignment of psychological patterns as form-creating (combining, central) elements in the process of choosing an appropriate option is highlighted [31]. Of the entire set of cognitive styles given in the work [32], we will consider only three cognitive styles, namely: the "field dependence/field independence" style, the "narrow/wide range of equivalence" style, the "impulsivity/reflectivity". Detailed justification and appropriateness of the choice of the above styles are given in the work [33].

4.2. Identifying the Cognitive-Style Characteristics

As follows, we briefly describe the cognitive styles studied and present the methods used for the research.

The style "field dependence/field independence" is traditionally considered as a way of an individual to solve perceptual problems, and the presence of "the ability to overcome a complex context" (according to G. Witkin). To diagnose cognitive-style features, G. Witkin's "*Included Figures*" technique was used (evaluation of field dependence - field independence, individual variant) [34].

The style "narrow/wide range of equivalence" reflects the predominant orientation of the individual to the features of similarity or differences of classified objects, their obvious or hidden features. To diagnose these cognitive-style features, the method "*Free sorting of objects*" by R. Gardner and V. Kolga was used.

The style "impulsivity/reflectivity" characterizes individual differences in the speed and correctness of decisions made in situations of uncertainty and the presence of many alternatives. To diagnose these cognitive-style features, the method "*Comparison of similar drawings*" by J. Kagan (assessment of impulsivity - reflectivity as the cognitive pace of decision-making) was used [35].

The choice of these particular styles for research is due to the fact that the team members united in the work on the project must have a good idea of the general structure of the entire project, understand the specifics of the work and the distinct (individual) tasks of other team members within the framework of this project, and have a proportionate cognitive pace of decision-making, carry out synthesis and analysis of project tasks.

In the framework of this study, the relationship between the cognitive-style characteristics of team members and the effectiveness of decision-making when working on a common project was studied.

5. Experimental results

To examine the cognitive-style characteristics of team members in the model, an experimental study was conducted. The most important phases of human interaction with the information system were modelled as the subject was needed to:

- familiarize s/himself with the content of the texts specially developed for this study,
- analyse the content of the texts,
- classify the content of the texts,
- then answer the proposed questions.

Also, during the study, the above mentioned cognitive-style characteristics were identified.

For this experiment, several texts from 2 to 8 pages in volume (250 - 300 words per one page) were prepared specifically. Throughout the experiment, the subject of investigation has to read these specifically arranged texts. After reading, the subject of the investigation was asked to answer questions about the structure of the text and to give a quantitative calculation of the discovered options. The volume of the presented material was taken into account to model the interaction with the information system. Gaze movements were recorded using specialized SMI equipment (http://www.smivision.com), which tracks the trajectory of the subject's gaze.

Several quantitative criteria for assessing the activity of information interaction have been established [1]. Statistical methods for data processing were applied together with using Student's t-test and Mann-Whitney U-test. Spearman's correlation coefficient was used to assess the relationship between variables. Student's t-test was used to analyse two independent data samples to compare the mean of the two populations. Mann-Whitney U-test determines whether the area of overlapping values between the two series is small enough.

The research results are shown in the Table. Questions of type 1 were used for the quantitative assessment, and questions of type 2 were questions about the structure of the text.

Note: Indicators for the assessment of the success and effectiveness of the activity are time for reading of the presented text (document); the keyword usage rate, i.e., how often the subject rereads the reference words; time for answering questions; coefficient of correct answer; coefficient of confidence in decision making i.e., how long the subject analyses the alternatives.

As an outcome of the analysis of the results obtained, the following interdependencies were revealed: 1) the more work experience, the less time during which the subjects look at the text of the document presented on the computer screen, and the less time spent on making a decision regarding the choice of an alternative, 2) on the contrary, the "coefficient of correctness of answers" is directly proportional to the indicator "work experience". That is, subjects with work experience more often solve problems correctly.

Table 1: Correlation relationships between performance criteria and characteristics of socio-demographic status.

Indicators	Gender	Age	Education	Experience
Stage I. Reading text without pivot words				
Reading time	0,61	0,54	0,21	-0,72
Answering time of quantitative questions	0,17	0,27	-0,03	-0,41
Correctness of answer to quantitative questions	-0,04	-0,41	0,28	0,68
Decision confidence factor	0,43	-0,05	-0,01	0,06
Answering time of questions about text structure	0,35	-0,16	0,31	0,10
Correctness of answer to questions about structure	-0,41	0,15	-0,07	-0,37
Coefficient of confidence of answer about text structure	0,05	0,15	-0,37	-0,22
Stage II. Reading text with pivot words				
Reading time	0,26	0,37	-0,03	-0,52
Answering time of quantitative questions	0,17	0,22	0,07	-0,52
Correctness of answer to quantitative questions	-0,61	-0,44	-0,41	0,41
Decision confidence factor	0,48	0,26	0,04	-0,46
Answering time of questions about text structure	-0,43	-0,32	-0,08	0,72
Correctness of answer to questions about structure	-0,10	0,20	0,40	0,17
Coefficient of confidence of answer about text structure	0,78	0,68	0,48	-0,68

It should also be noted that statistical data processing not only made it possible to reveal the relationship between the "coefficient of correctness of answers" and the availability of work experience - this fact is quite expected and natural, but it made it possible to use the cognitive characteristics of the user in developing the model, making them dependent on the style of decision-making in the process of collective activity, with the efficiency and effectiveness of collective decision-making.

6. Conclusion

This article proposes an approach to developing a model of collective decision-making, which makes it possible to consider the cognitive features of a user in the process of interacting with a distributed information system. In the course of the research, it was revealed that respondents characterized by the breadth of the equivalence range (i. e. "synthetics") were the most successful in dealing with the intended tasks on reading, analysing and classifying the proposed texts, as compared with the respondents, style features of which are more inherent in the area of "narrow range of equivalence" (i.e. "analytics"). The results obtained also indicate that such a property as "field independence" allows individuals to cope with tasks more successfully than "field dependent" research participants.

In the process of modelling, analysis and monitoring of information flows were carried out to support the processes of remote group interaction based on a distributed information system. Information flows are interconnected with collective decision-making processes, which allow monitoring and analysing the effectiveness of the team's activities. For this purpose, it is

possible to use the method of extracting specialized data samples from information arrays [36], where based on the analysis of the relationship of information flows; two classes-functions of collective information interaction were isolated:

- function-tasks - an interconnected sequence of information flows due to a sequence of actions team members aimed at solving a specific problem, as a result of which they have their own aspects and specifics in each case;

- functions-operations - an interconnected sequence of information flows due to the sequence of actions of team members, which are formal, standard and universal operations in the process of information interaction and are not aimed at solving a specific problem [37].

Based on the monitoring and analysis of the developed model, systematization, ranking and quantitative assessment of information flows were conducted.

Conflict of Interest

The authors declare no conflict of interest.

References

[1] A. Bakanov, T. Atanasova, N. Bakanova, "Cognitive Approach to Modeling Human-Computer Interaction with a Distributed Intellectual Information Environment," in 2019 Big Data, Knowledge and Control Systems Engineering, BdKCSE 2019, 2019, doi:10.1109/BdKCSE48644.2019.9010597.

[2] A. Tversky, D. Kahneman, "Judgment under uncertainty: Heuristics and biases," Science, 1974, doi:10.1126/science.185.4157.1124.

[3] M. Allais, "Le Comportement de l'Homme Rationnel devant le Risque:

Critique des Postulats et Axiomes de l'Ecole Americaine," Econometrica, 1953, doi:10.2307/1907921.

[4] O.I. Larichev, Current Methodological Problems of Systems Analysis and Its Application, 1984, doi:10.1016/b978-0-08-030830-2.50013-1.

[5] A.B. Petrovsky, "Multiple criteria decision making: Discordant preferences and problem description," Journal of Systems Science and Systems Engineering, 2007, doi:10.1007/s11518-007-5032-z.

[6] A.B. Petrovsky, "Multi-method technology for group multi-attribute choice," in RPC 2018 - Proceedings of the 3rd Russian-Pacific Conference on Computer Technology and Applications, 2018, doi:10.1109/RPC.2018.8482143.

[7] A.K. Goel, J. Davies, Artificial intelligence, Book, 2019, doi:10.1017/9781108770422.026.

[8] F. Hayes-Roth, "Knowledge Based Expert Systems," Computer, 1984, doi:10.1109/MC.1984.1658976.

[9] C. Fyfe, "Advanced Information and Knowledge Processing," General Systems, 2010.

[10] B.R. Gaines, "Modeling practical reasoning," International Journal of Intelligent Systems, 1993, doi:10.1002/int.4550080105.

[11] R. Axelrod, Structure of decision: The cognitive maps of political elites, 2015, doi:10.2307/2616237.

[12] J.H. Boose, "A survey of knowledge acquisition techniques and tools," Knowledge Acquisition, 1989, doi:10.1016/S1042-8143(89)80003-2.

[13] J.H. Boose, B.R. Gaines, "Knowledge Acquisition for Knowledge-Based Systems: Notes on the State-of-the-Art," Machine Learning, 1989, doi:10.1023/A:1022662924615.

[14] S.J. Grossman, O.D. Hart, "The Costs and Benefits of Ownership: A Theory of Vertical and Lateral Integration," Journal of Political Economy, 1986, doi:10.1086/261404.

[15] R. Kaluri, C.H. Pradeep Reddy, "An enhanced framework for sign gesture recognition using hidden markov model and adaptive histogram technique," International Journal of Intelligent Engineering and Systems, 2017, doi:10.22266/ijies2017.0630.02.

[16] R. Kaluri, C.H.P. Reddy, "Optimized feature extraction for precise sign gesture recognition using Self-Improved Genetic Algorithm," International Journal of Engineering and Technology Innovation, 2018.

[17] G. Lbov, V. Berikov, "Construction of an event tree on the basis of expert knowledge and time series," in Lecture Notes in Computer Science (including subseries Lecture Notes in Artificial Intelligence and Lecture Notes in Bioinformatics), 2011, doi:10.1007/978-3-642-22140-8_21.

[18] V. Desnitsky, I. Kotenko, "Expert knowledge based design and verification of secure systems with embedded devices," in Lecture Notes in Computer Science, 2014, doi:10.1007/978-3-319-10975-6_15.

[19] T. Atanasova, "Integrated semantic-based processes in digital home," Informatyka Ekonomiczna, 2014, doi:10.15611/ie.2014.3.02.

[20] H. Suzuki, R. Hishiyama, "An analysis of expert knowledge transmission using machine translation services", in SoICT '16 - Proceedings of the Seventh Symposium on Information and Communication Technology, 2016, doi.org/10.1145/3011077.3011085

[21] V.N. Golovachyova, G.Z. Menlibekova, N.F. Abayeva, T.L. Ten, G.D. Kogaya, "Construction of expert knowledge monitoring and assessment system based on integral method of knowledge evaluation," International Journal of Environmental and Science Education, 2016, doi:10.12973/ijese.2016.705a.

[22] T. Temel, F. Karimov, "Information systems model for targeting policies: A graph-theoretic analysis of expert knowledge," Expert Systems with Applications, 2019, doi:10.1016/j.eswa.2018.11.014.

[23] B. Kosko, "Fuzzy knowledge combination," International Journal of Intelligent Systems, 1986, doi:10.1002/int.4550010405.

[24] L.A. Ginis, "The use of fuzzy cognitive maps for the analysis of structure of social and economic system for the purpose of its sustainable development," Mediterranean Journal of Social Sciences, 2015, doi:10.5901/mjss.2015.v6n3s5p113.

[25] J.P. Carvalho, "Rule based fuzzy cognitive maps in humanities, social sciences and economics," Studies in Fuzziness and Soft Computing, 2012, doi:10.1007/978-3-642-24672-2_16.

[26] M. León, C. Rodriguez, M.M. García, R. Bello, K. Vanhoof, "Fuzzy cognitive maps for modeling complex systems," in Lecture Notes in Computer Science (including subseries Lecture Notes in Artificial Intelligence and Lecture Notes in Bioinformatics), 2010, doi:10.1007/978-3-642-16761-4_15.

[27] N. Abramova, Z. Avdeeva, S. Kovriga, D. Makarenko., Subject-formal Methods Based on Cognitive Maps and the Problem of Risk Due to the Human Factor, 2010, doi:10.5772/7118.

[28] N. Volkova, A. Gusev, "Cognitive styles: Controversial issues and research

problems," National Psychological Journal, 2016, doi:10.11621/npj.2016.0203.

[29] M. Kozhevnikov, C. Evans, S.M. Kosslyn, "Cognitive Style as Environmentally Sensitive Individual Differences in Cognition," Psychological Science in the Public Interest, 2014, doi:10.1177/1529100614525555.

[30] J.W. Atkinson, Motivation for achievement, 2015, doi:10.4324/9781315720951.

[31] A.R. Masalimova, M.N. Mikhaylovsky, A. V. Grinenko, M.E. Smirnova, L.B. Andryushchenko, M.A. Kochkina, I.G. Kochetkov, "The interrelation between cognitive styles and copying strategies among student youth," Eurasia Journal of Mathematics, Science and Technology Education, 2019, doi:10.29333/ejmste/103565.

[32] E.Y. Korjova, O. V. Rudykhina, "The possibilities of typological approach in the study of epistemological styles," Vestnik of Saint Petersburg University. Psychology, 2016, doi:10.21638/11701/spbu16.2016.302.

[33] A. Bakanov, M. Zelenova Cognitive Styles as Determinants of Success in Professional Activity, Социальная Психология и Общество, 2015, doi:10.17759/sps.

[34] H.A. Witkin, D.R. Goodenough, "Cognitive styles: essence and origins. Field dependence and field independence.," Psychological Issues, 1981.

[35] J. Kagan, "Reflection-impulsivity: The generality and dynamics of conceptual tempo," Journal of Abnormal Psychology, 1966, doi:10.1037/h0022886.

[36] N.B. Bakanova, V.M. Vishnevskii, "Modeling document movement in corporate systems document circulation," Automation and Remote Control, 2008, doi:10.1134/S0005117908090142.

[37] N. B. Bakanova, T. V. Atanasova, "Method for Automated Analysis of Users' Requests to Service Centre of Information Networks in OIS," Problems of Engineering Cybernetics and Robotics, 2020, doi: 10.7546/PECR.74.20.04.

Comparison of Machine Learning Parametric and Non-Parametric Techniques for Determining Soil Moisture: Case Study at Las Palmas Andean Basin

Carlos López-Bermeo[*], Mauricio González-Palacio, Lina Sepúlveda-Cano, Rubén Montoya-Ramírez, César Hidalgo-Montoya

Universidad de Medellín, Facultad de Ingenierías, Medellín, 050026, Colombia

A R T I C L E I N F O	A B S T R A C T
	Soil moisture is one of the most important variables to monitor in agriculture. Its analysis gives insights about strategies to utilize better a particular area regarding its use, i.e., pasture for cows (or similar), production forests, or even to answer what crops should be planted. The vertical structure of the soil moisture plays an important role in several physical processes such as vegetation growth, infiltration process, soil – atmosphere interactions, among others. Despite a set of tools are currently being evaluated and used to monitor soil moisture, including satellite images and in-situ sensor, several drawbacks are still persisting. In situ data is expensive for high spatial monitoring and vertical measurements and satellite data have low spatial resolution and only retrieval information of soil moisture for the top few centimeters of the soil. The present work shows an experiment design for collecting soil moisture data in a specific Andean basin with in-situ sensors in different kinds of soils as a promising tool for reproducing soil moisture profiles in areas with scarce information, employing only surface soil moisture and simple soil characteristics. Collected data is used to train machine learning supervised parametric (Multiple Linear Regression - MLR) and non-parametric models (Artificial Neural Networks - ANNs and Support Vector Regression - SVR) for soil moisture estimation in different depths. Conclusions show that parametric methods do not meet goodness of fit assumptions; so, non-parametric methods must be considered, and SVR outperforms parametric methods regarding regression accuracy allowing to reproduce the soil moisture content profiles. The proposed SVR model represents a high potential tool to replicate the soil moisture profiles using only surface information from remote sensing or in-situ data.

1. Introduction and problem statement

This paper is an extension of work originally presented in *CISTI 2020* [1]. Soil moisture is one of the most critical variables to be monitored in soils [2]. Understanding the behavior of the soil moisture makes it possible to determine the soil use [3], i.e., if it is suitable for cropping, for animal's pastures [4], and even, as a critical variable to understand if a particular terrain may be considered to real estate projects [5]. Another important application of soil moisture analysis belongs to risk management, such as landslides prevention and prediction [6]. For hydrologic applications, the soil moisture represents one of the most important variables controlling the interactions between the atmosphere and land through the evapotranspiration and evaporation processes. Additionally, the soil moisture represents a key variable for the infiltration process and direct surface runoff production in hydrological models.

In that way, different knowledge disciplines, such as hydrology [7], environmental management [8], geology [9], topography [10], among others, deal with soil moisture to deeply study its effects in plenty of different applications. Nonetheless, getting information about soil moisture is commonly a difficult task: available sources are scarce and are associated with satellite images, which causes low resolution regarding spatial distribution [11], that is, soil moisture is measured in broad areas and cannot be explicitly determined in points. During the last decades satellite images have emerged as a powerful tool to retrieve information about soil moisture in the superficial soil surface, even though data in other depth horizons is mandatory to model the behavior in a lot of applications.

---

[*]Corresponding Author: Carlos López-Bermeo, celopez@udem.edu.co

Given the importance and drawbacks mentioned above, several techniques based on Artificial Intelligence (AI) theory are currently employed to estimate and predict the soil moisture for several engineering and scientific applications. Knowledge-based systems that apply AI are considered as easy and user-friendly tools [12, 13], as they have advantages in terms of neither requiring a pre-defined conceptual relationship between the input-target parameters nor requiring expensive experimental and field measurement apparatus [14].

In this sense, several studies have been proposed to determine the best Machine Learning (ML) or (AI) model to estimate the soil moisture, considering different variables like meteorological data and satellite images, among others. There are two main ML models used: Support Vector Regression (SVR) and Artificial Neural Networks (ANN) in different configurations. It is the case of [15], three approaches are proposed to generate the SVR regression model for soil moisture estimation: in the first approach, the authors use the soil moisture and meteorological data (air temperature, relative humidity, average solar radiation, and soil temperature at five and 10cm) at time step $t-1$ and t for predict soil moisture at $t+4$ and $t+7$, where t is in days. For the second approach, they use only the meteorological data, while in the third approach, they use only soil moisture at the same time step. The results of this study show that the SVR models performed better forecasting than a simple ANN model. In the same line, [16] proposes the use of SVR for soil moisture prediction using remote sensing data coming from 10 sites in the Lower Colorado River Basin (US). The data includes backscatter and incidence angle from Tropical Rainfall Measuring Mission (TRMM), and Normalized Difference Vegetation Index (NDVI) from Advanced Very High-Resolution Radiometer (AVHRR). The authors trained an SVR with five years of data (time series) and tested on three years of data. The results show a Root Mean Square Error (RMSE) less than 2%. Additionally, results are compared with an ANN and a Multivariate Linear Regression Model (MLR), showing that the SVR has a better performance than the other models.

The latest studies show a tendency for the use of deeper ANN like shows [17] in their review. The authors classify the use of ANN in three categories according to the types of training data. For the first category, the ANN is trained with model-generated data. For the second category case, the ANN is trained with in-situ measurements, with the restriction that the spatial scale could mismatch between point-scale measurements. Finally, the third category encloses the ANN trained with global Land Surface Model (LSM) simulations for soil moisture estimation at large scales.

Other useful applications using ANN are related to the infilling missing soil moisture records such as the research presented in [18], who were using five statistical methods, and nine ANN categorized into Feedforward, Dynamic, and Radial Basis Network methods estimate missing soil moisture records. The obtained values were validated against known values for 13 soil moisture monitoring stations for three different soil layer depths in the Yanco region in southeast Australia. The results show that the nonlinear autoregressive neural network performs in similar quality than other typical methods such as the rough sets method, and monthly replacement. Other studies employing ANN for hydrologic variables are [19–22].

Although SVR and ANN are the most used techniques, several works can be found related to soil moisture prediction that use other techniques of AI and ML. Some authors include multiple techniques, like, where Classification and Regression Trees (CART), Boosted Regression Trees (BRT), Random Forest (RF), Multivariate Adaptive Regression Splines (MARS), and Flexible Discriminant Analysis (FDA), are tested, all with promising results. In this sence, [14] using several input variables such as dielectric constant, soil bulk density, clay content, and organic matter for 1155 soil samples, proposed a hybrid Adaptive Neuro-Fuzzy Inference System (ANFIS) - Grey Wolf Optimization (GWO) intelligent model for simulating soil moisture content. The results based on several statistical parameters verified the feasibility of these kinds of models improving accuracy by around 50% when compared with other similar models as ANN, SVR, and standalone ANFIS models.

Despite the increasing usage of Artificial Intelligence (AI) theory tools related to soil moisture estimation, most of the studies have the same thing in common; none of them is focused on the estimate of the soil moisture at different depths. The data estimate corresponds to a depth between 5 and 10 cm approximately or the root zone. Few studies such as [23], employed surface soil moisture (0–5 cm) values and Hydrological Soil Groups (HSGs) information to perform a Statistical Soil Moisture Profile (SSMP) model to transfer the spatial variations of soil moisture profile with the change in soil hydraulic properties. The proposed model was based on correlation techniques with preceding time steps of soil moisture fields. In another study, [24] employed multispectral imagery from Unmanned Aerial Vehicle (UAVs) and a method based on the combination of an evolutionary algorithm and artificial intelligence called genetic programming (GP), to propose a methodology to simulate soil moisture at different levels. The results were compared to ANN and SVR methods.

With this idea in mind, the present work shows a methodology to fit some ML models with in-situ sensor data, which transmit real-time information by using IoT tools and methods to overcome limitations associated with the number of sensors to determine soil moisture at different depths using surface topsoil moisture estimates. The proposed methodology represents a high potential tool for reproducing the soil moisture profiles using only surface information from satellite or in-situ data for scarce information areas. Specifically, we use the most known statistics-based parametric method: Multiple Linear Regression (MLR) and perform the corresponding Analysis of Variance (ANOVA) [25] as well as the Goodness of Fit metrics (normality, independence, homoskedasticity). We also use two widespread ML non-parametric methods: SVR and ANN [26, 27]. All the models are primarily assessed by a case study, with collected data in the Las Palmas basin, at the Andean region, in Medellín, Colombia.

The rest of this paper is organized as follows: section 2 shows a short theoretical framework; section 3 stands the methodology and experiment design; section 4 shows the models fitting; in

section 5, the analysis over results is carried out. Finally, conclusions, future work, acknowledgments, and references are presented.

2. Theoretical framework

In this section, some key concepts will be defined to understand the work better.

2.1. Soil moisture

A given portion of soil is composed of solid particles and the rest of the voids. A part of the holes is occupied by water and the rest by air. The volume occupied by water is measured using the soil moisture content, which is defined as θ as in equation (1) :

$$\theta = \frac{Volume_{water}}{Volume_{total}} \qquad (1)$$

The study and knowledge of soil moisture are essential due to its influence on hydrological processes and energy flows on the earth's surface. It is also critical because of its connection with precipitation, runoff generation, nutrient transport, and groundwater [28–30]. Recent research identifies that a surplus or lack of soil moisture can favor floods or droughts occurrence [31]. Likewise, the feedback of soil moisture on evapotranspiration is essential for temperature variation and the appearance and persistence of heatwaves, as well as for precipitation generation and location [32]. Besides, the role of soil moisture in photosynthesis, ecosystem dynamics, soil respiration, and the terrestrial carbon balance is undeniable.

Therefore, soil moisture variation is critical in hydrological, ecological, and environmental studies [33] and, in particular, as a support for agriculture and biomass production [34]. Combinations of the factors mentioned above cause variations in spatial and temporal soil moisture content, which makes it a significant limiting factor for crop growth. Indeed, low crop yields should be more often related to insufficient soil moisture than insufficient rainfall [35,36], which causes that soil moisture plays a vital role as a critical resource for vegetation growth that supports agricultural production. In this sense, it is identified that soil moisture contributes in a crucial way to understanding the global climate system. For this reason, it has been highlighted by the Global Climate Observing System (GCOS) as one of the "essential climate variables". Therefore, monitoring temporal and spatial soil moisture variability is essential to estimate water availability limits and to quantify its climatic variations sensitivity and human pressures [32].

2.1.1. Soil moisture sensing technologies

Currently, several techniques are used to measure soil moisture, allowing monitor of humidity on a large scale: in-situ sensors (to take humidity measurements at the site where the sensor is located), and remote sensing from towers, aircraft, and satellites, using radiometers in the microwave region, scatterometers, synthetic aperture radars, and radar combinations-radiometers. According to [28], the products obtained with passive and active sensors have different correlation values around the world, when compared with in-situ measurements.

Although there are many possible sources of information, in the case of the tropics and specifically in the study area, there could

be limitations for the use of satellite information. Some derive from the possibility or not of having reliable and spatially coherent in situ soil measurements of soil moisture, which makes it challenging to carry out a cohesive evaluation of the accuracy and information content of remote sensing products. Besides, the use of inadequate techniques for downscaling can generate alterations in data quality. Another difficulty could arise due to the impossibility of obtaining quality data with fair spatial and temporal resolution in the study area, primarily due to its geographical location, which may limit some sensors use, especially optical ones. In this sense, in the visual spectrum, one of the significant limitations is the limited surface penetration due to high cloudiness. However, visible and infrared sensors and microwave sensors are not limited by cloud cover and night conditions [35]. Observations can be made at any time of day and are not dependent on sunlight [37].

Soil moisture in-situ sensing, In Colombia and many other tropical regions, there is very little information available on soil moisture taken from in-situ monitoring stations that can be used to understand the behavior of this variable for different applications. Although it is true that in-situ measurements require a costly investment and have low coverage of the territory, they allow the analysis at a local scale (as is the case of a basin). Additionally, they are necessary to validate the data from remote sensors that generally have a low spatial resolution.

The primary function of a soil moisture sensor is to report its current state, by using an electric variable (commonly voltage), to any acquisition system, i.e., datalogger, or IoT end node. The voltage reported is scaled to get the corresponding measurement, which is commonly given in cubic meters of water over cubic meters of soil material (m^3/m^3).

The most used operation principle in soil moisture sensors is the variation of capacitance as the moisture changes. Soil acts as a dielectric material between two plates, and it changes when this variable varies. However, conductivity sensors are also applied to sense moisture. Water content allows flowing electric currents between two electrodes, and it is proportional to soil moisture.

2.2. Parametric and non-parametric methods for data fitting

To fit some models for regression of moisture data and perform the comparison, we have chosen some of the most used methods in the literature. MLR, SVR, and ANN algorithms will be reviewed in this section.

2.2.1. Multiple Linear Regression (MLR)

MLR is one of the most used parametric strategies for data fitting. The general model is shown in equation (2):

$$\hat{Y} = \sum_{i=0}^{n} [\hat{\beta}_i X_i] + \varepsilon \qquad (2)$$

Where $\hat{Y}$ is the regression value of the dependent variable, $\hat{\beta}_i$ is a set of n+1 predictors (coefficients) which are determined by using least-squares optimization, X_i are n independent (predicting) variables, and ε is the regression error. If a categorical variable is in the predictors, a set of dummy variables is included, depending

on the number of levels of the factor. The goal, then, is finding the values of each $\hat{\beta}_i$ such that the global error ε is minimal.

Once the predictors are determined, an Analysis of Variance (ANOVA) must be performed [25], to determine if the means of the prediction variables are equal, that is, if all the variables are representative for the analysis.

Finally, to check if the model is statistically valid, some goodness-of-fit tests must be performed: normality, by using the Kolmogorov-Smirnoff test [38]; autocorrelation, by using Durbin-Watson test [37]; and homoskedasticity, by using Breusch Pagan test [39]. Due to the model usage is limited to the goodness of fit, many datasets do not meet this strategy.

2.2.2. Support Vector Regression (SVR) [40, 41]

The goal of this supervised learning strategy is to find one (or more) hyperplanes that separate previously tagged classes. By finding the support vectors, it is possible to predict, in the case of regression, the value of a new continuous variable based on a set of inputs. Figure 1 shows the geometric concept for two input characteristics.
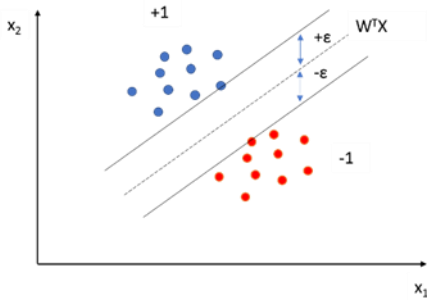
Figure 1: SVR geometric concept

The objective is to find the hyperplane that separates two classes with the maximum margin between them, therefore, finding the model is reduced to an optimization problem, where the coefficients w must be found, as shown in equation (3).

$$Min\ Z = \frac{1}{2}\|W\|^2 \tag{3}$$
$$St: |y_i - w_i x_i| \le \varepsilon$$

where y_i are the predicted variables, x_i are the independent variables (or features) and ε is the minimum tolerance between the separation hyperplanes and the features. For SVR, a slack variables set is added to equation (3), such that, for each value that falls outside ε, its deviation is recorded to make it minimal. The hyperparameter cost (C) is introduced to penalize said deviations, which is tuned through cross-validation. Thus, equation (3) is re-written, as shown in equation (4) (called the primal problem):

$$Min\ Z = \frac{1}{2}\|W\|^2 \ + C\sum_{i=0}^{n}|\xi_i| \tag{4}$$
$$St: |y_i - w_i x_i| \le \ \varepsilon + |\xi_i|$$

However, in many cases, the classes are not linearly separable, for this reason, it is recommended to use kernel functions, K [41, 42], to perform a transformation that increases the number of dimensions, allowing separating such classes, as shown in equation (5):

$$K(x_i, x_j) = \langle \phi(x_i), \phi(x_j) \rangle \tag{5}$$

where ϕ is a nonlinear mapping function and $\langle , \rangle$ is the inner product operator.

The dual problem to the primal problem is given by equation (6):

$$Min\ \frac{1}{2}\alpha^T Q\alpha \ - e^T\alpha \tag{6}$$
$$St: \begin{matrix} y^T\alpha = 0 \\ 0 \le \ \alpha_i \le C, i = 1, \dots, n \end{matrix}$$

where e is a vector of all ones, Q is a positive semidefinite matrix with $Q_{ij} = y_i y_j K(x_i, x_j)$ and α_i are the dual coefficients.

Using this model, the prediction function of the equation (7) is obtained:

$$f(x) = \sum_{i=1}^{n/2} y_i \alpha_i K(x_i, x) + b \tag{7}$$

where b is the bias term.

It is important to remark that the standard SVR model in equation (7) considers only real-valued functions [43]. Additionally, it is a discriminant method, i.e. produces a mapping from the data points to the class labels without computing probability distributions, allowing the method to be less computationally expensive, but more sensitive to noise than generative methods [44]. . The main advantage of SVR is that can deal with sparsity, non-linearity, and high dimensionality of the input data [45].

Regarding the SVR hyperparameter tuning (section 4.2), it is performed through cross-validation, and finally, the RMSE that exhibits the best results will be chosen. In the same way that MLR, if there are categorical variables in the set of X, *dummy variables* can be used.

2.2.3. Artificial Neural Networks (ANN). [40, 41]

This bio-inspired strategy is used in a lot of applications, where regression and classification are needed. The structure of a neural network emulates a meta-heuristic concept, based on interactions of neurons within the brain. The most known ANN is known as Multilayer Perceptron, and its architecture is shown in Figure 2. From this figure, a set of m input variables (x) in the Input layer are used to predict the values of n output variables (y) in the output layer. The prediction is achieved by choosing the correct number of neurons in different hidden layers h, which are fully connected with both previous and next layers. The effects of each connection are weighted by a set of constants W, which are determined by an optimization iterative method (commonly Gradient Descend). The main advantages of this kind of ANN (feedforward networks) are that they do not have a priori assumptions about the relationships between the independent and dependent variables [46], their

nonlinear modeling capability [47], and their minimal assumptions needed about the data [48]. In the same way that MLR, if there are categorical variables in the set of X, dummy variables can be used.
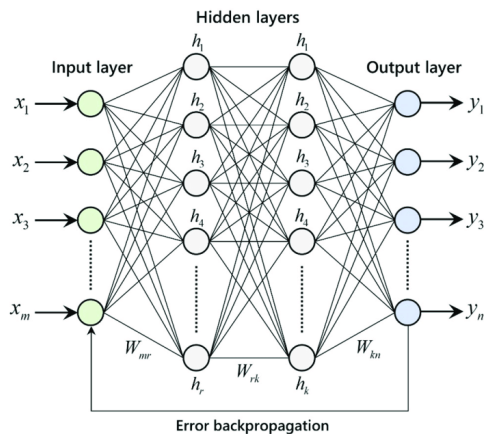
Figure 2: Multilayer Perceptron Architecture with backpropagation feedback [49]

Although using ANN can outperform other methods regarding its accuracy, its application must be extensively checked using cross-validation, since a common phenomenon known as *overfitting* makes that ANN cannot be a general model sometimes.

3. Methodology and experiment design

This section shows the steps to fit the different models. First, a measurement phase is proposed, where both instruments and locations are chosen. Then, with the set of data from in-situ sensors, some models are fitted. Finally, the performance evaluation is carried out, choosing the model which exhibits fewer regression errors.

3.1. Measurement phase

In this section, some considerations regarding the measurement are presented.

3.1.1. Location selection

Soil moisture is highly influenced by climatic characteristics of a region, specifically by rain amount and intensity, evapotranspiration [50], vegetation type, topography [51], soil properties (apparent density, porosity, organic matter content, texture, and structure), among other factors [52].

This is how changes in land use and land cover, in interaction with soil physical characteristics and climate, play a key role in soil moisture variations at different scales [53]. In the Colombian case, the soil moisture variability has been less studied and there is not enough information to understand its spatial and temporal dynamics, and much less has its contribution to water flows regulation been quantified.

This is the case in some areas of the Antioquia region, where precipitation is the only source of soil water and recharge of its surface layers. Therefore, soil moisture in deep layers cannot be replenished with contributions from rain and groundwater. For this reason, soil wet front movement study at different depths is key to understanding its variability and impact on agricultural production and ecosystems in tropical basins.

In different studies [54–56] it has been found that drought conditions affect variations in soil moisture content, while topography and vegetation type are the dominant factors that control the humidity in different soil layers. Specifically, soil water storage is mainly affected by topography at shallow depths, while in deep soil layers it is mainly controlled by vegetation type.

Considering the above, for the present study Las Palmas basin was selected, which has as characteristics of interest that it is in the tropical Andean zone of the municipality of Envigado, Antioquia, Colombia (coordinates: 6 ° 11'26.1 "N 75 ° 31'47.6" W), and which has undergone processes of change in land use and land cover, among which transition from crops and pastures to recreational and commercial uses stands out. There are also some small fragments of forest and secondary vegetation. This basin has an area of 31.31 km^2, with elevations from 2,500 to 2,600 meters above sea level and its predominant climate is cold humid to very humid and with an average annual rainfall of 2781 mm.

The basin also has different soil associations (Figure 3), which determine physical characteristics, as well as different depths in soil profiles [57]. The Tequendamita Association (TE) is found mainly in the Basin, formed by deep to moderately deep soils, well-drained, with medium textures, low to moderate fertility, mild to moderate erosion. A characteristic of these soils is that they are formed by metamorphic rocks (schists, gneisses) covered with volcanic ash. Soil samplings were made, and results were verified with previous studies such as the "General Study of Soils and Zoning of Lands of the Department of Antioquia" [58], and the" Semi-detailed study of soils in zone 13 of the municipality of Envigado for potential use purposes" [59].

Considering that the soil moisture content suitable for plant growth depends on the type of soil [60] and the physical explanation mentioned above related to the main variables affecting the soil moisture variability through the soil layers (vegetation, soil type, topography, among others), such parameters were considered to determine the sites where soil moisture monitoring stations were installed. Therefore, three types of vegetation cover representative of the basin (pastures, crops, and forest) were selected and combined with three different phases of the Tequendamita Association and one phase of the La Ceja Association (see Table 1). It is important to mention that the sensors were located having the characterization of soil profiles in the basin, which allowed determining the average depth of same, in each of the points where the monitoring stations were located. This means that an edaphological criterion was used for the location of each of the sensors. Additional criteria used to guarantee that the data collected were representative are the following: *i)* The points were located near access roads and agricultural areas located toward the higher part of the catchment where installation and security could be achieved with lower cost, *ii)* availability of connection to the telecommunications network to transmit data in real-time, *iii)* accessibility.

3.1.2. IoT end nodes

Soil moisture stations were designed and built using IoT tools and methods. Four stations are installed in the upper part of the basin, where a mobile network operator offers full 2G/3G coverage. At each point, three soil moisture sensors were put into

operation at different depths, depending on land cover (crops, pastures, and forest), and soil physical properties. The first layer, the depths per sensor, according to land cover, are shown in Table 1. Installed sensors are from the brand Meter Group, reference EC-5, measurement range from 0 up to 100%, with a resolution of 0.001 m^3/m^3 of Volumetric Water Content (VWC) and accuracy of ± 0.02 m^3/m^3. Sensor output is voltage, from 0 up to 2 Vdc, and is collected by a microcontroller unit ESP32, with an Analog-to-Digital Converter of 12-bit resolution. To ensure that the measurements are stable to be transmitted, the next conditioning protocol is used: *i)* take *n* measures from the sensor, *ii)* arrange samples from the lowest to highest, *ii)* extract the samples in the positions *n/2* and *1+n/2,* and *iii)* take the mean. Engineering units are scaled from ADC units to VWC by using a two-point scheme, by comparing readings of moisture in both water and air and using a Meter Group EM-50 as a calibration pattern. In-situ end-nodes are depicted in Figure 4.

Figure 3: Study area location in Antioquia and Colombia and soil associations present in the Las Palmas basin

After collecting measurements, data is sent to an IoT backend by using the protocol Message Queue Telemetry Transport (MQTT). The chosen IoT platform is Ubidots [61], and it also helps to store information and to provide a frontend user interface to visualize real-time indicators, as shown in Figure 5.

Table 1: Soil moisture sensor depths according to soil use

Land Cover	Soil association	Sensor 1 depth range (cm)	Sensor 2 depth range (cm)	Sensor 3 depth range (cm)
Crop	La Ceja Consociation (LCb)	0-23	23-37	>37
Pasture 1	Tequendamita Association (Ted2)	0-22	22-33	>33
Pasture 2	Tequendamita Association (Ted3)	0-33	33-60	>60
Forest	Tequendamita Association (Ted)	0-16	16-35	>35

Figure 4: IoT soil moisture end nodes in (a) crops, (b) pasture type 1, (c) pasture type 2 and (d) forest
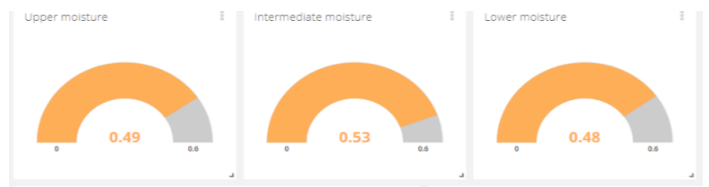
Figure 5: IoT backend / frontend platform [61]

3.2. Model fitting phase

First, all data is extracted from the Ubidots platform, using a temporal window from December of 2019 to June 2020, with an equi-temporal sampling rate of 15 minutes. All data is put together into a unique database table, including timestamp, moisture values per sensor, depths per sensor, and soil type. The models are fitted to output a moisture value at a particular depth, regarding the readings of the other two sensors, their corresponding depths, and the soil use.

To fit all the models, R Studio V 1.2.5019 was used. All the basic statistics measurements were inspected: quartiles, means, medians, and standard deviations (for continuous data), and counters (for categorical data). Regression expressions were adapted with *dummy variables* to allow that the categorical variable *soil type* could involve all the factors with different coefficients. Then, a preprocessing phase for continuous variables was carried out with two different strategies, according to the equations (8) and (9):

$$x_i' = \frac{x_i - \bar{x}}{s^2} \qquad (8)$$

$$x_i' = \frac{x_i - \min(x)}{\max(x) - \min(x)} \qquad (9)$$

where x_i' is the ith transformed sample, x_i is the ith sample of the continuous variable x from the dataset, $\bar{x}$ is the mean of x, s^2 is the standard deviation of x, $min(x)$ is the minimum value of x, and $max(x)$ is the maximum value of x.

Finally, the model fitting for MLR, SVN, and ANN was performed according to the corresponding method. The database has 77848 observations and is split into two sets, with a pseudo-random strategy: training (70%, that is, 54493 examples) and test (30%, that is, 23355 examples). Moreover, some additional tests were run for MLR, to ensure goodness of fit: Kolmogorov-Smirnov [38], Durbin-Watson [37], and Breusch Pagan [39].

3.3. Results analysis phase

After the models were fitted, the regression was carried out with each model, by using the test set. An initial graphical inspection was performed, and three performance metrics are used: RMSE (Root Mean Square Error), Index of Agreement (Willmott), and R^2. These metrics and the graphical approximation served to determine the accuracy of the models regarding field measurements. The pertinent analysis was developed.

4. Model fitting

For the sake of clearness, we will adopt the following notation: M_i is the ith sensor, D_i is the depth of ith sensor, i is an integer index to identify the sensor position ($i = 1$ is the superficial sensor, $i = 2$ is the middle sensor, and $i = 3$ is the deepest sensor), and P_1, P_2, and F are dichotomic *dummy variables* for representing the factors *pasture type 1*, *pasture type 2* and *forest*, in the categorical variable *soil type*. All the processes are executed in a laptop Lenovo G40, with a processor Intel Core i7 4500 @ 1.8 GHz and RAM = 12 GB.

A previous graphical inspection is performed to qualitatively behold if there are relationships among different moistures, as shown in Figure 6. Some statistical metrics are presented in Table 2.
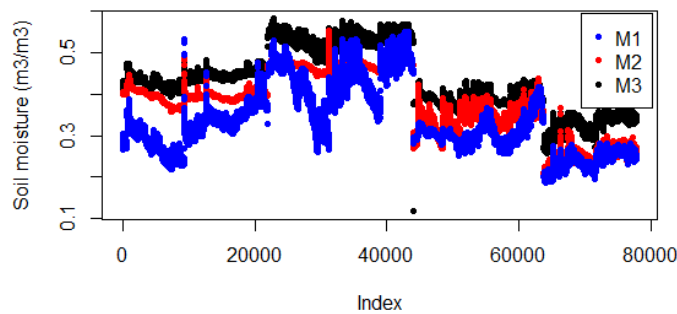
Figure 6. Trends of moisture data. M_1 is the superficial sensor, M_2 is the middle sensor, and M_3 is the deepest sensor. Index interval from 0 up to 21.000 corresponds to crops, from 21.000 to 44.000 corresponds to pasture 1, from 44.000 up to 64.000 corresponds up to pasture 2, and from 64.000 up to 79.000 corresponds to the forest.

From Figure 6, it can be noticed that effectively there is a relationship between the moistures at different depths since when an external variable, i.e., rainfall, causes a perturbation, each moisture varies. Moreover, according to Table 2, medians and means of moistures are arranged from M_1 to M_3 from the least to the greater, indicating that the deep the soil is, the high VWC is. It also can be noticed that the standard deviation of M_3 is the least, supporting that more superficial moisture changes in a wider range than the others, so external variables (rainfall or solar radiation) affect the most to the moistures closer to the soil surface. To validate the hypothesis of correlation among moistures, by using the Pearson correlation coefficient, the next results are obtained: $cor(M_1,M_2) = 0.85$; $cor(M_1,M_3) = 0.91$; $cor(M_2,M_3) = 0.97$.

Table 2: Statistical metrics for soil moistures

	M_1	D_1	M_2	D_2	M_3	D_3
Min	0.047	0.08	0.1918	0.255	0.117	0.33
Q1	0.27	0.11	0.332	0.275	0.382	0.33
Median	0.312	0.115	0.388	0.3	0.425	0.37
Mean	0.3308	0.1215	0.3772	0.3321	0.4322	0.4212
Q3	0.383	0.165	0.457	0.465	0.508	0.6
Max	0.552	0.165	0.553	0.465	0.582	0.6
SD	0.0786	0.029	0.0786	0.085	0.0735	0.113

4.1. MLR

Taking into account that there is a direct correlation among soil moistures, MLR can be fitted according to the process in section 2.2.1. So, the general model in equation (2) is re-written to the particular dataset, as shown in equation (10):

$$\widehat{M}_2 = \hat{\beta}_{0,2} + \hat{\beta}_{1,2}M_1 + \hat{\beta}_{2,2}D_1 + \hat{\beta}_{3,2}D_2 + \hat{\beta}_{4,2}P_1$$
$$+ \hat{\beta}_{5,2}P_2 + \hat{\beta}_{6,2}F + \varepsilon_2 \qquad (10)$$
$$\widehat{M}_3 = \hat{\beta}_{0,3} + \hat{\beta}_{1,3}M_1 + \hat{\beta}_{2,3}D_1 + \hat{\beta}_{3,3}D_3 + \hat{\beta}_{4,3}P_1$$
$$+ \hat{\beta}_{5,3}P_2 + \hat{\beta}_{6,3}F + \varepsilon_3$$

where all the $\hat{\beta}$ are the model estimators, and ε is the error model. Note that, in the first instance, it is needed to fit two models for M_2 and M_3, depending on the variables associated with the superficial moisture and the *soil type*. However, due to the high correlation between M_2 and M_3, it is essential to find the optimal $\hat{\beta}$ values, the strategy of minimization of *least squares* is applied [62], searching for a hyperplane that minimizes the cumulative errors from measurements and the predicted variable. The R function *lm* is used, getting the results in Table 3, for training data without preprocessing, and with the preprocessing strategies in the equations (8) and (9). From this table, the dichotomic coefficients $\hat{\beta}_{4,2}, \hat{\beta}_{5,2}, \hat{\beta}_{4,3},$ and $\hat{\beta}_{5,3}$ are not determined, due to there are a multicollinearity effect with the other variables; that is, such variables explain the effects thoroughly without needing the inclusion of the variable *soil type* if it is a crop, pasture 1, or pasture 2. The multicollinearity effect is tested by using the *alias* method proposed in [63]. This method shows how a collinear variable is explained by the others, as shown in Table 4.

According to Table 4, for example, the coefficient $\hat{\beta}_{5,2}$ (which corresponds to the binary variable P_2, pasture type 2) is explained by the others, being D_1 (superficial moisture sensor depth), the variable that explains the most the behavior of P_2. A similar analysis can be performed for other variables.

Table 3: Regressor values for the model in equation (8). P-values less than 0.05 indicate that the regressor is significative

Raw data			
Coefficient	Estimate	Std. Error	p-value
$\hat{\beta}_{0,2}$	0.6537	0.0019	<2 x 10^{-16}
$\hat{\beta}_{1,2}$	0.2615	0.1395	<2 x 10^{-16}
$\hat{\beta}_{2,2}$	-17.6344	0.0691	<2 x 10^{-16}
$\hat{\beta}_{3,2}$	5.6271	0.0203	<2 x 10^{-16}
$\hat{\beta}_{4,2}$	N/A	N/A	N/A
$\hat{\beta}_{5,2}$	N/A	N/A	N/A
$\hat{\beta}_{6,2}$	-0.4906	0.0015	<2 x 10^{-16}
$\hat{\beta}_{0,3}$	0.5464	0.0014	<2 x 10^{-16}
$\hat{\beta}_{1,3}$	0.3519	0.0010	<2 x 10^{-16}
$\hat{\beta}_{2,3}$	-8.8458	0.0356	<2 x 10^{-16}
$\hat{\beta}_{3,3}$	2.1546	0.0074	<2 x 10^{-16}
$\hat{\beta}_{4,3}$	N/A	N/A	N/A
$\hat{\beta}_{5,3}$	N/A	N/A	N/A
$\hat{\beta}_{6,3}$	-0.3496	0.0011	<2 x 10^{-16}
Max/Min preprocessing			
Coefficient	Estimate	Std. Error	p-value
$\hat{\beta}_{0,2}$	0.2479	0.0008	<2 x 10^{-16}
$\hat{\beta}_{1,2}$	0.3660	0.0019	<2 x 10^{-16}
$\hat{\beta}_{2,2}$	-4.1683	0.0162	<2 x 10^{-16}
$\hat{\beta}_{3,2}$	3.2853	0.0118	<2 x 10^{-16}
$\hat{\beta}_{4,2}$	N/A	N/A	N/A
$\hat{\beta}_{5,2}$	N/A	N/A	N/A
$\hat{\beta}_{6,2}$	-13634	0.0044	<2 x 10^{-16}
$\hat{\beta}_{0,3}$	0.1363	4.6 x 10^{-4}	<2 x 10^{-16}
$\hat{\beta}_{1,3}$	0.3834	0.0011	<2 x 10^{-16}
$\hat{\beta}_{2,3}$	-1.6136	0.0064	<2 x 10^{-16}
$\hat{\beta}_{3,3}$	1.2485	0.0042	<2 x 10^{-16}
$\hat{\beta}_{4,3}$	N/A	N/A	N/A
$\hat{\beta}_{5,3}$	N/A	N/A	N/A
$\hat{\beta}_{6,3}$	-0.7496	0.0024	<2 x 10^{-16}
SD/Mean preprocessing			
Coefficient	Estimate	Std. Error	p-value
$\hat{\beta}_{0,2}$	1.1298	0.0037	<2 x 10^{-16}
$\hat{\beta}_{1,2}$	0.2608	0.0013	<2 x 10^{-16}
$\hat{\beta}_{2,2}$	-6.6737	0.0261	<2 x 10^{-16}
$\hat{\beta}_{3,2}$	6.0411	0.0217	<2 x 10^{-16}
$\hat{\beta}_{4,2}$	N/A	N/A	N/A
$\hat{\beta}_{5,2}$	N/A	N/A	N/A
$\hat{\beta}_{6,2}$	-6.2131	0.0201	<2 x 10^{-16}
$\hat{\beta}_{0,3}$	0.8646	0.0029	<2 x 10^{-16}
$\hat{\beta}_{1,3}$	0.3761	0.0010	<2 x 10^{-16}
$\hat{\beta}_{2,3}$	-3.6	0.0144	<2 x 10^{-16}
$\hat{\beta}_{3,3}$	3.3201	0.0113	<2 x 10^{-16}
$\hat{\beta}_{4,3}$	N/A	N/A	N/A
$\hat{\beta}_{5,3}$	N/A	N/A	N/A
$\hat{\beta}_{6,3}$	-4.7565	0.0157	<2 x 10^{-16}

Table 4: Alias test for checking multicollinearity of non-determined coefficients in MLR

	$\hat{\beta}_{0,2}$	$\hat{\beta}_{1,2}$	$\hat{\beta}_{2,2}$	$\hat{\beta}_{3,2}$	$\hat{\beta}_{6,2}$
$\hat{\beta}_{4,2}$	-3.2352	0	58.8235	-11.7647	1.5294
$\hat{\beta}_{5,2}$	-9.3529	0	388.2353	-117.6471	8.2941
	$\hat{\beta}_{0,3}$	$\hat{\beta}_{1,3}$	$\hat{\beta}_{2,3}$	$\hat{\beta}_{3,3}$	$\hat{\beta}_{6,3}$
$\hat{\beta}_{4,3}$	-3.2352	0	47.0588	-5.8823	1.5294
$\hat{\beta}_{5,3}$	-9.3529	0	270.5882	-58.8235	8.2941

Once MLR models are fitted, an Analysis of Variance must be performed for the raw data and the two preprocessing strategies in the equations (8) and (9), to check if all the variables are significant. This analysis is carried out by using the R function *ANOVA,* obtaining the results in Table 5, showing that hypothesis tests performed to validate that all the model variables are significant, excepting the *soil type* for crops, pasture type 1, and pasture type 2.

Table 5: ANOVA for MLR in (a) estimation for M_2 and (b) estimation for M_3

(a)					
Raw data					
Variable	Df	Sum squares	Mean square	F value	p-value
M_1	1	244.84	244.8495	125163	<2 x10^{-16}
D_1	1	54.990	54.9909	281105	<2 x10^{-16}
D_2	1	9.8928	9.8928	50570	<2 x10^{-16}
soil type	1	18.6491	18.6491	95331	<2 x10^{-16}
Residuals	54488	10.6591	0.000195		
Max-Min preprocessing					
Variable	Df	Sum squares	Mean square	F value	p-value
M_1	1	1881.34	1881.34	125387	<2 x10^{-16}
D_1	1	422.75	422.75	281755	<2 x10^{-16}
D_2	1	76.29	76.29	50829	<2 x10^{-16}
soil type	1	144.07	144.07	96022	<2 x10^{-16}
Residuals	54488	81.75	0		
SD / Mean preprocessing					
Variable	Df	Sum squares	Mean square	F value	p-value
M_1	1	39213	39213	124894	<2 x10^{-16}
D_1	1	8779	8779	279632	<2 x10^{-16}
D_2	1	1594	1594	50777	<2 x10^{-16}
soil type	1	3005	3005	95714	<2 x10^{-16}
Residuals	54488	1711	0		
(b)					
Raw data					
Variable	Df	Sum squares	Mean square	F value	p-value

M_1	1	240.583	240.5830	230668	<2 x10^{-16}
D_1	1	37.9458	37.9458	363820	<2 x10^{-16}
D_2	1	0.3932	0.3932	70.236	<2 x10^{-16}
soil type	1	9.4532	9.4532	90636.	<2 x10^{-16}
Residuals	54488	5.6830	0.0001043		

Max Min preprocessing					
Variable	Df	Sum squares	Mean square	F value	p-value
M_1	1	1115.72	1115.72	234484	<2 x10^{-16}
D_1	1	174.04	174.04	365759	<2 x10^{-16}
D_2	1	1.78	1.78	3750	<2 x10^{-16}
soil type	1	43.53	43.53	91487	<2 x10^{-16}
Residuals	54488	25.93	0		

SD / Mean preprocessing					
Variable	Df	Sum squares	Mean square	F value	p-value
M_1	1	39213	39213	124894	<2 x10^{-16}
D_1	1	8779	8779	239632	<2 x10^{-16}
D_2	1	1594	1594	50777	<2 x10^{-16}
soil type	1	3005	3005	95714	<2 x10^{-16}
Residuals	54488	1711	0		

To assess the best preprocessing strategy, we calculate the R^2, the RMSE and the Index of Agreement for each model with the training data, for both M_2 and M_3 (Table 6). Because the preprocessing strategies change the scale of the measurements, it is evident that the R^2 and the Index of Agreement are similar for all the subsets, however, the RMSE is less for the raw data, since all the moistures are in the range 0.2 up to 0.6 m^3/m^3, and because the standard deviations are from 0.029 to 0.113 (Table 2), the span of the transformed sets is higher than the raw data, according to equations (8) and (9).

Table 6: Performance metrics for the sets of raw and preprocessed data for (a) M_2 and (b) M_3

(a)

	R^2	RMSE	Index of Agreement
Raw data	0.9685	0.14	0.9217
Max / Min	0.9685	0.0387	0.9217
SD / Mean	0.9683	0.177	0.9217

(b)

	R^2	RMSE	Index of Agreement
Raw data	0.9808	0.0101	0.9401
Max / Min	0.9808	0.0218	0.9402
SD / Mean	0.9807	0.1387	0.94

4.2. SVR

An SVR is trained to perform the regression of M_2 and M_3, based on M_1, D_1, D_2 or D_3, F, P_1, and P_2. Three types of kernels

are tested: linear, polynomial, and Radial Basis Function (RBF) [64]. A cross-validation process is carried out to determine which of the kernels exhibits better performance, by using the function *tune* in R Studio, considering the inverse of the regularization parameter cost, known as lambda (λ) and kernel width (γ) as hyperparameters. Since predictions with linear and polynomial kernels did not exhibit acceptable errors, we selected the RBF kernel to show the regressor tuning process. The steps developed to tune the SVR are as follows (for each preprocessing scheme): *i)* split raw data and preprocessed data into training and test sets, *ii)* configure a 2D grid with the values of the hyperparameters λ = (0.0001, 0.001, 0.01, 0.1, 1, 10, 100) and γ = (0.001, 0.01, 0.1, 1, 10, 100), *iii)* determine an SVR model for each subset of hyperparameters, *iv)* evaluate the regression errors of each model, and *v)* choose the model with the least regression error. After tuning all the SVRs, we found the best hyperparameters configuration. Regarding the training sets, Figure 7(a) shows the regression errors for the raw data of M_2 (which exhibited the least regression error = 4.36 x 10^{-6}), considering the hyperparameters λ =1 x 10^{-7} and γ = 0.001, and Figure 7(b) shows the regression errors for the raw data of M_3 (which exhibited the least regression error = 1.59 x 10^{-6}), considering the hyperparameters λ =1 x 10^{-5} and γ = 0.1. Besides, the regression errors for each preprocessing configuration (for the training sets) are shown in Table 7. Finally, for M_2, we obtained R^2= 0.985, RMSE = 0.0115, and Index of Agreement = 0.9422. Similarly, for M_3, we obtained R^2= 0.9885, RMSE = 0.0078, and Index of Agreement = 0.9542.
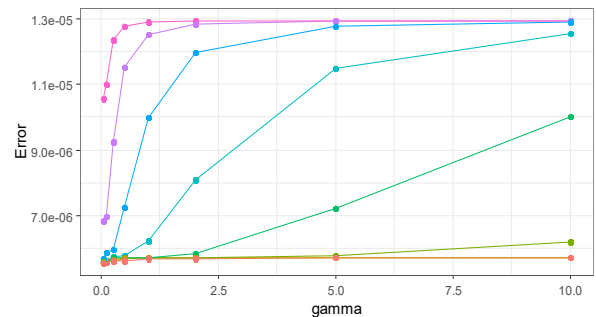
(a) Raw data for M_2
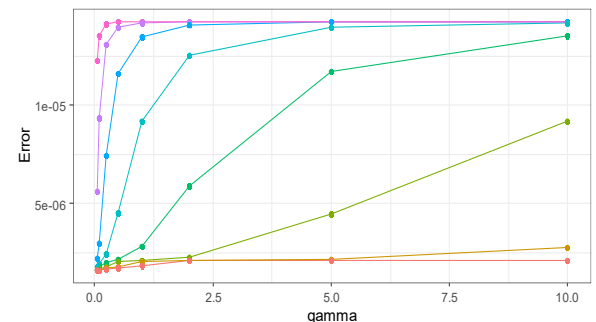
(b) Raw data for M_3

Figure 7: Hyperparameters selection for M_2 and M_3 for the training subset

Table 7: Regressor errors for each preprocessing scheme for the training subset

M_2	
Preprocessing	Regressor error
Raw	1.43×10^{-5}
Max/min	4.36×10^{-6}
SD/Mean	5.0387×10^{-6}
M_3	
Preprocessing	Regressor error
Raw	1.59×10^{-6}
Max/min	7.47×10^{-6}
SD/Mean	0.00032046

(a)

(b)

(c)
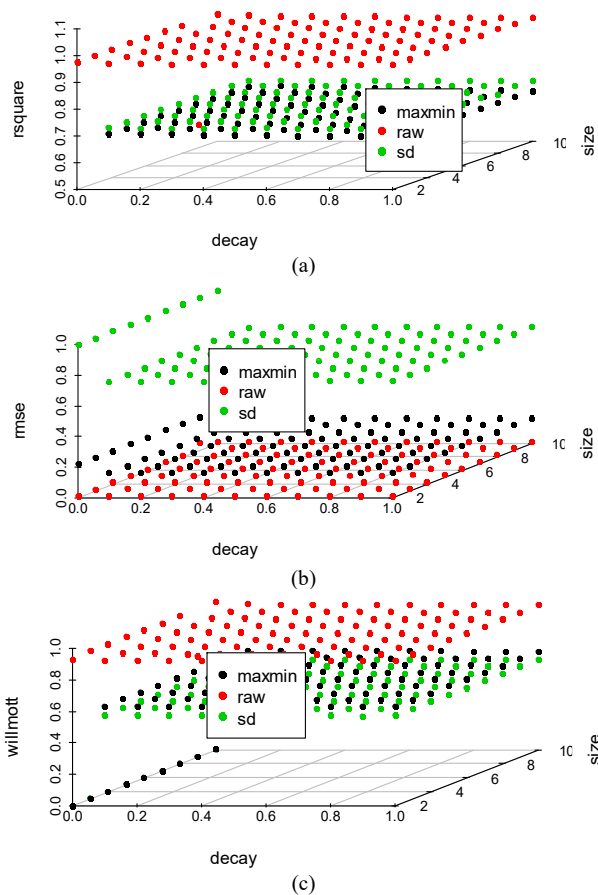
Figure 8: ANN regression performance for each preprocessing scheme for (a) R^2, (b) RMSE, and (c) Index of Agreement (Willmott) for M_2

4.3. ANN

An ANN is proposed to predict soil moisture. Two multilayer perceptrons are trained to perform the regressions of M_2 and M_3, based on M_1, D_1, D_2 or D_3, F, P_1, and P_2. A cross-validation process was carried out aiming to tune the hyper parameters of the ANN, i.e., *i)* best number of hidden layers, taking into account a tradeoff between low estimation error and simplicity, *ii)* weights values for each connection and *iii)* activation function the neurons (binary step, linear, sigmoid, tanh and Rectified Linear Unit -RELU- were considered). We have followed the next procedure to choose the best configuration: *i)* take raw data, or preprocessed data with the equations (8) or (9) and divide them into training

(70%) and test (30%) sets, *ii)* train a perceptron with a hidden layer and a number of neurons from 2 up to 10, and a decay from 0 up to 1 with steps of 0.1, *iii)* for each pair of hyperparameters, evaluate R^2, RMSE and the Index of Agreement (Willmott) for the training set, *iv)* inspect and select the best preprocessing scheme, *v)* plot errors for the selected preprocessing scheme according to the set of hyperparameters chosen, and *vi)* select the configuration of the neural network. Figure 8 and Figure 9 show different regression errors for the different preprocessing schemes for M_2 and M_3.

(a)

(b)

(c)
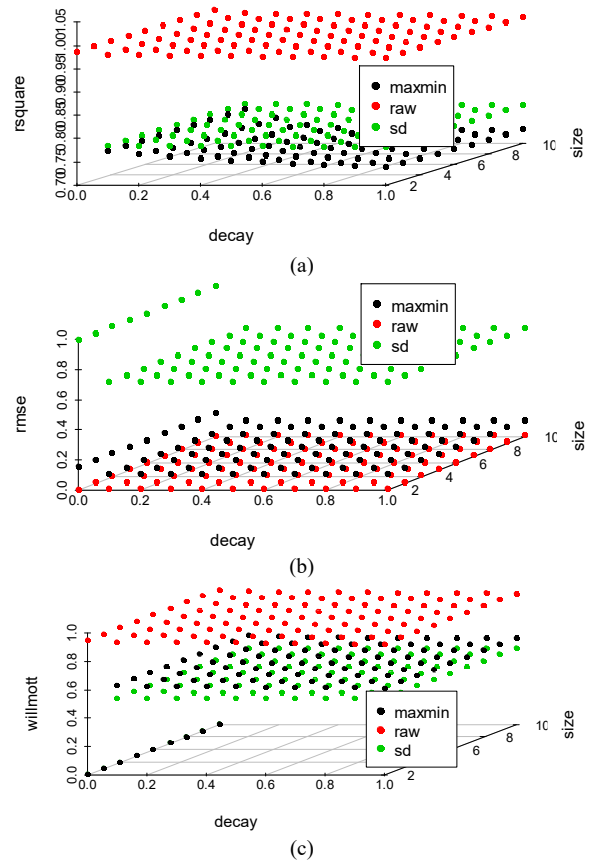
Figure 9: ANN regression performance for each preprocessing scheme for (a) R2, (b) RMSE, and (c) Index of Agreement (Willmott) for M_3

From Figure 8 and Figure 9, it can be seen that all the configurations of ANNs have better performance with raw data, since R^2 and Index of Agreement are close to 1, and RMSE is close to 0. Thus, we selected the raw data to get the best ANN configuration, as shown in Figure 10 and Figure 11.

(a)

(b)

(c)
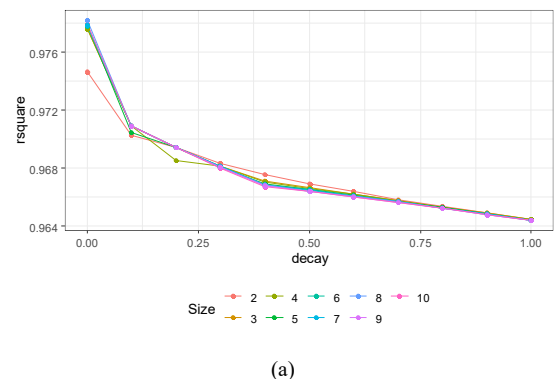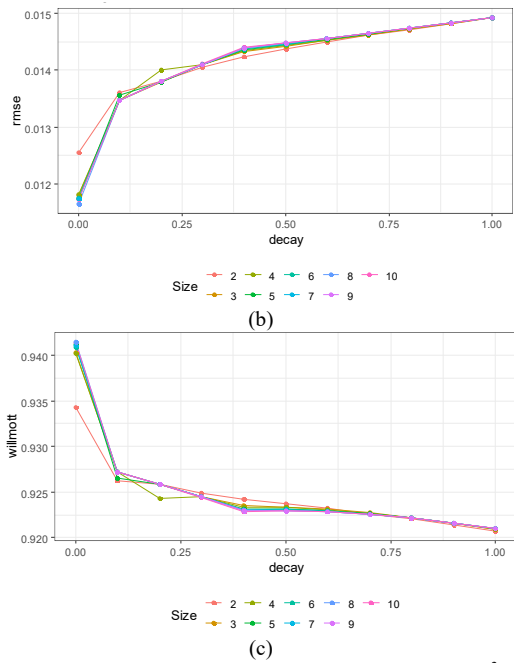
Figure 10: ANN regression performance for raw data for (a) R^2, (b) RMSE, and (c) Index of Agreement (Willmott) for M_2

(a)

(b)

(c)
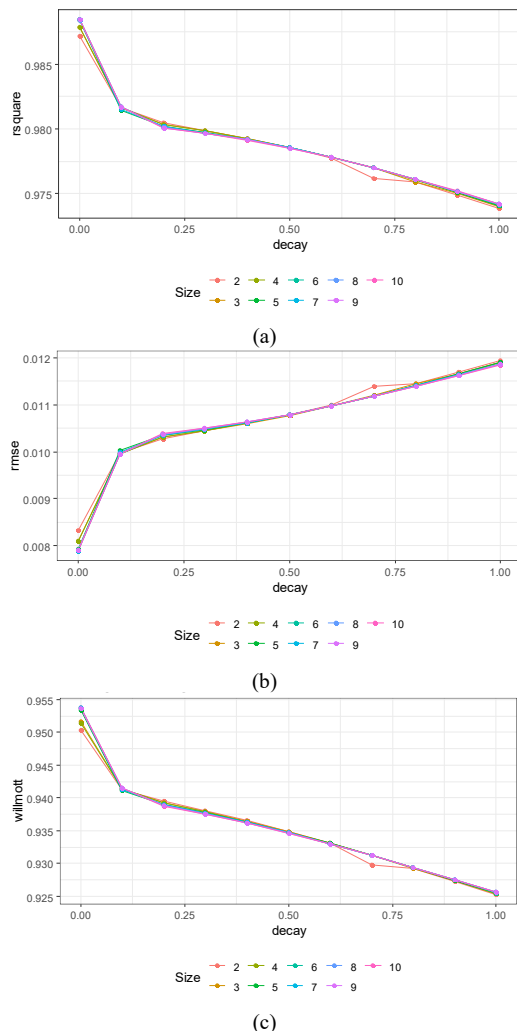
Figure 11: ANN regression performance for raw data for (a) R^2, (b) RMSE, and (c) Index of Agreement (Willmott) for M_3

From Figure 10, we obtained the best ANN configuration for M_2 as follows: an input layer with six neurons, a hidden layer with eight neurons, an output layer with one layer, and a decay = 0 (R^2=0.9781, RMSE=0.0116, and Index of Agreement=0.9414). Similarly, for M_3, we found the best configuration with a hidden layer of 7 neurons and a decay = 0 (R^2=0.9884, RMSE=0.0079, and Index of Agreement=0.9534). The ANNs' configurations are depicted in Figure 12.

(a)

(b)
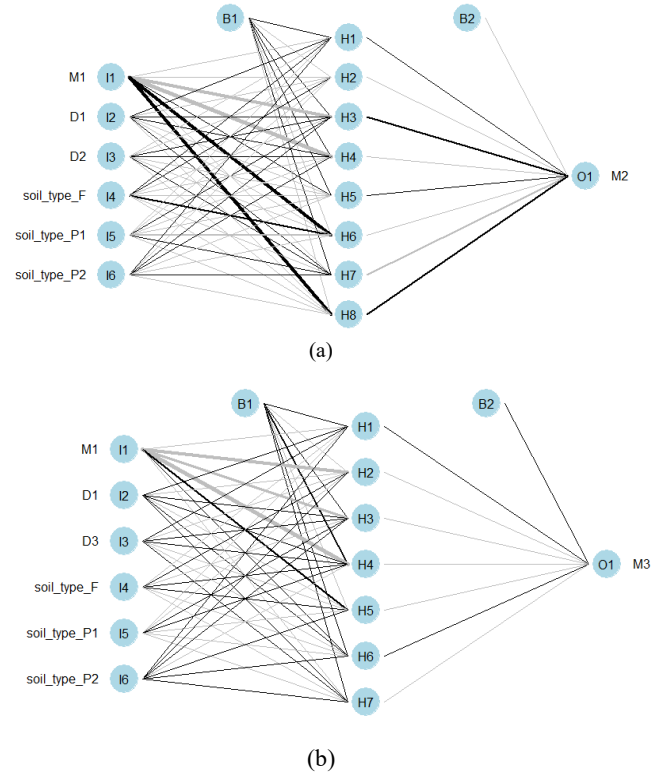
Figure 12: Multilayer perceptron ANN for (a)M_2 estimation and (b) M_3 estimation

In Figure 12, the darker and broader the line between two neurons is, the greater the weight is, which represents the relative importance (positive) of such connection. On the other hand, the grayer and broader the line between two neurons is, the lesser the weight is, which represents the relative importance (negative) of such connection. The tuned weights are shown in Table 8.

Table 8: Tuned weights for neurons connections of the ANN. Table (a) shows the weights from the input layer to the hidden layer for M_2 estimation, table (b) shows the weights from the hidden layer to the output for M_2 estimation, table (c) shows the weights from the input layer to the hidden layer for M_3 estimation, table (d) shows the weights from the hidden layer to the output for M_3 estimation.

(a)

	B1	I1	I2	I3	I4	I5	I6
H1	0.54	-2.61	0.15	-0.90	4.58	-8.25	1.71
H2	-5.51	-5.17	-0.63	-2.37	4.15	-6.48	-0.29
H3	11.76	-49.2	2.19	5.04	-9.21	8.75	0.46
H4	13.42	-54.7	1.68	2.96	-7.80	-11.8	0.25
H5	2.61	10.10	-0.60	-0.37	-2.94	-9.21	-5.50
H6	-13.4	52.54	-2.25	-6.89	14.50	-16.1	-0.90
H7	1.84	-2.64	0.86	1.68	-5.57	5.91	3.73
H8	-12.6	49.26	-2.26	-4.89	-5.09	-8.00	-0.66

(b)

	B2	H1	H2	H3	H4	H5	H6	H7	H8
O1	-2.9	7.86	-2.07	17.10	-7.78	2.27	-7.57	-14.44	16.95

(c)

	B1	I1	I2	I3	I4	I5	I6
H1	4.40	-6.37	0.81	1.36	-2.21	-0.84	0.66
H2	-1.44	-36.24	-0.70	-0.80	5.94	-0.48	2.11
H3	5.53	-24.60	0.78	4.76	-1.36	9.97	0.05
H4	15.28	-45.70	1.70	6.19	4.33	3.73	-4.13
H5	-4.00	17.68	-0.98	-2.84	2.12	-5.66	0.38
H6	0.14	11.19	0.51	-2.04	-8.67	-7.35	4.88
H7	2.07	-1.97	0.64	0.63	-9.89	-3.19	0.51

(d)

	B2	H1	H2	H3	H4	H5	H6	H7
O1	1.47	2.42	-11.36	-1.99	-0.28	-3.38	5.10	-6.77

Table 9: Performance metrics for regression models (test set) ANN, SVR and MLR

	R^2	RMSE	Index of Agreement
Test set ANN M_2	0.978	0.0116	0.9411
Test set MLR M_2	0.9686	0.014	0.9217
Test set SVR M_2	0.9786	0.0115	0.9423
Test set ANN M_3	0.988	0.008	0.9551
Test set MLR M_3	0.9885	0.01	0.9411
Test set SVR M_3	0.9808	0.007	0.9542
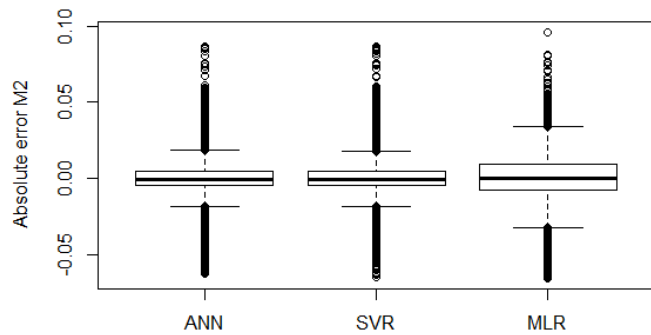
Figure 13: Absolute errors for the test set of M_2
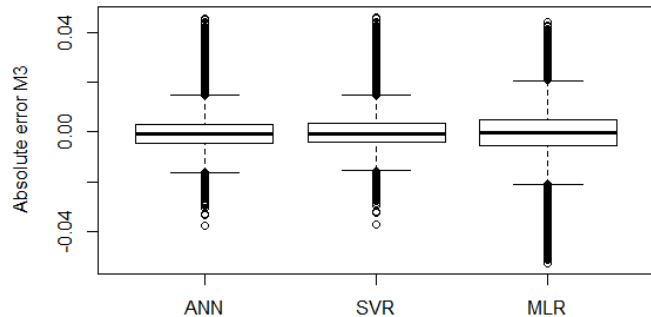
Figure 14: Absolute errors for the test set of M_3

5. Results

After fitting the parametric and non-parametric methods, some performance metrics will be applied to test what method could be used with better results to represent the soil moisture variability toward the soil profile for different type of soil and land cover configurations. It will indicate what model could be applied to extrapolate the soil moisture profiles toward areas with scarce information. To evaluate the models' performances, R^2, RMSE, and the Index of Agreement are proposed, as shown in Table 9. It can be noticed that, at first glance, the general performance of the

methods is almost the same with slightly worse results for the MLR method for the sites presented. A deeper analysis can be carried out from the error dispersions of each method, as depicted in Figure 13 and Figure 14, where it can be noticed that error dispersion is higher for MLR, and the absolute error performances of ANNs and SVR are similar. Furthermore, when plotting the time-series (Figure 15 and Figure 16), it can be noticed that a deeper analysis should be carried out regarding the soil types.
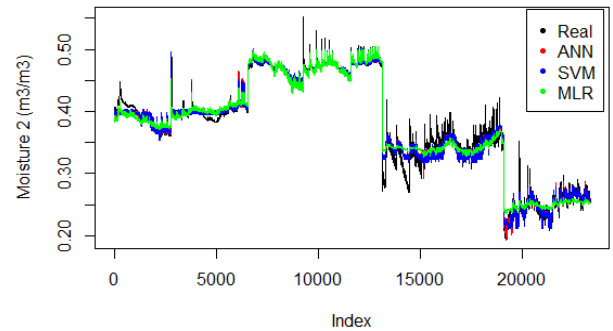
Figure 15: Regression results for the test set of M_2. Index interval from 0 up to 6.500 corresponds to crops, from 6.501 to 13.100 corresponds to pasture 1, from 13.101 up to 19.100 corresponds up to pasture 2, and from 19.101 up to 23.355 corresponds to the forest
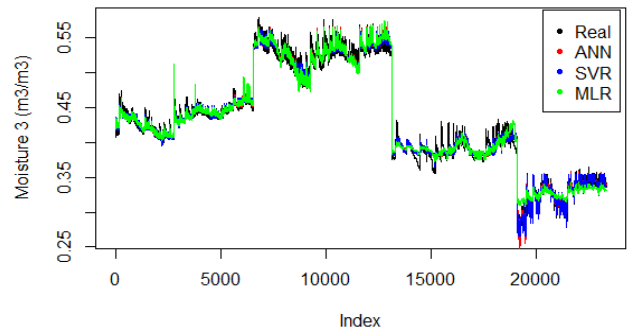
Figure 16: Regression results for the test set of M_3. Index interval from 0 up to 6.500 corresponds to crops, from 6.501 to 13.100 corresponds to pasture 1, from 13.101 up to 19.100 corresponds up to pasture 2, and from 19.101 up to 23.355 corresponds to the forest.

It can be noticed that the methods (ANN, MLR, and SVR) exhibit similar results for the crop, pasture 1, and pasture 2 in terms of average variability of the soil moisture (Figure 15 and Figure 16). Nonetheless, SVR outperforms the other two methods in terms of high variability when comparing versus the measured data. In the case of the forest, it is more evident that SVR can better predict the real values of both M_2 and M_3. On the other hand, none of the methods are accurate enough to predict behaviours in pasture 2. Due to this visual inspection, RMSE, R^2, and Index of Agreement are recomputed but segmented by each *soil type,* as shown in Table 10.

Table 10: Performance metrics for regression models ANN, MLR, and SVR differenced by *soil type*

Soil type – Moisture	Performance metric	R^2	RMSE	Index of Agreement
Crop M_2	Test ANN	0.8095	0.0425	0.7922
	Test MLR	0.8129	0.0424	0.8027
	Test SVR	0.6542	0.1168	0.6031

Crop M_3	Test ANN	0.9307	0.0044	0.8725	
	Test MLR	0.9325	0.0043	0.8782	
	Test SVR	0.9344	0.0044	0.8993	
Pasture 1 M_2	Test ANN	0.8176	0.0583	0.7722	
	Test MLR	0.8174	0.0588	0.7695	
	Test SVR	0.8246	0.0049	0.7715	
Pasture 1 M_3	Test ANN	0.8439	0.0077	0.7824	
	Test MLR	0.8444	0.0081	0.7902	
	Test SVR	0.8585	0.0074	0.8136	
Pasture 2 M_2	Test ANN	0.2836	0.0551	0.2526	
	Test MLR	0.2770	0.0551	0.2468	
	Test SVR	0.3386	0.0196	0.3121	
Pasture 2 M_3	Test ANN	0.3749	0.0125	0.3185	
	Test MLR	0.3560	0.0128	0.3054	
	Test SVR	0.4419	0.0119	0.4112	
Forest M_2	Test ANN	0.8247	0.0785	0.8063	
	Test MLR	0.8245	0.0795	0.7985	
	Test SVR	0.8264	0.0079	0.8111	
Forest M_3	Test ANN	0.8247	0.0185	0.7954	
	Test MLR	0.3245	0.0796	0.2212	
	Test SVR	0.9207	0.0059	0.8924	

It can be noted, according to Table 10, that SVR outputs better results in most of the cases, excepting for M_2 in the crop, where MLR fits better data with the test set. In the rest of the cases, ANN outperforms MLR. Since the R^2 value depends on the individual standard deviations, it is possible that the segmentations conducted for analyzing the individual performance regarding the soil type present different fitting values than the case of the whole dataset.

For the sake of statistical validity, some goodness-of-fit tests must be carried out for the parametric method (MLR): normality, autocorrelation, and homoskedasticity. All the tests are calculated using residual errors. For normality, the Kolmogorov Smirnov test [38] is applied, obtaining a p-value = 2 x 10^{-16}, so residuals are not normal. For autocorrelation, the Durbin test is applied, obtaining a DW = 0.02. According to [37], if the value is too far from 2, there is a autocorrelation. Finally, for homoskedasticity, the Breusch Pagan test [39] is carried out, obtaining a p-value=2 x 10^{-16}, which means that residuals are heteroskedastic. Because there is no normality, correlation, nor homoskedasticity, the linear regression model could not be applied.

6. Conclusions

In this paper, a comparison between parametric and non-parametric methods for fitting soil moistures in Las Palmas Andean Basin. This research was motivated due to scarce information from satellite images and in-situ measurements toward the tropical areas where the soil moisture plays an important role in climate variability, so more in-depth soil moisture research is not possible.

The proposed methodology based on parametric and non-parametric methods employing a database collected from three typical land covers: crop, pasture, and forest, and typical soil types demonstrated that there are high correlations between superficial and intermediate soil moistures, as well as superficial and deepest soil moistures, so it is possible to propose prediction models to avoid the need to install many instruments per point or even the high ability of the proposed method to use surface information from satellite data to obtain soil moisture profiles.

A model fitting using MLR, SVR, and ANN was carried out, aiming to predict the soil moisture, by using as predictor variables the superficial soil moisture, its depth, the depth of the soil moisture that wants to be predicted, and the *soil type*. All models offer similar performance metrics, except for forest, where the SVR outperforms the other methods. However, goodness-of-fit tests are not met by residual errors of the MLR model, so it cannot be used with statistical validity. In that way, SVR is the best model to fit moistures based on superficial soil moisture.

Finally, it is important to state that the traditional hydrological models had been calibrated employing few information of the full complex and non-linear hydrological rainfall runoff transformation process (normally flow in specific points), avoiding the understanding of the spatial variability along the full catchment and imposing calibration parameters representing just a small part of the physical phenomenon. The inclusion of distributed spatial parameters in the calibration process such as infiltration parameters or soil moisture profiles can increase strongly the quality of the results obtained along the full catchment or even increase the understanding of the physics involved. In this direction the proposed methodology represents an important contribution to several engineering and hydrological applications.

7. Future work

We are planning to install two additional soil moisture stations in another forest, and residential soil uses, to better tune the models.

Conflict of Interest

The authors declare no conflict of interest.

Acknowledgment

References

[1] M. Gonzalez-Palacio, L. Sepulveda-Cano, J.D. Valencia-Calvo, J. Quiza-Montealegre, "System dynamics baseline model for determining a multivariable objetive function in Wireless Sensor Networks," in CISTI 2020, 2020.

[2] V.R. Pauwels, R. Hoeben, N.E. Verhoest, F.P. De Troch, "The importance of the spatial patterns of remotely sensed soil moisture in the improvement of discharge predictions for small-scale basins through data assimilation," Journal of Hydrology, **251**, 88–102, 2001.

[3] H. Sharma, M.K. Shukla, P.W. Bosland, R. Steiner, "Soil moisture sensor

calibration, actual evapotranspiration, and crop coefficients for drip irrigated greenhouse chile peppers," Agricultural Water Management, **179**, 81–91, 2017, doi:10.1016/j.agwat.2016.07.001.

[4] S. Walther, G. Duveiller, M. Jung, L. Guanter, A. Cescatti, G. Camps-Valls, "Satellite Observations of the Contrasting Response of Trees and Grasses to Variations in Water Availability," Geophysical Research Letters, **46**(3), 1429–1440, 2019, doi:10.1029/2018GL080535.

[5] H. Janssen, G.A. Scheffler, R. Plagge, "Experimental study of dynamic effects in moisture transfer in building materials," International Journal of Heat and Mass Transfer, **98**, 141–149, 2016, doi:10.1016/j.ijheatmasstransfer.2016.03.031.

[6] L. Zhuo, Q. Dai, D. Han, N. Chen, B. Zhao, M. Berti, "Evaluation of Remotely Sensed Soil Moisture for Landslide Hazard Assessment," IEEE Journal of Selected Topics in Applied Earth Observations and Remote Sensing, **12**(1), 162–173, 2019, doi:10.1109/JSTARS.2018.2883361.

[7] L. Brocca, L. Ciabatta, C. Massari, S. Camici, A. Tarpanelli, "Soil moisture for hydrological applications: Open questions and new opportunities," Water (Switzerland), **9**(2), 2017, doi:10.3390/w9020140.

[8] X. Huang, Z.H. Shi, H.D. Zhu, H.Y. Zhang, L. Ai, W. Yin, "Soil moisture dynamics within soil profiles and associated environmental controls," Catena, **136**, 189–196, 2016, doi:10.1016/j.catena.2015.01.014.

[9] I. V. Florinsky, Digital Terrain Analysis in Soil Science and Geology: Second Edition, Elsevier Inc., 2016.

[10] J. Liu, B.A. Engel, Y. Wang, Y. Wu, Z. Zhang, M. Zhang, "Runoff Response to Soil Moisture and Micro-topographic Structure on the Plot Scale," Scientific Reports, **9**(1), 2019, doi:10.1038/s41598-019-39409-6.

[11] M. Pan, E.F. Wood, "Impact of Accuracy, Spatial Availability, and Revisit Time of Satellite-Derived Surface Soil Moisture in a Multiscale Ensemble Data Assimilation System," IEEE Journal of Selected Topics in Applied Earth Observations and Remote Sensing, **3**(1), 49–56, 2010, doi:10.1109/JSTARS.2010.2040585.

[12] B. Kuang, Y. Tekin, A.M. Mouazen, "Comparison between artificial neural network and partial least squares for on-line visible and near infrared spectroscopy measurement of soil organic carbon, pH and clay content," Soil and Tillage Research, **146**(PB), 243–252, 2015, doi:10.1016/j.still.2014.11.002.

[13] K. Were, D.T. Bui, Ø.B. Dick, B.R. Singh, "A comparative assessment of support vector regression, artificial neural networks, and random forests for predicting and mapping soil organic carbon stocks across an Afromontane landscape," Ecological Indicators, **52**, 394–403, 2015, doi:10.1016/j.ecolind.2014.12.028.

[14] S. Maroufpoor, E. Maroufpoor, O. Bozorg-Haddad, J. Shiri, Z. Mundher Yaseen, "Soil moisture simulation using hybrid artificial intelligent model: Hybridization of adaptive neuro fuzzy inference system with grey wolf optimizer algorithm," Journal of Hydrology, **575**, 544–556, 2019, doi:10.1016/j.jhydrol.2019.05.045.

[15] M.K. Gill, T. Asefa, M.W. Kemblowski, M. McKee, "Soil moisture prediction using support vector machines," Journal of the American Water Resources Association, **42**(4), 1033–1046, 2006, doi:10.1111/j.1752-1688.2006.tb04512.x.

[16] S. Ahmad, A. Kalra, H. Stephen, "Estimating soil moisture using remote sensing data: A machine learning approach," Advances in Water Resources, **33**(1), 69–80, 2010, doi:10.1016/j.advwatres.2009.10.008.

[17] Q. Yuan, H. Shen, T. Li, Z. Li, S. Li, Y. Jiang, H. Xu, W. Tan, Q. Yang, J. Wang, J. Gao, L. Zhang, "Deep learning in environmental remote sensing: Achievements and challenges," Remote Sensing of Environment, **241**, 2020, doi:10.1016/j.rse.2020.111716.

[18] G. Dumedah, J.P. Walker, L. Chik, "Assessing artificial neural networks and statistical methods for infilling missing soil moisture records," Journal of Hydrology, **515**, 330–344, 2014, doi:10.1016/j.jhydrol.2014.04.068.

[19] M. Khalil, U.S. Panu, W.C. Lennox, "Groups and neural networks based streamflow data infilling procedures," Journal of Hydrology, **241**(3–4), 153–176, 2001, doi:10.1016/S0022-1694(00)00332-2.

[20] F.D. Mwale, A.J. Adeloye, R. Rustum, "Infilling of missing rainfall and streamflow data in the Shire River basin, Malawi - A self organizing map approach," Physics and Chemistry of the Earth, **50**–**52**, 34–43, 2012, doi:10.1016/j.pce.2012.09.006.

[21] T.R. Nkuna, J.O. Odiyo, "Filling of missing rainfall data in Luvuvhu River Catchment using artificial neural networks," Physics and Chemistry of the Earth, **36**(14–15), 830–835, 2011, doi:10.1016/j.pce.2011.07.041.

[22] P. Coulibaly, N.D. Evora, "Comparison of neural network methods for infilling missing daily weather records," Journal of Hydrology, **341**(1–2), 27–41, 2007, doi:10.1016/j.jhydrol.2007.04.020.

[23] M. Pal, R. Maity, "Development of a spatially-varying Statistical Soil Moisture Profile model by coupling memory and forcing using hydrologic soil groups," Journal of Hydrology, **570**, 141–155, 2019, doi:10.1016/j.jhydrol.2018.12.042.

[24] M. Aboutalebi, N. Allen, A.F. Torres-Rua, M. McKee, C. Coopmans, "Estimation of soil moisture at different soil levels using machine learning techniques and unmanned aerial vehicle (UAV) multispectral imagery," SPIE-Intl Soc Optical Eng: 26, 2019, doi:10.1117/12.2519743.

[25] R. Girden, "ANOVA: Repeated measures," Computer Science, 1991.

[26] N. Rodríguez-Fernández, P. de Rosnay, C. Albergel, P. Richaume, F. Aires, C. Prigent, Y. Kerr, "SMOS neural network soil moisture data assimilation in a land surface model and atmospheric impact," Remote Sensing, **11**(11), 2019, doi:10.3390/rs11111334.

[27] X. Dai, Z. Huo, H. Wang, "Simulation for response of crop yield to soil moisture and salinity with artificial neural network," Field Crops Research, **121**(3), 441–449, 2011, doi:10.1016/j.fcr.2011.01.016.

[28] W.E.H. Blum, Functions of soil for society and the environment, Reviews in Environmental Science and Biotechnology, **4**(3), 75–79, 2005, doi:10.1007/s11157-005-2236-x.

[29] K. Liao, X. Lai, Z. Zhou, Q. Zhu, "Applying fractal analysis to detect spatio-temporal variability of soil moisture content on two contrasting land use hillslopes," Catena, **157**, 163–172, 2017, doi:10.1016/j.catena.2017.05.022.

[30] J. Geris, D. Tetzlaff, J.J. McDonnell, C. Soulsby, "Spatial and temporal patterns of soil water storage and vegetation water use in humid northern catchments," Science of the Total Environment, **595**, 486–493, 2017, doi:10.1016/j.scitotenv.2017.03.275.

[31] L. Brocca, T. Moramarco, F. Melone, W. Wagner, "A new method for rainfall estimation through soil moisture observations," Geophysical Research Letters, **40**(5), 853–858, 2013, doi:10.1002/grl.50173.

[32] W. Dorigo, W. Wagner, C. Albergel, F. Albrecht, G. Balsamo, L. Brocca, D. Chung, M. Ertl, M. Forkel, A. Gruber, E. Haas, P.D. Hamer, M. Hirschi, J. Ikonen, R. de Jeu, R. Kidd, W. Lahoz, Y.Y. Liu, D. Miralles, T. Mistelbauer, N. Nicolai-Shaw, R. Parinussa, C. Pratola, C. Reimer, R. van der Schalie, S.I. Seneviratne, T. Smolander, P. Lecomte, "ESA CCI Soil Moisture for improved Earth system understanding: State-of-the art and future directions," Remote Sensing of Environment, **203**, 185–215, 2017, doi:10.1016/j.rse.2017.07.001.

[33] H. Lin, H.J. Vogel, J. Phillips, B.D. Fath, Complexity of soils and hydrology in ecosystems, Ecological Modelling, **298**, 1–3, 2015, doi:10.1016/j.ecolmodel.2014.11.016.

[34] X. Jia, M. Shao, Y. Zhu, Y. Luo, "Soil moisture decline due to afforestation across the Loess Plateau, China," Journal of Hydrology, **546**, 113–122, 2017, doi:10.1016/j.jhydrol.2017.01.011.

[35] S. Zhang, W. Fan, Y. Li, Y. Yi, "The influence of changes in land use and landscape patterns on soil erosion in a watershed و تاثیر تغییرات کاربری اراضی و الگوی شکل شناسی زمین برروی فرسایش خاک در حوزه," Science of The Total Environment, **574**, 34–45, 2017.

[36] L. Gao, Y. Lv, D. Wang, T. Muhammad, A. Biswas, X. Peng, "Soil water storage prediction at high space-time resolution along an agricultural hillslope," Agricultural Water Management, **165**, 122–130, 2016, doi:10.1016/j.agwat.2015.11.012.

[37] K.J. White, "The Durbin-Watson Test for Autocorrelation in Nonlinear Models," The Review of Economics and Statistics, **74**(2), 370, 1992, doi:10.2307/2109675.

[38] M. F.J.Jr., "The Kolmogorov-Smirnov test for goodness of fit," Journal of the American Statistical Association, **56**(1951), 68–78, 1951.

[39] D.M. Waldman, "A note on algebraic equivalence of White's test and a variation of the Godfrey/Breusch-Pagan test for heteroscedasticity," Economics Letters, **13**(2–3), 197–200, 1983, doi:10.1016/0165-1765(83)90085-X.

[40] W.S. Noble, What is a support vector machine?, Nature Biotechnology, **24**(12), 1565–1567, 2006, doi:10.1038/nbt1206-1565.

[41] N. Deng, Y. Tian, C. Zhang, Support vector machines: Optimization based theory, algorithms, and extensions, CRC Press, 2012, doi:10.1201/b14297.

[42] T. Kavzoglu, I. Colkesen, "A kernel functions analysis for support vector machines for land cover classification," International Journal of Applied Earth Observation and Geoinformation, **11**(5), 352–359, 2009, doi:10.1016/j.jag.2009.06.002.

[43] W. Zhou, L. Zhang, L. Jiao, J. Pan, "Support vector regression based on unconstrained convex quadratic programming," in Lecture Notes in Computer Science (including subseries Lecture Notes in Artificial Intelligence and Lecture Notes in Bioinformatics), Springer Verlag: 167–174, 2006, doi:10.1007/11881070_27.

[44] M. Awad, R. Khanna, Support vector regression, Apress, Berkeley: 67–80, 2015, doi:doi.org/10.1007/978-1-4302-5990-9_4.

[45] L. Tian, X. ZHANG, A Convergent Nonlinear Smooth Support Vector Regression Model, 205–207, 2015, doi:10.2991/978-94-6239-102-4_43.

[46] Y.O. Ouma, C.O. Okuku, E.N. Njau, "Use of Artificial Neural Networks and Multiple Linear Regression Model for the Prediction of Dissolved Oxygen in Rivers: Case Study of Hydrographic Basin of River Nyando, Kenya," Complexity, **2020**, 2020, doi:10.1155/2020/9570789.

[47] A. Landi, P. Piaggi, M. Laurino, D. Menicucci, "Artificial neural networks for nonlinear regression and classification," in Proceedings of the 2010 10th International Conference on Intelligent Systems Design and Applications, ISDA'10, 115–120, 2010, doi:10.1109/ISDA.2010.5687280.

[48] A. Biglarian, E. Bakhshi, A.R. Baghestani, M.R. Gohari, M. Rahgozar, M. Karimloo, "Nonlinear survival regression using artificial neural network," Journal of Probability and Statistics, 2013, doi:10.1155/2013/753930.

[49] P.L. Fernández-Cabán, F.J. Masters, B.M. Phillips, "Predicting roof pressures on a low-rise structure from freestream turbulence using artificial neural networks," Frontiers in Built Environment, **4**, 2018, doi:10.3389/fbuil.2018.00068.

[50] B. Liu, M. Shao, "Modeling soil-water dynamics and soil-water carrying capacity for vegetation on the Loess Plateau, China," Agricultural Water Management, **159**, 176–184, 2015, doi:10.1016/j.agwat.2015.06.019.

[51] H. YiLong, C. LiDing, F. BoJie, H. ZhiLin, G. Jie, L. XiXi, "Effect of land use and topography on spatial variability of soil moisture in a gully catchment of the Loess Plateau, China.," Ecohydrology, **5**(6), 826–833, 2012.

[52] X. Fang, W. Zhao, L. Wang, Q. Feng, J. Ding, Y. Liu, X. Zhang, "Variations of deep soil moisture under different vegetation types and influencing factors in a watershed of the Loess Plateau, China," Hydrology and Earth System Sciences, **20**(8), 3309–3323, 2016, doi:10.5194/hess-20-3309-2016.

[53] C. Zhu, Y. Li, "Long-Term Hydrological Impacts of Land Use/Land Cover Change From 1984 to 2010 in the Little River Watershed, Tennessee," International Soil and Water Conservation Research, **2**(2), 11–21, 2014, doi:10.1016/S2095-6339(15)30002-2.

[54] L. Gao, M. Shao, "Temporal stability of soil water storage in diverse soil layers," Catena, **95**, 24–32, 2012, doi:10.1016/j.catena.2012.02.020.

[55] X. Mei, Q. Zhu, L. Ma, D. Zhang, H. Liu, M. Xue, "The spatial variability of soil water storage and its controlling factors during dry and wet periods on loess hillslopes," Catena, **162**, 333–344, 2018, doi:10.1016/j.catena.2017.10.029.

[56] B. Yang, X. Wen, X. Sun, "Seasonal variations in depth of water uptake for a subtropical coniferous plantation subjected to drought in an East Asian monsoon region," Agricultural and Forest Meteorology, **201**, 218–228, 2015, doi:10.1016/j.agrformet.2014.11.020.

[57] Soil Survey Staff, Keys to soil taxonomy, 2014.

[58] IGAC, General Study of Soils and Land Zoning: Department of Antioquia (In Spanish), Instituto Geografico Agustin Codazzi, Bogota, Colombia, 2007.

[59] IDEA, Semi-detailed Study of Soil in Zone 13 of the Municipality of Envigado for Potential Use Purposes (In Spanish), 2014.

[60] Y. Zhang, L. Qiao, C. Chen, L. Tian, X. Zheng, "Effects of organic ground covers on soil moisture content of urban green spaces in semi-humid areas of China," Alexandria Engineering Journal, 2020, doi:10.1016/j.aej.2020.08.001.

[61] Unidots, Ubidots IoT Platform, 2020.

[62] R.L. Burden, F. J.D., Numerical Analysis, Brooks/Cole, Cengage Learning, 2011.

[63] J.M. Chambers, A.E. Freeny, R.M. Heiberger, Analysis of variance; designed experiments, CRC Press: 145–193, 2017, doi:10.1201/9780203738535.

[64] S. Fine, K. Scheinberg, "Efficient svm training using low-rank kernel representations," Journal of Machine Learning Research, **2**(Dec), 243–264, 2002.

A Novel Blockchain-Based Authentication and Access Control Model for Smart Environment

Nakhoon Choi, Heeyoul Kim[*]

Department of Computer Science and Engineering, Kyonggi University, Suwon 16227, Republic of Korea

A B S T R A C T

With the increase of smart factories and smart cities following the recent 4th industrial revolution, internal user authentication and authorization have become an important issue. The user authentication model using the server-client structure has a problem of forgery of the access history caused by the log manipulation of the administrator and unclearness of the responsibility. In addition, users must independently manage the authentication method for each service authentication. In this paper, to solve the above problem, the researchers propose an integrated ID model based on a hybrid blockchain. The proposed model is implemented as two layers of Ethereum and Hyperledger Fabric: the former layer is responsible for integrated authentication, and the latter layer is responsible for access control. The physical pass or application for user authentication and authorization are integrated to one ID through the proposed model. In addition, the decentralized blockchain ensures the integrity and transparency of the stored access history, and it also provides non-repudiation of authority and access history.

1. Introduction

This paper is an extension of work originally presented in ICACT 2020 (International Conference on Advanced Communication Technology) [1].

With the increase of smart factories and smart cities in accordance with the 4th industrial revolution, user authentication and access control are emerging as important issues. A smart factory automates factory facilities to reduce process failure rates and is operated by a small number of employees [2]. However, there is a problem of responsibility in case of an accident. In addition, users of smart city may need different authentication means for each city service, and there is a risk of manipulation of access history.

The administrator of the centralized access control model of the existing server-client structure can modify and delete the access history. With the above problem, it is possible to avoid responsibility through internal corruption in case of an accident. In addition, the user proves the authority through different authentication methods including physical means and mobile applications for each service. This makes it inconvenient for users to issue and manage various authentication methods, and it is troublesome for users to prove their authority history and career.

[*]Corresponding Author: Heeyoul Kim, Department of Computer Science and Engineering, Kyonggi University, Suwon, 16227, Korea, Email: heeyoul.kim@kgu.ac.kr

To solve the above problem, the authors in [3] proposed integrated authentication using smart cards for integrated access control of various services. However, there is a problem that the administrator can modify the authority and access details arbitrarily, such as the access control list or the capability list.

In order to solve the above problem through the blockchain, the model in [4] stores the information in DHT(Distributed Hash Tables) and performs access control for information based on the Bitcoin system. However, it is not possible to store access details, and there is a problem of processing speed with low TPS(Transaction per Second) of Bitcoin. Also, it is necessary to verify practicality and suitability. These studies are inadequate for authentication and access control in smart environments.

This paper proposes an integrated authentication and access control model in smart environments that solves the problems above with the help of blockchain technology. The proposed model processes user authentication and access request through a hybrid blockchain system using private and public blockchain together. The proposed model enables users to acquire and prove various access rights through one authentication means, thus it integrates the authentication of various smart factory services and smart city services. In addition, the proposed model prevents problems such as access history manipulation that occurs in the existing central model based on the integrity and transparency of the blockchain. Moreover, the user's history recorded in the blockchain can be easily used as the proof of the user's career.

The rest of this paper presents the following. Section 2 introduces blockchain platforms utilized in the proposed model. Section describes the architecture and process of the model. Section 4 displays the results of implementing the model. Section 5 provides application scenario using the model and Section 6 contains conclusions.

2. Background

The flexible connection of vertical or horizontal organizations became important in the wake of the Fourth Industrial Revolution [5]. This paper uses blockchain platform to build reconfigurable network of existing organizations. The integrity of information is secured in the relationship of organizations through the decentralized characteristics of blockchain. Users can also benefit from all the benefits without noticing that the blockchain has been used on the surface.

2.1. Ethereum

Ethereum [6] is a representative public blockchain using PoW(Proof of Work) [7] consensus algorithm like Bitcoin. PoW consensus algorithm is the process of selecting block creators among unreliable participants on blockchain networks. Participants compete to find a hash value that matches the target condition to elect a miner. The public blockchain introduces the economic concept of cryptocurrency, which leads to the correct consensus by compensating the cryptocurrency to the miner elected. The block generated through the consensus is distributed to the participants of the blockchain network and is connected to the previous block through the 'previous block hash' included in the block header to ensure the integrity of the previous block. All blocks and transactions are open to the public with ensuring transparency, and the decentralized network evolves continuously without administrators.

Ethereum supports the creation and distribution of smart contract [8] for the development of DApp(decentralized Application). A smart contract is written in Solidity, a Turing completeness language, and recorded in the distributed ledger with ensuring the integrity of the results according to automated execution and input [9]. Figure 1 represents the operation of the smart contract in Ethereum. The smart contract made with Solidity is compiled and stored in the form of the EVM(Ethereum Virtual Machine)-bytecode in the ledger. Calling the code through Ethereum clients such as Geth(Go-Ethereum) is executed in the EVM environment.
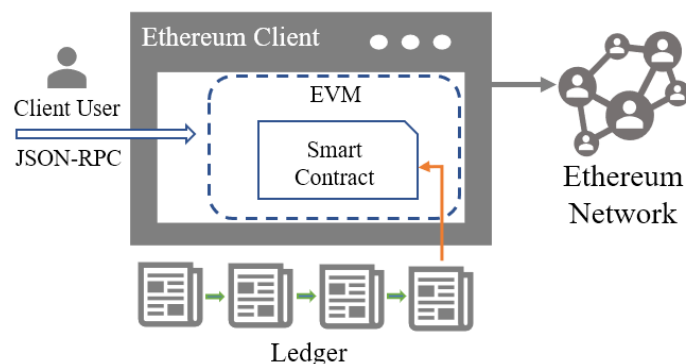
Figure 1: Operation of Smart Contract in Ethereum Client

2.2. Hyperledger Fabric

Hyperledger Fabric [10] (hereinafter referred to as "Fabric"), as part of the Linux Foundation's Hyperledger project, is a representative private blockchain platform commonly used for enterprise environments. Unlike public blockchains, it uses certificates and PKI(Public Key Infrastructure) to authenticate participants with a restricted network, and is managed through a MSP(Membership Service Provider), an authentication management system that defines the role and access rights of nodes in the network.

A peer is a node of organizations that compose the Fabric network and manages ledgers and chaincodes, and the peers are divided into endorser, committee, anchor, and leader according to their roles. Transactions for the execution of chaincodes in the network are performed through three steps: execution, ordering and validation. The chaincode plays the same role as Ethereum's smart contract and updates or queries data to the ledger. Currently, development of chaincodes is possible through Golang, Node.js, etc. Fabric does not require much resources in the consensus, unlike PoW, by ordering transactions through Ordering service to create blocks. Therefore, it has much better performance than the public blockchain platforms.

2.3. Metamask

The blockchain wallet stores the user's personal key as well as managing the balance of the blockchain account, and creates a transaction on behalf of the user and submits it to the network. In this sense, wallet is the easiest approach to using blockchain for normal users. The proposed model uses Metamask [11] for convenient use in PC or mobile environment.

Metamask is the most representative web-based Ethereum wallet extension program executed in browser, and is currently supported by Chrome, Firefox, Opera, etc., and beta test is being conducted in mobile environment. It supports Ethereum account management, digital signature generation, and transaction creation. users can easily access the smart contract of the blockchain through Metamask.

In order for users to access the Ethereum network, they must participate in the network as a blockchain node through the Ethereum client. This method lowers user accessibility, so Metamask uses Infura API [12], a cloud service for network connection to wallet users. Through the Metamask, users can access the Ethereum network in the web environment without operating the node directly, and operate the smart contract and receive the results.

3. A Blockchain-based Authentication and Access Control Model

3.1. Model Architecture

The proposed model uses a hierarchical hybrid blockchain where a public Ethereum network is connected to multiple private Fabric networks. Figure 2 shows the layered architecture of the proposed model. The public layer based on Ethereum is an integrated authentication management layer. The private layer is composed of various subsystems for smart factories and smart

cities (hereinafter referred to as "Organization"), and each organization operates Fabric network separately for authorization and access control.
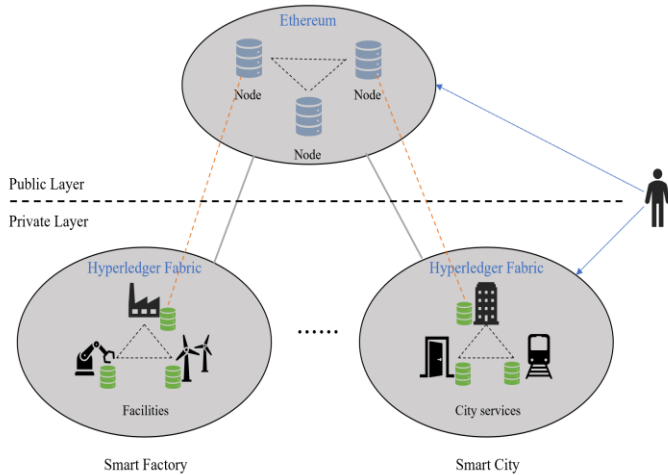
Figure 2: Layered Architecture of the Proposed Model

The proposed model uses a hierarchical hybrid blockchain where a public Ethereum network is connected to multiple private Fabric networks. Figure 2 shows the layered architecture of the proposed model. The public layer based on Ethereum is an integrated authentication management layer. The private layer is composed of various subsystems for smart factories and smart cities (hereinafter referred to as "Organization"), and each organization operates Fabric network separately for authorization and access control.

3.1.1. Public Layer - Integrated Authentication Management

Through this public layer, users create their own IDs based on their Ethereum accounts. The ID of a user is composed of the user's Ethereum account, a secret computed by hashing the user's personal information, a set of tokens used for user authentication by organizations, and a contact method (e.g., E-Mail) as shown in Figure 3. The proposed model provides a smart contract named IAM (Integrated Authentication Manager) utilized by the users to create and control their IDs. The functions in the IAM is described in Table 1, and these functions except for query functions have an access control mechanism on the IDs based on the function modifier in Solidity. In other words, it is guaranteed that only the legitimate owner of the ID can modify the secret and register tokens via these functions.

Figure 3: The structure of a user's ID

Table 1: Description of Functions in the IAM Smart Contract

Function	Purpose
createId(secret)	To create an ID and register the secret based on the user's Ethereum account
modifySecret(secret)	To modify the secret registered
regToken (token, tkName)	To register tokens and their aliases for the authentication by organizations
queryUser(secret)	To find the registered user by given secret and to retrieve user information
queryByToken(token)	To verify whether the token was successfully registered by the user

3.2.2. Private Layer – Access Control Management

In the private layer, there may be several Organizations managing smart environments respectively. Figure 4 represents the architecture of an Organization. Several nodes compose a Hyperledger Fabric network for the Organization. Among them, the admin node provides the ordering service for consensus and is handled by the administrator. The Ethereum sync node is connected to the Ethereum in the public layer and responsible for delivering the user's ID information for authentication.
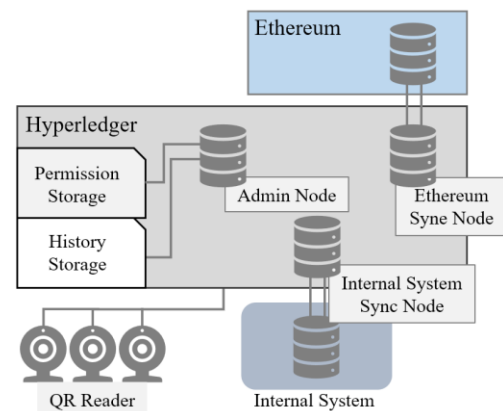
Figure 4: Architecture of an Organization in the Private Layer

Our model provides role-based access control (RBAC), and the role and access rights of each user are recorded in the Fabric blockchain via the chaincode named PM (Permission Manager). Table 2 shows the functions provided by the PM, and only the administrator can execute these functions for creation and modification of the authority. The access history is written by another chaincode called by the client application. The information stored in the Fabric blockchain is transparent and open to the legitimate participants in the Organization.

Table 2: Description of Functions in the PM Chaincode

Function	Purpose
userReg(secret)	To register a new user identified by the secret
permSet(account, role)	To set the role and authorization of the user having the given account
queryPerm(account)	To check and verify the user's role and access rights

3.2. Process Description

3.2.1. Creating an Integrated ID

A new user joining in the proposed model first performs the process of creating an integrated ID. The user first generates a secret by hashing his personal information as follows:

$$secret = Keccak\text{-}256(Birth,\ Name,\ Phone) \qquad (1)$$

Formula 1 shows the creation of the user's secret, and Keccak-256 is a hash function adopted in the SHA-3 competition of the NIST (National Institute of Standards and Technology) [13].

Then, with assuming that the user already has an Ethereum account, he makes a transaction via Metamask to request the smart contract IAM for the creation of his integrated ID. Since the transaction is signed by his Ethereum private key, the IAM can identify and authenticate the requester. The secret can be seen by anyone after recorded in the blockchain. However, his personal information is not exposed due to the one-wayness of the hash function.

3.2.2. Registering User's Access Rights in Organization

When a user who has completed creating his ID newly joins in a specific Organization, his access right is registered by the process shown in Figure 5. The detailed process is as follows.

1) A new user Alice provides his personal data used for computing secret to the Organization.
2) The internal system of the Organization computes secret of the user by Equation (1), and then send it to the Ethereum sync node in the Fabric network.
3) The Ethereum sync node approaches the smart contract IAM to obtain the user's ID with the received secret.

4) The admin node issues a user-specific validation token T_{Alice}. The purpose of this token is to verify the ownership of the ID obtained in step 3). This token is the hash value of a seed generated per each user, and it is signed by the private key of the admin node (Equation (2)). Then, the token is sent to the user.

$$T_{Alice} = Sign(Keccak\text{-}256(seed_{Alice}),\ Org\ admin) \qquad (2)$$

5) Alice registers the received token in his integrated ID through the smart contract IAM. This step only can be done by the creator of the ID because the IAM compares the requester of this register transaction with the owner of the target ID.
6) If the registration of T_{Alice} is successfully accepted by the IAM contract, the Ethereum sync node can recognize it and is convinced of Alice's ID ownership.
7) The administrator registers both the authority information of Alice and his Ethereum account in the permission storage of the organization.

3.2.3. Access Control

Our model provides a role-based access control with registered users' authorization information. Figure 6 shows the process when Alice requests access to the manufacturing control system in a smart factory. A QR reader attached to the control system is used to interact with the user. Our model determines whether the user's role has appropriate access right or not as follows.

1) Alice generates a QR code which includes both a timestamp for preventing replay attack and a digital signature generated by his Ethereum private key. Our model uses ECDSA [14] based on elliptic curve 'secp256k1' as well as Ethereum. Let G be the base point of the curve E where n is the order of G. Alice's private key is d, and his public key is $Q=dG$. The signature (r, s, v) is computed as follows.
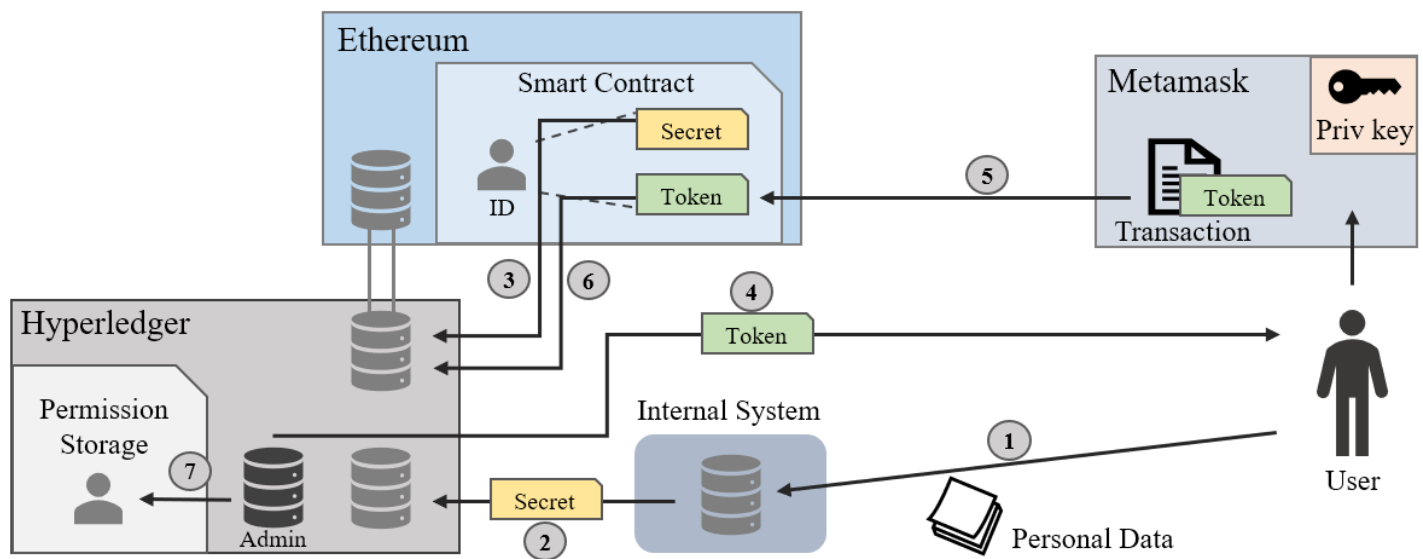
Figure 5: The Process of Registering User's Access Rights in an Organization

① Calculate the hash value $h = hash(m)$ of the message m to be signed, and let z be the l leftmost bits of h where l is the bit length of n.

② Generates a random number k within $[0 \sim n\text{-}1]$.

③ Compute $R = kG$ and obtain the x-coordinate r of point R.

④ Compute $s = k^{-1}(z + rd) \mod n$.

⑤ Compute $v = 27 + (y \% 2)$ (y: y-coordinate of Q).

⑥ (r, s, v) is the digital signature value.

2) The QR reader scans the QR code generated by Alice, and as a Fabric client it delivers the timestamp, signature, and the *object_serial* (ID of the QR reader) to the Fabric node.

3) The Fabric node verifies received signature (r, s, v) with the help of Ethereum's *ecRecover()* method. If it is valid, as a result of this method call, the node discovers Alice's Ethereum account.

4) The authority information of the discovered Ethereum account is retrieved from the permission storage.

5) If Alice's role has been approved for access to the subject to which the *object_serial* is assigned, this request is granted.

6) Alice's access attempt is recorded in the history storage.
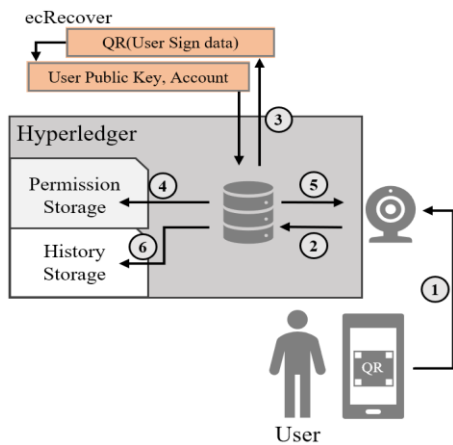
Figure 6: The Process of Access Control in an Organization

4. Implementation and Experiment

The proposed model was implemented, and its soundness was confirmed through an experiment. Table 3 describes the implementation environment of each component. The web dApp runs on the Chrome browser with Metamask installed, and it registers the user's secret for creating ID and the Organization's token for registering the user's access rights. The smart contract IAM and the chaincode PM provides the functions described in Section 3.1. QR generator is an application where the user's Ethereum private key is stored, and it generates a QR code containing the user's signature to obtain access right. QR reader is a Fabric client attached to the protected resources.

Table 3: Development Environment

	Environment	Chrome, Metamask
Web dApp		
	Language	JavaScript
Smart Contract IAM	Environment	Ethereum Ropsten Testnet
	Language	Solidity ^0.5.0

	Environment	Hyperledger Fabric 2.1
Chaincode PM		
	Language	Node.js
QR Generator	Environment	Android Emulator
	Language	Java
QR Reader	Environment	Raspberry Pi
	Language	Node.js

Figure 7 shows the screenshots when a user creates his integrated ID via the web dApp. As can be seen in Figure 8(a), a user inputs his personal data to compute secret. Then, the installed Metamask generates and transmits an Ethereum transaction requesting creation of the user's integrated ID.
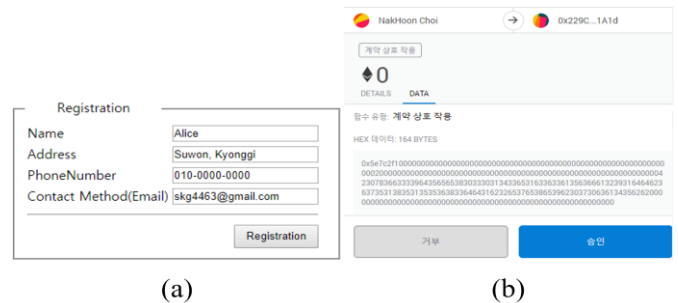
Figure 7: Screenshots when Creating Integrated ID. (a) Input of User Data for Computing Secret, (b) Generation of Ethereum transaction with Metamask

Figure 8 shows the logs when an organization registers a user Alice's role after verifying authentication. With given Alice's personal data, the organization computes Alice's secret (Figure 8(a)). Then, the organization checks whether Alice's integrated ID exists or not in the smart contract IAM by calling the *queryUser(secret)* function. If the ID exists, a validation token is issued for Alice (Figure 8(b)). After Alice successfully registers his token in his ID, the organization's Ethereum sync node can detect this event by implementing an event listener for IAM. As can be seen in Figure 8(c), the organization discovers Alice's Ethereum account from this event, and then assigns Alice's role and access right. In this experiment, the role 'level_2' is assigned to Alice and he is granted to access 'object 001'.

Figure 8: Logs when Registering Alice's Access Right in an Organization. (a) Computation of Alice's Secret by the Organization, (b) Issuance of a Validation Token for Alice, (c) Detection of Token Registration and Assignment of Alice's Role

Figure 9 shows an example QR code generated when Alice wants to access a protected resource in the organization. The QR generator installed in Alice's smartphone generates this QR code

by using of the stored private key (Figure 9(a)). As can be seen in Figure 9(b), the QR code contains two values (q0 and q1), where q0 is Alice's ECDSA signature and q1 is the Unix timestamp. Then, Alice provides this QR code to the QR reader attached to the resource.
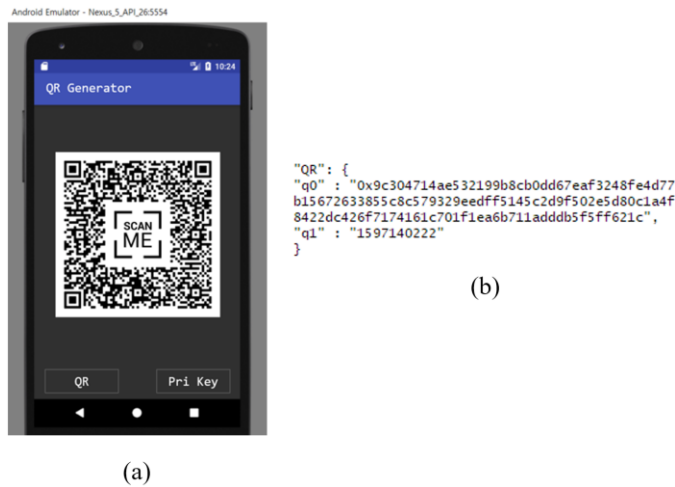
Figure 9: An Example QR Code Generated for Access. (a) Screenshot of QR Generator, (b) The Information stored in the QR Code

The QR reader transmits both its *object_serial* ('0001' in Figure 10) and the signature obtained by scanning the QR code to the Fabric node. The node recovers Alice's Ethereum account by using of the *ecRecover* function. Also, it verifies the validity of both ECDSA signature and timestamp. Then, it can get Alice's registered role from the permission storage with the account, as shown in Figure 10. Finally, the node decides whether to grant or deny Alice's access request based on his role, and then it informs the QR reader of the decision result.

Figure 10: Logs when Alice's Access Request is Granted

5. Application Scenario using the Proposed Model

To help understanding the proposed model and claim its usefulness, we provide an application scenario using the model from a user point of view in this section. Let us assume that a new user Alice having an Ethereum account Eth_A decided to use the proposed model. He visits the web dApp and creates his own integrated ID (ID_A) by registering both his email address and secret based on his personal data.

Since then, Alice has moved into the smart city K-city (Organization #1) to seek employment. The K-city already has adopted the model extensively, and it participates as an organization. He visits the government office of the city to register himself. The office checks the existence of ID_A and then issues a token T_{Alice}^{Org1}. Alice registers this token in his ID_A by using of his

Ethereum private key. Then, the office assigns the role 'citizen' to Alice and registers his access right to use various public facilities in the city.

Now Alice can prove his identity and use various facilities with his smartphone where the QR generator application is installed. Suppose Alice visits a public library to get hiring information. He just generates a QR code and shows it to the QR reader attached to the gate of the library. Then, his access is allowed, and he can enter the library.

Before long, Alice is hired by a smart factory F-factory (Organization #2). Similarly, in the enrollment process, he can easily register himself with a newly issued token T_{Alice}^{Org2}, without creating a new identity to be used in the factory. Then, the role 'engineer' is assigned to Alice and his access right for the control panel in the factory is registered. As a result, he can control the panel by generation a valid QR code whenever he needs to access it while at work.

Suppose someday Alice commits a mistake in operating some equipment in F-factory, which causes enormous damage to the factory. He gets into a panic, and he may try to avoid suspicion by deleting or manipulation evidences such as CCTV videos. However, since the access history of the users is stored in the immutable blockchain ledger of the F-factory nodes, he cannot hide the fact that he accessed the equipment at that time. Thus, the F-factory can identify Alice's behavior and call him to account.

In another case, suppose an attacker Trudy pretending as Alice tries to access the control panel. He cannot generate a valid QR code because he cannot discover Alice's private key. The attacker may eavesdrop Alice's QR code and try to use it later. However, the timestamp in the QR code prevents this kind of replay attack. Moreover, even if a security incident occurs, the factory can perform a security audit with the immutable access history.

6. Conclusion

Currently many companies and organizations use a centralized model for authentication and access control, so there is internal corruption caused by manipulating access history and it is possible to avoid responsibility in case of an accident. This paper proposes an access control model for smart factories and smart cities using blockchain, a decentralization platform, to solve the problems of existing centralized model and to ensure the integrity and immutability of access history.

The proposed model allows a user to prove their access rights through one integrated ID based on his Ethereum account without creating a new ID separately for each organization. In the aspect of an organization, it is needless to establish separate authentication mechanism, and the organization can easily authorize the users belong to it to access its protected resources. In addition, the proposed model records the access history in the internal blockchain of the organization not only to prevent arbitrary modification and deletion but also to provide non-repudiation.

The proposed model provides a clue to how various smart environments cooperate closely. Both the concept of integrated ID and the hybrid blockchain combining public blockchain and private blockchain can help secure, pragmatic, and user-friendly smart systems. In addition, flexible scalability in a smart environment is secured through a blockchain, and reliability of services and information provided to users is guaranteed.

Acknowledgement

References

[1] N. Choi, H. Kim, "Hybrid Blockchain-based Unification ID in Smart Environment," International Conference on Advanced Communication Technology, ICACT, **2020**, 166–170, 2020, doi:10.23919/ICACT48636.2020.9061430.

[2] G. Büchi, M. Cugno, R. Castagnoli, "Smart factory performance and Industry 4.0," Technological Forecasting and Social Change, **150**(October 2019), 119790, 2020, doi:10.1016/j.techfore.2019.119790.

[3] G. Moukhliss, R. Filali Hilali, H. Belhadaoui, "A smart card digital identity check model for university services access," ACM International Conference Proceeding Series, **Part F1481**, 3–6, 2019, doi:10.1145/3320326.3320401.

[4] G. Zyskind, O. Nathan, A.S. Pentland, "Decentralizing privacy: Using blockchain to protect personal data," Proceedings - 2015 IEEE Security and Privacy Workshops, SPW 2015, 180–184, 2015, doi:10.1109/SPW.2015.27.

[5] A. Mushtaq, I.U. Haq, "Implications of blockchain in industry 4.O," 2019 International Conference on Engineering and Emerging Technologies, ICEET 2019, 1–5, 2019, doi:10.1109/CEET1.2019.8711819.

[6] G. Wood, "Ethereum: A secure decentralised generalised transaction ledger," Ethereum Project Yellow Paper, **151**(2014), 1–32, 2014.

[7] S. Nakamoto, Bitcoin: A peer-to-peer electronic cash system, Manubot, 2019.

[8] N. Szabo, "Smart contracts: building blocks for digital markets," EXTROPY: The Journal of Transhumanist Thought,(16), **18**(2), 1996.

[9] K. Christidis, M. Devetsikiotis, "Blockchains and Smart Contracts for the Internet of Things," IEEE Access, **4**, 2292–2303, 2016, doi:10.1109/ACCESS.2016.2566339.

[10] C. Cachin, "Architecture of the hyperledger blockchain fabric," in Workshop on distributed cryptocurrencies and consensus ledgers, 2016.

[11] Metamask Inc, Metamask, Website Https://Metamask.Io/,.

[12] The Infura Inc, INFURA, Website Https://Infura.Io/,.

[13] S. Chang, R. Perlner, W.E. Burr, J.M. Kelsey, L.E. Bassham, "Third-Round Report of the SHA-3 Cryptographic Hash Algorithm Competition NISTIR 7896 Third-Round Report of the SHA-3 Cryptographic Hash Algorithm Competition."

[14] D.R.L. Brown, "SEC 1: Elliptic curve cryptography," Certicom Research, v2, 2009.

Multiple Machine Learning Algorithms Comparison for Modulation Type Classification Based on Instantaneous Values of the Time Domain Signal and Time Series Statistics Derived from Wavelet Transform

Inna Valieva[1,*], Iurii Voitenko[2], Mats Björkman[1], Johan Åkerberg[1], Mikael Ekström[1]

[1]*School of Innovation, Design, and Engineering, Mälardalen University, Västerås, 721 23, Sweden*

[2]*Electronics Development, Wireless P2P Technologies, 79140, Sweden*

A R T I C L E   I N F O

A B S T R A C T

Modulation type classification is a part of waveform estimation required to employ spectrum sharing scenarios like dynamic spectrum access that allow more efficient spectrum utilization. In this work multiple classification features, feature extraction, and classification algorithms for modulation type classification have been studied and compared in terms of classification speed and accuracy to suggest the optimal algorithm for deployment on our target application hardware. The training and validation of the machine learning classifiers have been performed using artificial data. The possibility to use instantaneous values of the time domain signal has shown acceptable performance for the binary classification between BPSK and 2FSK: Both ensemble boosted trees with 30 decision trees learners trained using AdaBoost sampling and fine decision trees have shown optimal performance in terms of both an average classification accuracy (86.3 % and 86.0 %) and classification speed (120 0000 objects per second) for additive white gaussian noise (AWGN) channel with signal-to-noise ratio (SNR) ranging between 1 and 30 dB. However, for the classification between five modulation classes demonstrated average classification accuracy has reached only 78.1 % in validation. Statistical features: Mean, Standard Deviation, Kurtosis, Skewness, Median Absolute Deviation, Root-Mean-Square level, Zero Crossing Rate, Interquartile Range and 75th Percentile derived from the wavelet transform of the received signal observed during 100 and 500 microseconds were studied using fractional factorial design to determine the features with the highest effect on the response variables: classification accuracy and speed for the additive white gaussian noise and Rician line of sight multipath channel. The highest classification speed of 170 000 objects/second and 100 % classification accuracy has been demonstrated by fine decision trees using as an input Kurtosis derived from the wavelet coefficients derived from signal observed during 100 microseconds for AWGN channel. For the line of sight fading Rician channel with AWGN demonstrated classification speed is slower 130 000 objects/s.

1. Introduction

This paper is an extension of the work "Multiple Machine Learning Algorithms Comparison for Modulation Type Classification for Efficient Cognitive Radio" originally presented in Milcom 2019 [1].

The global market of mobile devices and services actively using the electromagnetic spectrum is continuously growing.

Traditionally the electromagnetic spectrum utilization has been performed using a robust static approach developed almost a century ago: it rations access to the spectrum in exchange for the guarantee of interference-free communication spectrum is divided into the rigid, exclusively licensed bands, allocated over large, geographically defined regions. In conditions when some of these license bands are being nearly unused, while the others are overwhelmed, the problem of spectrum scarcity arises [2]. To cope with the increasingly populated spectrum, the electromagnetic spectrum utilization policies have been reformed

in recent years with the objective to allow the unlicensed secondary users to access licensed bands without causing interference to the licensed primary users [3].

Blind waveform estimation techniques can be used with an intelligent transceiver, yielding an increase in the transmission efficiency by reducing the overhead. Waveform information is critical to implement spectrum sharing scenarios like frequency hopping spread spectrum (FHSS) and dynamic spectrum access (DSA). Modulation type classification is a part of the waveform estimation together with the central frequency and symbol rate estimation. Multiple artificial intelligence algorithms have been successfully applied to solve the modulation classification problems. The availability of abundant data, breakthroughs of algorithms, and the advancements in hardware development during recent years have been driving forward vibrant development of deep learning [4]. Modulation classification using convolutional NN has been presented in [5] and [6]. Mathworks deployed a hands-on practical implementation of deep learning-based modulation classification in [7]. In [8], the authors have demonstrated successful launch of the optimized AlexNet on ZYNQ7045 FPGA: the inference execution times of CNNs in low density FPGAs has been improved using fixed-point arithmetic, zero-skipping and weight pruning. However, in this work the choice has been made to use less computationally demanding supervised ML algorithms. Conventional artificial intelligence (AI) algorithms like machine learning (ML) require preprocessing of the input signal and feature extraction. Received signal features used for the modulation classification could be classified into spectral-based and cyclostationary features. The spectral-based features exploit the unique spectral characters of different signal modulations in three physical aspects of the signal: the amplitude, phase, and frequency. The authors have summarized some of the well-recognized spectral features designed for modulation classification including the following and suggested a decision tree classification [9]. The authors have applied instantaneous amplitude, instantaneous phase, and spectrum symmetry together with the set of new features from both spectral and time domain including linear predictive coefficients, adaptive component weighting, zero-crossing ratio, linear frequency bank spectral coefficient for the classification of commonly used digital modulations including ASK, FSK, MSK, BPSK, QPSK, PSK, FSK4 and QAM-16 [10]. Gardner pioneered the area of cyclostationary signal analysis [11]. Gardner and Spooner first implemented cyclostationary analysis for modulation classification problems in [12].
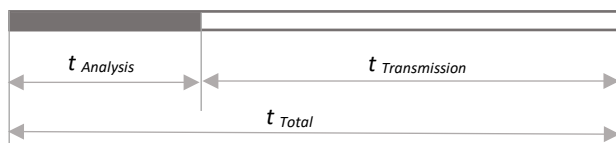
Figure 1: Optimizing sensing and transmission times.

The aim of this work is to determine the optimal modulation classification algorithm and suggest the subset of the strongest and robust features derived from the received signal that could be used to blindly classify the modulation type in our hardware application: a software-defined radio-based network consisting of multiple digital cognitive radio nodes. SDR-based nodes are operating in the frequency band from 70 MHz to 6 GHz with up to 56 MHz of instantaneous bandwidth are used as the hardware platform for the cognitive functionality deployment with FHSS capabilities. Available computational resources are Dual-core ARM Cortex A9 CPU, 2x512 MB of DDR3L RAM, and 512 MB of QSPI flash memory. The operation system is Embedded Linux. The radio part is based on Analog Devices AD9364 radio transceiver and Xilinx' Zynq-7020 FPGA. It is supporting multiple digital modulations including both linear: QPSK, BPSK, 8PSK, 16PSK, and non-linear: 2FSK. Symbol rate could be also adjusted between 10 KSymbols/s and 1 MSymbol/s to generate the cognitive waveform. Our target application predefines most of the boundary conditions and operational requirements such as required decision-making speed and computational resources available. In this work time required for radio scene analysis $t_{Analysis}$ is defined as a sum of time required for radio scene observation $t_{Observation}$ and processing $t_{Processing}$ for the received signal on the receiver front end. Time allocated for the active data transmission is data transmission time, $t_{Transmission}$ and total time is the sum of observation and transmission time as illustrated by Figure 8. Allocating the sensing time and transmission time at the MAC layer is involving a tradeoff between ensuring the PUs user's QoS requirements as opposed to maximizing the data throughput. To meet real-time operation requirements on the target hardware the following real-time performance characteristics must be met by the proposed algorithms. The maximum time available for radio-scene environment observation is $t_{observation}$=500×10^{-6} seconds. Our application is a time-slotted communication system, where 500 microseconds corresponds to one-time slot, also maximum processing time has been selected likewise $t_{processing}$=500×10^{-6} seconds, which requires the minimum classification speed of 2000 objects per second. Modulation classification is required to be performed for SNR values above the demodulation threshold of 12 dB, which corresponds to bit-error-rate BER=10^{-8} and BER=3.4×10^{-5} for BPSK and 2FSK, respectively.

The frequency of the radio scene environment sensing (how often sensing should be performed by the cognitive radio) and sensing time (the duration the sensing is performed) are key parameters affecting the throughput. While higher sensing times ensure more accurate radio scene environment sensing, this may result in a comparatively smaller duration for actual data transmission during the total time for which the spectrum may be used, thereby lowering the throughput [13]. To achieve the optimum between sensing time and throughput, for example, in IEEE 802.22 two-stage sensing (TSS) mechanism is implemented that includes: fast sensing, done at the rate of 1 ms/channel, and fine sensing performed on-demand. In this work, we have evaluated the possibility to perform the classification based on instantaneous values to shorten the spectrum sensing time and reduce computational costs. To improve classification accuracy, classification based on spectral-based statistical features derived from the wavelet transform of the received signal observed during the certain observation time frame has been proposed. In this study observation times of 100 and 500 microseconds have been used. The lowest observation time has been selected 100 microseconds to accommodate the lowest symbol rate of 10 KSymbols/second supported in our target application for cognitive waveform generation.
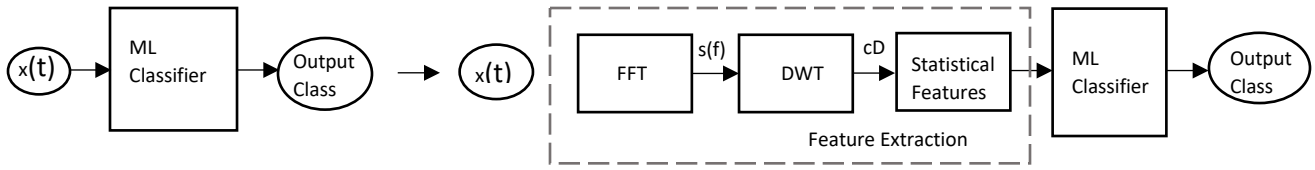
Figure 2: Modulation classification using a) instantaneous values of the time domain signal input; b) time series statistics input.
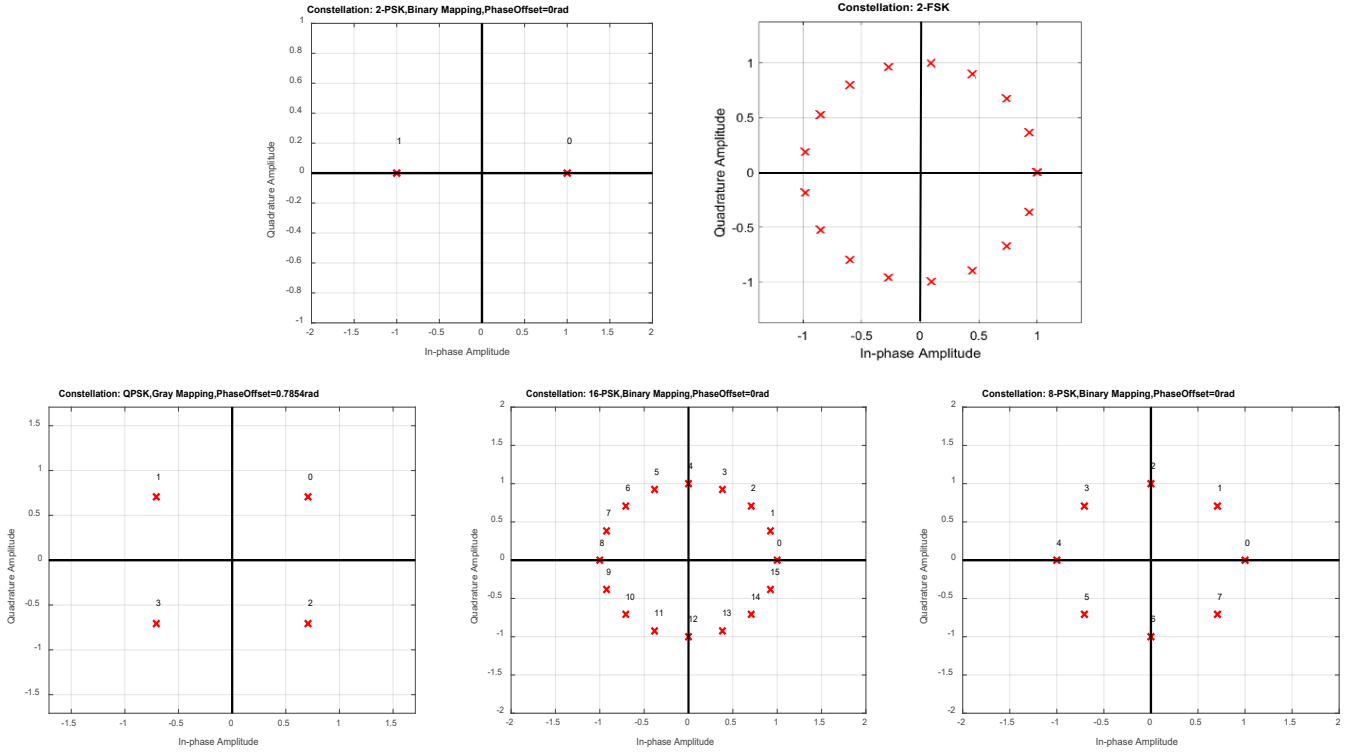
Figure 3: Constellation plots for studies modulation classes BPSK, 2FSK, QPSK, 8PSK, 16PSK.
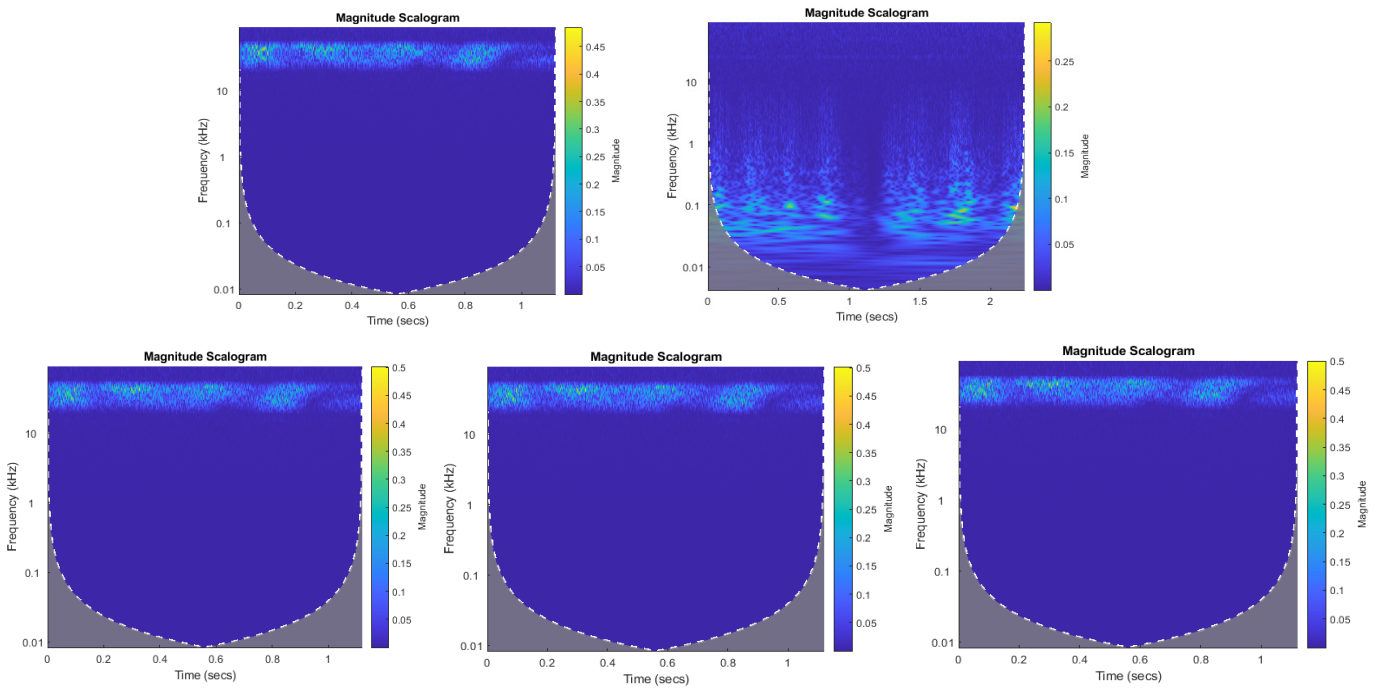
Figure 4: Scalograms obtained from Haar transform. wavelet coefficients for BPSK, 2FSK, QPSK, 8PSK, 16PSK. Observation time 500 microseconds signal.

The highest: 500 microseconds that correspond to one time slot in our time-slotted target application. Wavelet transform has been used in this work for the feature extraction, since obtained wavelet coefficients could be reused also to detect the vacant frequency channels and estimate the symbol rate, what could potentially save time and computational resources spent on radio scene analysis. Cyclostationary based algorithms have also been named in the literature as a powerful algorithm for modulation type and symbol rate estimation and vacant frequency channels detection. However, they are prone to cyclostationary noise and require longer observation time and is relatively computationally complex [14], and therefore this work has been focused on wavelet-based algorithms. Multiple supervised machine learning classifiers have been tested to perform classification based on instantaneous values and time-series statistics. The performance of tested classifiers has been evaluated in terms of classification accuracy and speed.

2. Methodology

Both feature extraction and classification algorithms applied in the literature to solve the modulation classification problem has been studied and evaluated. Primary, modulation type classification has been performed based on the input values of the instantaneous values of the in-phase and quadrature components of the time domain digital signal. Classification results have been satisfactory for the case of the binary classification between 2FSK and BPSK modulations. However, once the classification task has been extended to the higher-order modulations, the suggested classification approach has shown unacceptably low classification accuracy of 78.1 %. The highest classification accuracy of 84.9 % has been observed in the validation phase for classifying five modulations into two classes: linear and non-linear modulations using a fine SVM classifier.

Therefore, to improve the classification accuracy for higher-order modulations we have looked at multiple statistical features extracted from the time series containing the received signal observed during observation times of 100 and 500 microseconds. The following criteria have been considered when selecting classification features and feature extraction algorithm:

1. Robustness to noise; 2. Computational complexity; 3. Possibility to reuse preprocessed data for solving other radio scene environments observation tasks such as vacant bands detection and symbol rate estimation. Nine spectral-based statistical features derived from Haar wavelet transform coefficients calculated from the frequency domain signal observed during the selected observation time. The Haar transform has been selected as the simplest and less computationally demanding of all wavelet families. From the vector of wavelet coefficients, nine statistical features have been derived. To determine the strongest features to be used as inputs to ML classifier fractional factorial design analysis has been performed.

In statistics, a full factorial experiment is an experiment whose design consists of two or more factors, each with discrete possible values or "levels", and whose experimental units take on all possible combinations of these levels across all studied factors. Fractional factorial designs are experimental designs consisting of a carefully chosen subset or fraction of the experimental runs of a full factorial design. Significance is quantitively measured and referred to as the main effect [15]. A fractional factorial design approach has been used to analyze the main effects of every of nine statistical features and observation time on two studied response parameters: classification speed and accuracy in conditions of noise represented by two levels: AWGN and AWGN and multipath Rician channel model. Two levels have been applied and studied: first-level "-1" corresponds to not including the classification feature into classification and second level "+1" corresponds to including the studied feature into classification input. Observation time has also been varied according to two levels: first "-1" corresponds to 100 microseconds and the second level "+1" corresponds to 500 microseconds observation time. MATLAB and Simulink environment has been used for training and validation data sets generation including the modulator and propagation channel models, MathWorks classification learner ML Classification Learner tool has been used to train and validate classifiers. Twenty-four supervised ML classification algorithms have been studied and evaluated in terms of classification accuracy and classification speed for two studied channel models: AWGN and Rician multipath channels with AWGN.

3. Input data and feature extraction

To suggest optimal feature extraction and classification algorithms for our target radio application seven artificial data sets, consisting of signal samples modulated into 2FSK, BPSK, QPSK, 8PSK, 16PSK have been generated. Data sets are described in detail in Section 4. Figure 3 presents the constellation plots of five studied modulation types.

3.1. Classification using instantaneous values

The classification performed using instantaneous values of the time domain signal and SNR as classification inputs does not require any feature extraction: the raw values of the in-phase and quadrature component and SNR (recorded by transceiver as RSSI) have been used directly as an input to the classifier.
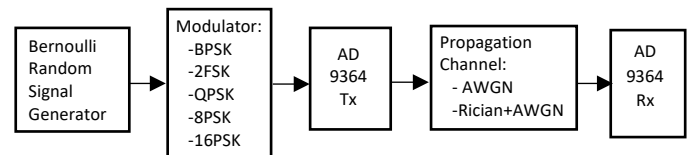
Figure 5: Generalized model used for data set generation.

Table 1: Spectral-based features derived from time series used for modulation type classification

N	Feature	Factor	Description
1	Mean	A	Mean value of the wavelet coefficients obtained from single-level discrete wavelet transform of the frequency domain signal.
2	Standard Deviation	B	Standard deviation of the wavelet coefficients obtained from single-level discrete wavelet transform of the frequency domain signal.

3	Kurtosis	C	Kurtosis is a statistical measure that defines how heavily the tails of a distribution differ from the tails of a normal distribution calculated from the wavelet coefficients obtained from single-level discrete wavelet transform of the frequency domain signal [16].
4	Skewness	D	Skewness is a measure of the asymmetry of the probability distribution of a real-valued random variable about its mean. Calculated from the wavelet coefficients obtained from single-level discrete wavelet transform of the frequency domain signal [16].
5	Median absolute deviation	E	It is a measure of the statistical dispersion: a robust measure of the variability of a univariate sample of quantitative data. It is more resilient to outliers in a data set than the standard deviation. It is calculated from the wavelet coefficients obtained from single-level discrete wavelet transform of the frequency domain signal [17].
6	Root-mean-square level	F	The RMS value of a set of values (or a continuous-time waveform) is the square root of the arithmetic mean of the squares of the values, or the square of the function that defines the continuous waveform [18].
7	Zero crossing rate	G	It is the rate of sign-changes along a signal: the rate at which the signal changes from positive to zero to negative or from negative to zero to positive [19].
8	Interquartile range	H	The interquartile range (IQR) is a measure of variability: calculated based on dividing a data set into quartiles [20].
9	75th Percentile	I	The percentile rank of a score is the percentage of scores in its frequency distribution that are equal to or lower than it [21].
10	SNR	J	Signal-to-Noise ratio corresponds to RSSI value for the received signal measured by transceiver.

Table 2: Classifiers performance reached in validation. Classification between FSK and BPSK modulations. AWGN channel (SNR ranging from 1 to30 dB). Data set 1

Classifier	With PCA (1 feature of 3)		No PCA (3 features of 3)		No PCA (2 features of 3, No SNR)	
	Average Accuracy, %	Prediction speed, Objects/s	Average Accuracy, %	Prediction speed, Objects/s	Average Accuracy, %	Prediction speed, Objects/s
Decision Trees: Fine	52.1	1600 000	86.0	1 200 000	84.2	2 000 000
Decision Trees: Medium	51.3	1200 000	85.2	1 000 000	83.3	2 100 000
Decision Trees: Coarse	50.7	1300 000	82.2	2 300 000	82.1	2 100 000
KNN: Fine	55.5	770 000	82.3	310 000	78.9	300 000
KNN: Medium	57.9	220 000	86.1	110 000	84.6	110 000
KNN: Coarse	61.5	55 000	86.8	28 000	85.5	27 000
KNN: Cosine	50.0	300	83.7	290	78.1	320
KNN: Cubic	57.9	150 000	86.1	29 000	84.6	46 000
KNN: Weighted	56.0	220 000	84.2	130 000	82.0	120 000
SVM: linear	50.1	47 000	55.3	3000	63.8	120 000
SVM: Quadratic	50.0	70 000	54.7	2300	42.8	92 000
SVM: Cubic	50.0	160 000	58.8	34 000	62.8	40 000
SVM: Fine Gaussian	49.5	230	86.9	790	85.4	970
SVM: Medium Gaussian	49.8	190	86.5	610	84.3	750
SVM: Coarse Gaussian	49.8	240	49.8	240	81.4	600
Ensemble Boosted Trees	51.3	110 000	86.3	120 000	85.0	120 000
Ensemble Bagged Trees	55.5	19 000	85.4	44 000	83.1	33 000
Ensemble Subspace Discriminant	49.8	100 000	50.3	86 000	50.5	120 000
Ensemble Subspace KNN	55.5	34 000	80.5	6100	69.5	17 000
Ensemble RUS Boosted Trees	51.3	120 000	85.1	150 000	83.3	130 000
Logistic Regression	49.8	1600 000	50.9	1 200 000	50.5	3 200 000
Linear Discriminant	49.8	1200 000	50.3	1 900 000	50.5	1 300000

3.2. Classification using time-series statistics.

Nine spectral-based statistical features have been derived from the received signal observed during the observation time. Primary fast Fourier transform has been applied to switch to the frequency domain. Then discrete wavelet transform has been applied to the frequency domain signal using Haar wavelet. This transform cross-multiplies a function against the Haar wavelet with various shifts and stretches. Figure 4 presents scalograms plots for studied modulations obtained by Haar wavelet transform. Then from the derived wavelet coefficients, nine spectral-based statistical features summarized in Table 1 have been calculated.

4. Data set

Seven data sets used for training and validation have been generated and are described briefly below. Three labeled artificial data sets consisting of three features: instantaneous values of in-phase and quadrature components of the time domain signal and SNR and four data sets consisting of nine statistical features extracted from time-series recorded during 100 and 500

microseconds and SNR for two channel models: AWGN and Rician channel with AWGN. Figure 5 describes the generalized model used to generate data sets.

Data Set 1: *Binary classification between BPSK and 2FSK using instantaneous values.* Data set for training and validation has been generated using a virtual model presented in Figure 5. The random input signal has been generated by Bernoulli binary random signal generator and modulated into BPSK or FSK. The modulated signal is transmitted by transmitter AD9364 TX. AWGN channel model has been selected to emulate the propagation environment, where SNR ranges from 30 to 1 dB. Data set consisting of 408000 rows and 4 columns, where two first columns correspond to the instantaneous values of the signal in the time domain: in-phase and quadrature components, the third column corresponds to SNR value and the fourth column represents the data label. 80 % of the data set has been used for training the classifiers and 20 % has been used for validation.

Data Set 2: *Classification of BPSK, 2FSK, QPSK, 8PSK, 16PSK into two classes linear and nonlinear using instantaneous values.* Data set of total size 910000 rows by 4 columns consisting of BPSK, 2FSK, QPSK, 8PSK, 16PSK has been generated in a similar way as Data Set 1: two first columns are corresponding to the instantaneous values of the signal in the time domain: in-phase and quadrature components, the third column corresponding to SNR value and the fourth column represents the data label corresponding to two classes: linear or non-linear modulation. Also, 80 % of the generated data set has been used for training the classifiers and 20 % of the generated data set has been used for validation of the classifiers.

Data Set 3: *Classification of BPSK, 2FSK, QPSK, 8PSK, 16PSK into five classes using instantaneous values.* Data set 3 consisting of five modulations described above has been used to train classifiers to classify all five modulation types. In this data set only the fourth column corresponding to the label has been changed to accommodate five output classes. Also, 80 % of the data set has been used for training of the classifiers and 20% for validation.

Table 3: Classifiers performance reached in validation. Classification between linear and non-linear modulations. Non-Linear: FSK, linear: BPSK, QPS, 8PSK, 16PSK modulations. AWGN channel (SNR ranging from 1 to 30dB). Data set 2.

Classifier	Average Accuracy, (%)	Prediction speed, (Objects/s)
Decision Trees: Fine	80.5	1 200 000
Optimized Trees	83.0	3 400 000
KNN: Fine	77.1	310 000
KNN: Medium	82.6	110 000
SVM: Fine Gaussian	84.9	790
Ensemble Boosted Trees	80.9	120 000
Ensemble Bagged Trees	81.8	44 000
Ensemble Subspace KNN	80.5	6100
Ensemble RUS Boosted Trees	78.1	150 000

Data Set 4: *Classification of BPSK, 2FSK, QPSK, 8PSK, 16PSK into five classes using statistical features derived from time series observed during 500 microseconds for AWGN channel.*

Data set 4 consists of 1500 samples (300 signal samples for every modulation type) resulting in a matrix of 1500 rows by 11 columns where the first nine columns correspond to statistical features column 10 corresponds to SNR and the last column corresponds to data class label. Statistical features for every signal sample have been derived from the received signal observed during 500 microseconds in conditions of the AWGN propagation channel (SNR ranging from 1 dB to 30 dB). Also, 80 % of the data set has been used for training, and 20 % for validation.

Data Set 5: *Classification of BPSK, 2FSK, QPSK, 8PSK, 16PSK into five classes using statistical features derived from time series observed during 100 microseconds. AWGN channel.* Data set 5 consisting of 1500 samples (300 signal samples for every modulation type) resulting in a matrix of 1500 rows by 11 columns where the first nine columns correspond to statistical features, column 10 corresponds to SNR and the last column corresponds to data class label. Statistical features for every signal sample have been derived from the received signal observed during 100 microseconds in conditions of AWGN propagation channel with

SNR ranging from 1 to 30 dB. Also, 80% of the data set has been used for training, and 20% for validation.

Data Set 6: *Classification of BPSK, 2FSK, QPSK, 8PSK, 16PSK into five classes using statistical features derived from the received signal observed during 500 microseconds for Rician multipath channel.* Data set 6 consisting of 1500 samples (300 signal samples for every modulation type) resulting in a matrix 1500 rows by 11 columns where the first nine columns correspond to statistical features, column 10 corresponds to SNR and the last column corresponds to data class label. Statistical features have been derived from time-domain signal observed during 500 microseconds in conditions of Rician multipath line-of-sight fading channel model with AWGN (SNR = 30). Three fading paths have been chosen with path delays selected for outdoor environments 0; 9×10^{-5} and 1.7×10^{-5}. Path delay ranging 10^{-5} is suggested for the mountains area. Average path gains have been chosen [0 -2 -10]. The Rician K-factor has been selected K-factor = 4, it specifies the ratio of specular-to-diffuse power for a direct line-of-sight path, it is usually in the range [1, 10] and 0 corresponds to Rayleigh fading. Maximum Doppler shift has been chosen 4 dB, which corresponds to a signal from a moving pedestrian [22]. Also, 80% of the data set has been used for training the classifiers and 20 % for validation.

Data Set 7: *Classification of BPSK, 2FSK, QPSK, 8PSK, 16PSK into five classes using statistical features derived from time series observed during 100 microseconds. Rician multipath channel.* Data set 7 consisting of 1500 samples (300 signal samples for every modulation type) resulting in a matrix 1500 rows by 11 columns where the first nine columns correspond to statistical features column 10 corresponds to SNR and the last column corresponds to data class label. Statistical features for every signal sample have been derived according to the steps summarized in feature extraction from time-domain signal observed during 100 microseconds in conditions of Rician multipath channel model with AWGN with SNR = 30 dB. The properties of the Rician channel have been selected the same as in data set 6. 80% of the data set has been used to train classifiers, 20% for validation.

Table 4: Classifiers performance reached in validation. Classification between FSK, BPSK, QPSK, 8PSK and 16PSK modulations using statistical features derived from the wavelet transform of the time series recorded during 500 microseconds. AWGN (SNR ranging from 1 to 30 dB) channel. Data set 4.

Classifier	With PCA (1 feature of 10)		No PCA (10 features of 10)		No PCA (5 features of 10)		No PCA Mean (1 features of 10)	
	Average Accuracy, %	Prediction speed, Objects/s	Average Accuracy, %	Prediction speed, Objects/s	Average Accuracy, %	Prediction speed, Objects/s	Average Accuracy, %	Prediction speed, Objects/s
Decision Trees: Fine	100	15000	100	21000	100	20000	100	12000
Decision Trees: Medium	89.3	13000	99.7	23000	90.6	21000	79.9	18000
Decision Trees: Coarse	82.9	15000	88.1	19000	68.9	23000	67.5	19000
KNN: Fine	100	22000	100	42000	100	48000	100	51000
KNN: Medium	98.1	22000	96.6	26000	98.2	38000	97.2	56000
KNN: Coarse	80.6	18000	61.1	13000	61.7	21000	69.1	36000
KNN: Cosine	38.3	18000	96.9	22000	97.2	33000	21.3	38000
KNN: Cubic	98.1	17000	96.6	7800	98.5	20000	97.2	52000
KNN: Weighted	100	18000	100	36000	100	52000	100	52000
SVM: linear	57.0	15000	93.8	18000	75.1	21000	63.8	28000
SVM: Quadratic	51.2	20000	100	17000	98.0	17000	51.8	22000
SVM: Cubic	59.5	16000	100	16000	100	17000	47.7	27000
SVM: Fine Gaussian	79.9	13000	100	12000	99.2	16000	75.9	18000
SVM: Medium Gaussian	81.4	9400	97.9	16000	85.0	18000	69.4	20000
SVM: Coarse Gaussian	52.1	8200	88.9	14000	67.8	14000	65.9	16000
Ensemble Boosted Trees	93.0	9200	52.8	27000	99.9	10000	82.1	11000
Ensemble Bagged Trees	100	8200	100	11000	100	11000	100	12000
Ensemble Subspace Discriminant	56.3	6100	69.9	5900	59.3	6200	70.6	9500
Ensemble Subspace KNN	100	4400	100	4500	100	5000	100	6700
Ensemble RUS Boosted Trees	90.5	9800	83.6	61000	95.3	13000	80.4	11000
Linear Discriminant	56.3	13000	77.4	17000	62.5	17000	70.6	17000
Naïve Bayes	48.8	28000	60.9	60000	86.0	4800	73.8	18000

Table 5: Classifiers performance reached in validation. Classification between FSK, BPSK, QPSK, 8PSK and 16PSK modulations using statistical features derived from the wavelet transform of the time series recorded during 500 microseconds for Richian multipath with AWGN (SNR =30dB) channel model. Data set 5.

Classifier	With PCA (1 feature of 10)		No PCA (10 features of 10)		No PCA (5 features of 10)		No PCA Mean (1 feature of 10)	
	Average Accuracy, %	Prediction speed, Objects/s	Average Accuracy, %	Prediction speed, Objects/s	Average Accuracy, %	Prediction speed, Objects/s	Average Accuracy, %	Prediction speed, Objects/s
Decision Trees: Fine	100	21000	100	27000	100	150000	93.0	160000
Decision Trees: Medium	49.5	98000	60.9	140000	55.6	150000	40.8	140000
Decision Trees: Coarse	41.6	11000	45.2	110000	41.5	120000	31.1	150000
KNN: Fine	100	22000	100	40000	100	79000	100	72000
KNN: Medium	95.7	23000	96	25000	95.7	45000	95.4	71000
KNN: Coarse	34.5	18000	36	16000	42.5	30000	37.7	36000
KNN: Cosine	37.7	17000	95.7	36000	95.7	30000	21.3	34000
KNN: Cubic	95.7	24000	95.6	2400	95.3	17000	95.4	54000
KNN: Weighted	100	29000	100	35000	100	38000	100	81000
SVM: linear	36.1	21000	36.6	26000	36.1	26000	21.8	40000
SVM: Quadratic	35.7	17000	66.6	21000	45.2	26000	23.5	29000
SVM: Cubic	36.5	19000	100	21000	61.4	30000	23.2	33000
SVM: Fine Gaussian	37.1	7800	91.8	11000	81.6	14000	38.0	11000
SVM: Medium Gaussian	36.2	8700	46.0	10000	44.2	11000	29.6	12000
SVM: Coarse Gaussian	35.0	8500	35.1	9700	34.9	11000	24.3	9700
Ensemble Boosted Trees	56.8	9400	86.4	12000	85.4	9700	49.9	12000

Ensemble Bagged Trees	100	9300	100	14000	100	8700	100	10000
Ensemble Subspace Discriminant	35.8	7800	39	8100	35.0	6400	22.5	8400
Ensemble Subspace KNN	100	5700	100	5300	100	4100	100	6100
Ensemble RUS Boosted Trees	61.7	11000	80.5	14000	86.0	14000	47.5	13000
Linear Discriminant	35.8	8600	37.9	18000	34.7	110000	22.5	100000
Naïve Bayes	39.9	9700	37.6	74000	37.9	110000	24.9	140000

5. ML classifiers training and validation results

Selected twenty-three classifiers have been trained and validated multiple times using every data set described above to investigate the effect of the extracted features and observation time on classification accuracy and speed. Among the trained classifiers we have studied decision trees, KNN with the various kernels, support vector machines (SVM), ensembles with bagging and boosting sampling, and discriminant methods. Also, principal component analysis PCA has been applied to keep enough components to explain 95 % of data variance for the dimension reduction. To protect against overfitting five-fold cross-validation method was used.

5.1. Classification using instantaneous values

Modulation type classification has been performed based on the input values of the instantaneous values of the in-phase and quadrature components of the time domain digital signal. Primary Classifiers have been trained three times using data set 1: 1. using PCA, 2. Using all three features: in-phase, quadrature components and SNR 3. Using two features including in-phase, quadrature components. Table 2 summarizes the validation results for the AWGN channel with SNR ranging from 1 to 30 dB. The effect of input features available in the data set 1 on classification accuracy, and speed has been studied. The highest classification accuracy has been achieved using all three available features: in-phase, quadrature components, and SNR. However, removing SNR from classification resulted in a reduction in the average classification accuracy by only 3 %. The highest average classification accuracy of 86.9 % was observed for the Fine Gaussian SVM, which on the other hand has been observed to be the slowest. Ensemble boosted trees with 30 decision trees learners trained using AdaBoost sampling and 20 splits and fine decision trees have shown optimal performance in terms of both classification accuracy and speed with an average classification accuracy of 86.3 % and 86.0 %, classification speed of 1200000 objects per second, which is faster than required 2000 objects per second.

Data set 3 containing also instantaneous values of the time domain signal and SNR consisting of five modulations has been used to train classifiers to classify all five modulation types. However, the average classification accuracy has not met the requirement of 85 %. The highest classification accuracy of 78.1 % has been reached by customized decision trees with the number of splits set to 2689, Gini's diversity index has been used as a split criterion.

Among the other tested classifiers, there were ensemble bagged trees, ensemble boosted trees, RUS boosted trees which have demonstrated even worse classification accuracy than decision trees. To capture more of the fine differences between the received signal modulated into different linear modulations it is suggested to use the spectral features derived from the signal observed during the selected observation time.

5.2. Classification using time-series statistics.

Training and validation for both propagation channels AWGN (SNR from 1 dB to 30 dB) and AWGN (SNR = 30 dB) with Rician fading have been performed using data sets 4-7. Primary, the training of the studied classifiers has been performed using time series recorded during observation time corresponding to 500 microseconds using data sets 4 and 5 for AWGN and Rician channel with AWGN, respectively. Classifiers have been trained four times: 1. using PCA, 2. Using all ten spectral-based statistical features 3. Using five features including mean, standard deviation, root-mean-square level, zero crossing rate, 75th percentile of a data set, and 4. Using only one input feature: the mean value of the wavelet coefficients. Tables 4-5 summarize the validation results for the AWGN channel with SNR ranging from 1 to 30 dB and Rician multipath with AWGN (SNR = 30 dB) channel. The best performing classifiers that have reached 100% classification accuracy have been retrained on the features derived from the time series observed during 100 microseconds. Tables 6 and 7 present the validation results for AWGN and multipath Rician channel trained and validated four times as for the time series recorded during 500 microseconds. Tables 6 and 7 show that four out of the five selected classifiers including fine decision trees, fine KNN, ensemble bagged trees, and ensemble subspace KNN that demonstrated classification accuracy of 100 % on the time series recorded during 500 microseconds have demonstrated classification accuracy close to 100 % when trained using PCA, using all ten features and using five features for both AWGN and multipath channel also when have been trained on time series recorded during 100 microseconds. However, SVM has shown worse performance when trained with a reduced number of features.

Applying PCA has resulted in a drastic decrease in the classification accuracy for ensemble subspace KNN for both AWGN and multipath Rician channels. For most classifiers, like fine decision trees, ensemble bagged trees applying PCA has resulted in the decreased classification speed. Fine KNN has shown 100% classification accuracy for classification using only one input to the classifier: mean value and the highest classification speed of 56000 and 91000 objects/s for AWGN and multipath fading channel, respectively. However, KNN is still slow even using only one feature than fine decision trees using five features classifying 110000 and 120000 for AWGN and multipath channel.

6. Classification feature analysis using fractional factorial design

The fractional factorial design has been applied to determine the most significant classification features referred to as the design.

Table 6: Classifiers performance reached in validation. Classification between FSK, BPSK, QPSK, 8PSK and 16PSK modulations using statistical features derived from the wavelet transform of the time series recorded during 100 microseconds for AWGN (SNR ranging from 1 to 30 dB) channel. Data set 6

Classifier	With PCA (1 feature of 10)		No PCA (10 features of 10)		No PCA (5 features of 10)		No PCA Mean (1 feature of 10)	
	Average Accuracy, %	Prediction speed, Objects/s	Average Accuracy, %	Prediction speed, Objects/s	Average Accuracy, %	Prediction speed, Objects/s	Average Accuracy, %	Prediction speed, Objects/s
Decision Trees: Fine	100	9500	100	18000	100	110000	100	120000
KNN: Fine	100	21000	100	37000	98.6	19000	100	56000
KNN: Weighted	100	22000	100	34000	100	47000	100	58000
SVM: Cubic	95.7	23000	100	19000	100	24000	38.7	31000
Ensemble Bagged Trees	100	7600	100	8700	100	6800	100	11000
Ensemble Subspace KNN	36.4	5500	100	4700	100	4800	100	5400

Table 7: Classifiers performance reached in validation. Classification between FSK, BPSK, QPSK, 8PSK and 16PSK modulations using statistical features derived from the wavelet transform of the time series recorded during 100 microseconds for Rician multipath with AWGN (SNR = 30dB) channel model. Data set 7

Classifier	With PCA (1 feature of 10)		No PCA (10 features of 10)		No PCA (5 features of 10)		No PCA Mean (1 feature of 10)	
	Average Accuracy, %	Prediction speed, Objects/s	Average Accuracy, %	Prediction speed, Objects/s	Average Accuracy, %	Prediction speed, Objects/s	Average Accuracy, %	Prediction speed, Objects/s
Decision Trees: Fine	100	15000	100	23000	100	120000	94.2	160000
KNN: Fine	100	27000	100	24000	100	55000	100	91000
KNN: Weighted	100	25000	100	27000	100	48000	100	58000
SVM: Cubic	100	7900	100	16000	69.9	28000	69.9	28000
Ensemble Bagged Trees	100	5700	100	9900	100	11000	100	11000
Ensemble Subspace KNN	36.4	6900	100	5200	100	5000	100	6500

Table 8: Experimental factors and levels

N	Factor	Unit	Symbol	Coded level	
				-1	+1
1	Mean	-	A	on	off
2	Standard Deviation	-	B	on	off
3	Kurtosis	-	C	on	off
4	Skewness	-	D	on	off
5	Median absolute deviation	-	E	on	off
6	Root-mean-square level	-	F	on	off
7	Zero crossing rate	-	G	on	off
8	Interquartile range	-	H	on	off
9	75th percentile of data set	-	I	on	off
10	SNR	dB	J	on	off
11	Observation time	μs	K	100	500

factors that have the highest main effect on the response parameters: classification accuracy and speed We have been looking at both the main effects of the independent variables and interactions between the input parameters (A-J) and observation time (K) for the best performing classifier in terms of accuracy and speed. We have 10 design factors corresponding to the features referred as (A-J) and observation time referred to as (K) with 2 levels for each design factor corresponding to: high (+1) the feature is used for classification or low (-1) the feature is not used for

classification. Observation time has been also varied at two levels (+1) high corresponding to 500 microseconds and (-1) low corresponding to 100 microseconds. We have considered one noise factor corresponding to the propagation channel model with two levels corresponding to the AWGN (-1) channel with SNR ranging from 1dB to 30 dB and Rician multipath propagation and AWGN with SNR=30 dB (+1). The full factorial design will result in 2^{10} number of experiments, to reduce the number of experiments this study has been limited to fractional factorial design with 13 experiment runs performed, where the first ten runs with only one feature used for classification independently from the others for 100 microseconds observation time, since we are mostly interested to study the performance for the shortest observation time. The eleventh run has been selected to investigate the effect of observation time; the twelfth and thirteenth runs have been included to study the effect of observation time independently from the classification features with all nine spectral-based statistical features used as classification input.

The main effect is defined as the overall effect of an independent variable in the complex design. The definition of an effect is the difference in the means between the high (+1) and the low level (-1) of a factor. From this notation, A is the difference between the mean values of the observations at the high level of A minus the average of the observations at the low level of A. Interaction is defined here as the effect of one independent variable

depending on the other independent variable, i.e it describes the combined effect of the independent variables considered simultaneously [15]. Tables 9-13 summarize the experimental design and results: main effect of every factor on classification accuracy and speed for five best performing classifiers: fine decision trees, fine KNN, weighted KNN, ensemble bagged trees with 59886 splits, and 30 learners and ensemble subspace KNN with 9 subspace dimensions and 30 learners.

The overall highest main effects on classification accuracy and speed have been observed for the fine decision trees classifier. In tables 9-13, we have obtained a relatively high main effect for using/not using SNR for classification. In tables 9-13, summarizing the performance of the classifier, it is possible to see that removing the SNR value as an input to the classifier does not affect the response parameters significantly, on the other hand using SNR value only for classification as in the experiment run N10 (what in reality does not make any sense) result in the very low classification accuracy. Since the main effect is a difference between the mean values of the high and low, we observe here the high main effect of SNR as a classification input parameter. For example, the main effect of using SNR (J) as classification input on classification accuracy for fine decision trees is –20.0, while for Kurtosis (C) it is 19.6. Classification accuracy if we use only (C) for classification experiment run N3 is 100% for both Rician and AWGN channels and if we use only (J) for classification is 8.6% for both Rician and AWGN channels. This makes the highest main effect of SNR input a questionable result for practical application. Also, the value of the main effect should be interpreted only in combination with the value of the response parameter: classification accuracy and speed.

The highest classification speed of 170 000 objects per second for 100% classification accuracy has been demonstrated by fine decision trees using only one classification input the skewness of the wavelet coefficients derived from signal observed during 100 microseconds for AWGN channel model. For Rician and AWGN, channel classification speed has been slower 130 000 objects/s. Both skewness and kurtosis has shown the highest main effect on classification accuracy for fine trees. Using mean value as the only input parameter to fine trees classifier, however, has shown less robust results in terms of the classification accuracy: 94.5% has been demonstrated for Rician and AWGN channel, while for AWGN channel 100%. The mean value shows the second-highest main effect on the classification accuracy 19.5 for the fine decision trees and the highest main effect of 10.9, 11.1, 11.5, and 10.9 for the other four classifiers including fine KNN, weighted KNN, ensemble bagged trees and ensemble subspace KNN, respectively. It also shows the highest main effect on the classification speed for all five selected classifiers.

Slightly slower classification speed has been demonstrated by KNN classifiers: 110000 objects per second have been observed for fine KNN for AWGN channel and 89000 objects per second for AWGN channel with Rician multipath. The slowest from all studied are ensembles, for example, ensemble subspace KNN has demonstrated a classification speed of 4500-6800 objects per

second. However, classification speed for ensembles does not decrease as much as for the fine trees with the increasing number of features. For ensemble bagged trees for AWGN channel the same classification speed of 11000 has been demonstrated for classification using only mean A and using all calculated features (A-J).

Interaction A-K

	1	2
A	78.9	98.4
K	82.5	98.3

Interaction B-K

	1	2
B	82.3	98.8
K	82.5	98.3

Interaction C-K

	1	2
C	80.4	100.0
K	82.5	98.3

Interaction D-K

	1	2
D	80.4	100.0
K	82.5	98.3
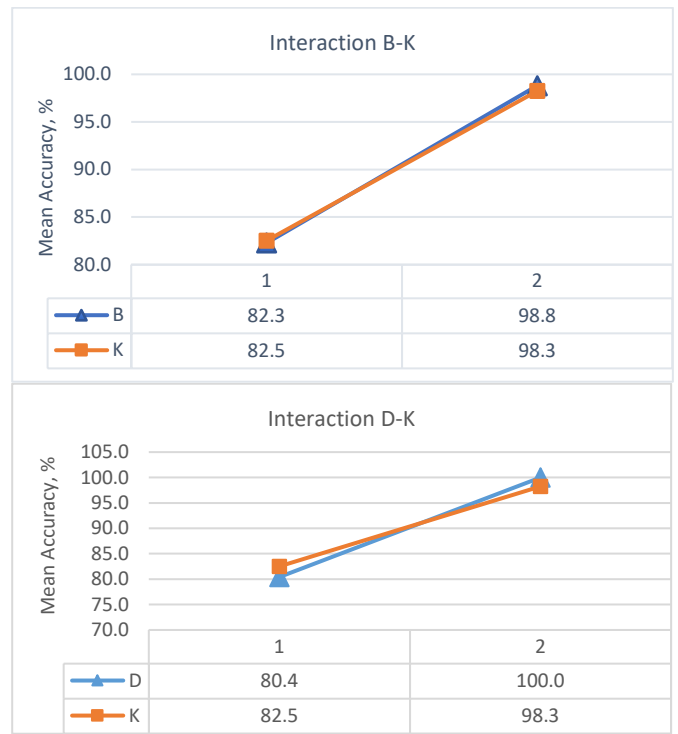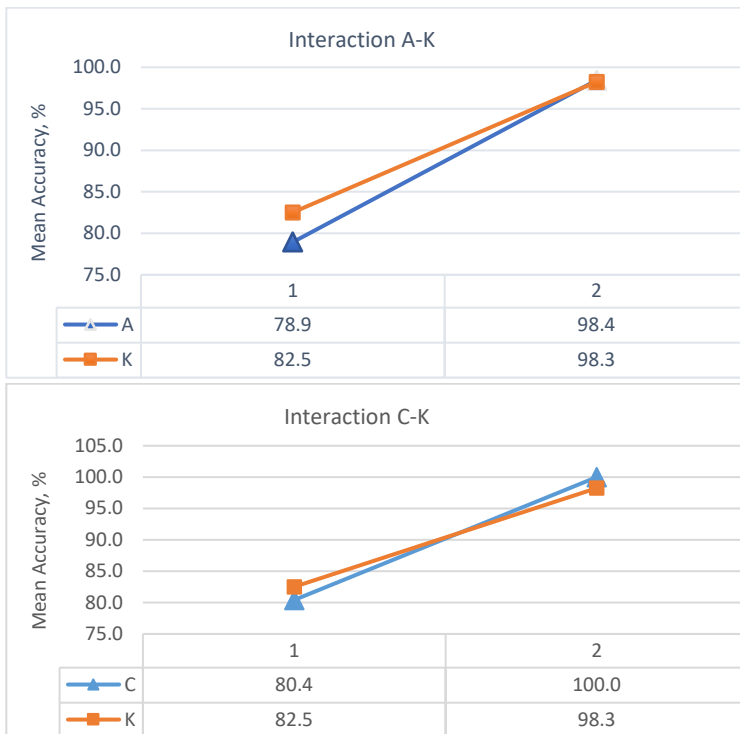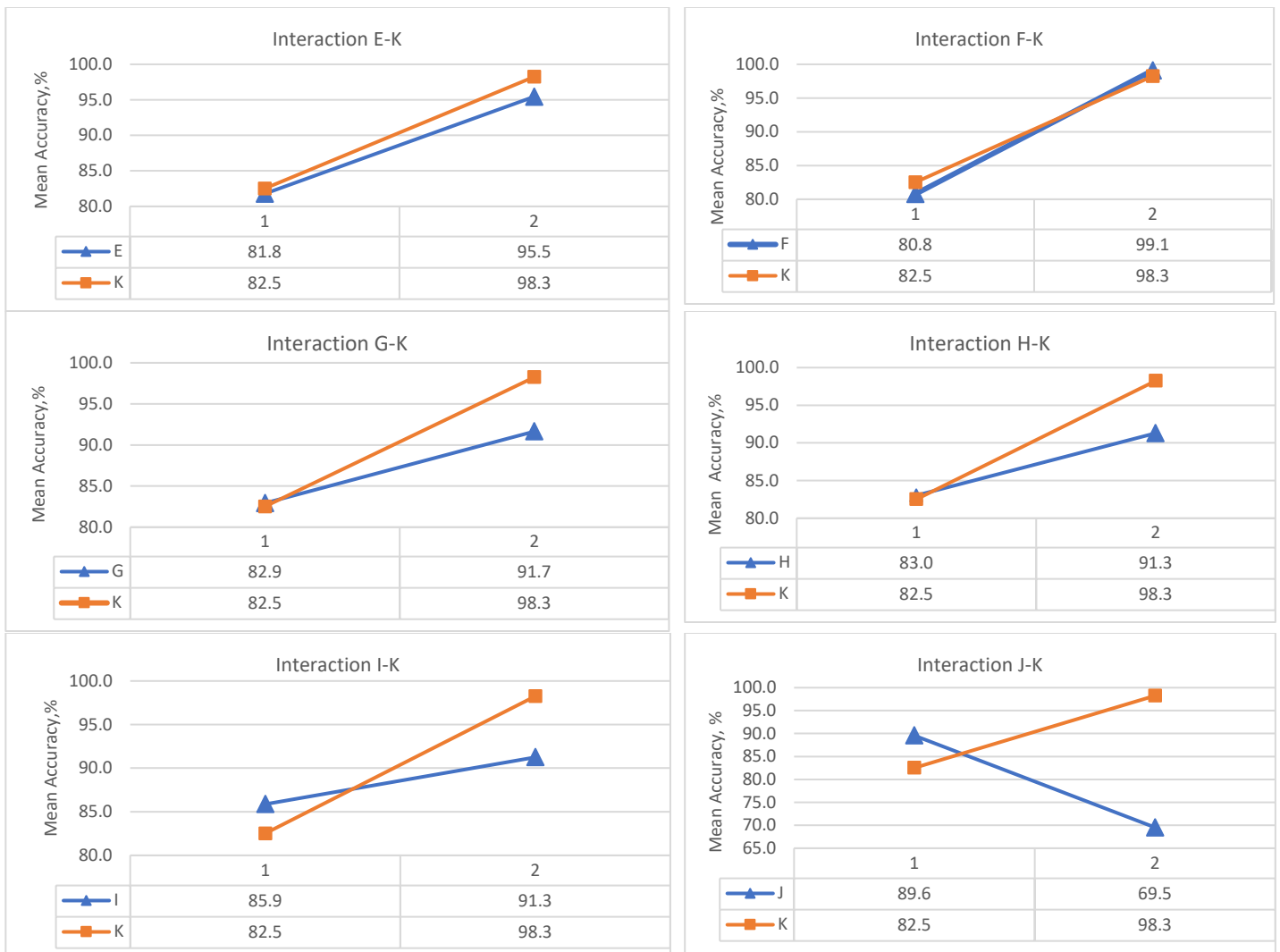
Figure 6: Main Effects and interactions between factors (A-J) and observation time (K) for fine decision trees

Table 9: Experimental design and results of fractional factorial design limited to 13 experimental runs for fine decision trees classifier

	Factors											AWGN		AWGN + Rician		Mean Accuracy	STD Accuracy	Mean Speed	STD Speed
Run	A	B	C	D	E	F	G	H	I	J	K	Speed	Accuracy	Speed	Accuracy				
1	+	-	-	-	-	-	-	-	-	-	-	100000	100	160000	94.5	97.3	3.9	130000	113068
2	-	+	-	-	-	-	-	-	-	-	-	140000	100	140000	92.9	96.5	5.0	140000	98927
3	-	-	+	-	-	-	-	-	-	-	-	110000	100	150000	100	100.0	0.0	130000	105995
4	-	-	-	+	-	-	-	-	-	-	-	170000	100	130000	100	100.0	0.0	150000	91853
5	-	-	-	-	+	-	-	-	-	-	-	130000	93.8	98000	78.9	86.4	10.5	114000	69235
6	-	-	-	-	-	+	-	-	-	-	-	110000	100	140000	92.9	96.5	5.0	125000	98927
7	-	-	-	-	-	-	+	-	-	-	-	170000	75.4	130000	74.5	75.0	0.6	150000	91871
8	-	-	-	-	-	-	-	+	-	-	-	130000	72.9	160000	74.9	73.9	1.4	145000	113085
9	-	-	-	-	-	-	-	-	+	-	-	120000	73.4	99000	74.1	73.8	0.5	109500	69951
10	-	-	-	-	-	-	-	-	-	+	-	110000	8.6	180000	8.6	8.6	0.0	145000	127273
11	+	-	-	-	-	-	-	-	-	-	+	12000	100	160000	93	96.5	4.9	86000	113069
12	+	+	+	+	+	+	+	+	+	+	-	18000	100	23000	100	100.0	0.0	20500	16193
13	+	+	+	+	+	+	+	+	+	+	+	21000	100	27000	100	100.0	0.0	24000	19021
Main Effects Accuracy	19.5	16.5	19.6	19.6	13.7	18.3	8.7	8.3	5.4	-20.0	15.7								
Main Effects Speed	-69.2	-29.6	-29.5	-27.5	-35.6	-31.1	-35.8	-36.7	-40.3	-58.4	-24.7								

Table 10: Experimental design and results of fractional factorial design limited to 13 experimental runs for fine KNN classifier

	Factors											AWGN		AWGN + Richian		Mean Accuracy	STD Accuracy	Mean Speed	STD Speed
Run	A	B	C	D	E	F	G	H	I	J	K	Speed	Accuracy	Speed	Accuracy				
1	+	-	-	-	-	-	-	-	-	-	-	73000	100	91000	100	100.0	0.0	36500	64276
2	-	+	-	-	-	-	-	-	-	-	-	69000	100	41000	100	100.0	0.0	55000	28921
3	-	-	+	-	-	-	-	-	-	-	-	83000	100	65000	100	100.0	0.0	74000	45891
4	-	-	-	+	-	-	-	-	-	-	-	54000	100	77000	100	100.0	0.0	65500	54377
5	-	-	-	-	+	-	-	-	-	-	-	91000	100	84000	100	100.0	0.0	87500	59326
6	-	-	-	-	-	+	-	-	-	-	-	110000	100	86000	100	100.0	0.0	98000	60740
7	-	-	-	-	-	-	+	-	-	-	-	72000	79.9	69000	80.6	80.3	0.5	70500	48734
8	-	-	-	-	-	-	-	+	-	-	-	80000	100	110000	100	100.0	0.0	95000	77711
9	-	-	-	-	-	-	-	-	+	-	-	83000	100	110000	100	100.0	0.0	96500	77711
10	-	-	-	-	-	-	-	-	-	+	-	93000	21.3	83000	21.3	21.3	0.0	88000	58675
11	+	-	-	-	-	-	-	-	-	-	+	51000	100	72000	100	100.0	0.0	61500	50841
12	+	+	+	+	+	+	+	+	+	+	-	37000	100	30000	100	100.0	0.0	33500	21142
13	+	+	+	+	+	+	+	+	+	+	+	42000	100	40000	100	100.0	0.0	41000	28214
Main Effects Accuracy	10.9	9.8	9.8	9.8	9.0	9.8	1.3	9.8	9.8	-24.3	9.0								
Main Effects Speed	-38.0	-34.1	-25.9	-29.6	-20.1	-15.5	-27.4	-16.8	-16.2	-19.8	0.0								

Table 11: Experimental design and results of fractional factorial design limited to 13 experimental runs for weighted KNN classifier.

	Factors											AWGN		AWGN + Rician		Mean Accuracy	STD Accuracy	Mean Speed	STD Speed
Run	A	B	C	D	E	F	G	H	I	J	K	Speed	Accuracy	Speed	Accuracy				
1	+	-	-	-	-	-	-	-	-	-	-	62000	100	58000	100	100.0	0.0	60000	40941
2	-	+	-	-	-	-	-	-	-	-	-	63000	100	67000	100	100.0	0.0	65000	47305
3	-	-	+	-	-	-	-	-	-	-	-	90000	100	63000	100	100.0	0.0	76500	44477
4	-	-	-	+	-	-	-	-	-	-	-	62000	100	77000	100	100.0	0.0	69500	54377
5	-	-	-	-	+	-	-	-	-	-	-	66000	100	55000	100	100.0	0.0	60500	38820
6	-	-	-	-	-	+	-	-	-	-	-	73000	100	79000	100	100.0	0.0	76000	55791
7	-	-	-	-	-	-	+	-	-	-	-	60000	79.4	67000	100	89.7	14.6	63500	47313
8	-	-	-	-	-	-	-	+	-	-	-	71000	100	79000	80	90.0	14.1	75000	55798
9	-	-	-	-	-	-	-	-	+	-	-	68000	100	72000	100	100.0	0.0	70000	50841
10	-	-	-	-	-	-	-	-	-	+	-	56000	20.4	73000	21.3	20.9	0.6	64500	51604
11	+	-	-	-	-	-	-	-	-	-	+	52000	100	81000	100	100.0	0.0	66500	57205
12	+	+	+	+	+	+	+	+	+	+	-	34000	100	23000	100	100.0	0.0	28500	16193
13	+	+	+	+	+	+	+	+	+	+	+	36000	100	35000	100	100.0	0.0	35500	24678
Main Effects Accuracy	11.1	9.9	9.9	9.9	9.9	9.9	5.5	5.6	9.9	-24.4	9.0								
Main Effects Speed	-21.3	-25.2	-20.2	-23.3	-27.2	-20.4	-25.9	-20.9	-23.0	-25.4	-14.1								

Table 12: Experimental design and results of fractional factorial design limited to 13 experimental runs for Ensemble bagged trees classifier.

	Factors											AWGN		AWGN + Rician		Mean Accuracy	STD Accuracy	Mean Speed	STD Speed
Run	A	B	C	D	E	F	G	H	I	J	K	Speed	Accuracy	Speed	Accuracy				
1	+	-	-	-	-	-	-	-	-	-	-	11000	100	11000	100	100.0	0.0	11000	7707
2	-	+	-	-	-	-	-	-	-	-	-	9400	100	9600	100	100.0	0.0	9500	6718
3	-	-	+	-	-	-	-	-	-	-	-	11000	100	12000	100	100.0	0.0	11500	8415
4	-	-	-	+	-	-	-	-	-	-	-	10000	100	11000	100	100.0	0.0	10500	7707
5	-	-	-	-	+	-	-	-	-	-	-	10000	100	10000	100	100.0	0.0	10000	7000
6	-	-	-	-	-	+	-	-	-	-	-	11000	100	10000	100	100.0	0.0	10500	7000
7	-	-	-	-	-	-	+	-	-	-	-	12000	76	7700	100	88.0	17.0	9850	5382
8	-	-	-	-	-	-	-	+	-	-	-	9800	100	8500	100	100.0	0.0	9150	5940
9	-	-	-	-	-	-	-	-	+	-	-	7600	100	7700	100	100.0	0.0	7650	5374
10	-	-	-	-	-	-	-	-	-	+	-	14000	8.9	1200	8.7	8.8	0.1	7600	842
11	+	-	-	-	-	-	-	-	-	-	+	12000	100	10000	100	100.0	0.0	11000	7000
12	+	+	+	+	+	+	+	+	+	+	-	8700	100	9900	100	100.0	0.0	9300	6930
13	+	+	+	+	+	+	+	+	+	+	+	11000	100	14000	100	100.0	0.0	12500	9829
Main Effects Accuracy	11.5	10.3	10.3	10.3	10.3	10.3	5.1	10.3	10.3	-29.2	9.4								
Main Effects Speed	1.4	0.6	1.4	1.0	0.8	1.0	0.7	0.4	-0.2	-0.3	2.1								

Table 13: Experimental design and results of fractional factorial design limited to 13 experimental runs for Ensemble subspace KNN classifier

	Factors											AWGN		AWGN + Rician		Mean Accuracy	STD Accuracy	Mean Speed	STD Speed
Run	A	B	C	D	E	F	G	H	I	J	K	Speed	Accuracy	Speed	Accuracy				
1	+	-	-	-	-	-	-	-	-	-	-	6100	100	6500	100	100.0	0.0	6300	4525
2	-	+	-	-	-	-	-	-	-	-	-	6200	100	6200	100	100.0	0.0	6200	4313
3	-	-	+	-	-	-	-	-	-	-	-	6800	100	7100	100	100.0	0.0	6950	4950
4	-	-	-	+	-	-	-	-	-	-	-	5600	100	6400	100	100.0	0.0	6000	4455
5	-	-	-	-	+	-	-	-	-	-	-	6700	100	6800	100	100.0	0.0	6750	4738
6	-	-	-	-	-	+	-	-	-	-	-	6600	100	6200	100	100.0	0.0	6400	4313
7	-	-	-	-	-	-	+	-	-	-	-	6500	79.9	7800	100	90.0	14.2	7150	5452
8	-	-	-	-	-	-	-	+	-	-	-	6100	100	5900	80.6	90.3	13.7	6000	4108
9	-	-	-	-	-	-	-	-	+	-	-	6800	100	5500	100	100.0	0.0	6150	3818
10	-	-	-	-	-	-	-	-	-	+	-	6200	21.3	5300	21.3	21.3	0.0	5750	3733
11	+	-	-	-	-	-	-	-	-	-	+	6700	100	6100	100	100.0	0.0	6400	4243
12	+	+	+	+	+	+	+	+	+	+	-	4700	100	5200	100	100.0	0.0	4950	3606
13	+	+	+	+	+	+	+	+	+	+	+	4500	100	5300	100	100.0	0.0	4900	3677
Main Effects Accuracy	10.9	9.8	9.8	9.8	9.8	9.8	5.5	5.6	9.8	-24.3	9.0								
Main Effects Speed	-0.7	-1.0	-0.7	-1.1	-3.0	-0.9	-0.6	-1.1	-1.1	-1.2	-0.6								

Since the decision trees are the fastest classifier reaching an accuracy of 100%, the study of the interactions has been limited only to fine decision trees. Interaction between observation time and every of the spectral-based statistical feature (A-J) has been studied and plotted in Figure 6. Non-parallel lines corresponding to the main effects in Figure 6 indicate the presence of interaction between spectrum observation time and all the studied features. The study of interactions between extracted features has been discarded because they have been extracted from the same source: Haar transforms coefficients derived from frequency domain signal and therefore are not considered to be fully independent variables. The most prominent interactions are observed between 75th percentile and observation time, SNR as a classification feature and observation time, root-mean-square level and observation time, skewness and observation time, kurtoses, and observation time.

7. Conclusions and future work

In the scope of this work we have studied the possibility to classify the modulation type using instantaneous values of the time domain signal and SNR as inputs to the classifier. The main advantage of this approach is that it has potential to increase throughput by shortening the spectrum observation time and decreases the computational complexity: the raw values of in-phase and quadrature components of the signal are used as an input to the classifier and therefore there is no need for any preprocessing or feature extraction. This approach is applicable for binary classification between BPSK and 2FSK modulations, however it fails in case the classification task is extended to multiple classes containing higher order modulations. The possible reason for this is the missing data that is not included in the pair of in-phase and quadrature component. If the input values pair lies on the x axis the modulation could be classified as any of four types: BPSK, 2FSK, 8PSK or 16PSK. In case of the input pairs are located on the y axis it could be classified as any of three modulation classes: 2FSK, 8PSK, 16PSK. We have confirmed that to reach the classification accuracy of at least 85% or higher for classification between multiple high order modulations it is required to observe the received signal and perform feature extraction. In this study we have studied nine spectral/based

statistical features derived from the wavelet coefficients obtained by applying the Haar wavelet transform to the frequency domain received signal. The highest classification speed of 170 000 objects/second and 100 % classification accuracy has been demonstrated by fine decision trees using as the single input kurtosis (C) derived from the wavelet coefficients derived from signal observed during 100 microseconds for AWGN channel. For line-of-sight fading Rician channel with AWGN demonstrated classification speed is slower 130 000 objects/s. Skewness and kurtosis have shown the highest main effect on classification accuracy for fine decision trees. The mean value demonstrated the highest main effects on classification speed for fine decision trees, fine KNN, weighted KNN, ensemble bagged trees, ensemble subspace KNN.

In the scope of the future work it is planned to implement the proposed fine decision trees classification algorithm on our target application hardware. Also, it is intended to extend this work to the multiple propagation channel models including Rayleigh and Rician for doppler shifts corresponding to target application embedded in the ground and aerial unmanned platforms moving with speeds 100-200 km/hour.

References

[1] I. Valieva, M. Björkman, J. Åkerberg, M. Ekström, I. Voitenko, "Multiple Machine Learning Algorithms Comparison for Modulation Type Classification for Efficient Cognitive Radio," in MILCOM 2019 - 2019 IEEE Military Communications Conference (MILCOM), 318–323, 2019, doi:10.1109/MILCOM47813.2019.9020735.

[2] D. Rosker, D. M., "DARPA Spectrum Collaboration Challenge (SC2).," DARPA Spectrum Collaboration Challenge (SC2), 2020.

[3] C. Xin, Spectrum Sharing for Wireless Communications, 2015.

[4] O. Fink, Q. Wang, M. Svensén, P. Dersin, W.-J. Lee, M. Ducoffe, "Potential, challenges and future directions for deep learning in prognostics and health management applications," Engineering Applications of Artificial Intelligence, **92**, 103678, 2020, doi:https://doi.org/10.1016/j.engappai.2020.103678.

[5] S. Peng, H. Jiang, H. Wang, H. Alwageed, Y.-D. Yao, "Modulation classification using convolutional Neural Network based deep learning model," 1–5, 2017, doi:10.1109/WOCC.2017.7929000.

[6] kaiyuan jiang, J. Zhang, H. Wu, A. Wang, Y. Iwahori, "A Novel Digital Modulation Recognition Algorithm Based on Deep Convolutional Neural Network," Applied Sciences, 2020, doi:10.3390/app10031166.

[7] Mathworks., Modulation Classification with Deep Learning., 2020.

[8] M. Véstias, R. Duarte, J. Sousa, H. Neto, "Fast Convolutional Neural

Networks in Low Density FPGAs Using Zero-Skipping and Weight Pruning," Electronics, **8**, 2019, doi:10.3390/electronics8111321.

[9] Z. Zhu, Automatic Modulation Classification: Principles, Algorithms and Applications, John Wiley & Sons, Incorporated, 2015.

[10] A. Kubankova, H. Atassi, A. Abilov, "Selection of optimal features for digital modulation recognition," 2011.

[11] W. Gardner, Cyclostationarity in Communications and Signal Processing, IEEE Press, New York, 1994.

[12] W.A. Gardner, C.M. Spooner, "Cyclic spectral analysis for signal detection and modulation recognition," in MILCOM 88, 21st Century Military Communications - What's Possible?'. Conference record. Military Communications Conference, **2**, 419–424, 1988, doi:10.1109/MILCOM.1988.13425.

[13] C. Cormio, K.R. Chowdhury, "A survey on MAC protocols for cognitive radio networks," Ad Hoc Networks, **7**(7), 1315–1329, 2009, doi:https://doi.org/10.1016/j.adhoc.2009.01.002.

[14] M. Raina, G. Aujla, "An Overview of Spectrum Sensing and its Techniques," IOSR Journal of Computer Engineering, **16**, 64–73, 2014, doi:10.9790/0661-16316473.

[15] K. Hinkelmann, Design and analysis of experiments., John Wiley & Sons, Inc., 2011.

[16] C. Rajan, Statistics for Scientists and Engineers, John Wiley & Sons, Incorporated, 2015.

[17] Mathworks, Mean or median absolute deviation, 2020.

[18] Mathworks, Root-mean-square level, 2020.

[19] Mathworks, Zero Crossing Rate, Nov. 2020.

[20] Mathworks, Interquartile range, 2020.

[21] Mathworks, 75th Percentile, 2020.

[22] Mathworks, Fading Channels, 2020.

An Enhanced Artificial Intelligence-Based Approach Applied to Vehicular Traffic Signs Detection and Road Safety Enhancement

Anass Barodi[*,1], Abderrahim Bajit[1], Taoufiq El Harrouti[2], Ahmed Tamtaoui[3], Mohammed Benbrahim[1]

[1]Laboratory of Advanced Systems Engineering, National School of Applied Sciences, Ibn Tofail University, Kenitra, 14000, Morocco

[2]Laboratory of Engineering Sciences (SI), National School of Applied Sciences, Ibn Tofail University, Kenitra, 14000, Morocco

[3]National Institute of Posts and Telecommunications (INPT-Rabat), SC Department, Mohammed V University, Rabat, 10000, Morocco

A R T I C L E   I N F O

A B S T R A C T

The paper treats a problem for detection and recognition objects in computer vision sector, where researchers recommended OpenCV software and development tool, it's several and better-remembered library resource for isolating, detecting, and recognition of particular objects, what we would find an appropriate system for detecting and recognition traffic roads signs. The robustness with optimization is a necessary element in the computer vision algorithms, we can find a very large number of technics in object detection, for example, shapes transformation, color selection, a region of interest ROI, and edge detection, combined all these technics to reach high precision in animated video or still image processing. The system we are trying to develop, is in high demand in the automotive sector such as intelligent vehicles or autonomous driving assist systems ADAS, based on intelligent recognition, applying Artificial Intelligence, by using Deep Learning, exactly Convolutional Neural Network (CNN) architecture, our system improves the high accuracy of detection and recognition of traffic road signs with lower loss.

1. Introduction

Computer vision belongs to a large family of Artificial Intelligence-based systems, more precisely, it is to AI what eyes are to humans, an extremely powerful tool capable of analyzing, recognizing an image pattern, and even analyzing several images simultaneously, in other words, a video stream. To achieve this, computer vision relies on different technologies, firstly image processing, which applies operations and algorithms directly on the image, and secondly Deep Learning through neural networks using a large amount of data. In the automotive world, Industry 4.0 [1] has already chosen its IoT camp, the automotive groups have announced that their autonomous vehicles will embed an onboard camera, and not only electronic sensors, aiming to reduce a maximum accident's risk and also helping the driver to safely control his car to avoid dangers. The re-manufacturing sector has also already started to conquer computer vision, the major

objective of the automotive industry, is to make non-polluting vehicles, e.g. electric or hybrid vehicles, to integrate intelligent options [2], to make vehicles easier, to move in and out of the city area, with road safety for both cars, users, and pedestrians. The procedure that we are going to follow in our system development, that integrates a series of automotive embedded systems, among the most famous of these systems, is the ADAS system that has accelerated the vehicle sector and improved its features, which has made the semi-automatic vehicles, to facilitate the tasks of conduction and avoid all possible dangers [3]. The human being is based essentially on his eyes, to make a description and a global analysis of his environment, because this description will allow him to manage these reactions, that he has to make either in the present or the future. Therefore, the equivalence of this behavior enters the field of computer vision or robotics, where it is called object detection [4, 5], which in our case are the traffic road signs, that help traffic management. Every year, researchers offer us a new advanced, highly precise technology, and slightly object detection error injection. Our traffic road signs system detection [5], which is based on the colors of the environment description, to detect the desired specific colors of the specified objects.

*Corresponding Author: Anass BARODI, Laboratory of Advanced Systems Engineering (ISA), National School of Applied Sciences, Ibn Tofail University. Kenitra, Morocco, barodi.anass@uit.ac.ma, https://orcid.org/0000-0003-3022-4761

The fact of making this description, therefore, required a test its effectiveness, based on onboard vehicle cameras, and then to integrate it into the developed algorithm. So detecting the colors of traffic roads signs with accuracy, is the necessary factor, so that we can recommend the approach, that can be applied in the future or improved, and applied to Industry 4.0 [6], but we're not going to stop only on the colors [7], we're also going to base it on the geometry of the traffic roads signs, to reduce detection errors. The general procedure of our system, is based on human characteristics, that it can easily detect objects, and avoids encountering difficulties due to light reflection. The performance will increase, if we have combined the colors and geometries of the traffic road signs, which will conduct us to reach an interesting and robust algorithm [8]. In computer vision and image processing, the detection or recognition of specific objects in movements, in unknown or a known environment, is commonly elaborate by different researches studies every year, the most technique based on the invariance properties of the interest objects, it can be the appearance of the objects, the geometry of the scene or objects, photometry or color, for example, space-time constraints.

Video is a media that poses complex problems, because of the large data volume to be processed, with the difficulty of extracting the representative information from its content. At present, indexing the content of images, and dividing the video into elementary unit shots, representative images only partially meets this growing need. But, the content of an image is often too rich in itself, and contains several objects of interest, i.e. semantic objects. When a target is located in a video frame, it is often useful to follow this object in the following images, each image target successfully tracked, can provide a lot of information or feature, about its activity with the identity, the visual characteristics most using are colors. Usually, the RGB represents color space, but this space doesn't a uniform perceptual, because the differences calculating between colors in this space by machines, do not correspond to the difference perceived by humans, besides, the RGB dimensions are highly correlated. But the HSV is an approximately uniform color space [9], with a high degree of sensitivity to the noise, for example, can be used to extract a characteristic for histogram-

based appearance, for detected the contour-based edges of all or specific objects; that existed in images, in general, many tracking algorithms in real-time uses and recommend this space.

Object recognition is an important topic in computer vision, it has a huge evolution during these years, combined with Artificial Intelligence, which has been finalized by the appearance of Deep Learning [10], Deep Learning has touched different areas, such as automotive, robotics, industry. In computer vision, object recognition or object classification is a method for identifying the presence of an instance, or a class of objects in a digital image, for example, the application face detection and the detection of persons [11]. These methods often involve supervised learning, and have applications in multiple fields, such as, Biometric recognition using biometric technology, Surveillance, Industrial inspection, Robotics, Medical analysis, our case is applied for Intelligent Vehicle Systems, which are necessary for recognize and tracking the traffic road signs, as well as autonomous vehicle [12].

2. Methodology

The strategy is to develop a homogeneous system for detection and recognize traffic road signs, the system combines three essential parts, the first, detection of traffic road signs by methods that are proposed, and well described later on. Secondly, when the sign detected, strongly is going to be cropped with dimensions defined in real-time, finally, the last phase, is the recognition of the traffic road using Artificial Intelligence, establishment an architecture has the same concept of the human being analyzes with his brain, for classification or recognize the correct place different objects in the environment.

The paper organized as follows; section 1 contains an introduction to the essential for detection and recognition. Section 2 presents a system diagram, then section 3 describes the detection approach. Section 4, related work for different work of detection and our proposed approach, section 5 and section 6 for the discussion and implementation in real-time. Section 7 with section 8, to recognize road signs by deep learning and evaluation the performance of the system proposed.
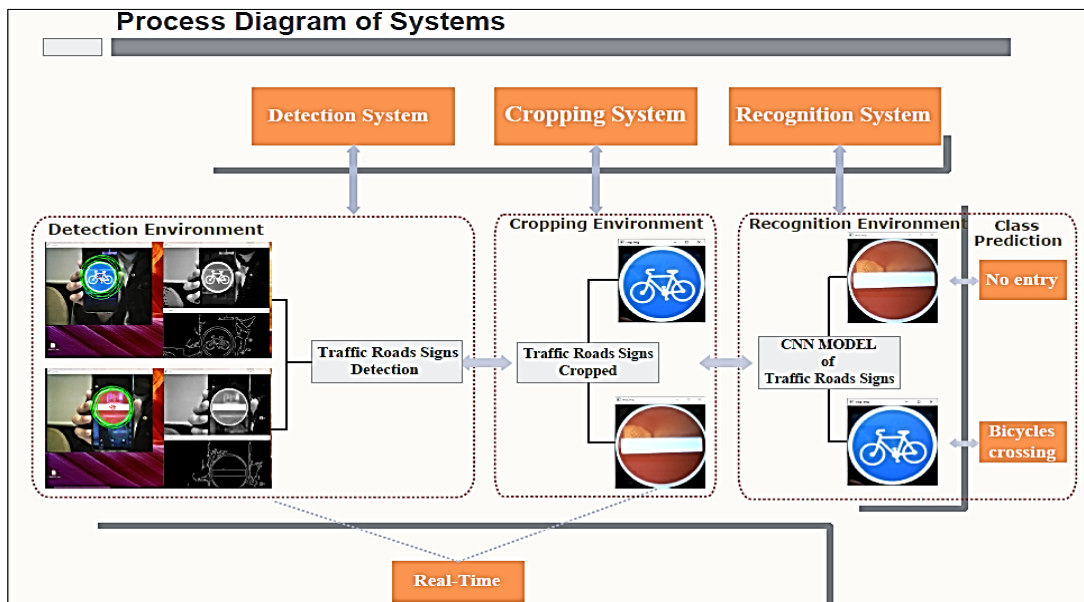
Figure 1: Traffic road signs detection and recognition System diagram
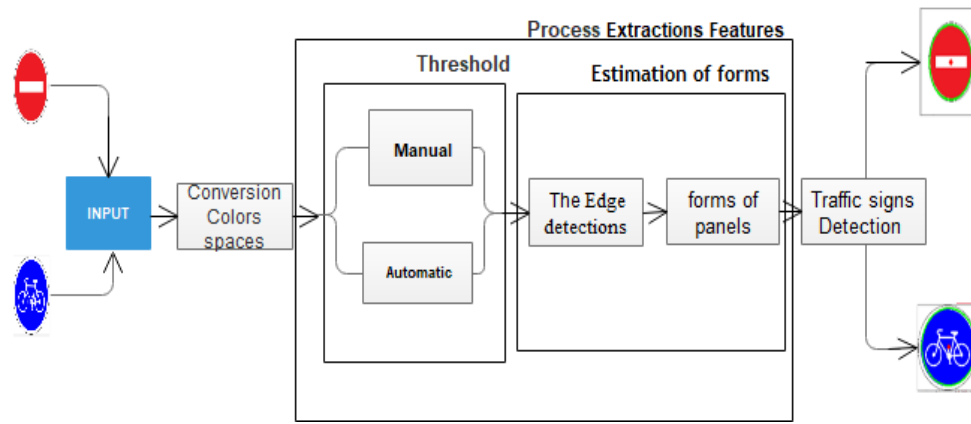
Figure 2: Traffic road sings detection diagram [5]

3. Road Signs Detection

In the figure. 2, the system tries to determine which road signs have a circular shape and specific colors.

The colors of the traffic road signs, are unique in the whole world, fixing the relevant colors or those that represent the majority, are blue and red. The second part, which is based essentially on the detection of the geometries of the traffic roads signs, which are also by default unique, can find either the geometry: rectangular, circular, triangular, and square, therefore for our study, based the circular, because it a percentage of 50% of the traffic roads signs, and at the same time contains the colors, to achieve our objective, it must to a play on the elements, that characterize the circular form, so the circle is described mathematically, by center position and radius.

4. Related Work

The paper has the main objective, to implement an application aiming to detect and recognize traffic signs in real-time, most of the techniques use the color detection presented in this paper [13], or based only on the shapes of signs treated in this paper [14], our approach combined between colors and shapes of traffic road signs, by applying the Canny matrix transformation. This approach uses the OpenCV library, because integrated powerful functions, to properly detect the edges in the image. Before the process detects shapes of signs, following sub-steps, firstly, the conversion input image from the RGB space to the HSV space for segmentation. secondly, applying the Gaussian smoothing filter, to minimize false detection results, as the color-based one just isolates red and blue colors of interest.

4.1. Color detection

The image can be represented by function G (X, Y), the X and Y are the spatial coordinates for two-dimension, besides this, the amplitude at any point G (X, Y) corresponding in general to gray level or mostly to intensity, and when the amplitude is discretized, the image is categorized to a digital image. The digital image also referred to as a scene, has a marker as an indication, each frame or image different from other mathematically, based mainly on its height (H) and width (W).

In image processing has several descriptions of images, for simplicity, can be a binary image, a rectangular matrix contains these values, 0 represented the blacks, or 1 represented the whites. Also, can be a grayscale image, the total number of pixels is 256,

distributed from 0 (black) to 255 (white), these values means that each pixel encoded on 8 bits, grayscales are very powerful for recognition or detection of the most objects in a complexed scene [15]. Finally, the color image has 3 color channels, described respectively in this order by pixels number of red (R), green (G), and blue (B), it's coded or ranging between 0 and 255, which results in 255^3=16,777,216 possible colors, that it takes 24 bits to code a pixel. In the general hierarchy of video data present in a sequence, which means that contents one or more images groups, and ends with an end-of-sequence code, this grouping of one or more images facilitating direct access, thus, the image is the elementary unit for coding the video sequence [16].

As shown in figure 2, the first step based on color detection, to have a system capable of detecting; the colors of road signs with high accuracy, our approach proposes the conversion from RGB to HSV space, this conversion is essentially, based on the equations above [5], the first one is used to normalize each color channel, which makes the interval ordered [0,255] to [0,1], to calculate delta, C_{min} and C_{max} [17].

$$R_1 = \frac{R}{255} \; ; \; G_1 = \frac{G}{255}; \; B_1 = \frac{B}{255} \tag{1}$$

$$C_{max} = \max(R_1, G_1, B_1) \tag{2}$$

$$C_{min} = \min(R_1, G_1, B_1) \tag{3}$$

$$\Delta = C_{max} - C_{min} \tag{4}$$

The HSV space is considered to be a natural representation model, which means has the same physiological color perception seeing by the eye of a human, in generally decomposing the colors consists of physiological criteria. This space decomposes the color, according to more intuitive characteristics close, to the current vocabulary to describe a color, based on pure color. Finally, these equations above serve to complete the conversion, to determine each channel: Hue, Saturation, and Value [5].

- The Hue Channel (H), corresponding to the perception of color:

$$H = \begin{cases} 0°, & \Delta = 0 \\ 60° \text{x} \left(\frac{G_1 - B_1}{\Delta} \bmod 6 \right), & C_{max} = R_1 \\ 60° \text{x} \left(\frac{R_1 - B_1}{\Delta} + 2 \right), & C_{max} = G_1 \\ 60° \text{x} \left(\frac{R_1 - G_1}{\Delta} + 4 \right), & C_{max} = B_1 \end{cases} \tag{5}$$

- The Saturation Channel (S), describing the color purity, which can be bright or dull:

$$S = \begin{cases} 0, & C_{max} = 0 \\ \dfrac{\Delta}{C_{max}}, & C_{max} \neq 0 \end{cases} \qquad (6)$$

- The Value Channel (V), indicating the light amount in the color, that can have a light or dark appearance:

$$V = C_{max} \qquad (7)$$

4.2. Canny matrix transformation

The deployment between the Canny filter and the Hough transformation, to detect edges and locate shapes wants, a well-known algorithm for pattern detection, Hough transform do a parametric estimation method. The pattern recognition method, proposed by Hough are morphological study methods, but they require a large computation time, in the case of complex geometrical shapes or discontinuous contours, the Canny contour detection method, allowed us to highlight rather wide contours, that are perfectly suited to pair correlation localization, to achieve the work with higher detection accuracy.

4.3. Edge Detection

Canny a multi-step process for edge detection, First of all, it is a question of reducing the noise of the image to optimize contour detection, this reduces strong responses during the gradient calculation, leading to false positives, the solution using Gaussian Filter, very powerful filter, has a kernel of convolution operator in a 2D Gaussian plan [18], this operation due to Gaussian probability law, demonstrated in equation (8), σ^2 represent the variance of each variables couple (x, y) with the peak (μ). The main condition for using this type of filter, whether the image is in gray level so that it can be processed to standard deviation Gaussian σ.

$$G_0(x,y) = A e^{\frac{-(x-\mu_x)^2}{2\sigma_x^2} + \frac{-(y-\mu_y)^2}{2\sigma_y^2}} \qquad (8)$$

A canny filter is based on Sobel's algorithm, it has additional steps that allow us to work on more complex images [19]. This method allows, by changing the intensity of edge detection, to eliminate linearization and noise defects and at the same time to have wide contours. The width is important for the correlation localization algorithm that follows this contour detection algorithm [20].

$$\text{Angle:} \ \ \theta = \tan^{-1}\left(\frac{G_y}{G_x}\right) \qquad (9)$$

$$\text{Edge:} \ \ G = \sqrt{G_x^2 + G_y^2} \qquad (10)$$

The Angle and Edge algorithm-based, has been designed to be optimal according to three criteria:

1) Good detection: low error rate in contour signaling;
2) Good localization: minimizing detected and real contours gap;
3) Answer clarity: one answer per outline, no false positives.

After calculating the norm and the direction of the gradient, in each pixel of the image, these methods extract contours of a single-pixel, thickness by selecting the local maxima of the gradient norms. One can mention the detectors of Canny, Deriche, Marr - Hildreth, or the more recent one of Bao [20]. For the operators of Canny and Deriche, an additional variable allows us to adjust the

detection sensitivity at the expense of the spatial precision of the contour and vice versa. Moreover, it can be noted that the contours detection in areas, with strong gradients does not necessarily, correspond to an object. In this case, post-processing can be effective, these useful methods yield good results for non-textured image analysis, high-contrast objects with marked contours.

4.4. Shape extraction

The international road safety regulations, are essentially based on laws, that must be respected by everyone, either drivers of automobiles or passengers, so the majority of its laws have been modeled by traffic road signs, that have unique shapes, for example triangular, rectangular, square, or circular, keeping only the circular shapes that exist in the images.

So, the objective of our approach, is to improve or increase the accuracy of the system, that based on artificial intelligence, will have accuracy to detect traffic road signs, we focus the studies on the circular shape, applying the Hough circles method of OpenCV [18] modeled by this equation:

$$(x - X_{center})^2 + (y - Y_{center})^2 = r^2 \qquad (11)$$

Paul Hough invented a pattern recognition technique, named Hough transform, this technique allows us to recognize any shape in an image, for example, the circles or lines, this technique will serve, to identify circles presences in an image, it can be very easily extended to circle recognition, compared to other models, the Hough technique is a simple mathematical model and robust. This produces sinusoids curves, can be accumulated in a space called Hough space, its role is to draw all points set of the circles, to find out the places when the curves intersect, which means the presence of a circle, mathematically the circle is characterized, by (r) radius and center (X_{center},Y_{center}) in equation (11).

For forming a cone with a vertex ($X_{center} = x$, $Y_{center} = y$, $r = 0$), based essentially on the set number of circles, passing through a given point N (x, y) according to the axis r, and the best points correspond to the maximum intersection of cones. On the other hand, if the circle radius is specified, in a two-dimensional the (a, b) plane, in this plane, the set of circles passing through a given point N is described by the circle of center ($X_{center} = x$, $Y_{center} = y$) and radius r, also the best points that bring together the intersection of several circles. Finally, in accumulation, an M matrix is constructed, each element M (i, j) contains the number of circles passing through the point, but the method consists to construct a hyper-matrix for accumulation when the radius is unknown, which each value of cells M (i, j, k), corresponds to a cubic space (a, b, r), characterized by scanning between 1 pixel up and the dimension of the image.

5. Implementation

5.1. The manual threshold applied to images
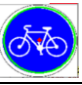
We have tried to roughly summarize the procedure or essential steps in the traffic road signs detection process. Based essentially on the colors by setting the lower and upper limit markers for each color, and the geometry of the signs- see the evolution in Table. I.

5.2. Manual thresholding in Real-time

At this level, we try to apply the detection in real-time, for evaluation of our algorithm the detection of traffic road signs,

especially circular shape, which have the colors either Red or Blue, been using a web camera of Asus laptop.

Color	HSV space	Canny Edge	Panel Detection
Red			
Blue			

The results obtained contains two essential windows: One window shows the color images conversions, that have several objects detected with Gaussian filtering to eliminate noise, to easily convert it into grayscale images, the other represents the Canny outlines that facilitate the detection of the desirable object outline, at each figure 4: (a) and (b). We took real-world images of two road signs of different colors: red for the "No-entry" sign and blue for the "Bicycle" sign, but the more relevant thing, the extraction or detection of objects were not perfectly detected. So, we ask several questions where this error comes from, but most probably the two HSV space filters are not perfectly established.

6. Discussion

The goal of our approach is to have or ensure high accuracy for the detection of traffic road signs, specific circular shapes, then we will be able to apply it to all geometric shapes. We have concluded from what we have obtained previously that the HSV space filter terminals did not prove our approach, indirectly the

manual thresholding. In image processing, to have a high resolution or in-depth studies on images, we establish a histogram to have an idea of distributions pixels, because our objective is to reach automatic thresholding for the two test images used previously.

If we have visualized well or focused our attention on the two histograms, we interpret the results obtained, that we have a peak that seems to be the maximum of the pixels distributed for each histogram, in an interval from 250 to 255, it is the V channel in blue concerning the other channels H and S, for the figure. 4 (a) and (b). So, what we can conclude is to look for new values of the HSV space filters and make tests until we get high precision, it's hard because there are several factors among these factors is the luminance, the solution, we will unproven our work by using the automatic thresholding, we use the most robust is the OTSU method.

6.1. Automatic thresholding

The OTSU method based on a histogram of images, uses discriminant analysis to separate the text from the background, its principle is to divide the image into classes, and then look for the optimal threshold, by minimizing the variance function inter or intra classes. Otsu's method [21] tries to find or to get the optimal threshold, by separate the histogram into two segments, that maximize the inter-segment variance or minimizes a measure of intra-segment variance, the determination of these variances, based on the histogram normalization. The variances σ_i^2 for each threshold is given by equation (12), The ω_i designed weights of the probability for each class (i), which means the threshold separation.

(a)   Red signs   (b)   Blue signs
Figure 3: Traffic Signs detection manual thresholding [5]
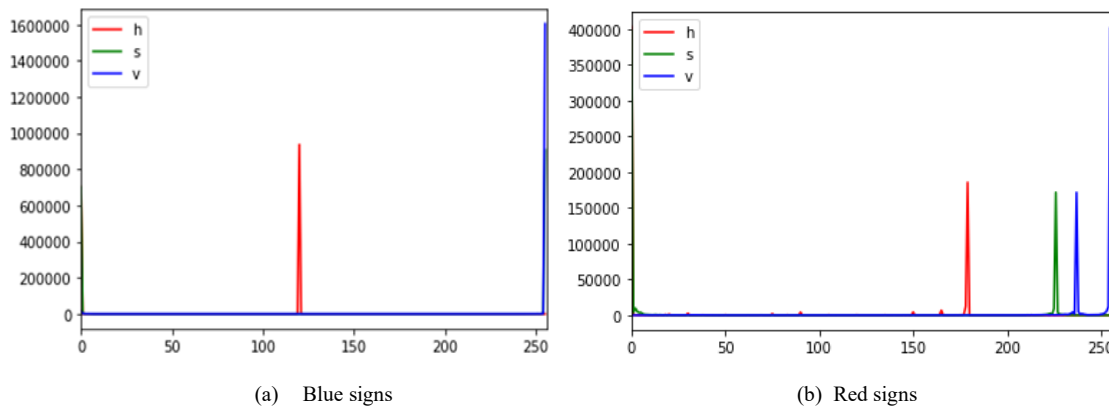
(a)   Blue signs   (b)   Red signs

Figure 4: Traffic road signs histogram [5]

$$\sigma_w^2(t) = \omega_1(t)\sigma_1^2(t) + \omega_2(t)\sigma_2^2(t) \qquad (12)$$

The Otsu method advises, for its technique to be effective, by minimizing the intra-class variance, due by maximizing the inter-class variance [20].

$$\omega_1(t) = \sum_{i=1}^{t} P(i) \quad \omega_2(t) = \sum_{i=t+1}^{I} P(i) \qquad (13)$$

$$\mu_1(t) = \sum_{i=1}^{t} \frac{iP(i)}{\omega_1(t)} \quad \mu_2(t) = \sum_{i=t+1}^{I} \frac{iP(i)}{\omega_2(t)} \qquad (14)$$

$$\sigma_1^2(t) = \sum_{i=1}^{t}[i - \mu_1(t)]^2 \frac{P(i)}{\omega_1(t)} \quad \sigma_2^2(t) = \sum_{i=t+1}^{I}[i - \mu_2(t)]^2 \frac{P(i)}{\omega_1(t)} \qquad (15)$$

The approach to detect regions of objects, therefore leads directly to a partition of the image, in this approach, we applied different methods consisting of manual or automatic thresholding, the simplest method for thresholding in image processing, through segmentation. From a grayscale image, image thresholding can be used to create an image with only two values, black or white, we have applied this method to the basic images that are shown below in Table. 1. The automatic thresholding applies a multi-level per Otsu's method, it consists to determine the number of regions, the optimal values of the different thresholds, based on the variance of the subdivisions. To have an algorithm for the detection of traffic roads signs with high efficiency and precision, from what we understood from the OTSU method, that is based on the classes average μ_1 and μ_2, also the class probabilities ω_i, which will be applied to the pixels of the road signs, either for blue or red, and we fly at the end of the binarized images.

Our strategy for the binary image was formed by the function of the OpenCV library, the bitwise function. Then we merged the three thresholds h, s, v resulting from the three binary images, to obtain at the end a single threshold value. Still, for the detection of traffic roads signs contours, we use Canny because it has proven its high precision in contour descriptions according to the previous tests, even when there is noise, it guarantees high detection and localization of objects for all two-dimensional applications. Before applying the Canny outline, it is preferable to apply a Gaussian filter. Table. 2 shows the manual thresholding values, which contain the bounds of the HSV space values and automatic thresholding.

Table 2: Identification signs for manual and automatic thresholding [5]

Threshold	HSV space	Canny Edge	Detection panels forms
Automatic			
Manual			

Starting from the fact that we are trying to detect the presence of the circle shape in an image, Firstly, the Hough transform consist of searching for the parameters of the structure to be detected, the second step aims to find the points of the image that may belong to the structure, typically the points where the gradient goes beyond a certain threshold. At each of these points, a representative of the structure will pass through and calculate its parameters, the values of these parameters correspond to a point in the parameter space, the third step consists of marking the curve represented by the calculated parameters as a possible representation of the structure being searched.

Table 3: Manual and automatic thresholding [5]

Threshold	Colors	Filter	Hue	Saturation	Value
Automatic	Red			Auto	
	Blue				
Manual	Red	Upper	180	255	255
		Lower	136	87	111
	Blue	Upper	130	255	255
		Lower	110	50	50

For the identification of colors in HSV space shown in the Table. 3, it is certainly necessary to specify very essential elements, for each color of the high and low filters. Our case is the colors that represent the majority of blue and red traffic roads signs, obtaining the values of channels H, S, and V after extensive experimentation and testing, but the trick is to note that these values can make a service or a work perfectly in an environment A and not sure certainly for an environment B. The solution is to apply automatic thresholding by applying the method of OTSU. OTSU adapts to each environment, to find optimal values for the HSV space that leads easily to the detection of traffic road signs. Finally, we are not only going to press on the color, but we are also going to combine the color and the detection of the circular geometry, it shows in table 3 we have an improvement that makes the algorithm more robust to detect the desired object with real-time optimization.

Practically, we are going to vote for parameters. The curve whose parameters obtain the most votes is therefore the one that best describes the structure. To collect the votes, we need an accumulator table, the size of this table is equal to the number of unknown parameters. The size of each dimension is equal to the maximum value of the corresponding parameter. Once the parameters have been calculated, they represent a cell of the accumulator table, we will increase the value of this cell by one unit. At the end of the process, we are going to explore the accumulator to find the boxes that have obtained the most votes, their corresponding parameters describe the occurrences of the structure we are looking at in table.2, which is the circular shape.

6.2. Real-time based Automatic thresholding

At this stage we try to make a real-time test for traffic road signs detection, we will produce the same scenario in an urban environment by using a webcam as shown in the two figures.5 (a) and (b). The relevant thing is that the detection of circular signs is made with high accuracy, so the automatic thresholding by the OTSU method has a great effect than the HSV space. For the three windows that make up the two figures, we have a very high image quality, which makes it easy for Canny to locate the outline of traffic road signs in a very powerful and robust. Otsu has a methodology able whatever the environments, to perform
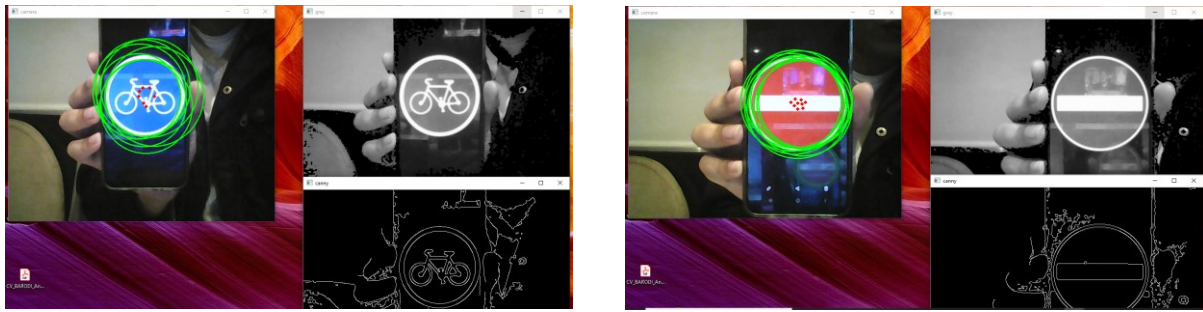
(a) Blue signs   (b) Red signs

Figure 5: Traffic road signs automatic thresholding [5]

automatic thresholding from the shape of the image histogram, so we deduce, that the conversion from gray-level space to binary space, makes it easier to calculate background and foreground classes, for optimal thresholding for each separate between classes, to comply with the condition, that intra-class variance to be minimal.

6.3. Cropping of the panels detected

The Hough feature descriptor used for road signs detection, calculated on a 32 × 32 patch of an image. Let an image of road signs with a size of 128 × 128. A patch with a size greater than 50 × 50 is selected for the calculation of the Hough descriptor. This patch is cropped from an image and resized to a size 32 × 32 in Table.4.

Table 4: Cropped traffic road signs

Cropped Blue Signs	Cropped Red signs
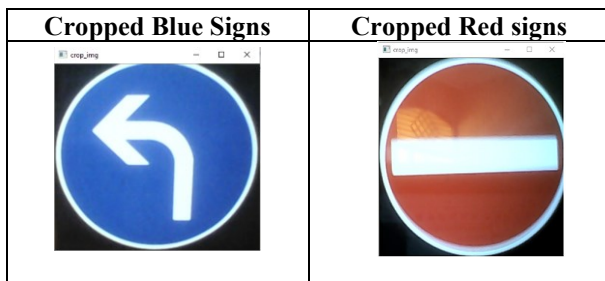
7. Recognizing Detected Road Signs

In the recognition part, applying model based on images of traffic road signs in Germany [22], the work is doing it with the Keras libraries for learning and classification, importing python

framework, by using some simple and efficient techniques, such as data augmentation [23] and dropout [24].

7.1. Deep Learning

Figure.6 clarify the second part of the approach, for recognizing images, exactly the traffic roads signs [22] using Artificial intelligence, these images cropped from the first part of detection, so this second part, demonstrate how to apply Convolution Neural Networks (CNN) architectures in general, we are going to use in our approach the field of Deep Learning (DL), because this family of architecture, has made it possible to make significant progress in the fields of image classification and recognize different objects, the DL models contains multi-layer of perceptron described above, with more intermediate layers. Each intermediate layer, subdivided all images datasets, for getting sub-parts of features, and providing simpler results to the next layer, CNN currently the powerful models for classifying images [25].

In figure.6 demonstrate two distinct parts of the CNN model, training and performance evaluation, for the first part, in input color images exist, which consist of pre-treatment, the conversion of the color space from RGB to grayscale, for providing a matrix of pixels has two dimensions for a grayscale image, and normalization by value 255 for each image, forget the images ranging between 0 and 1. After the step of pre-treatment, starts training the model, then select the best training model, and then choose based essentially, the curve of accuracy function and loss function. For the second part, the best model passed by strict steps, to evaluate performance; so, we use confusion matrix and rapport classification each class image.
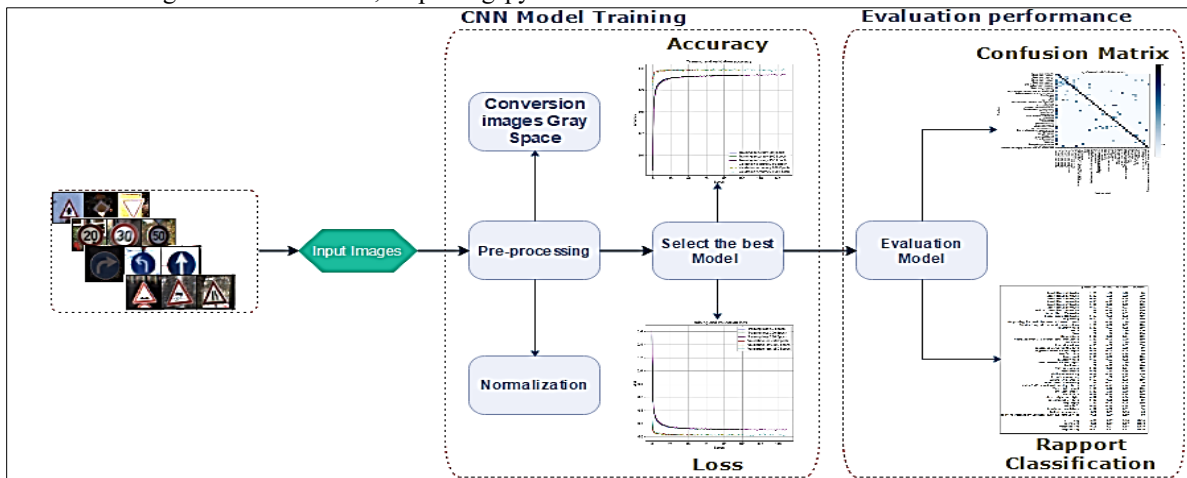
Figure 6: Traffic road signs CNN-based recognition model

(a)   Accuracy curves

(b) Loss curves
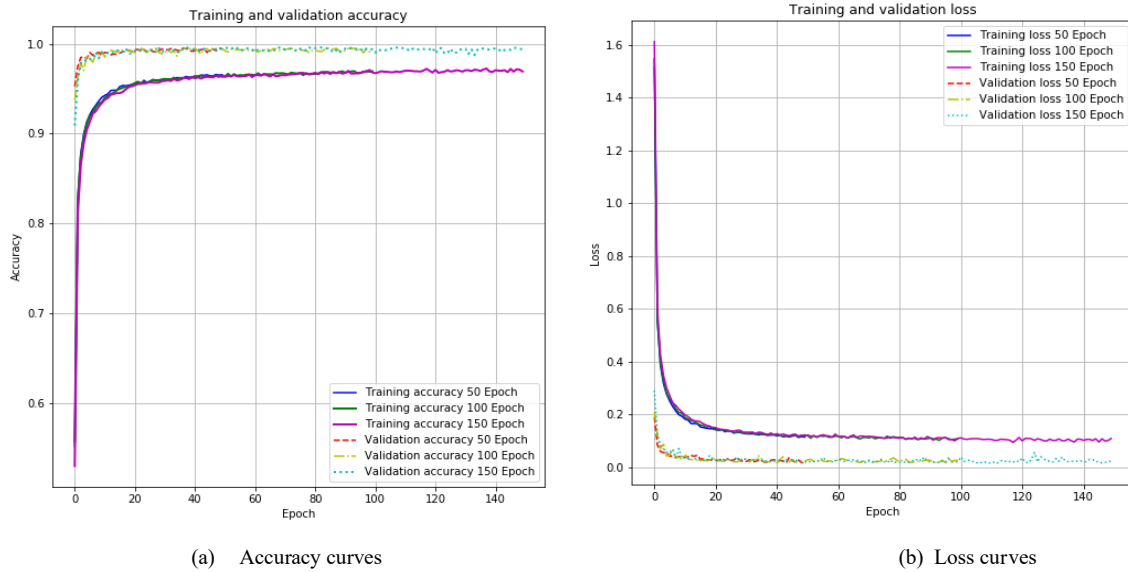
Figure 7: Results of training CNN Model proposed in Table.5

7.2. CNN-based Model Description

The first part of a CNN is the convolutional part, strictly speaking, functions as an extractor of the characteristics of the image, because the images pass through a succession of filters, or convolution cores, creating new images called convolution maps some broker filters reduce the images resolution, by using a local maximum of operation. After the convolution layers or maps, are flatteners and reassemble into a vector of features.

The CNN base on the MLP (Multi-Layer Perceptron) [26], and inspired by the behavior of the visual cortex, although effective for image processing, MLPs have great difficulty in handling large images, which are due to the exponential growth in the number of connections to the image size, for example, if taking an image size of 32x32x3, so the first hidden layer, need fully-connected neuron of the MLP, to have in inputs 3072 neuron, but for 224x224x3 size images, lead to being processed in inputs, need 150,528 neuron, which means when the images size are larger, the number becomes enormous of neurons.

A CNN architecture formed by an ensemble of different processing layers, the important layers are:

❖ The convolution layer (Conv2D) a receiver field the data, explained before.

❖ The pooling layer (MaxPooling2D) compresses or reduces the image size by subsampling.

Table 5: Architecture CNN Model

Layers	Output	Parameters
Conv2D	(None, 28, 28, 60)	1560
Conv2D	(None, 24, 24, 60)	90060
MaxPooling2D	(None, 12, 12, 60)	0
Dropout	(None, 12, 12, 60)	0
Conv2D	(None, 10, 10, 30)	16230
Conv2D	(None, 8, 8, 30)	8130
MaxPooling2D	(None, 4, 4, 30)	0
Dropout	(None, 4, 4, 30)	0
Flatten	(None, 480)	0
Dense	(None, 500)	240500
Dropout	(None, 500)	0
Dense	(None, 43)	21543
Total parameters: 378,023		
Trainable parameters: 378,023		
Non-trainable parameters: 0		

Table.5 is composed of four convolution layers, two layers of Max-pooling, and two layers of fully connected. The input image is 32*32 in size; goes to the first convolution layer, this layer composed of 60 filters of 5*5 size, with ReLU activation function forces neuron to return positive values, after this convolution, then 60 feature maps of size 32*32 are obtained, which represent the input of the second convolution layer, also composed of 60 filters. The Max pooling layer was applied afterward, to reduce the image size. At the output of this layer, we will have 60 feature maps of size 12*12. We repeat the same thing with the last convolution layers composed of 30 filters; the ReLU function always applies to each convolution, and Max-pooling layer valid all the time, at the output of these layers, the features vectors of sizes 480. Finally, using a neural network composed of two fully connected layers, the first layer composes of 500 neurons, where the ReLU activation function was used, the second layer uses softmax function, for calculating the probability distribution of the 43 classes of traffic roads signs.

7.3. Trained Model

According to Figure.7 (a), the curves of training accuracy increase when several epochs increases, the same observation for curves of validation accuracy, reflecting the fact of epochs, can conclude the model learns more information. If the validation

accuracy can't follow training accuracy, during the training model, this means that the CNN architecture, did not extract enough characteristics, for each class from the road sign images, called the underfitting, and when validation accuracy decreases during the training model, may result to overfitting, can conclude more features, allowing to model learn enough. Therefore, the curves of training loss decrease to achieve minimum error values, according to the number of epochs in the figure.7 (b), and the same for curves of validation loss. For all the graphs shown, the model does a very good job and powerful, according to the best scores shown in the figures previously during training, has reaches 11% in error rate and the totality for a 97% accuracy rate.

Table 6: Scores of accuracy and loss

Model	Epoch	Test Loss (%)	Test Accuracy (%)	Processor Type
CNN Model	50	06.93	97.91	NVIDIA GeForce 920M (GPU)
	100	11.64	97.05	
	150	11.31	97.11	

7.4. Training model description

Table.6 shows the results of scores accuracy and loss, using the test dataset, the execution time is too expensive, this comes

back to the large size of the base which requires to use GPU that CPU [27]. The model presented the best results found, the number of epochs and convolution layers reflect these good results; however, the execution time was very expensive because of the number of epochs.
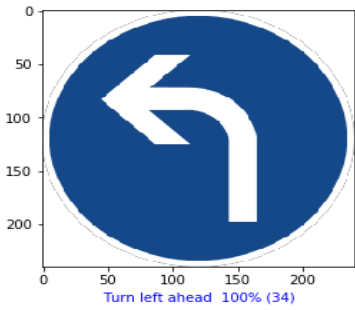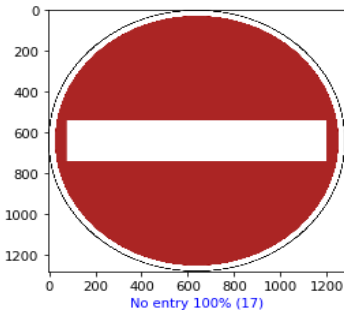
In general, a deep convolutional neural network gives good results and the performance of our network degrades, if the number of epochs increases. For example, according to the table, the increase leads to a loss of about 0.86% of the performance of the network. Therefore, depth is crucial to achieving good results. The results obtained have improved as we have deepened our network with the number of epochs. The learning base is also a crucial element in convolutional neural networks, you need a large learning base to achieve better results in the future.

8. System Performance Evaluation

8.1. Cropped images recognition

As can see in Table.7, after the detection of circular-shaped panels with high accuracy in a real-time environment. Then we cut the road signs, the next phase is the most important for our system, the recognition of the road signs, identifying it to which class or category belongs in an intelligent way using deep learning. The objects that contain both images have been classified correctly without any errors. The red sign has been classified or recognized with a prediction of 100% No-entry, the same for the blue sign with a percentage of 100% Turn left. So, we have good results that can be a basis for the improvement of ADAS systems in the automotive sector that will serve the evolution of industry 4.0.

Table 7: Recognition of TRAFFIC ROADS SIGNS cropped

Cropped Signs	Recognition Signs
	Turn left ahead 100% (34)
	No entry 100% (17)
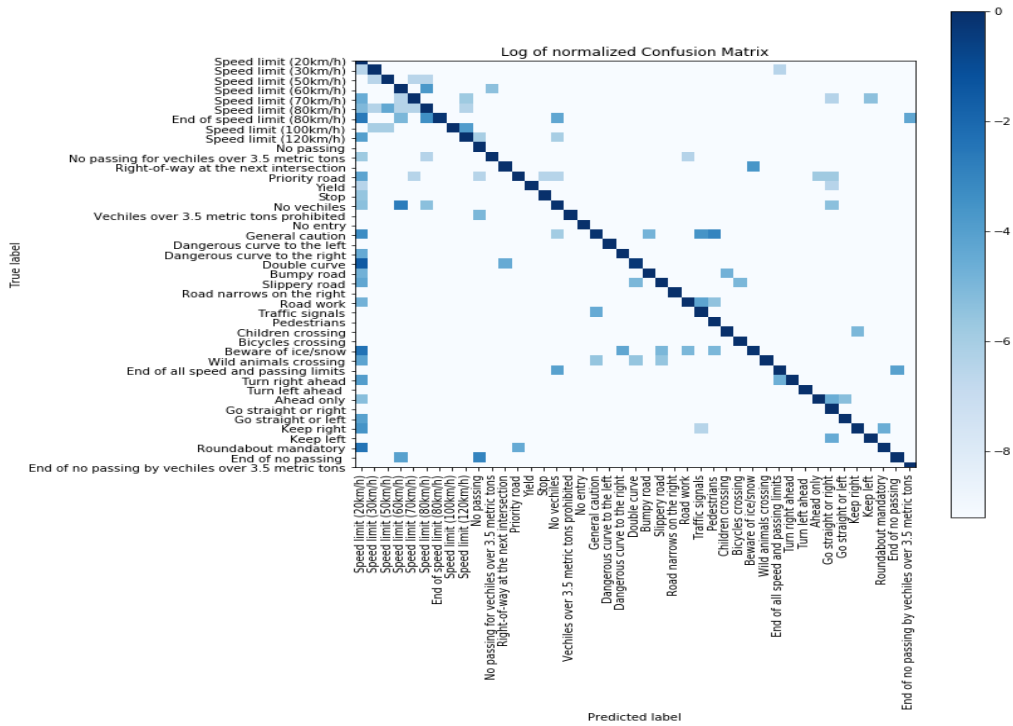
Figure 8: Confusion Matrix of CNN model

	precision	recall	f1-score	support
Speed limit (20km/h)	1.00	1.00	1.00	60
Speed limit (30km/h)	1.00	1.00	1.00	720
Speed limit (50km/h)	0.99	1.00	0.99	750
Speed limit (60km/h)	0.96	0.97	0.97	450
Speed limit (70km/h)	1.00	0.98	0.99	660
Speed limit (80km/h)	0.97	0.97	0.97	630
End of speed limit (80km/h)	1.00	0.86	0.92	150
Speed limit (100km/h)	1.00	0.98	0.99	450
Speed limit (120km/h)	0.97	0.98	0.98	450
No passing	0.99	1.00	0.99	480
No passing for vechiles over 3.5 metric tons	1.00	0.99	1.00	660
Right-of-way at the next intersection	1.00	0.97	0.99	420
Priority road	1.00	0.97	0.99	690
Yield	1.00	1.00	1.00	720
Stop	1.00	1.00	1.00	270
No vechiles	0.97	0.92	0.94	210
Vechiles over 3.5 metric tons prohibited	1.00	0.99	1.00	150
No entry	1.00	1.00	1.00	360
General caution	0.99	0.87	0.93	390
Dangerous curve to the left	1.00	1.00	1.00	60
Dangerous curve to the right	0.98	0.99	0.98	90
Double curve	0.97	0.77	0.86	90
Bumpy road	0.98	0.98	0.98	120
Slippery road	0.99	0.97	0.98	150
Road narrows on the right	1.00	1.00	1.00	90
Road work	1.00	0.97	0.98	480
Traffic signals	0.90	0.99	0.94	180
Pedestrians	0.73	1.00	0.85	60
Children crossing	0.99	0.99	0.99	150
Bicycles crossing	0.99	1.00	0.99	90
Beware of ice/snow	0.92	0.87	0.90	150
Wild animals crossing	1.00	0.97	0.99	270
End of all speed and passing limits	0.95	0.97	0.96	60
Turn right ahead	1.00	0.97	0.99	210
Turn left ahead	1.00	1.00	1.00	120
Ahead only	0.99	0.98	0.99	390
Go straight or right	0.92	1.00	0.96	120
Go straight or left	0.97	0.98	0.98	60
Keep right	1.00	0.96	0.98	690
Keep left	0.97	0.99	0.98	90
Roundabout mandatory	0.92	0.90	0.91	90
End of no passing	0.98	0.93	0.96	60
nd of no passing by vechiles over 3.5 metric tons	0.98	1.00	0.99	90
micro avg	0.99	0.97	0.98	12630
macro avg	0.98	0.97	0.97	12630
weighted avg	0.99	0.97	0.98	12630
samples avg	0.97	0.97	0.97	12630

Figure 9: The classification rapport of the CNN model

8.1. Confusion Matrix

The Confusion Matrix [28] is used to evaluate the performance of our model, since it reflects the metrics of True Positive, True Negative, False Positive, and False Negative. Figure.8 closely illustrates the position of these metrics for each class. For example, the model ranked the automotive images well and is ranked or confused by the images of the other classes. We notice that there is a little confusion in classification on everything for the first class, which reduced the classification rate a little.

The average classification rate, as shown in the figure. 9 is 98%, which indicates our good system, for precision and recall, and high classification values for all categories.

9. Conclusion

Object detection in images and more specifically the detection of road signs images is a problem addressed by artificial vision. Among its fields of application are video surveillance, road safety, detection assistance systems. In our work, we were interested in the detection of signs. A bibliographical study has been carried out to determine the possible detection adopted methods and the most used descriptors in this case. Image classification is an important task in the computer vision field, object recognition, and machine learning. Through Deep Learning, the future of artificial intelligence enhances large and very fast developing algorithms. We discussed how the detection process and image classification took by a camera device during the discussion of the concepts of the neural network. To realize our classification work we used deep learning, which has shown its performance in recent years and we chose the CNNs method as the classification method, this choice is justified by the method's simplicity and its efficiency. During the tests phase, the obtained result confirms our approach effectiveness. Our work is only in its initial version and remains open for comparison with other classification methods [29].

The objective was to create a system for the automotive sector that combines detection and recognition. Detection based on the color and geometry of road signs, recognition based on deep learning based on CNN architecture, we got a score of 100% for classifying the test images captured from a real environment. Our work to be complimentary for our next work of detected geometry: triangular and rectangular, and classified it using Artificial Intelligence. This approach can be applied to the development of embedded systems for the automobile, which will serve road safety for all road users, either the passenger or the driver.

References

[1] L. Li, "China's manufacturing locus in 2025: With a comparison of 'Made-in-China 2025' and 'Industry 4.0,'" Technological Forecasting and Social Change, **135**(February), 66–74, 2018, doi:10.1016/j.techfore.2017.05.028.

[2] K.M. Tan, V.K. Ramachandaramurthy, J.Y. Yong, "Integration of electric vehicles in smart grid: A review on vehicle to grid technologies and optimization techniques," Renewable and Sustainable Energy Reviews, **53**, 720–732, 2016, doi:10.1016/j.rser.2015.09.012.

[3] K. Armstrong, S. Das, J. Cresko, "The energy footprint of automotive electronic sensors," Sustainable Materials and Technologies, **25**, e00195, 2020, doi:10.1016/j.susmat.2020.e00195.

[4] S. Hossain, D.J. Lee, "Deep learning-based real-time multiple-object detection and tracking from aerial imagery via a flying robot with GPU-based embedded devices," Sensors (Switzerland), **19**(15), 2019, doi:10.3390/s19153371.

[5] A. Barodi, A. Bajit, M. Benbrahim, A. Tamtaoui, "An Enhanced Approach

[6] R.Y. Zhong, X. Xu, E. Klotz, S.T. Newman, "Intelligent Manufacturing in the Context of Industry 4.0: A Review," Engineering, **3**(5), 616–630, 2017, doi:10.1016/J.ENG.2017.05.015.

[7] K. Okuma, A. Taleghani, N. De Freitas, J.J. Little, D.G. Lowe, "A boosted particle filter: Multitarget detection and tracking," Lecture Notes in Computer Science (Including Subseries Lecture Notes in Artificial Intelligence and Lecture Notes in Bioinformatics), **3021**, 28–39, 2004, doi:10.1007/978-3-540-24670-1_3.

[8] Y. Lu, Z. Zhou, J. Zhao, "Visual Object Tracking Using PCA Correlation Filters," 2544–2550, 2018, doi:10.2991/caai-18.2018.10.

[9] S. Kolkur, D. Kalbande, P. Shimpi, C. Bapat, J. Jatakia, "Human skin detection using RGB, HSV and YCbCr color models," ArXiv, **137**, 324–332, 2017, doi:10.2991/iccasp-16.2017.51.

[10] A. Uçar, Y. Demir, C. Güzeliş, "Object recognition and detection with deep learning for autonomous driving applications," Simulation, **93**(9), 759–769, 2017, doi:10.1177/0037549717709932.

[11] R. Ranjan, V.M. Patel, R. Chellappa, "HyperFace: A Deep Multi-Task Learning Framework for Face Detection, Landmark Localization, Pose Estimation, and Gender Recognition,"IEEE Transactions on Pattern Analysis and Machine Intelligence, **41**(1), 121–135, 2019, doi:10.1109/TPAMI.2017.2781233.

[12] M. Rout, J.K. Rout, H. Das, Correction to: Nature Inspired Computing for Data Science, 2020, doi:10.1007/978-3-030-33820-6_12.

[13] V. Balali, A. Jahangiri, S.G. Machiani, "Multi-class US traffic signs 3D recognition and localization via image-based point cloud model using color candidate extraction and texture-based recognition," Advanced Engineering Informatics, **32**, 263–274, 2017, doi:10.1016/j.aei.2017.03.006.

[14] S. Houben, J. Stallkamp, J. Salmen, M. Schlipsing, C. Igel, "Detection of traffic signs in real-world images: The German traffic sign detection benchmark," Proceedings of the International Joint Conference on Neural Networks, 2013, doi:10.1109/IJCNN.2013.6706807.

[15] H. Zhang, T. Xu, H. Li, S. Zhang, X. Wang, X. Huang, D. Metaxas, "StackGAN: Text to Photo-Realistic Image Synthesis with Stacked Generative Adversarial Networks," Proceedings of the IEEE International Conference on Computer Vision, **2017-Octob**, 5908–5916, 2017, doi:10.1109/ICCV.2017.629.

[16] K. Muhammad, M. Sajjad, I. Mehmood, S. Rho, S.W. Baik, "Image steganography using uncorrelated color space and its application for security of visual contents in online social networks," Future Generation Computer Systems, **86**, 951–960, 2018, doi:10.1016/j.future.2016.11.029.

[17] G. Saravanan, G. Yamuna, S. Nandhini, "Real time implementation of RGB to HSV/HSI/HSL and its reverse color space models," International Conference on Communication and Signal Processing, ICCSP 2016, 462–466, 2016, doi:10.1109/ICCSP.2016.7754179.

[18] K. Preethi, K.S. Vishvaksenan, "Gaussian Filtering Implementation and Performance Analysis on GPU," Proceedings of the International Conference on Inventive Research in Computing Applications, ICIRCA 2018, (Icirca), 936–939, 2018, doi:10.1109/ICIRCA.2018.8597299.

[19] A. Barodi, A. Bajit, S. E. Aidi, M. Benbrahim, and A. Tamtaoui, "Applying Real-Time Object Shapes Detection To Automotive Traffic Roads Signs.", International Symposium on Advanced Electrical and Communication Technologies (ISAECT) , 1–6 ,2020-- Proceeding.

[20] B. Li, S.T. Acton, "Automatic active model initialization via poisson inverse gradient," IEEE Transactions on Image Processing, **17**(8), 1406–1420, 2008, doi:10.1109/TIP.2008.925375.

[21] M. Baygin, M. Karakose, A. Sarimaden, E. Akin, "An image processing based object counting approach for machine vision application," ArXiv, 18.

[22] J. Stallkamp, M. Schlipsing, J. Salmen, C. Igel, "The German Traffic Sign Recognition Benchmark for the IJCNN'11 Competition," Proc. of the International Joint Conference on Neural Networks, 1453–1460, 2011.

[23] A. Mikołajczyk, M. Grochowski, "Data augmentation for improving deep learning in image classification problem', Inter. Interdisciplinary PhD Workshop (IIPhDW), 117–122, 19, doi10.1109/IIPHDW. 2018.8388338."

[24] G.H. de Rosa, J.P. Papa, X.S. Yang, "Handling dropout probability estimation in convolution neural networks using meta-heuristics," Soft Computing, **22**(18), 6147–6156, 2018, doi:10.1007/s00500-017-2678-4.

[25] H.C. Shin, H.R. Roth, M. Gao, L. Lu, Z. Xu, I. Nogues, J. Yao, D. Mollura, R.M. Summers, "Deep Convolutional Neural Networks for Computer-Aided Detection: CNN Architectures, Dataset Characteristics and Transfer Learning," IEEE Transactions on Medical Imaging, **35**(5), 1285–1298, 2016, doi:10.1109/TMI.2016.2528162.

[26] V.F. Kuzishchin, V.A. Dronov, "The specific features of the algorithm for

in Detecting Object Applied to Automotive Traffic Roads Signs", IEEE International Conference on Optimization and Applications (ICOA), 1–6 ,2020 , doi:10.1109/ICOA49421.2020.9094457.

tuning controllers on the basis of the kvint firmware system," Thermal Engineering, **48**(10), 835–841, 2001.

[27] Y.D. Zhang, K. Muhammad, C. Tang, "Twelve-layer deep convolutional neural network with stochastic pooling for tea category classification on GPU platform," Multimedia Tools and Applications, **77**(17), 22821–22839, 2018, doi:10.1007/s11042-018-5765-3.

[28] M. Frid-Adar, I. Diamant, E. Klang, M. Amitai, J. Goldberger, H. Greenspan, "GAN-based synthetic medical image augmentation for increased CNN performance in liver lesion classification," Neurocomputing, **321**, 321–331, 2018, doi:10.1016/j.neucom.2018.09.013.

[29] A. Barodi, A. Bajit, M. Benbrahim, and A. Tamtaoui,'Improving the Transfer Learning Performances in the Classification of the AutomotiveTraffic Roads Signs', E3S Web Conf., 2020 -- Proceeding.

Dismantle Shilling Attacks in Recommendations Systems

Ossama Embarak*

Computer Information Science, Higher Colleges of Technology, Abu Dhabi, 51133 UAE

A R T I C L E I N F O	A B S T R A C T
	Collaborative filtering of recommended systems (CFRSs) suffers from overrun false rating injections that diverge the system functions for creating accurate recommendations. In this paper, we propose a three-stage unsupervised approach. Starts by defining the mechanism(s) that makes recommendation vulnerable to attack. Second, find the maximum-paths or the associated related items valued by the user. We then rule out the two attacks; we will need to pull two different measures. (a) We will pull user ratings across all reviews and measure their centre variance. (b) We will then pull each individual user rating and measure them according to the original rating. Detected attack profiles are considered untrusted and, over time, if the same user is detected as untrusted, the profile is classified as completely untrusted and eliminated from being involved in the generation of recommendations. Thus, protect CFRS from creating tweaked recommendations. The experimental results of applying the algorithm to the Extensive MovieLens dataset explicitly and accurately filter users considering that a user could seem normal and slightly diverge towards attack behaviours. However, the algorithm used assumes that the framework has already begun and manages user accounts to manage the cold start scenario. The proposed method would abstractly protect users, irrespective of their identity, which is a positive side of the proposed approach, but if the same user reenters the system as a fresh one, the system will reapply algorithm processing for that user as a normal one.

1. Introduction

This paper is an extension of work originally presented in 2019 Sixth HCT Information Technology Trends (ITT) [1]. Personalization Collaborative Filter Recommending Systems (CFRSs) is becoming increasingly popular in well-known e-commerce services such as Amazon, eBay, Alibaba, etc. [2]. Most people are rating products or services without even realizing it is something they can do [3]. However, CFRSs are highly vulnerable to "profile injection" attacks; often referred to as "shilling" attacks [4]. It is common for attackers to pollute the recommended systems with malicious ratings. They either demote a target item with the lowest rating; called a nuke attack or promote a target item with the highest rating; called a push attack to reach their target or minimize the recommendation's accuracy. It is therefore necessary to develop an effective detection system for detecting and removing attackers before the recommendation [5–7].

Detection methods based on the attacks gained much coverage. Since the similarities between attackers are higher than the actual users, some have been presented based on the similarity between users. Traditional similarity metrics, including the Pearson Correlation Coefficient (PCC),[8,9]. However, the detection efficiency of these methods relies

largely on the estimation of similarity. How to reduce the time consumption of the measurement of similarity is also a difficult problem, particularly when dealing with large datasets[10]. In addition, some attackers imitate the rating data of some legitimate users in order to increase their reliability. Only the use of similarities is difficult to discriminate incomplete [11]. In order to overcome these problems, a more efficient form of detection should be considered in the following aspects:

A. Applied algorithm complexity should be acceptable.

B. The proposed method should be able to defeat various kinds of "shilling" attacks.

This paper proposes an unsupervised detection method for detecting such attacks, consisting of three phases. The purpose of the proposed method is to filter out more legitimate users, and at the same time hold, all attackers step by step. Firstly, the recommendation system admin needs to understand the attacker's strategy based on the recommendations working mechanisms. Secondly, we constructed users' maximal paths that represent his/her loop less-visited nodes or rated items in an association, then calculate the maximal path's mean and standard deviation considering all ratings done by users visited that particular maximal path. Thirdly, we detected untrusted users by detecting the user's zone (normal, freeze or melt zone area) which reflect the gap between the user's ratings in the

*Corresponding Author: Ossama Embarak, oembarak@hct.ac.ae

maximal path (items) and the genuine profiles' ratings of the same path(items) considering the maximum expected calculated deviation. The proposed algorithm prevents untrusted users' maximal sessions should not be added to the system profiles used for generating recommendations, and the user is labelled as untrusted profiles in which the system should not consider such profiles towards generating recommendations.

Recommendation systems are massively used to support online systems provides services through the internet. As an alternative to passive search engines that simply accept as "true" the displayed results, these collaborative filtering systems attempt to take the perspective of the user's needs and what they are searching for and identify similar results based on that [12]. Decisions that depend on a user's previous demands can be made with a recommendation system; a recommendation system is a set of techniques used to process and generate recommendations. In order to inject the ratings of biased users into recommender systems, users attempt to influence the system by injecting biased ratings for a specific product they are interested or associated with. Through a process known as a rating bot attack, which can plough the ratings up or down, change the ratings of services or items to the highest or the lowest available levels, or launch attacks against them [13]. In order to avoid shilling attacks, the company has attempted to implement various suggestions, such as asking users to rate items by using certain code, or by only allowing ratings to occur after a certain amount of time, or by simply making profiles harder to create or by increasing the price of creating a profile? Because of the ways in which these methods can eliminate attacks, the participants in rating and evaluating services became much smaller than normal [14]. E-commerce web-systems suffer from attackers who push specific items to the recommendations list and promote the target item via manipulating recommendation systems [15]. The attackers create numerous profiles by injecting unusual identities and putting very high-ratings for their target items. An attacker's profile will camouflage itself by keeping track ratings for other non-target items, and the system will use that information to predict the attacker's targets. The manipulations of recommendations systems of injecting misleading and false data make a recommendation system's operation is negatively affected [16]. Recommendations systems powered by user-generated reviews will only be representative of individuals with very few reviews. Initial profiles will greatly affect future processing and output. Moreover, this system does not generate suitable recommendations, and occasionally, it breaks down the whole system; It causes the system to lose its credibility and respect by people in the community. Therefore, several research groups' main goal is to develop a system that can filter out fake profiles that could make those systems able to provide accurate recommendations [17].

This paper looks into a different type of attacks for recommendation systems and propose a solution to detect and isolate attackers. It contains the following sections: Section 1 introduction to recommendation systems and its attacks. Section 2, the background of recommendation systems different forms of attacks. Section 3, we discuss the previous researches and approaches for handling different attacks. Section 4 identify the study problem. In section 5, we explore the proposed solution. Section 6 demonstrate experimental results. Finally, The paper and the future work will be concluded.

2. Background

Numerous different sorts of recommenders are used on different sites. Studies in the past have shown dramatic growth in the methods used to improve recommendations. Recommendation systems can be broadly classified into content-based and collaboration-based [18]. Content-based filtering suggests products based on users browsing history. There are downsides to this type, such as over-specialization, which recommends only similar products to what was consumed before. Collaborative filtering takes into account past behaviour, considering that users will behave similarly. Shilling attacks manipulate recommendation systems by inserting malicious user profiles into the filter data [19]. The target item is either promoted or demoted. Attacks can be categorized as push or nuke strikes, a product may therefore be promoted or dismissed for advantages over competitors [20]. Over time, numerous attacks models have been developed. There are many detection techniques and algorithms to counter such attacks. All of the attack models are designed to generate vicious users. The discrepancies are recognized in how the strike profiles are established. Malicious users' domain items can be considered as $S = \{ I_s, I_p, I_n, I_\emptyset \}$, where I_s is the set of items that matched with the genuine users. *while* I_p is the set of items the malicious user promote, and I_n is the set of items he/she demote, and $I_\emptyset$ items that are not ranked yet by the trouble user.

Over the years, several attacks were developed. All such attacks can be classified either as a high-level attack or as a poor-knowledge attack based on their motivation and knowledge [21, 22]. Attacks with little knowledge are more practical and are more likely to impact the real world, but such attacks' effectiveness is also low. On the other hand, high-level attacks can have a huge impact on Recommender Systems' performance, but they are more difficult to pull out. *RandomBot attack* is the plainest form of a shilling attack. Items rated by the attackers selected in random, except for the target item. The rankings for such items are based on the overall system norm [22].

A maximum or minimum rating will be given on the basis that it is a push or a nuke attack. The purpose of a random attack is usually more effective in disrupting the Recommender Systems' performance than in promoting the target item. *Average Attack* is similar to Random Attack when selecting items. The randomized distribution of individual items is based on their distribution of ratings. The average rating of each filling item is assigned. This attack can only be carried out if the attacker knows the system's dataset. While random attack and average attack differ only from filler ratings, the average attack impact is much higher. *Bandwagon Attack* is the kind of attack where attacker profiles are filled with popular high rating items. Naturally, attack profiles are closer to many people. The highest value is given to the target item. Depending on the rating scheme used to provide the filler items, this attack can further be divided into random and bandwagon averages. Bandwagon is also classified as a low-knowledge attack since the attacker only needs public data. *Bandwagon Reverse Attack* is the exact reversal of an attack on a bandwagon. This attack is used to demote the target product by rating the items with high negative ratings low and giving the target item the least rating. *Segmented Attack* targets a particular group of users who can buy the target item in the e-commerce system. Segment attacks typically occur in collaborative item-based filtering [23, 24].

The ratings and items are based on knowledge of the segment from the attacker. The important benefit of this method is its ability to reach potential clients over other approaches. *Probe attack* occurs when an attacker provides genuine ratings for items based on their knowledge of the predicted rating scores. The attacker uses this detail to rate items, enabling it to appear similar to other ratings. The attacker composes the acceptable items list based on the rated items. This collaborative scheme allows attack profiles to remain close to their neighbours. It also facilitates an attacker in gaining more information about the system. *Love/Hate Attack,* where the attacker randomly chooses filler items and gives them the highest rating and lowest rating on the target item. It can also be known as a push attack by changing the highest ratings [25]. *Noise Injection attack* generates random numbers multiplied by a constant to each rating for a subset of rated profiles. The more obfuscation, the more constant. It can be effectively applied to obfuscate its signature to all standard methods. A slightly decreased ability to withstand an attack is observed in response to noise injection. *User-Shifting attack* where a subset of users revises ratings [26]. The attack subsets were selected randomly to reduce their similarities. Ratings are scaled differently for different subsets of the ratings [27]. *Target Shifting attacks* shift the targeted item rating to a lower level in push attacks than maximum. For nuke attacks, the minimum rating is shifted up by one. *The mixed attack* is made using the same proportions of random, average, bandwagon and segmented attacks. The detection technique should be able to detect all the standard attacks successfully. The various methods for attacking the same target item are used. It helps to avoid various methods of detection [28].
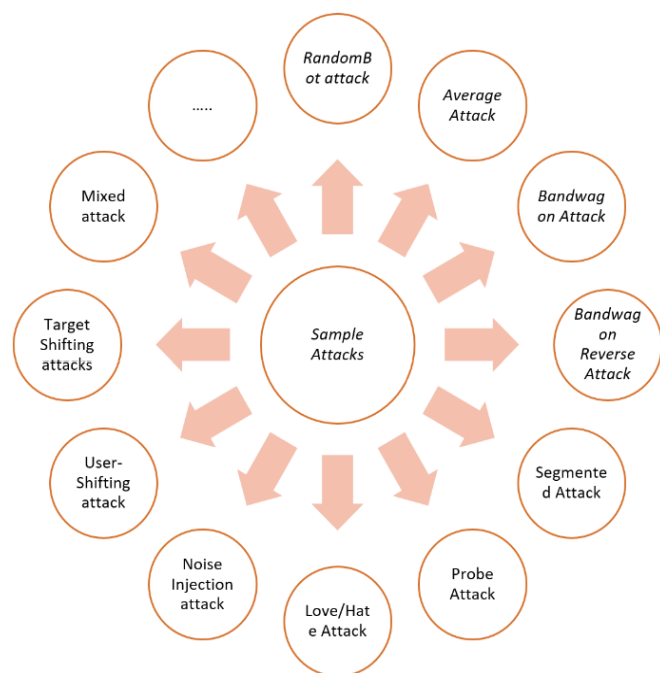
Figure 1: Sample Attacks Types

3. Related Works

A well-known class of attacks is called the Shilling attacks, which attempts to inject some profiles to influence the targeted system's performance [13]. This attack is divided into two attacks: push attack- which uses a malicious profile to rate a specific item highly (greater than most items) and nuke attack- which uses malicious profiles to lower rating for a specific item (s). Playbooks attacks reflect a series of actions undertaken to

maximize a certain item's importance and increase its profits [29]. Some systems produce low-quality recommendations, so that once the users discover such attacks, the system loses its users' respect and loyalty [30]. Unfair rating attack occurs when a system uses trusted agents' ratings and compares them against each other for a service entity. This attack leads to predictions that are not actually correct [31]. Re-entry attacks occur when an agent is transferred between accounts using different names to avoid low ratings [29]. Sybil attacks reflect a fake identity to give different ratings. So far, a robust recommendation system is essential for any application of a recommendation system. Robustness measures a model's ability to produce good predictions with noisy data [32]. Whenever a user rates something, the system updates its databases, which means we have no way of knowing if the ratings are real or not. Ratings can sometimes be tedious, which could be caused by users' carelessness, and malicious users may attack. In robustness, there are two different aspects, *the first* of which is the accuracy of recommendation, which are the products that were recommended by the systems after the attack took place. *The second thing a system must do is be very stable,* which means won't recommend slightly different products if it detects an anomaly or attack.

Before storing user ratings into the system, the attack type must be detected to maintain its good reputation before affecting its performance. Injecting profiles another example of forged data being injected by malicious users into recommendations systems to manage recommendations [33]. Collaborative filters are susceptible to profile attacks by user-based and item-based recommendations. In this sort of attack, the attackers try to evaluate target and non-target items to make ratings appear normal by forging rating profiles and injecting them in rating systems [34]. Studies show that group attack profiles manipulate the target object ranking recommendation. Many attackers work together in a given time frame to attack certain target items to quickly put some items into a preferred list. The next section will provide a breakdown of the experiment and its results.

4. Identifying the Problem

Recommendation systems may provide health recommendations that reflect the preferences of users. However, injecting false ratings or trying to push or nuke ratings of the offered items differs in the system's performance. Many proposed solutions are almost implemented after attacking or generating recommendations that burden many computations and increase system time complexity. Furthermore, depending on the specific fixed average rating, the dynamic change in items' ratings over time is not reflected. Therefore, we propose a new approach to filter users into normal, fully trusted and untrusted users based on their maximal traversing path or items movable threshold.

5. The Proposed Solution

Details of the proposed method are implemented in three stages in this section. In the first phase, we need to understand the attacker's strategy based on recommendations generation mechanisms. In the second phase, we constructed users' maximal paths and calculated the maximal path's mean and variance, considering all users' ratings visited that particular

maximal path. In the third stage, we detected untrusted users by detecting the user's zone (normal, freeze or melt zone area), which reflect the gap between the user's ratings in the maximal path (items) and the genuine profiles ratings of the same path(items) considering the maximum expected calculated deviation. All detected untrusted users' maximal sessions should not be added to the system profiles used for generating recommendations, and the user is labelled as untrusted profiles in which the system should eliminate his future participations.

5.1. Users Profiles

Recommendation systems collect user ratings – items used to form an object rating matrix that includes three elements: users, items and ratings.

$$U = \{ u_1, u_2, \ldots, u_{m-1}, u_m \}$$

where *U* refers to set of *m* users.

$$I = \{ I_1, I_2, \ldots, I_{n-1}, I_n \}$$

where *I* refers to a set of n items.

All users can rate few or all items; a user-item rating matrix generated from all the ratings is used to find attackers and make many recommendations.

$$\begin{bmatrix} I_{u_1}^1 & \cdots & I_{u_1}^n \\ \vdots & \ddots & \vdots \\ I_{u_m}^1 & \cdots & I_{u_m}^n \end{bmatrix}$$

Figure 2:   Items-users ratings matrix

where $I_{u_1}^1$ reflect the rating of the first item by the first user, while $I_{u_m}^n$ is the rating of the item number n by the user number m.

A regular user weight items in the overall round the norm. Similarly, both the push and nuke attackers aim to rate items extremely far from the item threshold. We call it a *freezing* zone, as the rates are very far from the item average rates measured, and the nuke attackers aim to rate items that are extremely low from the item thresholds, we call it a *melting* zone, as the rates are very far back from the item thresholds. We measure each user's ratings and can detect any change in weight in either "Freeze" or "Melting" zones by measuring the weighted mean of all ratings.

5.2. Attackers Background

The attackers usually deliberately attempt to change the efficiency of the recommendation system. They know how the system operates and use their expertise and understanding to affect the system's efficiency.

There are three types of systems in terms of user awareness of the Recommendation Mechanisms.

1. Systems that depend on the popularity threshold (like Insider) to produce recommendations are simply showing popularity to users. As a result, attackers know exactly what will be recommended, attempt to modify popularity

by revisiting the same path(route) or increase or decrease other paths' ratings.

2. Systems that depend on each item's popularity to produce a recommendation, the popularity displayed to users with a list of recommendations can also use the association rule to show that items x are frequently selected with item y, such as YouTube videos. As a result, attackers have full knowledge of how ratings are allocated in the recommended device profiles. Attackers attempt to manipulate the specific item(s) by raising or decreasing the item(s) ratings or increasing or decreasing the related items' ratings.

3. Systems that show recommended items without a strong indication of popularity or affiliation between items, such as Amazon. As a result, attackers have no understanding of the system mechanisms.

Recommendation system developers must consider the attacker tactics and program the system to identify and remove any untrusted users from being part of the profiles used to produce recommendations.

5.3. Constructing Maximal User Path

As shown in the figure below, each user targets items and gives their ratings of those items. The ratings influence those items to be the top choices. Others will probably allocate very little to nuke individual objects at the lowest level far below the average weighted μ of the item. An average is normally relative to all items rated.
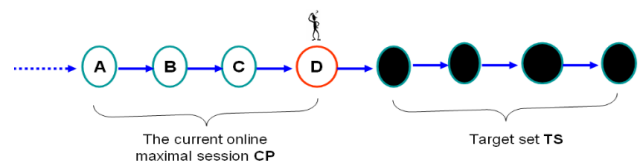
Figure 3:   User-Targeted Items

We consider a maximal route occurred during a visit (session), as shown in the figure below, where there is no loop happened in a maximal path. The user may have several visits during which the rating occurred, as shown in the below figure, the user might be a genuine or an attacker. Whether a genuine person or an attacker, a user tries to check certain nodes, so we need to assess his traversing rates.
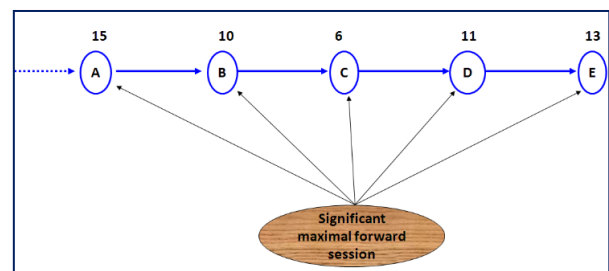
Figure 4:   User Maximal Path

We begin with each user session, and gradually explore the data, moving from s_i. And as for all of the rates R_i, they do not exceed the limits. The user session is entered into the system of that session.

$$s_i = \{ R_1, R_2, \ldots, R_{n-1}, R_n \}$$

By measuring the session maximal path average rate, we can find the rate deviation of the user's rating of the node's visited and rate by looking at the other user's ratings of the user rated objects.

$$\mu_{s_i} = \frac{\sum_{i=1}^{n} R_i}{n} \qquad (1)$$

$$\sigma(s_i) = \sqrt{\frac{\sum_{j=1}^{l}(|\mu_{s_i} - R_{u_j}^i|)^2}{n}} \qquad (2)$$

where μ_{s_i} represents the mean weight of that path by all users and $\sigma(s_i)$ represents the calculated standard deviation of all rates happened on that maximal path.

5.4. Detect Untrusted Users

The two types of attacks are very severe from average users, but this does not mean that a normal user does not score an object at a low or high rate. However, it is uncommon for the same user to rate multiple items with very low or very high ratings relative to other users that rate the same item on similar maximum paths.

We then found the following rule to use every rate state (melting, freezing, or normal).

where $F(s_i)$ is the evaluation function of each session as a collection of rankings made through a visit, $\Im_+$ represents the case when the user aims to push ratings far from the normal ratings (the freeze status), and $\Im$ reflects ratings happened within the threshold boundaries, while $\Im_-$ reflects the case when the user aims to downgrade target items (the melting status) as shown in the figure below.
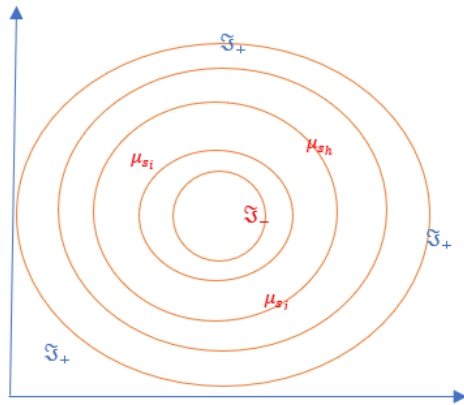
Figure 5: User Rates Zone

where,
Freeze case ($\Im_+$) = $\{R_i \mid R_i > \Im_+\}$
Meting case ($\Im_-$) = $\{R_i \mid R_i < \Im_-\}$
Normal case ($\Im$) = $\{R_i \mid R_i \cong \Im \text{ or } R_i \cong \mu_{s_i}\}$

Therefore, $\Im_+$ & $\Im_-$ users should be eliminated from being part of recommendation generation processing.

Table 1: Attack Status

Attack model	Zone	Status
push attack	Freeze zone	$\Im_+$
No attack	Normal	$\Im$
Nuke attack	Melting zone	$\Im_-$

Table 1 shows that $\Im_+$ reflects the highest rates could be reached by attackers in the rating; for specific items or maximal path, far beyond the standard deviation. And $\Im_-$ reflect the customer's minimum prices relative to the measured average rate and the selected products' standard deviations. While $\Im$ reflects the normal rates of the trusted user obtained by the recommendation systems.
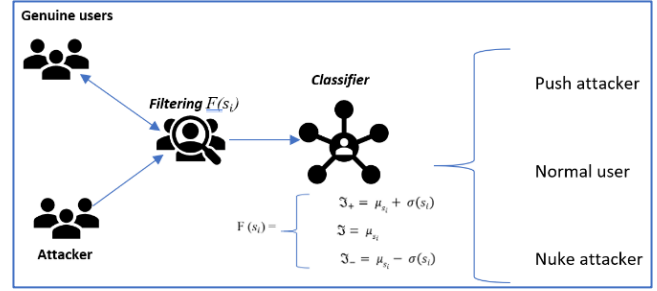
Figure 6: Suggested Model Stages

5.4.1. Algorithm for Detecting an Attack

The following algorithm demonstrates the followed steps to detect a user rating zone.

Input: users ratings or maximal path in a session.
Output: filter users into trusted, untrusted (melting, freeze).
1. Read a user u_i session s_i
2. $\forall_i \in s_i$, calculate μ_{s_i}, and $\sigma(s_i)$
3. Read **UT**
4. **While not UT**
   For R *in* s_i:
   a. *if* $R_i > \Im_+$
      i. *Detected Freeze case*
      ii. Refuse the whole session
      iii. Untrusted user is highlighted
      iv. **Update UT ← u_i**
   b. Else if $R_i < \Im_-$
      i. *Detected Melting case*
      ii. Refuse the whole session
      iii. Untrusted user is highlighted
      iv. **Update UT ← u_i**
   c. Else
      i. Detected Normal case
      ii. Accept the whole session ratings
      iii. Trusted user is highlighted
      iv. **Update U ← u_i**
5. Return zone

---

where R reflects items ratings in a session s, and **UT** reflects the untrusted users discovered and recorded on the system. The system would automatically maintain its functionality by upgrading any identified untrusted user to untrusted profiles that make sense of removing any ratings received from these users in the future. In contrast, the normal user ratings should be updated to the normal profiles used to produce recommendations.

5.5. The Contribution of the Manuscript

This paper's main contribution is implementing a new algorithm to filter user rating injections and item rating injections to prevent false similarities. A matrix of ratings is used in the processing to identify the trust of the user. Therefore, if the user ratings exceed a particular computed ceiling, the system routinely denies the user scores and moves

them in an untrustworthy category, and the user ratings are not considered in the recommendation creation.

6. Experimental Results

We use the available online Movie Lens 1M data set to apply and test the proposed algorithm, comprising 1,000,000,000 unidentified reviews of roughly 3,900 films received by 6,040 users of Movie Lens. All scores are 1 to 5 integers, with 1 being the lowest, and 5 being the highest. There are 18 separate domains in the data set and all users with at least 20 films rated. The proposed algorithm (see section 3.4.1) was able to detect cases near the freezing, and those were very close to the melting zone. Total cases were 11364): Normal ratings (2677), Malting near (3943), Freeze near (4611), found attacks (133) as demonstrated in the table below.

Table 2: Users- Malicious Detection

Domain name	Normal	Malting touch	Freeze touch	Detected Attacks
Action	240	158	154	3
Adventure	123	216	349	2
Animation	157	226	216	0
Children	125	152	173	9
Comedy	151	267	248	50
Crime	104	348	247	0
Documentary	177	326	536	4
Drama	173	158	195	15
Fantasy	123	234	165	0
Film-Noir	140	217	300	3
Horror	157	154	172	8
Musical	125	150	150	0
Mystery	141	148	141	11
Romance	177	178	272	0
Sci-Fi	173	353	467	12
Thriller	176	277	286	0
War	105	211	380	7
Western	110	170	160	9

In each movie domain, the following figure shows user patterns; it is clear that several freezes touch cases when user ratings exceed the normal ratings; the same is obvious in the melting zone. The experimental results showed that the algorithm detected 50 attacks from the comedy group, while many cases were under border conditions. The clearly reported attacks in the trained data showed that the attached percentage are as follows, in Action (2%) , Adventure(2%),Animation (0%), Children (7%), Comedy(38%), Crime(0%), Documentary(3%), Drama(11%), Fantasy(0%), Film Noir(2%), Horror(6%), Musical(0%), Mystery(8%), Romance(0%), Sci-Fi(9%), Thriller(0%), War(5%), Western(7%).
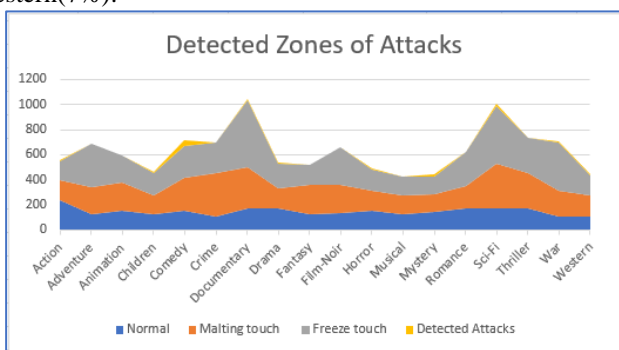
Figure 7:   Attacks Detections For 300 Users

We expanded the data set and considered 450 users; the algorithm could detect more attacks, as seen in the figure

below. This represents the incremental number of maximum paths that are being tested and the rise in the number of attacks observed by improvements in the slander of the deviation and the zones' size.
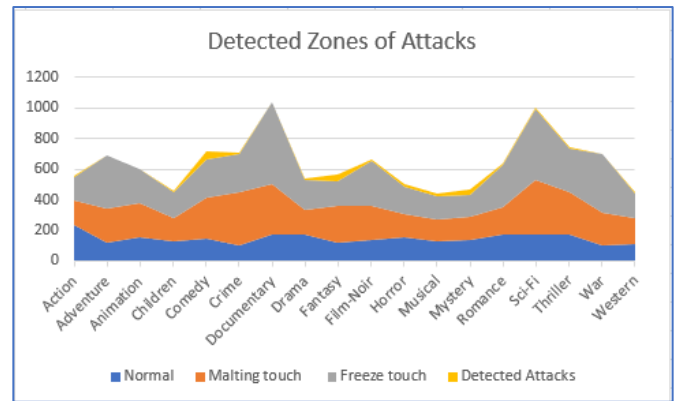
Figure 8:   Attack Detection For 450 Users

The following table demonstrates a comparison between the proposed algorithm and another two algorithms were used to detect malicious attacks in recommendation systems.

Table 3: Algorithms Comparison

Points	Proposed algorithm	Rating behaviour	Profile similarity
Processing	Find the maximal path or sequence of items ratings	Pinpoint lower rating values considering that it has a minimal contribution to the systems	Discover profiles similarity
System behaviour	Classify users in three zones Normal, Melting and Freeze before updating their datasets	Detect all lower rating profiles.	Detect all identical profiles in ratings
Actions	Use trustworthy users to make recommendations	Ignore low rate profiles and only use moderately to highly qualified profiles	Ignore all identical profiles
Privacy concerns	Users' demographic data are not collected, only their maximum routes or sequence of items are collected. No privacy concerns.	The issue of privacy is valid.	Privacy is a valid issue.
Effective against	Various attack forms.	Random and Reverse	Average, Segment,

		Bandwagon attacks	and Bandwagon attacks
System reacts	The system will continue to serve untrusted users but will ignore their preferences for making recommendations.	The system eliminates profiles of an attacker	The system removes the profiles of attackers

Different attacks can be conducted using the proposed algorithm by finding the maximum path and measuring how far it is from the abstract user path. This helps classify users into different three zones; Normal, Melting (extreme below the threshold), and Freeze (extreme high from the threshold). The system then can ignore both Melting& Freeze cases and maintain only the normal cases for recommendation processing.

7. Conclusion and Future Works

Shilling attacks are a significant challenge to collaborative filtering recommendation systems. These attack profiles are likely to have similar rating information to many legitimate profiles to make them difficult to identify. This paper proposed an unsupervised detection method for detecting attacks (or irregular ratings) consisting of three phases. In the first phase, we need to understand the attacker's strategy based on the recommendation generation mechanisms. In the second phase, we built users' maximal paths and calculated the maximal path's mean and standard deviation considering all users' ratings visited that particular maximal path. In the third stage, we detected untrusted users by detecting the user's zone (normal, freeze or melt zone area) which reflect the gap between the user's ratings in the maximal path (items) and the genuine users' ratings of the same path(items) considering the maximum expected calculated deviation. All detected untrusted users' maximal sessions should not be added to the system profiles used for generating recommendations, and the user is labelled as untrusted profiles in which the system should eliminate any future participation. Experimental results showed that with a greater number of maximum routes used by the recommendation systems, the model could detect more attacks and thus discover untrusted users and prevent them from affecting their performance. The proposed method's main limitations include the following two aspects: (a) How the system could work in the launching phase when there are no ratings in the system collected from users. However, in the beginning, various methods can be used to overcome such systems' cold start, such as developing a suggestion considering the like-minded users when navigating the system. (b) The proposed approach abstractly handles users regardless of their identities, representing a good side of the proposed approach, but if the same user joins the system as a new user, the system will perform the calculations again for that user. One of our future objectives is to apply the suggested algorithm on a larger data set and apply it to live stream data in collaborative systems.

Conflict of Interest

The authors declare no conflict of interest.

References

[1] O. Embarak, "Demolish falsy ratings in recommendation systems," in 2019 Sixth HCT Information Technology Trends (ITT), IEEE: 292–295, 2019.

[2] N. Sivaramakrishnan, V. Subramaniyaswamy, L. Ravi, V. Vijayakumar, X.-Z. Gao, S.L.R. J I.J. of B.-I.C. Sri, "An effective user clustering-based collaborative filtering recommender system with grey wolf optimisation," International Journal of Bio-Inspired Computation, **16**(1), 44–55, 2020. https://doi.org/10.1504/IJBIC.2020.108999

[3] Y. Pan, D. Wu, D.L. J D.S.S. Olson, "Online to offline (O2O) service recommendation method based on multi-dimensional similarity measurement," Decision Support Systems, **103**, 1–8, 2017. ttps://doi.org/10.1016/j.dss.2017.08.003

[4] Z. Yang, L. Xu, Z. Cai, Z. %J K.-B.S. Xu, "Re-scale AdaBoost for attack detection in collaborative filtering recommender systems," Knowledge-Based Systems **100**, 74–88, 2016.

[5] W. Zhou, J. Wen, Q. Xiong, M. Gao, J. J N. Zeng, "SVM-TIA a shilling attack detection method based on SVM and target item analysis in recommender systems," Neurocomputing **210**, 197–205, 2016.

[6] M. Si, Q. %J A.I.R. Li, "Shilling attacks against collaborative recommender systems: a review," Artificial Intelligence Review **53**(1), 291–319, 2020.

[7] S. Alonso, J. Bobadilla, F. Ortega, R. J I.A. Moya, "Robust model-based reliability approach to tackle shilling attacks in collaborative filtering recommender systems," EEE Access, **7**, 41782–41798, 2019. ttps://doi.org/10.1016/j.ds.2017.08.003

[8] Z. Yang, Z. Cai, X. %J K.-B.S. Guan, "Estimating user behavior toward detecting anomalous ratings in rating systems," Knowledge-Based Systems **111**, 144–158, 2016.

[9] K.G. Saranya, G.S. Sadasivam, M. %J I. journal of science Chandralekha, Technology, "Performance comparison of different similarity measures for collaborative filtering technique," Indian journal of science and Technology, **9**(29), 1–8, 2016.

[10] B. Li, Y. Wang, A. Singh, Y. Vorobeychik, "Data poisoning attacks on factorization-based collaborative filtering," in Advances in neural information processing systems, 1885–1893, 2016.

[11] M. Fang, G. Yang, N.Z. Gong, J. Liu, "Poisoning attacks to graph-based recommender systems," in Proceedings of the 34th Annual Computer Security Applications Conference, 381–392, 2018.

[12] M.N. TEKLEAB, RECOMMENDATION SYTEM ANALYSIS AND EVALUATION, NEAR EAST UNIVERSITY, 2019.

[13] A.M. Turk, A. %J E.S. with A. Bilge, "Robustness analysis of multi-criteria collaborative filtering algorithms against shilling attacks," **115**, 386–402, 2019.

[14] N. Nikzad–Khasmakhi, M.A. Balafar, M.R. %J E.A. of A.I. Feizi–Derakhshi, "The state-of-the-art in expert recommendation systems," **82**, 126–147, 2019.

[15] E. Çano, M. %J I.D.A. Morisio, "Hybrid recommender systems: A systematic literature review," **21**(6), 1487–1524, 2017.

[16] C. Wang, Y. Zheng, J. Jiang, K. %J E. Ren, "Toward privacy-preserving personalized recommendation services," **4**(1), 21–28, 2018.

[17] M. Sappelli, S. Verberne, W. %J J. of the A. for I.S. Kraaij, Technology, "Evaluation of context-aware recommendation systems for information re-finding," **68**(4), 895–910, 2017.

[18] J. Su, Content based recommendation system, 2017.

[19] L. Yang, W. Huang, X. %J I.E.T.I.S. Niu, "Defending shilling attacks in recommender systems using soft co-clustering," **11**(6), 319–325, 2017.

[20] V.W. Anelli, Y. Deldjoo, T. Di Noia, E. Di Sciascio, F.A. Merra, "Sasha: Semantic-aware shilling attacks on recommender systems exploiting knowledge graphs," in European Semantic Web Conference, Springer: 307–323, 2020.

[21] A.P. Sundar, F. Li, X. Zou, T. Gao, E.D. %J I.A. Russomanno, "Understanding Shilling Attacks and Their Detection Traits: A Comprehensive Survey," **8**, 171703–171715, 2020.

[22] P. Kaur, S.G. Goel, Shilling Attack Detection in Recommender Systems, 2016.

[23] X. Li, M. Gao, W. Rong, Q. Xiong, J. Wen, "Shilling attacks analysis in collaborative filtering based web service recommendation systems," in 2016 IEEE International Conference on Web Services (ICWS), IEEE: 538–545, 2016.

[24] M. Ebrahimian, R. Kashef, "Efficient Detection of Shilling's Attacks in Collaborative Filtering Recommendation Systems Using Deep Learning Models," in 2020 IEEE International Conference on Industrial Engineering and Engineering Management (IEEM), IEEE: 460–464, 2020.

[25] I. Gunes, H. %J I.R.J. Polat, "Detecting shilling attacks in private environments," **19**(6), 547–572, 2016.

[26] Y. Hao, F. Zhang, J. Wang, Q. Zhao, J. %J S. Cao, C. Networks, "Detecting shilling attacks with automatic features from multiple views,"

2019, 2019.

[27] V. Mohammadi, A.M. Rahmani, A.M. Darwesh, A. %J H.C. Sahafi, I. Sciences, "Trust-based recommendation systems in Internet of Things: a systematic literature review," **9**(1), 1–61, 2019.

[28] S. Khusro, Z. Ali, I. Ullah, "Recommender Systems: Issues, Challenges, and Research Opportunities," Lecture Notes in Electrical Engineering, **376**, 1179–1189, 2016, doi:10.1007/978-981-10-0557-2_112.

[29] O. Embarak, M. Khaleifah, A. Ali, "An Approach to Discover Malicious Online Users in Collaborative Systems," in International Conference on Emerging Internetworking, Data & Web Technologies, Springer: 374–382, 2019.

[30] Y. Cai, D. %J D.S.S. Zhu, "Trustworthy and profit: A new value-based neighbor selection method in recommender systems under shilling attacks," **124**, 113112, 2019.

[31] D. Lee, P. Brusilovsky, Recommendations based on social links, Springer Verlag: 391–440, 2018, doi:10.1007/978-3-319-90092-6_11.

[32] K. Christakopoulou, A. Banerjee, "Adversarial attacks on an oblivious recommender," in Proceedings of the 13th ACM Conference on Recommender Systems, 322–330, 2019.

[33] C.-M. Lai, Attackers' Intention and Influence Analysis in Social Media, University of California, Davis, 2019.

[34] O.H. Embarak, "Like-minded detector to solve the cold start problem," in 2018 Fifth HCT Information Technology Trends (ITT), IEEE: 300–305, 2018.

Optimal Hydrokinetic Turbine Array Placement in Asymmetric Quasigeostrophic Flows

Victoria Monica Miglietta[*], Manhar Dhanak

Department of Ocean and Mechanical Engineering, Florida Atlantic University, Boca Raton, Florida, 33431, USA

A R T I C L E   I N F O

A B S T R A C T

The Coriolis force in the ocean at mid to high latitudes can cause significant deviation of flow over bottom topography, including formation of Taylor columns. Structures in a tidal zone will experience zero inertial current between every tidal change. Around periods of directional change, the Coriolis force may be tapped into for energy. Factors like timescales and other environmental factors like local currents could influence the flow characteristics in an undesirable way and are outside of the scope of this study. The focus of this study is to assess how the design of a structure influences the asymmetric flow patterns produced around it by an incident quasigeostrophic flow. Analytical solutions existing for inviscid quasigeostrophic flow over isolated elongated elliptical topography are used for flows with small Rossby numbers. These solutions are used to predict and explore the characteristics of the flows expected during a change in the tidal cycle. Results show that a linear array placed perpendicular to a quasi-geostrophic flow will experience flow acceleration on the left-hand side when looking downstream. On the other hand, a linear array placed parallel to the quasi-geostrophic flow will experience a sharp velocity gradient over the array. This suggests that an array placed perpendicular to the quasi-geostrophic flow will provide for a more robust design when compared to a linear array placed parallel to the flow.

1. Introduction

Special considerations for large underwater turbine farms or arrays at mid and high latitudes will be necessary because at such latitudes the Coriolis force can measurably impact the dynamics of flow in asymmetric patterns. A thoughtful and robust array design can position turbines to harness the Coriolis force[1]. Array design requires knowledge of the local dynamics and an understanding of all forces including the Coriolis force. Tools for evaluating such an ocean engineering endeavor includes numerical solutions for flows moving past extended obstacles in instances when rotational forces are required to describe the flow [2].

The Coriolis force is a pseudo force caused by Earth spinning on its axis. Typical ocean engineering problems ignore Coriolis effects because they are minimal on the typical scale of ocean engineering problems. Also, local inertial forces often dominate engineering problems where a good approximation allows for the Coriolis force to drop out of consideration. But for tidal currents, the local inertial speeds will drop to zero at least twice daily, and it is at these periods where the Coriolis force may impact an array. A renewable energy system's array which produces electricity for

a municipal power grid will be sensitive to electrical and therefore environmental energy fluctuations. For locations with higher values of latitude the Coriolis force should be considered at periods surrounding slack tide.

Often tidal current power sites are limited to channels and bays [3-7], however tides are not limited to these locations. Tides occur throughout the Earth's oceans. Here the design of a turbine array in open water is analyzed. Vertical boundaries are far from the array and the domain's distinct boundaries are the surface of the water and the seafloor. A very long array, capable of being economically viable, composed of a single line of turbines is considered. The turbine array is taken to be 10,000m long. The large dimension is comparable to a topographic feature and certainly would allow for the array to meet a production goal on the order of megawatts of electricity. It is hypothesized that a very large array in the ocean would experience the same amplification of flow rate around it that a seamount experiences [8, 9].

Studies of seamounts, and underwater ridges indicate flow behavior around large obstructions in the ocean are influenced in a measurable way by the Coriolis force [2, 8, 10]. The largest dimension of 10,000m would put a turbine array on the scale of a

*Corresponding Author: Victoria Monica Miglietta, vmiglietta2013@fau.edu

small seamount and on par with the scale of a seamount [10]. It has been observed that flows past/around seamounts are amplified and that the flow above them is best described as stagnant [10]. These are rotational effects and have been of interest to marine biologists and oceanographers [9, 11].

The flow patterns and Coriolis effects on an underwater turbine array differ from those of wind turbine arrays because of the huge density difference between air and water. The nature of air and water differ in a way where the rotational phenomenon of Taylor columns are not found in the atmosphere for quasigeostrophic flow conditions [12, 13]. These Coriolis effects are not seen around wind farms or wind turbines because they disappear in a density gradient.

2. Background

2.1. Not a channel

Studies like [4-6] look at tidal channels being utilized for tidal current power. However, taking over an entire tidal channel or even a good portion of one for power generation would have serious consequences for the established use of a channel. Many channels have daily uses which include maritime traffic for shipping, fishing and recreation. Obtaining permits and backing of local communities to re-purpose heavily used tidal channels for power production would likely be a challenge. If the tidal power project was for a remote community or some remote operations then challenges could be different. However, for large coastal communities looking to harness tidal power across a tidal channel such challenges could be expected. For example, the offshore wind development off the coast of Massachusetts, Vineyard Wind, has experienced a lot of push back by the fishing industry in the area. The project has been on hold since 2019 while the Interior Department conducts a review. Harnessing tidal current power in more open areas, could be less oppressive to current users of waterways. In this study the ideal deployment area is far from boundaries like shorelines, piers, or breakwaters.

2.2. Static Obstruction in a Rotational Fluid

Here the effects of the static physical presence of an obstruction to flow in a changing tide were studied. The review of studies of the effects of seamounts on the flow around them shows that large obstructions, like that which could be expected from a tidal turbine array, produce asymmetric patterns seen in rotational fluids [14]. These rotational effects are caused by the spinning of the Earth. The fundamental physical dynamics for an obstruction to flow in a rotational fluid with a small inertial current is similar for a bottom seated obstruction and an obstruction suspended in the water column [14]. An array would have similar effects for both bottom seated and moored or suspended turbines in the water column.

Furthermore, the research presented here would be applicable to the tidal array design engineering as well as the deployment site assessment. The physical phenomenon of Taylor columns and their associated flow patterns could develop locally at the site of the engineered structure itself, and it could also develop on/around

a bathymetric feature like a ridge or seamount where an array or turbine is deployed. The University of Strathclyde encountered what was described as a spatial-temporal eddy with a 'calm' center when it was testing a tidal current turbine [15]. This could have been caused by a Taylor column which has a stagnant interior. The latitude for their deployment was approximately 55N.

2.3. Unchanging Coriolis Parameter in the f-plane

This study evaluates an array so large it can be viewed at the scale of topography, i.e. the array will define the 'landscape' in the area it is deployed. The *f*-plane approximation is made, where the Coriolis parameter does not change. If the array was to extend over several degrees of latitude the Coriolis parameter would change and a structure so great in size would need to be analyzed in the β-plane. For the *f*-plane approximation, the absolute velocity of the tidal current will be the parameter that changes the blocking parameter cyclically over time i.e. with the tidal cycle.

2.4. Blocking Parameter

The blocking parameter correlates the size of the obstruction with environmental parameters to indicate the degree of influence the structure has on the local flow patterns. A critical blocking parameter predicts the formation of a Taylor column. A Taylor column is a hydrodynamic phenomenon, parallel to the axis of rotation, which appears like an extension of an object, obstructing flow when the blocking parameter is at a critical value. The critical value of the blocking parameter S, is $O(1)$. There is no consensus on a more exact value for the blocking parameter. For the [10] observations the blocking parameter appeared to be approximately 0.7. The exact blocking parameter is likely to be site specific and will vary on a range of environmental parameters. Important parameters include the height of the array, h; the depth of the water, d, and the latitude which changes the Coriolis parameter, f.

This study uses the definition of the blocking parameter by [16],

$$S = h/(d \cdot R_0)$$

$$S = fhL/(d \cdot U) \qquad (1)$$

There is no consensus on the calculation of the blocking parameter or its critical value. The formation of a Taylor column was initially linked to the Rossby number dropping below the value of $1/\pi$ [12]. Effectively this original critical blocking parameter was when the Rossby number, R_0, was $1/\pi$ or smaller.

Further research [16] on rotational fluids added a coefficient to the inverse of the Rossby number, the ratio of the height of the obstruction to the depth of the water, h/d. Decades later [17] used the ratio of the greatest horizontal length of the obstruction to the water depth as the coefficient to the inverse of the Rossby number. The similar thread in all these blocking parameters is the Rossby number. The Rossby number is the ratio of inertial forces to rotational forces. The rotational forces are represented in the Rossby number by the terms fL. Where L is the characteristic length, the longest horizontal dimension of the object. The Coriolis parameter is larger for higher latitudes. The Rossby number will

decrease for higher latitudes because at these locations rotational forces are stronger. The Rossby number is inversely proportional to the Coriolis parameter

$$R_0 \propto 1/f \tag{1}$$

and the blocking parameter is proportional to the Coriolis parameter

$$S \propto f \tag{2}$$

Consequently, a structure located at a higher latitude will experience a higher blocking parameter; with velocity, and structure size, and water depth all remaining constant.

The Rossby number includes *L*, the characteristic length of an object. The [16] blocking parameter is the most complete because it not only includes the characteristic length of an object, but it also includes its height. The [17] blocking parameter is redundant in that it uses the length of the obstruction in its coefficient and the length also appears in the Rossby number. So effectively the [17] blocking parameter uses the square of the characteristic length. Returning to the perspective of a tidal current, the velocity will change and with it the blocking parameter will change. Recall that the blocking parameter is inversely proportional to the velocity

$$S \propto 1/U \tag{3}$$

Looking at the critical blocking parameter for various latitudes, faster speeds can bring about a critical blocking parameter at higher latitudes. This means that the period of the tidal cycle where the blocking parameter is critical will be longer at higher latitudes.

3. Problem Statement

Since it is during the slack tide that the Coriolis force could impact the dynamics of a turbine array, this period cannot be passed over simply as the period where tidal current turbines will not produce electricity. At slack tide, the water is in quasigeostrophic flow; meaning that the inertial current is minimal and the Coriolis force is needed to describe the flow. In quasigeostrophic flow, the consequence of a small inertial current is that it prevents the equilibrium of the pressure force and Coriolis force (this equilibrium is described as geostrophic flow).

During each tidal change the blocking parameter becomes critical. The critical value of the blocking parameter is associated with the formation of a Taylor column. When this happens the array (the obstruction) will behave like a taller structure, or it will have a sort of physical shadow above it (and possibly below it). Also, for a critical blocking parameter the flow can be described well by a 2-D approximation, where the velocity does not vary in the water column. This flow described by the 2-D approximation, i.e. a Taylor column, can appear almost instantaneously in a laboratory tank. The question addressed is what are the characteristics of the flow influenced by the Coriolis force in the immediate vicinity of a linear array? The equipment in a tidal zone is likely to experience rotational effects during periods when currents change direction. Asymmetric flow for quasigeostrophic conditions have been observed around seamounts and in this study modelling was used to predict how a large linear array would experience such conditions.

3.1. Method

The blocking parameter, *S*, will have a spiked value at every tidal change because it is inversely proportional to the velocity. Numerical [2] solutions were used to plot the velocity around a linear array when the blocking parameter was critical or *O(1)*. The solutions depend on the angle of the incident flow, *α*, and also depend on the ratio, *γ*, of the largest dimension, *L*, to the smallest dimension, *l*, in the X-Y plane.

$$\gamma = L/l \tag{4}$$

The solution is insensitive to the details of the shape of the obstacle [2]. Solutions model flow patterns closely to those in the oceans where the bathymetry is more complex than a simple ellipse [2]. The solution is for a homogeneous, inviscid, incompressible flow, with a constant depth, in a rotating frame, and it satisfies the conservation of potential vorticity. The stream function used [2] in elliptical coordinates (μ, θ) is:

$$\Psi = \begin{cases} \dfrac{1}{32} a^2 [(1 - e^{-2\mu_0} \cosh(2\mu)] \cos(2\theta) \\ \qquad\qquad + \dfrac{1}{32} a^2 [\cosh(2\mu) - \cosh(2\mu_0)], \quad \mu < \mu_0 \\ \dfrac{1}{32} a^2 \sinh(2\mu_0) \left(e^{-2\mu} \cos(2\theta) + 2(\mu - \mu_0) \right), \mu > \mu_0 \end{cases}$$

where $0.5a \sinh(\mu_0) = 1$, and $0.5a \cosh(\mu_0) = \gamma$.

4. Results

An idealized smooth diurnal tide, with equal peaks is considered for analysis. The far field velocity, *U*, changes the blocking parameter, *S*, as the tidal velocity changes. The height, *h*, is taken to be 10m, and the water depth, *d*, to be 35m. Aspect ratios between 1,000 and 250 do not vary the results remarkably. For steady quasigeostrophic flow the streamlines do not vary in the *Z* direction as long as there is no density gradient. The results show that directly at, or adjacent to, the structure is where the system could be impacted by the unique dynamics of periods dominated by quasigeostrophic flow. The character of the rotational effects is asymmetric and for the linear array placed in quasigeostrophic incident flow, the flow around it is distinctly asymmetrical when modelled with [2] analytical solutions. The results for different blocking parameters were considered as "snapshots" of what may occur over time because the time variability of these processes is not understood. The velocity fields at both ends of an array placed perpendicular to the quasi-geostrophic flow were examined for a number of velocities/blocking parameters and plotted against time. The plots reveal that the accelerations on the left-hand side looking downstream were greater than the decelerations on the opposite side, Figure 1. The corresponding effect on power over the period of quasi-geostrophic flow may be estimated from a plot of velocity cubed against time, Figure 2. The flow adjacent to the structure is most affected by the Coriolis force.

For such a perpendicular array (Figures 3 and 4) the flow is accelerated by a factor of 2 on one end, while on the opposite end it the flow rate is 1/2 to 1/5 of the far field velocity. The velocity coefficients at the end points do not change significantly as the blocking parameter increases. For blocking parameters larger than one, the location of the minimal flow (i.e. smallest velocity coefficient) moves away from the structure. The location of the most accelerated flow does not move away from the structure in the same manner. When the blocking parameter increases, flow adjacent to a greater area of the structure experiences acceleration. Furthermore, there is a steady decrease in velocity across the perpendicular array for critical blocking parameters of $O(1)$.

For an array placed parallel to the quasi-geostrophic flow (Figures 5 and 6) the velocity gradient is very sharp over the array. It is remarkable that for such a parallel array, the location of greatest flow deceleration moves significantly farther from the structure when the blocking parameter increases. The sharp velocity gradient appears unrealistic and indicates occurrence of flow separation and high turbulence.
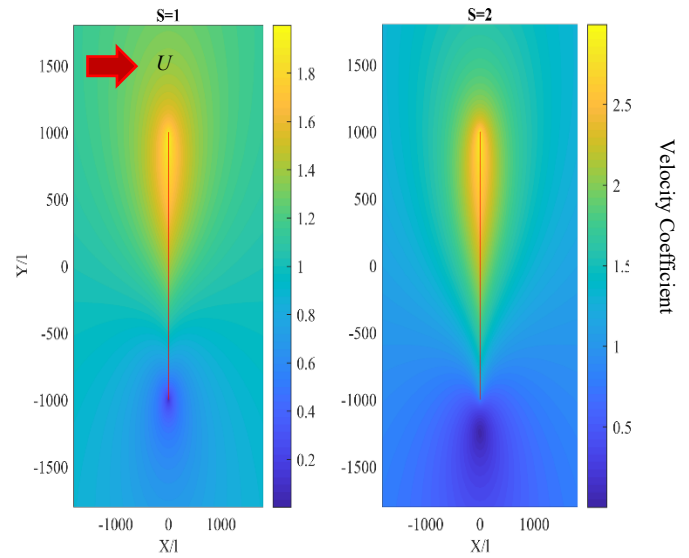
Figure 3: Modeled flow velocity change factors are plotted in color for flow at the depth of the array during quasigeostrophic flow with a blocking parameter, S, equal to 1 and 2. Flow direction is from the left to the right. The coordinate system is normalized using l, the minor axis of the elliptical body, which is 10m for the proposed array. The major axis L is 10,000m. A velocity coefficient of 1 corresponds to the far field velocity U.

Figure 1: Graph of the idealized far field tidal velocity U and the different velocities at both ends of a linear array aligned perpendicular to the tidal velocity. Solutions for perpendicular flow and $\gamma = 1,000$

Figure 4: Modeled flow velocity coefficients are plotted in color for flow at the depth of the array during quasigeostrophic flow with a blocking parameter equal to 2. A reduced velocity will increase the blocking parameter. The decelerated flow has moved away from the obstruction, as compared with S=1. More of the flow adjacent to the obstruction has a velocity coefficient >1 when compared with S=1. Flow direction is from the left to the right. The coordinate system is normalized using l, the minor axis of the elliptical body.

Figure 2: The power produced from an ocean current is proportional to the velocity cubed. A change in the flow around the structure during a tidal change may be experienced by sensitive power generation systems.
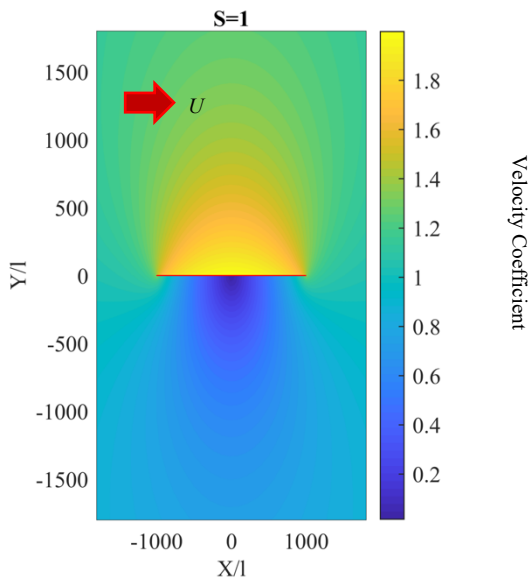
Figure 5: The asymmetry of the flow is striking for an array oriented perpendicular to the current. The area adjacent to the array has the greatest change in flow velocity. The array is modeled as static. Flow past the array has a blocking parameter, $S = 1$. The far field velocity has a velocity coefficient of one. The coordinate system is normalized using l, the minor axis of the elliptical body.
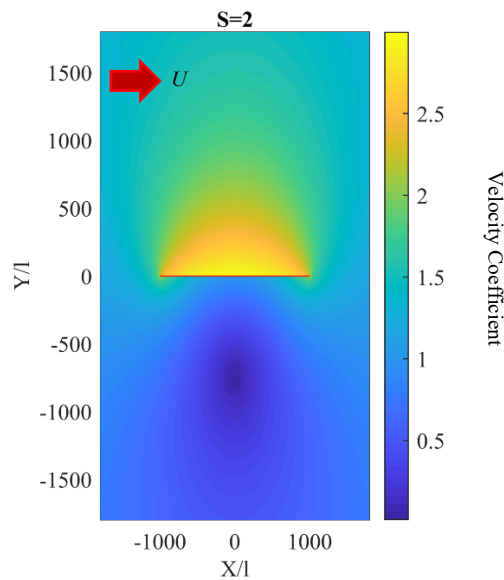
Figure 6: Flow past the array during quasigeostrophic flow with a blocking parameter, S = 2. The darkest blue point is the minimum velocity in the vicinity of the structure and this point has moved a significant distance, approximately half the characteristic length, *L*, away from the structure.

4.1. Design Plan

For a line of tidal current turbines at mid to high latitudes rotational flow effects caused by the Coriolis force can impact local dynamics at periods with small inertial currents. The strongest changes in flow dynamics can occur directly adjacent to a structure obstructing a quasigeostrophic flow. Flow acceleration and deceleration can occur around the structure asymmetrically. It appears prudent to make the following design considerations:

1) ensure that the linear array is placed perpendicular to the flow;

2) review local tidal current data and decide if both ebb and flood currents, or just one direction, will be used for power production;

3) prepare your system for an asymmetric velocity gradient, down the line of the array, at periods of tidal change.

One design recommendation for a site where both ebb and tide are utilized for energy production would be to separate the array into a minor and a major field with the two fields separated by supporting equipment. The major field placed on the left side of the array (looking downstream), for the strongest tidal direction. Dummy turbines could be included in the central field of supporting equipment to elongate the array if the asymmetric flow pattern is especially desirable for a production location.

An array parallel to the incident flow is not recommended because of the sharp velocity gradient modeled over it for quasi-geostrophic flow. The modeled gradient is not realistic and suggests occurrence of flow separation and high turbulence.

5. Final Comments

Site specific investigations are crucial for effective array design and deployment. All sites will have unique bathymetry and unique local currents. The variables affecting the layout of the array will include the angle of incident flow; the aspect ratio of the array; the water depth and height of the array; and the latitude at which the array is placed. Placement at higher latitudes will produce higher blocking parameters. The Taylor column phenomenon can be produced by an engineered structure, bottom seated or suspended in the ocean, or by a larger bathymetrical feature on which an engineered structure is placed.

Conflict of Interest

The authors declare no conflict of interest.

Acknowledgment

References

[1] V. Miglietta, M. Dhanak, "Current turbine array placement in quasigeosterophic flows over bottom topography," in Oceans Conference, Seattle, WA, USA, 2019.

[2] E. Johnson, "Quasigeostrophic flow over isolated elongated topography," Deep-Sea Research, **29**(9A), 1085-1097, Pergamon Press Ltd., Great Britain, 1982.

[3] C. Garrett, P Cummins, "The efficiency of a turbine in a tidal channel," Journal of Fluid Mechanics, **588**, 243–251, 2007, doi:10.1017/S0022112007007781.

[4] R. Vennell, "Tuning turbines in a tidal channel," Journal of Fluid Mechanics, **663**, 253-267, 2010, doi:10.1017/S0022112010003502

[5] R. Vennell, "Realizing the potential of tidal currents and the efficiency of turbine farms in a channel," Renewable Energy, **47**, 95-102, Elsevier, 2012, doi: https://doi.org/10.1016/j.renene.2012.03.036

[6] C. Christian, R. Vennel, "Efficiency of tidal turbine farms," Coastal Engineering Proceedings, **1**(33), structures.4, 2012, doi:https://doi.org/10.9753/icce.v33.structures.4

[7] S. Draper, T. Nishino, "Centered and staggered arrangements of tidal turbines," Journal of Fluid Mechanics, 739, 72-93, Cambridge University Press, 2014, doi:10.1017/jfm.2013.593

[8] G. Carter and M. Gregg and M. Merrifield. "Flow and mixing around a small seamount on Kaena Ridge, Hawaii," Journal of Physical Oceanography, **36**, 1036-1052, 2006.

[9] R.E. Brainard, "Fisheries aspects of seamounts and Taylor columns," Master's Thesis, Naval Postgraduate School. Monterey, California, 1986.

[10] W. Owens and N. Hogg. "Oceanic observations of stratified Taylor columns near a bump," Deep-Sea Research, **27A**, 1029-1045, Pergamon Press Ltd., Great Britain, 1979.

[11] A. Rogers, The biology of seamounts:25 years on., **79**, Advances in marine biology, 2018. Doi 10.1016/bs.amb.2018.06.001

[12] G.I. Taylor, "Motion of solids in fluids when the flow is not irrotational," Proc. Royal Society of London, Series A, Containing papers of a mathematical and physical character, **93**, 99-113, 1917.

[13] M. Buckley, "Taylor Columns," Course website for weather and climate laboratory at the Massachusetts Institute of Technology, 2004, Accessed June 2015. http://paoc.mit.edu/12307/reports/tcolumns.pdf

[14] J.W.M. Bush, H.A. Stone, J.P. Tanzosh, "Particle motion in rotating viscous fluids: Historical survey and recent developments," Current Topics in The Physics of Fluids, **1**, 337-355, 1994.

[15] J. Clarke et al. "Development and in sea performance testing of a single point mooring supported contra-rotating tidal turbine," in ASME 28th International Conference on Ocean Offshore and Arctic Engineering, 2009, doi:10.1115/OMAE2009-79995.

[16] R. Hide, "Origin of Jupiter's Great Red Spot." Nature, **190**, 895-896, 1961.

[17] P.J. Mason, R.I. Sykes, "A numerical study of rapidly rotating flow over surface-mounted obstacles," Journal of Fluid Mechanics, **111**, 175-195. Great Britain, 1981.

An Innovative Angle of Attack Virtual Sensor for Physical-Analytical Redundant Measurement System Applicable to Commercial Aircraft

Antonio Vitale[*], Federico Corraro, Nicola Genito, Luca Garbarino, Leopoldo Verde

CIRA – Italian Aerospace Research Centre, On-Board Systems and ATM, Capua (CE), 81043, Italy

A R T I C L E   I N F O

A B S T R A C T

The angle of attack is a critical flight parameter for commercial aviation aircraft, because automatic envelope protection systems rely on it to keep the aircraft within its safe flight envelope. Faulty measurements of the angle of attack could have catastrophic effects, leading to aircraft loss of control in flight and fatalities, as demonstrated by the recent accidents involving the Boeing 737-MAX. This paper presents a novel approach to the measurement of the angle of attack, which uses one virtual sensor and two physical sensors to implement a physical-analytical redundant system that is robust to a single fault of the physical sensors. The virtual sensor is based on an innovative and reliable estimator of the angle of attack. It was originally developed to provide General Aviation pilot with an accurate indication of trend toward stall, and has been suitably customized to fit its application to commercial aviation. One of the peculiarities of the redundant measurement system is that its implementation on-board several existing commercial aviation aircraft only needs the integration of a software code and does not require any installation of additional physical sensors. The proposed approach demonstrated very interesting performance, assessed in simulation through several Monte Carlo analyses. Its exploitation could contribute to reduce the angle of attack related accidents, improving the safety of the air transport system.

1. Introduction

This paper is an extension of work originally presented in SYSTOL'19 [1]. The original work defined an innovative method for the estimation of the angle of attack (AoA), which does not require any physical sensor dedicated to the measurement of the AoA. The present paper proposes a novel measurement system. It exploits the innovative estimator described in [1] and two physical sensors of the AoA, usually available on commercial aircraft, to compute a more reliable measurement of the angle of attack, which is robust to a single fault of the physical sensors. The paper defines the architecture and the algorithms of the proposed measurement system and discusses in depth its performance, which has been assessed through Monte Carlo simulations.

Loss of Control – In Flight (LOC-I) defines a condition in which the flight crew is unable to maintain the control of an aircraft while it is flying, resulting in an unrecoverable deviation from the intended flight path. LOC-I is the most significant cause of fatal accidents in General Aviation (GA): there are approximatively 37 fatal LOC-I accidents per year in Europe involving GA aircraft, leading to 67 persons on average losing their lives every year (for fixed-wing aircraft only) [2]. The LOC-I accidents can result from several contributing factors, which can act individually or in combination. They often result from failure to prevent or recover from a stall. An aircraft stalls if it exceeds the critical angle of attack and it may occur at any indicated airspeed. Hence, the only use of an airspeed indicator is unreliable to detect the proximity to stall. The measurement of the angle of attack could complement the airspeed information, prevent to enter an upset condition and allow performing safer manoeuvers. General Aviation aircraft often are not equipped with AoA sensors. The availability of suitable methods or affordable and reliable instruments to estimate or measure the angle of attack and to display its current value to the pilot would be dramatically beneficial for this aircraft category. Indeed, it could facilitate earlier detection of danger conditions and could permit adjusting power and configuration to avoid displacing the aircraft from the intended path. Additionally, the knowledge of the angle of attack could reduce the pilot workload [3], [4].

[*]Corresponding Author: Antonio Vitale, Italian Aerospace Research Centre, via Maiorise, 81043, Capua (CE), Italy, Email: a.vitale@cira.it

Based on these motivations, several methods for the estimation of the angle of attack are described in the literature. Many methods use the Kalman Filter [5]-[9], which exploits nonlinear kinematics equations for the propagation of the AoA estimation, and measurement models, coupled with suitable measurements, to correct the estimation. Usually, this approach is model-based and requires the knowledge of the aircraft aerodynamic model [5]-[7]. The estimator proposed in [8] does not need the aerodynamics of the aircraft neither other aircraft parameters; but the method works properly only if the aircraft dynamics are excited by continuously changing pitch and yaw angles. Model-based estimation methods that do not use the Kalman Filter are proposed in [10] and [11]; both these approaches require as input a detailed model of the aircraft aerodynamics. In [10] the data fusion of GPS (Global Positioning System) and IMU (Inertial Measurements Unit) sensors together with the aerodynamic information allow computing the angle of attack, whereas in [11] a Bayesian estimator provides it. In [12] the angle of attack calculation only relies on inertial data, but obtained estimation accuracy is not good in windy and turbulent conditions. The authors of [13] estimate the AoA by using a complementary filter. The steady state low frequency component of the estimation is obtained by solving algebraically the angle of attack kinematic equation, in which the AoA derivative is set equal to the pitch rate. The angle of attack high frequency content is considered coincident with the pitch rate. However, this simple method provides estimations which are characterized by high mean error and standard deviation. A Virtual Sensor is presented in [14]. It uses a Functional Pooling Non-linear Auto-Regressive with eXogenous excitation (FP-NARX) methodology that provides very good performance. However, this method requires the availability of a wide set of flight data, which shall cover the whole flight envelope of the aircraft in order to identify the NARX model that reconstructs the AoA behavior. Model-free virtual sensors for the angle of attack measurement are available in the literature, too. They mainly use neural networks [15], [16], which has the drawback to need huge amount of data for the training of the network.

This paper is an extension of the work presented in [1], which describes an innovative approach to estimate the angle of attack, developed and patented [17] by the Italian Aerospace Research Centre (CIRA) and ASPEN Avionics. The new AoA estimator aimed at dramatically improving the safety of GA aircraft, by providing an immediate, accurate, and clear visual display of trend toward stall and stall margin. It does not need the installation of external dedicated sensors, which is the key factor in limiting the adoption of angle of attack instruments by General Aviation pilots. The AoA computation exploits an Extended Kalman Filter and the measurements provided by navigation sensors that are more reliable than physical angle of attack sensors. The main innovative feature of the proposed method with respect to what already proposed in the literature is that it does not need detailed information about the aerodynamics of the aircraft neither huge amount of flight data for calibration/training. It only requires the knowledge of few aircraft parameters, easily gathered from the Pilot Operating Handbook (POH), and the execution of a short calibration flight, to carry out just once. This calibration flight is aimed at identifying the relevant aircraft aerodynamic parameters needed to tune the algorithm for the estimation of the angle of attack. The proposed estimator is operative on-board several

hundreds of private General Aviation aircraft since July 2015 without experiencing any problem.

The availability of reliable information about the angle of attack is very valuable to commercial aircraft, too. Higher levels of automation support the piloting tasks of commercial aircraft: the envelope protection systems exploit the angle of attack measurement to implement automatic corrective actions if the aircraft is approaching its flight envelope boundaries. These systems should improve the flight safety. However, in case of wrong angle of attack measurement, they could lead to LOC-I and fatalities, especially if the aircraft is performing critical flight phases such as take-off or landing. In fact, LOC-I is the leading cause of fatal accidents in commercial aviation and it is one of the accident categories with the lowest survivability ratio [18].

These statistics are confirmed by the recent flight accidents in March 2019 [19] and in October 2018 [20], which involved the Boeing 737-8 (MAX) operated by the Ethiopian Airlines and by the Lion Air, respectively. The investigation reports state that both the aircraft had a failure of one angle of attack sensor that dramatically affected the behavior of the envelope protection system. The Boeing 737 MAX has two independent physical sensors to measure the angle of attack, one sensor on each side of the forward fuselage. These sensors consist of an external vane, which rotates to align with the local airflow, connected to an internal resolver that measures the rotation angle. The aircraft is also equipped with a stability augmentation function, called the Maneuvering Characteristics Augmentation System (MCAS), which aims to improve the aircraft handling characteristics. Specifically, the MCAS was introduced to counteract the aircraft tendency to pitch-up when it flies at elevated angles of attack. This unwanted behavior is an effect of the new engines that were installed in the 737 MAX with respect to the previous 737 models. During the Ethiopian Airlines accident flight, soon after the lift-off, the left and right vanes provided different measurements of the AoA: the left measurement reached 74.5 degrees, while the right sensor showed a maximum value of 15.3 degrees. The difference between left and right AoA measurements (about 59 degrees) remained constant until the end of the recording [21]. The erroneous measurement of the angle of attack was not detected and it affected the pitch command. Indeed, the MCAS considered valid the left sensor's measurement and pushed down the nose of the aircraft several times. The crew tried to keep the aircraft along its planned flight path, but lost the control and the aircraft crashed. Figure 1, that is an excerpt of [21], shows the angle of attack measurements before the crash, pointing out the failure of the left sensor. The Flight Data Recorder of the Lion Air accident also registered differences between the measurements of the angle of attack (about 20 degrees) provided by the left and right sensors, as shown in Figure 2, taken from [22]. The erroneous angle of attack measurement produced multiple alerts and repetitive MCAS activations, which combined with pilot distractions due to numerous ATC communications contributed to the flight crew difficulties to control the aircraft and leaded to the crash after a steep dive.

Faulty angle of attack measurement was the cause of other incidents in the past, such as the crash of the Airbus A320-232 operated by XL Airways Germany on 27th November 2008 [23] and the incident of the Airbus A321-231 operated by Lufthansa

(flight 1829) on 5th November 2014. In this last case, the fault of the angle of attack sensor caused the anti-stall system to push down the nose of the aircraft, but since the aircraft was flying at high altitude, the crew was able to react, avoiding catastrophic results [24]. All these incidents remark that the availability of a fault tolerant system for the measurement of the angle of attack is very valuable. Triplex redundancy of physical sensors could be a solution to be robust with respect to a single sensor fault; however, triplex hardware redundancy is not always implemented for angle of attack sensor (the Boeing 737 MAX is an example).
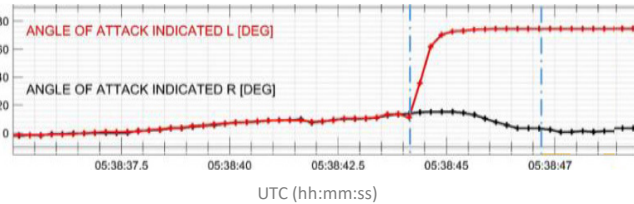
Figure 1: AoA measurements for the Ethiopian Airlines accident [21]
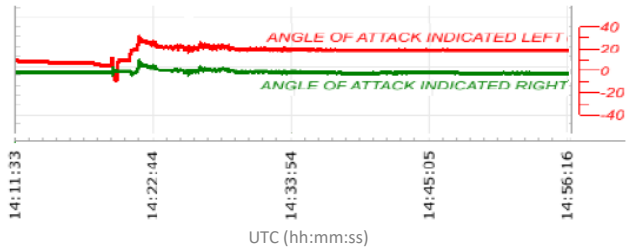
Figure 2: AoA measurements for the Lion Air accident [22]

The authors of the present paper deem that a suitable customization of the AoA estimator developed for GA aircraft and presented in [1] and [17] could help addressing the issues discussed for Commercial Aviation aircraft. Indeed, it could be exploited as an additional virtual sensor that, coupled with existing physical sensors and suitable voting algorithms [25]-[27], allows to implement a physical-analytical redundant measurement system that is robust to a single fault of the physical sensors. This measurement system could significantly improve the safety of the aircraft, reducing the occurrence of LOC-I related accidents, saving human lives, and avoiding the economic impact on the airliners and the aircraft manufacturers consequent to those accidents. The main benefit of this research to the industry consists in the possibility to achieve this result without the need for hardware modification to the existing aircraft, installation of additional physical sensors or change to the avionics hardware architecture. In fact, the proposed approach just requires the installation of the software code for the computation of the robust angle of attack measurement, which exploits as input the measurements provided only by the sensors already available on-board.

The next sections of the paper detail the proposed approach. The innovative AoA estimator is first described in section 2. Next, a possible application to commercial aviation aircraft is proposed, defining the architecture and the algorithms to implement a robust fault tolerant measurement system. Finally, section 4 shows the performance of the proposed method, assessed in simulation through Monte Carlo analysis. A section of conclusion ends the paper.

2. Angle of Attack Virtual Sensor

The design of the proposed angle of attack estimator was originally based on the following requirements:

- to be applicable to a wide set of aircraft;

- to exploit the information commonly available for GA aircraft;

- the installation of specific additional sensors shall not be required.

These requirements imply that the estimation method shall not require the knowledge of the detailed aerodynamic model, that is specific of each type of aircraft.

The proposed approach works in two steps. First, the parameters of the estimation algorithm are tuned through a calibration procedure, which consists in performing a flight test that shall be executed just once. Next, normal operations are carried out, that is, the estimator could compute the angle of attack during the flight.

The proposed method uses the measurements provided by sensors which are usually exploited for primary navigation and does not need a dedicated angle of attack sensor. It guarantees that the measurement's accuracy is independent upon the installation of the AoA sensor. It is worthy to note that the same set of sensors is used both for the calibration and in the normal operations. Figure 3 shows the basic concept of the virtual sensor. The following subsections details the calibration procedure and the angle of attack computation.
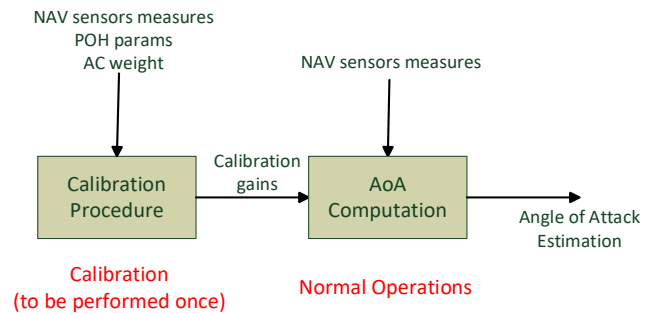
Figure 3: AoA virtual sensor basic concept

2.1. Calibration Procedure

The calibration procedure aims at identifying the lift curve of the aircraft and consists in flying steady and wing leveled at two different airspeed values (set points), which are close to the boundaries of the aircraft flight envelope. The test is repeated for each aircraft configuration that has significantly different aerodynamic characteristics. The calibration requires the knowledge of:

- few parameters available in the POH: MTOW (Maximum Take-off Weight), SEW (Standard Empty Weight), Stall Speed and Maximum Speed in clean and flapped configurations

- aircraft weight (it is worthy to remark that the weight shall be known only during the calibration flight and not during normal operations of the virtual sensor).

The lift (L) is assumed linear with respect to the angle of attack (α) and to the deflection of the longitudinal aerodynamic surfaces (δ_i):

$$L = QSC_L = QS\left(C_{L0} + C_{L\alpha}\alpha + \sum_i C_{L\delta}^i \delta_i\right) \quad (1)$$

where Q is the dynamic pressure, C_L is the lift coefficient, S is the aerodynamic reference surface, C_{L0}, $C_{L\alpha}$ and $C_{L\delta}^i$ are the lift aerodynamic derivatives. The contribution to the lift of all the longitudinal surfaces deflection is assumed negligible, except for the flaps (δ_F). Two flap configurations are considered for GA aircraft, clean and full flap. Each configuration has a different lift curve, which is still assumed linear and is uniquely identified by its slope ($C_{L\alpha}$) and intercept (C_{L0}). The calibration procedure is performed for both the configurations, the corresponding aerodynamic derivatives C_{L0}, $C_{L\alpha}$ are computed, and a linear variation for these derivatives is assumed to compute their values for intermediate configurations of the flaps. This approach implies that the values of C_{L0} and $C_{L\alpha}$ depend on the deflection of the flaps, whereas the explicit dependence in equation (1) of L on δ_F could be delated; therefore, the equation (1) could be reformulated as:

$$L = QS(C_{L0}(\delta_F) + C_{L\alpha}(\delta_F)\alpha) = QW\left(\hat{k}_0(\delta_F) + \hat{k}_1(\delta_F)\alpha\right) \quad (2)$$

where W is the aircraft weight and the parameters $\hat{k}_0, \hat{k}_1$, named calibration gains, are defined as follows (the dependence of C_{L0}, $C_{L\alpha}$, $\hat{k}_0$ and $\hat{k}_1$ on δ_F is not shown for the sake of conciseness):

$$\hat{k}_1 = \frac{S}{W} \cdot C_{L\alpha} \quad (3)$$

$$\hat{k}_0 = \frac{S}{W} \cdot C_{L0} \quad (4)$$

During the calibration flight, the aircraft weight is denoted as W_{cal} and the calibration gains (a set for each configuration) are computed as defined in [17]:

$$\hat{k}_{1cal} = \frac{S}{W_{cal}} \cdot C_{L\alpha} = \left(\frac{1}{Q_2} - \frac{1}{Q_1}\right) / (\vartheta_2 - \vartheta_1) \quad (5)$$

$$\hat{k}_{0cal} = \frac{S}{W_{cal}} \cdot C_{L0} = \left(\frac{1}{Q_1} - \frac{1/Q_2 - 1/Q_1}{\vartheta_2 - \vartheta_1} \cdot \vartheta_1\right) \quad (6)$$

where ϑ is the pitch angle. All the variables on the right-hand sides of the above equations represent measurements gathered during the calibration flight and the subscripts 1 and 2 refer to the set point index (two set points for each aircraft configuration). Therefore, the calibration gains could be easily evaluated.

Replacing (5) and (6) in (2) and rearranging, we get the lift equation applicable during normal operations [17]:

$$L = QW_{conv}(k_0 + k_1\alpha) \quad (7)$$

$$\hat{k}_{0cal} = \frac{S}{W_{cal}} \cdot C_{L0} = \left(\frac{1}{Q_1} - \frac{1/Q_2 - 1/Q_1}{\vartheta_2 - \vartheta_1} \cdot \vartheta_1\right) \quad (8)$$

where W_{conv} is the actual aircraft weight if it is known, otherwise it is a conventional weight given by [17]:

$$W_{conv} = max\{W_{cal}, [C_0 + W_{SEW} + C_1(W_{MTOW} - W_{SEW})]\} \quad (9)$$

The values of the constants C_0 and C_1 are computed with the aim to optimize the angle of attack estimation error.

2.2. Angle of Attack Computation

After the completion of the calibration procedure, the virtual sensor can estimate the angle of attack. The estimation algorithm exploits an Extended Kalman Filter (EKF), which combines the knowledge of the lift curve, identified during the calibration, with the measurements get from ADS (air-data system), GPS and IMU. The EKF state vector includes five variables, that is, the angles of attack (α) and sideslip (β) and the wind velocity components (W_N, W_E, W_D), expressed in North-East-Down (NED) reference frame. Classical kinematic equations in polar form [28] describe the dynamics of the aerodynamic angles, whereas stochastic zero-order Gauss-Markov processes [29] are used to represent the wind velocity behavior. These equations are applicable to any type of aircraft [17]:

$$\begin{aligned}
\dot{\alpha} = &\frac{1}{TAS\cos\beta}(a_z\cos\alpha - a_x\sin\alpha) + q \\
&- \tan\beta\,(p\cos\alpha + r\sin\alpha) \\
&+ \frac{1}{TAS\cos\beta}[u_w q\cos\alpha \\
&- v_w(r\sin\alpha + p\cos\alpha) \\
&+ w_w q\sin\alpha] + \eta_\alpha
\end{aligned}$$

$$\begin{aligned}
\dot{\beta} = &\frac{1}{TAS}(-a_x\cos\alpha\sin\beta + a_y\cos\beta \\
&- a_z\sin\alpha\sin\beta) + p\sin\alpha \\
&- r\cos\alpha \\
&+ \frac{1}{TAS}[-u_w(r\cos\beta \\
&+ q\sin\alpha\sin\beta) \\
&+ v_w(p\sin\alpha\sin\beta \\
&- r\cos\alpha\sin\beta) \\
&+ w_w(p\cos\beta \\
&+ q\sin\beta\cos\alpha)] + \eta_\beta
\end{aligned}$$

$$\dot{W}_i = \eta_{W_i} \qquad with\ i = N, E, D \quad (12)$$

where:

- a_x, a_y and a_z are the inertial acceleration components in the body reference frame (provided by the IMU);
- p, q and r are the angular rates components (roll, pitch and yaw rate) in the body reference frame (provided by the IMU);
- TAS is the module of the true air speed (provided by the ADS);
- $\eta_\alpha, \eta_\beta, \eta_{W_N}, \eta_{W_E}$ and η_{W_D} are process noises, which are assumed zero mean multivariate Gaussian with covariance matrix Q_{noise};
- u_w, v_w and w_w are the wind velocity components expressed in the body reference frame and computed as:

$$\begin{bmatrix} u_w \\ v_w \\ w_w \end{bmatrix} = \bar{\bar{R}}_{BI}^{-1} \times \begin{bmatrix} W_N \\ W_E \\ W_D \end{bmatrix} \quad (13)$$

- $\bar{\bar{R}}_{BI}$ is the Transformation matrix from body axes to NED axes.

The measurement vector is given by the inertial velocity components (V_N, V_E, V_D) in the NED reference frame (provided by the GPS) and the normal load factor (N_z) in body axes (provided by the IMU). The following equations are used [17]:

$$\begin{bmatrix} V_N \\ V_E \\ V_D \end{bmatrix} = \bar{\bar{R}}_{BI} \times \begin{bmatrix} TAS \cdot \cos\alpha \sin\beta \\ TAS \cdot \sin\beta \\ TAS \cdot \cos\beta \sin\alpha \end{bmatrix} + \begin{bmatrix} W_N \\ W_E \\ W_D \end{bmatrix} + \begin{bmatrix} v_{V_N} \\ v_{V_E} \\ v_{V_D} \end{bmatrix} \quad (14)$$

$$N_z = Q \cdot (k_1 \cdot \alpha + k_0) + tg(\alpha) \cdot N_x \quad (15)$$

where:

- N_x is the axial load factor;
- v_{V_N}, v_{V_E} and v_{V_D} are measurement noises, which are assumed zero mean multivariate Gaussian with covariance matrix R_{noise};
- k_1 and k_0 are the calibration gains.

The last measurement equation holds in the hypotheses of thrust aligned to the X-body axis (that is, with negligible contribution to the normal load factor) and small angle of attack approximation. If a measurement of the current thrust is available, then the contribution along the normal load factor could be added in the equation to remove the approximation. Finally, it is also worthy to note that if the calibration gains k_1 and k_0 are computed using the conventional weight instead of the actual one, then an approximation is introduced that affects the computation of the right-hand side of the equation (15) and consequently of the angle of attack. The availability of the measurement of the actual weight allows removing this approximation and improving the estimation results.
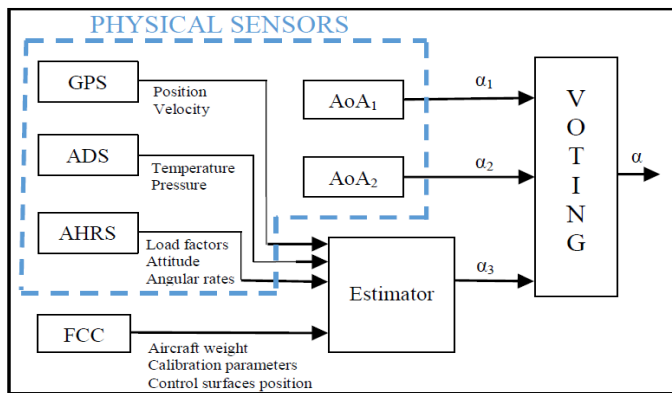
Figure 4: Physical-analytical redundant angle of attack architecture

3. Fault Tolerant Angle of Attack Measurement System for Commercial Aircraft

The proposed angle of attack estimator is applicable to commercial aviation aircraft after a suitable customization. Commercial aircraft are already equipped with one or more (but sometimes less than three [25]) physical angle of attack sensors. Indeed, the angle of attack measurement is nowadays a critical flight parameter as well as other primary navigation measurements. The introduction of a virtual sensor provides an

additional and independent measurement, which in conjunction with the physical sensors, allows implementing a single fault tolerant measurement system based on physical-analytical redundancy. Figure 4 shows a possible architecture of the proposed angle of attack measurement system, which exploits two physical sensors of the AoA.

The following subsections detail the customization of the estimator with respect to the one developed for GA aircraft and the voting algorithms applied to compute the consolidated AoA measurement out of the three AoA inputs.

3.1. Virtual Sensor Customization to Commercial Aviation

Some of the assumptions introduced in the design of the estimator for GA application can be removed if the estimator is applied to commercial aircraft.

First, in commercial flight an estimation of the aircraft weight is entered in the aircraft Flight Control Computer (FCC) before each flight, therefore it is a known parameter (although roughly) that can be provided as input to the AoA estimator. The use of a fuel consumption model allows computing the weight variation during the flight execution. Consequently, in the equations (7) and (8) the conventional weight can be replaced by the actual one and equation (9) is not used. Moreover, it is worthy to note that the availability of two physical sensors of the angle of attack allows improving the knowledge of the aircraft weight online while the aircraft is flying. Indeed, when the physical measurements coincide (that means supposedly the physical sensors are working properly), the value of the aircraft weight in the AoA estimation algorithm could be tuned (within a reasonable range) to force the virtual sensor measurement to converge to the physical ones. A suitable strategy can be defined to perform periodically this check and possibly to update the aircraft weight.

Second, commercial aircraft have several control aerodynamic surfaces and their configuration affects the lift curve of the aircraft. The deflection of each of these control surfaces is available to the FCC and it shall be used as an additional input to the AoA estimation algorithm. This consideration implies a modification to the aerodynamic modelling. The lift equation is more complex than the one defined by equation (7). It shall consider the effect of all the relevant aerodynamic surfaces, which in first approximation are assumed having a linear effect (however, quadratic, cubic or in general polynomial effects could be also used). Accordingly, the lift is given by:

$$L = QSC_L = QS\left(C_{L0} + C_{L\alpha}\alpha + \sum_i C_{L\delta}^i \delta_i\right)$$
$$= QW\left(k_0 + k_1\alpha + \sum_i k_\delta^i \delta_i\right)$$

where δ_i is the deflection of the i-th aerodynamic surface and k_δ^i is an additional calibration gain for each surface (more than one gain could be introduced for each surface if nonlinear effects are considered). Concerning the calibration process, the main differences with respect to the General Aviation aircraft are:

- an increased number of set points during the calibration flight shall be gathered, due to the increased number of calibration gains that shall be computed;

- the measurement of the deflection of each aerodynamic control surface is available and could be used as input to the calibration computation;

- the angle of attack measurement is available during the calibration (provided by the physical sensors), therefore it shall not be replaced by the pitch angle measurement.

The calibration test is performed first gathering two set points at different speeds (close to the aircraft's envelope limits) in clean configuration. The measurements in these set points allow the computation of the gains k_0 and k_1 by using equations (5) and (6), in which the angle of attack measurements replace the pitch angle ones. Next, two additional set points are gathered for each aerodynamic surface. These set points are collected again at two different speeds; only the aerodynamic surface related to the gain to be computed is deflected, whereas the deflections of all the other surfaces are null. Each gain is computed through:

$$k_\delta^i = \frac{S}{W_{cal}} C_{L\delta_i} = \left(\frac{Q_{i1} - Q_{i2}}{Q_{i2}\delta_{i2} - Q_{i1}\delta_{i1}}\right) k_0 + \left(\frac{Q_{i1}\alpha_{i1} - Q_{i2}\alpha_{i2}}{Q_{i2}\delta_{i2} - Q_{i1}\delta_{i1}}\right) k_1 \tag{17}$$

where the subscripts i_1 and i_2 identify the two set points related to the i-th surface; α, δ and Q are measured and k_0 and k_1 are already computed at this stage.

The availability of measurements of the actual weight of the aircraft and of the aerodynamic control surfaces deflection allows removing the approximations introduced in the estimator algorithm designed for GA application, leading to a significant improvement of the estimation accuracy.
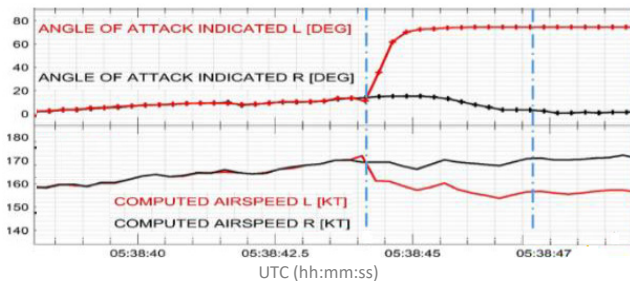
Figure 5: Effect of faulty AoA measurement on the airspeed computation [21]

Finally, it is worthy to remark that, during normal operations, the angle of attack computed by the estimator shall be completely independent from the AoA measurements provided by the physical sensors, in order to implement correctly the analytical redundancy. The estimator, as shown in Figure 4, exploits the measurements from GPS, AHRS and ADS sensors. GPS and AHRS are completely independent from the vane sensor. On the other hand, the AoA measured by the vane is usually exploited to correct the raw value of the static pressure measured by the ADS, in order to compensate for errors due to sensor position and aerodynamic effect. The corrected static pressure is then used by the air data computer to calculate the true airspeed, which therefore is influenced by the AoA measured by the vane. The effect of the AoA on the computation of the airspeed is pointed out by the data of the Ethiopian Airlines accident flight. Figure 5, excerpt of [21], shows the computed airspeed based on the static pressure corrected with left and right angle of attack measurements. The erroneous AoA values, provided by the left

sensor, produced corrected static pressure values greater than the true ones and consequently the computed airspeed values are lower than the true ones.

The row static pressure values (before applying the correction based on the AoA measurement) from both sides were identical, as shown in Figure 6 [21]. The different static pressure measurements highlighted in Figure 5 were therefore only due to the AoA correction. This effect should be considered in the selection of the inputs to the angle of attack estimation algorithm. Specifically, the uncorrected values of all the air data sensors shall be provided to the estimator. Possibly corrections of these inputs depending on the angle of attack shall be based on the AoA value computed by the estimator itself, at the previous computation time step. This approach guarantees the independence of the measurements provided by the analytical and physical sensors and used as input to the voting algorithm.
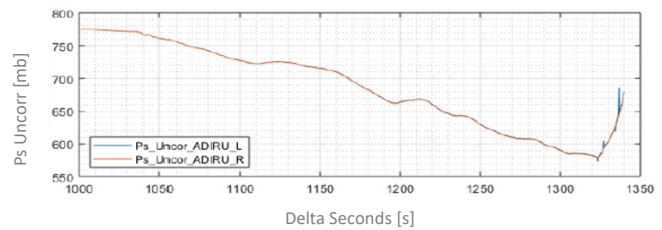
Figure 6: Static pressure reconstruction without AoA correction [21]

3.2. Voting and Signal Validity Check Algorithms

The voting algorithm consists in generating one single angle of attack measurement (consolidated value) out of three input signals of a triplex redundant architecture. Different voting techniques are available in the literature. The proposed approach applies a weighted voting, in which the consolidated signal is computed through a weighted mean of the valid inputs:

$$\alpha = \sum_{i=1}^{3} p_i \alpha_i \tag{18}$$

$$\sum_{i=1}^{3} p_i = 1 \qquad with \qquad 0 \le p_i \le 1 \tag{19}$$

where α is the consolidated value, α_i is the i-th measurement, and p_i is the i-th weight. Several choices could apply to the definition of the weights. They can be all equal, or a bigger weight could be assigned to the median input [25], or the weights could be all different, based on some metrics or criteria [26]. For each signal we define a weight that is inversely proportional to the supposed precision of the sensor providing the measurement. Assuming the input measurements are affected by a Gaussian error with standard deviation σ_i, the following weights are used:

$$p_i = F_i \frac{\frac{1}{\sigma_i}}{\sum_{i=1}^{3} \frac{1}{\sigma_i}} \tag{20}$$

where F_i is the validity flag of the i-th measurement, which is null if the input measurement is invalid, otherwise it values 1. To check the validity of each input, the algorithm computes at each time step the difference between the measurements of the angle of attack provided by the available sensors, and for each couple of sensors compares the difference (D_{ij}) with a suitable threshold (T_{ij}):

$$D_{12}(t_k) = |\alpha_1(t_k) - \alpha_2(t_k)| < T_{12} \qquad (21)$$

$$D_{13}(t_k) = |\alpha_1(t_k) - \alpha_3(t_k)| < T_{13} \qquad (22)$$

$$D_{23}(t_k) = |\alpha_2(t_k) - \alpha_3(t_k)| < T_{23} \qquad (23)$$

If both the differences related to the i-th measurement exceed the related thresholds (that is, the above relations involving the signal α_i are not satisfied) continuously for a predefined number of samples N_s, the i-th measurement is declared invalid and F_i is set equal to zero. Consequently, the computation of the consolidated value does not use the i-th measurement, because related weight is null. The thresholds are given by:

$$T_{ij} = C_{ij}(\sigma_i + \sigma_j) \qquad (24)$$

The values of both the constant C_{ij} and the number of samples N_s used to check conditions (21) to (23) are selected as a trade-off, in order to maximize the capability to detect invalid signals while minimizing the false alarm rate.

4. Angle of Attack Measurement System Performance

The performance of the proposed measurement system has been assessed in simulation through Monte Carlo analyses. The Monte Carlo technique is a procedure for numerically obtaining an estimation of the statistical characterization (mean, variance, cumulative probability, etc.) of a function's output. To this end, the input parameters of the function vary independently according to their statistical characterization, and the output of the function is computed for each realization of these inputs. The statistics of the output are then evaluated. Results presented in this section concern the angle of attack estimator (also including the calibration procedure) and the triplex redundant measurement system. A simulation tool was implemented as test harness to execute the analyses.

4.1. Simulation Tool

The simulation tool is implemented in Matlab/Simulink environment and is composed of:

- The main routine, which allows:
  o setting up the flight test manoeuver,
  o varying the inputs of the Monte Carlo analysis according to their statistical characterization
  o computing the performance metrics.
- A simulation model, presented in Figure 7, which includes:
  o AC Model – the detailed parametric models for the simulation of the aircraft, the atmosphere (winds and turbulence) and the on-board sensors.
  o AP – an autopilot that is able to perform automatically the requested test manoeuver.
  o Algorithms Feature – a module implementing the algorithms for the angle of attack estimation.
  o Save Results – a module that saves the simulated inputs and computed outputs.
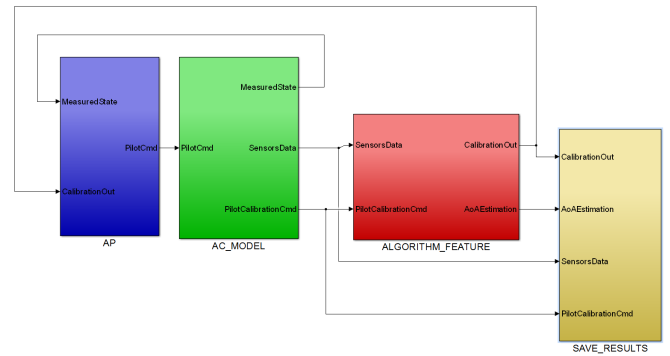
Figure 7: Simulation model for Monte Carlo analyses

- A routine that implements the triplex redundant AoA measurement system and computes the consolidated angle of attack.

The aircraft is modelled using the flight mechanics equations of a six degrees of freedom rigid body [30] and comprises a detailed aerodynamic model, also reproducing the stall phenomenon. The aircraft model has been validated in flight through the CIRA experimental aircraft [31]. The simulation of the relevant atmospheric phenomena is based on the ISA standard atmosphere [30] and the Dryden turbulence model [32]. The atmosphere model includes horizontal constant winds (variable with altitude), three-dimensional turbulence disturbances, and vertical gust (represented through "1-cosine" model) [32]. The three-dimensional turbulence is modelled by applying appropriate forming filters to band-limited white noise; the longitudinal, lateral, and vertical components (Φ_u, Φ_v, Φ_w) of the spectra of these forming filters are given by:

$$\Phi_u(\omega) = \frac{2\sigma_u^2 L_u}{\pi TAS} \frac{1}{1 + \left(\frac{L_u \omega}{TAS}\right)^2} \qquad (25)$$

$$\Phi_v(\omega) = \frac{2\sigma_v^2 L_v}{\pi TAS} \frac{1 + 12\left(\frac{L_v \omega}{TAS}\right)^2}{\left[1 + 4\left(\frac{L_v \omega}{TAS}\right)^2\right]^2} \qquad (26)$$

$$\Phi_w(\omega) = \frac{2\sigma_w^2 L_w}{\pi TAS} \frac{1 + 12\left(\frac{L_w \omega}{TAS}\right)^2}{\left[1 + 4\left(\frac{L_w \omega}{TAS}\right)^2\right]^2} \qquad (27)$$

where (L_u, L_v, L_w) and (σ_u, σ_v, σ_w) represent the turbulence scale lengths and intensities, respectively. The vertical gust velocity (V_{vg}) is computed through:

$$V_{vg}(x) = \begin{cases} 0 & x < 0 \\ \frac{V_m}{2}\left[1 - cos\left(\frac{\pi(x)}{d_m}\right)\right] & 0 \le x \le 2d_m \\ 0 & x > 2d_m \end{cases} \qquad (28)$$

where V_m is the maximum gust magnitude and d_m is the gust half-width.

The sensors model simulates actual sensors (ADS, AHRS, GPS) that measure the signals needed by the algorithms under test. The models of the ADS and AHRS compute the measurements of the generic signal (s_m) at time t_k by adding bias (b_s) and Gaussian noise (v_s) to the true signal value (s_t):

$$s_m(t_k) = s_t(t_k) + b_s + v_s(t_k) \qquad (29)$$

A low pass filter is then applied to the signal s_m, in order to emulate the sensors dynamics (frequency band limitation). The GPS model also introduces a data latency (δt) in the measurements, which is assumed negligible for the other sensors [33]:

$$s_{mGPS}(t_k) = s_t(t_k - \delta t) + b_s + v_s(t_k - \delta t) \qquad (30)$$

The data sheets of commercial off the shelf sensors are used to define bias, noise, latency and low pass filter characteristics. The sensors model allows injecting a failure in the measurement, such as additional bias, drift, or data freezing. In the Monte Carlo analyses, this feature was used only to simulate the failure of the angle of attack physical sensors.

4.2. Monte Carlo Analyses

Three different Monte Carlo analyses were performed to assess the performance of the following functionalities:

- calibration of the AoA estimation algorithm,
- AoA estimation,
- fault tolerant AoA measurement system.

The first two analyses were carried out considering three different classes of GA aircraft (light, medium and heavy airplanes). Indeed, the AoA estimation algorithm and its calibration procedure were originally designed for this category of aircraft. It is worthy to remark that this choice is conservative, because, as explained in the previous sections, improved results are obtained if the AoA estimator is applied to commercial aircraft. In the considered analyses the following parameters of the simulation model varied according to their statistical characterization, in order to obtain an accurate statistical assessment of the algorithms under investigation:

- aircraft weight, centre of gravity and inertia matrix;
- sensors' measurement error (bias and white noise);
- initial flight conditions;
- atmospheric conditions: horizontal wind (direction between 0 and 360 degrees, intensity up to 20Kts), turbulence (three levels of turbulence intensity), vertical gusts (cosine shape).

Uniform distribution is assumed for all these parameters, in order to get conservative results [34].

The last Monte Carlo analysis assumes the availability of a triplex AoA measurement (two physical sensors plus the AoA estimator) and assesses the performance of the proposed angle of attack measurement system, only considering the angle of attack trajectories and regardless of the aircraft being a GA or a commercial aircraft.

4.3. Performance Assessment Results

The first Monte Carlo analysis allowed getting a statistical characterization of the calibration gains and then of the aircraft lift model. The analysis comprised 1000 simulation runs for each of the considered aircraft classes. The actual aircraft weight, which is

required as input to the procedure, was corrupted with a measurement error

$$W_m = W_t(1 + v_W) \qquad (31)$$

where W_m and W_t are measured and true weights, respectively, and v_W is a random noise that varies from one simulation run to the other with uniform distribution in the range [-0.03, 0.03] (that is, the measurement error is in the range ±3% of the true weight). Concerning the model of the atmosphere, the turbulence level varied randomly between 0 and 1. Figure 8 and Figure 9 present the results for one of the considered aircraft categories, showing the estimation of the coefficients C_{L0} and $C_{L\alpha}$ normalized with respect to their true values, which are known in simulation.
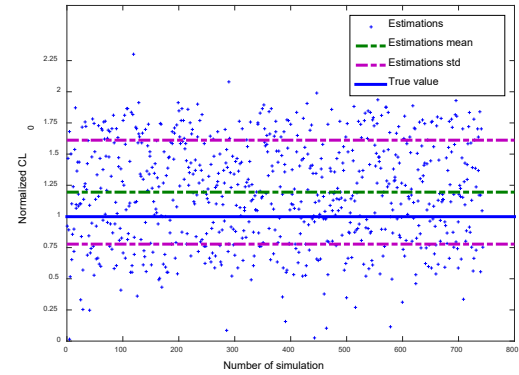
Figure 8: Normalized C_{L0} ceofficient computed in the calibration
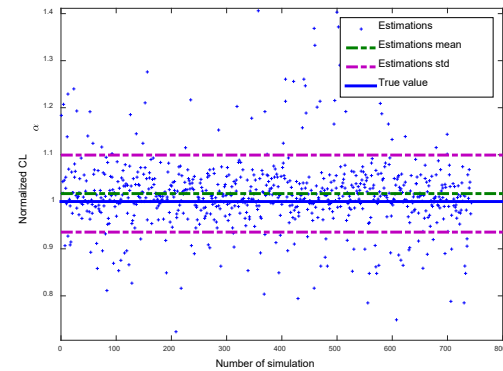
Figure 9: Normalized $C_{L\alpha}$ ceofficient computed in the calibration

Due to the turbulence and to the poor performance of the used autopilot, not all the 1000 calibrations were successful (the success rate was about 75%), that is, the aircraft was not able to keep the required stationary flight condition for a predefined period. The mean error on the C_{L0} estimation, computed on the successful tests, is about 20%, whereas the mean value of the estimated $C_{L\alpha}$ is very close to its true value. In order to assess the effect of these errors on the AoA estimation, a subset (250 samples) of the calculated couples (C_{L0}, $C_{L\alpha}$) was used to estimate the angle of attack in the same conditions flown to perform the calibration. The accuracy of the estimation, evaluated as the mean of the root mean square error (RMS), is 0.64 degree.

The second Monte Carlo focused on the AoA estimation. Several typical manoeuvers were considered, such as level flight, turn, climb, descend, stall, stall in sideslip, stall in turn. A dedicated Monte Carlo analysis was performed for each of these

manoeuvers. In each run, the calibration gains k_1 and k_0 were randomly drawn from the results obtained in the calibration Monte Carlo analysis for the same aircraft category. The number of simulations performed in each Monte Carlo Analysis was chosen in order to have a stable root mean square (RMS) error and to get the 95% confidence level on the probability to have the RMS below a given threshold. Indeed, given a condition P_X to check (such as, the RMS error is below the threshold), the confidence interval on the satisfaction of the condition can be computed as [35], [36]:

$$Low = \frac{k_{suc}}{N_{test}} + \frac{3}{4}\frac{1 - \frac{2k_{suc}}{N_{test}} - \sqrt{1 + 4\vartheta_P k_{suc}\left(1 - \frac{k_{suc}}{N_{test}}\right)}}{1 + \vartheta_P N_{test}} \quad (32)$$

$$Upp = \frac{k_{suc}}{N_{test}} + \frac{3}{4}\frac{1 - \frac{2k_{suc}}{N_{test}} + \sqrt{1 + 4\vartheta_P k_{suc}\left(1 - \frac{k_{suc}}{N_{test}}\right)}}{1 + \vartheta_P N_{test}} \quad (33)$$

$$\vartheta_P = \frac{9}{8log\left(\frac{2}{\varepsilon}\right)} \quad (34)$$

$$Pr\{Low < P_X < Upp\} > 1 - \varepsilon \quad (35)$$

where N_{test} is the number of tests performed in the Monte Carlo analysis, k_{suc} is the number of tests in which the condition P_X is satisfied, Pr denotes the probability, and ε is the fixed confidence parameter ($\varepsilon = 0.05$ in our case). Figure 10 and Figure 11 show the trend of RMS mean and standard deviation for one Monte Carlo, used to select the number of runs.

The metrics applied to assess the estimator performance are:

- the mean estimation error (MEE), which represents a measurement of the estimation accuracy in static conditions;
- the root mean square error (RMS), which indicates the overall accuracy of the estimation;
- the correlation between true and estimated angle of attack (CORR), which measures the capability of the estimator to track the dynamic behavior of the true value.

The assessment of the estimator's performance considers all the error's sources that are present during operative conditions, including unknown aircraft weight, sensors' error, and the effect of wind, turbulence and vertical gust. Of course, it produces a degradation of the accuracy with respect to ideal conditions. In level unaccelerated flight, under all possible aircraft configurations and turbulence levels, the MEE is lower than 1.5 degrees. The estimator is able to compute the angle of attack with RMS error varying from about 0.9 degrees for level flight under all possible environmental disturbances to less than 3 degrees for dynamic stall manoeuver, representing the worst-case condition. The average correlation factor between estimated and true angle of attack is bigger than 0.9, confirming the capability to track the dynamics. A sensitivity analysis highlighted that the main source of estimation error is the approximation introduced on the aircraft weight. Indeed, while actual aircraft weight in the simulator randomly varied with uniform distribution within the range [W_{SEW}, W_{MTOW}], the weight used by the estimator is constant in all the simulation runs and is equal to the conventional weight. The value of the conventional weight was selected to get conservative errors when approaching stall, that is, the angle of attack estimation is bigger than its actual value, also at cost of increasing maximum error.

This choice derives from the need to anticipate the stall condition. It also allows using optimized algorithms (not described in the present paper) to post process the error when the AoA increases, in order to get very reliable and accurate indication about stall approaching. The knowledge (also rough) of the actual aircraft weight (usually available for commercial aircraft) could significantly improve the estimation performance. Figure 12 presents the estimation of the angle of attack in level flight condition and in presence of a vertical gust, with length equal to 150 meters and maximum amplitude equal to 1600 feet per minute.
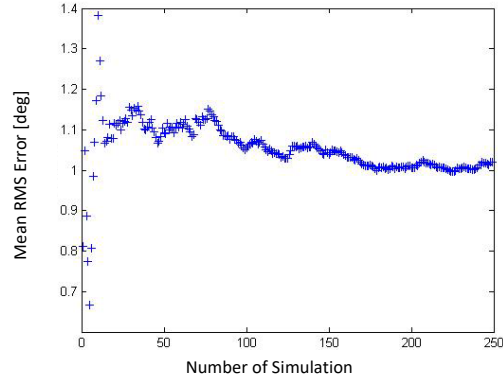
Figure 10: Mean of the RMS error versus number of simulation runs
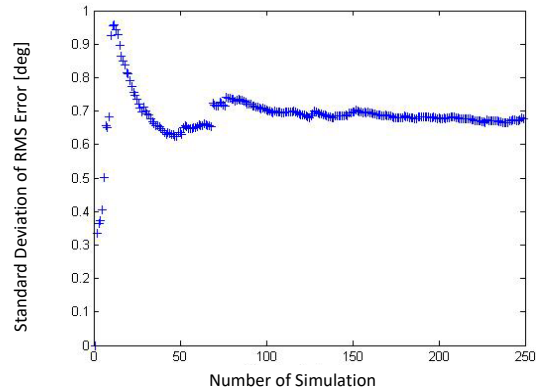
Figure 11: Standard deviation of the RMS error versus number of simulation runs

The final Monte Carlo aimed at assessing the capability of the redundant measurement system to detect a faulty sensor before its effects become significant and dangerous. To this end, one of the physical measurements of the angle of attack is corrupted by injecting one of the following faults, at a given time of the flight:

- constant bias, randomly selected in the range [5, 15] degrees;
- drift with slope randomly selected in the range [0.5, 5] degrees per second;
- signal freezing at a constant value.

The simulation lasts 90 seconds for each run (for the stall manoeuver it can end before 90 seconds if the aircraft stalls). The measurements are sampled at 10 Hz and the fault is injected 10 seconds after the start. The performance of the system is assessed by measuring the error of the consolidated angle of attack (output of the triplex redundant measurement system) with respect to the true angle of attack. Specifically, the mean and the standard deviation of the RMS error are evaluated. Moreover, the percentage of missed fault detections (that is, the percentage of faults that are not detected by the system) and of nuisance alarms

(that is, the percentage of declaration of invalid measurement when the fault is not present) are assessed. Monte Carlo analyses are carried out in four different flight conditions: climb, descent, cruise disturbed by a vertical gust, stall. In the first three conditions, the angle of attack is almost stationary; therefore, only bias and drift faults are added to the measurements of one physical AoA sensor (the freezing of the signal does not produce relevant errors). Bias, drift and signal freezing are used in the stall manoeuver, in which the angle of attack varies significantly during the test. All the Monte Carlo analyses are repeated twice. In the first set of analyses, the measurement system does not compensate for the estimation error due to the approximated aircraft weight (due to the use in the estimation of the conventional weight instead of the actual one). Table 1 shows the results for this test case. In the second set of Monte Carlo simulations, the estimated AoA is corrected by removing a constant offset, before providing it as input to the voting algorithm. The offset is computed as the mean difference, on a sufficiently long time, between the estimated AoA and the angle measured by the physical sensors, when these sensors measure about the same values (that means supposedly they are working properly). This procedure allows to compensate for, although roughly, the error due to the approximated weight. Table 2 presents the results for the second set of Monte Carlo analyses, whereas Figure 13 shows the results of one simulation run, in which the aircraft performs a stall manoeuver and one physical sensor of the angle of attack experiences a constant bias fault.
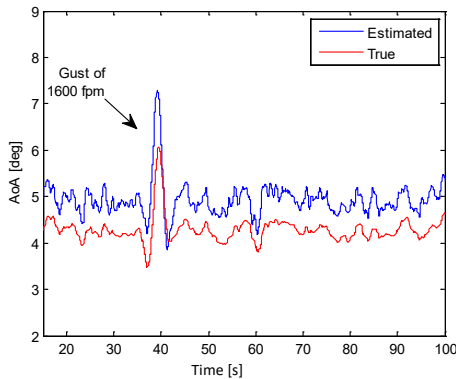
Figure 12: Angle of attack estimations for level flight with vertical gust

Table 1: Results of Monte Carlo analyses for the triplex redundant measurement system (without compensation for unknown aircraft weight)

	Fault	RMS mean [deg]	RMS std [deg]	False alarm %	Missed alarm %
Climb	Bias	0.67	0.18	6.4%	0%
	Drift	0.47	0.15	7.2%	0%
	None	0.24	0.09	1.6%	0%
Descent	Bias	0.68	0.19	0.8%	0%
	Drift	0.48	0.16	0.8%	0%
	None	0.23	0.08	0.4%	0%
Cruise	Bias	0.70	0.17	4.8%	0%
	Drift	0.49	0.16	4.0%	0%
	None	0.24	0.09	0%	0%
Stall	Bias	1.34	1.00	22.4%	5.6%
	Drift	1.08	1.11	26.4%	0%
	Freeze	1.08	1.06	28.8%	0%
	None	0.26	0.08	13.6%	0%

Table 2: Results of Monte Carlo analyses for the triplex redundant measurement system (with compensation for unknown aircraft weight)

	Fault	RMS mean [deg]	RMS std [deg]	False alarm %	Missed alarm %
Climb	Bias	0.62	0.16	0%	0%
	Drift	0.39	0.09	0%	0%
	None	0.20	0.06	0%	0%
Descent	Bias	0.63	0.16	0%	0%
	Drift	0.40	0.08	0%	0%
	None	0.20	0.06	0%	0%
Cruise	Bias	0.64	0.15	0%	0%
	Drift	0.40	0.08	0%	0%
	None	0.20	0.06	0%	0%
Stall	Bias	0.89	0.30	1.6%	0%
	Drift	0.63	0.22	2.4%	0%
	Freeze	0.73	0.23	2.8%	2.8%
	None	0.21	0.04	1.2%	0%
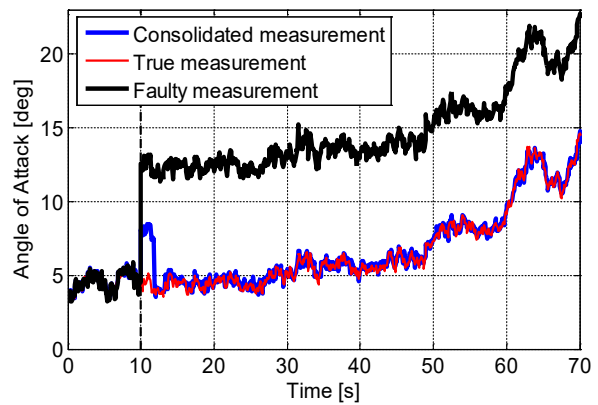
Figure 13: Angle of attack measurement for a stall manoeuver and a constant bias fault on one physical sensor

The improvements due to the weight error compensation are significant in all the examined metrics. As expected, a better estimation of the angle of attack leads to a reduction of the RMS error on the consolidated measurement and to a more effective detection of the faulty sensor. For all the considered flight phases and fault types, the mean RMS error is far below 1 degree also when the fault is present. The false alarm rate is always null, except for the stall maneuver in which however it is very low. The measurement system is able to detect all the injected faults, except for the case of measurement freezing, in which only 7 cases on 250 are missed (2.8%). Although these results are already very good, an optimization of the parameters of the voting and signal validity check algorithms could improve the result for both false and missed alarm percentage. Further investigations will be dedicated to this issue in the future.

5. Conclusion

This paper presented an original angle of attack measurement system applicable to commercial aviation aircraft. The system is based on a triplex physical-analytical redundancy, which only requires two physical sensors of the angle of attack. Indeed, the third sensor is virtual; it is an innovative angle of attack estimator, originally developed to provide General Aviation pilots with a maintenance free and low cost but accurate indication of trend toward stall and stall margin. This estimator does not require any angle of attack dedicated sensor, neither detailed information about

the aerodynamics of the specific aircraft, which is identified during a short calibration flight, carried out just once. The customization of the virtual sensor for the application to commercial aircraft, described in the present paper, allows getting better performance, due to the possibility to exploit additional information (such as, aircraft weight and deflection of the aerodynamic control surfaces), which usually are not available to General Aviation aircraft.

The physical-analytical redundant architecture defined in this paper provides a measurement system which is robust to a single fault of the angle of attack sensors. It could significantly improve the safety of the aircraft, reducing the occurrence of LOC-I related accidents, saving human lives, and avoiding the economic impact consequent to those accidents. It has the peculiarity to be applicable to the existing commercial aircraft by installing just a software code that implements the proposed algorithms, without the need to modify the on-board avionics instrumentation.

The performance of the proposed measurement system was assessed through Monte Carlo simulations. To this end, a high-fidelity simulation environment was implemented, which includes the models of aircraft, atmosphere, on-board sensors and an autopilot. The simulations highlighted very interesting results of both the angle of attack estimator and the overall measurement system. The latter is able to provide a consolidated angle of attack measurement with a mean RMS error far below 1 degree, also when a fault is present. Concerning the detection of the faults, it is generally successful; both missed and false alarm percentages are close to zero for all the examined cases. An optimized tuning of the proposed algorithms will probably further improve these results.

Future works will be focused on the validation of the system through real-time simulations and in-flight trials.

References

[1] A. Vitale, F. Corraro, N. Genito, L. Garbarino, L. Verde, "Innovative Real Time Estimator for Redundancy of Angle of Attack Sensors in Commercial Aircraft," in Proc. 4th Conference on Control and Fault Tolerant Systems SYSTOL'19, 2019, doi: 10.1109/SYSTOL.2019.8864783.

[2] General Aviation Joint Steering Committee - Loss of Control Working Groups, Final Report, 2014.

[3] M. Bromfield, B. Dillman, "The Effects of Using an Angle of Attack System on Pilot Performance and Workload during Selected Phases of Flight," Procedia Manufacturing, **3**, 3222-3229, 2015, doi: 10.1016/j.promfg.2015.07.873.

[4] ICAO, "Manual on aeroplane upset prevention and recovery training," Doc 10011, 2014.

[5] C. Ramprasadh, H. Arya, "Multi-stage fusion algorithm for estimation of aerodynamic angles in mini aerial vehicle," in Proc. 49th AIAA Aerospace Science Meeting, 2011, doi: 10.2514/1.C031322.

[6] A. Cho, Y.S. Kang, B.J. Park, and C.S. Yoo, "Airflow angle and wind estimation using GPS/INS navigation data and airspeed," in Proc. 13th Int. Conf. Control, Automation and Systems (ICCAS), 2013, doi: 10.1109/ICCAS.2013.6704159.

[7] S. Leutenegger, A. Melzer, K. Alexis, and R. Siegwart, "Robust state estimation for small unmanned airplanes," in Proc. IEEE Int. Conf. Control Applications, Antibes, France, 2014, doi: 10.1109/CCA.2014.6981466.

[8] T.A. Johansen, A. Cristofaro, K. Sorensen, J.M. Hansen, T.I. Fossen, "On estimation of wind velocity angle-of-attack and sideslip angle of small UAVs using standard sensors," in Proc. 2015 International Conference on Unmanned Aircraft Systems (ICUAS), 2015, doi: 10.1109/ICUAS.2015.7152330.

[9] A. Wenz, T.A. Johansen and A. Cristofaro, "Combining model-free and model-based angle of attack estimation for small fixed-wing UAVs using a standard sensor suite," 2016 International Conference on Unmanned Aircraft Systems (ICUAS), 2016, doi: 10.1109/ICUAS.2016.7502583.

[10] H. Long and S. Song, "Method of estimating angle-of-attack and sideslip angle based on data fusion," in Proc. International Conference on Intelligent Computation Technology and Automation, 2009.

[11] M. Shaqura, C. Claudel, "A hybrid system approach to airspeed, angle of attack and sideslip estimation in Unmanned Aerial Vehicles," in International Confonference on Unmanned Aircraft Systems ICUAS 2015, 2015, doi: 10.1109/ICUAS.2015.7152355.

[12] R.D. Colgren, "Method and system for estimation and correction of angle-of-attack and sideslip angle from acceleration measurements," U.S. Patent 6273370, November 1, 1999.

[13] Ramprasadh, S. Prem, L. Sankaralingam, Parag Deshpande, Ravi Dodamani, Suraj C S, "A Simple Method for Estimation of Angle of Attack," IFAC-PapersOnLine, **51** (1), 353-358, 2018, doi: 10.1016/j.ifacol.2018.05.048.

[14] P.A. Samara, G.N. Fouskitakis, J.S. Sakellariou, S. Fassois, "Aircraft angle-of-attack virtual sensor design via a functional pooling narx methodology," European Control Conference ECC2003, 2003, doi: 10.23919/ECC.2003.7085229.

[15] A. Lerro, M. Battipede, P. Gili, A. Brandl, "Survey on a Neural Network for Non Linear Estimation of Aerodynamic Angles," in Intelligent Systems Conference, 2017, doi: 10.1109/IntelliSys.2017.8324240.

[16] A. Lerro, M. Battipede, P. Gili, A. Brandl, "Aerodynamic angle estimation: comparison between numerical results and operative environment data," CEAS Aeronautical Journal, 11, 249–262, 2020, doi:10.1007/s13272-019-00417-x

[17] N. Genito, F. Corraro, L. Garbarino, A. Vitale, E. De Lellis, D. Bibby, S. Rieb, K. Jones, "System and method for angle of attack indication with no dedicated sensors and aircraft information," Patent WO 2016 / 164624, https://patents.google.com/patent/WO2016164624A1/en, October 13, 2016.

[18] IATA, "Loss of Control In-Flight Accident Analysis Report, 2019 edition," ISBN 978-92-9264-002-6, 2019.

[19] Aircraft Accident Investigation Bureau (AIB), "Aircraft Accident Investigation Preliminary Report - Ethiopian Airlines Group - B737-8 (MAX) Registered ET-AVJ - 28 NM South East of Addis Ababa, Bole International Airport - March 10, 2019," Report No. AI-01/19, 2019.

[20] Komite Nasional Keselamatan Transportasi, "Aircraft Accident Investigation Report - PT. Lion Mentari Airlines - Boeing 737-8 (MAX); PK-LQP - Tanjung Karawang, West Java - Republic of Indonesia - 29 October 2018," 2018.

[21] The Federal Democratic Republic of Ethiopia, Ministry of Transport, Aircraft Accident Investigation Bureau "Interim Investigation Report on Accident to the B737-8 (MAX) Registered ET-AVJ operated by Ethiopian Airlines on 10 March 2019," Report No. AI-01/19, 09 March, 2020.

[22] FINAL KNKT.18.10.35.04, "Aircraft Accident Investigation Report," PT. Lion Mentari Airlines, Boeing 737-8 (MAX), PK-LQP, Tanjung Karawang, West Java Republic of Indonesia, 29 October 2018.

[23] Bureau d'Enquêtes et d'Analyses pour la sécurité de l'aviation civile, "Report - Accident on 27 November 2008 off the coast of Canet-Plage (66) to the Airbus A320-232 registered D-AXLA operated by XL Airways Germany," 2010.

[24] German Federal Bureau of Aircraft Accident Investigation (BFU), "Interim Report," BFU 6X014-14, 2015.

[25] D. Ossmann, H.D. Joos, P. Goupil, "Enhanced Sensor Monitoring to Maintain Optimal Aircraft Handling in Case of Faults," Journal of Guidance, Control, and Dynamics, **40**(12), 3127-3137, 2017, doi: 10.2514/1.G002341.

[26] D. Berdjag, J. Cieslak and A. Zolghadri, "Fault detection and isolation of aircraft air data/inertial system," Progress in Flight Dynamics, GNC, and Avionics, **6**, 317-332, 2013, doi: 10.1051/eucass/201306317

[27] C. Seren, P. Ezerzer, G. Hardier, "Model-based techniques for virtual sensing of longitudinal flight parameters," Int. Journal of Applied Mathematics and Computer Science, **25**(1), 23-38, 2015, doi: 10.1515/amcs-2015-0002.

[28] R. E. Maine, K. W. Iliff, "Application of Parameter Estimation to Aircraft Stability and Control," NASA-RP-1168, June 1986.

[29] A. Gelb, Applied Optimal Estimation, M.I.T. Press, ISBN 0-262-20027-9, Cambridge, Massachusetts, 1989.

[30] B. Etkin, Dynamics of Atmospheric Flight, John Wiley & Sons, 1972.

[31] A. Fedele, N. Genito, A. Vitale, L. Garbarino, "Experimental aircraft system identification from flight data: Procedures and Results," CEAS 2013 Air & Space Conference, 2013.

[32] MIL-STD-1797A, "Flying Qualities of Piloted Aircraft," 1990.

[33] L. Garbarino, N. Genito, V. Baraniello, E. De Lellis, and A. Vitale, "Low Cost Air Data System For UAV In-Flight Experimentation," Society of Flight Test Engineers – 23rd European Chapter Symposium, 2012.

[34] B.R. Barmish, C.M. Lagoa, "The Uniform Distribution: A Rigorous

Justification for its use in Robustness Analysis," Mathematics of Control, Signals, and Systems, **10**, 203-222, 1997, doi: 10.1007/BF01211503.

[35] R. Tempo, G. Calafiore, F. Dabbene, Randomized Algorithms for Analysis and Control of Uncertain Systems, Springer-Verlag, New York, 2005.

[36] X. Chen, K. Zhou, J.L. Aravena, "Fast Universal Algorithms for Robustness Analysis," in Proceeding of the 42nd Conference on Decision and Control, 2003, doi: 10.1109/CDC.2003.1272897.

Eliminating Target *Anopheles* Proteins to Non-Target Organisms based on Posterior Probability Algorithm

Marion Olubunmi Adebiyi[*], Oludayo Olufolorunsho Olugbara

ICT and Society Research Group, Luban Workshop, Durban University of Technology, P.O Box 1334, Durban 4000, South Africa

A R T I C L E   I N F O

A B S T R A C T

Capturing similarity in gene sequences of a target organism to detect significant regions of comparison will most likely occur because genes share a related descendant. Local sequence alignment for the targeted organisms can help preserve associations among sequences of related organisms. Such homologous genes possess identical sequences with common ancestral genes. The genes may be similar to common traits, and varying purposes, but they descend from a common ancestor. Basic local alignment search tool (BLAST) from the National Center for Biotechnology Information. (NCBI) has been used by different researchers to resolve the various forms of alignment problems. However, much literature to bare the efficacy of standard protein-protein BLAST (BLASTp) on the MATLAB platform has not been seen. In this study, a position-specific iteration BLASTp of 20 anopheles insecticide target protein sequence was performed on NCBI Ensembl against genomes of Anopheles (target organism), then against humans, fruit-fly, zebrafish, and chicken genomes (non-target organisms) to eliminate the targets with homology to non-target organisms. Furthermore, the same iteration was repeated for the genomes of Anopheles and non-target organisms using a posterior probability algorithm built into MATLAB as a tool for protein to protein search BLAST. Outputs from NCBI and MATLAB were put forward to determine the optimality of an optimized search algorithm on MATLAB. The MATLAB-Blastp method based on the application of posterior probability has helped to avoid errors occurring in the early stages of alignment. Moreover, the same results were obtained for the sought features on NCBI Blastp with a refined understanding of how feature values are generated from MATLAB posterior probability built-in algorithm for position-specific BLAST.

1. Introduction

Local alignment algorithms are suitable for unrelated sequences that are assumed to comprehend areas of comparable sequence motifs within a larger sequence framework [1]. Alignment is a mutual procedure of two sequences exhibiting positions where sequences are similar or dissimilar. A sequence alignment establishes residue-to-residue correspondences among sequences such that the order of residue in each sequence is preserved. Sequence analysis is a subject of deoxyribonucleic acid (DNA), ribonucleic acid (RNA) or peptide sequence for wide variations of analytical techniques to comprehend its purpose, structure, and development [2].

Many dynamic programming algorithms such as Smith-Waterman, FASTA, and BLAST algorithms were developed for accomplishing local alignment. The Smith–Waterman algorithm

accomplishes the task of local alignment of sequences for defining comparable neighborhoods of regions between two nucleotides or protein sequences. The algorithm captures the segments of all likely lengths and optimizes a comparative measure, instead of stretching over the entire sequence being process [3]. FASTA program was written for comparing protein sequences but it was later modified to conduct searches on DNA [4]. FASTA software uses the principle of finding similarity between two sequences statistically. This software matches one sequence of DNA or protein with the other by local sequence alignment method. It searches for local region for similarity but not the best match between two sequences. Since this software compares localized similarities at a time, it can come up with a mismatch. FASTA takes a small part of a sequence known as k-tuples where a tuple can be from 1 to 6, matches it with k-tuples of other sequence and once a threshold value of matching is reached it generates result. It is a program that is used to shortlist prospects of matching large sequences because it is very fast.

BLAST is frequently used for relating data sequences, recovering, and extracting sequences from databases in bioinformatics [5]. It has shown useful contributions in molecular biology, computational biology, and molecular genetic [6]. BLAST presents reliable and fast statistical reports, flexible search algorithm, and heuristic search methods [7]. BLAST based algorithms seek to extract a snippet of a query sequence that has a perfect alignment with a fragment of a targeted sequence found in a database. In the original BLAST algorithm, the chopped fragment is becoming the input to extend alignment in both query and subject database. BLAST searches for short sequences in an input query that matches short sequences in a database [8]. The nucleotide-nucleotide search, megaBLAST, BLASTN, BLASTP, BLASTX, TBLASTN are other architypes of BLAST algorithms [9].

Dynamic programing through the BLAST algorithm with various variants has made homologous search on genome databases of organisms possible. The aim of such analysis was to predict genes that are homologous in similar or dissimilar species. Gene prediction depends mostly on comparing a genomic sequence with a complementary DNA (cDNA), or protein database. However, most results are inaccurate for several reasons, including incomplete reference databases and lack of contribution to analysis of species. Position specific iterative BLAST (PSI-BLAST) is a program that finds distance relative to a protein. It creates a list of all closely related proteins that were combined into a general "profile" sequence, and summarizes significant features found in protein sequences. A query against a protein database is performed with in-built profile to extract larger group of proteins. The posterior probability is implemented using Bayesian theorem that involves revising a prior profile sequence that is extracted by psi-blast. This algorithm takes into consideration a new sequence profile information, which is a larger profile sequence group used to construct a profile and the process was iterated for four identical non-target organisms. It is believed that PSI-BLAST is much more sensitive in picking up distance based evolutionary relationships than a standard normal protein-protein BLASTP [10].

In this study, a local alignment algorithm has been developed based on BLASTP (protein query sequence against protein database search) and PSI BLAST (for more sensitive protein–protein similarity searches) to determine the effectiveness of the two search algorithms. A literature review to extract one of the best local search algorithms (Smith Waterman algorithm) was conducted. The NCBI BLAST was used to implement a protein query against protein database with a known essential protein sequences with PSI-BLASTP combined with posterior probability to generate an updated list of corresponding homologous protein from four other closely identical organisms. NCBI BLAST is widely used to implement sequence alignment, but very few works have implemented the local BLAST on MATLAB environment. Consequently, we are proposing a distinct way of elucidating homologous genes of a target organism when compared to selected non-target organisms through sequence alignment. This work is relevant for predicting genes that must be targeted in anopheles when formulating new compounds for drug target. If such gene is tampered with in the target anopheles during insecticidal spray, what happens to non-target organisms such as human, fruit flies, chickens, and fishes.

There is a high tendency of harming non-targeted organisms during insecticidal spray if homologous genes are not eliminated in the target gene list before insecticidal compounds are formulated and recommended for use. Local sequence alignment for a targeted specie can help preserve associations among sequences of related specie. Such homologous genes possess identical sequences with common ancestral gene and are useful for function prediction and characterization.

2. Related Works

Orthologs are homologous genes that diverge after a speciation event, and still have their main functions conserved. A homologous gene is inherited from two species by a common ancestor and homologous genes can be similar in sequence. But homology is the existence of the same body morphological structures in different organisms. It is an important concept of evolution and comparative biology [11]. The availability of genome sequence of several species has provided an opportunity to elucidate the effects of evolution on every nucleotide and protein in a genome [12-14]. It is easy to identify nucleotide sets that descended from a common ancestral nucleotide with sequence alignment because the problem of identifying an evolutionary related nucleotide and protein is the sequence alignment [15]. Strategies for aligning multiple and entire genomes of organisms include 'local' alignment and 'global' alignment [13, 15]. Their work has demonstrated a typical example of evolutionary scenario that involved the replication of double-stranded DNA in a parent cell (target organism) and division into two child cells. Their result showed two positions of an undirected duplication because of slippage replication, and occurrence of a directed duplication involving an RNA intermediate.

Studies on efficiency of alignment algorithm for homologous sequence similarity search in a genomic database was performed on a single [3]. The dynamic programming was deployed to isolate similar regions in gene sequences as a form of comparative analysis [16]. The authors discovered a suitable technique to calculate similarity in protein gene sequences within and across related organisms. They proposed a technique that computes sequence similarity, and their algorithm was evaluated using data sets from various species. The 'best-in-genome' method has been introduced [17], where a pairwise local alignment [18] between rat (target genome) and human genome (non-target genome) was initiated. The filter kept the best alignment for each position in rat genome and generated many to one relationship between rat genome and human genome but did not capture all orthologous relationships. The result was a reference-based multiple alignment with a property that gave every column, at most one position from each genome. A vertebrate local aligner with a faster nucleotide and more sensitive cross-species protein alignments has been constructed [19]. A web-based BLAST server for human genome makes homologous search possible and serves the purpose multiple genome alignments for yeast, insects, and vertebrates [20]. Aligning human, mouse, and rat genome [21] with progressive extension pairwise alignment orchestrated for human to mouse alignment has been reported [22]. Researches have combined strategies and tools for whole genome alignments [23-27], but none of the previous works have been found to specifically provide the Psi-Blastp by Bayes theorem

posterior probability for generating homologous alignment of anopheles to human, fruit-fly, zebra-fish and chicken genomes as provided in this work.

3. Experimental

This work has been implemented using minimum hardware and software requirements of a computer system with at least 16GB of RAM, 1TB hard disk capacity, Intel Core i7 Microprocessor, with VGA monitor compatible of at least 640/480 resolution and enhanced keyboard with a mouse. The software requires windows operating 7, or higher version, a Blosum62, BLAST standalone database, MATLAB R2016B, and online Ensembl NCBI Database [28] and [29]. The 20 essential genes identified to be potential insecticidal targets for malaria vector were used as input data for Mosquito *Anopheles Gambiae* [30]. The original data for analysis were extracted from Kyoto Encyclopedia of Genes and Genomes (KEGG) database and AnoCyc database on BioCyc, https://biocyc.org/organism-summary?object=ANO [31]. The detailed summary of Anopheles gambiae, version 24.1 KEGG described a collection of databases dealing with genomes, biological pathways, diseases, drugs, and chemical substances. BioCyc is a swarm of about 5700 pathway/genome databases (PGDBs) specific to various organisms. Each PGDB houses a predicted metabolic network and full genome of a specific organism, including reactions, metabolites, metabolic pathways, enzymes, proteins, genes, and lots of other components [32]. The protein sequence of these genes was extracted from protein database at NCBI as flat file or FASTA format from Genebank. Table 1 shows the dataset features of twenty genes as enzyme name, protein name, gene name, enzyme commission (EC) number and gene identity (ID).

The implementation of a basic local alignment method using a query against protein database was performed in this study using posterior probability function in MATLAB. The goal was to ascertain the creation of position specific score profile matrix from an alignment. The BLASTp program in MATLAB Bioinformatic tool was designed to map sequences of 20 previously identified *Anopheles* gambiae insecticidal target genes unto all available protein sequence databases of a specified organism, disease, population, or proteome. Bayesian posterior probability was calculated from psi-blast output to capture the related proteins from distance species during its search. This has resulted into a larger profile sequence group used to construct the final profile information. The process was repeated for the four non-target organisms investigated in this study.

Table 1: Dataset Features

S/N	AnoCyc (BioCyc) Enzyme Name	Uniprot Protein Name	Gene Name (Uniprot)	EC Number	Gene ID
1	Alkyl hydroperoxide reductase subunit C Thiol specific antioxidant	Thioredoxin-dependent peroxidase	TPX1	1.11.1.15	AGAP000396
2	Cytochrome P450 B-class	AGAP012295-PA	CYP9L1	1.14.14.1	AGAP012295
3	Cytochrome P450	AGAP002429-PA	CYP314A1	1.14.99.22	AGAP002429
4	Betaine aldehyde dehydrogenase	AGAP003578-PA	1274242	1.2.1.3	AGAP003578
5	Ribosomal RNA adenine dimethylase	rRNA adenine N (6)-methyltransferase	1274612	2.1.1.183	AGAP004465
6	Methyltransferase type 11	2-methoxy-6-polyprenyl-1,4-benzoquinol methylase, mitochondrial	coq5	2.1.1.201	AGAP010488
7	tRNA (guanine9-N1)-methyltransferase	tRNA methyltransferase 10 homolog A	1271937	2.1.1.221	AGAP000324
8	MT-A70-like	AGAP002895-PA	1273072	2.1.1.62	AGAP002895
9	Cholineethanolamine kinase	AGAP000010-PA	1272266	2.7.1.82	AGAP000010
10	Diacylglycerol kinase catalytic domain	Sphingosine kinase	1270104	2.7.1.91	AGAP006995
11	Zn (II)-responsive transcriptional regulator	Phenylalanyl-tRNA synthetase beta subunit	1274174	6.1.1.20	AGAP003517
12	Galactose-binding domain-like	Beta-galactosidase	1281056	3.2.1.23	AGAP002055
13	Carbon-nitrogen hydrolase	AGAP012662-PA	1269132	3.5.1.3	AGAP012662
14	Formylmethionine deformylase	Peptide deformylase	1271597	3.5.1.88	AGAP003861
15	Threonyl-tRNA synthetase class IIa	Prolyl-tRNA synthetase	1274253	6.1.1.15	AGAP003589
16	Leucyl-tRNA synthetase	Leucyl-tRNA synthetase	1277687	6.1.1.4	AGAP008297
17	Ribosomal RNA methyltransferase Spb1 C-terminal	23S rRNA (uridine2552-2'-O)-methyltransferase	1274000	2.1.1.166	AGAP004177
18	Farnesyl diphosphate synthase	Polyprenyl synthetase	1269998	2.5.1.1	AGAP007104
19	Glucosaminegalactosamine-6-phosphate isomerase	6-phosphogluconolactonase	1271093	3.1.1.31	AGAP010866
20	FAD-binding type 2	Alkylglycerone-phosphate synthase	1274507	2.5.1.26	AGAP004358

Block substitution matrix (BLOSUM), which is the default matrix for a protein BLAST algorithm is a substitution matrix used for sequence alignment of protein. The matrix is based on local alignment. Based on block comparisons of sequence from database blocks, it contains multiple aligned un-gapped segments that correspond to the top-most conserved protein regions. The goals are to identify "biologically significant" patterns in protein families by emphasizing regions that are thought to be important to protein function. To look for good "discriminators" that emphasize and identify known family members, while excluding known non-members and to pro-site patterns of "motifs". The standalone BLAST is a suit of programs that were designed to mimic the NCBI BLAST server, and include "blastall"," megablast", and "blastp" that exist in NCBI BLAST suit. Its ease of use and user friendliness features are strong inspiration for its application in this study.

4. Results and Discussion

The protein sequences for each of the 20 insecticidal target genes was blasted against protein databases of four non-target organisms. The organisms are *Homo Sapiens* (Taxonomy ID: 9609) - human genome, *Drosophila* (Taxonomy ID: 7227) – fruit fly genome, *Danio Rerio* (Taxonomy ID:7955) – Zebra fish genome and *Gallus Gallus* (Taxonomy ID: 9031) – chicken genome. The selection procedure certifies that homologous gene of target organism (anopheles) exists in these four non-target organisms. There is possible homology match, which was identified and should be catered for in case of gene inhibition during insecticidal development. In fact, about 30 sequences were blasted against the whole genome per single iteration. The BLAST was matched with parameters before commencing on further BLASTP commands. The BLAST of proteins was run against the protein database of four targeted organisms. The BLASTP algorithm was implemented on Blosum62 Ensembl database section. During this process we were looking for homologs, which is a measure of relationship between two genes that descended from a common ancestral protein. Their various e-values and percentage identities were identified as the unique selection criteria. It confirmed the literature [33] that homologous

genes can be predicted and validated by sequence alignment method.

The e-value measures level of a likelihood that any match in sequences is purely by chance. Consequently, a lower e-value determines the less significant matches made but gives an idea of potential relations among query organisms and database organisms. This is a result of random chance and therefore the most significant gene matches in those non-target organisms were selected as the homologous. Selecting a homolog like the target sequence analyzed, the match with the lowest e-value and highest percentage was classified a significant match or hit. The e-value threshold was set at 0.00001 as a standard with NCBI Ensembl database that was deployed, while the position specific iteration BLAST threshold was set at 0.005. Figures 1 and 2 represent two sample result pages of 20-protein sequences blasted against the four non-target genome databases investigated with e-values and IDs of its homologous gene.

Different values were collected for various organisms blasted on ensembl platform. These values are the homolog, e-value, and percentage identity. Tables 2 and 3 show results of human and zebra fish homologous genes of the four organisms blasted in this study. The extracted database files from the Ftp site for the Anopheles was extracted from ftp://ftp.ncbi.nlm.nih.gov/genomes/ and available on Figure 3 shows this result for the case of human genomic information. The figure constitutes the precise data files and human genome information from NCBI genome databases and similar results were obtained for Zebrafish, Fruit-fly, and Chicken. The databases from the Ftp site were downloaded as GenBank files and converted to Microsoft (MS) Access database. The MS access file was linked as input to the MATLAB for implementation. BLASTP search was performed using MATLAB. A position specific iteration blast for protein query against protein (PSI–BLASTP) was completed for each sequence of anopheles against non-target organism (Human, Zebrafish, Fruit-fly, and Chicken) genome database. This was done to eliminate targets with homolog to non-target organism.
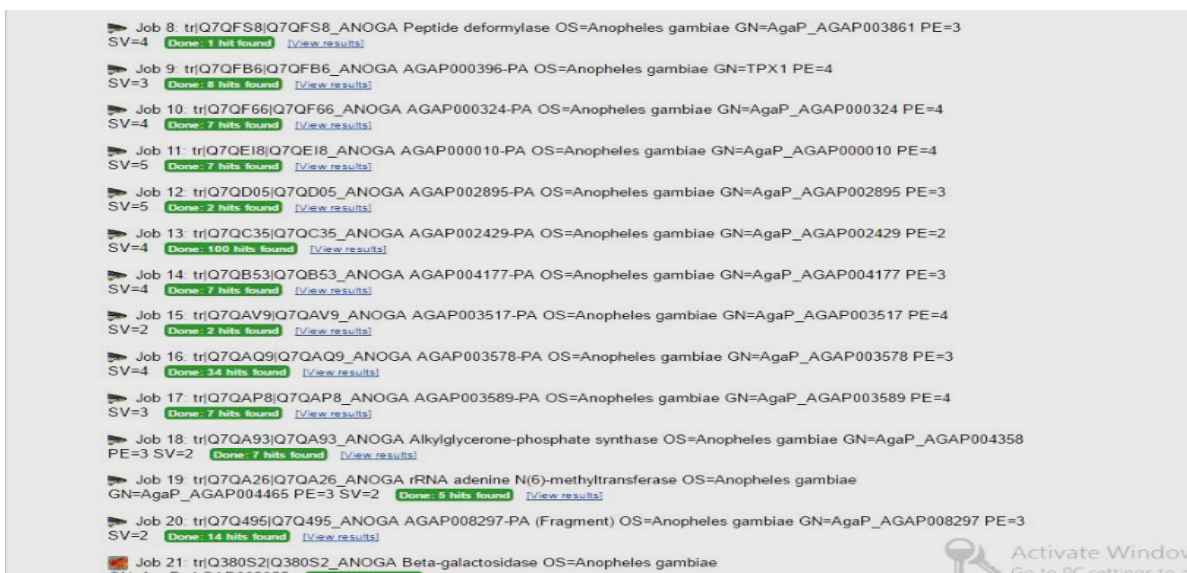
Figure 1: BLAST result page on ensembl.org
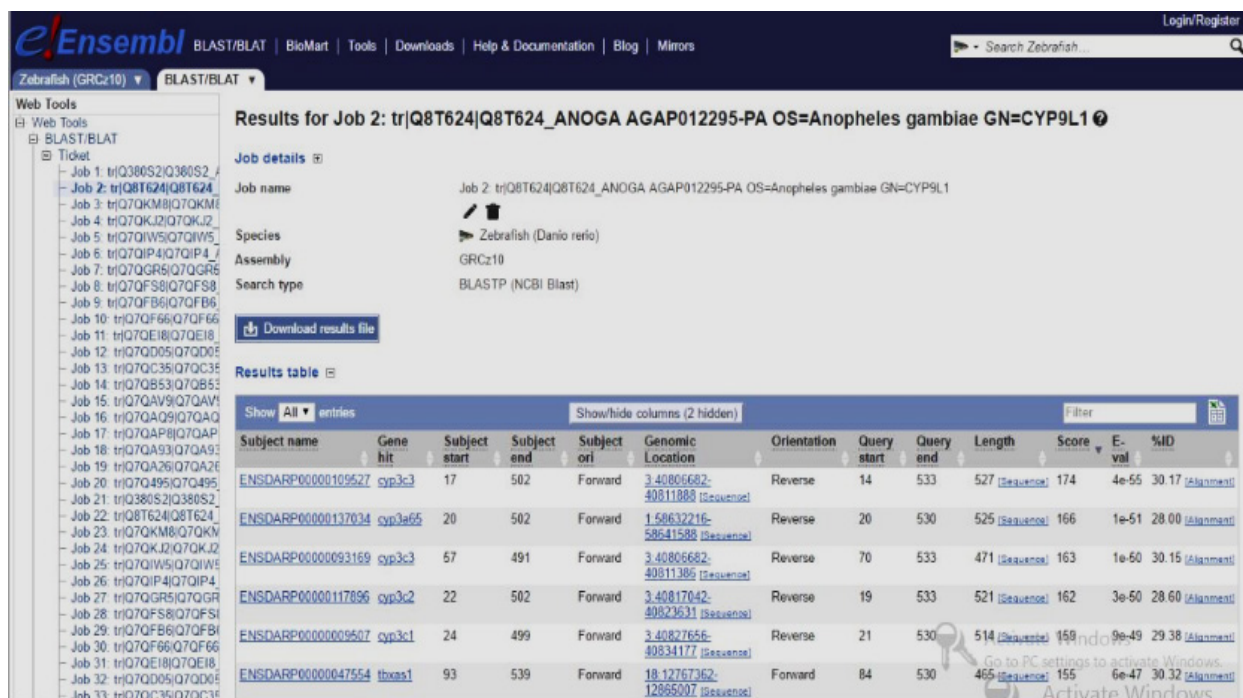
Figure 2: Extracted result with e-value and ID of its homologous gene

Finally, 20 anopheles protein targets were screened with two target genomes of Homo sapiens and Drosophila melanogaster. This was to identify isoforms from two organisms when screened with genomes of anopheles. The result of anopheles protein isoforms when screened with homo sapient and drosophila genomes is presented in Table 4. These isoforms can formulate a potential class of protein and can elucidate more molecular and functional variations ciphered in the genome by further functional analysis.

The search for protein isoform in this study may be out of scope because we do not have plans to conduct clinical or computational proteomics analysis and transcriptomic analysis. However, protein isoform is seen as the same protein existing in many different forms, rather it is a new class of protein that may be useful as biomarkers for early diagnostic of clinical proteomics [34]. Studies have shown that traditional methods of protein isoform determination have proved that isoforms can only be determined quantitatively at the transcript level, not in the protein level. Moreover, that condition came with several other disadvantages, high throughput analysis has made it possible, but the data used in this study are not confirmed transcriptomic dataset.

Table 2: Human (homo sapient) homologous gene

S/N	AnoCyc (BioCyc) Enzyme Name	EC Number	KEGG Gene ID	Homolog Gene ID	E-value	% ID
1	Alkyl hydroperoxide reductase subunit C Thiol specific antioxidant	1.11.1.15	AGAP000396	ENSP00000389047	1.00E-64	66.27
2	Cytochrome P450 B-class	1.14.14.1	AGAP012295	ENSP00000228606	1.00E-12	31.63
3	Cytochrome P450	1.14.99.22	AGAP002429	ENSP00000368079	1.00E-18	23.11
4	Betaine aldehyde dehydrogenase	1.2.1.3	AGAP003578	ENSP00000438296	1.00E-157	57.73
5	Ribosomal RNA adenine dimethylase	2.1.1.183	AGAP004465	ENSP00000421754	1.00E-107	77.91
6	Methyltransferase type 11	2.1.1.201	AGAP010488	ENSP00000449933	3.00E-11	58.82
7	tRNA (guanine9-N1)-methyltransferase	2.1.1.221	AGAP000324	ENSP00000423628	1.00E-14	35.77
8	MT-A70-like	2.1.1.348	AGAP002895	ENSP00000440598	1.00E-43	34.93
9	Cholineethanolamine kinase	2.7.1.82	AGAP000010	ENSP00000398091	1.00E-37	47.57
10	Diacylglycerol kinase catalytic domain	2.7.1.91	AGAP006995	ENSP00000471180	1.00E-14	38.25

11	Zn(II)-responsive transcriptional regulator	6.1.1.20	AGAP003517	ENSP00000367498	1.00E-20	30.49
12	Galactose-binding domain-like	3.2.1.23	AGAP002055	ENSP00000407365	1.00E-06	46.94
13	Carbon-nitrogen hydrolase	3.5.1.3	AGAP012662	ENSP00000356986	1.00E-37	33.21
14	Formylmethionine deformylase	3.5.1.88	AGAP003861	ENSP00000288022	1.00E-40	39.35
15	Threonyl-tRNA synthetase class IIa	6.1.1.15	AGAP003589	ENSP00000358060	1.00E-05	22.77
16	Leucyl-tRNA synthetase	6.1.1.4	AGAP008297	ENSP00000447763	1.00E-07	21.05
17	Ribosomal RNA methyltransferase Spb1 C-terminal	2.1.1.166	AGAP004177	ENSP00000384423	1.00E-22	37.41
18	Farnesyl diphosphate synthase	2.5.1.1	AGAP007104	ENSP00000417865	1.00E-05	27.04
19	Glucosaminegalactosamine-6-phosphate isomerase	3.1.1.31	AGAP010866	ENSP00000471446	2.00E-11	37.63
20		2.5.1.26	AGAP004358	ENSP00000417011	1.00E-11	25.58

Table 3: Zebra fish (danio rerio) homologous gene

S/N	AnoCyc (BioCyc) Enzyme Name	EC Number	Gene ID	Homolog Gene	E-value	% ID
1	Alkyl hydroperoxide reductase subunit C Thiol specific antioxidant	1.11.1.15	AGAP000396	ENSDARP00000120934	1.00E-49	72.5
2	Cytochrome P450 B-class	1.14.14.1	AGAP012295	ENSDARP00000122647	1.00E-06	34.07
3	Cytochrome P450	1.14.99.22	AGAP002429	ENSDARP00000091260	1.00E-19	24.52
4	Betaine aldehyde dehydrogenase	1.2.1.3	AGAP003578	ENSDARP00000012767	1.00E-154	57.91
5	Ribosomal RNA adenine dimethylase	2.1.1.183	AGAP004465	ENSDARP00000124704	1.00E-04	30.69
6	Methyltransferase type 11	2.1.1.201	AGAP010488	ENSDARP00000131342	1.00E-04	25.22
7	tRNA (guanine9-N1)-methyltransferase	2.1.1.221	AGAP000324	ENSDARP00000109893	1.00E-36	40.41
8	MT-A70-like	2.1.1.348	AGAP002895	ENSDARP00000022188	4.00E-154	48.34
9	Cholineethanolamine kinase	2.7.1.82	AGAP000010	ENSDARP00000019763	2.00E-93	46.37
10	Diacylglycerol kinase catalytic domain	2.7.1.91	AGAP006995	ENSDARP00000117613	1.00E-07	33.33
11	Zn(II)-responsive transcriptional regulator	6.1.1.20	AGAP003517	ENSDARP00000069614	4.00E-17	31.07
12	Galactose-binding domain-like	3.2.1.23	AGAP002055	ENSDARP00000047190	1.00E-120	38.75
13	Carbon-nitrogen hydrolase	3.5.1.3	AGAP012662	ENSDARP00000121828	1.00E-69	44.09
14	Formylmethionine deformylase	3.5.1.88	AGAP003861	ENSDARP00000013949	3.00E-43	40
15	Threonyl-tRNA synthetase class IIa	6.1.1.15	AGAP003589	ENSDARP00000103726	1.00E-04	22.57
16	Leucyl-tRNA synthetase	6.1.1.4	AGAP008297	ENSDARP00000106738	5.00E-127	63.76
17	Ribosomal RNA methyltransferase Spb1 C-terminal	2.1.1.166	AGAP004177	ENSDARP00000138990	1.00E-15	27.8
18	Farnesyl diphosphate synthase	2.5.1.1	AGAP007104	ENSDARP00000059927	1.00E-74	44.48
19	Glucosaminegalactosamine-6-phosphate isomerase	3.1.1.31	AGAP010866	ENSDARP00000124115	2.00E-13	29.92
20		2.5.1.26	AGAP004358	ENSDARP00000136279	1.00E-177	52.42
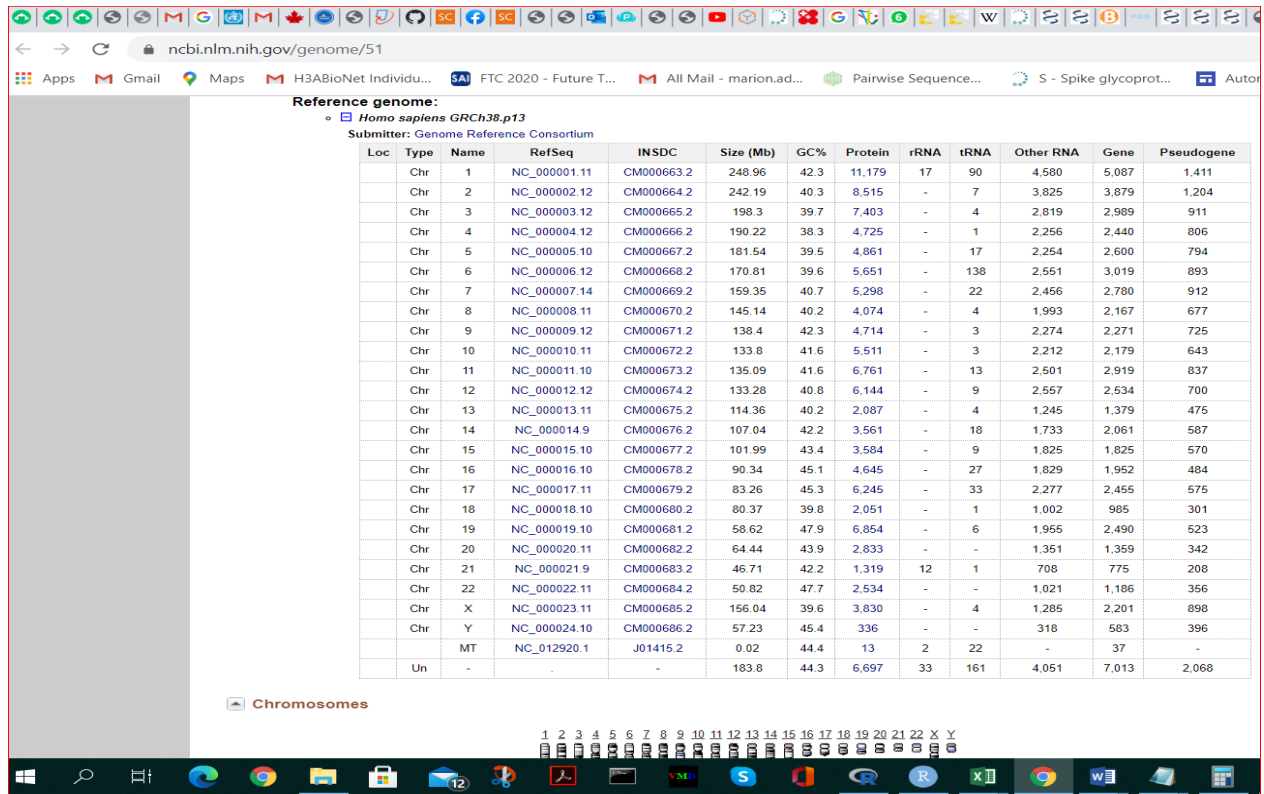
Figure 3: Database file genome information for Humans (Homo Sapiens)

Table 4: Anopheles protein isoforms when screened against *homo sapient* and *drosophila* genomes

Anopheles Gene ID	Number of Isoforms for Anopheles	Human Homolog/ Uniprot Gene ID	Number of Isoforms for Human homolog gene	Drosophila Homolog/ Uniprot Gene ID	Number of Isoforms for Drosophila homolog gene
AGAP000396	0	ENSP00000389047/ PRDX1	3	FBpp0082927/ Prx3	0
AGAP012295	0	ENSP00000228606/ CYP27B1	3	FBpp0088127/ Cyp9b1	0
AGAP002429	0	ENSP00000368079/ CYP4V2	2	FBpp0088437/ Cyp12d1-p	2
AGAP003578	0	ENSP00000438296/ ALDH1A2	10	FBpp0079406/ Aldh	2
AGAP004465	0	ENSP00000421754/ DIMT1	4	FBpp0291478/ mtTFB1	0
AGAP010488	0	ENSP00000449933/ COQ5	6	FBpp0073568/ Coq5	2
AGAP000325	2	ENSP00000423628/ TRMT10A	3	FBpp0077043/ trmt10a	0
AGAP002895	0	ENSP00000440598/ METTL3	6	FBpp0079219/ Mettl14	0
AGAP000010	0	ENSP00000398091/ ETNK2	7	FBpp0310123/ eas	5
AGAP006995	0	ENSP00000471180/ SPHK2	8	FBpp0073346/ Sk1	2
AGAP003517	2	ENSP00000367498/ LRRC47	2	FBpp0084021/ beta-PheRS	0
AGAP002055	0	ENSP00000407365/ GLB1	8	FBpp0078861/ Gal	2
AGAP012662	0	ENSP00000356986/ NIT1	5	FBpp0081507/ Dmel\CG8132	0
AGAP003861	0	ENSP00000288022/ PDF	0	FBpp0081794/ Dmel\CG31373	0
AGAP003589	0	ENSP00000358060/ TARS2	6	FBpp0072825/ ProRS-m	2
AGAP008297	0	ENSP00000447763/ VARS2	13	FBpp0291534/ IleRS-m	0

	0	ENSP00000364423/ PTCH1	12		0
AGAP004177				FBpp0082832/ CG5220	
AGAP007104	0	ENSP00000417865/ GGPS1	3	FBpp0087266/ Fpps	0
AGAP010866	0	ENSP00000471446/ PGLS	4	FBpp0297905/ Oscillin	4
AGAP004358	0	ENSP00000417011/ LDHD	3	FBpp0070365/ D2hgdh	3

5. Conclusion

In this study, BLAST which is a frequently used to determine sequence similarity by querying various sequences type against databases of various datatypes was experimented. BLAST with 20 *Anopheles* protein sequence was queried against four non-target organism databases. The results of this study have revealed the same e-values, which indicates that there is no significant homology (all e–values > 0.001) between the data on *Anopheles* when compared to humans, fruit-fly, zebrafish, and chicken databases. Posterior probability in MATLAB was used for experimentation in this study. The study results have shown obvious insecticidal targets in *Anopheles gambiae* with no significant homology to humans, fruit-fly, zebrafish, and chicken. Further analysis like synthesizing these targets in an experimental scenario can help close dangling ends in search for new insecticide compounds. This may be a useful endeavor for future research.

6. Data Availability Statement

The original source of data for this study is from a standard and structured public repository KEGG and AnoCyc on BioCyc, (https://biocyc.org/organism-summary?object=ANO). Protein sequence of these genes was extracted from the protein database at NCBI as flat file or FASTA format from Genebank. In addition, contents were extracted from UniProt Knowledgebase @ UniProtKB (https://www.uniprot.org/database/DB-0023). This represents some details from Cross-referenced databases on UniProtKB, Protein knowledgebase and UniParc Sequence archive. This is because our analysis involved fetching data from various public databases to generate outputs as the algorithm required in pursuit of research objective. Links to all data supporting the conclusions of this study is publicly available as indicated by web links.

Conflict of Interest

The authors declare no conflict of interest.

References

[1] V. G. Tumanyan, V. O. Polyanovsky, and M. A. Roytberg, "Comparative analysis of the quality of a global algorithm and a local algorithm for alignment of two sequences," Algorithms for Molecular Biology, **6**(25), 1748-7188, 2011, https://doi.org/10.1186/1748-7188-6-25.

[2] E. S. Donkor, N. T. K. D. Dayie, T. K. Adiku. "Bioinformatics with Basic Local Alignment Search Tool (BLAST) and Fast Alignment (FASTA)", Journal of Bioinformatics and Sequence Analysis, **6**(1), 1-6, 2014, https://doi.org/10.5897/IJBC2013.0086.

[3] T. O. Oladele, O. M. Bamigbola, and C. O. Bewaji, "On Efficiency of Sequence Alignment Algorithms," African Scientist, **10**(1), 9-14, 2009.

[4] D. J. Lipman, and W. R. Pearson, "Rapid and sensitive protein similarity searches", Science, **227**(4693), 1435-1441, 1985, https://doi.org/10.1126/science.2983426.

[5] C. A. Kerfeld, K. M. Scott. "Using BLAST to teach "E-value-tionary Concepts", PLoS Biology, **9**(2), 1-11, 2011.

[6] G. G. Syngai, P. Barman, R. Bharali, and S. Dey, "BLAST: An Introductory Tool for Students to Bioinformatics Applications", Keanean Journal of Science, **2**, 67-76, 2013.

[7] R. S. Neumann, S. Kumar, and K. Shalchian-Tabrizi, "BLAST output visualization in the new sequencing era", Briefings in Bioinformatics, **15**(4), 484-503, 2014, doi: 10.1093/bib/bbt009.

[8] D. W. Kim, N. R. Kim, D. S. Kim, S. H. Choi, S. H. Chae, H. S. Park, "easySEARCH: A user-friendly bioinformatics program that enables BLAST searching with massive number of query sequences", Bioinformation, **8**(16), 792–794, 2012, doi: 10.6026/97320630008792.

[9] M. Thomas. "The BLAST Sequence Analysis Tool", The NCBI Handbook, 2013.

[10] G. L, Rosen, R. Polikar, R., D. A. Caseiro, S. D. Essinger, B. A. Sokhansanj, "Discovering the unknown: Improving detection of novel species and genera from short reads", Journal of Biomedicine and Biotechnology, 2011, https://doi.org/10.1155/2011/495849.

[11] B. K. Hall, "Homology and embryonic development", In M. K. Hecht, R. J. Macintyre, M. T. Clegg, eds, Evolutionary Biology, Springer, Boston MA, **28**, 1–37, 1995, https://doi.org/10.1007/978-1-4615-1847-1_1.

[12] D. S. Moore "Importing the homology concept from biology into developmental psychology", Developmental Psychobiology, **55**(1), 13–21, 2013, https://doi.org/10.1002/dev.21015.

[13] I. Brigandt, "Essay: Homology", In: The Embryo Project Encyclopedia, ISSN: 1940-5030, 2011, https://embryo.asu.edu/view/embryo:124921.

[14] R. W. Scotland, "Deep homology: a view from systematics", BioEssays, **32**(5), 438–449, 2010, doi: 10.1002/bies.200900175.

[15] N. D. Colin, P. Lior, "Evolution at the nucleotide level: the problem of multiple whole-genome alignment", Human Molecular Genetics, **15**(1), R51–R56, 2006, https://doi.org/10.1093/hmg/ddl056.

[16] B. Shankar, D. Vinod, M. Basavaraj, and P. Manjunath. "Comparative analysis of dynamic programing algorithms to find similarity in gene sequences", International Journal of Research in Engineering and Technology, **2**(8), 312-316, 2013.

[17] W. J. Kent, R. Baertsch, A. Hinrichs, W. Miller, and D. Haussler, "Evolution's cauldron: duplication, deletion, and rearrangement in the mouse and human genomes", Proc. Natl Acad. Sci. USA, **100**(20), 11484 – 11489, 2003, doi: 10.1073/pnas.1932072100.

[18] S. Batzoglou, "The many faces of sequence alignment". Briefings in Bioinformatics, **6**(1), 6–22, 2005, doi: 10.1093/bib/6.1.6.

[19] W. J. Kent, "BLAT—the BLAST-like alignment tool", Genome Res., **12**(4), 656–664, 2002, doi: 10.1101/gr.229202.

[20] D. Karolchik, R. Baertsch, M. Diekhans, T. S. Furey, A. Hinrichs, Y. T. Lu, K.M. Roskin, M. Schwartz, C.W. Sugnet, D. J. Thomas, et al., "The UCSC

Genome Browser Database", Nucleic Acids Research, **31**(1), 51–54, 2003, https://doi.org/10.1093/nar/gkg129.

[21] M. Brudno, A. Poliakov, A. Salamov, G. Cooper, A. Sidow, E. Rubin, V. Solovyev, S. Batzoglou, and I. Dubchak, "Automated whole-genome multiple alignment of rat, mouse, and human", Genome Res., **14**(4), 685–692, 2004, doi: 10.1101/gr.2067704.

[22] O. Couronne, A. Poliakov, N. Bray, T. Ishkhanov, D. Ryaboy, E. Rubin, L. Pachter, and I. Dubchak, "Strategies and tools for whole-genome alignments", Genome Research, **13**(1), 73–80, 2003, doi: 10.1101/gr.762503.

[23] M. Brudno, C. Do, G. Cooper, M. Kim, E. Davydov, E. Green, A. Sidow, S. Batzoglou, "LAGAN and Multi-LAGAN: efficient tools for large-scale multiple alignment of genomic DNA", Genome Res., **13**(4), 721–731, 2003, doi: 10.1101/gr.926603.

[24] S. Zhao, J. Shetty, L. Hou, A. Delcher, B. Zhu, K. Osoegawa, P. de Jong, W. Nierman, R. Strausberg, and C. Fraser, "Human, mouse, and rat genome large-scale rearrangements: stability versus speciation", Genome Res., **14**(10a), 1851–1860, 2004, doi: 10.1101/gr.2663304.

[25] A. Siepel, G. Bejerano, J. Pedersen, A. Hinrichs, M. Hou, K. Rosenbloom, H. Clawson, J. Spieth, L. Hillier, S. Richards, G.M Weinstock, R. K Wilson, R. A Gibbs, W. J Kent, W. Miller, D. Haussler, "Evolutionarily conserved elements in vertebrate, insect, worm, and yeast genomes", Genome Res., **15**(8), 1034–1050, 2005, doi: 10.1101/gr.3715005.

[26] E. H. Margulies, M. Blanchette, D. Haussler, E. D. Green, "Identification and characterization of multi-species conserved sequences", Genome Res., **13**(12), 2507–2518, 2003, doi: 10.1101/gr.1602203.

[27] W. M. Fitch, "Distinguishing homologous from analogous proteins", Syst. Zool, **19**(2), 99-113, 1970, doi.org/10.2307/2412448.

[28] M. Mathur and Geetika, "Multiple Sequence Alignment Using MATLAB," International Research Publications House, **3**(6), 497-504, 2013.

[29] S. F. Altschul, T. L. Madden, A. A. Schäffer, J. Zhang, Z. Zhang, W. Miller, D. J. Lipman, "Gapped BLAST and PSI-BLAST: a new generation of protein database search programs", Nucleic Acids Research, **25**(17), 3389–3402, 1997, doi: 10.1093/nar/25.17.3389.

[30] M. Adebiyi, J. Oghuan, S. Fatumo, E. Adebiyi, R. Jason, "A Functional Workbench for Anopheles gambiae Micro Array Analysis", Proceedings - UKSim-AMSS 7th European Modelling Symposium on Computer Modelling and Simulation, 138-143, 2013, doi:10.1109/EMS.2013.24.

[31] R. Caspi, R. Billington, I. M. Keseler, A. Kothari, M. Krummenacker, P. E. Midford, W. K. Ong, S. Paley, P. Subhraveti, P. D. Karp, "The MetaCyc database of metabolic pathways and enzymes, a 2019 update", Nucleic Acids Res, **48**(D1), 445–453, 2020, doi: 10.1093/nar/gkz862.

[32] R. A. Holt, G. M. Subramanian, A. Halpern, G. G. Sutton, R. Charlab, D. R. Nusskern, P. Wincker, A. G. Clark, J. M. Ribeiro, S. L. Hoffman et al., "The genome sequence of the malaria mosquito Anopheles gambiae", Science, **298**(5591), 149-159, 2002, doi: 10.1126/science.1076181.

[33] T. Wiehe, S. Gebauer-Jung, T. Mitchell-Olds, R. Guigo. "SGP-1: prediction and validation of homologous genes based on sequence alignments," Genome Research, **11**(9), 1574-1583, 2001, doi.org/10.1101/gr.177401.

[34] F. Zhang, and Y. C. Chen, "A method for identifying discriminative isoform-specific peptides for clinical proteomics application", BMC genomics, **17**(S7), 522, 2016, doi: 10.1186/s12864-016-2907-8.

A Recommendation Approach in Social Learning Based on K-Means Clustering

Sonia Souabi[*], Asmaâ Retbi, Mohammed Khalidi Idrissi, Samir Bennani

RIME TEAM-Networking, Modeling and e-Learning Team- MASI Laboratory- Engineering 3S Research center. Mohammadia School of Engineers (EMI), Mohammed V University, Rabat, 10000, Morocco

A R T I C L E   I N F O

A B S T R A C T

E-learning, among the most prominent modes of learning, offers learners the opportunity to attend online courses. To improve the quality of online learning, social learning through social networks promotes interaction and collaboration among learners. As part of the learning process management in these environments, the implementation of recommendation systems facilitates the provision of content adapted to the needs and requirements of learners and generates recommendations likely to arouse their interest. Many researchers have been involved in several recommendation techniques such as the development of Machine Learning algorithms and the incorporation of social interactions between learners. However, the behavior within a learning environment can diverge from one learner to another. This must therefore be taken into consideration when generating recommendations, i.e., it is initially important to form groups of homogeneous learners prior to proposing recommendations. In this respect, the recommendations generated will be more appropriate to the learners' profiles and level of interaction. On this basis, we raise an important issue which is the importance of grouping learners into homogeneous groups in a recommendation system. In the recommendation system we advocate, we group learners based on the degree of interaction within the learning environment before generating the recommendation list based on a hybrid approach for each cluster. The overall system is, therefore, based on the identification of communities based on the k-means algorithm and the generation of recommendations list for each community separately. Finally, we compare the results of the system integrating the classification of learners as a preliminary step to the system excluding the k-means algorithm. The results reveal that the integration of the clustering algorithm leads to improvements in terms of performance and accuracy.

1. Introduction

This paper is an extension of the work originally presented at the Fourth International Conference on Intelligent Systems and Computer Vision [1]. Currently, e-learning is emerging on a large scale around the world. When face-to-face learning is not available, e-learning allows students to bring order to their ideas and to continue to lead students in their learning process [2], [3]. Social networks, a modernized version of learning, fully promotes interaction and collaboration among learners [4], [5]. When a traditional learning platform is sometimes unable to provide effective collaboration between learners, social networks offer a multitude of options for learners encouraging responsiveness between them. However, the availability of online courses is not the only factor that contributes to the success of the learning process. Learners require a more highly organized learning environment responsive to their needs and profile. In this respect, recommendation systems are the perfect medium to perform this task and to manage learning resources within e-learning [6], [7]. The role of recommendation systems is to filter the information that aims to present different learning objects. Through recommendation systems, a certain organization is implemented within the learning environment and learners are more able to explore what is most interesting to them. Many recommendation systems have been proposed in the literature, including: the content-based approach, collaborative filtering and hybrid approaches [8]-[10]. Within the e-learning context, each proposed recommendation system addresses specific questions and handles an underlying issue identified at the recommendation system level. By way of example, several researchers address collaborative filtering to generate recommendations to learners [11]. Others

*Corresponding Author: Sonia Souabi, soniasouabi@research.emi.ac.ma

focus their attention on hybrid approaches to improve the performance of their recommendation system. Machine Learning algorithms have also been proposed as part of learning recommendation systems, including supervised and unsupervised algorithms [12]. Most recommendation systems use explicit feedback from learners, i.e., assessment by learners to generate recommendations. However, explicit feedback is sometimes an unreliable indicator for recommendations. On the other hand, an e-learning environment can include hundreds or thousands of learners with varying degrees of interactivity, constituting divergent groups, interactive and non-interactive learners. Most studies conducted on recommendation systems do not consider that point with respect to online learning. In this regard, we propose to group learners into homogeneous groups before generating recommendations. Our work aims at implementing a preliminary step in the calculation of recommendations, namely the detection of communities with the same level of interactivity. In our previous work, we proposed a hybrid recommendation system based on the activities performed by the learners. Within the same framework, the current work presents a continuity of the previous work while improving the old system with a new recommendation strategy integrating the k-means algorithm as a preliminary step. In this sense, we propose to classify learners according to well-defined criteria of interactivity within a social learning network, and then generate recommendations for each community separately. In this way, each community will receive its own recommendations adapted to its specific needs. The approach we propose brings considerable added value as it categorizes learners according to their level of interactivity before calculating recommendations.

The document is divided as follows: Section 2 deals with the research work related to the recommendation systems proposed in e-learning, especially those that consider Machine Learning algorithms. Section 3 explains the global recommendation approach based on correlation, co-occurrence and the k-means algorithm, section 4 presents the results of the tests performed on the approach without k-means and the approach with k-means with interpretation, and section 5 summarizes the work done in the paper.

2. Literature review

2.1. Recommender systems in E-learning

There are several types of recommender systems: content-based recommender systems, collaborative filtering recommender systems and hybrid recommender systems. Hybrid recommender systems generally combines between content-based techniques and collaborative filtering approaches. In E-learning, all these types of recommendations were addressed, but differently from one proposition to another. Some researchers discuss the analysis of activities in collaborative filtering within the educational field [13]. This work aims to use ontology and the semantic web to provide efficient recommendations. Others propose a recommendation approach to guide learners in developed countries to select more appropriate resources [14]. Calculations are based on developed knowledge and rating predictions. A recommendation system was suggested based mainly on two primary steps: pre-processing and prediction [15]. Multiple algorithms was used: SVM, KNN, Random Forest, and Naïve Bayes. A personalized recommendation system was developed based mainly on ontology using the java programming language [16]. Learning style and level of knowledge were addressed in a proposed recommender system [17]. The approach contains four modules relating to courses and learners.

2.2. Related works

In Machine Learning, unsupervised learning includes algorithms that should perform based on unannotated examples. K-means, one of the important unsupervised algorithms, is used to identify clusters with the similar characteristics and properties by working with gravity centres. The optimal number of clusters is usually obtained through several methods, including: elbow method, average silhouette method, gap statistic method. In online learning, k-means is handled for many purposes, for instance classifying learners according to their attitudes, their performance, interaction rates (...). In the literature, there is a multitude of works addressing k-means as an algorithm for classifying not only learners, but also items, users, in different contexts and areas, such as recommender systems.

A learning content recommendation system was implemented within a learning platform to generate recommendations in an intelligent way based on the learners' interest [18]. The proposed system aims to combine ontology and clustering algorithms using the collected ontology. A new recommendation system that combines the content-based approach and the k-means algorithm simultaneously was proposed [19]. The approach consists of performing a transformation on user data. Then, learners are grouped into clusters based on the content approach and the clustering algorithm, and thus recommendations will be generated from the detected clusters. Some researchers focus on methods to optimize k in the clustering algorithms in order to maintain the variance of each cluster [20]. The clustering was based on movie genres and tags. The objective is to correctly evaluate the recommendation algorithm based on user classification and use sophisticated measures such as mean square error, proximity centrality. Abnormal profiles in the context of recommendation systems was detected. A hybrid recommendation system that integrates both the k-means algorithm and ant colony optimization was suggested [21]. The evaluation was based on several measures including precision, recall and accuracy. Several approaches are based on clustering techniques in recommendation systems that are mainly based on group preferences. Several algorithms were compared to identify which algorithm gives better accuracy and higher results [22]. Some use k-means, others use k-NN, and the results were compared in terms of performance and number of clusters obtained. Instead of working with a traditional clustering algorithm, a mutli-clustering approach working on a set of clusters was proposed [23]. The advantage of this algorithm is its ability to visualize the neighbourhood in a clearer and more refined way, and the time efficiency is high. Contextual information was used to generate more relevant recommendations [24]. The proposed technique seeks to use the k-means algorithm to cluster contexts and generate new user matrices.

Based on researches in terms on recommender systems based on clustering algorithms , it comes out that k-means has been approached in many areas, such as e-learning, e-commerce, movies in order to generate more appropriate recommendations. Thus, we can notice that clustering algorithms has been adopted in recommender systems for different purposes in all the cited works.

On the other hand, clustering algorithms have not been adequately addressed in e-learning. In our context, we propose to use the k-means algorithm within a pure learning context and to combine it with a hybrid recommendation approach in order to generate more relevant recommendations. Our goal is to classify learners according to their degree of interactivity before calculating recommendations to generate a more relevant list of recommendations.
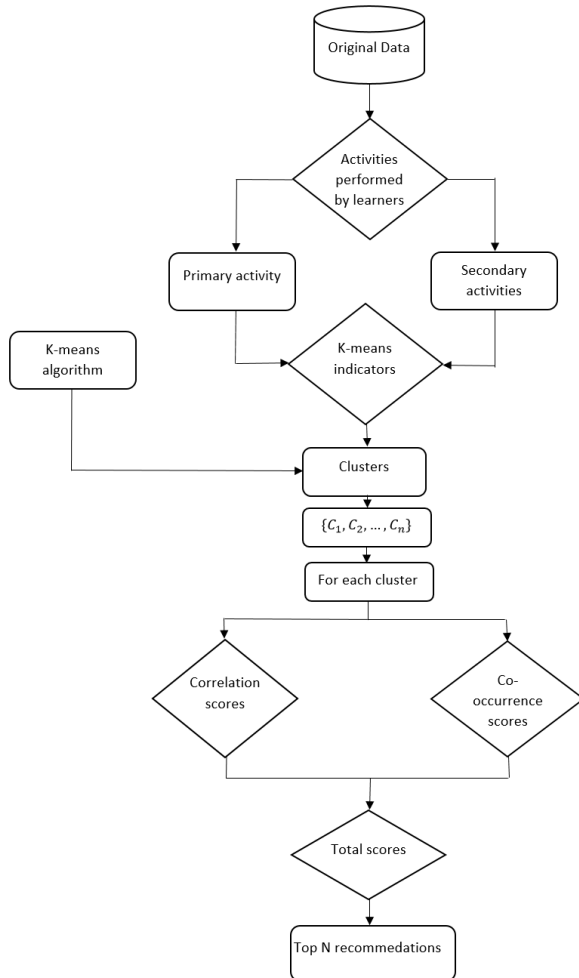
Figure 1: The recommendation system model proposed

3. Our proposed approach

3.1. K-means algorithm

Before proceeding to the description of our recommendation system, we will first define the k-means algorithm. The k-means algorithm is considered among the most widespread clustering algorithms. It consists of the analysis of a dataset containing several descriptors. The final goal is to group similar data in the same clusters. The idea is straightforward, all you need to do is to calculate the distance between the descriptors of two data to decide whether they are part of the same cluster. In a set of data, and to implement the k-means algorithm, there are the so-called centroids. Centroids are the key elements of the algorithm. The k-means relies on the centroids to detect the data closest to each centroid, and this loop continues until there is no further improvement in the distances between similar data, i.e. until the

algorithm converges. The algorithm below summarizes the different parts of the k-means algorithm (algorithm 1).

Algorithm 1: Concept of K-means Algorithm

Input
K optimum number of clusters
Output
Clusters or groups
Method
Selecting randomly K points. These are the centroids.
REPEAT
(1): Assign each point to the closest group according to centroids.
(2): Modifying centroids according to new clusters.
UNTIL CONVERGENCE

3.2. The proposed recommender system

The following flowchart (Figure 1) summarizes our recommendation approach.

The flowchart consists of several parts core to the proposed approach:

- The learners' actions in the database (sharing, communicating, downloading ...).
- The reconsideration of the initial data.
- The k-means algorithm.
- The different learning resources.
- The recommendation part.

In this part, we will describe each phase of the proposed approach separately:

a- First phase: The first phase consists in detecting the learners' actions in the database that have been carried out within the learning environment, for instance: sharing learning resources, sending private messages to other learners, downloading resources, exploiting resources. These actions are then grouped into two main categories: primary and secondary actions. The primary action is the action that can directly reflect learners' real preferences, for example, liking content, searching for content. It is through this indicator that we can ascertain learners' preferences. Secondary actions are also indicators of learner preferences, but are less consistent than the primary action.

b- Reconsideration of the initial data: This part consists in converging the data table into data that translate the interaction between learners and each learning object with respect to the selected actions, i.e. it is mandatory to restructure the database so that it meets our requirements for calculating recommendations.

c- The k-means algorithm: After restructuring the database, the next step consists in grouping the learners in clusters by selecting a number of descriptors. Each learner has a number of descriptors which are used to build the most similar clusters. Therefore, the choice of descriptors is an obvious prerequisite for applying the k-means algorithm.

d- Recommendations part: the last part consists of calculating the recommendations after detecting the clusters of the most similar learners. We will therefore generate the recommendations for each cluster separately. The idea is to consider the notions of correlation and co-occurrence in the calculation of recommendations, and thus to generate the final recommendations.

The hybrid recommendation algorithm combined with k-means algorithm is described below (algorithm 2).

Algorithm 2: Recommendation algorithm with k-means

Input
Learners data
Actions performed by learners
Output
Recommendations generated for each group
Method
1: Describing each learner by descriptors.
2: implementing the K-means algorithm based on previous list of learners and their descriptors.
3: Assign each learner to a specific cluster.
For each cluster
1: Calculate correlation and co-occurrence matrices.
2: Calculate recommendation scores based on previous step.
3: Find top N recommendations for each learner.
End for each

3.3. First stage: the k-means algorithm

➢ Define the descriptors

The database contains the learners' history, including the actions that are performed by the learners. We restructure the database to group learners according to two main descriptors:

- The first descriptor describes the level of interaction based mainly on the number of times an action has been performed.
- The second descriptor reflects the discrepancy between the actions performed by a learner.

Based on these two descriptors, it is possible to group learners into several clusters using the k-means algorithm within the learning platform. The indicators or descriptors are calculated as follows:

For a particular learner, the history of actions $\{a_1, a_2\}$ such as a_1 presents the primary action et a_2 is the secondary action, and the following resources $\{i_1, i_2\}$ (table 1 and table 2).

Table 1: Activities vs learning items structure

	a_1	a_2
i_1	x_1	x_2
i_2	x_3	x_4

Table 2: K-means descriptors

Learner 1	
First descriptor	$x_1 + x_3$
Second descriptor	$(x_1 + x_3) - (x_2 + x_4)/2$

For each learner, we will perform this operation, which allows us to classify learners according to these two indicators.

➢ Optimum number of K:

In order to properly apply the k-means algorithm, it is of paramount importance to define the optimal number k of clusters to be identified. One of the most successful methods for calculating the optimal number of k is the elbow method. It actually allows to specify the most adequate number of k to be considered since the

parameter k can change and can take several values. The elbow method consists in describing the variation according to the number of clusters. But in this case, what would be the optimal number? The optimal number k is simply the value from which the curve starts to take a constant value. So we will ensure that the value of k we selected represents the most accurate value for our context.

3.4. Second stage: The hybrid recommendation part

Now that the k-means algorithm is applied and clusters are detected, we now have the different groups of learners with similar behaviour in terms of interaction level. The rest of the work consists in generating recommendations through the calculation of recommendation scores for each learner pertaining to a given class. The proposed recommendation system is based on the calculation of correlation and co-occurrence scores through the analysis of the actions performed by the learners. In the following section, we will describe the mathematical model of our recommendation approach in detail:

The history matrix of learners =

	i_1			...			i_n		
l_1	a_1	...	a_m	a_1	...	a_m	a_1	...	a_m
⋮	⋮			⋮			⋮		
l_p	a_1	...	a_m	a_1	...	a_m	a_1	...	a_m

$\{i_1, \dots, i_n\}$: *Learner objetcs.*

$\{a_1, \dots, a_m\}$: *History actions performed by learners.*

$\{l_1, \dots, l_p\}$: *Learners.*

Referring to the basic matrix, which presents the learners' interaction with contents according to the selected actions, we generate recommendations for each cluster detected separately through the calculation of recommendation scores.

➢ Correlation

Correlation allows to identify the existing connection between two variables. Our context consists in calculating the correlation between the primary action and the secondary actions. The purpose is to situate the importance of the secondary actions in relation to the primary action to be used in the calculation of recommendations. We opted for the spearman correlation since it is the type of correlation that best suits our case, since it provides a way to evaluate the correlation in case of a non-normal distribution. We explain the notion of correlation in what follows (table 3 and eq. 1).

Table 3: General structure of correlation matrix

	a_1	...	a_m
a_1	1	...	$cor(a_1, a_m)$

⋮	⋮	⋮	
a_m	$cor(a_1, a_m)$	...	1

$$Correlation\ score = Total\ history\ matrix \times$$
$$\begin{bmatrix} 1 \\ \vdots \\ cor(a_1, a_m) \end{bmatrix} = \begin{bmatrix} s_{11} & \cdots & s_{1n} \\ \vdots & \cdots & \cdots \\ s_{l1} & \cdots & s_{ln} \end{bmatrix} \quad (1)$$

$\{(s_{11}, \ldots, s_{1n}), \ldots, (s_{l1}, \ldots, s_{ln})\}$ are scores of correlation for each particular learner towards each learning resource.

➢ Co-occurrence

Co-occurrence is defined as a measure to determine how many times two actions occur simultaneously in the same database. Learners generally do not react to the same actions in the same manner. They can be active in one action without engaging in another action. In this case, the co-occurrence between these two actions might be very weak. The role of co-occurrence is to define where two actions are linked at this level (table 4 and eq. 2).

Table 4: General structure of co-occurrence matrix

	a_1	...	a_m
a_1	$occurence(a_1)$	...	$co-occ(a_1, a_m)$
⋮	⋮	⋮	
a_m	$co-occ(a_1, a_m)$	...	$occurrence(a_m)$

$$Co-occurrence\ score \qquad\qquad (2)$$
$$= Total\ binary\ history\ matrix$$
$$\times \begin{bmatrix} occurrence(a_1) \\ \vdots \\ co-occ(a_1, a_m) \end{bmatrix} = \begin{bmatrix} p_{11} & \cdots & p_{1n} \\ \vdots & \cdots & \cdots \\ p_{l1} & \cdots & p_{ln} \end{bmatrix}$$

To generate the total recommendation scores, we proceed as follows (eq. 3).

$$Total\ score = Correlation\ score + co-occurrence\ score$$
$$= \begin{bmatrix} s_{11} + p_{11} & \cdots & s_{1n} + p_{1n} \\ \vdots & \cdots & \cdots \\ s_{l1} + p_{l1} & \cdots & s_{ln} + p_{ln} \end{bmatrix} \quad (3)$$

From the scores obtained, we extract the top N recommendations according to scores ranking.

4. Tests and results

In this work, we propose a recommendation system that aims to integrate the k-means algorithm within the system to generate more pertinent and reliable recommendations. Our intention is to prove that the k-means was efficient in generating more relevant recommendations and results. In order to test our recommendation approach for both cases, without k-means and with k-means, we selected two groups from a social network containing data on learners' interaction with the learning environment:

- The very first database consists of a set of 100 learners with many learning objects. We limited the number of learning objects to 10 and two actions, the primary action being the number of likes and the secondary action being the number of shares.
- The second database contains the same 100 learners from the first database, but interacting in a different social learning group. We selected some learning objects for the aforementioned actions: the number of likes and the number of shares.

The purpose of choosing these two databases is to highlight the performance of our recommendation system which incorporates the k-means algorithm, and which emphasizes the importance of grouping learners with similar attitudes in the same cluster. Homogeneity will be a major advantage in this case in terms of generated recommendations.

➢ Recommendation system evaluation:

The evaluation of the recommendation system is a prerequisite to measure its performance. In this respect, we divide the database into two major parts:

- The first part which consists in creating the recommendation model by referring to 80% of the data.
- The second part consists in measuring the accuracy and performance of the system by referring to 20% of the data.

We highlight the following measures (eq. 4 and eq. 5) according to specific parameters (Table 5).

$$Accuracy = \frac{TP + TN}{TP + TN + FP + FN} \quad (4)$$

$$Precision = \frac{TP}{TP + FP} \quad (5)$$

Table 5: Accuracy and precision parameters

	Recommended	Not recommended
Preferred	True positive (TP)	False positive (FP)
Not preferred	False positive (FP)	True positive (TP)

Before moving on to the application of k-means, it is important to identify the optimal number of clusters. In this sense, we use the elbow method which allows to plot the variation as a function of the K number. The optimal value we reach for both databases through the elbow method is 2.

In what follows, we will compare the results obtained through the application of the recommendation system not considering the k-means and the recommendation system identifying the number of clusters in the database before generating the recommendations (Table 6).

Table 6: Accuracy and precision for both recommender systems in the two databases

Database		Accuracy	Precision
First database	Without clustering	0,375	0,5
	Cluster 1	0,4	0,52
	Cluster 2	0,416	0,526
	Average between	0,408	0,523

	cluster 1 and cluster 2		
Second database	Without clustering	0,3	0,44
	Cluster 1	0,40625	0,55
	Cluster 2	0,406	0,525
	Average betwen cluster 1 and cluster 2	0,406	0,5375
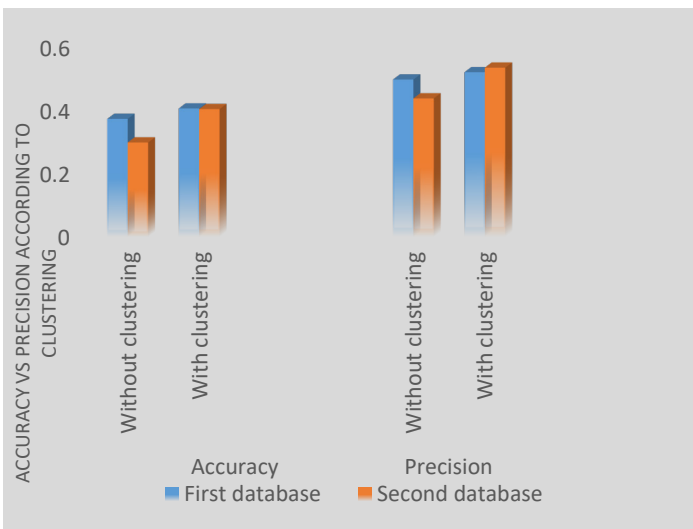
Figure 2: Accuracy and precision according to the two types of recommender systems (with k-means and without k-means)

Based on the results obtained (Figure 2), it appears that the recommendation system based on the classification of learners provides a higher performance compared to the recommendation system where community detection is not considered. A difference of 0.408-0.375=0.033 in terms of accuracy and 0.526-0.5= 0.026 in terms of precision. Apparently, the difference seems insignificant since the database is not of considerable size. Therefore, if the test is performed on a larger database the difference will be more noticeable. The same holds true for the second database where the difference in accuracy is 0.406-0.3=0.106 and the difference in precision is 0.5375-0.44=0.0975. These results highlight the importance of grouping learners according to their degree of interactivity before proceeding with the assignment of recommendations. Grouping learners with similar patterns of behaviour within the same community allows the generation of more adapted recommendations to their needs. Generating recommendations to learners with no prior classification reduces the performance of the recommendation system and provides recommendations that do not necessarily fit the needs of each community separately from the other. We recognize that the k-means algorithm brings considerable added value to the recommendation system due to the accuracy and performance improvements achieved. Grouping learners in homogeneous clusters facilitates the generation of recommendations.

5. Conclusion

The following work proposes a hybrid recommendation approach merging learner classification as a preliminary step before proceeding with recommendation calculations. In addition to the implicit feedback from learners that was integrated into the initial recommendation system, our approach proposes to group learners into communities with the corresponding degree of interactivity to improve the quality of the recommendations generated. Our approach consists in classifying learners according to specific interactivity criteria, then calculating recommendations for each community based on all the activities performed by the learners within the learning social network. On the one hand, the two notions of correlation and co-occurrence are combined in a unique hybrid recommendation system valuing the implicit feedback from the learners. On the other hand, the approach fosters the detection of homogeneous communities and clusters in order to generate recommendations more adapted to each community separately. The test was carried out on two databases of two different social learning groups, each consisting of 100 learners. The objective was to collect implicit feedback from learners within the learning environment. The results indicated that the recommendation approach based on the k-means algorithm leads to higher performance than the system without the k-means algorithm. This highlights the importance of classifying learners into homogeneous groups before generating recommendations. Our future work will consist of:

- Testing our recommendation approach on a larger database.
- Applying other algorithms other than k-means.

References

[1] S. Souabi, A. Retbi, M.K. Idrissi, S. Bennani, "A Recommendation Approach in Social Learning Based on K-Means Clustering," in 2020 International Conference on Intelligent Systems and Computer Vision (ISCV), IEEE, Fez, Morocco: 1–5, 2020, doi:10.1109/ISCV49265.2020.9204203.

[2] D.K. Abdul-Rahman Al-Malah, S. Ibrahim Hamed, H.Th.S. Alrikabi, "The Interactive Role Using the Mozabook Digital Education Application and its Effect on Enhancing the Performance of eLearning," International Journal of Emerging Technologies in Learning (IJET), 15(20), 21, 2020, doi:10.3991/ijet.v15i20.17101.

[3] E. Edelhauser, L. Lupu-Dima, "Is Romania Prepared for eLearning during the COVID-19 Pandemic?," Sustainability, 12(13), 5438, 2020, doi:10.3390/su12135438.

[4] A. Muradi, H. Hasanzada, "The Role of Social Networks in Learning English Language," 7(1), 10, 2020.

[5] C.G. Brinton, M. Chiang, "Social learning networks: A brief survey," in 2014 48th Annual Conference on Information Sciences and Systems (CISS), IEEE, Princeton, NJ, USA: 1–6, 2014, doi:10.1109/CISS.2014.6814139.

[6] A. Sekhavatian, M. Mahdavi, "APPLICATION OF RECOMMENDER SYSTEMS ON E-LEARNING ENVIRONMENT," 10, 2011.

[7] M.H. Ansari, M. Moradi, O. NikRah, K.M. Kambakhsh, "CodERS: A hybrid recommender system for an E-learning system," in 2016 2nd International Conference of Signal Processing and Intelligent Systems (ICSPIS), IEEE, Tehran, Iran: 1–5, 2016, doi:10.1109/ICSPIS.2016.7869884.

[8] D.M. Kandakatla, K. Bandi, "A Content Based Filtering and Negative Rating Recommender System for E-learning Management System," 7, 2018.

[9] S.K. Gorripati, V.K. Vatsavayi, "Community-Based Collaborative Filtering to Alleviate the Cold-Start and Sparsity Problems," 12(15), 9, 2017.

[10] A.N. Ngaffo, W.E. Ayeb, Z. Choukair, "A Bayesian Inference Based Hybrid Recommender System," IEEE Access, 8, 101682–101701, 2020, doi:10.1109/ACCESS.2020.2998824.

[11] S. Sharma, A. Mahajan, "A Collaborative Filtering Recommender System for Github," 5(8), 7, 2017.

[12] S.S. Khanal, P.W.C. Prasad, A. Alsadoon, A. Maag, "A systematic review: machine learning based recommendation systems for e-learning," Education and Information Technologies, 2019, doi:10.1007/s10639-019-10063-9.

[13] M. Brik, M. Touahria, "Contextual Information Retrieval within Recommender System: Case Study 'E-learning System,'" TEM Journal, 1150–1162, 2020, doi:10.18421/TEM93-41.

[14] J.-P. Niyigena, Q. Jiang, A Hybrid Model for E-Learning Resources Recommendations in the Developing Countries, Association for Computing Machinery, New York, NY, USA: 21–25, 2020.

[15] K. Chaudhary, N. Gupta, "E-Learning Recommender System for Learners: A Machine Learning based Approach," International Journal of Mathematical, Engineering and Management Sciences, **4**(4), 957–967, 2019, doi:10.33889/IJMEMS.2019.4.4-076.

[16] O.C. Agbonifo, M. Akinsete, "Development of an Ontology-Based Personalised E- Learning Recommender System," **38**(1), 12, 2020.

[17] Sunil, M.N. Doja, "An Improved Recommender System for E-Learning Environments to Enhance Learning Capabilities of Learners," in: Singh, P. K., Panigrahi, B. K., Suryadevara, N. K., Sharma, S. K., and Singh, A. P., eds., in Proceedings of ICETIT 2019, Springer International Publishing, Cham: 604–612, 2020.

[18] Saintgits College of Engineering, India, A. S Nath, "A Personalized Course Recommender System for E-Learning," International Journal of Networks and Systems, 11–14, 2019, doi:10.30534/ijns/2019/03832019.

[19] P. Cao, D. Chang, "A Novel Course Recommendation Model Fusing Content-Based Recommendation and K-Means Clustering for Wisdom Education," in: Zhang, J., Dresner, M., Zhang, R., Hua, G., and Shang, X., eds., in LISS2019, Springer Singapore, Singapore: 789–809, 2020.

[20] D. Cintia Ganesha Putri, J.-S. Leu, P. Seda, "Design of an Unsupervised Machine Learning-Based Movie Recommender System," Symmetry, **12**(2), 185, 2020, doi:10.3390/sym12020185.

[21] M.S. Kumar, J. Prabhu, "A hybrid model collaborative movie recommendation system using K-means clustering with ant colony optimisation," 18, 2020.

[22] Y. Yang, D. Hooshyar, J. Jo, H. Lim, "A group preference-based item similarity model: comparison of clustering techniques in ambient and context-aware recommender systems," Journal of Ambient Intelligence and Humanized Computing, **11**(4), 1441–1449, 2020, doi:10.1007/s12652-018-1039-1.

[23] U. Kużelewska, "Dynamic Neighbourhood Identification Based on Multi-clustering in Collaborative Filtering Recommender Systems," in: Zamojski, W., Mazurkiewicz, J., Sugier, J., Walkowiak, T., and Kacprzyk, J., eds., in Theory and Applications of Dependable Computer Systems, Springer International Publishing, Cham: 410–419, 2020.

[24] E. Kannout, "Context Clustering-based Recommender Systems," in 2020 15th Conference on Computer Science and Information Systems (FedCSIS), 85–91, 2020, doi:10.15439/2020F54.

Analysis of Gaze Time Spent at the Gazing Point that is Required During Reading

Yusuke Nosaka*, Miho Shinohara, Kosuke Nomura, Takuya Sarugaku, Mitsuho Yamada

Tokai University, Tokyo, 108-8619, Japan

A R T I C L E I N F O	A B S T R A C T
	This paper aims to clarify the lower limit of the gaze time required during reading by investigating at a display time of 98 msec or less using the visual information processing analyzer developed in the previous research. The image display range and display time at the point of gaze was controlled by moving the window in conjunction with the eye movement. As a result, it was found that normal reading, as if there were no window or visual field restriction, could not be performed with a display time of 42 msec or less, but that normal reading could be performed when sentences were displayed in a window of 7 characters at 56 msec. In this way, we believe we can obtain useful knowledge that is necessary for studying more effective methods of displaying text on electronic device.

1. Introduction

In recent years, information terminals such as smartphones and tablet terminals have been driving the spread of e-books. Before the popularization of smartphones and the like, many terminals exclusively for electronic books (e-books) were produced by various manufacturers, but since the introduction of the Apple iPhone in 2007, the use of e-books on smartphones rather than dedicated terminals has become mainstream. Not only does this make books highly portable, but books of various genres are also easily available online, making them more accessible.

Regarding research on electronic books, evaluations of the hardware include assessments of the size, weight, and resolution of the terminal on which the reading material is displayed, and the possibility of e-books replacing paper media has also been examined [1]-[3]. In addition, it has been reported that text on an electric display provides the same reading experience as text printed on paper if it is displayed at a high resolution [4]-[6]. Nevertheless, differences in reading between a display and paper, and differences in reading due to differences in display performance and operation have also been reported [7]-[9].

We have been studying e-books and traditional paper books, focusing on the differences in eye movements during reading. In particular, in the case of a paper book, the reader often gazes at the various places on the paper while turning a page and the reader's eye movements depend on how the page is turned. On the other hand, with an e-book, the reader's gaze moves linearly from the

end of the sentence of the previous page to the beginning of the next page [10]. By developing research on visual information processing with such eye movements, we will be able to develop a new display method for e-books that incorporates the characteristics of visual information that make it most easily absorbed by readers.

Human eye movements include saccade (intermittent and rapid step-like movement), smooth pursuit movement (smooth movement that occurs when following a moving object), and miniature eye movement (miniature involuntary movement that occurs when gazing at one point) [11]. The eye movement that occurs during reading is not a smooth pursuit eye movement that moves smoothly over the letters, but a repetition of a fixation, which is composed of miniature eye movements and occurs at a gazing point, and a saccade, which skips between fixation points. In addition to moving in the direction of sentence progression when reading, there is also a return movement, called regression, that moves in the opposite direction.

Research on eye movement during reading has a long history of more than a century, and many different researchers have reported useful results using various measurement methods.

In 1878, Javal, who observed and recorded eye movements reflected in a mirror, first reported that reading eye movements are repeated saccades and fixations [12]. Later measurement following Huey's method using an equipment like a contact lens made of a thin hardened layer of gypsum powder and a kymograph found that the number of fixations per line was 4 to 5 when the viewing distance was 33 to 42cm, and that that number did not change even

if the size of the characters was changed or the viewing distance was doubled; fixation duration likewise remained steady at about 200 msec. Furthermore, it has been reported that the average size of saccades is 3° to 4° [13]-[15]. Regarding fixation duration, Dearborn reports durations of 100 to 500 msec, with most falling between 200 and 300 msec [16]. Results for saccade and fixation similar to those in Huey's report have been found for reading in Japanese. It was reported that 2 to 8 characters are grasped observed in a single fixation and that the size of the saccade is also 2 to 8 characters [17], [18]. In addition, differences in the reading direction of sentences are being examined, and there have been many reports on eye movements during vertical and horizontal writing. Ohtomo reports that there was no difference in direction based on reading experiments of on vertical and horizontal writing in kanji and hiragana, kanji and katakana, hiragana, katakana, and romaji [19], [20]. Additionally, one report for a large influence of reading experience [21]. Although these studies were carried out early in the study of eye movements during reading, their results are still considered to be useful.

After the early research of the 1930s, the analysis of eye movements during reading received particular attention during the period from 1970 to 1980 with the development of computers and eye movement measurement devices. Past research on the perceptual range (effective visual field) during reading and the recognition of characters within the gazing point are considered to be highly compatible with e-books that can change display information in real time. In other research [2], a visual information processing analyzer that can control the image display range and display time at the point of gaze was also developed with reference to those eye movement studies. Furthermore, in experiments using this developed experimental device, it was reported that normal reading without restriction of the visual field can be performed by displaying images for 98 msec during gazing.

Therefore, this paper aims to clarify the lower limit of the gaze time required during reading by investigating at a display time of 98 msec or less using the visual information processing analyzer developed in the previous research. In this way, we believe we can obtain useful knowledge that is necessary for studying more effective methods of displaying text on electric device.

In this paper, previous research plays a major role. Therefore, Chapter 2 summarizes two similar studies on the perceptual range (effective field of view) that had significant effects on the previous study [22], and Chapter 3 describes the analyzers developed in the previous study and an experiment involving an image display time of 98 msec in detail. Chapter 3 indicates the approach of this research, Chapter 5 describes the method and results of this experiment, and Chapter 5 describes the conclusions and future developments.

2. Related Works

Since all parts of the visual field are not equally visible, it is thought that the amount of information processed is different if two locations in the field of view where information is presented are different. When performing various visual tasks, the part of the visual field from which information that is necessary for the tasks can be obtained is called the effective field of view. In this paper, "visual task" refers to reading.

There are various methods for investigating the effective visual field, including instantly presenting a character string or word using a tachistoscope (instantaneous presentation device) and estimating the readable range. Another method is that the number of characters viewed at a gazing point was estimated based on the record of eye movements in one line. All of these methods are based on estimation, and the departure from estimation is a method called windowing. The window is the area on the screen where the image is displayed. This method investigates the effective visual field by moving the window in conjunction with eye movement and changing the display information in the window during a period called saccadic suppression, in which the function of visual information processing in the brain decreases. If this window is smaller than the effective field of view, the reading time will be longer because less than the maximum amount of information will be obtained. Conversely, if the window is larger than the effective field of view, it will not be useful for reading, so the reading time becomes constant.

Research using the window method began with experiments by [23] and by [11], [24], [25]. The research by [22] solved the problems in these studies by developing a new analyzer. This section describes two studies of Saida and Ikeda and McConkie and Rayner and introduces the issues raised by Kushima and describes in detail the equipment developed by Kushima used in this study.

First, we explain the experiments of Saida and Ikeda. An image of the experimental equipment is shown in Figure 1. The subject's eye movements were acquired by the Limbus tracking method (a method of irradiating non-visible light such as near infrared rays to the black and white eye regions and calculating the difference of the reflected light). The acquired X-Y position information of the eye is input to the oscilloscope, and a rectangle is displayed at that position. Two TV cameras are prepared, the oscilloscope video is shot with TV camera 1, and a board with written text is shot with TV camera 2. The image of the rectangle shown on TV camera 2 is switched by the video switcher to the image on TV camera 1 using the wipe process. In this way, the displayed rectangular area, which is linked to eye movement, display the written text of the specified window width. The results of this experiment showed that if the size of the window exceeds 13 characters, it is possible for a viewer to read it as well as they would normally read without a window.
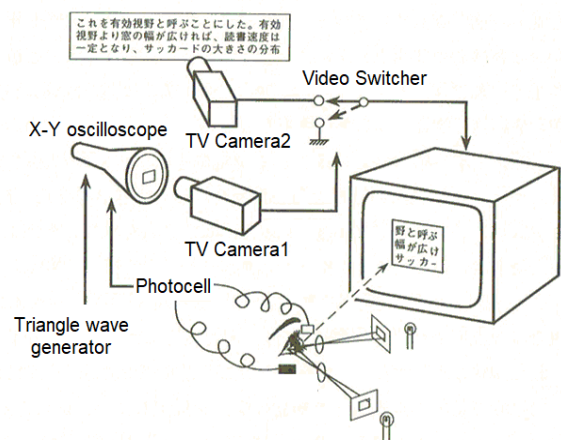
Figure 1: Experimental equipment by Saida and Ikeda [26]

Kushima point out the following issues regarding this experiment.

- In their experiment, a rectangle was displayed on the oscilloscope directly with the eye movement being the output, and the gaze area was not switched after the gazing point was detected.

- Since a camera and cathode ray tube (CRT) display were used at that time, it is expected that there would have been afterglow and an afterimage, but there was no description of this.

- Since the window moves in conjunction with eye movement, the display time of the window is considered to change depending on the gazing time, so the display time was not controlled.

On the other hand, in McConkie and Rayner's experiment the display (DEC Model 340) with built in uppercase and lowercase characters was controlled by inputting the eye movement acquired by the Limbus tracking method to a PDP-6 minicomputer. Since a character incorporated display was used, not only the masking of the gaze area, but also six patterns in which the characters in the window were replaced with X, x, characters with similar shapes, etc., were tested. The results of this experiment showed that the effective visual field was 13 characters, similar to the experiments of Saida and Ikeda. The following issues were raised in this experiment.

- Afterglow was only described as short afterglow, and it is not possible to determine how much afterglow or afterimage remained after switching.

- The saccade was not detected. If the eye movement exceeded a certain distance from the left edge of the sentence, the image in the window was switched, so the window was not displayed in the gaze area.

- There was no description of the display time of the characters in the window.

3. Research

An analyzer that overcomes the issues introduced in the previous chapter was developed in a previous study [22].

3.1. Overview of the developed analyzer used in this study

Table 1 shows the equipment used, Figure 2 shows the configuration diagram, and Figure 3 shows the flowchart.

Figure 2: System configuration diagram

Table 1: Experimental apparatus

Eye Movement Measuring Device	EMR-9 EYEMARK RECORDER (NAC Imaging Technology)
Sampling Rate	60Hz (serial communication), 120Hz, 240Hz
Resolution	0.1[degree]
Data Processing PC	OS Windows 7 Professional, Memory 32 GB, CPU core i7 3770
CRT Display	IIyama HM204A

The video output of the analyzer consists of a liquid crystal display for the experimenter and a CRT display (Figure 4; afterglow of 1 msec or less) for the subject. Liquid crystal displays are not used as displays for subjects because afterimages remain longer in the window after images are switched compared to CRT displays. The subject's CRT display shows only text, and the experimenter's LCD displays the EMR-9 (Figure 5) visual field camera image, allowing the subject's gazing point and text to be displayed. The system executes two threads in parallel. One thread acquires the position of the rectangle displayed on the CRT from the image of the EMR-9 field of view camera, and the other thread (on the left in Figure 3) obtains eye movement data from the EMR-9 by serial communication. Since the position of the rectangle shown on the CRT display is always obtained, head movement can be detected from the movement of the rectangle, and so the experiment can be performed in a natural posture without fixing the head. The saccade is detected by calculating the gazing point position, moving speed, rotation angle of eye movement, and

Figure 3: Flow chart

angular acceleration from the acquired eye movement data. When a saccade is detected, a window image is presented on the gazing point of the CRT display (Figure 3, left). When no saccade is detected, only the first three characters of each line are displayed. It was initially thought that it would be sufficient to display only the line that the subject is reading, but the subject does not always look at the center of the sentence. Since the size of the fovea, which has high visual acuity, is about 1°, the subject can read normally even if his or her gazing point deviates from the center of the character by ±1°. Since the center of the window is set at the center of the gazing point, in the case of horizontal writing the characters remain displayed in the window even if it shifts horizontally. However, if the window shifts vertically, part of each character may not be displayed inside the window when only one line is displayed. Furthermore, considering the accuracy of the EMR-9 (±0.1°), the upper and lower sentences were also displayed, so the size of the window was 3 lines in the vertical direction, and the number of characters in the horizontal direction was changed as a parameter.

Figure 6 shows an example of the change in the screen seen by the subject during the experiment. In Figure 6, the red filled circle represents the present gazing point (the red open circle represents the previous gazing point), and the blue frame shows the area displayed to the subject. When the gazing point moves and the termination of saccade is detected, a window image is displayed $\Delta t1$ seconds after the detection as shown in the lower right of Figure 6. The displayed window image is the text extracted from the sentence based on the size of the window. After the window image is displayed for $\Delta t2$ seconds, the masking image is displayed for one frame in the area where the window image was displayed. This process is repeated until the subject finishes reading, and the experimenter performs experiments by arbitrarily changing the values of $\Delta t1$ and $\Delta t2$. Kushima. measured eye movements during fixation to fixation movement imitating eye movements during reading, and suggest that eye movement speed (42 degrees/sec) is most appropriate for detecting the start and end of saccades as the threshold [22]. Therefore, eye movement velocity (42 degrees/sec) was used as the threshold value in the present study.

Since the retinal image is greatly blurred during the saccade, the perceptual function is reduced before and after the saccade so that the blurred image is not perceived. This phenomenon is called saccadic suppression [26]. The switching of the displayed image in the window must be performed within the period of saccadic suppression. Figure 7 shows the temporal ow of the processing. From Figure 7, it can be seen that there is a delay of 52 msec when the eye movement measurement device sends out the eye movement data by serial communication, and it takes about 2/60 sec (about 33 msec) to extract the gazing point; thus, it takes about 85 msec to detect the termination of a saccade. This means that the gazing period starts from 52 to 85 msec before the gaze point is extracted, and therefore the "fixation term" includes this period, as shown in Figure 7. Saccadic suppression continues after the saccade ends. The decrease in the detection rate due to the saccadic suppression recovers to 60% about 100 msec after the saccade, and to almost 100% in about 200 msec [27]. Considering this and the detection time of the saccade, Δ1 and Δ2 are varied.

Figure 4: CRT display

Figure 5: Eye movement analyzer
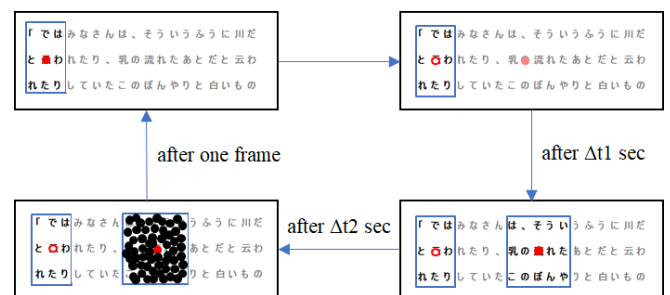
Figure 6: Example of screen change seen by the subject
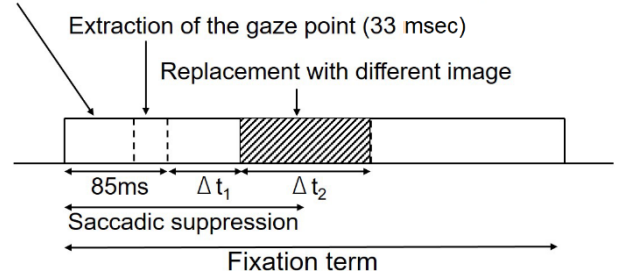
Figure 7: Time flow of processing

As described above, it is necessary to control the image replacement time of the gazing area in msec units. At a typical display refresh rate of 60 Hz, for example, drawing is performed approximately every 16.7 msec, so a delay of up to 16.7 msec is expected. In addition, if image switching of the gazing area occurs after the display is drawn, there is a possibility that image switching of gazing area does not occur on the display. To prevent this phenomenon, Kushima. implemented a vertical synchronization function to synchronize display drawing and program drawing.

Table 2 shows the differences between past research and research using the equipment developed by Kushima. First, in research by Saida and Ikeda, because the eye movement data are directly input into the oscilloscope and the rectangle is displayed, the window is not always displayed in the gazing area. However, since the gazing point is always acquired, a window can be displayed at the gazing point by the system developed by Kushima. Second, the study by Saida and Ikeda suggests that afterglow and an afterimage occurred because a camera and cathode ray tube (CRT) display were used together and, while McConkie and Rayner describe the afterglow as "short," they do not state how many characters remained when switching images. Under the system developed by Kushima, afterimages do not remain after image switching, and technological advances have reduced the afterglow time of CRT displays to less than 1 ms. Third, in the Saida and Ikeda's study, window display time was not controlled, and in McConkie and Rayner's research, since the gazing point is not detected, the image cannot be replaced for a certain period within the gazing time. However, since the gazing point is always acquired, the image can be switched within the gazing time, and the switching period can be controlled accurately by implementing the vertical synchronization function used in the system developed

by Kushima. Finally, because the gazing point is not detected, the image is switched in McConkie and Rayner's study according to the distance of the eye movement from the edge of the screen. In contrast, under the system developed by Kushima, the gazing point is always acquired, saccade detection is performed, and then the image is switched.

Here, we describe the experiments performed by Kushima in a previous study [2]. The subject in this experiment was a 21-year-old student. The experiment consisted of a training session and two main sessions. In the training session, the window width was changed from 17 characters to 3 characters at 2-character intervals for practice, and in the main session the window width was changed from 3 characters to 17 characters and from 17 characters to 3 characters. These experimental methods were based on the experiments of Saida and Ikeda, who conducted experiments using Japanese text. In the experiment, since the refresh rate of the CRT display was set to 72 Hz, image switching could be performed every 13.9 msec. Therefore, the experiment was performed with $\Delta 1$ set to 14 msec and $\Delta 2$ set to 98 msec.

Figure 8 shows the subjects' average reading time in the two main sessions. The horizontal axis in Figure 8 shows the window width, and the vertical axis shows the reading time(s). As shown in Figure 8, the reading time was greatly reduced between window widths of 3 and 5 characters, and the reading time did not change significantly when the window width was larger than 9 characters. Experiments by Saida and Ikeda showed that normal reading was possible when the window width was larger than 13 characters. As mentioned in the previous section, it was reported that the experiment by Kushima. showed the same tendency as the experiment by Saida, considering that the first three letters of each line were always displayed during Kushima' s experiment.

Table 2: Differences between past research issues and the equipment developed by Kushima

Issues in the research of Saida and Ikeda	Changes with the system developed by Kushima.
Because the eye movement data are directly input to the oscilloscope and the rectangle is displayed, the window is not always displayed in the gazing area.	Since the gazing point is always acquired, a window can be displayed at the gazing point.
It is thought that afterglow and an afterimage occurred because a camera and CRT display were used at that time.	Afterimages do not remain after image switching, and technological advances have reduced the afterglow time of CRT displays to less than 1 msec.
Window display time is not controlled.	Switching at the speed of the refresh rate of the CRT display is possible by implementing vertical synchronization function.
Issues in the research of McConkie and Rayner	**Changes with the system developed by Kushima.**
Description of the afterglow as "short" does not indicate how many characters were actually left when switching.	There is no afterimage when switching the display.
Since the gazing point is not detected, the image cannot be replaced for a certain period within the gazing time.	Since the gazing point is always acquired, the image can be switched within the gazing time, and the switching period can be controlled by implementing the vertical synchronization function.
Because the gazing point is not detected, the image is switched according to the distance of the eye movement from the edge of the screen.	The gazing point is always acquired, saccade detection is performed, and then the image is switched.
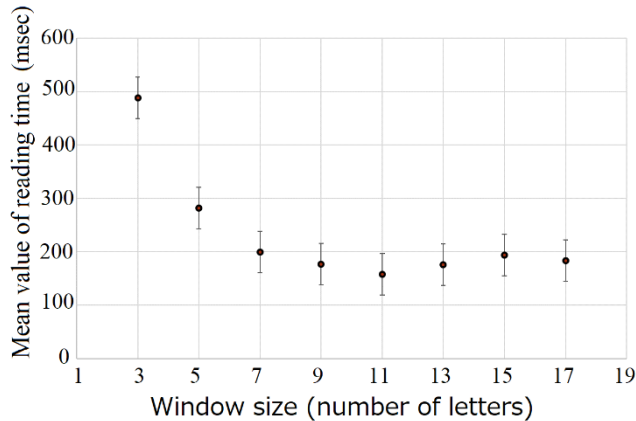
Figure 8: Average reading time [22]

4. The Approach of this research

In their research, only experiments with a display time of 98 msec were performed, and experiments with other display times were not performed. However, we think that reading is possible even with a shorter display time. Therefore, in this experiment, we decided to investigate the lower limit threshold of the gaze time that was necessary for reading by performing a similar experiment with a display time of 98 msec or less. The past research did not involve control of image switching time and display time, which are features of this device. Therefore, the approach in this paper is very novel, and we believe that it can show new possibilities for visual information processing during reading. In addition, since the experimental method was complicated and difficult, the authors deliberately described past research and Kushima' s research and clarified the position and purpose of the present research.

5. Experiments with variable window display time

5.1. Experimental method

An experiment was conducted to investigate the reading time at six different display times. The experimental method was based on the experiment of Kushima. In this experiment, it is necessary to align the literacy levels of the subjects and select the subjects who can acquire eye movements with high accuracy in advance. The measurement accuracy of the eye movement measuring device depends on the characteristics of the subject's eye, in addition to careful pre-calibration. That is, in order to maintain the accuracy of eye movement measurement at the character size level from the start to the end of the experiment, it is important to select the subject in addition to careful pre-calibration. Therefore, in a preliminary experiment conducted in advance, eight subjects aged 21 to 23 years (male) were selected from among many candidate subjects.

The experimental procedure consisted of a main session and two training sessions. The window width consisted of 8 images in the training session, and each window changed from 3 to 17 at 2-character intervals. Also, in the main session, 8 images were presented, and the characters were changed from 3 characters to 17 characters (up) and from 17 characters to 3 characters (down). The analysis was performed by averaging the reading times of the up series and down series measured in the main session for each

window width. The displayed images are excerpts from three novels from the copyright-free Aozora library: "Night on the Galactic Railway, "I Am a Cat," and "Bochan." As an example of the display image, "Night on the Galactic Railway," which was used in the training session, is shown in Figure 9. We used the early part of each novel to minimize any reading difficulty due to the content of the text. An example of the experimental environment is shown in Figure 10. The CRT display was placed at a viewing distance of 60 cm so that the subject's dominant eye was at the center of the image. The subject placed an eye patch on his or her non-dominant eye and stabilized his or her head on a chin rest. $\Delta t1$ was set at 14 msec, the same as in the previous study, and $\Delta t2$ was varied among 84, 70, 56, 42, 28, and 14 msec, all of which were 98 msec or less. A total of six types of $\Delta t2 \times 8$ different window sizes = 48 conditions. It is difficult to perform 48 experiments on a single subject with an eye patch on one eye. Therefore, we conducted experiments of 18 conditions per person so that reading times for 3 people could be obtained for each $\Delta t2$ and window size. We also experimented with combinations of subjects and sentences so that one subject did not read the same sentence multiple times. It has been found that the characteristics of saccades differ between reading with an emphasis on understanding sentences and reading with an emphasis on reading quickly [7]. In this experiment, in order to have the reader read in the former way, we informed the subjects before the experiment that they would perform a comprehension confirmation test after the experiment to align reading behavior among subjects.

5.2. Experimental result

Figure 11 shows a comparison of the average reading times measured for each display time. Here, the reading time was defined as the time from the start of reading to the end of reading. This comparison will clarify the display time that enables normal reading, and in the next step, additional subjects will be added to this display time for statistical examination. From Figure 11, it can be seen that the reading time is longer when the display time is shorter, and the reading time is shorter when the display time is longer. When the display time is 56 msec or more, the reading time does not change significantly when the window width is 7 characters or more, and when the display time is 42 msec or less, the reading time is longer than with the 56 msec display time, and the change in the reading time is large regardless of the window width expansion. In Kushima' s experiments, the reading time did not change significantly when the window width was 9 characters or more, so the tendency was similar to that in Saida's experiment. In the present experiment, the reading time converged when the display time was 56 msec or more and the window width was 7 characters or 9 characters or more, which is considered to be close to the tendency shown in Kushima' s results. On the other hand, when the display time was 42 msec or less, the reading time tended to be extended or to fluctuate without depending on the enlargement of the window width. This suggests that reading cannot be performed normally with a display time of 42 msec or less. However, from Figure 11, it is not possible to determine exactly whether the starting point at which the reading time did not change was the window width of 7 characters or 9 characters. Regardless of the window width, the trend remains the same as in previous studies, but a detailed investigation will improve the novelty of this experiment.

5.3. Examination of the minimum required number of characters in the window and display time

Further, experiment about a display time of 56 msec was performed with two new subjects, and a statistical study was performed on the data from all five sub jects. Here, based on the

「 で は み な さ ん は 、 そ う い う ふ う に 川 だ と 云 わ れ た り 、 乳 の 流 れ た あ と だ と 云 わ れ た り し て い た こ の ぼ ん や り と 白 い も の が ほ ん と う は 何 か ご 承 知 で す か 。」 先 生 は 、 黒 板 に 吊 し た 大 き な 黒 い 星 座 の 図 の 、 上 か ら 下 へ 白 く け ぶ っ た 銀 河 帯 の よ う な と こ ろ を 指 し な が ら 、 み ん な に 問 を か け ま し た 。 カ ム パ ネ ル ラ が 手 を あ げ ま し た 。 そ れ か ら 四 五 人 手 を あ げ ま し た 。 ジ ョ バ ン ニ も 手 を あ げ よ う と し て 、 急 い で そ の ま ま や め ま し た 。 た し か に あ れ が み ん な 星 だ と 、 い つ か 雑 誌 で 読 ん だ の で し た が 、 こ の ご ろ は ジ ョ バ ン ニ は ま る で 毎 日 教 室 で も ね む く 、 本 を 読 む ひ ま も 読 む 本 も な い の で 、 な ん だ か ど ん な こ と も よ く わ か ら な い と い う 気 持 ち が す る の で し た 。 と こ ろ が 先 生 は 早 く も そ れ を 見 附 け た の で し た 。「 ジ ョ バ ン ニ さ ん 。 あ な た は わ か っ て い る の で し ょ う 。」 ジ ョ バ ン ニ は 勢 よ く 立 ち あ が り ま し た が 、 立 っ て 見 る と も う は っ き り と そ れ を 答 え る こ と が で き な い の で し た 。 ザ ネ リ が 前 の 席 か ら ふ り か え っ て 、 ジ ョ バ ン ニ を 見 て く す っ と わ ら い ま し た 。 ジ ョ バ ン ニ は も う ど

Figure 9: Example of display image (Night on the Galactic Railway)

average reading time for a window width of 17 characters, we performed a t-test of the average reading times for other window widths at a significance level of 5%. Table 3 shows the results. The yellow cell in Table 3 is the p-value of the window width, which shows no significant difference from the average reading time of the 17-character window width. It shows that there is a significant difference between window widths of 3 characters and 5 characters, and it is clear that there is no significant difference when the window width is 7 characters or more. Comparing the p-values with those for window widths of 7 or more characters, it can be seen that there is a large difference between the 7-character and
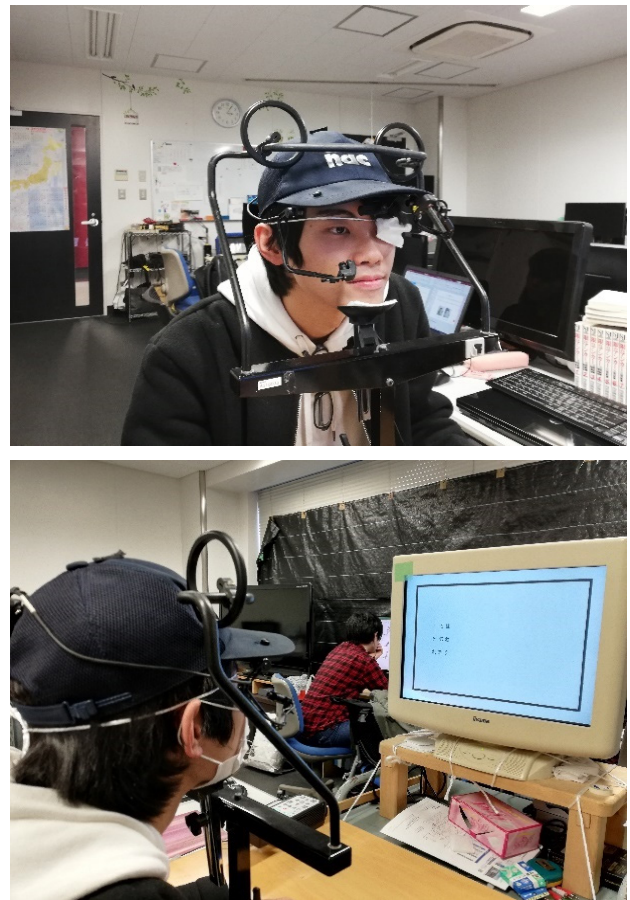
Figure 10: Example during experiment
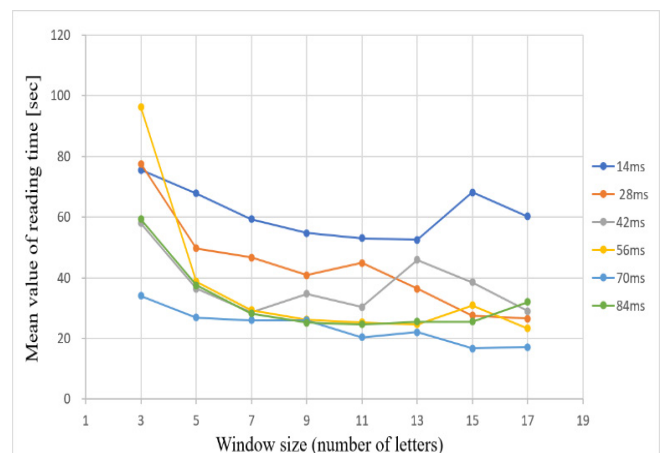
Figure 11: Comparison of average reading time at each display time

Table 3: Results of t-test of the average reading times for 17-character window width and other window widths (5%)

window width	3	5	7	9	11	13	15
p-Value	0.000299	0.008255	0.286812	0.801026	0.729294	0.941101	0.735377

9-character p-values, but they become almost constant at 9 or more characters.

According to the above results, it was shown in this experiment that reading can be performed in the same time required for normal reading without a visual field restriction only by displaying text in a window of 7 characters with a display time of 56 msec. The reason for the difference between our results and those of previous research is that while the previous research used sample texts extracted from a third grade, elementary school textbook, the present research used a text extracted from the Aozora Bunko (copyright-free Aozora library). Both texts were composed of the same level of kanji, hiragana, and katakana, but it is possible that the present study had slightly fewer kanji. It is extremely difficult to match the ratio among hiragana, katakana and kanji as well as the difficulty of the kanji, but doing so will be necessary to improve the accuracy of the experiment.

6. Conclusion

In recent years, the number of people reading e-books on smartphones and tablet terminals has been increasing. A major feature of these information terminals is that they can turn pages instantly, unlike conventional paper books. It has already been shown that this causes a difference in eye movement between e-books and paper books.

In this study, we conduct research on visual information processing during reading, and we believe that it is possible to develop a more efficient and easier to see method of displaying information on such terminals. In previous research, we identified problems with the use of windows in researching effective visual fields and developed a new visual information processing analyzer that overcomes them. Furthermore, experiments using the developed device showed that normal reading without any restriction of view was possible if images were displayed for 98 msec with a window width of 9 characters.

In this paper, we extended our previous research, and while the previous research only involved experiments with a display time of 98 msec, here we investigated the minimum display time required for reading. In this study, 18 experiments were performed to increase the variation of the display time and to collect data for three persons for each of six display times of 98 msec or less. As a result, it was found that normal reading, as if there were no window or visual field restriction, could not be performed with a display time of 42 msec or less, but that normal reading could be performed when sentences were displayed in a window of 7 characters at 56 msec. Additional subjects were added and the 56 msec display time was tested further, and this finding was statistically confirmed.

Although our previous research used only on a 98 msec display time because the main focus of that study was device development, in this experiment we investigated the lower threshold of the gaze time required for reading by changing the

display time. As mentioned in the experimental method, it is extremely difficult to select a subject who can maintain the accuracy of eye movement measurement at the character size level from the start to the end of the experiment, so this time we conducted an experiment using eight adult male subjects. We believe that advances in eye movement measuring devices will make it possible to acquire eye movements with greater accuracy with less dependence on the subject. We believe that it is necessary to further increase the number of subjects, add female subjects at the same time, and verify various age groups.

In the future, we would like to research visual information processing from additional angles, such as changing the composition ratio of hiragana, katakana, and kanji, the difficulty of the kanji, the length of the sentences, and the size of the characters. Furthermore, we think that this research not only proposes a display method on an electronic device, but also psychophysically can clarifies what kind of processing is performed in the brain and how long it takes for reading and character processing. We would like to develop it as an effective means to clarify information processing in the human brain in a non-invasive manner.

References

[1] H. Yaguchi: "A Study of e-book as Mobile Media," Japan Society of Publishing Studies, **40**, 45-62, 2009, doi : 10.24756/jshuppan.40.0_45.

[2] H. Yaguchi: "Conditions for the spread of e-book readers," Japan Printer, **93**, 11, 33-39, 2010-11-15.

[3] H. Shibata, Kentaro Takano, Kengo Omura: "Can electric reading devices replace paper," Fuji Xerox Technical Report, **21**, 98-109, 2012. in Japanese

[4] A. Dillon: "Reading from paper versus screens: a critical review of the empirical literature," Ergonomics, **35**, 10, 1297-1326, 1992, doi : 10.1080/00140139208967394.

[5] J. D. Gould, L. Alfaro, V. Barnes, R. Finn, B. Haupt, and A. Minuto: "Reading from CRT displays can be as fast as reading from paper," Human Factors, **29**, 5, 497-517, 1987, doi : 10.1177/001872088702900501.

[6] J. D. Gould, L. Alfaro, R. Finn, B. Haupt, and A. Minuto: "Why reading was slower from CRT displays than from paper," Proc. of CHI '87, 7-11, 1987, doi : 10.1177/001872088702900501.

[7] P. Muter, and P. Maurutto: "Reading and skimming from computer screens and books: The paperless office revisited," Behaviour and Information Technology, **10**, 4, 257-266, 1991, doi : 10.1080/01449299108924288.

[8] E. Wastlund, T. Norlandera, and T. Archerb: "The effect of page layout on mental workload: A dual-task experiment," Computers in human behavior, **24**, 3, 1229-1245, 2008, doi : 10.1016/j.chb.2007.05.001.

[9] A. Dillon, J. Richardson, and C. McKnight: "The effect of display size and text splitting on reading lengthy text from screen," Behaviour and

Information Technology, **9**, 3, 215-227, 1990, doi : 10.1080/01449299008924238.

[10] H.Takahira, R.Ishikawa, K.Kikuchi, T.Shinkawa, M.Yamada: "Analysis of Gaze Movement while Reading E-Books," IEICE Transactions on Fundamentals of Electronics, Communications and Computer Sciences, **E97-A**, 2, 530-533, 2014, doi : 10.1587/transfun.E97.A.530.

[11] G.W.McConkie, K.Rayner: "The span of the effective stimulus during a fixation in reading," Perception and Psychophysics, **17**, 6, 578-586, 1975, doi : 10.3758/BF03203972.

[12] E. Kowler: "Eye movements: The past 25 years," Vision Research, **51**, 13, 1457–1483, 2011, doi : 10.1016/j.visres.2010.12.014.

[13] K. E. Javal: "Essai sur la physiologic de la lecture, Annales d'oculistique," **79**, 97-117, 240-274, **80**, 135-147, 1878.

[14] E. B. Huey: "On the Psychology and Physiology of reading I," The American Journal of Psychology, **11**, 3, 283-302, 1900, doi : 10.2307/1412745.

[15] E. B. Huey: "On the Psychology and Physiology of reading II," The American Journal of Psychology, **12**, 3, 292-312, 1901, doi : 10.2307/1412280.

[16] E. B. Huey: "The psychology and pedagogy of reading," Macmillan, New York, 1908.

[17] W. F. Dearborn: "The psychology of reading," Columbia University Contributions to Philosophy and Psychology, **14**, 1, 1906.

[18] Kokishi Tanaka: "Basic research on language and reading," Meguro Shoten, Tokyo, 1916. in Japanese

[19] Chozo Matsuo: "Psychological Study of Reading," Psychological Series,**12**, Shinrigaku Kenkyukai, Tokyo, 1919.

[20] Shigeru Ohtomo: "Educational science issues," Toyo Tosho, Tokyo, 1927.

[21] Shigeru Ohtomo: "Educational Science Principles," Toyo Tosho, Tokyo, 1933.

[22] Tsuyoshi KUSHIMA, Miyuki SUGANUMA, Shinya MOCHIDUKI,and M itsuho YAMADA: "Development of a Novel Accurate Analysis System Re garding Information Processing Within the Gazing Point," IEICE Transacti ons on Fundamentals of Electronics, Communications and Computer Scien ces, **E102-A**, 9, 1205-1216, 2019, doi : 10.1587/transfun.E102.A.1205.

[23] Masaya SAIDA, Mitsuo IKEDA: "Sentence interpretation with limited field of view," Clinical ophthalmology, **29**, 8, 923-925, 1975, .

[24] K.Rayner: "The perceptual span and peripheral cues in reading," Cognitive Psychology, **7**, 1, 65-81, 1975, doi : 10.1016/0010-0285(75)90005-5.

[25] K.Rayner: "Parafoveal identification during a fixation in reading," Acta Psychological, **39**, 4, 271-282, 1975, doi : 10.1016/0001-6918(75)90011-6.

[26] Ryoji OSAKA, Yukio NAKAMIZO, Kazuo KOGA: "Experimental psychology of eye movement," Nagoya University Press, 1993.

[27] Volkmann, F.C., Shick,A.M. Riggs,L.A.: "Time course of visual inhibition during voluntary saccades," Journal of the Optical Society of America, **58**, 4, 562-569, 1968, doi : 10.1364/JOSA.58.000562.

Durability of Recycled Aggregate Concrete

Naouaoui Khaoula[*], Azzeddine Bouyahyaoui, Toufik Cherradi

Mohammadia School of Engineers, Mohamed V University Agdal, Rabat, 10000, Morocco

A R T I C L E I N F O	A B S T R A C T
	Many countries all over the world are promoting the recycled aggregate concrete for its advantage to solve the problem of shortage of natural resources in aggregates as well as promoting the recycling of waste and the reuse of materials. Recycled aggregate concrete replaces natural concrete with various rates of restitution of natural aggregates into recycled aggregates. The choice of rate is essential in the quality of the finished concrete and depends on the mechanical and durability characteristics. Tests in the civil engineering laboratory of the Mohammadia School of Engineers - Rabat Morocco have shown that above a rate of 30%, the mechanical characteristics drop. The addition of adjuvants / side products helps to increase this rate and a concrete with a 50% restitution can be used instead of natural concrete. Our study, the subject of this document, aims to study the durability of this concrete for various percentages of restitution. The experimental tests focused on determining the porosity of hardened concrete. The results were between 13 and 14% for all of the restitution percentages. This study concluded that for ordinary constructions, this concrete meets the criteria of the Perfertial Approach for durability. For projects with special criteria, other more in-depth studies will have to be carried out.

1. Introduction

Durability of concrete is the ability of concrete to resist to various types of damage, maintaining its strength and appearance integrity for its service period of exposure to its surrounding environment. Compared with nature aggregate concrete (NAC), the durability of recycled aggregate concrete (RAC) is usually weaker than NAC due to the adhered- mortar on the recycled aggregates (RA). The durability tests include deformation (drying shrinkage), impermeability, chloride penetration resistance, carbonation resistance, frost resistance and alkali aggregate reaction.

The benchmarking of many studies has demonstrated that the impermeability of RAC decreases with an increase of the replacement ratio of RA. Due to the capillary channels in the concrete system, fine elements of the recycled aggregates affects the impermeability more that the coarse ones [1-6]. In another side, the increase of coarse recycled aggregates increases the water absorption of concrete by immersion and capillarity regardless of the quality of RA.

For the chloride penetration resistance, the studies prove that it is lower in the RAC compared to NAC [7]. However, it was found that when RA was prepared with a low water /cement (w/c) ratio, it exhibits better performance than NAC in a chloride environment, probably due to the presence of higher C-S-H gels in RAC, which assists in chloride binding [8]. The carbonation depth increases, as many other durability properties, with the increase of RA replacement ratio. Many studies focused on the influence of different parameters on the carbonation resistance. They found that the increase of RA content, w/c ratio, and adhered mortar have a strong negative effect on it, the increase of exposure time or pozzolanic materials have negative effect when the presence of super-plasticizers, the pre-treatment of RA and the use of innovated mixing method affect positively the carbonation resistance.

Concerning the weak frost resistance, the RAC is not recommended in a harsh environment. However, the RAC, with a w/c ratio below 0.5 and incorporating 5% air content, can still be used in unsaturated and moderate cold climates [9]. The reduction of the amount of mixing water and the water saturation of the samples or the incorporation of a proper amount of fly ash and an air-entraining agent can help to improve the frost resistance [9-12].

[*]Corresponding Author: NAOUAOUI Khaoula, Mohammadia School of Engineers, Mohamed V university agdal Rabat, naouaoui.khaoula@gmail.com

Many methods have been proposed to improve the durability of concrete based on recycled aggregates [13-16] such us removing the adhered mortar of RCA. The adhered mortar content in RCAs has an obvious impact on strength and durability of RAC. Due to the presence of the adhered mortar, RCAs have a higher permeability than the natural aggregates.

Another method proposed is the use of the Two-Stage Mixing Approach (TSMA). The technique used is to divide the mixing process into two parts and proportionally splits the required water into two, which are added at different times us shown in Figure 1 illustrating the difference between normal mixing approach and TSMA mixing procedures [17].
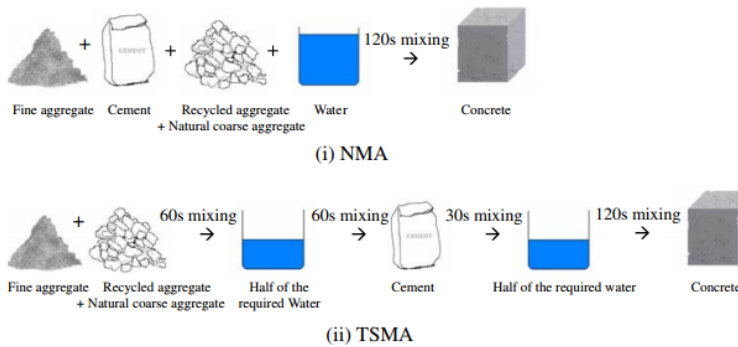
Figure 1: Mixing Procedures of the (i) Normal Mixing Approach and (ii) Two-Stage Mixing Approach

The Experimentation highlights that the deformation and permeability of RAC can be enhanced by adopting TSMA with up to 68.09% on shrinkage (with 100% RA substitution after 14 days of curing). The increase is up to 46.42% on creep (with 100% RA substitution after 14 days of curing), 35.41% on water permeability (with 100% RA substitution after 126 days of curing), 51.81% on air permeability (with 20% RA substitution after 56 days of curing) and 29.98% on chloride permeability (with 100% RA substitution after 126 days of curing).

The third improvement method proposed is to enhance the characteristics of RCA without removing adhered mortal by using physical and chemical methods. The main methods used are [18] the impregnation by a foreign chemical to block the open porosity of RCA or the Use of polyvinyl alcohol (PVA)-impregnated method to improve the resistance to chloride-ion penetration. We might also use materials as additives like pozzolanic materials (specially pulverized fly ash or ground granulated blast furnace slag) or water repellent to improve the cement matrix in RAC and enhance the durability by reducing the permeability of RAC. These techniques may have inconvenient like reducing the compressive strength of RAC [14, 15, 19, 20]. We can also adopt an accelerated carbonation technique to enhance the quality of RCA as well as the mechanical properties.

2. Compressive strength of recycled aggregate concrete: Overview of the experimental study

Recycled aggregate concrete is a large-scale concrete that has been used in several countries for years.

In Morocco, RCA is subject to several types of research in order to encourage its local use.

As part of the valuation of the RAC, a mechanical comparison was drawn up in order to highlight the technical possibility of replacing normal concrete with recycled aggregate concrete.

The study protocol is devised to three main parties: Study of the characteristics of recycled aggregates (water content, water absorption) in order to highlight the quality of the aggregates. The second step is the formulation of the RAC according to the Dreux-Gorisse method based on the desired characteristics in the concrete and on the particle size analysis of natural and recycled aggregates and finally the compressive strength experimental tests.

2.1. Water content (W %)

The water content is equal to the ratio of the mass of water contained in the sample to the mass; we can calculate it using the following relation:

$$W = 100 * \frac{M - M_S'}{M_S} \tag{1}$$

with

W: Water content

M: The mass of the sample

M's: The mass of the sample oven dried at 105 ° C to constant mass without prior washing.

M s: The mass of the sample washed on the 4 mm sieve and oven dried at 105 ° C to constant mass.

Table 1: Water content experimental results

Recycled aggregates 5-12.5			Recycled aggregates 12.5-31.5		
M (g)	M's (g)	M s (g)	M (g)	M's (g)	M s (g)
2000	197.6	1975.32	2000	1915	1963.8
W			W		
1.49%			4.32%		

The comparison between two recycled aggregates of two different classes: Recycled aggregates with particle size 5-12.5 and recycled aggregates with particle size 12.5-31.5 showed that the water content is greater for large aggregates. This is justified by the presence of several pores, which disappear during the fine crushing of the aggregates.

2.2. Water absorption rate (AB %)

Water absorption by definition is the quotient of the mass of a sample immersed in water for 24 hours at 20 ° C and atmospheric pressure, by its dry mass. It is determined according to the relation below:

$$A_b = 100 * \frac{M_a - M_S}{M_S} \tag{2}$$

where:

Ab: Water Absorption

Ms: The mass of the sample washed on the 4mm sieve and oven dried at 105 ° C to constant mass.

Ma: The mass of the sample immersed in water for 24 hours at 20 ° C at atmospheric pressure and carefully blotted with an absorbent cloth.

Table 2: Water absorption rate experimental results

Recycled aggregates 5-12.5		Recycled aggregates 12.5-31.5	
Ms (g)	Ma(g)	Ms(g)	Ma(g)
1975.32	2194.8	1963.8	2148.4
Ab		Ab	
11.11%		9.4%	

The comparison between the two recycled aggregates of two different classes has shown that the water absorption rate is higher for small aggregates. This is justified by the superiority of the contact surface.

2.3. Particle size analysis

The particle size analysis is the main experimental step to formulate the concrete and to compare the recycled aggregates with the natural ones, the results of the particle size analysis are as follows, and the graph represents the rate of cumulative sieves relative to each opening of the sieve. The sieves used are standards ranging from 0.08 to 31.5mm.

The four aggregates tested are: GR 5-12,5 relative to recycled aggregate with particle seize between 5 and 12,5 mm , GR 12.5-131.5 relative to recycled aggregate with particle seize between 12.5 and 31,5 mm, GN 5-12,5 relative to natural aggregate with particle seize between 5 and 12,5 mm GN 12.5-31.5relative to natural aggregate with particle seize between 12.5 and 31.5 mm.
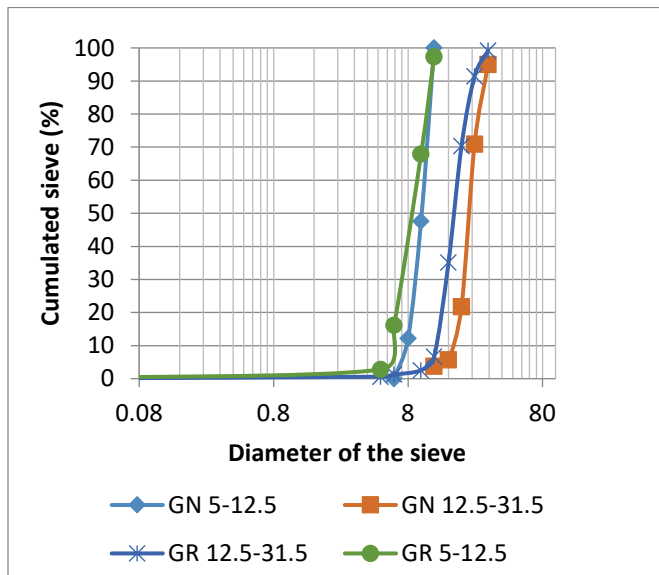
Figure 2: Granular curve for natural and recycled aggregates used in experimental study.

The interpretation of the granular curves shows that:

• The backbone of GR5-12.5 and GN5-12.5 is almost identical, at the opening 10 mm for example the percentage of the cumulative sieve of GN5-12.5 is almost 50% and of GR5-12.5 is 60%.

• The distribution of the various sizes of GR12.5-31.5 and GN12.5-31.5 aggregates is different.

Table 3: Differences between GR2 and GN2 in term of size analysis.

Diameter of the standard sieve	Cumulated sieve %	
	GN12.5-31.5	GR12.5-31.5
5	0,00	0,60
12,5	3,77	6,64
16	5,76	35,10
20	21,81	70,35
25	70,87	91,41
31,5	100,00	99,13

This distribution is favorable for GR12.5-31.5, it allows having less voids and pores in our concrete, which compensate for the defects of the recycled aggregates.

Based on the particle size analysis, the formulation chosen using Dreux-Gorisse method is:

Table 4: Concrete formulation

Component	Volume (m³)	Mass (kg)
Water	0.19	190
Cement	0.29	350
Sand	0,17	472,85
Gravel 5-12.5	0,15	376,14
Gravel 12.5-31.5	0,2	537,3

2.4. Compression test of pre-established concrete specimens

Compressive strength is the main characteristic of concrete in the medium term; identification tests and comparisons were carried out in the civil engineering laboratory of the Mohammadia School of Engineers and were based on changes in the replacement rate. Natural aggregates with recycled aggregates by opting for 0, 20, 30, 50, 75 and 100% recycled aggregates.
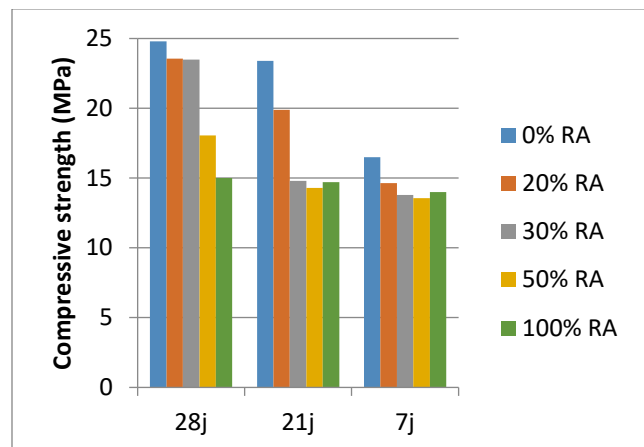
Figure 3: Compression test experimental results

The results interpretation is focused on the results at 28 days, we notice that with the increase in the replacement rate the compression decreases whether it is short term. We also notice that beyond 30% replacement the decrease in the value of compression exceeds 10%.

The second stage of the tests consists of improving the quality of the concrete in order to broaden its field of use and increase the replacement rate.

The proposed solution is to add various types of admixture in order to see the effect on the compressive strength of the type of admixture and the percentage of restitution used.

Our protocol is fixed on the use of three adjuvants: Plasticizer: BV 40, Super-plasticizer: Tempo 10M and the new generation super-plasticizer: SFR. These products are from the SIKA brand produced by SIKA MAROC installed in BOUSKOURA - Casablanca.

The choice of these three types is justified by the fact that we wanted to determine the effect of the type of admixture on our concrete.

Table 5: Compression test experimental results with and without adjuvant

% of RA	Compressive strength at 28 days without adjuvant – MPa	Compressive strength at 28 days with adjuvant (Tempo 10 M- 1%) - MPa
25	23.52	24,3
50	18,05	21,45
75	17,7	20,47
100	15	19,65

Results show that adding admixture improves compressive strength.

A comparison between various types of adjuvant proves that the plasticizer and super-plasticizer give better results than the new generation super-plasticizer as shown in table 5.

Table 6: Compression test experimental results with different adjuvants

% of RA	Type of adjuvant	% of adjuvant	Compressive strength at 7 days - MPa	Compressive strength at 28 days-MPa
50	BV40	1%	19,87	22,63
	SFR		11,50	16,65
	Tempo 10 M		17,47	21,45

The interpretation of these results is that adding a fairly complicated and developed formulation full of additive does not interact well with our attached cement.

The choice of the percentage of replacement of the binder by adjuvant is essential in the expected results. For each adjuvant, a recommended range of use is specified on the technical sheet for each product.

Experimental tests alone are able to choose the optimum value.

In our case, 1% constitutes our value chosen as being equivalent to the maximum of the test results (table 7)

Table 7: Compression test experimental results with different percentage of the adjuvant

% of RA	% of adjuvant	Type of adjuvant	Compressive strength at 7 days - MPa	Compressive strength at 28 days- MPa
50%	0.5%	Tempo 10 M	14,35	19,9
	1%		17,47	21,45
	1.5%		12,87	16,03

3. Porosity and density of hardened concrete

The porosity test was carried out according to NF P18-459 [21]

The test protocol is as follows:

- Formulation of concrete according to the quality required in test format,

- Leave 28 days in order to carry out tests on hardened concrete at 28 days of service life,

- After 28 days, place the test piece in a vacuum apparatus at a P <25 mbar for at least 4 hours,

- Reconnect the container to the vacuum pump and gradually introduce the imbibition liquid (drinking water) so that after 15 min the test pieces are covered with approximately 20 mm of water and maintain this pressure for a minimum of 44 hours.

Figure 3: the test pieces placed in the vacuum apparatus for 24 hours

The test carried out according to standard NF P 18-459 aims to determine the densities and porosities of various samples with different percentages of recycled aggregates replacing natural aggregates.

The density will thus be

$$\rho_d = \frac{M_{sec}}{M_{air} - M_{eau}} \times \rho_{eau} \qquad (3)$$

And the porosity

$$£ = \frac{M_{air} - M_{sec}}{M_{air} - M_{eau}} \times 100 \qquad (4)$$

with

M_{eau}: The mass of the specimen inhibited in the suspension system of the hydrostatic balance.

M_{air}: The mass of the test tube measured immediately after removing it from the water and wiping quickly to remove surface water without removing water from the pores.

M_{sec} : The mass of the oven-dried test piece.

The tests were carried out in an approved laboratory as part of the durability study of concrete made from recycled aggregates. The protocol is illustrated below:

Figure 4: Procedure for calculating M_{eau}

The results of the tests are collated in the following tables:

Table 8: The density experimental results

	M_{sec}	M_{air}	M_{eau}	ρ_d	
100%	2322,2	2464,1	1444,8	2,278	2,277
	2318,7	2459,4	1442,5	2,280	
	2310,3	2450,7	1434,8	2,274	
75%	2324,5	2465,6	1430,1	2,244	2,244
	2298,4	2439,9	1415,8	2,244	
	2298,3	2434,8	1410,9	2,244	
50%	2263	2423	1240,5	1,913	1,920
	2271,6	2429,4	1247,7	1,922	
	2284,1	2440,8	1254,3	1,925	

Table 9: The porosity experimental results

	M_{sec}	M_{air}	M_{eau}	£	
100%	2322,2	2464,1	1444,8	13,921	13,859
	2318,7	2459,4	1442,5	13,836	
	2310,3	2450,7	1434,8	13,820	
75%	2324,5	2465,6	1430,1	13,626	13,591
	2298,4	2439,9	1415,8	13,817	
	2298,3	2434,8	1410,9	13,331	
50%	2263	2423	1240,5	13,530	13,36
	2271,6	2429,4	1247,7	13,353	
	2284,1	2440,8	1254,3	13,206	

3.1. Results interpretation

The density increases with the increase in the rate of restitution. This is justified by the difference between the density of natural aggregates around 2000kg / m³ and the density of recycled aggregates from reinforced concrete with a density of 2500kg / m³

- Porosity, too, changes with the increase of recycled aggregates. This is justified by the characteristics of the recycled aggregates which consist of a natural aggregate coated in old cement, all coated in cement.

In order to interpret the results of our concrete in relation to its performance in terms of durability, the summary table of indicators following the Performantial Approach is used, based on various sustainability guides. (Table 10)

The buildings are subdivided into five categories according to the required lifespan:

- < 30 years

- From 30 to 50 years old: Building

- From 50 to 100 years: Building and civil engineering works

- From 100 to 120 years: Major works

- > 120 years: So-called exceptional works

Our study will be based on the first three categories due to the primary choice of the types of projects targeted by our concrete, which can be summed up in ordinary construction: Building or landscaping.

Based on durability indicators following the Performantial Approach, the recycled aggregates concrete might be used for all constructions with a lifespan of less than 30 years and all constructions with a lifespan of 30 to 50 years (Building) except those in:

• Tidal zone
• Immersion in water containing chlorides
• High exposure to sea salts or de-icing, but not in direct contact with seawater

Table 10: Summary table of indicators following the Performantial Approach[22] (P: porosity)

50 -100 Building and civil engineering works Level 3	30- 50 Building Level 2	< 30 Level 1	Required life Construction category Requirement level		Environment type →	
P < 14	P < 16	P < 16	- Dry and very dry (RH <65%) - Permanently wet (including immersion in fresh water)		1	Corrosion induced by carbonation (e = 30 mm)
P < 14	P < 16	P < 16	Wet, rarely dry (RH> 80%)		2	
P < 12	P < 14	P < 15	Moderate humidity (65 <RH <80%)		3	
P < 12(5)	P < 14(4)	P < 16	Periods of humidity alternating with dry periods without chloride (de-icing salts, spray, etc.)		4	
P < 14	P < 15	P < 16	5.1 : low [Cl-]	Exposure to sea salts or de-icing, but not in direct contact with seawater	5	Chloride induced corrosion (e = 50 mm)
•P < 11	P < 11	P < 14	5.2 : high [Cl-]			
•P < 13	P < 13	P < 15	Immersion in water containing chlorides		6	
•P < 11	P < 11	P < 14	Tidal zone		7	

Added to this, the possible use of the concrete is constructions with a lifespan of 50 to 100 years (Building and Civil Engineering Works) under the following conditions:

- Low exposure to sea salts or de-icing, but not in direct contact with sea water

- Humid environment, rarely dry (RH> 80%)

- Dry and very dry environment (RH <65%)

- Permanently humid environment (including immersion in fresh water)

Depending on the durability indicators, to use the concrete is other types of construction other in-depth studies should carry out and improvement in the concrete quality should be made.

4. Conclusion

This article is part of a series of test protocols carried out as part of the study of the performance of recycled aggregate concrete.

The study began with a mechanical comparison of ordinary concrete with recycled aggregate concrete with various replacement rates. These tests allowed us to deduce that for a basic concrete (without additions), the maximum replacement rate to meet the development conditions is around 25-30%. Beyond this value, training improvements will need to be made. In this sense, the addition of various admixtures has enabled us to deduce that super-plasticizers improve the quality of our concrete for replacement rates of 30 to 50%. Other changes might been used as explained in many researches studies: Change in the E / C ration, restitution of aggregates on one class only, primary sorting of aggregates.

The next step, the subject of this article, was to study the durability of recycled aggregate concrete. This study proves us that, overall, our new formulation complies with regulations in terms of manageability indicators for basic constructions.

At this stage, in order to finalize our protocol, an overview with a technical-economical comparison must be made in order to conclude the technical and economic reliability of the proposed product.

Conflict of Interest

The authors declare no conflict of interest.

References

[1] H. Guo, C. Shi, X. Guan, J. Zhu, Y. Ding, T.C. Ling, H. Zhang, Y. Wang , "Durability of recycled aggregate concrete – A review", Cement and Concrete Composites, **89**, 251-259, 2018, doi: 10.1016/j.cemconcomp.2018.03.008

[2] S.H. Liu, P.Y. Yan, "Properties and microstructure of high performance recycled aggregate concrete", Journal-chinese ceramic society, **35**(4), 456-460, 2007.

[3] J. de Brito, J. Ferreira, J. Pacheco, D. Soares, M. Guerreiro, "Structural, material, mechanical and durability properties and behaviour of recycled aggregates concrete", Journal of Building Engineering, **6**, 1-16, 2016, doi : 10.1016/j.jobe.2016.02.003.

[4] M. Bravo, J. de Brito, J. Pontes, L. Evangelista, "Durability performance of concrete with recycled aggregates from construction and demolition waste plants", Construction and Building Materials, **77**, 357-369, 2015, doi: 10.1016/j.conbuildmat.2014.12.103

[5] I. Martínez-Lage, F. Martínez-Abella, C. Vázquez-Herrero, J.L. Pérez-Ordóñez, "Properties of plain concrete made with mixed recycled coarse aggregate", Construction and Building Materials, **37**, 171-176, 2012, doi: 10.1016/j.conbuildmat.2012.07.045

[6] R. Kurda, J. de Brito, J. D. Silvestre, "Combined influence of recycled concrete aggregates and high contents of fly ash on concrete properties", Construction and Building Materials, **157**, 554-572, 2017, doi: 10.1016/j.conbuildmat.2017.09.128.

[7]   O. Nobuaki, M. Shin-Ichi, Y. Wanchai, "Influence of recycled aggregate on interfacial transition zone, strength, chloride penetration and carbonation of concrete", Journal of Materials in Civil Engineering, **15**(5), 443-451, 2003, doi: 10.1061/ (ASCE) 0899-1561(2003)15:5(443).

[8]   E. Vázquez, M. Barra, D. Aponte, C. Jiménez, S. Valls, "Improvement of the durability of concrete with recycled aggregates in chloride exposed environment", Construction and Building Materials, **67**, 61-67, 2014, doi : 10.1016/j.conbuildmat.2013.11.028.

[9]   R.M. Salem, E.G. Burdette, N.M. Jackson, "Resistance to freezing and thawing of recycled aggregates concrete", ACI Materials Journal, **100**(3), 216-221, 2003, doi:

[10]   J.Y. Sun, J. Geng, "Effect of partical size and content of recycled fine aggregate on frost resistance of concrete", Journal of Building Materials, **15**, 382-385, 2012, doi: 10.3969/j.issn.1007-9629.2012.03.017.

[11]   R.M. Salem, E.G. Burdette, "Role of c-hemical and admixtures on physical and frost resistance of recycled aggregate concrete", ACI Materials Journal, 95 (5), 558-563, 1998, doi: 10.14359/398.

[12]   Q.T. Liu, G.P. Cen, L.C. Cai, H.S. Wu, "Frost-resistant performance and mechanism of recycled concrete for airport pavement", Journal Huazhong University for science & Technology, **39**(12), 128-132, 2011.

[13]   D. Xuan, B. Zhan, C.S. Poon, "Durability of recycled aggregate concrete prepared with carbonated recycled concrete aggregates", Cement and Concrete Composites, **84**, 214-221, 2017, doi: 10.1016/j.cemconcomp.2017.09.015.

[14]   S.C. Kou, C.S. Poon, "Enhancing the durability properties of concrete prepared with coarse recycled aggregate", Construction Building Materials, **35**, 69-76, 2012, doi: 10.1016/j.conbuildmat.2012.02.032.

[15]   J.P. Hwang, H.B. Shim, S. Lim, K.Y. Ann, "Enhancing the durability properties of concrete containing recycled aggregate by the use of pozzolanic materials", Ksce Journal of Civil Engineering, **17**, 155-163, 2013, doi: 10.1007/s12205-013-1245-5.

[16]   S.C. Kou, C.S. Poon, "Properties of concrete prepared with PVA-impregnated recycled concrete aggregates", Cement and Concrete Composites, **32**, 649-654, 2010, doi: 10.1016/j.cemconcomp.2010.05.003.

[17]   V.W.Y. Tam, C.M. Tam, "Assessment of durability of recycled aggregate concrete produced by two-stage mixing approach", Journal of materials science, **42**, 3592-3602, 2007, doi: 10.1007/s10853-006-0379-y.

[18]   X.H. Li, L.G. David, "Mitigating alkali-silica reaction in concrete containing recycled concrete aggregate", Journal of the transportation research board, 1979, 30-35, 2006, doi: 10.1177/0361198106197900105.

[19]   P. Saravanakumar, G. Dhinakaran, "Durability aspects of HVFA-based recycled aggregate concrete", Magazine of Concrete Research, **66**(4), 186-195, 2014, doi: 10.1680/macr.13.00200.

[20]   Y.G. Zhu, S.C. Kou, C.S. Poon, J.G. Dai, Q.Y. Li, "Influence of silane-based water repellent on the durability properties of recycled aggregate concrete", Cement and Concrete Composites, **35**(1), 32-38, 2013, doi: 10.1016/j.cemconcomp.2012.08.008.

[21]   AFNOR, NF P18-459: Béton - Essai pour béton durci - Essai de porosité et de masse volumique, 2010.

[22]   Association Française de Génie Civil, Conception des bétons pour une durée de vie donnée des ouvrages : maîtrise de la durabilité vis-à-vis de la corrosion des armatures et de l'alcali-réaction Etat de l'art et Guide pour la mise en œuvre d'une approche performantielle et prédictive sur la base d'indicateurs de durabilité, 2004.

Recording of Student Attendance with Blockchain Technology to Avoid Fake Presence Data in Teaching Learning Process

Meyliana[1], Yakob Utama Chandra[1], Cadelina Cassandra[1], Surjandy[1,*], Erick Fernando[1], Henry Antonius Eka Widjaja[1], Andy Effendi[1], Ivan sangkereng[2], Charles Joseph[3], Harjanto Prabowo[4]

[1]*Information Systems Department, School of Information Systems, Bina Nusantara University, Jakarta, 11480, Indonesia*

[2]*Management Department, BINUS Online Learning, Bina Nusantara University, Jakarta, 11480, Indonesia*

[3]*PT. PineappleTech Multi Cemerlang, Jakarta, 11480, Indonesia*

[4]*Computer Science Department, Bina Nusantara University, Jakarta, 11480, Indonesia*

A B S T R A C T

University operational activities are a routine part of university operations and supervisory control and monitoring function. The low controlling and monitoring of operational activities can cause irrelevance in the teaching and learning process. A graduate may have a graduation document but has never attended the teaching and learning process. An official institution can issue this graduation document, but it is fake because no teaching-learning activity occurred. It happens because the data is easily being manipulated and changed in the current system. From the problem, this is what drives this research to be carried out. With the characteristics of distributed, secure, and traceable information, Blockchain will solve this problem. Based on a previous study, blockchain technology facilitates university operational activities so that it will solve the current problems. This research uses qualitative research methods. The research process starts with literature studies and forum group discussions conducted on nine universities in Indonesia (public and private universities). This study used the User-Centered Design Technique. This research focuses on the user, so the results possibly are applied. The research results prove that Blockchain technology can record student attendance as part of the graduation process's teaching and learning process. Blockchain's immutable, unchangeable, and distributed characteristics will ensure the student attendance record's validity in the teaching and learning process.

1. Introduction

The problem of graduation documents forgery has risen in various countries. Several previous studies have reported that graduation documents forgery requires a new solution, Blockchain technology uses to be a solution [1], [2]. Other research states that Blockchain technology uses record operation activity in a university to protect information [3], [4]. This research tried to simulate the use of Blockchain technology (multichain) [5] to record student attendance because Blockchain characteristics such as distributed [6], secure, and traceable

information [7], [8]. Blockchain will be a new solution to this problem [9], [10]. To prevent the falsification of graduation documents issued by the Institution (such as fake attendance report). The irregularity was found because several universities issue original graduation documents, but the graduate had never conducted academic activities [11]. The early research stated a similar issue regarding fake attendance [12].

Blockchain technology is expected to provide a solution to this problem. This qualitative research was conducted by involving 9 universities, private and public universities, to obtain input and validation of the simulation result. The technique used in the research is user-centered design (UCD) [13], [14]. By using the

UCD technique, the research results will prioritize the user needs. This study aims to test blockchain technology for student attendance recording. The simulation results found blockchain technology can facilitate record student attendance during the lecture process, which is very important as a control and supervision function over university operations. The limitations of the existing system capabilities such as user easily to update the data. But with Blockchain technology, which can record data and not easily be manipulated and changed, even the data will always be immutable. After obtaining validation from 9 universities, the final result of this study stated that blockchain technology can be used for recording the attendance lists. This systematic writing of this paper starts with an abstract, introduction, literature, method, result and discussion and finally, the conclusion. The research stages can be seen in Figure 1 below.
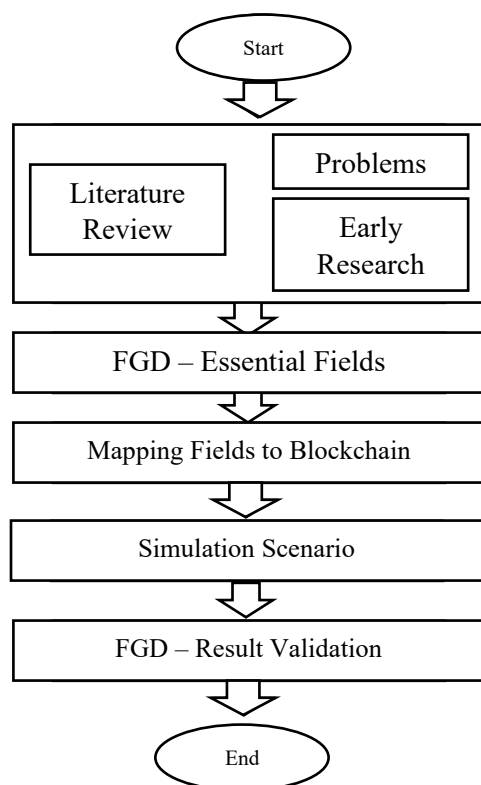
Figure 1: Research Stages

Exhibit at Figure 1, the first research stage began with a literature review. This literature review found graduates who had graduation documents, but graduates were never found to be present in lectures. Another study found that Blockchain can handle this problem. The next step was to conduct FGDs with nine private and public universities to find necessary fields to support attendance records. After determining the fields, mapping is carried out to record student attendance into the blockchain (multichain) application and directly written into the multichain application (Blockchain). After that, a simulation was carried out and validated to 9 universities through FGD.

2. Literature Review

This session will describe some of the theories used in this study.

2.1. Multichain

Multichain is a platform created in 2015[5]. Multichain made for cryptocurrency. Multichain is a blockchain with private and permission types. The simulation carried out is limited to a laboratory at the university, but the simulation data are real data from the current system.

2.2. Blockchain for Education

Blockchain technology discovers in 2008 [15], and after a cryptographer in 2014 [16] combines smart content features into Blockchain technology. Many previous studies have stated that blockchain technology can be used to improve the process and activities in education, such as borrowing books or libraries [17], students loan [18], for graduation documents [19], [20], and others in education [1], [21]. From previous research, it can be said that Blockchain is not only for cryptocurrency but also for support operations in education.

2.3. Blockchain Characteristics

Blockchain Technology's characteristics help monitor lecture activities to minimize the occurrence of fake graduation documents, especially those issued by institutions that have the authority to issue documents. The characteristics of Blockchain are [6], [16]:

- Immutable, which means that information that has been recorded on the Blockchain will always be there and never deleted. In this case, attendance records that occur as a result of students coming to attend lectures will continue to be recorded forever and cannot be removed.
- Unchangeable, which means the information that has been recorded on the Blockchain cannot be changed or updated forever. In this case, the attendance that occurs as a result of students coming to attend lectures will continue to be recorded forever and cannot be updated.
- Secure, it means that all data in blockchain technology will be stored safely. In this case, blockchain technology (multichain) uses unidirectional encryption. When the transaction (absence transaction) is recorded, it is encrypted with the hashing method. Besides that, the transactions also follow the Merkle tree method hashing, and it does not only occur in a transaction but the entire transaction.
- Transparent means that all nodes on the registered network can see all activities or activities recorded on the Blockchain (all parties can see the transaction/absence transaction).
- Peer-to-Peer means absence transactions that occur on the Blockchain are done peer-to-peer, meaning there is no intermediary party at the transaction time. In this case, regarding attendance, attendance is directly given by the university to students.
- Distribute factor means that all absence transaction information recorded on the Blockchain will be distributed to all nodes on the same network.

2.4. Previous Research

Previous research searches have been carried out using Publish and Perish applications[22] at Scopus database, with keyword attendance in the title paper, with a range of 2015-2021, and found 1 article discussing student attendance. The problems presented are the same as the problems found, such as manipulating attendance being the problems found[12]—solution found by using IoT. However, manipulation on the database level possibly occurred.

3. Methodology

The methodology used in this research is the qualitative method. Some techniques used are literature studies and focus group discussions. The details of the activity can be seen in Figure 1. The research process initially started with a literature review. In this stage, two things were found, namely existing problems and previous research. The problem found at this stage is focusing on university operations for monitoring lecture activities with a student attendance system. Another finding states that blockchain technology facilitates operational lecture activities and can even be used to prevent fake diplomas.

The next step is determining the essential fields to be written on the Blockchain (multichain). Figure 4 shows the existing attendance report, from which the report can be described which fields will be used. It also shows the students list who attended face-to-face meetings and made class attendance in rooms 521 and 523 on October 23, 2017, with subject codes comp6049 and comp6045.

Mapping fields will be written on the Blockchain (multichain), after mapping the fields, the attendance scenario is created. After the scenario is complete, the simulation is carried out using multichain.

3.1 Simulation Testing

This study using simulation techniques. This simulation technique uses because this technique has similarities to the actual situation or is close to the actual situation. This technique is also very quick and inexpensive to perform and makes it easy to judge whether it is appropriate [23].

3.2 Simulation Stages

The first step in this research is to look at the attendance reports generated from the running system by taking several samples and then analyzing the current system's attendance report. Map the running system's fields based on the log report to the Blockchain (multichain) fields that will be used. Enter data into the Blockchain (multichain) based on the information in the current attendance log report. The final step is to show the Blockchain results (multichain) to the expert as part of the result validation.
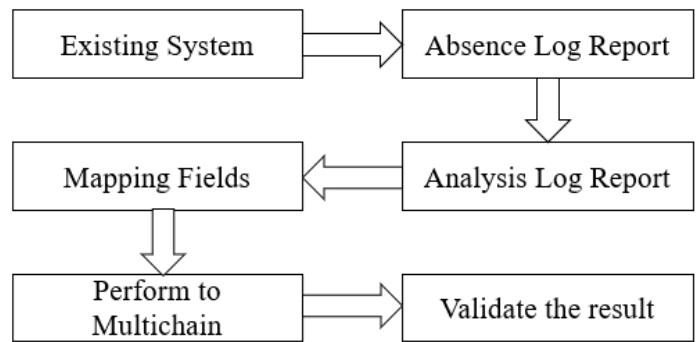
Figure 2: Simulation Stages
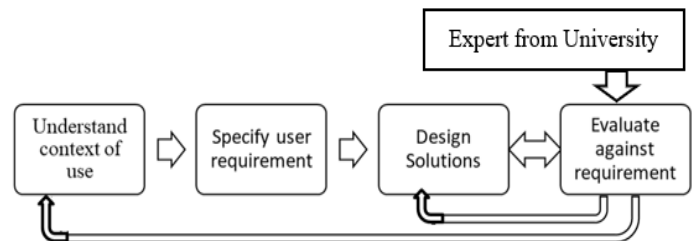
Figure 3: User-Centered Design

StudentID	STRM	Crse_id	Crse_code	Class_section	Start_dt	TappingTimeClass	Ispresent	N_Delivery_mode	Facility_ID
2101675432	1710	10545	COMP6049	LC01	10/23/2017	3:24:24 PM	Y	F2F	ANG523
2101675445	1710	10545	COMP6049	LC01	10/23/2017	3:28:36 PM	Y	F2F	ANG523
2101679456	1710	10545	COMP6049	LC01	10/23/2017	3:03:09 PM	Y	F2F	ANG523
2101684765	1710	10545	COMP6049	LC01	10/23/2017	3:18:05 PM	Y	F2F	ANG523
2101719592	1710	10545	COMP6049	LC01	10/23/2017	3:19:27 PM	Y	F2F	ANG523
2101719623	1710	10545	COMP6049	LC01	10/23/2017	3:18:49 PM	Y	F2F	ANG523
2101720354	1710	10545	COMP6049	LC01	10/23/2017	3:20:45 PM	Y	F2F	ANG523
2101724043	1710	10545	COMP6049	LC01	10/23/2017	3:21:55 PM	Y	F2F	ANG523
2101726944	1710	10545	COMP6049	LC01	10/23/2017	2:53:32 PM	Y	F2F	ANG523
2101727285	1710	10545	COMP6049	LC01	10/23/2017	3:03:21 PM	Y	F2F	ANG523
2001625995	1710	10548	COMP6065	LC01	12/22/2017	1:20:00 PM	Y	F2F	ANG521
2001626032	1710	10548	COMP6065	LC01	12/22/2017	1:20:00 PM	Y	F2F	ANG521
2001626000	1710	10548	COMP6065	LC01	12/22/2017	1:20:00 PM	Y	F2F	ANG521
2001625963	1710	10548	COMP6065	LC01	12/22/2017	1:20:00 PM	Y	F2F	ANG521

Figure 4: Student Absence Log from Recent System

3.3 User-Centered Design (UCD)

This qualitative research study uses the User-Centered Design (UCD) approach. This technique is chosen to ensure the simulation results are more focused on the user (user) and industry [7]. The UCD technique creates simulation scenarios where user interaction occurs by communicating with experts in operational fields. For details, see figure 3.

4. Result and Discussion

This research using the simulation technique begins with data collection from the current system to record student attendance. Figure 4 shows the attendance log of the student's attendance, and the detail is students with the id "2101675432" attend courses with the code "COMP6049" and class code LC01 on October 23, 2017 (10/23/2017) present in class at 3: 24.24 in room ANG523 face to face "F2F".

From the attendance log report, Figure 4 is then simulated into the Blockchain (multichain) application. There is no customization on multichain used.

The lab configuration can be seen in Figure 5, which shows a node with the name chain1 and the multichain version 1.0.9 using the 10011 protocol.

Figure 5: Multichain Node

Figure 6: Multichain Addresses

The address configuration represents a university and student entity. In this case, the entity functions are to send assets that record attendance transactions that occur during the teaching and learning transaction.

The address configuration shows in Figure 6, which describes all entities' addresses for simulating attendance transactions.

After address configuration, the next configuration is asset formation. Assets represent courses, classrooms, and schedules in face-to-face mode (model).

Figure 7 explains the teaching and learning preparation (courses, classrooms, and the schedule) by the lecturer (KD_Lec), lecture schedule shift (15:20-17:00), and student classes.

Figure 8 shows the success of recording the program schedule, which is represented as an asset on the multichain.

Figure 7: Input Dashboard 1 – Comp 6049

Figure 8: Success Result Input

745

Figure 9 shows a simulation for filling the lecture schedule of COMP6065 course in classroom 521 on December 22, 2017, by KD_Lec (D3730) teachers with a face-to-face model and class LC01 student classes.

Figure 9: Input Dashboard 2 – COMP6065

Figure 10 illustrates the lecture schedule that has been successfully recorded on multichain (Blockchain) as assets. Figure 10 shows the number of students in the class so the assets can be sent to students present, while the attendance date follows the recording date on multichain.

Name	ANG521-COMP6065-2017-12-22
Quantity	40
Units	0.01
Issuer	Univeristy Binus (1SH8oX3Eii3kE2KbYzkUYVVXGQhDV8QzYiHFEx, local)
KDLec	D3730
Time	13:20-15:00
Mode	F2F
Class	LC01

Figure 10: Success Result Input – Class 2

Figure 11 shows attendance transactions for a student 2101684765 - Name 3 with attendance at the COMP6049 course, on ANG campus with classroom 523 on October 23, 2017.

Figure 11: Attendance Activity

Figure 12 shows the transactions record of a student who attended the lecture. This recording proves that multichain (Blockchain) can facilitate to record student attendance activities in the face-to-face learning process that has occurred.

Label	2101684765 - Name 3
Address	1JFBKdvrGWYEzmZ53kyfv4bfD49FotC8wpKL8d
COMP6049-ANG523-2017-10-23	1

Figure 12: Attendance Record in Multichain

The simulation results reported in this paper are not all transactions shown in Figure 5, but the simulation is carried out thoroughly. The simulation involves experts from 9 universities, and all universities agree that the student attendance recording transaction can be done on the Blockchain (Multichain).

This research will complement previous research were using Blockchain (multichain) to become a database in recording student attendance transactions will be more robust because student attendance records cannot be manipulated.

5. Conclusion, Limitation and Future Research

This research uses qualitative methods using several techniques, such as FGD with experts and literature reviews. The simulation results are carried out directly by comparing the existing system's attendance logs with multichain results.

This research produces a product that can be used to implement and become solutions in recording student attendance.

Other things that still need to be improved such as multichain configuration using only one node (single node), which should be at least 3 (three) nodes (best practice). Another thing is that there is no wallet created so that students cannot see the simulation's results. It can be used to be developed in future research.

Conflict of Interest

The authors declare no conflict of interest.

References

[1] L.M. Palma, M.A.G. Vigil, F.L. Pereira, J.E. Martina, 'Blockchain and smart contracts for higher education registry in Brazil', International Journal of Network Management, (June 2018), 1–21, 2019, doi:10.1002/nem.2061.

[2] K. Al Harthy, 'The upcoming Blockchain adoption in Higher- education : requirements and process', 2019 4th MEC International Conference on Big Data and Smart City (ICBDSC), 1–5, 2019.

[3] H. Sun, X. Wang, X. Wang, 'Application of blockchain technology in online education', International Journal of Emerging Technologies in Learning, **13**(10), 252–259, 2018, doi:10.3991/ijet.v13i10.9455.

[4] Meyliana, Y.U. Chandra, C. Cassandra, Surjandy, H.A.E. Widjaja, E. Fernando, H. Prabowo, and C. Joseph, 'DEFYING THE CERTIFICATION DIPLOMA FORGERY WITH BLOCKCHAIN PLATFORM: A PROPOSED MODEL', in IADIS International Conference ICT, Society and Human Beings 2019 (part of MCCSIS 2019, 63–71, 2019.

[5] G. Greenspan, MultiChain White Paper | MultiChain, Multichain.Com, 2015.

[6] D. Bauman, P. Lindblom, C. Olsson, Blockchain - Decentralized trust, 2016, doi:http://entreprenorskapsforum.se/wp-content/uploads/2016/10/NaPo_Blockchain_webb.pdf.

[7] N. Kshetri, 'Blockchain's roles in strengthening cybersecurity and protecting privacy', Telecommunications Policy, (September), 1–12, 2017, doi:10.1016/j.telpol.2017.09.003.

[8] P.Y. Chang, M.S. Hwang, C.C. Yang, 'A blockchain-based traceable certification system', Advances in Intelligent Systems and Computing, **733**, 363–369, 2017, doi:10.1007/978-3-319-76451-1_34.

[9] M. Turkanovic, M. Holbl, K. Kosic, M. Hericko, A. Kamisalic, M. Turkanovi, 'EduCTX : A blockchain-based higher education credit platform', IEEE Access, **X**(January), 1–15, 2018, doi:10.1109/ACCESS.2018.2789929.

[10] T. Ahram, A. Sargolzaei, S. Sargolzaei, J. Daniels, B. Amaba, 'Blockchain technology innovations', 2017 IEEE Technology and Engineering Management Society Conference, TEMSCON 2017, (2016), 137–141, 2017, doi:10.1109/TEMSCON.2017.7998367.

[11] Fitri, Menteri Nasir: Jual Ijazah Palsu, 4 Kampus Dibekukan, Dua Rektor Dicopot (Minister Nasir: Selling fake diplomas certificate, 4 campuses frozen, two chancellors dismissed), Lldikti12.Ristekdikti.Go.Id, 2015.

[12] M.A. Safi'Ie, R. Hartono, G. Pratama, 'The development of Student Attandance System using RFID and Internet of Things (IoT) technology', IOP Conference Series: Materials Science and Engineering, **578**(1), 8–13, 2019, doi:10.1088/1757-899X/578/1/012084.

[13] I.D. Foundation, What is User Centered Design? | Interaction Design Foundation, Www.Interaction-Design.Org, 2020.

[14] T. Lowdermilk, User-Centered Design, O'Reilly Media, USA;, 2013.

[15] S. Nakamoto, Bitcoin P2P e-cash paper, 2008.

[16] M. Swan, Blockchain Blueprint for a New Economy, 1st ed., O'Reilly Media, Inc., 1005 Gravenstein Highway North, Sebastopol, CA 95472, USA, 2015.

[17] M.B. Hoy, 'An Introduction to the Blockchain and Its Implications for Libraries and Medicine', Medical Reference Services Quarterly, **36**(3), 273–279, 2017, doi:10.1080/02763869.2017.1332261.

[18] H.M. Gazali, R. Hassan, R.M. Nor, H.M.. Rahman, 'Re-inventing PTPTN study loan with blockchain and smart contracts', in 2017 8th International Conference on Information Technology (ICIT), IEEE: 751–754, 2017, doi:10.1109/ICITECH.2017.8079940.

[19] A. Srivastava, 'A Distributed Credit Transfer Educational Framework based on Blockchain', 2018 Second International Conference on Advances in Computing, Control and Communication Technology (IAC3T), 54–59, 2018.

[20] Meyliana, Y.U. Chandra, C. Cassandra, . Surjandy, E. Fernando, H.A.E. Widjaja, H. Prabowo, 'A Proposed Model of Secure Academic Transcript Records with Blockchain Technology in Higher Education', in ConRist 2019, 172–177, 2020, doi:10.5220/0009907401720177.

[21] T.M. Fernández-caramés, 'applied sciences Towards Next Generation Teaching , Learning , and Context-Aware Applications for Higher Education : A Review on Blockchain , IoT , Fog and Edge Computing Enabled Smart Campuses and Universities', 2019, doi:10.3390/app9214479.

[22] A.. Harzing, Publish or Perish, Harzing.Com, 2007.

[23] G. Hook, 'Business Process Modeling and simulation', in Proceedings - Winter Simulation Conference, 773–778, 2011, doi:10.1109/WSC.2011.6147804.

Comparation of Analytical Models and Review of Numerical Simulation Method for Blast Wave Overpressure Estimation after the Explosion

Alan Catovic[*], Elvedin Kljuno

Mechanical Engineering Faculty, Defense Technology Department, University of Sarajevo, Sarajevo, 71000, Bosnia and Herzegovina

ABSTRACT

A comparative analysis of formulas for blast wave overpressure is presented in the paper, and models were compared with available experimental data. The Kinney and Shin models show the best agreement with experimental data (Kingery-Bulmash) for free airburst, while for surface burst, Swisdak, Vanuci, and Jeon models predict test data most accurately. One of the novelties in the paper is introduction of new exponential and power functions for blast overpressure estimation, giving good agreement with experimental data. Also, several numerical simulations of free airburst explosions were performed to introduce methodology, and compare the data obtained with experimental data. A detailed description of the procedure for these simulations was provided – a contribution to numerical modeling of blast wave phenomena.

1. Introduction

There has been an increase in the research of explosive blast effects since numerous accidents (ie Beirut, 2020) happened, and terrorist attacks were carried out on civilians, with a large number of casualties during last decades. These include i.e. the bombing of US embassies (Ankara, 1958, Beirut, 1984), World Trade Center attack (New York, 2001), Mumbai attacks (2008), Mariott Hotel attack (Islamabad, 2008), Baghdad bombings (2016), Atatürk Airport attack in Turkey (2016), Nairobi hotel attack (Kenya, 2019), Jolo Cathedral bombings (Philippines, 2019), many attacks in Pakistan (Quetta, 2020) and also in larger area of Afganistan (lately Kabul, Kuz-Kunar, 2020) and many more.

An explosion presents violent release of energy. The detonation presents a rapid chemical reaction proceeding through the explosive charge at supersonic speed. The detonation wave converts explosive into a hot, dense, high-pressure gas, which is the source of powerful blast waves around explosion site (Figure 1).

Pressures at the Chapman-Jouguet point can go up to 400 kbar. Acceleration of the air particles (when the detonation is complete) beyond the face of the explosive is in order of 10^{11} g. Close to the face of the charge, at near-field scaled distance (where $Z=R/m^{1/3}$): $Z = 0,054$ m/kg$^{1/3}$, the maximal temperature is around 200 000 K. The temperature rises almost instantaneously with the shock front

arrival but the maximal temperature occurs at the expanding detonation products front [1].

In this paper, a comparison of analytical methods for blast wave overpressure is presented and compared to experimental data in Section 3. Also, numerical simulations of free airburst explosions were done in Ansys Autodyn for 1 kg, 10 kg, 10 T of TNT, and obtained data were compared with available empirical data, in Section 4. Section 5 presents conclusions.

Figure 1: Blast wave formation after the explosion [courtesy of Defence Research and Development Canada]

2. Explosion types and blast wave parameters

There are two main groups of blast loads, regarding explosive confinement: unconfined (free air blast explosions), an air burst close to the ground, and surface burst) and confined (fully vented, partially confined, and fully confined). In free air spherical explosions, shock wave moves from the center of the explosion

[*]Corresponding Author: Alan Catovic, Email: catovic@mef.unsa.ba

and hits the target with no amplification. Hemispherical explosions are surface explosions where the detonation is close to the ground, and where the incident shockwave is strengthened due to reflections from the ground. As the blast wave propagate, Mach front (Figure 2) can be formed by superposition of the incident and reflected waves [2]. Confined explosion relates to detonation inside structures.
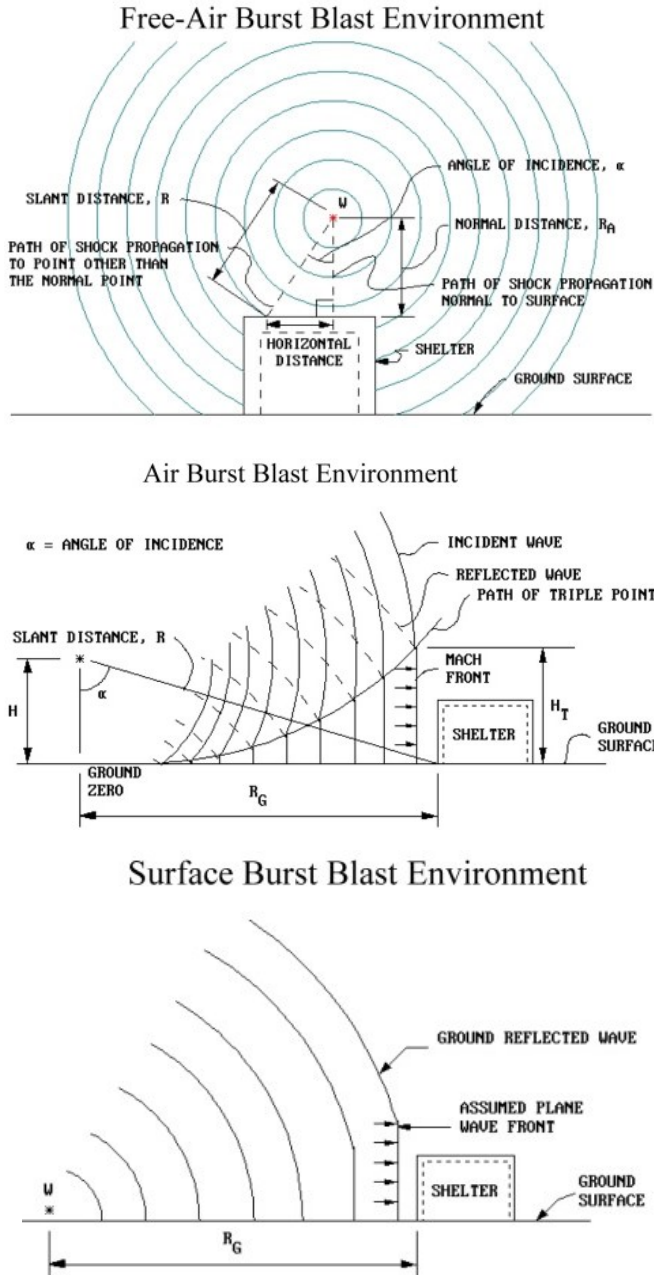
Figure 2: Free-air burst, air burst near ground and surface burst [2]

The pressure wave function in the air is schematicaly shown in Figure 3. There is a rapid rise from ambient pressure to a peak incident overpressure P_{so} which decays to the ambient value in time t_o (positive phase duration). The front arrives at a location in time t_A. Negative phase (duration t_{o-}) is characterized by underpressure P_{so-}. The incident impulse of the blast wave is the integrated area under the pressure-time curve (marked as i_s for the positive and i_{s-} for the negative phase) [2].
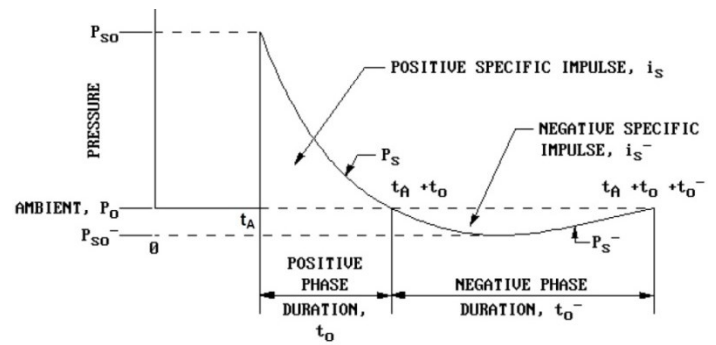
Figure 3: Free-field Pressure-Time variation [2]

In technical manuals [2], the overpressure exponential curve is often replaced by a linear curve. The negative phase is often ignored in structural calculations.

When the blast wave hits the surface, the reflected pressure value can be more than 20 times larger than the incident pressure value [3].

3. Prediction of blast wavefront parameters

A large number of studies were conducted in order to understand better blast effects after the explosion and the response of structures to blast loads. Empirical, semi-empirical, and numerical methods are mostly used for the prediction of blast effects.

Empirical methods are correlations with test data. The accuracy of empirical formula is usually lower for near-field explosions.

Semi-empirical methods are partly based on physical models. These methods rely also on experimental data and their accuracy is usually better than purely empirical methods. They are used in certain blast codes (programs)

Numerical (computational fluid dynamics, CFD) methods are usually the most accurate ones and are based on equations describing basic laws of continuum mechanics (conservation of mass, momentum, and energy). The physical behavior of materials is generaly described by constitutive equations [4].

Many programs such as BLASTX, CTH, SHAMRC, FEFLO, FOIL, DYNA3D, ALE3D, LS-DYNA, Air3D, CONWEP, AUTODYN, ABAQUS, 3D BLAST, SPEED have been developed to numericaly simulate the blast effects (Figure 4) and their load on structures.

Some of these programs (ie AUTODYN) can also be used to model the near-field explosion effects, in order to make new formulas for near-field air-blast estimations, and to update old formulas (ie. for reflection coefficients).
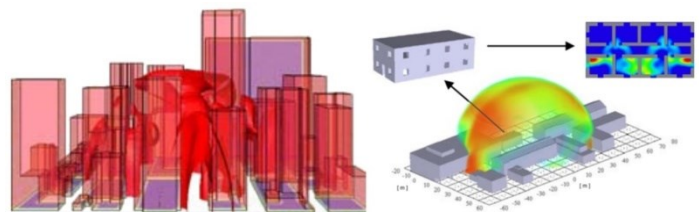
Figure 4: Simulations of shock wave in urban environment (AUTODYN and SPEED programs]
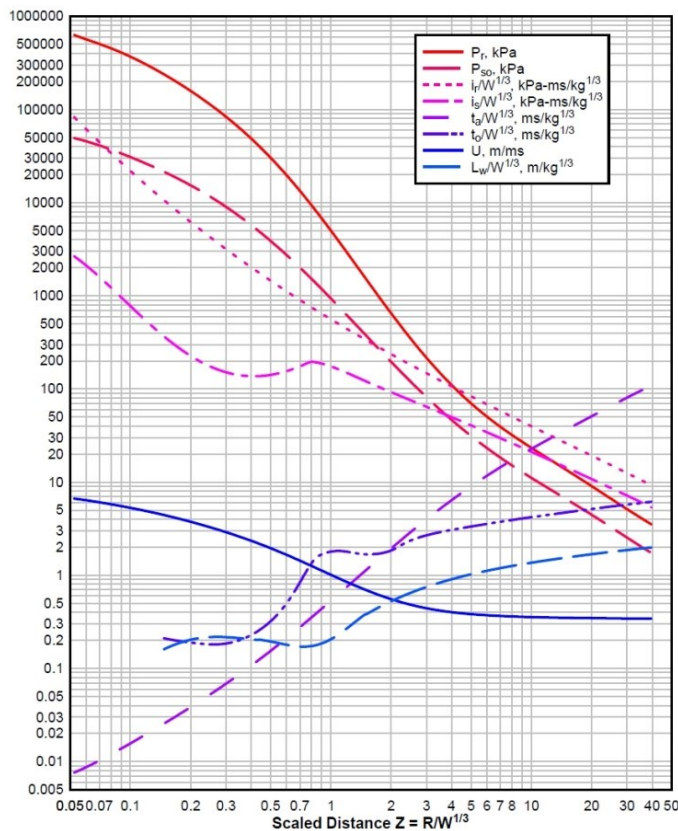
Figure 5: Positive phase parameters for spherical wave (TNT charges) from free-air bursts [4]
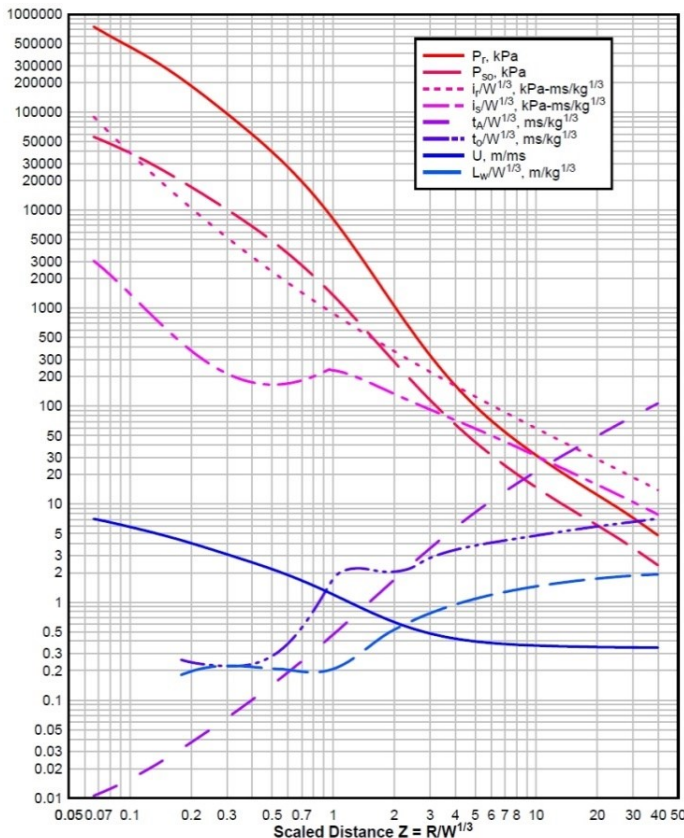
Figure 6: Positive phase parameters of hemispherical wave (TNT) from surface burst [4]

Reference [5] includes formulas for air bursts and surface bursts, for estimation of the values for incident and reflected pressures (and for other parameters as well). The positive phase pressures, impulses, durations, and other parameters of shock environment for free air and surface burst (for TNT) are given in Figs. 5 and 6 versus scaled distance Z (from Z=0,05 m/kg$^{1/3}$ to Z=40 m/kg$^{1/3}$).

According to Hopkinson-Cranz law, a dimensional scaled distance $Z = R/W^{1/3}$, where R is distance from the detonation point, and W is the mass of explosive charge (equivalent to TNT mass). The values of TNT equivalent mass factors can be found in papers and technical manuals.

Using diagrams, to obtain absolute value of particular parameter, their scaled value is multiplied by a $W^{1/3}$ to take the size of the explosive charge into calculation. Pressure and velocity are not scaled [5].

Calculations for surface burst are more straightforward than for airburst near the ground because of complex wave reflections in the latter case.

High-order polynomial equations functions made using regression analysis of test data [5] are used in the CONWEP.

In CONWEP (utilizes Kingery-Bulmash polynomials), following formula is used for defining P-t curve:

$$P(t) = P_{so}\left(1 - \frac{t - t_A}{t_o}\right)e^{-\left(\frac{A(t-t_A)}{t_o}\right)} \qquad (1)$$

Here A is decay coefficient, which can be calculated by curve fitting of experimental P(t) curve in positive phase [4]. Besides Eq (1), formulas of Flynn and Etheridge can be used for prediction of positive blast pressure profile.

Automated formulas for surface blast parameters can also be found in programs BECV4 and A.T. - Blast.

Table 1 below shows peak reflected overpressures P_r for surface burst (ie. in Figure 6) with different W-R (mass-distance) combinations. These values can be obtained using polynomial equations, or programs.

Table 1: Peak reflected overpressures P_r for surface burst

R (m)	Peak reflected overpressures (MPa)			
	100 kg	500 kg	1000 kg	2000 kg
1	165,8	354,5	464,5	602,9
2,5	34,2	89,4	130,8	188,4
5	6,65	24,8	39,5	60,2
10	0,85	4,25	8,15	14,7
15	0,27	1,25	2,53	5,01
20	0,14	0,54	1,06	2,13
25	0,09	0,29	0,55	1,08

Experiments have shown that human blast tolerance depends on magnitude of blast wave pressure and the shock duration. Tests showed that the lungs is the critical organ in injuries related to blast waves. The air bubbles release from damaged lung alveoli into the body vascular system accounts for most fatalities. The severe lung-haemorrhage occurs at pressure levels above 5,5 bar, while the lethality due to lung damage is for pressures 6,9 to 8,3 bar, Near

100 per cent deaths are confirmed for pressure levels 13,8 - 17,2 bar. Besides these primary effects of blast on humans, there are secondary (fragments from surrounding structures and buildings collapse), tertiary (blast wave and winds that can sweep people) and quaternary effects (other explosion-related injuries) [6].

Blast effects may damage structures by two main type of loading: diffraction and drag loading. Diffraction loading relates to loading the structure from all sides, where the blast overpressure is applied to sides of the object nearly simultaneously (i.e. on a building oriented towards explosion blast wave would arrive on the front sides and roof at nearly the same time). Ductile targets (i.e. made of metal) can be crushed. Brittle targets (i.e. made of concrete) will most likely shatter. The loading can be estimated from the peak overpressure [7].

Drag loading, related to dynamic pressure, is the force which acts on surfaces perpendicular to the pressure wave. The drag load is less than the diffraction loading, and it is applied for a longer time period. The drag load reverses direction, which can tear objects apart. Flexible targets are not damaged significantly by diffraction loading but can be prone to drag loading injuries. Objects not fixed can be thrown several meters away. Humans are quite vulnerable to this type of loading. Lightly protected equipment can also be damaged by drag loading [7].

Prediction formulas for blast loads on structures can be found in technical manuals.

Table 2 shows expected damage on structures loaded with the blast wave.

Table 2: Expected damage on objects loaded with blast wave [8]

Overpressure (kPa)	Expected damage
1,0 - 1,5	Window glass cracks
3,4 - 7,6	Minor damage in some buildings
7,6 - 12,4	Metal panels deformed
12,4 - 20	Concrete walls damaged
over 34,5	Wooden buildings demolished
27,6 - 48,3	Major damage to steel objects
41,4 - 62,1	Heavy damage to reinforced buildings
69 - 82,7	Probable demolition of most buildings

Blast overpressure is the most important parameter in blast effects modelling and many analytical relations can be found in the literature, most of them based on test data at different scaled distances and charge sizes.

The formulas for a free spherical airburst explosion can also be used for surface explosions by increasing the charge mass using the multiplication with a coefficient (reflection factor) 2η, where η takes into account energy used for deformation of the base material, with values ranging from 0,55 for water to 1 for steel.

The formulas for spherical airbursts and hemispherical surface burst blast wave pressure P_S, presented by several authors, are given in Tables 3 and 4.

Constants for polynomial formula by Kingery & Bulmash are omitted in Tables 3 and 4 because of space, but they can be found in their original paper [5]. Constants for formula by Jeon are also omitted from Table 4, and can be found in [9].

Table 3: Formulas for spherical airbursts blast wave pressure [10,11]

Author(s)	Formula for P_s (in MPa)	Applicability
Sadovskyi (1952)	$P_s = \dfrac{0,085}{Z} + \dfrac{0,3}{Z^2} + \dfrac{0,82}{Z^3}$ (2)	
Brode (1955)	$P_s = \dfrac{0,67}{Z^3} + 0,1$ (3)	$(1 < P_s)$
	$P_s = \dfrac{0,0975}{Z} + \dfrac{0,1455}{Z^2} + \dfrac{0,585}{Z^3} - 0,0019$ (4)	$(0,01 \le P_s \le 1)$
Naumyenko & Petroski (1956)	$P_s = \dfrac{1,050}{Z^3} - 0,0981$ (5)	$(Z \le 1)$
	$P_s = \dfrac{0,0745}{Z} + \dfrac{0,250}{Z^2} + \dfrac{0,637}{Z^3}$ (6)	$(1 < Z \le 15)$
Henrych & Major (1979)	$P_s = \dfrac{1,380}{Z} + \dfrac{0,543}{Z^2} - \dfrac{0,035}{Z^3} + \dfrac{0,000613}{Z^4}$ (7)	$(0,05 \le Z \le 0,3)$
	$P_s = \dfrac{0,607}{Z} - \dfrac{0,032}{Z^2} + \dfrac{0,209}{Z^3}$ (8)	$(0,3 < Z \le 1)$
	$P_s = \dfrac{0,0649}{Z} - \dfrac{0,397}{Z^2} + \dfrac{0,322}{Z^3}$ (9)	$(1 < Z \le 10)$
Held (1983)	$P_s = 2\dfrac{W^{2/3}}{R^2}$ (10)	
Kingery & Bulmash (1984)	$Y = C_0 + C_1 U + C^2 U^2 + ... + C_N U^N$ (11) (common logarithm of the pressure) $U = K_0 + K_1 \log(Z)$ (12) (C, K are constants, N is the polynomial order)	$Z \le 40,0$
Kinney & Graham (1985)	$P_s = \dfrac{808\left[1+\left(\frac{Z}{4,5}\right)^2\right]}{\sqrt{1+\left(\frac{Z}{0,048}\right)^2} \cdot \sqrt{1+\left(\frac{Z}{0,32}\right)^2} \cdot \sqrt{1+\left(\frac{Z}{1,35}\right)^2}}$ (13)	does not have limits on valid range
Mills (1987)	$P_s = \dfrac{1,772}{Z^3} - \dfrac{0.114}{Z^2} + \dfrac{0,108}{Z}$ (14)	
Hopkins-Brown & Bailey (1998)	$P_s = -1.245 + \dfrac{1,935}{Z} + \dfrac{0,2353}{Z^2} - \dfrac{0,01065}{Z^3}$ (15)	$(0,05 \le Z \le 1,15)$
	$P_s = \dfrac{0,0707}{Z} + \dfrac{0,3602}{Z^2} + \dfrac{0,4891}{Z^3}$ (16)	$(1,15 < Z \le 40)$
Gelfand & Silnikov (2004)	$P_s = 1700 \cdot e^{(-7,5 \cdot Z^{0,28})} + 0,0156$ (17)	$(0,1 \le Z < 8)$
	$P_s = 8000 \cdot e^{(-10,7 \cdot Z^{0,1})}$ (18)	$(8 \le Z)$
Bajić (2007)	$P_s = 0,102\dfrac{W^{1/3}}{R} + 0,436\dfrac{W^{2/3}}{R^2} + 1,4\dfrac{W}{R^3}$ (19)	
Shin (2015)	$Y = C_0 + C_1 U + C^2 U^2 + ... + C_N U^N$ (20) $U = K_0 + K_1 \log(Z)$ (21)	$0,0553 \le Z \le 40,0$

Table 4: Formulas for hemispherical surface burst blast wave pressure [10,11,12]

Author(s)	Formula for P_s (MPa)	Applicability
Newmark & Hansen (1961)	$P_s = 0,6784\dfrac{W}{R^3} + 0,294\sqrt{\dfrac{W}{R^3}}$ (22)	
Kingery & Bulmash (1984)	$Y = C_0 + C_1 U + C^2 U^2 + ... + C_N U^N$ (23) $U = K_0 + K_1 \log(Z)$ (24)	$Z \le 40,0$

Swisdak (1994)	$P_s = e^{(A_1 + B_1 \cdot \ln(Z) + C_1 \cdot \ln(Z)^2 + D_1 \cdot \ln(Z)^3 + E_1 \cdot \ln(Z)^4 + F_1 \cdot \ln(Z)^5 + G_1 \cdot \ln(Z)^6)} \cdot 10^{-3}$ (25) (A_1, B_1, C_1, D_1, E_1, F_1, G_1 are constants) (26)	$Z \leq 40,0$
Wu & Hao (2005)	$P_s = 1,059 Z^{-2,56} - 0,051$ (27) $P_s = 1,008 Z^{-2,01}$ (28)	$0,1 \leq Z \leq 1$ $1 \leq Z \leq 10$
Iqbal and Ahmad (2009)	$P_s = 1,026 \cdot Z^{-1,96}$ (29)	$1 \leq Z \leq 12$
Jeon (2017)	$P_s = 10^{(C_0 + C_1 \cdot \log(Z) + C_2 \cdot \log(Z)^2 + C_3 \cdot \log(Z)^3 + C_4 \cdot \log(Z)^4)}$ (30) (C_1, C_2, C_3, C_4 are constants) (31)	$Z \leq 40,0$
Vanucci (2017)	$P_s = e^{(0,14 - 1,49\ln(Z) - 0,08 \cdot \ln(Z)^2 - 0,62\sin(\ln(Z)))} \left(1 + \dfrac{1}{2e^{10Z}}\right)$ (32)	$Z \leq 40,0$

Figure 8: Positive blast wave incident overpressure values (vs scaled distance) for *surface* burst, obtained using formulas from different models, compared to experimental [5] curve (Kingery-Bulmash polynomials)

In this research, we conducted regression analysis (MatLab CF Tool) of test data [5] by using exponential and power functions, and for scaled distances range of $0,15 < Z < 40$. We propose exponential functions for surface burst wave pressure:

$$P_s = e^{(a_1 + b_1 \cdot \ln(Z) + c_1 \cdot \ln(Z)^2 + d_1 \cdot \ln(Z)^3 + e_1 \cdot \ln(Z)^4)} \quad \text{for } 0,15 < Z < 3 \quad (33)$$

$$P_s = e^{(a_2 + b_2 \cdot \ln(Z) + c_2 \cdot \ln(Z)^2 + d_2 \cdot \ln(Z)^3)} \quad \text{for } 3 < Z < 40 \quad (34)$$

Here, values of constants are: $a_1 = 0,3078$, $b_1 = -2,054$, $c_1 = -0,2916$, $d_1 = 0,06031$, $e_1 = 0,03571$, $a_2 = 0,906$, $b_2 = -3,514$, $c2 = 0,757$ and $d_2 = -0,08512$. Maximum relative difference between our formula (33) and test data [5] incident overpressure values is 3,3 % (Figure 9), and between formula (34) and test data values is 1,9 %. We propose, as a possible substitute equations, following power functions for hemispherical surface burst wave incident pressure, for different scaled distances:

$$P_s = 3,17 x^{-1,123} - 2,033 \quad \text{for } 0,15 < Z < 0,6 \quad (35)$$

$$P_s = 1,426 x^{-1,898} - 0,08057 \quad \text{for } 0,6 < Z < 2 \quad (36)$$

$$P_s = 1,448 x^{-2,371} + 0,01015 \quad \text{for } 2 < Z < 8 \quad (37)$$

$$P_s = 0,3396 x^{-1,366} + 0,0002888 \quad \text{for } 8 < Z < 40 \quad (38)$$

Maximum relative difference between formulas (35-38) and experimental data [5] for incident overpressure values is 3,4 % (Figure 9). Figure 9 presents comparison between our proposed

Figure 7: Positive blast wave incident overpressure values (vs. scaled distance) for *airburst*, obtained using formulas from different models, compared to experimental [5] curve (Kingery-Bulmash polynomials)

In this paper we made comparison of blast overpressures ($0,15 < Z < 10$) for airburst and surface (hemispherical) burst, using different models (presented in Table 3), and results are shown in Figs. 7 and 8. The experimental data [5] are included for reference as the widely approach for blast parameters prediction. Figure 7 shows most curves deviate from the test data for small scaled distances (ie for $Z < 0,4$). This may be since some of these equations (Brode, Mills) were developed for nuclear blast.

The Kinney (Eq. 13) and Shin (Eqs. 20 and 21) curves show the best agreement with Kingery-Bulmash data over the whole scaled distance. Figure 8 shows positive blast wave overpressure values for surface burst, obtained using formulas from different models (Table 4), compared to Kingery-Bulmash curve approximating test data.

Swisdak (Eqs. 25 and 26), Vanuci (Eq. 32), and Jeon (Eqs. 30 and 31) predict test data accurately, while other models struggle (i.e. Newmark model, used primarily for nuclear explosions, for scaled distances $Z < 0,4$).

functions and test data [5]. As can be seen, our formulas (33-38) adequately predict incident overpressure values for hemispherical surface burst, for all values of scaled distance (Z < 40).
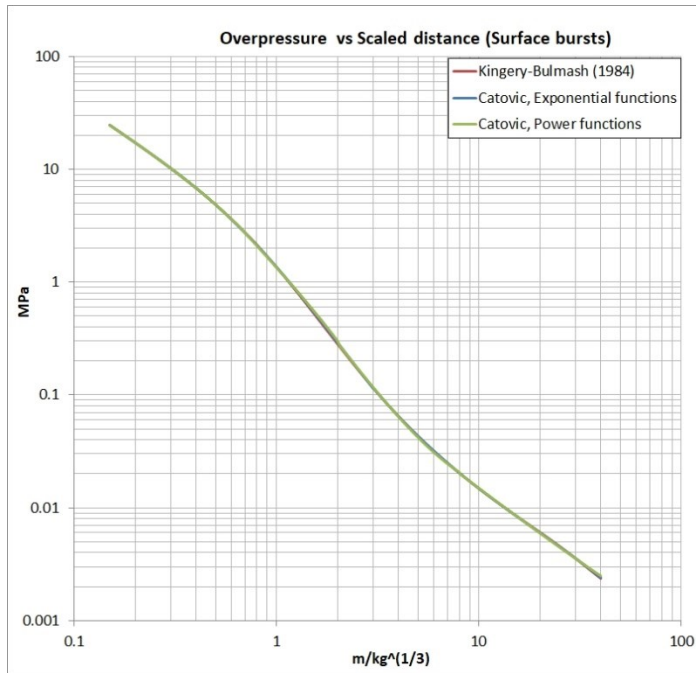
Figure 9: Positive blast wave incident overpressure values (vs. scaled distance) for surface burst, obtained using our models (formulas 33-38) compared to test [5] data (Kingery-Bulmash polynomials)

4. Numerical simulations

Numerical simulations of explosions were done in Ansys AUTODYN (version 2019), engineering software package that use finite difference, finite volume, and finite element techniques to solve a wide variety of non-linear problems in solid, fluid, and gas dynamics. This type of program is sometimes referred to as a hydrocode. The phenomena to be studied with such a program can be characterized as time-dependent with geometric nonlinearities (large strains and deformations) and material non-linearities (plasticity, failure, strain-hardening and softening, multiphase equations of state).

When simulating explosions, material properties can be selected from AUTODYN library (Table 5). Air uses Ideal gas equation of state, where the pressure P is related to the energy e (with adiabatic exponent γ) as:

$$P = (\gamma - 1)\rho e \qquad (39)$$

This form of an equation is useful for its simplicity and computation ease, where only the value of γ needs to be supplied.

For high explosives (i. e. TNT), there are different forms of equations of state (Ideal gas, Constant Beta, Wilkins, Becker-Kistiakowski-Wilson), but the one used in AUTODYN is Jones - Wilkins - Lee (JWL), in the following form:

$$p = A\left[1 - \left(\frac{\omega}{R_1 v}\right)\right] \cdot e^{-r_1 v} + B\left[1 - \left(\frac{\omega}{R_2 v}\right)\right] \cdot e^{-r_2 v} + \frac{\omega e}{v} \qquad (40)$$

The values of the constants A, R_1, B, R_2 and ω from Eq. (40) for some explosives have been estimated from experiments (cylinder test - expansion of a hollow metal cylinder filled with explosive), and are available in AUTODYN material library.

AUTODYN (1D, 2D, 3D) has been verified for use in blast effects estimation in many research papers.

In this research, we give an example of numerical simulation procedure of blast wave formation in the air after the detonation of 1 kg, 10 kg, and 10 T of TNT. Default values for the TNT and air equations of state were used, as well as other parameters specified in AUTODYN library (Table 5).

Table 5: Material properties of TNT and air in simulations (AUTODYN)

MATERIAL NAME: *TNT*	MATERIAL NAME: *AIR*
EQUATION OF STATE: JWL (det. products)	EQUATION OF STATE: Ideal Gas
Gamma: 1,35	Gamma: 1,4
Reference density (g/cm³): 1,63	Reference density (g/cm³): 1,225
Parameter A (kPa): 3,7377·10⁸	Pressure shift (kPa): 0
Parameter B (kPa): 3,7471·10⁶	Reference Temperature (K): 288,2
Parameter R_1: 4,15	Specific Heat (J/kgK): 717,59
Parameter R_2: 0,9	Thermal Conductivity (J/mKs): 0
Parameter ω: 0,35	
C-J Detonation velocity (m/s): 6,93·10³	
C-J Energy/unit volume (kJ/m³): 6,0·10⁶	
C-J Pressure (kPa): 2,1·10⁷	

Zones filled with the air were given initial energy of 2,068·10⁵ mJ/mm³ [13] to provide an ambient pressure of 101,3 kPa. A detonation point is located at the center of explosive (0,0,0) to start the explosion at time zero.

Gauge points (for pressure reading, Figure 10) were located at 0,5 m, 1 m, 2 m, 5 m from the detonation point of 1 kg TNT, 1m, 3 m, 6 m, 10 m for 10 kg TNT, and 3 m, 6 m and 9 m for 10 T simulation case.
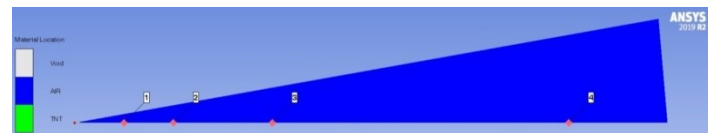
Figure 10: Location od detonation point and gauge points along the mesh

In AUTODYN, the programs' Euler solver was used in a wedge-shaped grid (1D model) at the apex of which the explosive charge (TNT) was located. For a mass of 1 kg, the explosive radius was 52,7 mm, for 10 kg TNT this radius was 113,56 mm, for 10 T it was 1135,6 mm. Outflow transmitting boundary condition was used to eliminate the wave reflection [13]. In reference [13], cell size values of 3 mm were recommended as a compromise between simulation duration and accuracy, but the results are dependent on the mesh so we used a cell size of 1 mm for comparison with the test data. Reference [1] suggests cell size equal to 0,002 times the distance to the monitoring location on the reflecting surface provided results within 10% of the converged value for 0,0553 ⩽ Z < 40 m/kg^{1/3}. The reference [13] suggests quadratic viscosity values of 0,1 which we adopted in our simulations.

As a part of the mesh size sensibility study, we first numerically simulated the blast wave formation after the explosion, with three different mesh sizes (1 mm, 10 mm, and 20 mm, quadrilateral cell

size) for 10 kg TNT charge, as an example. Results can be seen in Table 6, and in Fig 11. Table 6 shows that for coarser grid (20 mm) results deviate substantially from experimental data comparing to finer mesh (1 mm).

Table 6: Mesh size sensibility study results for 10 kg of TNT

R (m)		P (MPa)		Rel. diff. (%)
		P$_{AUTODYN}$	P$_{EXP}$ [5]	
1 mm cell	1	4,2715	4,4444	4,05
	3	0,4292	0,4420	2,98
	6	0,0919	0,0951	3,48
	10	0,0357	0,0355	0,56
10 mm cell	1	3,9991	4,4444	11,12
	3	0,4019	0,4420	9,99
	6	0,0890	0,0951	6,86
	10	0,0353	0,0355	0,88
20 mm cell	1	3,7079	4,4444	19,86
	3	0,3823	0,4420	15,63
	6	0,0864	0,0951	10,04
	10	0,0345	0,0355	3,22

Figure 11 shows mesh size influence on shock wave form at a distance of 1m, after detonation of 10 kg TNT. The coarser the grid, the slower the rate of rise of pressure front and the flatter the curve shape. Peak overpressure values are different for different cell sizes (smaller cell sizes giving larger pressure values).
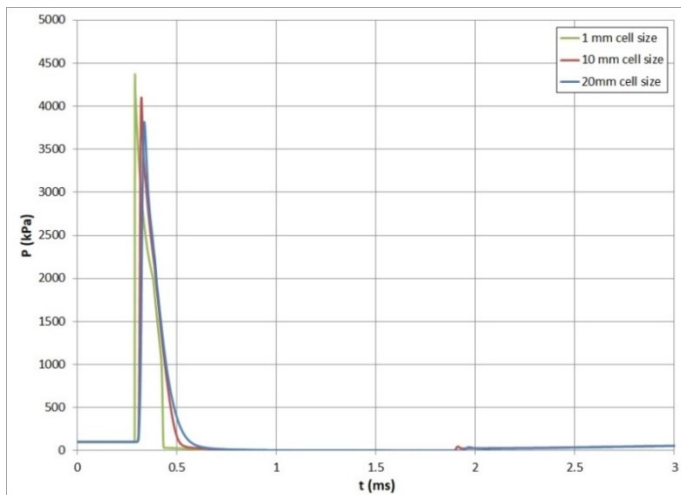
Figure 11: Mesh size influence on shock wave form at a distance of 1m, for 10 kg TNT explosive charge

Figure 12 shows the motion of a pressure wave along the mesh during simulation, for the case of 1 kg TNT.

During the simulation, AUTODYN shows rarefaction wave going toward detonation point (explosive charge). It reduces the pressures and density behind the front of the expanding detonation products.

This rarefaction wave, moving inward, is then reflected outward from the centre of the explosive forming, so called, secondary shock wave. Formation of a secondary shock wave, after the detonation of 10 kg explosive charge (TNT) can be seen in Figure 13.
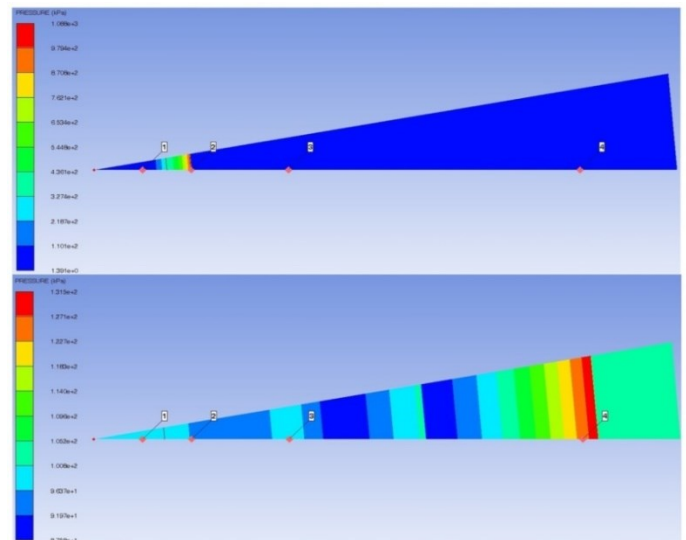
Figure 12: Motion of a pressure wave along the mesh during simulation for 1 kg of TNT
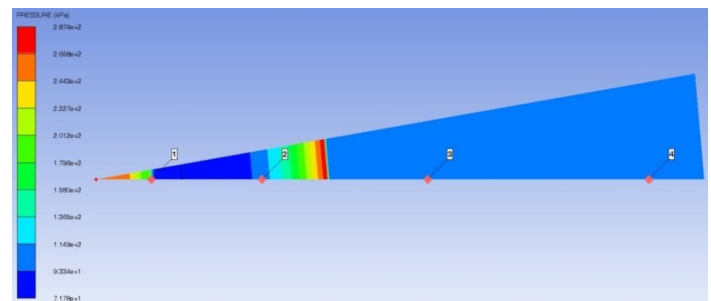
Figure 13: Formation of secondary shock wave (visible close to detonation point on the left) after the explosion of 10 kg TNT charge

AUTODYN can also provide 3D view of mesh by rotation of initial mesh with 360°), as shown in Figure 14.
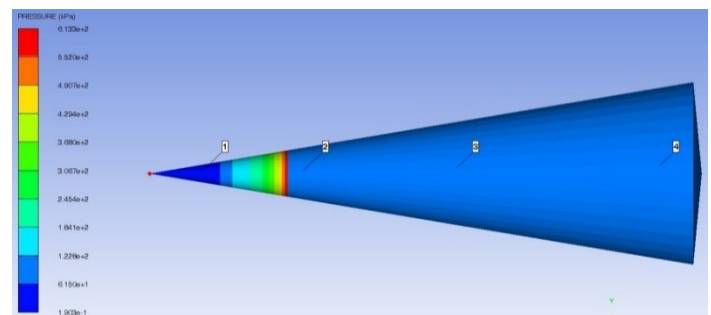
Figure 14: Rotation of initial mesh by 360°

Figure 15 illustrates the wave form P(t), obtained in simulations, at different distances from an explosion, for 1 kg and 10 kg TNT charges.

The second peak on the first (black) curve is likely caused by the blast wave reflection at the material interface (TNT/Air)

because of different acoustic impedances of these materials (it should be noted that this second peak is of little practical significance [13]).

We can see from Figure 15 that blast wave pressures drop significantly with distances in air.

Generally, when the blast wave moves through the atmosphere, pressures are rapidly decreased and have a brief existence span, (measured in milliseconds; as shown clearly in Figure 15).
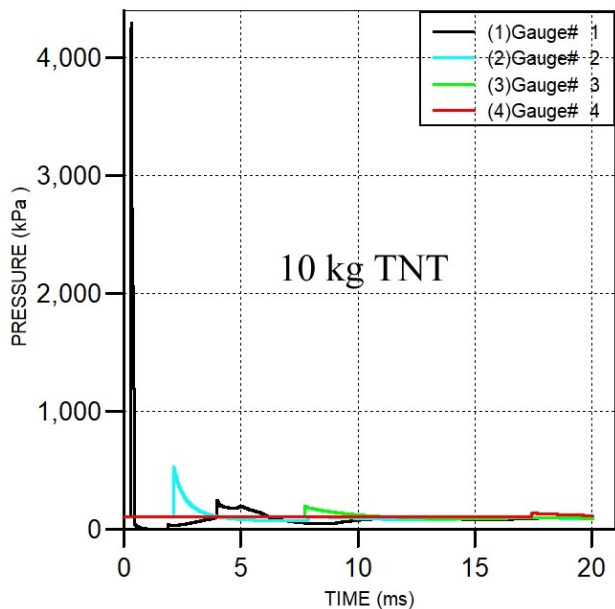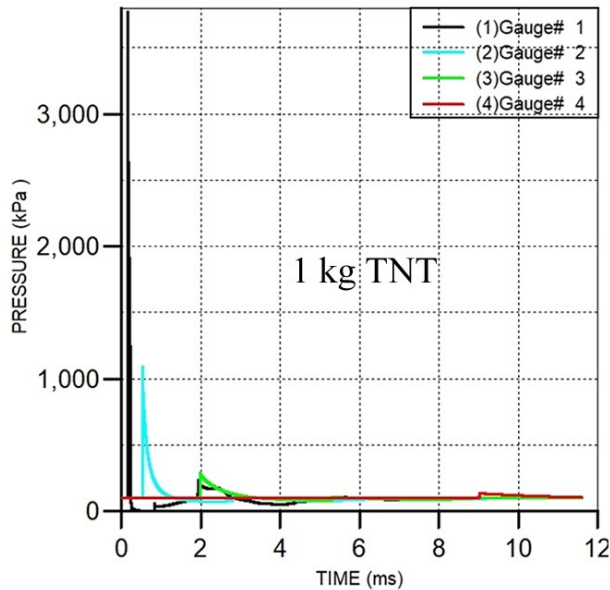
Figure 15: P(t) curves obtained in AUTODYN for 1 kg and 10 kg of TNT at different distances

The results from numerical simulations for 1 kg, 10 kg, and 10 T of TNT explosive charge were compared with experimental data [5], and relative differences presented in Table 7.

Relative differences observed between simulation results and test data were smaller than 5,9 % for all cases for 1 kg TNT,

smaller than 4 % for 10 kg TNT, and less than 2,1 % for 10 T charge.

AUTODYN User's Manual reports of errors around 4% for peak incident overpresure between numerical simulations and test data.

Table 7: Comparison of blast wave overpressure values obtained in numerical simulation (1 mm cell sized mesh) with experimental data [5], for 1 kg, 10 kg, and 10 T of TNT at different distances

R (m)		P (MPa)		Rel. diff. (%)
		$P_{AUTODYN}$	P_{EXP} [5]	
1 kg TNT	0,5	3,6661	3,8848	*5,96*
	1	0,9897	0,9349	*5,86*
	2	0,1843	0,1947	*5,64*
	5	0,0318	0,0313	*1,59*
10 kg TNT	1	4,2715	4,4444	*4,05*
	3	0,4292	0,4420	*2,98*
	6	0,0919	0,0951	*3,48*
	10	0,0357	0,0355	*0,56*
10 T TNT	3	22,2757	22,6409	*1,64*
	6	9,8847	10,0005	*1,17*
	10	4,3524	4,4445	*2,12*

As can be seen from the results, AUTODYN can successfully model blast wave formation in the air after the detonation of high explosive. Results from these simulations can be remapped into 3D urban scenario simulation of explosion, which can be follow-up research.

5. Conclusions

In this paper we made a comparation of available formulas for blast wave overpressure. These formulas were compared with available empirical data [5]. The Kinney and Shin models showed the best agreement with experimental data for free airburst, while for surface burst, Swisdak, Vanuci, and Jeon models predicted test data most accurately.

Also, we performed a numerical simulation of airburst detonation after the explosion of TNT charge in Ansys AUTODYN, for the cases of 1 kg, 10 kg, and 10 T of TNT explosive charge, with a fine mesh (1mm), where obtained data were compared with experimental data (Kingery & Bulmash). Relative differences observed between simulation results and test data were smaller than 5,9 % for all cases for 1 kg TNT, smaller than 4 % for 10 kg TNT, and less than 2,1 % for 10 T charge. In this part, we also gave a detailed description of the procedure for these simulations as a valuable tool for blast wave phenomena investigation.

The novelty in the paper is that we introduced new exponential and power functions for surface blast overpressure estimation, with small relative differences compared to experimental data [5]. These formulas, with acceptable accuracy, are somewhat simpler than many of the formulas used for blast overpressure estimation, and can be implemented faster.

The following work in this field can be pointed towards complex geometry urban scenario blast effect modeling, where surface burst effects dominate, with complex reflections of shock wave present.

Conflict of Interest

The authors declare no conflict of interest.

References

[1] J. Shin, A.S. Whittaker, A. J. Aref, D. Cormie, "Air-Blast Effects on Civil Structures ", New York, 2014, doi:10.13140/RG.2.1.3454.1686.

[2] Structures To Resist The Effects Of Accidental Explosions, UFC 3-340-02, Department of Defense, 2008.

[3] Engineering Design handbook: Explosions in Air, 1st ed., Army Materiel Command, Alexandria, Virginia, 1974.

[4] V. Karlos, G. Solomos, M. Larcher, "Analysis of blast parameters in the near-field for spherical free-air explosions", Ispra, Italy, 2016, doi:10.2788/778898.

[5] C. Kingery and G. Bulmash, Air blast parameters from TNT spherical air burst and hemispherical surface burst, Ballistic Research Laboratories, 1984.

[6] "Guidelines for Evaluating the Characteristics of Vapor Cloud Explosions", Flash Fires, and BLEVEs, 2nd ed., Center for Chemical Process Safety, American Institute of Chemical Engineers, New York, USA, 1994, doi:10.1002/9780470938157.

[7] J. Hall, Principles of Naval Weapons Systems, 1st ed., Kendall/Hunt, 2000.

[8] Explosive blast, GSA Security Reference Manual - Part 3: Blast Design and Assessment Guidelines, Federal Emergency Management Agency, 2001.

[9] J. DooJin, K. KiTae, H. SangEul, "Modified Equation of Shock Wave Parameters," Computation, **5**(3), 1–14, 2017, doi:10.3390/computation503004.

[10] G.F. Kinney, K.J. Graham, Explosive Shocks in Air, Springer, Berlin, Heidelberg, 1985, doi:10.1007/978-3-642-86682-1.

[11] P. Smith, J. Hetherington, Blast and Ballistic Loading of Structures, 1st ed., CRC Press, London, England, 1994, doi:10.1201/9781482269277.

[12] P. Vannucci, F. Masi, I. Stefanou, A study on the simulation of blast actions on a monument structure, HAL Archives-Ouvertes, France, 2017.

[13] T. C. Chapman, M.S. Rose, P.D. Smith, "Blast wave simulation using AUTODYN2D: A parametric study", International Journal of Impact Engineering, **16**(5), 777–787, 1995, doi:10.1016/0734-743X(95)00012-Y.

Deep Deterministic Policy Gradients for Optimizing Simulated PoA Blockchain Networks Based on Healthcare Data Characteristics

Achmad Ichwan Yasir, Gede Putra Kusuma[*]

Computer Science Department, BINUS Graduate Program - Master of Computer Science, Bina Nusantara University, Jakarta, Indonesia, 11480

A R T I C L E   I N F O

A B S T R A C T

Blockchain technology has proven to be the best solution for digital data storage today, which is decentralized and interconnected via cryptography. Many consensus algorithms can be options for implementation. One of them is the PoA consensus algorithm, which is proven to provide high performance and fault tolerance. Blockchain has been implemented in many sectors, including the healthcare sector that has different characteristics of larger and more diverse record sizes. Implementing blockchain costs a lot of money. We used a blockchain network simulator as the best alternative in our research. The main problems with blockchain implementation are having a dynamic characteristic network and providing a blockchain system that is adaptive to network characteristics. Therefore, we propose a method to optimize the simulated PoA blockchain networks using Deep Deterministic Policy Gradients by adjusting the block size and block interval. The simulation results show an increase in effective transaction throughput of up to 9 TPS for AIH and 5 TPS for the APAC data models, and without affecting other important aspects of the blockchain.

1. Introduction

Currently blockchain technology is penetrating to all sectors in the world. One of which is the health sector, where a lot of data exchange and access restrictions are very sensitive and important. On the other hand, the characteristics of the data are also challenging because they are larger in size and heterogeneous. Another important factor is the interoperability of healthcare record, how to provide open access to read and write to the right party with the best scalability [1]. By applying blockchain technology to medical records, patients as data owners can better maintain and control their data as personal data, and health care professionals, institutions, and hospitals can exchange certain patient data as needed to facilitate analysis of patient health [2]. In short, blockchain has the potential to enhance PHR solutions that provide privacy and interoperability [3].

Research on blockchain began a long time ago, and many fields have adapted this technology. Initially in the financial sector known as cryptocurrency and more recently in the health care field [4]. Many approaches have been proposed for applying blockchain technology to health records. Most of which is focused on the distributed medical record ledger and provide a useful framework for safeguarding patient privacy. Apart from that, another aspect

that is also important in the consideration of ensuring the adoption of blockchain technology is the distribution and integration performance of health data among healthcare organizations [5].

Electronic Health Records (EHRs) adoption increased over time for all specialties [6]. As the adoption of EHRs increases, the possibility of failure to execute on the promise of shared health records also increasing, and this is a serious issue that needs to be addressed in EHR systems [7]. Wider adoption of electronic health records can significantly affect performance and allow a previously unknown level of violation of health data [3]. The privacy and security of medical records are the main concerns of patients. Some patients withhold information from their healthcare providers because of concerns about their privacy [8].

On the other hand, bitcoin as the first knowledge based in cryptocurrency only confirms with mean and median average throughput is between 3.3 and 7 transactions per seconds (TPS) [9]. Even in theory Bitcoin can handle transaction process with throughput up to 27 TPS (transactions per second) [10] with an average transaction size of 0.25 KB (kilobyte) [11]. That throughput is far from enough to handle health record transactions base on ORBDA (openEHR benchmark dataset), which size per transaction within 7.9 KB on average for the Authorization for Hospital Admission (AIH) XML data model and 12.4 KB on

average for the Authorization for High Complexity Procedures (APAC) XML data model [12]. In simple calculation, if we assume blockchain technology is adapted from bitcoin and the data has the same characteristic with ORBDA, we will only have transaction transfer speed around (7 * 250) = 1750 KB/s so the throughput with AIH XML data model only around 1750/7900 = 0.22 TPS and APAC XML data model had around 1750/12400 = 0.14 TPS. The blockchain needs optimization to handle PHR cases. Therefore, we propose DDPG to optimize the blockchain factor to be able to adjust to network conditions and maximize throughput.

2. Related Works

We present some related works with concern about optimize simulated PoA blockchain networks using healthcare data characteristics and optimization methods to adjust blockchain parameters in a way to handle dynamic network characteristics. Recently many research and development to implement blockchain technology into the health records sector. Here are some recent frameworks that use blockchain technology. Firstly, OmniPHR model [13] is a PHR model design that is distributed with the openEHR standard. It is using a blockchain but not integrated with the source of the blockchain. you can say it can't be changed with dynamic network characteristics. Secondly, FHIRChain Model [14], which is also uses a Blockchain-Base and uses the Office of the National Coordinator for Health Information Technology (ONC) according to its development needs, as well as security and interoperability issues with standards HL7, however, also does not mention the overall blockchain aspect and the associated optimization of the node from the blockchain used [12]. After all, we did not find research/or framework regarding optimizing blockchain in the health sector, and that would be a state of the art of this research.

Regarding related research blockchain optimizations, In 2019, Liu proposed an optimization for Blockchain-enabled in general proposed for the Industrial Internet of Things (IIoT) systems using Deep Reinforcement Learning, and she did not consider area/regional distribution, like where is the region of nodes, the block producers only scattering over a 1km-by-1km area [15]. In the real implementation of a blockchain network, it is demanded to be able to handle a very wide and unlimited network. In the same year, Liu also proposed optimization for blockchain-enabled Internet of Vehicle, the difference between the previews proposal is the security factor based on a number of validators instead of consensus selectors [16]. The process of both optimization studies showed significant improvement. Therefore, in this study, we tried to adopt the research methodology, using the data characteristics of health records with the ORBDA specification (openEHR benchmark dataset for performance assessment) with the same scale node distribution and same characteristics of the bitcoin network.

In 2019, Distributed Systems Group from Tokyo Institute of Technology developed an open-source system called SimBlock, to simulate a blockchain Network. This system suitable for use in blockchain network research [17]. Besides, SimBlock is very easy to configure and resembles the conditions with the characteristics of the blockchain network, so we decided to use this SimBlock as a simulator of a blockchain network in our research.

3. Proposed Simulated Blockchain System

This chapter will explain the blockchain system with parameters involved and can be optimized, and the design of an optimization model using the Deep Deterministic Policy Gradients.

3.1. Blockchain

The blockchain is an arrangement by the sequence of blocks, which holds a complete list of transaction records [18]. Blockchain is the core technology for Bitcoin, which was the first blockchain proposed from Nakamoto in 2008 rather than being implemented to the public in 2009 [19], Blockchain was wildly developed to be applied in all sectors such as financial services such as digital assets, remittances, online payments , Industry, etc. including the health sector, which is the focus of our research.

There are various types of transaction data from PHR, and openEHR is an open-source framework which is commonly used as a standard specification for PHR. For experiments in this study using ORBDA as a dataset. The ORBDA dataset is available in compositions, versioned compositions, and openEHR EHR representations in XML and JSON formats. In total, the dataset contains more than 150 million composition records. and consists of 2 data types namely AIH and APAC [12]. which we will use the characteristics of the transaction in the simulator.

3.2. Blockchain Network Simulator

Blockchain life cycle is a collection of dependent events, based on the consideration of block creation and message transmission(send/receive) as events, we consider SimBlock as a simulator of this research. SimBlock allows us to easily implement the neighbor's algorithm node selection. Given that block creation times are calculated from the probability of successful block creation, it is unnecessary to reproduce mines requiring large calculating power, and networks involving multiple nodes can be simulated. [17].

The SimBlock has an easy-to-modify configuration based on actual network characteristics. including: 1). number of nodes (N): in the simulation can set the number of nodes involved in the blockchain network (i.e., block producer / validator candidates) and assume (V) notation for number of block validator. 2). Block Size (S^B) : the average size of each block that the node will propose. 3). Block Interval (T^I) : Block generation interval targeted by the blockchain. 4). Regional distribution: the percentage distribution of nodes according to the specified region. 5). node computation (c): manage and randomize the compute capacity of the node, 4). upload / download speed: important factor of a network which is this simulator can be configure based on the origin and destination regions.

3.3. Proof-of-Authority (PoA)

Proof of Authority (PoA) is a one of consensus algorithms for permissioned blockchain that was superiority is due to performance increases with character to typical BFT algorithms. Because PoA has a lighter message exchange [20]. Another advantage of proof of authority is its power to validate blocks based on a person's actual identity thus making the system more secure and efficient, the blockchain which achieves high

throughput and low latency [20], [21]. PoA is basically proposed for private networks as part of the Ethereum ecosystem and is implemented in 2 types; Aura and Clique. In this experiment, we consider using PoA Clique with a node / validator identity as the sequence. The PoA Clique algorithm proceeds in an epoch that is identified by a sequence of committed blocks. A transition block is broadcast when a new epoch starts. It defines a set of authorities (i.e., their id) and can serve as a snapshot of the current blockchain by new authorities who need to synchronize [20].

a). Time 1   b). Time 2
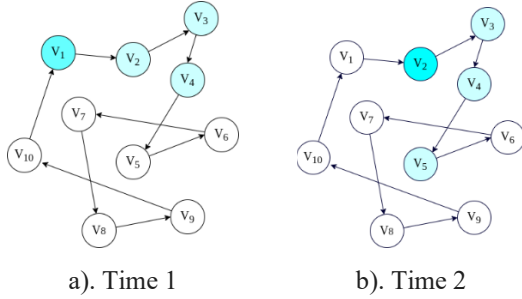
Figure 1: Regulatory authorities could issue a block on Clique

Figure 1 shows two consecutive steps and how current leaders and authorities allowed proposed blocks change. There are number of validators $(V) = 10$ authorities, hence $V - (V/2 + 1) = 4$ authorities allowed to issue a block at each step, and one of them perform as a leader (V_1 in Time 1, V_2 in Time 2). In Figure 1 (a), the V_1 is the leader while V_2, V_3, and V_4 can propose blocks. In Figure 1 (b), V_1 are no longer allowed to issue a block (already in the previous step, so it has to wait $V/2 + 1$ steps or epoch, while V_2 is operate as a leader and V_5 is now authorized to issue a block [20].

3.4. Performance Analysis

Transactional throughput is key to measuring blockchain scalability that's why we need optimization to make it able to handle openEHR records, In addition to scalability we also need to keep other parameters. i.e. decentralization, security , and latency. Other parameters act as scalability constraints to overcome the four-way trade-off issue.

3.4.1. Scalability

Blockchain is literally an arrangement of linked blocks in which a block be composed of a transactions sequence. Scalability is the key to measuring the performance of the blockchain, scalability is measured using throughput (Transactions per Second), calculated from number of transactions in a certain time (second) that can be processed by the blockchain system. Transactional throughput represented by Ω (transactions per second, i.e. TPS) is depend directly on the variable block interval and block size, and the notation will be

$$\Omega(S^B, T^I) = \frac{\lfloor S^B/x \rfloor}{T^I} \tag{1}$$

Block interval is notated by T^I, block size is notated by S^B, and x is represents the mean of transaction size. we will use a variable block size or time interval can find a way to optimize the throughput on the blockchain network and it can be seen from Eq. (1) shows that increasing value of block size or reducing value of block interval between blocks can increase throughput. However,

the adjustment must also consider the network conditions, to maintain parameters such as decentralization, security, and latency, so that we cannot arbitrarily adjust the block interval and block size.

3.4.2. Decentralization

In the simulation we reproduced the actual environment of bitcoin blockchain. And in order to measure decentralization factor, we consider Gini coefficient, which is recommended to measure of income inequality in this case is wealth of validator. The decentralization factor comes from the inequality of validator nodes, in an equation derived from the number of authority processes on the blockchain. and each block at least has been authorized by $V/2 + 1$ validator. To identify the notation The set of nodes is denoted as $\Phi_S = \{z_1, z_2, .. z_N\}$, Meanwhile, to denote set of validators, $\Phi_D = \{z_{d_1}, z_{d_2}, ... z_{d_V}\}$, $\Phi_D \subseteq \Phi_S$ and V is number of validator.

$$G(Y) = \frac{\sum_{z_{d_i} \in \Phi_D} \sum_{z_{d_j} \in \Phi_D} |Y_{d_i} - Y_{d_j}|}{2 \sum_{z_{d_i} \in \Phi_D} \sum_{z_{d_j} \in \Phi_D} Y_{d_i}} = \frac{\sum_{z_{d_i} \in \Phi_D} \sum_{z_{d_j} \in \Phi_D} |Y_{d_i} - Y_{d_j}|}{2K \sum_{z_{d_i} \in \Phi_D} Y_{d_i}} \tag{2}$$

Note i, j is link connection between validators, first validator (z_{d_i}) and seconds validator (z_{d_j}) and validate block next. (Y) is number of validation distribution calculated from the number of times the validator validates a block. The value of the Gini coefficient is on a scale of 0 to 1, where 0 is the highest decentralization and 1 is the highest centralization. In other words, the closer the coefficient is to 0, the more decentralized validation is processed. On the other hand, and the closer to coefficient 1, the validation process becomes more centralized. To ensure a decentralized block validator/producer of the validation distribution factor, it must meet the requirements as notation below.

$$G(Y) \leq \eta_s \tag{3}$$

where η_s is decentralization threshold and $\eta_s \in [0,1]$.

3.4.3. Latency

In order to calculate blockchain latency, We evaluate the system with TTF, that is, the time to finality denoted by T^F, is measured by many seconds will take to receive reasonable assurance that transactions written on the blockchain are immutable. Note that transaction processing includes two phases, i.e., the time span from block creation to block creation and time for blocks to be validated and time to reach consensus on the generated blocks among validators, so the TTF for a transaction is obtained from adding the time of block issued (block interval T^I) with the amount of time for the block validation process to reach consensus, notated below.

$$T^F = T^I + T^C \tag{4}$$

where T^C represented latency of consensus, that is, the time span for a new block to be authenticated by the block validator.

Furthermore, we divide the validation process into two-stage, specifically sending messages and verifying messages (verifying Validator, verifying features.). Therefore, the formula of T^C is

$$T^C = T^D + T^V \tag{5}$$

T^D is the spanning time for sending message and T^V represented time of validation process. In order to set the optimal delay time we prepared the blockchain network scenario delay requirements, assuming a block must be issued and validated in a (ω) number of consecutive block intervals where ω is greater than 1 ($\omega > 1$). In particular, the time span for transaction completion must meet the following constraint,

$$T^F \leq \omega \times T^I \tag{6}$$

3.4.4. Security

The PoA Clique consensus algorithm that we propose in this study has a default security configuration, security can be guaranteed in all network conditions during $N/2 + 1$ signers to be honest signers. Thas a simple majority is all that is needed to run a secure network. To ensure the security of the blockchain system, each validator must not submit no more than 3 times in every epoch. if we assume B as a block t represent as an epoch containing a set of blockchain then set of block producer denoted by, $\Phi_B = \{ z_{b_1}, z_{b_2}, \ldots z_{b_K}\}$, $\Phi_B \subseteq \Phi_D$ with K notated of number block producer of each (t). then we can denoted by:

$$F_i^{(t)} = \sum_{z_{b_i} \in \Phi_B}^V |z_{b_i}| \tag{7}$$

where $F_i^{(t)}$ = Total number of block validators i propose a block in one epoch (t). Specifically, the node validator should not be as block producer more than 3 times in each epoch.

$$F_i^{(t)} \leq 3 \tag{8}$$

3.5. Performance Optimization

Blockchain system optimization challenges are facing dynamic and large-dimensional characteristics, in the form of transaction size and node features on the blockchain system (e.g. distribution, transfer rate, computing resources), we propose the DDPG algorithm. Below is an identification of action space, state space and reward functions.

3.5.1. State Space

The state space that we identified at the time of the decision / epoch t ($t = 1,2,3,..$) is a combination of the average transaction size (χ), the distribution of the validation process (υ), the computation power of node (c), and transmission rate, the speed of data exchange between each node ($R = R_{(i,j)}$), which is denoted as

$$S^{(t)} = [\chi, \upsilon, c, R] \tag{9}$$

3.5.2. Action Space

Action Space is a parameter that needs to be adjusted to optimize throughput, we identified several parameters including block size (S^B) and block interval (T^I) in the blockchain simulator that can be adjusted in order to adapt with the dynamic network characteristic of blockchain system, $A^{(t)}$ denoted as

$$A^{(t)} = \left[S^{B'}, T^{I'}\right] \tag{10}$$

where block size $S^B \in 1, 2 \ldots, S^{B'}$ is normalized value from S^B in Mb and block interval. $T^I \in 1, 2 \ldots, T^{I'}$ is normalized value from T^I in minutes .

3.5.3. Reward Function

The reward function is identified to ensure decentralization, security, and finality of the blockchain system while also maximizing transactional throughput based on the reward value given, the decisions issued on each epoch must meet the requirements as the notation below.

$$P1: \max_A Q(S, A)$$
$$C1: G(Y) \leq \eta_s$$
$$C2: T^F \leq \omega \times T^I \tag{11}$$
$$C3: F^v \leq 3$$

The decentralization factor of validators or block producer, distribution of validation tasks is guaranteed by C1 (Eq. (3)), Time finality (TFF) is ensured by C2 (Eq. (6)) and security factors secured by C3 (Eq. (8)), We denote reward function as $R\left(S^{(t)}, A^{(t)}\right)$.

$$R^{(t)}\left(S^{(t)}, A^{(t)}\right) =$$
$$\begin{cases} \frac{\lfloor S^B/\chi \rfloor}{T^I}, & if \; C1 - C3 \; are \; satisfied \\ 0, & otherwiase \end{cases} . \tag{12}$$

If one or more of the notations is unsatisfying, it defines the blockchain as having poor performance in security, latency, or decentralization, so the reward value given is 0 because this case addresses this invalid situation. respectively, so that the action value function Q (S, A) is denoted by

$$Q(S, A) = E\left[\sum_{t=0}^{\infty} \gamma^t R^{(t)}\left(S^{(t)}, A^{(t)}\right) \Big| S^{(0)} = S, A^{(0)} = A\right] \tag{13}$$

with the discount factor $\gamma \in [0,1]$ that reflects the tradeoff between the immediate and future rewards, For a deterministic policy $\mu : S \to A$ we can write the Bellman Equation as

$$Q\left(S^{(t)}, A^{(t)}\right) = E\left[R^{(t)}\left(S^{(t)}, A^{(t)}\right) + \gamma Q^{(\mu)}\left(S^{(t+1)}, A^{(t+1)}\right)\right] \tag{14}$$

The off-policy algorithms like Q-Learning use the greedy policy $\mu(S) = \arg \max_A Q (S, A)$. Function approximators parameterized by Q, which is optimized by reducing the loss function:

$$L(\theta^Q) = E\left[\left(Q\left(S^{(t)}, A'|\theta^Q\right) - y^{(t)}\right)^2\right] \tag{15}$$

where:

$$y^{(t)} = R^{(t)} + \gamma \max_{A'} Q\left(S^{(t+1)}, A'\right) \tag{16}$$

3.5.4. Deep Deterministic Policy Gradient (DDPG)

DDPG is an actor-critic algorithm based on Deterministic Policy Gradient [22], [23]. The DPG algorithm consists of a parameterized actor function $\mu(S|\theta^\mu)$ which specifies the policy at the current time by deterministically mapping states to a specific action [24]. The critic $Q (S, A)$ is learned using the Bellman equation the same way as in Q-learning. The actor is updated by applying the chain rule to the expected return from the start distribution J with respect to the actor parameters:

$$\nabla \theta^\mu J \approx E\left[\nabla_A Q\left(S^{(t)}, A^{(t)}|\theta^Q\right)\right] =$$
$$E\left[\nabla_{\theta^\mu} Q\left(S^{(t)}, A^{(t)}|\theta^Q\right) \nabla_{\theta^\mu} \mu\left(S^{(t)}|\theta^\mu\right)\right] \tag{17}$$

DDPG combines the merits from its predecessor algorithms to make it more robust and efficient in learning. The samples obtained from exploring sequentially in an environment are not independently and identically distributed so DDPG uses the idea from Deep Q-Networks (DQN) called replay buffer [24]. Finally, we present the proposed DRL-based framework in **Algorithm 1**.

Algorithm 1: Pseudocode of the DDPG optimization algorithm

---

for each decision epoch t **do :**

Optimization process

1) Select a random action ε, with probability otherwise $A^{((t))} = arg(max_A Q (S)^{(t)}, A^{(t)})$ re $Q(\bullet)$ is estimated by the main Q network;

2) Run simulator $A^{((t))}$ with adjusted block size and interval;

Update

1) Observe the reward $R^{((t))}$ and the next state $S^{((t+1))}$;

2) Store the experience $(S^{(t)}, A^{(t)}, R^{(t)}, S^{(t+1)})$ in replay buffer D;

3) Randomly sample a mini-batch of state transitions $(S^{(i)}, A^{(i)}, R^{(i)}, S^{(i+1)})$ from experience memory D;

4) Calculate the target Q-value from the target Q network by:

$$y^{(i)} = R^{(i)} + \gamma max_{A'} Q(S^{(i+1)}, A')$$

5) Update critic by minimizing the loss by

$$L (\theta^Q) = [Qh(S^{(i)}, A' | \theta^Q) - y^{(i)}]^2$$

6) Update the actor using the sampled policy gradient by

$$\nabla_\theta J \approx \nabla_A Q(S^{(i)}, A^{(i)} | \theta^Q) \nabla_{\theta^\mu} \mu(S^{(i)} | \theta^\mu)$$

7) Update the target networks

$$\theta^{Q'} \leftarrow \tau\theta^Q + (1 - \tau)\theta^{Q'}$$
$$\theta^{\mu'} \leftarrow \tau\theta^\mu + (1 - \tau)\theta^{\mu'}$$

6) Update the actor using the sampled policy gradient by

$$\nabla_{\theta^\mu} L \approx \nabla_{\theta^\mu} Q(S^{(i)}, A^{(i)} | \theta^Q) \nabla_{\theta^\mu} \mu(S^{(i)} | \theta^\mu)$$

end

---

4. Experiments

This chapter explains details of the experiment. It begins with preparing the simulation process, then reporting and discusses the result.

4.1. Simulation Process

In the simulation, we consider a simulate blockchain in 2 types of Health records data model 1). AIH XML data model. 2). APAC XML data model. With characteristics of transactions that generate random size by given mean and standard deviation. Mean of AIH XML type is 7.9 Kb and 12.4 Kb for APAC XML type, and 1.0 Kb for both of them standard deviation, The scenario will involve 600 nodes with 100 nodes as block producer and assume all block procedures are block validators. The DDPG optimization algorithm was implemented using the PyTorch library, with

python as a programming language. and the SimBlock developed by Tokyo Institute of Technology system as a blockchain network simulator, with Java as the programming language, which can be run via the bash command. For the platform, we are using PyTorch 0.4.1 with Python 3.7.3 on Ubuntu 18.04.3 LTS. The geographic nodes distributions as in Table 1.

Table 1: Bitcoin node distribution and network characteristic [17]

	Percent nodes geographical distributions (%)	Upload Bandwidth in average (bit per second)	Download Bandwidth in average (bit per second)
North America	33.16	19200000	52000000
Europe	49.98	20700000	40000000
South America	0.90	5800000	18000000
Asia Pacific	11.77	15700000	22800000
Japan	2.24	10200000	22800000
Australia	1.95	11300000	29900000

Performance comparison of the four schemes considered: 1) The scheme by adjusting the block size and block interval, dynamically adjusting the block interval and block size as the action state in the learning process. 2) Scheme with fixed block size and dynamic block interval, the block produced by the block producer is the same size (5MB) and the block interval can be adjusted as an action state in the learning process. 3) Scheme with fixed block interval and dynamic block size. the block issuance time span is set regularly (every 10 minutes). And only the block size is set in the action state in the learning process. 4) no optimization, which is no variable set as action state, so the block issued is always the same size 5MB and frequency issuing block is every 10 minutes.

4.2. Experimental Results

From the simulation obtain a good result, where the implementation of the DDPG algorithm brings improvement transactions throughput of the blockchain.

4.2.1. Decentralization

Figure 2 represents the decentralization of AIH data model and Figure 3 represents the decentralization of APAC data model. Both graphs visualize the decentralized performance of the simulated blockchain network. Where to measure the decentralization factor, we use the number of validation processes of each block validator, we use the Gini coefficient metric, to capture the generalized decentralized of validation task distribution. proven that in the Lorenz curve is gradually approaching the ideal decentralization (stripe) with a decrease in the threshold, then the blockchain gets more decentralized, so it can be interpreted that the Gini coefficient is considered as an effective metric to quantitatively measure a decentralized blockchain [16].
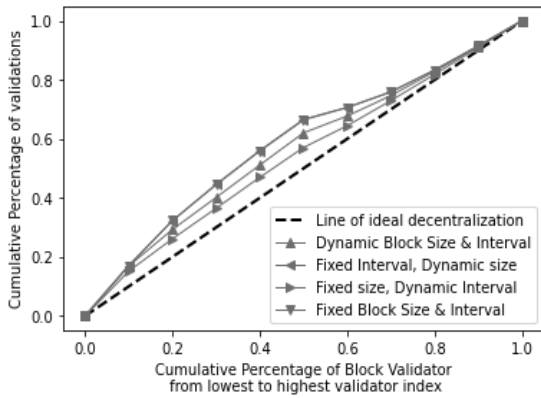
Figure 2: Lorenz curve of validation distribution of block validator with AIH data model
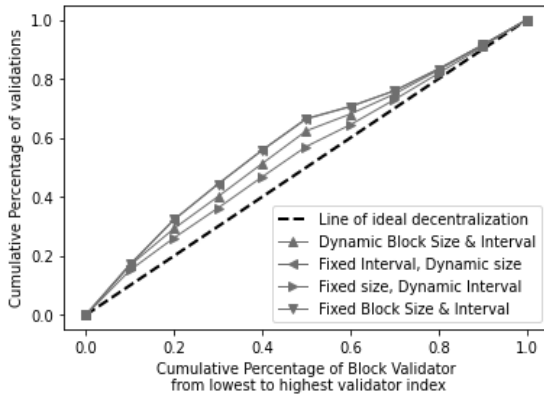
Figure 3: Lorenz curve, of validation distribution of block validator with APAC data model
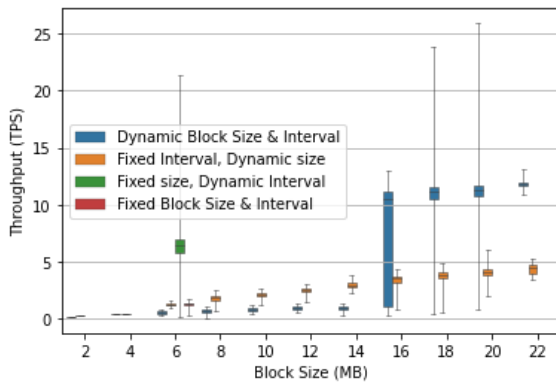
Figure 4: Median throughput vs. rounding up block size with AIH data model
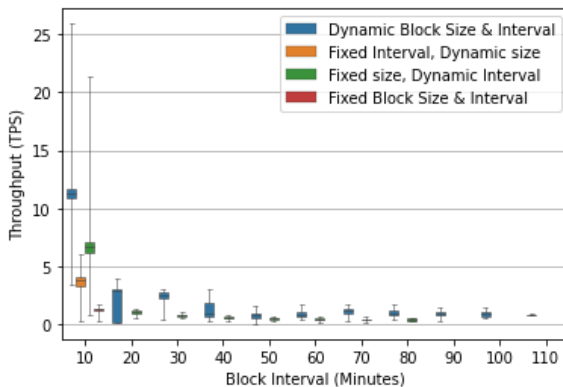
Figure 5: Median throughput vs. rounding up block interval with AIH data model

4.2.2. Baselines Performance

The correlation between block intervals and block size is very significant effect on throughput in AIH data models and can be shown in Figure 4 and 5.

The effect of the adjustment process in Simulation of Health records with AIH data model (Figure 4, Figure 5) showing significant correlations between transactional throughput with block size. Bigger block size, more likely it is to get a high throughput, but not guarantee the throughput will improve, and variable block intervals also have significant impact, the smaller the time interval proposed block, the more likely it is to get a high throughput. This correlation was also found in the blockchain health record simulation with the APAC data model depicted in Figure 6 and Figure 7.
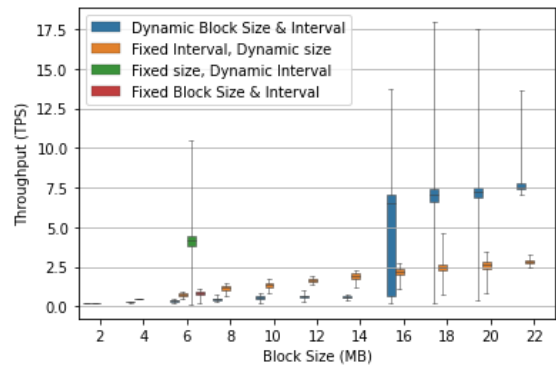
Figure 6: Median throughput vs. rounding up block size with APAC data model
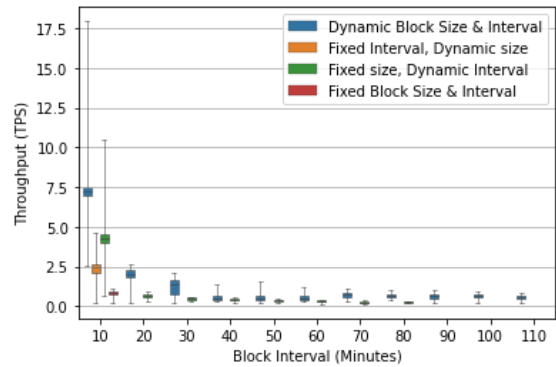
Figure 7: Median throughput vs. rounding up block interval with APAC data model

The effect of the adjustment process on block size and block interval on the transaction throughput is shown in Figures 4 - 7. We can see those graphs with 2 models AIH and APAC have the same pattern in the correlation between block size and throughput because the nodes validator can send and validate more transactions in one big block size but bigger block size needs more effort in sending a block into another node. Then, it can be seen that the Dynamic Block size and Block interval schemes achieve consistently higher throughput than other schemes with partially or completely fixed value parameters, because having a fixed value makes the system unable to adapt to network conditions. Meanwhile, it should be noted that fixed block size schemes perform better than fixed block interval schemes. A plausible explanation is in dealing with the situation of a low TTF threshold that a fixed block size scheme can be adjusted over the block interval. In addition, it makes sense when the results show that the

best performance of all schemes is a scheme whose block interval and block size can be adjusted according to network conditions, that reveals the advantages of a DDPG algorithm.

4.2.3. Throughput Performance

The simulation results show the performance of DDPG performance optimization scheme is presented in Figure 8 and Figure 9, the scheme we propose shows good convergence performance for both types of data models in AIH and APAC. At the beginning of the learning process, shows a very low throughput, and increases with increasing epoch, and reaches a stable state after about 750 episodes onwards. In addition, the proposed scheme can obtain the highest throughput results compared to other experiments with partially or completely fixed value parameters. The reasons behind these results are as follows: 1) In the DDPG Performance Optimization, the block interval and block size will be adjusted to optimize throughput adaptively based on network conditions; 2) For the proposed scheme with partially or completely fixed value parameters (block size / block interval), it fails to maximize throughput because the block interval or block size cannot adapt to dynamic networks.

In addition, based on the results of our research we also observe that the average TTF of a blockchain system decreases with an increase in the average source of computing power, and schemes with dynamic block size and block interval optimization require the lowest average TTF when compared with another partial optimized schema, or with a fixed block size and block interval scheme.
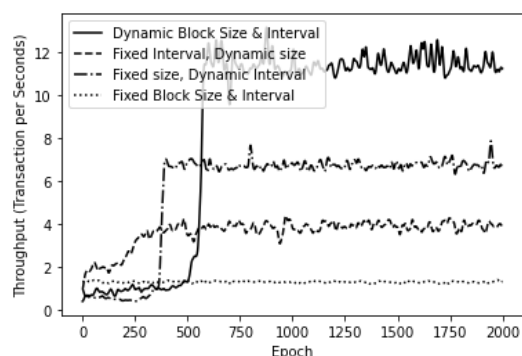
Figure 8: Convergence performance of different schemes with AIH data model
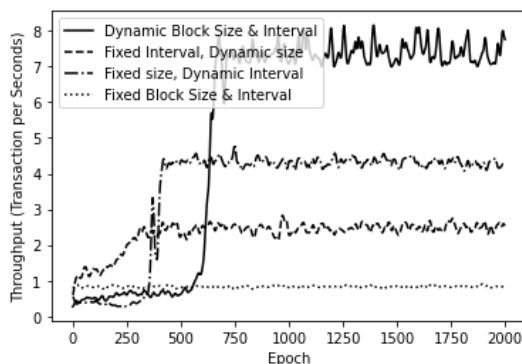
Figure 9: Convergence performance of different schemes with APAC data model

5. Conclusion

This paper presents the implementation of the DDPG algorithm performance optimization framework against the PoA Blockchain

Networks Simulation using Healthcare data characteristics in particular using the AIH and APAC data models, Scalability as the key to measuring blockchain networks can be increased effectively while ensuring other properties including decentralization, security, and latency. As we suggested, this research resulted in a framework combination of DRL based algorithm technic optimization and blockchain network characteristics of bitcoin in the simulator and applied with the healthcare data characteristics, the throughput of the blockchain was maximized by adjusting the block interval and block size based on the characteristics of the current network condition. The simulation results show that this framework can achieve maximum throughput than another experiment that has full or partial of the static parameter in blockchain system. The author realizes that this research still uses an emulator so, future work is in progress to consider adaptive in the real blockchain network and use types of Medical Records for blockchain.

Conflict of Interest

The authors declare no conflict of interest.

References

[1] E. Mezghani, E. Exposito, K. Drira, "A Model-Driven Methodology for the Design of Autonomic and Cognitive IoT-Based Systems: Application to Healthcare," IEEE Transactions on Emerging Topics in Computational Intelligence, **1**(3), 224-34, 2017, doi:10.1109/TETCI.2017.2699218.

[2] X. Liang, J. Zhao, S. Shetty, J. Liu, D. Li, "Integrating blockchain for data sharing and collaboration in mobile healthcare applications," in IEEE International Symposium on Personal, Indoor and Mobile Radio Communications, PIMRC, 1-5, 2018, doi:10.1109/PIMRC.2017.8292361.

[3] A. Goel, N. Chandra, "A prototype model for secure storage of medical images and method for detail analysis of patient records with PACS," in Proceedings - International Conference on Communication Systems and Network Technologies, CSNT 2012, 167-170 2012, doi:10.1109/CSNT.2012.217.

[4] G.G. Dagher, J. Mohler, M. Milojkovic, P.B. Marella, "Ancile: Privacy-preserving framework for access control and interoperability of electronic health records using blockchain technology," Sustainable Cities and Society, **39**, 283-297, 2018, doi:10.1016/j.scs.2018.02.014.

[5] A. Roehrs, C.A. da Costa, R. da Rosa Righi, V.F. da Silva, J.R. Goldim, D.C. Schmidt, "Analyzing the performance of a blockchain-based personal health record implementation," Journal of Biomedical Informatics, **92**, 103140, 2019, doi:10.1016/j.jbi.2019.103140.

[6] Z.M. Grinspan, S. Banerjee, R. Kaushal, L.M. Kern, "Physician specialty and variations in adoption of electronic health records," Applied Clinical Informatics, **4**(2), 225, 2013, doi:10.4338/ACI-2013-02-RA-0015.

[7] D. Ivan, "Moving Toward a Blockchain-based Method for the Secure Storage of Patient Records," NIST Workshop on Blockchain & Healthcare, 2016.

[8] G. Carter, D. White, A. Nalla, H. Shahriar, S. Sneha, "Toward Application of Blockchain for Improved Health Records Management and Patient Care," Blockchain in Healthcare Today, 1-6, 2019, doi:10.30953/bhty.v2.37.

[9] K. Croman, C. Decker, I. Eyal, A. Efe Gencer, A. Juels, A. Kosba, A. Miller, P. Saxena, E. Shi, E. Gün Sirer, D. Song, R. Wattenhofer, "On Scaling Decentralized Blockchains Initiative for CryptoCurrencies and Contracts (IC3)," International Conference on Financial Cryptography and Data Security, 2016.

[10] E. Georgiadis, D. Zeilberger, "A combinatorial-probabilistic analysis of bitcoin attacks *," Journal of Difference Equations and Applications, 2019, doi:10.1080/10236198.2018.1555247.

[11] J. Gobel, A.E. Krzesinski, "Increased block size and Bitcoin blockchain dynamics," in 2017 27th International Telecommunication Networks and Applications Conference, ITNAC 2017, 1-5, 2017, doi:10.1109/ATNAC.2017.8215367.

[12] D. Teodoro, E. Sundvall, M.J. Junior, P. Ruch, S.M. Freire, "ORBDA: An openEHR benchmark dataset for performance assessment of electronic health record servers," PLoS ONE, 2018, doi:10.1371/journal.pone.0190028.

[13] A. Roehrs, C.A. da Costa, R. da Rosa Righi, "OmniPHR: A distributed

architecture model to integrate personal health records," Journal of Biomedical Informatics, 2017, doi:10.1016/j.jbi.2017.05.012.

[14] P. Zhang, J. White, D.C. Schmidt, G. Lenz, S.T. Rosenbloom, "FHIRChain: Applying Blockchain to Securely and Scalably Share Clinical Data," Computational and Structural Biotechnology Journal, 2018, doi:10.1016/j.csbj.2018.07.004.

[15] M. Liu, F.R. Yu, Y. Teng, V.C.M. Leung, M. Song, "Performance optimization for blockchain-enabled industrial internet of things (iiot) systems: A deep reinforcement learning approach," IEEE Transactions on Industrial Informatics, 2019, doi:10.1109/TII.2019.2897805.

[16] M. Liu, Y. Teng, F.R. Yu, V.C.M. Leung, M. Song, "Deep Reinforcement Learning Based Performance Optimization in Blockchain-Enabled Internet of Vehicle," in IEEE International Conference on Communications, 2019, doi:10.1109/ICC.2019.8761206.

[17] Y. Aoki, K. Otsuki, T. Kaneko, R. Banno, K. Shudo, "SimBlock: A Blockchain Network Simulator," in INFOCOM 2019 - IEEE Conference on Computer Communications Workshops, INFOCOM WKSHPS 2019, 2019, doi:10.1109/INFCOMW.2019.8845253.

[18] Handbook of Digital Currency, 2015, doi:10.1016/c2014-0-01905-3.

[19] S. Nakamoto, Bitcoin: A Peer-to-Peer Electronic Cash System | Satoshi Nakamoto Institute, 2008.

[20] S. De Angelis, L. Aniello, R. Baldoni, F. Lombardi, A. Margheri, V. Sassone, "PBFT vs proof-of-authority: Applying the CAP theorem to permissioned blockchain," in CEUR Workshop Proceedings, 2018.

[21] O. Samuel, N. Javaid, M. Awais, Z. Ahmed, M. Imran, M. Guizani, "A blockchain model for fair data sharing in deregulated smart grids," in 2019 IEEE Global Communications Conference, GLOBECOM 2019 - Proceedings, 2019, doi:10.1109/GLOBECOM38437.2019.9013372.

[22] T.P. Lillicrap, J.J. Hunt, A. Pritzel, N. Heess, T. Erez, Y. Tassa, D. Silver, D. Wierstra, "Continuous control with deep reinforcement learning," in 4th International Conference on Learning Representations, ICLR 2016 - Conference Track Proceedings, 1-5, 2016.

[23] D. Silver, G. Lever, N. Heess, T. Degris, D. Wierstra, M. Riedmiller, "Deterministic policy gradient algorithms," in 31st International Conference on Machine Learning, ICML 2014, 1-5, 2014.

[24] A. Kumar, N. Paul, S.N. Omkar, Bipedal walking robot using deep deterministic policy gradient, ArXiv, 2018.

Blockchain Technology for Tracing Drug with a Multichain Platform: Simulation Method

Erick Fernando[1,*], Meyliana[1], Harco Leslie Hendric Spits Warnars[2], Edi Abdurachman[2]

[1]Information Systems Department, School of Information System, Bina Nusantara University, Jakarta, Indonesia 11480

[2]BINUS Graduate Program – Doctor of Computer Science, Bina Nusantara University, Jakarta, Indonesia 11480

A B S T R A C T

This study builds the implementation of the traceability process by conducting simulation tests using business process simulations with the implementation of blockchain technology to track drugs. This research focus involved stakeholders, including the pharmaceutical industry, pharmaceutical wholesalers (distributors/wholesalers), health services (drug stores, hospitals), consumers. Simulation methods are used to describe the distribution and traceability of drugs. Finally, the research contribution in incorporating blockchain technology to supply chain management could potentially help in drug traceability. This study provides an overview of blockchain technology capabilities to find out which stakeholders and assets are transacted on the blockchain system. A decentralized Autonomous Organization is an approach to organizing data on the blockchain that defines all stakeholders identities associated with different addresses. This process can organize each address's transactions on a special blockchain platform in this study using multichain. Furthermore, transactions that have occurred cannot be updated or deleted. This simulation also illustrates some of the blockchain characteristics that must exist, among others, transparent, distributed, immutable, and peer to peer transactions. This contribution gives supply chain management, in particular on drug distribution, stronger control over distribution.

1. Introduction

Supply chain management (SCM) is a system management process that occurs to stakeholders (in general: suppliers, wholesalers, retailers, consumers) starting from the process of receiving raw materials from raw material suppliers to manufacturers, to distributing from distributors, retailers to consumers [1–4]. In SCM, distribution is the most important part to bridge every stakeholder in the SCM system. The distribution process supports the company's profitability process because it has a real impact on the related stakeholders' costs and experiences [5]. This distribution occurs throughout the industry, especially in the pharmaceutical industry [6, 7]. The distribution process occurs in the pharmaceutical industry distributing drugs from the pharmaceutical industry to wholesalers, wholesalers to hospitals or pharmacies, from pharmacies to end consumers (patients or communities) [8]. This distribution process has several problems that occur in the distribution of drugs, including a lot of data that must be identified, namely drug data,

stakeholders (industry, pharmaceutical wholesalers, health services (drug stores, hospitals), consumers). Data must be integrated to ensure the distribution process is good and correct, and the most important thing is drug data tracing/tracking. The drug distribution process requires a trace process to make it easy to find out that drugs sold in the market are free from suspected counterfeit drugs. The problems that occur in distribution can be solved with blockchain technology. This technology has a more secure platform, which supports auditable storage, data exchange, data integration, data that is easy to trace, distributed data, validated data [9, 10].

Many other kinds of research have developed this blockchain technology. One of its features is the ability to trace and trace data on circulating drugs and is believed to minimize counterfeit drugs [11–16]. In its development, the existing literature is an enormous challenge to prove the implementation of blockchain technology for drug tracking/tracing in the market. Apart from the literature, this study also conducted a forum discussion group (FGD) of the pharmaceutical industry, pharmaceutical wholesalers

(distributors/wholesalers). The results of the FGD, one of the most important processes of drug distribution and following the drug distribution model in general, experienced the problem of suspected counterfeit drugs circulating in the market, which was difficult to trace. Another thing from the FGD is that the Food and Drug Supervisory Agency will register the identity of a drug circulating in the market but (In Indonesian country is BPOM), which is a representative of government institutions as a supervisory body. These data are used as the basis for the available drug data and become part of the simulation test.

This study builds the implementation of the traceability process by conducting simulation tests using business process simulations with the implementation of blockchain technology to track drugs. This research's focus involved stakeholders, including the pharmaceutical industry, wholesalers (distributors/wholesalers), health services (drug stores, hospitals), consumers. A decentralized Autonomous Organization is an approach to organizing data on the blockchain that defines all stakeholders identities associated with different addresses. This process can organize each address's transactions on a special blockchain platform in this study using multichain. The purpose of the research is to understand the supply chain comprehensively, its advantages, and challenges. Finally, the research contribution in incorporating blockchain technology to SCM could potentially help in drug traceability. This contribution gives SCM, in particular, on drug distribution stronger control over distribution.

2. Literature review

2.1. Pharmaceutical Supply Chain Management

The 1990s saw the beginning of the supply chain. The supply chain begins with interrelated activities in the product transformation process. Product transformation starts from raw materials into finished goods, which are then distributed to consumers. With the increasingly complex development of the supply chain system, further management is needed to get maximum results. Supply chain management (SCM) is a system management process that occurs to stakeholders (in general: suppliers, wholesalers, retailers, consumers) starting from the process of receiving raw materials from raw material suppliers to manufacturers, to distributing from distributors, retailers to consumers [1–4]. SCM is implemented in many companies and industries in various fields, one of which is in the pharmaceutical industry.

Pharmaceutical Supply Chain Management (PSCM) is growing rapidly and plays an important role in the supply of drugs needed by various stakeholders [17–19]. This role ensures the drug distribution process from industry to consumers. This process occurs in the pharmaceutical supply chain, which consists of raw material suppliers, drug manufacturers, pharmaceutical wholesalers (wholesalers/distribution), health services (pharmacies, hospitals, health centers, and drug stores), and customers [8].

2.2. Blockchain

The history of blockchain was originally introduced by [20]. At first, it started with financial transactions or cryptocurrency, namely bitcoin. Blockchain technology development has

developed from the first version to the latest 3.0 version [21]. The development of version 3.0 of blockchain technology with smart contracts provides enhanced features of blockchain that can support various enterprise systems such as supply chain management [21] to improve the performance of a system that implements it.
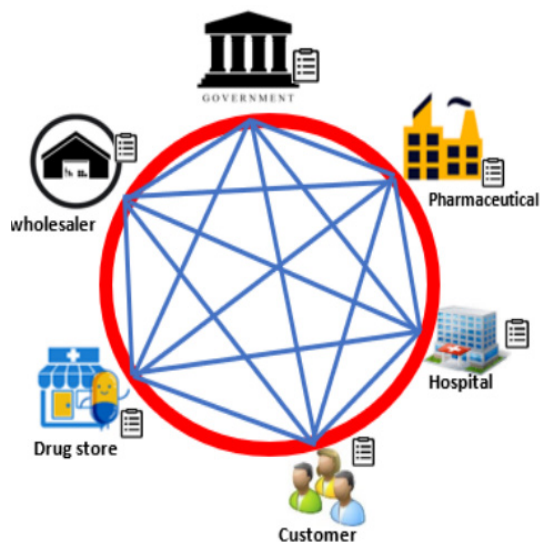
Figure 1: Blockchain Pharmaceutical, Supply Chain Management [5]

2.3. Multichain Platform

Multichain is a platform with the application of blockchain technology [22]. Multichain can be applied in all systems in various industries or companies [22,23]. Multichain has a structure by having one node in its implementation [24]. In that one node will be able to have several addresses and several assets. The structure of multichain to the user interface can be access by the blockchain in multichain with API.

Blockchain with multichain consists of 3 layers, namely: layer blockchain is Assets, stream, permissions, multi-sig. This layer describes what can use in multichain, Layer Chain, and API. This layer describes the data from layer blockchain how to save or to can read from the next layer is layer UI (multichain explorer). This describes in figure 2.
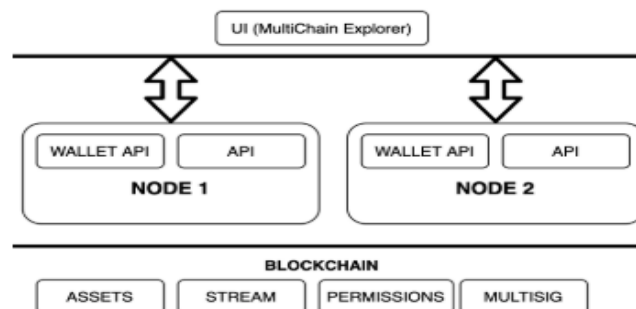
Figure 2: Structure Multichain [22]

3. Methodology

In this study, we use the design science research methodology (DSRM) approach. This method is primarily used in information systems [25]. The steps are taken to identify the problem with a focus group discussion (FGD) with the pharmaceutical industry,

pharmaceutical distributors/wholesalers. Then proceed with developing the model and then carry out the validation process. In this study, validation is carried out to ensure that blockchain technology is able to track drugs circulating in the market in the PSCM system so that the model built can match its purpose. The business model that will be developed will be carried out with a business process simulation (BPS) approach. BPS is a method of business process management to improve business processes and develop new business models. This BPS approach can reduce the costs required and perform system simulations on real business processes. The results can be used for future development considerations [5].
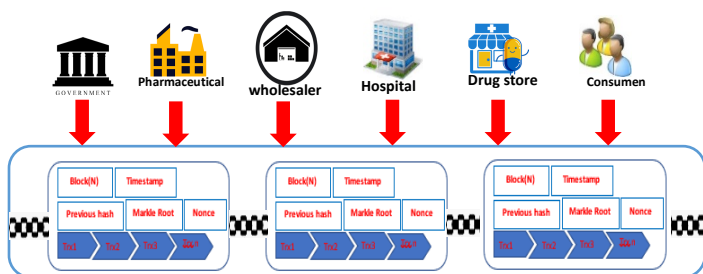
Figure 3: Process Distribution Model with Blockchain [5]

The simulation testing model in this study is based on the business model in Figure 2, which is in accordance with the results of the FGD. The stages start from implementing the script, then the script testing, testing the results, and finally validating the test results. This test is implemented in the blockchain application shown in Figure 4.
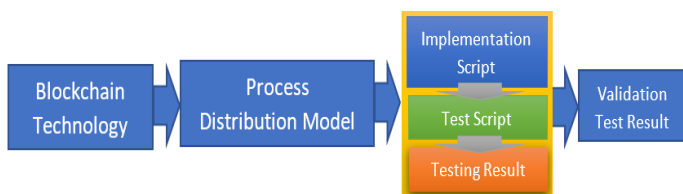
Figure 4: Simulation Process Model

Blockchain technology experiments using the following device environments:

1. Server O/S   : Ubuntu Server version 18 LTS
2. Blockchain platform : Multichain
3. Node name   : Blockchain
4. Version   : 2.0.2
5. Protocol   : 10012
6. Database   : SQLite
7. Node Address   : Blockhain@xxx.xxx.163.25:2681
8. Language   : JSON, C++, Python

4. Analysis and discussion

In this study, a strategy is to map each entity involved in the PSCM business process with an address on the blockchain system and pharmacy drugs as an asset on the blockchain system. Mapping these addresses on the blockchain is the process of creating a Decentralized Autonomous Organization (DAO). DAO is an organization of everything that wants to be related to the blockchain system where the relevant stakeholders, the data that you want to store, use computer code and programs. Thus this organization has the ability to function independently without a

centrally regulated authority. DAO designed on a multichain platform can be seen as follows fig 5 and described in table 1.
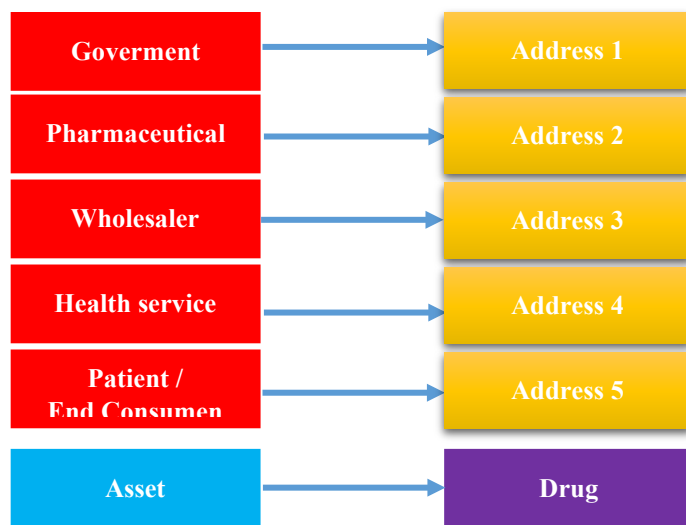
Figure 5: Implementation DAO

Table 1: DAO implementation for different stakeholders

Stakeholder	Address
Government	1WUU5Tmzp5Wr9WTB3UFSm8JaPFk WqmYQ5wSNoH
Pharmaceutical	1N1Jcv3TsUSuYWkADUtNKVeigdrpU Kititqtab
Wholesaler	1TCZSt6D5vZ3e6vMiaSsMLZ39umwRG JVbj7U2Z
Health service (drug store)	177QbpjwmTeFRfkCdHmVkiZQH4Wn MhYUPRS7jf
Patient / End Consumer	1GKkwSFs92174KZef37DibNx5b8ee4W ix1vhZS

These structures have only one identity stakeholders represented by 32 characters from the hashing result or can be known as a pseudo name on the blockchain.

4.1. Business processes that are implemented in the simulation

In the business process testing simulation, starting from the wholesaler/distributor receiving a shipment of 10000 DBL9624502804A1 drug assets (unique drug labels) from the pharmaceutical industry, then the distributor sends 100 DBL9624502804A1 drug assets to drug stores. Then the final consumer buys 10 DBL9624502804A1 drugs as the final process. This test is carried out with a multichain blockchain approach. From the simulation testing process, it can be seen that the process of the blockchain script is mapped one by one in the model for each step, and the simulations carried out can be seen in Table 2.

Table 2: Implementing Business Process to Blockchain

No	Business Process	Script Blockchain asset
1	pharmaceutical industry registers drug production DBL9624502804A1 of 20000 pack/batch (this drug code)	Issue 10000 assets named "DBL9624502804A1" from Pharmaceutical (1N1Jcv3TsUSuYWkADUtNKVeigd rpUKititqtab) to Wholesaler

		(1TCZSt6D5vZ3e6vMiaSsMLZ39u mwRGJVbj7U2Z)
2	Wholesaler sends 100 packs of DBL9624502804A1 drug production to drugstores	Issue 100 assets named "DBL9624502804A1" from Wholesaler (1TCZSt6D5vZ3e6vMiaSsMLZ39u mwRGJVbj7U2Z) to the drug store (177QbpjwmTeFRfkCdHmVkiZQH4 WnMhYUPRS7jf)
3	Drugstores deliver 100 packs of DBL9624502804A1 drug production to consumers	Issue 10 assets named "DBL9624502804A1" from the drug store (177QbpjwmTeFRfkCdHmVkiZQH4 WnMhYUPRS7jf) to Konsumen (1GKkwSFs92174KZef37DibNx5b8 ee4Wix1vhZS)

Figure 6: Implementing blockchain with a multichain platform
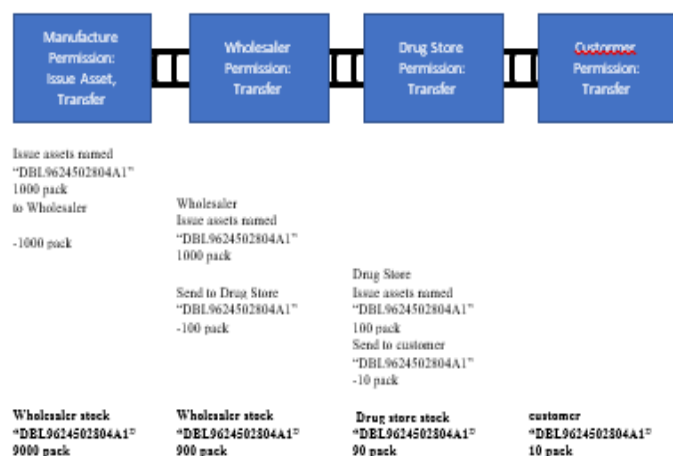
Figure 7: Blockchain transaction described in a block transaction

This business process maps to the blockchain system using a multichain platform where every process that is carried out will have one transaction, which is always recorded in a block. This process simulation shows that this platform can be appropriately used for the recording process of drug distribution.

Figure 8: Result tracing drug

4.2. Benefits of using blockchain in the pharmaceutical industry

Research an overview of the capabilities of the blockchain so that they can find out which stakeholders and assets are transacted on the blockchain system. Furthermore, transactions that have occurred cannot be updated or deleted. This simulation also illustrates some of the characteristics of the blockchain that must exist, among others, transparent, distributed, immutable, and peer to peer transactions.

This study implements peer to peer transactions that occur in related stakeholders in this system. With the results of technology simulation, testing with business processes serves to track drugs circulating in the market. This tracking also provides information on the final status of existing and circulating drug stocks in the market. The process of validating this simulation test results is carried out according to business processes that have been confirmed to domain experts such as the pharmaceutical industry and wholesalers.

4.3. Challenges of blockchain technology in the pharmaceutical industry

The challenge in this simulation process is that every data process that is published on the blockchain is in the form of a unique asset name (drug label name), and this process occurs sequentially to be validated on the blockchain system so it takes time and it is difficult to issue assets. The transaction can be many problem scalabilities.

5. Conclusion and Future Work

This study tested a business process simulation of the drug distribution process on the market from related stakeholders. This simulation explains how related stakeholders can interact with the blockchain system using DAO. With this, DAO initializes existing stakeholders with addresses that are formed using code and programming so that these stakeholders have a unique identity on the blockchain system. This study, using a multichain platform for simulation testing. This simulation test illustrates that the application of business processes in drug distribution can be implemented properly. So, that you can see the characteristics of the blockchain, including peer to peer (transactions that occur

directly with related stakeholders), cute (data cannot be changed because the transaction is hashing), and can be traced well to the drug distribution process.

This study is limited due to the pharmaceutical industry's lack of permission for various information related to the transaction process. The simulation testing system implements blockchain technology as it is by using multichain. The test process with this simulation has excellent results because it can describe the drug distribution business process that runs on blockchain technology using DAO. The next research will improve the blockchain technology infrastructure currently happening directly to multichain admin features. So that in the future, it is hoped that other support modifications can be made, such as a complete dashboard using API as integration with blockchain, implementable off-chain smart contracts, and direct development of business processes that occur in the pharmaceutical industry.

Reference

[1] J. Wu, M. Ulieru, M. Cobzaru, D. Norrie, "Supply chain management systems: state of the art and vision," in Proceedings of the 2000 IEEE International Conference on Management of Innovation and Technology. ICMIT 2000. "Management in the 21st Century" (Cat. No.00EX457), IEEE: 759–764, 2000, doi:10.1109/ICMIT.2000.916799.

[2] A.P. Barbosa-Póvoa, C. da Silva, A. Carvalho, "Opportunities and challenges in sustainable supply chain: An operations research perspective," European Journal of Operational Research, **268**(2), 399–431, 2018, doi:10.1016/j.ejor.2017.10.036.

[3] D.M. Lamberth, C. Cooper, M. Pagh, D. Janus, "Supply Chain Management : Implementation Issues and Research Opportunities," The International Journal of Logistics Management, **9**(2), 1998.

[4] R.H. Ballou, "The evolution and future of logistics and supply chain management," Production, **16**(3), 375–386, 2006, doi:10.1590/S0103-65132006000300002.

[5] E. Fernando, Meyliana, H.L.H.S. Warnars, E. Abdurachman, "Blockchain technology for pharmaceutical drug distribution in Indonesia: A proposed model," ICIC Express Letters, **14**(2), 113–120, 2020, doi:10.24507/icicel.14.02.113.

[6] E. Fernando, M. Meyliana, H.L. Hendric Spits Warnars, E. Abdurachman, "Key strategic issues pharmaceutical industry of SCM: A systematic literature review," Bulletin of Electrical Engineering and Informatics, **9**(2), 808–817, 2020, doi:10.11591/eei.v9i2.1264.

[7] E. Fernando, Meyliana, Surjandy, "Blockchain Technology Implementation in Raspberry Pi for Private Network," Proceedings of 2019 4th International Conference on Sustainable Information Engineering and Technology, SIET 2019, 154–158, 2019, doi:10.1109/SIET48054.2019.8986053.

[8] T.K. Mackey, G. Nayyar, "A review of existing and emerging digital technologies to combat the global trade in fake medicines," Expert Opinion on Drug Safety, **16**(5), 587–602, 2017, doi:10.1080/14740338.2017.1313227.

[9] R.Y. Garankina, E.R. Zakharochkina, I.F. Samoshchenkova, N.Y. Lebedeva, A. V. Lebedev, "Blockchain technology and its use in the area of circulation of pharmaceuticals," Journal of Pharmaceutical Sciences and Research, **10**(11), 2715–2717, 2018.

[10] R. Niblett, Higher education, Nature, **308**(5961), 683, 1984, doi:10.1038/308683b0.

[11] K. Fan, Y. Ren, Z. Yan, "Drugledger: A Practical Blockchain System for Drug Traceability and Regulation," 2018 IEEE International Conference on Internet of Things (IThings) and IEEE Green Computing and Communications (GreenCom) and IEEE Cyber, Physical and Social Computing (CPSCom) and IEEE Smart Data (SmartData), 1349–1354, 2018, doi:10.1109/Cybermatics.

[12] A. Jeppsson, O. Olsson, "Blockchains as a solution for traceability and transparency," Lund University Publications Journal, 1–102, 2017.

[13] R.B. Da Silva, C.A. de Mattos, "Critical success factors of a drug traceability system for creating value in a pharmaceutical supply chain (PSC)," International Journal of Environmental Research and Public Health, **16**(11), 2019, doi:10.3390/ijerph16111972.

[14] R. Kumar, R. Tripathi, "Traceability of counterfeit medicine supply chain through Blockchain," 2019 11th International Conference on Communication Systems and Networks, COMSNETS 2019, **2061**(1), 568–570, 2019, doi:10.1109/COMSNETS.2019.8711418.

[15] M. Pournader, Y. Shi, S. Seuring, S.C.L. Koh, "Blockchain applications in supply chains, transport and logistics: a systematic review of the literature," International Journal of Production Research, **58**(7), 2063–2081, 2020, doi:10.1080/00207543.2019.1650976.

[16] M. Benchoufi, R. Porcher, P. Ravaud, "Blockchain protocols in clinical trials: Transparency and traceability of consent," F1000Research, **6**, 1–66, 2017, doi:10.12688/f1000research.10531.1.

[17] S.R. Bryatov, A.A. Borodinov, "Blockchain technology in the pharmaceutical supply chain: Researching a business model based on Hyperledger Fabric," CEUR Workshop Proceedings, **2416**, 134–140, 2019.

[18] J.D. Evans, "Improving the Transparency of the Pharmaceutical Supply Chain through the Adoption of Quick Response (QR) Code, Internet of Things (IoT), and Blockchain Technology: One Result: Ending the Opioid Crisis," Pittsburgh Journal of Technology Law and Policy, **19**(1), 2019, doi:10.5195/tlp.2019.227.

[19] E. Fernando, H. Leslie, H. Spits, E. Abdurachman, "Blockchain Technology Factor for Improve Good Distribution Practice in the Pharmaceutical Industry," International Journal of Recent Technology and Engineering, **8**(6), 2174–2180, 2020, doi:10.35940/ijrte.f7181.038620.

[20] S. Nakamoto, "Bitcoin: A Peer-to-Peer Electronic Cash System," Www.Bitcoin.Org, 9, 2008, doi:10.1007/s10838-008-9062-0.

[21] M. Swan, Blockchain for a New Economy, 1st ed., O'Reilly Media, Inc., 1005 Gravenstein Highway North, Sebastopol, CA 95472, USA, 2015.

[22] A. Ismailisufi, T. Popovic, N. Gligoric, S. Radonjic, S. Sandi, "A Private Blockchain Implementation Using Multichain Open Source Platform," 2020 24th International Conference on Information Technology, IT 2020, (February), 24–27, 2020, doi:10.1109/IT48810.2020.9070689.

[23] D. Soto Setzke, M. Böhm, H. Krcmar, The role of openness and extension modularization in value capture for platform-based digital transformation, 2020, doi:10.1007/978-3-030-53337-3_11.

[24] multichain, Multichain, Www.Multichain.Com, 2020.

[25] K. Peffers, T. Tuunanen, M.A. Rothenberger, S. Chatterjee, "A Design Science Research Methodology for Information Systems Research," Journal of Management Information Systems, **24**(3), 45–77, 2008, doi:10.2753/mis0742-1222240302.

A Surface Plasmon Resonance (SPR) and Water Quality Monitoring: A System for Detecting Harmful Algal Bloom

Walvies Mc. Alcos[1], Mirador G. Labrador[2,*]

[1]*College of Engineering, Samar State University, Catbalogan City, 6700, Philippines*

[2]*Center for Engineering, Science and Technology Innovation, Samar State University, Catbalogan City, 6700, Philippines*

ARTICLE INFO	ABSTRACT
	Harmful algal blooms (HAB) or "Red tides" are organisms which produce toxins which are harmful to humans, fish, and other marine mammals. The said toxins come from dinoflagellates of genus Pyrodinium Bahamense var Compressum that cause Paralytic Shellfish Poisoning (PSP) and Dinophysis Caudata and Prorocentrum lima which results to Diarrhetic Shellfish Poisoning (DSP). In the coast of Western Samar, Philippines, there are reported occurrences of red tide toxins based on the laboratory result conducted by the Bureau of Fisheries and Aquatic Resources (BFAR) and the Local Government Unit (LGUs). HAB or Red tide has an impact on economy in terms of the loss of livelihood, sales, and exports, and also in terms of human life. This study developed a system that automatically detects the presence of red tide toxins and water quality parameters. Red Tide toxins and water quality parameters are determinant factors in detecting and forecasting the occurrence of HAB. In particular, the system utilizes a Surface Plasmon Resonance (SPR) and Water Quality parameter sensors used in detecting red-tide toxins and water quality. Data or information collected and generated by the system can be used for a faster, effective and efficient way of detecting and predicting the possible occurrence of HAB. Results positively indicate that the system performance can indeed be used as a Method in the detection and prediction of Harmful Algal Bloom. Specifically, for a time period of 80 minutes, 16 different sets of water parameters are captured and transmitted to the centralize system – making the system to be 100% functional as it is being set to operate in 5 minutes interval. Likewise, SPR bio toxin detection has a deviation rate of (+/-) 20%. Operational performance of the system is found to be 100%.

1. Introduction

Harmful algal blooms or HABs are organisms that produce toxins which are harmful to humans, fish, and other marine mammals. The said toxins come from Dinoflagellates of the genus Pyrodinium bahamense var compressum that is accountable for causing Paralytic Shellfish Poisoning (PSP) when ingested by mussels or oysters and also taken in by humans and for Diarrhetic Shellfish Poisoning (DSP) caused by the presence of Dinophysis caudata and Prorocentrum lima. In addition, this phenomenon has an enormous impact when it comes to economy since the production of supply of sea products, especially shellfish industry, is greatly affected.

There are over 4000 species algae (phytoplankton) and 2% (60 – 78 species) are known to produce toxins, and most of which are dinoflagellates. A proportion of these toxic dinoflagellates has a red-brown pigmentation-giving rise to the naming of algal blooms as 'red-tides', however, not all toxic algae are colored and incidents of poisoning have occurred in the absence of red blooms. Visible red tides may contain from 20,000 to 50,000 algal cells per l ml of seawater; however, concentrations as low as 200 cells per l ml may produce toxic shellfish [1].

In the coast of Western Samar, Philippines, there are reported occurrences of red tide toxins based on the laboratory result conducted by the Bureau of Fisheries and Aquatic Resources (BFAR) and the Local Government Unit (LGUs) from 2012 up to present. Based on their data, the most occurrence of red-tide was

in Irong-irong Bay, located in one of the costs of Samar Island, Philippines. It was followed by by Cambatutay Bay, Maqueda Bay, Villareal Bay of the same Island. The occurrence of this problem lasts for an average of 3 months with a longest recorded occurrence of 5 months for the past 5 years as indicated in 2016 Report of Bureau of Fishery and Aquatic Resources (BFAR).

On the contrary, various technologies were developed which are used in detecting HAB. One of these is the technology that utilizes fiber optic sensor in the detection of neurotoxin that causes harmful algal bloom. The technology makes use of the combination of absorption and reflection spectroscopy and the Principle Component Analysis (PCA) signal processing [2]. The process of sampling of the said technology starts with the gathering of contaminated water and put that sample on the device for analysis. But, there is no continuous monitoring mechanism on this part since there will be only testing of the sampled water if the user or researcher is on the site.

With this, the proposed system made use of ICT in achieving a real-time and low-cost monitoring of the different triggering factors of the occurrence of HAB. Specifically, a surface plasmon resonance multiplexer sensor and water quality parameter sensor was used coupled with that of the server-based monitoring software. Data gathered by the sensors were sent to a server-based program application. The same information are being stored in a cloud based services. Data captured and stored in a server based and cloud based application program will serve as a prime basis in the analysis and detection and prediction of HABs.

In particular, the study aims to develop an automated system that will capture the dynamics of the different parameters associated for the occurrence of HABs. Data captured in real-time basis will serve as inputs in the prediction. However, HABs prediction model based on the captured data by the developed system is not covered on this paper. Again, the intention of this study is to develop an automated mechanism that will detect the presence and dynamics of red-tide causing parameters.

2. Related Literature

The recurring occurrence of Harmful Algal Bloom in the coastal water of Samar, along with its adverse effect in human health and aquatic organisms necessitates the need to come-up an effective and efficient approaches, processes or technology that can be used to fast-tract the detection of the said phenomenon which is of paramount important. As such, several research and projects along on this area have been undertaken. On this, an analytical method has been developed for the quantitative analysis of marine biotoxins in shellfish – the main cause of the occurrence of harmful algal bloom.

One of such analytical method was made through the so called High Performance Liquid Chromatography (HPLC) with fluorescent detection using both pre-column oxidation as described in [3] and post column oxidation as described in [4]-[7]in addition to liquid chromatography tandem mass spectrometry. Similarly, HPLC with fluorescence detection in [8] have been utilized for the detection of Paralytic Shellfish Poisoning (SPS) toxins in algal and seawater samples with detection limits of nanograms per milliliter. Similarly, HPLC with fluorescence detection in [9] and LCMS/MS methods have been applied for the detection of the DSP toxins in

algal and seawater samples as described in [10]-[14]. Furthermore, the study of [15] describes a method incorporating HPLC with fluorescent detection of domoic acid with others using modified version as indicated in [16]-[18]. Indeed, the used of analytical method has been widely explored as evident to the number of researches undertaken as described previously; however, the said methods require skilled personnel and are labor intensive measuring only toxin group per method.

On the other hand, the study of [19], explored the used of near real-time ocean color data from the Sea-viewing Wide Field-of-view Sensor (SeaWiFS) to detect and trace HAB in Southwest Florida coastal water, its optical characteristics are influenced not only by phytoplankton and related particles, but also by the other substances, that vary independently of phytoplankton, notably inorganic particles in suspension and yellow substances. The results of the study showed that the SeaWiFS data provides an unprecedented tool for research and managers to study and monitor algal blooms in coastal environments. The existing study was also was not practical and expensive to be adopted by a rural area.

Accordingly, the study of [20], used the Early Warning Harmful Algae Bloom (HAB) Sensing System for use in Underwater Monitoring which utilizes Principal Component Analysis (PCA) to establish the complex linkages between ocean color, absorption and scattering, algae pigmentation and cell size, along the depth of bloom layers. The author proposed an optical fiber sensor based method of detecting the associated neurotoxins that cause Harmful Algal Blooms.

Another technology was developed by [21], a field deployable method that uses Surface Plasmon Resonance (SPR) and species-specific Peptide Nucleic Acid (PNA) probes to detect Alexandrium (a genus of dinoflagellate that is responsible for Paralytic Shellfish Poisoning at extremely low cell densities) rRNA. This instrument has been tested using synthetic nucleotide sequences designed to mimic two species of Alexandrium. The SPR is an optical detection method that measures the change in refractive index after binding (Hybridization) of a target to probe on a surface [22]. Changes in refractive index are measured in resonance units (RUs) [23] The samples are manually injected to the portable device, 100 uliters, and then starts to measure the sample.

The study of [24] developed a toolkit used rapid HABs detection and monitoring of maritime microalgae dubbed as Suitcase Lab. The toolkit enable rapid detection of specific microalgae associated with that of HABs as used in fields. In fact the toolkit can detect the presence of *A. catenella* – an HABs causing microorganism within the 2 hours of time sampling. Along with this, investigation and on micro phytoplankton community structure and abundance in two contrasted marine ecosystem has been explored in [25]. Results of such investigation indicates that the presence of such microorganism is prevalent in the commercially exploited environment.

The existing study does not have continuous monitoring mechanism on this part since there will be only manual testing of the sampled water if the user or researcher is on the site. With our technology, the testing of sample procedure is automated and will
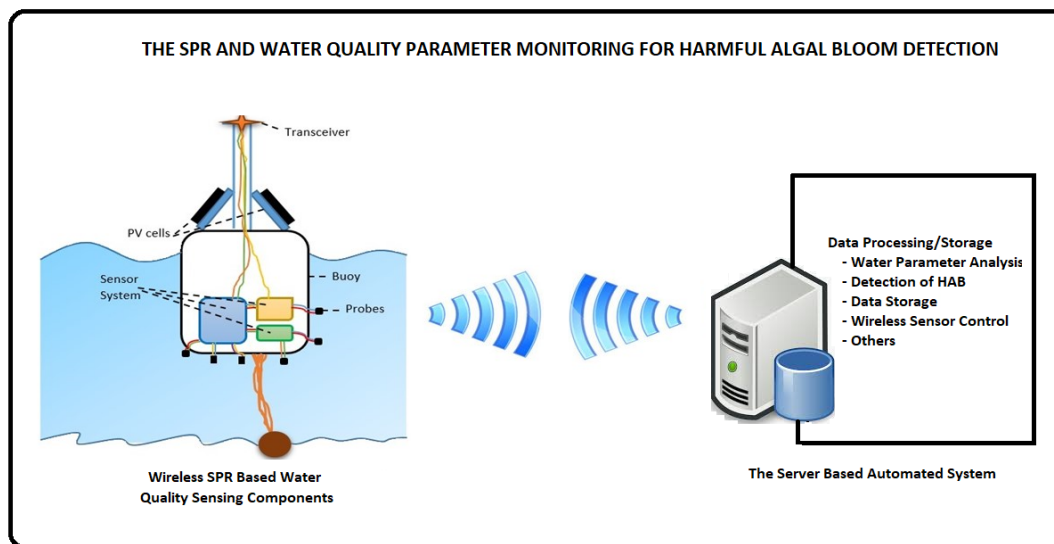
Figure 1: Developmental Model of the System

continuously be monitored depending on the necessary frequency of testing to be conducted.

Another method being explored in the detection of underwater biotoxins is the used of Surface Plasmon Resonance Technique described in [26]-[28]. Further, the study of [29] reported an situ SPR system using special optical fibers for measuring salinity of seawater using the determination of refractive index. The sensor was tested on a pelagic profiler and was successfully found to be functional. The study in [30] presented a similar optical fiber based SPR system for in situ measurement of reflective index and deployed it in 2013 in deep water.

3. System Development Model

A developmental research design approach following the Dynamic System Development Model (DSDM) has been adopted. DSDM is a project development concept consisting six phases as follows: (1) conceptualization, requirement and specification phase; (2) System Analysis Phase; (3) System Design – Hardware and Software Design phase; (4) Testing and Implementation Phase; and (5) Evaluation Phase.

In the conceptualization phase, benchmark information has been collected and analyzed. Benchmark information includes, but not limited to existing and similar technologies along water quality and harmful algal bloom detection; historical data on water quality and occurrence of harmful algal bloom in the specific site area; climate change and anthropogenic activities as causative factors to HAB occurrence; and other relevant information. This information becomes the basis in the formulation of the system conceptual model which is the outcome of the system analysis phase – the phase 2 of the DSDM. Figure 1 shows the conceptual model of the system.

In reference to the conceptual model shown in Figure 1, the operation and functional flow of the system has been developed following as one outcome of the system design process. The functional and operational flow indicated in Figure 2 shows the

graphical over-all workings of the proposed system. Figure 2 shows the detailed process, required and implied components – both hardware and software of the proposed system.

In particular, the system has been implemented utilizing the proposed backbone network articulated in [31] and [32]. The said network governs the communication and data transmission requirements of the sensing components s and that of the server-based automated system. Note that as indicated in Figure 1, detection of Harmful Algal Bloom via SPR, largely depends on the different water quality parameters that are being detected. The development model consist of two subsystems: (1) the wireless sensing component and (2) the server-based automated system.

The wireless sensing component consists of different sensors that detect the presence of HAB microorganisms in water and other water parameters such as the pH, turbidity, temperature, dissolved oxygen, and environmental parameters such as air temperature and humidity

The server-based automated system received all the information from the wireless sensing components and performs analysis of all received data including the determination of the so-called Harmful Algal Bloom.
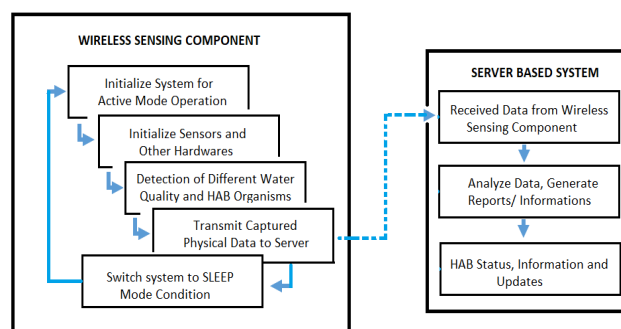
Figure 2: Operational and Functional Flow of the System
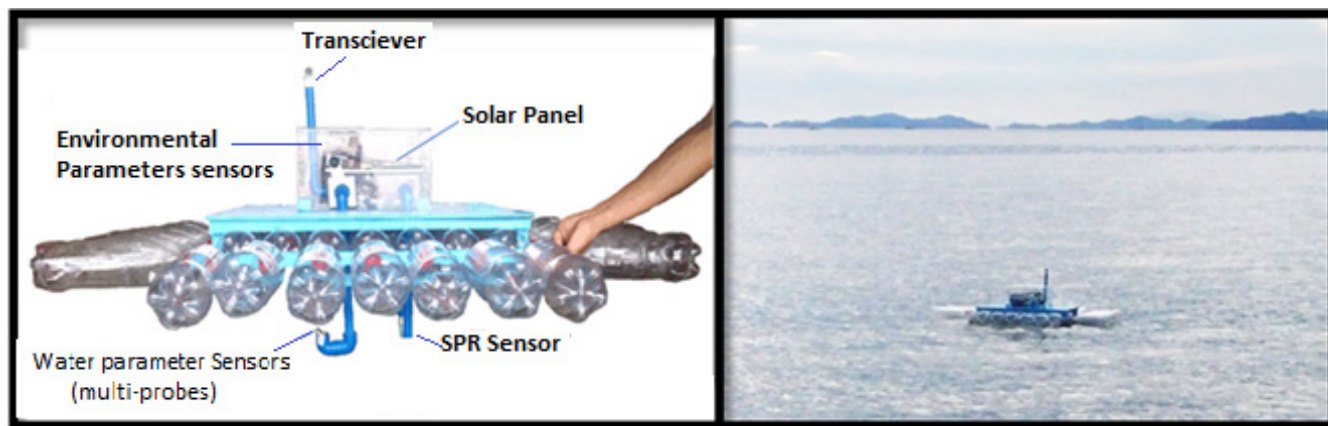
Figure 3: The Developed Wireless Sensors and SPR Based System

In particular, the Arduino uno, Xbee module, Spreeta Sensor, pH meter sensor, temperature sensor, humidity sensor, color - module, are used. Raspberry pie module. This hardware components form parts of the entire circuitry of the system. Further, a 5-watts solar panel is used to provide a 24/7 power supply to the wireless sensing component of the system. Note that a solar panel was specifically utilized in order to ensure a continuous power supply for the system and further ensure system continues operation.

The specific solar panel used was designed in conformity with the system required operational power where the current and voltage generated are auto-regulated. Voltage regulation was made possible with the use of LM317T and 1N4007 diode. In addition, considering the projected 24/7 operation of the system. Furthermore, the 1N4148 diode was also utilized to protect the LM317T and solar panel from reverse voltage generated by the battery. Reverse voltage is usually the main cause for the breakdown of the said component.

Figure 4: Water parameter sensor data

4. The SPR Based Harmful Algal Bloom System

4.1. The System Operation and Functional Flow

Figure 2 describes the operation and functions flow of the system. Once the system is on operational state condition – all sensors in the SPR based water quality monitoring automatically capture physical data and sends the same to the server-based automated system. Note that all sensors capture physical data and send the same to the central server for processing and analysis at

an interval of 4 hours. On this case, reports on the water quality and status of HAB are updated every after 4-hours period.

On the other hand, the server based system contains application and analytical software that performs the analysis of all received data. However, captured data by SPR sensors and water quality parameters sensor are collectively and comparatively analyze in order to determine the possible occurrence of HAB or if there is an existing occurrence of the same. Figure 2 shows the detailed operational and functional flow of the system.

4.2. System Development, Field Testing and Evaluation

Figure 3 shows the actual wireless sensing component of the system during deployment, testing and evaluation. Major electronics and circuits are enclosed in an air-tight box. A Polyvinyl Chloride (PVC) pipe was used as enclosure for probes that are submerged in the water. The same material was used as enclosure for environmental parameter sensors such as air humidity and temperature. Empty plastic bottles were used as buoy.

The system was deployed in Maqueda Bay Samar, Philippines. The buoy containing the wireless sensing component was stationed 50 meters off the shore of Maqueda Bay, where the server-side of the system was placed. The major focus of the field-testing is to determine the operation performance and functions of the system. For this particular purpose the sensing component was set to capture physical data and transmit the same to server-based component at an interval of 5 minutes.

Figure 4 depicts the captured physical water parameters being observed by the system as received by the server for a time period of 80 minutes. 16 different sets of collected data are received by the serve-based system on the said time period. The figure shows that when the air temperature decreases, air humidity increases.

These characteristics occurred from the received data set at 15:44 o'clock until the last received data set at 17:20 o'clock. In other words, the said results validates the general principle that as air temperature increases, air can hold more water molecules, and its relative humidity decreases. Thus, when temperatures drop, relative humidity increases. Note that there are two sets of temperature indicated on the figure – one is being represented in

Figure 5: SPR biosensor stability curve using the 0 ng/ml calibration standard

degree Fahrenheit and the other is represented in degree Celsius. Hence what is being referred on this particular discussion is the temperature represented in degree Fahrenheit. The degree Celsius represent the sea water temperature.

On the other-hand, the pH value of water does not significantly changes over the entire test and evaluation period. Figure 4 indicates that the pH water value ranges only from 5.61 to 5.66.

Moreover, the SPR sensor are actually multiplex biosensors that detects paralytic shellfish poisoning toxins, such as saxitoxin, okadaic acids and domoic acid. On this case, evaluation of the SPR sensors was based on biosensors response measured in RU monitored for a certain period of time. With this in order to ensure its operational and functional performance, test, monitoring and evaluation has been separately carried over an 8-week period. It is to be noted that, when the SPR biosensor is unstable, there would have been steady decrease in responses over time at each time point. However, from Figure 5, it can be seen that SPR sensors response time did not drop off significantly for any biotoxin, although fluctuation did occur having a (+/-) 20% deviation from system deployment until the end of experimental tests.

4.3. System Operational Performance

To further ensure the efficiency of the system operational performance. The system has been subjected to further evaluation by experts – emphasizing the extent of functionality of all components measured based on success or failure of operation over total number of test trials. Result of the said evaluation is shown in table 1. As reflected on table 1, the success of operation of all components is at 100%. The said results only implied that the develop system is indeed reliable once it would be adopted. In particular, the wireless sensing component of the system is programed to operate in two mode of operations – the ACTIVE mode and the SLEEP mode. The system is said to be in ACTIVE mode when it captures physical data and transmit the same to the central server. When the captured data are successfully transmitted, then the wireless sensing component switches to SLEEP mode and remains on that state for a period of 4-hours.

Furthermore, it can be seen in the figure that for over a 10 test trials of the different system components, no failure has been recorded. With the said result, the system operational capability can be considered as effective and efficient.

5. Conclusion and Recommendation

This study validates that real-time monitoring of sea-water quality parameters is feasible. These parameters include pH level, turbidity, temperature, dissolved oxygen, ambient air temperature and humidity among others. Also, the study was able to prove the capability and stability of the SPR biosensors as used in detecting paralytic shellfish poisoning toxins.

Thus, with the capability of the developed system to (1) monitor the real-time quality of sea water and (2) determine the presence of paralytic shellfish poisoning toxins in sea-water can be a good mechanism in the detection and prediction of the possible occurrence of Harmful Algal Bloom. Note that the HAB occurrence are correlated with that of water quality. Specifically, for a time period of 80 minutes, 16 different sets of water parameters are captured and transmitted to the centralize system – making the system to be 100% functional as it is being set to operate in 5 minutes interval. Likewise SPR biotoxin detection has a deviation rate of (+/-) 20%. Operational performance of the system is found to be 100%.

In conclusion, the developed system can be used as a mechanism to automate the detection and prediction of the possible occurrence of HAB. However, the need for the development of a comprehensive HAB prediction model software that will utilize the data captured by the develop system is recommended since the said is out-of-context of this study.

Table 1: Success and Failure of System Component Operations

Component and its Functions	Failure of Operation	Success Operation	No. of Test Trials	% of Success
The power supply and power system Acquisition of Sensor	0	10	10	100%
Node data for transmission	0	10	10	100%
pH level detection	0	10	10	100%
Water color detection	0	10	10	100%
Water Temperature detection	0	10	10	100%
Air temperature detection	0	10	10	100%
Reception/ Acquisition of sensors Data by Server Based system	0	10	10	100%
Analysis and Display of Sensor Data in Server	0	10	10	100%
Storage and retrieval of Data SPR multiplex sensors	0	10	10	100%
Average	**0**	**10**	**10**	**100%**

Conflict of Interest

The authors declare no conflict of interest.

Acknowledgment

research. Likewise, the same acknowledgement is extended to the Samar State University, College of Engineering

References

[1] A.C. Scoging, "Marine biotoxins.," Symposium Series (Society for Applied Microbiology), 1998.

[2] P.C. Chu, Y.H. Kuo, "Detection of red tides in the Southwestern Florida coastal region using ocean color data," in MTS/IEEE Seattle, OCEANS 2010, 1-5, 2010, doi:10.1109/OCEANS.2010.5663861.

[3] H.Z. He, H. Bin Li, Y. Jiang, F. Chen, "Determination of paralytic shellfish poisoning toxins in cultured microalgae by high-performance liquid chromatography with fluorescence detection," Analytical and Bioanalytical Chemistry, **383**(6), 1014-1017. 2005, doi:10.1007/s00216-005-0092-8.

[4] Y. Oshima, "Postcolumn Derivatization Liquid Chromatographic Method for Paralytic Shellfish Toxins," Journal of AOAC INTERNATIONAL, **78**(2), 528-532. 1995, doi:10.1093/jaoac/78.2.528.

[5] D.Z. Wang, S.G. Zhang, H.F. Gu, L. Lai Chan, H.S. Hong, "Paralytic shellfish toxin profiles and toxin variability of the genus Alexandrium (Dinophyceae) isolated from the Southeast China Sea," Toxicon, **48**(2), 138-151. 2006, doi:10.1016/j.toxicon.2006.04.002.

[6] N. Touzet, J.M. Franco, R. Raine, "Influence of inorganic nutrition on growth and PSP toxin production of Alexandrium minutum (Dinophyceae) from Cork Harbour, Ireland," Toxicon, 2007, doi:10.1016/j.toxicon.2007.03.001.

[7] N.G. Montoya, V.K. Fulco, M.O. Carignan, J.I. Carreto, "Toxin variability in cultured and natural populations of Alexandrium tamarense from southern South America - Evidences of diversity and environmental regulation," Toxicon, 2010, doi:10.1016/j.toxicon.2010.08.006.

[8] M. Halme, M.L. Rapinoja, M. Karjalainen, P. Vanninen, "Verification and quantification of saxitoxin from algal samples using fast and validated hydrophilic interaction liquid chromatography-tandem mass spectrometry method," Journal of Chromatography B: Analytical Technologies in the Biomedical and Life Sciences, 2012, doi:10.1016/j.jchromb.2011.11.015.

[9] I. Bravo, M.L. Fernández, I. Ramilo, A. Martínez, "Toxin composition of the toxic dinoflagellate Prorocentrum lima isolated from different locations along the Galician coast (NW Spain)," Toxicon, 2001, doi:10.1016/S0041-0101(01)00126-X.

[10] E. Fux, R. Bire, P. Hess, "Comparative accumulation and composition of lipophilic marine biotoxins in passive samplers and in mussels (M. edulis) on the West Coast of Ireland," Harmful Algae, **2009**, 1-5, 2009. doi:10.1016/j.hal.2008.10.007.

[11] E. Fux, J.L. Smith, M. Tong, L. Guzmán, D.M. Anderson, "Toxin profiles of five geographical isolates of Dinophysis spp. from North and South America," Toxicon, **2011**, doi:10.1016/j.toxicon.2010.12.002.

[12] J.D. Hackett, M. Tong, D.M. Kulis, E. Fux, P. Hess, R. Bire, D.M. Anderson, "DSP toxin production de novo in cultures of Dinophysis acuminata (Dinophyceae) from North America," Harmful Algae, **2009**, doi:10.1016/j.hal.2009.04.004.

[13] P. Vale, V. Veloso, A. Amorim, "Toxin composition of a Prorocentrum lima strain isolated from the Portuguese coast," Toxicon, 2009, doi:10.1016/j.toxicon.2009.03.026.

[14] A. Gerssen, P.P.J. Mulder, J. de Boer, "Screening of lipophilic marine toxins in shellfish and algae: Development of a library using liquid chromatography coupled to orbitrap mass spectrometry," Analytica Chimica Acta, **2011**, doi:10.1016/j.aca.2010.11.036.

[15] J.E. Milley, S.S. Batesf, C.J. Bird, A.S.W. De Freitas, M.A. Quilliamt, "Trace determination of domoic acid in seawater and phytoplankton by high-performance liquid chromatography of the fluorenylmethoxycarbonyl (fmoc) derivative," International Journal of Environmental Analytical Chemistry, 1990, doi:10.1080/03067319008026940.

[16] J. Fehling, K. Davidson, C.J. Bolch, S.S. Bates, "Growth and domoic acid production by Pseudo-nitzschia seriata (Bacillariophyceae) under phosphate and silicate limitation," Journal of Phycology, 2004, doi:10.1111/j.1529-8817.2004.03213.x.

[17] C.K. Cusack, S.S. Bates, M.A. Quilliam, J.W. Patching, R. Raine, "Confirmation of domoic acid production by Pseudo-nitzschia australis (Bacillariophyceae) isolated from Irish waters," Journal of Phycology, 2002, doi:10.1046/j.1529-8817.2002.01054.x.

[18] S. Besiktepe, L. Ryabushko, D. Ediger, D. Yilmaz, A. Zenginer, V. Ryabushko, R. Lee, "Domoic acid production by Pseudo-nitzschia calliantha Lundholm, Moestrup et Hasle (bacillariophyta) isolated from the Black Sea," Harmful Algae, **7**(4), 438-442, 2008, doi:10.1016/j.hal.2007.09.004.

[19] S.B. Hooker, C.R. McClain, The calibration and validation of SeaWiFS data,

Progress in Oceanography, 2000, doi:10.1016/S0079-6611(00)00012-4.

[20] E. O'Connell, W.B. Lyons, C. Sheridan, E. Lewis, "Development of a fibre optic sensor for the detection of harmful algae bloom and in particular domoic acid," in Conference Record - IEEE Instrumentation and Measurement Technology Conference, 1-5, 2007, doi:10.1109/imtc.2007.379024.

[21] A.R. Bratcher, L.B. Connell, P. Millard, "Portable biosensor detection of the harmful dinoflagellate Alexandrium using surface plasmon resonance and peptide nucleic acid probes," in OCEANS'11 - MTS/IEEE Kona, Program Book, **2011**, doi:10.23919/oceans.2011.6107116.

[22] P.E. Nielsen, M. Egholm, O. Buchardt, "Peptide Nucleic Acid (PNA). A DNA Mimic with a Peptide Backbone," Bioconjugate Chemistry, 1994, doi:10.1021/bc00025a001.

[23] E. Kretschmann, "Die Bestimmung optischer Konstanten von Metallen durch Anregung von OberflächenplasmaschwingungenThe determination of the optical constants of metals by excitation of surface plasmons," Zeitschrift Für Physik A Hadrons and Nuclei, 1971, doi:10.1007/bf01395428.

[24] S. Fujiyoshi, K. Yarimizu, Y. Miyashita, J. Rilling, J.J. Acuña, S. Ueki, G. Gajardo, O. Espinoza-González, L. Guzmán, M.A. Jorquera, S. Nagai, F. Maruyama, "Suitcase Lab: new, portable, and deployable equipment for rapid detection of specific harmful algae in Chilean coastal waters," Environmental Science and Pollution Research, 2020, doi:10.1007/s11356-020-11567-5.

[25] B. Rijal Leblad, R. Amnhir, S. Reqia, F. Sitel, M. Daoudi, M. Marhraoui, M.K. Ouelad Abdellah, B. Veron, H. Er-Raioui, M. Laabir, "Seasonal variations of phytoplankton assemblages in relation to environmental factors in Mediterranean coastal waters of Morocco, a focus on HABs species," Harmful Algae, 2020, doi:10.1016/j.hal.2020.101819.

[26] J. Melendez, R. Carr, D.U. Bartholomew, K. Kukanskis, J. Elkind, S. Yee, C. Furlong, R. Woodbury, "A commercial solution for surface plasmon sensing," Sensors and Actuators, B: Chemical, 1996, doi:10.1016/S0925-4005(97)80057-3.

[27] H. Kawazumi, K.V. Gobi, K. Ogino, H. Maeda, N. Miura, "Compact surface plasmon resonance (SPR) immunosensor using multichannel for simultaneous detection of small molecule compounds," in Sensors and Actuators, B: Chemical, 2005, doi:10.1016/j.snb.2004.11.069.

[28] A.N. Naimushin, S.D. Soelberg, D.U. Bartholomew, J.L. Elkind, C.E. Furlong, "A portable surface plasmon resonance (SPR) sensor system with temperature regulation," Sensors and Actuators, B: Chemical, 2003, doi:10.1016/S0925-4005(03)00533-1.

[29] N. Díaz-Herrera, O. Esteban, M.C. Navarrete, M. Le Haitre, A. Gonzalez-Cano, "In situ salinity measurements in seawater with a fibre-optic probe," Measurement Science and Technology, 2006, doi:10.1088/0957-0233/17/8/024.

[30] Y.C. Kim, J. Cramer, T. Battaglia, J.A. Jordan, S.N. Banerji, W. Peng, L.L. Kegel, K.S. Booksh, "Investigation of in Situ Surface Plasmon Resonance Spectroscopy for Environmental Monitoring in and around Deep-Sea Hydrothermal Vents," Analytical Letters, **46**(10), 1607-1617, 2013, doi:10.1080/00032719.2012.757701.

[31] M. Labrador, W. Hou, "Security mechanism for vehicle identification and transaction authentication in the Internet of Vehicle (IoV) scenario: A Blockchain based model," Journal of Computer Science, 1-6, 2019, doi:10.3844/jcssp.2019.249.257.

[32] M. Labrador, W. Hou, "Implementing blockchain technology in the Internet of Vehicle (IoV)," in Proceedings - 2019 International Conference on Intelligent Computing and Its Emerging Applications, ICEA 2019, 1-5, 2019, doi:10.1109/ICEA.2019.8858311.

ASTES

Mobile Application Design for Student Learning

Angelina, Weliati, Edwin Christian Jonatan Wardoyo, Sugiarto Hartono[*]

Information Systems Department, School of Information Systems, Bina Nusantara University, Jakarta, Indonesia 11480

A R T I C L E I N F O	A B S T R A C T
	The research objectives were to identify, analyze needs, as well as designing a mobile application for student online learning at PT. Ruang Raya Indonesia, particularly in the process of working on tasks assigned by the teacher. The methods used in this research are data collection method using Slovin theory, systems analysis by focusing on the current business processes, designing object-oriented systems (OOAD) method. The result is the design of mobile applications in the form of an application for students to be able to do the tasks assigned by the teacher, change private tutoring schedule, and view academic progress reports of the student during private tutoring. The Conclusion of this research is PT. Ruang Raya Indonesia requires a system that can provide students the information about student's private tutoring activity.

1. Introduction

PT. Ruang Raya Indonesia is a startup company engaged in educational technology. According to [1], the development of information and communication technology allows humans to exchange information in a short time without being limited by distance and time. As a result of globalization, there is free competition in the world of work, trade, and education. Advances in information and communication technology, especially in the field of education, have implications for how to use information and communication technology in the learning and teaching process as attractive as possible as a source of learning and improve the quality of education. Agreeing with Junaedi, [2] also argue that smartphones can be used for learning media, and one of the operating systems that can be run by smartphones is android. According to [3] smartphones have the impact of portability, namely practical and can be used to study anywhere and anytime.

According to [4], sometimes even though school teachers have taught well, students have the possibility of not understanding the material presented at school, so that additional material through tutoring may be needed by students to help students understand the material. In [5], the author revealed that private tutoring improves students' understanding of the subject matter, and has slightly better academic achievement than students who do not do private lessons.

Based on the percentage of APJII regarding the sector of internet service users, when viewed from the employment sector, the majority of the internet in Indonesia is used in the trade and service sector than in the 3rd place in education. The estimated increase in the number of smartphone users in Indonesia according to data quoted from [6] can reach 108 million users, taking into account this and also the opinions of users, all of these features will be developed on smartphones with the Android operating system. With this application, PT. Ruang Raya Indonesia has the hope of increasing student's interest in learning anywhere and anytime.

According to [7], there are 10 components that can be considered for an LMS, 2 of which are content development aimed at helping and also motivating students to learn, in this case, the teacher must be able to upload the teacher's notes. but the teacher also has to upload supporting material to increase student knowledge of certain materials. Apart from that students must be able to obtain supporting material, teachers must also be able to monitor student participation and development. The LMS must be able to record whether students take part in discussions or submit assignments.

Based on the results of data collection regarding the needs of users and stakeholders of the application at this time, it is found that the problems are both less supportive applications and lack of features to make users receive more information. Where current technology students feel uncomfortable with the current website because the page display is in the form of letters that can be very small and can be very large, writing that can overlap with other

*Corresponding Author: Sugiarto Hartono, shartono@binus.ac.id

writing and the layout of images that are not suitable so that it blocks other writing or images. The results of private lessons are not supported by documentation that can be seen directly by students. This results in a student not being able to know his academic progress while taking private lessons. The right place for doing assignments for students to do assignments given by private tutors. This allows students who take private lessons not to get enough enrichment assignments to improve students' academic abilities on the material taken. Then the private tutoring schedule that cannot be changed based on the situation at that time.

Seeing from all existing aspects, the application that is owned by PT. Ruang Raya can now be developed better to meet the needs of users. then it is proposed to do development that includes things such as acting classes, class history, online private tutor assignments, making student academic progress reports, making questions for student assignments, changing private teacher schedules.

The application developed aims to allow students to see a list of classes being taken by students and a list of classes that have been taken, allowing students to see the initial class plans taken and to view reports on academic progress during class, allowing students to change private tutoring schedules due to unpredictable obstacles, and allows students to do assignments given by private tutors and be able to see the value and discussion of this paper.

2. Research Method

In obtaining the data and information needed in this application design analysis, several methods are used as follows:

2.1. Data collection methodology

- Literature Review

Doing a literature study by looking at references from several books related to problems related to the problem, as well as looking for other references from the internet.

- Field Study

The first step will be observed. Where this observation is for data collection by observing directly about running business processes such as usage, and daily problems that occur with company applications.

The second step is to conduct interviews by holding direct questions and answers with related parties to obtain an overview of the ongoing business processes.

Then the third step is a questionnaire. This questionnaire was conducted using online distribution. Where the sample size taken is based on the Slovin formula. This questionnaire is distributed to students to obtain an overview of problems for the running system, to obtain student opinions on the application being developed, and to obtain information on the required features. Questions will be made open-ended and closed-ended questions, where closed questions are made and processed based on a Likert scale, that is, with questions measuring students' agreement and disagreement with a subject and have been arranged based on the need to obtain the required data and information.

2.2. Methods of Analysis and Application Design

The method used to develop applications is the Object-Oriented Analysis and Design (OOAD) method. The design stages are as follows:
Inception Phase
In this phase, determine the scope of the system to be designed and identify the system requirements. The focus in this stage is as follows:
- Identification and Analysis of Company and User Needs
- Observation of business processes and running applications
- Analyze the results of the questionnaire
- Determination of problems with the system and running application
- Recommended solutions on running systems and applications

All requirements obtained will be documented in the UML diagram as follows:
- Activity Diagram
- Use Case Diagram
- Domain Class Diagram
- Use Case Description
- State Machine Diagram

2.3. Elaboration Phase

In this phase, analysis and design of the system architecture is carried out, analysis of the system requirements is carried out in more depth and ensures that all user needs are identified. Documentation for Use Case Realization will be documented in the UML diagram used at this stage:
- User Interface
- Multilayer System Sequence Diagram
- Update Design Model Class Diagram
- Package Diagram

3. Result And Discussion

3.1. User Needs Analysis

Based on the user needs that have been obtained from the data collection process through questionnaires and interviews, it can be concluded that the needs of students who have not been met in the application are as follows:
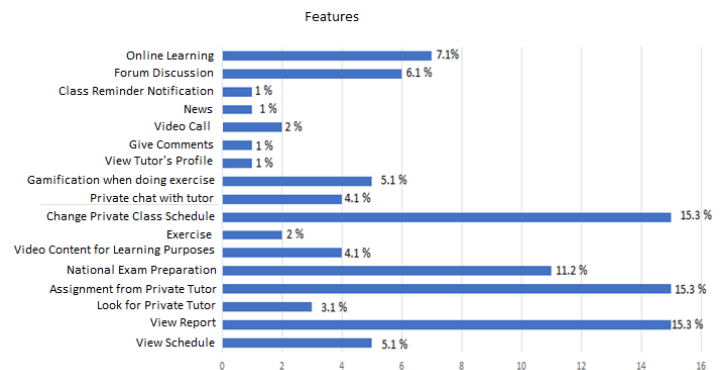
Figure 1: Graphics of desirability of features in smartphones

Judging from the level of user needs, the features that are needed by users who are in the top three are doing assignments,

changing schedules, and viewing academic reports with a percentage of 15.3%. By looking at these priorities, these features are the top priority for the design to be made in advance to meet the needs of the user.
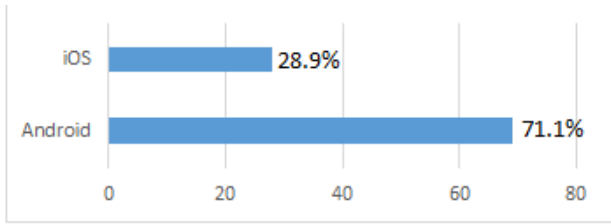
Figure 2: Graph of the operating system requirements on a smartphone

The development plan is made on the Android operating system because it sees the needs of the most selected users with a percentage of 71.1% so that development on the Android operating system becomes a development priority.

3.2. Problem Analysis

The problems faced in the current business process are as follows:

- Students who have taken private lessons can only be accessed on the official website where things that can be accessed are a list of active classes along with their details and class history. However, students feel uncomfortable with the current website because the appearance of the page is in the form of letters that can be very small and can be very large, the writing can overlap with other writing, and the layout of the images is not suitable so that it blocks other writing or images.
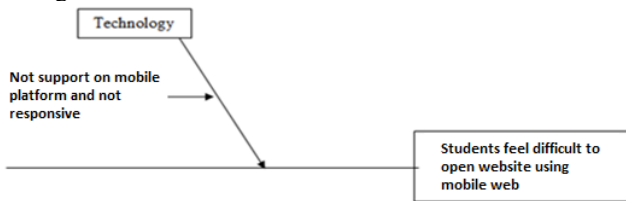
Figure 3: Fishbone Problem 1

- Currently, the results of private lessons are not supported by documentation that can be seen directly by students. This results in a student not being able to know his academic progress while taking private lessons.
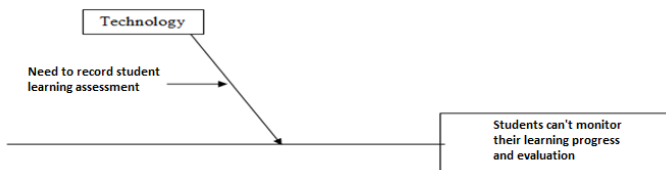
Figure 4: Fishbone Problem 2

- There is no proper place for performing assignments for students to do assignments given from private tutors. This allows students who take private lessons not to get enough enrichment assignments to improve students' academic abilities on the material taken. Where time is limited and
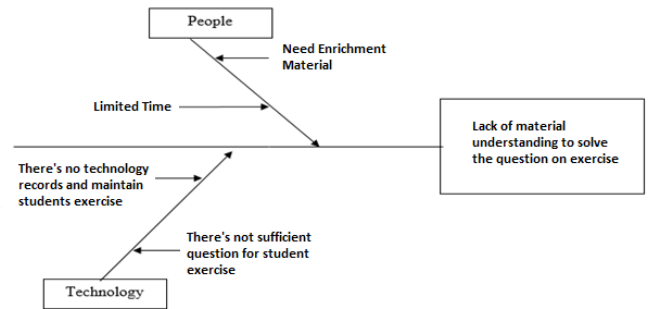
Figure 5: Fishbone Problem 3
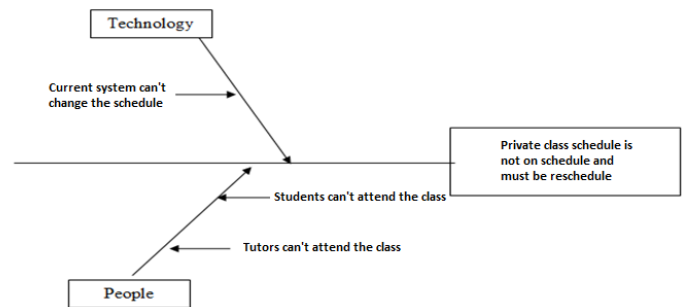
Figure 6: Fishbone Problem 4

4. Solutions

Proposals on Problems faced by PT. Ruang Raya Indonesia is as follows:

Table 1: Problem 1

Problem	Students who have taken private lessons can only be accessed on the official website. However, the page display is in the form of letters that can be very small and can be very large, text that can overlap with other writing, and the layout of the Figure is not suitable so that it blocks other text or figures.
Solution	Designed and built on mobile for this feature so students will be able to see the list by simply logging into the active class.
Reference	According to [5]: Strive for consistency, shortcuts to universal usability, offer informative feedback, design dialogue to generate closings, prevent errors, easy to reverse actions, support the internal focus of control, reduce short-term memory load
Features	- Students can see active Class - Students can view class history

Table 2: Problem 2

Problem	The results of private lessons are not supported by documentation that can be seen directly by students
Solution	Designed and made features to see student academic progress. This feature will be a place for students to see how their abilities are during class.
Reference	According to [5], all evaluation results must be reported to various interested parties, parents/guardians, school principals, supervisors, government, school partners, and the students themselves. This is intended so that the learning process, including the learning process and outcomes achieved by students and its development, can be known by various parties. The report on student learning progress is a means of communication between schools, students, and parents to develop and maintain a harmonious cooperative relationship between them. Broadly speaking, the purpose of reporting student learning outcomes is to provide accurate, clear information about the progress of student learning outcomes within a certain period, providing feedback for a student in knowing the strengths and weaknesses that give rise to motivation for learning outcomes, determine the progress of individual student learning outcomes in achieving competence.
Features	Students can view academic progress reports which consist of initial documentation reports, evaluation of sessions, evaluation reports

Table 3: Problem 3

Problem	Schedule that cannot be adjusted based on the conditions that occur
Solution	The features proposed are features of private tutoring schedule changes. This feature allows students or teachers to make changes to the private tutoring schedule that has been agreed upon in advance with the agreement of the two parties concerned. This feature is expected to help students or teachers to rearrange their private tutoring schedules so that private tutoring learning activities can run smoothly.
Reference	According to [5] states that "a schedule is defined as something that describes

where and when people and resources are at a time. Based on the Big Indonesian Dictionary, the schedule is the division of time-based on the work order arrangement plan. " Most people are familiar with lesson schedules presented as a table of days of the week and timeframes. It can be seen that each day is divided into periods. Each term has a list of courses being taught, by whom, and where. Schedules can be stated in several different ways, each student must have their schedule depending on the subject, as well as each teacher and room, all of these are different perspectives on the same schedule

Features	Student can reschedule

1. Application Design Result
- Use Case Diagram

Figure 7: Use Case Diagram

Activities that will be carried out in the application that are designed are doing assignments, viewing discussions - working on assignments, changing schedules, viewing reports, making reviews and ratings, changing reviews and ratings, viewing notifications (students), viewing discussions - active class (students), and see the discussion - history of class (students) where this activity will be carried out by students. Then make assignments, make initial documentation, make evaluation sessions, make evaluation reports, view notifications (teachers), see discussions (teachers), and decide on changes to private

tutoring schedules where this activity is carried out by the teacher. Furthermore, changing the initial documentation, changing the evaluation session, creating evaluation reports, changing assignments, and deleting tasks where this activity is carried out by the admin.

- Domain Class Diagram
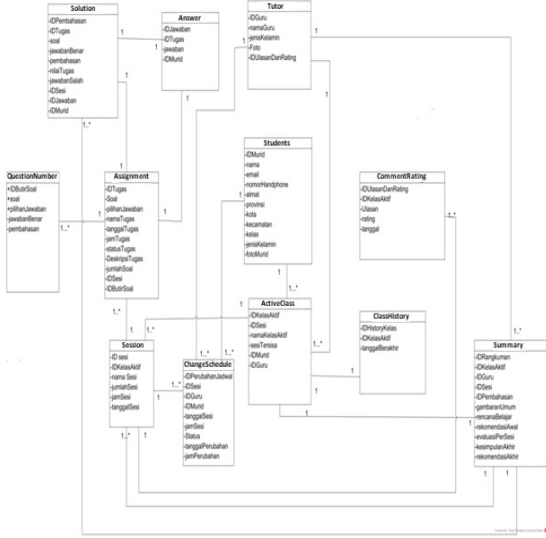
Figure 8: Domain Class Diagram

- User Interface
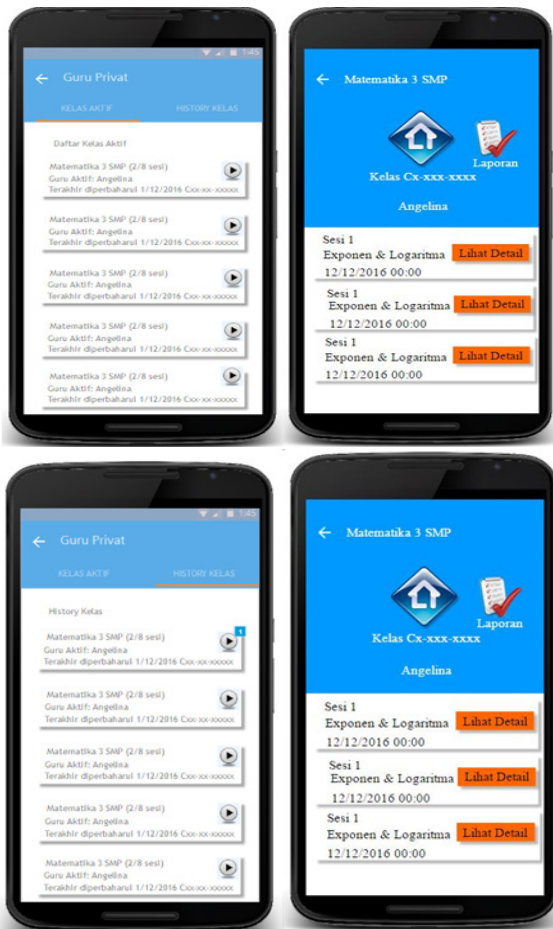
Figure 9: Active Class Look –Class history

Figure 10: Doing task
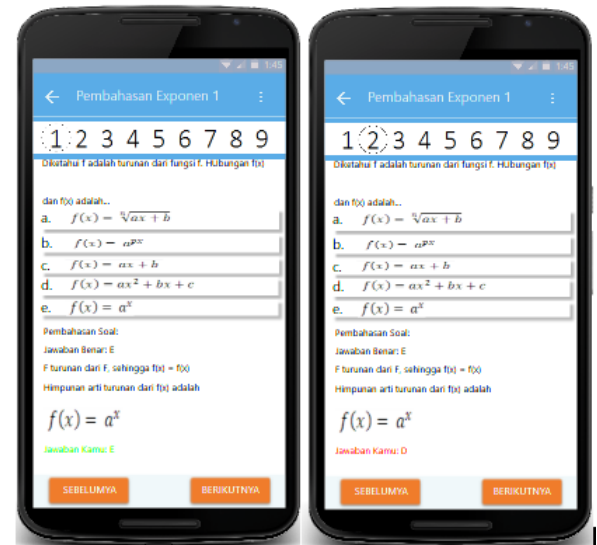
Figure 11: Discussion
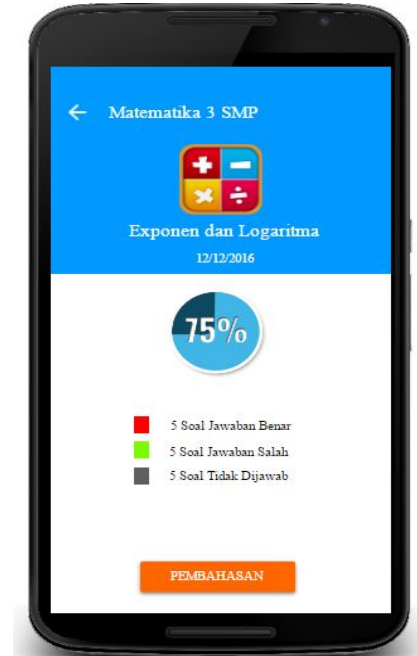
Figure 12: Result of Task
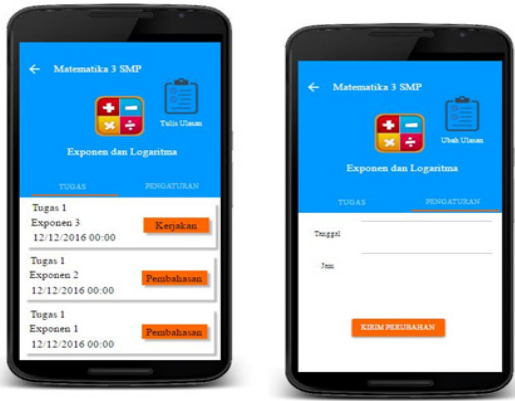
Figure 13: Reschedule

Figure 14: Report View

Figure 15: Making report-teacher

Figure 16: The view prompts for approval of a schedule change request

Figure 17: Making report-teacher

Figure 18: Making queestions-teacher

5. Conclusion

After analyzing the student application at PT Ruang Raya Indonesia, the following conclusions are obtained:

- PT. Ruang Raya Indonesia is a company that develops products and services in the field of educational technology. One of them is a mobile-based application with online chat features and can communicate and can ask questions that are not understood. However, the existing features still do not support students to interact more with mobile applications because there are very limited things students can do. With application development carried out, students will be able to interact more because students can see active classes taken, history of active classes that have been taken, work on assignments for student training, discussion of assignments that have been done, can change schedules, and can view reports - progress reports during private lessons.

- In the current running system, there are only a few features and features that do not meet user needs. As found there were no reports that could show the progress of students while taking private lessons. So it is proposed a development plan to view reports on academic progress. The report is filled in by private teachers in a special mobile-based application for teachers. In the teacher application, features are added to view the active class, make reports, make assignments, and make discussions which are used by the teacher as a basis for providing evaluation reports.

Based on the results of student application research at PT. Ruang Raya Indonesia, the advice that can be given to PT. Ruang Raya Indonesia is:

- To build an application design that has been made by PT. Ruang Raya Indonesia requires human resources who understand the use of Android Studio software.
- Make the features of the National Examination Practice Questions or tryouts so that students who need practice questions can carry out learning independently by working on questions from the question bank provided to prepare for future exams.
- Create a discussion forum so that students can have a community in the student application and can study groups online to explore existing material. With this forum students can also interact with each other with other students so that students who still have questions about a material can be assisted by other students in doing practice questions, learning modules and so on.
- Developing the search for private tutors because of the features to select and negotiate with the teacher directly regarding the teaching time schedule, and also the price per session for the total cost of teaching private tutors with students according to the existing private tutor ordering procedure.
- Make a learning video which contains a discussion of the material along with an explanation that students can understand. This video is useful for students to better understand the material by explaining it directly through the video.

References

[1] E. Junaedi, Pengaruh Modul Elektronik Berbasis Mobile Learning Terhadap Peningkatan Hasil Belajar Siswa Pada Mata Pelajaran Teknologi Informasi Dan Komunikasi, Universitas Pendidikan Indonesia, 2013.
[2] E. Supriyono, Heru., Saputra, Ardhiyatama Nur., Darsono, Ruswa., Sudarmilah, Rancang Bangun Aplikasi Pembelajaran Hadis Untuk Perangkat Mobile Berbasis Android, Universitas Muhammadiyah, Surakarta, 2014.
[3] D.P. Barakati, Dampak Pengguna Smartphone Dalam Pembelajaran Bahasa Inggris (Persepsi Mahasiswa), Universitas Sam Ratulangi, Manado, 2013.
[4] D.R. Das, Gunendra Chandra., Das, : ., Assam, 2013.
[5] J. Wittwer, "Discussion: Conditions, processes, and effects of private tutoring," Journal for Educational Research Online, 6, 125, 2014
[6] Indonesia, Raksasa Teknologi Digital Asia, 2015.
[7] B.A. Lewis et al., "Learning Management System Comparison," Proceedings of the 2005 Informing Science and IT Education Joint Conference, 18–25, 2005.

Text Mining Techniques for Cyberbullying Detection: State of the Art

Reem Bayari[*], Ameur Bensefia

CISAM Division, Higher College of Technology, Abu Dhabi, 4102, UAE

A B S T R A C T

The dramatic growth of social media during the last years has been associated with the emergence of a new bullying types. Platforms such as Facebook, Twitter, YouTube, and others are now privileged ways to disseminate all kinds of information. Indeed, communicating through social media without revealing the real identity has emerged an ideal atmosphere for cyberbullying, where people can pour out their hatred. Therefore, become very urgent to find automated methods to detect cyberbullying through text mining techniques. So, many researchers have recently investigated various approaches, and the number of scientific studies about this topic is growing very rapidly. Nonetheless, the methods are used to classify the phenomenon and evaluation methods are still under discussion. Subsequently, comparing the results between the studies and identifying their performance is still difficult. Therefore, the current systematic review has been conducted with the aim of survey the researches and studies that have been conducted so far by the research community in the topic of cyberbullying classification based on text language. In order to direct future studies on the topic to a more consistent and compatible perspective on recent works, we undertook a deep review of evaluation methods, features, dataset size, language, and dataset source of the latest research in this field. We made a choice to focus more on techniques that adopted neural networks and machine learning algorithms. After conducting systematic searches and applying the inclusion criteria, 16 different studies were included. It was found that the best accuracy was achieved when a deep learning approach is used particularly CNN approach. It was found also that, SVM is the most common classifier in both Arabic and Latin languages and outperformed the other classifiers. Also, the most widely used feature is N-Gram especially bigram and trigram. Furthermore, results show that Twitter is the main source for the collected datasets, and there are no unified datasets. There is also a shortage of studies in Arabic texts for cyberbullying identification in contrast with English texts.

1. Introduction

Online social media is now a part of everyday life activity; without a digital footprint, it has become increasingly difficult to survive in this new age of digital media. Cyberbullying is defined as an electronic form of intentional harm and hate to someone and it's considered as a crime [1]. The work presented in [2] reports that cyberbullying had a major and long-term impact on the victims. Cyberbullying leaves both the abuser (predator) and the victim with mental and physical consequences. Different researchers [2], [3] have reported that victims attempted suicide due to many cyberbullying incidents, where they have been mentally abused by offensive and violent messages received from abusers. Numerous studies have shown that adolescents are the primary victims [3], [4]. Despite the regulations, presented in most of the countries, that protect and help bullying victims, there are still many people who suffer from this phenomenon. Indeed, if the victim or his family doesn't report the case of bullying, the victim will keep suffering, and the abuser will continue making other victims. Therefore, the early detection of bullying will help in finding an effective solution by protecting the targeted person and punishing the abuser. Measures to track and identify potentially harmful online behavior must therefore be implemented. Because of the large number of daily posts, and the huge amount of information that circulates through the different social media platforms, manual checking for all posts is just impossible.

Consequently, several studies focused on finding a way to autodetect the presence of cyberbullying quickly and effectively in order to avoid any serious consequences [5], [6].

In this paper, we present an exhaustive list of the most recent research dedicated to autodetecting cyberbullying by focusing mainly on machine learning, neuronal networks and deep learning techniques. We undertook a deep review of evaluation methods, features, dataset size, language, and dataset source of the latest research in this field. In the following section we give the reader a background of cyberbullying, followed by section 3 where we discuss and present the cyberbullying approaches based or website is denigrated.

To accomplish the primary objective of this study, we identified our research questions as follows:

- RQ1: Which dataset was mainly used for the classification of cyberbullying?

- RQ2: What was the size and language of the dataset?

- RQ3: What was the method of classification used? And which one has been used most?

- RQ4: What were the metrics of quality used?

- RQ5: Which approach proved the most effective?

- RQ6: Which features were the most frequently used with classifiers?

2. Research Method

The main stages of the review methodology (research strategy, quality evaluation criteria) were outlined in this section, as in Figure 1.

2.1. Data Sources

In January 2020, we started this study, and we included most studies from 2016 to 2019 and some studies before that. We used the following databases: IEEE, Science Direct, ACM.

2.2. Inclusion and exclusion criteria

The inclusion and exclusion criteria were developed in the selection criteria stage to ensure that the research included in this study was valuable and relevant and would lead us to our main objective.

Inclusion criteria

- Papers that are purely for the classification of cyberbullying in texts.

- Papers that used neural networks / machine learning in the classification.

- Papers that explained the model and its performance measures.

- Papers which mentioned the size and language of the dataset.

Exclusion criteria

- Papers not for text classification

- Papers that didn't mention the findings' accuracy.
- Paper had not been published in journal or conference
- Paper did not use neural networks / machine learning in the classification.
- Paper that didn't mention the size and language of the dataset.
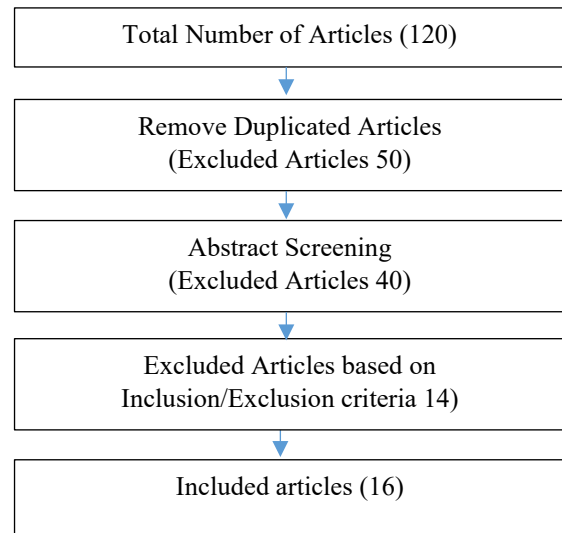
Figure 1: Data Sources

2.3. Search strategy

We used the bellow keywords to collect all the previous studies:

- "Cyberbullying" and "classification" and "neural networks" and "text"

- "Cyberbullying" and "classification" and "deep learning" and "text"

- "Cyberbullying" and "detection" and "deep learning" and "text"

- "Cyberbullying" and "classification" and "machine learning"

- "Cyberbullying" and "categorization" and "text"

- "Cyberbullying" and "classification" and "text"

2.4. Quality assessment evaluation

In this part, we designed quality assessment questions to make a checklist for the research and ensure that it would satisfy the aim of this systematic review.

- Q1: Was the corpus (size and language) identified and described well?

- Q2: Were the text classification approach described clearly?

- Q3: Was the performance of the method identified clearly?

3. Cyberbullying Background

The template is used to format your paper and style the text. All margins, column widths, line spaces, and text fonts are prescribed; please do not alter them. You may note peculiarities.

For example, the head margin in this template measures proportionately more than is customary. This measurement and others are deliberate, using specifications that anticipate your paper as one part of the entire proceedings, and not as an independent document. Please do not revise any of the current designations.

Cyberbullying is defined as the use of communication technology and information such as messages, photographs or videos in order to spread aggressive actions with the intention of harming others [1]. Unlike, bullying, cyberbullying does not require the presence of the victim in the same place or near the bully's place [7].Therefore, it differs from traditional bullying that depends on direct abuse towards victims who could be children, adolescents, or women through physical aggression and intentional, visible behavior [8]. Due to the development of technology and the increase of using smart devices, cyberbullying has become more common and represent a real problem, nothing seems to be able to stop. This is because it is done via the Internet, which involves unknown distances and sources, that allow users to speak without restrictions and it is easy to repeat the aggressive actions at any time and could spread rapidly. Cyberbullying it's not a new problem, in 2005, [2], indicated that the correlation between bullying and psychological symptoms is a reality. These symptoms may compromise risk factors involved in psychopathology. The authors indicate that bullying causes violence, delinquency, depression, anxiety, self-destructive, identity and suicidal issues, and that such symptoms could lead to psychopathology. Cyberbullying's effects are profound and could have major and long-term effects compared to traditional bullying, especially for teenagers who present the largest proportion of victims. According to statistics of [3], [4], several victims of cyberbullying tried to commit suicide because of the, degrading, and violent texts that abusers sent to them .

3.1. Cyberbullying Categories

There are several categories of cyberbullying as stated in [9], [10].

- Flooding: Consists of the bully giving the same one regularly comments, nonsense comments, or even by clicking on the enter key, in order not to let the victim contribute to the conversation.
- Masquerade: includes logging in to bully in a forum, chat room, or software using the account name of another person in order to bully a victim or tarnish the image of the victim.
- Flaming (bashing): involves two or more users attacking each other on a personal level. The conversation consists of a heated, short lived argument, and there is bullying language in all of the users' posts.
- Trolling (baiting): is intentionally posting opinion agreeing with other posts in an emotionally loaded thread in order to provoke a war, even though the comments do not actually reflect the actual opinion of the poster.
- Harassment: resembles conventional bullying most closely with the assumed relationship of the bully and victim. This form of cyberbullying involves sending the victim repeatedly abusive messages over extended periods of time.
- Cyberstalking and cyberthreats: involve sending messages that include harm attacks, which are threatening or extremely aggressive, or include extortion.

- Denigration: this kind of bullying includes Writing obscene, negative, or false rumors of someone to others or sharing them on a public forum or chat room, or website.
- Outing: this kind of bullying includes posting confidential, personal, or embarrassing information in a public chat room or forum. This type of bullying is close to denigration but requires the abuser and the victim to have a close relationship with each other either online or in person.
- Exclusion: this type of cyberbullying occurred most frequently in chat rooms or conversations between young people and adolescents by ignoring the victim.

3.2. Cyberbullying prevention methods and limitations

Due to the extreme worldwide prevalence of cyberbullying and it's direct link with many negative psychological symptoms, researchers have studied the relationship of cyberbullying with several factors in order to help in cyberbullying prevention. The work presented in [11], found that supplying sympathy and strengthening the relationship between caregiver and adolescents affect positively in cyberbullying prevention. On the other hand , the work that represented in [12], reports that the improving of awareness on cyberbullying issues played an important role in cyberbullying prevention. In addition, some countries considered the cyberbullying as a crime. Therefore, they put the laws in dealing with anyone doing such a crime as well as encouraged people to report any case of bullying, as in UAE. This is all to try to prevent children and teens from engaging in cyberbullying as well as to assist cyber victims to deal with the adverse effects of cyberbullying. Although, methods and tools continue to enhanced in cyberbullying detection , the access restrictions on high-quality data limit the applicability of state-of-the-art techniques. Consequently, much of the recent research uses small, heterogeneous datasets, without a thorough evaluation of applicability [13].

3.3. Cyberbullying automatic detection methods

The effective solution to detect bullying in the posts over social media is to build machine-based automated systems. It's for categorizing information and producing reports where cyberbullying is detected so that with fewer losses all recorded incidents can be quickly sorted out and addressed. Different methods are used to detect cyberbullying such as machine learning techniques, Natural Language Processing (NLP), and Deep Learning (DL). Examples include in [14], several NLP models such as Bag of Words (BoW), Latent Semantic Analysis (LSA) and Latent Dirichlet Allotment (LDA) used to detect bullying in Social Networks. On the other hand , some of the autodetection methods were based on word embedding, which expands a list of predefined offensive terms and assigns different weights to obtain bullying and latent characteristics [15].

4. Cyberbullying Detection Approaches Language-based

In this section, we present the most relevant works conducted in cyberbullying detection. We organized them based on the selected language, either Arabic or Latin, and both the features and the classification used in both cases.

4.1. Detection in Arabic language

Alakrot et al in [6], investigated of using word-level and N-gram features with common pre-processing methods, including

extra normalization effect on the efficiency of a trained SVM classifier .This is to detect offensive comments. Authors created dataset of 15,050 comments by collecting comments about the famous Arabic people from the YouTube platform. The dataset is available for public.As a result the stemming with pre-processing enhanced the detection of offensive language in casual Arabic text. In addition, the use of N-gram features increased the classifier efficiency. Despite the combination of stemming and N-gram features showed a negative impact on precision and recall ,pre-processing with stemming and N-grams (1-5) achieved the best performance as highlighted in Table 1.

Authors in [16], authors represented the first study in utilizing deep learning in Arabic cyberbullying detection .They utilized the same dataset in [17], with little changes. Changes include removing all hyperlinks, un-Arabic characters and emoticons. The dataset was tokenized into words to remove all unneeded characters before building the model's layers. Word Embedding was created after that. The dataset is divided into 80% for training and 20% for testing, then they trained a Feed Forward Neural Network FFNN. Authors considered the final decision of the accuracy 93.33 percent with validation accuracy 94.27, for the seven-layer network. Although it achieved an accuracy 94.56% with the three hidden layers.

In [17], it is suggested a system for detecting cyberbullying in English and Arabic text. The only features included in the first stage were text (content of tweet) and language (English, Arabic). In the second stage, authors used an affective tweets package, specifically the TweetToSentiStrength Feature Vector filter. SentiStrength used for weighting the tweets, (2 to 5) for positive feelings and (-2 to -5) for negative feelings ,(1 , -1) for representing neutral feelings. The English lexicon files were used by SentiStrength where subsequently replaced by custom-built Arabic files including weighted profane words .Haidar et al, built two datasets. First one was obtained from Facebook which reached 0.98GB of size in order to verify the system. Second one was collected from twitter to train and test the system. The Arabic dataset was collected from different dialects Lebanon, Syria, Gulf Area and Egypt mainly, it contains 35273 unique tweets after removing all duplicates. Authors show that there is a difference between the "yes" precisions between the two classifiers. In terms of precision, SVM was much higher with "yes" class. However, the overall system precision was 93.4 for SVM, 90.1 for NB.

A study by [18], utilized a collection of predefined obscene words as seeds words to collect another list from a large set of 175 million tweets . These were used to create a list of obscene words to detect offensive language and hate speech. Authors then generated new list from 3,430 words by performing Log Odd Ratio (LOR) method on unigrams and bigrams features. Authors evaluated the detection of offensive language by using five methods which are (seeds Words (SW),SW+LOR (unigram),SW+ LOR (bigram), LOR (unigram), LOR (bigram). The highest precision achieved from using the list generated by LOR(unigram).Authors have made the dataset public for research as well as the list of obscene words and hashtags.

Table 1 provides a comparative summary between the different approaches in Arabic cyberbullying detection discussed above.

4.2. Detection in Latin language

In [19], authors used sentiment analysis to detect instances of bullying in the social network using Naïve Bays classifier (NB). Authors worked on a balanced dataset consisting of 5000 English tweets. Authors collected messages that contained one of these words "Gay," "Homo," "Dike," and "Queer". For training data, queer word used to classify the positive tweets while the presence of any of these terms "Gay," "Homo," "Dike" used to classify the negative tweets. As a result, NB classifier achieved accuracy 67.3%.

Table 1: Comparative summary between the different approaches in Arabic cyberbullying detection

Ref	Dataset Size	Language	Platform	Performance			Approach	Features
				Prec	**Rec**	**F1**		
[6]	15,050 comments	Arabic	YouTube	88%	77%	82%	SVM	N-grams (1-5), word-level
				83%	80%	81%		
[16]	4.913 records	Arabic	Twitter	Accuracy: 93.33 with Validation accuracy: 94.27			FFNN	Unspecified
	30.890 records							
[17]	Arabic 35273	Arabic, English	Twitter, Facebook	90.1	90.9	90.5	NB	Text Language, SentiStrength Lexicon
	English 91431			93.4	94.1	92.7	SVM	
[18]	288 words and phrases. 127 Hashtag, 3.430 word	Arabic	Twitter, Al-Jazeera	98%	41%	58%	SW, SW+LOR (unigram), SW+LOR (bigram), LOR (unigram), LOR (bigram)	Predefined list, Unigram, Bigram

Table 2: Comparative summary between the different approaches in Latin cyberbullying detection

Ref	Dataset Size	Language	Platform	Performance				Approach	Features
				Precession	Accuracy	Recall	F1		
[19]	5000 tweets	English	Twitter		67.3%			NB	Predefined list
[20]	1000 tweets 3.045 posts 20.921 questions and answers.	English	Twitter, FormSpring.me, YouTube	60-81%	69-73%	26-94%	4-74%	GHSOM	Syntactic Semantic Sentiment Social
				60%	--	40%	--	C4.5	
				-	67 %	--	--	NB	
				---	--	67%	--	SVM	
[21]	1608 conversations	English	FormSpring.me	89.6%	77.65	91.1%	89.8%.	SVM	bigram, trigram,4-gram
[22]	900 messages written	Turkish	Twitter, Instagram	-	-	-	54%	J48	Undefined
				-	-	-	81%	NBM	
				-	-	-	84%	IBK	
				-	-	-	64%	SVM	
[23]	14,509 tweets	English	Twitter	--	78%	--	--	SVM	word skip-grams, and Brown clusters
[24]	25k tweets	English	Twitter	91%	--	90%	90%	logistic regression with L2 regularization	bigram, unigram, and trigram, syntactic structure sentiment lexicon, number of characters, words, and syllables in each tweet.
[15]	1762 tweets	English	Twitter	76.8		79.4	78.0	SVM	BOF, Latent Semantic Bullying

The authors in [20] , used an unsupervised approach for detecting cyberbully traces over social platforms. This is by utilizing Growing Hierarchical Self-Organizing Map. The suggested model is based on machine learning (decision tree C4.5, SVM, NB) as well as techniques derived from NLP (Natural Language Processing) such as semantic, syntactic features of textual sentences. Authors in this work tested the proposed model in three different datasets and platforms. The performance range for each classifier is covered in table 2.

The authors in [21], adopted a supervised approach for cyberbullying detection. Authors used different machine learning classifiers, TFIDF and sentiment analysis algorithms for features extraction. The classifications were evaluated on different n-gram language models. Authors found out, neural network with 3-grams achieved higher accuracy 92.8% compared to SVM with 4- grams that achieved 90.3%. Furthermore, NN exceeded other classifiers on the same dataset in another work. The dataset obtained from

Kaggle (Formspring.me) and consists of 1608 English instance conversations, labeled under two classes (Cyberbullying, non-Cyberbullying). Each class consists of 804 instances. The performance average rate for each classifier is highlighted in table 2.

A study by [22], authors adopted a supervised approach to the identification of bullying and harassment in posted messages in Turkish language. Authors used information gain and chi-square methods for features selection. Authors used the same labeled dataset. It was collected from Kaggle (Instagram and Twitter). Authors calculated the accuracy and running time for many machines learning classifiers, including SVM, Decision Tree (C4.5), Naïve Bayes Multinomial, and K Nearest Neighbors (KNN). Authors compared the accuracy of classifiers under different conditions, NBM classifier was the most efficient classifier before features selection is implemented, while IBk

achieved the most efficient when 500 features were selected. As shown in table two.

A study by [23] , authors used different methods of text classification to differentiate between hate ,profanity expressions, and other texts. In determining the baseline, authors used standard lexical characteristics and a linear SVM classifier. Authors applied a linear SVM classifier on three groups of features extracted surface n-grams, word skip-grams, and Brown clusters. The best accuracy (78%) achieved when authors used the character 4-gram model.

In [24], authors used a hate speech lexicon to collect tweets that containing hate speech keywords. It's used then to label a sample of these tweets under three categories (hate, offensive, normal) speech. Authors trained a multiclass classifier to distinguish these different categories. Authors used bigram, unigram, and trigram features as well as features for the number of characters, words, and syllables in each tweet. In addition, authors included binary and count indicators for hashtags, mentions, retweets, and URLs. Author then tested a variety of models; each model was tested by using 5-fold cross-validation. Authors found that the Logistic Regression and Linear SVM model outperformed other models. For the final model, logistic regression with L2 Regularization were used for the final model. The final model then trained by using the whole dataset to predict the label for each tweet. The best performance is highlighted in table 2.

In [15], authors introduced a novel learning method for cyberbullying recognition called Embedding Enhanced Bag-of-Words (EEBOW).EEBoW mixes BoW (Bag of Words) features, latent semantic features and bullying features .Bullying features are derived from word embedding, capturing the semantic details behind words. Authors reported that the EBoW model outperforms other comparable models, including Semantic-enhanced BOW (SEBOW), BoW, LDA(Latent Dirchilet Allocation), LSA(Latent Semantic Analysis) and BOW . The performance of best model (BoW) is highlighted in table two.

Table 2 provides a comparative summary between the different approaches in Latin cybe4rbullying detection as discussed above

5. Deep-Learning in Cyberbullying detection

Aauthors in [25] , proposed a novel algorithm to detect cyberbullying . The proposed algorithm is based on a convolution neural network (CNN) with semantics features by utilizing word embedding. It is to eliminate the needs for features extraction process. CNN-CB model consists of four layers: embedding, convolutional, max pooling and dense. Authors then applied the algorithm on dataset consist of about 39,000 English tweets .Authors then compared the accuracy result with the SVM classifier .Authors reported that the CNN-CB algorithm outperforms classical machine learning with accuracy 95 percent as shown in Table 3.

In [26], it is presented a novel approach to optimize Twitter cyberbullying detection based on deep learning (OCDD).The proposed approach eliminates the features extraction and selection phases . It's to preserve the semantics of words by replacing the tweet by a set of word vectors. Authors then fed it to a convolutional neural network (CNN) for classification phase along

with metaheuristic optimization a algorithm for parameter tuning. This is to find the optimal or near optimal values.

In [27], it is proposed an aggregate approach for the two deep learning models. The first one is character-level convolutional neural network (CNN). It's for capturing the low-level syntactic knowledge from the character series. The second is word-level (long-term recurrent convolutional networks) LRCN. It's to capture semantic high-level information from word sequence, complementing the CNN model. Authors used dataset contains in total 8,815 comments from Kaggle. Authors reported that the hybrid model's sensitivity and accuracy are 0.5932 and 0.7081, respectively. Also, the aggregated approach is significantly enhanced the performance as well as outperformed other machine learning methods in cyberbullying detection.

In [28], it is proposed a novel pronunciation-based neural network (PCNN) for cyberbullying detection .The proposed model is to overcome the misclassification that produced from using misspelled words. Authors phoneme text codes as interface for a coevolution neural network. This technique is to correct spelling errors which did not change the pronunciation. Authors then fed it to CNF in order to detect cyberbullying. Authors compared the performance of models using two datasets, collected from Twitter (1313 tweets) and Formspring.me (13,000 messages). Authors also solved the problem of datasets balance with different techniques in order to compare the result between balanced and imbalanced datasets. Authors compared PCNN performance with previous work and found PCNN outperform the other methods. Authors reported that PCNN performed better when it is applied on the Twitter dataset than Formspring.me dataset. In addition, PCNN and CNN Random model performed better than CNN with pre-trained.

6. Discussion

This section will present the results according to the language and method in three separate sections , following the same order of study that followed in section four.

6.1. Cyberbullying detection in Arabic language.

For Cyberbullying detection in Arabic language, the findings indicate that, SVM classifier is the most used classifier in the classification of Arabic text [6], [17]. Also, most of studies used Twitter platform as a source to collect the datasets[16]-[18]. For the surveyed papers, there was no unified dataset, and the maximum size of the dataset is 35273 tweets built by the writers in a study [17],and this size is small compared to the English dataset available. In addition, the results show that most common investigated feature is N-Grams particularly unigram and bigram [6], [18] . The common used method for measuring the accuracy are same to other languages (Precesion,Recall,F1). Furthermore, the highest accuracy achieved when authors used SVM classifier with Language SentiStrength Lexicon feature in [17] followed by NB classifier that is also investigated in the same study.Generally, it was found that deep learning algorithms have not been researched with the Arabic language as much as in English.

6.2. Cyberbullying detection in Latin language

The results of this analysis concluded that out of seven papers analyzed, the SVM classifier was tested five times, followed by the

NB classifier that was examined three times. Also, the most of the datasets are collected from Twitter platform , there is still no unified dataset and the maximum size of the dataset is 25k tweets in [24]. In addition, the results show that most common investigated feature is Bigram, Trigram. The commonly used methods for measuring the accuracy are same to other languages (Precession, Recall, F1).Also, the highest accuracy is archived by using SVM classifier that represented with bigram, trigram,4-gram features in [21].

6.3. Deep-Learning in Cyberbullying detection

After the deep systematic review, the results show that the CNN is the most common used method in the classification of cyberbullying. Also, CNN method had been investigated five times in different studies under different conditions . The results of review show also, that the most of datasets are collected from Twitter platform as well as there is no unified dataset and the maximum size of the dataset is 39,000 tweets, this is small to investigate the deep learning techniques. In addition for deep learning algorithms, the widely used approach for measuring the accuracy is the same for machine learning algorithms (Precession, Recall, F1). In addition, the highest accuracy is archived in [28] study when CNN is used, and outperformed the machine learning algorithms.

To conclude the result for both languages, the best accuracy was achieved when deep learning approaches were used particularly when CNN is applied in [28]. Also, deep learning algorithms were utilized more in the classification of cyberbullying in the English text, while machine learning used more with the Arabic text. Moreover, SVM is most common classifier in both Arabic and Latin languages and outperformed the other classifiers, it was examined seven times . Furthermore, N-Gram is the most widely used function for both Arabic and Latin languages with classifiers. The Twitter platform also primarily provides the origins of most of the datasets followed by FormSpring.me .

7. Conclusion

In this paper, we conducted an in-depth analysis of 16 studies on automatic cyberbullying detection methods based on text language. we undertook a deep review of evaluation methods, features, dataset size, language, and dataset source of the latest research in this field.We focused only on techniques that adopted neural network and machine learning algorithms. This is to direct future studies on this topic to a more consistent and compatible perspective on recent works, and to provide a practical and effective implementation for future systems. It was found that the best accuracy was achieved when a deep learning approach is used especially when CNN used. It was found also that, SVM is the most common classifier in both Arabic and Latin languages, and outperformed the other classifiers.Also, the most widely used feature is N-Gram especially bigram, trigram. In addition, Twitter is the main source for the collected datasets. Furthermore, there is no unified data sets. Although, cyberbullying prevention methods were adopted, largely, but most of the literature work aimed to enhance the detection by adding a new feature, as a number of features increased the process of features selection and extraction become more complicated. On the other hand, most of the work is

done to find automated English language solutions, although each language actually has different structures and rules. In addition, there is no standard dataset and list of bad words to be counted as being used in the cyberbullying detection efforts. Finding an effective solution to detect cyberbullying helps a lot in protecting the targeted person.

Conflict of Interest

The authors declare no conflict of interest.

References

[1] J.W. Patchin, S. Hinduja, "Bullies Move Beyond the Schoolyard: A Preliminary Look at Cyberbullying," Youth Violence and Juvenile Justice, **4**(2), 148–169, 2006, doi:10.1177/1541204006286288.

[2] T. Ivarsson, A.G. Broberg, T. Arvidsson, C. Gillberg, "Bullying in adolescence: Psychiatric problems in victims and bullies as measured by the Youth Self Report (YSR) and the Depression Self-Rating Scale (DSRS)," Nordic Journal of Psychiatry, **59**(5), 365–373, 2005, doi:10.1080/08039480500227816.

[3] P.W. Agatston, R. Kowalski, S. Limber, "Students' Perspectives on Cyber Bullying," Journal of Adolescent Health, **41**(6 SUPPL.), 59–60, 2007, doi:10.1016/j.jadohealth.2007.09.003.

[4] T. Beran, L.I. Qing, "Cyber-harassment: A study of a new method for an old behavior," Journal of Educational Computing Research, **32**(3), 265–277, 2005, doi:10.2190/8YQM-B04H-PG4D-BLLH.

[5] E.A. Abozinadah, A. V. Mbaziira, J.H.J. Jones, "Detection of Abusive Accounts with Arabic Tweets," International Journal of Knowledge Engineering-IACSIT, **1**(2), 113–119, 2015, doi:10.7763/ijke.2015.v1.19.

[6] A. Alakrot, L. Murray, N.S. Nikolov, "Towards Accurate Detection of Offensive Language in Online Communication in Arabic," Procedia Computer Science, **142**, 315–320, 2018, doi:10.1016/j.procs.2018.10.491.

[7] J.D. Marx, "Healthy communities: What have we learned and where do we go from here?," Social Sciences, **5**(3), 2016, doi:10.3390/socsci5030044.

[8] M.A. Campbell, "Cyber Bullying: An Old Problem in a New Guise?," Australian Journal of Guidance and Counselling, **15**(1), 68–76, 2005, doi:10.1375/ajgc.15.1.68.

[9] S. Nadali, M.A.A. Murad, N.M. Sharef, A. Mustapha, S. Shojaee, "A review of cyberbullying detection: An overview," International Conference on Intelligent Systems Design and Applications, ISDA, 325–330, 2014, doi:10.1109/ISDA.2013.6920758.

[10] Willard, "Parent Guide to Cyberbullying and Cyberthreats," 1–14, 2014.

[11] R.P. Ang, D.H. Goh, "Cyberbullying among adolescents: The role of affective and cognitive empathy, and gender," Child Psychiatry and Human Development, **41**(4), 387–397, 2010, doi:10.1007/s10578-010-0176-3.

[12] W. Cassidy, K. Brown, M. Jackson, "'Under the radar': Educators and cyberbullying in schools," School Psychology International, **33**(5), 520–532, 2012, doi:10.1177/0143034312445245.

[13] C. Emmery, B. Verhoeven, G. De Pauw, G. Jacobs, C. Van Hee, E. Lefever, B. Desmet, V. Hoste, W. Daelemans, "Current limitations in cyberbullying detection: On evaluation criteria, reproducibility, and data scarcity," Language Resources and Evaluation, 2020, doi:10.1007/s10579-020-09509-1.

[14] J.M. Xu, K.S. Jun, X. Zhu, A. Bellmore, "Learning from bullying traces in social media," NAACL HLT 2012 - 2012 Conference of the North American Chapter of the Association for Computational Linguistics: Human Language Technologies, Proceedings of the Conference, 656–666, 2012.

[15] R. Zhao, A. Zhou, K. Mao, "Automatic detection of cyberbullying on social networks based on bullying features," ACM International Conference Proceeding Series, **04-07-Janu**, 1–6, 2016, doi:10.1145/2833312.2849567.

[16] B. Haidar, M. Chamoun, A. Serhrouchni, "Arabic Cyberbullying Detection: Using Deep Learning," Proceedings of the 2018 7th International Conference on Computer and Communication Engineering, ICCCE 2018, 284–289, 2018, doi:10.1109/ICCCE.2018.8539303.

[17] B. Haidar, M. Chamoun, A. Serhrouchni, "A multilingual system for cyberbullying detection: Arabic content detection using machine learning," Advances in Science, Technology and Engineering Systems, **2**(6), 275–284, 2017, doi:10.25046/aj020634.

[18] H. Mubarak, K. Darwish, W. Magdy, "Abusive Language Detection on Arabic Social Media," 52–56, 2017, doi:10.18653/v1/w17-3008.

[19] H. Sanchez, "Twitter Bullying Detection," Homo, 2011.

[20] M. Di Capua, E. Di Nardo, A. Petrosino, "Unsupervised cyber bullying

detection in social networks," Proceedings - International Conference on Pattern Recognition, **0**, 432–437, 2016, doi:10.1109/ICPR.2016.7899672.

[21] J. Hani, M. Nashaat, M. Ahmed, Z. Emad, E. Amer, A. Mohammed, "Social media cyberbullying detection using machine learning," International Journal of Advanced Computer Science and Applications, **10**(5), 703–707, 2019, doi:10.14569/ijacsa.2019.0100587.

[22] S.A. Özel, S. Akdemir, E. Saraç, H. Aksu, "Detection of cyberbullying on social media messages in Turkish," 2nd International Conference on Computer Science and Engineering, UBMK 2017, 366–370, 2017, doi:10.1109/UBMK.2017.8093411.

[23] S. Malmasi, M. Zampieri, "Detecting hate speech in social media," International Conference Recent Advances in Natural Language Processing, RANLP, **2017-Septe**, 467–472, 2017, doi:10.26615/978-954-452-049-6-062.

[24] T. Davidson, D. Warmsley, M. Macy, I. Weber, "Automated hate speech detection and the problem of offensive language," Proceedings of the 11th International Conference on Web and Social Media, ICWSM 2017, 512–515, 2017.

[25] M.A. Al-Ajlan, M. Ykhlef, "Deep learning algorithm for cyberbullying detection," International Journal of Advanced Computer Science and Applications, **9**(9), 199–205, 2018, doi:10.14569/ijacsa.2018.090927.

[26] M.A. Al-ajlan, "Optimized Twitter Cyberbullying Detection based on Deep Learning," 2018 21st Saudi Computer Society National Computer Conference (NCC), 1–5, 2018.

[27] S. Bu, S. Cho, A Hybrid Deep Learning System of CNN and LRCN to Detect Cyberbullying from SNS Comments, Springer International Publishing, 2018, doi:10.1007/978-3-319-92639-1.

[28] X. Zhang, J. Tong, N. Vishwamitra, E. Whittaker, J.P. Mazer, R. Kowalski, H. Hu, F. Luo, E. Dillon, "Based Convolutional Neural Network," 2016 15th IEEE International Conference on Machine Learning and Applications (ICMLA), 740–745, 2016, doi:10.1109/ICMLA.2016.0132.

Simulating COVID-19 Trajectory in the UAE and the Impact of Possible Intervention Scenarios

Abdulla M. Alsharhan*

Faculty of Engineering and IT, The British University in Dubai, Dubai, 345015, United Arab Emirates

A R T I C L E I N F O	A B S T R A C T
	This paper aims to simulate the current trajectory of the pandemic growth in the UAE; when it is likely to end and at what cost? It also examines the current and additional possible measures to contain the second wave of the pandemic. The method used is a simple Susceptible-Infected-Recovered (SIR) model called covid19_scenarios. The key finding suggests current intervention is 35 – 45% and effective, and based on keeping them, the pandemic curve in the UAE is expected to be flattened around the fourth quarter of 2022 with the maximum saved lives and lowest burden on the healthcare system. In contrast, it can end earlier at the end of the second quarter of 2021 but at a much higher fatality rate and a health system ready with 3,600 intensive care units. It also revealed that country closure has a minor impact, and severe and fatal cases will continue to appear even after vaccinating the whole community.

1. Introduction

On 16th January, a Chinese family arrived from Wuhan in the United Arab Emirates (UAE) to spend their holiday. One week later, the family headed to a local clinic after feeling unwell. Four family members, including the grandmother, mother, father, and a nine-year-old girl, were confirmed to have the virus [1]. The next day, on 30th January 2020, [2] confirmed COVID-19 outbreak as a Public Health Emergency of International Concern, and on 11th March declared COVID-19 as a pandemic.

In response, the UAE announced its National Disinfection Programme, whereby public facilities and transportation were disinfected daily from 26th March – 24th June 2020. After the quarantine, the UAE carried on specific interventions related to COVID-19, including preventing public gatherings and family visits, keeping physical distance, wearing masks and gloves, and not exceeding the limit of three passengers per vehicle for non-family members.

Policy-makers in the UAE made some noticeable primary efforts to contain the pandemic. Significant interventions included implementing distance learning and remote work, suspending prayer in all worship places, postponing sports events, closing shopping malls, maintaining distance at entertainment venues, and suspending visas, flights, and even the entry of GCC citizens [3]. On 24th June 2020, the National Emergency Crisis and Disaster

Management Authority announced the end of the National Disinfection Programme with immediate effect.

These efforts paid off when the rate of daily confirmed cases started declining, reaching the lowest recorded number of daily cases on 3rd August 2020. However, after some rules of social distancing were relaxed, the daily numbers started rising again, indicating a second wave of the pandemic. By 25th November, the National Emergency Crisis and Disaster Management Authority reported that 161,000 cases had been diagnosed in the UAE. While 93% have recovered, there are still 10,000 active cases and 500+ deaths.

Figure 1: Intervention impact on daily cases in the UAE (NCEMA 2020)

2. Literature Review

After carefully searching the major databases, two papers were located that discuss simulating COVID-19 in the UAE. The search

*Corresponding Author: Abdulla M. Alsharhan, Alsharhan@outlook.com

databases included WorldCat, Google Scholar, and CrossRef. The search keywords included terms such as "COVID-19" AND ("simulation" OR "simulating") AND ("UAE" OR "United Arab Emirates").

In [4], the authors tried to estimate the number of required beds for both acute and critical cases in the UAE in addition to the possible infection of healthcare personnel. The simulation also predicted the peak time and the total infections before and after non-pharmaceutical interventions.

Assuming the UAE population is 9,631,000. The simulation revealed that UAE would reach the highest at t = 56 at April 2020, where on the 26th of May, it will reach its peak at a 1.67 per cent infection rate of the total population, an equivalent to 165,360 infections. After that, it will decrease dramatically. The infection should disappear on the 100th day, around the 9th of July. However, although the actual figures from NCEMA match the peak prediction of the first wave, it did not match the total infection at that time, which appears to be around 30,000 confirmed cases only, which could suggest the effectiveness of the measures used by the policy-makers during that period.
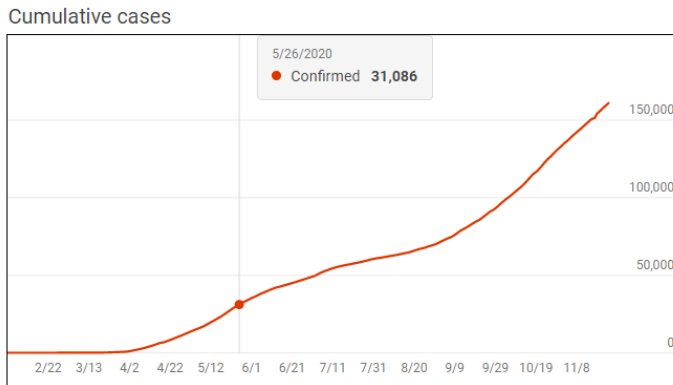
Figure 2: Actual cumulative cases in the UAE as of the 26th of May, 2020 (Microsoft Bing.com)

This study also predicted that the maximum number of required beds would be 63,138 at t=66, which is equivalent to that of the 6th of June, 2020. While it is difficult to validate this assumption; the study did not mention how many of them are needed to be for intensive care unit (ICU) beds. The simulation also concluded the UAE transmission rate and the basic reproduction number on the period between the 21st of April to the 15th of May, 2020 to be R0 = 1.7768.

In [5], the authors simulated the dynamics of COVID-19 in the UAE based on fractional derivative modelling using Riesz wavelets. The parameters used in this study were calculated based on official published data of COVID-19 in the UAE, while the dynamic of the virus transmission was considered from other sources due to the fact that the dynamic of the virus transmission from a country to another does not change much. The total UAE population used in this study was 9.666 million, which is close to the previous study. The study did not mention a clear transmission rate or the basic reproduction number, but the transmissibility multiple used is ψp at (0.1).

However, as the UAE is preparing to get back to normal, little is known on how the new relaxed interventions will impact the spread of the pandemic. This study objective is to support the policy-makers by analysing the impact of going back to normal by the beginning of 2021. In order to simulate the desired outcomes, the following hypothesis will be tested:

A. The UAE is ready to go back to normal at the beginning of 2021.

B. The UAE can go back to normal, and the current healthcare system can handle all the cases.

C. Suspending entry to the UAE is necessary to contain and end the pandemic.

D. Extending the current intervention should be the new normal, as it is essential to decreasing severe, deadly cases.

E. Vertical Isolation (isolating young and senior citizens) is similar to the "doing nothing" scenario.

F. The vaccine will end the pandemic, and we can go back to normal life.

G. We still need to keep the current interventions, even if the community is vaccinated.

3. Methods

A simple Susceptible-Infected-Recovered (SIR) model was used to simulate the COVID-19 outbreaks in the UAE. The model is called "covid19_scenarios".

This model was selected because of its unique ability to blend real and simulated data. It is also already loaded with each country default parameters, including the UAE. It is simple to use and provide a web-based user-friendly interface that allows real-time data adjustment, which reflects the output immediately on the model. Besides, it has different categories for individuals exposed to the virus that are not yet infectious. In addition, severely sick individuals in need of hospitalisation, people in critical condition, and a fatal category. The tool that was utilised was a computational biology tool developed by [6]. The source code of this tool is freely available at github.com/neherlab/covid19_scenarios and the web-based version is also available at https://covid19-scenarios.org.

3.1. Basic Assumptions

- Individuals are infected by contact with infectious persons. Each individual causes, on average, R0 secondary infections while they are infectious.

- Infection rates could change based on seasonal variations.

- Individuals who are infected go into a state after a latency period. This development occurs in three different stages, which will ensure that the distribution of time spent in the exposed compartment matches real-life scenarios.

- Positive individuals either recover or progress to a severe case. The ratio of progressing to recovery to severe case depends on age.

- Severe positive cases are hospitalised in the Intensive Care Unit (ICU) (if beds are available), placed in an overflow compartment, or receive palliative care. At the same time, younger age groups are given priority access to the ICU.

- Individuals in the ICU either recover and are transferred to standard hospital rooms or die. Fatality rate depends on the age group and ICU admission availability.

- Individuals in palliative care die, which could also represent death at home [6].
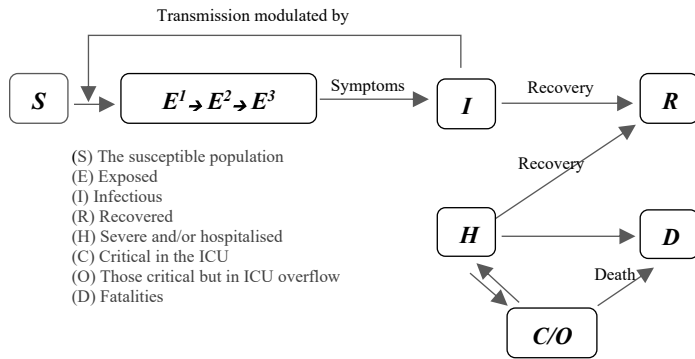
Figure 3: A schematic illustration of the underlying model

3.2. Parameters

The parameter values presented are based on the following assumptions:

Table 1: The UAE's Epidemiology and Population Parameters

Parameter	Value
Population [1]	9,935,374
Seroprevalence	8%
Initial number of cases	109,3962
Hospital Beds (est.) [2]	15,868
ICU/ICMU (est.) [3]	476
Imports per day [4]	22
Simulation time range	10th August 2020 – 31st December 2021
Number of Runs	15
Annual average R_0	0.89 – 1.16
Latency (days)	3
Infection period (day)	3
Seasonal forcing	1
Seasonal Peak	January
Hospital stay (days)	3
Intensive Care Unit (ICU) stay	14
Severity of ICU overflow	2

3.3. Basic assumptions about the UAE

1. According to [7], the current population of the UAE as of Tuesday 17th November 2020 is 9,935,374.

2. In reference to [8], the latest bed estimation goes back to 2013, since more recent numbers of beds are not provided. The total number of hospital beds in 2020 was estimated to be 15,868. Figure 2 shows the estimation is based on calculating the compound annual growth rate (CAGR) from 2013 (9,760 beds) to 2018 (13,811 beds), which is equivalent to 7.19%.

3. Intensive care units (ICU) were estimated with a common standard of 3% of the total hospital beds [6]. Therefore, the estimated ICU numbers are (3% x 15,868 = 476).
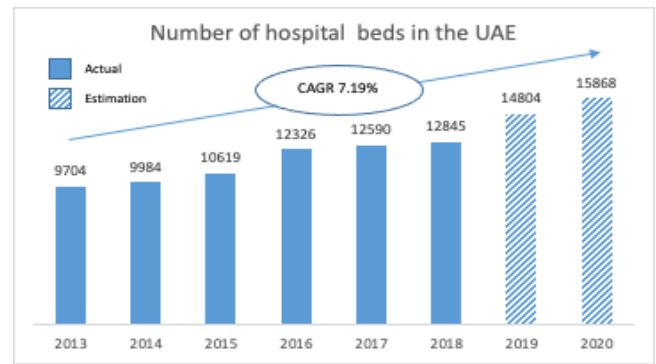
Figure 4: The total number of hospital beds in the UAE estimation

4. The latest available data about arrivals are not provided. The total number of passengers who arrived in the UAE in 2020 was estimated to be 15,868. Figure 3 shows that assumption is based on calculating the Compound Annual Growth Rate (CAGR) from 2011 (34 million passengers) to 2016 (58 million passengers) [8], which is equivalent to 7.19%. Then the growth rate was used to calculate the growth trajectory for 2017, 2018, 2019, and 2020. Since last February 2020, 59 airline companies stopped or reduced flights, and many countries, including the United States, Russia, Australia, and Italy, have introduced travel restrictions [9]. It is difficult to determine how much traffic is impacted by these interventions; therefore, we assumed international travel restrictions produce a 90% overall traffic reduction in the UAE, which result in an equivalent to 8 million (90 x 10% = 8).

5. The remaining data was based on the default setting of the model, which are based on the published epidemiological and clinical notes about each country, including the UAE.
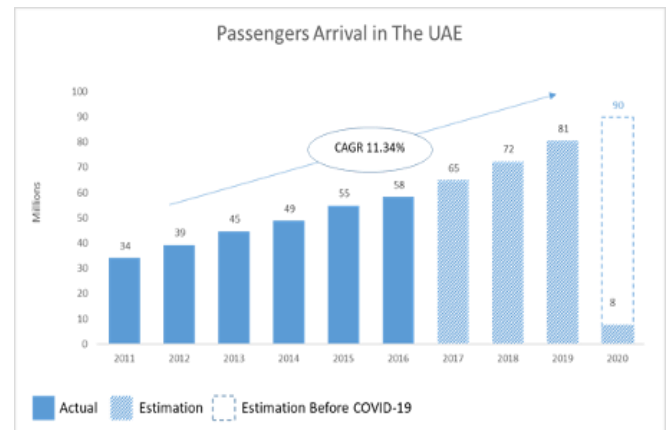
Figure 5: Estimated number of passenger arrivals in the UAE

3.4. Age-dependent parameters

Table 2 shows the UAE age-dependent parameters. The second column shows the number of individuals who falls under each age group category. The next columns summarise the COVID-19 intensity based on epidemiological and clinical notes from China, Spain, Switzerland, and Italy. The "Confirmed" column shows the assumption of what fraction of the previous category will impact the next [6]. Both "Confirmed" and "Isolated" columns are editable and can be adjusted to test different hypotheses.

Table 2: The UAE age-dependent parameters

Age group	Age distribution	Confirmed % total	Severe % of confirmed	Palliative % of severe	Critical % of severe	Fatal % of critical	Fatal % of all infections	Isolated % total
0–9	1011712	5	1	0	5	10	0	0
10–19	842993	5	3	0	10	10	0	0
20–29	2149345	10	3	0	10	10	0	0
30–39	3169316	15	3	0	15	10	0.01	0
40–49	1608106	20	6	0	20	10	0.02	0
50–59	797911	20	10	0	25	20	0.1	0
60–69	242705	25	25	5	30	30	0.88	0
70–79	55883	30	35	10	25	40	2.1	0
80+	12431	40	50	20	15	40	5.2	0

4. Results and analysis

This section shows the results for several scenarios. The simulations represent major possible interventions that could be made by the policy-makers in the UAE. In this study, the parameters are based on data from the UAE.

4.1. Scenario (A): Going back to normal at the beginning of 2021

This scenario simulates the behaviour without any additional intervention, as it will be used as a baseline for comparison with all the other scenarios. To generate this scenario, the current intervention is assumed to provide 35% – 45% protection (Table 5). As per Figure 5, the estimated annual visitors are expected to be 10% of the usual annual visitors. At least 8 million passengers are expected to arrive in the UAE annually. If we are assuming the current airport interventions are effective and are dedicating 99% of the cases, then the community will only import about 0.1% undedicated positive cases annually. This is equivalent to 8,000 positive cases per year, or 22 positive daily cases on average (Table 3).
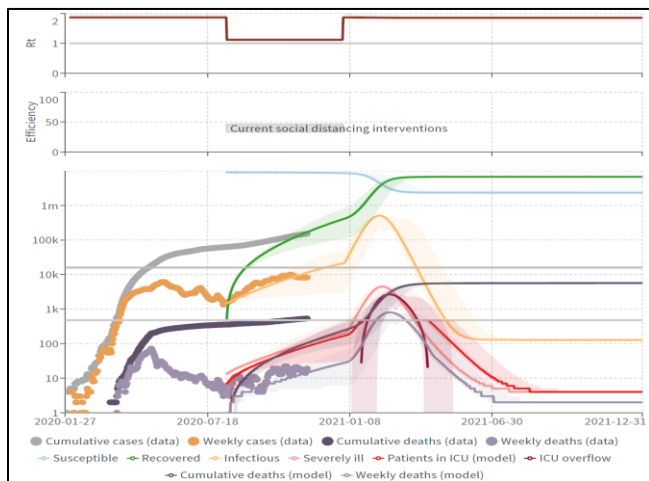
Figure 6: Scenario (A): Going back to normal at the beginning of 2021
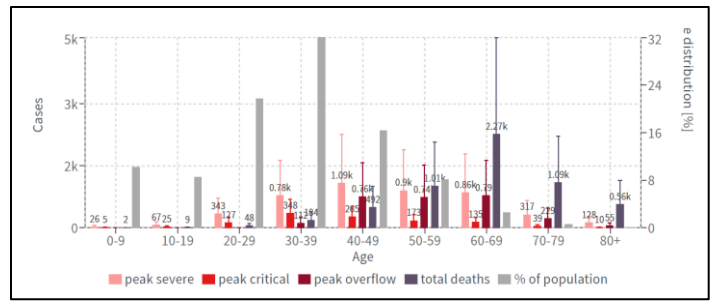
Figure 7: Scenario (A): Distribution across age groups

Table 3: The UAE population parameters, baseline

Population parameter	Value
Age distribution for	UAE
Case counts for	UAE
Number of hospital beds	15868
Number of available ICU beds	476
Cases imported into the community per day	22
Number of cases at the start of the simulation	3000
Population size	9935374
Seroprevalence [%]	8.5

Table 4: The UAE epidemiology parameters, baseline

Epidemiology parameter	Value
Average time in regular ward [days]	3
Average time in ICU ward [days]	14
Infectious period [days]	3
Latency [days]	3
Increase in death rate when ICUs are overcrowded	2
Seasonal peak in transmissibility	January
R0 at the beginning of the outbreak	1.8–2.2
Seasonal variation in transmissibility	0

Table 5: The UAE Mitigation parameters baseline

Intervention name	From	To	Reduction of transmission
Current social distancing interventions	Aug 10 2020	Dec 31 2020	35% – 45%

With this scenario, a new peak should be expected during the second week of February 2021 resulting in the number of severe cases to reach 55.76k, with deaths totalling 5.68k. Moreover, 40% of the deaths are estimated to be among the $60 – 69$ age group. The curve will then flatten during the second week of June after most of the community has immunity against the virus and weekly cases will continue to fluctuate between $127 – 142$, and the total weekly deaths will be two. It is noticeable that there are four months of overflow in ICUs.

4.2. Scenario (B): Increasing the ICU up to no overflow is happening

In these scenarios (Figure 8), the number of ICUs is increased up to a level where there is no overflow. After several runs, the required ICU numbers are 3,800, eight times more than the current estimated available ICUs. This scenario shows that the total severe cases did not change than the baseline. However, the total death has decreased to 4.75k, which is 16% less than Scenario (1).
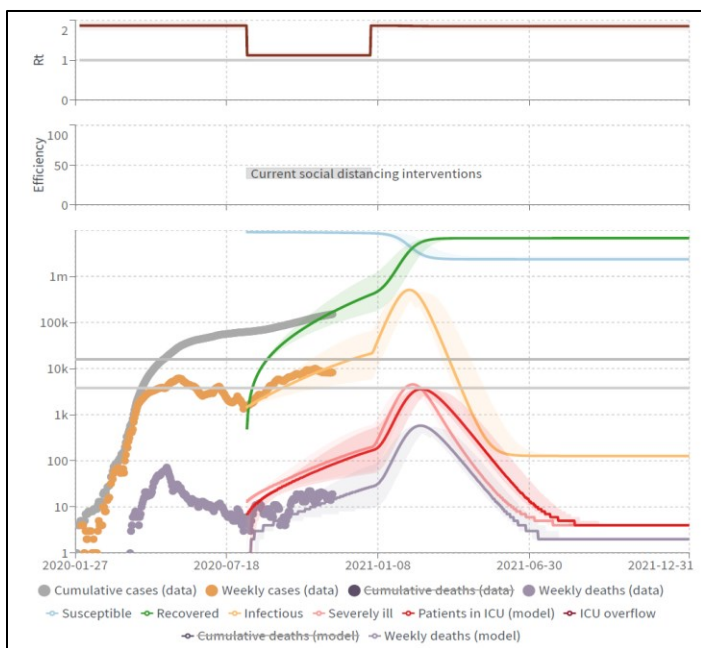
Figure 8: Scenario (B): Increasing the ICU units up to no overflow is happening
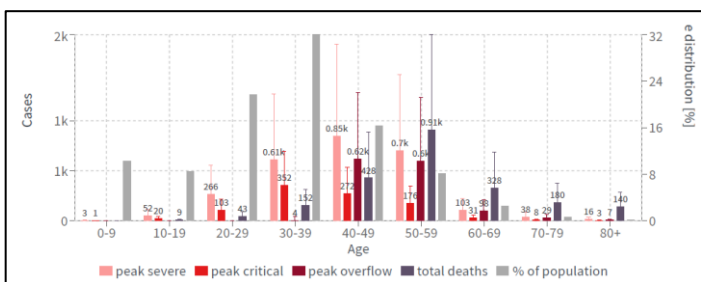
Figure 9: Distribution across age groups in scenario (C) shows decreased death rates in the 60 – 69 age group
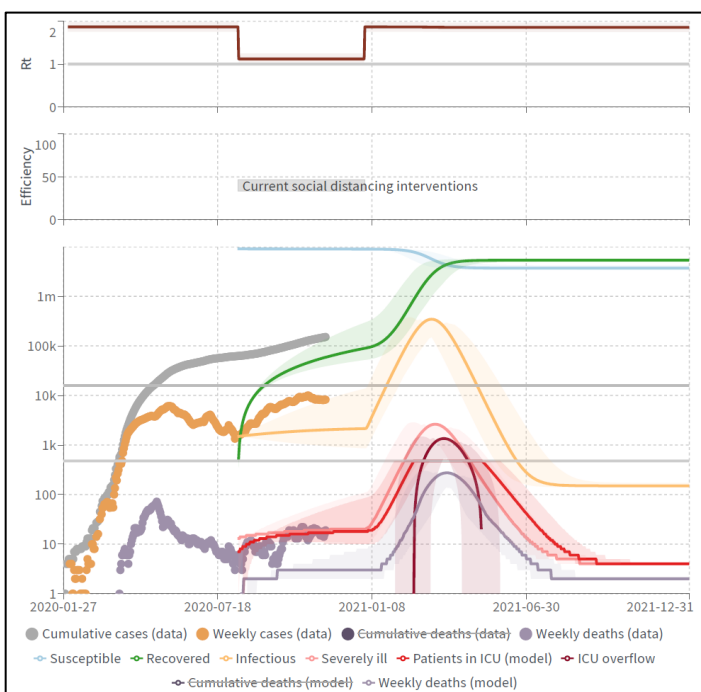
Figure 10: Scenario (C): Vertical Isolation shows that severe cases have decreased by 32%, and the death rates have decreased by 61%

4.3. Scenario (C): Vertical Isolation

In this scenario (Figure 10), some age groups were isolated to examine how this intervention will affect the model. The isolated age groups are 0 – 9 and 60 – 69. However, since full isolation will not be possible due to family and community contact, the isolation rate was kept at 90%. The result of this scenario shows the total severe cases decreased by 32% to 37.85k of the baseline, and the total death has decreased by 61% to 2.19k of the baseline. The following chart (Figure 9) shows how Scenario (C) decreased death rates in the 60 – 69 age group.

4.4. Scenario (D): Airport closure

In this scenario (Figure 11), the impact of new cases imported to the community was examined. Simulating this scenario, the number of imported daily cases was assumed to be zero. Scenario (D) shows that the impact of this intervention was only less than 1% on the outcome as total severe cases have decreased by 0.3% to 55.59k of the baseline. At the same time, the total death cases have decreased by 0.9% to 5.63k of the baseline. However, it shows the pandemic will end by the middle of 2021, probably after achieving herd immunity.
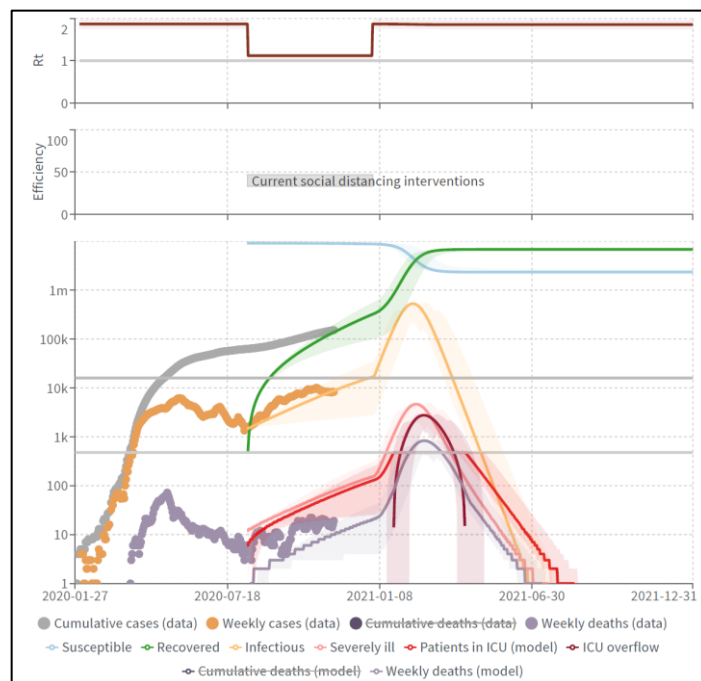
Figure 11: Scenario (D): Airport closure

4.5. Scenario (E): Extending the current intervention

This scenario examines extending the current intervention taken by the policy-makers and the community of the UAE. In order to simulate the impact of these interventions, several runs were conducted to create a similar growth trajectory for the actual weekly cases. It was found the actual weekly growth, starting from the second wave (10th August 2020), matches a 35% – 45% reduction, which means the current intervention is reducing transmission by 35% – 45%. In this scenario, the same rate was continued for as long as it took to flatten the curve. The result shows the peak will be reached by the second week of March 2021. However, it will take the curve much longer to flatten, which

should decrease the pressure on the health care system, as there will be no ICU overflow, and therefore, no extra ICU units will be needed. The simulation assumes the curve can be flattened by the second week of October 2022, regarding severe cases and deaths. Scenario (E) shows that the number of severe cases has decreased dramatically, by 68.8%, to 17.4k of the baseline, and the total deaths have decreased, by 73.1%, to 1.53k of the baseline.
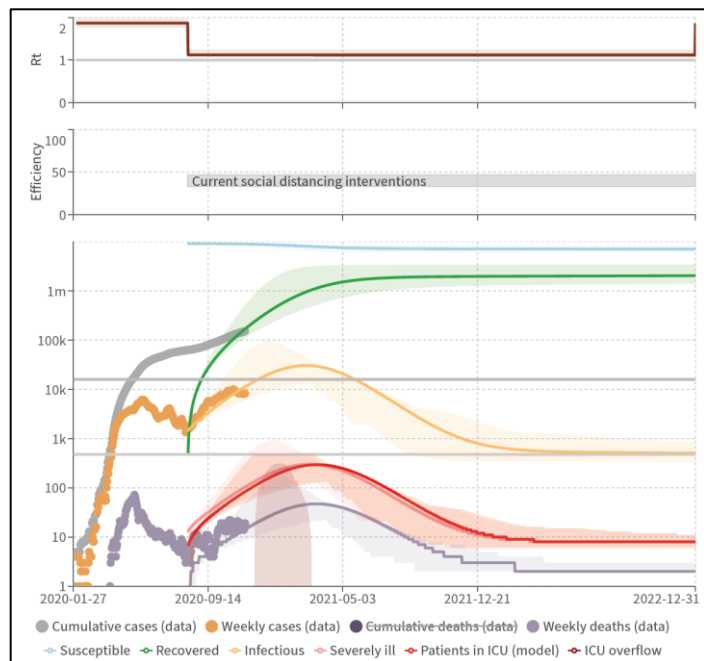
Figure 12: Scenario (E): Extending the Current Intervention
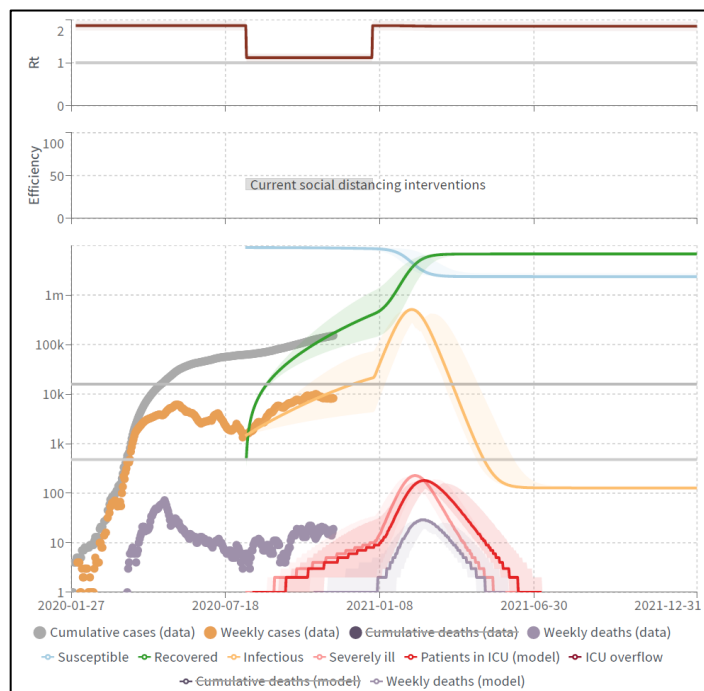
Figure 13: Scenario (F): Vaccinating the community

4.6. Scenario (F): Vaccinating the community

On 18th November 2020, [10] announced their COVID-19 vaccine to be 95% effective, beginning 28 days after the first dose. Many hope the vaccine will allow life to return to normal. The

scenario (F) simulation (Figure 13) assumes the entire community has been vaccinated against COVID-19. Therefore, all interventions are lifted at the beginning of 2021. The effectiveness of the vaccine was determined to be at 95%, meaning only 5% of the community could still be infected. The scenario, in this case, predicts the infection rate will reach its peak in the second week of February 2021, and a total of 501,000 people will have tested positive. However, most of these cases will be mild. This scenario shows that the total severe cases have decreased by 95% to 2.79k. In comparison, the total death cases have decreased by 96% to 228.5 of the baseline. The curve will be flattened in the third week of August 2021 at an average of 127 confirmed cases per week.

4.7. Scenario (G): Vaccinating the community and keeping the current interventions

In this scenario, we assume the whole community are vaccinated and have 95% immunity against the COVID-19. Nevertheless, the current interventions are still applied for as long as it takes to flatten the curve. The curve needed to be modelled for over three years. The outcome shows a 98.5% reduction in critical and death cases, with 910 critical cases and 82.5 death cases. The simulations also show the curve could be flattened in the second week of June 2022 at an average of 52k confirmed cases per week and 0 fatality rates afterwards.
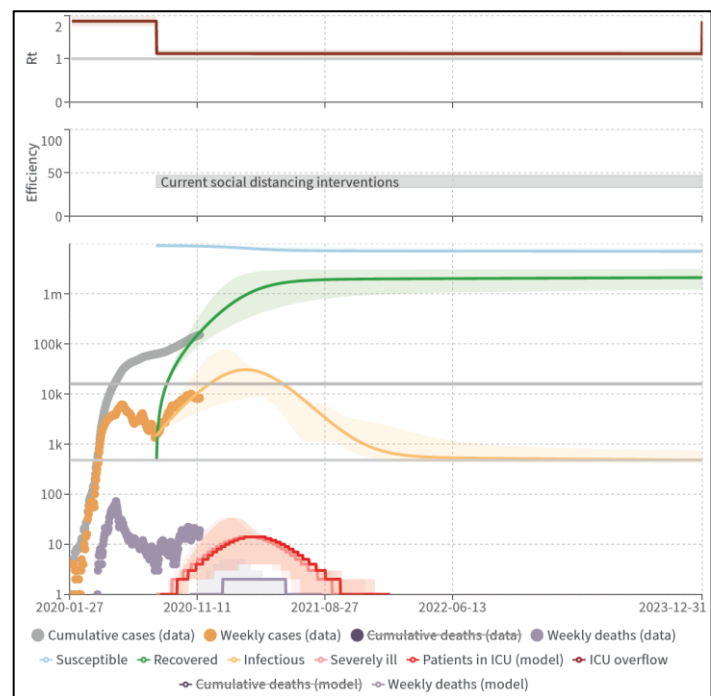
Figure 14: Scenario (G): Vaccinating the community and keeping the current interventions

5. Discussion

5.1. (A) The UAE is ready to go back to normal at the beginning of 2021.

The simulation shows it is still too early to go back to normal at the beginning of 2021. The going back to normal life scenario (A) shows that another wave is expected to rise, reaching a peak in 45 days with more than 5,000 deaths to be expected, part of which is caused by intensive care units' capacity overflow.

5.2. (B) The UAE can go back to normal, and the current healthcare system can handle all the cases.

Scenario (B) examines how many ICU units are needed to prevent death by lack of ICU capacities. The simulation indicates there will be a need of 3,124 additional ICU units (total of 3,600). Furthermore, that will only decrease the fatality rate by 16%. However, the scenario (A) is likely to be the shortest scenario to flatten the curve (Q3 2021), but it comes with the highest fatality rate.

5.3. (C) Vertical Isolation (isolating young and senior citizens) is similar to the do-nothing scenario.

On the other hand, the vertical isolation scenario (C) seems to have a noticeable impact on the simulation outcome. It decreases death rates by 61%, and the severe cases by 31%. Therefore, it cannot be assumed it is similar to the do-nothing scenario.

5.4. (D) Suspending entry to the UAE is necessary to contain and end the pandemic.

One significant finding of these simulations is the minor impact of the airport closure scenario (D). As it turns out, it only has a less than 1% impact on the simulation outcomes, which indicate it is not an effective intervention and has an insignificant impact in the context of the UAE parameters.

5.5. (E) Extending the current intervention should be the new normal, as it is essential to decrease severe and death cases.

Keeping the current interventions scenario (E) is still highly effective, as it has decreased both severe and fatality rates by nearly 70%.

5.6. (F) The vaccine will end the pandemic, and we can go back to normal life.

The long-awaited vaccine for COVID-19. However, the outcome of this scenario shows around a 95% decrease in severe and death rates. However, the remaining 5% can result in an average of 2.79k severe cases and 127 deaths. A significant finding of scenario (F) suggests the importance of keeping some sort of intervention for some time, even after getting vaccinated.

5.7. (G) We still need to keep the current interventions, even if the community is vaccinated.

The final tested hypothesis in this study is vaccinating the community while keeping the current interventions (G). The outcome of this simulation shows little impact as it decreased severe and deadly cases by only an additional 3.5% (total of 98%).

As an alternative, a key takeaway of this study is that no matter what interventions are taken, at least 154 cases will still be expected on a weekly bases. This is even under the assumption that the airport intervention is 99.9% effective, airline movement is 10% of normal (Figure 3), and 100% of positive cases are isolated.

6. Conclusion

George Edward Pelham once said, "All models are wrong, but some are useful". We hope this study will bring some useful insights to policy-makers in the community of the UAE.

Based on the current trajectory of the pandemic growth, the current intervention suggests its effectiveness is 35-45%. The pandemic daily cases curve is expected to be flattened around the fourth quarter of 2022. Moreover, relaxing intervention and going back to normal earlier than expected will cost the UAE health system to be ready with an average of 3,600 intensive care units. This assumption is not counting the different federal Emirates measures nor vaccine availability as there is still not enough data about when it will be made available.

It is highly encouraged to use the COVID-19 scenario model to simulate different parameters in different geographical locations. This simulation provides some key insights that can confirm some commonly known hypotheses and disapprove others.

Conflict of Interest

The authors declare no conflict of interest.

Acknowledgement

References

[1] G. Duncan, S. Gautam, "Coronavirus: UAE records first case – The National," The National News, 2020.

[2] WHO, Archived: WHO Timeline – COVID-19, World Health Organization, 2020.

[3] U.AE, National Disinfection Programme – The Official Portal of the UAE Government, 2020.

[4] S. Bentout, A. Tridane, S. Djilali, T.M. Touaoula, "Age-Structured Modeling of COVID-19 Epidemic in the USA, UAE and Algeria," Alexandria Engineering Journal, 2020, doi:10.1016/j.aej.2020.08.053.

[5] M. Mohammad, A. Trounev, C. Cattani, "The dynamics of COVID-19 in the UAE based on fractional derivative modeling using Riesz wavelets simulation," Zayed University, 2020.

[6] N.B. Noll, I. Aksamentov, V. Druelle, A. Badenhorst, B. Ronzani, G. Jefferies, J. Albert, R.A. Neher, "COVID-19 Scenarios: An interactive tool to explore the spread and associated morbidity and mortality of SARS-CoV-2," MedRxiv, 2020, doi:10.1101/2020.05.05.20091363.

[7] Worldometer, United Arab Emirates Population (2020) – Worldometer, 2020.

[8] FCSA, Statistics by Subject, Federal Competitiveness and Statistics Centre, 2020.

[9] M. Chinazzi, J.T. Davis, M. Ajelli, C. Gioannini, M. Litvinova, S. Merler, A. Pastore y Piontti, K. Mu, L. Rossi, K. Sun, C. Viboud, X. Xiong, H. Yu, M. Elizabeth Halloran, I.M. Longini, A. Vespignani, "The effect of travel restrictions on the spread of the 2019 novel coronavirus (COVID-19) outbreak," Science, **368**(6489), 395–400, 2020, doi:10.1126/science.aba9757.

[10] Pfizer, Pfizer and BioNTech Conclude Phase 3 Study of COVID-19 Vaccine Candidate, Meeting All Primary Efficacy Endpoints | Pfizer, 2020.

Model of Fish Cannery Supply Chain Integrating Environmental Constraints (AHP and TOPSIS)

Sana Elhidaoui[*, 1, 2], Khalid Benhida[1], Said Elfezazi[1], Yassine Azougagh[1], Abdellatif Benabdelhafid[3]

[1]*LAPSSII, EST of Safi, Cadi Ayyad University, 46000, Morocco*

[2]*DCS: Engineering Sciences, faculty of science and technology, Cadi Ayyad University Marrakesh, 40000, Morocco*

[3]*Universiapolis, Agadir, 80000, Morocco, & Le Havre Normandy University, France*

A R T I C L E I N F O	A B S T R A C T
	This paper proposes a modeling framework (analytical modeling) for the case of fish cannery supply chain (FCSC) to optimize the environmental impact of the set of its processes; indeed, for our knowledge, there were few studies attempting to address this case study as a model of green supply chain. Implementation of the proposed model is done using first MCDM methods (AHP, TOPSIS) in order to select and classify processes and the corresponding environmental impact, as well as dealing with environmental analysis. Furthermore; a flowchart is proposed as an addition to improve the other processes in terms of reducing environmental impact, and the numerical resolution is carried out using the LINDO software. The proposed framework will guide researcher both as well as practitioners in establishing an optimal model for the green fish cannery supply chain (FCSC).

1. Introduction

In logistic field, most of researchers aim to meet the challenge of integrating new scientific data in terms of methods, software, managerial solution, to support supply decision making, furthermore environmental dimension is among the most attractive area of study to deal with. Nowadays, a set of supply chain (SC) models have been proposed in the literature, integrating the environmental dimension, using various modeling tools and methods [1]-[4]. Mainly; this paper proposes a modeling framework of the fish cannery supply chain (FCSC), by integrating the environmental constraints and it contributes in helping and assisting researchers, as well as practitioners to establish a global model of the green fish cannery supply chain (FCSC), where few articles seek to tackle modeling studies in this area of study, particularly as an industrial supply chain [5]-[7], followed by a numerical resolution using the LINGO software. The remainder of the paper starts with a relevant literature review, which typically tackle the cannery fish supply chain (FCSC), and the main keywords in section 2.

And subsequent to a detailed description of the case study in Section 3. The model formalization and discussion are addressed in Section 4. Section 5 provides the numerical resolution, while

Section 6 addresses the conclusion, limitations and future research direction.

2. Literature Review

2.1. Fish cannery supply chain

The Agri-food industry, in particular the fish cannery industry, is chosen as a case study. Generally, there are many kinds of fish, such as sardines and mackerel, which are among the most consumed fish in the Mediterranean region [8]; While in tropical and subtropical oceans, western and central pacific ocean (in particular Asian country) tuna is the most common cannery industry, Southeast Alaska and Puget Sound, Washington State, USA are known by salmon fish etc. One must bear in mind the time constraint since this industry is almost seasonal, operation is limited to about 3 months in a year for salmon [7], and up to 9 months/year for the other types. In this case study objectives are established as to demonstrate the applicability of the model whatever the purposes, and to visualize its added value on the one hand, by treating a case of an area rarely addressed in research as an industrial SC.

The environmental constraints or impact resulting from this type of industry is treated separately from its modeling. Among the most significant and widespread environmental impact of this

industry: water pollution, or wastewater [9]-[11], waste fish [7], most of research works that deal with this impact propose solutions to minimize it. On the other hand, fish processing waste has an interesting energy value. The increase of the aforementioned wastes as well as the increasing of the renewable energy market confirms that this waste could have a place as a future source of biofuels [12].

Furthermore; and for our knowledge, there is no standard model for this type of industry as a whole SC case study. In [6] the authors have dealt with the fish cannery industry, notably the case of tuna, under a model that encompasses multiple fishing fleets including canneries, in the form of scenarios by exploiting the future results of the world tuna fishery through a simple presentation: climate change effects, changes in global tuna demand, and changes in access to fishing areas. Also an optimization, mathematical model is reported by authors of [7], which aims to optimize food portion in packaging, actually the model is presented in a case study of a cannery portion of fish. We notice well that these two examples consist in treating this type of SC in the manner that the raw material is of exhaustible nature (in the biological way also), which strongly supports the scarcity of research works dealing with a global model of the green industrial SC (including all environmental impact), particularly the proposed case study.

2.2. MCDM method: AHP and TOPSIS

MCDM (Multi-Criteria Decision Making) gathers a set of sophisticated methodological tools to assist in decision making to cope with complex decisions. It is a powerful method for evaluating and ranking one or more customized solution from a set of options that consider multiple indicators, which are typically contradictory. In particular, it allows us to highlight conflicts within the metric indicators, to identify an effective and structured framework and, finally, to make the holistic trade-offs necessary to reach a decision"[13].

AHP (Analytic hierarchy process) method is among the MCDM tools, to hierarchize criteria in order to achieve a specific goal, where scores of all criteria are grouped into a unique aggregate score. In literature, there is a considerable amount of research work that has used the AHP method either to evaluate performance of the green SC [14], [15] and for ranking the key performance indicators [16], also for assessment of the sustainability of the SC [17], or for the risk assessment [18], [19], commonly AHP is well-known for supplier selection [20]-[22], also it's applied in reverse logistics.

TOPSIS (technique for order preference by similarity ideal solution) has been proposed for the first time by [23]. TOPSIS is an effective method to solve existing problems of multi-attribute decision making with finite alternatives. The concept of this method is to classify the alternatives by calculating the distance of each alternative in relation to the ideal solution and the ideal negative solution of the problems in order to determine the optimal alternative. These ideal and negative-ideal solutions are calculated in considering other alternatives [24].

Most of papers utilized both AHP followed by TOPSIS which is preferred in comparison, [25]. In [26], authors applied the robust Analytical Hierarchy Process (AHP)-Fuzzy and TOPSIS for the

evaluation and selection of contractors [27] the Fuzzy Analytical Hierarchy Process (FAHP) and (TOPSIS) is used to evaluate performance, and particularly in the selection of reverse logistics service [28]. In notably, this paper exclusively applies these two methods for the classification of processes and their environmental impacts.

In the following paragraph, a model of the (FCSC) is presented. Furthermore, the two methods: AHP and TOPSIS would be used, in order to classify the environmental impacts and the SC's processes.

3. Case study

This section presents a case study of the fish cannery industry, this option of industry is exclusively treated as a SC model in this paper in addition most of the research works focus on the biological aspect in studying this case study. Data is collected from 4 anonymous companies of the fish cannery industry in the same city in Morocco, preserving all the needed information, with the aim to establish a model of green (FCSC), which may help industrialists in this field, in the one hand, and researchers in the future, in the other hand, by providing a global framework of green SC modeling. Therefore, this type of industry is characterized by a set of activities from fish procurement to distribution.

After a five-month visit to the four companies, we have collected data related to each process of this SC, these processes may change in terms of appointment from one company to another, but the activities remain the same. Reception of raw materials from suppliers (different) and distribution of final product to a limited number of destinations (clients, retailers…). These companies use only Small fish species such as sardines. The set of processes is presented in fig.1 below, we opted for this organizational chart in order to highlight the objective of this paper, namely to meet the optimization of environmental constraints in SC modeling. Particularly, the fig.1 below shows the impact of waste water at all levels (till the process of cooling):
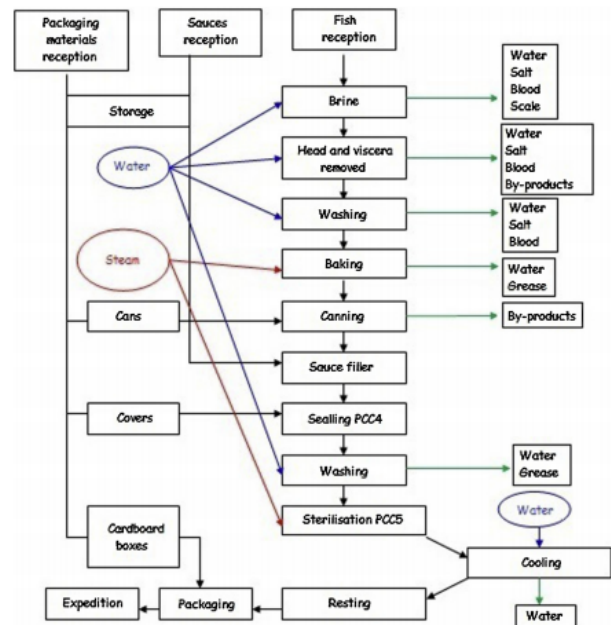
Figure 1: Fish canning industry supply chain (flow chart) [10]

3.1. Description

Hereafter a detailed description of the SC's characteristics, and the common elements between the four companies, all these data could be used in the resolution of the models, and to establish an action plan (improvement). In the next sections collected data are also used in AHP and TOPSIS (Water consumption, energy consumption, noise …).

Table 1: Case study data collection

Time sheet	- The delivery of final products and raw materials is done by a limited number of paths, and runs constantly 24h/24h -The plant works 8 hours a day, 6 days a week (8h/24h normal, 6d/7d)
Production site and platform	-Each company is composed of 2 production sites (only one site works when the total quantity doesn't exceed 8tonnes) -A physical systems for receiving the raw material from the logistics platform
Procurement	- Procurement of the fish quantity varies between 2 trucks to 4 trucks, each of which has a maximum capacity of 12 tonnes (minimum 4 tonnes).
Water and energy consumption	- The average monthly water consumption is 1400 m³ -Electrical energy(Total consumption per tonne): 86Kw/tonne
Processes	-10 processes (as shown in fig.1) only are taken into account
Raw materials	-Fish, brine and spices, oil, boxes, cartons, tomato sauce, detergents, coal, lead (for marking) -Total quantity of raw material (fish): [8tones, 48tonnes]

3.2. Material and Method

This type of SC promotes mathematical modeling, given the nature of its well-defined and flexible activities to model them mathematically. As evoked at the beginning of this paper, the analytical modeling has opted for, by proposing a mathematical model to an objective function which minimizes the environmental impacts, and helps in decision making, regarding the actions to be undertaken. For the mathematical model, only impacts whose parameters can be used in mathematical modeling are retained. In addition, for the identification of the significant impact, the TOPSIS method is used in order to hierarchize processes according to their criticality regarding environmental impacts as to classify

them from the worst alternative, also by further using the AHP method to classify the different environmental impacts and then using this ranking in TOPSIS method.

3.3. Identification of environmental Constraints

The environmental analysis presents a set of steps to be followed, to achieve a set of aspects, and significant impacts, of the different processes or activities of the SC. In addition the environmental analysis is required by ISO14001 standard, but it is indeed an optional direction. In this case study, we are interested in tackling, the most relevant significant impact regarding the critical activities or processes, and as we have previously mentioned, we opted for the AHP and TOPSIS methods which allows us to inherit the desired criteria, in a fuzzy environment to assist in the selection of processes and environmental impact.

Our main goal from AHP method is to classify criteria according to their criteria weight, the criteria adopted, according to the companies' experts of our case study, are the most relevant to prioritize in order to conduct a study of the most significant environmental impacts, namely: water consumption, energy consumption, noise, effluent discharge, air pollution, and then the ranking result are further used in TOPSIS, which is chosen to rate and compare processes alternatives in a fuzzy environment, to be taken into account in our modeling.
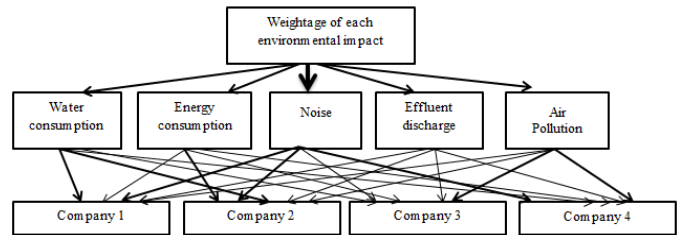
Figure 2: The structure of AHP method

3.4. AHP Method

A hierarchical structure is constructed using five criteria and four alternatives through the literature review and taking opinions from the four experts from each company. In order to achieve the main goal (namely: weight of the selected environmental impacts).

The pairwise comparison matrix determines the relative importance (table 2) of different attributes or criteria with respect to the goal, in table 3 below:

Table 2: Scale of relative importance

1	Equal importance
3	Moderate importance
5	strong importance
7	Very strong importance
9	Extreme importance
2,4,6,8	Intermediate value
1/3, 1/5, 1/7, 1/9	Value for inverse comparison

The normalized pair-wise matrix is elaborated in table 4. The new pair-wise matrix as shown below in table 5 is established by calculating the weighted sum value and each criterion weight with its rate:

Table 3: Pair-wise comparison matrix

	Water consumption	Energy consumption	Noise	Effluent discharge	Air pollution
Water consumption	1	1 /2	7	2	5
Energy consumption	2	1	5	2	5
Noise	1/7	1/5	1	1/5	1/3
Effluent discharge	1 /2	1 /2	5	1	3
Air pollution	1/5	1/5	3	1/3	1
Sum	3.84	2.4	21	5.53	14.33

Table 4: Normalized pair-wise matrix

	Water consumption	Energy consumption	Noise	Effluent discharge	Air pollution	Criteria weight
Water consumption	0.26	0.21	0.33	0.362	0.35	0.3024
Energy consumption	0.53	0.416	0.24	0.362	0.35	0.38
Noise	0.04	0.083	0.05	0.04	0.023	0.05
Effluent discharge	0.053	0.21	0.24	0.2	0.21	0.183
Air pollution	0.052	0.083	0.143	0.06	0.07	0.082
Sum	3.84	2.4	21	5.53	14.33	

Table 5: New pair-wise matrix (non-normalized)

	Water consumption	Energy consumption	Noise	Effluent discharge	Air pollution	Weighetd Sum Value	Criteria weight	Rate
Water consumption	0.302	0.19	0.35	0.366	0.41	1.62	0.3024	5.36
Energy consumption	0.604	0.38	0.25	0.366	0.41	2.01	0.38	5.29
Noise	0.043	0.08	0.05	0.0366	0.03	0.21	0.05	4.2
Effluent discharge	0.151	0.2	0.25	0.183	0.25	1.034	0.183	5.65
Air pollution	0.06	0.08	0.15	0.06	0.082	0.432	0.082	5.27

Table 6: Standard of RI

N	1	2	3	4	5	6	7	8	9	10
RI	0.00	0.00	0.58	0.90	1.12	1.24	1.32	1.41	1.45	1.49

The relative weights are given by the eigenvector (w) corresponding to the maximum eigenvalue (λmax), such as :

$$\lambda max = (5.36+5.29+4.2+5.65+5.27)/5 = 5.154$$

A consistency index (CI) is calculated. Equation (1) describes the formula for the coherence index. The consistency ratio (CR) is calculated. Indeed, the CR allows checking if the evaluations are

consistent or not. The CR can be determined by taking the ratio of the CI and the random index (RI).

Consistency index (C.I.)

$$(\lambda max - n)/(n-1)$$

$$C.I = (5.154-5)/(5-1) = 0.04$$

Consistency Ratio

C.I/ RI=0.04/1.12=0.034 <0.10 => so our matrix is **reasonably consistent**

Table 7 presents the result of criteria ranking:

3.5. TOPSIS Method

Define abbreviations and acronyms the first time they are used in the text, even after they have been defined in the abstract. Do not use abbreviations in the title or heads unless they are unavoidable. The TOPSIS method is used to classify (rate) processes according to the selected environmental impact, then to use them in the model formalization, for this case study only some environmental impacts are used in mathematical modeling, regarding priorities given by experts.

Table 7: Criteria ranking

Criteria	Criteria weights	Rank
Water consumption	0.3024	**2**
Energy consumption	0.38	**1**
Noise	0.05	**5**
Effluent discharge	0.183	**3**
Air pollution	0.082	**4**

Table 8: Selection of the best

	Attribute/criteria	Water consumption m3/tone	Energy consumption(l/tone; Kw/ton)	Noise	Effluent discharge	Air pollution
Alternatives	Transportation and reception	0,002	14,82	62	3	5
	Brine process	1,600	20	66	4	2
	Head and viscera removed process	0,71	12	64	5	2
	Washing	1,8	12	65	4	2
	Baking	2,68	22,22	92	5	5
	Canning	0,04	5	89	3	2
	Sauce filler	0,01	4,22	67	3	3
	Sealing PCC4	0,001	6,40	88	3	2
	Washing	0,48	6	89	4	2
	Sterilization	0,27	7	65	3	3
	Cooling process	0,003	16	64	2	4
	Packaging	0,001	6	62	4	2
	$\sqrt{\sum_{j=1}^{n} X_{ij}^2}$	3,7137	43,1524	255,0931	12,7671	10,5830

The transformation of units among various criteria into common measurable units to allow comparisons between criteria. Then, the normalized values of the alternatives are determined X_ij is the numerical score of alternative j on criterion i. The corresponding normalized value $\overline{X}_{ij}$ is defined as follows :

$$\overline{X}_{ij} \square \frac{x_{ij}}{\sqrt{\sum_{j=1}^{J} x_{ij}^2}} \text{ with: i=1,2, 3,....n and j=1,2, 3,....m ;}$$

Table 9: Non measurable criteria scale

Point scale	
Low	1
Below average	2
Average	3

Big	4
Very big	5

Vector normalization: $\overline{X}_{ij} = \frac{x_{ij}}{\sqrt{\sum_{j=1}^{n} x_{ij}^2}}$ (1)

The weighted normalized decision matrix vij can be calculated by multiplying the normalized evaluation matrix $\overline{X}_{ij}$ by its associated weight wi to obtain the result:

$$\text{vij} = \text{wi} * \overline{X}_{ij} \quad \text{with : i=1,2, 3,....n} \quad (2)$$

and j=1,2, 3,....m ;

$$\text{and } \sum_{i-1}^{n} w_i = 1 \quad (3)$$

Table 10: Normalized decision matrix

Attribute/ criteria	Water consumption m3/tone	Energy consumption (l/tone; Kw/ton)	Noise	Effluent discharge	Air pollution
Transportation and reception	0,0005	0,3434	0,2430	0,2350	0,4725
Brine process	0,4308	0,4635	0,2587	0,3133	0,1890
Head and viscera removed process	0,1912	0,2781	0,2509	0,3916	0,1890
Washing	0,4847	0,2781	0,2548	0,3133	0,1890
Baking	0,7217	0,5149	0,3607	0,3916	0,4725
Canning	0,0108	0,1159	0,3489	0,2350	0,1890
Sauce filler	0,0027	0,0978	0,2626	0,2350	0,2835
Sealing PCC4	0,0003	0,1483	0,3450	0,2350	0,1890
Washing	0,1293	0,1390	0,3469	0,3133	0,1890
Sterilization	0,0727	0,1622	0,2548	0,2350	0,2835
Cooling process	0,0008	0,3708	0,2489	0,1567	0,3780
Packaging	0,0003	0,1390	0,2430	0,3133	0,1890

Table 11: Weighted Normalized decision matrix

Weightage	0,3024	0,38	0,05	0,183	0,082	S_j^+	S_j^-	P_j
Attribute/ criteria	Water consumption m3/tone	Energy consumption (l/tone; Kw/ton)	Noise	Effluent discharge	Air pollution			
Transportation and reception	0,000163	0,131	0,012	0,043	0,039	0,097	0,229	0,702
Brine process	0,130285	0,176	0,013	0,057	0,015	0,193	0,094	0,329
Head and viscera removed process	0,057814	0,106	0,013	0,072	0,015	0,099	0,185	0,651
Washing	0,146571	0,106	0,013	0,057	0,015	0,164	0,118	0,419
Baking	0,218228	0,196	0,018	0,072	0,039	0,274	0,000	0,000
Canning	0,003257	0,044	0,017	0,043	0,015	0,017	0,266	0,940
Sauce filler	0,000814	0,037	0,013	0,043	0,023	0,016	0,271	0,943
Sealing PCC4	0,000081	0,056	0,017	0,043	0,015	0,024	0,261	0,914

Washing	0,039086	0,053	0,017	0,057	0,015	0,051	0,231	0,819
Sterilization	0,021986	0,062	0,013	0,043	0,023	0,037	0,240	0,867
Cooling process	0,000244	0,141	0,012	0,029	0,031	0,105	0,229	0,686
Packaging	0,000081	0,053	0,012	0,057	0,015	0,033	0,262	0,889
V_1^+	0,000081	0,037	0,012	0,029	0,015			
V_1^-	0,218228	0,196	0,018	0,072	0,039			

V_1^+ **Ideal best value**: correspond to the minimum value (because we are interested in minimizing impact)

V_1^- **Ideal worst value**: correspond to the maximum value (because we are not interested in maximizing impact)

Euclidean distance from ideal best and worst:

$$S_j^+ = \left[\sum_{j=1}^m \left(V_{ij} - V_j^+ \right)^2 \right]^{0.5} \quad (4)$$

$$S_j^- = \left[\sum_{j=1}^m \left(V_{ij} - V_j^- \right)^2 \right]^{0.5} \quad (5)$$

$$P_i = \frac{s_i^-}{s_i^+ + s_i^+} \quad (6)$$

For the P_j must be ranked in ascending order, as long as our goal is to classify the most activities that generate more environmental impacts. A set of alternatives can then be ranked in order of preference in descending order of P_i.

Table 12: Criteria (processes) ranking

Attribute/criteria	S_j^+	S_j^-	P_j	Rank
Transportation and reception	0,097	0,229	0,702	6
Brine process	0,193	0,094	0,329	2

Attribute/criteria	S_j^+	S_j^-	P_j	Rank
Head and viscera removed process	0,099	0,185	0,651	4
Washing	0,164	0,118	0,419	3
Baking	0,274	0,000	0,000	1
Canning	0,017	0,266	0,940	11
Sauce filler	0,016	0,271	0,943	12
Sealing PCC4	0,024	0,261	0,914	10
Washing	0,051	0,231	0,819	7
Sterilization	0,037	0,240	0,867	8
Cooling process	0,105	0,229	0,686	5
Packaging	0,033	0,262	0,889	9

Based on the results of the TOPSIS method, "baking" is identified as the most critical process to be considered in the modeling. The table 13 below contains the set of significant aspect and related significant impacts, according to each selected process, this study is carried out, with the help of expert panel:

Table 13: Significant aspects and impacts

Activities	Aspects	Impacts
Baking	-Water consumption -Energy consumption(coal) -Emission of gaseous pollutants (greenhouse gases, CO2 ... etc.) -Noise - Liquids or solid wastes -Coal splinters	-Wastewater -Consumption of non-renewable energy -Noise pollution -Pollution of ambient air - Destruction of the ozone layer, and global warming - Flow towards the natural environment
Brine process	-Water consumption -Energy consumption(electricity) - Liquids or solid wastes -Accidental spills	-wastewater -Exhaustion of non-renewable energies -Pollution of ambient air
Washing	-Water consumption -Energy consumption (electricity) -Noise	-Wastewater (Water stress)and water pollution -Contamination of ground, and water surface. -Noise pollution -Exhaustion of non-renewable energies

Head and viscera removed process	- Liquids or solid wastes -The raw material splinters -Energy consumption (electricity) -Water consumption	- Contamination of ground, and water surface. -Exhaustion of non-renewable energies -Wastewater (Water stress)and water pollution
Cooling process	-Use of refrigerant gases -Air pollution -Energy consumption (electricity) -Water consumption -Noise	-Using the product generated from persistent waste in the environment. -Wastewater -Noise pollution -Exhaustion of non-renewable energies
Transportation reception	-Emission of gaseous pollutants (greenhouse gases, CO2 exhaust gases, etc.) -Consumption of fuels -Possibility of accidental dispersion -Atmospheric emissions due to fuel combustion	- Destruction of the ozone layer, and global warming -Exhaustion of non-renewable energies - Damage for people -Atmospheric pollution -Contamination of soil, surface water. -Pollution of ambient air
Sterilization	-Energy consumption (electricity) -Emission of gaseous pollutants (greenhouse gases, CO2 exhaust gases, etc.) -Noise -Water consumption	-Exhaustion of non-renewable energies -Destruction of the ozone layer, and global warming -Noise pollution -Wastewater
Sealing PCC4	-Energy consumption (electricity) -Possibility of accidental dispersion -Noise	-Exhaustion of non-renewable energies -Contamination of soil, surface water. -Noise pollution
Canning	-Energy consumption (electricity) -Noise - Liquids or solid wastes	-Exhaustion of non-renewable energies -Noise pollution - Contamination of ground, and water surface.
Sauce filler	-Energy consumption (electricity) -The raw material splinters -Noise	-Exhaustion of non-renewable energies -Contamination of ground -Noise pollution

4. The model Formalization

In the model formalization phase, and after selecting the method/tool to be applied, as well as the identification of the significant impacts, all the model elements are presented below:

Hypothesis and constraints

-Non-regularity of procurement

-Persistence of the raw material

Sets

J: Set of processes j of the SC.

I: Total energy consumption (type)

Parameters

- W_j : Water consumption in process j.

- d_j : Processing time of the quantity Qj of raw material (product) used in process j.

- $E_{e,j}$: Electrical energy consumption in process j.

- $E_{f,j}$: Energy (fuel) consumed in process j.

Decision Variables

- Q_j : Quantity of raw material (product) used in process j.

Data

- $E_{f,tot}$: Total energy (fuel oil) consumed (l/tone).

- $E_{e,tot}$: Total electrical energy consumed (kw/tone).

- W_{Tot} : Total quantity of water consumed (m3/tone).

- Q_{Tot} : Total amount of raw material per day.

-n_0 : The number of baking ovens available at the plant.

-Q_0 : Maximum amount of raw material to be baked in n0 oven.

-P_j: Percentage of water consumption of process water j.

- **D**: Total processing time of Qj from raw material to final product

Objective Function

For environmental impact of noise and effluent discharge, a set of actions is proposed to improve and to optimize theses impacts in Fig.3 below. Hereafter the objective function "(1)" that minimizes the environmental impact of the selected processes, by taking into account various variables as the quantity of raw material, etc.

NB: The environmental impact of water consumption, in transport and reception process, is excluded due to the negligible volume of water consumed during this process.

$$Max(z) = \sum_{j=1}^{n} Q_j d_j \qquad \text{With } j=1,2,\ldots6 \qquad (7)$$

Constraints

- Constraint of electrical energy consumption

$$\sum_{j=1}^{n} E_{e,j}\, Q_j \le E_{e,tot} Q_{Tot} \qquad (8)$$

- Constraint of maximum quantity to be processed in the baking process:

$$Q_j \le n_0 Q_0 \qquad (9)$$

- Water consumption percentage constraint for all processes j:

$$\sum_{j}^{n} P_j\, Q_j \le 100 \times Q_{Tot} \qquad (10)$$

- Water consumption constraint for all processes j :

$$\sum_{j}^{n} W_j\, Q_j \le W_{Tot} \times Q_{Tot} \qquad (11)$$

- Constraint of energy consumption of transport and baking processes (fuel oil):

$$\sum_{j=1}^{n} E_{f,j}\, Q_j \le E_{f,tot} Q_{Tot} \qquad (12)$$

- Constraint on the total quantity of raw material to be processed Qj:

$$\sum_{j}^{n} Q_j \le Q_{Tot} \qquad (13)$$

- Constraint of the total processing time from raw material Qj to finished product:

$$\sum_{j=1}^{n} d_j \le D \qquad (14)$$

The objective function (1) maximizes the amount Qj of raw material to be transformed during each of the six processes in order to minimize the energy consumed and the amount of water consumed. Constraints (2) and (6) ensure that the energy consumed by each process for the transformation of the quantity Qj of raw material versus the total energy consumed is satisfied. Constraint (3) limits the available backing capacity. Constraints (4), (5) determine respectively the percentage and quantity of water consumed for each process j. Constraints (7) and (8) determine respectively the total daily quantity and the processing time.

The proposed model is a mathematical linear programming model whose objective function is to minimize the following environmental impact: Energy and water consumption. All parameters, data and decision variables may be adjusted according to the studied SC; it is also conceivable to include other constraints. Indeed, the proposed model is quite streamlined and has not addressed all potential conditions or assumptions. The flow chart in fig.3 below is designed as an improvement action to monitor all environmental impacts, in particular noise, and effluents discharge. In the next section, a numerical resolution of this model is proposed.

5. Numerical resolution

The numerical resolution is performed using the LINGO software (from LINDO SYSTEM INC).Data: (for the transformation of the quantity QJ of the raw material.

Table 14: Numerical data of the studied supply chain

Processes	J	Processing time of one tone of raw material (min)	Energy (electric, fuel oil) consumed (kw/tone, l/tone)	% of water consumption	Water consumption (m³/tone)
Baking	1	67	22.22	0.3	2.68
Brine process	2	60	20	0.2	1.6
Washning	3	15	6	0.8	0.48
Head and viscera removed process	4	60	12	-	-
Cooling process	5	120	16	-	-
Transport and reception	6	10	14.84	-	-
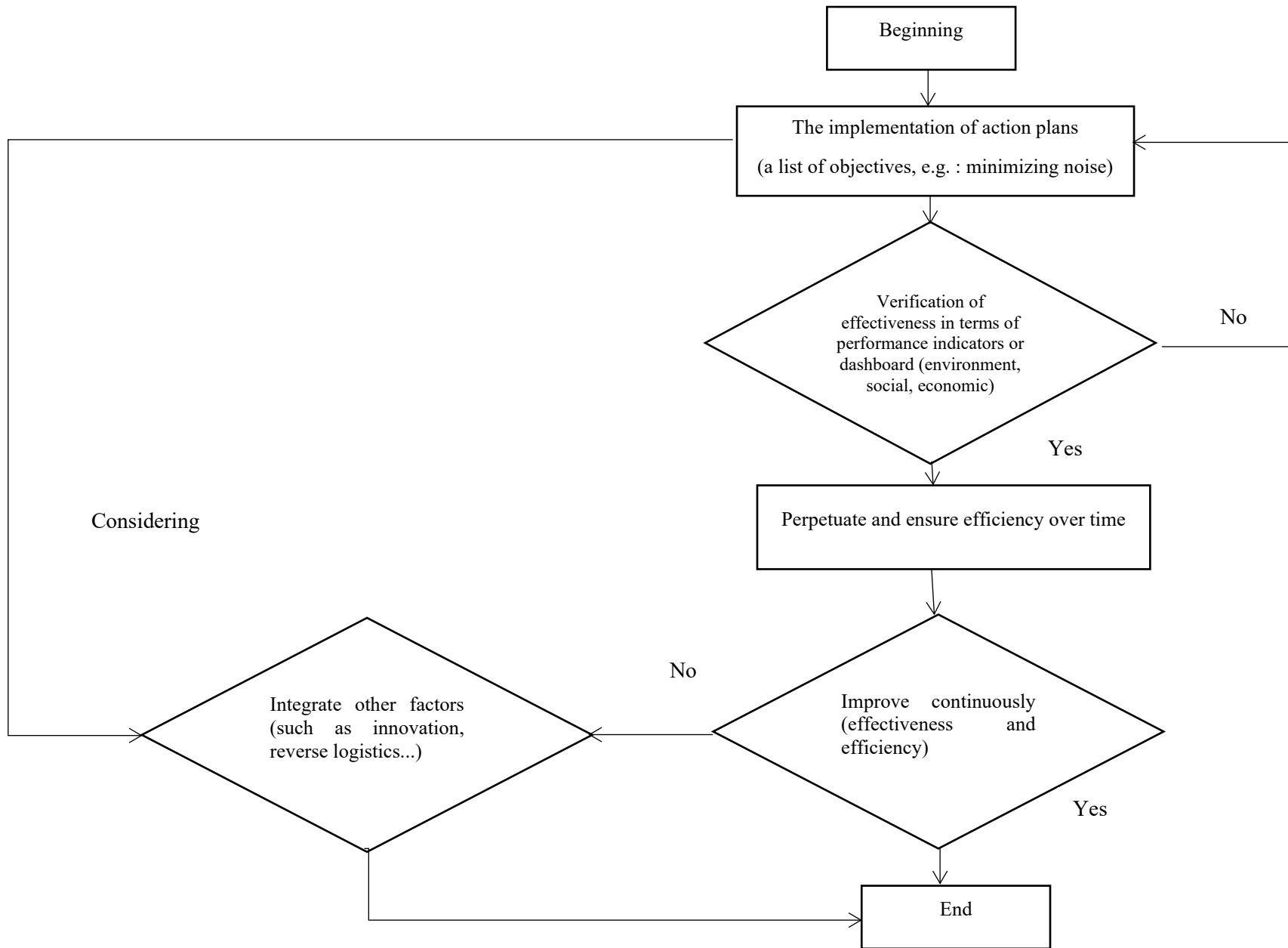
Figure 3:flow chart for the monitoring of the environmental impacts

The objective function :

$$MAX=67*Q1+60*Q2+15*Q3+60*Q4+120*Q5+10*Q6 \quad (15)$$

Contraints :

$$20*Q2+6*Q3+12*Q4+16*Q5<=86; \quad (16)$$

$$Q1<=4.032; \quad (17)$$

$$0.3*Q1+0.2*Q2+0.08*Q3<=1*QTot; \quad (18)$$

$$2.68*Q1+1.6*Q2+0.48*Q3<=6.63; \quad (19)$$

$$22.22*Q6+14.84*Q1<=37; \quad (20)$$

$$Q1+Q2+Q3+Q4+Q5+Q6<=28; \quad (21)$$

The objective of this section is to present the application of our mathematical model, by proposing numerical examples. The problem is solved by LINGO 18, on a computer with 1.83 GHz and 2 GB RAM:

Global optimal solution found.

Objective value:	810.8794
Infeasibilities:	0.000000
Total solver iterations:	4
Elapsed runtime seconds:	1.16

For the values of Qj:

Variable	Value	Reduced Cost
Q1	2.473881	0.000000
Q5	5.375000	0.000000

We notice that the optimal quantity (to reduce water and energy consumption) of the raw material or semi-finished product in the baking process is: Q1=2.473881tone, for the duration of 67min, and for the cooling process Q5=5.375000 tone for the duration of 120 min (2h).

6. Conclusion

The research on green SC modeling has been flourishing, in recent years, but continues to require more and more in-depth research for future studies. Nevertheless, when it comes to academicians, and industrialists, the aim of achieving an optimal model of the green supply chain is very challenging to decide which methods or tools are suitable. On the one hand, this paper provides a theoretical contribution to the body of literature, to our knowledge, there is virtually no model of the (FCSC) that takes into account all environmental impacts. In the other hand, it has some managerial implications, the proposed model can be deployed by supply chain managers, as it demonstrated in the case of fish cannery, and also the result of implementation of this model on this case study can be exploited in other fields of application.

The paper starts with literature review of the main terminology such as the (FCSC). Next, it invests in a case study which is less often dealt with as a whole supply chain, namely the case of a fish cannery, where the paper further uses relevant methods in doing so, like AHP and TOPSIS.

Moreover, the proposed mathematical model aims to minimize the identified significant impacts, and as for some directions of future research, it would be interesting to deal with other software for the model resolution, even further to include the social and economic hypotheses in order to address the whole sustainable (FCSC) modeling. The proposed framework may also serve as a preliminary approach for modeling the green supply chains regardless of their nature.

References

[1] A.J.C. Trappey, C. V. Trappey, C.T. Hsiao, J.J.R. Ou, C.T. Chang, "System dynamics modelling of product carbon footprint life cycles for collaborative green supply chains," International Journal of Computer Integrated Manufacturing, **25**(10), 934–945, 2012, doi:10.1080/0951192X.2011.593304.

[2] F. Gautier, P. Lacomme, P. Pariente, S.K. Tchomte, N. Tchernev, "Linear model for supply chain operational planning and carbon footprint optimization," Supply Chain Forum, **14**(2), 40–53, 2013, doi:10.1080/16258312.2013.11517314.

[3] Ole Ottemöller, "Modelling Change in Supply Chain Structures and its Effect on Freight Transport Demand," Schriftenreihe Des Instituts Für Verkehr, **38**(April 2017), 2017.

[4] W. Guo, Q. Tian, Z. Jiang, H. Wang, "A graph-based cost model for supply chain reconfiguration," Journal of Manufacturing Systems, **48**(March), 55–63, 2018, doi:10.1016/j.jmsy.2018.04.015.

[5] S. Tabrizi, S.H. Ghodsypour, A. Ahmadi, "Modelling three-echelon warm-water fish supply chain: A bi-level optimization approach under Nash–Cournot equilibrium," Applied Soft Computing Journal, **71**, 1035–1053, 2018, doi:10.1016/j.asoc.2017.10.009.

[6] C. Mullon, P. Guillotreau, E.D. Galbraith, J. Fortilus, C. Chaboud, L. Bopp, O. Aumont, D. Kaplan, "Exploring future scenarios for the global supply chain of tuna," Deep-Sea Research Part II: Topical Studies in Oceanography, **140**, 251–267, 2017, doi:10.1016/j.dsr2.2016.08.004.

[7] F.K. Omar, C.W. De Silva, "Optimal portion control of natural objects with application in automated cannery processing of fish," Journal of Food Engineering, **46**(1), 31–41, 2000, doi:10.1016/S0260-8774(00)00068-6.

[8] V. Ferraro, A.P. Carvalho, C. Piccirillo, M.M. Santos, P.M. Paula, M. E. Pintado, "Extraction of high added value biological compounds from sardine, sardine-type fish and mackerel canning residues - A review," Materials Science and Engineering C, **33**(6), 3111–3120, 2013, doi:10.1016/j.msec.2013.04.003.

[9] P. Chowdhury, T. Viraraghavan, A. Srinivasan, "Biological treatment processes for fish processing wastewater - A review," Bioresource Technology, **101**(2), 439–449, 2010, doi:10.1016/j.biortech.2009.08.065.

[10] R.O. Cristóvão, V.M.S. Pinto, A. Gonçalves, R.J.E. Martins, J.M. Loureiro, R.A.R. Boaventura, "Fish canning industry wastewater variability assessment using multivariate statistical methods," Process Safety and Environmental Protection, **102**, 263–276, 2016, doi:10.1016/j.psep.2016.03.016.

[11] A. Val del Rio, A. Pichel, N. Fernandez-Gonzalez, A. Pedrouso, A. Fra-Vázquez, N. Morales, R. Mendez, J.L. Campos, A. Mosquera-Corral, "Performance and microbial features of the partial nitritation-anammox process treating fish canning wastewater with variable salt concentrations," Journal of Environmental Management, **208**, 112–121, 2018, doi:10.1016/j.jenvman.2017.12.007.

[12] G.K. Kafle, S.H. Kim, K.I. Sung, "Ensiling of fish industry waste for biogas production: A lab scale evaluation of biochemical methane potential (BMP) and kinetics," Bioresource Technology, **127**, 326–336, 2013, doi:10.1016/j.biortech.2012.09.032.

[13] R. Gao, H.O. Nam, W. Il Ko, H. Jang, "Integrated system evaluation of nuclear fuel cycle options in China combined with an analytical MCDM framework," Energy Policy, **114**(December 2017), 221–233, 2018, doi:10.1016/j.enpol.2017.12.009.

[14] K. Govindan, S. Rajendran, J. Sarkis, P. Murugesan, "Multi criteria decision making approaches for green supplier evaluation and selection: A literature review," Journal of Cleaner Production, **98**, 66–83, 2015, doi:10.1016/j.jclepro.2013.06.046.

[15] C.H. Kuei, C.N. Madu, C. Lin, "Developing global supply chain quality management systems," International Journal of Production Research, **49**(15), 4457–4481, 2011, doi:10.1080/00207543.2010.501038.

[16] V.K. Sharma，P Chandana，A Bhardwaj, "Critical factors analysis and its ranking for implementation of GSCM in Indian dairy industry," J. Manuf. Technol. Manag., **5**(6), 911–922, 2014, doi:10.1108/JMTM-03-2014-0023.

[17] F. Dehghanian, S. Mansoor, M. Nazari, "A framework for integrated assessment of sustainable supply chain management," IEEE International Conference on Industrial Engineering and Engineering Management, 279–283, 2011, doi:10.1109/IEEM.2011.6117922.

[18] K. Zimmer, M. Fröhling, P. Breun, F. Schultmann, "Assessing social risks of global supply chains: A quantitative analytical approach and its application to supplier selection in the German automotive industry," Journal of Cleaner Production, **149**, 96–109, 2017, doi:10.1016/j.jclepro.2017.02.041.

[19] F.T.S. Chan, N. Kumar, "Global supplier development considering risk factors using fuzzy extended AHP-based approach," Omega, **35**(4), 417–431, 2007, doi:10.1016/j.omega.2005.08.004.

[20] K. Shaw, R. Shankar, S.S. Yadav, L.S. Thakur, "Supplier selection using fuzzy AHP and fuzzy multi-objective linear programming for developing low carbon supply chain," Expert Systems with Applications, **39**(9), 8182–8192, 2012, doi:10.1016/j.eswa.2012.01.149.

[21] V. Mani, R. Agrawal, V. Sharma, "Supplier selection using social sustainability: AHP based approach in India," International Strategic Management Review, **2**(2), 98–112, 2014, doi:10.1016/j.ism.2014.10.003.

[22] S. Gold, A. Awasthi, "Sustainable global supplier selection extended towards sustainability risks from (1+n)th tier suppliers using fuzzy AHP based approach," IFAC-PapersOnLine, **28**(3), 966–971, 2015, doi:10.1016/j.ifacol.2015.06.208.

[23] K.. Huwang, C.L., & Yoon, K.P "Multiple attribute decision making:methods and applications," Springer-Verlag, 1981.

[24] T.C. Wang, T.H. Chang, "Application of TOPSIS in evaluating initial training aircraft under a fuzzy environment," Expert Systems with Applications, **33**(4), 870–880, 2007, doi:10.1016/j.eswa.2006.07.003.

[25] S. Senthil, B. Srirangacharyulu, A. Ramesh, "A robust hybrid multi-criteria decision making methodology for contractor evaluation and selection in third-party reverse logistics," Expert Systems with Applications, **41**(1), 50–58, 2014, doi:10.1016/j.eswa.2013.07.010.

[26] M. Sonia, C. James, "response to demand uncertainty of supply chains: a value-focused approach with ahp and topsis," International Journal of Industrial Engineering, **25**(6), 739–756, 2018.

[27] P. Kumar, R.K. Singh, "A fuzzy AHP and TOPSIS methodology to evaluate 3PL in a supply chain," Journal of Modelling in Management, **7**(3), 287–303, 2012, doi:10.1108/17465661211283287.

[28] A. Jayant, P. Gupta, S.K. Garg, M. Khan, "TOPSIS-AHP based approach for selection of reverse logistics service provider: A case study of mobile phone industry," Procedia Engineering, **97**, 2147–2156, 2014, doi:10.1016/j.proeng.2014.12.458.

Ferromagnetic Core Reactor Modeling and Design Optimization

Subash Pokharel[*], Aleksandar Dimitrovski

Department of Electrical and Computer Engineering, University of Central Florida, Orlando, 32816, USA

A R T I C L E   I N F O

A B S T R A C T

This article presents an analytical model of a single-phase ferromagnetic core power inductor (reactor) based on a magnetic equivalent circuit (MEC). The MEC model consists of magnetomotive forces (MMFs) and reluctances for all flux paths: magnetic core and leakage flux paths. The MEC elements are found established on the characteristics of the ferromagnetic material and the reactor's dimensions. Then the inductances of the reactor are determined using the MEC for a group of Silicon Steel (Si-Fe) sheets, which are juxtaposed with the inductances obtained using the finite element analysis (FEA) method. This comparison corroborates the MEC presented here. Furthermore, for the unsaturated (linear) region of the B-H characteristics of the same sets of Si-Fe materials, the inductive reactance closed-form solution of the reactor is obtained as a function of the design parameters. As an application example of the presented analytical model, reactor design optimizations (single-objective and multi-objective) are formulated and solved based on the derived closed-form reactance expression resulting in a reactor not only optimized in reactance but also in terms of material use and size.

1   Introduction

This article augments the underlying work initially introduced in the 2019 North American Power Symposium (NAPS) [1].

Inductors (or the reactors in power engineering) are fundamental and most uncomplicated circuit elements that provide economical, sturdy, and efficient solutions to a spectrum of power system intricacies. The inductors have been used to limit fault and load current, compensate reactive powers, filter harmonics, damp the transients, and balance the loads, to mention a few applications in the electric power system. As a result of the significant expense and restricted usefulness for sufficient and optimal AC flow controls with FACTS devices, inductors are considered a superior alternative in power systems [2]. The use of reactors can be in conjunction with improving electric power quality, especially in the ever-changing contemporary power networks. The reactors can be connected either in series or parallel with the network based on a particular application. Contingent upon the voltage and power ratings, they can be either dry-type or oil-submerged sort. Usually, dry-type series reactors are made with air cores, and oil-immersed shunt types are made with ferromagnetic cores. Powdered core reactors, which are manufactured by the compression of the very fine particles of the magnetic materials, are preferred for high-reliability military and

space applications because they are robust against shocks, vibrations, and nuclear radiations. Also, flux containment is better in powdered core compared to the ferromagnetic cores [3]. A simple schematic of a single-phase $(1 - \Phi)$ ferromagnetic core reactor for use in power systems is shown in Figure 1.

The inductor is symmetrical with non-ferromagnetic (air) gaps in the center of the inner leg. Over the gaps, there is AC winding connecting to the AC circuit. The gaps are used to limit the magnetic flux in order to prevent reactor's saturation from the rated operating supply. The core of ferromagnetic reactors is made of a material with high permeability that acts as an excellent conductor for magnetic flux. The ferromagnetic core's ability to conduct and concentrate the magnetic flux flow and, consequently, the reactor's inductance is dictated by its permeability. The relationship between the flux flow in the ferromagnetic core and the current supply through the coils of an electromagnetic device (like the reactor) is nonlinear. The rate-of-change (ROC) of flux for the field strength shifts from moderate to rapid to low when the operating condition shifts from the inception to linear to the saturated region. Generally, magnetic power devices' operation is not recommended in the saturation region, where more increment in MMF supply produces a minuscule change in flux. The operation of such devices in the saturation region increases the magnetizing current, responsible for

increased losses and possible hazardous operating conditions. For some applications which work on the principle of the magnetic amplifier (MA), like continuously varying series reactor (CVSR) and fault current limiters (FCL), the inductance of the device is changed without any moving parts. The inductance variation is achieved with the help of DC bias supply by controlling the permeability and saturation of the ferromagnetic core as described in [2, 4]. The use of the laminated ferromagnetic core is the general practice to lower core losses; the ferromagnetic core in Figure 1 is shown as a solid rectangular core for simplicity only.Placing non-ferromagnetic gaps with magnetic properties similar to free space in the ferromagnetic core is also common. The effective permeability and the inductance of the device get reduced by such non-ferromagnetic gaps. However, the device's usable range of operation gets increased with dominant reluctance in the magnetic circuit. Likewise, the non-ferromagnetic gaps assume a crucial part in making the flux flow sensitivity lower to external conditions like temperature. The adequate selection of the air gap dimension is an essential job of the reactor designer because there is a need to struck an equilibrium between avoiding core saturation with a significant gap and imposed constraints to achieve the desired value of the inductance.
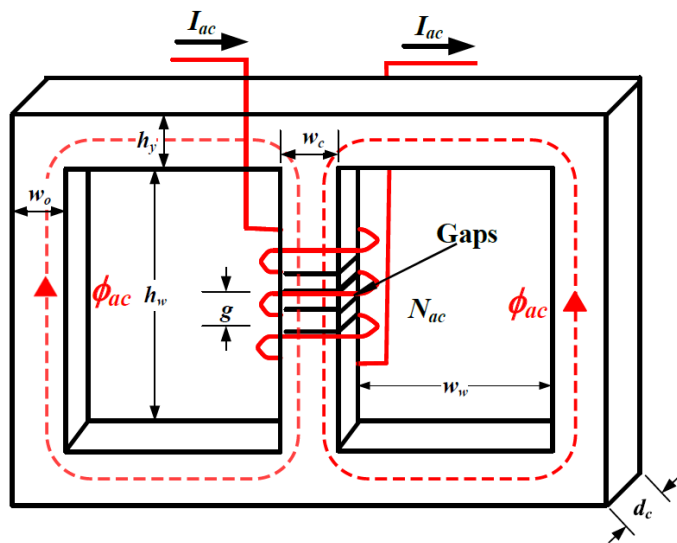
Figure 1: Ferromagnetic core reactor and its dimensions

FEA based methods are usually adopted for accurate parameter calculations and characterization of the electromagnetic devices. This numerical method can be tedious with a tremendous computational burden. It also lacks closed-form solutions. Therefore, it is not suitable for the repetitive design processes and dynamic analyses of magnetic power devices [5, 6]. In [7] and [8], the authors introduced the magnetic equivalent circuit (MEC) based method a long time ago. MEC is an alternative magnetic field modeling method for electromagnetic devices with a considerably reduced computational resources requirement. The MEC approach is based on the design inputs, material characteristics, and physical device geometry. It represents such devices with lumped magnetic circuit components: magnetomotive forces (MMFs) and reluctances. The MEC representation is considered coarser than the FEA but more acceptable than the electrical-equivalent lumped parameter models,

which are based on fundamental equations. Hence, MEC is considered a bargain between those approaches in terms of computational resource need and accuracy [9, 10]. MEC approach is based on the design inputs, material specifications, and geometry of the device. The inductance calculation of a device is straightforward with this approach. MEC has the ability to accommodate local saturation effects; however, because of the eddy current and skin effects, the MEC representation becomes challenging. A comprehensive understanding of the device in consideration and a significant engineering judgment is required to generate a reluctance network with spatial discretization [9]–[13].

A great deal of engineering time and experience can be avoided with the optimization-based design process, which can produce a better design with less engineering effort [14]. A reactor's design can involve many performance targets, some more important than others, with a set of constraints. With multi/many-objective design optimization, the feasible solution space might be discontinuous and non-convex. The evolutionary algorithms are typically chosen for such problems. A large number of design evaluations are necessary to produce a Pareto optimal front, and approximate analytical models make such computations efficient. In this article, the constrained single objective (SO) and multi-objective (MO) optimization design formulations, coupled with the detailed MEC-based analytical model that captures the reactor's electromagnetic behavior, are presented. These design examples signify the importance of computationally efficient and accurate analytical MEC models for the reactor's design optimization.

The article is structured as follows. Section 2 proposes an adequately precise yet simple MEC for a gapped ferromagnetic core reactor. The inclusion of the fringing fluxes in the MEC proposed in the previous section improves its accuracy. The methodology for the confirmation of the MEC model is presented in Section 3. The next section follows the methodology introduced with a case study for a set of Silicon Steel (Si-Fe) ferromagnetic materials. The design optimization examples are presented in Section 5, facilitated by the reactance expressions obtained from the validated MEC. Based on the proposed MEC, its validation, and optimization examples, conclusions are drawn in Section 6.

2 Magnetic Equivalent Circuit

The dimensions of the simple single-phase gapped ferromagnetic core reactor are shown in Figure 1. The gaps (air) in the core make the leakage flux not influential for the reactor's magnetostatic characterization. For this reason, an arbitrary winding configuration choice is made for this device. The reactor features two windows of width w_w and height h_w. w_o and w_c are the widths of the exterior and middle leg, respectively. The central leg has non-ferromagnetic gaps of elevation g which stretches d_c into the surface, which is the same throughout the reactor. Both top and bottom yokes have the same height of h_y.

Figure 2 represents one of the simplest possible MECs of the reactor. The reluctances (resembling resistors from electric circuits) in the proposed MEC are positioned to interpret the accurate reactor physical structure. Similarly, the MMF source position (resembling voltage source from the electric circuit) in the MEC indicates the

winding position in the reactor. The ferromagnetic core reluctances are denoted by $R_1 - R_7$, dependent on the magnetic flux through the corresponding elements. In MEC, these reluctance are shown to be a function of flux.
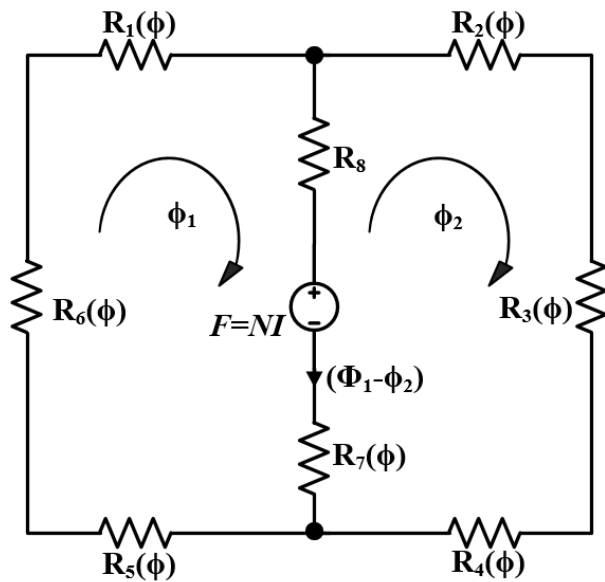
Figure 2: Magnetic equivalent circuit

However, the non-ferromagnetic air gap reluctance (R_8 in Figure 2) is fixed and does not depend on the corresponding flux. The MMF source in the middle leg of the proposed MEC is the product of the number of winding turns (N) and current supply through it (I), i.e., $F = NI$. In Figure 2, loop fluxes are represented by ϕ_1 and ϕ_2, making the inner leg branch flux to be ($\phi_1 - \phi_2$) in the specified direction.

For a representative branch k, the generalized reluctance is:

$$R_k = \frac{l_k}{A_k \mu} \tag{1}$$

In equation (1), A_k and l_k are cross-sectional area normal to the flux flow direction and length of branch element, respectively, and μ is the permeability (absolute) of the material used. The absolute permeability depends on the type of flux path, based on which the reluctances can be categorized into:

2.1 Core Piece Reluctance

The reluctances of ferromagnetic core pieces are intrinsically nonlinear. The reluctance of each ferromagnetic element in the MEC depends on the material property, physical geometry, and supply through the winding around the core. The core piece's absolute permeability can be demonstrated as a function of either flux density (B) or flux intensity (H). Considering the symmetry of the reactor, based on (1), the characteristic core piece reluctances can be written as:

$$R_1(\phi) = \frac{2w_w + w_o + w_c}{2d_c h_y \mu_B(\frac{\phi}{d_c h_y})} \tag{2a}$$

$$R_3(\phi) = \frac{h_y + h_w}{d_c w_o \mu_B(\frac{\phi}{d_c w_o})} \tag{2b}$$

$$R_7(\phi) = \frac{h_y + h_w - g}{d_c w_c \mu_B(\frac{\phi}{d_c w_c})} \tag{2c}$$

Also, $R_1(\phi) = R_2(\phi) = R_4(\phi) = R_5(\phi)$ and $R_3(\phi) = R_6(\phi)$. Each branch reluctance in (2) has absolute permeability represented as the functions of flux density through them. In [15], the author describes the process of finding these absolute permeabilities, which can be summarized by the following expressions.

$$\mu_B(B) = \mu_0 \frac{A(B)}{A(B) - 1} \tag{3}$$

where,

$$A(B) = \frac{\mu_r}{1 - \mu_r} + \sum_{k=1}^{K} \left\{ \alpha_k |B| + \frac{\alpha_k}{\beta_k} log \left(\frac{e^{-\beta_k \gamma_k} + e^{-\beta_k |B|}}{1 + e^{-\beta_k \gamma_k}} \right) \right\} \tag{4}$$

In equation (4), B represents the magnetic flux density; μ_r and μ_0 are the relative and absolute permeabilities, respectively. Here, anhysteretic characteristics are considered with the reactor operating in the linear region. Moreover, α, β, and γ are the permeability function parameters for select core materials.

An iterative numerical search is needed for each branch of the MEC corresponding to the core piece ferromagnetic components to find a value of reluctance, given some initial values for the flux density. Figure 3 shows the flowchart summarizing this iterative process. The absolute permeability calculation is the first step of the iterative process. For mesh circuit analysis, permeability as a function of flux density is preferred. Using the absolute permeability ($\mu \equiv \mu_B(B)$), the reluctance of each piece can be calculated using (1). In the next step, each branch is represented in the standard general form: a series combination of an MMF source and the reluctance. Based on the complete circuit element formation, mesh analysis is carried out to find the fluxes through each loop. Except for the first iteration, as indicated in the flowchart, the stopping criteria for the iterative process are the maximum number of iterations and branch flux relative error between consecutive iterations.

2.2 Air Gap Reluctance

In the MEC model of Figure 2, the reluctance R_8 is the air gap reluctance. It is a constant reluctance without any dependence on the flux passing through it. Following (1), the reluctance of the air gap is given by:

$$R_g = \frac{g}{d_w w_c \mu_0} \tag{5}$$

While getting reluctance in (5), it is assumed that the cross sectional flux flow between the top and bottom of the air gap is streamlined. However, there exists a portion of a flux that flows in the vicinity of the air-gap corners spreading in all directions,

which is known as the fringing flux. Because of this flux, the effective cross-sectional area of the air gap is increased, resulting in decreased air gap reluctance. The fringing fluxes should be incorporated into the air gap reluctance computation to make the MEC highly accurate.

Figure 3: Iterative non-linear reluctance calculation flowchart
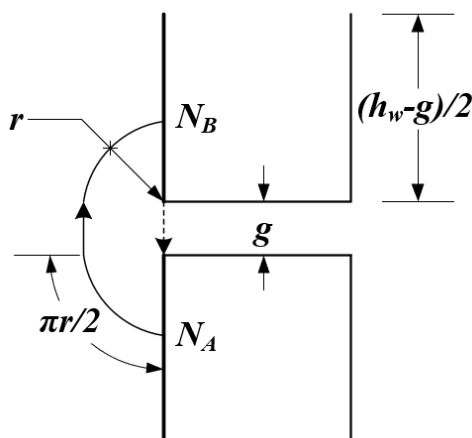
Figure 4: Fringing permeance calculation

The Ampere's circuital law, which relates the current to the associated magnetic field, can be described by (6) representing the magnetic field intensity H(A/m) over a closed path c to be equivalent to the current enclosed by that path ($I_{enclosed}$.)

$$\oint_c H \cdot dl = I_{enclosed} \tag{6}$$

The fringing effect can be captured by applying Ampere's law for the uniformly flowing flux from surface node N_A to N_B along the expanse of the flux route shown in Figure 4 as:

$$H(g + \pi r) = F \tag{7}$$

In (7), H and $F(= NI)$ are the magnetic field strength (intensity) and the MMF source respectively. Based on the relationship with H, the magnetic flux density ($B = \mu H$) can be represented as:

$$B = \frac{\mu_0 F}{(g + \pi r)} \tag{8}$$

The surface integration of the flux density gives the flux coming out of surface node N_A, given by (9).

$$\phi = \int B dS = \int_0^{(h_w - g)/2} \frac{\mu_0 F}{(g + \pi r)} d_c dr \tag{9}$$

Also, the fringing flux incorporated with the designated path can be linked to fringing permeance (P_{fring}) and MMF source as:

$$\phi = P_{fring} F \tag{10}$$

From equations (9) and (10):

$$P_{fring} = \frac{\mu_0 d_c}{\pi} log \left\{ 1 + \frac{\pi(h_w - g)}{2g} \right\} \tag{11}$$

For the central leg with air gap, the depth and the width are the same; therefore, the total fringing permeance is four times the P_{fring}. Hence, the air gap reluctance can be given by:

$$R_{air-gap} = R_8 = R_g \| \frac{1}{(4P_{fring})} = \frac{R_g}{1 + 4R_g P_{fring}} \tag{12}$$

3 MEC Validation Methodology

A meshed circuit analysis based on Kirchhoff's laws from electric circuits can be adopted to solve the proposed MEC once each MEC element is determined. This analysis gives flux through each branch and loop of the MEC. The physical law of energy conversation holds for the MEC. Therefore, a balance between the energy generated by the MMF source(s) and energy dissipated into the reluctances always exists. The energy balance principle can be exploited to find the overall equivalent inductance of the inductor directly. From [16] the reactor's inductance is:

$$L_{MEC} = \frac{1}{I^2} \sum_{k=1}^{n} \phi_k^2 R_k \tag{13}$$

Here, $1 \leq k \leq n$ is the index representing each branch in the MEC with a total number of branches being n; while R_k and ϕ_k are the reluctance and flux through the branch k respectively. Furthermore, the winding coil has current I following through it.

By performing different analyses (magnetostatic/transient) using the software packages based on FEA can give the inductance of a reactor. A three-dimensional (3-D) model of an inductor with minimal error tolerance set up can compute the inductance (apparent/incremental) accurately in the FEA software package.

The proposed MEC of the reactor is verified by comparing the equivalent inductances obtained from MEC as described in (13) using MATLAB®[1], and the FEA based approach using ANSYS Maxwell®[2]. The following case study presents the comparative analysis.

4 Case Study

A contextual analysis for the affirmation of the presented analytical model is carried out in this section, followed by the closed-form reactance calculation based on the validated model.
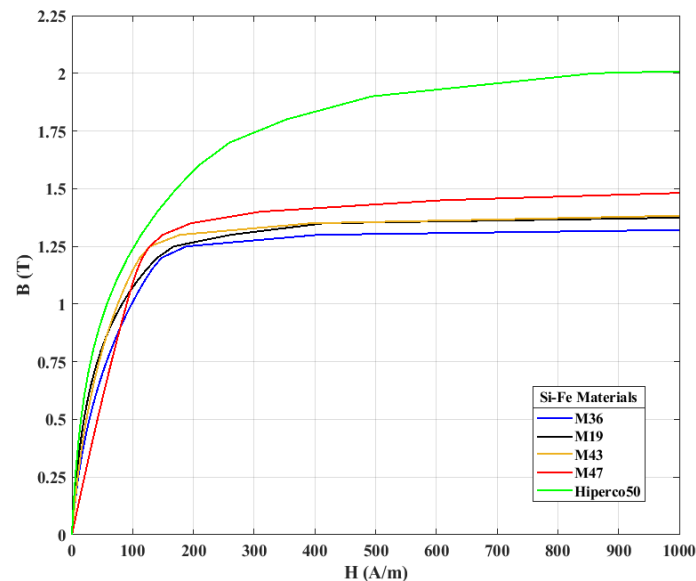
Figure 5: Candidate ferromagnetic material characteristics

4.1 MEC Validation

A single-phase reactor considered for the MEC validation has the parameters, as shown in Table 1.

Table 1: Gapped core reactor parameters

Parameters	Symbol	Value
Window height	h_w (m)	0.374
Window width	w_w (m)	0.056
Leg width	$w_o = w_c$ (m)	0.076
Yoke/base height	h_y (m)	0.076
Core depth	d_c (m)	0.076
Number of turns	N	39
Rated current	i (A)	$25\sqrt{2}$

[1]https://www.mathworks.com/products/matlab.html
[2]https://www.ansys.com/products/electronics/ansys-maxwell

A set of magnetic core materials (Si-Fe) is considered with accompanying qualities (relative permeability, permeability function parameters, and maximum flux densities) extracted from [17]. The magnetic properties (B-H curves) for these materials generated according to [18] are shown in Figure 5. The two approaches described in the previous section are applied to calculate and compare the inductance of the reactor made up of each of the given materials.

For both linear and non-linear regions of the magnetization characteristics of Si-Fe, it is clear that the anhysteretic curve of Hiperco50 is considerably different from the others, as can be seen in Figure 5.

(a) Adaptive mesh plot   (b) Flux density plot
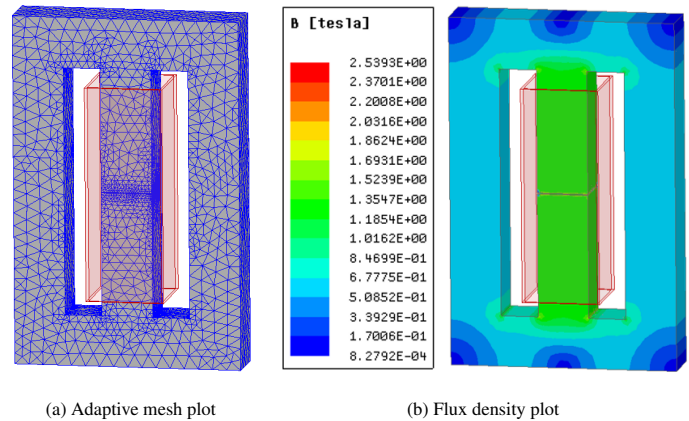
Figure 6: FEA simulation Results for Si-Fe Hiperco50 core

Figure 6 shows 3-D FEA results for the reactor with the Si-Fe Hiperco50 core with the parameters from Table 1. The adaptive meshing has been applied to the model to make the simulation more accurate. The figure also shows the flux density distribution throughout the core, and it can be seen that the middle leg has the highest flux density.

For every core materials from the group, the inductances using both approaches and relative error between them are summarized in Table 2. The errors are within 1% for each of the materials. This minimal range of errors across a group of Si-Fe materials confirms the accuracy of the proposed MEC.

Table 2: Inductance comparison

Si-Fe Materials	Inductance (mH)		% Error
	MEC	FEA	
M19	7.853	7.880	0.348
M36	7.905	7.871	-0.427
M43	7.910	7.935	0.310
M47	7.831	7.904	0.925
Hiperco50	8.012	8.081	0.850

4.2 Reactance Calculation

For a 60 *Hz* system, a single-phase inductor's reactance can be expressed as:

$$X_L = 120\pi L \tag{14}$$

where,

$$L = \frac{N^2}{\mathcal{R}_m} \tag{15}$$

here, $\mathcal{R}_m$ is the equivalent reluctance of the reactor. A circuit reduction on MEC can be applied to obtain it, as shown in Figure 7.

(a) Step I (b) Step II
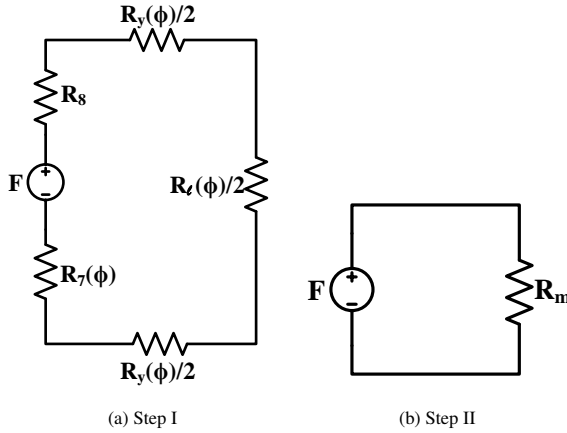
Figure 7: MEC reduction

As the design of the reactor is symmetrical, a circuit simplification by the parallel combinations of the reluctances corresponding to the yoke and vertical leg transforms the MEC from Figure 2 to Figure 7a. Furthermore, the series reluctances in a single loop MEC in Figure 7a can be combined to achieve the simplest MEC as in Figure 7b. Accordingly:

$$\mathcal{R}_m = R_y(\phi) + 0.5R_l(\phi) + R_7(\phi) + R_8 \tag{16}$$

In Figure 7, $R_y \equiv \{R_1 = R_2 = R_4 = R_5\}$ and $R_l \equiv \{R_3 = R_6\}$. A further break down of (16) for a linear operation region (in the magnetization characteristic curve) returns:

$$\mathcal{R}_m = \frac{6.25 \times 10^5 g}{0.7854 d_c w_o + g d_c \log\left(-0.5708 + \frac{1.5708 h_w}{g}\right)}$$
$$+ \frac{X\left\{-h_y g + w_o(w_o + w_w)\right\} + Y h_y(h_y + h_w)}{d_c h_y w_o} \tag{17}$$

A symbolic mathematical computation program called MATHEMATICA®[3] has been used to obtain this simplified expression. For different core materials, the coefficients X and Y in (17) are summarized in Table 3.

---

[3]https://www. wolfram.com/mathematica/

Table 3: Reactance coefficients

Si-Fe Materials	Coefficients	
	X	Y
M19	44.324	66.486
M36	58.996	88.494
M43	51.342	77.012
M47	86.369	129.554
Hiperco50	36.473	54.710

5 Design Optimization

5.1 Single Objective Optimization

An example of a single objective optimization problem is set up using the expression for the reactance of the reactor. The use of minimal material for the core is the objective while complying with several design constraints. Here, it is assumed that the reactor core is made up of Si-Fe M36 material. The design constraints include the target reactance, flux density limits for each element of MEC ($n = 8$), and minimum and maximum limits for the design parameters. The design parameter vector (19) consists of all design parameters. Their ranges and the initial points are summarized in Table 4.

$$\begin{aligned}
\min_{\mathbf{X}} \quad & V = d_c\{2h_w w_o + w_c(h_w - g) + 2h_y(2w_w + 2w_o + w_c)\} \\
\text{s.t.} \quad & X_L = x_{design}, \\
& B_k \le B_{max}, \ \forall k \in n, \\
& \mathbf{x}_{min} \le \mathbf{x} \le \mathbf{x}_{max}
\end{aligned} \tag{18}$$

In (18), $B_{max} = 1.25\ T$ is the maximum flux density in the linear region of the B-H curve for Si-Fe M36, and $x_{design} = 2\ \Omega$.

Table 4: Domain of design parameters

Parameters	$\mathbf{x}_{min}$ (m)	$\mathbf{x}_{max}$ (m)	$\mathbf{x}_{initial}$ (m)
w_o	0.0762	0.1016	0.0889
w_w	0.0559	0.0762	0.0635
h_y	0.0762	0.1016	0.0889
h_w	0.3739	0.5080	0.4572
d_c	0.0762	0.1016	0.0889
g	0.0015	0.0023	0.0020
w_c	0.0762	0.1016	0.0889

$$\mathbf{x} = [w_o \quad w_w \quad h_y \quad h_w \quad d_c \quad g \quad w_c]^T \tag{19}$$

A non-linear solver called 'Knitro' with YALMIP toolbox from MATLAB® has been used to solve this non-linear optimization problem. Table 5 summarizes the optimization results.

Table 5: SO optimization results

Parameters	Value (m)	Parameters	Value (m)
w_w	0.0559	$w_o = w_c$	0.0762
h_y	0.0762	h_w	0.3739
g	2.286×10^{-3}	d_c	0.0762

The optimal (minimum) ferromagnetic core material volume is found to be $1.0452 \times 10^{-2} m^3$. An approximate 'back-of-the-envelope' calculation for the volumetric minimization of the reactor with some educated guess regarding the constraints verifies the presented results. The air-gap (g) is very sensitive towards the reactance and the flux density in the core; however, it has a minimal impact on the reactor's total ferromagnetic volume. Therefore, the constraint set $\mathbf{x}$ other than g can be guessed towards the minimum limit to get the minimum ferromagnetic volume. If $\mathbf{x}$ is chosen to be x_{min}, the ferromagnetic volume would be $1.0457 \times 10^{-3} m^3$.

The optimal ferromagnetic volumes for different Si-Fe materials are summarized in Figure 8. In the figure, the ferromagnetic volumes are very near each other; however, the price difference between the materials will impact material selection.
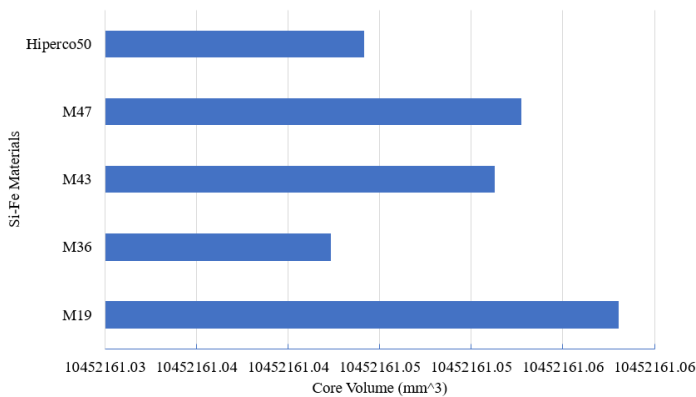
Figure 8: Optimal core volume comparison

5.2 Multi-Objective Optimization

Reactance is the most important characteristic of the ferromagnetic core inductor. In addition to the core material volume minimization, an additional objective of reactance maximization is introduced here. The multi-objective (MO) optimization searches a vast design space and is quite effective in finding optimal machine designs. An evolutionary population-based genetic algorithm [19] is implemented to solve a MO reactor optimization problem. A genetic algorithm (GA) can find multiple solutions from a population of solution candidates in one execution, which is not possible with classical optimization [14].

The goal of this design example is to come up with a single-phase power reactor design that has a reactance of at least X_{min}, and maximum ferromagnetic core flux density below B_{max}. It is desirable to minimize the reactor's ferromagnetic core material volume and maximize the reactance at the rated system conditions.

$$\min_{\mathbf{X}} \begin{bmatrix} V & \dfrac{1}{X_L} \end{bmatrix}$$
$$\text{s.t.} \quad X_L \geq X_{Lmin}, \tag{20}$$
$$B_m \leq B_{max},$$
$$\mathbf{x}_{min} \leq \mathbf{x} \leq \mathbf{x}_{max}$$

The ferromagnetic core material used in this optimization problem is the same material used for single objective optimization problem described in the previous section (Si-Fe M36). The optimal reactor would have a reactance of at least 1.5 Ω (X_{min}) and the flux density of the 1.25 T (B_{max}) so that the operation of the reactor is within the linear region of the characteristics curve of the selected core material for the rated supply. In 20, the flux density has been bounded only for the middle leg flux density because it is the dominant flux density region. The gapped middle leg flux density can be approximated by:

$$B_m = \frac{\phi_m}{A} = \frac{Ni}{\mathcal{R}_m A} \approx \frac{\mu_0 Ni}{g} \tag{21}$$

The parameter bounds are the same as in the previous section, given in Table 4. The free parameter vector is represented by (19). The symbols in parameter vector are as defined in Table 1. It is assumed that the window spaces are sufficient for the winding.

The fitness function for the MO optimization problem can be defined as:

$$f = \begin{cases} \varepsilon(\bar{c} - 1)[1 \quad 1]^T, & \bar{c} < 1 \\ \left[\frac{1}{V} \quad X_L\right]^T, & \bar{c} = 1 \end{cases} \tag{22}$$

In (22), ε–a small positive number (in order of 10^{-10})– does not have an influence on the optimization outcomes but is appropriate for the observation of the optimization progress.

And, $\bar{c}$ is the aggregate constraint of the MO problem, which is:

$$\bar{c} = \frac{1}{n_c} \sum_{i=1}^{n_c} c_i = \frac{c_1 + c_2}{2} \tag{23}$$

where, n_c is constraint number (here, $n_c = 2$). Once X_L and B_m have been evaluated using (14) and (21), constraint functions can be put together as (24):

$$c_1 = gte(X_L, X_{L_{min}}) \tag{24a}$$

$$c_2 = lte(B_m, B_{max}) \tag{24b}$$

where, $gte()$ and $lte()$ are greater-than-or-equal-to and less-than-or-equal-to functions, respectively. These functions are defined as:

$$lte(x, x_{max}) = \begin{cases} 1, & x \leq x_{max} \\ \frac{1}{1+x-x_{max}}, & x > x_{max} \end{cases} \tag{25a}$$

$$gte(x, x_{min}) = \begin{cases} 1, & x \geq x_{min} \\ \frac{1}{1+x_{min}-x}, & x < x_{min} \end{cases} \tag{25b}$$

The MO optimization is carried out using GOSET [20], a MATLAB-based genetic optimization toolbox. The optimization

has been performed with a population size of 1500 over 2000 generations with the specifications described by Table 6, and the parameter bounds given in Table 4.

Table 6: Genetic algorithm parameters

Parameters	w_o	w_w	h_y	h_w	d_c	g	w_c
Encoding	log	log	log	log	log	log	log
Chromosome	1	1	1	1	1	1	1

Table 7 summarizes the GA options carried out in the different steps of the MO optimization.

Table 7: Summary of GA options implemented

GA	Elitist nondominated sorting GA(NSGA-II) [21]
Selection	Tournament selection
Death	Random replacement
Gene repair	Hard limiting
Scaling	Offset scaling

Figure 9 represents the objective space at the end of the optimization, where each point represents the objectives of the corresponding design. The objective space plot is according to the fitness function definition. Therefore, reactance is plotted against the reciprocal of the ferromagnetic core material volume. The design points can be divided into nonviable, dominated, and nondominated design sets. The nonviable designs are near the origin and the negative axes of the objective space. The figure indicates the distinct design sets which are viable but dominated or nondominated.

Figure 10 shows only the nondominated designs with the axes representing the reactance and the material volume. This plot clearly shows the tradeoff between the objectives. A sample design on the Pareto optimal front is also indicated. The parameters representing the sample design are summarized in Table 8.
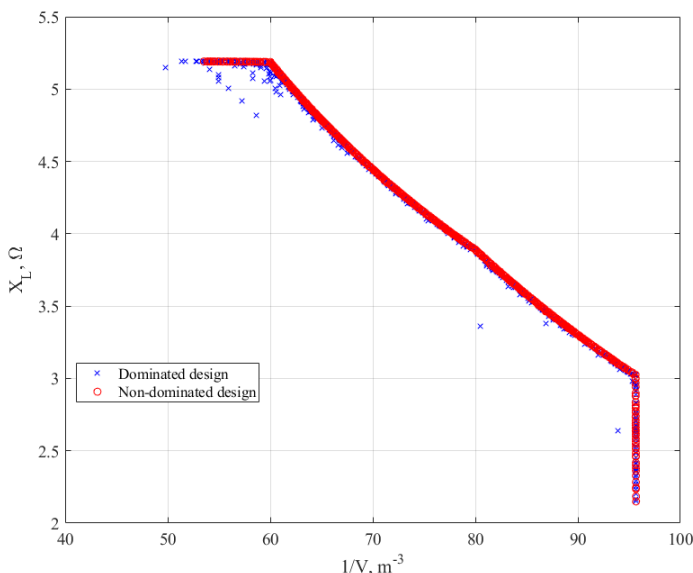
Figure 9: Objective design space
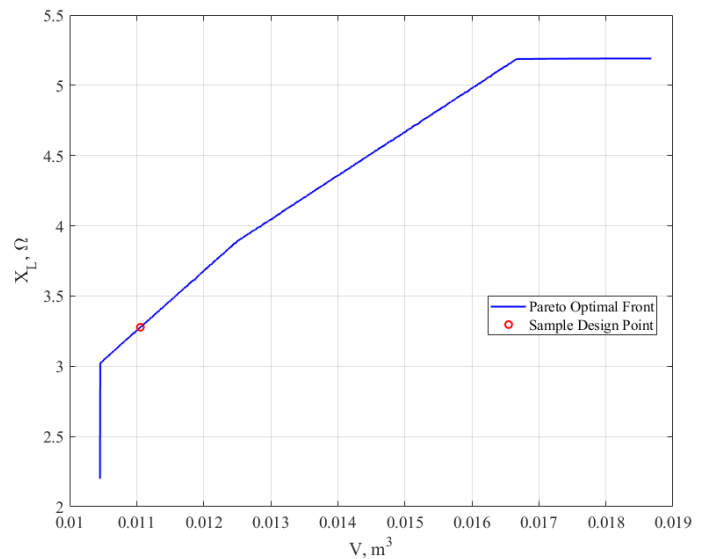
Figure 10: Pareto frontier boundary

Table 8: Sample design results

Parameters	Values (m)	Parameters	Values (m)
w_o	0.085	w_w	0.05589
h_y	0.076233	h_w	0.3739
d_c	0.0762	g	0.001524
w_c	0.0762		

For the sample design, the ferromagnetic material volume is 0.011176 m^3, and the reactance of the inductor is 3.32 Ω. This reactance is above the minimum limit X_{Lmin}, and the flux density is found to be 1.137 T, which is less than the flux density limit B_{max}.

To check the validity of the sample design obtained above, a 3-D FEA model is created again with the parameters from Table 8. The magnetostatic analysis from FEA shows that the reactance of the sample design is 2.96 Ω, which is ≈ 12% off from the MO optimization results. It is a fairly good result considering the simplicity of the model used, and more accurate than a spreadsheet-based design typically used by manufacturers.

6 Conclusions

In this article, a systematic analytical representation was proposed for a 1-Φ ferromagnetic core air-gapped inductor based on MEC. For a set of Si-Fe materials for core, the proposed MEC was substantiated after collating the inductances obtained by using the 3-D FEA method. The minuscule error of the inductance values throughout the entire group of materials validated the proposed model. Furthermore, when the ferromagnetic core is in the unsaturated (linear) region of the operation, an inductor reactance expression was derived as a function of design parameters. To illustrate one of the applications of the suggested systematic model, both SO and MO optimization problems were formulated and solved. They prove the MEC's applicability for obtaining optimal reactor designs for a specific application and highlight its efficiency and importance.

The future work will include reactor design improvements with more complex models, including more detailed flux leakages, and analyses (loss and thermal), as well as data from tests on the physical device with comparison of computational and experimental results.

Conflict of Interest   The authors declare no conflict of interest.

References

[1] S. Pokharel, A. Dimitrovski, "Analytical Modeling of A Ferromagnetic Core Reactor," in 2019 North American Power Symposium (NAPS), 1–6, 2019, doi:10.1109/NAPS46351.2019.9000352.

[2] A. Dimitrovski, Z. Li, B. Ozpineci, "Magnetic Amplifier-Based Power-Flow Controller," IEEE Transactions on Power Delivery, **30**(4), 1708–1714, 2015, doi:10.1109/TPWRD.2015.2400137.

[3] C. W. T. McLyman, Transformer and inductor design handbook, CRC press, 2017.

[4] A. Dimitrovski, Z. Li, B. Ozpineci, "Applications of saturable-core reactors (SCR) in power systems," in 2014 IEEE PES T&D Conference and Exposition, 1–5, 2014, doi:10.1109/TDC.2014.6863404.

[5] A. Deihimi, "Improved model of saturated regions in Magnetic Equivalent Circuits of highly saturated electromagnetic devices," in 2008 11th International Conference on Optimization of Electrical and Electronic Equipment, 45–50, 2008, doi:10.1109/OPTIM.2008.4602385.

[6] M. Moallem, G. E. Dawson, "An improved magnetic equivalent circuit method for predicting the characteristics of highly saturated electromagnetic devices," IEEE Transactions on Magnetics, **34**(5), 3632–3635, 1998, doi:10.1109/20.717858.

[7] E. Lwithwaite, "Magnetic equivalent circuits for electrical machines," in Proceedings of the Institution of Electrical Engineers, volume 114, 1805–1809, IET, 1967.

[8] C. Carpenter, "Magnetic equivalent circuits," in Proceedings of the Institution of Electrical Engineers, volume 115, 1503–1511, IET, 1968.

[9] M. Amrhein, P. T. Krein, "3-D Magnetic Equivalent Circuit Framework for Modeling Electromechanical Devices," IEEE Transactions on Energy Conversion, **24**(2), 397–405, 2009, doi:10.1109/TEC.2009.2016134.

[10] S. D. Sudhoff, B. T. Kuhn, K. A. Corzine, B. T. Branecky, "Magnetic Equivalent Circuit Modeling of Induction Motors," IEEE Transactions on Energy Conversion, **22**(2), 259–270, 2007, doi:10.1109/TEC.2006.875471.

[11] J. Cale, S. D. Sudhoff, Li-Quan Tan, "Accurately modeling EI core inductors using a high-fidelity magnetic equivalent circuit approach," IEEE Transactions on Magnetics, **42**(1), 40–46, 2006, doi:10.1109/TMAG.2005.859439.

[12] B. N. Cassimere, S. D. Sudhoff, D. H. Sudhoff, "Analytical Design Model for Surface-Mounted Permanent-Magnet Synchronous Machines," IEEE Transactions on Energy Conversion, **24**(2), 347–357, 2009, doi:10.1109/TEC.2009.2016139.

[13] A. Taher, S. Sudhoff, S. Pekarek, "Calculation of a Tape-Wound Transformer Leakage Inductance Using the MEC Model," IEEE Transactions on Energy Conversion, **30**(2), 541–549, 2015, doi:10.1109/TEC.2015.2390260.

[14] S. D. Sudhoff, Optimization-Based Design, 1–44, Wiley-IEEE Press, 2014, doi:10.1002/9781118824603.ch01.

[15] S. D. Sudhoff, Magnetics and Magnetic Equivalent Circuits, 45–112, Wiley-IEEE Press, 2014, doi:10.1002/9781118824603.ch02.

[16] S. Pokharel, A. Dimitrovski, "A Gapless Ferromagnetic Core Reactor - Magnetic Equivalent Circuit and Inductance," in 2019 IEEE Power Energy Society General Meeting (PESGM), 1–5, 2019, doi:10.1109/PESGM40551.2019.8973400.

[17] S. D. Sudhoff, Selected Magnetic Steel Data, 443–444, Wiley-IEEE Press, 2014, doi:10.1002/9781118824603.app3.

[18] G. M. Shane, S. D. Sudhoff, "Refinements in Anhysteretic Characterization and Permeability Modeling," IEEE Transactions on Magnetics, **46**(11), 3834–3843, 2010, doi:10.1109/TMAG.2010.2064781.

[19] D. S. Weile, E. Michielssen, "Genetic algorithm optimization applied to electromagnetics: a review," IEEE Transactions on Antennas and Propagation, **45**(3), 343–353, 1997, doi:10.1109/8.558650.

[20] S. Sudhoff, Y. Lee, "GOSET Manual Version 1.03," Available from Scott Sudhoff, Purdue University School of Electrical and Computer Engineering, 2004.

[21] K. Deb, A. Pratap, S. Agarwal, T. Meyarivan, "A fast and elitist multiobjective genetic algorithm: NSGA-II," IEEE Transactions on Evolutionary Computation, **6**(2), 182–197, 2002, doi:10.1109/4235.996017.

Contingency Plan in the Supply Chain of Companies in the Retail Industry in the Face of the Impacts of COVID-19

Carlos Juventino Ruiz Montoya[*], José Luis Martínez Flores

UPAEP University, 21 sur 1103 Barrio de Santiago CP. Puebla, 72410, México

A R T I C L E I N F O	A B S T R A C T
	The main issue that is being presented in 2020 is the impact that all organizations are having due to the COVID-19 pandemic, and it is not for less given the global collapse that is occurring in all aspects. Many organizations have been affected by this catastrophe and in the face of an unforeseen scenario, the disruptions in the different supply chains have revealed the lack of some essential products for human consumption. *For organizations that are looking for alternatives of what to do and that are constantly analyzing how to reinvent their processes to mitigate the impacts of the pandemic and thus stay current during the contingency, they have before them the challenge of strengthening their supply chains, however It is difficult to think that the contagion of this virus that has brought the great powers of the planet to their knees, collapsing their productive, economic and especially health systems.* *This research aims to propose a model that allows the development of an action plan in the event of the COVID-19 contingency in the sector of companies classified as essential, such as the retail industry. It is not enough to have well-defined and structured processes, these must also be dynamic and interconnected to privilege the distribution of essential products and for this it is important to be clear about the pillars of supply chain management and the key elements that they proposed.* *Organizations must learn to protect their supply chains and to achieve it research offers a perspective on how to assess the level of risk of the processes of the retail industry and thus have identified the opportunities that will have to improve to build a resilient supply chain and strengthened.*

1. Introduction

Throughout time humanity has faced a significant number of disruptions that have affected from basic aspects such as the very survival or health of human beings to the complete collapse of the productive and economic systems, some of these disruptions have been caused for decisions related to the political and economic interests of man, such as the armed conflicts of the two world wars of the last century and that meant significant changes in the way of life of the affected countries, mainly those of the defeated side. Like the group of disruptions caused by the hand of man, there are other disruptions that have occurred and that have their origin in sometimes predictable behavior, but in many other unpredictable ones in nature, in both cases destructive, causing the loss of human lives and the destruction of assets and infrastructure for the proper functioning of business operations. In this group of natural disasters are hurricanes, earthquakes, tsunamis and fires, in addition to others, associated with diseases in humans that become epidemics and at a higher level of severity due to the size of the contagion, in the devastating effect of a pandemic.

Unfortunately, and due to this type of disruption, organizations are part of a side effect of what happens in the environment in which they find themselves. Each of these impacts and their post-mortem analysis are on an undesirable list of scenarios that have already occurred at the time, such as the SARS disease that occurred in Asia from 2002 to 2003, the tsunami in Indonesia in 2004, Hurricane Katrina that The United States struck in 2005, the 2009 - 2010 H1N1 influenza that occurred in Mexico, and currently the living pandemic of the COVID-19 coronavirus that started in China and is already spread around the world in 2020.

[*]Corresponding Author: Carlos Juventino Ruiz Montoya,
cjruizmontoya@hotmail.com

The historical account of disruptions that humanity has faced is wide and with a diversity of origins, however, regardless of their origin, they have something in common, a collapse of the different supply chains in the territory, region or country. where it occurs, causing to the companies a series of disorders in their supply operation from suppliers, in-house manufacturing and in the supply of goods to customers. Businesses with a more robust supply chain will enable them to be better prepared to responded more effectively to the effects of a disruption.

A service oriented organization must take care that the processes of its supply chain, in addition to being efficiently structured, have haracteristics of agility, adaptability and alignment to dynamically translate the needs that are being presented to the customer and can be respond satisfactorily in [1] the author explained the Triple A as a model that allows the supply chain to be adequately managed.

The supply chain management processes do not remain fixed over time, they have to be transformed according to the needs of the market and the sales point where the customer goes adapting to the purchasing trends of the consumer customer. Currently, from a commercial point of view in the retail industry, it is common to classify or have segmented the type of consumer that goes by store, this is a work of market intelligence, an emerging area in the modern design of organizations who have the need to know the sensitivity of how the market behaves, it is precisely this area that is responsible for doing this type of study to better define the commercial strategy to follow. In [2], the author explained the importance of having the commercial strategy integrated to the supply chain.

When talking about processes implicitly you have to consider two elements or vectors that converge on the subject, on the one hand, the capacity of the processes that in turn represent the potential designed to offer by the process, and on the other, the indicators of performance or kpi´s (key performance indicators) of the processes.

To measure the performance of the processes, they must have indicators or metrics that provide feedback to the system for which they were designed. The indicators must be focused on the measurement of the operational processes and offer deliverables on what happens at the border of each process, maintain a standard of behavior that constantly aspires to excellence in performance and that are also consistent with the strategy of the organization supply chain. If the importance of the Triple A Model was previously highlighted, in [3] the author complemented the model by highlighting the importance of top management's commitment to agility, flexibility, efficiency and service. Metrics should provide feedback to the organization on the elements that make up the established strategy.

With the evolution of the supply chain, accelerated mainly by the digital era and e-commerce, organizations have focused their actions to maintain an efficient customer service process by establishing strategies that allow them to stay current in a highly competitive environment, however the backyard that integrate the supply network, the management of optimal inventories for the preparation of orders looks vulnerable or simply exposed to the risks that every organization faces in the midst of a pandemic. In [4] the author described the importance of having identified supply

chain segmentation and regionalization as a way to mitigate risk. The stage during which this situation occurs generates high uncertainty where many organizations are not clear on how to act. In [5] the author explained the fact of having clear and defined processes to mitigate the effect of uncertainty and to have a clearer direction to follow by taking disruptive measures integrated in a mitigation strategy.

The purpose of this research is to offer a perspective on how to classify for a better assessment of the risk level of the retail supply chain. The classification is supported by four management pillars and these in turn integrate seven key elements that will be addressed in the proposed research methodology.

2. Literature review

When addressing the issue of disruptions that have occurred in the past, that are present today and that will surely continue to occur in the future, and that affect the environment where the basic daily activities of the world population are carried out, and therefore that of organizations, on this topic you can find a great diversity of research work and a multivariate approach or point of view, which depends on the type of research that the author wants to highlight or highlight. Just as these perspectives are mentioned in the different investigations carried out and that will be cited throughout the work, this investigation has as its main contribution to offer organizations an analysis, diagnosis and proposal of contingency actions against the disruptions caused by catastrophes natural as the pandemic that we are currently experiencing with COVID-19 and that affects the supply chains of companies considered or classified as essential as the retail industry, due to the impact they have on society in the supply of food and products of first necesity.

This research would not be a complete work if it does not leave a learning that generates value to the society in which companies develop and is not accompanied by a proposal for organizations on how they should be better prepared to face unplanned situations such as disruptions of this type.

Before continuing and delving into such a relevant topic today, it is important to start with a proposal to classify the disruptions that occur in organizations and in general in the society where we live, even before making such a classification it is important to be clear the definition of this, disruption is the sudden or sudden interruption of something that presents an expected behavior.

Having clarity of the definition, now if we can have a classification on the different types of disruption that exist, this classification is part of the research that has been integrated by different researchers who have contributed to their work on the subject. As described, a disruption has to do with an unexpected scenario and behavior that causes human beings, in addition to uncertainty, a forced change in their behaviors and behaviors such as work, consumption, coexistence, socialization, fun , among others. According to this description that contemplates a change in people's behavior patterns, we cannot expect something different to happen in labor and social organizations where people are the central elements that integrate them and give them life.

2.1. Classification of disruptions affecting the supply chain

By ordering ideas we can then say that when speaking of a disruption that affects organizations it is closely linked to an

unexpected situation or scenario and therefore can be classified into two types of disruptions, (1) those that are in a controlled environment and that in many occasions they obey technological innovations, and (2) those that arise due to an uncontrolled situation caused by disasters or natural catastrophes and even human-induced situations without even having dimensioned the impact that this will cause, such as terrorists acts. In [6], the author explained that whatever the origin that causes a disruption brings with it impacts on the supply chain. Annex 1 shows the classification of controlled disruptive events most relevant to the retail industry.

There is, as already mentioned, another group of disruptive events that are uncontrolled and that are also worth classifying in order to have a systemic perspective of the disruptive events facing humanity. In recent years we have seen these types of incidents that affect a large part of our planet and that lead us to reflect on how to manage properly and how to be prepared to when they happen, to mention some of these incidents and their impacts, how to imagine that the eruption of a volcano in Iceland would paralyze much of Europe's air movements and with it the interruption of the flow of goods, a series of forest fires in The United States and Australia would lead to the closure of companies dedicated to the assembly of by-products or components in the United States and, in the case of Australia, the closure of companies and the displacement of the workforce to other areas of the country, the bird flu that occurred in Asia and that caused millionaire losses to many companies affected by this situation and the sanitary fence that was implemented. The hurricanes and tsunamis that have occurred in different parts of the world have caused, in addition to human tragedies, the paralysis of factories and even the complete disappearance of companies dedicated to the manufacture of inputs within different supply chains. Disruptive events caused by uncontrolled situations can be seen in Annex 2.

The focus of this research is directed to this group of disruptions in uncontrolled environments and to be more specific, to the impacts of pandemics and epidemics in supply chains, in this case to the affectation that COVID-19 is causing in the international market and in the different supply chains that integrate it, in [6] the author explained in his conceptual framework of supply chain disruptions, about disruptions in the behavior of demand and disruptions in the supply of products.

2.2. COVID-19 and its impact on supply chains

The effect of a pandemic like that of COVID-19 is anteceded by what happened more than two decades ago with the aforementioned H5N1 avian influenza and a few years later with the H1N1 influenza that occurred between 2009 and 2010, however, the prolonged effect by COVID -19 is unmatched in terms of economic, social and loss of life impacts.

COVID-19 has come to present itself as an evil that the present generation had not faced, it has come as a script taken from a horror movie in all aspects, a segment of the apocalypse that illustrates what the future of the world will be like after observing how the health systems of entire nations have collapsed, of the economy and not to mention the psychosocial aspect that this disease is causing. Various authors describe the current scenario using analogies that refer to a combination of interrelated variables, on the one hand the probability that it will happen and the impact that

it can cause when it happens. In [7] the author metaphorically described such events as the COVID-19 pandemic as a "black swan" for humanity, in [8] the author described in reference to the same hypothesis the rarity of seeing a "black swan" and on the other hand the high impact it represents for humanity in this case the pandemic that is sweeping the whole world.

As a member of a leading transnational organization in the retail industry, just a few months ago, to be exact the beginning of 2020, we did not imagine in our annual strategic planning process of the company the threat of facing a scenario like the one that is being presented by the effect of COVID-19, it was not a topic, much less a stage that our organization and many others imagined.

After a few months of experiencing this global collapse, it is possible to make a count of learning that has favored the operational continuity of the organizations that have remained standing to continue being a profitable option for their clients and consumers. Among these learnings we can mention some in which the research will be deepened:

1) Have a structure robust enough for management, seeking efficiency both in the execution of local operational functions and in staff functions.
2) Have an interconnected network of suppliers for each distribution center, with a solid alternative of local supply.
3) Having human resources and protecting them from the environment so that what has been previously described can take place, even becoming the most important aspect for the organization to remain current. Protecting people becomes a priority for organizations.

These three lessons help organizations have more resilient supply chains in order to get this complicated stage on track, affecting their operational continuity. The motivation to carry out an investigation to carry out this investigation is to contribute knowledge and learning in situations such as the one being experienced.

2.3. An overview of the retail industry as an essential company in the days of COVID-19

The COVID-19 crisis has affected the economy through different factors related to the health of the population, the mandatory blockades and interruptions to trade, as well as a series of collateral effects such as the decisions that organizations forced by the situation have had to make and which are related to maintaining sources of employment. In [9], the author explained about emotional factors such as the pessimistic feeling of consumers and companies derived from high uncertainty and financial stress.

For companies classified as essential due to the role they play before society for offering food products and other types of food considered basic for human consumption, it is a challenge to keep their supply chain processes active in a complicated environment and where many companies that are part of the supply chain gradually lose productive capacity given the situation of the pandemic and with it the available inventories. It is here at this point where presented the situation many organizations reflect on the design, the priorities and the strategy that they have followed to develop the business and where the supply chain and the supply network that integrates it become relevant, such as previously

described, "leverage" in the factors of people, network of providers, above all the development of the premises and lastly the operational and staff structure that it provides. In [10], the author explained about the key aspect of developing collaborative strategies with suppliers and together adopting best practices that help to have a better performance in the supply chain.

The pandemic shows that it may be too simplistic to base decisions about production locations solely on economic factors and many companies may not fully appreciate their vulnerability to global shocks through their supply chain relationships and the costs this imposes. In [11], the author explains the importance of having future risk assessments of companies before they decide to relocate production or when reconsidering their location options.

There is a social commitment to the population and to the government authorities to keep the supply network in force so that the population is not affected by the lack of basic necessities. In a situation like COVID-19, a strategy must be adopted to adequately manage the shortage and make efforts to carry out emerging actions to ensure the supply of essential products. This work proposes scenarios in which organizations classified as essential, such as the retail industry, can adopt a model based on a continuity matrix in the face of the loss of capacity of the logistics network.

The value chain for food or perishable products offered in the retail industry becomes more relevant in a scenario such as the one currently presented in the COVID-19 contingency. In [12], the author described that the supply chain must be designed in such a way that production, transformation and distribution generate the expected value in the supply chain and therefore to the consumer.

3. A structured proposal for supply chain management based on a contingency plan against COVID-19

The proposal that is developed in this work incorporates the key elements to take care of for the operational continuity of the supply chain of companies in the retail industry. Adequate management through the proposed contingency matrix will not only allow operating with well-defined criteria for decision-making based on the changes that the supply chain is having in the different processes that comprise it, but will also help to maintain an organization communicated at all organizational levels about the intention of senior management in the face of the pandemic. The group of researchers who have worked on the development of the document have had the opportunity to carry out the implementation of the tool in the leading company in the market in convenience stores in Mexico.

Talking about COVID-19 today is talking about a diversity of topics that converge on a macro issue such as the global collapse due to the effects of the pandemic that we had to live in this 2020 and that will surely go beyond this year. It is common to see the large number of articles suggesting how to bring life in all aspects to a new normal.

3.1. Method of assessing the level of risk of the supply chain

Faced with the impacts of the pandemic, supply chains have collapsed to a greater or lesser extent throughout the world, the network of suppliers has been compromised and, in worst case scenarios, disarticulated. This level of exposure highlights the importance of having a mechanism for assessing the level of risk

in the supply chain. As part of the research carried out, a method of assessing the level of risk of the supply chain is being proposed. For this, it is important to start from a statement that the authors of this work make based on the experience and consultations made in the works of other researchers. As a starting point it is necessary to start with the definition of the key, operational and service processes.

3.2. Operational and service processes of the supply chain

The key processes that make up the operation of the supply chain become a distinctive seal that gives identity to the organization and marks the success or failure in achieving the value proposition to the end customer.

Focused on the case of the retail industry where companies participate in an environment with some volatility and where business strategies change from one day to the next or in extreme cases, from morning to night with various promotions simultaneously and with packages or commercial combos from different suppliers, the supply chain must be directly connected to the commercial strategy in order to make each of its processes focused on providing the service work. The companies that make up the retail industry are considered essential due to the impact on the supply of food to the community where they are located.

Following are the key processes in the supply chain of a distribution center serving a network of convenience stores:

1. Supply
2. Receipt of merchandise from suppliers
3. Storage of merchandise
4. Order management and replenishment planning
5. Assortment of orders
6. Preparation and consolidation of orders
7. Loading and boarding
8. Delivery of orders to the store

The key processes of a distribution center operation can be seen in Figure 1. In [13], the author described the supply chain processes in the SCOR Model with the objective of having a valid reference for the construction of a proposal that offers visibility and focus on having an efficiency analysis of the supply chain processes. In [14], the author explained the approach to supply chain efficiency and the integration of best practices. In [15], the author contributed to the SCOR Model the hierarchy of processes for decision making and supply chain management. Table 3 shows the relationship of the proposed processes with those classified in the SCOR Model. Table 3 shows the relationship of the proposed processes with those classified in the SCOR Model.

3.2.1. Supply

It is the process by which all merchandise supply activities are managed from the supplier to the distribution center or directly to the stores. The supply process aims to guarantee the supply of goods in a timely manner, in the quantity required for sale and with the quality that meets the parameters of each product for sale to consumer customers.

This process groups a series of activities considered strategic by a team that is constantly analyzing inventories, sales behavior, in close communication with the categories in which the product catalog is classified and finally with the marketing part. for proper planning of promotions.

Table 1: Comparative relationship of SCOR Model processes and operating processes of the retail industry.

SCOR Model processes		Retail industry supply chain operational processes
Plan Supply Chain	Plan Source	Supply - Receipt of merchandise
	Source Stocked Product	Storage of merchandise
	Plan Make	Order management
	Make to stock	Assortment of orders
		Preparation and consolidation of orders
	Plan Delivery	Loading and boarding
		Delivery of orders to the store

3.2.2. Receipt of merchandise

It is the reception of merchandise orders from suppliers, they obey an appointment planning agreed with suppliers and must be in accordance with procedures and policies on the requirements to be met in the proper handling of products that in some cases require certain parameters of refrigeration, humidity and security, such as the height of the platforms where the merchandise arrives.

3.2.3. Storage of merchandise

Within sequential flow of operations, it is the process in which the merchandise is located in a site within the area destined for storage. This process aims to create the appropriate conditions for the safekeeping and control of different goods. Each movement of merchandise from its storage location to another point, obeys a merchandise flow instruction to send said merchandise to an assortment location that can be refrigerated boxes, pieces or parts assortment.

3.2.4. Order management

It is an administrative process that is carried out with merchandise replacement tools at the store and is practically the equivalent of having a production program or planning of order fulfillment activities, ordered by priority based on the criticality of inventories. in shop. This process represents the intelligence center that drives the operations of the distribution center and through which resources are allocated to fulfill store orders.

3.2.5. Assortment of orders

It is the process in which operation personnel carry out order fulfillment activities. There are three different areas of order assortment which are:

1. Refrigerated product area: The assortment of orders is made in a plastic container and each piece is placed inside.

2. Product assortment per box area: The order assortment is for a higher unit of measure and is defined for products with high turnover or high displacement at the point of sale. To carry out this type of assortment, the Operator uses mobile equipment

to place all the merchandise that is supplied per box on a pallet.

3. Product assortment area by piece, blister or minor packaging: The assortment is carried out online by assortment by pieces and the Assortment Operator uses a plastic container to place all the pieces that appear in the order of order.

After an order is filled from any assortment area, there is an assurance reliability check thread, offering feedback to the assortment team on the quality of the task performed.

3.2.6. Preparation and consolidation of orders

Process by which the orders already filled, both boxes and dry parts and refrigerated parts are ordered by store. It is consolidated by store and in the order in which they will be loaded in the transport unit; as well as how the orders will be delivered by store according to routing, which requires room temperature and which requires refrigeration.

3.2.7. Loading and boarding

Process in which the orders are loaded in the transport units according to a routing sheet and delivery order, as well as the invoicing of each order. It is important to keep a sequential control of the load so that the Distribution Operator does not have setbacks in deliveries.

3.2.8. Delivery of orders to the store

It is the transportation process by which the merchandise is transported and delivered from the distribution center to the store. The Distribution Operator delivers to the customer under certain conditions that have to do with product handling conditions such as maintaining the cold chain for products that require it and the corresponding administrative and control documents that support the order. Annex 3 shows the capacities of each process, as well as the associated unit of measurement.

3.3. System of metrics or performance indicators of key processes

As the key processes of the distribution center have been defined, each process has an associated performance standard and metrics to evaluate it. Table 5 shows the metrics for each process under the efficiency approach. In the context of the supply chain, the integration of the objectives in its different levels is an important factor for the correct selection of the indicators, which will provide a broader view of the business. In [16], the author described the importance of having identified key performance indicators, through which a reference will be available at all times to assess the resilience of the processes when a disruption occurs.

Of course, there will be other indicators that have to do with the result of the business if what you want to see is the economic contribution; however, these are more common to see throughout the chain. They are also described in Annex 5.

In order to have a level of detail that allows a better management of goods, it is essential to have an administration by product categories. In [10], the author explained the importance of interconnecting merchandise categories for efficient management of supply chain processes. Figure 1 shows the supply chain from the supplier to the store, passing through the distribution center.

3.4. Key elements to successfully respond to the COVID-19 pandemic

During the research conducted, we had the opportunity to analyze different contributions from other researchers related to the key elements of the supply chain, which date back almost two decades. Without a framework for action that allows visibility of these key elements, it will be difficult to promote the improvement of supply chain performance. In [17], the author explained the importance for organizations of designing an operating model that facilitates the management of supply chain processes and identifying their restrictions, in addition to these elements. There are other researches that based on their studies make another proposal from a different perspective, where a classification is made according to the relevant aspects of supply chain resilience. In [18] the author presented a proposal to categorize resilience actions using four main categories: systems, process, control and recovery.
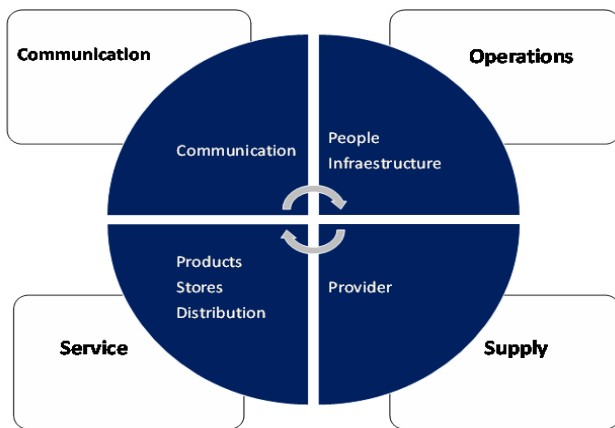
Figure 2: Key elements of the convenience store supply chain (source: self made)

The research proposal is contained in seven key elements, classified in turn into four supply chain management pillars comprising the proposed evaluation method, as shown in Figure 2. The key elements to consider in order to have A perspective and reference of the level of vulnerability of the supply chain to possible risks are grouped into four management pillars are described below:

- Operations: Refers to the group of activities that allow the continuity of the operation of the key processes. It includes the human resource, infrastructure and general facilities of the work unit.
- Supply: Includes the relationship and development of suppliers to guarantee the supply of goods from the supplier's facilities to the distribution center.
- Service: They are all the activities that allow the supply of goods from the distribution center to the store. The elements

that make up the service pillar are merchandise, distribution and stores.
- Communication: Refers to the strategy that the company intends to carry out to communicate its intention at all levels of the organization and even outside of it.

The key elements that, in turn, make up the supply chain management pillars and through which an evaluation of the level of response to the effects of a pandemic such as COVID-19 can be made are:

1. People

2. Facilities and infrastructure

3. Suppliers

4. Goods / Products

5. Stores / points of sale

6. Distribution / delivery to store

7. Communication

3.4.1. People

It comprises the most important resource at all levels of the supply chain, its well-being is a priority so that each of the supply chain processes can be carried out. Although it sounds like a very repeated cliche, "people are the most important thing" and they should know it and they should feel it, without a clear pronouncement from the organization of approach to people, it is difficult to advance in the other aspects.

Faced with a situation such as that of COVID-19, where the level of risk of contagion is present, there must be a consistency in the saying, in the being and in the doing from top management to the most basic positions in the structure. If there is no legitimate concern for the safety and health of people, there is no emotional bond that generates commitment.

3.4.2. Facilities and infrastructure

They are the assets of the organization necessary for the work units to be active. This element is closely related to human resources and must offer security and protection conditions so that personnel can carry out their activities without any distraction. It includes the industrial building or warehouse, the machinery and peripheral work equipment so that people can carry out their functions.

In the face of a pandemic like the one presented by COVID-19, maintaining the safety of the facilities becomes critical for the continuity of the operations of the companies that handle food and perishable products and that is why they are considered essential companies for society. Keeping the workplace pollution-free for employees represents a major challenge for companies and largely depends on the implementation of sanitation measures and / or protocols and strict compliance with government requirements for the preservation of hygiene standards.

3.4.3. Suppliers

It is the active network of suppliers that supply goods to the distribution centers or directly to the points of sale. It is important to have full knowledge of the conditions of each supplier in the

network, in [19], the author described the importance of having information from upstream suppliers several levels back. Companies that do not do so are less able to respond or estimate the potential impacts when a crisis erupts. Under the supply chain perspective, the objective is to maintain continuity in the supply of products in order to have them in a timely manner and in the quantity required in distribution centers and / or in stores or points of sale. A supply chain is as strong as is the capacity of alternative suppliers. Some researchers consider the supplier network as the benchmark to determine the level of resilience of the companies' supply chain, highlighting as a strategy the development of local suppliers to mitigate the risk of dependence on suppliers located outside their geographical area, of the country and even to the continent.

It should be borne in mind that in the face of a pandemic such as this one, companies must develop new supply alternatives, it is a fact that the companies that precede the chain will be affected in their operations.

3.4.4. Goods / products

Refers to the active catalog of items offered to the customer at the point of sale. When speaking of merchandise or articles, it is important to mention that the companies dedicated to the sale of basic necessities use for a better administration of these, a classification regularly called category. This classification consists of grouping the type of merchandise so that a group of people, regularly on a staff basis, can establish the marketing strategy that involves the relationship with suppliers, marketing, study of new developments and promotion plans. The categories together with the financial area determine the profit margin of each product to evaluate its performance, establishing for this purpose negotiations of costs and sale prices. In [20], the author explained the existence of algorithms or models that allow setting price points considering the market and the position as leader in the competition.

Faced with a situation such as COVID-19, organizations must be clear about the economic performance of each product, this will allow them to make better decisions about the profitability of the business and thus privilege the items that in their classification are considered essential for society but that are also profitable for the organization. In [21], the author explained the strategy of increasing inventories can be a measure to mitigate the risk posed by a disruption, however, it is reactive to an actual shortage; the strategy can include product substitution or back-up supply.

3.4.5. Stores / points of sale

These are the points of sale to the consumer customer or stores that the company has. They can be classified according to their location and format by the type of customer who regularly comes to buy. In [22], the author described that the complexity of the store as such lies in the number of stores in operation and the store formats it has with different sizes, catalog and price points.

The commercial and marketing team are the ones who carry out this classification of stores and thus be able to establish a catalog of products for each type of store. This classification of stores allows in addition to establishing a catalog of particular products, establishing the entire campaign of promotions, prices and launches, this differentiation is key to evaluating the performance of each store in its sales volume.

An example of differentiation in the classification of stores is the store that is located inside a high-density residential subdivision with the store that is located inside a hospital, it will be found that neither catalog of products for sale is the same and due to the location conditions, nor is the sale income.

3.4.6. Distribution or delivery to store

It is the transportation process by which the merchandise is delivered from the supplier or distribution center to the point of sale. The transport equipment used is conditioned for handling both merchandise that requires refrigeration and room temperature.

Under the store delivery conditions required in this contingency stage, the distribution personnel must have the necessary protective equipment to carry out the merchandise delivery tasks at the point of sale, as well as the sanitation measures for the units must be in accordance with certain regulatory measures for the handling of perishable product.

3.4.7. Communication

They are the means or mechanisms established by the organization to maintain timely and assertive communication at all levels of the organization, and even in the event of possible communication with the press and / or a statement to government authorities. Communication must at all times be reliable, truthful and above all timely about the organization's intentions in the face of the contingency it is facing.

There are different methodologies that help organizations to be prepared to face a contingency from the point of view of information management and what they want to communicate from a 360° perspective, as described above. We will mention that there is a methodology that helps coordinate and this is Incident Management and Crisis Resolution (IMCR), methodology developed in the United States.

3.5. Scenarios taken to a continuity actions matrix of COVID-19

Organizations are facing an unprecedented global crisis, human survival depends on essential elements during the pandemic and that can be met by properly utilizing key resources such as raw materials, employees and active logistics systems. In [23], the author described that the priority of nations during the pandemic is to save human lives, but shortages of essential commodities such as food, drugs, diagnostic equipment, clinical healing and personal protective equipment have made it difficult to fight the infection.

Having defined the priorities of nations and organizations to preserve the health of people as the most important priority, it remains for organizations to resolve the most important aspects to ensure the operational continuity of businesses, in [24], the author explained the importance of uncertainty management in the supply chain and how strategies can be established in inventory management. In [25], the author described that organizational leaders must urgently implement short-term strategies to be more resilient while making longer-term considerations that will reconfigure supply chains to protect against risks.

- Develop visibility of the entire value chain in primary, secondary and even tertiary players.

- Evaluate nearby options to shorten supply chains and increase proximity to customers.

- Take advantage of advanced manufacturing technologies to be more resistant. Another important point is to systematically evaluate the end-to-end value chain, to establish agile action plans.

Organizations are facing an unprecedented global crisis, and one approach that has not exactly been the most appropriate for supply chain management is to think about generating efficiencies and savings at the expense of eliminating slack or "margins of maneuver", such as operating with a diversity of suppliers for the same product, operating with safety inventories in the chain, etc., which in the face of a disruptive situation such as the COVID-19 pandemic leaves the organization exposed. In [26], the author explained that there has long been a focus on making the supply chain more efficient based on reducing costs, reducing inventories and increasing asset utilization, thus eliminating buffers and flexibility to absorb disruptions.

With the description of the key elements and their classification by management pillar, a continuity actions matrix can be integrated in a more practical way to evaluate possible scenarios and trigger actions focused on ensuring supply to stores.

In summary, after presenting the key elements for business continuity in companies classified as essential (and largely applicable to non-essentials as well), organizations will need to work on:

- Guarantee that people feel protected in a work environment that complies with the conditions and measures of control, sanitation and use of personal protective equipment that mitigates the risk of contagion, also keeping facilities and work tools under a protocol frequent cleaning. In [19], the author explained that employee welfare is paramount, and obviously people are a critical resource.

- Developing local suppliers for the supply of key merchandise, that implies redesigning the supply network to a great extent. If COVID-19 has revealed anything, it is the high level of risk represented by having a large number of suppliers in one place.

- Organizations should develop suppliers close to their main markets; this strategy will help mitigate the risk of centralized dependence, which can be maintained and alternatively explore other sources of supply. In [4], the author explained that another important factor to consider is that as transportation and other costs increase, global supply chains may be replaced by regional supply chains.

- Provide the service as far as the contingency allows and maintain the value proposition of the stores, without infringing the care of the workers and complying with the requirements established by the government agencies. As organizations considered essential, those products of first necessity for the population must be privileged and, on the other hand, they also represent a greater profitability for the organization, for this it is important that a detailed analysis of those products is made and that level is established with suppliers. priority in supply.

- Maintain communication at all levels of the organization about the decisions that the company is taking, from issues of personnel health and care of facilities}, to those that could be more critical as partial closure of operations and in in the worst case, the total closure of work units.

- For people, it is important to be informed about how the organization is facing the pandemic and what decisions are being made by senior management. To the extent that there is clear communication, the uncertainty will be combated and the staff will be focused on their care and the performance of their tasks.

- Assessing the level of risk in the supply chain is to have a preventive approach and it must be considered from the strategic planning process of organizations, that annual exercise that most organizations that describe themselves as preventive and that base their management under procedures and well-defined work systems, should consider in such planning an assessment of the risk level of their supply chain. Does this evaluation require an expense to be considered in the annual budget? The answer is yes, and excess spending due to not having an action plan to mitigate risks in the face of a disruptive event such as this pandemic may be much higher than the cost of a supply chain assessment.

- There will be many lessons learned from this disruption by COVID-19, even some organizations will not survive in order to capitalize on the learning it leaves. For the surviving companies it will be an opportunity to integrate the knowledge acquired and the recommendations that lead them to strengthen their processes and increase their resilience in the face of a disruptive event that submitted their performance and put their permanence at high risk.

The proposal made in this research is the COVID-19 business continuity matrix and is intended to provide a complete picture for organizations to evaluate the variables faced by organizations. In [27], the author described that robust strategies must be developed that integrate the purposes of reducing costs and improving customer satisfaction during and after a major disruption. In [28], the author described the importance of the design of the supply chain conceptual framework and the essential elements that have to do with resilience to disruptions that occur and supply chain resilience recovery policies. In [29], the author explained that the problem for top management of organizations is to choose a good strategy and quantify the benefits to develop a robust model for supply chain disruption analysis, for this it is important to identify and understand the overall behavior and intrinsic weaknesses of these systems and their components, especially in the face of negative events such as disruptions. In [30], the author presented that only a small minority of companies that invested in mapping and measuring the vulnerability of their supply chains are the best prepared to face this pandemic. Annex 5 shows the matrix of continuity actions to face the different impact scenarios of COVID-19.

3.6. Stabilization of the post-disruption operation

The stabilization stage of the operation is a continuation of the actions described in the continuity actions matrix as part of a plan where the regeneration or recovery of the resources of the supply

chain is taking place through the effect of the disruption has yielded. It is important to prepare a recovery plan and periodically review it by the management team so that the scenarios that require decision-making are updated. To the extent that there is an updated plan and communicated to the entire organization, the horizon will be visible when a total restoration of the organization and its supply chain will be presented and thus decisions can be made as to decide when to stop buying , when to stop transporting or when to stop producing, among other operations that have had to be implemented with an over cost justified by the disruption.

Another important aspect mentioned in the key elements is the communication that exists at all levels of the organization and which must be used to reach the collaborators with what they need to know, having a single source of information helps maintain the credibility of people when their health and that of their families is at stake.

Any action plan focused on treatment, solution or simply trying to coexist with a problematic situation, in this case a disruption of natural origin, must leave knowledge to organizations, considered essential or non-essential, if organizations do not learn from these lessons they will not have the opportunity to leave a legacy and an ABC of what was done as good practice to come out in front of a pandemic like that of COVID-19 and new managers, they will not be able to learn from those experiences to face the new challenges that they will surely have during their management when new disruptions arise.

Among the relevant contributions that integrate the research is a series of strategies that help stabilize operations and that focus on the objectives of identifying the level of risk in the supply chain, adequately managing resources and having an action plan to mitigate risks with suppliers and internal processes. In [31], the author explained that actions should be taken to improve internal capabilities, prepare inventory levels that meet projected sales and reserve logistical capacity.

4. Conclusions

The importance of having defined and structured processes for proper management of the supply chain offers a scenario that helps to better manage uncertainty and for this reason to mitigate disruptive environments that arise. Having performance metrics aligned to the strategy and capabilities of the processes help not to fall into the obsolescence of the supply chain. The processes and their metrics make it easier to be able to develop a proposal that allows evaluating the level of risk in the supply chain and consequently developing an emerging action plan for each scenario that presents a disruption of the magnitude of COVID-19.

Many organizations must be sensitive to the fact that the supply chain is a series of processes that have life and that must be evaluated periodically from the perspective of the level of risk to which they are exposed due to the dynamism of environmental variables. It will always be a successful and strategic alternative to diversify the sources of resources and related to this point, these types of decisions are what organizations must bear in mind when it comes to making decisions to pulverize the supply of goods from suppliers located in another region, in another country or even on another continent.

This research aims to offer a point of reference that allows evaluating the supply chain of organizations in the retail industry, from the perspective of the key elements raised throughout the work and that in the end is the main contribution that is made.

Finally, a supply chain oriented to service and to a value proposition committed to the customer allows creating a virtuous cycle to reinvent the increasingly resilient and anti-fragile supply chain. It is important to recognize that there are different investigations that focus on the management of disruptive stages in organizations, as well as these extremely valuable work carried out, there will be other future contributions that will come with new approaches and other variables to consider. Given this scenario, there is the commitment of those who collaborated in this scientific work to leave a documented learning for future generations of how to handle these disruptions, we will not be fulfilling a professional commitment, nor would our legacy be complete on how it was managed and left ahead of COVID-19.

Conflict of Interest

The authors declare no conflict of interest.

Acknowledgment

References

[1] H.L. Lee, "The Triple-A Supply Chain". Harvard Business Review, 102-112, 2004.

[2] U. Jüttner, M. Christopher, J. Godsell, "A strategic framework for integrating marketing and supply chain strategies," Cranfield University, UK. **21** (1), 104-126, 2010, DOI: 10.1108/09574091011042205.

[3] C. Chandra, J. Grabis, "Supply Chain Configuration: Concepts, Solutions and Applications", Springer Science + Business, 2016.

[4] S. Chopra, M. S. Sodhi, "Reducing the risk of supply chain disruptions," MIT Sloan Management Review, **55** (3), 72-80, 2014. https://www.researchgate.net/publication/271853432.

[5] K. Stecke, S. Kumar, "Sources of supply chain disruptions, factors that breed vulnerability and mitigating strategies", University Texas School of Management. Journal of Marketing Channels, **16**, 193-226, 2009, DOI: 10.1080/10466690902932551.

[6] B. Shen, Q. Li, "Market disruptions in supply chain: a review of operational models," Donghua University Shanghai, China. International Transactions in Operational Research 2017, 697-711, 2017. DOI: 10.1111/itor.12333.

[7] N. Taleb, "The black swan the impact of the highly improbable," https://www.researchgate.net/publication/46763446_The_Black_Swan_The_Impact_of_the_Highly_Improbable, 2010.

[8] S. Zwick, "Coronavirus is bad, but the green swan is worse," https://www.ecosystemmarketplace.com/articles/coronavirus-is-dangerous-but-the-green-swan-is-worse/, 2020.

[9] M. Meier, E. Pinto, "COVID-19 Supply chain disruptions," Universität Mannheim, Department of Economics. 2020.

[10] S. Ganesan, G. Morris, J. Sandy, R. W. Palmatier, B. Weitz, "Supply chain management and retailer performance: Emerging trends, issues, and implications for research and practice," University of Arizona. Journal of Retailing **85**, 84-94, 2009. doi:10.1016/j.jretai.2008.12.001.

[11] A. Serig, H. Görg, S. Mösle & M. Windisch, "COVID-19: Disruptions on the global value chain," https://www.weforum.org/agenda/2020/04/covid-19-pandemic-disrupts-global-value-chains/, 2020.

[12] R. Zhong, L. Wang, "Food supply chain management: systems, implementations, and future research," University of Auckalnd, New Zeland. Department of Mechanical Engineering, **117** (9), 2085-2114, 2017. DOI 10.1108/IMDS-09-2016-0391.

[13] P. Bolstorff, R. Rosenbaum, "Supply chain excellence: a handbook for dramatic improvement using the SCOR Model," Amacom, 2003.

[14] G. Reiner, P. Hofmann, "Efficiency analysis of supply chain processes," Vienna University of Economics and Business Administration, **44**(23), 5065-5087, 2006. DOI: 10.1080/00207540500515123.

[15] S. Huan, S. Sheoran, G. Wang, "A review and analysis of supply chain operations reference (SCOR) Model," University of Cincinnati, **9** (1), 23-29, 2004. DOI: 131139-158098434138188.

[16] A. Karl, J. Micheluzzi, C.R. Pereira, "Supply chain resilience and key performance indicators: a systemic literature review," Universidade do Estado de Santa Catarina, Joinville, SC, Brasil. **28**, 2018. DOI: 10.1590/01036513.20180020.

[17] H. Min, G. Zhou, "Supply chain modeling: past, present and future," University of Lousville. Computers & Industrial Engineering, **43**, 231-249, 2002. PII: S0360-8352(02)00066-9.

[18] M. M. Queiroz, D. Ivanov, A. Dolgui, S. Fosso Wamba, "Impacts epidemic outbreaks on supply chain: mapping research agenda amid the COVID-19 pandemic through a structured literature review," Operationes Research. 2020. doi.org/10.1007/s10479-020-03685-7.

[19] J. B. Rice, "Prepare your supply chain for coronavirus," https://hbr.org/2020/02/prepare-your-supply-chain-for-coronavirus. 2020.

[20] K. Chen, T. Xiao, "Demand disruption and coordination of the supply chain with a dominant retailer," Nanjing University, Jiangsu, China. **197**, 225-234, 2009. doi:10.1016/j.ejor.2008.06.006.

[21] L. V. Snyder, A. Zümbül, P. Peng, Y. Rong, A. J. Schmitt, B. Sinsoysal, "OR/MS Models for supply chain disruptions: a Review," University of Nebraska, USA, 2015. DOI: 10.1080/0740817X.2015.1067735.

[22] E. Ekinci, A. Baykasoglu, "Modelling complexity in retail supply chains," Dokuz Eylul University, Izmir, Turkey. **45** (2), 297-322, 2016. DOI 10.1108/K-12-2014-0307.

[23] S. Singh, R. Kumar, R. Panchal, M. Kumar Tiwari, "Impacto of COVID-19 on logistics systems and disruptions in food supply chain," National Institute of Industrial Engineering (NITIE), Mumbai, India. International Journal of Production Research, DOI: 10.1080/00207543.2020.1792000, 2020.

[24] S. Chopra, P. Meindl, "Supply chain management: strategics, plan and operations," Pearson 2013.

[25] F. Betti, Kristian Hong, "Coronavirus is disrupting global value chains. Here's how companies can respond," https://www.weforum.org/agenda/2020/02/how-coronavirus-disrupts-global-value-chains. 2020.

[26] J. Kirkpatrick, L. Barter, "COVID-19 Managing supply chain risk and disruption," https://www2.deloitte.com/global/en/pages/risk/articles/covid-19-managing-supply-chain-risk-and-disruption.html, 2020.

[27] C. Tang, "Robust strategies for mitigating supply chain disruptions," UCLA Anderson School, **9** (1), 33-45, 2006. DOI: 10.1080/13675560500405584.

[28] D. Ivanov, A. Dolgui, B. Sokolov, M. Ivanova, "Disruptions in supply chain and recovery policies: state of the art review," Berlin School of Economics and Law, Berlin, Germany, **49** (12), 1436-1441, 2016. 10.1016/j.ifacol.2016.07.773.

[29] M. F. Blos, P. F. Miyagi, "Modeling the supply chain disruptions: a study based on the supply chain interdependencie," Escola Politecnica da Universidade de Sao Paolo, SP, Brazil, **48** (3), 2053-2058, 2015. 10.1016/j.ifacol.2015.06.391.

[30] T. Choi, D. Rogers, B. Vakil, "Coronavirus is a wake-up call for supply chain management," https://hbr.org/2020/03/coronavirus-is-a-wake-up-call-for-supply-chain-management, 2020.

[31] D. Simchi-Levi, "Three scenarios to guide your global supply chain recovery, Even as the business climate remains deeply unpredictable, supply chain leaders should act now to plot their comebacks," https://sloanreview.mit.edu/article/three-scenarios-to-guide-your-global-supply-chain-recovery/, 2020.

Annex 1. Main disruptive events in a controlled environment in the retail industry.

Disruption	Description
Technological effect / e-commerce	Definitely the disruptive element with the greatest impact in the last decade, those who dominate networks and online shopping have ample possibilities to position themselves in a highly competitive market. Today it is a must for organizations to be in the online market.
Proximity, time dedicated to home purchase and delivery	Another disruptive element associated with the first, the famous last mile represents for the consumer customer a key decision factor to carry out the purchase. Delivering merchandise at the consumer's door is a battle that is being waged every day today.
Specialty market and lifestyle	Not all stores have the same product catalog, for different reasons or circumstances, the store's commercial design may change to serve certain types of customers who come to or are in that market. A convenience store located in a popular sector should have a differentiation from a store located in a university.
Catalog of products and services	With the passage of time the convenience store has become a strong competitor for large supermarkets, let's say that the evolution of the "corner store" has become a convenience store that offers the consumer customer a wide catalog of products and services.
Perishable management	Bet on handling products that require refrigeration such as prepared food, meat and fruits and vegetables. Even a growing market that procures organic products claims a segment for this type of product.

Annex 2. Main disruptive events in an uncontrolled environment in the retail industry.

Disruption	Description
Natural disasters such as earthquakes, hurricanes, tsunamis, volcanic eruptions, fires, among others.	Natural events that happen suddenly in different locations in the world and that cause a collapse in the flow of goods and in the economic aspect. Although they may be areas that have identified the level of risk, this type of natural disaster cannot be forecast.
Pandemics / epidemics and other health issues involving a sanitary fence	Condition where the health of the population of a country or countries that have a commercial relationship is affected by the exchange of goods among themselves. The effect of a global pandemic has an impact on the flow of goods of all the countries that are interconnected for the transfer of goods and other types of resources.
Terrorist acts	Premeditated or intentional actions that aim to cause destabilization through inflicting damage to a specific place or society and that through chaos there is an expected size of affectation. In general, the disruptive event that it causes has to do with reinforcing security measures and trade blockades.
Socio-political and economic decline	Aggravation of the socio-political conditions of a country which causes a recession or deceleration in the economic development of the industry and in general for the population. This type of disruption can take time to appear at the maximum level of affectation and as it is a slow process, it also usually takes time to mitigate the level of maximum affectation.
Armed conflicts	Like the disruptions considered as deterioration of the social and political fabric and as a consequence an adverse economic impact, in many cases society ends up rising up in arms before an unacceptable government. This type of disruption often takes a long time to find a solution that manages to offer social and economic stability.

Annex 3. Operational and service processes of a retail industry supply chain.

Processes	Capacity	Unit of measurement	Description
Supply	Active code catalog	No. active codes	It is the catalog of active product codes.
	Active providers	No. of active providers	The number of active suppliers supplying merchandise.
	Supply service for criticality of merchandise and supplier	% service level	It is the level of supply service that can be measured according to the criticality by merchandise and by supplier.
Merchandise reception	Merchandise reception	Pallets	Pallets received from the supplier.
Storage merchandise	Case storage positions	Pallets	Number of positions for storing product pallets in cases.
	Case assortment positions	Pallets	Number of positions for product pallets that will be supplied by cases.
	Dry parts storage positions	Pallets	Number of positions for storing product pallets in boxes. Shares storage with group of cases.
	Dry pieces assortment positions	Assigned positions / lanes	Number of positions fed by cases and to be supplied by pieces.
	Refrigerated parts storage positions	Pallets	Number of positions for storing product pallets in refrigerated product cases.
	Refrigerated parts assortment positions	Assigned positions / lanes	Number of positions fed by boxes and to be supplied by refrigerated pieces.

Order management	Assortment of cases on shift	Cases	Capacity considered for planning and assigning tasks of assortment cases.
	Assortment of pieces dry pieces on shift	Pieces	Capacity considered for planning and assigning dry parts assortment tasks.
	Assortment of refrigerated parts on shift	Pieces	Capacity considered for planning and assigning chilled parts assortment tasks.
Assortment of orders	Assortment of cases on shift	Cases	Assortment capacity per shift of the assortment staff of boxes assortment.
	Assortment of dry pieces on shift	Pieces	Assortment capacity per shift of operating personnel for assorting dry parts.
	Assortment of refrigerated parts on shift	Pieces	Assortment capacity per shift of assorted operating personnel for refrigerated parts.
Preparation and consolidation of orders	Lowing of containers (pieces)	Containers	Number of drops for containers that were supplied by dry pieces.
	Preparation of pallets on duty	Pallets	Number of pallets prepared in the convergence of the assortment of dry pieces and cases.
Loading and boarding	Staying of prepared pallets	Pallets	Ability to safeguard assorted orders waiting to be loaded on the platform.
	Pallet load per hour	Pallets	Loading capacity to transport units associated with mobile equipment movements.
Delivery of orders to store	Transport fleet	No. of units	Transport units that make up the vehicle fleet.
	Gates	No. of loading gates	Number of platforms enabled for loading and unloading operations.

Annex 4. Key performance indicators of supply chain processes.

Processes	Indicator	Unit of measurement	Description
Supply	Inventory level in distribution center	Days	This indicator represents the level of merchandise inventory expressed in days in the distribution center and is a function of the volume of daily movement or transfer to stores. From the perspective of the Abasto process, it measures the effectiveness of planning the supply of suppliers to the center of distribution. Calculation: The inventory of the merchandise is divided by the value of its daily trip to stores.
	Lost sale	%	It is the percentage of merchandise that is not in inventory or not available for sale in the store and that has a daily sales behavior based on statistics. Calculation: The shortage of each merchandise is divided by the projected daily sale behavior of each merchandise.
	Inventory level in store	Days	This indicator represents the level of merchandise inventory expressed in days in the store and is based on the store's sales volume. From the perspective of the Abasto process, it measures the effectiveness of planning the supply from the distribution center to the store. Calculation: The inventory of the merchandise in the store is divided by the daily sale value of the store.
Merchandise reception	Compliance with supplier receipt program	%	Level of compliance with the appointment schedule established with providers. Calculation: The number of arrivals within the window is divided by the number of scheduled appointments.
	Fill rate providers	%	Level of compliance that is carried with suppliers on the requested merchandise. Calculation: The quantity of merchandise received is divided by the quantity of merchandise scheduled to be received.
Storage of merchandise	Inventory days in the distribution center	Days	This indicator represents the days inventory of merchandise in the distribution center, is based on the volume of daily trips to stores. Calculation: The inventory of the merchandise is divided by the value of its daily trip to stores.
	Product wastage	%	This indicator shows the decrease generated in the warehouse due to internal handling and product obsolescence. Calculation: The value of the lost merchandise is divided by the value of the total inventory of the distribution center.
	Inventory rotation	Cycles or number	This indicator measures the efficiency with which you have the ability to rotate inventory in the cedis. Calculation: It is the number of cycles or times that stocks were turned over during a period of time that can be monthly.
Order management	Product missing	%	This indicator shows products scheduled to be shipped to the store and not in the inventory available from the distribution center. Calculation: The total number of missing merchandise is divided by the number of merchandise scheduled to be shipped to the store.
	Cycle time	Hours	This indicator shows the cycle time of an order, it is also known as lead time. Calculation: It is the time elapsed since the store order is generated until the distribution center delivers it to the store.

Assortment of orders	Assortment productivity	Units / hr	Efficiency indicator that shows the use of resources for the productive tasks of operating personnel in each work area. Calculation: The volume supplied (pieces or boxes) is divided by operator per hour of work. There are three work areas and there may be different productivity units.
	Assortment error rate	%	Quality indicator that shows the reliability of the assortment of the productive groups. Calculation: Divide the number of errors in the operating staff assortment by the total assortment volume per operator.
Preparation and consolidation of orders	Productivity in preparation	Units / pallet	Indicator that shows the performance in the preparation and consolidation of the order prior to loading it on the platform. It is intended that the integration of orders, both for parts (plastic basket) and boxes, is of maximum density per palle. Calculation: Number of packages placed per pallet prepared.
Loading and boarding	Productivity under load	Units / truck	This efficiency indicator aims to measure the load capacity of packages in the transport unit. The aim is to make the most of the volume of the transport unit. Calculation: Number of packages loaded per transport unit.
	Unit charging time	Hours	This indicator measures the time the transport unit remains on the loading platform. The objective is for the unit to be released as soon as possible so that it begins its journey. Calculation: It is the elapsed time from when the transport unit is assigned to the platform until it is released to start the journey.
Delivery of orders to store	Compliance to delivery windows	%	This service indicator reflects arrivals within the expected time period or store delivery window. Calculation: The number of orders arriving within the assigned time window is divided by the total number of scheduled orders.
	Fill rate	%	Level of fulfillment of the delivered merchandise vs. the merchandise requested in the store order. Calculation: The quantity of merchandise delivered to the store is divided by the quantity of merchandise scheduled to be delivered.
	Cycle time deliveries	Hours	This indicator seeks to measure the time it takes for the transport unit on its order delivery route until it returns to the distribution center to start another cycle. Calculation: It is the elapsed time from when the unit is released to start an order delivery trip to stores until it returns to the distribution center.

Annex 5. Economics indicators of supply chain processes.

Processes	Indicator	Unit of measurement	Description
Group of processes inside the distribution center	Warehouse expense	$ / package	Represents the expense incurred in the warehouse operations considering the direct labor related to the operation.
	Wastage expense	$ / package	It is the expense attributable to the loss of product and inventory differences in the warehouse.
Entrega de pedidos a tienda	Distribution expense	$ / package	It is the expense of the distribution and delivery of merchandise to the store.
All processes in the supply chain	Total logistics expenditure	$ / package	It is the integral expense of all the key processes that make up the supply chain of the distribution center.

Annex 6. Continuity actions matrix of COVID-19.

Health phase	Risk level	Capacity level	Operatives		Supply		Service			Communication and diffusion
			People	**Facilities and infraestructure**	**Providers**	**Merchandise**	**Stores**	**Distribution / delivery to store**		**Communication**
Does no apply	0	Normal operation 100%	● 100% operational team ● Recruitment of personnel as a protection measure against possible damages due to loss of labor	● Review and evaluation of risks of manipulation of equipment and infrastructure ● Survey of vulnerable areas to contagion	● Identification of suppliers with risk of shortage ● Communication and risk mapping with strategic suppliers ● Explore alternative vendor alternatives	● Normal marketing plan ● Normal releases and promotions ● Local and regional promotions in the normal way	● 100% supply of stores ● Monitoring of stores closed due to contingencies	● Strengthening of the transport fleet (own and contracted) ● Routing planning with sequential time windows		● Activation of the Incident Management and Crisis Resolution Committee (MIRC)
1	1	Operation with emergenging actions 90% - 100%	● Assignment of personnel to the operational workforce by 10% ● Identification of areas that require working overtime ● Isolation for personnel classified as vulnerable group ● Activation of health filters to identify symptoms in the staff	● Installation of health and safety measures such as health filters ● Restriction of access to confined areas or without adequate ventilation ● Cancellation of meeting places that do not comply with the distance measures	● Establish a supply plan for items considered to be in high demand due to contingencies ● Establish prioritization strategy with merchandise categories (privilege suppliers of basic products) ● Activation of alternative providers and privilege regional alternatives	● Normal marketing plan ● Normal releases and promotions ● Local and regional promotions in the normal way ● Identification of the articles considered essential to prioritize their supply from suppliers	● 100% supply of stores ● Monitoring of stores closed due to contingencies ● Monitoring of rejection of deliveries to store by contingency			

2	2	Operational performance 70% - 90%	● Exploration and activation of operating schedules, working days and shift duration
			● Activation of shifts on non-working days
			● Keep staff from vulnerable groups in isolation
			● Maintain health filters to identify symptoms in staff
				● Installation of health and safety measures such as health filters
				● Restriction of access to confined areas or without adequate ventilation
				● Cancellation of meeting places that do not comply with the distance measures
				● Installation of physical barriers in work areas to avoid the risk of contagion
					● Generation of advance purchases for items classified as essential
					● Prioritization of supplier receipts
					● Consider the exchange of merchandise between distribution centers and stores (optimally distribute shortages)
					● Activation of alternative providers and privilege of regional alternatives
						● Adjusted marketing plan and according to merchandise availability
						● Prioritize the marketing of essential contingency items, such as food and perishables, cleaning and hygiene
						● Management with capacity planning, inventory replacement adjust purchases according to demand and capacity level of the distribution center
							● Monitoring of stores closed due to contingencies
							● 100% supply of stores
							● Monitoring of rejection of deliveries due to contingencies
							● Decrease in the frequency of delivery of orders to stores
							● Financial analysis that favors sending orders to the best-selling stores
								● Extension of distribution days
								● Modify daily delivery plan to a less frequent one
										● Establishment of the crisis action plan
										● Establishment of communication roles in the management team
										  - Towards the staff
										  - Towards the client
										  - Towards the General Directorate
										  - Towards authorities and government
										  - With the press and social media
										● Carry out a follow-up session to the operation and review each element of the contingency matrix

	3	Operational performance 50% - 70%	● Balancing of operating loads according to staff availability, activation of extra shifts according to availability ● Keep staff from vulnerable groups in isolation ● Staff working remotely (for those who apply the scheme) ● Strengthening of established health filters, identification of symptoms in personnel	● Installation of health and safety measures such as health filters, sanitizing mats, sanitization application with authorized cleaning fluids ● Restriction of access to confined areas or without adequate ventilation ● Cancellation of meeting places that do not comply with the distance measures ● Installation of physical barriers in work areas to avoid the risk of contagion	● Generation of advance purchases for items classified as essential ● Prioritization of the receipt of strategic merchandise suppliers ● Consider the exchange of merchandise between distribution centers and stores (optimally distribute shortages) ● Activation of alternative providers and privilege regional alternatives ● Daily communication on the operational continuity of suppliers based on the priority classification of their products ● Evaluate the collection of merchandise at the supplier's facilities	● Prioritize the marketing of essential contingency items, such as food and perishables, cleaning and hygiene ● Management with capacity planning, inventory replacement adjust purchases according to demand and capacity level of the distribution center ● Carry out financial analysis to privilege the articles that provide the greatest economic benefit to the organization. ● Exchange of merchandise between operating units and stores	● Validation of stores that remain open and capable of receiving merchandise ● Supply to stores classified as private based on sale ● Decrease in the frequency of delivery of orders to the store	● Extension of delivery days to store ● Balancing operators in deliveries 24 hours ● Decrease the frequency of delivery of orders to the store ● Perform dynamic routing with priority stores and ● Eliminate restriction of order delivery windows		
3	4	Operational performance 30% - 50%	● Balancing of operating loads according to staff availability, activation of extra shifts according to availability ● Keep staff from vulnerable groups in isolation ● Staff working remotely (for those who apply the scheme) ● Strengthening of established health filters, identification of symptoms in personnel				● Validation of stores that remain open and capable of receiving merchandise ● Monitoring of rejection of deliveries due to contingencies ● Supply of stores that remain open and classified as high sales ● Delivery of orders according to availability and receipt capacity			

Customer Behavior of Green Advertising: Confirmatory Factor Analysis

Doni Purnama Alamsyah[1,*], Norfaridatul Akmaliah Othman[2], Rudy Aryanto[1], Mulyani[1], Yogi Udjaja[1]

[1]*Bina Nusantara University, Jakarta, 11480, Indonesia*

[2]*Universiti Teknikal Malaysia, Melaka, 75000, Malaysia*

A R T I C L E I N F O	A B S T R A C T
	The implementation of green advertising is relatively low for credibility but has an impact on green customer behavior. Based on the phenomenon, the purpose of this study is to examine factors affecting green advertising development, which is based on experienced customers towards products and advertisements and environmental issues. This research focuses on customers to create an implementation model for green advertising among companies. The study was conducted through a survey of 215 customers in West Java (Indonesia) who experienced green advertising and bought environmental-friendly products. Data were collected through a quantitative questionnaire and processed with SmartPLS to test and evaluate Confirmatory Factor Analysis (CFA). In emphasizing the study results, a fit test of the research model and research hypotheses were also being carried out by valuing the KMO. Research findings show several dimensions involved in developing green advertising, such as experience, theme, message, claim, emotion, interaction, and impact. The dimensions of green advertising were plotted in the CFA model so that the priority scale from the implementation of green advertising measurement can be detected. Customers assume green advertising as advertising that takes environmental issues of "global warming," and this issue can adopt by companies in implementing the green marketing strategy.

1. Introduction

Customer behavior has led to environmental sustainability; it is assessed from the increasing level of customer awareness of companies' environmental-friendly products [1]. This phenomenon provides opportunities for companies to adopt environmental-based advertising [2]. Advertisement can influence a customer to choose environmental-friendly products. Environmental-based advertising activities which also known as green advertising, is a marketing strategy that tackle the issue of environmental sustainability and health impacts among users [3]. The implementations of green advertising become important because customers have started to care about the environment with various movements, such as "green consumerism" [4], whereby the activities put forward to customer behavior in consuming and recommending environmental-friendly products [5]. Green customer behavior becomes an essential part of the company's attention in implementing marketing strategy today [6]. The issue of "green product" has become a world issue; people's behavior is changing in every country to be more

concerned about the environment as an effort to face the issue of "global warming" [5]. The efforts made by creating environmental-friendly products and decreased the production of goods and services that use chemical materials [7]. The development of environmental issues occurs in several sustainability concepts, including the concept of green living, which is an effort to live a healthier life with the attention and the use of environmental-friendly products [8]–[10].

Green advertising is part of the green marketing strategy that companies used to create awareness of green products [11]. However, the credibility of green advertising is considered low by customer. This is because customer behavior towards advertising is influence by extensive propaganda of mass media [12]. Therefore, the study of customer behavior in assessing advertising is necessary because previous research has demonstrated that the attitudes towards advertising has provided opportunities for brand attitudes changes [7]. In Indonesia, the green advertising concept was started in 2004 and has been implemented by the government to educate the environmental issue, while companies used it for corporate image [13]. The consumer's perceived value of green

advertising focuses on 3R issue (reduce, reuse, recycle), no plastic day, and earth hour. The impacts of green advertising on green lifestyle and green products is still low, even though this issue is essential for companies to achieve green advertising implementation [14]. The essence of green advertising is a campaign on environmentally friendly products which support sustainability [15]. The concept of sustainability is undoubtedly considered necessary by various parties, such as the government, companies, and society [16]. The education of advertising seems to involve environmental issues in green advertising [17]. Green advertising appears to change customer behavior who cares about the environment. Indonesian government starts to implement the sustainability concept, which was started in 2012 through a regional regulation on Green Building in Jakarta [18]. As the government concern about the environment, it has become a part of green advertising which has been carried out by the government, to serve public service advertisements about the global warming issue [19]. The regulations issued by the government certainly have an impact on marketing strategy whereby companies tackle environmental issues through the concept of green advertising [20]. The characteristics of green advertising are difference with the advertising concept in general; because companies has a goal towards the image and reputation on social responsibility [21]. Hence, companies prioritize green advertising concept, not only for educating environmental-friendly products but also strengthening the company's image and reputation.

Realizing the importance on reviewing the implementation issue of green advertising in Indonesia and its impact on customer behavior, this study focuses on factor analysis that forms green advertising performance from a customer's perspective. This study intends to put forward the green advertising concept, so that it can be references by companies to campaign environmental issues, through symbols or images that are valuable to society towards sustainability concept.

2. Literature Review

2.1. Green Customer Behavior

Green customer behavior refers to customer behavior in using healthy, environmentally friendly products, and it can protect environmental sustainability [22]. Green customer behavior has a level of concern; the higher is the extraordinary impact on loyal behavior for all the environmental issues [23] and trying to recommend to others [24]. The customer's awareness of the environment prioritizes green products and campaigns for healthy lifestyles [25]. However, green customer behavior is not easy to develop [26]; it is influence by the internal situation of customers such as knowledge and self-awareness [27], and external situation of customers such as the environment [28]. Environmental factor has an important role [29] because it has greater level of interaction with customers.

2.2. Green Customer Behavior

Technological developments and environmental issues provide a new perspective for companies in marketing strategies through advertising media, by adopting green advertising, both offline and online [30]. Due to stiff competition, companies have started to find more creative advertising alternatives through unexpected places, unconventional methods, or unusual

communication delivery [31]. It seems clear that the company's efforts are to provide awareness through advertising media, which is easy to remember and provides value for customers and the company [32]. Green advertising is believed to be a strategy that also provides opportunities to increase company's value both from the viewpoint of the product and its image [33]. It considers that green advertising has a concept that is not much different from advertising in general. However, environmental issues provide other opportunities that can be interpreted by a customer today [7]. Media in green advertising is delivered online, like social media or the internet, and offline like newspapers or billboards [34]. The previous concept states that "green advertising are advertisements that promote products, services, ideas or organizations' ability to help or reduce environmental harm" [5]. There are two elements discussed in green advertising, namely education on products or services and a positive impact on the environment [1]. The implementation of green advertising for companies is considered successful if it can provide a company's environmental image. At the same time, customers are assessed through understanding and practicing green living [7].

Green advertising is genuinely delivered by companies or the government to increase customer awareness of the environment [20]. It is undoubtedly in line with government and companies' views, which is trying to deal with the issue of "global warming" and environmental sustainability [35]. Customer care is captured in a consistent attitude that considers good or bad towards a product in the environment to recommend it to others. It seems clear that green advertising is considered effective if it can influence customers' perceptions and customer behavior in the environment [17]. In the previous studies, it has been known that the impact of green advertising on customer behavior such as concern [5], perception [17], attitude [12] to company's image [36]. However, the essential green advertising concept is the consequence of growing customer awareness of the environment [20]. There are many green marketing strategy research indicated the impact of environmental knowledge and the awareness on customer behavior towards the environment [37]. Several media become customer's references in examining the concept of green advertising, such as television, website, media social, radio, newspaper or magazine, billboards, banner dan brochure [5]. However, each media certainly provides a different level of preference; it depends on the level of persuasion given. In the end, the concept of green advertising needs to meet three main criteria, namely explicit or implicit about the correlation between products and environment [12], promoting a green lifestyle with or without products [38], and it explains company image that cares to environment [20].

2.3. Measurements of Green Advertising

Green advertising's implementation contains two prominent elements; informational claims and effective claims [3]. Informational claims are related to the use of environmentally friendly products advertised, while effective claims are the experiences relate to the environment. Indeed, informational and effective claims provide a positive view of customers in assessing green products [12]. There are many criterias in assessing and evaluating green advertising; several previous studies have explained that there is no definite measure that can represent green advertising [3]. All criteria depend on the objectives of green

advertising and customer's goals that determine the success or the failure of advertising done [2], [5], [11]. Some experts' opinions explained the measurement of green advertising. Firstly, it starts with green impact, which is the importance of advertising media that takes to environmental issues into a biophysical environment, green lifestyle, and an image of environmental responsibility [21]. Secondly is a green message, where advertising is assumed necessary to give a clear message related to ecological, environmental sustainability, or nature-friendly messages [39]. The third is a green theme, where advertising needs to provide an attractive theme to be enjoyed by customers on green products that are pleasant, convincing, believable, favorable, and goods [12].

Fourthly is green emotions, where advertising can conveye the emotional values for customers in terms of environment-protection emotion [2], [40]. Customer emotion in advertising is related to moral emotion, social emotion, and ecological fear related to climate change [2]. The fifth is related to customer's experience; it is undoubtedly essential; it is related to the green experience. Advertising is assumed as necessary to provide an experience that is assessed from the perspective of knowledge, perceived comfort, and information obtained by customers [41]. Next is assessed from green interaction related to the level of interaction that customers will feel on advertising, such as appeal, issue proximity, and environmental consciousness [42]. Finally, the measurement based on the previous studies is assessed to green claims. This measure puts forward the recognition of environmental friendly products that can meet customers' expectations in terms of degradable, recycled, recyclable, ozone friendly [43].

3. Research Methodology

The research method was conducted by surveying customers who purchased environmentally friendly products through a set of questionnaires. Customer were chosen from products categories that is convenient to customers, such as food and beverages. Data were carried out through online questionnaire among customer in West Java Province. The answers had been determined through Likert Scale approach, from "1" for strongly disagree and "7" for strongly agree. The questionnaire was distributed within three months, from August to October 2020, with a target of 300 respondents. This research was also included in experimental research where the respondents were given a treatment, which was the knowledge related to green advertising at the beginning of the questionnaire to find out their views regarding green advertising in Indonesia.

The data from respondents were processed through the Confirmatory Factor Analysis (CFA) technique; it intended to find-out the factors that determine the creation (or development?) of green advertising proposed by the research model. Meanwhile, the analysis tools used were SmartPLS, considering the ease of analyzing CFA on data below 300. Based on the previous theory study, several elements would be studied in determining green advertising, such as green impact, green message, green theme, green emotion, green experience, green interaction, and green claim. Each dimension was measured by an indicator as shown in Figure 1. Data analysis stages were started from data tabulation, research model fit test, and rearch hypothesis test. Considering

that this research used the CFA approach, only a fit model test through Outer Model would be conducted. It was tested for convergent validity, composite reability, average variance extracted, and discriminant validity [44], [45]. Meanwhile, the research hypothesis test was conducted by evaluating the value of Kaiser-Mayer-Olkin Measure of Sampling Adequacy (KMO MSA), where it must be more than 0.5, and the value of Bartlett's Test of Sphericity (Sig.) was smaller than 0,05 [46]. The final objective of the analysis was to find the determinant factors to develop green advertising that provide customers' value of customers'concern for environmentally friendly products.

From previous research studies, it appeared that several measurements can be assessed from green advertising. However, all of them have one goal: to increase customer awareness of green advertising implementation. In this study, the measurements that have been tested,were green impact, green message, green theme, green emotion, green experience, green interaction, and green claim [2], [21], [39], [41], [43], [47]. The essence of some of these measurements provide the same opportunity as a determining factor in assessing green advertising; before the Confirmatory Factor Analysis (CFA) is carried out, the assumptions are conveyed in the form of research hypothesis based on the CFA model as follows.

Hypothesis 1 (H1) Green impact is a dimension that can developed green advertising.

Hypothesis 2 (H2) Green message is a dimension that can developed green advertising.

Hypothesis 3 (H3) Green theme is a dimension that can developed green advertising.

Hypothesis 4 (H4) Green emotion is a dimension that can developed green advertising.

Hypothesis 5 (H5) Green experience is a dimension that can developed green advertising.

Hypothesis 6 (H6) Green interaction is a dimension that can developed green advertising.

Hypothesis 7 (H7) Green claim is a dimension that can developed green advertising.

4. Result and Discussions

Confirmatory Factor Analysis (CFA) research relates to green advertising; it starts by distributing an online questionnaire for three months (August, September, October).

Data from the questionnaire spread to 215 respondents who filled in the data correctly, then data was tabulated, and the research model was tested through SmartPLS. Data analysis begins with the research instrument test, research hypothesis test, and analysis of Confirmatory Factor Analysis test result.

4.1. Validity and Reliability Test

Before conducting data analysis through CFA, validity, and reliability tests were examined. Considering that analysis is carried out through CFA, the tests are conducted only using the outer model test for convergent validity, composite reliability, average variance extracted, discriminant validity, and outer weight. If all the outer model test results are adequate, it is stated to be fit, and a CFA study can be carried out.
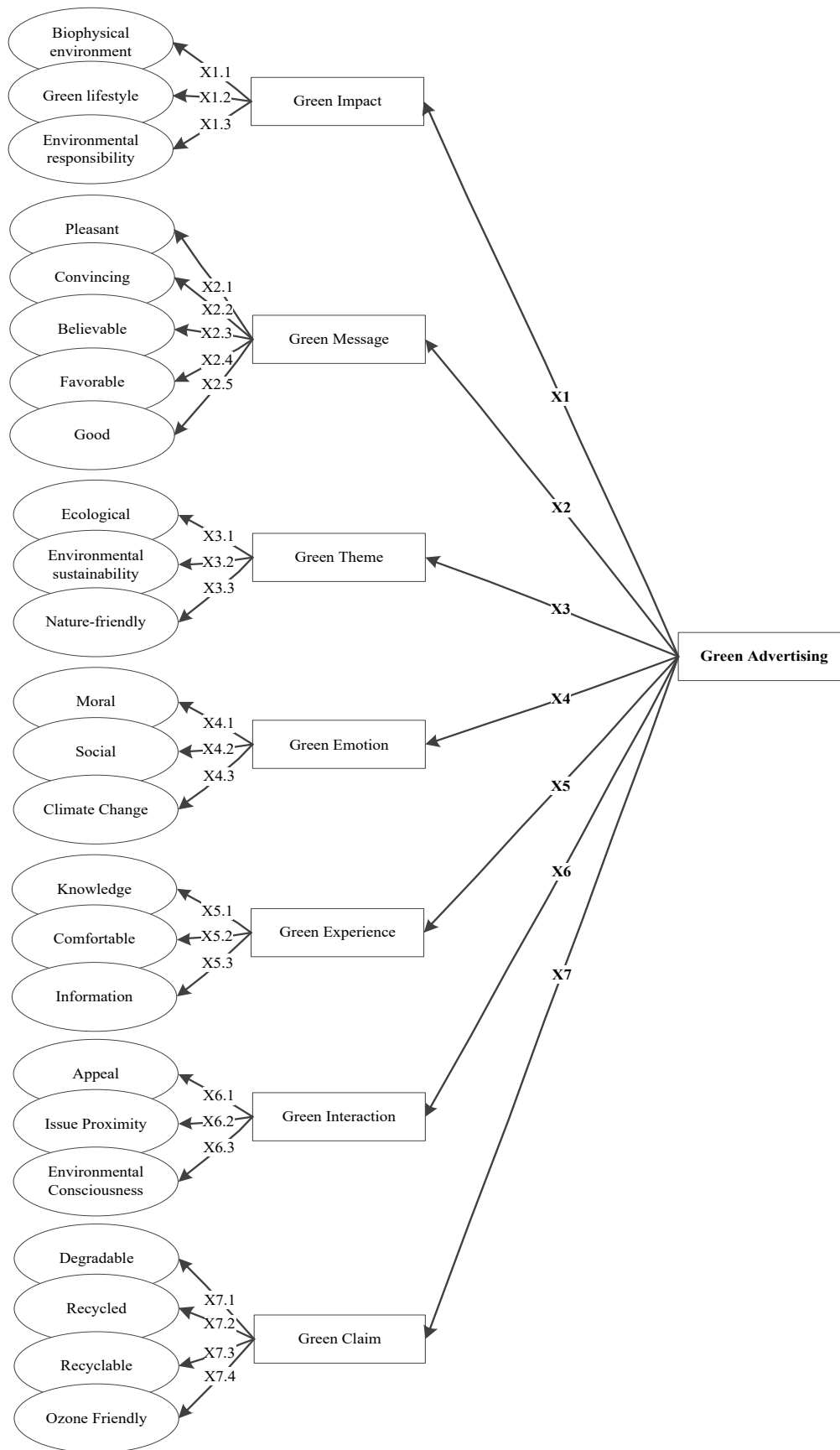
Figure 1: CFA Model

Convergent validity test is assessed by evaluating the correlation of outer loading results, which is more than 0.50 for the correlation. Furthermore, the discriminant validity test shows whether the measured variable has acceptable reliability. Discriminant validity has known through the evaluation of the composite reliability value, which must be above 0.8. The next test is the Average Variance Extracted (AVE) value, which is stated to be fair, and it fulfills the criteria when the value is more significant than 0.5. The next evaluation studied Cronbach's Alpha's value, which is one of the recommended discriminant validity measures to have a value above 0.7. The final test is carried out the outer weight, which is stated to fulfill the requirements if the outer weight value is above 0.20. The results of the first outer model test are summarized in Table 1, which

indicated that from all the previous tests, composite reliability, AVE, and discriminant validity are fulfill the requirements.

The second outer model test results which related to outer weight are summarized in Table 2, which evaluation of sample original value is above 0,20. It is stated to be fit, or it means that it fulfills the requirements. Finally, the results of the outer model test reviewed from convergent validity, where the results are summarized in Table 3 with all of the outer loading value are accepted because the correlation value is above 0.50. Based on all of the test results of the outer model, it can be stated that the research instrument can be accepted, and it can be analyzed further for CFA.

Tabel 1: Construct Validity and Reliability

	Cronbach's Alpha	rho_A	Composite Reliability	Average Variance Extracted (AVE)
Green Impact	0,924	0,926	0,939	0,688
Green Message	0,843	0,844	0,905	0,761
Green Theme	0,825	0,827	0,878	0,590
Green Emotion	0,796	0,796	0,880	0,710
Green Experience	0,747	0,747	0,856	0,665
Green Interaction	0,775	0,784	0,870	0,691
Green Claim	0,773	0,785	0,868	0,688

Tabel 2: Outer Weight Values

	Original Sample (O)	Sample Mean (M)	Standard Deviation (STDEV)	T Statistics (|O/STDEV|)	P Values
Biophysical Environment	0,368	0,369	0,017	21,769	0,000
Green Lifestyle	0,387	0,387	0,016	24,088	0,000
Environmental Responsibility	0,391	0,391	0,016	24,600	0,000
Pleasant	0,242	0,242	0,015	16,551	0,000
Convincing	0,276	0,276	0,016	17,230	0,000
Believable	0,270	0,271	0,014	18,720	0,000
Favorable	0,254	0,253	0,017	15,269	0,000
Good	0,259	0,259	0,016	15,899	0,000
Ecological	0,400	0,401	0,015	27,331	0,000
Environmental Sustainability	0,401	0,400	0,017	22,947	0,000
Nature-Friendly	0,386	0,386	0,015	25,172	0,000
Moral	0,421	0,420	0,022	18,967	0,000
Social	0,393	0,395	0,015	26,166	0,000
Climate Change	0,413	0,414	0,021	19,750	0,000
Knowledge	0,440	0,440	0,017	25,158	0,000
Comfortable	0,375	0,374	0,017	22,605	0,000
Information	0,386	0,386	0,017	23,110	0,000
Appeal	0,440	0,442	0,020	22,460	0,000
Issue Proximity	0,345	0,345	0,022	15,632	0,000
Environmental Consciousness	0,416	0,417	0,021	20,084	0,000
Degradable	0,256	0,256	0,016	16,240	0,000
Recycled	0,303	0,304	0,015	19,858	0,000
Recyclable	0,304	0,304	0,011	26,755	0,000
Ozon Friendly	0,308	0,308	0,014	21,757	0,000

Tabel 3: Outer Loading Values

Instruments	Green Impact	Green Message	Green Theme	Green Emotion	Green Experience	Green Interaction	Green Claim
Biophysical Environment	0,848						
Green Lifestyle	0,887						
Environmental Responsibility	0,882						
Pleasant		0,748					
Convincing		0,835					
Believable		0,820					
Favorable		0,721					
Good		0,708					
Ecological			0,848				
Environmental Sustainability			0,858				
Nature-Friendly			0,821				
Moral				0,826			
Social				0,835			
Climate Change				0,784			
Knowledge					0,878		
Comfortable					0,775		
Information					0,838		
Appeal						0,862	
Issue Proximity						0,779	
Environmental Consciousness						0,845	
Degradable							0,793
Recycled							0,890
Recyclable							0,860
Ozon Friendly							0,862

Table 4: Values of KMO

Hypotheses		KMO	Sig.	Result
Green Impact ← Green Advertising	H1	0,772	0,000	Accepted
Green Message ← Green Advertising	H2	0,791	0,000	Accepted
Green Theme ← Green Advertising	H3	0,705	0,000	Accepted
Green Emotion ← Green Advertising	H4	0,674	0,000	Accepted
Green Experience ← Green Advertising	H5	0,674	0,000	Accepted
Green Interaction ← Green Advertising	H6	0,694	0,000	Accepted
Green Claim ← Green Advertising	H7	0,826	0,000	Accepted

4.2. Factor Analysis of Green Advertising

This research focuses on green advertising, which is assessed from several criteria, including green impact, green message, green theme, green emotion, green experience, green interaction, and green claim. Based on the result in Table 3, it showed that all outer-loading values are accepted; with the value above 0.70. Outer loading values explained the level of closeness between the indicator and its dimensions because the determining indicator is better when it close to 1. The result indicated that several factors supported the creation of dimensions on green advertising. The first dimension is green impact with a sequence of determinants, which starts from green lifestyle, environmental responsibility to the biophysical environment. The green impact is a dimension for green advertising and can motivate customers who accept advertising [48]. The first measurement, which becomes a customer's attention, is green lifestyle, where customers assume that green advertising is expected to provide a new lifestyle for healthier customers. The next dimension is green message;

several supporting indicators with a sequence are convincing, believable, pleasant, favorable, and goods. Green messages can be a dimension that forms green advertising; it considers that advertising is full of messages; customers will receive advertisements recipients [39]. Customers prioritize convincing message or giving confidence because the advertisement is trustworthy and not an imaginary advertisement. Another dimension that becomes the determining factor of green advertising is green theme with indicators formed from environmental, ecological sustainability, and nature friendly. A green theme is related to a theme in online or offline advertising, considering that a theme will stimulate customers to understand the meaning of advertising [12]. In this case, a green theme that becomes the primary concern of customers is environmental sustainability issue. This is because the themes have more impact on customers' understanding in conveying the advertisement.

The next dimension is green emotion, which is formed from several indicators, such as climate change, social, and moral.

Green emotion is considered as dimension that represent green advertising related to customers' emotional level when look at the advertisement. These emotions are positively natural-friendly, and aim to believe more in advertising behind green advertising [2]. Based on loading factor value survey, it has been revealed that the size of climate change is the most important indicator that can change customers' emotional value because green advertising relates indirectly to the issue of climate change. Green advertising lead to the assumption of customers involvement; which is stated in the green experience dimension [7]. Green experience is assessed from information, knowledge, and comfortable. Customers certainly hope that in assessing green advertising, they can improve their experience, and this experience is considered essential when it comes to the information they need. The next dimension that becomes the determining factor for green advertising is green interaction; it is formed by several indicators, such as appeal, environmental consciousness, and proximity issues. Green interaction is related to customers' interactions with the advertisements [42]; the outer loading appeal stated that it is the most influencing indicators. It means that green advertising will be able to invite interaction from customers if the advertisement is attractive. It is the reason why people said that to create content of green advertising is quite challenging because it requires special attention that relates to the environment. The last dimension is related to green claims, which consist of recycled, ozone friendly, recyclable, and degradable. It means that green claims relate to customers' recognition for the advertisements [43]. This recognition is considered as the most important recognition, because it need to ensure environmental-friendly product to be easy recycled.

A hypothesis test surely to tests the analysis results of determinants factors of green advertising; it was intended to emphasize that all the dimensions have been determined, and it can be a measurement for green advertising. The hypothesis test results are conducted by evaluating the value of KMO presented in Table 4. All "accepted" dimensions can be dimensions for green advertising. It considers that the value of KMO is above 0.5, and the value of Bartlett's Test of Sphericity (Sig.) is smaller than 0,05. Therefore, the result stated that the indicator factors which consist of green impact, green message, green theme, green emotion, green experience, green interaction, and green claim can develop green advertising.

4.3. Model of CFA Green Advertising

In the research finding of the analysis factor, there are seven dimensions of green advertising; green impact, green message, green theme, green emotion, green experience, green interaction, and green claim. However, these dimensions certainly have a different standard value informing to green advertising assessed by customers. Therefore, to determine the highest and lowest standard in green advertising, value extractions based on commonalities process [49] has been conducted, as illustrated in Figure 2.

Based on Figure 2, it is clear that the highest extraction value is green experience, and the lowest extraction value is green impact. The extraction value determines the impact's size of dimensions in determining green advertising. The findings show a composition of dimensions that can develop green advertising,

which is started from experience, theme, message, claim, emotion, and interaction to impact. The dimensions need to be conducted priority scale by companies if companies decided to adjust green marketing to green advertising. These research findings explain the importance of adjusting green advertising implementation as part of marketing strategy.
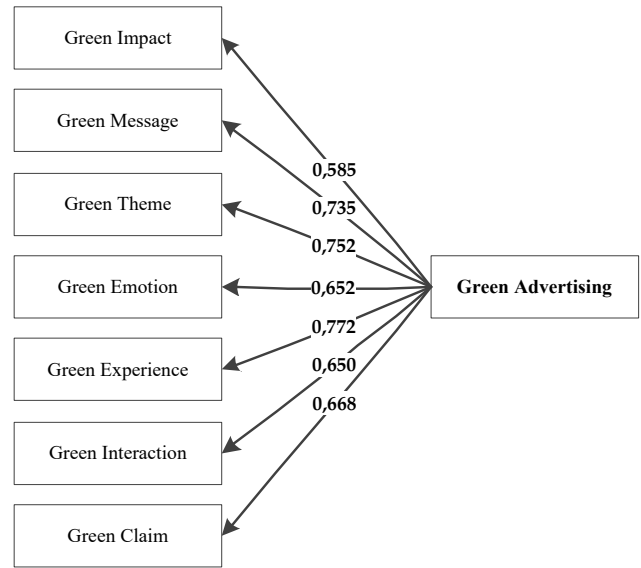
Figure 2: Model of Green Advertising

This study focuses on the behavior of customer who have purchased environmentally friendly products in Indonesia (West Java), which means that companies can utilise the model of green advertising (Figure 2) in promoting pure environmentally friendly products. All green advertising dimensions have meaningful content, so it would be better to develop green advertising. However, if the dimensions are to be reduced, it is advisable to start from the dimensions that have the lowest impact in developing green advertising. It means that the green advertising model's use of dimensions is adjusted to dimensional load in forming green advertising. The goal of green advertising can be achieved, namely product education that is friendly to the environment. The finding of this research can provide input for the government in advertising policies, for company in implementing green marketing and for society as customer who needs to get information related to a sustainable environment.

4.4. Customer Perceived of Green Advertising

Green advertising can give impacts on customer behavior by providing the assumptions and responses to environmental sustainability [1], [5]. In this case, customers of products and services offered by the company certainly need to understand the advantages and disadvantages of products they will choose, particularly for products that have a positive impact on the environment. Therefore, it is essential for company to implement green advertising. However, the implementation of green advertising needs to consider several dimensions which can develop the right customer's perception. In this study, a series of dimensions has been stated, namely: experience, theme, message, claim, emotion, and interaction. These findings are based on customers' assessment in evaluating green advertising received by them until now, and it refers to the evaluation on

environmentally friendly products. Based on green advertising results, it can be argued that a customer's experience of green products is controls by the customer perceived value of green advertising; the theme of the conveyed advertisement; the message of the conveyed advertisement; the advertisement claim which can change customer's confidence; customer emotion is positive after seeing the advertisements; customer interaction is optimistic after seeing the advertisements; and the impact of advertising which motivates to customers to live a healthy life.

The research findings depicted in Figure 2 can be implemented by companies to educate customer on environmentally friendly products and the government in educating the importance of environmental sustainability to society. However, the model of green advertising is not suitable when used in educating conventional products or is not purely environmentally friendly because the dimensions used in this study focused on green products and the selected consumers have an environmentally friendly concern. So it is necessary to consider green advertising that companies use is not only for environmental issues, but also for the products created. This research findings explained the importance of understanding customer behavior in supporting the implementation of marketing strategies; mainly, it takes environmental issues as green advertising. There is essential information for stakeholders such as the government, companies, and society in promoting green advertising.

5. Conclusions

This study aims to analyze the determining factors in deciding green advertising, in which there are several measurements have been presented by the previous studies. This study provides the appropriate measurement for green advertising which can be utilized to educate customers. Seven dimensions were tested in determining green advertising, namely: experience, theme, message, claim, emotion, interaction to impact. The implementation of green advertising has impacted customers' points of view; and it considered several customers' attention. Customers' attention means experience, which consist of information, knowledge, and comfort issues. A model of green advertising through Confirmatory Factor Analysis was developed in this research. Through this model, it can provide some input to the government in evaluating the policies to deal with "global warming" issues, as well as to companies in implementing green marketing.

This research, however, has certain limitations. It applied CFA based on each dimension and does not study the impact of green advertising implementation on customer behavior, for instance customer care. Therefore, future research should emphasizes on the utilization of exploratory factor analysis (EFA) and the impact of the study on customer behavior. In addition, this research does not examine the technology used in green advertising, so it is recommended that further research to examine the technical support in green advertising, taking into consideration that that the advertising model is utilizing electronic and digital media, which are related to the latest technology.

References

[1]   D. P. Alamsyah, N. A. Othman, and H. A. A. Mohammed, "The awareness of environmentally friendly products: The impact of green advertising and green brand image," *Manag. Sci. Lett.*, **10**, 1961–1968, 2020, doi: 10.5267/j.msl.2020.2.017.

[2]   T. F. Kao and Y. Z. Du, "A study on the influence of green advertising design and environmental emotion on advertising effect," *J. Clean. Prod.*, **242**, 118294, 2020, doi: 10.1016/j.jclepro.2019.118294.

[3]   P. Hartmann and V. Apaolaza-Ibáñez, "Green advertising revisited," *Int. J. Advert.*, **28**(4), 715–739, Jan. 2009, doi: 10.2501/S0265048709200837.

[4]   A. M. F. Paço, M. L. B. Raposo, and B. Interior, "Green Consumer Market Segmentation: Empirical Findings From Portugal," *Int. J. Consum. Stud.*, **34**(1996), 429–436, 2010, doi: 10.1111/j.1470-6431.2010.00869.x.

[5]   M. H. A. Rahim, R. Z. J. A. Zukni, F. Ahmad, and N. Lyndon, "Green advertising and environmentally responsible consumer behavior: The level of awareness and perception of Malaysian youth," *Asian Soc. Sci.*, **8**(5), 46–54, 2012, doi: 10.5539/ass.v8n5p46.

[6]   B. Cynthia and C. B. Hanson, "Environmental Concern, Attitude Toward Green Corporate Practices, and Green Consumer Behavior in The United States and Canada," *ASBBS eJournal*, **9**(1), 62–71, 2013.

[7]   P. Hartmann and V. Apaolaza-Ibáñez, "Green advertising revisted: Conditioning virtual nature experiences," *Int. J. Advert.*, **28**(4), 37–41, 2009, doi: 10.2501/S0265048709200837.

[8]   F. N. Jamal, N. A. Othman, R. C. Saleh, and S. Chairunnisa, "Green purchase intention: The power of success in green marketing promotion," *Manag. Sci. Lett.*, **11**, 1607–1620, 2021, doi: 10.5267/j.msl.2020.12.011.

[9]   F. N. Jamal, N. A. Othman, R. C. Saleh, and A. N. Putri, "Hybrid Structural Equation Model and Dynamic Simulation of Eco Label towards Green Marketing," *Syst. Rev. Pharm.*, **11**(12), 956–961, 2020.

[10] S. Omar, N. A. Othman, and J. Jabar, "Effect of eco-innovation practices on sustainable business performance," *Pertanika J. Sci. Technol.*, **25**(S5), 123–128, 2017.

[11] K. Chan, A. Ahmed, and S. Tih, "Green Advertising Appeal and Consumer Purchase Intention," *J. Pengur.*, **47**, 157–168, 2016.

[12] C. D'Souza and M. Taghian, "Green advertising effects on attitude and choice of advertising themes," *Asia Pacific J. Mark. Logist.*, **17**(3), 51–66, 2005, doi: 10.1108/13555850510672386.

[13] B. Wiryomartono, "'Green building' and sustainable development policy in Indonesia since 2004," *Int. J. Sustain. Build. Technol. Urban Dev.*, **6**(2), 82–89, 2015, doi: 10.1080/2093761X.2015.1025450.

[14] D. P. Alamsyah, N. A. Othman, M. H. Bakri, A. N. Adjie, K. Salsabila, and D. Syarifuddin, "Confirmatory factor analysis of green advertising and its impact on green awareness," *Manag. Sci. Lett.*, **10**(16), 3899–3906, 2020, doi: 10.5267/j.msl.2020.7.021.

[15] Y. Song and Y. Luximon, "Design for sustainability: The effect of lettering case on environmental concern from a green advertising perspective," *Sustain.*, **11**(5), 1333, 2019, doi: 10.3390/su11051333.

[16] M. Merad, N. Dechy, and F. Marcel, "A pragmatic way of achieving Highly Sustainable Organisation: Governance and organisational learning in action in the public French sector," *Saf. Sci.*, **69**, 18–28, 2014, doi: 10.1016/j.ssci.2014.01.002.

[17] C.-F. Wei, B. C. Y. Lee, T.-C. Kou, and C.-K. Wu, "Green Marketing: The Roles of Appeal Type and Price Level," *Adv. Manag. Appl. Econ.*, **4**(5), 63–83, 2014.

[18] Z. R. Anderson, K. Kusters, J. McCarthy, and K. Obidzinski, "Green growth rhetoric versus reality: Insights from Indonesia," *Glob. Environ. Chang.*, **38**, 30–40, 2016, doi: 10.1016/j.gloenvcha.2016.02.008.

[19] M. Sihite, "The Competitive Strategy in Green Building for Indonesian Stakeholder's," *Int. J. Innov. Manag. Technol.*, **6**(1), 2015, doi: 10.7763/ijimt.2015.v6.565.

[20] D. P. Alamsyah, T. Suhartini, Y. Rahayu, I. Setyawati, and O. I. B. Hariyanto, "Green advertising, green brand image and green awareness for environmental products," *IOP Conf. Ser. Mater. Sci. Eng.*, **434**(1), 012160, 2018, doi: 10.1088/1757-899X/434/1/011001.

[21] B. Banerjee and K. McKeage, "How green is my value: exploring the relationship between environmentalism and materialism," *ACR North Am. Adv.*, 1994.

[22] H. C. Huang, T. H. Lin, M. C. Lai, and T. L. Lin, "Environmental consciousness and green customer behavior: An examination of motivation crowding effect," *Int. J. Hosp. Manag.*, **40**, 139–149, 2014, doi: 10.1016/j.ijhm.2014.04.006.

[23] D. P. Alamsyah, O. I. B. Hariyanto, and H. Rohaeni, "Customer Green Awareness and Eco-Label for Organic Products," in *International Conference on Organizational Innovation (ICOI)*, 2019, 100), 64–68, doi: 10.2991/icoi-19.2019.12.

[24] D. L. Gadenne, J. Kennedy, and C. McKeiver, "An empirical study of environmental awareness and practices in SMEs," *J. Bus. Ethics*, **84**(1), 45–63, 2009, doi: 10.1007/s10551-008-9672-9.

[25] F. Fuerst and C. Shimizu, "Green luxury goods? The economics of eco-labels in the Japanese housing market," *J. Jpn. Int. Econ.*, **39**, 108–122, 2016, doi: 10.1016/j.jjie.2016.01.003.

[26] D. P. Alamsyah and D. Syarifuddin, "Store Image: Mediator of Social Responsibility and Customer Perceived Value to Customer Trust for Organic Products," *IOP Conf. Ser. Mater. Sci. Eng.*, **288**(1), 012045, 2017, doi: 10.1088/1757-899X/288/1/011001.

[27] Y. S. Chen and C. H. Chang, "Enhance environmental commitments and green intangible assets toward green competitive advantages: An analysis of structural equation modeling (SEM)," *Qual. Quant.*, **47**(1), 529–543, 2013, doi: 10.1007/s11135-011-9535-9.

[28] Y. Chen and C. Chang, "Enhance Green Purchase Intentions. The Roles of Green Perceived Value, Green Perceived Risk, and Green Trust," *Manag. Decis.*, 50(3), 502–520, 2012.

[29] C. Othman and M. S. Rahman, "Investigation of the relationship of brand personality, subjective norm and perceived control on consumers' purchase intention of organic fast food," *Mod. Appl. Sci.*, **8**(3), 92–106, 2014, doi: 10.5539/mas.v8n3p92.

[30] W. Y. Wu, H. Shih, and H. Chan, "A Study of Customer Relationship Management Activities and Marketing Tactics for Hypermarkets on Membership Behavior," *Bus. Rev. Cambridge*, **10**(1), 89–96, 2008.

[31] D. Y. Choi and E. R. Gray, "Socially responsible entrepreneurs: What do they do to create and build their companies?," *Bus. Horiz.*, **51**(4), 341–352, 2008, doi: 10.1016/j.bushor.2008.02.010.

[32] A. Davies, A. J. Titterington, and C. Cochrane, "Who buys organic food? A profile of the purchasers of organic food in Northern Ireland," *Br. Food J.*, **97**(10), 17–23, 1995, doi: 10.1108/00070709510104303.

[33] A.-I. Maniu and M.-M. Zaharie, "Advertising Creativity – The Right Balance between Surprise, Medium and Message Relevance," *Procedia Econ. Financ.*, **15**(14), 1165–1172, 2014, doi: 10.1016/s2212-5671(14)00573-5.

[34] D. Y. Rahmi, Y. Rozalia, D. N. Chan, Q. Anira, and R. P. Lita, "Green Brand Image Relation Model, Green Awareness, Green Advertisement, and Ecological Knowledge as Competitive Advantage in Improving Green Purchase Intention and Green Purchase Behavior on Creative Industry Products," *J. Econ. Bus. Account. Ventur.*, **20**(2), 2017, doi: 10.14414/jebav.v20i2.1126.

[35] R. Fernando, "Sustainable globalization and implications for strategic corporate and national sustainability," *Corp. Gov.*, **12**(4), 579–589, 2012, doi: 10.1108/14720701211267883.

[36] D. P. Alamsyah, T. Suhartini, Y. Rahayu, I. Setyawati, and O. I. B. Hariyanto, "Green advertising, green brand image and green awareness for environmental products," *IOP Conf. Ser. Mater. Sci. Eng.*, **434**(1), 012160, 2018, doi: 10.1088/1757-899X/434/1/011001.

[37] D. P. Alamsyah and H. A. A. Mohammed, "Antecedents of Green Awareness for Eco-Friendly Products," *ASEAN Mark. J.*, **10**(2), 109–126, 2019.

[38] Y. S. Chen, C. Y. Lin, and C. S. Weng, "The influence of environmental friendliness on green trust: The mediation effects of green satisfaction and green perceived quality," *Sustain.*, **7**(8), 10135–10152, 2015, doi: 10.3390/su70810135.

[39] G. M. Zinkhan and L. Carlson, "Green advertising and the reluctant consumer," *J. Advert.*, **24**(2), 1–6, 1995, doi: 10.1080/00913367.1995.10673471.

[40] C. D. Hopkins, K. J. Shanahan, and M. A. Raymond, "The moderating role of religiosity on nonprofit advertising," *J. Bus. Res.*, **67**(2), 23–31, 2014, doi: 10.1016/j.jbusres.2013.03.008.

[41] M. Rizwan, U. Mahmood, H. Siddiqui, and A. Tahir, "An Empirical Study about Green Purchase Intentions," *J. Sociol. Res.*, **5**(1), 290–305, 2014, doi: 10.5296/.

[42] C. Chang, "Are guilt appeals a panacea in green advertising ?," *Int. J. Advert.*, **31**(4), 741–771, 2012, doi: 10.2501/IJA-31-4-741-771.

[43] S. J. Grove and N. Kangun, "A content analysis of environmental advertising claims: A matrix method approach les carlson," *J. Advert.*, **22**(3), 27–39, 1993, doi: 10.1080/00913367.1993.10673409.

[44] N. M. Suki, N. M. Suki, and N. S. Azman, "Impacts of Corporate Social Responsibility on the Links Between Green Marketing Awareness and Consumer Purchase Intentions," *Procedia Econ. Financ.*, **37**(16), 262–268, 2016, doi: 10.1016/s2212-5671(16)30123-x.

[45] G. T. Yeo, V. V. Thai, and S. Y. Roh, "An Analysis of Port Service Quality and Customer Satisfaction: The Case of Korean Container Ports," *Asian J. Shipp. Logist.*, **31**(4), 437–447, 2015, doi: 10.1016/j.ajsl.2016.01.002.

[46] Y. Suh and M. S. Kim, "Internationally leading SMEs vs. internationalized SMEs: Evidence of success factors from South Korea," *Int. Bus. Rev.*, **23**(1), 115–129, 2014, doi: 10.1016/j.ibusrev.2013.03.002.

[47] C. T. Chang, "Are guilt appeals a panacea in green advertising? The right formula of issue proximity and environmental consciousness," *Int. J. Advert.*, **31**(4), 741–771, 2012, doi: 10.2501/IJA-31-4-741-771.

[48] S.-I. Wu and Y.-J. Chen, "The Impact of Green Marketing and Perceived Innovation on Purchase Intention for Green Products," *Int. J. Mark. Stud.*, **6**(5), 81–101, 2014, doi: 10.5539/ijms.v6n5p81.

[49] M. V. Oet and S. J. Ong, "From organization to activity in the US collateralized interbank market," *Res. Int. Bus. Financ.*, **50**, 472–485, 2019, doi: 10.1016/j.ribaf.2016.01.012.

Diagnosis of Tobacco Addiction using Medical Signal: An EEG-based Time-Frequency Domain Analysis Using Machine Learning

Md Mahmudul Hasan[1, *], Nafiul Hasan[2], Mohammed Saud A Alsubaie[3], Md Mostafizur Rahman Komol[1]

[1]*Centre for Accident Research and Road Safety- Queensland, Queensland University of Technology, Brisbane, QLD 4059, Australia*

[2]*Department of Electrical and Electronic Engineering, Bangladesh Army University of Engineering and Technology, Qadirabad, 6431, Bangladesh*

[3]*Department of Mathematics, Taif University, Taif, 26513, Saudi Arabia*

A R T I C L E   I N F O

A B S T R A C T

Addiction such as tobacco smoking affects the human brain and thus causes significant changes in the brainwaves. The changes in brain wave due to smoking can be identified by focusing on changes in electroencephalogram pattern, extracting different time-frequency domain features. In this aspect, a laboratory-based study has been presented in this paper, for assessing the brain signal changes due to the tobacco addiction. Four classifier models, namely, Logistic Regression (LR), K- Nearest Neighbor (KNN), Support Vector Machine (SVM) and Random Forest Classifier (RFC) were trained and tested for assessing the performance of the time domain, frequency domain and fusion of time-frequency domain features, with a five-fold cross-validation. Four different performance measures (sensitivity, specificity, accuracy, and area under the receiver operating characteristic curve) were used to measure the overall performance, and the results suggested that the classifiers based on time-frequency domain features perform the best while using combinedly. Using the utilized fusion of the time-frequency domain features, the classification models can identify the smoker group with an accuracy ranged from (86.5-91.3%), where the RFC shows the best accuracy of 91.3%, which is higher than the three other classifiers models.

1. Introduction

This paper is an extension of work originally presented in International Conference on Computer, Communication, Chemical, Materials and Electronic Engineering (IC4ME2) [1]. The presented paper [1] utilized electroencephalogram (EEG) for the diagnosis of tobacco smoking based on only one machine learning model (artificial neural network), where the current article is expanded further to validate the EEG based diagnosis using multiple machine learning models. Also, this paper examines the utility of the time domain and frequency domain, individually and their combination on the EEG based tobacco addiction diagnosis.

In this modern era of life science, research in the field of neuroscience and cognitive engineering is flourishing with technological evolution. Electroencephalogram (EEG) is being used in this sector to understand sophisticated conditions of the brain as this is sensitive and susceptible to any action, especially for drug addiction, for example, alcohol, morphine, heroin or Cannabis addictions. Different stages of drug addiction can be determined only through EEG analysis, and this is very much necessary in the treatment of drug addiction. Some drug elements, such as nicotine is found in nature (from Nicotiana tabacum and Nicotiana rustica). They also have good effects on health; for example, nicotine is being used in the treatment of cognitive disorder and depression. Its impact on the body depends on the way of its metabolism and absorption, such as P-450 pathway degrades several body parts. At a level, it strengthens/weaken other taken drugs. A review work has done to analyze the pros and cons of nicotine, where limitation they noted are the analysis of the complex way of changing cognitive function and host inflammatory response [2]. By analyzing the EEG response, the changing pattern can be determined easily. Drug elements like

*Corresponding Author: Md Mahmudul Hasan, 2 Rochester Terrace, Brisbane, QLD 4059, Australia; Email: mahmudul.hasan.eee.kuet@gmail.com

tobacco, tar and nicotine affect on mood and behavior, which is controlled by human brain consisting of neurons [3].

2. Literature Review

A significant amount of public awareness against tobacco addiction have been conducted to date, but not all the public announcements were effective. To know the degree of effectiveness of public service announcement against smoking, a pilot study was conducted in Rome by collecting EEG, heart rate and galvanic skin response. Based on approach withdrawal, effort and emotional indexes, it was found that these parameters that show notable differences between effective and ineffective perception [4].

In addition to the public awareness, several studies have been conducted on identifying the physical and mental changes due to the smoking habit and potential treatments. An analysis was performed by [5], who had experimented on 21 male smokers. The authors had analyzed the EEG wave of the participants before and after the horizontal rotation treatment. They found that the treatment is beneficial in improving the EEG Alpha band, which reduces the smoking effect. An increment in alpha rhythm denotes higher relaxation and concentration ability of subjects [5]. Another study was conducted on 19 smoker participants. The functional magnetic resonance imaging (fMRI) and EEG analysis represented the effect of nicotine on the brain while doing oddball tasks, which is a response time task [6]. The study suggested that the integrated EEG-fMRI system is better identifying the brainwave changes due to smoking.

Though most of the studies has investigated the effect of tobacco smoking on the brain using the EEG, very few studies had done the differentiation of EEG characteristics using machine learning algorithms. In a study [7], the authors have done an experiment on 20 participants having 10 smokers and 10 non-smokers, to observe the changes in the EEG signal due to the smoking effect. The authors had used a Support Vector Machine (SVM) classifier based on Radial Basis Function (RBF) kernel and found that the the power spectral density (PSD) features performed better than the Fast Fourier Transform (FFT) features. Another study developed an EEG-based architecture to determine the effect of tobacco in the brainwaves, using 3 participants in a laboratory-based work [1].

The authors extracted time, frequency domain features from the EEG and showed that the frequency domain features, especially the power spectral density (PSD) and the Fast Fourier Transform (FFT) are most sensitive to the smoking condition than the time domain features for the smoker detection. The study showed promising results but utilized only one classifier (ANN) for the classification approach and only one performance measure (mean square error) for the assessment of the system [1]. However, considering the sensitivity and specificity metrics are most important for an EEG based detection system. As higher sensitivity with lower specificity leads to the higher false detection and the opposite trend causes the missing of a lot of positive states (in this case, smokers), a compromise between the two metrics is crucial.

This paper embodies a methodology for the diagnosis of tobacco smoking, based on the time-frequency analysis of the EEG signal. Also, the analysis was conducted to find efficient analyzing

model and feature. BIOPAC® system was used for data collection, and Acknowledge-4.1® package [8] was used for extracting features. Later, python 3.6.9 version was used in Google Colab platform for data analysis. Most importantly, four supervised classification models, namely, Logistic Regression, K- Nearest Neighbor (KNN), Support Vector Machine (SVM) and Random Forest Classifier (RFC) were trained and tested for evaluating the performance of each of the EEG rhythm, with a five-fold cross-validation. Moreover, four different performance measures (sensitivity, specificity, accuracy and area under the receiver operating characteristic curve) were utilized to examine the performance of the diagnosis system. The following part of this paper is organized as follows- a brief methodology, including experimental design and tools, then the result section with the findings. Last, the paper was concluded, followed by a short discussion on the outcomes.

3. Methodology

3.1. Experimental Design

The methodology for building an electroencephalogram based tobacco addiction diagnosis system is shown in Figure 1. After selecting three participants, EEG were obtained by the BIOPAC® system. After that the removal of noise and artifacts were considered.
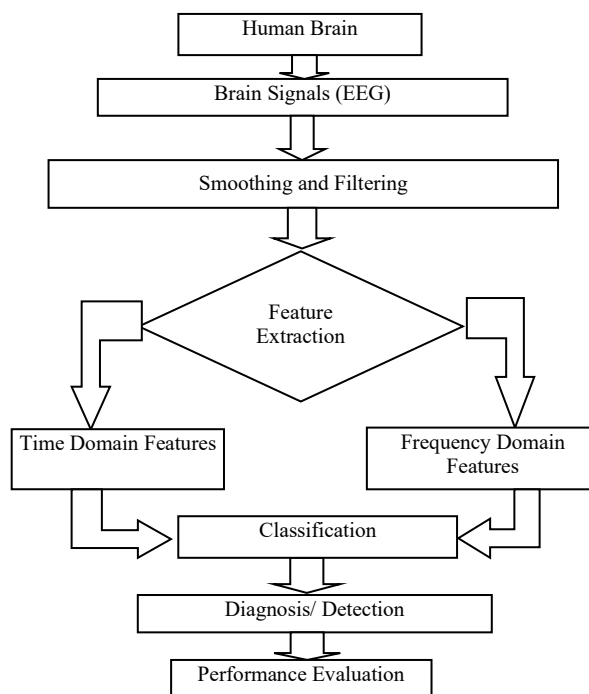
Figure 1: Block diagram for the proposed EEG based smokier / nonsmoker detection system

Afterwards, eight features were extracted for each domain, and the selected features were supplied towards the machine learning tools. Four different classification models, namely K-nearest neighbours (KNN), support vector machines (SVM), logistic regression (LR) and random forest classifier (RFC) models were developed in python 3.6.9 platform. The evaluation of the best classifier and domain was done by comparing their performance.

3.2. Experimental Equipment

3.2.1. Hardware tool

BIOPAC® MP 36 device was used at Biomedical Engineering lab, KUET for the experimentation purpose. The experimental setup is shown in Figure 2 [8].

3.2.2. Pre-processing and feature extraction software tool

Feature extraction was an important step in this study, which was done using the BIOPAC® student Lab Pro and Acqknowledge 4.1® software Google Colab research platform with the python 3.6.9 for developing the Machine learning-based classification models [9].

3.3. Participants

In total, three subjects participated in this experimental study, who were male, healthy and not suffering from psychological illness. The subjects were instructed to close their eyes while solving some simple arithmetic questions for 20 minutes. An interpreter used to ask the arithmetic question to the participants. In that respect, the brain response (EEG signal) is a result of cognitive event-related potential (ERP) type. A total of ten trials were taken for each subject. The cognitive event was selected because in that case, the participants can easily concentrate and in eye closed condition, there are no eye blinking/ EOG artefacts [9].

Electrodes placement was configured on the right central (C4), and the right occipital (O2) position as the regions are responsible for problem solving and cognitive function, respectively. It is to note that, the authors have selected the cognitive task from their experience from previous pilot studies where the cognitive task gives clear signals with less noise [10, 11].
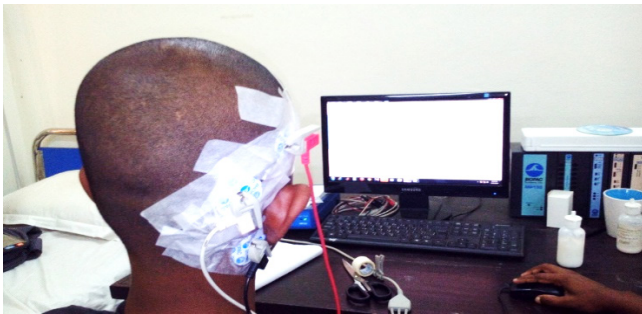
Figure 2: Representational view while conducting the experiment in BME lab, KUET

3.4. Experimental Procedure

3.4.1. Signal Preprocessing

The primarily obtained EEG signals could have contained noise due to muscle movement, eye blinking and hand movement. Along with line frequency was 50 Hz. To pre-process raw EEG was gone through bandpass finite impulse response (FIR) filter with a range of 0.5 to 44 Hz, as it removes the non-linear trends of the signals. Later the signal was further smoothed, taking a moving average over a short period of the signal.

3.4.2. Feature Extraction

Various features were extracted in time and frequency domain, including standard deviation (STDDEV), maximum value (E_{max}),

skew (sk), kurtosis (k), power spectrum density (PSD) mean, PSD max, Fast Fourier Transform (FFT) mean, FFT max (total eight feature) were extracted for each subject using the Acknowledge 4.1® software. For feature extraction was done using a 5-second epoch length.

3.4.3. Feature Scaling

The time and frequency domain features, which were extracted from the EEG signal, have different range in their magnitude. As the machine learning models work with various features putting them in the same matrix, it is essential to put all the features in a same range, which is referred to as feature scaling. Two common types of feature scaling is done in preliminary data: standardization and normalization [12, 13]. MinMaxScaling was done in this study in python 3.6.9 platform, as a part of the normalization process. *MinMaxscaler()* function from *sklearn* library was used fo this purpose. Here the data is shrunk within a range between [-1,1].

$$x_{new} = \frac{x - x_{min}}{x_{max} - x_{min}} \tag{1}$$

The formula of min-max scaling can be given by equation (1). Here, x_{new} is the normalized value of a feature point x, within a range x_{min} and x_{max} [14].

3.5. Classification

For the diagnosis of tobacco smoking, classification is the main and last step, which is done through machine learning. Machine learning is the application of artificial intelligence, which provides a system capable of learning nature from a given data. There are three categories of Machine Learning models and applications, supervised learning, unsupervised learning, and reinforcement learning. Supervised learning is extensively used for the classification and regression problem [15]. Previous studies worked with EEG have used supervised learnings, especially K-Nearest Neighbour [16], Support Vector Machine [17], Random Forest Classifier [18] and Logistic Regression [19]. Based on the previous studies, these four classifiers were chosen for the data classification in this research.

3.5.1. Logistic Regression (LR)

Logistic regression is a supervised learning model, which works based on the linear method, and the predictions are made using a logistic or sigmoid function σ(t). The sigmoid function is 'S' patterned curve that takes a real number and maps within a range between 0 and 1. Equation (2) represents the sigmoid function.

$$\sigma(t) = \frac{e^t}{e^t + 1} = \frac{1}{1 + e^{-t}} \tag{2}$$

Considering two types of variables, dependent and independent, Logistic regression predicts the dependant variable based on the independent variable. The 'C parameter' was tuned here in the Logistic regression model to reduce overfitting [20,21].

3.5.2. K-nearest neighbours (KNN)

KNN is a supervised learning algorithm, and a non-parametric method where k nearest training examples in the feature space is taken as input and neighbours vote do the classification generally used for classification and regression. At the very starting point,

KNN read the value of K, type of distance D and test data; then it finds the K nearest neighbours D to the test data and thus sets the maximum label class of K to test data. The same process is gone through an iterative process named looping. In details, its algorithm initializes the value of K from 1 (setting as initial iteration value). After loading data, iteration from initial K =1 (generally) to the total number of training data point while distances specifically Euclidean distance between test data and each row of training data is measured and sorted in ascending order to get topmost k rows from the sorted array and the most frequent class is returned as the predicted class [22]. The value of K was tuned, and the k for best efficiency was chosen in the classifier model in this research to reduce overfitting.

3.5.3. Random Forest Classifier (RFC)

Ensemble learning models, such as Random forests are made of individual decision trees with a logic of group of weak learners to finally make a strong learner while the decision trees operate as divided or conquer. A class is predicted from every decision tree and a final class is predicted by model depending on their vote [22]. Two parameters were tuned in the RFC models in this study, namely, '*n_estimate*', which implies the number of trees in the forest and 'max-depth' which signifies the depth of each tree.

3.5.4. Support Vector Machines (SVM)

An SVM is a supervised learning algorithm, which aims to obtain a hyperplane classifying the data point (data points can be at any side of hyperplane) in feature dimensional space while depending on both linear and non-linear regression. Data points distance across to hyperplane are called support vector whose detection can exchange hyper plane's location [22]. The model used a Gaussian kernel for SVM classifier in this research due to the non-linear trend of the dataset. Two parameters- 'C' and 'gamma' was adjusted within a set of values using the grid search algorithm to reduce overfitting.

3.6. Performance Measures

3.6.1. Sensitivity or True Positive Rate (TPR)

True positive rate or Sensitivity is the proportion of the true positives (desired factor), which is correctly identified from the given test set [23]. The definition of sensitivity can be provided by equation (3), where TP = True Positive and FN = False Negative. In this study, sensitivity is the measure of the proportion of successfully identifying a smoker.

$$\text{Sensitivity} = \frac{TP}{TP+FN} \qquad (3)$$

3.6.2. Specificity or True Negative Rate (TNR)

True negative rate Specificity is the proportion of true negative (undesired factor) in which was correctly excluded from the given test sets [23]. The definition of specificity can be provided by equation (4), where TN = True Negative and FP = False Positive. In the case of this study, specificity is the measure correctly identifying a non-smoker. In this study, accuracy is the proportion of successful identification, either smoker or non-smoker.

$$\text{Specificity} = \frac{TN}{TN+FP} \qquad (4)$$

3.6.3. Accuracy

The overall accuracy is the proportion of true results (either true positive or true negative) in an experiment [23,24]. The definition of accuracy can be provided by equation (5), given that TP = True positive, TN= True Negative, FP= False Positive and FN = False Negative. In this study, accuracy is the proportion of the successful identification, either a specific person or not being that person.

$$\text{Accuracy} = \frac{TP+TN}{TP+TN+FP+FN} \qquad (5)$$

3.6.4. Area under the receiver operating characteristic (ROC) curve (AUC)

ROC is the plot of the sensitivity (true positive rate) against the (1- specificity) or false positive rate, where all the possible combination of TPR and FPR are plotted, showing the trade-off between them [23–25]. As sensitivity and specificity are two major parameters of performance measures, AUC under ROC always provides a compromise between them. Though there are few methods for validation, five-fold cross-validation was done in this study while evaluating the performance measures. The mean value and the standard deviation (SD) were noted, considering the five experimental validations. Thus, the mean sensitivity, specificity and AUC was calculated from the obtained confusion matrix.

4. Results

4.1. Data visualization (Box plot and violine plots)

Data visualization is an important part to observe the data arrangement. Given data points found from the selected features were plotted in box and violin plots to observe the range of each of the features. The following Figure 3 and Figure 4 shows that the time and frequency domain features are having a versatile variation in the range. Range of the difference features varies among themselves either in the time domain or in the frequency domain, and therefore, the feature scaling was performed.
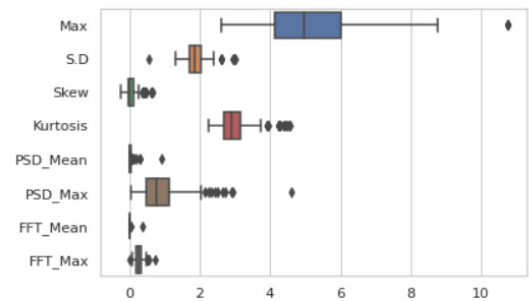
Figure 3: Box Plot of part EEG data showing varying magnitude of differnt features

4.2. Classification Performance

All the features were scaled and were supplied towards the machine learning models after necessary parameter tuning. Four different performance measures were evaluated, namely, sensitivity or true positive rate (TPR), specificity or True negative rate (TNR), accuracy and area under the receiver operating characteristic (ROC) curve (AUC). The obtained results are listed in the Table 1.
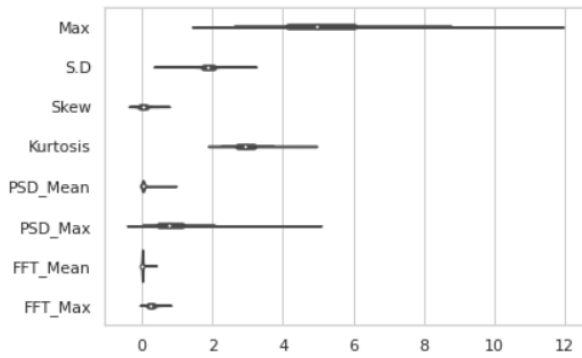
Figure 4: Violine Plot of part EEG data showing varying magnitude of differnt features

Table 1: Performance measures (mean value) for EEG based smoker detection using four different classifiers, five-fold cross-validation

Domain	Performance Measures	LR	KNN	RFC	SVM
Time Domain	Sensitivity	58.9	56.07	63.6	53.1
	Specificity	55.2	57.54	61.3	55.3
	Accuracy	57.4	55.53	62.4	59
	AUC	53.7	54.04	65	60.1
Frequency Domain	Sensitivity	70.7	77.14	81.2	70.9
	Specificity	70.7	71.35	83.7	76.3
	Accuracy	76.1	73.75	82.9	72.9
	AUC	71.4	77.59	83.2	77.1
Time-Frequency Domain	Sensitivity	89.2	83.75	94.3	85
	Specificity	86.3	91.25	92.1	87.2
	Accuracy	**87.2**	**87.5**	**91.3**	**86.5**
	AUC	78.3	80.7	92	88.2
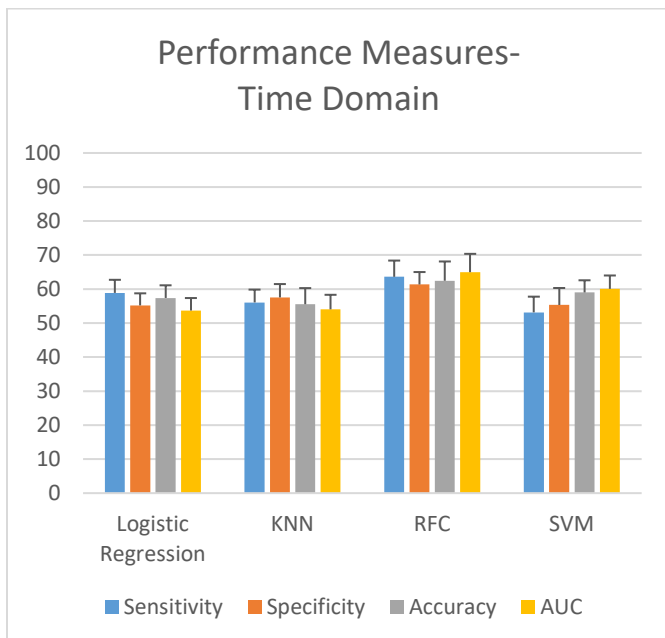
Figure 5: Performance measurement of time domain

4.2.1. Scenario-1: Classification using Time Domain Features

The following Figure 5 shows the plots of the performance measures (mean ± SD) obtained from the classification of smokers and non-smokers using the time domain features from four different classifiers, LR, KNN, SVM and RFC, respectively. The plots show that the gap between sensitivity and specificity is highest in LR (3.68%) and lowest in the case of KNN (1.44%). Overall, RFC gives an accuracy of 62.4%, which performs the best.

4.2.2. Scenario-2: Classification using Frequency Domain Features Domain

The following Figure 6 shows the plots of the performance measures (mean ± SD) obtained from the classification of subjects addicted to smoking using the frequency domain features from four different classifiers, LR, KNN, SVM and RFC, respectively. The plots show that the gap between sensitivity and specificity is higher in KNN (5.8%) and SVM (5.4%) and lowest in the case of LR (0.05%). Overall, RFC gives an accuracy of 82.9%, which performs the best.
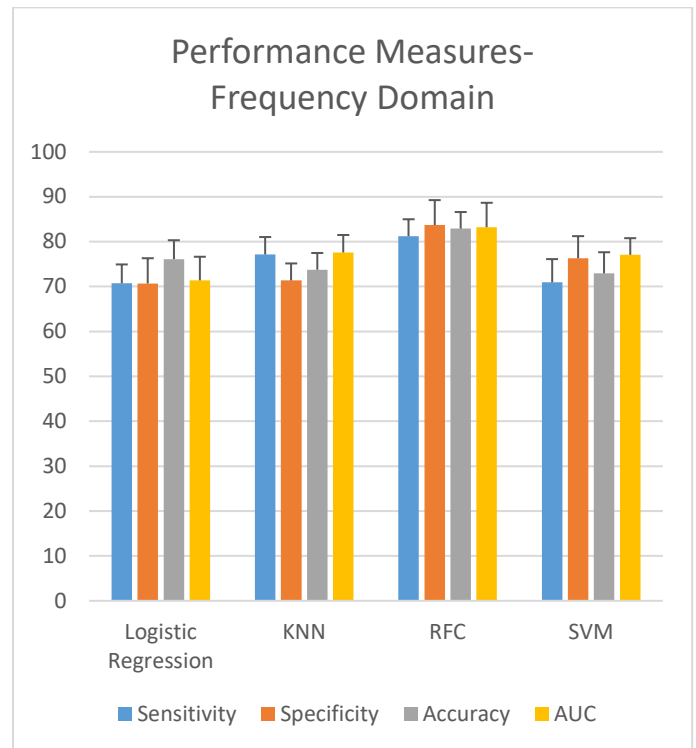
Figure 6: Performance measurement of frequency domain

4.2.3. Scenario-3: Classification using the Time-Frequency Domain Features Domain Features

The following Figure 7 shows the plots of the performance measures (mean ± SD) obtained from the classification of subjects addicted to smoking using the time domain features from four different classifiers, LR, KNN, SVM and RFC, respectively. The plots show that the gap between sensitivity and specificity is the highest in the case of SVM (7.5%) and lowest in the case of RFC (2.2%) and ANN (2.2%). Overall, RFC gives an accuracy of 91.3%, which performs the best.

Figure 7: Performance measurement of the time-frequency domain
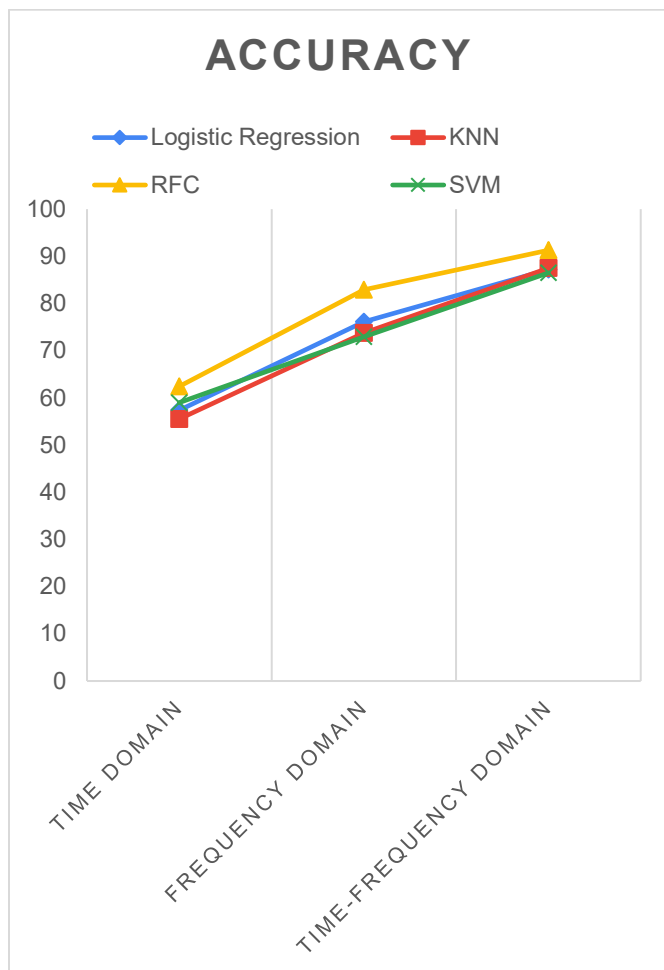
Figure 8: Comparison of accuracy metrics for four different classifiers

4.3. Choosing the best Scenario

The overall accuracy was considered as the reference metrics while finding out the best scenario, as it is difficult to compare different classifiers using several measures. The plots of the accuracy for four different classifiers corresponding to different domain are shown in the Figure 8 below. From the given figure, it is evident that the accuracy for random forest classifier is better than any other domains for all the four classifiers.

The accuracy plots also reveal the relative comparison among the time domain features, frequency domain features and the effect of the fusion of both time and frequency domain. It is evident that the frequency domain features perform better than the time domain features for all of the classifiers. Again, the time-frequency fusion outperforms the previous scenarios when the time or frequency domain feature were used individually. So, in the rest of the paper, the combined-time frequency domain features will be considered for further analysis.

4.4. Choosing the best classifier

The plots for the area under the ROC curve for the classifiers built using the time-frequency domain of EEG features are shown in the Figure 9 below. The figure illustrates that the RFC classifiers show the best compromise between sensitivity and specificity, with covering the highest area under the ROC curve (AUC= 0.92%).
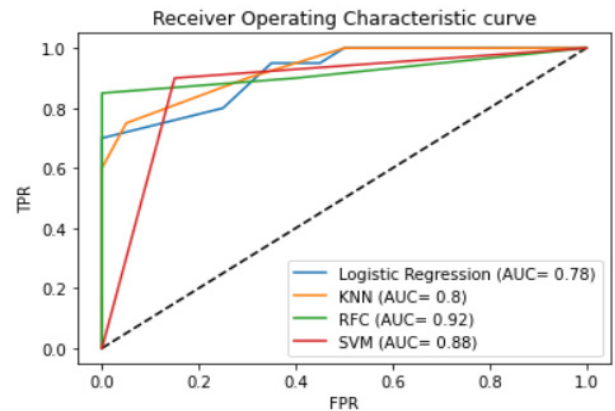
Figure 9: Comparison of AUC for four different classifiers for time-frequency domain
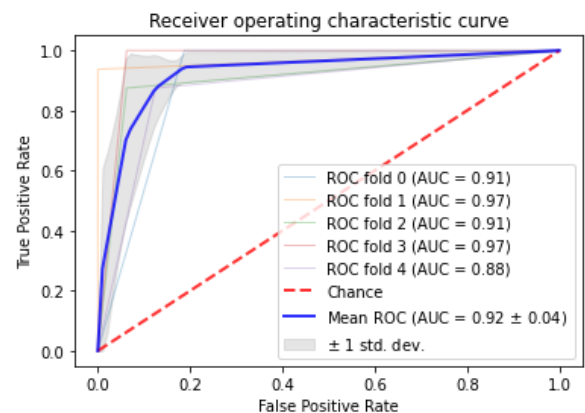
Figure 10: ROC Plots for time-frequency domain-based RFC model with 5-fold CV

Area under the AUC curve plots for 5 different experiments in 5-fold cross-validation with time frequency domain features using RFC classifier is shown in Figure 10. The AUC ranged from (0.78-0.92) for all the models with the time-frequency domain features, with a mean of 0.92 and 0.04 standard deviation. This signifies that the time-frequency domain shows an excellent performance than the other domains of EEG signal in tobacco smoking diagnosis.

5. Discussion

Four different classifiers were used in this study for assessing the performance of the EEG domains for the diagnosis of tobacco smoking. The results revealed that the time-frequency domain performs the best among the other domains. It also revealed that the maximum performance was obtained using the RFC Classifier, with a sensitivity, specificity and accuracy of 94.3%, 92.1% and 91.3%, respectively. Moreover, RFC based model time-frequency domain-based dataset shows promising AUC (0.92), which is a good compromise between sensitivity and specificity.

The finding of this study is consistent with some of the previous studies [1,7]. The study [7] achieved an accuracy ranged from 97.33-97.50%, while using the frequency domain features, such as, PSD and FFT features of EEG signal, which also supports the finding of the current study. Though the study of [7] used only RBF kernel based SVM, the current study validated the other classifiers which support the findings. In another study [1], where authors found the time-frequency domain as the best performing domain, though they have used only one classifier (ANN), and one performance metrics (Accuracy). Contrarily, the time domain performed the worst (RFC accuracy= 62.4%) in their study, while using a holdout approach for validation. The current study used a five-fold cross-validation and validated the outcome of the previous research with multiple classifiers.

Based on the results and analysis in the study, the following research implications and recommendations can be provided. First, using the frequency domain features is always recommended to diagnose tobacco smoking using the EEG signals. However, using time-frequency fusion is highly recommended as this combination provides a higher classification performance. Second, the given outcomes could be correlated with the drug-related impairment in the human brain, which could provide further insight into the correlation between the two addiction.

There are some feasibility issues with the study. First, using EEG sensors to detect the smoking habit could be a cumbersome procedure. However, the research could add value to observe the effect of different cigarettes depending upon their nicotine levels and their impact on the human brain. Second, the use of EEG as ground truth in tobacco-related experiments. If the setup is available in the lab, the EEG measurement could be used as ground truth when observing the effect of Tobaccos smoking on other factors. Third, the impact of drug addiction is more severe in the human brain than smoking. This experiment can add value to the relative comparison of the drug and tobacco addiction. However, the scope of the paper is not out of limitations. Inter-individual difference among participants is another factor, which is needed to be considered. As the paper represented a novel methodology of EEG based diagnosis of tobacco smoking, more research is required to find out the feasibility in real-world conditions as well.

6. Conclusion

To develop an EEG based diagnosis of tobacco addiction, an analysis was done in this study to find out the feasibility of the time and frequency domain features using this proposed model. Here, ultimate results were obtained after applying several steps- feature scaling, tuning of classifiers, and finally with five-fold cross-validation of the developed models. The research investigation found that the combination of the time-frequency domain features with RFC classifier showed the best accuracy while the time domain features showed the lowest accuracy. This analysis shows that time-frequency domain shows the best Accuracy with SVM (86.5 %), LR (87.2%), KNN (87.5%) and RFC (91.3%), Time-domain shows the lowest accuracy with all classifiers while the ffrequency domain shows higher accuracy than time domain, but still, this is less than the combined time-frequency domain performance. Among all the classifiers, RFC showed the best Accuracy and SVM showed the lowest accuracy. However, the experiment could be done on more number of participants to validate the model based on lave one participant out approach. Also, efficiency will increase with the addition of more EEG channels which could be considered for future implications.

Conflict of Interest

The authors declare no conflict of interest.

Acknowledgment

References

[1] M.M. Hasan, N. Hasan, A. Rahman, M.M. Rahman, "Effect of Smoking in EEG Pattern and Time-Frequency Domain Analysis for Smoker and Non-Smoker," in 2019 International Conference on Computer, Communication, Chemical, Materials and Electronic Engineering (IC4ME2), IEEE: 1–4, 2019. doi: 10.1109/IC4ME247184.2019.9036492

[2] C.N. Metz, P.K. Gregersen, A.K. Malhotra, "Metabolism and biochemical effects of nicotine for primary care providers," Medical Clinics, **88**(6), 1399–1413, 2004.

[3] R.C. O'reilly, Y. Munakata, Computational explorations in cognitive neuroscience: Understanding the mind by simulating the brain, MIT press, 2000.

[4] G. Cartocci, E. Modica, D. Rossi, A.G. Maglione, I. Venuti, G. Rossi, E. Corsi, F. Babiloni, "A pilot study on the neurometric evaluation of 'effective' and 'ineffective' antismoking public service announcements," in 2016 38th Annual International Conference of the IEEE Engineering in Medicine and Biology Society (EMBC), IEEE: 4597–4600, 2016.

[5] Z.M. Hanafiah, K.F.M. Yunos, Z.H. Murat, M.N. Taib, S. Lias, "EEG brainwave pattern for smoking behaviour after horizontal rotation treatment," in 2009 IEEE Student Conference on Research and Development (SCOReD), IEEE: 559–561, 2009. doi: 10.1109/SCOReD247184.2019.9036492

[6] T. Warbrick, A. Mobascher, J. Brinkmeyer, F. Musso, T. Stoecker, N.J. Shah, G.R. Fink, G. Winterer, "Nicotine effects on brain function during a visual oddball task: a comparison between conventional and EEG-informed fMRI analysis," Journal of Cognitive Neuroscience, **24**(8), 1682–1694, 2012.

[7] L.C. Chin, A.M. Zazid, C.Y. Fook, V. Vijean, S.A. Awang, M. Affandi, L.S. Chee, "Differentiate Characteristic EEG Tobacco Smoking and Non-smoking," in Journal of Physics: Conference Series, IOP Publishing: 12055, 2019, doi:10.1088/1742-6596/1372/1/012055.

[8] D. Acquisition, Analysis with BIOPAC MP Systems, AcqKnowledge 4 Software Guide. pdf, Biopac Systems, Inc. ISO 9001: 2008.

[9] N. Hasan, M.M. Hasan, M.A. Alim, "Design of EEG based wheel chair by using color stimuli and rhythm analysis," in 2019 1st International Conference on Advances in Science, Engineering and Robotics Technology (ICASERT), IEEE: 1–4, 2019, doi:10.1109/ICASERT.2019.8934493.

[10] M.M. Hasan, M.H.A. Sohag, M.E. Ali, M. Ahmad, "Estimation of the most effective rhythm for human identification using EEG signal," in 2016 9th International Conference on Electrical and Computer Engineering (ICECE), IEEE: 90–93, 2016, doi:10.1109/ICECE.2016.7853863.

[11] M.M. Hasan, M. AshfaqulIslam, S.A. Imtiyaz, M. MahbubHasan, "Presumption method for detecting and analyzing human mental behavior by employing EEG signal," in 2018 4th International Conference on Electrical Engineering and Information & Communication Technology (iCEEiCT), IEEE: 519–523, 2018.

[12] M. Wester, W. McMullen, A. Macy, "Biopac Student Lab Pro, Hardware and Software Reference Manual, ver. 2.1, BioPac Systems," Inc., Santa Barbara, CA.[Accessed on 26 April 2018], 1997.

[13] B.B. flow Monitor, Biopac Systems, Inc. ISO 9001: 2000.

[14] C. Colantuoni, G. Henry, S. Zeger, J. Pevsner, "SNOMAD (Standardization and NOrmalization of MicroArray Data): web-accessible gene expression data analysis," Bioinformatics, **18**(11), 1540–1541, 2002, doi:https://doi.org/10.1093/bioinformatics/18.11.1540.

[15] F. Pedregosa, G. Varoquaux, A. Gramfort, V. Michel, B. Thirion, O. Grisel, M. Blondel, P. Prettenhofer, R. Weiss, V. Dubourg, "Scikit-learn: Machine learning in Python," The Journal of Machine Learning Research, **12**, 2825–2830, 2011.

[16] F. Riaz, A. Hassan, S. Rehman, I.K. Niazi, K. Dremstrup, "EMD-based temporal and spectral features for the classification of EEG signals using supervised learning," IEEE Transactions on Neural Systems and Rehabilitation Engineering, **24**(1), 28–35, 2015, doi:10.1109/TNSRE.2015.2441835.

[17] S. Bhattacharyya, A. Khasnobish, S. Chatterjee, A. Konar, D.N. Tibarewala, "Performance analysis of LDA, QDA and KNN algorithms in left-right limb movement classification from EEG data," in 2010 International conference on systems in medicine and biology, IEEE: 126–131, 2010.

[18] H. Lee, S. Choi, "Pca+ hmm+ svm for eeg pattern classification," in Seventh International Symposium on Signal Processing and Its Applications, 2003. Proceedings., IEEE: 541–544, 2003.

[19] L. Fraiwan, K. Lweesy, N. Khasawneh, H. Wenz, H. Dickhaus, "Automated sleep stage identification system based on time–frequency analysis of a single EEG channel and random forest classifier," Computer Methods and Programs in Biomedicine, **108**(1), 10–19, 2012, doi:https://doi.org/10.1016/j.cmpb.2011.11.005.

[20] J. Kim, J. Lee, C. Lee, E. Park, J. Kim, H. Kim, J. Lee, H. Jeong, "Optimal feature selection for pedestrian detection based on logistic regression analysis," in 2013 IEEE International Conference on Systems, Man, and Cybernetics, IEEE: 239–242, 2013.

[21] H. Rajaguru, S.K. Prabhakar, "Non linear ICA and logistic regression for classification of epilepsy from EEG signals," in 2017 international conference of electronics, communication and aerospace technology (ICECA), IEEE: 577–580, 2017.

[22] K. AlSharabi, S. Ibrahim, R. Djemal, A. Alsuwailem, "A DWT-entropy-ANN based architecture for epilepsy diagnosis using EEG signals," in 2016 2nd International Conference on Advanced Technologies for Signal and Image Processing (ATSIP), IEEE: 288–291, 2016, doi:10.1109/ATSIP.2016.7523093.

[23] W. Zhu, N. Zeng, N. Wang, "Sensitivity, specificity, accuracy, associated confidence interval and ROC analysis with practical SAS implementations," NESUG Proceedings: Health Care and Life Sciences, Baltimore, Maryland, **19**, 67, 2010.

[24] A.-M. Šimundić, "Measures of diagnostic accuracy: basic definitions," Medical and Biological Sciences, **22**(4), 61, 2008.

[25] D. Justin, R.S. Concepcion, A.A. Bandala, E.P. Dadios, "Performance Comparison of Classification Algorithms for Diagnosing Chronic Kidney Disease," in 2019 IEEE 11th International Conference on Humanoid, Nanotechnology, Information Technology, Communication and Control, Environment, and Management (HNICEM), IEEE: 1–7, doi:10.1109/HNICEM48295.2019.9073568.

Multi-Layered Machine Learning Model For Mining Learners Academic Performance

Ossama Embarak[*]

Computer Information Science, Higher Colleges of Technology, Abu Dhabi, 51133, UAE

A B S T R A C T

Different colleges and universities have different approaches to dealing with low-performance learners. However, in most cases, analgesics do not deal with root problems. This research suggests a model of three layers of variables sequentially adaptable to a deep-root issue. The suggested model can identify early pupils who could be at risk because of inaccurate or lack of match sequences and suggest rehabilitation. The approach proposed was implemented at three levels. First, we examined the personality type for 180 learners from different majors: Security and Forensics, Networking, and Application Development, using the MBTI test. Second, we build a knowledge matrix for courses by dividing each learning outcome into its knowledge segments. Then, we build the skills matrix for courses by decomposing each learning outcome into its skills segments. We then use machine learning (SVM, DT and association rules) algorithms to mine student performance on a smaller scale of knowledge and skills, taking into account their personality types instead of measuring an entire course's holistic performance. Finally, we developed a system of recommendations to detect performance deviations in knowledge and skills and provide adaptive learning materials that fit the examined students' personality. The proposed approach demonstrates its validity and effectiveness. However, it needs regular updates on learners' performance, which could be automated and linked to evaluation tools. The framework also has a minor impact on learners' privacy since it exposes individual personalities to their advisors.

1. Introduction

This paper is an extension of work initially presented in 2018 Fifth HCT Information Technology Trends (ITT), IEEE [1]. On average, students have different talents, distinct attitudes, and different levels of enthusiasm in their educational programs. Although various students may share a major, it is, however, important to analyze students in many aspects, including the knowledge and skills they have learned. The students have a wide range of learning styles that reflect how they can analyze, plan, and respond to the learning environment [2]. Some students may be comfortable thinking of hypotheses and abstract ideas, while others feel better being a little more concrete with data. Some of the student body prefers active learning, interaction by taking notes and seeing the material presented [3]. It shows how different the students are to each other even within the same major. There are three learners of the course. One learner who has begun to learn by auditory means, another who has begun with tactile activities and finally another learner who is visually dominated [4]. The challenge of the day is to equip our students with the information and skills they will need to accomplish their goals into their future professional careers, regardless of their personal preference. There are many majors in computing that require different knowledge and essential skills than those

required for their future careers. To memorize everything here is not exactly effective; i.e., memorization is inefficient. An inability to memorize is a type of learning disorder. Students with such a condition do not expend much effort in studying or preparing for exams. There are two different behaviours that those students might do. Some students might adopt a more in-depth approach when understanding the meaning, whereas the others might make a more strategic approach to understand such type of knowledge, get the best knowledge of their peers and gain related skills [5,6]. As it should be, learners often have their own personal values that affect their own personal ability to absorb new knowledge and learn new functional skills [7].

Knowing students' personality patterns is extremely valuable in finding out their skills; the Myers-Briggs Type Indicator (MBTI) is very much in use. as a means to do just that. Neural dynamics testing techniques, as used in MBTI, helps with understanding the form of human personality. The four main personality traits are eye contact, emotional perception of facial expressions, sensitivity to language, and sensitivity to others' physical appearance [8].

The first pattern is the orientation of energy: Extroversion (E) is preferable to those who prefer to be energized for situations, people and things (that is, for the external world)

850

2

compared with their complement, preferring to direct their energy towards information, beliefs, ideas and explications (that is, the internal world) (I).

The second pattern is the information and things an individual wants to deal with; Those who prefer to deal with facts and describe clearly situations are sensitive (S). They prefer to deal with ideas, expectations and unknown factors that are not obvious, rather than their additions dependent on intuition. (N).

The third pattern is the sort of decision-making, People would rather make decisions based on objective logic and analysis- Thinking (T) than those who prefer to make decisions based on the values they believe important — feelings Feelings (F).

Fourth, how people make their planning, Those who prefer well-designed and planned lifestyles judge (J) against those who like flexibility, flow and react to things, i.e. perception (P) [9].

- ***Extraversion(E) vs Introversion (I)***
- ***Sensing (S) vs Intuition(N)***
- ***Thinking(T) vs Feeling(F)***
- ***Judging vs Perceiving(P)***

A person may be more inclined to be extroverted than an introvert. Likewise, a person could be more sensing than intuitive, more thoughtful than feeling and judging than perceived. The table below decipher examples of detected personalities.

Table 1:Sample types of personality

Personality Type	ISTJ	ISFJ	ESFP	INTP	ENTJ
Extraversion(E)	×	×	√	×	√
Introversion (I)	√	√	×	√	×
Sensing (S)	√	√	√	×	×
Intuition(N)	×	×	×	√	√
Thinking(T)	√	×	×	√	√
Feeling(F)	×	√	√	×	×
Judging(J)	√	√	×	×	√
Perceiving(P)	×	×	√	√	×

Each personality fits more than the others to a particular career; for example, the ISTJ personality type could fit more into the Systems administrator.

I: Propensity to think about things in the mind
S: Prefer ideas with practical applications
T: Take decisions on an impersonal basis, using a logical reasoning
J: Prefer detailed step-by-step instructions

Combining these four couples generates 16 alternative personality types that enable scientists to understand individuals and advance in a specific area through measurement (s). Students with a preference for introversion, probably doing a lot of thorough work or considering a problem, can find it difficult to live in a noisy or interactive environment [10]. Consequently, they can tend to pick less active and interrupted concentrations. The measurement of computer skills in vital terms and concepts, which are understandable and learning for students during their studies. We have to measure skills such as troubleshooting, network setup, audit protection framework, etc. In addition, it is possible to develop applications, systems, networks, etc.

Maintaining a system to ensure students' personality types is extremely important for understanding their emotions, thinking,

and behaviour. For example, understand if a student prefers to work alone or prefers to work with others. Prefers an extremely organized and fixed career, or someone who would like a flexible, open schedule, which allows him or her to be spontaneous. This information helps to determine which career(s) are appropriate for the preferences of students. There are no special advantages or disadvantages over these patterns as they complement each other. If a student has been detected as an Extroversion with a specific percentage, it is an Introversion of the supplement percentage; therefore, each pair is valid for each person but with different strength. The networking employee is expected to be self-driven to deal with network issues and not wait for outside directions. Extraverts tend to be more active when learning, while introverts tend to be more reflective when learning.
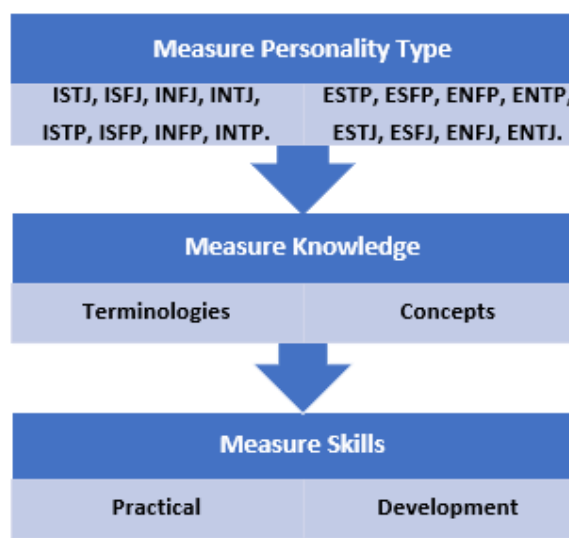
Figure 1:   Learner comprehension layers

3. Literature Review

We cannot think of a single method of teaching suitable for all pupils of the same major. Most academic institutions follow the same method, which relies on the delivery of lectures, where students have to absorb the material and then repeat it in the review. This approach does not solve the gaps in student skills, expertise and competencies. Different learning styles define students they prefer to interpret knowledge in different ways [11]. Several models were developed to classify the way people learn; Jung's psychological theory, also known as the Myers-Briggs Type Indicator, is the most famous model (MBTI) [12]. This test provides ample information about a person's personality and the consequences of his or her education. The engineering department of the University of Western Ontario has demonstrated that in the first year of engineering courses men introverts, intuition, thinkers and judges are more likely to excel than extraverts, felt, sensed, and interpreted people at the lower end of their range [13]. They used an MBTI test and performance test on 119 students to determine whether that particular group of seniors would perform very well later in a class like that. The type of personality that is more likely to drop out of the curriculum is recommended to be one that is not overly concerned with grades.

Sensors personality ratings were significantly lower than Intuitors in courses with few high abstractions, an especially important practical question posed by the tests. Introverts may be well-suited for team activities, but extraverts will enjoy working together. Persons who score highly in the Intuitive

cluster score higher on creativity and problem-solving skills than those with a Sensing personality [14]. For example, in understanding academic success, another model created in recent years is the Felder and Silverman [15]. Its purpose is to answer four questions, which are as follows.

On the student's preferred topic, what information do they preferentially perceive? For the student who has a sensory personality, they prefer to be focusing on interacting with what they see, hearing the sounds, and using their physical sensations as a way of experiencing. Those who think more specifically are more comfortable with their abstracts (theories, math, memories, thoughts, and are more likely to solve the problems faster and innovative. What kind of information are our senses perceived most effectively? That is visual personality (exhibited in the eyes) or verbal personality (expressed through speech). What process is the student used to incorporate this information into their outside learning?   Actively through participation in physical activity, or through meditation. How does the student characteristically   get   from   "not   understanding"   to "understanding?" The classroom needs to be set up with logical steps in place, with students thinking linearly and being able to only work with a partial understanding (logic step), or where students think globally and applying their knowledge until they fully understand the picture and have a holistic perspective (global system step) [16]. The Kolb Model assumes that every class possibly includes students of every category. This leads to the belief that these learners are often more likely to become better learners, leading them to perform better [17].

The key issue is how to find an appropriate method of learning for new students when the knowledge is lacking. There are numerous approaches that solutions tend to be used in solving a new state: a cold start problem, [18] Develop the algorithm that finds the closed likeminded learner, and so it generates its recommendations accordingly. [19] Researchers found that students with characteristics that esteem the parental world among students in technology majors were more likely to be of an ESFJ, ISFJ, ESFP, INTJ, and ISTP. On the other hand, students majoring in management information systems tend to be more ESTJ and ISTJ. In an article by [20]ISTJ, INTJ, and ISFJ are the most common personality types found in the computing industry. A study that was done by [21] shows that the relationship between the students' personality and their academic performance depends on the correspondence between the students' personality and the chosen major. Researchers have found, first of all, that system analysts are more extroverted than other thought-provoked people, that computer designers are more introverted and less extroverted than other thought-provoked people, and that programmers are more introverted and less extroverted than other thought-provoked people.

4.   The Proposed Approach

The details of the proposed approach are to be applied in four phases. In the first phase, we build the courses' knowledge and skills matrix by decomposing the course's learning outcomes into its knowledge and skills segments. This will help apply machine learning algorithms to mine learners' performance on a smaller scale of concept segments rather than on the entire course's performance or an entire block of concepts. In the second phase, we collected the personalities of students using the MBTI test. In the third level, we assess learners' success (Knowledge & Skills) considering their personality and

concentration. Finally, apply a recommendation framework to enhance the performance of learners using machine learning.

4.1. Construct a matrix of knowledge and skills

Analyze courses in terms of skill and knowledge. The starting point was to decompose the courses into their relevant knowledge and skills, representing all the concepts used in each CLO course and laid out in the PLO curriculum, as seen in the following analysis for CIS1403, fundamental to the programming course.

Table 2:Fundamental of programming knowledge & Skills

CLO Number	Description	knowledge	Skills
CLO1	Apply basic programming concepts to write simple programs that use data types, variables, constants, expressions, and statements, focusing on these constructs in Java.	Just remember data types. Recognize the appropriate parameters and values. Please, understand expressions.	Apply the data types. Read through the used data types Create a fully working application in which all variables are properly typed.
CLO2	Write programs that take control flow decisions by means of conditional statements and iterative decisions.	Understand how expressions work. Learn to understand Iteration statements.	Make use of iterations to accomplish control flow. Use conditionals to control the flow of a program.
CLO3	Write programs using unidimensional arrays for initialization, access, transversal, and searching for different data types.	Understand one-dimensional array	Write programs using single-dimensional arrays Write programs that access, update, and search one-dimensional arrays.
CLO4	Develop programs using built-in and user-defined functions with parameter lists.	Understand different user-defined functions {void and return}	Analyze user-defined functions Write functions with parameters
CLO5	Organize and document the program's source code in line with industry standards and best practices.	Recognize coding standers Recognize coding best practices	Apply coding best practices Analyze a programming problem Write a fully working program with function calls

The method retains four key components: intelligence, abilities, attitude and soft skills of the learner. The developed machine learning model used by these components to assess learners of the greatest importance, learners' key causes of At-risk, and we strive to calculate their employability ratio in the light of these core components.

4.2. Evaluation of student personalities

Understanding the personality type will help clarify the preferences, and how or why students may be different. Personality types are useful for understanding how a person can learn, manage, monitor, communicate, collaborate, compromise and cope with stress. Understanding the behaviours of learners helps prepare students to improve their knowledge and skills. This helps to apply a self-awareness tool to recognize strengths, consider and manage growth needs, and establish a career and personal development strategies.
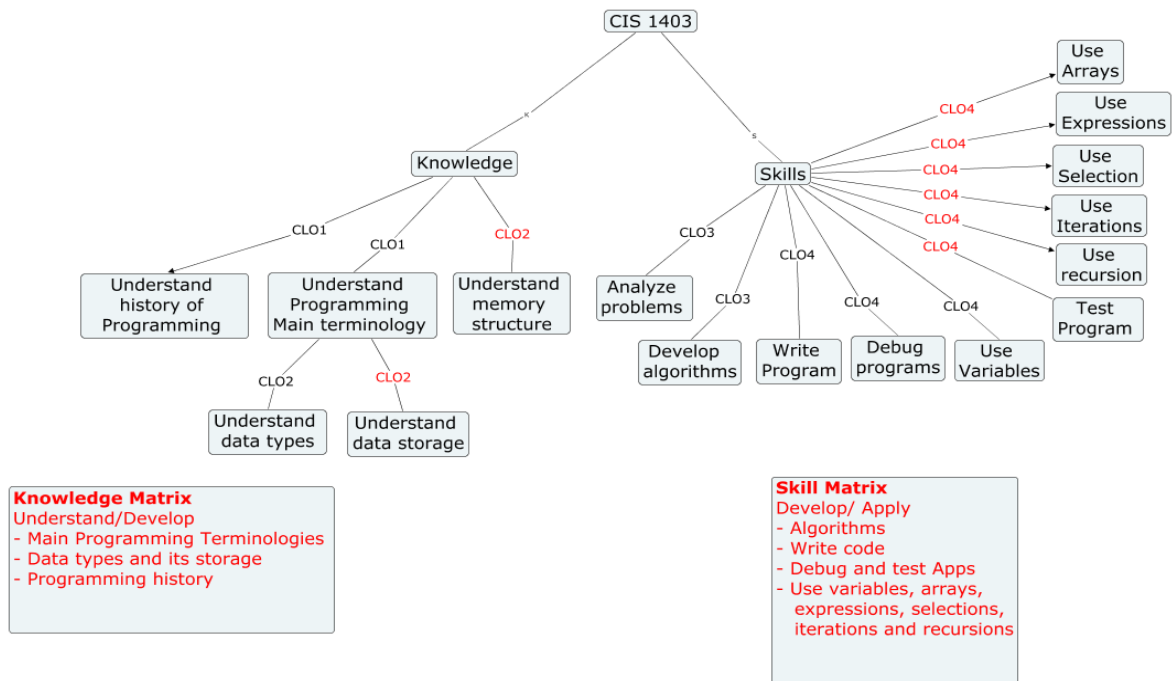
Figure 2: Course knowledge and skills decomposition

We collected data about students' personality using https://www.16personalities.com/, where students' future profession can be categorized into MBTI Sixteen Personality Types shown below [22].

Figure 3: Personality types main features

4.3. Build a recommendation system

Build a recommendation framework that considers learners' personalities from on the one hand and the knowledge and skills they have from the other, as shown in the figure below.
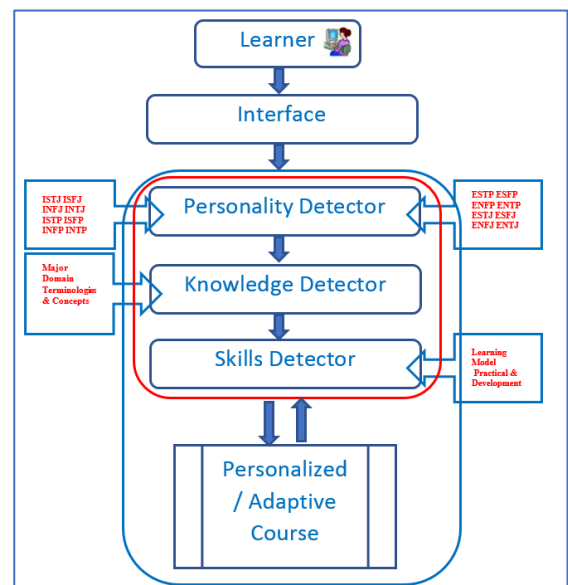
Figure 4: Three-layered course personalization model.

5. Research Procedures

For this research, 180 students were asked twice to use different platforms to take the Myers-Briggs Style Test. Eliminating all irregularities, only correct and clean data for treatment has been processed. Data collection incorporates the Type of Personality and the Personality Code; Extraversion (E), Introversion (I), Sensing (S), and Intuition (N) (P).

Variables

Three factors influence the development of students and thus their academic status in this research. First, we will consider the

personality type created through a four-letter combination, each of which represents a set of independent characteristics. : extroverted versus introduced, sensing versus intuitive, thought versus feeling and judging versus prospecting. The second factor is the students' knowledge based on each class: the third factor is the students' skills that meet their concentration needs. We can determine if a student is in good academic standing by considering their first-year grades, time in school, etc.

5.1. Create Learners profiles

We have developed student profiles that incorporate their personality style and academic knowledge and skills. The figure below shows the types of students, which is used to analyze whether the student's personality affects their achievements in the three majors of computer networking.

Table 3: Learners measured personality

Catalog	Academic Standing	Cgpa	Major	Emsat English Overall Score	Emsat Math	High School Average	Personality Type	Extraverted	Introverted	Intuitive	Observant	Thinking	Feeling	Judging	Prospecting	Assertive	Turbulent
201810	Very Good	3.12	CSF	1175	1225	86.24	ESTP-T	56	44	45	55	60	40	44	56	39	61
201620	Near At-Risk	2.29	CSF	1175	0	84.8	INFJ-T	12	88	55	45	43	57	61	39	42	58
201910	Near At-Risk	2.08	COM	1300	300	87.7	ISFJ-A	39	61	47	53	43	57	57	43	51	49
201910	Distinctive	3.81	COM	1050	850	88.57	INFJ-T	15	85	64	36	19	81	60	40	26	74
201920	Good Standing	2.6	COM	1075	725	89.59	ENFP-T	54	46	52	48	44	56	49	51	47	53
201810	At-Risk	1.8	CIN	1025	425	87.2	ENTJ-T	61	39	52	48	58	42	56	44	44	56
201520	Near At-Risk	2.34	FJM	0	0	81.5	ISFP-T	47	53	41	59	44	56	46	54	37	63
201820	Very Good	3.13	COM	1125	550	82.31	ESTJ-A	83	17	42	58	51	49	67	33	69	31
201810	Distinctive	3.67	CSF	1025	850	93.96	INFJ-T	43	57	53	47	43	57	56	44	46	54
201810	At-Risk	1.82	CIA	1150	375	87.6	INTJ-T	37	63	51	49	64	36	67	33	49	51
201810	Good Standing	2.66	CIN	1125	450	88.3	INFJ-T	39	61	74	26	56	44	56	44	42	58
201910	Good Standing	2.71	COM	1100	0	91.3	ESTP-T	56	44	45	55	28	72	71	29	56	44
201910	Near At-Risk	2.44	COM	0	0	78.6	ISFJ-T	32	68	30	70	49	51	69	31	42	58
201810	Good Standing	2.65	CSF	1150	300	87.3	ISFP-A	39	61	37	63	47	53	49	51	56	44
201810	Good Standing	2.79	CSF	1250	1050	88.85	INTP-T	39	61	55	45	56	44	42	58	49	51
201720	Near At-Risk	2.45	CIN	700	300	90.5	INTP-T	49	51	53	47	53	47	49	51	46	54
201820	At-Risk	1.84	COM	1100	325	76.92	ESFP-A	29	71	46	54	53	47	64	36	43	57
201810	At-Risk	1.78	FJW	1100	300	89.5	ESFJ-T	56	44	45	55	43	57	53	47	44	56
201910	Very Good	3.11	COM	1075	850	89.78	INFP-T	54	46	32	68	18	82	60	40	36	64
201810	Good Standing	2.76	CIA	1100	300	93.6	ISFJ-T	57	43	49	51	44	56	63	37	43	57

The following two tables show a sample of students' knowledge and skills performance in the programming course.

Table 4: Learners knowledge performance

Catalog	Academic Standing	Cgpa	Major	Remember Data Types	Understand Variables, Constants	Understand Expressions	Understand Selection Statements	Understand Iteration Statements	Understand One Dimensional Array	Understand Different User Defined Functions (Void And Return)	Knowledge Performamce
201810	Very Good	3.12	CSF	0.9	1.8	1.8	2	2	1.91	1.91	1.76
201620	Near At-Risk	2.29	CSF	0.925	1.85	1.85	1.775	1.775	1.89	1.89	1.71
201910	Near At-Risk	2.08	COM	0.9125	1.825	1.825	1.85	1.85	1.74	1.74	1.68
201910	Distinctive	3.81	COM	0.92	1.84	1.84	1.755	1.755	1.8	1.8	1.67
201920	Good Standing	2.6	COM	0.925	1.85	1.85	1.72	1.72	1.53	1.53	1.59
201810	At-Risk	1.8	CIN	0.725	1.45	1.45	1.6	1.6	1.9	1.9	1.52
201520	Near At-Risk	2.34	FJM	0.975	1.95	1.95	1.075	1.075	1.734	1.734	1.50
201820	Very Good	3.13	COM	0.87	1.74	1.74	1.24	1.24	1.83	1.83	1.50
201810	Distinctive	3.67	CSF	0.7275	1.455	1.455	1.46	1.46	1.89	1.89	1.48
201810	At-Risk	1.82	CIA	0.7275	1.455	1.455	1.46	1.46	1.89	1.89	1.48
201810	Good Standing	2.66	CIN	0.9375	1.875	1.875	1.12	1.12	1.7	1.7	1.48
201910	Good Standing	2.71	COM	0.8225	1.645	1.645	1.185	1.185	1.89	1.89	1.47
201910	Near At-Risk	2.44	COM	0.8225	1.645	1.645	1.185	1.185	1.89	1.89	1.47
201810	Good Standing	2.65	CSF	0.7875	1.575	1.575	1.72	1.72	1.442	1.442	1.47
201810	Good Standing	2.79	CSF	0.8625	1.725	1.725	1.32	1.32	1.63	1.63	1.46
201720	Near At-Risk	2.45	CIN	0.8	1.6	1.6	1.28	1.28	1.8	1.8	1.45

201820	At-Risk	1.84	COM	0.7625	1.525	1.525	1.52	1.52	1.46	1.46	1.40
201810	At-Risk	1.78	FJW	0.6	1.2	1.2	1.68	1.68	1.7	1.7	1.39
201910	Very Good	3.11	COM	0.7	1.4	1.4	1.44	1.44	1.6838	1.6838	1.39
201810	Good Standing	2.76	CIA	0.75	1.5	1.5	1.56	1.56	1.43	1.43	1.39
201820	Near At-Risk	2.16	COM	0.8	1.6	1.6	1.005	1.005	1.81	1.81	1.38
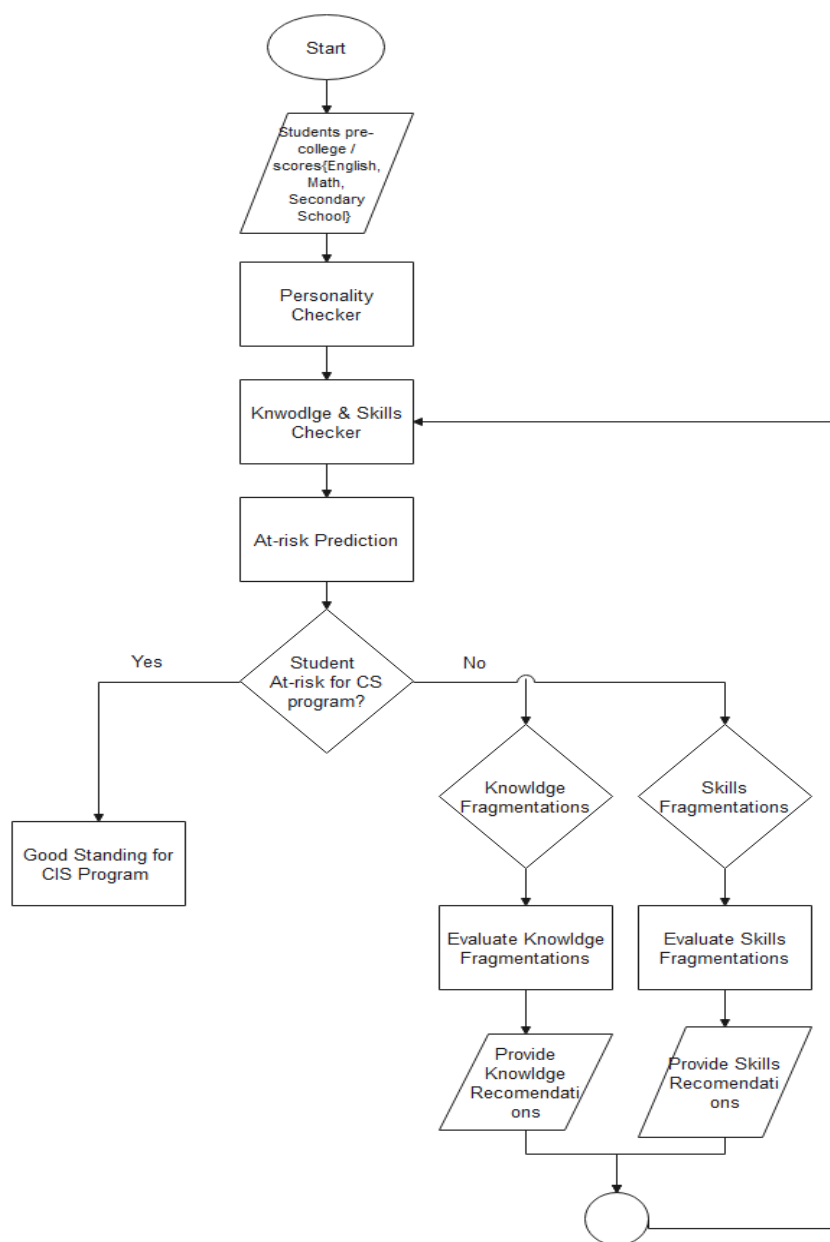
Figure 5:   Flow chart for detecting the best program

Table 5: Learners skills performance

Catalog	Academic Standing	Cgpa	Major	Apply Coding Best Practices	Analyse User Defined Functions	Analyse A Programming Problem	Apply Data Types	Evaluate The Used Data Types	Create A Fully Working Application Using Proper Variables Data Types	Apply Control Flow Via Conditional Statements	Apply Control Flow Via Iterations	Write A Program Using Selection And Iteration	Write Programs That Employ One-Dimensional Arrays Initialization	Write Programs That Employ One-Dimensional Arrays Accessing,	Write Functions With Parameters	Write A Fully Working Program With Function Calling	Skills Performance
201810	Very Good	3.12	CSF	2.01	3.82	3.82	2.865	4.775	2.865	3	3	5.73	6	5.73	4.02	4.02	3.97
201620	Near At-Risk	2.29	CSF	2.67	3.78	3.78	2.835	4.725	2.835	2.663	2.663	5.67	5.325	5.67	5.34	5.34	4.10
201910	Near At-Risk	2.08	COM	2.664	3.48	3.48	2.61	4.35	2.61	2.775	2.775	5.22	5.55	5.22	5.328	5.328	3.95

201910	Distinctive	3.81	COM	2.673	3.6	3.6	2.7	4.5	2.7	2.633	2.633	5.4	5.265	5.4	5.346	5.346	3.98
201920	Good Standing	2.6	COM	2.175	3.06	3.06	2.295	3.825	2.295	2.58	2.58	4.59	5.16	4.59	4.35	4.35	3.45
201810	At-Risk	1.8	CIN	2.588	3.8	3.8	2.85	4.75	2.85	2.4	2.4	5.7	4.8	5.7	5.175	5.175	4.00
201520	Near At-Risk	2.34	FJM	0.981	3.468	3.468	2.601	4.335	2.601	1.613	1.613	5.202	3.225	5.202	1.962	1.962	2.94
201820	Very Good	3.13	COM	2.481	3.66	3.66	2.745	4.575	2.745	1.86	1.86	5.49	3.72	5.49	4.962	4.962	3.71
201810	Distinctive	3.67	CSF	1.806	3.78	3.78	2.835	4.725	2.835	2.19	2.19	5.67	4.38	5.67	3.612	3.612	3.62
201810	At-Risk	1.82	CIA	1.806	3.78	3.78	2.835	4.725	2.835	2.19	2.19	5.67	4.38	5.67	3.612	3.612	3.62
201810	Good Standing	2.66	CIN	2.265	3.4	3.4	2.55	4.25	2.55	1.68	1.68	5.1	3.36	5.1	4.53	4.53	3.42
201910	Good Standing	2.71	COM	2.358	3.78	3.78	2.835	4.725	2.835	1.778	1.778	5.67	3.555	5.67	4.716	4.716	3.71
201910	Near At-Risk	2.44	COM	2.358	3.78	3.78	2.835	4.725	2.835	1.778	1.778	5.67	3.555	5.67	4.716	4.716	3.71
201810	Good Standing	2.65	CSF	1.8	2.884	2.884	2.163	3.605	2.163	2.58	2.58	4.326	5.16	4.326	3.6	3.6	3.21
201810	Good Standing	2.79	CSF	1.695	3.26	3.26	2.445	4.075	2.445	1.98	1.98	4.89	3.96	4.89	3.39	3.39	3.20
201720	Near At-Risk	2.45	CIN	2.454	3.6	3.6	2.7	4.5	2.7	1.92	1.92	5.4	3.84	5.4	4.908	4.908	3.68
201820	At-Risk	1.84	COM	1.845	2.92	2.92	2.19	3.65	2.19	2.28	2.28	4.38	4.56	4.38	3.69	3.69	3.15
201810	At-Risk	1.78	FJW	1.665	3.4	3.4	2.55	4.25	2.55	2.52	2.52	5.1	5.04	5.1	3.33	3.33	3.44
201910	Very Good	3.11	COM	2.19	3.368	3.368	2.526	4.21	2.526	2.16	2.16	5.051	4.32	5.0514	4.38	4.38	3.51
201810	Good Standing	2.76	CIA	1.86	2.86	2.86	2.145	3.575	2.145	2.34	2.34	4.29	4.68	4.29	3.72	3.72	3.14
201820	Near At-Risk	2.16	COM	2.538	3.62	3.62	2.715	4.525	2.715	1.508	1.508	5.43	3.015	5.43	5.076	5.076	3.60
201810	Near At-Risk	2.42	CSF	2.055	3.02	3.02	2.265	3.775	2.265	2.34	2.34	4.53	4.68	4.53	4.11	4.11	3.31
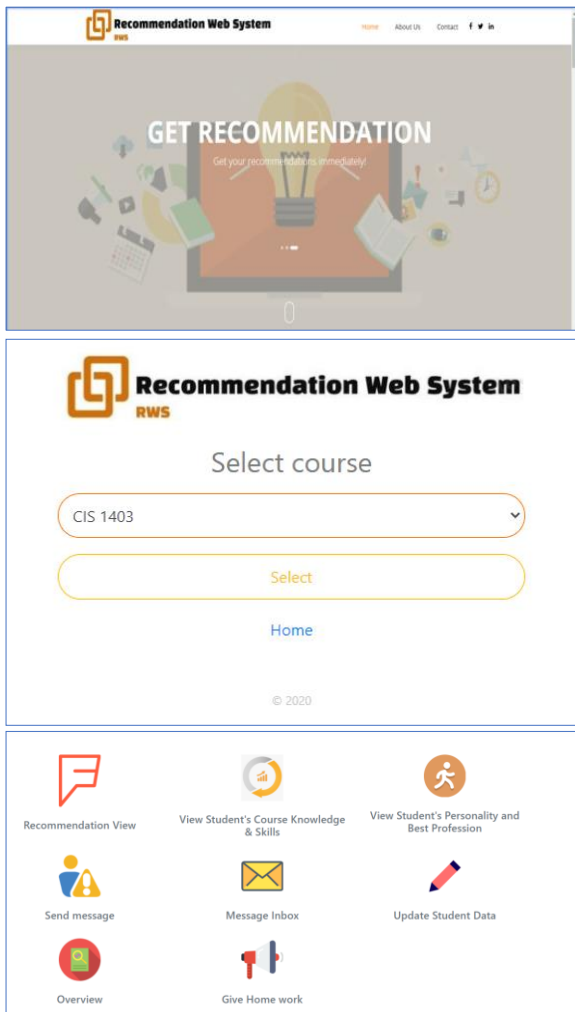
Figure 6: Recommendation Education system for At-risk learners

In order to find the best predictor for student performance, we have used different machine learning algorithms (Decision Tree, Random Forest, SVM and Association rules); then we evaluated and refined the used algorithm. The main aim is to develop a primitive platform that can be used to develop an education recommendation system to support At-risk learners 24/7 and teachers to coach students with poor knowledge, skills, and to provide them with the right advice.

Applying online coaching to at-risk students needs to build a recommendation framework that predicts at-risk students considering their knowledge and skills performance in segments of concepts rather than an entire course, considering their personality style. This helps to give coaching in the form of advice crumbs, as shown in the implementation figure 9 below, which may be tutorials, segment coding, exercises, peer discussions, etc.

The association rules are used to created recommendations considering student knowledge and skills performance.
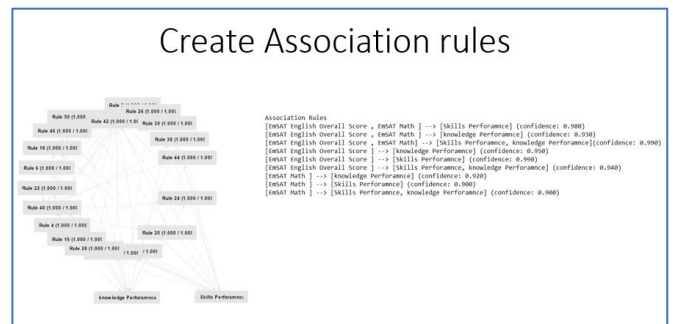
Figure 7: Applied Association rules for creating recommendations

5.2. Explore profiles of students

First, we purified information from all NA instances, measured the mean and variance and the range for each pattern.

As shown in the table below, we measured the mean and variance and the three majors' GPA quartile.

Table 6:   Descriptive statistical of the GPA - CIS three-concentrations

Major	count	mean	std	min	25%	50%	75%	max
Applications Development	32.00	3.10	0.40	2.15	3.00	3.20	3.25	3.90
Networking	56.00	2.69	0.61	1.40	2.27	2.56	3.20	3.74
Security and Forensics	126.00	2.69	0.54	1.30	2.40	2.68	3.00	3.68

In the application development department, the students typically have the highest average GPA, the Security and Forensics students have the second-highest average GPA, and the Networking students have the lowest average GPA. In the three conditions, we have been able to identify different personalities. Security and forensic students share the introverted sensing function type, which means they are more likely to feel, and judge - ISFJ.

It should be clear that, as demonstrated below, we have security students with various types of personalities, however, the GPA scores declined slightly accordingly.
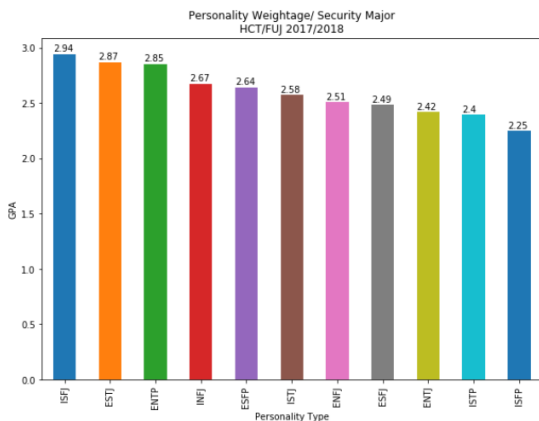
Figure 8:   Personality type's weight-Security and Forensics Major.

Students form Networking Major are more ISTJs, which means more Introduction (I), Sensing (S), Thinking (T), and Judging (J). As shown in the below figures, major students in the App development are more ISTJ.
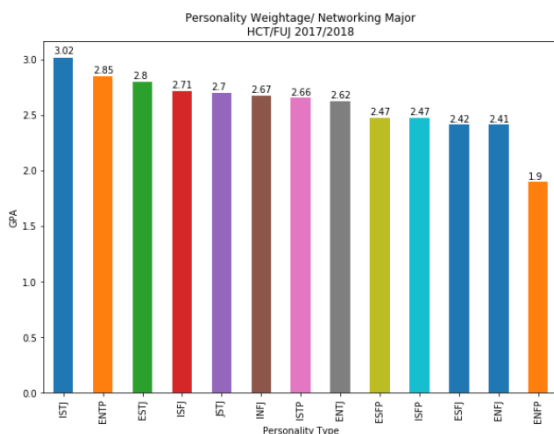
Figure 9:   Personality type-Networking major.
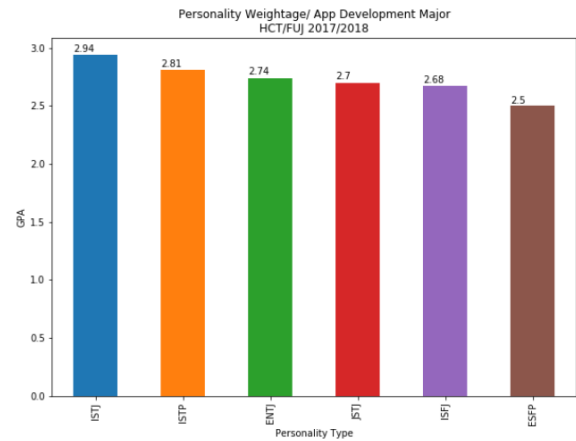
Figure 10: Personality type – App Development major.

6.   Experimental Results

In the following tables, we summarized the statistics on student success.

Table 7:   Four courses performance statistics for personality types - Security and Forensics major

	GPA	CIS 1403	CIS 2403	CIN 2003	CSF 3103	Extraverted	Introverted	Sensing	Intuitive	Thinking	Feeling	Judging	Prospecting
count	9.00	9.00	9.00	9.00	9.00	9.00	9.00	9.00	9.00	9.00	9.00	9.00	9.00
mean	2.44	1.84	1.92	2.18	2.81	42.78	57.22	56.96	43.04	52.70	47.30	59.08	40.92
std	0.30	0.47	0.50	0.51	0.48	20.61	20.61	8.62	8.62	10.82	10.82	16.78	16.78
min	1.87	1.33	1.52	1.00	2.00	7.00	30.25	40.50	34.00	36.00	35.50	32.00	24.50
25%	2.30	1.53	1.68	2.05	2.80	30.58	39.00	56.00	38.67	44.00	39.41	42.00	29.75
50%	2.50	1.73	1.75	2.33	2.84	34.71	65.29	60.00	40.00	57.67	42.33	67.19	32.81
75%	2.53	2.03	2.00	2.38	3.06	61.00	69.42	61.33	44.00	60.59	56.00	70.25	58.00
max	2.92	2.92	3.20	2.85	3.57	69.75	93.00	66.00	59.50	64.50	64.00	75.50	68.00

Table 8:   Four courses performance statistics for personality types- Networking major

	GPA	CIS 1403	CIS 2403	CIN 2003	CSF 3103	Extraverted	Introverted	Sensing	Intuitive	Thinking	Feeling	Judging	Prospecting
count	13.00	13.00	13.00	13.00	13.00	13.00	13.00	13.00	13.00	13.00	13.00	13.00	13.00
mean	2.50	1.80	1.79	2.56	2.71	51.81	48.19	53.47	46.53	49.63	50.37	50.01	49.99
std	0.40	0.53	0.49	0.56	0.53	21.06	21.06	7.47	7.47	11.28	11.28	18.07	18.07
min	1.90	1.00	1.30	1.71	1.90	25.33	19.00	41.10	38.00	40.25	34.10	33.95	24.25	24.50
25%	2.24	1.57	1.60	2.29	2.26	31.78	30.25	46.00	40.25	39.00	40.54	36.00	31.38
50%	2.50	1.71	1.68	2.40	2.88	55.57	44.43	56.38	43.62	51.00	49.00	46.00	54.00
75%	2.79	2.00	1.94	2.70	3.06	69.75	68.22	59.75	54.00	59.46	61.00	68.62	64.00
max	3.13	3.18	3.22	4.00	3.43	81.00	74.67	62.00	58.90	66.05	65.90	75.50	75.75

Table 9:   Four courses performance statistics of personality types-App Development major.

	GPA	CIS 1403	CIS 2403	CIN 2003	CSF 3103	Extraverted	Introverted	Sensing	Intuitive	Thinking	Feeling	Judging	Prospecting
count	4.00	4.00	4.00	4.00	4.00	4.00	4.00	4.00	4.00	4.00	4.00	4.00	4.00
mean	2.96	3.07	2.98	2.14	1.88	29.68	70.32	43.94	56.06	44.54	55.46	37.97	62.03
std	0.34	0.15	0.21	0.45	0.14	8.85	8.85	12.80	12.80	10.81	10.81	13.60	13.60
min	2.52	2.90	2.74	1.60	1.74	20.33	60.14	30.57	40.00	30.88	43.71	26.60	43.00

857

25%	2.79	2.98	2.86	1.86	1.78	23.53	64.58	35.79	49.25	39.22	49.18	29.15	57.04
50%	3.02	3.07	2.98	2.17	1.90	29.27	70.73	42.60	57.40	45.50	54.50	34.14	65.86
75%	3.19	3.16	3.10	2.45	2.00	35.42	76.47	50.75	64.21	50.82	60.78	42.96	70.85
max	3.27	3.23	3.22	2.60	2.00	39.86	79.67	60.00	69.43	56.29	69.12	57.00	73.40

The count feature shown in the above table should be clear, referring to each major's personality styles. In addition, the mean, minimum and standard deviation of GPA values from each course is calculated, and the four courses and personalities are also calculated. Apart from CSF 3103, the course for the security major, the App development students did not receive the results of NaN but took the networking course CIN-2003. We evaluated students' performance with their personalities in the four classes. In every course, according to the college grading system, we determined the GPA value of students.

Table 10: College GPA grades conversion values

Score	F	D	D+	C-	C	C+	B-	B	B+	A-	A
GPA	0	1	1.3	1.7	2	2.3	2.7	3	3.3	3.7	4

a) *The personalities patterns in the four courses for Security and Forensics major.*
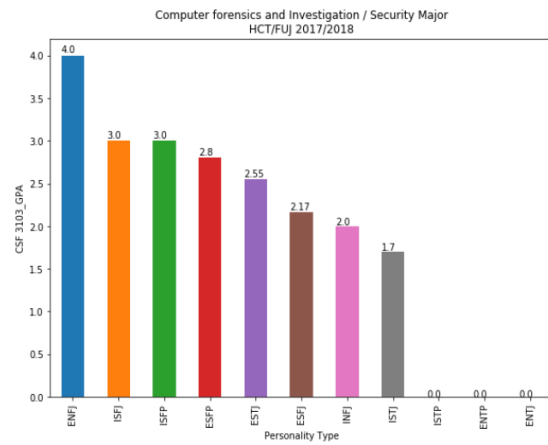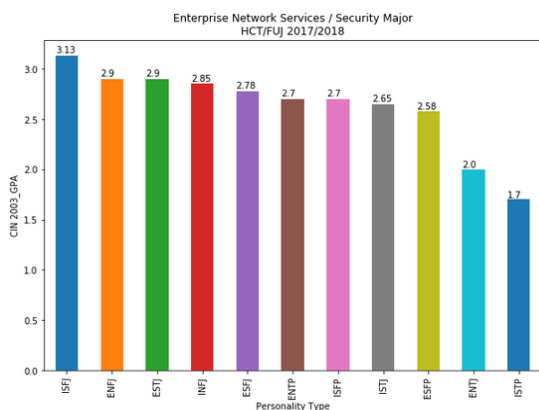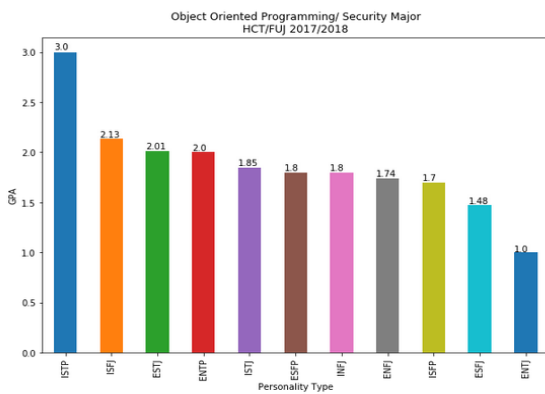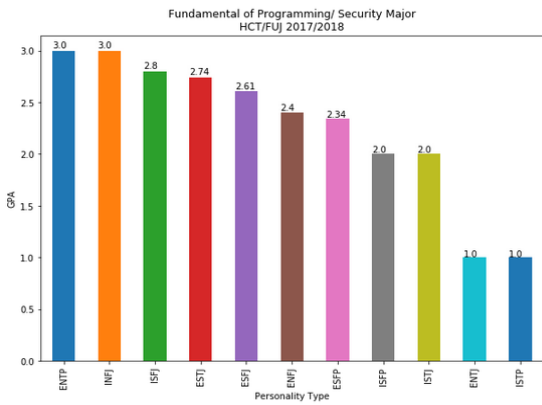
Figure 11: The impact of personality as a measure for four courses on security and forensics major.

b) *The personalities patterns in the four courses for Networking major.*

858
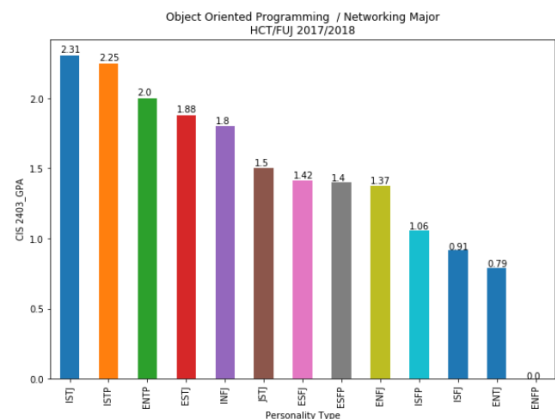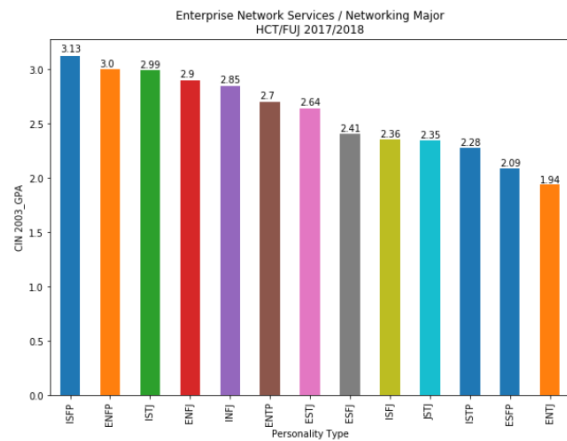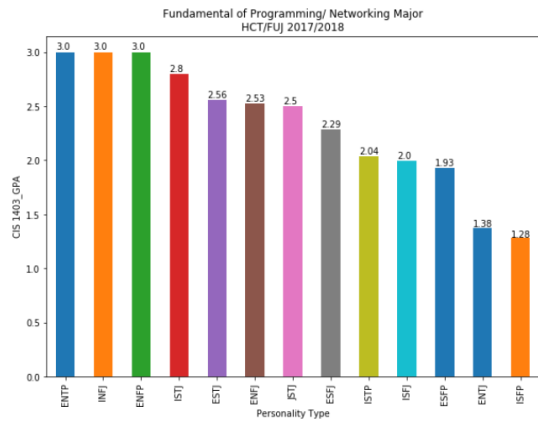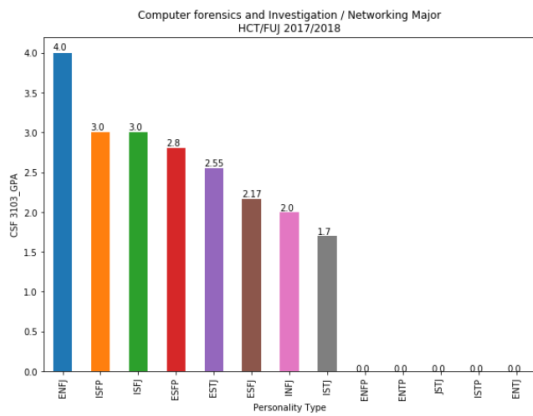
Figure 12: Impact of personality for Networking major as a measure on the four courses

c) *The personalities patterns in the four courses for App Development major*
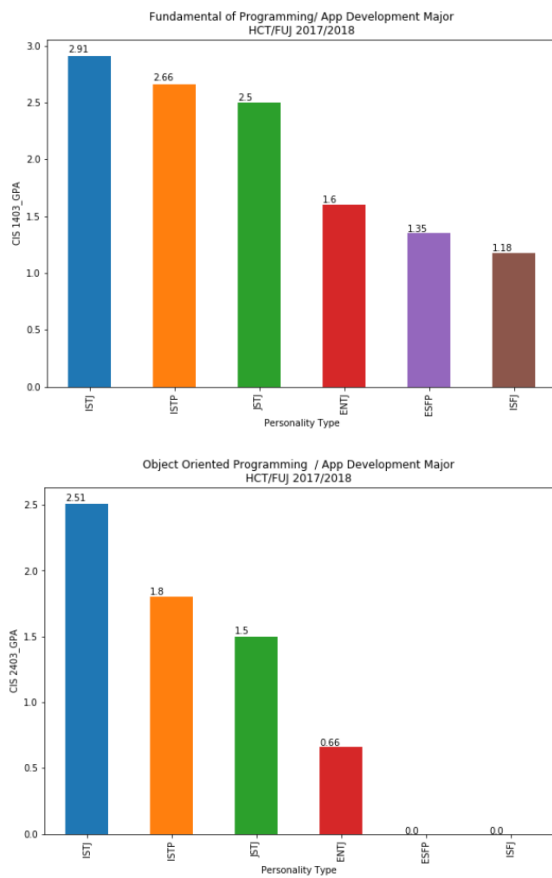
Figure 13: The personality impact on App Development as measured on the four courses.

In each major and different course, the following table summarizes the results of the best personalities.

Table 11: Personality performances in the four courses.

	GPA	Fundamentals of Programming	Object-Oriented Programming	Enterprise Network Services	Computer Forensics and Investigation
Security and Forensics	>=3.0	ENTP, INFJ	ISTP	ISFJ	ENFJ, ISFJ, ISFP
	>=2.5	ISFJ, ESTJ, ESFJ		ENFJ, ESTJ, INFJ, ESFJ, ENTP, ISFP, ISTJ, ESFP	ESFP, ESTJ
	>=2.0	ENFJ, ENFP, ISTJ, ISFP	ISFJ, ESTJ, ENTP	ENTJ	ESFJ, INFJ
Networking	>=3.0	ENTP, INFJ, ENFP		ISFP, ENFP	ENFJ, ISFP, ISFJ
	>=2.5	ISTJ, ESTJ, ENFJ, ISTJ		ISTJ, ENFJ, INFJ, ENTP, ESTJ	ESFP, ESTJ
	>=2.0	ESFJ, ISTP, ISFJ	ISTJ, ISTP, ENTP	ESFJ, ISFJ, ISTJ, ISTP, ESFP	ESFJ, INFJ
App Development	>=3.0				
	>=2.5	ISTJ, ISTP, ISTJ	ISTJ	ISTJ, ISTP	
	>=2.0			ISTJ	

Based on their personality, we may describe the conditions for a major choice to be made, or we have the ability to predict a student's GPA (grade point average). Take an example such as this study by the hospital and try to analyze it with the below algorithm.

If *"ISFJ" or "ESTJ"*
➔ *The best major is Security & Forensics*

ELSE IF *"ISTJ" or "ENTP"*
➔ *The best major is Networking*

ELSE IF *"ISTJ" or "ISTP"*
➔ *The best major is App Development.*

In the case of teaching computers to "understand" the best major, we can also rely on specific patterns, the systematic way, in the algorithm below.

If *"S" and "J"*
➔ *choose Security & Forensics*

ELSE IF *("S" or 'N') AND "T"*
➔ *The best major is Networking*

ELSE IF *"S" AND "T"*
➔ *The best major is App Development.*

It is important to have measured students' knowledge and skills to recognize getting into trouble students' academic status and their needs. Students are given an assessment in four courses that cover OOP, Enterprise Networks and Services. A breakdown of students' knowledge from various academic majors was compiled, and the numbers are listed below.

The factors that we looked at were the students' different academic performance, as well as the skills they demonstrated in the OOP course.

Table 12: The knowledge of OOP course over the three majors.

Knowledge		Object-Oriented Programming					
	GPA	Concepts of object-oriented programming	Terminology of methods	Terminology of functions	Terminology of inheritance	Terminology of encapsulation
Security and Forensics	>=3.0	82%	77%	76%	81%	83%
	>=2.5	0%	0%	0%	0%	0%
	>=2.0	74%	71%	71%	76%	75%
Networking	>=3.0	0%	0%	0%	0%	0%
	>=2.5	0%	0%	0%	0%	0%
	>=2.0	77%	68%	74%	69%	67%
App Development	>=3.0	0%	0%	0%	0%	0%
	>=2.5	77%	72%	76%	68%	81%
	>=2.0	0%	0%	0%	0%	0%

Table 13: OOP skills performance in the three major categories.

Skills		Object-Oriented Programming				
	GPA	Implement OOP tools	Use advanced features	Develop programs	Use Collections Framework	Test and evaluate a program
Security and Forensics	>=3.0	87%	79%	77%	76%	79%
	>=2.5	0%	0%	0%	0%	0%
	>=2.0	77%	65%	68%	72%	81%
Networking	>=3.0	0%	0%	0%	0%	0%
	>=2.5	0%	0%	0%	0%	0%
	>=2.0	80%	66%	71%	73%	72%
App Development	>=3.0	0%	0%	0%	0%	0%
	>=2.5	79%	69%	77%	80%	83%
	>=2.0	0%	0%	0%	0%	0%

7. Discussion and Conclusions

This study proposes a model for evaluating university students' academic status and GPA performance ambitions. Faculty and staff call upon these three factors in decisions: personality preferences, perceived knowledge and skills as well as what they expect from each student. In their attitudes, knowledge and skills, computing students are not identical. We see the disparities between students' grades because the universities lack an understanding of these disparities between learners' abilities and a special opportunity for creating a truly unique learning method that matches their individuality. This makes it difficult to apply the same philosophy and expects all students to be highly qualified.

This system allows for specific algorithms to be included, in the students' guidance, academic major choice or even the selection process. In a class on security, when we use sections for personality types, we can use an algorithm to predict the student's ranking automatically.

IF "Security & Forensics major."
  IF "ENFJ" or 'ISFP' or ISFJ'
    ➔ *Expected high grade*
  ELSE IF 'ENTJ' or 'ENPT'
    ➔ *Expected fail case*

ELSE
    ➔ *Expected low grade*

We did not look at all scenarios, only example algorithms.

IF "OBJECT-ORIENTED COURSE"
  IF "ISTP" or "ISTJ"
    ➔ *Expected high grade*
  ELSE
    ➔ *Expected low grade*

In general, consider how OOP awareness is summarized in Table 9. Security students have the ability to implement higher object-oriented concepts than those with a non-security background. Again, we want to emphasize the personality that makes these differences, not the selected major. This clarifies that major security students could perform well than other major students because of the difference in a student's personality that corresponds to the offered programming course. See the algorithm below that demonstrates it.

For a Major
  If Personality 'ISTJ' & 'FUNDAMENTAL OF PROGRAMMING'

    ➔ *Expect GPA >=2.0*

In view of the basics, the students in App developers major with the 'ISTJ' personality achieve round 2.91 GPA, while networking students are expected to achieve 2.8 GPA and security and forensics students 2.0 GPA. The differences are seen in the second and third levels as a result of other factors: knowledge and skills.

In the following sections, the benefits of implementing the three-layer model are listed.

1. Maintain high-quality graduates with an appropriate level in their technical knowledge and skills.
2. Minimize cases at risk.
3. Keep an eye on signs of inattentiveness and poor academic performance.
4. A decrease in the number of delayed graduate students.
5. Avoid the disproportionate dropout from prospective students in response to dismissal or academic warnings.
6. Make sure to have a high level of student retention.
7. Provide tools to assist individuals to become more effective in selecting courses and getting the right major.
8. Keep clear knowledge of each student's academic progress in case of a student falling behind.

8. The Conclusion & Future Work

Educational institutions have a tremendous burden of handling students with low academic performance (At-risk students). Many approaches support this group of pupils, such as psychological therapy, a proper timetable for vulnerable pupils, recall, personal training, mock-tests, direct private education, or success centres. However, these methods are not enough to solve the issue, since other factors could also influence the learner's success, which could be their family difficulties, cognitive style, prior academic performance, and the foundation of the college level. Learners personalities are the most important factor that needs a great deal of attention to understand students' individuality and natural abilities. This greatly helps to adapt the

materials supplied to their perceptions and offers solid support during the study programme. This paper proposes a recommendation system based on three key angles: personalities of the learner, skills of the learner and academic knowledge of the learner. The proposed layered model helps predict at-risk students, provide better advising, enhance learners' performance and skills, discover their employability competencies, and support learners with a recommendation in terms of tutorials, exercises, etc. during their study period. Based on the association rule, the proposed recommendation framework is structured to predict student success in different college programs and predict their academic status based on their personality analysis and academic performance. It is highly recommended that the admission and consultancy framework be maintained at the university level to fill the fragmentation of students' knowledge and skills. This improves student success and clearly identifies the study program's weaknesses and encourages students to address any observed fragmentations.

This pilot study offers further insight as to the strengths and weaknesses of the three specific majors who receive the most job postings, "Application Development, Networking and Security and Forensics." In addition to measuring a student's actual academic performance, the system also distributes personalized advice based on the student's digital profile. Collecting data from multiple learners from different programs allows us to understand what the program is trying to accomplish and what students need to know. The data completed throughout the learning process helps guide and get the learners to further levels of understanding. Future research will continue to create more trust in this advice through the study's continuation to include students from various other programs, like Business Solutions, Applied Media and Engineering. The proposed and implemented solution is very successful and leads to quick results, but it does not offer as much information because it does not account for the students' learning progress. Advisors constantly have access to learners' information about their personalities which affect their privacy.

Conflict of Interest

The authors declare no conflict of interest.

Acknowledgements

References

[1] O.H. Embarak, "Three Layered Factors Model for Mining Students Academic Performance," in 2018 Fifth HCT Information Technology Trends (ITT), IEEE: 219–226, 2018. https://doi.org/10.1109/CTIT.2018.8649491

[2] F. Martin, D.U. J O.L. Bolliger, "Engagement matters: Student perceptions on the importance of engagement strategies in the online learning environment," ERIC, **22**(1), 205–222, 2018.

[3] M. Salam, N. Ibrahim, M. J I.J. of I. Sukardjo, "Effects of Instructional Models and Spatial Intelligence on the Mathematics Learning Outcomes after Controlling for Students' Initial Competency," ERIC, **12**(3), 699–716, 2019.

[4] R.A. J O.J. of S.S. Faisal, "Influence of Personality and Learning Styles in English Language Achievement," **7**(8), 304–324, 2019.

[5] C.Y.R. Loh, T.C. J J. of E. Teo, S. Policy, "Understanding Asian students learning styles, cultural influence and learning strategies," **7**(1), 194–210, 2017.

[6] E. Care, H. Kim, A. Vista, K. J C. for U.E. at T.B.I. Anderson, "Education

System Alignment for 21st Century Skills: Focus on Assessment," 2018.

[7] J. Halberstadt, J.-M. Timm, S. Kraus, K. J J. of K.M. Gundolf, "Skills and knowledge management in higher education: how service learning can contribute to social entrepreneurial competence development," 2019.

[8] M. Gerlach, B. Farb, W. Revelle, L.A.N. J N. human behaviour Amaral, "A robust data-driven approach identifies four personality types across four large data sets," **2**(10), 735–742, 2018.

[9] A. Baumert, M. Schmitt, M. Perugini, W. Johnson, G. Blum, P. Borkenau, G. Costantini, J.J.A. Denissen, W. Fleeson, B. J E.J. of P. Grafton, "Integrating personality structure, personality process, and personality development," **31**(5), 503–528, 2017.

[10] A. Kamal, S. J E. Radhakrishnan, I. Technologies, "Individual learning preferences based on personality traits in an E-learning scenario," **24**(1), 407–435, 2019.

[11] H.T.-C. in human behavior, undefined 2016, "Integrating learning styles and adaptive e-learning system: Current developments, problems and opportunities," Elsevier,.

[12] R. Stein, A.B. %J S. Swan, P.P. Compass, "Evaluating the validity of Myers-Briggs Type Indicator theory: A teaching tool and window into intuitive psychology," **13**(2), e12434, 2019.

[13] Z.T. Ardakani, L. Samadi, "The Relationship between Introversion as Personality Trait and Job Satisfaction among EFL Teachers."

[14] L.S. Byrd, A study of an arts integration curriculum and its impact on academic achievement, University of South Alabama, 2019.

[15] S. J E.L.T. Alnujaidi, "The Difference between EFL Students' Preferred Learning Styles and EFL Teachers' Preferred Teaching Styles in Saudi Arabia," **12**(1), 90–97, 2019.

[16] H. J D.S. Demirkan, "An inquiry into the learning-style and knowledge-building preferences of interior architecture students," **44**, 28–51, 2016.

[17] G. J C. Falloon, Education, "Using simulations to teach young students science concepts: An Experiential Learning theoretical analysis," **135**, 138–159, 2019.

[18] O. Embarak, M. Khaleifah, A. Ali, "An Approach to Discover Malicious Online Users in Collaborative Systems," in International Conference on Emerging Internetworking, Data & Web Technologies, Springer: 374–382, 2019.

[19] J. Reynolds, D.R. Adams, R. Ferguson, P. Leidig, "The personality of a computing major: It makes a difference," in 2016 Proceedings of the EDSIG Conference. ISSN, 2473–3857, 2016.

[20] M.Z. Tunio, H. Luo, W. Cong, Z. Fang, A.R. Gilal, A. Abro, S. %J I.A. Wenhua, "Impact of personality on task selection in crowdsourcing software development: A sorting approach," **5**, 18287–18294, 2017.

[21] S.J.L. Foster, M.R. %J I.J. of E.S. Huml, "The relationship between athletic identity and academic major chosen by student-athletes," **10**(6), 915, 2017.

[22] Myers Briggs Assessment - Learn the Power of Personality Preferences.

A S T E S

Accounting Software in Modern Business

Lesia Marushchak[1,*], Olha Pavlykivska[1], Galyna Liakhovych[2], Oksana Vakun[2], Nataliia Shveda[3]

[1]Department of Accounting and Audit, Ternopil Ivan Puluj National Technical University, Ternopil, 46001, Ukraine

[2]Department of Accounting and Finance, Ivano-Frankivsk Education and Research Institute of Management Ternopil National Economic University, 76000, Ukraine

[3]Department Management and Administration Department, Ternopil Ivan Puluj National Technical University, 46001, Ukraine

A R T I C L E   I N F O

A B S T R A C T

The purpose of the research is an investigation of different accounting software products, their functions, and specific features to make easier choice among variety of similar products and analysis of their pros and cons that can influence on companies' performance. Authors classified accounting software according to its capabilities to serve the different managerial purposes. Because accounting software contains hundreds, some of them even thousands of features, the grouping method gave a possibility to assort similar models that might suit the company's specific requirements – size, cost, customizing, formats, appointments, models, and providers. Observation and comparing of data showed that the cost of accounting programs is critical to making the right choice. As the global accounting software market has a tendency to abrupt change to e-accounting, so that makes it impossible to predict the future behavior of accounting software users. To determine the objectives of this research statistical procedures are conducted. Received results can help potential users of accounting software products to choose the appropriate one based on listed advantages and disadvantages among the best sellers – customization tools, foreign currencies handling, financial and managerial reporting system and analytical capabilities. Lack of prior research studies on the topic and lack of available data have caused significant limitation of the analysis scope. The obtained results gave possibility to identified the main elements in formation the list of features necessary for making right choice of accounting software products. Facts showed managers, who don't consider specific needs and features of accounting software, encounter with problem of discrepancy to company's requirements.
The research is based on theoretical and empirical data. To collect the necessary data for research there was used a quantitative approach. Analytical method helped to analyze and evaluate the ponderable factors which must be considered in selecting process the most appropriate accounting software for companies. The research is dedicated to problems connected with an uncertainty that appears in the accounting software market. This research adds new knowledge to the accounting field as there was disproving theoretical and practical knowledge about accounting software.

1. Introduction

Accounting software has become an integral part of all types of business. Nowadays accounting and financial management became the scientific tools in running the business where software programs help to manage finance more effectively. Companies also spread their activities on international markets to get their

shares and as a result, there is an increased demand for new and more sophisticated accounting software packages capable for handling international accounting issues [1]. There are more than 150 well-identified software products around the world and most of them are targeted on large business. But the main stress must be made especially on small business as companies this size are most unprotected and cannot finance much in accounting programs. There are a number of vendors which serve this share

of market [2], but there is a very short list of scientific researchers conducted on this theme which would help business owners make the right and cost suitable choice.

As accounting systems are connected with other management platforms such as inventory management, warehouse management, order management, customer relationship management, enterprise resource planning, sales and production planning, enterprise quality management, supply chain and distribution systems, accounting software must be more than the simple programs for record and storage accounting information. Except this point, when it comes to select the right accounting product, the choices can be contradictory how to choose necessary speed, accuracy and reliability. The relationship between accounting software and company performance might be distinguished only in case when the accounting software program is suitable for some special company features. It also should be stressed that many specialists are involved in the accounting process. Many conducted researches showed that accounting information system adoption really influenced effectively on companies' performance, profitability and operations efficiency in some countries: Malaysia, Finland, Spain, Iran and Pakistan [3]-[6]. But there is also limitation in similar researches in the EU countries.

So, an accounting software program together with specialists and methods used to gather financial information about business events create the accounting information system. Accounting software without other components of AIS is the only device for recording and storage of information. Owners often buy simple accounting software with limited functional specification and do not get all possible results when it connects with other managerial systems. Choosing among cloud accounting and traditional accounting software is the main dilemma and problematic challenge for a lot of small and medium sized businesses and the important issue of current research.

Problems related to the right choice of accounting software programs could be solved only in complex: with selection of appropriate interconnected technical components – input and output devices, information storage and processors; and after deep examination of all accounting software pros and cons.

Current research has shown that it is important for companies to make special investigation to find what type of accounting software is necessary and suitable for satisfaction of accounting and managerial needs. There was made authors' contribution to develop knowledge in the theoretical and practical acquisition of accounting sphere. There have no researches been conducted which would show statistical analyses of companies produce accounting software according to different types, comparison of price policies and only few researches were conducted to evaluate the impacts of using accounting software on the companies' performance (only in separate countries).

2. Literature Review

Professional technologies have changed the way professionals conduct accounting. For past several decades accounting software has been used only to conduct monetary transactions between companies and with individuals but with time it became more complex. Nowadays accounting software is an effective tool in managing business processes. There are thousands of firms producing different kinds of accounting software. Managers collide with problems in choosing the most suitable accounting software to fit all companies' requirements.

Many scientists tried to investigate the influence of accounting information system (AIS) on the performance of all types of business. But most of them are connected to separate countries. Research [7] showed the influence of accounting information systems (AIS) on the performance of small and medium enterprises (SMEs) in Iraq and proved that AIS is one of the most important indicators for SMEs sustainability. Another author [8] investigated the impact of accounting software on the business performance of Malaysian firms. The research was based on participants' attitudes towards the importance of AIS. Results were positive and the author affirmed that accounting software has the significant importance and a great value to businesses, organizations and the economy. Some scientists [9] indicated that accounting software plays a critical role in the creation of quality accounting information and in storage necessary information to the decision-makers. In scientific paper was [10] investigated the impact of accounting information systems on organizational performance in the context of Saudi's SMEs and there was defined that it is a tool that helps to improve control of company's managers about business performance. It also can reduce the cost of accounting spending. Accounting software has a direct influence on the quality of financial statements submitted to the different state departments. Conducted investigation [11] showed the sufficient impact of accounting IS on the quality of financial statements, time of their preparation in Jordan and showed the positive result in case of its usage. Several scientists conducted research connected with defining the impact of AIS on performance measures in a case of Spanish SMEs, [12] and they found that it has a positive influence on outcome indicators and productivity. Other scientists went ahead and proved that with rapid technological development the transactions of a business are becoming more complex than it was ever that course more demand for control. Good accounting software can put a business in efficient control.

But in the literature, there are almost no scientific approaches to the classification of features and specifications of accounting software which can meet separate requirements of companies according to their sizes. Only a few accounting software types were analyzed according to their advantages and disadvantages.

3. Results: Theoretical Background

Accounting tasks are spreading each year; it is much than a booking, so many specialists have been thought about simplification of accountants' work and making storage of information more reliable. A computerized accounting system could be defined as an effective means of keeping accounting records in the electronic version. Accounting software is a special class of computer programs that helps to manage a business. The most suitable definition of 'accounting software' was given by Barron's Accounting Dictionary: 'Accounting software are programs used to maintain books of account on computers. The software can be used to record transactions, maintain account balances, and prepare financial statements and reports'[13]. Many accounting software programs are designed to create simple

money transactions (bookkeeping) between companies and others to record entire financial comings and goings for simplifying analysis procedures and decisions making processes. It depends on their scopes and functions.

History of accounting software. Most accountants affirm that accounting software is an invaluable tool for modern business but at first it was only appointed to simple operations storage. And the essential meaning of accounting software was recording financial data and later its function was extended to turning it into useful financial information [14]Error! Reference source not found.. With time professionals titled the accounting software as a 'magic wand', since before the computerizing of accounting transactions many tasks were conducted by hands and companies kept large transaction journals. The change happened only in the 20th century when computers transformed accounting significantly. The first computer for accounting purposes was sold in 1955 [15]. Later, **Peachtree Software** introduced the first accounting software in 1978 – a package for the early personal compute [16]. The Internet era has caused a significant increase in demand for accounting software. A list of companies and competitiveness among them has been increasing each year. Such innovation gives a real picture of the company's performance or as it is modishly to talk 'fair view' and 'health status of company'.

Functions, features and requirements to users. But even though the automated program **makes mach manual accounting and bookkeeping easier processes,** all software should meet the necessary requirements for legal and ethical characteristics of each country. The general functions of accounting software in IAS are analyzed in Figure 1.
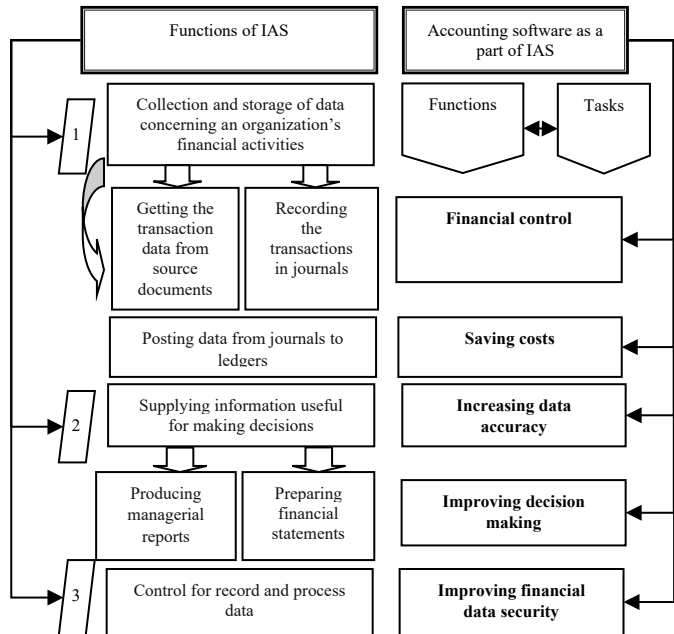
Figure 1: Managerial functions and tasks of accounting software in complex with IAS [17]; [14]

Accounting software has standard functions in the accounting field reflected in Figure 2.

The speed and accuracy of operations are the main characters of accounting software. Scientists also emphasize two other features of such computer programs; one of them is the managing

of resources more efficiently in accounting departments and other reducing of costly bookkeeping mistakes [18]. Calculation of math figures and sums in the accounting process became far easier with new computer technology.
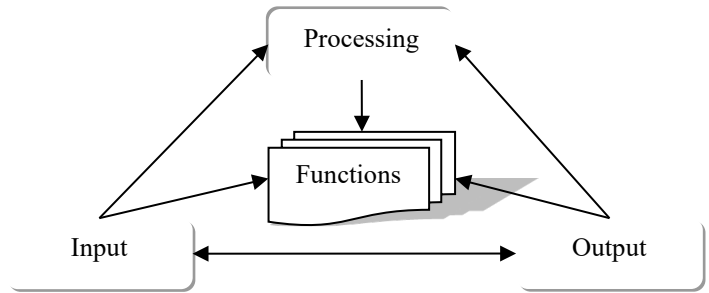
Figure 2: Productive (basic) functions of accounting software
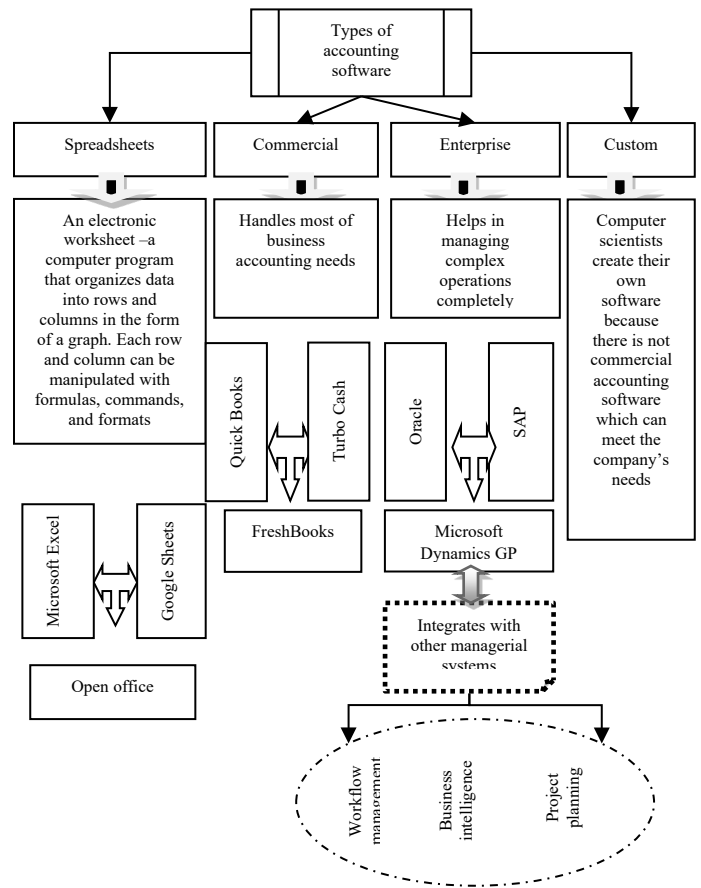
Figure 3: Types of accounting software [20]

But there was not proved how much time was reduced in an accounting cycle after computer programs appeared. Overall work from all departments is faster because a computer can keep and calculate thousands of indicators simultaneously. Most of managers and business owners separate another controversial dilemma – the requirement of qualified accountants on each stage of the accounting process. In past years accountants had to obtain necessary education, knowledge and experience in the accounting sphere and then they could work with accounting procedures for a long period, only changes in Government Standards on the state level required of Certification training or additional educational programs (courses). Accounting computer programs work faster

but only after clearly defined tasks. Computerized accounting procedures require accountants who can use specific software and therefore special computer skill. Only few accountants have possibilities to obtain the necessary qualification and experience themselves. Others need special education or training. But it is additional expense for many business owners. This problem is also connected with the high cost of training courses. But, the future benefit is higher than temporary expenses. Moreover, AIS can easily integrate with other management systems of enterprises.

Accounting software has a row of advantages and disadvantages. But most practitioners do not take into account them; this is evidenced by fact that almost all organizations and companies have used computer programs for accounting purposes in everyday business [19]. Scientists predict that computerization of accounting work will continue in the future as managers have value benefit from it – a stable source of information expressed in three forms – a document query, report and results of calculation (mostly expenses and income).

The effectiveness level of accounting software units depends on many factors such as types, appointments and their functions (Figure 3).

It is also necessary to stress on other classification of accounting software [22], where the author excreted three types of accounting software – database, installed and cloud. Large companies and corporations need to secure own data so owners install database software that has a higher level of security, fulfills more complex tasks, integrates with large network and complicated accounting functions (ex. Oracle). Installed accounting software is useful for businesses where internet connection is limited or absent. Meanwhile, cloud accounting is becoming more popular among startups and small-sized companies (ex. Freshbooks, Quickbooks, Xero and Sage 50 Premium Accounting in different versions). Currently, 6% of SMEs use a 'cloud-based' accounting system worldwide [23]. There is also another classification of software which fits accounting purposes [24], and it is reflected in Figure 4.

Figure 4: Types of accounting software serving the different purposes [24]

Table 1: Advantages and disadvantages of accounting software

Advantages and disadvantage of separate accounting software					
Cloud accounting software		Commercial accounting software (Peachtree)		Enterprise accounting software	
Pros	Cons	Pros	Cons	Pros	Cons
Lower operational costs (investment, maintenance is absent), this type of accounting software is cheaper then purchasing software	Stable demand in access to the internet connection	Offer a set of the most widespread features to perform accounting tasks	Comparable high cost	Easy to install on a system and deploy to end-users quickly	Comparable high cost
Higher reliability	There is the risk of data confidentiality (hacking – there is no guarantee that data is 100% safe)	Affordability for companies' owners – the average cost	There is a small but real possibility to lose information if the system is attacked by computer viruses in case it is not enough protected	Easy to customize	There is a small but real possibility to lose information if the system is attacked by computer viruses in case it is not enough protected
Higher accuracy (fewer mistakes). Much easier tools then other types propose	Technical problems	There is no demand in well-experienced skills	Increasing of productivity	Meet almost all user requirements	The necessity of high qualified personals
Pay only for subscription	Vendor lack-in/ lack-of control	High level of security	Flexibility and timeliness	Increasing productivity	On-going support
24/7 access and possibilities to recover data (restore)	In some cases limits to the data that can be freely store	Low risk	The necessity of high qualified personals	Management information	Mistakes in data entry can throw off a whole set of data
Collaboration	A lack of specialized tools	Flexibility and timeliness	Mistakes in data entry can throw off a whole set of data	Flexibility and timeliness	Can be inflexible

Table 2: Cost comparison of 12 top accounting software programs and description of their capabilities [27]**Error! Reference source not found.**; [28]; [29]; [30]; [31]; [32]; [33]

№	Accounting software	Form	Manufacturer	Cost, $ per month/y	Appointment
			For start-ups, small and medium-sized businesses		
1	QuickBooks	Online	Intuit United States	20-150	Easy for working accounting software with features that can satisfy complex accounting needs: reconciliation, taxes, reporting and inventory management. 4,5 million customers globally use QuickBooks
		Desktop		299, 95	
2	FreshBooks		Designed by Mike Mc Derment in Toronto, Ontario	6-20	FreshBooks is a cloud-based accounting designed software. It is ideal for freelancers (accountants) and small businesses that look to fast track their sales cycle and keep their processes in line with standards and regulations. Over 12 million users in 120 countries
3	Accounting by Wave	Online	Wave (Wave Apps)	Free (only several payroll services)	It is a very suitable and free accounting software for many owners of small companies. It is a powerful bookkeeping. Easily integrates with other management systems of companies
		Mobile version			
4	FreeAgent	Cloud-based	FreeAgent Central	Free	It is the accounting software for small business in the UK. There are over 80 000 small business users.
5	Manager	Online	NGSoftware	Free	For a small business, all industries, 70 languages
		Desktop			
			For mid-sized and large businesses		
6	QuickBooks Enterprise	–	Intuit United States	1419-3442	The end-to-end accounting software designed for growing business. Usage of the program helps to manage inventory, run payrolls, track sales and report. This type of software manages accounting transactions from start to finish. 135 000 companies chose QuickBooks Enterprise. There is another version QuickBooks Desktop Enterprise 20.0. Users: manufacturers, wholesalers, retailers and nonprofit (for different industries)
7	Xero	Online	Xero (New Zealand)	20-40	It is the smart online accounting for small business. Experts consider this type of accounting software one of the best for growing companies. It is also suited for mid and large businesses.
8	Finsync	Cloud-based	Finsync	From 40	It is a powerful accounting software (all-in-one) with different options. All types of business can use it.
9	NetSuite	Cloud-based	Oracle	–	It is suitable accounting software for companies that have grown out of their accounting software and are ready for full ERP[1] software
10	Zoho Books	Online	Zoho	9-29	The main features of accounting software are: end-to-end accounting, easy collaboration and integrated platform
11	FinancialForce accounting	Cloud-based	FinancialForce	From 175	This accounting software is designed for the companies with employees 100 +. It allows managing company's accounting and it works with a large amount of data. It also boasts powerful features. Experts prove that accounting software can satisfy complex enterprise requirements. The main characters of the product are multicurrency and global tax
12	*MYBOS Accounting & Billing*	Desktop	SBSCC Sri Lanka	249	Full integrated multi-user accounting software. In general, this accounting software is for medium-sized business. It is also accounting management that helps companies' owners to control sales and purchases, inventory, and journal entries. For companies, it is possible to obtain a hybrid cloud system
	MYBOS Accounting on Cloud	Online		199	

Some special industries order to design separate accounting software which belongs to Commercial off-the-shelf software. These are positive determinates of selecting accounting software. But other features might influence the appropriate choice of accounting software. Owners must choose among free, paid, or online accounting software. Most of the producers give a trial period for testing their products. In [25], the author stressed that selecting the most appropriate accounting software package has become one of the most critical decisions for most organizations in the fast-changing business world. A choice depends on the advantages and disadvantages of accounting software packages.

Vendors of accounting software try to advertise the main positive aspects of their products and it is very hard to exaggerate meaning of benefit from the accounting software. But many owners have a predisposition to make choice among types of software which give not only gain inside of companies but competitive advantages in the marketplace. In the question of

---

[1]ERS – enterprise resource planning.

choice among accounting software advantages must overweight completely disadvantages (Table 1).

The list of some of the best accounting software for three groups of business according to size is reflected in Figure 5.
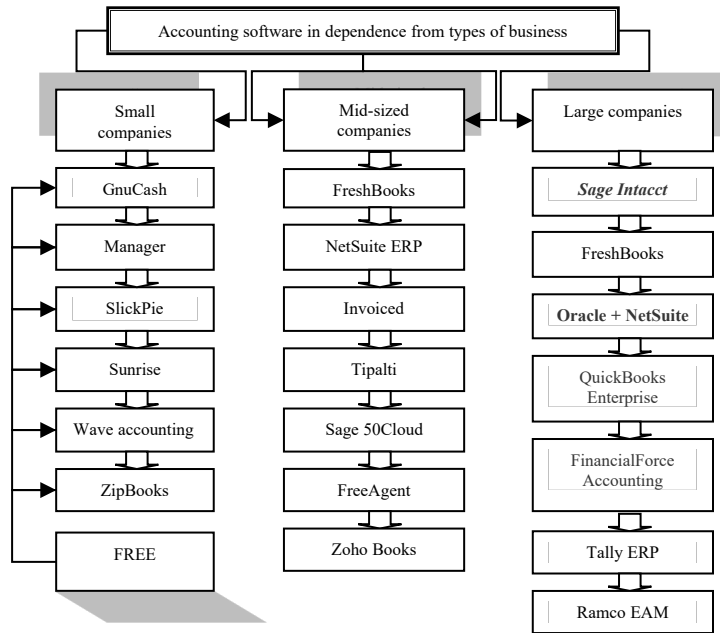
Figure 5: Different accounting software for three types of business
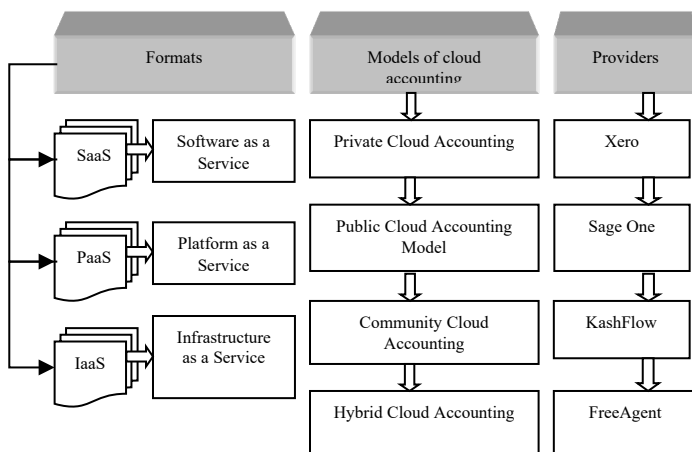
Figure 6: Brief characteristic of cloud accounting system [26]

There are other suitable accounting software programs for different types of business. More and more consumers need special software that contains features of effective management. Nowadays, true and fast information for external and internal users is only one of the main reasons for the purchase of accounting software. Cloud accounting software: This term appeared in far 2011. It gives the possibility to perform all accounting functions through internet-based devices. The main features of cloud accounting are shown in Figure 6.

Cloud accounting is a more flexible system with one strong requirement – connection to the internet. It is appointed to work with traditional accounting functions, updates financial information automatically and provides complex financial reports.

4. Practical aspects of accounting software choice

Cost of accounting software: The world market is full of different accounting programs with a variety of capabilities. Prices for accounting programs vary from several dollars to thousand. It depends on many factors and the number of users supported it. The cost of accounting software includes installation, implementation, training programs for users, customizing the software, and operational costs. Nowadays, many producers offer accounting programs on a cloud base and the number of venders who sell licenses has been decreasing each year. It is better for producers to get charge a monthly subscription fee from users. For small businesses and start-ups, the most appropriate accounting software is QuichBooks, Wave, Manager and FreshBooks, but some of their manufactures offer packages for growing business and thriving firms with competitive items. For large companies, there are several worldwide famous accounting software producers such as Intuit (USA), Xero (New Zealand) and Oracle (USA), (Table. 2).

The price is the second indicator which influences on the right choice. For small companies the price is affordable, it varies from $5 to $500 (Figure 7). But companies with multinational transactions and a large amount of staff need accounting software with additional opportunities and integration capabilities. The scientist [34] advised to choose optional enterprise-class accounting software that can meet the company's specific needs but the price is higher accordingly.
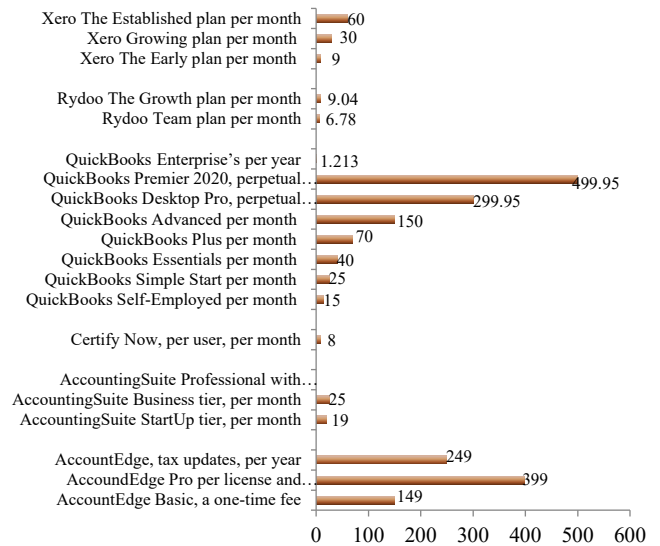
Figure 7: Compression of the prices for different accounting software products [35]

Many manufactures of accounting software offer additional payment options for some special requirements. Byers also desire to combine accounting software with human resources management (HRM) and POS[2] (software) systems; integration with the last one is limited in many accounting products. The right

---

[2]POS – point of sale.

accounting system must be adopted not only for information gathering but for synchronizing transactions, serving with oversight into the company's position, and proposing accounting solutions. The other point which must be accounted by users is a pricing policy for accounting software. Venders offer two popular pricing models: subscription-based on a cloud platform or 'pay-as-you-go' model[3] and perpetual licensing. Subscription price must be made monthly/year and it guarantees necessary support and maintenance. Some venders give buyers a choice to use all components, special modular components or features they need and pay for them. Many designers of accounting software include additional services and support in the base price of core products but others offer additional features, or modules for an extra payment. Before making the eventual choice for any type of accounting software it is very important to learn whether venders have professionals who are specializing in installation, supporting, and integrated with other company's systems processes or they involve the third party. Third-party consultants sometimes have divergences. It is worldwide accepted to provide the basic training services for free but there are some exceptions.
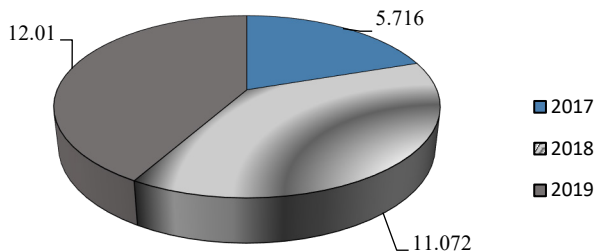
Figure 8: Global accounting software market in 2017-2019, Bn, USD dollars [36]-[38]
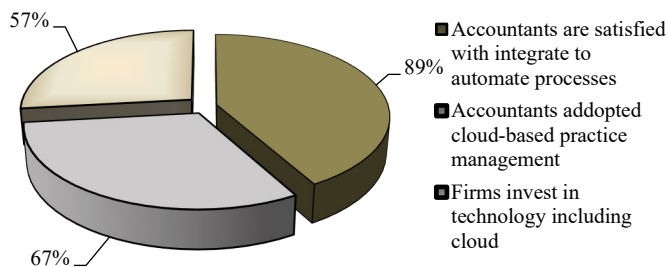
Figure 9: Perception of cloud technologies by accountants, 2017 [39]

The global market of accounting software: The market size of accounting software has been increasing each year and scientists predict the continuation of this tendency for the next few years (Figure 8)**.** Most of the rising is observing in the cloud-based sector. Now, cloud accounting replaced the old desktop versions. Many business owners invest in the cloud accounting system that gives the future long-term benefit in a case when they plan to expand their activity. It is always useful to exploit such type of software when a lot of employees work on the same data. Large companies which are represented by foreign branches perceive

cloud-based accounting software more flexible. Most of the users are worried by one main question – is it enough safe? It's protected by the individual password. Accounting software providers also create backup servers in different locations for reinsurance if one server would go down, users can access to necessary data. Excess to cloud accounting software is more protected than the traditional one. The team of 'Finances Online' investigated that more than 50 % of owners and accountants are satisfied by the cloud accounting platform (Figure 9).

Other useful statistical data shows that companies have increased their profits after adopted online accounting (Figure 10).
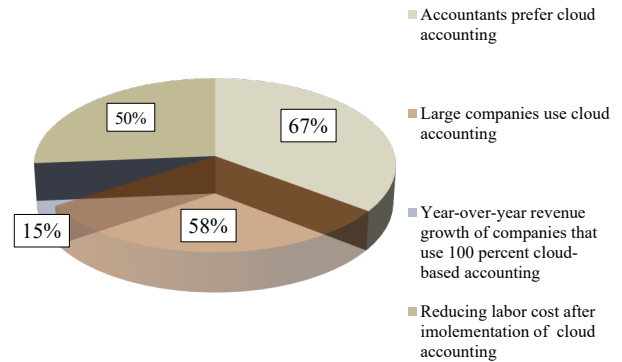
Figure 10: Cloud accounting statistics in 2018 [40]

Any type of accounting software is a great solution for each business as its advantage's overweight disadvantages. There is a huge variety of accounting software, producers, and venders. Many specialists try to model the best one or make the most suitable for all businesses. But the best accounting product for one company might not be the best for another even with similar features. The main character which must fit all customers is trust in it.

5. Accounting Software Influence on Companies Performance

Accounting software provides companies' owners and managers with quick and easy reports for decision making [41]. Accounting system can effect on all spheres of activity [42] and has positive influence on companies' performance. Appropriate accounting software gives some benefits, the most important among them are affordability, time savings, higher accuracy and one place for all financial tasks; they are all available to each form of business.

6. Generalization of Results

Accounting software in modern business plays very important role and it is a great progress made in the accounting sphere. The main goal of accounting software is tracking financial transactions and generating various financial reports. It is a p a r t of w h o l e accounting systems which might include different types of software from simple transaction-entry programs to advanced accounting systems integrated with other management

---

[3] Pay-as-you-go system is one in which you pay for a service before you use it and you cannot use more than you have paid for. Cambridge Dictionary.

programs of the company. Accounting software makes accountants work easier and gives information about the 'true health' of business, companies' owners agree to pay a substantial sum for complicated and advanced accounting technologies. Companies with foreign branches have always troublesome issues with coordination among them (mainly a time of reports' delivery that could cause a delay in decision making process) but after cloud technologies appeared, most problems have solved. Cloud accounting or e-accounting is rather a new type of service than IT. The main advantage of cloud accounting software is no time and place limitation as well as putting the whole accounting system to the cloud-based platform.

Analyzed scientific researches proved the positive interrelationship between accounting software and business performance. But in this relationship, many factors have an indirect influence. There are several benefits for companies' owners who use such software: the establishment of financial control, saving costs, increasing data accuracy, and improving data security. With a good accounting system, accountants and business owners can make financial forecasting and improve the decision-making process.

Nowadays, the global accounting market is represented by a lot of producers who offer from traditional old desktop accounting software to the modern cloud-based platforms on license subscription conditions. The tendency of the global market has a positive and stable increasing character. Research showed that more than 60% of accounting specialists are satisfied with their current accounting programs and most of them are ready to invest in accounting technologies for getting future benefits. Most specialists affirm that cloud-based accounting software together with other intelligent online programs is the future of accounting.

7. Conclusion

Research showed a significant increasing of accounting software popularity and that fact has caused sufficient diversification in computer accounting programs. And it's becoming difficult to decide which one to choose. There was grouping of accounting software programs of the most famous world producers using affordable and easy-to-use approaches, listed their advantages and disadvantages, analyzed price policy parameters. There were indicated items to keep in mind when selecting accounting software for companies: special features (accounts receivable and accounts payable tools, track inventory, time tracking, project management, payroll or advanced reporting capabilities), usability (desktop software, cloud software or mobile version and number of users) and costs (inexpensive, average price or expensive with extra features). Also research reports about some risks which connect with storage accounting date and information. As recommendation there are some offers for each type of accounting software program – to give detail explanation on its security level, use multi-business support, find providers with additional services and possible training programs.

Conflict of Interest

The authors declare no conflict of interest.

References

[1] M.I. Ajay Adhikari, "Firm characteristics and selection of international accounting software," Journal of International Accounting and Taxation, **13(1)**, 59–63, 2004.

[2] M. Burns, "Customer survey roundup," CA Magazine, Retrieved June 15, 2013.

[3] B. Gullkvist, "Towards Paperless Accounting and Auditing," E-Business Research Centre, 87–98, 2002.

[4] H. Sajady, M. Dastgir, H. Hashem Nejad, "Evaluation of the effectiveness of accounting information systems," International Journal of Information Science and Management, **6**(2), 49–59, 2008.

[5] K. Saira, M.A. Zariyawati, M.N. Annuar, "Information System and Firms," International Business Research, **3**(4), P28, 2010.

[6] R. Kouser, A. Awan, Gul-e-Rana, F.A. Shahzad, "Firm size, leverage and profitability: Overriding impact of Accounting Information System," Business & Management Review, **1**(10), 58–64, 2011.

[7] E. Harash, "Accounting performance of SMEs and effect of of accounting information system: A conceptual model," Global Journal of Management and Business Research (D), **17**(3), 21–26, 2017.

[8] I.N. Ch.Yvonne, "The impact of accounting software on business performance," International Journal of Information System and Engineering, **6 (1)**(November 2017), 2018, doi:10.24924/ijise/2018.04/v6.iss1/01.26.

[9] D.M.J. Wickramsinghe, R. Pemarathna, N. Cooray, T. Dissanayake, "Impact of accounting software for Business Performance," Imperial Journal of Interdisciplinary Research (IJIR), **3**(5), 1–6, 2017.

[10] Trabulsi, "The Impact of Accounting Information Systems on Organizational Performance : The Context of Saudi ' s SMEs," International Review of Management and Marketing, **8**(2), 69–73, 2018.

[11] A.A.J. Abdallah, "The impact of using accounting information systems on the quality of financial statements submitted to the income and sales tax department in Jordan," European Scientific Journal, **1**(December), 41–48, 2013.

[12] E.U. Grande, R.P. Estébanez, C.M. Colomina, "The impact of accounting information systems (AIS) on performance measures: Empirical evidence in spanish SMEs," International Journal of Digital Accounting Research, **11**(June 2010), 25–43, 2011, doi:10.4192/1577-8517-v11_2.

[13] J.K.S. J.G. Siegel, Dictionary of Accounting Terms, Third Edit, 2000.

[14] Accounting Information System, Aziroff, 2019.

[15] B. Scott, The Accounting Journal: 60 years of accounting software, MYOB, 2015.

[16] F. Sherman, The History of Computerized Accounting, Career Trend, 2019.

[17] Kanya, The Importance of Accounting Software for Businesses, Businesstech, 2019.

[18] U.D. Dr Mahesh, "Role of accounting software in today scenario," International Journal of Research in Finance and Marketing, **6**(6), 25–34, 2016.

[19] V.N.T. İ. Dalci, Benefits of Computerized Accounting Information Systems on the JIT Production Systems, Eastern Mediterranean University, 21–36.

[20] T. James, Types of Accounting Software, Chrone, 2019.

[21] What is a Spreadsheet?, My Accounting Course, 2020.

[22] K. Coloso, Best Accounting Software for Startups, Founders Guide, 2015.

[23] P. Griffiths, Accounting in the Cloud – Pros and Cons, Accru Chartered Accountants, 2020.

[24] What are the types of accounting software?, Shoebooks Team, 2012.

[25] A.A. Abu-Musa, "The Determinates Of Selecting Accounting Software: A Proposed Model," Review of Business Information Systems (RBIS), **9**(3), 85–110, 2005, doi:10.19030/rbis.v9i3.4456.

[26] S.A. Tarboush, "Cloud Accounting As a New Business Model and Its Influence on Accounting Process," (2), 1–14, 2017.

[27] Ch. Krause, QuickBooks Online VS QuickBooks Desktop: Which Is Better?, Merchant Maverick, 2019.

[28] The way you work is changing. Our dedication to small business has not., QuickBooks, 2020.

[29] Accounting software that's free and powerful, Wave Accounting, 2020.

[30] Xero is online accounting software for your small business, Xero, 2020.

[31] Looking for accounting software?, Manager, 2020.

[32] E. Seppala, Best Accounting Software For Large Businesses, Merchant Maverick, 2020.

[33] Accounting software world, FinancialForce, 2020.

[34] J. Martinez, 5 Mistakes to Avoid When Choosing Accounting Software, PC, 2017.

[35] M. Pardo-Bunte, How Much Does Accounting Software Cost? 2020 Pricing Guide, BetterBuys, 2020.

[36] Global Accounting Software Market to be worth US$ 11,771.6 Mn by 2026: Transparency Market Research, Cision, 2018.

[37] Hardware and software IT services / Accounting software market, Fortune

Business Insights, 2019.

[38] Accounting software market – growth, trends, and forecast (2020-2025), Mordor Intelligence, 2020.

[39] D. Epstein, What is Accounting Software? Analysis of Features, Types, Benefits and Pricing, FinancesOnline, 2020.

[40] M. Gigante, 30+ Important Accounting Statistics You Need to Know in 2019, 2018.

[41] M.M. Thottoli, K. V. Thomas, R.A. Essia, "Adoption of Audit Software by Audit Firms: A Qualitative Study," Journal of Information and Computational Science, **9**(9), 768–776, 2019.

[42] H. Rkein, "Saudi Journal of Business and Management Studies Impact of Automation on Accounting Profession and Employability: A Qualitative Assessment from Lebanon," Journal of Business and Management Studie, **4**(4), 372–385, 2019, doi:10.21276/sjbms.2019.4.4.10.

ASTES

Gene Selection for Cancer Classification: A New Hybrid Filter-C5.0 Approach for Breast Cancer Risk Prediction

Mohammed Hamim[*,1], Ismail El Moudden[2], Hicham Moutachaouik[1], Mustapha Hain[1]

[1]*ENSAM-Casablanca Université Hassan II, Casablanca, 20070, Morocco*

[2]*EVMS-Sentara Healthcare Analytics and Delivery Science Institute, Norfolk, 23324, United States*

ARTICLE INFO

ABSTRACT

Despite the significant progress made in data mining technologies in recent years, breast cancer risk prediction and diagnosis at an early stage using DNA microarray technology still a real challenging task. This challenge comes especially from the high-dimensionality in gene expression data, i.e., an enormous number of genes versus a few tens of subjects (samples). To overcome this problem of data imbalance, a gene selection phase becomes a crucial step for gene expression data analysis. This study proposes a new Decision Tree model-based attributes (genes) selection strategy, which incorporates two stages: fisher-score-based filter technique and the gene selection ability of the C5.0 algorithm. Our proposed strategy is assessed using an ensemble of machine learning algorithms to classify each subject (patients). Comparing our approach with recent previous works, the experiment results demonstrate that our new gene selection strategy achieved the highest prediction performance of breast cancer by involving only five genes as predictors among 24481 genes.

1 Introduction

Ranked second among 36 kinds of cancers, breast cancer has the greatest number of incidences and moralities among females worldwide. As per a recent publication of the WHO (World Health Organization), in 2018, 627,000 females were estimated to lose their lives from this disease, representing approximately 15% of all cancer deaths among females worldwide. According to the same source, early detection is becoming a critical tool to reduce breast cancer morbidity and mortality [1]. At present, breast mammogram and ultrasound images are the most traditionally used breast cancer detection techniques. However, besides their high computational cost, these techniques may lead to an overdiagnosis (false positives), which can cause serious clinical consequences, including death from the side effects of a potential Overtreatment [2]. An alternative to this technique is to take the advantages of both data mining and gene expression technology to predict breast cancer. However, this alternative is not without challenges since the significant number of non-informative features in gene expression data may increase the search space size, which makes gene analysis an impossible task [3]. In the context of this new alternative, a gene selection phase is mandatory to deal with the problem of high-dimensionality in gene

expression data. The gene selection process aims at getting rid of any irrelevant and redundant genes in gene expression data, which can simplify the learning model by using a strict minimum number of predictors, and thus improving breast cancer risk prediction performance [4]. In terms of contribution to this research field, this study proposes a new Decision Tree model-based gene selection approach, which incorporates two stages: fisher-score-based ranked technique and the gene selection capability of the C5.0 algorithm. The ranked method consists in reducing the computational cost by removing non-informative genes from the original gene expression data, while the C5.0 algorithm consists in identifying the optimal subset of genes, which are quite informative to classify patients. Finally, the genes contained in the obtained gene subset are used as predictors to construct an ensemble of predictive models using 6 learning algorithms: Random Forests (RF), Support Vector Machine (SVM), Logistic Regression (LR), K-Nearest Neighbors (KNN), Artificial Neural Network (ANN) , and C5.0 Decision Tree algorithm. In the next section, we briefly outline existing approaches. Methodology and Materials are described in section 3. Section 4 is devoted to discussing all experiment results. The final section concludes the proposed work.

*Corresponding Author: Mohammed Hamim, ENSAM-CASABLANCA, & mohamed.hamim@gmail.com

2 Existing literature

From different approaches, a variety of studies have been proposed on breast cancer risk prediction.

Through the implementation of Random Forest(RF) and Extreme Gradient Boosting (XGBoost) , S. Kabiraj et al. predicted breast cancer with an accuracy of 74.73% and 73.63%, respectively[5].

Using the breast cancer Coimbra dataset provided by the University of California Irvine (UCI), Naveen et al., proposed 6 machine learning-based prediction models. The learning process was initialized by a Z-Normalization and cross-validation technique. Experimental results show that the Decision tree and KNN algorithms achieved the highest prediction performance [6]. Agarap proposed a deep learning-based approach on normalized features implementing rectified linear units (ReLU) as the activation function, while the Softmax function as the classifier function. The average cross-validation performance using 10-fold does not exceed 87.96% in terms of accuracy on WBCD (Wisconsin Breast Cancer Data) dataset[7]. S. S. Prakash and K. Visakha also proposed a deep neural network-based approach to predict breast cancer. The authors optimized the neural network model using the early stopping mechanism and dropout layers to avoid overfitting problems. The selected predictors were obtained from the WBCD provided by UCI [8].

Using gene expression signature, Turgut et al., in their work, first proposed 8 machine learning-based predictive models without using any gene selection algorithms. Then they combined the proposed machine learning algorithms with two feature selection methods: RLR (Randomized Logistic Regression) and RFE (Recursive Feature Elimination). The most striking results concern the SVM algorithm since it achieved the best accuracy of 88.8% after using the selection process [9]. In the same context of gene expression data, Al-Quraishi et al. presented a breast cancer prediction model based on an ensemble classifier using FCBF (Correlation-based filter) algorithm. Compared to the existing works, their framework achieved an accuracy of 96.11% by involving 112 genes [10]. Aldryan et al. developed a prediction framework using MBP (Modified Backpropagation) with Conjugate Gradient Polak-Ribiere and the standard ACO (Ant Colony Optimization). The MBP was used as a classifier, while the ACO as a gene selection technique. For breast cancer classification using MBP without gene selection, they get the average F-Measure score of 0.2328. After combined with the feature selection using the ACO algorithm, it obtains an average of 0.6412 in terms of performance by involving 2448 genes [11]. Jain et al. presented a two phases-based hybrid feature selection strategy. Their approach combines the Correlation-based Feature Selection (CFS) with the improved-Binary Particle Swarm Optimization (iBPSO) algorithm. The proposed strategy was assessed using Naïve–Bayes (NB) algorithm, and the experiments results showed an accuracy of 92.75% for breast cancer classification using an average of 32 genes [12]. To overcome class imbalance issue and time consumption of their old gene selection approach, Li et al. introduced a more efficient implementation of linear support vector machines based recursive feature elimination system (SVM-RFE). Their proposed approach was assessed on 6 public gene expression datasets, and results demonstrated a slight enhancement in terms of

time consumption and prediction performance [13].

3 Research methodology

3.1 Description

Using gene expression data, the present paper proposes a new framework that improves breast cancer prediction performance. Figure 1 summarizes the main steps of the proposed framework, where fisher score combined with C5.0 are used to select a small number of informative features, and ANN, SVM, KNN, LR, RF , and C5.0 algorithms are applied to the new gene subset to assess the effectiveness of the proposed gene selection approach. The overall pseudo-code of the whole prediction system is illustrated in Algorithm 1 . -discussed in the following sections.

Algorithm 1: Our proposed prediction system

Function *Classification(Training_set, Test_set)*:

  List_Classifiers = [SVM, LR, C5.0, ANN, KNN, RF]

  /* iterate over all proposed machine learning algorithms   */

  for *each Classifiers in List_Classifiers* **do**

    Model ←Train *classifier* on the Training set

    Test the *Model* on the Test set

    Calculate average performance (Accuracy , F1-score, and the AUC).

  Return All obtained *Models* with their average performances

/* Main program   */

Input :-A p-diemsional DNA microarray dataset $D = [y, x_1, x_2, ..., x_p]_{n \times 1}$, with n is the number of samples, x is the gene vector , y is the target vector and p is the number of genes

Output : List of generated prediction models with their average performance and running time for each one.

1 Split data D using the stratified K-fold cross-validation technique.;

2 **for** *each fold in D* **do**

3    $D_{test} \leftarrow fold$;

4    $D_{train} \leftarrow$ remaining $(K - 1) folds$;

    /* Standardization of D_{train} and D_{test} using (12)   */

5    $SD_{train}, SD_{test} \leftarrow Standardization(D_{train}, D_{test})$;

    /* Filtering data using Fisher ratio using (1)   */

6    $F_{train}, F_{test} \leftarrow Filter(SD_{train}, SD_{test})$;

    /* Selection of the optimal gene subset using C5.0   */

7    $Sub_{train}, Sub_{test} \leftarrow C5.0(F_{train}, F_{test})$;

    /* Classification using the optimal gene subset   */

8    $Models \leftarrow Classification(Sub_{train}, Sub_{test})$;

9 **Return** all generated prediction models "*Models*"

3.2 Genes selection strategy

Feature selection is an important stage in intelligent systems modeling, especially in prediction systems [14, 15]. The feature selection or gene selection in the context of microarray data analysis
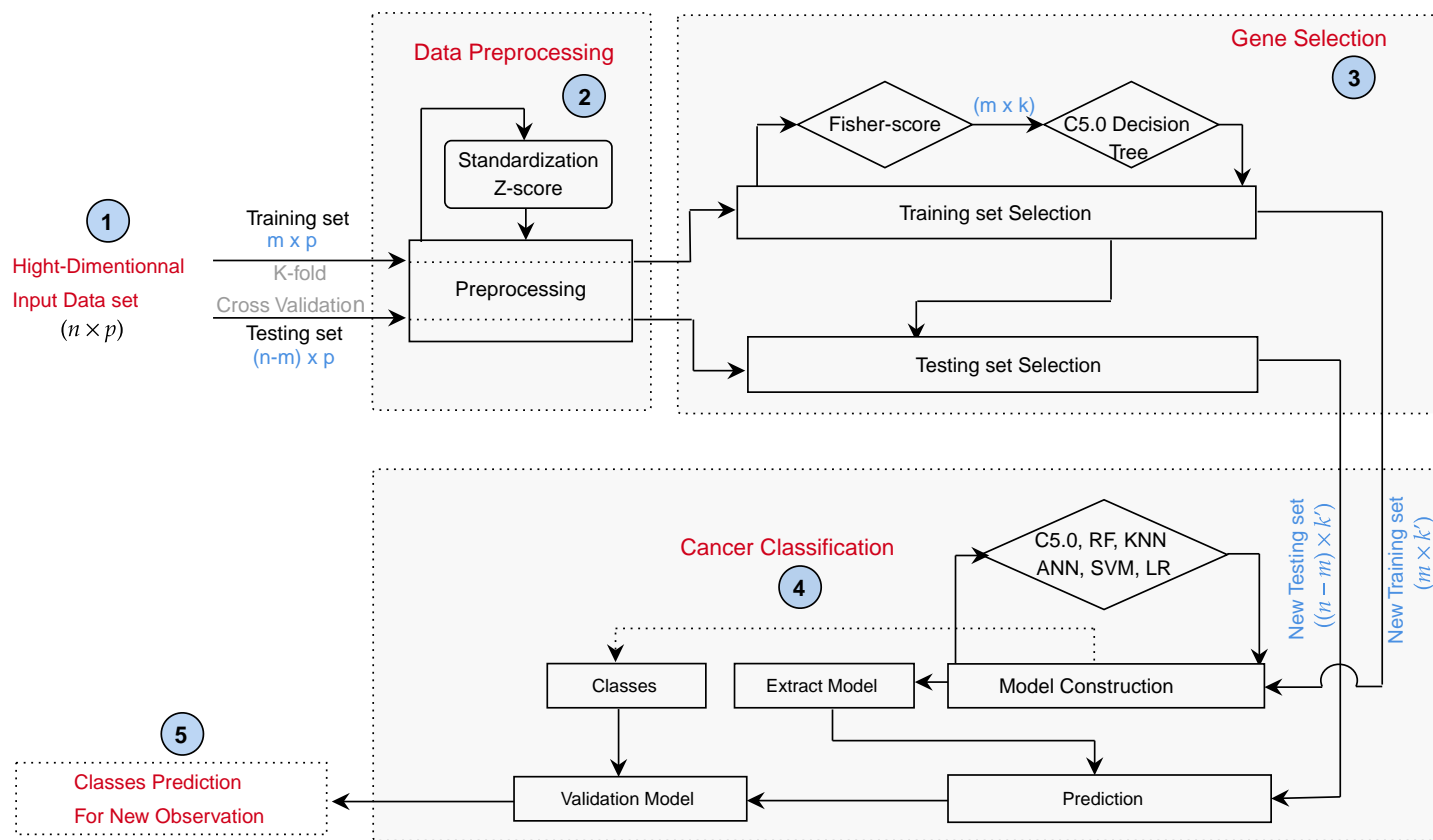
Figure 1: The proposed Framework

is a useful technique that can reduce dimensionality by removing any redundant, irrelevant, or noisy genes, which can lead to improve the classification performance and reduce the cost of computation [4], [16]–[18]. As shown in Figure 2, gene selection process can be reformulated as follows: given an original set of p genes, $X = (X_1, X_2, .., X_p)$, find a subset of genes $X_{sub} = (X_{i1}, X_{i2}, .., X_{ik<<p})$ such that the most informative genes are selected.
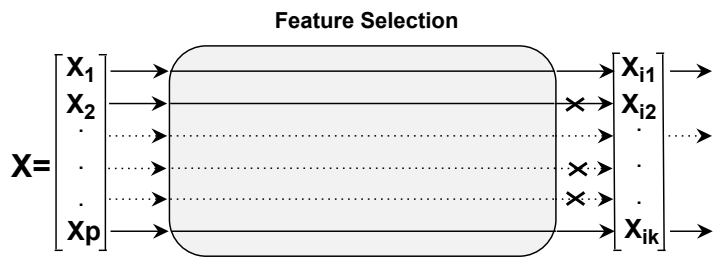
Figure 2: Feature Selection process

Here we present a novel gene selection strategy composed of two steps -Fisher score combined with the C5.0 algorithm- presented into the sequel.

3.2.1 Filter method using Fisher score

Because it acts independently of any classification process, Fisher score-based filter technique is considered as a fast supervised fea-

ture selection technique, the reason why it is frequently used when it comes to working with a large number of features (genes) [19]. It can be reformulated as follows: given an input data matrix G of genes, then the Fisher score of each gene (denoted by F) j can be represented by (1) :

$$F\left(G^j\right) = \frac{\sum_{k=1}^c \eta_k \left(\mu_k^j - \mu^j\right)^2}{\sum_{k=1}^c \eta_k \left(\sigma_k^j\right)^2} \qquad (1)$$

With μ_k^j, σ_k^j are the mean and standard deviation of k-th class, corresponding to the j-th feature. μ^j denotes the mean of the whole j-th gene in the G matrix.

As the F of each gene is calculated independently from original genes, only 10% of the highest-ranked genes were selected to achieve the second round of our proposed gene selection strategy.

3.2.2 C5.0 Decision Tree

C5.0 is a new decision tree algorithm developed from C4.5, which has proved its high detection accuracy in many research fields. Compared to C4.5, C5.0 can handle different types of data, deal with missing values, and support boosting to improve classification accuracy [20]. Besides its ability in classification tasks, C5.0 was was used as an efficient feature selection technique in many research Fields [21]–[24]. In the present work, we take both advantages of C5.0, its ability as a powerful feature selection method combined

with the Fisher score-based filter technique, and as a classifier to achieve the classification task in our whole prediction framework.

In the context of gene selection using C5.0 Decision Tree, all genes were initially compared by using the following process: first of all, we set the pruning degree (Pruning is an inherent technique that consists in reducing the size of decision trees by getting rid of branches of the tree that provide little information which can reduce the complexity of the classifier, thus improving classification performance) to 75% as a default value to prevent overfitting. Then, the information gain ratio of each gene is calculated using the formula (2).

$$GainRatio(G) = \frac{Info(S) - Info(S/G)}{Split(G)} \quad (2)$$

Where :

-$Info(S)$ is the Information Entropy which calculated as in (3) :

$$Info(S) = -\sum_{i=1}^{m} p_i log_2(p_i) \quad (3)$$

With m the number of classes in the training set (in our case m=2), S a given set of n samples ($|S| = n$) , and $p_i = \frac{n_i}{|S|}$ the probability that an object in S belongs to the class C_i (with n_i the number of samples that belong to the class C_i)

-$Info(S/G)$ denotes the Conditional Information Entropy which is defined as in (4):

$$Info(S/G) = -\sum_{j=1}^{v} \frac{|S_j|}{|S|} \sum_{i=1}^{m} \frac{n_{ij}}{|S_j|} log_2(\frac{n_{ij}}{|S_j|}) \quad (4)$$

Assuming that G divide the set S into v subsets ($S_1, S_2, ..., S_v$), then n_{ij} denotes the number of classes C_i samples in the subset S_j with $|S_j| = \sum_{i=1}^{m} n_{ij}$ and $|S| = n$.

-$Split(G)$ is defined as in (5) :

$$Split(G) = -\sum_{j=1}^{v} \frac{|S_j|}{|S|} log_2(\frac{|S_j|}{|S|}) \quad (5)$$

The most informative gene (best predictor) with the maximum information gain is selected to be the root node of the whole tree. Then, the root node in each level of the tree is selected from remained genes using the same principle. The gene selection process continues until a maximum depth is meet. As the tree was pruned, the optimal gene subset is determined [20, 25].

4 Classification Algorithms

4.1 Artificial Neural Network

The ANN is a form of distributed computation inspired by networks of human biological neurons. Typically, an ANN consists of a set of interconnected artificial neurons that are organized in several layers called, input, output, and one or several hidden layers. In a typical 3-layer network as shown in Figure fig :ANN, each neuron in a layer is connected to the all next layer neurons with no interconnectivity among the neurons of the same layer and no connection back. All the connections are defined by weight values denoted by w. In the input layer, all nodes get information from the outside and pass it to

the nodes of the next layer. Each node computes the weighting sum of all the N neurons of the previous layer and passes it through an activation function (usually logistic) [26]
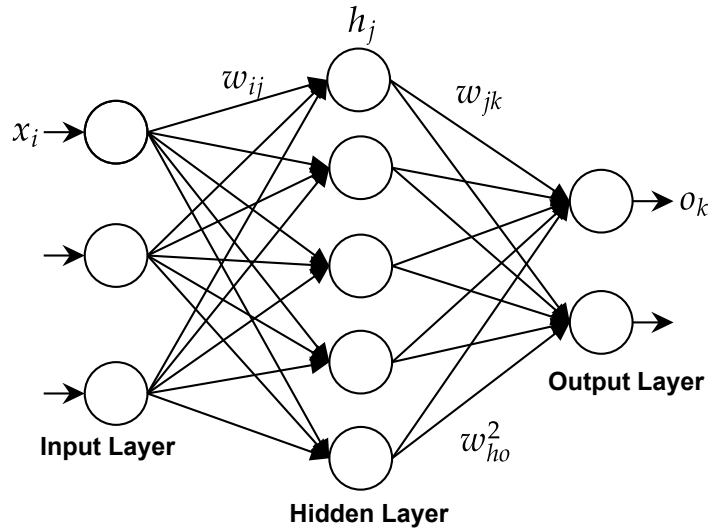
Figure 3: Artificial Neural Network diagram

4.2 Random Forest

As a powerful supervised pattern classification algorithm, RF is used in many intelligent systems. Random Forest is viewed as a combination of several independent decision tree classifiers. Each decision tree is constructed using a randomly selected subset of features. In RF, a majority voting process is used to affect samples to one of the classes by taking the most popular class among all predicted classes by all the tree predictors in the RF [27]. Many processes are used to construct a decision tree classifier; the most commonly used are the Information Gain (IG) and the Gini Index (GI) [28]. In the present paper, we used the GI for the random feature selection measure.

4.3 K-Nearest Neighbors

K-Nearest Neighbors is an easy and simple machine learning algorithm that is widely used in many domains of pattern classification. As the KNN is a non-parametric classifier, new samples are affected to the class represented by a majority of its K-nearest neighbors using a feature similarity rule; since there is no mathematical model to predict labels for new samples. The similarity process is defined using different distance metrics such as Hamming Distance, Euclidean Distance, and Minkowski distance [29] . In the present work, the similarity is measured between K-nearest neighbors using the Euclidean distance metric as in(6), and the number of neighbors K is set to k=4.

$$d(S_1, S_2) = \sqrt{\sum_{i=1}^{p} (s_{1i} - s_{2i})^2} \quad (6)$$

Where S_1 and S_2 are two given samples and p is the number of features .

4.4 Logistic Regression

As an extension of the linear regression algorithm for classification problems, Logistic Regression aims to find the best fitting model, which squeezes the output of a linear equation between 0 and 1 using the logistic function. In linear regression, the relationship between output and features is modeled by using a linear equation. However, in a classification problem, it is strongly recommended to have probabilities between 0 and 1, which can force the outcome to be only between 0 and 1 using (7).

$$L(x) = \frac{1}{1 + e^{-(a_0 + a_1 x_1 + a_2 x_2 + ... + a_n x_n)}} \qquad (7)$$

4.5 Support Vector Machine

The SVM is a binary classifier algorithm that has been successfully applied in many pattern recognition areas. In linear classification, SVM constructs a classification hyper-plane that separates the data into two sets by maximizing the margins and minimizing the classification error. The hyper-plane is constructed in the middle of the maximum margin. Thus, samples above the hyper-plane are classified positives. Otherwise, they are classified as negatives (Figure 4). SVM is a linear classifier algorithm, meaning that it uses a linear separation to classifier samples. However, in real intelligent systems, datasets are often linearly non-separable. To overcome this problem of non-linearity, a nonlinear transformation of the input vectors into a new feature space is performed, and then a linear separation is performed using the new feature space. In this work, the Gaussian kernel using (8), was used to overcome the non-linearity issue.

$$k(x_i, x_j) = \exp(-\frac{\| x_i - x_j \|^2}{2\sigma^2}) \qquad (8)$$

Where: $\| x_i - x_j \|^2$ denotes the Euclidean distance and σ a positive parameter which denotes the smoothness of the kernel.
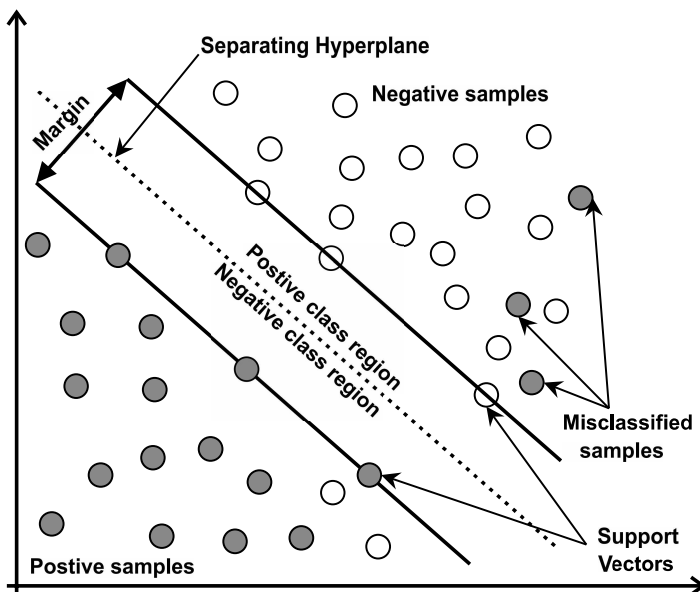
Figure 4: SVM diagram

4.6 Evaluation Metrics

The data mining process has several ways to check the performance of any classification model. The quality of any classification model is built from the confusion matrix (see Figure fig :CM), which summarizes the comparison between predicted and observed classes for all samples. Different types of evaluation measure are calculated from the confusion matrix, and the most commonly used in practice are the classification accuracy as in (9), and F1-score as in (10).

$$Accuracy = \frac{TP + TN}{TP + TN + FP + FN} \times 100 \qquad (9)$$

$$F1 - score = \frac{2TP}{2TP + FP + FN} \qquad (10)$$

		Predicted classes	
		Positives	**Negatives**
Observed classes	**Positives**	**TP** (True Positive)	**TN** (True Negative)
	Negatives	**FP** (False Positive)	**FN** (False Negative)

Figure 5: Confusion Matrix for binary classification

Another common evaluation metric used in Machine Learning is the receiver operating characteristic (ROC) curve, which is created by plotting the True Positive Rate (TPR=TP/(TP+FN)) against the False Positive Rate (FPR=FP/(FP+TN)). The Area Under the ROC Curve (AUC) provides a good idea about model performance. The model that gives 100% of corrects predictions has an AUC of 1, while the model that gives 100% of wrong predictions has an AUC of 0.

In the present paper, the average of each evaluation metric (described above) in training and test sets is calculated to evaluate the quality of each prediction model using (11).

$$metric = \frac{metric_{train} + metric_{test}}{2} \qquad (11)$$

5 Experimental results and discussion

Before presenting our experimental results in the next section, we describe the gene expression data set used in this paper, K-Fold cross-validation, data preprocessing, and the system configuration.

5.1 Breast cancer dataset details

The proposed prediction framework was conducted on the public available microarray breast cancer dataset [30], which includes 24,481 features with 97 samples, 51 (52.58%) of which are healthy and 46 (47.42%) are diagnosed with breast cancer. Details of our used microarray dataset are given in Table 1.

Table 1: Microarray datasets details

Dataset	Genes	Samples	Classes	Ref
Breast cancer	24481	97	Relapse/Non-relapse	[30]

5.2 Stratified 10-fold Cross-validation

In order to avoid overestimating prediction, a stratified 10-fold cross-validation technique was employed. By using this technique, samples are split into five equal folds (subset) of samples. One of the 10- fold is used for the testing step, and the remaining four folds are put together to form the training data. This process is repeated ten times. The stratification process was used to ensure that all folds are made by preserving the same percentage of samples for each class.

5.3 Preprocessing

Before supplying the datasets to our analysis system (Figure 1), it was necessary to perform a data preprocessing as it is an important step to overcome data imbalance issue. In the present paper, Gene expression levels for each gene were standardized using (12). The result is that expression levels for each feature have a mean 0 and variance 1.

$$X = \frac{X - \overline{X}}{\sigma} \tag{12}$$

Where: $\overline{X}$ the overall mean of the feature X and σ its standard deviation.

5.4 System configuration

By using parallel processing, our proposed framework was implemented in Python 3.7 language under Ubuntu 18.04.3 with v5.0 based Linux kernel 64bits operating system. All of the experiments were carried out using an Intel Xeon E5-2637 v2 3.5 GHz PC with 64 GB of RAM.
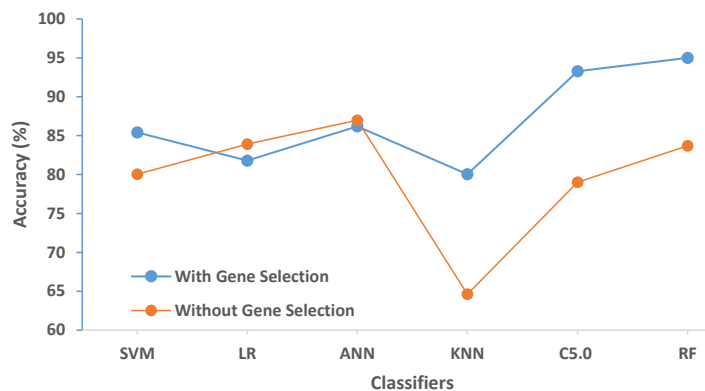
Figure 6: Classification performance with and without our proposed gene selection approach

5.5 Results and discussion

In order to see how good our new approach behaves in situations where there is a large number of genes versus few observations, this section aims at analyzing the results of our proposed framework in terms of classification accuracy, degree of dimensionality reduction, and the running time.

To prove the power of our gene selection approach in terms of prediction performance, we first applied our six proposed machine

learning algorithms on the whole breast cancer gene expression data set (without using any feature selection process). Table 2 presents the experimental results and shows the classification performance in terms of accuracy, F1-score, and AUC of each constructed classifier. As we can notice, the most striking performance was achieved by the ANN classifier, which does not exceed 86.99%, while the KNN algorithm shows the lowest performance rate of 64.62%. Almost the classification performances of all constructed classifiers do not exceed the eighties in terms of all evaluation metrics.

Table 2: Performance measurement without gene selection

Classification Model	Time (s)	Accuracy (%)	F1-score	AUC
ANN	42	86.99	0.84	0.85
KNN	1	64.62	0.65	0.65
LR	13	83.91	0.83	0.84
RF	1	83.71	0.86	0.84
SVM	1	80.05	0.79	0.8
C5.0	25	79.01	0.79	0.8
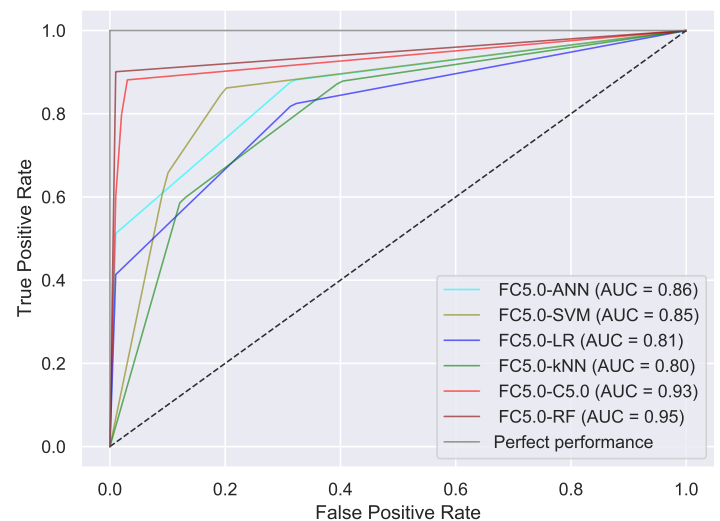
Figure 7: ROC curve of our shrinkage models using the proposed gene selection approach

Table 3 shows the experimental results of our gene selection method when used along with our proposed machine learning algorithms. The results are presented in terms of classification performance matched with the number of selected genes. As we can notice, using our approach, the dimensionality of our research space (the number of genes) was reduced in two phases. First, the number of genes passed from p=24481 (the original number of the gene as shown in Table 1) to k=2448 using the Fisher ratio-based filter method, the new k represents 10% of the original number of genes that have the highest score. In the second phase, the number of previously selected genes k was reduced for a second time using the inner feature selection ability of C5.0 Decision Tree algorithm; thus, the k passed from 2448 genes to five genes (k'=5). Thereafter, the new subspace of k'=5 predictors (genes) was used to construct the ensemble of classifiers (SVM, KNN, LR, ANN, C5.0, and RF). As

Table 3: Performance measurement using our framework

Input Data	Original Genes Number	Gene Selection approach		Selected Genes	Classification Model	Time (s)	Accuracy (%)	F1-score	AUC
		Fisher score (F)	C5.0						
Breast Cancer gene expression data	p=24481	k=2448	k'=5	NM_013438, AL137615, NM_003477, Contig26768_RC, Contig55662_RC	**FC5.0-RF**	**31**	**95.00**	**0.94**	**0.95**
					FC5.0-C5.0	31	93.28	0.94	0.97
					FC5.0-ANN	31	86.21	0.89	0.86
					FC5.0-SVM	31	85.4	0.86	0.85
					FC5.0-LR	31	81.78	0.82	0.81
					FC5.0-KNN	31	80.4	0.82	0.8
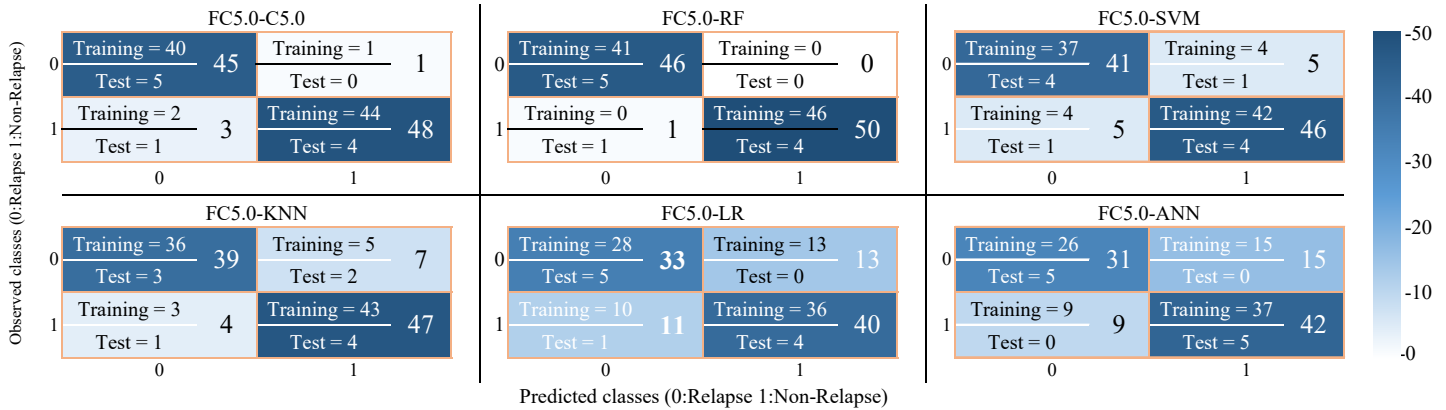
Figure 8: Confusion Matrix of our shrinkage models

we can see from experiment results (Table 3 and Figure 6), almost all constructed shrinkage models produced a classification performance that could exceed the eighties; and the most striking result concerns the FC5.0-RF and FC5.0-C5.0 models since they achieved the best prediction performance that could reach respectively to 95% and 93.28% in terms of all evaluation metrics, which is much better than what was reported in the first experiment (without applying gene selection Table 2). In contrast, the prediction performance has slightly deteriorated when it comes to LR and ANN classifiers when using our gene selection approach.

In Figure 7, the ROC curves are plotted to estimate the AUC of each constructed classifier model when using our gene selection method, which can help to compare their prediction performances. As we can see from this figure, ROC curves of FC5.0-RF and FC5.0-C5.0 models are the closest to the perfect performance curve, which can explain the quality of these models reported in Table 3. In the same context of the second experiment using our gene selection approach, Figure 8 gives a better overview of the relations between our generated prediction models outputs and the true labels. As we can notice, for our favorite model (FC5.0-RF) all samples in the training set are correctly classified, while in the test set, only one sample out of 10 is miss-classified, which confirms the achieved average classification accuracy of 95%.

According to all results reported above, it can be summed up that the power of our whole system (illustrated in Figure1)) comes from its ability to predict breast cancer risk with high performance by involving a bar minimum of genes predictors (only five genes).

Table 4 compares the performance (in terms of accuracy and the number of selected genes) of our gene selection-based breast cancer classification technique with existing gene selection methods. The comparison is made to demonstrate the capability of our

approach over other techniques in predicting breast cancer. As it can be noticed, the proposed approach led to a higher prediction performance by involving only five genes, which is much better than was reported for the other techniques.

Table 4: Comparison of the proposed FC5.0 approach with other feature selection-based approaches

Paper	Approach	# Selected genes	Best accuracy (%)
[9]	RFE+SVM	50	88,82
	RLR+SVM		87,87
[10]	FCBF+DNN+SVM	112	96.11
[11]	ACO+MBP	2448 (10%)	64.12
[12]	CFS+iBPSO+NB	32	94.00
[13]	SVM-VSSRFE	-	90.03
Ours	FC5.0-RF	5	95.00

6 Conclusion

By using gene expression data to improve breast cancer risk prediction, this study proposed a new Decision Tree model-based gene selection strategy, which incorporates two stages: fisher score-based filter method and the feature selection capability of the C5.0 algorithm. The prefiltering phase using the Fisher score aims at reducing the dimensionality of breast cancer gene expression data by getting rid of any irrelevant or redundant genes in the predictive genes. Then in the second stage, we make use of the obtained low-dimensional research space to find the best gene subset that maximizes the prediction performance by using the feature selection capability of the C5.0 decision tree algorithm. The optimal genes subset was used as the input for cancer classification using six machine learning algorithms. To prove the impact of our approach on breast cancer

risk prediction, we compared the classification performance of our generates models between them and with the performance of classifiers without using any gene selection process. Experimental results show that our gene selection approach led to a higher prediction performance that reached 95% using FC5.0-RF model by taking fewer genes, which is better than what was reported in Table 2 and Table 4 .

This work can be enhanced in two different aspects: the classification models and the search engine. For the classification model, we intend to propose the use of other supervised machine learning algorithms in order to achieve more accurate results in terms of prediction. For the search engine, other gene selection approaches can be proposed or combined with our proposed one. We expect these improvements to predict breast cancer risk with high accuracy, which may guide further breast cancer researches.

References

[1] "WHO | Breast cancer," Publisher: World Health Organization.

[2] "Determining relevant biomarkers for prediction of breast cancer using anthropometric and clinical features: A comparative investigation in machine learning paradigm," Biocybernetics and Biomedical Engineering, **39**(2), 393–409, 2019, doi:10.1016/j.bbe.2019.03.001, number: 2 Publisher: Elsevier.

[3] J. Cao, L. Zhang, B. Wang, F. Li, J. Yang, "A fast gene selection method for multi-cancer classification using multiple support vector data description," Journal of Biomedical Informatics, **53**, 381–389, 2015, doi:10.1016/j.jbi.2014.12.009.

[4] H. Moutachaouik, I. El Moudden, "Mining Prostate Cancer Behavior Using Parsimonious Factors and Shrinkage Methods," SSRN Electronic Journal, 2018, doi:10.2139/ssrn.3180967.

[5] S. Kabiraj, M. Raihan, N. Alvi, M. Afrin, L. Akter, S. A. Sohagi, E. Podder, "Breast Cancer Risk Prediction using XGBoost and Random Forest Algorithm," in 2020 11th International Conference on Computing, Communication and Networking Technologies (ICCCNT), 1–4, 2020, doi:10.1109/ICCCNT49239.2020.9225451.

[6] Naveen, R. K. Sharma, A. Ramachandran Nair, "Efficient Breast Cancer Prediction Using Ensemble Machine Learning Models," in 2019 4th International Conference on Recent Trends on Electronics, Information, Communication Technology (RTEICT), 100–104, 2019, doi:10.1109/RTEICT46194.2019.9016968.

[7] A. F. Agarap, "Deep Learning using Rectified Linear Units (ReLU)," CoRR, **abs/1803.08375**, 2018.

[8] S. S. Prakash, K. Visakha, "Breast Cancer Malignancy Prediction Using Deep Learning Neural Networks," in 2020 Second International Conference on Inventive Research in Computing Applications (ICIRCA), 88–92, 2020, doi:10.1109/ICIRCA48905.2020.9183378.

[9] S. Turgut, M. Dağtekin, T. Ensari, "Microarray breast cancer data classification using machine learning methods," in 2018 Electric Electronics, Computer Science, Biomedical Engineerings' Meeting (EBBT), 1–3, 2018, doi:10.1109/EBBT.2018.8391468.

[10] T. Al-Quraishi, J. H. Abawajy, N. Al-Quraishi, A. Abdalrada, L. Al-Omairi, "Predicting Breast Cancer Risk Using Subset of Genes," in 2019 6th International Conference on Control, Decision and Information Technologies (CoDIT), 1379–1384, IEEE, Paris, France, 2019, doi:10.1109/CoDIT.2019.8820378.

[11] D. P. Aldryan, Adiwijaya, A. Annisa, "Cancer Detection Based on Microarray Data Classification with Ant Colony Optimization and Modified Backpropagation Conjugate Gradient Polak-Ribiére," in 2018 International Conference on Computer, Control, Informatics and its Applications (IC3INA), 13–16, IEEE, Tangerang, Indonesia, 2018, doi:10.1109/IC3INA.2018.8629506.

[12] I. Jain, V. K. Jain, R. Jain, "Correlation feature selection based improved-Binary Particle Swarm Optimization for gene selection and cancer classification," Applied Soft Computing, **62**, 203–215, 2018, doi:10.1016/j.asoc.2017.09.038.

[13] Z. Li, W. Xie, T. Liu, "Efficient feature selection and classification for microarray data," PLOS ONE, **13**(8), e0202167, 2018, doi:10.1371/journal.pone.0202167, number: 8.

[14] I. El Moudden, H. Jouhari, M. Ouzir, S. bernoussi, "Learned Model For Human Activity Recognition Based On Dimensionality Reduction," 2018.

[15] I. El Moudden, S. Lhazmir, A. Kobbane, "Feature Extraction based on Principal Component Analysis for Text Categorization," 2017, doi:10.23919/PEMWN.2017.8308030.

[16] I. El Moudden, M. Ouzir, S. ElBernoussi, "Feature selection and extraction for class prediction in dysphonia measures analysis: A case study on Parkinson's disease speech rehabilitation," Technology and health care: official journal of the European Society for Engineering and Medicine, **25**, 1–16, 2017, doi:10.3233/THC-170824.

[17] M. Hamim, I. E. Moudden, H. Moutachaouik, M. Hain, "Decision Tree Model Based Gene Selection and Classification for Breast Cancer Risk Prediction," in Smart Applications and Data Analysis, 165–177, Springer, Cham, 2020, doi:10.1007/978-3-030-45183-7_12.

[18] M. Hamim, I. El Mouden, M. Ouzir, H. Moutachaouik, M. Hain, "A NOVEL DIMENSIONALITY REDUCTION APPROACH TO IMPROVE MICROARRAY DATA CLASSIFICATION," IIUM Engineering Journal, **22**(1), 1–22, 2021, doi:10.31436/iiumej.v22i1.1447.

[19] Q. Gu, Z. Li, J. Han, "Generalized Fisher Score for Feature Selection," arXiv:1202.3725 [cs, stat], 2012.

[20] R. Rathinasamy, L. Raj, "Comparative Analysis of C4.5 and C5.0 Algorithms on Crop Pest Data," International Journal of Innovative Research in Computer and Communication Engineering, **5**, 2017, 2019.

[21] Y. Y. Wang, J. Li, "Feature-Selection Ability of the Decision-Tree Algorithm and the Impact of Feature-Selection/Extraction on Decision-Tree Results Based on Hyperspectral Data," Int. J. Remote Sens., **29**(10), 2993–3010, 2008, doi:10.1080/01431160701442070.

[22] D. McIver, M. Friedl, "Using Prior Probabilities in Decision-Tree Classification of Remotely Sensed Data," Remote Sensing of Environment, **81**, 253–261, 2002.

[23] Z. Qi, A. G.-O. Yeh, X. Li, Z. Lin, "A novel algorithm for land use and land cover classification using RADARSAT-2 polarimetric SAR data," Remote Sensing of Environment, **118**, 21 – 39, 2012, doi:https://doi.org/10.1016/j.rse.2011.11.001.

[24] L. Deng, Y.-n. Yan, C. Wang, "Improved POLSAR Image Classification by the Use of Multi-Feature Combination," Remote Sensing, **7**, 4157–4177, 2015.

[25] S.-l. PANG, J.-z. GONG, "C5.0 Classification Algorithm and Application on Individual Credit Evaluation of Banks," Systems Engineering - Theory & Practice, **29**(12), 94 – 104, 2009, doi:https://doi.org/10.1016/S1874-8651(10)60092-0.

[26] S. Rajasekaran, G. A. V. Pai, Neural networks, fuzzy logic, and genetic algorithms : synthesis and applications, New Delhi : Prentice-Hall of India, eastern economy ed edition, 2003, includes bibliographical references and index.

[27] A. Chowdhury, T. Chatterjee, S. Banerjee, "A Random Forest classifier-based approach in the detection of abnormalities in the retina," Medical & Biological Engineering & Computing, **57**, 2018, doi:10.1007/s11517-018-1878-0.

[28] M. Pal, "Random forest classifier for remote sensing classification," International Journal of Remote Sensing - INT J REMOTE SENS, **26**, 217–222, 2005, doi:10.1080/01431160412331269698.

[29] R. O. Duda, P. E. Hart, D. G. Stork, Pattern classification, Wiley, New York, 2nd edition, 2001.

[30] L. J. van 't Veer, H. Dai, M. J. van de Vijver, Y. D. He, A. A. M. Hart, M. Mao, H. L. Peterse, K. van der Kooy, M. J. Marton, A. T. Witteveen, G. J. Schreiber, R. M. Kerkhoven, C. Roberts, P. S. Linsley, R. Bernards, S. H. Friend, "Gene expression profiling predicts clinical outcome of breast cancer," Nature, **415**(6871), 530–536, 2002, doi:10.1038/415530a, number: 6871.

A S T E S

Cyclic Evaluation of Capacity of Recovered Traction Battery after Short-Circuit Damage

Matus Danko[*], Marek Simcak

University of Zilina, Faculty of electrical engineering and information technologies, Department of mechatronics and autotronics, Zilina, 010 26, Slovakia

A R T I C L E I N F O	A B S T R A C T
	Presented paper discusses possibilities related to the recovery of the damaged lithium batteries after the short-circuit. The recovery procedure was applied on the selected traction LiFePO4 40Ah cell which was initially short-circuited. After the short-circuit, the damaged cell has visible damage of the electro-mechanical properties. For the recovery of damaged traction cell as much as possible, the experimental recovery procedure has been proposed. For the realization of this recovery procedure, the automated workplace for the cell discharging and charging with the proposed algorithm was created. For verification of the proposed recovery algorithm, the traction cell was tested with a delivered ampere-hour test at the various discharging currents. Results of the delivered ampere-hour test of the recovered cell were compared to results of delivered ampere-hour tests of the new cell. From the final evaluation is seen that the proposed recovery algorithm can recover up to 90% of capacity within a wide range of discharge and charge current.

1. Introduction

Batteries (in general form) are increasingly applied in fully electric vehicles or hybrid electric vehicles, energy storage systems, and other consumer product. The increasing of usage lithium batteries requires their bigger production and minimization of their ecological impact like footprints of carbon dioxide. Moreover, the raw materials access must be ensured, and the cost of materials must be kept low, then production rates will dramatically rise in the next several years. To secure enough battery materials, the spent lithium for batteries, especially those for hybrid electric vehicles or electric vehicles, must be recycled or recovered and used in other energy storage systems [1-5].

In present, complete recycling of lithium batteries is very costly so recycling is unprofitable. Production of batteries from recycled materials is unattractive for manufacturers because is up to 5 times more expensive than the new battery production from newly extracted materials. One of the ways to increase number of reused batteries is to regenerate them. The batteries used in cars are unusable in a vehicle when its usable capacity falls below 60%, but can still be used, for example, like energy storage in the photovoltaic system. In this simpler application, battery can safely

serve until the real end of life comes. It is assumed that up to 60% of li-ion batteries from vehicles can be used in this way [6-10].

Currently, the R&D institutions are not only involved into the research on recovery of raw materials, but also on reuse or second life of batteries which cannot fulfil the requirements of their original application area but are highly usable in less demanding application. Best example of battery second life is application of batteries from hybrid electric vehicles (HEV) or fully electric vehicles (EV) in small or medium battery storage systems (BSS) for example photovoltaic systems [11–13].

On the other side, there is also an issue that is common if operation of battery cells is considered. We can talk about improper storage or operation of cells which can resulting into the damage caused for example by deep discharge, over current discharging or short-circuit. Therefore, recovery or regeneration of such cells or harmed batteries is an important topic, due to the environment and the price of new batteries [14–18]. Nowadays, the recovery processes mainly used for NiMH and batteries lead-acid which was used in hybrid electric vehicles or large electricity storage systems. In present, lithium-based cells are largely used for e-mobility, so the topic of lithium battery recovery is more and more important, because of high lithium price [19–22].

Therefore, within the presented paper, the recovery procedure of damaged battery caused by application of long-term short-

[*]Corresponding Author: Matus Danko, University of Zilina, Faculty of electrical engineering and information technologies, Department of mechatronics and autotronics, Zilina, 010 26, Slovakia, +421 41 513 1610, matus.danko@feit.uniza.sk

circuit is being presented. The focus is given on the traction battery cell Sinopoly LiFePO4 - 40Ah/128Wh because LiFePO4 battery type are often used as traction batteries for electric or hybrid electric vehicles. Initially is being described the procedure of the application of long-term short-circuit, followed by the detection and evaluation of the damages caused by this improper operation. Consequently, the proposal procedure of regeneration is being described, while it is based on the pulsed charging with defined amplitude of charging current and durations of pluses, followed by adequate regeneration breaks. As an evaluation of suitability of proposed regeneration approach, the experimental test of the recovered battery capacity was realized, while received results have been compared to the similar tests of undamaged new cell.

2. Short-circuit damage of traction battery

During the operation of traction batteries, several hazardous conditions which are related to the behavior of the batteries can occur. These conditions can cause damage to the battery itself. Results of operation in inappropriate conditions primarily reflect into the open-circuit voltage (OCV) drop and significant loss of the capacity. If battery operation in hazardous condition is lasting, it can cause damage to the internal structure which can lead to damage of the package of the battery. In this paper is focus on operation at long-term short-circuit. Because unwanted hazardous operational conditions result in damage of battery structure, it is important to find the most suitable recovery procedure which can be applied for battery regeneration as near as possible to its nominal state.

In this paper, the attention is focused on the investigation of regeneration 40 Ah-128 Wh Sinopoly LiFePO4 3.2 V cell after short-circuit. In Table 1 are listed main parameters of tested cell.

Table 1: Parameters of selected cell

Electrical Parameter	Sinopoly LiFePO$_4$ 3.2 V 40 Ah	
Nominal voltage	3.2	(V)
Maximum charging voltage	3.65	(V)
Minimum voltage	2.5	(V)
Discharge current - maximum (continuous)	3	(C)
Discharging current - optimal	13	(A)
Charging current - maximum	60	(A)
Charging current - optimal	20	(A)
Operating temperature	−45 to +85	(°C)
Capacity	40	(Ah)
Package material	plastic	(-)

2.1. Experimental application of the short-circuit

For obtain a reference cell which can be used for recovery with proposal algorithm, selected LiFePO$_4$ 3.2 V, 40 Ah, 128 Wh battery cell was selected. Therefore, selected cell was short-circuited for obtaining reference short-circuited cell. Short-circuit, which is worst scenario of operation from safety point of view. On Figure 4 shown test set-up used for experiment of the short-circuit. This configuration uses mechanical switch rated for very high current for star of short-circuiting test. Thermo-vision camera

FLIR E5 and thermo-vision camera FLIR SC 660 used for thermal analysis during short-circuit.
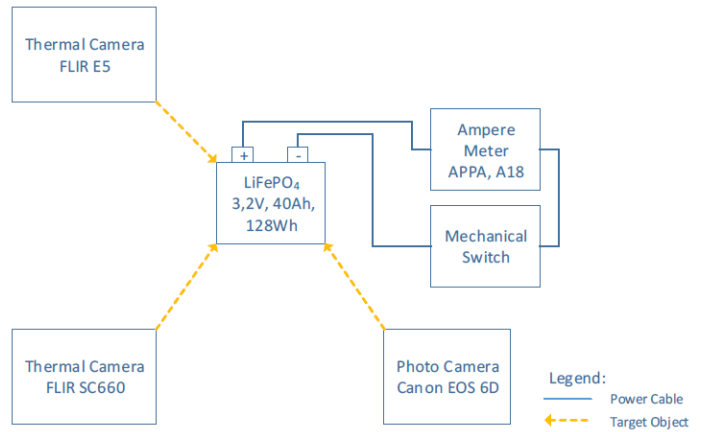
Figure 1: Block diagram of set-up for short-circuit test

The measurement of current during short circuit test was provided by current meter APPA A18, while measured values were stored on NI PXI with measurement cards NI PXI 1031 using LabVIEW. For the evaluation of battery dimensions and shape changes from pictures, camera Canon EOS 6D was used.
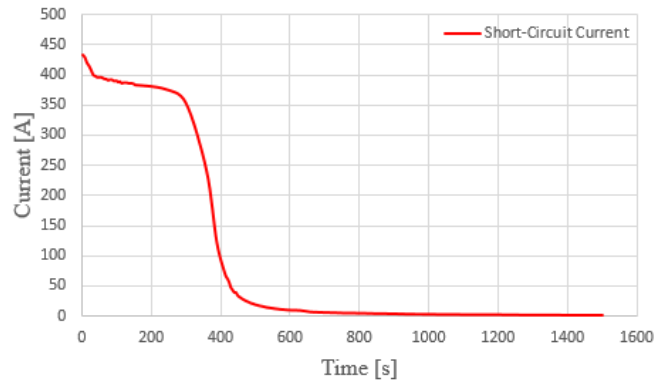
Figure 2: Current profile during the short-circuit experiment

On new battery cell which was formatted during manufacturing process was used for short-circuiting test. Secondary formatting was realized before short-circuiting test within laboratory conditions. Before short-circuiting test, battery open circuit voltage was 3,24 Vdc.

Figure 2 shows the current waveform during the short-circuit experiment. From this figure we can see that after short-circuiting, discharging current of the battery reached up to 430 A. Following more than 300 s, discharging current of the battery was over 350 A, than in next 100s is visible rapid fall of discharging current. After more than 600 s of test, current was reduced to the value of 11.5 A and finally to 2.7 A. The duration of this test was 25 min.

During short-circuited test, the battery discharging current reached more than 10C what is 3-times higher than maximal continuous discharging current determined from manufacturer. Even due to this critical operational condition, the maximum surface temperature recorded during experiment reached 49.2 °C (Figure 3), while during short-circuit test the ambient temperature was 18 °C. This maximum temperature was measured at the end

of the short-circuit test and the safety pressure valve was inactive during whole duration of short-circuit.
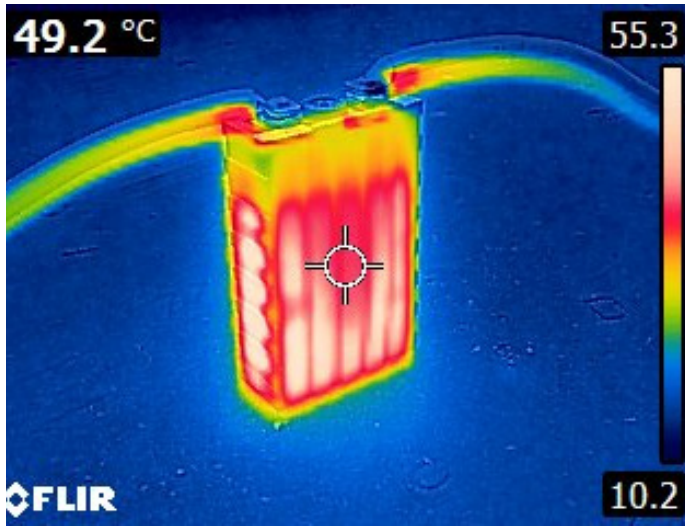
Figure 3: Maximal temperature during short-circuit test

The result of the short-circuit was visible mechanical change of the battery internal structure which cause change dimension of package. Figure 4 indicates structural damage after the end of the experiment, whereby depth of the package raised from 46 mm up to 54 mm, height of the package has risen from 186 mm up to 186.5 mm, and width had changed by 0.5 mm, i.e. from 116 mm down to 115.5 mm.
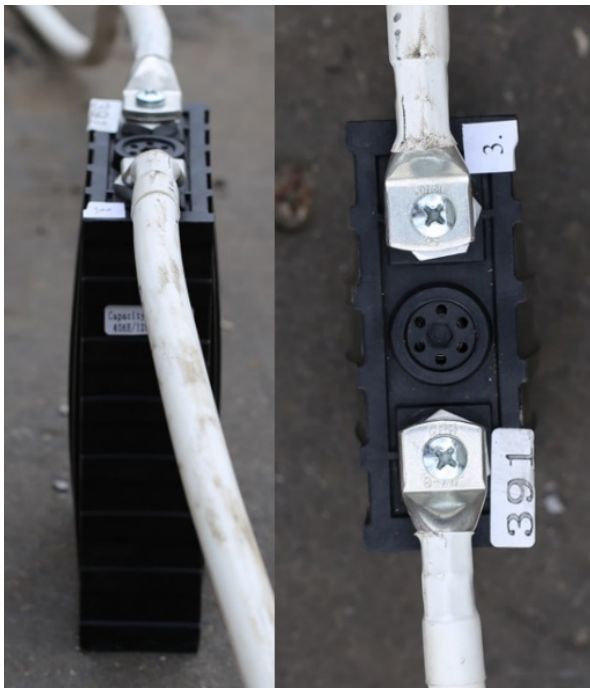
Figure 4: Changes of dimensions of the tested cell after experiment of long-term short-circuit

3. Regeneration procedure application after long-term short-circuit

After the short-circuit test, the tested cell was left resting for 22 days. After this rest period, geometrical dimension of cell was checked again while no dimensional or shape change was observed

compared to measured dimensions immediately after the short-circuit test. Consequently, the regeneration procedure which is explained by table 2. Was applied. The proposal procedure is based on the sequential charging with pulse charging current. This charging sequence is split into six subsequences. After finish of each subsequence, approximately 16 h resting period is applied. Each pulse subsequence duration is 100 min is divided into four cycles which duration is 25 min. The main difference between the cycles is the charging current amplitude (Table 2).

Table 2: Parameters of the regeneration procedure after long-term short-circuit.

Subsequence	Duration	Charging current amplitude	Maximal charging voltage
1	25 min × 4 cycle = 100 min	Increasing after each cycle = 0,5 – 2A	3.65 V
2	25 min × 4 cycle = 100 min	Increasing after each cycle = 2,5 – 4A	3.65 V
3	25 min × 4 cycle = 100 min	Increasing after each cycle = 4,5 – 6A	3.65 V
4	25 min × 4 cycle = 100 min	Increasing after each cycle = 6,5 – 8A	3.65 V
5	25 min × 4 cycle = 100 min	Increasing after each cycle = 8,5 – 10A	3.65 V
6	25 min × 4 cycle = 100 min	Increasing after each cycle = 10,5 – 12A	3.65 V

Capacity of cell was tested with delivered ampere-hour test after regeneration and after formatting procedure, while the results have been presented within [23].

During initial capacity testing the cell showed similar performance to reference, unused new cell up to 80 A of discharge current. However, for maximal 3C discharging current, the recovered cell showed just less than half of the capacity (Figure 5).
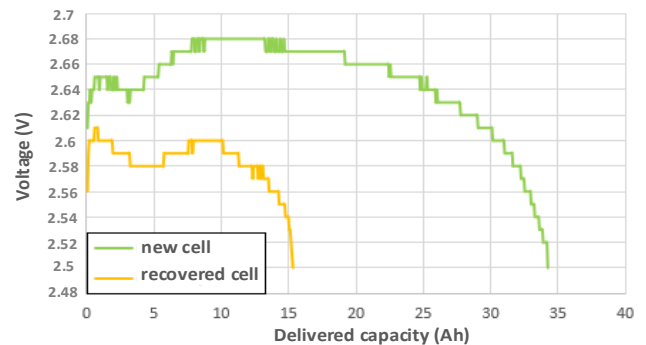
Figure 5: Voltage waveform during discharge with 3C discharging current for regenerated (yellow) and referenced cell (green)

After 28 days of storage, recovered battery was tested ten times in a row with delivered ampere-hour test. Differences in capacity values between repeated delivered ampere-hour tests were under

2%. The main issue, which was not satisfactory for the recovered cell, was the fact that for higher currents (above 2C) the battery lost its performance by more than 50 %. Therefore, second regeneration was applied once more, consequently resting period of 22 days was applied followed by formatting procedure. After this second regeneration procedure, once the cyclic testing of the capacity of regenerated battery was realized.

4. Cyclic testing of the capacity of recovered LiFePO$_4$ traction cell

Before this cycling testing, it is necessary to charge recovered batteries as well as reference one (non-damaged, unused and formatted cell). CC&CV charging (Constant Current and Constant Voltage) is recommended for selected types of batteries. Capacity of both batteries was verified by test of delivered ampere-hours.

For the battery capacity test, five discharging and charging strategies were chosen. Each strategy is specific by a different value of discharging and charging current, while the values of discharging currents was chosen based on manufacturer recommendations of selected cell 13A-120A (0.3-3C). Cyclic experiments have been made, i.e. recovered battery had continuously undertaken verification for each of charging and discharging test for 5 times to prove robustness of proposed regeneration procedure [24-25].
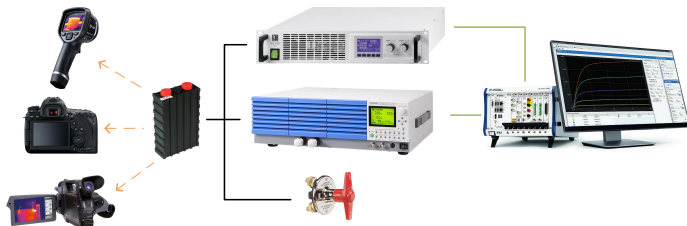
Figure 5: Block diagram of set-up for capacity testing with delivered ampere-hour test

4.1. Test of the discharged capacity

In figures 6 to Figure 10 can be seen voltage waveforms of battery cell during constant current discharge for 5 different current values (0.3C-3C). Each situation compares the situation for recovered cell and for reference (new) cell. From individual results is visible, that recovered battery exhibits the same performance as undamaged new cell.
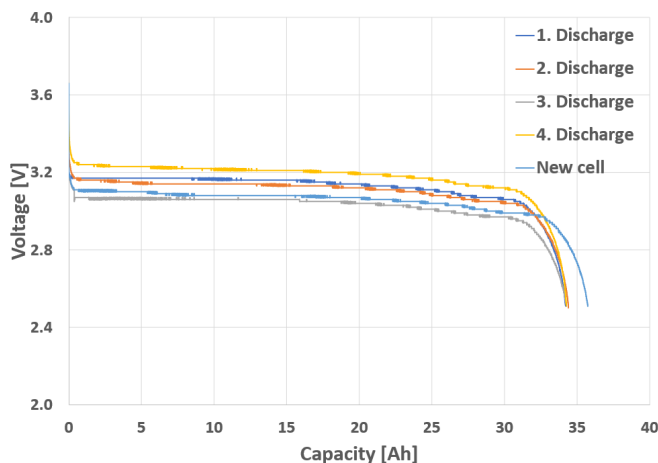
Figure 6: Cyclic discharging (I = 13A)
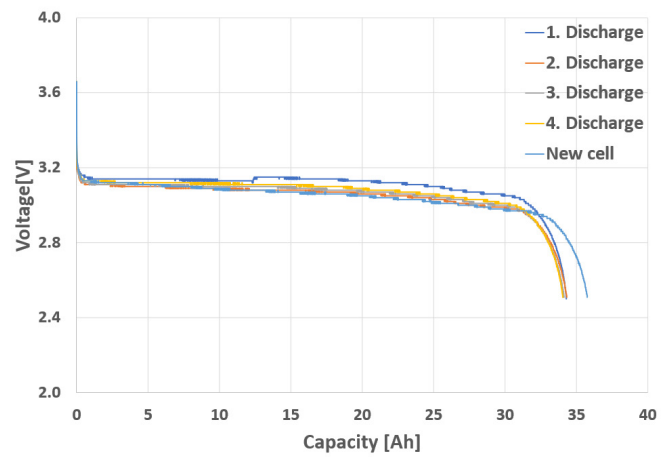
Figure 7: Cyclic discharging (I = 20A)
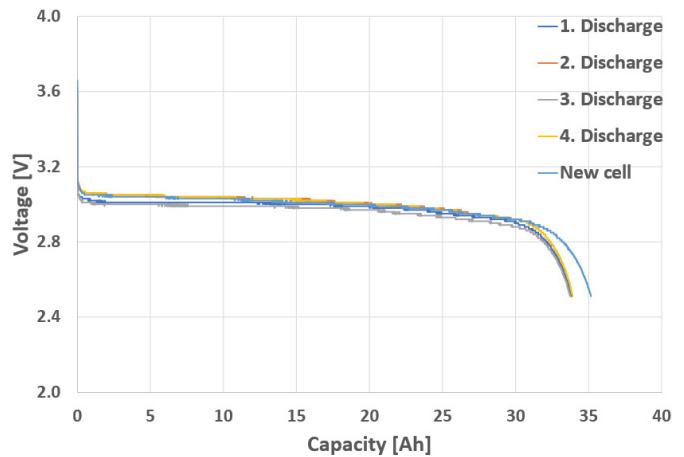
Figure 8: Cyclic discharging (I = 40A)
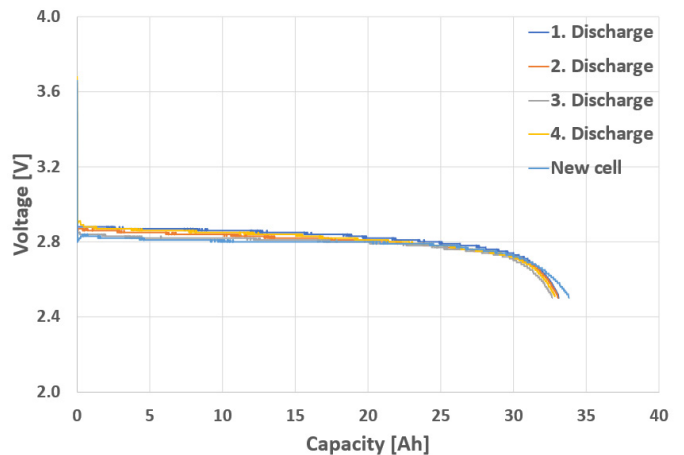
Figure 9: Cyclic discharging (I = 80A)

Each discharging test of recovered cell, i.e. for each value of discharge current, the measurement was validated for 4 times in order to prove stable value of recovered capacity. Simultaneously, there is a small difference between new and recovered cell. When comparing capacity for individual discharging currents, the highest difference of app. 2 Ah is visible for low discharging currents (Figure 6 – Figure 8). For higher values difference is reduced /Figure 9 – Figure 10).
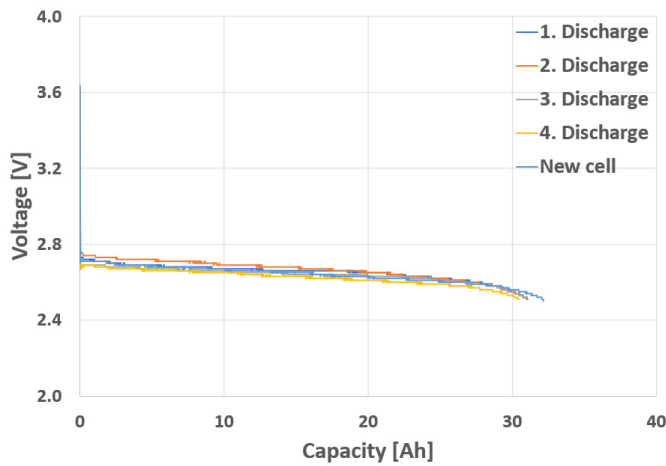
Figure 10: Cyclic discharging (I = 120A)

Within the datasheet of tested battery type it states that it is necessary to monitor the value of the temperature when discharging the cell with a current of 120 A. Temperature profile during whole discharging process by current of 120 A of recovered cell can be seen in Figure 11. From this figure is can be seen that temperature is reaching approximately 37.3 °C at the end of the discharging process. The value is much lower than critical discharging temperature listed in datasheet, which value is 85°C. This temperature profile was recorded for each discharging sequence.
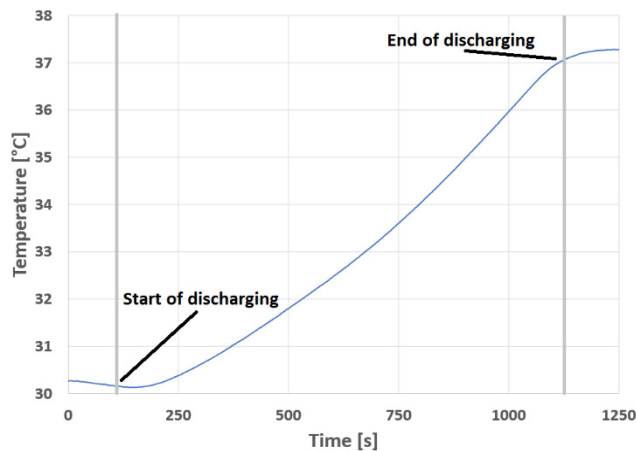
Figure 11: Temperature profile of recovered cell during discharge with 120A

The other two figures (Figure 12 and Figure 13) are representing reference results for individual situations, while independently the results for recovered and undamaged, new formatted cells are interpreted. Here the voltage waveforms are being showed during discharge with different discharging current values. At the beginning of discharging process there is a voltage drop. Voltage drop magnitude depends on the magnitude of the discharge current. The higher value of the discharge current cause the greater the voltage drop. This is caused by the effect of internal resistance of the cell. The difference between Figure 12 and Figure 13 is not markedly great, i.e. recovered cell exhibits similar behavior to undamaged. Therefore, it can be said that application of proposed capacity recovery algorithm has positively influenced the internal resistance of the cell as well.
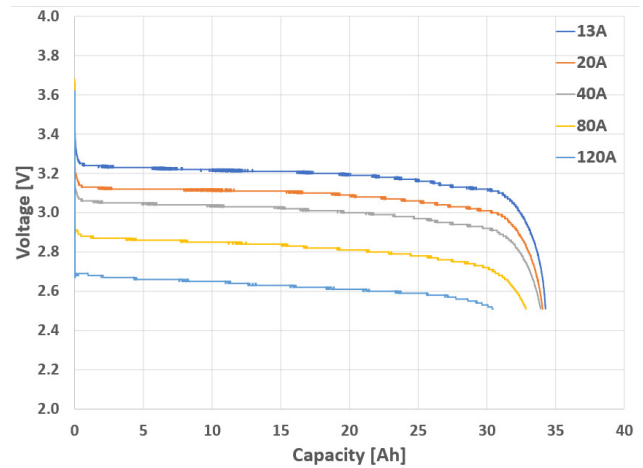
Figure 12: Voltage profile waveforms of recovered cell for various discharging currents
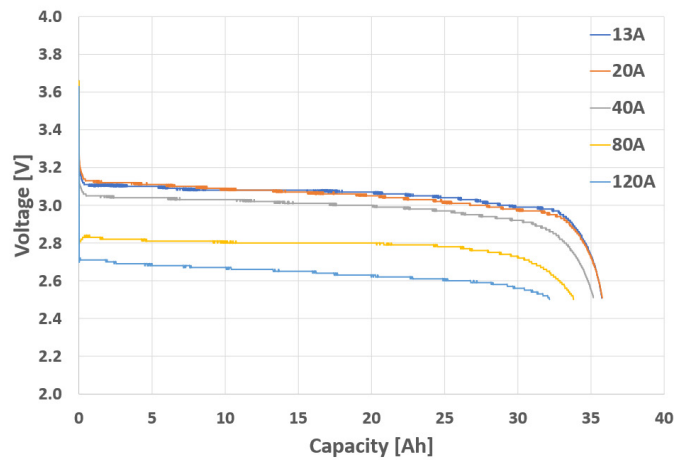
Figure 13: Voltage profile waveforms of new cell for various discharging currents

4.2. Test of charged capacity

Similary to the test of the discharging process, the test of the charging process was realized for recovered and new cell.
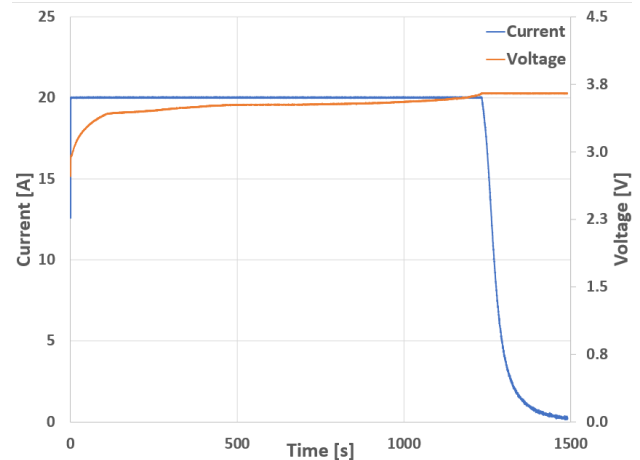
Figure 14: Charging waveforms of voltage and current (I_{CC} = 20A)

The recovered cell was tested several times to prove stability of the recovered capacity once again. Figure 14 shows the cell voltage and current waveforms during charging profile. Here we

can see the value of the constant current (in this case 20A) and the value of the charging voltage (3.65V). The charging profile is reflecting constant current, constant voltage procedure (CC/CV), what is an optimal charging method of tested type of bateries.
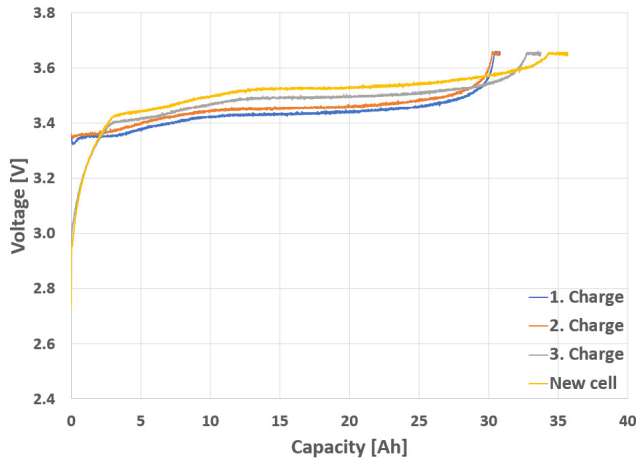
Figure 15: Cyclic charging (I = 20A)
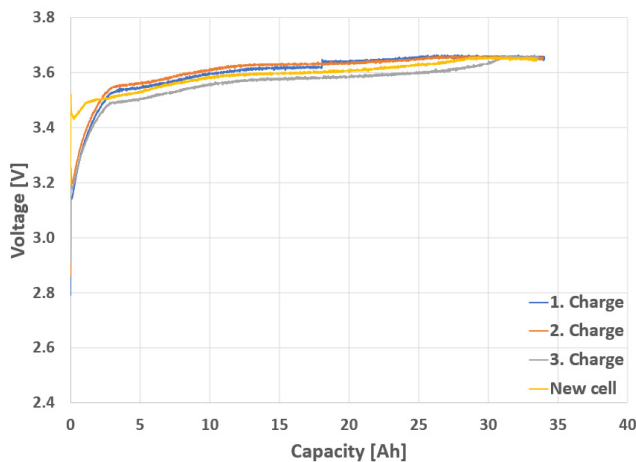
Figure 16: Cyclic charging (I = 40A)
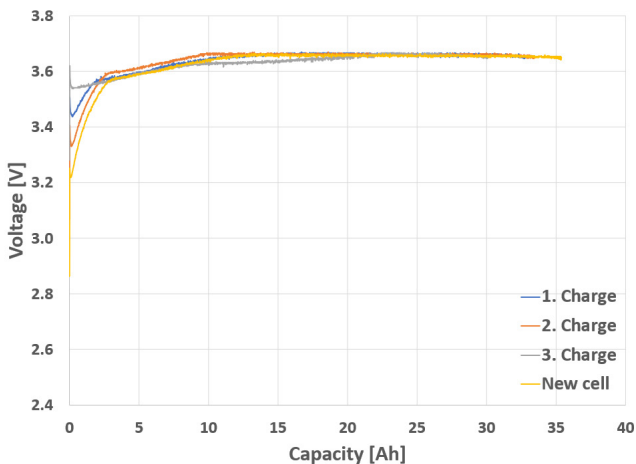
Figure 17: Cyclic charging (I = 60A)

In Figure 15 to Figure 17 are the voltage waveforms during charging proces. Individual figures are specific by the value of charging current. Each graph shows 3 measurements for recovered cell and one measurement for new cell. The graphs show that

charging process of new cell exhibits higher capacity if low value of charging current is applied (Figure 15). This process was also visible during discharge process by low values of current. The higher the charging current, the smaller the capacity differences between the recovered and new cell.

Figure 18 and Figure 19 are representing reference voltage profiles during charging process. Figure 18 is shown that maximum capacity of recovered cell is achieved at 33 Ah, while voltage is at the level of 3,65 V. From figure 19 can be seen that the capacity of new cell achieves approximately 37 Ah at maximum voltage level 3,65 V. Based on this results we can state, that recovered cell lost about 10% of its nominal capacity. This result is also confirmed by the voltage waveform from Figure 12 and Figure 13 where is seen, that recovered cell provides less capacity than new. However, even due to reduction of available capacity, the recovery algorithm enables to recover more than 90% of damaged cell capacity.
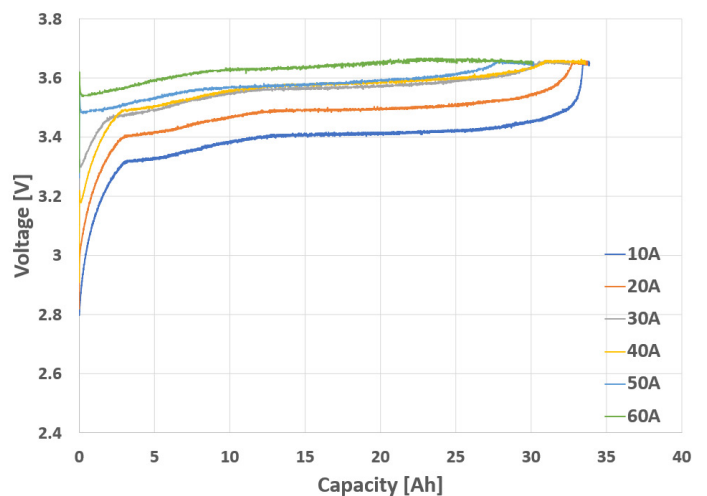
Figure 18: Reference waveforms of shorted cell based on the current
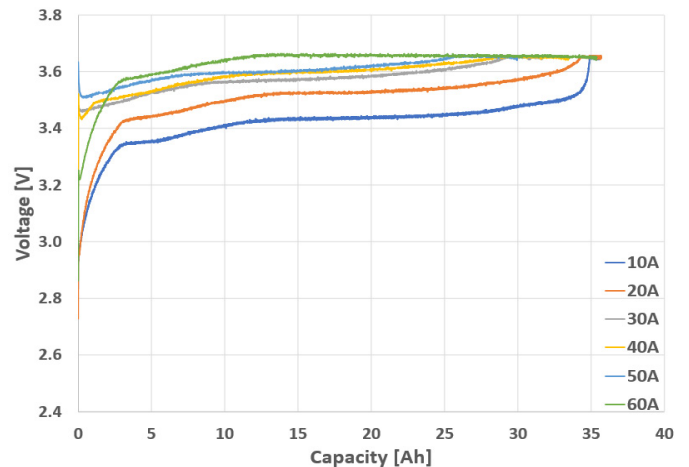
Figure 19: Reference waveforms of new cell based on the current

5. Conclusion

This paper present charging algorithm for recovery of lithium phosphate traction batteries after long-term short circuit. This recovery algorithm was applied to short-circuited Sinopoly LiFePO4 3.2V 40Ah cell. Proposal algorithm was verified with

delivered ampere-hour tests. Result of these tests was compared to delivered ampere-hour test of same type battery which was, new and formatted. From comparison of tests of new and recovered battery was found that proposed algorithm can recover up to 90% within wide range of discharge and charge currents.

Conflict of Interest

The authors declare no conflict of interest.

Acknowledgment

References

[1] M. Frivaldsky, J. Cuntala, P. Spanik, A.Kanovsky, "Investigation of thermal effects and lifetime estimation of electrolytic double layer capacitors during repeated charge and discharge cycles in dedicated application," ELECTRICAL ENGINEERING, **100**(1), 11-25, 2018

[2] S. Chamnan-arsa, K. Uthaichana, B.Kaewkham-ai, "Modeling of LiFePO₄ battery state of charge with recovery effect as a three-mode switched system," Proceedings of the 2014 13th International Conference on Control, Automation Robotics & Vision (ICARCV), Singapore, 1712–1717, 2014, doi:10.1109/ICARCV.2014.7064574.

[3] J. Koscelnik, M. Frivaldsky, M. Prazenica, R. Mazgut, "A Review of Multi-elements Resonant Converters Topologies," ELEKTRO 10th International Conference, Rajecke Teplice, SLOVAKIA, 2014

[4] H.D. Yoo, E. Markevich, G. Salta, D. Sharon, D. Aurbach, "On the challenge of developing advanced technologies for electrochemical energy storage and conversion," Materials Today, **17**(3), 110-121, ISSN 1369-7021, 2014, https://doi.org/10.1016/j.mattod.2014.02.014

[5] P. Spanik, J. Cuntala, M. Frivaldsky, P. Drgona, "Investigation of Heat Transfer of Electronic System through Utilization of Novel Computation Algorithms," ELEKTRONIKA IR ELEKTROTECHNIKA, **123**(7) , 31-36, 2012

[6] V. D'Angelo, S. Cannavacciuolo, S. Lecce, V. Bendotti, O. Pennisi, "Enhanced hotplug protection in BMS applications. Part I: Theoretical Aspects and Practical Issues," 2019 AEIT International Conference of Electrical and Electronic Technologies for Automotive (AEIT AUTOMOTIVE), Torino, Italy, 1-5, 2019. doi: 10.23919/EETA.2019.8804513.

[7] M. A. Boukhal, I. Lagrat, O. Elbannay, "Implementation of a lithium-ion battery state of charge estimation algorithm for BMS on the real time target NI myRio," 2019 International Conference on Wireless Technologies, Embedded and Intelligent Systems (WITS), Fez, Morocco, 1-5, 2019. doi: 10.1109/WITS.2019.8723849.

[8] M. Frivaldsky, B. Dobrucky, G. Scelba, P. Spanik, P. Drgona, "Bidirectional Step-Up/Step-Down DC-DC Converter with Magnetically Coupled Coils," Communications - Scientific Letters of the University of Zilina, 15(3), 21-25, 2013

[9] C. Huang-Jen, L. Li-Wei, P. Ping-Lung, T. Ming-Hsiang, "A novel rapid charger for lead-acid batteries with energy recovery," IEEE Trans. Power Electron. **21**(3), 640–647, 2006, doi:10.1109/TPEL.2006.872386.

[10] C. Sen, N. C. Kar, "Battery pack modeling for the analysis of battery management system of a hybrid electric vehicle," Vehicle Power and Propulsion Conference, 207– 212, 2009, doi: 10.1109/VPPC.2009.5289848

[11] P. Spanik, R. Sul, M. Frivaldsky, "Performance Investigation of Dynamic Characteristics of Power Semiconductor Diodes," ELEKTRONIKA IR ELEKTROTECHNIKA, 3, 3-6, 2010

[12] A. F. Moghaddam, A. Van Den Bossche, "An active cell equalization technique for lithium ion batteries based on inductor balancing," in 2018 9th International Conference on Mechanical and Aerospace Engineering (ICMAE). IEEE, 274–278, 2018

[13] M. Cacciato, G. Nobile, G. Scarcella, G. Scelba, A. G. Sciacca, "Energy management optimization in stand-alone power supplies using online estimation of battery SOC," 18th European Conference on Power Electronics

and Applications (EPE'16 ECCE Europe), Karlsruhe, 1-10, 2016 doi: 10.1109/EPE.2016.7695559

[14] M. Galad, P. Spanik, M. Cacciato, G. Nobile, "Comparison of common and combined state of charge estimation methods for VRLA batteries, " 2016 ELEKTRO, Strbske Pleso, 220-225, 2016, doi: 10.1109/ELEKTRO.2016.7512069

[15] Y. Cai, Z. Zhang, Y. Zhang, Y. Liu, "A self-reconfiguration control regarding recovery effect to improve the discharge efficiency in the distributed battery energy storage system," Proceedings of the 2015 IEEE Applied Power Electronics Conference and Exposition (APEC), Charlotte, NC, USA,, 1774–1778, 2015. doi:10.1109/APEC.2015.7104587.

[16] P. Spanik, R. Sul, M. Frivaldsky, P. Drgona, "Performance Investigation of Dynamic Characteristics of Power Semiconductor Diodes," ELEKTRONIKA IR ELEKTROTECHNIKA, **3**, 3-6, 2010

[17] M. E. Orchard, M. Lacalle, B. E. Olivares, J. F. Silva, R. Palma-Behnke, P. Estevez, B. Severino, W. Calderon-Muoz, M. Cortez, "Information-Theoretic Measures and Sequential Monte Carlo Methods for Detection of Regeneration Phenomena in the Degradation of Lithium-Ion Battery Cells," IEEE Transactions on Reliability. **64**(2), 701–709, 2015, doi:10.1109/TR.2015.2394356.

[18] M. Cacciato, G. Nobile, G. Scarcella, G. Scelba, "Real-Time Model-Based Estimation of SOC and SOH for Energy Storage Systems," IEEE Transactions on Power Electronics, **32**(1), 794-803, 2017. doi: 10.1109/TPEL.2016.2535321

[19] P. Drgona, A. Prikopova, M. Frivaldsky, M. Priecinsky, "Simulation Based Method for Design and Application of Digital Control System, "Communications - Scientific Letters of the University of Zilina, **13**(2A), 32-37, 2011

[20] J. Koscelnik, M. Prazenica, M. Frivaldsky, S. Ondirko, "Design and Simulation of Multi-element Resonant LCTLC Converter with HF Transformer," ELEKTRO 10th International Conference, Rajecke Teplice, SLOVAKIA, 2014

[21] B. Dobrucky, M. Frivaldsky, P. Drgona, I. Kurytnik, "Measurement of swtitching losses in power transistor structure," ELEKTRONIKA IR ELEKTROTECHNIKA, **2**, 75-78, 2008

[22] M. Frivaldsky, P. Drgona, P. Spanik, "Experimental analysis and optimization of key parameters of ZVS mode and its application in the proposed LLC converter designed for distributed power system application," INTERNATIONAL JOURNAL OF ELECTRICAL POWER & ENERGY SYSTEMS, **47**, 448-456, 2013

[23] M. Frivaldsky, J. Adamec, M. Danko, P. Drgona, "Traction battery (40 Ah LiFePO4) recovery after long-term short circuit," 2020 International Symposium on Power Electronics, Electrical Drives, Automation and Motion (SPEEDAM), Sorrento, Italy, 299-304, 2020. doi: 10.1109/SPEEDAM48782.2020.9161868.

[24] M. Frivaldsky, B. Dobrucky, M. Prazenica, J. Koscelnik, "Multi-tank resonant topologies as key design factors for reliability improvement of power converter for power energy applications," ELECTRICAL ENGINEERING, **97**(4), 287-302, 2015

[25] P. Spanik, M. Frivaldsky, P. Drgona, J. Kandrac, "Efficiency Increase of Switched Mode Power Supply through Optimization of Transistor's Commutation Mode," In: ELEKTRONIKA IR ELEKTROTECHNIKA, **9**, 45-52, 2010

ASTES

Method of Technological Forecasting of Market Behaviour of R&D Products

Vasyl Kozyk[1], Oleksandra Mrykhina[1], Lidiya Lisovska[2,*], Anna Panchenko [1], Mykhailo Honchar [3]

[1]*Department of Business Economics and Investment, Lviv Polytechnic National University, Lviv, 79013, Ukraine*

[2]*Management of Organizations Department, Lviv Polytechnic National University, Lviv, 79013, Ukraine*

[3]*Department of Management and International Business, Lviv Polytechnic National University, Lviv, 79013, Ukraine*

A R T I C L E I N F O	A B S T R A C T
	The current concept of open innovation corresponds to the R&D products transfer model – "role changes". One of the fundamental provisions of the model is that R&D products are considered for commercialization not only at the final stage of technological readiness, but at any of them. In today's changing market environment, special attention is paid to the transfer and commercialization of R&D products at the early stages of readiness, but this process is characterized by significant problems from the point of view of technological forecasting. To solve the problems, the article substantiates the method of technological forecasting of market behaviour of R&D products at the early stages of technological readiness, which is based on taking into account the strengths and weaknesses, development factors and limiting factors of R&D product. The method allows you to predict indicators of product behaviour relative to the market where its commercialization is planned. *As a component of the above method and in order to increase the level of reliability of calculations and validity of results, a method for determining the correction factor of indicators of market behaviour of R&D product has been developed. The method was developed on the basis of fuzzy set theory algorithms using the fuzzy logic toolbox (MATLAB), which made it possible to integrate a set of different types of forecast data on the market behaviour of an R&D product, taking into account the relationships and interdependencies between them, into one correction factor. This coefficient contains the characteristics of signs of the impact of R&D product on the market (in particular, market effects, types of market changes) and the impact of market effects on R&D product (effects generated by R&D products, organizational and technological changes in R&D products). To justify the correction factor, a knowledge base of responses from subject area experts has been formed. In order to further select a commercialization strategy for R&D product, a system with normative indicators has been developed that interpret the following types of strategies: zero-level commercialization of R&D product; first-level commercialization of R&D product; commercialization of the second level of R&D product.* *The author's method of technological forecasting of market behaviour of R&D products and choosing a commercialization strategy for a product is universal, can be applied to R&D product of any type of economic activity, transfer method, etc. Testing of the method on the example of a number of R&D products presented by the developers of the Lviv Polytechnic National University (Lviv, Ukraine) showed the validity of the author's method and its relevance in modern conditions of market singularity.*

1. Introduction

1.1. Framework of theme relevance

   This work is a continuation of a number of our scientific papers in the framework of research on the transfer of R&D products, in particular, presented at the 14th International Scientific and Technical Conference on Computer Sciences and Information Technologies (2019) [1].

   In recent years, there has been a change in a number of models

of R&D products transfer, due to changes in the models of the innovation process, globalization and digitalization. The current concept of open innovation corresponds to the R&D products transfer model – "role changes". One of the fundamental provisions of the model is that R&D products are considered for commercialization not only at the final stage of technological readiness, but at any of them. This position is important from several positions. First, depending on the stage of R&D product readiness for commercialization, both its original purpose and the level of consumer value may change (for example, when R&D products converge at the stage of idea justification).

Secondly, in the context of the spread of digitalization, the commercialization of R&D product is much faster, compared to the similar situation that was inherent in the global economy several decades ago.

In general, the level of technological readiness of an R&D product indicates its presence at a certain stage (research, development, etc.), which is compared with the planned (or final) stage, and, taking into account the features of R&D product development, predict the duration, cost and nature of market behaviour of the product. In other words, the market behaviour of a commercialized R&D product, which is evaluated at different stages of its technological readiness, will be different.

The above actualizes the need to pay attention to the study of approaches, methods and models of technological forecasting of market behaviour of R&D products. The success of implementing the R&D products commercialization strategy will depend on the reasonable choice of methodological tools for technological forecasting. The development of such methodological tools is relevant both from the point of view of the needs of the modern economy, and from the point of view of predicting the market behaviour of R&D products in the conditions of a market singularity.

1.2. Statistical Background

The relevance of the above problem is confirmed by numerous statistical data. In particular, among the problems that will befall R&D products in the form of startups, there is insufficient funding in the early stages of product development – 29 %, which is the second significant reason in the list of their failures (the first reason is the lack of market demand – 42 %) [2]. At the same time, startups are characterized by a growth trend. For example, for two dozen top universities in the United States, the number of startups has more than tripled in 20 years-from 306 units in 1998, up to 1098 units in 2018 [3], which explain the focus of universities to generate R&D products in the early stages with the help of startups. At the same time, 20 % of startups fail in the first year, 50% of startups fail in the first five years [4].

Traditionally, among small business owners, about 77 % of early-stage product financing is done by raising their own funds [4], which requires careful technological forecasting of the development and payback of R&D products. However, only 2 – 3 % of development funding belongs to alternative sources (Venture Investors, Business Angels, crowd funding, etc. [4]).

The importance of paying attention to technological forecasting of market behaviour of R&D products in the early stages of technological readiness is confirmed by the results of the NanoCom Consortium study [5], in which 214 people were interviewed about barriers to commercialization of R&D products

in the field of nanotechnology. Among them, 63 people noted significant barriers at 3 – 5 levels of TRL (technology readiness level), where R&D is conducted. Other significant barriers included commercially available at TRL levels 8 – 9 (93 responses). The participants of this organization also argue that the most significant impact of barriers occurs in the early stages of TRL – domain technological, and in subsequent stages TRL gives way to marketing and strategic domain.

R&D is one of the defining components of the structure of a number of global country competitiveness indices (Bloomberg Innovation Index, Global Competitiveness Index, Creativity Index, etc.), so technological forecasting of market behaviour of R&D products can be a strong argument for explaining other components of such indices (market perception, productivity, added value, etc.).

1.3. Formulation of the problem

Without a sound approach to technological forecasting of market behaviour of R&D products, there is a high probability that they will not forget or partially acquire the utility function that turns the product into a market innovation.

To develop a method of technological forecasting of market behaviour of R&D product in modern economic conditions, and, based on this, to justify the commercialization strategy for it, it is necessary to conduct a comprehensive study of both the product and the market. We should learn trends and patterns of the market, the readiness of R&D product for commercialization, and so on.

In this paper, we consider R&D product from the point of view of customer-oriented marketing, that is, the focus is on the consumer value of the product. Product R&D marketing is directly related to the consumer's consciousness. Therefore, in order to assess the level of technological readiness of an R&D product, it is necessary to keep in mind the readiness of the consumer (or market) to accept this technology. Starting from the first stage of evaluating the technological readiness of an R&D product it is necessary to formulate evaluation tasks in such a way that in the end we reach such technological, economic and other indicators that will best satisfy the business structures to which this technology will be transferred.

2. Theoretical Background

2.1. Approaches to substantiating R&D product development strategies

The development and commercialization of an R&D product requires considerable effort and resources from all participants in innovation activities. At the same time, one of the most important tasks is technological forecasting of changes that can occur with an R&D product and affect its commercialization and market distribution.

In modern scientific works on the problems of technological forecasting of R&D product development, various approaches, methods and models of research of R&D product and their market development are presented. In particular, to truly manifest innovation and reap its benefits, one must recognize that innovation is three different things: innovation is an outcome, innovation is a process, and innovation is a mindset [6].

A number of models of market development of R&D product

have been developed. The new technological innovations are changing the ways businesses are being operated. The sharing economy – based new business models (SEBMs) using technology have many benefits, it is paramount to understand these SEBMs models and the behaviour of the market, particularly on how to influence the market's attitude [7] this approach actualizes the importance of tasks to justify and choose a strategy for market development of R&D products.

The formation of a market development strategy should include forecasting factors and the dynamics of their impact on the market success of R&D products, sources of change and inertia that issue from the introduction of innovations in the market [8], business logic as consequence of far-reaching technological developments [9] using technological forecasting methods. Such factors should be systemic and complex, because focusing solely on the effectiveness of the technological innovation is detrimental to long-term operational benefits [10].

The above-mentioned problem is quite complex, since, as scientists note, chain reactions from one innovation can have effects so significant that the entire world alters its way of life to incorporate the new technology. Often times, the effects of a new type of technology build upon existing technology with future innovations building on the inventions of today. This constant evolution and growth forces businesses to adapt or expire [11].

In addition, scientists distinguish the interdependence between the introduction of different types of innovations, which determine the market prospects for each other's development, as in the case of the introduction of technological and organizational innovations [12]. Sustainability, adoption of various types of innovation [13], accounting for the environment in the agenda of companies [14]. The success of innovations depends in part on the business models used to distribute them [15]. Also important is the impact of specific types of information on commercialization rates of technologies [16].

Scientific papers note that the innovation adoption is a process, rather than a dichotomic choice [17]. Therefore, for a rational and effective process of adapting R&D products to the market, it is necessary to develop and implement strategic solutions.

For the formation of innovation development strategies, many approaches justify strategic management decisions from different positions. Marketing strategies and particularly brand associations with brand awareness, perceived quality, and brand loyalty [18], co-branding strategies become important [19].

In addition, market opportunities for innovation are associated with the implementation of competitive strategies and market-based assets (customer orientation, competitor orientation, and marketing creativity) were assessed for their ability to help an innovating firm deal with dysfunctional competition and improve the returns from innovation [20].

In connection with the development of the open innovation model, the following factors are becoming important: intellectual property strategy, the shaping of complementary and substitute appropriability regimes is central when strategizing in dynamic and systemic innovation contexts [21].

2.2. Tools for justifying R&D product development strategies

The study of tools for the formation of strategies for the development of technological innovations has led to a revision of methods of technological forecasting, that can be useful for bringing a new perspective to explain and generalize properties of the evolution of technology and predict which innovations are likely to evolve rapidly in society [22]. The tasks of modern technological forecasting are strategic foresight, sustainability, technology transfer, entrepreneurship, and absorptive capacity can be explored further [23].

When justifying the R&D products development strategy, scientists highlight two generative cognitive processes- analogical reasoning and conceptual computation [24].

More and more scientists are using matrix approach to technological innovations based on design science research, entrepreneurship, and innovation theories, especially in digital innovation [25].

Combined methods of forming strategic decisions based on MULTIMOORA (Multi-Objective Optimization on the basis of Ratio Analysis plus full multiplicative form) is a somewhat new multi criteria decision-making (MCDM) method which provides high efficiency and effectiveness in problem solving [26].

In order to avoid the subjectivism of expert assessments, the authors suggest novel approach for forecasting method selection and a recommendation-based ensemble forecasting approach [27].

Determination of the weighting coefficients of factors influencing the development of technological innovations can be carried out based on exponential smoothing; autoregressive integrated moving average and neural network are chosen to form the combined approach [28].

2.3. Theoretical generalization

The considered approaches to development strategies allow us to approach the justification of strategic decisions on the market development of R&D products from the standpoint of priority of a specific factor. However, according to successful practices, the market perception of R&D products is interdisciplinary in nature. In addition, the scientific and practical developments discussed above are based on the consideration of mostly completed innovations as objects, that is, the results of the completed innovation process. However, the object of this research is the intermediate result of the innovation process, namely, R&D product at the early stages of technological readiness.

These objects have different parameters of technological readiness [29] and features of market application. Therefore, it is necessary to take a differentiated approach to the development of methods for technological forecasting of market development of R&D products, choosing a strategy for their commercialization, and so on.

The author's method must be defined:

— the ability to differentiate in the projected period of market development of R&D products their functional advantages and weaknesses, factors that will restrain or stimulate the development of the product;

— the ability to take into account the features and characteristics of R&D product of various types of economic activity and business areas;

— with the ability to objectively predict market drivers and anti-drivers of R&D product development;

— it is an opportunity to take into account the dynamic nature

of the market development of R&D product in relation to the satisfaction of consumer needs;

— flexibility in changing input data, managerial maneuverability, and so on.

3. Research design

3.1. Methodology approach

The aim of the work is to develop a method for technological forecasting of market behaviour of R&D products at the early stages of their technological readiness.

The basis for conducting such a study is a number of hypotheses.

Hypothesis 1. The method of technological forecasting of market behaviour of R&D products is universal and can be applied to products of any type of economic activity, business sector, etc.

Hypothesis 2. Fuzzy set theory algorithms allow us to take into account changes in the market behaviour of R&D products in the short, medium and long term.

Hypothesis 3. Justification of the R&D product market behaviour indicator based on the author's method should correlate with the early stages of technological readiness of the product.

To prove / refute hypotheses and develop this method, it is advisable to conduct a study of the problems of technological forecasting of R&D products development at the empirical, theoretical and applied levels.

3.2. Methodology

3.2.1. Fundamentals of technological forecasting of market behaviour R&D product

When evaluating an R&D product for the purpose of market launch and developing strategies for its commercialization, analysts mainly use methods and models of technological forecasting of product *market development*.

Most of the known methodological tools for technological forecasting of market development of R&D products are based on the justification of its strengths and weaknesses, risks and chances, etc. [30–32]. However, the category "market development" is a general concept that implies a process that results in a change in the quality of a product, its transition from one qualitative state to another (higher). In the situation with technological forecasting of R&D product development, the category "market behaviour" will give a more accurate description of the above change. Within the framework of neobehaviourism, behaviour is considered visible manifestations that can be observed, internal states associated with external manifestations. Moreover, market behaviour is a set of states (characteristics) of an R&D product that a product reveals under the influence of certain environmental factors (market). However, the market behaviour of R&D products is not often taken into account by analysts in the context of technological forecasting. Therefore, traditional approaches to technological forecasting for R&D products do not always allow us to justify effective strategies for their commercialization.

If an R&D product is in the early stages of technological readiness, it is not always correct to assess the chances and risks

of a product. Odds are the probability of such market behaviour of an R&D product that will contribute to its success in the market. Risks are a combination of the probability and consequences of adverse events based on the market behaviour of an R&D product. To determine the chances and risks, first of all, it is necessary to assess the future consumer value of an R&D product. However, when an R&D product is only in the process of development, significant errors may occur when determining the level of its consumer value. The assessment of chances and risks can be more reliable when evaluating R&D products at the stages of appropriability high technological readiness – then it is possible to predict the market behaviour of R&D product and its perception by the market environment with a significant degree of reliability. Therefore, in the case of evaluating an R&D product at the early stages of readiness, it is advisable to clarify the categories "*chances*" and "*risks*" in a meaningful way. It is proposed to replace them with "*development factors*" and "*limiting factors*". These factors determine the probability of events occurring in the R&D product market (events that will determine the chances or risks of R&D product spreading in the market).

When making technological forecasting of the market behaviour of R&D product, it is advisable to pay attention, on the one hand, to the stage of technological readiness of R&D product on the other – to the perception of R&D product by the market environment.

To determine the early stages of technological readiness of R&D products, we will use the NASA approach [33]:

— basic principles observed and reported;
— technology concept and / or application formulated;
— analytical and experimental critical function and / or characteristic proof-of-concept;
— component and / or breadboard validation in laboratory environment;
— component and / or breadboard validation in relevant environment.

In the early stages of R&D product readiness, it is advisable to conceptually determine the level of compatibility of the current market data set with the corresponding set of knowledge about the technological readiness of R&D product.

The set of data (characteristics) obtained based on studying the technological readiness and market perception of R&D product can be systematized into stimulants and destimulants of R&D product, highlighting from them – strengths and weaknesses, development factors or limitations of R&D product. To organize the characteristics of an R&D product, you can use the following list.

Strengths / weaknesses of R&D product
— stage of technological readiness;
— functional indicators of the main and additional purpose of R&D product;
— indicators of the value of technical / analytical / marketing support from the developer;
— the level of environmental safety of the product;
— the level of economic efficiency of investment in R&D product (commercialization);
— the level of costs for the use and disposal of R&D product;
— R&D product patent protection level;
— the level of uniqueness / standardization of the R&D product;

— the level of complexity of implementing an R&D product;
— the time level of expected use of the R&D product before replacement or improvement;
— the level of novelty / improvement of the main functional characteristics of the R&D product;
— scale of implementation and use of R&D products, etc.

Development factors / limitations for R&D product
— the nature and number of direct / indirect competitors of the R&D product;
— nature and number of substitutes R&D product;
— market capacity;
— stage of the R&D product lifecycle;
— dependence on R&D product participants / developers;
— the level of access to resources for using the R&D product;
— the level of availability of R&D product information, etc.

These characteristics can be adjusted according to the scope of R&D product, market specifics, comparison with market analogues, and so on.

In order to substantiate the method of technological forecasting of market behaviour of R&D product, we have proposed the following sequence of actions:
1) systematize the evaluation basis (reference matrix) of technological forecasting of market behaviour of R&D product;
2) develop a methodological approach to correcting indicators of market behaviour of R&D product;
3) substantiate the method of evaluating the results of technological forecasting of market behaviour of R&D product;
4) develop a system for selecting strategies for commercializing an R&D product based on technological forecasting of its market behaviour.

Systematization of existing methodological approaches to technological forecasting and the application of development factors and limitations of R&D product allowed us to develop a reference matrix for technological forecasting of market behaviour of R&D product – table 1.

Table 1: Reference matrix for technological forecasting of market behaviour of R&D product

Characteristics		Significance of the parties (Z)	Evaluation of parties (A)	Rank (F)
Strengths (S)	S_1	Z_{S_1}	A_{S_1}	$F_{S_1} = \dfrac{Z_{S_1} \times A_{S_1}}{\sum_{i=1}^{n} Z_S \times A_S}$
	S_2	Z_{S_2}	A_{S_2}	$F_{S_2} = \dfrac{Z_{S_2} \times A_{S_2}}{\sum_{i=1}^{n} Z_S \times A_S}$
	...	...	...	...
	S_n	Z_{S_n}	A_{S_n}	$F_{S_n} = \dfrac{Z_{S_n} \times A_{S_n}}{\sum_{i=1}^{n} Z_S \times A_S}$
	Σ	$\sum_{i=1}^{n} Z_S \times A_S$		1
Weaknesses (W)	W_1	Z_{W_1}	A_{W_1}	$F_{W_1} = \dfrac{Z_{W_1} \times A_{W_1}}{\sum_{i=1}^{n} Z_W \times A_W}$
	W_2	Z_{W_2}	A_{W_2}	$F_{W_2} = \dfrac{Z_{W_2} \times A_{W_2}}{\sum_{i=1}^{n} Z_W \times A_W}$
	...	...	...	...
	W_n	Z_{W_n}	A_{W_n}	$F_{W_n} = \dfrac{Z_{W_n} \times A_{W_n}}{\sum_{i=1}^{n} Z_W \times A_W}$
	Σ	$\sum_{i=1}^{n} Z_W \times A_W$		1
Development factors (D)	D_1	Z_{D_1}	A_{D_1}	$F_{D_1} = \dfrac{Z_{D_1} \times A_{D_1}}{\sum_{i=1}^{n} Z_D \times A_D}$
	D_2	Z_{D_2}	A_{D_2}	$F_{D_2} = \dfrac{Z_{D_2} \times A_{D_2}}{\sum_{i=1}^{n} Z_D \times A_D}$
	...	...	...	...
	D_n	Z_{D_n}	A_{D_n}	$F_{D_n} = \dfrac{Z_{D_n} \times A_{D_n}}{\sum_{i=1}^{n} Z_D \times A_D}$
	Σ	$\sum_{i=1}^{n} Z_D \times A_D$		1
Limiting factors (L)	F_{L_1}	Z_{L_1}	A_{L_1}	$F_{L_1} = \dfrac{Z_{L_1} \times A_{L_1}}{\sum_{i=1}^{n} Z_L \times A_L}$
	F_{L_2}	Z_{L_2}	A_{L_2}	$F_{L_2} = \dfrac{Z_{L_2} \times A_{L_2}}{\sum_{i=1}^{n} Z_L \times A_L}$
	...	...	...	...
	F_{L_n}	Z_{L_n}	A_{L_n}	$F_{L_n} = \dfrac{Z_{L_n} \times A_{L_n}}{\sum_{i=1}^{n} Z_L \times A_L}$
	Σ	$\sum_{i=1}^{n} Z_L \times A_L$		1

Table 2: Correlation matrix of strengths, weaknesses, development / limiting factors and indicators of R&D product market behaviour

Characteristics of R&D production			Development factors (D)				Limiting factors (L)				Market behaviour indicators (P)
			D_1	D_2	...	D_n	L_1	L_2	...	L_n	
		Ранг	F_{D_1}	F_{D_2}	...	F_{D_n}	F_{L_1}	F_{L_2}	...	F_{L_n}	
Strengths (S)	S_1	F_{S_1}	$K^{SD}_{1,1}$	$K^{SD}_{1,2}$	...	$K^{SD}_{1,m}$	$K^{SL}_{1,1}$	$K^{SL}_{1,2}$	...	$K^{SL}_{1,m}$	P^{SDL}_1
	S_2	F_{S_2}	$K^{SD}_{2,1}$	$K^{SD}_{2,2}$	...	$K^{SD}_{2,m}$	$K^{SL}_{2,1}$	$K^{SL}_{2,2}$	...	$K^{SL}_{2,m}$	P^{SDL}_2
	...	...	...	...	...	...	...	...	...	...	...
	S_n	F_{S_n}	$K^{SD}_{n,1}$	$K^{SD}_{n,2}$	...	$K^{SD}_{n,m}$	$K^{WL}_{n,1}$	$K^{WL}_{n,2}$	...	$K^{WL}_{n,m}$	P^{SDL}_n
Weaknesses (W)	W_1	F_{W_1}	$K^{WD}_{1,1}$	$K^{WD}_{1,2}$	...	$K^{WD}_{1,m}$	$K^{WL}_{1,1}$	$K^{WL}_{1,2}$	...	$K^{WL}_{1,m}$	P^{WDL}_1
	W_2	F_{W_2}	$K^{WD}_{2,1}$	$K^{WD}_{2,2}$	...	$K^{WD}_{2,m}$	$K^{WL}_{2,1}$	$K^{WL}_{2,2}$	...	$K^{WL}_{2,m}$	P^{WDL}_2
	...	...	...	...	...	...	...	...	...	...	...
	W_n	F_{W_n}	$K^{WD}_{n,1}$	$K^{WD}_{n,2}$	...	$K^{WD}_{n,m}$	$K^{WL}_{n,1}$	$K^{WL}_{n,2}$	...	$K^{WL}_{n,m}$	P^{WDL}_n

In order to assess the strengths and weaknesses, development factors and limitations of an R&D product, it is necessary to involve experts in the relevant subject area and skill level. Experts determine the significance of the parties to the R&D product (Z) and evaluate them (A) according to the expressions in table. 1.

Significance is a non – repeating indicator for each of the characteristics (according to the principle: highest value-highest significance). A rating can be assigned, for example, from the interval 1…10, where 1 is the weakest manifestation of the characteristic, and 10 is the strongest. After that, the rank of ratings is determining. It is the specific weight of the impact of each characteristic on their entire group.

When making calculations, the priority should be the value of the R&D product for the consumer, its market competitiveness, as well as the expected efficiency of commercialization.

After establishing the ranks, we determine the pairwise correlation coefficients (C) of factors influencing the R&D product and calculate the indicator of its market behaviour (P). The matrix of relationships between indicators is shown in table 2.

Therefore, K [x; y], where x and y are in the range 0…1, is the correlation coefficient of strengths and weaknesses, development factors, and limitations of the R&D product. The sum of "x + y" placed in the corresponding cells will reflect the strength of the influence of a particular pair of factors: *SD, SL, WD* and *WL,* respectively, on the indicator of market behaviour.

The market behaviour indicator shows the strength of the manifestation of R&D product characteristics, due to the corresponding development factors or restrictions on it. This indicator is relative and is measured in fractions of units. Calculating the market behaviours indicator helps determine the level of R&D ability of a product in relation to market development.

To determine the indicator of market behaviours of an R&D product, it is advisable to follow the following systematic procedure:
1) summarize the correlation coefficients (K) separately for the strengths, weaknesses, development factors, and limitations of the R&D product. Use expressions to determine the indicator of market behaviour of an R&D product to set its value. For this purpose, expressions (1) – (2):

$$P^{SDL}_{n,m} = \sum_{i=1}^{n} K^{SD}_{n,m} - \sum_{i=1}^{n} K^{SL}_{n,m} , \qquad (1)$$
$$P^{WDL}_{n,m} = \sum_{i=1}^{n} K^{WD}_{n,m} - \sum_{i=1}^{n} K^{WL}_{n,m} ; \qquad (2)$$

2) interpret the obtained values of market behaviour indicators. In particular, $P^{SDL}_{n,m}$ shows how much the strengths of an R&D product supported by development factors can withstand limiting factors, $P^{WDL}_{n,m}$ reflects how much the weaknesses of an R&D product supported by developmental factors can overcome limiting factors. The "−" and "+" signs of the indicators indicate the dominance of the influence of factors of restriction or development, respectively. In general, the level of the indicator indicates the strength of influence of the characteristics used in the assessment.

In practice, when evaluating an R&D product, such important indicators of technological forecasting as trends and features of market development that will affect the market behaviour of an R&D product often fall out of sight. In particular: technology diffusion, convergence of products and markets, synergy of R&D products, multiplier and spillover effect of R&D product, etc. Such indicators are practically not taken into account by modern appraisers, which is due to the complexity of their determination. It is even more difficult to identify interdisciplinary factors influencing R&D products and their relationships. However, you cannot ignore them either. Market effects can determine the market behaviour of an R&D product and the choice of its commercialization strategy.

To take into account these aspects, it is advisable to introduce a correction factor for indicators of market behaviour of R&D product. In our opinion, the correction factor should consist of two interrelated components: I (the impact of R&D product on the market) and II (the impact of market effects on R&D product). In order to justify such a correction factor, it is advisable to apply an economic and mathematical apparatus that would be based on not only quantitative estimates, but also take into account qualitative assessments of the market behaviour of R&D product. To do this, you can apply the algorithms of fuzzy set theory.

The criterion for the effectiveness of correcting indicators of market behaviour of an R&D product based on fuzzy set theory algorithms can be expressed by maximizing the degree of suitability of the result in each specific case of technological forecasting.

The correction factor (M) of R&D product market behaviour indicators can be described by the function (3):

M = f (I – Impact of R&D product on the market;
II – impact of market effects on R&D product), (3)

which is a next-level system of functions (see table 3).

Table 3: Signs of adjustment of indicators of market behaviour of R&D products and their linguistic terms

Signs of adjustment of R&D products market behaviour indicators	Characteristics of signs of adjustment of indicators of market behaviour of R&D product	Meaning of linguistic terms of signs of adjustment of market behaviour indicators R&D product
I – Market impact of R&D product	a) *market effects:* market convergence, spillover effect, Diffusion, synergy, crowd effect, etc.	*Low* [− 100; − 80; − 60], *L; Admissible* [− 59; − 29.5; 0], *A; Middle* [0; 29.5; 59], *M; High* [60; 80; 100], *H*
	b) *types of market changes:* the level of market renewal; the number and types of market participants affected by R&D product; the level and depth of market changes that accompany the introduction of R&D product; barriers to market entry, etc.	*Low* [− 100; − 80; − 60], *L; Admissible* [− 59; − 29.5; 0], *A; Middle* [0; 29.5; 59], *M; High* [60; 80; 100], *H*
II – Impact of market effects on R&D product	a) *effects generated by R&D products:* convergence of R&D products; multiplier effect, etc.	*Low* [− 100; − 80; − 60], *L; Admissible* [− 59; − 29.5; 0], *A; Middle* [0; 29.5; 59], *M; High* [60; 80; 100], *H*
	b) *organizational and technological changes of R&D products:* flexibility (adaptation) of individual parameters of R&D product; the level of novelty of R&D product; the number and access to marginal resources that need to be attracted for the market development of R&D product and the level of costs for them; environmental friendliness of R&D product; scale of R&D product monetization; level of intellectual property protection, etc.	*Low* [− 100; − 80; − 60], *L; Admissible* [− 59; − 29.5; 0], *A; Middle* [0; 29.5; 59], *M; High* [60; 80; 100], *H*

To output the desired correction factor, use the Fuzzy Logic Toolbox (MATLAB). Within the framework of fuzzy set theory algorithms (based on the Mamdani model), the characteristics of signs of correction of market behaviour of R&D product are systematized by types (a, b, c, d), which are assigned the value of linguistic terms – table 3.

The correction factor of market behaviour is within the same limits as the characteristics of its features.

We have formed a knowledge base – a set of ratios of linguistic terms of adjustment features, taking into account their impact on the indicator of market behaviour of R&D product. In figure 1 shows a fragment of this knowledge base using the fuzzy logic toolbox (MATLAB).

1. If (a is Low) or (b is Admissible) or (c is Admissible) or (d is Low) then (Correction_factor is Admissible) (1)
2. If (a is Low) and (b is not Middle) and (c is Middle) and (d is Admissible) then (Correction_factor is Admissible) (1)
3. If (a is Low) and (b is Low) and (c is Low) and (d is Low) then (Correction_factor is Low) (1)
4. If (a is Low) or (c is High) or (d is Low) then (Correction_factor is Middle) (1)
5. If (a is Low) and (b is Low) and (c is Low) and (d is Low) then (Correction_factor is Low) (1)
6. If (a is Admissible) or (b is Admissible) or (c is Admissible) or (d is Admissible) then (Correction_factor is Admissible) (1)
7. If (a is Admissible) or (b is Admissible) or (c is Middle) or (d is Middle) then (Correction_factor is Middle) (0.7)
8. If (a is Admissible) and (b is Middle) and (c is Admissible) and (d is High) then (Correction_factor is Middle) (0.3)
9. If (a is Admissible) and (b is Low) and (c is High) and (d is Admissible) then (Correction_factor is Middle) (0.3)
10. If (a is Admissible) and (b is High) and (c is High) and (d is Middle) then (Correction_factor is Admissible) (0.7)
11. If (a is Middle) or (b is Admissible) or (d is Low) then (Correction_factor is Admissible) (0.7)
12. If (a is Middle) and (b is Admissible) and (c is Middle) and (d is High) then (Correction_factor is Middle) (0.7)
13. If (a is High) or (b is not High) or (c is High) or (d is High) then (Correction_factor is High) (0.5)
14. If (a is Low) and (c is Middle) and (d is Admissible) then (Correction_factor is Middle) (0.8)
15. If (a is High) and (b is Middle) and (c is High) and (d is High) then (Correction_factor is Middle) (0.8)
16. If (a is High) and (b is Low) and (c is Admissible) and (d is High) then (Correction_factor is Middle) (0.5)
17. If (a is High) and (b is not High) and (c is Admissible) and (d is Admissible) then (Correction_factor is Middle) (1)
18. If (a is Low) and (b is not Middle) or (c is Admissible) then (Correction_factor is Admissible) (1)
19. If (a is Low) or (b is Low) or (c is Low) or (d is Low) then (Correction_factor is Low) (1)

Figure 1: Knowledge base of relations of linguistic terms of adjustment features, considering their impact on the indicator of market behaviour of R&D product (fragment)

Visualization of the ratio of signs of adjustment of indicators of market behaviour of R&D product is shown in figure 2 – 3.

Implementing the described sequence, we obtain a relative correction factor, by the value of which we specify the indicators of market behaviour R&D product $P_{n,m}^{SDL}$ and $P_{n,m}^{WDL}$.
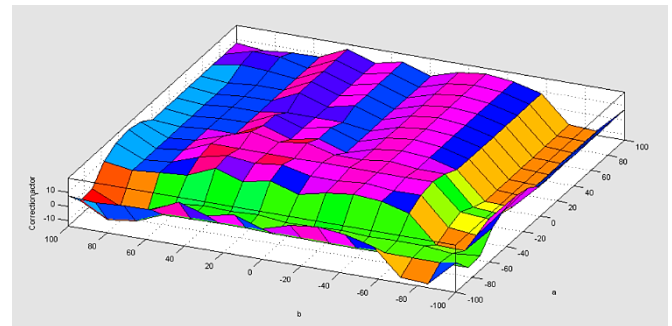
Figure 2: Visualization of the ratio of *a* and *b* signs of adjustment of R&D product market behaviour indicators
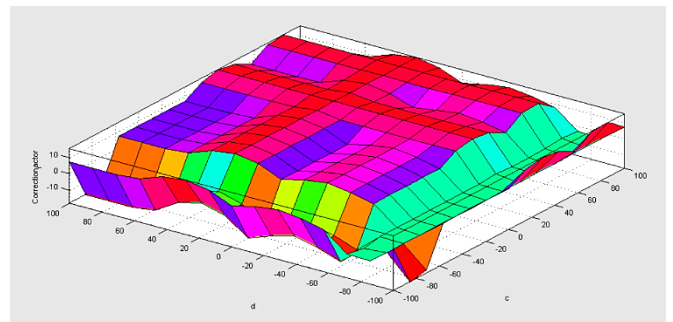
Figure 3: Visualization of the ratio of *c* and *d* signs of adjustment of indicators of market behaviour of R&D product

3.2.2. Evaluating results

There are many approaches to choosing an R&D product commercialization strategy, but none of the current ones takes into account technological forecasting of R&D product market behaviour. Taking into account the best practices of scientists [34 – 39], we have formed a system for choosing the strategy of

commercialization of R&D product, based on three methods of commercialization:

1) zero-level commercialization of R&D product;
2) commercialization of the first level of R&D product;
3) commercialization of the second level of R&D product.

If an R&D product is at the first or second stages of technological readiness (*basic principles observed and reported; technology concept and / or application formulated*), it is obvious that a zero-level commercialization strategy will be suitable for it. This strategy is the most efficient way to make a profit, since its object is the idea of an R&D product.

The object of the first – level commercialization strategy is an R&D product that is at the third or fourth stages of technological readiness: *analytical and experimental critical function and / or characteristic proof-of-concept; component and / or breadboard validation in the laboratory environment.*

The second – level commercialization strategy is possible for an R&D product at the fifth stage of technological readiness-*component and / or breadboard validation in a relevant environment.*

Calculated and adjusted values of market behaviour indicators (clause 3.2.1) should be noted in the system developed for this purpose (figure 4).
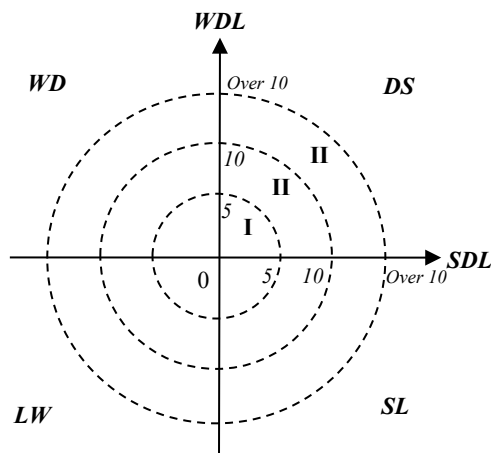
Figure 4: A system for selecting an R&D product commercialization strategy based on technological forecasting of market behaviour indicators*

* Symbols: I-zero-level commercialization strategy, II-first-level commercialization strategy; III-second-level commercialization strategy

The system is based on a Cartesian coordinate system (on the abscissa – *SDL* axis, on the ordinate – *WDL* axis), described by three circles – the boundaries of the choice of a particular strategy for commercialization of an R&D product, according to technological forecasting of its market behaviour.

The explanation of the choice of this form of representation of the system is justified by us in [38]. All circles have a centre at the zero point. The radius of the smallest circle is 5 units, average – 10 units. For the largest circle of Radius, it is established that its radius must be more than 10 units.

According to Figure 4, the division of scenarios within certain commercialization strategies is as follows: *DS* sector – measures that are necessary to use the strengths of R&D product for its development; *WD* sector – measures that need to be carried out, overcoming the shortcomings of R&D product and using development factors in relation to it; *LW* sector – measures that minimize the shortcomings and take into account the limiting factors of R&D product; *SL* sector – measures that use the strengths of R&D product and take into account the limiting factors in relation to it.

3.3. Data analysis

The author's method has been tested on a number of developments of Ukrainian business entities. Here is an example of technological forecasting of market behaviour of R&D product – OSL dosimetry of ionizing radiation (IR) based on Yap:Mn crystals. The main purpose of R&D product is individual passive (cumulative) IR dosimetry of people working with IR sources or may be exposed to radiation from such sources. The technology was developed by scientists of the Department of semiconductor electronics of the Lviv Polytechnic National University (Ukraine) [40, 41]. The R&D product includes a dosimeter with several detectors in a cassette; detectors (based on single crystals of yttrium-aluminum oxide activated with manganese); a device for determining the radiation dose absorbed by the cassette with detectors (reader); a method for performing measurements that provides determination of dosimetric values with a given degree of accuracy and reliability.

Research of the global market of OSL dosimetry of IR in the field of security and defense and the study of this R&D product allowed us to form strengths and weaknesses, development factors and limitations in relation to it (table 4).

Table 4: Evaluation of the characteristics of OSL dosimetry of IR technology for technological forecasting of their market behaviour

	Characteristics	Z	A	$Z_n \times A_n$	F
S	Increased level of product functionality for rescuers	8	10	80	0.229
	Tissue equivalence of the dosimetric detector material and localization of dose measurements	6	9	54	0.154
	Ability to record the dose of different types of IR in a wide range of values	7	9	63	0.180
	Ability to identify the IR source type	3	8	24	0.068
	Dosimetric material with extremely high sensitivity	4	7	28	0.080
	The material of the dosimetric detector allows you to measure the absorbed dose of IR in a wide range (from units of micrograms to several tens of kg), is a more stable and stable material, compared to analogues	5	7	35	0.100
	Ability to perform a rapid assessment of radiation energy and determine the type of unknown source	2	6	12	0.034
	The ability to quickly determine the radiation dose (important for portable readers, allows you to save the dosimeter with the accumulated dose after its partial reading, makes it possible to re-read multiple times)	9	5	45	0.128

	Synthesizer of OSL dosimetry of IR technology. Package patenting	1	8	8	0.022
	Σ			**349**	**1**
	Inflation, currency instability in the global IR dosimetry market	1	9	9	0.073
	Capital and knowledge intensity of product production	3	6	18	0.146
W	Difficulty in finding a qualified workforce to start product production	5	10	50	0.406
	Significant need for investment to start production	4	8	32	0.260
	Undeveloped sales channels in the country of origin (Ukraine) [42]	2	7	14	0.113
	Σ			**123**	**1**
	The North American region is promising from the point of view of the market launch (it is characterized by the largest global market share of manufacturers of IR dosimetry equipment and technology of 93.32 %, but the region's market is not saturated with these products) [38]	9	9	81	0.231
	Significant opportunities for product differentiation by Application Area	6	10	60	0.171
	In the country of producer (Ukraine), competitive products are presented in fragments; they are significantly more expensive than the analyzed product. The market of individual IR dosimetry in Ukraine is unsaturated today: up to 23,000 units. / year, or about $1.1 million (15.33 %) [43]	1	5	5	0.014
	Zoom effect	3	4	12	0.034
	The global dosimeters market will grow at a CAGR of 6.8% with a base value of $2.92 billion in 2020 to $4.36 billion in 2026 during the forecast period of 2020 – 2026 [44]	4	7	28	0.080
D	There is a tendency to increase demand for IR dosimetry products and technology in the medical field (the radiotherapy market is projected to grow from an estimated $5.6 billion in 2018 to $6.8 billion by 2023, at a CAGR of 4.1% during the forecast period) [45]	8	8	64	0.182
	The market of manufacturers and consumers of IP dosimetry equipment is characterized by an increase in demand for OSL dosimetry of IR and a tendency to replace TLD dosimetry with OSL dosimetry, due to the expanded list of opportunities that OSL dosimetry provides	5	5	25	0.071
	The OSL dosimetry of IR market is 25% of the world market	2	6	12	0.034
	The OSL dosimetry of IR market is characterized by the expansion of the personal dosimetry segment, due to the improvement of the "performance / cost" ratio and wider application opportunities	7	9	63	0.180
	Σ			**350**	**1**
	Low demand elasticity	1	4	4	0.024
	Insufficient communication between consumers and the manufacturer	3	5	15	0.093
	High level of specialization of competitive analogues presented in the markets	2	7	14	0.086
	Dependence on strategic relationships	4	7	28	0.173
L	Product complexity, production	5	8	40	0.248
	The OSL dosimetry of IR market is monopolistic (the main market operator is LANDAUER, Inc. (USA)), which is due to the scale of production of this enterprise and legal barriers to other market participants (patent protection of technology, etc.)	6	10	60	0.372
	Σ			**161**	**1**

Table 5: Indicators of market behaviour of OSL dosimetry of IR technology

		D										L							P Σ₁-Σ₂
		0.231	0.171	0.014	0.034	0.080	0.182	0.071	0.034	0.180	Σ₁	0.024	0.093	0.086	0.173	0.248	0.372	Σ₂	
	0.229	0.46	0.4	0.243	0.263	0.309	0.411	0.3	0.263	0.409	**3.058**	0.253	0.322	0.315	0.402	0.477	0.601	**2.37**	0.688
	0.154	0.385	0.325	0.168	0.188	0.234	0.336	0.225	0.188	0.334	**2.383**	0.178	0.247	0.24	0.327	0.402	0.526	**1.920**	0.463
	0.180	0.411	0.351	0.194	0.214	0.260	0.362	0.251	0.214	0.36	**2.617**	0.204	0.273	0.266	0.353	0.428	0.552	**2.076**	0.541
	0.068	0.299	0.239	0.082	0.102	0.118	0.250	0.139	0.102	0.248	**1.579**	0.092	0.161	0.154	0.241	0.316	0.440	**1.404**	0.175
S	0.080	0.311	0.251	0.094	0.114	0.130	0.262	0.151	0.114	0.260	**1.687**	0.104	0.173	0.166	0.253	0.328	0.452	**1.470**	0.211
	0.100	0.331	0.271	0.114	0.134	0.150	0.282	0.171	0.134	0.280	**1.867**	0.124	0.193	0.186	0.273	0.348	0.472	**1.596**	0.271
	0.034	0.265	0.205	0.048	0.068	0.084	0.216	0.105	0.068	0.214	**1.273**	0.058	0.127	0.120	0.207	0.282	0.406	**1.200**	0.073
	0.128	0.359	0.299	0.142	0.162	0.178	0.31	0.199	0.162	0.308	**2.119**	0.158	0.221	0.214	0.301	0.376	0.500	**1.320**	0.799
	0.022	0.253	0.193	0.036	0.056	0.072	0.204	0.093	0.056	0.202	**1.165**	0.046	0.115	0.108	0.195	0.270	0.394	**1.128**	0.037
	Σ																		**3.258**
	0.073	0.304	0.244	0.087	0.107	0.153	0.255	0.144	0.107	0.253	**1.654**	0.097	0.166	0.159	0.246	0.321	0.445	**1.434**	0.220
	0.146	0.377	0.317	0.160	0.179	0.226	0.326	0.217	0.180	0.326	**2.308**	0.170	0.239	0.232	0.319	0.394	0.518	**1.872**	0.436
W	0.406	0.637	0.577	0.520	0.440	0.486	0.588	0.477	0.440	0.586	**4.751**	0.430	0.499	0.492	0.479	0.654	0.778	**3.332**	1.419
	0.260	0.491	0.431	0.274	0.294	0.340	0.442	0.331	0.294	0.440	**3.337**	0.284	0.353	0.346	0.433	0.508	0.632	**2.556**	0.781
	0.113	0.144	0.284	0.127	0.147	0.193	0.295	0.184	0.147	0.293	**1.814**	0.137	0.206	0.199	0.286	0.361	0.485	**1.674**	0.166
	Σ																		**3.022**

The results obtained are used to determine pairwise correlation coefficients of factors influencing the R&D product, based on which indicators of its market behaviour (table 5) are calculated.

Using the author's method for determining the corrective coefficient of market behaviour of an R&D product, with the involvement of a group of expert appraisers from the subject area and based on the fuzzy logic toolbox (MATLAB), the desired coefficient is determined for the OSL dosimetry of IR technology (figure 5).
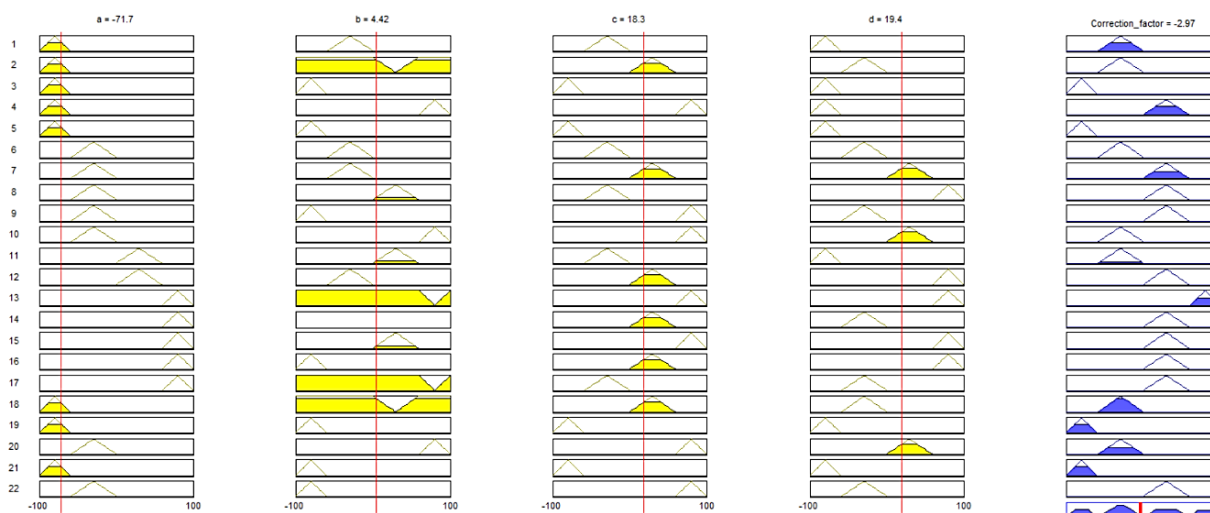
Figure 5: Results of determining the correction factor of indicators of market behaviour of OSL dosimetry of IR technology

The correction factor M for OSL dosimetry of IR technology will be − 2.97 %. The coordinates of the market behaviour indicator of this product, taking into account the correction factor, will be:

WDL: 3.258 * (− 2.97 %) = − 3.161;

SDL: 3.022 * (− 2.97 %) = − 2.93.

So, an indicator of the market behaviour of OSL dosimetry of IR technology in the R&D product commercialization strategy selection system (see figure 4) will have the coordinates – K [− 3.161; − 2.93], that is, it falls into the second matrix circle. In this case, a zero-level commercialization strategy is proposed for the product.

Since the product is located in the *LW* sector, as part of the chosen commercialization strategy for it, it is advisable to consider in detail for which positions of the correction factor the

market development of the product may slow down. Based on this, appropriate corrective measures can be developed.

The result obtained correlates with the stage of technological readiness of OSL dosimetry of IR technology – *technology concept and / or application formulated* (second stage).

Testing of a reasonable method of technological forecasting of market behaviour of R&D product and the choice of commercialization strategy based on this, carried out on the example of a number of R&D products presented by the development teams of the Lviv Polytechnic National University (Lviv, Ukraine), showed the following results (table. 6).

So, in the case of technological forecasting of market behaviour for the 1st and 4th R&D products, a zero-level commercialization strategy is defined, for the 2nd, 6th and 7th – a first-level commercialization strategy, for the 3rd, 5th – a second-level commercialization strategy.

Table 6: Results of technological forecasting of market behaviour of OSL dosimetry of IR technology using the author's method

№	R&D products	Technological readiness stage of R&D product [1…5]*	Value of the correction factor, %	Coordinates (K) in the strategy system	Type of commercialization strategy
1	Technology of optically-stimulated luminescent dosimetry	2	− 2.97	[− 3.161; − 2.93]	Zero-level commercialization strategy
2	Continuation of the life of machine parts by the method of surfacing under a layer of flux	3	4,48	[5.45; 6.89]	First-level commercialization strategy
3	Autonomous smoke and leak detection system carbon monoscope	5	7.14	[10.38; 14.91]	Second-level commercialization strategy
4	Forecasting and providing a given value of the initial resistance of dissimilar and homogeneous materials of small thicknesses and cross sections during point capacitor contact micro welding	2	− 1.6	[− 2.85; − 4.03]	Zero-level commercialization strategy
5	Contact point capacitor micro welding equipment	5	6.31	[10.03; 11.82]	Second-level commercialization strategy
6	Technology of surface friction strengthening of working surfaces of machine parts	4	3.56	[7.21; 8.025]	First-level commercialization strategy
7	Technology of surface friction displacement of working surfaces of machine parts	4	− 1.56	[− 5.01; − 5.87]	First-level commercialization strategy

* Stages are defined according to the NASA approach [33].

Based on the R&D products that were taken to test the method, it can be applied to products of any type of economic activity, transfer method, etc. However, the use of the author's method is characterized by reservations:

1) in a situation where the chosen strategy has a marginal value (it is on the edge of the circles that determine the choice of strategies for commercialization of R&D product), decisions should be made based on the current market situation, the overall strategy of the business entity and the objective vision of the analyst;

2) to obtain reliable results when applying the correction factor of market behaviour based on the fuzzy logic toolbox (MATLAB), it is advisable to review and, if necessary, correct the set of data involved in the assessment in each evaluation situation.

4. Conclusions

The method of technological forecasting of market behaviour of R&D products at the early stages of their technological readiness is substantiated. The method is based on taking into account the strengths and weaknesses, development factors and limiting factors of the product R&D, which allows you to predict indicators of market behaviour of the product relative to the market where its commercialization is planned.

The market is characterized by an array of different types of factors that in one way or another influence the market behaviour of R&D products. Therefore, within the framework of the method of technological forecasting of market behaviour of R&D products and in order to increase the level of reliability of calculations and validity of results, a method for determining the correction factor of indicators of market behaviour of R&D product has been developed. The method is developed on the basis of fuzzy set theory algorithms using the fuzzy logic toolbox (MATLAB). This made it possible to integrate a set of data on the market behaviour of an R&D product, taking into account their relationships and interdependencies, into one correction factor. This coefficient contains the characteristics of signs of the impact of R&D product on the market (in particular, market effects, types of market changes) and the impact of market effects on R&D product (effects generated by R&D products, organizational and technological changes in R&D products). To justify the correction factor, a knowledge base was formed based on the answers of experts who have knowledge of trends, patterns and features of market development in the subject area.

To select the R&D product commercialization strategy, a system with normative indicators that interpret the types of strategies has been developed. In particular, this allowed us to offer the following types of strategies: commercialization of the zero level of R&D product; commercialization of the first level of R&D product; commercialization of the second level of R&D product.

Due to the clarification of content categories (development factors and limitations) and the introduction of a correction factor for market behaviour indicators, the results of choosing an R&D product commercialization strategy are more accurate and reliable.

The **hypothesis 1** put forward in this paper is justified. The method of justifying the indicator of market behaviour of R&D products for the purpose of technological forecasting is universal, can be applied to products of any type of economic activity,

transfer method, etc.

The method of justifying the indicator of market behaviour of R&D products for the purpose of technological forecasting can only give errors if S, W, D, and L are poorly defined, compared, and weighed. Therefore, experts are recommended to pay thorough attention to studying the features of the product and market in each evaluation situation.

Hypothesis 2 is not fully justified. The proposed correction factor for indicators of market behaviour of R&D products based on fuzzy set theory algorithms makes it possible to take into account changes in the market behaviour of products only in the short term. The characteristics of the features that this coefficient is based on can only be relevant at the time of technological forecasting. To apply such methods in the medium and long term, it is necessary to take into account the volatility and singularity of the market.

Hypothesis 3 is true. Justification of the indicator of market behaviour of R&D product based on the principles of the author's method correlates with the early stages of technological readiness of the product, since: 1) the economic content of the stages of technological readiness of R&D products was laid in the author's method of technological forecasting of market behaviour of R&D products; 2) the characteristics of the signs of the correction factor of market behaviour indicators are based on phenomena, market effects, etc., which are characteristic of R&D product at a specific stage of technological readiness.

The economic interpretation of the obtained indicators of market behaviour of R&D products and the commercialization strategies selected based on this showed the validity of the author's method and its relevance in the changing conditions of the modern market. The study of the characteristics of the features of the correction factor of market behaviour indicators is the subject of the following scientific work.

Conflict of Interest

The authors declare no conflict of interest.

Acknowledgment

References

[1] N. Chukhray, N. Shakhovska, O. Mrykhina, M. Bublyk, L. Lisovska, "Consumer Aspects In Assessing The Suitability of Technologies for the Transfer", in 2019 IEEE 14th International Scientific and Technical Conference on Computer Sciences and Information Technologies, 142–147, 2019, https://doi:10.1109/STC-CSIT.2019.8929879

[2] N. McCarthy, "The Top Reasons Startups Fail", 2017

[3] D. Nag, A. Gupta, A. Turo, "The Evolution of University Technology Transfer: By the Numbers", 2020

[4] T. Tetreault, "10 Surprising Startup Statistics", 2019

[5] NanoCom Consortium, Best Practices to Lower the Barriers for Commercialisation of Nanotechnology Research. NanoCom Lowering Barriers for Nanotechnology Commercialisation. Barriers and Success Factors; Commercialisation Readiness Scale

[6] ", Business Horizons, 61(3), 453–460, 2018, https://doi.org/10.1016/j.bushor.2018.01.011

[7] S. S. Dadwal, A. Jamal, T. Harris, G. Brown, S. Raudhah, "Technology and Sharing Economy-Based Business Models for Marketing to Connected Consumers", in Handbook of Research on Innovations in Technology and Marketing for the Connected Consumer, IGI Global, 62–93, 2020.

[8] S. Sarasini, M. Linder, "Integrating A Business Model Perspective into Transition Theory: The Example of New Mobility Services", Environmental Innovation and Societal Transitions, **27**, 16–31, 2018, https://doi.org/10.1016/j.eist.2017.09.004

[9] K. E. Bosbach, J. F. Tesch, U. C. M. Kirschner, "A Business Model Perspective on Innovation Susceptibility", in: Tesch J. (eds) Business Model Innovation in the Era of the Internet of Things. Progress in IS. Springer, Cham, 2019, https://doi.org/10.1007/978-3-319-98723-1_6

[10] R. Santa, M. Ferrer, L. M. Jørsfeldt, A. Scavarda, "The Impact of the Quality of the Service From IS/IT Departments on the Improvement of Operational Performance: the Point of View of Users of Technological Innovations", International Journal of Business Information Systems, **28**(2), 125–146, 2018, https://doi.org/10.1504/IJBIS.2018.10012923

[11] S. T. McKnight, B. Maniam, J. Robertson, "Effects of Technology Innovations on Business", Journal of Business and Behavioral Sciences, **31**(1), 84–101, 2019.

[12] G. Azar, F. Ciabuschi, "Organizational Innovation, Technological Innovation, and Export Performance: the Effects of Innovation Radicalness and Extensiveness", International Business Review, **26**(2), 324–336, 2017, https://doi.org/10.1016/j.ibusrev.2016.09.002

[13] T. Rantala, J. Ukko, M. Saunila, J. Havukainen, "The Effect of Sustainability in the Adoption of Technological, Service, and Business Model Innovations", Journal of Cleaner Production, **172**, 46–55, 2018, https://doi.org/10.1016/j.jclepro.2017.10.009

[14] E. Martínez-Ros, "Revisiting Product and Process Innovations", International Journal of Business Environment, **10**(3), 270–280, 2019, https://doi.org/10.1504/IJBE.2019.097983

[15] T. B. Long, V. Blok, K. Poldner, "Business Models for Maximising the Diffusion of Technological Innovations for Climate-smart Agriculture", International Food and Agribusiness Management Review, **20**(1030-2017-2134), 5–23, 2016, https://doi.org/10.22434/IFAMR2016.0081

[16] J. T. Eckhardt, M. P. Ciuchta, M. Carpenter, "Open Innovation, Information, and Entrepreneurship Within Platform Ecosystems", Strategic Entrepreneurship Journal, **12**(3), 369–391, 2018, https://doi.org/10.1002/sej.1298

[17] F. Damanpour, F. Sanchez-Henriquez, H. H. Chiu, "Internal and External Sources and the Adoption of Innovations in Organizations", British Journal of Management, **29**(4), 712–730, 2018, https://doi.org/10.1111/1467-8551.12296

[18] D. S. de Oliveira, M. Caetano, "Market Strategy Development and Innovation to Strengthen Consumer-based Equity: The case of Brazilian airlines", Journal of Air Transport Management, **75**, 103–110, 2019. https://doi.org/10.1016/j.jairtraman.2018.12.006

[19] M. Grębosz-Krawczyk, J. Pointet, "Co-branding Strategy as a Source of Innovation on International Market", Journal of Intercultural Management, **9**(3), 63–77, 2017, https://doi.org/10.1515/joim-2017-0014

[20] W. Liu, K. Atuahene-Gima, "Enhancing Product Innovation Performance in a Dysfunctional Competitive Environment: the Roles of Competitive Strategies and Market-based Assets", Industrial Marketing Management, **73**, 7–20, 2018, https://doi.org/10.1016/j.indmarman.2018.01.006

[21] M. Holgersson, O. Granstrand, M. Bogers, "The Evolution of Intellectual Property Strategy in Innovation Ecosystems: Uncovering Complementary and Substitute Appropriability Regimes", Long Range Planning, **51**(2), 303–319, 2018, https://doi.org/10.1016/j.lrp.2017.08.007

[22] M. Coccia, "The Theory of Technological Parasitism for the Measurement of the Evolution of Technology and Technological Forecasting", Technological Forecasting and Social Change, **141**, 289–304, 2019, https://doi.org/10.1016/j.techfore.2018.12.012

[23] S. Singh, S. Dhir, V. M. Das, A. Sharma, "Bibliometric Overview of the Technological Forecasting and Social Change journal: Analysis from 1970 to 2018", Technological Forecasting and Social Change, **154**, 119963, 2020, https://doi.org/10.1016/j.techfore.2020.119963

[24] R. Amit, C. Zott, Business Model Innovation Strategy: Transformational Concepts and Tools for Entrepreneurial Leaders, John Wiley & Sons, 2020.

[25] A. Hevner, S. Gregor, "Envisioning Entrepreneurship and Digital Innovation Through a Design Science Research Lens: A Matrix Approach", Information & Management, 103350, 2020, https://doi.org/10.1016/j.im.2020.103350

[26] J. H. Dahooie, E. K. Zavadskas, H. R. Firoozfar, A. S. Vanaki, N. Mohammadi, W. K. M. Brauers, "An Improved Fuzzy MULTIMOORA Approach for Multi-criteria Decision Making Based on Objective Weighting Method (CCSD) and its Application to Technological Forecasting Method Selection", Engineering Applications of Artificial Intelligence, **79**, 114–128, 2019, https://doi.org/10.1016/j.engappai.2018.12.008

[27] M. Züfle, A. Bauer, V. Lesch, C. Krupitzer, N. Herbst, S. Kounev, V. Curtef, "Autonomic Forecasting Method Selection: Examination and Ways Ahead", in 2019 IEEE International Conference on Autonomic Computing (ICAC), 167–176, 2019, https://doi.org/10.1109/ICAC.2019.00028

[28] L. Zhou, "Prediction of a Service Demand Using Combined Forecasting Approach", Journal of Physics: Conference Series, **887**(1), 012075, 2017, https://doi.org/10.1088/1742-6596/887/1/012075

[29] O. Mrykhina, L. Lisovska, I. Novakivskyj, A. Terebukh, V. Zhukovska, "Method of Modelling Prices for R&D Products in the Case of their Transfer from Engineering Universities to the Business", Advances in Science, Technology and Engineering Systems, **5**(5), 80–93, 2020, https://doi.org/10.25046/aj050512

[30] R. M. Elavarasan, S. Afridhis, R. R. Vijayaraghavan, U. Subramaniam, M. Nurunnabi, "SWOT Analysis: a Framework for Comprehensive Evaluation of Drivers and Barriers for Renewable Energy Development in Significant Countries", Energy Reports, **6**, 1838–1864, 2020. https://doi.org/10.1016/j.egyr.2020.07.007.

[31] N. I. Chukhrai, L. S. Lisovska, "Formation of Innovation's Consumer Utility", Actual Problems of Economics, **149**(11), 27–34, 2013.

[32] R. Puyt, F. B. Lie, F. J. De Graaf, C. P. M. Wilderom, Origins of SWOT Analysis. Academy of Management Proceedings (Ed: Atinc G.), 2020 [online] Available at: https://doi.org/10.5465/AMBPP.2020.132

[33] NASA, "Technology Readiness Levels (TRLs)", 2020

[34] H. Pylypenko, V. Prokhorova, O. Mrykhina, O. Koleshchuk, S. Mushnykova, "Cost Evaluation Models of R&D Products of Industrial Enterprises", Naukovyi Visnyk Natsionalnoho Hirnychoho Universytetu, **5**, 163–170, 2020, https://doi.org/10.33271/nvngu/2020-5/163

[35] V. Dimitrova, "Commercialization of the Academic Scientific Product in Bulgaria, Economic Science, Education and the Real Economy: Development and Interactions in the Digital Age", Publishing House Science and Economics Varna, **1**, 343–356, 2020

[36] S. K. Daneshjoovash, P. Jafari, A. Khamseh, "Effective Commercialization of High-technology Entrepreneurial Ideas: a Meta-synthetic Exploration of the Literature", Journal of Small Business & Entrepreneurship. 2020

[37] W. Sutopo, R. W. Astuti, R. T. Suryandari, "Accelerating a Technology Commercialization; with a Discussion on the Relation Between Technology Transfer Efficiency and Open Innovation", Journal of Open Innovation: Technology, Market, and Complexity, **5**, 95, 2019, https://doi.org/10.3390/joitmc5040095

[38] O. Mrykhina, Technology Transfer from Universities to the Business Environment: Paradigm, Concept and Tools of Evaluation, Lviv Polytechnic Publishing House, 440, 2018.

[39] L. Halkiv, O. Karyy, I. Kulyniak, S. Ohinok, "Modeling and Forecasting Of Innovative, Scientific and Technical Activity Indicators under Unstable Economic Situation in the Country: Case Of Ukraine", Communications in Computer and Information Science, **1158**, 79-97, 2020. https://doi:10.1007/978-3-030-61656-4_5

[40] S. Ubizskii, D. Afanassyev, Y. Zhydachevskii, A. Luchechko, V. Rabyk, "Technique and Apparatus for Pulsed OSL Readout of YAP:Mn Dosimetric Detectors with Enhanced Dynamic Range," in 2019 International Conference on Information and Telecommunication Technologies and Radio Electronics (UkrMiCo), Odessa, Ukraine, 1–6, 2019, https://doi.org/10.1109/UkrMiCo47782.2019.9165365

[41] D. Afanassyev, S. Ubizskii, Ya. Zhydachevskyy, A. Luchechko, A. I. Popov, A. Suchocki, "Time-resolved Pulsed OSL of Ceramic YAP:Mn phosphors", Integrated Ferroelectrics, 196:1, 24–31, 2019, https://doi.org/10.1080/10584587.2019.1591980

[42] L. Halkiv, O. Karyy, I. Kulyniak, S. Ohinok, "Innovative, Scientific and Technical Activities in Ukraine: Modern Trends and Forecasts" in 2020 IEEE 3rd International Conference on Data Stream Mining and Processing, 9204148, 321-324, DSMP 2020. https://doi:10.1109/DSMP47368.2020.9204148

[43] Ministry of Defense of Ukraine, 2020

[44] Global Dosimeter Market Forecast to 2026 by Technology, End User, Device and Geography. Dublin, Aug. 25, 2020 (GLOBE NEWSWIRE) 2020

[45] Radiotherapy Market by Type (External (IGRT, IMRT, 3D-CRT, Stereotactic), Brachytherapy (LDR, HDR)), Product (LINAC, CyberKnife, Gamma Knife, Tomotherapy, Particle Therapy, Cyclotron), Application (Prostate, Breast), End User (Hospital) – Forecasts to 2023, 2020

Active Disturbance Rejection Control Design for a Haptic Machine Interface Platform

Syeda Nadiah Fatima Nahri[1], Shengzhi Du[1,*], Barend Jacobus van Wyk[2]

[1]*Department of Electrical Engineering, Tshwane University of Technology, Pretoria, 0001, South Africa*

[2]*Faculty of Engineering, the Built Environment and Technology, Nelson Mandela University, Port Elizabeth 6031, South Africa*

A R T I C L E I N F O	A B S T R A C T
	This paper proposes an active disturbance rejection control (ADRC) design for a haptic display platform structure. The motivation for the following scheme originates from the shortcomings faced by classical proportional integral derivative (PID) controllers in control theory. The ADRC is an unconventional model-independent approach, acknowledged as an effective controller in the existence of total plant uncertainties, and these uncertainties are inclusive of the total disturbances and unknown dynamics of the plant. The design and simulation for ADRC are established in MATLAB/ Simulink. The concerned electro-mechanical platform consists of dual ball screw driving system and DC motors. This overall physical system constitutes the haptic interface. Modelling of the two-dimensional physical platform is also explained in this article. Designing of ADRC controller and the human-machine interface (HMI) is followed by their integration, in order to obtain simulation results, thus proving the practicality and validity of the overall system. The results of the proposed controller are compared with the Proportional Integral (PI) controller, which suggests that the ADRC controller performs better as compared to the conventional PI controller.

1. Introduction

This paper is an extension of work originally presented in *2020 International SAUPEC/RobMech/PRASA Conference* [1]. Haptic feedback control systems containing human- in- the- loop (HITL) is relatively a young field of research, that display the interaction between human-machine systems. A typical bilateral teleoperation system consisting of the master device (human operator), communication channel and slave teleoperator, provide human operator's necessary interface and the experience of 'telepresence' [2, 3]. In simple text, the human perceives direct control and manipulation of the environment with their own hands, which is achieved by having their actions mediated physically by means of a robot, communication channel and control systems (i.e., controller), by providing the haptic sensing feedback signals (mostly interaction forces and position constraints) to the operators. Thus, the human operator can execute tasks remotely without physically being present there. Potential applications of teleoperation systems include highly specialized professions like telesurgery, mining, micro, and nanoparticles handling and artificial intelligence to name just a few [4]. These operations are performed globally, mainly to aid and assist the population with special needs.

The block diagram shown in Figure 1 gives a control system viewpoint of haptic teleoperation system. The main purpose of this system is the operator's ability to interact with the remote environment via haptic feedback. In this haptic teleoperation system, a human operator gets the feel of telepresence in the form of force operation and vibrations (sensations) from the haptic interface system, for instance, a simulator. Thus, the movement of the human arm is based on the haptic feedback signals received from the haptic interface device. Accordingly, the human arm will send force and position signals to the controller (highlighted in the top red circle) which will forward the modified force and position signals to the robot system. The robot will then exert the received control signal to the concerned object present in the remote environment. The measured signals (force, position, and vibration) are then fed back to the haptic interface (highlighted in the bottom red circle) resulting in haptic feedback and HITL system. Thus, the human operator feels they are directly executing control operation of the remote side themselves.
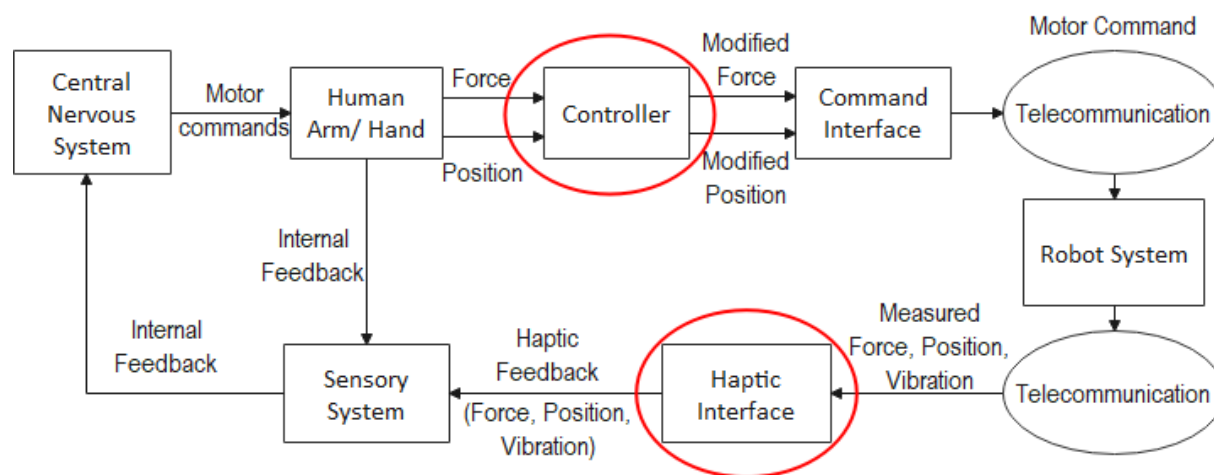
Figure 1: Control system viewpoint of haptic teleoperation system

In teleoperation systems, stability and transparency are both critical properties and conflicting to each other [5]. One of the main concerns relating to control systems design, is to achieve a decent tradeoff between these two contrasting goals. Stability can be achieved using Proportional integral derivative (PID) controls [6], wave-variables based passivity control [7] and time-domain passivity approach [8]. Whereas transparency is related to the human operator's potential to sense the slave side interaction with the environment. To enable this, force sensors are installed at the end effector providing force feedback control. Conversely, these force sensors impose measurement limitations due to their high cost, restricted area of contact and noise/ disturbances in the environment. Hence, disturbance observers were introduced [9]. On the contrary, these observers do not consider specific knowledge of the system like unmodelled dynamics and parameter uncertainties, resulting in narrowing the effectiveness of model-based controllers. Thus, these shortcomings have motivated the application of a model independent approach in the domain of bilateral teleoperation systems. Hence, an Active disturbance rejection control (ADRC) has been proven effective to tackle the limitations of both PID and model-based approaches [10,11]. ADRC's dynamic structure components, such as, the ESO (Extended state observer) and TD (Tracking differentiator), are used to compensate for internal and external disturbance(s) respectively. Therefore, the total system from the outside looks linear. The ADRC takes into account the time-varying nature of the system, unlike the PID controller, that considers particular time instants only. References [12–14] are survey papers that review the development of ADRC from its early beginning, along with, the controller's analysis being conducted from its methodology and theoretical perspective.

This paper aims to addresses and release the above mentioned constraints related to model- based approaches in control theory. This can be attained by introducing a model free approach (ADRC controller) for the physical interface platform (HMI) developed for this research. The objective of this paper includes the study of the disturbance rejection performances and control variable responses of the ADRC and PI controllers. The former provides a

better understanding on the system response curves obtained, whereas the latter depicts more information on controller behaviour. Contributions of this paper include the algorithmic innovation of the ADRC controller and development of a controlled object that serves as a movable two- dimensional (2D) interface platform. Based on this platform, we propose an ADRC for the system shown in Figure 1. Furthermore, this paper focusses on the integration of the designed controller with the human machine interface platform, followed by their experimental analysis and comparison with the previously obtained PI controller results in [1]. This integration and analysis serves as the main focal point of the paper. Thus, by this comparison, the effectiveness of the total proposed system is measured. All the simulations will be conducted via MATLAB and Simulink in this study. Apart from MATLAB/ Simulink, experimental analysis for ADRC based applications have been conducted using other softwares, like LabView, Scilab/ Xcos and OpenPCS, to name a few.

The rest of the paper is structured in this way: Initially, the related work is briefly explained in Section 2, subsequently the proposed hardware platform is addressed in Section 3. Furthermore, Section 4 discusses the design and simulation of an ADRC controller, followed by results and discussions in Section 5. Lastly, Section 6 closes the paper.

2. Related Works

2.1. ADRC Controller

For almost a century, the PID controller has dominated the control technology to meet the ever-increasing demands of the automation industry. However, the PID controller design being system-dependent falls under the category of error-based empirical design paradigm (EDP) [11]. Tuning of such controllers is challenging due to model mismatch between the actual system and approximate model. Other challenges include computational error, noise deterioration caused by derivative control, performance degradation in the control law (linear weighted sum) and complications by integral control due to accumulation of

errors [10]. These conditions necessitated the introduction of a special type of nonlinear controller being system model-independent, called the ADRC. This controller possesses features of strong robustness, fast response speed, high accuracy control, minimum overshoot (smooth curve) and capability to estimate and compensate the overall effects of uncertainties and is thus minimized. These uncertainties include unknown plant dynamics, external disturbances and internal disturbances, in real-time. The capability to control uncertainties in a given system is one of the principal concerns in the field of modern control theory. The ADRC design was first proposed in [15], followed in 1998 [16], for plants with a large number of uncertainties. The same was introduced in [17], followed by an extension in [11]. An adequate transient response is attained using an ADRC design, which possesses a relatively simple framework.

2.1.1. Disturbance Rejection Mechanism

The existing paradigms in the field of control engineering, are the Modern Control Paradigm (MCP) (model-based approach) and error-based Empirical Design Paradigm (EDP) (classical trial and error approach) [11]. But there is a significant gap between theory and practice in the field of feedback control engineering. This calls for a paradigm shift introducing a new paradigm, namely, Disturbance Rejection Paradigm (DRC) [18].

The basic idea of ADRC can be put straight in the following train of thoughts. Firstly, cascade integral design of the canonical (ideal) configuration of the plant. Secondly, portion of the plant that is distinct from the ideal form can be called the 'total disturbance', and is rejected. This includes internal disturbance (i.e. variations in plant dynamics) and external disturbance (i.e. arises from the environment). Lastly, estimate and compensate the total disturbance using an extended state observer (ESO), so as to reduce the nonlinear time-varying system to the canonical form. In short, two main characteristics of modern control theory on which the fundamentals of ADRC are set: Firstly, the concept of canonical form; Secondly, the objective of a state observer [12]. Thus, with such a unique design concept, ADRC provides exceptional outstanding solutions to various pressing problems in the engineering field. Thus, practical applications of ADRC include robot motion control and aerial robotic systems [19], control tool for practitioners [20], control of humanoid robot [21], quadrotor helicopter [22], in several chemical processes, MEMS systems and power converters [23,24], to name a few.

2.2. Haptic Feedback Control

Over the last four decades, several bilateral teleoperation architectures were developed serving as the key technology for human interaction with the remote environment, by supplying the operator with haptic feedback. This haptic feedback control improves the quality of human-robot interaction, on the other hand, stability and transparency parameters are greatly affected due to time delay and packet loss in the communication channel, between the master side (operator) and slave side (remote robot interaction with the environment), as shown in Figure 2.
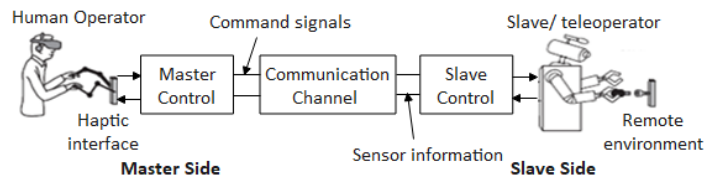
Figure 2: A basic haptic teleoperation system

Some of the important teleoperation architectures, along with their methods, studied and analysed in the past include Wave-variable (WV) approach [25,26], Time-domain passivity approach (TDPA) [27,28], and Model- mediated teleoperation (MMT) approach [29]. A detailed survey on the bilateral teleoperation algorithms and model-based control architectures for haptic interfaces is given in [3]. Such model-based methods represent input-output relationships using mathematical expressions, like the state-space model, Lagrange model, and transfer function model. They are also represented using various control laws, for example, the proportional integral (PI), proportional derivative (PD), PID, model predictive, sliding mode, and energy-based controllers [8,30].

The haptic teleoperation system control and design experience certain shortcomings, such as, uncertainties related to the communication channel and human operational dynamics, along with unsteady human operator decisions [31]. These uncertainties are time-varying and distinctive among individuals. Such inaccuracies make the model-based controller operation challenging and stimulate the use of model-free controllers, like the ADRC for smooth operations [10]. Thus, ADRC can contribute to the development of applications in connection with feedback control systems in man- machine interface systems. Recent studies on ADRC controller for teleoperation systems based on distinct parameters, and for nonlinear systems, have been explained in [32] and [33,34] respectively.

3. Hardware design and modelling

3.1. Proposed Hardware Platform

The basic idea behind the platform shown in Figure 3, is to manoeuvre the operating handle in a rectangular coordinate system.
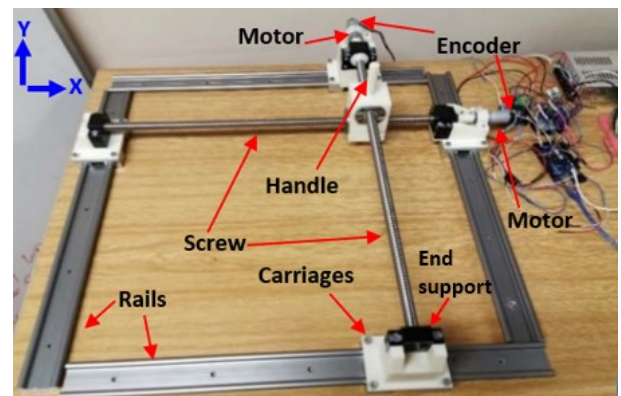
Figure 3: Experimental setup of the assembled hardware platform- 2 degree of freedom (2 DOF)

3.1.1. Mechanical components of the HMI design

Mechanical and electrical components constitute the experimental platform. The mechanical components used are stated in this subsection. The operating handle is a three-dimensional (3D) printed object, obtained using a designing software called Onshape. Both X-axis and Y-axis have a ball screw feed drive system (SFU1605) aligned parallel to each of the axis, with the operating handle assembled over the lead screw system. The ball-lead screws and nut dimensions are 600mm (length) x 16mm (diameter) x 5mm (pitch). Ball screw nuts provide the required linkage between the lead screws and the operating handle. Hence, ball lead-screw's rotational motion is transformed to operating handle's linear translation motion. As seen in Figure 3, two pairs of linear guide rails of dimensions 600mm (length) x 4mm (width) hold up the handle and screws. The guide rails used are called the Igus W series (WS-10-40-600), which possess benefits like low wear and tear, low friction, low noise system, and requires no maintenance being resistant to dust and dirt. The 3D printed carriages that firmly hold both ends of the lead screws, together with the sliding rails, are all mounted on a levelled surface. The end supports used for the ball screw (SFU16XX - BK 12 + BF 10) contains two parts, one for the front and the other for the rear of the lead screw. The fixed part is 10mm in diameter, whereas the floating part is 12mm in diameter. Also includes circlips and deep groove ball bearings. A DC motor mounted on one end-support component, and the motor shaft mechanically connected to the lead screw, help to drive the lead screw system.

3.1.2. Electrical components of the HMI design

The electrical components used in the experimental setup are explained in this subsection. As seen in Figure 3, a DC motor shaft equipped with an encoder is incorporated at one end of both the lead screws. The motors chosen are called the Metal Gearmotor 75:1 (gear ratio), with a 48 CPR quadrature encoder integrated on each motor, which provides 3592 counts per revolution of the gearbox's output shaft. Size of the motor is 25mm (diameter) x 66mm (length), with a shaft diameter of 4mm. These motors are intended for comfortable operation in the 3- 9V range. The encoders are connected to the Arduino MEGA 2560 board. Both motors are provided with a specific motor driver called the BTS7960 High Power H- Bridge motor driver. The motor driver has the following specifications, 43A of maximum current and input voltage range of 6V to 27V. According to the inout voltage received from the Arduino board, the motor drivers will adapt to these incoming signals, and then apply the appropriate voltage to the motor. The system contains two ACS714 current sensors, one for each motor driver, to aid in measuring the strength applied on the operating handle.

On accomplishing the hardware installation, signal transmission between MATLAB and the proposed interface system (HMI) was performed using Arduino 2560. This Arduino board was powered by an external power supply. Currently, only a single axis movement of the lead screw drive system is considered in this paper.

3.2. Mathematical Modelling of the Assembled Hardware Platform

Two of the single-axis electro-mechanical platform shown in Figure 3 are coupled together to implement the 2D movement. Torque (T_M) generated by the DC motor is transmitted to the ball screw shaft via coupling, which in turn causes the operating handle to move. Transmission ratio 'i' of ball screw system is defined as the distance travelled 'h' during one revolution of the shaft [35], also denotes, the transformation of rotational movement of screw shaft into linear motion of the operating handle. 'i' is given by the following equation,

$$i = {}^h\!/_{2\pi} \tag{1}$$

The lumped mass model (LMM) developed in [35,36] is adopted to derive the mathematical model for this structure. Such a model indicates several functions related to the system, by simplifying the simulation model to a reduced number of DOF system. As seen in Figure 4, all the rigidity parameters (k), inertial components (M), and damping parameters (c) are denoted in terms of axial and rotational components of the same parameter, i.e., total rotational and axial rigidity components, represented as (k_{rot}) and (k_{ax}) respectively.
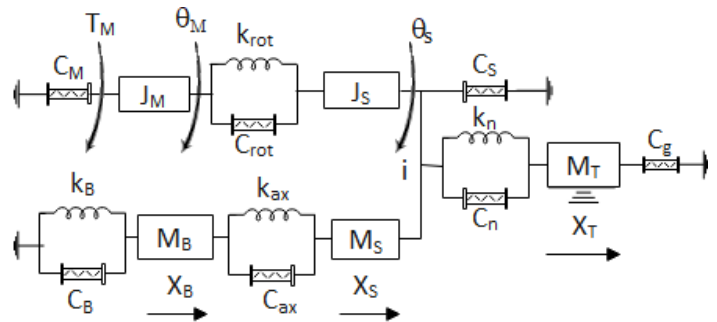
Figure 4: The LMM of the recommended HMI platform

The LMM parameters in Figure 4 consists of screw shaft rotary inertia J_S, base mass M_B, motor inertia J_M, screw shaft side equivalent mass M_S, handle mass M_T, equivalent torsional rigidity k_{rot}, ball screw nut rigidity k_n, axial base rigidity k_B, equivalent axial rigidity k_{ax}, DC motor torsional damping C_M, equivalent rotational damping C_{rot}, sides screw shaft damping C_S, ball screw nut damping C_n, axial guide damping C_g, axial base damping C_B, and equivalent axial damping C_{ax}.

Parameters (DOF) of the model shown in Figure 4 include,

θ_M- Angular rotation of the DC motor

θ_S- Angular rotation of screw shaft at handle position

X_B- Axial base displacement

X_S- Axial displacement of the screw shaft at handle position

X_T- Operating handle position

Equation 2 represents the mathematical model of a DC motor,

$$\dot{T}_M = \frac{-K_{bm}K_t}{L_a}\dot{\theta}_M - \frac{R_a}{K_t}T_M + \frac{K_t}{L_a}E_a \tag{2}$$

where, K_t and K_{bm} denote motor torque and back emf constants, L_a is winding leakage inductance, $\dot{\theta}_M$ is the angular velocity of the

rotor inside motor, E_a is the voltage source, and R_a is the armature resistance. References [1,36] provide a detailed step by step Lagrange and state-space mathematical modelling for the physical structure in Figure 4.

3.2.1. Lagrange Model

Second order Lagrange's equations are employed to develop the ball screw feed drive system's dynamic model. Lagrange function is defined by the variation between kinetic and potential energies of a physical system. Equation (3) gives the mathematical relations for total kinetic energy (T), potential energy (U) and dissipation function (D), associated with the total system.

$$\begin{cases} T = \frac{1}{2}J_M\dot{\theta}_M^2 + \frac{1}{2}J_S\dot{\theta}_S^2 + \frac{1}{2}M_B\dot{X}_B^2 + \frac{1}{2}M_S\dot{X}_S^2 + \frac{1}{2}M_T\dot{X}_T^2 \\ U = \frac{1}{2}k_{rot}(\theta_M - \theta_S)^2 + \frac{1}{2}k_B X_B{}^2 + \frac{1}{2}k_{ax}(X_S - X_B)^2 + \frac{1}{2}k_n(X_T - X_S - i\theta_s)^2 \\ D = \frac{1}{2}C_M\dot{\theta}_M^2 + \frac{1}{2}C_{rot}(\dot{\theta}_M - \dot{\theta}_S)^2 + \frac{1}{2}C_S\dot{\theta}_S^2 + \frac{1}{2}C_B\dot{X}_B^2 + \frac{1}{2}C_{ax}(\dot{X}_S - \dot{X}_B)^2 + \frac{1}{2}C_n(\dot{X}_T - \dot{X}_S - i\dot{\theta}_s)^2 + \frac{1}{2}C_g\dot{X}_T^2 \end{cases} \quad (3)$$

Lagrange equation, $L = T - U = \frac{1}{2}J_M\dot{\theta}_M^2 + \frac{1}{2}J_S\dot{\theta}_S^2 + \frac{1}{2}M_B\dot{X}_B^2 + \frac{1}{2}M_S\dot{X}_S^2 + \frac{1}{2}M_T\dot{X}_T^2 - \frac{1}{2}k_{rot}(\theta_M - \theta_S)^2 - \frac{1}{2}k_B X_B{}^2 -$
$$\frac{1}{2}k_{ax}(X_S - X_B)^2 - \frac{1}{2}k_n(X_T - X_S - i\theta_s)^2 \quad (4)$$

Equation (5) represents the Lagrangian function of a system. This function is calculated about force 'Q' and the generalized coordinate 'q'.

$$\frac{d}{dt}\left(\frac{\partial L}{\partial \dot{q}}\right) - \frac{\partial L}{\partial q} - \frac{\partial D}{\partial \dot{q}} = Q \quad (5)$$

Coordinates 'q' and 'Q' indicate independent coordinates and force inputs to the physical system respectively, given by the following relations in (6),

$$\begin{cases} q = (\theta_M \ \theta_S \ X_B \ X_s \ X_T)^T \\ Q = (T_M \ 0 \ 0 \ 0 \ 0)^T \end{cases} \quad (6)$$

On solving (4) using (5) and (6), the following set of equations were obtained,

$$\begin{cases} J_M\ddot{\theta}_M + k_{rot}(\theta_M - \theta_S) + C_M\dot{\theta}_M + C_{rot}(\dot{\theta}_M + \dot{\theta}_S) = T_M \\ J_S\ddot{\theta}_S - k_{rot}(\theta_M - \theta_S) - ik_n(X_T - X_S - i\theta_S) + C_S\dot{\theta}_S + C_{rot}(\dot{\theta}_M + \dot{\theta}_S) + iC_n(\dot{X}_T + \dot{X}_S + i\dot{\theta}_S) = 0 \\ M_B\ddot{X}_B + k_B X_B - k_{ax}(X_S - X_B) + C_B\dot{X}_B + C_{ax}(\dot{X}_S + \dot{X}_B) = 0 \\ M_S\ddot{X}_S + k_{ax}(X_S - X_B) - k_n(X_T - X_S - i\theta_S) + C_{ax}(\dot{X}_S + \dot{X}_B) + C_n(\dot{X}_T + \dot{X}_S + i\dot{\theta}_S) = 0 \\ M_T\ddot{X}_T + k_n(X_T - X_S - i\theta_S) + C_n(\dot{X}_T + \dot{X}_S + i\dot{\theta}_S) + C_g\dot{X}_T = 0 \end{cases} \quad (7)$$

After rearranging the terms in (7), a set of five equations are obtained, that is given in (8). Based on these equations, the Simulink model is built on the MATLAB software, this software-based mathematical model is displayed in Figure 5.

$$\begin{cases} \ddot{\theta}_M = \frac{1}{J_M}[T_M - k_{rot}(\theta_M - \theta_S) - \dot{\theta}_M(C_M + C_{rot}) - C_{rot}\dot{\theta}_S] \\ \ddot{\theta}_S = \frac{1}{J_S}[-\dot{\theta}_S(C_{rot} + C_S + i^2 C_n) - \theta_S(k_{rot} + i^2 k_n) - C_{rot}\dot{\theta}_M + k_{rot}\theta_M + ik_n X_T - ik_n X_S - iC_n\dot{X}_T - iC_n\dot{X}_S] \\ \ddot{X}_B = \frac{1}{M_B}[-X_B(k_{ax} + k_B) + k_{ax}X_S - C_{ax}\dot{X}_S - \dot{X}_B(C_B + C_{ax})] \\ \ddot{X}_S = \frac{1}{M_S}[k_{ax}X_B - X_S(k_{ax} + k_n) + k_n X_T - ik_n\theta_S - C_{ax}\dot{X}_B - \dot{X}_S(C_{ax} + C_n) - C_n\dot{X}_T - iC_n\dot{\theta}_S] \\ \ddot{X}_T = \frac{1}{M_T}[-k_n X_T - \dot{X}_T(C_n + C_g) + k_n X_S + ik_n\theta_S - C_n\dot{X}_S - iC_n\dot{\theta}_S] \end{cases} \quad (8)$$

LMM of the proposed design, is given in matrix form by the following relation in (9),

$$m\ddot{q} + c\dot{q} + kq = Q \quad (9)$$

Equations (10), (11) and (12) indicate the values for matrices m, k and c respectively. These matrix values are acquired from (7).

$$m = \begin{bmatrix} J_M & 0 & 0 & 0 & 0 \\ 0 & J_S & 0 & 0 & 0 \\ 0 & 0 & M_B & 0 & 0 \\ 0 & 0 & 0 & M_S & 0 \\ 0 & 0 & 0 & 0 & M_T \end{bmatrix} \quad (10)$$

$$k = \begin{bmatrix} k_{rot} & -k_{rot} & 0 & 0 & 0 \\ -k_{rot} & (k_{rot}+i^2 k_n) & 0 & i k_n & -i k_n \\ 0 & 0 & (k_B+k_{ax}) & -k_{ax} & 0 \\ 0 & i k_n & -k_{ax} & (k_{ax}+k_n) & -k_n \\ 0 & -i k_n & 0 & -k_n & k_n \end{bmatrix} \tag{11}$$

$$c = \begin{bmatrix} (C_M+C_{rot}) & C_{rot} & 0 & 0 & 0 \\ C_{rot} & (C_{rot}+C_S+i^2 C_n) & 0 & i C_n & i C_n \\ 0 & 0 & (C_B+C_{ax}) & C_{ax} & 0 \\ 0 & i C_n & C_{ax} & (C_{ax}+C_n) & C_n \\ 0 & iC_n & 0 & C_n & (C_n+C_g) \end{bmatrix} \tag{12}$$

3.2.2. State-Space Model and Transfer Function

Matric values given in (10-12), are substituted in (13), to provide the state-space representation of system model.

$$\ddot{q} = \frac{1}{m}(Q - c*\dot{q} - k*q) \tag{13}$$

For the state-space model, we first determine the number of states. In this experiment, each of the five equations in (7) are second-order differential equations, i.e, each equation will include at least two states.

State-state model is represented as, $\dot{x} = Ax + Bu$ and $y = Cx + Du$. In this system A is (11x11) matrix, B is (11x1) matrix, C is (1x11) matrix and D matrix is 0.

Equations (14) and (15) represent the State- space model and Transfer function of the system.

$$\dot{X} = \begin{bmatrix} \frac{-(C_M+C_{rot})}{J_M} & \frac{-k_{rot}}{J_M} & \frac{-C_{rot}}{J_M} & \frac{k_{rot}}{J_M} & 0 & 0 & 0 & 0 & 0 & 0 & 0 \\ 1 & 0 & 0 & 0 & 0 & 0 & 0 & 0 & 0 & 0 & 0 \\ \frac{-C_{rot}}{J_S} & \frac{k_{rot}}{J_S} & \frac{-(C_{rot}+C_S+i^2 C_n)}{J_S} & \frac{-(k_{rot}+i^2 k_n)}{J_S} & 0 & 0 & \frac{-i C_n}{J_S} & \frac{-i k_n}{J_S} & \frac{-i C_n}{J_S} & \frac{i k_n}{J_S} & 0 \\ 0 & 0 & 1 & 0 & 0 & 0 & 0 & 0 & 0 & 0 & 0 \\ 0 & 0 & 0 & 0 & \frac{-(C_B+C_{ax})}{M_B} & \frac{-(k_B+k_{ax})}{M_B} & \frac{-C_{ax}}{M_B} & \frac{k_{ax}}{M_B} & 0 & 0 & 0 \\ 0 & 0 & 0 & 0 & 1 & 0 & 0 & 0 & 0 & 0 & 0 \\ 0 & 0 & \frac{-i C_n}{M_S} & \frac{-i k_n}{M_S} & \frac{-C_{ax}}{M_S} & \frac{k_{ax}}{M_S} & \frac{-(C_{ax}+C_n)}{M_S} & \frac{-(k_{ax}+k_n)}{M_S} & \frac{-C_n}{M_S} & \frac{k_n}{M_S} & 0 \\ 0 & 0 & 0 & 0 & 0 & 0 & 1 & 0 & 0 & 0 & 0 \\ 0 & 0 & \frac{-i C_n}{M_T} & \frac{i k_n}{M_T} & 0 & 0 & \frac{-C_n}{M_T} & \frac{k_n}{M_T} & \frac{-(C_n+C_g)}{M_T} & \frac{-k_n}{M_T} & 0 \\ 0 & 0 & 0 & 0 & 0 & 0 & 0 & 0 & 1 & 0 & 0 \\ \frac{-K_{bm}K_t}{L_a} & 0 & 0 & 0 & 0 & 0 & 0 & 0 & 0 & 0 & \frac{-R_a}{L_a} \end{bmatrix} X + \begin{bmatrix} 0 \\ 0 \\ 0 \\ 0 \\ 0 \\ 0 \\ 0 \\ 0 \\ 0 \\ 0 \\ \frac{K_t}{L_a} \end{bmatrix} E_a \tag{14}$$

$$Y = [\,0\,0\,0\,0\,0\,0\,0\,0\,0\,1\,0\,]X \tag{15}$$

where $X = [\,x_1\,x_2\,...\,x_{11}\,]$. The output is the operating handle position (X_T), which is assigned to the state variable x_{10}.

The transfer function (G) stated in (16) is obtained from the state-space model by using the following MATLAB codes,

```
Sys = ss(A,B,C,D);G= tf(Sys)
```

$$G = \frac{0.001122\,s^6 - 1.1*10^8 s^5 + 3.453*10^{12}s^4 - 7.294*10^{14}s^3 + 2.29*10^{19}s^2 - 1.896*10^{19}s + 5.954*10^{23}}{\substack{s^{11} + 407.7s^{10} + 1.817*10^7 s^9 + 7.334*10^9 s^8 + 4.094*10^{13}s^7 + 1.552*10^{16}s^6 + 9.493*10^{18}s^5 + 3.353*10^{21}s^4 + \\ 3.329*10^{23}s^3 + 7.323*10^{25}s^2 + 3.045*10^{27}s + 1.138*10^{16}}} \tag{16}$$

The Controllability and Observability of the system can be obtained from its state- space model in (14). The Controllability matrix (C_M) and Observability matrix (O_M) were calculated using the following MATLAB commands, '$ctrb(A,B)$' and '$obsv(A,C)$' respectively. Both the matrices were found to be invertible with their determinant values not equal to zero. Thus, this shows that the system is controllable and observable.
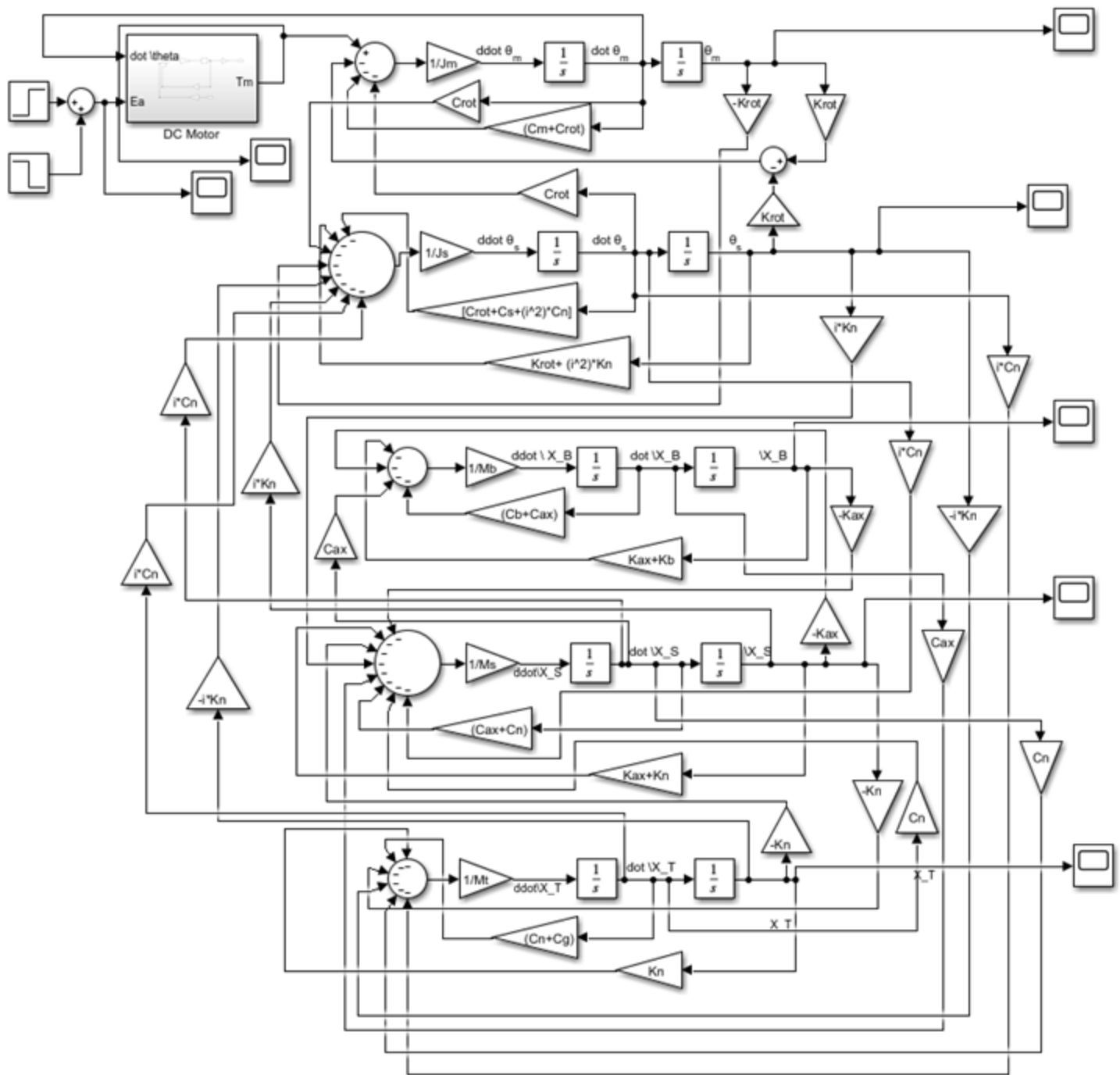
Figure 5: Simulink Block of the concerned Haptic Machine Interface (hardware platform)

4. Algorithm and Simulink Modelling of ADRC

ADRC originates from the classical PID controller, retaining the central idea of error feedback control. The drawbacks of the PID controller are overcome by the significant dynamic structure of ADRC. As seen in Figure 6, an ADRC architecture is composed of three parts, namely, the Tracking Differentiator (TD), Extended State Observer (ESO) and Nonlinear State Error Feedback (NLSEF). Each of the subsystems is explained here, followed by their Simulink model created on MATLAB.
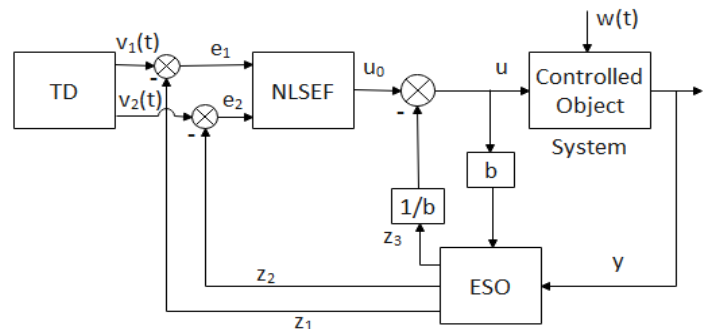
Figure 6: Basic ADRC structure of a two- order system
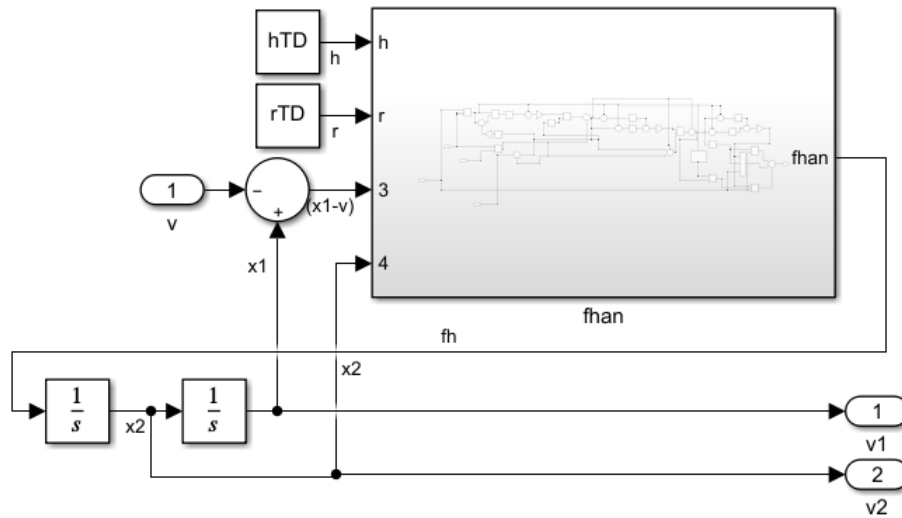
Figure 7: Simulink Model of TD subsystem

Definitions of parameters used for ADRC design: $v_1(t)$ or v_1 is the tracking signal, and $v_2(t)$ or v_2 is the differential signal of the given input signal. The output signal of the system and input signal of ESO is given by 'y'. u is called the control volume, it is the input signal of the controlled object and the ESO. z_1 and z_2 are variables of the estimated state. z_3 is the estimated signal of the total disturbance, i.e., both internal disturbance and the external interference present. $w(t)$ is the external disturbance acting on the concerned system. e_1 and e_2 are the error signals fed to the NLSEF.

$$\begin{cases} e_1 = v_1 - z_1 \\ e_2 = v_2 - z_2 \end{cases} \tag{17}$$

4.1. Tracking Differentiator (TD)

TD determines the transition process for the system input, in order to obtain a smooth input signal $v_1(t)$ which is the desired trajectory and its differential signal $v_2(t)$. Consider the input signal $v(t)$ is to be differentiated, thus, TD provides the fastest tracking $v(t)$ given by (18). By solving the following differential equation, the required transient profile is obtained.

$$\begin{cases} \dot{x}_1 = x_2 \\ \dot{x}_2 = -r\, sign(x_1 - v(t) + \frac{x_2\,|x_2|}{2r}) \end{cases} \tag{18}$$

The parameter r is chosen according to the speed of the transient profile, i.e., to expedite or moderately slow down the transient profile. v is the desired value for x_1. The Simulink model of TD is shown in Figure 7, wherein $fhan$ is a nonlinear function denoted as $fhan(x_1 - v, x_2, r, h)$. h is the simulation step, also called the sampling period.

$$fh = fhan(v_1 - v, v_2, r_0, h_0) \tag{19}$$

The function $fhan$ is presented later in this paper. Equation (19) is a time-optimal solution provides no overshoot and fastest

convergence from v_1 to v. Parameters r_0 and h_0 are equated to r and h respectively [10].

4.2. Nonlinear State Error Feedback (NLSEF)

The control law of PID controller implements a linear combination of the present, past and future predictive kinds of the tracking error. For an infinite time, the tracking error attains zero value for linear feedback systems. Whereas, for a nonlinear feedback function given in (20), the error can reach zero value much earlier in a finite time ($\alpha < 1$). Such a mechanism significantly alleviates the steady-state error in comparison to an integral control [10]. Thus, in an ADRC control framework, the nonlinear feedback functions fal and $fhan$ play a significant role during operation.

$$fal(x, \alpha, d) = \begin{cases} \frac{x}{d^{1-\alpha}}, |x| \le d \\ |x|^\alpha sign(x), |x| > d \end{cases} \tag{20}$$

The Simulink model of NLSEF seen in Figure 8, has been developed using the mathematical relations from (20-23).

$$u = k_0 e_0 + fhan(e_1, c * e_2, r, h_0) \tag{21}$$

Parameter c denotes the damping coefficient. And function $fhan(x_1, x_2, r, h)$ is represented using the following set of equations [37],

$$fhan = -r\left(\frac{a}{d} - sign(a)\right) s_a - r sign(a) \tag{22}$$

where,

$$s_a = \frac{[sign(a + d) - sign(a - d)]}{2} \tag{23}$$

$$\begin{cases} a = (a_0 + y - a_2)s_y + a_2 \\ d = rh^2 \\ a_0 = hx_2 \\ y = x_1 + a_0 \\ a_2 = a_0 + [sign(y)(a_1 - d)/2] \\ s_y = [sign(y + d) - sign(y - d)]/2 \\ a_1 = \sqrt{d(d + 8|y|)} \end{cases} \tag{24}$$
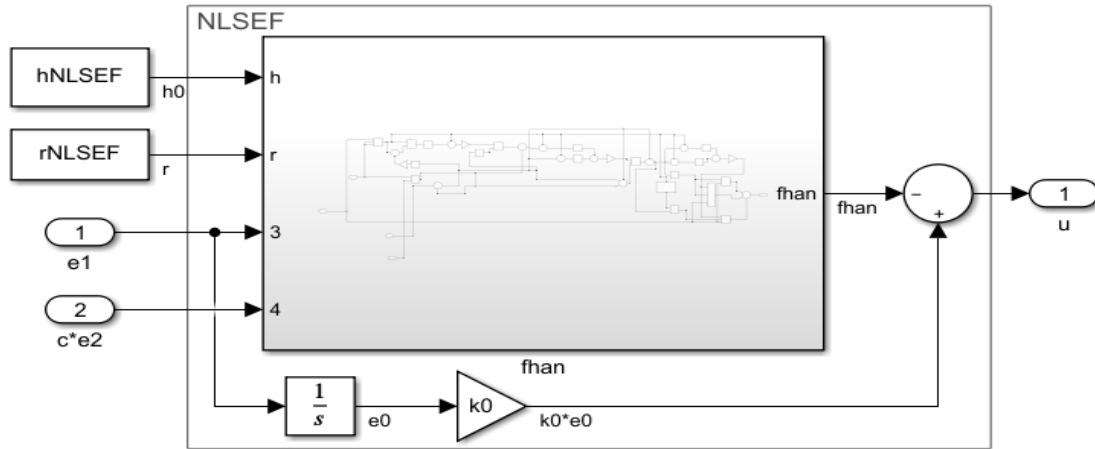
Figure 8: Simulink Model of NLSEF subsystem

4.3. Extended State Observer (ESO)

ESO estimates full system states and the total effect of disturbances (or extended states) in real-time. These disturbances may arise from unknown or nonlinear system dynamics of the manipulator, external disturbances, and mismatch of control parameters. Thus, in robot control, ESO present in the feedback loop is used to estimate and cancel the effects of these uncertainties. Figure 9 gives a detailed Simulink model of the ESO block. This subsystem constitutes of the nonlinear feedback function fal defined in (20). The algorithm for ESO is characterized as follows [37,38]:

$$\begin{cases} fe_1 = fal(e, 0.25, h) \\ fe = fal(e, 0.5, h) \end{cases} \tag{25}$$

$$\begin{cases} e = z_1 - y \\ \dot{z}_1 = z_1 + h(z_2 - \beta_{01}e) \\ \dot{z}_2 = z_2 + h(z_3 - \beta_{02}fe + b_0u) \\ \dot{z}_3 = z_3 + h(-\beta_{03}fe_1) \end{cases} \tag{26}$$

where, $\beta_{01}, \beta_{02}, \beta_{03}$ are parameters of ADRC that can be obtained from the system's sampling step. Thus, four main parameters to be controlled are, simulation step (h), control gain (r), damping coefficient (c) and compensation factor (b_0).
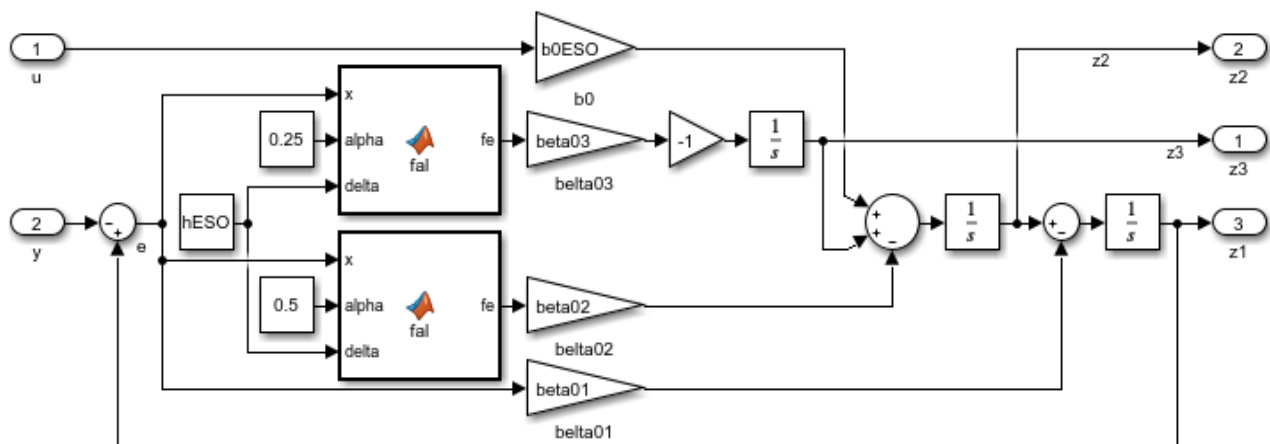
Figure 9: Simulation Model of ESO subsystem
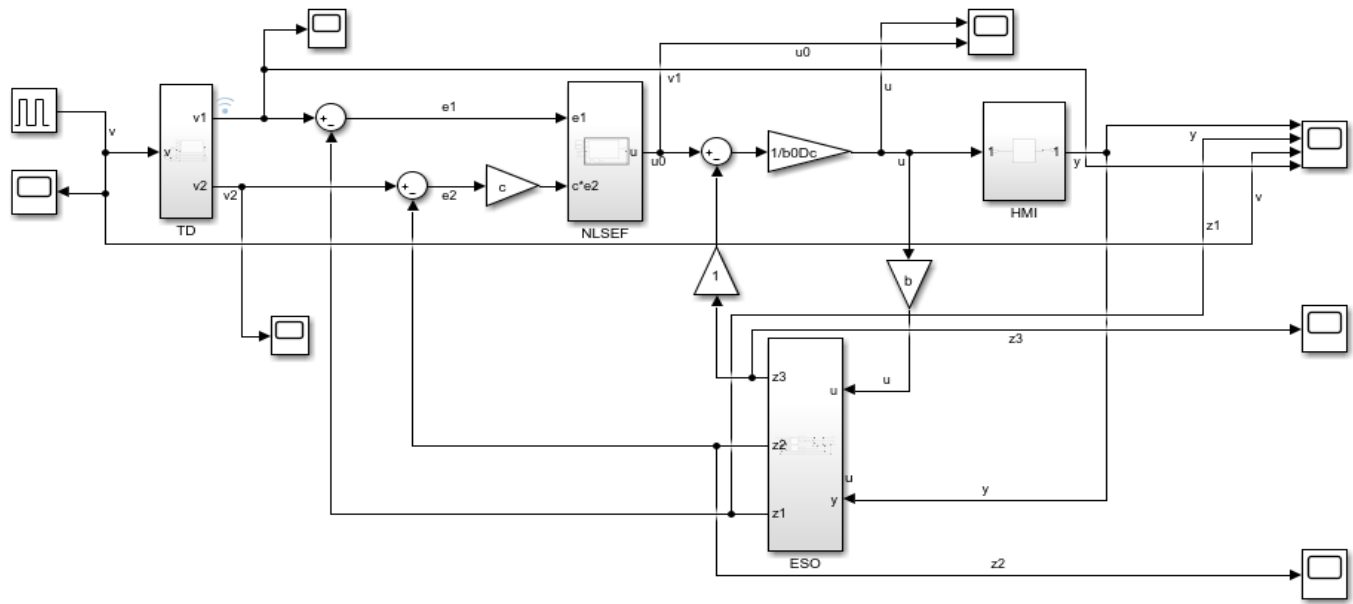
Figure 10: Simulink model of ADRC system including the HMI as the Controlled object

4.4. Controlled Object

The integration of TD structure, with the NLSEF structure, followed by the nonlinear ESO structure (which provides total disturbances estimation and rejection), altogether constitute the ADRC system. This controller is integrated with the HMI system. The Simulink model of HMI shown in Figure 5, is called the Controlled object in the ADRC system as seen in Figure 10.

5. Results and Discussions

5.1. Validation of the consistence between the physical interface system and the Simulink model

Figure 11 depicts the output response of the proposed physical system with PI controller, and Figure 12 depicts the LMM's response executed via MATLAB and Simulink.
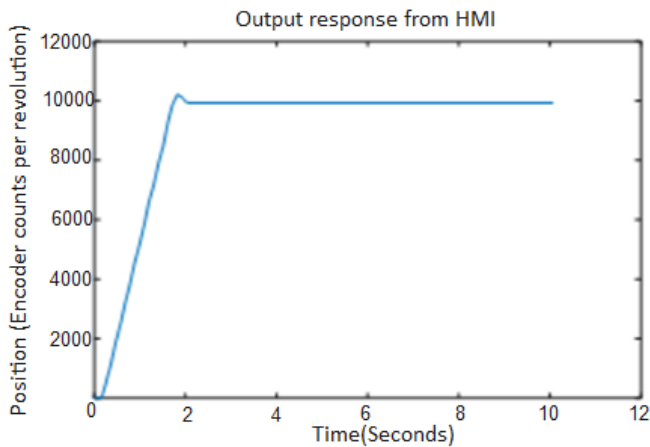
Figure 11: Output response of handle position from the physical system

As seen in Figures 11 and 12, except for the magnitude, output response curves obtained from the physical interface platform and from the Simulink model respectively, are found to be similar. Dissimilarity in magnitude is mainly because, firstly, the units of the Y-coordinates are distinct. Secondly, it is difficult to measure

the lumped parameter values of the physical platform. Thus, the proposed platform's parameter values are slightly different from the simulation model values (i.e. designed via Simulink). Yet the simulation model substantiated the fundamental characteristic of the recommended HMI platform. The parameter values that were used in the Simulink model are listed in Table 1.
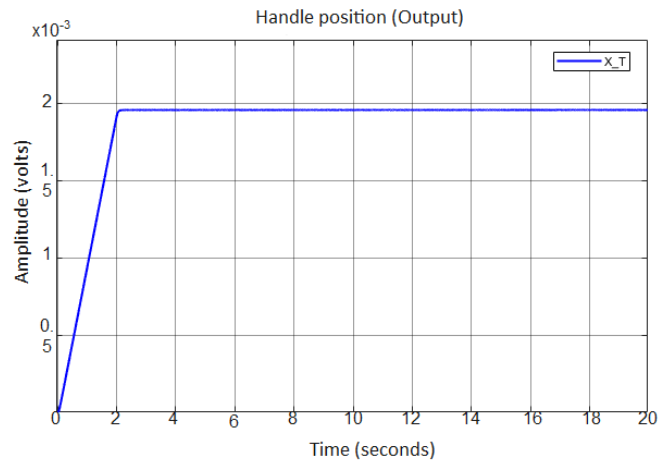
Figure 12: Output response of the Handle position (X_T) from Simulink model

Table 1: Parameter values of HMI used in Simulink Model

Parameters	Value
J_M	$6.75 * 10^{-3} (kg \cdot m^2)$
J_S	$1.7 * 10^{-3} (kg \cdot m^2)$
M_B	$3820 (kg)$
M_S	$11.28 \ (kg)$
M_T	$206 (kg)$
k_{rot}	$3.14 * 10^3 (N \cdot m \cdot rad^{-1})$
k_n	$9.8 * 10^7 (N \cdot m^{-1})$
k_B	$1 * 10^8 (N \cdot m^{-1})$
k_{ax}	$0.743 * 10^8 (N \cdot m^{-1})$
C_M	$0.001 (N \cdot s \cdot m^{-1})$
C_{rot}	$0.1 (N \cdot s \cdot m^{-1})$

C_n	$0.001\ (N \cdot s \cdot m^{-1})$
C_S	$0.001\ (N \cdot s \cdot m^{-1})$
C_B	$0.1\ (N \cdot s \cdot m^{-1})$
C_{ax}	$0.001\ (N \cdot s \cdot m^{-1})$
C_g	$0.001\ (N \cdot s \cdot m^{-1})$
L_a	$1.5 * 10^{-3}(H)$
R_a	$0.5\ (\Omega)$
K_t	$0.05\ (N \cdot m \cdot A^{-1})$
K_{bm}	$0.05\ (V \cdot rad^{-1} \cdot s^{-1})$
T	$0.01\ (s)$
i	$7.96 * 10^{-4}(m \cdot rad^{-1})$

5.2. Disturbance rejection performance of the designed ADRC controller and comparison with PI controller

Experimental analysis of the comparison between ADRC and PI controllers is based on the following performance indices, that is, the system response obtained in the vicinity of disturbance present in the motor voltage, and controller variable values of both the controllers. The volatage unstability in the motor is one of the primary disturbance to the control system. In this experiment, the disturbance on the voltage supply to the motor is added to validate the disturbance rejection performance of the designed ADRC and PI controllers. The disturbance is added at the 5th second with an amplitude of 5000mV and lasting 0.2s, as shown in Figure 13.

Figure 14 shows the system response of the system controlled by ADRC and PI controllers. For the sake of fair comparison, the ADRC and PI controllers are tuned to have similar overshoot values. From Figure 14, one can find the system response with ADRC (Figure 14(a)) goes back to the reference value quickly after the overshot, however, the PI controller takes longer time to

do so. Both system responses are affected by the disburance (starting from 5s in Figure 14), but the ADRC controlled system gets much smaller shift from the reference value than the PI controller.

Figure 15 demonstrates the control variable values of the two controllers, which depicts more details on controller behaviour. From Figure 15(a), one finds the ADRC controller starts with a mild control at the beginning due to the soften effect obtained in the tracking differentiator, which makes a smaller peak value on the control (Figure 15(a)). When the disturbance happens, the designed ADRC depresses the shift from reference value greatly, which leads to only a small change on the system response (refer to Figure 15(a)) from 5s. The PI controller is much more rigid when compared with the designed ADRC, which makes the controller start with an aggressive control (Figure 15(b)) at the beginning, and bigger shift from the reference value after the disturbance (refer to Figure 15(b)) from 5s.

These advantages of the system response controlled by ADRC can be explained in Figure 16, i.e. the total disturbances estimated by the ADRC. From Figure 16, one finds at the beginning of the control, the intial stage of the input step signal is considered as a disturbance (around 0s in Figure 16) which is compensated to obtain a soft rise of the system. This is obtained by the TD. When the disturbance occurs (around 5s in Figure 16), it is considered as disturbance (z_3 in (26)) as well and is compensated accordingly. Now the ESO observes the disturbance, and is compensated to the control variable generated by the NLSEF. This mechanism is shown in Figure 10. Thus, this disturbance rejection property of ADRC controller makes it unique in operation as compared to the PI controller.
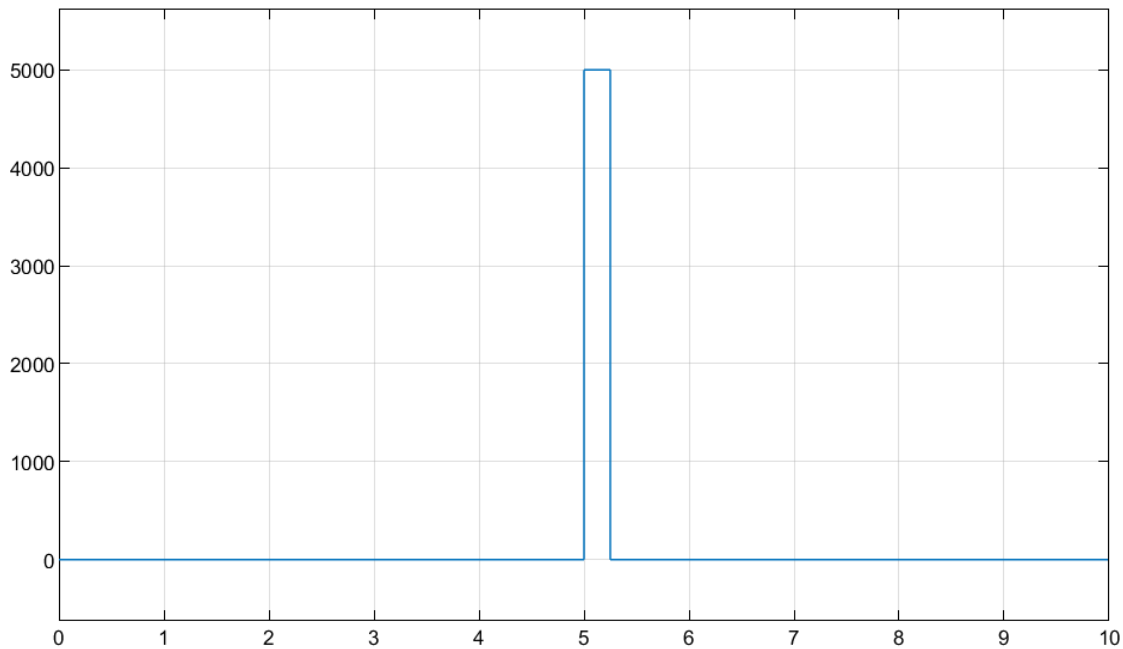
Figure 13: The added voltage disturbance in motor

(a)   ADRC controller

(b) PI controller
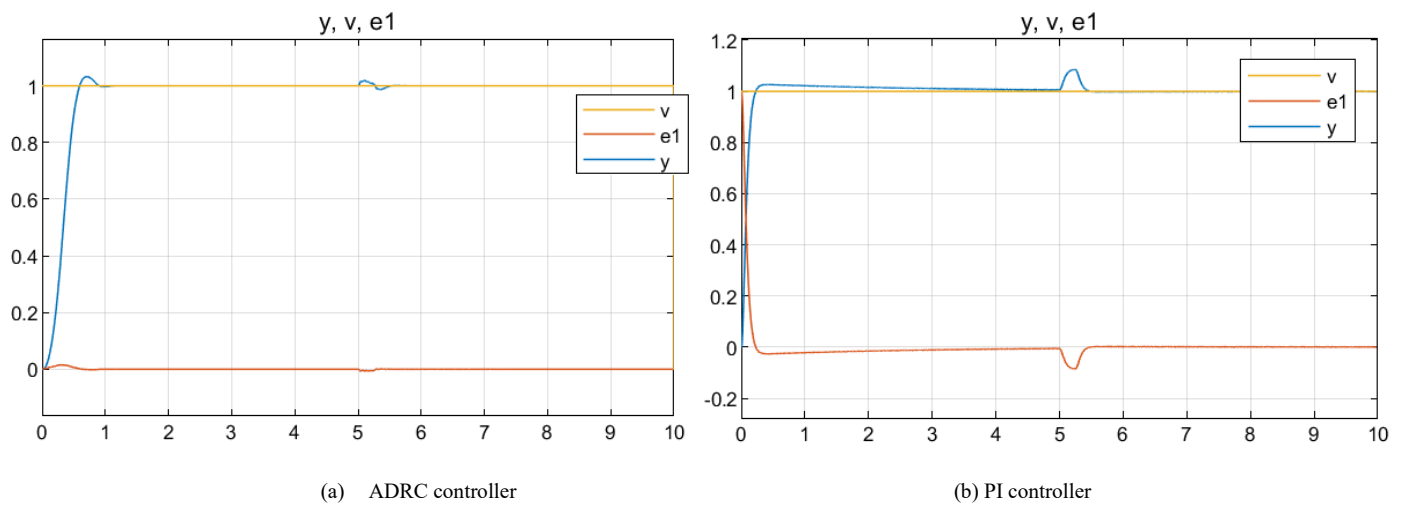
Figure 14: System response

(a) ADRC controller

(b) PI controller
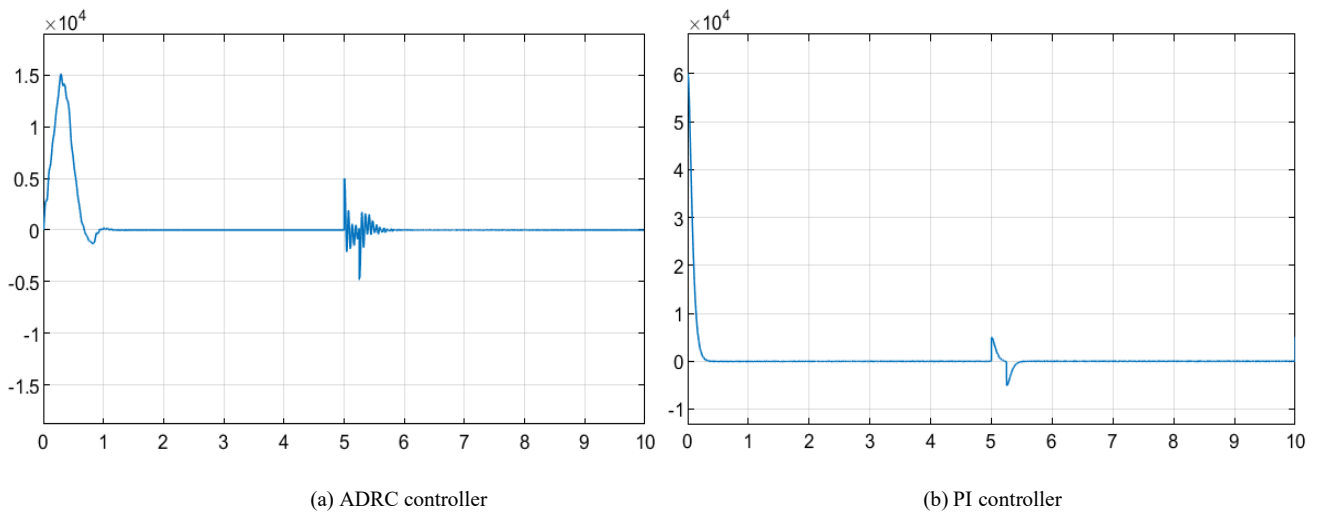
Figure 15: Control variable values
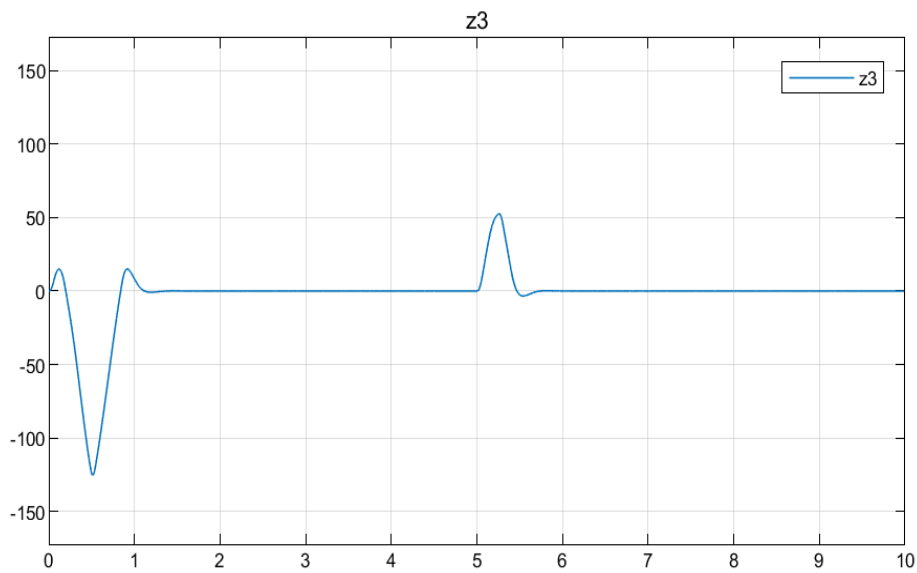
Figure 16: Estimated total disturbances by the ADRC

Table 2: Parameter values of the ADRC system

Parameters	Value
Tracking Differentiator (TD)	
hTD	0.03
rTD	10
Extended State Observer (ESO)	
beta01	100
beta02	300
beta03	1000
hESO	0.01
b0ESO	0.01
Nonlinear State Error Feedback (NLSEF)	
c	0.1
rNLSEF	20000
hNLSEF	0.001
k0	0
Disturbance Compensation	
b	1
b0Dc	1

6. Conclusions and Future work

The shift of feedback control paradigm design has been extensively studied over the past few decades. With a huge potential of disturbance rejection control method, this paradigm shift will play a critical role in the migration from the primitive PID controller to an ADRC. A PID controller passively responds to disturbances, causing zone oscillations. But on the other hand, ADRC actively rejects disturbances, delivering a smooth control system. In an ADRC, the unmeasurable states and total disturbances are actively compensated by the ESO present in the feedback loop. Whereas TD effectively acquire the continuous and differential form of signals from a measurement signal containing random noise, or from a discontinuous signal. It is easy to tune the parameters of TD due to its model independence property. The nonlinear feedback combination (NLSEF) of the two nonlinear functions play a significant role in this recently proposed control framework. Thus, considering the system parameters and model uncertainties, ADRC shows higher tolerance with merits of simple and intuitive model-free control design methods. Along with, it needs less energy in control in comparison to other control strategies.

This paper gives a detailed step by step design and mathematical modelling of the proposed HMI system developed for the research. After installation of the mechanical and electrical hardware components, Lagrange equations were derived based on the LMM of the system. An ADRC controller was designed and integrated with the haptic display platform Simulink model. Simulation studies were conducted to illustrate the efficiency and robustness of the ADRC controller.

However, up to date, debates and inconsistencies on the new paradigm concept still exist, and reports and validation on the successful integration of ADRC into the field of control theory are quite limited. This work pushes the realms of ADRC integration with actual physical plants for practical applications, and potentially opens up new realms constituting of new control laws formulated through experimentation.

Future research of this project will include the analysis of ADRC controller for a two-axis ball screw driving system dealing with time delay, and coupling between the two axes of the experiment. This analysis will be conducted with the modelling environment created on MATLAB/ Simulink.

Conflict of Interest

The authors declare no conflict of interest.

Acknowledgment

References

[1] S.N.F. Nahri, S. Du, B. Van Wyk, "Haptic System Interface Design and Modelling for Bilateral Teleoperation Systems," in 2020 International SAUPEC/RobMech/PRASA Conference, IEEE: 1–6, 2020, doi:10.1109/SAUPEC/RobMech/PRASA48453.2020.9041010.

[2] K. Abidi, Y. Yildiz, B.E. Korpe, "Explicit time-delay compensation in teleoperation: An adaptive control approach," International Journal of Robust and Nonlinear Control, **26**(15), 3388–3403, 2016, doi:10.1002/rnc.3513.

[3] P.F. Hokayem, M.W. Spong, "Bilateral teleoperation: An historical survey," Automatica, **42**(12), 2035–2057, 2006, doi:10.1016/j.automatica.2006.06.027.

[4] D.S. Nunes, P. Zhang, J. Sa Silva, "A Survey on Human-in-the-Loop Applications Towards an Internet of All," IEEE Communications Surveys & Tutorials, **17**(2), 944–965, 2015, doi:10.1109/COMST.2015.2398816.

[5] D.A. Lawrence, "Stability and transparency in bilateral teleoperation," IEEE Transactions on Robotics and Automation, **9**(5), 624–637, 1993, doi:10.1109/70.258054.

[6] L.Y. Ang K, Chong G, "PID control system analysis, design, and technology," IEEE Transactions on Control Systems Technology, **13**(4), 559–576, 2005, doi:10.1109/tcst.2005.847331.

[7] D. Sun, F. Naghdy, H. Du, "Wave-Variable-Based Passivity Control of Four-Channel Nonlinear Bilateral Teleoperation System Under Time Delays," IEEE/ASME Transactions on Mechatronics, **21**(1), 238–253, 2016, doi:10.1109/TMECH.2015.2442586.

[8] E. Nuño, L. Basañez, R. Ortega, "Passivity-based control for bilateral teleoperation: A tutorial," Automatica, **47**(3), 485–495, 2011, doi:10.1016/j.automatica.2011.01.004.

[9] A. Gupta, M. Kilchenman, O.' Malley, M.K. O'malley, "Disturbance-Observer-Based Force Estimation for Haptic Feedback MRI-compatible robotics View project Haptic Paddle View project Disturbance-Observer-Based Force Estimation for Haptic Feedback," Article in Journal of Dynamic Systems Measurement and Control, **133**(1), 2011, doi:10.1115/1.4001274.

[10] J. Han, "From PID to Active Disturbance Rejection Control," IEEE Transactions on Industrial Electronics, **56**(3), 900–906, 2009, doi:10.1109/TIE.2008.2011621.

[11] Z. Gao, "Active disturbance rejection control: a paradigm shift in feedback control system design," in 2006 American Control Conference, IEEE: 7, 2006, doi:10.1109/ACC.2006.1656579.

[12] Y. Huang, W. Xue, "Active disturbance rejection control: Methodology and theoretical analysis," Elsevier, **53**(4), 963–976, 2010, doi:10.1016/j.isatra.2014.03.003.

[13] H. Feng, B.-Z. Guo, "Active disturbance rejection control: Old and new results," Annual Reviews in Control, **6**, 1–11, 2017, doi:10.1016/j.arcontrol.2017.05.003.

[14] H. Jin, W. Lan, Y. Chen, "Replacing PI Control With First-Order Linear ADRC," in 2019 IEEE 8th Data Driven Control and Learning Systems Conference (DDCLS), IEEE: 1097–1101, 2019, doi:10.1109/DDCLS.2019.8908981.

[15] J. Han, "A class of extended state observers for uncertain systems," Control and Decision, **10**, 85–88, 1995.

[16] J.Q. Han, "Auto Disturbance Rejection Controller and It's Applications," Control and Decision, **13**, 19–23, 1998, doi:NII Article ID (NAID) 10007201534.

[17] Z. Gao, Y. Huang, J. Han, "An alternative paradigm for control system design," in Proceedings of the 40th IEEE Conference on Decision and Control (Cat. No.01CH37228), IEEE: 4578–4585, 2001, doi:10.1109/CDC.2001.980926.

[18] Z. Gao, "On the centrality of disturbance rejection in automatic control," ISA Trans, **53**(4), 850–857, 2014, doi:10.1016/j.isatra.2013.09.012.

[19] Q. Zheng and Z. Gao, "On practical applications of active disturbance rejection control," in Proceedings of the 29th Chinese control conference, 6095–6100, 2010, doi:INSPEC Accession Number: 11572423.

[20] G. Herbst, "A Simulative Study on Active Disturbance Rejection Control (ADRC) as a Control Tool for Practitioners," Mdpi.Com, **2**(4), 246–279, 2013, doi:10.3390/electronics2030246.

[21] A. Ortiz, S. Orozco, I. Zannatha, "ADRC controller for weightlifter Humanoid robot," in 2019 International Conference on Electronics, Communications and Computers (CONIELECOMP), IEEE: 41–46, 2019, doi:10.1109/CONIELECOMP.2019.8673147.

[22] Z.Q. W. Chenlu, C. Zengqiang, S. Qinglin, "Design of PID and ADRC based quadrotor helicopter control system," in 2016 Chinese Control and Decision Conference (CCDC), 5860–5865, 2016, doi:https://doi.org/10.1109/CCDC.2016.7532046.

[23] W.T. C. Fu, "Tuning of linear ADRC with known plant information," ISA Trans, **65**, 384–393, 2016, doi:doi:10.1109/access.2018.2805782.

[24] Z. Chen, Q. Zheng, Z. Gao, "Active Disturbance Rejection Control of Chemical Processes," in 2007 IEEE International Conference on Control Applications, IEEE: 855–861, 2007, doi:10.1109/CCA.2007.4389340.

[25] G. Niemeyer, J.-J.E. Slotine, "Stable adaptive teleoperation," IEEE Journal of Oceanic Engineering, **16**(1), 152–162, 1991, doi:10.1109/48.64895.

[26] Z. Chen, F. Huang, W. Sun, W. Song, "An Improved Wave-Variable Based Four-Channel Control Design in Bilateral Teleoperation System for Time-Delay Compensation," IEEE Access, **6**, 12848–12857, 2018, doi:10.1109/ACCESS.2018.2805782.

[27] C.P. J. H. Ryu, J. Artigas, "A passive bilateral control scheme for a teleoperator with time-varying communication delay," Mechatronics, **20**, 812–823, 2010, doi:doi:10.1016/j.mechatronics.2010.07.006.

[28] L. Sheng, U. Ahmad, Y. Ye, Y.-J. Pan, "A Time Domain Passivity Control Scheme for Bilateral Teleoperation," Electronics Mdpi.Com, **8**(3), 325, 2019, doi:10.3390/electronics8030325.

[29] X. Xu, B. Cizmeci, C. Schuwerk, E. Steinbach, "Model-Mediated Teleoperation: Toward Stable and Transparent Teleoperation Systems," IEEE Access, **4**, 425–449, 2016, doi:10.1109/ACCESS.2016.2517926.

[30] E.J. RodrIguez-Seda, Dongjun Lee, M.W. Spong, "Experimental Comparison Study of Control Architectures for Bilateral Teleoperators," IEEE Transactions on Robotics, **25**(6), 1304–1318, 2009, doi:10.1109/TRO.2009.2032964.

[31] S. Hirche, M. Buss, "Human-Oriented Control for Haptic Teleoperation," Proceedings of the IEEE, **100**(3), 623–647, 2012, doi:10.1109/JPROC.2011.2175150.

[32] L. Zhao, L. Liu, Y. Wang, H. Yang, "Active Disturbance Rejection Control for Teleoperation Systems with Actuator Saturation," Asian Journal of Control, **21**(2), 702–713, 2019, doi:10.1002/asjc.1767.

[33] Q. Wang, M. Ran, C. Dong, "On Finite-Time Stabilization of Active Disturbance Rejection Control for Uncertain Nonlinear Systems," Asian Journal of Control, **20**(1), 415–424, 2018, doi:10.1002/asjc.1558.

[34] C. Zhang, J. Yang, S. Li, N. Yang, C. Zhang, N. Yang, J. Yang, S. Li, "A generalized active disturbance rejection control method for nonlinear uncertain systems subject to additive disturbance," Nonlinear Dynamics, **83**(4), 2361–2372, 2016, doi:10.1007/s11071-015-2487-1.

[35] S. Frey, A. Dadalau, A. Verl, "Expedient modeling of ball screw feed drives," Production Engineering, **6**(2), 205–211, 2012, doi:10.1007/s11740-012-0371-0.

[36] L. Luo, W. Zhang, Electromechanical Co-Simulation for Ball Screw Feed Drive System, IntechOpen, 2019, doi:10.5772/intechopen.80716.

[37] Y.D. YV Wen-bin, "Modeling and Simulation of an Active Disturbance Rejection Controller Based on Matlab/Simulink," International Journal of Research in Engineering and Science (IJRES), **3**(7), 62–69, 2015, doi:www.ijres.org.

[38] Z. Gao, Q. Zheng, L.Q. Gao, "On Validation of Extended State Observer Through Analysis and Experimentation ADRC: a new paradigm of the science of automatic control View project ADRC: Problem Solving View project On Validation of Extended State Observer Through Analysis and Experimentation," Article in Journal of Dynamic Systems Measurement and Control, **134**(2), 2012, doi:10.1115/1.4005364.

ASTES

Procrustes Dynamic Time Wrapping Analysis for Automated Surgical Skill Evaluation

Safaa Albasri[1,*], Mihail Popescu[2], Salman Ahmad[3], James Keller[1]

[1]*Electrical Engineering and Computer Science, University of Missouri, Columbia, 65211, USA*

[2]*Health Management and Informatics, University of Missouri, Columbia, 65211, USA*

[3]*Acute Care Surgery, University of Missouri, Columbia, 65211, USA*

A R T I C L E I N F O	A B S T R A C T
	Classic surgical skill evaluation is performed by an expert surgeon examining an apprentice in a hospital operating room. This method suffers from being subjective and expensive. As surgery becomes more complex and specialized, there is an increase need for an automated surgical skill evaluation system that is more objective and determines more exactly the skills (or lack thereof) the apprentice has. The main purpose of our proposed approach is to use an existing skill database with known proficiency levels to evaluate the skills of a given apprentice. The skill of the apprentice will be assessed to be similar to the closest skill example found in the database (case-based reasoning). A key element of the system is the skill distance measure employed, as each skill example is a multidimensional time series (sequence) with widely varying values. In this paper, we discuss a new surgery skill distance measure denoted as Procrustes dynamic time warping (PDTW). PDTW integrates the search for exact alignment between two skill sequences using DTW and Procrustes distance as a measure for the similarity. The Procrustes approach is a shape distance analysis that involves rotation, scaling, and translation. We evaluated our proposed distance on three surgical motion data, a widely used JIGSAWS robot surgery dataset, a wearable sensor dataset, and a Vicon motion system dataset. The results showed that the proposed framework produced a better performance for surgeon skill assessment when PDTW was used compared to other time series distances on all three datasets. Also, some experimental results for the JIGSAWS dataset outperformed existing deep learning-based methods.

1. Introduction

This paper is an extension of work initially presented in the E-Health and Bioengineering Conference (EHB) [1] . Recently, the need for objective surgical skills assessment has captured the interest of practitioners and medical institutions due to the ever-increasing complexity and degree of specialization of the surgical procedure [2]. Traditionally, a senior expert surgeon performs direct observation, scores, assess, and gives feedback to the trainee surgeon (apprentice) with less practice in the hospital operating room. This traditional surgical proficiency evaluation approach is problematic due to its subjectivity, time consumption and cost. Furthermore, it is prone to errors and sometimes insufficient as

lacking details related to deficiencies. To address these difficulties, an automated skill assessment procedure is needed for an objective and detailed measure of proficiency levels [3, 4].

As any healthcare domain, surgery is continuously changed by technological advances and medical innovations that alter everyday surgical procedures. The challenge is to assist surgical procedure via the quantifiable data analysis to a better understanding of the surgical operating and to obtain more knowledge about human activities during surgery for advance and further study [5]. A reasonable solution to these challenges is to use technological advances like Robotic Minimally Invasive Surgery (RMIS) that improve overall operating room efficiency [5]. For instance, da Vinci surgical technology provides data-driven that potentially helps optimize and develop training skills

* Corresponding Author: Safaa Albasri, University of Missouri, USA.
saaxfc@mail.missouri.edu

for surgeons [6]. This information includes kinematic and video data that conduct a useful resource of quantifiable human motion during surgical operating [7, 8]. Wearable sensing devices that provide detailed motion information for surgical activities are a further example [9]. These recorded data give spacious resources to assess surgical proficiencies by modeling and analyzing descriptive mathematical approaches. The emergence of using machine learning methods with recent robotic surgery systems such as da Vinci and wearable sensing devices via data-driven enable and encourage developers to build and analyze automatic models for evaluating surgeon expertise and may help better coaching potential apprentices [10–12] .

Different earlier works focused on the automated surgical assessment seen good progress. The current techniques for objective surgical evaluation can be divided into three main research areas [10, 13]: 1) surgeon skill assessment, 2) surgical task analysis, and 3) surgemes recognition. These methods considered the surgeon movement using either: 1) kinematic information recorded by a robotic surgical system, 2) video records and 3) wearable sensors data. In this paper, we focused on the surgical skill evaluation based on kinematic and wearable sensors information. One of the initial works used Hidden Markov models (HMM) [14] to evaluate the surgical skills. This approach is structured-based and depends on the number of training samples, tuning parameters and it takes massive pre-processing. This type of model needs complicated preprocessing [3] and leads to low performance with a low number of samples [14]. Another method was proposed by [3] to predict the surgeon skill level (expert and novice) based on movement features of the surgical arms using logistic regression (LR) and support vector machines (SVM) classifiers for suturing surgical task. They extended their work to include eight global movement features (GMF) in [15], they applied LR, SVM, and kNN classifier to distinguish between the previous expertise levels for suturing and knot tying surgical tasks. In [16], a framework based on trajectory shape using DTW and k-nearest neighbor classifier proposed for surgical skill evaluation. This model can also provide online performance feedback through training. More recently, [13] proposed an approach based on symbolic aggregate approximation (SAX) and vector space model (VSM) to identify distinctive patterns of surgical procedure. They used the SAX to obtain the sequence of letters by discretizing the time series first. Then they utilize the VSM to find the discriminative patterns that represent a surgical motion which finally used them to be classified. A variety of holistic analysis features and a weighted features integrated approach proposed by [9] for automated surgical skill evaluation and GRS score prediction. These holistic features include approximate entropy, sequential motion texture, discrete Fourier and discrete cosine transform. They used the nearest neighbor as a classifier and linear support vector regression (SVR) for prediction. The works of literature mentioned above used the kinematic data information obtained from RMIS for surgical skill assessment. However, none of these methods were applied to the wearable sensors data like accelerometer which might give more information about the surgeon's motion during a surgical practice.

Recently, several advanced techniques applied the convolution neural network and deep learning methods for automated surgical skill evaluation. A parallel deep learning framework was proposed by [17] to identify the surgeon skill and task recognition. In their approach, they used a fusion technique between convolution neural networks and gated recurrent networks. Alternative deep convolution neural architecture based on ten layers proposed by [12] for surgical expertise evaluation. Another parallel deep learning approach was proposed in [18] by combining the LSTM recurrent network and CNN to indicate the skill levels. Additionally, recent studies have suggested approaches that use motion from videos [19,20] and wearable sensors to evaluate surgical skills [21,22]. These methods platform various features to perform Objective Structured Assessment of Technical Skills (OSATS) assessments. An approach proposed for surgical skill assessment is based on the acceleration data of both hands performing a basic surgical procedure in dentistry [2]. Also, an entropy-based features technique that utilizes both video and accelerometer data proposed for surgical skill assessment [4]. Despite these techniques which are building the basis and inspire performance results in the surgical skill area, however, some limits and drawbacks occur for the existing methods. some methods need predefined boundaries of the surgemes which done usually by a chief surgeon, i.e., consuming a large time. In other methods, decomposing the motion sequence requires a massive and complicated preprocessing in addition to a deficiency of robustness. Alternatively, the need to developing a new distance measure might have an advantage to a more robust and accurate assessment framework.

In this paper, our contribution to this work can be abridged as follows: 1) we defined a new surgical skill distance combined the best alignments between two multidimensional signals using DTW and measuring the distance between the two aligned sequences using Procrustes analysis 2) we proposed an automated skill classification framework based on using PDTW and kNN technique in the proposed framework to distinguish between the expertise levels focusing on overall performance 3) we investigated the proposed framework on a wearable sensor data for a surgical task. The purpose of this work is to present a technique that handles different kinds of sensor data in addition to the existing public JIGSWAS dataset. Some surgery motion results obtained by a Vicon camera with a 3D marker-based system and wearable device data are examples of the data we use.

2. Methodology

In this section, we illustrate the main components of our proposed framework, which are: motion alignment, Procrustes distance, and skills classifier, as shown in Figure 1. First, DTW is used to align two multidimensional time series performed by surgeons, while the Procrustes distance calculates similarity measure. Lastly, the skill levels of the surgeon are classified by kNN.

2.1. Similarity Measure

To obtain a useful classification, defining a reasonable distance is a crucial element to measure between two surgery tasks. Each

surgery task is represented by a set of features obtained from the traces (time series) of the motion capture sensors. One possible method is the Euclidean distance.
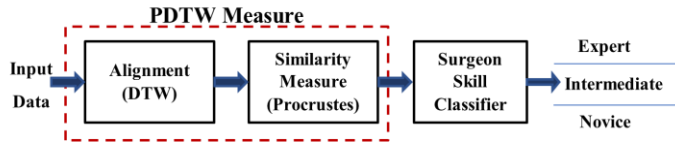
Figure 1: kNN based PDTW evaluation Framework

Euclidian distance is simple and widely used, whereas, it has some limitations and disadvantages. The Euclidean method is very sensitive to outlier and it is suffering from noise, shifting, and requires both signals to have the same length. Thus, we need a measure that can handle sequences with different lengths because the same surgery task might have different lengths even when operated by the same surgeon. A warping distance measure such as the Dynamic Time Warping (DTW), is one solution to do the job. The DTW can process time series with different lengths, it expands or contracts both signals (aligns them) such that their length becomes equal [23].

Let $X_{n \times v} = [X_1, X_2, \dots, X_n]$ and $Y_{m \times v} = [Y_1, Y_2, \dots, Y_m]$ be two sequences having v features and of length n and m respectively. To align X and Y, we form a two-dimensional ($n \times m$) grid distance. Each point d_{ij} of the grid corresponds to the distance measure (usually Euclidean) between every possible combination of two instances x_i from X and y_j from Y of the same features length (v) as follow [24]:

$$d_{ij}(x_i, y_j) = \sqrt{\sum_{k=1}^{v} (x_{ik} - y_{jk})^2} \tag{1}$$

The next step is to find the warping path through the grid, the path that attempts to minimize the total distance (warping cost) and give the best match between two signals and satisfy boundary conditions, continuity, and monotonicity constraints. It is usually achieved by using a dynamic program to calculate the cumulative distance $\gamma(i, j)$, which is the distance of the current cell (d_{ij}) and the minimum of the cumulative distance of the adjacent cells [24]:

$$\gamma(i, j) = d_{ij} + \min\{\gamma(i-1, j-1), \gamma(i-1, j), \gamma(i, j-1)\} \tag{2}$$

Despite the wide use of DTW in many applications and is a more robust distance measure than Euclidean distance, it fails for complex multidimensional signals. Also, when the unevenness occurred in the Y-axis, DTW can produce singularities by warping the X-axis. Inflection points, valleys, and peaks features can cause DTW to fail to align two signals properly [24].

The Procrustes analysis is a standard method in statistical analysis to compare the similarity of shape objects [25, 26]. The Procrustes distance is a shape metric that involves matching two shapes using similarity transformations (rotation, reflection, scaling, translation) to be as close as possible in the least-squares sense [27]. The Procrustes analysis also can estimate the mean shape to examine the shape variability in a dataset [28].

Assume X_1 and X_2 be two configuration matrices of the same $k \times m$ dimension (k points in m dimensions) that can be centered (normalized) using the following equation [28]:

$$(X_i)_c = CX_i \quad, \quad i = 1,2 \tag{3}$$

$C = H^T H$ is the centering matrix and H is the Helmert submatrix, let Z_1 and Z_2 be the pre-shapes unit size of X_1 and X_2 respectively, where the original configuration is invariant under the scaling and translation with the pre-shape [28]:

$$Z_i = \frac{(X_i)_H}{\|(X_i)_H\|} = \frac{H(X_i)}{\|H(X_i)\|} \quad, \quad i = 1,2 \tag{4}$$

$$(X_i)_H = HX_i \quad, \quad i = 1,2 \tag{5}$$

The full Procrustes distance between X_1 and X_2 is achieved by fitting the pre-shape Z_1 and Z_2 as closely as possible as the following [25]:

$$D_P(X_1, X_2) = \inf_{s,a,b,\theta,} \|Z_1 - Z_2\, s\, e^{j\theta} - (Z_2 + jb)1_k\| \tag{6}$$

where $\|.\|$ is the Euclidean norm, s is the scale, θ is the rotation, and $(a + jb)$ is the translation, 1_k is a k-dimensional vector of ones.

This work presents a distance measure PDTW based on a pairwise synchronization between two time series by utilizing a combination of Procrustes distance and DTW to overcome the drawbacks of using DTW alone. First, we use DTW as an alignment approach and then use Procrustes as a distance measure. DTW is used to locate the best matching between two signals, whereas Procrustes is used to minimize the distance.

2.2. Classification

The simplicity of the k-Nearest Neighbors (kNN) method and its reasonable results made it a handy feature classifier. It predicts the new unlabeled query point by using the labels of training data based on their similarity measure. kNN classifier assigns a label for the test point to the majority label of the k-closet neighborhoods [29]. We found k = 3 is a reasonable value and the one we utilize in this paper.

3. Experimental Evaluation

We used three datasets to evaluate the proposed PDTW-kNN model on the public surgical data JIGSAWS [7], and our two data MU-EECS [30], and EM-Cric. The JIGSAWS is a minimally invasive surgical skill assessment working set consist of various fundamental surgical tasks. Each task performed by a surgical surgeon with a different proficiency degree; an expert surgeon who performs the da Vinci Surgical System (dVSS) more than 100 hours of training, a novice surgeon who practice less than 10 hours on dVSS, and an intermediate surgeon (practice on dVSS between 10 and 100 hours). A motion capture based on markers, a Vicon system is used to collect the data from a resident surgeon in the MU-EECS data. The surgeon presented a tracheostomy surgery performed the same procedure six times. The EM-Cric data includes data from four surgeons with different expertise levels who performed the Emergency Cricothyrotomy task. Each surgeon performs the task four times, where the wrist wearable sensors are used to capture both hand motions. More details about the three datasets in the following parts:

3.1. JIGSAWS Data

We evaluate the proposed PDTW-kNN method for surgical proficiency assessment on a public widely used JIGSAWS dataset [7]. Moreover, we use this dataset for direct comparisons with other state-of-the-art approaches for surgical skill evaluation. MIS surgeons performed many types of elementary procedures on Da Vinci robotic systems because it gives confidence, precision, and real-time feedback to improve overall surgical treatment for the patient in the operation room [31].

JIGSAWS dataset consists of kinematic and video data collected from surgical surgeons with various surgical robotic skills performing basic surgical training curricula. All surgeons were right-handed: two expert surgeons (E) with > 100 robotic surgical practice hours, four novice trainee surgeons (N) having < 10 practice hours, and four intermediate surgeons (I) reported between 10 and 100 surgical robotic experience practice hours. The dataset provides two types of data: video and kinematic records for each trail get done by a subject in each task. All the subjects were required to do three fundamental surgical tasks five times repetitively. In this work, we use only kinematic data captured as 76-dimensional time series at 30 Hz from the da Vinci Surgical System (dVSS) using its Application Programming Interface (API). The three elementary surgical tasks are identified as suturing (SU), knot-tying (KT), and needle-passing (NP). Figure 2 presented sample frames of the three surgical tasks achieved by a surgical surgeon and defined them as follows [7]:

- Suturing: the surgeon picks the needle up, first and advances it to the bench-top model toward the incision. Then, the subject stitches up the needle through a dot-marked tissue on one aspect of the incision and extracts it out from the corresponding dot-marked on the other part of the incision. Lastly, the surgeon passes it to the right-hand and repeats the same process till the surgeon gets four times in total.

- Knot Tying: the surgeon makes one tie after selecting one side of a stitch that is tied to an elastic tube connected by its rims to the surface of the bench-top model.

- Needle Passing: the surgeon selects the needle. Then, passes the needle from the right side to the left through 4 tiny metal hoops that are placed over the surface of the bench-top model.
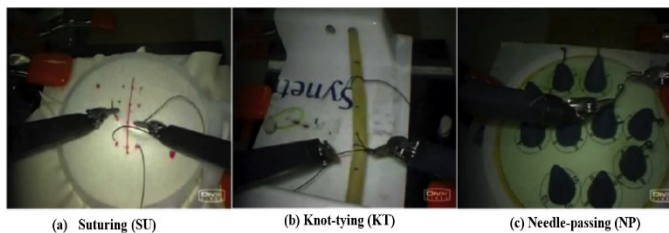
Figure 2: RMIS basic surgery tasks [7].

This dataset consists of a surgical manual annotation for the surgical skill of each trial. An annotating surgeon, with extensive robotic surgical experience, watched the entire trial and appointed a score based on a modified global rating score (GRS). GRS is the measure of the surgical technical skill of the surgeon who

performed the trial. GRS presents the total score of six elements illustrated in Table I. Where each component rating scale is between 1 and 5 and the best with a higher total score [7].

Table 1: Elements of Global Rating Score (GRS) [7]

Element	Rating scale		
Respect for tissue	Force on tissue	Careful tissue handling	Consistent handling
Suture/needle handling	Poor knot tying	Majority appropriate	Excellent suture
Time and motion	Unnecessary moves	Efficient time/ unnecessary moves	Economy moves/ Max efficiency
Flow of operation	Frequent interrupted	Reasonable progress	Planned operation/ efficient transitions
Overall performance	Very poor	Competent	Superior
Quality of the final product	Very poor	Competent	Superior
Rating score	**1**	**3**	**5**
Min. score =	∑ = 6	Max. score =	∑ = 30

3.2. MU-EECS Vicon Data

In this dataset, a Vicon system and IR reflective markers were used synchronously to trace and visualize the arms movement of the surgeon while carrying out a surgical procedure. Ten IR reflective markers were placed in different positions on both surgeon's arms as displayed in Figure 3 (a). Also, we can see seven Vicon cameras were located inside the lab to capture the resident surgeon's motions. The MU-EECS includes data presented by a resident surgeon who performed the same tracheostomy surgical procedure six times repeatedly. The earliest three procedures repeat in a consistently appropriate manner, whereas the remaining practices were performed with inaccurately way. This working set was collected through a project at the Center for Eldercare and Rehabilitation Lab in the Dept. of EECS at the University of Missouri Columbia [30].
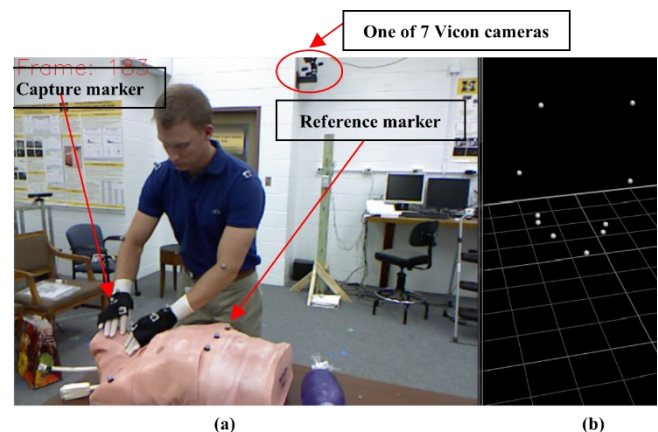
Figure 3: Tracheostomy surgery with Vicon Camera

3.3. EM-Cric Dataset

Emergency Cricothyrotomy (Cric) is a procedure for potentially lifesaving a human being under a high-stress situation, it happens when a person fails to restore enough oxygenation. Cric

is an incision through the skin and cricothyroid, which results in a better patient airway [32]. There are three main steps of the surgical Cric procedure skin incision, incision cricothyroid, and endotracheal tube placement membrane [33].

The EM-Cric dataset includes data from four surgical surgeons (subjects) who performed the Cric procedure with varying expertise levels to study skilled surgical human motion. Two residents reported as Novice (N) surgeon, one intermediate (I) surgeon, and one expert (E) surgeon, respectively. All surgeons are reportedly right-handed except one lefty hand. All surgeons perform the Cric procedure five times on a Trauma Man Surgical Simulator at the Medical Intelligent System Laboratory (MISL) in the Medicine School at the University of Missouri-Columbia. We placed the wristband sensors on both wrists of the surgeon's hands to capture the data, as shown in Figure 4. We use low cost synchronized data transmission MetaMotionR (MMR) sensors introduced by MbientLab. MMR is a 9-axis IMU wearable device that provides continuous monitoring of movement and real-time sensor data [34].

Figure 4: Cric surgical operation on TraumaMan Simulator by a medical surgeon.

The data was conducted for a total of three male right-handed, and one female left-handed participants with different expertise levels were recruited for this study. Two MMR sensors were used for the Cric procedure task, one attached to each wrist of the surgeon's hand. The captured data consists of three-dimensional acceleration with respect to time for each accelerometer, and result in 6-dimensional time series for both sensors. For this study, we use only raw accelerometer data which range was set to ±16 g. The sampling rate of data collection was set to 100Hz.

3.4. Performance Evaluation

We used different cross-validating schemes to evaluate our skill assessment framework on both kinematic and accelerometer data to compare our results with other approaches.

- Leave-One-Trial-Out (LOTO): For each surgical task, training all the trials except one i-th trial reserved for testing ($i = 1, .., N$). N is the total number of trials in a task.

- Leave-One-Supertrial-Out (LOSO): Different from LOTO setup, where we created five folds ($j = 1, 2..5$). The j-th fold combines all the j-th trials from all the surgeons for a given surgical task. Then, we repetitively training on four sets and keeping a single set for testing and reporting the average

classifying results. The fold j-th is known as supertrial j-th. In this scheme, the robustness of a technique can be assessed by keeping a supertrial out each time [7]. Also, repeating the task in a row can possibly impact the performance of the surgical apprentice in terms of boredom or tiredness, hence keeping the supertrial out perhaps catch that effect on the surgeons.

To evaluate the performance of our proposed technique and to quantitatively compare with other methods, we used the mean accuracy of surgical classification for each output class on the data-driven to validate the performance. The average accuracy, defined in (10), is the percentage of the sum of accurately predicted (TP+TN) over the total number of predictions (TP+TN+FP+FN) [35]:

$$ACC = \frac{T_P + T_N}{TP + TN + FP + FN} \tag{10}$$

where T_P, T_N, F_P, and F_N represent the number of true positive (predicted correctly belong to the target class), true negative (correctly classified not belong to the target class), false positive (incorrectly predicts to the target class), and false negative (incorrectly predict not belong to the class level) respectively [35].

4. Results and Discussions

In this part, the proposed approach and evaluation metrics described in the preceding sections were evaluated on kinematic and accelerometer data. Also, the results for all the datasets that were explained previously were reported in the following sections, respectively.

4.1. JIGSAWS Dataset

For JIGSAWS data, we perform two sets of experiments for the LOSO validation set up to identify the three expertise levels (E, I, and N) on our proposed approach. For the first assortment, we made use of all the 76-dimensional movement features of the time series. Whilst, in the second set we utilized just the coordinates features (x, y, z) of the two hands.

Figure 5 (a) illustrates the comparison of classification accuracy for surgical expertise levels versus k (the number of neighborhoods) in each task using all kinematic information. For the LOSO scheme, the improvement in accuracy for almost all cases of k of our kNN classifier based PDTW for all surgical tasks. e.g., the mean accuracy for all tasks at k = 3 is 95.7%. Also, kNN-PDTW provide an advantage over the traditional method (DTW) with a reduction in sensitivity to changing the number of neighbors (k) in k-NN.
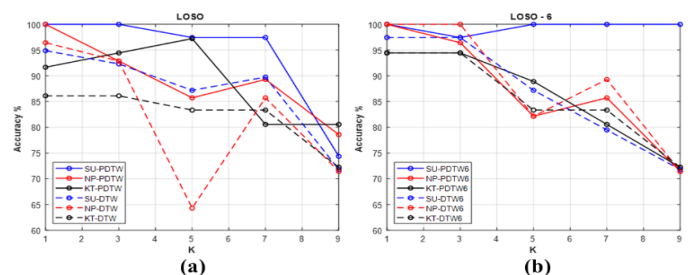
Figure 5: Accuracy of the proposed approach using PDTW and DTW as a function of k.
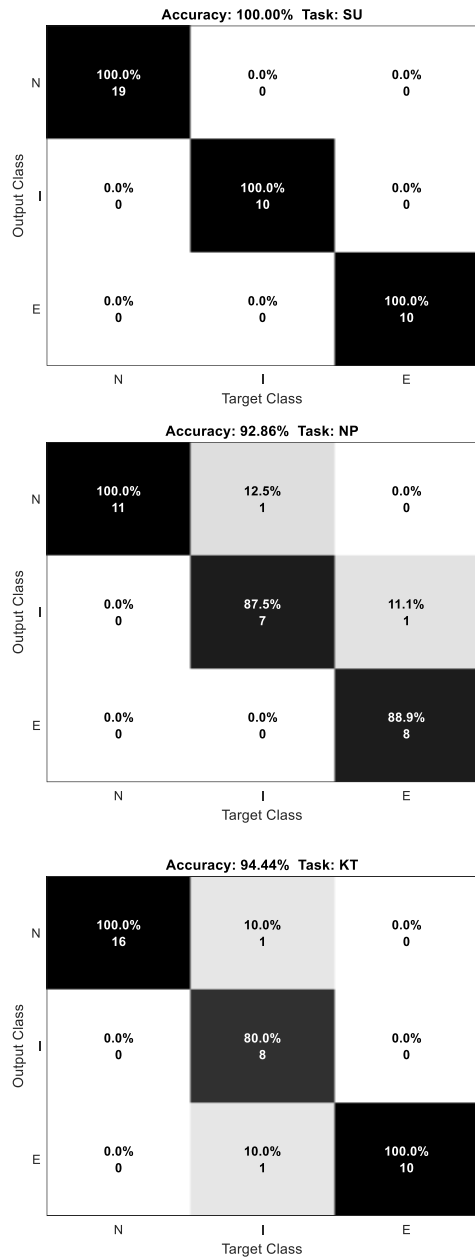
Figure 6: kNN-PDTW Confusion matrix of the three tasks SU, NP, KT for LOSO at k=3.

We also perform another experiment by using only 3D location information of the two hands for the LOSO scheme. Some interesting intuitions results can be seen in Figure 5(b). The accuracy results of the proposed kNN-PDTW6 using the Cartesian coordinates almost achieved the same results as using all the 76-dimensional motion data. This can be explained by the fact that Procrustes analysis works on the similarity of shapes and the motion data are traces in three dimensions space, which encourages us to use the wearable sensors later.

For a further comprehensive comparison, the confusion matrices result for each task is shown in Figure 6 at k=3. For the suturing task, surgeon expertise levels are 100% correctly classified. However, for the other tasks, the misclassifying happened when distinguishing between intermediate level and

other levels which in turn reduced the average accuracy to about 94% and 93% for knot tying and needle passing tasks, respectively. We must put into our perspective that each surgeon performs the task in a different style from other surgeons, even within the same expertise level regardless of the hours spent on practice. Because individual surgeons like to improve their proficiencies following their mentor. Thus, small differences between an intermediate surgeon and an expert make the classifier to introduce an error to recognize their skill levels and vice versa. The same case between intermediate and novice surgeons happened.

Another interest intended of our analysis, that we calculate the pairwise PDTW distance inside a group of expert-expert, expert-intermediate, and expert-novice surgeons, separately for each task. Figure 7 illustrates the boxplot of each group distance in each task. From the results, it is clear that the smallest distance is among expert surgeons, and then between expert-intermediate surgeons followed by the expert-novice group for each task. Also, we can see that the differentiating among expert-intermediate surgeons is more complicated in needle-passing than other tasks. one explanation is the needle-passing might be more challenging to learn or more complicated than suturing or knot tying. This might be related to the complication level of the task as can be seen in Figure 6 for the needle-passing task where an expert surgeon classified as intermediate surgeon mistakenly.
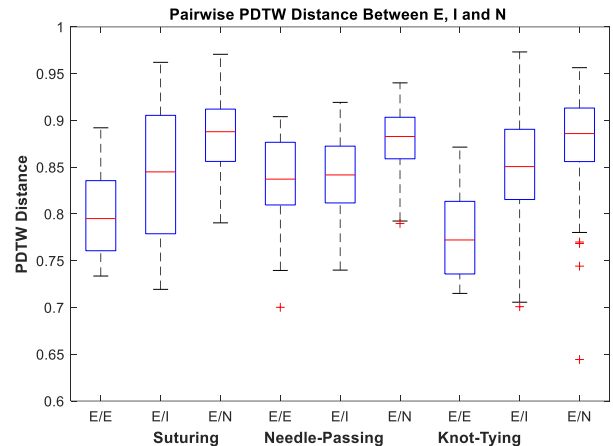
Figure 7: PDTW-distance within E/E, E/I, and E/N surgeons in each task.

Table 1 shows the classification accuracy results of our proposed skill assessment for the JIGSAWS dataset using the kinematic data only. Also, we report the state-of-the-art results for comparative intent under the LOSO validation scheme for each task separately. The results show that the proposed kNN-PDTW properly recognizes the surgeon skill levels and matched the work from CNN [36] for suturing. From Figure 7 we can see that it is straightforward to differentiate between the expertise levels with the help of using PDTW measure. Additionally, the NN classifier learned the dynamic information which already comes from various motion patterns of the surgeons that might benefit this result. In knot-tying, our proposed kNN-PDTW approach outperforms both CNN [36] and Deep Learning [12] approaches in terms of accuracy. Also, our results were near the CNN+LSTM+SENET method [18]. Our results were improved more for suturing and knot-tying tasks than the needle-passing

task, and we did slightly better than [12] in this task. The small distinctions between intermediate surgeons with other surgeons in this task illustrated in Figure 7 might explain the less performance on the needle-passing task. Furthermore, we can notice from Table I that no technique is suitable for the three tasks. In other words, an integration methodology of various approaches is needed for surgical proficiency assessment purposes for these tasks.

Table 2: Skill Assessment Classification Comparative of kNN-PDTW Performance using LOSO for JIGSAWS Data.

Approach		Accuracy		
		SU	NP	KT
Farad [15]	kNN	89.7%	-	82.1%
	LR	89.9%	-	82.3%
	SVM	75.4%	-	75.4%
Wang [12]		93.4%	89.8%	84.9%
Forestier [13]		89.7%	96.3%	61.1%
Fawaz [36]		**100%**	**100%**	92.1%
Anh [18]		98.4%	98.4%	**94.8%**
kNN-PDTW (proposed)		**100%**	92.8%	94.4%

As mentioned previously in section 3.1, the modified global rating score measures the surgical technical skill done by the annotation surgeon for the entire trial provided in the JIGSAWS dataset. Figure 8 presents the boxplot of the surgeons' GRS scores for each task. We can see from this figure, the consistency of the expert surgeons compared to the novice and intermediate surgeons in all tasks. Where the lowest variance the expert surgeons have ultimately implied their steadiness. Another interesting viewpoint from Figure 8, that we can see the scores challenge to differentiate among the surgeon's proficiency in the needle-passing task, which produces the misclassifications. One more thing to be observed in Figure 8, some intermediate subjects score better than expert subjects. This means that these surgeons might be eligible to be in a higher skill level or position.
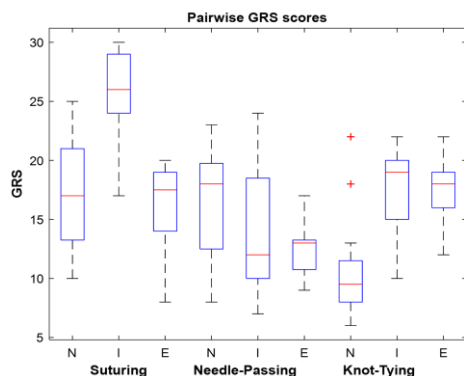
Figure 8: Boxplot of GRS scores for each task.

4.2. MU-EECS dataset

We experiment on the tracheostomy dataset to classify the trial level as either *Good* or *Bad*. In this experiment, we calculate the pairwise PDTW distance among the six trials that operated by a

resident surgeon [30]. Figure 9 presents the resulting distance of this experience for the MU-EECS dataset, where the yellow color is the farthest and the closer trials to each other are in darker blue.
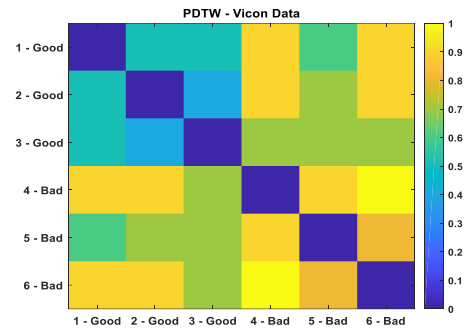
Figure 9: PDTW distance matrix for MU-EECS data.

Overall, the *Good* trials, which are the first three trials in Figure 9, has a similarity less than or equal to 0.5. e.g., about 0.3 is the difference between trials 2 and 3. On the other hand, the pairwise distance between *Bad* procedures, the last three trials, is greater than 0.7 in distance to each other. Also, we can see those *Good* procedures are nearly 0.7 far away from *Bad* trials except among trial-Good 1 and trial-Bad 5 about 0.55 difference.

Another insight from Figure 9, it is straightforward to cluster the trials into *Good* (the upper left corner) and *Bad* (in the lower right corner). That means the PDTW distance helps accurately to identify between the trials in this task where each group looks to cluster together. Finally, the boxplot of the PDTW measure among the Good and Bad trials separately is presented in Figure 10. In this figure and from a statistical viewpoint comparison, the mean and variance of the *Good* procedures ($\mu_{G-G} = 0.12$, $\sigma_{G-G} = 0.08$) is less than the *Bad* procedures ($\mu_{B-B} = 0.21$, $\sigma_{B-B} = 0.16$) which is consistent along with prior results.
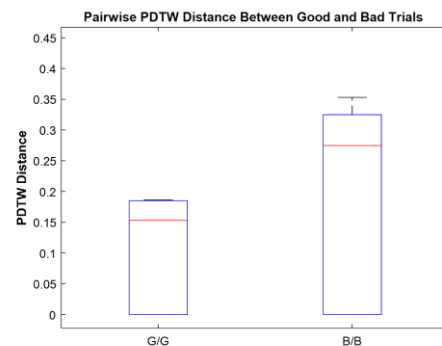
Figure 10: Boxplot of PDTW distance for MU-EECS dataset.

4.3. EM-Cric dataset

For the EM-Cric dataset, we performed two sets of cross-validation schemes, the LOTO for the trial level and the LOSO to identify the surgical proficiency levels (Expert, Intermediate, or Novice) of the subjects. As we mentioned previously in section 3.3, this dataset includes accelerometer data collected from four surgeons (expert, intermediate, and two novices) who performed the same task five times repetitively.

Before evaluating the classification accuracies, we calculate the pairwise distance among all the collected trials. Figure 11 (a) and (b) illustrate pairwise distance matrices comparison between DTW and PDTW measures, respectively. The first five trials represent the expert surgeon procedures, the second five stand for the intermediate surgeon trials, and the remaining ten trials are for the two novice surgeons, all performing the same task. Where the similar performances made by participants are indicated in strong blue squares in this figure. Also, the three separate square blocks in Figure 11 (b) give a visual insight for the possibilities of clustering expertise levels where the task is performed by different surgeons for this data using only the accelerometer data. Also, we can notice from this figure that PDTW distance separates well between expertise levels better than using DTW distance alone. The results in Figure 11 (b) shows that the expert surgeon has a dissimilar pattern to both intermediate and novice surgeons. Moreover, novice surgeons themselves are quite like each other.
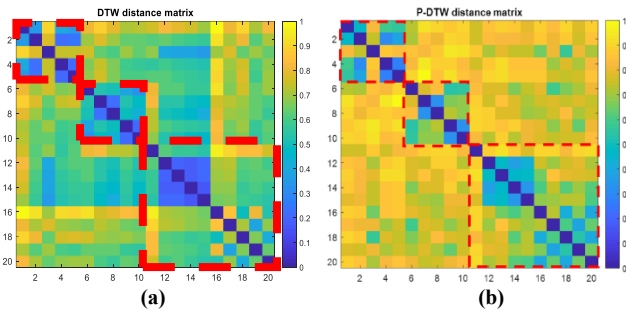
Figure 11: The pairwise distance for each trial on EM-Cric using (a) DTW and (b) P-DTW
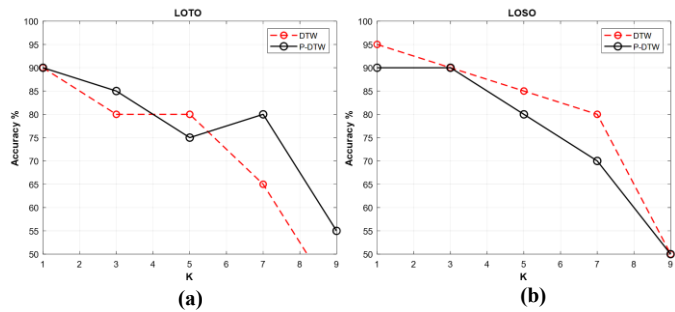
Figure 12: Classification accuracy as a function for k (a) LOTO and (b) LOSO cross-validation for Cric data

First, we performed experiments to compare how DTW and PDTW perform for classifying surgeon levels on Cric data using both LOTO and LOSO configurations. Figure 12 presents comparisons of the classification accuracy results of the proposed model for different values of K (number of neighbors) using LOTO and LOSO cross-validations, respectively. Figure 12 (a) shows that the results of our method based on PDTW performs better compared to using only DTW distance. These results indicate that our approach can identify the surgical skill levels well at trial levels because it utilizes the Procrustes analysis. Secondly, Figure 12 (b) presents the kNN-PDTW performance for the LOSO setup for the Cric dataset. The kNN based DTW approach performs slightly better for the accelerometer data. Whereas our approach results were improved, and the performance was

reasonably well and still having a higher classification accuracy of 90% at k = 3.

Figure 13 shows the confusion matrix of our kNN based PDTW for surgeon expertise at k = 3 for Cric data using LOSO configuration. We can see that the intermediate surgeon was classified correctly, whereas both expert and novice surgeons were misclassified in one trial. From Figure 11 (b), we can notice that there is one trial (#3) from the expert surgeon that seems far from other trials with Expert trials and the same for novice surgeons with the trial (#11) in the same figure. The average classification accuracy was 90%.
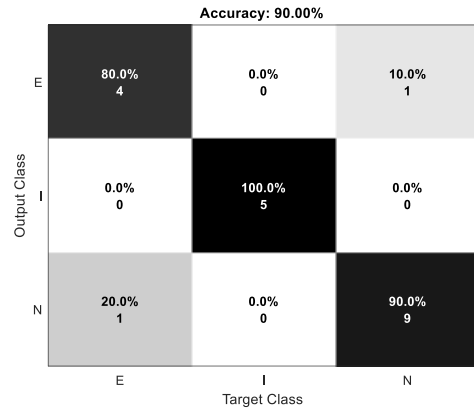
Figure 13: kNN-PDTW Confusion matrix for LOSO at k=3 for Cric data
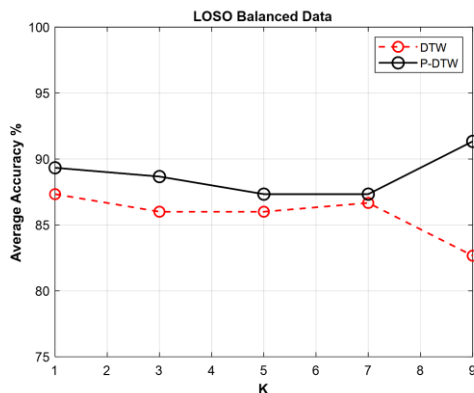
Figure 14: Balanced data classification results for the Cric data

Lastly, for a more thorough comparison, we perform another experiment for Cric data by using balanced data and evaluating using LOSO with a k-fold cross-validating scheme. The balanced data was obtained by having equal trials from each surgeon level. The reason we chose the balanced data experiment because we had two novice surgeons, one expert, and one intermediate surgeon. In this conduct experiment, we pick five trials randomly from a total of ten novice surgeon's trials and put them together with other trials from the expert surgeon and the intermediate surgeon trials. Then repeat the process ten times and report the average classification accuracy. Figure 14 shows the comparison classification accuracy as a function of k between PDTW and DTW based kNN classifier. Furthermore, Figure 15 presents the confusion matrix of kNN-PDTW predictions of the surgical skill classes. We can see from both above figures that the average accuracies of using PDTW much better than using DTW for all

values of k. Also, our approach using balanced data achieved average classification accuracy about 3% higher than using unbalanced data. the balancing data helps classified the novice surgeon's skill correctly with 100%.

Figure 15: Balanced data confusion matrix for the Cric data

5. Conclusions

In this paper, we define a new surgery skill distance measure PDTW. It incorporates the exploration for best alignment using DTW and the similarity measure using Procrustes distance among two multidimensional time series. We show that the proposed framework based PDTW can enhance the overall performance for surgical proficiency evaluation. We attain an average accuracy of 97% for the JIGSAWS dataset and the results outperform most state-of-the-art methods using kinematic data and are comparable to techniques based on deep schemes.

Also, here we have examined the use of wearable motion sensor devices in proficiency assessment to achieve an entirely objective evaluation. Although our results are encouraging, there are quite a few limitations. The number of subjects is relatively small, not as desired. Furthermore, only one surgical task the subjects were asked to work on and there is no break between the trials which might impact the performing of the trials. Despite the limitations, our results indicate that PDTW distance can be used by classifying techniques to categorize the expertise levels accurately. In the future, we plan to increase the number of participants with a variety of expertise which might have the potential to give more information and robustness to our method. Also, more tasks to be utilized instead of only a given surgical task. Furthermore, consider using another or a combination of classifiers to improve the overall classification accuracy for skill assessment.

References

[1] S. Albasri, M. Popescu, J. Keller, "A novel distance for automated surgical skill evaluation," in 2019 7th E-Health and Bioengineering Conference, EHB 2019, 2019, doi:10.1109/EHB47216.2019.8970029.

[2] G. Arbelaez-Garces, D. Joseph, M. Camargo, N. Tran, L. Morel, "Contribution to the objective assessment of technical skills for surgery students: An accelerometer based approach," International Journal of Industrial Ergonomics, **64**, 79–88, 2018.

[3] M.J. Fard, S. Ameri, R.B. Chinnam, A.K. Pandya, M.D. Klein, R.D. Ellis, "Machine learning approach for skill evaluation in robotic-assisted surgery," Lecture Notes in Engineering and Computer Science, **2225**, 433–437, 2016.

[4] A. Zia, Y. Sharma, V. Bettadapura, E.L. Sarin, I. Essa, "Video and accelerometer-based motion analysis for automated surgical skills assessment," International Journal of Computer Assisted Radiology and

Surgery, **13**(3), 443–455, 2018.

[5] F. Lalys, P. Jannin, "Surgical process modelling: A review," International Journal of Computer Assisted Radiology and Surgery, **9**(3), 495–511, 2014, doi:10.1007/s11548-013-0940-5.

[6] Intuitive Surgical, 2020, doi:https://www.intuitive.com/en-us.

[7] Y. Gao, S.S. Vedula, C.E. Reiley, N. Ahmidi, B. Varadarajan, H.C. Lin, L. Tao, L. Zappella, B. Béjar, D.D. Yuh, C.C.G. Chen, R. Vidal, S. Khudanpur, G.D. Hager, "JHU-ISI Gesture and Skill Assessment Working Set (JIGSAWS): A Surgical Activity Dataset for Human Motion Modeling," Modeling and Monitoring of Computer Assisted Interventions (M2CAI) – MICCAI Workshop, 1–10, 2014.

[8] C.E. Reiley, H.C. Lin, D.D. Yuh, G.D. Hager, "Review of methods for objective surgical skill evaluation," Surgical Endoscopy, **25**(2), 356–366, 2011.

[9] A. Zia, I. Essa, "Automated surgical skill assessment in RMIS training," ArXiv, **13**(5), 731–739, 2017.

[10] M. Jahanbani Fard, Computational modeling approaches for task analysis in robotic-assisted surgery, Ph. D. Thesis, Wayne State University, 2016.

[11] H.C. Lin, I. Shafran, D. Yuh, G.D. Hager, "Towards automatic skill evaluation: Detection and segmentation of robot-assisted surgical motions," Computer Aided Surgery, **11**(5), 220–230, 2006, doi:10.1080/10929080600989189.

[12] Z. Wang, A.M. Fey, "Deep learning with convolutional neural network for objective skill evaluation in robot-assisted surgery," ArXiv, **13**(12), 1959–1970, 2018.

[13] G. Forestier, F. Petitjean, P. Senin, F. Despinoy, A. Huaulmé, H.I. Fawaz, J. Weber, L. Idoumghar, P.A. Muller, P. Jannin, "Surgical motion analysis using discriminative interpretable patterns," Artificial Intelligence in Medicine, **91**(July), 3–11, 2018, doi:10.1016/j.artmed.2018.08.002.

[14] L. Tao, E. Elhamifar, S. Khudanpur, G.D. Hager, R. Vidal, "Sparse hidden Markov models for surgical gesture classification and skill evaluation," Lecture Notes in Computer Science (Including Subseries Lecture Notes in Artificial Intelligence and Lecture Notes in Bioinformatics), **7330 LNCS**, 167–177, 2012, doi:10.1007/978-3-642-30618-1_17.

[15] M.J. Fard, S. Ameri, R. Darin Ellis, R.B. Chinnam, A.K. Pandya, M.D. Klein, Automated robot-assisted surgical skill evaluation: Predictive analytics approach, International Journal of Medical Robotics and Computer Assisted Surgery, **14**(1), 2018, doi:10.1002/rcs.1850.

[16] M.J. Fard, S. Ameri, R.D. Ellis, "Skill Assessment and Personalized Training in Robotic-Assisted Surgery," CoRR, 2016.

[17] Z. Wang, A.M. Fey, "SATR-DL: improving surgical skill assessment and task recognition in robot-assisted surgery with deep neural networks," in 2018 40th Annual International Conference of the IEEE Engineering in Medicine and Biology Society (EMBC), IEEE: 1793–1796, 2018.

[18] X.A. Nguyen, D. Ljuhar, M. Pacilli, R.M. Nataraja, S. Chauhan, "Surgical skill levels: Classification and analysis using deep neural network model and motion signals," Computer Methods and Programs in Biomedicine, **177**, 1–8, 2019, doi:10.1016/j.cmpb.2019.05.008.

[19] Y. Sharma, V. Bettadapura, T. Ploetz, N. Hammerla, S. Mellor, R. McNaney, P. Olivier, S. Deshmukh, A. McCaskie, I. Essa, "Video Based Assessment of OSATS Using Sequential Motion Textures," in Fifth Workshop on Modeling and Monitoring of Computer Assisted Interventions (M2CAI), Georgia Institute of Technology, 2014.

[20] Y. Sharma, T. Plötz, N. Hammerld, S. Mellor, R. McNaney, P. Olivier, S. Deshmukh, A. McCaskie, I. Essa, "Automated surgical OSATS prediction from videos," in 2014 IEEE 11th International Symposium on Biomedical Imaging, ISBI 2014, IEEE: 461–464, 2014, doi:10.1109/isbi.2014.6867908.

[21] N. Ahmidi, M. Ishii, G. Fichtinger, G.L. Gallia, G.D. Hager, "An objective and automated method for assessing surgical skill in endoscopic sinus surgery using eye-tracking and tool-motion data," in International forum of allergy & rhinology, Wiley Online Library: 507–515, 2012.

[22] A.L. Trejos, R. V. Patel, M.D. Naish, A.C. Lyle, C.M. Schlachta, "A sensorized instrument for skills assessment and training in minimally invasive surgery," in Journal of Medical Devices, Transactions of the ASME, IEEE: 965–970, 2009, doi:10.1115/1.4000421.

[23] F. Gómez-Vela, F. Martínez-Álvarez, C.D. Barranco, N. Díaz-Díaz, D.S. Rodríguez-Baena, J.S. Aguilar-Ruiz, "Pattern recognition in biological time series," Lecture Notes in Computer Science (Including Subseries Lecture Notes in Artificial Intelligence and Lecture Notes in Bioinformatics), **7023 LNAI**, 164–172, 2011, doi:10.1007/978-3-642-25274-7_17.

[24] E.J. Keogh, M.J. Pazzani, "Derivative dynamic time warping," in Proceedings of the 2001 SIAM international conference on data mining, SIAM: 1–11, 2001.

[25] J.T. Kent, "New directions in shape analysis," The Art of Statistical Science,

115, 1992.

[26] K. V Mardia, P.E. Jupp, Directional statistics, John Wiley & Sons, 2009.

[27] M.B.B. Stegmann, D.D.D. Gomez, "A brief introduction to statistical shape analysis," Informatics and Mathematical …, (March), 1–15, 2002.

[28] I.L. Dryden, K. V. Mardia, Statistical shape analysis, with applications in R: Second edition, John Wiley & Sons, 2016, doi:10.1002/9781119072492.

[29] J.M. Keller, D. Liu, D.B. Fogel, Fundamentals of computational intelligence: neural networks, fuzzy systems, and evolutionary computation, John Wiley & Sons, 2016.

[30] M. Popescu, C.J. Cooper, S. Barnes, "Automated Operative Skill Assessment Using IR Video Motion Analysis," in AMIA, 2014.

[31] B.J. Dlouhy, R.C. Rao, "Surgical skill and complication rates after bariatric surgery," The New England Journal of Medicine, **370**(3), 285, 2014.

[32] M.G. Katos, D. Goldenberg, "Emergency cricothyrotomy," Operative Techniques in Otolaryngology-Head and Neck Surgery, **18**(2), 110–114, 2007.

[33] A. MacIntyre, M.K. Markarian, D. Carrison, J. Coates, D. Kuhls, J.J. Fildes, "Three-step emergency cricothyroidotomy," Military Medicine, **172**(12), 1228–1230, 2007.

[34] INC, MBIENTLAB, 2020, doi:https://mbientlab.com/metamotionr/.

[35] T. Fawcett, "ScienceDirect.com - Pattern Recognition Letters - An introduction to ROC analysis," Pattern Recognition Letters, **27**(8), 861–874, 2006.

[36] H.I. Fawaz, G. Forestier, J. Weber, L. Idoumghar, P.A. Muller, "Evaluating surgical skills from kinematic data using convolutional neural networks," in arXiv, Springer: 214–221, 2018.

The Mediating Role of Entrepreneurial Orientation on the Knowledge Creation-Firm Performance Nexus: Evidence from Indonesian IT Companies

Desman Hidayat[1,*], Edi Abdurachman[2], Elidjen[2], Yanthi Hutagaol[3]

[1]BINUS Entrepreneurship Center, Management Department, Bina Nusantara University, Jakarta, Indonesia 11480

[2]Management Department, BINUS Business School Doctor of Research in Management, Bina Nusantara University, Jakarta, Indonesia 11480

[3]International Accounting & Finance Program, Accounting Department, Faculty of Economics & Communication, Bina Nusantara University, Jakarta, Indonesia 11480

A R T I C L E   I N F O

A B S T R A C T

Disruptive innovation has created fast changes in the business environment and competition among companies, especially on information technology companies. Knowledge creation and entrepreneurial orientation are two variables that can improve firm performance. There is still limited study on how knowledge creation and entrepreneurial orientation both affects firm performance. This study aims to discuss how to effectively apply knowledge creation and entrepreneurial orientation to develop firm performance. A questionnaire has been conducted to 55 medium-large IT companies in Jakarta, Indonesia, and analyzed using structural equation modeling (SEM). The result showed that knowledge creation did not directly affect firm performance but indirectly affected entrepreneurial orientation. Knowledge creation also had a positive and significant effect on entrepreneurial orientation, and so does entrepreneurial orientation towards firm performance. Therefore, IT companies should consider both variables to improve their performance. Future studies may consider using qualitative or mixed-method approaches, conducting research for small IT companies and in other countries.

1. Introduction

The world is changing fast with the innovation that happens in the world. Disruptive innovation, where a new market disrupts and replaces the old market, shows how quickly the world is changing [1]. This situation raises the competition among companies as well [2].

Disruptive innovation heavily impacts the information technology (IT) sector. As the largest economy in South East Asia, Indonesia has many growing industries, especially in the digital sector [3]. Nevertheless, IT companies need to prepare themselves for disruption and the competitive environment to survive.

According to dynamic capabilities theory, companies need to explore their knowledge assets to face rapid technological change [4]. Knowledge is an essential part of IT companies that focus

more on intangible assets to compete. Knowledge creation is a way to create value for IT companies.

Technology advancement that changes rapidly can help companies find new opportunities to improve their performance [5]. One of the sectors that are affected by these changes is the IT sector. So, IT companies need to find a way to seek opportunities within this condition. Entrepreneurial orientation can be one way where they will be able to survive the competition and to increase their performance [6].

Although there are a lot of previous studies talking about how knowledge creation is related with entrepreneurial orientation [7, 8] and how each of those variables are related with firm performance [9], [10], but there is still limited study on how knowledge creation and entrepreneurial orientation both affects firm performance. It is also interesting to see how the variables will be related in IT sector that relies on intangible assets, such as knowledge. These explanations show the novelty of this study.

* Corresponding Author: Desman Hidayat, Email: d4906@binus.ac.id

This study aims to enrich the literature by investigating the interaction between knowledge creation, entrepreneurial orientation, and firm performance. Overall, this study makes two contributions: (1) It expands the understanding of the knowledge creation-firm performance relationship in IT companies, and (2) It explores how entrepreneurial orientation can be related to knowledge creation and firm performance.

2. Literature Review

2.1. Firm Performance

Firm performance is a variable that is often used to measure how good companies run. Researches often use firm performance as a dependent variable [11]. This study used firm performance to measure how good IT companies manage their businesses.

Firm performance is derived from the organizational effectiveness theory [12]. The performance of a company can show the effectiveness of that organization [13]. It takes more than just the financial factor to measure performance [12].

In this study, the firm performance was measured using financial and non-financial performance. It used five indicators: revenue, ROI, employees, products, and development [14, 15]. Financial performance was measured by using revenue and ROI, while non-financial performance was measured using employees, products, and development.

2.2. Knowledge Creation

Knowledge creation is an activity or process of developing new knowledge by sharing and combining tacit and explicit knowledge [16]. It enables firms to improve efficiency and create value [17]. Knowledge creation needs participation from individual members of an organization to be effective [18].

Knowledge-based view of the firm is the most common foundation used to define knowledge creation theory [19]. This view argued that firms' significant resources are mainly intangible and dynamic, such as knowledge [20]. This view is derived from dynamic capabilities.

Socialization, Externalization, Combination, and Internalization (SECI) are indicators to measure knowledge creation [18]. These indicators are representing the interaction between tacit and explicit knowledge [19]. This study used SECI as indicators to measure knowledge creation.

2.3. Entrepreneurial Orientation

Entrepreneurial orientation is one of the most researched topics in entrepreneurship literature [21]. It is the processes, practices, philosophy, and decision-making activities that help companies innovate [22]. Companies with the right entrepreneurial orientation continuously try to find new opportunities and strengthen their competitive positions [8].

The foundation of entrepreneurial orientation was based on entrepreneurship theory itself, where the main point of entrepreneurship is to understand how companies can seek and exploit opportunities [23]. Opportunities do not have to be related to something new, but they can focus on optimizing the existing framework. To discover the opportunities, companies must possess prior information related to the opportunities and cognitive properties to value them.

Five indicators are commonly used to measure entrepreneurial orientation. Those indicators are autonomy, innovativeness, risk-taking, proactiveness, and competitive aggressiveness [6]. The earlier concept of entrepreneurial orientation used three aspects: innovativeness, proactiveness, and risk-taking [24], but now it has been improved by adding the other two indicators. This study used the five indicators mention above to measure entrepreneurial orientation.

2.4. Hypothesis Development

Knowledge is one of the critical intangible resources that can help companies develop their performance [9, 25]. A lot of previous studies discuss how vital knowledge creation in relationship with performance [19]. High-tech companies need to have adequate knowledge resources in order to remain competitive [26]. Hence the hypothesis:

H1: There is a positive effect of knowledge creation towards firm performance.

Entrepreneurial orientation has been known to have a positive association with firm performance [8,9]. It has been tested in different contexts and countries [27]. This statement is also argued to be true for technological companies [28]. Therefore, hypothesis two is predicted as below.

H2: There is a positive effect of entrepreneurial orientation towards firm performance.

Knowledge creation and entrepreneurial orientation are often researched together. Previous studies showed that both variables are related [7, 8]. IT companies need to pay attention to both variables to maximize their performance. Therefore, hypothesis three states:

H3: There is a positive effect of knowledge creation towards entrepreneurial orientation.

Even though most of the previous research discussed how knowledge creation and entrepreneurial orientation separately affect firm performance, some studies talked about how they can simultaneously affect firm performance by having entrepreneurial orientation as the mediating variable [29]. This study argued that innovativeness and competitive aggressiveness as part of entrepreneurial orientation play the mediator between knowledge and performance. Hence the hypothesis:

H4: There is a positive indirect effect of knowledge creation towards firm performance mediated by entrepreneurial orientation.
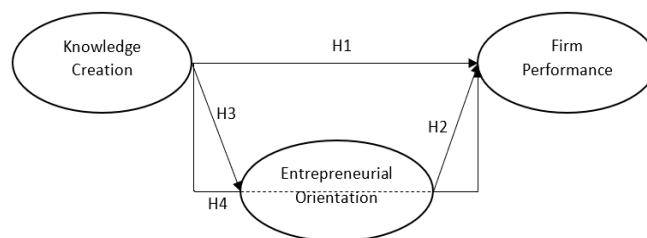
Figure 1: Research Model

3. Research Methodology

This study was conducted using an online survey with quantitative analysis. The unit analysis of this study is medium-

large IT companies in Jakarta. Indonesian Micro, Small, and Medium Enterprise Regulation No.20 (2008) defined medium enterprises as companies with 2.5-50 billion IDR revenues per year or 178-3.5 million USD and large enterprises as companies that have >50 billion IDR revenues per year or >3.5 million USD. According to 2016 Economic Census by Statistics Indonesia, the population of medium-large IT companies in Jakarta, the capital of Indonesia, is 303 companies [30].

This study used probability sampling design with simple random sampling. The samples for this study were 55 companies. The minimum sample size was 33 data, calculated using two arrows pointing at a construct, 5% significance level, and minimum R Square 0.25 [31]. Therefore, the samples are sufficient for this study. The survey was conducted for three months, from August to November 2020. The unit of observation in this study was a managerial level employee. Only one employee per company participated in this study.

Based on the companies' established period, most of the respondents (42%) were companies that have already been established for at least twenty years, and the smallest frequency came from new companies that have only been established for less than five years (7%). This data shows that many medium and large IT firms in Jakarta took a long time to develop their business into a medium-large company. Table 1 shows the details of the company establishment period.

Table 1: Companies' Established Period

Established Period	Frequency	Percentage
<5 years	4	7%
5-9 years	11	20%
10-14 years	9	16%
15-19 years	8	15%
>=20 years	23	42%
TOTAL	55	100%

Most of the company respondents have 11-50 employees (40%). Only one respondent has less than ten employees, while seven companies have more than five hundred employees. This data shows that medium or large companies do not mean that they must have many employees. Table 2 below shows more details on the numbers of employees.

Table 2: Companies' Number of Employees

Number of Employees	Frequency	Percentage
<=10 employees	1	2%
11-50 employees	22	40%
51-200 employees	20	36%
201-500 employees	5	9%
>500 employees	7	13%
TOTAL	55	100%

This study was done by using exploratory empirical research. The data analysis was done by partial least squares structural equation modeling (PLS-SEM). PLS-SEM is mainly used for the development of theories and exploratory research [31]. The analysis for this study was done using the smartPLS program. This study used a five-point Likert scale on the questionnaires. A five-point scale increases the response rate and quality of the responses while reduces the stress of the respondent [32].

4. Results and Discussion

4.1. Results

Validity was measured by removing items with less than 0.7 outer loadings. From the result, the risk-taking indicator measuring entrepreneurial orientation is not valid. Other indicators are all proven to be valid. Cronbach's Alpha, Composite Reliability (CR), and Average Variance Extracted (AVE) measure reliability. Variables should have Cronbach's Alpha >0.5, CR >0.6, and AVE >0.5 to be considered reliable [31]. The result showed that all the variables are reliable. More details on validity and reliability test result on entrepreneurial orientation (EO), firm performance (FP), and knowledge creation (KC) can be seen in table 3.

Table 3: Validity & Reliability Test Result

Variables	Indicators	Items	Instrument	Outer Loading	Cronbach's Alpha	CR	AVE
EO	Autonomy	EO11	Our company gives freedom to employees or team to express their business concept and vision, and oversees them until finish	0.783	0.892	0.913	0.569
		EO12	Our company has the self-directed ability and willingness to seek for opportunities	0.809			
	Innovativeness	EO21	Our company supports employees' creativity	0.771			
		EO22	Our company has a lot of new marketable products/services within the last five years	0.723			
	Proactiveness	EO41	Generally, our company's top managers have the tendency to lead the competition with new idea or product	0.721			
		EO44	Our company reacts quickly on the market demand	0.743			
	Competitive Aggressiveness	EO51	Our company is very aggressive	0.756			
		EO52	Our company is very competitive	0.723			
FP	Employee	FP12	Our company has good planning towards the future of employees	0.706	0.865	0.899	0.597

KC	Product	FP22	Our company's automation is higher than our competitors in the same industry	0.830			
	Development	FP31	Our company is very keen on investing in new market development	0.733			
		FP32	Our company is very keen on investing in new technology development	0.778			
	Revenue	FP41	Our company's income is higher than our competitors in the same industry	0.779			
	ROI	FP51	Our company's Return on Investment is higher than our competitors in the same industry	0.803			
KC	Socialization	KC11	Our company emphasizes on the creation of working environment that helps employees learn skills	0.700	0.930	0.939	0.586
		KC12	Our company arranges employee meetings to share and trade knowledge and experiences	0.742			
	Externalization	KC21	Our company uses collaborative learning tools	0.741			
		KC22	Our company usually develops working group discussion by using several techniques through internet	0.775			
		KC23	Our company usually share information, experiences, best practice, and learning to solve problems	0.732			
	Combination	KC31	Our company emphasizes on manual and document creation on products and services	0.835			
		KC32	Our company emphasizes content creation from management data gathering	0.791			
		KC33	Our company emphasizes content creation from technical information gathering	0.872			
	Internalization	KC41	Our company emphasizes on value seeking and sharing	0.764			
		KC42	Our company emphasizes on new thoughts seeking and sharing	0.709			
		KC43	Our company usually use on the job training to enrich knowledge	0.744			

Based on the result of Fornell-Lacker criterion, discriminant validity, all three variables are valid. Correlation between items and the square root of AVE shown no problem with the top numbers being the biggest one. Table 4 shows the details of discriminant validity.

Table 4: Fornell-Lacker Criterion

	EO	FP	KC
EO	**0.754**		
FP	0.752	**0.773**	
KC	0.689	0.570	**0.766**

The last part of discriminant validity measure beside loading factor and Fornell-Lacker criterion is Heterotrait-Monotrait Ratio (HTMT). The score for HTMT ratio should be <1.00 [31]. Based on the result, all variables are valid. Table 5 shows the HTMT result.

Table 5: HTMT Ratio

	EO	FP	KC
EO			
FP	0.848		
KC	0.703	0.616	

R Square shows the proportion of variation of dependent variables towards independent variables. Results showed that 57,1% of firm performance could be described through entrepreneurial orientation and knowledge creation, while 47.5% of entrepreneurial orientation can be described through knowledge creation. R square result can be seen in table 6.

Table 6: R Square

	R Square	R Square Adjusted
EO	0.475	0.465
FP	0.571	0.554

Goodness of fit can be seen from the value of Standardized Root Mean Square Residual (SRMR) and Normal Fit Index (NFI). On this study, the result of SRMR estimated model is 0.108 while the NFI score is 0.555. Although there are several PLS-SEM based model fit measures, but those measures are still in development [31].

After testing the validity and reliability, the next step was to test the path between variables. The test was done using SmartPLS. How the research model looked with the path coefficient and t-value can be seen in Figure 2.
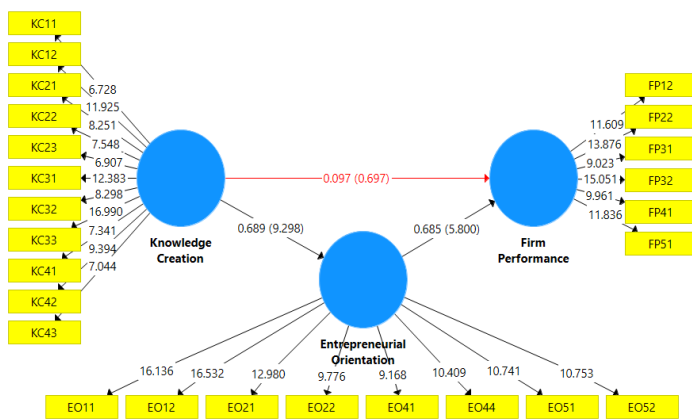
Figure 2: Research Model with Path Coefficient and T-Value

T-value should be >2.021 and p-value <0.050 for a significant path on a 5% error rate [33]. From the result, the direct effect of entrepreneurial orientation is positive and significant towards firm performance, and the direct effect of knowledge creation is positive and significant towards entrepreneurial orientation. However, knowledge creation has an insignificant direct effect on firm performance. By measuring the indirect effect, knowledge creation has a positive and significant effect on firm performance mediated by entrepreneurial orientation. Details on the structural equation model (SEM) test result can be seen in table 7.

Table 7: SEM Test Result

	Path Coef.	T-Stat	P-Value	Sig.
KC-> FP	0.097	0.697*	0.486*	Insignificant
EO -> FP	0.685	5.800	0.000	Positive & Significant
KC->EO	0.689	9.298	0.000	Positive & Significant
KC->EO->FP	0.472	4.873	0.000	Positive & Significant

4.2. Discussion

Based on this study, knowledge creation does not have a significant effect on firm performance. This argument supported previous research [34]. IT companies should not only be focusing on knowledge creation if they want to raise their performance. They should also think about other factors to make the knowledge creation effective. Therefore, hypothesis 1 is rejected.

Entrepreneurial orientation in this study is proved to have a positive and significant effect on firm performance. This statement strengthened the arguments done by previous researches [21,35,36]. By focusing on entrepreneurship, IT companies can find and exploit opportunities to improve their performance. Therefore, hypothesis 2 is accepted.

Knowledge creation has a positive and significant effect on entrepreneurial orientation, according to this study. This result strengthened previous research that argued the correlation between knowledge creation and entrepreneurial orientation [37] and supported the argument that showed knowledge creation affected entrepreneurial orientation [7]. IT companies must pay attention to

knowledge creation to increase their entrepreneurial orientation. Therefore, hypothesis 3 is accepted.

This study showed that knowledge creation has a positive and significant effect on firm performance when it is mediated by entrepreneurial orientation. This result supported the previous research on the same topic [29]. Both knowledge creation and entrepreneurial orientation are essential factors to improve IT company performance. Therefore, hypothesis 4 is accepted.

4.3. Implication

IT companies generally rely on intangible resources such as knowledge as their important asset. Nevertheless, the result of this study showed that knowledge alone is not enough to make the company perform better. Therefore, medium-large IT companies in Jakarta should think about other factors while focusing on their knowledge creation.

Technology changes rapidly. IT companies should think about a way to face this challenge. Entrepreneurial orientation can help the companies to seek opportunities and adapt to changes. The result of this study showed that it is important to develop entrepreneurial orientation in the companies to increase their firm performance.

Another important result from this study is the relation between knowledge creation and entrepreneurial orientation. This study showed that knowledge creation is important to develop entrepreneurial orientation, which in the end raise the firm performance. Therefore, IT companies should develop both their knowledge creation and entrepreneurial orientation.

5. Conclusion

5.1. Conclusion

The results of this study indicate the factors that can increase IT firm performance. This study's main conclusion is that knowledge creation and entrepreneurial orientation are essential antecedents of firm performance, especially for companies in the IT sector. However, knowledge creation alone is not enough to raise firm performance. It must also be mediated by entrepreneurial orientation.

The interesting finding in this study is that entrepreneurial orientation mediates the relationship between knowledge creation and firm performance. It indicates that IT companies should create an environment that supports knowledge creation for the employees. Companies should also have entrepreneurial orientation to adapt with the fast-changing environment.

5.2. Limitation and Future Work

This study has several limitations. The analysis in this study was done by quantitative approach. Adding qualitative approaches by having interview or focus group discussion on future research will enrich this study. Mixed-method research is also a good approach to understand more about the industry.

The companies observed is also limited to medium-large IT companies. Future research can be done to small IT companies. The knowledge creation might be different in small companies and their way to face the changes can also be different. Therefore,

doing study in small IT companies or conducting comparative study between small, medium, and large IT companies will enrich this study.

Other limitation is the scope of this research. This study used IT companies in Jakarta, Indonesia. Therefore, it will be hard to generalize this result to other countries. Future research ought to be held on other countries as well.

References

[1] C.M. Christensen, The Innovator's Dilemma: When New Technologies Cause Great Firms to Fail, Harvard Business School Press, Boston, Massachussets, USA, 1997.

[2] J.R.L. Kaivo-oja, I.T. Lauraeus, "The VUCA approach as a solution concept to corporate foresight challenges and global technological disruption," Foresight, **20**(1), 27–49, 2018, doi:10.1108/FS-06-2017-0022.

[3] K. Das, M. Gryseels, P. Sudhir, K.T. Tan, Unlocking Indonesia's Digital Opportunity, 2016.

[4] D.J. Teece, G. Pisano, A. Shuen, "Dynamic Capabilities and Strategic Management," Strategic Management Journal, **18**(7), 509–533, 1997.

[5] S. Venkataraman, "The Distinctive Domain of Entrepreneurship Research," Advances in Entrepreneurship, Firm Emergence and Growth, **3**, 119–138, 1997.

[6] G. Lumpkin, G.G. Dess, "Linking two dimensions of entrepreneurial orientation to firm performance," Journal of Business Venturing, **16**(5), 429–451, 2001, doi:10.1016/S0883-9026(00)00048-3.

[7] C. Weerakoon, A.J. McMurray, N. Rametse, P. Arenius, "Knowledge creation theory of entrepreneurial orientation in social enterprises," Journal of Small Business Management, **58**(4), 834–870, 2020, doi:10.1080/00472778.2019.1672709.

[8] N.A. Omar, K. Professional, M.A. Nazri, "The Effect of Entrepreneurial Orientation , Innovation Capability and Knowledge Creation on Firm Performance : A Perspective on Small Scale Entrepreneurs," Jurnal Pengurusan, **48**, 187–200, 2016.

[9] M.S. Aliyu, H.B. Rogo, R. Mahmood, "Knowledge Management , Entrepreneurial Orientation and Firm Performance : The Role of Organizational Culture Knowledge Management , Entrepreneurial Orientation and Firm Performance : The Role of Organizational Culture," Asian Social Science, **11**(23), 2015, doi:10.5539/ass.v11n23p140.

[10] B. Liu, J. Wang, "Demon or angel: an exploration of gamification in management," Nankai Business Review International, **11**(3), 317–343, 2020, doi:10.1108/NBRI-02-2018-0013.

[11] J.B. Santos, L.A.L. Brito, "Toward a subjective measurement model for firm performance," BAR - Brazilian Administration Review, **9**(SPL. ISS), 95–117, 2012, doi:10.1590/S1807-76922012000500007.

[12] K. Cameron, "A STUDY OF ORGANIZATIONAL EFFECTIVENESS AND ITS PREDICTORS," Management Science, **32**(I), 87–112, 1986.

[13] T. Connolly, E.J. Conlon, S.J. Deutsch, "Organizational Effectiveness: A Multiple-Constituency Approach.," Academy of Management Review, **5**(2), 211–218, 1980, doi:10.5465/amr.1980.4288727.

[14] R.L. Daft, Management, 10th ed., Cengage Learning, Ohio, 2012.

[15] S.M. Tseng, P.S. Lee, "The effect of knowledge management capability and dynamic capability on organizational performance," Journal of Enterprise Information Management, **27**(2), 158–179, 2014, doi:10.1108/JEIM-05-2012-0025.

[16] P.C. Izunwanne, "Developing an Understanding of Organisational Knowledge Creation: A Review Framework," Journal of Information & Knowledge Management, **16**(2), 2017, doi:10.1142/S0219649217500204.

[17] M. Tsai, Y. Li, "Knowledge creation process in new venture strategy and performance," **60**(1), 371–381, 2007, doi:10.1016/j.jbusres.2006.10.003.

[18] I. Nonaka, "A Dynamic Theory of Organizational Knowledge Creation," Organization Science, **5**(1), 14–37, 1994, doi:10.1287/orsc.5.1.14.

[19] D. Hidayat, E. Abdurachman, Elidjen, Y. Hutagaol, "Empirical Studies on Knowledge Creation and Performance : a Literature Review," in 2020 International Conference on Information Management and Technology (ICIMTech) 533, Bandung, Indonesia: 533–537, 2020.

[20] C. Curado, "The Knowledge Based-View of the Firm: From Theoretical Origins To Future Implications," Igarss 2014, (1), 1–5, 2006, doi:10.1007/s13398-014-0173-7.2.

[21] H. Montiel-Campos, "Entrepreneurial orientation and market orientation: Systematic literature review and future research," Journal of Research in Marketing and Entrepreneurship, JRME-09-2017-0040, 2018, doi:10.1108/JRME-09-2017-0040.

[22] M. Madhoushi, A. Sadati, H. Delavari, M. Mehdivand, R. Mihandost, "Entrepreneurial Orientation and Innovation Performance: The Mediating Role of Knowledge Management," Asian Journal of Business Management, **3**(4), 310–316, 2011.

[23] S. Shane, S. Venkataraman, "The Promise of Entrepreneurship as a Field of Research," The Academy of Management Review, **25**(1), 217, 2000, doi:10.2307/259271.

[24] D. Miller, "The Correlates of Entrepreneurship in Three Types of Firms," Management Science, **29**(7), 770–791, 1983, doi:10.1287/mnsc.29.7.770.

[25] P. Heisig, O.A. Suraj, A. Kianto, C. Kemboi, G. Perez Arrau, N. Fathi Easa, "Knowledge management and business performance: global experts' views on future research needs," Journal of Knowledge Management, **20**(6), 1169–1198, 2016, doi:10.1108/JKM-12-2015-0521.

[26] F. Zouaghi, M. Sánchez, M.G. Martínez, "Did the global financial crisis impact firms' innovation performance? The role of internal and external knowledge capabilities in high and low tech industries," Technological Forecasting and Social Change, **132**(April 2016), 92–104, 2018, doi:10.1016/j.techfore.2018.01.011.

[27] R. Basco, F. Hernández-Perlines, M. Rodríguez-García, "The effect of entrepreneurial orientation on firm performance: A multigroup analysis comparing China, Mexico, and Spain," Journal of Business Research, **113**(May), 409–421, 2020, doi:10.1016/j.jbusres.2019.09.020.

[28] Y. Liu, M. Wang, "Entrepreneurial orientation, new product development and firm performance: the moderating role of legitimacy in Chinese high-tech SMEs," European Journal of Innovation Management, 2020, doi:10.1108/EJIM-05-2020-0204.

[29] R. Zacca, M. Dayan, T. Ahrens, "Impact of network capability on small business performance," Management Decision, **53**(1), 2–23, 2015, doi:10.1108/MD-11-2013-0587.

[30] Badan Pusat Statistik, Sensus Ekonomi 2016 Direktori Usaha/Perusahaan Menengah Besar Kategori Informasi dan Komunikasi, 2017.

[31] J. Hair Jr, G.T. Hult, C. Ringle, M. Sarstedt, A Primer on Partial Least Squares Structural Equation Modeling (PLS-SEM), 2017.

[32] S. Sachdev, H. Verma, "Relative importance of service quality dimensions: a multisectoral study," Journal of Services Research, **4**(1), 93, 2004.

[33] U. Sekaran, R. Bougie, Research Methods for Business, 7th Editio, Wiley, West Sussex, UK, 2016, doi:10.1007/978-94-007-0753-5_102084.

[34] C.E. Lucier, J.D. Torsilieri, "Why knowledge programs fail: A CEO's guide to managing learning," Strategy & Business, **9**(4), 14–28, 1997.

[35] M.I. Hanif, F. Malik, A.B. Abdul Hamid, A.B.A. Hamid, "The effect of knowledge management and entrepreneurial orientation on organization performance," Journal of Entrepreneurship Education, **21**(4), 2651, 2018.

[36] R. Masa'deh, J. Al-Henzab, A. Tarhini, B.Y. Obeidat, "The associations among market orientation, technology orientation, entrepreneurial orientation and organizational performance," Benchmarking, **25**(8), 3117–3142, 2018, doi:10.1108/BIJ-02-2017-0024.

[37] F. Vidic, "Entrepreneurial Orientation (EO) and Knowledge Creation (KC)," International Journal of Economic Sciences and Applied Research, **6**(2), 103–124, 2013.

The Impact of eLearning as a Knowledge Management Tool in Organizational Performance

Abdulla Alsharhan[1], Said Salloum[2,3,*], Khaled Shaalan[1]

[1]*Faculty of Engineering & IT, The British University in Dubai, 345015, UAE*

[2]*School of Science, Engineering, and Environment, University of Salford, M16ORY, UK*

[3]*Research Institute of Sciences & Engineering, University of Sharjah, 27272, UAE*

A R T I C L E   I N F O

A B S T R A C T

This paper aims to understand the impact of eLearning capabilities on organizational performance. It also addresses the obstacles of organizational learning using eLearning methods and highlighting some emerging trends and technologies that will impact the eLearning experience in organizations. It examines a brief history of knowledge management and how it is related to learning, organizational learning, and performance. It also explores different eLearning technologies and trends. A systematic literature review was used to examine previous papers between 2016–2020. Results show eLearning can impact organizational performance in many ways, and human factors can be one of the most challenging obstacles in deploying eLearning solutions in organizations, and many emerging eLearning trends were explored including open educational resources, gamification, flipped classrooms, and many others.

1. Introduction

The fast-paced growth of information communication and technology is changing the world we live in into a knowledge-based society [1–3]. Within the context of the fourth industrial revolution and the knowledge-based economy, knowledge and learning systems play an important role in countries' competitiveness and organizational performance (OP).

Knowledge capturing has become a strategic priority for many countries as an essential asset [4–8], especially if they want to remain competitive, driven by rapid development in knowledge creation and high demand for skilled human capital [9–12]. In the past, countries and organizations could achieve that by traditional educational and vocational training systems; however, the new era requires faster and shorter innovation cycles to remain innovative, which increases the need for continuous skilled and trained human capital with constant knowledge updates and skillsets.

The current workforce is transforming the traditional "single-skilled personnel to multi-skilled employees" who can manage multi-tasks under one job title. Such a goal will be possible only through new disruptive learning models and life-long learning

(LLL) [13]. One of the knowledge-capturing and sharing tools is eLearning, where organizations and educational institutes can conduct training via electronic media via the internet. The COVID-19 pandemic has forced many institutes and organizations to carry out their training and education activities via eLearning tools [14,15]. These activities revealed some limitations in current eLearning practices such as quality of interaction, lack of natural discussions, and limited nonverbal communication [16]. The reason can be anything, ranging from the use of old-fashioned eLearning practices to poor content and connection quality.

Alternatively, the use of technology-enhanced learning (TEL) via mobile is changing the learning process for many. Language learning apps, for example, are impacting how learning is taking place. A recent study concluded that Duolingo is fostering vocabulary and grammar development [17]. Other fun and engaging examples include fitness training apps from Adidas and Nike and musical instrument training apps like Yousician. TEL is becoming one of the trending topics in computer science as it utilizes the use of computers, mobile, software and apps to assist learning [6].

The advantage of TEL is that it guarantees learning continuity in different circumstances such as during pandemics, natural

disasters, extreme weather conditions or for learners with disabilities. It frees the instructor from creating redundant lessons and devotes more time to developing quality learning materials. It also allows learners to engage in active and independent play-based learning and life-long learning [18].

Organizations need to encourage LLL via on-the-job training and eLearning methods. These learning methods will ensure that the current workforce is well equipped with the latest skills. Before knowledge is transformed into learning materials (eLearning), it is necessary to manage such knowledge first. Learning is an essential part of the Knowledge Management's (KM) life cycle, which complements the process of establishing, distributing, implementing, and managing the knowledge and information of an organization. It refers to a multidisciplinary approach to achieve organizational objectives by making the best use of knowledge. The most recent studies uncover the massive significance of presenting KM insights into eLearning frameworks. KM is believed to encourage an eLearning framework, where the joint effort between eLearning and KM will provide the single objective of hierarchical learning [19].

In this paper, we have included papers that are relevant to the role of KM, eLearning, and OP. We have reported a systematic review of the advances in eLearning in KM in response to OP. The objective is to provide overviews of the research studies within this field, how these concepts interact with each other, the main obstacles, and the recent emerging trends. More specifically, we have asked the following questions:

Table 1: Research question.

#	Research question
RQ1	How is eLearning capabilities in KM impacting OP?
RQ2	What are the challenges in implementing eLearning in organizations?
RQ3	What are some of the emerging trends and technologies in eLearning?

2. Literature Review

This section will highlight the recent contribution that focuses on the subject of this study, including the discussion of the latest practices related to KM, eLearning, training technologies, organizational learning, and performance.

2.1. Origin of KM

KM started within the management consulting community. They had realized how the internal networks in their organization is a vital tool to share and access information with their units, especially when these units were scattered in different geographical locations. While these consulting groups were working on facilitating their network to their use, they have gained some knowledge and recognized some good practices, such as developing and building these tools, expertise locators, lesson-learned databases, and designing dashboards.

They have realized the newly acquired expertise can be packaged, marketed, and sold to other similar entities, who might have multiple locations and experienced the same challenges. However, the new product needed a name. It seemed the term

"Knowledge Management" had appeared in this context for the first time in 1987. The KM term was spotted in an internal study in McKinsey on how to handle and utilize their information.

In 1993, the knowledge management went public at a conference organized by Ernst and Young. A young man at Ernst and Young came up with one of the first classic one-line definitions of KM. Tom Davenport defined KM as the process of capturing, distributing, and effectively using knowledge [20].

In 1998, the authors of [21] worked on a revised definition. They described KM as the activities related to utilizing and developing organization knowledge assets in line with organizational objectives. Early work by [22] in 2005 was among the first to link KM with innovation, as he defined KM as the purposeful and systemic coordination of an organization's individuals, technology, process, and structure to create values via reuse and innovation [23].

There were many models aroused around coordination between people, process, technology, and organization structure, including Wigg Model (1993), Zack Model (1996), Bukowitz and William Model (2000), and McElroy Model (2003). The following table explains the KM lifecycle steps, according to the four proposed models [24].

Table 2: KM lifecycle steps according to the four proposed models.

WIGG 1993	Zack 1996	Bukowitz & Williams 2000	McElroy 2003
Creation	Acquisition	Get	Learning
Sourcing	Refinement	Use	Validation
Compilation	Store	Learn	Acquisition
Transformation	Distribution	Contribute	Integration

In [24], the author summarizes the steps in seven steps: Identity, Create, Store, Share, Use and Learn. For this review, the focus has been on the learning aspect and knowledge sharing with more details.

2.2. KM & learning

A study by [25] explained how KM and learning work together. The knowledge assets used and shared in the past could be the foundation for creating new and improving current ones. In situations where experts provide a certain understanding in a context, the employees gain and learn a new experience and apply that knowledge to their workplace. If the knowledge resources have been found insufficient or incomplete, the researcher goes back to the identity/creation phase where additional resources are created based on the gaps found. This repeatable process creates double-loop learning. Some of the activities that assist the learning stage are benchmarking, best practices, lessons learned, and knowledge gap analysis. Technological applications and examples can be found in learning management and help desk systems [24].

2.3. KM in organizations

In addition to organizations' ability to learn and unlearn, collective knowledge is an essential asset in improving OP. It would also increase profitability, which will eventually create and maintain a competitive advantage. A study by [26] defines

organizational learning (OL) as using a purposeful learning process on individual, group, and system levels while changing the organization to satisfy its stakeholders. Scholars of [27] describe organizational learning as a social process where individuals engage in practices and speeches that reproduce the OL and expand it simultaneously.
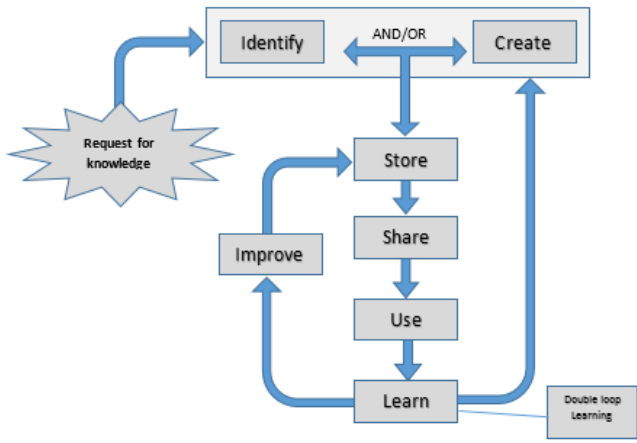
Figure 1: The KM Cycle (KMC) Model [24]

Four major vital areas were identified in [12]. These areas are the business drivers for the increased importance of KM in the organization today.

1. *Globalization of business:* The organization today is more global, multisite, multilingual, and multicultural.
2. *Leaner organizations:* Productivity is increasing faster, but it also needs to be done smarter as workers in KM are adapting to an increasing work pace and load.
3. *Organization amnesia:* Workforces are becoming mobile, which creates a challenge in sustaining knowledge in the organization and requires continuous learning. Employees are no longer expected to spend their entire lives in the same organization.
4. *Technology advancement:* People are connected seamlessly. The connections are not only ubiquitous but have radically changed expectations. Workers are expected to be "on" all the time, and response turnarounds are now measured by minutes, not weeks or even days [24].

One of the key challenges organizations face is the uncertainty of how exactly learning and KM impact OP. A dilemma that might create an ambiguity among leaders is how to optimize resources from KM. KM has no choice but to demonstrate how exactly they add value to the stakeholder [28]. A study by [29] examined the impact of KM on organizational learning, using OL in a mediating role. Results taken from 150 random samples show a close relationship between KM and OP. A critical insight is that OL is playing a mediating role between OP and KM. The study also revealed a positive relationship between emotional intelligence and OP.

In contrast, [30] investigated the effects of KM strategy and the effects of OL on OP. This study was conducted using a 5-point Likert-scale questionnaire on all levels of management in oil cooperation. The data collected from 161 managers confirmed that KM strategy is one of the preconditions and impactful factors

regarding OP and innovation. In contrast, OL does not seem to have correlated with organizational innovation.
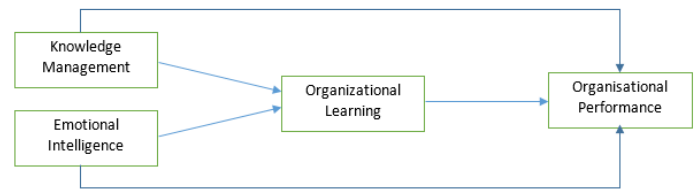
Figure 2: Relation between KM and OP [29].

2.4. eLearning

If we want to take a closer look at learning and training in the organization today, technology will be found as the driving force in workplace training. ATD's state of the industry report (2018) indicated that eLearning accounted for 40 percent of the formal learning hours used in 2017 [31]. The commonly known eLearning definition usually describes the activities of conducting learning using information and communication technologies. The authors of [32] identified that the most important remarkable milestones in learning are the evolution from distance learning to electronic learning to mobile learning. These three stages are in line with the impact of the Industrial Revolution in the eighteenth and nineteenth centuries and the Electronic Revolution in the last decade of the twentieth century [32].

Recent studies suggest that Massive Online Open Courses (MOOCs) will play a prominent role in organizational learning, provided these courses are relevant to the workplace and integrated effectively into the current training systems [33]. For many leaders and human resources trainers, eLearning is an easy way to provide workplace gamification content. The challenge remains that most training courses are theoretical and based on college courses, and they might not meet the corporate training version yet (except Udemy). However, a few work particularly with corporations to tailor-make their business knowledge into user-friendly courses, similar to ones we can identify with MOOCs platforms.

2.5. Computer-Assisted Learning

Computer-Assisted Learning (CAL) is one of the top 5 emerging trends in computer science in recent years [18]. This term can also be referring to Computer-Based Instruction (CBI), Computer-Aided Learning (CAL), or Computer-Aided Instruction (CAI) [34]. CAL can be defined as "learning that supplements regular classroom activities with computer activities during or surrounding classroom time" [35]. Apps are one well-known form of CAL applications. The authors of [36] found that educational apps can have added values to the learning process not available in the conventional eLearning tool, including repetitions, swift feedback, fun, creative tools, variety of methods, and pronunciation.

For this review, we can simply define CAL as "the learning procedures and environments facilitated through computers" [34]. The application of CAL is unlimited. One example of CAL applications can be seen in the medical field, which has recently become "a truth universally acknowledged" as a proven way to enhance the student learning process. In contrast, some instructors and trainers may lack the basic computer science skills needed to

fully utilize technology in learning. Lacking key ICT skills might be one of the obstacles that limit the use of TEL tools [36].

2.6. Technology-Enhanced Learning

The emerging term Technology-Enhanced Learning (TEL) is a broad category that does not have a particular definition. It can refer to any type of technology that enhances the learning experience [37]. "Mentimeter" is an example of an interactive presentation platform that utilizes the capabilities of TEL. The trainer can build an interactive presentation; collect polls, data, and opinions from learners; and export the insights, data, and trends from participants' input. Media Technology and Interaction Design have identified many research areas around TEL, including learning analytics, the interplay of learning design and technology, design-based research, computer-supported collaborative learning, blended learning, sustainable design, and visualization for TEL-related issues [38]. A study by [39] provided an interesting application in eLearning. The Georgia Institute of Technology in the United States provided some of their online courses using virtual teaching assistants (TAs). The chatbot was developed using IBM *Watson*; the TAs can reply to student questions without informing the learner that they are artificial intelligence agents.

2.7. eLearning in Information Technology (IT) Companies

When it comes to technology companies and IT organizations, one can assume they are already ahead of others when it comes to their eLearning capabilities. There is little known about how they transform knowledge internally. One of the interesting findings that high-tech companies like Microsoft, Google, IBM, Cisco, Canon and Microsystems are using gamification capabilities to motivate and train their people. Canon technicians are learning how to fix and repair by literally dragging and dropping parts virtually, while Cisco has a platform called MyPlanNet, where employees play the role of a company's manager. Additionally, IBM developed a game simulation that allows employees to run an entire city [40].

Another common practice among technology companies is to share their online training materials externally. In other words, they focus on training individuals before they hire them, particularly because high-tech companies require highly skilled human resources already trained in their preferred way of working. For example, IBM- and Google-certified specializations can be found on eLearning platforms like Coursera, Microsoft courses, Edx and Udacity. This practice not only cuts training costs for IT organizations but may also become an additional profit centre as they license these certificates. In addition, companies can access a pool of talented full-stack programmers when needed.

2.8. Life-long Learning and eLearning

Life-long learning (LLL) sometimes gets confused with adult learning. LLL is a process where individuals seek learning opportunities to develop their knowledge, skills and life (Richardson, 1978 in Mouzakitis & Tuncay, 2011). Individuals who have an interest in LLL have a continuous ambition to learn and are responsible for their self-learning. According to the European Commission (briefing paper 20, 2001), LLL has become a targeted objective for learning policies at the national and international levels in recent years. In [41], the author conducted

empirical research on 138 employees and found that seven out of ten employees prefer eLearning course delivery over classroom attendance. These data support how eLearning should play a vital role in executing lifelong training, especially for employees between 55 and 64 years old in all sectors.

3. Methodology

In an attempt to follow a preferred reporting items for systematic reviews and meta-analyses (PRISMA), research should provide an explicit statement and form questions including participants, interventions, comparisons, outcomes, and study design (PICOS) [42]. Therefore, the research questions (Table 1) have been formed based on PICOS principles. The following detailed systematic review is based on results from research papers obtained in different online journals and databases that focus on eLearning, KM, and OP, in addition to CAL.

3.1. Data sources and Search Strategies

Different articles were found to match the searching criteria. In particular, 211 materials were found in credible online journals. All the results were found using WorldCat.org, Google Scholar and Crossref databases, as shown in Figure 3. The searching algorithms used included the presence of the required elements in the research objective; additionally, the exclusion aided to sort out the sources which were undesirable, and no organizational context was side-lined, leaving only the required data. The following keywords have been used to locate information from the journal kw: ("computer-assisted education" OR "computer-assisted learning" OR "computer-assisted training" AND "knowledge management" AND "computer science") AND kw: ("e-learning" OR "eLearning" OR "online learning") AND (yr: 2016–2020). Additional keywords used to refine the search are "eLearning" AND "organizational performance" OR "organizational performance". Table 3 gives more insights on the inclusion and exclusion criteria.

Table 3: Inclusion and exclusion criteria

Inclusion	Exclusion
Articles published in 2016 or later	Articles published before 2016
Should be related to KM methodologies, processes, or lifecycles	Related to KM or OP but not linked to eLearning
Should be related to computer-assisted learning or techniques	Related to eLearning but not linked to KM or OP
Should have five or more citations	Has fewer than five citations
Papers are in English	Papers are not in English
Articles	Books or book chapters

3.2. Challenges faced

There is no one clear definition of the field of computer-assisted learning, making it challenging to locate all the research about it and its relation to the eLearning and KM cycle. Some related terms are computer-assisted education, computer-assisted instruction and TEL. The category of TEL may be too broad or have no direct relation with eLearning and OP yet.
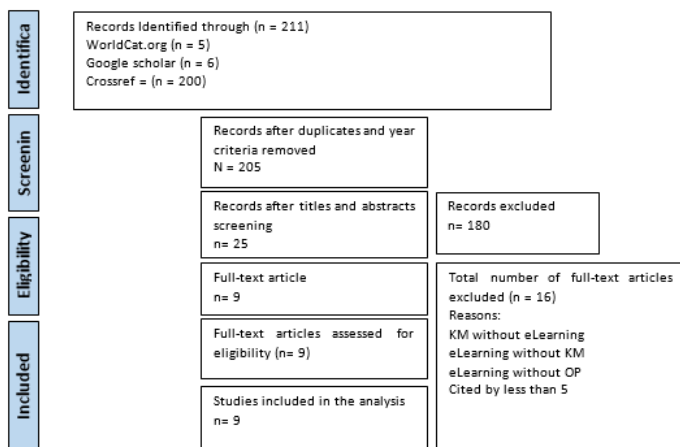
Figure 3: Research PRISMA model [43]

4. Results

The following is the result of reviewing the shortlisted nine research articles published between 2016 and 2020 on the impact of KM strategy and learning capabilities on OP.

4.1. RQ1. How are eLearning capabilities in KM impacting OP?

Previous studies mentioned that organizational eLearning capabilities in their KM context could enhance OP in many ways. Table 4 summarizes the main findings of the analysed KM researches in the context of eLearning and OL.

The finding revealed the many ways eLearning capabilities can impact OP. eLearning is a scalable tool that can increase individuals' competency levels on large scales. Every single individual can contribute to their organizational competitiveness, accelerate innovation rate and ultimately achieve a knowledge-based economy for their societies [19]. eLearning can also cut training and travel costs and ensure consistent training for all, increasing the quality and ensuring everyone is getting the same high-quality training [44]. Using the right eLearning capabilities can make a difference in the impact of the performance and quality result. eLearning Management Systems such as Moodle have proven to be the most effective tool in knowledge transferring compared to other distance learning tools such as email and teleconferences. Picking the right eLearning tool is essential because it increases the knowledge sharing among individuals and eventually increases performance and productivity [45]. Developing and sharing eLearning content on open platforms can also lead to gaining customer trust, attracting talent and enhancing organizational reputation. eLearning can also work as a new revenue stream for organization setting on knowledge assets [33].

Table 4: Analysis of KM research with regards to eLearning and OL.

Ref.	Purpose	methods	Finding	Country
[19]	KM and eLearning in Organisations.	Literature review	eLearning will not run alone without the KM.	Malaysia
[33]	The role of open educational resources (OER) in the eLearning movement	Literature review	Opportunities and advantages and limitation of OERs	Iran
[44]	E-Training & employees' performance.	Survey	Significant relationship between e-training (including e-training infrastructure & methods) and job performance,	Bahrain
[45]	The effectiveness of eLearning on change management and KM strategy in the organization using "Moodle".	Case Study	eLearning is the most effective method of knowledge transfer.	Canada
[46]	Study deep learning applications for developing resource for eLearning platform.	Qualitative	Deep learning enables the reusing repurposing current eLearning resources to create more personalized experience.	Saudi Arabia
[47]	How mobile learning experiences can support the co-creation of new knowledge.	Qualitative	That mobile technology is an excellent way to stimulate the social co-creation of new knowledge.	Thailand
[48]	A review of the current literature on digitally based serious games & gamification using digital tools in corporate training.	Literature review	Design principles for a game-based training methodology.	United States
[49]	The role of OL in employee engagement. The role of eLearning resources quality in bank sector.	Survey	OL positively impacts employee engagement, and eLearning resources quality partially impact employee engagement.	India
[50]	To integrate inquiry learning and KM into a flipped classroom to programming students in a higher education setting.	Quantitative	Integrating KM and inquiry-based approach into a flipped classroom can improve students' performance.	Thailand

4.2. RQ2. What are some obstacles to organisation learning using eLearning?

There are many factors that could undermine eLearning's effectiveness in any organisation. The first factor is the human factor. Some employees will resist sharing or allowing knowledge to transform because it might threaten their existence and will make them replaceable. Another factor related to human nature is the willingness to learn. Employees being in their comfort zones too long will not benefit from eLearning materials, and they might need some explanation on how eLearning can be useful for their career advancement [19]. Another human-related factor is the widespread belief that free and accessible content is worthless. The language [33] and the user interface can also be an obstacle to accessing the eLearning platform. The platform needs to be easy and straightforward to use, or the employee should be trained on it if necessary [44]. The quality source of the eLearning is also vital to ensure that useful and accurate messages are being delivered. This factor is particularly critical in some industries, such as the financial sector [49].

Content high initial development cost can also be a challenging factor in some small and medium organisations. However, the long-term impact can be scalable and widely accessible [46]. Intellectual properties of the content itself can also be restricted in some cases and limit the opportunity of sharing it, and this can go both ways [33]. Finally, the top management endorsement is vital to ensure that a knowledge-sharing and learning culture is in place [19,44].

4.3. RQ3. What are some of the emerging trends and technologies in eLearning?

Many significant trends emerged in eLearning in the last decade (Table 5). Some of them impact learners' outcomes and enhance their learning experience. These trends include Mobile Computer-Supported Collaborative Learning (mCSCL) [47], game-based learning - Gamification [48], flipped classroom [50], using Deep learning and artificial Inelegance in the eLearning field [46] and Open Educational Resources (OER) [36]. What the majority of these trends have in common can be summarized in their ability to provide social interaction, fun, and interactive and unlimited access. The instructor becomes a facilitator; learners are in control, and they co-create the new knowledge [47].

Table 5: The main trends and technologies eLearning found in the reviewed papers

Ref.	eLearning	Knowledge-Based Economy	eTraining	Moodle	Deep Learning	mCSCL / mLearning	Gamification / Serious Gaming	Flipped Classroom	OER / MOOC
[19]	X	X							
[33]	X								
[44]			X						
[45]	X			X					
[46]	X				X				
[47]						X			
[48]			X				X		
[51]	X							X	
[50]	X								X

5. Discussion

5.1. eLearning capabilities & OP

In [19], the study discussed the impact from an economic development perspective. As the economic evolution is witnessing a shift from an industrial-based economy to a knowledge-based economy, the whole country's performance, and not just the organization's, depends on the human capital being equipped with the necessary academic skills. Learning capabilities remained the

key challenge in a country like Malaysia to fully transform its economy into a knowledge-based one. This study valued learning capability as a vital role for remaining competitive. Successful organizations are those that can capture intalactual assets by managing their knowledge. The paper also acknowledged the critical role of top management, as they need to understand the best way to combine and share the knowledge sources to improve the company's performance. Once learning capabilities are rooted and embraced as part of the organizational culture; it will lead to increasing the competency level of every single individual, driven by the role of its KM system. Only then can the organization reach its full potential and increase its competitiveness performance [19]. However, the author did not specify what methodology was used to reach his findings, and he did not support his findings with examples or case studies.

The study by [33] pointed out how eLearning capabilities could reduce training costs and have a long-term impact on reducing operational expenses, which would lead eventually to better financial performance. Some researchers think organizations that create and share open-learning resources should be exempt from taxes.

The results of [44] also confirmed the [33] finding in cost savings. The study highlighted the importance of eLearning and its impact on individual performance. One direct impact of endorsing eLearning capability can be a huge amount of saving in training. This saving includes travel expense and training time. Other advantages include flexibility in self-based training and the variety and availability of training content. The eLearning model can also guarantee unified training for all, which will keep the resource inside the organization. The business will not be interrupted by those who take leave for training. This will increase the workers' productivity and the number of skilled and trained human capital, which ultimately will allow the business to remain competitive [44]. In addition, long-term organizational success is linked to embracing a learning culture among employees. One significant finding is the role of the eLearning infrastructure on employee performance.

The results of [45] are in line with the above findings, as the authors also found that eLearning is the most effective method of knowledge transfer. The authors examined how different learning capabilities can impact executing a successful KM strategy and improve the chance of knowledge sharing among individuals, which ultimately will lead to improving an individual's productivity and OP.

Three knowledge transfer types were used (email, teleconference, and eLearning), and eLearning proved to have the most significant impact. It created a sharing culture and a common place to retrieve information, but the authors also pointed out that further investigation was needed to ensure that the reuse of this module would lead to performance improvement [45]. Although the study used Moodle, an open-source eLearning platform, it did not discuss the security issues associated with open systems and platforms.

The study also highlighted the importance of matching learning modules with the right organizational needs; this will result in improving OP. In addition, the learning capabilities involving the use of eLearning modules can constitute a useful tool for sharing knowledge. This system will allow "just in time" training that will enable employees to cope with the necessary changes to their overall performance.

Another way in which an organization can use eLearning to stimulate their performance involves sharing their knowledge in an open platform or on the company's website, where they can attempt to gain customers' trust and attract talent's confidence. It is also a way to enhance the organizational image and reputation. In addition, the distribution of free learning materials can lead to an individual doing something for free in return. A study [33] has also highlighted the increased willingness of individuals to engage in an activity associated with a company after benefitting from free services such as knowledge sharing.

The results of [46] support the proposal of [33]. Deep learning applications in eLearning can automate this process and boost the repurposing of current organizational learning resources to create more customized experiences and content using the power of the natural language process (NLP) and machine learning.

5.2. Challenges in eLearning

In [19], the authors pointed out that, as everyone could imagine, eLearning practices were not a comfortable ride. The biggest obstacle in this paper was not the technology or the KM itself. Surprisingly, it lay in the human factor of the process. It has been found that employees can resist sharing the necessary knowledge. Individuals in organizations may argue that sharing the knowledge they have will threaten their existence in the organization, leading to their replacement with younger, cheaper staff. In addition, the embracing of comfort zone culture in organizations can be a barrier to making use of the full potential of eLearning tools. However, this finding could have been enhanced if it is supported by more concrete evidence. Further studies are needed to support this claim.

In [33], the study referred to an unfortunate widespread belief that if something like eLearning is free and accessible by all, such as OER, it might mean it is worthless. However, these concerns are not in line with those of [52], who found OER improves students' grades and addresses attainment gap concerns. They also offer opportunities for part-time students and populations historically underserved by higher education.

Intellectual properties were also raised in this study, where content producers restricting the reuse, editing, combining, or distributing of training materials. Language can also be a barrier for those who do not speak English as a second language. The same also applies to cultural diversity; the contextual gap can be another challenge that will result in a barrier for understanding not only the words but the context of the concept expressed through them.

The results of [44] are consistent with that, as the findings pointed out the importance of the simplicity and the accessibility of the eLearning platform as it might be an obstacle of the user interface was not interactive or attractive enough [44].

In [53] the authors have discussed the role of the eLearning resource quality and how the message of the content can be lost in the process. The issue related to updating multiple organizations, scattered in different locations from one credible source. Banks industries, for example, are impacted by several changes based on the economic situation. This industry is regulated by government economic policies that keep constantly changing to respond to the economic situation. Delivering these new updates effectively and swiftly is essential to bank employees. Banks are usually developing eLearning capabilities to inform their employees with these continuous updates; however, lacking a suitable mechanism to understand the quality of the learning resources can affect the understanding of these updates, resulting in outdated products and services, and eventually effects the bank's performance [53]. Unfortunately, high-quality content is usually associated with high cost. The results of [46] reinforce that by flagging out the cost involved in developing learning content. Although eLearning facilitates learning anytime and anywhere, the initial cost of developing eLearning resources can be a barrier to further deployment on an organizational level [46]. However, [46] also suggests tackling the cost linked with content development by using deep learning applications in reusing and purposing existing content, and save cost for the long-run.

5.3. eLearning emerging trends

In [47], the paper has discussed the mobile devices as one of the learning tools enhancing corporative learning. They describe the mobile learning operationally by a cooperative social process, supported by handsets, where the participant uses their handsets to interact internally and externally, to share and generate new knowledge. They used the terminology "mobile computer-supported collaborative learning" (mCSCL) to describe these activities. The paper also found six emerging perspectives on what learners are experiencing in mobile learning nowadays. They summarised their finding in the following points: 1) Social interaction is necessary, 2) Unlimited learning experience, 3) Learning becomes fun and interactive, 4) Instructor is becoming facilitator, 5) Learners control their learning between each other, 6) Learners value the co-creation of new knowledge [47].

A study by [48] highlighted another emerging field in adapting eLearning in an organization using game-based learning. These learning tools utilize the psychological readiness of individuals to engage in games. Game-based learning uses the same motivational and addiction mechanism used in video games and applies it to real-world activities to make them more enjoyable and attractive. The efforts focused on employing gamification techniques in the workplace to motivate, training and recruiting. Game-based training increases engagement, motivation, performance, and retention.

The study uses some empirical evidence as a successful application of game-based learning in the workplace environment.

Including L'Oreal, IBM, Cisco, Deloitte, and McDonald's. Whereby these companies have developed and implemented gamification and serious games as part of their overall training strategy. The impact has been measured by reducing lost time, an increase in engagement, and an increase in revenue up to USD 30 million [48].

In [50], the results suggested a flipped-classroom approach to improve learning outcomes. Flipped classroom or flipped workshop is considered an effective learning way by many researchers. The flipped classroom concept focuses on post-course activity, forcing learning to prepare and preview the material outside the class hours. For example, online learning tools are usually utilized, and learners have to attend online learning materials provided by the trainer before joining the actual class. The early finding indicates an improvement in learner's performance.

Authors of [46] have highlighted deep learning using artificial intelligence as one of the emerging trends in many eLearning fields. The value of deep learning comes in its ability to offer learners intuitive algorithms, automated delivery of content, the ability to swiftly reuse the current resource, and decrease the cost of content development. Some deep learning applications in eLearning includes Personalized learning path, Chatbots Performance indicator and Virtual teaching assistant.

The study of [33] discussed the role of OER in eLearning applications. The advantages of OER have gained increased attention worldwide; this could be for OER's potential in overcoming educational, demographic, economic, and geographic limitations. OER can come with various models, for example, the 4A model characterizes OER in the following As Accessible, appropriate, accredited, and affordable. In contrast, the 4R model characterized it in a 4R model, these Rs are: Reuse (open license of applying all or part for an individual goal), Revise (Editing, translating and modifying the content, Remix (Combining two materials to create a new resource and Redistribute (sharing with others).

The MOOC is one of the well-known concepts that has emerged from OERs. MIT's open courseware, for example, is the largest provider of such courseware. Up to 2015, MIT has successfully archived 2,250 training courses, and 450 training courses are being added annually. Many educational institutes have followed MIT's practices policy in publishing free open courses on MOOC platforms, such as Coursera, Edx, and Udacity platforms. Some corporations have even started to follow that practice, including IBM, Microsoft, and Google [33].

6. Conclusions

This paper has explained the importance of eLearning as a knowledge transfer tool on OP. It has also discussed the challenges and obstacles of applying eLearning tools and has highlighted the recent eLearning trends from 2016 to 2020. This study has further shown how individual LLL is critical in creating a knowledge-based economy and how eLearning capabilities provide an ideal solution for that mission. The research has shown that eLearning can impact OP in many ways. Also shown was the importance of matching learning modules with the right organizational needs in order to achieve the desired performance. One of the more significant findings is that sharing knowledge externally on an open eLearning platform can lead to gaining customers, attracting talent, and increasing a company's reputation and value. However, many of the findings discussed need further investigation. There is little known on how eLearning capabilities have impacted organizations during and after COVID-19 in different regions. Further study suggested studying the impact of eLearning as an LLL practice. Moreover, researchers must look at how students, young people, and senior employees engage in the eLearning platform, determine what motivates them, and decide how to validate their learning outcomes.

Acknowledgement

References

[1] S.A. Salloum, K. Shaalan, "Adoption of e-book for university students," in International Conference on Advanced Intelligent Systems and Informatics, Springer: 481–494, 2018.

[2] S.A. Salloum, C. Mhamdi, B. Al Kurdi, K. Shaalan, "Factors affecting the Adoption and Meaningful Use of Social Media: A Structural Equation Modeling Approach," International Journal of Information Technology and Language Studies, **2**(3), 96–109, 2018.

[3] S.A. Salloum, M. Al-Emran, S. Abdallah, K. Shaalan, "Analyzing the Arab Gulf Newspapers Using Text Mining Techniques," in International Conference on Advanced Intelligent Systems and Informatics, Springer: 396–405, 2017, doi:10.1007/978-3-319-64861-3_37.

[4] S.A. Salloum, M. Al-Emran, K. Shaalan, "The Impact of Knowledge Sharing on Information Systems: A Review," in 13th International Conference, KMO 2018, Slovakia, 2018.

[5] S.K. Al Mansoori S., Salloum S.A., "The Impact of Artificial Intelligence and Information Technologies on the Efficiency of Knowledge Management at Modern Organizations: A Systematic Review.," In: Al-Emran M., Shaalan K., Hassanien A. (Eds) Recent Advances in Intelligent Systems and Smart Applications. Studies in Systems, Decision and Control, Vol 295. Springer, Cham, 2021.

[6] A. Almansoori, M. AlShamsi, S.A. Salloum, K. Shaalan, Critical Review of Knowledge Management in Healthcare, 99–119, 2021, doi:10.1007/978-3-030-47411-9_6.

[7] S.K. Areed S., Salloum S.A., "The Role of Knowledge Management Processes for Enhancing and Supporting Innovative Organizations: A Systematic Review.," In: Al-Emran M., Shaalan K., Hassanien A. (Eds) Recent Advances in Intelligent Systems and Smart Applications. Studies in Systems, Decision and Control, **295**, Springer, Cham, 2021.

[8] A.A.A. Mehrez, M. Alshurideh, B.A. Kurdi, S.A. Salloum, Internal Factors Affect Knowledge Management and Firm Performance: A Systematic Review, 2021, doi:10.1007/978-3-030-58669-0_57.

[9] S.K. Habeh O., Thekrallah F., Salloum S.A., "Knowledge Sharing Challenges and Solutions Within Software Development Team: A Systematic Review.," In: Al-Emran M., Shaalan K., Hassanien A. (Eds) Recent Advances in Intelligent Systems and Smart Applications. Studies in Systems, Decision and Control, **295**, Springer, Cham, 2021.

[10] A.Y. Zainal, H. Yousuf, S.A. Salloum, "Dimensions of Agility Capabilities Organizational Competitiveness in Sustaining," in Joint European-US Workshop on Applications of Invariance in Computer Vision, Springer: 762–772, 2020.

[11] S.A. Salloum, M. Alshurideh, A. Elnagar, K. Shaalan, "Mining in Educational Data: Review and Future Directions," in Joint European-US Workshop on Applications of Invariance in Computer Vision, Springer: 92–102, 2020.

[12] S.A. Salloum, W. Maqableh, C. Mhamdi, B. Al Kurdi, K. Shaalan, "Studying the Social Media Adoption by university students in the United Arab Emirates," International Journal of Information Technology and Language Studies, **2**(3), 83–95, 2018.

[13] M. Raman, S. Gopinathan, "Role of knowledge and learning systems in fostering work-life balance," Knowledge Management & E-Learning: An International Journal, **8**(2), 213–215, 2016.

[14] A.S. Alnaser, M. Habes, M. Alghizzawi, S. Ali, "The Relation among Marketing ads, via Digital Media and mitigate (COVID-19) pandemic in Jordan The Relationship between Social Media and Academic Performance: Facebook Perspective View project Healthcare challenges during COVID-19 pandemic View project," Dspace.Urbe.University, (July), 2020.

[15] R.S. Al-Maroof, S.A. Salloum, A.E. Hassanien, K. Shaalan, "Fear from COVID-19 and technology adoption: the impact of Google Meet during Coronavirus pandemic," Interactive Learning Environments, 1–16, 2020.

[16] J.P. Lahti, T. Shinasharkey, "Corporate eLearning Position in Finnish Energy Business-Power Market Perspective."

[17] K.R. Finardi, R.G. Leao, G.B. Amorim, "Mobile assisted language learning: Affordances and limitations of Duolingo," Education and Linguistics Research, **2**(2), 48–65, 2016.

[18] M. Frot, 5 Trends in Computer Science Research | Top Universities, Top Universities, 2019.

[19] A.S.M. Zahari, S.M. Salleh, R.M.R. Baniamin, "Knowledge Management and e-Learning in Organisations," in Journal of Physics: Conference Series, IOP Publishing: 22051, 2020.

[20] M.E.D. Koenig, "What is KM? Knowledge management explained," KM World, **4**, 2012.

[21] T.H. Davenport, L. Prusak, Working knowledge: How organizations manage what they know, Harvard Business Press, 1998.

[22] K. Dalkir, "The knowledge management cycle," Knowledge Management in Theory and Practice. Oxford: Elsevier, 25–46, 2005.

[23] D. Hislop, R. Bosua, R. Helms, Knowledge management in organizations: A critical introduction, Oxford university press, 2018.

[24] M. Evans, K. Dalkir, C. Bidian, "A holistic view of the knowledge life cycle: the knowledge management cycle (KMC) model," The Electronic Journal of Knowledge Management, **12**(1), 47, 2015.

[25] M.M. Evans, N. Ali, "Bridging knowledge management life cycle theory and practice," in International Conference on Intellectual Capital, Knowledge Management and Organisational Learning ICICKM 2013–Conference Proceedings, 156–165, 2013.

[26] M.D. Nancy, The Organizational Learning Cycle: How We Can Learn Collectively - Nancy M. Dixon - Google Books, 2000.

[27] I. V Popova-Nowak, M. Cseh, "The meaning of organizational learning: A meta-paradigm perspective," Human Resource Development Review, **14**(3), 299–331, 2015.

[28] D. Wilkinson, "The 3 key issues for learning and knowledge management - Research.," in The OR Briefing - - Oxcogntia LLC., 2017.

[29] H. Mubeen, H. Ashraf, Q.A. Nisar, "Impact of emotional intelligence and knowledge management on organizational performance: Mediating role of organizational learning," Journal of Management Info, **11**(2), 35–52, 2016.

[30] M.S. Nikabadi, S. Bagheri, S.A. Mohammadi-Hoseini, "Effects of knowledge management strategy and organizational learning capability on innovation-driven performance in an oil company," Knowledge Management & E-Learning: An International Journal, **8**(2), 334–355, 2016.

[31] ATD Research, 2018 State of the Industry, 2018.

[32] D. Keegan, "The Future of Learning: From eLearning to mLearning.," 2002.

[33] M. Mosharraf, F. Taghiyareh, "The role of open educational resources in the eLearning movement," Knowledge Management and E-Learning, **8**(1), 10–21, 2016, doi:10.34105/j.kmel.2016.08.002.

[34] M. Schittek, N. Mattheos, H.C. Lyon, R. Attström, "Computer assisted learning. A review," European Journal of Dental Education: Review Article, **5**(3), 93–100, 2001.

[35] G. Hussain, I. Farooque, "Evaluation of the Effectiveness of Computer Assisted Learning to Improve the Clinical Examination Skills of First Year Medical Undergraduates," Original Research Article, **3**(8), 391–96, 2016, doi:10.16965/ijims.2016.144.

[36] L. Kolås, H. Nordseth, R. Munkvold, "Learning with educational apps: A qualitative study of the most popular free apps in Norway," in 2016 15th International Conference on Information Technology Based Higher Education and Training (ITHET), IEEE: 1–8, 2016.

[37] E. Cullen, What is Technology Enhanced Learning, and why is it important? - Mentimeter, Mentimeter, 2018.

[38] O. Bälter, Technology Enhanced Learning | KTH, Media Technology and Interaction Design, 2019.

[39] B.Y. Ekren, V. Kumar, "Next Generation Digital Engineering Education: MOOCs," in 5th NA International Conference on Industrial Engineering and Operations Management , Michigan: 1–11, 2020.

[40] J. Witte, R. Westbrook, M.M. Witte, "Gamification and Training," Global Conference on Education and Research , **1**, 56–58, 2017, doi:10.5038/2572-6374-v1.

[41] G. Mouzakitis, N. Tuncay, "E-Learning and lifelong learning," Turkish Online Journal of Distance Education, **12**(1), 166–173, 2011.

[42] A. A. Mohammed, Raj Gururajan, A.H. Baig, "Primarily Investigating into the Relationship between Talent Management and Knowledge Management in Business Environment," Knowledge Management in Business Environment., 2–8, 2017, doi:10.1145/3106426.31094441.

[43] D. Moher, L. Shamseer, M. Clarke, D. Ghersi, A. Liberati, M. Petticrew, P. Shekelle, L.A. Stewart, "Preferred reporting items for systematic review and meta-analysis protocols (PRISMA-P) 2015 statement," Systematic Reviews, **4**(1), 1, 2015, doi:10.1186/2046-4053-4-1.

[44] K.B. Kamal, M. Aghbari, M. Atteia, "E-training & employees' performance a practical study on the ministry of education in the Kingdom of Bahrain," Journal of Resources Development and Management, **18**, 2016.

[45] D. Tessier, K. Dalkir, "Implementing Moodle for e-learning for a successful knowledge management strategy," Knowledge Management & E-Learning: An International Journal, **8**(3), 414–429, 2016.

[46] A. Muniasamy, A. Alasiry, "Deep Learning: The Impact on Future eLearning.," International Journal of Emerging Technologies in Learning, **15**(1), 2020.

[47] G. Lim, A. Shelley, D. Heo, "The regulation of learning and co-creation of new knowledge in mobile learning," Knowledge Management & E-Learning: An International Journal, **11**(4), 449–484, 2019.

[48] K. Larson, "The Corporate Playground: A Review on Game-Based Learning in Enterprise Training," in E-Learn: World Conference on E-Learning in Corporate, Government, Healthcare, and Higher Education, Association for the Advancement of Computing in Education (AACE): 737–748, 2019.

[49] I.Y.A. Durairaj, T. Thiruvenkadam, M. Subrahmanian, "THE ROLE OF ORGANIZATIONAL LEARNING IN EMPLOYEE ENGAGEMENT AND THE MEDIATING ROLE OF E-LEARNING RESOURCES QUALITY," The Online Journal of Distance Education and E-Learning, **6**(4), 2018.

[50] K. Thongkoo, P. Panjaburee, K. Daungcharone, "Integrating inquiry learning and knowledge management into a flipped classroom to improve students' web programming performance in higher education," Knowledge Management and E-Learning, **11**(3), 304–324, 2019, doi:10.34105/j.kmel.2019.11.016.

[51] T. Thiruvenkadam, M. Subrahmanian, "THE ROLE OF ORGANIZATIONAL LEARNING IN EMPLOYEE ENGAGEMENT AND THE MEDIATING ROLE OF E-LEARNING RESOURCES QUALITY," The Online Journal of Distance Education and E-Learning, **6**(4), 78, 2018.

[52] N.B. Colvard, C.E. Watson, "The Impact of Open Educational Resources on Various Student Success Metrics The Impact of Open Educational Resources on Student Success Metrics," International Journal of Teaching and Learning in Higher Education, **30**(2), 262–276, 2018.

[53] M. Durairaj, C. Vijitha, "Educational data mining for prediction of student performance using clustering algorithms," International Journal of Computer Science and Information Technologies, **5**(4), 5987–5991, 2014.

Strategic Management of Brand Positioning in the Market

Oksana Garachkovska[*,1], Oleksii Sytnyk[2], Diana Fayvishenko[3], Ihor Taranskiy[4], Olena Afanasieva[5], Oksana Prosianyk[5]

[1]*Department of Public Relations and Journalism, Kyiv National University of Culture and Arts, Kyiv, 01601, Ukraine*

[2]*Department of Multimedia Technologies and Mediadesign, Taras Shevchenko National University of Kyiv Institute of Journalism, Kyiv, 02000, Ukraine*

[3]*Department of Journalism and Advertising, Kyiv National University of Trade and Economics, Kyiv, 02000, Ukraine*

[4]*Department of Marketing and Logistics, Lviv Polytechnic National University, Lviv, 79000, Ukraine*

[5]*Department of Management of Social Communications, Simon Kuznets Kharkiv National University of Economics, Kharkiv, 61166, Ukraine*

ARTICLE INFO

ABSTRACT

In the modern marketing system in a mass consumer society, the central place is given to the formation and promotion of brands. Professional conceptual approaches to brand management are able to preserve and increase the value and stability of the brand and allow the brand to survive in the most difficult competitive and crisis market conditions. In view of the fact that there is a fairly large number of theoretical developments, the purpose of the study was to develop practical recommendations regarding the strategic management of brand positioning in the market. The authors have developed an Algorithm for the strategic management of brand positioning in the market, which consists of 5 stages and 11 tasks. The tools proposed by the authors, which were discussed in detail and clearly demonstrated in the article, are of practical value. The product positioning process is not an easy process, and therefore even experienced professionals are not immune from mistakes. This research will help better to understand the brand positioning strategy in the market.

1. Introduction

Transformation processes in the economy in recent years have led to significant economic changes. With the transition to a market system, business entities' conditions have changed significantly, so the existing management and marketing technologies are no longer sufficient for successful management in market management conditions.

Given the saturation of the market with goods and services to stand out from the competition and take a worthy place in the minds of not only consumers but also all market participants, companies focus their efforts on differentiating offers, based on which they position their products. Branding in modern society is more than just creating a name, company logo or product. Thanks to the successful development and implementation of strategic

management of brand positioning in the market today, brands can become not only consumer market products, but also corporations, law firms, cities, countries, universities, hospitals, museums, restaurants and even individuals [1]. It is not surprising that consumers are willing to buy, first of all, well-known and high-quality so-called branded items or use the services of branded companies. They can increase the company's rating, on the one hand, and consumer status in society – on the other. Understanding the need and effectiveness of creating and positioning a product or corporate brand, the number of domestic brands consulting agencies – specialized companies for the strategic management of brand positioning in the market. Despite the growing interest in the problem of positioning by marketing theorists and practitioners, the main approaches to the selection and implementation of positioning strategies are still not systematized; there is no single approach to their classification and complementarity and mutual

avoidance, which complicates the positioning of products, brands and enterprises in practice.

Thus, branding is a relevant and demanded marketing tool for the formation of consumer demand, sales promotion and sales. The brand regulates the buyer's behaviour, creates a stable favourable image of the company and the product, and guarantees long-term stable relations with a loyal consumer. It is the relevance that explains the purpose of the study - the development of practical recommendations for the strategic management of brand positioning in the market.

2. Theoretical aspects of brand positioning management in the market

Jack Trout coin the term product positioning. Trout detailed the product positioning theory in his Industrial Marketing article, which was published in June 1969 [2]. The article aroused great interest in the marketing community, and later, in 1981, in their book Positioning, Battle for Minds, Jack Trout and Al Rice elaborated on the concept of "product positioning", supplementing it with many examples and illustrative business cases [3].

The reason for the emergence of the positioning theory is the desire to find a way to distinguish a product among products with similar properties and characteristics through marketing communications. Positioning theory says that the consumer cannot remember all goods' characteristics on the market due to their large number; therefore he remembers by the method of associations, endowing each product with certain attributes that are important to him when buying a product [4].

Branding is activity on development and brand management. Brand (from the English brand – stigma) – is the "brand name", the name of the enterprise, product, product group, service, etc., the official trademark. The brand provides wide popularity of the object, the ability to recognize it, uniqueness, deep penetration into the consciousness/subconscious of many members of the target audience, and significant value in consumers' eyes. This is a correctly and effectively constructed image, embodied, first of all, in the name. A brand is an information about the company, product or service; popular, easily recognizable and legally protected symbols of the manufacturer or product. Creativity is the most critical moment in the life of a brand. It is necessary to be noticed and to achieve the maximum positive perception of the market offer [5].

Branding requires high financial costs that are justified only for specific products. Also, relevant issues are related costs – inventory management [6, 7], human resources [8], innovations [9], etc. Thus, among branded goods without branding, victory is impossible in competition. Such goods, in turn, due to the high cost, contribute to the growth of profits and the formation of a producer's successful image [10]. There are various methods of brand evaluation, which are used to determine the ratings of the latter. Annual brand ratings illustrate certain phenomena and their patterns that occur in the economy and allow you to predict certain future events [11]. Marketing strategy, which also includes product positioning, is an area where practice prevails over theory. Due to the limited volume of the article, the authors decided to focus on the practical aspects of strategic management of brand positioning

in the market, namely, to develop an algorithm and tools for its effective use.

3. Results: an algorithm for the strategic management of brand positioning in the market

Based on the literature and existing practices analysis, the authors present an algorithm for developing brand positioning in the market (Fig. 3).
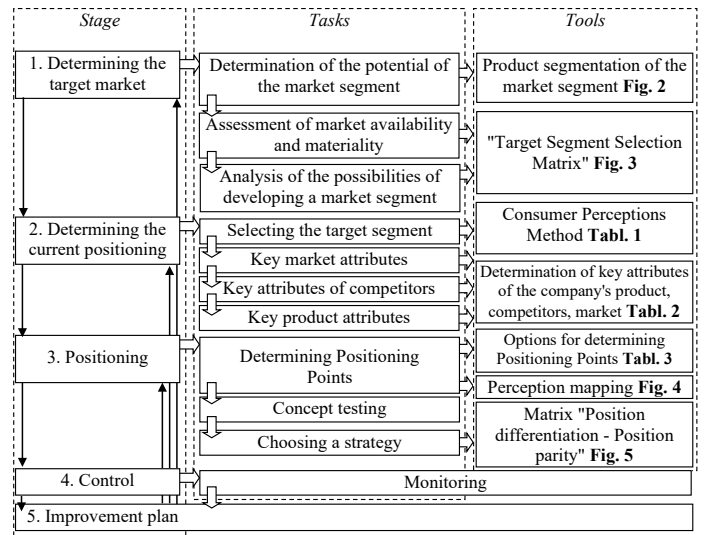
Figure 1: Algorithm for the strategic management of brand positioning in the market

The process of developing brand positioning consists of the following stages: determining the target market, assessing the current perception of the brand and competitors, developing and testing possible product positioning concepts, as well as monitoring the competitiveness of the approved strategy in the future and ways for further improvement if necessary. Let's consider the stages in more detail.

Stage 1. Selecting the target market. Setting a target market is the process of deciding which market segments a company should actively work to increase sales. Companies choose between an undifferentiated or differentiated approach or prefer a so-called concentrated approach.

The target market is the most suitable and profitable group of market segments (or one and the only segment) for the company, to which its marketing activities are directed.

Step 1.	List all the products available on the market: in the listing it is not necessary to be a maximalist and try to cover the market by 100%. It is enough to list all the products of large and medium players.
Step 2.	Determine all the characteristics by which the listed products differ. These characteristics can be: properties, volume, packaging, price, special taste, smell, etc.
Step 3.	Survey of consumers of the target market: what characteristics do they actually divide the goods on in the market. Target audience polling is a very important point in any market segmentation.
Step 4.	Compilation of a complete list of segmentation criteria based on Steps 2 and 3.
Step 5.	Description of each product from the list according to the listed characteristics.

Figure 2: Algorithm for product segmentation of the market segment (developed by the authors)

Suppose the company is faced with the task of conducting product segmentation of the industry. In that case, we propose to use the following algorithm (Fig. 2), with which it is possible not only to assess in detail the structure of the market but also to find free market niches for expanding the scope of the company.

The choice of the target market is closely related to the issues of product positioning, identifying its distinctive features and characteristics and determining its place in the market among other similar products from the perspective of the consumer himself. Positioning makes the product recognizable in the market. "Target Segment Selection Matrix" (Fig. 3) will allow a better understanding of the availability for the company of the materiality of the market and analyze the possibilities of developing a market segment.
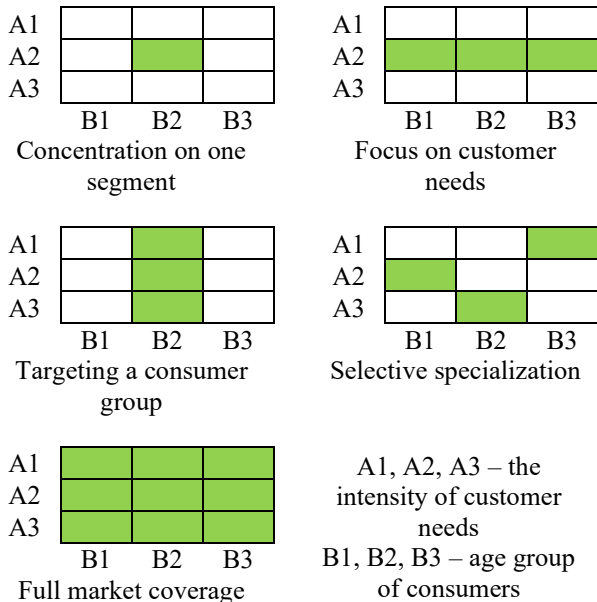
Figure 3: Target Segment Selection Matrix

In practice, these strategies can be implemented in the following ways:

1. Narrow specialization, concentration on one market segment, for example, on the production of one type of gadgets for adolescent girls.

2. Focus on consumer needs, for example, the production of one type of gadgets for all age groups of consumers.

3. Targeting a consumer group, such as producing a wide range of gadgets for teenage girls.

4. Selective specialization, such as the production of certain types of gadgets for certain age groups.

5. Full coverage of the market, namely: production of all types of gadgets for all age groups of consumers.

When selecting the optimal market segments, it is recommended to give preference to the largest segments, segments with clearly defined boundaries and not intersecting with other market segments, segments with new, potential demand, etc. It is considered to be the most optimal segment, where there are about 20% of buyers of this market, purchasing about 80% of the goods offered by the company.

Stage 2. Determination of the current position The stage involves assessing how the target audience (= target market) perceives the company's product and competitors' product. It is necessary to determine from 5-10 definitions that best characterize the goods in the opinion of consumers (Table 1).

Table 1: An example of determining the current positioning of a product of a company and main competitors based on consumer perception

Current perception of the company's product	Current perception of competitor's product 1	Current perception of competitor's product 2	Current perception of competitor's product 3
modern	traditional	known	expert
fashionable	known	widely advertised	high quality
young	widely advertised	recommended by experts	expensive
plain	recommended by experts	quality	recommended by experts
cheap	quality	safe	innovative
dynamic	safe	innovative	foreign
safe	family	dynamic	
A modern product without unnecessary additions for the younger generation at an affordable price	*Renowned Recommended Brand for the Whole Family*	*A well-known innovative brand recommended by experts*	*Innovative import brand expert*

To determine the key attributes of a product is necessary to decide on the properties of the product, which are essential in the industry and can become the basis for positioning the company's product (Table 2) ensuring the security of the region.

Market properties – mandatory properties for each product;

Distinctive properties of the company and competitors - characteristics of the product that are unique and not found elsewhere on the market;

Consumer properties is a description of the ideal product in the words of the consumer. The last column indicates the basic needs that the consumer seeks to solve using the desired product property (based on his motivation).

Stage 3. Positioning Now that all the preparatory stages have been passed, you can proceed directly to the very process of developing product positioning, which consists of four sequential phases: determining points of differentiation (= positioning points), building perception maps and testing the developed positioning concepts and choosing a strategy.

Points of differentiation. All good profitable markets have been occupied for a long time; they are highly competitive. In such markets, some companies are "first and best"; in such industries, all market niches are usually occupied, and it takes a lot of effort to find a competitive positioning for a new product. Points of differentiation (= positioning points) will help a company find vacant niches and look at the market from different angles (Table 3).

Table 2: Determination of the key attributes of the company's product, competitors, market

Properties of goods on the market	Market properties of goods	Company product properties	Competitor properties	Consumer properties	Problems and needs that the consumer seeks to solve with this property
Property 1	+	+		+	need 1
Property 2		+	+	+	need 2
Property 3			+		
Property 4	+	+		+	need 3
Property 5		+	+		
Property 6		+	+	+	need 4
Property 7	+			+	need 5
Property 8		+	+	+	need 6
Property 9		+			
Property 10	+	+	+	+	need 7

Table 3: Examples of positioning points

Options			Could it be a positioning point?
Option for creating a new subcategory on the market			
Product category improvement options	How can this sound? O1	How can this sound? O2	PP
improvement 1	not just (product category), but (improved product category)	The first in ...	yes/no
improvement 2	not just (product category), but (improved product category)	The first in ...	yes/no
EXAMPLE: new brand	Not just a brand, but a changing perception	Not just a brand, but a changing perception	yes
Option for Solving Consumer Needs			
Needs and problems of the target audience	Are the current market players solving this problem?	Is leadership possible in solving the problem?	PP
problem 1	yes/no	yes/no	yes/no
problem 2	yes/no	yes/no	yes/no
problem 3	yes/no	yes/no	yes/no
permanent breakdowns	no	yes	yes
inaccurate measurement	yes	yes	yes
impractical design	yes	no	no
The Option to Create the Opposite Image			
Perceptions and properties of competitors	Opposite	Attractive to the target audience?	PP
perception 1	…	yes/no	yes/no
property 1	…	yes/no	yes/no
traditional	innovative	yes	yes
known	little known	no	no
widely advertised	unadvertised (not overpriced)	yes	yes
Market Leadership Option			
Market properties of goods	Will it be valuable to the consumer if the product performs this property best?	Is there a product that best implements this property?	PP
property …	yes/no	yes/no	yes/no
ease of use	yes	yes	yes
memory	yes	no	yes
the ability to change the design	no	no	no

It is also possible to search for positioning points by opposition to the main competitor, by the method of product use, etc.

Choosing of strategy is one of the most important decisions in brand positioning. We propose using the matrix "Position differentiation – Position parity" (Fig. 5).

	Strong	Neutral	Weak
Strong	Raising the parity of the position	Maintaining a differentiated position	Maintaining a leading position
Neutral	Increasing the parity of the position and creating additional points of differentiation	Adjustment of position in the direction of strengthening parity and (or) differentiation of position	Maintaining a parity position
Weak	Repositioning	Creation of additional points of parity and strengthening of position differentiation	Enhancing position differentiation

Position differentiation (Y-axis label) — *Position parity* (X-axis label: Strong, Neutral, Weak)

Figure 5: Matrix "Position differentiation - Position parity"

The construction of the matrix is based on the following indicators.

1. Differentiation of the organization's position for consumers (Y-axis):

$$D = \sum_{i=1}^{n} W_i O_i \qquad (1)$$

where D is an indicator of differentiation of position for consumers;

W_i is the rank of the i-th differentiation point for the consumer (ranking in descending order, where the highest rank is the most significant differentiation point);

O_i is the assessment of the i-th point of differentiation by consumers (in points, from 1 to 5);

n is the number of points of differentiation;

2. Parity of the organization's position for consumers (plotted along the X-axis):

$$P = \sum_{i=1}^{m} W_i Q_i \qquad (2)$$

where P is the position parity indicator;

W_i is the rank of the i-th categorical point for the consumer (ranking in descending order, where the highest rank is the most significant point of differentiation);

O_i is the assessment of the i-th categorical point by consumers (in points, from 1 to 5);

m is the number of categorical points.

According to the matrix, the following types of strategies can be used [5].

Leadership strategies:

The strategy of maintaining a leading position assumes that the position of an educational organization is unique and contains the main characteristics associated by consumers with its activities – an optimal set of points of parity and differentiation. With distinct differences from the competition, the educational organization offers consumers exactly what they expect. It is the strongest and most attractive position in the minds of consumers.

The strategy of maintaining a differentiated position provides that the position is strong enough and has unique points of differentiation, but requires the educational organization to clearly understand why it has fewer parity points than the leading organization. The parity points taken as a basis are not very significant for consumers, or not all consumer expectations regarding these points are fully satisfied.

The strategy of maintaining a parity position assumes that the existing position is beneficial to the educational organization, since, despite the absence of unique characteristics (points of differentiation), consumers rate it highly and consider it attractive in terms of the proposed set of parity points.

Market Follower Strategies:

The strategy of increasing the parity of the position is a strategy in which the position of an educational organization is unique and has certain points of differentiation. Still, it is not significant enough for consumers. In this situation, the educational organization, as a rule, concentrates its marketing communication efforts on demonstrating to consumers those points of differentiation that do not matter to them. As a result, it is necessary to adjust the position, supplementing it with points of parity that are important for consumers.

The strategy of adjusting the position in the direction of increasing parity and (or) differentiation of the position assumes that the position of the educational organization is represented by characteristics that are different from competitors. Still, they are not of particular importance to consumers. The author has proved that in this case the position can be considered as promising, provided that the educational organization directs marketing efforts to increase its attractiveness - increasing the level of implementation of existing points of parity and points of differentiation through a significant set of marketing communications.

The strategy to enhance position differentiation is a strategy whereby a position is attractive in the short term because it is highly regarded by consumers. Nevertheless, in the context of continuously increasing competition in the market, it can "get lost", which dictates the need to direct marketing efforts to find points of differentiation to form a position in the long term.

Market Challenger Strategies:

The strategy of increasing the parity of the position and creating additional points of differentiation is used if the current status of the educational organization is not entirely attractive to consumers, since it does not contain a set of mandatory points of parity with which they associate its activities. As a result, the position does not have significant points of differentiation to attract the attention of consumers, which requires adjustments to complement the points of parity and differentiation that are meaningful to them.

The strategy of creating additional points of parity and strengthening the differentiation of the position is applied if the position of the educational organization does not stand out among others and is of little interest to consumers since it is not represented by points of differentiation and does not include all characteristics and points of parity that are important for consumers. In this situation, it is necessary to optimize the position by a set of parity points.

The repositioning strategy is used if the position does not have parity and is not differentiated, which requires an educational organization to make immediate marketing efforts to change it significantly.

The choice of an adequate strategy makes it possible to match the position transmitted using marketing communications and the position that has developed in the perception of consumers, thereby increasing the efficiency of brand management. This is possible using a set of communications for brand promotion on the market, developed by the chosen positioning strategy and implemented in marketing practice.

Stage 4. Control The product positioning process is not an easy process, and therefore even experienced professionals are not immune from mistakes. Therefore, after choosing a positioning control strategy, it is necessary to check it for compliance with the following criteria:

- positioning is based on 2-3 essential product characteristics;

- the target group of the product is clearly defined, it is evident from the positioning that the product is designed "not for all consumers";

- if the positioning is based on price, then it is not the only parameter;

- if a product is positioned against the prominent market leader, then it has absolute superiority in a particular area;

- for one target market, only one type (strategy) of product positioning is used;

- positioning is based on promises and product properties that the company is able to fulfil;

- positioning does not provide for cardinal repositioning of the product, or intermediate product positioning has been developed;

- if the existing positioning of the product was successful, then the new positioning only improves it, and does not change it;

- when developing positioning, a sufficient number of alternatives were considered, and the first successful option was not chosen.

Monitoring also includes tracking possible changes in market conditions, the emergence of new consumers, the strengthening of competitors, etc. The company can choose the different frequency of monitoring various components depending on the rate of their change.

Stage 5. Improvement plan Almost any company strives to maximize profits, sometimes this is not a primary goal, but it is also essential; therefore it is periodically necessary, after monitoring the current situation, to make forecasts for the future and improve the positioning strategy. Over time, the strategy can transform into a company's diversification strategy. When drawing up an improvement plan, it is necessary to go through stages 1-3 especially carefully, because sometimes top management makes the main mistake in this, considering these stages "passed" and does not go through them in detail again.

Thus, the proposed algorithm for the strategic management of brand positioning in the market and tools for its effective use will allow business entities to understand better and implement marketing tools to strengthen their competitive positions.

4. Conclusion

The basis of the success of any business is the presence of sustainable competitive advantages of goods and services, which consists of the consumer's understanding of their distinctive properties. The application of strategic positioning management significantly contributes to the solution of this problem. Brands and trademarks bring significant benefits to producers and consumers, which guarantees producers additional profits, ensuring consumer loyalty, and thus reducing the impact of competition on fluctuations in sales. The presence of a brand and consumer loyalty shows that one or another business entity is more competitive, especially in crisis conditions, and has greater advantages compared to other entities. This significantly mitigates the reaction of consumers to possible price fluctuations, opens up new opportunities for expanding markets for enterprises of the national economy.

Strategic management of brand positioning in the market is one of the most important marketing processes, which determines the adequate market position of the product and/or the company as a whole. The positioning strategy is multifaceted and requires separate consideration; tactics indicate the relationship with the marketing mix, and in the latter, the main role is given to promotion.

In the study, the authors focused on the development of practical recommendations for brand management: The proposed algorithm for the strategic management of brand positioning in the market and tools for its effective application will allow business entities to better understand and implement marketing tools, reduce costs, expand market share to strengthen their competitive positions.

Areas of further research may be the approbation of the proposed tools at domestic enterprises and the development of theoretical and methodological recommendations for rebranding.

Conflict of Interest

The authors declare no conflict of interest.

References

[1] N. Shmygol, O. Cherniavska, T. Pulina, R. Zavgorodniy, "Economic assessment of the implementation of the resource-efficient strategy in the oil and gas sector of the economy on the basis of distribution of trade margins between extracting and processing enterprise," Polityka Energetyczna, **23**(3), 135–146, 2020, doi:10.33223/epj/126998

[2] J. Trout, "Positioning is a game people play in today's me-too market place," Industrial marketing, **54**(6), 51–55, 1969.

[3] A.Ries, J. Trout, Positioning, The battle for your mind, Warner Books

McGraw-Hill Inc., 1981.

[4]   G.M. Caporale, A. Plastun, V. Oliinyk, "Bitcoin fluctuations and the frequency of price overreactions," Financial Markets and Portfolio Management, **33**(2), 109–131, 2019, doi:10.1007/s11408-019-00332-5

[5]   D.Schultz, S.Tannenbaum, R.Lauterborn. The New Marketing Paradigm: Integrated Marketing Communications, McGraw-Hill Education Inc., 1994.

[6]   S. Mishra et al., "Fuzzyfication of supplier-retailer inventory coordination with credit term for deteriorating item with time-quadratic demand and partial backlogging in all cycles," in Journal of Physics: Conference Series 1531:012054, 2020, doi:10.1088/1742-6596/1531/1/012054

[7]   Y. Krykavskyy, "Industrial supply chains: Between efficiency and responsibility," Actual Problems of Economics, **179**(5), 30–41, 2016.

[8]   E. Kostelijk, K. J. Alsem, "Brand positioning and employees," in book: Brand Positioning, 2020, doi: 10.4324/9780429285820-15

[9]   A. T. Ahmedova, "System of innovative business strategic management of the enterprise," Middle European Scientific Bulletin, **4**, 2020, 10–13, 2020, doi: 10.47494/mesb.2020.4.31

[10] B. Al-alak, A. Tarabieh, "Gaining competitive advantage and organizational performance through customer orientation, innovation differentiation and market differentiation," International Journal of Economics and Management Sciences, **1**(5), 80–91, 2011.

[11] R. Allen, M. Helms, "Linking Strategic Practices and Organizational Performance to Porter's Generic Strategies," Business Process Management Journal, **12**(4), pp. 433–454, 2006, doi:10.1108/14637150610678069

A S T E S

Redlich-Kister Finite Difference Solution for Solving Two-Point Boundary Value Problems by using Ksor Iteration Family

Mohd Norfadli Suardi[*], Jumat Sulaiman

Mathematics with Economics Programme, Faculty of Science and Natural Resources, Universiti Malaysia Sabah, 88400 Kota Kinabalu, Sabah, Malaysia

A R T I C L E I N F O	A B S T R A C T
	In this paper, we are concerned to investigate the efficiency of the second-order Redlich-Kister Finite Difference (RKFD) discretization scheme together with the Four Point Explicit Group Kaudd Successive Over Relaxation (4EGKSOR) iterative method for solving two-point boundary value problems (TPBVPs). In order to apply this block iteration to solve any linear system, firstly we discretize all derivative terms via the second-order RKFD discretization scheme over the proposed problem in order to get the second-order RKFD approximation equation. Due to the main characteristics of the coefficient matrix for the generated linear system which are large-scale and sparse, the best choice for solving this linear system is using one of the iterative methods. Therefore, the formulation of the Kaudd Successive Over Relaxation method together with the Explicit Group iteration method mainly on the Four-Point Explicit Group Kaudd Successive Over Relaxation (4EGKSOR) iterative method has been presented to solve this linear system iteratively. In order to show the efficiency of the 4EGKSOR, another two iterative methods have also been considered which are the Gauss-Seidel (GS) and the Kaudd Successive Over Relaxation (KSOR) to solve three examples of the proposed problems in which all numerical results obtained were recorded based on the number of iterations, execution time and maximum norm. Based on the performance analysis, clearly, the 4EGKSOR iterative method shows substantiated improvement in terms of the number of iterations and execution time.

1. Introduction

The successful of the development of numerical techniques for boundary value problems has been growing rapidly in the past few decades. Many researchers give more attention to this problem numerically and show the capability of their numerical techniques in solving this problem especially TPBVPs; due to its application, this problem can be found in science, engineering and physics fields including optimal control, beam deflection and heat flow [1-4]. In initial works on obtaining the numerical solutions of TPBVPs, many authors attempted to achieve higher accuracy by using the various numerical methods. It was done either by suggesting the families of spline methods for solving second-order two-point boundary value problem, see in [5-9]. The basic approach of these methods is dividing the interval into subinterval and at the same time, the construction of spline, B-spline and extended B-spline in each subinterval considered. For achieving better accuracy, these methods are required to solve a system of equations. Another numerical method is to solve TPBVPs by

developing the innovative method based on the Galerkin method see in [10-12]. Numerous numerical methods are used to solve the boundary value problems related TPBVPs for obtaining the approximation equation can be seen in [13-17].

Besides of using the above numerical methods to solve the proposed problem (1) as stated in the first paragraph, many studies were also introduced via the use of the concept of finite difference method (FDM). As a result, several numerical discretization schemes mainly in a family of the finite difference schemes have been proposed to form a new finite difference discretization scheme. For example, the standard finite difference [18], Chebyshev finite difference [19] and Rational Finite Difference [20] are imposed for solving TPBVPs. Clearly, the development of Chebyshev finite difference and Rational Finite Difference schemes has been encouraged by the combination of the standard finite difference concept together with the Chebyshev and rational approximation functions respectively. In conjunction with these combinations, the author in [20] also introduced a new finite difference scheme via the combination of exponential

954

approximations and finite difference discretization schemes which is known as exponential finite difference discretization schemes to show its capability for solving TPBVPs [21].

Apart from the use of Chebyshev, rational and exponential approximation functions as mentioned in the previous second paragraph, this paper attempts to investigate the feasibility of the Redlich-Kister polynomial as a numerical method for solving TPBVPs. Based on the previous studies on the application of the Redlich-Kister polynomial, the findings have pointed out that various types of Redlich-Kister polynomial functions have successfully been used to develop the appropriate mathematical models in physics and chemistry fields [22-24]. In addition to these functions, only one study has been explored to investigate the application of the Redlich-Kister approximation function in the numerical analysis particularly on constructing the mathematical model. For instance, in [25], the authors investigated the construction of two mathematical models based on the piecewise third-order Redlich-Kister polynomial model and the piecewise first-order polynomial model respectively to show the relationship of the number of iterations for Gauss-Seidel towards its corresponding grid size. The findings of their work concluded that the results of the piecewise third-order Redlich-Kister polynomial model gave highly accurate solutions as compared with the first-order polynomial solution. Inspired by the high accuracy of the Redlich-Kister (RK) function based on high-order approximation function, we present a feasibility study of two newly established Redlich-Kister Finite Difference (RKFD) discretization schemes for solving TPBVPs.

In order to solve the proposed problem, firstly, the RKFD discretization scheme will be used to discretize TPBVPs to form the RKFD approximation equation. After that, the approximate equation was obtained will lead us to construct a linear system. Since the generated linear system has a large and sparse matrix, the use of iterative methods is the best linear solver [26-28]. For instance, the implementation of the point iteration family namely SOR [29], AOR [30] and KSOR [31] can be used to solve this linear system. In addition to this point iteration family, Evans [32] introduced the Explicit Group (EG) iterative method which is faster than the Gauss-Seidel (GS) iterative method to get the numerical solution of this linear system. Despite the speed up the convergence rate for Explicit Group (EG) iteration, many researchers also developed new variants of the EG iteration family such as 9-Point EG [33], EGSOR [34], EDGSOR [35] and MEGSOR [36] in which all these block iterations have significantly reduced their convergence rate. Therefore, further discussion of this paper focuses on investigating the efficiency of the 4EGKSOR iterative method which is inspired by the paper research [37] and apply together with the newly established RKFD discretization scheme for solving the system of Redlich-Kister approximation equations. The formulation of the 4EGKSOR iterative method can be established via the combination of the EG and KSOR iterative methods.

Before applying and investigating the performance of this 4EGKSOR method, we need to do the process of discretization and let us consider the general equation for TPBVPs, which are given as follows

$$\frac{d^2U}{dx^2} + Z(x)\frac{dU}{dx} + G(x)U(x) = r(x), \quad x \in [0, \phi] \tag{1}$$

with the Dirichlet conditions,
$$U(0) = \varphi_0, \qquad U(\phi) = \varphi_1.$$

2. Redlich Kister Finite Difference Approximation Equation

The previous section has mentioned that the use of the RK function to introduce two newly established RKFD discretization schemes for approximating the proposed problem (1). To start the discretization process, firstly let us consider the RK approximation function of order n as follows

$$U_n(x) = \sum_{k=0}^{n} a_k \cdot T_k(x) \tag{2}$$

where $a_k, k = 0,1,2,...,n$ are the unknown parameters to be determined.

Figure 1: Distribution of grid network considered.

To facilitate us in discussing the use of this approximation function, let us construct the distribution of uniformly node points as indicated in Figure 1. Based on Figure 1, let us consider the first three RK functions that need to consider the number of node points as shown in Figure 2.

Figure 2: The path for T_1, T_2 and $_3$.

Then to derive the new second-order RKFD approximation equation, let us consider $n = 2$ in equation (2) and applying the concept in Figure 2, the second-order RK approximation function can be written as

$$U(x) = a_0 T_0(x) + a_1 T_1(x) + a_2 T_2(x) \tag{3}$$

where the first three RK functions are defined as

$$T_0(x) = 1,$$
$$T_1(x) = x,$$
$$T_2(x) = x(1-x).$$

Referring to Figure 1, let us define the node points, $x_c = x_0 + ch, c = 0,1,2,...,n$ where $h = \frac{\phi - 0}{n}, n = 2^p, p \geq 1$ donates the uniform step size. Then $U(x_k) = U_k, k = c-1, c, c+1$ and $T(x_k) = T_k, k = c-1, c, c+1$ represent the approximation value of functions, $U(x)$ and $T(x)$. By considering any group of three node points, x_{c-1}, x_c and x_{c+1} for equation (3), we have the following equations

$$U_{c-1} = a_0 T_{0,c-1} + a_1 T_{1,c-1} + a_2 T_{2,c-1}, \tag{4}$$

$$U_c = a_0 T_{0,c} + a_1 T_{1,c} + a_2 T_{2,c}, \tag{5}$$

$$U_{c+1} = a_0 T_{0,c+1} + a_1 T_{1,c+1} + a_2 T_{2,c+1}. \tag{6}$$

After that, the expression of three parameters $a_k, k = 0,1,2$ in equation (3) can be determined by solving the equations (4), (5) and (6) via a matrix approach. With these three parameters, we rewrite the second-order RK approximation function, $U(x)$ in equation (3) in which it can be shown as follows

$$U(x) = N_0(x)U_{c-1} + N_1(x)U_c + N_2(x)U_{c+1} \tag{7}$$

where the second-order RKFD shape functions, $N_k(x), k = 0,1,2$ are defined respectively as

$$\begin{cases} N_0(x) = \dfrac{1}{2h^2}\left(x^2 - 2xhc - xh + h^2c^2 + h^2c\right), \\ N_1(x) = \dfrac{1}{h^2}\left(2xhc - x^2 - h^2c^2 + h^2\right), \\ N_2(x) = \dfrac{1}{2h^2}\left(x^2 - 2xhc + xh + h^2c^2 - h^2c\right), \end{cases} \tag{8}$$

Then the first and second derivative of these RK shape functions can be shown as

$$\begin{cases} N_0'(x) = \dfrac{1}{2h^2}(2x - h - 2hc), \\ N_1'(x) = \dfrac{1}{h^2}(2hc - 2x), \\ N_2'(x) = \dfrac{1}{2h^2}(2x + h - 2hc), \end{cases} \tag{9}$$

and

$$\begin{cases} N_0''(x) = \dfrac{1}{h^2}, \\ N_1''(x) = -\dfrac{2}{h^2}, \\ N_2''(x) = \dfrac{1}{h^2}. \end{cases} \tag{10}$$

Then, by applying the first derivative concept into the function (7) with respect to x_c, it can be shown that the second-order RKFD discretization scheme of the first derivative of the function, $U(x)$ is given as

$$\left.\frac{\partial U}{\partial x}\right|_c = N_0'(x_c)U_{c-1} + N_1'(x_c)U_c + N_2'(x_c)U_{c+1} \tag{11}$$

and for the second derivative of the function $U(x)$ with respect to x_c can be approximated by

$$\left.\frac{\partial^2 U}{\partial x^2}\right|_c = N_0''(x_c)U_{c-1} + N_1''(x_c)U_c + N_2''(x_c)U_{c+1} \tag{12}$$

where $U(x_c) = U_{c,c=0,1,2,...,n}$ represent the approximation solution of function $U(x)$. Clearly, equations (11) and (12) are known as two newly established Redlich-Kister finite difference discretization schemes.

From the proposed problem (1), it needs to be rewritten in the discrete form at a node point, x_c and then we get

$$\left.\frac{d^2 U}{dx^2}\right|_c + Z(x_c)\left.\frac{dU}{dx}\right|_c + G(x_c)U(x_c) = r(x_c), \tag{13}$$

Then by considering both equations (11) and (12) and substitute them into equation (13), it can be pointed out that the newly established RKFD approximation equation of TPBVPs can be formulated as follows

$$\alpha_c U_{c-1} + \beta_c U_c + \gamma_c U_{c+1} = r_c, \tag{14}$$

where

$$\begin{aligned} \alpha_c &= N_0''(x_c) + Z_c N_0'(x_c), \\ \beta_c &= N_1''(x_c) + Z_c N_1'(x_c) + G_c, \\ \gamma_c &= N_2''(x_c) + Z_c N_2'(x_c). \end{aligned}$$

and

$$Z_c = Z(x_c), G_c = G(x_c), r_c = r(x_c), \quad c = 1,2,3,...,n-1.$$

Referring to the RKFD approximation equation (14) and considering $c = 1,2,...,n-1$, it is obvious that we can construct a generated linear system with its large-scale and sparse coefficient matrix as follows

$$W \cdot U = r \tag{15}$$

where

$$W = \begin{bmatrix} \beta_1 & \gamma_1 & 0 & 0 & 0 & 0 \\ \alpha_2 & \beta_2 & \gamma_2 & 0 & 0 & 0 \\ 0 & \alpha_3 & \beta_3 & \gamma_3 & 0 & 0 \\ 0 & 0 & \ddots & \ddots & \ddots & 0 \\ 0 & 0 & 0 & \alpha_{n-2} & \beta_{n-2} & \gamma_{n-2} \\ 0 & 0 & 0 & 0 & \alpha_{n-1} & \beta_{n-1} \end{bmatrix},$$

$$U = \begin{bmatrix} U_1 & U_2 & U_3 & \cdots & U_{n-2} & U_{n-1} \end{bmatrix}^T,$$

$$r = \begin{bmatrix} r_1 - \alpha_1 \cdot \varphi_0 & r_2 & r_3 & \cdots & r_{n-2} & r_{n-1} - \gamma_{n-1} \cdot \varphi_1 \end{bmatrix}^T.$$

3. Derivation of 4EGKSOR Iterative Method

Since the characteristics of the coefficient matrix of the linear system (15) are large-scale and sparse, the family of iterative methods can be chosen to be the best linear solver as stated in the first section. To solve this linear system, the Kaudd Successive Over Relaxation (KSOR) iterative method was developed by [38] as one of more efficient point iterative methods by using one weighted parameter which is used to speed up its convergence rate and show to be more economical computationally than the Gauss-Seidel (GS) iterative method. Due to the advantage of lower

computational complexity, we establish the formulation of the Four-Point Explicit Group Kaudd Successive Over Relaxation (4EGKSOR) iterative method, which is a combination between a standard Kaudd Successive Over Relaxation (KSOR) iterative method and Explicit Group approach by using the newly established RKFD approximation equation (14). To derive the formulation of 4EGKSOR, let us consider the grid network in Figure 1 and a group of block node points concept in Figure 3. Figure 3 illustrates the finite grid network of the RKFD approximation equation where block approach has been done until iteration convergence is achieved.
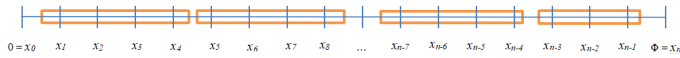
Figure 3: Distribution of grid network for 4EGKSOR method.

Before discussing more details on the formulation of the 4EGKSOR method, let us consider the coefficient matrix W (15) being defined as

$$W = F + J + L \tag{16}$$

where J is diagonal matrix, F and L are strictly lower and upper matrices of the generated linear system (15). Then, the large-scale and sparse linear system (15) becomes

$$(F + J + L) \cdot U = r \tag{17}$$

In drive to achieve the linear system (17) based on the point iteration approach, the implementation of the KSOR method over the linear system can be stated in matrix form as follows [31,39]

$$U^{(q+1)} = [(1-\omega)J - \omega F]^{-1}(J+L)U^{(q)} + [(1-\omega)J - \omega F]^{-1}r \tag{18}$$

where $U^{(q+1)}$ indicates the current value of U at the $(q+1)^{th}$ iteration.

Again, imposing the KSOR method (18) can also be rewritten in the point iteration approach as follows

$$U_c^{(q+1)} = \frac{1}{(1+\omega)} U_c^{(q)} + \frac{\omega}{(1+\omega)} \left(r_c - \alpha_c U_{c-1}^{(q+1)} - \gamma_c U_{c+1}^{(q)} \right) \tag{19}$$

for $c = 1,2,3,...,n-1$, whereas the optimum value of ω the different value subject to the size value of n. The range value of ω is given [31] by $\omega \in R - [-2,0]$.

By using the same steps to obtain equation (19), let us begin to introduce the KSOR block iteration approach. To start this discussion, let us consider again a sequence of a group of four and three node points in Figure 3. As we can see that two types of blocks were used to form during the implementation of the 4EGKSOR iteration. Firstly, the four-point block iteration is applied for the completed group of four and three point block is imposed into the ungrouped case. Referring to equation (15), the 4EGKSOR iterative method is defined as [37]

$$\begin{bmatrix} U_c \\ U_{c+1} \\ U_{c+2} \\ U_{c+3} \end{bmatrix}^{(q+1)} = \frac{1}{(1-\omega)} \begin{bmatrix} U_c \\ U_{c+1} \\ U_{c+2} \\ U_{c+3} \end{bmatrix}^{(q)} + \frac{\omega}{(1-\omega)} \begin{bmatrix} \beta_c & \gamma_c & 0 & 0 \\ \alpha_{c+1} & \beta_{c+1} & \gamma_{c+1} & 0 \\ 0 & \alpha_{c+2} & \beta_{c+2} & \gamma_{c+2} \\ 0 & 0 & \alpha_{c+3} & \beta_{c+3} \end{bmatrix}^{-1} \begin{bmatrix} S_1 \\ S_2 \\ S_3 \\ S_4 \end{bmatrix} \tag{20}$$

where

$$\begin{cases} S_1 = r_c - \alpha_c U_{c-1}, \\ S_2 = r_{c+1}, \\ S_3 = r_{c+2}, \\ S_4 = r_{c+3} - \gamma_c U_{c+1}, \end{cases}$$

Meanwhile, for the ungrouped case has been applied for only one group of three points block is shown as follows

$$\begin{bmatrix} U_{n-3} \\ U_{n-2} \\ U_{n-1} \end{bmatrix}^{(q+1)} = \frac{1}{(1-\omega)} \begin{bmatrix} U_{n-3} \\ U_{n-2} \\ U_{n-1} \end{bmatrix}^{(q)} + \frac{\omega}{(1-\omega)} \begin{bmatrix} \beta_{n-3} & \gamma_{n-3} & 0 \\ \alpha_{n-2} & \beta_{n-2} & \gamma_{n-2} \\ 0 & \alpha_{n-1} & \beta_{n-1} \end{bmatrix}^{-1} \begin{bmatrix} S_{n-3} \\ S_{n-2} \\ S_{n-1} \end{bmatrix} \tag{21}$$

where

$$\begin{cases} S_{n-3} = r_{n-3} - \alpha_i U_{n-4}, \\ S_{n-2} = r_{n-2}, \\ S_{n-1} = r_{n-1} - \gamma_n U_n, \end{cases}$$

Thus, Algorithm 1 describes a summary of the 4EGKSOR iterative method, which has been implemented for solving the proposed problem (1).

Algorithm 1:4EGKSOR iteration
i.   Set the initial value $U = 0$.
ii.   Calculate the coefficient matrix, W.
iii.   Calculate the vector, r.
iv.   For $c = 1,5,9,...,n-7$, calculate the equation (20).
v.   For $c = n-3$, calculate the equation (21).
vi.   Check the convergence test, $\left\| U_c^{(q+1)} - U_c^{(q)} \right\| < \varepsilon = 10^{-10}$. If yes, go to step (vii). Otherwise, go back to step (iv).
vii.   Display approximate solution.

4. Numerical Problem and Discussion

In this section, we investigate the feasibility of the 4EGKSOR iterative method for solving three examples of one-dimensional TPBVPs and then compared with GS and KSOR methods which are set up as a benchmarking for this study. All the results that have been obtained by imposing these three methods considered into these three examples are analyzed based on three comparison parameters such as the number of iterations (Iter), execution time (Time) in seconds and maximum norm (MaxNorm) at five different sizes, $n = 256, 512, 1024, 2048, 4096$. In this study, we also set up the value of tolerance error, $\varepsilon = 10^{-10}$ for all grid sizes are considered.

Example 1 [40]

Consider one-dimensional TPBVPs as

$$\frac{\partial^2 U}{\partial x^2} - \frac{\partial U}{\partial x} = -e^{(x-1)^{-1}}, \tag{22}$$

The analytical solution of problem (22) is $U(x) = x\left(1 - e^{(x-1)}\right)$.

Example 2 [41]

Consider one-dimensional TPBVPs

$$\frac{\partial^2 U}{\partial x^2} + xU(x) = \left(3 - x - x^2 + x^3\right)\sin(x) + 4x\cos(x), \qquad (23)$$

The analytical solution of problem (23) is $U(x) = \left(x^2 - 1\right)\sin(x)$.

Example 3 [42]

Consider one-dimensional TPBVPs

$$\frac{\partial^2 U}{\partial x^2} + U(x) = -1, \qquad (24)$$

The analytical solution of problem (24) is

$$U(x) = \cos(x) + \frac{1 - \cos(1)}{\sin(1)}\sin(x) - 1.$$

All results of GS, KSOR and 4EGKSOR iterative methods in solving these three examples are stated in Tables 1, 2 and 3 and illustrated in Figure 4, 5, and 6 respectively. Table 4 shows that the reduction percentage of KSOR and 4EGKSOR iterative methods which compared with GS method for three examples considered.

Table 1: Numerical results based on comparison criteria considered for Problem 1.

n	Method	Iter	Time	MaxNorm
256	GS	82043.0	7.92	4.0343e-07
	KSOR	769.0	0.75	2.4866e-07
	4EGKSOR	364.0	0.17	2.3889e-07
512	GS	292276.0	16.23	2.5291e-06
	KSOR	1526.0	1.67	6.7370e-08
	4EGKSOR	759.0	0.44	8.0806e-08
1024	GS	1025489.0	76.67	1.0346e-05
	KSOR	2853.0	3.19	2.5732e-08
	4EGKSOR	1295.0	0.78	4.7925e-08
2048	GS	3527433.0	409.03	4.1443e-05
	KSOR	5792.0	6.63	1.7614e-08
	4EGKSOR	2545.0	1.50	5.9857e-08
4096	GS	11811519.0	2359.09	1.6579e-04
	KSOR	10221.0	10.41	9.8302e-08
	4EGKSOR	5369.0	3.13	7.2651e-08

Table 2: Numerical results based on comparison criteria considered for Problem 2.

n	Method	Iter	Time	MaxNorm
256	GS	92156.0	19.79	9.0029e-07
	KSOR	796.0	0.81	1.5811e-06
	4EGKSOR	414.0	0.30	1.5584e-06
512	GS	329819.0	58.89	2.4116e-06
	KSOR	1559.0	1.69	3.7928e-07
	4EGKSOR	756.0	0.39	4.0320e-07
1024	GS	1164082.0	257.58	1.1096e-05
	KSOR	3073.0	3.56	1.0466e-07
	4EGKSOR	1450.0	0.82	6.2177e-08
2048	GS	4035615.0	1345.67	4.4746e-05

	KSOR	6145.0	7.18	3.8252e-08
	4EGKSOR	2826.0	1.71	4.3353e-08
4096	GS	13659733.0	2913.87	1.7907e-04
	KSOR	11571.0	11.03	5.2215e-08
	4EGKSOR	5181.0	3.06	1.0216e-07

Table 3: Numerical results based on comparison criteria considered for Problem 3.

n	Method	Iter	Time	MaxNorm
256	GS	89973.0	19.88	5.4091e-07
	KSOR	782.0	0.37	1.9062e-07
	4EGKSOR	381.0	0.17	2.0338e-07
512	GS	318924.0	60.80	2.9059e-06
	KSOR	1537.0	0.89	5.2948e-08
	4EGKSOR	724.0	0.40	2.5886e-08
1024	GS	1111808.0	256.86	1.1810e-05
	KSOR	3057.0	1.82	1.5546e-08
	4EGKSOR	1387.0	0.79	6.1722e-08
2048	GS	3791677.0	1260.25	4.7285e-05
	KSOR	5734.0	3.43	2.5772e-08
	4EGKSOR	2753.0	1.75	8.8766e-08
4096	GS	12544476.0	2681.69	1.8915e-04
	KSOR	10655.0	5.78	1.0642e-07
	4EGKSOR	5463.0	3.21	1.1934e-07

Table 4: Reduction percentage for the KSOR and 4EGKSOR in term of the iteration and time.

n	Method	Iter	MaxNorm
Problem 1	Iter	99.06-99.84	99.56-99.95
	Time	89.71-99.56	97.29-99.87
Problem 2	Iter	99.14-99.92	99.55-99.96
	Time	95.91-99.62	98.48-99.89
Problem 3	Iter	99.13-99.92	99.57-99.96
	Time	98.13-99.92	99.14-99.96
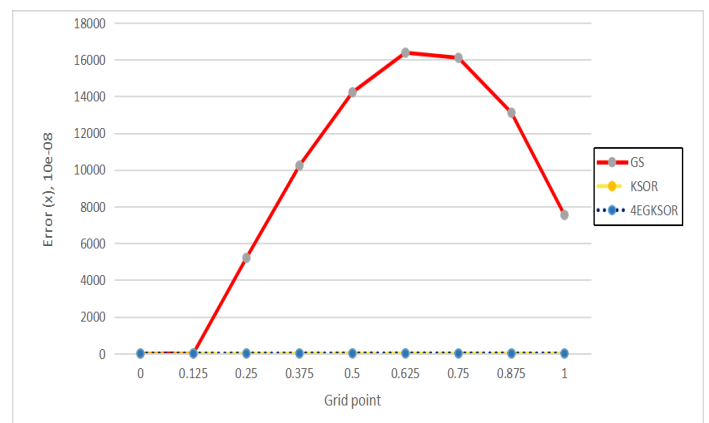
Figure 4: Comparison of three iterative methods based on error over the solution domain of Problem 1 at n = 4096.

All results are presented in Tables 1 to 4, the KSOR method gives reduced iteration and speeds up its execution time as compared with GS iterative method. Then, in terms of a reduction percentage, the KSOR iteration in Example 1 has significantly reduced number of iterations approximately by 99.06-99.84% and

speed up by 89.71-99.56%. For Examples 2 and 3 also give the pattern as same as Example 1 in which KSOR iteration is better than GS iteration. However, the 4EGKSOR iteration gives tremendously improved either in the number of iterations or execution time which are 99.56-99.95% and 97.29-99.87% for Example 1, 99.55-99.96% and 98.48-99.89% for Example 2 and 99.57-99.96% and 99.14-99.96% for Example 3 respectively. In conclusion, it shows that the KSOR iteration has greatly reduced its number of iterations and execution time as compared to the GS iteration. It means that the 4EGKSOR iteration has the least amount compared to GS and KSOR iterations in terms of the number of iterations and execution time. In addition to these findings, for the maximum norm, KSOR and 4EGKSOR iterative methods show a good agreement and become close to their analytical solution compared to GS iterative method, see in Figures 4, 5 and 6.
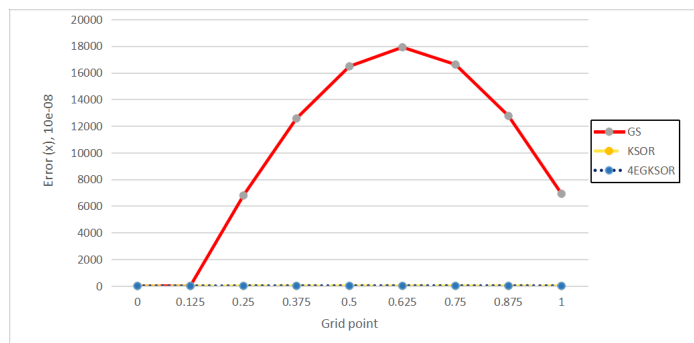
Figure 5: Comparison of three iterative methods based on error over the solution domain of Problem 2 at n = 4096.
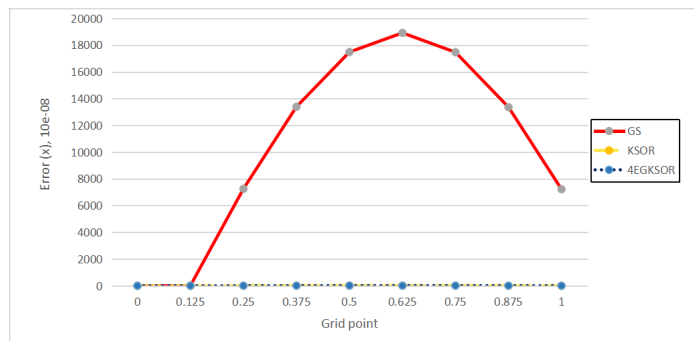
Figure 6: Comparison of three iterative methods based on error over the solution domain of Problem 3 at n = 4096.

5. Conclusions

The formulation of GS, KSOR and 4EGKSOR iterative methods have been successfully derived by using two newly established RKFD discretization schemes for solving TPBVPs. Then, the generated large-scale and sparse linear system based on two newly established RKFD approximation equations have been solved by using three iterative methods in which all results were recorded. Based on the implementation of these three iterative methods, the 4EGKSOR iterative method has tremendously reduced the iteration and Time as compared with GS and KSOR methods. Therefore, the combination of the KSOR block technique with the standard EG iterative method can reduce iteration and Time compared to the KSOR point approach. For

further study, this paper can be extended to perform the use of the newly established RKFD discretization scheme for solving the multi-dimensional boundary value problems by using the two-step iteration family [43,44], and the half-sweep [45,46] and quarter-sweep [47,48] iteration families.

Acknowledgment

References

[1] J. Aarao, B. H. Bradshaw-Hajek, S. J. Miklavcic, and D. A. Ward, "The extended domain eigen-function method for solving elliptic boundary value problems with annular domains." Journal of Physics A: Mathematical and Theoretical, **43**, 185-202, 2010, doi:10.1088/1751-8113/43/18/185202.

[2] T. N. Robertson, "The linear two-point boundary value problem on an infinite interval." Mathematics Of Computation, **25**(115), 475-481, 1971, doi:10.1090/s0025-5718-1971-0303742-1.

[3] Y. M. Wang, and B. Y. Guo, "Fourth-order compact finite difference method for fourth-order nonlinear elliptic boundary value problems." Journal of Computational and Applied Mathematics, **221**(1), 76-97, 2008, doi:10.1016/j.cam.2007.10.007.

[4] Y. Gupta, "A numerical algorithm for solution of boundary value problems with applications." International Journal of Computer Applications, **40**(8), 2012, doi:10.5120/4988-7252.

[5] C. Nazan, and C. Hikmet, "B-spline methods for solving linear system of second order boundary value problems." Computers and Mathematics with Application, **57**(5), 757-762, 2008, doi:10.1016/j.camwa.2008.09.033.

[6] B. H. Lin, W. H. Huan, and C. Yanpeng, "Polynomial spline approach for solving second-order boundary-value problems with neumann conditions." Applied Mathematics and Computation, 32, 6872-6882, 2011, doi:10.1016/j.amc.2011.01.047.

[7] N. N. A. Hamid, A. A. Majid, and A. I. M. Ismail, "Extended cubic B-spline method for linear two-point boundary value problems." Sains Malaysiana, **40**(11), 1285-1290, 2011,doi:10.5281/zenodo.107900.

[8] J. Rashidinia, and S. Sharifi, "B-spline method for two-point boundary value problems." International Journal of Mathematical Modelling and Computations, **5**(2), 111-125, 2015, doi:10.1016/j.cam.2010.10.031.

[9] M. N. Suardi, N. Z. F. M. Radzuan, and J. Sulaiman, "Cubic b-spline solution for two-point boundary value problem with aor iterative method." Journal of Phiysics: Conference Series, **890**, 012015, 2017, doi:10.1088/1742-6596/890/1/012015.

[10] M. El-Gamel, "Comparision of the solution obtained by Adomian decomposition and wavelet-galerkin methods of boundary-value problems." Applied Mathematics and Computation, **186**(1), 652-664, 2007, doi:10.1016/j.amc.2006.08.010.

[11] A. Mohsen, and M. E. Gamel, "On the galerkin and collocation methods for two point boundary value problems using sinc bases." Computer and Mathematics with Applications, 56, 930-941, 2008, doi:10.1016/j.camwa.2008.01.023.

[12] M. M. Rahman, M. A. Hossen, M. N. Islam, and M. S. Ali, "Numerical solutions of second order boundary value problems by Galerkin method with Hermite polynomials." Annals of Pure and Applied Mathematics, **1**(2), 138-148, 2012, doi:10.1.684.13.

[13] B. Jang, "Two-point boundary value problems by extended adomian decomposition method." Computational and Applied Mathematics, **219**(1), 253-262, 2007, doi:10.1016/j.cam.2007.07.036.

[14] S. M. Roberts, and J. S. Shipman, "Continuation in shooting methods for two-point boundary value problems." Journal of mathematical analysis and applications, 18(1), 45-58, 1967, doi:10.1016/0022-247x(67)90181-3 .

[15] C. F. Price, "An offset vector iteration method for solving two-point boundary-value problems." The Computer Journal, 11(2), 220-228, 1968, doi:10.1093/comjnl/11.2.220 .

[16] R. P. Agarwal, "On the method of complementary functions for nonlinear boundary-value problems." Journal of Optimization Theory and Applications, 36(1), 139-144, 1982, doi:10.1007/bf00934344 .

[17] Q. Fang, T. Tsuchiya, and T. Yamamoto, "Finite difference, finite element and finite volume methods applied to two-point boundary value

problems." Journal of Computational and Applied Mathematics, 139(1), 9-19, 2002, doi:10.1016/s0377-0427(01)00392-2 .

[18] M. M. Chawla, and C. P. Katti, "Finite difference methods for two-point boundary value problems involving high order differential equations." BIT Numerical Mathematics, **19**(1), 27-33, 1979, doi:10.1007/bf01931218 .

[19] E. M. Elbarbary, and M. El-Kady, "Chebyshev finite difference approximation for the boundary value problems." Applied Mathematics and Computation, 139(2-3), 513-523, 2003, doi:10.1016/s0096-3003(02)00214-x .

[20] P. K. Pandey, "Rational finite difference approximation of high order accuracy for nonlinear two point boundary value problems." Sains Malaysiana, **43**(7), 1105-1108, 2014.

[21] P. K. Pandey, "Solving two point boundary value problems for ordinary differential equations using exponential finite difference method." Boletim da Sociedade Paranaense de Matemática, **34**(1), 45-52, 2016, doi:10.5269/bspm.v34i1.22424 .

[22] S. Babu, R. Trabelsi, T. Srinivasa Krishna, N. Ouerfelli, and A. Toumi, "Reduced redlich–kister functions and interaction studies of dehpa+ petrofin binary mixtures at 298.15 k." Physics and Chemistry of Liquids, **57**(4), 536-546, 2019, doi:10.1080/00319104.2018.1496437 .

[23] A. Gayathri, T. Venugopal, and K. Venkatramanan, "Redlich-kister coefficients on the analysis of physico-chemical characteristics of functional polymers." Materials Today: Proceedings, 17, 2083-2087, 2019, doi:10.1016/j.matpr.2019.06.257.

[24] N. P. Komninos, and E. D. Rogdakis, "Geometric investigation of the three-coefficient redlich-kister expansion global phase diagram for binary mixtures." Fluid Phase Equilibria, 112728, 2020, doi:10.1016/j.fluid.2020.112728 .

[25] M. K. Hasan, J. Sulaiman, S. Ahmad, M. Othman, and S. A. Abdul Karim, "Approximation of iteration number for gauss-seidel using redlich-kister polynomial." American Journal of Applied Sciences, 7, 956-962, 2010, doi:10.3844/ajassp.2010.969.975 .

[26] D. M. Young, Iterative Solution Of Large Linear Systems. London: Academic Press, 1971.

[27] W. Hackbusch, Iterative Solution of Large Sparse Systems of Equations. Springer-Verlag, 1995.

[28] Y. Saad, Iterative Methods for Sparse Linear Systems, International Thomas Publishing, 1996..

[29] R. Rahman, N. A. M. Ali, J. Sulaiman, and F. A. Muhiddin, "Caputo's finite difference solution of fractional two-point boundary value problems using SOR iteration." In AIP Conference Proceedings, 2013, 1, 2018, doi:10.1063/1.5054233 .

[30] A. Sunarto, J. Sulaiman, and A. Saudi, "Implicit finite difference solution for time-fractional diffusion equations using AOR method." In Journal of Physics: Conference Series, 495, 1, 2014, doi:10.1088/1742-6596/495/1/012032 .

[31] N. Z. F. M. Radzuan, M. N. Suardi, and J. Sulaiman, "KSOR iterative method with quadrature scheme for solving system of Fredholm integral equations of second kind." Journal of Fundamental and Applied Sciences, **9**(5S), 609-623, 2017, doi:10.4314/jfas.v9i5s.43 .

[32] D. J. Evans, "Group explicit iterative methods for solving large linear systems." International Journal of Computer Mathematics, **17**(1), 81-108, 1985, doi:10.1080/00207168508803452 .

[33] A. Saudi, and J. Sulaiman, "Robot path planning using four point-explicit group via nine-point laplacian (4EG9L) iterative method." Procedia Engineering, **41**, 182-188, 2012, doi:10.1016/j.proeng.2012.07.160 .

[34] K. Ghazali, J. Sulaiman, Y. Dasril, and D. Gabda, "Application of Newton-4EGSOR Iteration for solving large scale unconstrained optimization problems with a tridiagonal hessian matrix." In Computational Science and Technology, 401-411, Springer, Singapore, 2019, doi:10.1007/978-981-13-2622-6_39 .

[35] A. Saudi, and J. Sulaiman, "Path Planning Simulation using Harmonic Potential Fields through Four Point-EDGSOR Method via 9-Point Laplacian." Jurnal Teknologi, **78**(8-2), 2016, doi:10.11113/jt.v78.9537.

[36] J. Sulaiman, M. K. Hasan, M. Othman, and S. A. A. Karimd, "MEGSOR iterative method for the triangle element solution of 2D Poisson equations." Procedia Computer Science, **1**(1), 377-385, 2010, doi:10.1016/j.procs.2010.04.041 .

[37] F. A. Muhiddin, J. Sulaiman, and A. Sunarto, "Implementation of the 4EGKSOR for Solving One-Dimensional Time-Fractional Parabolic Equations with Grünwald Implicit Difference Scheme." In Computational Science and Technology, 511-520, Springer, Singapore, 2020, doi:10.1007/978-981-15-0058-9-49.

[38] I. K. Youssef and A. A. Taha, "On modified successive overrelaxation method." Applied Mathematics and Computation, **219**, 4601-4613, 2013, doi:10.1016/j.amc.2012.10.071 .

[39] I. Youssef, "On the successive overrelaxation method." Journal of Mathematics and Statistics, **8**(2), 176-184,2012, doi:103844/jmssp.2012.176.184.

[40] H. N. Caglar, S. H. Caglar, and K. Elfaituri, "B-spline interpolation compared with finite difference, finite element and finite volume methods which applied to two point boundary value problems." Applied Mathematics and Computation, **175**(1), 72-79, 2006, doi:10.1016/j.amc.2005.07.019.

[41] Y. Li, J. A. Enszer, and M. A. Stadtherr, "Enclosing all solutions of two-point boundary value problems for odes." Computer and Chemical Engineering, **32**(8), 1714-1725, 2008, doi:10.1016/j.compchemeng.2007.08.013 .

[42] M. A. Ramadan, I. F. Lashien, and W. K. Zahra, "Polynomial and nonpolynomial spline approaches to the numerical solution of second order boundary value problems." Applied Mathematics and Computation, **184**, 476-484, 2007, doi:10.1016/j.amc.2006.06.053 .

[43] A. A. Dahalan, M. S. Muthuvalu, and J. Sulaiman, "Numerical solutions of two-point fuzzy boundary value problem using half-sweep alternating group explicit method." American Institute of Physics, **1557**(1), 103-107, 2013, doi:10.1063/1.4823884 .

[44] A. A. Dahalan, J. Sulaiman, and M. S. Muthuvalu, "Performance of HSAGE method with Seikkala derivative for 2-D fuzzy Poisson equation." Applied Mathematical Sciences, **8**(17-20), 885-899, 2014, doi:10.12988/ams.2014.311665.

[45] M. K. Hasan, J. Sulaiman, S. A. Abdul Karim, and M. Othman, "Development of some numerical methods applying complexity reduction approach for solving scientific problem.", 2010.

[46] A. Saudi, and J. Sulaiman, "Red-black strategy for mobile robot path planning." In World Congress on Engineering 2012. July 4-6, 2012. London, UK, International Association of Engineers, 2182, 2215-2219, 2010.

[47] N. I. M. Fauzi, and J. Sulaiman, "Quarter-Sweep Modified SOR iterative algorithm and cubic spline basis for the solution of second order two-point boundary value problems." Journal of Applied Sciences (Faisalabad), **12**(17), 1817-1824, 2012, doi:10.3923/jas.2012.1817.1824.

[48] J. V. Lung, and J. Sulaiman, "On quarter-sweep finite difference scheme for one-dimensional porous medium equations." International Journal of Applied Mathematics, **33**(3), 439, 2020, doi:10.12732/ijam.v33i3.6.

ASTES

Non–Performing Loans' Effect on the Loans' Shrinkage in Albanian Banking Sector

Arjan Tushaj[1], Valentina Sinaj[2,*]

[1]Faculty of Economics, Department of Economics, University of Tirana, Tirana, 1000, Albania

[2]Faculty of Economics, Department of Applied Statistics and Informatics, University of Tirana, Tirana, 1000, Albania

A R T I C L E I N F O	A B S T R A C T
	The article investigated the banking determinants of loans' growth using the quarterly data of Albanian banking sector during 2003-2018. We estimated the linear model of control variables to examine the bank's sound effects on loan's capacity. Empirical results demonstrated the initial positive outcome of the growth of non – performing loans on the loans' growth, but negative effect incorporating with the structural changes. This divergence emphasized the optimum loans' supply through the existence of U relationship amongst them and confirming the banking shrinking behavior related to the lending policy. Also, we confirmed the negative impact of capital regulation and long run correlation to capital regulation growth and growth ratio of loans.

1. Introduction

The economic progress of emerging economies affected by bank lending to attain the essential growth. Otherwise, the lending activity demonstrated the convinced hazard due to the bad credits and it would be one more reason to examine and to assurance the quality of lending in banking sector. The lending activity in banking sector associated with more theoretic and practical investigations particularly to the evolving economies past to the 2008's crisis. These investigations focused to the examination of theoretic and practical assessments according to the bad credits due to the borrower's defaulting. The bank lending has no option to avoid completely the phenomena of adverse selection and moral hazard. In [1], the authors analyzed the determinants of banking credit related to the emergent economies before and after the periods of 2008's crisis. They emphasized that the national and foreign funding affected positively the credit growth. Also, authors concluded that the economic growth, inflation growth and loose monetary policy induced the credit's increase. Meanwhile in [2], the authors examined the determinants of lending activity of banking sector pre – global crisis and post – global crisis in Central Eastern and Southeastern European countries. They emphasized that the economic growth, credit quality, financial intermediation level and foreign and domestic financing sources affected the credit's expansion.

The author in [3] analyzed the linkage among the cost's efficacy and non – performing credits related to banking sector in Zimbabwe during $2009 – 2014$. Author concluded the inefficiency of credit managers related to the non – performing growth. He recommended to applying the international best practical approach by credit managers in order to avoid the fragile policy and detrimental impact in long run on the banking loan's quality. His results approved the bad management hypothesis. Also, [4] highlighted that the significance of banking supervision joining to the large activities restrictions and expanding the market power decreased thoughtfully the threat of banking failure. These outcomes proved that banking procedures marked synchronously the banking effective environment and the banking performance.

The banking sector in Albania has been operated into a dynamic growth and induced the more exertions by banks to take the more appropriate position in the market. This goal of banks induced the enlarge lending strategy contributing to the increasing of non- performing loans ratio. These surroundings marked by the precise banking determining factors, mostly the decision – making procedures and the macroeconomic changes. Otherwise, these outcomes relied to the performance of principal economic segments.

The article followed by this structure: First section included the outline. Section 2 provided the literature review according to the determinants of bank lending and the linkage with non-performing loans. Section 3 demonstrated the empirical view

*Corresponding Author: Valentina Sinaj, sinajv@yahoo.com

related to banking loan's growth and non – performing loans in Albanian banking sector. Section 4 analyzed the description of econometric methodology and empirical results using in this article. The last section summarized the last remarks of this article.

2. Literature Review

The bank lending has always correlated with several kinds of banking risks which they investigated according to the theoretic and practical background of banking sector. This examination will focus to hypothetical and applied evaluations related to the determinants of bank loan's growth and the effect of non-performing loans to banking behavior related to lending. The bank lending has always associated with the phenomena of adverse selection and moral hazard.

In [5], the author examined the non-performing loans' effect towards the loan growth. He highlighted the banking lending behavior could restrain the economic activity particularly during the stress periods linked to the large ratios of non – performing loans. His outcomes using regression analysis concluded the robust effect of non – performing credits ratios on the loaning decisions referring to the upper and under threshold.

In [6], the author investigated the factors of banking loan related to 146 states during 1990 – 2013. His empirical results suggested the crucial effects of economic growth and healthy domestic banking sector related to bank lending. He highlighted that the dependence of foreign capital inflows exposed the domestic banking sector to external shock and faced to credit boom – bust cycles.

In [7], the author estimated the determining factors of lend evolution in Montenegro related to the demand stimulus and supply stimulus simultaneously. She confirmed that the positive economic developments and increasing banks' deposits potential induced the credit growth. Also, she emphasized that the bad credits and low soundness ratio affected negatively the lend supply and banking sector soundness was more influential according to the promoting of banks' lending. She found that the significance of supply factors related to credit growth during the post –crisis, meanwhile she provided the significance of both supply and demand factors to explain the credit growth during pre- crisis.

In [8], the author investigated the Italian bank lending behavior during financial crisis if the increase of credit risk would reduce the bank lending. Also, she analyzed the cooperative and commercial banks behaviors related to lending activity during 2007 - 2103. She found the negative impact linked to the bad loans and ratio of credit loss provision like the measurement of credit risk on bank lending behavior.

In [9], the authors investigated the endogenic and exogenic determinants related to the loan growing in selected Western Balkan economies and Turkey through a multiple regression analysis during 2007 – 2017. Their results emphasized the reverse relationship between non – performing credits ratio and credit rising's ratio according to each economy. Also, they concluded the positive effects of economic growth and deposits growth ratio on banking credit growth for all sample, except Croatia which it demonstrated the positive effect of return on equity on it.

In [10], the authors analyzed the impact of nonperforming loans (NPLs) related to the banking loan supply towards the nonfinancial businesses in Italy during 2008 - 2015. They found that the banks' lending behavior did not affect by NPL ratios using time-varying firm fixed effects to control meant for demand shifts and changes related to the borrower characteristics. Their results demonstrated the negative correlation among NPL ratios and loan growth. Although the exogenous appearance of new NPLs and the linked enhance within provisions could reflect the negative adjustment in loan supply.

In [11], the authors investigated the credit growing and banking behavior according to risk-taking during the expansive lending of 2006 – 2014 in Pakistan. They confirmed the loan's growth associated with increasing bad credits and decreasing the bank's creditworthiness due to the frail provident guideline amongst participants and unequal information of debtors, particularly the underestimated risk of lending through credit booms.

In [12], the authors investigated the determining factors of banking loan to business sector and they found the positive relationship among bank lending and economic growth according to Albanian banking sector. Also, they found that banking and financial intermediation and financial liberalization induced the increasing of lending demand. Authors emphasized the positive effect of exchange rate on banking loan and negative impact of crowding – out effect on it in the long run. Also, they concluded that the decreasing of bad loans and loaning's efficiency increased the loan's supply.

In [13], the author investigated the results of tight lending into banking sector related to innovation relying on German firms' data. Author confirmed the restriction of firms' capacity to enhance their external financial sources through banking sector during the financial crisis. He emphasized the increasing of firm's probability related to suspending innovation projects due to tight policy of banking sector and its negative outcome in long run.

Theoretic outcomes and functional results proved the convergence of non – performing loans towards the loans' ratios in banking sector despite of diverse backgrounds.

3. Loans growth and non-performing loans in Albanian banking sector

The banking solidity in Albania has sustained despite of sporadic tremors linked to effects of 2008's crisis. Figure 1 confirmed the subtleties of the growing ratio of non-performing loans and total gross loans during 2008 – 2018 relied on trimestral figures. According to the figure 1 the non – performing loans linked to the explosive propensity leading by the descendent propensity, especially after last quarter of 2008. The last quarter of 2008 demonstrated the outlier highlighting the contagious effects of 2008's crisis in Albanian banking sector and political cycles. Meanwhile the downward trend of non-performing loans' growing ratio related to the restrictive banks' loaning policy and the loans' rearrangement by the involvement through Bank of Albania. However, the flat propensity of loans' growth ratio affected by the restricted loaning policy of banks due to the increasing ratio of bad credits to total gross loans after 2008. The growth ratio of whole loans associated with the convergent trend

toward zero percentage, but the growth ratio of non-performing loans ratio linked to divergent trend compare to loan's growth ratio. Meanwhile the figure 2 demonstrated the comparative analysis amongst Western Balkan countries related to non – performing loans into banking sector during to 2009 - 2017. Figure 2 highlighted the upward trend of non – performing loans for each Western Balkan until 2013. It confirmed the largest ratio for Albania and Serbia until 2016 compare to others countries, especially Albania along entire period despite of trend and volatility.
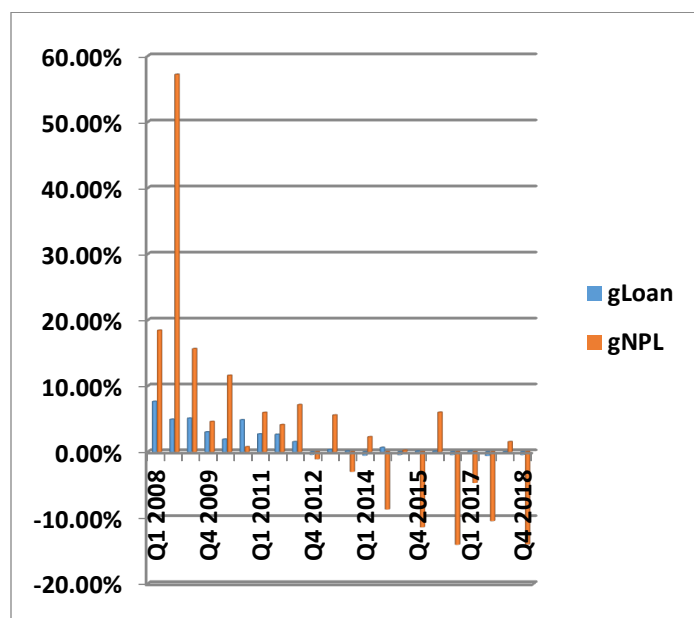
Figure 1: Growth rates of non-performing loans and total loan in banking sector, Source: Authors' calculations on dataset of Bank of Albania
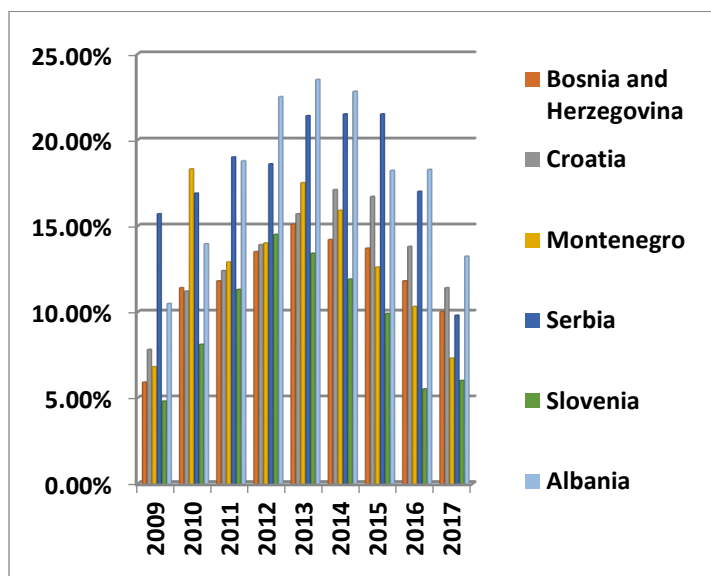
Figure 2: Non-performing loans ratios in banking sector of Western Balkan countries, Source: Central banks of individual countries

However, the banking sector in our country runs into a progressive growth and persuades the extra controls by banks concluding to their conduct. The banking concentration has contributed to the common advancement of banking sector.

Figure 3 demonstrated the banking concentration using Herfindahl–Hirschman Index (HHI) related to the total loans and non – performing loans in the banking sector through individual banks and banks' size (G1, G2 and G3) during 2005 - 2017. It exposed the stability of the loans' concentration and non – performing loans' concentration relied on individual banks along this period. Despite of convergence related to moderated concentration, non – performing loans demonstrated the higher concentration compare to loans according to individual banks. Meanwhile the concentration of total loans and non – performing loans through banks' size demonstrated the large values and approximately identical values during the specified period. Also, the concentration related to banks' size revealed the similar propensity according to total loans and non – performing loans despite of slight volatility, but higher concentration and large gap compare to the concentration of individual banks.
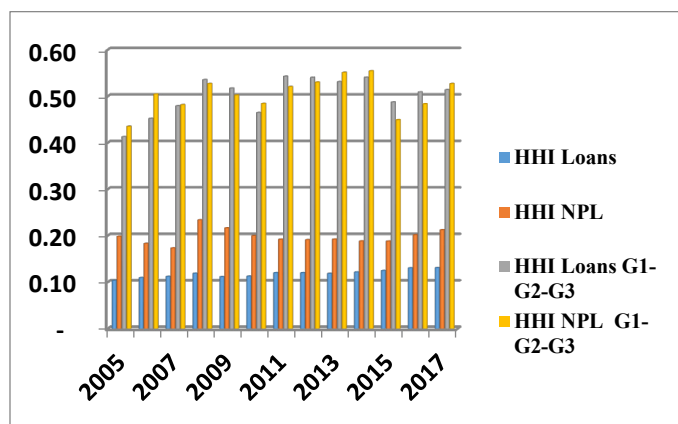
Figure 3: Concentration of loans and non-performing loans ratios in Albanian banking sector Source: Authors' calculations on dataset of Bank of Albania

4. Methodology and empirical results

4.1. Data description and econometric methodology

The loans' growth estimated to the linear model by least squares method referring on the quarterly data of Albanian banking sector during 2003-2018. The general linear model is following:

$$G\_loans_t = \beta_0 + \beta_1 G\_NPL_t + \beta_2 G\_deposits_t + \beta_3 G\_Cap.\,Re\,g_t + \beta_4 ROE_t + u_t$$

for t=1,…,64, and the residual completed the Ordinary Least Squares assumption and $u_t \sim N(0, \sigma^2)$ [14].

The linear model includes the variables controlling for bank sound effects on loan's capacity. The model used the growth ratio of banking control variables including the non-performing loans' growth (G_NPL), deposit's growth (G_Deposit), regulator capital's growth (G_Cap.Reg.) and return on equity (ROE). We expected the negative relationship among growth of non-performing loans and loans' growth supporting by theoretical and empirical view. Meanwhile we should investigate the U-shaped relationship between loans' growth and non – performing loans' growth supporting by the empirical model [5]. Ambiguous results of this correlation clarified the inverted conduct through the optimum of loans' growth affecting by non performing loans' growth. Furthermore, we expected the positive impact of return

on equity related to the loans' growth due to profitability in order to maximize banking profitability. Also, we expected the positive effect of deposits' growth on the loans' growth due to the deposits meant the probable loans' capacity and loans' source for banking sector. Moreover, the indicator of regulatory capital anticipated the negative outcome due to the banking capability to cover with capital the losses' risk exposure by the bad loans. This expectation supported that the capital rigidity merely confirmed the frail negative results on loan's growth, but the components of capital rigidity demonstrated the strongest negative effect related to loan's growth [15]. Also, the regulatory capital required the comprehensive fulfilment the Basel's criterions in order to be the well – capitalized banks and consequently inducing the banks' lending shrinkage. We proved our expectations related to the variables' impact on the loans' growth using R software.

4.2. Results of examination

We used the "Student test" related to the significance of coefficients' model. The null hypothesis demonstrated the non – significance of variable, and if the p-value of "T test" was less than the significance level meaning the rejection of null hypothesis. Meanwhile the model's significance was testing by Fisher statistics meaning the null hypothesis related to non – significance of model. Table 1 demonstrated the statistical significance of model and variables. Referring to the p-values we confirmed that the model was significant and all of variables were significant according to 5% level despite of ROE. The only non-significant variable was ROE, which it resulted to p-value of 6.8%. We selected the good – fit model using stepwise method based on the model selection criteria. We choose the model with the highest value of adjusted R^2 and related to Information Criteria, Akaik criterion (AIC, [16]), and Baeysian criterion [17], we decided the model with the smallest value of each criterion. Referring to the selection of regression Mallow's criterion [18], if the model is correct then Cp will tend to be close to or smaller than p. We used R software according to the whole evaluations and selections.

Also, we used variables and their lags and investigated the structural break[1] according to first quarter of 2008. Due to this reason, we used the dummy variable for year 2008 (value 1 before this moment and otherwise zero after this moment) related to the growth of non-performing loans and ROE. We applied several tests to examine the significance and consistence of model (see more details for results of tests in the appendix (table 2-5)). The estimated results referring to table 1 demonstrated the initial positive effect of non – performing loans' growth on the loans' growth. Otherwise, when we incorporated both the structural changes using dummy variable with non – performing loans' growth, we observed the negative effect of non – performing loans' growth. This result emphasized the change of banks' behavior related to loans' supply meaning the demonstration of U-form relationship among loans' growth and non – performing loans' growth.

The outcome supported the several empirical results due to contagious effect of 2008's crisis linked to the structural deviations. Meanwhile our estimated outcomes verified the

positive correlation amongst the growth of credits and deposits due to the deposits remain the main banking loans' source. Banks inclined to increase the loans' supply in order to add to their interest incomes and to maximize their profitability. This result supported our expectations and theoretical and empirical views. Also, ROE demonstrated the positive effect on the loans' growth and has continued the similar effect when we incorporated both the structural changes using dummy variable with ROE. This effect explained by banks' propensity to enhance the loans' supply due to higher profitability. Empirical results have testified the sustainable ROE's effect on loans' growth despite of structural changes due to 2008's crisis. Otherwise, our estimations proved the adverse effect of regulatory capital on the loans' growth. This result supported other empirical outcomes and converged to banks' lending shrinkage towards the intended well – capitalized banks due to rigid Basel's standards and contagious effects of 2008's crisis.

Table 1: Estimated results

Coefficients:				
	Estimate	Std. Error	t value	Pr(>|t|)
(Intercept)	0.04841	0.01818	2.663	0.010045 *
G_NPL	0.13796	0.03629	3.802	0.000352 ***
G_Deposit	0.33138	0.14747	2.247	0.028518 *
ROE	0.13613	0.07330	1.857	0.068475 .
G_Cap.Reg.	-0.33869	0.09508	-3.562	0.000751 ***
G_NPL*D	-0.21776	0.05355	-4.067	0.000148 ***
ROE*D	0.42841	0.06424	6.669	1.13e-08 ***
Signif. codes:	0 '***' 0.001 '**' 0.01 '*' 0.05 '.' 0.1 ' ' 1			
Residual standard error: 0.0252 on 57 degrees of freedom				
Multiple R-squared: 0.7948,		Adjusted R-squared: 0.7732		
F-statistic: 36.79 on 6 and 57 DF, p-value: < 2.2e-16				

Source: R, authors' estimations

In [19], the author emphasized if two time series have stochastic trends (i.e., they are nonstationary), a regression of one other may cancel out the stochastic trends, which it may advice the coexistence in the long-run, or equilibrium, among them even though individually the two series are nonstationary. We verified the stationarity of series using Augmented Dickey-Fuller test[2] (ADF) to determine the presence of unit roots. According to the ADF test, the null hypothesis is the series has a unit root. We used T-test to test the hypothesis and if the p-value was less than 5% significance level than null hypothesis rejected. Table 8 demonstrated the results of ADF test and it confirmed three series which they were the first order integration or I(1), particularly series of ROE, G_L and G_Cap.Reg. According to [20], the economic interpretation of cointegration states that if two (or more) series are linked to form an equilibrium relationship spanning the long run, then even though the series themselves may contain stochastic trends and thus be non-stationary, they will nevertheless move closely together over time and the difference between them will be stable or stationarity.

---

[1] See results in Table 7 in Appendix.

[2] See results in Table 8 in Appendix.

We examined the long run relationship amongst variables' series through the co-integration procedure using Granger causality test[3] to investigate empirically the direction of relation between variables. The null hypothesis emphasize that the first variable demonstrates no Granger causality to the second variable. The null hypothesis rejects, if p-value of Fisher test is less than the significance level. Table 9 demonstrated the empirical results of Granger causality test and it confirmed the short run relationship amongst variables, ROE, G_L and G_Cap.Reg at 10% level of significance.

Meanwhile the Johansen Procedure is used for co-integration of three non-stationary series, ROE, G_L and G_Cap.Reg. According to the results of Trace statistic in table 10 and their critical value, we confirmed only one couple of series which are co-integrated. Table 11 related to Engel – Granger procedure with one-equation, we derived one coupled variable which they were co-integrated, precisely the loans' growth and the growth of capital regulation demonstrated the long run correlation. This result emphasized the significance of capital regulation to take into more considerations by banking managers and policy makers due to its impact in long run. Also, we investigated the U shape relationship amongst loans' growth and non – performing loans' growth [4]. We calculate the minimum (turning point) of the parabola defined as in which corresponds to the averaged level loans' growth and non – performing loans' growth. The second order polynomial demonstrated its general form through the following equation:

$f(x)=ax^2+bx+c$ where $x\epsilon$ (0; $+\infty$) and at least $a\neq0$. Thus, the minimum (turning point) is defined as: $\left(-\frac{b}{2a}, f\left(-\frac{b}{2a}\right)\right)$.

Otherwise, it can be calculated by using the first derivative of function f(x): $f'(x)=2ax+b$ and by solving the equation: $f'(x)=2ax+b=0$. The solution of second equation estimated the level of non – performing loans' growth. Related to the threshold at which the relationship among the loans' growth and non – performing loans' growth turns from positive to negative. The empirical results of table 12 demonstrated the optimum value of loans' growth by 321 basis points when we included the structural changes of 2008's global financial crisis. This result explained the negative impact pending the non – performing loans' growth ratio and the loans' growth curvature was curved to 321 basis points due to the structural break point of 2008. The propensity of banks' behavior adjusted subsequent to optimum point in order to compensate the loss due to non – performing loans. Also, this result confirmed the banking shrinking behavior correlated to the lending policy consequently of non – performing loans subsequent to optimum loans.

5. Concluding remarks

The propensity of the growing ratio linked to the non-performing loans and total gross loans in Albanian banking sector during 2008 – 2018 has sustained its stability excluding the effects of contagious effects of global financial crisis, particularly subsequent to last quarter of 2008. The growth rate of total loans

and non-performing loans ratio diverge amongst them during this period. This divergence described by the restraining loaning strategy of banks and the credits' restructuring through Bank of Albania contribution. Meanwhile Albania demonstrated one of the largest ratios of non – performing loans into banking sector during to 2009 – 2017 despite of volatility referring to the comparative analysis amongst Western Balkan countries. Also, the non – performing loans and loans converged to the moderated concentration related to individual banks even though the high concentration of non – performing loans compare to the loans. However, the total loans and non – performing loans correlated to banks' size demonstrated the high concentration compare to the individual banks' concentration. This discrepancy justified the tight lending policy due to the increasing propensity of non – performing loans' concentration by banks' size.

We examined the initial positive outcome of growth ratio linked to non – performing loans towards the loans' growth. Meanwhile we tested the negative effect of non – performing loans' growth related to the dual incorporation by dummy variable of the structural changes. Ambiguous results confirmed by the contagious effect of 2008's crisis linked to the structural changes. This reversal of behavior confirmed the optimum of loans' growth affecting by non-performing loans' growth.

The optimum break demonstrated the U shape relationship amongst loans' growth and non – performing loans' growth through empirical result and explained the dual effect. The negative relationship was curved to the optimum of loans' growth by 321 basis points incorporating the structural break of 2008's global financial crisis. The propensity of banks' behavior adjusted subsequent to optimum loans to compensate the loss due to non – performing loans and converged to the banking shrinking behavior correlated to the lending policy. Policymakers should be monitoring continuously the non-performing loans' growth in the forthcoming to control the optimal loans' growth ratio.

The regulatory capital illustrated the negative effect on the loans' growth and proved the convergence to banks' lending shrinkage to retain the well – capitalized banks due to rigid Basel's standards and contagious effects of 2008's crisis. Empirical result tested the long run correlation amongst growth of loans and growth of capital regulation and highlighted to take into more considerations related to the capital regulation by banking managers and policy makers.

Meanwhile the deposits growth demonstrated the positive effect on the loans' growth confirming the core source of banking loans' supply. Furthermore, ROE confirmed the dual positive effect on the loans' growth with and without incorporation of the structural changes. This effect explained the banks' propensity to enhance the loans' supply due to higher profitability and testified the sustainable ROE's effect despite of 2008's crisis.

References

[1] K. Guo, V. Stepanyan, "Determinants of Bank Credit in Emerging Market Economies," IMF Working Paper, WP/11/51, 2011.

---

[3] See results in Table 9 – 11 in Appendix.
[4] See results in Table 12 in Appendix.

[2] S. Note, E. Suljoti, "Assessment of banks' lending determinant in Central Eastern and Southeastern European countries," Working Paper, Bank of Albania, 2017.

[3] S. Abel, "Cost efficiency and non-performing loans: An application of the Granger causality test," Journal of Economic and Financial Sciences, 11(1), May 2018, doi: 10.4102/jef.v11i1.170.

[4] G. Jiménez, J.A. Lopez, J. Saurina, "How Does Competition Impact Bank Risk-Taking," Journal of Financial Stability, 9(2), 185-195, 2007, doi:https://doi.org/10.1016/j.jfs.2013.02.004.

[5] M. Tracey, "The Impact of Non-performing Loans on Loan Growth: an econometric case study of Jamaica and Trinidad and Tobago," WP, September 2011.

[6] T. H.H. Pham, "Determinants of Bank Lending," May 2015, hal-01158241, Available at: https://hal.archives-ouvertes.fr/hal-01158241.

[7] M. Ivanović, "Determinants of Credit Growth: The Case of Montenegro," Journal of Central Banking Theory and Practice, 2016, 2, 101-118, 2016.

[8] D. Cucinelli, "The Impact of Non-performing Loans on Bank Lending Behavior: Evidence from the Italian Banking Sector," Eurasian Journal of Business and Economics 2015, 8(16), 59-71, 2015.

[9] A. Alihodžić, I.H. Ekşi, "Credit growth and non-performing loans: evidence from Turkey and some Balkan countries," Eastern Journal of European Studies, 9(2), 229-249, 2018.

[10] M. Accornero, P. Alessandri, L. Carpinelli, A.M. Sorrentino, "Non-performing loans and the supply of bank credit: Evidence from Italy," Questioni di Economia e Finanza (Occasional papers), 374, 2017, doi: 10.2139/ssrn.2954995.

[11] M. Kashif, S.F. Iftikhar, K. Iftikhar, "Loan growth and bank solvency: Evidence from the Pakistani banking sector," Financial Innovation, 2016.

[12] G. Shijaku, I. Kalluci, "Determinants of Bank credit to the Private sector: The case of Albania," Working Paper, Bank of Albania, 2013.

[13] S. Kipar, "The Effect of Restrictive Bank Lending on Innovation: Evidence from a Financial Crisis," Ifo Working 39, 2011.

[14] F.J. Fabozzi, S.M. Focardi, S.T Rachev, G.A. Bala, "The Basics of Financial Econometrics," John Wiley & Sons Inc., 2014.

[15] Y. Deli, I. Hasan, "Real effects of bank capital regulations: Global evidence," MPRA Paper, No. 79065, 2017, https://mpra.ub.uni-muenchen.de/79065/

[16] H. Akaike, "Information theory and an extension of the maximum likelihood principle," 199-213, 1973. In B. N. Petrov & B. F. Csaki (Eds.), Second International Symposium on Information Theory, 267–281. Academiai Kiado: Budapest.

[17] G. Schwarz, "Estimating the Dimension of a Model," Annals of Statistics, 6, 461-464, 1978.

[18] C.L. Mallows, "Some Comments on Cp.," Technometrics, 15, 661-675, 1973.

[19] D.N. Gujarati, D.C. Porter, "Basic Econometrics," Fifth Edition, McGraw-HILL International Editions Economics Series, Singapore, 2009.

[20] M.N. Harris, L.R. Macquarie, "A comparison of some introductory and undergraduate econometric textbooks," Journal of Economic Surveys, September 1995.

Appendix

Table 2: Results of functional form's selection

RESET test
data: model
RESET = 1.9149, df1 = 3, df2 = 54, p-value = 0.1381

Source: R, authors' estimations

Table 3: Results of dataset's distribution

Rainbow test
data: model
Rain = 1.3795, df1 = 32, df2 = 25, p-value = 0.2056

Source: R, authors' estimations

Table 4: Results of serial correlation

Breusch-Godfrey test for serial correlation of order up to 1
data: model
LM test = 0.055086, df = 1, p-value = 0.8144

Source: R, authors' estimations

Table 5: Results of heteroskedasticity

Studentized Breusch-Pagan test
data: model
BP = 13.354, df = 6, p-value = 0.03775

Source: R, authors' estimations

Table 6: Results of residual's distribution

Jarque Bera Test
data: res
X-squared = 4.8123, df = 2, p-value = 0.09016

Source: R, authors' estimations

Table 7: Results of structural breakpoint

Chow Breakpoint Test: 2008Q1			
Null Hypothesis: No breaks at specified breakpoints			
Varying regressors: All equation variables			
Equation Sample: 2003Q2 2018Q4			
F-statistic	8.92570	Prob. F(4,55)	0.0000
Log likelihood ratio	31.51608	Prob. Chi-Square(4)	0.0000
Wald Statistic	35.7028	Prob. Chi-Square(4)	0.0000

Source: Eviews 10, authors' estimations

Table 8: Results of series' stationarity

Seri	t-stat	Prob.	Result
G_L	-2.20678	(0.4773)	I(1)
D(G_L)	-14.5715	0	
G_NPL	-3.682	0.000497	I(0)
G_Dep.	-3.95877	-0.003	I(0)
ROE	-2.11681	-0.2389	
D(ROE)	-8.934263	0	I(1)
G_Cap.Reg.	-2.666251	-0.0856	
D(G_Cap.Reg.)	-8.601801	0	I(1)

Source: R, authors' estimations

Table 9: Results of series' casuality

Granger causality test	Fisher	P value	Result causality
G_L~G_Dep.	7.3719	0.00864	yes

G_L~ROE	4.5253	0.03752	yes
G_L~G_Cap.Reg.	3.2491	0.07648	yes

Source: R, authors' estimations

Table 10: Results of cointegration test according to the Johansen-Procedure

Test type: trace statistic, with linear trend
Eigenvalues (lambda):
0.42295174 0.33752592 0.14281396 0.06470381
Values of test statistic and critical values of test:
test 10pct 5pct 1pct
r <= 3 | 4.15 6.50 8.18 11.65
r <= 2 | 13.70 15.66 17.95 23.52
r <= 1 | 39.23 28.71 31.52 37.22
r = 0 | 73.32 45.23 48.28 55.43

Source: R, authors' estimations

Table 11 Results of cointegration test according to Engel-Granger (single-equation)

Dependent	tau-statistic	Prob.*	z-statistic	Prob.*
G_Cap. Reg.	-5.776400	0.0000	-19.18336	0.0444
G_L	-1.234115	0.8501	-3.435963	0.8470

Source: Eviews 10, authors' estimations

Table 12 Results of non – performing loans' impact on loans' growth

Dependent Variable: Loans' Growth				
Method: Least Squares				
Sample (adjusted): 2003Q2 2018Q4				
Included observations: 63 after adjustments				
Convergence achieved after 11 iterations				
Variable	Coefficient	Std. Error	t-Statistic	Prob.
C	0.017293	0.009384	1.842800	0.0705
G_NPL	-0.063087	0.028205	-2.236727	0.0292
(G_NPL)^2	0.098883	0.007466	13.23983	0.0000
D2008	0.083252	0.016147	5.155936	0.0000
[21] AR(1)	0.610183	0.104695	5.828215	0.0000
R-squared	0.788686	Mean dependent var		0.042558
Adjusted R-squared	0.774113	S.D. dependent var		0.053339
S.E. of regression	0.025351	Akaike info criterion		-4.435962
Sum squared resid	0.037275	Schwarz criterion		-4.265872
Log likelihood	144.7328	Hannan-Quinn criter.		-4.369065
F-statistic	54.11839	Durbin-Watson stat		2.381783
Prob(F-statistic)	0.000000			

Source: Eviews 10, authors' estimations

ASTES

Transient Stability Enhancement of a Power System Considering Integration of FACT Controllers Through Network Structural Characteristics Theory

Akintunde Alayande[1], Somefun A.O[1], Tobiloba Somefun[*,2], Ademola Ademola[2], Claudius Awosope[3], Obinna Okoyeigbo[2], Olawale Popoola[4]

[1]Department of Electrical and Electronics Engineering, University of Lagos, Akoka, Yaba, 220282, Nigeria

[2]Department of Electrical and Information Engineering, Covenant University, Ota, 112107, Nigeria

[3]Department of Electrical Engineering, Kanni Samab Consultants, Ilupeju, 100252, Nigeria

[4]Department of Electrical and Electronics Engineering, Tshwane University of Technology, Pretoria, 0008, South Africa

A R T I C L E   I N F O

A B S T R A C T

Modern power systems are topologically and structurally complicated due to their complex interconnections. Consequently, the complexity of the dynamic stability assessment be-comes more tedious, most especially, when considering a power electronics-based power system operating under faulty conditions. This paper, therefore suggests an alternative approach of Network Structural-Based Technique (NSBT) for the analysis and enhancement of transient stability of a power system considering Flexible Alternating Current Transmission Systems (FACTS) devices integration. The mathematical formulations based on the NSBT as well as the dynamic swing equations, required for carrying out the stability analysis, are presented. The structural characteristics of the network are captured by considering the interconnections of the network elements and the impedances between them. The eigenvalue analysis is then explored to identify suitable and possibly weak load node locations where the influence of FACTS device placement within the network, could be most beneficial. The transient stability analysis before and after critical outage conditions is investigated. The transient stability of the network operating under critical outage condition is then enhanced considering the integration of a multi- UPFC controller, which is suitably located as identified by NSBT. The effectiveness of the suggested approach is tested using the modified standard IEEE 5-bus, 30-bus networks as well as the practical Nigerian 28-bus grid incorporating a multi-FACTs controller. The results obtained show that the FACTS device contributes significantly to improving the transient stability of a multi-FACTS-based power network. The information provided by this study is highly beneficial to the system operators, utilities investors and power engineers, most especially, for predicting system collapse during critical outage conditions.

1. Introduction

The dynamic stability assessment of most practical power systems, which are topologically weak, has been a major concern to most power system engineers and researchers in recent times [1]. This becomes inevitable as a result of the ever-increasing demand for electric energy, which is causing the system to operate close to its capacity limits. In order to avoid system collapse without sacrificing the integrity of the network, it is expected that economic efficiency and the reliability of the network are maintained [2]. With the aim of achieving these, the power networks are faced with challenges such as overloading, voltage instability, and excessive transfer of power along transmission lines, to mention a few [3, 4]. Moreover, the frequent voltage collapse recorded in most modern power system networks is due to the fact that the networks are structurally weak [5]. This effect could be as a result of the reactive power deficit in the network. It

could also be traced to networks with very high resistance to reactance ratio, which is a characteristic of a distribution network or a radial transmission network. According to authors in reference [5], the least eigenvalue is approximately zero, and the magnitude of the elements of eigenvector associated to the least eigenvalue are approximately equal [5]. This constant magnitude shows that the network is a topologically weak power system, and it is due mainly to a wide relative electrical distance gap between the network load buses. A topologically weak network cannot be loaded up to its full capability limit without yielding a lower power transfer capability, and most power systems exhibit these structural characteristics, which make them be operated close to or beyond their permissible operating limits [6]. Therefore, there is a need for adequate compensation in order to enhance the transient stability of topologically weak power systems operating under critical contingencies and thereby enhancing the transfer capability of the network. This paper, therefore, attempts to provide an alternative approach to the enhancement of the transient stability of structurally weak power networks, which are operating under fault conditions considering the integration of FACTS devices.

Several contributions have been proposed by different authors for improving the transient stability of power systems undergoing disturbances through the integration of these FACTS devices [3]. FACTS devices are unique for their ability to preserve synchronism of generators whenever a major fault occurs within the network [7]. However, in order to obtain optimum performance of these FACTS devices, it is important to ensure that they are optimally placed within the power network under consideration. Traditionally, the problem is usually formulated as an optimisation problem, which is iterative in nature. For instance, the Modified Salp Swarm Optimization Algorithm (MSSOA) is used in [8] for the location of the UPFC (Unified Power Flow Controller. Another method proposed is the Particle Swarm Optimization algorithm in [7] for the optimal location of the STATCOM. Authors in reference [1] proposed a scheme using the zero dynamic approach to control the Thyristor Controlled Series Capacitors (TCSC) for its optimal location. The scheme controls the TCSC to investigate the transient stability of a multi-machine power system. The authors of [9] also present a hybrid BBO-DE algorithm to examine the performance of the system using the Static Var Compensator (SVC) and Power System Stabilizer (PSS). However, these iterative-based solution methods are not without challenges. The problem is formulated as a non-linear problem, which is a bit difficult to solve. Other problems include the existence of local minimal, non-convergence, time and space complexities etc. This influences to a greater extent, the results obtained, most especially, when dealing with a large practical network with multiple of contingency situation.

In this paper, a non-iterative method which solely depends on the structural interconnections of the network elements and their impedance values is suggested. This is because the study has shown that obtaining an effective solution to the problem actually lie in the structural interconnections of the network elements [10]. The main merit of this approach lies in the fact that the problem formulation as a linear and simple based on the fundamental circuit theory laws. Consequently, the solution is obtained in just one computation time. Hence, time and space complexities issues are totally eliminated. Also, the problem associated with the slack bus identification in the iterative-based methods is totally avoided.

Among the available FACTS controllers, UPFC has some inherent characteristics that are highly beneficial to solving some power system operational problems. For example, it can be used to control the flow of both active and reactive powers independently. Another benefit that could be derived from using UPFC is that it is a good controller for regulating the network load node voltages. These benefits are explored in this paper.

It has been shown, in the existing study that obtaining an effective solution to most power system problems does not depend on the loading conditions of the system but actually lie in the structural interconnections of the network elements [10]. Consequently, in this paper, a non-iterative method which solely depends on the structural interconnections of the network elements and their impedance values is proposed. The contributions of this paper to the active stream of research are as follows: The existing methods formulates the problem considered in this paper as an optimization problem which are without drawbacks such as local minimal issues, divergence problem etc. This present study, however, reformulates the problem of identifying UPFC placement as a linear problem based on the fundamental circuit theory laws. Consequently, the solution is obtained in just one computation time. Hence, time and space complexities issues are totally eliminated. Also, the problem associated with the slack bus identification in the iterative-based methods is totally avoided.

The remaining parts of the paper are structure as follows: section 2 presents the theoretical framework as well as the mathematical formulations to the problem, in section 3, the descriptions of the networks used are presented. The programming tools used are also presented in section 3. Section 4 presents the numerical results obtained and the discussion of the results. The paper is concluded in section 5.

2. Theoretical Background and Mathematical Formulations

This section provides the mathematical formulations and methodology used in building the numerical approach for the study. In this paper, the Newton-Raphson method used in carrying out the load-flow analysis is briefly revisited, the derivation of swing equation is presented, the mathematical formulation of the non-iterative dependent approach for identifying suitable load nodes where FACTS Devices could be placed for enhancement of the transient stability is presented, and the formulation for enhancing a structurally weak network is presented.

2.1. Static and Dynamic Modelling for Transient Stability Assessment

The steady-state analysis of power system is usually studied by solving the static power flow equations. Various approaches to solving these equations abound in the literature. However, the prominent solution techniques include Gauss-Seidel method [11], Fast Decoupled method and Newton – Raphson method [11, 12]. For the purpose of this study, the Newton – Raphson method is used because of its fastest rate of convergence as well as its self-correcting mechanism [13]. The complex power equations at any node i of an n-bus power system can easily be expressed as [14].

$$P_i + jQ_i = \dot{V}_i \sum_{j \in i} \hat{Y}_{ij} \hat{V}_j \qquad (1)$$

$$\forall j \in i (i = 1, 2, \ldots, n)$$

$$\dot{V}_i = V_i e^{j\theta_i} \tag{2}$$

where V_i and θ_i are the magnitude and phase angle of voltage at bus i.

The elements of admittance matrix can be expressed as

$$Y_{ij} = G_{ij} + jB_{ij} \tag{3}$$

From (1), the real and reactive power at any bus i respectively can be formulated as

$$P_i = V_i \sum_{j \in i} \widehat{V}_j \left(G_{ij} \cos \cos \theta_{ij} + jB_{ij} \right. $$
$$\left. \sin \sin \theta_{ij} \right) \tag{4}$$

$$Q_i = V_i \sum_{j \in i} \widehat{V}_j \left(G_{ij} \sin \sin \theta_{ij} - jB_{ij} \right.$$
$$\left. \cos \cos \theta_{ij} \right) \tag{5}$$

such that $(i = 1, 2, \ldots, n)$

where $\theta_{ij} = \theta_i - \theta_j$, which is the voltage phase angle difference between bus i and j.

The result is a linear system of equations that can be expressed as follow:

$$[\Delta\theta \, \Delta|V\,|\,] = J1[\Delta P \, \Delta Q\,] \tag{6}$$

where ΔP and ΔQ are mismatch equations given by (7) and (8) respectively as

$$\Delta P_i = -P_i + V_i \sum_{j \in i} \widehat{V}_j \left(G_{ij} \cos \cos \theta_{ij} + jB_{ij} \right.$$
$$\left. \sin \sin \theta_{ij} \right) \tag{7}$$

$$\Delta Q_i = -Q_i + V_i \left(G_{ij} \sin \sin \theta_{ij} - jB_{ij} \right.$$
$$\left. \cos \cos \theta_{ij} \right) \tag{8}$$

and J is a matrix of partial derivatives known as a Jacobian given as

$$\left[\frac{\partial \Delta P}{\partial \theta} \; \frac{\partial \Delta P}{\partial |V\,|} \; \frac{\partial \Delta Q}{\partial \theta} \; \frac{\partial \Delta Q}{\partial |V\,|} \right] \tag{9}$$

The linearised system of equations is solved to determine the next guess $(m + 1)$ of voltage magnitude and angles as follows:

$$\theta^{m+1} = \theta^m + \Delta\theta \tag{10}$$

$$|V\,|^{m+1} = |V\,|^m + \Delta|V\,| \tag{11}$$

where m is the iteration count. The process is iterated with a common stopping condition where the mismatch result is less than a given tolerance, ε.

For effective evaluation of power system transient stability assessment, the rotor angle dynamics provides a helpful insight into the behaviour of the system, most especially, when a sudden disturbance occurs. The sudden occurrence of a disturbance in a power system usually causes an increase in the mechanical torque (T_m) of the prime mover, and an acceleration torque (T_a) is developed if the mechanical torque is greater than the electromagnetic torque (T_e). Mathematically,

$$T_a = T_m - T_e \tag{12}$$

The machine is accelerated with an inertia J which consists of the inertia of the generator and prime mover. Therefore,

$$J\frac{d\omega_m}{dt} = T_a = T_m - T_e \tag{13}$$

where t is time in seconds and ω_m is the angular velocity of the rotor in mechanical rad/s. Expressing J in terms of inertia constant H results to

$$J = \frac{2H}{\omega_{0m}^2} VA \tag{14}$$

Therefore,

$$\frac{2H}{\omega_{0m}^2} VA \frac{d\omega_m}{dt} = T_m - T_e \tag{15}$$

Introduction of a new angular velocity of the rotor, ω_r (rad/s) results to

$$2H \frac{d\omega_r}{dt} = T_m - T_e \tag{16}$$

Alternatively,

$$\frac{d\omega_r}{dt} = \frac{d^2\delta}{\omega_0 dt^2} \tag{17}$$

where δ is the angular position of the rotor (elect. rad/s) with respect to a synchronously rotating reference frame.

By combining (16) and (17), the dynamics model of the rotor angle known as the swing equation can, therefore, be easily obtained expressed as

$$\frac{2H}{\omega_0} \frac{d^2\delta}{dt^2} = T_m - T_e \tag{18}$$

2.2. Identification of Suitable Load Nodes for Facts Device Placement: A Network Structural Perspective

The mathematical formulation for the problem considered in this paper is viewed from the fundamental circuit theory laws perspective. This is employed to develop the inherent structural

properties of power network considering the interconnectivity of the network elements and the impedance between them [15]. Though this theory has been extensively applied to solve various power system problems in the literature [16–19], there are more to the theory than we have had in the past. For instance, the application of this topological-based concept in resolving transient stability issues has not been holistically investigated. This is the main focus of this paper.

First, let us consider a simple power system network, to depict the structural interconnections of various power network elements, as shown in Figure 1.
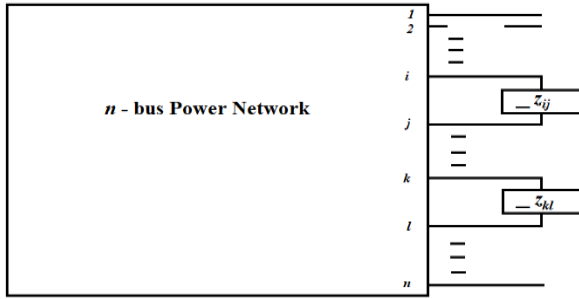
Figure 1: Interconnections of power network elements [4]

The matrix equation that relates the node voltages and line currents in terms of the line parameters can be written in its compact form as [5]

$$[A_c][V'] = \begin{bmatrix} z_{ij} \ 0 \ 0 \ z_{kl} \end{bmatrix} \begin{bmatrix} I_{ij} \\ I_{kl} \end{bmatrix} \tag{19}$$

where

$$[V'] = \begin{bmatrix} V'_1, V'_2, \dots, V'_i, V_j, \dots, V'_l, \dots, V'_n \end{bmatrix} \tag{20}$$

where

A_c is termed as the coupling matrix, $[V']$ represents the vector of the nodal voltage within the network after the enhancement through the identification of suitable nodes for placement of reactive power supports, I_{ij} and I_{kl} are the currents through the network branches $i-j$ and $k-l$ respectively.

For instance, the coupling matrix, based on Figure 1 can be formulated as

$$[A_c] = [\ 0 \ 0 \ 0 \ . \ . \ . \ 0 \ . \ . \ .1 \ 0$$
$$-1 \ . \ . \ . \ 0 \ . \ . \ . \ 0 \ \ 1 \ \ 0 \ . \ . \ .$$
$$-1 \ . \ . \ .0 \ 0 \ ] \tag{21}$$

Since a change in current causes a change in bus voltages, we can therefore write

$$[V'] = [Z_l][l_o + \Delta l] \tag{22}$$

Alternatively,

$$[V'] = [V] + [\Delta V] \tag{23}$$

where $[V]$ represents the voltage profile of the original power network.

$[\Delta V]$ denotes the change in the vector of the voltage profile for the network before the enhancement, which can easily be expressed as

$$[\Delta V] = -[Z_l][A_c^T]\begin{bmatrix} I_{ij} \ I_{kl} \end{bmatrix} \tag{24}$$

From equation (24),

$$\begin{bmatrix} I_{ij} \ I_{kl} \end{bmatrix} = [Y_{bus}]\begin{bmatrix} V_i -V_j \ V_k -V_l \end{bmatrix} \tag{25}$$

$$[Y_{bus}] = \{z^{new} + [A_c][Z_l][A_c^T]^{-1}\} \tag{26}$$

$$z^{new} = \begin{bmatrix} z_{ij} \ 0 \ 0 \ z_{kl} \end{bmatrix} \tag{27}$$

Obviously, the structural interconnections that exist between the network nodes of the enhanced network is fully captured in (26)

In order to investigate the influence of the network structural properties on the location of the FACTs devices for effective enhancement of the network, the eigenvalue decomposition approach is applied to (26) as [15]

$$[Y_{bus}] = W \sum W^T = \sum_{i=1}^{n} \omega_i \rho_i \omega_i^T \tag{28}$$

where W and $W^T = n$–by–n orthogonal eigenvectors of $[Y_{bus}]$.

ρ_i = The eigenvalue at any bus i, ω_i and ω_i^T respectively.

The inverse relationship between the bus voltage and their respective eigenvalues can be expressed as

$$[V] = \sum_{i=1}^{n} \frac{\omega_i^T \omega_i}{\rho_i} [I] \tag{29}$$

Various methods have been identified to determine the eigenvalue of the power network. They are broadly classified under iterative and no-iterative based methods. More recently, network structural characteristics based approach presents a model which provides a clear distinction between generation and load buses, as presented in reference [19]. This is shown by formulating the generator voltage and the load current as functions of their respective generator currents and load voltages as

$$[V_G \ I_L \ ] = [Z_{GG} \ H_{GL} \ W_{LG} \ C_{LL} \ ][I_G \ V_L \ ] \tag{30}$$

where

$$Z_{GG} = Y_{GG}^{-1} \tag{31}$$

$$H_{GL} = -Y_{GG}^{-1}Y_{GL} \tag{32}$$

$$W_{LG} = Y_{LG}Y_{GG}^{-1} \tag{33}$$

$$C_{LL} = Y_{LL} - Y_{LG}Y_{GG}^{-1}Y_{GL} \tag{34}$$

Obviously, from (30), it can be seen that the relationship between the vector of generator node voltages and the load node currents is governed by the matrix CLL, which captures the influence of all the interconnections of load buses after the influence of generator buses has been eliminated. Application of the eigenvalue presented in (29) can, therefore, be used to decompose CLL, which gives an inverse relationship between the load bus voltage and the associated eigenvalue. This relationship is used in this paper to identify the weak load nodes within the network [19].

3. Numerical illustrations

Case 1: The Standard IEEE 5-Bus Network

The standard IEEE 5- bus system network consists of two-generation nodes and three load nodes, which are interconnected by seven transmission lines. The one-line diagram is presented in Figure 2 using the PSAT interface. The line data are adapted from reference [20] and are sampled for determining the eigenvalues of the nodes and their corresponding eigenvectors.
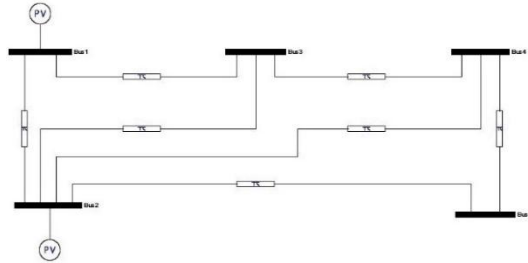
Figure 2: Single-line diagram of the standard IEEE 5-bus network

Case 2: The Standard IEEE 30 – Bus Network

Figure 3 shows the single line diagram, drawn in the PSAT environment, for the standard IEEE 30-bus network. This is used, as the second case study considered, in order to verify the effectiveness of the methodology suggested in this study. It comprises of six generator buses, twenty-four load buses, which are interconnected by forty-one transmission lines. In this study, the PSAT environment is used in conjunction with the MATLAB 2016a as the programming tools.

Case 3: The Nigerian 28-Bus Network

In order to investigate the effectiveness of the proposed approach in this study to practical power systems, the Nigerian 28-bus is considered whose one-line diagram is shown in Figure 4. The network comprises ten generator buses, eighteen load buses, which are connected by thirty-one transmission lines. It worth noting that the sizing of the UPFCs used in this study is adapted from the work of Melodi [21].

4. Results and Discussion

This section presents and discusses the simulation results in this study obtained based on the approach suggested. Three power system networks are considered to verify the efficiency of the method. The standard IEEE 5-bus network is first considered, then the standard IEEE 30-bus system using PSAT simulation and then the Nigerian 28-bus system using MATLAB programming tools. The data used is on 100MVA base. The graphical representation as well as the tabular presentation of the results are displayed and explained. The transient stability of the networks before reinforcement and before the integration of UPFC are presented, which serve as the base case. These results are then compared with the transient stability, of the system, after the reinforcement and integration of UPFC.

Figure 3: Single-line diagram of the standard IEEE 30-bus network
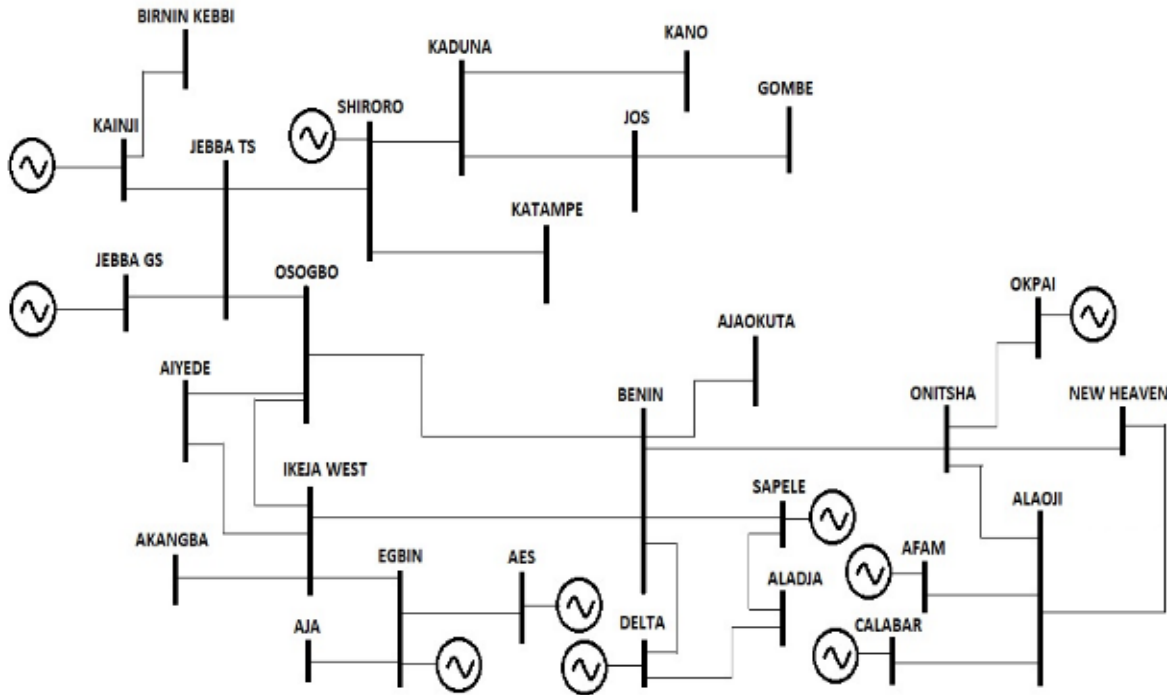
Figure 4: Single-line diagram of the Nigerian 28-bus network

4.1. Investigation of The Network Strength and Identification of The Suitable Load Nodes for Network Reinforcement

The eigenvalue analysis, on the reduced bus admittance of the network, based on the CLL matrix, is first performed. In this matrix, the interaction of the generators has been eliminated. So, the output of this matrix contains only the load-to-load interaction.

The IEEE 5-bus and the IEEE 30-bus networks are subjected to tests of determining the eigenvalues and the corresponding eigenvector, measured to confirm or ascertain the strength of the network. The network data are from reference [20]. The same procedures are extended to the Nigerian 28-bus network whose line data are adapted from reference [22]. The MATLAB 2016a is used as the programming tool to determine the eigenvalues and their corresponding eigenvectors in each case. It should be iterated that the sizing of the UPFCs employed in this study is carried out based on the existing work presented by the authors of reference [21]. The results obtained, for each case, are presented and discussed in the subsections that follow:

Case 1: The Standard IEEE 5-Bus Network

The modified network of the IEEE 5-Bus power network is shown in Figure 5. The transmission line where the multi-UPFC is located is first identified using eigenvalue analysis and then integrated into the network at the identified location, as shown in Figure 5. This UPFC is controlled such that appropriate compensation is delivered to the network, in steps, in order to maintain the network voltage profile such that the integrity of the network is maintained. This is carried out using the Newton-Rapson power-flow-based technique. The load-flow analysis is performed in this study to determine the base case voltage profile of the two networks considered. Figure 6 shows the graphical representation of the voltage profile obtained for the power-flow analysis using the standard IEEE 5-bus system.
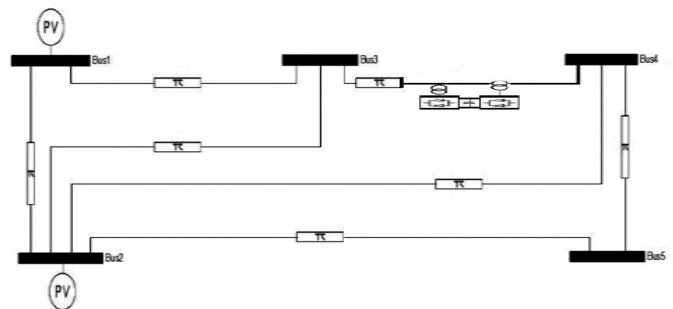
Figure 5: Single-line diagram of the modified IEEE 5-bus network
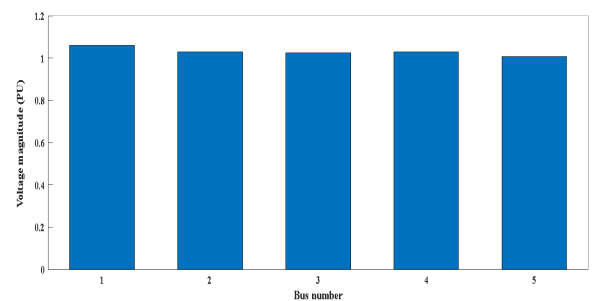
Figure 6: Base case voltage profile for the standard IEEE 5-bus network

The study then investigates the influence of FACTS device (UPFC) integration into the network during a disturbance. This is carried out by considering the transient stability of the network with and without FACTS. The simulation results for the two scenarios (with and without UPFC) are then compared. The results obtained from the eigenvalue analysis is ranked in ascending order, as shown in Table 1. The load node associated with the least eigenvalue is the suitable bus where the placement of the FACTS device would be of the highest benefit to the network. From Table 1, it can be seen that the least eigenvalue is ranked 1st, and this corresponds to load node 4 within the

network. In other words, as evident from Table 1, Bus 4 has the least eigenvalue of 0.1120, and this makes it the weakest bus in the system. This implies that the FACTS device will provide better compensation to the network if placed on the transmission line connecting buses 4 and 5. The eigenvector elements associated with the least eigenvalue of 0.1120 at bus 4 are found to be approximately equal to 0.571, as shown in Figure 7. This confirms the structural weakness of the network.

Table 1: Identification of a suitable location of FACTS device in the IEEE 5-Bus

Load node	Eigenvalue	Ranking
4	0.1120	1st
5	15.6029	2nd
3	71.4702	3rd
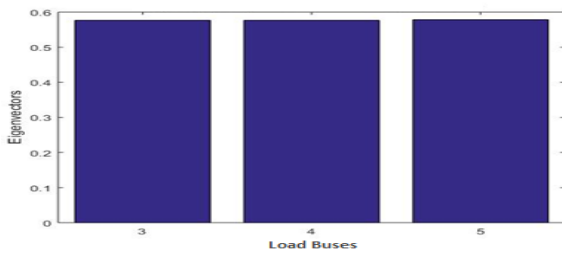
Figure 7: Eigenvectors associated with the least eigenvalue of the IEEE 5-bus network

Case 2: Standard IEEE 30-Bus Network

When the analysis of the eigenvalues is performed using the standard IEEE 30-bus power network, the transmission line, which is most suitable for placement of the multi-UPFC controller is determined. The modified network for the standard IEEE 30-bus network, when the UPFC is integrated, using the PSAT interface is shown in Figure 8. The same procedures, as explained in the preceding section, are repeated for the standard IEEE 30-bus network. The base case voltage profile using the standard IEEE 30-bus system is presented in Figure 9.

The same procedural steps followed in the case of the IEEE 5-bus network are also followed using the standard IEEE 30-bus network for identifying the suitable load nodes where the reactive power supports should be located within the network. Similar simulations are also carried out using the standard IEEE-30 bus system. The ten buses with the least eigenvalues within the network are selected, ranked and presented in Table 2.

Bus 23 is the load bus associated with the least eigenvalue of 0.00216, as shown in Table 2. The corresponding eigenvectors for this least eigenvalue are found to be equal in magnitude with a value of 0.235, as shown in Figure 10. This constant eigenvector magnitude shows that a very wide electrical distance exists between the load nodes, which accounts for the topological weakness within the network under consideration. This has a greater influence on the power-flow through the transmission lines within the network.

Table 2: Identification of a suitable location of FACTS device in the IEEE 30-Bus

Load node	Eigenvalue	Ranking of eigenvalue
21	7.3285	10th
22	6.7473	9th
23	0.0216	1st
24	0.7491	2nd
25	5.5871	8th
26	1.5335	3rd
27	2.1872	4th
28	4.5805	7th
29	3.2186	6th
30	3.0953	5th
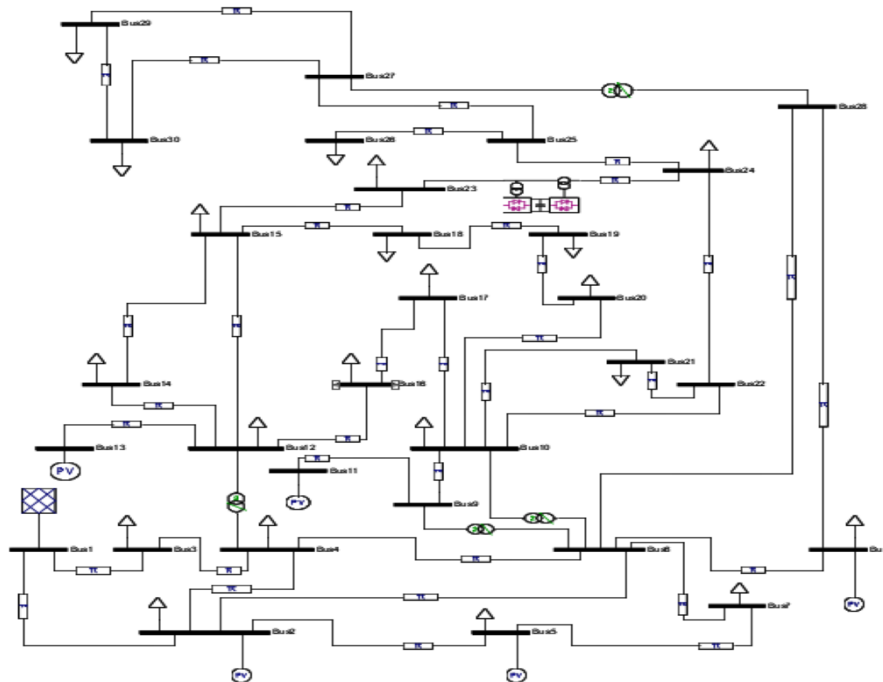
Figure 8: Single-line diagram of the modified IEEE 30-bus Network
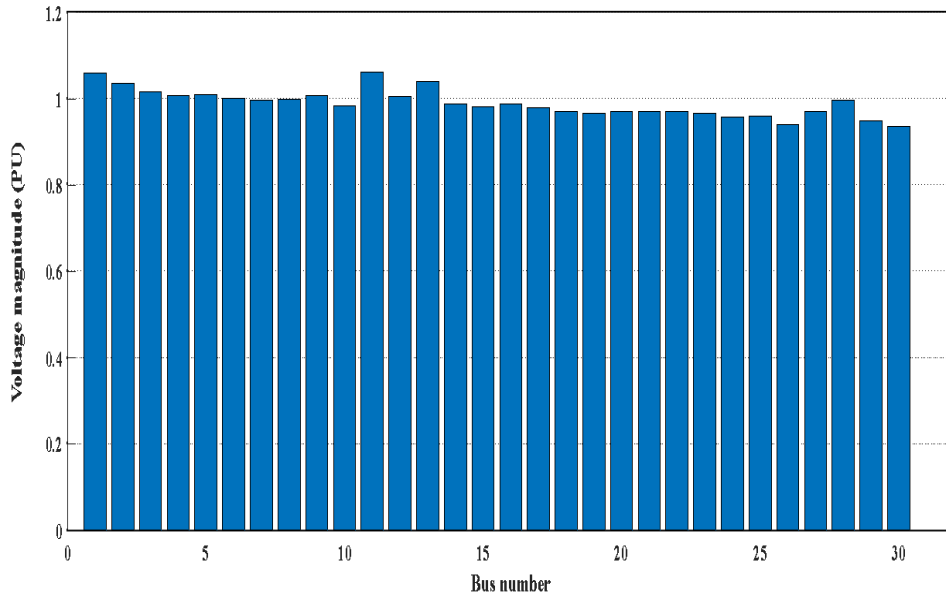
Figure 9: Base case voltage profile of the standard IEEE 30-bus network
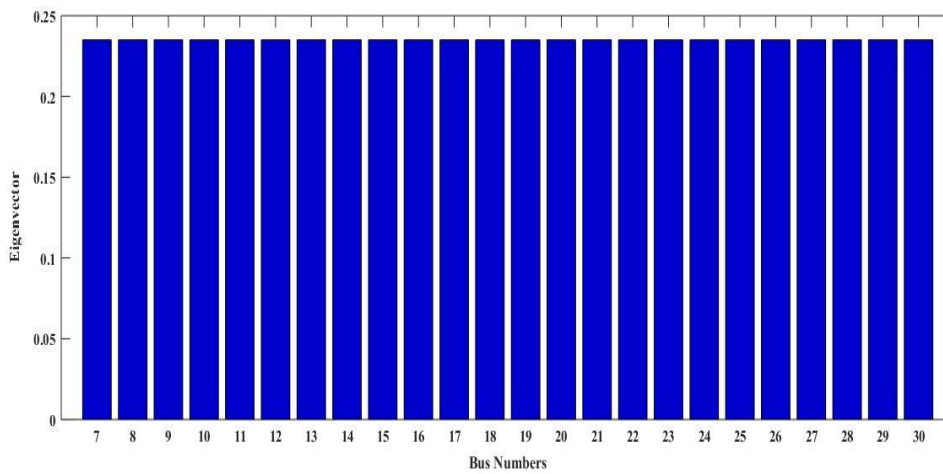
Figure 10: Eigenvectors of the least eigenvalue of the standard IEEE 30-bus network
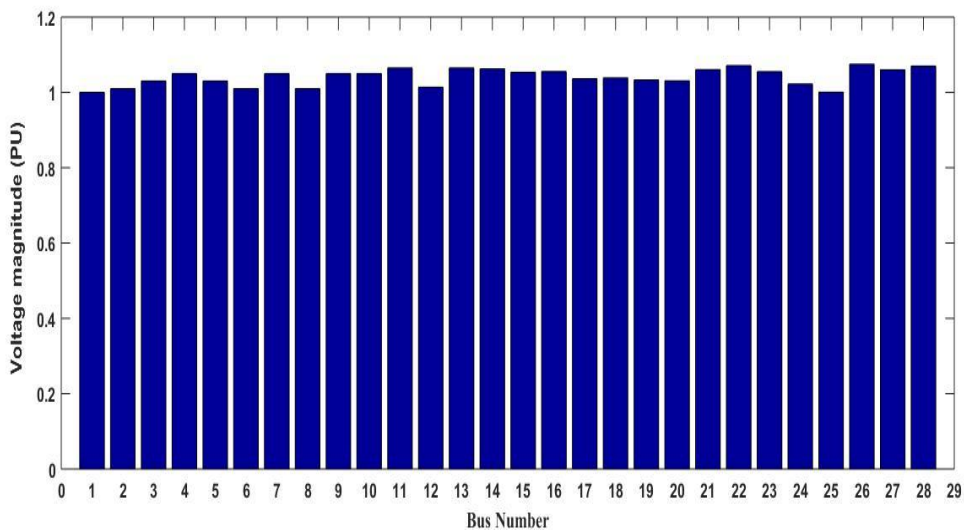
Figure 11: Base case voltage profile of the Nigeria 28-bus network

Table 3: Identification of a suitable location of FACTS device in the Nigerian 28-Bus

Load node	Name	Eigenvalue	Ranking of eigenvalue
19	Akangba	143.3201	10th
20	Ikeja West	103.4449	9th
21	Onitsha	98.5211	8th
22	New Haven	2.8253	1st
23	Alaoji	3.8524	2nd
24	Aladja	54.0964	7th
25	Aja	19.7755	3rd
26	Birnin Kebbi	32.3796	5th
27	Kaduna	29.6417	4th
28	Kano	51.5486	6th

The results of the eigenvalues, which are associated with the network load buses, as presented in Table 3, are then ranked in increasing order from the least value to the largest value. It is revealed based on the results that the weakest node within the network is bus 22 (New Haven) whose eigenvalue is 2.8253 and the next to it is bus 23 (Alaoji), with the eigenvalue of 3.8524. The implication of this is that a large electrical distance exists between the load buses 22 (New Haven) and 23 (Alaoji). This, therefore, suggests that the load bus 22 (New Heaven) is the weakest bus within the network. With this, the critical line is determined and the transmission line (New Haven - Alaoji), through which the UPFC is connected, is as therefore identified. The UPFC placement is, therefore, located between the buses 22 (New Haven) and 23 (Alaoji) as shown in the modified network shown in Figure 12. The eigenvectors that correspond to the least eigenvalue of 2.8253 is found to be approximately constant with a value of 0.2371, and the results are shown graphically in Figure 13 in which all the load buses are seen to maintain equal values of eigenvector.
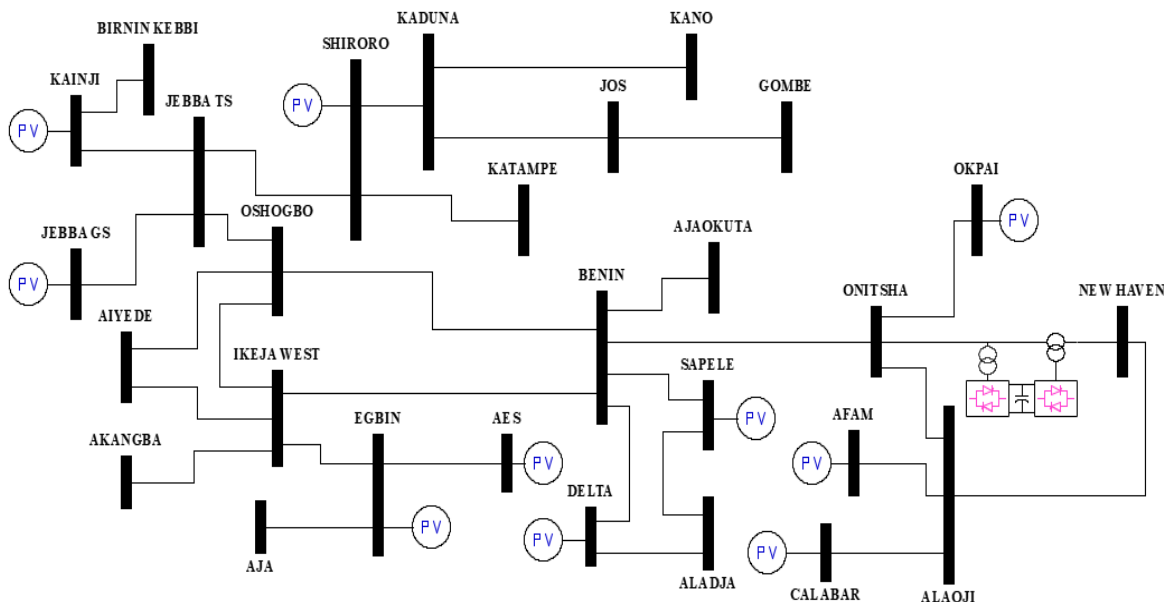
Figure 12: Single-line diagram of the modified Nigerian 28-bus Network
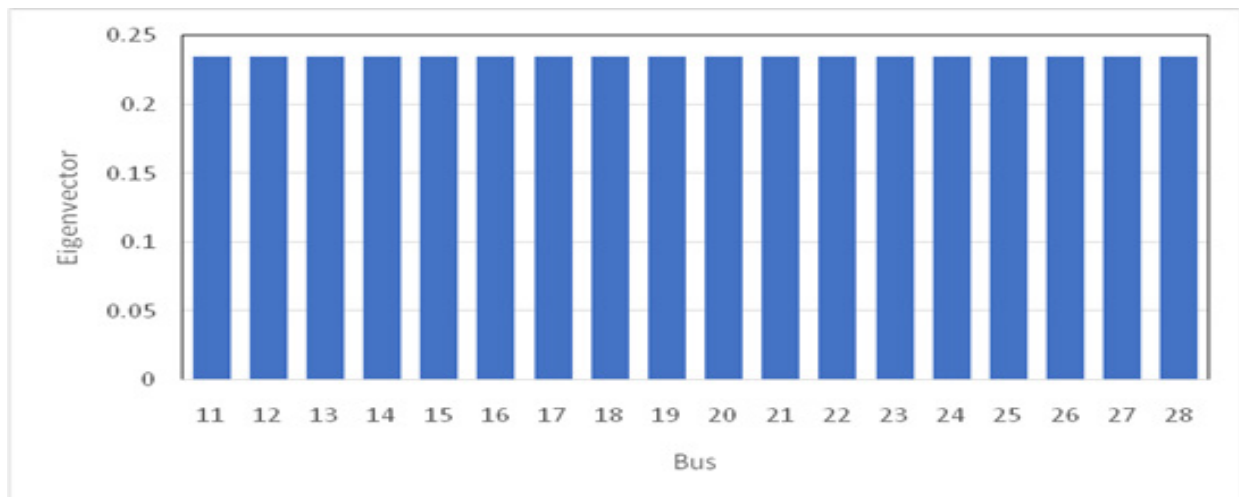
Figure 13: Eigenvectors corresponding to the least eigenvalue of New Heaven in the Nigerian 28-bus network

4.2. Transient Stability Assessment

In this section, the assessment of the system transient stability, when subjected to disturbances, is investigated. The responsiveness of the power systems to the sudden occurrence of faults are assessed. This serves as the base case solution, and the results obtained are presented. Based on the phase difference and the angle of convergence, the time taken by the power systems to regain stability and return to a normal mode of operation is considered. The transient stability assessment, considering the reinforcement of the network through the integration of multi-UPFC, is then carried out. The comparison of results is then made in order to investigate the impact of the FACTS device on the reinforcement of the topologically weak power networks. The results obtained from the simulations are presented in the sections that follow.

Case 1: Transient Stability Assessment of The IEEE 5-Bus System

This power network is subjected to a fault on bus 4 being the most critical load bus as identified based on the eigenvalue analysis. The contingency analysis is then performed by the removal of the transmission lines connected to it based on the N-1 criterion to determine the impact of the transmission line outages on the stability of the system. The results obtained from the simulations before the integration of the UPFC are shown in Figure 14.

Figure 14 (a) – (c) show the dynamic response for the transient stability assessment before the integration of UPFC for possible upgrading of the network. In Figure 14 (a), it can be seen that the effect of the disturbance during which line 2-4 is removed causes the rotor angle to fluctuate between the values of -2.5o and -22.5o. The phase angle after returning to synchronism, is found to become stable at -12.5o. However, the result of the transient assessment for the outages of line 3-4 and line 4-5 shows similarities in the phase angle difference, as shown in Figure 14 (b) and (c) respectively. The rotor angles fluctuate between -4o and -22.5o in both cases and the stable phase angle difference after returning to synchronism is -13.25o.

In order to investigate the impact of the multi-UPFC on the transient stability of the network, the transient stability assessment of the network is carried out considering the integration of the multi-UPFC into the network. From the eigenvalue results presented earlier in Table 1, suitable locations for the placement of multi-UPFC are identified based on the magnitude of the eigenvalues of the network load buses. It is seen that the bus with the least eigenvalue is identified as the most critical bus (bus 4) within the network. The transmission line connecting the most critical bus and the next ranked eigenvalue bus (bus 5) is identified as the most critical transmission line in the system. In other words, the most critical line in the IEEE 5-bus system, based on the approach suggested in this work, the critical line is the line connecting buses 4 and 5. In this paper, we assumed the worst scenario and therefore suggested that when a fault occurs at the most critical bus, the line connecting buses 4 and 5 should be removed to clear the fault. Furthermore, as presented in Table 1, the next ranked eigenvalue bus after bus 5 is bus 3. This implies that the network under consideration can easily be enhanced or upgraded by placing the multi-UPFC controller in series with the

line which connects the most critical bus (bus 4) and bus 3. It is noteworthy that the third line (line 2-5) is connected to bus 2, which is a generator bus. This is not considered for the muti-UPFC as the generator is capable of reinforcing the line with the needed compensation.

After the integration of FACTS devices into the network, the same procedure carried out without the incorporation of UPFC is repeated. The reactive power is then improved in steps, and the transient stability of the system is analysed. The most significant variation is observed when the reactive load demand is compensated to 30.5MVAR. The results obtained, considering the N-1 criterion within the network is shown in Figure 15.

It is observed that an improvement in the phase angle difference occurs after integrating the UPFC between the lines. Also, the angle of convergence is seen to have been improved. Figure 15 shows that the phase angle difference is found between -4 and -20 and the angle of convergence after the system regains synchronism is -12o, which is a significant improvement from the base case examined.
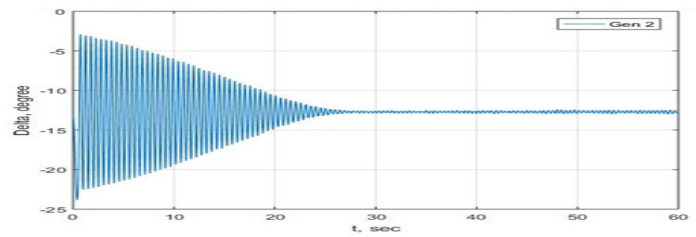
(a): Phase angle difference with line 2-4 removed
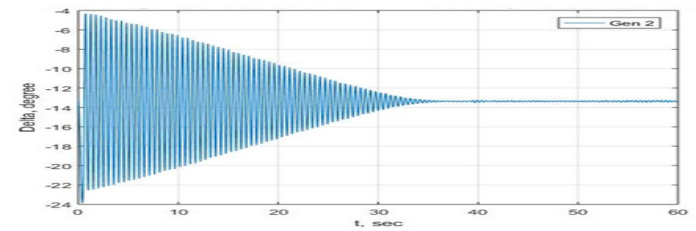
(b): Phase angle difference with line 3-4 removed
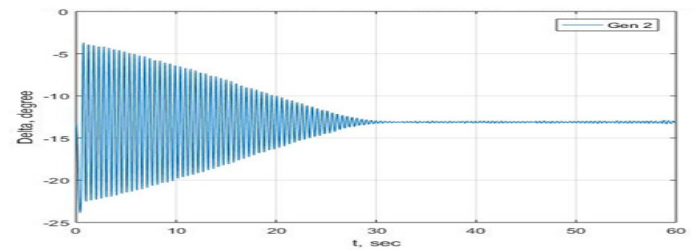
(c): Phase angle difference with line 4-5 removed

Figure 14: IEEE 5-bus transient stability assessment before the integration of UPFC
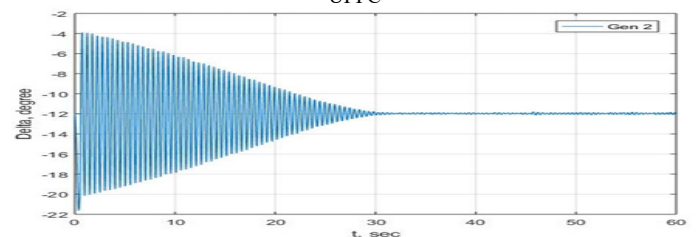
Figure 15: IEEE 5-bus transient stability assessment considering UPFC integration

Case 2: Transient Stability of The IEEE 30-Bus System

In this subsection, the transient stability assessment of the standard IEEE 30-bus power network is carried out. The simulation results obtained when the critical load bus (bus 23) with the least eigenvalue is subjected to a fault are presented and discussed in this section. The N-1 criterion is also taken into consideration as explained for the IEEE 5-bus network. To determine the Critical Clearing Time (CCT) for the network, the transient stability assessment of the network is first performed using a small clearing time and increase in steps to determine the actual clearing time the network becomes unstable. This maximum clearing time at which the network becomes stable is taken as the CCT.

The dynamic responses obtained from the simulation before integrating the multi-UPFC are shown in Figures 16 (a) and (b). Based on the simulation results obtained, the Critical Clearing Time (CCT) of 0.01s is obtained for the network. Figure 16 (a) shows the transient analysis when line 15-23 is removed. The network regains transient stability after 30 seconds. Similarly, when line 23-24 is removed, the time taken to regain transient stability is 50 seconds, as presented in Figure 16 (b).

The most critical line based on the results presented in Table 2 is line 23-24. Based on the eigenvalue analysis results obtained, the line on which the series UPFC is placed is identified to be the one connecting buses 23 and 15. Considering the N-1 contingency conditions, when a fault occurs at the most critical bus (bus 23), the most critical transmission line (the line connecting buses 23 and 24), as identified by the approach suggested in this study, is disconnected. For faults on bus 23, the reactive power is increased in steps, and the critical line attached to it, based on N-1 criterion is removed, and the transient stability analysed. The dynamic response obtained from the simulation is shown in Figure 17

It is evident from results obtained in Figure 17 that the inclusion of the multi-UPFC controller causes the network to regain transient stability faster than the time taken without the UPFC controller. Figure 17 confirms the improvement in time to 20 seconds from the base case of 50 seconds which it takes the system to regain transient stability when the critical line (line 23-24) is disconnected. The result shows that by the integration of the FACTS device, the transient stability of the power system improves significantly. The improvement is evident in the time-reduction of the distortion period, and this goes a long way at avoiding total system collapse during any major disturbance, usually faults.
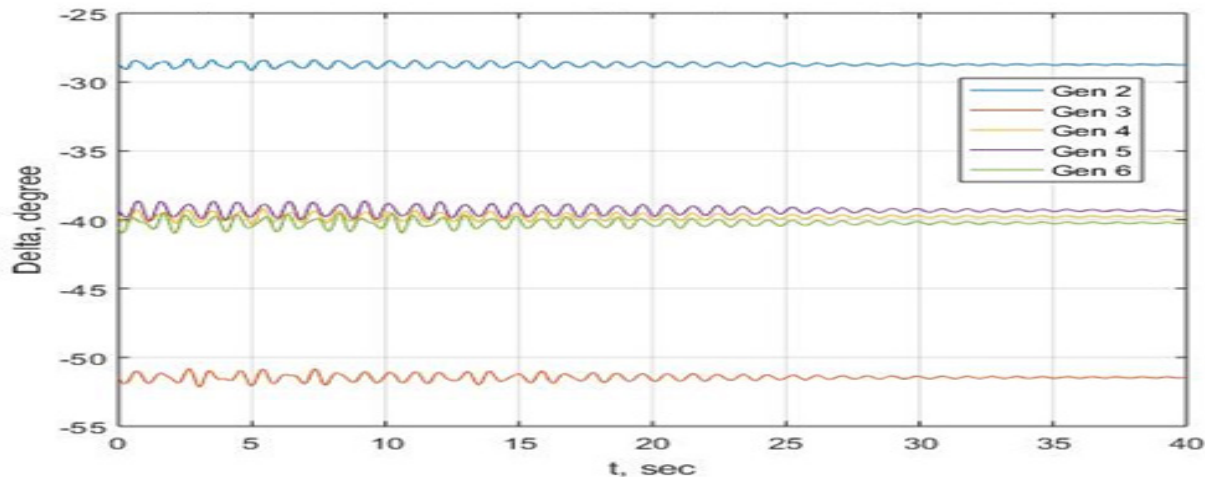
(a): Phase angle difference with line 15-23 removed
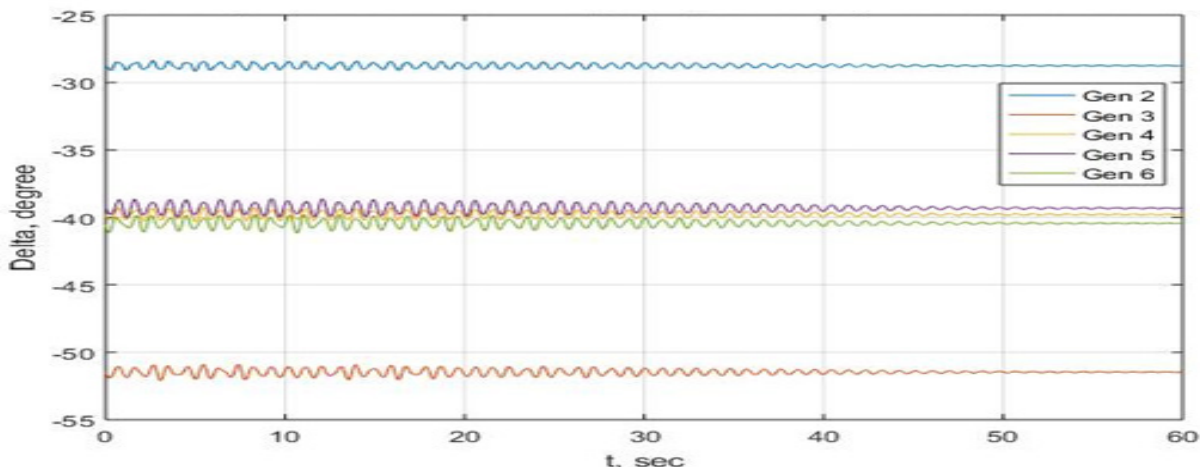
(b): Phase angle difference with line 23-24 removed
Figure 16: IEEE 30-Bus transient stability assessment before integrating UPFC
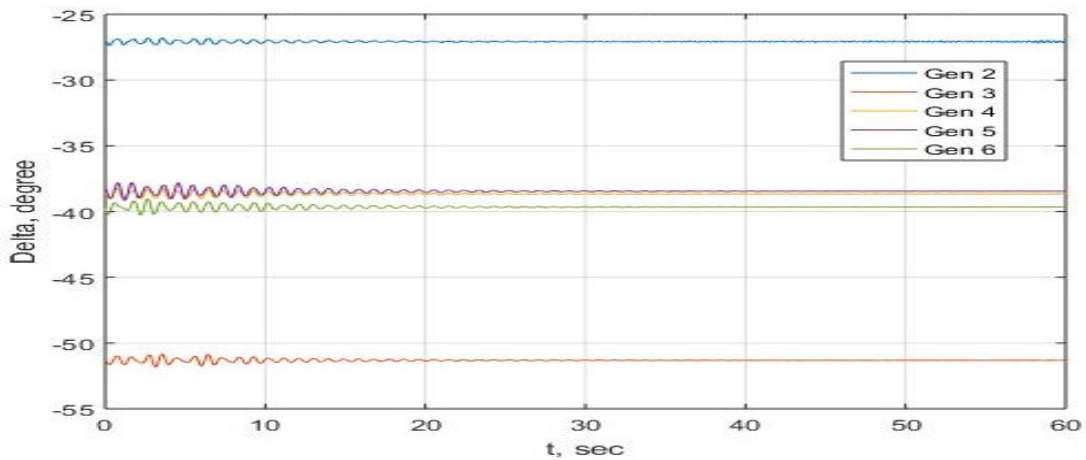
Figure 17: IEEE 30-bus transient stability assessment considering UPFC integration

Case 3: The Nigerian 28-Bus System

The same simulation procedures, as earlier discussed, are followed in this case. The total simulation time of 50 seconds and the clearing time of 0.08 second are considered for the simulation. The results obtained are presented in Figures 18 (a) and (b). By considering the N-1 criterion, the transmission line connecting New Heaven to Onitsha (line 22-21) is first disconnected with reference to a fault occurring on the bus 22 and the simulation result obtained is shown in Figure 18 (a). The simulation result obtained when the transmission line connecting New Haven to Alaoji (22-23) is disconnected is shown in Figure 18 (b).

The base cases show that three generators are significantly out of synchronism with the others, with reference to the generator at Egin. The worst scenario is seen at a phase angle of -10.75o. The procedure is once again repeated after the integration of the UPFC to examine the impact of ingesting reactive power into the system through the UPFC.
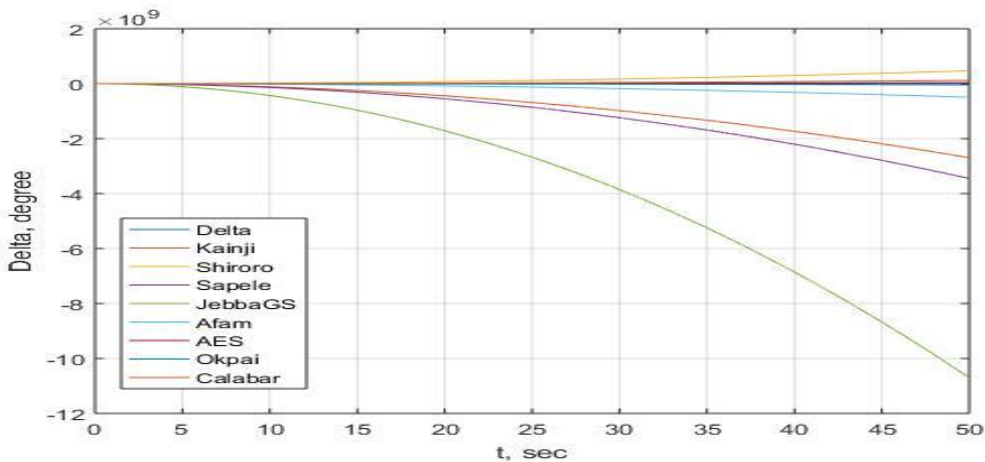
(a): Phase angle difference with line 21-22 removed
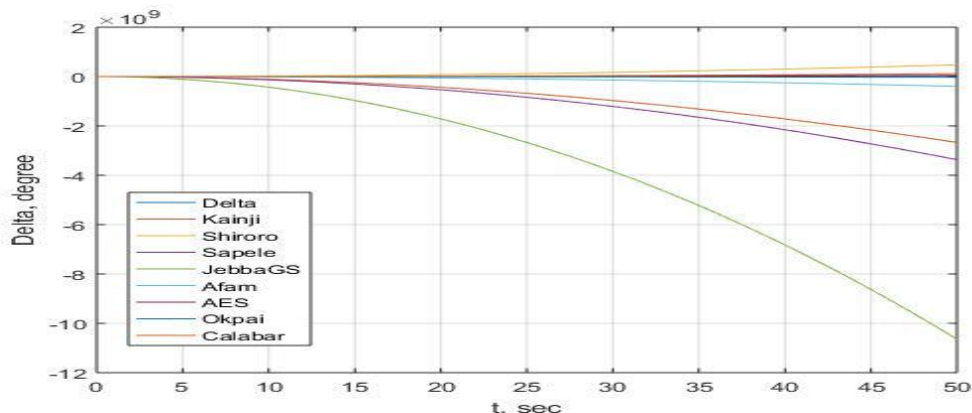
(b): Phase angle difference with line 22-23 removed

Figure 18: Nigerian 28-Bus Transient Stability Before Integrating FACTS Device

From the results of the eigenvalue presented in Table 3, the placement of the UPFC is identified based on the magnitude of the eigenvalues of the network load buses. The bus with the least eigenvalue, within the network, is identified to be bus 22 (New Haven). The transmission line connecting this bus and the next ranked eigenvalue bus 23 (Alaoji) based on the approach suggested in this work is identified as the most critical transmission line in the system. In other words, the most critical line in the Nigerian 28-bus system is the transmission line connecting New Haven and Alaoji buses (bus 22- bus 23). This, therefore, suggests that from the worst scenario when a fault occurs, the line connecting buses 22 and 23 should be removed to clear the fault. Furthermore, as presented in Table 3, the next ranked eigenvalue bus, connected to the critical bus, after Alaoji bus (bus 23) is Onitsha bus (bus 21). This implies that the network can easily be reinforced by placing the UPFC controller in series with the line which connects the most critical bus 22 and bus 2 (New Haven and Onitsha).

The impact of the multi-UPFC when the transmission line connecting New Haven and Alaoji (bus 22- bus 23) is removed is shown in Fig. 19. The results show that two more generators are caused to get into synchronism to make it a total of eight generators with reference to the generator at Egbin. Only one generator was thrown out of synchronism, and this shows a notable improvement in the system by reinforcing with multi-UPFC.
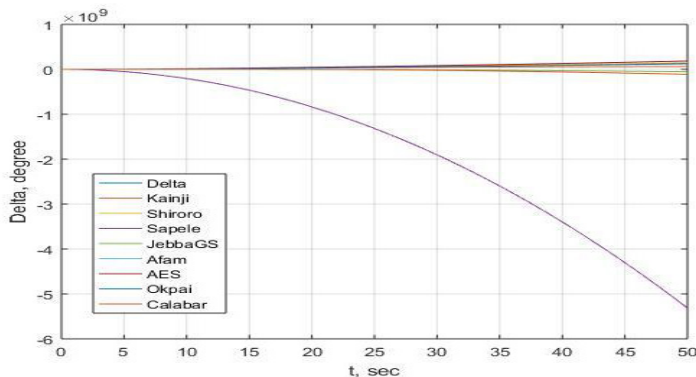
Figure 19: Transient stability for the phase angle difference with line 22-23 removed

When the generator bus at Sapele, which is out of synchronism with the critical line (line 22-23) is removed, a phase difference of -5.2o (as against -10.75o of the base cases) is obtained. This is evidence of the improved stability of the Nigerian 28-bus power network by reinforcing with the multi-UPFC controller.

5. Conclusion

In this paper, the influence of FACTS device integration on the assessment and enhancement of power system transient stability, in topologically weak power networks, have been presented. An extensive review of the existing studies on various approaches for solving the problem has been presented. The theoretical framework, as well as the mathematical formulations required for the analysis, are presented. Based on the mathematical formulations presented, a non-iterative based technique, which identifies the critical parts of the network where FACTS devices could be suitably located, for reinforcement of weak network, is

suggested. The multi-UPFC is employed for this purpose in this study. The standard IEEE 5-bus and 30-bus, as well as the Nigerian 28-bus networks, are used as case studies in order to test the effectiveness of the method suggested in this study. The results obtained before and after the integration of UPFC are compared. From the comparison of results obtained, it is clearly revealed that the UPFC also has a great influence on the simulation times. More conclusively, this study has shown that the integration of FACTS devices into a power system is effective for improving transient stability when the system faults occur in any part of the system. It is shown, in this study, that the integration of FACTS Devices reduces, to the barest minimum, the total time taken for the system to regain balance and return to its normal operating conditions without experiencing system collapse.

Conflict of Interest

The authors declare no conflict of interest.

Acknowledgment

References

[1] A. Halder, N. Pal, D. Mondal, "Transient Stability Analysis of a Multimachine Power System with TCSC Controller – A Zero Dynamic Design Approach," International Journal of Electrical Power and Energy Systems, **97**, 51-71. 2018, doi:10.1016/j.ijepes.2017.10.030.

[2] C. Zambrano, S. Arango-Aramburo, Y. Olaya, "Dynamics of power-transmission capacity expansion under regulated remuneration," International Journal of Electrical Power and Energy Systems, **104**, 924-932. 2019, doi:10.1016/j.ijepes.2018.07.029.

[3] A. AL Ahmad, R. Sirjani, Optimal placement and sizing of multi-type FACTS devices in power systems using metaheuristic optimisation techniques: An updated review, Ain Shams Engineering Journal, 2019, doi:10.1016/j.asej.2019.10.013.

[4] T.S. Shomefun, A. Ademola, C.O.A. Awosope, A.I. Adekitan, "Critical review of different methods for siting and sizing distributed-generators," Telkomnika (Telecommunication Computing Electronics and Control), **16**(5), 2018, doi:10.12928/TELKOMNIKA.v16i5.9693.

[5] A.S. Alayande, A.A.G. Jimoh, A.A. Yusuff, "Reinforcement of Topologically Weak Power Networks Through Network Structural Characteristics Theory," International Journal of Emerging Electric Power Systems, 2018, doi:10.1515/ijeeps-2017-0219.

[6] T.H. Sikiru, A.A. Jimoh, Y. Hamam, J.T. Agee, R. Ceschi, "Classification of networks based on inherent structural characteristics," in Proceedings of the 2012 6th IEEE/PES Transmission and Distribution: Latin America Conference and Exposition, T and D-LA 2012, 2012, doi:10.1109/TDC-LA.2012.6319055.

[7] K. Karthikeyan, P.K. Dhal, "Optimal Location of STATCOM based Dynamic Stability Analysis tuning of PSS using Particle Swarm Optimization," in Materials Today: Proceedings, 2018, doi:10.1016/j.matpr.2017.11.122.

[8] B. Vijay Kumar, V. Ramaiah, "Enhancement of dynamic stability by optimal location and capacity of UPFC: A hybrid approach," Energy, 2020, doi:10.1016/j.energy.2019.116464.

[9] K. Karthikeyan, P.K. Dhal, "A Hybrid BBO-DE optimization with Eigen value analysis based transient stability improvement by coordinated design of SVC," in Materials Today: Proceedings, 2018, doi:10.1016/j.matpr.2017.11.207.

[10] A.A. Jimoh, T.H. Sikiru, I.G. Adebayo, A.S. Alayande, "Influence of loading conditions in solving power system problems," in 2014 Australasian Universities Power Engineering Conference, AUPEC 2014 - Proceedings, 2014, doi:10.1109/AUPEC.2014.6966597.

[11] M. Tostado, S. Kamel, F. Jurado, An effective load-flow approach based on

Gauss-Newton formulation, International Journal of Electrical Power and Energy Systems, 2019, doi:10.1016/j.ijepes.2019.06.006.

[12] M. Karimi, A. Shahriari, M.R. Aghamohammadi, H. Marzooghi, V. Terzija, Application of Newton-based load flow methods for determining steady-state condition of well and ill-conditioned power systems: A review, International Journal of Electrical Power and Energy Systems, 2019, doi:10.1016/j.ijepes.2019.05.055.

[13] H. Yang, F. Wen, L. Wang, "Newton-Raphson on power flow algorithm and Broyden method in the distribution system," in PECon 2008 - 2008 IEEE 2nd International Power and Energy Conference, 2008, doi:10.1109/PECON.2008.4762737.

[14] Modern Power Systems Analysis (Power Electronics and Power Systems) | Xi-Fan Wang, Yonghua Song, Malcolm Irving | download, Dec. 2020.

[15] T.H. Sikiru, A.A. Jimoh, J.T. Agee, "Inherent structural characteristic indices of power system networks," International Journal of Electrical Power and Energy Systems, 2013, doi:10.1016/j.ijepes.2012.11.011.

[16] T.E. Somefun, C.O.A. Awosope, A. Abdulkareem, A.S. Alayande, "Deployment of power network structural topology to optimally position distributed generator within distribution system," Journal of Engineering Science and Technology Review, **13**(1), 2020, doi:10.25103/jestr.131.2.

[17] A.S. Alayande, A.A. Jimoh, A.A. Yusuff, "An alternative algorithm for solving generation-to-load matching and loss allocation problems," International Transactions on Electrical Energy Systems, 2017, doi:10.1002/etep.2347.

[18] A.S. Alayande, A.A. Jimoh, A.A. Yusuff, "Solution to network usage allocation problem in power networks," in 2016 IEEE International Conference on Renewable Energy Research and Applications, ICRERA 2016, Institute of Electrical and Electronics Engineers Inc.: 719–725, 2017, doi:10.1109/ICRERA.2016.7884428.

[19] A.S. Alayande, A.A. Jimoh, A.A. Yusuff, "Identification of critical buses and weak transmission lines using inherent structural characteristics theory," in Asia-Pacific Power and Energy Engineering Conference, APPEEC, 2016, doi:10.1109/APPEEC.2015.7380974.

[20] P.K. Gouda, A.K. Sahoo, P.K. Hota, "Optimal power flow including unified power flow controller in a deregulated environment," International Journal of Applied Engineering Research, 2015.

[21] A.O. Melodi, B.O. Akinloye, "Transmission Capacity Enhancement for Nigerian Power Transmission Grid using TCSC and UPFC," **8**(2), 82–90, 2014.

[22] Akwukwuegbu IO, Nosiri OC, Agubor CK, Olubiwe M, "Comparative Power Flow Analysis of 28 and 52 Buses for 330KV Power Grid Networks in Nigeria Using Newton-Raphson Method," IJRERD International Journal of Recent Engineering Research and Development, Dec. 2020.

A S T E S

Open Energy Distribution System-Based on Photo-voltaic with Interconnected- Modified DC-Nanogrids

Essamudin Ali Ebrahim[1,*], Nourhan Ahmed Maged[1], Naser Abdel-Rahim[2], Fahmy Bendary[3]

[1]*Power Electronics and Energy Conversion Department, Electronics Research Institute, Cairo, 12622, Egypt*

[2]*Department of Electrical Engineering, Future University, Cairo, 12622, Egypt*

[3]*Department of Electrical Engineering, Faculty of Engineering at Shoubra, Benha University, Benha, 13511, Egypt*

A R T I C L E I N F O	A B S T R A C T
	This manuscript exhibits a perfect design for a flexible number of modified DC nanogrids within an open energy distribution network (OEDN) that interconnected via a DC bus. Each modified nano-grid implies a single-input multi-output switched boost inverter (SIMO-SBI). The DC-output for each inverter is robustly controlled to keep the DC-bus interconnected voltage constant. The proposed control uses model reference technique to defeat the non-linearity of the system. In addition, a control algorithm is proposed to manage the optimum power flow and increase the system reliability. The MATLAB/Simulink program is used in modelling and simulation of the suggested arrangement to achieve the robustness of the proposed OEDN with multiple 5-Kw interconnected nanogrids fed from photovoltaic (PV) arrays. Several simulation results are introduced for both open and closed loop control to verify the robustness and validity of the system against the main parameters' changes. In accession, the smoothing power flow between nanogrids indicates that the proposed algorithm for the controller is sophisticated and able to supervise the power among all nanogrids of an OEDN.

1. Introduction

AC generation, distribution and transmission for long distances had been in existence for even more than a century with the high spread for the AC loads in the markets [1].

Conventional AC grid depends mainly on traditional energy sources - such as oil, coal and natural gas - that are permeable and polluting the environment. Also, this classical grid uses a centralized control system that is sensitive to any fault occurrence and cause an outage for the whole network such as New York blackout in Aug. 2003. So, decentralized control techniques are good solutions for this traditional network [2].

Renewable energies such as solar, wind, geothermal, biomass are environmental friendly distributed generation (DG) resources. Most of these renewable resources such as photovoltaic systems and fuel cells produce a DC output power that can directly feed to the DC loads without AC conversion. Unfortunately, the generated power from those renewable resources is limited and intermittent. These small-rated resources can be classified according to its rating capacity as: mini grid rate from 50 kW to 1.5 MW, micro grid rate from 5 kW to 50 kW, nano grid rate from 1.5 kW to 5.0 kW, and the smallest one is a pico grid rate less than 1.5 kW [3].

These compact DC grids can be interconnected with each other via a simple-configuration DC bus instead of AC interconnections. DC-interconnection don't need to synchronization, quickly integrated with distributed generation (DG), and no skin effect for transmission lines [4].

Classical DC nano-grid has large numbers of two-stage converter-inverter set. The interconnection of this combined set causing some problems such as communication interference with noise. In addition, the main disadvantage of the two-stage converter-inverter set is that it needs to be protected against overlapping of the two inverter-switches on the same arm [5].

The authors in [6-8] described a new modified model for the DC nanogrid with the help of single-input multi-output switched boost inverter (SIMO-SBI). It improves the system efficiency and increase its reliability. In addition, it produces simultaneously DC and AC voltages in a single stage.

In [9], the authors presented a complete analysis for SBI, control circuits, and open-loop control strategy fed from photovoltaic (PV) generator was proposed. Also, in [10], The authors proposed a closed-loop control technique to ensure the robustness of the system against main parameter variations. In addition, the authors introduced a buck-boost converter as a host controller for a battery management system utilized within an autonomous nanogrid.

So, this study is an extension of the previous work of references [9, 10] as a part of an internal research project at Electronics Research Institute, Egypt. It utilizes the features of DC-interconnection to join between several autonomous nanogrids within an OEDN. Before interconnection, a model reference robust control scheme is tested to keep the interconnection dc-link voltage constant. Also, a sophisticated control algorithm is proposed for power management between two-interconnected nanogrids as a case study. This guarantees an optimal and smooth bi-directional power flow between nanogrids even though one of them has been disrupted. This algorithm depends mainly on load demands for each nanogrid. The performance and robustness of the proposed system is tested after modelling and simulation of mathematical models with the help of Matlab/ Simulink software program. Test results ensure the robustness of the proposed system against parameter variations and the validity of the proposed system to be applied for several off- or on-grid DC interconnection.

This manuscript is organized as follows: section 2 compares between the classical AC grid and the OEDN. But, section 3 involves the proposed interconnection of multiple modified DC nanogrids within an OEDN. Section 4 discusses the single input - multi output switched boost inverter (SBI) topology with its open and closed loop algorithms. Section 5 introduces the design of the proposed OEDS as a case study. It also includes the test results of the proposed OEDN control technique to evaluate its performance and check the robustness against load variations. Finally, section 6 is the conclusion.

2. The Classical AC Network via OEDN

There are three stages in the AC-grid cycle: generation, transmission, and utilization. If a fault occurs in any part of this network, it will cause a trip for the whole system. Moreover, the classical power grid can't accommodate the rapid rise in electricity demand. It is also unyielding to promote the introduction of clean energy or other types of technology that will make it more competitive. To solve these mentioned problems, figure 1 proposes some guides. It also shows that the valuable solution for delivering effective, sustainable, safe and reliable power to the customer is the decentralized renewable grids. So, this paper introduces one of these solutions by interconnecting nanogrids with each other's via a DC link to form an open energy distribution network (OEDN) [4] as described in Figure 2.

The OEDN is a modern type of the decentralized network that described by building up several numbers of interconnected modified DC nanogrids via a local DC power bus and managed in a distributed way to form a reliable OEDN [4]. The authors in

In [11, 12], the author studied the main advantages of interconnecting grids. They also proposed a multi-level grid system in the form of interconnecting renewable energy microsystems.

So, this framework proposed an alternate control mechanism for interconnecting scattered modified islanded nanogrids to form a complete OEDN. Table 1 shows a comparison between a single designed nanogrid system and a complete OEDN.

The OEDN gives many benefits rather than the separated single DC nanogrid as it improves the grid performance and guarantees stability of the system. It ensures the continuity of the load feeding even though one of the nanogrid had been disrupted. Since, this allows a power management through nanogrids to all loads without interruption from other available nanogrids [11]. The OEDN structure relies on the two main DC layers [4]. The first layer implies a group of interconnected modified DC nanogrids based-on the single input-multi output switched boost inverter (SBI). And the second layer is a DC power bus that interconnects nanogrids to each other. The DC links are chosen for both levels due to their advantages such as: the DC link is more simpler to integrate than the AC link. The DC link makes mathematical model analysis simpler since there is no need for synchronization (no frequency, no phase shift and no AC-complex control). In addition, the DC link increases the reliability of the transmission lines and enhances the safety of the grid due to lack of reactive power [11].
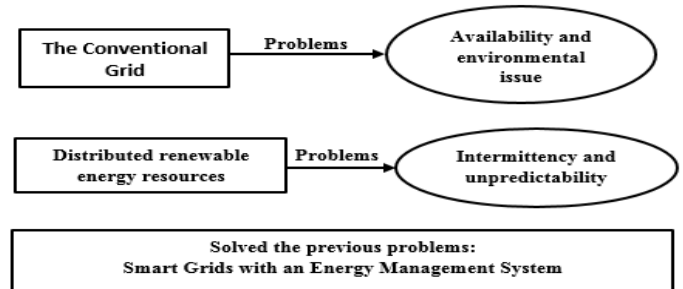
Figure 1: several problems with solutions for the classical grid
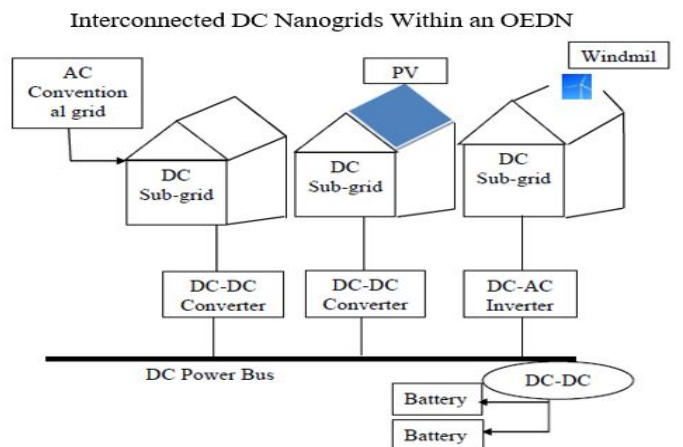
Figure 2: The structure of interconnected DC Nano grids within an OEDS

3. A Modified DC-Nanogrid against Traditional One

The standard DC nano-grid requires a 2-stage AC-DC power conversion system to support both DC and AC loads. So, its

design has several challenges as it involves a great number of converters and inverters, as seen in Figure 3. Moreover, different separated security and control algorithms are needed for each stage. This series of conversions rises the system total cost and losses.

But on the other hand, a single-stage conversion system was proposed to overcome some drawbacks mentioned in the standard one. Those updated nanogrids are modified with few numbers of conversion stages [12-14].
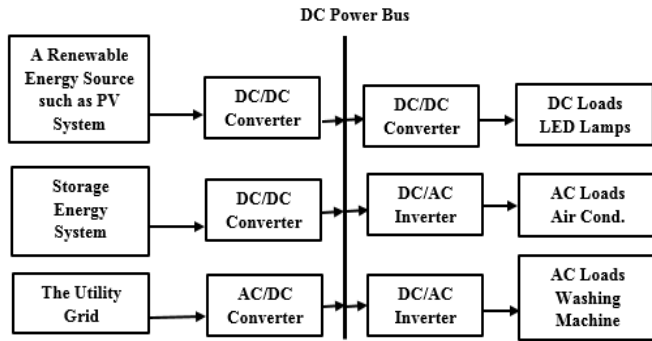
Figure 3: The standard nanogrid structure

Table 1: Show a comparison between OEDN and single nanogrid system

An OEDS	Single nanogrid
Power generated is uncentralized	Power generated at the end user
50 – few hundred households	Less than 50 households
Coverage ranges from a few hundred meters to 1-2 kilometres	Coverage ranges less than 100 metres
Need a few large numbers of DC / AC conversion sets	A few numbers of DC/AC inverters are required

4. A Single Input Multi Output - Converter

The suggested modified DC nanogrid system is based on a single entry switched boost inverter (SBI) as shown in figure 4. SBI is a single-stage power converter capable of providing DC and AC loads simultaneously from the same DC input voltage. It can also provide an output AC voltage whether higher (boosting) or lower (bucking) than its DC input voltage. It prevents noise due to electromagnetic interference (EMI) compared with the classical two stage power converters [14]. Moreover, SBI doesn't need to a dead time circuit as its operation technique depends on the shoot-through state. The SBI operation is originated its basic concept from the Inverse Watkins topology and the Z-source inverter (ZSI) operating idea. But, the SBI has many benefits compared with the ZSI - as explored in table 2 [15-19].

4.1. Topology of a Single Stage Switched Boost Inverter

The circuit diagram of the SIMO-SBI contains five IGBT switches, two passive elements (an inductor (L) with capacitor (C)), two diodes (D_a, D_b), and a low pass LC passive filter is connected across the AC output of the inverter to mitigate un-desirable harmonic components as shown in figure 5. SBI has

two operating modes non-shoot through state mode and shoot through state mode. The AC Output voltage of the SBI can be controlled by the following equations:

$$V_{AC} = M.V_{DC} \qquad (1)$$

$$V_{AC} = M. (1-D/1-2.D).V_G \qquad (2)$$
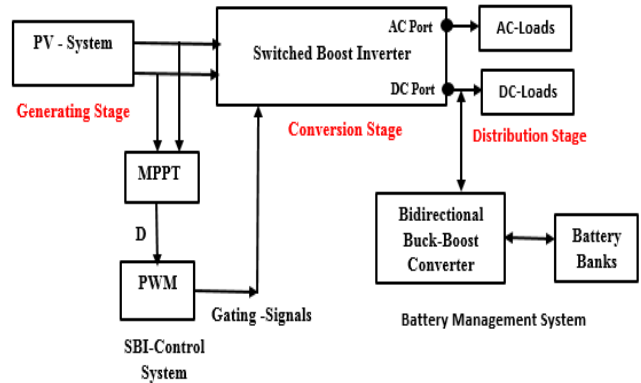
Figure 4: Block diagram for the suggested modified DC nanogrid

Table 2: Comparison between ZSI and SBI

SIMO Inverters	Active Switches	Reactive switches	Noise Interference	Accuracy
SBI	More	Less	Less	More
ZSI	Less	More	More	Less
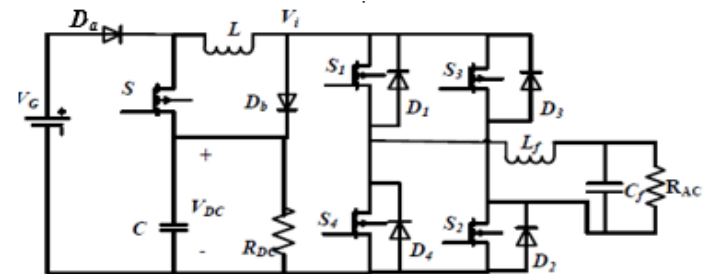
Figure 5: The Circuit diagram of the SIMO-SBI

So, M and D are chosen in such a way to control its peak output AC voltage V_{AC}. Also, the sum of shoot-through duty ratio (D) and the modulation index (M) should be less than or equal to unity, i.e.

$$M + D \leq 1 \qquad (3)$$

4.2. Open Loop Control Algorithm for a SIMO-SBI

The SBI open loop control technique derives its basic idea from the traditional sinusoidal pulse width modulation (PWM) technique. But, the standard PWM scheme should be changed in order to allow use of its shooting-through mode territory. So, this new approach has been used during the positive and negative half periods of the sinusoidal modulation signal Vm (t). The SBI open loop control algorithm was discussed in details in [9, 20]. SBI doesn't need to a dead time circuit in its operation technique. On the other hand, its main drawback was summarized in its limiting duty ratio (D) (0-0.5) which cause high harmonics in its output voltages when the duty ratio gets closer to the end of the range (0.4 - 0.5).

Figures 6 and 7 are included as samples in the process of main-parameter changes manually for SBI to adjust its performance before interconnection. Figure 6 demonstrates the performance of the switched boost inverter as a buck converter to obtain an AC output voltage less than its DC input at duty ratio equal 0.22.
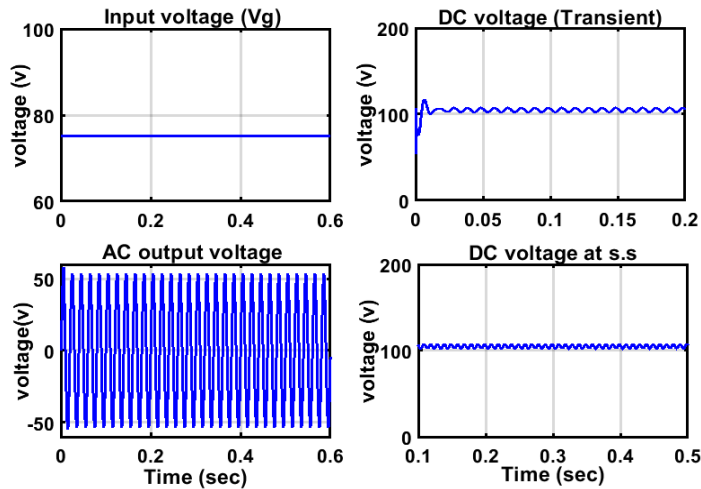
Figure 6: The SBI operation in a bucking mode (with D=0.22)
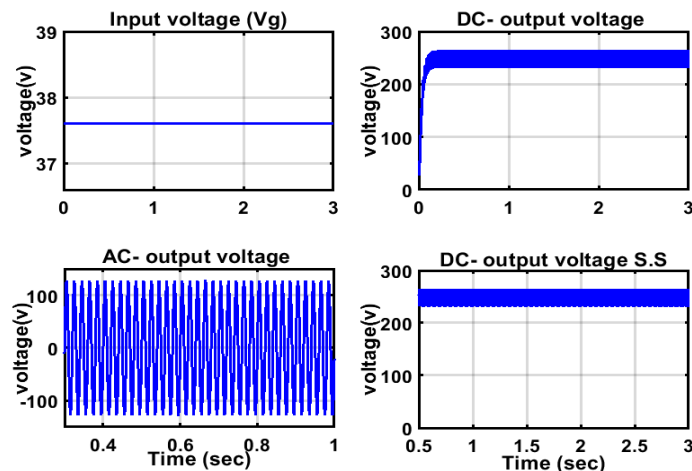
Figure 7: The SBI operation in a boosting mode with (D=0.4515)

While, figure 7 illustrates the performance of the inverter as a boost converter and to raise AC output voltage higher than its DC input with a duty ratio equal 0.4515. So, the robust closed loop control should be used to maintain the SBI output voltages constant, especially through the critical range of the duty ratio (0.4 – 0.5).

4.3. Closed Loop Control Algorithm for a SIMO-SBI

The purpose of the closed loop control is to keep the system stable even after it has been subjected to a certain variety. The output of the inverter is highly sensitive to any slight change in its duty ratio [19].

As, the output of the inverter will go to infinity if the system duty ratio (D) is 0.5. And the system output is observed to be erratic with a very high percentage of harmonics when its duty ratio becomes closer to 0.45. So, the system DC output voltage of

the SBI should be controlled by using a robust closed-loop control algorithm to keep it constant.

This control algorithm is mainly depending on comparing the DC output voltage and the DC reference voltage and the resulting error is managed by a PID control strategy. The PID controller was chosen due to its simplicity, easy in continuous tuning, provides good stability, and rapid response. The parameters of the PID controller were designed based on the Ziegler-Nichols formulas. The proportional, integral, and derivative gains are selected as [20]:

$$K_P = 5 \times 10^{-7}, K_I = 5 \times 10^{-7}, K_D = 1 \times 10^{-6}$$

The output of this controller is used to readjust the PWM pattern applied to the inverter switches. This controller strategy is applied to overcome the disadvantages of the inverter and to monitor its DC output value. As a consequence, its AC output voltage will regulate according to Equation 2, at a constant modulation index (M=0.5), as discussed in details in [10].
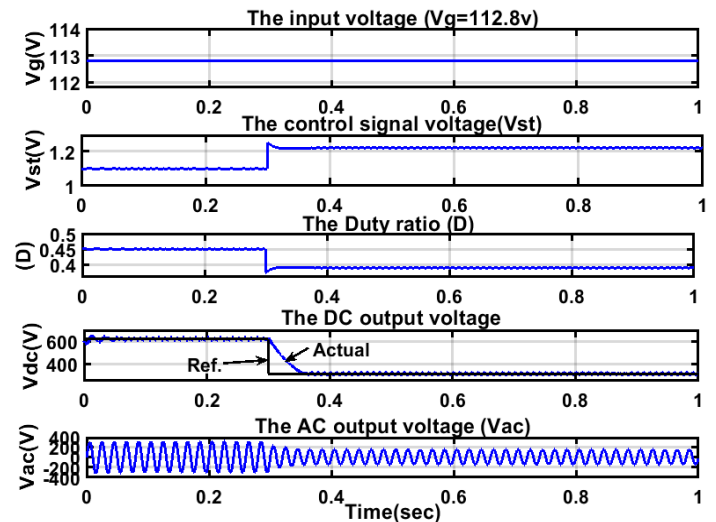
Figure 8: The input voltage, control signal, the duty ratio, the DC/AC output voltages respectively by decreasing the reference voltage from 622 to 311v.
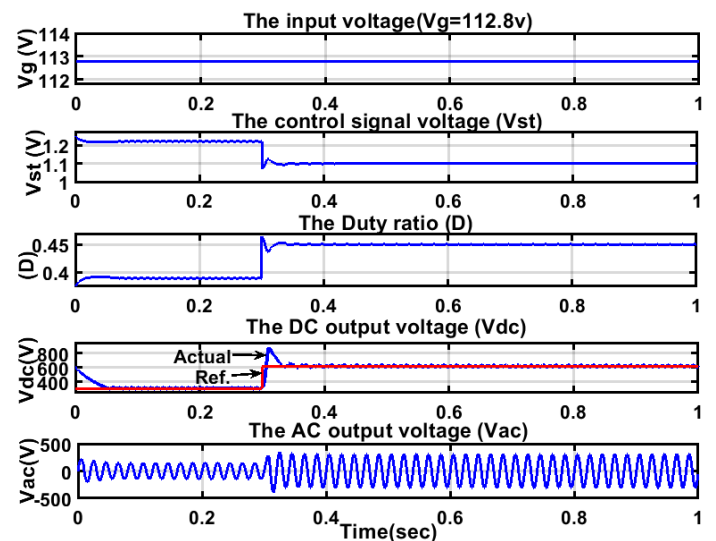
Figure 9: the input voltage, control signal, the duty ratio, the DC/AC output voltages respectively by increasing the reference voltage from 311 to 622v.

For insurance of the robustness of the controller in maintaining the DC-link voltage constant before interconnection the following sample figures test the time response of the closed loop control under disturbances. Figures 8 ,9 demonstrates the system response to the sudden increase/ decrease in the DC reference output voltage of the SBI (V_{ref}) from (622 to 311 V) and vice versa (with step time 0.3). This robustness of the controller keeps the inverter DC output voltage constant. This can be achieved for each interconnected modified DC nanogrid to form a complete stable OEDN.

Hence, each proposed modified DC nanogrid in the OEDN contains solar photovoltaic (PV) arrays supply as a renewable energy distributed generation (DG). Although PV is a clean, pure, natural replenished resource, and environmental friendly, but also is an intermittent resource that is very sensitive to the sun's heat, temperature, humidity and climatic conditions. So, this standalone system will require a power storage scheme such as batteries to retain the excess energy produced from the renewable PV systems. Also, storage system supplies energy in the load peak hours, or through nights and cloudy days.

However, the battery storage system is connected to the system via a bi-directional buck-boost converter that control the battery loading / unloading algorithm. This converter interconnects between both sides of the SBI DC-bus and the lead acid battery banks. This will happen during the charging process of the battery bucking the voltage of DC-link from 622 V to 240V of the battery-bank voltage. On the other hand, through discharging process, it operates as a booster to raise battery voltage form 240V to the DC-link voltage (i.e., 622V). This process can be achieved through a sophisticated algorithm discussed in [10, 20]. This technique guarantees consistency of operation of the scheme without a lack of load requirements. The block diagram for the battery management system is shown in figure 10.

5. The Open Energy Distribution Network (OEDN) Control Algorithm

The SBI robust closed loop control technique allows to maintain the DC-nanogrid output voltages constant under different system operating conditions. It allows for smooth power transfer from one nanogrid to another by applying a simple additional control algorithm to manage the load demands [21,22]. The OEDN control algorithm is depending on a bi-directional controlled-switch that is used to allow power flow between the adjacent nanogrids as seen in Figure 11.

In the proposed system, the control signal turns the switch Sng1 on when any of either the DC or AC load requirements of nanogrid 1 is lower than that obtained from its PV source. So, The Sng1 is turned on to allow the excess power to transfer easily and smoothly from grid 1 to grid 2. While, the control signal turns the switch Sng2 on when any of either the DC or AC loads requirements of nanogrid 2 is lower power than that obtained from its PV source.

In other words, nanogrids with different values of generated power will able to transfer excess power between them according to load demands. As a consequence, this control algorithm allows the smooth flow of excess power from one grid to another. The

regulation of the working switches is relying mainly on the signal from the output of the comparator control algorithm is facilitating the energy swap between several interconnected nanogrids in an OEDN. Figure 12 introduced the control schematic diagram and Figure 13 provides in details the flow chart for this proposed algorithm.
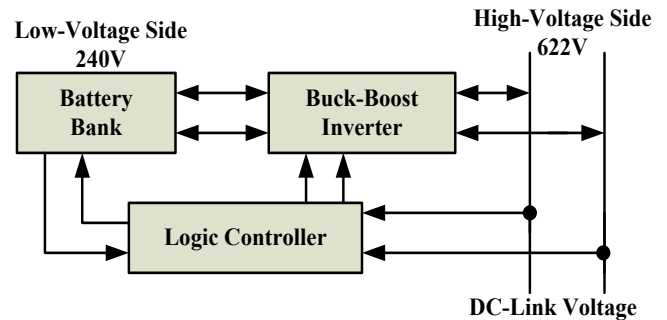
Figure 10: Battery management system
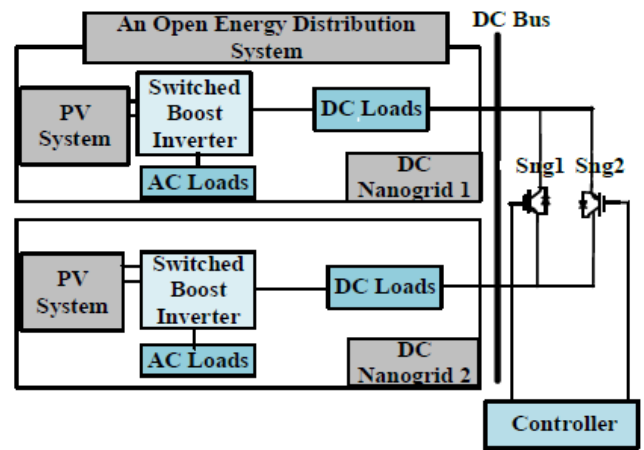
Figure 11: The block diagram for an OEDS control system
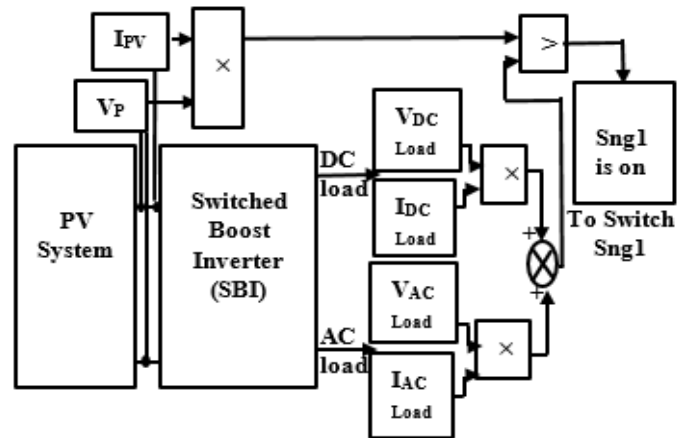
Figure 12: The two interconnected nanogrids control algorithm

5.1. Case study: an OEDN-based two DC-nanogrids

The following results introduce the efficiency of the proposed OEDN control algorithm to operate stably under various conditions. They also demonstrate the performance of the SBI output voltages with its rigorous robust closed loop control

technique. Matlab / Simulink software package was used in modelling and simulation of the proposed system [23].
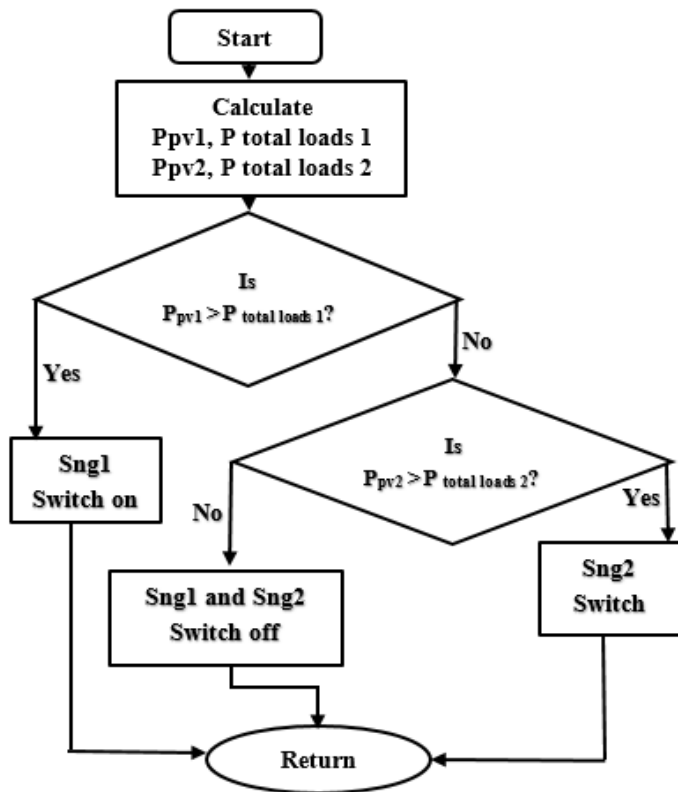
Figure 13: The OEDS controller flow chart

The Following test results demonstrate the system robustness under different conditions. Figures 14 and 15 show the flow of power in a full OEDN with two interconnected grids from separate solar generators. All nanogrids are energized from independent solar generators with checking stability of the overall control system under any fault conditions within the same OEDN. Each figure shows the AC, DC output and the total load powers for the two DC-interconnected nanogrids within an OEDN .

Figure 14 shows that the generating power of one grid PV source is 6 kW and 4.5 kW for other. If the load of the first one will consume the full power in the first 0.4 sec. Then, if the power of that load are distributed abruptly and minimizing its consumption to just 4.5 kW. At the same time, the demands of the other load in (NG2) increased and need to this excess power to its load.

So, the extra power of the first nanogrid will transfer in the same time to the load of other grid to compensate the power shortage. At this instant (i.e., t=0.4 Sec.), the demand power for other grid will be increased to 1.5 kW. As a sequence, figures 14 ((a) and (b)) represents the AC and DC output powers of both interconnected nanogrids followed by the total load power with their different requirements at 0.4 sec (as shown in figure 14c).

While, figure 15 shows two other nanogrids with different generating powers. As, the first nanogrid with a PV source of rating 6.5 kW. The utilities of this nanogrid consume all power through 0.4 sec. Then, Its consumption is reduced to just 5.5 kW. So, the extra power of the first nanogrid will transfer in the same

time to satisfy the shortage of power in the other nanogrid loads. The previous two cases ensured the system ability of the exchange power stably between the interconnected modified DC nanogrids in an OEDN.

Note: if there is a surplus power from Ng1 and Ng2, then this excess power will be transferred to the battery banks for storage and emergency use.
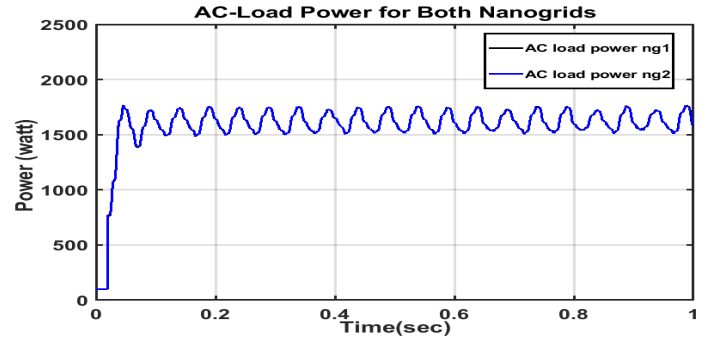
(a) The power consumed by AC- loads for both nanogrids
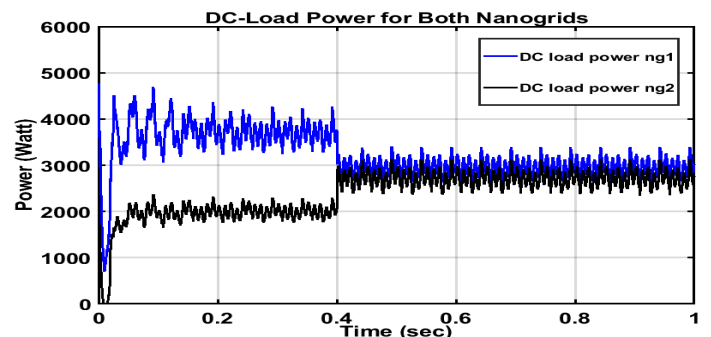
(b) The power consumed by DC- loads for both nanogrids
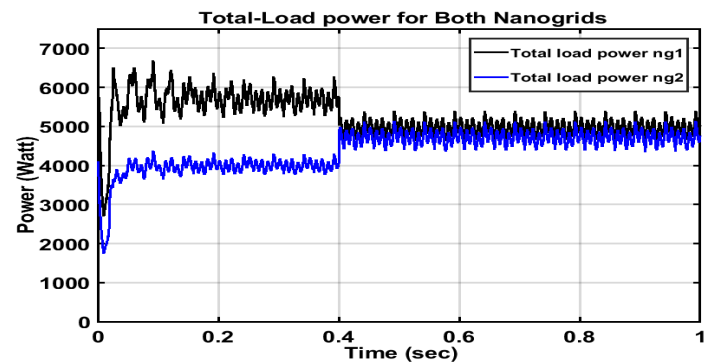
(c)The total interconnected power transferred for both nanogrids

Figure 14: AC,DC and total power of the two PV-based nano-grids with rated generated power of values 6 and 4.5 kW respectively

6. Conclusion

This paper explored the importance of the DC interconnection and DC distribution systems. It identified a perfect design for the OEDN with interconnected DC grids. A bi-directional robust control technology was introduced to assure an efficient energy transmission between the linked DC nanogrids. It guarantees the system optimum operation even if any of the grid generating sources are cut off. Thusly, it converted the centralized scheme to a decentralized one with high reliability of mental process.

Moreover, The modified, adapted SIMO power electronic SBI with its adaptive monitoring control system was carried out in each nano-grid. It tends to ameliorate the performance of the inverter by adjusting its outputs to high levels. In this mode, it allows the AC output voltages to be grown to a value (220 V rms) which is suitable for the loads in EGYPT.

Also, DC-interconnection among nanogrids is suitable and efficient more than AC in the two cases (autonomous off – and on-grid) systems.
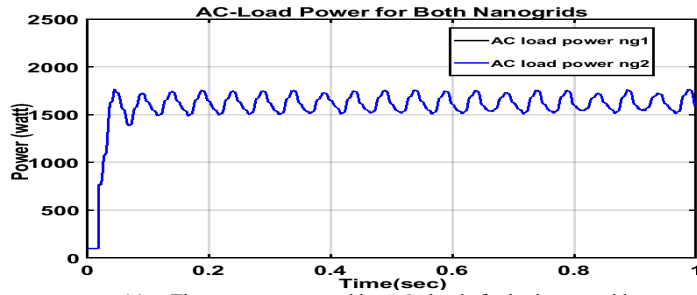
(a)   The power consumed by AC- loads for both nanogrids
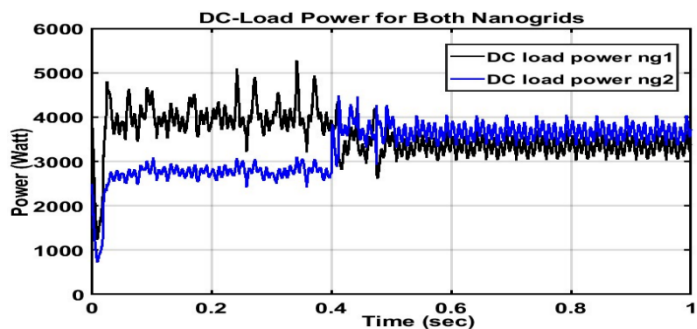
(b)   The power consumed by DC- loads for both nanogrids
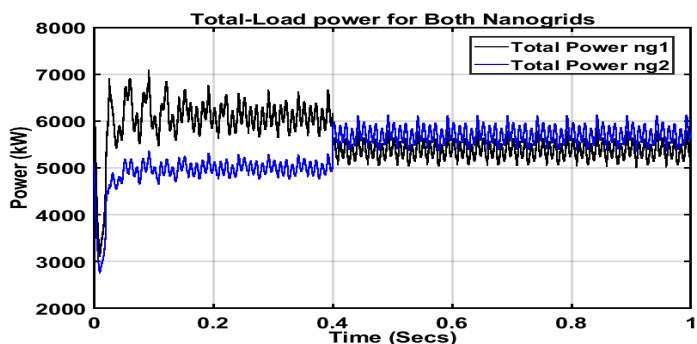
(c)   The total interconnected power transferred for both nanogrids

Figure 15: AC,DC and total power of the two PV-based nano-grids with rated generated power of values 6.5 and 5 kW respectively

Conflict of Interest

The authors declare no conflict of interest.

Acknowledgment

References

[1] P. Asmus, "Microgrid, virtual power plants and our distributed energy future," The Electricity Journal, **23**(10), 72–82, 2010, doi: 10.1016/j.tej.2010.11.001.

[2] A. Raheem, S.A. Abbasi, A. Memon, S.R. Samo, Y. H. Taufiq-Yap, M.K. Danquah, R. Harun, "Renewable energy deployment to combat energy crisis in Pakistan.," Energy, Sustainability and Society, **6**(1), 1-13, 2016,

doi: 10.1186/s13705-016-0082-z.

[3] C. Marnay, B. Nordman, J. Lai, "future roles of milli-micro and nano-grids," CIGRÉ International Symposium, the Electric Power System of the Future-Integrating Super-Grids and Microgrids, Bologna, Italy, 2011.

[4] A. Werth, N. Kitamura, K. Tanaka, "conceptual study for open energy systems: distributed energy network using interconnected DC nanogrids," IEEE Transactions on Smart Grid, **2**(4), 1621- 1630, 2015, doi:10.1109/TSG.2015.2408603.

[5] R. Adda, O. Ray, S. Mishra, "implementation and control of switched boost inverter for DC nano-grid applications", IEEE Energy Conversion Congress and Exposition, USA, 15-20, 2012, doi: 10.1109/ECCE.2012.6342289.

[6] D. Burmster, R. Rayudu, W. Seah, D. Akinyele, "A review of nanogrid topologies and technologies," Renewable and Sustainable Energy Reviews, **67**, 760-775, 2017, https://doi.org/10.1016/j.rser.2016.09.073.

[7] O.D. Castle, A. El Shahat. "Single-input-multi-output (SIMO) converter for nano-grids applications," South east Con IEEE, 1-5, 2017, doi: 10.1109/SECON.2017.7925282.

[8] R.Adda, O. Ray, S. Mishra," synchronous-reference-frame-based control of switched boost inverter for standalone DC nanogrid applications," IEEE Transactions on Power Electronics, **3**(28), 1219-1233, 2013, doi: 10.1109/TPEL.2012.2211039.

[9] E. A. Ebrahim, N.A. Maged, N. Abdel-Rahim, F. Bendary, "a novel approach of a single input multi output switched boost inverter," JEE Journal of Electrical Engineering, **3**(3), 90-101, 2018, Corpus ID: 220422035.

[10] E. A. Ebrahim, N.A. Maged, N. Abdel-Rahim, F. Bendary, "Closed-loop Control of a Single-Stage Switched-Boost Inverter in Modified DC-Interconnected Nano-grids," IET, The Journal of Engineering (JoE), **2020**(10), 843-853, 2020, doi: 10.1049/joe.2019.1248.

[11] M. C. Falvo, L. Martirano, "From smart grids to sustainable energy microsystems," Proc. 10th Int. Conf. Environ. Elect. Eng., Rome, Italy, May 2011, doi: 10.1109/EEEIC.2011.5874756.

[12] M. Brenna, M. Falvo, F. Foiadelli, L. Martirano, D. Poli, "sustainable energy microsystem (SEM): preliminary energy analysis," IEEE PES Innov. Smart Grid Technol. (ISGT), Washington, DC, USA, 1–21, 2012, doi: 10.1109/ISGT.2012.6175735

[13] A.S. Shilpa, H.V. Shetty," Switched Boost Inverter with PWM Control and Development of a Prototype Model," International Journaln of Advanced Research in Electrical , Electronic and Instrumentation Engineering, **8**(3), 2014. doi: 10.15662/ijareeie.2014.0308011

[14] R. Adda, S. Mishra, A. Joshi, "A PWM Control Strategy for Switched Boost Inverter," IEEE Energy Conversion Congress and Exposition (ECCE), 991-996, 17 Sep. 2011, doi: 10.1109/ECCE.2011.6063880.

[15] P.C. Loh, D.M. Vilathgamuwa, Y.S. Lai, G.T. Chua and Y. Li, "Pulse-Width Modulation of Z-Source Inverters," IEEE 39th IAS Annual Meeting. Conference in Industry Applications Conference, **20**(6), 1346 – 1355, 2004, doi: 10.1109/IAS.2004.1348401.

[16] B. Ebrahim, M.H. Nozadian, E.S. Asl and S. Laali. "Developed embedded switched-Z-source inverter," IET Power Electronics, **9**(9), 1828-1841, 2016. doi: 10.1049/iet-pel.2015.0921.

[17] Y. Huang, M, Shen, FZ. Pengand and J. Wang, "Z -Source Inverter for Residential Photovoltaic Systems," IEEE Transactions on Power Electronics, **3**(6), 1776-1782, 2006, doi: 10.1109/TPEL.2006.882913.

[18] J. Liu, J. Hu, L. Xu, "Dynamic Modeling and Analysis of Z - Source Converter—Derivation of AC Small Signal Model and Design-Oriented Analysis," IEEE Transactions on Power Electronics, **7**(5), 1786-96, 2007, doi: 10.1109/TPEL.2007.904219.

[19] M.K. Nguyen, Y.C. Lim, S.J. Park, "A Comparison between Single-Phase Quasi- Z-Source and Quasi-Switched Boost Inverters," IEEE Transactions on Industrial Electronics, **62**(10), 6336-6344, 2007, doi: 10.1109/TIE.2015.2424201.

[20] N.A. Maged, DC-based energy distribution system for Inter-connected nano-grids, M.Sc. thesis, Benha University, Egypt, 2018.

[21] E. A. Ebrahim, N.A. Maged, N. Abdel-Rahim, F. Bendary, Photovoltaic-Based Interconnected-Modified DC-Nanogrids within an Open Energy Distribution System.," 6th International Conference on Advanced Control Circuits and Systems (ACCS) & 2019 5th International Conference on New Paradigms in Electronics & information Technology (PEIT). IEEE, 253-258, 2019, doi: 10.1109/ACCS-PEIT48329.2019.9062843.

[22] E. A. Ebrahim, N.A. Maged, N. Abdel-Rahim, F. Bendary, " DC-Based Interconnected-Modified Nanogrids within an Open Energy Distributed System (OEDS)," CIRED conference, 25th International Conference on Electricity Distribution, 2019, http://dx.doi.org/10.34890/992.

[23] Math Works, Matlab / Simulink User's Guide, Math Work Co., USA, 2014.

Classifying Garments from Fashion-MNIST Dataset Through CNNs

Alisson Steffens Henrique[*,1], Anita Maria da Rocha Fernandes[2], Rodrigo Lyra[2], Valderi Reis Quietinho Leithardt[3,4], Sérgio D. Correia[3,4], Paul Crocker[5], Rudimar Luis Scaranto Dazzi[2]

[1]*Master in Applied Computing, Univali, School of the Sea Science and Technology, Itajaí, 88302-901, Brazil*

[2]*Laboratory of Applied Intelligence, School of the Sea Science and Technology, Itajaí, 88302-901, Brazil*

[3]*VALORIZA, Research Center for Endogenous Resources Valorization, Instituto Politécnico de Portalegre, 7300-555 Portalegre, Portugal*

[4]*COPELABS, Lusófona University of Humanities and Technologies, Campo Grande 376, 1749-024 Lisboa, Portugal*

[5]*Departamento de Informática, Universidade da Beira Interior, Instituto de Telecomunicações, Delegação da Covilhã, 6201-601 Covilhã, Portugal*

A B S T R A C T

Online fashion market is constantly growing, and an algorithm capable of identifying garments can help companies in the clothing sales sector to understand the profile of potential buyers and focus on sales targeting specific niches, as well as developing campaigns based on the taste of customers and improve user experience. Artificial Intelligence approaches able to understand and label humans' clothes are necessary, and can be used to improve sales, or better understanding users. Convolutional Neural Network models have been shown efficiency in image classification. This paper presents four different Convolutional Neural Networks models that used Fashion-MNIST dataset. Fashion-MNIST is a dataset made to help researchers finding models to classify this kind of product such as clothes, and the paper that describes it presents a comparison between the main classification methods to find the one that better label this kind of data. The main goal of this project is to provide future research with better comparisons between classification methods. This paper presents a Convolutional Neural Network approach for this problem and compare the classification results with the original ones. This method could enhance accuracy from 89.7% (the best result in the original paper, using SVM) to 99.1% (with a new cnn model called cnn-dropout-3).

1. Introduction

This paper is an extension of work originally presented in the Iberian Conference on Information Systems and Technologies [1].

The fashion market has changed dramatically over the last 30 years, resulting in an evolution in that industry [2]. Understanding customer tastes and better-directing sales are the way to increase profit [3].

The rise of internet business lets people buy their clothes through websites, faster and easier. The introduction of methods to improve user's experience when searching for items in these platforms is decisive [4].

Classifying clothes is part of the broad task of classifying scenes [5–9]. The automatic generation of image labels that describe those products can alleviate human annotators' workload [10]. This kind of information may also help labeling scenes and better understanding users' tastes, culture, and financial status [5].

In [11], the authors present Fashion – MNIST data set based on images from Zalando, which is the Europe's largest online fashion platform. Fashion MNIST has 70,000 products with 28x28 pixel grey scale images divided into 10 categories: t-shirt, trouser, pullover, dress, coat, sandals, shirt, sneaker, bags and ankle boots.

[*]Corresponding Author: Alisson Steffens Henrique, ash@edu.univali.br

Those images were formerly thumbnails on their web store. This dataset is widely used in Artificial Intelligence (AI) benchmarks, and it is preloaded in Keras [12].

The original work used different AI models on this dataset to discover which one is better suited for the data labeling [11]. The evaluated implementations (from scikit-learn) were: Decision Tree, Extra Tree, Gaussian Naive Bayes, Gradient Boosting, k Neighbors, Linear Support Vector Classification, Logistic Regression, Multilayer Perceptron, Passive Aggressive Classifier, Perceptron, Random Forest, Stochastic Gradient Descent and Support Vector Classification. Their best result was using SVM, and they could achieve 89.7% of accuracy.

CNNs can have better results when compared to SVM [13]. Knowing that, this paper proposes the use of Convolutional Neural Networks (CNN) to label FashionMNIST dataset. The main goal is to compare those results with the original one, providing future research to be able to easily choose the most suitable classification method. In this paper, we present the development of four different CNN models and compared the results with the original ones. Our original work [1], used these four models with TensorFlow 1 (TF1) to get the results. Now, we present this extension using TensorFlow 2 (TF2) and GPU computing (with tensorflow-gpu and keras).

2. Background

2.1. Feature Learning

Machine Learning refers to computer systems capable of learning and modifying their behavior, in response to external stimuli or through experiences accumulated during their operation [14].

The main objective of Machine Learning is to generalize beyond the existing examples in training set, because regardless the amount of existing data, it is very unlikely that during the tests, the same examples will appear [15].

Conventional Machine Learning techniques are limited to processing natural data in its raw form. To build a model capable of doing pattern recognition, it is necessary to develop a feature extractor, which transform raw data into a representation that the classifier can detect [16, 17].

The group of methods that allow systems (based on Machine Learning) to discover the necessary representations for detecting and classifying raw data is known as Feature Learning [18].

These methods can not only learn how to map the feature to a result, but also to build the representation itself, often resulting in better performance than the representations developed by a specialist [19].

The growing scientific interest in this topic has been followed by a notable success, both in academia and industry. Mainly in areas of speech recognition, signal processing, object recognition and natural language processing [20].

Some of the Feature Learning techniques that have been producing promising results refer to Deep Learning. As more data becomes available, the more successful this technique will be [19].

2.2. Deep Learning

There are several techniques capable of Feature Learning, some are known as Deep Learning. They are models made by multiple nonlinear transformations, to produce abstract and more useful representations.

These models transform a representation into another, more abstract than the previous. In classification models, for example, more representation layers tend to amplify aspects of the data that are important for classification and hide irrelevant variations. By adding more layers, these models can represent more complexes functions [21].

The key aspect of Deep Learning is that layers of representations are not specified by a human specialist. They are learned through data, using common Machine Learning procedures. In the Deep Learning context, we can use Convolutional Neural Networks for this.

2.3. Convolutional Neural Network

Convolutional Neural Networks [22], refer to a variation of MLP (Multilayer Perceptron) and are based on the visual cortex behavior, where the neurons of the initial regions are responsible for detecting simple geometric shapes in the image, such as corners and edges, and the final neurons detect more complex graphic shapes. The process is repeated throughout the cortex until neurons in the final region detect characteristics of higher abstraction level, such as specific faces [23].

CNNs are used in problems where it is necessary to find relevant information implicit in data set, through operations that occur in convolution and pooling layers. In relation to the image classification task, variants of Convolutional Neural Networks that have been prevalent in the literature [24], and they demonstrate excellent results in the MNIST, CIFAR and ImageNet datasets [11, 25].

A convolutional layer is composed by several neurons, each one is responsible for applying a filter to a piece of the input matrix [23]. The convolution operation consists of applying a series of filters, sliding over the entire input matrix, and the result of applying the filters is called a feature map [22].

A pooling layer implements a nonlinear sub sampling function to dimensional reduction and small invariances capture. Pooling reduces the dimensionality of the input feature map and produces a new feature, creating something like a summary of the input.

For each filter, the highest value (max pooling) is selected, or the average (average pooling) is calculated. The pooling application speeds up training and reinforces CNN's strength in relation to position and size of most important characteristics of the training data.

2.4. Dropout

One of the most common challenges in training a Convolutional Neural Network is overfitting. There are several ways to mitigate this problem in a Deep Learning model: increasing the number or size of layers, or use a technique known as dropout.

The term dropout refers to "dropping" units (neurons) from a neural network, which means, temporarily removing them from model. The choice of which neuron to remove is random, and the amount can be fixed using a constant, for example, the constant 0.5 defines that half of the neurons will be removed.

This technique has considerably improved the accuracy and performance of neural network in several applications, such as object classification, speech recognition and document classification, among others [6]. This shows that this technique can be generalized for any problem.

3. Related Work

In [6], the authors presented a context sensitive grammar in an And-Or graph representation, that can produce a large set of composite graphical templates of cloth configurations.

In [5], the authors introduce a pipeline for recognizing and classifying clothes in natural scenes. To do so, they used a multi-class learner based on a Random Forest. Data was extracted features maps which were converted to histograms and used as inputs for a Random Forest (for clothing types) and an SVM (for clothing attributes) classifier. As result, their pipeline can describe the clothes on a scene, as show in Figure 1. They also created their own dataset with 80000 images labeled in 15 classes.
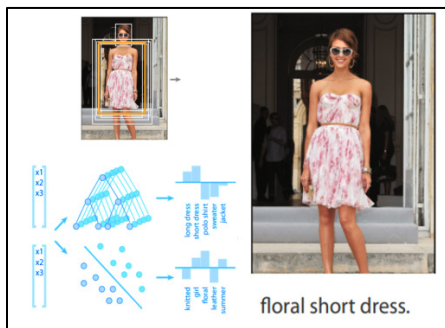
Figure 1: Model presented in [5].

In [26], the authors propose a knowledge-guided fashion analysis network for clothing landmark localization, and classification. To do so, they used a Bidirectional Convolutional Neural Network. As results, the model can not only predict landmarks, but also category and attributes, as shows Figure 2.
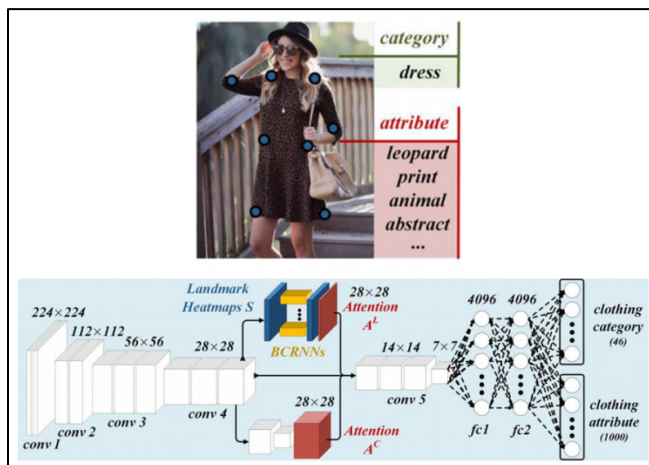
Figure 2: Model proposed [25].

4. Data Set

Fashion-MNIST is a direct drop-in alternative to the original MNIST dataset, for benchmarking machine learning algorithms [11]. MNIST [27] is a collection of handwritten digits, and contains 70000 greyscale 28x28 images, associated with 10 labels, where 60000 are part of the training set and 10000 of the testing. Fashion-MNIST has the exact same structure, but images are fashion products, not digits. A sample of this set can be seen in Figure 3.
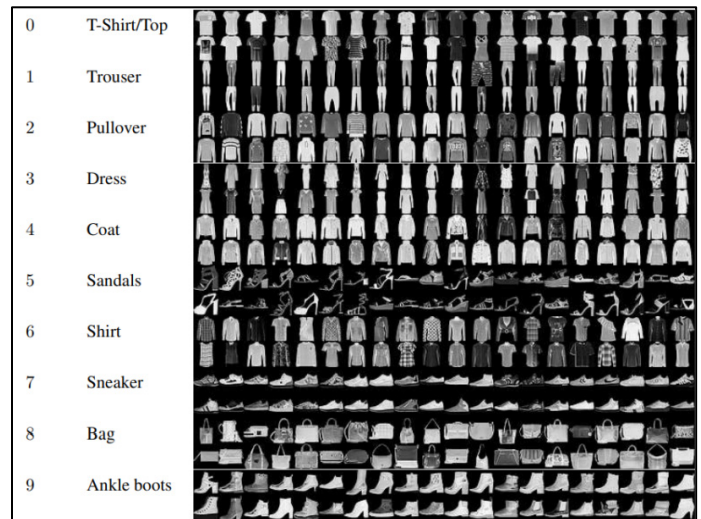
Figure 3: Fashion-MNIST sample

The dataset can be obtained as two 785 columns CSV, one with training images, and the other with testing ones. Each CSV row is an image that has a column with the label (enumerated from 0 to 9) and 784 remaining columns that describe the 28x28 pixel image with values from 0 to 255 representing pixel luminosity.

To make data access easier, we generated images divided in directories by usage, and labels. This way, we are able, to easily obtain image information by using only its path e.g., resources/test/dress/10.png.

5. CNN Models

To label this dataset, four CNN models were done in Python with Keras and TensorFlow. Training was executed in a Jupyter notebook, using GPU. We also used Weights and Biases [14] to grab information about training and hardware usage.

Proposed models were named: cnn-dropout-1, cnn-dropout-2, cnn-dropout-3 and cnn-simple. The goal of those models was to be able to label the dataset without the need of too much training or processing on activation, so developers can use it on real time applications such as online stores and searching websites.

5.1. cnn-dropout-1 and cnn-dropout-3

Both models use two consecutive blocks containing: a convolution, a max pooling, and finally a drop out. These blocks are connected to two more fully connected layers, who are connected to an output layer of ten neurons, each one representing a category. The only difference between these two models is that cnn-dropout-3 has considerably lower dropout values, as show in Figure 4.
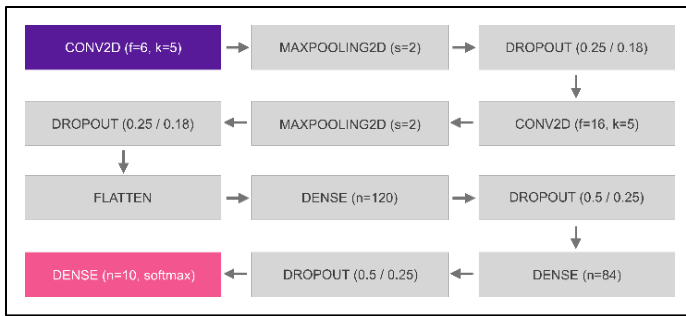
Figure 4: Topology of cnn-dropout-1 and cnn-dropout-3.

where the first drop out values is for model 1, and the second one for model 3. This topology has 44426 trainable parameters.

5.2. cnn-dropout-2

This proposed model is very similar to the cnn-dropout-1 model. However, it has two layers of convolutions before each max pooling. This model has about 32340 trainable parameters as shows Figure 5.
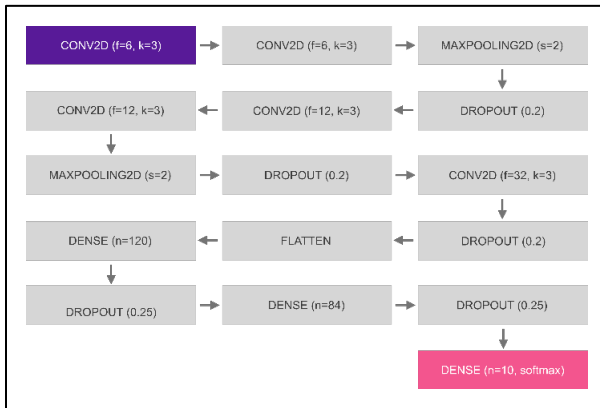
Figure 5: Topology of cnn-dropout-2.

5.3. cnn-simple

Cnn-simple is a model with less layers. It has only two convolutions, followed by a fully connected layer, in addition to the respective dropout and max pooling like other models. This model has 110968 trainable parameters and is shown in Figure 6.
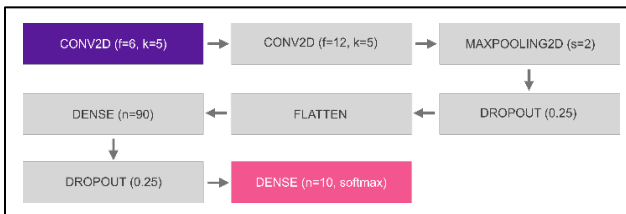
Figure 6: Topology of cnn-simple.

Since this model has only one max pooling, the image gets to the dense layer with 14x14 pixels in size (four times the size of other models which is 7x7). So, de dense layer training is expected to be slower.

All those models were modeled based on Keras Sequential model. Convolutional and dense layers used Rectified Linear Unit (ReLU) activation functions, except by the last dense layer on each

model (output layer), were Softmax was used. The optimizer used was Adadelta [28] Batch size was 128 and we trained the models for 12 epochs. To improve results, image pixel luminosity values were normalized to float numbers between 0 and 1.

6. Results

On the training dataset, the most accurate model was cnn-simple, with 98.95% of accuracy. Figure 7 shows that other models were also acceptable, based on the results obtained: 98,06% (cnn-dropout-3), 97.51% (cnn-dropout-2), and even the worst model (cnn-dropout-1), got an accuracy of 96,46%.
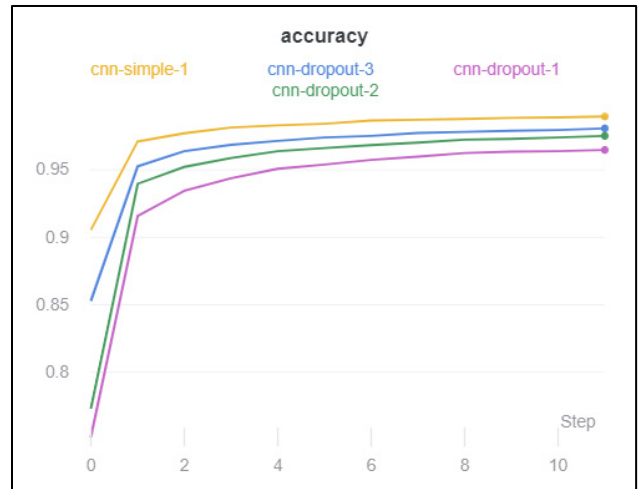
Figure 7: Accuracy

Validation accuracy had different results (as shows Figure 8), with cnn-dropout-3 having the best results 99.1%, followed nearly by cnn-dropout-2 (99.08%) and cnn-simple (99.05%). Cnn-dropout-1 still the one with the worst results (98.69%).
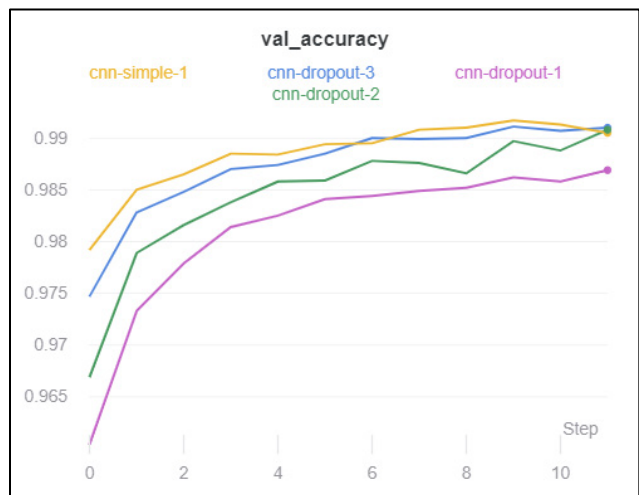
Figure 8: Validation Accuracy

Loss had good results, with cnn-simple having the best results both in training and validation loss, followed by cnn-dropout-3, cnn-dropout-2, and cnn-dropout-1. Results are shown in Figure 9.

When evaluating time, the two more accurate models, were also de faster in training. Figure 10 presents the relation between time and the training epoch. The lines tilt angle shows how fast the training was.
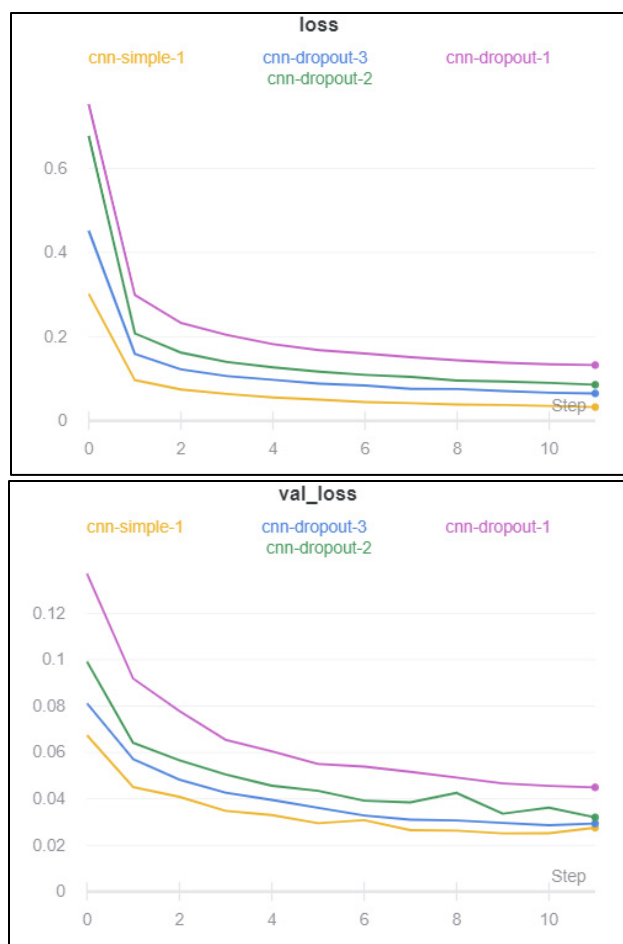
Figure 9: Training and Validation Loss
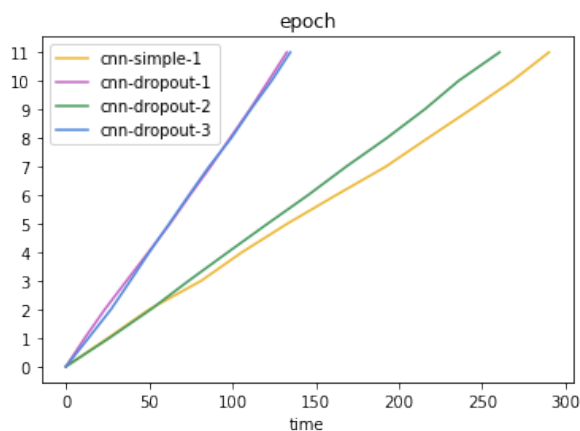
Figure 10: Training Time

Since we are using the same dataset, it is possible to compare these models with traditional non-convolutive machine learning algorithms presented in [11]. Table 1 presents the comparison among our model with theirs.

Table 1: Models Comparison

Model	Accuracy
cnn-dropout-3	99.10%
cnn-dropout-2	99.08%
cnn-simple-1	99.05%
cnn-dropout-1	98.69%
support vector classification	89.70%
gradient boosting	88.00%
random forest	87.30%
multilayer perceptron	87.00%
k neighbors	85.40%
logistic regression	84.20%
linear support vector classification	83.60%
stochastic gradient descent	81.90%
decision tree	79.80%
Perceptron	78.20%
passive aggressive classifier	77.60%
extra tree	77.50%
gaussian naive bayes	51.10%

Results shows that even our worst results (cnn-dropout-1) got better results than the best result in [11] (SVC, 89.70%).

7. Conclusions

Obtained results evidence that classifying fashion products with CNN can be more accurate than by using other conventional machine learning models. In addition, it was observed that the dropout technique together with more convolutive layers are effective when it comes to reducing the bias of a model.

Using TensorFlow 2 and GPU for training, we could reach not only a better training time, but also, better accuracies. Table 2 shows the differences between our original work and the present.

Table 2: Version Comparison

Model	TF1				TF2			
	Loss		Accuracy		Loss		Accuracy	
	Train	Test	Train	Test	Train	Test	Train	Test
cnn-dropout-1	0.21	0.26	91.87	90.35	0.13	0.04	96.47	98.69
cnn-dropout-2	0.19	0.25	92.59	90.81	0.08	0.03	97.51	99.08
cnn-dropout-3	0.14	0.25	94.53	90.86	0.06	0.02	98.06	99.10
cnn-simple-1	0.04	0.26	98.91	91.72	0.03	0.02	98.95	99.05

We also could decrease loss and bias, which were our main problems. We could not evaluate improvements in runtime since we used different hardware than in the original run.

Our original work found that the best model was cnn-simple, but now, with these new results, we discovered that cnn-dropout-3 is better (using TF2). This is good news because this model is faster to train, since it has an extra max-pooling layer that decreases dense layer inputs by a quarter.

About our goals, we could compare obtained results with the ones from the original FashionMNIST paper, and they show that CNNs can be great classifiers for garments. Table 1 contains our main results about it and can be used in future works to help researchers and developers finding the best classification technique.

Conflict of Interest

The authors declare no conflict of interest.

Acknowledgment

References

[1] A. Hodecker, A.M.R. Fernandes, A. Steffens, P. Crocker, V.R.Q. Leithardt, "Clothing Classification Using Convolutional Neural Networks," in Iberian Conference on Information Systems and Technologies, CISTI, IEEE Computer Society, 2020, doi:10.23919/CISTI49556.2020.9141035.

[2] R. Boardman, R. Parker-Strak, C.E. Henninger, "Fashion Buying and Merchandising," Fashion Buying and Merchandising, 2020, doi:10.4324/9780429462207.

[3] Y. Zhong, S. Mitra, "The role of fashion retail buyers in China and the buyer decision-making process," Journal of Fashion Marketing and Management, **24**(4), 631–649, 2020, doi:10.1108/JFMM-03-2018-0033.

[4] K.V. Madhavi, R. Tamilkodi, K.J. Sudha, "An Innovative Method for Retrieving Relevant Images by Getting the Top-ranked Images First Using Interactive Genetic Algorithm," Procedia Computer Science, **79**, 254–261, 2016, doi:10.1016/j.procs.2016.03.033.

[5] L. Bossard, M. Dantone, C. Leistner, C. Wengert, T. Quack, L. Van Gool, "Apparel classification with style," in Lecture Notes in Computer Science (including subseries Lecture Notes in Artificial Intelligence and Lecture Notes in Bioinformatics), 321–335, 2013, doi:10.1007/978-3-642-37447-0_25.

[6] H. Chen, Z.J. Xu, Z.Q. Liu, S.C. Zhu, "Composite templates for cloth modeling and sketching," Proceedings of the IEEE Computer Society Conference on Computer Vision and Pattern Recognition, **1**, 943–950, 2006, doi:10.1109/CVPR.2006.81.

[7] K. He, X. Zhang, S. Ren, J. Sun, Delving deep into rectifiers: Surpassing human-level performance on imagenet classification, 2015, doi:10.1109/ICCV.2015.123.

[8] Z. Song, M. Wang, X.S. Hua, S. Yan, "Predicting occupation via human clothing and contexts," Proceedings of the IEEE International Conference on Computer Vision, 1084–1091, 2011, doi:10.1109/ICCV.2011.6126355.

[9] K. Yamaguchi, M.H. Kiapour, L.E. Ortiz, T.L. Berg, "Parsing clothing in fashion photographs," Proceedings of the IEEE Computer Society Conference on Computer Vision and Pattern Recognition, 3570–3577, 2012, doi:10.1109/CVPR.2012.6248101.

[10] K. Meshkini, J. Platos, H. Ghassemain, "An Analysis of Convolutional Neural Network for Fashion Images Classification (Fashion-MNIST)," in Advances in Intelligent Systems and Computing, Springer: 85–95, 2020, doi:10.1007/978-3-030-50097-9_10.

[11] M. Kayed, A. Anter and H. Mohamed, "Classification of Garments from Fashion MNIST Dataset Using CNN LeNet-5 Architecture," in 2020 International Conference on Innovative Trends in Communication and Computer Engineering (ITCE), Aswan, Egypt, 2020, 238-243, doi: 10.1109/ITCE48509.2020.9047776.

[12] A. Jain, A. Fandango, A. Kappor, TensorFlow Machine Learning Projects : Build 13 real-world projects with advanced numerical computations using the Python ecosystem, Packt Publishing Limited, Birmingham, United Kingdom, 2018. ISBN13: 9781789132212.

[13] Y. Shin, I. Balasingham, "Comparison of hand-craft feature based SVM and CNN based deep learning framework for automatic polyp classification," Proceedings of the Annual International Conference of the IEEE Engineering in Medicine and Biology Society, EMBS, 3277–3280, 2017, doi:10.1109/EMBC.2017.8037556.

[14] S. Vieira, W.H. Lopez Pinaya, A. Mechelli, Introduction to machine learning, 2019, doi:10.1016/B978-0-12-815739-8.00001-8.

[15] O. Theobald, Machine Learning for Absolute Beginners, Scatter Plot Press, 169, 2017. ISBN: 1549617214.

[16] S. Shalev-Shwartz, S. Ben-David, Understanding machine learning: From theory to algorithms, Cambridge university press, 2013, doi:10.1017/CBO9781107298019.

[17] E.L. De Oliveira, "Machine learning techniques applied to predict the performance of contact centers operators," Iberian Conference on Information Systems and Technologies, CISTI, 2019, doi:10.23919/CISTI.2019.8760665.

[18] J. Maindonald, "Pattern Recognition and Machine Learning," Journal of Statistical Software, **17**, 2007, doi:10.18637/jss.v017.b05.

[19] I. Goodfellow, Y. Bengio, A. Courville, Deep learning, MIT Press Cambridge, 2016. ISBN: 9780262035613.

[20] A. Peña, I. Bonet, D. Manzur, M. Góngora, F. Caraffini, "Validation of convolutional layers in deep learning models to identify patterns in multispectral images: Identification of palm units," in Iberian Conference on Information Systems and Technologies, CISTI, IEEE Computer Society, 2019, doi:10.23919/CISTI.2019.8760741.

[21] N. Buduma, N. Locascio, Fundamentals of deep learning : Designing Next-Generation Machine Intelligence Algorithms, O'Reilly Media, Inc., 2017. ASIN: B0728KKXWB.

[22] Y. Lecun, Y. Bengio, G. Hinton, Deep learning, Nature, **521**(7553), 436–444, 2015, doi:10.1038/nature14539.

[23] K. Fu, D. Cheng, Y. Tu, L. Zhang, Credit card fraud detection using convolutional neural networks, Lecture Notes in Computer Science, **9949**, 483–490, 2016, doi:10.1007/978-3-319-46675-0_53.

[24] C. Szegedy, W. Liu, Y. Jia, P. Sermanet, S. Reed, D. Anguelov, D. Erhan, V. Vanhoucke, A. Rabinovich, "Going deeper with convolutions," in Proceedings of the IEEE Computer Society Conference on Computer Vision and Pattern Recognition, 1–9, 2015, doi:10.1109/CVPR.2015.7298594.

[25] A. Baldominos, Y. Saez, P. Isasi, "A Survey of Handwritten Character Recognition with MNIST and EMNIST," Applied Sciences, **9** (15), 3169, 2019, doi:10.3390/app9153169.

[26] W. Wang, Y. Xu, J. Shen, S.C. Zhu, "Attentive Fashion Grammar Network for Fashion Landmark Detection and Clothing Category Classification," in Proceedings of the IEEE Computer Society Conference on Computer Vision and Pattern Recognition, 4271–4280, 2018, doi:10.1109/CVPR.2018.00449.

[27] L. Deng, "The MNIST database of handwritten digit images for machine learning research," IEEE Signal Processing Magazine, **29**(6), 141–142, 2012, doi:10.1109/MSP.2012.2211477.

[28] E. M. Dogo, O. J. Afolabi, N. I. Nwulu, B. Twala and C. O. Aigbavboa, "A Comparative Analysis of Gradient Descent-Based Optimization Algorithms on Convolutional Neural Networks," in Proceedings of 2018 International Conference on Computational Techniques, Electronics and Mechanical Systems (CTEMS), Belgaum, India, 2018, 92-99, doi: 10.1109/CTEMS.2018.8769211.
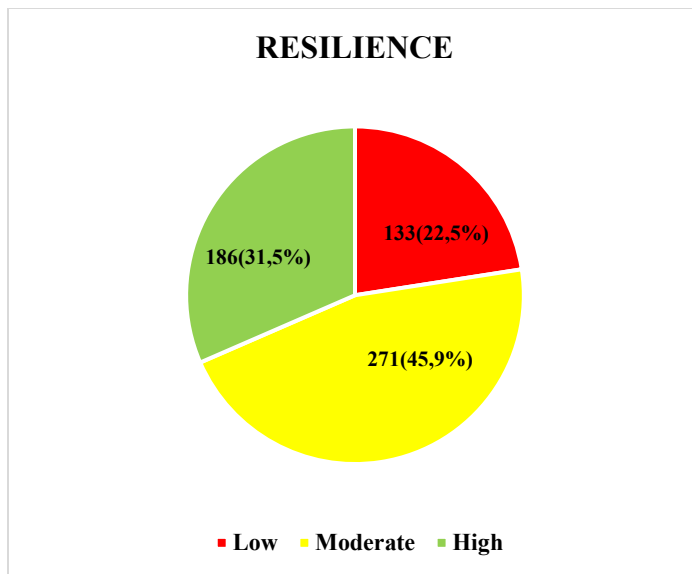
Resilience During the COVID-19 Pandemic in Female Heads of Household Residing in a Marginal Population in Lima

Rosa Perez-Siguas[1,*], Anne Tenorio-Casaperalta[2], Lucy Quispe-Mamani[2], Luis Paredes-Echeverria[2], Hernan Matta-Solis[1], Eduardo Matta-Solis[1]

[1]*Research and Intellectual Creativity Direction, Universidad María Auxiliadora, 15408, Lima-Perú*

[2]*Faculty of Health Sciences, Universidad María Auxiliadora, 15408, Lima-Perú*

A R T I C L E   I N F O

A B S T R A C T

Resilience is the way in which the person develops their self-determination to solve conflicts that compromise their physical and mental well-being in the face of a crisis such as the COVID-19 pandemic, therefore the objective of this study is to determine resilience during the COVID-19 pandemic in female heads of household residing in a marginal population in Lima. It is a quantitative, non-experimental, descriptive, and cross-sectional study, with a total population of 650 and a sample of 590 in the study, who answered a questionnaire with sociodemographic data and the Connor and Davidson Resilience Scale in its short version of 10 items. The results show the total resilience of female heads of households, 271 (45.9%) of women heads of households have moderate resilience, 186 (31.5%) have high resilience and 133 (2.5%) have low resilience. In conclusion, it is recommended to seek strategies that allow women to improve resilience since this will benefit them to be able to overcome and face what is experienced by the COVID-19 pandemic.

1. Introduction

In the world, the coronavirus pandemic (COVID-19) has taken the entire population by surprise [1], where they are mainly reflected in the capacities that individuals have to face this stressful situation, where personality and psychological functioning are seen affected in the well-being of each individual [2].

In the same way, the population in the world has had to take measures to have the capacity to face these situations due to the COVID-19 pandemic that compromise their mental and emotional health as a result of social isolation and by not doing their daily routines [3], in such a way so that the resilience that each individual possesses decreases [4]. Resilience is the capacity of each individual to face traumatic circumstances caused by COVID-19, but this decreases due to the fact that anxiety, depression and post-traumatic stress are evident in the population as a result [5], [6].

As a result, the resilience that each individual possesses to face this global crisis is not adequate, because contagion in one of its

family negatively compromises facing it, leading to factors of depression, anguish, sadness [7].

Resilience is of vital importance to cope with stress and to maintain balance in mental health [8], where it acts against the effects generated by stress and also on sleep quality [9]. For this reason, the resilience that is sought to be acquired during the COVID-19 pandemic will improve each individual and allow them to face this situation in a healthy way that helps mentally both in their person and family [10], [11].

In a study in Spain [12], it was observed in 459 participants that resilience in 139 (30.6%) of the participants had a low resilience, while 115 (25.4%) had a high level of resilience, but that the scores falls were more related to obsessive thoughts and fear due to the pandemic that compromised sleep.

In a study from the United Kingdom [13], the author mention in their results of 250 female participants, they stated that 18.9% of the participants presented a lower level of resilience, but 65% obtained a moderate and high resilience, where it means that the Participants have resilience characteristics that they do not

necessarily need to strengthen in order to improve their ability to cope with any situation that compromises their health.

In a study from Peru [14], the authors presented in the results of 315 female heads of household surveyed on resilience, it was observed that 49% of women presented a moderate level of resilience, 27.9% presented a high level of resilience and 22.9% a low level of resilience, this is due to the fact that the pandemic generates a situation of conflict, where the lives of women become more compromised because they live in an area where the economic crisis is present long before the pandemic.

In a study from Israel [15], in their results of 300 participants they verified a relationship between resilience and individual well-being where they significantly and negatively interpreted the feeling of danger and symptoms of distress, where the greater the individual resilience and well-being, the lower the feeling of danger and symptoms of distress in the population.

Therefore, this study seeks strategies that improve resilience in women heads of households where it allows them to face this COVID-19 pandemic in a way that does not harm their physical and mental health.

The objective of the research work is to determine the resilience during the COVID-19 pandemic in women heads of households who reside in a marginal population in Lima. In which it will give us important data that allow us to observe how resilience is in women heads of household.

2. Methodology

In this part, the type and design of the research was developed, also he population which the research work was carried out, the inclusion and exclusion criteria will also be given in detail and finally the technique and instrument of data collection.

2.1. Research type and Design

In the study, due to its characteristics, way of collecting data and measuring the variables involved, has a quantitative approach. Regarding the methodological design, it is a non-experimental, descriptive, cross-sectional study [16].

2.2. Population and sample

The total population was 650 female heads of household who were identified, of which 590 agreed to participate voluntarily and signing the informed consent.

Inclusion Criteria

- Women heads of households who have leadership and decision-making in the family within the household.
- Female heads of household who reside at least 6 months in the area.
- Women who participate voluntarily and who gave their informed consent.

2.3. Technique and Instrument

The technique used is the virtual survey of the Google form, in which, through the data collection instrument, the Connor and Davidson Resilience Scale in its short version of 10 items (CD-RISC 10) that aim to measure the Resilience during the COVID - 19 pandemic in female heads of household residing in a marginal population of Lima.

For data collection, it has been structured in 2 blocks: 1. Sociodemographic data such as age, marital status, level of education and current occupation; 2. CD-RISC 10 that comprises 10 items in which it presents a one-dimensional dimension with the 10 respective items, in which it is assessed with a Likert-type scale with 5 response options: "0 = never", "1 = almost never" , "2 = sometimes", "3 = almost always" and "4 = always", obtaining a total score by adding all its items, so that its score would be from 0 to 40 points, where "0 to 9" is a low resilience, "10 to 30" moderate resilience and "31 to 40" high resilience, the higher the score corresponds to a higher resilience in female heads of household [17].

The validity of the instrument was determined based on the exploratory factor analysis technique with Varimax rotation. The Kaiser-Mayer-Olkin sample adequacy measure obtained a coefficient of 0.894 (KMO> 0.5), while the Bartlett sphericity test obtained significant results (X^2 approx. = 10708.291; gl = 45; p = 0.000). The measures of sampling adequacy of the anti-image diagonal obtained significant coefficients for the 10 items (MSA> 0.8). The principal components analysis determined that there is a single factor that explains the variance by 85.125%. Since there is only one factor, the matrix of rotated components could not be extracted. For all the above, the instrument is considered valid.

The reliability of the instrument was determined based on Cronbach's Alpha statistical test, the same one that obtained a coefficient of 0.980 (α> 0.8) for all the items (i = 10).

In this research, the data to be entered was given in a data matrix that was designed in the statistical program IBM SPSS Statistics Base 25.0, its corresponding analysis was carried out, in which it will allow us a better processing of data to make tables and statistical graphics so that they are later described and interpreted in results and discussions, respectively.

2.4. Place and Application of the Instrument

The virtual survey was carried out to measure resilience during the COVID-19 pandemic in women heads of households who reside in a marginal population of Lima, in which it was carried out in the district of Comas in the Carmen Alto area, which is a vulnerable area where they do not have basic services (water, electricity, sewage), where most of the families live in poverty and extreme poverty, since most of the family members do not have stable jobs, everything is done eventually.

3. Results

The results of the surveys carried out following the guidelines corresponding to the study will be shown in figure 1:

Figure 1 shows the results of the total resilience of women heads of households where 271 (45.9%) of women heads of

households have moderate resilience, 186 (31.5%) have high resilience and 133 (2.5%) have low resilience. Regarding high resilience, it is the person who faces extreme situations such as COVID-19 and that leads to maintaining their emotions, maintains their self-confidence and self-motivates to get ahead, moderate resilience, is the person who keeps their impetus to go out forward in the face of the COVID - 19 crisis and low resilience is the person who does not face the situation due to the COVID - 19 pandemic, leading to depressive symptoms and anxiety due to this fact.

In relation to the total resilience and the marital status of women heads of household, it was verified using Pearson's Chi-square test (X^2) to determine the relationship between both variables, where the level of significance of the test obtained a value of 1.35 (p> 0.05) $(X^2 = 3.632; df = 6)$. Therefore, emphasis is placed on a hypothesis of association between both variables. Therefore, we interpret that women heads of household in relation to their single marital status have a moderate resilience 61 (43.9%), as does the marital status married 51 (49%), cohabiting 156 (45.7%) and widowed marital status 3 (50%) have moderate resilience and 3 (50%) have high resilience.

Figure 1: Resilience during the COVID - 19 pandemic in female heads of household residing in a marginal population of Lima

Table 1: Resilience during the COVID - 19 pandemic in female heads of household in relation to marital status residing in a marginal population of Lima

| | | | MARITAL STATUS | | | | |
			Single	Married	Cohabiting	Widow	Total
RESILIENCE	LOW	Count	30	21	82	0	133
		% within marital status	21,6%	20,2%	24,0%	0,0%	22,5%
	MODERATE	Count	61	51	156	3	271
		% within marital status	43,9%	49,0%	45,7%	50,0%	45,9%
	HIGH	Count	48	32	103	3	186
		% within marital status	34,5%	30,8%	30,2%	50,0%	31,5%
Total		Count	139	104	341	6	590
		% within marital status	100,0%	100,0%	100,0%	100,0%	100,0%

Chi-square tests

	Value	df	Asymptotic significance (bilateral)
Pearson's Chi-square	3,632[a]	6	,726
Likelihood ratio	4,875	6	,560
Linear by linear association	,250	1	,617
N° of valid cases	590		

a. 3 cells (25.0%) have expected a count less than 5. The minimum expected count is 1.35.

Table 2: Resilience during the COVID-19 pandemic in female heads of household in relation to the level of education who reside in a marginal population of Lima

| | | | Level of Education | | | | | |
			Without Instruction	Primary	Secondary	Superior University	Superior Technical	Total
RESILIENCE	LOW	Count	14	25	59	2	33	133
		% within Level of instruction	20,9%	27,8%	19,7%	33,3%	26,0%	22,5%
	MODERATE	Count	31	38	145	2	55	271
		% within Level of instruction	46,3%	42,2%	48,3%	33,3%	43,3%	45,9%
	HIGH	Count	22	27	96	2	39	186

	% within Level of instruction	32,8%	30,0%	32,0%	33,3%	30,7%	31,5%
Total	Count	67	90	300	6	127	590
	% within Level of instruction	100,0%	100,0%	100,0%	100,0%	100,0%	100,0%

Chi-square tests

	Value	df	Asymptotic significance (bilateral)
Pearson's Chi-square	4,456[a]	8	,814
Likelihood ratio	4,388	8	,821
Linear by linear association	,184	1	,668
N° of valid cases	590		

a. 3 cells (20.0%) have expected a count less than 5. The minimum expected count is 1.35.

Table 3: Resilience during the COVID-19 pandemic in female heads of household in relation to the occupation that reside in a marginal population in Lima

				Current Occupation		
			Stable worker	Temporary worker	No occupation	Total
RESILIENCE	LOW	Count	1	65	67	133
		% within current occupation	10,0%	24,5%	21,3%	22,5%
	MODERATE	Count	5	111	155	271
		% within current occupation	50,0%	41,9%	49,2%	45,9%
	HIGH	Count	4	89	93	186
		% within current occupation	40,0%	33,6%	29,5%	31,5%
Total		Count	10	265	315	590
		% within current occupation	100,0%	100,0%	100,0%	100,0%

Chi-square tests

	Value	df	Asymptotic significance (bilateral)
Pearson's Chi-square	4,088[a]	4	,394
Likelihood ratio	4,258	4	,372
Linear by linear association	,217	1	,642
N° of valid cases	590		

a. 3 cells (33.3%) have expected a count less than 5. The minimum expected count is 2.25.

In relation to the total resilience and the level of education of women heads of household, it was verified using Pearson's Chi-square test (X^2) to determine the relationship between both variables, where the level of significance of the test obtained a value of 1.35 (p> 0.05) ($X^2 = 4.456$; df = 8). Therefore, emphasis is placed on a hypothesis of association between both variables. Therefore, we interpret that women heads of households without education show moderate resilience 31 (46.3%), at the primary education level 38 (42.2%) have moderate resilience, at the secondary education level 145 (48.3%) have moderate resilience, in university 2 (33.3%) have low resilience, 2 (33.3%) have moderate resilience and 2 (33.3%) have high resilience and in technical 55 (43.3%) have resilience moderate.

In relation to the total resilience and the level of education of women heads of household, it was verified using Pearson's Chi-square test (X^2) to determine the relationship between both variables, where the level of significance of the test obtained a value of 2.25 (p> 0.05) ($X^2 = 4.088$; df = 4). Therefore, emphasis is placed on a hypothesis of association between both variables.

Therefore, we interpret that female heads of household with stable work have moderate resilience 5 (50%), with temporary work 111 (41.9%) have moderate resilience and no occupation 155 (49.2%) have moderate resilience.

4. Discussion

In this research work, the approach to mental health of women heads of household was revealed, emphasizing the ability to resolve conflicts or face situations that compromise their health due to the COVID-19 pandemic.

In the results of resilience during the COVID-19 pandemic in women heads of households present a moderate level of resilience, in our findings it has been observed that due to the coping with the danger caused by COVID-19 in the society and in the families, women who are heads of households have anticipated this great change and have sought a way to resolve this conflict in order to maintain the well-being of their children, also, it has been foreseen that the resilience in families has been maintained without the financial support of the state, but that the state does need social or

family support to support it at home. In [12], the authors maintain that mainly in women who do not have family support, they tend to manifest depressive symptoms and anxiety because they cannot support their family and this leads to poor health in them. Similarly in [13], the authors identify that depression and anxiety manifest themselves because the individual cannot cope with the problems caused by the COVID-19 pandemic, where one of their relatives is infected or has died, all this has repercussions on the head of the household and can compromise their physical and mental well-being.

In the results of resilience with marital status, it is interpreted that in family's resilience is important since this will allow them to reorganize and recover their optimal levels of functioning and well-being in the family that is subjected to stress because of the pandemic of the COVID - 19. In [15], the authors argue that resilience within the family is very important because supporting each family member will allow them to maintain a balance in their mental health during the COVID - 19 pandemic, since this has generated symptoms such as depression, anxiety and stress due to social isolation and quarantine.

In the results of resilience with the level of education, we can interpret that it is important to be resilient since it favors the person for their self-determination process in the face of any coping situation, especially during the health crisis due to COVID - 19. In [4], the authors argue that being resilient during the COVID-19 pandemic will allow them to improve their coping skills and self-determination in any dangerous situation and allow them to overcome any circumstance within the family.

5. Conclusions

It is concluded that resilience is important since it is a protective factor to an adaptation response to stressful situations such as the COVID-19 pandemic.

It is concluded that psychological support should be given to the population according to their needs and vulnerability due to the COVID-19 pandemic.

It is concluded that the present study emphasizes the understanding of female heads of households who have an inappropriate state of mind during the COVID-19 pandemic.

It is recommended to look for strategies that allow to improve the resilience of women since this will benefit them to be able to overcome and face what is experienced by the COVID - 19 pandemic.

The limitation of this research work is that there are few studies in our country and that access to the mothers' homes was not adequate since some were not present or did not want to be present in the study.

Conflicts of Interest

The authors declare no conflict of interest.

References

[1] C. Jacques, T. López, L. Medina, J. de Bont, A. Gonçalves, T. Duarte, A. Berenguera, "Gender-based approach on the social impact and mental health in Spain during COVID-19 lockdown: a cross-sectional study," BMJ Open, **10**(11), e044617, 2020, doi:10.1136/bmjopen-2020-044617.

[2] G. Zager, T. Kavčič, A. Avsec, "Resilience matters: Explaining the association between personality and psychological functioning during the COVID-19 pandemic," International Journal of Clinical and Health Psychology, **21**, 100198, 2020, doi:10.1016/j.ijchp.2020.08.002.

[3] A. Havnen, F. Anyan, O. Hjemdal, S. Solem, M. Gurigard, K. Hagen, "Resilience moderates negative outcome from stress during the COVID-19 pandemic: A moderatedmediation approach.," International Journal of Environmental Research and Public Health, **17**(18), 1–12, 2020.

[4] J. Blanc, A. Briggs, A. Seixas, M. Reid, J. Girardin, P. Perumal, R. Seithikurippu, "Addressing psychological resilience during the coronavirus disease 2019 pandemic: a rapid review," Current Opinion in Psychiatry, **34**(1), 29–35, 2021, doi:10.1097/yco.0000000000000665.

[5] A. Dodesini, A. Caffi, M. Spada, R. Trevisan, "Resilience in pregnant women with pre-gestational diabetes during COVID-19 pandemic: the experience of the Papa Giovanni XXIII Hospital in Bergamo, Italy," Acta Diabetologica, 10–12, 2020, doi:10.1007/s00592-020-01640-3.

[6] T. Kavčič, A. Avsec, G. Zager, "Psychological Functioning of Slovene Adults during the COVID-19 Pandemic: Does Resilience Matter?," Psychiatric Quarterly, 2020, doi:10.1007/s11126-020-09789-4.

[7] X. Ma, Y. Wang, H. Hu, X. Tao, Y. Zhang, H. Shi, "The impact of resilience on prenatal anxiety and depression among pregnant women in Shanghai," Journal of Affective Disorders, **250**, 57–64, 2019, doi:10.1016/j.jad.2019.02.058.

[8] C. Vinkers, T. van Amelsvoort, J. Bisson, I. Branchi, J. Cryan, K. Domschke, O. Howes, M. Manchia, L. Pinto, D. de Quervain, M. Schmidt, N. van der Wee, "Stress resilience during the coronavirus pandemic," European Neuropsychopharmacology, **35**, 12–16, 2020, doi:10.1016/j.euroneuro.2020.05.003.

[9] H. Preis, B. Mahaffey, C. Heiselman, M. Lobel, "Vulnerability and resilience to pandemic-related stress among U.S. women pregnant at the start of the COVID-19 pandemic," Social Science and Medicine, **266**, 113348, 2020, doi:10.1016/j.socscimed.2020.113348.

[10] C. Jacob, D. Briana, G. Di Renzo, N. Modi, F. Bustreo, G. Conti, A. Malamitsi, M. Hanson, "Building resilient societies after COVID-19: the case for investing in maternal, neonatal, and child health," The Lancet Public Health, **5**(11), 624–627, 2020, doi:10.1016/S2468-2667(20)30200-0.

[11] A. Ayed, A. Embaireeg, A. Benawadth, W. Al-Fouzan, M. Hammoud, M. Alhathal, A. Alzaydai, M. Ayed, "Maternal and perinatal characteristics and outcomes of pregnancies complicated with COVID-19 in Kuwait," BMC Pregnancy Childbirth, **20**, 754, 2020.

[12] D. Lubián, C. Butrón, J. Arjona, M. Fasero, J. Alcolea, V. Guerra, M. Casaus, A. Bueno, A. Olvera, B. Rodríguez, A. Cuevas, J. Presa, P. Coronado, R. Sánchez, E. González, "Mood disorders and resilience during the first COVID-19 pandemic wave in Spain: Conclusions of the first Spanish survey.," Journal of Psychosomatic Research, **140**, 110327, 2020, doi:10.1016/j.jpsychores.2020.110327.

[13] N. Roberts, K. McAloney, K. Lippiett, E. Ray, L. Welch, C. Kelly, "Levels of resilience, anxiety and depression in nurses working in respiratory clinical areas during the COVID pandemic," Respiratory Medicine, **176**(August 2020), 106219, 2021, doi:10.1016/j.rmed.2020.106219.

[14] A. Tenorio, L. Paredes, L. Quispe, "Resiliencia durante la emergencia sanitaria por COVID - 19, en mujeres jefas de hogar residentes en una zona de Carabayllo.," Revista de Investigación Científica Ágora, **07**(2), 88–93, 2020.

[15] S. Kimhi, H. Marciano, Y. Eshel, B. Adini, "Recovery from the COVID-19 pandemic: Distress and resilience," International Journal of Disaster Risk Reduction, **50**(June), 101843, 2020, doi:10.1016/j.ijdrr.2020.101843.

[16] C. Fernández, P. Baptista, Metodología de la Investigación. 6ta ed. México: Mc Graw-Hill/Interamericana., 2015.

[17] B. Notario, M. Solera, M. Serrano, R. Bartolomé, J. García, V. Martínez, "Reliability and validity of the Spanish version of the 10-item Connor-Davidson Resilience Scale (10-item CD-RISC) in young adults.," Health and Quality of Life Outcomes, **9**(1), 63, 2011, doi:10.1186/1477-7525-9-63.

Underwater Computing Systems and Astronomy–Multi-Disciplinary Research Potential and Benefits

Ayodele Periola[*], Akintunde Alonge, Kingsley Ogudo

University of Johannesburg, Electrical and Electronic Engineering Technology, Johannesburg, 2092, South Africa

ARTICLE INFO	ABSTRACT
	The Ocean plays an important role in hosting investigations in underwater astronomy and enabling the realization of new research prospects. This paper discusses synergistic prospects of the blue economy from the perspective of underwater astronomy and scientific inquiry, technological and economic development. The presented research investigates how the synergy enhances computing applications. The paper presents the overloaded application paradigm that explores the ability of underwater telescope networks to accommodate additional applications. The investigated metrics for computing applications are the accessible computational resources, and power usage effectiveness (PUE) that is investigated in a scenario where onshore computing stations used in underwater astronomy observations are integrated with existing terrestrial data centers. This is necessary as onshore computing stations benefit from free cooling being located near natural maritime resources. The performance evaluation investigates how the proposed synergy and the emerging crowd–sourcing can enhance the observation resolution for underwater astronomy observations. Investigation shows that the synergy enhances accessible computational resources, PUE and observation resolution by an average of 48.8%, 1.6% and 41.3%, respectively.

1. Introduction

Knowledge discovery and the conduct of research is an important goal that can be realized via the emergence of new paradigms that aim to answer existing and new research questions. An important research aspect in this regard is that of astronomy observations. The role of the ocean in expanding research frontiers is relatively under–explored in comparison to earth's terrestrial environment with respect to astronomy. There are different forms of astronomy such as optical astronomy, X–ray astronomy, gamma astronomy, and radio astronomy.

A new frontier for the conduct of astronomy is the ocean that enables the realization of underwater astronomy. Underwater astronomy focuses on the study of neutrinos and uses underwater telescopes (i.e., scientific underwater vehicles). The conduct of underwater astronomy requires the launch of underwater telescopes (scientific underwater vehicles) into the ocean at varying locations and altitudes. In underwater astronomy, the concerned telescopes are organized into a network that observes different aspects of the underwater environment with the aim of detecting neutrinos.

In similarity to other aspects of astronomy, underwater astronomy is a scientific endeavour that aims to advance human knowledge. This can create a false notion that underwater astronomy does not enhance the conduct of other technologies and applications. The result of this is a reduced participation in the conduct of underwater astronomy observation. This leads to lack of or reduced collaboration between scientists in astronomy and other disciplines. A significant effect of this reduced or lack of collaboration is an increased paucity of funds required to develop and deploy underwater astronomy systems. The paucity of funds reduces the chances of underwater astronomy systems in realizing its full potential in contributing to knowledge and also enhancing other application areas. It is important to address this challenge as a conduct of astronomy has enabled technological breakthroughs resulting in useful applications in other domains [1–6]. Nevertheless, it is important to note that the breakthroughs in [1–6] do not consider the new domain of underwater astronomy [7–9].

The discussion in [7–9] presents an outline of the development of the science of underwater astronomy. In addition, the discussion in [9] identifies other sources that were previously thought to be neutrino sources in the universe. Some of these sources are X-ray binaries and gamma ray bursts. In addition, Spiering recognized that the use of underwater neutrino detectors has been considered

[*]Corresponding Author: Ayodele Periola, periola@hotmail.com

suitable since 1960. However, the consideration of an approach in which underwater astronomy concerns forms a synergy with other applications requires further research consideration.

The focus of the research presented in this paper is to demonstrate the usefulness and value potential of underwater astronomy. The non–consideration of underwater astronomy in [1–6] alongside the need to demonstrate the usefulness of underwater astronomy to other application is addressed in this paper.

Contribution: The discussion in the presented research focuses on the conduct of underwater astronomy. The research recognizes that it is challenging to provide a societal basis to justify the conduct of scientific investigations via underwater astronomy observations. The provision of a societal basis is important to convince other applications and disciplines to donate resources in designing and deploying systems for conducting underwater astronomy observations. The realization of this goal requires the identification of other applications that benefit from the conduct of underwater astronomy observations. This goal is realized by identifying applications that can potentially benefit from the launch of systems intended for use in underwater astronomy observations. Two applications i.e., underwater surveillance, and computing systems have been identified. The consideration of the applications of underwater surveillance and computing alongside the concerns in underwater astronomy shares the system realization costs amongst these applications. This reduces the cost associated with the realization of underwater astronomy systems. In addition, the conduct of underwater astronomy while accommodating the concerns of underwater surveillance and computing enhances these applications by improving their performance. This paper also explores how the conduct of underwater astronomy observations provides a platform enabling the conduct of scientific enquiry in reducing pseudo–science towards verifying the existence of aquatic humanoids. In addition, the paper presents a case from the public health perspective to justify the need to continue the conduct of investigation in this direction. Furthermore, the consideration of the applications in underwater surveillance, and computing increases the potential of underwater astronomy in other areas leading to an overloaded application context.

The contribution of this paper is the presentation of the overloaded application paradigm. In the proposed overloaded application paradigm, the ability of underwater astronomy observations to provide support to new research motives and computing applications is examined. The contributions of this paper are:

1) Firstly, the paper proposes the probe of the ocean with the aim of enhancing knowledge discovery and reducing the propagation of pseudo – science. This is important in investigating the existence of aquatic humanoids. The proposed investigation aims to answer questions from two perspectives. The first perspective is that of providing scientific and technical answers to a long-standing concern. The second perspective aims to provide a platform to further investigate how aquatic humanoids have developed immune response to marine viral outbreaks. This paper provides and discusses the rationale and presents a design of the system for conducting the proposed scientific investigation.

2) Secondly, the paper recognizes that the deployment of underwater telescopes increases the coverage of the ocean thereby enabling the realization of underwater surveillance applications. The conduct of underwater astronomy also necessitates the design of novel computing networks for data processing. The discussion in this paper proposes a novel underwater surveillance network that re–uses the infrastructure and network deployed to realize underwater astronomy applications. In addition, the paper proposes a novel computing network architecture enabling the integration of onshore computing platforms with existing terrestrial cloud computing platforms. The paper also recognizes the potential of underwater astronomy to spur technological development in other areas.

In addition, the paper formulates and investigates benefits arising from the synergy in the proposed paradigm. The performance benefits are analysed from the perspectives of computing applications and astronomy investigations. The formulated and investigated metrics from the computing perspective are the accessible computing resources and the PUE. The observation resolution metric has received consideration from the astronomy investigation perspective.

2. Background

The value potential of conducting astronomy observations with a focus on Africa receives consideration in [10]. In their discussion, astronomy is considered from a broad perspective i.e. it comprises the use of terrestrial and space-based telescopes. Technological advances in astronomy are recognized to enhance education (for students and teachers), healthcare (eye care), and fostering skills development and; ensure equal gender participation in science, technology, engineering and mathematics.

The discussion in [10] recognizes that additional work is needed to increase astronomy's relevance in Africa. This can be achieved by directing the effort of researchers in astronomy system design to other potential impact areas. The conduct of collaborative research is required to maximize the developmental profits obtainable from astronomy. However, the potential of driving multi–disciplinary research via an examination of multi–domain problems are not done in [10]. This can be addressed in additional research.

The development motive underlying the participation of African nations in Astronomy is discussed in [11]. The Ethiopian initiative uses space science and technology to address challenges being faced in accessing water and enhancing agricultural productivity. The drive by Kenya and Zambia to engage in radio astronomy has motivated the need to develop capacity in converting satellite earth stations to terrestrial radio telescopes. The Sudanese institute of Space Research and Aerospace also aims to establish an astronomy exploration centre and terrestrial telescope. The drive to conduct astronomy research in this case motivates aerial surveillance systems development and; advances small satellite application in education. The drive to conduct astronomy also drives development in remote sensing, satellite meteorology, information and communication technology; and security and defence.

Astronomy has prospects to enable technological development and advance research in information and communication technology, and security and defence. The discussion in [11] is themed towards developing terrestrial and space-based astronomy assets. It also recognizes the potential of astronomy research to enhance the future of life in Africa. However, this does not consider new areas of astronomy such as aerial astronomy [12] and underwater astronomy observations. The knowledge values and development potential of these aspects should also be examined.

The African Union in [13] discusses the developmental role of space science and astronomy in technological development. The conduct of astronomy has enabled the development of technologies such as the geographical positioning systems, space geodesy, and key roles in analyzing ocean and ice level measurements and continental drifts analysis. The conduct of astronomy observations enables development of conceptual and practical skills that can be transferred to other areas like meteorology, and; information and communication technology. These conceptual skills are useful in other domains such as technology research thereby enabling astronomy to have a significant knowledge value. However, exploring this aspect requires further research.

It is recognized in [14] that most astronomy observatories are located in terrestrial and space-based locations. This view is shared with [11] and [13]. The perspective does not consider underwater astronomy. The conduct of terrestrial astronomy and space astronomy is recognized to drive the development of supercomputing technology and big data analysis methods. Though [12], recognizes the importance and role that terrestrial and space-based astronomy plays in driving technological development; its role in role in designing future computing platforms architecture for distributed terrestrial and space-based astronomy requires further consideration.

The development potential of the square kilometer array is considered in [15] where it is recognized that the square kilometer array enables advances in big data processing algorithms and supercomputing. These developments enhance human capital development and positions South Africa as an emerging knowledge economy. It also enables the emergence of private sector spin–offs that participate in the high-tech global value chain. A similar perspective can be found in [16].

The growing interest in underwater astronomy as seen in [17] positions it to address puzzles in physics such as the origin of the cosmic rays. Developmental efforts are required to realize the design of KM3NeT array [16]. However, lessons that can be learnt from the development of digital optical modules and associated software are not deemed to be useful in addressing underwater research and development concerns.

The study in [18] describes procedures required to determine the suitability of an underwater site for hosting an underwater telescope. A desired site should have suitable optical properties, low background noise and bioluminescence. The optical property of water is influenced by its chemical properties. However, the potential of using the optical properties in other applications has not been examined.

This section shows that the desire to conduct astronomy observations drives technological development. This technology advancing role has been motivated mainly by space-based and terrestrial-based astronomy observations. This has not considered underwater astronomy as recognized and addressed in this paper.

3. Underwater Astronomy – Support for Scientific Inquiry

This section explores how ocean exploration and underwater astronomy influences the conduct of investigations in seeking answers to scientific inquiry. It has two aspects. The first and second discuss the motivation for scientific inquiry and the associated system design respectively.

3.1. Rationale for Scientific Investigation

The ocean is a vast resource whose exploration is a key goal of scientific investigation. Being explored to a lesser extent in comparison to earth's terrestrial plane, the ocean serves as a platform enabling the conduct of investigations for the purpose of verifying different claims. An important scientific inquiry being considered is verifying the existence of aquatic humanoids biological species. This is deemed necessary to reduce the propagation of pseudo–science [19–21] in the public domain. In addition, the successful detection (thereby proving their existence) or non–existence is deemed important to enhance knowledge discovery in the information age. The discussion in this section also discusses the implications on future global health.

The launch of underwater telescopes enables increased ocean exploration. This provides access to new ocean regions and opportunities to probe for answers to scientific questions such as verifying the actual existence of aquatic humanoids. The research in [20–21] shows that there is the need to conduct additional research to verify this claim. This can potentially provide answers to questions on public health as the ocean is recognized to host a significant number of marine viruses [22–24]. A potential research step is to investigate how aquatic humanoids (if detected) have developed resilience to marine viruses and marine viral outbreaks.

A successful detection of aquatic humanoids is an advantageous step in studying their adapted and developed immune response to viruses. This is helpful in understanding how to develop new systems and solutions to manage viral outbreaks, epidemics and pandemics. A study in this regard is potentially useful in developing solutions to enhance human viral immunity in the future. This is important for future global public health and human welfare.

3.2. Scientific Investigation–System for Executing Scientific Search

The execution of a search to scientifically provide an answer on the existence of aquatic humanoids requires a probe of the ocean. This probe can be realized via the launch of scientific payload integrated in a system designed for this purpose. However, this approach incurs a high expense making it prohibitive for developing nations and other capital constrained contexts where underwater telescopes have already been deployed. The approach being proposed in this paper is to re–use the existing framework provided by already deployed underwater telescopes to find answers to the scientific inquiry under investigation. This is being considered as it enables the re–use of hardware and computing

infrastructure initially deployed for the purposes of underwater astronomy.

Underwater telescopes comprise photomultipliers that are embedded in digital optical modules [25]. These modules are deployed in a string configuration with a pre-defined separating distance. The strings have 15 m separating distance at depths lying between 745 m to 1270 m. Additional payload to support other scientific investigations in the underwater environment can be placed in the gap i.e. separating distance lying between digital optical modules. For example, the ANTARES neutrino telescope is at a depth of 2475 m [26]. The neutrino telescope in [27] is located in the ocean's bathypelagic zone extending between the depths of 1 km to 4 km. The siting of ANTARES in the bathypelagic zone makes it feasible to conduct ocean related research in this zone. The distance between strings on average in the KM3Net underwater telescope is about 90 m. In addition, the KM3Net underwater telescope has an information and communication network, and supporting infrastructure. The infrastructure is used to transmit acquired results on the scientific search from the ocean.

The payload that executes the search under consideration is hosted in the string gap (separating distance between digital optical modules). It is located in the string gap to prevent disturbance to digital optical module observation. The payload comprises underwater camera (capturing image and video); and underwater acoustic camera. The realization and use of underwater video camera systems is now technologically feasible [28–30]. The underwater video cameras are accompanied with underwater acoustic cameras. The use of underwater acoustic cameras is also feasible because of technology maturation. The underwater acoustic camera detects bio-acoustic signatures from previously undetected biological sources. The underwater video camera [28–30] and acoustic underwater camera [30–32] are deployed to scan the underwater environment. The use of the acoustic underwater camera is deemed suitable because biological sources have acoustic bio-signatures [33]. The deployed cameras are immobile and utilize the computing resources aboard the onshore computing station.

A combination of the acoustic bio–signature, picture (alongside video) at a given epoch is sent to the onshore computing facility. Relations between the digital optical modules, underwater (video), underwater acoustic cameras and the onshore computing facility (hosting several servers) is shown in Figure 1. The servers host computing resources used for algorithm execution and data processing. The digital optical modules and cameras are connected to a central module that is linked to the onshore computing facility.

In Figure 1, the cameras are deployed in a network and have varying coverage in various directions within the underwater environment. The deployed cameras and sensors incorporate the benefit of viewing diversity. The limited viewing capabilities of
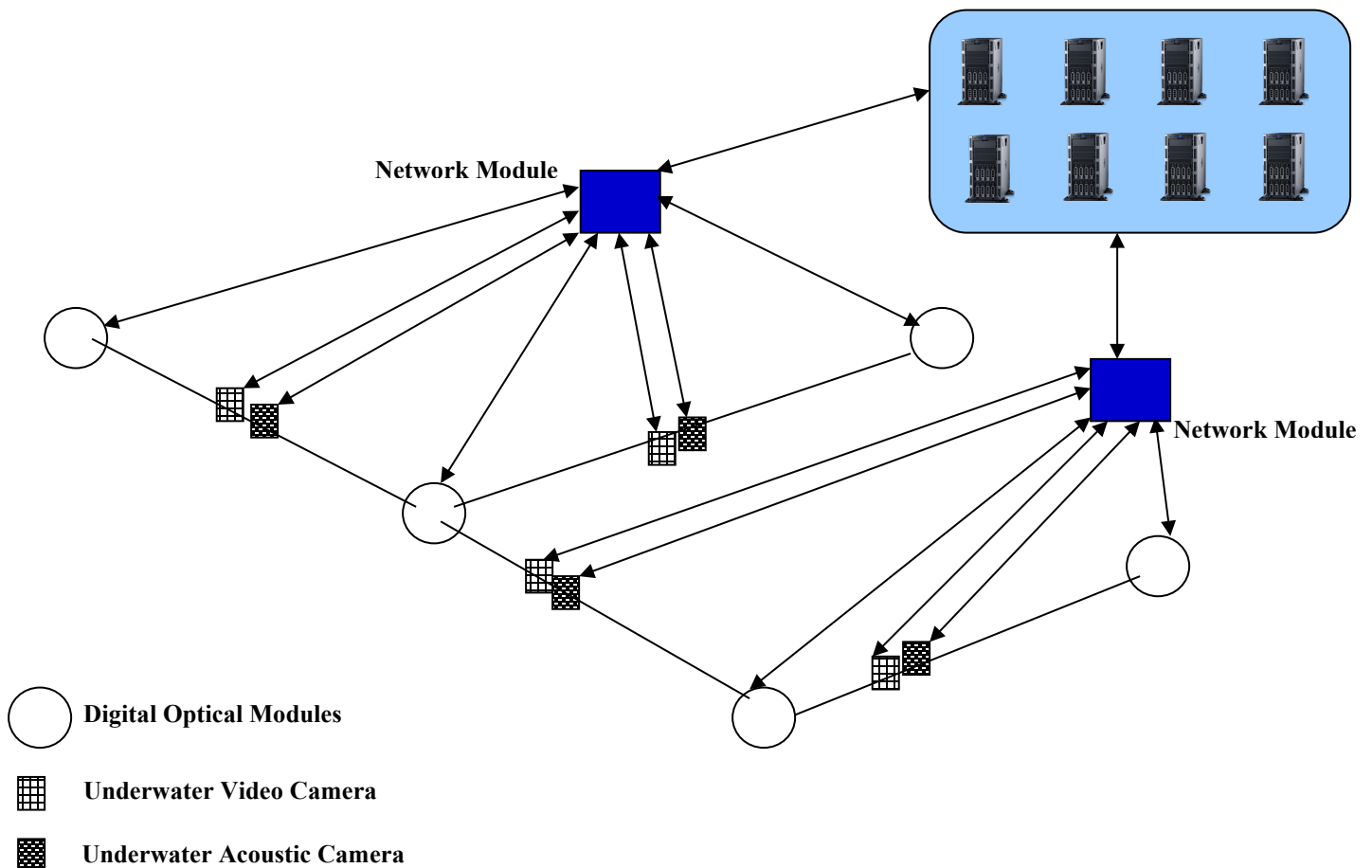
Figure 1: Network Scenario showing the role of the Network Module and Onshore Computing Entity

some cameras and sensors are compensated by cameras and sensors with improved capabilities. Viewing diversity implies the ability of either an acoustic or video camera being able to detect objects that cannot be detected by another acoustic or video camera. This is feasible considering the heterogeneous capabilities of sensors and cameras in a large spatial underwater network.

The consideration of viewing diversity reduces the need to explicitly consider the detecting ranges of sensors and the cameras being presented in Figure 1. This reduces underwater surveillance network design complexity because additional details on the individual technical capabilities of each underwater acoustic sensor and underwater video camera need not be individually considered. In Figure 1, the underwater camera sensors and underwater acoustic camera are stationary. The underwater camera sensors and underwater acoustic cameras differ from the underwater telescope. The underwater telescope is stationary, executes the functionality of the scientific underwater vehicle and is realized by the digital optical module.

As seen in Figure 1, the deployment of the underwater telescopes is considered at different ocean depths. Each depth is also associated with a distance from a reference shore. The underwater cameras and sensors are integrated in the string gaps existing between underwater telescopes. Hence, they constitute the sensors that are placed in the string gaps. String gaps are the spaces un-utilised between conductors that link the digital optical modules intended to capture neutrino radiation in underwater astronomy observation.

Therefore, the sensors placed in the string gaps are also deployed at different ocean depths. The data on the ocean depths are acquired and accessed while planning for the deployment of the underwater telescopes. The underwater cameras and sensors acquire information from a three dimensional perspective. The considered dimensions are the: (1) concerned ocean depth, (2) distance from the reference shore and (3) Epoch of observation. The information on the concerned ocean depth, distance from the reference shore and epoch of observation are associated with each observation by the concerned sensor or camera.

Figure 2: An acoustic camera capable of underwater operation [34]

Figure 3: An underwater video camera suitable for proposed use [35]

The illustration in Figure 4 shows the execution of observation by the underwater acoustic camera and underwater video camera in the string gap. Figure 4 shows the three dimensional

representation as seen in the varying distances of the considered regions from a reference shore and the differing depths. Each region of the underwater environment is being observed by the digital optical module. The combination of each region alongside the underwater acoustic camera and underwater video camera is known as the logical observation group. In Figure 4, there are four logical observation groups i.e. logical observation group 1, logical observation group 2, logical observation group 3 and logical observation group 4. In each observation group, underwater acoustic cameras and underwater video cameras that are integrated into the string gap observe the concerned area. The observation is accompanied with data recording alongside the information on the depth (distance along the vertical i.e., y–axis), distance from the reference shore (along the x–axis) at different epochs (being the time dimension). An observation in this manner results in a three–dimensional observation.
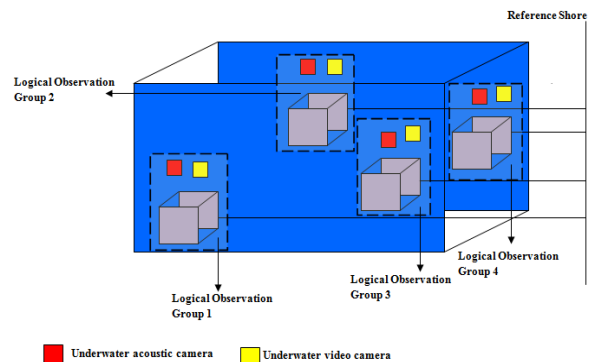
Figure 4: Scenario describing the role of underwater acoustic camera and underwater video camera in observing selected area of the underwater environment. These sensors are integrated into the string gap.

4. Underwater Astronomy – Knowledge Advances and Benefits to Computing Systems Design

The discussion in this section describes how the conduct of underwater astronomy enhances knowledge advances in near ocean and underwater computing systems design. The underwater environment hosts a significant number of applications besides underwater astronomy such as networking and computing. This section has two parts. The first describes the rationale for considering the impact of underwater astronomy in computing networks. The second presents the supporting system model.

4.1. Underwater Astronomy and Computing Systems – A Rationale

The emergence of underwater astronomy necessitates the design of onshore computing station networks. The processing of data arising from underwater astronomy requires designing onshore computing station networks. This is capital intensive. Therefore, it is important to design solutions that reduce the associated costs. The ability of underwater astronomy's computing station to potentially address this challenge is considered in this aspect.

4.2. Underwater Astronomy and Computing – Architecture and System Design Concerns

The advent of underwater astronomy increases the amount of ocean data requiring processing. This increases the volume of data

requiring access to computing resources for processing. The need to enable data processing has necessitated the deployment of onshore computing stations to receive and process data from underwater neutrino telescopes [36–37]. In [36], the trigger and data acquisition system is not integrated with cloud computing systems. Therefore, organizations seeking to deploy underwater telescopes require ownership of onshore computing platforms. The drawback to this perspective is that it increases the cost of conducting underwater astronomy. This is because all organizations desiring to conduct underwater astronomy have to deploy own computing platforms and do not subscribe to existing terrestrial cloud computing platforms. Therefore, it is desirable to design novel network architecture linking onshore computing entities to existing cloud computing platforms. This is because cloud computing has been recognized to be beneficial to astronomy [37]. In the case of underwater astronomy, underwater data centres such as those in [38] are useful. This contributes to knowledge in the area of wireless network architecture.

The use of underwater computing platforms also enhances the PUE in comparison to terrestrial computing platforms [39–40]. The use of underwater computing platforms in data processing is suitable for processing scientific data as seen in [41]. However, designing architecture and network enabling the underwater astronomy telescopes to utilize underwater data centres requires research attention. The need to integrate underwater telescope data processing with underwater computing platforms is beneficial in two aspects. The first is that it enables the design of integrated systems that connect underwater telescope arrays with underwater computing platforms. This is advantageous in terms of contributing to knowledge in systems architecture. The second is that the use of underwater computing platforms opens a new vista for sub–marine application data processing. Therefore, underwater astronomy has prospects in advancing research in network architecture and integrated systems.

5. Underwater Astronomy – Enabling Underwater Surveillance

Deploying underwater telescopes over a vast sub–ocean area provides vast ocean coverage thereby enabling the development of an underwater surveillance strategy. The resulting large area coverage provides a potential underwater surveillance application. This enables the realization of an underwater surveillance network. The discussion here has two aspects. The first discusses the rationale for considering how underwater astronomy can enable underwater surveillance. The second presents a potential system model.

5.1. Underwater Astronomy and Surveillance Applications – Rationale

The deployment and maintenance of underwater telescopes necessitates and increases human–ocean interaction. The maintenance of underwater telescopes can be done at the ocean shore or aboard an ocean vessel at the expense of high logistics costs; and reduced underwater telescope observation time. The maintenance can also be conducted in the underwater environment with reduced degradation in the observation ability of other underwater telescopes. However, this is at the expense of hiring ocean divers for the execution of maintenance procedures. This is challenging because telescope engineers and technicians are not

trained ocean divers. Alternatively, submarines can also be used at the expense of high costs. Nevertheless, these approaches facilitate human–ocean interaction which is useful for underwater surveillance. Underwater surveillance approaches are considered from two perspectives. The first and second considers that maintenance of underwater telescopes is done on the surface (shore or aboard an ocean vessel) and in the underwater environment, respectively.

5.2. Underwater Astronomy–Architecture and System Design Concerns

Underwater surveillance and maritime security are closely related [42–43]. Underwater security can be realized via the use of submarines or autonomous underwater vehicles which is capital intensive. The high cost makes it challenging to ensure adequate underwater maritime security. A conservative estimate shows that a sum of about \$20B is required to design and realize an operational submarine [44]. This is beyond the reach of capital constrained organizations.

Therefore, developing nations have challenges in using submarines for underwater surveillance and security. Autonomous underwater vehicles are a feasible low-cost alternative to submarines. However, deploying multiple autonomous underwater vehicles also has high costs. The scenario shown in Figure 1 describes how cameras can be integrated in the string gap of underwater telescopes. These cameras can be integrated during the execution of a scheduled telescope maintenance manoeuvre.

The deployment of underwater telescopes alongside underwater cameras is suitable for realizing underwater surveillance. In this case, the underwater cameras give a video output that is processed by the organization(s) deploying the underwater cameras and owns the copyright to the video content. The resulting video is processed to extract security related information from the received underwater data. The network of video cameras is also suited for underwater surveillance and is cheaper than using multiple autonomous underwater vehicles. The realization of an underwater surveillance network enables advances in: (i) Video acquisition via underwater camera networks, (ii) Video processing with focus on preference of underwater surveillance, and (iii) integration of video processing results with cloud computing platforms.

Underwater surveillance can also be addressed when the maintenance is conducted in the underwater environment. The design of an underwater vehicle with lower acquisition and operational costs in comparison to submarines is proposed. The required capability can be realized via variable duration short mission manned underwater vehicles. The proposed variable duration short mission underwater vehicle serves as an underwater habitat that hosts telescope technicians and engineers. It hosts the payload used to execute the maintenance procedures. The variable duration short mission underwater vehicle operates for a maximum of 3 hours in the underwater environment before returning to the surface/shore. The telescope technicians and engineers execute the maintenance via robotic arms and do not exit the variable duration short mission underwater vehicle's interior.

The proposed variable duration short mission underwater vehicle is suitable for use by naval authorities for underwater

surveillance applications. In this case, the robotic arms host camera payload and enables the operator to record image and video of the underwater environment. Therefore, regional and national organizations such as the Navy can benefit from technological advancements arising from the need to conduct underwater astronomy.

6. Value Addition – Aspects of the Blue Economy

The development of the blue economy enhances future economic growth [45, 46] and can be realized via marine spatial planning [47, 48]. Marine spatial planning determines the suitability of marine resources for use in different ocean applications. The integration of sensors in the 'string gap' makes it easy to monitor the ocean. The acquired data can be used to determine the best way for allocating ocean resources.

The locating of multiple underwater telescopes in the ocean requires the conduct of ocean survey [47, 48]. This enables the determination of best ocean zones to site underwater telescopes. For example, it is noted in [49] that water composition influences the variation of water's optical parameters. This implies that ocean site selection for placing underwater telescopes involves the acquisition of knowledge on sea water's instantaneous optical and chemical properties. The chemical properties of water influence other factors such as the time varying underwater specific heat capacity. This is useful in the determination of the suitable location for siting underwater data centres.

The discussion in [50] notes that the exploration of maritime resources such as Lake Baikal (Domogatsky, Bezrukov), Atlantic Ocean, Black Sea, Indian Ocean, Pacific Ocean and Mediterranean Ocean (with sites in Zheleznyk and Petrukhin). The exploration of maritime resources in these locations enables the acquisition of data on the maritime resources at the mentioned locations. The acquired underwater maritime underwater data provides a significant amount of underwater and oceanographic big data. The data is suitable for use in determining the physical properties of different aspects of the underwater environment at different epochs. The role of such data in marine spatial planning (for different ocean zones) is recognized in [51, 52].

The blue economy encompasses a significant number of opportunities such as seabed mining [53], large scale fishing, maritime transportation, underwater tourism and seaweed farming. The conduct of underwater astronomy observations provides an opportunity to explore the sub-surface ocean environment. This makes it feasible to determine underwater ocean zones suitable for deploying the applications identified in [54, 55].

The prospects and challenges of underwater technological development has motivated by the conduct of underwater astronomy is shown in Table I. Table I focuses on the prospects and benefits associated with underwater surveillance and the blue economy. The information presented in Table I focuses on how the desire to conduct underwater astronomy can make contributions to underwater surveillance and the blue economy.

7. Performance Formulation

This section examines the benefit of the proposed solution and has two parts. The first and second aspects discuss the performance benefits and formulate the performance model, respectively.

Table 1: Potential Benefits to Ocean Surveillance, Underwater Security and Blue Economy

S/N	Sector	Potential Contributions
1	Underwater Security (infrastructure Acquisition)	Variable duration short mission manned underwater vehicles can be used as low cost entities with capabilities similar to a submarine and suitable for short length missions by a Naval force.
2	Naval Security Services	The use of cameras integrated in the string gap for underwater surveillance improves the naval surveillance services because of the use of a distributed underwater camera network.
3	Technological Development–Robotics	The need to design robotic arms for underwater maintenance and camera positioning contributes to research and technological development.
4	Astronomy Organizations	Sharing of onshore computing facility costs with Naval organizations reduces the cost burden on astronomy organizations.
5	Entertainment: Underwater Media	Acquired underwater video can be sold to channels where it can be viewed as entertaining video content.
6	Marine Spatial Planning	The obtained images and video of the underwater environment can be used to characterize the ocean environment. This is useful for marine spatial planning purposes
7	Blue Economy–Application Identification	A successful marine spatial planning process helps in determining suitable revenue earning applications that can be hosted in a given ocean zones.
8	Knowledge Contribution – Chemical and Optical Properties	The study of the optical properties of ocean water for determining the viability of an underwater location for hosting telescopes provides opportunity to understand the relations between chemical composition of water and its optical properties at an epoch.
9	Computing–Future Computing Platforms	The acquisition of information on chemical properties is suitable for determining the viability of a given maritime resources for hosting underwater data centres; determining number of suitable hosting locations.
10	Knowledge Contribution–Ocean Maps	The information obtained via cameras and used to develop a profile of different underwater ocean zones can be used to develop an ocean profile or underwater map. This is a novel contribution to knowledge.
11	Human Capital Development–Naval Infrastructure	The development of variable length duration manned underwater vehicles (with submarine capability) enables the development of human capital in the aspect of underwater vehicle hardware design and manufacture; as well as software design and realization.
12	Human Capital Development–Software	Processing of Video from underwater environment for security preferences enables skill acquisition with regard to video editing software design and development.

7.1. Performance Benefits

The discussion has proposed the adoption of a multi-domain approach to ocean exploration with a focus on underwater astronomy. In the proposed consideration, external technological and scientific interests are recognized to benefit from the conduct of underwater astronomy. The resulting crowd–sourcing effort reduces the costs of conducting underwater astronomy. In addition, the launch of multiple underwater telescope units' results in an array that enhances the resolution of underwater astronomy observations. This is because multiple entities that were previously unconsidered now launch additional logical underwater telescope units. The benefit of this is an increase in the baseline of the resulting underwater interferometer system. From a perspective of general observation, a longer baseline is beneficial to obtain improved resolution in astronomy observations [56–57]. The launch of additional logical underwater telescope unit at low costs due to the incorporation of a crowd–sourced approach increases the interferometer size and baseline. This improves the observation resolution of underwater astronomy systems.

The integration of onshore computing platforms into the existing cloud computing platform framework increases the computational resources accessible to computing applications. Two computing applications are recognized in this regard. These are underwater astronomy and wireless computing applications. In addition, onshore computing platforms are located at vantage locations where they can easily benefit from free cold air cooling. This is because onshore computing platforms are able to take advantage of the cold air and cold water available in nearby maritime resources such as rivers and the ocean shore. This reduces the reliance on the use of conventional cooling methods that uses components such as air conditioners, pumps and chillers. Therefore, the integration of onshore computing platforms into existing data centers can enhance the PUE.

Therefore, the proposed multi–domain perspective has three benefits. These are: (i) increasing the computational resources accessible to underwater astronomy, wireless networks and computing applications, (ii) Enhancing the PUE of existing cloud computing platforms and (iii) improving the resolution of underwater astronomy.

7.2 Performance Formulation

Let α and β denote the set of vessels and cameras (integrated in the string gap), respectively.

$$\alpha = \{\alpha_1, \alpha_2, \dots, \alpha_A\} \tag{1}$$
$$\beta = \{\beta_1, \beta_2, \dots, \beta_B\} \tag{2}$$

In addition, let γ and Υ be the set of onshore computing platforms and data centers (cloud computing platforms), respectively.

$$\gamma = \{\gamma_1, \gamma_2, \dots, \gamma_C\} \tag{3}$$
$$\Upsilon = \{\Upsilon_1, \Upsilon_2, \dots, \Upsilon_D\} \tag{4}$$

The set of servers associated with the onshore computing platform $\gamma_c, \gamma_c \in \gamma$ and data centers (cloud computing platforms) $\Upsilon_d, \Upsilon_d \in \Upsilon$ are given as:

$$\gamma_c = \{\gamma_c^1, \gamma_c^2, \dots, \gamma_c^I\} \tag{5}$$
$$\Upsilon\Upsilon_d = \{\Upsilon\Upsilon_d^1, \Upsilon\Upsilon_d^2, \dots, \Upsilon\Upsilon_d^J\} \tag{6}$$

Let $C_2(\gamma_c^i, t_y)$, $\gamma_c^i \in \gamma_c$, $t_y \in t$ denote the computational resources accessible on i^{th} server aboard the cth onshore computing platform γ_c at the yth epoch t_y. The computational resources accessible on the jth server aboard the dth computing platform $\Upsilon_d^j, \Upsilon_d^j \in \Upsilon_d$, $t_y \in t$ at the yth epoch t_y is denoted $C_2(\Upsilon_d^j, t_y)$. In the case, where cloud computing platforms are not accessed by underwater astronomy applications, the accessible computing resources, θ_1 is

$$\theta_1 = \sum_{c=1}^{C} \sum_{i=1}^{I} \sum_{y=1}^{Y} C_2(\gamma_c^i, t_y) \tag{7}$$

In the case where cloud computing platforms are accessible by underwater astronomy applications, the accessible computing resources, θ_2 is:

$$\theta_2 = \sum_{c=1}^{C} \sum_{i=1}^{I} \sum_{y=1}^{Y} C_2(\gamma_c^i, t_y) + \sum_{d=1}^{D} \sum_{j=1}^{J} \sum_{y=1}^{Y} C_2(\Upsilon_d^j, t_y) \tag{8}$$

The power required to operate the servers γ_c^i and Υ_d^j at the epoch t_y are denoted as $P_1(\gamma_c^i, t_y)$ and $P_1(\Upsilon_d^j, t_y)$, respectively. In addition, the power required to cool the servers γ_c^i and Υ_d^j at the epoch t_y are denoted as $P_2(\gamma_c^i, t_y)$ and $P_2(\Upsilon_d^j, t_y)$, respectively. The PUE of a cloud computing platform comprising only servers in existing data centers ν_1 is:

$$\nu_1 = \sum_{c=1}^{C} \sum_{i=1}^{I} \sum_{y=1}^{Y} \left(\frac{P_1(\gamma_c^i, t_y) + P_2(\gamma_c^i, t_y)}{P_1(\gamma_c^i, t_y)} \right) \tag{9}$$

When the cloud platform comprises both non–onshore based servers and onshore based servers, the PUE of the resulting cloud computing platform, ν_2 is:

$$\nu_2 = \sum_{c=1}^{C} \sum_{d=1}^{D} \sum_{i=1}^{I} \sum_{j=1}^{J} \left(\sum_{y=1}^{Y} \frac{A + B}{P_1(\gamma_c^i, t_y) + P_1(\gamma\Upsilon_d^j, t_y)} \right) \tag{10}$$

$$A = P_1(\gamma_c^i, t_y) + P_1(\gamma\Upsilon_d^j, t_y) \tag{11}$$

$$B = P_2(\gamma_c^i, t_y) + \left(1 - \acute{\Gamma}(j, d, t_y)\right) P_2(\gamma\Upsilon_d^j, t_y) \tag{12}$$

$\acute{\Gamma}(j, d, t_y)$ is the reduction in the cooling energy on the server Υ_d^j due to the maritime resource at the yth epoch t_y.

Furthermore, let ς denote the set of organizations that benefit from the proposed integration approach such that:

$$\varsigma = \{\varsigma_{ao}, \varsigma_{nao}\} \tag{13}$$

$$\varsigma_{ao} = \{\varsigma_{ao}^1, \varsigma_{ao}^2, \dots, \varsigma_{ao}^F\} \tag{14}$$

$$\varsigma_{nao} = \{\varsigma_{nao}^1, \varsigma_{nao}^2, \dots, \varsigma_{nao}^M\} \tag{15}$$

ς_{ao} and ς_{nao} are the set of underwater astronomy organizations and non–underwater astronomy organizations respectively.

$\varsigma_{ao}^f, \varsigma_{ao}^f \in \varsigma_{ao}$ and $\varsigma_{nao}^m, \varsigma_{nao}^m \in \varsigma_{nao}$ are the fth underwater astronomy organization and m^{th} non–underwater astronomy organization, respectively.

The underwater telescopes associated with the fth underwater astronomy and m^{th} non–underwater astronomy organizations are given as:

$$\varsigma_{ao}^{f} = \{\varsigma_{ao}^{f,1}, \varsigma_{ao}^{f,2}, \dots, \varsigma_{ao}^{f,Q}\} \qquad (16)$$

$$\varsigma_{nao}^{m} = \{\varsigma_{nao}^{m,1}, \varsigma_{nao}^{m,2}, \dots, \varsigma_{nao}^{m,L}\} \qquad (17)$$

The baseline for underwater telescopes $\varsigma_{ao}^{f,q-1}, \varsigma_{ao}^{f,q-1} \in \varsigma_{ao}^{f}$, $(q-1) \geq 1$ (the $(q-1)^{th}$ underwater telescope belonging to the underwater astronomy organization) and $\varsigma_{ao}^{f,q}, \varsigma_{ao}^{f,q} \in \varsigma_{ao}^{f}$ (the $(q)^{th}$ underwater telescope belonging to the underwater astronomy organization) at the epoch t_y is denoted $\ddot{Y}(\varsigma_{ao}^{f,q-1}, \varsigma_{ao}^{f,q}, t_y)$.

The underwater interferometer baseline without and with the synergy are B_1 and B_2 , respectively and given as:

$$B_1 = \sum_{y=1}^{Y} \left(\sum_{f=1}^{F} \sum_{q=2}^{Q} \ddot{Y}(\varsigma_{ao}^{f,q-1}, \varsigma_{ao}^{f,q}, t_y) \right) \qquad (18)$$

$$B_2 = \sum_{y=1}^{Y}(C + D) \qquad (19)$$

$$C = \sum_{f=1}^{F} \sum_{q=2}^{Q} \ddot{Y}(\varsigma_{ao}^{f,q-1}, \varsigma_{ao}^{f,q}, t_y) \qquad (20)$$

$$D = \sum_{m=1}^{M} \sum_{l=2}^{L} \ddot{Y}(\varsigma_{nao}^{m,l-1}, \varsigma_{nao}^{m,l}, t_y) \qquad (21)$$

The resolution of the underwater astronomy radiation if λ is the Cherenkov radiation wavelength, without and with the proposed synergy is denoted $\hslash_1$ and $\hslash_2$, respectively:

$$\hslash_e = \frac{\lambda}{B_e} , e \in \{1,2\} \qquad (22)$$

8. Performance Evaluation and Analysis

The performance evaluation of the proposed mechanism is done using the parameters in Table 2. The computational resource aboard the servers used in the simulation has been chosen considering the parameters used in [58]. The proportion of energy used in cooling servers aboard terrestrial data centers is considered to have a value of 40% as seen in [59]. The value of the power consumption used in servers is motivated by information obtained from [60]. In Table 2, the coverage of underwater telescopes from participating organizations differs from the coverage of telescopes deployed by underwater astronomy organizations. In addition, the baseline in both cases has been selected to have a similar range of values. This is done to prevent a scenario where a greedy approach is used when adding underwater telescopes from participating organizations. The performance simulation and analysis has been performed with the MATLAB software package.

The results for the simulated accessible computational resources and PUE performance is shown in Figure 5 and Figure 6, respectively. The results obtained and presented in Figure 5

shows that the joint usage of onshore computing platforms alongside existing terrestrial computing platforms increases the accessible computational resources. In the existing case, a server unit is a server in an existing terrestrial computing platform. A server unit in the proposed case is a logical combination of individual servers in the onshore and existing terrestrial computing platforms.

Figure 6 shows that the use of the onshore computing platforms with the existing terrestrial computing platforms improves the PUE (a lower PUE is better) because of the reduced cooling energy in onshore computing platforms as they are closer to maritime resources. Onshore computing platforms are sited in near long term low temperature environments such as rural maritime resources. This increases the available cold water that can be freely accessed for server cooling. Such a performance benefit can be seen in the Google Hamina onshore computing platform [60].

Analysis of the results shows that leveraging on a synergy between underwater astronomy organizations and identified technology interests enhance the accessible computational resources, and the PUE. The accessible computational resources and PUE are enhanced by an average of 48.8% and 1.6%, respectively.

The influence of the proposed synergy on the observation resolution is also investigated and the obtained result is in Figure 7. Figure 7 shows that observation resolution improves with an increase in the number of logical telescope units. A lower observation resolution implies that more details can be obtained from the observation procedure and is better than a higher observation resolution. In the proposed case, a telescope deployed by a participating organization and the one telescope deployed by the underwater astronomy organization comprises a logical telescope. However, the logical telescope unit has a longer baseline (i.e. telescope separation) thereby resulting in a lower observation resolution. The simulation uses an observation wavelength of 450 nm for the Cherenkov radiation as obtained from [61]. Analysis shows that the synergy enhances the observation resolution by 41.3% on average.

Table 2: Parameters used for Performance Evaluation

S/N	Parameter	Value
1	Quantity of Servers in the Onshore Computing Platform	70
2	Quantity of Servers in the Existing Terrestrial Computing Platform	120
3	Minimum Computational Resources in the Onshore and Existing Terrestrial Computing Platform Server	[2.02, 0.99] Gbytes
4	Maximum Computational Resources in the Onshore and Existing Terrestrial Computing Platform Server	[78.75,95.95] Gbytes
5	Average Computational Resources in the Onshore and Existing Terrestrial Computing Platform Server	[35.47,44.52] Gbytes
6	Minimum Power Consumed by Server in the Onshore and Existing Terrestrial Computing Platform Server	[0.38, 1.48] W
7	Maximum Power Consumed by Server in the Onshore and Existing Terrestrial Computing Platform Server	[46.29, 71.78] W

8	Average Power Consumed by Server in the Onshore and Existing Terrestrial Computing Platform Server	[19.53, 36.84] W
9	Proportion of power used in cooling servers in existing terrestrial data centers	40%
10	Minimum proportion of cooling power reduction due to onshore location	0.1%
11	Maximum proportion of cooling power reduction due to onshore location	4.92%
12	Average proportion of cooling power reduction due to onshore location	2.54%
13	Number of Underwater Astronomy Organizations	1
14	Number of Participating Organizations	1
15	Minimum Baseline of Underwater Telescopes from Underwater Astronomy Organizations	9.50 m
16	Maximum Baseline of Underwater Telescopes from Underwater Astronomy Organizations	1.99 km
17	Average Baseline of Underwater Telescopes from Underwater Astronomy Organizations	1.01 km
18	Minimum Baseline of Underwater Telescopes from Participating Organizations	114.98 m
19	Maximum Baseline of Underwater Telescopes from Participating Organizations	1.43 km
20	Average Baseline of Underwater Telescopes from Participating Organizations	0.79 km
21	Wavelength of the Cherenkov Radiation under observation ([61])	450 nm.

Figure 5: Simulation results obtained for accessible computational resources

Figure 6: Simulation results obtained for the PUE.
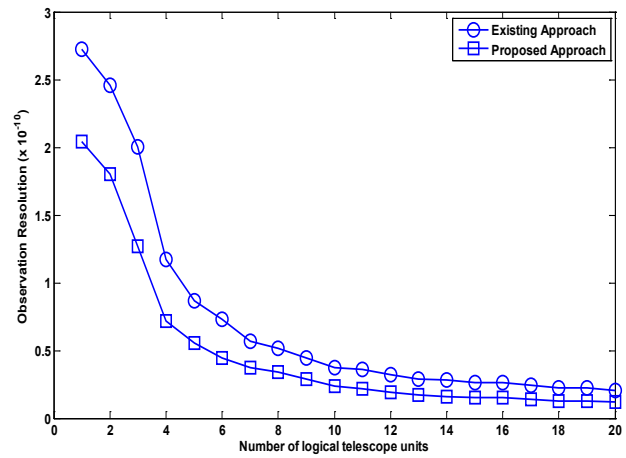
Figure 7: Simulation results obtained for observation resolution

9. Conclusion

This paper recognizes that the future conduct of underwater neutrino astronomy has significant research and knowledge value prospects. The knowledge prospect advances scientific research and knowledge. The identified aspects constitute areas where additional research is required. The paper describes the synergy between underwater astronomy and other applications in computing and scientific investigations. In addition, the performance evaluation examines performance improvements that can be obtained by using the proposed synergistic approach. This is done using computing and observation related metrics. The computing related metrics are the PUE and accessible computational resources. The observation related metric is the observation resolution. Investigation shows that the use of the collaborative approach improves accessible computational resources, PUE and resolution by 48.8%, 1.6% and 41.3% on average, respectively.

Conflict of Interest

The authors declare no conflict of interest.

Acknowledgment

References

[1] J. Baars, T.Beasley, D. Bisikalo, G.Bladon, M.Burton, A.G.de Castro, L.L. Christensen, G.Giovannini, J.M.van der Hulst, C.Keller, A.M. Magalhães, M.Rosenberg and F. Snik, 'From Medicine to Wi–Fi : Technical Applications of Astronomy to Society', (eds) B.Downer, M.Burton, E.van Dishoeck and P.Russo, International Astronomical Union, 2019, [Online] https://www.iau.org/static/archives/announcements/pdf/ann19022a.pdf, Accessed August 4, 2020.

[2] M. Backes, R. Evans, E.K. Kasai, and R. Steenkamp, 'Status of Astronomy in Namibia', Afr. Rev. Phys. **13**, 90-95, 2018, eprint 1811.01440.

[3] M.Rosenberg, P.Russo, G.Bladon and L.L.Christensen, 'Why is Astronomy Important?' [Online], https://arxiv.org/ftp/arxiv/papers/1311/1311.0508.pdf, 2013, Accessed, August 4, 2020.

[4] D.Farrah, K.E. Smith, D.Ardilla, C.M.Bradford, M.Dipirro, C.Ferkinhoff, J.Glenn, P.Goldsmith, D.Leisawitze, T.Nikola, N.Rangwala, S.A.Rinehart, J.Staguhn, M.Zemcov, J.Zmuidizinas, J.Bartlett, S.Carey, W.J.Fisher, J.Kamenetz, J.Kartaltepe, M.Lucy, D.C.Lis, L.Locke, E.L.Rodriguez, M.MacGregor, E.Mills, S.H.Moseley, E.J.Murphy, A.Rhodes, M.Richter,
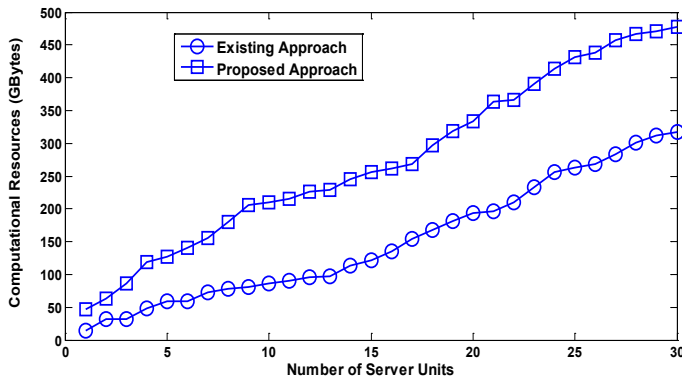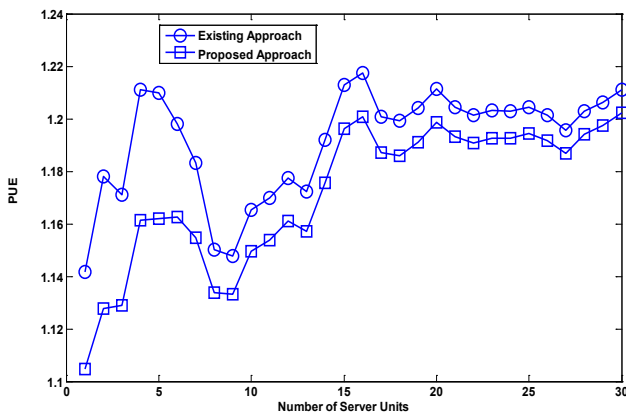
D.Rigopoulos, D.Sanders, R.Sankrit, G.Savini, J.D.Smith and S.Sherwalt, 'Review: - Far Infrared Instrumentation and Technological Development for the next decade', Journal of Astronomical Telescopes, Instruments and Systems, **5**(2), 020901–020901, 2019, https://doi.org/10.1117/1.JATIS.5.2.020901

[5] United Nations, 'Exploring Space Technologies for Sustainable development and the benefits of international research collaboration in this Context Report of the Secretary – General', Commission on Science and Technology for Development, Twenty – Third Session, Geneva, 23–27 March 2020, Item 3(b) of the Provisional Agenda, https://unctad.org/system/files/officialdocument/ecn162020d3amend1_en.pdf

[6] C.Walker, D.Chingo and S.Dubow, 'Karoo Futures: Astronomy in Place and Space – Introduction', Journal of Southern African Studies, **45**(4),627 – 639, 2019, https://doi.org/10.1080/03057070.2019.1654664

[7] M.Boehmer, J.Bosna, D.Brussow, L.Farmer, C.Fruck, R.Gernhauserm, A.Gartner, D.Grant, F.Henningsen, S.Hiller, M.Hoch, K.Holzapfal, R.Jenkyns, Ni, Khera, K.Krings, C.Kopper, I.Kulin, K.Leismuller, J.Little, P.Macroun, J.Michel, M.Morley, L.Papp, B.Pirenne, C.Qiu, I.C.Ree, E.Resconi, A.Round, A.Ruskey, C.Spannfellner and M. Traxler, 'STRAW (STRings for Absorption Length in Water) : Pathfinder for a neutrino telescope in the deep Pacific Ocean', Journal of Instrumentation, 14, 1 – 30 , P02013, 2019, https://doi.org/10.1088/1748-0221/14/02/P02013

[8] S.Aiello, S.E.Akrame, F.Ameli, E.G.Anassontzis, M.Andre, G.Androulakis, M. Anghinolfi, G.Anton, M.Ardid, J.Aublin, T.Avigtals, C.Bagatelas, G.Barbarino, B.Baret, J.Barrios-Marti, A.Belias, E.Berbee, A.van der Berg and J.Zuniga, 'Sensitivity of the KM3Net/ARCA neutrino telescope to point – like neutrino sources', Astro-particle Physics, **111**, 100 – 110 ,2019, https://doi.org/10.1016/j.astropartphys.2019.04.002

[9] C.Spiering, 'History of high energy neutrino astronomy', International Conference on History of the Neutrino: 1930-2018 Paris, France, September 5-7, 2018, (2019), ISBN: 9791096879090

[10] V.McBride, R.Venugopal, M.Hoosain, T.Chingozha and K.Govender, 'The Potential of Astronomy for Socioeconomic Development in Africa', Nature Astronomy, **2**, 511–514, 2018, https://doi.org/10.1038/s41550-018-0524-y

[11] M.Pović, M.Backes, P. Baki, D.Baratoux, S.B Tessema, Z.Benkhaldoun, M.Bode, N.A. B. Klutse, P.Charles, K. Govender, E.van Groningen, E. Jurua, A.Mamo, S.Manxoyi, V.McBride, J.Mimouni, T.Nemaungani, P. Nkundabakura, B.Okere, S.Saad, P.C. Simpemba, T.Walwa and A.Yilma,' Development in astronomy and space science in Africa', Nature Astronomy, 2, 507- 510, 2018, https://doi.org/10.1038/s41550-018-0525-x

[12] AA Periola and O.E. Falowo, 'Instrumentation Location Diversity Paradigm for Future Astronomy Observations, Wireless Personal Communications, **103**, 2475–2499, 2018, https://doi.org/10.1007/s11277-018-5940-x

[13] African Union, 'African Space Strategy – For Social, Political and Economic Integration', [Online] https://au.int/sites/default/files/documents/37434-doc au_space_strategy_isbn-electronic.pdf, Accessed 31/07/2020.

[14] J.Retre, P.Russo, H.Lee, E.Penteado, S.Salimpour, M.Fitzgerald, J.Ramchandani, M.Possel, C.Scorza, L.Lindberg, E.Arends, S.Pompea and W.Schrier, 'Big Ideas in Astronomy - A Proposed Definition of Astronomy Literacy', [Online] https://www.iau.org/static/archives/announcements/pdf/ann19029a.pdf, May 2019, Accessed August 31, 2020.

[15] M.Gastrow and T.Oppelt, 'Big Science and human development–what is the connection?' South African Journal of Science, **114**(11/12), , 1–7, November/December 2018, DOI: https://doi.org/10.17159/sajs.2018/5182

[16] M.J.Sousa, 'Skills to Boost Innovation – In the Context of Public Policies', SWS Journal of Social Sciences and Art, **1**, 90 – 103 , 2019, https://doi.org/10.35603/ssa2019/issue1.09

[17] S.Klein, 'Invest in neutrino astronomy', Nature, **533**, 462 – 464, 2016, doi:10.1038/533462a

[18] C.Fruck and I.C. Rea, 'STRAW: STRings for Absorption length in Water', 36TH International Cosmic Ray Conference, ICRC 2019, **358**, 1–9, PoS, (ICRC2019) 890,July 24TH – August 1ST, 2019, Madison, WI, U.S.A, http://inspirehep.net/record/1701337

[19] A.D.Thaler and D.Shiffman, 'Fish tales: Combating Fake Science in Popular Media', Ocean & Coastal Management, **115**, 88-91, 2015, https://doi.org/10.1016/j.ocecoaman.2015.04.005

[20] V.Scribner, 'Such Monsters Do Exist in Nature? Mermaids, Tritons and the Science of Wonder in Eighteenth Century Europe', Itinerario, **41**(3), 507 – 538, 2017, Cambridge University Press, DOI: https://doi.org/10.1017/S0165115317000663

[21] G.Fauville, 'Ocean Literacy in the Twenty – First Century' in Exemplary Practices in Marine Science Education: A Resource for Practitioners and Researchers (eds), G.Fauville, D.L.Payne, M.E.Marrero, A. Andersson and

F.Crouch, Springer, 2019, 3–11, DOI:10.1007/978-3-319-90778-9

[22] J.E.Welsh, P.Steenhuis, K.R.Moraes, J.V.D.Meer, D.W.Thieltges,and C.P.D.Brussard, 'Marine Virus Predation by non – host organisms', Scientific Reports, 2020, **10**(1),1 -9, 5221, DOI: 10.1038/s41598-020-61691-y

.[23] D.L.Kirchman, 'A marine virus as foe and friend', Nature Microbiology, **5**, 982 – 983, 2020, DOI https://doi.org/10.1038/s41564-020-0764-3

[24] E.Laanto, 'Viruses – The Invisible Majority of the Oceans', 05 Feb 2019, [Online] Accessed 26/07/2020, https://microbiologysociety.org/publications/past-issues/oceans/article/viruses-the-invisible-majority-of-the-oceans.html

[25] A.D.Avrorin, A.V.Avrorion, R.Bannash, I.A. Belolaptikov, V.R.Brudanin, N.M.Budner, N.S.Gorshkov, A.A. Doroshenko, G.V.Domogatsky, R.Dvornicky, A.N.Dyachok, Zh.A.M.Dzhilikibaev, L.Fajt, S.V.Fialkovsky, A.R.Gafarov, K.V.Golobkov, T.I. Gres, K.G.Kebkal, O.G.Kebkal, E.V.Khramov, M.M.Kolbin, K.V.Konischea, A.V.Korobchenko, A.P.Kosheckin, V.A.Kohzim, M.V.Krughov, M.K.Kryukov, V.F.Kulepov, D.A.Kuleshov, M.B.Milenin, R.A.Mirgazov, V.Nazari, A.I.Panfilov, D.P.Petukhov, E.N.Phikovsky, M.I.Rozamov, E.V.Rjabov, V.D.Rushay, G.B.Safronov, F.Simkovic, A.V.Skurichin, B.A.Shaybonov, A.G.Solovjev, M.N.Sorokovikov, A.V.Skurichin, B.A.Shaybonov, A.G.Solovjev, M.N. Sorokovikov, M.D.Shelepov, G.V.Suvrova, I.Shtekl, V.A. Tabolenko, B.A.Tarashanky, S.A.Yakolev, and A.V.Zagorodnikov, 'Spatial Positioning of Underwater Components for Baikal – GVD', EPPJ Web of Conferences, **207**, 1–4, 07004, 2019; VLVnT–2018, https://doi.org/10.1051/epjconf/201920707004.

[26] M. Sanguineti, 'ANTARES and KM3Net: The Latest Results of the Neutrino Telescopes in the Meditterranean', Universe, 2019, **5**(65), 1 – 9, doi:10.3390/universe5020065

[27] B.C.O'Leary, and C.M.Roberts, 'Ecological Connectivity across ocean depths: Implications for Protected Area Design', Global Ecology and Conservation, **15**, 1–10, 2018, e00431, https://doi.org/10.1016/j.gecco.2018.e00431

[28] R.Garcia and N.Gracias, T.Nicosevici, R.Prados, N.Hurtos, R.Campos, J.Escartin, A.Elibol, R.Hegedus and L.Neumann, 'Exploring the Seafloor with underwater robots', Chapter 4, in Land, Sea & Air (eds) A.M.Lopez, A.Imiya, T.Pajdla, and A.M. Alvarez, Feb 10, 2017, https://doi.org/10.1002/9781118868065.ch4

[29] V.Vogler, S.Schneider and J. Willmann, 'High-Resolution Underwater 3-D Monitoring Methods to Reconstruct Artificial Coral Reefs in the Bali Sea: A Case Study of an Artificial Reef Prototype in Gili TrawanganIn Journal of Digital Landscape Architecture , **4**, 275–289. doi:10.14627/537663030.

[30] F.Ferreira, and D.Machado, G.Ferri, S.Dugelay and J.Potter, 'Underwater Optical and Acoustic Imaging: A Time for Fusion? A Brief overview of the State of the Art, Science and Technology' Organization Centre for Maritime Research and Experimentation, Reprint Series, June 2019, CMRE –PR-2019 – 078, doi: 10.1109/OCEANS.2016.7761354

[31] Underwater Acoustic Cameras, https://dosits.org/galleries/technology-gallery/observing-and-monitoring-marine-animals/underwater-acoustic-cameras/

[32] Y.Wang, Y.Ji, H.Woo, Y.Tamara, H.Tsuchiya, A.Yamashita and H.Asama, 'Rotation Estimation of Acoustic Camera Based on illuminated Area in Acoustic Image', IFAC PapersOnline, **52**(21), 163 – 168, 2019, https://doi.org/10.1016/j.ifacol.2019.12.301

[33] M.Thomas, B.Martin, K.Kowarski, B.Gaudet and S.Matwin, 'Marine Mammal Species Classification using Convolutional Neural Networks and a Novel Acoustic Representation', in U.Brefeld, E.Fromont, A.Hotho, A.Knobbe, M.Maathuis, and C.Robardet (eds), Machine Learning and Knowledge Discovery in Databases, ECML, PKDD 2019, Lecture Notes in Computer Science, 11908, 290–305, 2019, DOIhttps://doi.org/10.1007/978-3-030-46133-1_18

[34] 3D Acoustic Camera 3D Array [Online] https://www.cae-systems.de/fileadmin/CAEpage/Datenblaetter/datasheet-acoustic-camera-3D-array.pdf, Accessed: Jan 09, 2020.

[35] R. Bailey, 'The Best Underwater Cinema Cameras: An overview of cinema cameras for underwater use',[Online] Available: https://www.uwphotographyguide.com/cinema-cameras-underwater-review, Accessed: Jan 09, 2020.

[36] C.Pellegrino, 'The Trigger and Data Acquisition System (TriDAS) of the KM3Net experiment', Nuovo Cim.C, **39**(1), 1–4, 2016, 10.1393/ncc/i2016-16250-9

[37] M.Favaro, T.Chiarusi, F.Giacomini, M.Manzali, A.Margiotta and C.Pellegrino', The Trigger and Data Acquisition System for the KM3Net – Italia Towers', EPJ Web of Conferences, **116**(05009), 05009–15, 2016, DOI: 10.1051/epjconf/201611605009

[38] A.M.Smith, R.Pike, W.O'Mullane, F.Economov, A.Bolton, I.Momcheva, A.E.Bauer, B.Becker, E.Bellm, A.Conmolly, S.M.Crawford, N.Hathi, P. Melchior, J.Peek, A.Solmaz, R.Thomson, E.Tollerud, and D.W.Liska, 'Astronomy should be in the clouds', In Bulletin of the American Astronomical Society , **51**, 55, 2019, arXiv:1907.06320

[39] A.A Periola, 'Incorporating diversity in cloud-computing: a novel paradigm and architecture for enhancing the performance of future cloud radio access networks', Wireless Networks, **25**(7), 3783–3803, 2019, , DOIhttps://doi.org/10.1007/s11276-018-01915-2

[40] A.A Periola, A.A Alonge and KA Ogudo, 'Architecture and System Design for Marine Cloud Computing Assets', The Computer Journal, **63**(6), 927 – 941, https://doi.org/10.1093/comjnl/bxz169

[41] J.Roach, 'Microsoft's Undersea Data Centre Helps the hunt for a COVID – 19 Vaccine', [Online], https://news.microsoft.com/innovation-stories/project-natick-covid-19/, June 16, 2020, Accessed: 27/07/2020.

[42] N.Klein, 'Maritime Autonomous Vehicles within the International Law Framework to Enhance Security International Law Studies', Maritime Autonomous Vehicles, **95**, 244–271, 2019, https://digital-commons.usnwc.edu/cgi/viewcontent.cgi?article=2907&context=ils, ISSN: 2375-2831

[43] T.Prodan, J.Kasum, M.Stosic, and C.Ugrin, 'Security Challenges and Guideline Proposals for the Development of Underwater Security', National Security and the Future, **1–2**(20), 2019, 71 – 84, https://hrcak.srce.hr/231824

[44] M. Hellyer, 'the Cost of Defence: ASPI Defence Budget Brief', 2019 – 20, Australian Strategic Policy Institute, 2019, http://nla.gov.au/nla.obj-770022340

[45] N.J.Bernett, A.M.Montemayor, J.Blythe, J.J.Silver, G.Singh, N.Andrews, A.Calo, P.Christie, A.D.Franco, E.M.Finkbeiner, S.Gelgich, P.Guidetti, S.Harper, N.Hotte, J.N.Kittinger, P.C.Bilton, L.Lister, R.L.Lama, E.McKinley, J.Scholtens, A.M.Solas, M.Sowman, N.T.Alvarez, L.C.L.Teh, M.Voyer and U.R.Sumaila, 'Towards a sustainable and equitable blue economy', Nature Sustainability, **2**, 991–993, 2019, DOI: https://doi.org/10.1038/s41893-019-0404-1.

[46] I.Ertor, and M. Hajimichael, 'Editorial: Blue degrowth and the politics of the sea: rethinking the blue economy', Sustainability Science, **15**, 1–10, 2020, DOI: https://doi.org/10.1007/s11625-019-00772-y.

[47] I. Lukic and M.Rabaut, 'Marine Spatial Planning to Create Space for a sustainable economy', [Online] https://www.gstic.org/inspiration/marine-spatial-planning-sustainable-blue-economy/ Jan 27, 2020, Accessed July 28, 2020.

[48] Kira Gee, 'The Ocean Perspective' in Marine Spatial Planning – Past, Present and Future (eds) Jacek Zaucha, and Kira Gee, 2018, 23 – 45, DOI 10.1007/978-3-319-98696-8

[49] K.G.Balasi, D.Lenis, M.Maniatis, N.Moragos, and G.Stavropoulos, 'A Method for measuring the optical parameters of Deep Sea Water', frontiers in Physics, **6**, Nov 2018, Article 132, 1–11, https://doi.org/10.3389/fphy.2018.00132

[50] C.Spiering, 'History of Neutrino Astronomy and Neutrino Telescopes', 2018, [Online], neutrinohistory2018.in2p3.fr/talks/07_spiering.pdf, Accessed 28/07/2020.

[51] R.Retzlaff and C.LeBleu, 'Marine Spatial Planning: Exploring the Role of Planning Practice and Research', Journal of Planning Literature, **33**(4) 466–491, 2018, https://doi.org/10.1177/0885412218783462

[52] C.F.Santos, C.N.Ehler, T.Agardy, F.Andrade, M.K.Orbach, and L.B.Crowder, 'Marine Spatial Planning 'in World Seas: an environmental evaluation, Academic Press, 571–592, 2019, eBook ISBN: 9780128052037

[53] Rosanna Carver, 'Lessons for blue de-growth from Namibia's emerging blue economy', Sustainability Science, **15**, 131–143, 2020, DOI: https://doi.org/10.1007/s11625-019-00754-0.

[54] I.O.Yarwood, N.I.Kadagi, N.A.F.Miranda, J.Uku, I.O.Elegbede and I.J.Adewumi, 'The Blue Economy – Cultural Livelihood – Ecosystem Conservation Triangle: The African Experience', Frontiers in Marine Science, **7**(586), 1–18, 2020, https://doi.org/10.3389/fmars.2020.00586

[55] C.M.Rogerson and J.M.Rogerson, 'Emergent Planning for South Africa's blue economy: Evidence from Coastal and Marine Tourism', Urbani izziv, **30**, 24–36, Supplement, 2019, DOI: 10.5379/urbani-izziv-en-2019-30-supplement-002

[56] R.M. Roettenbacher, 'Interferometry with Meter – Class Telescopes', 2019, Contrib. Astron. Obs. Skalnat´e Pleso, **49**, 97–106, https://ui.adsabs.harvard.edu/abs/2019CoSka..49...97R/abstract

[57] G.Bourdarot, H. G.deChatellus and J.P. Berger, 'Toward a large bandwidth photonic correlator for infrared heterodyne interferometer: A first laboratory proof of concept', Astronomy and Astrophysics, **639**, A53, 1–7, https://doi.org/10.1051/0004-6361/201937368

[58] Y.Yamato, 'Server Selection, Configuraton and Reconfiguration Technology for Iaas Cloud with Multiple Server Types', Journal of Network and Systems Management, **26**, 339-360, 2018, DOI: https://doi.org/10.1007/s10922-017-9418-z

[59] J.Kyathsandra, and C. Rego, 'The Efficient Data Center: Improving Datacenter Efficiency Through Intel Technologies and High Ambient Temperature Operation', [Online] https://www.intel.co.jp/content/dam/doc/technology-brief/efficient-datacenter-high-ambient-temperature-operation-brief.pdf, Accessed September 16, 2020.

[60] Z.Zhou, 'GreenEdge : Greening Edge Datacenters with Energy–Harvesting IoT devices', IEEE International Conference on Network Protocols, 8 – 10 Oct 2019, 1–6, Chicago IL, USA, USA, DOI: 10.1109/ICNP.2019.8888103

[61] U.F Katz, 'Cherenkov light imaging in astroparticle physics', Nuclear Instruments and Methods in Physics Research Section A: Accelerators, Spectrometers, Detectors and Associated Equipment, **952**, 161654, 2020, DOI: 10.1016/j.nima.2018.11.113

ASTES

Text Mining Techniques for Sentiment Analysis of Arabic Dialects: Literature Review

Arwa A. Al Shamsi[*], Sherief Abdallah

The British University in Dubai, Faculty of engineering and IT, Dubai, 345015, UAE

A R T I C L E I N F O	A B S T R A C T
	Social media attracts a lot of users around the world. Many reasons drive people to use social media sites such as expressing opinions and ideas, displaying their diaries and sharing them with others, social communication with family and friends and building new social relationships, learning and sharing knowledge. Written text is one of the most common forms used for communication while using social media sites. People use written texts in different languages, and due to the increased usage of social networking sites around the world, the amount of texts and data resulting from this use is large. These generated data considered as a valuable source of information that attracted business owners, companies, government institutions, and of course, it attracts researchers and data scientists as well. Researchers and data scientists increasingly presented great efforts in investigating and analyzing Arabic Language texts. Most of these efforts targeted the Modern Standard form of Arabic Language. While exploring the social media sites, most of the Arab users tend to use their dialects while utilizing Social Media sites, which results in generating a massive amount of Arabic Dialects texts. The number of researches and analysis of Dialects' form of the Arabic language are limited, however, it is increasing recently. This literature review aims to explore approaches and methods used for Sentiment Analysis of Arabic Dialects text.

1. Introduction

Social Media sites have become very popular in society, the popularity of social media is increasing day by day. Recently, many people prefer to spend their time using various applications in smart devices and using the Internet as well. Perhaps social media may take the majority of this usage. People use social media for various reasons such as online shopping, learning, communication, expressing opinions and ideas, sharing their diaries, and many different reasons. People tend to express their opinions, thoughts, feelings, and comment on the various topics that are posted on social media using their dialects. Dialects are the informal form of the language. Each country of the Arab world has its Dialect, and each dialect has many sub-dialects. In [1], the author stated that the population of the Arab world prefer to utilize their dialects in their daily communication, Arabic dialects increasingly utilized online for communications and in social media, moreover, Arabic dialects utilized in TV shows as well as radio programs. As social media usage increased sharply, the amount of data generated as a result of this usage is increasing as well. In [2], the author stated that due to the great amount of data in the form of Natural Language generated in a daily manner online, there is a great need to process this kind of data. This huge amount of generated data attracted companies' owners, marketers

and business owners, government institutes and, scientists and researchers as well.

Recently, the world witnesses the revolution of Artificial Intelligence, Data Science, and Machine Learning. Researchers and data scientists are increasingly interested in studying and analyzing natural language texts. Great efforts and researches increasingly targeted the Modern Standard form of Arabic Language, however, researches that targeted the dialects form of Arabic language are limited. In [1], the author stated that due to the limited tools and software that can be utilized for Dialects, researches that targeted dialects are very limit. Many factors affected this limitation, such as the dialect's complexity. Authors in [3] stated that the Dialectal form of the Arabic language has no standard written format which is considered a challenge for analyzing and processing Arabic Dialects. Authors in [4] added to the Arabic Dialects challenges the Diacritical issue and explained how it may change the meaning of the same word, moreover, authors explained how negation may be considered as a challenge while dealing with Arabic Dialects.

This literature review aims to explore researches that involve constructing resources for Arabic Dialects and investigate approaches and methods used for Sentiment Analysis of Arabic Dialects text, focusing on machine learning approaches and Lexicon-based approaches.

[*]Corresponding Author: Arwa Ahmed Al Shamsi, 20180935@student.buid.ac.ae

2. Literature Review

2.1. Arabic Language Background

Arabic is one of the most popular languages that are spoken by millions of people all around the world. In [5], the author stated that the Arabic language is considered the fifth most common language that is spoken by more than 420 million people all around the world. The Arabic language has its unique features. It consists of 28 letters and it is written from the right side to the left side. In [6], the author mentioned that based upon statistics presented by Wikipedia in 2018; the Arabic language is the official language of 25 nations and 380 million is the approximate number of Arabic speakers. In [7], the author mentioned that the Arabic language is one of the Semitic languages meaning that it is written from the right side to left, moreover, Arabic language letters shape changed according to the position of the letter in the word itself. In [1], the author stated that Arabic language letters are used as well in Malay, Urdu, and Persian languages. The Arabic Language is written from right to left. The Arabic language has three types i.e. Classical Arabic which is the language of the Holy Qur'an, Modern Standard Arabic, and Dialectal Arabic form. The Arabic language attracted researchers due to the increased usage of this language over the internet. In [7], the author stated that Arabic users over social media are increasing year after year according to official statistics, this increase resulted in a massive amount of data generated daily online that are in Arabic language. Hence, there is an increasing need for powerful tools and effective approaches for processing Arabic language texts that are in either the Modern Standard Arabic form or in the Arabic Dialects form.

2.1.1. Modern Standard Arabic

Modern Standard Arabic (MSA) is the standard form of the Arabic language that is used in formal papers, schoolbooks, education, TV news, newspapers, street signs, etc. Modern Standard Arabic has a written standard format while the dialects are not. As mentioned earlier, the Arabic language attracted researchers due to the increased use of this language over the internet. Most of the researches that targeted the Arabic language focused on the Modern Standard Arabic form of the Arabic language. In [8], the author stated that NLP tools and applications are mostly based upon the Modern Standard Arabic form of the Arabic language. Modern Standard Arabic is closer to Classical Arabic compared to Arabic Dialect that is less related to classical Arabic. In [9], the author attracted by NLP for Arabic Language and most of the researches done concentrated on MSA as reported in a systematic review.

2.1.2. Arabic Dialect

Arab World consists of 22 countries. Each of these Arab countries has a special Arabic dialect that their population used for daily conversations and talk. In [1], the author mentioned some of the most common Arabic Dialects such as Levantine Arabic, Egyptian Arabic, Gulf Arabic, North African Arabic, and many other Arabic Dialects are spoken by the Arab population. It stated that the Arab population prefers to use their dialects in their daily communication, Arabic dialects increasingly used online in social media sites, moreover, Arabic dialects appeared and utilized in TV shows as well as radio programs. The main dialect for each country can be divided into more sub-dialects. It stated that Arabic Dialects consists of Arabic and non-Arabic words that exist as a result of many reasons; an example of the reasons: Gulf people traveling to India and Iran, moreover, European traders came to Gulf countries after oil discovery, these reasons resulted in non-Arabic words existence in Gulf dialects. In [10], the author interested in their research in studying Arabic dialects. The authors described how Gulf Arabic dialect is the language of the population of Gulf Cooperation, however, this Gulf Arabic dialect is differing slightly between the population of each of the Gulf Cooperation Countries. In [1], the author mentioned that the limited number of Dialects software and NLP tools resulted in limited works and researches that studied and analyzed Dialects. However, [9] in a systematic review presented some research papers that have studied Arabic Dialects. Authors presented valuable researches done in the field of basic language analysis such as ADAM which is an Analyzer for Dialectal Arabic Morphology of Egyptian and Levantine dialectal language, and CALIMA which is an analyzer for Egyptian dialects morphological. Authors as well presented researches and works that have been concentrated on building resources such as Curras which is a dataset of Palestinian dialects and it consists of 56,000 morphologically annotated tokens, DART which is a dataset of around 25000 Arabic tweets, ArabicWeb16 which is a dataset of 10.8 TB of Arabic dialects, CALYOU which is a dataset of Algerian dialect, NileULex which is an Arabic sentiment lexicon of Egyptian and Levantine dialects in addition to Modern Standard Arabic, and TSAC dataset which is sentiment analysis dataset for Tunisian dialects.

2.2. Machine. Learning

Machine Learning involves constructing systems and models that can be improved over experience. It stated that Machine Learning involves machines and systems that can program themselves to learn and get the knowledge needed for better performance. The most common machine learning methods are Classification, Clustering, Regression, Deep Learning and Neural Networks, Transfer Learning, Word Embeddings, Natural Language Processing, Dimensionality Reduction, Reinforcement Learning, and Ensemble Methods. Deep Learning and Neural Networks, Word Embeddings, Transfer Learning, and Natural Language Processing methods of Machine Learning will be further explained below.

2.2.1. Deep Learning and Neural Networks

Deep Learning and Neural Networks are considered a revolutionary approach in the Machine Learning domain. In [6], the author explained that Artificial Neural Network utilized for complex problem solving as it functions in a way similar to Neural Network in brains of humans. Deep Neural Networks are known for their accuracy as well as outstanding performance. Deep Learning approaches are used increasingly for NLP tasks. Researchers utilized Deep Learning approaches for Arabic NLP. As an example of researches used Deep Learning for Arabic NLP: [6] used nine Deep Learning models for text categorization. Moreover, they utilized Word Embeddings approaches and evaluated performance and accuracy. Results showed that all of the nine Deep Learning models presented very good performance and high accuracy, moreover, the use of Word embeddings increased the accuracy and improved the performance. Additionally, in [11] the author investigated different Deep Learning models for Arabic Dialects text classification. Authors concentrated on Egyptian, Levantine, and Gulf dialects and reported that for Egyptian-Gulf pair; Bi-Directions LSTM offered better performance than other Deep Learning models, while for other dialects pairs; LSTM presented better performance.

2.2.2. Transfer Learning

Transfer learning involves using tasks or models that have been learned and transfer the learned knowledge along with applying improvements for a new task or model. In [12], the author defined transfer learning as the process of using data from a source domain to solve problems in another domain. The problem aimed to be solved is related to the data from the source domain, but it is different. In [13], the author successfully presented a model in which Transfer Learning can be used effectively in the case of multiple source domains used for solving problems in multiple target domains. In [14], authors used the Transfer Learning method for ANLP. Transfer learning was used as an extension for the word embeddings model. Authors investigated the effectiveness of the extension applied to skipgram model, the extension involved incorporation of lemmas and efficient use of word2vec word embedding model. The authors reported that the extended model presented better performance than word2vec and fastText on the Arabic word similarity task.

2.2.3. Word Embeddings

Word embeddings is an emerging field that involves distributed word representations which mean representing words as vectors in space. Word Embeddings models are either monolingual or bilingual. The most common is the monolingual models. In [15], the author stated that monolingual word embedding models can be utilized for word order and morphology, while bilingual word embedding models can be utilized for machine translation and parallel sentence extraction. The authors explained that bilingual word embedding models are vector representations of two languages, these languages are mapped into the same space. Word Embeddings have been implemented and utilized for NLP purposes. In [16], the author stated that word embeddings involve using semantic features for representing words as vectors, word embeddings utilized in NLP most commonly for classification and sentiment analysis. In [17], the author stated that the most common Word Embeddings methods are Word2Vec and GloVe. In [18], the author mentioned that there are 4 Arabic word Embeddings which are CBOW, GloVe, Skip-gram model, and Arabic part of the Polyglot word embeddings. The authors evaluated 4 Arabic word embeddings models utilizing benchmark and reported that the best performance achieved from the CBOW model, while the least performance was achieved from the Polyglot model of word embeddings. In [5], the author defined Word Embeddings as vectors used to represent words in continuous space to find any relation between them. The authors presented AraVec which is an open-source Word Embeddings project utilized in the ANLP field. In [19], authors enlarged the informative content of the training sentences by efficient adaptations to word embeddings tools which result in improving the accuracy and performance. Authors as well were able to successfully utilize one embedding space to represent disparate dialects.

2.2.4. Natural Language Processing NLP

Language is the way of communication between people. Language helps us to understand the world around us. The languages that are spoken by people all around the world are known as natural languages. Natural Language Processing (NLP) involves the use of computers to understand and deal with natural languages. In [70], the author define NPL as a section of Artificial Intelligence and Computer Science that involves studying the interactions between human natural languages and computers, moreover, NLP involves Natural Language understanding and generation. The authors mentioned that the increased information in natural language form increased the need for understanding and processing this kind of information. In [2], the author agreed that the massive amount of Natural Language form of data generated daily online increased the need for processing this kind of data. The authors identified NLP as the process of automatic analysis, understanding, and presentation of human Natural Languages.

2.2.4.1. Arabic Natural Language Processing ANLP

ANLP is short for Arabic Natural Language Processing and it involves automatic analysis and processing of Arabic Natural Language. As mentioned earlier, the Arabic Language has three main forms; Classical Arabic, Modern Standard Arabic (MSA), and Arabic Dialects (AD). ANLP tools are supposed to have the ability to deal with the three forms of the Arabic language. However, Classical Arabic is rarely targeted by researchers as it represents the Arabic form of the Holy Qur'an. Tools and techniques are mostly utilized for MSA compared to AD. In [10], the author stated that the use of ANLP tools for AD may be hard due to the nature of AD and the differences between MSA and AD i.e. phonological differences and morphological differences.

2.3. Researches and works on Arabic Dialects

Recently, Arabic Dialects AD attracted researchers. The need to analyze, classify and process the Arabic dialects is increasing due to the fact of increasing the content of Dialect texts, especially in Social Media as stated in [10] . The authors stated that efforts done on MSA are big compared to the works on AD which are limited and mostly targeted Egyptian and Saudi Dialects. However, researchers increasingly do researches and studies that targeted AD. Researches conducted on AD involve basic language analysis, building resources, language identification, and Semantic level analysis. One of the most common examples of semantic level analysis is Sentiment Analysis.

2.3.1. Basic Language Analysis

Basic language analysis for Arabic Dialects involves Orthographic Analysis, Morphological Analysis, and Syntactical Analysis. Sections below present a brief description of each of the basic language analysis type.

2.3.1.1. Arabic Dialects Orthographic Analysis

Arabic dialects have no standard orthographic format meaning that the same word can be written in two or more different ways which may release challenges for NLP tools. In [8], the author stated that MSA and AD are phonologically different, AD have no standard orthographic, i.e. there is no standard format for written AD, Arabic Dialects usually written based upon its phonetics which makes it difficult for analyzing and processing AD. Researchers presented efforts in orthographic analysis for the Arabic language. In [20], the author introduced CODA which is a Conventional Orthography for Dialectal Arabic. CODA offered a computational model that can be utilized for AD. In [21], the author presented valuable efforts in providing conventional orthography that can be utilized for Tunisian Arabic. The presented conventional orthography is based upon CODA that was mentioned earlier. In [10], the author introduced Gumar Corpus which is a Gulf dialects corpus that consists of 110 million words. The corpus was annotated, and the authors presented guidelines for standard orthography analysis.

2.3.1.2. Arabic Dialects Morphological Analysis

The Arabic language is recognized as a rich language of Morphology. In [22], the author defined morphology as the science that involves extracting the word's branches from the word's source. In [8], the author explained how the morphology of MSA is different from the morphology of AD even the grammar, as well as stems of words, may differ. The exploration of Arabic dialects morphology attracted researchers early. In [23], the author introduced MAGEAD which is an Arabic Language Morphological analyzer. MAGEAD is considered as an online morphological generator as well as an analyzer. In [24], the author presented an accurate Egyptian dialect morphological analyzer which is an extension for the Egyptian Colloquial Arabic Lexicon. In [25], the author constructed a lexicon for Tunisian dialects and proposed an approach for Tunisian dialects morphological analysis. Researchers presented efforts as well in constructing a corpus that is morphologically annotated. In [26], the author successfully constructed a morphologically annotated Emirati dialects corpus that consists of about 200,000 words.

2.3.1.3. Arabic Dialects Syntactical Analysis

Dialects are different syntactically, the syntax in dialects affected by many factors, the most common factor that affect the syntax of Arabic dialects is the foreign languages. Syntactical analysis for Arabic dialects has been addressed in several research papers. In [27], the author explored the difficulties in Arabic dialects syntactic analysis, the authors proposed an approach for constructing treebank for Tunisian dialects. In [28], the author proposed a method that involves integration between syntactic analysis and morphological tagging for automatic diacritization of the Arabic language. The method is applied through the case and features prediction improvements. In [29], the author presented guidelines used for syntactic annotation for the treebank of Quranic Arabic dependency which is part of Quranic Arabic Corpus. In [30], the author proposed CamelParser which is a syntactic dependency analysis system for the Arabic language. The proposed system can be used for Morphological Disambiguation.

2.3.2. Building Resources

Researchers worldwide have done great efforts on collecting corpus for Modern Standard Arabic MSA, researchers increasingly attracted by Dialectal Arabic, Great efforts as well have been done to collect corpus for Arabic Dialects.

2.3.2.1. Modern Standard Arabic Corpus Resources

Researchers are increasingly attracted by the Arabic language analysis. One of the most important efforts conducted in the field of ANLP is building resources for the Arabic language. Most of the resources that have been built for the Arabic language are in the form of MSA. In [8], the author stated that almost all available Arabic datasets are for MSA form. Below are some of the researches in which great efforts have been conducted to create corpora of MSA. In [6] the author created two corpora of Modern Standard Arabic text i.e. SANAD and NADiA from Arabic news articles and offered the created corpora as open-source for the public to be utilized for further researches. Moreover, in [31] the author constructed a corpus of MSA that is manually annotated on the sentence level. The corpus was collected from newswire documents. In [32], the author presented AWATIF which is a corpus of MSA that is labeled for Sentiment Analysis purposes at the sentence level. In [33], the author presented noticeable efforts for creating a corpus of MSA from online newspapers.

2.3.2.2. Arabic Dialect Corpus Resources

Dialectal Arabic involves all the dialects that the population of the Arab World use. Arabic Dialects can be categorized according to the region and similarity into: (1) Gulf Dialects which include the Arabic Dialects Spoken by Arab Gulf people, (2) Egyptian Dialect, (3) Levantine Dialect which involves dialects spoken by the population of Palestine, Jordan, Syria, and Lebanon, (4) North African Dialect which include dialects spoken by Morocco, Algeria, Libya and Tunis people. In [8], the author stated that social media websites are considered as one of the most precious sources of AD as people tend to express their thoughts and opinions in written forms using their dialects. In [34], the author stated that although the Arabic Language has been used in a wide range online, the available Arabic datasets are still limited. Internet World Stats statistics represented that the Arabic Language is the fourth most common language used across the internet. Recently, researchers tend to present efforts in ANLP and especially in creating an Arabic corpus that can benefit researches in the ANLP domain. In [10], the author constructed corpus for Gulf Dialects that made up of 100 million words collected from 1200 forum novels, and this Gulf Dialects corpus called Gumar Corpus. In [26], utilized Gumar Corpus to collect a corpus of Emirati dialects. The Collected Emirati dialects consist of around 200,000 words of Emirati Dialects. In [8], the author created a Dialectal Arabic Dataset that include Gulf Dialects, Egyptian Dialect, Levantine Dialects, and North African Dialects. In [34], the author presented BRAD 2.0 which is an extension to BRAD 1.0 corpus. BRAD 1.0 is a dataset of Arabic book reviews that can be utilized for Sentiment Analysis as well as Machine Learning. While BRAD 2.0 is a dataset that is much bigger than BRAD 1.0 and it consists of more than 600,000 Arabic book reviews written in both Modern Standard Arabic and Dialectal Arabic. The Arabic dialects in BRAD 2.0 dataset are Gulf, Egyptian, and Levantine. In [35], the author successfully constructed a corpus of MSA and Saudi Dialect from Twitter and manually annotate the constructed corpus, and offered the constructed corpus for the research community. The authors named the generated corpus AraSenTi-tweet corpus, number of tweets collected were 2.2 million tweets while after annotation the remaining tweets are 17,573 tweets. In [36], the author constructed a corpus of Arabic Dialects. The sources for the corpus text are from Twitter, Facebook, and Newspapers comments. The corpus consisted of Gulf, Egyptian, North African, Levantine, and Iraqi dialects. Twitter texts are classified based upon either seed words, or coordinate points. While Comments from Facebook and Newspapers are classified depending on the nationality of the page owner and country of Newspapers respectively. The authors as well presented an online game that is utilized for text annotation. In [37], the author constructed two corpora i.e. News Corpus (NC) and Arts Corpus (AC) both corpora consist of Arabic Dialects texts from Facebook that can be utilized for Sentiment Analysis. From the above, it is clear how researchers are increasingly interested in building resources for Arabic Dialects. In this literature review, the author targeted research papers that are published in the period from 2014 onward. The databases the author utilized are IEEE, Springer, ScienceDirect, ACM, and WorldCat. The keywords mentioned below have been used for collecting the research papers:

- "Arabic Dialects" and "lexicon"
- "Arabic Dialects" and "dataset"
- "Arabic Dialects" and "corpus"

The inclusion criteria for research papers:

- Must involve constructing resources (dataset / corpus / lexicon) for Arabic Dialects.

- Must be for Arabic Dialect texts only.
- Must be published in the period from 2014 onward.
- Research paper published in journal or conference

Table 1: research and studies that involve constructing a dataset for Arabic Dialects texts

Ref	Data size	Platform or Source	Dialect type	Annotated	Features Extracted
[10]	Gumar Corpus: 110 million words	from 1,200 forum novels	Gulf Arabic	Yes, for sub-dialects at document level for the dialect, novel name and writer name for each	
[26]	about 200,000 words	from eight Gumar corpus novels in the Emirati Arabic variety	Emirati Dialect	Yes, manually annotated	
[8]	13,876,504 word	Twitter, comments from online newspapers, and Facebook	Gulf, Iraqi, Egyptian, Levantine, and North African.	Yes, manually using annotation tool	
[34]	BRAD 2.0 : 692586 annotated reviews	Arabic Book Reviews from www.goodreads.com	MSA and DA (Egyptian, Levantine, and Gulf)	Yes	Yes, unigrams and bigrams
[38]	8000 tweets	Twitter	Arabic and mostly Egyptian	Yes, tweets were labelled into positive, negative, neutral and both	
[71]	Arabic Online Commentary Data set AOC : 52.1M words	Three online newspapers Al-Ghad from Jordan, Al-Riyadh from Saudi Arabia, and Al-Youm Al-Sabe' from Egypt	MSA and Arabic Dialects	Yes, at sentence level	
[35]	AraSenTi-Tweet Corpus: 17,573 tweets	Twitter	Saudi Dialect	Yes, manually and lablled into: positive, negative, neutral and mixed	
[36]	200K tweets, 10K online newspaper comments, and 2M comments from Facebook → total words= 13.8M words	Twitter, Facebook, and Online newspaper	Gulf Dialect, Iraqi Dialect, Egyptian Dialect, Levantine Dialect, and North African Dialect.	Yes, using online game	
[37]	2000 posts, (1000 posts News Corpora NC), and (100 post Arts Corpora AC)	(NC) Al Arabiyya News Facebook page posts, and (AC) collected from The Voice Facebook page	Arabic Dialects	Yes, manual annotation	
[39]	Egyptian Dialect Gender Annotated Dataset (EDGAD) : 70000 tweets	Twitter	Eygptian Dialects	Yes, manually	N-Gram Feature Vector (NFV)
[40]	438,931 tweets	Twitter	Arabic Dialects	Yes, automatically	Ngrams feature
[41]	7698 comments	Facebook	Algerian Vernacular Arabic	Yes, manually	
[42]	1800 tweets	Twitter	MSA and Jordanian Dialect	Yes, manually	N-grams TF-IDF TF
[43]	ArSentD-LEV: 4000 tweets	Twitter	Levantine Dialect	Yes, via crowdsourcing	
[44]	Curras: more than 56 K tokens	Facebook, Twitter, Blogs, and Forums	Palestinian Dialect	Yes, manually	
[45]	194 negative comments & 194 positive comments	Three Algerian newspapers	Algerian Dialect	Yes, by two Arabic native speakers	
[46]	8000 messages	Facebook	Algerian dialect (Arabic and Arabizi)	Yes, automatically	
[47]	151,548 tweets	Twitter	MSA and Egyptian Dialect	Yes, manually	
[48]	Around 6 million tweets	Twitter	MSA and Arabic Dialects	Yes, automatically	

Table 1 illustrates some of the research and studies that involve constructing a dataset for Arabic Dialects texts. Table 2 below illustrates some of the research and studies that involve constructing a Lexicon for Arabic Dialects texts.

Table 2: research and studies that involve constructing a Lexicon for Arabic Dialects texts

	Data size	Platform or Source	Dialect type	Method
[38]	8000 tweets	Twitter	Arabic and Egyptian	lexicon was created by the human annotators from tweets
[7]	1527 idioms and 7358 Words	From NileULex [51]	MSA and Egyptian Dialect	Extend NileULex which is an Arabic sentiment lexicon
[51]	NileULex: 5953 unique terms	Perivoulsy available lexicons	MSA and Egyptian Dialect	Automatically and manually update to lexicons that are developed earlier
[37]	2817 lexemes	(NC) Al Arabiyya News Facebook page posts, and (AC) collected from The Voice Facebook page	Arabic Dialects	Lexemes were extracted from the posts
[50]	words lexicon, idioms lexicon, emoticon lexicon and special intensified word lexicon	Constructed from different datasets based on manual annotation	Arabic Dialects	Lexicons were built by tool dynamically and expanded incrementally over time.
[41]	Keywords lexicon (L1): 2380 negative polarity and 713 positive polarity	Arabic and Egyptian Lexicon	Algerian Vernacular Arabic	Lexicons built by translating words from Arabic and Egyptian Lexicons
	Negation words lexicon (L2)	MSA dictionary		
	Intensification words Lexicon (L3)	MSA dictionary		
[52]	2000 topics (1000 tweets and 1000 comments)	Twitter and Arabic microblogs	MSA and Egyptian Dialect	Basic lexicon is manually collected and annotated, then synonym set and antonym set are used for automatic expansion of the lexicon
[53]	25086 words	Dialect Lexicon	Algerian dialect	Construct a dialect lexicon then merge two lexicons (a dialect and a sentiment lexicon)
[54]	AIPSeLEX: 3632 idioms/ proverbs	Websites and books	MSA and Egyptian Dialect	Collected and annotated manually at sentence level

2.3.2.1. Arabic Dialect lexicon

Great researches and studies have been conducted in the field of creating lexicon for the English Language texts that can be used for the NLP domain while a limited number of research papers considered creating lexicon for Arabic Language either in its Modern Standard Arabic form or Arabic Dialects form. In [37], the author defined lexicon as a set of lexemes utilized for text classification. In [49], the author created a lexicon of MSA form of Arabic Language. The created lexicon used for text classification and the accuracy was high and reached around 97% of classification accuracy. In [37], the author successfully developed a lexicon that can be utilized for Sentiment Analysis. In [50], the author utilized 5 datasets for lexicon construction. All the utilized datasets are constructed from Twitter i.e. consisted of tweets that are annotated. the generated lexicon is dynamic as it is updated automatically to include new words. Table 2 below illustrates some of the research and studies that involve constructing a Lexicon for Arabic Dialects texts.

2.3.3. Language Identification: Arabic Dialect Identification

Language Identification involves the automatic identification of the language from speech or text. Researchers are increasingly interested in exploring approaches for dialects identification. Arabic Dialect Identification involves dialect automatic identification either dialectal text identification or dialectal speech identification. Some of the researches and studies in the domain of dialect identification are mentioned below. In [55] authors identified and classified Arabic Dialects text of 25 cities of the Arab world. Results were promising as the accuracy of the developed system was 67.9% for sentences of about 7 words length and 90% accuracy in the case of utilizing 16 words. Additionally, in [71] the author utilized an annotated dataset of online newspaper contents to train classifiers for the identification of Arabic dialects. The proposed system determines whether the given sentence is in Modern Standard Arabic form or Gulf, Levantine, Egyptian, Iraqi, Maghrebi dialects forms.

2.3.4.   Semantic-level Analysis

The semantic-level analysis involves Machine Translation and Sentiment Analysis. In this literature survey, the author concentrated on Sentiment Analysis for Arabic dialects.

2.3.4.1. Sentiment Analysis Literature

One of the most common implementations that involve the use of NLP is Sentiment Analysis (SA). SA involves classifying text to describe whether its expressions are positive or negative. In some cases, the text is classified into positive, negative, or neutral. In [38], the author mentioned that Sentiment Analysis involves the text classification based upon its polarity or emotion. In [17], the author stated that people recently tend to express their thoughts, ideas, and opinions about products, services, etc. on websites, blogs, social media, and many other channels through the web. This massive content generated by users all over the world attracted NLP researchers. In [34], the author mentioned how Sentiment Analysis is important for investigating public attitudes

toward product or services, Sentiment Analysis as well can be used for exploring wider public opinions. In [56], the author agreed that online websites and applications recently considered as a valuable source of opinions that can benefit business owners, services providers as well as customers who aim to explore public reviews about different products or facilities, etc. In Arab world, Arab people usually tend to use dialect language in their daily life rather than MSA form. Moreover, Arab people express their ideas and opinions as well thoughts through the web most commonly using their dialectal form of language which results in generating a massive amount of dialectal Arabic texts that are considered a challenge for ANLP researchers.

2.3.4.1.1. Sentiment Analysis Approaches

There are different approaches used for Sentiment Analysis; Lexicon-based approach for Sentiment Analysis in which lexicon is utilized, Machine learning approach for Sentiment Analysis, or in some cases, researchers utilized an approach that is a combination of both Lexicon-based approach and Machine Learning approach. In [7], the author mentioned that the Sentiment Analysis approaches are the Lexicon-based approach, machine

learning approach, and hybrid approach which is a mix of both approaches. In this literature review, the author targeted research papers that are published in the period from 2014 onward. The databases the author utilized are IEEE, Springer, ScienceDirect, ACM, and WorldCat. The keywords mentioned below have been used for collecting the research papers:

- "Arabic Dialects" and "Sentiment Analysis"
- "Arabic Dialects" and "Sentiment Analysis" and "approach"

The inclusion criteria for research papers:

- Must involve Sentiment Analysis experiment study
- Must be for Arabic Dialect texts only.
- Must be published in the period from 2014 onward.
- Research paper that is published in journal or conference.

Table 3 below presents a comparative summary between the different approaches that are used so far in recent researches and studies for Sentiment Analysis of Arabic Dialects.

Table 3: Approaches that are used so far in recent researches and studies for Sentiment Analysis of Arabic Dialects

Ref	Data size	Platform	Dialect type	Features	Approach		Performance			
							Accuracy	Precision	Recall	F-Measure
[38]	8000 tweets	Twitter	Arabic and mostly Egyptian	unigrams, bigrams and trigrams	Lexicon-based approach		0.665	0.485	0.845	N/A
					machine learning approach: Naive Bayes		0.7	0.47	0.35	N/A
[34]	BRAD 2.0 : 692586 annotated reviews	Arabic Book Reviews from www.goodreads.com	MSA and DA (Egyptian, Levantine, and Gulf)	unigrams and bigrams	Naive Bayes (NB)		87.14	N/A	N/A	N/A
					Decision Tree (DT)		83.80	N/A	N/A	N/A
					Random Forest (RF)		86.18	N/A	N/A	N/A
					XGBoost		88.71	N/A	N/A	N/A
					Support Vector Machines (SVM)		90.68	N/A	N/A	N/A
					Convolutional Neural Networks (CNN)		89.61	N/A	N/A	N/A
					Recurrent Neural Networks (RNN)		90.05	N/A	N/A	N/A
[7]	2067 tweets	Twitter	MSA and Egyptian Dialect	Ngrams	Lexicon + Look-Up stemmer		82.58	N/A	N/A	N/A
					Lexicon + Look-Up stemmer + idioms list		90.8	N/A	N/A	N/A
					Lexicon + Look-Up stemmer + idioms list + SVM		96	N/A	N/A	N/A
[50]	No of tweets: 1-ASTD: 9,174 2-MASTD: 1850 3-ArSAS: 19,762 4-GS: 4,191 5-Syrian Tweets	Twitter	Arabic Dialects	Feature Vector	Hybrid system apply Machine Learning approaches and Lexicon based approaches	Unbalanced 3-Class Results	73.67 (RNN)	N/A	N/A	68.57 (L2R2)
						Balanced 3-Class Results	66.83 (L2R2)	N/A	N/A	66.55 (L2R2)
						Unbalanced 2-Class Results	83.73 (L2R2)	N/A	N/A	82.03 (L2R2)
						Balanced 2-Class Results	79.87 (SVM)	N/A	N/A	79.86 (SVM)

Ref	Corpus	Source	Dialect	Features	Method	Classifier				
	Corpus: 2000 6- ArTwitter: 2000 tweets					Lexicon Update Results	85 (RNN)	N/A	N/A	84.95 (RNN)
[40]	75,774 positive tweets and 75,774 negative tweets	Twitter	Arabic Dialects	Ngrams	ML classifiers	NB	95.91	96.15	95.90	95.90
						BNB	98.00	98.00	98.00	98.00
						MNB	98.19	98.21	98.18	98.18
						ME	94.18	94.44	99.31	94.17
						Ada-Boost	73.76	78.95	73.75	72.53
						SVM	99.31	99.32	99.31	99.31
						LR	98.96	98.98	98.97	98.97
						SGD	99.11	99.12	99.11	99.11
						RR	99.96	99.96	99.96	99.96
						PA	99.96	99.96	99.96	99.96
[17]	-Health services dataset: 2026 tweets	Twitter	Arabic Dialects	TF, TF-IDF, POS, Lex, Auto-Lex	-Word2Vec model used to build an Automatic Arabic Lexicon that used with different Machine Learning methods		0.85 to 0.92	N/A	N/A	N/A
	-subset of the dataset: 1732 tweets				- Word2Vec used apart from of the lexicon in Convolutional Neural Networks in order to expand the vocabularies		0.87 to 0.95	N/A	N/A	N/A
[41]	7698 comments	Facebook	Algerian Vernacular Arabic	Code-Switched; French encoded in Arabic letters; combination of the two first features; words written in a form that most Algerians generally used	Lexicon Based Approach		79.13%	N/A	N/A	N/A
[57]	7287 comments — Tunisian dialect-TSAC corpus; 10254 comments — Morocco dialect-ElecMorocco2016; 200 words — Magrebi dialect-Northafrica corpus		Algerian Dialect	Bag of Words (BOW), word2vec and doc2vec	Best result on different corpus presented in tis table	Shallow Learning	N/A	94%	86%	78%
						Deep Learning	N/A	84%	83%	83%
[42]	1800 tweets	Twitter	MSA and Jordanian Dialect	N-grams TF-IDF TF	NB		83.61	79.38	93.11	84.73
					SVM		88.72	92.10	84.89	88.27
[58]	(ASTD): 10006 tweets	Twitter	Arabic Dialect	-	narrow convolutional neural network (NCNN): classification at sentence level		N/A	N/A	N/A	75.90
[45]	SANA: 194 negative comments & 194 positive comments	Three Algerian newspapers	Algerian Dialect	N-grams TF-IDF TF TO BTO	SANA dataset	SVM	72.16	N/A	N/A	N/A
						NB	75.00	N/A	N/A	N/A
						KNN	66.49	N/A	N/A	N/A
	OCA: 250 positive reviews and 250 negative reviews				OCA dataset	SVM	82.80	N/A	N/A	N/A
						NB	89,80	N/A	N/A	N/A
						KNN	88.40	N/A	N/A	N/A
[59]	22550 tweets	Twitter	MSA and Jordanian Dialect	-	Dialectal words translated	SVM	N/A	0.878	0.868	0.867
						NB	N/A	0.905	0.997	0.876

					into MSA form using Dialects lexicon then classifiers were used				
[60]	3550 tweets	Twitter	Jordanian Dialect	N-grams	SVM	0.84	0.85	0.84	0.84
					NB	0.58	0.71	0.58	0.54
[61]	17,573 tweets	Twitter	MSA and Saudi Dialect	Semantic, Stylistic, and Tweet-specific features	Lexicon-based approach (calculates TweetScore) and corpus-based approach (SVM along with features)	N/A	N/A	N/A	69.9
[62]	Five datasets	Twitter and Facebook	MSA and Arabic Dialects	N-gram Embeddings	Embeddings were composed and learned using unordered composition function and a shallow neural model.	88.2	87.4	88.4	87.8
[63]	3 datasets	Twitter and Facebook	MSA nd Tunisian Dialect	N-grams TF	Lexicon-Based Approach	81.9	83.2	83.4	81.9
					Supervised approach — SVM	94.0	93.9	93.8	93.9
					Supervised approach — NB	82.7	83.9	82.5	82.5
[47]	151,548 tweets	Twitter	MSA and Egyptian Dialect	TF-IDF	NB	95.98	96.22	95.98	95.97
					AdaBoost	72.83	77.27	72.82	71.66
					SVM	98.94	98.95	98.94	98.94
					ME	94.22	94.48	94.22	94.21
					RR	99.90	99.90	99.90	99.90

* only best classification results in term of accuracy, recall, Precision, and F-measure are included in this table

2.3.4.1.2. Applications of Sentiment Analysis

Companies, Government authorities, institutions as well show great interest in Sentiment Analysis. In [64], the author explained in detail some of the most common applications of Sentiment Analysis. In the field of business, Sentiment Analysis can be utilized for consumer reviews analysis. Such implementations of Sentiment Analysis witnessed in Google Product search and Amazon websites. Moreover, Business owners and companies value the information retrieved from Sentiment Analysis as it would positively affect their production and help them apply required improvements. On the other hand, in the business field, Sentiment Analysis can be utilized for advertising and commerce online as well as for brand reputation. While in the political field, Sentiment Analysis can be used for monitoring public opinions about government practices and services provided. Sentiment Analysis can be utilized as well in the finance field to monitor financial situations and avoid financial risks. These are some of the applications in which Sentiment Analysis can be effectively used.

2.3.4.1.3. Sentiment Analysis of Arabic Dialect

Huge works for Sentiment Analysis have been conducted and targeted the English language, moreover, researches in the field of Sentiment Analysis for the Arabic Language are increasing as well. In [56], the author stated that limited works and researches have been conducted for Arabic Sentiment Analysis due to many reasons such as the morphological complexity nature of the Arabic Language, the requirement for pre-processing, feature representation, spam opinion elimination and handling the negation in Arabic language. The authors explained how the Arabic language has complex morphological nature such as words with different meanings that may have the same root. Sentiment Analysis for Arabic dialects has been addressed by several research papers. Below are some of the researches and studies that investigated Sentiment Analysis for Arabic Dialects. In [7], the author perform automatic extraction of opinions over social media that are written in MSA and Egyptian Dialects, Authors analyzed

Sentiment automatically into either positive or negative. In [50], the author successfully generated hybrid system that can be utilized for Sentiment Analysis for Arabic language. The developed system offered high accuracy and great performance as lexicon was generated from five datasets and it intelligently allows for an automatic update to include new words. In [65], the author utilized OCA freely available corpus and generated ARMD corpus, both are for movie reviews analysis. The authors utilized both supervised and unsupervised approaches for Sentiment Analysis, after that, the authors combined both approaches. The authors reported that the hybrid approach in which supervised and unsupervised methods are used offered the best results in terms of precision, recall, and F-measure. In [22], the author stated that the most common classifiers for Sentiment Analysis of Arabic language are Support Vector Machine and Naïve Bayes. Authors found that the hybrid approach for Sentiment Analysis presented the best results in terms of preciseness both at the document level and sentence level. In [1], the author proposed a rule-based stemmer that can be utilized for gulf dialects. The performance of the offered stemmer is better than other algorithms. The offered stemmer as well showed acceptable accuracy. In [38], the author presented valuable efforts in creating a web-based tool that can be utilized for Sentiment Analysis of Arabic text. The presented web-based tool was developed using the R language and it showed good performance in term of Accuracy. To perform Sentiment analysis for Arabic dialects, some important steps should be taken into consideration such as Pre-Processing and Feature Extraction.

2.3.4.1.3.1. Pre-Processing

Pre-processing is a critical step; sometimes it is referred to as normalization and it involves transforming the word into its standard form. In [38], the author define the pre-processing step as the process of cleaning data to reduce errors and improve Sentiment Analysis performance. In [34], the author mentioned that the pre-processing step for the dataset would allow classifiers to efficiently learned the dataset. In [16], the author stated that pre-processing is essential for Arabic Natural Language Processing

implementations such as sentiment analysis and summarization tasks. Authors explained that pre-processing for Dialectal Arabic involves the following steps: Tokenization, Remove Diacritics, remove non-Arabic words and letters, Remove Punctuations, replace Arabic Letters (أ,إ,آ), (ة), (ئ,ي) and (ؤ) with (ا), (ه), (ي) and (و) respectively. [56] as well described the pre-processing steps and mentioned that it involves Tokenization, non-Arabic words removal, Normalization, stop words removal, and light stemming. In [7], the author stated that the steps of pre-processing involve Tokenization which means text splitting into separated words, Normalization which involve return letters into the same form, all stop words are removed, and finally words stemming.

2.3.4.1.3.2. Feature Extraction

Sentiment Analysis involves text classification. The classification of texts requires the selection and extraction of text features. Features are the classifier's input. In [39], the author stated that feature selection is the process of extracting features that would affect the classification process. In [38], the author explained how features can be utilized for analyzing raw data. In [66], the author stated that features include part of Speech, frequency, opinion words, and negation. In [38], the author stated that the most common features utilized are N-grams which is frequency (terms presence) features, and the most commonly utilized type of N-grams is unigram followed by bigram and trigram. In [34], the author stated that bigram features consider two words, and these words most commonly come together. Authors mentioned as well that bigram tokens can be effectively utilized for negation detection for either MSA or AD as well. In [55], the author effectively extracted words n-grams and characters n-grams and utilized them as features for AD identification.

2.3.4.1.4. Machine Learning Approaches for Sentiment Analysis of Arabic Dialects

Machine Learning techniques have been widely used for Sentiment Analysis purposes for Many Languages. Machine Learning techniques as well have been used for Sentiment Analysis for the Arabic Language. In [22], the author stated that machine learning techniques can be used in sentiment analysis for Arabic text and SVM presented good performance when used for the sentiment analysis of Arabic texts. In [40], the author utilized Machine learning approaches for Sentiment Analysis for Arabic Dialects. The authors utilized different classifiers for Sentiment Classification of a labeled dataset and reported that PA and RR classifiers presented the best results in terms of accuracy, recall, F-measures, and precision. However, in [6] the author stated that the utilization of Deep Learning approaches recently for NLP tasks presented better performance and results. Table 3 above presents a comparative summary between the different approaches that are used so far in recent researches and studies for Sentiment Analysis of Arabic Dialects.

2.3.4.1.5. Sentiment Analysis for Arabic Dialects Challenges

In [22], the authors mentioned several challenges encountered while working with ANLP such as its complexity. Moreover, fewer works and researches have been done in the field of the Arabic Language compared to English language. In [10], the author presented how Dialectal Arabic does not have a standard orthographic written form. In [3], the author described how dialectal Arabic has no standard written form which results in a lack of NLP tools for Arabic Dialects. In [1]. the author mentioned challenges while working with Arabic dialects; Arabic dialects

have no standard written format, moreover Arabic Dialects have complicated morphological forms. In [7], the author agreed that the Arabic language has complex nature; for MSA each word has a root and the task of finding the root for words is not easy and may reduce the accuracy, moreover, the Dialectal Arabic represents the language of different regions, meaning that each Dialect has its collection of words and this would add further challenges to Dialectal Arabic processing and analyzing tasks. In [4], the author mentioned several challenges while dealing with the Arabic language, first, Diacritical may change the meaning of the same word, second, the negation in Arabic may be challenging compared to English language in which negation is presented mostly using the prefix, moreover, the use of dialectal Arabic may present spelling errors since there is no standard written form for Arabic dialects.

3. Conclusion

Social media attracts people all around the world. Due to the increased utilization of Social Media, a massive amount of written text is generated daily and considered as a valuable source of information that attracted business owners, companies, government institutions, and of course, it attracts researchers and data scientists as well. Natural Language Processing NLP is an important field of science that involves studying and analyzing Natural language texts. Increasing efforts were presented in investigating and analyzing the Modern Standard form of Arabic Language as well as the Arabic Dialects. This literature review aims to explore researches that involve constructing resources for Arabic Dialects and investigate approaches and methods used for Sentiment Analysis of Arabic Dialects text, focusing on machine learning approaches and Lexicon-based approaches.

4. References

[1] B. Abuata, A. Al-Omari, "A rule-based stemmer for Arabic Gulf dialect," Journal of King Saud University - Computer and Information Sciences, **27**(2), 104–112, 2015, doi:10.1016/j.jksuci.2014.04.003.

[2] P.D. Kilmer, "Review Article: Review Article," Journalism: Theory, Practice & Criticism, **11**(3), 369–373, 2010, doi:10.1177/1461444810365020.

[3] F. Mallek, B. Belainine, F. Sadat, "Arabic Social Media Analysis and Translation," Procedia Computer Science, **117**, 298–303, 2017, doi:10.1016/j.procs.2017.10.121.

[4] L. Almuqren, A.I. Cristea, "Framework for sentiment analysis of Arabic text," HT 2016 - Proceedings of the 27th ACM Conference on Hypertext and Social Media, 315–317, 2016, doi:10.1145/2914586.2914610.

[5] A.B. Soliman, K. Eissa, S.R. El-Beltagy, "AraVec: A set of Arabic Word Embedding Models for use in Arabic NLP," Procedia Computer Science, **117**, 256–265, 2017, doi:10.1016/j.procs.2017.10.117.

[6] A. Elnagar, R. Al-Debsi, O. Einea, "Arabic text classification using deep learning models," Information Processing and Management, **57**(1), 2020, doi:10.1016/j.ipm.2019.102121.

[7] H. H. Mustafa, A. Mohamed, D. S. Elzanfaly, "An Enhanced Approach for Arabic Sentiment Analysis," International Journal of Artificial Intelligence & Applications, **8**(5), 1–14, 2017, doi:10.5121/ijaia.2017.8501.

[8] A. Alshutayri, E. Atwell, "A social media corpus of Arabic dialect text," Computer-Mediated Communication and Social Media Corpora. Clermont-Ferrand: Presses Universitaires Blaise Pascal, 1–23, 2019.

[9] I. Guellil, H. Saâdane, F. Azouaou, B. Gueni, D. Nouvel, "Arabic natural language processing: An overview," Journal of King Saud University - Computer and Information Sciences, (xxxx), 2019, doi:10.1016/j.jksuci.2019.02.006.

[10] S. Khalifa, N. Habash, D. Abdulrahim, S. Hassan, "A large scale corpus of Gulf Arabic," Proceedings of the 10th International Conference on Language Resources and Evaluation, LREC 2016, 4282–4289, 2016.

[11] L. Lulu, A. Elnagar, "Automatic Arabic Dialect Classification Using Deep Learning Models," Procedia Computer Science, **142**, 262–269, 2018, doi:10.1016/j.procs.2018.10.489.

[12] S.J. Pan, J.T. Kwok, Q. Yang, "Transfer learning via dimensionality reduction," Proceedings of the National Conference on Artificial

Intelligence, **2**, 677–682, 2008.

[13] Y. Yoshida, T. Hirao, T. Iwata, M. Nagata, Y. Matsumoto, "Transfer learning for multiple-domain sentiment analysis - Identifying domain dependent/independent word polarity," Proceedings of the National Conference on Artificial Intelligence, **2**, 1286–1291, 2011.

[14] P. Shapiro, K. Duh, "Morphological Word Embeddings for Arabic Neural Machine Translation in Low-Resource Settings," 1–11, 2018, doi:10.18653/v1/w18-1201.

[15] A. Erdmann, N. Zalmout, N. Habash, "Addressing noise in multidialectal word embeddings," ACL 2018 - 56th Annual Meeting of the Association for Computational Linguistics, Proceedings of the Conference (Long Papers), **2**, 558–565, 2018, doi:10.18653/v1/p18-2089.

[16] E.H. Almansor, A. Al-Ani, "Translating dialectal Arabic as low resource language using word embedding," International Conference Recent Advances in Natural Language Processing, RANLP, **2017-Septe**, 52–57, 2017, doi:10.26615/978-954-452-049-6-008.

[17] A.M. Alayba, V. Palade, M. England, R. Iqbal, "Improving Sentiment Analysis in Arabic Using Word Representation," 2nd IEEE International Workshop on Arabic and Derived Script Analysis and Recognition, ASAR 2018, 13–18, 2018, doi:10.1109/ASAR.2018.8480191.

[18] M. Elrazzaz, S. Elbassuoni, C. Helwe, K. Shaban, "Methodical evaluation of Arabic word embeddings," ACL 2017 - 55th Annual Meeting of the Association for Computational Linguistics, Proceedings of the Conference (Long Papers), **2**, 454–458, 2017, doi:10.18653/v1/P17-2072.

[19] A. Erdmann, N. Zalmout, N. Habash, "Addressing noise in multidialectal word embeddings," ACL 2018 - 56th Annual Meeting of the Association for Computational Linguistics, Proceedings of the Conference (Long Papers), **2**, 558–565, 2018, doi:10.18653/v1/p18-2089.

[20] N. Habash, M. Diab, O. Rambow, "Conventional orthography for dialectal Arabic," Proceedings of the 8th International Conference on Language Resources and Evaluation, LREC 2012, 711–718, 2012.

[21] I. Zribi, R. Boujelbane, A. Masmoudi, M. Ellouze, L. Belguith, N. Habash, "A conventional orthography for tunisian Arabic," Proceedings of the 9th International Conference on Language Resources and Evaluation, LREC 2014, 2355–2361, 2014.

[22] A. Alsayat, N. Elmitwally, "A comprehensive study for Arabic Sentiment Analysis (Challenges and Applications)," Egyptian Informatics Journal, (xxxx), 4–9, 2019, doi:10.1016/j.eij.2019.06.001.

[23] N. Habash, O. Rambow, "M Agead : C #@," **M**(July), 681–688, 2006.

[24] N. Habash, R. Eskander, A. Hawwari, "A Morphological Analyzer for Egyptian Arabic," Proceedings of the Twelfth Meeting of the Special Interest Group on Computational Morphology and Phonology SIGMORPHON2012, 1–9, 2012.

[25] I. Zribi, M.E. Khemakhem, L.H. Belguith, "Morphological Analysis of Tunisian Dialect," International Joint Conference on Natural Language Processing, (October), 992–996, 2013.

[26] S. Khalifa, N. Habash, F. Eryani, O. Obeid, D. Abdulrahim, M. Al Kaabi, "A morphologically annotated corpus of Emirati Arabic," LREC 2018 - 11th International Conference on Language Resources and Evaluation, 3839–3846, 2019.

[27] A. Mekki, I. Zribi, M. Ellouze, L.H. Belguith, "Syntactic analysis of the Tunisian Arabic," CEUR Workshop Proceedings, **1988**, 2017.

[28] A. Shahrour, S. Khalifa, N. Habash, "Improving Arabic diacritization through syntactic analysis," Conference Proceedings - EMNLP 2015: Conference on Empirical Methods in Natural Language Processing, (September), 1309–1315, 2015, doi:10.18653/v1/d15-1152.

[29] K. Dukes, E. Atwell, A.B.M. Sharaf, "Syntactic annotation guidelines for the quranic Arabic dependency treebank," Proceedings of the 7th International Conference on Language Resources and Evaluation, LREC 2010, 1822–1827, 2010.

[30] A. Shahrour, S. Khalifa, D. Taji, N. Habash, "CamelParser: A system for Arabic syntactic analysis and morphological disambiguation," COLING 2016 - 26th International Conference on Computational Linguistics, Proceedings of COLING 2016: System Demonstrations, 228–232, 2016.

[31] M. Abdul-Mageed, M.T. Diab, "Subjectivity and sentiment annotation of modern standard Arabic newswire," ACL HLT 2011 - LAW 2011: 5th Linguistic Annotation Workshop, Proceedings, (3), 110–118, 2011.

[32] M. Abdul-Mageed, M. Diab, "AWATIF: A multi-genre corpus for modern standard Arabic subjectivity and sentiment analysis," Proceedings of the 8th International Conference on Language Resources and Evaluation, LREC 2012, 3907–3914, 2012.

[33] A. Abdelali, J. Cowie, H. Soliman, "Building A Modern Standard Arabic Corpus," Workshop on Computational Modeling of Lexical Acquisition. The Split Meeting. Croatia, 25th to 28th of July, 2005.

[34] A. Elnagar, L. Lulu, O. Einea, "An Annotated Huge Dataset for Standard and Colloquial Arabic Reviews for Subjective Sentiment Analysis," Procedia Computer Science, **142**, 182–189, 2018, doi:10.1016/j.procs.2018.10.474.

[35] N. Al-Twairesh, H. Al-Khalifa, A. Al-Salman, Y. Al-Ohali, "AraSenTi-Tweet: A Corpus for Arabic Sentiment Analysis of Saudi Tweets," Procedia Computer Science, **117**, 63–72, 2017, doi:10.1016/j.procs.2017.10.094.

[36] O. Newspapers, E. Twitter, O. Newspapers, I. Proceedings, A. Alshutayri, E. Atwell, "This is a repository copy of Creating an Arabic Dialect Text Corpus by Exploring Twitter , Version : Accepted Version Creating an Arabic Dialect Text Corpus by Exploring Twitter , Facebook , and Online Newspapers," 2018.

[37] M. Itani, C. Roast, S. Al-Khayatt, "Developing Resources for Sentiment Analysis of Informal Arabic Text in Social Media," Procedia Computer Science, **117**, 129–136, 2017, doi:10.1016/j.procs.2017.10.101.

[38] M. El-Masri, N. Altrabsheh, H. Mansour, A. Ramsay, "A web-based tool for Arabic sentiment analysis," Procedia Computer Science, **117**, 38–45, 2017, doi:10.1016/j.procs.2017.10.092.

[39] S. Hussein, M. Farouk, E.S. Hemayed, "Gender identification of egyptian dialect in twitter," Egyptian Informatics Journal, **20**(2), 109–116, 2019, doi:10.1016/j.eij.2018.12.002.

[40] D. Gamal, M. Alfonse, E.S.M. El-Horbaty, A.B.M. Salem, "Implementation of Machine Learning Algorithms in Arabic Sentiment Analysis Using N-Gram Features," Procedia Computer Science, **154**, 332–340, 2018, doi:10.1016/j.procs.2019.06.048.

[41] M. Mataoui, O. Zelmati, M. Boumechache, "A Proposed Lexicon-Based Sentiment Analysis Approach for the Vernacular Algerian Arabic," Research in Computing Science, **110**(1), 55–70, 2016, doi:10.13053/rcs-110-1-5.

[42] K.M. Alomari, H.M. Elsherif, K. Shaalan, Arabic tweets sentimental analysis using machine learning, Lecture Notes in Computer Science (Including Subseries Lecture Notes in Artificial Intelligence and Lecture Notes in Bioinformatics), **10350 LNCS**, 602–610, 2017, doi:10.1007/978-3-319-60042-0_66.

[43] R. Baly, A. Khaddaj, H. Hajj, W. El-Hajj, K.B. Shaban, "ArSentD-LEV: A Multi-Topic Corpus for Target-based Sentiment Analysis in Arabic Levantine Tweets," (1), 2019.

[44] M. Jarrar, N. Habash, F. Alrimawi, D. Akra, N. Zalmout, "Curras: an annotated corpus for the Palestinian Arabic dialect," Language Resources and Evaluation, **51**(3), 745–775, 2017, doi:10.1007/s10579-016-9370-7.

[45] H. Rahab, A. Zitouni, M. Djoudi, "SANA: Sentiment analysis on newspapers comments in Algeria," Journal of King Saud University - Computer and Information Sciences, (xxxx), 2019, doi:10.1016/j.jksuci.2019.04.012.

[46] I. Guellil, A. Adeel, F. Azouaou, A. Hussain, "SentiALG: Automated Corpus Annotation for Algerian Sentiment Analysis," Lecture Notes in Computer Science (Including Subseries Lecture Notes in Artificial Intelligence and Lecture Notes in Bioinformatics), **10989 LNAI**(Ml), 557–567, 2018, doi:10.1007/978-3-030-00563-4_54.

[47] D. Gamal, M. Alfonse, E.-S. M.El-Horbaty, A.-B. M.Salem, "Twitter Benchmark Dataset for Arabic Sentiment Analysis," International Journal of Modern Education and Computer Science, **11**(1), 33–38, 2019, doi:10.5815/ijmecs.2019.01.04.

[48] H. Abdellaoui, M. Zrigui, "Using tweets and emojis to build TEAD: An arabic dataset for sentiment analysis," Computacion y Sistemas, **22**(3), 777–786, 2018, doi:10.13053/CyS-22-3-3031.

[49] F.H.H. Mahyoub, M.A. Siddiqui, M.Y. Dahab, "Building an Arabic Sentiment Lexicon Using Semi-supervised Learning," Journal of King Saud University - Computer and Information Sciences, **26**(4), 417–424, 2014, doi:10.1016/j.jksuci.2014.06.003.

[50] K. Elshakankery, M.F. Ahmed, "HILATSA: A hybrid Incremental learning approach for Arabic tweets sentiment analysis," Egyptian Informatics Journal, **20**(3), 163–171, 2019, doi:10.1016/j.eij.2019.03.002.

[51] S.R. El-Beltagy, "NileULex: A phrase and word level sentiment lexicon for Egyptian and modern standard Arabic," Proceedings of the 10th International Conference on Language Resources and Evaluation, LREC 2016, 2900–2905, 2016.

[52] H.S. Ibrahim, S.M. Abdou, M. Gheith, "Automatic expandable large-scale sentiment lexicon of modern standard Arabic and colloquial," Proceedings - 1st International Conference on Arabic Computational Linguistics: Advances in Arabic Computational Linguistics, ACLing 2015, (July 2016), 94–99, 2016, doi:10.1109/ACLing.2015.20.

[53] I. Guellil, F. Azouaou, "Bilingual Lexicon for Algerian Arabic Dialect Treatment in Social Media," WiNLP, 1–4, 2017.

[54] H. S.Ibrahim, S. M. Abdou, M. Gheith, "Idioms-Proverbs Lexicon for Modern Standard Arabic and Colloquial Sentiment Analysis," International Journal of Computer Applications, **118**(11), 26–31, 2015, doi:10.5120/20790-3435.

[55] M. Salameh, H. Bouamor, N. Habash, "Fine-Grained Arabic Dialect Identification," Processdings of the 27th International Conference on Computational Linguistics Santa Fe, New Mexico, USA, 1332–1344, 2018.

[56] R.M.K. Saeed, S. Rady, T.F. Gharib, "An ensemble approach for spam detection in Arabic opinion texts," Journal of King Saud University -

Computer and Information Sciences, (xxxx), 2019, doi:10.1016/j.jksuci.2019.10.002.

[57] I. Guellil, M. Mendoza, F. Azouaou, "Arabic dialect sentiment analysis with ZERO effort. Case study: Algerian dialect," Inteligencia Artificial, **23**(65), 124–135, 2020, doi:10.4114/intartif.vol23iss65pp124-135.

[58] M. Alali, N. Mohd Sharef, M.A. Azmi Murad, H. Hamdan, N.A. Husin, "Narrow Convolutional Neural Network for Arabic Dialects Polarity Classification," IEEE Access, **7**, 96272–96283, 2019, doi:10.1109/ACCESS.2019.2929208.

[59] R.M. Duwairi, "Sentiment analysis for dialectical Arabic," 2015 6th International Conference on Information and Communication Systems, ICICS 2015, (April), 166–170, 2015, doi:10.1109/IACS.2015.7103221.

[60] J.O. Atoum, M. Nouman, "Sentiment analysis of Arabic Jordanian dialect tweets," International Journal of Advanced Computer Science and Applications, **10**(2), 256–262, 2019, doi:10.14569/ijacsa.2019.0100234.

[61] N. Al-Twairesh, H. Al-Khalifa, A. Alsalman, Y. Al-Ohali, "Sentiment Analysis of Arabic Tweets: Feature Engineering and A Hybrid Approach," 2018.

[62] H. Mulki, H. Haddad, M. Gridach, I. Babaoğlu, "Syntax-Ignorant N-gram Embeddings for Sentiment Analysis of Arabic Dialects," 30–39, 2019, doi:10.18653/v1/w19-4604.

[63] H. Mulki, H. Haddad, C.B. Ali, I. Babaoglu, "Tunisian dialect sentiment analysis: A Natural Language Processing-based Approach," Computacion y Sistemas, **22**(4), 1223–1232, 2018, doi:10.13053/CyS-22-4-3009.

[64] A. D'Andrea, F. Ferri, P. Grifoni, T. Guzzo, "Approaches, Tools and Applications for Sentiment Analysis Implementation," International Journal of Computer Applications, **125**(3), 26–33, 2015, doi:10.5120/ijca2015905866.

[65] B. Brahimi, M. Touahria, A. Tari, "Improving sentiment analysis in Arabic: A combined approach," Journal of King Saud University - Computer and Information Sciences, (xxxx), 2019, doi:10.1016/j.jksuci.2019.07.011.

[66] W. Medhat, A. Hassan, H. Korashy, "Sentiment analysis algorithms and applications: A survey," Ain Shams Engineering Journal, **5**(4), 1093–1113, 2014, doi:10.1016/j.asej.2014.04.011.

[69] Biermann A.W. (1986) Fundamental mechanisms in machine learning and inductive inference. In: Bibel W., Jorrand P. (eds) Fundamentals of Artificial Intelligence. Lecture Notes in Computer Science, **232**, Springer, Berlin, Heidelberg

[70] Abhimanyu Chopra, Abhinav Prashar, Chandresh Sain, 2013. Natural Language Processing. INTERNATIONAL JOURNAL OF TECHNOLOGY ENHANCEMENTS AND EMERGING ENGINEERING RESEARCH, VOL 1, ISSUE 4, ISSN 2347-4289

[71] Omar F. Zaidan and Chris Callison-Burch, 'Arabic Dialect Identification', Computational Linguistics. **40**(1), 171-202, 2014

Variation in Self-Perception of Professional Competencies in Systems Engineering Students, due to the COVID -19 Pandemic

Teodoro Díaz-Leyva*,1, Nestor Alvarado-Bravo[2], Jorge Sánchez-Ayte[1], Almintor Torres-Quiroz[2], Carlos Dávila-Ignacio[1], Florcita Aldana-Trejo[3], José Razo-Quispe[3], Omar Chamorro-Atalaya[1]

1University National Technological of Lima Sur, Faculty of Engineering and Management, Lima, Peru

2University National of Callao, Faculty of Chemical Engineering and Faculty of Economic Sciences, Callao, Peru

3San Juan Bautista Private University, Faculty of Communication and Administrative Sciences, Lima, Peru

A R T I C L E   I N F O

A B S T R A C T

The objective of this article is to determine if the self-perception of professional competences has been affected, in systems engineering students, during the health emergency declared in Peru by Covid-19; The results will allow the public university of Peru to make corrective decisions and formulate proposals to improve the functioning of the variable under study. Initially, the comparative analysis was carried out, where it is observed that in the academic semester 2020-I (during the health emergency), there is a greater number of students who present a better self-perception of the 10 indicators of the professional skills dimension, compared to the semester 2019-II (before the health emergency). Likewise, the indicators "To solve problems and cases of the specialty" and "To master practical professional skills" present a higher rate of improvement in self-perception, of 8.14% and 10.37%, respectively. Finally, when carrying out the statistically validation of the association of the two mentioned indicators, using the contingency table, it is observed, by the Chi-square statistic, a significance (bilateral) lower than α = 0.05, with this, it is verified , the significant association of the indicators; This is supported by the percentage obtained in the contingency table, where it is shown that 90.6% of the systems engineering students in the 2019-II semester and 95.5% of the students in the 2020-I semester , who are satisfied with the indicator "To master practical professional skills", have experienced a positive impact with the indicator "To solve problems and cases of the specialty".

1. Introduction

A commonly perceived scenario in many universities in Latin American countries is one in which students who graduate from their professional careers do not seem to be sufficiently prepared for the challenges that arise in real life; In this regard in [1], the author highlights that many students lack skills that allow them to take risks, organize and go beyond what they have learned in class.

That is why it is almost necessary for the model in which the teacher is the center of attention in a class, to be totally displaced. In this regard, in [2], the author states that emphasis should be placed on the figure of the teacher as a tutor or facilitator, and the center of attention in a class session should be on the student, on their ability to learn and learn by doing; hence, many universities have redefined the teaching objectives in terms of competencies.

In [3], the author points out that in the context of education in which we find ourselves, the great paradigm that students face is to move from traditional models in learning processes, towards more open models in which the student is part of their own learning process.

In this regard, in [4], the author points out that university higher education currently poses multiple challenges, among them: raising quality, relevance, equity, greater links with the community

*Corresponding Author: Teodoro Díaz-Leyva, Edif. R Dpto. 202 Sec.I A.M.C, Ventanilla, Lima, 982716223, isdiazl@hotmail.com

and emphasis on research; all this obtained from the competences that students are acquiring in their professional training period.

From a general perspective in relation to professional competences, in [5], the author affirms that when the professional competencies that a student must acquire to carry out a task are investigated, not only those inherent to knowledge are recreated, knowledge or particular practice, but those that are linked to thoughts; therefore, controlling the former will make the latter more efficient.

In relation to the aforementioned, in [6], the author establishes that a professional competence is the set of skills, attitudes and responsibilities that describe the learning outcomes of a subject or educational program, which enable the student to develop a professional activity.

In [7], the author points out that changes in the world of work, information management processes and knowledge production, ways of knowing and researching, characteristics of today's society, traversed by ICT (Technology of Information and Communication), permanently generate new training needs that the classroom and the university do not always seem to be able to satisfy.

In [8], the author points out that higher education institutions that are in charge of training systems engineering professionals must remain attentive to the reality of their environment and continually verify the profile of their graduates to be trained; since the contents based on technological tools are quite changeable over time.

Another outstanding contribution in relation to the competences in the training of students in systems engineering is indicated in [9], so that systems engineers are prepared to take on the challenges of the new knowledge society that they express in their mission, they must possess skills to transmit information, select the ideal medium, possess skills in the use of ICT, ability to select and classify information, among others.

In this regard in [10], the author specifies that in order for university students to have a positive perception in relation to the professional skills acquired during their university days, these must represent tools that allow them to effectively face the challenges that await them, giving significant contribution to society.

In [11], the author defines the university student's self-perception as the way in which he perceives himself within the educational process. Also in [12], the author points out that the university student's self-perception indicates how the student or students feel about themselves, how they see themselves in the field they are developing.

Perhaps all of the above is seen from a non-pandemic context, with classroom development in person, making use of laboratories or equipment installed at the University; However, today we are in the midst of a Covid-19 pandemic; In this regard in [13], the author points out that the unexpected expansion of Covid-19 has forced university classes to take place virtually or not in person in many countries, which at a certain point results in knowing whether through These platforms the student manages to develop the

professional competences, typical of the professional career of systems engineering.

In this sense, the objective of this article is to carry out a comparative analysis of the variation of the self-perception of students of the systems engineering professional career of the academic semesters before (2019-II) and after (2020-I) the declared health emergency in Peru due to Covid-19. In addition, to identify which were the indicators that make up the self-perception variable that have experienced a greater impact on their satisfaction; whose association validation will be carried out through contingency tables.

2. Investigation methodology

2.1. Research design

The design is non-experimental, of a cross-sectional type, because the variable is studied simultaneously in a single year, in a single time, in which the survey of students from the 7th to the 10th cycle the Public University of Peru. The diagram that presents the cross-sectional design under study is as follows. It should be noted that the data collection period is carried out at different times, and at different samples, because the number of students surveyed is not the same in the 2019-II semester, as in the 2020-I semester.

Figure 1: Research design

where:

M1 and M2, represent the systems engineering students of the academic semester 2019-II and academic semester 2020-I, respectively

T1 and T2, represent the data collection period, both in the academic semester 2019-II, and in the academic semester 2020-I

O1 and O2, represents the observation made of the self-perception of the professional competencies of systems engineering students, both in the 2019-II semester and in the 2020-I semester.

2.2. Research level

The research level is descriptive, because the variables are not altered, and what is intended to be highlighted are the aspects related to the variation of the self-perception of those of the professional competences established in Public University located in Peru satisfaction survey, which was validated in [14].

2.3. Population and sample

The population is made up of students from the 7th to the 10th cycle Public University, in both the 2019-II and 2020-I semesters; Likewise, the sample is made up of all students, these being 149 and 140, students respectively; because there is no equality in the number of students per semester, the sample is not the same; It

should be noted that, as it is the mandatory survey at Public University of Peru, it has been carried out on all students.

2.4. Data Collection Technique and Instrument

The data collection, as indicated in [15], it is carried out by applying the instrument, using various techniques or tools, for this case the survey technique is used and the instrument is the questionnaire, 6 dimensions are established (professional competencies, teaching staff, library services, administrative services of the faculty and professional school, university support service and personal and social attitudes), which will identify student satisfaction in the education Public University of Peru. In this research, the dimension "professional competences" has been chosen.

Data collection, as indicated in [16], is a selective process since it cannot be all-encompassing; Given the aforementioned, it is established that the sample is composed of students from the 7th to the 10th cycle Public University of Peru both in the 2019-II and 2020-I semester; Regarding this, in [17] it is pointed out that the results are more valid when the survey is applied to students in the last cycles, because they are more aware of the understanding of the competences they must acquire.

Likewise, the data collected were processed and transformed, initially using the scale of attitudes and opinions, known as the Likert scale; Since the questionnaire has two self-perception options to choose from, these being unsatisfied and satisfied, each one was valued with the numeral 1 and 2, respectively.

To carry out the data analysis, initially the validation test of the data collection instrument will be carried out by means of the SPSS software, then the comparative analysis of the results will be carried out using the Microsoft Excel software, finally, to carry out the validation of the data. association of the indicators, the contingency table that indicates the Chi-Square value will be used, this test is performed with the SPSS software.

3. Results of the Investigation

3.1. Validation of the data collection instrument

There are various models of reliability, for this research we will use Cronbach's Alpha, as indicated in [18], this model is based on the correlation between the study variables, through this test, it will be demonstrated statistically by means of the software IBM SPSS V25, that the data collection instrument, which is applied is reliable. This test has established the following criteria:

- 0.9 - 1 = The measuring instrument is excellent
- Between 0.89 - 0.8 = The measuring instrument is very good
- Between 0.79 - 0.7 = The measuring instrument is acceptable
- Between 0.69 - 0.6 = The measuring instrument is weak
- Between 0.59 - 0.5 = The measuring instrument is poor
- <0.5 = The measuring instrument is not acceptable

Table 1: Reliability Analysis

Reliability statistics	
Cronbach's alpha	N of elements
.894	20

As can be seen in table 1, the Cronbach's Alpha coefficient is equal to 0.894, this means that the data collection instrument is very good, therefore, its use and the data collected are reliable. It should be noted that the number of elements equal to 20 corresponds to the 10 indicators of the "professional competences" dimension, both for the 2019-II and 2020-I semesters.

3.2. Comparing indicators that are part of professional skills

At this point, the results that respond to the objective of this article are shown, which is to perform a comparative analysis of the variation of the self-perception of students of the systems engineering professional career of the academic semesters before (2019-II) and after (2020-I) of the health emergency declared in Peru by Covid-19.

Initially, in figure 2, the results of the self-perception of the professional competences dimension and its 10 indicators are presented; These results belong to the 149 systems engineering students from the 2019-II academic semester, before the health emergency declared in Peru by Covid-19, and when the classes were held in person.
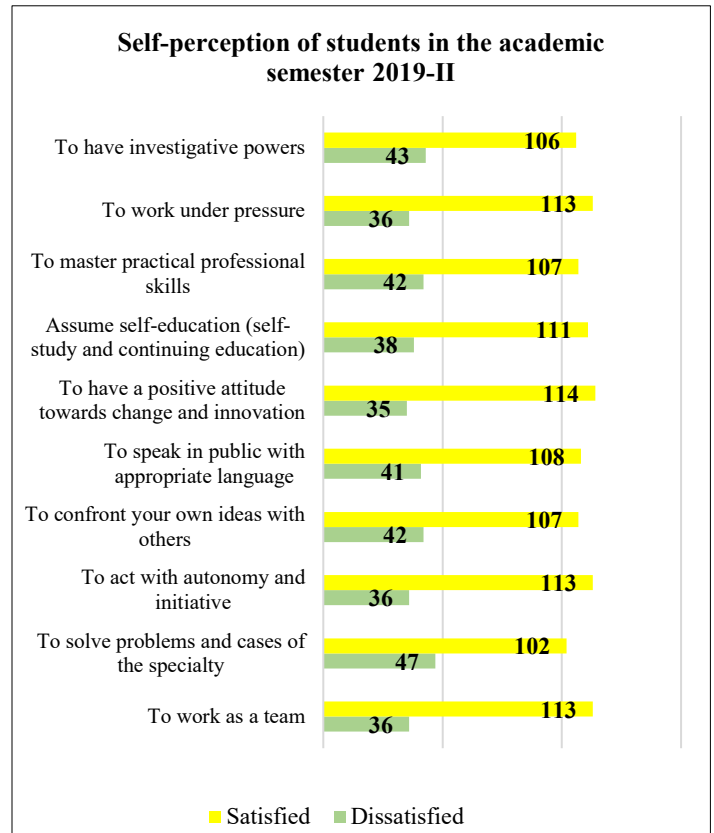
Figure 2: Self-perception of students in the academic semester 2019-II

Next, in the following figure 3, the results of the self-perception of the professional competences dimension and its 10 indicators are presented; These results belong to the 140 systems engineering students of the 2020-I academic semester, during the health emergency declared in Peru by the Covid-19, and when the classes were held virtually or not in person.
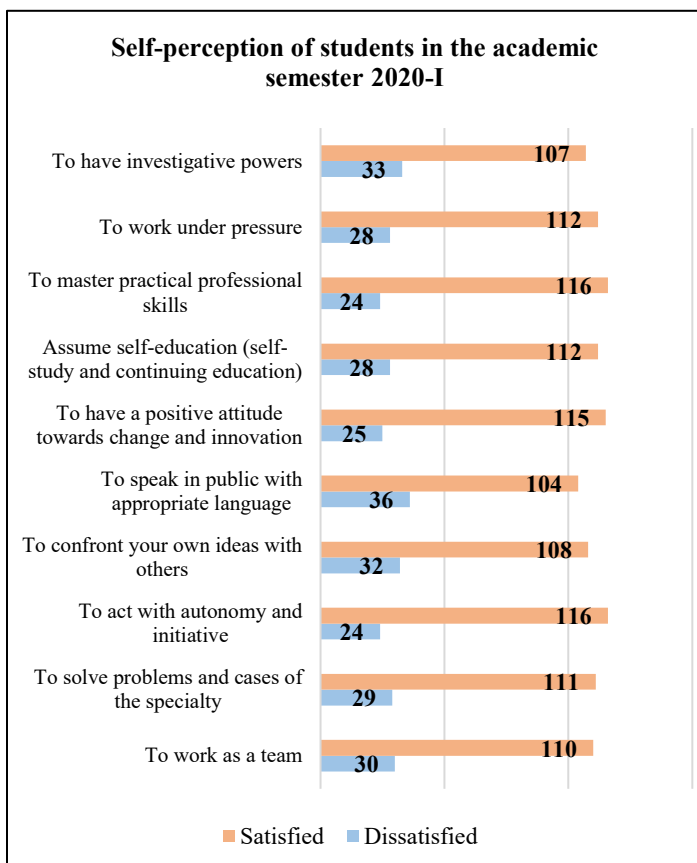
Figure 3: Self-perception of students in the academic semester 2019-II

Table 2: Percentage of variation of the variable self-perception of professional competences

		To solve problems and cases of the specialty	To master practical professional skills
2019 - II	Satisfied	102	107
	% Satisfied	71.14%	72.48%
2020-I	Satisfied	111	116
	% Satisfied	79.29%	82.86%
% OF VARIATION		8.14%	10.37%

Figure 4 shows the increase in these two indicators.
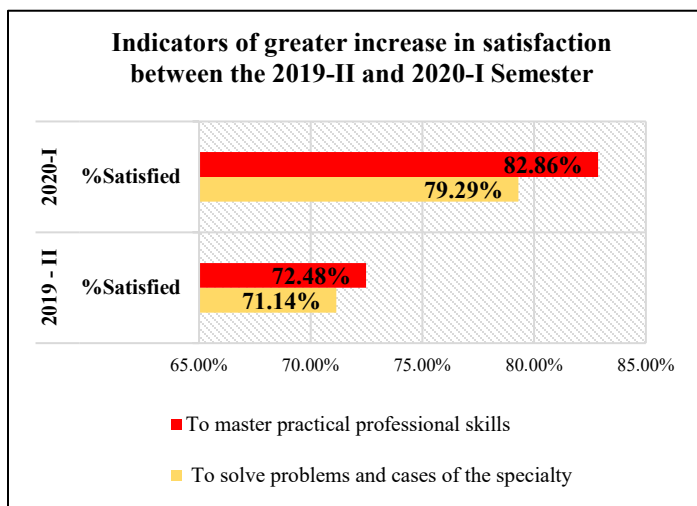
Figure 4: Indicators with the greatest increase in satisfaction (2019-II - 2020-I)

As shown in the results obtained (figure 2 and 3) in the systems engineering career, in the 2020-I semester, there is a greater number of students who present a better self-perception of the 10 indicators of the professional competences dimension, compared to the academic semester 2019-II, where there was no health emergency declared in Peru by Covid-19, and classes were held in person.

3.3. Identifying the two indicators with the highest increase post Covid-19 pandemic

Continuing with the research, and once the number of students with a better self-perception of the professional competences dimension has been determined in the comparative analysis, both in the academic semester 2019-II and in the semester 2020-I; Through the results obtained, we proceed to identify the indicators that make up the professional competences variable, which have experienced a greater increase in satisfaction, post-Covid-19 pandemic. These results are shown in Table 2.

Table 2 shows that, in the systems engineering career, in the 2020-I semester, during the Covid-19 pandemic, students have experienced a greater impact of the satisfaction of the indicators "To solve problems and cases of the specialty" and "To master practical professional skills"; As can be seen, the satisfaction index for these two indicators has improved by 8.14% and 10.37%, respectively. It should be noted that this test counts the number of students who coincide with the perception of satisfaction of the indicators, therefore, the total sample is not reached.

3.4. Analysis of indicators through contingency table

Once the results are obtained, at this point the statistical validation of the association between the two indicators with the greatest increase in satisfaction in the systems engineering career is carried out, during the Covid-19 pandemic; These indicators are "To solve problems and cases of the specialty" and "To master practical professional skills".

This validation is carried out using the IBM SPSS V25 statistical software, in which the contingency table tool will be used.

It should be noted that the contingency table is used to validate an association between two variables, and thus, to test the hypothesis. In this sense, once the indicators with the greatest increase in satisfaction after the Covid-19 pandemic have been identified, the null (Ho) and alternative (Ha) hypotheses of the research are established.

Ho: Mastering practical professional skills does not allow problem solving and specialty cases in systems engineering students.

Ha: Mastering practical professional skills allows students to solve problems and specialty cases in systems engineering.

Table 3 shows the validation results of the association of the indicators in the 2019-II semester.

Table 3: Contingency table of the association of the indicators with the greatest increase in satisfaction in the 2019-II semester

	Value	gl	Significance (bilateral)
Pearson's Chi-square	60.217	1	.000
Likelihood ratio	57.117	1	.000
N of valid cases	149		

Likewise, table 4 shows the validation results of the association of the indicators in the 2020-I semester.

Table 4: Contingency table of the association of the indicators with the greatest increase in satisfaction in the 2020-I semester

	Value	gl	Significance (bilateral)
Pearson's Chi-square	60.259	1	.000
Likelihood ratio	50.145	1	.000
N of valid cases	140		

As can be seen in Table 3 and 4, the value of the Chi-square statistic is 60.217 and 60.259, respectively, and the likelihood ratio 57.117 and 50.145, as established by different authors, if these values differ significantly from 5 for levels of significance greater than 0.05, it is stated that there is an association. Likewise, the significance (bilateral) of Chi-square is less than $\alpha = 0.05$, due to this, the null hypothesis is rejected, thereby accepting the alternative hypothesis.

As the value of p is less than 0.05, it is shown that there is a significant association between the two indicators; Therefore, table 5 shows the percentage of satisfaction between the association of the analyzed indicators, for the 2019-II semester.

Table 5: Contingency table of the percentage of satisfaction among the indicators with the greatest increase in satisfaction in the 2019-II semester

Contingency table			
% within to solve problems and cases of the specialty			
		To master practical professional skills		Total
		Dissatisfied	Satisfied	
To solve problems and cases of the specialty	Dissatisfied	72.1%	27.9%	100.0%
	Satisfied	9.4%	90.6%	100.0%
Total		27.5%	72.5%	100.0%

In the same way, supporting the result, Table 6 shows the percentage of satisfaction between the association of the analyzed indicators, for the 2020-I semester.

Table 6: Contingency table of the percentage of satisfaction among the indicators with the greatest increase in satisfaction in the 2020-I semester

Contingency table			
% within to solve problems and cases of the specialty			
		To master practical professional skills		Total
		Dissatisfied	Satisfied	
To solve problems and cases of the specialty	Dissatisfied	65.5%	34.5%	100.0%
	Satisfied	4.5%	95.5%	100.0%
Total		17.1%	82.9%	100.0%

As shown in table 5 and 6, 90.6% and 95.5% of systems engineering students who are satisfied with the indicator "To master practical professional skills", have experienced a positive impact with the indicator " To solve problems and cases of the specialty".

Through these results, it can be stated that there is a significant association between the indicators; establishing that students of systems engineering by mastering practical professional skills, can solve problems and cases of the specialty.

4. Discussion of results

It is important to indicate that the systems engineering career was chosen, for the present investigation why in the context of the pandemic it was sought to determine the impact, on student satisfaction, with respect to the dimension of self-perception of acquired competences, taking into account that the development of it, lies in its vast majority in the use of a PC.

Given the development of the research, it was obtained that, in the systems engineering career, in the 2020-I semester, during the Covid-19 pandemic, there is a greater number of students who present, a better satisfaction of the 10 indicators of the professional competences dimension, compared to the academic semester 2019-II; This is supported by the fact that, in the face-to-face classes, it was evident that the laboratories were deficient in terms of the number of computers per student, therefore, the practical learning of the subjects was not the most efficient, while in the context After the pandemic, each student uses their own PC at home, thus achieving greater use of the software used.

What is described in the previous paragraph reaffirms the following result, which reveals that, in the systems engineering career, in the 2020-I semester, during the Covid-19 pandemic, students have experienced a greater impact of the satisfaction of the indicators "To solve problems and cases of the specialty" and "To master practical professional skills"; As can be seen in table 2, the satisfaction index for these two indicators has improved by 8.14% and by 10.37%.

In relation to the indicators obtained, in [19], it is pointed out that to obtain an ideal professional performance, the specialty problems that are most often presented to the student must be taken into account, as well as the contents and tools that are counted for the development of the subjects; the correct handling of it must be visualized in the integration of knowledge that allows the student

to solve professional problems according to their rigor and complexity; Likewise, the academic organization provided by the educational institution in relation to the environment with which the professional counts for its development, allows the teacher to efficiently carry out his evaluation of said professional competencies.

Due to the (bilateral) significance of Chi-square is less than α = 0.05, it can be verified statistically that there is a significant association between the analyzed indicators, with this it can be affirmed that systems engineering students have mastered practical professional skills, can solve specialty problems and cases. Regarding this, in [20] it is indicated that universities must integrate in their academic decisions, plans that allow keeping the contents taught in classrooms up to date, as well as tools for their development, in order to keep up with what the labor market dictates; For example, the student by learning properly, the programming languages most used for the design of solution software or tools mostly used in communication networks of companies, will be able to solve problems and cases of the specialty, thus managing to face the problem. working market.

Reaffirming everything described, the results expressed in the contingency table indicate that 90.6% of the systems engineering students in the academic semester 2019-II and 95.5% of the students in the 2020-I semester, who are satisfied with the indicator "To master practical professional skills", have experienced a positive impact with the indicator "To solve problems and cases of the specialty".

5. Conclusions

When carrying out the comparative analysis of the variation in the self-perception of students of the systems engineering career of the academic semesters before (2019-II) and after (2020-I) of the health emergency declared in Peru by Covid-19 , it is concluded that in the systems engineering career, in the 2020-I semester, there is a greater number of students who present a better satisfaction of the 10 indicators of the professional competencies dimension, compared to the 2019-II academic semester.

When carrying out the identification of the indicators that make up the self-perception variable, which have experienced a greater impact on their satisfaction, it is concluded that the indicators "To solve problems and cases of the specialty" and "To master practical professional skills" present a higher index improvement in satisfaction, of 8.14% and 10.37%, respectively.

When carrying out the validation of the association of the indicators that have experienced a greater impact on their satisfaction, through contingency tables, it is concluded that 95.5% of the students who are satisfied with the indicator "To master professional skills practices", have experienced a positive impact with the indicator "To solve problems and cases of the specialty". Likewise, the Chi-square statistic gives us a (bilateral) significance lower than α = 0.05, due to this, the significant association of the indicators is statistically verified, stating that systems engineering students by mastering practical professional skills they can solve specialty problems and cases.

Conflict of Interest

The authors declare no conflict of interest.

References

[1] V. Flores, Scientific Competences and Educational Quality of Students in the Professional School of Systems Engineering, Thesis, University National of Education, 2019.

[2] M. Pinto, D. Guerrero-Quesada, "How Spanish university students perceive informational competences: a case study," Investigation Librarian, **31**(73), 213-236, 2017, doi: dx.doi.org/10.22201/iibi.24488 321xe.2017.7 3.57854.

[3] M. Gonzales-Alonso, R. Fernandez-Díaz, M. Simon-Martin, "Evolution of the self-perception of the level of acquisition of competences of the students of an engineering degree subject," Childhood, Education and Learning, **3**(2), 441-447, 2017, doi: 10.22370/ieya.2017.3.2.762

[4] J. Larrea, L. alonso, R. Tejeda, "Strategy for the evaluation of professional competencies in students of systems engineering," Electronic Journal Training and Educational Quality, **5**(2), 17-32, 2017, doi: http://refcale.uleam.edu.ec/index.php/refcale/article/view/1114.

[5] A. Mortigo, D. Rincón, "Emotional competences in higher education students: self-perception and demographic correlation," University of Rioja, **10**(21), 430-448, 2018, doi: https://dialnet.unirioja.es/servlet/artic ulo?codigo=6934960.

[6] I. Cruz, SICPE Information Systems for the Continuous Evaluation of the Achievement of the profile of the graduate of the Systems Engineering career, Thesis, University Peruvian Union, 2017.

[7] S. Fulgueira, Information systems teachers' competencies in educational processes measured by technologies for the development of professional competences in industrial engineering, Thesis, University National of Cordova, 2017.

[8] C. Martínez, "Certification model based on competencies for the career of engineering in computer systems in El Salvador," Journal Inventum, **11**(21), 2016, doi:10.26620/uniminuto.inventum.11.21.2016.

[9] L. Coronel-Rojas, "Selection and use of information as generic competencies in the professional training of systems engineers," Journal Perspectives, **2**(1), 6-17, 2017, doi:10.22463/25909215.1280.

[10] M. Perez, A. Tufiño, "Teleeducation and Covid-19," CienciAmerica Journal, **9**(2), 58-64, 2020, doi:10.33210/ca.vgi2.296.

[11] U. Ramírez, J. Barragaán, "Self-perception of university students on the use of digital technologies for learning," Apertura Journal, **10**(2), 94-109, 2018, doi: 10.32870/Ap.v10n2.1401.

[12] L. Dunai, J. Alfonso, I. lengua, G. Peris-Fajarnés. Tufiño, "Study of the self-perception of academic performance of first year university students," INNODOCT 2018, **4**(1), 905-910, 2018, doi: 10.4995/TNN201 8.2018.8906.

[13] I. Panadero, C. Bocos, J. Sevillano, "From face-to-face to virtual in labs: the good, the ugly and the bad," CIVINEDU 2020, **4**(1), 54-55, 2020, doi: http://www.civinedu.org/wp-conten/tuploads/2020/11/C IVINEDU2020.

[14] E. Gallardo, "Investigation methodology," Huancayo: University Continental, 72, 2017, ISBN 978-612-4196-

[15] F. Arias, "The research project," Mercantil: Episteme, **7**, 76, 2016, ISBN 980-07-8529-9

[16] M. Tobón, M. Durán, A. Áñez, "Academic and professional satisfaction of university students," REDHECS Electronic journal of Humanities, Education and Social Communication, **11**(22), 110-129, 2016, ISSN-e 1856-9331

[17] J. Rodríguez-Rodríguez, M. Reguant-Álvarez, "Calculate the reliability of a questionnaire or scale using the SPSS: Cronbach's alpha coefficient," REIRE Revista d'Innovació i Recerca en Educació, **13**(2), 1–13, 2019, https://doi.org/10.1344/reire2020.13.230048

[18] R. Ramírez-Fernández, J. Machado-Licona, O. Fernández-Ramírez, "Evaluation of professional competences in university students," 8th International Scientific Conference, University of Holguín

[19] R. Ramírez-Fernández, J. Machado-Licona, O. Fernández-Ramírez, "Quality in university education, from the systems engineering program: a qualitative vision of higher education," Amphibian Scientific Journal, **2**(2), 41–50, 2019, https://doi.org/10.37979/afb.2019v2n2.49

Simulated IoT Based Sustainable Power System for Smart Agriculture Environments

Shahenaz S. Abou Emira[1,2], Khaled Y. Youssef [3,*], Mohamed Abouelatta[1]

[1]*Faculty of Engineering, Electronics and Electrical Communication, Ain Shams University (ASU), Cairo, 39827, Egypt*

[2]*Faculty of Engineering, Electronics and Electrical Communications, October University for Modern Sciences and Arts (MSA), Cairo, 39827, Egypt*

[3]*Faculty of Navigation Science and Space Technology, Beni-Suef University (BSU), Beni-suef, 62511, Egypt*

ARTICLE INFO	ABSTRACT
	In vital energy applications especially the agricultural environments, the service of adaptive power utilization plays an essential role in facilitating the usage of Internet of Things systems. Such environments are distinguished by the large range of lands where most of the region lacks the commercial power lines. Reaching some high or deep sensing points is also difficult in such environments. The adaptive power system will pave the way to make a smart service for users to create a platform for real time interaction. It can enhance the reliability, stability and sustainability of power supply, and provide more humanized and various intelligent services for the users. The usage of adaptive power can be improved effectively using IoT technology with its strong data processing and reliable communication. In this paper, an algorithm is proposed to offer a sustainable power service for smart agriculture system to guarantee continuous system operation. It mainly rely on controlling the load demands and managing the renewable energy. A model is built on Matlab that governs the proposed algorithm and the results of the simulation are discussed.

1. Introduction

This paper is an extension of work originally presented in 15th International Computer Engineering Conference (ICENCO) [1]. The food demand increased due to the huge growth in population so it is essential to increase the food production and try to avoid any production losses. Agriculture has a major impact on food production so monitoring the plants' performance is very important. In order to avoid any crop losses, agro systems were designed. Remote sensors were used in these systems to measure light, humidity, soil moisture and temperature. The measured data will indicate whether the plants' performance is good or not and the data will be collected and sent to the user for further action[2, 3]. IoT is a new technology that is used recently in most of the smart systems. Using IoT technology in agro systems allow the plants to express its needs only when it is needed which will allow the efficient usage of resources. There are some challenges that appears in IoT systems, energy optimization is one of the main challenges that faces IoT. It is a major challenge due to the high number of devices that exist in the network which need high

energy to keep it active for long time. It is essential to study this challenge as wireless sensors are commonly used in precision agriculture in remote areas and the agro systems depend mainly on sensors' power so battery drainage will cause the system to stop which isn't desired [4, 5].

The life time of sensor nodes needs to be long in order for the network to be active and to avoid battery drainage. In this paper, an energy management technique based on intelligent load scheduling is introduced for agro-applications. The battery state of charging and the solar power are the main parameters used in the proposed algorithm to activate or deactivate the loads. Based on the loads' priority and the availability of power provided by the battery or solar, loads are activated for specific time. The loads' priority is standard defined as the applications that need to be operating due to criticality are defined based on the standards of agro.

2. Literature Review

Researchers have implemented and introduced some systems using various methods and sensors to monitor the status of plants' health. It improved the agricultural production and helped in

preventing crop losses. In [6], the author illustrated the demonstration of a smart plant monitoring system. The system was enabled to discover any changes occurred in the measurements of light, moisture level and temperature. The plant received its required irrigation and illumination using a machine based curation. An Android device was used by the user in order to enable the user to override an operation which is a machine curated and in this case it is shifted to user based curation instead of machine based curation. In [7], the author explained a system that uses IoT technology in order to control and monitor an agricultural production. The sensors' data was gathered in the monitoring system from IoT devices and then stored at the database of the cloud in order to be accessible by the users. The users could control the actuators in the controlling system over the internet with the usage of IoT devices.

The main source of power for the systems presented previously is the sensors' batteries so systems that uses energy efficiently are studied. Energy plays a significant role in monitoring the environment of agriculture. Researchers presented various algorithms which assure the efficient usage of energy using energy harvesting, load scheduling and power reduction techniques. In [8], the author presented a method used in wireless sensor network for managing power efficiently. The system model consisted of three parts: sensing unit, transmitter unit , and power unit. Energy harvesting was used in the power unit as the power source used for charging the battery is the solar energy. Sending and collecting the data was the responsibility of the other two units. The microcontroller is utilized to monitor the sensed signal and if any disorder detected, it would be transmitted to the receiver.

In [9], the author concentrated on elongating the sensor nodes' life time by minimizing the consumption of energy. A solar cell was utilized to power the system to assure energy sustainability. The minimization of power consumption was achieved by proposing two methods of power reduction. Sleep/wake based on duty cycling was utilized and the second method was integrating the redundant data of the soil moisture with sleep/wake scheme. This research introduced the Sleep/wake on redundant data (SWORD).

In [10], the author presented an algorithm based on devices scheduling in order to optimize and reduce the electricity cost. Two methods were tested for load scheduling optimization either without the usage of renewable energy or with the usage of it. The results of the implementation showed that the cost is reduced up to 53% when combining the proposed algorithm with renewable energy and in case no renewable energy is combined with the algorithm, the cost is reduced up to 40%.

In [11], the author illustrated an algorithm that depends on electricity cost changes and renewable sources real time output in order to schedule the loads. The scheduling and management of energy was established according to the exchange of sensor data and control demands. It would update the real time output of the renewable sources and determine the devices' priority. After the sensed data was received, the energy management unit in the system updated the devices' priority status and the output of renewable sources. The energy management unit would transfer the devices to on or off status if required depending on the energy management and devices scheduling.

In [12], the author discussed various ways to utilize renewable energy in order to assure the efficient usage of energy, ,cost reduction, and handling loads. The scheduling of loads in the used algorithm was depending on time and overload management using multilevel priority. Based on the need of load scheduling during peak demand hour, a duration of time was determined. The loads with medium and high priorities would be activated during this time and the load with low priority would be deactivated. All load would be deactivated in case the limit was exceeded.

3. Proposed Architecture for Energy Efficient Agro Systems

As shown in Figure 1, the proposed architecture consists of four sensors: light sensor, color sensor, soil moisture sensor and temperature/humidity sensor. The proposed architecture is used for monitoring plants' performance in agro systems. The data measured by the soil moisture sensor and temperature/humidity sensor will be sent to Central Processing Server (CPS) to decide the proper time for irrigation after comparing it with the threshold values. Regarding the other two sensors, the user will take the action required based on the received data that were measured by these sensors in case there were any up normal values detected at the CPS. The goal is to ensure the continuous operation of this system by using energy efficiently to increase the life time of the system. Figure 2 shows a proposed architecture for sensor area network (SAN1) using energy efficient technique. It depends mainly on two parts:

3.1. Solar panel or battery used as a power source

- The source of power during day is the solar panel. It is used for supplying the loads during day as it is working and the power needed by the loads is available. Some loads will be switched off in case that the solar power isn't enough for suppling all loads and the rest will be on depending on the available solar power.

- The source of power during night is the battery. The active loads will be supplied by the battery and some loads will be off during night as these loads will not highly affect the system's operation.

3.2. The loads (sensors and actuators) which are divided into categories according to priority.

- Load 1 (High priority): the high priority loads highly affect the system's operation. This load must be on most of the time so the deactivation will be during night only in case that the state of charging of the battery is less than the threshold value.

- Load 2 (Medium priority): if the power is enough for supplying medium and high priority loads, this load will be active. It will be deactivated when the power isn't enough to supply all loads and this will occur mostly during night.

- Load 3 (Low priority): it doesn't have a huge impact on the system's operation so it can be deactivated during night. The user can activate this load upon his request if needed during night after checking the battery state of charging if it is within threshold values or not.

The soil moisture sensor is considered a high priority load due to its high criticality in precise agriculture applications as stated in

[13] .The soil moisture sensor is used in the proposed system to change the concept of scheduled irrigation to be on demand irrigation as its measured values help in deciding whether plants needs to be watered or not and based on these values irrigation takes place .The light sensor is considered a medium priority load in the proposed system due to its medium criticality as it needs to be active at specific time as it is used in the proposed algorithm to indicate whether the weather is sunny or cloudy and to indicate also whether it is day or night. Accordingly, the algorithm will switch to the power source that can be used in the current situation to supply the loads. The water quality sensor is considered a low priority load as irrigation is applied mostly during day so there is no need to schedule it to work during night but in the proposed algorithm it can be activated during night if needed upon the user request.
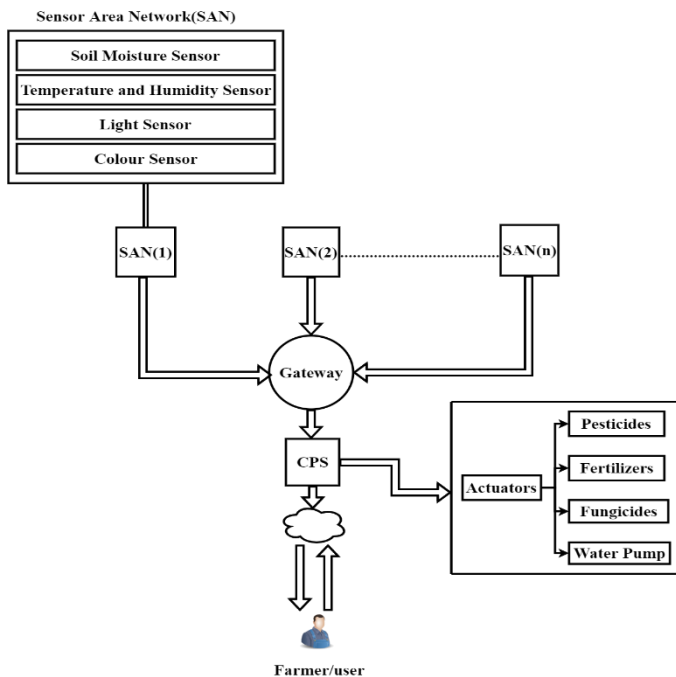
Figure 1: Architecture for Monitoring Agro Systems
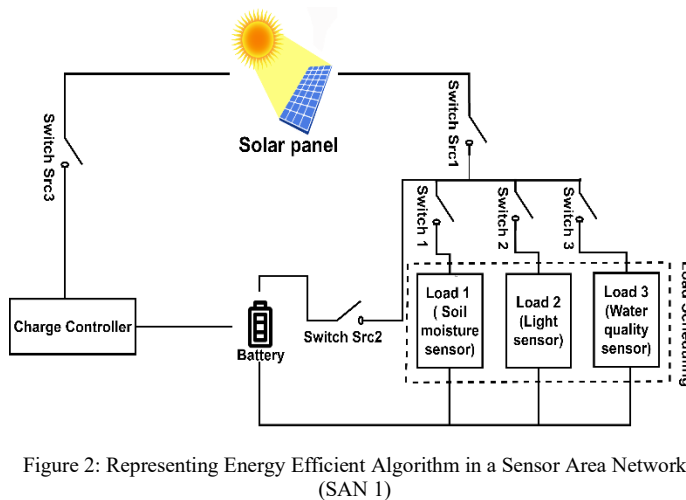
Figure 2: Representing Energy Efficient Algorithm in a Sensor Area Network (SAN 1)

4. Proposed Energy Efficient Algorithm

The proposed algorithm uses energy efficiently in agricultural applications to elongate the sensor nodes life time. The agro

devices' dormant mode will be synchronized and controlled by the proposed algorithm based on the change of day/night. This algorithm doesn't depend on the marketable power supplies so it will guarantee a sustainable environment. The battery drainage issue will be solved to some extent which will enable a sustainable power system. The proposed energy efficient algorithm is dependent on the load scheduling technique and solar energy. There are two other methods for powering the system either by using battery only or by using battery along with load scheduling.

The proposed algorithm is compared with these two methods. In the first method as shown in Figure 3, there is no enough power for supplying the loads as they are active for only five consecutive hours. In the second method, load scheduling technique is used which saves more power therefore the loads are active for longer time as shown in Figure 3. However. The problem of battery drainage still exists and the battery needs to be replaced but it is not easy to replace it in agro-applications. Replacing the battery is not necessary in the proposed algorithm as the solar panel is used during day to recharge the battery. The loads are supplied by the battery only during night. The solar panel is used to supply the loads during day therefore the battery state of charging is maintained for longer time in the proposed algorithm as shown in Figure 3. As a result of using the proposed algorithm, the life time of the sensor nodes is increased due to the increase of the battery life time.
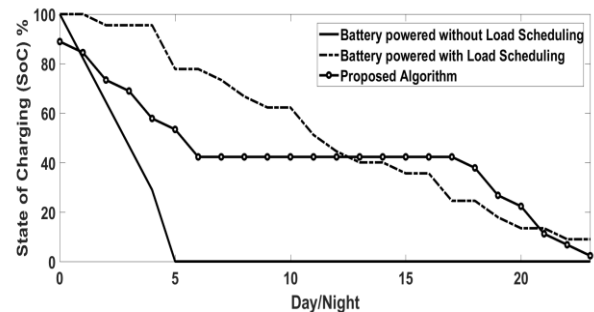
Figure 3: State of Charging versus Day/Night for The Two Power Methods Compared with The Proposed Algorithm.

The two main parameters used in the proposed algorithm are the availability of power and the criticality index of the load. The first parameter is represented as solar irradiance or State of Charging (SoC) of the battery. The second parameter indicates whether the load is critical or not to operate in the non-scheduled time. Based on these two main parameters, the agricultural ecosystems loads are transferred to on or off state. Intelligent load Scheduling and solar power are combined in this algorithm to efficiently implement the system using IoT.

Figure 4 represents a flow chart for a combined energy efficient technique using intelligent load scheduling and solar energy. The algorithm initially checks the capacity of solar power during day to decide whether to activate or deactivate the load. It is proven in the simulation that the idle duration varies based on the availability of solar power. For example, when the solar irradiance is reduced from 1000 W/m^2 to 500 W/m^2, the idle duration is increased by Δt. The battery is the source of power during night and it takes the lead in the absence of the sun to supply all the needed loads.

The loads are transferred to on or off state based on their criticality index as the loads are classified according to priority. The loads with high and medium priority are activated if SoC of battery is more than or equal to 75% and the unnecessary loads are deactivated. According to the availability of power, the loads' idle time is tuned and calculated. By time, the idle duration increases as a function of the battery drainage. If SoC is below 40%, the load with high priority is activated and the load with medium priority is deactivated and the idle duration increases based on the drainage rate of the battery. The inactive loads can be transferred to on state if needed during night based on user request.

The idle duration levels during day and night are shown in Table 1. The first level is selected during day as it is devoted for the dynamic solar irradiance scenario in which it varies during day hours from 100 W/m^2 to 1000 W/m^2. The other levels are devoted for the battery SoC variations. According to the availability of power, the idle duration for each load changes by Δt. Table 1 shows different scenarios where the idle duration level for each load changes by Δt and according to this change, the power gain is calculated for each load. The power gain shows the state of the consumed power at the current level compared to the previous level. As shown in Figure 5, the power gain increases as the Δt increases.

Figure 4: The Flow Chart Illustrates That the Decision of Activating or Deactivating the Loads is Taken After Checking State of Charging (SoC) of The Battery and the Availability of Light.

Table 1: Representing the Power Gain and The Changes in Idle Time for Different Scenarios

Level	Scenario	Load Priority	Active Hours	Δt (Hours)	Power Gain (dBm)
1	Dynamic Irradiance	High	11	10	46.48
		Medium	5	5	45.22
		Low	4	4	44.25
2	100%	High	12	1	36.47
		Medium	6	1	38.23
		Low	0	4	44.25
3	≥75%	High	10	2	39.48
		Medium	4	2	41.25
		Low	0	0	0
4	≥50%	High	6	4	42.49
		Medium	2	2	41.25
		Low	0	0	0
5	≥40 %	High	4	2	39.48
		Medium	1	1	38.23
		Low	0	0	0
6	<40 %	High	1	3	41.25
		Medium	0	1	38.23
		Low	0	0	0

Figure 5: Power Gain versus The Change in Idle Time (Δt) for The Three Loads

It is very essential to choose the optimum sleep time (T_s) that will not affect the system operation. There are three significant parameters that must be taken into consideration while choosing T_s, State of Charging (SoC), Load current (I_L), and Load index (η). The load index (η) ranges from 0.1 to 1. The value 1 indicates high priority, 0.5 indicates medium priority and 0.1 indicates low priority. The SoC is the difference between the battery rated capacity (C_{rated}) and the used capacity by loads (C_{used}) divided by the battery rated capacity. SoC can be calculated using (2):

$$T_s = fn(SoC, I_L, \eta) \tag{1}$$

$$SoC = \frac{C_{rated} - C_{used}}{C_{rated}} \times 100 \tag{2}$$

Figure 6 represents the charging stage of the battery which shows that the battery state of charging is increasing with time. As a result the sleep duration for the loads is decreasing due to the increase of the amount of power available in the battery. Therefore the sleep duration is inversely proportional to the SoC as shown in Figure 7. Figure 8 shows that the increase in load current results in a decrease in the battery state of charging.
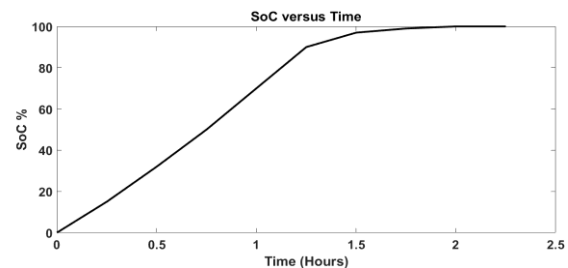
Figure 6: SoC Represented in a Charging Stage versus Time
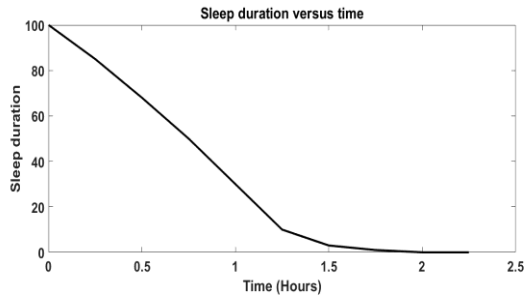
Figure 7: Sleep Duration versus Time
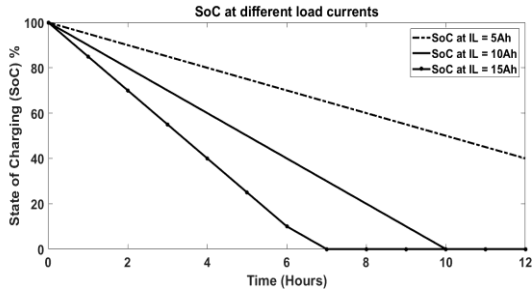
Figure 8: State of Charging at Different Load Currents versus Time

The active duration for each load depends on the maximum current consumed by the loads (I_{Lmax}), the current consumed by load 1 (I_{L1}) and the load index (η). Equation (3) is used to calculate the active duration for each load then calculate the sleep duration using (4). The active and sleep durations for the three loads are shown in Figure 9 and 10. Figure 11 represents the sleep duration for each load versus the battery SoC.

$$T_a = \frac{I_{Lmax} \times 60 \times \eta}{2 \times I_{L1}} \tag{3}$$

$$T_s = 60 - T_a \tag{4}$$
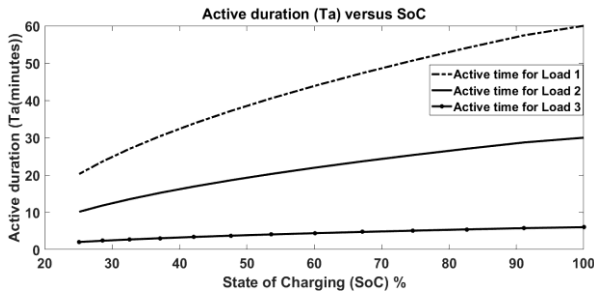
Figure 9: Active Duration for Three Loads versus State of Charging (SoC)
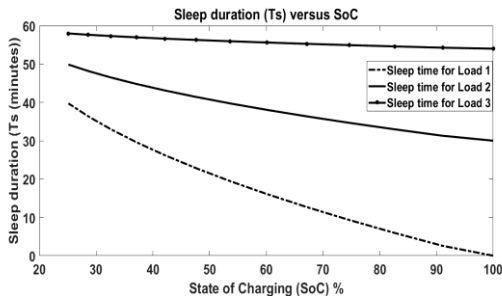
Figure 10: Sleep Duration for Three Loads versus State of Charging (SoC)

a

b

c
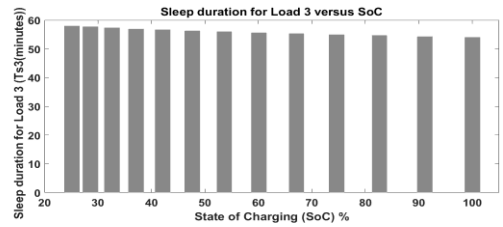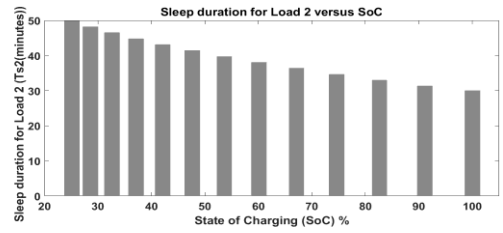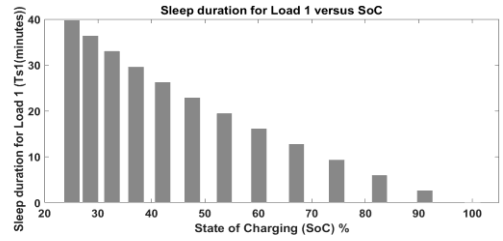
Figure 11: Sleep Duration for Each Load versus State of Charging (SoC)

a

b

c
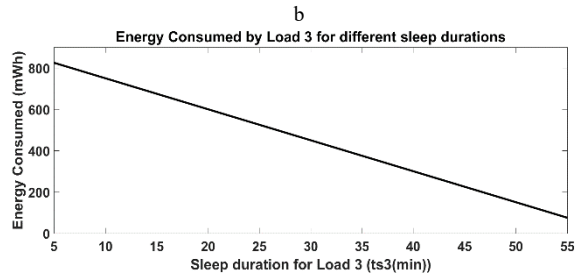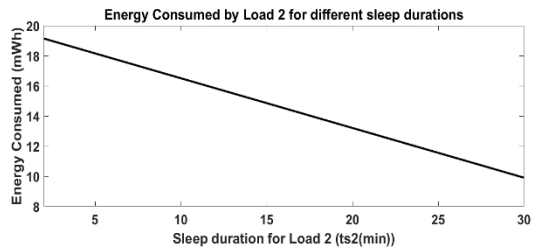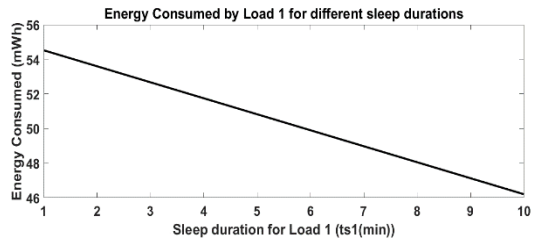
Figure 12: Energy Consumed by Each Load versus Sleep duration for Each Load

1034

The energy consumed by each load for a uniform sleep duration depends on the power consumed by the load (P), the operating time (T_o), Sleep time for each load (T_s) and the number of sleep durations (n). The energy consumed by each load is calculated using (5). As shown in Figure 12, the energy consumed by each load decreases by increasing the sleep duration.

$$E = P \times T_o - P \times T_s \times n \qquad (5)$$

5. Simulation Model Results

An agro environment is simulated on a Matlab Model that is designed using one node consisting of battery, three loads and solar panel. The designed model is used to test the algorithm by testing it at different scenarios that are shown in Tables 2 and 3. The solar irradiance and the state of charging must be checked first to enable the model to select the optimal scenario based on these two parameters. This scenario selection will guarantee the efficient use of energy which will increase the battery life time. The current and power of the solar panel is affected by solar irradiance so a decrease in solar irradiance causes a decrease in the current and power as shown in Figure 13. Low solar irradiance occurs as a result of the small amount of solar energy absorbed by the solar panel which results in a decrease in power and current. Due to the change in climatic conditions as shown in Table 2, solar irradiance changes. The solar power is affected by these changes and it will have an effect during day on deciding whether to switch loads on or off.
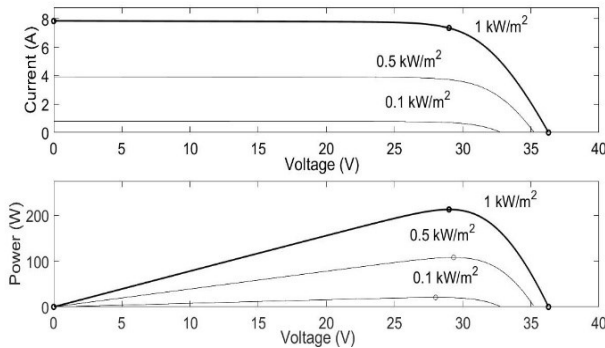
Figure 13: Power and Current at Different Solar Irradiances

Table 2 and 3 show the different scenarios that are designed depending on the battery state of charging and the changes in solar irradiance during day. The loads are activated or deactivated based on the availability of energy provided by battery or solar panel. High priority load is represented as load 1, medium priority load is represented as load 2 and low priority load is represented as load 3. Table 2 shows the four scenarios that are used usually during night. These scenarios are designed depending on the state of charging of the battery. During night, load 1 and load 2 are active for specific hours based on priority while load 3 is deactivated.

Table 2: Represents Different Scenarios of Load Scheduling During Night

Scenario #	Scenario Description	SoC (%)	hrs	Load Scheduling Scenarios		Load Active hours (hrs)
				Priority	Status	
1		100	12	High	On	12
	Fully charged			Medium	On	6
				Low	Off	0
2	Partially charged	75	12	High	On	10
				Medium	On	4
				Low	Off	0
3	Half charged	50	12	High	On	6
				Medium	On	2
				Low	Off	0
4	Battery draining	<40		High	On	1
				Medium	Off	0
				Low	Off	0

Figure 14 shows the battery state of charging as it decreases with time. It is essential to monitor the battery state in order to select the best scenario for supplying loads during night based on amount of power remained.
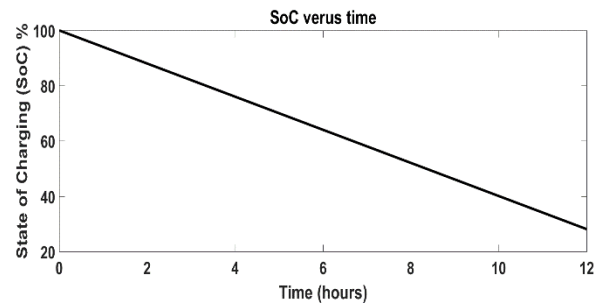
Figure 14: Battery State of Charging versus Time

The solar irradiance is divided into two types static and dynamic. Static solar irradiance is represented in the first three scenarios that are shown in Table 3. These scenarios are designed for various cases that might occur during day in case of static solar irradiance. The duration is constant for the first three scenarios as it is estimated to be 12 hours.

In case the solar irradiance is dynamic during day, this is represented in the fourth scenario shown in Table 3. Scenario 4 is designed due to the change of solar irradiance during day hours. The values of solar irradiance in the previous scenarios might happen in one scenario at different hours. The first scenario in Table 2 and the fourth scenario in Table 3 are simulated and shown in Figure 16 and 17.

Figure 15 shows the changes in solar irradiance during day while during night the loads are supplied by the battery. These variations have an effect on solar power provided to the loads which will decide the status of the load.
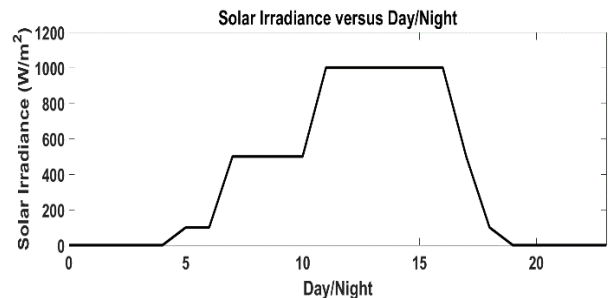
Figure 15: Solar Irradiance versus Day /Night

Table 3: Represents Different Scenarios of Load Scheduling During Day

Scenario #	Scenario Description	Climatic Conditions	Solar Irradiance	hrs	Load Scheduling Scenarios		Load Active hours (hrs)
					Priority	Status	
1	Static Irradiance	Direct sunlight	1000 W/m2	12	High	On	12
					Medium	On	10
					Low	On	8
2	Static Irradiance	Cloudy sunlight	500 W/m2	12	High	On	6
					Medium	On	4
					Low	On	2
3	Static Irradiance	Very cloudy	100 W/m2	12	Powered by Battery Only		
4	Dynamic Irradiance	Clear direct sunlight	1000 W/m2	6	High	On	6
					Medium	On	3
					Low	On	3
		Cloudy sunlight	500 W/m2	5	High	On	5
					Medium	On	2
					Low	On	1
		Very cloudy	100 W/m2	3	Powered by Battery Only		

The loads' status shown in Figure 16 has an effect on its total consumed energy as it changes due to the change in loads' status during day and night. The compensation factor (CF) is shown in Figure 22 as it is calculated for the eight scenarios. It is defined as the ratio between the loads' consumed energy and the energy supplied. During day hours, the solar irradiance changes and at noon, it reaches the maximum point. The solar power at the maximum point will be enough to supply all the loads as shown in Table 3 for specific hours.
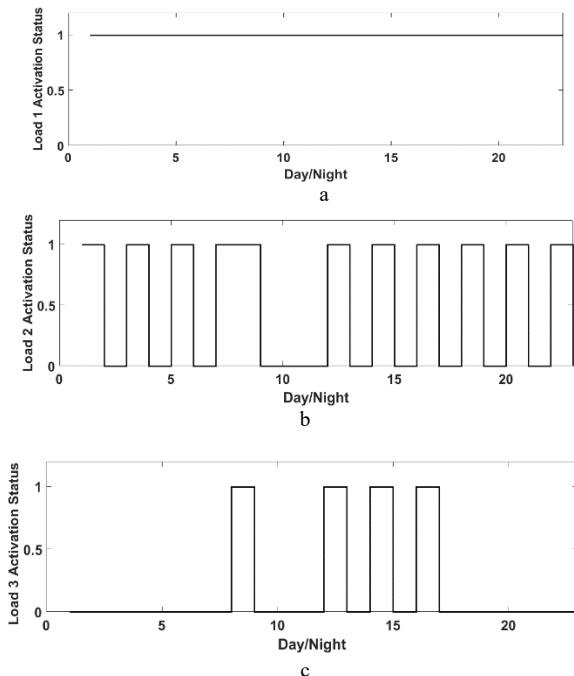
Figure 16: Loads (On/Off Status) versus Day/Night (Scenario 1 in Table 2 and Scenario 4 in Table 3)

Figure 16(a) shows the status of load 1 during day and night. During day hours, load 1 is supplied by solar and in this case the load is active. While during night, it is supplied by the battery.

Figure 16(b) shows the status of load 2, it is activated during day for only 5 hours. Load 2 is activated during night for 6 hours. Figure 16(c) shows the status of load 3, it is activated during day for only 4 hours and it is deactivated at night.

The calculation of load's consumed energy is according to the status of loads shown in Figure 16. The supplied energy either by solar or battery is efficiently consumed using the load scheduling scenarios to provide a sustainable system as shown in Figure 17.
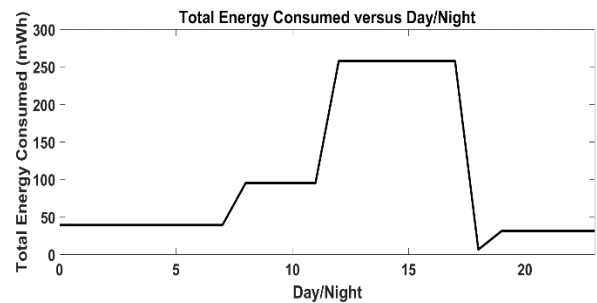
Figure 17: Total Energy Consumed versus Day/Night (Scenario 1 in Table 2 and Scenario 4 in Table 3)

Scenario 2 in Table 2 along with scenario 4 in Table 3 are tested and shown in Figure 18 and 19. Figure 18 shows the loads on/off status during day and night. The total consumed energy by the loads is calculated based on the status of loads as shown in Figure 19.

Figure 18(a) shows that during day hours, load 1 is activated as the power is provided by solar in this case while at night, the load

is still activated and supplied by the battery. Figure 18(b) shows that during day, load 2 is activated for only 5 hours and it is activated for 4 hours at night. Figure 18(c) shows that during day, load 3 is activated for only 4 hours but at night it is deactivated.

a

b

c
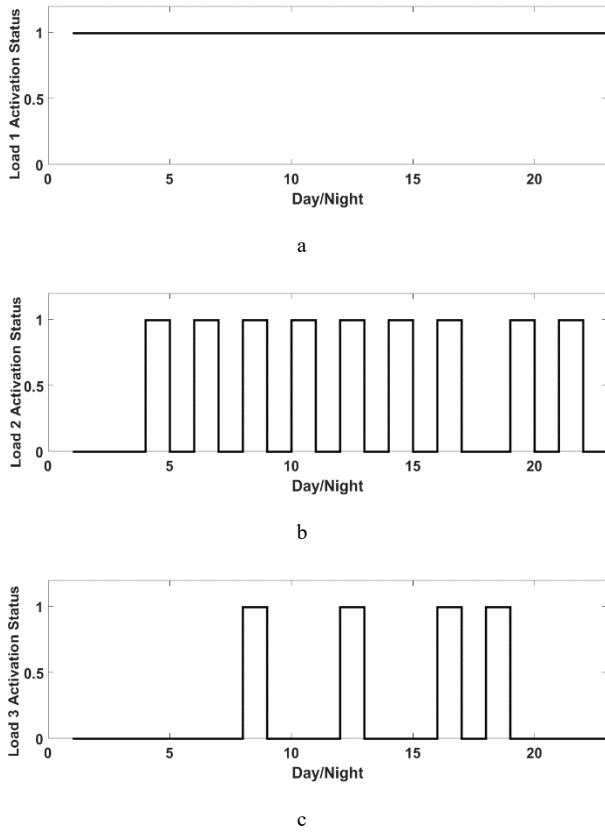
Figure 18: Loads (On/Off Status) versus Day/Night (Scenario 2 in Table 2 and Scenario 4 in Table 3)

The efficient usage of energy during day and night will provide a sustainable system. The total consumed energy by the loads during day and night in accordance to the loads' status is shown in Figure 19.
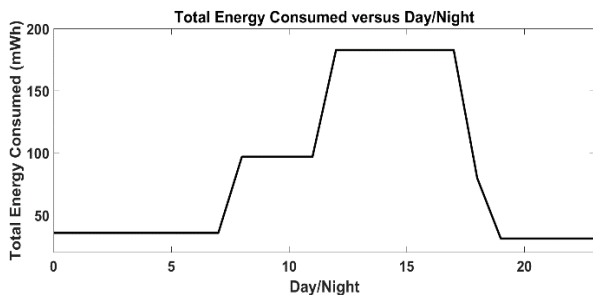
Figure 19: Total Energy Consumed versus Day/Night (Scenario 2 in Table 2 and Scenario 4 in Table 3)

Scenario 3 in Table 2 along with scenario 4 in Table 3 are simulated and represented in Figure 20 and 21. Figure 20 shows the status of the loads which indicates whether it is on or off during day and night. Figure 21 shows the total consumed energy by the loads during day and night based on the status of the loads.

Figure 20(a) shows the status of load 1 during day and night. During day, load 1 is activated by solar power for only 10 hours.

During night, it is activated for only 6 hours as it is supplied by the battery. Figure 20(b) shows the status of load 2 during day and night. During day, load 2 is activated for only 5 hours and at night it is inactive. Figure 20(c) shows the status of load 3 during day and night. During day, load 3 is activated for only 4 hours and at night it is inactive. The supplied energy is consumed efficiently by the loads using the designed scenarios of load scheduling. The total consumed energy by the loads during day and night is shown in Figure 21.

a

b

c
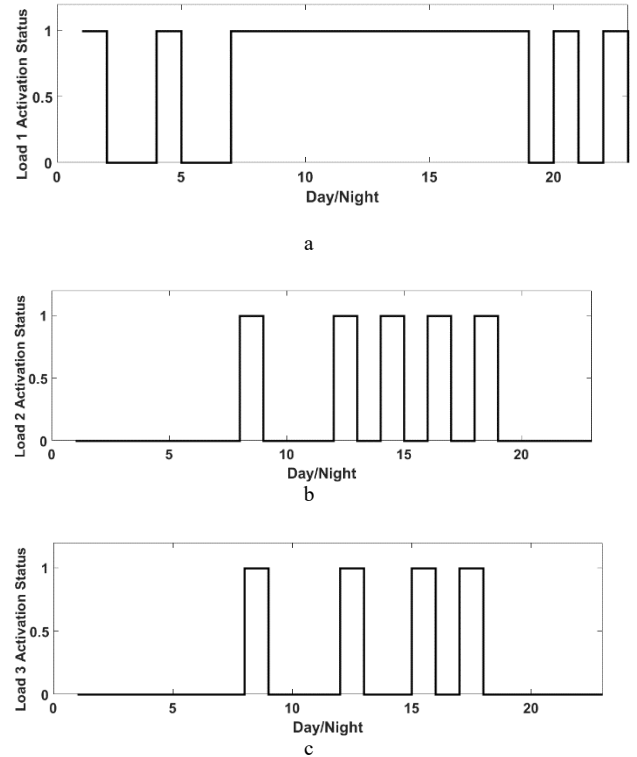
Figure 20: Loads (On/Off Status) versus Day/Night (Scenario 3 in Table 2 and Scenario 4 in Table 3)
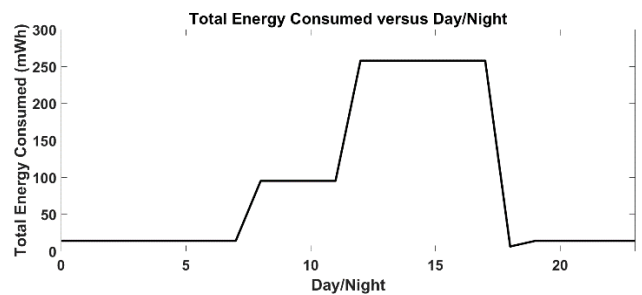
Figure 21: Total Energy Consumed versus Day/Night (Scenario 3 in Table 2 and Scenario 4 in Table 3)
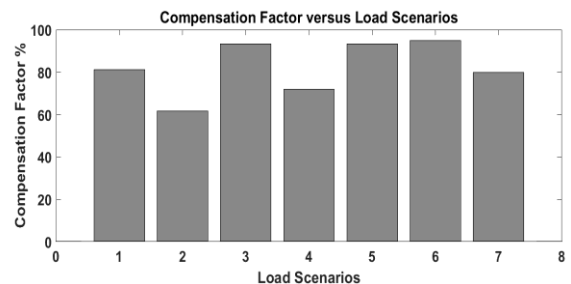
Figure 22: Compensation Factor (CF) versus Load Scenarios

Figure 22 represents the compensation factor (CF) which is calculated for all the designed scenarios. It is the consumed energy by the loads relative to the energy supplied by solar or battery. The compensation factor (CF) is used to show whether there will be an amount of remaining energy that can be used for battery charging or all the supplied energy is fully consumed by the loads.

6. Discussion

The proposed algorithm was simulated and its results are shown in Table 4. The main source that was used for supplying power to the loads during day is the solar panel. During day, there are four designed scenarios for load scheduling. In scenario 1, the three loads will be activated based on priority for a certain time and the energy consumed by the loads is 671.94 mWh at 1000 W/m^2. When the solar irradiance changes to 500 W/m^2, the solar power in this case isn't enough for supplying all loads so scenario 1 isn't suitable for this case as the loads activation period must be reduced.

In this case, scenario 2 is chosen as load 1 (highest priority) is activated for 6 hours while load 2 (medium priority) is activated for 4 hours and load 3 (lowest priority) is activated for 2 hours. In this scenario, the energy consumed by the loads is 184.32 mWh, the battery can be recharged during day using the remaining solar power. At 100 W/m^2, scenario 3 is selected as the loads are supplied by the battery because the solar power is not enough for supplying the loads in this case. The three solar irradiances 1000, 500 and 100 W/m^2 can vary during day so they are combined and represented in scenario 4. In scenario 4, the solar irradiance is 100 W/m^2 for 3 hours, 500 W/m^2 for 5 hours, and 1000 W/m^2 for 6 hours.

Table 4: Simulation Results for Energy Efficient Algorithm

Power Source	Scenario #	Power (mw)			Energy (mwh) for different scenarios	CF %
		Load 1	Load 2	Load 3		
Solar	1	4.62	1.65	75	671.94	81.26
	2	4.62	1.65	75	184.32	61.64
	3	4.62	1.65	75		
	4	4.62	1.65	75	359.07	71.77
		4.62	1.65	75		
		4.62	1.65	75		
Battery	1	4.62	1.65	75	65.34	93.33
	2	4.62	1.65	75	52.8	94.73
	3	4.62	1.65	75	31.02	79.93
	4	4.62	1.65	75		

During night, the algorithm was simulated by using the battery as the main source of power for supplying the loads. There are also four designed scenarios for load scheduling at night. In scenario 1, the loads are supplied by a fully charged battery so load 1 is activated for 12 hours while load 2 is activated for 6 hours as it is active for 1 hour every 2 hours and load 3 is inactive. In scenario 2, the battery SoC is 75 % so load 1 is active for 12 hours, load 2 is active for 4 hours as it is active for 1 hour every 3 hours and load 3 is inactive. Load 3 can be activated based on the user demand or it remains inactive till the availability of light. In scenario 3, the battery SoC is 50% so load 1 is active for 6 hours as it is active for 1 hour every 2 hours while load 2 is active for 2 hours as it is active for 1 hour every 6 hours and load 3 is inactive. In scenario 4, the

battery SoC is below 40% so load 1 is active for 1 hour while load 2 and 3 are switched off till the availability of light in order for the loads to be powered by the solar and for the battery to be recharged. The proposed algorithm guarantees the efficient usage of energy by using the designed scenarios for load scheduling during day and night. It provides a sustainable system as it avoids the drainage of the battery which will prolong the system life time.

7. Conclusion

As a conclusion, it is essential to monitor plants' performance as it helps in increasing and saving the agricultural production. Monitoring the performance of plants is facilitated using IoT technology as it uses wireless sensors that enables the plants to talk and express its requirements. Energy optimization is a major challenge that faces IoT. In agriculture, wireless sensors are utilized in remote areas therefore they consume high energy for continuous operation. An energy efficient technique was proposed in this paper to avoid battery drainage in order to guarantee system sustainability and continuous operation. Solar power and intelligent load scheduling are combined in the proposed algorithm. The results showed that the system operation adapts to the availability of power represented as solar irradiance or battery SoC. It operates using solar panels during day based on solar irradiance but during night, it depends on the battery SoC. During day and night, intelligent load scheduling based on priority is applied to ensure continuous operation. The proposed algorithm elongates the sensors' batteries life time as it efficiently uses energy to ensure the system sustainability. The proposed algorithm enhanced the battery life time by 79.2 %.

References

[1] S.S. Abou Emira, K.Y. Youssef, M. Abouelatta, "Adaptive power system for IoT-based smart agriculture applications," in ICENCO 2019 - 2019 15th International Computer Engineering Conference: Utilizing Machine Intelligence for a Better World, IEEE: 126–131, 2019, doi:10.1109/ICENCO48310.2019.9027393.

[2] S.S. Sarmila, S.R. Ishwarya, N.B. Harshini, C.R. Arati, "Smart farming: Sensing technologies," in Proceedings of the 2nd International Conference on Computing Methodologies and Communication, ICCMC 2018, 149–155, 2018, doi:10.1109/ICCMC.2018.8487571.

[3] S. Rawal, "IOT based Smart Irrigation System," International Journal of Computer Applications, 159(8), 7–11, 2017, doi:10.5120/ijca2017913001.

[4] S. Naveen, S. Hegde, "Study of IoT: Understanding IoT Architecture, Applications, Issues and Challenges," in 1st International Conference on Innovations in Computing & Networking (ICICN16), CSE, RRCE, 477–482, 2016.

[5] D.A. Vyas, D. Bhatt, D. Jha, "IoT : Trends , Challenges and Future Scope," International Journal of Computer Science & Communication, 7(1), 186–197, 2016, doi:10.090592/IJCSC.2016.028.

[6] S. Sadasivam, V. Vadhri, Smart Plant Monitoring System, Informatik, Technische Universitat Darmstadt, Darmastadt, 2015.

[7] D. Markovic, R. Koprivica, U. Pesovic, S. Randic, "Application of IoT in monitoring and controlling agricultural production," Acta Agriculturae Serbica, 20(40), 145–153, 2015, doi:10.5937/aaser1540145m.

[8] K.Y. Chan, H.J. Phoon, C.P. Ooi, W.L. Pang, S.K. Wong, "Power management of a wireless sensor node with solar energy harvesting technology," Microelectronics International, 29(2), 76–82, 2012, doi:10.1108/13565361211237662.

[9] H.M. Jawad, R. Nordin, S.K. Gharghan, A.M. Jawad, M. Ismail, M.J. Abu-Alshaeer, "Power reduction with sleep/wake on redundant data (SWORD) in a wireless sensor network for energy-efficient precision agriculture," Sensors (Switzerland), 18(10), 3450–3475, 2018, doi:10.3390/s18103450.

[10] H. Swalehe, P.V. Chombo, B. Marungsri, "Appliance scheduling for optimal load management in smart home integrated with renewable energy by using whale optimization algorithm," GMSARN International Journal, 12(2), 65–75, 2018.

[11] X. Liu, L. Ivanescu, R. Kang, M. Maier, "Real-time household load priority scheduling algorithm based on prediction of renewable source availability," IEEE Transactions on Consumer Electronics, **58**(2), 318–326, 2012, doi:10.1109/TCE.2012.6227429.

[12] S. Trivedi, K. Parkh, K. Agrawal, "Load Scheduling for Smart Energy Mangement in Buildings with Renewable Power Generation," International Journal of Engineering Research And, **6**(03), 322–326, 2017, doi:10.17577/ijertv6is030349.

[13] M.R. Mohd Kassim, I. Mat, A.N. Harun, "Wireless sensor network in precision agriculture application," in 2014 International Conference on Computer, Information and Telecommunication Systems, CITS 2014, 1–5, 2014, doi:10.1109/CITS.2014.6878963.

Simulating Get-Understand-Share-Connect Model using Process Mining

Shahrinaz Ismail[*,1], Faes Tumin[2]

[1]*Universiti Kuala Lumpur (UniKL), Process Mining Research Cluster (PMineReC), Malaysian Institute of Information Technology (MIIT), Kuala Lumpur, 50250, Malaysia*

[2]*Permodalan Nasional Berhad, Technology Division, Core Application Systems Department (CASD), Kuala Lumpur, 50400, Malaysia*

A R T I C L E   I N F O

A B S T R A C T

This paper presents the method of simulating the personal knowledge management (PKM) processes, based on Get-Understand-Share-Connect (GUSC) Model, using real event logs data from an online learning platform. The method used in here is process discovery and conformance, which are the process mining techniques. Having the model proven at granular level of multi-agent system, this research is found significant in proving that PKM indeed exists in students' online learning behavior and needs to be monitored to ensure that they are managing knowledge in a complete cycle, to support their credibility as future graduates and knowledge workers in organizations. The ideal process starts from Get, then Understand, and followed by Share and Connect, but this study proves that the sequence may vary although the original theory is construed. This depends on the way the online activities being mapped to the Get, Understand, Share and Connect processes during the data processing stage. The results from this paper include the simulation of the GUSC model as discovered from real event logs data.

1. Introduction

Due to the habit and intuitive that they possess, the digital natives, i.e. the generation that grows up with the Internet technologies, are used to independent learning and do not rely much on physical classroom learning. It is a competition of being the most knowledgeable to them, to be able to gain more knowledge and manage their personal knowledge in as many means as they can through the Internet, hence the shift from traditional classrooms to online learning environment in many universities today.

Looking at the need to ensure that learners gained the right knowledge at the right time, and being competitive and marketable graduates, it is necessary to also ensure that they could well manage their personal knowledge. With the current experience in managing classes and teaching materials online, the data is available for analysis on online learning behavior of learners using the university online learning platform. Instead of relying on questionnaire and interview surveys that highly depend on respondents' feedback that could be bias and distorted from truth,

it is a better way to approach the case of online learning behavior directly from the data source on the server.

Recent research has proven the existence of personal knowledge management (PKM) in online learning platforms, including social media and learning management system provided by universities. However, these studies were mostly done using surveys. One significant research developed an agent-based simulation to visualize the PKM processes based on those surveys. There is a gap between these two types of previous research, in which this study intends to close this gap with its findings visualized directly from the original source, which is the event logs data from the online learning server. In doing so, this research aims to achieve the following objectives:

- to discover PKM model by visualizing the process flow in online learning environment; and

- to simulate the PKM processes using real case data for further verification on conforming the model.

This paper is an extension of work originally presented in the 6th International Conference On Research & Innovation In Information Systems (ICRIIS2019), Malaysia [1].

*Corresponding Author: Shahrinaz Ismail, Universiti Kuala Lumpur City Campus, 1016 Jalan Sultan Ismail, +603-21754435, shahrinaz@unikl.edu.my

2. Related Works

2.1. GUSC Model Simulation

As mentioned in the introduction, a recent research has developed an agent-based simulation on GUSC Model, a model that is proven in quite a number research before this. The abbreviation "GUSC" comes from the words Get, Understand, Share and Connect, which are the processes deem necessary for personal knowledge management (PKM). The GUSC Model was simplified from a handful of previous models on PKM by renowned authors since 2009 [2]-[4]. The only difference between GUSC Model and other models before this is the proven suitability of this model for intelligent agents modelling, in which the PKM processes can be developed at granular level for software agents to perform.

In lieu to the previous models, this PKM model is based on the following processes [4], [5]:

- *Get or Retrieve knowledge (G)*: This process simulates how learners retrieve knowledge in explicit form, in which that knowledge has been converted from tacit form by the person who shared it;

- *Understand or Analyze Knowledge (U)*: This process simulates how learners analyze the explicit knowledge that they have retrieved, and convert it to a tacit form in a way that they understand;

- *Share or Publish Knowledge (S)*: This process demonstrates how learners share or post the knowledge that they have understood in an explicit form, so that others can gain knowledge from it;

- *Connect to Knowledge Source (C)*: This process is about connecting learners to sources of knowledge, including materials and people, which may involve communication between the two, resulting in a transformation from tacit form of knowledge to another tacit form.

The decision of adopting GUSC Model for this research is due to its credibility in proving the existence of PKM in learning environment [6], smart classroom [7], [8] , social network [9] , and social messaging applications [10], [11]. In addition to that, prototypes have been developed to prove that GUSC Model can be used to design PKM platforms for individuals [12], and a simulation of GUSC Model in learning environment is developed to show and prove PKM processes among learners [13].

It was suggested in the recent research on GUSC simulation [14] to relook into the simulation itself by improving the way the measurement of each PKM process is done. There is a trend discovered from the simulation, in which there are some "learning sessions" that are not used, or termed as "non-usage". This is a significant finding that is found interesting for this research to investigate using real event logs data.

2.2. Process Model Discovery

Derived from business process management domain, process mining helps the analysis of business process based on actual data of event logs. It is often thought as the same as data mining, but it is not. Data mining algorithm is significant to process mining but the latter provides more comprehensive benefits in terms of the organizational system as a whole.

Event logs are analysed in the context of process-aware system [15], in which the full view of the case situation is being understood, hence the importance of the event logs to researchers. Process mining techniques are expected to be non-trivial because it is based on extraction of only useful information from the logs [16], which in turn could provide truthful, real data without biasness. Nevertheless, process mining can show that a real process in a system is more complex than the way it is planned to be in documents. The event logs from e-learning environments might contain huge amounts of fine granular events and process-related data, which consist of different categories that make the whole process messy and prone to producing waste of resources and useless data [17].

There are three different techniques suggested for process mining [18], as follows:

- *Process Model Discovery*: By using the event logs retrieved from the database, fuzzy miner algorithms are applied by the process mining software to produce a process model. This requires data to be readily available, in a situation where process model is not yet planned or developed in documentation.
- *Conformance Checking*: When a process model is available (either from the plans and documentation or from the discovery), the retrieved event logs are analysed to conform whether the real activities happening in the system is as how the process is modelled for, or not.
- *Process Improvement*: The purpose of this technique is to improve the existing process model using the information retrieved from the event logs. It is different than conformance checking because it measures the alignment between the model and the real online activities, hence producing an improved model that fits the condition deemed necessary.

There are several algorithms that can be used to perform process discovery including Fuzzy miner and Heuristic miner [19]. Fluxicon Disco is a recommended tool for automated process model discovery based on fuzzy miner algorithms. The strength of the fuzzy miner is the seamless process simplification and highlighting of frequent activities that are very useful for the research purpose [20]. The process model could be messy and fuzzy mining will come in handy in terms of filtering out the data and adjusting the level of details available in the model, in order to better perceive the process model.

3. Methodology

For this research, process model discovery will be used to initiate the process of discovering the GUSC Model in online learning environment and achieving the first objective. This is followed by conformance checking, to prove that GUSC processes really happen in the online environment, by simulating the processes through animated visualization, to achieve the second objective.

3.1. Case Settings

This research has chosen a case university that implements a Moodle-based online learning environment called "VLE", i.e.

virtual learning environment. The event logs data from year 2016 to 2017 was extracted from the VLE database for the purpose of this study. The event log consists online activities data that the students went through every day in the VLE. The extracted fields from the event logs data are date and time, case ID, and activity.

The students who performed the online learning activities in the selected case are those from semester three to six. They were chosen because they have experience using the VLE for more than one semester.

The selected courses for this study are from software engineering and business technology. These courses are selected to ensure that both technical and less technical contents are covered in the process model discovery, since the lecturers or instructors of both courses have their own way of delivering teaching materials online and assigning activities. For example, business technology may have a more theoretical contents compared to software engineering, hence the instructor may use discussion forum and wiki more than the latter.

Other important matters to be identified during case settings are the activities in the event log and the relevance of data to this research. Irrelevant data of less or non-relevant activities need to be omitted out, for example "register", "delete comment" and "update profile". Since the purpose of this research is to analyze PKM processes in VLE, the activities selected for analysis are those related to PKM activities only, such as "course module viewed", "quiz attempt started" and "quiz attempt summary viewed".

3.2. Process Discovery

In process discovery, the event log was extracted and imported into the chosen process mining tool (i.e. Fluxicon Disco), in which the log is automatically transformed to create a newly discovered process model using fuzzy miner algorithm. There are two ways of process discovery: play-in, i.e. from event log to process model; and play-out, i.e. from process model to event log [21].

The first step in classification of requirement is the extraction of the event log from VLE database and importing the event log into the Fluxicon Disco. Figure 1 shows the interface after the event log is imported into the tool.

From Figure 1, the event log (in *.CSV file format) that is inserted into the process mining tool needs to be classified according to the requirement, i.e. ID, Activity and Timestamp. Due to the difficulty of having process instances scattered over multiple rows (i.e. in *.CSV file), it is found that the Fluxicon Disco is a suitable tool for data extraction compared to a normal spreadsheet.

The basic data requirement for process mining is to look into the historical process data precisely, such as a "process lens". The three requirements are as follows:

i) *Case ID*: A case identifier, else called as process case ID, is important to recognize various executions of a similar process. The correctness of case ID relies on the domain of the process. For this research case, the case ID are *Get*, *Understand*, *Share* and *Connect*, i.e. the GUSC processes.

ii) *Activity*: There ought to be names for various procedure steps or status changes as activities were performed in the process. In the event that the information only appears once or in a single passage (i.e. one row) for each procedure occasion, then it could be concluded that at that point the information is not detailed enough.

iii) *Timestamp*: From the timestamp, the delays between activities can be identified as it could show the duration of each activities in a process. This could be further related to the process of a series of activities and its duration across time.

Figure 1: Event log being imported into Fluxicon Disco
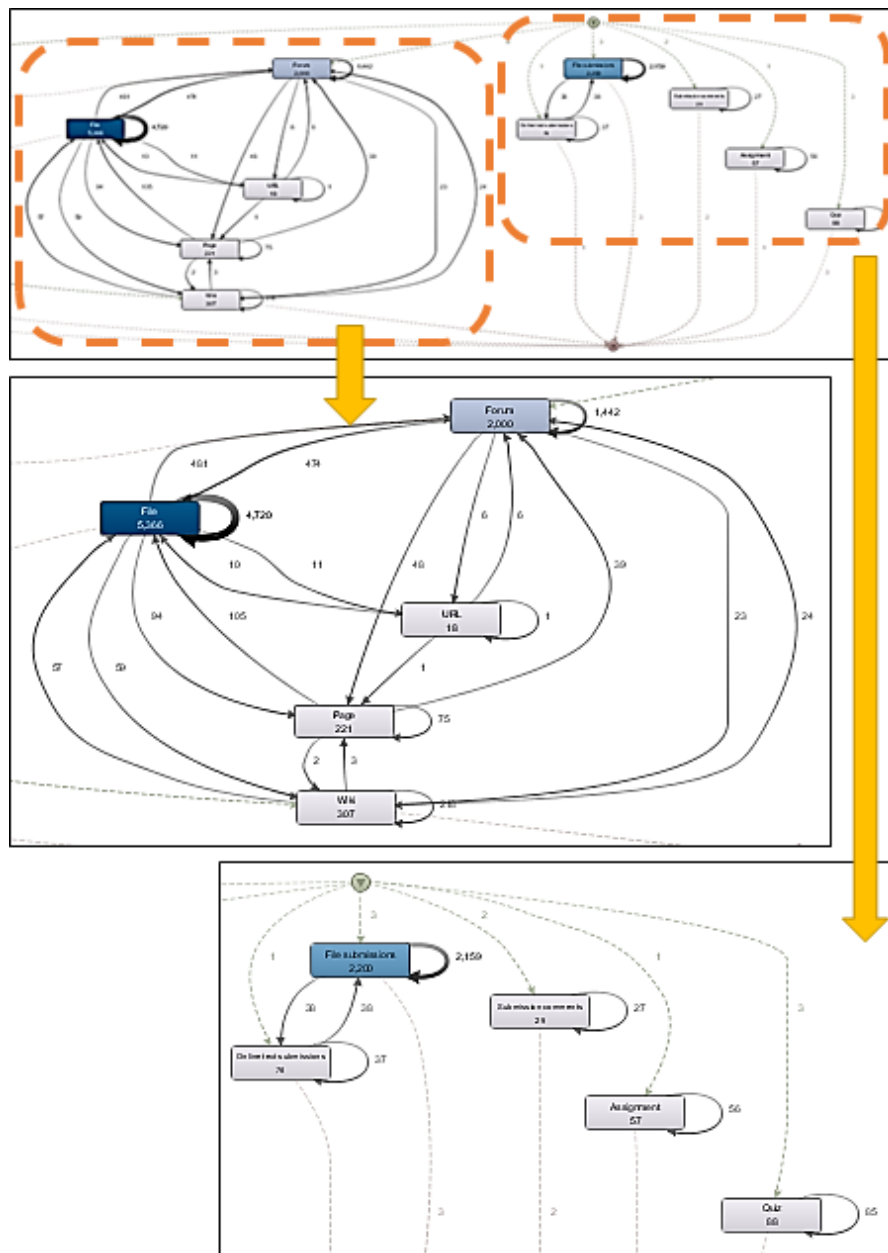
Figure 2: Results after classification of requirement

3.3. Process Mapping

Figure 2 shows the result after classification of requirement has been confirmed. From the classification, a process model is developed based on the mapping that has been assigned in the event log. This process model can be manipulated by adjusting its part and activity frequency. This is to ensure that the process model is better understood, instead of merely showing the full process that involves so many paths and activities that will often be displayed as spaghetti-like process. Adjusting the activities to lower the frequency would not make the process model unreliable, but it could hide some activities that may not seem fit to the process model.

In a glance as shown in Figure 2, it is observed that there are two groups of activities being defined in the overall process. The left part of the process flow shows the learning activities over forum, file, URL, webpage and wiki, whereas the right part of the

process flow shows the assessment related activities, mainly file submission, assignment and quiz.

Filtering of data can be easily done in Fluxicon Disco, as compared to using spreadsheet. Data that is identified to be useless for the process model simulation is filtered out. The Timeframe can also be filtered according to year, month and/or day, according to the time an active process happened. For this research, the whole timeframe is taken into account to see active months and years, so that none of the activities are left behind, e.g. student logging in to VLE during mid-semester break or in semester break. Figure 3 shows the interface of filtering process in Fluxicon Disco.

The statistics interface shown in Figure 4 displays an overview of the data, which can be in a huge amount. The statistics table shows which case is frequently active in the process, and the connection between each data. The *Connect* process is identified throughout the process in a more understandable way. This table

generated in Fluxicon Disco also shows the frequency of each activity that consists the number of events data. The duration of each activity can also be viewed here.
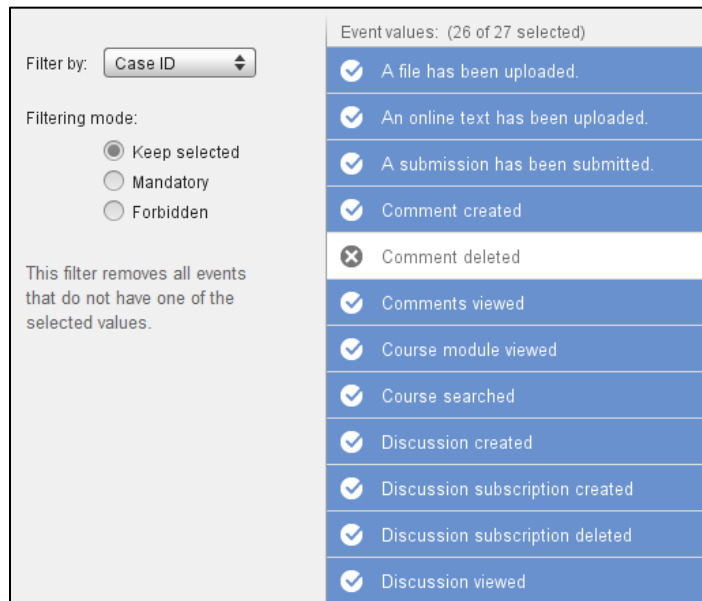
Figure 3: Filtering of data in Fluxicon Disco

activities and their frequencies. The results shown here are presented according to three types, i.e. process model by components, by PKM process variables, and by activities that happened in the VLE.
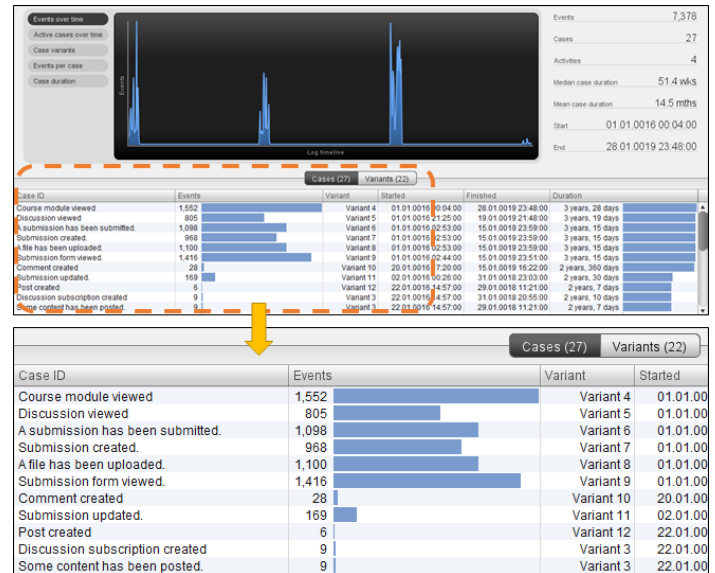
Figure 4: Statistics of activities in Fluxicon Disco

4. GUSC Model Simulation

This section presents the results of the GUSC Model simulation using the fuzzy miner algorithm in Fluxicon Disco. The simulation results are displayed in two modes: static view of GUSC process flow; and animated view of GUSC process flow.

The process model presented here basically shows the actual process that happened in VLE, which consists of the numbers of

4.1. Static View of GUSC Process Flow

Figure 5 shows the process model that was developed according to components from the event log. In general, there are 10 components analyzed for process model discovery simulation: File; File submissions; Submission comments; Quiz; Assignment; Forum; Wiki; Online text submissions; URL; and Page.
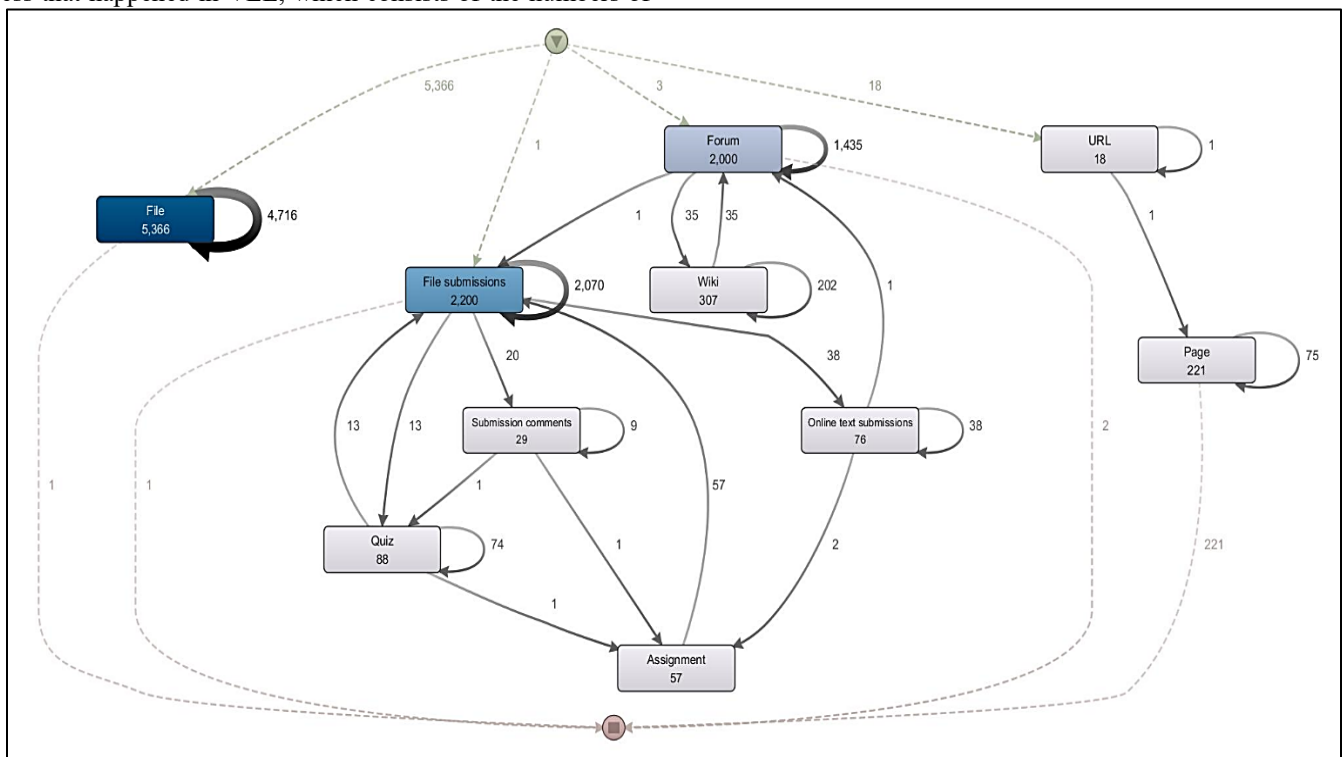
Figure 5: GUSC process model by components

The 'File' component (shown in darkest shade in Figure 5), is the dominant one because the activities that happened on a 'File' is frequently active (i.e. 5,366 occurrences). Students' activities of downloading or uploading files would fall under this 'File' component. Activities like 'downloading notes' are quiet common in the event logs and it happens quite frequently among the students.

'URL' (18 occurrences) is a component that is posted by the lecturers, in which the URL or hyperlink of a website is shared in the VLE for students to click on and be directed to the landing page with materials to learn. A 'Page' (221 occurrences) or webpage serves the same purpose as the 'URL', but instead of directly bringing the users to an external website, it is an internal webpage created by the lecturers, in which the students can view notes and multimedia contents like a page in a website within the VLE.

Each activity has different component and each component may share the same activity name. For example, the component 'File' may have two activities in it that are 'Course module viewed' and 'Wiki page viewed', and these two activities share the same component with 'Forum', 'Page', 'URL', and 'Wiki'. This is due to the way the 'File' component is used within the other activities.

Table 1 shows the number of occurrences for each component shown in Figure 5. It also presents the number of recurrences for each component, which happened when students return to the same component during a session. Figure 5 also shows the frequencies of inflow and outflow processes, which are not presented in Table 1. However, the total number of recurrences, inflow and outflow processes for each component should be the same as the number of occurrences for each component.

Table 1: Component Occurrences in VLE

Component	Occurrence	Recurrence
File	5,366	4,716
File submissions	2,200	2,070
Submission comments	29	9
Quiz	88	74
Assignment	57	-
Forum	2,000	1,435
Wiki	307	202
Online text submissions	76	38
URL	18	1
Page	221	75

Figure 6 shows the process model that was developed according to PKM processes, based on the GUSC model. The processes are *Get*, *Understand*, *Share* and *Connect*, as stated in Section 2. These processes are mapped to the VLE activities in the imported event log data (i.e. in the *.CSV file), as the mapping was developed according to the PKM process model requirements made prior to this study.

As shown in Figure 6, the number shows the frequencies of the VLE activities that are mapped to the GUSC processes. The *Get* activity is the dominant one as compared to the other processes (shown in darkest shade in Figure 6). This result is as expected

because the *Get* activities is common to happen more frequently than *Share* or *Connect* activities. The basic idea of having VLE is to provide a platform for students to *Get* information and knowledge shared by others, especially in the form of learning materials and notes.
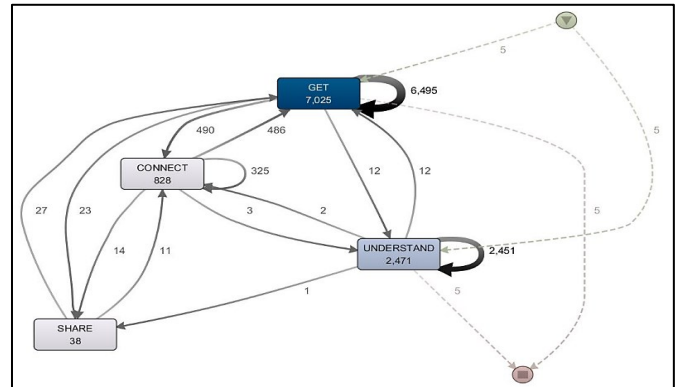
Figure 6: GUSC process model by PKM processes

The looping arrow displayed on *Get* process shows a number of reworks that occurred in the event. An activity that keeps looping like this basically means that students kept downloading the same notes or materials, e.g. for three days in a row. The same pattern is seen on the *Understand* process, in which the process keeps looping on the same activity as the students attempt to understand the information and knowledge in VLE. An example of this is uploading of assignment, in which students are allowed to keep uploading an assignment, or attempt multiple submissions of an assignment, as long as the deadline has not yet past.

Table 2 shows the number of occurrences and recurrences for each GUSC process derived from Figure 6. As described for Table 1, the inflow and outflow processes are not shown here, but the number of occurrences should show the total number of inflow processes, outflow processes and recurrences as a whole.

Table 2: GUSC Process Occurrences in VLE

Process	Occurrence	Recurrence
Get	7,025	6,495
Understand	2,471	2,451
Share	38	-
Connect	828	325

Figure 7 shows the overall view of the GUSC process model according to VLE activities. The most dominant activity is "File – Course module viewed – Get" with 5,366 occurrences (shown in darkest shade in Figure 7). This is followed by "Forum – Course module viewed – Get" (1,167 occurrences) and "File submissions – A file has been uploaded – Understand" (1,100 occurrences). In other words, the *Understand* process does happen in an online learning environment like VLE, even if can only be proven by uploading of files to VLE.

In a glance, the process model presented in Figure 7 looks quite structured. Unlike the previous two views, Figure 7 shows no recurrences of any activity. Recurrences only happened between two activities, e.g. between "Forum – Course module viewed – Get" and "Forum – Discussion viewed – Connect" (470 occurrences to, and 473 occurrences return). Table 3 shows the summary of occurrences according to the activities derived from Figure 7.
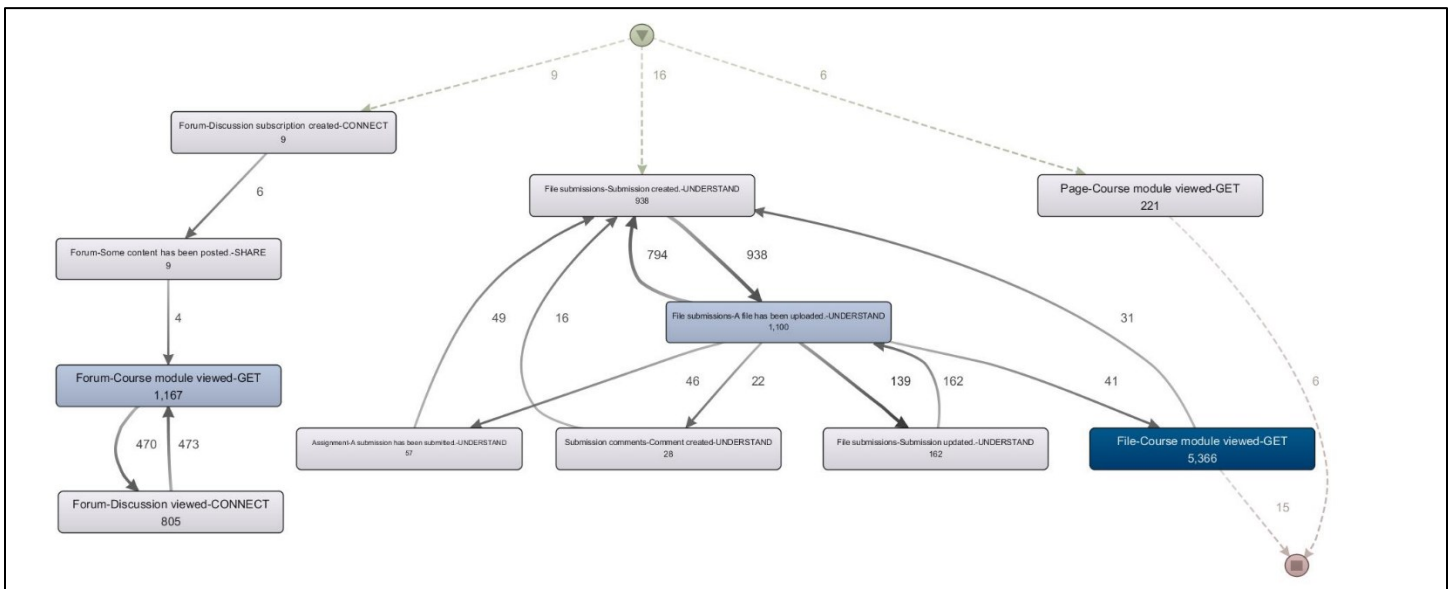
Figure 7: GUSC process model by activities

Table 3: Activity Occurrences in VLE

Activity	Occurrence
Forum – Discussion subscription created – Connect	9
Forum – Some content has been posted – Share	9
Forum – Course module viewed – Get	1,167
Forum – Discussion viewed – Connect	805
File submissions – Submission created – Understand	938
File submissions – A file has been uploaded – Understand	1,100
Assignment – Submission has been submitted – Undestand	17
Submission comments – Comment content – Understand	28
File submissions – Submission updated – Understand	102
Page - Course module viewed – Get	221
File - Course module viewed – Get	5,366

4.2. Animated View of GUSC Process Flow

The GUSC model simulation shows the movement of the processes in 'blobbing' shapes. The movement can be seen with different rhythm and speed depending on the time duration and frequency of the running processes. The thicker the line movement of the process travels, the frequent the process is. Figure 8 shows the snapshot of this animation of GUSC process model, in which the thicker line in red is where a process travels, and the yellow 'blobbing' shape shows the high volume per time unit.

As shown in Figure 8, the *Understand* process does not travel to other variables except for one way towards *Share* process, while *Get*, *Connect* and *Share* processes travel to each other. This can be explained that *Get*, *Connect* and *Share* processes happen before the *Understand* process can happen. The situation supports the findings of previous research that proved the *Get*, *Connect* and

Share are connected to each other and they are the main processes of PKM [6]. This was statistical proven to justify that an *Understand* process can only happen when a *Share* process happens (the one-way line shown from *Understand* to *Share* in Figure 8), and *Share* process happens when *Get* and *Connect* processes happen (shown in darker lines in Figure 8).
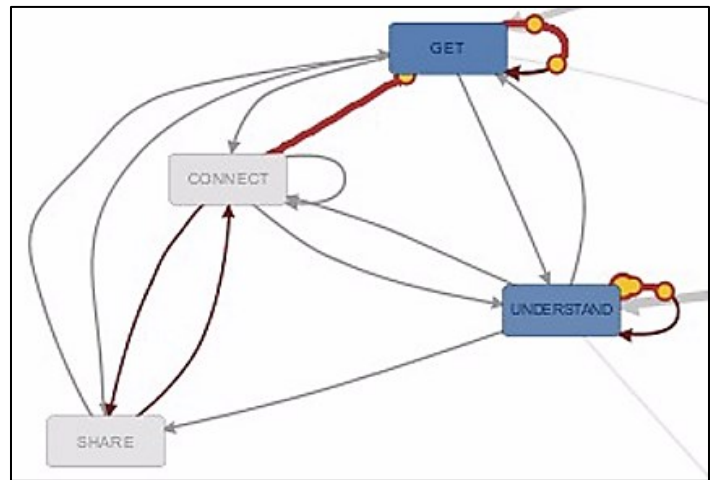
Figure 8: Animated view of GUSC process model

Figure 9: Frequency of occurrences and recurrences on Forum and Wiki

1	Time	User full name ▼	Event context ▼	Component ▼	Event name ▼
2	24/03/19, 19:54	NURAIN NAZIEAN BINTI CHAPERI &#22;	Forum: Announcement	Forum	Course module viewed
3	23/03/19, 15:02	NUR NAJIHAN BINTI ABDUL MANAF 	Forum: Announcement	Forum	Course module viewed
4	23/03/19, 11:26	NURAIN NAZIEAN BINTI CHAPERI &#22;	Forum: Announcement	Forum	Course module viewed
5	22/03/19, 23:44	NUR NAJIHAN BINTI CHAPERI &#22;	Forum: Announcement	Forum	Course module viewed
6	22/03/19, 21:14	NURAIN NAZIEAN BINTI CHAPERI &#22;	Forum: Announcement	Forum	Course module viewed
7	22/03/19, 12:33	NUR NAJIHAN BINTI ABDUL MANAF 	Forum: Announcement	Forum	Course module viewed
8	22/03/19, 10:18	NUR NAJIHAN BINTI ABDUL MANAF 	Forum: Announcement	Forum	Course module viewed
9	19/03/19, 21:48	NUR NAJIHAN BINTI ABDUL MANAF 	Forum: Announcement	Forum	Discussion viewed
10	19/03/19, 21:47	NUR NAJIHAN BINTI ABDUL MANAF 	Forum: Announcement	Forum	Discussion viewed
11	19/03/19, 21:46	NUR NAJIHAN BINTI ABDUL MANAF 	Forum: Announcement	Forum	Course module viewed
12	19/03/19, 19:22	NURALIYA FARHANNAH BINTI NORAZLAN &#82	Forum: Announcement	Forum	Discussion viewed
13	19/03/19, 19:22	NURALIYA FARHANNAH BINTI NORAZLAN &#82	Forum: Announcement	Forum	Discussion viewed
14	19/03/19, 19:22	NURALIYA FARHANNAH BINTI NORAZLAN &#82	Forum: Announcement	Forum	Course module viewed
15	19/03/19, 19:05	NURAIN NAZIEAN BINTI CHAPERI &#22;	Forum: Announcement	Forum	Discussion viewed
16	19/03/19, 19:05	NURAIN NAZIEAN BINTI CHAPERI &#22;	Forum: Announcement	Forum	Course module viewed
17	19/03/19, 15:37	NUR DAYANA BINTI RADZUAN &#22;	File: Chapter 3: The PM Process Groups	File	Course module viewed
18	19/03/19, 15:34	NUR AFIQAH BINTI ZAKARIA R	File: Chapter 3: The PM Process Groups	File	Course module viewed

Figure 10: Timestamp in event log data

5. Discussions

Among the features available in VLE, forum is a powerful platform that can facilitate students in performing all PKM processes. It has been mapped to all four PKM processes, namely GUSC processes, and the results have shown that Forum receives high occurrences and recurrences in certain areas of PKM. Although Wiki has similar strength in providing the same PKM facilities, the exposure on its usage is still low, in which students do not find that Wiki could help in enhancing their learning capacity through collaboration and knowledge sharing. Both of these features or components require high commitment and interaction among the students, and thus the processes of *Connect* and *Understand* could be well performed on top of *Get* and *Share*.

The process model discovered through this simulation research has shown the real scenario of processes that occurred in VLE, but it is far from the expectation this research earlier perceived. A simple activity as downloading lecture notes is actually an important activity in VLE to achieve the process of *Get* knowledge, but it happens as a looping activity. In business process view, a looping activity is not good because it shows that the first time of performing the activity is not done properly. As a result, it can be concluded that the students are not managing their knowledge very well because they keep on downloading the same notes several times.

This research shows that using Forum and Wiki in VLE will not only let the students interact with each other but it can also boost the full potential of the VLE itself. Not many users know all the features in VLE that can provide the full potential benefits of managing knowledge, hence time is wasted on available precious resources. Figure 9 shows the frequency of the activities happened on Forum and Wiki, in which the process travels a lot between these two components that all the PKM processes happened in this loop simultaneously. In contrast, components like Assignment only fall under *Understand* process, as students only tend to submit their assignments once they have understood on how to complete them.

Figure 10 shows the event log data when it was first retrieved from the database. It does not show the start and end time of a process, but only the overall time when a process happened. The unavailability of both start and end timestamp in the VLE event log data has caused this limitation. This limitation has caused some difficulties in analyzing further on students' activities, especially when the duration of each activity can produce significant measurement and findings for this research, in which the duration can be derived from having two timestamps.

Overall, the use of process mining has helped in proving a theoretical model like personal knowledge management processes, without biasness of respondents' feedback. This research has proven that the same event log data can be used to analyze different theoretical models, as the same data was used in a research on self-regulated learning (SRL) model prior to this [22].

6. Conclusion

In a nutshell, this research has achieved its objectives of discovering PKM model by visualizing the process flow in online learning environment, and simulating the PKM processes using real case data for further verification on conforming the model. With the simulation views (i.e. both static and animated views), it is expected that online learning environment users can benefit in terms of knowing their status of managing knowledge. It should benefit both the lecturers (who can use the simulation to gauge students' learning behavior as well as improving teaching initiatives) and students (who can know where they can improve in terms of responding to the learning system for own future benefits). Nevertheless, the process model discovered in this research is highly dependent on how the online learning environment is used in the case organization, in which the features used by both lecturers and students reflect whether the PKM model is fully complied or not. Missing features or activities may affect the learners' capability of managing personal knowledge, as they depend on the features to exist for them to have more choices and fully utilize as part of their learning sessions.

It is recommended that the future work could improve the way this research is conducted, in terms of activity and component mapping to the PKM processes (i.e. GUSC), as well as identifying the start and end time for each activity in an online learning system to better analyze the overall PKM processes. Other opportunities

include adopting suitable techniques to perform the process mapping to activities and extending this research on other courses and case settings.

Acknowledgment

References

[1] S. Ismail, F. Tumin, "Analysis on online learning environment using process mining technique for personal knowledge management mapping," in International Conference on Research and Innovation in Information Systems, ICRIIS, 2019, doi:10.1109/ICRIIS48246.2019.9073269.

[2] L. Razmerita, K. Kirchner, F. Sudzina, "Personal knowledge management: The role of Web 2.0 tools for managing knowledge at individual and organisational levels," Online Information Review, **33**(6), 1021–1039, 2009, doi:10.1108/14684520911010981.

[3] H. Jarche, From observation to breakthrough, Adapting to Perpetual Beta Blog, 2012.

[4] S. Ismail, M.S. Ahmad, Z. Hassan, "Emerging personal intelligence in collective goals: Data analysis on the bottom-up approach from PKM to OKM," Journal of Knowledge Management, **17**(6), 2013, doi:10.1108/JKM-08-2013-0313.

[5] S. Ismail, T.D. Nguyen, M.S. Ahmad, "A multi-agent knowledge expert locating system: A software agent simulation on personal knowledge management (PKM) model," in International Conference on Intelligent Systems Design and Applications, ISDA, 2014, doi:10.1109/ISDA.2013.6920705.

[6] S. Ismail, A. Othman, M.S. Ahmad, "Knowledge Management in Learning Environment: A Case Study of Students' Coursework Coordination," in Knowledge Management International Conference (KMICe), 2014.

[7] S. Ismail, S.F.M. Suhaimi, M.S. Ahmad, "The GUSC model in smart notification system: The quantitative analysis and conceptual model," in 2013 8th International Conference on Information Technology in Asia - Smart Devices Trend: Technologising Future Lifestyle, Proceedings of CITA 2013, 2013, doi:10.1109/CITA.2013.6637581.

[8] S. Ismail, M.S. Ahmad, "Knowledge Management in Agents of Things: A case study of smart classroom management," in International Conference on Research and Innovation in Information Systems, ICRIIS, 2013, doi:10.1109/ICRIIS.2013.6716685.

[9] S. Ismail, Z. Mohammed, N.W. Yusof, M.S. Ahmad, "Personal Knowledge Management among Adult Learners: Behind the Scene of Social Network," International Journal of Humanities and Social Sciences, 2013.

[10] S. Ismail, M.S. Ahmad, "Personal Knowledge Management among Managers: Mobile Apps for Collective Decision Making," Journal of Information Systems Research and Innovation, 2015.

[11] S. Ismail, N. Jamaludin, "Managing knowledge over social messaging application: The case of an event management project group," in 2016 3rd International Conference on Computer and Information Sciences, ICCOINS 2016 - Proceedings, 2016, doi:10.1109/ICCOINS.2016.7783184.

[12] S. Ismail, M.F. Ghazali, "Mobile coursework coordination deploying the concept of agent-mediated personal knowledge management in learning environment," in ICICTM 2016 - Proceedings of the 1st International Conference on Information and Communication Technology, 2017, doi:10.1109/ICICTM.2016.7890797.

[13] S. Ismail, "Simulating Get-Understand-Share-Connect model for personal knowledge management in learning environment," in 2nd International Symposium on Agent, Multi-Agent Systems and Robotics, ISAMSR 2016, 2017, doi:10.1109/ISAMSR.2016.7809995.

[14] S. Ismail, "Simulating Get-Understand-Share-Connect model for personal knowledge management in learning environment," in 2nd International Symposium on Agent, Multi-Agent Systems and Robotics, ISAMSR 2016, 2017, doi:10.1109/ISAMSR.2016.7809995.

[15] W. Van Der Aalst, T. Weijters, L. Maruster, "Workflow mining: Discovering process models from event logs," IEEE Transactions on Knowledge and Data Engineering, 2004, doi:10.1109/TKDE.2004.47.

[16] W.M.P. Van Der Aalst, "Process-aware information systems: Lessons to be learned from process mining," in Lecture Notes in Computer Science (including subseries Lecture Notes in Artificial Intelligence and Lecture Notes in Bioinformatics), 2009, doi:10.1007/978-3-642-00899-3_1.

[17] A.H. Cairns, B. Gueni, M. Fhima, A. Cairns, S. David, N. Khelfa, "Process Mining in the Education Domain," International Journal on Advances in Intelligent Systems, 2015.

[18] W. Van der Aalst, Process mining: Data science in action, 2016, doi:10.1007/978-3-662-49851-4.

[19] K. Rattanathavorn, W. Premchaiswadi, "Analysis of customer behavior in a call center using fuzzy miner," in International Conference on ICT and Knowledge Engineering, 2015, doi:10.1109/ICTKE.2015.7368485.

[20] V.A. Rubin, A.A. Mitsyuk, I.A. Lomazova, W.M.P. Van Der Aalst, "Process mining can be applied to software too!," in International Symposium on Empirical Software Engineering and Measurement, 2014, doi:10.1145/2652524.2652583.

[21] W.M.P. Van Der Aalst, "Relating process models and event logs 21 conformance propositions," in CEUR Workshop Proceedings, 2018.

[22] M.H.B.A. Bakar, S. Ismail, S.H.S. Ali, "A process mining approach to understand self regulated-learning in moodle environment," International Journal of Advanced Trends in Computer Science and Engineering, 2019, doi:10.30534/ijatcse/2019/1581.32019.

Formal Proof of Properties of a Syntax-Oriented Editor of Robotic Missions Plans

Laurent Nana*, François Monin, Sophie Gire

Univ Brest, Lab-STICC, CNRS, UMR 6285, F-29200 Brest, France

A R T I C L E   I N F O

A B S T R A C T

This article copes with the formal verification of properties of the missions building module of PILOT's software. PILOT is a language dedicated to remote control of robots. An incremental syntax-oriented editor was built in order to increase the dependability of PILOT's missions and we showed that, under a maximum size of plan, this editor allows building only all plans that are syntactically correct. The limitation in size was due to state space explosion problem inherent to the Model-checking approach used for the proof. In order to extend the proof to all plans without any limitation in size, we investigated the theorem-proving approach, and especially PVS (Prototype Verification System). This paper therefore focuses more on modeling of PILOT plans and related building operations and the use of PVS to verify properties of the built models, in view of proving the aforementioned properties of PILOT software's missions building module.

1. Introduction

This paper extends the work originally presented in [1]. In the prolongation of preceding works aiming at enhancing the dependability of robotic applications [2-12], it targets the use of verification systems, and especially PVS (Prototype Verification System), for properties verification of a syntax-oriented editor of missions plans conceived for PILOT, a programming language devoted to the control of robots from remote. PILOT is developed within the Laboratory of Sciences and Techniques of Information, Communication and Knowledge (Lab-STICC). Proof systems rest on methods of formal proof or verification that can be described as approaches enabling to define systems properties and check their correctness using mathematics techniques and inference rules. In an earlier work, with the help of Prolog and University of Amsterdam's SWI-Prolog tool, we proved that the syntax-oriented editor allows building all and only plans having a correct syntax. Nevertheless, we could only do this proof for plans whose size was under a maximum limit, due to the explosion of state-space inherent to the model-checking approach implemented using the SWI-Prolog tool. Theorem proving approaches and related tools such PVS should make it possible to get rid of the constraint on plans size, and to extend the proof to all plans whatever their size. PVS has been chosen because of our experiment in its use for protocol verification [13, 14]. The formal verification of properties of PILOT's syntax-oriented editor involves a proper formalization of the language syntax and of the editor's working. This article is dedicated to the modeling of PILOT plans and building operations of plans, and the use of PVS to verify properties of the built models, in view of proving the correctness of PILOT's incremental syntax-oriented editor.

The rest of this paper is structured as follows. A state of the art of robotic systems' formal verification is presented in the second section. The third section addresses preliminaries on formal proof methods and gives an overview of PVS. The language PILOT as well as PILOT plans construction and checking method are presented in the fourth section. The fifth section deals with verification of properties with the help of SWI-Prolog tool. The sixth section is dedicated to the modeling of plans and building operations of plans, and verification of properties on the models using PVS. Conclusions are presented in the seventh and last section.

2. Related works

In [15], the authors reminded, firstly that formal methods of verification were only recently introduced in the control community to assist developers in the construction of complex robotic systems' control architectures, and secondly that the hybrid nature of such systems (combination of discrete and continuous behaviors) makes their formal treatment hard and necessitates new methods that are both operational and efficient.

In [16], the authors tackle issues and outlooks in robotics. One of the issues they pinpoint is long-term mission execution

*Corresponding Author: Laurent NANA, Univ. of Brest, Computer Science Department, 20 Avenue Le Gorgeu, 29238 Brest, +33298052283, nana@univ-brest.fr

capability. Despite the fact that dependability, formal verification and fault tolerance methods are not directly referred, they are needed to reach that objective.

In [17], the authors address the inclusion of operations into the control architecture of a UUV (unmanned underwater vehicle) for the mapping and the watching of the ocean. The proposed control system integrates safety mechanisms to lessen hazards at the Mission level and necessitates to use formal verification approaches.

In [18], the authors portray an approach for the use of formal tools to verify the controllers of unmanned autonomous vehicles (UAV) working in congested areas. They mention that the design of controllers of such systems is difficult, in consequence of the required speed and responsiveness. They also notify that, since it is costly to test and compare distinct UAV controllers, formal verification is the number one phase for their performance and efficiency optimization.

In [19], the authors propound a model-checking tool for user assistance in properties checking of systems having complex behaviors. The system modeling is done with the help of a finite-state automaton. The latter is very large and its manual verification is therefore very difficult. The model-checking tool helps the user by automating part of the verification process.

In [20], the authors propose a review of research works related to the application of formal specification and verification methods to the autonomous robotic domain. They pinpoint the insufficiency of testing on real deployment or simulation of autonomous robots. Indeed, the complexity of these robotic systems and their use in safety critical applications do not allow to test some of their behaviors. The authors claim the necessity to use formal methods to guarantee the exactness of such systems.

In [21], the authors propose an integration of the modeling language Timed Rebeca in ROS, a middleware for mobile robots' program development. A conceptual model of ROS programs in Timed Rebeca is proposed and used to verify the correctness of properties defined by users on ROS programs. Timed Rebeca is based on a model checking approach.

In [22], the authors deal with the formal proof of a robotic system. Model checking approach is applied as well as theorem proving approach of higher-order logic. The first one requires the discretization of the differential equations describing the continuous dynamics of the system and therefore limits the model to an abstracted view of the system, whereas the second one allows using it in its true form and makes it possible to take into account all the real possibilities of the dynamics of the system. Different techniques used for the analysis of the robotic system are compared, based on expressiveness, accuracy and automation.

Above works show the usefulness of formal verification approaches in robotics. They also show that solutions and tools are needed to facilitate the use of formal verification methods in the robotic domain. Analysis of state of the art reveals that the majority of works on formal verification of robotic systems use model checking techniques. In [20], only 3 between 49 works related to formal verification of robotic systems use theorem proving, despite their ability to avoid the state-space explosion issue that sometimes occur when using model checking. It is necessary to develop the use of theorem provers for robotic systems, given their complexity that makes their verification with model checkers prone to the state-space explosion problem.

In the next section, preliminaries on formal proof methods are first introduced, then the theorem prover PVS is presented.

3. Preliminaries on formal proof methods and Prototype Verification System

3.1. Formal proof methods

Two main formal proof methods exist: model-checking and demonstration also called theorem proving.

In the model checking approaches (illustration in figure 1), system's state-space model is built and its properties are first specified. Both are then input to the model checking system that goes through the state space exhaustively and checks if the system satisfies the given properties. When a property is not satisfied, the model checker generates error information.
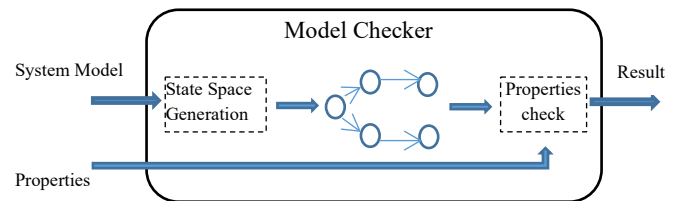
Figure 1: Model checking

In the theorem proving approaches (illustration in figure 2), system's mathematical model is built and its properties are formalized using a well-defined logic. Both are then input to the theorem proving system as theorems. Using axioms, hypothesis and deductive reasoning (inference rules), the theorem prover helps the user to develop his proof and to verify if the system satisfies the given properties. Inference rules together with theorems that have already been verified make it possible to prove new theorems. When the theorem proving relies on a decidable (propositional) logic, it can be automatic. When it is based on an un-decidable (higher-order) logic, it is interactive.
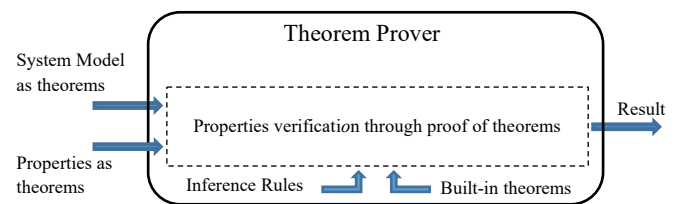
Figure 2: Theorem proving

In comparison to theorem proving, the advantage of model-checking is its entire automation. Its disadvantage is that it is subject to state-space size explosion that could cause problems due to limited computer memory space and limited computational resources.

3.2. Prototype Verification System

PVS [23] is a deductive verification system. It manages a tree of proofs and helps the user to build a full proof tree, i.e. a tree whose terminal nodes are all admitted as being true. Each non-terminal node is a goal from which children nodes are obtained by

a step of the proof. Goals are sequents having each the following shape:

$$p_1, p_2, \ldots, p_n \vdash q_1, q_2, \ldots, q_m$$

where the p_i are the antecedents and the q_i are the consequents.

PVS system uses backward reasoning: each proof step results in sequents that are at least as strong as previous ones. The root of the proof is the sequent $\vdash q$ where q is the theorem to prove.

PVS system furnishes a specification language that is strongly typed [24] as well as an interface that makes it possible to specify systems under Emacs, to formally specify properties on those systems and to prove them with the help of the proof system of PVS [25].

PVS's specification language is founded upon a logic of higher order. It provides various types and subtypes, including elementary ones (strings, numbers, predicates, etc.), abstract data and compound types (records, union, etc.). PVS system offers several useful functions for the process of formal verification. The main commands implementing the decision procedures are the following:

- *typecheck:* it makes it possible to analyze the file containing the specification of the system and to detect semantic errors.

- *prove:* it makes it possible to start the proof of properties that are non-trivial for the system.

- *flatten*: enables to flatten the structure of the current goal

- *split*: enables to separate a goal into subgoals

- *inst*: makes it possible to instantiate variables with given terms

- *expand*: enables to expand/develop a definition or an expression

- *skolem*: it makes it possible to "skolemize" quantified variables (quantifiers are removed and quantified variables are replaced by skolem constants).

- *grind/ground*: enable to launch the process of decision/simplification of a rule.

- *induct*: makes it possible to perform an induction on a variable.

- *undo*: enables to go back in the proof.

- *lemma*: makes it possible to add a lemma to the assumptions.

- More elaborated commands, such as *skosimp* that iterates the application of *skolem* and *flatten* commands on the current rule.

The next section presents the language PILOT and the method of construction and checking of plans.

4. Language PILOT and method of incremental construction and checking of missions' plans

4.1. The language PILOT

PILOT [5, 26, 27] is founded on the action concept. An action is composed of an order that the robot can execute, a rule of precondition and rules of supervising each having a tied treatment. An action is either elementary or continuous. Elementary actions

end by themselves, in general once they reach their goal, while continuous actions' termination is provoked by a parallel or a preemption primitive. Whether elementary or continuous, an action only executes if its precondition is true. Similarly, when a supervision rule of an action becomes true during its execution, the corresponding treatment is launched. For each supervising rule, the default treatment consists in stopping the related action. Precondition and supervision rules are usually conditions expressed on values of sensors. Figure 3 shows the graphical representation of elementary and continuous actions.

Figure 3: Elementary action and continuous action

In PILOT language, the following control primitives are available for missions' plans programming:

- Sequentiality: it starts by a "sequence beginning" and ends by a "sequence end". It enables to define an order of execution on other primitives of the language (actions and control primitives). A graphical symbol named "intersequence" is used to connect the primitives of the sequence. Figure 4 illustrates a sequence comprising 2 elementary actions.
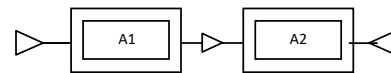
Figure 4: Sequentiality

- The conditional: it is formed by branches, each composed of a Boolean expression and a sequence following it. Starting from top, the first sequence whose condition is true is the only one to be executed. Figure 5 shows an example of conditional primitive with 2 alternatives.
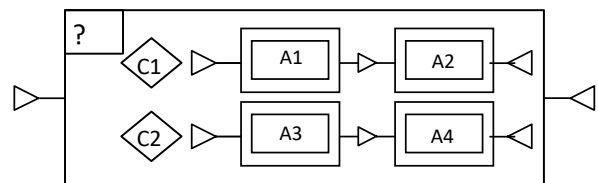
Figure 5: Conditional

- Iteration: it is constituted of a criterion of continuation and a sequence following it. Depending on the continuation criterion, the iteration is said to be fixed or to be conditional. In the first case, the criterion is a number of loops. In the second one, the criterion is a boolean condition. Figure 6 shows and example of fixed iteration on the left and an example of conditional iteration on the right. In the example of fixed iteration, elementary action A1 is executed 3 times. In the example of conditional iteration, elementary action A2 is executed while condition s>2 is true.
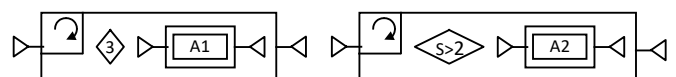
Figure 6: Fixed and conditional iterations

- Parallelism: it is composed of sequences executed in parallel. It terminates its execution when all its sequences have ended theirs. Figure 7 illustrates an example of parallel primitive. In this

example, elementary actions A1 and A2 are executed in parallel and the parallel execution ends when both actions reach the end of their execution.
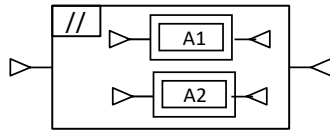
Figure 7: Parallelism

• Preemption: it is composed of sequences executing in parallel, but unlike parallelism structure, the termination of its execution occurs as soon as one of the sequences ends. Figure 8 illustrates an example of preemption with 2 sequences. In this example, once one of the sequences ends, it causes the termination of the second one and leads to the end of the parallel execution.
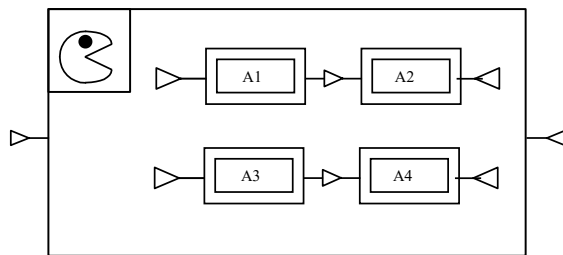
Figure 8: Preemption

After the above presentation of the language PILOT, the next subsection describes the incremental syntax-oriented building approach of missions' plans.

4.2. Method of construction and checking of PILOT missions' plans

The syntax-oriented edition of PILOT plans guarantees that the plan is syntactically correct at each step of plan building. When the programmer starts building a mission plan, he obtains a sequence that is empty. In order to continue the construction of the plan, he uses operations *insert*, *erase* or *modify*. The *modify* operation makes it possible to change elements such as the Boolean expression of a conditional primitive, etc. Whenever an operation is applied by the user, the editor checks the syntactic validity of the plan obtained and only takes the modification into account in the positive case. When the syntax is incorrect, the editor informs the user through a message. For the purpose of ensuring the syntactic correctness of the plan whenever insertion operation is performed, the following default primitives are associated with the structures of PILOT language:

• The default conditional structure which contains a unique alternative consisting in a condition set to "false" followed by an empty sequence.

• The default iteration structure that contains a continuation criterion set to 0 followed by an empty sequence.

• The default parallelism structure which contains a unique empty sequence.

• The default preemption structure that contains a unique empty sequence.

These default structures are illustrated in the example of plan shown in Figure 11.

Assuming that:

• *plan* is the current mission plan,

• *elt* is the element to insert in the plan,

• *sel* is the element of the plan selected by the user to indicate where to insert the new element (i.e. he wants *elt* to be inserted just before *sel*),

• *cont* represents the immediate encapsulating structure containing *sel*.

• Type *(<param>)* represents the type of <param>. Type values are BS, ES, BE, NL, EA, CA, CP, IP, PP. They respectively correspond to "Beginning of Sequence", "End of Sequence", Boolean Expression", "Number of Loops", "Elementary Action", "Continuous Action", "Conditional Primitive", "Iteration Primitive", and "Parallel Primitive". Here, parallelism and preemption primitives are considered of type PP.

• PredecessorOf (<param>) represents the element preceding <param> in the plan.

• SetOfSequencesOf (<param>) defines the set of sequences of <param>. In this case <param> is supposed to be a parallel primitive.

• IsContinuousActionSequence (<param>) is true if <param> is a sequence made of a beginning of sequence, followed by a continuous action followed by an end of sequence. Otherwise, it is false.

The precondition of the implemented insertion operation can be represented as follows:

$$
\begin{aligned}
&\exists\ elt\ \wedge \\
&(\neg\exists\ sel \Rightarrow (\exists\ cont \Rightarrow (\text{Type}\ (cont) \neq \text{IP}\ \wedge \\
&\quad (\text{Type}\ (cont) = \text{PP} \Rightarrow \text{Type}\ (elt) = \text{BS})\ \wedge \\
&\quad (\text{Type}\ (cont) = \text{CP} \Rightarrow \text{Type}\ (elt) = \text{BE})))) \wedge \\
&(\exists\ sel \Rightarrow ((\text{Type}\ (sel) = \text{BS} \Rightarrow \\
&\quad (\exists\ cont \wedge \text{Type}\ (cont) = \text{PP} \wedge \text{Type}\ (elt) = \text{BS})) \wedge \\
&\quad (\text{Type}\ (sel) = \text{BE} \Rightarrow \\
&\quad (\exists\ cont \wedge \text{Type}\ (cont) = \text{CP} \wedge \text{Type}\ (elt) = \text{BE}) \wedge (\text{Type}\ (sel) \neq \text{NL}))) \wedge \\
&(\text{Type}\ (elt) = \text{CA} \Rightarrow \\
&\quad ((\exists\ cont \wedge \text{Type}\ (cont) = \text{PP})\ \wedge \\
&\quad (\exists\ sel \wedge \text{Type}\ (sel) = \text{ES} \wedge\ \text{Type}\ (\text{PredecessorOf}\ (sel)) = \text{BS})\ \wedge \\
&\quad (\exists\ seq\ /\ seq \in \text{SetOfSequencesOf}(cont) \wedge sel \notin seq\ \wedge \\
&\quad \neg\text{IsContinuousActionSequence}\ (seq))))
\end{aligned}
$$

After this presentation of PILOT and the description of the method of construction and checking of PILOT missions' plans, the next section deals with properties' proof of the latter, based on Prolog and an associated tool.

5. Verification of the method of construction and checking of PILOT missions' plans using Prolog and an associated tool

It is necessary demonstrating that the implementation of the syntax-oriented editor enables the construction of all but solely plans whose syntax is valid. For the sake of simplicity, only the

case of plans building using insertion operations is considered. In this case, the approach used for the validation can be illustrated by the colored Petri net of Figure 9. In colored Petri nets [28], colors are represented by associating values to tokens.
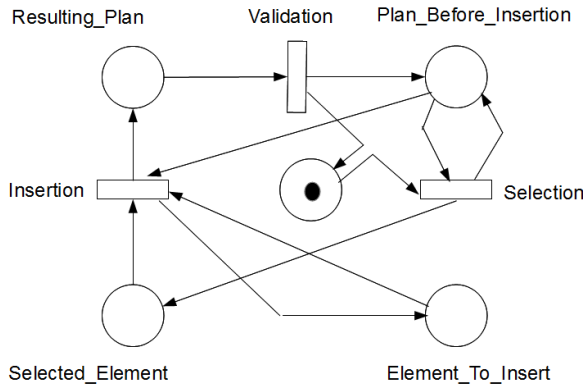
Figure 9: Validation approach

The initial marking of places "Plan_Before_Insertion" and "Element_To_Insert" are respectively {[beg_seq, end_seq]} and {beg_seq, end_seq, cont_act, elem_act, par, pre, iter, cond, bool_exp, loops_num}. Initially, place "Selected_Element" has an empty marking and so is place "Resulting_Plan".

The transition "Selection" (respectively "Insertion") models an element selection (respectively insertion) of (respectively in) the plan. As far as transition "Validation" is concerned, it represents the formal syntax analyzer of the language PILOT. The mechanism implemented for the syntax-oriented building of plans is free of errors if the Petri net of Figure 9 does not contain any deadlock.

For the application of this certification method to the syntax-oriented editor of PILOT plans, a syntax-checker has been built in PROLOG based on the approach suggested in [29]. Thereafter, the plan construction has been modeled and the properties hereafter have been checked:

- Are there insertions that lead to plans whose syntax is not correct?

- Are there plans with correct syntax whose construction is not possible with the proposed insertion model?

The first property aims at ensuring that the proposed syntax-oriented building mechanism disallows the construction of plans whose syntax is not correct. Regarding the second property, the goal is to make sure that the mechanism does not disallow the building of correct plans. Indeed, the checking mechanism may be too restrictive and lead to the rejection of plans that are syntactically correct.

Due to the working of PROLOG, it was necessary to limit the size of the set of plans built. If not, the PROLOG tool would have tried to generate all syntactically correct plans and this would have led to memory space problems. PROLOG parser and plan construction models were therefore modified to solely generate plans of size under a threshold. Here, the size is that of the list modeling the plan. Figure 10 shows the translation of the above properties in PROLOG, taking the size constraint into account. In this PROLOG code, *convert* converts a model representing the

graphic plan into a model which the syntax analyzer can process. *convert_set* works similarly, but applies to set of models.

```
inserion_issue (Size_Max, NG_Plan, G_Plan):-
    automated_insertions (Size_Max, G_Plans_List),
    member (G_Plan, G_Plans_List),
    convert (G_Plan, NG_Plan),
    not valid_syntax (NG_Plan,[]).
anomalous_rejection (Size_Max, NG_Plan):-
    automated_insertions (Size_Max, G_Plans_Set),
    convert_set (G_Plans_Set, NG_Plans_Set),
    valid_syntax_plans (Size_Max,Valid_NG_Plans_Set),
    member (NG_Plan, Valid_NG_Plans_Set),
    not member (NG_Plan, NG_Plans_Set).
```

Figure 10: Syntax analyzer' properties validity translation in Prolog

SWI-Prolog tool of University of Amsterdam were used for the programming. The tests performed for plans of size under 15 showed no insertion problem and no anomalous rejection. Consequently, for plans whose size is under 15, the proposed syntax-oriented building mechanism enables constructing only but all plans whose syntax is valid. For greater sizes, an exception related to lack of memory space is raised. The lack of space is caused by the exponential increase of the set of plans.

The next section presents the modeling of PILOT plans' properties as well as the modeling of plans' building operations, for their verification using Prototype Verification System. As indicated in the third section, Prototype Verification System offers a theorem proving system which enables to avoid the aforementioned memory space problem.

6. Plans and operations modeling for properties verification using Prototype Verification System

6.1. Prolog approach model analysis

In the approach used for PILOT's syntax-oriented editor properties' proof using SWI-Prolog, plan's model is a numbered elements list, so as to be able to locate components of the plan as in its graphical version. Indeed, for operations such as insertion, it is necessary identifying where insertion is wished. In PILOT's Graphical User Interface (Figure 11), in order to insert an element in a plan, the user selects the element among the operators list on the left, then he clicks on the location of the plan before which he wants to insert the element.
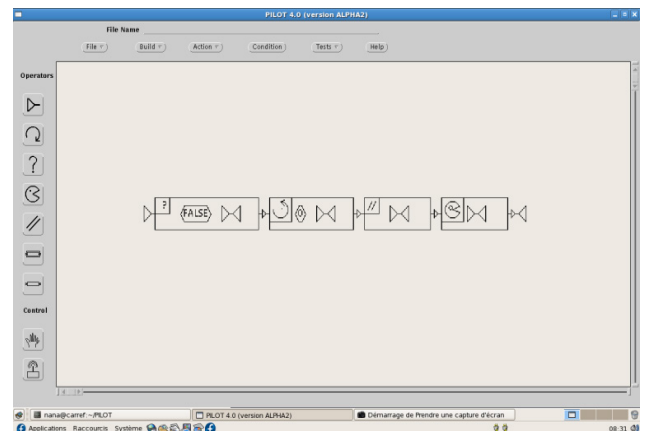
Figure 11: Graphical User Interface of PILOT

The use of numbers to locate the components of the plan is suitable to produce all the plans buildable by insertion of a unique primitive of the language within a plan. Nonetheless, it becomes an obstacle to the generalization needed for theorem proving with the help of Prototype Verification System, the reasoning being done independently of the size of the plan. One of the main difficulties was therefore to find a model of representation of the plan, not based on the numbering of its elements, and making it possible to uniquely locate its elements.

Building and syntax-checking operations necessitate identification of each plan element's container. Indeed, the behavior of operations such as insertion is container-dependent. Mechanisms such as that provided by SWI-Prolog through the notation "par: number: List" make it easy to isolate blocks and locate the containers. PVS offers no similar mechanism. Therefore, the design of a solution for containers' identification is needed for PVS.

6.2. Models proposal for the proof of properties with PVS

Proving PILOT editor's properties with PVS, necessitates defining various models notably for PILOT plan, selection's container and operation "selection" that specifies where to perform the insertion in the plan. The models proposed for these different entities are presented hereafter.

a) Plan model

The plan is represented as a list of elements belonging to the set {*bs, es, e, c, exp, par, pre, condi, iter*} (see example on Figure 12). These elements refer to PILOT' syntax terminals. *bs* denotes sequence beginning, *es* sequence end, *e* (respectively *c*) elementary (respectively continuous) action, *exp* expression of conditional. *pre, par, condi* and *iter* respectively denote preemption, parallelism, conditional and iteration primitives.

Plan	PVS model
Empty sequence	cons (bs, cons (es, null))
Sequence with a single conditional primitive	cons (bs, cons (condi, cons (exp, cons (bs, cons (es, cons (es, null))))))
Sequence with a single elementary action	cons (bs, cons (e, cons (es, null)))

Figure 12: Examples of plans modeled in PVS

b) Modeling properties of syntactically correct plans

In the proposed approach, each rule of the grammar of the language is represented using a two parameters function whose first parameter is the part of the plan submitted for parsing and the second is the remainder expected after retrieving the pattern matching the rule. The output of the function is true when the real and expected remainders are identical. Otherwise, it is false. In Prolog's case, this approach enables to automatically generate the program that recognizes the language, as shown in Table 1.

Using the same approach under PVS, the program recognizing the language PILOT has the shape shown in Figure 13.

It turns out that this solution cannot be used as such under PVS. Indeed, in PVS's description language, a function call can only be done after the definition of the function. So, in figure 13, the call to seq_base in the definition of validplan isn't concretely allowed. An approach to solve this problem could be just to specify (declare) the function before the call without defining it completely, but it is disallowed in Prototype Verification System.

A first method adopted to overpower these drawbacks has been to elaborate PILOT syntax rules' dependencies graph, then using it to define the functions in the order of dependency, beginning by the functions not involving cross recursive calls, and then using the passing of functions as parameters to define functions involved in calls with cross recursion. The principle is shown hereafter through a definition of even and odd parities:

Table 1: Description of PILOT's syntax with Prolog

PILOT Syntax rules		Description in Prolog	
S	: SEQ_BASE	validplan (A,B)	:- seq_base (A,B).
SEQ_BASE	: bs L_PRIMI_BASE es	seq_base ([bs|A],B)	:- l_primi_base (A, [es|B]).
L_PRIMI_BASE	: ε |	l_primi_base (A,A).	
	PRIMI_BASE L_PRIMI_BASE	l_primi_base (A,B)	:- primi_base (A,C), l_primi_base (C,B).
PRIMI_BASE	: PRIMI_PARALLEL |	primi_base (A,B)	:- primi_parallel (A,B).
	PRIMI_PREEMPTION |	primi_base (A,B)	:- primi_preemption (A,B).
	PRIMI_CONDITIONAL |	primi_base (A,B)	:- primi_conditional (A,B).
	PRIMI_ITERATION |	primi_base (A,B)	:- primi_iteration (A,B).
	PRIMI_ACT_ELEM	primi_base (A,B)	:- primi_act_elem (A,B).
PRIMI_PARALLEL	: par '(' LIST_SEQ ')'	primi_parallel ([par,'('|A],B)	:- list_seq (A, [')'| B]).
LIST_SEQ	: LIST_SEQ_A SEQ_BASE LIST_SEQ_A	list_seq (A,B)	:- list_seq_a (A,C), seq_base(C,D), list_seq_a (D, B).
LIST_SEQ_A	: ε |	list_seq_a (A,A).	
	SEQ_LIST_SEQ_A	list_seq_a (A,B)	:- seq (A, C), list_seq_a (C,B).
SEQ	: SEQ_BASE |	seq (A,B)	:- seq_base (A,B).
	SEQ_SPECIFIC	seq (A,B)	:- seq_specific (A,B).
SEQ_SPECIFIC	: bs PRIMI_ACT_CONT es	seq_specific ([bs|A],B)	:- primi_act_cont (A,[es|B]).
PRIMI_ACT_CONT	: c	primi_act_cont ([c|A],A).	
PRIMI_PREEMPTION	: pre '(' LIST_SEQ ')'	primi_preemption ([pre,'('|A],B)	:- list_seq (A, [')'| B]).
PRIMI_CONDITIONAL	: condi '(' LIST_CONDITIONAL ')'	primi_conditional ([cond,'('|A],B)	:- list_conditional (A,[')',B]).
LIST_CONDITIONAL	: CONDITIONAL LIST_CONDITIONAL |	list_conditional (A,B)	:- conditional (A,C), list_conditional (C,B).
	CONDITIONAL	list_conditional (A,B)	:- conditional (A,B).
CONDITIONAL	: exp SEQ_BASE	conditional ([exp|A],B)	:- seq_base (A,B).
PRIMI_ITERATION	: iter '(' SPEC_ITER ')'	primi_iteration ([iter,'('|A],B)	:- spec_iter (A, [')'|B]).
SPEC_ITER	: CONDITIONAL |	spec_iter (A,B)	:- conditional (A,B).
	nb SEQ_BASE	spec_iter ([nb|A],B)	:- seq_base (A, B).
PRIMI_ACT_ELEM	: e	primi_act_elem ([e|A],A).	

```
% definition of types and declaration of variables
primi: type = {bs, es, …}
t: type = list [primi]
a, b, c, x, y: t
% representation of rules
validplan (a, b): bool = seq_base (a, b)
seq_base (a, b): bool = (car (a) = bs) and l_primi_base (cdr (a),
    cons (es, b))
l_primi_base (a, b): recursive bool = ((a = b) or (a /= b and a /=
    null and exists c: (primi_base (a, c) and l_primi_base (c, b))))
    measure lambda (x, y): length (x)
primi_base (a, b): bool = primi_parallel (a, b) or
    primi_preemption (a, b) or primi_conditional (a, b) or
    primi_iteration (a, b) or primi_act_elem (a, b)
```

Figure 13: Specification of PILOT syntax in PVS with same method as Prolog

$$\text{Even } (n: N): \text{Boolean} = n{=}0 \text{ or } (n \neq 0 \text{ and odd } (n{-}1))$$

$$\text{Odd } (n: N): \text{Boolean} = n{=}1 \text{ or } (n \neq 1 \text{ and even } (n{-}1))$$

This definition of even and odd functions can be transformed in PVS as shown in figure 14.

```
Even_1 (n: N, od: N -> Boolean): Boolean = n = 0 or (n ≠ 1
    and od (n-1))
Odd (n : N) : Boolean = n=1 or (n ≠ 1 and Even_1 (n-1,
    Odd))
Even (n: N) : Boolean = Even_1 (n, Odd)
```

Figure 14: Representation of even and odd functions for PVS with resolution of recursive crossed calls

Nevertheless, the syntax of PILOT contains several complex crossed calls involving more than 2 crossed calls. For example, "seq_base" refers to "l_primi_base" that refers to "primi_base" which refers in turn to "primi_parallel" that also refers to "seq_base".

Under PVS, defining a function that is recursive also necessitates adding a function called *measure* which decreases in the course of recursive calls and having a down side limit, so as to ensure recursive calls ending.

Figure 15 illustrates the representation proposed in order to solve the problem related to recursive cross calls for the example mentioned above.

A representation of PILOT's syntax under PVS has been generated with the help of this approach. For its validation, the obligations of proofs produced by Prototype Verification System were proven and a few plans' definition theorems, among which those in Figure 16, have been defined and proved with the help of PVS.

a) Modeling of plan element selection

The intention is to design a model representing the point of insertion in the PILOT plan. The following two components can

be used for characterizing the point of insertion: the clicked element and its container. The proposed model of representation of the selected element is the couple (Lbe, Laf) where Lbe corresponds to the head of the plan list ending just before the selected element, and Laf is the remaining of the plan starting from the selected element. This solution makes it possible to take advantage of the properties of concatenation of lists in the design of the models of operations that apply to the selected element. It also provides a good consistency with the syntactic rules modeling where two parts of the list representing the plan have to be distinguished, namely the part recognized by the rule and the remainder.

```
primi_parallel_i (a, b, lsq): bool = (a/= null and b /= null and
    car (a) = par and lsq (cdr (a), b))
primi_base_i (a, b, lsq): bool = primi_act_elem (a, b) or
    primi_parallel_i (a, b, lsq) or …
l_primi_base_i (lsq) (a, b): recursive bool = (a = b) or (a /=
    b and exists c: (primi_base_i (a, c, lsq) and
    l_primi_base_i (lsq) (c, b)) measure lambda (lsqf) (x, y):
    length (x)
seq_specific (a, b): bool = a = cons (bs, cons (c, cons (es,
    b)))
seq_base_i (a, b, lsq): bool = a /= null and car (a) = bs and
    l_primi_base_i (lsq) (cdr(a), cons (es, b))
seq_i (a, b, lsq): bool = seq_base_i (a, b, lsq) or seq_specific
    (a, b)
l_seq_a (a, b): recursive bool = a = b or (a /= b and exists c:
    seq_i (a, c, l_seq_a) and l_seq_a (c, b))
measure lambda (x, y): length (x)
l_seq (a, b): bool = exists c, d: (l_seq_a (a, c) and
    seq_base_i (c, d, l_seq_a) and l_seq_a (d, b))
seq_base (a, b): bool = seq_base_i (a, b, l_seq)
validplan (a): bool = seq_base (a, null)
```

Figure 15: Excerpt of PILOT's syntax description in PVS with cross recursive calls solving

In the proposed modeling, the selected element's container is frequently split in two parts, one belonging to Lbe and the other to Laf. Plan element selection model is shown in Figure 17. In this model, Lcon is the tail of the plan that starts from the selected element's container.

An extract of the PVS model of the selection operation is given in Figure 18. It shows the specification of the selection of an outermost plan's element (i.e. an element of the main sequence of the plan), as well as the case of a selection within a parallel box. In the first case, there is no container, whereas in the second case, the parallel box is the container.

P01: theorem validplan (cons (bs, cons (es, null)))

P02: theorem validplan (cons (bs, cons (e, cons (es, null))))

P03: theorem validplan (cons (bs, cons (e, cons (e, cons (es, null)))))

P04: theorem validplan (cons (bs, cons (par, cons (bs, cons (es, cons (es, null))))))

P05: theorem validplan (cons (bs, cons (par, cons (bs, cons (es, cons (e, cons (es, null)))))))

P06: theorem validplan (cons (bs, cons (par, cons (bs, cons (e, cons (es, cons (bs, cons (es, cons (es, null)))))))))

P07: theorem validplan (cons (bs, cons (condi, cons (exp, cons (bs, cons (es, cons (es, null)))))))

P08: theorem validplan (cons (bs, cons (e, cons (condi, cons (exp, cons (bs, cons (e, cons (es, cons (e, cons (es, null)))))))))

P09: theorem validplan (cons (bs, cons (iter, cons (exp, cons (bs, cons (es, cons (es, null)))))))

P10: theorem validplan (cons (bs, cons (iter, cons (exp, cons (bs, cons (e, cons (es, cons (e, cons (es, null)))))))))

Figure 16: Samples of PVS demonstrated theorems
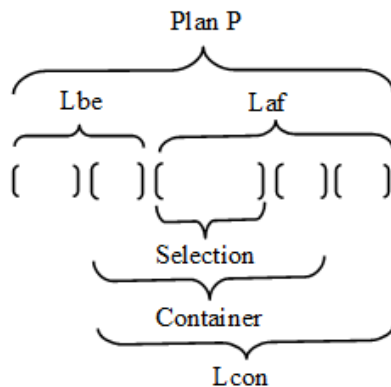
Figure 17: Selection model of a plan element

In this selection operation, "fusion" is an operation that performs the fusion of two lists and "seq" is such that its first parameter is a list L starting by a sequence S followed by a list LS2 of primitives.

7. Conclusion

As shown in the state of the art part of this paper, it is necessary to develop the use of theorem provers for robotic systems, given their complexity that makes their verification with model checkers prone to the state-space explosion problem. This work is a step forward in this direction, through a case study showing the limits of model-checking for the proof of properties of a robotic system, namely the syntax-oriented editor of a robotic missions programming language (PILOT), and investigating the use of the PVS theorem proving system to overcome the problem encountered with the model-checking approach.

Another goal of the work was to check out the appropriateness of Prototype Verification System for accomplishing complicated demonstrations that involve the design of models for different kinds of entities frequently encountered in robotics and more generally in control-command systems (language syntax, operations ...).

```
selection (P, Lbe, Laf, Lcon): recursive bool =
  P = fusion (Lbe, Laf) and
  ( % sequence element selected
    ( Lcon = null and (Laf = cons (es, null) or
      % sequence beginning selected
      Lbe = null or
      % another element of sequence selected
      (l_primi_base (Laf, cons (es, null))))) or
    % selection into a parallel box of the sequence
    % w: parallel box, x: list of primitives after the parallel box
    ( exists Lpar, Lbepar, w, x, y :
      ( P = fusion (Lbepar, Lpar) and primi_par (Lpar, w, x) and
        l_primi_base (x, y, cons (es, null)) and
        ( ( Laf = Lpar and Lcon = Lpar and Lbe = Lbepar) or
          % S: sequence of the parallel box
          % Ls1: list of sequences before S
          % Ls2: list of primitives after S
          % Lcon1: list from the container to the end of S
          ( Exists S, Ls1, Ls2, L, Lbe1, Laf1, Lcon1:
            ( list_seq_a (cdr (Lpar), Ls1, L) and
              seq (L, S, Ls2) and
              selection (S, Lbe, Laf1, Lcon1) and
              ( % element at the top level of S selected
                ( Lcon1 = null and Lcon = Lpar) or
                % selection of an element within a box of the
                sequence S
                ( Lcon1 /= null and Lcon = fusion (Lcon1, Ls2))
              ) and
              ( Lbe = fusion (Lbepar, cons (par, fusion (Ls1, Lbe1)))
              and
                Laf = fusion (Laf1, Ls2))))))
  ) or
  % code for the other encapsulating primitives
  …
)
measure lambda (s, s1, s2, s3): length (s)
```

Figure 18: Extract of selection operation's PVS model

In order to reach these goals, PVS functions have been used to represent PILOT's syntax. The proposed model has been validated notably by verifying the obligations of proofs produced by Prototype Verification System and proving some theorems defined on PILOT plans. The modeling of recursive cross-calls has been the major issue faced during PILOT's syntax specification in PVS.

As matter of fact, contrary to Prolog, the language of specification provided by PVS disallows to use a function before its full definition. Consequently, a PVS model without cross recursivity was proposed. The specification in PVS of the selection operation of the syntax-oriented editor of PILOT has also been presented in this paper.

The results obtained at this step of the work (the representation model of the syntax rules of the language PILOT under PVS and its validation, the modeling of operations of the syntax-oriented editor of PILOT), enables to conclude in a good capacity of PVS for the modeling of aforementioned entities of control-command systems and for the achievement of further formal proofs.

Conflict of Interest

The authors declare no conflict of interest.

Acknowledgment

References

[1] L. Nana, F. Monin, S. Gire, "Proof of properties of a syntax analyzer of robotic mission plans" in Proceedings of 4th International Conference and Workshops on Recent Advances and Innovations in Engineering –ICRAIE 2019, IEEE, Kedah, Malaysia, 2019.

[2] M. Barbier, J. F. Gabard, D. Vizcaino, O Bonnet-Torrès, "ProCoSA: a software package for autonomous systems supervision" in Proceedings of 1st National Workshop on Control Architectures of Robots: software approaches and issues, Montpellier, France, 2006.

[3] C. Barrouil, J. Lemaire, "Advanced Real-Time Mission Management for an AUV" in Proceedings of SCI NATO RESTRICTED Symposium on Advanced Mission Management and System Integration Technologies for improved Tactical Operations, Florence, Italy, 1999.

[4] L. Laouamer, A. Benhocine, L. Nana, A Pascu, "Motion JPEG Video Authentication based on Quantization Matrix Watermarking: Application in Robotics" Int. Journal Computer Application, **47**(24), 1-5, 2012.

[5] L. Nana, "Investigating safety mechanisms for robotics applications" IPSI BGD Transaction Internet Res., **3**(1), 45-50, 2006.

[6] L. Nana, L. Marcé, J. Opderbecke, M. Perrier, V. Rigaud, "Investigation of safety mechanisms for oceanographic AUV missions programming" in Proceedings of the IEEE OCEANS'05 Europe Conference, Brest, France, 2005.

[7] L. Nana, F. Singhoff, J. Legrand, J. Vareille, P. Le Parc, F. Monin, D. Massé, L. Marcé, J. Opderbecke, M. Perrier, V. Rigaud, "Embedded intelligent supervision and piloting for oceanic AUV" in Proceedings of the IEEE OCEANS'05 Europe Conference, Brest, France, 2005.

[8] L. Nana, J. Legrand, F. Singhoff, L. Marcé, "Modelling and Testing of PILOT Plans Interpretation Algorithms" in Proceedings of Multi-conference on Computational Engineering in Systems Applications, CESA'03, IEEE, Lille, France, 2003.

[9] L. Nana Tchamnda, V-A. Nicolas, L. Marcé, "Towards a formal approach for the regeneration of PILOT control system" in Proceedings of 6th World Multiconference on Systemics, Cybernetics and Informatics, SCI'2002, IEEE Venezuela, Orlando, Florida, USA, 2002.

[10] F. Py, F. Ingrand, "Dependable Execution Control for Autonomous Robot" in Proceedings of IROS 2004 (IEEE/RSJ International Conference on Intelligent Robots and Systems), Sendai, Japan, 2004.

[11] E. Rutten, "A framework for using discrete control synthesis in safe robotic programming", Research report, INRIA, 2000.

[12] N. Turro N, "MaestRo: Une approche formelle pour la programmation d'applications robotiques", PhD Thesis, Université de Nice, Sophia Antipolis, 1999.

[13] J. F. Groote, F. Monin, J. C. Van de Pol, "Checking verifications of protocols and distributed systems by computer" in Proceedings of Concur'98, Sophia Antipolis, France, 1998.

[14] J.F. Groote, F. Monin, J. Springintveld, "A computer checked algebraic verification of a distributed summation algorithm". Form. Asp. Comput. **17**(1), 2005, 19–37. DOI:https://doi.org/10.1007/s00165-004-0052-7.

[15] D. Bresolin, L. Di Guglielmo, L. Geretti, R. Muradore, P. Fiorini, T. Villa, "Open problems in verification and refinement of autonomous robotic systems" in Proceedings of the 15th Euromicro Conference on Digital System Design, pp. 469-476, Cesme, Izmir, Turkey, 2012.

[16] E. Zereik, M. Bibuli, N. Miskovic, P. Ridao, A. Pascoal, "Challenges and future trends in marine robotics" Annu. Rev. Control, **46**, 2018, 350-368, ISSN 1367-5788. https://doi.org/10.1016/j.arcontrol.2018.10.002.

[17] M. Ludvigsen, A. J. Sørensen, "Towards integrated autonomous underwater operations for ocean mapping and monitoring". Annu. Rev. Control, **42**, 145-157, 2016.

[18] A. J. Barry, A. Majumdar, R. Tedrake, "Safety verification of reactive controllers for UAV flight in cluttered environments using barrier certificates" in Proceedings of 2012 IEEE International Conference on Robotics and Automation, Saint Paul, MN, USA, 484-490, 2012. doi: 10.1109/ICRA.2012.6225351

[19] C. Armbrust, L. Kiekbusch, T. Ropertz, K. Berns, "Tool-assisted verification of behavior networks" In proceedings of 2013 IEEE International Conference on Robotics and Automation, Karlsruhe, Germany, 1813-1820, 2013. doi: 10.1109/ICRA.2013.6630816

[20] M. Luckcuck, M. Farrell, L. A. Dennis, C. Dixon, M. Fisher, "Formal Specification and Verification of Autonomous Robotic Systems: A Survey" ACM Comput. Surv. **52**(5), 2019, DOI: https://doi.org/10.1145/3342355

[21] S. Dehnavi, A. Sedaghatbaf, B. Salmani, M. Sirjani, M. Kargahi, E. Khamespanah. "Towards an Actor-based Approach to Design Verified ROS-based Robotic Programs using Rebeca" Procedia Computer Science, **155**, 59-68, 2019, https://doi.org/10.1016/j.procs.2019.08.012.

[22] A. Rashid, O. Hasan, I. T. Bhatti, Formal Verification of Robotic Cell Injection Systems, Editor(s): Ahmad Taher Azar, Control Systems Design of Bio-Robotics and Bio-mechatronics with advanced applications, Academic Press, 2020.

[23] S. Owre N. Shankar, J. M. Rushby, D. W. J. Stringer-Calvert, "PVS System Guide", Technical Report, SRI International, Menlo Park, CA, 1999.

[24] S. Owre N. Shankar, J. M. Rushby, D. W. J. Stringer-Calvert, "PVS Language Reference", Technical Report, SRI International, Menlo Park, CA, 2001.

[25] N. Shankar S. Owre, J. M. Rushby, and D. W. J. Stringer-Calvert, "PVS Prover Guide", Technical Report, SRI International, Menlo Park, CA, 1999.

[26] J.-L. Fleureau, "Vers une méthodologie de programmation d'un système de télérobotique : comparaison des approches PILOT et Grafcet", PhD Thesis, Université de Rennes 1, 1998.

[27] E. Le Rest, "PILOT : un langage pour la télérobotique", PhD Thesis, Université de Rennes 1, 1996.

[28] K. Jensen, Coloured Petri Nets - Basic Concepts, Analysis Methods and Practical Use, Springer-Verlag Berlin Heidelberg, 1997

[29] F. Giannesini, H. Kanoui, R. Pasero, M. Van Caneghem, Prolog, InterEditions, 1985.

Modeling and Design of a Compact Metal Mountable Dual-band UHF RFID Tag Antenna with Open Bent Stub Feed for Transport and Logistics Fields

Hajar Bouazza[1, 2,*,] Aarti Bansal[3], Mohsine Bouya[2], Azeddine Wahbi[4], Antonio Lazaro[5], Abdelkader Hadjoudja[1]

[1]Electrical and Energetic Systems laboratory Ibn Tofail University Kenitra, 14000, Morocco

[2]TIC laboratory, College of Engineering & Architecture, International University of Rabat, 11100, Morocco

[3]Electronics and communication Engineering, Thapar Institute of Engineering and Technology, Patiala, 147001, India

[4]Laboratory of Industrial Engineering, Information Processing and Logistic, Faculty of sciences Ain Chock, Hassan II University, Casablanca, 20000, Morocco

[5]Department of Electronics, Electrics and automatics Engineering Universitat Rovira I Virgili (URV) Tarragona, 43001, Spain

A R T I C L E   I N F O

A B S T R A C T

In this paper, we have modeled and designed a metal mountable tag antenna that is applied to cover two major UHF RFID bands, i.e., European (EU) (865-867 MHz) and U.S. bands (902-928 MHz). It is applied for many applications, especially in the transport and logistics fields. The tag antenna configuration utilizes microstrip configuration with open bent stub feed network to attain conjugate matching w.r.t. Monza R6 chip impedance. The proposed microstrip patch-based tag antenna structure is simple without using any shorting pin/holes, thus making it easy and inexpensive to manufacture. Additionally, the proposed tag's impedance has been easily tuned in order to achieve conjugate matching in regard to the employed chip impedance. The presented tag antenna has been fabricated and experimentally characterized to measure its read-range performance in the desired bands. Further, the differential probe set up is used to measure the designed tag's impedance. Also, the designed tag read-range is measured using a reader setup and is observed to exhibit read-range up to 11 m and 9 m in European and U.S. UHF RFID bands, respectively. The tag exhibits an impedance of 9.7 – j 130 ohms at 866 MHz and 8.7 – j 124 ohms at 915 MHz. The proposed tag antenna design's performance is verified, analyzed, and optimized by CST Studio Suite software. The performances of the designed tag are evaluated and analyzed in terms of conjugate matching, reflection coefficient, and read range measurement. From the results, it is noticed that the designed tag exhibit dual-band behavior with good impedance matching, Reflection coefficient, and high read range.

1. Introduction

Ultra-High Radio Frequency Identification (UHF-RFID) technology has emerged as an efficient technique to track the objects/items/products without needing to be in the line of sight. The major RFID applications are in access control, logistics, healthcare, asset tracking owing to its advantage of long read range and compact size in comparison to Low (L.F.) and High Frequency (H.F.) bands [1]. The UHF RFID band is further divided between two major regions, i.e., European and North America/U.S.

covering (865-867 MHz) and (902-928 MHz) bandwidth with a maximum allowed transmitted power of 3.28 W and 4 W, respectively [2], [3]. To operate the tag reliably in both the regions, it is required that the designed tag must exhibit dual-band operation covering European and U.S. UHF RFID bandwidth.

The RFID tag has to be affixed on a different type of conductive and non-conductive object to be tracked. Further, the performance of the tag deteriorates significantly especially when placed on conductive items such as metals. This is attributed to the cancellation of radiations resulting from phase electromagnetic

wave reflections from the underlying metal surfaces [4-6]. To track the metallic objects efficiently, some of the recent work utilizes a microstrip patch antenna with a full ground beneath to overcome the influence of conductive objects such as metal, liquids, etc. as depicted in ref [7] and [8]. Further, the planar inverted-F antenna (PIFA) incorporating vias/ holes for the compact-sized tag is presented in [9], [10]. However, the employed vias/holes contribute to increased fabrication cost and complexity to the tag structure.

In this article, the work presented in [11] is extended further. Here, a dual-band metal mountable tag antenna having a planar structure covering European and North American UHF RFID bands is designed. The proposed tag antenna utilizes a microstrip patch antenna having a bent open stub feed. This bent feed structure offers the benefit of easy impedance tuning of the designed tag considering the complex chip impedance.

In this paper, we propose an RFID tag antenna to be integrated to track items in fundamental applications such as in the supply chain for the transport and logistics field. Effective management of this chain leads to very concrete results. To increase this efficiency, the implementation of an RFID based container-tracking system is necessary. This will contribute to real-time identification and reaching new levels of traceability and control.

To that end, and to test the performances of the UHF RFID tag developed, a real test is planned on the metal containers in airports; this test requires the deployment of a chain of readers and tags attached to the objects.

The container is the basic loading unit, usually made of aluminum alloys, with different sizes, the largest, exclusively on cargo aircraft, and the means are loaded in the holds of passenger aircraft.

For better optimization of airfreight, goods are transported in containers designed for safety reasons and to facilitate loading and unloading operations. These goods can be easily tracked using a metal mountable RFID tag. Thus, in this article, a UHF RFID tag is proposed, designed and tested for metallic objects. The designed tag is able to operate on two frequency bands EU and US to ensure interoperability of the system. This work is an extension of the work presented in [11], In this paper, the designed tag antenna's working performance on the basis of circuit analysis is represented. Further the simulated results of the tag presented in [11] are verified experimentally in terms of differential impedance and read range. Also, the designed tag's read range performance is compared for two different heights of the substrate. It is observed from a comparison table (Table II) that the designed tag has better performance with respect to other recently designed tags covering two major RFID bands at UHF range i.e., ETSI and U.S. Further, the tag is specifically designed for metal mountable applications. Also, the designed tag covers a better-measured read range of 11 m and 9.7 m in ETSI and U.S. band when mounted on metal objects.

The paper is organized as follows. The proposed tag antenna structure is introduced in Section 2. The section 3 discusses the equivalent circuit of the patch antenna. The parametric study to show its tuning capability for conjugate impedance matching is shown in Section 4. Further, the simulation performance of the

designed tag antenna is shown in Section 5. The impedance measurements for the employed RFID chip i.e. Monza R6, and the designed tag antenna is carried out in Section 6. Also, Section 7, presents the designed tag's measured read range performance. Finally, Section 8 concludes the work.

2. Proposed design

2.1. Antenna structure

The tag antenna proposed here has been designed using a microstrip patch antenna. The proposed tag antenna geometry and its dimensions are illustrated in Fig.1 and Table 1, respectively as described in [11]. It consists of two simple microstrips, a patch, and a bent feed line [8].
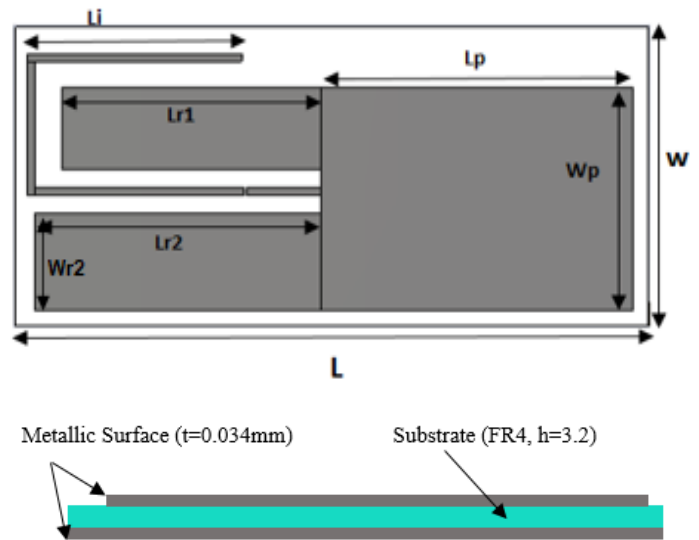
Figure 1: The proposed tag antenna design (Top View and Side view).

Table 1: The proposed antenna dimensions (units in mm)

Par.	L	W	Lp	W_p	L_{r1}	L_i	L_{r2}	W_{r2}
Value	85	40	42	30	30	25	36	11

The tag structure is designed with a full ground plane beneath to be mountable on metallic objects. It is fabricated using FR4 substrate having $\varepsilon r = 4.69$, $\tan \delta = 0.02$, and a thickness h=3.2 mm, with a total dimension of W*L (40 mm * 85 mm). As the size is a critical factor in designing RFID tags, and in order to reduce tag size, the bent feed line structure has been adopted for feeding the patch. The antenna size can also be reduced by opting for higher permittivity substrates. However, they lead to higher costs. Also, the open stub feed line inserted into the patch decreases the input impedance of the patch. The RFID chip is connected to the feed line and its position is optimized to obtain conjugate impedance matching. The parameters L_1 and L_{r1} are optimized to obtain conjugate matching.

3. Equivalent Circuit Model

Figure 2 illustrates the transmission line model of the designed antenna. From the figure, the global structure of the antenna model has been modeled as two transmission lines connected in series configuration [12] comprising of microstrip patch and the feed line of lengths l_1 and l_2 respectively. The antenna input impedance at the feed port can be calculated as:

$$Z_{in} = Z_{in}^1(l_1) + Z_{in}^2(l_2) \qquad (1)$$

where Z_{in}^1 represents the input impedance of the radiation patch, and Z_{in}^2 represents the input impedance of the bent open stub line.

Further, the microstrip patch input impedance is given as in [13]:

$$Z_{in}^1(l_1) = Z_0^1 \frac{R_r + jZ_0^1 \tan(\beta l_1)}{Z_0^1 + jR_r \tan(\beta l_1)} \qquad (2)$$

where R_r , Z_0^1 and β are the resistance and characteristic impedance and the propagation constant of the radiation patch.
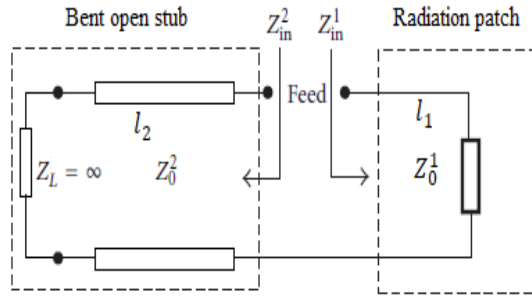
Figure 2: Open stub patch antenna transmission line model representation

Also, the employed open stub feed's input impedance is represented by:

$$Z_{in}^2(l_2) = -jZ_0^2 \frac{1}{\tan(\beta l_2)} \qquad (3)$$

where the characteristic impedance of the open stub line is represented by Z_0^2 .

For a preliminary design of the radiating patch antenna, and before proceeding with the optimization, the dimensions were calculated using the classic rectangular patch equations expressed bellow:

$$L = Leff - \Delta L \qquad (4)$$

where L is the physical length, ΔL is the extended length due to fringing field effects and $Leff$ is its effective length. The extended length, ΔL is given by [14] as shown in equation (5).

$$\frac{\Delta L}{h} = 0.412 \frac{(\varepsilon_{eff} + 0.3)(\frac{w}{h} + 0.264)}{(\varepsilon_{eff} - 0.258)(\frac{w}{h} + 0.8)} \qquad (5)$$

where w is the width of the patch, h is the substrate height, and εeff is the effective dielectric constant.

Also, the effective dielectric constant of the patch is represented as follows:

$$\varepsilon_{eff} = \frac{(\varepsilon_r + 1)}{2} + \frac{(\varepsilon_r - 1)}{2}(1 + \frac{12h}{w})^{-1/2} \qquad (6)$$

where, ε_r is the relative dielectric constant of the substrate.

4. Parametric Study

The conjugate impedance matching is optimized by tuning the lengths of the stub, i.e., L_i and L_{r1}, respectively as explained in [11].

Further, the parametric study to investigate the influence of varying the antenna dimensions, i.e., L_{r2} and W_{r2} in order to tune the second resonant frequency, i.e., 915 MHz, is shown in Fig. 3.

It has been observed that the resonance shifts towards the right by varying these parameters simultaneously and keeping the other parameters constant.
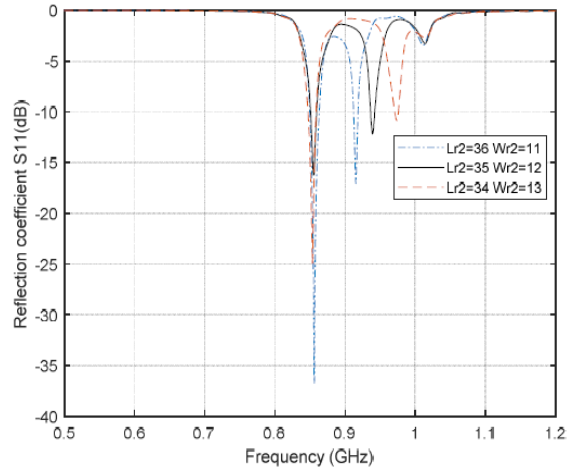
Figure 3: Simulated reflection coefficient versus frequency of the for different values of Lr2 and Wr2.

5. Simulation results

In this context, we have designed, analyzed, simulated, and optimized the proposed tag antenna using CST Studio Suite software.

The tag antenna must exhibit conjugate impedance that matches the employed chip impedance, i.e., Impinj Monza R6 [15]. The simulated and measured S_{11} results for the designed tag antenna are shown in Fig. 4.
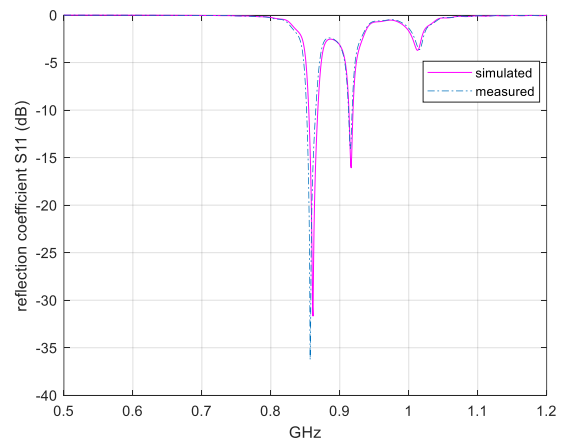
Figure 4: Antenna measured reflection coefficient comparison

6. Impedance Measurement of Designed Tag Antenna and Chip

The Monza R6 chip is employed here at the feeding port of the designed tag antenna and its equivalent circuit is shown in Fig. 3. The chip has a resistance, R_p, of 1200 Ω in parallel to the capacitance, C_p, of 1.43 pF and a chip sensitivity of -20 dBm. The equivalent circuit values for the chip are provided in the datasheet

for the die chip and do not take into account the parasitic impedance that includes substrate, packaging, and input power dependence. The packaged chip, i.e., LXMS21ACMF-183 from Murata is used in the designed tag prototypes. Thus, it is important to consider the chip impedance dependence with respect to frequency.
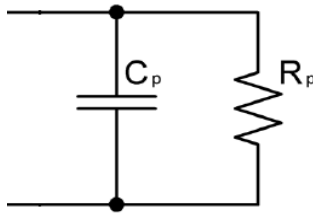
Figure. 5: Tag Chip Linearized R.F. Model

The measurements of the tag antenna and the chip impedances are obtained using vector network analyzer E5062A from Agilent. The tag antenna impedance cannot be directly measured using a 50 Ohms port directly. Therefore, to measure the differential impedance, the tag antenna has been considered as a two-port network and to measure its reflection coefficient, its differential impedance input impedance, Z_{in}, has been calculated represented as:

$$Z_{in} = \frac{2Z_0\,(1-S_{11}S_{22}+S_{12}S_{21}-S_{12}-S_{21})}{(1-S_{11})(1-S_{22})-S_{21}S_{12}} \quad (7)$$

here, Z_0 represents the coaxial cable's characteristic impedance. Figure 6 illustrates the setup to measure the impedance. The differential balun with short-circuited semi-rigid coaxial cables using λ/4 was constructed to measure the impedance. The terminals of constructed balun are soldered to the feed terminals of the designed tag antenna Further, the port extension technique has been applied while measuring differential impedance as detailed in [16].
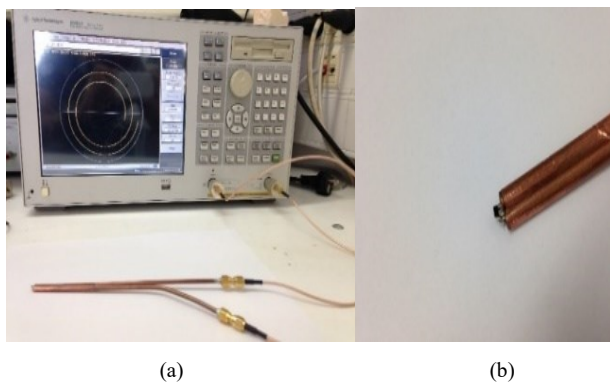
(a)   (b)
Figure 6: Equipment for chip and antenna characterization. (a) VNA, (b) Balun

Figure 7 and fig. 8 shows the used chip input impedance measurements versus the frequency. The chip impedance is measured to be 9.7 – j 130 Ω at 866 MHz and 8.7 – j 124 Ω at 915 MHz, respectively. In comparison, the input impedances given in the datasheet are 13.6-j 127 Ω at 866 MHz and 12.2-j 120 Ω at 915 MHz [17]. As observed, the packaged chip input impedance is slightly different and also depends on the input power.

Finally, the reflection coefficient (Γ) is further calculated using measured tag antenna impedance i.e., Zin and chip impedance, i.e., Zchip respectively, and is represented as:

$$\Gamma = \frac{Z_{in}-Z_{chip}^*}{Z_{in}+Z_{chip}} \quad (8)$$

(a)

(b)
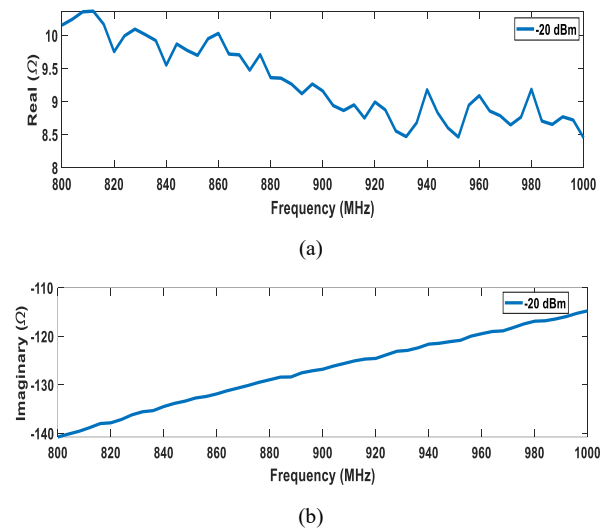
Figure 7: Chip input impedance for -20 dBm input power
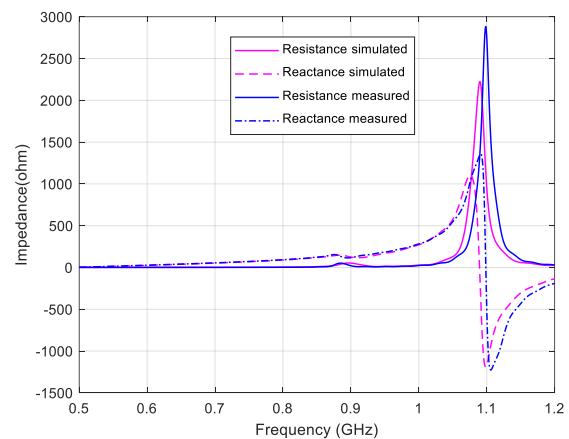
Figure 8: Representation of simulated and measured results of the antenna input impedance

Figure 9 shows a comparison of the simulated and measured reflection coefficient results in the 2 required frequency bands i.e. ETSI & FCC.
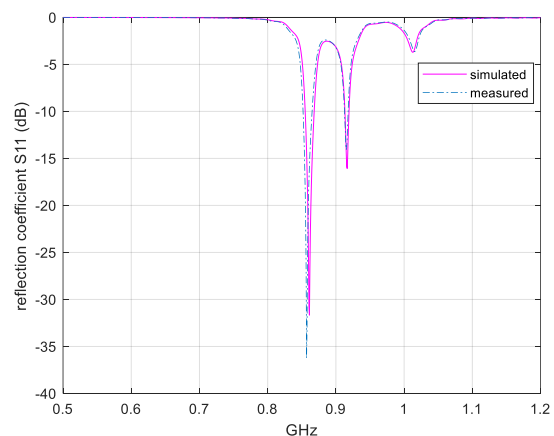
Figure 9: Results of the antenna's reflection coefficient.

It can be seen that a reasonably good value for the reflection coefficient is obtained, which validates the existence of a suitable conjugate impedance matching between the chip' and the designed tag antenna impedance.

7. Read Range Measurements

The reading range or the tag range is defined as the maximum distance from which the tag can be recognized [18], and is the most important parameter for evaluating the RFID tag performance. The equation below shows this reading range following the Friis formula for free space:

$$R = \frac{\lambda}{4\pi} \sqrt{\frac{P_{EIRP} \times G_{tag} \times (1-|\Gamma|^2)}{P_{th}}} \qquad (9)$$

where PEIRP is the equivalent isotropic radiated power specified as 3.3 W in the E.U. band and 4 W in the U.S. band.

Further, λ represents the operating free-space wavelength and P_{th} indicates the chip sensitivity at the resonant frequency. The G_{tag} is defined as the antenna tag's gain and Γ is the reflection coefficient defined above in equation (8). The tag's read range can be maximized by achieving a lower-power reflection coefficient defined by $|\Gamma|^2$ and a high-gain antenna G_{tag}.

Also, the ability of the tag to transfer power to the connected chip is represented by $(1-|\Gamma|^2)$ which is also known as the power transmission coefficient of the tag.

Figure 10 describes the devices used for experimental measurement of the reading range in an anechoic chamber.

Figure 10: The Read range measurement setup

The measuring setup consists of an RFID reader, i.e., CAEN RFID, circularly polarized Reader antenna with a realized gain Gr of 8 dBi. The reader is connected to the reader antenna and a host computer. The cable losses and attenuator losses were taken into consideration.

From the measurement results, we deduced that the tag has a reading range of approximately 11 m and 9.7 m at 866 MHz and 915 MHz with an EIRP of 3.3 W, respectively, as illustrated in Fig. 11.

The gain of the tag antenna, as well as the height of the chosen substrate, strongly influences the read range of the tag. a comparison of the read range for two different substrate heights

i.e., 3.2 and 1.6 is shown in Figure 12. The read distance was observed to degrade from 11m to 4 m at 866 MHz and 9.7 m to 3.7 m at 915 MHz.
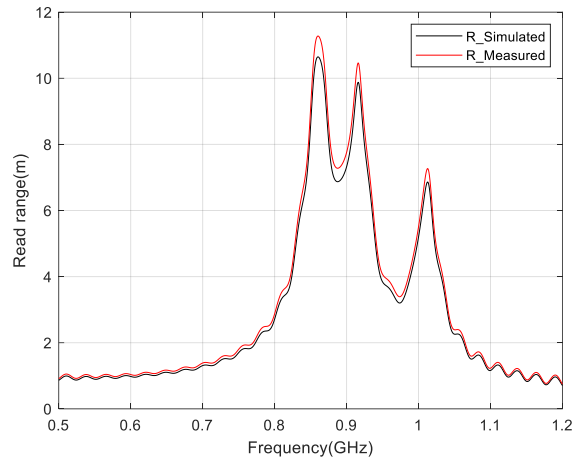
Figure 11: Results of simulated and measured antenna read range
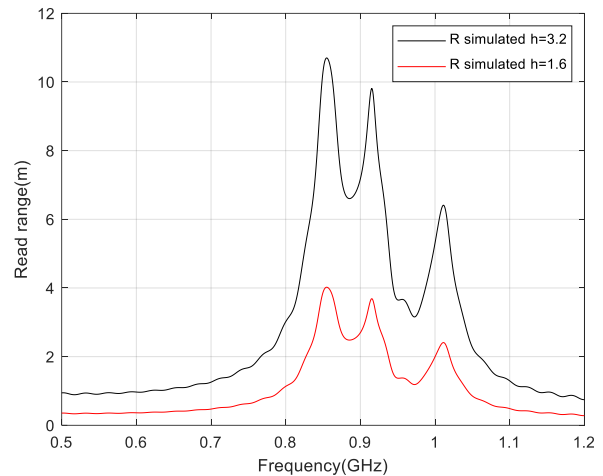
Figure 12: Read-range for two different substrate thickness.

7.1. 3D-Radiation Pattern

As already mentioned, impedance matching between antenna and chip impedances, is a key design requirement. Therefore, its radiation pattern cannot be measured directly using a 50-ohm port. Hence, the performance of the tag antenna is also assessed based on its simulated 3 D (Dimensional) gain and radiation pattern as shown in Figure 13. It has been observed from the figure that the tag antenna exhibits a realized gain of -3 dBi. Also, to minimize the effect of mounted objects, the tag should exhibit a unidirectional radiation pattern. Thus, it is depicted from Fig. 14, that the designed tag antenna exhibits a directional radiation pattern with a directivity of 4.2 dBi. This feature is mainly desirable to design the platform tolerant tag and hence validates its application for metal mountable tracking objects.

A performance comparison of our proposed tag antenna with some previous research studies representing metal-mountable UHF RFID tags is shown in Table 2. From the table, it has been observed that the tags designed in [18-22] are larger as compared to the tag proposed in this work. Moreover, our proposed tag is

characterized by its operability in the two main frequency bands with a better reading range. On the other hand, all the other tags shown in the table cover a single UHF RFID band. Further, the tag designed in [20] is compact, however, still it covers a lower read range in a single UHF RFID band.
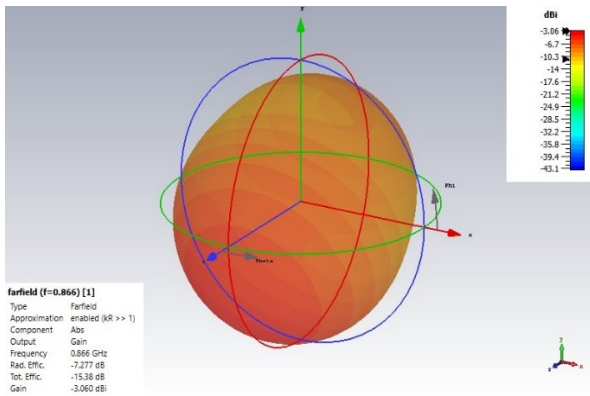
Figure 13: 3 D Gain pattern of the designed tag at 866 MHz
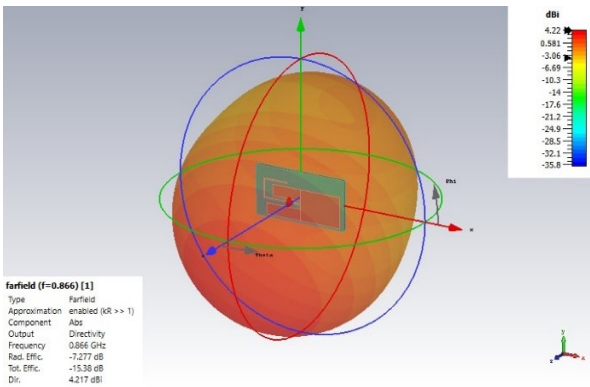
Figure 14: 3 D directivity pattern of the designed tag at 866 MHz

Table 2: A comparison table performances of UHF tags mounted on metallic items

Ref.	Transmitting EIRP Power	Circuit Size (mm)	Backing Plate Size (cm)	Max. Read Range (m)
This work	4 W	85×40×3.2	20×20	11 m (ETSI) 9.7 m (FCC)
[19]	4 W	86×41×3.2	20×20	5.6
[20]	3.3 W	88×60×0.76	15×15	5.4
[21]	4 W	30×30×3	20×20	7.2
[22]	4 W	120×60×0.4	15 × 30	10
[23]	N/A	84×126×1.28	N/A	2.5

Thus, better performances in regard to reading range, size and also covered bands, characterize our proposed RFID tag. Also, it is deduced that the designed tag may be employed for different applications such as health monitoring, logistics, and transport supply chains, and IoT (Internet of Things) network applications, etc.

8. Conclusion

In this research paper, a new planar dual-band compact platform tolerant UHF RFID tag antenna presented in [11] has been simulated, fabricated, and tested for its impedance and read range performance experimentally. To measure the real performance of metallic objects, the tag is mounted on a metal sheet. (20 m x 20 m) while measuring. Our tag antenna is modeled and designed using CST Studio Suite software. The designed tag is specifically designed to be mountable on metallic items by considering a full ground plane. The tag comprises a simple structure and does not include any vias, thus facilitating low-cost, efficient design for mass production. Further, the simulated and measured impedance, reflection coefficient, and read ranges of the tag structure have been presented and are observed to be well in agreement with each other. From the tag antenna reflection coefficient, it is realized that the designed antenna covers both major UHF RFID bands i.e., European (E.U., 865-867 MHz) and North American (the U.S., 902-928 MHz). The designed tag exhibits a read range up to 11 m at 866 MHz and 9 m at 915 MHz.

Hence, the designed tag antenna is observed to perform better in terms of conjugate impedance matching, unidirectional radiation pattern, and high read range in both the required resonant bands. Thus, it is validated that the designed tag is suitable for use in real-time applications such as transport and logistics fields and IoT network applications.

Conflict of Interest

The authors declare no conflict of interest.

Acknowledgment

References

[1] K. Finkenzeller, RFJD handbook, 3rd ed Wiley, New York, 2010

[2] I. Any et al., "Regulatory status for using RFID in the EPC Gen2 (860 to 960 MHz) band of the UHF spectrum," **2**(November), 1–18, 2016.

[3] V. D. Hunt, A. Puglia, and M. Puglia, RFID: A Guide to Radio Frequency Identification. New York: Wiley, 2007.

[4] T. Björninen, L. Sydänheimo, L. Ukkonen, and Y. Rahmat-Samii, "Advances in antenna designs for UHF RFID tags mountable on conductive items," IEEE Antennas Propagation Magazine, **56**(1), 79–103, 2014. doi: 10.1109/MAP.2014.6821761.

[5] D. M. Dobkin, S. M. Weigand, W. J. Communications, and S. Jose, "Environmental Effects on RFID Tag Antennas," 135–138, 2005.

[6] K. Penttilä, M. Keskilammi, L. Sydänheimo, and M. Kivikoski, "Radio frequency technology for automated manufacturing and logistics control. Part 2: RFID antenna utilization in industrial applications," The International Journal of Advanced Manufacturing Technology, **31**(1–2), 116–124, 2006. doi.: 10.1007/s00170-005-0174-y

[7] H. Chen, S. Member, C. Sim, and S. Kuo, "Compact Broadband Dual Coupling-Feed Circularly Polarized RFID Microstrip Tag Antenna Mountable on Metallic Surface," IEEE Transaction Antennas and Propagation, **60**(12), 571–5577, 2012. doi: 10.1109/TAP.2012.2210273.

[8] L. Mo and C. Qin, "Planar UHF RFID Tag Antenna With Open Stub Feed for Metallic Objects," IEEE Transaction Antennas and Propagation, **58**(9),3037–3043, 2010. doi: 10.1109/TAP.2010.2052570

[9] M. Hirvonen, P. Pursula, K. Jaakkola, and K. Laukkanen, "Planar inverted-F antenna for radio frequency identification," ELECTRONIC LETTERS, **40** (14), 2004. doi: 10.1049/el:20045156

[10] H. Chen, S. Member, and Y. Tsao, "Low-Profile PIFA Array Antennas for

UHF Band RFID Tags Mountable on Metallic Objects," IEEE Transaction Antennas and Propagation, **58**(4), 1087–1092, 2010. doi: 10.1109/TAP.2010.2041158

[11] H. Bouazza, A. Lazaro, M. Bouya and A. Hadjoudja, "Dual-band UHF RFID tag for metallic items," 2019 IEEE-APS Topical Conference on Antennas and Propagation in Wireless Communications (APWC), 090-092, 2019, doi: 10.1109/APWC.2019.8870474.

[12] L. Mo and C. Qin, "Tunable compact UHF RFID metal tag based on cpw open stub feed PIFA antenna," International Journal of Antennas and Propagation 2012. doi: 10.1155/2012/167658

[13] L. Reinhold and B. Pavel, RF Circuit Design: Theory and Applications. New York: Pearson Education, 2000. doi: 10.1155/2012/167658

[14] C. A. Balanis, Antenna Theory Analysis and Design, 3rd ed. New Jersey: John Wiley & Sons, 2005.

[15] Datasheet Impinj Monza R6, https://support.impinj.com/hc/en-us/articles/202765328-Monza-R6-Product-Brief-Datasheet

[16] A. Bansal, S. Sharma, Khanna, "platform tolerant dual-band UHF RFID tag antenna with enhanced read range using artificial magnetic conductor structures". Int. J RF Microw Comput Aided Eng. 2019. doi: 10.1002/mmce.22065

[17] H. Bouazza, A. Lazaro, M. Bouya, and A. Hadjoudja, "A Planar Dual-Band UHF RFID Tag for Metallic Items", Radioengineering, **29**(3), 505. 2020, doi: 10.13164/re.2020.0504

[18] A. Bansal, S. Sharma and R. Khanna, "A Spiral Shaped Loop Fed high Read Range Compact Tag Antenna for UHF RFID Applications," 2019 IEEE International Conference on RFID Technology and Applications (RFID-TA), 212-215, 2019, doi: 10.1109/RFID-TA.2019.8892203.

[19] A. P. Sohrab, Y. Huang, M. N. Hussein and P. Carter, "A Hybrid UHF RFID Tag Robust to Host Material," in IEEE Journal of Radio Frequency Identification, **1**(2), 163-169, June 2017, doi: 10.1109/JRFID.2017.2765623.

[20] POLIVKA, M., SVANDA, M. "Stepped impedance coupled patches tag antenna for platform tolerant UHF RFID applications. IEEE Transactions on Antennas and Propagation", **63**(9), 3791–3797. 2015, doi: 10.1109/TAP.2015.2447034

[21] F. Bong, E. Lim and F. Lo, "Flexible Folded-Patch Antenna With Serrated Edges for Metal-Mountable UHF RFID Tag," in IEEE Transactions on Antennas and Propagation, **65**(2), 873-877, 2017, doi: 10.1109/TAP.2016.2633903.

[22] Y. Lin, M. Chang, H. Chen and B. Lai, "Gain Enhancement of Ground Radiation Antenna for RFID Tag Mounted on Metallic Plane," in IEEE Transactions on Antennas and Propagation, **64**(4), 1193-1200, 2016, doi: 10.1109/TAP.2016.2526047.

[23] M. Abu, E. E. Hussin, A. R. Othman, F. M. Johar, N. M. Yatim, and R. F. Munawar, "Design of 0.92 GHz artificial magnetic conductor for metal object detection in RFID tag application with little sensitivity to incidence of angle," Journal of Theoretical and Applied Information Technology., **60**(2), 307–313, Feb. 2014. Id: 73550079

Using a safety PLC to Implement the Safety Function

Karol Rástočný, Juraj Ždánsky, Jozef Hrbček[*]

Department of Control and Information Systems, University of Žilina, Faculty of Electrical Engineering and Information Technology, Žilina, 010 26, Slovak Republic

A R T I C L E   I N F O

A B S T R A C T

Nowadays almost every PLC manufacturer offer a so-called safety PLC. It is a specific category of PLC, which in recent years have become a commonly used means of performing safety functions, especially in industrial applications. In this area of specific applications, a maximum of SIL 3 is normally required. However, the guaranteed safety features of the PLC lead to the consideration or discussion, whether they could be used in applications with higher safety requirements. This paper deals with the possibility of using the safety PLC to implement safety functions with SIL 4. The paper presents the long-term experience of the authors in the development of control systems for railway applications with the required level of SIL4.

1. Introduction

This paper is an extension of the work originally presented at the conference [1]. Extension relates to elaboration of the impact of random and systematic failures to the safety of the safety function (SF) realized on the Safety Programmable Logic Controllers (sPLC) in the dual architecture, which is realized by this architecture. The part of realized extension is a specific application example of the realization of SF with the safety integrity level 4 (SIL 4) using two safety PLCs certified to SIL 3.

In practice (in industry, transport, medicine ...) we can quite often encounter that the ongoing process or operation of a machine or equipment can pose a risk to assets (people, environment, property damage, ...), which fall within its remit. It is necessary to deal with the risk analysis in this case. This means identifying hazards, their consequences and calculating (or estimating) the risk. Generally, the risk (R) is given by the sum of the combinations of the occurrence frequency of the i - th hazard (h_i) and its consequences (c_i), it means:

$$R = \sum_{i=1}^{n} h_i \times c_i, \tag{1}$$

where n is the number of identified hazards.

The appropriate safety measures (technical, organizational) must be applied to reduce this risk to at least a predefined tolerable value (Figure 1), if the calculated (estimated) risk is greater than the predefined tolerable risk ($R>R_T$). The technical safety measures can be passive (covers, fencing, ...) or active. Safety-relevant systems (SRSs) are used as active technical safety measures, which realize the safety functions (SFs).

Total risk (R)	
Acceptable risk (R_T)	Risk to be reduced
Residual risk (R_R)	Reduced risk
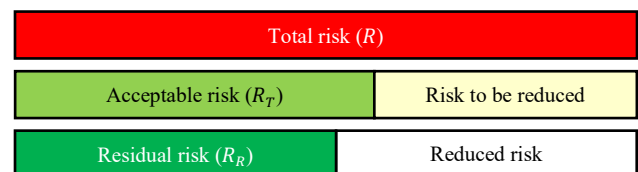
Figure 1: Relations between individual components of risk

A process (equipment, machine) is considered safe if it is valid that

$$SR_R \leq R_T. \tag{2}$$

The application of safety measures can be focused on:

- only to reduce the frequency of individual hazards;

- only to reduce the consequences of individual hazards;

- to reduce the frequency of occurrence and also to reduce the consequences of individual hazards.

[*]Corresponding Author: Jozef Hrbček, University of Žilina, +421 041 513 3354,
Email: jozef.hrbcek@uniza.sk

This paper deals with the issue of using the technical active measures to reduce the frequency of hazards.

Based on the risk analysis, the safety functions are defined within the specification of safety requirements so that ordinarily one SF covers one hazard (or even more hazards). The aim of SF realization is to achieve risk reduction to the required value (for example, by reducing the frequency of hazards). In order to achieve this objective, the SRS must be characterized by the fact that during fault-free operation it performs the specified SFs and in case of failure the SRS must ensure that the ongoing process either remains in the given operating state (if this state does not endanger the assets within its operation), or has entered a predefined safe state (for example, disconnecting power from the motor and stopping the machine). This is a feature called "fail-safe".

Since safety cannot be understood in absolute but relatively, the possibility of SF failure must also be taken into the account. The degree to which SF is able to achieve the fail-safe property is expressed by SIL. Standard [2] defines four levels of SIL (1 to 4), SIL 4 means the most stringent safety requirements (for continuous operation, the mean frequency of a dangerous safety function failure PFH $10^{-9} \leq$ to $< 10^{-8}$ h^{-1} is required; i.e. an average of one dangerous SF failure is about 11 416 years). The required SIL for SF is determined depending on the size of the risk that SF reduces.

One of the suitable technical means for the implementation of SRS based on processor technology are also sPLCs. These are especially modified PLCs to have a fail-safe feature. These are usually modular systems with which SFs can be implemented not only with the required safety properties (with the required SIL), but also with the required reliability properties (with the required availability).

Commonly available sPLCs are mainly used for the implementation of SFs with a requirement for maximally SIL 3. This is because they are primarily developed for industrial applications where this requirement is usually sufficient (normally the SFs are implemented with desired SIL 2 or SIL 3 in the industry).

However, there are special cases of applications (e.g. in railway transport) where the implementation of SFs with SIL 4 is required, but these sPLCs are relatively expensive and do not always meet the functional requirements of the customer (for example, they do not have suitable I/O modules for wiring special components that are used in a given area of a specific application). Therefore, several manufacturers of the safety-related electronic signaling systems for railway applications are developing their own modular systems (such as generic products), which they use to realize specific applications (for example sPLC type NEXUS from the company PrvíSignalní [3]).

The efforts to increase the efficiency of the development of generic products of electronic signaling systems for railway applications have caused some manufacturers (e.g. [4], [5]) decided to develop a product for the implementation of SFs with SIL 4, which consists of two sPLCs (intended for the realization of SFs with SIL 3). It is a dual structure based on composite fail-safety with fail-safe comparison. A block diagram of such a structure is shown in Figure 2. The Equipment Under Control

(EUC) block represents the controlled equipment, resp. monitored equipment (either as a separate element or as a part of the controlled or monitored process).
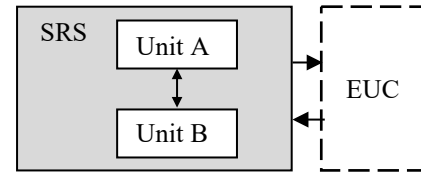
Figure 2: Block diagram of a general dual structure

The technical safety principle of such a solution (Figure 2) is based on mutual exchange and comparison of the data between the unit A (one sPLC) and unit B (second sPLC). The positive result of the comparison is the sign of the correct operation of the system.

Standards [2] and [6] require to prove not only functional safety (correct performance of the function in a fault-free state), but also technical safety of SRS (represents the fail-safe feature). Although functional safety can be in principle proved by the tests, it is impossible to prove technical safety in the same way. Making technical safety prove encounters the problems that are pointed out in this article. Since the safety proves must be performed individually for each SF (SRS can generally be implemented by several SFs, whereas a different SIL may be required for each SF and each SF may be implemented by different parts of the SRS). To clarify the considerations presented in this paper, the authors accepted the simplification that the SRS implements only one SF. Under this assumption is valid, that a dangerous failure of the SRS (due to the occurrence of a failure) is equal to a dangerous failure of the SF.

2. Realization of SF with SIL 4 using sPLCs with SIL 3

SF with SIL 4 must be realized in such a way that the requirements for safety integrity (SI) level 4 are met, which result from [2] resp. [6]. These are the requirements for safety integrity against random failures (RanF-SI) and also for integrity against systematic failures (SysF-SI). In the case of RanF-SI a failure of hardware components is supposed; in the case of SysF-SI it means the software errors, whether embedded software (firmware) or application software, but the hardware failures with a common cause cannot be ruled out (one hardware failure will affect the operation of both units A and unit B).

In principle, the influence of both systematic and random faults to SF failure can be illustrated by the fault tree shown in the Figure 3.

The fault tree in Figure 3 can be described by a logical function:

$$S\_DF = S\_DRF + S\_DSF, \tag{3}$$

whereas:

$$S\_DRF = A\_RF . B\_RF, \tag{4}$$

$$S\_DSF = (A\_SFA + A\_SFE) . (B\_SFA + B\_SFE), \tag{5}$$

where S_DF is a dangerous fault of SRS (top event), S_DRF is the dangerous random failure of SRS, S_DSF is the dangerous systematic failure of SRS, A_RF (B_RF) is a random fault of unit A (B), A_SFE (B_SFE) is a systematic failure of the application software of unit A (B), A_SFE (B_SFE) is a systematic failure of the embedded software or hardware of unit A (B).

The logical function (3) expresses the fact that SRS dangerous failure can be caused by the random or systematic failure.

Figure 3: Fault tree for SRS in Figure 2

2.1. The influence of random failures on SF safety integrity

The primary construction elements of PLCs are the electronic components, which are characterized by the occurrence of the random failures. It is generally accepted that the occurrence of random failures of electronic components can be described by the exponential distribution rule. Manufacturers usually declare the failures rates for individual modules (in the case of sPLC, the dangerous failures rate). Based on this information and knowledge of the structure of SRS, the dangerous failures rate of SRS (dangerous failure rate of SF) can be calculated.

If the manufacturer declares the dangerous failure rate for the electronic system or its part (for example, the sPLC module for the implementation of SF with SIL 3), which is designed for industrial applications, then calculating the dangerous failure rate accept to assume that every second failure either alone or in combination with another failure (other failures) is dangerous [7]. Such an assumption may not be in accordance with the requirements for other applications. For example, for railway applications [6], if SIL 4 is required for an SF that is implemented

with an electronic SRS, then it is considered that any failure may be potentially dangerous. This fact must be taken into account when calculating the failure rate of SF for a specific application.

If the units A and B are physically independent of each other, then the basic events A_RF and B_RF from the fault tree in Figure 3 are independent too. The probability of the dangerous random failure of the SRS can be expressed by relation 6:

$$SP_{S\_DRF}(t) = P_{A\_RF}(t).P_{B\_RF}(t),$$

$$P_{S\_DRF}(t) = \left(1 - e^{-\lambda_{A\_RF}.t}\right).\left(1 - e^{-\lambda_{B\_RF}.t}\right), \qquad (6)$$

where the $P_{S\_DRF}(t)$ is the probability of dangerous random failure of SRS, $P_{A\_RF}(t)$ is the probability of dangerous random failure of unit A, $P_{B\_RF}(t)$ is the probability of dangerous random failure of unit B, λ_{A_RF} (λ_{B_RF}) is the dangerous random failures rate of unit A (B).

The dangerous random failure rate of SRS can be calculated using the equation:

$$\lambda_{S\_DRF}(t) = \frac{\frac{dP_{S\_DRF}(t)}{dt}}{1 - P_{S\_DRF}(t)}, \qquad (7)$$

after substituting (6) into (7) and adjusting, it can be determined that:

$$\lambda_{S_{DRF}}(t) =$$

$$\frac{\lambda_{A\_RF}.e^{-\lambda_{A\_RF}.t} + \lambda_{B\_RF}.e^{-\lambda_{B\_RF}.t} - \left(\lambda_{A_{RF}} + \lambda_{B_{RF}}\right).e^{-\left(\lambda_{A_{RF}} + \lambda_{B_{RF}}\right).t}}{e^{-\lambda_{A\_RF}.t} + e^{-\lambda_{B\_RF}.t} - e^{-\left(\lambda_{A_{RF}} + \lambda_{B_{RF}}\right).t}}. \quad (8)$$

Assuming that $\lambda_{A\_RF}.t \ll 1$ and $\lambda_{B\_RF}.t \ll 1$, then the SRS dangerous failure rate is:

$$\lambda_{S\_DRF}(t) \le 2.\lambda_{A\_RF}.\lambda_{B\_RF}.t. \qquad (9)$$

The mutual physical independence of unit A and unit B can be achieved by applying appropriate technical measures (e.g.: galvanic separation of the units, separate the power supply of unit A and unit B, ...).

SRS consists not only of sPLC, but also other elements necessary for obtaining information from the monitored (or controlled) process (equipment, machine) and elements for the realization of SF outputs. An example of a frequently used SRS wiring with sensors (S_A, S_B) and contactors (C_A, C_B) represents the Figure 4. Safe disconnection of the EUC from the power supply after affecting the sensors is the purpose of this wiring.

The wiring of sensors and contactors follows the sPLC manufacturer's recommendations and their selection depends on the specific application. In this case, contactors are used which, in addition to the coil (W_A, W_B) and the main contacts (c_{1A}, c_{1B}), also contain control contacts (c_{2A}, c_{2B}). The manufacturer must guarantee the co-operation of the main contact and the mechanically coupled auxiliary contact (it is the characteristic of relay type C according to [8]). The correct function of the

contactor is checked using feedback through application diagnostics. The feedback data is compared with the commands for the contactor in the application software. Test diagnostics in the application software and comparison of feedback data are discussed in more detail, e.g. [9] and [10]. Diagnostics can be performed in distinct forms and can cover a whole system [11], [12] or be specifically oriented on selected system parts [13], [14].
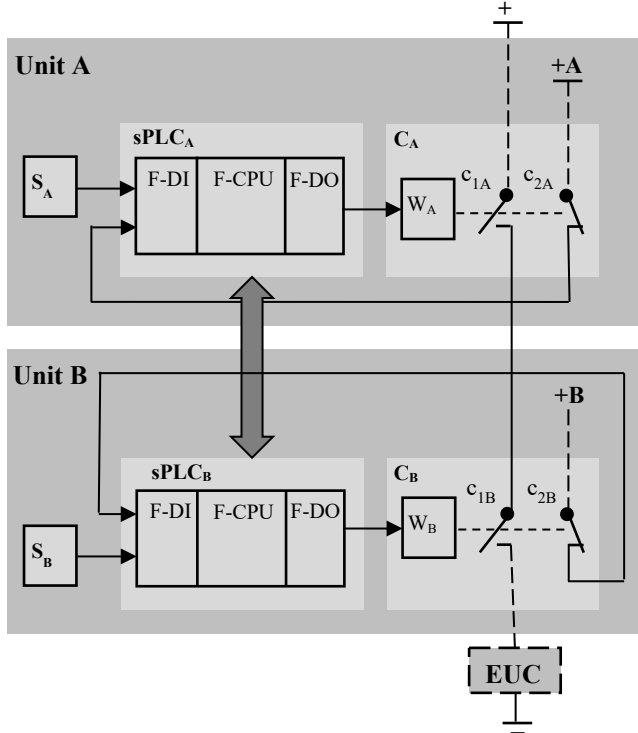
Figure 4: Wiring of the SRS

Occurrence of the dangerous failure due to random failure of SRS in Figure 4 can be described by a fault tree (Figure 5).

If the basic events of the fault tree in Figure 5 are independent (realistic and feasible assumption) then according to (9) it is valid that:

$$\lambda_{S\_DRF}(t) \leq 2.\lambda_{SA}.\lambda_{SB}.t + 2.\lambda_{SA}.\lambda_{sPLCB}.t + 2.\lambda_{SA}.\lambda_{CB}.t + 2.\lambda_{sPLCA}.\lambda_{SB}.t + 2.\lambda_{sPLCA}.\lambda_{sPLCB}.t + 2.\lambda_{sPLCA}.\lambda_{CB}.t + 2.\lambda_{CA}.\lambda_{SB}.t + 2.\lambda_{CA}.\lambda_{sPLCB}.t + 2.\lambda_{CA}.\lambda_{CB}.t, \quad (10)$$

whereas:

$$\lambda_{sPLCA} = \lambda_{D_{FDIA}} + \lambda_{D_{FCPUA}} + \lambda_{D_{FDOA}},$$
$$\lambda_{sPLCB} = \lambda_{D\_FDIB} + \lambda_{D\_FCPUB} + \lambda_{D\_FDOB}, \quad (11)$$

where λ_{SA} (λ_{SB}) is the sensor A (B) random failure rate, λ_{sPLCA} (λ_{sPLCB}) is dangerous random failure rate of sPLC$_A$ (sPLC$_B$), λ_{CA} (λ_{CB}) is random failure rate of the contactor A (B), λ_{D_FDIA} (λ_{D_FDIB}) is the module F-DI random failure rate of the unit A (B), λ_{D_FCPUA} (λ_{D_FCPUB}) is the module F-CPU random failure rate of the unit A (B), λ_{D_FDOA} (λ_{D_FDOB}) is the module F-DO random failure rate of the unit A (B).
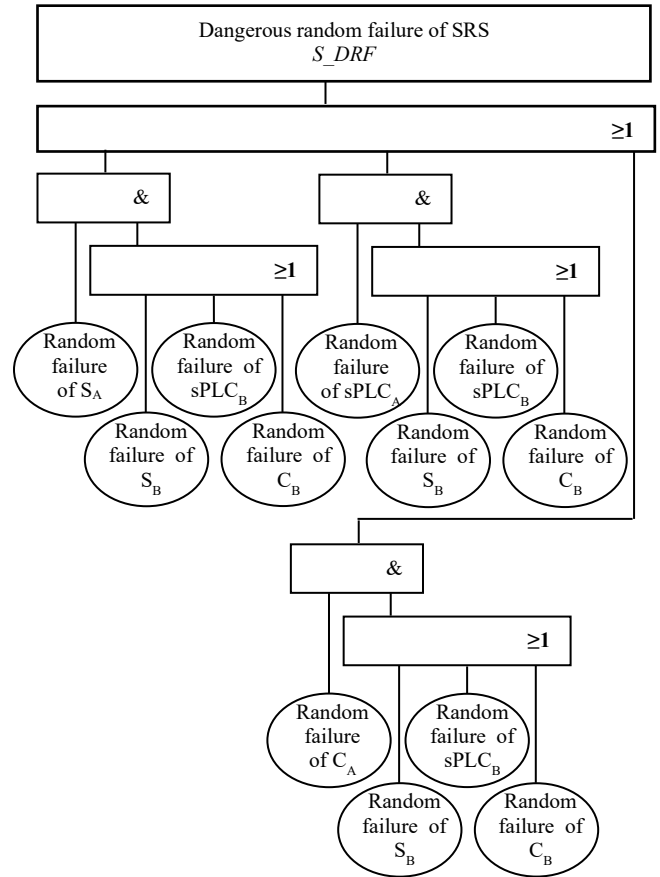
Figure 5: The fault tree of the SRS from Figure 4

If the SF realized by SRS (Figure 4) is to meet the RanF-SI requirement for SIL 4, then it must be true that

$$\lambda_{S\_DRF}(t) \leq \lambda_{SIL4}. \quad (12)$$

It follows from (10) and (12) that

$$t_O \leq \frac{\lambda_{SIL4}}{2.X},$$
$$X = (\lambda_{SA}.\lambda_{SB} + \lambda_{SA}.\lambda_{sPLCB} + \lambda_{SA}.\lambda_{CB} + \lambda_{sPLCA}.\lambda_{SB} + \lambda_{sPLCA}.\lambda_{sPLCB} + \lambda_{sPLCA}.\lambda_{CB} + \lambda_{CA}.\lambda_{SB} + \lambda_{CA}.\lambda_{sPLCB} + \lambda_{CA}.\lambda_{CB}), \quad (13)$$

where t_O is the maximum allowed time of failure detection and negation.

2.2. Results of modeling the impact of random failures on the SF safety integrity - a case study

Let the SRS in Figure 4 implements one SF, in the implementation of which all elements participate. The failures rate, or dangerous failures rate of these elements are listed in the Table 1. Figure 6 shows the dependence of the SRS dangerous random failures rate ($\lambda_{S\_DRF}(t)$) depending on the time of failure detection and negation (t_O) calculated according to the relation (9) - curve 1 and calculated according to the relation (8) - curve 2. Maximum tolerable dangerous failure rate for SIL 4 is shown by a horizontal line. The intersection of curve 1 or 2 with this line

determines the maximum allowed time of fault detection and negation. For curve 1 it means the time 3830 h and 3845 h for curve 2. The difference between determined times is relatively small and acceptable from a safety point of view because the time determined from the simplified relationship (9) is shorter.

Table 1: The failures rates and dangerous failures rates of realized SF

Element	Failure rate	Dangerous failure rate
S_A	5.10^{-7} h^{-1}	
S_B	5.10^{-7} h^{-1}	
sPLC$_A$		4.10^{-9} h^{-1}
F-DI 16x24VDC		1.10^{-9} h^{-1}
F-CPU 1516F-3PN/DP		1.10^{-9} h^{-1}
F-DQ 8x24VDC/2A PPM		2.10^{-9} h^{-1}
sPLC$_B$		4.10^{-9} h^{-1}
F-DI 16x24VDC		1.10^{-9} h^{-1}
F-CPU 1516F-3PN/DP		1.10^{-9} h^{-1}
F-DQ 8x24VDC/2A PPM		2.10^{-9} h^{-1}
C_A	$6,4.10^{-7}$ h^{-1}	
C_B	$6,4.10^{-7}$ h^{-1}	

The diagnostic mechanisms available to the SRS must guarantee that all potentially dangerous faults are detectable (diagnostic coverage DC = 100%). Another approach must be used to calculate the dangerous failure rate of SRS if this condition is not fulfilled - for example, a model based on the Markov chain [15] (in this paper, the fault tree analysis (FTA) is used). The issue of using different methods to assess the dangerous failure rate of SRS as well as considering the influence of other factors (besides the random failures rates and DC) on the dangerous failure rate of SRS is discussed in [15]. For the sake of clarity, the fault tree analysis (FTA) method is used in this article.

It can be stated that the realization of SF with SIL 4, with respect to RanF-SI, using a dual structure is realistically achievable.
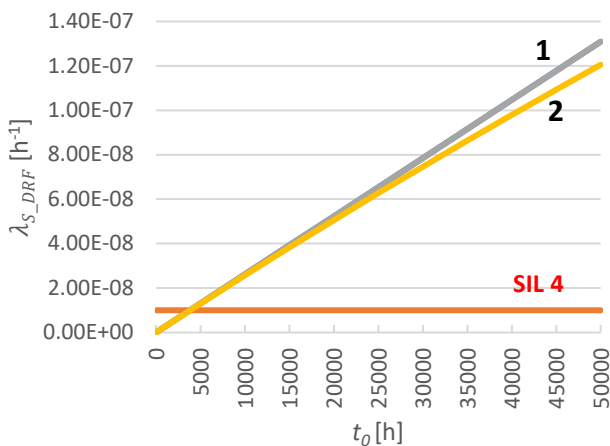
Figure 6: Dependence of the SRS dangerous random failures rate on the failure time detection and negation

2.3. The impact of systematic failures on the safety integrity of SF

While RanF-SI is a quantifiable part of SI, SysF-SI is a non-quantifiable part of SI. Probability calculations cannot be used for its evaluation (assessment), because the rate of the occurrence of the systematic failures is not known (practically, the occurrence of systematic failures is impossible to identify) and the distribution of systematic failures is not known. Achieving the required SysF-SI is based on the effective prevention of failures by applying appropriate and suitable safety measures (depending on the required SIL for SF), which are defined in the relevant standards for the given areas of applications. The evaluation (assessment) of SysF-SI is based on the assessment that the prescribed safety measures are effective and have been applied at a sufficient level [2].

The fault tree in Figure 3 shows the influence of systematic failure on the occurrence of the SRS dangerous failure. This influence is expressed by a logical function (5). In general, it should be assumed that unit A and unit B have only some mutual systematic failures, and thus it cannot be valid that the basic events A_SF, B_SF are mutually interdependent. Therefore, in this case, it must be evaluated by the general relation that:

$$P_{S\_DSF}(t) = P_{A\_SF}(t).P_{(B\_SF/A\_SF)}(t), \text{ resp.}$$
$$P_{S\_DSF}(t) = P_{B\_SF}(t).P_{(A\_SF/B\_SF)}(t), \tag{14}$$

where $P_{S\_DSF}(t)$ is the probability of dangerous systematic failure of the SRS, $P_{A\_SF}(t)$ ($P_{B\_SF}(t)$) is the probability of systematic failure of unit A (B), $P_{(B\_SF/A\_SF)}(t)$ is the conditional probability of systematic failure of unit B provided that the systematic failure of unit A has occurred and $P_{(A\_SF/B\_SF)}(t)$ is the conditional probability of systematic failure of unit A provided that the systematic failure of unit B has occurred.

In general, it is valid that

$$P_{A\_SF}(t) \leq P_{(A\_SF/B\_SF)}(t) \leq 1, \text{ resp.}$$
$$P_{B\_SF}(t) \leq P_{(B\_SF/A\_SF)}(t) \leq 1, \tag{15}$$

where $P_{(A\_SF/B\_SF)}(t) = 1$, resp. $P_{(B\_SF/A\_SF)}(t) = 1$, if the units A, B are identical (have the same systematic failures) and $P_{(A\_SF/B\_SF)}(t) = P_{A\_SF}(t)$, resp. $P_{(B\_SF/A\_SF)}(t) = P_{B\_SF}(t)$, if unit A and unit B are mutually independent (units do not have the same systematic failures).

Figure 7 shows in principle the influence of safety measures to prevent of systematic failures in consideration of the degree of interdependence of units A, B and therefore also to the on SI.

If the units A and B are HW and also SW identical (same sPLC and the same application software; Figure 7a), then it can be stated that the units A, B are dependent and the SF, which is realized by these units has the same level of SysF-IS as would have SF if it were realized only by one unit (unit A or unit B). This means that if the sPLC manufacturer states that using this sPLC can be realized SF with max. SIL 3, it must be assumed that the SysF-IS level is 3. The fact is that in such a case it does not make sense to use a dual structure.

Increasing the SysF-IS level can be in principle achieved in the following ways (safety measures):

$A\_SF = B\_SF$

$P[(A\_SF) \cap (B\_SF)] = 1$

A_SF B_SF

A_SF B_SF

$0 < P[(A\_SF) \cap (B\_SF)] \leq 1$ $P[(A\_SF) \cap (B\_SF)] = 0$
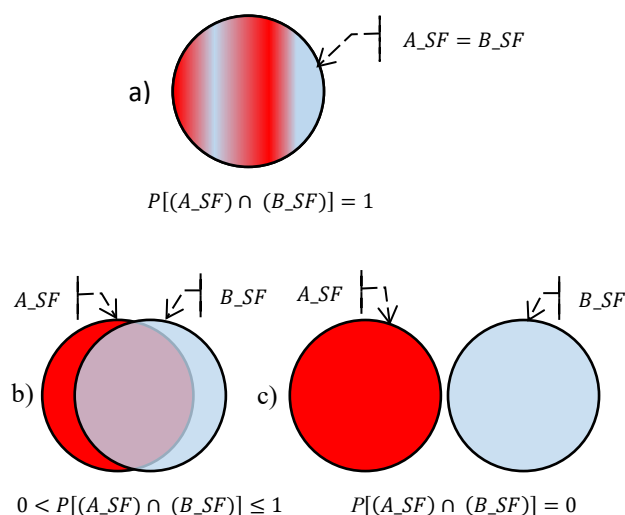
Figure 7: The illustration of the "overlapping" of the sets of systematic failures of unit A and unit B

- software diversification (different software in unit A and in unit B);
- hardware diversification (different hardware in unit A and in unit B, i.e. using of different sPLCs in unit A and in unit B);
- diversification of hardware and software.

Modifying the embedded software is a very effective safety measure to increase the SysF-IS level. However, when using sPLC, such a solution is practically impossible because this software is inaccessible to the user (this is information that the sPLC manufacturer does not provide). Diversification of application software is possible. In addition to functional algorithms related to the realized SFs, the application software can also implement mechanisms that allow the detection of a part of the systematic failures operating in a given unit. These are, for example, the following mechanisms:

- a clear, complete, and verifiable specification of requirements;
- registration of requirements using semi-formal or formal methods;
- compliance with coding standards;
- use of verified function blocks that are verified by "good" practice;
- consistent testing.

The fact is that the number of reduced systematic failures can be expected, but it cannot be demonstrated that the level of remaining systematic failures is acceptable. This is also related to the fact that the set of systematic failures is not known and therefore it is impossible to implement safety measures for their detection and subsequent negation in a targeted manner. In reality, some safety mechanisms implemented in application software may be redundant.

The aim of diversification is not to reduce the number of systematic failures in unit A, resp. unit B, but the goal is to minimize the mutual dependence (Figure 7b). This minimization is achieved by the fact that existing systematic failures do not affect the data manipulated in these units in the same way and

at the same time (by acquiring or processing or transforming or storing or transmitting data). In association with diversification, it should be noted that a powerful diagnostic tool in the dual structure presented here is the comparison of data. The larger volume of data that is the subject of the comparison and the frequency of comparison make a greater probability of detecting a failure. Diversification brings the problems of ensuring the compatibility of different sPLCs and with the synchronization requirement to be comparison possible at all. Comparison of output signals only is not considered sufficient.

The ideal situation is shown in Figure 7c, when the interpenetration of systematic failures of unit A and unit B is zero.

3. Conclusion

The use of sPLCs in dual architecture (certified to SIL 3) primarily eliminates random hardware failures. In this way, it is possible to achieve the final SIL of the realized safety functions at level 4.

Fight against the systematic failures can be done best at the embedded software level. Due to the fact that the embedded software is fixed from the user's point of view, the use of sPLC from two different manufacturers and the subsequent application of discrepancy diagnostics may be a suitable solution. Discrepancy diagnostics must be focused on a thorough comparison of internal states, memory states, etc.

Manufacturers of the sPLCs certified to SIL 4 are already starting to appear (e.g. HIMatrix product from the HIMA Company [16]). However, such products are rare and their use is precisely limited to a particular area of application. It can be assumed that in the future, the development of sPLCs will be aimed at increasing their safety and expanding their application possibilities.

Conflict of Interest

The authors declare no conflict of interest.

Acknowledgment

References

[1] K. Rástočný, J. Ždánsky, J. Hrbček, "The problems related to realization of safety function with SIL4 Using PLC," in Proceedings of the 30th International Conference on Cybernetics and Informatics, K and I 2020, Institute of Electrical and Electronics Engineers Inc., 2020, doi:10.1109/KI48306.2020.9039878.

[2] EN 61508 - European Standards, Functional Safety of Electrical/ Electronic/Programmable Electronic Safety-Related Systems, 2010.

[3] 1sig - Zabezpečovací systémy pro železnice, tramvaje a metro, První Signální, a.s.

[4] Schneider Electric - Orbus Hardwired Safety Systems, Schneider Electric Global.

[5] Pilz - Automation solution in the railway industry, Pilz GmbH & Co. KG.

[6] EN 50129 - European Standards, Railway Application. Communication, Signalling and Processing Systems. Safety-Related Electronic Systems for Signalling, 2018.

[7] EN 62061 - European Standards, Safety of Machinery – Functional Safety of Safety-Related Electrical, Electronic and Programmable Electronic Control Systems, 2016.

[8] EN 50578 - European Standards, Railways Applications. Direct Current Signalling Relays, 2013.

[9] J. Ždánsky, K. Rástočny, J. Hrbček, "Influence of architecture and diagnostic to the safety integrity of SRECS output part," International Conference on Applied Electronics, **2015**–**Octob**, 297–301, 2015.

[10] K. Rástočný, J. Ždánsky, J. Balák, P. Holečko, "Diagnostics of an output interface of a safety-related system with safety PLC," Electrical Engineering, **99**(4), 1169–1178, 2017, doi:10.1007/s00202-017-0624-1.

[11] A.H. Naghshbandy, H.M. Shanechi, A. Kazemi, I. Pourfar, "Study of fault location effect on the inter-area oscillations in stressed power systems using modal series method," Electrical Engineering, **92**(1), 17–26, 2010, doi:10.1007/s00202-010-0154-6.

[12] W. Velten-Philipp, M.J. Houtermans, "The effect of diagnostic and periodic proof testing on the availability of programmable safety systems," WSEAS Transactions on Systems, **5**(8), 1861–1867, 2006.

[13] J.C. Urresty, J.R. Riba, L. Romeral, J.A. Ortega, "Mixed resistive unbalance and winding inter-turn faults model of permanent magnet synchronous motors," Electrical Engineering, **97**(1), 75–85, 2014, doi:10.1007/s00202-014-0316-z.

[14] M. Moujahed, H. Ben Azza, K. Frifita, M. Jemli, M. Boussak, "Fault detection and fault-tolerant control of power converter fed PMSM," Electrical Engineering, **98**(2), 121–131, 2016, doi:10.1007/s00202-015-0350-5.

[15] K. Rástočný, J. Ždánsky, M. Franeková, I. Zolotová, "Modelling of diagnostics influence on control system safety," Computing and Informatics, **37**(2), 457–475, 2018, doi:10.4149/cai_2018_2_457.

[16] HIMatrix - The Compact Safety Solution, HIMA Paul Hildebrandt GmbH.

Prioritization of Sustainable Supply Chain Management Practices in an Automotive Elastomer Manufacturer in Thailand

Saruntorn Mongkolchaichana, Busaba Phruksaphanrat*

Thammasat University Research Unit in Industrial Statistics and Operational Research, Industrial Engineering Department, Faculty of Engineering Thammasat University, Pathum-thani, 12121, Thailand

A B S T R A C T

Nowadays the sustainable awareness trend is increasing. The consumers' attitude has changed, causing companies to pay more attention to management in a sustainable way. Effective sustainable supply chain management (SSCM) can increase social, economic, and environmental benefits. Important factors from literatures were gather and organized to be a framework for SSCM. The proposed framework incorporates the whole supply chain for both internal and external activities, which can be applied to a manufacturer. The case study factory, which is an automotive elastomer producer has planned to adopt SSCM, so it needs to know the main factors for its operations. Logarithmic fuzzy preference programming method (LFPP) was used to rank SSCM criteria. The results of ranking important criteria showed that external factors (government and competition) were the most significant criteria that the factory has determined. Government and competitors are significant drivers that initiate the company to implement SSCM. Regulations and standards were good guidelines to SSCM for the factory. Next, the Triple Bottom Line (TBL) criteria (social, economic, environment) were considered in the overall operations. Not only concerning about cost and profit, but also environmental effect and social responsibility are cooperated. Finally, internal factors (supplier, consumption, and company) were considered with low level of importance. The proposals of actions of the company were also shown as a guideline for a manufacturer.

1. Introduction

This paper is an extension of work of a similar concept presented initially in the ICIEA 2019 conference [1]. The previous work considered the criteria for green supply chain management (GSCM), while the current work extended the scope to sustainable supply chain management (SSCM). In this research, the main criteria for SSCM were collected and organized to be a new framework for an automotive elastomer factory [1–4].

The evolution of process flow management from raw materials to finished goods is known as supply chain management (SCM). SCM plays an important role in any organization's success. However, there are many operations in the supply chain, which cause environmental impact to the social communities. The concept of sustainability has gained increased popularity due to

the increase in environmental problems. Organization's management strategies have to improve and adjust to the current world situation for survival and friendly environment by not destroying the environment and not harming social communities. The use of environmentally friendly raw materials in the most effective way is one of the interesting practices [5]. Moreover, the participation of communities by corporate social responsibility (CSR) activities or developing community projects, helps to ensure the longevity of the organization.

SSCM is effective management that considers economic, environmental, and social performances at the same time in the supply chain. The basic aim of GSCM is to eliminate all wastes within the industrial system and limit use of hazardous substances. The aims of SSCM concern not only profit but also environmental and social dimensions, called a Triple Bottom Line (TBL). Companies must consider environmental effects from

processes in the supply chain such as purifying the toxic water or air emitted by the manufacturing process before releasing it to the environment to maintain good health in the community [6]. There are many pieces of research on case studies of SSCM. Some of them consider the specific operation in the supply chain such as supplier selection, reverse logistics, packing, etc [7–9]. However, the overall framework for SSCM for a supply chain needs to be clarified and important factors also need to be highlighted.

SSCM has various factors that affect the operations, which differ in each organization; also, the levels of action within each organization need to be considered differently too. Sari (2017) recommended considering inbound operations, production operations, outbound operations, and reverse logistics as primary criteria for the decision making in GSCM practices [10]. Uygun and Dede (2016) suggested a green design, green purchasing, green transformation, green logistics, and reverse logistics criteria. These activities are mainly concerned with environmental awareness [11]. Wu et al. (2020) and Mastrocinque et al. (2020) considered TBL as primary criteria throughout the SCM [12,13]. These criteria need to prioritize and formulate appropriate internal management strategies to achieve more benefit for the stakeholders in the most efficient way.

Multi-criteria decision making (MCDM) method is one of the most commonly used methods for ranking [14]. There are many methods of MCDM such as Analytical Hierarchy Process (AHP), Fuzzy Set Theory, Case-based Reasoning, Data Envelopment Analysis (DEA), Simple Multi-Attribute Rating Technique, Goal Programming, Simple Additive Weighting (SAW), and Technique for Order of Preference by Similarity to Ideal Solution (TOPSIS) [15,16]. However, in evaluation criteria, the decision-maker may not be able to precisely decide the value for the decision, so the fuzzy set concept was proposed [17]. Then, many fuzzy methods for prioritization were presented [18]; these include the logarithmic least-squares method, geometric mean method, extent analysis method, lambda-max method, fuzzy preference programming method (FPP), linear goal programming method, and logarithmic fuzzy preference programming method (LFPP). Nevertheless, these methods still have some pitfalls to avoid [19–21]. The LFPP method has been chosen in this research to prioritize the criteria for three main reasons. The first reason is realistic computation; there is not an argument about this method from literature reviews. The second reason is that the data's consistency can be calculated, and can be re-evaluated over a short evaluation time. Finally, LFPP can maintain Saaty's AHP assessment rules in all aspects.

In this research, a case study of an automotive elastomer manufacturer was studied. Currently, the case study factory has already applied GSCM, but the management team desire to get a higher level of consideration about sustainability to survive in rapidly changing societies. The new goal of the factory is to implement SSCM in order to focus on social, economic, and environmental aspects. So, the main criteria that influence SSCM implementation should be investigated initially. A new framework of SSCM for the factory is presented. The

organization's main objective is to achieve the lowest internal costs (the most profitable) and the least impact on the environment (using environmentally friendly raw materials and the most efficient use) to ensure that the product is green before releasing it to the market and consumers. Criteria were used to construct a new framework composed of SSCM factors for both internal and external factors, it can be used with any factory. All critical factors are integrated into the framework, which can satisfy the qualified policy of the factory. This research aims to prioritize the important criteria that affect the SSCM of the case study factory by use of LFPP, so that the factory can know which criteria should be emphasized and invested firstly. Then, the goals and direction can be clearly set. The proposals of actions of the factory also present in this research.

This research is organized as follows: Section 2 mentions the definition of SSCM and the detail about SSCM activities involved in the operations. Relevant literature was reviewed to determine the important criteria for SSCM of the case study. Section 3, calculation procedure by LFPP method is discussed. Section 4, the results from prioritization of the important criteria that affect the SSCM in this case study are deliberated. Conclusion, discussion, and future research are presented in section 5.

2. Sustainable Supply Chain Management

SSCM is an extension of GSCM, which mainly focuses on environmental, economic, and social dimensions [7]. These three dimensions are related to the Triple Bottom Line (TBL) principles [22], in which the perspectives are focused on the achievement and success of an organization in the economy, environment, and society as shown in Figure 1. They are the key to success of sustainable development, which needs to be balanced [13,22,23].
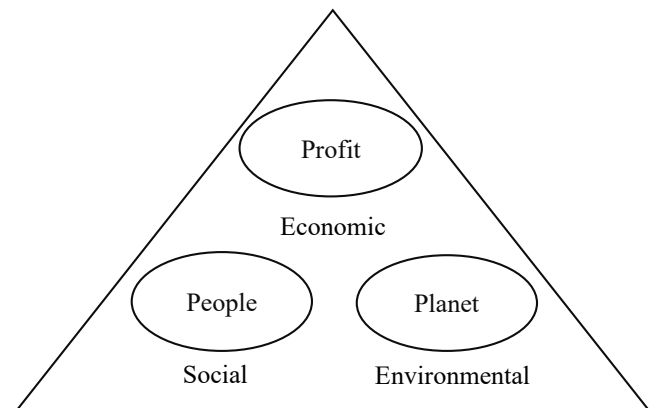
Figure 1: Triple bottom line for SSCM [24]

The objective of the organization previously only focused on profit, which cannot maintain sustainability. Many companies have turned to concern about people, societies, stakeholders, planet, and environmental responsibility. The TBL-based business aim is not only high profit, but also more consideration about the social and environmental problems. TBL shows profit at the top of the triangle. It is an economic dimension that almost all organizations desire.

The concept of people or humans in TBL is to emphasize fair business practices to the communities, employees, and societies by not causing harm to workers and people in the communities, but at the same time, the business has to make a profit for shareholders. Moreover, fair trade must be performed for the people dimension to balance with a social perspective.

Planet or natural dimension means a business should support sustainability and the diversity of the environment. The operations of the company must produce as little waste as possible from resources and must use recycling methods and reduce toxic gas and wastes to secure the environment and biodiversity, so the planet dimension is identical with an environmental perspective.

2.1. Sustainable activities

SSCM has comprehensive activities throughout the workflow processes. SSCM activities must care about social, economic, and environmental dimensions at the same time. These three perspectives incorporated with administrative activities start from planning strategies through to reverse logistics activities. They are described as follows:

- Sustainable strategy and planning: Strategic planning by top management is essential for organizations' initiative to improve and change [25]. If there is no strategic planning or goal setting, there is no direction that makes people understand the management intent [29, 30]. The implementation of SSCM defines the company's goal to sustainability, in which everyone should adhere to the three perspectives: social, economic, and the environment in all operations.

- Sustainable design: The design is not only for recyclable packaging or readily biodegradable products [8,28,29]; SSCM's sustainability design goes beyond that. Green design is a comprehensive design across SCM that is the best starting point for green purchasing, green production, green packaging, and green logistics. In recent years, biodegradable materials from renewable natural resources have received extensive government support.

- Sustainable purchasing: The purchasing managers need to be aware of sustainable raw materials that have to be compared among suppliers. There are many factors to be concerned about, which are cost, delivery, quality, environmentally friendly products, and value. Besides, the company also has the freedom to choose suppliers and avoid bribery from suppliers [7].

- Sustainable production: The production process design has many points to consider [8], such as a suitable location for machinery to reduce energy consumption or less fuel consumption and to get the best performance, type of source of energy, the amount of waste produced by the production [30].

- Sustainable packaging: The essential feature of product packaging is the ability to protect products from contamination damage, and deterioration. The packaging design may include special techniques to make good quality packaging, which is designed according to the 3R theory, which is recyclable (the product can be modified and reuse),

reduce (reduce the use of raw materials in the production of packaging or the product itself), and reuse (the product or packaging can be reused). Also, packaging design should be easily disassembled for digestibility and create as low waste material percentage as possible [8,28,30]. Moreover, biodegradable packaging is also a favorite choice for manufacturers.

- Sustainable logistics: The green logistics design process has many points to consider, such as the design of the distribution route for the most efficient transportation, the minimization of the number of trips [31,32], the reduction of transport cost, the volume of the empty return transport called backhauling [33], the selection of transport vehicles to reduce CO_2 emissions that cause environmental impact [34], the selection of third-party logistics service providers [35], the warehouse design for convenient loading and unloading of products without congestion, and the reduction of waiting time and administrative costs [28]. If sustainable logistics can be applied, it can cover three perspectives, which are social perspectives such as management of traffic congestion, economic perspective by reducing the transportation cost and transportation fuel consumption, and environment perspective by reducing the number of transportation trips and distances to reduce the greenhouse gas emission.

- Sustainable consumption: Determine how to consume the raw materials in the right way to minimize the processes that bring environmental pollution. The instructions must be written in words that are easily understood. The company must analyze consumer trends, consumer characteristics [36], customer green preference [37,38], and consumer purchase behavior [39] of the new generation of people who are becoming increasingly influential in the global green and sustainable market [40].

- Sustainable reverse logistics: Due to the increasing environmental impact today, various industries need more control over the amount of waste from the production processes [9]. Controlling waste is a waste management process that needs to delve into great detail to achieve the most efficient reduction in pollution and use resources efficiently [28]. Therefore, setting up a waste center is needed to receive the used products to facilitate consumers and initiate reverse logistics to be more successful [40].

2.2. Sustainable criteria for implementation

Every activity consists of essential components; for example, green purchasing has a vital role in choosing which supplier is suitable to deliver material that satisfies the company's qualification standards. Therefore, a review of the critical criteria that directly affect SSCM activities must be compiled to cover all management practices. In the previous work, the guidelines for GSCM were proposed [1]. There are 6 criteria: government, competitor, social, supplier, customer, and company to prioritize the criteria that are important to GSCM. Further pieces of literature have proposed more criteria for SSCM. These criteria can be incorporated to construct the SSCM framework for defining an action plan as shown in Table 1.

Table 1: The main criteria for SSCM implementation.

Criteria	company	supplier	competition	consumption	government	social	economic	environment
[2]	✓	✓	✓	✓	✓	✓	✓	✓
[3]	✓	-	-	-	-	✓	✓	✓
[4]	✓	✓	✓	-	-	✓	✓	✓
[5]	✓	-	✓	✓	✓	✓	✓	✓
[8]	✓	-	-	-	✓	✓	✓	✓
[13]	✓	-	-	-	✓	✓	✓	✓
[26]	✓	-	✓	-	-	-	-	✓
[27]	✓	✓	-	✓	✓	-	✓	-
[29]	✓	✓	-	-	-	-	✓	✓
[41]	✓	✓	-	✓	-	-	-	-
[42]	✓	-	-	-	-	✓	✓	✓
[43]	✓	-	✓	✓	-	-	✓	-
[44]	✓	✓	-	✓	-	-	-	✓
[45]	✓	✓	-	✓	✓	-	-	✓
[46]	✓	-	-	-	-	-	-	✓
[47]	✓	-	-	-	✓	✓	✓	✓
[48]	✓	✓	✓	✓	-	-	-	✓
[49]	✓	-	-	-	-	✓	-	✓
[50]	✓	✓	-	-	-	✓	✓	✓
[51]	✓	✓	✓	-	✓	✓	✓	✓
[52]	✓	✓	-	-	-	-	✓	-
[53]	✓	✓	-	-	-	-	✓	✓
[54]	✓	-	-	✓	✓	-	✓	-

There are 8 main criteria related to SSCM; company, supplier, competition, consumption, government, social, economic, and environment.

2.3. The sustainable supply chain management framework

In the past, the SCM of an organization was not complicated and consisted of a few stakeholders. Most companies focused on developing economic efficiency, such as technical quality development, reducing cost, and improving delivery performance. However, today, business operations are more complicated, leading to a broader range of stakeholders [55]. Supply chain activities are transformed into a complicated network model [56]. The suppliers, manufacturers, distributors, and logistic providers

must work together to enhance their competitiveness. Meanwhile, other stakeholders such as consumers, investors, employees, and society pressure the manufacturers to be concerned about social and environmental issues that affect them. Therefore, nowadays organizations have adopted a sustainable development approach to their SCM [6,33], which considers whole parts of the operation throughout the supply chain known as SSCM. SSCM helps the organization to reduce the risk rate and enhances the competitiveness of the business. Promoting good corporate governance throughout the life cycle of products and services can improve environmental performance, social performance, operations performance, and competitiveness of an organization [57].
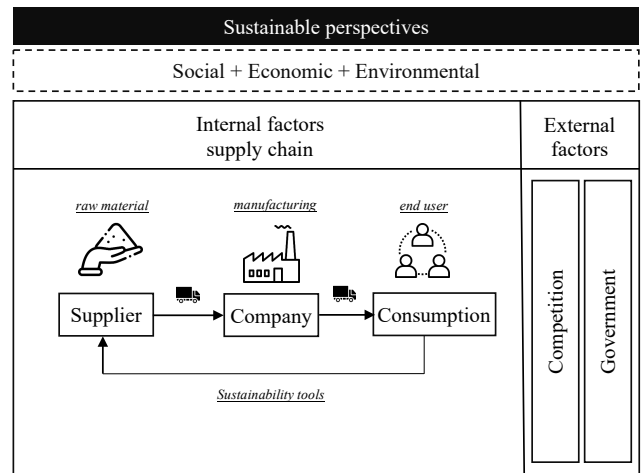
Figure 2: A framework of an SSCM for a manufacturer

A new framework of an SSCM is proposed in this research as shown in Figure 2. It consists of three parts. The first part is external factors, referring to surrounding factors that can indirectly affect the corporate supply chain, which are competition and government. The second part is internal factors, referring to the composition of the main parts of the supply chain, which start from supplier, to company, and end at consumption. Next, the TBL consists of environmental, social, and economic aspects. They are the basis for sustainability. Sustainability tools can be applied to the framework to support the implementation. Whitehead et al. (2020) proposed the tools, which consist of 3 groups; tools for action, tools for analysis and evaluation, and tools for communication [58]. It is also summarized tools and approaches for sustainability, which are cradle to cradle, GSCM, life cycle analysis (LCA), eco-design, reverse logistics, design for environment (DFE), Quality Function Deployment (QFD) for the environment, sustainable value analysis tool (SVAT), sustainability balanced scorecard (SBSC), corporate social responsibility (RSC) and sustainable value stream mapping (Sus-VSM) [59]. These sustainability tools can help an organization's supply chain to achieve successful SSCM. Criteria based on the framework are summarized in Figure 3. They can be described as follows.

Government is the criterion related to enacting laws to enforce and setting standards or regulations that industrial factories must follow. Government criterion is divided into two parts: enforcement of laws or policies and recommendations for

manufacturers from the government. Industries must follow the government laws; if any factory fails to follow the laws, there are penalties. Policies and recommendations from the government might be disregarded if the company is not willing to implement them. It depends on the individual organization's willingness or the opinions of executives within the organization. Many policies require action and enforcement that a business may select by itself or by the government. The role whereby a government can facilitate sustainability will depend on its authority which is different in each country. For example, a government with strong political leaders may generate models which benefit the local community and focus on supporting economic growth. In welfare-state models, the government provides services to firms and nonprofit organizations or takes on social-economic development [60]. Manufacturers determine their profit and level of energy efficiency. The government has sustainable goals that relate to saving energy, seeking profit, and increasing social welfare. Therefore, sustainability is a fundamental issue for both organizations and the government [61].

Competition in the market is one of the critical factors. Competition may be in the form of price, quality, variety of products, responsiveness, or environmental awareness, etc. In the case of SSCM implementation, social trends and substitute goods can affect consumers in making a decision. The organization should be concerned about the market trend to adapt to the competitive market. If the organization does not become active or is slow to adjust to consumption flow, it will lose market share. Competition in each type of market is different. Every organization needs fair competition as an ideal, but in the real situation, it may not be. Therefore, the rapid change of the organization is an advantage and benefit for the organization. The company's choices can affect the decisions of the firm's competitors. The firm invests in sustainability only if it can gain more revenue or reduce cost [62].

Economic sustainability has been defined as gaining more income and stability for society. In the current situation, an economy which does not disturb natural, social, and human societies is needed for sustainability [63]. If the current situation of the economy is getting worse, the investment in SSCM operations will be debated at management board level, and the SSCM operations may be delayed. On the other hand, if the economy is good, a high profit from operations or good cash flow may allow an organization to be able to start SSCM operation quickly. Moreover, the policy formulation from the government is an important factor. For example, if the government requires less tax on the green product, the product price will not be high, it will generate more incentives for consumption and produce more profit. The organization also wants to make more of the products that are best-sellers in the market. All the above result from the first criterion, which is government.

The social factor has direct and indirect effects on SSCM that start with employees on the production line. If the organization has sustainable production management, such as equipped with technology to optimize the use of resources as needed and get the most efficient outputs, minimize energy consumption and air polluting emissions [64], employees do not have the risk of direct exposure to volatile chemicals during production, production accidents will be reduced and the operators of manufacturing plant should have a good quality of life as well. Furthermore, supposing the organization has a policy to apply CSR, it will benefit the surrounding communities. The government is very important in supporting the policy by reducing tax for industrial factories that implement CSR [65, 66], which makes companies willing to undertake CSR projects.

The environment is related to various problems concerning pollutants from water [67], air, and other wastes from factories, which create increasing problems. Reduction of CO_2 emissions, energy consumption [71, 72] and wastes from the processes, products, packaging, and any substances that can increase the world's temperature, are critical issues. Different environmental regulations have started to emerge and be proposed to companies by governments. Companies must comply with environmental legislation existing in each country. Moreover, standards related to environmental consideration are one of the effective tools for the company to apply.

Selecting suppliers that market environmentally friendly raw materials without affecting the surrounding communities can help when implementing SSCM. However, this criterion is difficult to apply in order to make a significant impact on SSCM because organizations cannot enforce or control all suppliers, so choosing a supplier is yet another option in implementing SSCM within the organization. The selection of suppliers requires several factors to be considered [22, 70]. The key principles are the high quality of raw materials, reasonable prices, and on-time delivery.

Consumption can take place only if consumers are more aware of the environment and communities. The eco-label campaign is part of the approachability that can greatly appeal to consumers who are passionate about green consumption. Using its features is an important selling point. Currently, the consumer has a greater preference for healthy and environmentally friendly products [71]. Consumer perspective in sustainability is the driver for a company in the caring economy [72].

The company, including the management team, realize that the operation of SSCM requires a budget for investment [62]. Furthermore, employees within the organization have to adjust to the work with more responsibilities [73]. They must also cooperate to achieve the company strategic goal of SSCM. Moreover, organizations should provide support such as services, knowledge, information, training and facilities for them to achieve efficiency and effectiveness as soon as possible.

Criteria	
Company • Information • Top management support and motivation • Process /System operation • Strategy and goal • Incentives and rewards • Reputation loss • Business characteristics • Organizational culture • Innovation	**Government** • Laws / Regulation / Standard • Government support • Disposal green policies • Environmental policies of government • Transparency • Pressure
Supplier • Raw material use (material toxicity and chemicals) • Trade groups • Certification	**Social** • Communities • Corporate social responsibility
	Economic • Cost and benefit • Tax on green product • Production cost
Consumption • Green image • Green product • Consumers' characteristics • Reverse logistics • Feedback	**Environment** • CO_2 emission • Risk management • Pollution prevention • Energy reduction • Waste reduction
Competition • Market segment • Product pricing • Competitive advantage • Fair competition	

3. Logarithmic fuzzy preference programming method

Wang and Chin (2011) have proposed a logarithmic fuzzy preference programming method (LFPP) for finding the weight to prioritize the fuzzy number by comparing pairs of the dataset from the decision matrix [74]. The basis of this method was developed from the FPP method of Mikhailov (2004) by using nonlinear functions computation to find the weight with the following [75]:

$$ln\ \tilde{a}_{ij} \approx (ln\ l_{ij}, ln\ m_{ij}, ln\ u_{ij}), i,j = 1,..., n. \quad (1)$$

where $\tilde{a}_{ij}$ is an approximate triangular fuzzy number.

The membership function is shown below.

$$ \mu_{ij}\left(ln\left(\frac{w_i}{w_j}\right)\right) = \begin{cases} \dfrac{ln\left(\frac{w_i}{w_j}\right) - ln\ l_{ij}}{ln\ m_{ij} - ln\ l_{ij}}, ln\left(\frac{w_i}{w_j}\right) \leq ln\ m_{ij} \\ \dfrac{ln\ u_{ij} - ln\left(\frac{w_i}{w_j}\right)}{ln\ u_{ij} - ln\ m_{ij}}, ln\left(\frac{w_i}{w_j}\right) \geq ln\ m_{ij} \end{cases} $$

$$(2)$$

$\mu_{ij}(ln\ (w_i/w_j))$ is a membership of function $ln\ (w_i/w_j)$ belonging to the approximate triangular fuzzy judgment $ln\ \tilde{a}_{ij}$. A crisp priority vector to maximize the minimum membership degree $\lambda = min\{\mu_{ij}(ln(w_i/w_j)) \mid i = 1,…, n - 1; j = i + 1,.., n\}$. The subsequent model can be constructed as

Maximize λ

$$ \text{Subject to} \begin{cases} \mu_{ij}\left(ln\left(\frac{w_i}{w_j}\right)\right) \geq \lambda, i = 1,…,n-1; j = i+1,…,n, \\ w_i \geq 0, i = 1,…,n, \end{cases} $$

$$(3)$$

or as

Maximize 1 - λ

$$ \text{Subject to} \begin{cases} ln\ w_i - ln\ w_j - \lambda ln(m_{ij}/l_{ij}) \geq ln\ l_{ij}, \\ -ln w_i + ln w_j - \lambda ln(u_{ij}/m_{ij}) \geq -ln u_{ij}, \\ i = 1,…,n-1; j = i+1,…,n, \\ w_i \geq 0, i = 1,..,n. \end{cases} $$

$$(4)$$

To avoid λ from taking a negative value, Wang and Chin (2011) proposed nonnegative deviation variables δ_{ij} and η_{ij} for $i = 1,…,n-1$ and $j = i + 1,…, n$ such that they meet the following inequalities:

$\ln w_i - \ln w_j - \lambda\ln(m_{ij}/l_{ij}) + \delta_{ij} \geq \ln l_{ij}$, $i = 1,…, n - 1; j = i + 1,…, n$,

$- \ln w_i + \ln w_j - \lambda\ln(u_{ij}/m_{ij}) + \eta_{ij} \geq - \ln u_{ij}$, $i = 1,…, n - 1; j = i + 1,…, n$.

Then, the model to maximize the minimum membership degree becomes

MODEL: LFPP

$$Minimize J = (1 - \lambda)^2 + M \cdot \sum_{i=1}^{n-1} \sum_{j=i+1}^{n} \left(\delta_{ij}^2 + \eta_{ij}^2\right)$$

$$Subject\ to \begin{cases} x_i - x_j - \lambda ln\ (m_{ij}/l_{ij}) + \delta_{ij} \geq ln l_{ij}\ , \\ \quad i = 1,…, n - 1; j = i + 1,…, n, \\ -x_i + x_j - \lambda ln\ (u_{ij}/m_{ij}) + \eta_{ij} \geq -ln u_{ij}\ , \\ \quad i = 1,…, n - 1; j = i + 1,…, n, \\ \lambda, x_i \geq 0, i = 1,…, n, \\ \delta_{ij}, \eta_{ij} \geq 0, i = 1,…, n - 1; \\ \quad j = i + 1,…, n, \end{cases}$$

(5)

Let $x_i = ln\ w_i$ for $i = 1,…, n - 1$,

M is a large constant value, x_i^* is an optimal solution, λ is a membership degree, δ_{ij}, η_{ij} are nonnegative deviation variables for $i = 1,…, n-1$ and $j = i + 1,…, n$ and

$l_{ij} = 1/u_{ji}, m_{ij} = 1/m_{ji}, u_{ij} = 1/l_{ji}$ and $0 < l_{ij} \leq m_{ij} \leq u_{ij}$ for all $i,j = 1,. . .,n; j - i$.

Normalize the value of x_i^* and sorting fuzzy pairwise comparison matrices by (6)

$$w_i^* = exp(x_i^*)/ \sum_{j=1}^{n} exp(x_i^*), i = 1,…, n. \qquad (6)$$

where $exp(\ )$ is the function of exponential for which the calculation is $exp(x_i^*) = e^{x_i^*}$ for $i = 1,…, n$.

w_i^* is the weight of each criterion from $i = 1,…, n$.

The following equation is used to check the consistency of data.

$$l_{ij} \leq w_i/w_j \leq u_{ij}, i = 1,…, n-1, j = i + 1,…, n. \qquad (7)$$

4. Prioritizing of SSCM criteria for the case study

The SCM process of an automotive elastomer manufacturer has a flow chart as shown in Figure 2. The supply chain flow process begins with the purchasing process, where sources of the best raw materials for the company such as a polymer, fillers, softeners, and other additives are procured. A supplier who has the lowest cost, which high-quality products and delivery on time was selected. After receiving raw materials, the production is done according to production planning. After the products are finished and pass the quality inspection, they are transferred to the packing process. Then, finished goods are delivered to customers.

There are environmental concerns in all of the above activities, which need to be reviewed through three aspects: social, economic, and environmental. These processes are internal factors of the SCM. Additionally, the process would not be complete if it did not take the external factors into account. The external factors are competitors and the government. The competition between the companies is considered in terms of price, quality, strategies, and market share. Also, the company needs to follow the laws and regulations of the government. However, the government also provides support to the company to reach international standards. The three sustainable perspectives are integrated with both internal and external factors. The company can control all processes by setting the procedures for each aspect by using sustainability tools that can help an organization's supply chain to achieve successful SSCM.

The automotive elastomer manufacturer has decided to apply SSCM in the company, so the importance of each criterion needs to be clarified. Then, everyone in the company can move in the same direction emphasizing the critical criteria. Eight criteria in the previous section were considered and ranked. A fuzzy decision matrix was constructed and evaluated by five experts who are key men in the factory: the procurement supervisor, planning supervisor, quality control supervisor, production engineer, and research and development engineer who has worked in this company for more than 10 years. The decision matrix is shown in Table 2. Model in equation (5) for this fuzzy pairwise comparison matrix can be written as

$$Minimize\ J = (1 - \lambda)^2 + M \cdot \sum_{i=1}^{7} \sum_{j=i+1}^{8} \left(\delta_{ij}^2 + \eta_{ij}^2\right)$$

$$Subject\ to \begin{cases} x_1 - x_2 - \lambda \ln\left(\frac{0.35}{0.26}\right) + \delta_{12} \geq \ln(0.26), \\ -x_1 + x_2 - \lambda \ln\left(\frac{0.57}{0.35}\right) + \eta_{12} \geq -\ln(0.57), \\ x_1 - x_3 - \lambda \ln\left(\frac{0.34}{0.24}\right) + \delta_{13} \geq \ln(0.24), \\ -x_1 + x_3 - \lambda \ln\left(\frac{0.46}{0.34}\right) + \eta_{13} \geq -\ln(0.46), \\ x_1 - x_4 - \lambda \ln\left(\frac{1.52}{0.80}\right) + \delta_{14} \geq \ln(0.80), \\ -x_1 + x_4 - \lambda \ln\left(\frac{2.41}{1.52}\right) + \eta_{14} \geq -\ln(2.41), \\ \quad\quad\quad\quad \vdots \\ x_7 - x_8 - \lambda \ln\left(\frac{2.09}{0.99}\right) + \delta_{78} \geq \ln(0.99), \\ -x_7 + x_8 - \lambda \ln\left(\frac{3.19}{2.09}\right) + \eta_{78} \geq -\ln(3.19), \\ \lambda, x_1, x_2, x_3, …, x_8 \geq 0, \\ \delta_{12}, \delta_{13}, \delta_{14}, …, \delta_{78} \geq 0, \\ \eta_{12}, \eta_{13}, \eta_{14}, …, \eta_{78} \geq 0. \end{cases}$$

(8)

Taking a sufficiently large number for M, say M=1000, to solve this model with Lingo 17.0 as shown in Figure 4, the optimal solution can be obtained as

Table 2: Fuzzy comparison matrix of the aggregated weights of the criteria

| Criteria | | C_1 | | | C_2 | | | C_3 | | | C_4 | | |
		Company			Supplier			Competition			Consumption		
C_1	Company	1.00	1.00	1.00	0.26	0.35	0.57	0.24	0.34	0.46	0.80	1.52	2.41
C_2	Supplier	1.74	2.83	3.87	1.00	1.00	1.00	0.29	0.37	0.51	1.25	2.00	3.06
C_3	Competition	2.19	2.93	4.11	1.97	2.69	3.47	1.00	1.00	1.00	1.32	2.05	3.10
C_4	Consumption	0.42	0.66	1.25	0.33	0.50	0.80	0.32	0.49	0.76	1.00	1.00	1.00
C_5	Government	1.55	2.64	3.68	2.76	3.82	4.85	0.49	0.80	1.35	2.30	3.32	4.34
C_6	Social	1.64	2.09	3.13	1.07	1.52	2.22	0.40	0.64	0.94	1.00	1.52	2.46
C_7	Economic	1.43	2.00	5.00	1.05	1.28	2.78	0.45	0.81	1.00	1.01	1.56	2.56
C_8	Environment	1.59	2.94	3.33	1.27	1.61	2.50	0.45	0.66	0.99	1.28	1.79	4.35
Criteria		C_5			C_6			C_7			C_8		
		Government			Social			Economic			Environment		
C_1	Company	0.27	0.38	0.64	0.32	0.48	0.61	0.20	0.50	0.70	0.30	0.34	0.63
C_2	Supplier	0.21	0.26	0.36	0.45	0.66	0.93	0.36	0.78	0.95	0.40	0.62	0.79
C_3	Competition	0.74	1.25	2.05	1.06	1.55	2.49	1.00	1.23	2.21	1.01	1.51	2.22
C_4	Consumption	0.23	0.30	0.44	0.41	0.66	1.00	0.39	0.64	0.99	0.23	0.56	0.78
C_5	Government	1.00	1.00	1.00	1.52	2.27	3.37	1.49	2.07	3.07	1.09	1.98	2.98
C_6	Social	0.30	0.44	0.66	1.00	1.00	1.00	0.98	0.99	1.00	1.01	1.12	1.32
C_7	Economic	0.33	0.48	0.67	1.00	1.01	1.02	1.00	1.00	1.00	0.99	2.09	3.19
C_8	Environment	0.34	0.51	0.92	0.76	0.89	0.99	0.31	0.48	1.01	1.00	1.00	1.00

Figure 4: The result obtained from Lingo 17.0.

$$x_1^* = 0, x_2^* = 0.4656, x_3^* = 1.1459, \dots, x_8^* = 0.5329,$$

$$\delta_{12}^*, \delta_{13}^*, \delta_{14}^*, \dots, \delta_{78}^* = 0,$$

$$\eta_{12}^* = 0.0889, \eta_{13}^*, \eta_{14}^*, \dots, \eta_{78}^* = 0,$$

based on which, normalization of LFPP priorities as

$$w_1^* = \frac{EXP(x_1^*)}{\sum_{i=1}^{8} EXP(x_i^*)} = 0.0620,$$

$$w_2^* = \frac{EXP(x_2^*)}{\sum_{i=1}^{8} EXP(x_i^*)} = 0.0988,$$

$$w_3^* = \frac{EXP(x_3^*)}{\sum_{i=1}^{8} EXP(x_i^*)} = 0.1951,$$

$$\dots,$$

$$w_8^* = \frac{EXP(x_8^*)}{\sum_{i=1}^{8} EXP(x_i^*)} = 0.1057.$$

According to (7), the results of the consistent test found that there were four pairs outside the specified limits: a_{12}, a_{15}, a_{23}, and a_{25}, so the decision-makers needed to reevaluate the pairwise comparison judgment as shown in Table 3.

After reevaluating, weights were found and the importance could be sorted as shown in Table 4 and Figure 5. Lingo 17.0 with Intel (R) Core (TM) i5-3570 CPU @ 3.40GHz RAM 8.00 GB 64-bit was used to calculate weights of each criteria. The total calculation time for weights criteria was 0.06 seconds.

The prioritizing results clearly show that external factors, which are government and competition, are the main criteria for applying SSCM in the factory. Then, the economic, social, and environment criteria, which are TBL factors for sustainability, are considered. Their weights are similar which means that the emphasis of the factory on TBL is balanced. Finally, supplier, consumption, and company, which are internal factors have lower weightings.

Table 3: Reevaluate fuzzy comparison matrix

Criteria		C_1 Company			C_2 Supplier			C_3 Competition			C_4 Consumption		
C_1	Company	1.00	1.00	1.00	0.26	0.35	0.65	0.24	0.34	0.46	0.80	1.52	2.41
C_2	Supplier	1.54	2.83	3.87	1.00	1.00	1.00	0.29	0.37	0.52	1.25	2.00	3.06
C_3	Competition	2.19	2.93	4.11	1.92	2.69	3.47	1.00	1.00	1.00	1.32	2.05	3.10
C_4	Consumption	0.42	0.66	1.25	0.33	0.50	0.80	0.32	0.49	0.76	1.00	1.00	1.00
C_5	Government	1.55	2.64	4.55	2.50	3.82	4.85	0.49	0.80	1.35	2.30	3.32	4.34
C_6	Social	1.64	2.09	3.13	1.07	1.52	2.22	0.40	0.64	0.94	1.00	1.52	2.46
C_7	Economic	1.43	2.00	5.00	1.05	1.28	2.78	0.45	0.81	1.00	1.01	1.56	2.56
C_8	Environment	1.59	2.94	3.33	1.27	1.61	2.50	0.45	0.66	0.99	1.28	1.79	4.35
Criteria		C_5 Government			C_6 Social			C_7 Economic			C_8 Environment		
C_1	Company	0.22	0.38	0.64	0.32	0.48	0.61	0.20	0.50	0.70	0.30	0.34	0.63
C_2	Supplier	0.21	0.26	0.40	0.45	0.66	0.93	0.36	0.78	0.95	0.40	0.62	0.79
C_3	Competition	0.74	1.25	2.05	1.06	1.55	2.49	1.00	1.23	2.21	1.01	1.51	2.22
C_4	Consumption	0.23	0.30	0.44	0.41	0.66	1.00	0.39	0.64	0.99	0.23	0.56	0.78
C_5	Government	1.00	1.00	1.00	1.52	2.27	3.37	1.49	2.07	3.07	1.09	1.98	2.98
C_6	Social	0.30	0.44	0.66	1.00	1.00	1.00	0.98	0.99	1.00	1.01	1.12	1.32
C_7	Economic	0.33	0.48	0.67	1.00	1.01	1.02	1.00	1.00	1.00	0.99	2.09	3.19
C_8	Environment	0.34	0.51	0.92	0.76	0.89	0.99	0.31	0.48	1.01	1.00	1.00	1.00

Table 4: Comparison result for reevaluate

Criteria		Weight
C_5	Government	0.2314
C_3	Competition	0.1811
C_7	Economic	0.1337
C_6	Social	0.1336
C_8	Environment	0.1150
C_2	Supplier	0.0885
C_4	Consumption	0.0628
C_1	Company	0.0539
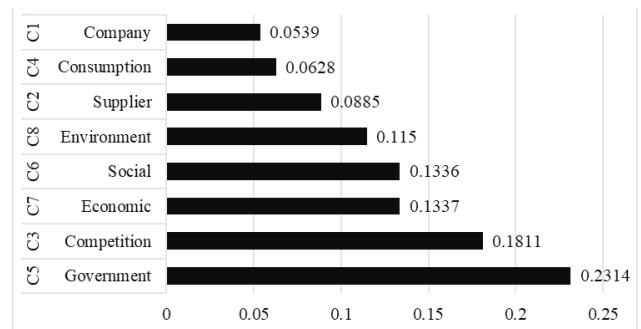
Figure 5: SSCM criteria weights

External pressures from the government and competitors' impact on SSCM for the automotive elastomer manufacturer in Thailand. There are some regulations and laws that control environmental problems that are caused by small particles and hazardous chemicals. The factory has followed the standards of the Ministry of Industry and certified ISO 14001:2015 for many years. The environmental issue is one of the company's strategies. It has an operation plan to protect the environment such as use fewer chemical substances, reduce wastes and pollution, etc. These two factors are very important in leading the factory to the implementation of SSCM.

In the competitive market with rapid change, the factory needs to adjust itself to satisfy the target market, which is the global market. Most of the management team in this factory are foreigners who mainly focus on the global trend. Sustainable awareness for the manufacturer is currently in practice.

The economic issue is important for all profit organizations to survive. However, it should be balanced with social and environment issues. Every project about sustainable management in the factory has to be evaluated by feasibility analysis before implementing it.

The company implemented GSCM before desiring to switch to SSCM, so environmental concerns have existed in almost all of the supply chain. It has been certified to ISO14001:2015 for many years and still keeps track to reduce environmental problems of the factory.

The factory has a policy to select high-quality suppliers. These selected suppliers can help the company to improve the firm's competitiveness across its supply chain. Reasonable price, high quality of raw materials, and fast response are the main factors of the selection. The existing suppliers rarely consider sustainability.

Most customers of the factory are foreign customers, who have less concern about the sustainability of the products. The company products are small parts for automotive manufacturers. Most of the automotive manufacturers are considering clean technology involving combustion in the engine, which is not related to the case study company's products.

The company has the least weight of importance for SSCM. It operates for maximizing profits but the regulations, standards, laws, and stakeholders have forced the company to be concerned not only with profit but also the environment and social issues.

5. Conclusions

This research proposes a framework for SSCM that combines the whole supply chain. It is applied to the case study factory, which is an automotive elastomer producer. Criteria are collected and factors (government and competition), TBL factors (environment, rearranged into the framework, which is suitable for a manufacturer. Three main groups of criteria, which are external social, and economic), and internal factors (supplier, company, and customer) are reviewed. These factors are prioritized by the LFPP method, which has advantages over other methods. Government and competition are the most important criteria for the case study factory that force it to implement SSCM. Laws, regulations, and standards are carefully determined and set for the company to achieve. They are set has the highest priority for the company to achieve. Market and competitors are studied and the operation plan related to these criteria is defined. Environment, social, and economic criteria are the next factors that the factory is concerned about. They are considered to be at the same level of importance, which is balanced according to the concept of SSCM. Profit is still the goal that the factory wants to achieve, but there is also an environmental concern and the certified environmental standard to be satisfied. Moreover, the factory has plans for corporate social responsibility activities with the communities in its action plan. Existing SCM involves suppliers, the company, and customers. They are considered as the less important criteria. The proposals of actions of the case study factory was shown as an example for the other factories.

For future research, the level of SSCM performance in each practice tool should be evaluated to know the efficient tools for the implementation of SSCM.

References

[1] S. Mongkolchaichana, B. Phruksaphanrat, "A Comparison of Prioritization Methods for Green Supply Chain Management Criteria Evaluation," 2019 IEEE 6th International Conference on Industrial Engineering and Applications, ICIEA 2019, (2015), 313–317, 2019, doi:10.1109/IEA.2019.8715191.

[2] S. Seuring, M. Müller, "From a literature review to a conceptual framework for sustainable supply chain management," Journal of Cleaner Production, **16**(15), 1699–1710, 2008, doi:10.1016/j.jclepro.2008.04.020.

[3] C.R. Carter, D.S. Rogers, "A framework of sustainable supply chain management: Moving toward new theory," International Journal of Physical Distribution and Logistics Management, **38**(5), 360–387, 2008, doi:10.1108/09600030810882816.

[4] M. Pagell, Z. Wu, "Building a more complete theory of sustainable supply chain management using case studies of 10 exemplars," Journal of Supply Chain Management, **45**(2), 37–56, 2009, doi:10.1111/j.1745-493X.2009.03162.x.

[5] M. Pakseresht, B. Shirazi, I. Mahdavi, N. Mahdavi-Amiri, "Toward sustainable optimization with stackelberg game between green product family and downstream supply chain," Sustainable Production and Consumption, **23**, 198–211, 2020, doi:10.1016/j.spc.2020.04.009.

[6] S.A.R. Khan, Z. Yu, H. Golpira, A. Sharif, A. Mardani, A state-of-the-art review and meta-analysis on sustainable supply chain management: Future research directions, Journal of Cleaner Production, **278**, 2021, doi:10.1016/j.jclepro.2020.123357.

[7] J. Li, H. Fang, W. Song, "Sustainable supplier selection based on SSCM practices: A rough cloud TOPSIS approach," Journal of Cleaner Production, **222**, 606–621, 2019, doi:10.1016/j.jclepro.2019.03.070.

[8] L. Meherishi, S.A. Narayana, K.S. Ranjani, "Sustainable packaging for supply chain management in the circular economy: A review," Journal of Cleaner Production, **237**, 117582, 2019, doi:10.1016/j.jclepro.2019.07.057.

[9] J. Jemai, B. Do Chung, B. Sarkar, "Environmental effect for a complex green supply-chain management to control waste: A sustainable approach," Journal of Cleaner Production, **277**, 122919, 2020, doi:10.1016/j.jclepro.2020.122919.

[10] K. Sari, "A novel multi-criteria decision framework for evaluating green supply chain management practices," Computers and Industrial Engineering, **105**, 338–347, 2017, doi:10.1016/j.cie.2017.01.016.

[11] Ö. Uygun, A. Dede, "Performance evaluation of green supply chain management using integrated fuzzy multi-criteria decision making techniques," Computers and Industrial Engineering, **102**, 502–511, 2016, doi:10.1016/j.cie.2016.02.020.

[12] C. Wu, Y. Zhang, H. Pun, C. Lin, "Construction of partner selection criteria in sustainable supply chains: A systematic optimization model," Expert Systems with Applications, **158**, 2020, doi:10.1016/j.eswa.2020.113643.

[13] E. Mastrocinque, F.J. Ramírez, A. Honrubia-Escribano, D.T. Pham, "An AHP-based multi-criteria model for sustainable supply chain development

in the renewable energy sector," Expert Systems with Applications, **150**, 2020, doi:10.1016/j.eswa.2020.113321.

[14] X. Yu, S. Zhang, X. Liao, X. Qi, "ELECTRE methods in prioritized MCDM environment," Information Sciences, **424**, 301–316, 2018, doi:10.1016/j.ins.2017.09.061.

[15] M. Alvandi, S. Fazli, L. Yazdani, M. Aghaee, "An Integrated MCDM Method in Ranking BSC Perspectives and key Performance Indicators (KPIs)," Management Science Letters, **2**(3), 995–1004, 2012, doi:10.5267/j.msl.2012.01.024.

[16] M. Velasquez, P. Hester, "An analysis of multi-criteria decision making methods," International Journal of Operations Research, **10**(2), 56–66, 2013.

[17] C. Kahraman, B. Öztayşi, I. Uçal Sari, E. Turanoğlu, "Fuzzy analytic hierarchy process with interval type-2 fuzzy sets," Knowledge-Based Systems, **59**, 48–57, 2014, doi:10.1016/j.knosys.2014.02.001.

[18] R.R. Kumar, S. Mishra, C. Kumar, "Prioritizing the solution of cloud service selection using integrated MCDM methods under Fuzzy environment," Journal of Supercomputing, **73**(11), 4652–4682, 2017, doi:10.1007/s11227-017-2039-1.

[19] S. Kubler, J. Robert, W. Derigent, A. Voisin, Y. Le Traon, "A state-of-the-art survey & testbed of fuzzy AHP (FAHP) applications," Expert Systems with Applications, **65**, 398–422, 2016, doi:10.1016/j.eswa.2016.08.064.

[20] Y.M. Wang, Y. Luo, Z. Hua, "On the extent analysis method for fuzzy AHP and its applications," European Journal of Operational Research, **186**(2), 735–747, 2008, doi:10.1016/j.ejor.2007.01.050.

[21] K. Zhü, "Fuzzy analytic hierarchy process: Fallacy of the popular methods," European Journal of Operational Research, **236**(1), 209–217, 2014, doi:10.1016/j.ejor.2013.10.034.

[22] K. Rashidi, A. Noorizadeh, D. Kannan, K. Cullinane, Applying the triple bottom line in sustainable supplier selection: A meta-review of the state-of-the-art, Journal of Cleaner Production, **269**, 2020, doi:10.1016/j.jclepro.2020.122001.

[23] C.S. Goh, H.Y. Chong, L. Jack, A.F. Mohd Faris, Revisiting triple bottom line within the context of sustainable construction: A systematic review, Journal of Cleaner Production, **252**, 2020, doi:10.1016/j.jclepro.2019.119884.

[24] M.C. Arslan, H. Kisacik, "The Corporate Sustainability Solution: Triple Bottom Line," The Journal of Accounting and Finance, (July), 18–34, 2017.

[25] H.L. Lam, W.P.Q. Ng, R.T.L. Ng, E.H. Ng, M.K.A. Aziz, D.K.S. Ng, "Green strategy for sustainable waste-to-energy supply chain," Energy, **57**, 4–16, 2013, doi:10.1016/j.energy.2013.01.032.

[26] J. Dai, F.L. Montabon, D.E. Cantor, "Reprint of 'Linking rival and stakeholder pressure to green supply management: Mediating role of top management support,'" Transportation Research Part E: Logistics and Transportation Review, **74**, 124–138, 2015, doi:10.1016/j.tre.2014.12.003.

[27] S.M. Lo, S. Zhang, Z. Wang, X. Zhao, "The impact of relationship quality and supplier development on green supply chain integration: A mediation and moderation analysis," Journal of Cleaner Production, **202**, 524–535, 2018, doi:10.1016/j.jclepro.2018.08.175.

[28] Stella Despoudi, Green supply chain, Elsevier Inc., 2020, doi:10.1016/b978-0-12-816449-5.00002-3.

[29] P. Du, X. Yang, L. Xu, Y. Tan, H. Li, "Green design strategies of competing manufacturers in a sustainable supply chain," Journal of Cleaner Production, **265**, 121853, 2020, doi:10.1016/j.jclepro.2020.121853.

[30] M. Kharaji Manouchehrabadi, S. Yaghoubi, J. Tajik, "Optimal scenarios for solar cell supply chain considering degradation in powerhouses," Renewable Energy, **145**, 1104–1125, 2020, doi:10.1016/j.renene.2019.06.096.

[31] L. Ren, S. Zhou, X. Ou, "Life-cycle energy consumption and greenhouse-gas emissions of hydrogen supply chains for fuel-cell vehicles in China," Energy, **209**, 118482, 2020, doi:10.1016/j.energy.2020.118482.

[32] J. hua Zhao, D. lin Zeng, L. ping Che, T. wei Zhou, J. yi Hu, "Research on the profit change of new energy vehicle closed-loop supply chain members based on government subsidies," Environmental Technology and Innovation, **19**, 100937, 2020, doi:10.1016/j.eti.2020.100937.

[33] H. Allaoui, Y. Guo, J. Sarkis, "Decision support for collaboration planning in sustainable supply chains," Journal of Cleaner Production, **229**, 761–774, 2019, doi:10.1016/j.jclepro.2019.04.367.

[34] Y. Cao, Y. Zhao, L. Wen, Y. Li, H. li, S. Wang, Y. Liu, Q. Shi, J. Weng, "System dynamics simulation for CO2 emission mitigation in green electric-coal supply chain," Journal of Cleaner Production, **232**, 759–773, 2019, doi:10.1016/j.jclepro.2019.06.029.

[35] H. Baligil, S.S. Kara, P. Alcan, B. Özkan, E. Gözde Alar, "A distribution network optimization problem for third party logistics service providers," Expert Systems with Applications, **38**(10), 12730–12738, 2011,

doi:10.1016/j.eswa.2011.04.061.

[36] S. Wei, T. Ang, V.E. Jancenelle, "Willingness to pay more for green products: The interplay of consumer characteristics and customer participation," Journal of Retailing and Consumer Services, **45**(June), 230–238, 2018, doi:10.1016/j.jretconser.2018.08.015.

[37] Y. Wang, G. Hou, "A duopoly game with heterogeneous green supply chains in optimal price and market stability with consumer green preference," Journal of Cleaner Production, **255**, 120161, 2020, doi:10.1016/j.jclepro.2020.120161.

[38] X. Zhang, H.M.A.U. Yousaf, "Green supply chain coordination considering government intervention, green investment, and customer green preferences in the petroleum industry," Journal of Cleaner Production, **246**, 118984, 2020, doi:10.1016/j.jclepro.2019.118984.

[39] V. Carfora, C. Cavallo, D. Caso, T. Del Giudice, B. De Devitiis, R. Viscecchia, G. Nardone, G. Cicia, "Explaining consumer purchase behavior for organic milk: Including trust and green self-identity within the theory of planned behavior," Food Quality and Preference, **76**(March), 1–9, 2019, doi:10.1016/j.foodqual.2019.03.006.

[40] D. Chen, J. Ignatius, D. Sun, S. Zhan, C. Zhou, M. Marra, M. Demirbag, "Reverse logistics pricing strategy for a green supply chain: A view of customers' environmental awareness," International Journal of Production Economics, **217**(May 2018), 197–210, 2019, doi:10.1016/j.ijpe.2018.08.031.

[41] H. Gholizadeh, H. Fazlollahtabar, "Robust optimization and modified genetic algorithm for a closed loop green supply chain under uncertainty: Case study in melting industry," Computers and Industrial Engineering, **147**(January 2019), 106653, 2020, doi:10.1016/j.cie.2020.106653.

[42] M. Ramirez-Peña, A.J. Sánchez Sotano, V. Pérez-Fernandez, F.J. Abad, M. Batista, "Achieving a sustainable shipbuilding supply chain under I4.0 perspective," Journal of Cleaner Production, **244**, 2020, doi:10.1016/j.jclepro.2019.118789.

[43] M.A.N. Agi, X. Yan, "Greening products in a supply chain under market segmentation and different channel power structures," International Journal of Production Economics, **223**(October 2019), 107523, 2020, doi:10.1016/j.ijpe.2019.107523.

[44] A.Y. Uemura Reche, O. Canciglieri Junior, C.C.A. Estorilio, M. Rudek, "Integrated product development process and green supply chain management: Contributions, limitations and applications," Journal of Cleaner Production, **249**, 119429, 2020, doi:10.1016/j.jclepro.2019.119429.

[45] T. Hadi, S.K. Chaharsooghi, M. Sheikhmohammady, A. Hafezalkotob, "Pricing strategy for a green supply chain with hybrid production modes under government intervention," Journal of Cleaner Production, **268**(December 2015), 121945, 2020, doi:10.1016/j.jclepro.2020.121945.

[46] P. Gautam, A. Kishore, A. Khanna, C.K. Jaggi, "Strategic defect management for a sustainable green supply chain," Journal of Cleaner Production, **233**, 226–241, 2019, doi:10.1016/j.jclepro.2019.06.005.

[47] A.C. Ng, Z. Rezaee, "Business sustainability factors and stock price informativeness," Journal of Corporate Finance, **64**(June), 101688, 2020, doi:10.1016/j.jcorpfin.2020.101688.

[48] S. Shoukohyar, M.R. Seddigh, "Uncovering the dark and bright sides of implementing collaborative forecasting throughout sustainable supply chains: An exploratory approach," Technological Forecasting and Social Change, **158**(April), 120059, 2020, doi:10.1016/j.techfore.2020.120059.

[49] C.R. Carter, P.L. Easton, "Sustainable supply chain management: Evolution and future directions," International Journal of Physical Distribution and Logistics Management, **41**(1), 46–62, 2011, doi:10.1108/09600031111101420.

[50] S. Seuring, M. Müller, "Core issues in sustainable supply chain management - A Delphi study," Business Strategy and the Environment, **17**(8), 455–466, 2008, doi:10.1002/bse.607.

[51] E. Koberg, A. Longoni, "A systematic review of sustainable supply chain management in global supply chains," Journal of Cleaner Production, **207**, 1084–1098, 2019, doi:10.1016/j.jclepro.2018.10.033.

[52] G. Yadav, S. Luthra, S.K. Jakhar, S.K. Mangla, D.P. Rai, "A framework to overcome sustainable supply chain challenges through solution measures of industry 4.0 and circular economy: An automotive case," Journal of Cleaner Production, **254**, 120112, 2020, doi:10.1016/j.jclepro.2020.120112.

[53] M. Abdel-Basset, R. Mohamed, "A novel plithogenic TOPSIS- CRITIC model for sustainable supply chain risk management," Journal of Cleaner Production, **247**, 119586, 2020, doi:10.1016/j.jclepro.2019.119586.

[54] S. Yadav, S.P. Singh, "Blockchain critical success factors for sustainable supply chain," Resources, Conservation and Recycling, **152**(May 2019), 104505, 2020, doi:10.1016/j.resconrec.2019.104505.

[55] J.R. Brown, R.P. Dant, C.A. Ingene, P.J. Kaufmann, "Supply chain management and the evolution of the 'Big Middle,'" Journal of Retailing, **81**(2 SPEC. ISS.), 97–105, 2005, doi:10.1016/j.jretai.2005.03.002.

[56] M.S. Shaharudin, Y. Fernando, C.J. Chiappetta Jabbour, R. Sroufe, M.F.A. Jasmi, "Past, present, and future low carbon supply chain management: A content review using social network analysis," Journal of Cleaner Production, **218**, 629–643, 2019, doi:10.1016/j.jclepro.2019.02.016.

[57] D. Das, "The impact of Sustainable Supply Chain Management practices on firm performance: Lessons from Indian organizations," Journal of Cleaner Production, **203**, 179–196, 2018, doi:10.1016/j.jclepro.2018.08.250.

[58] J. Whitehead, C.J. MacLeod, H. Campbell, "Improving the adoption of agricultural sustainability tools: A comparative analysis," Ecological Indicators, **111**(June 2019), 106034, 2020, doi:10.1016/j.ecolind.2019.106034.

[59] C.A.L. Vanegas, G.A. Cordeiro, C.P. de Paula, R.E.C. Ordoñez, R. Anholon, "Analysis of the utilization of tools and sustainability approaches in the product development process in Brazilian industry," Sustainable Production and Consumption, **16**, 249–262, 2018, doi:10.1016/j.spc.2018.08.006.

[60] E. Dawkins, K. André, K. Axelsson, L. Benoist, Å.G. Swartling, Å. Persson, "Advancing sustainable consumption at the local government level: A literature review," Journal of Cleaner Production, **231**, 1450–1462, 2019, doi:10.1016/j.jclepro.2019.05.176.

[61] M. Rasti-Barzoki, I. Moon, "A game theoretic approach for car pricing and its energy efficiency level versus governmental sustainability goals by considering rebound effect: A case study of South Korea," Applied Energy, **271**(May), 115196, 2020, doi:10.1016/j.apenergy.2020.115196.

[62] J. Veldman, G. Gaalman, "On the design of managerial incentives for sustainability investments in the presence of competitors," Journal of Cleaner Production, **258**, 120925, 2020, doi:10.1016/j.jclepro.2020.120925.

[63] M. Mofidi Chelan, A. Alijanpour, H. Barani, J. Motamedi, H. Azadi, S. Van Passel, "Economic sustainability assessment in semi-steppe rangelands," Science of the Total Environment, **637–638**, 112–119, 2018, doi:10.1016/j.scitotenv.2018.04.428.

[64] Y. Zhao, Y. Tan, S. Feng, "Does reducing air pollution improve the progress of sustainable development in China?," Journal of Cleaner Production, **272**(September 2013), 122759, 2020, doi:10.1016/j.jclepro.2020.122759.

[65] B. Xia, A. Olanipekun, Q. Chen, L. Xie, Y. Liu, "Conceptualising the state of the art of corporate social responsibility (CSR) in the construction industry and its nexus to sustainable development," Journal of Cleaner Production, **195**, 340–353, 2018, doi:10.1016/j.jclepro.2018.05.157.

[66] E. Staniškienė, Ž. Stankevičiūtė, "Social sustainability measurement framework: The case of employee perspective in a CSR-committed organisation," Journal of Cleaner Production, **188**, 708–719, 2018, doi:10.1016/j.jclepro.2018.03.269.

[67] H. Ding, H. Huang, O. Tang, "Sustainable supply chain collaboration with outsourcing pollutant-reduction service in power industry," Journal of Cleaner Production, **186**, 215–228, 2018, doi:10.1016/j.jclepro.2018.03.039.

[68] S.A. Neves, A.C. Marques, J.A. Fuinhas, "Is energy consumption in the transport sector hampering both economic growth and the reduction of CO2 emissions? A disaggregated energy consumption analysis," Transport Policy, **59**(May), 64–70, 2017, doi:10.1016/j.tranpol.2017.07.004.

[69] M. Olfati, M. Bahiraei, F. Veysi, "A novel modification on preheating process of natural gas in pressure reduction stations to improve energy consumption, exergy destruction and CO2 emission: Preheating based on real demand," Energy, **173**, 598–609, 2019, doi:10.1016/j.energy.2019.02.090.

[70] S. Hendiani, H. Liao, R. Ren, B. Lev, "A likelihood-based multi-criteria sustainable supplier selection approach with complex preference information," Information Sciences, **536**, 135–155, 2020, doi:10.1016/j.ins.2020.05.065.

[71] J.M. Polimeni, R.I. Iorgulescu, A. Mihnea, "Understanding consumer motivations for buying sustainable agricultural products at Romanian farmers markets," Journal of Cleaner Production, **184**, 586–597, 2018, doi:10.1016/j.jclepro.2018.02.241.

[72] B. Hartl, T. Sabitzer, E. Hofmann, E. Penz, "'Sustainability is a nice bonus' the role of sustainability in carsharing from a consumer perspective," Journal of Cleaner Production, **202**, 88–100, 2018, doi:10.1016/j.jclepro.2018.08.138.

[73] H. Dixon-Fowler, A. O'Leary-Kelly, J. Johnson, M. Waite, "Sustainability and ideology-infused psychological contracts: An organizational- and employee-level perspective," Human Resource Management Review, **30**(3), 100690, 2020, doi:10.1016/j.hrmr.2019.100690.

[74] Y.M. Wang, K.S. Chin, "Fuzzy analytic hierarchy process: A logarithmic fuzzy preference programming methodology," International Journal of Approximate Reasoning, **52**(4), 541–553, 2011, doi:10.1016/j.ijar.2010.12.004.

[75] L. Mikhailov, "A fuzzy approach to deriving priorities from interval pairwise comparison judgements," European Journal of Operational Research, **159**(3), 687–704, 2004, doi:10.1016/S0377-2217(03)00432-6.

Design of Platform to Support Workflow Continuity in Multi-Device Applications

Oscar Chacón-Vázquez[1], Luis G. Montané-Jiménez[1,*], Carlos Alberto Ochoa-Rivera[1], Betania Hernández-Ocaña[2]

[1]FEI, Universidad Veracruzana, Xalapa, 91020, México

[2]Universidad Juárez Autónoma de Tabasco, Villahermosa, 86040, México

A R T I C L E   I N F O

A B S T R A C T

Nowadays, the Internet has become an indispensable tool for the realization and continuity of activity at a different time, place, and technological context (e.g., mobile, pc, tablet), so that interaction techniques through the use of multi-device support have become of great interest. From this perspective, continuity in interactions is an essential concept in the face of changes in context environments where an interaction develops. There are works related to the continuity and support of multi-device environments through software platforms that are useful to improve continuity support; however, reducing steps to resume an activity on a different device is an aspect that needs to be studied in greater detail. In support of the above, this paper presents an exploratory study that shows that continuity is a useful feature for users; however, there are still aspects that need to be studied. Therefore, in this paper, we propose a platform to implement continuity in a workflow that reduces the steps necessary to continue and resume activity in a different device context and a case study which serves as a method to evaluate the platform proposal and the models on which it is based.

1. Introduction

The Internet has become one of the main tools for carrying out different activities in various sectors, for example, work, entertainment and communication [1]. The evolution of the Internet has had effects in many areas of information and communication technologies such as computers [2] that make use of it, and the paradigms and models of software development [3].

The evolution of computers towards small devices with considerable computing capacity and intelligence, have brought about changes in the design and interaction paradigms seeking a better integration in our environments [4]. The constant evolution of computers towards small devices with considerable computing capacity and intelligence, have brought about changes in the design and interaction paradigms seeking a better integration in our environments [5]. In general, these developments use tools that make it easier to carry out software projects.

Interaction techniques through the use of platforms with support for multi-device environments have become one of the fields of greatest interest thanks to the great adoption of the internet and the evolution of information and communication technologies, taking advantage of its advantages [6]. The tools that have emerged derived from these techniques are broad and useful, focusing on different areas of interaction such as the use

of single sign-on systems, the use of multiple devices to interact with the same system at the same time, and the ability to continue certain activities with a long duration across different contexts [2].

In multi-device interactions, an activity can be carried out through different devices and in other contexts; this is much more complex to keep a user-focused on an activity and recover the activity's status was left. For example, a student who writes a document on a computer at his school may interrupt his work and continue it later from a different computer at home. This activity implies having to transfer the information from one computer to another and recovering the last state (e.g., page of a document where the student was, available tools, and information on the clipboard).

Continuity has become an essential concept in recent years for commercial information systems. We can find these systems such as Netflix, Amazon Video, and Spotify, which allow through a login and constant synchronization between devices to maintain a state between them and allowing the user to resume their activity (playback of some content multimedia) in a different context. Similarly occurs with Apple operating systems, which, in the case of system-specific applications, allow resuming an activity between devices, omitting several additional steps to do so.

Continuity has been one response to the interruptions brought by changes in context, reducing the number of steps necessary to

*Corresponding Author: Luis G. Montané-Jiménez, Email: lmontane@uv.mx

continue an activity; however, its implementation is complex due to multiple aspects [4], [6]. Therefore, we propose a conceptual platform that helps implement continuity in a software project, and it helps reduce the number of steps necessary to continue an activity when changing context. This proposed platform allows programmers and designers to focus their efforts completely on said design and reducing the workload to implement continuity. It also reduces the users' cognitive load in applications complex by quickly migrating an activity between different devices, reducing interruptions in the workflow.

This paper is structured as follows. Section 2 reviews the terms related to continuity in the workflow, and Section 3 presents a comparison of the work related to continuity and workflow. Section 4 presents a study of continuity in commercial applications. Section 5 presents a conceptual model of continuity in software projects. Section 6 presents a case study where the platform was implemented for testing. Finally, Section 7 presents the conclusions and future work.

2. Continuity in workflow

2.1. Workflow

The term workflow is a concept applicable to all areas where the human being develops. Specifically, information systems refer to a series of tasks that must be followed and completed so that a user can obtain a result (e.g., complete an activity). In [7], the authors refer to the workflow simply as flow. The workflow tends to be confused with the activity itself. This activity is the aim pursued by the user. For example, when someone to read a book, the workflow is necessary to complete it: i) read chapter 1, ii) read chapter 2, among others. The workflow has the characteristics shown in Table 1.

2.2. Interaction between devices

Adopting multiple devices in people's daily lives creates an environment where information is easily shared between them [8]. Currently, users are not limited to owning only a computer and a mobile phone, systems that in most cases are isolated from each other. In these environments, a user can have multiple computers that are used in different places and with other devices such as tablets or Smart TVs that have tools and applications that have the ability to interact and communicate with each other to offer the user a user interface that is seen as a whole, regardless of the equipment or device where users perform an activity.

Interaction between devices is an emerging branch of Human-Computer Interaction (IHC) focused on the way in which users interact between the different devices to which they have access, as well as the way in which applications take advantage of these forms interaction to offer much more dynamic user experiences [9]. There are two types of interaction between devices, i) interaction with multiple devices and ii) interaction across multiple devices [6]. The i) interaction with multiple devices is based on the ability of each of the devices to operate a system or application at the same time [10], allowing to create an environment where each device takes a specific role within the application and thereby better distributing the options and capabilities of the system. It focuses especially on collaborative environments where each person can take a specific role within the application, adapting the interface to each role and thereby

avoiding overloading the interface with unnecessary elements. On the other hand, ii) interaction through multiple devices focuses especially on monitoring activities that were started on a certain device, and due their duration, it may need to be interrupted and continued on a different device [7], facilitating the change of context for the user using concepts such as continuity and workflow to provide better user experiences.

Table 1: Workflow characteristics

Characteristic	Description
Divisible in tasks	The activities can be divided into more specific and shorter tasks, the completion of these tasks has the consequence of approaching the end of the activity.
Duration	It is an important factor in the definition of an activity and its flow, it defines the time that is invested in carrying out the activity and generally greatly affects the methods and moments of interaction.
Focus	It refers to the number of people involved in the activity; it affects the way in which the activities are carried out. It is possible to catalog the activity flows in two: one user and multi-user.

2.3. Continuity

The continuity term is defined as the ability to perform an activity on devices used sequentially and without presenting major interruptions in their workflow (context changes) [6]. It is a capacity and characteristic that we can find present in many commercial systems and applications and that take advantage of the benefits of the Internet and the capabilities of the devices with which we interact to reduce the steps necessary to continue an activity between them.

The experiences that implement continuity have 6 main characteristics that can be seen as objectives to be achieved [6]: i) Privacy, provide the user with the assurance that the data is safeguarded. ii) Appropriation, operate inherently in conjunction with the user and their work context. iii) Personalization, provide users with the possibility to choose which and when the continuity functions are activated. iv) Awareness, ability to "infer" the next steps that the user will perform. v) Inclusion, broad compatibility with current and future devices of the user, increasing interaction possibilities. Finally, vi) Troubleshooting, offering the ability to solve problems arising from the use of continuity to the user.

In a specific context in which a user interacts with a system that implements continuity and requires interrupting their work and continuing it in a different context, it is possible to distinguish two types of continuity [7]: monoactivity, and sequential activities. In monoactivity, continuity refers to activities such as: reading a book, watching a movie, or writing a text that may require a long time to complete. The advent of technology and the great expansion of mobile devices have contributed significantly to users changing how they performed these actions [2]. These activities can be carried out in short periods, where the context of use and the time available have an essential effect on the

interaction. Continuity in one-time activities focuses on this type of interaction, trying to minimize the necessary steps so that a user who left an activity pending completion can resume it when he deems it appropriate.

Continuity in sequential activities refers to when the user faces activities whose time and necessary effort allow them to be divided into the performance of sub-activities [7]. The continuity in these types of activities does not depend on being able to carry out the same activity through different contexts, but rather on maintaining a state between all the sub-activities, allowing the user to minimize the mental processes necessary to continue working. The design of these interactions is not based on its duration but rather on the place where a sub-activity occupies the general activity. In general, these types of interaction focus on offering the user information related to the last time they interacted with the system rather than minimizing the steps necessary to continue with the activities.

3. Continuity related work analysis

Multi-device environments and the accelerated evolution of information and communication technologies have led to the development of a great variety of works with multi-device and continuity implications; each of them has its characteristics and qualities. Among the works carried out, the most noteworthy include frameworks, development tools, and evaluations of applications that implement continuity.

3.1. Frameworks

The frameworks are a recurring theme in computer science because they allow us to establish future work bases and propose different approaches to solve a problem. In the multi-device and continuity field, there are several works where proposals for theoretical frameworks are presented. Recent works conceptually propose a framework for co-located devices in the same environment distributing the interface of an application through the users' roles when using the interface simultaneously [10].

In [11] propose a conceptual framework where for each device a role must be established and used in some way within the adaptation process, continuity is included at the conceptual level. More recent works introduce the concept of continuity as in "Design a framework to support the development of smart cross-device applications" [9], where a framework is proposed which provides guidelines and tools to distribute interfaces through nearby devices. Continuity is introduced as a state maintenance that improves the user experience.

A recurring theme in framework development is maintaining state through different methods. In [12,13] present frameworks that allow data to be automatically migrated between applications. However, they do not have current tools that maintain the state completely. On the other hand, [14] propose a tool to migrate data through interaction with Kinect to migrate data during a work session with several devices easily.

3.2. Development tools

Application development is a complex task that uses many tools to facilitate the process. In the field of continuity and multi-device interaction, work has also been carried out based on tools' development.

In [15] present a studio-type tool focused on the design of multi-device interfaces, and focused on its interactivity. The tool focuses on designing web-based interfaces that can be distributed and function in a coordinated manner between various devices; it also allows defining contexts for the devices to adapt according to them.

Several tools focus on data migration; among them, we can find tools that allow data to be migrated between "neighboring" applications of a mobile device [16]. In [2] propose a tool that allows for migrating information searches between different devices while maintaining history. On the other hand, there are works such as present in [17–19] that allow for migrating the state through different triggers such as biometric sensors and JavaScript methods. Finally, in [20] present a tool that allows data to be migrated through NFC tags, mainly focused on web searches.

Other authors have focused on the development of tools that support the internal procedures of the applications. In [5], the author propose a middleware type tool to implement a single sign-on between devices; continuity is a crucial part of the tool since, through this sign-on, the state can be transferred between devices.

3.3. Evaluations to applications

Continuity is a tool that has been implemented in both software projects and projects for the commercial field, verifying the effectiveness of applications that implement continuity. A multimedia application prototype to continue multimedia consumption through different devices was developed in [21]. This prototyping's main objective is to demonstrate the interaction techniques' effectiveness between the most used devices. Through the study and the prototype, it was possible to demonstrate that it developed software with a user-centered approach is necessary. However, there are still processes that can be implemented to improve interaction.

On the other hand, a conceptual model is presented in [22] where long-term searches on the web are supported across different devices; their approach is not just based on allowing long-term searches across different devices. It also provides intelligence by offering suggestions based on search patterns. The study carried out on the model showed significant differences in user interaction, depending on the context and type of device used.

In [6], the author evaluated one of the most representative applications of continuity in a commercial context: *Apple Continuity*. The study carried out contrasts the characteristics of Apple's service against user comments; the results indicate that continuity is accepted and desired by users in general. However, adapting to these new interaction methods can become complex, so the focus on user-based development is important to avoid such complexity. Further, [23] present an evaluation of automatic code generation to implement continuity with a strong emphasis on commercial applications.

Finally, there are work that present the applications of a method developed by authors to evaluate the migratory aspect of multi-device application such as presented by [24], [25].

3.4. Continuity related work comparative

By reviewing the work related to continuity and multi-device applications, Table 2 is presented, which shows that several

elements come into play when continuity is implemented in devices and systems.

The concept of multi-devices is applied in many ways throughout the different jobs, allowing the creation of different forms of interaction in the systems. It is also proven that it is a key point to give way to the continuity of activities in applications.

Table 2: Comparative of papers related to continuity

Paper	Year	Type	Emphasis	Multi-device	Continuity	
					Explicit	Implicit
Mobile to TV migration	2008	Tool	Backend	Yes	Yes	Yes
Remote AppBus	2009	Tool	Backend	Yes	Yes	No
Flexible framework	2009	Framework	Backend	Yes	No	Yes
JavaScript state	2011	Tool	Frontend	No	No	Yes
Multimedia prototype	2011	Evaluation	Frontend	Yes	Yes	Yes
Deepshot	2011	Framework	Backend	Yes	Yes	Yes
Single session start	2012	Tool	Backend	Yes	No	Yes
Virtual Browser	2012	Tool	Backend	No	Yes	No
Taskshadow-W	2013	Tool	Backend	No	Yes	Yes
Communication evaluation	2013	Evaluation	Backend	Yes	Yes	Yes
Interface IDE	2014	Tool	Frontend	No	No	No
XDKinect	2014	Framework	Backend	Yes	Yes	Yes
Search model for continuity	2015	Evaluation	Backend	Yes	Yes	No
Code generator	2015	Evaluation	Backend	Yes	Yes	No
Apple Continuity	2016	Evaluation	Frontend	Yes	Yes	Depends
CustomConsole	2016	Framework	Backend	Yes	No	No
Moving context kit	2017	Framework	Backend	Yes	Yes	No
Yanux framework	2018	Framework	Frontend	Yes	No	Yes
CORMORANT	2019	Tool	Backend	Yes	Yes	Yes
Model 4C's	2019	Framework	Backend	Yes	No	Yes

In the same way, works have been created that support the implementation of a part of continuity in applications. The main problem found in them is the poor compatibility with applications due to their focus on a specific aspect makes it difficult for continuity to be implemented by developers except in the aspects for which these tools were developed. It is also noteworthy that, in recent years, jobs such as [9–11] have focused on the creation of frameworks both at a conceptual and technical level for the creation of tools with interactions in continuity, showing a huge advantage over applications because they allow developers to expand the range of end uses that may have an application.

Based on the information presented in Table 2 and the reviewed works, we can see that, although explicit continuity and implicit continuity (called by many authors as maintenance of a state) are characteristics that do not always go hand in hand. The results, especially from those studies focused on evaluations of continuity implementations, suggest maintaining a state in applications that implement continuity is a very desirable feature.

With the analysis of the related works, it can be affirmed that one of the ways to implement continuity in the applications is through a framework or technological platform that provides developers with the necessary tools to create ecosystems with continuity characteristics. Although forays into these types of work have previously been made, there are aspects that remain to be covered, such as compatibility with modern platforms and with future platforms and the generalization of activities.

One of the most desirable features in continuity is maintaining an application state, which, in the long run, reduces the steps to resume an activity. This aspect is a topic little explored by researchers.

4. Exploratory study

In support of the points identified in the review of works, an exploratory study was designed to identify points of improvement in the user experience in multi-device applications, with a specific focus on applications that implement one or more aspects of continuity. The methods and materials used for this study are described below.

4.1. Experiment design

For this study, an exploratory experiment was designed and executed using the Google Forms tool; a questionnaire was constructed with a total of 20 items or questions that encompassed four different categories. Users were chosen randomly, regardless of their age, gender, or degree of academic studies. A total of 30 people were chosen for the application of the study.

The categories considered for the exploratory study are the following: i) general user data for classification and future consideration during data analysis; ii) continuity analysis in multi-device applications focused on music streaming; iii) continuity analysis in multi-device video streaming applications; and iv) continuity analysis in multi-device applications for document editing.

4.2. Evaluation tools

For the study, a questionnaire with 20 items was designed, the first four dedicated to categorical information from the user; the rest are described in Table 3. For its execution, the Google Docs tool was used; specifically, the Google Forms application allowed the questionnaire to be distributed quickly and effectively to the respondents. Another reason for its choice is that it provides a graphical analysis of the results and avoids the results' repetition by monitoring the respondents with their email.

Table 3: Questions applied in the exploratory study

ID	Question	Detail
5	How often do you use these devices to play music?	Question on Likert 5 points scale

6	It would be useful if the application automatically changes places to play your music on the most suitable device	Question on Likert 5 points scale
7	Would you like the application to be displayed as you interrupted it on another device when changing devices?	Question on Likert 5 points scale
8	What would you expect your player app to do when you want to switch devices?	Multiple option question
9	How often do you use these devices to play video?	Question on Likert 5 points scale
10	Of the following characteristics of an application for video playback, which of them are most important to you	Multiple option question
11	Is it useful to you that a video player application allows you to continue a movie / series right where you left off?	Question on Likert 5 points scale
12	You would like a video application to allow you to continue with a movie / series on another device only by turning it on and opening the application	Question on Likert 5 points scale
13	When it comes to playback across multiple devices, what would you improve on a video app?	Open question
14	How often do you use these devices to work on a document?	Question on Likert 5 points scale
15	Have you ever used the "pick up where you left off" feature in Microsoft Office	Multiple option question
16	How useful is this feature for you when switching from one workplace to another or between different devices?	Question on Likert 5 points scale
17	How much would you like Microsoft Office to allow you to continue a document without having to indicate it using the "continue where you left off" function?	Question on Likert 5 points scale
18	Would it be useful for you if, in addition to taking you to the section where you worked in the document, also the settings, clipboard and tools kept their last state?	Question on Likert 5 points scale
19	Would you like that when you open the Microsoft application (Office, Excel, PowerPoint) it would automatically open the last document you had open?	Question on Likert 5 points scale
20	When it comes to writing documents, what would you expect from an application when switching between contexts or devices?	Open question

4.3. Process

The participants' selection was carried out randomly, a short introduction to the subject of the study was given, and the instructions for filling out the tool; their participation was completely voluntary.

The tool was sent by electronic means to the users chosen for the test who had the approximate time of 1 day to answer them without affecting their working hours or daily activities. Finally, after a week, the data obtained through the platform was collected for subsequent analysis.

4.4. Results

Regarding music playback applications, it is notable that one of the characteristics most sought after by users is the "intelligence" of the application to play on the most suitable device available.

The results translate into that it would be instrumental for most users if they are playing music, and this automatically chooses the most appropriate device to play on. For example, a user who plays content on their cell phone, and when they get to Your home could automatically transfer this playback to your TV or computer, without the need for intermediate steps.
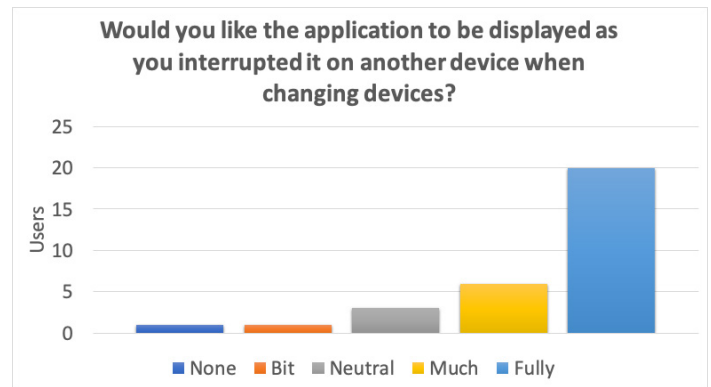
Figure 1: Opportunities of continuity in music streaming apps
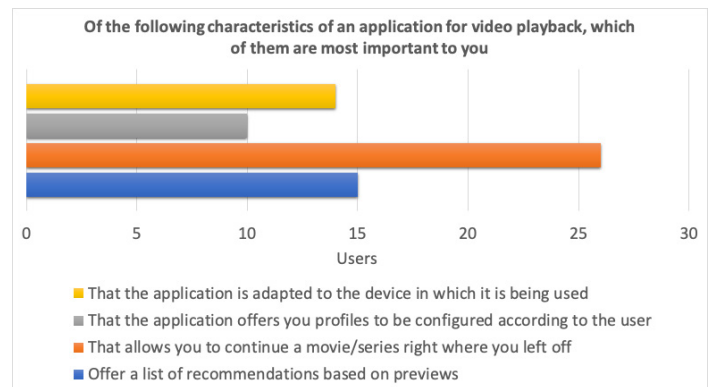
Figure 2: Continuity in video streaming apps

In addition, an aspect that music applications lack and that users expect from applications is the maintenance of a state, that is, that the application remembers where it was stopped the last time it was used, as can be seen in the second graph of Figure 1.

Regarding video applications, continuity has a greater presence in the application processes and turns out to be one of the characteristics that users like the most, as shown in Figure 2. In the same way as playback applications, music users are interested in the possibility of maintaining the state of the content reproduction when exchanging between devices. However, the approach applied in implicit continuity is not as relevant for users as seen in the second and third graphs of the survey conducted. Finally, for productivity applications, an analysis of the continuity implementation was carried out for an office suite widely used in the world and whose continuity implementation is explicit. Each time the user starts the application and opens a document you have been working on recently, you are presented with a button to go directly to the place where you last edited the document.
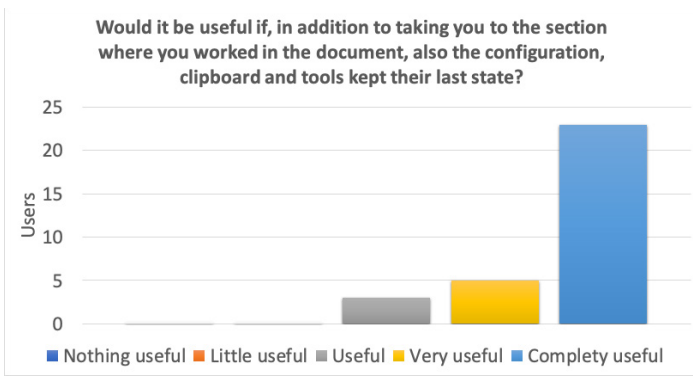
Figure 3: Continuity in document edition apps

In this type of application, two important aspects can be distinguished with regard to continuity. An important aspect mentioned by users is that the application directly remembers the status of the application with the documents they are working on, without the need for this function to be explicitly activated by the users. On the other hand, users would also find it useful to retrieve the configuration of tools for editing documents such as clipboards, temporary settings of the application, and additional tools such as a calculator or a browser; the results of the latter can see in Figure 3. With what was previously described, some users differ in the case that the application implements implicit continuity. It could be noted in the review of the comments made by the users; not all agree that the last document worked should be opened.
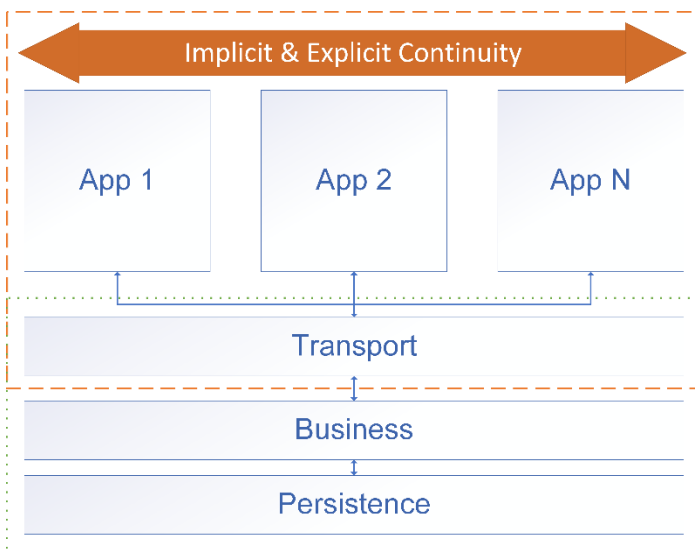
Figure 4: General model of the platform for implementation of continuity

5. Conceptual model for continuity implementation in software projects

Based on the models proposed by [5,9–11,15] and in the results of the continuity study carried out, a technological platform proposal was made at a conceptual level for the implementation of continuity in the activity flows shown in Figure 4 and detailed in its components in Figure 5. This model proposes an architecture for a platform where applications compatible with different devices can be easily implemented, and one of its goals is to allow its users to continue their task in a simple way when faced with a context change. The objective and the structure of the model for

the platform allows the reduction of steps necessary to continue an activity between several devices, that is, to facilitate the implementation of implicit continuity in several applications.

In Figure 4, the general behavior of the platform can be observed. Through a set of layers, the necessary support is provided to create multi-device environments, taking advantage of the possibilities of explicit continuity and, above all, of implicit continuity, regardless of the type and number of applications being developed.

The persistence layer focuses on the storage of information corresponding to the application domain and the context where it operates (for example, the type of device used and the environment where it is done), typically composed of three elements, i) the application's usage status data, that is, configuration and usage information, this data contains information about how the last device was used ii) the device status data that considers device-specific details such as type of last device or the app version used which helps to adapt the interface of next used device and iii) the domain data referring to the application's own information (documents, photos, among others) which is used to present the data that were working, is based on unstructured language for the storage of information. This layer also contains the basic operational engine, which provides essential functions (create, update, delete, and read) over the data storage in order to operate with the basic application information.
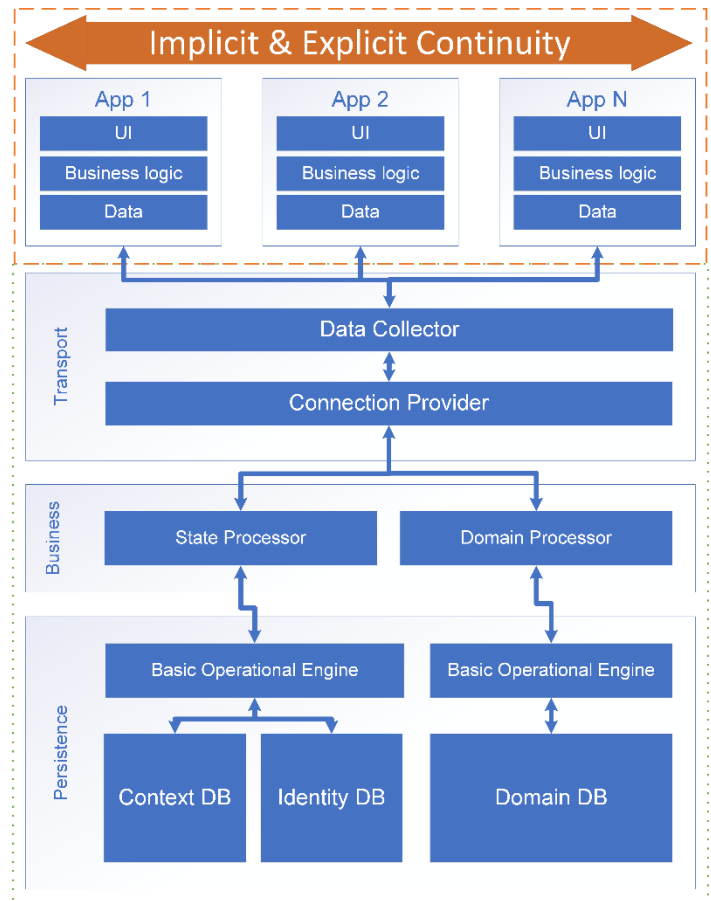
Figure 5: Components of the technological platform for the implementation of continuity in software projects

Table 4: Description of the conceptual model of a technological platform for the implementation of continuity in workflow

Characteristic	Description
Context DB	Storage component that allows to save the information of the context of use of the devices, it is a long-term data storage software, it contains elements that function as tools for the selection of device sequence and the configuration of interfaces
Identity DB	Storage component that stores information corresponding to users and that is used as a starting point to create state representations, this database must contain data from the user that help to identify the information that is stored in the context and domain database, its purpose is to maintain control over the information that the platform operates
Domain DB	Storage component focused on the operational information of the applications, it contains representations of the information that the user enters or obtains from the application.
Basic Operational Engine	It is a logical component that provides access to the basic functions on the storage components, the proposed implementation design defines an engine for domain data and another for identification and context information in order to reduce workloads over other components.
State Processor	Logical component that allows composing and decomposing the state representations and the information obtained from the operational engines and sending that information to the next layer depending on whether it is retrieved or entered into the platform, its purpose is to offer an interpreter for both directions of the platform.
Domain Processor	Logical component that provides functionality on domain information and that must establish the data transformation bases for the changes that are necessary between the jumps of multiple applications. This element works as a translator when it is necessary. It must also be responsible for communicating the domain data to the upper and lower layers in order to reduce the information contained by state representations
Connection provider	High-level component that functions as a data input to the lower layers, receives the information from the data collector and is responsible for passing it to one of the two processors of the business layer. This component is proposed to function as an API in order to be able to be integrated into software projects without having to modify the base structure of the project
Data Collector	Its a high-level component that is proposed to be responsible for direct communication with the final applications, it must be in charge of obtaining the necessary information to create the representation of the state that will be sent to the connection provider and also of presenting the information when a representation is retrieved from the platform towards a final device, It is proposed that this element be built as libraries for the specific programming languages of each final application
App 1,2… N	These are the final applications where the platform can be implemented, which can go from 1 to N, each one can have its own logic processes, information storage media and graphic interface.

The persistence layer communicates with the business layer, which comprises two processing services (state and domain logic). These processing elements are responsible for making the necessary changes to the data; being the most important elements since a large part of the adaptation depends on them. Finally, in the highest part, the transport layer is composed of two elements (data collector and connection provider). These elements are those that are exposed to the developers and are integrated into the final applications, built in the form of APIs, extracting the necessary information from the applications and sending them to the processing models so that the rest of the platform works. It is also are responsible for making the necessary changes to the application interfaces. It is through these two elements that applications reduce the steps necessary to resume activities. These elements have to be able to scale to serve as many final applications as a program has been developed.

In order to support the understanding of this platform, a diagram was developed with the components of the model and which is presented in Figure 5, as well as the description of these components which is found in Table 4.
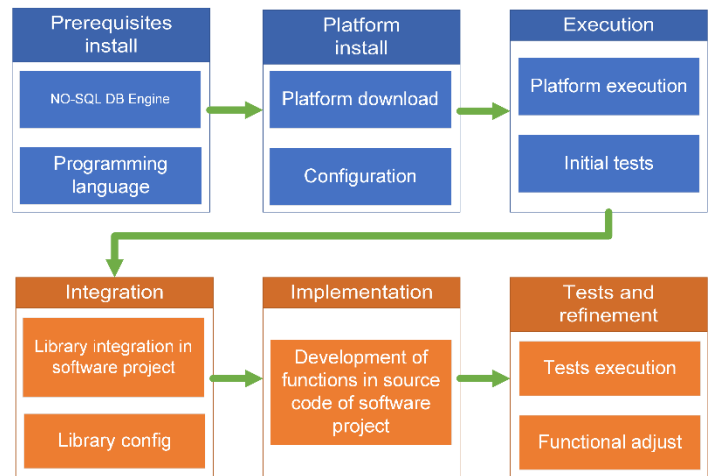
Figure 6: Platform implementation roadmap

In Figure 6, the platform implementation is shown; in the upper part the work stages are shown directly on the platform which are: i) pre-requisite installation in which the execution environment of the platform through the configuration of tools for database management and the programming language used by the platform, ii) installation of the platform that consists of downloading the platform code and its configuration with the database management tool, iii) Execution which consists of the start-up and rapid tests of the correct operation of the platform.

At the bottom of the implementation sheet, the steps after the installation of the platform are shown, which apply directly to the software project; these steps are: iv) Integration where the libraries that are added to the software projects allow communication to the platform and its configuration, v) Implementation where the views and functions of the software are developed, and it is indicated where the platform libraries will work and vi) Testing and refinement where the tests should be carried out on each final application and adjusting functions in case these changes are necessary.

6. Case Study

The platform is an intermediate software that communicates with the different components of other applications; due to the nature of this type of software. It is impossible to carry out functional and use tests directly on its construction, so the software is implemented in a Case study where both the function and the user experience when using continuity could be evaluated.
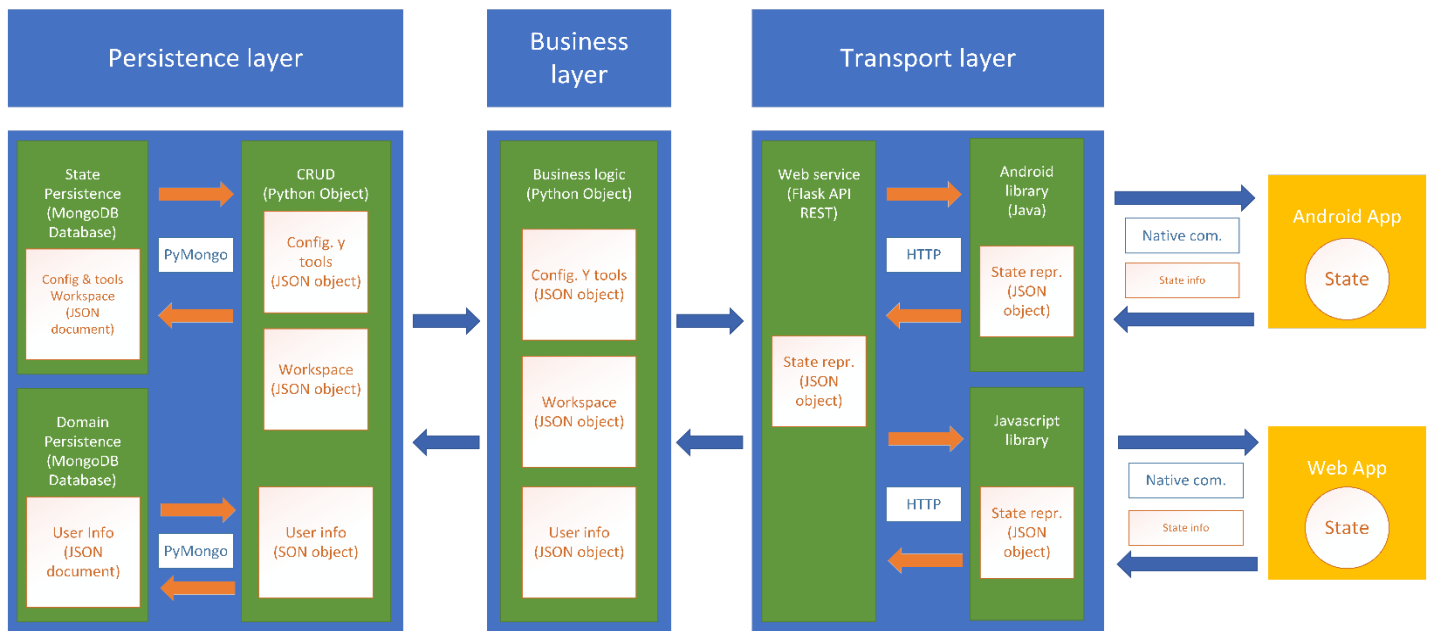
Figure 7: Implementation architecture for study case

The selected case study is an application that allows you to create exams according to a catalog of questions previously evaluated and approved. The process of editing an exam can be a complex task for those who take it, and because of this, in many cases, it is necessary to move it between one device and another.

The case study has three elements: a direct administration system that allows the question catalog to be generated, edited, and debugged. A web application is attached to the administration system to generate the exams from any browser. Finally, an Android application that also allows generating the exams.

The structure of the selected application makes it perfect to test the proposed solution because it's possible to change between two different types of apps and two different contexts, also, the selected applications can be executed in many modern mobile devices and even in any device that can accessing internet through a web browser.

On the other hand, the limitations of this case study are that it does not allow the analysis of an interaction that is too deep, such as using a text editor, in addition to the fact that it is an application in its final stages of development, so an error that is not related to the use of continuity and biases the study in a certain way.

Two libraries were built that allowed to integrate the platform in the case study, the first in JavaScript for the web sections and the second in Java-Android for the android section of the case study. Figure 7 shows in detail the structure and elements that make up the platform in its implementation for the case study.

The persistence layer is implemented through two databases that represent the storage components, one for the domain and one for the state. These connect a first layer of python that offers basic functions on databases (basic functional engines). At the second level there is a business layer that implements methods and processes to arm and disarm the state representations and finally the transport layer is responsible for implementing a RESTful-type web service and the two libraries mentioned above, while the REST service receives and sends the information when the

libraries so require, the libraries control directly and in a practically automatic way the events in the applications of the case study that save and retrieve the information.

7. Conclusions and future work

The development of computer systems has changed over time, adapting to the different tools that arise daily. The notable increase in the use of mobile devices is one of the main reasons that have led to the emergence of new interaction and development paradigms.

One of the main topics that researchers and the market related to systems development have focused on is multi-device interaction. Continuity arises as part of the multiple ways in which a multi-device interaction occurs. The possibilities that continuity offers to improve the different ways in which a user interacts with a system are vast, yet there is still a long way to go.

One of the problems that researchers currently focus on solving through the use of continuity is the minimization of interruptions in the flow of an activity, something that could be seen through the review of works related to this research and the exploratory study carried out is a feature that users are beginning to expect from the systems.

The design of a platform to implement this type of interaction is complex due to the components that are required for correct operation, as well as the very logical structure that is required to maintain the state of the applications between the changes made by the user.

The results obtained once the implementation was carried out in the case study were favorable, the platform facilitated the continuity implementation in the case study and also allowed to reduce the necessary steps to resume an activity, which facilitated context changes for users.

In contrast to other works that were reviewed during the writing of this document, we can see that a platform that provides full support for continuity has a deeper impact than applications such

as [2,4,5,12–14], whose emphasis is strongly focused on the login and the migration of user data over the migration of operation data.

On the other hand, a better performance can also be noted than the proposals made by authors such as [3,9,11,16,18], where migration Information is a present feature, but small details such as the configuration or the last view requested are not considered, forcing the user to have to remember this when resuming an activity. It is still necessary to make improvements with respect to the platform's ability to adapt based on usage preferences and configurations that affect continuity, as well as to carry out tests that guarantee its effectiveness, with continuity being a useful tool in different contexts of use. However, it still requires a long and dedicated development process.

Finally, as part of the future work, it is expected to carry out a series of tests through the case study in order to validate the functionality and design of the Platform.

Conflict of Interest

The authors declare no conflict of interest.

Acknowledgment

References

[1] L. Tan, N. Wang, "Future Internet: The Internet of Things," in ICACTE 2010 - 2010 3rd International Conference on Advanced Computer Theory and Engineering, Proceedings, 2010, doi:10.1109/ICACTE.2010.5579543.

[2] B. Cheng, "Virtual browser for enabling multi-device web applications," Proceedings of the Workshop on Multi-Device App Middleware - Multi-Device '12, 1–6, 2012, doi:10.1145/2405172.2405175.

[3] C. Ye, J. Wei, H. Zhong, T. Huang, "Middleware Support for Internetware : A Service Perspective," Systems Research, 2010, doi:10.1002/ardp.201300158.

[4] H. Kim, E.A. Lee, "Authentication and Authorization for the Internet of Things," IT Professional, **19**(5), 27–33, 2017, doi:10.1039/b904090k.

[5] P.A. Cabarcos, F. Almenares, R. Sánchez Guerrero, A. Marin, D. Díaz-Sánchez, "Multi-device Single Sign-on for cloud service continuity," Digest of Technical Papers - IEEE International Conference on Consumer Electronics, 644–645, 2012, doi:10.1109/ICCE.2012.6162011.

[6] D. Raptis, J. Kjeldskov, M.B. Skov, "Continuity in Multi- - Device Interaction: An Online Study," Proceedings of the 9th Nordic Conference on Human-Computer Interaction - NordiCHI '16, 2016, doi:10.1145/2971485.2971533.

[7] M. Levin, Designing Multi-Device Experiences, First, O'Reilly Media, Inc, 2014.

[8] J. Schöning, H. Reiterer, C. Holz, J. Vermeulen, N. Marquardt, C. Klokmose, S. Houben, "Opportunities and challenges for cross-device interactions in the wild," Interactions, **24**(5), 58–63, 2017, doi:10.1145/3121348.

[9] A. Pedro, C. Nuno, N. Rui, "Designing a framework to support the development of smart cross-device applications," Mum18 Rw, 367–374, 2018.

[10] A. Marzo, "CustomConsole : A Framework for Supporting Cross-device Videogames," 1952–1958, 2016.

[11] K. O'Leary, T. Dong, J.K. Haines, M. Gilbert, E.F. Churchill, J. Nichols, "The Moving Context Kit: Designing for Context Shifts in Multi-Device Experiences," Proceedings of the ACM Conference on Designing Interactive Systems (DIS 2017), 309–320, 2017, doi:cshg.

[12] M. Barisch, J. Kögel, S. Meier, "A flexible framework for complete session mobility and its implementation," Lecture Notes in Computer Science (Including Subseries Lecture Notes in Artificial Intelligence and Lecture Notes in Bioinformatics), **5733 LNCS**, 188–198, 2009, doi:10.1007/978-3-642-03700-9_20.

[13] T.H. Chang, Y. Li, "Deep shot: A framework for migrating tasks across devices using mobile phone cameras," in Conference on Human Factors in Computing Systems - Proceedings, 2011, doi:10.1145/1978942.1979257.

[14] M. Nebeling, E. Teunissen, M. Husmann, M.C. Norrie, "XDKinect: Development framework for cross-device interaction using kinect," in EICS 2014 - Proceedings of the 2014 ACM SIGCHI Symposium on Engineering Interactive Computing Systems, 2014, doi:10.1145/2607023.2607024.

[15] M. Nebeling, T. Mintsi, M. Husmann, M. Norrie, "Interactive development of cross-device user interfaces," Proceedings of the 32nd Annual ACM Conference on Human Factors in Computing Systems - CHI '14, 2793–2802, 2014, doi:10.1145/2556288.2556980.

[16] N. Narasimhan, C. Janssen, M. Pearce, "Remote AppBus - Enabling seamless access to short term memory on mobile devices," 2009 6th IEEE Consumer Communications and Networking Conference, CCNC 2009, 1–5, 2009, doi:10.1109/CCNC.2009.4784773.

[17] D. Hintze, J. Kepler, "CORMORANT : Ubiquitous Risk-Aware Multi-Modal Biometric Authentication across Mobile Devices," **3**(3), 2019.

[18] F. Bellucci, G. Ghiani, F. Paternò, C. Santoro, "Engineering JavaScript state persistence of web applications migrating across multiple devices," in Proceedings of the 2011 SIGCHI Symposium on Engineering Interactive Computing Systems, EICS 2011, 2011, doi:10.1145/1996461.1996502.

[19] F. Paternò, C. Santoro, A. Scorcia, "User interface migration between mobile devices and digital TV," Lecture Notes in Computer Science (Including Subseries Lecture Notes in Artificial Intelligence and Lecture Notes in Bioinformatics), **5247 LNCS**, 287–292, 2008, doi:10.1007/978-3-540-85992-5-28.

[20] S. Li, G. Pan, Y. Xu, Z. Ye, L. Chen, "Taskshadow-W: NFC-triggered migration of web browsing across personal devices," in UbiComp 2013 Adjunct - Adjunct Publication of the 2013 ACM Conference on Ubiquitous Computing, 2013, doi:10.1145/2494091.2494119.

[21] R. Bernhaupt, M. Abdellatif, T. Mirlacher, "Cross-device continuous media consumption," 217, 2011, doi:10.1145/1941007.1941046.

[22] S. Han, Y. Zhen, H. Daqing, "Understanding and supporting Cross-Device Web Search For Exploratory Task with Mobile Touch Interactions," ACM Transactions on Information Systems, **33**(4), 2015.

[23] E. Umuhoza, H. Ed-Douibi, M. Brambilla, J. Cabot, A. Bongio, "Automatic code generation for cross-platform, multi-device mobile apps: Some reflections from an industrial experience," in MobileDeLi 2015 - Proceedings of the 3rd International Workshop on Mobile Development Lifecycle, 2015, doi:10.1145/2846661.2846666.

[24] R. De A. Maués, S.D. Junqueira Barbosa, "Cross-communicability: Evaluating the meta-communication of cross-platform applications," Lecture Notes in Computer Science (Including Subseries Lecture Notes in Artificial Intelligence and Lecture Notes in Bioinformatics), **8119 LNCS**(PART 3), 241–258, 2013, doi:10.1007/978-3-642-40477-1_15.

[25] T. Dong, E.F. Churchill, J. Nichols, "Understanding the Challenges of Designing and Developing Multi-Device Experiences," Designing Interactive Systems, 62–72, 2016, doi:10.1145/2901790.2901851.

Evolution of Cardiovascular Risk Indicators in Elderly Hypertensive Men from a Health Facility in North Lima

Rosa Perez-Siguas[*], Hernan Matta-Solis, Eduardo Matta-Solis

Research and Intellectual Creativity Direction, Universidad María Auxiliadora, 15408, Lima-Perú

A R T I C L E   I N F O

A B S T R A C T

Cardiovascular risk today is one of the non-communicable diseases that occurs in the population of the third age where risk factors further compromise its health, therefore the objective of the study is to determine the evolution of the Cardiovascular Risk indicators in hypertensive elderly from a facility in North Lima. This is a quantitative, non-experimental, descriptive, and cross-sectional study, with a population of 47 hypertensive elderly people over 60 years of age, whose cardiovascular risk was determined with the PAHO cardiovascular risk calculator. In the results, we can see that in the month of January, 17 (36.2%) presented a moderate risk, 19 (40.4%) presented high risk, 8 (17%) presented very high risk and 3 (6.4 %) presented critical risk, in June, 17 (36.2%) presented low risk, 24 (51.1%) presented moderate risk, 4 (8.5%) presented high risk, 2 (2.1 %) presented very high risk and 1 (2.1%) presented critical risk and in December, 25 (53.2%) presented low risk, 17 (36.2%) presented moderate risk, 4 (8.5%) presented high risk and 1 (2.1%) presented critical risk. In conclusion, prevention of cardiovascular problems in the elderly should be expanded, to contribute to their health status and quality of life due to the increase in population.

1. Introduction

Cardiovascular risk is the probability that the individual presents cardiac problems in a certain time, and this will depend fundamentally on factors that predispose the individual's risk, these factors can be modifiable and non-modifiable, whose function varies in relation to the present risk, which can be qualitatively (high, intermediate or low) or quantitatively (numerical probability of suffering a complication in a given period) [1].

In the population, aging worldwide is increasingly accelerated, whereas of 2015 the amount of the population of older adults in the world has doubled, going from 12% to 22%, it is also underestimated that within 2 years the number of the age group of the elderly will be higher than children under 5 years of age. Likewise, in the near future, the majority of older adults will be concentrated in countries with low to middle income [2], therefore it should be taken into account that the aging process is usually accompanied by chronic diseases, among which stand out heart disease [3].

Worldwide, cardiovascular diseases (CVD) are responsible for approximately 17 million deaths per year, among them

complications from high blood pressure produce 9.4 million deaths annually. The worldwide prevalence of hypertension (HT) is estimated to be 35% [4]. For its part, the Pan American Health Organization (PAHO) estimates that hypertension affects between 20-40% of the adult population in the Americas. At the Peruvian level, 16.5% are affected [5]. Focusing on the elderly, HT affects 67% of those over 60 years of age in the United States and in Peru the prevalence is 43.3% in those over 60 years of age. The foregoing shows that hypertension is a growing public health problem, in the context of epidemiological transition that the country is going through [6].

In a study carried out in Peru [7], they observed that in patients older than 80 years of age with a history of HT, the main risk factors were that 10.07% of older adults were smokers and it was more frequent in men. As for women, 33% had high cholesterol in both sexes, diabetes mellitus in 16.63% and 14.29% were obese, these last two risk factors were seen more in women than men.

In a study carried out in Brazil [8], they showed in their results cardiovascular factors in patients older than 60 years in relation to the cardiovascular disease they suffered and their lifestyle habits, where 53% had high blood pressure, 25% diabetes mellitus and 8% already suffered from a cardiovascular disease,

in relation to their life habits, 68% of older adults carried out physical activity, 35% were alcoholics and 50% were smokers, therefore risk factors such as alcoholism and smoking occurred more in men than women, and therefore cardiovascular diseases appeared early in men.

In a study carried out in Brazil [9], they observed in their results that 64.9% of adults older than 60 years with a history of arterial hypertension were obese, also it was found that 70.8% of older adults had a metabolic syndrome, 27.2 % had a low cardiovascular risk, 46.8% moderate and 26% high, interpreting that older adults who presented metabolic syndrome had a high probability of having a high cardiovascular risk.

The present study is important because it will provide relevant and real data about the cardiovascular risks of hypertensive elderly people since the elderly makes them more vulnerable to contracting metabolic and cardiovascular diseases.

2.   Methodology

It is an applicative study where the evolution of cardiovascular risk indicators in hypertensive older adults will be detailed, also 3 measurements will be given in their assessment in the months of January, June, and December, to analyze the evolution and observe if hypertensive older adults present cardiovascular risk factors.

2.1. Research type and Design

The present study, due to its characteristics, way of collecting data and measuring the variables involved, has a quantitative approach. Regarding the methodological design, it is a non-experimental, descriptive, cross-sectional study [10].

2.2. Population

In the present study, the population is made up of 47 hypertensive elderly men over 60 years of age who attend a health facility in North Lima.

2.3. Inclusion Criteria

- Older adult patients suffering from arterial hypertension
- Patients who attend at least 3 check-ups at the health facility.
- Older adult patients who have signed the informed consent according to the principles of ethics of charity, non-maleficence, justice, and autonomy.

2.4. Technique and Instrument

To carry out this research work, the Cardiovascular Risk Calculator of the Pan American Health Organization (PAHO) was used, which aims to determine the risk in the elderly, this instrument was used because the study was exploratory and only required the use of the PAHO Calculator. The Cardiovascular Risk Calculator is administered to assess whether the patient has a cardiovascular risk, this calculator will determine the risk depending on sex, age, blood pressure, history of diabetes mellitus, cholesterol and risk factors such as smoking, in this way it is determined whether the patient is at low, moderate, high, very high, and critical risk; when calculating the parameters, it is estimated that there may be a risk of presenting some

cardiovascular disease - to establish the values, the incidence of less than 10% at 10 years is considered low risk, that is, less than 1% per year. Another way to read it is to consider that of a group of 100 people in this situation, one will develop a disease each year, thus reaching 10 people in a decade. At the other extreme, very high risk greater than 40% at 10 years, indicates that of 100 people in this condition, 4 will have events annually and 40 will have them in the next 10 years; almost one in two [11].

The Calculator is more accurate if cholesterol levels are reported, although it may not be considered if the data is not reported. Once the risk estimate has been obtained, it can be evaluated to what extent the risk could be modified by correcting factors such as smoking, high blood pressure and hypercholesterolemia. It is considered ideal not to smoke, blood pressure values less than 140/90 mmHg and total cholesterol less than 200 mg / dl. In some cases, it is possible that the desired cholesterol may be much lower than that, depending on the presence of other risk factors. In such a way that the person may notice that when they quit smoking their risk drops by half, or that it transforms from very high to low by correcting the three factors that we can influence in this calculator. Age and gender cannot be changed, and diabetes status is taken upon knowledge of its diagnosis but is not based on blood glucose levels or other parameters.

It refers to low risk to carry out all its preventive control activities; moderate risk when it performs its controls but not daily; high risk, when the patient barely performs its preventive controls; very high risk when the patient scarcely performs its preventive controls and presents symptoms product of the disease; and critical risk when the patient does not perform any preventive control and the symptoms present to the disease tend to complicate.

2.5. Place and Application of the Instrument

To carry out the Development of the cardiovascular risk calculator in hypertensive elderly patients, it was carried out in a Health Facility in North Lima

First, the permits were coordinated with the head of the establishment to carry out the research, then the permission to the patient explaining about what was going to be developed and why the research work will be carried out.

It was developed during the mornings with an approximate time of 10 minutes for each elderly hypertensive patient, concluding a good satisfaction since they supported the research work.

It is important to emphasize the presence of health personnel during the development of the research work, because the patient as an older adult with hypertension there is the possibility that signs, and symptoms of the disease may occur and thus the necessary treatment can be administered to be able to stabilize it.

3.   Results

The results of hypertensive elderly patients corresponding to the research work will be shown below:

CARDIOVASCULAR RISK IN HYPERTENSIVE ELDERLY
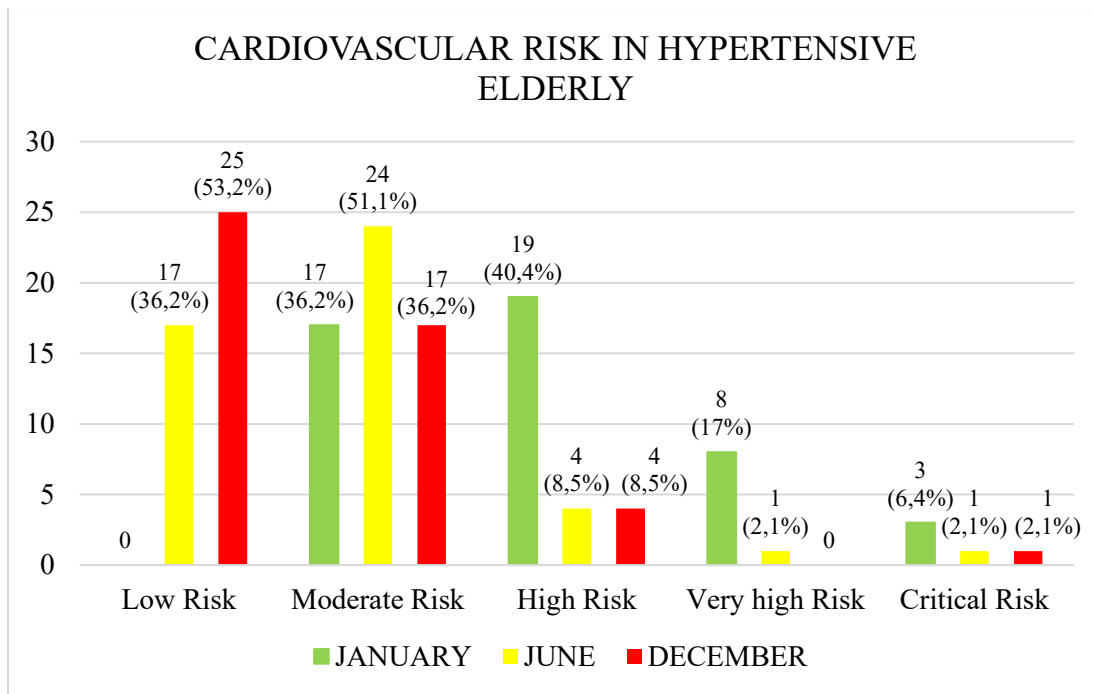
Figure 1: Semiannual comparison of the Evolution of cardiovascular risk indicators in hypertensive elderly from a facility in North Lima

Figure 1 shows the six-monthly comparison of the evolution of cardiovascular risk indicators in hypertensive elderly people from a health facility in North Lima, where in January, 17 (36.2%) presented a moderate risk, 19 (40.4%) presented high risk, 8 (17%) presented very high risk and 3 (6.4%) presented critical risk, in June, 17 (36.2%) presented low risk, 24 (51.1%) presented moderate risk, 4 (8.5%) presented high risk, 2 (2.1%) presented very high risk and 1 (2.1%) presented critical risk and in the month of December, 25 (53.2%) presented low risk, 17 (36.2%) presented moderate risk, 4 (8.5%) presented high risk and 1 ((2.1%) presented critical risk.

In Table 1, it is observed that in moderate cardiovascular risk, within the hypertensive elderly population, 17 (100%) do low physical activity, at high cardiovascular risk, 9 (47.4%) do low physical activity and 10 (52.6%) do not do physical activity, at very high cardiovascular risk, 3 (37.5%) do low physical activity and 5 (62.5&) do not do physical activity, and at critical risk 3 (100%) do not do physical activity, in relation to weight, the hypertensive elderly had a weight between 70 kg and 99 kg respectively with a height of 155 cm to 171 cm, taking their BMI where in moderate cardiovascular risk 17 (100%) were overweight, in high cardiovascular risk 19 (100%) were obese, at very high cardiovascular risk 5 (62.5%) were overweight and 3 (37.5%) were obese, in relation to smoking, at moderate cardiovascular risk 8 (47.1%) were smokers and 9 (52.9%) were not smokers, in relation to cardiovascular risk and diabetes mellitus, at moderate risk 13 (76.5%) suffered of diabetes and 4 (23.5%) do not have diabetes, at high risk 17 (89.5%) have diabetes and 2 (10.5%) do not have diabetes, at very high risk 6 (75%) suffer from diabetes and 2 (25%) do not have diabetes and at critical risk 3 (100%) do not suffer from diabetes, in relation to blood pressure in hypertensive elderly, they had a blood pressure between 120 mmHG to 180 mmHG and in relation to cholesterol, the hypertensive elderly had a cholesterol level between 180 mg/dl and 300 mg/dl.

In Table 2, it is observed that in low cardiovascular risk within the hypertensive elderly population, 14 (82.4%) do medium physical activity, 3 (17.6%) do low physical activity, and moderate cardiovascular risk 2 (8.3%) do medium physical activity and 22 (91.7%) do low physical activity, at high cardiovascular risk 2 (50%) do low physical activity and 2 (50%) do not do physical activity, in very high cardiovascular risk 1 (100%) does not do physical activity and in critical cardiovascular risk 1 (100%) does not do physical activity, in relation to weight, hypertensive elderly had a weight between 60 kg and 91 kg respectively with a height from 155 cm to 171 cm, taking their BMI where the low cardiovascular risk 6 (35.3%) were within the normal range, 10 (58.8%) were overweight and 1 (5.9%) was obese, at moderate cardiovascular risk, 1 (4.2%) is within the normal range and 23 (95.8%) were overweight, at high cardiovascular risk, 4 (100%) were obese, at very high cardiovascular risk 1 (100%) was obese and at critical cardiovascular risk 1 (100%) was obese, in relation to smoking, at low cardiovascular risk 1 (5.9%) was a smoker and 16 (94.1%) were non-smokers, at moderate cardiovascular risk 13 (54.2%) were smokers and 11 (45.8%) were non-smokers, at high cardiovascular risk 1 (25%) was a smoker and 3 (75%) were not smokers, at very high cardiovascular risk 1 (100%) was a smoker and at critical cardiovascular risk 1 (100%) was a smoker, in relation to cardiovascular risk and diabetes mellitus, at low cardiovascular risk 12 (70.6 %) suffer from diabetes and 5 (29.4) do not have diabetes, at moderate cardiovascular risk 21 (87.5%) have diabetes and 3 (12.5) do not have diabetes, at high cardiovascular risk 4 (100 %) suffer from diabetes mellitus, at very high cardiovascular risk 1 (100%) suffers from diabetes and at critical cardiovascular risk 1 (100%) suffers from diabetes, in relation to blood pressure in hypertensive elderly, they had a blood pressure between 112 mmHG to 155 mmHG, and lastly, in relation to cholesterol in the hypertensive elderly, they presented a cholesterol level between 178 mg/dl to 285 mg/dl.

Table 1: Cardiovascular Risk in Hypertensive elderly in relation to Risk Factors for the Month of January of a Health Facility in North Lima

Cardiovascular risk	Physical Activity		Weight (KG)	Height (cm)	Body Mass Index (BMI)		Smoking		Diabetes		Maximum Systolic Pressure (mmHg)	Cholesterol
	Low	Do not			Overweight	Obese	YES	NO	YES	NO		
Low risk	-	-			-	-	-	-	-	-		
Moderate risk	17 (100%)	0	≥70KG a ≤99KG	≥155cm ≤171 cm	17 (100%)	0	8 (47,1%)	9 (52,9%)	13 (76,5)	4 (23,5%)	≥120 mmHG a ≤180mmHG	≥188mg/dl a ≤300mg/dl
High risk	9 (47,4%)	10 (52,6%)			0	19 (100%)	12 (63,2%)	7 (36,8%)	17 (89,5%)	2 (10,5%)		
Very high risk	3 (37,5%)	5 (62,5%)			5 (62,5%)	3 (37,5%)	5 (62,5%)	3 (37,5%)	6 (75%)	2 (25%)		
Critical risk	0	3 (100%)			0	3(100%)	3(100%)	0	3 (100%)	0		

Table 2: Cardiovascular Risk in Hypertensive Elderly in relation to Risk Factors for the Month of June in a Health Facility in North Lima

Cardiovascular risk 2	Physical Activity			Weight (KG)	Height (cm)	Body Mass Index (BMI)			Smoking		Diabetes		Maximum Systolic Pressure (mmHg)	Cholesterol
	Medium	Low	Do not			Normal	Overweight	Obese	YES	NO	YES	NO		
Low risk	14 (82,4%)	3 (17,6%)	-	≥ 60 Kg a ≤ 91 Kg	≥ 155 cm a ≤ 171 cm	6 (35,3%)	10 (58,8%)	1 (5,9%)	1 (5,9%)	16 (94,1%)	12 (70,6%)	5 (29,4%)	≥ 112 mmHG a ≤ 155 mmHG	≥ 178 mg/dl a ≤ 285 mg/dl
Moderate risk	2 (8,3%)	22 (91,7%)	-			1 (4,2%)	23 (95,8%)	0	13 (54,2%)	11 (45,8%)	21 (87,5%)	3 (12,5%)		
High risk	0	2 (50%)	2 (50%)			0	0	4 (100%)	1 (25%)	3 (75%)	4 (100%)	0		
Very high risk	0	0	1 (100%)			0	0	1 (100%)	1 (100%)	0	1 (100%)	0		
Critical risk	0	0	1 (100%)			0	0	1 (100%)	1 (100%)	0	1 (100%)	0		

Table 3: Cardiovascular risk in hypertensive elderly in relation to risk factors for the month of December in a health facility in north lima

Cardiovascular risk 3	Physical Activity			Weight (KG)	Height (cm)	Body Mass Index (BMI)			Smoking		Diabetes		Maximum Systolic Pressure (mmHg)	Cholesterol
	Medium	Low	Do not			Normal	Overweight	Obese	YES	NO	YES	NO		
Low risk	23 (92%)	2 (8%)	0	≥55 Kg a	≥ 155 cm a	22 (88%)	2 (8%)	1 (4%)	2 (8%)	23 (92%)	18 (72%)	7 (28%)	≥ 100mmHG a	≥160 mg/dl a ≤ 265
Moderate risk	6 (35,3%)	11 (64,7%)	0			1 (5,9%)	16 (94,1%)	0	11 (64,7%)	6(35,3%)	17 (100%)	0		
High risk	0	3 (75%)	1 (25%)			0	1 (25%)	3 (75%)	4 (100%)	0	3 (75%)	1 (25%)		

Very high risk	-	-	-	≤ 92Kg	≤171 cm	-	-	-	-	-	-	-	≤ 150mmHG	mg/dl
Critical risk	0	1 (100%)	0			0	0	1 (100%)	1 (100%)	0	1 (100%)	0		

In Table 1, it is observed that in low cardiovascular risk, within the hypertensive elderly population, 23 (92%) do medium physical activity and 2 (8%) do low physical activity, in moderate cardiovascular risk 6 (35.3%) do medium physical activity and 11 (64.7%) do low physical activity, at high cardiovascular risk, 3 (75) do low physical activity and 1 (25%) do not perform physical activity, at risk Critical cardiovascular 1 (100%) do low physical activity, in relation to weight, hypertensive elderly had a weight between 55 kg to 92 kg respectively with a height of 155 cm to 171 cm, taking their BMI where in low cardiovascular risk, 22 (88%) are within the normal range, 2 (8%) were overweight and 1 (4%) was obese, at moderate cardiovascular risk, 1 (5.9%) is within the normal range and 16 (94.1 %) were overweight, at high cardiovascular risk, 1 (25%) was overweight and 3 (75%) were obese, at critical cardiovascular risk 1 (100%) was obese, in relation to smoking, at low cardiovascular risk 2 (8%) were smokers and 23 (92%) were non-smokers, at moderate cardiovascular risk 11 (64.7%) were smokers and 6 (35.3%) were not were smokers, at high cardiovascular risk 4 (100%) were smokers and at critical cardiovascular risk 1 (100%) was a smoker, in relation to cardiovascular risk and diabetes mellitus, at low cardiovascular risk, 18 (72%) suffered from diabetes and 7 (28%) do not suffer from diabetes, at moderate cardiovascular risk 17 (100%) have diabetes, at high cardiovascular risk, 3 (75%) have diabetes and 1 (25%) does not have diabetes, at cardiovascular risk Critical 1 (100%) suffers from diabetes, in relation to blood pressure in hypertensive elderly, they had a blood pressure between 100 mmHG to 150 mmHG and lastly in relation to cholesterol in hypertensive elderly, they had a cholesterol level between 160mg / dl to 265mg / dl.

Among the results obtained, it is important to consider the months of difference in which it will allow us if hypertensive elderly people can reduce cardiovascular risk by performing physical activities such as passive exercises, walks, yoga, muscle stretching, and the communication with the family as it will allow to see if have any symptoms that decrease their health well-being.

4. Discussion

In this research work, an approach is given to the public health of hypertensive elderly people in a health facility, where factors and conditioning factors in them, such as the elderly population, increase the probabilities of having cardiovascular risks.

In the results on the cardiovascular risks distributed every six months in the months of January, June, and December, we can verify that in the initial month of January, the patients presented a high cardiovascular risk, this is because as adults of the third age, because of their gender male, increases the chances of suffering some type of cardiovascular risk. In [8], they argued that life habits in the elderly population related to cardiovascular risk are influenced by sociodemographic and clinical factors, where sex, smoking and alcoholism; the presence of diabetes mellitus and

arterial hypertension were more associated with the patient's desire to be able to control the disease and the alteration of blood pressure, where they do physical activities and control their own disease. Likewise, in [12], they argued that arterial hypertension is a cardiovascular risk factor with the greatest burden in the male population, therefore, with regard to chronic diseases, it is associated with diseases such as cardiovascular mortality and ischemic heart disease that can compromise the individual's health.

In the same way, the factors that put the health of hypertensive elderly at risk make available the probabilities that they suffer from heart disease or even die as a result. In [7], the authors mentioned that risk factors such as high blood pressure, smoking, diabetes, overweight or obesity and physical inactivity, are factors that compromise the elderly to be vulnerable and increase the chances of dying from heart disease. Likewise, in [13], the authors argued that older adults with cardiovascular risk factors are more associated with suffering an acute myocardial infarction since sedentary lifestyle and arterial hypertension can happen

For this reason, physical activity, a healthy diet, not consuming products that compromise your health, allow the elderly to have a better quality of life, a good life expectancy, all of which will allow the elderly to improve and live a life healthy. In the same way, in [14], the authors maintain that a change in lifestyle, regular physical activity, having a balanced diet, will allow the elderly to improve their quality of life. In [15], the authors argued that a good quality of life in the elderly is due to the fact that the level of physical activity is associated with a lower prevalence of presenting a cardiovascular risk factor. In [16], the authors mentioned in their systematic review that increasing the level of physical activity, balancing the diet, and eliminating tobacco and alcohol habits allows older adults to improve their quality of life.

For all this to be carried out, a plan is needed that allows it to be put into practice in the elderly to maintain a healthy life and that cardiovascular risks can be prevented. For this, 4 steps have been carried out as a plan to prevent cardiovascular risks:

- Reduction or elimination of tobacco consumption: Quitting smoking and not using smokeless tobacco is one of the best options for the heart, since the chemical substances in tobacco damage the heart and blood vessels reducing oxygen in the blood, thereby increasing blood pressure and the heart must work more than it does usually. Although the cardiovascular risk decreases in the person one day after they stop smoking, so if after a year without tobacco, it will decrease half the risk of a smoker.

- Daily physical activity: In the elderly, regular physical activity is important since it allows them to reduce cardiovascular risk, since it allows weight control, and reduces other conditions

such as high blood pressure, high cholesterol, and type 2 diabetes mellitus; so, they should do aerobic exercises a week, and activities that strengthen their muscles, since these activities offer benefits for the heart.

- Healthy Eating: A balanced diet helps protect the heart, prevents high blood pressure, cholesterol and reduces the risk of contracting type 2 diabetes mellitus, limiting the intake of salt, sugar, carbohydrates, alcohol, and saturated fat, all of which will allow them to have a good health.

- Maintain a healthy weight: For one to have a healthy lifestyle, one must perform physical activities along with a healthy diet, since physical activity helps maintain weight, lowers high blood pressure, reduces the risks of type 2 diabetes, among other risks All this with a healthy diet that is low in calories, and more nutritious, allows their weight to be preserved and stay healthy.

5. Conclusions

It is concluded that primary prevention strategies should be considered in elderly patients with high cardiovascular risk and have secondary prevention

It is concluded that prevention of cardiovascular problems should be expanded in the elderly, to contribute to their health and quality of life due to the increase in the population.

It is required to provide counseling on food and nutrition that motivates the elderly and their family to learn about the benefits of a healthy diet.

It is concluded that an adequate diagnosis and control of risky diseases must be carried out, especially acting on the risk factors identified at an early age, to achieve a better quality of life when one is an older adult.

The limitation of this research work is due to the situation due to the COVID-19 pandemic that could not take more elderly patients for the study, since the population depended only on one health center, so it was taken only 47 elderly patients who were the most recurrent to their controls in the same.

Conflicts of Interest
The authors declare that they have no conflict of interest.

References

[1] B. Pérez, E. García, A. Graciani, P. Guallar, E. López, L. León, J. Banegas, F. Rodríguez, "Social Inequalities in Cardiovascular Risk Factors Among Older Adults in Spain: The Seniors-ENRICA Study.," Revista Española de Cardiología (English Edition), **70**(3), 145–154, 2017, doi:10.1016/j.rec.2016.05.010.

[2] Organización Mundial de la Salud, Envejecimiento y salud., OMS, 2020.

[3] A. Rosas, V. Narciso, M. Cuba, "Atributos de la Atención Primaria de Salud (A.P.S): Una visión desde la Medicina Familiar.," Acta Médica Peruana, **30**(1), 42–47, 2013.

[4] J. Machline, R. Marques, L. Petri, "Effect of a Multifaceted Quality Improvement Intervention on the Prescription of Evidence-Based Treatment in Patients at High Cardiovascular Risk in Brazil: The BRIDGE Cardiovascular Prevention Cluster Randomized Clinical Trial.," JAMA Cardiology, **4**(5), 408–417, 2019, doi:10.1001/jamacardio.2019.0649.

[5] J. Álvarez, A. Álvarez, W. Carvajal, M. González, J. Duque, O. Nieto, "Determinación del riesgo cardiovascular en una población.," Revista Colombiana de Cardiologia, **24**(4), 334–341, 2017,

doi:10.1016/j.rccar.2016.08.002.

[6] J. Sacramento, G. Duarte, S. Gómez, M. Romero, M. Begoña, "Herramientas de evaluación del riesgo cardiovascular: una revisión del alcance.," Australian Critical Care, **32**(6), 540–559, 2019.

[7] E. Ruiz, H. Ruiz, L. Guevara, H. Ortecho, R. Salazar, C. Torres, C. Vasquez, "Factores de riesgo cardiovascular en mayores de 80 años.," Horizonte Médico (Lima), **15**(3), 26–33, 2015, doi:10.24265/horizmed.2015.v15n3.05.

[8] A. Brandão, J. Dantas, I. Costa, M. Santos, E. Galvão, P. Brandão, "Riesgo de enfermedades cardiovasculares en ancianos: hábitos de vida, factores sociodemográficos y clínico.," Gerokomos, **28**(3), 127–130, 2017.

[9] M. Gomes, L. Ramos, I. Rodrigues, T. Barbara, S. Schwerz, M. Morato, "Increased cardiovascular risk and role of metabolic syndrome in hypertensive elderly.," Esc Anna Nery, **25**(1), 1–8, 2021.

[10] C. Fernández, P. Baptista, Metodología de la Investigación. 6ta ed. México: Mc Graw-Hill/Interamericana., 2015.

[11] WHO/PAHO, Calculadora Riesgo Cardiovascular., OPS, 2020.

[12] F. Félix, L. Lozano, P. Alvarez, M. Grau, J. Ramírez, D. Fernández, "Impacto de los factores de riesgo cardiovascular en la población extremeña: aportación de la cohorte HERMEX para una estrategia preventiva.," Atención Primaria, **52**(1), 3–13, 2020, doi:10.1016/j.aprim.2018.11.006.

[13] J. Alvarez, V. Bello, G. Pérez, O. Antomarchi, M. Bolívar, "Factores de riesgo coronarios asociados al infarto agudo del miocardio en el adulto mayor.," Medisan, **17**(1), 54–60, 2013.

[14] R. Rondanelli, R. Rondanelli, "Prevention of Cardiovascular Disease in Older Adults," Revista Média Clínica Condes, **23**(6), 724–731, 2012, doi:10.1007/978-3-642-37078-6_57.

[15] C. Celis, C. Salas, J. Leppe, C. Cristi, E. Duran, N. Willis, "Un mayor nivel de actividad física se asocia a una menor prevalencia de factores de riesgo cardiovascular en Chile: resultados de la Encuesta Nacional de Salud 2009-2010.," Revista Medica de Chile, **143**(0), 1435–1443, 2015.

[16] J. Ramírez, D. Chaparro, H. León, J. Salazar, "Efecto del ejercicio físico para el control de los factores de riesgo cardiovascular modificables del adulto mayor: revisión sistemática.," Rehabilitacion, **49**(4), 240–251, 2015, doi:10.1016/j.rh.2015.07.004.

Investigation of the LoRa Transceiver in Conditions of Multipath Propagation of Radio Signals

Dmytro Kucherov[1,*], Andrei Berezkin[2], Volodymyr Nakonechnyi[3], Olha Sushchenko[4], Ihor Ogirko[5], Olha Ogirko[6], Ruslan Skrynkovskyy[7]

[1]*Department of Computerized Control Systems, National Aviation University, Kyiv, 03058, Ukraine*

[2]*Pukhov Institute for Modelling in Energy Engineering, National Academy of Science of Ukraine, Kyiv, 03164, Ukraine*

[3]*Department of Cyber Security and Information Protection, Taras Shevchenko National University, Kyiv, 01033, Ukraine*

[4]*Department of Aerospace Control Systems, Institute, National Aviation University, Kyiv, 03058, Ukraine*

[5]*Department of Mathematic, Kazimierz Pułaski University of Technology and Humanities in Radom, Radom, 26600, Poland*

[6]*Department of Information Technologies, Lviv State University of Internal Affairs, Lviv, 79020, Ukraine*

[7]*Department of Business Economy and Information Technology, Lviv University of Business and Law, Lviv, 79021, Ukraine*

A B S T R A C T

The article presents some results of the research of the LoRa module. These modules can be the basis of possible IoT technologies are implementing, providing enough good range of receiving and transmitting messages. The SX1276 transceiver has been testing to determine the signal loss in the propagation channel. These experiments took in a highly-populated Kyiv district and one of the passageways of a Podbryantsevsky salt mine near the Solar town. The measured parameters are the maximum radio communication range in the mine, the signal-to-noise ratio, the number of bit errors and losses of the signal transmission. The data of the study we plan to use for the engineering of the radio-messaging networks based on LoRa radio modules.

1. Introduction

Multipath propagation is obtaining as a result of re-reflections of the signal source antenna beam from ground objects. Namely from buildings, a large number of rooms and corridors inside them, hills, vegetation, mine tunnels, etc., which create except the one direct some indirect directions of arrival of the beam. The receiving signal is an additive mixture of signals with different amplitudes, phases, and arrival directions. Multipath propagation of radio signals results in signal fading and frequency shift of the receiving signal.

Multipath propagation decreases the quality of the data reception. In the same circumstances, radar reception is resolved by introducing a small frequency additive into the low power oscillator of the frequency converter then receiving signal frequency deviation is synchronous with the transmitting signal frequency. The next way is the creation of additional reception channels. Another situation arises in technique for communicating, where noise has a strong effect, and the signal-to-noise ratio (SNR) is less than unity. A natural solution pointed problem is the complication of the receiving set by introducing additional receive channels and complex signal processing. However, this approach is not acceptable for the Internet of Things (IoT) technology. The peculiarity of the application of this technology in mines is the small size of antennas and equipment, also low power consumption.

Optimal filtering is one way to expand the SNR at the receiver output. However, in processing technology, this approach is not always suitable. The signal spectrum expands due to interference, and by increasing the acceptance threshold, and the signal may be lost. In this case, for improving the signal quality at the input of the matched filter, the noise protection is offered. Unluckily, well-known methods of suppression of narrow-band interference do not apply as well.

Due to its ability to maintain communications and lighting simultaneously, some authors consider the visible light communications (VLC) system like potential opportunity to implement effective communications in mines, which is basing on the phenomenon of light propagation. In this case, the quality of communication devices is highly dependent on the available channel propagation models, including long-term fading, which was critical for the project and assessing the operation of VLC systems. But, the basic features of the VLCs have not yet been enough explored. Also, dust and moisture block the propagation of light signals.

This paper is an extended version of our work [1] presented at the 2019 IEEE International Scientific-Practical Conference Problems of Infocommunications, Science and Technology (PIC S&T) in which the research purpose was to study the features of LoRa (Long Range) signal processing in multipath propagation. The remaining part of the paper is organized as follows: Section 2 presents the works that provide an overview of the subject area; Section 3 devotes the general formulation of the problem; Section 4 briefly describes the features of the radio module when used in free space. Section 5 presents the results of module tests in multipath conditions, and conclusions from the studies are presented in Section 6.

2. Paper Review

Due to frequent disasters that occur in mining sites caused by landslides and rockslides of underground mine workings, the creation of a reliable system for communication in places of underground mining has recently become important.

In this case, the traditional solution is the use of radio communication systems. In the document [2], prepared in response to the MINER Act, an analysis of existing communication systems in different frequency ranges has been presented, and the basic requirements for existing radio communication facilities are formulating. Their functions are not only messaging but also tracking the actions of miners. Thus, radio communication is recognizing as the principal method of communication. In this respect, it is also worth noting that the work to establish the requirements for frequency ranges and radio communication range based on the study of the average attenuation characteristics of radio signals in mines of various types of minerals by this time was partially done (for example, see [3, 4]).

Reviews of communication facilities in underground mines have also presented in papers [5, 6], where were manifest the problems of wireless communication under the ground, associated with attenuation and loss of communication that is greater than when they have on the surface. The attenuation parameter for a frequency of 900 MHz has been refined in [7] and was concluding the possibility of using mobile communications in coal mines.

Recently, as an alternative to conventional wired and radio transmitting systems, researchers [8-11] are considering the possibility of using visible light as a means of communication for mine communication. So, in the article [8], based on this approach, a method is proposed for modeling the visible light propagation channel for two types of underground utilities: directly at the bottom hole and on the roadway, and the results of studies of the number of indicators spread signal in the visible light channel have presented. The main achievement of the authors of [9] is assessment loss as a function of distance.

In [10], the use of angular diversity receivers has been proposed that was focus on reducing inter-cell interference. It also considers new mathematical models of light distribution: pyramidal and hemi-dodecahedral. Numerical values for data rate, signal energy, and signal-to-noise-plus-interference ratio have also been presented, which can be useful for evaluating new solutions.

It is worth noting, the use of optics for communication has studied earlier. One of the earliest sources for time division multiple access (TDMA) broadcast communications dates back to 2005 [11]. Described here are a malfunction resistant system start and restart of the system with the dynamic self-configuration capability and a controlled internal diagnostic system.

The authors of [12, 13] propose the technology of detecting personnel and equipment in tunnels of underground manufactories by data transmission through light-emitting diodes and a photodetector; their approach also uses the trilateration method. So, in [12], an algorithm for determining the location of targeting objects is proposed. It is built based on data from several VLC systems located on the cover of an underground tunnel, as well as VLC mobile devices placed in the interests of ensuring the safety of miners, and the same problem is solved in three-dimensional space by authors [13].

To detect underground facilities, it is also possible to use ground penetration radar (GPR). So, in [14], it is proposed to divide the transmission paths into two types of signals: blocked and unblocked. Since the volume of blockaded signals is less than the estimated signal space, their routes are using in signal processing. A similar approach was proposed by the authors [15] based on the ULF (Ultra Low Frequency) radio channel for a mine specializing in the extraction of non-ferrous metals. In [16], GPR was used to assess soil moisture in the interests of agriculture. However, the range of propagation of electromagnetic waves underground is not long, does not exceed several meters; their use is advisable only in the interests of agriculture, which has been established by numerous studies and is confirming in [17 - 19]. The article [20] discusses the problems of robot navigation for coal mines.

This research continues the work presented in [21, 22].

3. Problem Statement

A multipath reception for a receiver based on LoRa technology is considering. In an open space, the module manufacturer guarantees the service of remote users at a distance of up to 20 km for a long life of the time, which makes the technology comparable with common Wi-Fi and LTE (Long-Term Evolution) [1].

The set of modules forms a system for picking reports from users and transmitting them to the server for further treatment and, maybe, answering queries. The messages exchanged between users; the service is providing by the open air at frequencies below GHz.

A message is a data package, which includes a preamble, a header and a payload, its size is dependent on the spreading factor

(S_f). Length of the package varied from 51 to 256 bits. The information transfer rate is between 22 and 27 kbps. The selection of this parameter depends upon the range, bandwidth and expansion factor. The signal that is emitted is a chirp signal, which is now assumed as the standard in the area of short-range wireless communication systems (IEEE 802.15.4a).

A distinguishing characteristic of signal receiving in multipath propagation is a significant deterioration in the signal quality, up to its complete loss. Examples of single radiation without interference and the total effect of four chirp signals without interference shown in Fig. 1, 2.
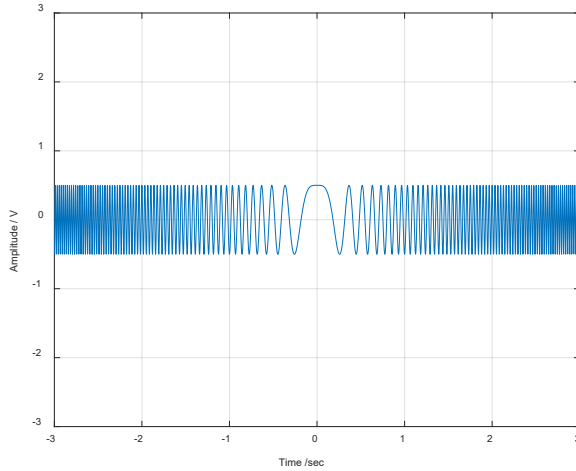
Figure 1: The one chirp signal
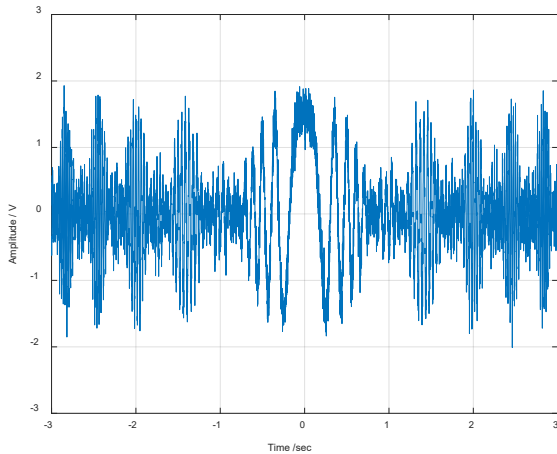
Figure 2: The four chirp signal with different phase shifts

A traditional study in the course of multipath reception is to clarify losses in the transmitter-receiver section and guarantee the receiving range [23]

$$R = \sqrt{\frac{P_t F(\theta) G_t A_r e^{-2\alpha d}}{4\pi P_r}}$$

(1)

where R is the radio communication range; P_t is the transmitter signal power; $F(\theta)$ is the antenna directivity in the θ direction, $F(0) = 1$; G_t is the transmitting antenna gain; A_r is the effective receiver area; P_r is the signal power at the receiving set input; α is

the attenuation of the signal along the path of the beam propagation, taking into account the free space and propagation environment; d is the distance between two antennas.

Channel losses determine the budgeting of the wireless communication channel, which is calculated by the formula [23]:

$$P_r = P_t + G_t - L_s - L_{ch} - M$$

(2)

where G_t is the gain determined by the directivity of the antennas, L_s is the system's loss (for instance, in short antennas used in most remote devices), etc.; L_{ch} is the loss in the signal spillover channel, M is the attenuation signal is computed by empirical data. All values in the equation are expressing in dB.

If we know value R radio communication ranges in free space and the range in the loss conditions D, the value of losses in dB can be specified using the formula

$$L = 40 \lg\left(\frac{D}{R}\right)$$

(3)

SNR and bit error (BER) rates are auxiliary indicators of reception quality. The SNR is determining as follows

$$SNR = P_{signal} / P_{noise} = (a_{signal} / a_{noise})^2$$

(4)

The purpose of the research is to assess the effectiveness of using LoRa modules in a confined space, where it is possible to observe multipath propagation.

4. Preliminary remarks

A typical LoRaWAN radio network integrates end devices into architecture type a star. Messages are underlying double encrypted to ensure security. Devices that have small power consumption are ensuring by using a short time for transferring in a comparatively long time interval when the terminal device is in a "sleep" regime. Information is transferring both asynchronous and synchronous modes. The information from the end node of the network is spreading through the gateway to the network server and then deliver to the application server. LoRa modules have better receiver sensitivity because it uses chirp signals, error correction, high transmit noise immunity and insensibility to frequency changes of resonators.

In experiments, we used a module based on the SX1276 microcircuit (Fig. 3), in which messages are transmitting at a frequency of 868 MHz. Other parameters of the transceiver based on the SX1276 microcircuit [24] are presented in Table 1.

Table 1: Some parameters of SX1276

Option	Value
Δf, kHz	20.8
S_f	8
BR, bps	1562
P_r, dBm	− 128

The channel budget, calculated by the formula (2), for a transmitter with a power of 100 mW in the case of ideal transmit-receive dipoles, for which the gain was chosen to be 2.1 dB and the minimum loss and signal attenuation turns out to be 130 dB.

The maximum range of radio communication in line-of-sight conditions for a lifting height of the receiving and transmitting antennas of 1 m under experiment conditions and normal refraction does not exceed 25 km.
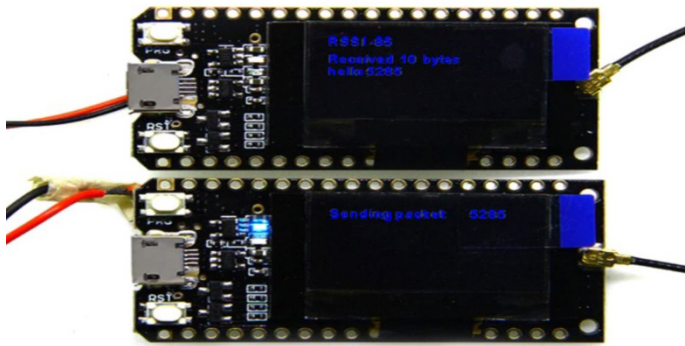
Figure 3: The module SX1276

The force of the received signal as a function of the range without interference [25, formula (5.15)] has shown in Fig. 4 with a blue line; the threshold sensitivity of the studied module is a black straight line. Crossing the lines gives the radio communication range corresponding to the real sensitivity of the receiving module, which turns out to be 4.8 km.
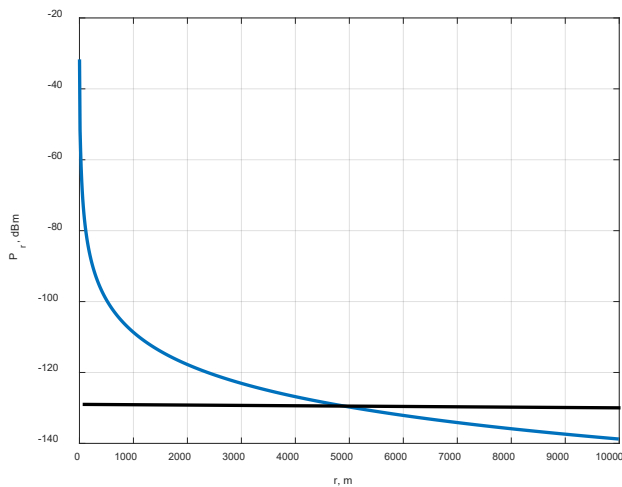
Figure 4: Estimation of the maximum radio communication range for a given sensitivity

5. Research results

The LoRa chipset study consisted of a sequence of surface experiments in a highly-populated city spot, where mobile communications and radio internet interfere with the receiving channel, and underground, in a mine where spurious radiation is absent. Ground tests based on a point-to-point scheme and a point-gateway with treatment on a remote server and underground tests were according to a point-to-point layout.

5.1. Interference radio

In the beginning, the transmitter installs on the last floor of a hard-wall building in Kyiv. A few Wi-Fi networks were deploying inside this building, on the roof of the building were also installed antennas of three operators' mobile communication. The indicator

of the receiving device showed the message quality. At the experiment, the LoRa radio module was deposited from the 11th floor of the building to the first floor and to the downstairs located two floors below the first floor for creating multipath reception. The measurement framework reveals in Fig. 5. In Fig. 5, the abbreviations MS are used for the marking of the antenna of the stations of mobile operators, Tr is the transmitting module, Rc is the receiving device.
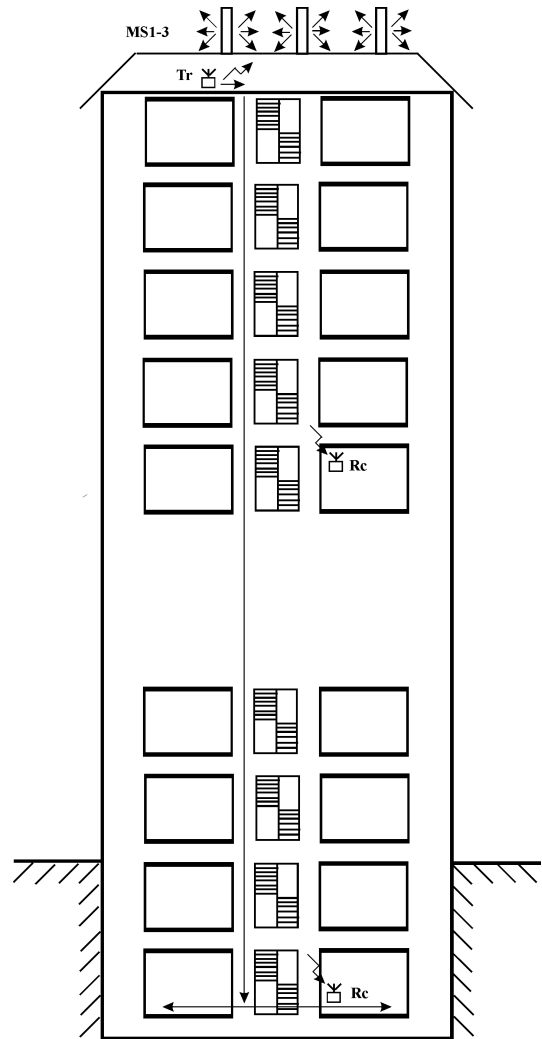
Figure 5: Layout of devices in the experiment

Rooftop antennas of mobile communications and Wi-Fi routers causing interference. These signals create a noise background, which chose as the "white". Crosstalk is causing by multiple reflections of beams inside the building from reinforced concrete structures. Using signal and noise level were fixed on every building floor, and the legibility of the text message was controlled as well. Additional documenting of the measurements has been carried out by a panoramic receiver, which chose as a reference. A initial report of the interference condition presents in Table 2.

The functioning of the transceiver in the "point-to-gateway" regime is fundamentally no different from the "point-to-point." The main difference is data processing, which carries out on a cloud server, and therefore the information has been slightly delayed (tens of milliseconds) compared to the point-to-point regime. In measurements, an auxiliary radio communication

channel was used by a mobile phone. The results of measurements of the BER and SNR for the LoRa radio module shows in Fig. 6, 7.

Table 2: Interference Condition

Type of sources	Frequency, MHz	Power, W	Effect
CDMA	800-900	2-60	strong
LTE	900-2400	2-60	middle
Wi-Fi	2400	0,1	weak
Other	400-5000	<0,01	weak
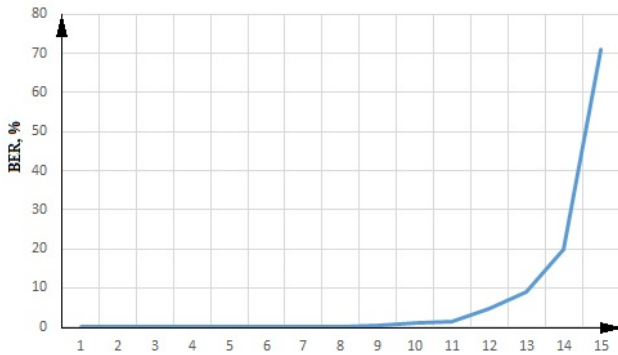
Figure 6: BER as a function of the number of the floor
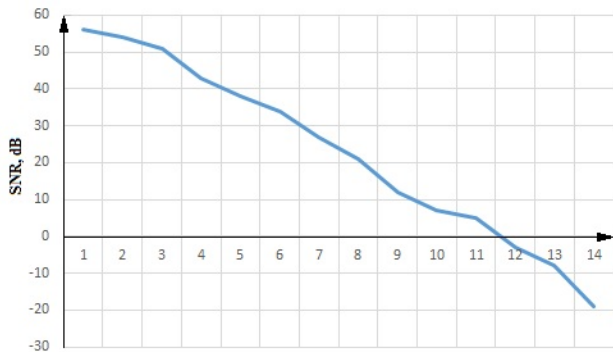
Figure 7: SNR as a function of the number of the floor.

By the experiment results, it has established that text messages receive on all floors and within 2 m from the staircase in the basement; the loss connection was at a distance of 8-10 m from the stairs.

5.2. Using the LoRa module in a mine

This subsection contains data on the results of measurements of the quality of message reception by the LoRa radio module at the conveyor slope of the Podbryantsevsky salt mine, located in the vicinity of the Soledar town.

The measurements were fulfilled in tunnels of the mine, in which are two parallel corridors connected by passages, Fig. 8. The experiment was carried out by step-by-step removal of the receiving set from a stationary transmitter with a fixed distance. The motion has been done from the initial point, corresponding to

the transmitter location, clockwise around the salt layer 23 m wide. The transmitter has installed 100 m from the comer.
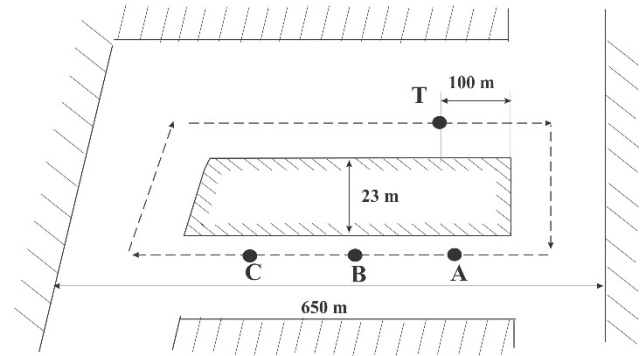
Figure 8: Section of the Podbryantsevsky formation mine, where measurements have been done

Point A in the diagram corresponds to a growth in the signal level around the comer, point B matches the signal maximum, and point C to a total signal loss. Also, the information in the mine was transmitted by voice; it was also repeated by the Motorola radio station functioning in the decimeter range and its output signal power of 1 W.

The quality of communication in LoRa assesses by the number of packets received and by voice; the last way was estimated according to the degree of intelligibility of radio phrases. The results of the measurements present in Table 3, where value D is the distance from the LoRa receiving set to the transmitter antenna (T); Received Signal Strength Indicator (RSSI) serves as an indicator of the signal level at the receiving set input; Packets is the number of transmitted packets; Quality of Receiving is a category parameter of reception. The last parameter was the estimated sign "+" in case of satisfying reception, and "-" otherwise.

Table 3: Report of Receiving Quality

D, m	RSSI, dBm	Packets	Quality of Receiving
100	-94	4	+
115	-96	4	+
129	-107	4	+
162 (A)	-98	4	+
187	-97	4	+
211	-96	4	+
230 (B)	-93	4	+
243	-101	4	+
263	-113	4	+
283	-124	-	±
303 (C)	-128	-	−

Based on the measurement data, a graph of the loss function $L(D)$ is built, where D is the range from the signal source to the

measurement point, Fig. 9. The resonant character of the curve in Fig. 9 is a consequence of the superposition of beams resulting from multipath propagation. Signal power losses in the section of indirect signal propagation with a length of 150-230 m have an average value of 15 dB.
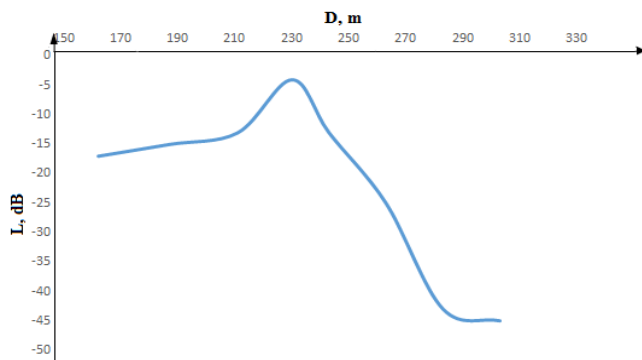
Figure 9: Graph of the function *L* (*D*).

Analysis of various forms of communication in mine made it possible to establish that the range of voice communication, with due regard for phrasal awareness, no more than 30 m; the distance of radio communication no more than 100 m; the transmission range by LoRa reached 150 m.

6. Conclusions

The paper presents a study of the LoRa module on two models of multipath propagation with external interference in a city building and without them in a salt mine. In the course of the studies carried out in a high-rise building, it was found that for the LoRa transmitter with a decrease in the SNR by 70 dB, the BER deteriorates by only 15%. The transmission range of messages in the mine with indirect beam propagation (Rayleigh channel) exceeded the distance of conventional radio communications by 30%, voice communications by five times. The average loss at the frequency under consideration is 15 dB for a Rayleigh radio propagation channel, provided the messages are intelligible. These results are planning to be the basis for the choice of the LoRaWAN radio network topology as an element of mine communication.

Conflict of Interest

The authors declare no conflict of interest.

Acknowledgment

The authors thank both the authorities of the Taras Shevchenko National University, and National Aviation University the especially leadership of the Faculty of Cybersecurity, Computer and Software Engineering for their support during the preparation of this paper. The authors also thank the anonymous reviewers, whose comments significantly improved the content of the paper.

References

[1] D. Kucherov; A. Berezkin; O. Sushchenko, "Features of Signal Processing by Means of LoRa Technology," in 2019 IEEE International Scientific-Practical Conference Problems of Infocommunications, Science and Technology (PIC S&T), Kyiv, Ukraine, 19-24, 2019. https://doi.org/10.1109/PICST47496.2019.9061410

[2] "Basic Tutorial on Wireless Communication and Electronic Tracking: Technology Overview," https://www.cdc.gov/niosh/mining/content/emergencymanagementandresponse/commtracking/commtrackingtutorial1.html

[3] T.S. Cory, Propagation of EM Signals In Underground Mines, Rockwell International Commercial Telecommunications Group, 1977. https://www.cdc.gov/niosh/mining/works/coversheet331.html

[4] T.S. Cory, R.J. Mahany, Mining Publication: Propagation of EM Signals in Underground Metal/Non-Metal Mines, U.S. Bureau of Mines, 1981. https://www.cdc.gov/niosh/mining/works/coversheet828.html

[5] J.N. Murphy, H.E. Parkinson, "Underground Mine Communications," P IEEE, **66** (1), 26–50, 1978. https://www.cdc.gov/NIOSH/mining/UserFiles/works/pdfs/umc.pdf

[6] S. Yarkan, S. Guzelgoz, H. Arslan, R.R. Murphy, "Underground Mine Communications: A Survey," IEEE COMMUN SURV TUT, **11**(3), 125–142, 2009. https://doi.org/10.1109/SURV.2009.090309

[7] Y.P. Zhang; G.X. Zheng; J.H. Sheng, "Radio propagation at 900 MHz in underground coal mines," IEEE T ANTENN PROPAG, **49**(5), 757–762, 2001. https://doi.org/10.1109/8.929630

[8] J. Wang, A. Al-Kinani, W. Zhang, and C.-X. Wang, "A New VLC Channel Model for Underground Mining Environments," in 2017 13th International Wireless Communications and Mobile Computing Conference (IWCMC), Valencia, Spain, 2017. https://doi.org/10.1109/IWCMC.2017.7986613

[9] J. Wang, A. Al-Kinani, J. Sun, W. Zhang, and C.-X. Wang, "A Path Loss Channel Model for Visible Light Communications in Underground Mines," in 2017 IEEE/CIC International Conference on Communications in China (ICCC), Qingdao, China, 2017. https://doi.org/10.1109/ICCChina.2017.8330479

[10] P.P. Játiva, M.R. Cañizares, C.A. Azurdia-Meza, D. Zabala-Blanco, A.D. Firoozabadi, F. Seguel, S. Montejo-Sánchez and I. Soto, "Interference Mitigation for Visible Light Communications in Underground Mines Using Angle Diversity Receivers," Sensors, **20** (2), 367, 1-29, 2020. https://doi.org/10.3390/s20020367

[11] T.-P. Wilfredo, Malekpour, Mahyar R., Miner, Paul S., "ROBUS-2: A Fault-Tolerant Broadcast Communication System," in NASA technical report, 2005, p. 188, https://ntrs.nasa.gov/citations/20050158766

[12] D. Iturralde, F. Seguel, I. Soto, C. Azurdia, S. Khan, "A new VLC System for Localization in Underground Mining Tunnels," IEEE LAT AM T, **15**(4), 581-587, 2017. https://doi.org/10.1109/TLA.2017.7896341

[13] A.D. Firoozabadi, C. Azurdia-Meza, I. Soto, F. Seguel, N. Krommenacker, D. Iturralde, P. Charpentier and D. Zabala-Blanco, "A Novel Frequency Domain Visible Light Communication (VLC) Three-Dimensional Trilateration System for Localization in Underground Mining," APPL SCI, **9**(7), 1488; 1-15, 2019. https://doi.org/10.3390/app9071488

[14] S. Suherman, A.H. Rambe, E. Wijayanto and N. Mubarakah, "Received signal consideration for the through the earth radiobased underground object detection," J PHYS CONF SER, **1566**, 1-7, 2020. https://doi.org/10.1088/1742-6596/1566/1/012003

[15] D.S. Kudinov, O.A. Maikov, E.A. Kokhonkova and V.S. Potylitsyn, "Development of a mathematical model and analysis of the receiver for emergency alerts in a mine," IOP CONF SER-MAT SCI, **862**, 1–7, 2020. https://doi.org/10.1088/1757-899X/862/3/032111

[16] A. Salam, A. Ahmad, "Underground Soil Sensing Using Subsurface Radio Wave Propagation," Purdue e-Pubs, 255–260, 2019. https://docs.lib.purdue.edu/cit_articles/19

[17] I.F. Akyildiz, E.P. Stuntebeck, "Wireless Underground Sensor Networks: Research Challenges," Ad Hoc Networks, **4**, 669–686, 2006. https://doi.org/10.1016/j.adhoc.2006.04.003

[18] I.F. Akyildiz, Z. Sun, M.C. Vuran, "Signal Propagation Techniques for Wireless Underground Communication Networks," PHYS COMMUN-AMST, **2**(3), 167–183, 2009. https://doi.org/10.1016/j.phycom.2009.03.004

[19] N. Saeed, M.-S. Alouini, T.Y. Al-Naffouri, "Towards the Internet of Underground Things: A Systematic Survey," IEEE COMMUN SURV TUT, **21**(4), 2019, 3443–3466. https://doi.org/10.1109/COMST.2019.2934365

[20] X. Chen, R. Liu, S. Zhang, H. Zeng, X. Yang, H. Deng, "Development of millimeter wave radar imaging and SLAM in underground coal mine environment," J CHINA COAL SOC, **45**(6), 2182-2192, 2020. https://doi.org/10.13225/j.cnki.jccs.ZN20.0316

[21] D. Kucherov, A. Berezkin, L. Onikienko, V. Nakonechnyi, "Processing Signals in The Receiving Channel for the Lora System," Data-centric business and applications. ICT Systems-Theory, Radio-Electronics, Information Technologies and Cybersecurity, **5**, 423–445. https://doi.org/10.1007/978-3-030-43070-2_19

[22] D. Kucherov, A. Berezkin, "Identification approach to determining of radio signal frequency," in Int. Conf. Antenna Theory and Techniques (ICATT), Kyiv, Ukraine, 2017. https://doi.org/10.1109/ICATT.2017.7972668

[23] B. Sklar, Digital Communications Fundamentals and Applications, Second Ed, Prentice Hall PTR, USA, 2002.

[24] SEMTECH SX1276. https://pdf1.alldatasheet.com/datasheet-pdf/view/800239/SEMTECH/SX1276.html

Challenges and New Paradigms in Conservation of Heritage-based Villages in Rural India-A case of Pragpur and Garli Villages in Himachal Pradesh

Preeti Nair[1,*], Devendra Pratap Singh[1], Navneet Munoth[2]

[1]School of Architecture and Planning, Amity University, Noida, 201301, India

[2]Maulana Azad National Institute of Technology, Department of Architecture and Planning*, Bhopal, 462003, India*

A R T I C L E I N F O	A B S T R A C T
	The research paper aims to focus on the issues and challenges in developing a sustainable model of an ideal heritage village project by using descriptive and empirical investigation methods. To capture the perception and understanding of the concept of sustainability of a Heritage Village, a mixed-methods approach was conducted by the researcher where document where reviewed, observations were done, structured interviews and a questionnaire survey was conducted involving resident's in the heritage villages of Pragpur and Garli in Himachal Pradesh, India. Through this research, the objective was to catalogues the resident's outlook and understand their belongingness towards their rural settlement. The analysis conducted, was also to understand their attachment to the heritage fabric which would act as a catalyst for their sustainable development. Due to the diversification in terms of architecture, social and cultural aspects, it was important to analyze the resident's perception towards the built heritage as it may vary to be more or less important to different people, community groups, or generations.

1. Introduction

The term "Heritage" proposes a wider based concept that includes both tangible and intangible heritage as well as the natural ecosystem of the settlement. It includes built environment, historic places and monuments, settlement pattern, settlement morphology, heritage collections, past and present cultural practices including living experiences of the residents of these villages. It can act as a catalyst for the overall sustainable growth and change in these rural settlements [1]. The collective memory of each locality or community or a particular heritage is unique. The preservation, conservation, documentation, presentation of the built heritage, and cultural diversity of any particular place are important challenges.

Manmade structures which possess heritage character and significance should become a part of the built heritage of any settlement and the society [2]. Due to the rapid modernization of the built environment, there is a need for focusing attention to preserve the cultural and architectural heritage, before it disappears completely. Buildings and settlements of historic or architectural value in all urban and rural areas are disappearing

very fast due to neglect and decay or reconstruction in newer materials which results in changing the specific characters of these village cores, leading to monotonous and repetitive new modern constructions.

The built heritage is the prominent aspect to transform the current situation of rural areas because it has the potential to diversify people's perception and acts as a common denominator for the development of these settlements. Heritage can act as a catalyst for the future development and sustainability of a village [3]. It indicates that by enhancing the heritage character of a village, a sustainable tool can be devised for the residents who live in these settlements to make them part of the rural development process. Additionally, the tool is likely to give rural areas a positive, vibrant image and in this way, a trend can be developed for bringing the migrated youth back into these rural areas. It also indicates that cultural meanings and construction assets such as vernacular construction techniques can be mobilized for rural and regional development, and cultural identities can become important for uplifting local economies.

[*]Preeti Nair, Research Scholar, Amity School of Architecture and Planning, Amity University, Noida, Uttar Pradesh, India, +91 -9711433201, preetinair30@gmail.com
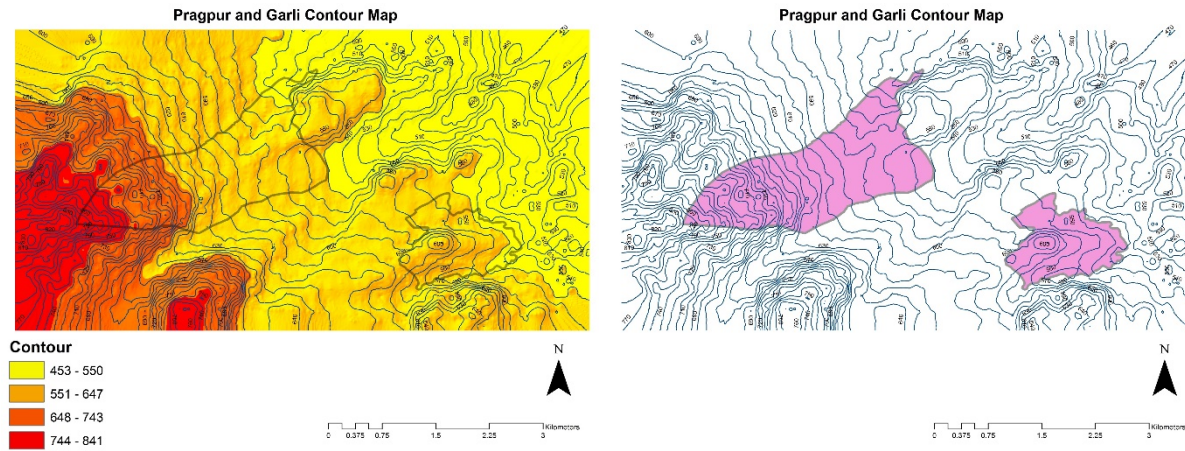
Figure1: Contour Map of Pragpur and Garli geo-referenced on GIS

2. Methodology

In the following study, a mixed method of analysis is conducted to investigate the status quo of these villages and also to understand the perception of the residents. In this mixed method of analysis, a three-stage layered analysis is conducted where the first stage is to conduct a spatial analysis using GIS, and then a descriptive and empirical analysis is conducted upon the responses received from the entire sample area. Questionnaire Surveys and interview-based surveys were used as tools to obtain variables. The relevance and public reaction to the concept of being a "Heritage village "models and theories regarding the sustainable built environment were questioned primarily. A total of 100 responses were gathered from these two villages and Turkey Post-Hoc test was conducted on the responses gathered using a five-point Likert scale. The questionnaire was developed on seven major parameters as Economic Viability, Infrastructure, Heritage, Social and cultural Character, Governance/ Policy framework, Environment, Settlement Pattern.

3. Study Area

The villages of Pragpur and Garli in Himachal Pradesh are situated at two thousand feet which are approx. 550 Meters above sea level, it comes under the region of district Kangra, Himachal Pradesh. The heritage-based settlement of Pragpur and Garli with a pristine view ideally suited to explore the distinct characteristics of Kangra valley. This area has several water channels that mix into river Beas with its pleasant and comfortable climate, better connectivity, rich flora, and fauna (Figure 1). The Dhauladhar mountain range raised behind this picture of pastoral perfection and needy frames it with tall peaks that are draped with snow for the better part of the year. Recognized as Heritage Village by a notification dated 9th December 1997 the state Government has classified Pragpur and Garli as a "Heritage Zone".

Heritage villages of Pragpur and Garli also fall under the ecozone, ideal for the development of tourism. These villages are also promoted by the administration as an example for community development in the hospitality sector. The core area of Pragpur is notified as "Heritage Villages" by the state government. This makes it one of the villages in India with such a distinctive title. Understanding the unique architectural style and settlement pattern the Government has declared the creation of SADA

(Special Area Development Authority) for improving the infrastructure in the area in the field of tourism[4][5].
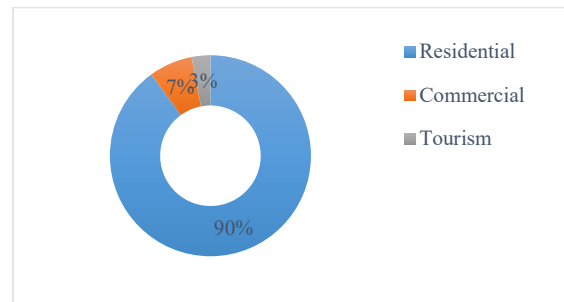
Figure 2: Land use percentage for the village of Pragpur and Garli

4. Architectural features of the built form

Pragpur and Garli can be divided into three major sectors based on the activities, such as residential, commercial, and tourism-based buildings (Figure 2). The Residential area is the zone where all the heritage-based residences are built[6]. The commercial area is where all the small-scale activities such as retail activity, weavers, shoemakers, etc. are housed. Tourism based infrastructure is where the residential houses have been converted into small scale hotel. Some of the major features that can be observed within the settlement are,15ft. that main street is around 15 feet in width which also acts as the main spine for connectivity from the urban centres.7-10 ft wide secondary streets are used for core connectivity towards the interior of the settlement having around 6010 feet width. Low height structures can be observed along the main street usually used for retail purposes.

The layout of the streets is in a linear pattern and the secondary roads radiate from the main street along the natural contour of the settlement. The main axial road of the village consists of built with variable land uses. As per the land use characteristics observed it was seen that the ground floors are used for commercial and retail. The lower floors are designed such as to create a recessed structure and the above floors act as cantilevers. A row of the columnar corridor is constructed supporting the projected floors of the upper storey. A colonnaded facade is recessed which provides easy entry and forms a semi-

transparent visual screen that creates a unified image of the structures. These plinth areas or semi-open areas act as recreational spots for the shop owners. The upper cantilever storey is used for residential purposes. Most of the residential and commercial structures are not more than two stories. A series of residences having vernacular architectural characteristics are built along the connecting streets of the village which diverge from the main spine. Many of these houses have a central courtyard. The common material used for the construction of these heritage houses are mud plaster, dry and seasoned bamboos with a layer of bitumen for roofing purposes. In the case of repetitive floors, the floors are finished with mud mixed with reed or bhusa to create a thick paste-like consistency. Wood is primarily used for doors and windows. The balustrades on all floors are constructed using seasoned timber. The doors, windows, and even the railings have magnificent ornamentation and carvings designed on them. The door frames are also adorned with carved patterns such as local flowers and flowering buds, animal frescos, and geometrical patterns. Window and door arches are constructed to support the lintel beams. A mixed variety of arches are observed such as segmental arches, flat arches, gothic spires, etc. The chajjas over the openings are also intricately carved. The streets are designed using cobbled stone in interesting patterns. The verandas are also constructed using stones in various patterns like linear, rectangular and circular patterns. The houses are arranged in a row formation around an open to sky courtyard. On the upper floors, the windows are reduced gradually in size. Half-timbered construction is mainly observed in these villages for the construction of residential buildings.

The half-timber construction method is, in which the external and internal walls are constructed using the timber-framed structure and the space between them is filled with materials such as mud plaster, brick, or daub and wattle. In these hilly regions the half-timber construction is usually made of squared oak timbers joined by rafters, tenons, mortises, and wooden pegs; the building's structural skeleton is strengthened using braces in the corners (Table 1).

To understand the evolution of the rural settlement and to catalogue its existence in the rural areas, the help of GIS (Geographic Information System) is taken. First, we created a base map of the spatial database of the Garli village. Then specific attributes such as the timeline of the construction, the year of the last restorations or reconstructions over time, etc. were attached to each vector. The main objective was to identify the residential buildings which were constructed through vernacular style and which residential buildings were renovated with their material study used in construction. In this way, it was possible to generate several maps that emphasize the old village system and the houses which have been abandoned by its residents (Figure 3 and 4). This attribute and the database are updated in real-time, and in this way the government can decide their restoration policies in a more precise way, comparing with the traditional methods. The updated data regarding the preservation and conservation status of residential houses represent an important factor in monitoring, protection and documentation of local heritage and, at the same time, offer the possibility to involve the local community in heritage management for sustainable development.

Table 1: Visual Survey of Pragpur and Garli depicting architectural features

Parameters	Images	Architectural Features
Settlement pattern		1. Streets paved with dressed cobbled stone.
Buildings		2. Gothic spires 3. Gables with decorative and ornate finials 4. Wooden pillars and heavy wooden beams 5. Roofs are sloping, made of local slate on wooden framework 6. Gabbled and cross gabbled
Materials		7. Mud plastered 8. Slate roofed houses 9. Bamboo 10. Reed or bhusa 11. Cobbled stone
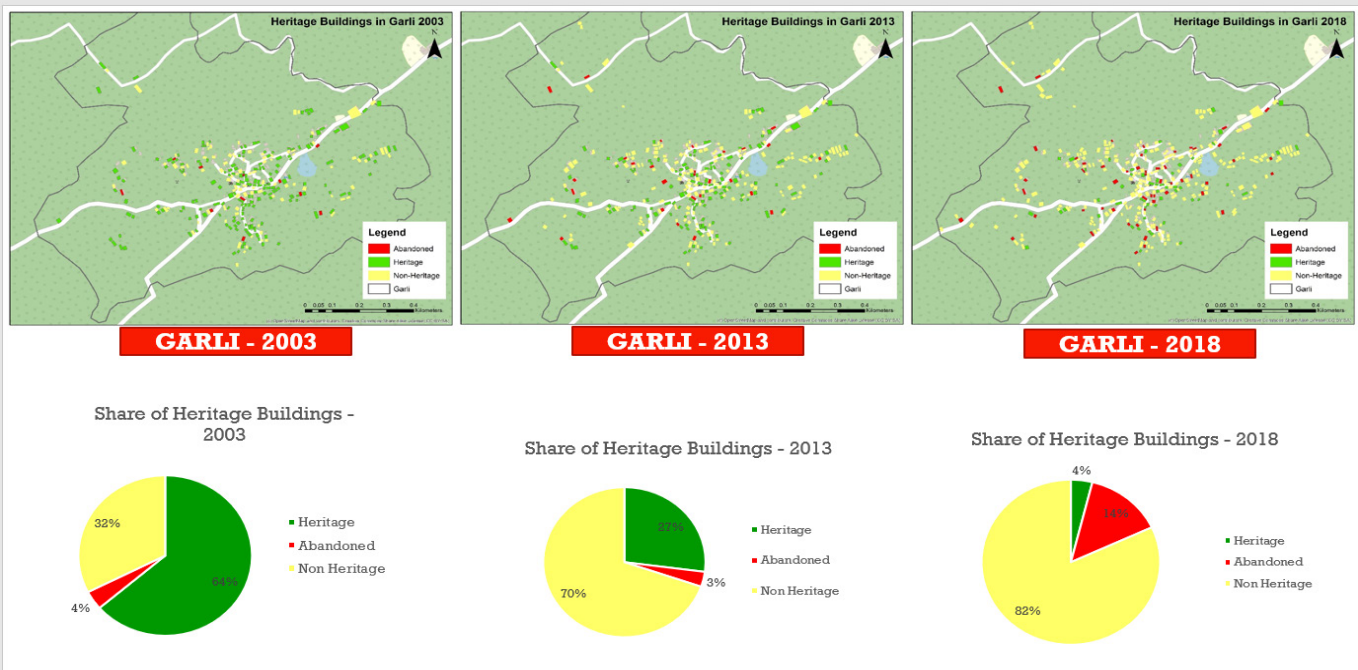
Figure 3- Settlement mapping of built heritage for year 2003,2013,2018 of Garli
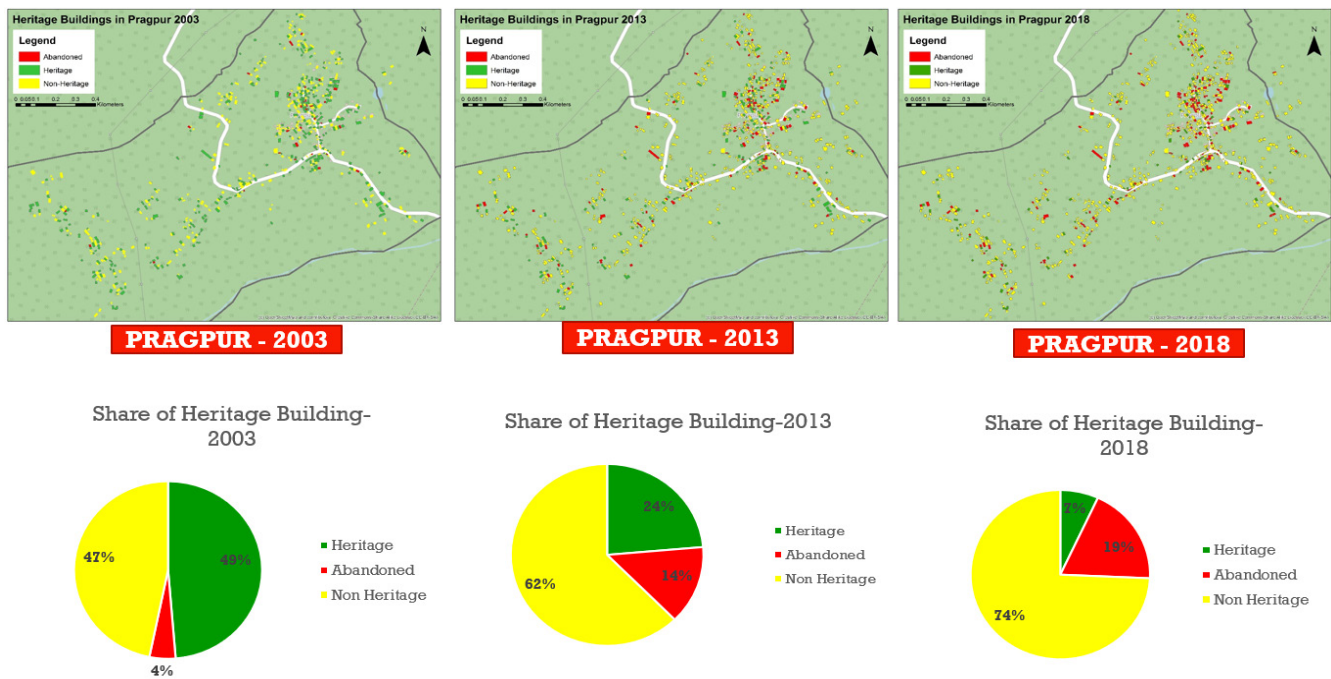
Figure 4: Settlement mapping of built heritage for year 2003,2013,2018 of Pragpur

5. Data Collection

To attain a holistic view, 100 interviews (50 in Pragpur and 50 in Garli) were carried out with groups of specialists (including academicians and conservationist), cultural reference groups (including community heads or chieftains, heritage managers, cultural groups, the private hospitality sector, and local NGOs). It is also important to understand that these traditional villages are located near the core and buffer zones of their urban district[7]. The composition of the sample of respondents was taken according to people who have a direct impact due to the development of these villages (Table 2).

The respondents were asked varied questions regarding the status of a "Heritage Village". Also, it reflects the understanding of the respondents as to whether after getting the said status whether the employment opportunities have increased[8]. This study also aims to enrich the literature with an empirical investigation on issues and challenges in developing a sustainable model of heritage village projects[9]. Thus, the objectives are to identify the most common and fundamental issues and challenges that currently exist in these villages and to determine if these issues can be resolved with certain interventions[10].
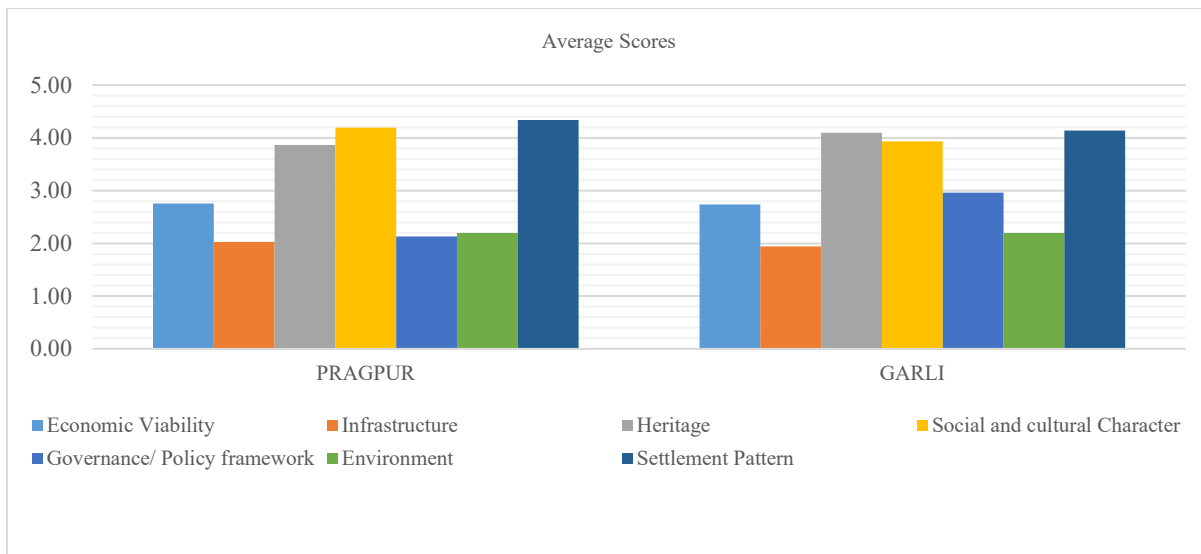
Figure 5: Descriptive analysis for the responses

Table 2: Sample size for the questionnaire survey in Pragpur and Garli

	Pragpur	Garli
Total Residential Buildings	354	118
Heritage Building	93	21
New Construction	261	97
Abandoned Residences	67	17
Sample Size for Survey	50	50

5.1. Statistical analysis

Statistical analysis is performed by using descriptive and inferential statistics. Pearson correlation was applied to see the relationship between the variables. One-way Anova followed by Tukeys HSD post-hoc test for multiple comparisons was applied to see the mean difference between the villages.

Correlation in the broadest sense is a measure of an association between variables. In correlated data, the change in the magnitude of 1 variable is associated with a change in the magnitude of another variable, either in the same (positive correlation) or in the opposite (negative correlation) direction. The Pearson correlation coefficient is typically used for jointly normally distributed data. Then to understand the study One-way Anova was used.

- To compute large and varied data sets, which included data collected from two different villages and having varied responses. It was also done to verify the variability of the data acquired.

- To test which method yields the most suitable result in the sample of data collected. The sample consisted of stakeholders comprising of the residents, government officials, and tourists in these two villages.

If data are analyzed using ANOVA, and a significant F value obtained, a more detailed analysis of the differences between the

treatment means will be required. In this case, the P-value is less than 0.05 considered as significant at 95% confidence level.

The statistical software SPSS version 24.0 was used in the analysis. The questions in the questionnaire invited them to indicate the level of agreement of each factor in relation to the seven main parameters based on a five-point scaling, i.e., Strongly Agree = 5, Agree = 4, neutral = 3, Disagree = 2, and Strongly disagree = 1.

6. Result and Discussion

The Economic Viability parameter, the focus was to correlate the economic fabric [11]of these villages as a community and whether this can act as a prominent factor that governs the sustainable development of a rural area[12]. The Infrastructure parameter focuses on the infrastructure needed for developing a sustainable village model which may include roads, tourism infrastructure, connectivity, etc. The parameter also addresses the negative impact of creating an ideal village model and that may hamper the heritage fabric of the villages[13]. Understanding the relationship and assessing the loss and degradation of the core's-built heritage is the focus behind the Heritage parameter. This is to analyse, investigate, and discuss, the concerns, obstacles, and issues of sustainability to this rural heritage conservation. In the Social and cultural Character parameter the focus is to examine the influence of socio-cultural factors on the formation of architectural spaces in Heritage based villages by applying a descriptive-analytical method and using literature study.

The results of this study indicate that the structural system of traditional houses is based on a hierarchical system and is intricate for the development of the settlement. The Governance/Policy Framework parameter attempts to focus on the holistic system or dynamic model to analyze the interaction of the social–economic–heritage sectors to examine policies to achieve the goal of development and conservation. The Literature study shows that conservation alone cannot lead to its own goal. Economic development strategies or policies could be a better choice if the development is carefully planned and effectively controlled to avoid over-consuming resources.

Table 3: Statistical analysis

		N	Mean	Std. Deviation	Std. Error	95% Confidence Interval for Mean		Minimum	Maximum	p-value
						Lower Bound	Upper Bound			
Economic Viability	PRAGPUR	50	19.28	3.33	0.47	18.33	20.23	14.00	32.00	<0.001
	GARLI	50	19.18	2.97	0.42	18.33	20.03	12.00	25.00	
Infrastructure	PRAGPUR	50	16.20	2.74	0.39	15.42	16.98	11.00	23.00	<0.001
	GARLI	50	15.54	2.21	0.31	14.91	16.17	11.00	20.00	
Heritage	PRAGPUR	50	23.20	3.16	0.45	22.30	24.10	15.00	29.00	<0.001
	GARLI	50	24.58	3.14	0.44	23.69	25.47	15.00	29.00	
Social and cultural Character	PRAGPUR	50	16.78	1.64	0.23	16.31	17.25	13.00	20.00	<0.001
	GARLI	50	15.74	2.42	0.34	15.05	16.43	10.00	20.00	
Governance/ Policy framework	PRAGPUR	50	4.26	1.69	0.24	3.78	4.74	2.00	7.00	<0.001
	GARLI	50	5.92	2.15	0.30	5.31	6.53	2.00	9.00	
Environment	PRAGPUR	50	2.20	1.03	0.15	1.91	2.49	1.00	4.00	0.017
	GARLI	50	2.20	0.97	0.14	1.92	2.48	1.00	4.00	
Settlement Pattern	PRAGPUR	50	4.34	0.80	0.11	4.11	4.57	3.00	5.00	0.012
	GARLI	50	4.14	0.93	0.13	3.88	4.40	2.00	5.00	

Understanding the influence of human behavior on the landscape is the prime objective of the Environment parameter. Also, to analyze the reason for village landscape transition which come from road construction, the transformation of building materials, higher living level, the inflection of family structure and social relationship, different culture and self-identity [14]. To investigate or to identify the challenges and hurdles towards the growth or deterioration of the settlement of heritage villages, it was gathered that through cataloguing the settlement pattern the evolution of the community and its historical background can be documented with its various changes in all its bearings.

To understand the aim of the Economic Viability parameter was to determine their economic status of the respondents and whether they have benefitted from the status of "heritage village" [15]. The respondents of the villages of Garli and Pragpur had major concerns while developing their residential buildings. The families owning these houses lacked the economic resources and finances to maintain these houses [16]. While enquiring about the infrastructure development the residents were not content and strongly disagrees with the increase in any land value in villages of Garli and Pragpur in Himachal where the circle rate for 100 sq. meters are around 886 Rs and 1751 Rs (District Kangra, Government of India website) respectively from last one decade.

It indicated the stagnation in terms of development. In these villages, it was also observed that mostly the migrant population is residing in the heritage houses were on a rental basis [17]. They are mostly not aware of the heritage status and do not have the economical means to maintain these residential buildings. The infrastructure needed to sustain and develop a heritage village was not visible in these Villages.

Community Participation has been observed as a major factor for the sustainable development of a settlement [18]. In villages like Garli, some residential patrons have tried to restore their residential buildings and convert them into commercial and recreational spaces for the tourist, parallel developing the village

and generating employment for the locals. The basic amenities such as fire protection and police protection also lack in these villages. The villagers were governed under Panchayat System and they themselves resolve the petty issues related to the governance of the villages [19].

The villages lacked the basic infrastructure to support a tourist influx. It was determined by the study that, many people outside of these villages are not aware of the heritage status. The upkeep the vernacular architectural style of the residences, not many skilled labours are available. The construction and maintenance in these villages are done according to the new construction style using materials such as RCC and Bricks. In Pragpur and Garli, timber construction and wood such as teak and sheesham were used for the construction of residential houses.

7. Findings

The major factors highlighted in this study were as detailed below:

- The first major criteria were to identify the heritage-based settlements through the extensive literature study. A multidisciplinary approach was initiated where along with the architectural characters certain parameters were combined such as economy, social conditions, settlement morphology, etc.

- It was also observed that different policy development schemes or frameworks for the inclusion of rural heritage preservation measures is not highlighted or mentioned. There is no incorporation of heritage-based rural development in the physical planning processes as part of a holistic approach towards sustainable development [20]. This research wants to focus on and promote the inclusion of preservation of heritage-based residential buildings representing the local architectural style.

- Finally the study wants to highlight the importance of heritage in rural development. Through the descriptive and empirical study of the data, it was found that for the development of these types of settlements the role of the local residents and community plays an important part [21]. There is a need for introducing public awareness as a tool to generate employment in these rural areas.

The data acquired through the questionnaire survey along with the interview survey gave many insights to identify the hurdles and challenges while implementation of heritage-based development policy. A multidisciplinary approach as mentioned earlier can be used where collaboration with tourism, hospitality industry all related sectors can be initiated [22]. This was considered important to resolve any issues which may cause the undermining preservation of the built resources. It is also stressed that preservation of cultural and natural heritage should be perceived together and they must not be promoted with activities that can cause hindrances towards sustainability. To make the residents conscious about the values of rural heritage certain programs can be initiates such as studies on vernacular architecture, promotion of knowledge, and training about traditional techniques and materials.

It was also observed during the survey that the majority of participants were of the suggestion that a balance should be maintained between the retained heritage-built fabric and its economic viability. The entire exercise was conducted to understand the importance of the residential buildings and should actually be protected. Secondly, it was to address its importance for the future generations of these villages. The second factor also ponders upon the different methods of adaptability and reuse of these heritage buildings. The process also helped to understand the hurdles along with the decision-making towards the protection and conservation of these buildings. Many respondents have also agreed that the policymakers and government officials should ensure that if the value of a residential building is under heritage significance then relevant heritage policies and bye-laws should be formulated.

8. Conclusion

Through the extensive literature study regarding the preservation of this built heritage, the researcher had identified core parameters that are vital for sustainable development. The qualitative study and empirical study evaluated the study and the observation done to understand the ground reality. The major parameters were categorized into several sub-parts depending on the focus, such as historical value, economic viability, infrastructure, socio-cultural characteristics, and the overall aesthetic value. The research aimed to understand the perception of the local community and analyse their approach and consensus to further develop a holistic policy framework. The detailed analysis led to the determination that the infrastructure lacks the capacity to promote tourism or hospitality industry to create a sustainable model to promote the heritage of that area. In very few cases, the architectural value (vernacular architectural style) is also considered but all are linked to the history of a particular settlement along with its cultural values.

It is evident from the analysis from the sample groups and interviews that diversity plays an important role when discussing the importance of their heritage settlement. It varies across the communities, geographical location. It also varied because of their economic status, socio- cultural parameters as seen in these villages of Pragpur and Garli. As per the investigation, it was also highlighted that administration plays an important role as policymakers and implementors. It is important for the local government to create awareness towards the importance of these heritage-based residential buildings and that they may gain value in the future.

9. References

[1] S.H. Zolfani, E.K. Zavadskas, "Sustainable development of rural areas' building structures based on local climate," Procedia Engineering, **57**, 1295–1301, 2013, doi:10.1016/j.proeng.2013.04.163.

[2] E. Erdogan, S.D.B. Erkiş, "Sille settlement in the context of sustainable historical fabric and façade analysis of its traditional houses," Archnet-IJAR, **8**(3), 117–135, 2014, doi:10.26687/archnet-ijar.v8i3.214.

[3] I. Syahrul, M. Radzuan, N. Fukami, Y. Ahmad, "Cultural heritage, incentives system and the sustainable community: lessons from Ogimachi Village, Japan.," Cultural Heritage, Incentives System and the Sustainable Community: Lessons from Ogimachi Village, Japan., **10**(1), 130–146, 2014.

[4] R.P.B. Singh, M. Fukunaga, "The {World} {Heritage} {Villages} of {Shirakawa}-{Gō} and {Gokayama}, {Japan}: {Continuing} {Culture} and {Meeting} {Modernity}," Heritagescape and Cultural Landscapes. Planet Earth & Cultural Understanding Series, Pub, **6**(Special Lecture 3), 129–150, 2010.

[5] S. Kim, "World Heritage Site designation impacts on a historic village: A case study on residents' perceptions of Hahoe Village (Korea)," Sustainability (Switzerland), **8**(3), 2016, doi:10.3390/su8030258.

[6] C. Holtorf, "Embracing change: how cultural resilience is increased through cultural heritage," World Archaeology, **50**(4), 639–650, 2018, doi:10.1080/00438243.2018.1510340.

[7] N. Mitsche, F. Vogt, D. Knox, I. Cooper, P. Lombardi, D. Ciaffi, "Intangibles: Enhancing access to cities' cultural heritage through interpretation," International Journal of Culture, Tourism, and Hospitality Research, **7**(1), 68–77, 2013, doi:10.1108/17506181311301381.

[8] N.A. Haddad, L.A. Fakhoury, "Towards developing a sustainable heritage tourism and conservation action plan for irbid's historic core," Archnet-IJAR, **10**(3), 36–59, 2016, doi:10.26687/archnet-ijar.v10i3.1035.

[9] S. Prompayuk, P. Chairattananon, "Preservation of Cultural Heritage Community: Cases of Thailand and Developed Countries," Procedia - Social and Behavioral Sciences, **234**, 239–243, 2016, doi:10.1016/j.sbspro.2016.10.239.

[10] R. Askarizad, "Influence of Socio-Cultural Factors on the Formation of Architectural Spaces (Case Study : Historical Residential Houses in Iran) Influence of Socio-Cultural Factors on the Formation of Architectural Spaces," **1**(May), 44–54, 2019.

[11] O.S. Asfour, A.T. Hathat, "Strategies of Sustainable Rural Development in the Gaza Strip : Wadi Gaza Town as a Case Study STRATEGIES OF SUSTAINABLE RURAL DEVELOPMENT IN THE GAZA STRIP : WADI GAZA TOWN AS A CASE STUDY," (August), 2016.

[12] G.A.. Tanguay, E. Berthold, J. Rajaonson, "A Comprehensive Strategy to Identify Indicators of Sustainable Heritage Conservation," Les Cahiers Du CRTP (Workin Paper), (September), 2014.

[13] S. Roy, "Regional Disparities in Growth and Human Development in India," (September), 2012.

[14] I.S. Mat Radzuan, S. Inho, Y. Ahmad, "A rethink of the incentives programme in the conservation of south korea's historic villages," Journal of Cultural Heritage Management and Sustainable Development, **5**(2), 176–201, 2015, doi:10.1108/JCHMSD-02-2014-0006.

[15] M. A. S., "Efficient Rural Development Strategies for the Improvement of Indian Economy," International Journal of Pure & Applied Bioscience, **5**(6), 566–570, 2017, doi:10.18782/2320-7051.5462.

[16] N.A. Haddad, F.Y. Jalboosh, L.A. Fakhoury, R. Ghrayib, "Urban and rural umayyad house architecture in Jordan: A comprehensive typological analysis at Al-Hallabat," Archnet-IJAR, **10**(2), 87–112, 2016, doi:10.26687/archnet-ijar.v10i2.835.

[17] I.K. Suarthana, N. Madiun, S.O. Yuniarsa, "Exploring The Community Participation, Tourism Village, And Social-Economic To Environment Impact (Case Study: Pentingsari Village, Yogyakarta)," International Journal of Business and Management Invention, **4**(9), 85–90, 2015.

[18] A.J. Imperiale, F. Vanclay, "Using Social Impact Assessment to Strengthen Community Resilience in Sustainable Rural Development in Mountain Areas," Mountain Research and Development, **36**(4), 431–442, 2016, doi:10.1659/MRD-JOURNAL-D-16-00027.1.

[19] I.S. Mat Radzuan, Y. Ahmad, "Synthesising an effective incentives system in safeguarding the heritage village of melaka and george town," Planning Malaysia, (5), 157–168, 2016, doi:10.21837/pmjournal.v14.i5.200.

[20] X. Honggang, "Exploring Sustainable Policies for Xidi, the World Heritage Village ," Proceedings of the 28th International Conference of the System Dynamics Society, 1–16, 2010.

[21] J. Hosagrahar, J. Soule, L.F. Girard, A. Potts, "International Council on Monuments and Sites (ICOMOS) Cultural Heritage, the UN Sustainable Development Goals, and the New Urban Agenda," 2016.

[22] L. Yan, C. Liang, H. Zhiwen, "Conservation of Historical and Cultural Towns and Villages in China," Aussie-Sino Studies, **3**(4), 85–97, 2017.

A S T E S

Electronically Tunable Triple-Input Single-Output Voltage-Mode Biquadratic Filter Implemented with Single Integrated Circuit Package

Natchanai Roongmuanpha, Taweepol Suesut, Worapong Tangsrirat[*]

School of Engineering, King Mongkut's Institute of Technology Ladkrabang (KMITL), Bangkok 10520, Thailand

A R T I C L E I N F O	A B S T R A C T
	This article proposes a compact and simple design of electronically adjustable voltage-mode biquadratic filter using fundamental active cell implemented on a single integrated circuit (IC) package as LT1228. The proposed circuit having triple inputs and single output (TISO) employs namely one resistor and two capacitors as the passive components. All the five possible biquadratic filtering responses, namely low-pass (LP), band-pass (BP), high-pass (HP), band-stop (BS) and all-pass (AP), are realized by the appropriate selection of the relevant input signals. The pole angular frequency and the quality factor of the proposed TISO filter are electronically tunable through the bias current of the IC chip LT1228. Non-ideal effects and sensitivity performance are carried out. The theoretical results are satisfactorily validated by both PSPICE simulation results and experimental measurements using commercially available LT1228.

1. Introduction

Over the decade, analog filters always play a role in many important analog signal processing applications, i.e. communication systems, measurement and instrumentation systems, etc. Nowadays, the realization of an active analog filter using versatile active building blocks has been focused by many researchers due to many advantage features, such as simple circuitry, high linearity, and wide dynamic range. In the literature, many modern active electronic elements have been utilized in analog active filter design, such as current conveyor (CC) [1–7], differential difference current conveyor (DDCC) [8–12], differential voltage current conveyor (DVCC) [13–16], fully differential second-generation current conveyor (FDCCII) [17], current differencing buffered amplifier (CDBA) [18–20], current feedback operational amplifier (CFOA) [21–27], current follower transconductance amplifier (CFTA) [28–29], operational transconductance amplifier (OTA) [30–34], voltage differencing buffered amplifier (VDBA) [35–36], voltage differencing inverting buffered amplifier (VDIBA) [37], fully balanced voltage differencing buffered amplifier (FB-VDBA) [38], voltage differencing transconductance amplifier (VDTA) [39–41], and voltage differencing gain amplifier (VDGA) [42–44]. However, so many of them require at least two or more active elements for

their realizations [1–5, 7, 8, 10, 11, 13, 18–27, 30–39, 41, 43, 44]. Moreover, the voltage-mode filters presented in [1–17, 19–29, 38, 42] need a large number of passive resistors, while the articles in [1, 4, 16, 22] also contain three passive capacitors. It is also to be emphasized that the realizations of [1–27] suffer from the lack of electronic tuning capability of their important parameters. Even though some similar works were developed by based on various active building blocks in either bipolar junction transistor or (BJT) or complementary metal oxide semiconductor (CMOS) technologies, they are not commercially available chips and reachable in general. Besides, the performances of the research developments in [1–4, 7–20, 22, 24, 25, 28–37, 39–44] have been demonstrated through only simulation results.

In this communication, an electronically tunable voltage-mode biquadratic filter with three input and one output terminals (TISO) consisting of only single active IC package LT1228, one resistor and two capacitors is introduced. The proposed TISO filter can realize the five standard biquadratic filtering responses, namely low-pass (LP), band-pass (BP), high-pass (HP), band-stop (BS) and all-pass (AP), all at a single output terminal without modifying a circuit structure. It also provides an electronic adjustability of its pole angular frequency (ω_o) and quality factor (Q) via the external bias current of the LT1228 IC chip. The theoretical propositions are confirmed by PSPICE simulations with LT1228's model parameters, and the simulated results corroborate the theory. In addition, all conclusions discussed in this work are also verified by

the measurement results of an experimentally test circuit with a single IC package LT1228, and the experimental findings are found to be in agreement with the theoretical values.

2. Description of IC Package LT1228

Our design utilizes only one active cell of a commercially available IC LT1228 from Linear Technology Company [46]. An active cell LT1228 is internally a combination of an operational transconductance amplifier (OTA) and a current feedback operational amplifier (CFA) in 8-pin IC package, as demonstrated in Figure 1. This device has three high impedance input terminals (p, n, and z), and one low impedance output terminal (o). It provides the output current i_z at intermediate terminal z which is the difference of two input voltages v_p and v_n ($v_p - v_n$) multiplied by transconductance gain (g_m). An external impedance Z_z is connected to the terminal z, and the potential v_z developed across Z_z will transfer to the output voltage v_o at the terminal o by the CFA. Its ideal terminal characteristics can be described as:

$$\begin{bmatrix} i_p \\ i_n \\ i_z \\ v_o \end{bmatrix} = \begin{bmatrix} 0 & 0 & 0 & 0 \\ 0 & 0 & 0 & 0 \\ g_m & -g_m & 0 & 0 \\ 0 & 0 & 1 & 0 \end{bmatrix} \cdot \begin{bmatrix} v_p \\ v_n \\ v_z \\ i_o \end{bmatrix} . \qquad (1)$$

Thanks to the LT1228 manufacturing, the g_m-value can be altered to the desired value through the external DC bias current I_B by the following relation: [46]

$$g_m = 10 I_B . \qquad (2)$$

(a)

(b)

(c)
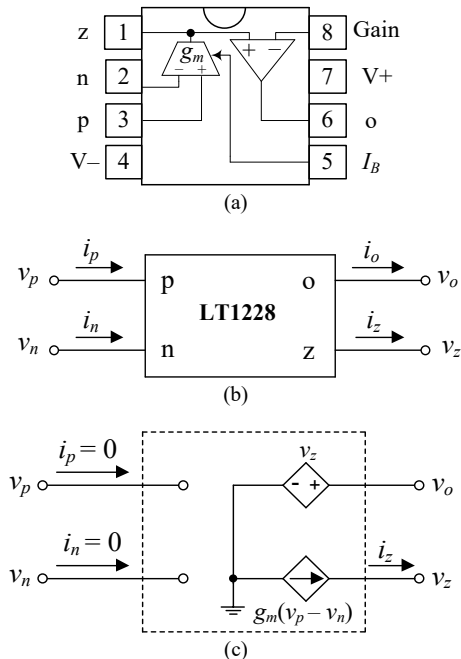
Figure 1: IC device LT1228.
(a) active elements in LT1228 (b) schematic representation
(c) equivalent circuit.

3. Proposed TISO Biquadratic Filter

The realization of an electronically tunable TISO voltage-mode biquadratic filter is given in Figure 2. The proposed TISO filter is implemented with a single LT1228 together with one resistor and two capacitors. A straightforward analysis of the proposed TISO filter reveals the following output voltage function:

$$V_{out}(s) = \frac{s^2 R_1 C_1 C_2 V_3 + s C_1 V_2 + g_m V_1}{D(s)} , \qquad (3)$$

where the denominator $D(s)$ is found to be:

$$D(s) = s^2 R_1 C_1 C_2 + s C_1 + g_m . \qquad (4)$$

From an inspection of Equations (3)-(4), it appears the five standard biquadratic filter functions can be obtained all at the terminal v_{out} of the proposed circuit by the following conditions.

(i)   The LP response is obtained by setting $v_{in} = v_1$ (input voltage signal) and $v_2 = v_3 = 0$ (grounded).

(ii) The BP response is obtained by setting $v_{in} = v_2$ and $v_1 = v_3 = 0$.

(iii) The HP response is obtained by setting $v_{in} = v_3$ and $v_1 = v_2 = 0$.

(iv) The BS response is obtained by setting $v_{in} = v_1 = v_3$ and $v_2 = 0$.

(v)   The AP response is obtained by setting $v_{in} = v_1 = -v_2 = v_3$.
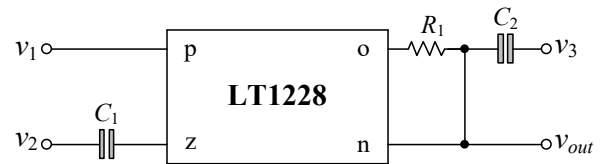
Figure 2: Proposed electronically tunable TISO biquad implementation employing single LT1228.

Therefore, the proposed TISO filter of Figure 2 does not require any element matching conditions or equality constraints for the desired filter function realizations. In all types, the important characteristics ω_o, and Q are respectively found as:

$$\omega_o = 2\pi f_o = \sqrt{\frac{g_m}{R_1 C_1 C_2}} , \qquad (5)$$

and

$$Q = \sqrt{\frac{g_m R_1 C_2}{C_1}} . \qquad (6)$$

In case of practical design, if $C = C_1 = C_2$, then the ω_o and Q simplify to:

$$\omega_o = \frac{1}{C}\sqrt{\frac{g_m}{R_1}} , \qquad (7)$$

and

$$Q = \sqrt{g_m R_1} . \qquad (8)$$

In view of the above expressions, the parameters ω_o and Q of the proposed TISO filter can be altered electronically by means of g_m-value. According to Equation (2), the g_m variation can be obtained by an adjustment of the bias current. Also note that since the major contribution of this work is to design a compact and

minimum configuration voltage-mode TISO filter with electronic tunability, an orthogonal control of ω_o or Q is not expected.

4. Non-Ideal Analysis and Sensitivity Performance

In consideration of the non-ideal behavior, the terminal behaviors of LT1228 can be rewritten as:

$$
\begin{bmatrix} i_p \\ i_n \\ i_z \\ v_o \end{bmatrix} = \begin{bmatrix} 0 & 0 & 0 & 0 \\ 0 & 0 & 0 & 0 \\ \alpha g_m & -\alpha g_m & 0 & 0 \\ 0 & 0 & \beta & 0 \end{bmatrix} \cdot \begin{bmatrix} v_p \\ v_n \\ v_z \\ i_o \end{bmatrix} , \tag{9}
$$

where $\alpha = (1 - \varepsilon_{gm})$ and $\beta = (1 - \varepsilon_v)$, where $|\varepsilon_{gm}| << 1$ and $|\varepsilon_v| << 1$ are the transconductance inaccuracy and the voltage transfer error, respectively. Taking this effect into account, the characteristics ω_o and Q given in Equations (5) and (6) are modified to:

$$
\omega_o = \sqrt{\frac{\alpha\beta g_m}{R_1 C_1 C_2}} , \tag{10}
$$

and

$$
Q = \sqrt{\frac{\alpha\beta g_m R_1 C_2}{C_1}} . \tag{11}
$$

In this case, all sensitivity coefficients of ω_o and Q with respect to the active and passive components are derived and found to be as follows:

$$
S_\alpha^{\omega_o} = S_\beta^{\omega_o} = S_{g_m}^{\omega_o} = \frac{1}{2} , \tag{12}
$$

$$
S_{R_1}^{\omega_o} = S_{C_1}^{\omega_o} = S_{C_2}^{\omega_o} = -\frac{1}{2} , \tag{13}
$$

$$
S_\alpha^Q = S_\beta^Q = S_{g_m}^Q = S_{R_1}^Q = S_{C_2}^Q = \frac{1}{2} , \tag{14}
$$

and

$$
S_{C_1}^Q = -\frac{1}{2} . \tag{15}
$$

It is clear from Equations (12)-(15) that the absolute values of the ω_o- and Q-sensitivities are all equal to 0.5. These values ensure that the sensitivity performance of the circuit is to be of low value.

5. Simulation Results

In this section, the proposed circuit and its filtering responses are simulated and discussed through the PSPICE simulation program. For ideal simulation, the LT1228 macro-model parameters obtained from Linear Technology Company and DC supply voltages of ±5V were employed. To demonstrate the functionality of the proposed filter, the circuit is designed for $f_o = 159.15$ kHz and $Q = 1$. In this case, the various component values have been set as $I_B = 100$ μA for $g_m = 1$ mA/V, $R_1 = 1$ kΩ and $C_1 = C_2 = 1$ nF. The simulation results for all filter responses are shown in Figures 3-7, which demonstrates very close agreement with the theoretical responses. For time-domain responses, a 159-kHz sine-wave input voltage with 50 mV peak amplitude was applied to the filter. The simulation results show that the error in f_o-value was found to be less than 1%.
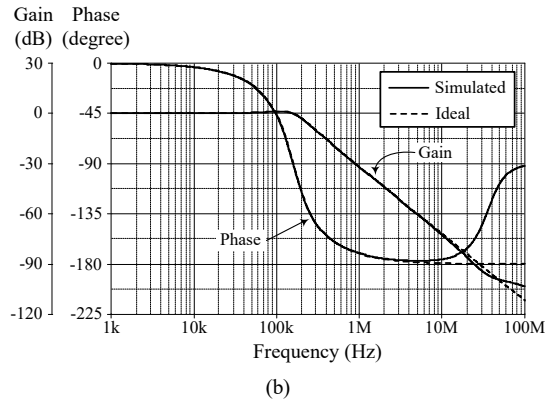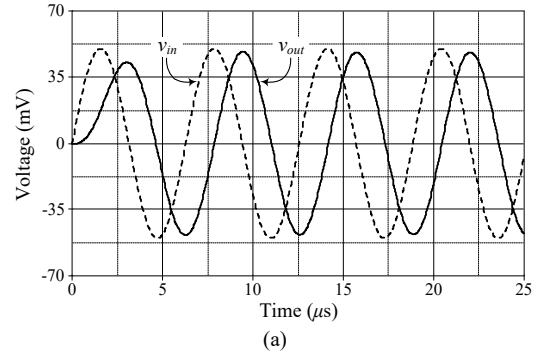
Figure 3: Ideal and simulated LP characteristics
(a) time-domain responses   (b) frequency responses
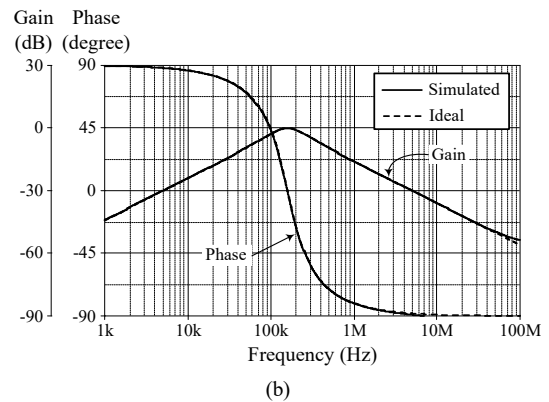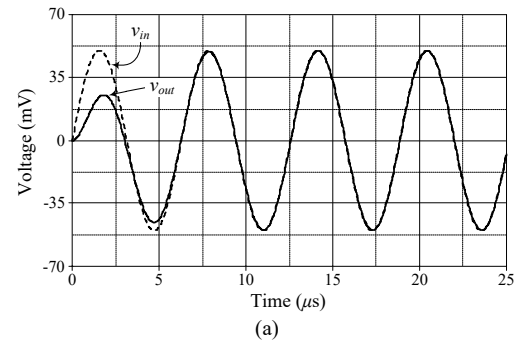
Figure 4: Ideal and simulated BP characteristics
(a) time-domain responses   (b) frequency responses
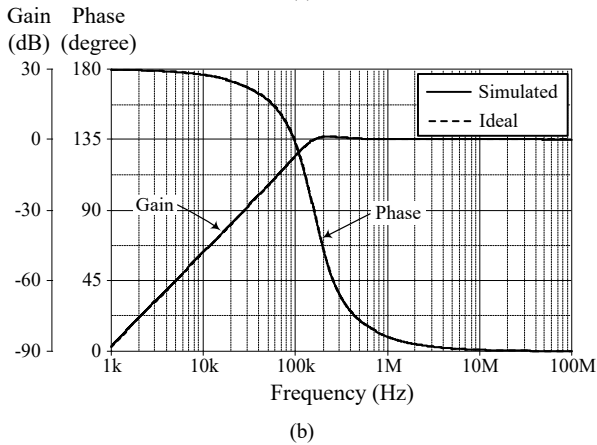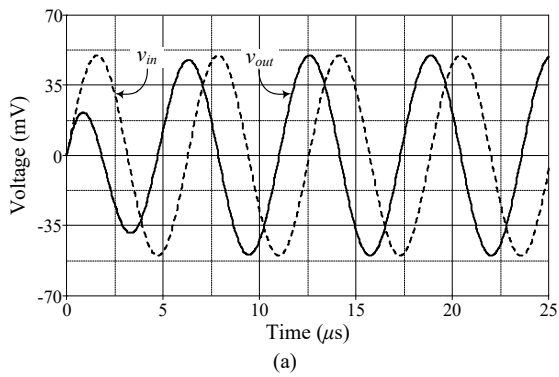
Figure 5: Ideal and simulated HP characteristics
(a) time-domain responses   (b) frequency responses

Figure 6: Ideal and simulated BS characteristics
(a) time-domain responses   (b) frequency responses

Figure 7: Ideal and simulated AP characteristics
(a) time-domain responses   (b) frequency responses

Furthermore, the electronic tuning of gain characteristic for BP filter concerning I_B is observed. The related gain expressions of the proposed BP filter, as shown in Figure 8, are plotted for $I_B = 50$ μA, 200 μA, and 500 μA, which resulted in $g_m = 0.5$ mA/V, 2 mA/V, and 5 mA/V, respectively. From Figure 8, the simulation conditions, and corresponding theoretical and simulated f_o and Q are summarized in Table 1.
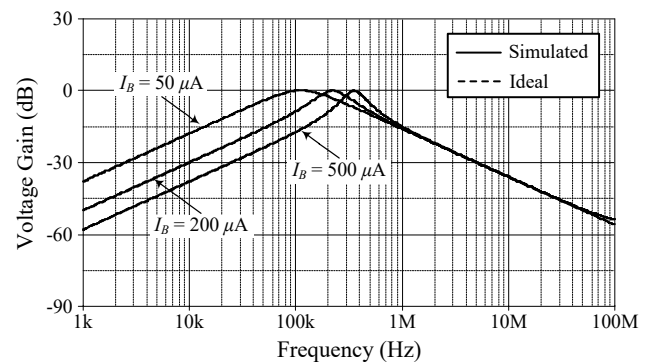
Figure 8: Ideal and simulated frequency responses of the proposed BP filter with an adjustment of I_B.

6. Experimental Results

To further validate the practical workability of the TISO biquadratic filter in Figure 2, the prototype circuit built with readily available IC element LT1228 and discrete passive elements were used to execute experimentally laboratory tests. The circuit was measured using Keysight EDUX1002G digital storage oscilloscope. All of the measured results were performed

Table 1: f_o and Q adjustment of the proposed filter by varying I_B

I_B (μA)	g_m (mA/V)	R_1 (kΩ)	C (nF)	Q	f_o (kHz) Simulated	f_o (kHz) Ideal	% f_o deviation
50	0.5	1	1	0.7	111.43	112.54	0.99
100	1	1	1	1	157.70	159.15	0.91
200	2	1	1	1.4	222.84	225.08	0.99
500	5	1	1	2.2	352.37	355.88	0.99

at symmetrical supply voltages of ±5 V, and I_B = 100 μA (g_m = 1 mA/V), R_1 = 1 kΩ, and $C_1 = C_2 = 1$ nF. This results in f_o = 159.15 kHz and Q = 1. To observed transient response, the measurement was carried out with a 159-kHz sine-wave signal input of 50 mV peak amplitude. The experimental results for the transient and frequency responses as well as the associated frequency spectrums are displayed in Figures 9-13. Also from Figures 9(c)-13(c), the measured results of the percentage total harmonic distortion (%THD) of the v_{out} for each filtering responses are noted in Table 2. It can be concluded that the measured results are close to the theoretical analysis, and also verify the functionality of the proposed circuit.

Table 2: Total harmonic distortions of v_{out} in Figure 2.

Filter	THD (%)
LP	0.67
BP	4.47
HP	0.73
BS	2.4
AP	0.32

Another set of measurements have been carried out to examine the electronic adjustability of the proposed TISO filter. BP filter response is used for illustrative purposes. Figure 14 illustrates the measured BP frequency responses for various bias current I_B. The g_m-values of the considered filter have been set as 0.5 mA/V, 2 mA/V, and 5 mA/V, for I_B = 50 μA, 200 μA, and 500 μA, respectively. As follows from Equations (5) and (6), the f_o values have been obtained as 112.54 kHz, 225.08 kHz, and 355.88 kHz, while the Q values have been obtained as 0.7, 1.4, and 2.2, respectively.

(b)
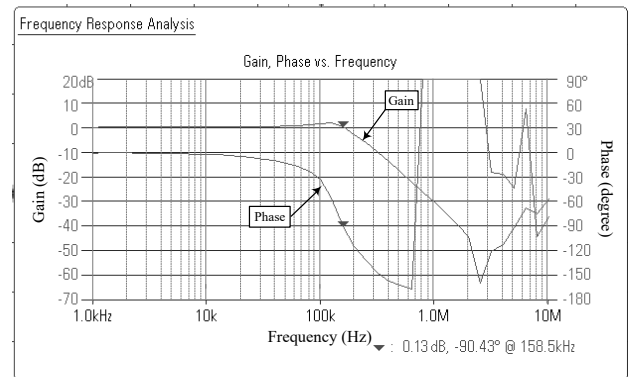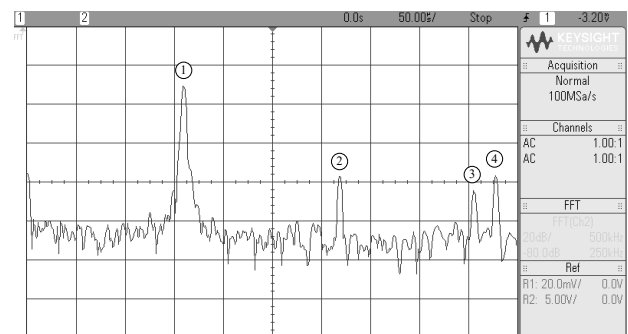
	Frequency (kHz)	Gain (dB)
①	159.1	-30.625
②	318.5	-78.875
③	455.8	-84.375
④	477.7	-76.250

(c)

Figure 9: Experimental results of the proposed LP filter.
(a) time-domain responses (b) frequency responses
(c) frequency spectrum

(a)

(a)

(b)

	Frequency (kHz)	Gain (dB)
①	159.1	-29.375
②	318.5	-90.625
③	454.9	-83.750
④	477.7	-72.500

(c)

Figure 11: Experimental results of the proposed HP filter
(a) time-domain responses   (b) frequency responses
(c) frequency spectrum

(c)

	Frequency (kHz)	Gain (dB)
①	159.1	-30.000
②	318.5	-72.500
③	455.1	-84.375
④	477.7	-57.125

Figure 10: Experimental results of the proposed BP filter
(a) time-domain responses   (b) frequency responses
(c) frequency spectrum

(a)

(b)

(a)

(b)

	Frequency (kHz)	Gain (dB)
①	159.1	-57.500
②	318.5	-100.625
③	365.8	-100.000
④	434.0	-100.625
⑤	477.7	-91.250

(c)
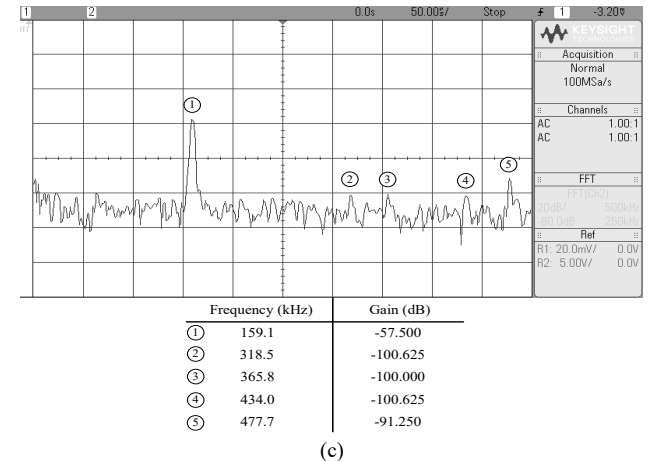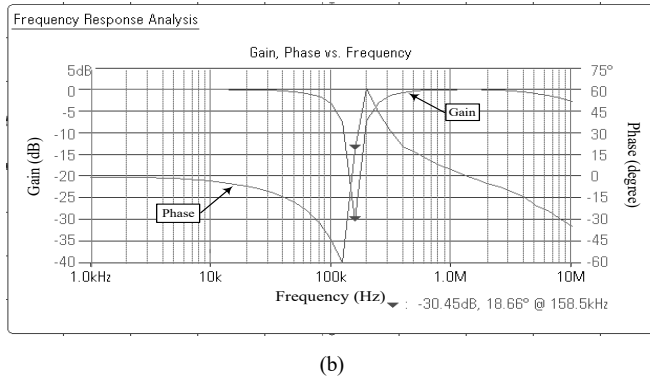
Figure 12: Experimental results of the proposed BS filter
(a) time-domain responses   (b) frequency responses
(c) frequency spectrum

(a)

(b)
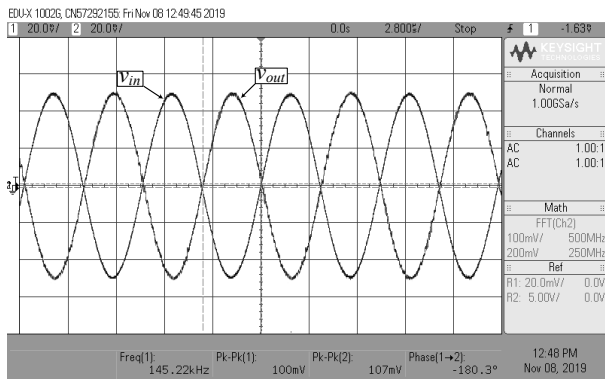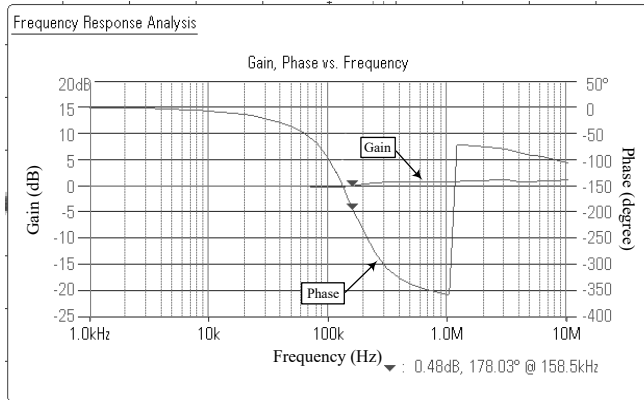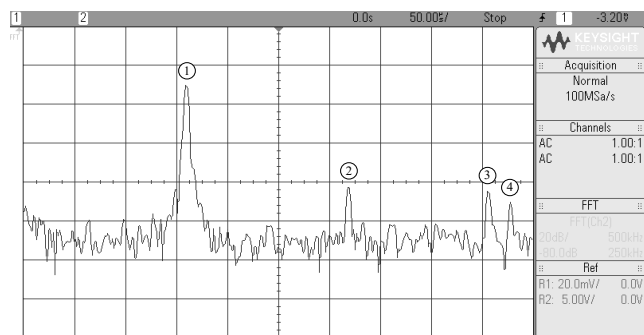
	Frequency (kHz)	Gain (dB)
①	159.1	-30.000
②	318.5	-82.500
③	455.8	-84.375
④	477.7	-90.000

(c)

Figure 13: Experimental results of the proposed AP filter
(a) time-domain responses   (b) frequency responses
(c) frequency spectrum
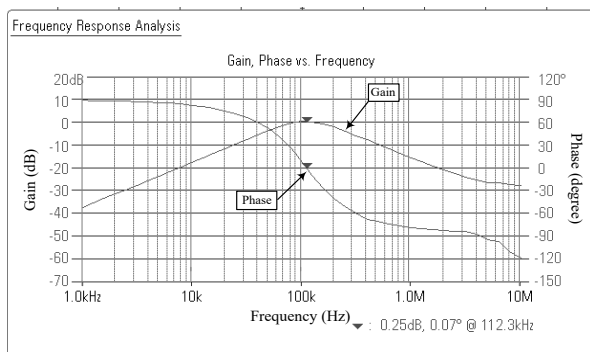
(a)
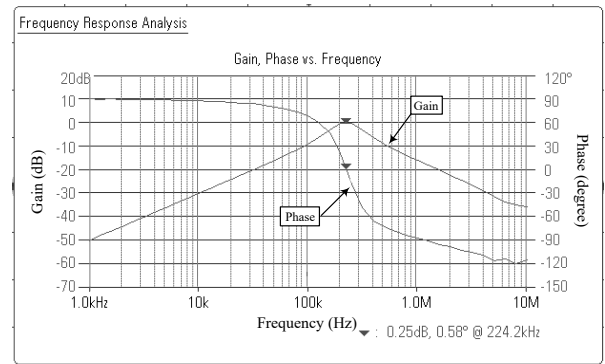
(b)
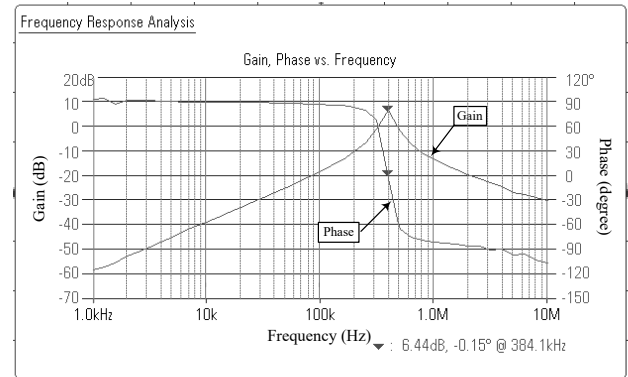
(c)

Figure 14: Measured gain responses for the proposed BP filter
with an adjustment of I_B.
(a) $I_B = 50\ \mu A$ (b) $I_B = 200\ \mu A$ (c) $I_B = 500\ \mu A$

7. Conclusions

This contribution describes the practical implementation of an electronically tunable voltage-mode biquadratic filter with triple input terminals and single output terminal. The proposed filter employs only a single commercially available IC LT1228 together with one resistor and two capacitors. The filter can realize all five standard biquadratic filtering functions all at a single output terminal by an appropriate input signal selection. The characteristics of ω_o and Q can be controlled electronically and linearly in an electronic manner via the external bias current. Simulation results obtained from the PSPICE macro-model of the LT1228 by Linear Technology as well as constructed in prototype hardware using commercially available IC LT1228 are performed to confirm the properties of the proposed circuit.

Conflict of Interest

The authors declare that they have no conflict of interest.

Acknowledgment

References

[1] M. Higashimura, "Realisation of voltage-mode biquads using CCIIs" Electron. Lett., **27**(15), 1345–1346, 1991. https://doi.org/10.1049/el:19910847

[2] A.M. Soliman, "Kerwin-Huelsman-Newcomb circuit using current conveyors" Electron. Lett., **30**(24), 2019–2020, 1994. https://doi.org/10.1049/el:19941368

[3] M. Higashimura, Y. Fukui, "Universal filter using plus-type CCIIs" Electron. Lett., **32**(9), 810–811, 1996. https://doi.org/10.1049/el:19960518

[4] J. W. Horng, J. R. Lay, C. W. Chang, M. H. Lee, "High input impedance voltage-mode multifunction filters using plus-type CCIIs" Electron. Lett., **33**(6), 472–473, 1997. https://doi.org/10.1049/el:19970297

[5] C. M. Chang, M. J. Lee, "Voltage-mode multifunction filter with single input and three outputs using two compound current conveyors" IEEE Trans. Circuits Syst.-I: Fundamental Theory and Applications, **46**(11), 1364–1365, 1999. https://doi.org/10.1109/81.802827

[6] J. W. Horng, "Voltage/current-mode universal biquadratic filter using single CCII+" Indian J. Pure & Appl. Phys., **48**(10), 749–756, 2010.

[7] J. W. Horng, Z. R. Wang, C. C. Liu, "Voltage-mode lowpass, bandpass and notch filters using three plus-type CCIIs" Circuits and Systems, **2**(1), 34–37, 2011. https://doi.org/ 10.4236/cs.2011.21006

[8] J. W. Horng, W. Y. Chiu, H. Y. Wei, "Voltage-mode highpass, bandpass and lowpass filters using two DDCCs" Int. J. Electronics, **91(8)**, 461–464, 2004. https://doi.org/10.1080/00207210412331294603

[9] M. A. Ibrahim, H. Kuntman, O. Cicekoglu, "Single DDCC biquads with high input impedance and minimum number of passive elements" Analog Integr. Circ. Sig. Process., **43**, 71–79, 2005. https://doi.org/10.1007/s10470-005-6572-0

[10] W. Y. Chiu, J. W. Horng, "High-input and low-output impedance voltage-mode universal biquadratic filter using DDCCs" IEEE Trans. Circuits Syst.-II: Express Briefs, **54**(8), 649–652, 2007. https://doi.org/10.1109/TCSII.2007.899460

[11] H. P. Chen, "Universal voltage-mode filter using only plus-type DDCCs" Analog Integr. Circ. Sig. Process., **50**, 137–138, 2007. https://doi.org/10.1007/s10470-006-9005-9

[12] W. Y. Chiu, J. W. Horng, "Voltage-mode highpass, bandpass, lowpass and notch biquadratic filters using single DDCC" Radioengineering, **21**(1), 297–303, 2012.

[13] H. P. Chen, S. S. Shen, "A versatile universal capacitor-grounded voltage-mode filter using DVCCs" ETRI Journal, **29**(4), 470–476, 2007. https://doi.org/10.4218/etrij.07.0106.0335

[14] E. Yuce, "Voltage-mode multifunction filters employing a single DVCC and grounded capacitors", IEEE Trans. Instrum. Meas., **58**(7), 2216–2221, 2009. https://doi.org/10.1109/tim.2009.2013671

[15] W. Tangsrirat, O. Channumsin, "Voltage-mode multifunctional biquadratic filter using single DVCC and minimum number of passive elements" Indian Journal Pure & Applied Physics, **49**(10), 703–707, 2011.

[16] J. W. Horng, "Voltage-mode multifunction bi-quadratic filter employing single DVCC", Indian Journal Pure & Applied Physics, **99**(2), 153–162, 2012. https://doi.org/10.1080/00207217.2011.623268

[17] F. Kaçar, A. Yeşil, "Voltage mode universal filters employing single FDCCII" Analog Integr. Circ. Sig. Process., **63**, 137–142, 2010. https://doi.org/10.1007/s10470-009-9440-5

[18] K. N. Salama, A. M. Soliman, "Voltage mode Kerwin-Huelsman-Newcomb circuit using CDBAs" Frequenz, **54**(3–4), 90–93, 2000. https://doi.org/10.1515/FREQ.2000.54.3-4.90

[19] W. Tangsrirat, T. Pukkalanun, W. Surakampontorn, "CDBA-based universal biquad filter and quadrature oscillator" Active and Passive Electron. Components, **2008**, (247171, 6 pages), 2008. https://doi.org/10.1155/2008/247171

[20] J. Pathak, A. K. Singh, R. Senani, "New voltage mode universal filters using only two CDBAs" ISRN Electronics, **2013**(12), (987867, 6 pages), 2013. https://doi.org/10.1155/2013/987867

[21] S. I. Liu, D. S. Wu, "New current-feedback amplifier-based universal biquadratic filter" IEEE Trans. Instrum. Meas., **44**(4), 915–917, 1995. https://doi.org/10.1109/19.392891

[22] J. W. Horng, M. H. Lee, "High input impedance voltage-mode lowpass, bandpass and highpass filter using current-feedback amplifiers" Electron. Lett., **33**(11), 947–948, 1997. https://doi.org/10.1049/el:19970618

[23] J. W. Horng, "New configuration for realizing universal voltage-mode filter using two current feedback amplifiers" IEEE Trans. Instrum. Meas., **49**(5), 1043–1045, 2000. https://doi.org/10.1109/19.872927

[24] N. Shah, M. F. Rather, S. Z. Iqbal, "CFA-based three input and two outputs voltage-mode universal filter" Indian J. Pure & Appl. Phys., **43**(8), 636–639, 2005.

[25] S. Topaloglu, M.Sagbas, F.Anday, "Three-input single-output second-order filters using current-feedback amplifiers" Int. J. Electron. Commun. (AEÜ), **66**(8), 683–686, 2012. https://doi.org/10.1016/j.aeue.2011.12.009

[26] V. K. Singh, A. K. Singh, D. R. Bhaskar, R. Senani, "New universal biquads employing CFOAs" IEEE Trans. Circuits Syst.-II: Express Briefs, **53**(11), 1299–1303, 2006. https://doi.org/10.1109/TCSII.2006.882345

[27] S. F. Wang, H. P. Chen, Y. Ku, P. Y. Chen, "A CFOA-based voltage-mode multifunction biquadratic filter and a quadrature oscillator using the CFOA-based biquadratic filter" Appl. Sci., **9**(11), 2019. https://doi.org/10.3390/app9112304

[28] W. Tangsrirat, "Novel Current-mode and voltage-mode universal biquad filters using single CFTA" Indian Journal Pure & Applied Physics., **17**(2), 90–104, 2010.

[29] J. Sirirat, W. Tangsrirat, W. Surakampontorn, "Voltage-mode electronically tunable universal filter employing single CFTA" in 2010 International Conference on Electrical Engineering/Electronics, Computer, Telecommunications and Information Technology (ECTI-CON), Chiang Mai, Thailand, 2010.

[30] R. Nawrocki, U. Klein, "New OTA-capacitor realisation of a universal biquad" Electron. Lett., **22**(1), 50–51, 1986. https://doi.org/10.1049/el:19860034

[31] J. Wu, E. I. E. Masry, "Universal voltage- and current-mode OTAs based biquads" International Journal Electronics, **85**(5), 553–560, 1998. https://doi.org/10.1080/002072198133842

[32] J. W. Horng, "Voltage-mode universal biquadratic filter using two OTAs" Active and Passive Elec. Comp., **27**, 85–89, 2004. https://doi.org/10.1080/0882751031000116160

[33] M. Kumngern, M. Somdunyakanok, P. Prommee, "High-input impedance voltage-mode multifunction filter with three-input single-output based on simple CMOS OTAs" in 2008 International Symposium on Communications and Information Technologies (ISCIT), Lao, China, 2008. https://doi.org/10.1109/ISCIT.2008.4700228

[34] J. Sarasri, B. Knobnob, M. Kumngern, "Electronically tunable voltage-mode universal filter using simple OTAs" in 2011 IEEE International Conference on Computer Science and Automation Engineering (CSAE), Shanghai, China, 2011. https://doi.org/10.1109/CSAE.2011.5952912

[35] F. Kaçar, A. Yesil, A. Noori, "New CMOS realization of voltage differencing buffered amplifier and its biquad filter applications" Radioengineering, **21**(1), 333–339, 2012.

[36] J. Pimpol, N. Roongmuanpha, W. Tangsrirat, "Low-output-impedance electronically adjustable universal filter using voltage differencing buffered amplifiers" in 2019 International Conference on Informatics, Environment, Energy and Applications (IEEA), Osaka, Japan, 2019. https://doi.org/10.1145/3323716.3323738

[37] O. G. Sokmen, S. A. Tekin, H. Ercan, M. Alci, "A novel design of low-voltage VDIBA and filter application" Elektronika Ir Elektrotechnika, **22**(6), 51–56, 2016. https://doi.org/10.5755/j01.eie.22.6.17224

[38] V. Biolkova, Z. Kolka, D. Biolek, "Fully balanced voltage differencing Buffered amplifier and its applications" in 2009 52nd IEEE International Midwest Symposium on Circuits and Systems (MWSCAS), Cancun, Mexico, 2009. https://doi.org/10.1109/MWSCAS.2009.5236157

[39] J. Satansup, T. Pukkalanun, W. Tangsrirat, "Electronically tunable single-input five-output voltage-mode universal filter using VDTAs and grounded passive elements" Circuits Syst. Signal Process., **32**, 945–957, 2013. https://doi.org/10.1007/s00034-012-9492-0

[40] D. Prasad, D. R. Bhaskar, M. Srivastava, "Universal voltage-mode biquad filter using voltage differencing transconductance amplifier" Indian J. Pure & Appl. Phys., **51**, 864–868, 2013.

[41] W. Tangsrirat, "Linearly tunable CMOS voltage differencing transconductance amplifier (VDTA)" Informacije MIDEM, **49**(2), 61–68, 2019. https://doi.org/10.33180/InfMIDEM2019.202

[42] O. Channumsin, W. Tangsrirat, "SITO-type high-input impedance voltage-mode multifunction filter using single active element" in 2019 5th International Conference on Engineering, Applied Sciences and Technology (ICEAST), Luang Prabang, Laos, 2019. https://doi.org/10.1109/ICEAST.2019.8802603

[43] N. Roongmuanpha, T. Dumawipata, W. Tangsrirat, "Triple-input single-output electronically controlled voltage-mode biquadratic filter" in 2019 5th International Conference on Engineering, Applied Sciences and Technology (ICEAST), Luang Prabang, Laos, 2019. https://doi.org/10.1109/ICEAST.2019.8802540

[44] P. Moonmuang, T. Pukkalanun, W. Tangsrirat, "Voltage differencing gain amplifier-based shadow filter: a comparison study" in 2020 6th International Conference on Engineering, Applied Sciences and Technology (ICEAST), Chiang Mai, Thailand, 2020. https://doi.org/10.1109/ICEAST50382.2020.9165352

[45] N. Roongmuanpha, T. Pukkalanun, W. Tangsrirat, "Three-input one-output voltage-mode biquadratic filter using single VDBA" in 2020 8th International Electrical Engineering Congress (iEECON), Chiang Mai, Thailand, 2020. https://doi.org/10.1109/iEECON48109.2020.229503

[46] Linear Technology, "100MHz current feedback amplifier with DC gain control", LT1228 datasheet, 1994.

ASTES

The Performance of Project Teams Selected Based on Student Personality Types: A Longitudinal Study

Svitlana Ivanova[1], Lubomir Dimitrov[2], Viktor Ivanov[*,3], Galyna Naleva[4]

[1]*South Ukrainian National Pedagogical University named after K.D. Ushynsky, Department Mathematics and its teaching methods, Odesa, 65020, Ukraine*

[2]*Technical University of Sofia, Department Mechanical Engineering, Sofia, 1000, Bulgaria*

[3]*Odessa National Polytechnic University, Department Mechanical Engineering and elements of machine, Odesa, 65044, Ukraine*

[4]*Ukraine National University "Odesa Maritime Academy", Department of Higher Mathematics, Odesa, 65029, Ukraine*

A R T I C L E   I N F O

A B S T R A C T

The use of heuristic methods in teaching is not possible without the cooperation of all or part of the students' academic group. That is, the teacher who made the decision to apply the heuristic method de facto solves the issues of organizing project method in teaching. There are a large number of indications on the relationship between the effectiveness of the use of heuristic methods, taking into account the personality differences of students. As well as the importance of taking into account the personality differences in the project method. However, there is a lack of information about experimental studies in which three components: the project method, the heuristic method and the Myers Briggs personality types methodology, would be considered simultaneously. This prompted us to conduct this study. As part of the project method, a tournament among students of prospective mathematics teachers was held during 2014-2020. Teams of three types to participate in the competition were formed. There was a team whose members were not previously trained. The team whose members studied the heuristic method - "Creativity enhancement method". And also a team whose members, along with the study of the heuristic method, were selected in a special way. Students included in this group had personality types most suitable for performing heuristic techniques, which are components of the heuristic method. The task of the tournament was to compile a set of educational problems in geometry that can be used in the school curriculum. The problems developed by the team were evaluated by the panel. Members of other teams acted as opponents and reviewers. Using the heuristic method allowed teams to prepare more problems and systematize them. The best results in the use of the heuristic method showed the team, the composition of which was selected in a special way. The survey conducted according to the results of the tournament showed an increase in students' interest both in the studied discipline and in the project method, as well as a willingness to use the project method in their future work.

1. Literature review

1.1. Problem-based learning

The experiment on the application of the project method in the study of the discipline "Mathematics training methodology" was carried out from 2014 to 2020 year. This article is a generalization and continuation of the work originally presented at the International Conference on High Technologies for Sustainable Development, which describes the 2014-2018 experiment [1].

Problem-based learning (PBL) is a widely spread teaching method. This method has the following features: using collaboratively work in groups or teams, using principle "learning by doing", increased motivation and interest in learning outcomes [2].

*Corresponding Author: Viktor Ivanov, Email: ivv@opu.ua

Creative techniques are also used [2]. In its turn, principle "learning by doing" include such techniques: learning by trial and error, evidence in practice, experience versus book learning, discovery versus instruction [3]. Another point of view on the main features of PBL in [4] is as follows: the method involves solving a problem posed by the student, initiative of a group of students by the form of study, results of research and activities in the form of the final product, long-term project, and teachers are used only as consultants. The PBL is considered as three principal approaches: learning, contents and social [5]. The term learning means cognitive learning, which have follows peculiarities: the problem is focused on learning, learning versus experiment, enhancement motivation and study within the framework of the project. These peculiarities are the same that point out above. The content approach first of all implies interdisciplinary learning. The social approach is mean that student organize in project team and get project management skills.

At all source mentioned above indicate such features of PBL; cognitive character of learning (including heuristic methods [5]); student should be organized in group; the goal is to solve the problem (this solution to the problem is carried out within the framework of the project [4, 5]). One author is using term a group [4], another is using both term group and team [2]. It is more clearly stated in [5] - the project team is working on the project. Direct link to project management is here.

1.2. Elements of role-playing projects in PBL

In this and other publications, the project method is equated to PBL. But, according to [6], there are four types of projects: construction, enjoyment, problem and specific learning. Thus PBL is only a third type of project. The "construction" project constructs the interaction of the project team members according to certain circumstances. This means that role projects, as well as their well-known variety - a business game - are construction projects. We believe that all types of projects include elements of construction project and PBL. When considering PBL projects, at least the role of the teacher and the role of the team leader are highlighted. Also, the size of the team is usually taken into account.

In [2] the team contract is considered to be an interesting PBL tool. This contract contains the project rules namely: objective of the project, communication between team members, rules and procedures for meetings, etc. At this contract experience of project method is used. As example, a resource and time management elements are include. The team role distribution is considered at item - define the responsibilities of each team member. The role of the teacher is described as a facilitator of the learning process in [2]. Group size guidelines are given. Students which study engineering in framework of PBL perform project tasks in industry. The teacher acted as a mediator among the student group and employees of the firm. The number of assistant lecturers should be limited [7].

In the case of real project, special employee of the company – an instructor can be assigned. He selects a project topic, prepares the presentation of the project for a group of students with a statement of the problem and meets regularly with the members of the group [7]. But inspector should not execute the project instead of students or impose their opinion on them. It is also considered necessary to have an instructor who must prepare important data

and organize information for students [2]. The instructor ensures a link between educational tasks with real problems. Another problem is that the use of the project method to solve real problems presupposes the existence of a core of good academic standing and conscientious students. Lack such of core creates an incredible administrative struggle to compensate for lack of student's motivation and to maintain the quality of the final product for the client [7]. Also, the potential problem for the implementation of real projects should be limited in scope so that the task does not exceed academic terms - a quarter or a semester.

In [8] example of student's group from 5 to 45 is provided. But note that more often groups of 5-7 are applied. It is point out that two faculty advisers should provide the work of student's group [8]. In [9] teaching roles in problem-based learning is described as a process-oriented supervisor.

PBL uses the results of research in the field of cognitive psychology to enhance creativity and increase interest [10]. The size of group is considered; note that for most purposes 3-5 members feasible is recommended. But this recommendation is not based on scientific analysis, but only on experience. Regarding the long-term project, it is indicated that most of the project terms are four years, when the whole process of studying at the university is performed on one project [10]. It should be noted that the work of the project team is provided by one or two teachers [10].

1.3. The role of teacher

The role of teachers is advisory, rather than authoritarian. Teachers used teaching assistant as mentors. On a final stage the report to the client is prepared with help a research assistant [10]. In [11] it was concluded that the group size and team tenure don't influence at the team performance. Note that both the term group and command are used in [10] and [11].

At the each publication mention above the role of a teacher is discussed. In detail the teacher's role is investigated in [12]. This role changes according to stage of a project. At the preparatory stage, the teacher motivates the students, helps in setting the goals of the project. When performing the main stage teacher directs the process. At the final stage the teacher is involved in summarizing works as an independent expert [12]. There are notes that it is very difficult for a teacher to plan or execute projects with students and control them at the same time. In [10] for decided this problem the senior seminar students as mentors are used. In order to avoid the monitoring problems, the teacher may assign a leader for each group of students. Collective execution of the project may lead to the fact that the poor academic standing students avoid academic work. Therefore, the teacher can use individual evaluations, along with a general evaluation of the performance of the group [7]. Such an evaluation can also be given by the instructor (research assistant) and each member of the group can evaluate the contribution of his colleagues during the various stages of the project [7]. In [13] identifies various ways of organizing the work of the teacher: with open (explicit) coordination or with hidden coordination (including the coordinator in the work on the project). In [14] refer different options for the distribution of roles between the teacher and students. In the case that the total amount of work can be divided into independent parts for each student, the role of the co-ordinator falls upon the teacher. In the case when it is possible to identify the main and auxiliary tasks, and also when the

final distribution of tasks between students occurs in the process of performing assignments, the role of the co-ordinator falls upon the teacher and one of the students. Such a distribution of roles exists when performing of integrated master's theses when several students develop one topic [14].

The main sources mentioned above are connected project approach with creating a group. In [15] note that obviously, the group is fundamentally and, when possible, students should be grouped. It is important to give students time to study group behaviour and performance. A study of the work in the student group showed that although the teacher's intervention and management led to improved student satisfaction with the results of the project, this negatively affected group unity [15]. An interesting variant in which the function of the co-ordinator is entrust to one of the students. This student co-ordinator is usually chosen from among the most successful students [16]. In general, many researchers distribute students into "strong" and "week", meaning only their academic achievements. For election of co-ordinator, such a feature as a high sense of responsibility, can take into account, for example [15].

In [11] pays attention to the need to take into account the personal differences of students while monitoring their academic achievements. So, students in different ways can show themselves in oral or written evaluation. To take account of these differences is proposed to use socionics typology [17]. Refer that the project method is also assumed control of academic achievements. In [18] insists that the same teaching method gives different results for students with different personality types. He invited to divide students into small groups so that each group included representatives of only one personality types. [18].

1.4. Student competition

The foregoing article consider different aspect of project method at education; these are: increasing creativity, "learning by doing", increased motivation, results of research and activities in the form of the final product, teacher's role, size of group and selection team members in according there personality types. Depending on the type of project, this or that moment turns out to be very important. It is consider the projects, which included this entire item. These projects are based on student's competitions.

The Formula Student team includes from 40 to 50 members typically [19]. This large team is parted into sub-teams of 3 or 4 participants. A large project team has a leader called the captain. Usually this role is performed by a graduate student. The formalized roles are systems engineer and managers responsible for marketing and financial matters [19]. The captain and faculty member is controlled financial issues, also. An adviser and industry mentor supported each large team. In this case is realized problem learning study: team solve problem of automobile design with final product - racing car. As well role-playing project is realized. The students are performed role of design division of automobile company.

The same examples when there is a PBL project and a role project and also the final product are World Robot Olympiad and Robot Soccer World Cup. Another example is student tournaments. International Natural Sciences Tournament (INST) is including following specializations: Chemistry, Material Science,

Geography, and Engineering. University students can participate in the team. The researcher or doctoral student acts as a trainer. Separate tournaments in mathematics (International Tournament of Young Mathematicians) and physics (International Physicists' Tournament) are held.

The International Physicists' Tournament (IPT) has the most established and regulated rules for conducting [20]. The IPT preparatory work on the formation of tasks carried out group of teachers, which is then not in contact with students. The other teachers, usually four of them, are panel members. Each team has the adviser - PhD student. Team is headed by the captain; he is one of a student. Teams of six students receive a list of tasks that can be solved experimentally or theoretically. In a round of a tournament, each team plays one of the following roles: speaker, opponent, and reviewer. Each task consists of three rounds, i.e. each team must play all three roles. Along with the team competition, the participant's personal contribution is assessed. Speakers and Opponents who receive an above average grade for their performances receive personal points. Individual winners of the Tournament are determined by the total amount of personal points.

Point out that in a number of cases, the work result of the project team may be not only in obtaining certain knowledge and skills, but it have practical result. Practical result is important when:

- A project is real and results of which will be used in practice;
- Competition between projects groups, for example - Formula Student, IPT, INST, etc.;
- Business games, when the insufficient level of results breaks the plot of the game and does not allow achieving the necessary knowledge and skills;
- This is the study of heuristic methods, when the absence of a result will not allow to fully revealing the content of the topic.

1.5. The results of the review and the objectives of the study

The effectiveness of the application of project method, as reviewed by the literature sources, is related to the features of the formation and work of project teams. Recommendations for the size of the project team are very different - from 2 to 12 members. Note that there are usually 15-25 students in an academic group. The size of the project team depends on the size of the academic group, due to organizational factors. Conveniently if all students of an academic group are included in the project team or two teams are formed from this academic group. The most common recommendation is that the project team should be small, but for more teams, more teachers should be involved than a lecturer and assistant.

In two cases, it is important to distribute roles between students in the project team - in the implementation of long-term projects and in student team tournaments. Long-term projects can be implemented for execution of a bachelor's degree project, a master's degree project and a term paper formed to work for a long period of time. The project team can be formed for a year or more for implementing collaborative interdisciplinary or research projects. In [11], it was concluded that group size does not affect team performance. We assumed this was due to the fact that team members were selected without regard to their personal

differences. Extensive experience in the formation and organization of project team interaction has been accumulated in project management. As a rule, the distribution of roles between students of the team members is spontaneous: someone is chosen for the role of leader, someone is a generator of ideas, and someone is responsible for processing the results of the work. Sometimes students themselves are called to perform certain functions in the team. However, there are various scientifically valid typologies of team roles. This distribution can be performed on the basis of the project management theory. The terminology accepted in project management, namely: project team, teamwork, team roles, is also expedient to use. The heuristic nature of the design method is often noted. The content of the project method can be the work of the team to study and apply the heuristic method [21]. In this case the distribution of team roles should be performed on the basis of personality type's methodologies [21]. The important question is about the role of the teacher in the project method. The roles of teachers vary. Teachers prepare material and project rules. They are advisers and evaluate students. Is teacher outside the project team or its member? Usually it depends on which project we are considering. In a short-term project, the teacher is out of the project. If the subject of the study is a long-term project, then the teacher can be an advisor and even be a member of the project team.

The study includes a preparatory stage, which consists of building project teams, teaching students to use the heuristic method and surveys to determine their personality type. The experiment itself included the organization of a tournament, work with the use of a heuristic method, including taking into account the personality type of students. As well as the panel's assessment of the teams' work results and a survey of the participants about the experiment results. At the analysis stage, the performance of the project teams, and the effectiveness of using individual techniques of the heuristic method by students with certain personality types were compared.

2. The methodology of experiment

2.1. The hypothesis of the study

The project method is widely used in education. The scientific basis of this method was developed in project management. The guidelines for team size and selection of team members were generally developed based on the team role methodology. Often the purpose of forming a project team is to ensure teamwork within the heuristic method. The methodology of personality types is more suitable for selecting group members and organizing the interaction of team members in the case when the application of the heuristic method is the reason for the formation of the project team. The lack of data on the combination of personality type's methodology, heuristic method and project method should make up for this experiment.

The following statement is accepted as hypotheses of a study:

- H_a - The use of the heuristic method, allows to improve the performance of the team.
- H_b - The formation of a project team, taking into account the personality types of students, allows to improve the performance of the team.

- H_c - The use of the project method in the form of team competition increases the interest of team members in the application of this method.

2.2. Tools are used to test these hypotheses of a study

The Keirsey Temperament Sorter. Student's personality types were determined using the Keirsey questionnaire [22]. The first test was conducted six months before the tournament. The second test was performed immediately before the tournament. Along with personality types, their brightness was determined. The test was carried out on the basis of an adapted version of the test in Ukrainian (http://ibib.ltd.ua/2211-test-keyrsi-tekst-35784.html). Two academic groups consisting of 15-20 students in each took part in testing. The coincidence of the results of the first and second tests was in the range of 76–81%, which is within the acceptable range (75–90%) in accordance with [23]. Students with personality types necessary for the execution of the heuristic method algorithm were selected to the first group. Of the students with the same personality types, preference was given to the participants with the brighter type.

The expert evaluation. The teacher and two PhD students prepared tasks for the tournament and became members of the panel. The panel members evaluate each problem based on a report and discussion. The maximum score is 100 points. The problem was evaluated on four items: correctness of composing and solving the problem (40), completeness of methodological recommendations (20), compliance with the requirements of the educational set of problems (20), consistency, clarity and validity of each stage in the presentation of the problem (20).The maximum number of points for each item is indicated in parentheses. The individual contribution of each participant was also assessed. The maximum score also is 100 points. The problem was evaluated on five items: ability to report, ability to debate, quickness in correcting your mistakes, finding mistakes in opponents, the ability to analyze the proposed sets of problems from a methodological point of view. The maximum score of each item is 20 points.

The survey. A survey was conducted following the experiment. All students answer the questions "Do you like the project method?" and "Will you use the project method in your future work?". The members of first and second team answer the questions "Do you like the heuristic method?" and "Will you use the heuristic method in your future work?". The members only of first team answer the questions "Do you like the distribution team role due personality type?" and "Will you use the distribution team role due personality type in your future work?".

2.3. The heuristic method

It was decided to use as a heuristic method "creativity enhancement method" [21]. This method included several heuristic techniques, namely: collective discussion, pause between the presentation of ideas and their criticism, random associations, analogy, expert evaluation, using a matrix. The sequence of heuristic techniques is follow. At first is applied three techniques collective discussion, pause between the presentation of ideas and their criticism, expert evaluation. This three techniques is represented a all known brainstorming. The main difference of a creativity enhancement method in contradistinction to another

method based on brainstorming is using matrix. The purpose of the first three heuristics is to determine what sense should be given to the row and column. Second part of heuristic techniques follows. These are random associations, analogy and expert evaluation. The goal of techniques random associations and analogy is to generate ideas about the semantic content of the first row and first column elements. Expert evaluation technique is used to select better variant of ideas. Third part of heuristic techniques grouped around the matrix. These are using a matrix, collective discussion and expert evaluation. The combination of elements first row and first column give a content of each matrix cells [24]. Each cells can contain a possible solve of problem. But in fact, many combinations give impossible options or options that are not implemented under given restrictions. The cells that are have sense the material of collective discussion. The final selection is performed using expert evaluation techniques.

2.4. The personality types selection

The preparation of students to use creativity enhancement method one lecture session and one practical session were provide.

According to the method especially selected students performed determination techniques. The moderator of discussion should be with personality type ENTJ or ESTJ [21, 22]. For collective discussion the ENTJ, ENTP, ESTJ and INTJ personality types are recommended [22, 25, 26]. These types are arranged in the order in which they are best suited for this technique. For criticism the types sequences in order of their degree of preferable: ISTP, INTP, ISTJ, ESTJ [25, 27, 28]. For expert evaluation the same type can be used only at another sequences their degree of preferable. For technique of random associations the types ENTP and ENTJ should be added to discussion group [21, 26]. For technique of analogy a type INTJ should be used [22, 25].

3. The results of the experiment

The experiment was attended by students of SUNPU - prospective teachers of mathematics. Every year, the subject studied two academic groups. The experiment was carried out during 2014-2020. Students were assigned to two or three project teams. The academic group was reorganized into a project team if the number of students was less than 15 or two project teams if the number of students was more than 15. Thus, there were two or three project teams. The teams were of three types. The third project team were participants, who were doing methodical task without special preparatory training for this task. The members of the first project team took additional sessions to learn the creativity enhancement method. The participant of this team especially selected on the base of their personality type. The types, which corresponded with personality type to need a heuristic technique of method, were included in team. Members of the second project team are also studying the heuristic method. Students of the third project team didn't have additional classes. In total, sixteen project teams were created: a fifth team of the first type, three teams of the second type, and three teams of the third type (Table 1).

The total number of problems prepared by the teams is presented in Figure 2. The tournament was organized for project teams as part of the study of the discipline «Mathematics training methodology». IPT rules were used for the competition. If there were three teams, then each of the teams consistently acted as a

speaker, opponent and reviewer. In the competition between the two teams, there were only speakers and opponents. The teams were tasked with developing a set of geometric problems, namely, a planimetry subsection. The topic of these problems set is established the same for all teams. This set of problems can be used in the school curricula. Specific requirements for this set are established: definite purpose of using, the arrangement of the problems in increasing order of difficulty and the availability of the alternate problems (with the same level of difficulty as well as methodical recommendations).

Table 1: Types of team per year

Year / Types of team	2014	2015	2016	2017	2018	2019	2020
First type	■	■	■	■	■	■	■
Second type	■			■		■	■
Third type	■	■	■		■		■

The work of teams of the first and second types was organized in accordance with the heuristic method algorithm. The collective discussion group included from 5 to 10 people, depending on the number of project team members. The ideas put forward by them were discussed by a group of critics of 3-5 people, together with some of discussion group participants. The final decision is made by an expert evaluation group of three people, one of whom is a moderator. Then the team was divided into two parts, one discussed the specific content of the rows, the second columns. Groups is performed this task using free association and analogy techniques. Based on the results of the discussion, a matrix was drawn up. Schemes of problems were depicted in the corresponding cells of the matrix. The discussion group is selected problems for further development. Then, the team, to increase productivity, split into parts and worked on selected problems. For each problem it was necessary to find several solutions and develop methodological recommendations. The expert evaluation group with high-achieving students selected problems that could be presented.

Figure 1: Example of a table with options for problems

An example of a fragment of one of the matrices obtained by the command of the second team type is presented in Figure 1. The

elements that need to be found are marked in red. These are the medians drawn to the three sides of the triangle. The first row of the matrix is location options of medians (LOM). The first column contains the given triangle elements (GTE). Each cell of the second row corresponds to a triangle with all sides are given.

Of the three options for the location of the median, only one was chosen, since in all three cases the solution algorithm is the same. In the third row, there are triangles in which two sides and the angle between them are known. Two options are selected when the median is drawn from a known angle and when it is drawn from an unknown angle. In the fourth row, there are triangles in which two sides and angle are known but the angle is not located between them. Two variants are also chosen when the median is drawn from a known angle and when it is drawn from an unknown angle. Further, in the matrix considered triangles in which one side is known. These rows are not shown. For each of the triangles marked with a yellow background, the team developed several solutions with explanations, as well as recommendations for the teacher on how to apply these problems in the school curricula.

The total number of problems prepared by the teams is presented in Figure 2 and Table 2. The team reported the results, usually there were several speakers. Students preparing the problem presented it. The panel evaluated the team members who participated in the presentation individually. The members of the opponent's team who participated in the discussion were also individually assessed. The participants of the opposing team looked for inaccuracies in the solution and deficiencies in the explanation. They raised objections to methodological recommendations and to the possibility of using the problem in the school course. On the basis of the report and discussion, the panel evaluated each of a set of problems. Problems with more than 100 points were selected for use in the school course. The number of problems selected by the panel is shown in Figure 3 and Table 2.
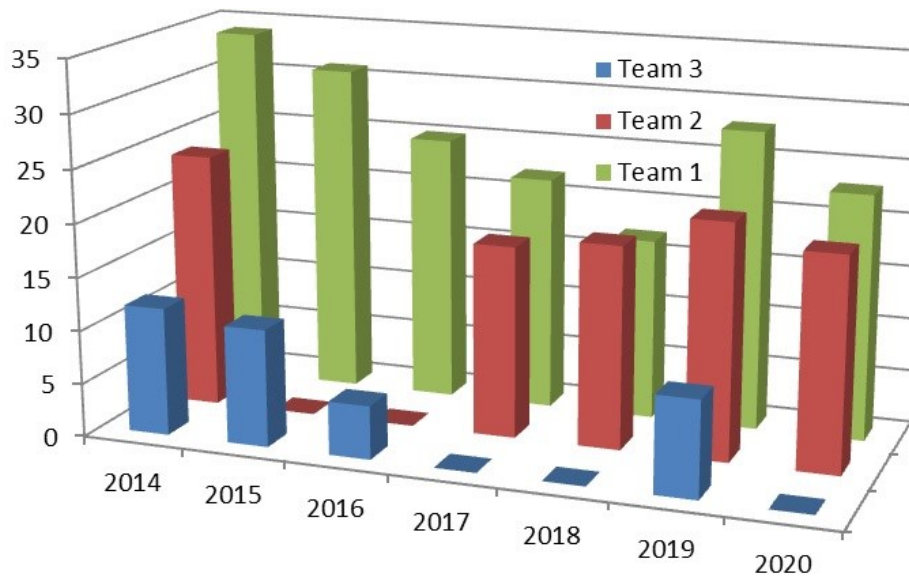
Figure 2: Total number of problems by year
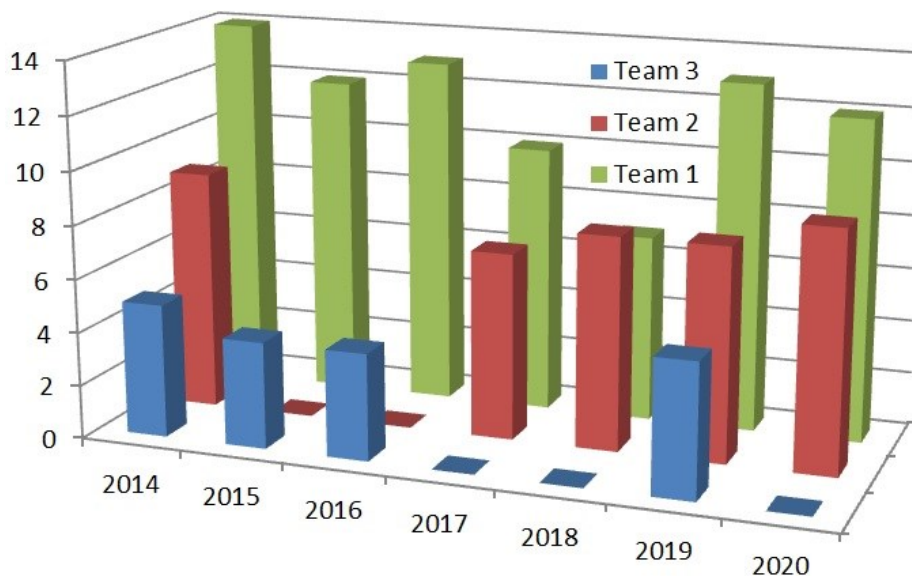
Figure 3: Selected number of problems per year

Table 2: Team performance

Team No \ Year	Team 1		Team 2		Team 3	
	Total	Se-lected	Total	Se-lected	Total	Se-lected
2014	34	14	24	9	12	5
2015	31	12	-	-	11	4
2016	25	13	-	-	5	4
2017	22	10	18	7	-	-
2018	17	7	19	8	-	-
2019	29	13	22	8	9	6
2020	24	12	20	10	-	-

The results of the student survey showed an increase in the interest of team's members of all types in the project method and the heuristic method. The students of the first type of team showed enthusiasm for defining their personality types and organizing the team work based on this data. As for the prospects for using the acquired skills in further work, everything is not so unequivocally. Most of the students of the first type team are not going to use the knowledge gained about personality types in their further work. Almost half of them are ready to use the heuristic method in the future, in contrast to participants from teams of the second type. The project method of work was assessed by the students of teams of three types as the most deserving of use in the work of a teacher (Table 3).

Table 3: Types of team per year

Survey questions \ Team types	First team	Second team	Third team
Do you like the project method?	89%	84%	73%
Do you like the heuristic method?	77%	69%	-
Do you like the distribution team role due personality type?	82%	-	-
Will you use the project method in your future work?	65%	71%	58%
Will you use the heuristic method in your future work?	44%	24%	-
Will you use the distribution team role due personality type in your future work?	23%	-	-
Has interest in studying the discipline increased due to innovations in the form of education?	81%	73%	67%

4. Analysis of experiment result and discussion

The performance of the second type team, which used the heuristic method, is higher than the performance of the third type team. Teams of the second type developed 24 problems. The average number of problems in a set is 8. The third type team developed 13 problems. The average number of problems in a set is 4,3. Thus, the results of the experiment confirmed the hypothesis H_a.

The application of the heuristic method requires special training. One lecture and one practical session are the minimum time to explain the essence of the method. It would be desirable to have more time for this. But there is a problem associated with the allocation of even this short time. If the heuristic method were used in teaching several disciplines, then there would be an opportunity for additional training. The method is quite complex, and several times the teams invented the contents of the matrix during brainstorming and heuristic techniques of random associations and analogies are not used. Heuristic techniques of random associations and analogies can be used to search for the contents of rows and columns. If one technique does not work, the other can be used additionally. It is promising to use the heuristic method in long-term projects carried out during a semester or longer.

The performance of the first type team, which was formed taking into account the personality types of students, is higher than the performance of the second type team and much higher than the performance of the third type team. The first type of team developed sets of 56 problems. The average number of problems in a set is 11,2. The experimental results confirmed the hypothesis of H_b. This means that the selection of performers for the execution of heuristic techniques was performed correctly.

It is very difficult to select the necessary personality types for the project teams, considering the level of knowledge, motivation and the personal interaction and relationships due to the small number of students learning a certain subject. For to form first type team in some cases it was necessary to include the students that had rare personality types ENTJ (moderator) ENTP (discussion group) from another academic group. This reduced the performance of teams of the second and third types. Experience has shown the academic achievements of the students can be more important than the exact matching of their personality types with their role in the creativity enhancement method. Sometimes we had to include the students from different academic groups into the project teams to strike a balance between the levels of their knowledge. The correct selection of team members of the first type allows students to understand the advantages of the method through a successful result. The project team included not only students with a personality type that is suitable for performers of heuristic techniques. Thus, it was necessary to find a model of participation for those who have a different personality type. Experience shows that the ENFP can act as a moderator, facilitating discussion through one's own imagination and enthusiasm. The personality type ENFJ can substitute INTJ in the discussion group because of their ability to generate the ideas. The personality type ENFJ can also fulfil the role of the teacher assistant when teaching creativity enhancement method. Having the big number of the representatives of personality types ISTJ, INTJ, INTP, ISTP, in the discussion group, it makes sense to give the students time to make the record of their ideas before the beginning of the discussion. A higher level of students' knowledge is created the prerequisites for the effective execution of the chosen role when working in a project team. However, this students, who did not have high grades earlier with the matching of their personality type with the appointed role surprisingly enough showed a better efficiency. For example, a student of personality type ISTJ, with an average level of academic achievement, working as a critic in a project team, enthusiastically is joined the work in detail analyzing the proposals of other team members. This

is allowed him to systematize and deepen his knowledge and skills appropriate way for him. The personality types of students, who show high results in the experiment, usually coincide with the typical personality types for STEM specialties: ISTJ, INTP, ESTJ, INTJ, ENTP, and ENTJ.

The survey showed that the members of the three types of teams were enthusiastic about the project method implemented in the form of competition. 82% of the total number of students liked the participation in the project. Students, who are going to use the project method in their profession - 64,7%. Thus, hypothesis H_c is confirmed.

The number of students in project teams is higher than recommended by the majority of research. This is due to the lack of teachers to conduct the research. Another problem of the project method was the organization of teamwork in such a way that all team members took an active part in it. We did not have this problem with the work of the first type of teams, unlike the second and third type teams. This serves as an indirect confirmation of the success of team interaction based on personal types. When using project method, there has always been the problem of assessing the personal contribution of team members and, accordingly, evaluating their academic achievements. Not all students presented solutions to problems and participated in the discussion. In the first type team, the students, in particular, the moderator, were involved in the assessment, which contributed to its objectivity and validity. The fact that students who solved the problem represent it is good for their self-realization, but it can be bad for the team score. From the point of view of higher score of the team, it is advisable to entrust the presentation of problems to students with high academic achievements.

5. Conclusion

The experiment was conducted in the form of a tournament, which made it possible to implement the PBL project and at the same time the role-playing project. The project had the final product - a set of geometry problems. Students studied the creativity enhancement method using the principle of "learning by doing". Thus, the project was comprehensive. Three types of project team took part at competition. Students of first and second project team are learned the heuristic method. Students of third project team haven't special training. It was found that the use of the project method in the form of a team competition aroused increased interest among students. It has been established also that the use of the heuristic method improves the performance of the project team. Members of first project team were selected according to their personality types. It was proven that the selection of students with certain personality types to the project team, the most suitable for the implementation of the heuristic techniques of the method, allowed increasing the performance of the project team. This confirms the correctness of the recommendations for the selection of personality types corresponding to a certain heuristic techniques. It is best to choose students with the ENTJ personality type for the role of moderator. It is recommended to choose personality types ENTP, ENTJ, INTJ for discussion and generation of ideas. The ISTP, INTP and ISTJ personality types should be used as criticisms. Several members of a collective discussion group must necessarily be at the group of critics. However, among the critics, there should be several

members of the project team who did not participate in the discussion, for unbiased analysis of the proposed solutions. Academic achievement affects the performance of teams along with the personality types of students. This is important to consider when choosing a moderator and discussion group members. For this reason, the preferred ENTJ types can be replaced with ESTJ as the moderator, and ENTP can be replaced with INTP in the discussion group.

Conflict of Interest

The authors declare no conflict of interest.

References

[1] S. Ivanova, L. Dimitrov, V. Ivanov and G. Naleva, "An Experiment on the Joint use of the Heuristic and Project Methods at the University," in 2019 IEEE International Conference on High Technology for Sustainable Development (HiTech), 1-5, doi: 10.1109/HiTech48507.2019.9128248.

[2] R. Seidel, E. Godfrey, "Project and team based learning: An integrated approach to engineering education," In 4th ASEE/AaeE Global Colloquium on Engineering Education, №146, 2005.

[3] H. W. Reese, "The learning-by-doing principle. Behavioral development bulletin, " 17(1), 1-19, 2011. doi.org/10.1037/h0100597.

[4] J. Adderley, Project Methods in Higher Education, Research into Higher Education Monograph 24 London: Society for Research into Higher Education, 1975.

[5] A. Kolmos, E. De Graaff, X. Du, "Diversity of PBL–PBL learning principles and models," In Research on PBL practice in engineering education, 9-21, 2009, doi.org/10.1163/9789087909321_003.

[6] W.H. Kilpatrick, "The project method," Teachers college record, 19(4), 319-335. 1918.

[7] N.K.Malhotra, A. Tashchian, A.K. Jam, "The project method approach: An integrated teaching tool in marketing research," Journal of Marketing Education, 11(2), 32-40, 1989, doi.org/10.1177/027347538901100206.

[8] J. E. Mills, D. F. Treagust, "Engineering education—Is problem-based or project-based learning the answer," Australasian journal of engineering education, 3(2), 2-16, 2003.

[9] A. Kolmos, "Reflections on project work and problem-based learning,: European journal of engineering education, 21(2), 141-148, 1996, doi.org/10.1080/03043799608923397.

[10] L. Helle, P. Tynjälä, E. Olkinuora, "Project-Based Learning in Post-Secondary Education – Theory, Practice and Rubber Sling Shots," High Educ., 51, 287–314, 2006, https://doi.org/10.1007/s10734-004-6386-5.

[11] R. Harms, "Self-regulated learning, team learning and project performance in entrepreneurship education: Learning in a lean startup environment," Technological Forecasting and Social Change, Elsevier, 100, 21-28, 2015, doi: 10.1016/j.techfore.2015.02.007.

[12] Е.С. Полат, Новые педагогические и информационные технологии в системе образования. Академия. 2009.

[13] Т.И. Гречухина, А.В. Меренков, С.В. Куньщиков, И.Ю. Вороткова, А.В. Усачева, Самостоятельная работа студентов: виды, формы, критерии оценки, Екатеринбург: Издательство Уральского университет, 2016.

[14] А.Т. Ашеров, В.І. Шеховцова, "Проектна культура будущих инженеров–педагогов компьютерного профиля: сущность понятия," Теорія і практика управління соціальними системами, 4, 70-79, 2007.

[15] G. Kirkpatrick, "Online 'chat' facilities as pedagogic tools: a case study," Active Learning in Higher Education, 6(2), 145-159, 2005, doi.org/10.1177/1469787405054239.

[16] S.A Barab, T.M. Duffy, "From practice fields to communities of practice," Theoretical foundations of learning environments, 25–55, 2000.

[17] О.П. Кальнік, "Індивідуалізація контролю навчальних досягнень студентів вищих навчальних закладів на основі використання соціонічних типів та установки на вид діяльності. Педагогіка та психологія." **53**, 66-74, 2016.

[18] D. Prorak, T. Gottschalk, M. Pollastro, "Teaching method and psychological type in bibliographic instruction: effect on student learning and confidence," RQ, **33(4)**. 484-495. 1994.

[19] I. Talmi, O. Hazzan, R. Katz, "Intrinsic Motivation and 21st-Century Skills in an Undergraduate Engineering Project: The Formula Student Project," Higher Education Studies, **8(4)**, 46-58, 2018.

[20] V. Vanovskiy, "International Physicists' Tournament - the team competition in physics for university students," European Journal of Physics, **35(6)**, 064003, 2014. doi: 10.1088/0143-0807/35/6/064003.

[21] V. Ivanov, L. Dimitrov, S. Ivanova and O. Olefir, "Creativity enhancement method for STEM education," 2019 II International Conference on High Technology for Sustainable Development (HiTech), Sofia, Bulgaria, 1-5, 2019, doi: 10.1109/HiTech48507.2019.9128255.

[22] D. Keirsey, M. Bates, Please understand me. Del Mar, CA: Prometheus Nemesis, 1978.

[23] R.M. Capraro, M.M. Capraro, "Myers-Briggs Type Indicator score reliability across studies: A metaanalytic reliability generalization study," Educational and Psychological Measurement, **62**(4), 590-602, 2002, doi.org/10.1177/0013164402062004004.

[24] V. Ivanov, G. Urum, S. Ivanova, G. Naleva, "Analysis of Matrix and Graph Models of Transmissions for Optimization Their Design." Eastern-European Journal of Enterprise Technologies, **4(1)**, 11-17, 2017, doi:10.15587/1729-4061.2017.107182

[25] M.H. McCaulley, "Myers-Briggs Type Indicator: A bridge between counseling and consulting". Consulting Psychology Journal: Practice and Research, 2000. https://dx.doi.org/10.1037/1061-4087.52.2.117]

[26] L. Moller, C. Soles, "Myers Briggs type preferences in distance learning education", International Journal of Educational Technology, **2(2)**, 2001.

[27] C.F. Yokomoto, R. Ware, "Applications of the Myers-Briggs Type Indicator in engineering and technology" Education--part II. Indiana University-Purdue University Indianapolis. Session, **2230**, 4.88.1-4.88.10, 1999.

[28] D.W. Salter, N.J. Evans, D.S. Forney, "A longitudinal study of learning style preferences on the Myers-Briggs type indicator and learning style inventory", Journal of College Student Development, **47(2)**, 173-184, 2006.

Artificial Neural Network Approach using Mobile Agent for Localization in Wireless Sensor Networks

Basavaraj Madagouda[1,*], R. Sumathi[2]

[1]*Department of Computer Science and Engineering, Jain College of Engineering and Research Belagavi, VTU Belagavi, 590001, India*

[2]*Department of Computer Science and Engineering, Siddaganga Institute of Technology Tumkur, VTU Belagavi, 590001, India*

A B S T R A C T

Wireless sensor networks (WSNs) are having large demands in enormous applications for the decade. The main issue in WSNs is estimating the exact location of unknown nodes. All applications are dependent on the location information of unknown nodes in WSNs. Location information of mobile anchor node is used to estimate the location of unknown nodes. A new approach is implemented in this paper for the localization of unknown nodes using Artificial Neural Networks. Specifically, a neural feed network is used for the indoor position process. Also several neural network configuration sets have been tested, which includes Bayesian regularisation (BR), Levenberg-Marquardt (LM), resilient back propagation (RP), Scaled Conjugate Gradient (SCG) and Degree Descent (SCG),etc. At the end results are simulated using MATLAB and Mean Square Error is calculated and compared with other existing approaches. The proposed approach is energy efficient and uses only a two-way message to obtain inputs for the localization. Even the cost is minimized as in the proposed system only one mobile anchor node is used.

1. Introduction

With the development of new applications in numerous areas, wireless sensor networks (WSNs) have gained a vast reaction from academia and industry. Applications for the future include monitoring of vegetation and the environment, search and rescue processes, object tracking in hospitals, monitoring of patients, and military applications. Because of technological development, small, cheaper sensor nodes have been developed that consume less power and feature capabilities like sensing, data storage, computer technology, and wireless communication.

Localization among others, architecture, deployment, synchronization, calibration, quality of service, and security are the key and difficult part of many WSN applications. The sensor data has to be attached to measured data in order to make this important for location since it is essential to monitor and record broad information like acoustic, visual, thermal, and seismic or any other type of measured observation. For example, the place or part of the farm from which the data is collected would be required for the person monitoring a big vegetation farm, with a wide variety of vegetables, since various vegetables have different special needs. Reporting Object origin, node location is required so as to support or answer group querying, routing and network coverage questions. Research into the problem of node location has provided a number of solutions over the course of the decade.

Overall, most of the time there is a compromise between localization accuracy, computer complexity, and technology energy efficiency according to their application needs.

A large number of space-dispersed sensor nodes is usually used in a WSN such that the location of the sensor node when the nodes are used is unable and inefficient. Sensor nodes may also be relocated from their original position. An algorithm is therefore necessary for an independent assessment of the location of the node. In this research paper, a new location scheme for neural network-based nodes is proposed. In order to address the node location problem, the Received Signal Strength Indicator (RSSI), is utilized to evaluate the coordinates and location of WSN nodes. Contributions are as follows:

Is RSSI an appropriate component for WSN node location? We use RSSI to determine where the sensor nodes are located and explain how RSSI is suitable for locations. There will not be a need for additional hardware because sensor nodes are openly outfitted with RF modules for wireless communication. Multi track fading and noise, however, can contaminate the RF signal and thus affect the RSSI value through a noise-to-signal correction.

Also, of the utmost importance is the choice of the evaluation model. A 2D indoor environment that is determined by the x and y co-ordinates is considered in this research. A single node of anchor requires directional steering antennas, which directly

boosts the sensors' cost and electricity consumption. Therefore, the two or more anchor nodes with different configurations explain the best configuration used for the anchor nodes.

A new 2D indoor locating system based on a neural network is introduced. For an accurate localization, the global positioning system can be used. The use of GPS does require the attachment of external hardware to the sensor nodes, thereby increasing cost and electricity consumption. In addition, a GPS viewing line is required and is therefore not applicable to indoor environments.

A neural feed network is used for the proposed indoor position process. A variety of neural network configuration sets have been tested, and Bayesian regularisation (BR), Levenberg-Marquardt (LM), resilient back propagation (RP), Scaled Conjugate Gradient (SCG) and Degree Descent (SCG) are the best neural network training and implementation (GD).

2. Literature survey

In [1], the authors presented a survey on machine learning algorithms for WSNs. They have presented techniques to identify intrusion by merging clustering and deep neural network methods and discussed machine learning-based localization techniques for WSN such as fuzzy logic, k-means + fuzzy-c-means, CNN+SVM, ANN, SVM. Also discussed ML-based congestion control strategies. Logic-based cram detection and control systems have been configured for efficient and active queue management as the basis for minimizing packet loss. It can be carried out in three stages. Second, it senses congestion in the second it modifies congestion control and by balancing the flow it recovers from the congestion.

In [2], the authors have suggested a new distance measuring capability using the Adaptive Neural Fuzzy Inference Scheme to render model, map RSSI to the precise T-R distance and experiments prove feasible.

In [3], the authors has proposed an adaptable model dependent on the neural organization and lattice sensor preparing stage for exact limitation of sensors. Recreation results show that the area exactness can be expanded by expanding the framework sensor thickness and the number of passages. The author proposed and explored a confinement procedure for WSNs utilizing NN. They think about NN for building adaptable planning among RSS and the situation of the sensor hubs. In this method, the NN is prepared to utilize the RSS estimations of the lattice sensors. The positive highlights of the framework are its dependence against the adjustment in the RSS estimations with time and no requirement for the additional course of action of equipment. The organization's preparation is refreshed with a standard timespan to limit area mistake. Simulation experiments demonstrate that the area exactness can be expanded by expanding the matrix sensors' density and APs.

Nowadays for enhancing the accuracy of localization in the Range-Free approach is more focused. In [4], the authors introduced many algorithms to improve accuracy such as BP artificial neural network (BP ANN). Rather than the amorphous algorithm is very easy to develop, and it will generate huge errors in the localization procedure. For resolving the issue and to diminish localization error, presented an improved localization algorithm. A widely utilized model in neural networks (NN) is BP NN. BP algorithm is a NN of three-level. The methodology used for the detection of network weight and the threshold between BP algorithms with minimal error and recursive technology is known

as the deepest descent. BP ANN practitioners are incredibly self-organizing and self-learning, error replication, and a minimal theory of error in error optimization.

In [5], authors presented a study on localization in WSN by utilizing neural networks (NN). This study analyses localization algorithms and their advantages and disadvantages. They Discussed localization, localization classification methods, localization classification algorithms, and the pros and cons.

In [6], authors submitted comparable analyses of the localization WSN localization networks of Sigmoidal Feed ANN (SFFANNs) and Radial Base Function (RBF). The system proposed uses the Obtained Signal Force Indicator (RSSI), a static node calculated on a grid of 100 x 100 m2 of the three anchor nodes. The key aim of the SFFANNs' and RBF network system comparative analysis is the development of an efficient WSN localization structure. Both ANN models approximate the position error by using RSSI values. Quality comparison has been done with respect to standard deviations, mean position errors, and statistical parameters of R-square. MLP has the best efficiency, shown by simulation outcomes, where accuracy is considered.

In [7], the RBF network has been reviewed by the authors for the implementation of the WSN position method. For reasons of faster convergence and the lowest measurement rate, the RBF-based localization architecture should be evaluated. The analyses of RBF in this paper have been a probabilistic NN and general regression NN. For designing an efficient localization method, the suggested technique may be used. To minimize position errors, the predictive location algorithm proposed by the authors [8] relies on RBF NN. An algorithm detains moving node standards inherent in it and learns them from them. A field of mobile nodes can be expected by removed traveling highlights. Reproduction findings confirm that these calculations will be more reliable in the visually impaired interval to understand detailed localizations.

In [9], the authors proposed computationally – cheap arrangements rely upon support vector machine (SVM) and twin SVM learning algorithms where network nodes right off wanted signal. At that point, the network is trained to determine nodes in the region of source; subsequently, locale of the function is distinguished. At last, centroid of event region is assessment of source area. Re-enactments show the productivity of the proposed techniques. SVMs are integral tools for regression and classification which depend on the statistical learning hypothesis. Contrasted and other ML strategies, for example, ANNS, SVMs have a superior speculation ensure. SVM separates the data tests of 2 classes by deciding a particular hyperplane in input space. This hyperplane boosts the partition among 2 classes by taking care of a quadratic programming issue whose arrangement is around the globally optimal.

In [10], the author has examine the reasonableness of a portion of these algorithms while investigating diverse compromises. In particular, authors initially figure new method of characterizing many feature vectors for planning localizing issues onto diverse AI models. Instead of regarding localization as a classification issue, as accomplished in the majority of detailed work, authors treat it as a regression problem. Authors have contemplated an effect of varying network parameters, for example, anchor population, network size, transmitted signal power, and remote channel quality, on confining precision of the models. Authors have additionally considered the effect of sending anchor nodes in the framework as opposed to putting the nodes arbitrarily in

deployment areas. Their outcomes have uncovered fascinating experiences while utilizing the multivariate regression model and SVM regression model with an RBF. Various models have been characterized for various ML algorithms. A portion of the normally utilized models incorporates neural networks, multiple linear regression model, linear regression model, SVM with various kinds of kernels, Logistic regressions or classifications, k-nearest neighbours (KNN), and random forest (RF) clustering.

In order to address the Wireless Sensor Networks (WSN) localization accuracy problem in [11], the authors have suggested the latest Methodology for Localization Backpropagation Network (BPNN). At first, node localization calculations are provided with range intervals and signal power, and on BPNN the parameters solve easily. In a simulation experiment, the main factors of NS2 and MATLAB are also evaluated. The results show that this technique is successful in comparison with other localization algorithms and can minimize localization errors effectively.

In [12], the authors proposed ANNs way to deal with localization in WSN through change of ANNs structures utilizing Genetic Algorithms. Populace of feed forward ANNs composing their structure in genetic code is developed more than 20 ages. Every individual is assessed through the preparation of training of ANN and further estimation of its root mean square error for all testing set. The RSSI estimations were utilized as ANN inputs to localize hubs. The methodology is to collect information from the ANNs under an input reactivated static 26 x 26 meter indoor organizational climate, which consists of eight anchor hubs, under a reactivation of the static 26x26 meter indoor organization environment. The methodology has been used. Hereditary calculations of MATLAB and fake neural organizations were used for stashing tools.

In [13], the authors emphasise the comparison and study of MLPNN and RBFNN for the creation of a position system in WSNs. Various sensor node collection were evaluated using both MLPNN and RBFNN along with the mean square error of various input data sets. Their simulation findings effectively suggest that MLPNN is more reliable with respect to localization than RBFNN.Use the "Insert Citation" button to add citations to this document.

In [14], the authors suggest a new algorithm for localizing the sensor nodes using virtual anchor nodes. VAN is located in its system with minimum anchor nodes. The goal of their work is to improve the accuracy of the position by optimizing the location ratio and minimizing the costs of several anchor nodes.

In [15], the author explained the localization based on ANN in WSN. Localization refers to the issue of finding the location or position of sensor nodes in a network. But localization problem is still an open challenge in WSN. Author analyzed and classified existing works on localization algorithms that uses ANN. ANN algorithms were identified based on how they were utilized in the localization processes; noise characterization, model construction, training phase optimization, clustering, and prediction. Author also discussed about the features and related work about it and how to improve the accuracy of previous localization using ANN.

In [16], the authors proposed an approach known as ANN approach for moderating the reaction of mixed noise sources and harsh factory conditions on the localization of the wireless sensors. They have focused on investigating the effect of blockage

and ambient conditions on the accuracy of mobile node localization. They have added a simulator for simulating the noisy and dynamic shop conditions of manufacturing environments, also for analyzing the proposed neural network.

In particular, in networks with sparse anchor deployment, cooperative localization improves the accuracy of position estimates. In [17], the authors presented implementation of it in low-cost WSN that are low-power. A WSN hardware platform with ultra-wideband range and communication is shown and the implementation of a cooperative localization algorithm based on belief propagation is addressed. The key sources of error are addressed and indoor tests of the device are performed using a simple channel access scheme and a standard ranging process.

In [18], the authors presented an enhanced centroid localization algorithm for WSN. One of the main technologies in the WSN is node localization. The center position algorithm depends entirely on the size and distribution density of the anchor nodes, but they are distributed randomly and their density is small. Given the conventional centroid localization algorithm, an enhanced centroid localization algorithm is vulnerable to the effect of network deployment status and the current situation of low positioning accuracy. Second, the idea of reference anchor nodes is implemented by bringing weight thought into the measurement method of node coordinates.

This template, modified in MS Word 2007 provides authors with most of the formatting specifications needed for preparing electronic versions of their papers. All standard paper components have been specified for three reasons: (1) ease of use when formatting individual papers, (2) automatic compliance to electronic requirements that facilitate the concurrent or later production of electronic products, and (3) conformity of style throughout the conference proceedings. Margins, column widths, line spacing, and type styles are built-in; examples of the type styles are provided throughout this document and are identified in italic type, within parentheses, following the example. Some components, such as multi-leveled equations, graphics, and tables are not prescribed, although the various table text styles are provided. The formatter will need to create these components, incorporating the applicable criteria that follow.

3. Methodology

An ANN, also known as the network of neurons, offers a simple way of revealing valued and true functions as examples. ANN uses a supervised curriculum. Inputs and outputs to the ANN are given to learn and create a correct model. The classification and regression dilemma is normally tackled. Typically, the artificial neuron network has 3 layers, input layer, hidden layer(s), and finally output layers.

Neural feedback and feedback networks form two classes of neural networks. In a neural feed network, the outcome is fed from one layer of neurons to the next layer, no layers are skipped during this process, and the system has no feedback. The position is composed of three major neural networks: MLP, the Recurrent Neural Network and, the RBF.

It is to be noted that RSSI values are very unpredictable and vary under ambient noise and sensor mobility. The benefit of a neural network is that prior environmental and noise propagation is not needed. More precision is achieved through a neural network compared to other approaches such as Kalman filters. Comparing other neural network types, for the study the

compromise between MLP neural accuracy and the network memory requirement was chosen.
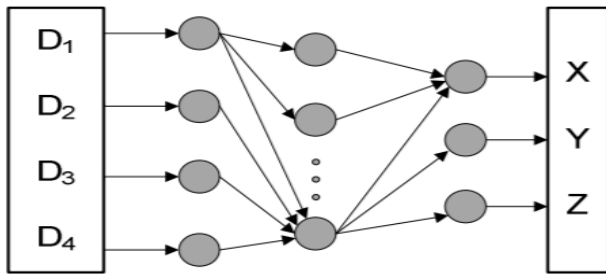
Figure 1: A general feed-forward neural network structure with four inputs and three outputs.

3.1. Network Model

WSN model for region assessment of static sensor nodes. Static nodes are moved to region of recognition and the node of mobile
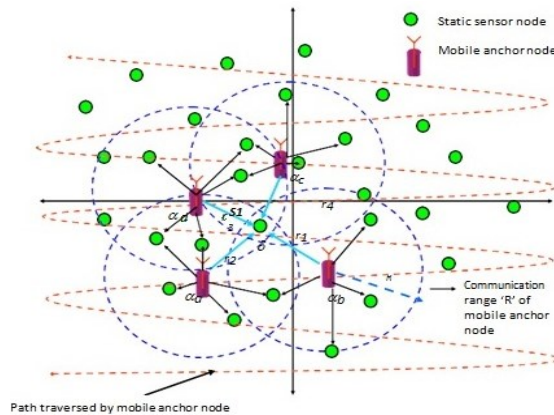
Figure 2: Illustration of broadcasting and reception of beacon signal from a Mobile Anchor and static sensor node respectively.

anchor (MA) ready for intersection. In addition, in the fig, the way MA navigates. 2.

It is assumed that R is a contact range of the MA hub. MA has a GPS recipient and knows its location often. The MA is sending beacon signal at a fixed "Live" interval with an id, transmission radius, current location, transmission power and format shown in figure 2. Before the MA node moves around the sensor area, the administrator determines the 'alternative' intervals.

Figure 3: Packet format of beacon message

Any static sensor node in MA node's "R" range receives a signal from the beacon. A table called Mobil Anchor Location (MAP), as represented in Table 1, is retained in every static sensor Node.

When static sensor node beacon signals are obtained, X-y coordinate values are extracted from signal and stored in the MAP table in corresponding fields. The distance is determined according to the signal power obtained and stored in the Chart Table.

Consider scenario in Figure 2, let $\alpha_a, \alpha_b, \alpha_c$ and α_d be the MA positions throughout its traversal time and having (x_1, y_1),

(x_2, y_2), (x_3, y_3) and (x_4, y_4) as their coordinates. Static sensor node S1, at position δ whose co-ordinate is (x_0, y_0), receives beacon signals when MA is at position $\alpha_a, \alpha_b, \alpha_c$ and α_d and stores their x-y co-ordinate values into MAP table. Similarly, S1 receives beacon signals when it comes into MA node proximity. Eventually, x-y co-ordinate values are extracted from received signal and stored into MAP table.

3.2. RSS Measurement

Distance from the MA node at position I to the static node S1 at position (x0, y0) is referred to as a correspondence to r (i), as seen in the following equations; (R2) The noise free RSS or received power at S1, denoted by P_i^r

$$P_i^r = k_i \frac{P_i^t}{d_i^\alpha}, i = 1,2,3, \ldots., m \qquad (1)$$

$$d_i^\alpha = k_i \frac{P_i^t}{P_i^r}, i = 1,2,3, \ldots., m \qquad (2)$$

If the beacon signals received by the static node i=1, 2... m number, the transmitted power is P_i^t, the power received is P_i^r, and the propagation constant is α, k (i)denotes other environmental variables that influence the received power. Range related measurement can be modeled, as expressed in (R1)

$$r_i = k_i \frac{P_i^t}{P_i^r} \qquad (3)$$

$$r_i = d_i^\alpha + \eta_i \qquad (4)$$

Every static node calculates r_i for each received beacon signal and stores into MAP table as demonstrated in table 1.

Table 1: MA Positions stored at static sensor node

X-co-ordinate	Y-co-ordinate	Distance (r)
(x_1)	(y_1)	r_1
(x_2)	(y_2)	r_2
(x_3)	(y_3)	r_3
(x_4)	(y_4)	r_4
•	•	•
•	•	•
(x_m)	(y_m)	r_m
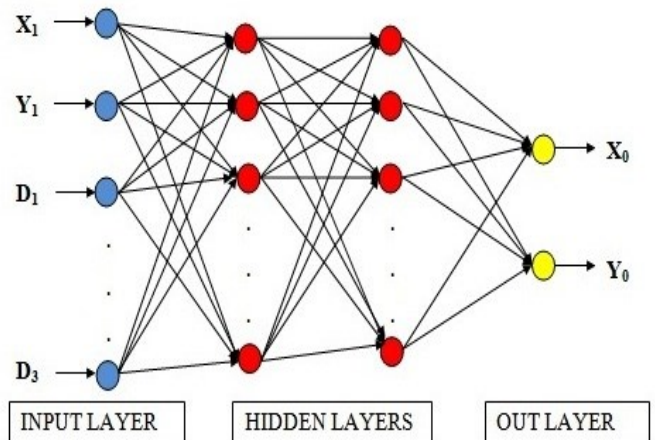
Figure 4: Multi-layer perceptron neural network

3.3. Multi-Layer Perceptron Neural Network Model

Neural network model (framework), initially trained with training dataset. Proposed system consisting of Multilayer Perceptron neural network [MLPNN] model having input layer, one or more hidden layers and output layer.

Nine inputs are passing to MLPNN, consisting of three different positions of MA with respect to distance from sensor node. Hidden layer having various neurons. Each neuron, having transfer function to find out weights of each connection between inputs to hidden layer neurons. Output layer having two neurons produces the location coordinates of unknown sensor node. Activation function (linear or nonlinear) is used to calculate location of sensor nodes.

3.4. Algorithm

The multilayer perceptron algorithm is as follows:

Step 1: Initialization: Arbitrary values are used to trigger all networks and thresholds, which are consistently distributed across a limited range. If these values are 0, gradients will also be computed to 0, if and only if there will be no direct relation between input and output and network. More training trials, with various initial weights, are planned to have the best cost-effectiveness. If the initial values are sufficiently high, however these units appear to be saturated.

Step 2: A new period of formation: an era means all the examples are presented in the training set. Training on the network typically requires further training times. The weights are calibrated for statistical rigour, only after the test vectors are applied on the network. Therefore, after each model in the training set and after the end of the training stage, weights must be memorised and adjusted, the weights changed only once. There is a "online version, simpler, which directly updates weights, in which case there may be the order in which the network vectors are displayed. Both weight gradients and current error have been initialised at 0 (alternative to 0) and E=0).

Step 3: The forward propagation of the signal

An example from the training set is applied to the inputs. Outcomes of neurons from hidden layer are computed:

$$y_j(p) = f\left(\sum_{i=1}^{n} x_i(p) . w_{ij} - \theta_j\right) \quad (5)$$

Where n is hidden layer number of inputs for neuron j and f is sigmoid activation.

Real network outputs are measured:

$$y_k(p) = f\left(\sum_{i=1}^{n} x_{jk}(p) . w_{jk} - \theta_k\right) \quad (6)$$

Where m is the input number from the output layer of neuron k.

Error updated by epoch:

$$E = E + \frac{(e_k(p))^2}{2} \quad (7)$$

Step 4: Backward error propagation and weight correction. Neuron error gradients are computed in the output layer:

$$\delta_k(p) = f'e_k(p) \quad (8)$$

where f' is the activation derivative function. A mistake occurs as

$$e_k(p) = y_{d,k}(p) - y_k(p) \quad (9)$$

If we use the single-pole sigmoid (equation 1, its derived is:

$$f'(x) = \frac{e^{-x}}{(1+e^{-x})^2} = f(x).(1 - f(x)) \quad (10)$$

Furthermore, the single-pole sigmoid is the function used. Then it becomes equation (10):

$$\delta_k(p) = y_k(p).(1 - y_k(p)).e_k(p) \quad (11)$$

The weight gradients from the secret layer to the output layer are updated:

$$\Delta w_{jk}(p) = \Delta w_{jk}(p) + y_j(p).\delta_k(p) \quad (12)$$

The gradients of the neuron errors are determined in the secret layer:

$$\delta_j(p) = y_j(p).\left(1 - y_j(p)\right).\sum_{k=1}^{l} \delta_k(p) w_{jk}(p) \quad (13)$$

where l is the number of network outputs.
The weight gradients of the input layer are modified with the hidden stage.

$$\Delta w_{ij}(p) = \Delta w_{ij}(p) + x_i(p).\delta_j(p) \quad (14)$$

Step 5: A new version. A new one. If the current training cycle still has test vectors, pass stage 3. If not the weights of all the links are changed according to the weight gradients:

$$w_{ij} = w_{ij} + \eta . \Delta w_{ij} \quad (15)$$

Where μ is the rate of analysis. When a stage is over, we check if it meets the termination condition ($E < E_{max}$ or a maximum number of periods of training have been achieved). Otherwise, we will move on to phase 2. If so, the MLP algorithm is over.

3.5. Simulations

On a PC with an i5 processor with an 8 GB RAM processing speed of 3.50 GHz, simulations can be brought. Sensor nodes are positioned on the grid intersection points and are first learned to locate as seen in the Figure. 5.
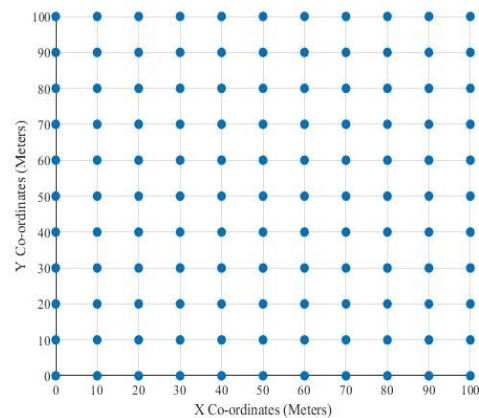
Figure 5: Illustrate the deployment of Sensor nodes and Mobile anchor node

The trained network with numerous training algorithms has placed localised sensor nodes on arbitrary points on the grid. The research is conducted. The node position is determined with the positioning information of the moving anchor node. The network is taught and checked using a handheld anchor node with the initial position to determine network efficacy (0.5, 0.5).

The sensor nodes are initially installed in a fixed location on the grid during testing. The handheld anchor node that has a set network gap has been deployed. Each mobile anchor node interval 't' sends its present position (X and Y coordinates) to sensor nodes that fall within its radio frequency spectrum. Each sensor node shall compute its current position using the proposed position algorithm by obtaining a minimum of three separate location information from mobile anchor node positions.

To determine the position of sensor nodes in the same grid, a further test of the qualified network is carried out. The nodes of the sensor were spread around the test grid uniformly. The testing is seen via the coordinate grid.

4. Results and discussion

For this study 5 different training algorithms BR, LM, RP, GD and SCG have been used for formation of the neural network, requiring supervised learning.
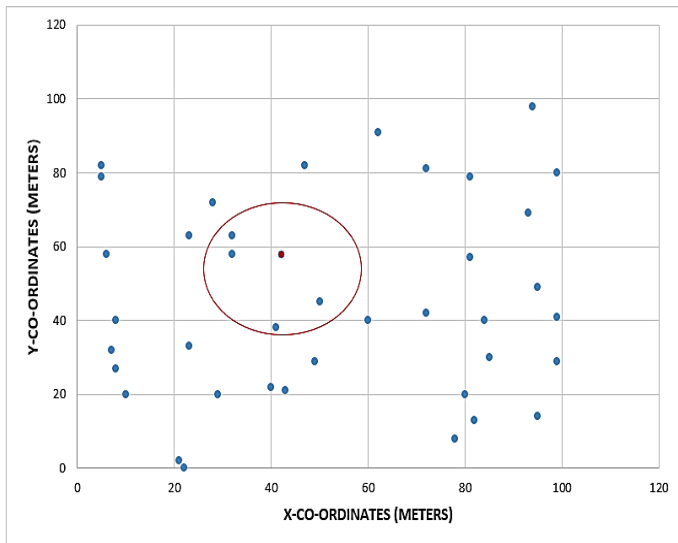
Figure 6: Illustration of Mobile anchor node with random deployment of sensor nodes

A neural network. Several testing functions with a different number of layers and nodes have been conducted. There are optimal results from network of 3 layers with a 9-12-2 structure. There were 9 neurons in input layer, hidden layer with 12 neurons and two in the output layers. Hyperbolic sigmoid tangent activation function for hidden layers, whereas pure line function in output layer has been used. This structure was utilized for the evaluation of the performance of the following anchor node configurations with different numbers of anchors.

An experiment was performed. 5 different BR, LM, RP, GD and SCG training algorithms for the formation of a neural

network that require supervised learning have been used to this study. A network of neural components. A number of test functions have been performed with different layers and nodes. A network of three layers with a structure 9-12-2 produces optimal results.

$$e = \sum_{i=1}^{n} \frac{1}{n} \sqrt{(x_i - x_{oi})^2 + (y_i - y_{oi})^2}$$

where n is the overall number of test sets and exact position (x_{oi}, y_{oi}) and estimated position of sensor node in i^{th} test dataset is (x_i, y_i).

The above mobile anchor node configurations were used for assessments of the performance of various anchor numbers. The average location error during this phase is illustrated in Figure 7. Figure 8 shows the time required for the network to train using different training algorithms.
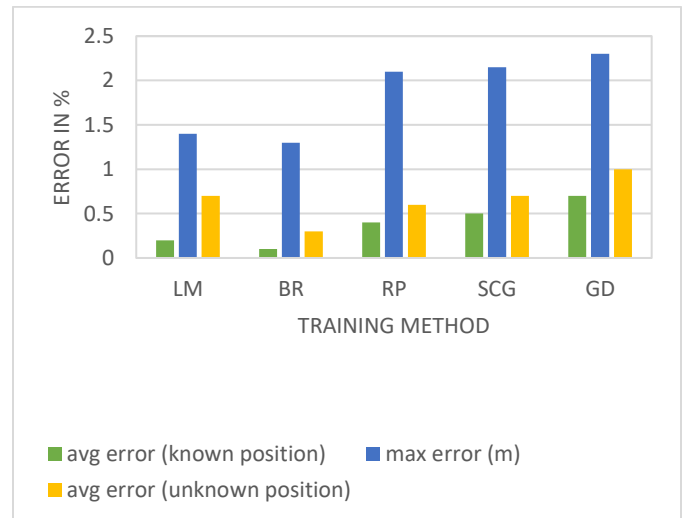
Figure 7: Illustration of localization error of different training algorithm with mobile anchor.

In Figure 7, Depicts different training algorithms have compares with localization error. The BR training algorithm is having less average error as compared to other training algorithms.
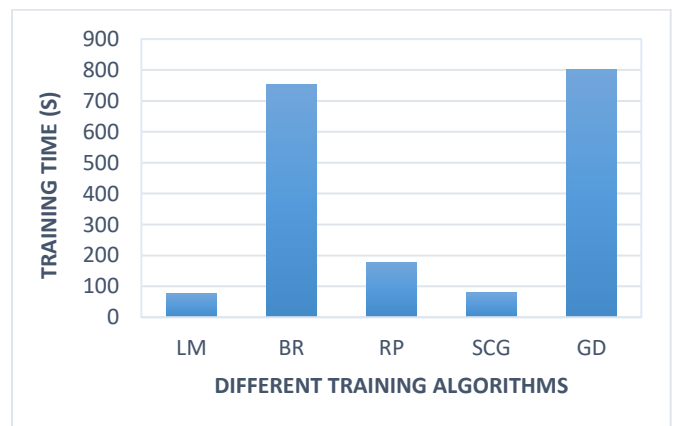
Figure 8: Illustrate time taken to train neural network for different training algorithms with mobile anchor

In Figure 8. Shows the training time taken by the ANNN model for different training algorithms. LM, RP and SCG are taking less training time and BR and GC training algorithms are taking more training time.

Cost of the network will be reduced with using one mobile anchor agent. Estimated Mean Localization Error (Meters) for different number of sensor nodes using BR training algorithm is shown in Figure 9 for the communication range of mobile anchor node that is R=40 meters, 60 meters and 80 meters.
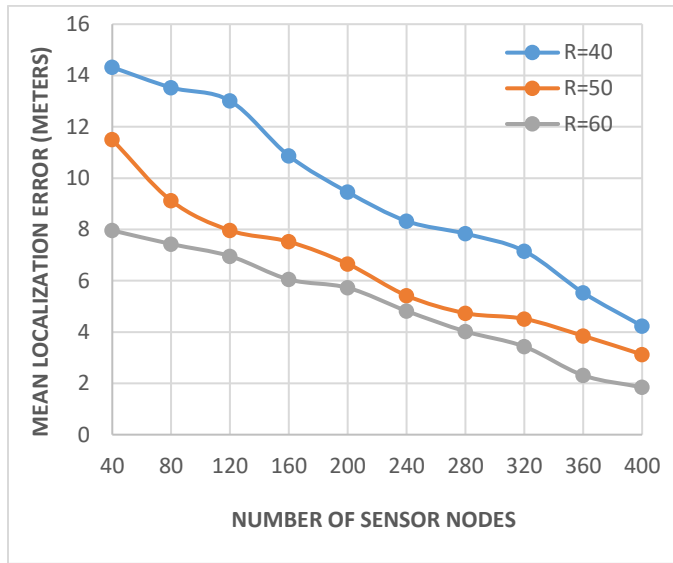
Figure 9: Estimation error when varying communication range.

In Figure 10. Depicts convergence accuracy of mobile anchor node with different time stamps for broadcasting their location information to static sensor nodes using BR training algorithm.
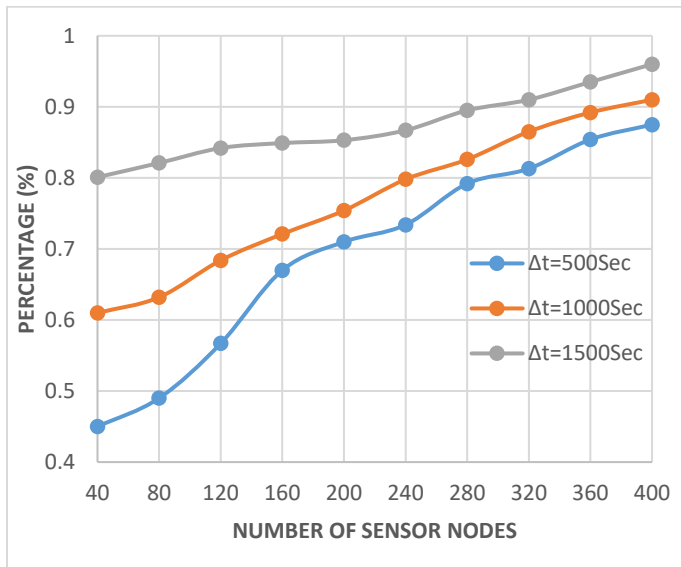
Figure 10: Convergence accuracy for various regular intervals.

5. Conclusions

The use of ANN has been suggested for an effective 2D localization algorithm for WSN. The RSSI signal values from the mobile anchor node are the entry to the proposed process. Since every mobile anchor node is fitted with wireless RF modules, no

external hardware is necessary. The approach proposed is therefore , energy-efficient and uses just a two-way message to obtain the location inputs. As in the proposed system, only one mobile anchor node is used, even the cost is minimized. It is however, advisable to use the RSSI value of the mobile-based anchor Node beacon request signals, which may further reduce the location error. The following is recommended.

In order to obtain the finest neural network for localization, the BR training algorithm is evaluated to give the best results. Hence, the training time for this algorithm is quite high compared to other methods such as LM, RP, and SCG. It is therefore recommended that the BR method is used when offline training is performed as in this case. The LM method is recommended for applications requiring online training.

Conflict of Interest

The authors declare no conflict of interest related to this paper.

References

[1] D. Praveen Kumar, T. Amgoth, C. S. R. Annavarapu, "Machine learning algorithms for wireless sensor networks: A survey," Information Fusion, 49, https://doi.org/10.1016/j.inffus.2018.09.013.

[2] X. Feng, Z. Gao, M. Yang, S. Xiong, "Fuzzy distance measuring based on RSSI in Wireless Sensor Network," 2008 3rd International Conference on Intelligent System and Knowledge Engineering, https://doi.org/10.1109/iske.2008.4730962.

[3] M. S. Rahman, Y. Park, K. D. Kim, "Localization of Wireless Sensor Network using artificial neural network," 2009 9th International Symposium on Communications and Information Technology, https://doi.org/10.1109/iscit.2009.5341165.

[4] L. Zhao, X. Wen, D. Li, "Amorphous Localization Algorithm Based on BP Artificial Neural Network," International Journal of Distributed Sensor Networks, 11(7), https://doi.org/10.1155/2015/657241.

[5] K. Madhumathi, Dr. T Suresh, "Localization of Mobile Wireless Sensor Node Using Randomized Feature Sample of Estimated RSSI Value," Journal of Advanced Research in Dynamical and Control Systems, **11**(11-SPECIAL ISSUE), https://doi.org/10.5373/jardcs/v11sp11/20192943.

[6] A. Payal, C. S. Rai, B. V. R. Reddy, "Comparative Analysis of Sigmoidal Feedforward Artificial Neural Networks and Radial Basis Function Networks Approach for Localization in Wireless Sensor Networks," International Scholarly and Scientific Research & Innovation, **10**(7), https://doi.org/doi.org/10.5281/zenodo.1125123.

[7] A. Payal, C. S. Rai, B. V. R. Reddy, "Analysis of Some Feedforward Artificial Neural Network Training Algorithms for Developing Localization Framework in Wireless Sensor Networks," Wireless Personal Communications, **82**(4), https://doi.org/10.1007/s11277-015-2362-x.

[8] C. Xiao, & N. Yu," A predictive localization algorithm based on RBF neural network for wireless sensor networks," 2015 International Conference on Wireless Communications & Signal Processing (WCSP), https://doi.org/10.1109/wcsp.2015.7341145.

[9] S. Javadi, H. Moosaei, D. Ciuonzo, "Learning Wireless Sensor Networks for Source Localization," Sensors, 19(3), https://doi.org/10.3390/s19030635.

[10] G. Bhatti, "Machine Learning Based Localization in Large-Scale Wireless Sensor Networks," Sensors, **18**(12), https://doi.org/10.3390/s18124179.

[11] C. Zhou, L. Wang, L. Zhengqiu, "The Study of WSN Node Localization Method Based on Back Propagation Neural Network," Advances in Intelligent Systems and Computing, https://doi.org/10.1007/978-3-319-67071-3_54.

[12] S. H. Chagas, J. B. Martins, L. L. De Oliveira," An approach to localization scheme of wireless sensor networks based on artificial neural networks and Genetic Algorithms," 10th IEEE International NEWCAS Conference, https://doi.org/10.1109/newcas.2012.6328975.

[13] B.K. Madagouda & R. Sumathi, "Analysis of Localization Using ANN Models in Wireless Sensor Networks," 2019 IEEE Pune Section

International Conference (PuneCon), https://doi.org/10.1109/punecon46936.2019.9105871.

[14] B.K. Madagouda, R. Sumathi, A. H. Shanthakumara, "Localization of Sensor Nodes Using Flooding in Wireless Sensor Networks," Communications in Computer and Information Science, https://doi.org/10.1007/978-3-642-29219-4_72.

[15] R. Dela Cruz, "Artificial Neural Network-based Localization in Wireless Sensor Networks".

[16] M. Gholami, N. Cai, R. W. Brennan, "An artificial neural network approach to the problem of wireless sensors network localization," Robotics and Computer-Integrated Manufacturing, **29**(1), https://doi.org/10.1016/j.rcim.2012.07.006.

[17] B. Etzlinger, A. Ganhor, J. Karoliny, R. Huttner, A. Springer, "WSN Implementation of Cooperative Localization," 2020 IEEE MTT-S International Conference on Microwaves for Intelligent Mobility (ICMIM), https://doi.org/10.1109/icmim48759.2020.9299096

[18] X. Yang, X. Wang, W. Wang, "An Improved Centroid Localization Algorithm for WSN," 2018 IEEE 4th Information Technology and Mechatronics Engineering Conference (ITOEC), https://doi.org/10.1109/itoec.2018.8740471.

Allocation of Total Congestion Cost and load participation to Generators for a PoolCo Market in Deregulated Power System

Yashvant Bhavsar[1,*], Saurabh Pandya[2]

[1]*Electrical Engineering Department, Vishwakarma Government Engineering College, Ahmedabad, 382424, India*

[2]*Electrical Engineering Department, Lukhdhirji Engineering College, Morbi, 363641, India*

ARTICLE INFO	ABSTRACT
	The objective of this paper is to allocate transmission congestion cost to responsible generators using a novel method. Deregulation of the electrical power system leads to the compulsion of open access to the transmission system for all entities of the power system. There is a trend to utilize cheaper generators by all loads. This leads to a violation of the operational and physical constraints of transmission corridors connected to those generators. It is not possible to utilize cheaper generators all the time due to the operational and physical constraints of the transmission lines. Hence there is an increase in the cost of energy produced. This increase in energy cost is taken into account as total congestion cost. Allocation of total congestion costs among various entities is always a complex task. Here, generators liable for the increase in total congestion cost identified using Bialek's algorithm. Bialek's upstream algorithm was applied to allocate congestion costs to generators. Results are obtained on IEEE-14 bus and IEEE-30 bus standard test systems.

1. Introduction

The electric power industry was operated as a *"regulated monopoly"* up to the nineties decade. Then after the structure of the electric power industry took a major shift and all its operations were unbundled, i.e. de-regulated. Because of the restructuring of the power utilities, the power industry is becoming turbulently competitive, and going through technological and regulatory changes, which affect its planning, operation, control, and services to customers. It is important to spot the consequences and impacts of those changes on the planning, operation, control and cost of the power system. In a deregulated power system, the transmission system must be available to all users without any discrimination. Due to physical and operating constraints of transmission corridors, not all the load be served by the cheaper generators, leading to the increased generation cost. The system operator (SO) must identify the responsible entity for this increase in cost. Determination of congestion cost and distribution of this among all participants is a crucial issue with the operation of a deregulated power grid.

Market-based methods are methods that used either dispatch methods, generator rescheduling, load management or nodal pricing based methods. Pool and contract dispatch models with a priority of load curtailment applied using social welfare and contracts between generators and load [1, 2]. Optimal bus price-based simple methods were proposed [3] to calculate congestion cost supported the very fact that additional flow increases congestion. Various dispatch methodologies introduce [4] for open access of transmission line by representing a conceptual model of pool dispatch, bilateral dispatch and multilateral dispatch alongside the need for dispatch coordination between these models. Effectiveness of congestion clusters method for congestion management discussed for cost and loss minimization [5] with the definition of transmission congestion distribution factors (TCDFs) which used to evaluate the change in the flow of a rise in the injection of power at any bus. Two sets of sensitivity indices: Real Power transmission Congestion distribution Factors (PTCDFs) and Reactive Power transmission Congestion Distribution Factors (QTCDFs) used for congestion management [6] during which selection and participation of generators depend upon both their reactive sensitivity and bid price for up/downregulation. A simplified approach proposed [7] for

security-oriented power system operation in which the first contribution of each generator for a particular overloaded line is identified and then based on the relative electric distance (RED) concept the specified proportion of generation for the specified overload relieving obtained. A combined objective function [8] was obtained using the generation cost function and congestion management cost function incorporating additional penalty factors that were further solved by a bacterial foraging algorithm. A multi-objective congestion management framework with optimization of congestion management cost, voltage security and dynamic security called augmented ε-constraint technique discussed in which the first objective function is that the cost of congestion management while the second and third objective function is of voltage stability margin (VSM) and Corrected Transient Energy Margin (CTEM) [9]. Simple indices introduced [10] for effective and agreeable load curtailment in congested lines because of the sensitivity of load to a congested branch, economic incentives to reduce consumption and customer willingness to curtail load during congestion. These indices are achieved by mathematical formulation for maximizing social welfare, the overall index for possible load management and generator re-dispatch. Zonal congestion management approach discussed in[11,12], using real and reactive power sensitivity index as well as balancing energy up/down service settlement and other similar factors. Based on the calculation of the congestion cost index (CCI) total congestion cost index (TCCI) is minimized for a given number of buses [13]. CCI is obtained by difference of bidding rate and power during the pre-dispatch and re-dispatch era. Security constraint optimal power flow (SCOPF) with and without line flow constraints [14] used to determine total congestion cost which further distributed into line-wise congestion cost, whereas same SCOPF with inputs from energy management system (EMS) and state estimator applied iteratively [15] with contingency analysis used to estimate the actual cost of congestion. The participation of generators and loads within the use of the transmission network is decided employing a modified z-bus matrix [16]. The modified z-bus matrix is formed by modeling both generators and loads as constant admittances in the network considering them separately. A novel topological approach to MW-Mile proposed based on electricity tracing method [17]. The equation for topological generation distribution factor almost like that of generalized generation distribution factor defined, which further used for formation of supplement transmission charge of any generator in the network. Distributed energy sources (DERs) plays important role for alleviating transmission congestion cost. The usage based transmission cost division method is introduced in which transmission capacity is divided into four capacities to gauge the contribution of DERs to transmission cost [18]. A modified inage domain method for power flow tracing [19] used to allocate transmission cost and advance congestion management. Power tracking coefficient developed [20]with the help of kirchof's law for the active power flow tracking and revenue collected by individual generator determined. A method [21] suggested allocating the transmission fixed charge based on the modification of the impedance matrix in which real power flow through the line expressed in terms of load current also as electrical distance and voltage injection at the bus. Iteratively one by one impact of every generator selected on the network using the z-bus of the network [22] and transmission congestion cost determined based on the current decomposition method. A DC power flow based problem [23] using generation

shift factor is defined as a lossless system to work out contribution-based congestion cost allocation methods in a bilateral market.

A fair allocation of transmission congestion cost to the generation companies is required in poolco market where generator dispatch pattern changes due to congestion. Here in this work transmission line congestion is identified by observing the value of the dual variable associated with constraints [14]. Total congestion cost (TCC) evaluated by generator re-dispatch method with and without constraints. The dual variable associated with the congested line is utilized to find the line allocation factor. Line-wise congestion cost (LWCC) of each congested line is evaluated with help of the line allocation factor. For power flow tracing, results obtained from common methods like graph method and node method are not accurate and it takes more computational time. To allocate congestion cost, the cost associated with congested lines should only be considered. A novel method discussed here using bialek's upstream algorithm [17,24] to allocate this TCC to all generators as well as the generator's contribution to supplying the load of the system.

2. Problem formulation

2.1. Total Congestion Cost (TCC) and Allocation to Line

A simple method to evaluate TCC is the generator re-dispatch method. In this method, optimal power flow (OPF) is applied with and without line flow constraints. The difference in evaluated costs of both cases is identified as TCC. This TCC is allocated to the lines under congestion. Generalized optimal power flow problem with constraints is formulated as:

$$C(P_{Gi}) = \sum_{i \in N_{gi}}(a_i P_{Gi}^2 + b_i P_{Gi} + C_i) \qquad (1)$$

where,

N_{Gi} = Number of generators in the system

The above optimized problem is with several constraints as follows:

$$P_{Gi} - P_{Di} - P_{loss} = 0 \qquad (2)$$

$$P_{Gimin} \leq P_{Gi} \leq P_{Gimax} \qquad (3)$$

$$Q_{Gimin} \leq Q_{Gi} \leq Q_{Gimax} \qquad (4)$$

$$V_{imin} \leq V_i \leq V_{imax} \qquad (5)$$

$$P_{ij} \leq P_{ijmax} \qquad (6)$$

where,

P_{Gi} = Active power generation in *MW* at bus *i*.

P_{Di} = Load in *MW* at bus *i*.

P_{Gimin} = Minimum limit of active power generation at bus *i*.

P_{Gimax} = Maximum limit of active power generation at bus *i*.

Q_{Gimin} = Minimum limit of reactive power generation at bus *i*.

Q_{Gimax} = Maximum limit of reactive power generation at bus *i*

V_{Gi} = Voltage at bus *i*

V_{Gimax} = Maximum voltage limit at bus *i*

V_{Gimin} = Minimum voltage limit at bus *i*

P_{ij} = Power flow in MW between bus i and j

P_{ijmax} = Power flow limit in MW between bus i and j

In the above constraints (2) is power balance constraint whereas (3) to (6) are inequality constraints.

Following are steps to evaluated TCC and its allocation to the congested line:

1. Run optimal line flow without and line flow constraints and obtain total generation cost (*TGC*) as per (1).

2. With line flow constraints, repeat optimal power flow for obtaining a revised total generation cost (*TGC'*).

3. Total congestion cost (*TCC*) is evaluated as:

$$TCC = TGC' - TGC \qquad (7)$$

4. The dual variable associated with the constraint of (6) is utilized to obtain the line allocation factor L_{ij} as [14],

$$L_{ij} = \frac{\mu_{ij}(S_{ijmax} - S_{ij})}{\sum \mu_{ij}(S_{ijmax} - S_{ij})} \qquad (8)$$

where,

μ_{ij} = Dual variable associated with constrained line

S_{ij} = Actual line flow between bus i and j

S_{ijmax} = Maximum line flow limit between bus i and j

5. Congested cost allocated to the constrained line is evaluated as:

$$LWCC_{ij} = TCC * L_{ij} \qquad (9)$$

Equation (9) determines the line-wise congestion cost allocated to the constrained line from that of TCC.

2.2. Generator share to line congestion cost

In poolco model of the deregulated power system, it requires to identify generators (suppliers) liable for line congestion as well as the allocation of congestion cost to those generators is equally important. For fair allocation of congestion cost to the generators, generator share to line flow is to be determined. Here bialek's upstream algorithm [17,24] is employed to spot generators participation for the corresponding line flows from congested lines. The subsequent steps demonstrate to determine the sharing of line congestion cost to generators:

1. After carrying out OPF, convert net real power into lossless line flows $|P_{i-j}|$.

2. Next to determine node injection power as,

$$P_i = \sum_j |P_{i-j}| + P_{Gi} \qquad (10)$$
For $i = 1, 2 \dots n$ n = number of buses

where,

n = number of buses
j = node directly supplying to the node I

3. The ratio of line flow to the node injection power, Generation cost coefficient (GCC), determined as,

$$C_{ji} = \frac{|P_{j-i}|}{P_i} \qquad (11)$$

4. An up-stream distribution matrix A_u evaluated whose elements are determined as,

$$[A_u]_{ji} = \begin{cases} 1 & for\ i = j \\ -C_{ji} & for\ j\ supplyinng\ to\ node\ i \\ 0 & other\ wies \end{cases} \qquad (12)$$

5. Take the inverse of the upstream distribution matrix evaluated with help of (12).

6. Determine the topological distribution factor by,

$$D_{i-l,k}^{g\ fact} = \frac{|P_{i-l}|[A_u^{-1}]_{ik}}{P_i} \qquad (13)$$

7. Generator share to line flow is determined as,

$$|P_{i-l}| = \sum_{k=1}^{n} (D_{i-l,k}^{g\ fact}) P_{GK} \qquad (14)$$

8. Line congestion cost allocated to generators as,

$$P_{gcc} = \frac{|P_{i-l}|}{P_{ij}} LWCC_{ij} \qquad (15)$$

Distribution of line congestion cost to the generators on the proportional sharing base is obtained by (15).

2.3. Generator participation to supply each load

With help of the same upstream algorithm suggested by bialek, generator participation to supply the load can be determined. Following are steps to be followed for evaluating the same.

1. Power outflow from each node is determined as,

$$P_i^{ndout} = \sum_j P_{i-j} \qquad (16)$$
For every node j connected to node i.

2. The ratio of net power flow to the node injection power P_i is given as,

$$P_i^{ndration} = \frac{P_i - P_i^{ndout}}{P_i} \qquad (17)$$

3. Generator at node I participation to each load at bus j is calculated as,

$$P_{i-j}^{GL} = [A_u]_{j,i}^{-1} P_j^{ndratio} P_{Gi} \qquad (18)$$

where,

P_{Gi} = Power generation at bus i
$[A_u]_{j,i}^{-1}$ = Upstream distribution matrix evaluated in section 2.2

3. Results and Analysis

The problem formulated during the previous section was solved with help of MATLAB programming. Initially, test results are obtained on small test bus systems like 6-bus and 9-bus test systems. Then after standard IEEE-14 and IEEE-30 test bus systems are used for obtaining results. In this section, the results of higher test bus systems are discussed. These test results are obtained for TCC, line congestion cost, and share of generators to TCC as well as line congestion cost.

3.1. IEEE-14 bus test results

IEEE-14 bus test system is with 20 lines and 5 generators. Figure 1 shows the line diagram of IEEE-14 bus system. OPF is

carried out without line flow constraints then after imposing line flow on line number 1 (connecting bus 1 and 2) and 4 (connecting bus 2 and 4). Generators' cost function is of 3rd order polynomial function. Bus number 1 is considered as slack bus for OPF. After that TCC, line congestion cost and generator share to the TCC as well as generator participation to each load are obtained as described in the previous section.
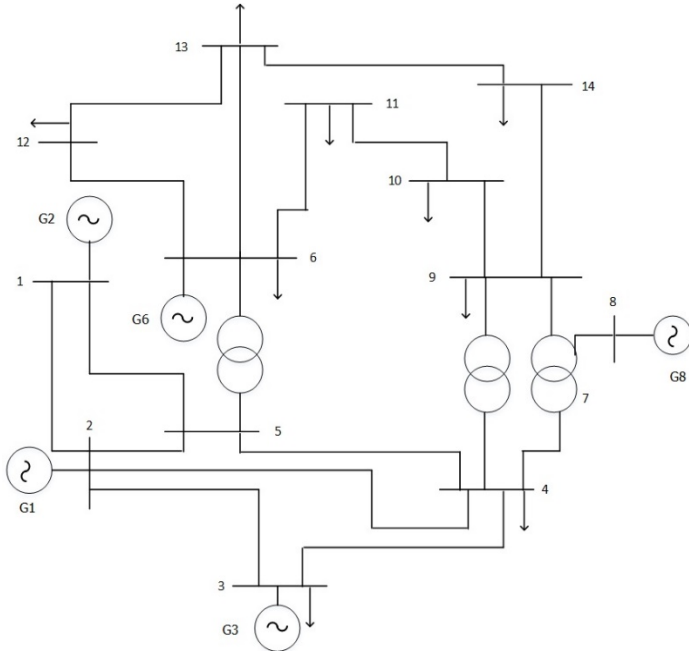
Figure 1: IEEE-14 bus test system

Table 1 shows the results obtained for the line congestion cost. Power flow without line flow constraints is 129.667 MW through line 1. With an imposing line flow limit of 110 MW, it is reduced to 109.94 MW. Similarly, for line number 4, after imposing a line flow limit of 40 MW, line flow is reduced to 38.392 MW from that of 55.3137 MW.

Table 1: IEEE-14 bus results for line congestion cost

Line no	Fbus	Tbus	Pflow w/o constraints in MW	Pflow with constraints in MW	Max line flow in MW	Line constraints allocation factor	Line congestion cost in $/hr	Total congestion cost in $/hr
1	1	2	129.667	109.94	110	0.493	28.53	57.88
4	2	4	55.3137	38.392	40	0.507	29.34	

Total congestion cost is 57.88 $/hr, further allocated to the congested line from line constraints allocation factor is 28.53 $/hr and 29.35 $/hr. Equation (14) is for identifying generator share to line flows. For IEEE-14 bus system, the generator share to the line flows is shown in Figure 2.

As shown in Figure 2, generator 1 at bus 1 is responsible for the major contribution to the line flow because the generation of the generator is remarkably high compared to all other generators. Subsequent contributor to the line flow is generator 2 connected at bus 2, whereas other generators are contributing very less to the line flow. Table 2 shows the allocation of congestion cost to the generators from that of line congestion cost.
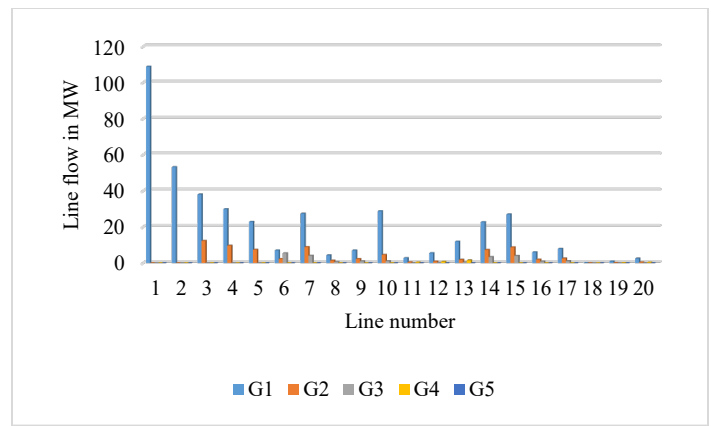
Figure 2: IEEE-14 bus generator share to line flows

Table 2: IEEE-14 bus line congestion cost allocated to generators

From bus	To bus	G1	G2	G3	G6	G8	Total	Line Cong Cost
1	2	28.532	0	0	0	0	28.532	28.532
2	4	22.175	7.173	0	0	0	29.348	29.348
Total Cost		50.707	7.173	0	0	0	57.880	57.880

All congestion costs are in $/hr in Table 2. As described in Table 2, generator 1 is sharing most of the line congestion cost as it is a major supplier to the load. It is observed that the summation of congestion cost shared by generators is equal to the total of the line congestion cost as well as that of TCC. Hence results of TCC and line congestion costs allocated to generators are self validated.

Generation participation to the system load is identified with help of bialek's upstream algorithm described in section 2.3. . The total load of the IEEE-14 bus system is 259 MW and the total generation of the system is 264.13 MW. Following Figure 3 is depicting how each load of the system is shared by individual generators.
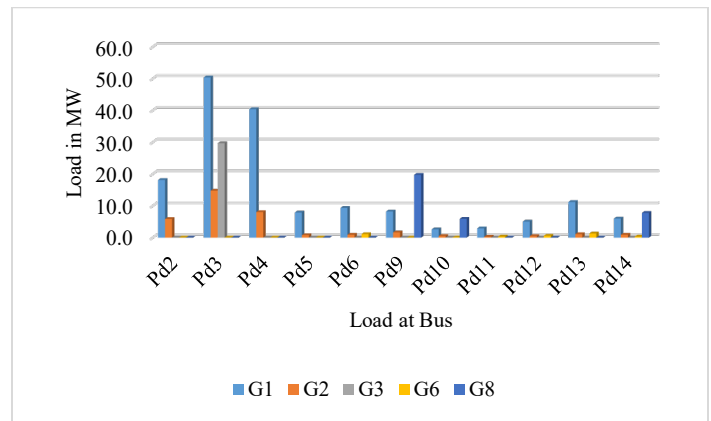
Figure 3: IEEE-14 bus load share by individual generators

Pd2, Pd3… Pd14 are the power demands (loads) at corresponding buses of the system. It is observed that generator 1 is sharing most load of the system followed by generator 2. This is in line with the sharing of line flow by all generators. Generation of generator 1 is 162.15 MW and so it serves a total load of 162.15 MW of the system with maximum sharing of 50 MW load connected at bus 2. Generators connected at bus numbers 1, 2 and

3 are supplying a load of 227.03 MW load, almost 85% of the system load.

3.2. IEEE-30 bus test results

Another standard test bus system, IEEE-30 bus system is used to get similar results as obtained on IEEE-14 bus system. As shown in Figure 4, IEEE-30 bus system having 41 lines along with six generators. The entire load connected to the system is 283.4 MW.
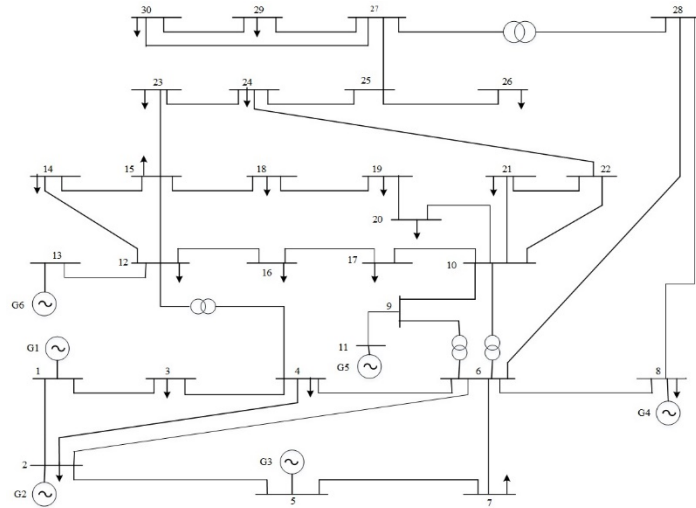
Figure 4: IEEE-30 bus system

TCC and line congestion costs are evaluated for the IEEE-30 bus system and the result obtained are tabulated in Table 3. Here, OPF is carried out without line flow constraints and then imposing line flow constraints on line one (connecting bus 1 and 2) and seven (connecting bus 4 and 6) to identify TCC. Allocation of TCC to line congestion cost is shown in Table 3.

Table 3: IEEE-30 bus results for line congestion cost

Line no	Fbus	Tbus	Pflow w/o constraints in MW	Pflow with constraints in MW	Max line flow in MW	Line constraints allocation factor	Line congestion cost in $/hr	Total congestion cost in $/hr
1	1	2	139.115	99.997	100	0.0511	8.16	159.48
7	4	6	55.314	38.393	40	0.9489	151.32	

Here it is revealed that after imposing line flow limits, power flow reduced to 99.99 MW and 38.39 MW through line numbers one and seven. TCC evaluated is 159.48 $/hr due to congestion. With help of line allocation factors of every congested line, this TCC was further allocated as 8.16 $/hr for line number 1 and 151.32 $/hr for line number 7.

Figure 5 shows the line flow share of generators up to line number 20. Again in this case also generator 1 is sharing the remarkable load of the system, hence the line flow share of generator 1 is high compared to all other generators. For the remainder of the lines, it is noticed that only except that of generator 2, a generator connected at bus 4 (generator 4) is sharing somewhat of line flow particularly of line number 36 and 40.
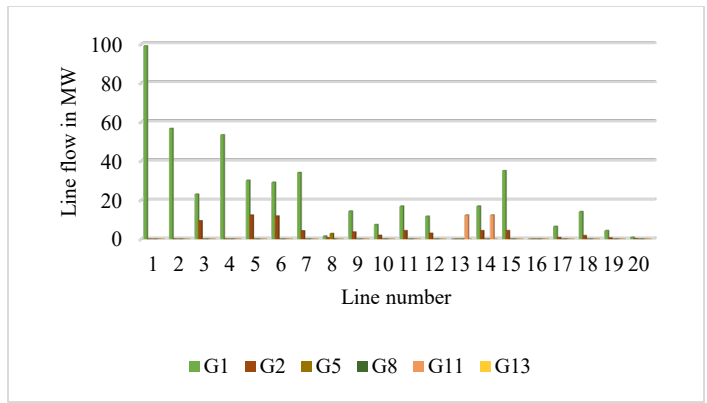
Figure 5: IEEE-30 bus generator share to line flows (up to line 20)

Table 4: IEEE-30 bus line congestion cost allocated to generators

From bus	To bus	G1	G2	G3	G4	G8	Total	Line Cong Cost
1	2	8.16	0	0	0	0	8.16	8.16
4	6	134.84	16.48	0	0	0	151.32	151.32
Total Cost		143.0	16.48	0	0	0	159.48	159.48

Table 4 states line flow congestion cost allocation to individual generators. Although IEEE-30 bus system contains a total of six generators, Table 4 shows five generators as only two generators (at bus numbers 1 and 2) are sharing line congestion cost. Here also the summation of individual sharing of line congestion cost by generators is equal to TTC and summation of line congestion cost.
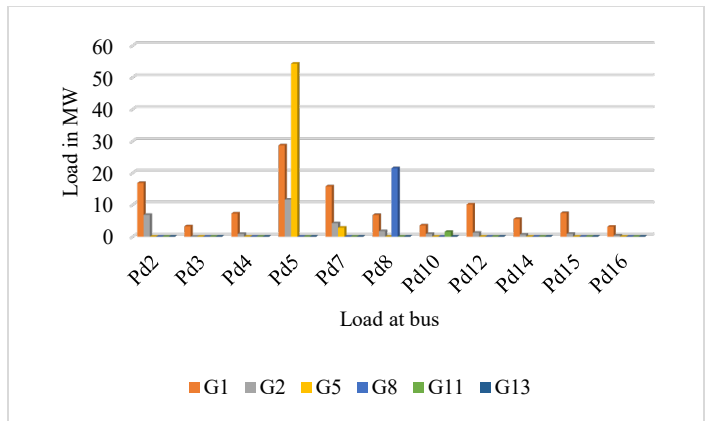
Figure 6: IEEE-30 bus load share by individual generators (first 11 loads)
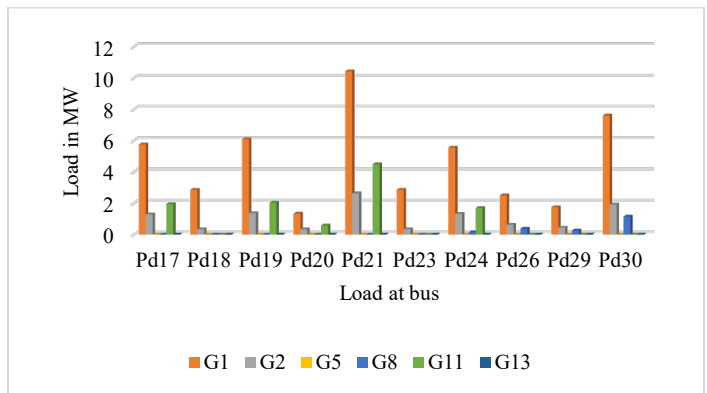
Figure 7: IEEE-30 bus load share by individual generators (Rest 10 loads)

Figure 6 and Figure 7, show the load participating by all generators of IEEE-30 bus system. There are a total of 21 loads connected to various buses as shown in Figure 5 and Figure 6. Out of a total system load of 283.4 MW, generator 1 is sharing 155.2 MW of load, and generator 3 is connected at bus 5 sharing a load of 57.13 MW.

4. Conclusion

In this paper, a method is proposed to allocate TCC to congested lines with help of a dual variable associated with these congested lines. Further, a novel method discussed to allocate these line congestion costs to generators with help of bialek's upstream algorithm of tracing the flow of electricity. Also, with help of the same algorithm formulation is done for the participation of system generators to each load connected to the system. Results are obtained for IEEE-14 bus and IEEE-30 bus test systems. Results obtained are self-validictory, and reveal that TCC is equal to the summation of individual line congestion cost as well as equal to the summation of individual congestion cost shared by all accountable generators.

References

[1] A.K. David, R.S. Fang, "Congestion management of electric power systems under open transmission access," IEE Conference Publication, (450), 469–474, 1998, doi:10.1049/cp:19971879.

[2] R.S. Fang, A.K. David, "Transmission congestion management in an electricity market," IEEE Transactions on Power Systems, 14(3), 877–883, 1999, doi:10.1109/59.780898.

[3] T.W. Gedra, "On transmission congestion and pricing," IEEE Transactions on Power Systems, 14(1), 241–248, 1999, doi:10.1109/59.744539.

[4] A.K. David, "Dispatch methodologies for open access transmission systems," IEEE Transactions on Power Systems, 13(1), 46–53, 1998, doi:10.1109/59.651612.

[5] S. Charles Raja, P. Venkatesh, B. V. Manikandan, "Transmission Congestion Management in restructured power systems," 2011 International Conference on Emerging Trends in Electrical and Computer Technology, ICETECT 2011, 23–28, 2011, doi:10.1109/ICETECT.2011.5760085.

[6] E. Muneender, D.M. Vinod Kumar, "Optimal rescheduling of real and reactive powers of generators for zonal congestion management based on FDR PSO," Transmission and Distribution Conference and Exposition: Asia and Pacific, T and D Asia 2009, 1–6, 2009, doi:10.1109/TD-ASIA.2009.5356989.

[7] G. Yesuratnam, M. Pushpa, "Congestion management for security oriented power system operation using generation rescheduling," 2010 IEEE 11th International Conference on Probabilistic Methods Applied to Power Systems, PMAPS 2010, 287–292, 2010, doi:10.1109/PMAPS.2010.5528719.

[8] A. Ramesh Kumar, L. Premalatha, "Security constrained multi-objective congestion management in transactional based restructured electrical network using bacterial foraging algorithm," Proceedings of IEEE International Conference on Circuit, Power and Computing Technologies, ICCPCT 2013, (1), 63–67, 2013, doi:10.1109/ICCPCT.2013.6528913.

[9] M. Esmaili, N. Amjady, H.A. Shayanfar, "Multi-objective congestion management by modified augmented ε-constraint method," Applied Energy, 88(3), 755–766, 2011, doi:10.1016/j.apenergy.2010.09.014.

[10] Y. Niu, Y.L. Cong, T. Niimura, "Transmission congestion relief solutions by load management," Canadian Conference on Electrical and Computer Engineering, 1, 18–23, 2002, doi:10.1109/ccece.2002.1015168.

[11] J. Yu, J. Galvin, "Zonal congestion management and settlement," Proceedings of the IEEE Power Engineering Society Transmission and Distribution Conference, 1(SUMMER), 249–254, 2001, doi:10.1109/pess.2001.970021.

[12] A. Kumar, S.C. Srivastava, S.N. Singh, "Congestion management in competitive power market: A bibliographical survey," Electric Power Systems Research, 76(1–3), 153–164, 2005, doi:10.1016/j.epsr.2005.05.001.

[13] K.Y. Lee, S. Manuspiya, M. Choi, M. Shin, "Network congestion assessment for short-term transmission planning under deregulated environment," Proceedings of the IEEE Power Engineering Society Transmission and Distribution Conference, 3(WINTER MEETING), 1266–1271, 2001, doi:10.1109/pesw.2001.917258.

[14] A. Jana, "A new approach to transmission congestion cost calculation," 2008 Joint International Conference on Power System Technology POWERCON and IEEE Power India Conference, POWERCON 2008, 9–12, 2008, doi:10.1109/ICPST.2008.4745363.

[15] T.J. Overbye, "Estimating the actual cost of transmission system congestion," Proceedings of the 36th Annual Hawaii International Conference on System Sciences, HICSS 2003, 2003, doi:10.1109/HICSS.2003.1173857.

[16] Y.P. Molina, O.R. Saavedra, C. Portugal, "Allocation of transmission network cost using modified Zbus matrix," International Journal of Electrical Power and Energy Systems, 63, 323–330, 2014, doi:10.1016/j.ijepes.2014.06.007.

[17] J. Bialek, "Topological generation and load distribution factors for supplement charge allocation in transmission open access," IEEE Transactions on Power Systems, 12(3), 1185–1193, 1997, doi:10.1109/59.630460.

[18] J.X. Wang, H.W. Zhong, Q. Xia, "A usage-based transmission cost allocation scheme considering impacts of DERs," IET Conference Publications, 2016(CP705), 2016, doi:10.1049/cp.2016.1184.

[19] A. Baczynska, W. Niewiadomski, "Power flow tracing for active congestion management in modern power systems," Energies, 13(18), 2020, doi:10.3390/en13184860.

[20] D. Bhowmik, A.K. Sinha, "An efficient cost based allocation approach for individual generators associated with the system," Computers and Electrical Engineering, 70, 212–228, 2018, doi:10.1016/j.compeleceng.2017.12.040.

[21] J. Nikoukar, M.R. Haghifam, A. Parastar, "Transmission cost allocation based on the modified Z-bus," International Journal of Electrical Power and Energy Systems, 42(1), 31–37, 2012, doi:10.1016/j.ijepes.2012.03.002.

[22] H. Zein, "Cost allocation of transmission usage based on current magnitude," 2013 International Conference on Quality in Research, QiR 2013 - In Conjunction with ICCS 2013: The 2nd International Conference on Civic Space, 175–179, 2013, doi:10.1109/QiR.2013.6632560.

[23] M.P. Abdullah, M.Y. Hassan, F. Hussin, "Assessment of contribution-based congestion cost allocation using AC and DC for bilateral market," PECon2010 - 2010 IEEE International Conference on Power and Energy, (2), 897–901, 2010, doi:10.1109/PECON.2010.5697706.

[24] J. Bialek, Tracing the flow of electricity, IEE Proceedings: Generation, Transmission and Distribution, 143(4), 313–320, 1996, doi:10.1049/ip-gtd:19960461.

Parameters Degradation Analysis of a Silicon Solar Cell in Dark/Light Condition using Measured I-V Data

Dominique Bonkoungou[1,*], Toussaint Guingane[1], Eric Korsaga[1], Sosthène Tassembedo[1], Zacharie Koalaga[1], Arouna Darga[2], François Zougmore[1]

[1]Laboratory of Materials and Environment (LAME), University of Ouagadougou, Ouagadougou, 7021 Burkina-Faso

[2]Group of electrical engineering, Paris (LGEP) 11, rue Joliot Curie, Plateau de Moulon, 91192, Gif sur Yvette

A R T I C L E I N F O	A B S T R A C T
	In this paper, we investigate and analyze parameters degradation in a typical photovoltaic (PV) cell, which lead to power loss under dark as well as light condition using measured current-voltage (I-V) data. A nonlinear least squares method to extract the parameters such as the reverse saturation currents, the ideality factors, the series and shunt resistances of the cell from the dark current-voltage (I-V) curves is used. In order to analysis the sensitivity of the dark current-voltage (I-V) measurement to each of the six extracted parameters as a function of the voltage as well as the temperature and the density current, we simulate the operation of a silicon solar cell (KXB0022-12X1F). The analysis of the dark current-voltage (I-V) curves permit us to detect variation as small as 15% in the series resistance. We also extends the use of dark as well as light current-voltage (I-V) measurements to modules configurations of cells and uses a nonlinear least squares method to evaluate the cell efficiency parameters in the modules. Results obtained show a degradation of the values of the maximum power (Pmax) as compared to initial values by about 12, 3%, 12, 06% and 10, 21 % respectively in Total-Cross-Tied (TCT), Bridge-Link (BL) and Honey-Comb (HC) configurations.

1. Introduction

The analysis of the current-voltage curves of solar cells parameters is an important tool for quality control and evaluation of their efficiency. Though photovoltaic (PV) cells are a very important source of electrical energy, some studies [1-5] show that in a number of ways, the photovoltaic (PV) cells/modules can fail. In the circumstances; it is very important to understand the origin and behavior of these faults, before trying to improve them. However, the analysis approach required for determining the source of power loss within a solar cell depend on the fault itself, and may necessitate an analysis process which adds to system operation costs and may not always be feasible [6-8]. Authors in [9] have classified the degradation of PV cells into groups such as early degradation and long-term degradation. Early degradation are defined as encapsulant discoloration and delamination; cracks in the cell [7, 8], burnt cell caused by hot spot; soiling and shading cell, defect in anti-reflective [9]. The early degradation are also inspected in long-term field-aged PV cells/modules. Long-term degradation can be defined as corrosion of solar joint or crack in

solder joint of the PV cells connection [9]. Understanding the cause of PV cell fault and how they affect the efficiency of the PV cells is essential to improve their dependability.

In this paper, we will focus on investigating and analyzing some parameters degradation that lead to power loss in PV cells under dark/light condition using measured I-V data. The 2-diodes equivalent circuit is used to describe the electronic properties of the solar cell. A set of analyzed parameters are determined from the dark/light I-V characteristics that can identify some fault of the PV modules aggregation of electrical components and solar cells, as well as shunting and recombination losses occurring due to cell cracks, shading cell [8, 10]. An experimental setup for measuring both dark and light I-V characteristics of solar cells is performed for this purpose. It is a complementary study of a previous work in which parameters of a typical solar cell named KX0B22-12X1F have been extracted under dark condition. This work also extends the use of dark as well as light I-V measurements to modules configurations of cells and uses a nonlinear least squares method [11] to evaluate the cell efficiency parameters in the modules. Results obtained are used to analyze

*Corresponding Author D. Bonkoungou, P.O. Box 243 Ouaga 10, contact: 00226 78 61 52 85 & Email: dominique.bonkoung@gmail.com

the shade impact in the PV cell efficiency and the effect of the cell imperfection on PV module efficiency.

2. Experiment

We have made measurement on 270 mm² silicon solar cell (KXB0022-12X1F). The I-V characteristics of the cell have been measured with a system according to international standard consisting of a Keithley 2400 multimeters; a sol-UV simulator (Oriel 81192/ 1000 W); an arc lamp source (Oriel -68920). A desktop computer is used to processes the measured data using LABVIEW. To measure the I-V curve under dark we used the procedure described into [11]. For light I-V curve measurements, the cell is illuminated by a halogen (ORIEL) .This last is fed by a halogen power supply. We performed two experiments for the measurements with homogeneous as well as heterogeneous impacts on light I-V curves. Pictures of the experiment approach are displayed in figure 1. Under dark condition, the data are measured in the forward and reverse direction using a power supply. For the power supply, the voltage is measured from – 5 Volts to 1 Volt with a resolution of 0.01 Volt. The maximum current was 1 A, which corresponds to 42.4 mA/cm².

Figure 1: Experimental setup

3. Parameters extraction and fault analysis

3.1. I-V characteristics under dark condition

The 2-diodes model is used to describe the dark I-V curves of the PV cell [11].

$$I = \frac{V - R_S I}{R_p} + I_{02}\left[\exp\left(\frac{V - R_S I}{n_2 U_{th}}\right) - 1\right] + I_{01}\left[\exp\left(\frac{V - R_S I}{n_1 U_{th}}\right) - 1\right] \quad (1)$$

where $U_{th} = \frac{KT}{q}$ is the thermal voltage, q is the electron charge, K is the Boltzmann's constant, T is the temperature; R_s is the series resistance; $I_{0i}(i=1,2)$ is the dark saturation current of the diode; R_p is the shunt resistance; $n_i(i=1,2)$ is the ideality factor. In our previous work [11], the six parameters like $[I_{0i}(i=1,2); n_i(i=1,2); R_s; R_p]$ are obtained by fitting (1) to a set of measured data using a nonlinear squares method of dark I-V measurement data. The standard deviation (SD) between computed and measured data is less than 3% [11].

3.2. I-V characteristics under illuminated condition

To analyze the results obtained for the various parameters $[I_{0i}(i=1,2); n_i(i=1,2); R_s; R_p]$ under dark condition [11], we have made additional measurements in light condition. Under illuminated condition, the PV cell generate a photocurrent I_{light} and this last has to be added to (1) expressed by (2):

$$I + I_{light} = \frac{V - R_S I}{R_p} + I_{02}\left[\exp\left(\frac{V - R_S I}{n_2 U_{th}}\right) - 1\right] + I_{01}\left[\exp\left(\frac{V - R_S I}{n_1 U_{th}}\right) - 1\right] \quad (2)$$

All the parameters are defined previously. To study the efficiency of the PV cell in light condition, it is important to analyze the following parameters such as: the open circuit voltage (V_{OC}), the short circuit photo-generated current (I_{SC}) and the fill factor (FF) [3]. For the determination of the cell parameters under illumination, we proceeded as follows. We have determined the I_{SC} value by assuming that the short circuit condition is verified i.e. for $V = 0$ and $I = I_{SC}$. We get the following equation:

$$I_{SC} + I_{light} = \frac{0 - R_S I_{SC}}{R_p} + I_{02}\left[\exp\left(\frac{0 - R_S I_{SC}}{n_2 U_{th}}\right) - 1\right] + I_{01}\left[\exp\left(\frac{0 - R_S I_{SC}}{n_1 U_{th}}\right) - 1\right] \quad (3)$$

Likewise, for $V = V_{OC}$ and $I = 0$ at open circuit condition, we obtain:

$$I_{light} = \frac{V_{OC}}{R_p} + I_{02}\left[\exp\left(\frac{V_{OC}}{n_2 U_{th}}\right) - 1\right] + I_{01}\left[\exp\left(\frac{V_{OC}}{n_1 U_{th}}\right) - 1\right] \quad (4)$$

Using (3) and (4), we yield a relationship between V_{OC} and I_{SC} given by equation 5:

$$V_{OC} + R_S I_{SC} = R_P[I_{01}(\exp(-\beta_1 R_S I_{SC}) - \exp(\beta_1 V_{OC})) + I_{02}(\exp(-\beta_2 R_S I_{SC}) - \exp(\beta_2 V_{OC}))] \quad (5)$$

where $\beta_i = \frac{1}{n_i U_{th}}$ $(i=1,2)$. To fitting the illuminated I-V characteristics, we inserted the parameters values obtained in dark condition into (2) and determined V_{OC} as well as I_{SC}. For I_{light}, we have exploited the value of I given by (1) whose expansion for low voltages allows us to establish the following relation:

$$I_{Light} = I_{SC}\left(1 + \frac{R_S}{R_P}\right) \quad (6)$$

The fill factor (FF) can be calculated by means of the definition:

$$FF = (V_{mp} I_{mp})/(V_{OC} I_{SC}) \quad (7)$$

where $(V_{mp}.I_{mp})$ is the upper value of the voltage-current (V.I) product.

4. Results and Discussion

4.1. PV cell parameters sensitivity analysis both in dark and light condition

In order to analysis the sensitiveness of the dark current-voltage measurement to each of the six parameters as a function

R_P, R_S are relatively neglected. We analyze the different power losses by progressively degrading the parameters of the cell, one at a time. We varied the parameters such as I_{01}, I_{02}, R_S and n_2 by increasing their value. During this time, we decreased the value of R_P and n_1. It can be seen in Figure.2 that increased I_{02} impact the low value voltage as well as the medium voltage region of the dark I-V curve. This phenomenon can be explained by the increase of the number of fault in the cell junction. Unlike I_{02}, the increase in I_{01} affects both the medium and the high voltage ranges of the dark I-V curve. The sensitivity to R_P and n_2 are important at low and medium voltage ranges. We can conclude that the increase in I_{01}, I_{02}, R_P and n_2 affect and present distinct curvatures in the low and medium voltage ranges of the curve.

Figure 3: Sensitivity analysis of each extracted parameter $\left[I_{0i} (i=1,2); n_i (i=1,2); R_s; R_p \right]$ as a function of density current

The increase of the value of R_S drastically affect the high current and voltage regions shown in Figure 4. This shows that the analysis of the dark I-V characteristics of a solar cell is a very important tool which permit us to detect variations as small as 15% in R_S. Besides, the disturbance of R_S under dark condition made it possible to identify the faults which hinder the proper functioning of the PV cell, when we realize that the R_S in a particular PV cell as well as module would have to double before a 5% drop in power resulted [12]. The analysis of disturbances in the other parameters such as $I_{0i} (i=1,2); n_i (i=1,2); R_p$ can allow us to identify certain operating faults. And it could make easier to modify the manufacturing process to improve cell performance.

Figure 2: Dark I-V curves of a particular solar cell (KX0B22-12X1F) affected by variant faults

Then, an exhaustive analysis of these different variations (see Figure 1) can make it possible to detect operating faults. Using the measured dark I-V characteristics, we analyzed the sensitivity of each extracted parameter as a function of the current, shown in Figure 3. The parameter β is defined as being the sensitivity ratio described as follow: $\beta = \dfrac{\delta V}{\delta \alpha_i} * \alpha_i$ where $\alpha_i (i=1,2,3,4,5,6)$ represents the different parameters i.e. $\alpha_1 = I_{01}$, $\alpha_2 = I_{02}$, $\alpha_3 = R_P$, $\alpha_4 = R_S$, $\alpha_5 = n_1$ and $\alpha_6 = n_2$. These sensitivity coefficients show the dependencies of the solar cell parameters on the current level. As can be observed that for currents smaller than 400 mA/cm² , the sensitivity coefficient to R_P rises to 0, 3% as well as 0, 45% for n_2. And at high current ranges, the sensitivity to R_S increases from 0% to 0, 15% in the studied interval.

Figure 4: Effects of series resistance on the semilog plot of the dark I-V curves

Figure 5 presents the fitted and measured I-V characteristics of the PV cell in light condition. As can be noted that the fitted I-V curve agreed very well to the measured I-V characteristic. From this figure, one has determined the values of I_{SC} and V_{OC} by extrapolation to $V = 0$ axis respectively to $I = 0$ and FF by using equation 7.

The different parameters V_{OC}, I_{SC} and FF are directly obtained from the light I-V curve. The values of these parameters are given in Table1. In this table, we compares the fitted and

measured data at room temperature. We can remark that the results obtained reveal a good approximation with the two I_{sc}-V_{oc} characteristics.
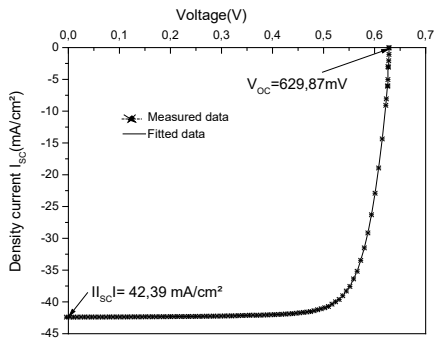
Figure 5. Fitted and measured light I-V curves at 300K.

Table 1: Measured and fitted parameters of the studied PV cell under illumination condition

Parameters	I_{SC} (mA/cm²)	V_{OC} (mV)	FF (%)
Measured data	-42,39	629,87	72, 21
Fitted data	-42,39	628,76	71,32
Deviation (%)	0	-0,27	-1,2

The plots in Figure 6 present the effects of temperature on the light I-V characteristics of a particular silicon solar cell. The plot clearly demonstrates that the open circuit voltage (V_{OC}) decreases with increasing temperature; whereas the short circuit current (I_{SC}) remains unchanged throughout the temperature range studied i.e. $I_{SC} \cong 42,40$ mA/cm². This shows that V_{OC} considerably depends on the temperature.
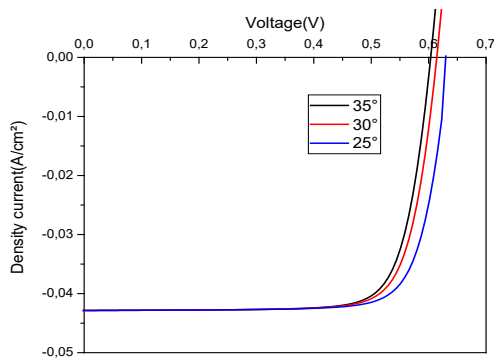
Figure 6: Density current I_{SC} versus voltage V_{OC} for variant temperatures

In order to analyze the effect of partial or total shading on the studied PV cell, we performed two experiments for the measurements with homogeneous as well as heterogeneous impacts on light I-V curves. Firstly, we measured the light I-V curves of the PV cell with uniform irradiances at Standard Test Condition (STC: 1000 W/², 25° C; AM.1.5) shown in Figure 7; these data are used as a baseline for the future analysis.
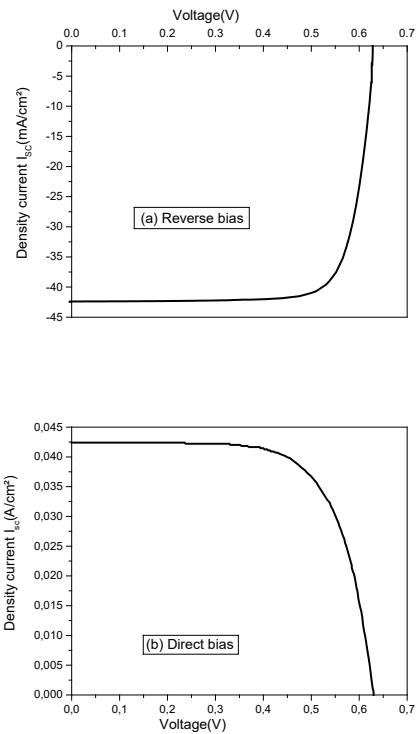
Figure 7: measured I-V characteristic of the studied PV cell under illumination in direct (a) and reverse (b) bias at STC

Secondly, we covered 25% (respectively 50% and 75%) of the area of the PV cell with a light-tight lid. Afterwards, the PV cell was illuminated over about 25% (respectively 50% and 75%) of its area. Results can be observed in Figure 8. It can be noted that the increase in the rate of shading of the cell produces a higher reduction of short circuit current I_{SC}, which causes a reduction in maximum power. It clearly demonstrate that the cell generated current is a function of the rate of light transmittance.
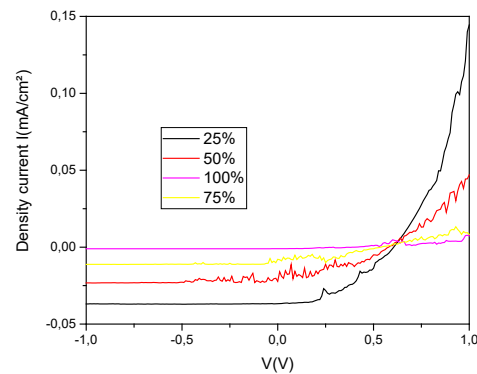
Figure 8: effect of partial shading of the studied PV cell on light I-V characteristics

4.2. Analysis of three (3) types cell interconnections under partial shade conditions

This section offers an extensive study of different reconfigurations of PV cells operating under partial shade conditions. For this purpose, we have studied the shading rate of 3 types of configurations such as Total-Cross-Tied (TCT),

Bridge-Link (BL) and Honey-Comb (HC) of PV cells shown in Figure 9.

a)   TCT

b)   BL

c)   HC
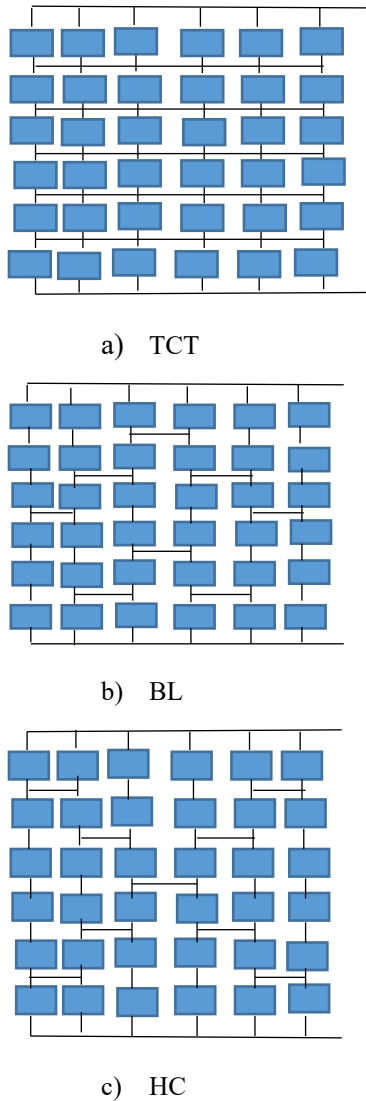
Figure 9: Types of 36 PV cells interconnection in a typical PV module

The results of shading rate of these configurations have been analyzed by shading completely selected cells in the PV module. Two experiments are made: firstly, one of the 6 X 6 PV cells is 100% shade for each type of configuration; secondly, nine (9) cells are 100% shaded and twenty-seven (27) working properly. I-V and P-V characteristics of these conditions are shown in Figures 10 and 11. First thing that can be observed is that there is a degradation of the power produced depending of the type of configuration. For the first experiment, shading one cell involve an efficiency decrease; for the second case, shading nine (9) cells involve efficiency to decrease further. We can note that in Figure 10, the values of the maximum power (Pmax) decreased as compared to initial values by about 12, 3%, 12, 06% and 10, 21 % respectively in TCT, HC and BL interconnections. Figure 11 proves that the decrease of Pmax can be imputed to the decrease of the short circuit current I_{SC}. The reduction in I_{SC} is explained by the rate of shading cells which limit the light transmittance. The influence of the number of shaded cell is presented in bar

chart form in Figure 12. The TCT and BL configurations exhibit themself as the most
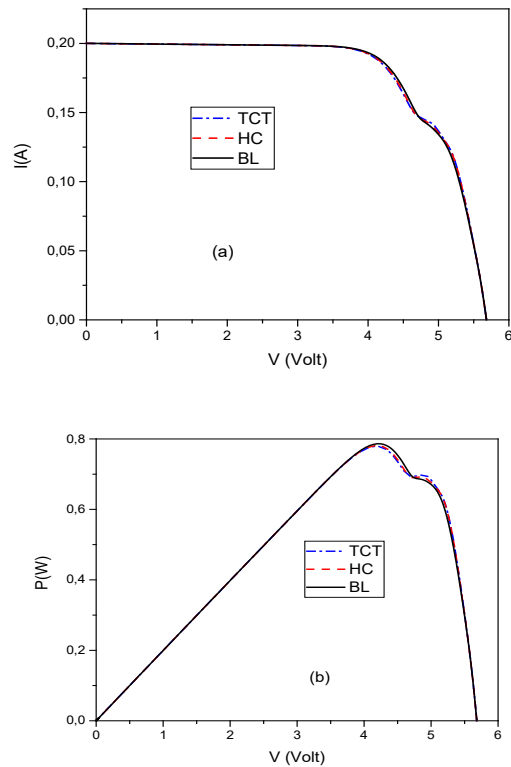
Figure 10: effect of shading one cell in a typical PV module (36cells) for three various configurations: (a) I-V curve and (b) P-V curve
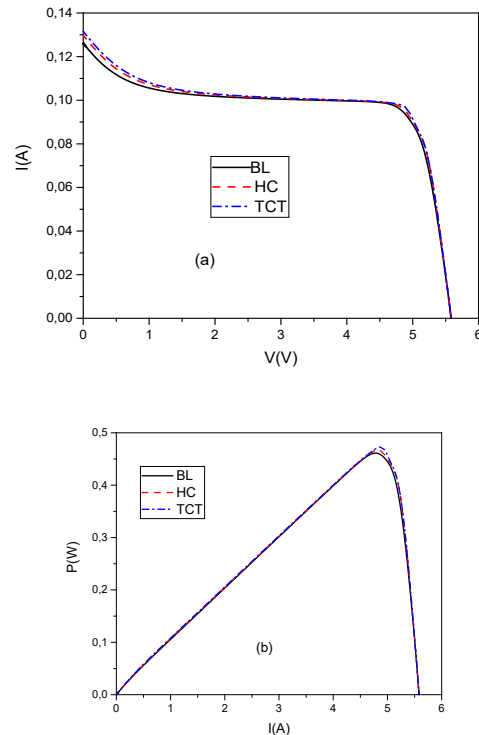
Figure 11: effect of shading nine cells in a typical PV module (36cells) for three various configurations: (a) I-V curve and (b) P-V curve
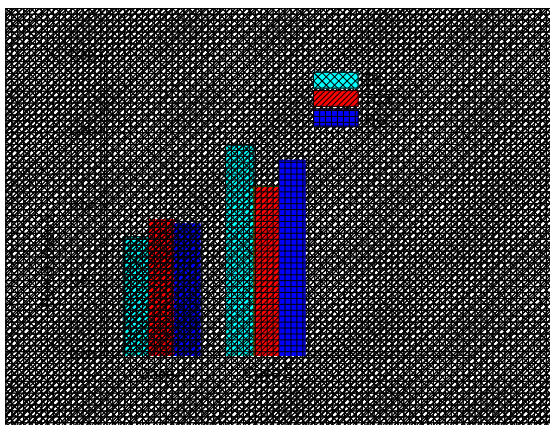
Figure 12: effect of the number of shaded cells on power losses

5. Conclusion

In this paper, an analysis parameters degradation in a typical PV cell, which lead to power loss under dark as well as light condition using measured I-V data was made. In order to analysis the sensitivity of the dark I-V measurement to each of the six extracted parameters as a function of the voltage as well as the temperature and the density current, we simulated the operation of a silicon solar cell (KXB0022-12X1F). The analysis of the dark I-V curves permit us to detect variation as small as 15% in the series resistance. We have also extended the use of dark as well as light I-V measurements to modules configurations of cells and uses a nonlinear least squares method to evaluate the cell efficiency parameters in the modules. Results obtained have shown a degradation of the values of the maximum power (Pmax) as compared to initial values by about 12, 3%, 12, 06% and 10, 21 % respectively in Total-Cross-Tied (TCT), Bridge-Link (BL) and Honey-Comb (HC) configurations. The decrease of Pmax could be imputed to the decrease of the short circuit current Isc. The reduction in Isc is explained by the rate of shading cells which limit the light transmittance.

Conflict of Interest

The authors declare no conflict of interest.

References

[1] S. K. Firth; K.J. Omas, S.J. Rees," A simple model of PV system performance and its use in fault detection " Solar Energy, **84** (4), 2009, 624-635, doi:10.1016/j.solener.2009.08.00

[2] M.A. Munoz, M.C Alonso-Gracia, N. Vela, F. Chenlo.," Early degradation of silicon PV modules and guaranty conditions " Solar Energy, **85**(9), 2011, 2264- 2274 doi:10.1016/j.solener.2011.06.011

[3] J.I Van Molken, U.A. Yusufoglu, A. Safiei, H. Windgassen, R. Khandelwal, T. M. Pletzer, H. Kurz," Impact of micro-cracks on the degradation of solar cell performance based on two-two model parameters" SiliconPV: April 03-05, Leuven, Belgium, Energy Procedia 27, 2012, 167- 172 doi:10.1016/j.egypro.2012.06.046

[4] E.L. Meyer and E.E. Van Dyk,"Assessing the reliability and degradation of photovoltaic module performance parameters", **53**(1), 83-93, 2004, doi:10.1109/TR.2004.824831.

[5] P. Hacke, R. Smith, K. Terwiliger, S. Glick, D. Jordan, S. Johnson, M. Kempe and S. Kurtz," Testing and analysis for lifetime prediction of crystalline silicon PV module undergoing degradation by system voltage stress", 38 th IEEE Photvoltaic specialists conference, Austin, TX, 2012, 001750-001755 doi:10.1109/PVSC.2012.6317933.

[6] D. Sera, S. Spataru, L. Mathe, T. Kerekes, R. Teodorescu," Sensorless PV array Diagnostic method for residential PV system" 26 th European photovoltaic Solar Energy conference and exhibition, 2011, 3776- 3782, doi:10.4229/26thEUPVSC.2011-4AV.3.37

[7] A. Drews, A. C. de Keizer, H.G. Beyer, E. Lorenz, J. Betcke, W. G. J.H. van Sark, W. Heydenreich, E. Wiemken, S. Stettler, P. Toggweiler, S. Bofinger, M. Schneider, G. Heilscher, D. Heinemann," Monitoring and remote failure detection of grid connected PV systems based on satellite observations " Solar Energy, **81**(9), 2007, 548- 564, doi:10.1016/j.solener.2011.06.011

[8] S. V. Spataru, D. Sera, P. Hacker, T. Kerekes, R. Teodorescu " Fault identification in crystalline silicon PV modules by complementary analysis of light and dark current-voltage characteristics " Progress in photovoltaics: research and applications., 2015, doi:10.1002/pip.2571.

[9] N.C Park, J.S. Jeong, B.J. Kang, D.H. Kim, "The effect of encapsulant discoloration and delimination on the electrical characteristics of photvoltaics module," Microelectronics reliability **53**(2013), , 1818-1822, doi:10.1016/j.microrel.2013.07.062.

[10] P. Hacke, K. terwilliger, R. smith, S. Glick, J. Pankow, M. Kempe, S. Kurtz, I. bennett, M. Kloos," System voltage potential-induced degradation mechanisms in PV modules an methods for test" 37 th IEEE Photovoltaic Specialists Conference, Seatle WA, 2011, 000814-000820,, doi:10.1109/PVSC.2011.6186079.

[11] D. Bonkoungou, T. Guingane, E. Korsaga, S. Tassembedo, K. Zacharie, A. Darga, F. Zougmore" Measurement and analysis of the I-V-T characteristics of a photovoltaic cell: KX0B22-12X1F", 8 International conference on smart Grid (icSmartGrid), Paris, France, 2020, 157-162 doi:10.1109/icSmartGrid49881.2020.9144904

[12] D.L.King, B. R. Hansen, J.A. Kratochvil, and M. A. Quintana, "Dark current-voltage measurement on photovoltaic modules as a diagnostic or manufacturing tool". conference record of the twenty sixth IEEE Photvoltaic specialists conference, Anaheim, CA, USA, 1997, 1125-1128 doi:10.1109/PVSC.1997.654286.

An Operational Responsibility and Task Monitoring Method: A Data Breach Case Study

Saliha Assoul[1], Anass Rabii[*, 2], Ounsa Roudiès[2]

[1]ENSMR, Siweb, E3S, Mohammed V University, Rabat, 10010, Morocco

[2]EMI, Siweb, E3S, Mohammed V University, Rabat, 10010, Morocco

ARTICLE INFO	ABSTRACT
	As a result of digitalization, services become highly dependent on information systems thus increasing the criticality of security management. However, with system complexity and the involvement of more human resources, it becomes more arduous to monitor and track tasks and responsibilities. This creates a lack of visibility hindering decision making. To support operational monitoring, we propose a method composed of i) a core of security concepts from International Standard Organization (ISO) standards ii) a graphical modeling language iii) a guiding process and iv) a tool that provides verification through formal Object Constraint Language (OCL) queries. Applying this method to the case of the Capital One data breach showcases incident prevention through task supervision. The resulting work product is a formal comprehensive map of assets, actors, tasks and responsibilities. The SysML formalism allows different actors to extract information from the map using OCL queries. This allows for regular task and responsibility verification thus closing any window of attack possible.

1. Introduction

With the advent of digitalization era, the widespread dependence on information systems (IS) rose as well. This new age was kick started by technological developments especially in IoT, Big Data and Cloud, paving the way for newer services and spreading IS use to more diverse fields (Industry-science research alliance). However, this dependence translated into an increase in criticality levels of assets and tasks. Fields such as health, energy, or e-Government, which were already dealing with critical information or physical assets, are facing greater challenges in security management. As a response, practices of security management had been thoroughly addressed by corporations, standardizing organizations and academia. The quest for security approaches and methods to apply systematically to specific situations fueled the creation of best practices, standards and maturity models. The popular ISO 27000 standard series stood out for the creation and management of Information Security Management Systems (ISMS) (ISO 27000). ISO provides baseline requirements in ISO 27001, best practices in ISO 27002, security risk management in ISO 27005 or even specialized recommendation for network security in ISO 27033. Additionally, a plethora of security maturity models were created between 2007

and 2018 to support continuous improvement of security in diverse fields. However, our systematic review [1] of the literature showed that even if many standards and approaches are available, implementation remains problematic. The lack of implementation feedback further makes the study of a real case such as the Capital One Financial Corporation breach [2] more appealing to discuss. We postulate that this issue is due to two major aspects: system complexity and human behavior.

Dealing with increased complexity created between interacting systems, we find it necessary to adhere to a high level of formalism to ensure rigor and precision to tackle one of the four dimensions of human factors in information security: responsibility [3]. Taking root in the system engineering paradigm, our solution is based on the standard system formalization language SysML. We propose a scalable formal representation of security responsibilities in accordance with complex system composition that supports traceability and management. This formalism provided by extended SysML profiles, enables the use of formal verification languages such as OCL to support supervision. We also provide a guiding procedure based on continuous improvement for iterative applications as well as a supporting tool. This method would provide security managers with proper knowledge to track fundamental causes, such as asset vulnerabilities, unaccomplished tasks and accountabilities. In our previous studies, we described

our generic framework dedicated to information security management, extracted security concepts for SysML profiles [4] as well their application in security requirement management [5]. In this paper, we examine the responsibility issue and illustrate it using a case study.

We present and discuss the case of a data breach that occurred in Capital One in order to analyze the consequences of an informal specification of responsibilities and therefore prove the relevance of the problem we tackle. Next, we apply our method to the case to highlight its advantages. Through the Capital One case study we will address the following research questions:

- RQ1: How did Capital One track the chain of responsibility for their data breach?
- RQ2: How did Capital One security managers verify the implementation of security controls?
- RQ3: How to model tasks and responsibilities in a multi-scale information system?
- RQ4: How to formalize operational monitoring in a multi-scale information system?

In the following sections, we detail the context of our study highlighting the problem that our method aims to solve and how it fits within the existing body of work. Next, we present the components of our proposed method. Lastly, we present the Capital One Case followed by the application of our solution to highlight its applicability and its ability to prevent similar cases.

2. Related Works & Problematic

Information system complexity introduced heterogeneous components with a high connectivity level. In the complex system paradigm [6,7], systems can be decomposed into smaller autonomous collaborating sub-systems. This entails that security breaches and by consequence security management become pervasive. This means that measures taken to address security matters must be propagated to other collaborating systems. Similarly, this complexity makes responsibility harder to pinpoint and necessary tasks less apparent. On the other hand, the transition from theoretical and generic standard recommendations or requirements to practical application by human resources reveals a substantial gap. In 1996, including human behavior was considered as a novel conceptual stance within security management [8]. Since then, both academia and standardizing organizations have provided a plethora of references for security management that take human behavior as an important variable.

On one hand, standardizing organizations such as NIST and ISO provide thorough and well recognized references like the NIST Cybersecurity Framework, ISO 27001 and ISO 21827. These standards have either stood the test of time or have been periodically updated. We consider these standards as an important body of knowledge and procedures for our studies. We position ourselves as an extension of these standards providing the method to guide implementation that is out of their scope. On the other hand, academia has also produced countless information security maturity models such as SOASMM for SOA architecture [9], MMISS-SME [10] for small and medium enterprises, CCSMM for American governmental entities [11] or ISMM-PCI [12] for the payment card industry. Through our systematic literature review [1], we became aware of the lack of implementation and validation

results for academic security maturity models. We also perceived that the academic shift towards specialization is also related to the implementation issue, hence why our solution intervenes at the implementation phase.

This implementation issue was due to the impact of human behavior on information security as asserted by both academia and standardizing organizations. According to research [13], human resources are considered the weakest link in securing information systems. In studying the impact of habits in following security policy [14], the authors highlight the effect of individual beliefs, thoughts, actions, attitudes, awareness, and training among others on policy compliance. ISO 27001 and 21827 standards also emphasize the importance of awareness building and skill development for all interested parties. In addition, as system complexity also entails more stakeholders, responsibilities become pervasive and contain multiple levels of accountability. In this context, the problem, firstly, is that actors have difficulties proficiently managing their responsibilities within their own scope of action. While the standard recommendations are clear, organizations have difficulties down-scaling them into actionable tasks and responsibilities [15]. Secondly, managers don't have a multi-scale visibility over the system to insure monitoring adapted to scalability. In fact, we currently rely on individual manager capability for tracking tasks using natural language management tools and renowned methods such as responsibility assignment matrices [16].

As the Design Science [17] method entails, the next step is the production of artifacts to put this knowledge to use. Our method aims to bridge this gap by addressing operational monitoring for security management with a scalable vision, focusing on human behavior. In their study of non-malicious security violations, the authors [18] clear up that while employees are goal centered, job performance is the end goal rather than security. Sharing this view, we perceive that providing managers with the adequate tool to operate is the way forward. Also, studies on the social impact on information security address the influence of external systems in their culture models [19] demonstrating the need for the multi-scale visibility our solution provides. Finally, formalizing human involvement in applying security processes as well as supporting diversity of security approaches through genericity are essential. In order to achieve this, we rely on the prevalent system modeling language SysML. As a matter of fact, several studies use SysML as their basis for security risk assessment [20], secure system design [21] for model transformations [22]. We share the same system engineering vision for security management as these studies to address a different aspect of security that is operational management. Other modeling languages such as KAOS [23] offer the possibility for responsibility modeling but lacks the formalism necessary for supervision. Whereas, our solution enables a formal and complete representation of security related information. As a result, it will help test and verification using OCL, allowing for day to day monitoring, the cornerstone of Agile's [24] success in software engineering.

3. The operational responsibility and task monitoring method

As information systems' complexity blurs the lines of responsibility, we provide a generic method for responsibility, task

and vulnerability traceability. By definition, a method is composed of a set of concepts, a language, a procedure and a tool to support it all. In the following sub-sections, we will detail each component as well as their provenance.

3.1. Core concept

In order to populate our modeling language, we need to introduce information security concepts. We can rely on existing references such as standards or prominent security maturity models in order to extract these concepts. In fact, we analyzed and compared the main security concepts used in the security maturity models we found through our systematic literature review [1]. We have found that these models are highly connected to the ISO 27001 and ISO 27002 standards [4]. Seeing that the ISO standards are aligned, we compared the security concepts used in ISO 21827 to prominent academic and governmental security maturity models. We concluded that the ISO standards are comprehensive sources for information security concepts. The concepts that we put to use in this monitoring method are listed in Table 1.

Table 1: Core of Information security concept list

Concept Name	Semantic Meaning	Example
System	Smart building, Energy grid, Network	Smart building, Energy grid, Network
Asset	Anything of value to the organization	Software, Building, Server, Information, Process
Human Resource	An actor implicated with the system	Client, Chief of security, System Owner
Task	A set of actions assigned to a human resource that must be executed	Log data analysis, Configuration update
Responsibility	The obligation to oversee, take care of a specific asset	Security responsibility, Maintenance responsibility, Access responsibility
Vulnerability	The state of exposure to the possibility of being attacked, damaged or tampered with	ragility, Open port, Plain text storage, Weak password

3.2. Language

In order to provide a graphical modeling language tailored to our concepts, we chose to extend SysML, the standard system modeling language. It supports specification, analysis, modeling, verification and validation of complex systems. It is defined as an extension of the well-known UML language used in software engineering. Another upside for choosing UML is the Object Constraint Language (OCL). OCL is a formal textual language that

allows constraint and object query expressions. It is a key point to the testing needed for monitoring. In addition, we can extend the SysML basic concepts by adding our security core concepts by the mean of profiles. This leads to define a new block diagram that includes security concepts. It allows us to define newer associations between these concepts for the necessary interactions. This ensures that we profit fully from the richness of the predefined SysML block diagram concepts. Our profile consists of the security concepts in Table 1 coupled with five new associations added to define new relationships between them. In Table 2 we specify the composition of our profile as well as the properties required for traceability.

Table 2: Security Responsibility Profile Elements

Concept Name	Relationship	Properties
System	Systems contain one or many Assets. Systems can interact with one another.	Owner Purpose
Interact With	Association linking two systems	Influence StartDate EndDate
Asset	Assets collaborate with one another. Assets Belong to one or many systems. Assets have one or many responsibles. Assets have one or many vulnerabilities.	ID Description IsActive LastActiveDate
Belong To	Association between assets and systems	Criticality level
Collaborate With	Association between assets	Nature Description CollabDuration CollabStartDate
Vulnerability	A Vulnerability belongs to one or many assets	Existence likelihood Description Recommendation
Human Resource	A human resource can be responsible for one or many assets. A human resource is a specialization of an asset. A human resource can execute one or many tasks.	Organizational unit
Responsible for	Association linking a human resource to one or many assets.	RespDuration RespStart LastResp RespNature

Execute	Association linking a task to a human resource.	StartDate EndDate
Task	A task can be executed by a human resource. An influence from an external system can impact a task.	ID Description IsExecuted Deadline Nature Criticality level
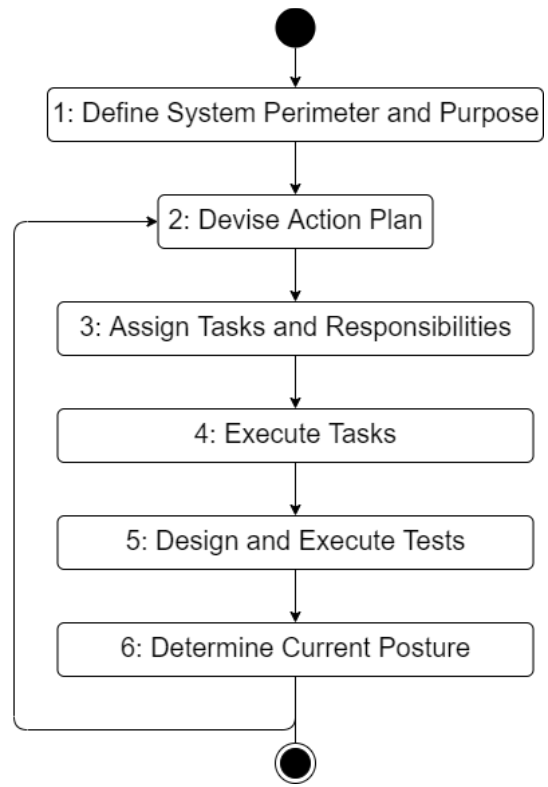
3.3. Procedure

The third part of our operational monitoring method is a procedure to guide step by step the usage of the modeling language. Drawing from the existing base of knowledge, continuous improvement is a central aspect of the ISO security standards. This translates into a cyclical security management procedure [5]. Using a PDCA cycle [25], operational monitoring would take place during the "Do" and "Check" phases. However, with the facilities enabled by the formal language, we can have a higher frequency of verification.

This is reflected in more frequent cycles of verification and testing. In Figure 1, we zoom into the "Do" and "Check" phase of the overall security management in order to highlight the usage of our method in operational monitoring.

First Step: The system definition resembles that of a general security management approach. It allows us to determine the scope of the system we plan to assess and aim to protect. This also clarifies the borders of the system properly defining the flow of interactions with other systems. The resulting work product is a mapped out system through a security block diagram. This diagram would present assets including their characteristics and collaborations, human resources involved and systems with which the system in question interacts.

Second Step: The organizations must devise an action plan that aligns with their internal goals and security requirements. That action plan is then adapted depending on existing resources and human resources capabilities.

Third Step: The action plan is down-scaled into actionable assignments. These duties and responsibilities are then allocated to the different actors within the system bounds with specific deadlines. This is where, traditionally, managers would use classic management tools defining tasks using User Stories that can be translated into model elements: "As a *Responsibility* I must *Task* by *Deadline*". This information is used to complete the previously mentioned security diagram.

Fourth Step: Human resources execute the tasks allocated to them. Task execution duration is task dependent and supervisions needs to be adapted accordingly.

Fifth Step: Supervisors and managers can design OCL tests to monitor task execution or do bulk monitoring. These tests can immediately yield undone tasks, return human resource work load or other tasks where manual verification would be arduous.

Sixth Step: These managers can determine, through multiple pre-designed tests, the current operational posture for their responsibilities within the system. The cycle then restarts, devising a new action plan based on previous results and future goals.

Figure 1: Operational monitoring procedure steps

3.4. Tool

In order to produce a functioning graphic editor for our language to support our method, we set out to find an existing well renowned modeling tool to extend. In Table 3, we set out to find a free and open source modeling solution.

Table 3: Renowned Modeling Tool Comparison

Modeling Tool	Author	OpenSource	Free
Modelio	Modelio Corp.	Yes	No
Entreprise Architect	Sparx Systems	No	No
MagicDraw	NoMagic	No	No
Eclipse Papyrus	Eclipse Foundation	Yes	Yes
Eclipse Sirius	Eclipse Foundation	Yes	Yes

Both Sirius and Papyrus are adequate choices, the scale tipped in favor of Papyrus for the availability of support and documentation. After this selection, the profile for the security SysML extension is created in a separate project. It is meant to act as a new extension point to be added to the profile list. This gives us, through the option of palette configuration, the possibility to add the profile elements. We can also define their graphical syntax

i.e. new shapes if needed, we elected to leave the original block shape with their respective stereotype. The resulting palette is shown in Figure 2. As it is for tests through OCL, Eclipse Papyrus supports the addition and execution of any OCL queries written in all Papyrus projects. By right clicking within the project, Eclipse allows the addition of OCL files, their execution and validation through the drop-down menu in Figure 3.
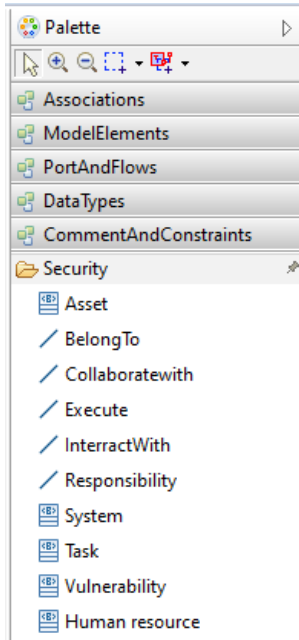
Figure 2: Security Responsibility Palette
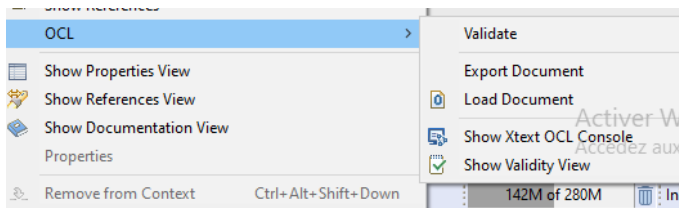
Figure 3: Dropdown Menu for OCL

4. Capital One Breach Case Study

In this section, we follow the operational responsibility and task monitoring method in analyzing the Capital One data breach. At first, we analyze the impact of Capital One's monitoring practices. Secondly, we use the data breach as a case study to apply the steps of this method. Finally, we highlight the lessons learned from this case study.

4.1. Methodological Consideration

Because of the rarity of details concerning information security management, analyzing the detailed study [2] would yield interesting insights. Their study aligns with our vision since their initial hypothesis: Renowned standards do not provide enough guidance for organizations for implementation nor incident management. Also, organizations aren't capable of implementing and maintaining security controls. One of the recommendations made was to find a way to manage the time frame between control implementation, evaluation and audit. This is precisely where our study intervenes analyzing task and responsibility operational

monitoring. As per the typology provided in [26] and [27], our units of analysis in this "Descriptive Case Study" are the tasks or responsibilities of a single human resource. Our conceptual framework is that of our proposed solution, detailed in section 3. 1., as we will be studying the different human resources and assets intervening in Capital One's systems as well as the different responsibilities and tasks. We will address them through the research questions previously presented in the introduction:

- RQ1: How did Capital One track the chain of responsibility in their data breach?

- RQ2: How did Capital One security managers verify the implementation of security controls?

- RQ3: How to model tasks and responsibilities in a multi-scale information system?

- RQ4: How to formalize operational monitoring in a multi-scale information system?

4.2. Procedure

Capital One is ranked eighth largest bank overall with a revenue of around 28 billion dollars in 2018. Technology implementation and consistent progress are considered driving ideologies within Capital One. As it is the case in banking, they abide by several security standards such as the New York Stock Exchange corporate governance rules, as well as being one of the participants in supplementing the NIST security standards. Capital One are considered pioneers in migrating their data centers to a cloud environment, environment from which the breach stemmed later. In spite of all their efforts, a breach disclosing the personal data of around 106 million individuals was discovered in July the 19th, 2019. According to the investigations that followed, an employee for the cloud storage service provider Amazon Web Service (AWS) created a scanning tool that allowed the culprit to recognize servers with firewall misconfigurations allowing access to buckets of data. This permitted the later execution of a set of scripts to retrieve access credentials then copy the now available data.

4.3. Analysis

Following the steps of our procedure described in section 3.3, we address primarily the failure in the implementation of technical security controls from Capital One's side. In the **First step**, we describe the contents of the Capital One Security Management System. They have invested in hiring a renowned Chief Information Security Officer (CISO), talented security engineers as well as on other security related investments for tool development.

Secondly, the bank's action plan allegedly revolves around implementing information security standards such as the NYSE requirement or NIST security controls. This meant that the CISO had the duty of choosing the security controls he deems adequate to protect his system. He then had to specify the time and resources allocated for each security control as well as defining the evaluation and audit periodicity. This is also when he's supposed to decide the means by which the controls are to be satisfied. First of all, a Web Application Firewall (WAF) needs to be implemented and configured to block any entry from malicious

proxy servers or from TOR exit nodes. Secondly, set up proper periodic vulnerability scans for the WAF. Lastly, revoke administrative account access credentials in case of internal changes. In the *third step*, the CISO should assign these duties to the security engineer and the security manager. In the case as we understand it, there was time window in which the attack occurred and that is between task execution in *step four* and the monitoring test that would have identified the failed NIST controls in *step five*.

Research Question 1: In an article by The Wall Street Journal, Capital One attributes the problem to an error in its own infrastructure. However, in a second article in the same journal, interviewing Capital One employees reported that multiple issues are at the root of this breach. Prior to the incident, there have been complaints that employees have raised concerns that they required more software to spot breaches. This delay is caused by the difference in skillset between IT professionals and governance professionals. As systems become more interconnected, all involved parties must acquire multidisciplinary skills so that governance professionals understand the necessary requirements in terms of technology to be able to provide them within a smaller timeframe. This could also be linked to failures to stay within budget lines despite hefty investments. This shows that Capital One failed to trace back the source of their infrastructural issues that is managerial and financial at its core.

Research Question 2: A second issue voiced by employees was low morale due to an increase in number of employee terminations. This is also due to budget issues that later became detrimental to routine security control implementation. Employees also reported an internal practice giving liberties to programmers the freedom to code in whatever language they choose if it would help complicate breaking into their systems in turn complicating pen-testing. These two incidents reflect that Capital One also lacked visibility as well as control over the tasks executed inside its scope. The Capital One security managers knew the necessary security controls to implement, however, they lacked regular verification of their implementation. This is what created the timeframe the culprit needed to execute his attack.

4.4. Lessons Learned

In the previous subsection, we clarified that Capital One had issues regarding task and responsibility tracking. Now, we will address these issues through discussing the second set of research questions.

Research Question 3: In our previous analysis, the first issue was the lack of multi-scale visibility coupled with lack of understanding between engineers in the security management system and their higher-ups in top management. This an aspect that our solution addresses via a complex system vision, where multiple systems interact with one another and therefore influencing one another. Using our method, in the first step, we can model Capital One as two systems "Governance System" and "Security Management System" each containing their respective human resources. As is shown in Figure 4, we can model the budget that the first system provides to the next or how the financial issues can influence security management. In this case, any employee dismissed must be removed from the model. Carrying on, we add to each human resource their set of tasks to which we assign deadlines and the attribute *Isexecuted* to be set to

"True" when it's done. Figure 5 shows the different security tasks and their responsible. Each task is the implementation of a necessary NIST security control [2]. In the case of the layoffs and human resource removal, the tasks would remain and it would be apparent that they need to be reassigned in order to maintain security controls. Verification for human resource task load and tasks with no *responsible* association can be done through OCL tests. In addition, each human resource can find her own tasks by executing a script. This script would return all tasks that are assigned to the human resource with a *responsible* association.
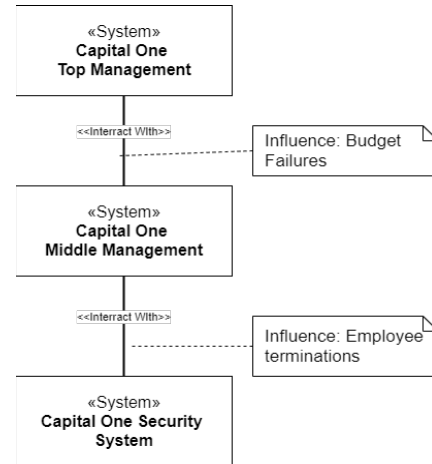
Figure 4: System Influence Diagram

Research Question 4: Following task modeling and responsibility assignment, it is the managers' duties to design tests for task supervision. This would normally be achieved by individually verifying each task accomplishment manually. Through the formal modeling of each task and responsibility, we now have the possibility of designing tests where we can list all tasks that have the attribute *IsExecuted* set to "False" and compare the current date to the deadlines. This would also link us immediately to the person responsible for this task execution. Since the day to day supervision tests don't have to be re-written, this makes monitoring less time consuming and therefore more efficient opening the possibility for day to day supervision. In the case of Capital One, this would have resulted in the revocation of the culprit's access credentials earlier as well as reassigning other employee's tasks in time. In turn, this would have closed any timeframe required to conduct the attack.
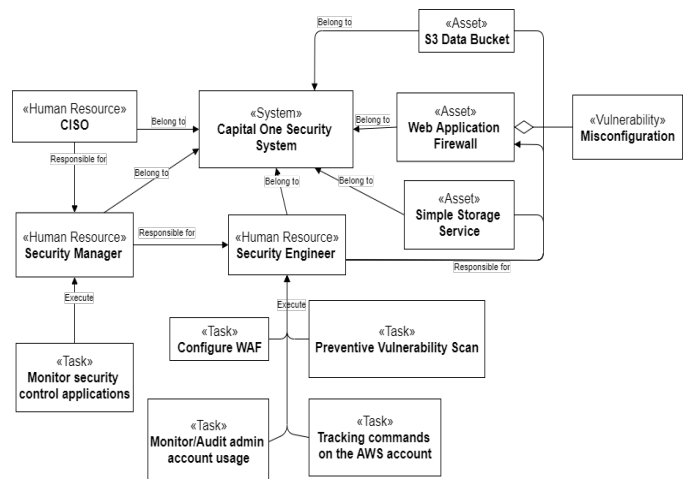
Figure 5: Operational Traceability diagram for Capital One Case

5. Conclusion

This paper presents a method for operational security monitoring applied to a security breach case. It aims to bridge the gap identified between security control identification and implementation. We have presented the components of our method that provide a much-needed formalism in security management. We have built this method using prominent modeling and security management standards in the base of knowledge. We have chosen to extend the SysML modeling standard with security monitoring concepts. This allows the creation of specialized block diagrams that model the actors and assets within a system as well as the tasks and responsibilities. The resulting diagram is a map capable of capturing complex system composition and interaction. Furthermore, this formalism provides the ability to use OCL for proper monitoring and supervision even for complex systems. In fact, the information depicted is of different use to different actors. OCL queries allow managers to regularly verify task execution and manage task loads. They also allow security engineers to see which new tasks were assigned to them or whether undone tasks still remain. Moreover, we have highlighted through our procedure the issues usually faced during the "Do" and "Check" phases of the Deming wheel. This allowed us to showcase the importance and applicability of our method for security management onto a high profile case. The described case study provided a high level of detail that allowed us to properly study the applicability and utility of our proposed method. Our method does not circumvent the complexity of the systems studied, it retains all the necessary information for operational monitoring. It aims to provide the tools that different actors need to carry out their roles in security management.

For future studies, we intend to include this study within a bigger whole designed for security management to reach "security by design". We also plan to further improve the modeling tool facilitating tests and creating a plugin to be featured in Eclipse Marketplace for public usage.

References

[1] A. Rabii, S. Assoul, K. Ouazzani Touhami, O. Roudies, "Information and cyber security maturity models: a systematic literature review," Information and Computer Security, **28**(4), 627–644, 2020, doi:10.1108/ICS-03-2019-0039.

[2] N. Novaes Neto, S.E. Madnick, A. Moraes G. de Paula, N. Malara Borges, "A Case Study of the Capital One Data Breach," SSRN Electronic Journal, (January), 0–24, 2020, doi:10.2139/ssrn.3542567.

[3] A. Alhogail, "Design and validation of information security culture framework," Computers in Human Behavior, **49**, 567–575, 2015, doi:10.1016/j.chb.2015.03.054.

[4] R. Anass, A. Saliha, R. Ounsa, "A Concept & Compliance Study of Security Maturity Models with ISO 21827," in Proceedings of the 22nd International Conference on Enterprise Information Systems, SCITEPRESS - Science and Technology Publications: 385–392, 2020, doi:10.5220/0009569703850392.

[5] A. Rabii, S. Assoul, O. Roudies, "Security requirements elicitation: A smart health case," Proceedings of the World Conference on Smart Trends in Systems, Security and Sustainability, WS4 2020, 776–781, 2020, doi:10.1109/WorldS450073.2020.9210330.

[6] F. Lahboube, O. Roudies, N. Souissi, "Extending supervision metamodel to complex system context," in 2015 Third World Conference on Complex Systems (WCCS), IEEE: 1–7, 2015, doi:10.1109/ICoCS.2015.7483242.

[7] Y. Bar-Yam, "General Features of Complex Systems," Knowledge Management, Organisational Intelligence and Learning and Complexity, **I**(1), 1–10, 1997.

[8] J. Backhouse, G. Dhillon, "Structures of responsibility and security of

information systems," European Journal of Information Systems, **5**(1), 2–9, 1996, doi:10.1057/ejis.1996.7.

[9] M. Kassou, L. Kjiri, "SOASMM: A novel service oriented architecture Security Maturity Model," in 2012 International Conference on Multimedia Computing and Systems, IEEE: 912–918, 2012, doi:10.1109/ICMCS.2012.6320279.

[10] MMISS-SME Practical Development: Maturity Model for Information Systems Security Management in SMEs, in Proceedings of the 5th International Workshop on Security in Information Systems, SciTePress - Science and and Technology Publications: 233–244, 2007, doi:10.5220/0002430402330244.

[11] G.B. White, "The community cyber security maturity model," in 2011 IEEE International Conference on Technologies for Homeland Security (HST), IEEE: 173–178, 2011, doi:10.1109/THS.2011.6107866.

[12] S. Yulianto, C. Lim, B. Soewito, "Information security maturity model: A best practice driven approach to PCI DSS compliance," in 2016 IEEE Region 10 Symposium (TENSYMP), IEEE: 65–70, 2016, doi:10.1109/TENCONSpring.2016.7519379.

[13] K.D. Mitnick and William L. Simon, The Art of Deception: Controlling the Human Element of Security, John Wiley & Sons, Inc., 2003, doi:10.5555/861316.

[14] J.P. Jeretta Horn Nord,Alex Koohang,Kevin Floyd, "IMPACT OF HABITS ON INFORMATION SECURITY POLICY COMPLIANCE," Issues in Information Systems, **21**(3), 217–226, 2020, doi:https://doi.org/10.48009/3_iis_2020_217-226.

[15] A. Longras, T. Pereira, P. Carneiro, P. Pinto, "On the Track of ISO/IEC 27001:2013 Implementation Difficulties in Portuguese Organizations," in 2018 International Conference on Intelligent Systems (IS), IEEE: 886–890, 2018, doi:10.1109/IS.2018.8710558.

[16] K.H. Rose, "A Guide to the Project Management Body of Knowledge (PMBOK® Guide)-Fifth Edition," Project Management Journal, **44**(3), e1–e1, 2013, doi:10.1002/pmj.21345.

[17] R.B. Fuller, "A comprehensive anticipatory design science," **34**, 357–361, 1957.

[18] K.H. Guo, Y. Yuan, N.P. Archer, C.E. Connelly, "Understanding Nonmalicious Security Violations in the Workplace: A Composite Behavior Model," Journal of Management Information Systems, **28**(2), 203–236, 2011, doi:10.2753/MIS0742-1222280208.

[19] K. Huang, K. Pearlson, "For What Technology Can't Fix: Building a Model of Organizational Cybersecurity Culture," 2019, doi:10.24251/HICSS.2019.769.

[20] S. Ouchani, O.A. Mohamed, M. Debbabi, "A Security Risk Assessment Framework for SysML Activity Diagrams," in 2013 IEEE 7th International Conference on Software Security and Reliability, IEEE: 227–236, 2013, doi:10.1109/SERE.2013.11.

[21] L.A. Yves Roudier, "SysML-Sec - A Model Driven Approach for Designing Safe and Secure Systems," in Proceedings of the 3rd International Conference on Model-Driven Engineering and Software Development, SCITEPRESS - Science and and Technology Publications: 655–664, 2015, doi:10.5220/0005402006550664.

[22] F. Lugou, L.W. Li, L. Apvrille, R. Ameur-Boulifa, "SysML Models and Model Transformation for Security," in Proceedings of the 4th International Conference on Model-Driven Engineering and Software Development, SCITEPRESS - Science and and Technology Publications: 331–338, 2016, doi:10.5220/0005748703310338.

[23] A. Dardenne, A. van Lamsweerde, S. Fickas, "Goal-directed requirements acquisition," Science of Computer Programming, **20**(1–2), 3–50, 1993, doi:10.1016/0167-6423(93)90021-G.

[24] J.A. Highsmith, Adaptive Software Development: A Collaborative Approach to Managing Complex Systems, Dorset House Publishing Co., Inc., 2000, doi:10.5555/323922.

[25] W.E. Deming, Out of the Crisis, The MIT Press, 2018, doi:10.7551/mitpress/11457.001.0001.

[26] T. Hollweck, "Robert K. Yin. (2014). Case Study Research Design and Methods (5th ed.). Thousand Oaks, CA: Sage. 282 pages.," The Canadian Journal of Program Evaluation, 2016, doi:10.3138/cjpe.30.1.108.

[27] P. Baxter, S. Jack, "The Qualitative Report The Qualitative Report Qualitative Case Study Methodology: Study Design and Qualitative Case Study Methodology: Study Design and Implementation for Novice Researchers Implementation for Novice Researchers," Number 4 Article, **13**(4), 12–13, 2008.

Performance Evaluation of a Gamified Physical Rehabilitation Balance Platform through System Usability and Intrinsic Motivation Metrics

Rosula Reyes[*,1], Justine Cris Borromeo[1,2], Derrick Sze[1]

[1]*Ateneo de Manila University, Department of Electronics, Computer, and Communications Engineering, Quezon City, 917, Philippines*

[2]*Scuola Superiore Sant'Anna, Pisa PI, 56127, Italy*

A R T I C L E   I N F O

A B S T R A C T

Motivation significantly influences the outcome in the rehabilitation of patients. Several developments have been made to assess and increase patient motivation by addressing factors linked to motivation such as the personality of the patient, professional administering rehabilitation, and the rehabilitation environment. The main objective of the study is to evaluate the reliability of a gamified environment for the rehabilitation of stroke patients by testing its functionalities within standard physical therapy time and intervals. To achieve this, calibration was characterized. Also, user feedback was taken in the form of questionnaires based on the System usability scale (SUS) and Intrinsic Motivation Inventory (IMI). Based on the SUS scale, results show that the game manipulability is good, the game concept and design is satisfactory, and the game comprehensibility is also good based on the qualitative conclusion per SUS score. For the IMI ratings, it was found out that the highest rating was the perceived choice which indicates their voluntary participation in the game. Some improvements can still be added to the game itself to increase the motivation of patients. The balance board manipulability and the recalibration time interval can be further improved for comfort and ease of use by the patients.

1. Introduction

Balance deficiency is one of the common issues for post-stroke and post-injury patients, as well as for individuals who wish to train his/her balance even without deficits (e.g. athletes). Out-patients who had such deficiency will undergo a balance therapy program. In the current setting, a patient will attend therapy sessions about six to ten times. Each session, the patient will perform various balance exercises such as static balance, dynamic balance, and manual perturbation exercises using balance board, wobble board, balance rails, and mirrors extensively assisted by physical therapists. The patient will then perform the exercise, but most of the time, the patient will feel the pain of such exercises as well as boredom due to its repetitive nature. Also, the therapist will record the patient's balance quality according to what is observed, making several corrections to the number of balance sessions as well as the physician's initial observation. This also introduces an inconsistency problem when a different therapist observes the patient and records the score for interpretation. Finally, the patient has to rely on his/her safety on

the therapist, since the current tools do not have robust feedback for the patient to observe his/her balance performance. With these, the patient is usually discouraged and unmotivated to attend another therapy session as well as not trying to perform them by himself/herself.

In line with this, one of the determinants that greatly affect the success rate of undergoing physical rehabilitation is the motivation level of the patient. Motivation has been identified to be influenced by a variety of factors such as the personality of the patient, the professional administering rehabilitation, and the rehabilitation environment. Research work integrating the use of the Microsoft Kinect or the Wii Fit Board with various games to change the rehabilitation environment has proven to be effective in increasing patient motivation and overall affecting the outcomes on a more positive result [1, 2]. However, improvements on these previous researches can still be made, such as creating a more affordable and open-sourced design of the hardware and incorporating more game elements that engage the patient which will aid in the success rate of the physical rehabilitation.

[*]Corresponding Author: Rosula Reyes, rsjreyes@ateneo.edu

Balance-on-action-Team (BOAT) implements affordable hardware and open-source software to enable a wider reach in the utilization of gamification in physical rehabilitation. It is an automated balance board medical device with a gamified element for conducting balance exercises for patients undergoing balance rehabilitation therapy. The overall goal is to provide rehabilitation centers, sports clinics, and personal trainers with safer, faster, and more engaging means of conducting balance training and therapy. In this way, balance exercises in the Philippines setting will become faster, more consistent from therapist-to-therapist, and more fun to perform.

The main objective of the study is to evaluate the reliability of the equipment (calibration and functionalities) based on the standard physical therapy time and intervals. Furthermore, conduct surveys to evaluate the game's impact on motivation.

This paper describes the various studies related to rehabilitation and patient motivation in Section 2 of the Review of Related Literature. Section 3 discusses the Methodology which focuses on the hardware and software implementation in Section 3.1 and the testing procedure in Section 3.2, using different metrics. The results are shown and discussed in Section 4 which includes the calibration in Section 4.1, Game Self Evaluation in Section 4.2, Motivation Analysis in Section 4.3, and Game Walkthrough Evaluation in Section 4.4. Lastly, the Conclusion and Recommendation can be found in Section 5.

2. Review of Related Literature

Several studies have been conducted on the rehabilitation of stroke patients using varying platforms, approaches, and frameworks. A similar balancing platform was studied by [3] where the focus is on utilizing the Nintendo Wii Balance Board for rehabilitation. The study developed a *WeHab* system that added visual biofeedback based on the center of pressure location. This system also allows for multiple balanced boards to be used together, customization of activities and difficulty level, and integration with a webcam to capture video footage during the sessions. Similarly, visual biofeedback was also used by [4] using Microsoft Kinect for postural rehabilitation. This allows the system to determine if the patient performed the correct postural exercises through the built-in capabilities of the Kinect in movement and gesture recognition. Another type of balancing platform that can be used is a wobble board which was studied by [5]. Here, the instrumented wobble board is used to create multidirectional perturbations and obtain vibrotactile feedback for training dynamic sitting balance. This research work also uses a microprocessor and an inertial measurement unit but has an added eight vibrating tractors. Aside from these approaches, the rehabilitation of patients can also be monitored using EMG on the lower limbs, such as in the work of [6]. In this case, a balance board was also used but accompanied with obtaining sEMGs signals to analyze how the muscle activity reacts from dynamic leaning caused by balance reactions.

Assessing patient motivation and system usability have been determined to help improve rehabilitation for chronic stroke patients. Instead of balance exercises used in this research, the study by [7] evaluates the feasibility of a new technology-supported task-oriented arm training regime (T-TOAT) for chronic stroke patients. The system is comprised of movement tracking sensors, an exercise board, and a software-based toolkit used for skills training. The patient motivation was assessed on the Health Care Self Determination Questionnaire (HCSDT) based on the self-determination theory. Furthermore, system usability was also assessed and was found to be rated good by the users. After performing various tests, it was discovered that the T-TOAT approach improved arm-hand performance significantly for the duration of the post-training. Similar to this work, system usability and motivation were evaluated through various questionnaires and assessment tools for improving rehabilitation.

Another patient motivation assessment tool applied in this work is the Intrinsic Motivation metrics which was also conducted in a study by [8]. This study aims to characterize motivation based on the information of activities for smart wearable health equipment applications. The participants in the study were tasked to solve a computer-generated puzzle under one of the four random conditions including the long-term feedback (LFB), long term graphical feedback (LGFB), short term feedback (SFB), and non-feedback for the trend of correct answers. Intrinsic motivation was then measured using both a 12-item version of the Intrinsic Motivation Inventory and the time it takes the participant to solve the puzzle. Based on these, it was observed that the most desirable type of feedback is one that improves perceived competence, which can then be adapted to health equipment displaying methods.

The BOAT is a research project that was conceptualized and developed through the collaboration between the Ateneo de Manila University and the Philippine Orthopedic Center. The gamified environment was initially developed by [9] using an inertial measurement unit. The goal was to provide the gamified elements in the form of quests and rewards system for providing an interactive and fun rehabilitation process. The hardware prototype was developed and tested in [10] using intervention techniques, motivation, and game design analysis. This was then continued by [11] through a comparative game design analysis. Several changes have been made for the hardware design, shown in Figure 1, and software game mechanics implementation by [12]. The research work added more customizability, and personalized information from the patients to help the physician perform better assessments. This research focuses on evaluating the gamified rehabilitation platform of [12] through various metrics such as system usability and intrinsic motivation metrics.
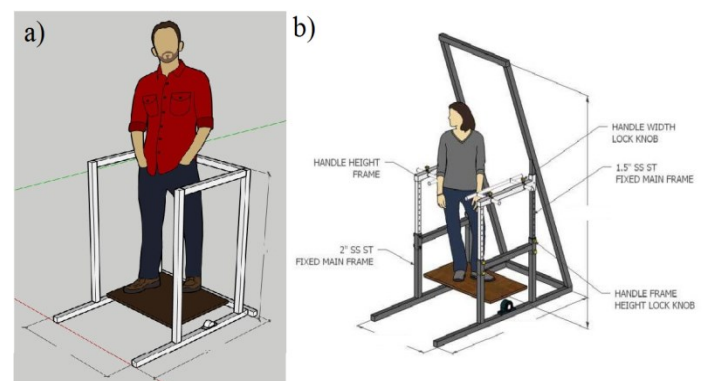
Figure 1: Hardware Changes from the Prototype [6] to the Commercialized [8]

3. Methodology

3.1. Design of the System

For the software, the gamified environment of the balance board lets the user experience a seamlessly integrated, open-world seafaring game integrated with a quest system [12]. The quest system allows the patient to perform physical rehabilitation exercises under the guise of the game. There are three quests or game modes designed to correspond with different physical rehabilitation exercises and specific metrics from the Tinetti Balance Assessment Tool and the Equilibrium Score. Each game mode and its corresponding mechanics are shown in Table 1.

Table 1: Game Modes and Mechanics [12]

Game Mode	Mechanics	Player Input
Collect the Crates	The player must be able to collect as much trash (in the form of crates) as possible within a certain amount of time	Lateral Dynamic Balance Exercise. The player must be able to challenge himself/herself a postural sway and recover from it as much as possible using lateral movements.
Avoid the Bombs	The player must be able to avoid all possible bombs within the boat's path in a certain amount of time	Static Balance Exercise. Players must be able to stand still as much as possible to avoid the bombs.
Follow the Light	The player must be able to follow the light in front of the boat without getting too near or too far from it	Posterior-Anterior Dynamic Balance Exercise. The player must be able to challenge himself/herself a postural sway and recover from it as much as possible using posterior-anterior movements.

The hardware design includes the following components: the frame, balance board, accelerometer, and Gizduino Uno. Most of the hardware components were mounted on the frame which features adjustable mechanisms and can be disassembled. The balance board is commonly used in physical rehabilitation for static and dynamic exercises, especially in the Philippine Orthopedic Center. There are two types of balance boards, the two-directional balance board which was used in this study, and the multi-dimensional balance board or wobble board. Relatively, the bidirectional balance board provides more accurate data from the accelerometer readings since only two directions are measured and the rest are disregarded. Several adjustable components are used to cater to different characteristics and categories of patients. One of these is the stopper which adjusts the maximum tilting angle of the balance board for both sides with increments of 5°. This allows the physician to change the maximum angle depending on the patient's capabilities. Furthermore, this helps in stabilizing the platform at 0° before running the application. Also, the handrails where the patient will hold on to when playing the game can be raised or lowered to compensate for patients with different heights. Each consecutive hole for moving the handrail is about 2 inches apart. Lastly, the friction of the balance board can be altered using the tension control knobs with a range of 1 to

8 for each side. Adjusting the magnitude of the sway of the board will help more balance-challenged patients gradually adapt to the game mechanics.

As a safety precaution, the patient is advised to wear a harness that is attached to an adjustable lanyard, presented in Figure 2. The lanyard is then mounted on the hooks of a metal bar which can be rotated 360° along the vertical axis to allow a smoother transition for the dynamic posterior-anterior to lateral sway and vice versa. Moreover, wearing the harness greatly minimizes the risk of falling from the balance board.

Figure 2: Harness for Lateral (a) and Posterior-Anterior (b) Movement

For the improvements tracking, the calibration of the equipment is accomplished through linear regression using two data points from the sensor readings. From the generated equation in slope-intercept form, the slope and y-intercept will be saved in a .txt file inside the Results folder on the desktop. This will enable the user to see any variations in calibration.

Similarly, the game metrics are recorded in the form of a .txt format in the Results folder. It publishes the patient's name, the date and time when the exercise is completed, the quest played, the type of balance exercise, their in-game score, the Equilibrium Score (ES), the maximum posterior-anterior sway, maximum lateral sway, and game settings information. This information allows the physician to track and evaluate the progress of the patients after engaging in the physical rehabilitation procedure.

Data from each game mode are recorded in the form of the ES, shown in (1), which indicates their quality-of-balance progress as patients play the game. The ES is the probability of fall in which a score of 100 indicates a 0% chance of fall while a score of 0 indicates a 100% chance of fall.

$$\text{ES} = \frac{\gamma - (\theta_{max} - \theta_{min})}{\gamma} \text{ X } 100\% \qquad (1)$$

where θ_{max} is the maximum postural sway relative to the vertical

θ_{min} is the minimum postural sway relative to the vertical (natural standing angle)

γ is the limits of stability angle for the clinical setting

3.2. Testing the System

To fully test the reliability of the system, several methodologies were adapted based on metrics related to the study, which includes the following:

An SUS (System Usability Scale) is a self-rated scoring system that measures the usability of a certain device or software. It is usually a ten-item test that has open-ended statements with user responses from "Strongly Disagree" to "Strongly Agree". Each item is scored on a 5 (or 7) point scale. To prevent purely positive or purely negative responses, this questionnaire is designed to have alternate positive-worded and negative-worded statements. Thus, the following rules for computing the SUS are the following:

- For every negative statement (odd-numbered items for this test): take the max score (e.g. 7) and subtract it by the raw score (e.g. raw score = 3, SUS score = 7 – 3 = 4)
- For every positive statement (even-numbered items for this test): take the raw score then subtract by 1 (e.g. raw score = 6, SUS score = 6 – 1 = 5)
- Add all of the SUS scores of every item. The maximum score should be:

$$(\text{max points} - 1) * \text{max items} \qquad (2)$$

- Depending on the maximum number of items, the overall SUS score should be on a scale of 0 to 100. Therefore, for a 10-item questionnaire with 7 as maximum points, the entire sum should be divided by 0.6 since the maximum score is 60.
- The overall SUS score is then tallied and averaged. Normalization is considered for the average therefore a score of 68 and above is a favorable result, while a score of below 68 is an unfavorable result. Figure 3 shows how the scores will be interpreted qualitatively in the conclusion.

SUS Score						
0 - 50	51 - 60	61 - 67	68	69 - 74	75 - 85	86 - 100
Poor	Bad	Unsatisfactory	Average	Satisfactory	Good	Excellent
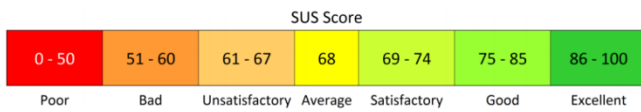
Figure 3: SUS Score Equivalent

The Intrinsic Motivational Inventory (IMI) measures the motivation of the test subjects in playing the game. All 22 questions are modified from the template provided by the Self-Determination Theory Organization but have the same measurement (http://www.selfdeterminationtheory.org). For determining the IMI Score of the test subjects, the following procedures are done.

- The responses for items 2, 9, 11, 14, 19, and 21 are reversed. That is, the item score is equal to 8 minus the response (item score = 8 – response).
- These subscale scores in Table 2 are added together:

Table 2: IMI Subscales

Interest/Enjoyment	Items 1, 5, 8, 10, 14, 17, 20
Perceived Competence	Items 4, 7, 12, 16, 22
Perceived Choice	Items 3, 11, 15, 19, 21
Pressure/Tension	Items 2, 6, 9, 13, 18

- The subscale scores are analyzed as follows:
- o Interest/Enjoyment, Perceived Competence, and Perceived Choice is summed up into the IMI score for the subject's motivation. This sum is high if the test subject is motivated enough to perform the balance exercises through the game
- o Pressure/Tension is the IMI score for the subject's loss of motivation. This score is high if the test subject is not motivated enough to do the balancing exercise even if the game is played.

The Motivation-to-No-Motivation (MNM) ratio is then determined to check how much the test subjects are motivated based on their responses on the IMI. MNM is achieved by applying the equation:

$$\text{MNM} = \frac{IE+PCT+PCH}{IE+PCT+PCH+PT} \qquad (3)$$

where MNM = Motivation-to-no-Motivation ratio,

IE = IMI subscale score for Interest/Enjoyment,

PCT = IMI subscale score for Perceived Competence,

PCH = IMI subscale score for Perceived Choice, and

PT = IMI subscale for Pressure/Tension.

4. Results and Discussion

The reliability of the prototype was evaluated to assess the accuracy and precision of the components based on the calibration values before and after using the balance board. The test was also conducted with twenty (20) healthy test subjects consisting of 10 males and 10 females within an age range of 20-30 years old. Each subject has no history of stroke and no injury 6 months prior.

4.1. Calibration

Calibration evaluates and adjusts the precision and accuracy of the balance board. In calibrating, the balance board was referenced at +20 and -20 degrees, and sensor values of the MPU 6050 were then recorded on these angles to calculate the slope.

For the reliability of the balance board based on calibration, the slope was recorded before and after the game based on the following parameters: 10min (Game)-15min (Rest), 15min (Game)-20min (Rest), varying tension control, and varying weight of the test subjects.
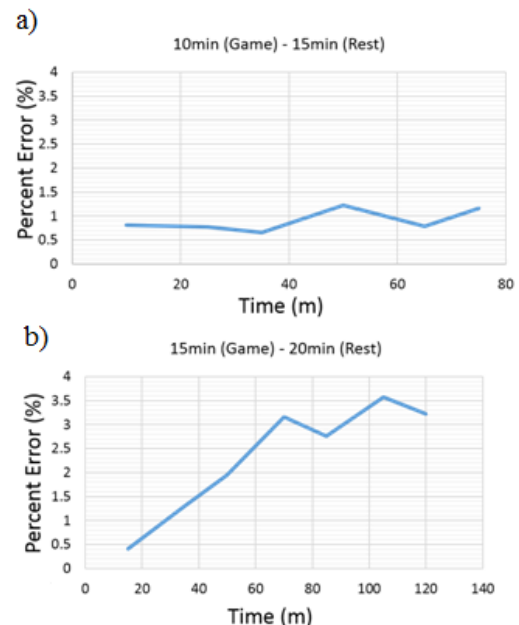
Figure 4: Slope Percentage Error vs. Time Graph: (a) 10min (game) – 15min (rest), (b) 15min (game) – 20min (rest)

Figure 4 shows the percentage error of the balance board slope as time increases. The percentage error was computed using this equation

$$\text{Error (\%)} = \frac{2\,|x-y|}{x+y} *100 \qquad (4)$$

where *x* is the initial slope while *y* is the value of the slope after some time. With *3.5%* as the maximum percentage error (4) at around *105 minutes*, it is safe to say the calibration of the prototype is still precise after turning it on for around *1 hour and 30 min.*

The slope of the balance board was also recorded as the tension control adjusts from 1(low friction) to 8(high friction). The correlation between the percentage error of the slope and the tension control is shown in Figure 5. Since the maximum percentage error is around *0.8%*, it shows that the calibration value is still precise even if the tension control is varied.
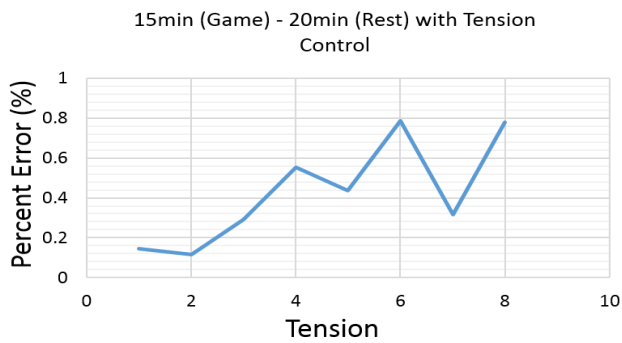
Figure 5: Slope Percentage Error vs Tension

Figure 6 shows the percentage error of the slope before and after doing the game testing as the weight (kg) of the test subject varies. Based on the figure, we can say that there is no correlation between the weight of the person doing the test and the slope percentage error. It also shows that the person's weight doesn't affect the calibration of the balance board with a maximum error of around *1.5%.*
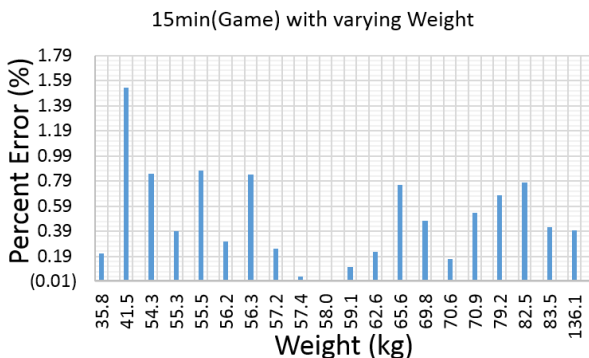
Figure 6: Slope Percentage Error vs Weight

4.2. Game Self Evaluation

Game Self Evaluation is an SUS questionnaire to be filled out by the test subjects for their evaluation of both the hardware and the game. It is divided into four groups: Balance Board Manipulability Measures, Game Manipulability Measures, Game Concept and Design Measures, and Game Comprehensibility Measures.

The Balance Board Manipulability Measures is a self-rated survey on how the balance board is used to them. This is collated and calculated based on SUS. For Balance Board Manipulability Measures, the average SUS for all 20 test subjects is 64.06, which is 5.89% lower than the average SUS score of 68. Overall, the result is unsatisfactory and the balance board manipulability measures can be improved.

The lowest SUS is 35.42 while the highest is 93.75. The highest-rated item is #1 (I thought the board was too high for me to use) with an average SUS of 5 (0 being the lowest and 6 being the highest). This is because the handle on the sides of the balance board can be adjusted depending on the height of the test subject. The lowest rated item is #8 (I felt it did not need any much muscle effort in using this platform) with an average SUS of 2.55. This is because the platform was tested for healthy patients while the level of difficulty of the game was intended for post-stroke and post-injury patients. Improvements can be made by adding a motor on the balance board to assist the test subjects when they feel tired or when they executed too much muscle effort.

The Game Manipulability Measures part of the evaluation is based on how playable the game is for the test subjects. The results are also collated and calculated on an SUS basis. The average SUS for all 20 test subjects on Game Manipulability Measures is around *75.94%,* which is *11.67%* higher than the average SUS score of *68.* Based on the results, we can say that game manipulability is good.

The lowest SUS is *47.92* while the highest is *100.* Item #8 (I thought the game was simple and uncomplicated) is the highest rated item with an average SUS rate of 5.65. The lowest rated item is #7 (My legs got tired very easily when playing the game) with an average SUS rate of 3.6.

The Game Concept and Design Measures is a self-rated survey on how enjoyable and how appropriate the game is for balance board rehabilitation. The results are collated and calculated on an SUS basis. The average SUS for all 20 test subjects on Game Concept and Design Measures is around *70.64%,* which is *3.88%* higher than the average SUS score of *68.* Based on the results, we can say that the game's concept and design are satisfactory.

The lowest SUS is *51.28* while the highest is *96.15.* Item #1 (I thought the game was too hard for me) is the highest rated item with an average SUS rate of 5.7. This proves that the game is easy to play and understand by the test subjects. The lowest rated item is #3 (I got bored at this game) with an average SUS rate of 2.75. This might be because the gameplay was a bit easy for healthy test subjects but it might be challenging for post-stroke and post-injury patients.

The Game Comprehensibility Measures is a self-rated survey on how easy and understandable the instructions of the game when playing, which is collated and calculated based on SUS. Based on the results of 20 test subjects, the average SUS is around *80.42,* which is *18.26%* higher than the average SUS of *68.* This shows that the game comprehensibility measures are on a good level based on the qualitative conclusion per SUS score.

The lowest SUS is *63.89* while the highest is *100*. Item #2 (I thought the amount of information to follow this game was enough) is the highest rated item with an average SUS rate of 5.39. The lowest rated item is #11 (The sound was too loud or too soft, or had an annoying burst of sound) with an average SUS rate of 4.17, which is still above the average possible score of 3.

4.3. Motivation Analysis

In this project, all twenty (20) test subjects' responses had been collated and analyzed based on the IMI subscales. Table 3 shows the IMI results while Figure 7 shows a graph of the IMI rate in each IMI subgroup.

Table 3: IMI Results

IMI Subscale	Average	IMI rate (%)	Highest Score	Lowest Score
Interest/Enjoyment	35.25	71.94 %	49	21
Perceived Competence	29.7	84.86 %	35	19
Perceived Choice	30.3	86.57 %	35	18
Pressure/Tension	12.5	35.71 %	22	5
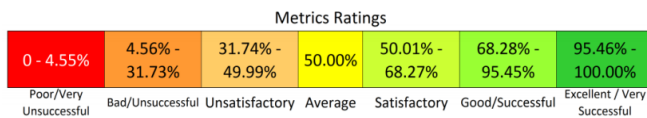
Figure 7: Qualitative Conclusion per Metrics Reading for MNM

In calculating their IMI scores, the average MNM is *0.88* with a minimum MNM of *0.78* and a maximum MNM of *0.95*. Results show that the average motivation of all 20 test subjects is in Good/Successful rating based on qualitative conclusion on metrics rating (Figure 7). This indicates that overall, the test subjects have good motivation in performing the balance exercises.

On all the IMI subscales as shown in Figure 8, the perceived choice is their highest response rate with *86.57%*, which indicates that they rated their voluntary participation and continued participation of playing the game. It is followed by perceived competence with *84.86%*. This means that the test subjects are skilled and they felt competent in playing the game. Interest/enjoyment which is another motivation subscale is also rated high with *71.94%*. The graph also shows that the test subjects didn't feel any pressure/tense and they feel relaxed while playing the game since the Pressure/Tension subscale only has a rate of *35.71%* and is below the average rate of *50%.*
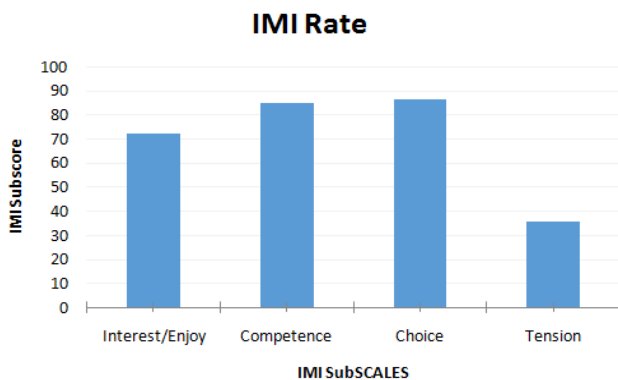
Figure 8: IMI Bar Graph

Game Walkthrough Evaluation is a self-rated survey consisting of short answers on what the test subjects thought of the game. Each item is analyzed and compared with other metrics to find out which part of the game is easy or hard, and what would be the difficulty in using the game.

4.4. Game Walkthrough Evaluation

Figure 9 shows the feedback of the test subjects while playing the game. The figure shows that most of the test subjects enjoyed while experimenting. They considered "Collect the crates" as their favorite part of the game while Follow the light was the most disliked one. Also, "Collect the crates" was the easiest part of the game while "Avoid the bombs" and "Follow the lights" tied to be the hardest part of the game. Additionally, the participants considered "Follow the lights" as the most tiring game, and difficult to control.
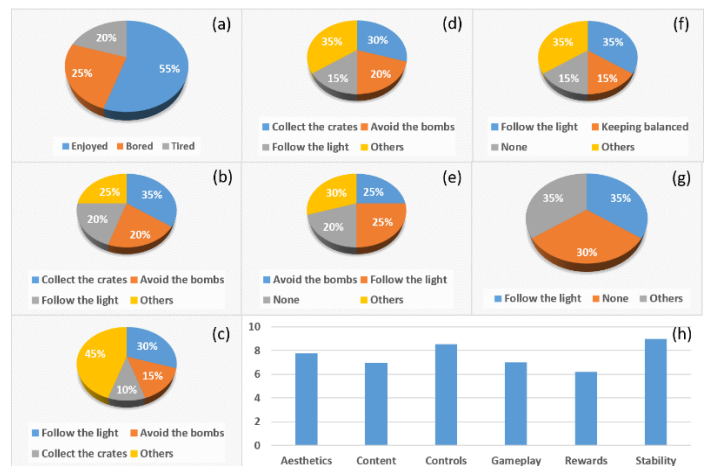
Figure 9: Game Walkthrough Evaluation Results: (a) Feeling after playing the game, (b) Favorite part of the game, (c) Disliked part of the game, (d) Easiest part of the game, (e) the hardest part of the game, (f) Tiring part of the game, (g) Control difficulty in the game, (h) Game overall Score.

The game is scored 7.58 over 10 (shown in Figure 9 (h)), with stability being the strongest feature (9) and rewards being its weakest feature (6.2). The participants also noticed some bugs/errors while playing like delayed movement on the projector screen, squeaking noise during the game, slow pace on the levels, monotonous gameplay, small text on the screen, etc. These need to be improved to increase overall game satisfaction.

5. Conclusion

The gamified environment and balancing platform were successfully tested on twenty individuals in compliance with the standard physical therapy time and procedures. Based on tests with varying tensions and weights, the equipment was observed to require recalibration every 1 hr and 30 minutes. The users also gave feedback based on a rating from the System usability scale (SUS) and IMI (Intrinsic Motivation Inventory) with regards to the different aspects of the game and equipment. The overall evaluation of the game got a score of *7.58* with stability as the strongest feature and rewards as the lowest one.

Further improvements can be made on the overall system such as the need for technical adjustments in the current build such as bugs, glitches, and sounds, adding a "Congratulations" instead of "Game Over" to increase motivation, integrating more natural

special effects (e.g. fish, seagulls, rain, etc.) and also, make the subject immersed in a relaxing-natural coastal area where the endpoint is a docking area/lighthouse. Lastly, testing the system with post-stroke and post-injury patients of different age groups, height, and body mass index (BMI) instead of healthy individuals would yield a more accurate and better reliability evaluation of the platform.

Conflict of Interest

The authors declare no conflict of interest.

Acknowledgment

References

[1] B. Lange, C. Chang, E. Suma, B. Newman, A. Rizzo, M. Bolas, "Development and Evaluation of Low Cost Game-Based Balance Rehabilitation Tool Using the Microsoft Kinect Sensor," in IEEE Engineering in Medicine and Biology Society, 1831-1834, 2011, doi:10.1109/IEMBS.2011.6090521

[2] A. Reinthal, K. Szirony, C. Clark, J. Swiers, M. Kellicker, S. Linder, "ENGAGE: Guided Activity-Based Gaming in Neurorehabilitation after Stroke: A Pilot Study," Stroke Research and Treatment, 1-10, 2012, doi:10.1155/2012/784232

[3] M. W. Kennedy, J. P. Schmiedeler, C. R. Crowell, M. Villano, A. D. Striegel and J. Kuitse, "Enhanced feedback in balance rehabilitation using the Nintendo Wii Balance Board," 2011 IEEE 13th International Conference on e-Health Networking, Applications and Services, Columbia, MO, 2011, 162-168, doi: 10.1109/HEALTH.2011.6026735.

[4] L. Neri, G. Adorante, G. Brighetti and E. Franciosi, "Postural rehabilitation through Kinect-based biofeedback," 2013 International Conference on Virtual Rehabilitation (ICVR), Philadelphia, PA, 2013, 218-219, doi: 10.1109/ICVR.2013.6662110.

[5] A. D. Williams, A. Kumawat, K. Agarwal, Q. A. Boser, H. Rouhani and A. H. Vette, "An instrumented wobble board for assessing and training dynamic sitting balance," 2017 IEEE International Conference on Systems, Man, and Cybernetics (SMC), Banff, AB, 2017, 2249-2254, doi: 10.1109/SMC.2017.8122955.

[6] K. Song, S. Shin, H. Kim, S. Chung, J. An and C. Lim, "Effect of balance board training on lower limb muscle activity," 2012 5th International Conference on BioMedical Engineering and Informatics, Chongqing, 2012, 515-518, doi: 10.1109/BMEI.2012.6513165.

[7] A. Timmermans, H. Seelen, R. Geers, P. Saini, S. Winter, J. Vrugt, H. Kingma, "Sensor-Based Arm Skill Training in Chronic Stroke Patients: Results on Treatment Outcome, Patient Motivation, and System Usability,"in IEEE Transactions on Neural Systems and Rehabilitation Engineering, 18(3), 284-292, 2010, doi:10.1109/TNSRE.2010.2047608.

[8] M. Yonei, K. Tanaka, "Toward measurement display content for improving instrinsic motivation in smart health equipment," in 2019 IEEE 1st Global Conference on Life Sciences and Technologies (LifeTech 2019), 206-209, 2019,doi:10.1109/LifeTech.2019.8884067.

[9] H. Lim, M. Tan, R. SJ-Reyes, Aiding Physical Rehabilitation Through Gamification: Development of a Gamified Environment Utilizing an Inertial Measurement Unit mounted on a Balance Board for Physical Therapy, M.S. Thesis, Ateneo de Manila University, 2016.

[10] J. Garcia, M. Rigor, R. SJ-Reyes, Intervention Study of an Enhanced Serious Game: A Comparative Game Design Analysis between Previous and Latest Version, M. S. Thesis, Ateneo de Manila University,2017.

[11] J. Chua, R. SJ-Reyes, A Pre-Clinical Study of Gamification of Balance Exercises with Intervention Techniques and Feedback System using Intervention, Motivation, and Game Design Analyses, M. S. Thesis,Ateneo de Manila University, 2017.

[12] M. Retirado, R. SJ-Reyes, "Development of an Active Balance Training Platform for a Gamified Physical Rehabilitation," in2nd European Conference on Electrical Engineering and Computer Science (EECS),279-289, 2018, doi:10.1109/EECS.2018.00059.

An algorithm for Peruvian counterfeit Banknote Detection based on Digital Image Processing and SVM

Bryan Huaytalla, Diego Humari, Guillermo Kemper[*]

Faculty of Engineering, School of Electronic Engineering, Universidad Peruana de Ciencias Aplicadas, Lima 15023, Peru

A R T I C L E I N F O	A B S T R A C T
	In this work we propose an algorithm for Peruvian counterfeit banknotes detection. Our algorithm operates in banknotes with 50, 100 and 200 soles denominations that were manufactured from 2009 onwards. This algorithm offers an automatic diagnosis based on digital image processing and support vector machines (SVM). Current Peruvian counterfeit detection systems are specially designed to analyze relevant characteristics in dollars and euros. Then, some counterfeiters can fool these systems. We made our detection system robust because we focus on the image acquisition and the segmentation of intaglio marks engraved over the banknotes. After segmentation, we applied embossing and Sobel filters followed by an aperture morphological operation to obtain special characteristics that were then classified by an SVM. We have validated our methodology using real and fake banknotes from a dataset of 240 samples provided by Central Reserve Bank of Peru (BCRP). Our final identification accuracy was 96.5%.

1. Introduction

In order to properly introduce the proposed algorithm, it's been divided into three sections: motivation and incitement, literature review and contribution.

1.1. Motivation and incitement

In Peru, counterfeiting money is a well-known fraud method. In fact, according to the Central Office Against Counterfeiting Money from Peru, the amounts of fraudulent banknotes have reached millionaire quantities (Oficina Central de Lucha contra la Falsificación de Numerario – OCN – Peru: "Principales operativos contra la falsificación" Available: http://www.ocn.gob.pe). As a result, the annual report of the United States Secret Service, an entity with which the Peruvian National Police works together to combat national and foreign banknote counterfeiting, places Peru as the main banknote counterfeiter country worldwide, surpassing other South American countries such as Colombia , which had this title before.

In Peru, this type of practice is especially problematic and constitutes an attack on society, because it makes people to lose trust on currency in circulation which increases money transaction time. Even worse, this distrust in Peruvian money hurts the economic growth and, in the long term, it could also lead to inflation because, as there is more money circulating than the amount the government can handle, people purchasing power increases, which would turn into an increase in prices. Finally, this ends up affecting the economy of any person or any company that receives the fradulent banknotes, especially when those banknotes are the ones with the highest denomination.

In this context, some enterprises offer solutions in the form of counterfeit banknote detectors. However, most of these detectors are based on foreign banknote manufacturing technologies, such as the "Elwic BC 3500 UV / MG next-generation banknote counter" or "PREZZOPAZZO DST-38D banknote detector", which use verification parameters such as magnetism, infrared or banknote thickness, all of which have already been fooled by Peruvian banknotes counterfeiters.

A common method used by scammers is to discolorate low-denomination banknotes (i.e. 10 or 20 soles banknotes), and then overprint them with high-denomination banknote values (i.e. 50, 100 or 200 soles banknote values). These overprints can be of very high detail so they successfully fool the aforementioned verification parameters used by commercial detectors. However these type of techniques are less common on lower denomination banknote (10 and 20 soles) as they would be less cost effective.

Our algorithm focuses on intaglio marks which are distinctive for Peruvian banknotes and whose imitations have not reached such a high level of sophistication.

[*]Corresponding Author: Guillermo Kemper, Av. Prolongación Primavera 2390, Monterrico, Santiago de Surco, Lima 15023, Peru, email: guillermo.kemper@upc.pe

The focus of the algorithm is on the higher denomination banknotes (50, 100 and 200 soles) since these are the more commonly counterfeited and the more damaging to the victims.

Some other commercial detectors are aimed to serve more as inspection tools for the user, using ultraviolet lights or magnifying glasses as is in the case of "Elwic Professional Banknote Detector IRD-2200" or the "Anizun Magnifying glass mini microscope". These solutions do not provide a clear detection verdict. Rather, they are based on users' prior knowledge of the distinctive marks and details that a legitimate banknote must have. By relying on the human senses, these methods have an intrinsic error. Furthermore, counterfeiters are capable of mimicking several of the most distinctive characteristics of authentic banknotes, such as fluorescent markings or some images that give the illusion of being seen against the light (Arjowiggins Security. "Security features: Watermarks, security fibres and security threads" Available: https://securitypapers.arjowiggins.com). Compared to these detection tools, our method offers a clear and readable verdict on the denomination and legitimacy of the analyzed banknote.

Another common counterfeit technique used in Peruvian banknotes is the removal of security bands from 100 and 200 soles banknotes. These bands are manually removed from a legitimate banknote and placed on a falsified one, then the legitimate but damaged banknote can be exchanged for a new one in banks. This way, counterfeiters have a fake one with a security band that would pass even a meticulous examination. Our algorithm can tackle this problem as it uses banknotes intaglio marks that cannot be removed and placed in falsified ones.

1.2. Literature review

We reviewed various scientific publications related to banknote analysis.

For example in [1] and [2] the authors tackled the automatic banknote denomination recognition problem by using digital image processing techniques. However in our proposed algorithm we not only determine banknote denomination but, in addition, perform a procedure aimed to identify the veracity of the banknote by analyzing intaglio marks with digital image processing techniques.

On the other hand, in [3] and [4] the authors were concerned about banknotes veracity but did not contemplate the use of an enclosure to standardize image light conditions. In comparison, our proposed solution does use an enclosure to ensure uniform illumination across all processed training and validation images.

Publications such as [5] and [6] that are based on digital image processing techniques have some flaws, as they did not consider the use of supervised learning algorithms to solve the classification task. On the contrary, our proposed solution uses a support vector machine (SVM) to tackle the classification problem after a training process performed with labeled images.

Some recent publications include the use of artificial intelligence [7] and deep learning [8] to detect counterfeit currency. However, these algorithms were designed and tested to work on other currencies such as dollars, euros, etc. Its performance on peruvian banknote has not been tested and they

don't use the intanglio marks as a classification parameter, which is the most difficult detail to forge.

Likewise, convolution techniques and neural networks are used in [8] which demand a lot of computational load and therefore requires to be implemented in hardware boards such as Jetson TX2. In contrast, we propose a low complexity algorithm that can be easily implemented on a small single-board computer (such as Raspberry Pi 3) with very satisfactory results.

1.3. Contribution and paper organization

Given that intaglio marks (Banco Central de Reserva del Perú, BCRP: "Elementos de seguridad de los billetes de 100 soles", Available: http://www.bcrp.gob.pe) are banknotes difficult-to-falsificate features we decided to design an algorithm that analyzes them (see Figure 1 for a view of some intaglio marks). In order to analyze intaglio marks we capture banknote images using a digital camera and an enclosure to guarantee proper light conditions. These images are then analyzed and enhanced using image processing techniques and a support vector machine (SVM) to determine whether the image corresponds to a legitimate or a fake banknote. Thus, our proposed system offers an automatic diagnostic on the veracity of the banknote analyzed.
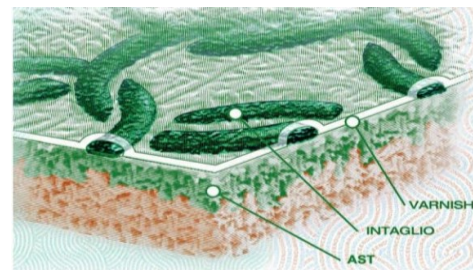
Figure 1: Intaglio marks [9].

Taking all these considerations into account, our methodology was able to perform a 96.5% of detection over the image dataset comprising 240 banknotes provided by the Central Reserve Bank of Peru (BCRP).

The amount of 240 samples was the result of the source of information provided by the Central Reserve Bank of Peru.

The selection of these samples had the following filters.

- The number of samples for the indicated denominations is reduced to 2 groups.
- The first group is confirmed by banknotes that did not enter into circulation, i.e., that did not deceive people.
- The second group of banknotes belongs to the group that entered circulation, i.e. the user did not detect the counterfeit banknote at the beginning.

For the validation process the second group was selected. In this case, BCRP specialists selected the banknotes that presented the greatest difficulty in detecting counterfeits. The details of the proposed algorithm, the results of the tests and the conclusions will be described in the following sections.

2. Proposed algorithm

For a better understanding, the distinctive characteristics of Peruvian banknotes will be first described and then a discussion of the main blocks of our algorithm will be presented.

(a)   (b)   (c)
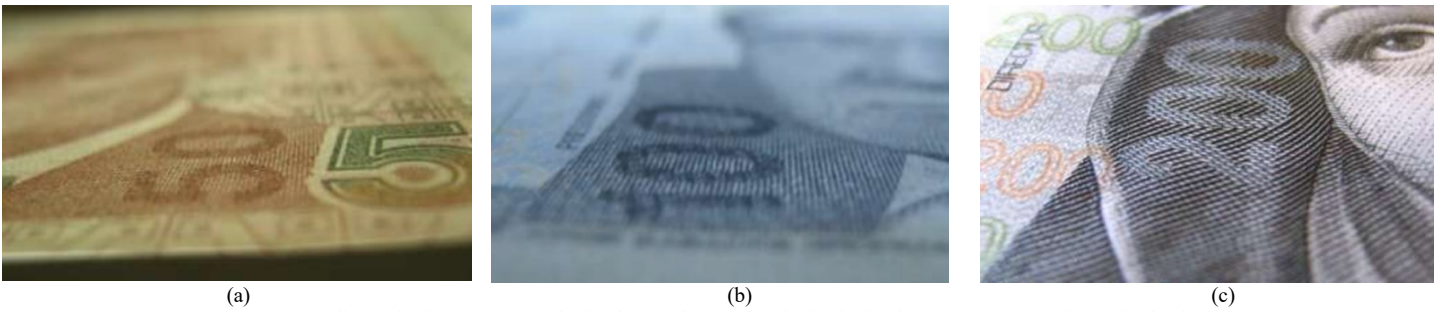
Figure 2: Intaglio marks for a (a) Fifty soles banknote, (b) One-hundred soles banknote, (c) Two-hundred soles banknote.
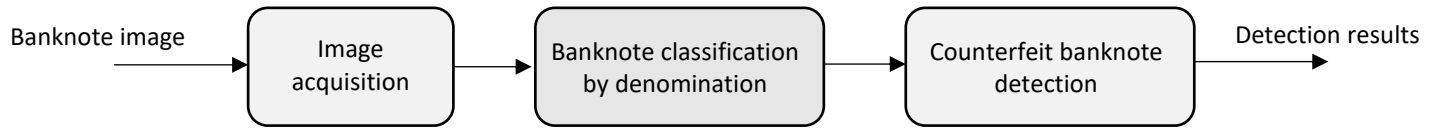
Figure 3: Block diagram of the proposed algorithm

2.1. Banknotes characteristics

We will focus our analysis on the intaglio marks from 50, 100 and 200 soles banknotes (Banco Central de Reserva del Perú, BCRP: "Nuevos billetes de 50, 100 y 200 soles", Available: http://www.bcrp.gob.pe). These marks can be appreciated by the human eye only if banknotes are positioned as in Figure 2 and with good illumination conditions. These marks depend on the banknote denomination, for this reason it is important to first determine the banknote denomination before proceeding with the analysis of intaglio marks.

In Figure 3 we present the block diagram of the proposed algorithm. In the following sections we will describe each block.

(a)   (b)

(c)

Figure 4: Sample of acquired images for (a) Fifty soles banknote, (b) One-hundred soles banknote, (c) Two-hundred soles banknote.

2.1. Image acquisicion

We used a closed enclosure to control light conditions, the enclosure was illuminated by a 3W white light LED. To capture the intaglio marks, every picture was taken from the right side of the banknote obverse. The sample banknotes are placed into the enclosure using mechanical guides that help with their correct and quick placement. LED lights were positioned so the area of interest would be distinguished more clearly.

A Raspberry v1 camera was used to take the picture, this camera has a CMOS OmniVision OV56476 with 5 megapixels (2592 x 1944 pixels resolution). The banknotes region of interest has RGB format (true color, 24 bits per pixel). Each primary component is defined as $I_R(x,y)$, $I_G(x,y)$ and $I_B(x,y)$, where (x,y) are the spatial coordinates.

All the computations were made by the Raspberry Pi 3B + single board computer which is compatible with the camera used and can perform all the required processing steps in less than 3 seconds with low power consumption (5 V /2.5 A). The acquired image is set to M=1644 rows and N=2592 columns.

In Figure 4 we showed 50, 100 and 200 soles banknotes taken under the described conditions.

2.2. Banknote classification by denomination

Given the captured images, we defined three regions of interest that were fixed so we can identify relevant characteristics in each banknote. These regions of interest can be expressed as:

Region 1:

$$I1_R(x,y) = I_R(x+400, y+500) \tag{1}$$

$$I1_G(x,y) = I_G(x+400, y+500) \tag{2}$$

$$I1_B(x,y) = I_B(x+400, y+500) \tag{3}$$

where:

$$x = 0,1,\dots,600$$
$$y = 0,1,\dots,500$$

Region 2:

$$I2_R(x,y) = I_R(x+780, y+750) \tag{4}$$

$$I2_G(x,y) = I_G(x+780, y+750) \tag{5}$$

$$I2_B(x,y) = I_B(x+780, y+750) \tag{6}$$

where:

$$x = 0,1,\dots,519$$
$$y = 0,1,\dots,699$$

Region 3:

$$I3_R(x,y) = I_R(x + 780, y + 1500) \qquad (7)$$

$$I3_G(x,y) = I_G(x + 780, y + 1500) \qquad (8)$$

$$I3_B(x,y) = I_B(x + 780, y + 1500) \qquad (9)$$

where:

$$x = 0,1, \dots, 519$$
$$y = 0,1, \dots, 1024$$

These regions were chosen because they allow us to differentiate between banknotes denomination by their coloration (See Fig. 5 for an example in a 200 soles banknote).

Figure 5: Two-hundred soles banknote with the three regions of interest (red boxes).

We averaged color components in every region of interest as features. To compute these averages, we use the following equations:

$$P1_R = \frac{1}{M1 \times N1} \sum_{x=0}^{M1-1} \sum_{y=0}^{N1-1} I1_R(x,y) \qquad (10)$$

$$P1_G = \frac{1}{M1 \times N1} \sum_{x=0}^{M1-1} \sum_{y=0}^{N1-1} I1_G(x,y) \qquad (11)$$

$$P1_B = \frac{1}{M1 \times N1} \sum_{x=0}^{M1-1} \sum_{y=0}^{N1-1} I1_B(x,y) \qquad (12)$$

where M1 = 601 and N1 = 501

$$P2_R = \frac{1}{M2 \times N2} \sum_{x=0}^{M2-1} \sum_{y=0}^{N2-1} I2_R(x,y) \qquad (13)$$

$$P2_G = \frac{1}{M2 \times N2} \sum_{x=0}^{M2-1} \sum_{y=0}^{N2-1} I2_G(x,y) \qquad (14)$$

$$P2_B = \frac{1}{M2 \times N2} \sum_{x=0}^{M2-1} \sum_{y=0}^{N2-1} I2_B(x,y) \qquad (15)$$

where M2 = 520 and N2 = 650

$$P3_R = \frac{1}{M3 \times N3} \sum_{x=0}^{M3-1} \sum_{y=0}^{N3-1} I3_R(x,y) \qquad (16)$$

$$P3_G = \frac{1}{M3 \times N3} \sum_{x=0}^{M3-1} \sum_{y=0}^{N3-1} I3_G(x,y) \qquad (17)$$

$$P3_B = \frac{1}{M3 \times N3} \sum_{x=0}^{M3-1} \sum_{y=0}^{N3-1} I3_B(x,y) \qquad (18)$$

where M3 = 520 and N3 = 1025

We compound this averages in a feature vector V_{C1} defined as:

$$V_{C1} = [P1_R \ P1_G \ P1_B \ P2_R \ P2_G \ P2_B \ P3_R \ P3_G \ P3_B] \qquad (19)$$

The compound feature vector V_{C1} is then classified using a Support Vector Machine (SVM) with a radial basis function kernel [10]. This kernel, which is described as a Gaussian function, was chosen because of its high performance to classify nonlinear data, as it is in our case. SVM was selected as the classifier because of its better performance compared with other techniques like KNN and because of its robustness to classify nonlinear data [11]. We used 70% of the banknotes for training and 30% for testing. We obtained a 99% of accuracy in this task as will be detailed in the results section.

2.3. Counterfeit banknote detection

After banknote classification by denomination, we now proceed to determine if the banknote is false or legitimate. To do so, we first isolate a counterfeit detection region of interest per banknote denomination as follows:

For fifty soles banknotes:

$$I4_R(x,y) = I_R(x + 760, y + 1460) \qquad (20)$$

$$I4_G(x,y) = I_G(x + 760, y + 1460) \qquad (21)$$

$$I4_B(x,y) = I_B(x + 760, y + 1460) \qquad (22)$$

where:

$$x = 0,1, \dots, 520$$
$$y = 0,1, \dots, 365$$

For hundred soles banknotes:

$$I4_R(x,y) = I_R(x + 630, y + 465) \qquad (23)$$

$$I4_G(x,y) = I_G(x + 630, y + 465) \qquad (24)$$

$$I4_B(x,y) = I_B(x + 630, y + 465) \qquad (25)$$

where:

$$x = 0,1, \dots, 295$$
$$y = 0,1, \dots, 550$$

For two-hundred soles banknotes:

$$I4_R(x,y) = I_R(x + 200, y + 545) \qquad (26)$$

$$I4_G(x,y) = I_G(x + 200, y + 545) \qquad (27)$$

$$I4_B(x,y) = I_B(x + 200, y + 545) \qquad (28)$$

where:

$$x = 0,1, \dots, 500$$
$$y = 0,1, \dots, 255$$

In Figure 6, we zoom in these regions of interest.

After the selection of the counterfeit detection region of interest, we compute averages in each component using the following equations:

$$P4_R = \frac{1}{M4 \times N4} \sum_{x=0}^{M4-1} \sum_{y=0}^{N4-1} I4_R(x,y) \tag{29}$$

$$P4_G = \frac{1}{M4 \times N4} \sum_{x=0}^{M4-1} \sum_{y=0}^{N4-1} I4_G(x,y) \tag{30}$$

(a)   (b)

(c)
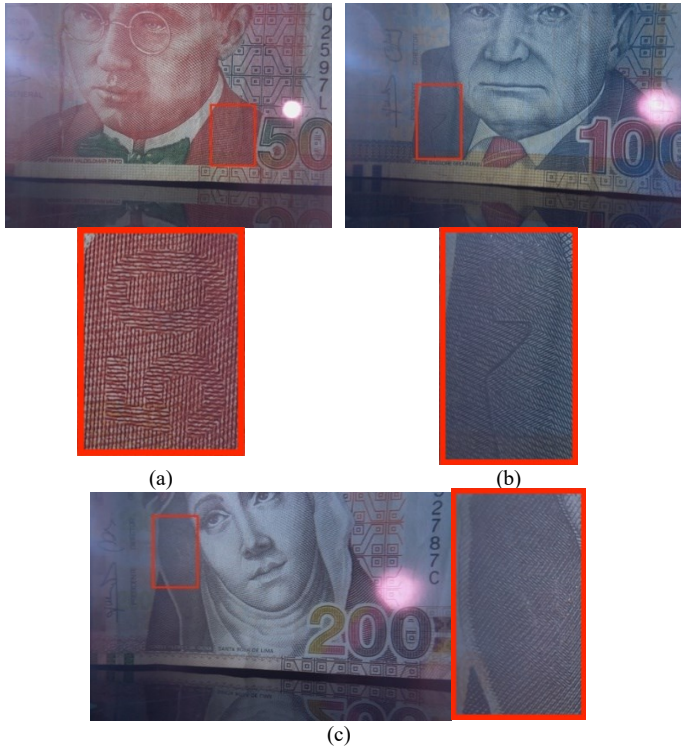
Figure 6: Amplified regions of interest for counterfeit banknote detection in the case of a (a) Fifty soles banknote, (b) One-hundred soles banknote, (c) Two-hundred soles banknote.

$$P4_B = \frac{1}{M4 \times N4} \sum_{x=0}^{M4-1} \sum_{y=0}^{N4-1} I4_B(x,y) \tag{31}$$

Every color component is then enhanced using an embossing filter [12] which is designed according to the banknote denomination, as is shown in equations (32), (33) and (34).

$$H1_{50} = \begin{bmatrix} -2 & 0 & 0 \\ 0 & 1 & 0 \\ 0 & 0 & 2 \end{bmatrix} \tag{32}$$

$$H1_{100} = \begin{bmatrix} -3 & 0 & 0 \\ 0 & 1 & 0 \\ 0 & 0 & 3 \end{bmatrix} \tag{33}$$

$$H1_{200} = \begin{bmatrix} -2 & 0 & -2 \\ 0 & 1 & 0 \\ 2 & 0 & 2 \end{bmatrix} \tag{34}$$

We then obtain the filtered components $I4'_R(x,y)$, $I4'_G(x,y)$ and $I4'_B(x,y)$ which have highlighted textures as can be seen in Figure 7.
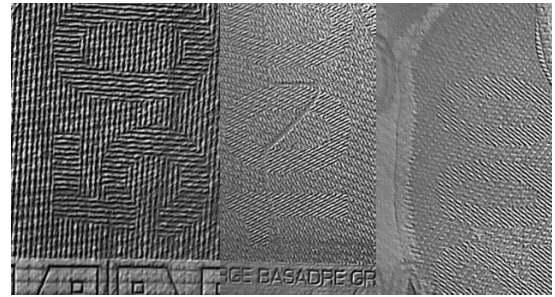
Figure 7: Results of the embossing filter in every region of interest for 50,100 and 200 soles banknotes.

To magnify edges, we applied Sobel filters [13] over the embossing components. In the case of the one-hundred banknote, we used a sobel variation filter due to the diagonal orientation of intaglio marks in this banknote. Final sobel filters are defined in equations (35), (36) and (37).

$$H2_{50} = \begin{bmatrix} 1 & 2 & 1 \\ 0 & 1 & 0 \\ -1 & -2 & 1 \end{bmatrix} \times 0.5 \tag{35}$$

$$H2_{100} = \begin{bmatrix} 2 & 0 & 0 \\ 2 & 0 & -10 \\ 0 & 0 & 2 \end{bmatrix} \times 0.7 \tag{36}$$

$$H2_{200} = \begin{bmatrix} 1 & 2 & 1 \\ 0 & 1 & 0 \\ -1 & -2 & -1 \end{bmatrix} \times 0.5 \tag{37}$$

After this step, we obtain as results $I4''_R(x,y)$, $I4''_G(x,y)$ and $I4''_B(x,y)$. Sobel filters are designed to sharp edges and variations [14], as we can see in Figure 8.

Figure 8: Sobel filter results for 50, 100 and 200 soles banknotes.

Now, the components are binarized using a threshold that varies with the banknote denomination [15]. Since constant illumination conditions are guaranteed, constant thresholds are used for each denomination in the binarization process. The resulting components are expressed using the following equations:

For fifty soles banknotes:

$$V4_R(x,y) = \begin{cases} 1, & I4''_R(x,y) \geq 40 \\ 0, & I4''_R(x,y) < 40 \end{cases} \tag{38}$$

$$V4_G(x,y) = \begin{cases} 1, & I4''_G(x,y) \geq 40 \\ 0, & I4''_G(x,y) < 40 \end{cases} \tag{39}$$

$$V4_B(x,y) = \begin{cases} 1, & I4''_B(x,y) \geq 40 \\ 0, & I4''_B(x,y) < 40 \end{cases} \tag{40}$$

For one-hundred soles banknotes:

$$V4_R(x,y) = \begin{cases} 1, & I4''_R(x,y) \geq 130 \\ 0, & I4''_R(x,y) < 130 \end{cases} \tag{41}$$

$$V4_G(x,y) = \begin{cases} 1, & I4''_G(x,y) \geq 130 \\ 0, & I4''_G(x,y) < 130 \end{cases} \tag{42}$$

$$V4_B(x,y) = \begin{cases} 1, & I4''_B(x,y) \geq 130 \\ 0, & I4''_B(x,y) < 130 \end{cases} \tag{43}$$

For two-hundred soles banknotes:

$$V4_R(x,y) = \begin{cases} 1, & I4''_R(x,y) \geq 150 \\ 0, & I4''_R(x,y) < 150 \end{cases} \tag{44}$$

$$V4_G(x,y) = \begin{cases} 1, & I4''_G(x,y) \geq 150 \\ 0, & I4''_G(x,y) < 150 \end{cases} \tag{45}$$

$$V4_B(x,y) = \begin{cases} 1, & I4''_B(x,y) \geq 150 \\ 0, & I4''_B(x,y) < 150 \end{cases} \tag{46}$$

The binarization process allowed us to reduce information from grayscale images [16]. Instead of an 8-bit image, now we have a 1-bit image, as seen in Figure 9.

Figure 9: Results from the binarization process

After this, we filtered the results using the aperture morphological operation. We do this to eliminate some noisy elements and enhance visibility of objects of interest (intaglio marks) [17]. Structuring elements are designed depending on the banknote denomination as follows.

$$\mathbf{H3_{50}} = \begin{bmatrix} 1 & 1 & 1 & 1 & 1 & 1 & 1 & 1 \\ 1 & 1 & 1 & 1 & 1 & 1 & 1 & 1 \end{bmatrix} \tag{47}$$

$$\mathbf{H3_{100}} = \begin{bmatrix} 0 & 0 & 1 \\ 0 & 1 & 0 \\ 1 & 0 & 0 \end{bmatrix} \tag{48}$$

$$\mathbf{H3_{200}} = \begin{bmatrix} 1 & 1 & 0 \\ 1 & 0 & 1 \\ 0 & 1 & 1 \end{bmatrix} \tag{49}$$

$$\mathbf{I4'''_n} = (\mathbf{V4_n} \ominus \mathbf{H3_n}) \oplus \mathbf{H3_n} = \mathbf{V4_n}°\mathbf{H3_n} \tag{50}$$

Thus, we obtain new image components $\mathbf{I4'''_R}$, $\mathbf{I4'''_G}$ and $\mathbf{I4'''_B}$. Figure 10 shows some results.

We then apply connectivity 4 to count the number of objects in each component. The number of objects per component are denominated $K4_R$, $K4_G$ y $K4_B$. We use these values to create a new compound feature vector V_{C2} as follows:

$$V_{C2} = [P4_R \ P4_G \ P4_B \ K4_R \ K4_G \ K4_B] \tag{51}$$

This feature vector is classified using an SVM trained per each banknote denomination (i.e. we used 3 SVMs). Thus, we used independent hyperplanes to perform our classification for our 6-dimensional vector [18]. Again, we used a radial basis function kernel [11] and 70% of the banknotes for training and 30% for testing.

Figure 10: Results after aperture morphological operation using specially designed structural elements.

3. Results

In this section we present our results for the classification and detection tasks using our 240 banknote dataset which are distributed as shown in Table 1. The ground-truth veracity of the banknotes was determined by a specialist of the BCRP.

Result for the banknote classification by denomination task are presented in Table 2. As we used 70% of the data to train the SVM classifier these results correspond to the remaining 30%. To compute our performance metric we divide the number of correct results by total number of samples.

As we can see, the results from this step were almost perfect, we only had one mistake in the classification of a one-hundred soles banknote.

In Table 3 we show the results for the detection process.

Results obtained in the detection process are satisfactory. There was only one mistake on a 50 soles banknote and another one on a 100 soles banknote.

Table 1: Banknotes distribution

Denomination	Veracity	Number of samples
50	Legitimate	32
	Fake	50
100	Legitimate	40
	Fake	49
200	Legitimate	32
	Fake	37

Table 2: Results for the classification process

Denomination	Number of test samples	Correctly classified samples	Performance
50	22	22	100%
100	33	32	97%
200	21	21	100%

Table 3: Results for the detection process.

Denomination	Number of test samples	Correctly detected samples	Percentage of correct detection
50	25	24	96%
100	28	27	96.4%
200	21	21	100%

In Tables 4, 5 and 6, we show correct and incorrect detections of the true and false banknote by denomination. In Table 4, a legitimate 50 soles banknote was incorrectly detected as false. This was caused by a deteriorated banknote that was bent on several places. In Table 5, a legitimate 100 soles banknote was incorrectly detected as false. This was caused by an incorrect insertion of the banknote on the image acquisition zone.

Table 4: Results for the 50 soles banknote detection process

Sample\Result	Legitimate	Fake
Legitimate	14	1
Fake	0	10

Table 5: Results for the 100 soles banknote detection process

Sample\Result	Legitimate	Fake
Legitimate	14	1
Fake	0	12

Table 6: Results for the 200 soles banknote detection process

Sample\Result	Legitimate	Fake
Legitimate	7	0
Fake	0	14

The average performance (according with Table 3) is then 97.47%. We observed that mistakes were generated because of banknote positioning problems (they were not inserted correctly or maybe the banknote was bent so its image could not be acquired correctly).

According to Table 3, the average detection performance of the proposed algorithm is 97.47%. The detection errors were mainly generated by banknote positioning problems, i.e. the banknotes were not inserted correctly or perhaps the banknote was bent, so its image could not be acquired correctly.

These problems could be solved by the use of additional hardware or by training the SVM classifier with images with these imperfections.

Finally, the total effectiveness of our algorithm $P_{(A)}$ (including classification and detection) is computed using the following equation:

$$P_{(A)} = P_{(B)} \times P_{(C/B)} \qquad (52)$$

where $P_{(B)}$ is the percentage of correct classifications, $P_{(C/B)}$ is the percentage of correct detections given a correct classification. Table 7 summarizes our final results.

Then, the total effectiveness average is 96.5%, which are results that could improve with a bigger sample. Compared to other studies with different currencies, it reached a higher percentage than Ballado's (95%) [6] and a lower percentage than Han's (100%) [7].

Table 7: Total effectiveness

Denomination	$P_{(B)}$	$P_{(C/B)}$	$P_{(A)}$
50	100%	96%	96%
100	97%	96.4%	93.5%
200	100%	100%	100%

4. Conclusions

The proposed algorithm was able to identify the denomination and veracity of Peruvian banknotes that were manufactured from 2009 onwards using the intanglio marks as a deciding factor, and support vector machines (SVM). The practical operation of this algorithm was validated by specialists from the Central Reserve Bank of Peru (BCRP). The few cases in which the algorithm failed were caused by the deteriorated state of the banknote. It is suggested not to use banknote that is ripped or folded in order to avoid missreadings.

Our automatic algorithm was efficient and can be used by any user who needs to determine the veracity of Peruvian 50, 100 or 200 soles banknotes.

The algorithm was entirely developed in Python and was embedded into a Raspberry single board computer. Additionally, does not consume high computational resources.

As we increase the number of training samples we can improve SVM performance for classification.

Conflict of Interest

The authors declare no conflict of interest.

Acknowledgment

References

[1] G. Ramasamy and S. Subramanian, "Identification of currency denomination using image processing," International Journal of Advanced Research, Ideas and Innovations in Technology, **5**(2), 2019.

[2]   S. Guzmán, Detector de billetes para personas con discapacidad visual, BSc. Thesis, Universidad Tecnológica del Perú, 2012.

[3]   D. Alekhya, G. Prabha, G. D. Rao, "Fake currency detection using image processing and other standard methods," International Journal of Research in Computer and Communication Technology, **3**(1), 2014.

[4]   J. L. Estela, Análisis comparativo de algoritmos de reconocimiento de imágenes por descriptores de color para la identificación de billetes, BSc. Thesis, Universidad Señor de Sipán, Chiclayo, Peru, 2016.

[5]   Abdullah M. Shoeb, Hadeer M. Sayed, Norah F. Saleh, Ehab I. Khafagy, Sameh Neji, "Software system to detect counterfeit Egyptian currency," in International Conference on Control, Instrumentation, Communication and Computational Technologies, 2016, doi:10.1109/ICCICCT.2016.7988010.

[6]   A. H. Ballado, J. C. Dela Cruz, G. O. Avendaño, N. M. Echano, J. E. Ella, M.E.M. Medina, B.K.C. Paquiz, "Philippine currency paper bill counterfeit detection through image processing using Canny Edge Technology," in 8th IEEE International Conference on Humanoid, Nanotechnology, Information Technology, Communication and Control, Environment and Management (HNICEM), 2015, doi:10.1109/HNICEM.2015.7393184.

[7]   M. Han, J. Kim, "Joint banknote recognition and counterfeit detection using explainable artificial intelligence," Sensors, **19**(16), 3607, 2019, doi.org/10.3390/s19163607.

[8]   T. D. Pham, C. Park, D. T. Nguyen, G. Batchuluun, K. R. Park, "Deep learning-based fake-banknote detection for the visually impaired people using visible-light images captured by smartphone cameras," IEEE Access, **8**, 63144 – 63161, 2020, doi:10.1109/ACCESS.2020.2984019.

[9]   T. Crane, "Some observations on technological developments in durable substrates," Billeteria: International review on cash management, **5**(9), 2011.

[10]   D. Duvenaud. Automatic model construction with Gaussian processes, Ph.D. Thesis, Pembroke College, England, 2014.

[11]   C. M. Bishop, Patter recognition and machine learning, Springer, 2006.

[12]   S. Umbaugh, Computer imaging: Digital image analysis and processing, CRC Press, 2010.

[13]   J. Álvarez, J. Fernández, "Procesamiento de imágenes bajo Windows CE utilizando el procesaror ARMv 4I," ITECKNE Innovación e Investigación en Ingeniería, **8**(2), 2008, doi: 10.15332/iteckne.v8i2.41.

[14]   R. Muthukrishnan, M. Radha, "Edge detection techniques for image segmentation," International Journal of Computer Science and Information Technology, **3**(6), 2011, doi:10.5121/ijcsit.

[15]   R. Gonzalez, R. Woods. Digital Image Processing, Pearson, 2018.

[16]   C. Solomon, T. Breckon, Fundamentals of digital image processing: A practical approach with examples in Matlab, John Wiley & Sons, 2010.

[17]   G. Aguilar, Procesamiento digital de imágenes utilizando filtros morfológicos, BSc. Thesis, Escuela Politécnica Nacional, Quito, Ecuador, 1995.

[18]   C. C. Chang, C. J. Lin, "LIBSVM: A Library for Support Vector Machines," ACM Transactions on Intelligent Systems and Technology, **2**(3), 2011, doi.org/10.1145/1961189.1961199.

Quality of Life in People with Type 2 Diabetes Residing in a Vulnerable Area in the Los Olivos district - Lima

Rosa Perez-Siguas*, Eduardo Matta-Solis, Hernan Matta-Solis

Research Directorate, Universidad María Auxiliadora, 15408, Lima-Perú

ABSTRACT

Non-communicable chronic diseases are more frequent in developing countries, having a significant impact on morbidity, mortality, health care costs and productivity. A study indicates that physical exercise, glucose control, complications, hypertension, duration of diabetes, diet and depression are associated with the quality of life in patients with type 2 diabetes. The purpose of the study is to determine the quality of life in people with Type 2 Diabetes who reside in a vulnerable area of Los Olivos. The focus of this study is quantitative, its design is descriptive because it allows the study population to be described at a given moment. The population was 173 people with type 2 diabetes, from the Juan Pablo II Confraternity Maternal and Child Center in Los Olivos. The diabetes 39 questionnaire (D-39) was applied, made up of 39 items grouped into five dimensions, which measures the quality of life in diabetes. The results showed a half quality of life (51.4%), followed by high (26%) and low (22.5%). These results support the importance of promoting and educating about healthy habits in the diabetic patient, so that they can maintain an adequate quality of life. Type 2 diabetes is a silent and progressive disease in its initial stage, public health systems must increase efforts to make timely diagnoses, where the disease can be controlled avoiding the presence of complications and sequelae that can be fatal for the patient.

1. Introduction

Worldwide, the total number of people detected with type 2 diabetes mellitus (DM2) has increased considerably in the last three decades, although we know that diabetes mellitus is one of the noncommunicable diseases that can cause death [1].

DM2 is well known globally, since the rapid increase in the prevalence of this disease is evidenced and it has been confirmed that in 2019, 488 million in the ages of 20 to 99 years old suffer from this disease. Where the last decade the countries of type two diabetes mellitus have been the countries of China, India, the United States, Pakistan and Brazil respectively [2].

Diabetes is an incessant chronic condition where it causes a high level of sugar in the blood [3]. This is due to the decrease in the mechanism of beta cells of the pancreas [4], generating various stimuli in various parts of the body, among them, they are pancreatic failure, increased risk of cardiovascular system diseases, hypertension, kidney failure, neuropathy, problems with foot vascularization, ketoacidosis, visual problems, among others [5], [6].

The International Diabetes Federation (IDF) warned that the number of people with T2DM disease will rise worldwide from 325 million in 2017 to 629 million with diabetes in 2045 [7].

In Latin America, the IDF estimated that 9.4% of adults had diabetes and 7.9% had impaired fasting blood glucose (IFG) in 2015, and these numbers are expected to increase to 11.9 % and 9.4%, respectively, in 2040 [7].

In Latin America and the Caribbean, since 2015 it has been calculated in people aged 20 years and over, who suffered from DM2. Therefore, DM2 has represented an economic burden in the countries of Latin America and the Caribbean in 2015 [8].

The factors that mainly compromise health and cause DM2 worldwide are overweight and obesity, sedentary lifestyle and an inadequate diet [9][10]. Also, complications at the cardiovascular level in people with DM2 due to the factors that compromise their health are the main causes of morbidity and mortality, in addition to the kidney complications present in diabetic people [1].

Although, when you have DM2 and other cardiovascular diseases that occur at a younger age, they tend to develop

aggressively, compromising the health of the diabetic person [11]. It can also lead to low life expectancy and this as a consequence causes a decline in quality of life [12].

In the same way, heart disease and other cardiovascular diseases can be generated quickly if the diabetic patient is depressed, mental health in diabetic patients is important since it maintains life expectancy and thus there is no complications in the patient [13].

In [14], the authors mentioned differences between social overload and sexual behavior, where they specified that sexual behavior had a high impact on the quality of life of the Brazilian population in the study and that social burden affected the quality of life, out of shame to present DM2, to be called diabetic and to present DM2 interrupting their family life.

In [15], the authors mentioned in their study the evaluation of the quality of life in people with DM2 and that in their results it is observed that the social burden domain is the one that has the highest incidence in quality of life (56.26 ± 12.07) followed by the domain of sexual functioning (54.35 ± 9.47), the domain of anxiety and worry (54.33 ± 7.76), the domain of energy and mobility (51.46 ± 8.73) and the domain of diabetes control (50.08 ± 10.84) concluding that the Sex life and mobility of the diabetic person is affected by age.

In [16], it was observed in the results of quality of life in the participants where 62.3% had an average quality of life, regarding the subjective perception of the state of health, 46.7% considered having adequate health well-being, expressing that a healthy diet, physical activities and a controlled treatment will allow an improvement in the quality of life in diabetic patients in the long term.

In [17], the authors interpreted that patients who have regular consultations and treatments for diabetes control, expressed that they improved their quality of life, on the other hand, in patients with comorbidities they demonstrated a considerable decrease in their quality of life. Its systematic review study, it was observed in 31 studies in patients with DM2, that 50% of the studies reported that diabetic patients received some treatment to control their disease.

In [18], the authors in their study of quality of life and depression in patients with diabetes, interpreted that 54.1% of the majority of participants perceived depression with the Patient Health Questionnaire-9 (PHQ-9)score of 6.15 ± 5.01 on a scale of 0-27. On a scale of 0 to 100, the highest mean quality of life score was reported in the social relationship domain (57.32 ± 11.83), followed by the environment domain (54.71 ± 7.74), psychological health (53.25 ± 10.32) and physical health (50.74 ± 11.83). Concluding that a study should be carried out on depression, since this factor affects more the quality of life, being associated with negativity, affecting its treatment and glycemic control of diabetes. In the absence of a timely and pertinent detection of depression, emotional problems may be exacerbated, and therefore the quality of life and well-being would be affected, all this will ultimately trigger an oversight in the health of the diabetic, and their adherence to treatment and control of the disease will not be fully assumed. This could be translated into the presence of hyperglycemia symptoms, which is the beginning for the irreversible damage to the target organs of the disease to be evident.

Diabetes is a health problem that affects global public health, in Perú, the care and monitoring of people affected with this disease is essential, since it will allow this disease not to evolve and generate sequelae or death in the person. Valuing the quality of life allows generating scientific evidence that serves as a basis to improve health strategies aimed at the care and care of these patients who become vulnerable due to the systemic damage that is characteristic of this type of metabolic disease. This non-communicable disease is considered one of the 11 health problems (health problem no. 3: metabolic and cardiovascular diseases) indicated in the document Prioridades Nacionales de Investigación en Salud en Perú 2019-2023, prepared by the Instituto Nacional de Salud and the endorsement of the Ministerio de Salud of our country.

The main objective of the research work is to determine the quality of life in people with Type 2 Diabetes who reside in a vulnerable area of Los Olivos. Due to the complications and costs that type 2 diabetes generates for the patient, the family, and the country; it is of utmost importance to take care of the health of these patients, it is necessary that they come to their medical control periodically where their levels of glycemia, weight and the impact of the medication are mainly valued. But it knows that the disease and its pathophysiology generate an impact in other areas such as social, emotional, limitations in the development of activities of daily living, etc., therefore it is important to assess the quality of life related to the health of these people, because, it will have evidence of how the disease affects other dimensions of the patient's life. It means a scientific evidence that allows health and nursing personnel to improve their professional practice aimed at the care and self-care of these people affected by this systemic disease.

Therefore, the objective of the research work is to determine the quality of life in people with Type 2 Diabetes living in a vulnerable area of Los Olivos - Lima.

The hypothesis of the research work is that type 2 diabetes mellitus negatively affects the quality of life of the patient, even though they have knowledge about the risk of the disease reported in their routine controls.

2. Methods

2.1. Research type and Design

The present study is of a quantitative approach, since the main variable will be measured with a quantitative data collection instrument and will be used for the analysis of the data collected, mainly descriptive statistical processes. The methodological design is a descriptive and cross-sectional research, it is descriptive because reality is described as it is presented and it is transversal because the process of measuring the variable was carried out only once in time by each participant [19].

2.2. Population and sample

We worked with the sample of the total population of diabetic patients in the jurisdiction of each health center. According to the

initial standard, 187 participants with type 2 diabetes were identified, then 14 of them did not decide to participate by their own decision or did not meet some of the selection criteria (inclusion and exclusion) indicated below, finally the population was made up of 173 patients diagnosed with type 2 diabetes.

Table 1: Sociodemographic data in people with type 2 diabetes residing in a vulnerable area in Los Olivos (n=173)

Information of the participants	Total		Value Sig. (p)
	n	**%**	
Total	173	100	
Age			0.000
Adult (30 to 59 years old)	91	52.6%	
Older Adult (60 and over)	82	47.4%	
Sex			0.730
Female	88	50.9	
Male	85	49.1	
Marital Status			0.171
Single	6	3.5	
Married	92	53.2	
Widowed	9	5.2	
Cohabitant	55	31.8	
Divorced	11	6.4	
Types of Family			0.578
Nuclear	104	60.1	
Extended	32	18.5	
Expanded	26	15.0	
Single Parent	9	5.2	
Reconstituted	2	1.2	
Degree of Study			0.093
No Education	1	0.6	
Primary Education	18	10.4	
Secondary Education	140	80.9	
Higher University Education	2	1.2	
Higher Non-university Education	12	6.9	
Occupation Condition			0.138
Stable Worker	4	3.2	
Eventual	114	65.9	
No Occupation	44	25.4	
Retired	11	6.4	

In Table I, it has the sociodemographic data of the study participants, there were 173 people affected with diabetes. The minimum age was 38 years old; the maximum was 77 years old and the mean was 58.35 years.

Regarding the participant's sex, 88 that represent 50.9% correspond to female and 85 that represent 49.1% correspond to male. Regarding the degree of study, 140 participants representing 80.9% have secondary education, 18 participants representing 10.4% have primary education, 12 participants representing 6.9% have Higher non-university education, 2 participants representing 1.2% have higher university education and 1 participant representing 0.6% have no education. Regarding marital status, the married with 92 (53.2%) cases predominate, followed by the

cohabitant with 55 (31.8%) cases, divorced with 11 (6.4%) cases, widowed with nine (5.2 %) cases and finally single with 6 (3.5%) cases. Regarding the type of family, nuclear families predominate with 104 (60.1%) cases, followed by extended families with 32 (18.5%) cases, expanded with 26 (15%) cases, single parent with nine (5.2%) cases and reconstituted with two (1.2%) cases. Regarding the occupation condition, the eventual prevails with 114 (65.9%) cases followed by the no occupation with 44 (25.4%) cases, retired with 11 (6.4%) cases, and finally stable worker four (2.4%) cases.

One aspect to highlight is that within the sociodemographic data. It was found that there is a significant relationship between age and quality of life with a (p=0.000).

2.3. Inclusion Criteria

The inclusion criteria are adults (30 to 59 years old) and older adults (60 to more years old) with a medical diagnosis of type 2 diabetes, also who are in treatment and are continuing patients (have at least one control medical consultation) in the health center of the jurisdiction. Moreover, participants who are residents in the area with their own home, also who voluntarily agreed to participate in the study and agreed to sign the informed consent and finally, those who did not meet at least one of the selection criteria were not included in the study.

2.4. Technique and Instrument

To measure the quality of life in Diabetes, the data collection instrument called the Diabetes 39 questionnaire was used. Before its application in the field work, its validity and reliability were verified.

To measure the quality of life in Diabetes, the data collection instrument called the Diabetes 39 Questionnaire was used, this is an instrument originally developed in the English language and specifically designed to determine the health-related quality of life of people with diabetes type 2 mellitus. It has currently been validated and translated into the Spanish language and its use is widespread in many other languages. This instrument is made up of 39 items which are distributed in 5 dimensions or factors: Energy-Mobility, which refers to the limitation of the level of energy and daily activities, decrease in visual acuity and disturbed sleep (consisting of 15 items); Diabetes control, which refers to the impact of medical treatment based on the therapeutic plan, glycemic control and diet (consisting of 12 items); Anxiety-concern, which are the concerns that the person has about economic issues, life stresses and future life (consisting of 4 items); Social burden, which refers to the limitations of diabetes mellitus that interfere with family and friends life (made up of 5 items) and sexual functioning, which refers to the impact of diabetes on sexual abilities and functioning (made up of three items) [20][21].

Validity was determined by expert judgment, consulting five health professionals about the content and statements of the instrument used in this study. The content validity of the instrument was 86.2%, which is interpreted as good. Then a pilot study was developed in which 30 people between adults and older adults participated. Statistical validity and reliability were calculated with this sample. Statistical validity was obtained using the Kaiser-Meyer-Olkin (KMO) sample adequacy tests and the

Bartlett sphericity test. The sample adequacy test gave a score of 0.963 (KMO>0.5) and the Bartlett specificity test gave a significance level of 0.000 (p<0.001). Both tests affirm the instrument's validity hypothesis. The reliability of the instrument was determined based on the Cronbach's alpha coefficient. A high value of internal consistency was obtained between the results of the instrument which is 0.996 (α>0.6), confirming the reliability of the measuring instrument.

Participants answer how much their quality of life has affected in the last month by an action expressed by each item, marking an X on a modified visual analog type scale, whose scale of values goes from one to seven, where one corresponds if it is not affected at all and seven corresponds to extremely affected quality of life [20].

2.5. Place and Application of the Instrument

The data collection process was carried out during the last quarter of 2019. Prior, coordination was carried out to obtain data on patients with type 2 diabetes who live in the jurisdiction of the Health Establishment called the Centro Materno Infantil Confraternidad - Juan Pablo II located in the Los Olivos district. Each participant was visited at home, spending with each of them an approximate time of 15 to 20 minutes to complete the data sheet. Nursing staff was the one who mainly participated in the work of filling in data sheets, this due to their important participation in Primary Health Care areas such as Family Health, Community Health and Health Promotion. In addition, it had the support of the health promoters in the area, who facilitated the identification of the participants' homes. At the end of completing each data sheet, it was revised to ensure that it has its complete data coding and entry.

For the data analysis, a guide to the diabetes instrument Diabetes 39 was used, which gives details of how the quality of life in diabetes is evaluated for each of the five dimensions. The software used for data entry and management were Excel and the Statistical Package for the Social Sciences (SPSS).

3. Results

In Table 2, it can see the quality of life in people with type 2 diabetes, where the medium quality of life predominates with 51.4% (n = 89), followed by the high quality of life with 26% (n=45), and finally the low quality of life with 22.5% (n = 39).

Table 2: Quality of Life in people with Type 2 Diabetes residing in a vulnerable area in Los Olivos (n=173)

Quality of life	n	%
Low quality of life	39	22.5
Medium quality of life	89	51.4
High quality of life	45	26.0
Total	173	100.0

In Table 3, it can see the quality of life in its energy and mobility dimension, where the medium quality of life predominates with 69.4% (n = 120), followed by the high quality of life with 26% (n = 45), and finally the low quality of life with 4.6% (n = 8).

In Table 4, it can see the quality of life in its diabetes control dimension, where the medium quality of life predominates with

51.4% (n = 89), followed by the high quality of life with 26% (n = 45), and finally the low quality of life with 22.5% (n = 39).

Table 3: Quality of life according to its energy and mobility dimension, in people with type 2 Diabetes residing in a vulnerable area in Los Olivos (n=173)

Energy and mobility	n	%
Low quality of life	8	4.6
Medium quality of life	120	69.4
High quality of life	45	26.0
Total	173	100.0

Table 4: Quality of life according to its diabetes control dimension, in people with type 2 diabetes residing in a vulnerable area in Los Olivos (n=173)

Diabetes control	n	%
Low quality of life	39	22.5
Medium quality of life	89	51.4
High quality of life	45	26.0
Total	173	100.0

In Table 5, it can see the quality of life in its anxiety and concern dimension, where the medium quality of life predominates with 52% (n = 90), followed by the high quality of life with 26% (n = 45), and finally the low quality of life with 22% (n = 38).

Table 5: Quality of life according to its anxiety and concern dimension, in people with type 2 Diabetes residing in a vulnerable area in Los Olivos (n=173)

Anxiety and concern	n	%
Low quality of life	38	22.0
Medium quality of life	90	52.0
High quality of life	45	26.0
Total	173	100.0

In Table 6, it can see the quality of life in its social burden dimension, where the medium quality of life predominates with 52% (n = 90), followed by the high quality of life with 26% (n = 45), and finally the low quality of life with 22% (n = 38).

Table 6: Quality of life according to its social burden dimension, in people with type 2 Diabetes residing in a vulnerable area in Los Olivos (n=173)

Social Burden	n	%
Low quality of life	38	22.0
Medium quality of life	90	52.0
High quality of life	45	26.0
Total	173	100.0

The results of this study constitute scientific evidence that allows to understand the health situation of these patients with type 2 diabetes in a greater dimension, which allows a more holistic and comprehensive assessment of the evolution of their disease, thus the professional health will make more timely and relevant decisions that translate into improving their well-being.

4. Discussion

This research work on quality of life in diabetes is part of the research line of chronic non-communicable diseases, this one has an approach from the perspective of health promotion that should be promoted from primary health care.

Regarding the quality of life in people with diabetes, the medium quality of life prevailed, therefore, the hypothesis established in the research work is accepted, that is, the person

with diabetes mellitus has an unsatisfactory quality of life, even though they have knowledge about the risks that this disease generates.

The results interpret that diabetes mellitus negatively exposes the quality of life of the person, factors such as sedentary lifestyle and inadequate nutrition further compromise the well-being of the person. In [16], the authors argue that the quality of life in people with diabetes mellitus is not only based on rigorous treatment and physical activity in order to maintain their health, but also on the emotional support they have from their family in order to maintain their mental health and thus allow them to improve their quality of life.

In [15], the authors observed that the diabetes control dimension is affected by the time of the disease and the degree of education of the patient.

The results of glycemic control observed in patients with DM2 is low, so an approach is considered where a strategy is sought to improve knowledge about their disease and their adherence to treatment [4]. DM2 is one of the diseases that is most associated with cardiovascular diseases; studies have shown that glycemic control reduces diabetic vascular complications [3]. In [17], the authors reported that the control of diabetes and continuous treatment is very important because it allows the prevention of certain comorbidities since patients with DM2 are exposed to contracting diseases that are mainly cardiovascular.

In [14], they indicated that the quality of life was greatly affected in the items related to the social burden dimension: shame of having diabetes, being called diabetic and having diabetes interfering in their family life. This result deserves special attention in diabetes, where educational programs are carried out, to incorporate strategies that facilitate the approach of aspects related to the impact of diabetes.

Life-altering change is a diagnosis of type 2 diabetes, people must cope with the diagnosis to accept type 2 diabetes. Anxiety, depression, stress, and angst from diabetes were identified as key influential psychosocial factors. The emotional responses to the diagnosis were related to depression and anxiety. Negative styles of resignation, protest, or isolation were higher in women and were associated with poorer quality of life, while avoidance was associated with increased diabetes-related distress and depressive symptoms [10]. In [18], they argued that depression and anxiety are factors that predispose diabetic patients to a poor quality of life, because their psycho-emotional health is altered by suffering from the disease and also having a negative attitude, sadness and shame as this interrupts their daily routines.

People with DM2 express concern due to insulin prices, therefore, it generates a negative impact on their state of mind [11], since personal care and living with complications related to DM2, causes negativity at a psychosocial level affecting health in it.

The frequency of depression in patients with diabetes raises the need to consider depression as an additive factor to the disease burden of this condition. Type 2 diabetes is a silent and progressive disease in its initial stage, public health systems must increase efforts to make timely diagnoses, where the disease can be controlled avoiding the presence of complications and sequelae that can be fatal for the patient [13].

5. Conclusions

It is concluded that the nursing staff has an important role in educating and guiding diabetics, with its science of care, it must contribute to generating behavioral changes in this type of patients, only in this way, it could guarantee that they have a controlled disease and carry a full and quality life.

It is concluded that nutritional counseling for patients should be considered mainly for the families of older adults and thus they are oriented in what needs the older adult is going to present at home.

It is concluded that patients must have a correct management of the disease, as well as psychological support, both family and professional, to improve their quality of life.

The limitation in the present research work is that it was considered that in Peru there is little research on quality of life in patients with diabetes, so it is necessary that several studies be carried out to improve knowledge about the quality of life in patients with diabetes.

Conflicts of Interest

The authors declare that they have no conflict of interest.

References

[1] Y. Zheng, S. Ley, F. Hu, "Global aetiology and epidemiology of type 2 diabetes mellitus and its complications.," Nature Reviews Endocrinology, **14**(2), 88–98, 2018, doi:10.1038/nrendo.2017.151.

[2] P. Saeedi, I. Petersohn, P. Salpea, B. Malanda, S. Karuranga, N. Unwin, S. Colagiuri, L. Guariguata, A. Motala, K. Ogurtsova, J. Shaw, D. Bright, R. Williams, "Global and regional diabetes prevalence estimates for 2019 and projections for 2030 and 2045: Results from the International Diabetes Federation Diabetes Atlas, 9th edition.," Diabetes Research and Clinical Practice, **157**, 107843, 2019, doi:10.1016/j.diabres.2019.107843.

[3] S. Reddy, E. Bhatia, "Intensive glycaemic control in type 2 diabetes mellitus: Does it improve cardiovascular outcomes?.," National Medical Journal of India, **24**(1), 21–27, 2011, doi:10.3810/pgm.2011.11.2501.PMID.

[4] A. Abdullah, A. Alkandari, J. Longenecker, S. Devarajan, A. Alkhatib, R. Al-Wotayan, Q. Al-Duwairi, J. Tuomilehto, "Glycemic control in Kuwaiti diabetes patients treated with glucose-lowering medication.," Primary Care Diabetes, **14**(4), 311–316, 2020, doi:10.1016/j.pcd.2019.12.001.

[5] N. Sneha, T. Gangil, "Analysis of diabetes mellitus for early prediction using optimal features selection.," Journal of Big Data, **6**, 1–13, 2019, doi:10.1186/s40537-019-0175-6.

[6] D. Azañedo, G. Bendezú, M. Lazo, D. Cárdenas, G. Beltrán, N. Thomas, R. Ceballos, G. Málaga, "Calidad de control metabólico en pacientes ambulatorios con diabetes tipo 2 atendidos en una clínica privada," Acta Medica Peruana, **34**(2), 106–113, 2017, doi:10.35663/amp.2017.342.318.

[7] International Diabetes Federation, Atlas de la Diabetes de la FID. Novena edición 2019, 2019.

[8] A. Barcelo, A. Arredondo, A. Gordillo, J. Segovia, A. Qiang, "The cost of diabetes in Latin America and the Caribbean in 2015: Evidence for decision and policy makers.," Journal of Global Health, **7**(2), 20410, 2017, doi:10.7189/jogh.07.020410.

[9] L. Bautista, G. Zambrano, "La calidad de vida percibida en pacientes diabéticos tipo 2.," Investigación En Enfermería: Imagen y Desarrollo., **17**, 131–148, 2015.

[10] M. McCoy, L. Theeke, "A systematic review of the relationships among psychosocial factors and coping in adults with type 2 diabetes mellitus.," International Journal of Nursing Sciences, **6**(4), 468–477, 2019, doi:10.1016/j.ijnss.2019.09.003.

[11] A. Ahne, F. Orchard, X. Tannier, C. Perchoux, B. Balkau, S. Pagoto, J. Harding, T. Czernichow, G. Fagherazzi, "Insulin pricing and other major diabetes-related concerns in the USA: A study of 46 407 tweets between 2017 and 2019.," BMJ Open Diabetes Research and Care, **8**(1), 1–11, 2020, doi:10.1136/bmjdrc-2020-001190.

[12] T. Çolak, G. Acar, E. Elçin, B. Özgül, İ. Demirbüken, Ç. Alkaç, M. Polat,

"Association between the physical activity level and the quality of life of patients with type 2 diabetes mellitus.," Journal of Physical Therapy Science, **28**(1), 142–147, 2016, doi:10.1589/jpts.28.142.

[13] K. Dennick, J. Sturt, J. Speight, "What is diabetes distress and how can we measure it? A narrative review and conceptual model.," Journal of Diabetes and Its Complications, **31**(5), 898–911, 2017, doi:10.1016/j.jdiacomp.2016.12.018.

[14] R. Zulian, M. dos Santos, V. Veras, F. Rodrigues, C. Arrelias, M. Zanetti, "Quality of life in patients with diabetes using the Diabetes 39 (D-39) instrument.," Revista Gaúcha de Enfermagem, **34**(3), 138–146, 2013, doi:10.1590/S1983-14472013000300018.

[15] S. Thapa, P. Pyakurel, D. Baral, N. Jha, "Health-related quality of life among people living with type 2 diabetes: A community based cross-sectional study in rural Nepal.," BMC Public Health, **19**(1), 1–6, 2019, doi:10.1186/s12889-019-7506-6.

[16] L. Bautista, G. Zambrano, "La calidad de vida percibida en pacientes diabéticos tipo 2," Investigación En Enfermería: Imagen y Desarrollo, **17**(1), 131–148, 2015, doi:10.11144/javeriana.ie17-1.lcdv.

[17] J. Sánchez, D. Morales, T. González, C. Tovilla, I. Juárez, L. López, Y. Hernández, J. Ble, N. Pérez, J. Rodriguez, "Quality of life of Latin-American individuals with type 2 diabetes mellitus: A systematic review.," Primary Care Diabetes, **14**(4), 317–334, 2020, doi:10.1016/j.pcd.2019.09.003.

[18] S. Mishra, A. Sharma, P. Bhandari, S. Bhochhibhoya, K. Thapa, "Depression and health-related quality of life among patients with type 2 diabetes mellitus: A cross-sectional study in Nepal.," PLoS ONE, **10**(11), 1–13, 2015, doi:10.1371/journal.pone.0141385.

[19] C. Manterola, G. Quiroz, P. Salazar, N. García, "Metodología de los tipos y diseños de estudio más frecuentemente utilizados en investigación clínica.," Revista Médica Clínica Las Condes, **30**(1), 36–49, 2019, doi:10.1016/j.rmclc.2018.11.005.

[20] J. López, R. Rodríguez, "Adaptación y validación del instrumento de calidad de vida Diabetes 39 en pacientes Mexicanos con diabetes mellitus tipo 2.," Salud Publica de Mexico, **48**(3), 200–211, 2006, doi:10.1590/S0036-36342006000300004.

[21] J. Boyer, L. Earp, "The Development of an Instrument for Assessing the Quality of Life of People with Diabetes: Diabetes-39.," Medical Care, **35**(5), 440–453, 1997, doi:10.1097/00005650-199705000-00003.

ASTES

Psychological Anguish in Families due to Positive Cases of COVID-19 in the Puente Piedra District Home

Rosa Perez-Siguas*, Eduardo Matta-Solis, Hernan Matta-Solis

Research Directorate, Universidad María Auxiliadora, 15408, Lima-Perú

ARTICLE INFO

ABSTRACT

The psychological impact is alarming in families since they are exposed to high risks of contagion because their mental health is altered, therefore, the objective of the research study is to determine the Psychological Impact on families due to positive cases of COVID - 19 in the Puente Piedra district, 2020. This is a quantitative, non-experimental, descriptive, and cross-sectional study, with a population of 22 families with household members infected with COVID - 19 from the Puente Piedra district, who answered a questionnaire with sociodemographic data and the Depression, Anxiety and Stress Scale (DASS-21). In the results where can be observed, with respect to the sex data of the head of the family to whom the questionnaire was carried out, where we can observe with respect to the psychological impact on families by positive cases of COVID-19 at home in the district of Puente Piedra, where the male head of the family 13 (76.5%) of the total have a medium psychological impact and 4 (23.5%) have a low psychological impact, in the female head of the family 4 (80 %) of the total have a medium psychological impact and 1 (20%) have a low psychological impact. In conclusion, greater attention should be paid to vulnerable groups such as the young, the elderly, and women since they are more prone to contracting the disease.

1. Introduction

Concerns about the new coronavirus (COVID - 19) in the world population are becoming more alarming, because it has negative psycho-emotional and psychosocial effects on them [1], therefore the World Health Organization (WHO), maintains that the psychological impact has generated an increase in anxiety, depression and stress in the population as a result of isolation and quarantine as a result of the coronavirus pandemic [2].

In this way, the world population has had a strong impact on their daily lives, likewise while the isolation and quarantine due to the pandemic continues, the population will be experiencing different mental disorders such as nervousness, fear, anxiety, depression and insomnia, all of which can long-term impact if the pandemic can be extended for a long time [3], [4]. More concern in public health is increasing due to the increase in COVID-19 cases in the country, which has generated physical, socioeconomic and psychological impacts on the entire population [5].

Likewise, the pandemic not only affects the daily life of the world population but also has negative impacts on the person as a result of unemployment and the closure of businesses [6], and on

the family as a result of isolation at home without any visit, all this has been planned to stop the rapid spread of the coronavirus, still interrupting the daily routines of the person and family where it plays an important role in their health and physical and mental well-being [7], [8].

All this generates on a large scale forms of prevention or strategies that allow protection against this disease [9], [10], where the government implemented measures that allow the population to take care of themselves, therefore strategies such as personal protection measures, correct hygiene hands, home isolation and social distance, are measures that the population will choose in their prevention of contagion by COVID – 19 [11].

In China, it was evidenced in 1210 participants on the mental health of the general population in China, where the results showed that 53.8% had moderate and severe psychological impact, 16.5% with depressive symptoms, 28.8% with anxiety symptoms and 8.1% presented stress and each of them was between moderate and severe, concluding that women are more likely to present psychological impact than men [12].

In India, an online survey was conducted with a total of 1106 among male and female participants from 64 cities in the country,

where the data obtained in their results, the majority of respondents 66.8% presented a minimal psychological impact, 15% mild psychological impact, 5.5% moderate psychological impact and 12.7% severe psychological impact, finding that the psychological impact in women is considerably higher than in men [13].

In Spain, through a questionnaire, it was observed in 1014 participants of the general population, in relation to the threat of COVID-19 and their emotional state during quarantine, giving in their results that 51% of the population presented sadness and depression, 54.7% anxiety and 29.3% hostility; product of the threat of the coronavirus, which is reflected in the population at a cognitive and emotional level (affective and mental) as a result of the quarantine in prevention of the pandemic [14].

Another study in Spain, a study was carried out in 1161 participants between the ages of 19 to 84 years of age, which, in the results, it was observed that the psychological impact was more reflected in the fear of COVID-19, sleep problems , stress, anxiety and depression are factors that were prioritized more because they alter the mental health of the participants during confinement by COVID – 19 [15].

The objective of the research work is to determine a psychological impact on families due to positive cases of COVID-19 in the Puente Piedra district, 2020, in which, it will allow us to observe what is the psychological impact that exists in families of in the Puente Piedra district.

Therefore, the hypothesis maintains that the psychological impact on families with positive cases for COVID-19 considerably affects the psycho-emotional level in family members.

This study is important since it provides us with data based on the reality of families that are mentally vulnerable caused by the COVID-19 pandemic.

2. Methodology

2.1. Type of Study

It is a study with a quantitative approach, with a descriptive, non-experimental and cross-sectional study methodology [16].

2.2. Population

In the research work, it was made up of 22 families from the Puente Piedra district of the Micaela Bastidas Association.

2.3. Inclusion criteria

- Families with one or more family members infected with COVID - 19 at home.
- Families who signed the informed consent.

2.4. Technique and instrument

The survey was used as a data collection technique, including the DASS - 21 instrument with the objective of measuring the psychological impact in families with positive cases of COVID - 19.

The depression, anxiety, and stress scale (DASS-21), each of the three DASS scales contains 14 items, divided into subscales of 2 to 5 items with similar content. The depression scale assesses dysphoria, hopelessness, devaluation of life, self-loathing, lack of interest or participation, anhedonia, and inertia. The anxiety scale assesses autonomic arousal, skeletal muscle effects, situational anxiety, and the subjective experience of anxious affect. The stress scale is sensitive to levels of non-specific chronic arousal. It evaluates the difficulty to relax, the nervous excitement and the discomfort, agitation, or irritation, over reactivity and impatience. It consists of 4 answer alternatives, 0 "not at all", 1 "sometimes", 2 "most of the time" and 3 "most of the time" that serve to rate the degree to which they have experienced each state during last week. To obtain the final score of the DASS-21, the total score obtained must be multiplied by two (data x2) [17].

At the statistical level, the instrument was validated using the Kaiser-Meyer-Olkin (KMO) test, resulting in a sample adequacy of 0.203 and the Bartlett's Sphericity Test of 0.000 ($x^2 = 353.725$; gl = 210; p <0, 05), and to determine the reliability of the instrument, it was performed using Cronbach's Alpha statistical test, determining an internal consistency index of 0.802 ($\alpha > 0.6$).

For data processing, a matrix drawn up in the statistical program Statistics Base 26.0 (SPSS) was entered, where the analysis was carried out for the elaboration of tabulations and figures for the interpretation in their respective results and discussions.

2.5. Place and application of the instrument

The questionnaire carried out to measure the psychological impact on families due to positive cases of COVID-19 at home, was carried out in North Lima, in the Puente Piedra district, of the Micaela Bastidas - Zapallal Association.

It was coordinated respectively for the study with the head of the family to carry out the survey, once this, it was explained what the study is about and why the research survey was carried out.

The survey was carried out during the presence of the head of the household with a certain time for filling in the survey of approximately 15 minutes, concluding with satisfaction when collecting the surveys since the families supported our study.

It is important to emphasize the presence of the family at the time of filling in the questionnaire, since they were also given information about questionnaire, and why it is being carried out, all this was done to generate trust with the family allowing to carry out the present research work.

3. Results

Below is a summary table of the surveys carried out following the guidelines corresponding to the research work:

In Table I, the psychological impact in relation to the sex of the head of the family is related, in which it is determined with the Pearson chi-square test (X^2), the significance level of the test obtained a value of 1.14 (p > 0.05) ($X^2 = 0.869$; df = 1). therefore, a hypothesis of association between variables is not rejected, which is why it is verified that there is a relationship between the psychological impact and the sex of the head of the family.

Table 1: Psychological Impact on Families in relation to the head of the family for positive cases of COVID - 19 in the Puente Piedra district, 2020

			Total psychological impact		
			Low	Medium	Total
Sex of the Head of Household	Male	Count	4	13	17
		% within Sex of the Head of Household	23,5%	76,5%	100,0%
	Female	Count	1	4	5
		% within Sex of the Head of Household	20,0%	80,0%	100,0%
Total		Count	5	17	22
		% within Sex of the Head of Household	22,7%	77,3%	100,0%

Chi-square tests

	Value	df	Asymptotic significance(bilateral)	Exact significance (bilateral)	Exact significance (unilateral)
Pearson's Chi-square	,027[a]	1	,869		
Continuity correction[b]	,000	1	1,000		
Likelihood ratio	,028	1	,867		
Fisher's exact test				1,000	,687
Linear by linear association	,026	1	,872		
N° of valid cases	22				

a. 3 cells (75.0%) have expected a count less than 5. The minimum expected count is 1.14.
b. It has only been calculated for a 2x2 table
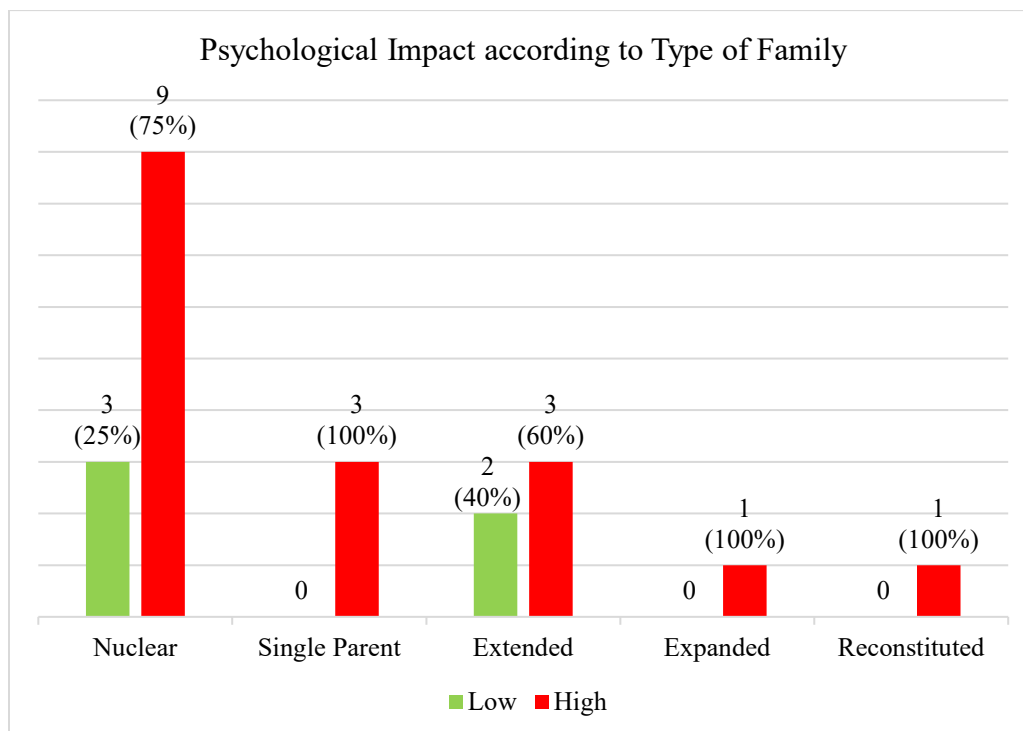
Figure 1: Psychological Impact on Families in relation to the Type of Family for positive cases of COVID-19 in the Puente Piedra district Home, 2020

Therefore, it can be interpreted that the sex data of the head of the family to whom the questionnaire was carried out, where we can observe with respect to the psychological impact on families due to positive cases of COVID-19 in the Puente Piedra district, where the Male head of household 13 (76.5%) of the total have a medium psychological impact and 4 (23.5%) have low psychological impact, in the female head of household 4 (80%) of the total have an impact medium psychological impact and 1 (20%) has low psychological impact.

Figure 1 shows the data in relation to the type of family, where it can see that 9 (100%) of the nuclear family type has a high psychological impact, 3 (25%) of the nuclear family type has a low psychological impact , 3 (100%) of the single parent type have a high psychological impact, 3 (60%) of the extended family type have a high psychological impact, 2 (40%) of the extended family type have a low psychological impact, 1 (100%) of the expanded family type has a high psychological impact and 1 (100%) of the reconstituted family type has a high psychological impact.
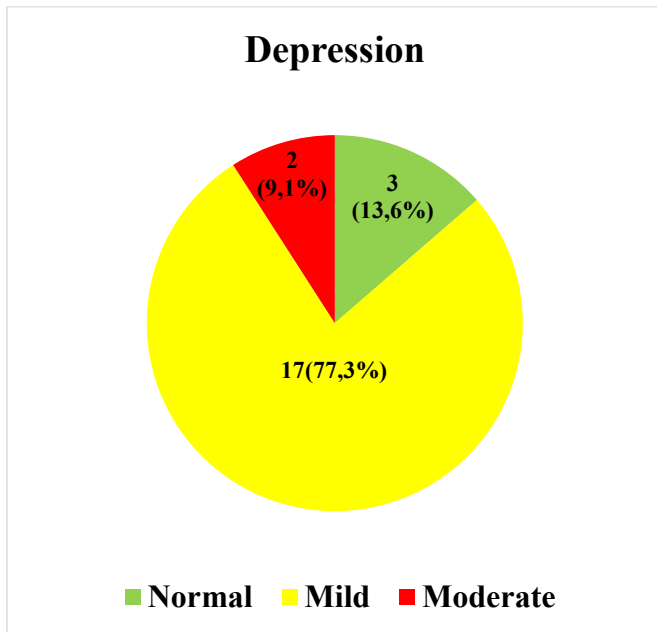
Figure 2: Psychological Impact on its Depression Dimension in families due to positive cases of COVID-19 in the Puente Piedra district, 2020

In Figure 2, the data are shown in relation to the depression dimension, where 17 (77.3%) of the total presented mild depression, 3 (13.6%) of the total presented normal depression and 2 (9.1%) of the total presented moderate depression.

In Figure 3, the results of the anxiety dimension are observed, where 13 (59.1%) of the total presented moderate anxiety, 6 (27.3%) of the total presented mild anxiety and 3 (13.6%) of the total presented normal anxiety.

In Figure 4, the results of the stress dimension are observed, where 19 (86.4%) of the total presented normal stress and 3 (13.6%) of the total presented mild stress.

4. Discussion

In this study, emphasis the psychological impact from the point of view of promoting mental health in families, in which it

seeks to contribute programs that allow families to benefit to face situations that generate an alteration in their mental health allowing cope with this emergency due to the COVID - 19 pandemic.
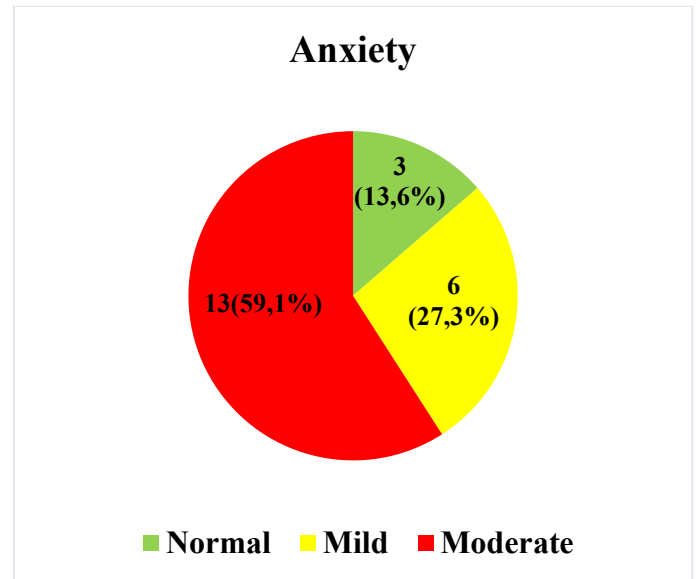
Figure 3: Psychological Impact on the Anxiety Dimension in Families due to positive cases of COVID-19 in the Puente Piedra District, 2020
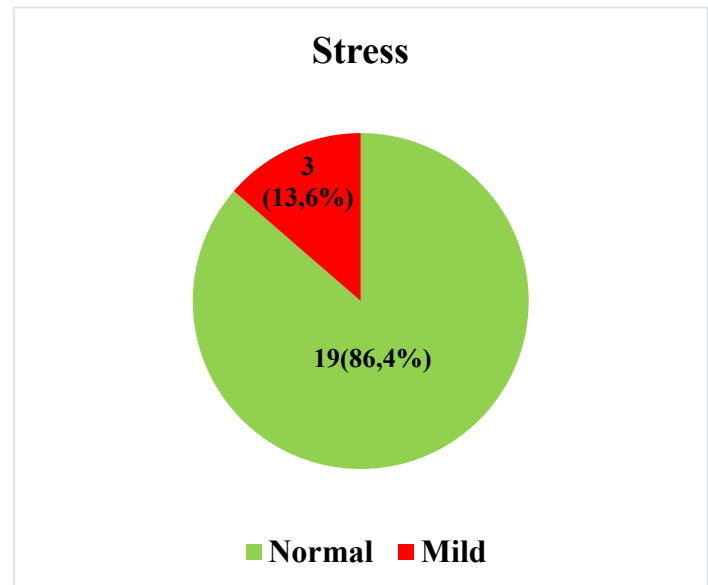
Figure 4: Psychological Impact on the Stress Dimension in Families due to positive cases of COVID-19 in the Puente Piedra district, 2020

These results that were obtained reflect the mental health that families have during the outbreak of the COVID-19 pandemic in Peruvian families, making them susceptible to depression, anxiety, and stress. In the head of the family, it was observed that the psychological impact occurred more in men than in women, this is since the male as head of the family must support the family economically and emotionally, therefore when he sees that one of his relatives infected by COVID - 19, their mental health is altered. In [12], they argue that women are the most vulnerable than men, since age, sex, being a student and presenting some physical symptoms of their own health, are factors of high psychological impact and that increase anxiety levels, stress and

depression. In the same way in [13], they argue that women have a greater psychological impact due to the COVID-19 pandemic than men because physical comorbidities were predictors of having a greater psychological impact in response to the pandemic. Comparing the results with the studies discussed, we can see that in the statistical samplings in our results it is observed that men have more psychological impact than women, on the other hand, in the studies that are discussed, women represent the majority of the population with a high psychological impact where the pictures of depression, anxiety and stress turn out to be highly elevated.

In relation to the type of family, the nuclear type of family is the most altered, because the COVID-19 pandemic has been crucial in the family, factors such as isolation within the home, unemployment, job instability due to the pandemic, the fear of contracting the disease when leaving the home have generated a certain degree of anxiety and stress in the parents. In [4], they argue that single mothers without support during the pandemic have had high rates of depression, anxiety and stress, therefore, this implies the importance of family support to face the COVID-19 epidemic. In [18], argue that loneliness, social isolation and financial stress are risk factors that affect poor physical and mental health, where the well-being of the person and the family are vulnerable to becoming infected with COVID - 19.

In its dimensions, the most altered was anxiety, this is because the family must face this crisis product of the COVID-19 pandemic where one of their relatives has been infected, where the isolation of the family member infected by COVID-19 has generated a feeling of nervousness and tension in the family members who take care of it, likewise in [12], they maintain that the female sex as the main member of the household at the same time that the male sex presents symptoms such as myalgia, dizziness, coryza, maintaining that they do not have an adequate perception of their well-being of their own health that avoids contagion by COVID - 19. In [14], they argue that the cognitive and emotional states of people as a result of quarantine, make people perceive the threat of COVID - 19 in a highly negative way, where emotional states, such as sadness, depression, anxiety and irritability, aggravate the psychological well-being of the person, damaging their well-being of the same and of the s family members. In the studies discussed, it is observed that in China 28.8% of its population shows a high index of anxiety and in Spain 54.7%, in comparison with our study 59.1% have a moderate index of symptoms anxiety, all this is based on how they can handle or face quarantine without affecting their mental health, therefore the management of strategies that allow them to maintain their mental health in perfect condition.

5. Conclusion

It is concluded that the family due to COVID-19 must have the ability to cope when one of their relatives contracts the disease and be able to emotionally cope with this situation without disturbing the other members of the family.

It is concluded that greater attention should be paid to vulnerable groups such as the young, the elderly, and women since they are more prone to contracting the disease.

It is concluded that the accessibility of health services for the family on prevention and coping strategies on mental health due to the COVID-19 pandemic should be considered.

We can conclude that in our country the susceptibility of presenting symptoms of depression, anxiety and stress is higher than in comparison to other countries

It is concluded that anxiety is a primary factor that more compromises people who already have a mental condition for this reason, in our study we can observe that the majority of the population presents symptoms of anxiety compared to other studies that manage strategies that allow to reduce the anxiety.

Health strategies that allow families to have access to virtual mental health care are recommended

The importance of preventive measures focused on the mental health of people during epidemics, which are developed by mental health personnel, is recommended, suggesting that mainly risk groups be identified for their care.

This research work will be beneficial for future studies, since the COVID-19 pandemic will leave consequences on people's mental health, and thus the consequences that COVID-19 will allow the development of research strategies that allow establish preventive measures on themselves.

Conflict of Interest

The authors declare no conflict of interest.

References

[1] S. Dubey, P. Biswas, R. Ghosh, S. Chatterjee, "Psychosocial impact of COVID-19.," Diabetes & Metabolic Syndrome: Clinical Research & Reviews, 779–788, 2020.

[2] Organización Mundial de la Salud, Mental health and COVID-19., OMS, 2020.

[3] F. Inchausti, N. García, J. Prado, S. Sánchez, "La psicología clínica ante la pandemia COVID-19 en España," Clinica y Salud, 31(2), 105–107, 2020, doi:10.5093/CLYSA2020A11.

[4] H. Wang, Q. Xia, Z. Xiong, Z. Li, W. Xiang, Y. Yuan, Y. Liu, Z. Li, "The psychological distress and coping styles in the early stages of the 2019 coronavirus disease (COVID-19) epidemic in the general mainland Chinese population: A web-based survey.," PLoS ONE, 15(5), 233410, 2020, doi:10.1371/journal.pone.0233410.

[5] K. Poudel, P. Subedi, "Impact of COVID-19 pandemic on socioeconomic and mental health aspects in Nepal," International Journal of Social Psychiatry, 66(8), 748–755, 2020, doi:10.1177/0020764020942247.

[6] J. Hernández, "Impacto de la COVID-19 sobre la salud mental de las personas," Medicentro Electrónica, 24(3), 578–594, 2020.

[7] F. Chacón, J. Fernández, M. García, "La Psicología ante la Pandemia de la COVID - 19 en España. La respuesta de la Organización Colegial," Clínica y Salud, 31(2), 119–123, 2020.

[8] Ontario Agency for Health Protection and Promotion, "Negative Impacts of Community-Based Public Health Measures During a Pandemic (e . g ., COVID-19) on Children and Families Key Findings.," Public Health Ontario, 1–26, 2020.

[9] N. Valero, M. Vélez, A. Duran, M. Torres, "Afrontamiento del COVID-19: estrés, miedo, ansiedad y depresión?," Enfermeria Investiga. Investigacion, Vinculacion, Docencia y Gestion, 5(3), 63–70, 2020, doi:10.1111/inm.12726.

[10] A. Sutin, M. Luchetti, D. Aschwanden, J. Lee, A. Sesker, J. Strickhouser, Y. Stephan, A. Terracciano, "Change in five-factor model personality traits during the acute phase of the coronavirus pandemic.," PLoS ONE, 15(8 August), 1–13, 2020, doi:10.1371/journal.pone.0237056.

[11] H. Seale, A. Heywood, J. Leask, M. Sheel, S. Thomas, D. Durrheim, K. Bolsewicz, R. Kaur, "COVID-19 is rapidly changing: Examining public perceptions and behaviors in response to this evolving pandemic.," PLoS ONE, 15(6 June), 1–13, 2020, doi:10.1371/journal.pone.0235112.

[12] A. Lozano, "Impacto de la epidemia del Coronavirus (COVID-19) en la salud mental del personal de salud y en la población general de China.," Revista de Neuro-Psiquiatria, **83**(1), 51–56, 2020, doi:10.20453/rnp.v83i1.3687.

[13] M. Varshney, J. Parel, N. Raizada, S. Sarin, "Initial psychological impact of COVID-19 and its correlates in Indian Community: An online (FEEL-COVID) survey.," PLoS ONE, **15**(5), 1–10, 2020, doi:10.1371/journal.pone.0233874.

[14] M. Pérez, M. Molero, Á. Martínez, J. Gázquez, "Threat of COVID-19 and emotional state during quarantine: Positive and negative affect as mediators in a cross-sectional study of the Spanish population.," PLoS ONE, **15**(6), 1–11, 2020, doi:10.1371/journal.pone.0235305.

[15] B. Sandín, R. Valiente, J. García-Escalera, P. Chorot, "Psychological impact of the COVID-19 pandemic: Negative and positive effects in Spanish people during the mandatory national quarantine," Revista de Psicopatologia y Psicologia Clinica, **25**(1), 1–22, 2020, doi:10.5944/RPPC.27569.

[16] C. Fernández, P. Baptista, Metodología de la Investigación. 6ta ed. México: Mc Graw-Hill/Interamericana., 2015.

[17] A. Lovibond, Depression Anxiety Stress Scale (DASS-21). Psychology Foundation of Australia. Sydney - Australia., 1995.

[18] J. Newby, K. O'Moore, S. Tang, H. Christensen, K. Faasse, "Acute mental health responses during the COVID-19 pandemic in Australia.," PLoS ONE, **15**(7), 1–21, 2020, doi:10.1371/journal.pone.0236562.

A Novel Approach to Design a Process Design Kit Digital for CMOS 180nm Technology

Thinh Dang Cong[1,2], Toi Le Thanh[1,2], Phuc Ton That Bao[1,2], Trang Hoang[1,2,*]

[1]*Department of Electronics Engineering, Ho Chi Minh City University of Technology (HCMUT), Ho Chi Minh City, 72506, Vietnam*

[2]*Vietnam National University, Ho Chi Minh City, 71308, Vietnam*

A B S T R A C T

In this paper, a novel approach to design a Process Design Kit Digital for CMOS 180nm process is presented. This work proposes a detailed flow to design a PDK Digital using Ocean language, which is a vital element in the semi-custom design and applied in education purposes in universities in Vietnam. The PDK digital includes Standard Cell Library containing 47 standard cells and Wire-Load Model. The library is designed based on the CMOS 180nm process with a supply voltage of 1.8V.

1   Introduction

CMOS technology has been developing in recent years due to its benefits such as high integration density, low fabrication cost, etc. Many new techniques of circuit design have been given ranging from RFIC [1]–[5] to mm-Wave IC design [6], [7].

In the past, the full custom design took many resources, efforts, and design time for designing a big chip. Meanwhile, the semi-custom design has significant decreased in the design and verification time for chip design by using the Electronic Design Automation (EDA) tools and PDK digital [8]. Especially, the latter provides a considerable decrease in design time, decreasing around 25% to 50%. Moreover, the latter would be applying for many more complex designs than the former [9].

Focusing on the PDK digital, the one consists of Synopsys library and P&R library [10]. While the former is applied for timing, power consumption, and noise analysis, the latter is used for place and route design in a design flow [11]. There are two ways to design an SCL. The first one uses the Liberty NCX tool of Synopsys. The Liberty NCX determines the function of standard cells. Following this, the tool creates the complete simulations by using HSPICE that would make the liberty file for each logic cell in the library [12], [13]. The second way performs characterization for all standard cells manually using the Spectre tool. The process of characterization consists of many simulations where the transition of the input and the capacitance of output load are varied. Timing and other parameters would be extracted, and outputted as a liberty format file.

The license of the Liberty NCX tool is unavailable at universities in developing countries due to its cost. Therefore, designing an SCL using this tool is almost impossible [13]. With regards to the manual characterization, the challenge is that we have to do many simulations to generate timing, power consumption, etc [14]. This way takes much time to design each logic cell. For instance, to design an INV logic cell, we have to do 7x7 simulations and 49x6 calculations to generate all parameters for the liberty file.

In this work, the Ocean language is proposed to solve problems about the licensing and running manually many simulations. The language is an extension of the Skill language used to control Analog simulation. The flow automatically performs parametric simulations of each logic cell and generates output parameters with the format as the liberty file [15]. Regarding the Wire-Load Model (WLM), this paper proposed a method and used accuracy formulas to design a complete model.

The authors presented ideas about designing a PDK Digital for CMOS technology in the "2019 19th International Symposium on

*Corresponding Author: Trang Hoang, Department of Electronics Engineering, Ho Chi Minh City University of Technology (HCMUT), VNU-HCM, Ho Chi Minh City, 72506, Vietnam, Tel: (+84) 988 071 579 & Email: hoangtrang@hcmut.edu.vn

Communications and Information Technologies (ISCIT)" [1] and the following paper is an extension of this work.

The remainder of this paper is organized as follows: Section II shows the SCL design flow from the transistor level. This section also gives the schematic design, Euler rules for layout design, DRC/LVS definition, etc. A detailed liberty format generation flow is given in section III. Section IV shows how to design a wire-load model. Finally, section V presents the conclusion.

2   Standard Cell Library Design

An SCL is made up of combinational logic cells such as INV, AND, FA, sequential logic cells such as DFF, Latch, and physical cells, etc. The design flow is composed of many steps. To begin with the front-end design stage, firstly, the schematic of all standard cells in the library are designed from transistor level. After that, symbol creation and do simulation at corners [16]. Next, in the back-end design stage, to optimize the layout design in term of area and routing, the layout design needs to have some rules as follows:

1. All the input and output pins must be placed on the intersections of the vertical and horizontal routing tracks with the special exception for power and ground pins.

2. All the cells in the library are designed to be multiple of the unit tile which is defined by a library developer. The height of the cells must be equal and be multiple of the unit tile's height.

3. This work uses M1 and M2 for the layout design.

4. Minimize the width of all standard cells in the library.

5. Optimize pins access to prevent the routing congestion in place and route stage.

6. Some special cells such as filler, decap cells can be put in the library to make sure the connection of supply trails and N-well.

The figure below shows the schematic, Euler path for optimization, and layout design of an AOI22 cell in the library. The layout should follow the considerations as above.
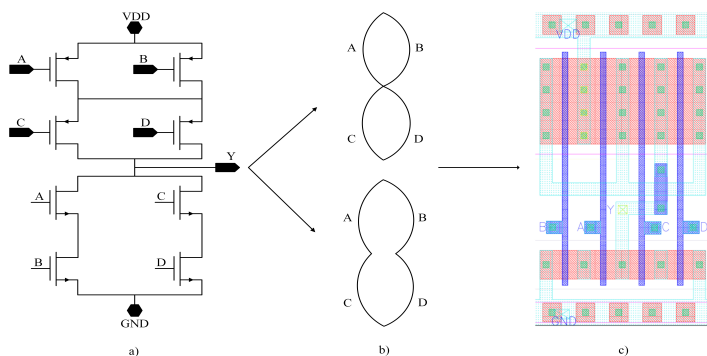
Figure 1: a. Schematic design, b. Euler path, c. Layout design

The Physical Verification process will be performed after the layout design. This process will accomplish sequentially Design Rule Check (DRC) verification and Layout Versus Schematic (LVS) verification.

Firstly, by using the rules from the fabricators, the layout design is checked to ensure no potential violation, which is called DRC verification. The design rules are supplied by the manufacturers to ensure the chip will function properly when fabricated. The design rules include many rules such as the minimal critical dimensions, shape angles, pattern density requirements, etc [17]. The DRC flow chart is shown in Figure 2 and the example design rules are presented in Figure 3.
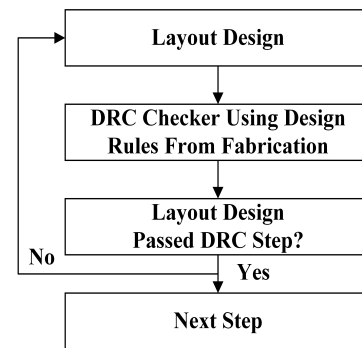
Figure 2: DRC flow chart

For example, the resolution rules for metal 1 and metal 2 layers are 0.23μm and 0.28μm, respectively. With regards to the rules for poly layer, the min.poly width is 0.18μm, min.gate to contact spacing is 0.375μm, and the min.poly overlap of diffusion is 0.22μm. For contact rules, the exact size and min.contact overlap are 0.22μm and 0.12μm, respectively.
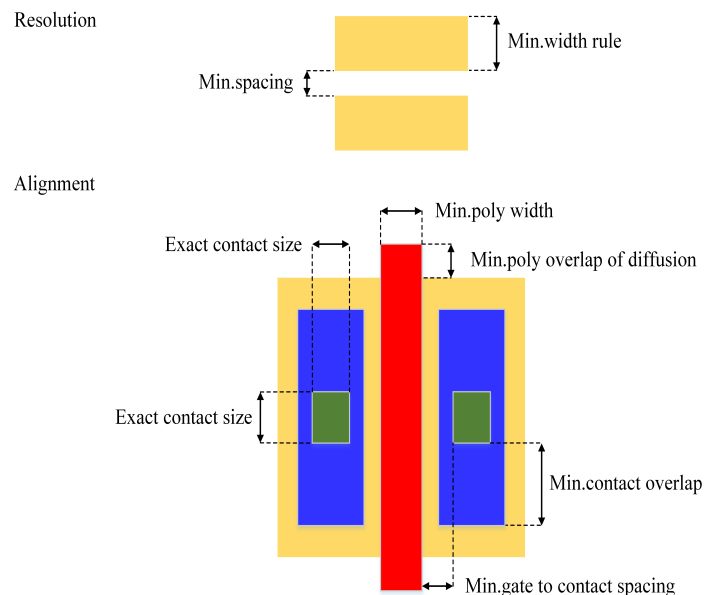
Figure 3: The example rules are used for DRC check

Followed by the LVS verification, which is the more critical verification step. Particularly, the LVS compares any combination of physical or schematic designs.

Depending on the layout design, so different parasitic components can be generated. These parasitic parameters can make the functionality and characteristic of the layout design different from schematic design. For that reason, if the whole parameters in the schematic design are different from the parasitic parameters of the layout design, which makes it impossible to complete the LVS step. Hence, this verification proves the chip after being fabricated will function as the schematic design [17]. When the LVS errors occur, we have to fix the layout design and perform the DRC step again to complete the LVS step without errors. The LVS flow chart is shown in Figure 4.
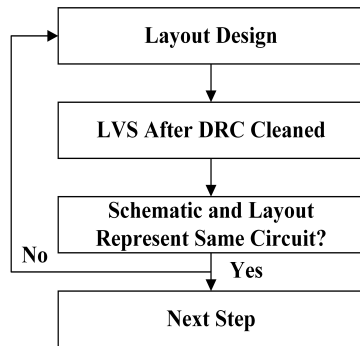
Figure 4: LVS flow chart

The Physical Verification process plays a vital role in the design flow. Therefore, the designers ensure that each cell in the library passed the DRC and LVS without any violations [18]. After the Physical Verification process, the post-layout simulation at corners will be executed before the cell characterization step. Next, Layout Parasitic Extraction (LPE) step is performed. Afterward, the post-layout simulations at corners are performed by using the parasitic parameters extracted. Therefore, the characterization of the standard cells will be calculated [19]. The post-layout simulation becomes possible and correct only after the LVS step is completed, then the extracted parameters are accurate. The post-layout simulation process will be shown in Figure 5.
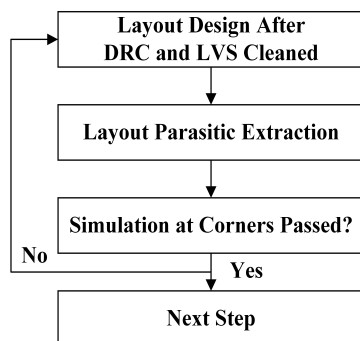
Figure 5: Post Layout Simulation Process Flow chart

Finally, the characterization step is divided into Liberty Format Generation step and Abstract View & GDS step. While the timing models, power models including dynamic and static power are extracted by the former to make the liberty file (*.lib) [20]. The Synopsys internal database format (*.db) may be translated from the

liberty file by the Library Compile tool of Synopsys. The latter is used to create the library exchange format (*.lef) file by abstracting from the layout design, and the last step is the generating GDS file [21]. The block diagram in the figure below (Figure 6) illustrates the SCL design flow.
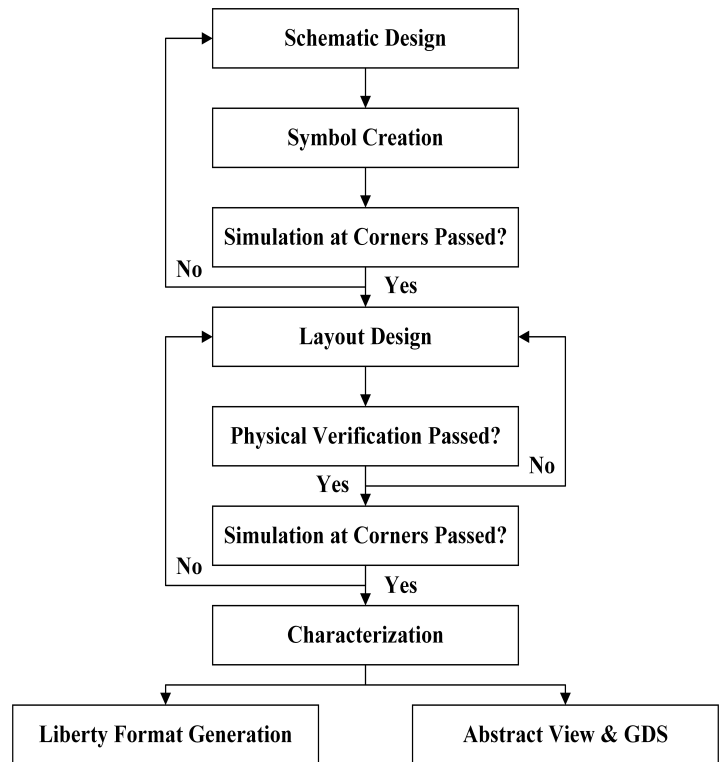
Figure 6: SCL design flow chart

3 Liberty Format Generation

After the post-layout simulation process, the standard cell characterization process is performed. Especially, the liberty format generation process, this process will generate an output file (*.lib) which is one of the most important files in the standard cell library design. The liberty file includes structural information, functional information, timing information, power information, and environmental information of each standard cell.

Firstly, the structural one declares connectivity of a logic cell including cell, bus, and in-out pin descriptions. Secondly, the functional one describes the logical function of each output pin of each cell. Thirdly, timing models are given including cell rise delay, cell fall delay, rise transition, fall transition. Next, power models give the dynamic and static power consumption of each cell. Finally, environmental information describes the manufacturing process, temperature of operation, supply voltage, etc.

In this part, to perform cell characterization and generate output file same as the liberty file's format, all cells in the library will have the same load capacitance C_{load} = 2 fF, 5 fF, 6 fF, 7 fF, 8 fF, 9 fF, 9.5 fF, the input slew of the waveform $slope$ = 0.01 ns, 0.02 ns, 0.04 ns, 0.06 ns, 0.08 ns, 0.09 ns, 0.095 ns [22]. The load capacitance and input slew are declared in the Ocean file to create 7x7 = 49 simulation times and extract the timing model and dynamic power

consumption for each cell.

These figures below (Figure 7 and Figure 8) show the testbench circuits for the Ocean script run and the results of a NAND gate cell with two inputs.

(a)

(b)
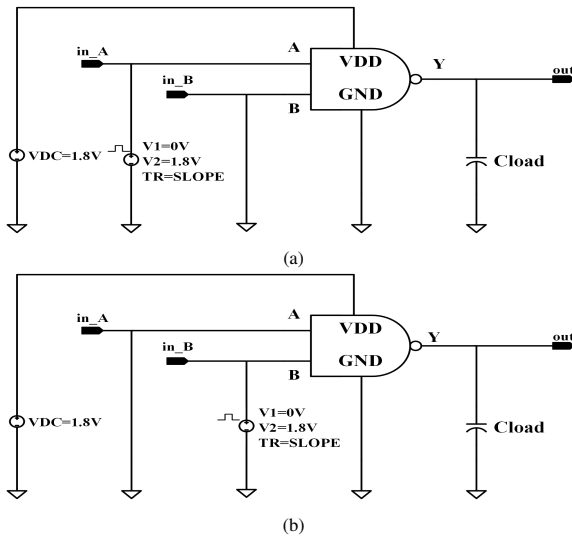
Figure 7: Testbench circuits for characterization
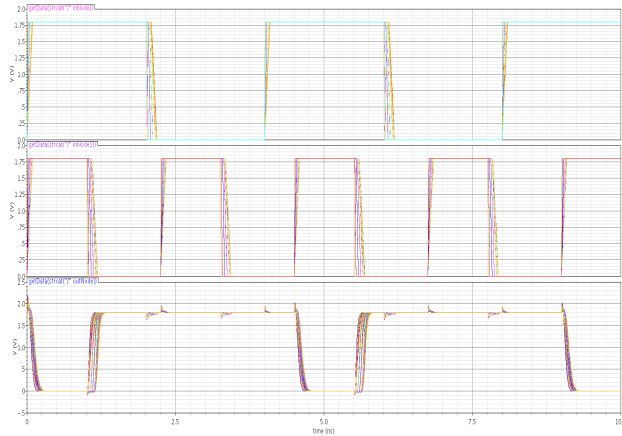
Figure 8: Waveform results

3.1 Input capacitance

In SCL design, one of the most important parameters that we need to calculate is input capacitance. The output capacitance of each cell can be determined but in most cases, the capacitance is specified only for the inputs and not for the outputs, which means that the output pin capacitance is zero in the library design [23].

The following formula illustrates the relationship between input capacitance, current, and supply voltage at an input pin.

$$I = C\frac{dV}{dt} \tag{1}$$

where I is the current at the input pin, V is the supply voltage and it is equal to 1.8V in this paper. By inputting a pulse power to the

input pin and calculating the current, the input capacitance value is determined as the formula below:

$$C_{input} = \frac{\int_t^{t+\Delta t} I dt}{\int_t^{t+\Delta t} dV} = \frac{\int_t^{t+\Delta t} I dt}{VDD} = \frac{\int_t^{t+\Delta t} I dt}{1.8} \tag{2}$$

where Δt is the time when the voltage at each input pin changes the logic level.

The two tables below show the capacitance of each input pin of the NAND2 cell. These tables also provide the rise power and fall power which are presented in the next section.

Table 1: PIN A

t_n(ns)	0.01	0.02	0.04	0.06	0.08	0.09	0.095
RISE POWER	0.001098	0.001099	0.001101	0.001098	0.001100	0.001093	0.001097
FALL POWER	0.002029	0.002049	0.002053	0.002040	0.002044	0.002045	0.002044
INPUT CAPACITANCE = 3.079fF							

Table 2: PIN B

t_n(ns)	0.01	0.02	0.04	0.06	0.08	0.09	0.095
RISE POWER	0.001404	0.001406	0.001407	0.001405	0.001412	0.001409	0.001407
FALL POWER	0.001552	0.001534	0.001516	0.001504	0.001491	0.001483	0.001478
INPUT CAPACITANCE = 2.774fF							

3.2 Timing models

All the timing arcs of the cell are declared in the timing model. There are two types of timing models that are linear and non-linear timing. Whereas the former provides less accurate for the sub-micron process, the latter is better. Therefore, most standard cell libraries use the latter. [20]. The definitions of all the timing arcs in the timing model are given in these figures as follows (Figure 9-11):
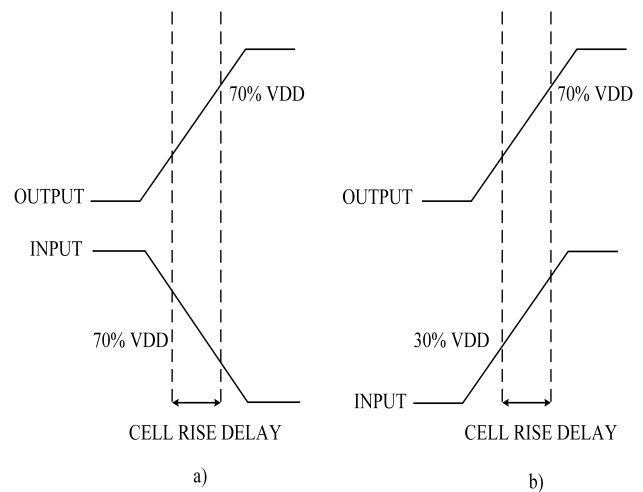
Figure 9: a. Cell rise delay at negative unate case, b. Cell rise delay at positive unate case
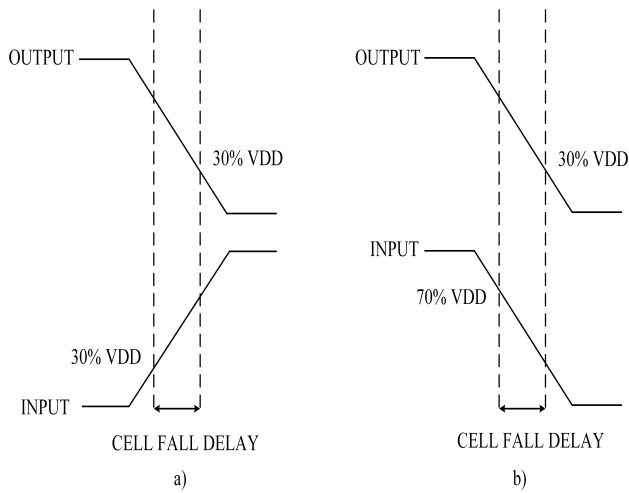
Figure 10: a. Cell fall delay at negative unate case, b. Cell fall delay at positive unate case
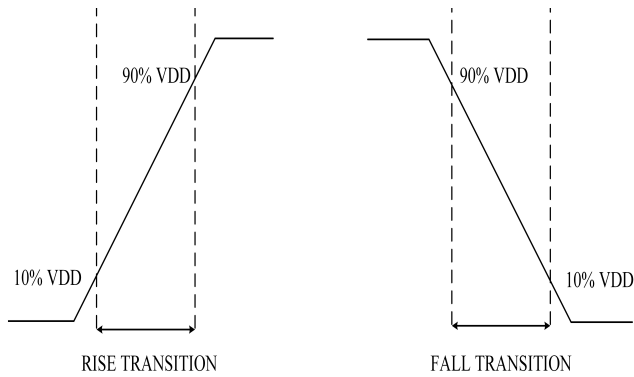
Figure 11: a. Rise transition time, b. Fall transition time

Table 3: Cell Rise Delay

C_{load} \ t_n	0.01	0.02	0.04	0.06	0.08	0.09	0.095
2	0.0284388	0.0459522	0.0481537	0.0503347	0.0524551	0.0545356	0.0555650
5	0.0430937	0.0497589	0.0518424	0.0538036	0.0562515	0.0583046	0.0593685
6	0.0506982	0.0573539	0.0592578	0.0614723	0.0635472	0.0659118	0.0670066
7	0.0587234	0.0650961	0.0671953	0.0692366	0.0712060	0.0733503	0.0744634
8	0.0665493	0.0729249	0.0751495	0.0772798	0.0793351	0.0813871	0.0825202
9	0.0706249	0.0768656	0.0790399	0.0810872	0.0832540	0.0854972	0.0864483
9.5	0.0726732	0.0790870	0.0809977	0.0832278	0.0853940	0.0873195	0.0882354

Table 4: Cell Fall Delay

C_{load} \ t_n	0.01	0.02	0.04	0.06	0.08	0.09	0.095
2	0.0352318	0.0874551	0.0911567	0.0954046	0.0996116	0.103758	0.105814
5	0.0779892	0.0903443	0.0936665	0.0979536	0.1021390	0.105976	0.108099
6	0.0836045	0.0958160	0.0996820	0.1035520	0.1078860	0.112125	0.114218
7	0.0899048	0.1018210	0.1061800	0.1103530	0.1144480	0.118486	0.120481
8	0.0966727	0.1086380	0.1126100	0.1169130	0.1210420	0.125246	0.127239
9	0.1002420	0.1123940	0.1164030	0.1203470	0.1240760	0.128452	0.130556
9.5	0.1019340	0.1139970	0.1181590	0.1222040	0.1261880	0.130108	0.131898

Table 5: Rise Transition

C_{load} \ t_n	0.01	0.02	0.04	0.06	0.08	0.09	0.095
2	0.0285015	0.0525788	0.0565313	0.0590775	0.0617117	0.0643864	0.0657346
5	0.0444646	0.0525918	0.0556488	0.0590963	0.0622286	0.0641798	0.0666422
6	0.0454360	0.0532991	0.0566497	0.0593233	0.0623244	0.0653851	0.0665893
7	0.0483083	0.0564303	0.0588248	0.0616149	0.0644307	0.0672005	0.0683990
8	0.0519840	0.0593587	0.0620207	0.0648213	0.0673532	0.0702575	0.0715643
9	0.0544479	0.0608779	0.0637309	0.0668407	0.0693130	0.0715348	0.0725691
9.5	0.0554892	0.0626609	0.0649285	0.0673040	0.0697900	0.0727158	0.0742639

Table 6: Fall Transition

C_{load} \ t_n	0.01	0.02	0.04	0.06	0.08	0.09	0.095
2	0.0294817	0.0918175	0.0966698	0.102074	0.107603	0.113067	0.115792
5	0.0765303	0.0921913	0.0968935	0.102306	0.107671	0.112408	0.115192
6	0.0763769	0.0914495	0.0964209	0.102027	0.107571	0.113009	0.115709
7	0.0763993	0.0916860	0.0970722	0.102287	0.107523	0.112521	0.115014
8	0.0779230	0.0930608	0.0984027	0.103380	0.108256	0.113244	0.115654
9	0.0789342	0.0936807	0.0983939	0.103534	0.108970	0.114131	0.116615
9.5	0.0800157	0.0946327	0.0993140	0.104174	0.108800	0.113987	0.116831

Table 7: Rise Power Consumption

C_{load} \ t_n	0.01	0.02	0.04	0.06	0.08	0.09	0.095
2	-3.460e-05	-5.033e-05	-5.365e-05	-5.692e-05	-6.020e-05	-6.348e-05	-6.512e-05
5	-4.006e-05	-5.040e-05	-5.376e-05	-5.703e-05	-6.031e-05	-6.351e-05	-6.485e-05
6	-4.021e-05	-5.025e-05	-5.357e-05	-5.691e-05	-6.019e-05	-6.347e-05	-6.510e-05
7	-4.022e-05	-5.011e-05	-5.339e-05	-5.680e-05	-6.010e-05	-6.329e-05	-6.497e-05
8	-4.043e-05	-5.025e-05	-5.353e-05	-5.673e-05	-6.013e-05	-6.327e-05	-6.495e-05
9	-4.050e-05	-5.033e-05	-5.357e-05	-5.686e-05	-6.015e-05	-6.342e-05	-6.508e-05
9.5	-4.051e-05	-5.030e-05	-5.356e-05	-5.685e-05	-6.013e-05	-6.350e-05	-6.515e-05

Table 8: Fall Power Consumption

C_{load} \ t_n	0.01	0.02	0.04	0.06	0.08	0.09	0.095
2	-2.729e-06	-1.502e-05	-1.504e-05	-1.506e-05	-1.506e-05	-1.507e-05	-1.507e-05
5	-1.384e-05	-1.407e-05	-1.404e-05	-1.413e-05	-1.414e-05	-1.424e-05	-1.407e-05
6	-1.276e-05	-1.296e-05	-1.312e-05	-1.305e-05	-1.310e-05	-1.311e-05	-1.316e-05
7	-1.229e-05	-1.246e-05	-1.240e-05	-1.247e-05	-1.251e-05	-1.255e-05	-1.256e-05
8	-1.190e-05	-1.219e-05	-1.222e-05	-1.226e-05	-1.224e-05	-1.222e-05	-1.222e-05
9	-1.209e-05	-1.207e-05	-1.213e-05	-1.204e-05	-1.212e-05	-1.219e-05	-1.223e-05
9.5	-1.211e-05	-1.209e-05	-1.214e-05	-1.219e-05	-1.224e-05	-1.229e-05	-1.230e-05

In this work, threshold values for timing arc calculation are 30%, 70% for cell rise/fall delay calculation and 10%, 90% for rise/fall transition calculation. These values are declared in the header section of the liberty file [24]. These four tables below show the timing arc results of the NAND2 cell after the characterizing step.

3.3 Power models

There are two types of power in the power model that are dynamic power and static power consumption. For dynamic power, this one

includes rise power and fall power. While the former is calculated in the time when output changes from 0 to VDD. The latter is determined when output goes from VDD to 0. The formula below shows the dynamic power calculation.

$$VDD^* integ(i("/V0/PLUS"), t, t + \Delta t)/(1e - 9) \tag{3}$$

These two tables (Table 7 and Table 8) above give the dynamic power consumption of the NAND2 cell after the characterizing step.

In contrast, the static power consumption occurs when the cell is in inactive condition. There are many leakage currents caused the cell has this power consumption such as sub-threshold current which is the main component of the currents, tunneling current through the gate oxide [25]. Static power consumption can be shown as the following formula:

$$LEAKAGE\ POWER = \sum I_{LEAKAGE}.VDD \tag{4}$$

With regards to calculate the static power, firstly, a testbench circuit is designed with all inputs are pulled down as Figure 12a and calculate the power. Next, a testbench circuit is designed with all inputs are pulled up as Figure 12b and then calculate the power. Finally, taking the bigger power number to represent the static power of a cell.
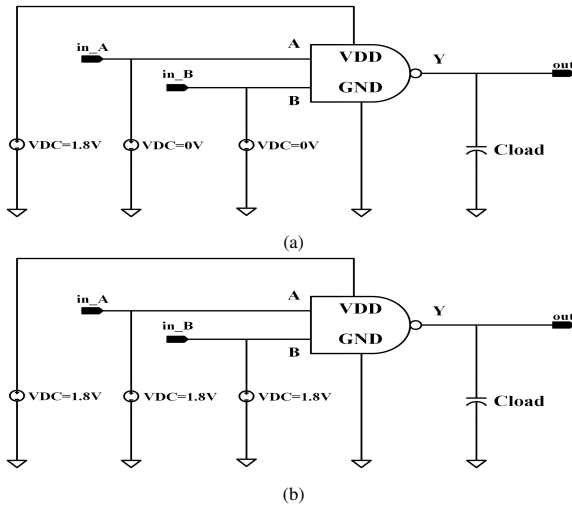
Figure 12: Testbench circuits for static power calculation, (a) Testbench circuit for static power calculation in pull down condition, (b) Testbench circuit for static power calculation in pull up condition

4 Wire-Load Model Design

The wire delays must be estimated during the timing analysis before placement and routing. Using a wire-load model is the simplest method of estimation. The wire-load model gets a rough value of the total wire capacitance based on the size of the chip and the fanout of the net [26]. The wire-load model is specified in the Liberty file.

In this work, the wire capacitance is computed by using the results of T. Sakurai and K. Tamaru's paper [27]. The accuracy of these formulas is practically sufficient for a wide range of wire thickness, wire width, and inter-wire spacing. When two or three nets are placed on bulk silicon, the total capacitance of one net includes the "coupling" capacitance between lines C_{side} and "ground"

capacitance between the net and the ground C_{plate}. Below are the detailed steps to determine the wire capacitance of a net.

First, the coupling capacitance C_{plate} between line and bulk silicon is given as formula:

$$C_{plate} = E_{ox}(1.15(\frac{W_{int}}{T_{fox}}) + 2.8(\frac{T_{int}}{T_{fox}})^{0.222}) \tag{5}$$

Next, the coupling capacitance C_{side} between lines is shown as:

$$C_{side} = 2E_{ox}(0.03\frac{W_{int}}{T_{fox}} + 0.83\frac{W_{int}}{T_{fox}} - 0.07\frac{W_{int}}{T_{fox}}^{0.222})(\frac{W_{sp}}{T_{fox}})^{-1.34} \tag{6}$$

Where E_{ox} is a dielectronic constant of SiO_2. It is given as:

$$E_{ox} = E_0 K_r = 3.9x8.85xE^{-03} = 0.035(\frac{fF}{\mu m}) \tag{7}$$

Final, the total capacitance or wire capacitance is determined as:

$$C_{total} = C_{plate} + MFC.C_{side} (\frac{fF}{\mu m}) \tag{8}$$

Where Miller Coupling Factor (MFC) is equal to 1.5 in this work.

Regarding the resistance of a interconnect net, this value is computed by the formula as below:

$$R_{total} = \rho\frac{L}{S} = \rho\frac{L}{W_{int}T_{int}} (\frac{\Omega}{\mu m}) \tag{9}$$

The figure below defines all variables used in the formulas above.
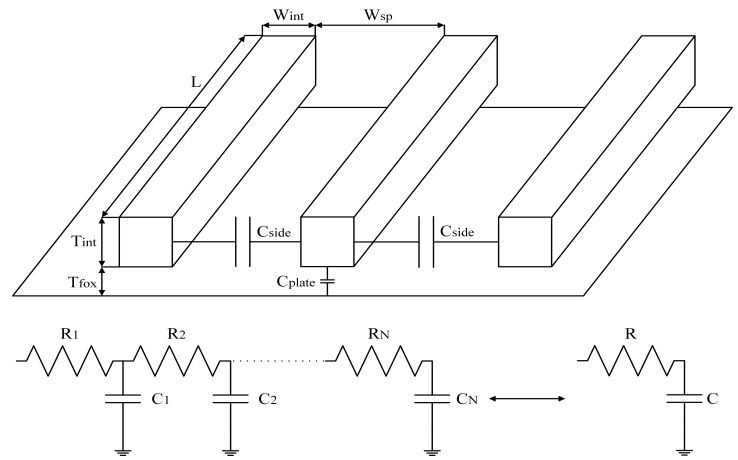
Figure 13: Variables definition used to compute the wire capacitance

This work is performed based on the CMOS 180nm process which has six metal layers. The following table provides the values of all variables defined in the formulas above.

Table 9: Values Of Variables For Wire Capacitance Calculation

Metal Layer	W_{INT} (μm)	W_{SP} (μm)	T_{INT} (μm)	T_{FOX} (μm)	C_{side} ($\frac{fF}{\mu m}$)	C_{plate} ($\frac{fF}{\mu m}$)
M1	0.23	0.23	0.53	0.003981	0.019	1.456
M2	0.28	0.28	0.53	0.003981	0.015	1.737
M3	0.28	0.28	0.53	0.003981	0.015	1.737
M4	0.28	0.28	0.53	0.003981	0.015	1.737
M5	0.28	0.28	0.53	0.003981	0.015	1.737
M6	1.50	1.50	2.34	0.003981	0.007	8.665

The table below shows the results of wire capacitance and resistance with the unit length of $1\mu m$. In addition, the delay of each metal layer is computed by the following formula:

$$t_{delay} = 4^*RC \tag{10}$$

Table 10: Values Of Wire Capacitance, Resistance, Delay

Metal Layer	Length (μm)	Capacitance (fF)	Resistance ($ohms$)	Delay (ps)
M1	1	1.484	0.164	0.097
M2	1	1.759	0.135	0.095
M3	1	1.759	0.135	0.095
M4	1	1.759	0.135	0.095
M5	1	1.759	0.135	0.095
M6	1	8.675	0.006	0.020

Based on the results above, the resistance and capacitance of a net will be calculated as the following formulas:

$$R = length.R_{unitlength} \tag{11}$$

$$C = length.C_{unitlength} \tag{12}$$

The tool in the timing analysis stage, especially the synthesis stage will calculate the capacitance and resistance of a interconnect net based on the particular *length* value.

5   Conclusion

In this paper, a novel approach to design a Process Design Kit (PDK) Digital for CMOS 180nm process is presented. For the Standard Cell Library design, by using the Ocean language, this work solved the problems about the licensing of the Liberty NCX tool which is unavailable in universities in developing countries, especially Vietnam, and running manually many simulations when the tool is not applied. Regarding the Wire-Load Model, this paper proposed a method and used accuracy formulas to design a complete model.

Conflict of Interest   The authors declare no conflict of interest.

References

[1] C. THINH Dang, T. TOI Le, H. TRANG, "Technology Education Challenges and Solution to Design a Process Design Kit for Digital CMOS Technology in Vietnam," in 2019 19th International Symposium on Communications and Information Technologies (ISCIT), 381–385, 2019, doi: 10.1109/ISCIT.2019.8905155.

[2] X. He, X. Zhu, L. Duan, Y. Sun, C. Ma, "A 14-mW PLL-Less Receiver in 0.18- μm CMOS for Chinese Electronic Toll Collection Standard," IEEE Transactions on Circuits and Systems II: Express Briefs, **61**(10), 763–767, 2014, doi:10.1109/TCSII.2014.2345303.

[3] J. Sun, C. C. Boon, X. Zhu, X. Yi, K. Devrishi, F. Meng, "A Low-Power Low-Phase-Noise VCO With Self-Adjusted Active Resistor," IEEE Microwave and Wireless Components Letters, **26**(3), 201–203, 2016, doi: 10.1109/LMWC.2016.2521167.

[4] H. Liu, C. C. Boon, X. He, X. Zhu, X. Yi, L. Kong, M. C. Heimlich, "A Wideband Analog-Controlled Variable-Gain Amplifier With dB-Linear Characteristic for High-Frequency Applications," IEEE Transactions on Microwave Theory and Techniques, **64**(2), 533–540, 2016, doi:10.1109/TMTT.2015.2513403.

[5] H. Liu, X. Zhu, C. Boon, X. He, "Cell-Based Variable-Gain Amplifiers With Accurate dB-Linear Characteristic in 0.18 μm CMOS Technology," Solid-State Circuits, IEEE Journal of, **50**, 586–596, 2015, doi:10.1109/JSSC.2014.2368132.

[6] X. Tong, Y. Yang, Y. Zhong, X. Zhu, J. Lin, E. Dutkiewicz, "Design of an On-Chip Highly Sensitive Misalignment Sensor in Silicon Technology," IEEE Sensors Journal, **17**(5), 1211–1212, 2017, doi:10.1109/JSEN.2016.2638438.

[7] S. Chakraborty, Y. Yang, X. Zhu, O. Sevimli, Q. Xue, K. Esselle, M. Heimlich, "A Broadside-Coupled Meander-Line Resonator in 0.13- μm SiGe Technology for Millimeter-Wave Application," IEEE Electron Device Letters, **37**(3), 329–332, 2016, doi:10.1109/LED.2016.2520960.

[8] M. A. Capilayan, R. Minguez, J. A. Hora, "Analysis on HSpice performance trade-off versus simulation time," in 2015 International Conference on Humanoid, Nanotechnology, Information Technology,Communication and Control, Environment and Management (HNICEM),1–6, 2015, doi: 10.1109/HNICEM.2015.7393176.

[9] A. Sadhu, P. Bhattacharjee, "Methodology of Standard Cell Library Design in .LIB Format," Journal of VLSI Design Tool & Technology, 30–38, 2014.

[10] J. Hu, J. Wang, "Low power design of a full adder standard cell," in 2011 IEEE 54th International Midwest Symposium on Circuits and Systems (MWSCAS), 1–4, 2011, doi:10.1109/MWSCAS.2011.6026457.

[11] S. Srinivasan, M. Hogan, "Physics to Tapeout: The Challenge of Scaling Reliability Verification," in 2019 IEEE International Reliability Physics Symposium (IRPS), 1–5, 2019, doi:10.1109/IRPS.2019.8720440.

[12] Y. Kuo, L. J. Arana, L. Seva, C. Marchese, L. Tozzi, "Educational design kit for synopsys tools with a set of characterized standard cell library," in 2018 IEEE 9th Latin American Symposium on Circuits Systems (LASCAS), 1–4, 2018, doi:10.1109/LASCAS.2018.8399907.

[13] M. S. I. bin Hussin, Y. W. Lim, N. A. Kamsani, S. J. Hashim, F. Z. Rokhani, "Development of automated standard cell library characterization (ASCLIC) for nanometer system-on-chip design," in 2017 IEEE 15th Student Conference on Research and Development (SCOReD), 93–97, 2017, doi:10.1109/SCORED.2017.8305414.

[14] S. Jain, M. Alioto, "A closed-form energy model for VLSI circuits under wide voltage scaling," in 2016 IEEE International Conference on Electronics, Circuits and Systems (ICECS), 548–551, 2016, doi:10.1109/ICECS.2016.7841260.

[15] C. K. Jha, S. N. Ved, I. Anand, J. Mekie, "Energy and Error Analysis Framework for Approximate Computing in Mobile Applications," IEEE Transactions on Circuits and Systems II: Express Briefs, **67**(2), 385–389, 2020, doi: 10.1109/TCSII.2019.2910137.

[16] M. Li, C.-I. Ieong, M.-K. Law, P.-I. Mak, M. Vai, R. Martins, "Sub-threshold standard cell library design for ultra-low power biomedical applications," Conference proceedings : ... Annual International Conference of the IEEE Engineering in Medicine and Biology Society. IEEE Engineering in Medicine and Biology Society. Conference, **2013**, 1454–1457, 2013, doi: 10.1109/EMBC.2013.6609785.

[17] M. U. Khan, Y. Xing, Y. Ye, W. Bogaerts, "Photonic Integrated Circuit Design in a Foundry+Fabless Ecosystem," IEEE Journal of Selected Topics in Quantum Electronics, **25**(5), 1–14, 2019, doi:10.1109/JSTQE.2019.2918949.

[18] M. Lee, S. Cho, N. Lee, J. Kim, "Design for High Reliability of CMOS IC With Tolerance on Total Ionizing Dose Effect," IEEE Transactions on Device and Materials Reliability, **20**(2), 459–467, 2020, doi:10.1109/TDMR.2020.2994390.

[19] B. Contreras, G. Ducoudray, R. Palomera, C. Bernal, "Automated Parameter Extraction and SPICE Model Modification For Gate Enclosed MOSFETs Simulation," in 2019 16th International Conference on Synthesis, Modeling, Analysis and Simulation Methods and Applications to Circuit Design (SMACD), 189–192, 2019, doi:10.1109/SMACD.2019.8795289.

[20] J. Bhasker, R. Chadha, Static timing analysis for nanometer designs: A practical approach, 2009, doi:10.1007/978-0-387-93820-2.

[21] T. J. Chang, Z. Yao, B. P. Rand, D. Wentzlaff, "Organic-Flow: An Open-Source Organic Standard Cell Library and Process Development Kit," in 2020 Design, Automation Test in Europe Conference Exhibition (DATE), 49–54, 2020, doi:10.23919/DATE48585.2020.9116540.

[22] B. Gupta, W. R. Davis, "Characterization of Fast, Accurate Leakage Power Models for IEEE P2416," in 20th International Symposium on Quality Electronic Design (ISQED), 39–44, 2019, doi:10.1109/ISQED.2019.8697565.

[23] M. Olivieri, A. Mastrandrea, "Logic Drivers: A Propagation Delay Modeling Paradigm for Statistical Simulation of Standard Cell Designs," IEEE Transactions on Very Large Scale Integration (VLSI) Systems, **22**(6), 1429–1440, 2014, doi:10.1109/TVLSI.2013.2269838.

[24] K. Vaidyanathan, D. H. Morris, U. E. Avci, H. Liu, T. Karnik, H. Wang, I. A. Young, "Improving Energy Efficiency of Low-Voltage Logic by Technology-Driven Design," IEEE Journal on Exploratory Solid-State Computational Devices and Circuits, **4**(1), 10–18, 2018, doi:10.1109/JXCDC.2018.2812242.

[25] N. Karagiorgos, S. Nikolaidis, "Application of the power contributors method for the AOI22 CMOS cell," in 2019 8th International Conference on Modern Circuits and Systems Technologies (MOCAST), 1–4, 2019, doi:10.1109/MOCAST.2019.8742028.

[26] M. R. F. Abingosa, C. Receno, J. Imperial, J. A. Hora, "Interconnect modeling of global metals for 40nm node," in 2015 International Conference on Humanoid, Nanotechnology, Information Technology,Communication and Control, Environment and Management (HNICEM), 1–6, 2015, doi: 10.1109/HNICEM.2015.7393172.

[27] T. Sakurai, K. Tamaru, "Simple formulas for two- and three-dimensional capacitances," IEEE Transactions on Electron Devices, **30**(2), 183–185, 1983, doi:10.1109/T-ED.1983.21093.

Performance Evaluation Reprogrammable Hybrid Fiber-Wireless Router Testbed for Educational Module

Muhammad Haqeem bin Mohd Nasir[1], Wan Siti Halimatul Munirah binti Wan Ahmad[1], Nurul Asyikin binti Mohamed Radzi[*,1,2], Fairuz Abdullah[1,2]

[1]*Institute of Power Engineering (IPE), Universiti Tenaga Nasional, Kajang Selangor, 43000, Malaysia*

[2]*Department of Electrical and Electronic Engineering, College of Engineering, Universiti Tenaga Nasional, Kajang Selangor, 43000, Malaysia*

A R T I C L E   I N F O

A B S T R A C T

Fiber-Wireless (FiWi) network is an integration of fiber optic and wireless connections in the same network. It is one of the best solutions to overcome rapid increment of Internet users and bandwidth-hungry services. To facilitate fundamental knowledge and further understanding on FiWi for students and researchers at the university level, this article proposes the development of a fast integration and scalable FiWi router testbed using Raspberry Pis as the embedded system-based hardware for lab-scale experiments. The performance of the router testbed in terms of end-to-end delay and throughput for upstream and downstream are evaluated. The delay values comply with IEEE 802.15.4 routing scheme. The performance of the router testbed is compared with the industrial grade off-the-shelf router in terms of throughput for each network. A testbed stress test is conducted by sending two data traffics simultaneously, and the performance test is repeated for Wireless-Fiber-Wireless and Fiber-Wireless-Fiber network architecture. The results show the proposed router testbed is scalable, flexible, and capable of fast integration.

1. Introduction

This paper is an extension of work originally presented in 2020 IEEE 8th International Conference on Photonics (ICP) [1]. However, in that work, fiber connection alone would not be able to accommodate all connections, especially to mobile and smart devices that are rapidly increasing. Furthermore, the demand for Internet and leased line bandwidth are growing continuously at more than 20% per year due to more video streaming, cloud computing, social media and mobile data delivery [2]. By 2020, the bandwidth demand will continue to grow due to an enhancement of video quality such as 8K Ultra High Definition (UHD) and increasing number of user subscriptions. Because of that, the estimated traffic in terms of mobile data and fixed systems will be 2600 times more than the traffic in 2010 [2]. This growth is accelerated by the new type of communication services such as device-to-device (D2D) and machine-to-machine (M2M) [3]. Therefore, to ensure users experience are at the same level of Quality of Service (QoS) regardless the time and location while the

demand is increasing, Fiber-Wireless (FiWi) deployment has become a necessity because it can cover a large area and support large number of users. According to [4], FiWi is still an ongoing study and there are plenty of rooms for improvement.

It is important to equip fundamental knowledge and further understanding on FiWi for students and researchers at the university level. Therefore, to facilitate this, it is essential to have a scalable FiWi testbed with fast integration capability, which is proposed in this article. FiWi network is a combination of fiber and wireless connection in the same network [5, 6] to provide fixed and mobile services [7-11]. A typical FiWi network consists of high-capacity passive optical network (PON) as backhaul comprising of Optical Line Terminal (OLT) and multiple Optical Network Units (ONU), connected to a cluster of wireless front end routers [12]. ONU is integrated with a wireless gateway that provides wide-area connectivity to users. At the optical backhaul, the OLT at the central office (CO) forms a root connected to the optical backbone via fiber link to provide cloud computing services. ONU is connected to the OLT via 1 : N (N = 32, 64) splitter to form a leaf-shaped nodes. The CO is responsible to manage the information

*Corresponding Author: Nurul Asyikin Mohamed Radzi, Universiti Tenaga Nasional, 43000 Kajang, Selangor, Malaysia, +603-89212020 ext. 3286, email: asyikin@uniten.edu.my

transmission between mobile devices with ONUs and acts as a gateway to other networks [13]. In the wireless end of FiWi network, mobile devices such as smart phones [14, 15], virtual reality (VR) glasses [16], smart watches and other Internet of Things (IoT) devices [16-18] have access to the Internet either via ONU or multi-hop wireless mesh network. Based on a study by [19], one of the advantages of FiWi is that it provides high speed optical backhaul for a wireless mesh network. In [20] stated that the network has a broadband access where it uses wide range of frequencies enabling a large number of data to communicate simultaneously. Whereas, mobile backhaul combines reliability and capacity of Ethernet-based optical backhaul with the wide range of coverage and flexibility of Ethernet-based wireless devices. By utilizing the efficacy of both optical fiber and wireless, a fast speed and low cost of service areas can be achieved [21]. It provides cost effectiveness, robustness, flexibility, high capacity, reliability and self-organization compared to fiber or wireless connection alone [22-24] Another advantage of having FiWi network is the combination of fiber optic and radio access technologies in multi-tier Radio Access Network (RAN) [2].

Radio access technologies will be used to deliver wireless services with high capacity, high link speed, and low latency [25]. The multi-tier RAN will improve the cell edge performance for mobile fronthaul and backhaul, resource sharing, and centralization of multiple standards with different frequency bands and modulation formats. FiWi network is a promising technology to support high demand of bandwidth and large number of users in different types of topologies and geographical environments.

Over the years, research communities have been working hard to improve the performance of FiWi network. Hence, in order to study and perform an extensive performance evaluation, testbeds are needed. Testbed is known as a prototype for proof-of-concept of any technology features where further studies can still be conducted [26]. There are various types of testbed in various platforms such as lab-scale testbed and field testbed. According to [27], built in lab-scale testbed is portable, which means, it can easily be packed away, securely stored and safely transported. The testbed can also be reused and assembled by other researchers in the future. For field testbeds, they consist of high-end setup which require installation by trained professionals and usually require large spaces. For example, in [28], an experiment was conducted consisting of 64 massive multiple-input multiple-output (MIMO) antennas for the FiWi testbed setup. The setup is comparing with collocated massive MIMO to simultaneously serves many users using the same time-frequency resource. For educational module, a simpler setup is preferable because fast integration capability is an important criterion for an educational testbed. This will speed up the installation of the testbed and the lecturers can have more time on explaining rather than focusing on testbed installation.

A testbed can have flexible architecture to be connected to any devices such as multiple sensors [29]. Despite of its compactness, it has powerful local computation unit. A testbed can also be reconfigured to different topologies as required. A review on two types of router testbeds (commercial-based and embedded system-based) were presented in [30]. The commercial-based are store-bought off-the-shelf routers [31, 32]. Some examples of embedded system-based routers are using netFPGA [33], Banana Pi [34] and Raspberry Pi [35-37]. From the study in [30], the embedded

system-based routers are reconfigurable, reprogrammable, scalable and cost less than the commercial routers. These advantages will be a suitable choice for the lab-scale router testbed in research and academic field.

Developing a lab-scale testbed is also one of the practical ways of studying and experimenting a particular technology before an actual implementation due to its portability and flexibility. This article describes the development of a FiWi router testbed with the said advantages, with several additional features: fast integration capability, scalable and flexible. The proposed router testbed uses Raspberry Pi for its programmable function (coded in Python language) to be a router. The details of the router structure will be described in the following section.

2. Hybrid Fiber-Wireless Router Testbed

Figure 1 shows a flowchart that reflects the overview of technical development for the proposed router testbed. Firstly, after the proposed routers in the testbed are connected with one another in FiWi architecture, connection reliability test is done by sending a packet from one client to another client. If the packet is not received by the client, an additional processing delay is increased in the proposed router. This delay is an additional time for the router to process the packets including label injecting, label checking, and packet forwarding. The process is repeated until the clients are able to receive the packet without fail. Afterwards, the performance of the proposed router is tested in FiWi architecture in terms of throughput and end-to-end delay in order to validate its correctness and comply with the current communication standards. After it is validated, a stress test is done by sending two traffics at a time to test the stability of the proposed router. Then, the architecture is changed to Fi-WiFi and Wi-FiWi in order to test its flexibility and scalability.

The proposed FiWi router testbed is using Raspberry Pi 3B+ to support data transmission for research and education purposes. It consists of four routers that are connected in tree topology and may be varied accordingly, as shown in Figure 2. It is a typical topology for FiWi network [12, 13]. Each router is an integration of four Raspberry Pi 3B+; one Header Pi and three Forwarding Pis. The three Forwarding Pis are to emulate the real router, with each of them having a unique static IP address. To form a router, the Raspberry Pis will be connected to two Ethernet switches via CAT5e Ethernet cable, as illustrated in Figure 3. Ethernet Switch 1 is to represent the internal connection of the routers (between Header Pi and Forwarding Pis). While Ethernet Switch 2 representing the external connection between routers. An Access Point (AP) is added as an element to the router structure to support wireless transmission.

2.1. Topology

The router testbed is set up in tree topology consisting of four proposed routers for the default FiWi architecture, as shown in Figure 2. The connection between routers is using single mode fiber optic patch cord. Since Raspberry Pi has only one Ethernet port, a Fiber Media Converter (FMC) is needed as an adapter. Then, the architecture is expanded to Fi-WiFi and Wi-FiWi as shown in Figure 4 and Figure 5, respectively. Compared to other topologies such as ring and mesh, the flexibility and stability of the proposed router can be observed after going through a number of

medium changes from wireless to fiber and vice versa in tree topology. Moreover, the purpose of these setups is to test the scalability of the testbed.
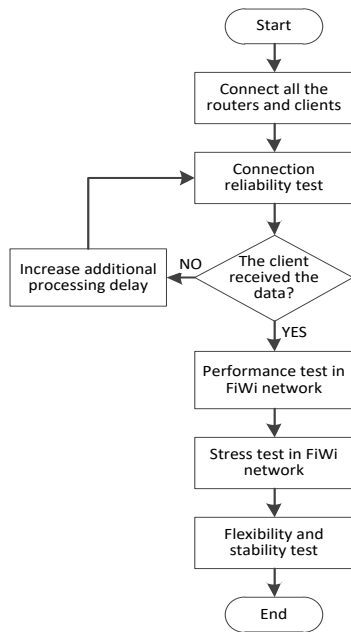
Figure 1: The overall flowchart of this work
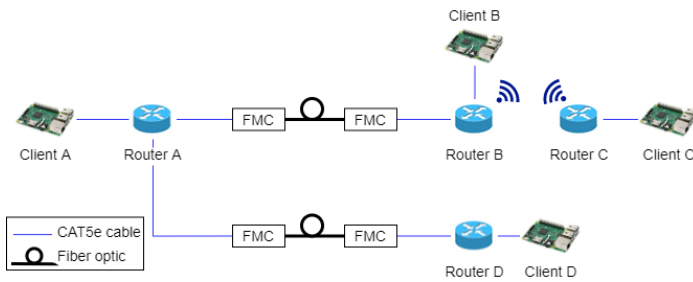
Figure 2: The architecture of FiWi router testbed

The architecture of this testbed can be scaled easily to Fi-WiFi and Wi-FiWi without any tedious hardware rearrangement. The routing mechanism for FiWi, Fi-WiFi and Wi-FiWi can be achieved by changing the label for each client, Header Pi and Forwarding Pi in the router program code. The labels for routers and clients in any of the three architectures (FiWi, Fi-WiFi and Wi-FiWi) must be unique to prevent misinterpretation of data destination by the router.

2.2. Routing Mechanism

The flowcharts of the testbed routing mechanism are shown in Figure 6, 7 and 8, for the client, Header Pi and Forwarding Pi, respectively. When a client sends a packet of data to the destination, a pre-label is added to the payload of the packet to indicate where the data should end. The client sends the data to Header Pi. Then, the Header Pi checks the label to know the beginning (source) and end (destination) of the data. After the Header Pi has identified the destination of the data, it replaces the old label with a new label onto the payload and then broadcast the data to each Forwarding Pis. Each of the Forwarding Pi has its own unique label because each identity label corresponds to one destination only. When the Forwarding Pi receives data from

Header Pi, it will check the label on the payload of the packet with its own identity label. If both labels are the same, the Forwarding Pi will continue to forward the data to desired destination set by the client. Otherwise, if both labels are not the same, the Forwarding Pi turns the data to zero and drops the packet.
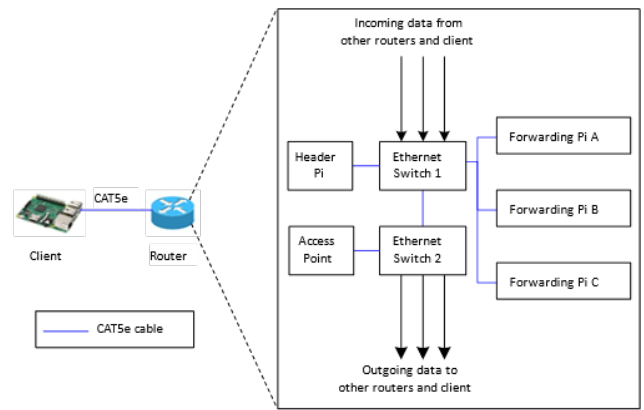
Figure 3: The structure of proposed router
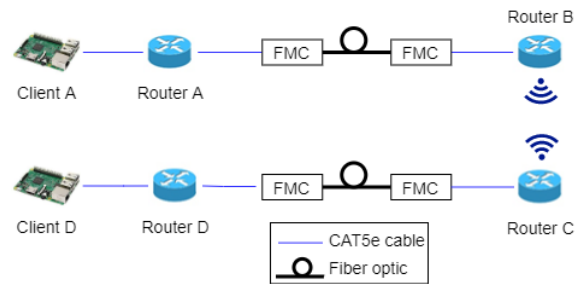
Figure 4: The architecture for Fi-WiFi router testbed
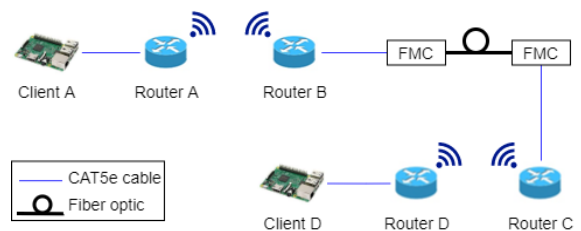
Figure 5: The architecture for Wi-FiWi router testbed

2.3. Experimental Setup

2.3.1. FiWi Router Testbed Performance Test

For this test, Raspberry Pi client is used to send a packet to another client via a combination of fiber and wireless transmission as in Figure 2. The initial data size transmitted is at 100 bytes for proof of concept [38]. Then, the data size is increased by 100 bytes each time until 1445 bytes. The performance of the experiment in terms of end-to-end delay and throughput are plotted on the graph. The proposed router is compared with industrial grade router to check its functionality and to observe its correctness. The setup for the industrial grade router is using the same topology as the proposed testbed. The upstream and downstream transmissions are done by using two computers. The throughput of the proposed router testbed is validated with industrial grade router. The bandwidth of the industrial grade router is set to 1 Gbps. However,

the initial data size is set to 10 kB and increased by 10 kB for each transmission until 100 kB. This is because the industrial grade router is connected to an access point with similar specification to the proposed testbed setup, limiting the actual bandwidth to 1 Mbps. Then, the throughput of the experiment for upstream and downstream are captured using Wireshark.

Figure 6: Client flowchart

Figure 7: Header Pi flowchart

Figure 8: Forwarding Pi flowchart (label example for A)

2.3.2. FiWi Router Testbed Stress Test

The limit of the FiWi router testbed is tested by sending two traffics simultaneously from one router to another. This stress test is done by connecting two clients for each proposed router. The performance will be analysed in terms of the end-to-end delay and throughput for downstream and upstream for two simultaneous traffic transmission. The purpose of this test is to evaluate the stability of the proposed testbed.

2.3.3. Scalability Test

Scalability is defined as the ability for the testbed to adapt to a new architecture or arrangement easily and its ability to expand the number of new components. In order to add or remove a component in the testbed, minor changes need to be done to its arrangement. In this case, the testbed architecture is changed to Fi-WiFi and Wi-FiWi to test its scalability performance and to prove the testbed is flexible to work in various architecture. The scalability test presents the performance for Fi-WiFi and Wi-FiWi in terms of end-to-end delay and throughput. Hence, the purpose of this section is to analyse the scalability performance and to compare which architecture is better for the testbed.

2.4. Parameters

2.4.1. Design

Design parameters are defined as the input for the testbed; the data size and the end-to-end delay. The data size is the length of data in bytes (B). It can be varied easily by the user at the client side. In this experiment, the increment of the transmitted data size is 100 bytes for each transmission. The summary of data size and corresponding throughput scale used in the experiment are listed in Table 1. The data size affects the end-to-end delay where greater data size may result in greater end-to-end delay. The end-to-end delay is used to study the throughput of the testbed.

Table 1: Summary of data size and throughput scale used in the testbed experiment

	Start	Data size increment	End	Throughput scale
Proposed testbed	100 bytes	100 bytes	1445 bytes	linearly
Industrial grade router	10 kB	10 kB	100 kB	1

2.4.2. Performance

Performance parameters are the output of the testbed which indicate its performance. Two performance parameters are taken into consideration; end-to-end delay and throughput. End-to-end delay is the time taken when the user sends the data from a client to another client. Throughput is the overall performance of the testbed in bit per second (bps) when the data size in bit (b) is divided by end-to-end delay, L, in second (s). The throughput, Th_{TL} calculation is summarized in (1) [39], where D_T is data transmitted and D_L is data loss.

$$Th_{TL} = \frac{D_T - D_L}{L} \qquad (1)$$
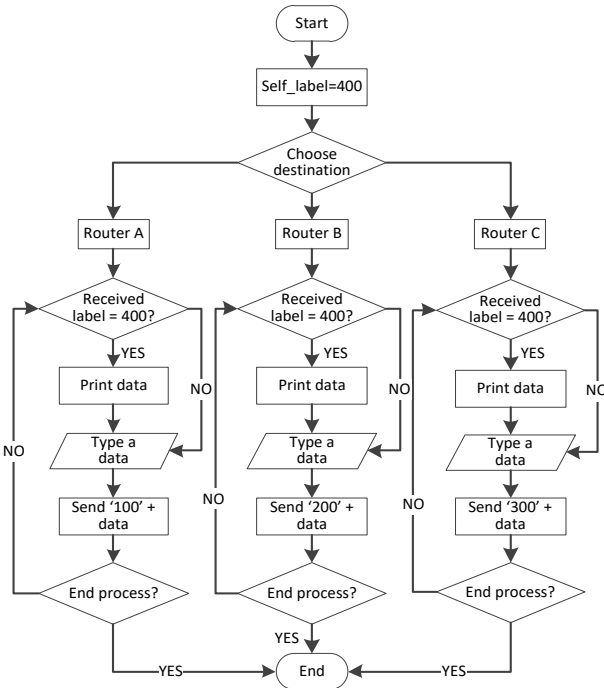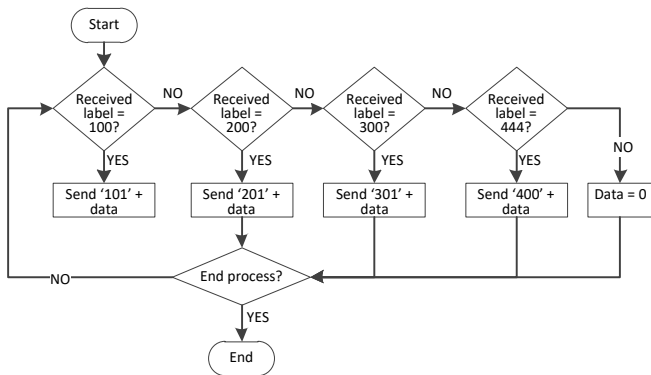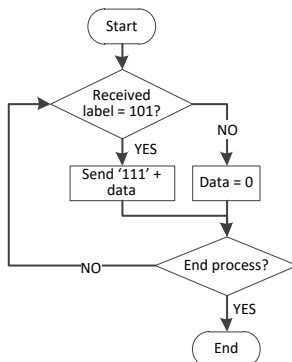
3. Results and Discussion

3.1. Fiber-Wireless Performance Test

Figure 9 shows the throughput for downstream and upstream transmissions. The purpose of this validation is to observe the correctness of the router testbed. The throughput of the testbed is scaled up to match the throughput industrial grade router. Based on the figure, the throughput of the proposed testbed has similar increasing trend as the industrial grade router, thus validates the correctness. The downstream throughput for proposed testbed increases from 0 bps at 0% offered load to 719 kbps at 100% offered load. The throughput of industrial grade router increases from 0 bps at 0% offered load to 697 kbps at 90%, then decreases at 100% offered load when reaching its bandwidth limit. This situation is due to the QoS algorithm in the industrial grade router limits the maximum throughput.

Similar trend is observed for upstream transmission, where the throughput of the proposed testbed increases as the offered load increases from 0 bps to 770.351 kbps at 0% to 100% offered load. The throughput for industrial grade router is also increasing from 0 bps to 774 kbps at 0% to 100% offered load.

For both downstream and upstream transmissions, industrial grade router is able to transmit data up to 700 kbps and 774 kbps respectively at 100% offered with 1445 bytes of in each packet. But the proposed testbed can only transmit for one packet of 1445 bytes, up to 52.097 kbps for downstream transmission and 54.335 kbps for upstream transmission. Hence, if the proposed testbed sends as many packets as the industrial grade router, the transmitted data in the proposed testbed is vertically scaled up by factor of 13.436 (700 kbps/59.097 kbps = 13.436) for downstream and 12.883 for upstream (774 kbps/59.097 kbps = 13.436). Vertical scaling is a method to translate a graph without losing the original properties where all y-values in the graph are multiplied by a specific factor. Therefore, for the proposed testbed, the throughput for each offered load is multiplied with 13.436 and 12.883 for downstream and upstream respectively.

Overall, the throughput of the proposed testbed is slightly lesser than the industrial grade router due to its lower technical specification, bandwidth and processing power but is adequate enough for lab-scale experiment. From the graphs, we can conclude that the trend of the proposed testbed is correct.
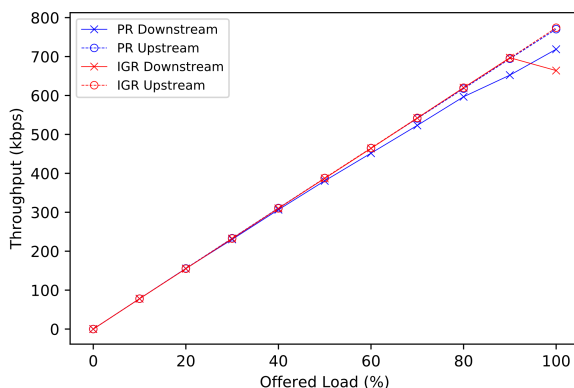
Figure 9: FiWi downstream and upstream throughput for the proposed router (PR) testbed and the industrial grade router (IGR)

Figure 10 shows the end-to-end delay for downstream and upstream transmission in FiWi architecture. For downstream, the minimum and maximum end-to-end delay are 0.1246 s and 0.14484 s at 100 bytes and 1445 bytes, respectively. For upstream, the minimum end-to-end delay is 0.12193 s at 100 bytes, and the maximum is 0.12430 s at 1445 bytes. The increased delay is due to testbed takes longer time to process the data. The subtle differences in the graphs caused by very small data size for a large bandwidth of fiber (1 Gbps). Furthermore, the data is transmitted by using light pulses in fiber. Hence, it transmits faster compared to electrical pulses in copper. For example, during downstream transmission, the end-to-end delay at 100 bytes is 0.1246 s, whereas at 200 bytes the end-to-end delay is 0.1250 s. The end-to-end delay is expected to be higher in the proposed router testbed compared to a typical fiber-supported router like industrial grade router, also because of hardware limitation. This is acceptable as part of the aim of this article is to create a reconfigurable router testbed that supports fiber-wireless transmission for educational module.
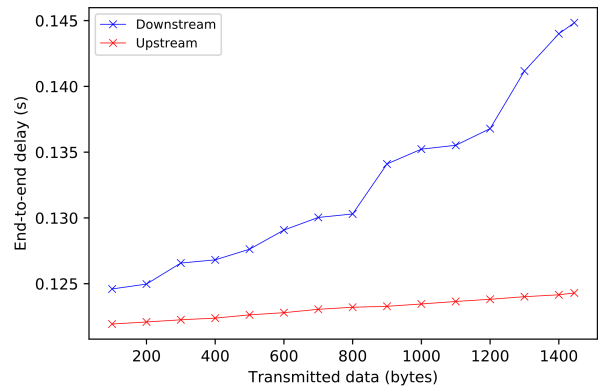
Figure 10: FiWi downstream and upstream end-to-end delay
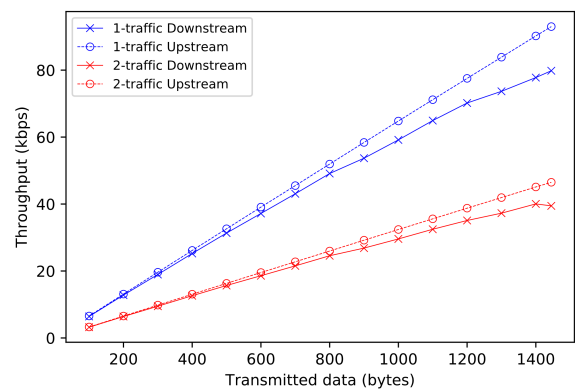
Figure 11: FiWi stress test downstream and upstream throughput for 1-traffic and 2-traffics transmissions

3.2. Fiber-Wireless Stress Test

Figure 11 shows the throughput for downstream and upstream transmissions. The throughput is still increasing gradually with the data size. The minimum and maximum throughput are 3.210 kbps at 100 bytes and 40.047 kbps at 1400 bytes. For downstream

with 2 traffics, the throughput decreases at 1445 bytes from 40 kbps to 39.5 kbps due to the end-limit of the testbed. Compared with the throughput of a single traffic, the throughput of two traffics is about half of the throughput of single traffics. The reason of this occurrence is two traffics causing the proposed testbed to process the data twice. For example, at 100 bytes in downstream transmission, the throughput for a single traffic is 6.42 kbps whereas the throughput for two traffics is 3.21 kbps. This statement is supported by [40] where more traffics contribute to less throughput.

Figure 12 shows the downstream and upstream end-to-end delay graphs. For downstream, the trend of the graph is increasing with the data size, from 0.249 s at 100 bytes to 0.293 s at 1445 bytes. At 1445 bytes, there is a sudden increase of end-to-end delay, due to the testbed's end-limit. Theoretically, when number of traffics increases, the end-to-end delay also increases [41]. Therefore, comparing the plots for downstream, the end-to-end delay of two traffics is twice as big as single traffic, because testbed needs to process the data twice. For example, the end-to-end delay at 1445 bytes for single traffic and two traffics are 144.838 ms and 293.01 ms, respectively.

The trend for upstream end-to-end delay is also similar where the delay increases from 243.863 ms at 100 bytes to 248.591 ms at 1445 bytes. At 1445 bytes, the end-to-end delay for two traffics and single traffic are 248.591 ms and 124.296 ms, respectively. Even though the trends of the graphs are almost constant, it is actually increasing as the data increases. The constant trends of the graphs are due to the presence of fiber which make the difference in end-to-end delay between two data such as 100 bytes and 200 bytes are not significant.
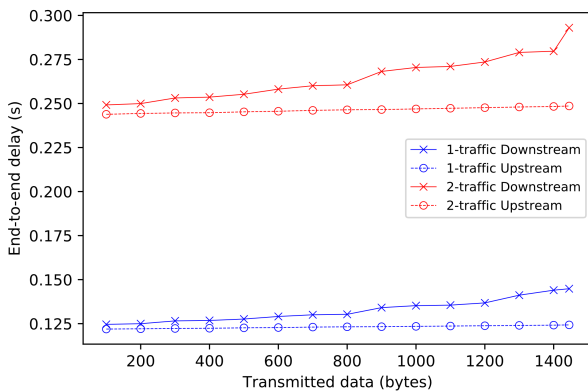
Figure 12: FiWi stress test downstream and upstream end-to-end delay for 1-traffic and 2-traffics transmissions

3.3. Scalability Test

3.3.1. Fiber-Wireless-Fiber

The plot for Fi-WiFi downstream and upstream throughput is shown in Figure 13. The downstream throughput increases with the data size from 2.626 kbps at 100 bytes to 22.403 kbps at 1445 bytes. For upstream, the throughput is increasing up until 1100 bytes only, unstable at 1200 bytes to 1300 bytes, then continue to decrease from 1400 bytes to 1455 bytes. Even though the

downstream throughput is increasing, but the graph gradient is gradually decreasing starting at 700 bytes. Whereas the upstream throughput becomes unstable at 1200 bytes to 1300 bytes because the proposed testbed is almost at its limit, resulting in greater graph gradient. Then, the throughput decreases at 1400 bytes and 1445 bytes due to the sudden increase of upstream end-to-end delay at 1400 bytes in and the delay continues to increase until 1445 bytes.

The downstream and upstream end-to-end delay for Fi-WiFi architecture is shown in Figure 14. The downstream delay increases with the data size from 0.609 s at 100 bytes to 1.032 at 1445 bytes. For upstream, the increases from 0.505 s at 100 bytes to 0.948 s at 1445 bytes. The end-to-end delay for this setup is higher than the FiWi architecture because the data has to undergo multiple routers and medium conversions from fiber to wireless and then wireless to fiber [42]. For downstream transmission, there is a sudden increase in end-to-end delay at 1400 bytes due to the end-limit of the proposed testbed, thus the longer processing time.

3.3.2. Wireless-Fiber-Wireless

The downstream and upstream throughput for Wi-FiWi architecture can be seen in Figure 13. The trend of the downstream throughput increases with the transmitted data size from 2.833 kbps at 100 bytes to 38.09 kbps at 1445 bytes. For upstream, the throughput increases from 2.81 kbps at 100 bytes to 38.348 kbps at 1445 bytes. At 100 bytes, the throughput for upstream transmission is slightly lower than downstream. However, as the transmitted data increases, the throughput for upstream transmission is higher than downstream: the throughput at 1100 bytes is 29.754 kbps (upstream) and 29.941 kbps (downstream). However, starting 1200 bytes, the throughput for upstream transmission is 32.276 kbps, while for downstream is 32.087 kbps. At 1445 bytes, the performance for both transmissions are slightly decreased due to the end-limit of the testbed, referring to the slope of the graph at this point. The slight differences in the throughput values proving that the proposed testbed in Wi-FiWi architecture is stable for both transmissions. This proposed router testbed is therefore suitable to be a scalable testbed.

Figure 14 shows the end-to-end delay of downstream and upstream transmissions respectively for Wi-FiWi architecture. The downstream end-to-end delay increases with the transmitted data size from 0.565 s at 100 bytes to 0.607 s at 1445 bytes. There is a sudden increase to the downstream end-to-end delay at 1200 bytes, because the proposed testbed is approaching its limit. Hence, the data processing time takes longer at this point. For upstream, the end-to-end delay is also increasing with the transmitted data, from 0.569 s at 100 bytes to 0.603 s at 1445 bytes. It can be observed that the downstream and upstream end-to-end delay for Wi-FiWi architecture is also higher than the FiWi because there are more medium changes in between clients. Therefore, the process of medium conversion contributes to higher end-to-end delay.

3.3.3. Fi-WiFi versus Wi-FiWi

Figure 13 clearly shows the comparisons in terms of throughput between Fi-WiFi and Wi-FiWi architectures for downstream and upstream transmissions from 100 bytes to 1445 bytes. The performance for Wi-FiWi is more stable than Fi-WiFi based on the behaviour of the graphs. This is because Fi-WiFi has more conversion from electrical pulses to light pulses and vice versa compared to Wi-FiWi causing the instability in Fi-WiFi.

Thus, the overall performance in Wi-FiWi is more stable because it has better observable graphs compared to Fi-WiFi.

Figure 14 shows the end-to-end delay comparisons between Fi-WiFi and Wi-FiWi architectures for downstream and upstream transmissions. Both have increasing end-to-end delay when the transmitted data size increased from 100 bytes to 1445 bytes. However, Fi-WiFi architecture has higher delay than Wi-FiWi because of the higher number of FMCs in Fi-WiFi. Hence, the medium conversions from light pulses to electrical pulses or vice versa is more than Wi-FiWi, thus contributes to more delay. From the graphs, we can conclude that Wi-FiWi has more stable transmission because throughout the transmissions, the end-to-end delay changes subtly. The summary of the throughput and end-to-end delay results at full load (1445 bytes) for all experiments using the proposed router testbed are listed in Table 2. Throughput results for FiWi architecture are not scaled, to fairly compare with other experiments.
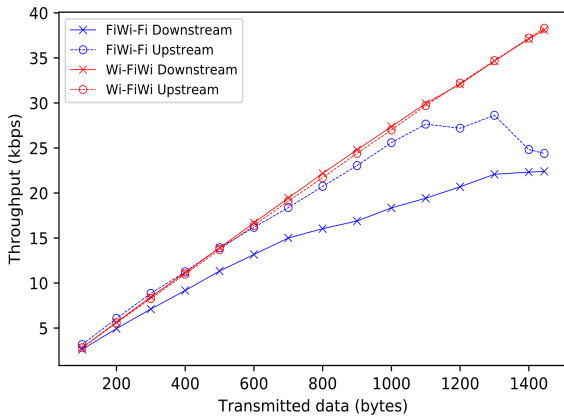
Figure 13: Fi-WiFi vs Wi-FiWi throughput
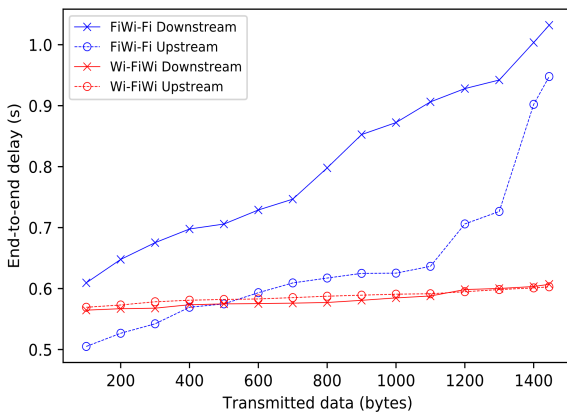
Figure 14: Fi-WiFi vs Wi-FiWi end-to-end delay

4. Conclusion

FiWi is seen to be one of the best technologies for future global data communication network architecture due to the advantages of providing robustness and mobility to the consumers by deploying FIber and wireless in one network. To equip fundamental knowledge and further understanding on FiWi for students and researchers at the university level, this article proposed a FiWi router testbed. It is a fast integration and scalable, which is essential for an educational module testbed. The focus of this research is on lab-scale environment router testbed in FiWi architecture to provide a proof-of-concept solution on reconfigurable router testbed in FiWi network. Raspberry Pi is chosen to be the embedded system hardware in this research for the development of scalable and reconfigurable FiWi router testbed. It has a socket module which enables the user to program Raspberry Pi to communicate with each other using IP addresses.

The proposed FiWi testbed throughput performance has been validated with industrial grade router to prove the correctness. As the proposed testbed approaches its limit, the throughput is maintained with no further increment. For the end-to-end delay, it increases with the data size with acceptable measure and its behaviour satisfies the end-to-end delay of IEEE 802.15.4 routing scheme. Hence, the proposed testbed is suitable to serve as an educational module FiWi testbed due to its simplicity, reconfigurable and fast implementation. A stress test shows that the end-to-end delay for two traffics is twice as high as single traffic due to the twice data processing. This causes the throughput for two traffics is halved of the single traffic throughput. For scalability performance test, the end-to-end delay in Fi- WiFi is higher than Wi-FiWi architecture due to more electrical pulses to light pulses conversion and vice versa from FMC in Fi-WiFi. Furthermore, Wi-FiWi is more stable compared to Fi-WiFi, thus making the testbed flexible and scalable for various possible setups. The proposed router testbed also shows a promising stability, a huge advantage to test various architectures.

Table 2: Summary of throughput and end-to-end delay results at full load (1445 bytes) for all experiments

| Experiment | Parameters | | | |
| | Throughput (kbps) | | End-to-end delay (s) | |
	Up stream	Down stream	Up stream	Down stream
FiWi	54.34	59.10	0.124	0.144
FiWi stress test	46.50	39.45	0.250	0.290
Fi-WiFi	24.40	22.40	0.948	1.030
Wi-FiWi	38.35	38.09	0.600	0.610

Conflict of Interest

The authors declare no conflict of interest.

Acknowledgment

References

[1] M. H. M. Nasir, W. S. H. M. W. Ahmad, N. A. M. Radzi, F. Abdullah, A. Abdullah, A. Ismail, and M. Z. Jamaludin, "Raspberry Pi as Reconfigurable Fiber-based Router and Its Performance Analysis," in 2020 IEEE 8th International Conference on Photonics (ICP), 30-31, 2020, doi:10.1109/ICP46580.2020.9206497.

[2] M. Tornatore, G.-K. Chang, and G. Ellinas, Fiber-wireless convergence in next-generation communication networks, Springer, 2017.

[3] E. A. Kosmatos and N. D. Tselikas, "Dominant handover algorithms for vehicular radio-over-fiber networks at 60 GHz: a performance Evaluation study" Performance Evaluation, **102**, 21-33, 2016, doi: 10.1016/j.peva.2016.05.001.

[4] M. Ridwan, N. A. M. Radzi, F. Abdullah, N. M. Din, and C. Rashidi, "Feasibility study of a reconfigurable fiber-wireless testbed using universal software radio peripheral" International Journal of Engineering and Technology Innovation, **8**(4), 274-283, 2018,

[5] N. Ghazisaidi and M. Maier, "Fiber-wireless (FiWi) access networks: challenges and opportunities" IEEE Network, **25**(1), 36-42, 2011, doi:10.1109/MNET.2011.5687951.

[6] M. Maier and N. Ghazisaidi, FiWi access networks, Cambridge University Press, 2011.

[7] B. P. Rimal, M. Maier, and M. Satyanarayanan, "Experimental testbed for edge computing in fiber-wireless broadband access networks" IEEE Communications Magazine, **56**(8), 160-167, 2018, doi:10.1109/MCOM.2018.1700793.

[8] V. Mishra, R. Upadhyay, and U. R. Bhatt, Progress in Advanced Computing and Intelligent Engineering, Springer, 2018.

[9] J. Liu, H. Guo, H. Nishiyama, H. Ujikawa, K. Suzuki, and N. Kato, "New perspectives on future smart FiWi networks: scalability, reliability, and energy efficiency" IEEE Communications Surveys & Tutorials, **18**(2), 1045-1072, 2015, doi:10.1109/COMST.2015.2500960.

[10] Y. Liu, L. Guo, B. Gong, R. Ma, X. Gong, L. Zhang, and J. Yang, "Green survivability in fiber-wireless (FiWi) broadband access network" Optical Fiber Technology, **18**(2), 68-80, 2012, doi: 10.1016/j.yofte.2011.12.002.

[11] Q. Dai, G. Shou, Y. Hu, and Z. Guo, "A general model for hybrid fiber-wireless (FiWi) access network virtualization," in 2013 IEEE International Conference on Communications Workshops (ICC), 858-862, 2013, doi:10.1109/ICCW.2013.6649354.

[12] Y. Yu, C. Ranaweera, C. Lim, L. Guo, Y. Liu, A. Nirmalathas, and E. Wong, "Hybrid fiber-wireless network: An optimization framework for survivable deployment" Journal of Optical Communications and Networking, **9**(6), 466-478, 2017, doi: 10.1364/JOCN.9.000466.

[13] H. Guo and J. Liu, "Collaborative computation offloading for multi-access edge computing over fiber–wireless networks" IEEE Transactions on Vehicular Technology, **67**(5), 4514-4526, 2018, doi:10.1109/TVT.2018.2790421.

[14] Z. Zhang, J. Kong, C. Huang, Q. Wu, J. Wu, and J. Li, "Virtual network embedding algorithm considering resource fragmentation in virtualized industrial fiber-wireless (FiWi) access network," in Proceedings of the International Conference on Imaging, Signal Processing and Communication, 148-152, 2017, doi: 10.1145/3132300.3132328.

[15] H. Beyranvand, W. Lim, M. Maier, C. Verikoukis, and J. A. Salehi, "Backhaul-aware user association in FiWi enhanced LTE-A heterogeneous networks" IEEE Transactions on Wireless Communications, **14**(6), 2992-3003, 2015, doi:10.1109/TWC.2015.2399308.

[16] P. Porambage, J. Okwuibe, M. Liyanage, M. Ylianttila, and T. Taleb, "Survey on multi-access edge computing for internet of things realization" IEEE Communications Surveys & Tutorials, **20**(4), 2961-2991, 2018, doi:10.1109/COMST.2018.2849509.

[17] W. Sun, J. Liu, and H. Zhang, "When smart wearables meet intelligent vehicles: Challenges and future directions" IEEE wireless communications, **24**(3), 58-65, 2017, doi:10.1109/MWC.2017.1600423.

[18] B. P. Rimal, D. P. Van, and M. Maier, "Mobile edge computing versus centralized cloud computing over a converged FiWi access network" IEEE Transactions on Network and Service Management, **14**(3), 498-513, 2017, doi:10.1109/TNSM.2706085.

[19] P.-Y. Chen and M. Reisslein, "FiWi network throughput-delay modeling with traffic intensity control and local bandwidth allocation" Optical Switching and Networking, **28**, 8-22, 2018, doi: 10.1016/j.osn.2017.11.001.

[20] B. P. Rimal, D. P. Van, and M. Maier, "Mobile edge computing empowered fiber-wireless access networks in the 5G era" IEEE Communications Magazine, **55**(2), 192-200, 2017, doi:10.1109/MCOM.2017.1600156CM.

[21] H.-H. Lu, C.-Y. Li, T.-C. Lu, C.-J. Wu, C.-A. Chu, A. Shiva, and T. Mochii, "Bidirectional fiber-wireless and fiber-VLLC transmission system based on an OEO-based BLS and a RSOA" Optics Letters, **41**(3), 476-479, 2016, doi: 10.1364/OL.41.000476.

[22] P. Singh and S. Prakash, "Optical network unit placement in Fiber-Wireless (FiWi) access network by Moth-Flame optimization algorithm" Optical Fiber Technology, **36**, 403-411, 2017, doi: 10.1016/j.yofte.2017.05.018.

[23] B. Kantarci, N. Naas, and H. T. Mouftah, "Energy-efficient DBA and QoS in FiWi networks constrained to metro-access convergence," in 2012 14th International Conference on Transparent Optical Networks (ICTON), 1-4, 2012, doi:10.1109/ICTON.2012.6253908.

[24] M. Lévesque, M. Maier, F. Aurzada, and M. Reisslein, "Analytical framework for the capacity and delay evaluation of next-generation FiWi network routing algorithms," in 2013 IEEE Wireless Communications and Networking Conference (WCNC), 1926-1931, 2013, doi:10.1109/WCNC.2013.6554859.

[25] J. Liu, H. Guo, Z. M. Fadlullah, and N. Kato, "Energy consumption minimization for FiWi enhanced LTE-A HetNets with UE connection constraint" IEEE Communications Magazine, **54**(11), 56-62, 2016, doi:10.1109/MCOM.2016.1600169CM.

[26] N. Choosri, Y. Park, S. Grudpan, P. Chuarjedton, and A. Ongvisesphaiboon, "IoT-RFID testbed for supporting traffic light control" International Journal of Information and Electronics Engineering, **5**(2), 102-106, 2015, doi:10.7763/IJIEE.2015.V5.511.

[27] W. Hurst, N. Shone, A. El Rhalibi, A. Happe, B. Kotze, and B. Duncan, "Advancing the micro-CI testbed for IoT cyber security research and education," in The Eighth International Conference on Cloud Computing, GRIDs, and Virtualization, 129-134, 2017.

[28] S. T. Abraha, D. F. Castellana, X. Liang, A. Ng'oma, and A. Kobyakov, "Experimental study of distributed massive MIMO (DM-MIMO) in in-building fiber-wireless networks," in 2018 Optical Fiber Communications Conference and Exposition (OFC), 1-3, 2018,

[29] Z. Gong, W. Xue, Z. Liu, Y. Zhao, R. Miao, R. Ying, and P. Liu, "Design of a reconfigurable multi-sensor testbed for autonomous vehicles and ground robots," in 2019 IEEE International Symposium on Circuits and Systems (ISCAS), 1-5, 2019, doi:10.1109/ISCAS.2019.8702610.

[30] M. H. M. Nasir, N. A. M. Radzi, W. S. H. M. W. Ahmad, F. Abdullah, and M. Z. Jamaludin, "Comparison of router testbeds: embedded system-based, software-based, and multiprotocol label switching (MPLS)" Indonesian Journal of Electrical Engineering and Computer Science, **15**(3), 1250-1256, 2019, doi:http://doi.org/10.11591/ijeecs.v15.i3.pp1250-1256.

[31] S. M. Blair, F. Coffele, C. Booth, B. De Valck, and D. Verhulst, "Demonstration and analysis of IP/MPLS communications for delivering power system protection solutions using IEEE C37. 94, IEC 61850 sampled values, and IEC 61850 GOOSE protocols," in 2014 CIGRE Session, 1-8, 2014.

[32] K. Tantayakul, R. Dhaou, B. Paillassa, and W. Panichpattanakul, "Experimental analysis in SDN open source environment," in 2017 14th International Conference on Electrical Engineering/Electronics, Computer, Telecommunications and Information Technology (ECTI-CON), 334-337, 2017, doi:10.1109/ECTICon.2017.8096241.

[33] V. Sivaraman, A. Vishwanath, D. Ostry, and M. Thottan, "Greening router line-cards via dynamic management of packet memory" IEEE Journal on Selected Areas in Communications, **34**(12), 3843-3853, 2016, doi:10.1109/JSAC.2016.2600412.

[34] D. Posch, B. Rainer, S. Theuermann, A. Leibetseder, and H. Hellwagner, "Emulating NDN-based multimedia delivery," in Proceedings of the 7th International Conference on Multimedia Systems, 1-4, 2016. doi: 10.1145/2910017.2910626.

[35] S. Y. Jang, B. H. Shin, and D. Lee, "Implementing a dynamically reconfigurable wireless mesh network testbed for Multi-Faceted QoS support," in Proceedings of the 11th International Conference on Future Internet Technologies, 95-98, 2016, doi: 10.1145/2935663.2935678.

[36] X. Piao, L. Huang, K. Yuan, J. Yuan, and K. Lei, "The real implementation of NDN forwarding strategy on android smartphone," in 2016 IEEE 7th Annual Ubiquitous Computing, Electronics & Mobile Communication Conference (UEMCON), 1-6, 2016, doi:10.1109/UEMCON.2016.7777909.

[37] V. Gupta, K. Kaur, and S. Kaur, "Developing small size low-cost software-defined networking switch using Raspberry Pi," in 50th Annual Convention of Computer Society of India : Next-Generation Networks, 147-152, 2018, doi: 10.1007/978-981-10-6005-2_16.

[38] S. Brown, "An analysis of loss-free data aggregation for high data reliability in wireless sensor networks," in 2017 28th Irish Signals and Systems Conference (ISSC), 1-6, 2017, doi:10.1109/ISSC.2017.7983622.

[39] J. Padhye, V. Firoiu, D. Towsley, and J. Kurose, "Modeling TCP throughput: a simple model and its empirical validation," in Proceedings of the ACM SIGCOMM'98 Conference on Applications, Technologies, Architectures, and Protocols for Computer Communication, 303-314, 1998, doi: 10.1145/285237.285291.

[40] H. Xu, X.-Y. Li, L. Huang, H. Deng, H. Huang, and H. Wang, "Incremental deployment and throughput maximization routing for a hybrid SDN" IEEE/ACM Transactions on Networking, **25**(3), 1861-1875, 2017, doi:10.1109/TNET.2017.2657643.

[41] Q. T. Minh, T. K. Dang, T. Nam, and T. Kitahara, "Flow aggregation for SDN-based delay-insensitive traffic control in mobile core networks" IET Communications, **13**(8), 1051-1060, 2019, doi:10.1049/iet-com.2018.5194.

[42] M. A. Abidini, O. Boxma, C. Hurkens, T. Koonen, and J. Resing, "Revenue maximization in optical router nodes" Performance Evaluation, **140**, 102-108, 2020, doi: 10.1016/j.peva.2020.102108.

Factors Impacting Digital Payment Adoption: An Empirical Evidence from Smart City of Dubai

Anas Najdawi[*,1], Zakariya Chabani[2], Raed Said[2]

[1]*Faculty of Management, Amity University, Dubai, 12346, UAE*

[2]*Faculty of Management, Canadian University of Dubai, Dubai, 12346, UAE*

ARTICLE INFO	ABSTRACT
	The emergence of new digital payment technologies has introduced both opportunities and challenges across all industries. This research aims to examine the significant factors that influence the adoption of new e-payment technologies, specifically in smart cities, as in Dubai. A comprehensive theoretical framework based on several previous studies included the following factors; Perceived Usefulness, Perceived Trust, Perceived Personal Innovativeness, Perceived Ease of Use, Perceived Risk, and Generation Cohort. The results of this research confirm that all proposed factors significantly affect the adoption of e-payment in Dubai as a case of a smart city; however, the perceived usefulness is not as significant as the other factors. Moreover, comparative analysis across the three generations showed almost similar patterns of adopting e-payment systems.

1. Introduction

E-payment is among the revolutionary changes caused by technology in the field of financial services that tremendously changed humans' life by making them simpler and easier than before. Currently, e-payments have taken over the entire world of financial transactions whether these are meant for personal or commercial use [1] because it offers numerous benefits to the consumers including cost-effectiveness and conservation of time and energy. The UAE in general, and Dubai in particular, has extensively adopted new innovative e-payment systems with over 25 e-payment service providers offering more than 250 payment services for traffic fines, electricity bills, parking fines, university fees, etc... [2]. Moreover, the e-payment transactions in the UAE increased by 21% between 2015 and 2016, which represents $12.4 billion of goods and services [3] due to the Dubai government's vision of creating the perfect smart city.

Despite their rapid growth, e-payment systems are not perfect. Some disfavors easily noticed, such as hacking risks, the high cost of setting-up, and upgrading the system. These disadvantages prevent some individuals from adopting e-payment systems. This paper investigates the key factors that influence the adoption of new e-payment technologies across several generations in smart cities such as Dubai. Consequently, help the organizations in

Dubai, facilitating the adoption of innovative e-payment services through smart and effective design that is more conscious about the essential factors in the adoption criteria. The expansion of new e-payment adoption research allows companies and organizations to spend less effort and time, which can be invested in developing new e-payment services with more significant opportunities in the market.

A large number of studies employed the TAM or UTAUT models to investigate the factors affecting e-payment adoption. However, the framework proposed in [4] is considered more suitable for the goals of the current research. The study investigated the Malaysian consumers' perception of e-payment and recommended the Benefits, Trust, Self-Efficacy, Ease of Use, and Security as the most critical factors affecting the consumers' perception of e-payment. This research extended the previous frameworks by proposing the following factors: Perceived Usefulness, Perceived Trust, Perceived Personal Innovativeness, Perceived Ease of Use, and Perceived Risk. Moreover, the effect of age cohorts (X, Y, and Z Generations) on the previous factors and the users' perception to adopt the e-payment system in Dubai is to be examined.

The research in [5], is the sole study among past studies that shed light on how Age influences the factors of e-payment adoption. However, only some of the factors (Perceived Ease of Use and Perceived Usefulness) were considered by the researchers, overlooking the impact of other significant factors.

[*]Corresponding Author: Anas Najdawi, Amity University, Dubai, UAE, anajdawi@amityuniversity.ae

In [6], the authors explored the factors affecting the adoption of e-payment systems among university students in the UAE. In this study, the researchers employed a modified TAM model in which the factor of trust was also incorporated. However, the population studied in this paper is limited to the university's students only. Therefore, the age factor was not being taken into consideration. The authors addressed students residing in all the emirates of UAE.

In [7], the authors adds to the previous work the demographic variables and e-payment channel adoption in the UAE. The current paper is organized as follows. Section 2 is dedicated to reviewing the previous works. Section 3 will represent our framework. The next section will be the description of the methodology used in order to accept or reject the proposed hypotheses. After that, the results are listed and discussed in Sections 5 and 6. The conclusions and different implications are provided in Section 7. Finally, the research limitations and recommendations for future studies are stated in Section 8.

2. Literature Review

2.1. E-payment systems

Similarly to all e-services, an electronic platform is essential for the functioning of e-payment systems. The e-payment supports various kinds of monetary transactions [1], including regular transactions like paying for grocery or utility bills as well as B2B transactions besides others, and thus, it enables the buyer and seller to reap the benefits of a faster and more convenient payments system [2].

Various modes of payment, including e-money, debit or credit cards, and internet banking, may be considered as E-payment [3]. Moreover, another important revolution in this context is the introduction of mobile money by various organizations. For instance, two of the most successful companies in terms of mobile money are Apple pay and Samsung pay [4].

The e-payment systems have numerous advantages. For instance, they offer faster monetary transactions waiving the need for long queues and waiting periods for payments and receipt of money. People can remotely perform the payment and receipt of money through their cell phones or another mode of payment. Additionally, the fees related to financial transactions when using e-payment systems are far less than transaction fees when using traditional ways in most countries, especially in Dubai. Even in the absence of direct fees, the consumer may have to bear indirect fees, such as transportation fees, to go to the bank to withdraw money or go to the store to buy goods and services.

However, e-payment systems also have some disadvantages, for instance, the security threat that users face when using the e-payment system, the Risk of hacking the system, which causes a loss of money and personal information. Another disadvantage would be the cost; although the cost will be less for users, some costs related to securing the system and installing or upgrading it could be relatively high.

2.2. Generations X Y Z characteristics

The ICTs are changing and transforming individuals and society in general. Various generations are characterized by different traits, preferences, behaviors, principles, and concerns [5]. Therefore, all people with the same characteristics are grouped in what is called a cohort.

The author serves as the bridge that connects the previous and current generations [8]. One of the prominent attributes of Gen X is its reliance on reviews of other people. They make purchase decisions only after thorough research and review of feedback posted by others to make better decisions regarding the purchase [9]. However, they witnessed ICT development and then information society; hence, they became more familiarized with technology [10]. They are adapting to technology very fast.

The author evolved amidst technological advancements and internet growth, allowing them to acquire tons of information without hassle. Gen Y has been introduced to the internet and technology since childhood; hence, they are thoroughly familiar with technology [11], [10], and Media is part and parcel of their lives since they grew in the era of information [12]; therefore, they are comfortable with technology and would prefer to communicate with e-mail or text than talking face-to-face [13] and focus significantly on technical information [14].

Using computers and the internet is part and parcel of Gen Z's lives, who deem social media platforms as the basis of communication and interaction [10]. Therefore, they are excellent with all the digital devices, and they are almost unable to exist without these devices [15].

2.3. Related frameworks and theories

TAM stands for Technology Acceptance Model, which was developed by Davis with the aim to determine and forecast the factors that affect a system before implementing it. TAM was employed by the majority of researchers to develop the framework in order to investigate the factors that influence e-payment adoption. The TAM model identified two major factors; Perceived Usefulness and Perceived Ease of Use, which can be affected by external variables [16]. Later, it was adapted to include more factors; some researchers included Perceived risk, Security, Perceived advantage, Trust, Web assurance seals and Usability [17]. Others, adopted the Perceived Risk and Information on e-payment as additional factors. Adopted Trust, Self-efficacy, and Security as additional factors [18].

In [19], the author performing research on the e-payment adoption in the context of Iran, the factors of Usability (Perceived Ease of use) and Technological and transaction system, as well as access to protection rules (Perceived Usefulness), were used by the authors. Moreover, Technical security, Security reports, Transaction system, and Personal experience pertaining to e-payment systems were identified in [20] as external variables. While the Age was added as a moderating factor in [21].

Other researchers adapted the UTAUT model to incorporate the factor of trust while discarding the factor of user behavior. Another change made in this model was the substitution of Behavioral intention with Continuance Intention [22]

3. Research model and hypotheses

The theoretical framework employed for the current research is shown in Figure 1. This study is carried out to investigate the

factors affecting the Emirate of Dubai residents' perception of using e-payment. The relationships between the factors affecting the residents' perception of using e-payment are used to develop the hypotheses in the following subsections. The factors we used in our conceptual model in light of prior findings from the literature are the following:
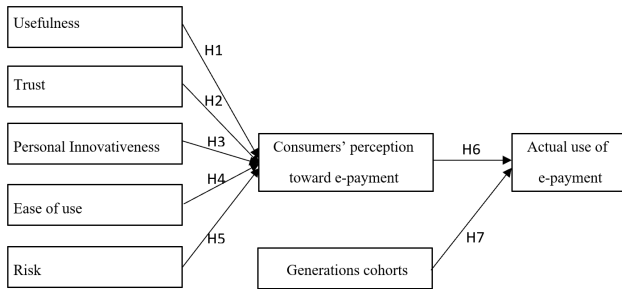
Figure 1: The Extended and Adopted Conceptual Framework

3.1. Perceived usefulness

Perceived usefulness implies the consumer's perception regarding the effectiveness and convenience offered by e-payment systems in simplifying his daily transactions [23]. In other words, it is the benefits that a person can get from e-payment systems. E-payment systems provide the user with a convenient mean of payment and the ability to store and transport a currency value [24].

Moreover, e-payment systems can provide other benefits such as time and cost-saving. Usefulness is one of the most important factors for e-payment systems use [17], [18], [25], [26]. However, as per some researchers, considerable time and effort may have to be invested by the consumer to learn how to use the e-payment system [27]; therefore, e-payment systems may be costly rather than cost-saving systems. Thus, it is hypothesized that:

H1 - There is a significant relationship between perceived usefulness and consumers' perception toward e-payments.

3.2. Perceived Trust

Perceived Trust in the context of e-payment systems implies the confidence bestowed by the user in the system regarding the reliability of the system in protecting the user's personal data and money from misuse and theft [28] , [29].

Many researchers stated that a high level of trust is essential for an e-payment system adoption [29], [22]. Similarly, users' concern over data privacy, internet security, etc., leads to a low level of trust, and thus, it will impact the adoption of e-payment systems negatively [32].

However, some researchers argue that trust alone is not sufficient to attract individuals adopting e-payment systems; for instance, if a reputed organization offers e-payment functions, the consumer will willingly use them; However, the user will hesitate in using the e-payment services provided by an untrustworthy organization [17]. Others found that trust is not significantly associated with individuals' perception toward e-payment [20] [31]. Thus, it is hypothesized that:

H2 - There is a significant relationship between consumers' perceived trust and perception toward e-payments.

3.3. Perceived personal innovation

Innovativeness is defined as the extent to which individuals consider themselves as technology leaders and pioneers [33]. This factor has been considered as an important factor influencing user's adoption of e-payment systems [18], [34], [35]. Thus, it is hypothesized that:

H3 - There is a significant relationship between perceived personal innovativeness and consumers' perception toward e-payments.

3.4. Perceived ease of use

Ease of use is defined as to which extent a person will not spend effort while using an e-payment system [23]. It can be attained via several factors, such as the content, design [29], information management, and speed [36]. E-payments systems can be affected significantly by these factors [37]. Previous researchers found that ease of use has a positive effect on the adoption of e-payment systems [18], [21]. Thus, it is hypothesized that:

H4: There is a significant relationship between perceived ease of use and consumers' perception toward e-payments.

3.5. Perceived Risk

Risk is defined as the individual's uncertainty about e-payment systems [38], due to their concern about fraud, theft, hacking, misuse of personal information, etc... Individuals may feel hesitant about the e-payment system due to Risk as an important factor influencing the adoption of the e-payment systems [39]. And the individuals' concern about the system may be a barrier to its adoption [40].

Contrary to most studies, some researchers argue that there is no relation between Risk and intention to adopt e-payment systems; although the Risk affects the payment system's adoption, it has no direct link; thus, individuals may use the system despite their concern [17]. Therefore, it is hypothesized that:

H5: There is a significant relationship between the perceived Risk and consumers' perception toward e-payments.

3.6. Consumer's perception towards the actual use of e-payment

User's attitudes toward IT systems represent a paramount factor that influences a particular system's actual use by individuals [16]. Thus, it is hypothesized that:

H6: Consumers' perception toward e-payment has a positive effect on the actual use of e-payments

3.7. Generations XYZ

In the current study, the generation cohorts will be defined based on the results from the literature review as follow:

- Generation X (Gen X), born between 1965 and 1979

- Generation Y (Gen Y), born between 1980 and 1994, this generation is also commonly known as 'Millennials' and sometimes as 'the children of Globalization' [41].

- Generation Z (Gen Z), born between 1995 and Nowadays, this generation is also known as the "silent generation," the iGeneration, generation quiet, and the next generation" [13].

The researchers believe that people from different generations do things differently when it comes to adopting e-payment systems in Dubai. Thus, it is hypothesized that:

H7: There are no significant differences among different generations toward the actual use of e-payments.

4. Methodology

The participants in this study were using e-payment in the emirate of Dubai. In this research, a nonprobability sample technique is used for collecting responses. Convenience sampling is a type of non-probability sampling where population elements are selected for inclusion in the sample based on access ease. In some cases, judgment sampling is used where the researchers' judgment is used for selecting participants who are considered as representative of the population.

The survey was carried out using a self-administered online questionnaire, which consisted of two major sections. The first section comprises 10 questions intended to collect demographic information and some information about the use of e-payment. The second section contains 28 statements meant to examine those factors that influence the perception of using the e-payment. This section's items essentially required the respondents to choose to what extent they agreed with each statement. The items were close-ended questions based on a 5-point Likert scale that each spectrum includes strongly disagree, disagree, no idea, agree, and strongly agree.

The proposed factors in accordance with the above hypotheses and the conceptual research framework constructed in section 3 are; Perceived Usefulness (abbreviated as PU), Perceived Trust (PT), Perceived Personal Innovation (PPI), Perceived Ease of Use (PEOU), Perceived Risk (PR), and Consumers' Perception toward e-payment (CP). Notably, items of the questionnaire for each one of these factors were cautiously adapted from prior studies. However, the wording was kept as similar as possible across studies.

The pilot study was done on 20 consumers prior to its dissemination to satisfy face validity. Cronbach Alpha, which is a measure of reliability based on the internal consistency of the constructs, was calculated for each factor. The reliability for each factor was higher than the acceptable 0.75 limit that [42] suggests. The Cronbach Alpha for the data instrument in total was 0.913, indicating that the questionnaire has attained a rather high level of reliability. Hence, all items are retained.

Before the regression analysis, 7 variables were created. The items relating to each factor were added together for each respondent, and the average was found. The mean scores ranged from a possible score of 1 to 5, with 1 representing total

disagreement with all stated items, and 5 representing total agreement with all stated items—two types of variables available in the research - dependent variable and independent variables. The main objective of this research is to investigate the predictors/variables that would determine the consumers' perception of the use of e-payment in Dubai. In this study the independent variables are the PU, PEOU, PT, PR, PPI, and CP. These six independent variables would be tested to identify whether these variables possess an influence on the dependent variable, which is the actual use of e-payments (UEP).

5. Analyses and Results

5.1. Descriptive findings

We conducted an online survey to investigate factors affecting consumers' perception of e-payment differences via generations based on our proposed conceptual framework. A total of 379 respondents visited the survey's link, and 242 respondents (63.8%) completed the survey. Of the 242 respondents, 207 respondents (85.5%) were considered eligible for this study after we removed respondents who answered that they are not currently using any of the e-payment methods.

Table 1. Shows the demographic characteristics of the e-payment users in the Emirate of Dubai who use e-payment. From the respondents to the questionnaire, 52.9 % were male, and 47.1 % were female. 12.6 % of the participants have a year of birth less than 1980 (Generation X), 33.3% between 1980 and 1994 (Generation Y), and 54.1% born in 1995 or above (Generation Z). Twenty-two percent of the participants were married, and in terms of the current professional position, 12.1 % were Executive, 10.1% Non-executive, 2.4% Housewife, 61.4% students, 5.3% Self-employed, and 8.7% were in other positions. Also, 30 % of the participants had High school or lower, 12.6 Diploma, 37.7% Bachelor's degree, 10.1% Masters and 9.7% Ph.D. holders. In term of the monthly income, the study found that 55.2% of the respondents having income below 10000 Dirhams, 14.3% between 10000 and 20000, 18.2% between 20000 and 30000, 5.9% between 30000 and 40000 and 6.3% having a monthly income above 40000 Dirhams

Table 1: Demographic characteristics of the sample (n=207)

Criterion	Category	Frequency	%
Gender	Male	109	52.9
	Female	97	47.1
Generation	X	26	12.6
	Y	69	33.3
	Z	112	54.1
Marital Status	Single	161	77.8
	Married	46	22.2
Current Professional Position	Executive	25	12.1
	Non-executive	21	10.1
	Housewife	5	2.4
	Student	127	61.4
	Self-employed	11	5.3
	Others	178	8.7
Education	High school or lower	62	30.0

	College (2 years program)	26	12.6
	Bachelor's degree	78	37.7
	Masters	21	10.1
	Ph.D.	20	9.7
Monthly Income	Below 10000	113	55.2
	10000 up to less than 20000	29	14.3
	20000 up to less than 30000	38	18.2
	30000 up to less than 40000	12	5.9
	40000 or above	14	6.4
Total:		207	100

5.2. Relationships between the factors affecting the Consumers' perception towards e-payment

Table 2 shows the results of the regression model we have done so far using SPSS after we checked the assumptions of regression analysis. From these outputs, we conclude that the factors under investigation explained 78.2% of the variance of the consumers' perception to use e-payments in Dubai. The remaining 21.8% of the variance can be explained by other factors not listed in our conceptual framework. As shown in the ANOVA table (Table 3), the minimal significance F indicates that our regression model is valid at a 0.05 significant level.

Table 2. Regression Model Summary

Model	R	R Square	Adjusted R Square	Std. Error of the Estimate
1	.782[a]	.611	.602	.40269
a. Predictors: (Constant), PR, PEOU, PPI, PT, PU				

Table 3. ANOVA Table

Model		Sum of Squares	Df	Mean Square	F	Sig.
1	Regression	51.303	5	10.261	63.274	.000[b]
	Residual	32.595	201	.162		
	Total	83.898	206			
a. Dependent Variable: CP						
b. Predictors: (Constant), PR, PEOU, PPI, PT, PU						

Table 4 shows the estimations of regression coefficients along with their t-ratios and probability values. It is seen that PEOU, PT, and PPI have a positive and statistically significant effect on the CP. In contrast, the PR has a negative and statistically significant effect on the CP. However, the results of Table 4 indicate that there is no significant relationship between PU and the CP (p-value 0.057). Therefore, hypotheses H2, H3, H4, and H5 of the present research have been validated, but there is no strong evidence to accept H1 at a 5% level of significance.

The sixth hypothesis of the study assumes that the consumers' perception toward e-payment has a positive effect on the actual use of e-payment. To test this hypothesis, we used a correlation analysis. The result of the Pearson's correlation coefficient between the consumers' perception toward e-payment and the actual use of e-payments is significant at 0.01 level (r = 0.452, p-value=0.000). The findings support the stated hypothesis H6 and confirm that consumers' perception toward e-payment has a positive effect on the actual use of e-payments

Table 4: Regression coefficients of the factors affecting consumers' perception of e-payment

Model		Unstandardized Coefficients		Standardized Coefficients	T	Sig.
		B	Std. Error	Beta		
1	Constant	.656	.239		2.742	.007
	PU	.144	.076	.143	1.911	.057
	PT	.116	.056	.110	2.073	.039
	PEOU	.446	.077	.452	5.782	.000
	PPI	.219	.048	.238	4.529	.000
	PR	-.096	.034	-.127	-2.797	.006
a. Dependent Variable: CP						

5.3. Differences among generations towards the use of e-payments

This section discusses the differences among generations towards the use of e-payments. As indicated in Table 5, the findings show that the respondents of generation X have a better agreement in using e-payments (average 4.10) than that of generation Y (with an average of 3.88) and of generation Z (with an average of 3.99). However, the value of the standard deviation (SD), reveals no significant differences between the respondents of generation X (SD=0.69) and the respondents of generation Z (SD=0.65). This contrasts with the respondents of generation Y (SD=0.97). This means there is a more significant difference among generation Y than the two other generations in regards to their perception to use e-payments.

Moreover, we used ANOVA test to verify the seventh and final hypothesis (H7). The hypothesis assumes a statistically significant difference in the consumers' perception of respondents from different generations toward the use of e-payment. As illustrated in Table 6, the p-value is above 0.05 (Sig. = 0.425). This indicates that there are no significant differences in the consumers' perception of respondents from different generations toward the use of e-payment. Therefore, the seventh hypothesis H7 is supported.

Table 5: Averages and Std. deviations of respondents from different generations toward the use of e-payment

Gen.	N	Mean	Std. Deviation	Std. Error	95% Confidence Interval for Mean		Min.	Max.
					Lower Bound	Upper Bound		
X	26	4.1026	.69134	.13558	3.8233	4.3818	2.33	5.00
Y	69	3.8841	.97991	.11797	3.6487	4.1195	1.00	5.00
Z	112	3.9970	.65070	.06149	3.8752	4.1189	2.33	5.00
Tot.	207	3.9726	.77987	.05420	3.8658	4.0795	1.00	5.00

Table 6: ANOVA Table of the respondents from different generations toward the use of e-payment

	Sum of Squares	df	Mean Square	F	Sig.
Between Groups	1.047	2	.523	.859	.425
Within Groups	124.242	204	.609		
Total	125.289	206			

6. Discussion

In the first hypothesis H1, Perceived Usefulness was found not to have a significant relationship with the consumers' actual use of

e-payment in Dubai. The finding was consistent with previous studies [27]. The result implied that regardless of the persons' belief that using an e-payment system will enhance the performance of his day to day activities; consumers are more likely to use e-payment.

In the second hypothesis, H2, Perceived Trust was found to have a significant relationship with the consumers' actual use of e-payment in Dubai. Similar results were demonstrated from previous studies [22], [29]-[32]. And this implied that a high level of trust is essential for an e-payment adoption.

Perceived personal innovation was found to have a significant relationship with the consumers' actual use of e-payment in Dubai, which supported the third hypothesis H3, which was in line with many past studies. [18], [34], [35]. And this implied that the extent to which individuals consider themselves as technology leaders and pioneers is considered an important factor influencing the user's adoption of e-payment.

Perceived Ease of Use was found to have a significant relationship with the consumers' actual use of e-payment in Dubai, which supported the fourth hypothesis H4, which was in line with many past studies [18], [21], [37]. And this implies that ease to use of handling e-payment, such as convenience, speed, flexibility, simplicity, accessibility, and availability, is also considered a vital factor influencing the user's adoption of e-payment.

Perceived Risk was found to have a significant negative impact found to have a significant relationship with the consumers' actual use of e-payment in Dubai, which supported the fifth hypothesis H5. This was in line with many past studies [39], [40]. This implies that individuals' concern about the system may be a barrier to its adoption.

In the sixth hypothesis, H6, the Consumers' Perception toward e-payment was found to have a significant positive relationship with the consumers' actual use of e-payment in Dubai. And this implied that the user's attitude toward IT systems represents a paramount factor that influences the actual use of e-payment.

Finally, this study's results did not show significant differences among the different generations toward the use of e-payment, which supported our seventh hypothesis, H7. This might be indicated that most consumers in Dubai, as a smart city, are sufficiently familiar with using e-payment and accepting any new technologies easily.

7. Conclusion and implications

In this paper, the researchers studied the effect of some factors that might affect the adoption of new e-payment services and technologies. Based on an extended framework that captures the unique status of smart cities such as Dubai that move faster in digital transformation rather than less developed ones. The extended framework included all of Perceived Usefulness, Perceived Trust, Perceived Personal Innovativeness, Perceived Ease of Use and Perceived Risk on the adoption of e-payment systems in Dubai while considering the age cohorts (X, Y, and Z generations).

The results show that most of the factors used in the study are indeed critical and significant to the users' adoption of e-payment systems in Dubai. However, perceived usefulness is not as

significant as the other factors; we think it is because some users care more about the system being easy to use than to be useful.

Unexpectedly, we found no serious differences between the generation cohorts regarding the adoption of e-payment in Dubai. We think that this due to the government of Dubai's efforts to in digital transformation of all of its E-Government services, and the adoption of digital payments toward a cashless economy might be a reason. The results imply that the government's strategies encourage consumers to use technologies in general as e-payment systems are working fine. This research will help future studies that focus on more recent technologies in the region based, such as adopting cryptocurrencies by individuals and businesses in the Middle East's smart city context.

8. Study limitations and recommendation for future work

This study is not free from some limitations. And to begin with, the sample employed in our empirical analysis is collected by nonprobability sampling techniques. The use of a convenient sample limits the research results to the specific sample, which means that the findings cannot be generalized to a larger population [43]. Other factors and dimensions, including the individual differences, system characteristics, social influence, and facilitating conditions missing in this study, will be considered in future research.

Additionally, the exact e-payment channels and factors toward adoption in Dubai and the preferred e-payment methods should be conducted to understand how Dubai as a smart city is moving toward the digital transformation of e-payment channels and their diffusion among the consumers; this will compared to other smart cities in the region including Saudia Arabia and Singapore [44], [45] and my be focused on specific sector such as banking [46]. The expected results will be useful to financial institutions, government, and e-payment technology providers in this region and marketers and, will encourage the innovative design of e-payment services that are most likely will be adopted by individuals, businesses, and governments.

Conflict of Interest

The authors declare no conflict of interest.

References

[1] Z. J. Zuopeng and J. M. Sajjad, "Knowledge market in organizations: incentive alignment and IT support," Industrial Management & Data Systems, 1101 - 1122, 2012. doi:10.2991/ijcis.d.191025.002

[2] T. Pikkarainen, K. Pikkarainen, H. Karjaluoto and S. Pahnila, "Consumer acceptance of online banking: An extension of the technology acceptance model," Internet Research , 224-235, 2004. DOI: 10.1108/10662240410542652

[3] W. Chaiyasoonthorn and W. Suksa-ngiam, "The diffusion and adoption of electronic payment systems in bangkok," International Journal of e-Business Research, **15**(2), 102-115, 2019.doi:10.1086/261933

[4] J. M. Gray, "How apple pay coincides with the consumer financial protection act: will apple become a regulated entity," Journal of High Technology Law, 170-194, 2015.

[5] S. Lissitsa and O. Kol, "Generation X vs. Generation Y – A decade of online shopping," Journal of Retailing and Consumer Services, **31**, 304-312, 2016. DOI: 10.1016/j.jretconser.2016.04.015

[6] S. A. Salloum and M. Al-Emran, "Factors affecting the adoption of e-payment systems by university students: extending the TAM with trust,"

International Journal of Electronic Business, 371-390, 2018. DOI: 10.1504/IJEB.2018.098130

[7] A. Najdawi, . Z. Chabani, . S. Raed and O. Starkova, "Analyzing the Adoption of E-Payment Technologies in UAE Based on Demographic Variables," in 2019 International Conference on Digitization (ICD), Sharjah, 2019. DOI: 10.1109/ICD47981.2019.9105908

[8] J.-G. Heaney, "Generations X and Y's Internet banking usage in Australia," Journal of Financial Services Marketing, 196-210, 2007.doi: 10.1057/palgrave.fsm.4760052

[9] E. Peralta, "Generation X: The Small But Financially Powerful Generation," 17 September 2015. [Online]. Available: https://www.centro.net/blog/generation-x-the-small-but-mighty-generation/.

[10] E. Csobanka, "The Z Generation," Acta Technologica Dubnicae, 6-10, 2016. doi: 10.1515/atd-2016-0012

[11] I. BAKANAUSKIENĖ, R. BENDARAVIČIENĖ and I. BUČINSKAITĖ, "EMPLOYER'S ATTRACTIVENESS: GENERATION Y EMPLOYMENT," Human Resources Management & Ergonomics, **X**(1), 2016.

[12] M. Muda, R. Mohd and S. Hassan, "Online Purchase Behavior of Generation Y in Malaysia," Procedia Economics and Finance, **37**, 292 – 298 , 2016.doi: 10.1016/S2212-5671(16)30127-7

[13] J. G. Harber, "Generations in the Workplace: Similarities and Differences.," East Tennessee State University, Johnson City, 2011.

[14] M. Rahulan, O. Troynikov, C. Watson, M. Janta and V. Senner, "Consumer behavior of generational cohorts for compression sportswear," Journal of Fashion Marketing and Management: An International Journal, 87–104, 2015. doi: 10.1108/JFMM-05-2013-0072

[15] A. Kolnhofer-Derecskei, R. Zs. Reicher and A. Szeghegyi, "The X and Y Generations' Characteristics Comparison," Acta Polytechnica Hungarica, **14**(8), 2017. doi: 10.12700/APH.14.8.2017.8.6

[16] F. D. Davis , "Perceived usefulness, perceived ease of use, and user acceptance of information technology," MIS Quarterly, 19-340, 1989. doi: 10.2307/249008

[17] S. Ozkan , G. Bindusara and R. Hackney, "Facilitating the adoption of e-payment systems: theoretical constructs and empirical analysis," Journal of Enterprise Information Management, 305 - 325, 2010. doi: 10.1108/17410391011036085

[18] C. Lin and C. Nguyen, "Exploring E-Payment Adoption in Vietnam and Taiwan," Journal of Computer Information Systems, **51**(4), 41-52, 2011.doi: 10.1080/08874417.2011.11645500

[19] M. Barkhordari, Z. Nourollah, H. Mashayekhi, Y. Mashayekhi and M. S. Ahangar, "Factors influencing adoption of e-payment systems: an empirical study on Iranian customers," Information Systems and e-Business Management, **15**(1), 89–116, 2017.doi:10.1007/s10257-016-0311-1

[20] E. Oney, G. O. Guven and W. H. Rizvi, "The determinants of electronic payment systems usage from consumers' perspective," Economic Research-Ekonomska Istraživanja, **30**(1), 394-415, 2017. doi: 10.1080/1331677X.2017.1305791

[21] A. Riskinanto, B. Kelana and D. R. Hilmawan, "The Moderation Effect of Age on Adopting E-Payment Technology," Procedia Computer Science, 536–543, 2018. doi: 10.1016/j.procs.2017.12.187

[22] Indrawati and D. A. Putri, "Analyzing Factors Influencing Continuance Intention of E-Payment Adoption Using Modified UTAUT 2 Model," in 6th International Conference on Information and Communication Technology, 2018. doi: 10.1109/ICoICT.2018.8528748

[23] S. Roy and I. Sinha , "Determinants of Customers' Acceptance of Electronic Payment System in Indian Banking Sector – A Study," International Journal of Scientific & Engineering Research, 177- 187, 2014.

[24] S. Chakravorti, "Theory of Credit Card Networks: A Survey of the Literature," Review of Network Economics, 50-68, 2003. doi: 10.2139/ssrn.419944

[25] S. San Martín , B. López-Catalán and M. A. Ramón-Jerónimo , "Factors determining firms' perceived performance of mobile commerce," Industrial Management & Data Systems, 946-963, 2012. doi: 10.1108/02635571211238536

[26] Y. Chou, C. Lee and J. Chung, "Understanding m-commerce payment systems through," Journal of Business Research, 1423 – 1430, 2004. doi:10.1016/S0148-2963(02)00432-0

[27] C. Kim, W. Tao, N. Shin and K.-S. Kim, "An empirical study of customers' perceptions of security and trust," Electronic Commerce Research and Applications, 84–95, 2009. doi:10.1016/j.elerap.2009.04.014

[28] T. Kongprapunt and N. Pupat, "FACTORS INFLUENCING GENERATION Y'S ONLINE PURCHASE INTENTION TOWARD XYZ ONLINE STORE IN THAILAND," Assumption University GSB e-journal, 94-106, 2018.

[29] D. Abrazhevich, Electronic Payment Systems: a User-Centered Perspective and Interaction Design, Eindhoven: Eindhoven University of Technology, 2004.doi: 10.6100/IR575913

[30] S. Kurnia and B. Lim, "Exploring the Reasons for a Failure of Electronic Payment," Journal of Research and Practice in Information Technology, 231-243, 2007.doi: 10.1007/s10660-011-9083-3

[31] W. M. Teoh, S. C. Chong, B. Lin and J. W. Chua, "Factors affecting consumers' perception of electronic payment: An empirical analysis," Internet Research, **23**(4), 465-485, 2013.doi: 10.1108/ IJBM-05-2013-0048

[32] N. B. Tasin, "Factors Influecing Customer's Trust in Online Shopping Among Executives in a Bank," Malaysian Journal of Social Sciences and Humanities, 47-60, 2017.doi: 10.47405/mjssh.v2i3.47

[33] A. Parasuraman and C. Colby, Techno-Ready Marketing: How and Why Your Customers Adopt Technolog, New York: The Free Pres, 2002.

[34] E. M. Rogers, Diffusion of Innovations, 5th edition, New York: Free Press, 2003.

[35] C. Kim , K. Takashima and S. Newell , "How do retailers increase the benefits of buyer innovativeness?," Asia Pacific Journal of Marketing and Logistics, 571-586, 2018.

[36] M. Jun and S. Cai, "The key determinants of Internet banking service quality: a content analysis," International Journal of Bank Marketing, 276-291, 2001.doi: 10.1108/02652320110409825

[37] P. Guriting and N. O. Ndubisi , "Borneo online banking: evaluating customer perceptions and behavioural intention," Management Research News, 6-15, 2006. doi: 10.1108/01409170610645402

[38] S. Ram and J. .. sheth, "Consumer resistance to innovations: the marketing problem and its solution," Journal of Consumer Marketing, 5-14, 1989. doi:10.5281/zenodo.1094243

[39] S. L. Jarvenpaa, N. Tractinsky and M. Vitale, "Consumer trust in an Internet store," Information Technology and Management, 45-71, 2000. doi: 10.1023/A:1019104520776

[40] S. Sarin, T. Sego and N. Chanvarasuth, "Strategic Use of Bundling for Reducing Consumers' Perceived Risk Associated with the Purchase of New High-Tech Products," Journal of Marketing Theory & Practice Theory & Practice, 71-83, 2003. doi:10.1080/10696679.2003.11658502

[41] S. B. Berkup, "Working With Generations X And Y In Generation Z Period: Management Of Different Generations In Business Life," Mediterranean Journal of Social Sciences, **5**(19), 218-229, 2014. doi: 10.5901/mjss.2014.v5n19p218

[42] J. C. Nunnally, Assessment of Realibilty, IN: Pschometric Theory, New York: McGraw-Hill, 1978.

[43] J. Hair, R. Anderson, R. Tatham and W. Black, Multivariate data analysis, NY: Macmillan, 1998.

[44] K. Baskaran, "The impact of digital transformation in Singapore e-tail market," International Journal of Innovative Technology and Exploring Engineering (IJITEE), **8**(11), 2320-2324, 2019.

[45] A. R. Chaudhry, B. Rajput and R. Mishra, "Influence of IoT &AI in place making and creating Smart Cities," in 2019 10th International Conference on Computing, Communication and Networking Technologies (ICCCNT), Kanpur, 2019.

[46] A. Mehrotra, "Artificial Intelligence in Financial Services – Need to Blend Automation with Human Touch," in 2019 International Conference on Automation, Computational and Technology Management (ICACTM), London, 2019.

ASTES

Comparison between Collaborative Filtering and Neural Collaborative Filtering in Music Recommendation System

Abba Suganda Girsang[*], Antoni Wibowo, Jason, Roslynlia

Computer Science Department, BINUS Graduate Program – Master of Computer Science, Bina Nusantara University, Jakarta, 11480, Indonesia

A R T I C L E I N F O	A B S T R A C T
	Music is one of the most popular entertainments, and the music industry continues to increase over time. There are many types of genres in music, and everyone has their own choice of the type of music they want to listen to. The recommendation system is an important function in the application, especially when there are a large number of choices for a particular item. With a good recommendation system, users will be able to get help from the suggestions given and can improve the user experience of the application. By using collaborative filtering (CF) methods to recommend products related to personal preference history, this feature can be better provided. However, the CF method still lacks in integrating complex user data. Hybrid technology may be a solution to perfect the CF method. The combination of neural network and CF also called NCF is better than using CF alone. The focus of this research is a CF method combined with neural networks or neural collaborative filtering. In this study, we use 20,000 users, 6,000 songs, and 470,000 records of ratings then predict the score using CF and NCF approach. We aim to compare the recommendation systems using CF and NCF. The study shows that NCF is better in gathering certain playlists according to one's preferences, but it takes more time to build compared to user-based collaborative filtering.

1. Introduction

Music is one of the most popular entertainments. There are 1.15 trillion users who stream video and audio-based music on digital platforms in 2019 and increased by 29.3% from the previous year. The increasing number of users are based on the fact that music could control people's emotions, moods, or physiological arousal [1]. Besides users, music content also increases a lot every year. Large numbers of music content are making it hard for people to search relevant music, especially when it is unorganized. Therefore, there is a need to organize all music content, but it is very time consuming to do manually. In order to simplify this process, some music applications like Spotify and Youtube Music implement recommendation mechanisms or systems [2]. This recommendation system can suggest a list of relevant music from the library and becoming popular nowadays and crucial to prevent their customer to move on to another service [3].

Recommendation systems use two main approaches, content based and collaborative filtering (CF). Content based approach focuses on item metadata or attributes. For example, a music described by genre, singer, producer, etc. Otherwise, CF approaches focus on user preferences and are called as personalized recommendation systems. This approach analyzes the relationship between user and item. Similar users tend to be interested in similar items. User similarity can be measured by their history or review. Afterwards, user-item relation is used to predict what item might be liked by other users similar to him. Suggested items may vary for each user, due to different interests. Thus, CF approach has become popular and widely used in recommending items [4].

In CF, matrix factorization (MF) becomes one of the most popular techniques besides neighbour-based using similarity metric. Unfortunately, MF performance impeded due to inadequately capturing an advanced structure of user interaction data. Thus, it is required to develop another technique by using MF approach to obtain better results [5]. Recommendation system nowadays widely implements hybrid techniques in order to overcome limitations of the CF approach [2, 3]. An approach by combining both CF and neural networks is one of the hybrid

techniques used widely for learning the interaction function from data [5].

Collaborative filtering approach combined with neural network or called neural collaborative filtering (NCF) enthrall this study. The aim of this study is to compare NCF with user-based CF. In this paper, we also implement collaborative filtering and neural collaborative filtering in a digital online music application. After a user logged in, the system will provide recommendations with the two methods along with the predicted rating.

This paper consists of 5 sections starting from the review from previous work in section 2, followed by methodology in section 3. In section 4, we discuss the experiment results of neural collaborative filtering compared with user-based collaborative filtering. Finally, we concluded our study with suggestions for future research in section 5.

2. Related Work

Recommendation system is a system that is used to predict an object as a suggestion to a related user. Suggested item expected to be liked or relevant to user's interest. It consists of two different strategies, which are the content-based approach and CF. Content-based approach, did its job by distinguishing the product's nature. CF on the other hand relies only on past user behavior. It then complicates the use in the beginning since it is unable to address products new to the system, and so called the cold start problem [6].

Collaborative filtering uses two types of input, those are explicit and implicit feedback. Those feedbacks are used as user-item interaction. For explicit feedback, data acquired explicitly from user input in response to portray if the user is interested in an item. However, not every user likes to give their thoughts about an item, so explicit data is not always available. This underlines the reason why we need to observe user behavior to acquire the implicit feedback. Examples of implicit feedback are mouse click, the number of times a video or music played, etc. An implicit feedback has an inherently noisy nature, it requires appropriate measures for evaluation, and the numerical value indicates confidence [6].

The CF approach is widely used in e-commerce, movie/video/music platform, food application, and social media - Facebook, Instagram, Twitter. There are two types in CF approach, those are: user-based and item-based. User and item-based CF are alike, where user-based search the items that a user interacted with. While item-based search which users interacted with this item. Collaborative filtering approaches are used widely nowadays. Research by [5,7–11] implemented CF and showed that CF resulted in high accuracy and suitable for recommendation systems. This approach has for about 2 thousand users, and the accuracy is 80-90% [9]. While research by [12] gives 0.8 and 4.5 as the highest RMSE and MAE value, respectively.

The principal in creating a neighbour-based CF recommendation system is to identify user similarity from their preferred items, then select top most similar k users [5,10,11]. Neighbour-based CF provides good recommendations. Research by [12] shows that multiple processes to predict rating with k=1 and use the average of item's ratings gives better performance in terms of precision, recall, accuracy, MAE, MSE, etc. Research by [3,11] shows that a recommendation system with kNN-based CF does well in predicting rating of song given the attributes with a small error value. Another method for CF is using latent vectors to represent users and items, called matrix factorization (MF) [7]. In this process, the inner product of those latent vectors become the interaction between user and item, or ratings. Latent-vectors factors are learned in MF method by minimizing the loss or difference between actual and predicted ratings [13]. Deep learning like recurrent neural network (RNN) can represent better user interest from the latent-vectors factors [14].

Even though those techniques perform well, it also has its deficiency. Therefore, fusing one technique to the others could be more promising in providing better recommendation. Nowadays, combining/hybrid techniques are used widely in machine learning and also recommendation systems. By combining technique, each technique is expected to overcome others' limitations [2,3,15]. One of which is by combining with neural networks for learning the interaction function from data. It is supported by a paper that stated that neural collaborative filtering (NCF) or combination of MF with neural network shows that NCF with 4 layers results in greater HR@10 and NDCG@10 value [5]. Another hybrid approach proposed by [14] called multiple user interest representation (MUIR), combined CF and content based filtering aspects using deep learning which resulted in better precision, recall, NDCG values compared to content based filtering and other methods. Based on those hybrid techniques, it shows that combined techniques produce better results and complement one's weakness.

3. Methodology

In this section, we will explain our steps on building a song recommendation system using user-based collaborative filtering and neural collaborative filtering as shown in Figure 1.
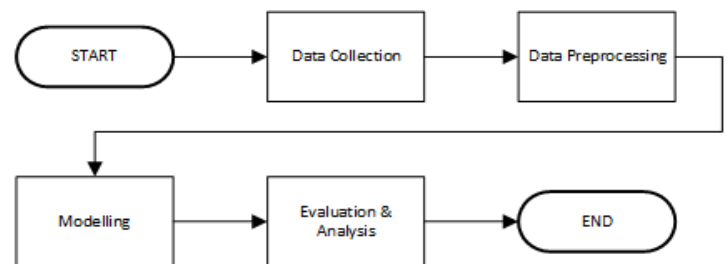
Figure 1: Steps of the Music Recommendation System Research

3.1. Data Collection

Data used in this study consist of users, music, and the total number of times the music was played. There are over 20,000 users, 6,105 music, and 470,759 records about the number of times music was played.

Figure 2 shows the ERD used in our digital online music application. The "playlistcount" (3rd) table contains the implicit feedback of the number of times each user heard a song. The "playlistrating" (4th) table shows the rating data of each user for a song that is heard. The 3rd table has a close relationship with 4th table where the rating is obtained from normalizing the number of times a user listens to a song. Calculation of normalization will be discussed in Chapter 3.2.
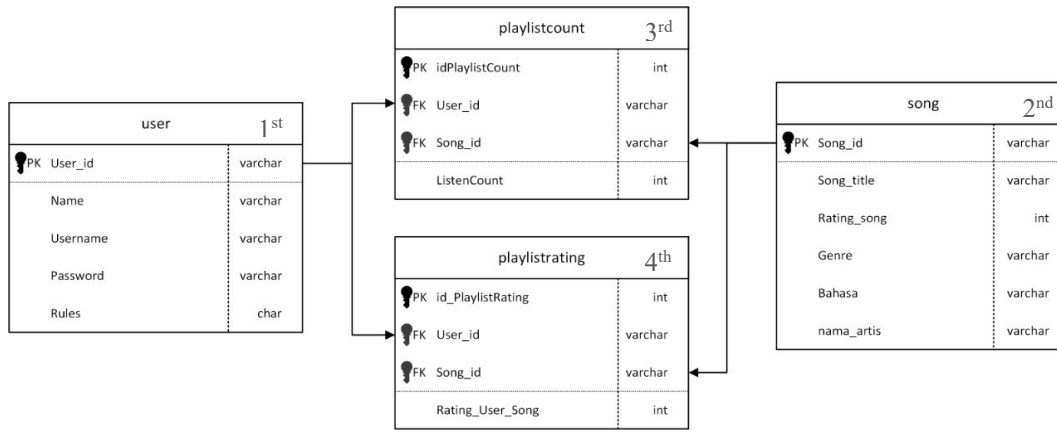
Figure 2: Entity Relationship Diagram of Music Data

3.2. Data Preprocessing

We need to normalize the number of times the music is played c_{ui} due to different habits each user is likely listening to. The normalize value then considered as rating r_{ui} – the rating from user u for item i as shown in Eq. (1):

$$r_{ui} = \frac{c_{ui}}{Max(c_u)} \times 100 \qquad (1)$$

The denominator of Eq. (1) search maximum number of times user u listened to a music. The rating value is then stored in the database on the 4th table as shown in Figure 2 and used for suggesting music content to each user. It is ranging from 0-100.

3.3. Modelling

To predict personalized music rating, we use two techniques, that is: user-based collaborative filtering and neural collaborative filtering. For those techniques we use the same preprocessed data discussed before. All models were run on Google Colaboratory with its GPU runtime.

3.3.1. User-based Collaborative Filtering

For user-based collaborative filtering, we first choose a user u, then we find similar user candidates by seeing if they have listened to the same music. Due to lots of users in the database, we use sample candidates of n users. Next, compute correlation or similarity between user u and similar users' candidate. In calculating the similarity of two objects, we can use similarity metrics, such as cosine similarity, pearson correlation coefficient (PCC), and mean square distance (MSD). In this study, we use PCC formula [7–9,12] as shown in Eq. (2):

$$r = \frac{\sum_{i=1}^{n}(x_i - \bar{x})(y_i - \bar{y})}{\sqrt{\sum_{i=1}^{n}(x_i - \bar{x})^2}\sqrt{\sum_{i=1}^{n}(y_i - \bar{y})^2}} \qquad (2)$$

In Eq. (2), x represents ratings from user 1, while y represents ratings from user 2. The output of pearson correlation (r) ranges from -1 to 1 representing how similar is user 1 and user 2. The value of r = -1 when there is a perfect negative correlation, r = 0 means there is no correlation at all, and r = 1 means there is a perfect correlation. Next, we sort similarity users in descending order as it represents the most similar preference with user u and choose the top 50 users. After that, we predict the rating.

There are several methods for predicting rating, such as weighted average (WA), mean centering (MC), and Z-Score (ZS) [12]. In this study, we use the weighted average method. Correlation value with the top 50 users then used as a weighting factor in order to calculate predicted rating by weighted average as shown in Eq. (3) [12]:

$$\dot{r}_{ui} = \frac{\sum_{j=1}^{n_{ui}} sim(i,j) * r_{ju}}{\sum_{j=1}^{n_{ui}} |sim(i,j)|} \qquad (3)$$

where:

- $sim(i,j)$ is the output of PCC of user i and j similarity
- r_{ju} is actual rating from user j of item u
- $\dot{r}_{ui}$ is predicted rating from user u of item i

In CF, we split data into two sections: training and testing. First, we take 5 given ratings by each user and use it as a testing data. Therefore, we have 376,617 as training data and 100,000 as testing data. While predicting test data, the model could output NaN values, so we do not consider when calculating errors.

3.3.2. Neural Collaborative Filtering

Neural collaborative filtering approaches combine general matrix factorization with neural network matrix factorization as shown in Figure 3. This model combines linearity of GMF and non-linearity of neural network in modelling user-item interaction. This model was built by using Keras. Extra preprocessing was implemented when building this model because our input data consist of strings. We then use labelencoder provided by the sklearn library to encode and decode user and music id. Encode is necessary to build the model while decode is used when predicting rating for the user.

For each input, that is: users and music, we create embedding or latent factor with a size of 64 for each item. Then, we multiply item and user embedding as a layer for general matrix factorization (GMF). For the neural network layer, it aims to learn user-item interaction representing predicted rating matrix. Concatenating the item vector with the user vector has been widely used in multimodal deep learning network. However, it does not consider user-item interaction [5]. So, we use a multi layer perceptron (MLP) to learn the interaction function. First, we concatenate item and user embedding and use four hidden layers

with 0.25 as a dropout rate. For each hidden layer we implement a linear activation function, ReLu R(x) as shown in Eq. (4). The value of R(x) ranges from 0 to infinite. Then, we concatenate GMF results with the matrix generated from the MLP layer as NeuCF layer. Last, the output of NCF is given by using ReLu activation function on NeuCF layer's output. The formula used in NCF model are shown in Eq. (5) - Eq. (7) [5].
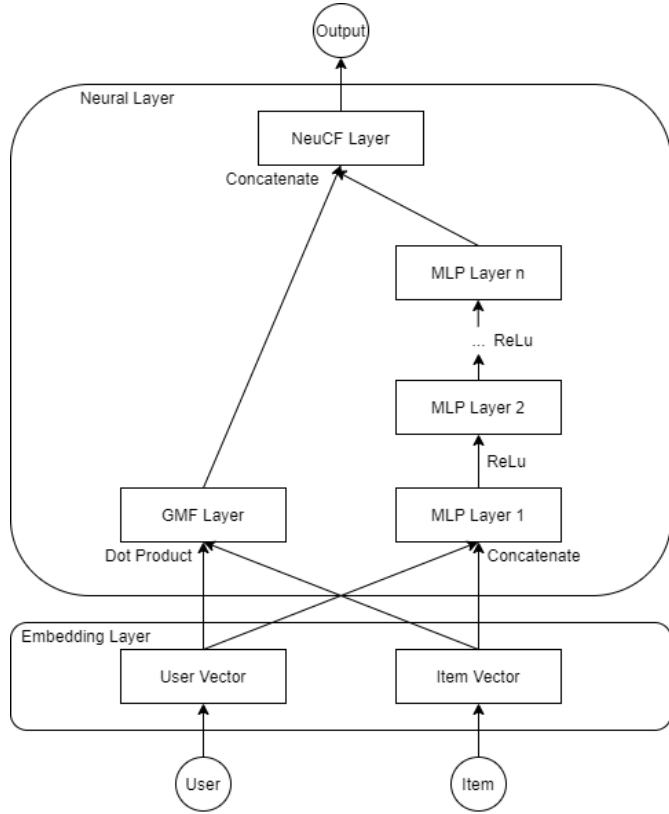
Figure 3: Structure of Neural Collaborative Filtering

$$R(x) = \max(0, x) \tag{4}$$

$$GMF = p_u \cdot q_i \tag{5}$$

$$\text{MLP} = \alpha_L \left(W_L^T \left(\alpha_{L-1} \left(\dots \alpha_2 \left(W_L^T \begin{bmatrix} p_u \\ q_i \end{bmatrix} + b_2 \right) .. \right) \right) + b_L \right) \tag{6}$$

$$y_{ui} = R \left(h^T \begin{bmatrix} GMF \\ MLP \end{bmatrix} \right) \tag{7}$$

For all formulas above, p_u and q_i denotes user and item embedding respectively. We define this task as a linear regression problem as we intend the output of NCF is the predicted rating value. Therefore, we use mean square error (MSE) as the loss function. Parameters used in this model are shown in Table 1.

Table 1: NCF Model Parameters

Variable	Value
Batch size	64
Epoch	10
Learning rate	0.001
Optimizer	ADAM

In the neural collaborative filtering approach, we split the data into training, validation, and testing data. The percentage of testing data is 20% of all data and 80% for training. The training data is then split into training and validation, with a percentage of the total data validation of 20% of the training data. Therefore, we have 301,285 as training data, 75,322 as validation data, and 94,152 as testing data.

3.4. Evaluation

Since the recommendation system output is predicted rating, we use regression evaluation metrics. We use mean absolute error (MAE), Mean Absolute Percentage Error (MAPE), mean square error (MSE), and root mean square error (RMSE) for the calculation. The evaluation and comparison of our music recommendation system presented as a value of actual and predicted music rating. The formula of each evaluation metrics is shown in Eq. (8) - Eq. (11):

$$\text{MAE} = \frac{\sum_{i=1}^{n} |y_i - x_i|}{n} \tag{8}$$

$$\text{MAPE} = \frac{\sum_{i=1}^{n} \frac{|y_i - x_i|}{y_i}}{n} \times 100\% \tag{9}$$

$$\text{MSE} = \frac{\sum_{i=1}^{n} (y_i - x_i)^2}{n} \tag{10}$$

$$\text{RMSE} = \sqrt{\frac{\sum_{i=1}^{n} (y_i - x_i)^2}{n}} \tag{11}$$

Where x and y represent predicted and actual value respectively.

4. Experiments

Our experiments take two steps, which are searching the best architecture used for NCF and comparing it with user-based CF. Table 2 and Figure 4 below shows the performance of NCF given different architecture on validation data. We test the model using 32, 64, and 128 latent vector factors or dimensions with 3 and 4 hidden layers. We use 3 and 4 hidden layers based on experiments by [5] which shows that 4 hidden layers results in better NDCG@10 value and 3 hidden layers once give the best NDCG@10 value. For every number of latent vector dimension, it is true that 4 hidden layers model gives less error than with 3 hidden layers. It also showed that 64 latent factor dimensions gives better error performance with about 5 value difference between the lowest error of 32 and 64 latent factors.

Table 2: Neural Collaborative Filtering Performance with Different Architecture

Layers	Factor	Highest Error	Lowest Error	Average Time to Build
3	32	29.123	20.271	13 minutes
	64	26.097	16.480	29 minutes
	128	25.655	24.086	55 minutes
4	32	25.799	15.879	15 minutes
	64	25.201	15.697	30 minutes
	128	25.397	23.676	57 minutes
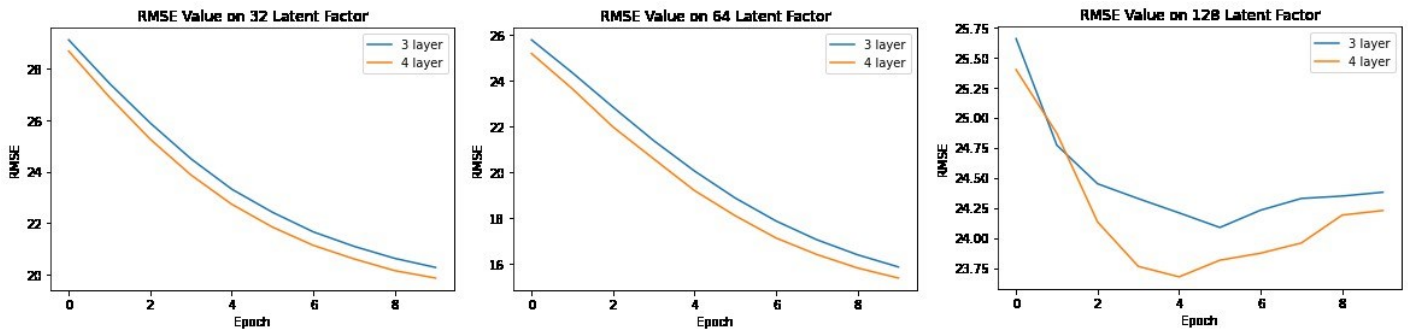
Figure 4: RMSE of Neural Collaborative Filtering on Testing Data

Evaluation metrics of CF and NCF shown in Table 3 below are calculated based on the 94,152-test data. Based on the result, it is shown that NCF is better than user-based CF, as it has lower error calculated with MAE, MAPE, MSE, and RMSE. Other than that, CF error has a big difference with NCF with about two times larger. These errors seem to be larger than other research mentioned before because we use a wider range of 0-100 for each rating. It is not surprising since there are some limitations in PCC. Some of the important limitations by PCC are that similar users could only be calculated if there is an overlap over the rated items and due to CF sparse data makes PCC results NaN measure [15].

Table 3: Collaborative Filtering and Neural Collaborative Filtering Performance

Method	MAE	MAPE	MSE	RMSE
CF	14.866	66.118	645.786	26.107
NCF	7.933	28.591	246.422	15.697

Table 4 below shows the predicted rating by using CF and NCF. We use 3 users given 7 sample music to see the difference between actual and predicted rating by both CF and NCF. The closest difference means that the framework predicts better results. NCF framework gets a 21/27 score and reflects that NCF provides more appropriate and optimal recommendations compared to CF.

Table 3: Sample of Recommendation Score

# User	# Song	Actual	CF Score	NCF Score	Winner
1	1	34	43.666	25.124	NCF
	2	13	28.5	10.368	NCF
	3	20	54.75	40.449	NCF
	4	17	13.3	18.745	CF
	5	17	19.66	22.226	CF
	6	3	27	25.456	NCF
	7	6	26.8	25.338	NCF
2	1	5	20.4	17.052	NCF
	2	50	58	51.9	NCF
	3	20	54.75	40.449	NCF
	4	5	13.5	13.961	CF
	5	5	17.666	6.296	NCF
	6	5	23.375	6.747	NCF
	7	11	85	34.424	NCF
3	1	33	30.2	26.475	CF
	2	33	23.25	29.868	NCF
	3	66	44	26.472	CF
	4	33	16.666	30.487	NCF
5		33	37.5	39.8	CF
6		33	13.666	40.82	NCF
7		66	33.2	44.707	NCF

Table 3 and 4 represent NCF framework is better than CF alone as it gets less error in predicting rating. Unfortunately, NCF needs more time to build a model with approximately 25-30 minutes with our model using Google Colaboratory GPU runtime. However, it is worth implementing NCF as it predicts more accurately and faster than user-based CF when using pre-build NCF model. The NCF model needs 5.24 seconds while CF needs 12.16 seconds in recommending music. Therefore, the NCF model must be trained first and stored so that in its application, it is only necessary to load the model.

The experimental results were obtained by following the stages, methods, and architecture described in Chapter 3. The parameters described in Chapter 3 are the best parameters to get optimum results based on several experiments such as changing the number of latent factor dimensions and the number of hidden layers. Other than that, we also consider the time to build the model with the difference of the errors.
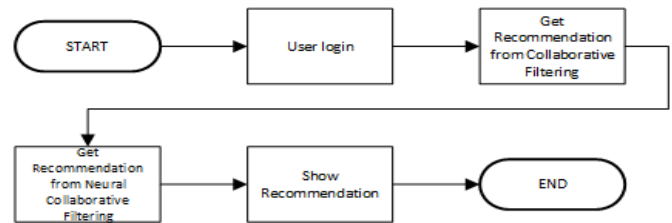
Figure 5: Application Workflow

The disadvantage of doing a load model is that it cannot cope with significantly changing conditions. The model is trained with existing data, if there is a change in behaviors, the model cannot handle it. To overcome this, the model must be trained regularly so that changes in user habits can be learned and the system provides appropriate recommendations. In this application, model training is carried out periodically using recurring jobs. With the recurring jobs that carry out training with the latest data, it is hoped that it can overcome significant changes in user behaviours.

An example of a user interface of our application can be seen in Figure 6. After the user logs in, 2 recommendation options will be given, using CF and NCF, this process on our application shown in Figure 5. On that page, the predicted rating for each recommended music is also displayed. There is no identical music on the top 9 recommendations based on CF and NCF. In NCF the predicted ratings are more varied rather than CF results.
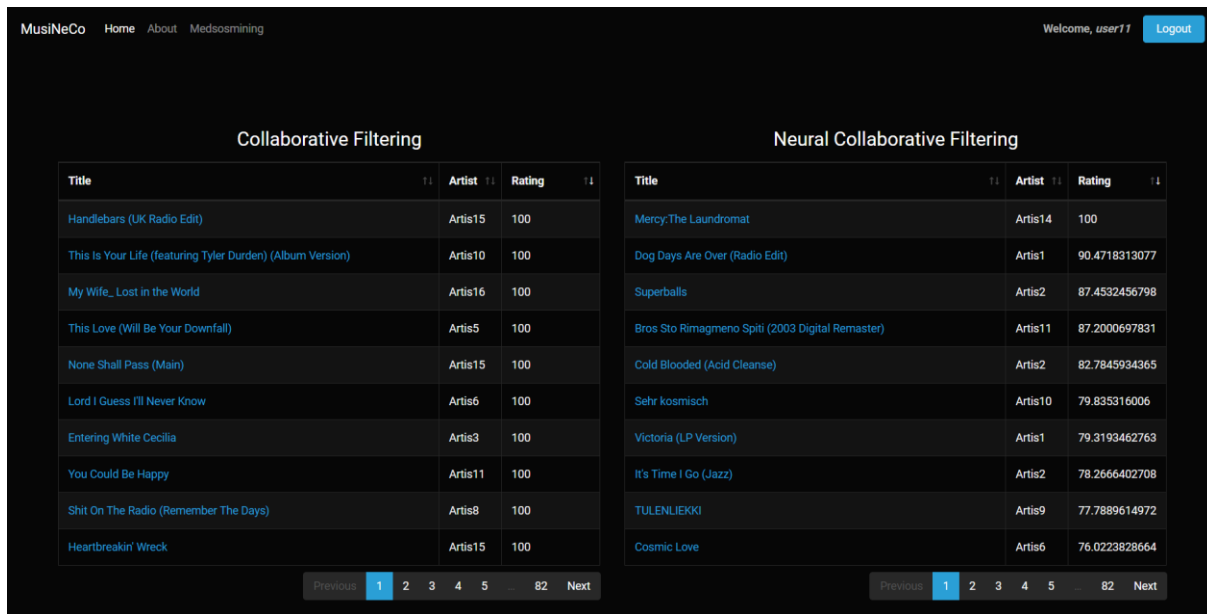
Figure 6: Music Recommendation Application

5. Conclusion

Our study focuses on NCF then compared with CF approach on music dataset. From the results discussed in Chapter 4, it can be concluded that NCF produces better recommendations than CF in terms of errors, predicting ratings, and time used to predict. It is unsurprising that NCF gives better performance since it learns the user and music embeddings that more similar users in the context of preferred music are closer to each other in the embedding space rather than single correlation calculation performed on CF. Moreover, recommendation model from NCF could be used repeatedly on giving recommendation without recalculating similarity between users when needed. However, building NCF model needs more powerful computation power due to massive matrix manipulation needed.

In addition to making comparisons between CF and NCF, we also make comparisons with several model parameters to the NCF model in order to obtain an optimal model. Model with more hidden layer may converge in a higher level of abstraction. It is proved in this study that four hidden layers model gives smaller error paired with small time difference when building the model compared with three hidden layers model. The result of this study can be implied to increase people's engagement with digital online music applications as it provides sufficient recommendations according to the user preference.

Although neural collaborative filtering has better results than collaborative filtering, this method has a weakness in terms of preparation time because it has to go through the build and training model stages. This stage takes a long time, so the alternative is to save the trained model and load the model to get recommendations. To solve the process time problem, the implementation of the application does not do real-time training instead, it loads a trained model. Further research on recommendation systems could contribute in proposing a new approach or combining several approaches to improve system performance, either in terms of times, effectiveness, errors, accuracy, or other performance metrics.

Conflict of Interest

The authors declare no conflict of interest.

Acknowledgment

References

[1] T. Schäfer, "The goals and effects of music listening and their relationship to the strength of music preference," PLoS ONE, **11**(3), 1–15, 2016, doi:10.1371/journal.pone.0151634.

[2] D. Sánchez-Moreno, A.B. Gil González, M.D. Muñoz Vicente, V.F. López Batista, M.N. Moreno García, "A collaborative filtering method for music recommendation using playing coefficients for artists and users," Expert Systems with Applications, **66**, 1339–1351, 2016, doi:10.1016/j.eswa.2016.09.019.

[3] D. Jayashree, S. Goutham Manian, C. Pranav Srivatsav, "Music recommendation system," Asian Journal of Information Technology, **15**(21), 4250–4254, 2016, doi:10.3923/ajit.2016.4250.4254.

[4] H. Liu, Z. Hu, A. Mian, H. Tian, X. Zhu, "A new user similarity model to improve the accuracy of collaborative filtering," Knowledge-Based Systems, **56**, 156–166, 2014, doi:10.1016/j.knosys.2013.11.006.

[5] X. He, L. Liao, H. Zhang, L. Nie, X. Hu, T.S. Chua, "Neural collaborative filtering," 26th International World Wide Web Conference, WWW 2017, 173–182, 2017, doi:10.1145/3038912.3052569.

[6] Y. Hu, C. Volinsky, Y. Koren, "Collaborative filtering for implicit feedback datasets," Proceedings - IEEE International Conference on Data Mining, ICDM, 263–272, 2008, doi:10.1109/ICDM.2008.22.

[7] N. Sivaramakrishnan, V. Subramaniyaswamy, S. Arunkumar, A. Renugadevi, K.K. Ashikamai, "Neighborhood-based approach of collaborative filtering techniques for book recommendation system," International Journal of Pure and Applied Mathematics, **119**(12), 13241–13250, 2018.

[8]   A. Gunawardana, G. Shani, "A survey of accuracy evaluation metrics of recommendation tasks," Journal of Machine Learning Research, **10**, 2935–2962, 2009.

[9]   A.S. Girsang, A. Wibowo, Edwin, Song Recommendation System Using Collaborative Filtering Methods, 2019, doi:10.1145/3369199.3369233.

[10] A.K. Azmi, N. Abdullah, N.A. Emran, "A hybrid knowledge-based and collaborative filtering recommender system model for recommending interventions to improve elderly wellbeing," International Journal of Advanced Trends in Computer Science and Engineering, **9**(4), 4683–4689, 2020, doi:10.30534/ijatcse/2020/71942020.

[11] S. Ayyaz, U. Qamar, "Improving collaborative filtering by selecting an effective user neighborhood for recommender systems," Proceedings of the IEEE International Conference on Industrial Technology, **1**(2), 1244–1249, 2017, doi:10.1109/ICIT.2017.7915541.

[12] P.K. Singh, M. Sinha, S. Das, P. Choudhury, "Enhancing recommendation accuracy of item-based collaborative filtering using Bhattacharyya coefficient and most similar item," Applied Intelligence, **50**(12), 4708–4731, 2020, doi:10.1007/s10489-020-01775-4.

[13] Y. Zhang, D. Liu, G. Yang, L. Hu, "Quantization-based hashing with optimal bits for efficient recommendation," Multimedia Tools and Applications, **79**(45–46), 33907–33924, 2020, doi:10.1007/s11042-020-08705-z.

[14] X. Chen, D. Liu, Z. Xiong, Z.-J. Zha, "Learning and Fusing Multiple User Interest Representations for Micro-Video and Movie Recommendations," IEEE Transactions on Multimedia, **9210**(c), 1–1, 2020, doi:10.1109/tmm.2020.2978618.

[15] L. Sheugh, S.H. Alizadeh, "A note on pearson correlation coefficient as a metric of similarity in recommender system," 2015 AI and Robotics, IRANOPEN 2015 - 5th Conference on Artificial Intelligence and Robotics, 2015, doi:10.1109/RIOS.2015.7270736.

ASTES

Analysis of the Bolivian Universities Scientific Production

Natalia Indira Vargas-Cuentas[*,1], Avid Roman-Gonzalez[2]

[1]*Image Processing Research Laboratory (INTI-Lab), Universidad de Ciencias y Humanidades (UCH), Lima, 15314, Peru*

[2]*Business on Engineering and Technology S.A.C. (BE Tech), Lima, 15076, Peru*

A R T I C L E I N F O	A B S T R A C T
	The Bolivian higher education system comprises 59 universities; these institutions have the challenge of increasing their scientific production since it is one of the factors to provide quality education and meet one of the 17 Sustainable Development Goals (SDGs). But currently, the GDP assigned to the research and development (R&D) sector of Bolivia is 0.16%. In this regard, this research aims to develop a scientific production assessment of the publications generated by Bolivian universities and indexed in SCOPUS in the last ten years. On the other hand, the universities included in the 2020 SIR World and SIR Iber rankings will be identified, and their scientific production will be reviewed. After conducting the analysis, it was observed that the country still has a low scientific production compared to the rest of the countries in the region, with a total of 3,451 publications indexed in SCOPUS and 303.97 publications per million inhabitants in the last ten years. The 2020 SIR World ranking shows that only one Bolivian university is in the ranking and holds the 774th position. For their part, 26 Bolivian universities entered the 2020 SIR Iber ranking. Among all these institutions, they produced 1,010 publications indexed in SCOPUS for the five years analyzed.

1. Introduction

The United Nations (UN) indicates that one of the 17 sustainable development goals is to provide quality education [1]; it is essential to speak of higher education for sustainable development in this context. That is why universities are encouraged to fulfill the mission of becoming centers of learning and research for sustainable development within their communities [2].

However, according to [3, 4], Bolivia's universities, together with other countries of the Andean region such as Ecuador and Peru, have not been structured in their beginning from substantial scientific communities. For this reason, the higher education systems of the three countries did not develop enough scientific bases, so they suffer from academic weakness at the institutional level [5].

Bolivia is a country located in South America; it is an Andean country with 11,353,100 inhabitants, according to data from the World Bank [6]. The GDP assigned to the research and development (R&D) sector in Bolivia is 0.16%, according to

UNESCO (United Nations Educational, Scientific and Cultural Organization) [7]. The country's higher education system comprises 59 universities registered in the Vice Ministry of Higher Education for Professional Training [8]. Bolivian universities are classified into autonomous public universities (11), private universities attached to the Executive Committee of the Bolivian University - CEUB (3), private universities (39), indigenous universities (3), and exceptional regime universities (3).

According to [9], one of the challenges of the Bolivian higher education system is that there is a difference between Bolivian public universities since they try to focus on three functions of higher education: training, research, and interaction, and contrarily private universities tend to focus on their teaching activities without focusing on doing research. The main reason [2, 10] is that most university teachers, especially in private universities, do not work full-time, which prevents them from getting involved in scientific research development. It is also mentioned in [5] that university teachers are overloaded with teaching hours and administrative work.

Given this limitation, according to [5] until 2006, many universities have promoted research infrastructure creation.

According to records, 17 research centers belong to private universities, 25 research institutes belong to government organizations, and 141 belong to the public university system, giving 183 research and development centers located mainly in three departments La Paz, Cochabamba, and Santa Cruz.

Besides, according to [11], there have been national policies to increase human resources in research, for example, the increase in postgraduate programs, both masters and doctoral programs in Bolivia, which left a total of 1,015 research professors and 631 research assistants, in addition to 4,014 completed investigations until 2014. However, these statistics do not include data from private universities. According to UNESCO, for the year 2020, the country has 2,218 full-time equivalent researchers [7].

Another important aspect is the number of Bolivian academic-scientific journals indexed in SciELO, RedALyC, and SCOPUS databases. According to [12], until 2011, Bolivia had six journals indexed in SciELO and one journal indexed in SCOPUS; these shows a scarce presence and not in all sources. However, these seven scientific journals included in prestigious databases for the scientific community at the regional and international levels increase Bolivian scientific production's visibility.

In this sense, scientific research and production are essential not only because they allow innovation, the resolution of social demands, and the country's technological development. Also, because there are metrics to classify universities, in which scientific production is an essential factor. This situation is the case of the Scimago Institutions Rankings (SIR) that develops two annual reports. One is SIR World, an institutional ranking of organizations from different sectors that produce research in the world. The other is SIR Iber, which shows the scientific activity of higher education institutions in Ibero-America [13, 14]. For an institution to enter SIR World, it needs a scientific production of at least 100 research articles indexed in the SCOPUS database per year. Also, to enter SIR Iber, the institution must have at least one document published and indexed in SCOPUS. Additionally, the Academic Ranking of World Universities (ARWU) uses different indicators, including the number of former students and staff who won Nobel prizes, scientific production, and the citation index [15].

The present research seeks to analyze the scientific production developed by Bolivian universities and indexed in SCOPUS from 2010 to mid-2020 and compare it with other countries' scientific production in the South American region. Moreover, the SIR World and SIR Iber report for 2020 will be analyzed to identify the Bolivian universities included in these rankings. Finally, the scientific production indexed in SCOPUS in 2019 and part of 2020 of the five Bolivian universities with the highest scientific production in Bolivia according to SIR Iber 2020 will be presented.

2. Methodology

2.1. Data sources

The data necessary for the development of this research work are the following:

- Scientific production: The data on scientific production in Bolivia and the rest of South American countries were extracted from SCOPUS, which is an international database that indexes scientific publications, covers scientific journals

and books from various publishers [12, 16]. SCOPUS belongs to Elsevier, a modern global information analysis publisher specializing in science and health [17].

Scientific production data were extracted from 2010 to the end of July 2020. Moreover, due to the constant updating of the database, it was decided to collect scientific production data on the same date, 07/27/2020, for all countries and institutions analyzed in this study.

- Population data: The number of inhabitants of the South American countries was extracted from the open-access data catalog prepared by the World Bank data team [6]; this catalog contains world population data. In all the South American countries analyzed in this study, the population data are updated until 2018.

- Bolivian universities: The list of Bolivian universities was extracted from the guide of universities of the Plurinational State of Bolivia [8], prepared by the Vice-Ministry of Higher Education for Professional Training; this Vice-Ministry is part of the Ministry of Education of Bolivia. This guide is the latest version published and is updated to the year 2016.

- Classification of Bolivian universities by scientific production, this list was extracted from Scimago Institutions Rankings (SIR) from both the SIR World report and the SIR Iber report; both reports correspond to the year 2020 and can be consulted at https://www.scimagoir.com/rankings.php. It should be mentioned that, although both rankings correspond to 2020, they are prepared based on data from five years from 2014 to 2018 [13].

2.2. Data preparation and analysis

In South America, there are 13 countries, all of which are culturally diverse, and their higher education systems have gone through different historical processes, so they present different scientific production levels. These factors added to the fact that all the regional countries have different sizes and amounts of inhabitants.

Therefore, to develop a fair comparison, this study proposes comparing South American countries' scientific production per million inhabitants.

$$P_i = \frac{P_S}{N_i} \, x \, 1\,000\,000 \qquad (1)$$

where:

P_i = Publications per million of inhabitants
P_S = Number of Publications indexed in SCOPUS
N_i = Number of inhabitants

As can be seen, the previous equation will allow a proper classification of the countries by their scientific production indexed in SCOPUS.

3. Results

The results obtained after processing and analyzing the collected data were divided into two sections for better understanding. The first section will show a comparative analysis of the scientific production indexed in SCOPUS in the 13 countries of South America. The second section will show the Bolivian

universities' scientific production indexed in SCOPUS and how they are positioned in Ibero-America and the country.

3.1. Scientific Production in South America

It is intended to analyze and compare the entire scientific South American region's scientific production to observe its evolution over the last ten years and, above all, to identify and diagnose the growth of scientific production in Bolivia.

Therefore, to develop a fair comparison, this study proposes comparing South American countries' scientific production per million inhabitants. As mentioned in the methodology section, the scientific production data was consulted on July 27, 2020.

According to the data obtained in the last column of Publications per million inhabitants (Pi), it can be observed that the country in the region with the highest scientific production per million inhabitants is Chile, with a total of 6,597.13 articles per million inhabitants. Secondly is Uruguay, with a total of 4,427.85 articles per million inhabitants. In the third position is Brazil, with 3,567.35 articles per million inhabitants. Then, there is Trinidad and Tobago, with 3,205.99 articles per million inhabitants. Argentina follows it with 3,193.68 articles per million inhabitants.

Subsequently, it is located in Table 1 Colombia, with 2,024.73 articles per million inhabitants. After Colombia, Ecuador can be found with 1,378.45 articles per million inhabitants. In the eighth position is Peru, with 791.61 articles per million inhabitants. Subsequently, Suriname is found with 776.05 articles per million inhabitants. Venezuela follows with 664.87 articles per million inhabitants. In the eleventh position is Guyana, with 587.93 articles per million inhabitants. Afterward is Paraguay with 343.58 scientific articles per million inhabitants and finally Bolivia with 303.97 articles per million inhabitants.

Figure 1 shows the difference between the total scientific production of the South American countries from 2010 to 2020 (A) and the scientific production per million inhabitants (B) during the same period.

As shown in Fig. 1 A), if only the total number of scientific publications were counted, Brazil would be found in the first place by a significant difference. However, when considering the

population factor, it can be observed in Fig 1. B) that Chile rises to first place. Another compelling case to comment on is one of Peru and Ecuador. It can be seen in Table 1 that Peru, until 2015, had higher scientific production than Ecuador. But as can be observed in 2016, Ecuador begins to increase its scientific production and exceeded the Peruvian scientific production. Additionally, it can be observed that Trinidad and Tobago, despite having a reduced scientific production that remains relatively constant throughout the ten years of study. When considering the number of inhabitants to calculate scientific production per million of inhabitants, this country is located in a good position within Table 1. Finally, Venezuela, unlike the rest of the countries in the region that are increasing their scientific production year after year, can be observed that Venezuela is decreasing its scientific production.
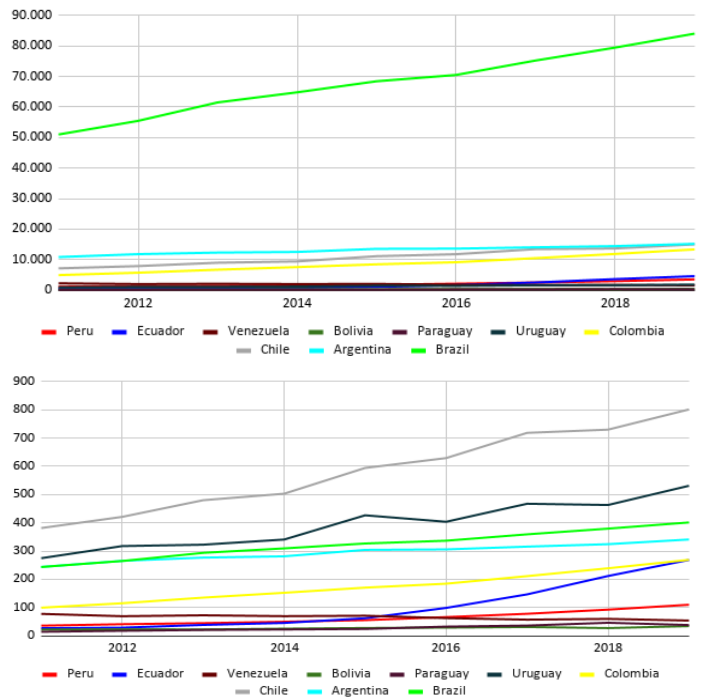
Figure 1: Scientific Production in the South American countries A) Total number of publications from 2010 to 2020 B) Publications per million of inhabitants (Pi)

Table 1: Scientific Production in the South American countries

Country	Number of inhabitants	2010	2011	2012	2013	2014	2015	2016	2017	2018	2019	2020	TOTAL	Pi
Chile	18,729,200	7,147	7,889	8,994	9,426	11,134	11,788	13,462	13,675	15,016	15,818	9,210	123,559	6,597.13
Uruguay	3,449,300	948	1,096	1,113	1,176	1,472	1,393	1,613	1,598	1,833	1,935	1,096	15,273	4,427.85
Brazil	209,469,300	51,028	55,492	61,532	64,848	68,472	70,543	75,270	79,505	84,090	86,815	49,655	747,250	3,567.35
Trinidad and Tobago	1,389,900	399	441	403	355	493	357	421	448	444	447	248	4,456	3,205.99
Argentina	44,494,500	10,851	11,807	12,322	12,526	13,539	13,616	14,052	14,437	15,177	14,800	8,974	142,101	3,193.68
Colombia	49,648,700	4,943	5,721	6,713	7,564	8,469	9,161	10,492	11,872	13,359	14,438	7,793	100,525	2,024.73
Ecuador	17,084,400	460	492	657	777	1,061	1,687	2,506	3,618	4,591	4,970	2,731	23,550	1,378.45
Peru	31,989,300	1,149	1,313	1,432	1,591	1,774	2,117	2,493	2,964	3,519	4,409	2,562	25,323	791.61
Suriname	575,991	15	12	27	40	23	40	65	51	67	71	36	447	776.05
Venezuela	28,870,200	2,240	2,002	2,096	2,006	2,052	1,807	1,650	1,729	1,558	1,355	700	19,195	664.87
Guyana	779,004	42	25	36	34	33	39	45	40	64	54	46	458	587.93
Paraguay	6,956,100	99	123	144	156	168	226	252	321	265	413	223	2,390	343.58
Bolivia	11,353,100	251	262	254	286	314	329	353	310	388	430	274	3,451	303.97

Source: SCOPUS database

In Bolivia's case, it can be observed that, although it is in the last position concerning the other countries of the region if the number of inhabitants is taken into account Fig. 1 B). However, it climbs ranks in Table 1, reaching the tenth position if only the total scientific production over ten years is taken into account Fig. 1 A), with a total of 3,471 scientific articles indexed in SCOPUS from 2010 to mid-2020.

Besides, from 2010 to 2017, Bolivia shows a growth in scientific production that remained relatively constant over time; Bolivia presents two decreases registered, one in 2012 with a reduction of 3.05% and another reduction of 12.18% in 2017. Also, it can be observed that there has been a growth in scientific production, especially during the last two years, since Bolivia presented an increase of 25.16% in 2018, which is the highest percentage of growth registered in the previous ten years. It has been possible to observe another increase reported in 2019 of 10.82%.

Finally, it can be seen that by the end of July 2020, Bolivia already presents a total of 274 publications indexed in SCOPUS, which represents 63.72% of the total scientific production of 2019. This percentage leads to thinking that this year will present growth in scientific production compared to what was obtained the previous year.

3.2. Scientific Production in the Bolivian Universities

As explained in the methodology section, the SIR World and SIR Iber reports were consulted to identify Bolivia's higher education institutions with the necessary scientific production to enter one or both rankings.

Consulting the SIR World 2020 report, it was found that only one Bolivian university is present in the ranking, in the 774th position was the Universidad Mayor de San Andrés (UMSA). This university is an autonomous public university located in La Paz, which is the seat of Bolivia's government. It is essential to mention that it is the first time that a Bolivian university has managed to overcome the fence of 100 publications and enter this ranking. The UMSA in 2018 managed to reach 110 scientific publications

indexed in SCOPUS, the reason that allowed it to represent the country in this ranking.

As consulted in SIR World [18], the Universidad Mayor de San Andrés published in 85 scientific journals and different areas of research, as can be seen in Fig. 2:
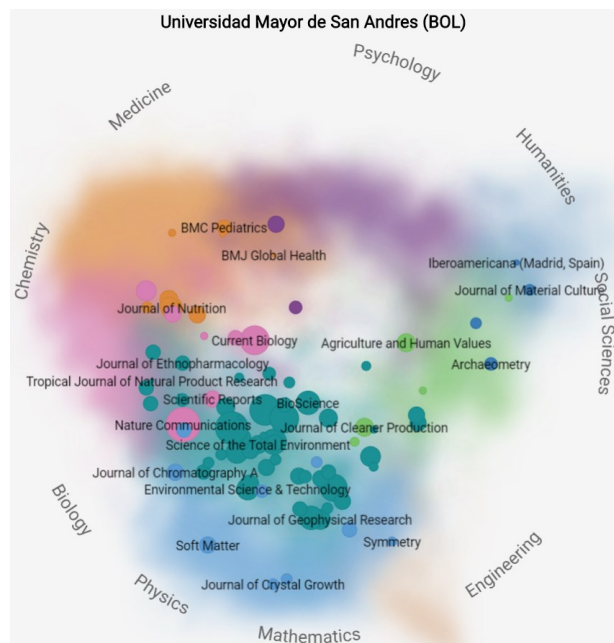
Figure 2: Research topics of the Universidad Mayor de San Andrés (UMSA) [18]

In Fig. 2, each circle's spatial position represents the scientific article's research topic; for its part, the colored spots indicate the research areas. The circles' size represents the value of the SCImago Journal & Country Rank (SJR) of the publication. It can be seen that there is a predominance of publishing in the areas of biology and medicine.

Furthermore, when consulting the SIR Iber 2020 report, the list of 26 Bolivian universities that accomplished to enter that Ibero-American ranking was compiled, as can be seen in Table 2:

Table 2: Bolivian universities in SIR Iber 2020

IBE	LAC	CO	Organization	Country	O	IC	%Q1	%Lead
343	255	1	Universidad Mayor de San Andrés	BOL	497	89.34	60.36	32.39
463	369	2	Universidad Mayor de San Simón	BOL	214	90.65	55.61	37.85
559	462	3	Universidad Autónoma Gabriel Rene Moreno	BOL	86	91.86	70.93	20.93
559	462	3	Universidad Católica Boliviana San Pablo	BOL	86	84.88	39.53	27.91
607	509	4	Universidad San Francisco Xavier de Chuquisaca	BOL	35	94.29	48.57	17.14
608	510	5	Universidad Privada Boliviana	BOL	34	91.18	38.24	20.59
616	518	6	Universidad Autónoma del Beni José Ballivián	BOL	26	92.31	73.08	19.23
625	527	7	Universidad Autónoma Tomas Frías	BOL	17	100	64.71	0
625	527	7	Universidad Técnica de Oruro	BOL	17	88.24	23.53	17.65
631	533	8	Universidad Autónoma Juan Misael Saracho	BOL	11	90.91	45.45	9.09
631	533	8	Universidad Privada de Santa Cruz de la Sierra	BOL	11	81.82	63.64	18.18
634	536	9	Universidad Amazónica de Pando	BOL	8	100	62.5	0
634	536	9	Universidad Andina Simón Bolívar, Bolivia	BOL	8	50	12.5	62.5
635	537	10	Universidad Privada Franz Tamayo	BOL	7	71.43	57.14	71.43
636	538	11	Universidad Pública de El Alto	BOL	6	100	33.33	0

637	539	12	Universidad Privada del Valle	BOL	5	100	60	20
638	540	13	Universidad de Aquino Bolivia	BOL	4	75	0	25
639	541	14	Escuela Militar de Ingeniería	BOL	3	100	33.33	66.67
639	541	14	Universidad Nuestra Señora de La Paz	BOL	3	66.67	66.67	66.67
640	542	15	Universidad de la Cordillera	BOL	2	100	50	0
640	542	15	Universidad Nacional Siglo XX	BOL	2	100	50	0
640	542	15	Universidad Nur	BOL	2	50	0	50
640	542	15	Universidad San Francisco de Asís	BOL	2	100	0	0
641	543	16	Universidad de los Andes, Bolivia	BOL	1	0	0	100
641	543	16	Universidad Privada Abierta Latinoamericana	BOL	1	100	0	0
641	543	16	Universidad Tecnológica Boliviana	BOL	1	0	0	100

Source: SIR Iber 2020 [14]

Table 2 shows the 26 Bolivian universities present in the SIR Iber 2020 ranking. Also, it can be seen in the respective position of the institution in Ibero-America (IBE) in Latin America (LAC) and in the country itself (CO) according to its scientific production. Besides, in column (O), the institution's total number of publications indexed in SCOPUS can be observed. Also, in the column (IC), the percentage of the institution's international collaboration with other scientific networks can be seen to develop joint research. Likewise, in the column (% Q1), it can be observed the percentage of scientific publications produced by the institution that are published in journals that are located in the highest quartile of each category of knowledge, according to the SCImago Journal Rank. Finally, in the column (% Lead), it can be seen the percentage of papers published by the institution whose principal researcher, that is, the corresponding author of the document belongs to that institution.

Also, it can be observed that the university in the first place is the Universidad Mayor de San Andrés, with a total of 497 publications indexed in SCOPUS. Followed by the Universidad Mayor de San Simón with 214 publications and in third place in the country is the Universidad Autónoma Gabriel René Moreno with a total of 86 publications indexed in SCOPUS.

It is essential to mention that most institutions have a high percentage of international collaboration (IC), except for four universities. This factor is favorable for Bolivian scientific production since it is crucial to forming scientific networks to carry out research and inter-institutional publications.

Besides, it can be observed that in the case of the Universidad Autónoma del Beni Jose Ballivián presents a total of 26 publications indexed in SCOPUS, of which 73.08% are published in journals that are located in the first quartile of the SCImago Journal Rank. This factor is an indicator of its scientific production's institutional capacity to reach a high expected impact level.

Finally, an essential aspect of analyzing is institutional leadership in scientific production. It can be seen that of the five institutions that lead the ranking in the country that the Universidad Mayor de San Simón is the one that presents the highest percentage of leadership with 37.85%. However, it can be observed that it is a low percentage, which means that although the institution is developing publications, the principal author, the corresponding author of the scientific publications, does not belong to the institution. Contrarily, there are universities with less scientific

production but with high leadership percentages, such as the Universidad Privada Franz Tamayo.

As consulted in the SIR Iber 2020 report and as summarized in Table 2, it can be indicated that six higher education institutions represent the first five places in the ranking of scientific production in Bolivia. There are six because there is a third-place tie between the Universidad Autónoma Gabriel René Moreno and the Universidad Católica Boliviana San Pablo with 86 publications indexed in SCOPUS.

Consequently, in Table 3, it can be seen the scientific production for 2019 and 2020 of the institutions corresponding to the top five positions in the country:

Table 3: Scientific production of Bolivian universities

University	Scientific Production indexed in SCOPUS	
	2019	2020
Universidad Mayor de San Andrés	99	84
Universidad Mayor de San Simón	51	27
Universidad Autónoma Gabriel Rene Moreno	14	14
Universidad Católica Boliviana San Pablo	21	11
Universidad San Francisco Xavier de Chuquisaca	10	3
Universidad Privada Boliviana	23	12

Source: SCOPUS Database

As previously mentioned, the SIR Iber report is a ranking that takes into account five years to perform its analysis. In this case, the 2020 report was prepared to take into account indicators corresponding to five years from 2014 to 2018. For this reason, Table 3 has been compiled the total number of publications indexed in SCOPUS for the year 2019 and part of 2020 to be able to observe the scientific production developed by the universities located in the top five positions in the country in recent years.

Therefore, in Table 3, it can be observed that the Universidad Mayor de San Andrés has registered for 2019 a total of 99 publications indexed in SCOPUS and for 2020 a total of 84 publications. If this institution keeps working, in the same way, it could reach the 100 scientific publications to be included again in the ranking SIR World.

Moreover, it can be seen that the Universidad de San Simón has a total of 51 and 27 indexed publications for the years 2019 and 2020, respectively. It can also be observed that the Universidad Autónoma Gabriel René Moreno had 14 indexed publications for

2019 and 14 publications so far in 2020. Subsequently, the Universidad Católica Boliviana San Pablo can be observed. It is essential to mention that this university is the first private university in the top five; this university has a scientific production of 21 indexed publications for 2019 and 11 publications for 2020. Also, it can be seen that the Universidad San Francisco Xavier de Chuquisaca presents a scientific production of 10 and 3 publications indexed in SCOPUS for 2019 and 2020, respectively. Finally, the second private university in the top 5 is the Universidad Privada Boliviana, with a scientific production of 23 indexed publications for 2019 and 12 indexed publications so far in 2020. If this university maintains the same production rhythm can ascend positions in the next SIR Iber report.

4. Discussion and Conclusions

Higher education institutions are called to guarantee the sustainable development goal of quality education, for which, in addition to teaching activities, they must concentrate on research and scientific production.

The scientific production in Bolivia is compared with the production of the other countries of the South American region for ten years from 2010 to the present; it can be seen that the country is among the last positions with a total of 3,451 publications indexed in SCOPUS and 303.97 publications per million inhabitants.

As has been observed, the scientific production indexed in SCOPUS of Bolivia has had a growth of 71.32% from 2010 to 2019. Still, to know if this growth has been accelerated or slow, it is necessary to compare Bolivia's case with another country's scientific production. For developing this comparison, Peru was chosen, an Andean and neighbor country. Peru presents a growth of 283.72% from 2010 to 2019; it could be said that its scientific production indexed in SCOPUS has almost quadrupled.

To analyze Peru's growth, it is necessary to mention that there have been fundamental changes in two of the three pillars that support research; since there have been changes at the State level and at the university level that strengthen its scientific production. Starting in 2013, the National Council of Science, Technology, and Innovation (CONCYTEC) have provided more funds for two large programs. The first is the development of theoretical and applied research by Peruvian universities, and the second is aimed at the repatriation of Peruvian scientists. Likewise, in 2014 the new university law was approved. With this, it was urged that all Peruvian universities could comply with the necessary quality conditions (CBC) to obtain a license granted by the National Superintendency of Higher University Education (SUNEDU) and continue in operation [19]. This law's critical point is that one of the necessary quality conditions required by SUNEDU is research. This condition has allowed the creation of research lines related to professional careers, increased teachers who carry out research, students with research skills, and a more significant presence of Peruvian universities in international rankings.

The low growth in Bolivia's scientific production could be due to several factors. For example, the Vice Ministry of Science and Technology (VCyT), which belongs to the Ministry of Education, focuses on strengthening science education programs and scientific dissemination. Still, it must expand its scope to the management and distribution of competitive funds for research. Furthermore, most university teachers, especially in private universities, do not work full-time. Additionally, teachers are overloaded with teaching hours and administrative work [2, 5, 10]. Besides, there is a lack of a repatriation program for Bolivian scientists specialized abroad, causing the loss of Bolivian talents. The impact of these factors is evidenced in the low quantity of full-time equivalent researchers in the country, which, according to UNESCO, are 2,218 full-time equivalent researchers for the year 2020 [7]. Finally, it can also be mentioned scarce funds to finance research projects and centralization of research infrastructure, since 183 research and development centers are located mainly in three Bolivia departments: La Paz, Cochabamba, and Santa Cruz [5].

However, the Bolivian government has identified some aspects that it must strengthen to increase its scientific production. In that sense, in 2016, it organized the First Meeting of Bolivian Scientists Living Abroad for Scientific and Technological Liberation [20], in which 54 researchers based in different parts of the world have participated together with representatives from ministries and private companies. This meeting had the objective of exchanging proposals and ideas to identify actions and mechanisms to strengthen science, technology, and innovation in Bolivia in the short, medium, and long term. It is essential to follow up and begin to implement the suggested strategic mechanisms.

Besides, it could be seen that of a total of 59 universities that constitute the university higher education system in Bolivia, only one institution could enter the SIR World report for the year 2020, ranking in the position 774th. Also, 26 universities are present in the SIR Iber 2020 report, which means that only 44.07% of the country's existing higher education institutions entered this ranking. They produced a total of 1,010 publications indexed in SCOPUS for the period analyzed. These scientific publications from higher education institutions represent 61% of the national total.

Besides, it was possible to observe that of all the institutions present in the SIR Iber ranking, 11 were autonomous public universities, 12 were private universities, and 3 were private universities attached to CEUB. This situation shows that 100% of autonomous public universities and private universities attached to CEUB managed to enter the SIR Iber 2020 report. Only 30.77% of Bolivian private universities managed to enter the ranking. Moreover, it has been possible to establish, as can be seen in Fig.3, that autonomous public universities have developed 84.36% of scientific production. In comparison, private universities attached to the CEUB have produced 8.92% of publications. Private universities have generated only 6.72% of the scientific production reported in the five years analyzed, which shows that 27 of the 39 private universities in Bolivia are not prioritizing research. This situation is evidence that, for the moment, private universities are not taking advantage of the existing relationship that some of these institutions have in a more significant way with the business production system of Bolivia. This factor is essential since a synergy could be generated; it would create spaces for research, innovation, and learning for both companies and universities.

It is essential to mention that at the time of compiling Bolivian universities' scientific production data in the SCOPUS database, it was possible to reveal that 89.83% of the country's universities

have not created their institutional profile. This factor is challenging to verify each institution's number of publications; in this sense, it is recommended that all higher education institutions in the country create their institutional profile in SCOPUS.
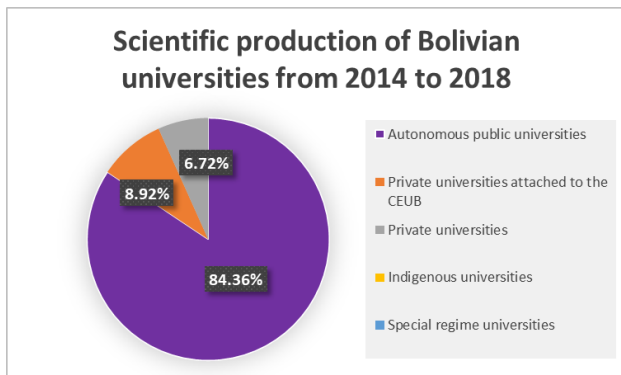
Figure 3: Scientific production of Bolivian universities from 2014 to 2018

Finally, analyzing the scientific production indexed in SCOPUS of 2019 and 2020, it can be observed that the Universidad Mayor de San Andrés is emerging to overcome the fence of 100 publications once again and represent Bolivia in the SIR Wolrd ranking.

We believe that Bolivia should begin to propose changes in a country's research tripod's policies and mechanisms, including the Bolivian state, universities, and industry, to strengthen scientific and research activities. It is also crucial to enhance the Vice Ministry of Science and Technology activities, which should begin by identifying national strategic priorities and calling on universities and other entities to develop research in those defined lines to achieve sustainable development.

It is crucial that in the future, the country can define national policies to promote scientific activities in higher education institutions, both in public universities and private universities.

Moreover, it is essential to start considering the implementation of programs for the repatriation of scientists to avoid the brain drain, which is a phenomenon that is currently observed in Bolivia. It is also necessary to strengthen existing postgraduate programs and create new ones, as this will allow increasing the research-trained resources in the country.

Finally, other countries' steps in the region can be analyzed and followed. For example, Ecuador and Peru's case, whose firsts steps were to define priority research lines in the country and develop calls for competitive funds to finance research projects following those research lines.

Conflict of Interest

The authors declare no conflict of interest.

References

[1] UNESCO, Education for Sustainable Development Goals: Learning Objectives, UNESCO, 2017. ISBN 978-92-3-100209-0

[2] L. I. Litzner Ordóñez, W. Rieß, "La Educación para el Desarrollo Sostenible en la universidad boliviana. Percepciones del profesorado". Teoría de la Educación. Revista Interuniversitaria, 31, 149–173, 2019, DOI: http://dx.doi.org/10.14201/teri.19037.

[3] C. Weise, La construcción de políticas públicas universitarias en el período neoliberal: estado y universidad, contradicciones en una década de desconcierto: el caso de Bolivia, Master's Thesis, FLACSO, Argentina. 2005. http://hdl.handle.net/10469/1057.

[4] C. Weise, J. L. Laguna, "La educación superior en la región andina: Bolivia, Perú y Ecuador" Revista da Avaliação da Educação Superior (Campinas), **13**(2), 425-450, 2008, https://doi.org/10.1590/S1414-40772008000200009.

[5] G. Rodríguez Ostria, C. Weise Vargas, Educación Superior Universitaria en Bolivia –Estudio Nacional, Cochabamba: Iesalc-Unesco-Editorial Talleres Gráficos «Kipus», 2006.

[6] World Bank Data Team (2018). World population 2018. World Bank open access data catalog. Available in: http://databank.worldbank.org/data/download/POP.xls [30 July 2020]

[7] UNESCO (2020). Global Investments in R&D. Fact Sheet No. 59. FS/2020/SCI/59. Consulted: [21 August 2020]. Available in: http://uis.unesco.org/sites/default/files/documents/fs59-global-investments-rd-2020-en.pdf

[8] Viceministerio de Educación Superior de Formación Profesional – Ministerio de educación de Bolivia (2016). Guía de Universidades del Estado Plurinacional de Bolivia. Available in: https://www.minedu.gob.bo/files/publicaciones/vesfp/dgesu/GUIA-UNIVERSIDADES-2016.pdf [29 July 2020]

[9] G. R. Ostria, "Debates y desafíos: Reformas de la educación superior en Bolivia, una sociedad multicultural" Policy Futures in Education, **7**(5), 513-531, 2009, https://doi.org/10.2304/pfie.2009.7.5.513.

[10] A. Martínez Barrientos, S. Santillán Butrón, M. Loayza Melgarejo (2016). Educación Superior en Iberoamérica. Informe Nacional: Bolivia.

[11] UNIVERSIA (2016). Educación superior en Iberoamérica. Informe nacional: Bolivia [Online]. Consulted: [14, July, 2020] Available in: https://cinda.cl/wp-content/uploads/2019/01/educacion-superior-en-iberoamerica-informe-2016-informe-nacional-bolivia.pdf

[12] S. E. Miguel, "Revistas y producción científica de América Latina y el Caribe: su visibilidad en SciELO, RedALyC y SCOPUS" Revista Interamericana de Bibliotecología, 34 (2), 187-199, 2011, ISSN: 0120-0976.

[13] Scimago Institutions Rankings (2020). Ranking Methodology. [Online]. Consulted: [21 July 2020]. Available in: https://www.scimagoir.com/methodology.php

[14] F. De-Moya-Anegón, E. Herrán-Páez, A. Bustos-González, E. Corera-Álvarez, G. Tibaná-Herrera, F. Rivadeneyra. Ranking iberoamericano de instituciones de educación superior 2020 (SIR Iber). Granada: Ediciones Profesionales de la Información, 2020. ISBN: 978 84 120239 3 0 https://doi.org/10.3145/sir-iber-2020

[15] Academic Ranking of World Universities (2019). ARWU 2019 Methodology. [Online]. Consulted: [26 July 2020]. Available in: http://www.shanghairanking.com/ARWU-Methodology-2019.html

[16] Elsevier (2020). All solutions: SCOPUS. [Online]. Consulted: [06 August 2020]. Available in: https://www.elsevier.com/solutions/scopus

[17] Elsevier (2020). Elsevier history. [Online]. Consulted: [10 August 2020]. Available in: https://www.elsevier.com/about/history

[18] Scimago Institution Rankings (2020). Institution Universidad Mayor de San Andres. [Online]. Consulted: [14 August 2020]. Available in: https://www.scimagoir.com/institution.php?idp=609

[19] Superintendencia Nacional de Educación Superior Universitaria. (2015). Modelo de licenciamiento institucional y su implementación en el sistema universitario peruano.

[20] E. A. G. Rocha, M. G. G. Alvestegui, A. S. G. Amaya, U. F. M. Covarrubias, S. A. Q. Condoretty, L. L. Torres, M. M. SupAgro, "Encuentro de Científicos Bolivianos Radicados en el Exterior, para la Liberación Científica y Tecnológica: Comentarios Breves", (2016).

Wireless Sensor Networks Simulation Model to Compute Verification Time in Terms of Groups for Massive Crowd

Naeem Ahmed Haq Nawaz[*,1], Musab Bassam Al-Zghoul[2], Hamid Raza Malik[2], Omar Radhi Aqeel Al-Zabi[2], Bilal Radi Ageel Al-Zabi[2]

[1]*Department of Computer Science, Umm Al-Qura University, Makkah Al-Mukarmah, 24381, Saudi Arabia*

[2]*Department of Computer Science, Umm Al-Qura University, Al-Qunfida, 28821, Saudi Arabia*

A R T I C L E I N F O	A B S T R A C T
	Everyone needs fast response or output against its request or need. Therefore, technologies are used to make the processing fast and accurate according to our needs. But in some situations, still we need to do more. Especially, when we need to process a massive or huge crowd of people in limited time frame such as at airport, religious gatherings, at stations etc. As the verification time increases crowd also increases and causing problems such as missing of the next flight, causality in religious gathering. Also, percentage of usefulness of verification system decreases and vice versa. Currently, different approaches are being employed to reduce verification time such as decentralized, distributed, queuing etc. But each of the approach has its merits and demerits. In order to minimize this problem, one of the solutions is to perform group (cluster) based verification. The reason behind is that as religious or tourist visits are done in groups, therefore, we can easily perform the group verification to make the verification fast in context of time. Further, we can set the limit where we need the group verification and where we can go through the normal verification (one by one). In this paper, we presented a Wireless Sensor Network (WSN) simulation model to calculate verification time in the groups form for massive crowd. We discussed the different scenarios for a group such as all group (cluster) members (CMs) are same and within the range or out of the range of cluster head (CH), CMs and non-CMs are within the range or out of range of the CH. We considered the pilgrimage as use case to compare the verification time taken by existing system and proposed system in context of time. We also compared the verification time with respect to verified and unverified CMs (CMs) in a group verification model. By optimizing the number of CM members in a group will decrease the number of unverified CMs (the drop rate), hence the performance of the group verification will be increased by minimizing the group verification time.

1. Introduction

We need to develop a new system or setup to achieve some important factors such as reducing the time, cost, improving the quality and increasing the security. Time is an important factor among the other factors to measure the usefulness of a system. In the verification systems, if verification time is increased its percentage of usefulness is decreased and vice versa. Especially, in time constrained or real time systems, margin for time delay is very low among the other systems. Nowadays, everyone needs fast response or output against its request or need. We are using

* Corresponding Author: Naeem A Nawaz, Ummal Qura University, nanawaz@uqu.edu.sa

technologies to make the verification fast and accurate according to our needs. But in some situations, still we need to improve, especially, when we need to process a massive or huge crowd of people in context of time. When a crowd exceeds from its given limit in term of capacity then it is called massive crowd. Standard size of massive crowd varies according to the nature of the crowd as given in [1]. Some places cause congestion or bottle neck when verification is required such as at airport, at stations, religious gatherings etc. In order to make the verification fast, distributed verification is introduced and it requires verification at different places. For instance, in case of airport, verification will be done first at country of departure and then at country of arrival. As the verification is done one by one by using the new technologies, it

makes the verification fast but not fast enough in case of massive crowd. Even then there become long queues and cause problems such as missing of the next flight at airports, causality in at religious places during religious gathering or sports gathering in stadiums. To minimize this problem one of the solutions is to verify the crowd in in group form. The group verification will provide help to reduce the time for crowd verification at public area hence provides safety from causality, stampede and terrorist attacks. In order to adjust the massive crowd according to the capacity of the area an approach is discussed in which capacity estimation is done by counting the number of the persons getting in and out from the specific area according to capacity by using WSN [2]. In WSN based identification model, grouping technique and different operational phases are discussed and has been compared with existing system [3]. WSN architecture is an efficient solution to problem by exploiting the capabilities of wireless sensor network to collect required data in the form of clusters. Supplying of food is done in cluster form according to a given limit of time [4]. The time series clustering is presented it also include general-purpose clustering algorithms. In time series clustering studies, general-purpose clustering algorithms are used to evaluate the performance of the clustering results. Results can be obtained either in the forms of raw data, extracted features, or some model parameters. On the basis of results, comparison between two time series can be done [5]. The conceptual model for WSN based smart movement is discussed by [6]. At node level energy is consumed by sensing-module to sense the data, microprocessor process the data and data is forwarded by radio communication. This consumption of energy causes other limitation such as network life- time and limited abilities to perform different task. To increase the performance of WSN, one of the solutions is to make the clustering of sensors [7].

The cities of Makkah and Madinah are crowded during Hajj and Umrah. Therefore, the crowd needs to be managed in these days. The problem of such a crowd is that how to make verification of pilgrims at different place as pilgrims are moving from place to place and between cities. This goal can be achieved by verifying the crowd in group form with the help of WSN.

Other technologies will also provide help to achieve the goal. For example Cloud computing system can facilitate the pilgrims to access data, it does not matter how far away are they from the physical location of the resources of the hardware and software. [8]. Internet of Things (IoT) allows pilgrims to connect with anyone, at any time, at anyplace with the help of devices by using Internet services [9]. In the same way, it helps the government to used management approach not only optimizing data but also considers prominent governance structures planning [10].

In this paper, single group scenarios, their designs and simulations are discussed to calculate the verification time for optimal number of CMs (pilgrims) in a single group. At the end, comparison of the existing system and proposed system verification time is performed.

1.1. Paper Layout

In section 2, we briefly discuss the background. Section 3 presents verification of the crowd approaches or strategies. Section 4 depicts the proposed group (cluster) verification model according to single Group (cluster) approach and operational

phases. Section 5 elaborates the proposed scenarios for single group (cluster) verification approach, section 6 offers design of algorithms for CH and CMs, section 7 gives the simulation setup for proposed model. Section 8, simulation scenarios in Contiki/Cooja and a brief review of the existing system. Section 9 explains the simulation results and comparison between existing and proposed system verification time. Section 10 represents the conclusion and future directions.

2. Background

In this section, we present the previous work and the technologies involved to improve the verification time for massive crowd. A solution is proposed to solve the storage problem by using the distributed collection of the data collection [11]. An Adaptive Collection scheme based on Matrix Completion (ACMC) is proposed and compared with other data collection schemes to reduce delay and to improve the energy utilization of the network. [12]. Manufacturing Internet of Things (MIoT), provides the data analytics about massive volume of data, heterogeneous data and real-time velocity of manufacturing data [13]. The clustering of the WSN is a problem because of diversity of WSN applications. In order to evaluate clustering different parameters are considered. After comparisons with different techniques they concluded that with low energy consumption, high data delivery rate centralized clustering solutions based on the Swarm Intelligence paradigm are more efficient for applications [14], [15]. The concept of local density to find each point of density to avoid the connecting the clusters having different capacities. They used Hadoop platform running MapReduce, clustering big data with varied density [16]. Nearest Point with Indexing Ration (NPIR) tries to solve some limitations of clustering by using non-spherical clusters, clusters with unusual shapes, or clusters with different densities. NPIR is evaluated real and artificial data sets of different levels of complexity, number of clusters and points. Results showed that NPIR performance is good Homogeneity Score, Completeness Score, V-measure, and Adjusted Rand Index [17]. A review and analysis the method is used to find the better clustering mechanism to get high efficiency. Different methods have been studied and discussed their advantages are highlighted to provide help the selection of and efficient clustering mechanism [18]. The possibilities of a Wireless Sensor Network support (WSN) for a Fog computing system in disposable intelligent wireless sensors is presented. With the coordination of augmented reality, an environmental monitoring system and communication infrastructure, in the framework of a next-generation emergency management system can be developed. [19]. A strategy Wireless Power Transfer (WPT) is used to divide the load of the CH. Each CM node in the cluster will transfer a specific amount of energy to get red the CH from a whole load instead it will bear a part of the whole load in this way lifetime of WSN is increased [20]. The concept of mobile as a service model is explored as "tri-opt". "Tri-Opt" means electric powertrains, new model cars and growth in smart cities [21]. The capacity estimation in the context of dynamic position and events by using zones and levels is done to process the crowd [1].

The definition of the IoT covering the different application from different field such healthcare, transport, verification, education, transport, and also provide help to crowd [22].

Simulator can be used efficiently if we evaluate the things from the top level. Because topologies, data collection and protocols give better performance at top level and are the best for simulation [23]. An emulator is used to run the test bed to evaluate WSN applications in primarily level. If test bed is successful, then large scenario is used in real time environment. We will work on the software level for the implementation, but in future, the same scenario can be implemented on a hardware device. Full Function Devices (FFDs) and Reduced Function Devices (RFDs) are two standard classes of an LR-WPAN devices. FFDs have the advanced capabilities such as synchronization of nodes and forward data packets in multi-hop communications. But the job RFDs is to communicate with FFD [24]. Link layer acknowledgments do not result from packets that are sent a broadcast. But in principle of Contiki MAC, during full wake-up interval, the sender sends the packets repeatedly to make ensure that it is received by all neighbors [25]. An inexpensive Clear Channel Assessment (CCA) mechanism used by Contiki MAC wake-up. It checks an indication of radioactivity on the channel with the help of Signal Strength Indicator (RSSI) of the radio transceiver. It compares RSSI with a given threshold and returns positive if the RSSI is below. This indicates that the channel is clear. If RSSI is above the given threshold then it returns negative result. This indicates that the channel is busy [26]. If it is considered that each receiver has a specific time period of wake-up interval, then sender can optimize the sending of data by using the wake-up phase time period. The receiver can read the link layer acknowledgement to get information about receiver's wake-up time. To overcome this problem, we have used multi-hop communication between CMs and their respective CH [27].

Due to one by one individual verification, the existing system is unable to process the crowd speedily or it goes for random identification and verification. Furthermore, if crowd verification is done in group (cluster) form and data is pre-written on the devices, the crowd verification time can be reduced. By using group (cluster) verification for crowd, we do not need the random identification and verification because group (cluster) verification minimizes the time.

3. Present Implementation of Crowd Verification

The present verification process for crowd or religious crowd is done person by person at different points such as entrance points of the country borders, airports of departure and airports of arrival, entry points at city or the entry points of the religious places. This verification process is needed again and again because after verification people travel on the routes or stay at the places where other unverified people are staying. For example, in case of Hajj (Pilgrimage) crowd stays among the people without Hajj permit. Therefore, on crossing the city of the Holy Makkah border again, they need verification of Hajj permit again. When the pilgrims go to the Hajj events places (Al-mushier), they again need verification so that people without Hajj permit can be prohibited. Currently verification process is divided among the airport of departure and airport of arrival for some countries. But in case of any internet problem or hacking among the countries of departure and arrival, it causes a big problem.

We mused about the other technologies such as smart cards, mobile phone and WSN devices with queue verification to handle the crowd but as mentioned the nature of the crowd they are not good users of technologies and also smart mobile will increase the cost that is not affordable for every pilgrim. Subsequently, we pondered about cluster approach and pre-stored data because data are collected and stored a long time before the pilgrimage process. Group (cluster) of pilgrims will be controlled by the well-trained person as a CH. Each CM has the simple reusable sensing device and proactive approach to pre-stored the data on CM device for verification. Simple reusable device means it has few buttons with different color and functions, there is no special expertise required to use it. Reusable means on the return of the device data can be burnt for new pilgrims and it is a cost-effective solution.

4. Proposed Group Verification for Massive Crowd

The proposed group (cluster) verification for crowd is an idea taken from sensing as a service model to minimize the crowd verification time by performing the verification in group (cluster) form not one by one. The distinguishing feature of this proposed group verification model is that it enables the verification of pre-stored data in cluster form. Consequently, we minimize the verification time for crowd. The use of sensor devices is multiple purposes other than data collection and transmission. The current crowd verification implementations usually take more time and therefore at some checkpoints it is done randomly. However, the proposed model can benefit in many ways, the most important of which is cluster verification, pre-stored data storage and fast crowd verification. For instance, if the proposed model is unable to implement to the whole crowd then it can be implemented at a specific part or aged pilgrims. It can be implemented according to the nature of the crowd where fast verification is required and it is compulsory such as in case of COVID-19. Because verification is slow it causes massive crowd according to the space available and it became difficult to maintain social distancing.

The proposed group verification for crowd (Pilgrims) steps at the airport as a use case are:

- At the time of biometric, identification along with CM device and passport interchange is done. CM devices are already indexed according to the arrival schedule of pilgrims.
- Data verification from CMs to CH
- Data verification from Cluster Head (CH) to server (immigration system)

The step to verify visa number by scanning the passport or entering the visa number of pilgrims will be done automatically in group (cluster) form by CH, as CH has pre-stored data of pilgrims. After group (cluster) verification by immigration, pilgrims will be free to collect their luggage. The remaining steps, printing of sticker for schedule, pasting of schedule, writing of reference number and entry stamp on passport will be done by the immigration in cluster (bulk) form. The passport, after entry stamp will be collected by the company from the immigration department. Because as a rule, passports of the pilgrims are possessed by the company not by the pilgrims. In this way, group verification will minimize the waiting time for pilgrims and further steps minimize the significant amount of crowd verification time.

In the last decade a lot of research has been done to improve the WSNs architecture and protocols to get efficient results in the implementation of different applications. Technologies are on the way and have provided cheaper, powerful and smaller wireless devices. These cheaper, powerful and smaller wireless devices are supporting to the multiplicity applications of WSNs in low-power standard [28].

The combination of different technologies with WSN will provide strength to different applications in different fields of life such as smart home, smart cities, smart cars, healthcare, education, online smart marketing etc. The time verification process involves different phases such as; sensor registration, sensor dispatching, sensor grouping or clustering [3]. Our main focus is on the group (cluster) verification with respect to time. As mentioned in the previous phases that the sensor devices are registered from the servers. The CH will generate the list of its CMs by using the CM_ID and CM will response its request. When CM_ID will be verified, then status will be updated by the name of entry point.

5. Group Verification Scenarios for Massive Crowd

In a single group verification approach, we discussed different for a single group (cluster) with CH and its CMs. In different group verification scenarios, we used different numbers of the CMs within a single CH transmission range. Further, we discussed the scenarios to check the performance, if some of the CMs are out of the transmission range of the CH, if there are CMs and non-CMs, but within and out of range of the single CH transmission range. We write the algorithms to handle different scenarios for a single group.

5.1. Different number of CMs (5, 10, 15, …, 50) within single CH range

We used different numbers of the CMs (5, 10, 15, ….) within a single CH transmission range, as illustrated in Figure 1. This provides us the maximum number of CMs that can be supported by a single CH. It also provides us with the maximum number of the CM verified by a single CH. By this approach, we can fix the number of the pilgrims (people) in one group for the best or optimize group scenario. Implementation of this scenario as a use case is at the airport in the immigration hall where group (cluster) formation area is allocated.
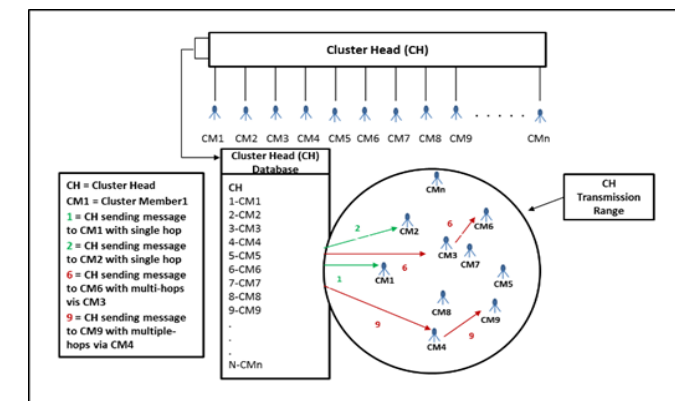
Figure 1: Different Number of CMs (5, 10, 15, …, 50) Within Single CH Range

5.2. CM Devices Belong to Single Group (cluster) but some out of CH Range

The scenario given in Figure 2 is considered at the places where CMs of the single CH are in scattered form. Some of them may be out of transmission range of the CH. For example, CMs are scattered or misplaced at the airport and are waiting in lounge. In such situations, the out of transmission range CMs can be communicated via nearby CMs with the help of multi-hop communication to pass the message. In this way, all CMs can be communicated for any activity or verification. If we want to identify our CMs, then the verification message can be generated and as a verification, CM_LED turns green (flag sets to 1).
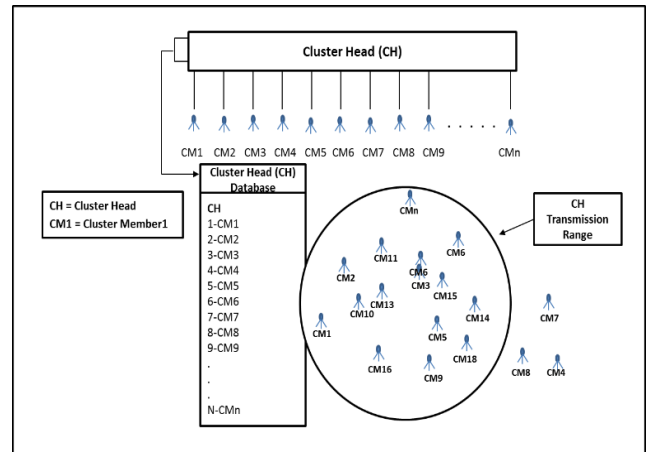
Figure 2: CMs Devices Belong to Single Group (cluster) but Some Out of CH Range
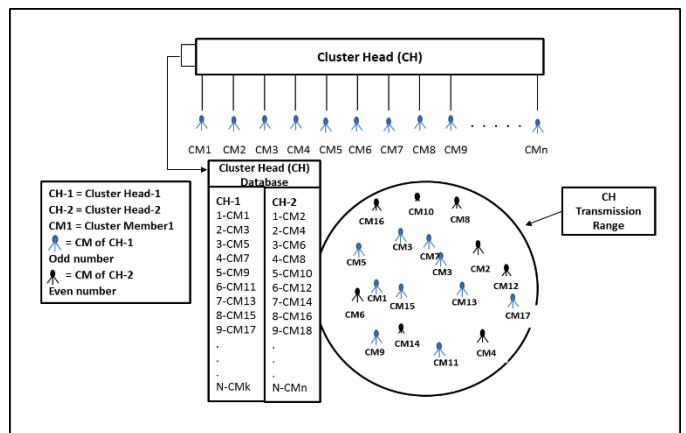
Figure 3: Single CH Having Different CMs Devices Within Range

5.3. CH having different CMs devices within range

The scenario given in the Figure 3, discussed to check the performance of the CH, if some non-CMs become within the transmission range of a CH. With the help of this scenario not only we check the performance, but also in the future we extend the feature that the CH identifies the non-CM's CH and inform to the concerned CH via server that one of CMs is within my group (cluster) range. This will provide help, in case the pilgrims lost and mixed with another group, then it can be easily identified by the current location. For example, CM_2 belongs to the CH-2 but currently, it is under the CH-1, then CH-1 will inform CH-2 that

one of your CM_2 is with me at this location. In another case, CH-1 can detect the location of CH-2 and guide CM_2 about the location of its original CH (CH-2). CMs belong to different groups (clusters) are represented by light and dark color scheme.

5.4. Different CMs devices but some out of CH range

The scenario given in the Figure 4, discusses the performance if there are CMs and non-CMs and some CMs remain outside the CH transmission range. By this scenario, we see the communication effect between CH and CMs outside the transmission range in presence of non-CMs. This scenario is applicable when CMs of the different group (cluster) mixed with each other and some of them are out of range.
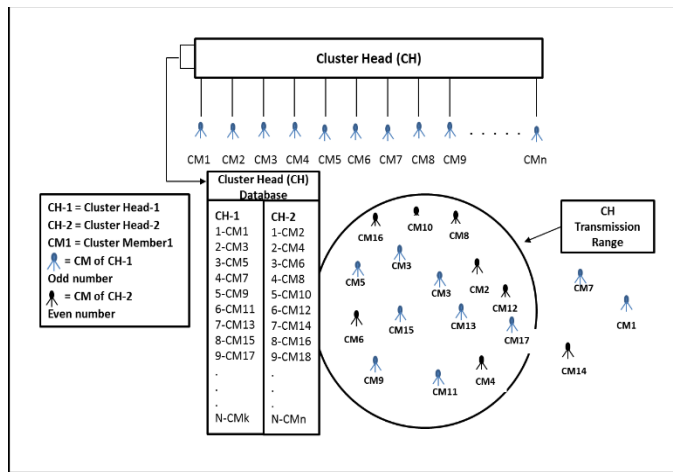
Figure 4: Different CMs Devices but Some out of CH Range

6. Design of Algorithm

There are different ways of verifying pilgrims (people) in a crowd: manual checking, biometric verification, facial recognition, scanners and by querying from the database system. These processes do verification one by one and consume a lot of time. In this section, we discuss the algorithm for group (cluster) verification to minimize verification time for crowd. In order to achieve the objective of the research, we need to write some algorithms for different scenarios of the proposed model. The algorithm is written to send, receive, store, forward, verify and drop the unverified packet. To make a better understanding, we write pseudo code so that latter on code can easily be run on the simulation tool and we can get the results. The algorithm representing different scenario is given in the next section. The multi-hop group (cluster) verification algorithm is developed after the study of [29] concept of multi-hop and [30] collaboration by neighbor table.

6.1. Single group (group) verification algorithms

In single group (cluster) verification algorithm, we discuss the algorithm that represents the different situations (scenarios) of a single group and its CMs. Different group (cluster) situations (scenarios) represented such as; all CMs those belong to the same group (cluster) and are within the transmission range of the CH; all CMs those belong to the same CH, but some are out of the

transmission range of CH; CMs and non-CMs within the range of a single CH; and some CMs are outside the CH range. According to the given algorithm, we write code to handle the different scenarios.

Algorithm 1 Verification by CH	
Step-1	Begin
Step-2	GET value for Max NCM
Step-3	GET list of the CMs and Broadcast
Step-4	While(Simulation on AND Number of CM <= Max NCM)
Step-5	IF(CM_ID (In CH list) == CM_ID (Response from CM)
Step-6	Add CM_ID in the verified list
Step-7	GOTO Step-4
Step-8	ELSE
Step-9	Drop the packet
Step-10	GOTO Step-4
Step-11	Endif
Step-12	Endwhile
Step-13	End

Algorithm 1 discusses the CH side verification. The CH has a list of CMs with maximum number of CMs (Max NCM) and CH broadcast the list CM_ID. If the response received from CM (CM_ID) matches with CH list, then CH adds the CM_ID in verified list. Otherwise drops the data packet. This verification process carries on until Max NCM verified or simulation time is out.

Algorithm 2 Response by CM	
Step-1	Begin
Step-2	GET value for Max Hops
Step-3	While(Simulation is On)
Step-4	IF(CM_ID (Received) == CM_ID (Current CM))
Step-5	Response to CH
Step-6	Store in Log
Step-7	Display the LED Green
Step-8	ELSE
Step-9	IF(Number of Hops <= Max Hops)
Step-10	Store in neighbor Table
Step-11	Forward To next CM
Step-12	ELSE
Step-13	Drop packet
Step-14	Endif
Step-15	Endif
Step-16	Endwhile
Step-17	End

Algorithm 2 discusses the scenario in CM side. CMs set by the maximum number of the hops (Max Hops). If the CM_ID receive from the CH matches the CM_ID of the current CM then its response to CH, store it in log file and turn LED into Green for CM device. Otherwise it checks current number of hops is less than the Max Hops then it stores information in the neighbor table, and forward data packet to the next CM. If it exceeds the maximum number of hops, then it drops the packet. This process carries on until the simulation time is out.

7. Simulation Setup for Proposed Group Verification for Crowd

Contiki OS is a lightweight open source operating system for sensor network. It was designed by Adam Dunkels, at the Swedish Institute of Computer Sciences. C programming language is used in both Contiki OS and its programs. Contiki is flexibly portable OS and it has been ported to different platforms. Cooja is Java based Contiki network simulator with a graphical user interface
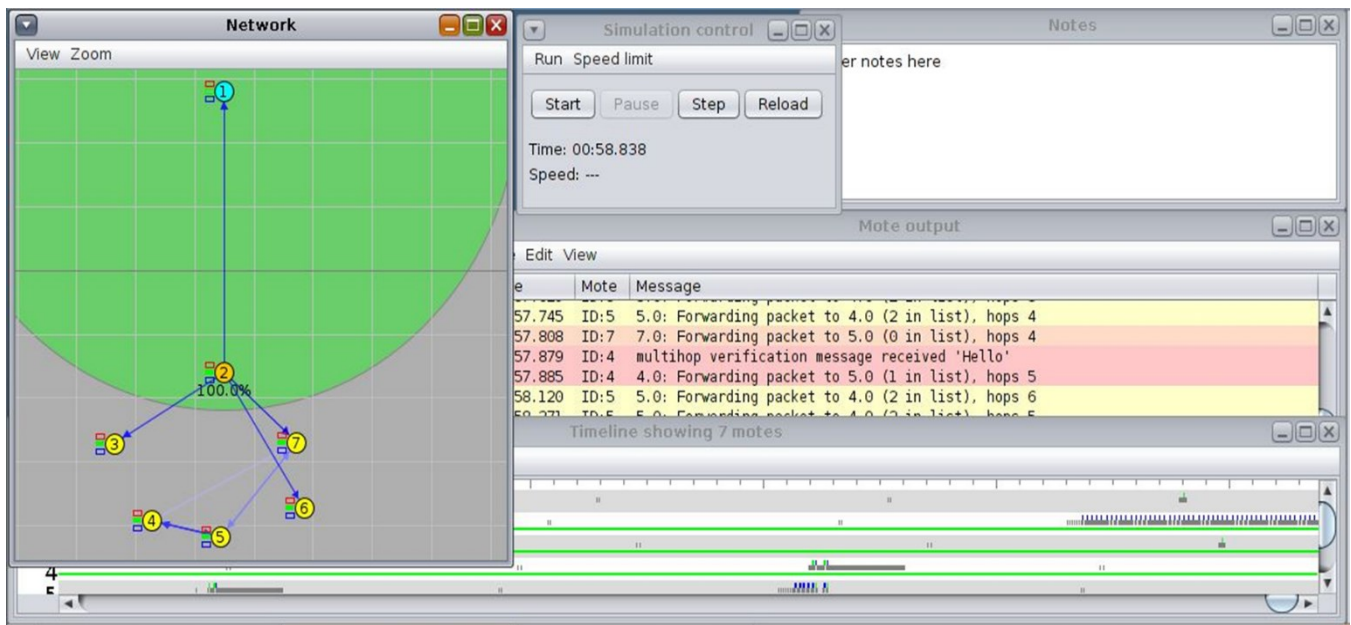
Figure 5: Full view of the Contiki/Cooja simulator

(GUI). It integrates to simulate with the external tools to provide additional features to the large and small networks. Motes can be emulated, which is faster and allows simulation of larger networks, or at the hardware level. Two emulator software packages are contained by this tool: Avrora and MSPSim. Cooja can emulate multiple platforms like: TelosB/SkyMote, MicaZ mote, Zolertia Z1 mote, ESB, Wismote [31].

The Figure 5 shows full screen view of Contiki/Cooja simulator. Network simulator "Contiki/Cooja" is separated into small windows such as: Network Window, Notes Window, Simulation Control Window and Mote Output Window.
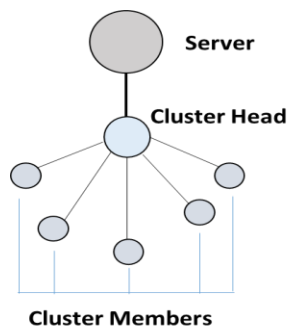
Figure 6: Scenario for Flow and Functions of Nodes

We took the simple scenario to make understanding of the flow and function of each node as given in Figure 6. Server function is to keep the record and status of the pre-registered CMs. Antelope is a relational database management system (RDBMS) and it facilitate a sensor to work as a database server. It provides help to create dynamic databases and to run complex queries [1].

7.1. Client Interface

The client interface to insert data in the Antelope database is shown in the Figure 7. Client interface in Antelope DBMS provides help to store the record by using the client interface.

Figure 7: CLIENT Interface to Insert Data

7.2. Server Interface

The server interface displays the output result in Mote output screen for each query is shown in Figure 8. The function of the CH node is to keep a list of CM IDs, send, receive, verify CM IDs. We fetch the group of CM IDs by compiling the code on the CH node.

7.3. Multi-Hop Communication for Nodes

The multi-hop communication initializes the memory and initializes the list for the neighbor table entries used for the neighbor table. Open a multi-hop connection on Rime channel and Register an announcement ID. As multi-hop connection is set open sensor buttons are Activated. Sensor buttons are used to

drive the traffic. When button click option is used sensor device transmit the data. Multi-hop also has a function to check the neighbor table. If the neighbor is not present in the list, a new neighbor table entry is added to the neighbor table. CM function is to verify the CM_ID by replying I am here, and to update the memory storage.
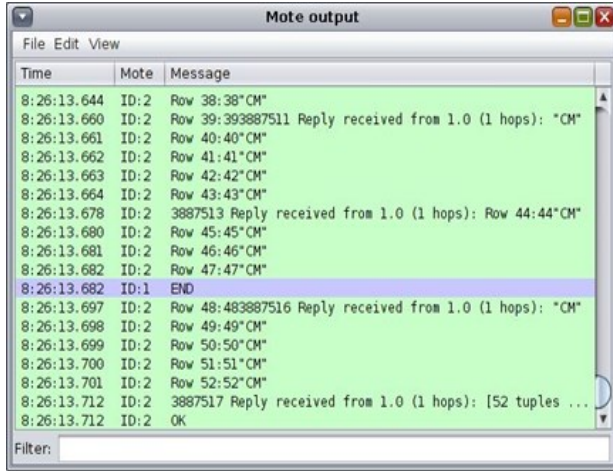
Figure 8: Server Interface Showing Query Process

Table 1: Simulation parameters

Simulation Parameters	Values
Number of Group (cluster) Members	5, 10, 15, 20, 25, 30, 35, 40, 45, 50
Transmission Range	50 m X 100 m
Startup Delay	1000 ms (1 sec)
Neighbor Timeout	60 sec
Max Neighbor	16
Position	Random
Simulation Time	5 min
Communication	Multi hop
Radio Channel	26
Protocol	CSMA MAC Contiki

7.4. Simulation Parameters

The algorithms are implemented on WSN based scenarios that are developed to validate the proposed simulation model. At first, the results for different number of CMs a group (cluster) are presented. The optimal number of CMs in a group is 20, where all of the CMs are verified and unverified number of CMs (drop rate) is zero. As then number of CMs increases from 20 to 25, unverified number of CMs increases which increases the group verification time for a crowd. The verified and unverified rate shows that WSN based model can verify CMs in group (cluster) form that leads to minimize group verification time and hence minimize crowd verification time. The results for verified and unverified CMs in a group (cluster) are explained by controlling and varying the number of CMs in group (cluster). The results for proposed system are calculated and estimated in terms of total number of CMs verified and unverified. The verification time

results have shown in Table 2 and Figure 17 only include the verified CMs. But the verification time results have shown in Table 3 and Figure 18 include both verified and unverified CMs. The simulation environment with parameters is given in the Table 1.

To study the validity of proposed model, Cooja/Contiki Simulator is used. In Table 1, the simulations parameters are mentioned for simulating the proposed group verification to calculate the number of verified, unverified CMs and verification time for crowd in group (cluster) form.

- **Number of CMs:** The number of CMs existing (populated) in a single group (cluster)
- **Transmission Range:** The coverage area of the CH
- **Startup Delay:** Simulation startup delay to get ready for communication
- **Neighbor Timeout:** The time at which the old neighbor entry will be removed so that the table doesn't overflow.
- **Max Neighbor:** The maximum number of neighbors that can be supported. As the number of neighbors is increased, the number entry in the table will increase. It will require more memory and causes more delay.
- **Position:** The x and y coordinate of the CM's position. It can be defined as linear, elliptical, random or manually.
- **Simulation Time:** The time at which the simulation is completed to get required results.
- **Communication:** The multi-hop communication will help to forward the packet to the next neighbor if the destination CM is at a longer distance and in this way save the energy of CM. It will also help deliver the packet if the node is out of the CH's range.
- **Radio Channel:** Cooja/contiki support different radio channels for communication.
- **Protocol:** CSMA MAC is a Contiki lightweight protocol designed for low power, low memory and low verification power wireless sensor network.

8. Contiki/Cooja Simulation Scenarios

There are different performance metrics to evaluate crowd verification in group (cluster) form. Most of them include number of verified and unverified CMs in a group (cluster).

8.1. Different number of CMs (5, 10, 15, ..., 50) within single CH range

In a single group (cluster) scenario, the number of CMs increases by multiples of 5 in each simulation. The maximum number of the CMs support by the Contiki/Cooja is 45 CMs in our scenario. Some of the scenarios are shown in the Figures 9, 10 and 11. Results are obtained from log file taken from Contiki/Cooja.

In Figure 8, there is one server, one CH and 5 CMs. The CH has generated the signals (CM_ID) for verification. All 5 CMs are verified and as a result of verification their LED color turns into Green (flag sets to 1).

In Figure 10, There are 25 CMs for group verification. Out of 25 CMs, 22 CMs are verified but CMs having CM_ID 23, 24 and

27 remain unverified. LEDs of Verified CMs turn into green while LEDs of unverified CMs remains off.
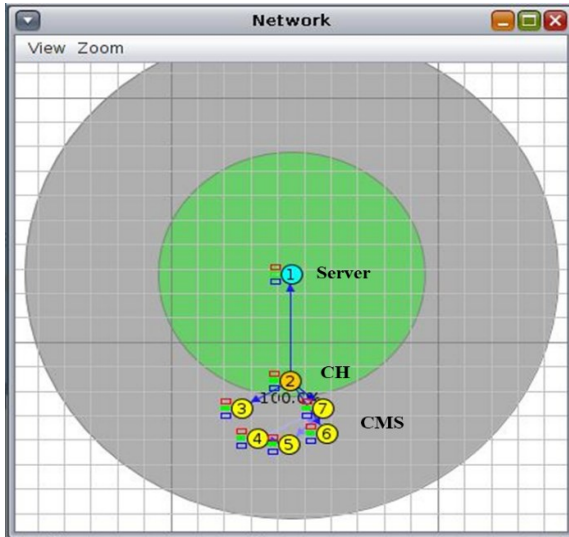
Figure 9: Single Group (cluster) Having 5CMs

Figure 10: Single Group (cluster) Having 25

Figure 11: Single Group (cluster) Having 45 CMs

In Figure 11, only 14 out of 45 CMs verified but 31 CMs remain unverified. LEDs of Verified CMs turn into Green while for unverified CMs they remain off.

8.2. CM Devices Belong to Single Group (cluster) but some out of CH Range

In Figure 12, CMs number 4, 14, 15, 17, 19, 20, 23 and 24 are out of transmission range of CH. CMs number 4, 15, 20 and 24 are verified but CMs number 14, 17, 19 and 23 remain unverified. This means 4 out of 8 CMs out of transmission range of CH are verified. This showed that multi-hop also works out of transmission range but the number of verified CMs decreased and time for verification increased. The best result for the single group (cluster) is provided when CMs are within the transmission range of CH.

Figure 12: Out of 25 CMs Some are Out of CH Range

Figure 13: CH having CMs and non-CMs

8.3. CH having different CMs devices within range

In Figure 13, CH having 10 CMs and 5 non-CMs. All CMs from CM 3 to 12 are verified but all non-CMs from CMs13 to 17 remain unverified. This means CH can verified the CMs in the presence of the non-Ms.

8.4. Different CMs devices but some out of CH range

In Figure 14, 15, and 16, different views of CH having CMs, non-CMs and some out of range are shown. All the CMs within the range are verified and their LEDs turn into green. But in case of non-CMs all non-CMs remain unverified and their LEDs remain off either within the range or outside the range of CH. The CMs 18, 19 and 20 are out of range. The CMs 18 and 19 are verified but CM 20 remain unverified. That means 2 out of 3 are verified outside of CH range by using the multi-hop communication.

Figure 14: Coverage area by server

Figure 15: Coverage area by CH
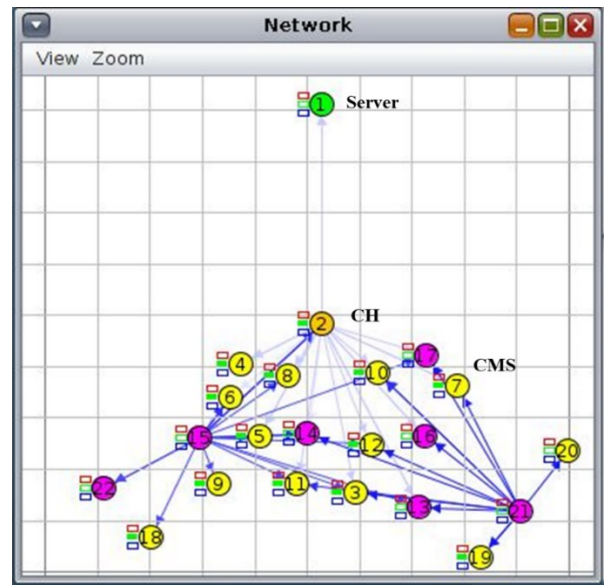
Figure 16: Without coverage area

9. Verification Time for Existing and proposed Systems

Currently verification is done in queue form one by one or person by person. There are different steps involved for the process of verification. This verification of crowd in queue form causes a long queue and delay. Time Taken by Verified CMs by existing system is given in Table 2 and 3 columns have heading "Time Taken by Verified CMs in Min" is calculated by observation and well-planned interview is given in "Unpublished" [33].

Verification time is compared with the existing system verification time. In first step, verification times for only verified number of CMs in a group (cluster) are compared. In the second step, verification times for verified and unverified (go through the normal process) CMs in a group (cluster) are compared.

9.1. Verification Time for Single Group (cluster) by Proposed Vs Existing System (Only Verified CMs)

In this case, we evaluated the single group (cluster)'s verification time by proposed and existing systems, but only considered the number of verified CMs. As represented in Table 2 and Figure 17, we found the number of verified CMs by proposed system and calculated the verification time on the basis of simulation from log file generated by the Contiki/Cooja tool. By data collection, we calculated the existing system minimum, average and maximum verification time per person and are 5 minutes, 7 minutes and 12 minutes respectively. But we considered minimum verification time (5 minutes) by the existing system to compare with proposed system verification time. Therefore, to get total verification time taken by the existing system, we multiply the number of verified CMs by 5. As represented in the Figure 17, the minimum verification time is 0.4 minutes by the proposed system, but by existing system is 25 minutes, when number of verified CMs for the single group (cluster) are 5. The maximum verification time by the proposed system is 4.9 minutes, but the existing system has a maximum verification time of 110 minutes. The optimal time for verification by the proposed system is 3.3 minutes, when numbers of verified
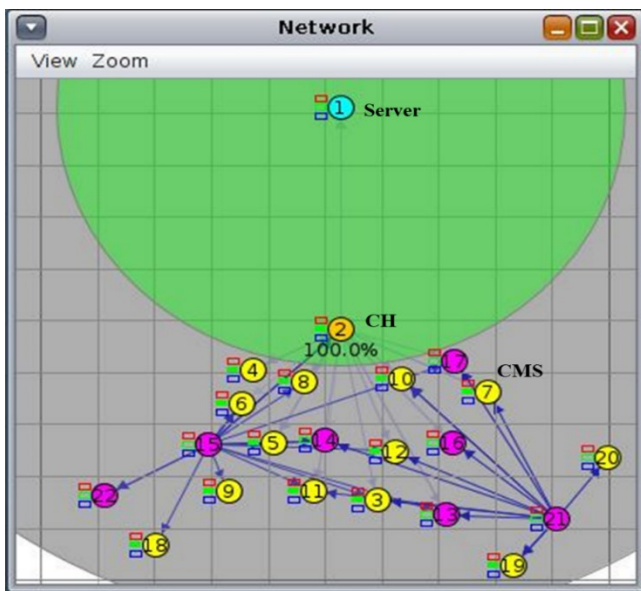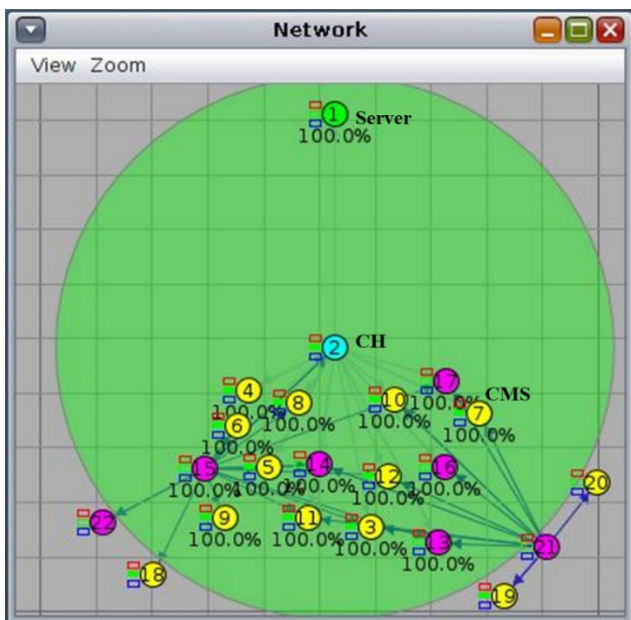
Table 2: Verification Time for Single Group (cluster) by Proposed VS Existing System (Only Verified CMs)

Number of CMs in a Group (cluster)	Number of Verified CMs	Time Taken by Verified CMS in Min (Proposed System)	Time Taken by Verified CMs in Min (Existing System)
5	5	0.4	25
10	10	0.9	50
15	15	2.5	75
20	20	3.3	100
25	22	3.9	110
30	17	4.2	85
35	15	4.7	75
40	15	4.9	75
45	14	4.6	70
50	13	4.6	65
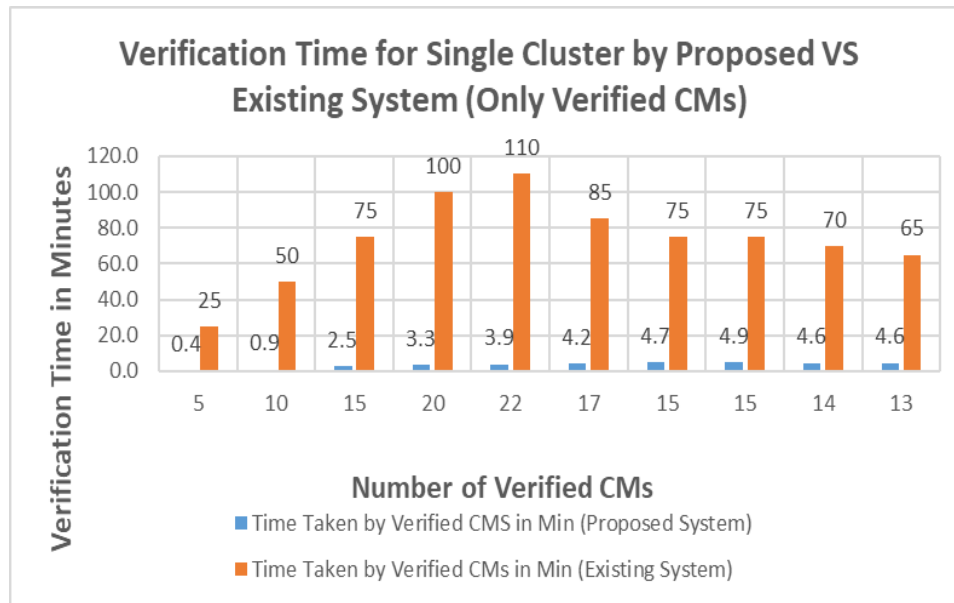
Figure 17: Verification Time for Single Group (cluster) by Proposed VS Existing System (Only Verified CMs)

CMs are 20. But when number of verified CMs are 20, the verification time by the existing system becomes 100 minutes. Such a large difference validates our proposed system.

From this analysis, we conclude that our proposed system is better and suitable for the single group (cluster) having 20 CMs. The maximum number of CMs verified is 22 out of 25 and the verification time is 3.9 Minutes by the proposed system but for the existing system is 110 minutes. If we increase the number of CMs in a group (cluster), it affects the performance of the proposed system and verification time increases. The reasons for this increase are discussed in section 9.3.

9.2. Verification Time for Single Group (cluster) by Proposed vs. Existing System (Verified &Unverified CMs)

In this case, we evaluated the crowd verification time by proposed and existing system, but we considered both verified and unverified number of CMs. As represented in Table 3 and Figure 18, we found the number of verified and unverified CMs by the proposed system on the basis of simulation from log file generated by Contiki/Cooja tool. We calculated the total verification time by the proposed system by the addition of time taken for verification by verified CMs on the base of simulation and time taken for verification by unverified CMs on the base of minimum time by data collection (existing system). To get total verification time taken by the existing system, we multiply the

number of verified and unverified CMs by 5, as per person verification time by existing system is 5 minutes. As represented in the Figure 18, when number of verified CMs are 5, the minimum verification time is 0.4 minutes by the proposed system and that of the existing system is 25 minutes. The maximum verification time by the proposed system is 184.6 minutes and that of the existing system 250 minutes, when the number of CMs in the group (cluster) is 50.

The optimal time for verification by the proposed system is 3.3 minutes, when the number of verified CMs is 20. But verification time by the existing system is 100 minutes. Such a large difference validates our proposed system. If we increase the number of CMs to more than 20 i.e. 25 in a group (cluster), then some CMs are unverified. These CMs have to go for verification by an existing system which increases the verification time to 18.9 minutes.

After 18.9 minutes, verification time of the proposed system increases with big differences, 69.2, 109.7, 129.9, 164.6 and 184.6 minutes because the number of unverified CMs increases into 13, 20, 25, 31 and 37 CMs. As the number of CMs increases, the unverified CMs rate also increases and that increases the verification time. In this way, unverified CMs affect the performance and verification time increases. Reasons for this increase in verification time are discussed in the section 9.3.

Table 3: Verification Time for Single Group (cluster) by Proposed VS Existing System (Verified & Unverified CMs)

Number of CMs in a Group (cluster)	Time for Verified CMs (Min)	Time for Unverified CMs (Min)	Total Time for Verified and Unverified CMs (Min)	Total Time Taken by Existing system (Min)
5	0.4	0	0.4	25
10	0.9	0	0.9	50
15	2.5	0	2.5	75
20	3.3	0	3.3	100
25	3.9	15	18.9	125
30	4.2	65	69.2	150
35	4.7	105	109.7	175
40	4.9	125	129.9	200
45	4.6	160	164.6	225
50	4.6	180	184.6	250
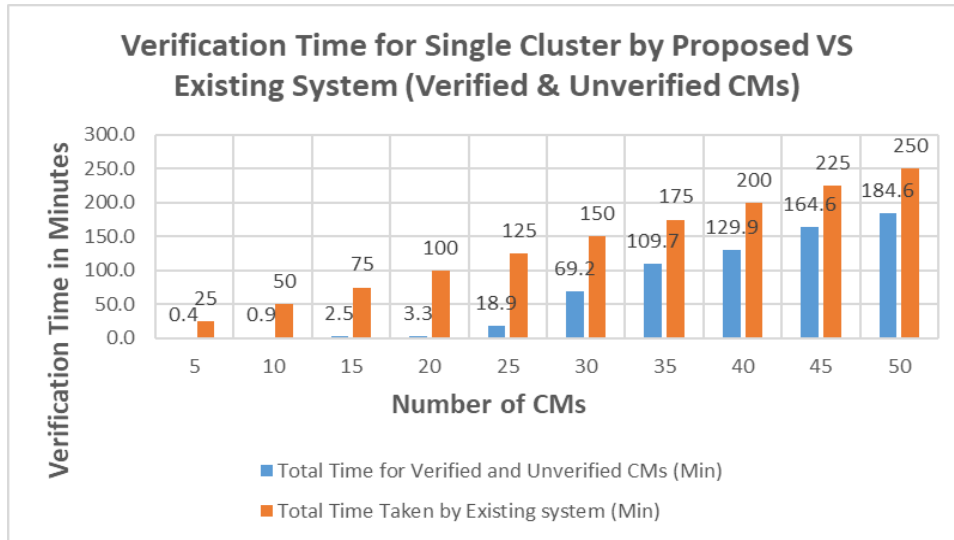
Figure 18: Verification Time for Single Group (cluster) by Proposed VS Existing System (Verified & Unverified CMs)

9.3. Reasons of Increment and Decrement of Group (cluster) Verification Time

First reason, by increasing the number of CMs increases the number of neighbor's entries in the neighbor table (The table in which each CM keeps a record of its neighbor). When it exceeds the maximum number of entries in a neighbor table or neighbor time out, it causes dropping or removing of the entries from the neighbor table. The dropping of entries causes the incomplete route to destination, therefore, packet drops. The second reason is that the packet is forwarded neighbor to neighbor and it exceeds the maximum number of neighbors and hence drops the packet to save the energy. In our case, the limit of maximum number of the neighbors is 16.

The third reason is that the group (cluster) verification model works on the MAC layer and it uses the CSMA Contiki protocol. CSMA does not support collision detection, but when collision happens, it retransmits the packets after a certain time period. It causes a delay in packet delivery and hence increases the crowd verification processing time. As we increase the number of CMs, it increases the traffic that increases the chances of greater number of collisions and hence packet drops before reaching the destination.

10. Conclusion and Future Directions

This article provides an overview of the simulation model for group (cluster) verification and its application. We discussed the present verification approaches and proposed a model to calculate the verification time for verified and unverified CMs. We also explain the different scenarios of CMs and as well algorithms for CMs and CH. If simulation-based group (cluster) time verification model is implemented, it provides many application scenarios. In time specific verification application, such as at stadium, airports, trains etc. To avoid the CVID-19, after taking the temperature, verification can be done in group (cluster) form (while maintaining the social distance) to minimize the verification time. To optimize the number of CMs in group (cluster) for fast verification to reduce the massive crowd.

This research shows some simulation results and on the basis of simulation results, needs to be further expanded to test the WSN sensing emulation model into the laboratory and then in real environment. According to our knowledge, this is the one of the limitations that there is no such complete practically implemented model. The Internet and WSN communication causes dropping of packets due to low memory, less processing power and low energy. Therefore, factors affecting the packet dropping need to be identified and improved for efficient packet delivery. Furthermore, there is no such mechanism to identify that the person carrying the CM device is his own device or it has taken from another person (friend) or it is using lost device. In any case misplace or misuse of CM device causes a great risk in security viewpoint. An algorithm can be designed to maintain the social distance to avoid the COVID-19 attack.

Reference

[1] https://anrg.usc.edu/contiki/index.php/Antelope (Database_Management_System)_-_Contiki (Accessed online: 27-Aug-2020)

[2] N.A. Nawaz, H.R. Malik, A.J. Alshaor, "A framework for smart capacity estimation at crowded area using WSN," in Proceedings - 2019 International Arab Conference on Information Technology, ACIT 2019, 159–164, 2019, doi:10.1109/ACIT47987.2019.8991037.

[3] N.A. Nawaz, A. Waqas, Z.M. Yusof, A.W. Mahesar, A. Shah, "WSN based sensing model for smart crowd movement with identification: An extended study," Journal of Theoretical and Applied Information Technology, 95(5), 975–988, 2017.

[4] N.A. Nawaz, A. Waqas, Z.M. Yusof, A. Shah, "A framework for smart estimation of demand-supply for crowdsource management using WSN," in ACM International Conference Proceeding Series, 1–5, 2017, doi:10.1145/3018896.3025140.

[5] T. Warren Liao, "Clustering of time series data - A survey," Pattern Recognition, 38(11), 1857–1874, 2005, doi:10.1016/j.patcog.2005.01.025.

[6] N.A. Nawaz, A. Waqas, Z.M. Yusof, A. Shah, "WSN based sensing model for smart crowd movement with identification: A conceptual model," in Proceedings of the International Conferences on ICT, Society, and Human Beings 2016, Web Based Communities and Social Media 2016, Big Data Analytics, Data Mining and Computational Intelligence 2016 and Theory and Practice in Modern Computing 2016 - Part o, 2016.

[7] M.N. Khan, H.U. Rahman, M.A. Almaiah, M.Z. Khan, A. Khan, M. Raza, M. Al-Zahrani, O. Almomani, R. Khan, "Improving Energy Efficiency With Content-Based Adaptive and Dynamic Scheduling in Wireless Sensor Networks," IEEE Access, 2020, doi:10.1109/access.2020.3026939.

[8] G. Aceto, V. Persico, A. Pescapé, Industry 4.0 and Health: Internet of Things, Big Data, and Cloud Computing for Healthcare 4.0, Journal of Industrial Information Integration, 2020, doi:10.1016/j.jii.2020.100129.

[9] P.J. Nesse, S.W. Svaet, D. Strasunskas, A.A. Gaivoronski, "Assessment and optimisation of business opportunities for telecom operators in the cloud value network," Transactions on Emerging Telecommunications Technologies, 2013, doi:10.1002/ett.2666.

[10] C. Lindkvist, A. Temeljotov Salaj, D. Collins, S. Bjørberg, T.B. Haugen, "Exploring urban facilities management approaches to increase connectivity in smart cities," Facilities, 2020, doi:10.1108/F-08-2019-0095.

[11] S. a Aly, A. Ali-Eldin, H. V Poor, "A Distributed Data Collection Algorithm for Wireless Sensor Networks with Persistent Storage Nodes," 2011 4th IFIP International Conference on New Technologies, Mobility and Security, 1–5, 2011, doi:10.1109/NTMS.2011.5721066.

[12] J. Tan, W. Liu, T. Wang, N.N. Xiong, H. Song, A. Liu, Z. Zeng, "An adaptive collection scheme-based matrix completion for data gathering in energy-harvesting wireless sensor networks," IEEE Access, 7, 6703–6723, 2019, doi:10.1109/ACCESS.2019.2890862.

[13] H.N. Dai, H. Wang, G. Xu, J. Wan, M. Imran, "Big data analytics for manufacturing internet of things: opportunities, challenges and enabling technologies," Enterprise Information Systems, 2020, doi:10.1080/17517575.2019.1633689.

[14] D.W. Sambo, B.O. Yenke, A. Förster, P. Dayang, Optimized clustering algorithms for large wireless sensor networks: A review, Sensors (Switzerland), 2019, doi:10.3390/s19020322.

[15] B.P. Rimal, A. Jukan, D. Katsaros, Y. Goeleven, "Architectural Requirements for Cloud Computing Systems: An Enterprise Cloud Approach," Journal of Grid Computing, 2011, doi:10.1007/s10723-010-9171-y.

[16] J. Santos, T. Syed, M. Coelho Naldi, R.J.G.B. Campello, J. Sander, "Hierarchical Density-Based Clustering using MapReduce," IEEE Transactions on Big Data, 2019, doi:10.1109/tbdata.2019.2907624.

[17] R. Qaddoura, H. Faris, I. Aljarah, "An efficient clustering algorithm based on the k-nearest neighbors with an indexing ratio," International Journal of Machine Learning and Cybernetics, 2020, doi:10.1007/s13042-019-01027-z.

[18] I. Kumari, V. Sharma, A review for the efficient clustering based on distance and the calculation of centroid, International Journal of Advanced Technology and Engineering Exploration, 2020, doi:10.19101/IJATEE.2020.762021.

[19] L. Campanile, M. Gribaudo, M. Iacono, M. Mastroianni, "Performance evaluation of a fog WSN infrastructure for emergency management," Simulation Modelling Practice and Theory, 2020, doi:10.1016/j.simpat.2020.102120.

[20] A. Hassan, A. Anter, M. Kayed, "A robust clustering approach for extending the lifetime of wireless sensor networks in an optimized manner with a novel fitness function," Sustainable Computing: Informatics and Systems, 2021, doi:10.1016/j.suscom.2020.100482.

[21] P. Cooper, T. Tryfonas, T. Crick, A. Marsh, "Electric Vehicle Mobility-as-a-Service: Exploring the 'Tri-Opt' of Novel Private Transport Business Models," Journal of Urban Technology, 2019, doi:10.1080/10630732.2018.1553096.

[22] L. Da Xu, W. He, S. Li, Internet of things in industries: A survey, IEEE Transactions on Industrial Informatics, 2014, doi:10.1109/TII.2014.2300753.

[23] A. Abuarqoub, M. Hammoudeh, F. Al-Fayez, O. Aldabbas, "A Survey on Wireless Sensor Networks Simulation Tools and Testbeds," Sensors, Transducers, Signal Conditioning and Wireless Sensors Networks, 2016.

[24] U. Raza, P. Kulkarni, M. Sooriyabandara, "Low Power Wide Area Networks: An Overview," IEEE Communications Surveys and Tutorials, 2017, doi:10.1109/COMST.2017.2652320.

[25] G.Z. Papadopoulos, V. Kotsiou, A. Gallais, P. Chatzimisios, T. Noel, "Low-power neighbor discovery for mobility-aware wireless sensor networks," Ad Hoc Networks, 2016, doi:10.1016/j.adhoc.2016.05.011.

[26] E. Ancillotti, R. Bruno, M. Conti, "Reliable data delivery with the IETF routing protocol for low-power and lossy networks," IEEE Transactions on Industrial Informatics, 2014, doi:10.1109/TII.2014.2332117.

[27] E. Yaacoub, A. Kadri, A. Abu-Dayya, "Cooperative wireless sensor networks for green internet of things," in Q2SWinet'12 - Proceedings of the 8th ACM Symposium on QoS and Security for Wireless and Mobile Networks, 2012, doi:10.1145/2387218.2387235.

[28] H.M.A. Fahmy, Wireless Sensor Networks Essentials, 2020, doi:10.1007/978-3-030-29700-8_1.

[29] H. Kim, E.H. Kim, "Hop-based activation scheduling in wireless sensor networks," International Journal of Multimedia and Ubiquitous Engineering, 2014, doi:10.14257/ijmue.2014.9.4.01.

[30] T. Higuchi, H. Yamaguchi, T. Higashino, M. Takai, "A neighbor collaboration mechanism for mobile crowd sensing in opportunistic networks," in 2014 IEEE International Conference on Communications, ICC 2014, 2014, doi:10.1109/ICC.2014.6883292.

[31] Sharad, E.N. Kaur, I.K. Aulakh, "Evaluation and implementation of cluster head selection in WSN using Contiki/Cooja simulator," Journal of Statistics and Management Systems, 23(2), 407–418, 2020, doi:10.1080/09720510.2020.1736324.

Evaluation of Facebook Translation Service (FTS) in Translating Facebook Posts from English into Arabic in Terms of TAUS Adequacy and Fluency during Covid-19

Almahasees Zakaryia[*,1], Al-Taher Mohammad[1], Helene Jaccomard[2]

[1]*Applied Science Private University, Department of English Language and Translation, Faculty of Arts and Science, Amman, 00962, Jordan*

[2]*University of Western Australia, Department of Translation, School of Humanities, Perth, 0061, Australia*

A R T I C L E   I N F O

A B S T R A C T

The study aims to verify the capacity of Facebook Translation Service in translating English Facebook posts into Arabic in terms of two criteria: adequacy and fluency in line with the Translation Automation User Society (TAUS) scales. To ensure consistency and objectivity as recommended by TAUS, six evaluators, native speakers of Arabic and near-native speakers of English, rated the same data on each scale. The evaluators were acquainted with fluency and adequacy scales along with MT limitations and potentials. Once the corpus was uploaded and sent to the evaluators using TAUS tools, they had to assign scores online on 1-4 rating scales. Then, each report was displayed online on the TAUS reports tool. Evaluators' responses were combined in thematic categories and were calculated to obtain frequencies and percentages. The study found that FTS provided fluent output with highest percentage of the scale good equal to 3 on a scale from 1 to 4, where the output is assessed as flowing smoothly with minor linguistic errors. Moreover, FTS succeeded in generating an adequate output with the highest percentage of responses as 'most' equal to 3 on a scale from 1 to 4, where almost the full meaning of the source is deemed to be transferred in the target language. This study is useful since it highlights the role of Facebook Translation service in translating, educating the public and fighting COVID-19. Consequently, such research would encourage the use and research on the potentiality of MT and FTS in dealing with abrupt crises, such as COVID-19.

1. Introduction

Translation is a medium of human communications. It bridges the gap between human communities and ensures the best way of communicating among global communities[1]. Nowadays, the world is facing the most frightening Coronavirus (COVID-19) outbreak in the last decade. The health authorities, international health organizations, political leaders, healthcare providers and the public have social media sites at their disposal. They post information regarding COVID-19 daily. The flow of social media posts about COVID-19 is unprecedented, and would be beyond the capacity of human translation, let alone an economically viable proposition to have them translated by humans. During lockdowns around the globe, Machine Translation (MT) helped to translate such posts into Arabic. The author in [2] states, "The challenge is how to communicate rapidly changing data across language

borders so that essential information is not lost in translation". In this regard, he goes as far as stating that machine translation is a strong ally in the fight against COVID-19. Social media sites have become popular among young Arabs, who tend to use them daily. The [3] shows that Facebook is the most popular social media site in the Middle East with 200 million daily users, representing almost 70% of Middle East population. Facebook has a translation service, which offers translation for more than 80 languages.

Facebook wide use makes it necessary to evaluate the content and verify its effectiveness and limitations to the end users. English ranks as the top language of social media with 25% of internet.

This means that many Arab Facebookers will be exposed to posts written in English with some able to read and understand it, and a large portion of those who are not competent in English. Facebook has been offering their own translation service since 2011, FTS.

Users can easily activate the translation service on their profiles in two ways. They can click on top right hand of their page and select setting and privacy, then choose language and region. After that, users have to click on the language into which they would like to have posts translated into. The current study scrutinizes FTS in terms of adequacy and fluency in rendering English posts into Arabic during the COVID-19 lockdown.

1.1. Machine Translation

Machine Translation (MT) is the study of the computer systems or online applications in transferring the Natural Languages from one language into another. Author in [1] shows that MT systems are "applications or online services that use machine-learning technologies to translate large amounts of text from and to any of their supported languages. The service translates a "source" text from one language to a different "target" language". The availability of such online systems for free or at low costs makes it necessary to verify the effectiveness of MT systems in dealing with natural languages especially with the languages which belong to different families such as English and Arabic.

Translation has been integrated into technology thanks to the giant technological progress of the last 70 years, starting with the first successful MT project at the University of Georgetown in 1954 as a result of collaboration between Georgetown University and International Business Machines (IBM). The [2] indicates that the success of the first experiment "attracted a great deal of media attention in the United States. Although the system had little scientific value, its output was sufficiently impressive to stimulate the large scale funding of MT research in the USA and to inspire the initiation of MT projects elsewhere in the world and notably in the USSR".

Research in [3] shows that 1980 is considered a flagship moment of MT with new developments emerging whilst "more dramatic development took place in MT in the 1990 since computers became more powerful with much higher storage capabilities". This crowned with the invention of the internet, a source of translation for the general public [4]. Automatic translation tools available on the Internet translate billions of documents daily, which would take human translators months. Whereas MT service was not free in the early history of the Internet, nowadays, we have a set of MT platforms that provide translation service for free such as Google Translate, Microsoft Translator, FTS and others. The author in [5] states, "Machine Translation (MT) is being deployed for a range of use-cases by millions of people on a daily basis. Google Translate and Facebook provide billions of translations daily across many languages".

1.2. Facebook Translation

The author in [5] indicates that Google translate and Facebook Translation users reach more than 1 billion monthly. The research in [6] shows that Facebook, firstly, used Google Translate service to translate comments into 50 languages. Facebook launched its first Translation Service in 2011, called In-line Translation Facebook Tool [7]. Where [8] states, "After Google integrated the "translate" feature into its social network, which allows users to translate posts and comments into 50 different languages, Facebook, as usual has followed the footprints of Google+, and quietly announced the launch of "translate" button – powered by Microsoft's Bing", setting itself apart from Google. The author in [9] describes the first Facebook Translation tool, "Facebook has quietly introduced a new tool that makes instant inline language translations appear with a single click". For instance, if a non-Spanish user on a Facebook public page gets across a post in Spanish, then he/she will click on the translation button and then he/she will be able to see the translation of the post in his/her language. FTS works on individual posts on Facebook and not on users' profiles yet, including comments. Currently, FTS offers translation service for 89 languages and they will continue to add more languages.

FTS adopted phrase to phrase MT approach, thus translating whole sequences of words of differing lengths. The author in [10], the founder of Facebook, explained that translation is the best mean to connect human globally. "Understanding someone's language brings you closer to them, and I'm looking forward to making universal translation a reality. To help us get there faster, we're sharing our work publicly so that all researchers can use it to build better translation tools". In the same year, Facebook research team developed a new MT approach using Convolutional Neural Networks (CNNs), allowing to translate languages more accurately (read: increase quality on a BLEU scale) and up to nine times faster than the traditional Recurrent Neural Networks (RNNs). The author in [11] describes the new MT approach as "Today we're publishing research on how AI can deliver better language translations. With a new neural network, our AI research team was able to translate more accurately between languages, while also being nine times faster than current methods", a superior speed confirmed by [12]. The author in [13] has shown that "CNNs have been very successful in several machine learning fields, such as image processing. However, Recurrent Neural Networks (RNNs) are the incumbent technology for text applications and have been the top choice for language translation because of their high accuracy".

In the late of 2019, Facebook research has declared new advances in NLP, which boost the accuracy of Facebook Translation. They have also introduced a new self-supervised pretraining approach, RoBERTa, that surpassed all existing Natural Language Understanding (NLU) systems on several language comprehension tasks. They have also collaborated with New York University (NYU), DeepMind Technologies, and the University of Washington (UW) to promote their future research [14].

In a first study on Facebook Translation evaluation, it evaluated Facebook translation service in handling low-resources languages: Lao, Kazakh, Haitian, Oromo, and Burmese. They evaluated the translation of English posts into these languages. They implemented different strategies: LASER, back-translations, self-training, multilingual modeling, to improve the translation from English to low source languages. "For instance, Sinhala to English and Nepali to English translations on Facebook have improved from "useful," which are just accurate enough to understand the meaning, to "good," which generate full meaning but may have typos or grammatical errors"[15].

The study is mainly concerned with Facebook translation of English posts related to COVID-19 released by international

organizations such as WHO, political leaders, medical specialists and the general public. The study aims to verify the efficiency of FTS in translating posts from English into Arabic and provides constructive feedback about the degree of fluency and adequacy of FTS and whether FTS is considered a reliable source of information or not.

1.3. Machine Translation Evaluation

MT systems Evaluation (MTE) is crucial to the development of MT systems. The author in [4] shows that the evaluation of MT is central to determine the effectiveness and performance of MT systems. Machine Translation Evaluation is essential to all end-users: researchers, designers and users to select the best system to use [16]. In similar way, the development of MT systems depends on the evaluation of MT systems, limitations and strengths of the systems. MT evaluation sheds light on the capacity of the system: what the system can or cannot do. The author in [17]emphasizes that the evaluation of MT system shows accuracy and fluency sought for the audience and purpose and complies with the other features negotiated between the requester and supplier, taking into consideration end-user needs".

Many evaluation methods have been used over the history of MTE. The first MT evaluation dated back to 1954 to assess the ability to translate 250 words from Russian into English, and they succeeded in translating this small number of words. The success of the experiment attracted a lot of funding. Consequently, in 1962 the first committee, the Automatic Language Processing Advisory Committee (ALPAC), was formed for evaluation. They found that it was not worthy to spend more money on useful MT system. The report ended with nine recommendations to evaluate MT, three of them encouraged to do further research on MT systems [18].

MT systems have achieved high performance close to human accuracy. The authors in [19], [20] shown that MT systems 'performance have achieved near human level performance. Moreover, the widespread of MT reached millions and therefore it has become a source of information for millions of people. In [3] Google Translate has been used by 500 million daily. However, many studies have highlighted the shortcomings of MT in dealing with Natural language processing (NLP). The have indicated that the main challenge of MT is having large parallel corpora. However, these corpora are not available in all NL [21]-[23]. There are very limited parallel corpora for the majority of language pairs. On the other hand, most of the previous studies depend on monolingual corpora in each language [24], [25]. According to [23] the success of the previsions of MT research is about using inferred bilingual dictionary. Moreover, it is indicated that the success of the previous studies is about using model training in sequence to sequence systems [26]-[28]. Previous studies have adopted back translation strategy in supervising i.e. generating inputs to train the target models and vice versa. Despite the fact that there are many methods designed for evaluation, there is still no generally accepted methodology to evaluate MT systems. Yet, MT needs evaluation, which can be done manually and automatically [22].

To assess MT system, there are three stages to evaluate their performance and efficiency: firstly, the design of the system; secondly, the development of the system; and thirdly, the evaluation of the system by potential customers [27]. With regards to the third point, MT evaluation is divided into three categories. The first is adequacy, which is used to assess the end user's needs, such as readability and costs. The second is diagnostic evaluation, where the designers and developers examine the output of MT and its relevance to the input. The third is the performance evaluation in order to assess the systems' performance in specific areas to assist the developers and the designers of the system [28].

MT could be evaluated manually and automatically [29], [30]. The author in [31] states manual evaluation investigates the systems' usability via human participants by means of Error Analysis […], whereas automatic evaluation examines MT outputs through the text's similarity to a referenced translation. Similarly, MT evaluation has two aspects: intrinsic and extrinsic. The former highlights the language quality, while the former highlights the capacity and efficiency of the system. He also adds that there are two ways to evaluate MT output: automatic and manual evaluation. Automatic evaluation relies on the usage of metrics that could approximate the similarity between the output and the human referenced translation without human interventions, while manual evaluation depends on human evaluators to assess and rank MT output [32]. The author in [15] sums up the advantages of automatic evaluation as fast and cheap: there is no need for bilingual speakers, it requires minimal human labor and can be used as an ongoing evaluation process during the design of the system.

MT could be evaluated automatically in terms of Edit-Distance metrics, Precision and Recall, F-Measure and Word Order. The author in [33] indicates that Edit Distance evaluates MT in terms of additions, omissions, substitutions, which are the requirements for adequate output. Precision and Recall evaluates the degree of n-gram matching between MT and human translation based on referenced translation, such as BLEU and NIST. The F measure is used to measure the overall quality performance. The word order counts the word order sequence between the source sentence and the output of MT. The author in [34] reminds us why BLEU is the most popular metrics among researchers:

> *one of the reasons why the metric is popular in the community seems to be for its simplicity for MT developers at least. Another reason why BLEU is widely used is that it has the best correlations with human judgments of translation quality. It estimates the similarity between the translated sentence and the referenced sentence.*

In fact, automatic evaluation has some advantages, but its shortcomings outweigh its advantages. Automatic evaluation assesses the text similarity between the output and the referenced human translation. It does not look for the meaning transference from the ST to the TT, which is a fundamental requirement for accuracy in translation. Bilingual Evaluation Understudy (BLUE) looks for n-gram similarity not meaning [35]. The author in [36] further argues that BLEU evaluates text similarity rather than meaning. Moreover, the Translation Automation User Society [37] agrees that automatic evaluation could provide one side of quality, which could not reflect the genuine quality of MT output. For these reasons and others, the current study adopts manual methods in evaluating MT output holistically in terms of adequacy and fluency scales provided by TAUS, rather than automated evaluations using BLEU for instance.

In fact, manual evaluation of MT is considered as golden standard to evaluate MT and cannot be overwhelmed by automatic evaluation. Manual evaluation of MT could be done in terms of quality assessment, translation ranking, error analysis, information extraction, comprehension test and post editing. Translation ranking results provide the end users with the degree of the output intelligibility.

In the same vein, [36] developed several tools for MT quality evaluation. They offered these tools on their website to conduct MT evaluation in terms of adequacy and fluency. The adequacy tool enables the evaluators to assess the output based on 1-4 rating scales to verify how much of the meaning is contained in the TT as shown in Table 1 & 2.

Table 1: Adequacy Rating Scale [34]

Adequacy Rating Scales		
4	Everything	All of the meaning in the source is contained, no more, no less
3	Most	Almost all the meaning in the source is contained in the translation.
2	Little	Fragments of the meaning in the source are contained in the translation.
1	None	None of the meaning in the source is contained in the translation.

On the other hand, [36] also provides a fluency tool to evaluate MT output in terms of structural rules as accepted by native speakers of the TL. Fluency evaluates MT output in terms of 1-4 rating scales.

Table 2: Fluency Rating Scale [34]

Fluency Rating scales		
4	Flawless	Refers to a perfectly flowing text with no errors.
3	Good	Refers to a smoothly flowing text even when a number of minor errors are present.
2	Disfluent	Refers to a text that is poorly written and difficult to understand.
1	Incomprehensible	Refers to a very poorly written text that is impossible to understand.

The present study aims to verify the best results of MT output in terms of adequacy and fluency scales provided by TAUS. The study has adopted TAUS since it provides a constructive feedback of the Facebook Machine Translation. Such feedback helps the system's developers to improve the efficiency of the systems and provide the users with insights about how much is the FTS is adequate and fluent.

2. Literature Review

As discussed above, MTE is essential in evaluating MT output to provide the end users with feedback about the strength and limitations of the systems. Facebook is the most prominent social media sites globally. It is also classed as the most popular social media site in the Arab region. Therefore, Facebook has become a major source of information for the majority of Facebookers during the COVID-19 outbreak. No research to date has been conducted to evaluate the efficiency of Facebook Translation in rendering English posts into Arabic in general and COVID-19 in particular.

The author in [37] conducted a study to trace the percentage of FTS usage among Jordanian during COVID-19 lockdown. They found that 94.3% use Facebook daily; 87.1% of the participants activated Facebook Translation Service (FTS). Moreover, 62.2% of the participants considered Facebook as a primary source of information regarding COVID-19 and 27.8% as secondary source. The authors in [38] have conducted a descriptive study on medical students in Jordan to assess knowledge, attitude, perceptions and precautionary measures toward COVID-19 among a sample of students in Jordan. They have found that 83.4% used social media sites as their preferred source of information regarding COVID-19. Moreover, [39] have conducted another study in Jordan to assess knowledge, practice and attitude of university students regardless of their majors. They have found that the sources of information for the University students are social media, internet and television. No significant difference was noticed between medical and non-medical college students on the sources of their information.

On the other hand, [40] has shown the social media sites have become a useful tool in confronting the crisis and connecting people together during the crisis. Moreover, public health experts have used social media sites to educate the public about the effects of COVID-19 and to discuss COVID-19 with specialists. The acceleration in the digital life changes the way of approaching the health information. She shows public health experts will use social media sites to spread correct information regarding health problems [41]. The author in [42] shows that Facebook has become a source of discussion and information exchange for 100,000 health care providers regarding the COVID-19 outbreak.

Social media sites have become platforms for survival against social isolation during the COVID-19 to "help people avoid the detrimental effects of social isolation during this pandemic" [42], with Facebook playing a major role as well. Social networks usage has rocketed covering different aspects of our life, including medicine, geography and business growth. Facebook has been used widely during COVID-19 as a platform for business, charity, and community service [43]. The [44] goes as far as suggesting that social media sites during the crisis preached religion to the followers and provided a form of religious instruction and support. On the other hand, social media have become the platform for sharing hurtful messages for people of China. They blamed China as a source of the crisis [45]. However, Facebook and other social media clamped down the spread of fake news concerning COVID-19 and fake news

This research brings the importance of MT systems in handling translation across languages during world crises. The next part highlights the methodology used in assessing MT role during COVID-19 Crisis.

3. Methodology

The study evaluates the effectiveness FTS has in providing adequate and fluent output for English posts related to Coronavirus into Arabic. It provides an answer to the following question: To what extent is FTS capable in providing adequate and fluent translation for English COVID-19 posts into Arabic? To answer this question, six evaluators evaluated the output of FTS in terms of the above TAUS adequacy and fluency scales.

The corpus of the study consists of 300 English posts related to COVID-19, collected over March and April 2020, the peak months of the pandemic. The posts were selected from various Facebook pages that belonged to political leaders, healthcare providers, medical specialists and the public. To ensure consistency and objectivity as recommended by TAUS creators, six evaluators, native speakers of Arabic and near-native speakers of English rated the same data on each scale. The evaluators were acquainted with fluency and adequacy scales along with MT limitations and potentials. Once the corpus was uploaded and sent to the evaluators using TAUS tools, they had to assign scores online on 1-4 rating scales. Then, each report was displayed online on the TAUS reports tool. The data were analyzed using SPSS Statistics to get Pearson interrater agreement among evaluators in ranking the output at two different times. The results showed that there is a high inter-rater reliability among the rators.

Table 3. Interrater correlation

N	Fluency	Adequacy
1	.947**	.969**
2	.973**	.936**
3	.931**	.967**
4	.839**	.782**
5	.976**	.867**
6	.944**	.985**

The above table shows Interrater correlation using Person Correlation between first and second evaluation for each rater, resulting in a statistically significant strong correlation between first and second evaluations for each rater.

4. Results and Discussion

4.1. Fluency

The following example illustrates how FTS translated a World Health Organization (WHO) COVID-19 instructional post into Arabic.

Example 1

Source Text: Many people are making great sacrifices to stay home and protect their health and that of others from COVID-19.

FTS output: الكثير من الناس يقدمون تضحيات كبيرة للبقاء في المنزل وحماية صحتهم وصحة الاخرين من كوفيد-19

alkthyr mn alnas yqdmwn tdhyat kbyrh llbqa' fy almnzl whmayh shthm wshh alakhryn mn kwfyd-19

Back translation: many people are offering great sacrifices to stay home and protect their health and that of other from COVID-19.

This example shows how FTS rendered the English WHO post into Arabic. The analysis shows that FTS rendered the posts fluently. Moreover, four of the raters gave the above example a rate of 4, flawless, while two of them ranked it as 3, Good. The analysis shows that FTS provided intelligible and fluent output.

Example 2

Source Text: Now, anyone returning from overseas is being forced into quarantine for 14 days when they arrive back in Australia. This is mostly occurring in hotels, and at Government expense.

FTS output: الان، اي شخص عائد من الخارج يجبر الى الحجر الصحي لمدة 14 ايام عندما يعود الى استراليا. يحدث هذا في الغالب في الفنادق، وعلى نفقة الحكومة.

alan, ay shkhs 'ea'ed mn alkharj yjbr ala alhjr alshy lmdh 14 ayam 'endma y'ewd ala astralya. yhdth hda fy alghalb fy alfnadq, w'ela nfqh alhkwmh.

Back Translation: Now, anyone returning from abroad is being forced into quarantine for 14 days when they return to Australia. This is mostly occurring in hotels, and at Government expense.

The above example shows how FTS rendered into Arabic a Facebook post of Mark McGowan, Premier of Western Australia, regarding the quarantine for arrivals to Australia. The analysis shows that the raters rated the post in a balanced way. Three of raters rated the output as flawless, where the post is perfectly translated. Moreover, three of them ranked FTS output as Good, where the sentence is fluently translated despite minor errors. In fact, these minor errors did not inhibit the intelligibility of the text.
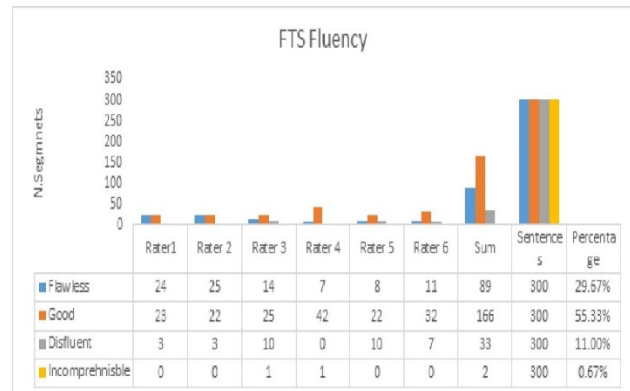
Figure 1: FTS Fluency

The above chart illustrates the degree of fluency obtained by FTS in providing fluent translation for English posts related to COVID-19 into Arabic. The highest fluency scale goes for *good* among the six evaluators with a percentage of 55.33%, where FTS output is easily understood without difficulty even when a number of minor errors are present. The lowest scale goes for incomprehensible scale, where the output is poor and impossible to understand which is equal to 0.67%. The first and second raters had similar evaluation. They indicated that the FTS output is held between *good* where the output has minor errors with 55.33% and *flawless* with 29.67%, a perfect output with no errors. The other four raters ranked FTS as *good*, followed by Flawless and then *disfluent*, where the text is poorly written and difficult to understand. According to the raters, FTS is mostly adequate in

conveying Source the ST to the TT where the target side translation is grammatically well informed, without spelling errors and experienced as using natural/intuitive language by a native speaker.

Adequacy

Example 3

Source Text: The conclusion I reached is that the Government should end the lockdown after Easter and return to a mitigation strategy,   with
self-quarantining limited to those most at risk" writes Toby Young.

FTS Output: الاستنتاج الذي توصلت اليه هو انه ينبغي للحكومة انهاء الاغلاق بعد عيد الفصح والعودة الى استراتيجية التخفيف، مع الحجر الصحي الذاتي, يقتصر على اولئك الاكثر عرضة للخطر, يكتب توبي يونغ.

alastntaj aldy twslt alyh hw anh ynbghy llhkwmh anha' alaghlaq b'ed 'eyd alfsh wal'ewdh ala astratyjyh altkhfyf, m'e alhjr alshy aldaty, yqtsr 'ela awl'ek alakthr 'erdh llkhtr, yktb twby ywngh.

Back Translation: The conclusion I reached is that the government should end the lockdown after Easter and returned to mitigation strategy, with self-quarantining limited to those at most risks, writes Toby Young.

This example shows how FTS rendered the Telegraph Facebook Posts into Arabic. The results show that the source text meaning is contained in the output translation. The four raters rated the FTS output as Most, where almost all the meaning in the source text is contained in the translation. However, two raters gave a scale of 4 Everything. The current study concurs with the last rating, Everything, that all the information contained in the source text is found in the target output.

Example 4

Source Text: When the world's doctors come together, amazing things can happen. We're all hopeful that plasma therapy can help treat COVID-19.

I'm glad Bloomberg Philanthropies can play our part to support Arturo Casadevall's research.

FTS Output:

عندما يجتمع اطباء العالم معا، يمكن ان تحدث اشياء مذهلة. نحن جميعا نامل ان العلاج بالبلازما يمكن ان يساعد في علاج كوفيد-19.

Bloomberg Philanthropies يمكن ان يلعب دورنا لدعم ابحاث ارتورو كاسادفال انا سعيد ان

'endma yjtm'e atba' al'ealm m'ea, ymkn an thdth ashya' mdhlh. nhn jmy'ea naml an al'elaj balblazma ymkn an ysa'ed fy 'elaj kwfyd-19.

ymkn an yl'eb dwrna ld'em abhath artwrw kasadfal Bloomberg Philanthropies ana s'eyd an

Back Translation: When the world's doctors come together, amazing things can happen. We are hopeful that Plasma thereby can help cure COVID-19. I happy that Bloomberg Philanthropies can take part in supporting Arturo Casadevall's research.

The example shows how FTS transferred the English post into Arabic. The six assessors ranked the output differently. Four of them rated it as Most, while the other two raters ranked it as Little. The study correlates with the four raters that almost all the meaning in the source text is contained in the translation. However, the study indicates that keeping the noun 'Bloomberg Philanthropies' untranslated does not inhibit the intelligibility of the text
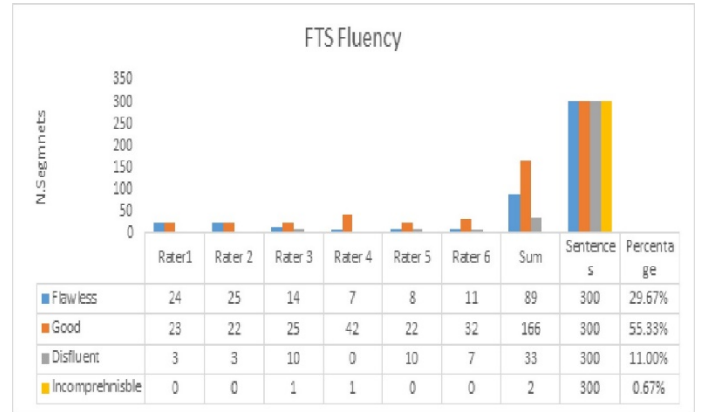
Figure 2: Adequacy Scales
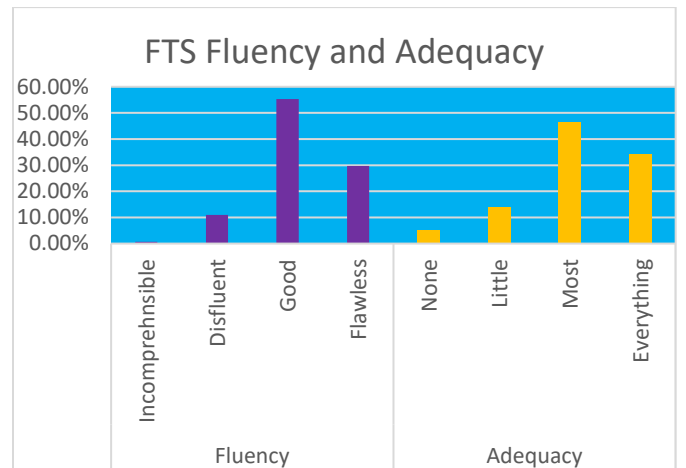
Figure 3: FTS Fluency and Adequacy Performance

The above chart shows the degree of adequacy obtained by FTS in providing adequate translation for English Facebook Posts related to COVID-19 into Arabic. The analysis shows that the highest adequacy scale goes for *most* scale with a percentage of 47%%, where almost all of source text meaning is contained in the target text, while the lowest scale goes for *none*, none of the meaning is contained in the translation which is equal to 5.33%. The six raters had similar views that most of the outputs are scaled as *most*, followed by *everything*, all the meaning of the source text is contained in the translation, and then little in the third rank and None with lowest rate. The chart below illustrates FTS performance based on TAUS adequacy and Fluency.

The above chart illustrates the ratings of fluency and adequacy obtained by FTS in rendering English Facebook posts related to COVID-19 into Arabic. The analysis shows that the highest degree of adequacy achieved by FTS is Most, with a percentage of 46.33, followed by Everything and then Little and None, indicating that almost all of the ST meaning is contained in

the TL. Similarly, the highest degree of fluency achieved by FTS is Good, where FTS succeeded in providing Fluent output with minor grammatical categories, followed by Flawless, Disfluent and then Incomprehensible. These two degrees indicate the FTS could provide fluent and adequate translation to the end users.

The results of the study have indicated that Facebook have conducted rigorous research to ensure the best translation quality for the end users. The study has shown that FTS has achieved a high degree of fluency starting with **good** scale, followed by *flawless*, **disfluent and *incomprehensible***. The study has shown that FTS achieved a higher degree of adequacy starting with **most**, followed by **everything**, **little** and **none**. These results agree with [11] that Facebook introduced Neural Machine Translation (NMT) to provide an accurate translation for the end users. Moreover, the study confirms the findings by [37], that the NMT introduction enhances the accuracy and the speed of MT across languages. The study correlates with [13] that back-translations, self-training, multilingual modeling could improve Facebook translation accuracy across human languages.

5. Conclusion

This research is the first research to fill a gap in the literature about the FTS degree of adequacy in contributing to translate the English Facebook posts related to COVID-19 into Arabic. It provides useful data on FTS adequacy and fluency criteria.

Overall, Facebook translation service obtained a high degree of adequacy and fluency. This is because FTS is trained well to deal with Arabic content. More importantly, we could benefit from FTS with Human Assisted Machine Translation (HAMT), in which a computer system does most of the translation, appealing in case of difficulty to a human translator for post editing services. Therefore, FTS helps in fighting COVID-19 since it facilitates the process of information exchange. Moreover, the study recommends further studies to conduct diachronic evaluation for FTS output over a period of time, since the current study is limited to assess FTS output during the COVID-19 outbreak in Jordan. Despite the fact that FTS achieved a higher degree of adequacy and fluency scales, the current analysis does not cover all genres and therefore there is a lack of integrative evaluation studies that pave the research for the holistic analysis and the error analysis studies. The FTS is still far from reaching fully adequate and fluent translation of a quality obtained by human translators.

6. Limitation and Study Forward

This study has some limitations as it investigates the adequacy and fluency of Facebook Translation Service during COVID-19 on a particular topic, namely COVID-19, from the instructors' perspective, within a defined timeframe (post COVID-19 era), and geographical context (Jordan) to answer three research questions. Consequently, further research will be necessary to examine the adequacy and fluency of FTS in other fields and different timeframes. That the current study focuses on the period of the outbreak of the COVID-19 pandemic, it is recommended that other researchers examine the long-term adequacy and fluency of FTS in all fields. It is also recommended that researchers conduct similar research on the adequacy and fluency of FTS in translating from English into their languages at different situations.

References

[1] Microsoft.com, Machine Translation - Microsoft Translator for Business, 2020.

[2] J. Hutchins, Compendium of Translation Software Compendium of Translation Software Directory of commercial machine translation systems and computer-aided translation support tools behalf of The International Association for Machine Translation by The European Associat, 2010.

[3] Z. Almahasees, Diachronic Evaluation of Google Translate, Microsoft Translator and Sakhr in English-Arabic Translation — the UWA Profiles and Research Repository, 2020.

[4] F. Gaspari, J. Hutchins, "Online and Free ! Ten Years of Online Machine Translation : Origins , Developments , Current Use and Future Prospects," 2007.

[5] Bernard Scott, Machine Translation: Technologies and Applications | SpringerLink, 2018.

[6] C. Amendola, How to Use Facebook Translate Button – Multilizer Translation Blog, 2020.

[7] Singh, How to enable new Facebook In-Line Translation Tool on Facebook Pages | Tech 24 Hours, 2020.

[8] T. Martín-Blas, A. Serrano-Fernández, "The role of new technologies in the learning process: Moodle as a teaching tool in Physics," Computers and Education, **52**(1), 35–44, 2009, doi:10.1016/j.compedu.2008.06.005.

[9] White, Facebook Launches New In-Line Translation Tool, 2011.

[10] M. Zuckerberg, Mark Zuckerberg - Today we're publishing research on how... | Facebook, 2017.

[11] J. Gehring, M. Auli, D. Grangier, D. Yarats, Y.N. Dauphin, "Convolutional sequence to sequence learning," in 34th International Conference on Machine Learning, ICML 2017, International Machine Learning Society (IMLS): 2029–2042, 2017.

[12] Facebook Engineering, A novel approach to neural machine translation - Facebook Engineering, 2017.

[13] Facebook AI, New research awards in NLP and machine translation, 2019.

[14] EuroMatrix, [PDF] 1.3: Survey of Machine Translation Evaluation | Semantic Scholar, 2009.

[15] G.S. Koby, P. Fields, D.R. Hague, A. Lommel, A. Melby, "Defining Translation Quality," Tradumàtica: Tecnologies de La Traducció, (12), 413, 2014, doi:10.5565/rev/tradumatica.76.

[16] N.R. Council, Language and Machines, National Academies Press, 1966, doi:10.17226/9547.

[17] H. Hassan, A. Aue, C. Chen, V. Chowdhary, J. Clark, C. Federmann, X. Huang, M. Junczys-Dowmunt, W. Lewis, M. Li, S. Liu, T.-Y. Liu, R. Luo, A. Menezes, T. Qin, F. Seide, X. Tan, F. Tian, L. Wu, S. Wu, Y. Xia, D. Zhang, Z. Zhang, M. Zhou, "Achieving Human Parity on Automatic Chinese to English News Translation," arXiv preprint arXiv, 2018.

[18] Y. Wu, M. Schuster, Z. Chen, Q. V. Le, M. Norouzi, W. Macherey, M. Krikun, Y. Cao, Q. Gao, K. Macherey, J. Klingner, A. Shah, M. Johnson, X. Liu, Ł. Kaiser, S. Gouws, Y. Kato, T. Kudo, H. Kazawa, K. Stevens, G. Kurian, N. Patil, W. Wang, C. Young, J. Smith, J. Riesa, A. Rudnick, O. Vinyals, G. Corrado, et al., "Google's Neural Machine Translation System: Bridging the Gap between Human and Machine Translation," arXiv preprint arXiv 2016.

[19] P. Koehn, "Neural Machine Translation," Tradumàtica: Tecnologies de La Traducció, (15), 66, 2017.

[20] P. Isabelle, C. Cherry, G. Foster, "A Challenge Set Approach to Evaluating Machine Translation," EMNLP 2017 - Conference on Empirical Methods in Natural Language Processing, Proceedings, 2486–2496, 2017.

[21] R. Sennrich, B. Haddow, A. Birch, "Improving Neural Machine Translation Models with Monolingual Data," 54th Annual Meeting of the Association for Computational Linguistics, ACL 2016 - Long Papers, **1**, 86–96, 2015.

[22] G. Lample, A. Conneau, L. Denoyer, M. Ranzato, "Unsupervised Machine Translation Using Monolingual Corpora Only," ArXiv, 2017.

[23] M. Artetxe, G. Labaka, E. Agirre, K. Cho, "Unsupervised Neural Machine Translation," ArXiv, 2017.

[24] D. Bahdanau, K.H. Cho, Y. Bengio, "Neural machine translation by jointly learning to align and translate," in 3rd International Conference on Learning Representations, ICLR 2015 - Conference Track Proceedings, International Conference on Learning Representations, ICLR, 2015.

[25] I. Sutskever, O. Vinyals, Q. V. Le, "Sequence to Sequence Learning with Neural Networks," Advances in Neural Information Processing Systems, **4**(January), 3104–3112, 2014.

[26] P. Vincent, H. Larochelle, Y. Bengio, P.A. Manzagol, "Extracting and composing robust features with denoising autoencoders," in Proceedings of the 25th International Conference on Machine Learning, Association for

Computing Machinery (ACM), New York, New York, USA: 1096–1103, 2008, doi:10.1145/1390156.1390294.

[27] W. Hutchins, H. Somers, "An introduction to machine translation," Undefined, 1992.

[28] L. Hirschman, L. Hirschman, H.S. Thompson, "Overview of Evaluation in Speech and Natural Language Processing," 1997.

[29] S. Chan, Routledge Encyclopedia of Translation Technology - 1st Edition - Sin-W, 2014.

[30] Z.M. Almahasees, "Assessing the Translation of Google and Microsoft Bing in Translating Political Texts from Arabic into English," International Journal of Languages, Literature and Linguistics, **3**(1), 1–4, 2017, doi:10.18178/ijlll.2017.3.1.100.

[31] M. Przybocki, G. Sanders, A. Le, Edit Distance: A Metric for Machine Translation Evaluation, 2006.

[32] E. Stephens, "Human Evaluation on Statistical Machine Translation," Undefined, 2014.

[33] E. Reiter, A structured review of the validity of BLEU, Computational Linguistics, **44**(3), 393–401, 2018, doi:10.1162/COLI_a_00322.

[34] TAUS, Adequacy/Fluency Guidelines - TAUS - The Language Data Network, 2019.

[35] R. Tatman, Evaluating Text Output in NLP: BLEU at your own risk | by Rachael Tatman | Towards Data Science, 2019.

[36] TAUS, TAUS Quality Dashboard. An Industry-Shared Platform for Quality Evaluation and Business Intelligence September, PDF Free Download, 2015.

[37] Z. Mohammad, Adam Benvie, Improving the accuracy & speed of translations with Neural Machine Translation - Watson Blog, 2018.

[38] A.I. Khasawneh, A.A. Humeidan, J.W. Alsulaiman, S. Bloukh, M. Ramadan, T.N. Al-Shatanawi, H.H. Awad, W.Y. Hijazi, K.R. Al-Kammash, N. Obeidat, T. Saleh, K.A. Kheirallah, "Medical Students and COVID-19: Knowledge, Attitudes, and Precautionary Measures. A Descriptive Study From Jordan," Frontiers in Public Health, 2020, doi:10.3389/fpubh.2020.00253.

[39] H. Alzoubi, N. Alnawaiseh, A. Al-Mnayyis, M. Abu-Lubad, A. Aqel, H. Al-Shagahin, "Covid-19 - Knowledge, attitude and practice among medical and non-medical university students in Jordan," Journal of Pure and Applied Microbiology, 2020, doi:10.22207/JPAM.14.1.04.

[40] Zakrzweski, The Technology 202: Coronavirus could change how social networks approach public health - The Washington Post, 2020.

[41] H. Ouyang, "At the Front Lines of Coronavirus, Turning to Social Media," The New York Times, 2020.

[42] A. Ertzioni, The Sociology of Surviving the Coronavirus | The National Interest, 2020.

[43] Goldstein, Facebook Unveils New Feature to Help Those in Need amid Coronavirus | PEOPLE.com, 2020.

[44] Heilweil, Coronavirus social distancing leads to empty churches and a rise in apps - Vox, 2020.

[45] Wong, Coronavirus sparks a different kind of problem for social networks - CNET, 2020.

ASTES

Determinants that Influence Consumers' Intention to Purchase Smart Watches in the UAE: A Case of University Students

Nasser Abdo Saif Almuraqab[*]

Dubai Business School, University of Dubai, Dubai, 14143, UAE

A R T I C L E I N F O	A B S T R A C T
	It has been observed that the smartwatches have emerged quickly on the digital era with the ability to significantly influence daily life and improve users' wellbeing, decisions, and behaviour. Nonetheless they are in their stages of adoption, smartwatches are marked the most widespread type of wearable technologies. Considering this, present work has been carried out to intensify the scholarly understanding of determinants that affecting consumers' behaviour of purchasing intention, to reach this objective, an integrated model based on Technology Acceptance Model (TAM) was designed and examined. An online questionnaire was utilized for the collected data (n=106). The empirical analysis based on partial least square method, using SmartPLS software. The findings exposed that visibility, social influence, and perceived ease of use are the proximate factors that drive adoption intention. Further, the analysis reveals that Consumers' purchasing intention is significantly influenced by intention to use and cost. The extent of these factors is influenced by consumers' perception of smartwatches as a technology and as a fashion accessory. Present study has also attempted to scholarly discuss the theoretical and managerial implications.

1. Introduction

The contemporary technological improvements and global penetration of mobile devices such as smartwatches and smartphones have resulted in anytime-anywhere real time accessibility to information. In addition, the concept of 'mobility' is advancing from simply carriable to seamlessly wearable technology. Consequently, expanding the ubiquity of personal communication to higher level. Technically, wearables are those smart electronic devices and computers that can be integrated into various kinds of daily used accessories of clothing and can be wore on or attached to the body [1]. Such devices are designed to provide consumers with a seamless and integrated experience. The major function of wearable gadgets is to help users achieve a state of self-connected by using sensors and software that simplify communication, data exchange, and instantaneously information access. Consequently, wearable devices have become a prominent part of internet of things (IOT) [2–5].

In particular, smartwatches by e.g. (Samsung, Apple, Huawei) have been highly publicized for many features and functions that attract wide range of consumers' interests, containing health-monitoring, fitness, and location tracking and extended smart features such as communications [6]. As per the results revealed

by different recent surveys regarding smartwatch adoption, the marketplace for smartwatches will continue to grow exponentially by 2020 to be around 373 million units will be sold out globally [7, 8].

Regardless Of smartwatches' high scores on the 'hype-o-meter', empirical examinations on how consumers' view and behavior of purchasing intention of these devices have not been satisfactorily conducted, and related research are still precursive. To fill this identified gap, present research has examined number of proximate psychological factors such as social influence, visibility, and cost that how these factors affect the determination of the user adoption and purchasing intention of smartwatches by assimilating them with technology acceptance model. This research thus aims to design a research model permitting a systematic estimation of smartwatch adoption and purchasing intention, with significant implications for manufacturers, marketing, and policy makers toward future wearable technology adoption.

2. Literature review

2.1. Wearable devices and smartwatches

A study conducted by [1] exposed that the terms 'wearable devices' or 'Wearable technologies', or just 'wearables' refers to

contemporary micro-electronics or even computers that are smartly integrated into daily use accessories relevant to clothing and hence can be wore or attached to body. These characteristics deliver the consumers a seamless and integrated experience. It has been commonly observed that wearable devices provide significant convenience when compared to laptops and mobile phones. This quality can be rightly attribute to their light weight, easily accessible in nature, can be used while moving, non-keyboard commands and control such as voice and gesture. Another worth mentioned significance of these devices is that they are simultaneously considered as technology and fashion by large number of users [9]. Further, in terms of performance, these devices can outperform than laptops and a smart phone, consequently the researcher thinks that they can easily replace the competitors in future. The author in [10] argues that awareness and knowledge these devices have been increased, which is positively affecting manufacturers intentions to release new versions of wearable technologies to the market. It has been argued that wearable devices possess significant potential for dramatically changing the landscape for societies and businesses as they can largely add to individuals' wellbeing and ultimately help them to make relatively batter and rational decision. Such as, smart wearable's in medical centers can help through providing most accurate health information that will ultimately increase patients' safety and success of medical operations.

The relevant published research does not provide any clarifying description of smartwatch technology. Such as, [8] discussed number of wearable's involving Samsung Galaxy Gear and Fitbit Flex, as smartwatches. While most of these are wrist-worn technologies, and technically other distinctions are required to mark them as smartwatches. Such as smart bracelets, smart wristband or fitness tracker are technically made for tracking the physical functions of the user and provide limited information in small displays. Hence these devices are primarily designed for compilation of limited data that a user can perform some analysis using laptop or smartphone. Further the capabilities of these are very limited in terms of presentation of information's such as pulse or time; also, the wristbands do not allow the installation of new applications. Contrary to that the smartwatches have relatively larger display and are mostly designed in larger size then traditional watches. In-addition, smartwatches are equipped with advance technology of touch screens, they allowed the users to install new apps. Another remarkable difference in wristband and smartwatches is that the latter provide extra functionality when user is connected to Internet. Smartwatches are capable for providing Facebook notifications, emails etc. while the primary function of wristbands is to gather data. In line with the conclusion of [11] our discussion reveals that smartwatches are relatively good choice as compare to wristbands hence, present work defines smartwatches as a device that is wore similar to regular watch and permits for apps installation and utilize the relevant features. In addition, an academic work was conducted by [12] on the wearable technologies and smartwatches' adoption, highlighting the impact of usefulness and visibility, their study revealed that perceived usefulness and visibility are important determinants that influence adoption among consumers. However, their study didn't test or examine consumers' intention to purchase the smartwatches, and the impact of adoption intention on purchasing

decision. Which this study will reveal and tend to contribute and fill this literature gap.

2.2. Theoretical framework and research model development

The contemporary era has been experiencing the invention and innovation of different types of technologies; the technologies are commercialized on large scales that are leading to the development of different theoretical and conceptual models to explain the technology acceptance. One of the frequently discussed and used theoretical models is Technology Acceptance Model (TAM) that provides insights into final user's acceptance of ICT. This model postulate that the primary and prominent psychological factors of intention to use (ITU) are perceived ease of use (PEOU) and perceived usefulness (PU) [13,14]. It has been argued that when final end users perceived that a service is relatively easy to use and operate, they will use the technology. Number of earlier works done in the current area of interests suggests that TAM framework has the advantage of explanatory power and follow a parsimonious approach, this has been proved through many research works on the user adoption of several mobile-services and technologies, including m-government or smart government apps, tablet computers, e-book readers, mobile cloud computing, long-term evolution services (LTE), and digital currencies [8,15–21]. Consequently, TAM has been adopted as the primary theoretical framework to investigate the user acceptance of smartwatches. The following hypotheses have been developed in the current study.

H1: Perceived usefulness (PU) will have positive effect on users' intentions to use smartwatches (ITU).
H2: Perceived ease of use (PEOU) will have positive effect on users' intentions to use smartwatches (ITU).

2.3. Visibility

In contemporaneous societies, clothing, trinkets, and makeup are considered as important and prominent determinants of persons' imprint development e.g., [22–24]. A study carried out by [25] outlined first person verdicts as instant rejoinders during first meetings and considered that the noticeable factors of ones' personality plays an important role in impression structure. Earlier studies on possessions and branding exposed the ideology that visible components of personality can be used for impression and gathering data about others e. g. [26,27]. Hence, a user using a brand, or possession or product to reveal a facet of her/himself to others, wants to make sure that other people acknowledge such possession. As concluded by [28] "visible products and services are the bases for inferences about the status, personality, and disposition of the owner or consumer of these goods." As a contemporary trend, people tend to purchase products with high social status [29], the study presumes that people with more information's and awareness regarding visibility have a positive mindset towards a technology, others' influence may enhance consumers' intention [12,30–32]. Following this prior explanation, it is hypothesized:

H3: Visibility (VB) will have a positive effect on users' intention to use smartwatches (ITU).

2.4. Social influence

It has been observed that social influence is a significantly important factor, considering the technology has fashion factor

involved as well. This is the case with most of the wearable devices such as smartwatches. Consequently, as soon as users tend to buy something, they do consider their social circles and social networks. Number of earlier relevant studies included social influence as a critical factor of the consumer buying behavior [15,33]. Two independent studies conducted by [34,35] investigate the adoption of wearable devices by passengers and concluded that social influence significantly affect behavioral intention. They further discussed that the social influence can greatly affect these systems because people normally tend to notice and that these devices will greatly increase their survival chances. Other studies have also confirmed that same for other wearable technologies such as smart clothing [36], smart glasses [37,38], and fitness/health wearable technologies [39–42]. Hence, it is hypothesized:

H4: Social influence (SI) will have a positive effect on users' intention to use smartwatches (ITU).

2.5. Cost

Cost is also considered as a vital factor in previous studies. whether consumers think that the smartwatches are costly or reasonable? whether they are willing to pay or not? Manufactures and all those concerns give high weightage to these questions because they know that consumer buying behavior is greatly influenced by consumers' opinions of cost. In fact, [43] attempted to analyze the nexus between cost and acceptance of m-banking. They reach to the conclusion that higher the cost of a service, less the consumers will be willing to purchase it. Similar results were exposed by number of other studies such as in case of m-commerce [44,45]. Considering the above, cost of smartwatches has been included as an explanatory variable with the following hypothesis to test its validity:

H5: Cost (CT) will have negative effect on intentions to purchase smartwatches (PI).

2.6. Purchase intention

Attitudes towards technology (i.e. intention to use) are the only determinants of purchasing intention, claims [46]. Costa-Font, [47] also articulate that certain attitudes encourage consumers' choice of a product. These claims are widely supported in literature on technology adoption. These claims are well validated by empirical results showing strong associations [48,49]. Also, based on Davis' technology acceptance model, the author will test the correlation between intention to use and purchase intention. **H6:** Intention to use (ITU) smartwatches will have a positive effect on consumers' purchasing intention (PI).
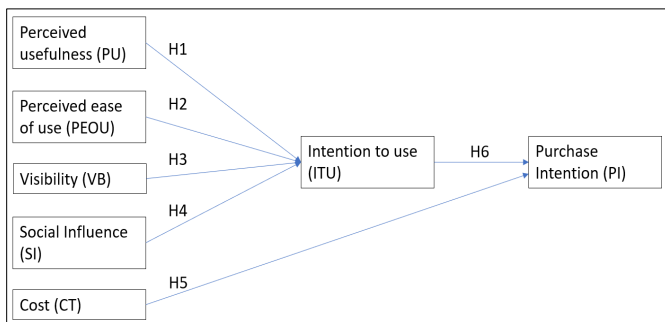
Figure 1: Conceptual framework of the research

3. Methodology

To the best of author's awareness, this is a pioneering empirical study that has exclusively attempted to scholarly examined the determinants of smartwatches buying intention of the people in the context of UAE. Present study has adopted an empirical approach for testing the model used, a well-designed and pretested questionnaire has been used for collecting the desired data on the proposed variables.

3.1. Instruments

The questionnaire served in this study has been divided into three sections. Introduction to the study and objectives of the study are given in first section, this was inevitable as respondents were UAE citizens (expats and locals). The next section was composed of questions related to demographic information's such as age, education, gender, and possession. And the final section was composed to 23 questions that measured seven variables drawn from relevant studies. All this has added significantly to the validity of instrument and ultimately to the reliability. Present study has extended the TAM model through inclusion of PU and PEOU to the predicted variables from the available literature, which are cost, social influence, and visibility. Table 2 has been allocated to the items' distribution that contains means and standard deviations of the items. It has been observed that this technique has added significantly in enhancement the consistency and strength of study's model.

3.2. Sampling process

The survey used in this research has been developed as follow: initially the researcher conducted a reliability test through collecting data from limited number participant from the target population (50 to 60) minimum. For this purpose, Cronbach's alpha was obtained from SmartPLS3. For justification of and deciding upon sample size, the researcher pre-planned that the survey will be distributed through electronic targeting to connect minimum 50 responses if possible. Consequently, to compel with the SmartPLS3 criteria of 10-times larger formative indicator for measuring single construct, or even highest order structural path that was indicated by the construct in the structural model.

Followed by that, the scholar has shared the survey link to the participants using the email list given by the University of Dubai. This simple random sampling method resulted in 106 responses after discarding incomplete responses, that is sufficient for the generalization and of results and sustainability of terms. Table 1 has been allocated to presents the sample demographics.

3.3. Analysis of the results

Partial least squares analysis which is based on structural equation modelling (SEM) [50]. SEM methodology has the advantage of assessing the measurement and structuring model simultaneously, hence factor analysis and hypothesis testing are done concurrently [51]. Further, PLS was used instead of covariance-based SEM as it is more appropriate for exploratory study [51]. For ensuring significant perceivability of the items used in the model, the Likert scale with responses recorded from 1 to 5 has been used. Table 2 presents information regarding loadings, cross-loadings, standard deviation, and means of all the variables used in the model.

Table 1: Sample Table

Gender	Frequency	Percentage
Male	65	61%
Female	41	39%
Education		
High school	3	3%
Diploma	8	8%
Bachelor	52	49%
Postgraduate	43	41%
Age		
>18	1	1%
18-24	26	25%
25-34	32	30%
35-44	38	36%
45-54	7	7%
55-64	2	2%

The scholar has properly measured the discriminant and convergent validities for examining the research model used in the research. For verification and validity of convergent strength, the average variance extracted was performed, for internal consistency Cronbach's Alpha and item loadings were obtained. All of these statistics were higher than 0.70 for composite reliabilities, the Cronbach's Alpha was above 50 percent, the statistic for item loadings was 0.70 [52] all these are given in Table 2 and 3. Further, Table 2 shows that average loading of variables is higher than 70 percent; this is desirable in social sciences. Further, the acceptable level dependency of all variables has been shown by Cronbach's alpha (suggested value 0.8, acceptable value 0.6) the details of these values are given in Table 2.

Technically, prior to responding the research question, the scholar should examine and test for the possible correlation. Agreeing to [53] for the discriminant validity, as compare to a construct correlation with other variables, the AVE must be larger for every construct. Table 3 present the results for inter-construct correlation matrix, with bold values representing the respective square root AVE.

A Simultaneous equation model test has been applied using SmartPLS3 to add further to the results shown and to properly achieve the research aim. Technically, the non-parametric bootstrapping procedure is used by PLS-SEM for statistically testing the model under consideration. In simple words, numbers of sub-samples out of the study sample are produced and are tested for the verification and validity of model best fit. The University of Dubai has its own licensed SmartPLS3 tool that is used by the scholars. The output is presented in Table 3.

A great significance of SmartPLS3 tool is that it simultaneously computes the t-statistic and exact probability value p-value for each hypothesis tested. The results are provided in Table 4.

For obtaining the t-values, the bootstrapping procedure was utilized. The coefficient of determination R^2 value of 0.69

suggests that the model is good fit. Further, Figure 2 provides partial coefficient values along with their respective 't' and 'p' values.
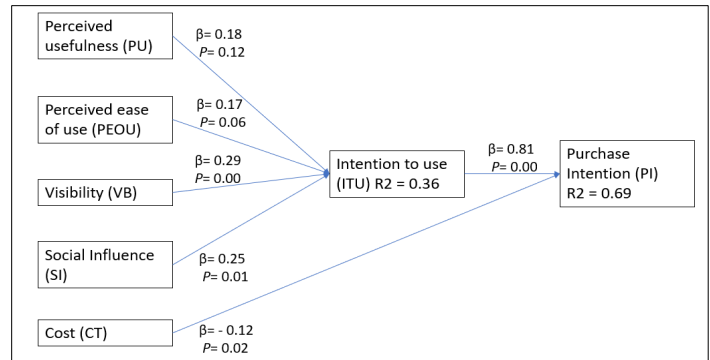
Figure 2. Hypotheses' *b*- and *p*-values

4. Discussion

As users' interest in smartwatches has lately become obvious, increasing assurance has been placed on the determinants that facilitate consumers' experience and boost greater adoption of smartwatches. Consequently, this research investigates smartwatches' key psychological and technological determinants trying to understand consumers' behavior, and explores their effect on smartwatches purchasing intention, by designing and confirming an integrated user adoption model. The model explains that people at the UAE will tend to purchase smartwatches for less cost (CT) of course, and other factors mediated by intention to use (ITU), which are visibility (VB), social influence (SI) and of course such technology should be easy to use (PEOU). The first variable (PI) is a well-explored construct that is used as a surrogate for smartwatch purchasing. In this study, PI was predicted by two major variables (ITU) and (CT), with a varying degree of significance. It was found that three out of four variables mediated by (ITU) which have significant indirect effect on (PI), these are (PEOU), (SI), and (VB). Only one of the variables was found not to be significant, which is (PU).

The analysis reveals that the prominent construct of PI is the intention to use (ITU), with partial coefficient value of 0.81. This suggests that the more the people of UAE have the intention to use technology, the more they will purchase smartwatches. Further, the analysis shows that, cost (CT) is another dominant explanatory factor of PI, with partial coefficient value of -0.12. This suggests that higher the cost, lower will be purchase intent of the people and vice versa, as the peoples in UAE consider price or cost to be a major factor that shape their future buying decision. In addition, and as per the results analysis above, there were critical predictors have significant indirect influence on people purchasing intention, mediated by ITU. These are VB, SI, PEOU in order. Visibility found to be important predictor with beta value 0.29. This suggests that in the context of UAE, people care about visibility (VB) of wearable technologies, i.e., they care about how people will notice in case they wear smartwatch and they do believe that smartwatches are more visible and prominent. Consequently, they have greater intention to use smartwatches. Similar finding was discussed by [12] on the significance of VB on ITU. These results support the findings of [12] that smartwatches, merge technology and fashion aspects.

Table 2: Means, standard deviations, and item measurement loadings and cross loadings of the variables. And internal validity

Item	Measurement item outer loadings						
	ITU	CT	PEOU	PI	PU	SI	VB
ITU1	0.917	-0.137	0.356	0.688	0.44	0.328	0.366
ITU2	0.955	-0.111	0.372	0.805	0.437	0.393	0.329
ITU3	0.895	-0.079	0.311	0.786	0.381	0.377	0.422
PC1	-0.103	0.862	-0.022	-0.167	0.058	0.072	0.076
PC2	-0.122	0.925	-0.099	-0.226	0.019	-0.048	-0.019
PC3	-0.077	0.834	0.002	-0.159	-0.037	0.017	0.025
PEOU1	0.379	-0.099	0.88	0.426	0.405	0.243	0.249
PEOU2	0.339	0.026	0.911	0.346	0.323	0.194	0.182
PEOU3	0.266	-0.068	0.887	0.322	0.438	0.178	0.145
PI1	0.861	-0.117	0.344	0.901	0.471	0.393	0.365
PI2	0.768	-0.159	0.436	0.916	0.461	0.464	0.252
PI3	0.675	-0.302	0.424	0.914	0.409	0.371	0.262
PI4	0.726	-0.225	0.362	0.924	0.382	0.444	0.336
PI5	0.808	-0.194	0.362	0.942	0.46	0.43	0.291
PI6	0.702	-0.212	0.373	0.933	0.446	0.505	0.226
PU1	0.366	0.047	0.397	0.375	0.714	0.216	0.31
PU2	0.358	0.041	0.239	0.311	0.829	0.352	0.209
PU3	0.42	0.049	0.382	0.434	0.87	0.439	0.235
PU4	0.336	-0.013	0.365	0.372	0.853	0.455	0.228
PU5	0.391	-0.057	0.401	0.473	0.876	0.444	0.184
SI1	0.343	0.02	0.225	0.482	0.462	0.897	0.025
SI2	0.351	0.014	0.188	0.357	0.358	0.939	0.079
SI3	0.388	-0.009	0.222	0.443	0.435	0.889	0.121
VB1	0.389	0.07	0.198	0.328	0.257	0.126	0.885
VB2	0.297	0.059	0.193	0.206	0.197	-0.045	0.855
VB3	0.359	-0.06	0.191	0.278	0.272	0.117	0.878
Cronbach's alpha	0.91	0.85	0.87	0.97	0.89	0.89	0.84
Composite reliability	0.95	0.91	0.92	0.97	0.92	0.93	0.91
AVE	0.85	0.76	0.80	0.85	0.69	0.83	0.76

Table 3: Discriminant validity

	ITU	CT	PEOU	PI	PU	SI	Visibility
ITU	**0.923**						
CT	-0.117	**0.874**					
PEOU	0.375	-0.053	**0.893**				
PI	0.826	-0.215	0.415	**0.922**			
PU	0.454	0.017	0.432	0.477	**0.83**		
SI	0.398	0.008	0.234	0.471	0.461	**0.909**	
Visibility	0.403	0.026	0.222	0.316	0.28	0.085	**0.873**

Table 4: *T*-values and *p*-values with hypothesis status

Hypotheses	Path coefficient	*T*-value	*P*-value	Hypothesis status
PU ⟶ ITU	0.18	1.55	0.12	Not supported
PEOU ⟶ ITU	0.17	1.84	0.06	Supported *
SI ⟶ ITU	0.25	2.46	0.01	Supported **
VB ⟶ ITU	0.29	3.42	0.00	Supported ***
CT ⟶ PI	-0.12	2.25	0.02	Supported **
ITU ⟶ PI	0.81	23.05	0.00	Supported ***

* p≤0.1 -- ** p≤ 0.05 -- *** p≤ 0.01

The analysis exposed that social influence (SI) has significant impact on PI with the partial coefficient value of 0.25. This outcome leads us to conclude that in the context of UAE economy, peoples attach more importance to social influence and will have more intention to purchase smartwatches if they consider the influence of closed or important ones, such as family, relatives, colleagues, and important people at the society such as social influencers. A person in UAE will purchase smartwatch, if s/he notice that people important in her/his life thinks that s/he should have a smartwatch. Technically, bandwagon effect can be observed in case of smartwatches purchases in UAE.

Similarly, the analysis suggests that perceived ease of use (PEOU) significantly influence ITU with a partial coefficient value of 0.17, suggesting that ease of use is as major determinant of buying behavior in UAE. People give importance to acquiring knowledge about how to use and operate smartwatches. It has been observed that perceived usefulness (PU) has no significant relationship with (PI) in the context of UAE economy. This outcome can be explained by number of factors involved, first, most of the peoples think that smartwatches are not important as have already been receiving notifications through their mobile phones, further facilities such as heartbeat rate is available in most of the smart phones as well as in most of other wearable technologies. Further, battery drain is a significant problem as people do not like to charge their smartwatches on daily basis or even every next day. All these explains why PU is not a significant factor in the context of UAE economy, and Similar finding was reported [8].

The analysis suggests that 69% of the variation in PI is explained by the included variables in the model, in social sciences that is considered as a substantial level of prediction. Out of the six variables included in the model as predictors of intention to use (ITU), four variables namely CT, PEOU, SI, were found to have statistically significant relationship with ITU and one variable PU was found not significant. Further, table 5 suggests that all but (H1) of the proposed hypotheses were supported.

Most the variables included in the present study are significantly important for analyzing smartwatch adoption and purchasing behavior in the context of UAE. The findings of the current study are in line with the findings of the earlier studies in the field.

The study suggests that visibility and social influence play critical roles in shaping purchasing intention of the peoples in UAE; people are close together and influence each other via social perceptions. Further, in the context of UAE, people also care about others' impression on their wearable devices. Moreover, prior research works have also reported that cost of smartwatches is also important and is negatively influencing purchasing decision. Hence, manufacturers should give significant importance to prices of their products and should try to produce different types of products with different prices. Finally, it has been found that ease of use is another important determinant and consumer mostly prefers simple and easy to use smartwatches in terms of features and applications. However, perceived usefulness does not influence consumers' intention to use smartwatches, subsequently buying behavior them. As many people believed that smartwatches are not mature enough to replace some or main functions of smart phones yet, and it has some drawbacks discussed earlier.

5. Conclusion

5.1. Theoretical Contribution

This research contributes two-folds to the existing stock of knowledge on the present area of interest. First, published scholarly research on smartwatches is relatively limited, and this study is an addition to limited research. Specifically, it added and validated the importance of technology acceptance utilizing (TAM) to predict the purchasing intention. In addition, TAM was combined with more variables such as cost, social influence to explain consumers' purchasing intention. Second, this work provides technical insights for understanding smartwatches, which are observed as from a technology and psychology viewpoint. Analysis suggests that most people consider smartwatches to be a combination of technology and fashion. Hence, visibility is an important determinant of adoption intention, and subsequently influence consumers' purchasing decision. However, TAM has not yet tackled the visibility part, while related aspects, such as image have been shown to be relevant in some contexts. The outcomes of the this study are in line with the previous work, which suggest that consumers perceive smartwatches on two dimensions: technology and fashion [12,33]. Generally, when exploring the adoption of purchasing intention of wearable technologies, using TAM, other variables i.e. (social influence, visibility, and cost) should be considered. Just as, any smart T-shirt or smart shoes may be considered relatively more fashion related than technology. Consequently, the relevant

theories about fashion adoption may work more appropriately in this case.

5.2. Practical contribution

It has been argued that smartwatches are a combination of technology and fashion, and they are supposed to accordingly be well-designed, affordable, and meet social needs of their targeted consumers. Despite limited customization of the design, majority of smartwatches offer technical customizations through installation of applications. To take full advantage of their market competitiveness, manufacturers are offering their products in variety of colors or wristband, whereas other are advertising various virtual background on the screen. In addition, manufacturers, should pay attention to the cost factor, which is critical, or they might introduce different models with differ prices. While the focus of this study is on smartwatches, it provides a guidance and managerial implications for decision makers for manufacturers and their marketing, not only on smartwatches, but also, on other wearable devices, for example smart glasses, smart shoes, or smart clothing.

6. Limitation and Future Research

Similar to other scholarly works, present study has number of delimitations that needs to be addressed in future research. First, as current study has taken sample from single country, the allows the researcher to control number of exogenous factors, which results an increase in internal validity, and thus limits the generalizability of the study. Although, previous studies carried out in this regard exposed that TAM [54] and other models associated with visibility [55,56] are considerably steady in varying samples and contexts, making this restriction less threatening for the sustainability of present study. furthermore, the inclusion of non-branded smartwatches allows consumers to express openly the influence on their intention without being potentially biased by a particular smartwatches brand.

Nevertheless, this advantage relates to the limitation with brand related issues, for instance brand loyalty, was not considered. For example, it was argued that a user with high brand attachment [57] or brand love [58] to Apple, would purchase any product of Apple. Upcoming studies should concentrate on tackling such limitations. Moreover, further evaluation of the significance of visibility is necessary. For example, particular design features i.e., color, shape, size) might be examined to verify the ideal strategy and improve the understanding of the desired visibility.

Correspondingly, the functions of smartwatches and its benefits, could be further studied to expose perceived usefulness (PU). Lastly, forthcoming studies might apply resistance models i.e. [59] to recognize the resistance to smartwatches and/wearable technologies. These models might be crucial in situation where smartwatches substitute conventional watches.

Conflict of Interest

The authors declare no conflict of interest.

References

[1] R. Wright, L. Keith, "Wearable technology: If the tech fits, wear it," Journal of Electronic Resources in Medical Libraries, **11**(4), 204–216.

[2] M. Swan, "Sensor mania! the internet of things, wearable computing, objective metrics, and the quantified self 2.0," Journal of Sensor and Actuator Networks, **1**(3), 217–253.

[3] P. Castillejo, J.F. Martínez, L. López, G. Rubio, "An internet of things approach for managing smart services provided by wearable devices," International Journal of Distributed Sensor Networks, **9**(2), 190813.

[4] S. Hiremath, G. Yang, K. Mankodiya, "Wearable Internet of Things: Concept, architectural components and promises for person-centered healthcare," in 2014 4th International Conference on Wireless Mobile Communication and Healthcare-Transforming Healthcare Through Innovations in Mobile and Wireless Technologies (MOBIHEALTH, IEEE: 304–307.

[5] A. Sun, T. Ji, J. Wang, H. Liu, "Wearable mobile internet devices involved in big data solution for education," International Journal of Embedded Systems, **8**(4), 293–299.

[6] A. McIntyre, Wearable computing in the workplace to be dependent on apps and services, 19–24.

[7] T. Danova, "Why the smart watch market is poised to explode as it draws millions of consumers into wearable computing," Business Insider, 1–18.

[8] K.J. Kim, D.H. Shin, "An acceptance model for smart watches," Internet Research,.

[9] D.W. Hein, P.A. Rauschnabel, Augmented reality smart glasses and knowledge management: A conceptual framework for enterprise social networks, Springer Gabler, Wiesbaden: 83–109.

[10] S. Park, K. Chung, S. Jayaraman, Wearables: Fundamentals, advancements, and a roadmap for the future, Academic Press: 1–23.

[11] M.E. Cecchinato, A.L. Cox, J. Bird, "Smartwatches: the Good, the Bad and the Ugly?," in Proceedings of the 33rd Annual ACM Conference extended abstracts on human factors in computing systems, 2133–2138.

[12] S.H.W. Chuah, P.A. Rauschnabel, N. Krey, B. Nguyen, T. Ramayah, S. Lade, "Wearable technologies: The role of usefulness and visibility in smartwatch adoption," Computers in Human Behavior, **65**, 276–284. https://doi.org/10.1016/j.chb.2016.07.047

[13] F.D. Davis, "Perceived usefulness, perceived ease of use, and user acceptance of information technology," MIS Quarterly, 319–340.

[14] F.D. Davis, "User acceptance of information technology: system characteristics, user perceptions and behavioral impacts," International Journal of Man-Machine Studies, **38**(3), 475–487.

[15] J. Jung, S. Chan-Olmsted, B. Park, Y. Kim, "Factors affecting e-book reader awareness, interest, and intention to use," New Media & Society, **14**(2), 204–224.

[16] E. Park, K.J. Kim, "User acceptance of long-term evolution (LTE) services," Program,.

[17] E. Park, A.P. Pobil, "Technology acceptance model for the use of tablet PCs," Wireless Personal Communications, **73**(4), 1561–1572.

[18] J. Joo, Y. Sang, "Exploring Koreans' smartphone usage: An integrated model of the technology acceptance model and uses and gratifications theory," Computers in Human Behavior, **29**(6), 2512–2518.

[19] K.J. Kim, S.S. Sundar, "Does screen size matter for smartphones? Utilitarian and hedonic effects of screen size on smartphone adoption," Cyberpsychology, Behavior, and Social Networking, **17**(7), 466–473.

[20] N.A.S. Almuraqab, "M-Government adoption factors in the UAE: a partial least squares approach," International Journal of Business and Information, **11**(4).

[21] N.A. Saif Almuraqab, "Predicting determinants of the intention to use digital currency in the UAE: An empirical study," The Electronic Journal of Information Systems in Developing Countries, **86**(3), 12125. https://doi.org/10.1016/j.cb.2016.078956

[22] H.L. Douty, "Influence of clothing on perception of persons," Journal of Home Economics, **55**(3), 197–202.

[23] N. Judd, R.H.C. Bull, D. Gahagan, "The effects of clothing style upon the reactions of a stranger," Social Behavior and Personality: An International Journal, **3**(2), 225–227.

[24] R.H. Holman, Clothing as communication: an empirical investigation, ACR North American Advances.

[25] H.W. Bierhoff, R. Klein, Reasoning in Impression Formation, Springer, Berlin, Heidelberg: 77–105.

[26] R.W. Belk, Effects of consistency of visible consumption patterns on impression formation, ACR North American Advances.

[27] B.M. Fennis, A.T.H. Pruyn, "You are what you wear: Brand personality influences on consumer impression formation," Journal of Business Research, **60**(6), 634–639. https://doi.org/10.1016/j.jbusres.2006.06.013

[28] R.W. Belk, Assessing the effects of visible consumption on impression formation, ACR North American Advances.

[29] K. Wilcox, H.M. Kim, S. Sen, "Why do consumers buy counterfeit luxury

brands?," Journal of Marketing Research, **46**(2), 247–259.

[30] H. Nysveen, P.E. Pedersen, H. Thorbjørnsen, "Intentions to use mobile services: Antecedents and cross-service comparisons," Journal of the Academy of Marketing Science, **33**(3), 330–346. https://doi.org/10.1177%2F0092070305276149

[31] A. Eckhardt, S. Laumer, T. Weitzel, "Who influences whom? Analyzing workplace referents' social influence on IT adoption and non-adoption," Journal of Information Technology, **24**(1), 11–24, 2015. https://doi.org/10.1057%2Fjit.2008.31

[32] S. Sawang, Y. Sun, S.A. Salim, "It's not only what I think but what they think! The moderating effect of social norms," Computers & Education, **76**, 182–189.

[33] H. Yang, J. Yu, H. Zo, M. Choi, "User acceptance of wearable devices: An extended perspective of perceived value," Telematics and Informatics, **33**(2), 256–269, 2016. https://doi.org/10.1016/j.tele.2015.08.007

[34] L.H. Wu, L.C. Wu, S.C. Chang, "Exploring consumers' intention to accept smartwatch," Computers in Human Behavior, **64**, 383–392.

[35] S.T. Kwee-Meier, J.E. Bützler, C. Schlick, "Development and validation of a technology acceptance model for safety-enhancing, wearable locating systems," Behaviour & Information Technology, **35**(5), 394–409.

[36] G. Turhan, "An assessment towards the acceptance of wearable technology to consumers in Turkey: the application to smart bra and t-shirt products," Journal of the Textile Institute, **104**(4), 375–395.

[37] P.A. Rauschnabel, A. Brem, B.S. Ivens, "Who will buy smart glasses? Empirical results of two pre-market-entry studies on the role of personality in individual awareness and intended adoption of Google Glass wearables," Computers in Human Behavior, **49**, 635–647, 2010. https://doi.org/10.1016/j.chb.2015.03.003

[38] M. Kalantari, P. Rauschnabel, Exploring the early adopters of augmented reality smart glasses: The case of Microsoft HoloLens, Springer, Cham: 229–245.

[39] L. Wu, J.Y. Li, C.Y. Fu, "The adoption of mobile healthcare by hospital's professionals: An integrative perspective," Decision Support Systems, **51**(3), 587–596.

[40] K. Jang Yul, Determinants of Users Intention to Adopt Mobile Fitness Applications: an Extended Technology Acceptance Model Approach.

[41] X. Wang, L. White, X. Chen, Y. Gao, H. Li, Y. Luo, "An empirical study of wearable technology acceptance in healthcare," Industrial Management & Data Systems,.

[42] A.I. Canhoto, S. Arp, "Exploring the factors that support adoption and sustained use of health and fitness wearables," Journal of Marketing Management, **33**(1–2), 32–60.

[43] P. Luarn, H.H. Lin, "Toward an understanding of the behavioral intention to use mobile banking," Computers in Human Behavior, **21**(6), 873–891.

[44] S.Y. Hung, C.Y. Ku, C.M. Chang, "Critical factors of WAP services adoption: an empirical study," Electronic Commerce Research and Applications, **2**(1), 42–60.

[45] J.-H. Wu, S.-C. Wang, "What drives mobile commerce?: An empirical evaluation of the revised technology acceptance model," Information & Management, **42**(5), 719–729. https://doi.org/10.1016/j.cb.2015.03.003

[46] L. Bredahl, "Determinants of consumer attitudes and purchase intentions with regard to genetically modified food–results of a cross-national survey," Journal of Consumer Policy, **24**(1), 23–61.

[47] M. Costa-Font, J.M. Gil, W.B. Traill, "Consumer acceptance, valuation of and attitudes towards genetically modified food: Review and implications for food policy," Food Policy, **33**(2), 99–111.

[48] C. Yue, S. Zhao, C. Cummings, J. Kuzma, "Investigating factors influencing consumer willingness to buy GM food and nano-food," Journal of Nanoparticle Research, **17**(7), 283.

[49] F.A. Yamoah, R. Duffy, D. Petrovici, A. Fearne, "Towards a framework for understanding fairtrade purchase intention in the mainstream environment of supermarkets," Journal of Business Ethics, **136**(1), 181–197.

[50] C.M. Ringle, S. Wende, S. Will, SmartPLS 2.0 (M3) Beta.

[51] D. Gefen, D. Straub, M.C. Boudreau, "Structural equation modeling and regression: Guidelines for research practice," Communications of the Association for Information Systems, **4**(1), 7.

[52] J.F. Hair, W.C. Black, B.J. Babin, R.E. Anderson, R. Tatham, Multivariate data analysis.

[53] C. Fornell, D.F. Larcker, "Evaluating structural equation models with unobservable variables and measurement error," Journal of Marketing Research, **18**(1), 39–50.

[54] W.R. King, J. He, "A meta-analysis of the technology acceptance model," Information & Management, **43**(6), 740–755.

[55] J.L. Nueno, J.A. Quelch, "The mass marketing of luxury," Business Horizons, **41**(6), 61–61.

[56] F. Vigneron, L.W. Johnson, "Measuring perceptions of brand luxury," Journal of Brand Management, **11**(6), 484–506.

[57] S. Belaid, A.T. Behi, "The role of attachment in building consumer-brand relationships: an empirical investigation in the utilitarian consumption context," Journal of Product & Brand Management,.

[58] R. Batra, A. Ahuvia, R.P. Bagozzi, "Brand love," Journal of Marketing, **76**(2), 1–16.

[59] P. Spreer, P.A. Rauschnabel, "Selling with technology: understanding the resistance to mobile sales assistant use in retailing," Journal of Personal Selling & Sales Management, **36**(3), 240–263, 2015. https://doi.org/10.1016/j.chb.2015.03.01203

ASTES

SIFT Implementation based on LEON3 Processor

Nasr Rashid[*,1,2], Khaled Kaaniche[1]

[1]*College of Engineering, Department of Electrical Engineering, Jouf University, Sakaka, 72388, Saudi Arabia*

[2]*Faculty of Engineering, Department of Electrical Engineering, Al-Azhar University, Cairo, 11751, Egypt*

A R T I C L E I N F O	A B S T R A C T
	This paper proposes a new method of implementation of the part of SIFT (Scale-Invariant Feature Transform) algorithm used to extract the feature of an image of a size 256×256 of pixels, which is mainly based on the using the LEON3 soft core processor .With this method it is possible to detect points of interest and so perform matching. This process allows several real time applications as robotic navigation, stereovision, object recognition etc. Obtained results show a very robustness in rotation, scale invariant as well as luminosity change. SIFT algorithm saw big success in various applications of computer vision. However, its high computation complexity has been a challenge for the most part of embedded implementations. This paper presents a partial implementation of the SIFT algorithm, which is to implement just the extraction of the characteristics that is based on the LEON3 processor. This implementation method overcomes the existing problems, in particular, the high dependence of existing implementations on the hardware architecture used. Indeed, the high flexibility of the processor allows the possibility to develop the application independent of the target board.

1. Introduction

The detection and the description of stable local features are two fundamentals components of many object recognition algorithms. In this context, Moravec and Harris were the first who proposed algorithms for the detection of interest points. Over time, several improvements have been applied to these algorithms until the appearance of the SIFT algorithm. This was a big success in various applications of computer vision.

In the computer vision field, it is interesting to extract features of an image for use in various applications such as image recognition, autonomous navigation of robots, and face recognition.

A significant progress has been developed in this axis. One of the most interesting works of characterization that gives good results was carried out in 2004 [1]: Features extracted by SIFT (Scale Invariant Feature Transform) are largely invariant to rotation, change of scale, change illumination, noise and small changes in views.

The main disadvantage of the SIFT algorithm is its high computational cost. This is the result of the complex iterative process used to obtain the invariance to changes and transformations mentioned above. An effective solution to this problem is to move to embedding this algorithm on hardware platforms, to improve the execution time.

In the second section of this paper, related works are presented. Section 3 shows briefly explanation of the principles of SIFT algorithm. In section 4, proposed method is developed. The experimental results are shown in Section 5, and a conclusion summarizes proposed work and suggests some ways to improve results.

2. Related works

The SIFT algorithm has succeeded in a large number of applications; however, its high computational complexity has been a challenge for embedded implementations. Several works have overcome this problem while developing hardware architectures based on very powerful development platform, which allows improving the running time and the precision of the results. In fact, they have benefited from the hardware parallelism offered by (Field-Programmable Gate Arrays) FPGAs. Some studies have only implemented the detection portion of points of interest based

*Corresponding Author: Nasr Rashid, +201001652392 & Email: nasrrashid34.el@azhar.edu.eg

only on a purely hardware architecture. Other works are based on a mixed architecture (hardware /software), where the software part is designed using a softcore (Nios II) or a Digital Signal Processor (DSP). A full hardware implementation was presented in 2008 [2].

The author proposed a parallel hardware architecture for detecting of points of interest based on the SIFT algorithm applied to the Simultaneous Localization and Map-building (SLAM) problem. That architecture was based on specific hardware optimizations considered fundamental to include such a robotic control system on a chip. The proposed architecture was completely independent and able to detect features from 30 images/second. They calculated the descriptor through the Nios II processor. Another architecture was proposed in 2009 [3]. Authors modified the original version of the SIFT algorithm to increase the processing speed and reduce the used hardware resources. They used two octaves where each one was formed by four scales, instead of three octaves each one was formed by five scales. This choice has degraded the mapping results, but it has optimized the use of material resources. They also reduced the size of the descriptor, in order to reduce the execution time; they went from a size of 128 to a size of 72. With this optimization, the proposed system was able to detect the features of an image of a size of 640 × 480 pixels in 31 milliseconds. In [4], the authors presented a partial implementation of the SIFT algorithm, where they only implemented a feature extraction part. The proposed architecture is able to detect points of interest from an image of 320 × 240 pixels in 11 ms.

In [5], the author described a low-cost embedded system based on a new architecture that successfully integrates an FPGA and a DSP. The step of detecting characteristics was implemented using a fully parallel architecture based on FPGA. However, the description step was performed using a fixed-point DSP. With this new design, it allowed both reducing the used hardware resources and to accelerating treatment. It was able to detect characteristics in 10ms from images of a size of a 320 × 256 pixels (without convolution step). Despite the optimizations made by the authors during the design of their architecture, the latter mismatched compared with the result obtained by the executable in [6]. This defect was caused by the loss in accuracy due to the representation of the data relating to the magnitudes and orientations in a fixed point format.

All these works have benefited from hardware parallelism offered by FPGAs to optimize the computation time and increase accuracy. But the developed architectures are dedicated to a very specific FPGA [2], [7], [8] and if you want to change the target FPGA card, you must make changes that can take a lot of time; as the example of [2] where architecture will be implemented on the FPGA of the Altera family. This paper presents a partial implementation of the SIFT algorithm, which is to implement just the extraction of the characteristics that is based on the LEON3 processor. This implementation method overcomes the existing problems in the methods presented above. Indeed, the high flexibility of the processor allows the possibility to develop the application independent of the target board.

3. Description of SIFT Algorithm

The SIFT algorithm was proposed in 2004 [1], it has been used mainly in the field of computer vision for recognizing object, people and faces. This algorithm is decomposed into four parts:

- Detection of extrema in the scale space
- Precise localization of points of interest
- Assignment orientations
- Descriptor Calculation

In this article, only the first and second step of the algorithm are considered.

3.1. Detection of extrema in space scales

This step is to determine the location of the invariant point scale change through a continuous scaling function called scale space. This function was provided in 1984 [9]. In fact, it is the result of the convolution of the Gaussian function $G(x, y, \sigma)$ with an $I(x, y)$ input image:

$$L(x,y,s) = G(x,y,s) * I(x,y) \tag{1}$$

$$G(x,y,s) = \frac{1}{2ps^2}e^{-(x^2+y^2)/2} \tag{2}$$

After determining the scale space, Lowe proposed to calculate the difference of the Gaussian (DOG) to determine the points of interest invariant to scale changes. Unlike the Gaussian is calculated from the difference between two adjacent scales separated by the constant factor k.

$$D(x,y,s) = (G(x,y,s) - G(x,y,ks)) * I(x,y) \tag{3}$$

Below is a detailed demonstration of this approximation:

$$\frac{\P G}{\P s} = s \tilde{N} G^2 \tag{4}$$

then

$$\frac{\P G}{\P s} = \frac{(G(x,y,s) - G(x,y,ks))}{ks - s} \tag{5}$$

from (3) and (5):

$$G(x,y,s) - G(x,y,ks) = s(k - 1)\tilde{N} G^2 \tag{6}$$

The factor *(k−1)* in the equation is a constant that affects neither the location nor the stability of the points of interest.
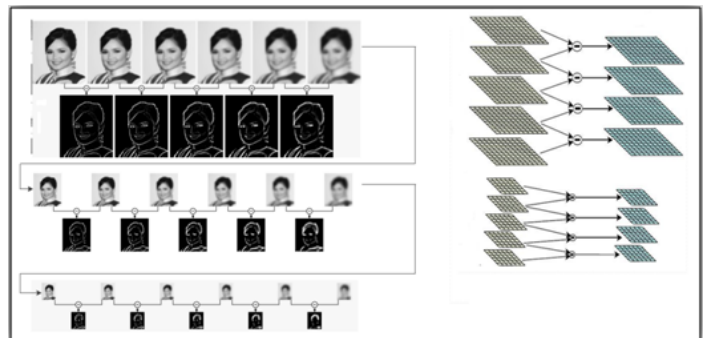
Figure 1: Detection of extrema in space scales: steps of forming the pyramid

The above steps will form a single octave. However, Lowe proposed to determine the point of interest within a pyramid which is a set of octaves. So, to form a new octave, it reduces the size of the original image of the previous octave and the process is repeated. Figure 1 shows the steps of forming the pyramid.

Indeed, the original image is sampled down by a factor of two, and then by a factor of four in order to form the basic image of each octave. Then, inside each octave, the initial image is convolutional   with a Gaussian is to produce all the images of the scale space. Finally, the adjacent images of the same octave are subtracted to produce difference of Gaussian (DOG).

To detect the local maxima and minima of *D(x, y, σ)*, each point is compared with its eight neighbors in the current image and the scale in its nine neighbors in the above and below scales. It will be chosen only if it is larger or smaller than all of these neighbors. Figure 2 shows a detailed explanation of this step.
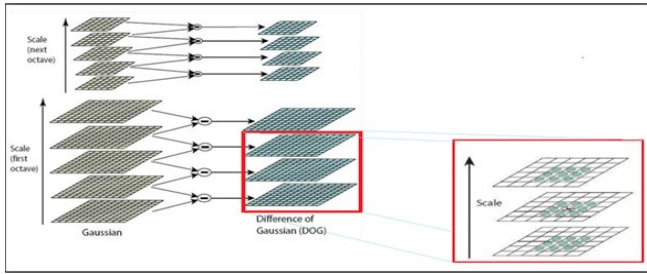
Figure 2: Detection of extrema in space scales: detailed explanation

3.2. Precise localization of points of interest

The previous step has generated a set of points, some of which are unstable. For this, an elimination should be performed for low contrast points and points situated on the edges because they are unstable. To eliminate weak points of contrast, the Taylor expansion to order one of the DOG functions is performed. A point of interest is considered unstable if $D(X) < 0.03$. A point of interest that is located in the edges is removed if the primary curve along the contour of which it is positioned is greater than the curvature in the orthogonal direction. The main curve is represented by the eigenvalues of the Hessian matrix H of 2×2 sizes given by the following expression:

$$Tr(\mathbf{H}) = D_{xx} + D_{yy} = a + b \qquad (7)$$

To avoid the calculation of eigenvalues, users exploited, in general, the approach proposed by Harris and Stephens (1988). Let α is the largest eigenvalues and β the smallest:

$$Tr(\mathbf{H}) = D_{xx} + D_{yy} = a + b \qquad (8)$$

$$Det(\mathbf{H}) = D_{xx}D_{yy} - (D_{xy})^2 = ab \qquad (9)$$

Let *r* be the ratio between the two eigenvalues ($\alpha = r\beta$), using two expressions (8) and (9), then:

$$\frac{[Tr(\mathbf{H})]^2}{Det(\mathbf{H})} = \frac{(a+b)^2}{ab} = \frac{(rb+b)^2}{rb^2} = \frac{(r+1)^2}{r} \qquad (10)$$

A point is retained if it satisfies the following condition:

$$\frac{[Tr(\mathbf{H})]^2}{Det(\mathbf{H})} < \frac{(r+1)^2}{r}$$

4. Proposed Method

To implement the feature extraction part, a C code is developed which allows the creation of space DOG space and extract the features of an image of a size of 256 × 256 pixels. The code is developed in accordance with the original version of the SIFT algorithm, where there is three octaves and where each

consists of five scales. Also, a Gaussian filter with size 7 × 7 is used. This code is implemented on the FPGA cyclone that hosts the LEON3 processor.

4.1. LEON3 processor

LEON3 [10] is a 32-bit RISC processor provided as a synthesizable VHDL model on digital ASIC or FPGA circuits. The model is highly configurable. In fact, the user can set many features of LEON3 according to his needs. The LEON3 version can be used under the GPL, allowing free use for research. ASIC LEON3 versions have been developed specifically to operate ionizing medium VHDL model and a fault tolerant LEON3-FT. Figure 3 shows the architecture of the LEON3 processor which is formed by two separate and reconfigurable cache instruction and data, 7 pipeline stages, and cabled MAC unit, multipliers and dividers. LEON3 is supplied with an IP grouped together in the "GRLIB IP" library [11] which includes a set of VHDL libraries from which the cores (IP) are instantiated in a local design. The architectures provided by this library are based on the AMBA (Advanced Microcontroller Bus Architecture) bus. There are two distinct types of buses at the AMBA. The AMBA / AHB bus used for the interconnection between the IP that requires a high data throughput as the LEON3 processor, the memory controller and the JTAG. The AMBA/APB bus (AMBA Advanced Peripheral Bus) on which the units that require a low data rate as timers and UART connect. These two buses are interfaced through the AHB/APB Bridge. Furthermore, it contains several LEON3 models designated for different FPGA board. This ensures the LEON3 processor great flexibility. The GRLIB also contains a configurable design for a multiprocessor architecture based on the LEON3. LEON3 makes available to the designer tools facilitating its rapid development (e.g.; through graphical configuration utility). This prevents wasted time in an arduous and time consuming development. For embedded applications, it is fully synthesizable, and can be implemented with a number up to 16 hearts.

4.2. Development platform

NIOSII is a dedicated embedded hardware platform application. Figure 4 shows the development platform, which is formed equipped with a EP1C20400C700 FPGA. It is also equipped with a set of memory media: flash memory (8 Moctet) SRAM (1 MB) and SDRAM (16 Moctet). In addition, this kit includes a set of communication tools: JTAG, two serial communication ports. Figure 5 shows algorithm flowchart. Step 1 presents convolution product computing. Step 2 compute the difference of Gaussians DoG. Finally, step 3 is dedicated to interest point extraction.

5.   Test and verification

To test proposed approach, LEON3 processor should be configured ; this step can be performed either under UNIX or Windows with Cygwin. Then the VHDL code of the processor is compiled in the Altera Quartus environment and finally the transfer to the card is done using the Altera programmer. Now to transfer the code to the card and run it by the LEON3 processor the GRMON tool [12] is employed, this is a debug monitor used for debugging SoC based on the LEON3 processor. The latter supports the following debugging interfaces: UART, PCI, JTAG and Ethernet. JTAG is selected for this step.
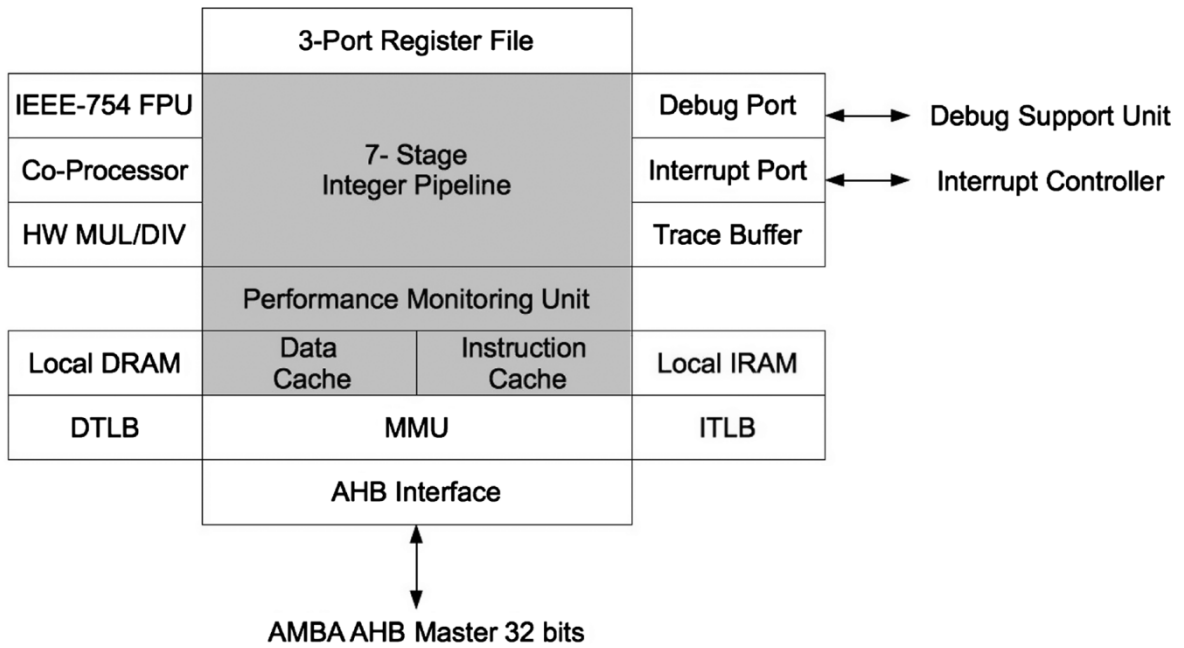
Figure 3: Architecture of the LEON3 processor
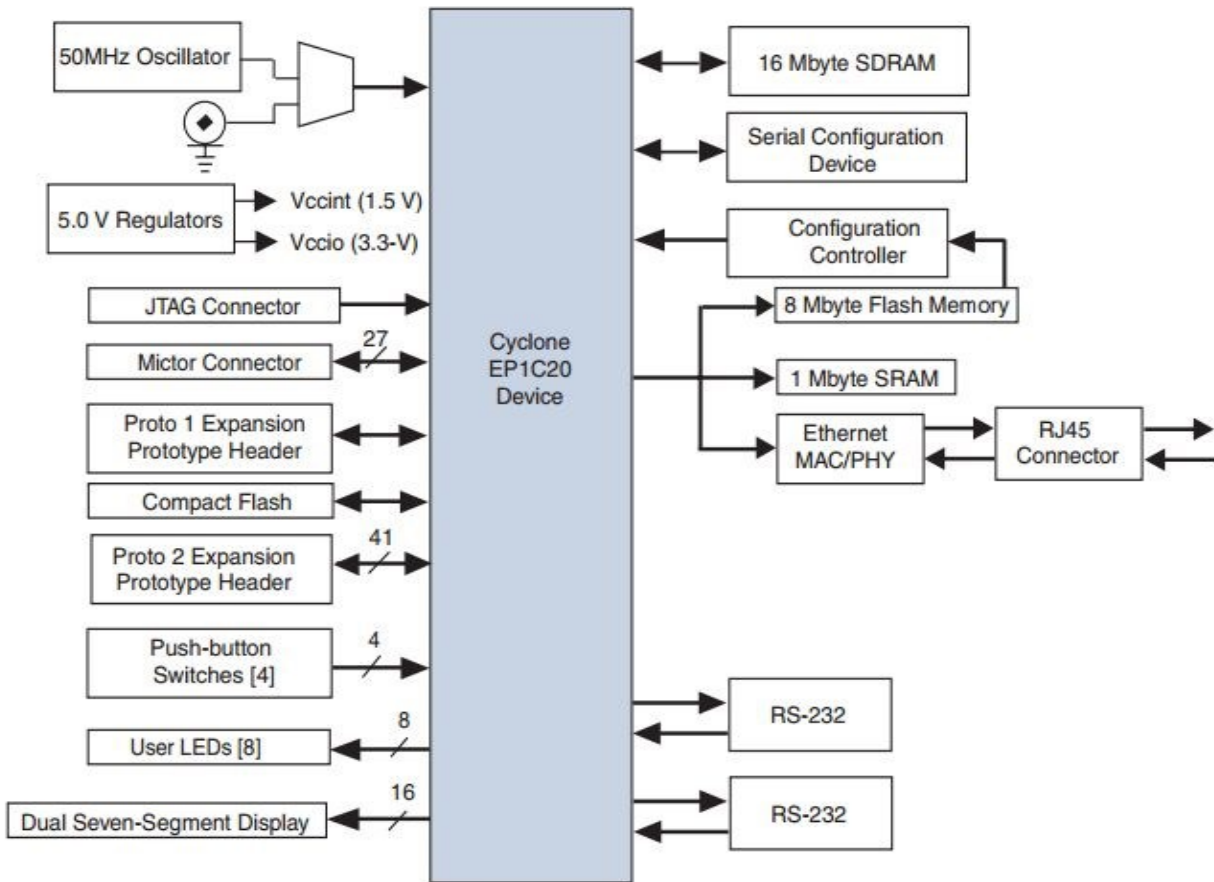
Figure 4: Development platform
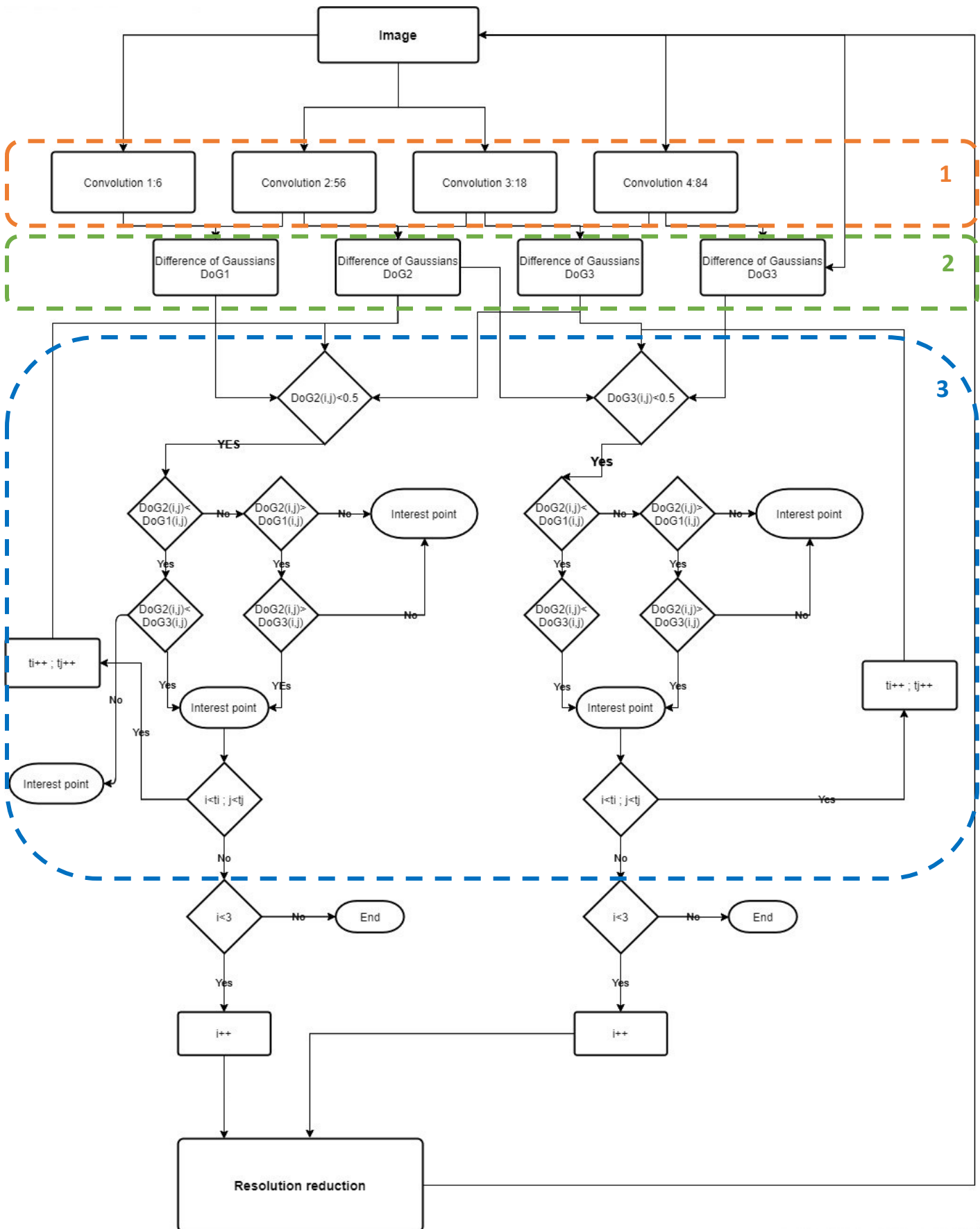
Figure 5: Algorithm flowchart
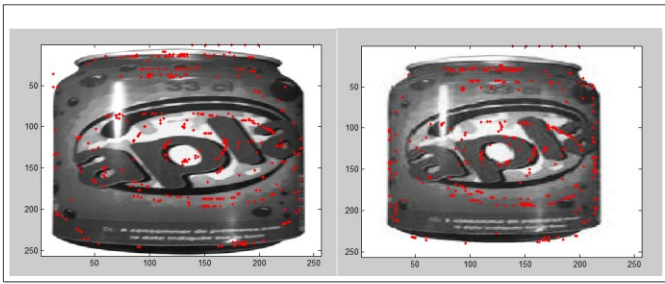
(1) Scale change 15%
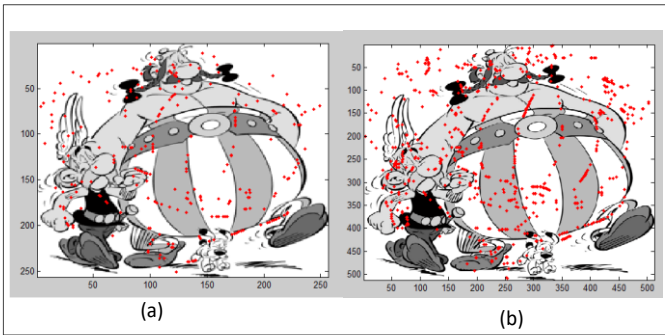
(2) 256×256 vs 512×512
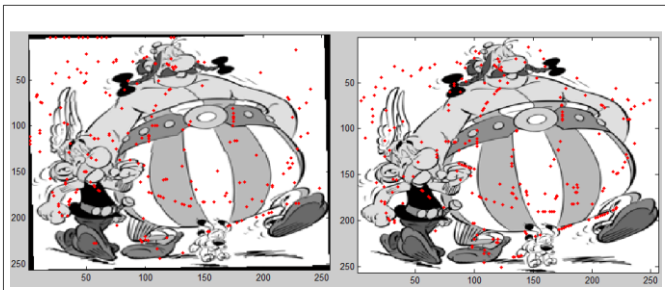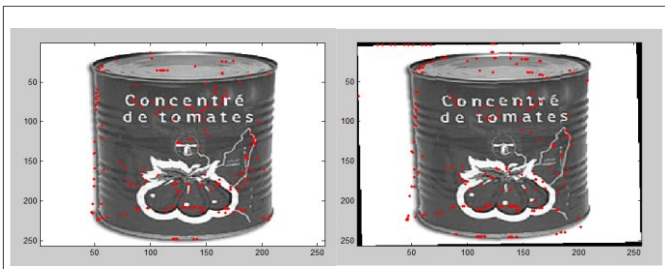
(3) Rotation -10°

(4) Rotation -10°

Figure 6: Experimental Results

For validation, proposed algorithm is performed on a set of images that have undergone various transformations such as: scaling, rotation, brightness and also images that are taken randomly from the internet. The test results are given in Figure 6. To judge the results; a visual inspection as well as quantitative measures are used. The objective of this evaluation is to locate points of interest on the same position at the same image that undergoes different processing. All these tests confirm that have been able to successfully implement the detection points of interest. SIFT code is running on the FPGA card reliably, but with an execution time equal to 3.06mn. To reduce the execution time, we benefit from a high configurability offered by the LEON3 processor that allows us to quickly design a multiprocessor architecture. This approach consists in subdividing the image into a set of blocks where each block will be executed by a single processor. Thus the run time is equal to the time taken by one processor to determine the points of interest at a single block. The Convolution was included. Process input was a grey level image and process output was SIFT points coordinate. Point description was not included (vector with 128 values) as like the majority of similar work. Embedded code stops at the generation of points. To validate this approach image is divided into four blocks, each of a size of 64×64 pixels. Where the execution time becomes 9s instead of 3.06 mn. It is to be mentioned that at this article we have used the FPGA Cyclone I, whereas nowadays the FPGA cards are performed in terms of frequency and the number of logical blocks programmable this card as Cyclone III, Vertex V, etc.... In fact, the use of this card increases over the size of the LEON3 processor cache hence reducing memory access time and thus decreasing the execution time. Figure 7 and Figure 8 show statistical result of the detection process as well as matching rate results. Matching rate is computed by dividing number of matched points by minimum between right and left detected points. Obtained rate allows any ego-motion model estimation using rejection sampling for example. It can be used as a recognition support as well.
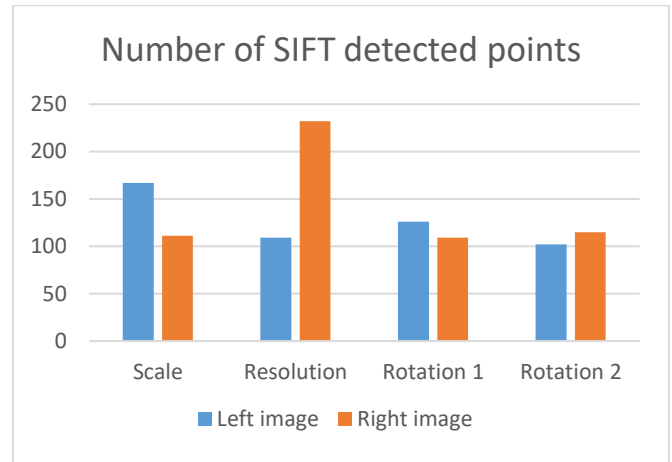
Figure 7: Number of SIFT detected points
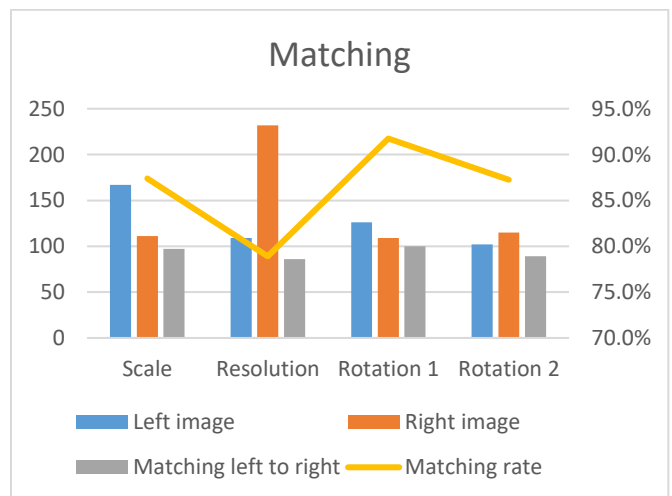
Figure 8: Matching rate

6. Conclusion

The objective in this work is to establish a detailed study of the SIFT algorithm and to propose a solution to implement it on a reconfigurable platform. This paper presented the different methods of extracting and describing points of interest, before focusing the study on the SIFT algorithm. SIFT is characterized by a very high algorithmic complexity due to the intensive use of iterative operations in order to guarantee invariance to the different types of change Rotation, scale ..., etc.

Thus, a new method was proposed based on LEON3 which has enabled us, through software programming in C language, to embed the part of extracting points of interest on an FPGA platform. Once the method is implemented, its validation will take place while being based on multiple images. The proposed approach showed very encouraging results.

In order to improve obtained results, a number of perspectives can be considered. In order to increase the size of the processor cache, FPGA boards which have a high integration capacity such as Virtex V, startixII can be used. In order to embed the FPGA platform supporting the SIFT algorithm on board a mobile robot, we propose to refine the results of the point of interest extraction step and program the description part. The main objective still to guarantee the robot's autonomous navigation (trajectory monitoring, obstacle detection, SLAM…etc.).

References

[1] D. G. Lowe, "Distinctive image features from scale-invariant keypoints", International Journal of Computer Vision, 60, 91–110, 2004, doi: 10.1023/B:VISI.0000029664.99615.94.

[2] V. Bonato, E. Marques, G. A. Constantinides,"A parallel hardware architecture for scale and rotation invariant feature detection", IEEE Transaction Circuits and Systems for Video Technology, **18**(12), 1703-1712, 2008. doi: 10.1109/TCSVT.2008.2004936

[3] L. Yao, H. Feng, Y. Zhu, Z. Jiang, D. Zhao, W. Feng, "An architecture of optimised SIFT feature dection for an FPGA implimentation of image processing", in 2009 International Conference on Field Programmable Technology, 30-37, 2009, doi: 10.1109/FPT.2009.5377651.

[4] L. Chang, J. H. Palancar, L. E. Sucar, M. Arias-Estrada, "FPGA-based detection of SIFT interest keypoints", Machine Vision and Applications, **24** (2), 371-392, 2013, doi: 10.1007/s00138-012-0430-8

[5] S. Zhong, J. Wang, L. Yan, L. Kang, Z. Cao, "A real-time embedded architecture for SIFT", Journal of Systems Architecture , **59**(1), 16-29, 2013, doi: 10.1016/j.sysarc.2012.09.002

[6] SIFT demo program. www.cs.ubc.ca.

[7] S. A. Li, W. Z. Pan, C. C. Hsu, C. K. Lu, "FPGA-based hardware design for scale-invariant feature transform". IEEE Access, 6, 1-1, 2018, doi: 10.1109/ACCESS.2018.2863019.

[8] J. J. Koenderink, "The structure of images". Biological Cybernetics. 50, 363-370, 1984, doi: 10.1007/BF00336961

[9] A. Fejér, Z. Nagy, J. Benois-Pineau, P. Szolgay, A. de Rugy and J. Domenger, "FPGA-based SIFT implementation for wearable computing", in 2019 IEEE 22nd International Symposium on Design and Diagnostics of Electronic Circuits & Systems (DDECS), Cluj-Napoca, Romania, 1-4, 2019, doi: 10.1109/DDECS.2019.8724653.

[10] LEON3 processor. www.gaisler.com

[11] GRLIB IP Library User's Manual [online]. www.gaisler.com

[12] GRMON Evaluation version [online]. www.gaisler.com.

ASTES

The Ecosystem of the Next-Generation Autonomous Vehicles

Saleem Sahawneh[*,1], Ala' J. Alnaser [2]

[1]*Computer Science Department, Florida Polytechnic University, Lakeland , FL 33805-8531, USA*

[2]*Department of Applied Mathematics, Florida Polytechnic University, Lakeland , FL 33805-8531, USA*

ARTICLE INFO

ABSTRACT

Autonomous vehicles (AVs) technology is expected to provide many benefits for the society such as providing safe transportation to the community and reducing the number of accidents on the roads. With the emergence of AVs, the conventional safety infrastructure in which humans drive their vehicles will need to be upgraded in order to take full advantage of the new technology. AVs are responsible for the different aspects of driving, namely: perception, decision making and taking action. Capturing data and diagnosing issues becomes imperative in this new transportation system because an error might be an indication of a systemic problem which may lead to future accidents or failures. Therefore, any AV accident must be dealt with seriously. Unfortunately, current procedures and the type of data collected during the investigation of an accident is not sufficient; For example, AV minor accidents are not investigated in depth as it is with AV major accidents and therefore, if the cause of the accident is a systemic issue, then it might cause more accidents in the future. The main goal of this paper is to explore the requirements for accident reports for incidents involving AVs and the procedures to escalate issues to avoid systemic risks. All the information available about AV accidents, regardless of the severity of the accident, will be analyzed and studied. This paper will present three recommendations; An updated law enforcement accident report, an escalation procedure that depends on the diagnosis of the fault and a database of AV accidents to enable ongoing learning to find systemic issues.

1 Introduction

1.1 Conventional Automobile Regulation

There is a desire everywhere to reduce the number of car accidents on our roads due to its effects on the communities and the economy. This paper is an extension of work originally presented in [1] in which we studied a number of autonomous vehicle's accidents and analyzed them in order to understand the behaviour of autonomous vehicles and to locate the root causes of these accidents. Studying traffic accidents is not new. Actually, accidents have been a concern for societies since the first recorded fatality back in 1869 [2]. There are different causes of accidents such as the weather, obstructions on the roads, mechanical problems with the vehicles, etc. However, the main causes are the drivers themselves who might be drowsy, intoxicated or over speeding [3]–[4]. Problems of traffic congestion and road accidents have increased due to the increase in the demands of vehicles [5]. Nowadays, over a million people lose their lives due to road traffic crashes world wide and these

crashes cost most countries 3% of their gross domestic product [6]. Some advanced driving assistance systems helped in improving the safety of vehicles on the roads such as Adaptive Cruise Control. The current goal that manufactures are working on now is to have fully automated vehicles on roads within the foreseeable time and this will reduce the number of accidents significantly on the roads [7]. These autonomous vehicles are in their experimental phase where they operate on the roads along with a backup (safety drivers) to take control as needed and to avoid accidents.

In order to manage automobile accidents, one must consider a number of involved parties, such as local law enforcement, insurance companies, state licensing authorities and federal authorities [1]. The driving process can be divided into three aspects: Perception, Decision Making and Action. Currently, the human driver operating a traditional vehicle is responsible of the perception as well as the decision making of the driving process. The manufacturer of the vehicle is responsible for the action aspect of the driving process. When an accident occurs, an accident report is produced by the law enforcement who are the first engagement entity in the

creation of the accident report. Law enforcement investigate the accident and includes the following information:

- Location and timing of the accident.

- Identifying information of drivers and vehicles.

- Description of the accident based on drivers, passengers, and other witnesses.

- Description of property damages and medical issues.

- Occasionally, weather conditions are included

The investigation of the accident determines the direct cause of the accident and determines which party is at fault. The fault can be related to drivers or the vehicle itself. Then the other entities, including insurance companies, lawyers and court system, would intervene to solve the financial consequences of the accident. However, if the vehicle itself is at fault then the National Highway Traffic Safety Administration (NHTSA) gets involved [8]. One of the main tasks of NHTSA is to license vehicles, offer feedback on safety of vehicles and to locate systemic vehicle issues and fix them. The Crash Investigation Sampling System (CISS) or the Office of Defects Investigation (ODI) are usually the initiators of the NHTSA investigations.

It is note worthy that the Federal Aviation Administration (FAA) has been very successful in their accident investigation methods where there is a requirement to include a flight data recorder (FDR) and a cockpit voice recorder (CVR) inside what is referred to as "a black box". Besides that, safety concerns are confidentially gathered for further analysis.

Vehicles have similar technology to the FDR, namely, the Event Data Recorder (EDR). The EDR is a device installed in a motor vehicle to record technical vehicle and occupant information for a brief period of time before, during and after a crash [9]. However, it is not required by the Federal Government to install it in all vehicles [10]. The official definition of the EDR and the minimal list of parameters that must be recorded was produced by the NHTSA in 2019. The recorded parameters include longitudinal and latitudinal speeds and accelerations, engine throttle and RPM, time, ABS activity, air bags deployment status, role angle of the vehicle, occupants position and many more which are recorded until a fraction of a second before an event or accident [11]. Furthermore, EDR technology has been voluntarily used with almost 92% of new light automobiles since 2012.

1.2 AV Accident Reports

The traditional driving system assumes that the perception and decision making aspects of the driving process are the responsibility of the human driver. However, with an AV system, the responsibility for perception and decision making is shifted to the vehicle itself. This transition from humans to AVs requires developing new procedures and laws (regulations) that can answer some of the new challenging questions such as how to determine who owns liability in case of an accident, how to license AVs, and how NHTSA can certify a fleet of AVs.

In the United States, a number of local states authorities have adopted different laws to regulate AV as a driver. For example, California's Department of Motor Vehicle (DMV) adopted regulations for testing AVs in 2014. In a followup amendment in 2018 [12], the laws requires the manufacturers to submit an AV collision report within a period 10 days of any accidents (minor or major). The report includes the following information: Manufacturer's information, cars involved (time, location of the accident, description of damage, etc.), property damage, a description of the accident, a check list that contains information about the weather, lightning, road way surface (wet, ery, etc) and road way conditions (flooded, holes, etc). Moreover, for each vehicle involved in the collision, the report contains information about movement preceding collision (stopped, backing, etc), type of collision (head-on, side swipe, etc) and associated factors (such as vision obstruction).

Besides the collision reports, every manufacturer is required to submit an annual report, by January 1st of each year, that contains all the disengagements of the AV technology during testing their AVs on California's public roads. These reports show how often the vehicles were disengaged from autonomous mode during test. The disengagements could be because of technology failures or simply because the backup driver wanted to safely operate the vehicle.

Beyond California, none of the other states provide guidance on AV accident reports.

1.3 Related Work

Different aspects related to Autonomous vehicle's accidents and safety have been studied such as Collision Avoidance [13], the ethical decision-making during crashes [14] and the Automated Vehicles Safety in Lane-Change Scenarios [15]. However, studies of real AV's crashes have been limited to collecting and analyzing AV crash data from a limited number of accident's reports [16], [17]. There is an agreement between the researchers in this field that the current AV crash reports are unstructured and sparse which results in impeding the learning and analysis work. The importance of the information in the accident reports help in capturing systemic problems that might exist even in what seems to be minor accidents.

In [1], a database was built using reports collected on 94 minor and major accidents involving AVs. The data was statistically analyzed and that helped in building a foundation for a proposed accident report that meets the AV needs. In this work, we expanded the database to include 200 accidents and the analysis has been performed on all of these accidents.

This paper focuses on suggestions and mechanisms to determine and capture the necessary data that is needed in order to capture any systemic issues. This is important in the verification of AVs where the accidents can be simulated by creating the same scenarios which led to the accidents. This is helpful to determine if the decision made by the AV involved in the accident was as expected or not. The real crash data is valuable with this regard.

This paper follows the following outline; Section 2 describes the core architecture of AV systems. The analysis of current crashes from the point-of-view of developing a safety methodology is in Section 3. Our recommendations for an improved AV ecosystem infrastructure is presented in Section 4 and finally, Section 5, offers conclusions.

2   The AV system Architecture

The key to understanding the reasons behind the accidents that involve AVs is understanding the structure of the systems that the AV is comprised of. As mentioned briefly before, the AV operates using the three standard stages of driving: Perception, Decision Making and Action. Figure 1 presents the major components of the AV system where the components are divided with respect to their contribution to each of the driving stages. When a human driver is in control of a traditional vehicles, the perception stage and decision making stage are the responsibility of the driver, while the action is performed by the vehicle. The automotive industry has over 100 years of experience in making certain that the action is performed in an optimum manner. Comparatively, the perception phase through the use of sensors is very recent. Sensing the environment is accomplished using sensors such as cameras, radar and lidar technologies. All the inputs of these components are combined with object recognition artificial intelligence engines. Perception also combines the sensory input with communication from other vehicles (V2V) and the surrounding infrastructure (V2I). The internal model of the surrounding environment of the AV is finally created by combining all these inputs.
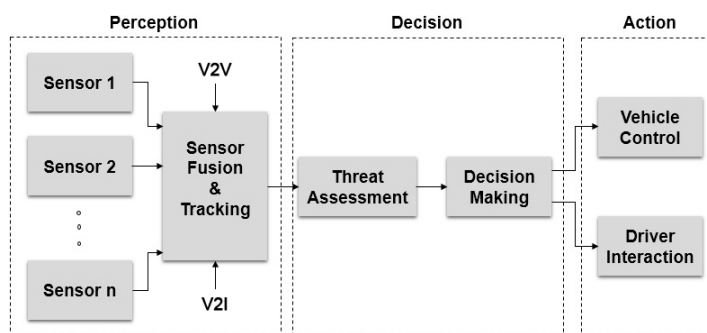
Figure 1: Autonomous vehicle technology architecture

In the context of reports on accidents involving AV's, the gathering of sufficient amount of information is imperative so that it can be analyzed to understand what the AV perceived and the reason behind the decision it made. Looking at the architecture of AVs, when an accident occurs, several open questions arise. These include:

- Are the sensors functioning as required and as intended ?
- What is the accuracy level of the the sensor fusion/object recognition?
- Is the threat assessment and the analysis of any obstruction correct?
- Assuming perfect input, is the AV making the correct decision?
- What is the accuracy of the internal maps?
- Is the communication between the vehicle and the environment (V2I) and between the vehicle and other vehicles (V2V) understood properly?

We will now examine whether we can diagnose these issues with current information.

3   Analysis of Current Accidents

An analysis of all reported AV accidents up to the present date was carried out with the objective being to understand the needs of future accident reports regardless of the automation level at this point. These AVs are being tested on the roads and they require a safety driver while the AVs perform driving.

3.1   Data collection

After mining the public records of the Department of Motor Vehicles in California in addition to multiple sources from the press, a database of accidents involving AVs was built. The database included details in the following categories:

- Information about the road and environment

    - The location of the accident using GPS coordinates
    - Atmospheric and weather conditions
    - Types of the roads and road structure (intersections, highways, etc)

- Information about the accident

    - Description of the traffic at the time of the accident
    - Manner of accident (rear-ending, side swiped, etc)
    - Date and time of the incident
    - The speeds of the involved vehicles
    - The road speed limit
    - Severity/fatality level of accident

- Information about the AV

    - The manufacturing company operating the AV
    - Vehicles' models
    - The autonomous mode used during the incident

As faced by other researchers in this area, converting the unstructured loose textual data into formats which would enable analysis on a deeper level is vital but quite challenging. The database was populated with all the information that was available, however, the data was incomplete in many cases, specially in the cases of minor accidents. To fill in some of the missing information, such as the type of roads and number of lanes , Google Earth was used based on the location of accidents provided in the accident reports (location of an accident is given as an address or as a cross street in the report).

3.2 Detailed review of minor accidents

The earliest record we have of an accident involving an autonomous vehicle dates back to May of 2010, since then there has been many other accidents. However, getting access to up-to-date information and records of these accidents to create a database has been quite challenging. We have looked and gathered information on about 200 accidents with 189 of these accidents in the state of California. That is due to the fact that the state of California was one of the first states to put into place a law that allows the AVs to be tested on public roads and that allows police officers to write accident reports for all accidents involving AVs and make these reports available as public records. In addition, most of the manufacturers and Technology Developers are based in California and they were testing vehicles close to their facilities. In Figure 2, is a list of all manufacturers and developers we have in our database and their percentages of accidents. As anticipated, manufacturers and developers with larger fleets of AVs, such as GM Cruise and Google (Waymo), have had bigger share of accidents with 46% and 37% (combined) respectively. It is also worth noting that the number of companies investing and working in this field has increased in the last 2 years [1].
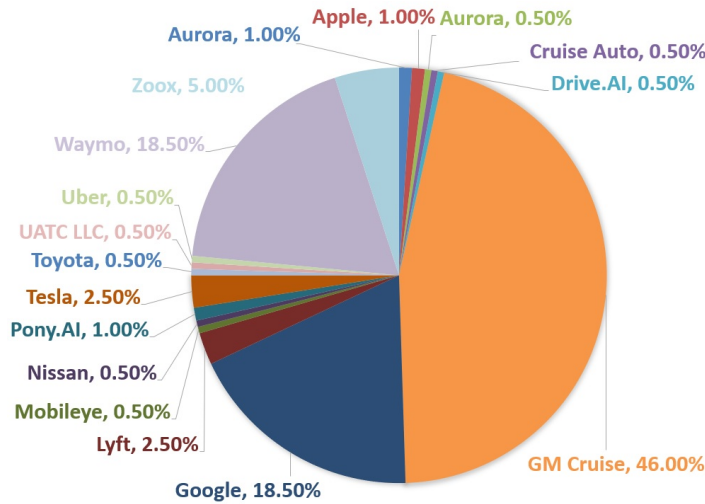
Figure 2: Percentages of crashes by AV Developers

The accident reports were not consistent, and in many cases the reports were missing many pieces of information which are necessary to truly understand what caused the accident and all the parameters that were involved.

There are many characteristics of an accident that will be much more important now that AVs are on the roads performing the perception, decision making, and the mechanics of the driving process. Characteristics such as speeds of all vehicles involved in the accident and the speed limit, as well as the road structure, just to name a few, are specially important, to be able to simulate the accidents accurately and understand the cause. Even minor accidents could be caused by a systemic error in the decision making algorithms which could cause much bigger issues later. However, many of these characteristics are either missing or not required by the current accidents report forms.

In the construction of our database, much effort and time was spent analyzing accident reports and filling in missing information. We

have found that the AV speed was unknown in 51% of the accidents, 63.5% of the accidents speed of the second elements in the crash (vehicle or object) was not listed. In 83.5% of the accidents, the speed limit for the road on which the accident happened was not recorded. Also, the type of road on which the accident occurred was not clear in 6.25% of the reports.

Figure 3, illustrates the accidents sorted by road type as listed on the accidents' reports. The majority of the accidents happened at intersections, especially at four-way intersections where 68.5% of all the crashes occurred. These accidents could be caused by a failure of the sensors or the algorithms which are supposed to gather sensor input and fuse it together in order for the AV to have an accurate model of the environment around it. Furthermore, it is worth noting that the environment at intersections is quite complex.
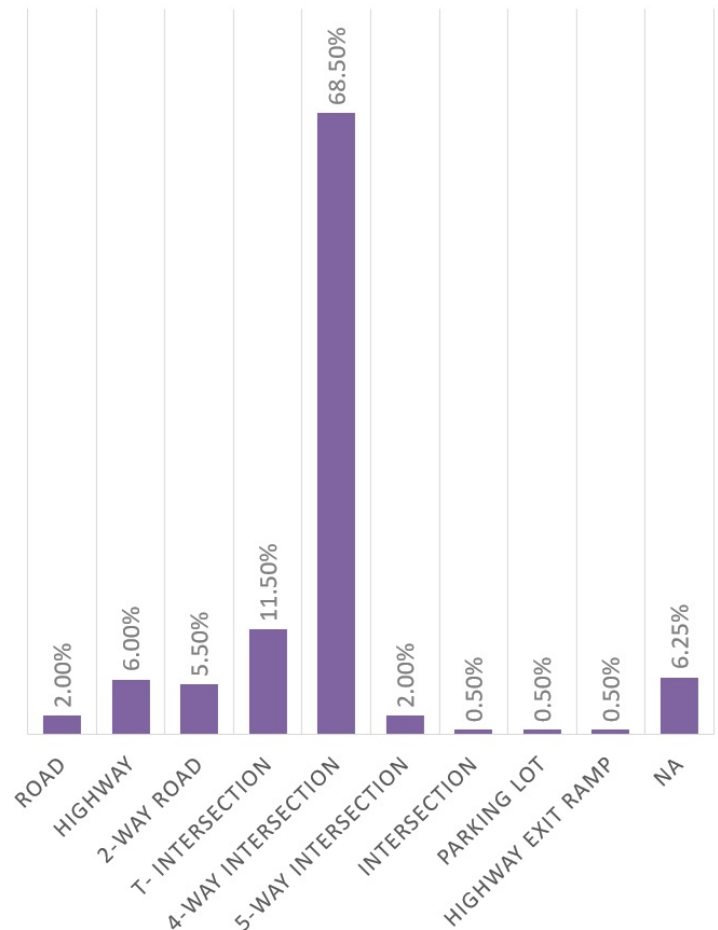
Figure 3: Types of roads where accidents happened

The chart in Figure 4 shows the speed ranges of vehicles (elements) involved in the crashes and the percentage of crashes that happened in these ranges. As mentioned previously, the speeds for AV and the other element or vehicle was not recorded in many reports. However, out of the ones that were recorded we observed that the majority of crashes happened at low to idling speeds. This was not surprising since the vast majority of accidents happened at intersections where the vehicles were either stopping or just starting to move from a full stop. In addition, AV testing has been limited to nice weather and low speed situations.
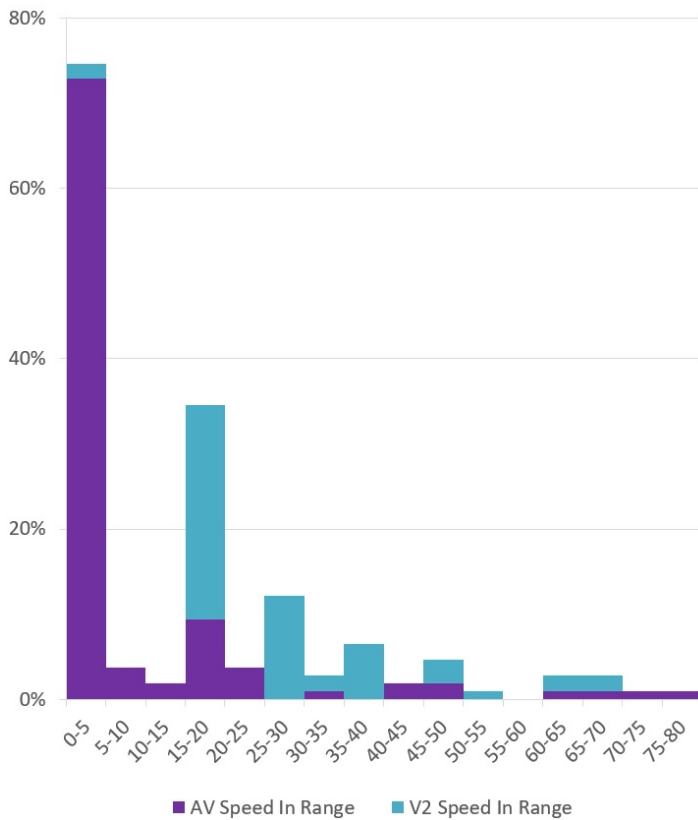
Figure 4: The percentage of accidents corresponding to speed range

Table 1: Accidents types and percentages and the status of the AV system.

Type of Accident	AV Mode	
	Engaged	Disengaged
Taxi Driver slapped a window	0.0%	1.3%
A vehicle backed into AV	0.0%	1.3%
A vehicle rear ended the AV	67.8%	38.0%
Angle	9.1%	7.6%
A vehicle struck the AV's rear bumper	0.0%	1.3%
AV Backed into another vehicle	0.0%	1.3%
AV rear ended another car	0.8%	2.5%
Broadside	2.5%	7.6%
Head-on	0.0%	5.1%
Hit by Pedestrian	0.8%	1.3%
Hit Object	0.8%	3.8%
Perpendicular	1.7%	3.8%
Rear end, Head on	0.0%	2.5%
Side swipe	9.1%	22.8%
A car made slight contact AV's side	0.8%	0.0%
A pedestrian struck.	0.8%	0.0%
Radar Clipped by a passing truck	0.8%	0.0%
AV Front to back of firetruck	0.8%	0.0%
Rear ended a fire truck	0.8%	0.0%
The AV crossed the red light	0.8%	0.0%
NA	2.5%	0.0%

It was surprising to find that the vast majority of AV accidents are actually humans hitting AVs (see Table 1). Furthermore, when also considering the type of accident and speeds at which the accidents happen, one may conjecture that a portion of these accidents could have happened because of a lack of understanding of the behavior of the AV. For instance, 67.8% of the crashes were involving another vehicle rear-ending the AV while it was slowing down to turn right at an intersection. The AV's are required to make a full stop before turning right when there is a red light or a stop sign while the human driver in the vehicle behind it might have predicted that the AV will just slow down and make the turn.

3.3 Major accidents

Autonomous Vehicle's major accidents with severe damage, injury or fatalities occurrence are very important to analyze. The information obtained from any accident can be used to understand the behavior (actions) of AVs under different circumstances. In [1], three fatal accidents were analyzed. These accidents took place in three different states in USA and were reported in media: Florida, California and Arizona between 2016 and 2018. Each major accident happened under different scenarios from the other ones. For instance, the autonomous vehicles were driving at different speeds ranging from 43 up to 74 mph at the time of the accident. However, we noticed one common thing between these accidents which is that the object (truck, road barrier or a pedestrian) that the AVs collided with was either stopping or moving at very low speed.

Upon analyzing these major accidents, we found out the following findings:

- Autonomous Vehicles, in some cases, were able to sense the objects in front of them few seconds before the accident but did not recognize it as a threat. For example, the software on Uber's AV system, back in 2018, initially classified the pedestrian crossing the road in front of Uber as an another vehicle moving in the same direction before reclassifying the pedestrian as a bicycle that was static.

- Some procedures for risk assessment were not appropriate including oversight of the backup drivers.

- Threat analysis is a critical in the development of AVs.

- When the autopilot is used to follow a leading car, while navigating other traffic and road curvature conditions, there is a need for continuous perception and a stable feedback system with the leading car under all conditions. If that feedback is interrupted then a back up plan should be implemented.

- Autonomous vehicles, under experimental driving, issue warnings to the human back up drivers in some situations. An action plan must be implemented when the human driver ignore these warnings. For example, in Uber accident, The National Transportation Safety Board (NTSB) determined that one of the main causes of the accident was the failure of the Uber backup driver to monitor the road.

- There is a lack of system prevention measures to prevent the possibility of misuses of technology by the drivers specially when drivers lack the understanding of the limitations of the autopilot.

- There is a need to record and take instant action when complains are received from the users of the vehicles because that could reveal a systemic problem. As an example, in California's Tesla accident, the driver had complained few times that his Model X vehicle would drift of its lane in the same location where the collision occurred while using the autopilot.

- Manufacturers should be involved in order to get an independent analysis and verification of the data associated with the vehicle's crashes. Also, the data must be standardized and retrievable. This retrieved information is extremely important to detect if an issue is an indication of a systemic risk.

In 2019, another fatal major accident took place in Florida, USA and it is discussed in this paper.

Details of Accident: On March 1, 2019, about 6:17 a.m, A fatal crash occurred when a 2018 Tesla Model 3 under-rode a truck (truck-tractor in combination with a semitrailer) which resulted in the death of the Tesla driver. This accident took place in State Highway 441 in Delray Beach, Florida. The accident happened when Tesla, driving southbound at 68 mph on a 55 mph speed limit road, came across a truck that pulled out of a private driveway on the right hand side of the road and blocked Tesla's path. The NTSB's preliminary report stated that the truck slowed down as it crossed Tesla's lane and blocked Tesla's path. The truck was trying to make a left turn into northbound lanes and Tesla's ADAS didn't execute an evasive maneuvers to stop or change direction of the car. The car came to a stop on the highway's earthen median, about 1,600 feet away [18]. Besides that, the NTSB report states that the driver of Tesla engaged the autopilot 10 seconds before the impact and that the driver's hands weren't detected on the steering wheel from less than 8 seconds to the crash. This accident reminds us of the 2016 Tesla crash that took place in Florida. Both of the accidents involved tractor-trailer trucks with similar scenarios and both resulted in the unfortunate death of the drivers. In both accidents, the autopilots were engaged.

The accident in 2016 took place when a semi-autonomous Tesla Model S70D collided with a tractor-trailer while approaching an intersection. The tractor was making a left turn across the path of the Tesla, but Tesla did not stop and crashed into the trailer [1]. Tesla was using a black and white camera and there is a possibility that the computer was believed incorrectly that the road in front of the Tesla was clear. This accident might have been avoided if a LIDAR sensor was used instead of the camera since the colors would not have mattered [19]. Also, the autopilot system was tuned to ignore more of the radar inputs at high speed in order to avoid false positives.[20].

Similarities of both accidents: Despite the time difference between the two accidents and also despite the software updates that have been applied to the autopilot (AP1 to AP2) since the first accident [21], there are major similarities between the two accidents: both of accidents involved hitting stationary truck-trailers at high speed and the semi-autonomous vehicles didn't attempt to stop. Also, both of the accidents happened in sunny and clear skies days.

These two accidents show that a safety challenge still exists with the autopilots and how they deal with stationary objects at high speeds. Correct AV's perception of the environment is critically im-

portant for safety. In the above mentioned crashes, it seems that the autopilot failed to perceive the truck-trailors as objects blocking the path of the AV. On the other hand, a false perception could also lead to dangerous accidents. For example, an AV mistakenly perceives a moving object as a stationary object. This situation could trigger the autopilot to stop the car completely and that is a dangerous action specially if the vehicle is travelling at high speed on the freeway which might cause other vehicles to rear end the AV.

These accidents highlight the need to understand the perception aspect of the AV. If the perception engine is fooled then that might lead to accidents. The communication between vehicles themselves on the road (vehicle to vehicle,V2V) and also with the infrastructure (V2I) might be necessary to avoid accidents. Also, it might be useful to use more accurate sensors such as LIDARS instead of cameras in order to reduce the risk of misconception by the vehicle.

Analysing the accident and understanding why the AV took the decision is extremely important to locate the problem and work on solving it to prevent it from happening again in the future. Therefore, the data collected from these accidents are important.

4 Recommendations on AV EcoSystem Infrastructure

The creation of an ecosystem or road environments in which AVs can operate at a higher level of efficiency requires upgrades in three major areas. This is based on analysing the accidents up to the present date and the methods by which information was gathered, as well as, the operational fundamentals of AVs. The areas in need of improvement are:

- Utilization of data from Event Data Recorders (EDRs) for vehicles and infrastructure

- Update and supplement Vehicle Accident Report

- Upgrade Fatality Analysis Reporting System (FARS) and an Automated Storage Retrieval System (ASRS) system

4.1 EDR Information

As mentioned earlier, Event Data Recorders are currently available in over 92% of vehicles on the road. However, EDRs are needed as a requirement for all AVs. Regardless of the model, an EDR collects and record the current vehicle dynamics. However, an EDR in an AV (AV-EDR) need to capture additional AV critical data. The AV critical data include raw sensor inputs, all communications (V2V and V2I), the ongoing object model of the surrounding environmental produced by the perception stage, and finally the threat annotations of the object model.

The time-based unmodified recordings of all the sensors (Camera, Lidar, Radar, etc) together with the vehicle dynamics produce the mathematical model for the AV. Using this mathematical model and information, issues or faults related to manufacturing, electromagnetic interference, or weather can be detected.

One of critical components for understanding faults of object recognition is details and accurate recording of the perceived object model and its corresponding threat annotations. The core AI sitting

at the center of the AV systems are possibly the most challenging to construct and test. If the AI system has a fundamental error, then it is likely that this error will reveal itself in other circumstance. Therefore, such errors can give rise to systemic risks beyond the current incident.

Moreover, recording all the communication between the vehicles and with the environment (V2V and V2I) information is essential to identify issues in the case where communication was planned but failed. Also, to determine if errors occurred due to the actual message contained within the communication is faulty or if communication is compromised.

Finally, AV-EDR data should be recorded locally and on the cloud in standard formats. The combination of EDR recordings for the AV and the environment form a reasonably complete package information for any accident of that is automatically collected. In the case of an accident, law enforcement at the scene should have instant access to the EDR information.

4.2 AV Police Accident Report

The current accident report procedure has been optimized to handle human related traffic accidents. However, in order to deal with this upcoming technology, the accident procedure needs to be updated in three main areas; severity, the interview with the driver, and interviews with other humans. For severity, since the human beings behaviour is well understood, current minor accidents are treated lightly. On the other hand, when an AV is involved in minor incidents it could be an indication of a systematic fault or safety issues that may cause major accident in the future. Hence, law enforcement will need to put additional focus on all accidents involving AVs even the minor accidents.

Normally, law enforcement officers interview the drivers of all vehicles involved in an accident. However, the driving AI of an AV cannot be interviewed. Therefore, police officers need to understand what the AV was "seeing" to understand the decision that was made. To understand the perception, our recommendation is pictures to be taken from the point of view of the AV. Determine if there is any significant activity that might affect the Lidar, Radar or any other sensor of the AV. For instance weather conditions, radio equipment, or power lines could have some influence on the sensors. Moreover, to understand the decision made by the AV, the officers may need to consider all activities in the surrounding environment that may deceive the AV. Examples of activities include actions made by pedestrians or small animals on the side of the road or on the road itself, as well as the actions of trucks or scooters or other vehicles that may move in way different than the AV.

Lastly, when accidents are caused by other humans due to their perception of an AV then it is imperative to know what the AV did to communicate its intent to the other humans in the surrounding environment. If someone perceives the AV as behaving erratically then it is as dangerous as any other erratic driver. Additionally, interviewing other drivers is of particular importance in instances where the other drivers collide with an AV even if it a minor scrape or a fender bender.
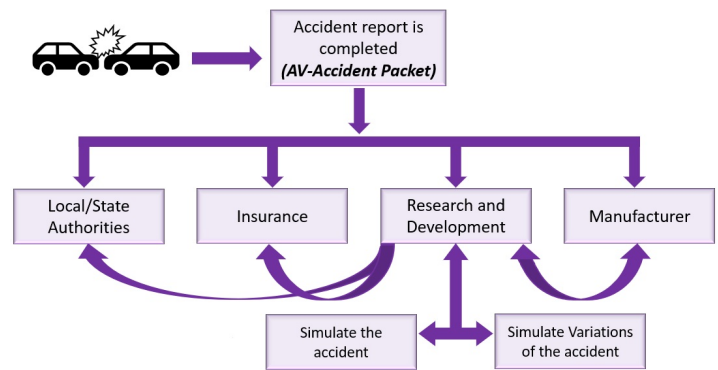
Figure 5: The accident report and the information flow

4.3 Learning Flow

By including the EDR recordings of the AV and environmental parameters along with the law enforcement input in the accident report, which we will call the *AV-Accident Packet*, we can analyze and understand how an accident happened and its causes. In this manner, systemic errors can be identified early and procedures can be created to escalate the issues and find remedies for it. The most critical concerns are those caused by algorithmic issues since they would be replicated across all the vehicles sharing the same software. These types of concerns need to be determined and the issues need to have a swift escalated response. On the other hand, hardware failures such as sensors or other components are also very important and can indicate reliability issues on the long term. However, hardware issues are very unlikely to be the reason behind systemic errors. Additionally, if an accident occurs where a human driver hit an AV then it is not probable that the cause requires to be escalated immediately, although the accident should be carefully considered.

To establish an overall safety model, manufactures and other involved parties must be able to utilize all the accidents' data efficiently in the production and testing of AVs. Furthermore, a database of accidents should be built and made available to be mined for possible systemic errors that wouldn't be easily identified if the data is just considered locally.

4.4 Importance of Completed Accident reports (AV-Accident Packet)

The rate at which automotive technology is growing is very rapid. The addition of all of this technology into the vehicles has had an affect on the way traffic is understood. Finally, the introduction of AVs in normal traffic is going to continue to change traffic behaviour which requires the reassessment of the procedures used to report accidents and how the information within the report flows (see Figure 5).

The importance of the AV-Accident Packet, as defined above, includes, but not limited to, the following main points:

- Research and Development:
  - Analyzing the data to understand the causes of the accident.

– Recreate accidents by simulation using similar scenario and extend that to include variations of parameters included (actors, road types, weather, etc.)

– Expanding the database of accidents to be used for verification and validation of AV systems.

• Manufacturers and developers

– In addition to the items listed above, the makers of AVs will have the highest interest in the performance of their product.

– Provide software updates and maybe hardware replacements.

• Insurance

– Determine Liability.

– Run risk assessments to determine the cost of insurance. For example, a company with lots of AV accidents means the cost will be higher.

• Local/State Authorities

– Collect data and analyze the statistics about accidents.

– Provide policies and regulations based on accurate information.

– Organize appropriate response in case of an accident; For instance, AVs communicate with the authorities upon the occurrence of accidents and provide an initial report.

Once the AV-Accident Packets are available, accidents can then be re-created within a simulation, and this is indispensable for multiple reasons. One is to improve the process of diagnosing errors. Also, when a correct decision is achieved which would avoid the accident or at least reduce its severity, then a validation platform, such as the one discussed in [22], can be used to check the validity of decision or action. Additionally, various test cases can be derived and simulated easily to find similar issues and fix them. Hence, this approach generates an essential feedback loop in the verification of the safety of AVs.

Presently, traditional accident data is collected and used by FARS to find systemic problems. However, this database must be enlarged to keep records and follow issues for AVs. For instance the database must include parameter measuring the reliability of sensors, conditions for edge-cases causing problems in the perception or threat recognition. It is also reasonable to have a weather index similar to the heat index of boating safety index that would give a measure on the effect of extreme weather phenomenon on the AV systems.

There is still a need to learn the process of building, deploying and regulating AV systems. Therefore, there is a substantial need that all parties involved must share information and thus build a system of gathering input and data which can provide a confidential way for any source to share input in order to help insure the public does not have to face unsafe conditions.

5 Conclusion

Stakeholders will sooner or later transform the complete picture of our roads into a fully AV-controlled environment. Undoubtedly, this promises immense range of benefits including safe transportation, to our community. Because of the differences between conventional driving and AV driving, we should treat AV accidents differently. In the AV world, the risk of systematic problems exist and it is extremely important to capture these problems at an early stage. One of the methods to capture these problems and risks is by the analysis of the current AV accidents regardless of their severity. The nature of AV systems requires capturing an incredible amount of date in order to operate (perception, decision making and action). Therefore, in order to understand the cause of an accident, a prior to the accident data must be available. In this paper, we looked at the architecture of an AV system, collected data for almost 200 AV accidents and then we analyzed them in order to understand the root cause of these accidents. The accidents can be simulated by using the collected data to create similar scenarios of the accidents and that is vital in the verification and validation of AV systems.

However, with the current accident reports, some important information related to AV systems is still missing from the current accident reporting system. The current conventional automobile infrastructure must be upgraded to meet the AV needs and this paper proposes three upgrades: First, an updated law enforcement accident report that incorporates the EDR recording and sufficient details on the environment surrounding the accident. Second, a procedure for escalation which depends on the analysis of the error. Lastly, a well organized database of related AV accidents must be available to stakeholders to enable ongoing learning to find systemic issues.

References

[1] S. Sahawneh, A. J. Alnaser, M. . Akbaş, A. Sargolzaei, R. Razdan, "Requirements for the Next-Generation Autonomous Vehicle Ecosystem," in 2019 SoutheastCon, 1–6, 2019, doi:10.1109/SoutheastCon42311.2019.9020400.

[2] I. Fallon, D. O'Neill, "The world's first automobile fatality," Automobiles; Accidents; Traffic; History of medicine, **37**, 601–603, 200, doi:10.1016/j.aap.2005.02.002.

[3] S. Nanda, H. Joshi, S. Khairnar, "An IOT Based Smart System for Accident Prevention and Detection," in 2018 Fourth International Conference on Computing Communication Control and Automation (ICCUBEA), 1–6, 2018, doi:10.1109/ICCUBEA.2018.8697663.

[4] S. Chandran, S. Chandrasekar, N. E. Elizabeth, "Konnect: An Internet of Things (IoT) based smart helmet for accident detection and notification," in 2016 IEEE Annual India Conference (INDICON), 1–4, IEEE, 2016, doi:10.1109/TITS.2016.2582208.

[5] U. Alvi, M. A. K. Khattak, B. Shabir, A. W. Malik, S. R. Muhammad, "A Comprehensive Study on IoT Based Accident Detection Systems for Smart Vehicles," IEEE Access, **8**, 122480–122497, 2020, doi:10.1109/ACCESS.2020.3006887.

[6] "Road traffic injuries," 2020.

[7] H. Wang, Y. Huang, A. Khajepour, Y. Zhang, Y. Rasekhipour, D. Cao, "Crash mitigation in motion planning for autonomous vehicles," IEEE transactions on intelligent transportation systems, **20**(9), 3313–3323, 2019, doi:10.1109/TRANS.2019.2582208.

[8] Y.-K. Bae, H. BENÍTEZ-SILVA, "The effects of automobile recalls on the severity of accidents," Economic Inquiry, **51**(2), 1232–1250, 2013.

[9] "Event Data Recorder," 2020.

[10] U. Bose, "The black box solution to autonomous liability," Wash. UL Rev., **92**, 1325, 2014.

[11] "U.S. Federal Regulations in CFR Title 49, Subtitle B, Chapter V, Part 563," 2019.

[12] "Testing of Autonomous Vehicles with a Driver," 2019.

[13] K. Lee, D. Kum, "Collision avoidance/mitigation system: Motion planning of autonomous vehicle via predictive occupancy map," IEEE Access, **7**, 52846–52857, 2019, doi:10.1109/Access.2019.2582208.

[14] K. Lee, D. Kum, "Collision avoidance/mitigation system: Motion planning of autonomous vehicle via predictive occupancy map," IEEE Access, **7**, 52846–52857, 2019, doi:10.1109/ACCESS.2020.3005887.

[15] D. Zhao, H. Lam, H. Peng, S. Bao, D. J. LeBlanc, K. Nobukawa, C. S. Pan, "Accelerated evaluation of automated vehicles safety in lane-change scenarios based on importance sampling techniques," IEEE transactions on intelligent transportation systems, **18**(3), 595–607, 2016, doi:10.1109/TITS.2016.2582208.

[16] F. M. Favarò, N. Nader, S. O. Eurich, M. Tripp, N. Varadaraju, "Examining accident reports involving autonomous vehicles in California," PLoS one, **12**(9), e0184952, 2017.

[17] B. Schoettle, M. Sivak, "A preliminary analysis of real-world crashes involving self-driving vehicles," University of Michigan Transportation Research Institute, 2015.

[18] "PRELIMINARY REPORT, HIGHWAY, HWY19FH008," 2020.

[19] "Tesla Autopilot Car Crash Kills Driver," 2018.

[20] "Tesla Autopilot Crashes and Causes," 2020.

[21] "Tesla Autopilot AP1 vs AP2 vs AP3 – Differences Explained," 2021.

[22] A. J. Alnaser, M. I. Akbas, A. Sargolzaei, R. Razdan, "Autonomous vehicles scenario testing framework and model of computation," SAE International Journal of Connected and Automated Vehicles, **2**(4), 2019.

Recording of Academic Transcript Data to Prevent the Forgery based on Blockchain Technology

Meyliana[1], Cadelina Cassandra[*,1], Yakob Utama Chandra[1], Surjandy[1], Erick Fernando[1], Henry Antonius Eka Widjaja[1], Harjanto Prabowo[2]

[1]*Information Systems Department, School of Information Systems, Bina Nusantara University, Jakarta, 11480, Indonesia*

[2]*Computer Science Department, Bina Nusantara University, Jakarta, 11480, Indonesia*

A B S T R A C T

Diploma certificate and transcript forgery is a serious issue in education. The government is still finding the best way to prevent and minimize this issue in the future. The diploma certificate and transcript are very easy to duplicate, not only from third parties. Even the university can easily produce a fake diploma certification and transcript for their benefit. Blockchain technology is a new technology and now can be used to prevent the fake graduation documents. This research shows the simulation of blockchain technology used (Multichain) for data recording of academic transcript as one of the graduation documents. FGD has been carried out by inviting several reputable universities to validate the prototype. As a result, the FGD participants validated the prototype and agreed if it possible to be implemented in university, especially for recording the academic transcript data. Recording the academic transcript on blockchain technology can contribute to prevent forgery.

1. Introduction

Diploma Certification forgery is not a new issue in Indonesia. Recently, in 2020 as reported from serambinews.com, it involved a Rector Candidate from one of Higher Education in Indonesia. A diploma certificate is still important in Indonesia for several positions. It is easy for university to produce the certification without any data validation [1]. This is not a new problem in Indonesia. Since 2015, there are many cases of diploma certification forgery. Many people got in this case and public figure and people in government too [2]. The publisher of this fake graduate information can be from a third party or even a legal university.

Looking at this problem, producing a certification for people that not even come and study to the university is very easy. The information is easily manipulated, and the user only needs to enter and create the data without any validation. So, data integrity is very important, every process that happens during university study needs to be locked, approved, and validated by stakeholder inside the university. Any data is not approved cannot be processed and every data in the application is immutable and unchangeable.

If this integrity is maintained in University, the graduation document will be hard to be duplicated or be falsified. Talking about this data integrity, blockchain is a technology that sure make this happen, mainly because of the features and capabilities of blockchain such as the security, reliability, integrity, and the concept of decentralization. Founded in 2008 by a group or person called Satoshi Nakamoto, blockchain is very popular and used in many areas, not only cryptocurrency [3]. Several studies show blockchain technology can be used as technology that can prevent the graduation documents forgery [4]-[7]. Blockchain also can be combined with IoT (Internet of Things) to support the educational systems and create more interactive communication among students, teachers, employers, and other stakeholders [8]. Despite blockchain's ability and ensuring data integrity, there is still lack of research showing how this blockchain can prevent the fake diploma and academic transcript. This study simulates the process of academic transcript record using blockchain technology (multichain). This research used a qualitative method and conducted lab as a media to show the blockchain implementation on transcript data records.

This research is continuing from the previous study [9]. The previous study discussed about the process and value chain in academic transcript. The process was confirmed by all users in

Focus Group Discussion. This research will show the simulation of data recording of academic transcript in Blockchain (Multichain) after all process is done.

The structure of this paper divided into several sections. The first section is introduction, which describes the background of the study and the issue or problem discussed and solved in this research. The second section is Literature Review which discuss about the theoretical background to support this research. The third section is Methodology which explain the research design and technique used in this research. The fourth section is Result and Discussion, which describes the prototype and result of Focus Group Discussion. The last section is conclusion as the overall information, contribution, and further research.

2. Literature Review

2.1. Blockchain in Higher Education

Blockchain is the concept of a decentralized network and was first found in 2008 by a group or person named Satoshi Nakamoto [3]. It was first used for cryptocurrency and bitcoin was the first cryptocurrency and gained popularity for years by using blockchain technology. Since then, blockchain is popular and widely used. Blockchain using peer – to – peer ledger for all transaction registration. Blockchain is still categorized as a new technology but the popularity makes many other fields want to adopt blockchain, this mainly because of its capabilities such as immutable, unchangeable, data integrity and transparency. There are several studies discussed about blockchain technology and education, many application proposed such as application to issue diploma certificate, student academic transcript, and other students track record [4].

Blockchain in education field can be found critically important because of the asset is student. They need to be recognized for every track record they made during their study. Not only for the internal university, this data also used by government and company [9].

Some current applications of blockchain in education such as: Open Blockchain for Digital certificate application [10] which provide controls to student certificate for storing and keep the credential. Also support service application and Earning Application which connect between learning and earning [11].

2.2. Multichain

Multichain is a blockchain platform first introduced in [12]. Multichain is categorized as private blockchain. Multichain could solve privacy problems, and the management of user permissions by ensuring all activity and transaction inside the blockchain is only visible to the chosen users who have permission. In multichain, user will randomly generate their private key which has a mathematical public address.

Multichain can also be implemented for many blockchain technology based and successfully implemented agricultural food for food tracking, food tracing, and the lifecycle of the food production [13].

2.3. User Centered Design Method

User-Centered Design is a methodology that aims to gaining deep understanding about the user needs [14]. User Centered Design (UCD) can be done by using questionnaires, focus group discussions, interviews, paper prototyping, and so on as long as users contribute in the process [15]. UCD will engage user closely with the project in designing the solution and put the user as the center of design. This research using User Centered Design Method and several Focus Group Discussion is done for this research.

UCD contains of four phases, they are [16]:

- Phase 1 is Specify Context of Use, in this phase, observation and literature review was carried out to gather the requirements.
- Phase 2 is Specify Requirement, in this phase, after all information is gathered, Focus Group Discussion (FGD) with users is conducted to specify the requirements and make categorization based on the result in the first phase
- Phase 3 is Produce Design Solution. After knowing about the requirements, the design prototype is created in this phase and Focus Group Discussion is also conducted to show the prototype to users and gather the feedback.
- Phase 4 is Evaluate Design, this phase is the evaluation phase after the prototype is created. This evaluation will involve the user as the center of this methodology.

2.4. Simulation

Simulation is a process for conducting trials close to the actual situation and is often used because they are fast and cheap [17]. Simulation is used to ensure the information can be recorded in blockchain (Multichain).

Focus group discussion was conducted by inviting 7 universities. FGD aims to show the prototype flow simulation to the users/participants and get the feedback for future development.

The overall process of the simulation is shown in figure 2 below:
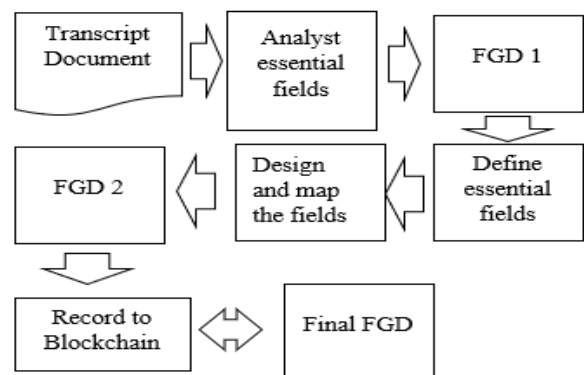
Figure 1. Simulation Phase

- Transcript Document used for this simulation is the original transcript provided from one university, it is used to resemble the real condition
- Analyst essential fields & FGD 1, the important fields were discussed in the document transcript and FGD confirmed the results with other people who have the same interest.
- Define essential fields, at this stage a decision has been made on which fields are important in this simulation
- Design and Map the fields. At this stage the fields that have been agreed are mapped into the blockchain (Multichain)
- Record to Blockchain, at this stage all information is entry directly into the Blockchain
- Final FGD, in this process the final data or information validation is carried out in the system to ensure that the data or information stored is following user needs and has been agreed upon.

3. Methodology

This research also using User Centered Design (UCD) concept and method by exploring the user needs and requirements [14]. Using this concept, users will understand the technology and the prototype built more easily, and we will easily get what the users need the most. We conducted several Focus Group Discussion (FGD) to know more about the user needs, by inviting 7 universities and to validate and confirm the process in their universities.

The research design and simulation steps using User Centered Design (UCD) are explained in this figure for more details:
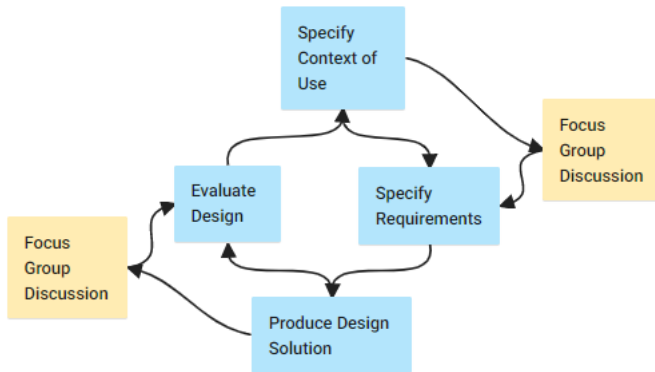
Figure 2: Research Design & Simulation Steps

4. Result and Discussion

This research is the continue study from the previous research. The previous research discussed about the value chain and activity process in producing academic transcript [9]. This research will not discuss about the process and raw data before the data recording (smart contract process), meanwhile, the discussion is about the simulation of data record in Blockchain (Multichain).

The diploma certificate also recorded in this multichain of blockchain from previous research [3]. Diploma certificate is defined as the asset in Blockchain (Multichain) and this research

will discuss another asset of graduation document, which is academic transcript.

To highlight the business process of how academic transcript is created will be described on figure 3 [9]:
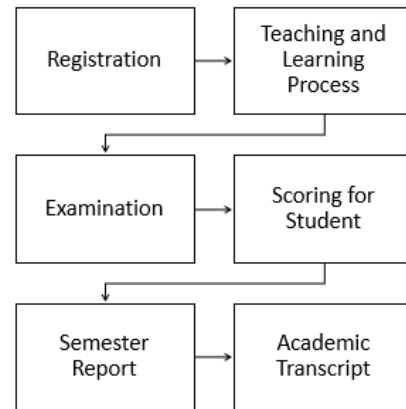
Figure 3: Process of Academic Transcript

To highlight the application process, can be seen on figure 4:
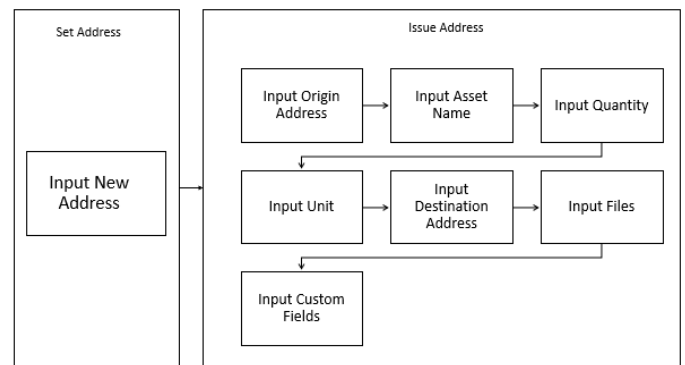
Figure 4. System Process

The more detail explanation of each component will be described below.

Figure 5: Node

4.1. Node and Address

Just review about the Node and Address in the Blockchain (Multichain), the node is one private blockchain and many

addresses can be created in this node. Every address can have several assets, example: diploma certificate, academic transcript, achievement certificate, etc.

The configuration for this simulation using Node name "chain1", version 1.0.9, protocol 10011, node address represents the entity (university, student). The more detail is shown on figure 5. As presented in Figure 5, it is the node used in the blockchain.

Exhibit at Figure 6, presenting the example of address in blockchain node, this address could be represented the university or students.

Figure 6: Address in Blockchain

Once the address is recorded on the blockchain, the user can create asset for each address. The Asset for example diploma certificate, academic transcript, etc.

Exhibit at Figure 7 and 8, show the process of data entry for academic transcript.

In this simulation (using as-is Multichain), to process the data record into Blockchain (Multichain), the academic transcript data is divided into two assets. The first asset describes the student general information, and the second asset describe about the detail grade and course information. The figure 4 and 5 show the input process.

This simulation is done manually for easy process understanding. The first step, user need to ensure the first entity (From Address) is the university, then create the asset name (ex: TranscriptSeri1). User also need to determine the quantity and unit of the Asset. Then choose the address (to Address which represent student). The field can be seen on Figure 7. The first transcript named TranskripSeri1

Figure 7 (a): Issue Asset TranscriptSeri1 Part 1

User then need to fill out the fields as the important parameter on the academic transcript. For more detail information of the

fields to be entry. It exhibits in figure 7b. The data is presented in Indonesian Language as real data.

Figure 7 (b): Issue Asset TranscriptSeri1 Part 2

Figure 8 (a): Issue Asset TranscriptSeri2 Part 1

Figure 8b: Issue Asset TranscriptSeri2 Part 2

Based on FGD Result, some fields are important in Academic Transcript. The fields are then filled to the blockchain as exhibit in figure 5b, all fields on figure 7b presented in Indonesian Language as the real simulation:

- Paper No (No_Surat)
- Name (Nama)

- Student ID (NIM)
- Date of Birth (Tempat Tgl Lahir)
- Faculty (Fakultas)
- Study Program (Prodi)
- Program (Program)
- Streaming (Peminatan)
- Degree (Jenjang)
- Total Credit (Total Credit)

Name	TranskripSeri1
Quantity	1
Units	0.01
Issuer	Univeristy Binus (1SH8oX3Eii3kE2KbYzkUYVVXGQhDV8QzYiHFEx, local)
No_Surat	FM-BINUS-AA-FPU-000/V00
Nama	MMMMMM
NIM	00000000
Tmpt Tgl Lahir	<<tempat>><<Tgl Lahir>>
Fakultas	School of IS
Prodi	Sistem Informasi
Program	Sistem Informasi
Peminatan	E-Business
Jenjang	S1
Total Credit	146

Figure 9: Asset Created

Next, on Figure 8a and 8b show the other part of Academic Transcript named as TranscriptSeri2 which have the same flow with figure 7a and 7b. The data is presented in Indonesian Language as real data.

The explanation of the detailed fields:

- GPA

- University No (SK_PT)
- Accreditation (Akreditasi)
- Transcript Number (No_Transkrip)
- Diploma Certificate No (Nomor Ijazah)
- Course Code (Kode Mtk)
- Course Name (Matakuliah)
- Credit (Kredit)
- Grade
- Thesis Title (Judul Thesis)

After the Academic Transcript is created and issued, this academic transcript is recorded and cannot be update. Figure 9 and 10 show the successful of data entry.

Name	TranskripSeri2
Quantity	1
Units	0.01
Issuer	Univeristy Binus (1SH8oX3Eii3kE2KbYzkUYVVXGQhDV8QzYiHFEx, local)
GPA	4
SK_PT	55/55/55555
Akreditasi	55/55/55555
No_Transkrip	00000000000
Nomor Ijazah	00000000001
KodeMtk	ISYS0000
Matakuliah	<<Matakuliah>>
Kredit	2
Grade	A
Judul_Thesis	<<Judul Thesis>>

Figure 10: Another Asset Created

Figure 10 is the real example of Academic Transcript published from university to students that was successfully recorded to Blockchain (Multichain).

Figure 11: Example of Real (Current) Printed Academic Transcript
The data on the picture was blurred for confidential purpose

The simulation and the result are presented to the FGD participant on November 5th and 12th 2020. Several feedbacks from FGD regarding to the issue of security, training for university users, and the data synchronization with government. The participants of FGD are from Binus University, Indonesia Open University, Darma Persada University, Pelita Harapan University, Kalbis University, STP Trisakti, and Universitas Negeri Jakarta with all total of 17 participants.

5. Conclusion

Blockchain in education is quite popular recently. Blockchain in education can be used to validate the data records and asset for students such as diploma certificate and academic transcript. This paper simulates the application prototype for recording Academic Transcript Data to prevent the forgery as many cases happen because of fake diploma dan academic transcript. Using blockchain technology will ensure the data integrity. The Focus Group Discussion gives positive results. All participants agree and approved the application. The users also think it is appliable to their university, but another improvement needs to be made regarding data standardization and infrastructure. Based on the simulation, Blockchain (Multichain) is possible to be implemented in University for Academic Transcript record.

The limitation of this research is because this is still in very initial stage of development, this prototype simulation is using Multichain with no modification and only implemented with one node so there is no backup if any error or crash happened. Next project will improve this research.

Conflict of Interest

The authors declare no conflict of interest.

References

[1] Amirullah, Dipenjara karena Kasus Ijazah Palsu, Ini Perjalanan Karir Nurul Qomar, Dari Pelawak hingga Politisi (Arrested due to Fake Diploma Certificate, this is the career journey of Nurul Qomar, from Comedian to Politician), 2020.

[2] Y. Linggasari, Menteri Nasir: 187 Pemilik Ijazah Palsu Punya Jabatan Penting (187 Fake Diploma Certificate Owner has important Position), 2015.

[3] Meyliana, Y.U. Chandra, C. Cassandra, H.A.E. Widjaja, . Surjandy, E. Fernando, J.A. Sunandar, H. Prabowo, "Blockchain Technology for University Diploma Certificate," (Conrist 2019), 193–198, 2020, doi:10.5220/0009907801930198.

[4] A. Alammary, S. Alhazmi, M. Almasri, S. Gillani, "Applsci-09-02400.Pdf," 2019.

[5] Meyliana; Cadelina Cassandra; Surjandy; Henry Antonius Eka Widjaja; Harjanto Prabowo; Erick Fernando; Yakob Utama Chandra, "A Blockchain Technology-Based for University Teaching and Learning Processes," 2020 International Conference on Information Management and Technology (ICIMTech), **4**, 2020, doi:10.1109/ICIMTech50083.2020.9211209.

[6] D. Tapscott, A. Tapscott, "THE BLOCKCHAIN REVOLUTION & Higher Education.," Education Review, **52**(2), 10–24, 2017.

[7] M.B. Hoy, "An Introduction to the Blockchain and Its Implications for Libraries and Medicine," Medical Reference Services Quarterly, **36**(3), 273–279, 2017, doi:10.1080/02763869.2017.1332261.

[8] T. Alam, M. Benaida, "Blockchain and internet of things in higher education," Universal Journal of Educational Research, **8**(5), 2164–2174, 2020, doi:10.13189/ujer.2020.080556.

[9] Meyliana, Y.U. Chandra, C. Cassandra, . Surjandy, E. Fernando, H.A.E. Widjaja, H. Prabowo, "A Proposed Model of Secure Academic Transcript Records with Blockchain Technology in Higher Education," in ConRist 2019, 172–177, 2020, doi:10.5220/0009907401720177.

[10] G. Chen, B. Xu, M. Lu, N.-S. Chen, "Exploring blockchain technology and its potential applications for education," Smart Learning Environments, **5**(1), 1–10, 2018, doi:10.1186/s40561-017-0050-x.

[11] B. Awaji, E. Solaiman, A. Albshri, "Blockchain-based applications in higher education: A systematic mapping study," ArXiv, (June), 2020.

[12] G. Greenspan, "MultiChain Private Blockchain — White Paper," 1–17, 2013.

[13] A. Ismailisufi, T. Popović, N. Gligorić, S. Radonjić, S. Šandi, "A Private Blockchain Implementation Using Multichain Open Source Platform," (February), 2020, doi:10.1109/IT48810.2020.9070689.

[14] Interaction Design Foundation, User Centered Design, 2020.

[15] J. Sujan, S. Roy, D. Fels, "User Centered Design Methods and Their Application in Older Adult Community USER CENTERED DESIGN METHODS AND THEIR Introduction :," (July), 2016, doi:10.1007/978-3-319-40349-6.

[16] Z. Almeraj, "A User Centered Design Roadmap for Researchers and Designers Working with Visually Impaired and Blind Children A User Centered Design Roadmap for Researchers and Designers Working with Visually Impaired and Blind Children," (February), 2019.

[17] H. Leslie, H. Spits, E. Abdurachman, "A Proposed Supply Chain Model of Blockchain Technology-Based in Automotive Component Industry," (January), 2020, doi:10.35940/ijrte.E6440.018520.

Fault Diagnosis and Noise Robustness Comparison of Rotating Machinery using CWT and CNN

Byeongwoo Kim[*], Jongkyu Lee

Department of Electrical, Electronic and Computer Engineering University of Ulsan, Ulsan, KS016, South Korea

A B S T R A C T

For systems using rotating machinery, diagnosing the faults of the rotating machinery is critical for system maintenance. Recently, a machine learning algorithm has been employed as one of the methods for diagnosing the faults of rotating machinery. This algorithm has an advantage of automatically classifying faults without an expert knowledge. However, despite a good training performance of the deep learning model, there remains a challenge of performance degradation arising from noise when the model is applied in a real environment. In this study, to solve this problem, we identified the faults of a rotating machinery after applying the continuous wavelet transform (CWT) and then we extracted the images for detecting the faults of rotating machinery and apply y them to the convolution neural network (CNN). Subsequently, we compared it with a commonly used artificial neural network technique according to load and noise. When we added the white noise from 1dB to 20dB to vibration signal, the proposed method converged to 100% accuracy from 8dB at no load, at 10dB at presence of load. we verified that the proposed method improved the performance in diagnosing the faults of rotating machinery.

1. Introduction

With the development of industry and technology, various industrial rotating machines have become capable of handling high speeds and heavy loads, which cause massive mechanical and thermal loads, resulting in their breakdown [1]. When a rotating machine fails, fault diagnosis is very important as time and economic loss can occur. Therefore, a countermeasure is required to check the condition of rotating machines and to diagnose faults. According to statistical data, 45%–55% of failures in rotating machines are due to faults in the bearings [2]. Monitoring the condition of the rotating machine to detect its faults helps reduce losses [3]-[5].

Machine learning algorithm is a common method of diagnosing faults of rotating machines.

In general, the fault diagnosis method of rotating machines using a machine learning algorithm is divided into four steps: (1) data acquisition, (2) feature extraction, (3) machine learning algorithm training (neural network training), and (4) classification [6]-[9].

The data acquisition step is the process of obtaining a signal that indicates the state of a rotating machine using a sensor. A noise-measuring device, the electric current signals of the motor, and vibration signals are used to obtain signs that indicate the state of the rotating machine [10]-[12]. Among them, the commonly used method detects the fault of the rotating machine by obtaining vibration signal data that are the easiest to measure and can clearly indicate the state of the rotating machine [13].

In the feature extraction step, signs that indicate the state of the rotating machine are extracted from the vibration signals. In general, a signal measured from the rotating machine consists of a mixture of noise and a sign indicating the state of the rotating machine. If vibration signals containing noise are used as input values in the machine learning algorithm, it is difficult to accurately diagnose the state of the rotating machine due to the noise. Hence, noise should be removed from the vibration signals through feature extraction to use them as input values for the machine learning model.

The most common feature extraction methods use filters and signal decomposition [14]-[16]. The widely used methods of diagnosing faults in vibration signals include empirical mode decomposition (EMD) technique, which uses intrinsic mode function (IMF) to decompose the signals, and wavelet transform method, which uses the wavelet function to decompose the signals.

The EMD technique yields outstanding performance when detecting faults of rotating machines [17]. However, it requires to

combine sub-band signals because the sub-bands decomposed by IMF are generally not orthogonal to each other [18].

The wavelet transform method has the advantage of adjusting the cycle and amplitude to show the features more clearly in the vibration signals of rotating machine and to remove the noise included in the vibration signals [19], [20].

In the machine learning algorithm training step, the algorithm is trained by using the features extracted from the vibration signals as input values for the machine learning algorithm. Among the various machine learning algorithms, the algorithms using deep learning show better performance, and among the deep learning algorithms, convolution neural network (CNN) shows superior performance.

In the classification step, the test data, which are not used in the training step, are used to classify the state of the rotating machine, and the indicator showing the performance of the model can be derived.

Eren used CNN to diagnose faults of rotating machines but diagnosed their faults based solely on the performance of the CNN model without considering the method of removing the noises [21]. Meanwhile, Yuan used discrete wavelet transform and CNN to improve the performance of the existing rotating machine fault diagnosis model. However, there was a limitation in showing the suitable performance in a poor environment where noise can be measured substantially because the experiment was conducted without reflecting noise [22].

In this study, we used continuous wavelet transform method, to decompose vibration signals into noise, and signals indicating the state of the rotating machine to detect its faults, and extracted signals that can be used to detect the faults of the rotating machine, from the decomposed signals. The extracted features were used as input values of CNN, a deep-learning technique, to classify the faulty state of the rotating machine. Furthermore, we added white Gaussian noise to investigate the effectiveness of the corresponding algorithm through performance comparison between the model and conventional machine learning methods in a poor environment where a large amount of noise can be observed.

2. Theory

2.1. Continuous wavelet transform

The advantage of the wavelet transform method is that the wavelet function with dynamic resolution can be used to efficiently analyze the vibration signals, unlike Fourier transform, which cannot accurately display the characteristics of non-cyclic signals due to the fixed resolution [23][24]. The time series analysis using the wavelet transform is defined as follows.

$$\psi_{s,\tau}(t) = \frac{1}{\sqrt{s}}\psi(\frac{t-\tau}{s}) \tag{1}$$

In Eq. (1), the signal is decomposed by shifting the wavelet function to the time axis by τ and scaling by a. If the mother wavelet is given, then continuous wavelet transform (CWT) of the signal f(t) is defined by Eq. (2).

$$W(s,\tau) = \int_{-\infty}^{+\infty} f(t)\frac{1}{\sqrt{s}}\psi^*(\frac{t-\tau}{s})dt \tag{2}$$

The wavelet coefficient obtained in Eq. (2) indicates the similarity between f(t) and $\psi(t)$. The wavelet transform produces the decomposition of the time scale of f(t), but the time-frequency region can be obtained by the pseudo-frequencies.

The relationship between the scale and the pseudo-frequencies changes depending on the center of the wavelet function, performance of the scale, and sampling cycle and maximizes the spectrum of the wavelet function with the given scale. The relationship of these parameters is expressed by Eq. (3).

$$f_s = \frac{f_c}{s \cdot \Delta} \tag{3}$$

In Eq. (3), f_c denotes the center frequency, Δ is the sampling cycle, and f_s shows the result of the pseudo-frequency. The entire signal is synthesized by applying the inverse continuous wavelet transform (ICWT) defined in Eq. (4) as follows:

$$f(t) = \frac{1}{C_\psi}\int_{-\infty}^{+\infty}\int_{-\infty}^{+\infty} W(s,\tau)\psi_{s,\tau}(t)\frac{dsd\tau}{s^2} \tag{4}$$

here, C_ψ is the acceptance constant obtained when the mother wavelet satisfies all requirements.

2.2. Convolutional Neural Network

CNN was inspired by the principle of recognizing objects in the visual cortex of the brain and was derived from the field of deep learning. It consists of convolutional layer, pooling layer, and fully connected layer [25].

The main function of a convolutional layer is to obtain a feature map through the convolutional operation of filter for the input. The convolutional layer typically consists of learnable kernel and bias. The size of the kernel corresponds to the size of the filter, and the depth of the kernel corresponds to the number of channels in the feature map. The input of the convolutional layer can be calculated by the weight and the inner product of cognitive region, as expressed by Eq. (5).

$$y_{l,j}^{conv} = \sum_{i=1}^{k} w_{i,j}^l * y_{l-1}^{pool} + b_j^l \tag{5}$$

In Eq. (5), $y_{l,j}^{conv}$ refers to the convolutional value of ith channel in the convolutional layer l, y_{l-1}^{pool} refers to the ith output of the pooling layer l-1, $w_{i,j}^l$ refers to the kernel of the convolutional layer l, b_j^l refers to the bias of the jth channel in the convolutional layer l, and * refers to the convolutional operation.

After the convolutional operation is completed, the value of convolutional layer is calculated according to the activation function. The role of the activation function is to perform the nonlinear projection for the input of the neuron. Rectified linear unit (ReLU), one of activation functions, is used for pattern recognition. The ReLU function shows excellent performance in accelerating convergence and solving vanishing gradient problems. Therefore, the ReLU is used as the activation function of a convolutional layer, and the output of convolutional layer 1 can be expressed by Eq. (6).

$$y_{l,j}^{ReLU} = f(y_{l,j}^{conv}) = \max[0, y_{l,j}^{conv}] \tag{6}$$

Here, $y_{l,j}^{ReLU}$ represents the output of the jth channel in the convolutional layer l, and $f(\cdot)$ refers to the activation function.

After the convolutional layer operation, the pooling layer is used to extract additional features. It plays a role of reducing the dimensions of the output of the previous layer. Therefore, the key purpose of this layer is to reduce the volume of data to reduce the computation time on the computer. Types of pooling layer include max pooling, average pooling, logarithmic pooling, and weight pooling.

Max pooling is used to classify operation because it can speed up the convergence and improve the generalization. Max pooling function can be expressed by Eq. (7).

$$y_{l,j}^{pool} = \max\left(w(s_1, s_2) \cap y_{l-1,j}^{ReLU}\right) \qquad (7)$$

$w(s_1, s_2)$ represents the window of the pooling layer that can shift to a certain step, and s_1 and s_2 correspond to the dimensions of the pooling layer. Further, $y_{l-1,j}^{ReLU}$ refers to the output of jth channel in the convolutional layer, and $\cap$ refers to the overlap between the pooling layer and the channel's output.

In general, the CNN model contains multiple convolutional and pooling layers and extracts feature maps sequentially. The extracted feature map is transformed into a vector, which is used as an input of a fully connected layer. The main function of the fully connected layer is to extract additional features and connect the output step to the softmax classifier. A fully connected layer usually consists of 2 or 3 hidden layers, and all neurons of a hidden layer can be shown by Eq. (8).

$$y = \sigma\left(\left(w_f\right)^T s_m + b_f\right) \qquad (8)$$

w_f refers to the weight matrix of the fully connected layer, b_f represents the bias, and $\sigma(\cdot)$ represents the activation function of the fully connected function.

2.3. Batch normalization

In general, as the depth of the neural network structure increases, the distribution of features changes, and the overall distribution gradually approaches both ends of the nonlinear function value interval. This phenomenon is called gradient diffusion, which causes a problem with the convergence of the model. To resolve this problem, the Google DeepMind team proposed batch normalization technique in 2014 [26].

The key purpose of the batch normalization technique is to revert the distribution of all neurons to the standard normal distribution through a specific normalization method. Batch normalization can re-parameterize almost all neural networks and, thus, can be used for any hidden layer. Batch normalization, which optimizes neural networks, can improve the performance of neural networks, such as faster convergence, faster learning time, ability to allow higher learning rate, and easier initialization of weights.

First, normalization can make each scalar feature with the mean 0 and the unit variance, as expressed in Eq. (9).

$$\hat{x} = (x_i - E[x_i])/\sqrt{Var[x_i]} \qquad (9)$$

However, if Eq. (9) is used to directly normalize the features of a certain layer, the learned features can be affected, thereby reducing the performance of the neural network. To overcome this problem, each normalized x_i is modified based on two adjustment parameters, γ_i and β_i, aiming at scaling and shifting the normalized values. This process can be expressed by Eq. (10).

$$f_i = \gamma_i \hat{x} + \beta_i \qquad (10)$$

here, γ_i and β_i are parameters that can be used to learn the method of recovering the characteristic distribution of the existing neural network. By setting $\gamma_i = \sqrt{Var[x_i]}$ and $\beta_i = E[x_i]$, the existing activation can be restored. In this case, the activation values are stably distributed during learning.

Second, because the mini-batch technique is used in training process, the specific activation x_i that possesses the B value in the mini-batch is $\varphi = \{x_{1\dots B}\}$, and the corresponding transformation is $y_{1\dots B}$. Therefore, the batch normalization transform $BN_{\gamma,\beta}: X_{1\dots B} \rightarrow y_{1\dots B}$ can be represented by Eqs. (11), (12), (13), and (14).

$$E[X_\varphi] = \frac{1}{B}\sum_{p=1}^{B} x_p \qquad (11)$$

$$Var[x_\varphi] = \frac{1}{B}\sum_{p=1}^{B}(x_p - E[x_\varphi])^2 \qquad (12)$$

$$\widehat{x_p} = (x_p - E[x_\varphi])/\sqrt{Var[x_\varphi] + \varepsilon} \qquad (13)$$

$$\widehat{y_p} = \gamma\widehat{x_p} + \beta \qquad (14)$$

here, ε is a constant and is used to avoid undefined gradient values.

3. Experiment setup

This study required constructing a variety of dataset to enhance the accuracy of the fault detection of the rotating machine. Thus, we utilized the Case Western Reserve University Bearing Fault Database, which is widely used for fault detection of conventional rotating machines [27]. Because various researchers have conducted experiments using this database, there are several advantages: the data are reliable, and the performance comparison can be conducted with other learning algorithms. As shown in Figure 2, the test bench consists of a motor on the left, a torque transducer/encoder on the center, and a dynamometer on the right.

The vibration signals were measured in a total of four types: normal, ball fault, inner race fault, and outer race fault. The levels of crack consisted of 0.007, 0.014, and 0.021 inch, and the levels of load consisted of 0 HP, 1 HP, 2 HP, and 3 HP.

Figure 1 shows the fault detection process of rotating machine using vibration signals. Data having cracks of 0.007 inch were used, and the dataset was classified into Case 1 (0 HP), Case 2 (1 HP), Case 3 (2 HP), and Case 4 (3 HP), depending on the level of load. Each case consisted of 4,368 data: 1,092 for normal data, 1,092 for ball faults, 1,092 for inner race faults, and 1,092 for outer race faults. In addition, white Gaussian noise was increased in the vibration signals having cracks of 0.007 inch to verify the robustness to noise by CWT. As shown in Figure 3, the sample

data were constructed to train the CNN model by performing the segmentation with 4,392 signals where white Gaussian noise was added in the actual vibration signals. For each sample data, continuous wavelet functions, such as morse, morlet, and bump wavelet, were applied, and CWT was used. The conversion to images with the size of 224 × 224 was performed to use them as inputs of CNN after signal preprocessing, as shown in Figure 2.
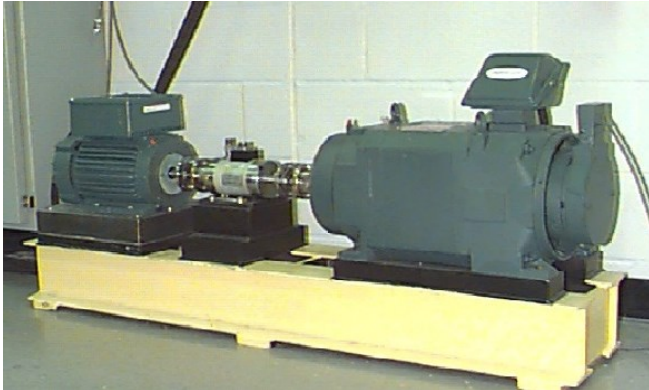
Figure 1: Experiment setup

The CNN was constructed with 8 3 × 3 filters for the first layer of the CNN model, 16 3 × 3 filters for the second layer, and 32 3 × 3 filters for the third layer. Additional features were extracted through the fully connected layer, and the faults of rotating machine were classified using the softmax classifier. After the convolutional operation was completed in each layer, batch normalization and max pooling, a type of pooling layer, were applied.

To conduct the training of the constructed CNN model, 70% of 4,368 data in the entire dataset were used for the training process of the CNN model, and the rest were used to validate the trained CNN model. To validate the performance of the trained model, comparative analysis was performed with the DNN technique, a conventional vibration signal analysis method using artificial neural network (ANN).
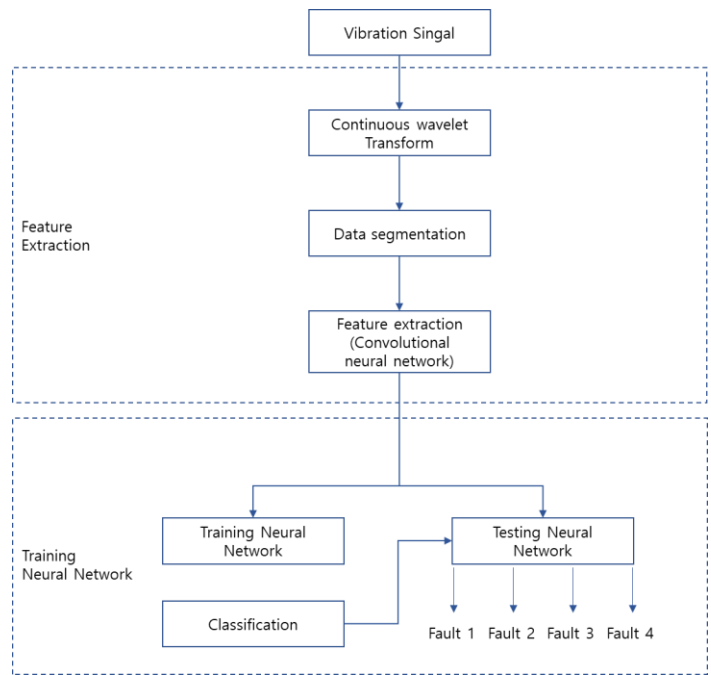
Figure 2: Representation of proposed fault diagnosis structure

4. Simulation

As shown in Fig 3, CWT was performed through the continuous wavelet functions—namely, morse, morlet, and bump wavelet—using the white Gaussian noise-added vibration signals, and the results were used as input values of the CNN model.

To compare the performance of the generated CNN model, comparative analysis was performed using the ANN model by extracting statistical parameters, such as peak, entropy, skewness, kurtosis, variance, and rms, and using them as the input values of the ANN, as shown in Figure 4.
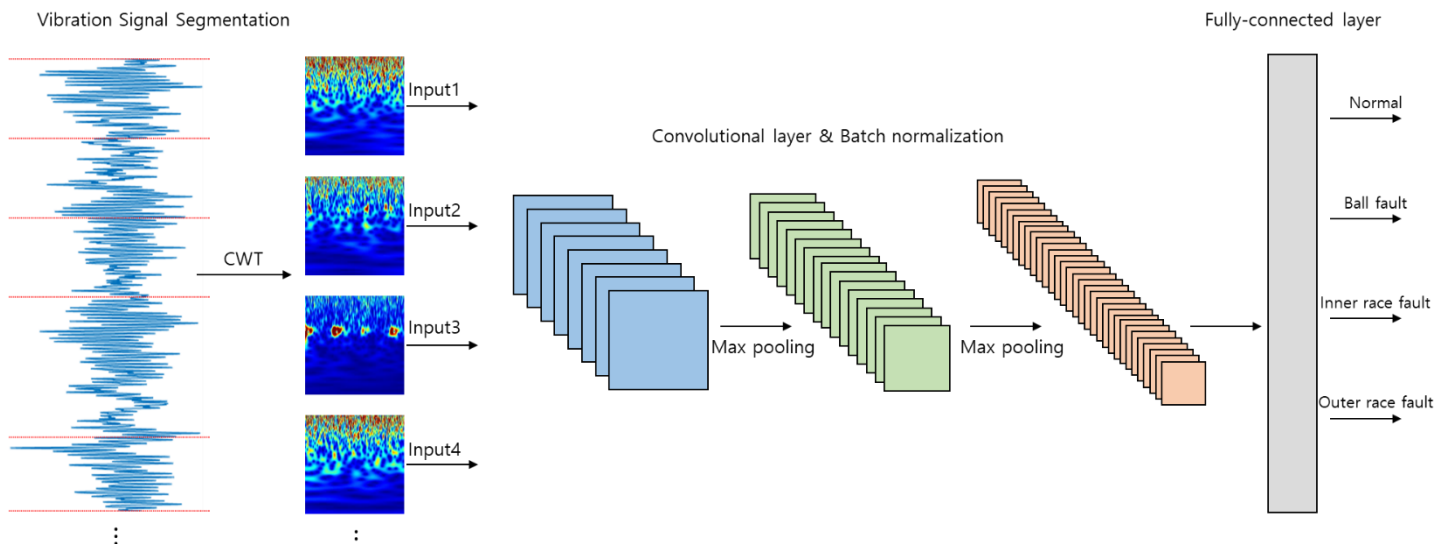
Figure 3: The process of fault diagnosis in vibration signal using CWT & CNN.
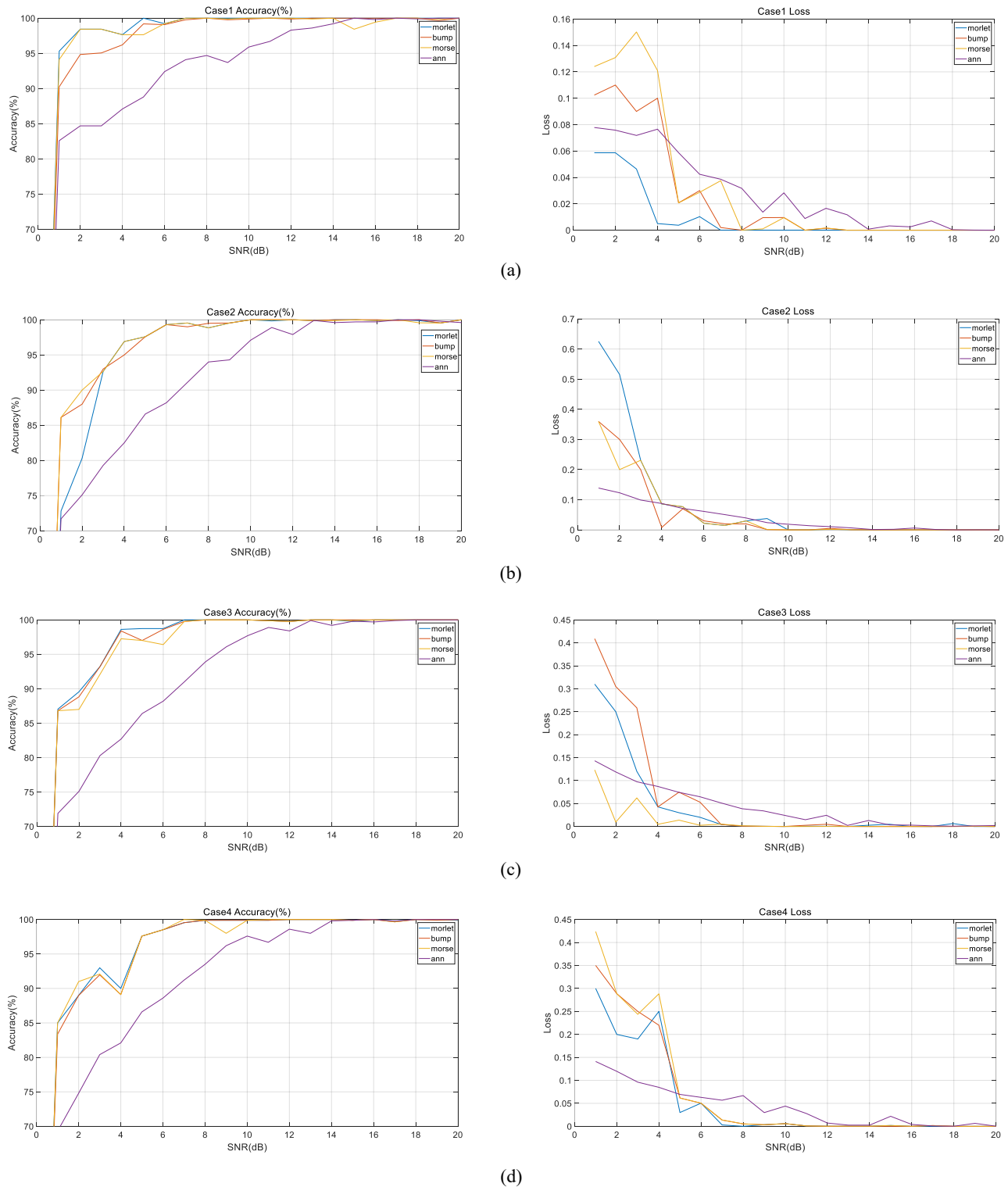
Figure 4: Result of fault diagnosis (accuracy & loss) – (a) Case1(=0HP), (b) Case2(=1HP), (c) Case3(=2HP), (d) Case4(=3HP)

To compare the performance of the CNN model and the CWT for noise removal, we compared the accuracy and loss for each signal-to-noise ratio (SNR) level with those of the existing method, in which the parameters are extracted from the vibration signals and then used as inputs of the ANN, as shown in Figure 4.

When the SNR was 1 dB in the Case 1 (0 HP) dataset, the accuracy of the CNN model using morlet wavelet was 95.31% with a loss of 0.05869, that of the CNN model using bump wavelet was 90.25% with a loss of 0.11, and that of CNN model using morse wavelet was 90.13% with a loss of 0.124. Therefore, the performance was excellent compared to that of the ANN model.

Furthermore, when the SNR level was reduced step by step, the CNN model using CWT showed that the accuracy converged to 100% at the SNR level of 8 dB, whereas the ANN model showed that the accuracy converged to 100% when the SNR level was 15 because of performance degradation in the denoising function.

In terms of loss, the CNN model using CWT showed the convergence close to 0 when the SNR level was 11 dB. However, the model using the ANN showed the convergence to 0 when the SNR level was 18 dB, indicating that the performance was lower than that of the CNN model.

When SNR was 1 dB in the Case2 (1 HP) dataset, the accuracy of the CNN model using morlet wavelet was 72.82% with a loss of 0.6254, that of the CNN model using bump wavelet was 86.12% with a loss of 0.3602, and that of the CNN model using morse wavelet was 86.09% with a loss of 0.3597. The differences were not large compared to those of the ANN model (accuracy: 71.7% and loss: 0.1388). When the SNR level was reduced, the accuracy converged to 100% at the SNR level of 10 dB in the CNN model using CWT. Conversely, the accuracy converged to 100% when the SNR level became 14 dB in the ANN model. Furthermore, in terms of loss, the CNN model using CWT showed the convergence to 0 when the SNR level was 10 dB, whereas the ANN model showed the convergence to 0 when the SNR level was 14 dB.

When the SNR level was 1 dB in the Case 3 (2 HP) dataset, the accuracy of the CNN model using morlet wavelet was 87.04% with a loss of 0.31, that of the CNN model using bump wavelet was 86.72% with a loss of 0.409, and that of the CNN model using morse wavelet 86.61% with a loss of 0.1232. Therefore, the performance was excellent compared to that of the ANN model (accuracy: 71.9% and loss: 0.1432).

When the SNR level was 1 dB in the Case 4 (3 HP) dataset, the accuracy of the CNN model using morlet wavelet was 85.13% with a loss of 0.2947, that of the CNN model using bump wavelet was 83.37% with a loss of 0.34924, and that of the CNN model using morse wavelet was 85.03% with a loss of 0.4238. Meanwhile, the accuracy and loss of the ANN model were 69.3% and 0.1431, respectively. As the noise signal decreased, the CNN model using CWT showed that the accuracy and the loss converged to 100% and 0, respectively, when the SNR level was 10 dB. However, the ANN model showed that the accuracy converged to 100% when the SNR level was 14 dB, and the loss converged to 0 when the SNR level was 16 dB. Based on these results of the vibration signal analysis, we have confirmed that the CNN model using CWT is more robust to noise than the existing method. Furthermore, we used the pooling layer and batch normalization to reduce the training time of the CNN model and improve the performance, thereby confirming the effectiveness and stability of the method, in comparison with the conventional signal analysis method.

5. Conclusion

In this study, vibration signal analysis was conducted to diagnose faults of rotating machines. Furthermore, to investigate the performance in actual work site environment, we conducted vibration signal analysis. Hence, we added white Gaussian noise in the vibration signals step by step and applied CWT. Subsequently, we extracted the images to use them as input values of the CNN. When we added the white noise from 1dB to 20dB

to vibration signal, the proposed method converged to 100% accuracy from 8dB at no load, at 10dB at presence of load. The analysis results confirmed that CWT-applied CNN model showed superior performance compared to the existing signal analysis method.

6. Acknowledgment

References

[1] A. H. Bonnett, G. C. Soukup, "Cause and analysis of stator and rotor failures in three-phase squirrel-cage induction motors", IEEE Transaction on Industry Applications, **28**(4), 921-937, 1992, 10.1109/PAPCON.1991.239667

[2] Nandi, S., Toliyat, H. A., & Li, X., "Condition monitoring and fault diagnosis of electrical motors – a review", IEEE Transactions on Instrumentation and Measurement, **65**(11), 2646-2656, 2005, 10.1109/CMD.2008.4580260

[3] B. Dolenc, P. Boskoski, D.Juricic , "Distributed bearing fault diagnosis based on vibration analysis", Mech. Syst. Signal Process, 66-67, 521-532, 2016, DOI: 10.1016/j.ymssp.2015.06.007

[4] L. Barbini, A.J. Hillis, J.L. du Bois, "Amplitude-cyclic frequency decomposition of vibration signals for bearing fault diagnosis based on phase editing", Mech. Syst. Signal Process, 103, 76-88, 2018, DOI: 10.1016/j.ymssp.2017.09.044

[5] E. EI-Thalji, Jantunen, "A summary of fault modeling and predictive health monitoring of rolling bearings", Mech. Syst. Signal Process, 60-61, 252-272, 2015, DOI: 10.1016/j.ymssp.2015.02.008

[6] W.K. Xi, Z.X. Li, Z. Tian, et al., "A feature extraction and visualization method for fault detection of marine diesel engines", Measurement, 116, 429-437, 2018, DOI: 10.1016/j.measurement.2017.11.035

[7] J.B. Yu, J.X Lv, "Weak fault feature extraction of rolling bearings using local mean decomposition-based multilayer hybrid denoising", IEEE Trans. Instrum. Meas., **66**(12), 3148-3159, 2017, 10.1109/TIM.2017.2751878

[8] M. Amar, I. Gondal, C. Wilson, "Vibration spectrum imaging: a novel bearing fault classification approach", IEEE Trans Ind. Electron., **51**(1), 494-502, 2015, 10.1109/TIE.2014.2327555

[9] B. Madahian, L.Y. Deng, R. Homayouni, "Development of a literature informed Bayesian machine learning method for feature extraction and classification", BMC Bioinform, 16. , 2015, DOI: 10.1186/1471-2105-16-S15-P9

[10] Chacon, J.L.F., Kappatos, V., Balachandran, W., & Gan, T.-H., 2015 "A novel approach for incipient defect detection in rolling bearings using acoustic emission technique", Applied Acoustics, 89, 88-100., 2015, DOI: 10.1016/j.apacoust.2014.09.002

[11] S. Singh, Kumar, A., & Kumar, N., " Motor current signature analysis for bearing fault detection in mechanical system", Procedia Materials Science, 6, 171-177, 2014, DOI: 10.1016/j.mspro.2014.07.021

[12] J. Zarei, J. Tajeddini, M. A., & Karimi, H. R., "Vibration analysis for bearing fault detection and classification using an intelligent filter", Mechatronics, **24**(20), 151-157, 2014, DOI: 10.1016/j.mechatronics.2014.01.003

[13] P. Kharche, P. Ksgirsagar, S. V., "Review of fault detection in rolling element bearing", International Journal of Innovative Research in Advanced Engineering, **1**(5), 169-174, 2014, https://ijirae.com/images/downloads/vol1issue5/JNME10092(33).pdf

[14] W. He. Z.N. Jiang., K. Feng, "Bearing fault detection based on optimal wavelet filter and sparse code shrinkage", Measurement, **42**(7), 1092-1102. 2009, DOI: 10.1016/j.measurement.2009.04.001

[15] X. L. An, H. T. Zeng, W. W. Yang, et al., 2017, "Fault diagnosis of a wind turbine rolling bearing using adaptive local iterative filtering and singular value decomposition", T. I. Meas. Control., **39**(11), 1643-1648, 2017, DOI:

10.1177/0142331216644041

[16] X. An, Weiwei Yang, Xuemin An, "Vibration signal analysis of a hydropower unit based on adaptive local iterative filtering", P. I. Mech. Eng. C-J Mec. **231**(7), 1339-1353, 2017, DOI: 10.1177/0954406216656020

[17] Y. Li, M. Xu, X. Liang, "Huang Application of bandwidth EMD and adaptive multiscale morphology analysis for incipient fault diagnosis of rolling bearings", IEEE Trans. Ind. Electron., **61**(8), 6506-6517, 2017, 10.1109/TIE.2017.2650873

[18] J.P. Yang, P.Z. Li, Yang, et al., "An improved EMD method for modal identification and a combined static-dynamic method fir damage detection", Sound Vib., 240, 242-260, 2018, DOI: 10.1155/2014/317954

[19] Q.B. He, "Vibration signal classification by wavelet packet energy flow manifold learning", J. Sound Vib., **332**(7), 1881-1894, 2013, DOI: 10.1016/j.jsv.2012.11.006

[20] Q. Pan, L. Zhang, G. Dai, H. zhang, "Two denoising methods by wavelet transform", IEEE Trans. Signal Processing, **47**(12), 3401-3406, 1991, DOI: 10.1109/78.806084

[21] L. Eren, "Bearing Fault Detection by One-Dimensional Convoltional Neural Networks", Mathematical Problems in Engineering, DOI: 10.1155/2017/8617315

[22] Y. Xie, Tao Zhang, "Feature Based on DWT and CNN for Rotating Machinery Fault Diagnosis", IEEE Transaction, CCDC, **29**, 3861-3866, 2017 10.1109/CCDC.2017.7979176

[23] V. Pichot, J.M. Gaspoz, S. Molliex, A. Antoniadis, Wavelet transform to quantify heart rate variability and to assess its instantaneous changes, Journal Applied Physiol, **86**(3), 1081–1091, 1991, DOI: 10.1152/jappl.1999.86.3.1081

[24] L.G. Gamero, J. Vila, F. Palacios, Wavelet transform analysis of heart rate variability during myocardial ischaemia, Med. Biol. Eng. Comput. 40, 72–78, 2002, DOI: 10.1007/BF02347698.

[25] X. Li, W. Zhang, Deep learning-based remaining useful life estimation of bearings using multi-scale feature extraction, Reliab. Eng. Syst. Saf. 182 208–218, 2019, DOI: 10.1016/j.ress.2018.11.011.

[26] J. Wang, S. Li, B. Han, et al., Construction of a batch-normalized autoencoder network and its application in mechanical intelligent fault diagnosis, Meas. Sci. Technol. 30, 1–14, 2019, DOI: 10.1088/1361-6501/aaf319.

[27] K.E. Loparo, "Bearing fault diagnosis based on wavelet transform and fuzzy inference", Mechanical System and Signal Processing, 2005, DOI: 10.1016/S0888-3270(03)00077-3

Improved Fuzzy Time Series Forecasting Model Based on Optimal Lengths of Intervals Using Hedge Algebras and Particle Swarm Optimization

Nghiem Van Tinh[*,1], Nguyen Cong Dieu[2], Nguyen Tien Duy[1], Tran Thi Thanh[1]

[1]*Faculty of Electronics, Thai Nguyen - University of Technology, Thai Nguyen, 250000, Vietnam*

[2]*Thang Long University, Hanoi, 100000, Vietnam*

A R T I C L E   I N F O

A B S T R A C T

Recently, numerous scholars have suggested fuzzy time series (FTS) models to forecast many different fields. One of the vital issues for high accurate forecasting in FTS model is method of partitioning in Universe of discourse (UoD). In this research, we propose a novel FTS model, which is established by using hedge algebra (HA) and particle swarm optimization (PSO) for forecasting the different problems. In this model, HA is considered an algebraic structure for partitioning the UoD into unequal - size intervals based on optimal parameters which is determined by PSO. After making the intervals with unequal - length, the data values of times series on each interval are symbolized by fuzzy sets and then, these fuzzy sets are utilized to make fuzzy relation groups. Lastly, we keep using the PSO to adjust the size of each interval with view to reaching the better accurate prediction rate. The effectiveness of the proposed method is demonstrated on two datasets which are often applied in many studies in literature as enrolments data of the University of Alabama and Car road accident data in Belgium. The obtained results show that the proposed model produces higher accuracy forecasting when compared with the some of the recent FTS prediction models for all orders of model.

1. Introduction

The time series forecasting problem is an attractive and vital research issue. This forecasting problem has been often handled by using a variety of methods like mathematical statistics, artificial neural networks, etc. The downsides of the traditional time series forecasting models are that they extensively dependent on historical data or require having the linearity assumption and cannot solve prediction problems in which the values of time series are linguistic terms. To overcome these difficulties, the authors in [1, 2] first produced the concepts of FTS, which have the ability to deal with vague and incomplete data sets by utilizing the fuzzy set theory [3]. They have proposed the two FTS forecasting models to implement on university enrolments of Alabama with a forecasting schema consisting of main five steps: (1) defining UoD, (2) Partitioning of the UoD into intervals, (3) determining the fuzzy sets and fuzzifying the time series, (4) Establishing fuzzy logical relationship, and (5) forecasting and defuzzifying the forecasting values.

However, their approaches take a lot of time to build forecasting model because of using the complex max– min operations in fuzzy relationship matrix and lack of persuasiveness in partitioning the UoD. These limitations led research [3] to develop a new FTS forecasting model using simple arithmetic operations to replace the complex matrix operations [1, 2] in the determination of fuzzy relationship matrix and defuzzification output values. In addition, research works [5, 6] found out the importance of assigning weights to deal with the issue of recurrent fuzzy relationship and to reflect the difference in their importance. Expansion of the framework [3] into a high-order FTS schema [7], and the influence of the length of intervals in article [8] come with the development from the one-factor FTS models into two-factor FTS model [9]. These forecasted approaches are the basis for the strong development of many FTS models in the next time periods. Recently, many authors have applied different advanced data mining techniques in each stage of FTS model with view to enhancing forecasting accuracy. Study in article [10] used the automatic clustering technique for partitioning the UoD into unequal - size intervals at the fuzzification stage in their forecasting model. Some other researches apply soft computing

techniques(especially evolutionary computing, clustering techniques) for adjusting and selecting intervals with unequal-size, can be found as genetic algorithm [11, 12], simulated annealing [13], PSO [14-22], K-mean [23, 24], fuzzy C-means [25, 26]. Just recently, a completely different way from fuzzy approach, several works with regards to HA have been published. In [27], the authors have presented a forecasting method based on the theory of hedge algebra [28] for forecasting university enrolments, to be a typical option. In which, the hedge algebra was used to construct linguistic domains and variables instead of performing data fuzzification and defuzzification in the fuzzy approach. In addition, researches in [29, 30] proposed the HA-based forecasting models to obtain unequal – length intervals in the UoD by mapping the semantics of linguistic variables into fuzziness intervals. However, two these research works only focus on building the first-order forecasting model to apply the number of students annually at the University of Alabama. In addition, their forecasting models have not yet applied the optimal techniques, so the obtained forecasting results are not really good enough.

Based on analyzing of the aforementioned research works showed that determining of the length of interval and the order of fuzzy relationships affect strongly forecasting performance of the model. To avoid the above - mentioned limitations and promote the advantage of combination with methods of partitioning in the UoD. The purpose of this study is to suggest a new partition method which uses PSO algorithm to optimize parameters of HA in the FTS prediction model. Therefore, we develop a novel hybrid prediction model using method of fuzzy relation group [17], integrating with HA and PSO algorithm in the identification of optimal intervals with view to enhancing the forecasting performance of the proposed model. For making it become reality, HA has been used to divide the UoD into intervals with unequal – size based on the parameters optimized by PSO. After obtaining the intervals, the time series data is put into the intervals by fuzzy sets and used them to create the FLRs, group of FLRs. Later, all information in FLR groups are utilized to produce the final prediction results based on the our defuzzification principle [31]. Finally, to enhance the accuracy of the model, we continue applying PSO algorithm to readjust the initial interval lengths which are obtained by fuzzy parameters of HA into intervals with the more proper length. Our forecasting model is examined on two following real-world datasets: 1) the historical enrolment dataset of University of Alabama [3], 2) the dataset of car road accident [32]. The examined results point out that our forecasting model outperforms the some of the recent FTS models in terms of prediction accuracy rate.

The next content of this paper introduces brief fundamental theories related to FTS model such as, fuzzy time series, Hedge Algebras and PSO algorithm. A method using PSO technique which has never been applied before in the selecting optimal parameters of HA and optimal length of intervals simultaneously, is presented in Section 3. Section 4 discusses the forecasting performance by comparing the obtained results of the proposed model with ones of the previous models. The last section gives conclusions and directions for future work.

2. The Fundamental Theories and Algorithms

In this section, we briefly introduce general knowledge related to FTS which is proposed in [1, 2] and improved by study [3]. In addition to, the hedge algebras [28] and PSO algorithm [33] is also reviewed.

2.1. Fuzzy time series

The concepts of FTS were proposed in [1, 2], in which the historical time series data are given in the form of fuzzy sets [3].

Assume that $Y(t)$ $(t = . . , 0, 1, 2 . .)$ a real subset R $(Y(t) \subseteq R)$, regarded as the UoD on which the fuzzy sets $f_i(t)$ $(i = 1,2 ...)$ are defined. If $F(t)$ including the collection of $f_1(t), f_2(t), ...$, then $F(t)$ is namely a FTS which is defined on $Y(t)$ [1, 2]

If there exists fuzzy logical relationship (FLR) between $F(t-1)$ and $F(t)$, namely R(t-1, t), such that they can be expressed as $F(t) = F(t-1) * R(t-1, t)$ or $F(t-1) \rightarrow F(t)$; Where R(t-1, t) is the first-order fuzzy relationship between $F(t)$ and $F(t-1)$ and "$*$" represents the max–min composition operator. Here $F(t)$ and $F(t-1)$ are fuzzy sets. If, let $A_i = F(t)$ and $A_j = F(t-1)$, the relationship between $F(t)$ and $F(t-1)$ is replaced by $A_i \rightarrow A_j$, where A_i and A_j are called the current state and the next state of fuzzy relationship, respectively [1, 2, 4]

Let $F(t)$ be a fuzzy time series. If $F(t)$ is derived by more fuzzy sets $F(t-1)$, $F(t-2)$,…, $F(t-\beta+1)$, $F(t-\beta)$, then fuzzy relationship between them can be represented as $F(t-\beta)$, …, $F(t-2)$, $F(t-1) \rightarrow F(t)$. This relationship is called the β - order FTS model [1, 2, 7]

Suppose that $F(t)$ is derived from $F(t-1)$, then the relationship can be denoted as $F(t-1) \rightarrow F(t)$. If, let $A_i(t) = F(t)$ and $A_j(t - 1) = F(t-1)$. The FLR of them can be replaced as $A_j(t - 1) \rightarrow A_i(t)$. In addition, at the time t, there are also exists fuzzy relationships as $A_j(t1 - 1) \rightarrow A_{i1}(t1), . ., A_j(tn - 1) \rightarrow A_{in}(tn)$ with $t1, t2, . ., tn \le t$. It is noted that $A_i(t1), A_i(t2), …,$ and $A_i(tn)$ having the same fuzzy set A_i, but look at different times $t1, t2, …,$ and tn, respectively. If these FLRs appear before $A_j(t - 1) \rightarrow A_i(t)$, they can be grouped into a fuzzy relationship group as follows: $A_j(t - 1) \rightarrow A_{i1}(t1), A_{i2}(t2), … , A_{in}(tn), A_i(t)$, and it is called TV-FRG [17].

2.2. Some basis concepts of Hedge Algebras

Hedge Algebras are introduced by N.C. Ho in 1990. It is considered as a new approach to solve forecasting problems in which it is used to quantify the linguistic variables. Each of linguistic variable $\mathcal{X}$ is represented by an algebraic structure, which is built on the inherent semantic order of the linguistic terms [28] and defined as follows:

Definition 1: The linguistic variable $\mathcal{X}$ is a set including 5 components $\mathcal{AX} = (X, G, C, H, \le)$ and called HA;

In which, X is the basic set in $\mathcal{AX}$; " $\le$ " is a natural semantically ordering relation on X; $G = \{c^-, c^+\}$, $c^- \le c^+$ is the set of generating elements (eg., Low $\le$ High) ; $C = \{\mathbf{0}, \mathbf{w}, \mathbf{1}\}$ is a set of constants, with $(\mathbf{0} \le c^- \le \mathbf{W} \le c^+ \le \mathbf{1})$; $H = H^- \cup H^+$, with $H^- = \{ h_i : -q \ge i \ge -1\}$ denotes the set of all negative hedges of X, and $H^+ = \{h_i : 1 \le i \le p\}$ denotes the set of all positive hedges;

Definition 2. Let $\mathcal{AX} = (X, G, C, H, \le)$ be a HA. The function $fm: X \rightarrow [0, 1]$ is named to be a fuzziness measure of elements in X, if:

1) $fm(c^-) + fm(c^+) = 1$ and $\sum_{h \in H} fm(hx) = fm(x)$ with $\forall x \in X$;

2) $f(x) = 0$ with $\forall x \epsilon X$ so that $fm(0) = fm(W) = fm(1) = 0$

3) For $\forall x, y \in X, \forall h \in H, \frac{fm(hx)}{fm(x)} = \frac{fm(hy)}{fm(y)}$, this equation does not depend on x; y and it is called fuzziness measure of the hedge h and namely by $\mu(h)$. The properties of $fm(x)$ and $\mu(h)$ are given as below:

Proposition 1. The fm denotes the fuzziness measurement on X, the following statements hold.

With $\in X, x = h_n h_{n-1} \dots h_1 c, h_j \in H, c \in G$

1) $fm(hx) = \mu(h)fm(x), \forall x \in X$

2) $\sum_{-q < i < p, i \neq 0} fm(h_i c) = fm(c)$

3) $\sum_{-q < i < p, i \neq 0} fm(h_i x) = fm(x)$

4) $fm(x) = fm(h_n h_{n-1} \dots h_1 c) = \mu(h_n)\mu(h_{n-1})\dots\mu(h_1)fm(c)$

5) $\sum_{i=-1}^{-q} \mu(h_i) = \alpha$ and $\sum_{i=1}^{p} \mu(h_i) = \beta$, with $\alpha, \beta > 0$ and $\alpha + \beta = 1$

$fm(h_p c^-)\ fm(h_1 c^-)\ fm(h_{-1} c^-\ fm(h_{-q} c^-)\ fm(h_{-q} c^+\ fm(h_{-1} c^+\ fm(h_1 c^+\ fm(h_p c^+)$
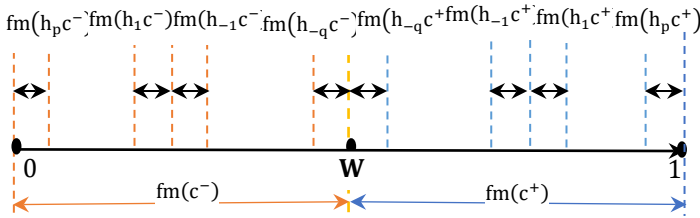
Figure 1: The order of fuzziness measure of elements $x \in X, h_j \in H, c \in G$.

2.3. Particle swarm optimization

PSO is an evolutionary computation algorithm which is introduced by article [33] for searching the global optimum solution. It is developed by work [14] for applying in the forecasting field. Each particle in the swarm represents a potential solution to the global optimization problem. When particles move from this position to other position in q-dimensional space, all particles (i.e, N particles) have fitness values which are estimated according to fitness function. In the moving process of particles. The position of the best particle among all particles found so far is saved and each particle maintains its individual best position which has passed previously. Each individual particle kd ($1 \leq kd \leq N$) is composed of three components: its position $P_{kd} = [p_{kd,1}, p_{kd,2}, \dots, p_{kd,q}]$, the velocity vector $V_{kd} = [v_{kd,1}, v_{kd,2}, \dots, v_{kd,q}]$ and the best position that it has individually found so far $\mathcal{P}_{best,kd} = [\mathcal{P}_{kd,1}, \mathcal{P}_{kd,2}, \dots, \mathcal{P}_{kd,q}]$. Then the best position global $G_{best} = \min(\mathcal{P}_{best,kd}^t)$ found by the overall best out of all the particles in the swarm. The briefly summarizes steps of the standard PSO algorithm in Algorithm 1 as follows:

Algorithm 1: The PSO algorithm

Initialize: learning factors $C_1 = C_2$; ω_{max}, ω_{min}; random positions $P_{kd,i}$; random velocities $V_{kd,i}$ in q-dimensional space (i= 1,2,…,q);
▪ Positions of each kd^{th} (kd = 1,2, …, N) particle's positions are randomly determined:
$$P_{kd} = [p_{kd,1}, p_{kd,2}, \dots, p_{kd,q}]$$

---

where; $p_{kd,i}$ denotes i^{th} position of kd^{th} particle; N is the number of particles in a swarm
▪ Velocities are randomly determined:
$$V_{kd} = [v_{kd,1}, v_{kd,2}, \dots, v_{kd,q}]$$
▪ Let $\mathcal{P}_{best,kd} = P_{kd}$
while *(t ≤ iter)* **do** // iter is maximal iteration number
  for each particle kd in swarm **do**
  ▪ **Calculate** the fitness value of particle kd: $f(x_{kd})$
  ▪ **Update** the personal best position of particle kd
$$\mathcal{P}_{best,kd}^{t+1} = \begin{cases} \mathcal{P}_{best,kd}^{t+1}; & \text{if } f(P_{kd}^{t+1}) > \mathcal{P}_{best,kd}^t \\ f(P_{kd}^{t+1}); & \text{if } f(P_{kd}^{t+1}) \leq \mathcal{P}_{best,kd}^t \end{cases}$$
  End for
  ▪ **Update** the global best position G_{best} according to the fitness value.
  for each particle kd in swarm **do**
  ▪ **Update** the velocity: $V_{kd,i}^{t+1} = \omega^t * V_{kd,i}^t + c_1 * R1() * (\mathcal{P}_{best,kd} - P_{kd,i}^t) + c_2 * R2() * (G_{best} - P_{kd,i}^t)$ (1)
  ▪ **Update** the position: $P_{kd,i}^{t+1} = P_{kd,i}^t + V_{kd,i}^{t+1}$ (2)
  End for
  Update inertia weight ω : $\omega^t = \omega_{max} - \frac{t*(\omega_{max} - \omega_{min})}{iter}$ (3)
End while

3. The FTS Proposed Model Using HA and PSO

The aim of this section is to present a new FTS forecasting model based on the advantage of using PSO to get optimal parameters of HA and optimal intervals in the UoD simultaneously. Firstly, PSO is selected in the proposed model to optimize parameters of HA like fuzziness measure of the hedges and fuzziness measure of primary generator for attaining initial intervals in the UoD. Then, we continue to apply PSO algorithm to readjust the initial interval lengths in fuzzy time series obtained by HA into optimal intervals with view to obtaining the better forecasting accuracy rate. Finally, from these optimal obtained intervals, we produce the forecasting results of model by defining fuzzy sets, fuzzy historical data on each divided interval, determinizing the FLRs, establishing fuzzy relationship groups and calculating the forecasting values from the defuzzification method [31]. The step-by-step of the our model is given as follows.

Step 1: Define UoD of historical time series

Assume that $U = [d_{min} - n_1, d_{max} + n_2]$ is UoD. For defining U, the minimal value d_{min} and the maximal value d_{max} in the time series data is determined; n_1 and n_2 are two proper positive numbers, respectively to let the U cover the noise of the testing data. Then, partition UoD into several adjoining intervals based on optimal parameters of HA obtained by PSO algorithm.

Step 2: Call the proposed algorithm "**Optimizing parameters of HA based on PSO algorithm**" to obtain the initial partition of the intervals. This algorithm is introduced in the next part:

This study uses HA with structure which is presented in Definitions 1 and 2 as $\mathcal{AX} = (X, G, C, H, \leq)$, in which G = $\{c^-, c^+\}$ ={**Low, High**} with **Low** (Lw) ≤ **High** (Hi); C = {**0, w, 1**} a set of constants, with $(0 \leq c^- \leq W \leq c^+ \leq 1)$ and H = {**Little, Very** }. Here, HA is applied as basis to partition data of time series into initial intervals with unequal-size [29] and PSO is used for optimizing the parameters of HA with elements fm(Low)

and μ(little), in which fm(Low) + fm(High) =1 and μ(little) + μ(very) =1. From the optimal parameters obtained, q initial adjoining intervals with different lengths which are defined $u_1 = [d_{min} - n_1, x_1]$, $u_2 = [p_1, p_2]$,…, $u_k = [p_{q-1}, d_{max} + n_2]$, respectively.

Step 3: From on the intervals obtained in Step 2, Call the algorithm "**PSO-based optimal lengths of intervals finding algorithm**" to achieve the unequal intervals with optimal length.

This step applies PSO to adjust the initial intervals which are obtained from HA.

Step 4: From the optimal intervals achieved in Step 3, define the fuzzy sets A_i as follows:

From q intervals, there are q fuzzy sets to represent various intervals on U. Determine the fuzzy sets A_i ($1 \le i \le$ q) as follows:

$$A_1 = \frac{a_{11}}{u_1} + \frac{a_{12}}{u_2} + \cdots + \frac{a_{1q}}{u_q}$$
$$A_1 = \frac{a_{21}}{u_1} + \frac{a_{22}}{u_2} + \cdots + \frac{a_{2q}}{u_q}$$
$$\cdots\cdots\cdots\cdots\cdots\cdots\cdots\cdots$$
$$A_q = \frac{a_{q1}}{u_1} + \frac{a_{q2}}{u_2} + \cdots + \frac{a_{qq}}{u_q}$$

Where, $a_{ij} \in [0,1]$ ($1 \le i \le$ q, $1 \le j \le$ q), u_j is the jth interval of the UoD. The value of a_{ij} denotes the degree of membership of u_j in the fuzzy set A_i which are defined by the triangular membership function with three values 0, 0.5 and 1.

Step 5: Fuzzy the historical time series data into fuzzy sets A_i

Fuzzy time series is generated by converting each historical data into a fuzzy set. If a time series datum depends on interval u_j and the maximal membership value of fuzzy set A_i occurs at u_j, then the historical datum is considered as fuzzy set A_i. In this way, all historical data of time series is fuzzified into A_i.

Step 6: Define all β – order fuzzy logical relations ($\beta \ge 1$).

The fuzzy logical relationship can be construct by two or several consecutive fuzzified values, respectively. To create an β- order FLR, we need to explore any relationship - type as F(t − β), F(t − β + 1),…, F(t − 1) → F(t) , in which F(t − β), F(t − β + 1),…, F(t − 1) and F(t) are called the "current state" and the "next state" of the fuzzy logical relationship, respectively. Then, it has been obtained by replacing the corresponding fuzzy sets A_i.

Step 7: Establish all β - order fuzzy relationship groups (FRGs)

We use fuzzy relationship group [17] to form FRGs in this study. To clarify this, we consider three first - order FLRs at three different times t-2, t-1 and t as follows: $A_i \rightarrow A_j$; $A_i \rightarrow A_k$ and $A_i \rightarrow A_j$, respectively. Suppose that we want to forecast the value of time series data of time t-1, the appearance of the fuzzy sets on the right-hand side of FLRs having the same left - hand side is considered to form into together G1 as $A_i \rightarrow A_j, A_k$. The same way, if forecasting time t, the FLRs which have the same right-hand side are grouped into a group G2 as $A_i \rightarrow A_j, A_k, A_j$.

Step 8: Calculate and defuzzify the forecasted output values

To defuzzify the fuzzified time series data which are based on the established FRGs, we apply two rules which are introduced in papers [31, 14] to calculate the forecasting output values at time t as follows:

Rule 1: Applying for computing output values in the training stage

Our defuzzified principle in article [31] is employed to calculate value based on information of each group. For each group in the training stage, we divide each corresponding interval with regards to the fuzzy sets in the next state of the TV- FRGs into three sub-intervals with equal- length as calculated in (4)

$$\text{Forecasted\_output} = \frac{1}{2*n} \sum_{i=1}^{n} (subm_{ik} + Value\_lu_{ik}) \quad (4)$$

where, n denotes the total number of fuzzy sets on the left-hand side of TV-FRG.

✓ $subm_{ik}$ denotes the medium value of one of three sub-intervals ($1 \le k \le 3$) with regards to i-th fuzzy set in the next state of FRG that the real data at forecasting time falls into this sub-interval.

✓ $Value\_lu_{ik}$ denotes the one of two values belongs to lower or upper bound of one of three sub-intervals which has the real data at forecasting time ranges from L_{ik} to U_{ik} of sub-interval. **If** the real data value at forecasting time minor the mid-point value of sub-interval u_{ik}, then $Value\_lu_{ik}$ is allocated as the lower bound of sub-interval u_{ik} ; **else** $Value\_lu_{ik}$ is allocated as the upper bound of sub-interval u_{ik}

Rule 2: Applying for calculating output value in the testing stage

In the testing stage, prediction value of each group which has the unknown linguistic value on the next state is estimated by the master vote scheme [14]. Assume there a β - order FRG which has type as $A_{t-\beta}$, $A_{t-(\beta+1)}$, $A_{t1} \rightarrow$ #, the prediction value is estimated according to (5) as follows:

$$Forecated\_output = \frac{(M_{t-1}*w_h) + M_{t-2} + \cdots + M_{t-\beta}}{w_h + (\beta - 1)} \quad (5)$$

Where , the symbol w_h is the highest votes predefined by user; is the order of the FLRs; the symbols $M_{t-1}, M_{t-2} \ldots$ and $M_{t-\beta}$ are the medium values corresponding to intervals in accordance to the latest fuzzy set and other fuzzy sets on the current state of FRG having the maximal membership values of $A_{t-1}, A_{t-2}, \ldots,$ and $A_{t-\beta}$ occur at intervals $u_{t1}, u_{t2}, \ldots,$ and $u_{t-\beta}$, respectively.

Step 9: Evaluate the performance of the proposed model

The forecasting performance of the proposed model estimated by two following criterions as: Mean Square Error (MSE) and Mean Absolute Percentage Error (RMSE).

$$\text{MSE} = \frac{1}{n} \sum_{k=\beta}^{n} (F_k - R_k)^2 \quad (6)$$

$$\text{RMSE} = \sqrt{\frac{1}{n} \sum_{k=\beta}^{n} (F_k - R_k)^2} \quad (7)$$

Here, R_k and F_k are the actual and forecasted value at time k, respectively, n is number of observations to be forecasted, β is the order of fuzzy relationship.

In the following, we propose a new approach for optimizing parameters of Hedge Algebras, called "Optimizing parameters of HA based on PSO". This approach is utilized in Step 2 of the proposed model to get the optimal parameters of HA. Details of this approach are shown in Algorithm 2.

Algorithm 2: Optimizing parameters of HA based on PSO algorithm

Step 1: Initialize; Generate P particles in two - dimensional space

- ✓ Assume that the fuzziness interval of "Low" term denotes the first dimension and fuzziness intervals of "Little" hedge denotes the second dimension in the construct HA.
- ✓ Let kd be a particle including two elements $l_{kd,1}$ and $l_{kd,2}$, represented by the position vector $L_{kd} = [l_{kd,1}, l_{kd,2}]$; where $l_{kd,i} \in [0, 1], 0 \leq i \leq 1$ and $l_{kd,1} + l_{kd,2} = 1$. These two elements act as the fuzziness intervals of fm(Low) and μ(Little) of HA, as given in Figure 2(a). The velocity of each particle kd is denoted by the velocity vector $V_{kd} = [v_{kd,1}, v_{kd,2}]$ including two elements $v_{kd,1}$ and $v_{kd,2}$ as shown in Figure 2(b).
- ✓ In th PSO, the initial position vector L_{kd} and the initial velocity V_{kd} of each particle kd are generated randomly in range [0, 1], the personal best position vector $P_{best,kd} = [p_{kd,1}, p_{kd,2}]$ of each particle kd denoting the best position which has the minimum objective value found so far. Initially, the personal best position vector $P_{best,kd}$ of each particle kd like its initial position vector L_{kd}.

$l_{kd,1}$	$l_{kd,2}$

a) Position vector of particle *kd*

$v_{kd,1}$	$v_{kd,2}$

b) Velocity vector of particle *kd*
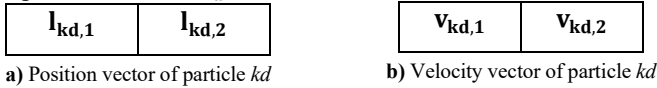
Figure 2: The graphical representation of particle kd

Step 2:   while *(t ≤ iter)* **do** // *iter is a predefined number of iterations*

For each particle *kd* **do** the following steps:

Step 2.1: Calculate the objective value MSE_{kd} of each particle kd, as given by following sub-steps:

Step 2.1.1: Generate q linguistic terms corresponding to q intervals From the position vector $L_{kd} = [l_{kd,1}, l_{kd,2}]$ or two parameters fm(Low) and μ(Little) of HA, divide the U into q intervals as $u_1 = [d_{min} - n_1, p_1]$, $u_2 = [p_1, p_2]$,..., $u_k = [p_{q-1}, d_{max} + n_2]$, respectively.

Step 2.1.2: Based on the obtained intervals, define q fuzzy sets as $A_1, A_2, ..., A_{q-1}$ and A_q

Step 2.1.3: Fuzzy the historical time series data into fuzzy sets A_i

Step 2.1.4: Establish fuzzy relationships based on the fuzzy sets A_i defined and fuzzified data

Step 2.1.5: Establish all TV-FRGs based on FLRs defined

Step 2.1.6: Defuzzify and calculate the forecasting output values

Step 2.1.7: Compute the objective value MSE_{kd} of each particle based on formula (6)

Step 2.2: Update the private best position vector $\mathcal{P}_{best,kd}$ of each particle kd, if $MSE^t(kd) \leq MSE^{t-1}(kd)$; $p_{kd,1} = l_{kd,1}$ and $p_{kd,2} = l_{kd,2}$

Step 2.3: Choose the best particle *Gbest* among all *P* particles, (which has the minimum MSE value), set $P_{Gbest} = [l_{Gbest,1}, l_{Gbest,2}]$ be the position vector of the Gbest

Step 2.4: Update the velocity V_{kd} and the position L_{kd} of each particle k*d* according to (1) and (2), respectively; update ω in (3).

end for
Step 3: **Check the stopping criterion**

If (t < iter), then let **t = t+1** and go to ***Step 2.1 else***, print the results (the position vector $P_{Gbest} = [l_{Gbest,1}, l_{Gbest,2}]$ be the optimal parameters of HA by letting Fm(Low) = $l_{Gbest,1}$ and μ(Little) = $l_{Gbest,2}$)).

end while

To sum up, the flowchart of the proposed algorithm "**Optimizing parameters of HA based on PSO**", which is shown in Figure 3.

Next, we present algorithm **"Finding optimal intervals using PSO"** which has been called in Step 3 of the proposed model to find the best length of each interval with view to getting the better accurate forecasting.

Finding optimal intervals using PSO

In this algorithm, PSO is used to adjust the initial interval lengths which are determined by Algorithm 2. The briefly explanations of this algorithm are given as below: Each particle of PSO in q-dimensional space is used to represent the partitioning of time series data, where q is the number of intervals in the *UoD*. Assume that the lower bound and upper bound of UoD be $p_0 = (d_{min} - n_1)$ and $p_q = (d_{max} + n_2)$, respectively. Each particle represents a vector including q-1 elements as $p_{kd,1}, p_{kd,2}, ..., p_{kd,q-2}$ and $p_{kd,q-1}$, where $(1 \leq i \leq q - 1)$ and $p_{kd,i} \leq p_{kd,i+1}$. From q-1 elements, attain the q adjoining intervals as $u_1 = [p_0, p_{kd,1}], u_2 = [p_{kd,1}, p_{kd,2}], ..., u_q = [p_{kd,q-1}, p_{kd,q}]$, respectively. If particles in a swarm move to from current position to another, the elements of the new vector with regards to position of particles that need to be adjusted in an ascending order $(p_{kd,1} \leq p_{kd,2} \leq \cdots \leq p_{kd,q-1})$. In the training phase, position of each particle is changed by using (1) and (2), and repeated the steps until the repeated value (t) equal to the predefined number of iterations (iter). If (t = iter), then all the FRGs obtained by the (Gbest) among all personal best positions $(\mathcal{P}_{best\_kd})$ of all particles which used to forecast the new data in testing phase and presented in Algorithm 4. Here, the MSE function in (6) is used to represent the forecasting accuracy of each particle in the training stage. The steps of the algorithm **"Finding optimal intervals using PSO"** are shown in **Algorithm 3** as follows:

Algorithm 3: Finding optimal intervals using PSO

Input: Historical time series data
Output: Optimal intervals and the MSE value

Initialize:

- ✓ P particles in q-dimensional space, the maximum iteration (iter)
- ✓ The initial position P_{kd} and the velocity V_{kd} of all particles, respectively. Where, the intervals in position vector is created by the particle 1 be the same as the one which are created from HA as $u_1 = [p_0, p_{1,1}]$, $u_2 = [p_{1,1}, p_{1,2}], ..., $ and $u_q = [p_{1,q-1}, p_{1,q}]$,
- ✓ The initial personal best position vectors of the kd^{th} particle is the same as its initial position vector at the beginning: let $\mathcal{P}_{best,kd} = P_{kd}$

while *(t ≤ iter)* **do** // *iter is maximum iteration number*

    for each particle kd $(1 \leq kd \leq P)$ **do**

- **Calculate** the objective value MSE_{kd}, of each particle kd by performing the steps from Step 4 to Step 8 above, such as: defining fuzzy sets, fuzzify time series data, determining all $\beta -$ order fuzzy relations, establishing all $\beta -$ order TV- FRGs, computing forecasted values
- **Update** $P_{best,kd}$ value of particle kd by the MSE values

$$\mathcal{P}^{t+1}_{best,kd} = \begin{cases} \mathcal{P}^{t+1}_{best,kd}\ ; & \text{if } MSE\left(P^{t+1}_{kd}\right) > \mathcal{P}^{t}_{best,kd} \\ MSE\left(P^{t+1}_{kd}\right)\ ; & \text{if } MSE\left(P^{t+1}_{kd}\right) \le \mathcal{P}^{t}_{best,kd} \end{cases}$$

End for

- **Update** the global best position G_{best} by the MSE value.

for each particle kd $(1 \le kd \le P)$ **do**

- **Update** the velocity: $V^{t+1}_{kd,i} = \omega^t * V^t_{kd,i} + c_1 * R1() * \left(\mathcal{P}_{best,kd} - P^t_{kd,i}\right) + c_2 * R2() * \left(G_{best} - P^t_{kd.i}\right)$
- **Update** the position: $P^{t+1}_{kd.i} = P^t_{kd,i} + V^{t+1}_{kd,i}$

End for

- **Update** inertia weight ω : $\omega^t = \omega_{max} - \frac{t*(\omega_{max}-\omega_{min})}{iter}$

End while

Instance: Explanation of the optimization process of the proposed model using Algorithm 3 on the enrolments data [4] is given as follows: the number of intervals and particles corresponding be (q = 7 and P=4, respectively. From the historical enrolments data, we define the UoD as U = [13000, 20000], where lower bound p_0 =

13000 and upper bound p_7= 20000, respectively. For finding the optimal solution, the parameters in PSO is defined as: the values of $p_{kd,i}$ fall within the range of (13000, 20000], the values of $v_{kd,i}$ fall within the range of [-100, 100], $(1 \le i \le 7, 1 \le kd \le 4)$, the values of C_1 and C_2 be 2, and the ω value ranges from 0.9 to 0.4 and maximum number of iterations be 2, respectively. The positions and velocities of all particles are initialized randomly and listed in Tables 1 and 2, respectively.

Algorithm 4: The forecasting algorithm in the testing stage

The optimal lengths of intervals and order of FLRs obtained in Algorithm 3 that are used to estimate untrained data in the testing stage based on the Principle 2 in the forecasting model.

In Table 1, we have given the 7 intervals for 4 particles which are $u_1 = [p_0, p_1]$, $u_2 = [p_1, p_2]$,..., and $u_7 = [p_6, p_7]$, respectively. Where, the initial position of particle 1 act as the intervals are created as the same the one which are obtained from HA in Algorithm 2 and listed as u_1= [13000, 14470.47), u_2= [14470.47, 15149.8) , u_3= [15149.8, 15829.15), u_4=[15829.15, 16143), u_5= [16143, 16528.14), u_6 = [16528.14, 17361.8), u_7= [17361.8, 20000]. The MSE value of particles is considered according to equation (6). From the corresponding MSE values, every particle records its own personal best positions ($\mathcal{P}_{best}$) so far.
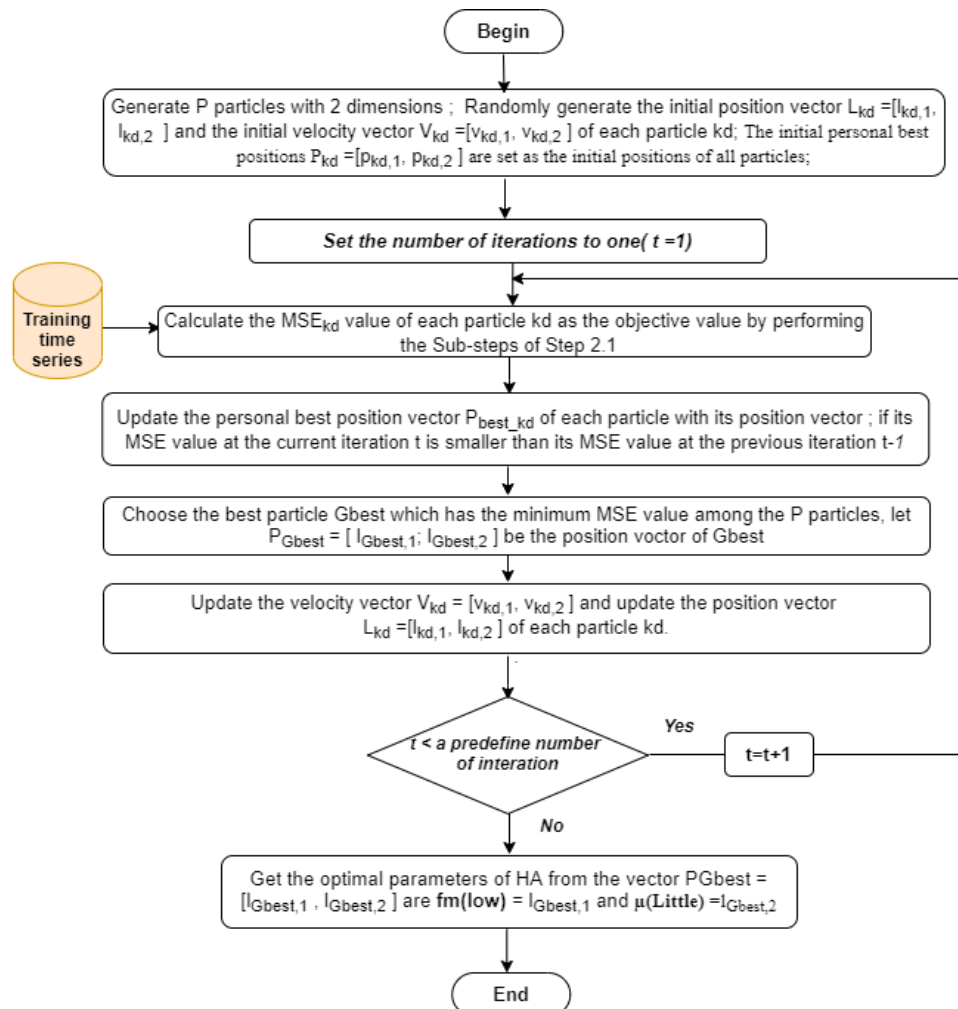
Figure 3: Flow chart of the proposed algorithm "Optimizing parameters of HA based on PSO"

Table 1: The randomized initial positions of all particles

P	p_1	p_2	p_3	p_4	p_5	p_6	MSE
1	14470.47	15149.8	15829.15	16143	16528.14	17361.8	103486.13
2	14188.81	14232.49	15853.02	16448.05	16905.66	18224.27	183494.58
3	13951.02	14390.22	15579.73	16510.86	17408.76	18386.16	145004.74
4	16098.76	17518.15	18332.49	18779.17	18995.24	19826.96	558449.1

Table 2: Randomly generated initial velocities of all particles

P	v_1	v_2	v_3	v_4	v_5	v_6
1	32.16	-60.62	97.31	86.1	-51.3	-26.34
2	-81.93	88.23	-94.65	54.95	-1.92	26.4
3	-56.46	-12.85	33.18	74.45	94.08	-27.5
4	-71.06	-70.14	85.8	-92.89	-56.09	-53.16

Table 3: The initial Pbest of all particles; the Gbest value is created by particle 1.

P	p_1	p_2	p_3	p_4	p_5	p_6	MSE
1	**14470.47**	**15149.8**	**15829.15**	**16143**	**16528.14**	**17361.8**	**103486.13**
2	14188.81	14232.49	15853.02	16448.05	16905.66	18224.27	183494.58
3	13951.02	14390.22	15579.73	16510.86	17408.76	18386.16	145004.74
4	16098.76	17518.15	18332.49	18779.17	18995.24	19826.96	558449.1

Table 4: The second positions of all particles

P	p_1	p_2	p_3	p_4	p_5	p_6	MSE
1	14499.41	15095.24	15916.73	16220.49	16481.97	17338.09	160447.25
2	14288.81	14332.49	15762.27	16348.05	16805.66	18124.27	99566.34
3	14051.02	14490.22	15679.73	16410.86	17308.76	18286.16	135650.18
4	15998.76	17418.15	18232.49	18679.17	18895.24	19726.96	600250.48

Table 5: The second Pbest of all particles; the Gbest value is obtained by particle 2

P	p_1	p_2	p_3	p_4	p_5	p_6	MSE
1	14470.47	15149.8	15829.15	16143	16528.14	17361.8	103486.13
2	**14288.81**	**14332.49**	**15762.27**	**16348.05**	**16805.66**	**18124.27**	**99566.34**
3	14051.02	14490.22	15679.73	16410.86	17308.76	18286.16	135650.18
4	16098.76	17518.15	18332.49	18779.17	18995.24	19826.96	558449.1

Firstly, the $\mathcal{P}_{best}$ values are initialized to the same as the initial position of all particles. Table 3 presents the $\mathcal{P}_{best}$ values of all particles so far and the global best position Gbest = min ($\mathcal{P}_{best}$) which is particle 1. After the first iteration, all particles change its positions based on (1) and (2). The second positions and the corresponding new MSE values of all particles are presented in Table 4.

Comparing the MSE values in Table 3 with the MSE values in Table 4, it can be seen that particle 2 and particle 3 in Table 4 attained a better position than their own $\mathcal{P}_{best}$ values so far. Thus, the two particles are updated in Table 5. The new Gbest is obtained by particle 2, because of the its smallest MSE value. The proposed model is accomplished by repeating the steps in Algorithm 3 until the maximal number of iterations is reached. Finally, the proper lengths of intervals are achieved corresponding to Gbest value that the particle 2 gets so far. These obtained intervals are employed to forecast the final output results.

4. Experiments and analysis

In this paper, our forecasting model has been implemented on two datasets as enrolments data of University of Alabama [3] and number of deaths in car road accidents in Belgium [32]. These two datasets have been applied for forecasting with the huge amount of research works in the literature. Before implementing the proposed forecasting model, two time series datasets are briefly described. Then, the simulated results and analyses related to these datasets are given, respectively. Description of time series data and evaluation of the proposed model are discussed as follows.

4.1. Prepare data for experiments

4.1.1. Time series description

This study, we focus on two time series datasets which are often used to demonstrate validity and performance of the FTS forecasting model. The statistical characteristics of two these time series are expressed as follows.

(a) The enrolments dataset of university of Alabama

This time series data consists of 22 values between 1971 and 1992, see Figure 4(a). This dataset has utilized to examined with the huge amount of reseach works which are presented in the articles [1, 2, 4, 6 - 7, 10 -12, 14, 15, 17, 21 - 24, 29 - 31]. The obtained results among these works are choosed for comparing with our proposed model. Some of results among these studies are considered for comparing with that of the proposed model in this paper. The UoD of enrolments time series is determined as U = [$d_{min} - n_1$, $d_{max} + n_2$] = [13000, 20000].

(a) Real data of enrolments time series

(b) Real data of car road accidents time series
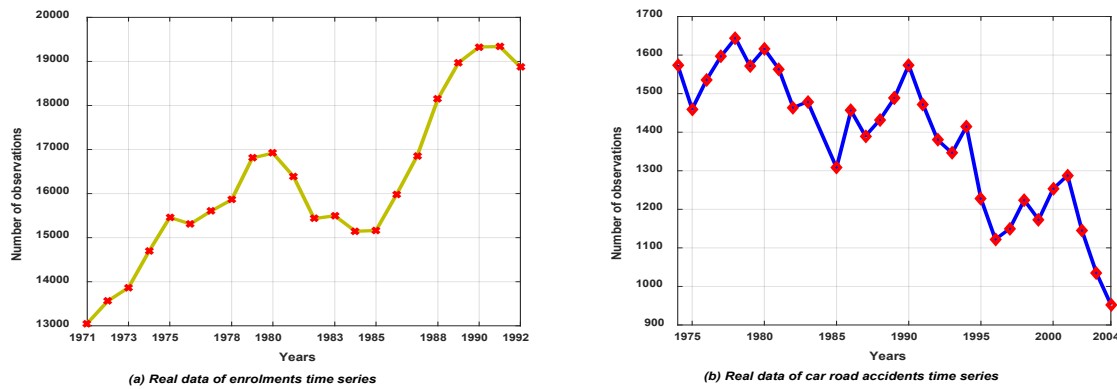
Figure 4: Plots of the amplitude of time series used in experiments

In which, the minimal value and the maximal are $d_{min}=13055$ and $d_{max}=19337$, respectively, and two proper positive values n_1 and n_2 are set as 55 and 663, respectively

(b) The dataset of car road accidents in Belgium

There are 31 observations about the car road accidents ranges from 1974 to 2004 that taken from National Institute of Statistics, Belgium. Figure 4(b) depicts the yearly deaths in car road accidents in Belgium. This time series data is investigated in the research works [6, 32, 40 - 42]. The obtained results from these works have been also selected to compare with our proposed model. In this time series, the minimal value and the maximal are $d_{min}= 953$ and $d_{max}=1644$, and two proper positive values n_1 and n_2 are set as 3 and 6, respectively. Therefore, the UoD can be defined as $U = [d_{min} - n_1, \ d_{max} + n_2] = [950, 1650]$.

Table 6: The parameters of PSO are applied to the enrolments data and car road accidents data

The parameters in PSO	Enrolments	Car road accidents
The number of particles N	50	50
The max number of iterations *iter*	150	150
The inertial weight ω is decreased by	ω_{max}= 0.9 to ω_{min} = 0.4	ω_{max}= 0.9 to ω_{min} = 0.4
The coefficient C1 = C2	2	2
The positions P in search space	[13000, 20000]	[950, 1650]
The velocities V in search space	[-100, 100]	[-100, 100]
Number of intervals q	Defined by HA	Defined by HA
The number of particles N	50	50

4.1.2. Setup parameters for experiments

For implementing the experiments, we use C# programming tool on an Intel Core i7 PC with 8GB RAM. From parameters of each time series data in Table 6, our forecasting model is tested 30 independent runs on each of dataset with various number of orders and intervals to make forecasting results. Then, the best result of among testing runs is recorded to compare with most well-known models in the same dataset with regards to MSE (6) and RMSE (7) functions. The selected parameters of the PSO are used in

experiments for receiving optimal intervals and final forecasting results are placed in Table 6.

4.2. Application of forecasting and comparing results

In this section, we give out results of two experiments with regards to real-world time series datasets which are described in Section 4.1. Then, comparison of results between the proposed model and well-known FTS models in the literature are also presented.

4.2.1. Applying for Experiment 1

Case (1): Forecasted results obtained by the first – order FTS

The forecasting results obtained from this experiment are compared with the ones of the current models [34-37, 27, 29] under the same number of intervals equal to 7. A comparison with regards to RMSE value between the proposed model and the different forecasting models are given in Table 7. Considering the Table 7, the results show that the proposed model has the smallest forecasting errors with regards to RMSE value equal to 188.8 among all its counterparts. There are significant differences between the proposed model and the compared models above. It is the way which determining of the fuzzy relationship group and method of partitioning the UoD are applied in the forecasting model. Three models in works [34-36] are constructed according to the framework [3] to forecast different problems and apply information granules for partitioning, respectively, whereas the proposed model uses hedge algebras for determining unequal-sized interval lengths. Comparing with two models in articles [27, 29]. These models apply the fuzzy relation groups [3] to structure the forecasting model, in which the proposed model uses the fuzzy relation groups that we have proposed in article [17] to build the forecasting model. Comparing the model [37], the proposed model employs the HA combining with PSO to select the optimal intervals, whereas the model [37] applies the maximum spanning tree based fuzzy clustering for dividing intervals with different lengths in the intuitionistic FTS model. In addition, the proposed model is also given to compare with other models which are presented in [6, 11, 14, 15, 17, 36, 38] under the number of intervals of 14. The forecasting results and MSE values between our model and other models are given in Table 8. Table 8 shows that our model has capable of more accurate forecasting and obtains the MSE value 5938.8 which is the smallest among all the existing models.

Table 7: Comparative results of proposed model with the current models based on first – order FTS under seven intervals

Year	Real data	[34]	[35]	[36]	[27]	[37]	[29]	Proposed model
1972	13563	13486	13944	14279	13820	13500	13865	13703.74
1973	13867	14156	13944	14279	13820	14155	14082	13844.48
1974	14696	15215	19344	14297	13820	14155	14514	14155.49
1975	15460	15906	15328	15392	15402	15539	15391	15485.7
---	---	---	---	---	---	---	---	---
1990	19328	18808	18933	19257	19135	18780	19165	19260
1991	19337	18808	18933	19257	19135	19575	19165	19321.7
1992	18876	18808	18933	19257	19135	18855	15219	19167.5
RMSE		578.3	506	445.2	441.3	350.9	210.9	188.8

Table 8: Comparative results of the proposed model with the current models based on first – order FTS with number of intervals of 14

Year	Real data	[38]	[6]	[11]	[14]	[15]	[17]	[36]	Proposed model
1971	13055								
1972	13563	14436.5	13653	13714	13555	13579	13434	13512	13605.8
1973	13867	14000	13653	13714	13994	13812	13841	13998	13753.55
----	----	----	----	----	----	----	----	-----	----
1991	19337	19500	19059	19149	19340	19260	19340	19666	19292.14
1992	18876	19500	19059	19014	19014	19031	18820	18718	19043.13
MSE		297788	31684	35324	22965	8224	7475	14534	5938. 8

Case (2): *Forecasting results obtained by the high – order FTS*

In this case, all historical enrolments dataset [4] covering a period from year 1971 to 1992 are separated into two parts. The first part including 19 observations between 1971 and 1989 is used for training and the second part consists of 3 observations is utilized for testing. The forecasting performance of our model and the compared models are evaluated using the MSE and RMSE function.

a) The obtained results in the training stage

To authenticate the superiority of our prediction model based on the different high - order FLRs, the research works [7, 12, 14, 15, 17] are cited for comparing. The comparative results for all forecasting models under the number of intervals equal to 7 are shown in Table 9. From Table 9 shows that the proposed model outperforms in term of forecasting accuracy the other existing models under different high-order fuzzy relationships at all. In particularly, our model has the smallest average MSE value of 1608.26 among all of compared models. Among all fuzzy relationships is done in the model, the proposed model obtains the lowest MSE value equal to 111.6 by 6th- order fuzzy relationships. The major difference between our model and the compared models is approach of forming FRGs and optimization method they used. In optimization method, the model [12] performs genetic algorithm but the models in articles [14, 15, 17] and the proposed model proceed the PSO algorithm to achieve the best intervals, respectively. Also using PSO to find suitable intervals, our model incorporates HA to partition the different initial intervals of the UoD instead of equal length intervals. In the determining of FRGs, our model is constructed from model [17], the remaining models in articles [7, 12, 14, 15] are created from structure [3]. From the above analysis, it is clearly seen that our model provides more convincing forecasted results when compared to five models considered above.

In addition, our proposed model has been also applied to compare with other existing models based on the different high–order FTS under number of intervals equal to 14. These compared models which are presented in papers [7, 39,12, 14, 15]. The comparative results of the proposed model with its counterparts are placed in Table 10. Comparing model [39] with the proposed model, the proposed model provides the better MSE value. In addition, comparing the forecasting model in article [7] and the proposed model, both of them use the 5th-order fuzzy relationship but our model is much more superior in term of forecasting accuracy. When compared with remaining forecasting models in articles [12, 14, 15]. Although these modes use the fuzzy logical relationship with number of orders is larger, but the results obtained from our model are also better than the existing competing models. In particular, from Table 10, our model obtains the forecasting error MSE of **16.9** which is the lowest among five compared models above. This can conclude that the proposed model not only provides superior forecasting results but also shows the best stability based on the various high-order FLRs, for all cases. To be clearly imagined, Figure 5 describes the trend in term of forecasting accuracy between our model and the previous models for different orders. Viewing these curves, it is clearly seen that forecasting accuracy of our model is more accurate than those of compared models under dissimilar high-order FLRs at all. To sum up, the comparisons above is enough to demonstrate the effectiveness of our model which outpace the previous models based on high - order model with unlike number of intervals in the forecasting the enrolments of University of Alabama.

Table 9: The results of the our model and the compared models with 7 intervals

Orders	[7]	[12]	[14]	[15]	[17]	Proposed model
2	89093	67834	67123	19594	19868	10824.85
3	86694	31123	31644	31189	31307	533.2
4	89376	32009	23271	20155	23288	441.36
5	94539	24984	23534	20366	23552	289.6
6	98215	26980	23671	22276	23684	111.6
7	104056	26969	20651	18482	20669	143.46
8	102179	22387	17106	14778	17116	251.6
9	102789	18734	17971	15251	17987	270.4
Average MSE	95867.63	31377.5	28121.38	20261.38	22183	1608.26

Table 10: The obtained results of our model and the compared models with 14 intervals

Years	Real data	[7]	[39]	[12]	[14]	[15]	Proposed model
1971	13055						
1972	13563						
1973	13867		14934.5				
1974	14696		15590				
1975	15460		15422.9				
1976	15311	15500	15603				15311.38
1977	15603	15500	15861				15605.19
1978	15861	15500	16807				15856.73
1979	16807	16500	16919	16846			16808.78
1980	16919	16500	16388	16846	16890	16920	16917.96
1981	16388	16500	15553.9	16420	16395	16388	16386.01
---	---	---	---	---	---	---	---
1991	19337	19500	18876	19334	19337	19335	19332.48
1992	18876	18500	14934.5	18910	18882	18882	18875.09
MSE		86694	53084	1101	234	173	16.9
RMSE		294.44	230.4	33.18	15.3	13.15	4.11
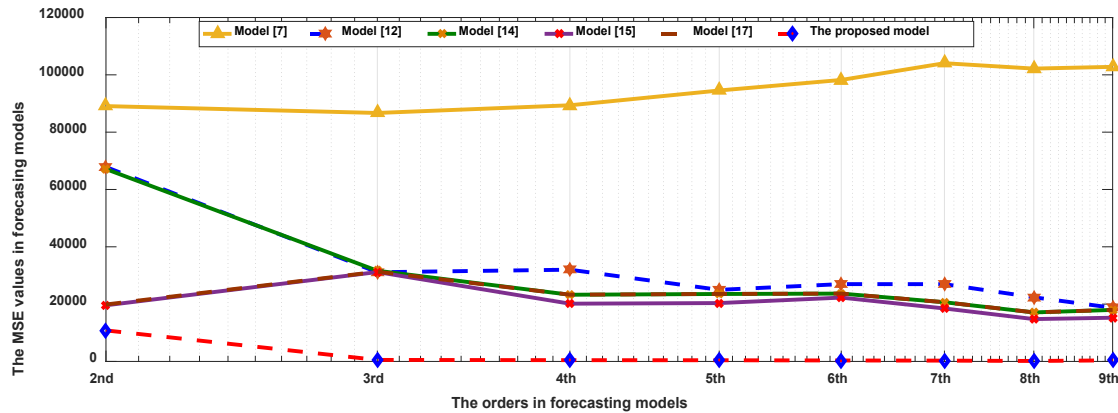
Figure 5: The curves of the MSE values between the our model and the compared models

b) *The obtained results in the testing stage*

From enrolments time series from 1971 to 1992, to forecast the new enrolments for the next year with one head - step. Can be explained through the examples as below: the historical data of enrolments from year 1971 to 1989, is utilized to forecast the new enrolment of year 1990. In the same way, the enrolments data between 1971 and 1990 are used to forecast data of year 1991. Thereafter the enrolments data have been well trained by our model, the future enrolments values could be accomplished to compare to the future ones of the forecasting models proposed in articles [4, 11, 14, 39]. A comparative forecasting results produced by the 3rd - order FTS with different number of intervals and the highest vote W_h=15 [14] which are shown in Table 11 and 12. From these Tables show that our model obtains the smallest RMSEs value equal to 99.2 and 60.28 among five competing models, respectively.

Table 11: Comparative results of our model with other models under the number of intervals of 7 and which use vote W_h=15

Year	Real data	[3]	[11]	[14]	ATVF-KM [39]]	ATVF-PSO [39]	Proposed model
1990	19328	18168	18059	18326	19525	19226	19246.4
1991	19337	18909	18669	19212	19150	19182	19267.5
1992	18876	19609	19083	19203	18933	18876	19010.2
RMSE		**773.66**	**576.66**	**484.16**	**160.43**	**107.29**	**99.2**

Table 12: Comparative results of our model with other models under the number of intervals of 14 and which use vote W_h=15

Year	Real data	[3]	[11]	[14]	ATVF-KM [39]	ATVF-PSO [39]	Proposed model
1990	19328	18162	17862	18120	19287	19238	19278.3
1991	19337	18721	18633	19027	18811	19224	19363.2
1992	18876	19221	19085	19137	18836	19224	18964
RMSE		**709**	**653.66**	**621.91**	**305.7**	**92.35**	**60.28**

Table 13: The obtained results between our model and the competing models using the different number of intervals and various orders

Year	Real data	[40]	[41]	[42]	[32]	[6]	Proposed model	
							1st - order	3rd - order
1974	1574	----	---	----	----	----	----	----
1975	1460	1497	----	1458	----	1506	1463.02	----
1976	1536	1497	----	1467	----	1553	1529.42	----
1977	1597	1497	1497	1606	1594	1598	1593.24	1596.94
1978	1644	1497	1497	1592	1643	1584	1643.7	1645.18
---	----	----	----	----	----	----	----	----
2002	1145	1095	1098	1114	1146	1143	1137.48	1143.68
2003	1035	995	97 10	1097	1036	970	1087.35	1034.44
2004	953	995 9	7 929	929	954	970	958.54	951.95
MSE		**83.12**	**46.78**	**37.66**	**19.2**	**41.61**	**29.4**	**0.85**

4.2.2. Applying for Experiment 2

In this section, our proposed model have been implemented for forecasting the car road accidents in Belgium [32] ranges period from 1974 to 2004. We also test 30 times and take the best forecasting result to compare with the results from the other five forecasting models in articles [40 - 42, 32, 6]. The comparative results based on the different number of intervals and the various orders of FTS are shown in Table 13. Comparing between models [40, 6] and our proposed model, our model achieves the far better MSE value of 29.4 in two compared models based on the first - order FTS with different number of intervals. Also, from Table 13, we can be seen that, comparing model [41] and model [32], our proposed model produces the far smaller MSE value of 0.85 in two considered competing models using the 3rd - order FTS with different number of intervals. To summarize, the our model provides better forecasting results and higher accuracy than the models in [40 – 42, 32, 6] corresponding to the number of orders of FTS and number of intervals equal to 14 as shown in Table 13.

5. Conclusions and upcoming work

In this paper, a novel model for predicting enrolments and car road accident is developed. To remedy the downside of the conventional FTS model, the FTS proposed model combines hedge algebras and PSO is developed to resolve two issues which are considered to be important and greatly affect the forecasting accuracy is that the length of intervals and fuzzy relationship group. By utilizing the concept of time variant fuzzy relationship group, the proposed model has handled the more persuasive historical data and has been demonstrated to be more appropriate for real-world applications. In addition to that the parameters of HA are modified by PSO algorithm to get the initial intervals partitioning of the UoD. In data mining and finding of optimal solution, PSO is considered to accomplish better compared to other heuristic techniques with regards to success rate and solution quality. Furthermore, the forecasting efficiency of the proposed model is significantly improved in adjusting the lengths of intervals. The forecasting performance of the proposed model is demonstrated by forecasting the enrolments at University of Alabama and the car road accidents in Belgium. Details of the comparison in Tables 7-13 indicate that the proposed model achieves the lowest forecasting errors when compared with other forecasting models., for many cases. Also, from Figure 5, it can be observed that the amount of error rate in terms of MSE obtained by our high - order FTS model are smaller than all other models considered in this research. Even though our model shows that the greater forecasting capability when compared with some of recent ones based on the high-order FLRs. Determining of the high-order FLR spends a lot of computational time than first-order FLR. Therefore, development of new approaches that can automatically select out the optimal degree of the high-order FLRs is a worthy idea in FTS forecasting model. Those will be the work closely related to this research in the coming time.

Acknowledgment

References

[1] Q. Song, B.S. Chissom, "Fuzzy time series and its models", Fuzzy Sets and Systems, **54**(3), 269-277, 1993a, DOI: 10.1016/0165-0114(93)90372-O.

[2] Q. Song, B.S. Chissom, "Forecasting Enrollments with Fuzzy Time Series – Part I," Fuzzy set and systems, **54**(1), 1-9, 1993b, DOI: 10.1016/0165-0114(93)90355-L.

[3] L.A. Zadeh, "Fuzzy sets", Information systems, 8, 338–353, 1965, DOI: 10.1016/S0019-9958(65)90241-X.

[4] S.M. Chen, "Forecasting Enrollments based on Fuzzy Time Series," Fuzzy set and systems, **81**, 311-319, 1996, DOI: 10.1016/0165-0114(95)00220-0.

[5] H.K. Yu "Weighted fuzzy time series models for TAIEX forecasting ", Physica A, **349**, 609–624, 2005.

[6] V.R. Uslu, E. Bas, U.Yolcu, E. Egrioglu, "A fuzzy time series approach based on weights determined by the number of recurrences of fuzzy relations", Swarm and Evolutionary Computation, **15**, 19-26, DOI: 10.1016/j.swevo.2013.10.004, 2014.

[7] S. M. Chen, "Forecasting Enrollments based on hight-order Fuzzy Time Series", Int. Journal: Cybernetic and Systems, **33**(1), 1-16, 2002, DOI: 10.1080/019697202753306479.

[8] K. Huarng, "Effective lengths of intervals to improve forecasting in fuzzy time series". Fuzzy Sets and Systems, **123** (3), 387–394, 2001b, DOI: 10.1016/S0165-0114(00)00057-9

[9] L. W. Lee, L. H. Wang, S. M. Chen, Y.H. Leu, "Handling forecasting problems based on two-factors high-order fuzzy time series". IEEE Transactions on Fuzzy Systems, **14**, 468–477, 2006. DOI: 10.1109/TFUZZ.2006.876367

[10] S.M. Chen, K Tanuwijaya "Fuzzy forecasting based on high- order fuzzy logical relationships and automatic clustering techniques", Expert Systems with Applications, **38**, 15425–15437, 2011. Doi: 10.1016/j.eswa.2011.06.019

[11] S.M. Chen, N.-Y. Chung, "Forecasting enrollments of students by using fuzzy time series and genetic algorithms", International Journal of Information and Management Sciences, **17**, 1–17, 2006a.

[12] S.M. Chen, N.-Y. Chung, "Forecasting enrollments using high-order fuzzy time series and genetic algorithms", International of Intelligent Systems, **21**, 485–501, 2006b. doi: 10.1002/int.20145

[13] L.-W. Lee, L.-H. Wang, S.M. Chen, "Temperature prediction and TAIFEX forecasting based on high order fuzzy logical relationship and genetic simulated annealing techniques," Expert Systems with Applications, **34**, 328–336, 2008. Doi: 10.1016/j.eswa.2006.09.007

[14] I. H. Kuo, S. J. Horng, T.W. Kao, T.L, C.L. Lee, Y. Pan, "An improved method for forecasting enrollments based on fuzzy time series and particle swarm optimization", Expert systems with applications, **36**, 6108–6117, 2009, DOI: 10.1016/j.eswa.2008.07.043.

[15] Y.L. Huang, S. J. Horng, M. He, P. Fan, T.W. Kao, M.K. Khan, J.L. Lai, I. H.Kuo, "A hybrid forecasting model for enrollments based on aggregated fuzzy time series and particle swarm optimization". Expert Systems with Applications, **38**, 8014–8023, 2011. Doi: 10.1016/j.eswa.2006.09.007

[16] L.Y. Hsu, S.J. Horng, T.W. Kao, Y.H. Chen, R.S. Run, R.J. Chen, J.L. Lai, I. H.Kuo, "Temperature prediction and TAIFEX forecasting based on fuzzy relationships and MTPSO techniques", Expert Syst. Appl., **37**, 2756–2770, 2010.

[17] N.C. Dieu, N.V. Tinh, "Fuzzy time series forecasting based on time-depending fuzzy relationship groups and particle swarm optimization", In: Proceedings of the 9th National conference on Fundamental and Applied Information Technology Research (FAIR'9), Can Tho, Vietnam, 125-133, 2016, doi: 10.15625/vap. 2016.00016.

[18] J.I.Park, D.J. Lee, C.K.Song., M.G. Chun, "TAIFEX and KOSPI 200 forecasting based on two-factors high-order fuzzy time series and particle swarm optimization", Expert Systems with Applications, **37**, 959–967, 2010.

[19] S.M. Chen, H.P. Bui Dang, "Fuzzy time series forecasting based on optimal partitions of intervals and optimal weighting vectors", Knowledge-Based Systems, **118**, 204–216, 2017. Doi: 10.1016/j.knosys.2016.11.019

[20] S.M. Chen, W.S. Jian, "Fuzzy forecasting based on two-factors second-order fuzzy-trend logical relationship groups, similarity measures and PSO techniques", Information Sciences, 391–392, 65–79, 2017.

[21] M. Bose, K. Mali, "A novel data partitioning and rule selection technique for modelling high-order fuzzy time series", Applied Soft Computing, **17**, 1-15, https://doi.org/10.1016/j.asoc.2017.11.011, 2017.

[22] Z.H. Tian, P. Wang, T.Y. He, "Fuzzy time series based on K-means and particle swarm optimization algorithm", Man-Machine-Environment System Engineering. Lecture Note in Electrical Engineering. 406, 181-189, Springer 2016.

[23] Z. Zhang, Q. Zhu. "Fuzzy time series forecasting based on k-means clustering", Open Journal of Applied Sciences, **2**, 100-103, 2012.

[24] N.V. Tinh, N.C. Dieu, "Improving the forecasted accuracy of model based on fuzzy time series and k-means clustering", journal of science and technology: issue on information and communications technology, **3**(2), 51-60, 2017.

[25] E.Bulut, O. Duru, S.Yoshida, "A fuzzy time series forecasting model formulti-variate forecasting analysis with fuzzy c-means clustering", WorldAcademy of Science, Engineering and Technology, **63**, 765–771, 2012.

[26] S. Askari, N. Montazerin, "A high-order multi-variable Fuzzy Time Series forecasting algorithm based on fuzzy clustering", Expert Systems with Applications, **42**, 2121–2135, 2015.

[27] N.C. Ho, N.C. Dieu, V.N. Lan. "The application of hedge algebras in fuzzy time series forecasting", Journal of science and technology, **54**(2), 161-177, 2016.

[28] N.C. Ho., W. Wechler,"Hedge algebra: An algebraic approach to structures of sets of linguistic truth values", fuzzy Sets and Systems, **35**, 281-293, 1990.

[29] H.Tung, N.D. Thuan, V.M. Loc, "The partitioning method based on hedge algebras for fuzzy time series forecasting", Journal of Science and Technology, **54** (5), 571-583, 2016.

[30] N.D. Hieu , N.C. Ho, V.N. Lan, "Enrollment forecasting based on linguistic time series", Journal of Computer Science and Cybernetics, **36**(2), 119-137, 2020.

[31] N.V. Tinh, "Enhanced Forecasting Accuracy of Fuzzy Time Series Model Based on Combined Fuzzy C-Mean Clustering with Particle Swam Optimization", International Journal of Computational Intelligence and Applications, **19**(2), 1-26, 2020.

[32] S M. Yusuf, M.B. Mu'azu, O. Akinsanmi, " A Novel Hybrid fuzzy time series Approach with Applications to Enrollments and Car Road Accident", International Journal of Computer Applications, 1**29**(2):37 – 44, 2015.

[33] J. Kennedy, R. Eberhart, "Particle swarm optimization", Proceedings of IEEE international Conference on Neural Network, 1942–1948, 1995.

[34] L.Wang, X. Liu, W. Pedrycz. "Effective intervals determined by information granules to improve forecasting in fuzzy time series". Expert Systems withApplications, **40**, pp.5673–5679, 2013.

[35] L. Wang, X. Liu, W. Pedrycz, Y. Shao, "Determination of temporal information granules to improve forecasting in fuzzy time series". Expert Systems with Applications, **41**(6), 3134–3142, 2014, DOI: 10.1016/j.eswa.2013.10.046.

[36] W. Lu, X. Chen, W. Pedrycz, X. Liu, J. Yang, "Using interval information granules to improve forecasting in fuzzy time series". International Journal of Approximate Reasoning, 57, 1–18, 2015.

[37] Y. Wang, Y. Lei, X. Fan, Y. Wang, "Intuitionistic Fuzzy Time Series Forecasting Model Based on Intuitionistic Fuzzy Reasoning", **2016**, Article ID 5035160 , pp 1-12, 2016, DOI: 10.1155/2016/5035160.

[38] Abhishekh, S. S. Gautam, S. R. Singh, "A refined weighted method for forecasting based on type 2 fuzzy time series", International Journal of Modelling and Simulation, **38**(3), 180-188, 2018, doi.org/10.1080/02286203.2017.1408948.

[39] K. Khiabani, S.R. Aghabozorgi, "Adaptive Time-Variant Model Optimization for Fuzzy-Time-Series Forecasting", IAENG International Journal of Computer Science, **42**(2), 1-10, 2015. Doi: 10.1016/j.knofgsys.2016.11.019

[40] T A. Jilani, S. M .Burney., C. Ardil, "Multivariate high order FTS forecasting for car road accident", World Acad Sci Eng Technol, **25**, 288 - 293, 2008.

[41] Jilani T A, Burney S M A. Multivariate stochastic fuzzy forecasting models". Expert Syst Appl, **353**, 691–700, 2008

[42] E. Bas, V. Uslu. , U.Yolcu, E. Egrioglu, "A modified genetic algorithm for forecasting fuzzy time series", Springer, Appl Intell, **41**, 453-463, 2014.

ASTES

Robust Adaptive Feedforward Sliding Mode Current Controller for Fast-Scale Dynamics of Switching Multicellular Power Converter

Rihab Hamdi[*,1], Amel Hadri Hamida[1], Ouafae Bennis[2], Fatima Babaa[3]

[1]LMSE Laboratory, Electrical Engineering Department, Biskra University, Biskra, 07000, Algeria

[2]PRISME Institute, University of Orléans, 21 rue Loigny La Bataille, Chartres Orléans, 28000, France

[3]LEC Laboratory, Electrical Engineering Department, Constantine1 University, Constantine, 49042, Algeria

A R T I C L E I N F O	A B S T R A C T
	Higher efficiency and lower losses are widely considered as the best metrics to optimize, in a high-power converter performance context. To provide a solution to the ever-increase of high switching frequencies challenges, we must explore soft-switching technologies to resolve interface issues and reduce the switching losses. This manuscript describes a comparative analysis between the fixed-bandwidth (FBW) and the variable-bandwidth (VBW) of the hysteresis modulation (HM) based on the conventional sliding mode (CSM) strategy. The two adopted techniques are applied to a bidirectional multichannel DC-DC asynchronous Buck converter. The cells are parallel-connected and operating in continuous conduction mode (CCM). The objective is to have a system that is more stable, more efficient and able to cope with variations in input voltage, load and desired output voltage. That requires, first, to attenuate the non-linearity phenomenon of the conventional sliding mode by placing a hysteresis modulation. Then, after applying this technique, we confronted the dilemma of the variable switching frequency. Our hypothesis was to incorporate a variable bandwidth of the hysteresis modulation. The results obtained under parametric variation clearly show the areas where significant differences have been found between the two approaches. Likewise, they both share several key features. Simulation studies in the MATLAB® / Simulink™ environment are performed to analyze system performance and assess its robustness and stability.

1. Introduction

DC-DC converters, with many different topologies, represent a hotspot in modern technology and have revolutionized switching control. Although the characteristics of power electronics, in terms of nominal voltage and current values, continue to improve, the range of applications continues to expand in several areas including energy storage, automation, transport, high power industrial drives and transmission / distribution of electrical energy [1], [2]. Whereas the needs for higher efficiency, reliability, modularity in high electronics power, multicellular converters are on the rise. Studies [3–6] based on a parallel multiphase topology have shown that the latter provides better performance, lower losses, reduced cost, and fast dynamic responses. Parallel-connected multi-cell DC-DC converters have an important role in

several applications such as inverters, powertrain systems and equipment of the power factor correction and they have countless advantages, the major one is to enhance performances such as energy efficiency and high capacity [7–11]. One approach dedicated to small converters is to run them at a higher switching frequency, this will reduce the size of reactive components (inductors and capacitors) and it contributes to the improvement of the output voltage's quality of the converter. High losses in the IGBT switches remains the major limitation of the high frequencies, which reduces efficiency. Significant information and in-depth investigations in the same framework can be found in these studies [12–18].

Higher efficiency and more stringent control features of power electronics become very attractive. Nonlinear Sliding mode controllers applied to parallel multi-cell converters combine control concepts with multiple sliding surfaces and integral

*Corresponding Author Rihab Hamdi, Email: rihab.hamdi2012@gmail.com

variable structure. They are easy to design, robust and shows good transient and stable performances. Furthermore, they restrict the switching frequency variation, mitigate the undesired transient response and achieve a good compromise between transient and stationary performances. Hence, there are two ways of control involved for multicellular converters. The first consists in controlling the multi-commutations with phase shifting from one another, one therefore speaks of interleaving. The second is to apply the same control signal simultaneously to the multi-switchings, it is therefore synchronicity. The controllers developed for paralleled multiphase converters take into consideration most of the characteristics mentioned above [19]. To date, several researchers have reported that these control schemes have many desirable features: easy-designed because each sliding surface is independently controlled, smooth transient responses tested under parametric variations, eliminate the problem of chattering, the impact of high switching frequencies is managed by the integrators. All these promising results have been experimentally proven on a closed loop system. Previous studies proposed to use the extended linearization method for the design of the sliding mode controller, and then improving robustness using the combined controllers. Thus, they developed a procedure to choose the high-pass filter parameters of the sliding mode-controlled converters. In addition, they presented derivatives of sliding mode control, including the direct /indirect sliding mode, the integral sliding mode, the proportional sliding mode and the high order sliding mode [20–28]. As far, sliding mode control has been widely studied and has proven to be a future solution for generations of power converters, yet, it suffers from the problem of high frequency oscillation (chattering) due to the practical limitations of system components and the problem of switching frequency variation by applying the traditional sliding mode.

This leads us to propose an implementation of the sliding mode controller by hysteresis function. The implementation is easy to reproduce and does not require additional auxiliary circuits or complex calculations. The introduction of a hysteresis band as the limit conditions of the sliding mode, delays the period of states exchange and gives a sign to control the switching frequency of the system, and therefore, the trajectory of the system variates in close proximity to the excesses of the band. So, the practical problem of chattering will be solved. Particularly, boundary layer-based control schemes allow multicell converters to operate with a fixed switching frequency [29–35]. This strategy will be fully covered in the rest of our work. The remainder of the paper is organized as demonstrated: In Section II, the adopted system is described and modeled. Section III reviews the control mechanism based on the sliding mode controller. Section IV is devoted to analyze the simulation results and to discuss the effectiveness of the control strategies. The conclusion is reported in Section V.

2. Paralleled Non-Isolated Multi-Cell Converter

The studied three-cell DC-DC buck converter is shown in Figure 1. It consists of a constant DC input voltage source V_{in} connected to three similar modules sharing a resistive load R and a filter capacitor C. Each module is based on an implemented controllable power MOSFETs S, the antiparallel diode D that authorizes the embedded switch to exhibit a bidirectional current conduction property and a filter inductor L. Note that the parallel

switching buck converter operates in continuous conduction mode (CCM). The three cells are identical, in other words, $L_1=L_2=L_3$.
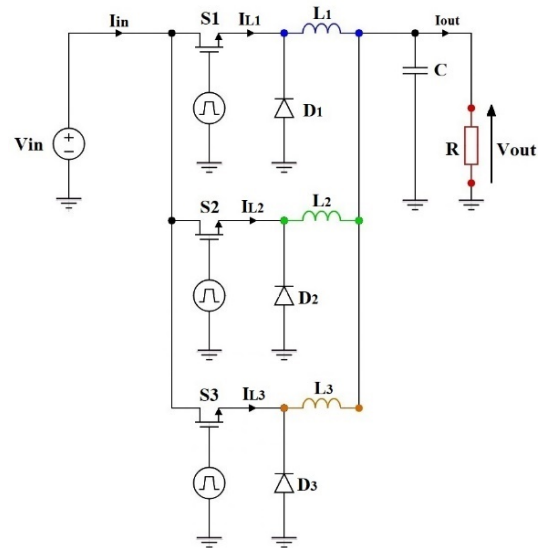
Figure 1: Three-channel Buck converter parallel-associated

The converter can be represented by a system of equations based on a model with mean values, then the system dynamics of the studied converter can be expressed as:

$$L\frac{dI_{Lj}}{dt} = V_{in}D - V_{out} \tag{1}$$

$$C\frac{dv_{out}}{dt} = I_L + \frac{V_{out}}{R} \tag{2}$$

Where I_{Lj} is the current flowing through inductance $j = 1,2,3$, I_L the current at the output of the converter, V_{in} is the input voltage and V_{out} is the output voltage of our converter and V_{ref} is the desired output voltage. The state of space can be expressed as:

$$
\begin{aligned}
x_1 &= V_{ref} - V_{out} \\
x_2 &= \dot{x}_1 = -\frac{dV_{out}}{dt} = \frac{1}{C}\left(\frac{V_{out}}{R} - \int \frac{uV_{in} - V_{out}}{L}dt\right)
\end{aligned}
\tag{3}
$$

This model can be used directly to simulate the converter, in MATLAB / Simulink type environment.

3. Hysteresis Modulation-Based Sliding Mode Controller

We propose two different control schemes, developed in the continuous domain, to stabilize parallel multi-phase standalone converter and compare them. The proposed sliding mode control (SMC) strategy based on hysteresis modulation (HM) automatically compensates for the parametric variations of the converter and the variation of the line impedance, such that it allows the three-cell paralleled converter to share the load and does not require the modules to be interconnected. We illustrate the fixed-bandwidth of the hysteresis modulation technique-based sliding mode control; however, this approach has accentuated the problem of variable switching frequencies that requires a high-bandwidth current sensor. At this point in our work, we are interested in an adaptive and feedforward current control solution to overcome this problem and adapt a variable-bandwidth of the

hysteresis modulation to mitigate the nonlinearity phenomenon in conventional sliding mode control to fix the switching frequency.

Describing the mathematical model of the system in question, operating in CCM, and especially its states of space necessary for the design of the sliding mode voltage control (SMV), the reformed expression of the state of space is:

$$\begin{bmatrix} \dot{x}_1 \\ \dot{x}_2 \end{bmatrix} = \begin{bmatrix} 0 & 1 \\ -\dfrac{1}{LC} & -\dfrac{1}{RC} \end{bmatrix} \begin{bmatrix} x_1 \\ x_2 \end{bmatrix} + \begin{bmatrix} 0 \\ -\dfrac{V_{in}}{LC} \end{bmatrix} u + \begin{bmatrix} 0 \\ \dfrac{V_{ref}}{LC} \end{bmatrix} \quad (4)$$

Employing the sliding mode voltage control (SMVC) and taking into account the state trajectory that includes the control parameters x_1 and x_2, we can determine the switching function u.

$$S = \alpha x_1 + x_2 = Jx \quad (5)$$

$$\begin{cases} J = [\alpha, 1] \\ x = [x_1, x_2]^T \end{cases} \quad (6)$$

That forms the control law:

$$u = \begin{cases} 1 = \text{'ON'} & When\ S > k \\ 0 = \text{'OFF'} & When\ S < k \end{cases} \quad (7)$$

The convergence conditions are the criteria that allow the dynamic errors of the system to converge towards the sliding surface. They are ensured by a judicious choice of the function of LYAPUNOV, which guarantees the attraction of variables to regulate to their references, to build the discontinuous control size and meet the stability criterion:

$$\lim_{S \to 0} S.\dot{S} < 0 \quad (8)$$

Thus, the existence condition for the adopted control strategy is:

$$\dot{S} = \begin{cases} J\dot{x} < 0 & for\ 0 < S < \xi \\ J\dot{x} > 0 & for\ -\xi < S < 0 \end{cases} \quad (9)$$

where ξ is a positive quantity, infinitely small and arbitrarily chosen.

Substituting (3) and (5), we find:

$$S = \frac{1}{R}(V_{ref} - V_{out}) - i_C \quad (10)$$

The sliding coefficient is set as (11) and thus the above equation is valid:

$$\alpha = \frac{1}{RC} \quad (11)$$

We can therefore deduce the conditions of existence:

$$\lambda_1 = (\alpha C - \frac{1}{R})x_2 - \frac{1}{L}x_1 + \frac{V_{ref} - V_i}{L} < 0 \quad (12)$$

$$\lambda_2 = (\alpha C - \frac{1}{R})x_2 - \frac{1}{L}x_1 + \frac{V_{ref}}{L} > 0$$

The bandwidth of the FBW regulator based sliding mode controller has been selected according to the following equation:

$$B_{Fixed-Width} = \frac{(V_{in0} - V_{out})}{2.L.fw} \cdot \left(\frac{V_{out}}{V_{in0}} \right) \quad (13)$$

$$V_{in0} = \frac{3 \cdot V_{in} \cdot \sqrt{6}}{\pi} \quad (14)$$

Hence, we focus on the adaptive feedforward current control technique in continuous conduction mode (CCM). So that, the expression of the current variation ΔI_L, as a function of the input voltage V_{in}, the output voltage V_{out}, the switching frequency fw, and the value of the inductance L, can be shown as:

$$\Delta I_L = \frac{(V_{in} - V_{out})}{L.fw} \cdot \left(\frac{V_{out}}{V_{in}} \right) \quad (15)$$

Still with the aim of ensuring the operation at fixed frequency of the proposed hysteresis modulator, a requirement is imposed, and that the hysteresis bandwidth must satisfy it, is:

$$B_{Variable-Width} = \frac{\Delta I_L}{2} = \frac{(V_{in} - V_{out})}{2.L.fw} \cdot \left(\frac{V_{out}}{V_{in}} \right) \quad (16)$$

The dynamic performance of the two schemes needs to be demonstrated under conditions when some changes are imposed and a feedforward transient occurs. Simulations are performed for various cases of the circuit parameter variations: load changes, input voltage changes and reference voltage changes.

4. Simulation Results and Robustness Assessment

In this part, and to properly study the behavior and performance evaluation of the closed-loop converter and the various control techniques synthesized in the previous section, particularly when modifying the operating conditions, we will simulate the behavior of a 3-cell chopper connected to an R load. A robustness test was carried out to analyze the sensitivity of the strategies and the correctors implemented with regard to possible variations in the parameters of the model. For the parameter's identification of the studied converter, we determine the nominal values of the inductance L and the capacitance C using the conditions below:

➢ The current through the inductance, must be within a reasonable interval, for all the conditions of charge, because our converter is operating in continuous conduction mode.

➢ The maximum ripple of the output voltage should not exceed a small percentage, usually 5% of the output voltage V_{out}.

Taking these conditions into account, the LC filter must obey the conditions of the relationships below, where fw corresponds to the switching frequency and β is the duty cycle.

$$L \geq \frac{V_{in}}{\Delta I_{out,\max} \cdot f_w} \beta (1 - \beta) \quad (17)$$

$$C \geq \frac{(1-\beta)}{8L.f_w^{\,2}}\left(\frac{V_{out}}{\Delta V_{out}}\right) \qquad (18)$$

Table 1 shows the specifications that we adopted of the studied buck converter simulated in the MATLAB® environment.

Table 1: Specifications of The Paralleled Three-Channel Buck Converter

Description	Parameters	Nominal Value
Input voltage	V_{in}	*24 V*
Capacitance	*C*	*60 µF*
Inductance	*L*	*50 mH*
Resistance	*R*	*12 Ω*
Switching frequency	*fw*	*400 kHz*
Desired output voltage	V_{ref}	*12 V*

Figure 2 duplicates the variation of the average switching frequency as a function of the input voltage variation. The VBW HM-based SMC adaptive feedforward control reduces switching frequency variation compared to the FBW HM-based SMC control. This result highlights the major contribution of our work, thanks to the developed strategy, we achieve a significant reduction in the variation of the switching frequency.

Figure 3 and Figure 4 show the output voltage response for the two control strategies used. it seems clear that the system operating with VBW HM-based SMC achieves the best compromise passing from the transient regime to the stationary regime. Thus, its transition response is smoother, more stable, without overshoot and with less chatter, on the other hand, the response of our system under the control of the FBW HM-based SMC is faster but it represents more variation in amplitude of the oscillations, with an overshoot.

It appears clearly from Figure 5 and Figure 6, during an increase/decrease in resistance (50% variation) every 0.2s, that the closed-loop output voltage response reacting with the FBW HM-based SM exhibit an undesired transient drop that lasts a few seconds and disturbs the smoothness of the output voltage followed abruptly by a steady-state. While, in the other case, the system compensates for a transient drop in a soft way. Through the output current simulation results, we can observe that the VBW

HM-based SM goes perfectly with the load changes to even almost assure that there is no transient regime. Figure 7 and Figure 8 point-out the output voltage response and the output load current response for the two controllers when the system undergoes a change in the input supply (V_{in} varied from 24V to 50V) at 0.2s. For the two cases, the chattering increase, however, the output voltage and the output load current vary around the reference values. The zoom in clearly shows an increase in the amplitude of the oscillations accompanied by an upward shift of the output voltage in steady-state regime when the input voltage increases, it comes down to the variation of the switching frequency.

Figure 9, Figure 10, Figure 11 and Figure 12 present the output voltage response and the output load current response for the two controllers when the system undergoes a change in the output reference (V_{ref} varied from 12V to 20V). Switching from one value to another is almost similar, there is no big difference except that the VBW HM-based SM is more precise. The carried-out simulations show extremely encouraging outcomes as far as reference tracking effectiveness and robustness, a quick estimation of the control law permits a quicker dismissal of the unsure load impact. They demonstrate the propriety of sliding mode control for such sort of framework.

The results in terms of stability assessment and performance analysis under system parameters variation are recapitulated in Table 2.
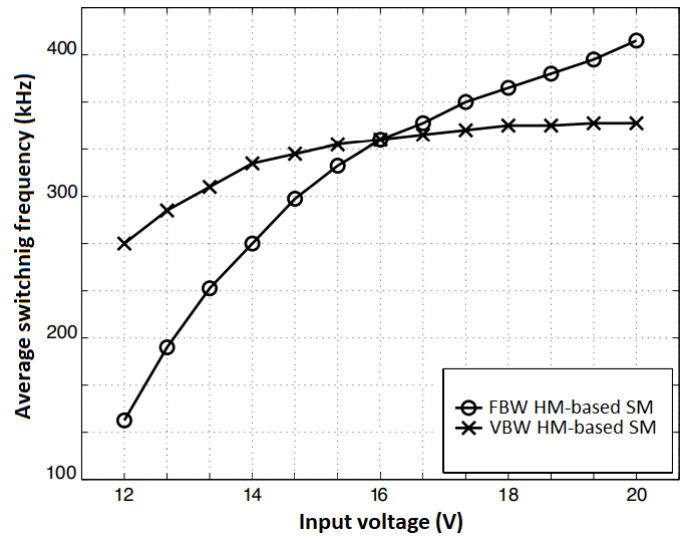
Figure 2: The variation of the average switching frequency as a function of the input voltage variation.

Table 2: Comparative Performances of FBW HM-SMC with VBW HM-SMC

	FBW HM-based SMC	VBW HM-based SMC
Load variation		
Time of compensation	*0.01 s*	*0.015 s*
The drop width	*0.22 V*	*0.13 V*
Amplitude of oscillations	*±0.15 V*	*±0.1 V*
Response time	*0.02 s*	*0.03 s*

Input variation		
Amplitude of oscillations		
For t < 0.2 s	*±0.14 V*	*±0.12 V*
For t > 0.2 s	*+0.3 V*	*±0.12 V*
	-0.15 V	
Reference variation		
Time of transition	*0.015 s*	*0.03 s*
Amplitude of oscillations	*±0.14 V*	*±0.12 V*
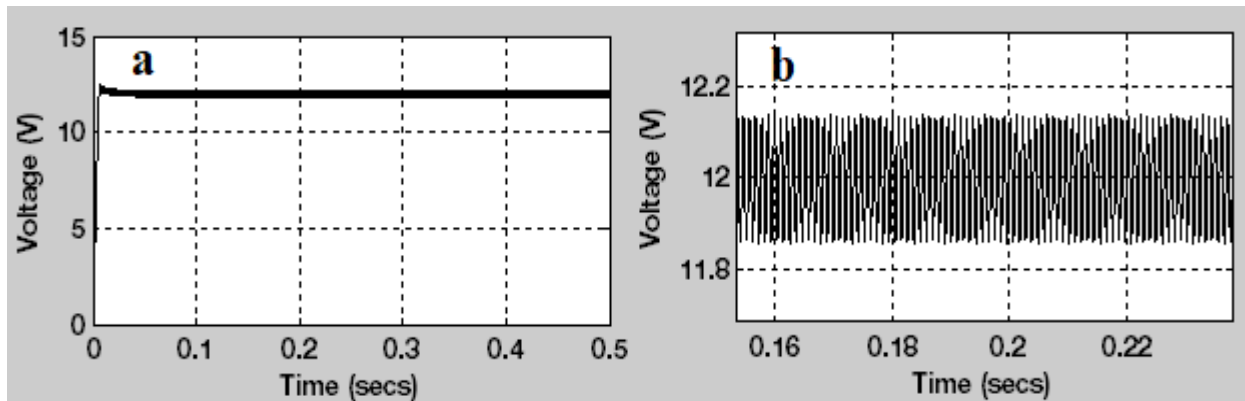
Figure 3: (a) The Output voltage response for the FBW HM-based SMC. (b) Zoom in
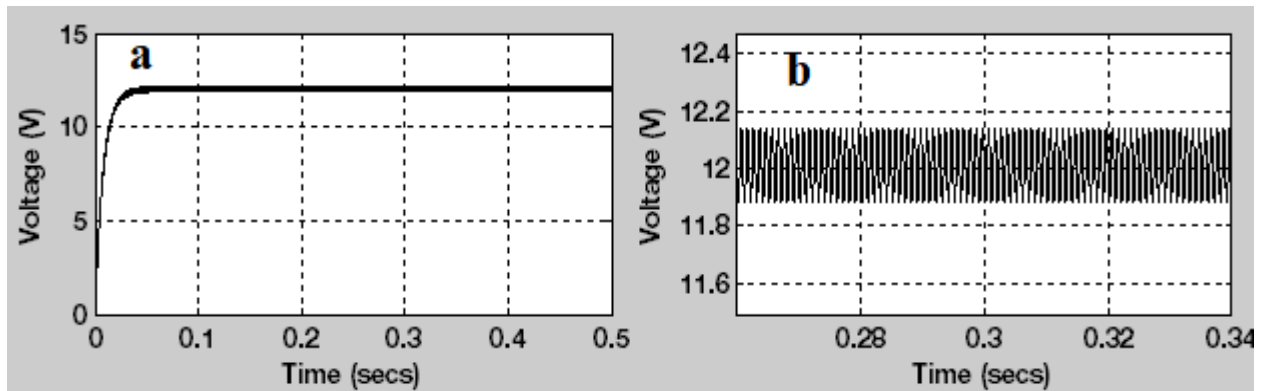
Figure 4: (a) The Output voltage response for the VBW HM-based SMC. (b) Zoom in
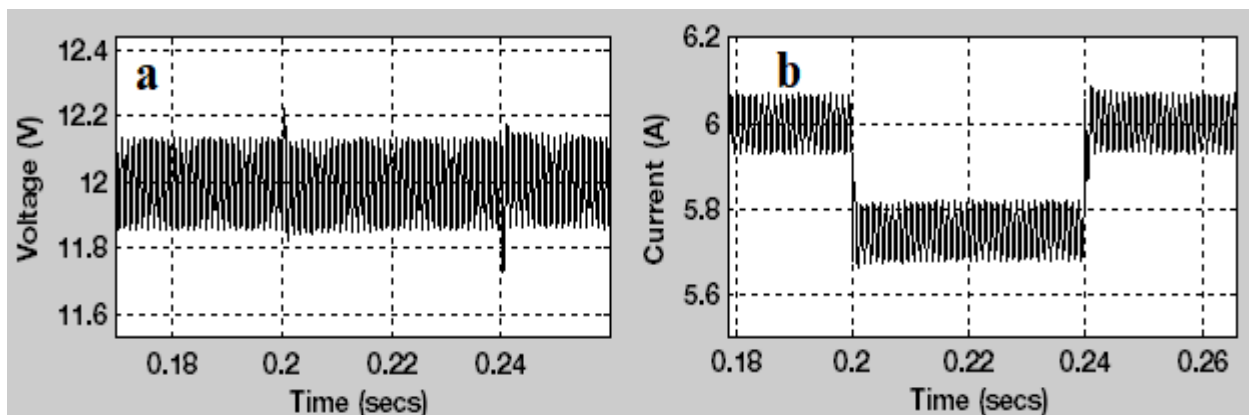
Figure 5: (a) The output voltage response. (b) The output load current response.
Both for the FBW HM-based SMC when the system undergoes a slight change in the load resistance.
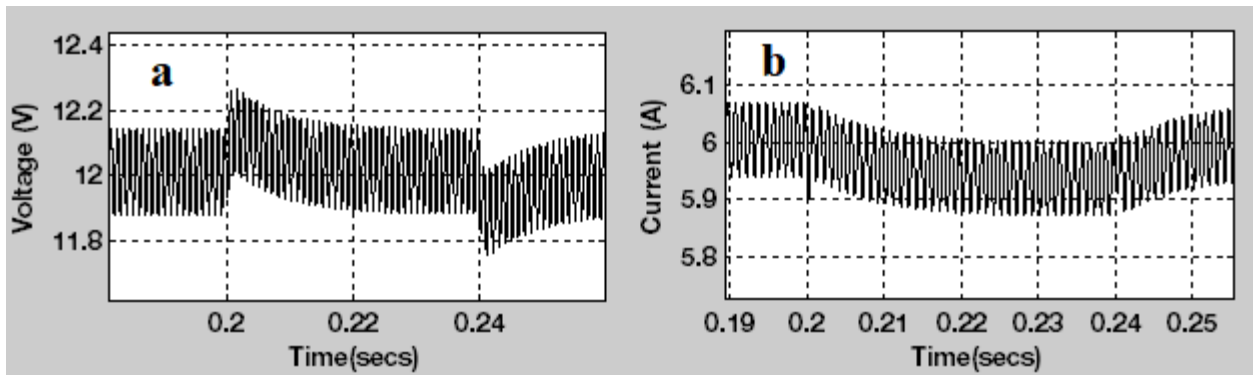
Figure 6: (a) The output voltage response. (b) The output load current response.
Both for the VBW HM-based SMC when the system undergoes a slight change in the load resistance.
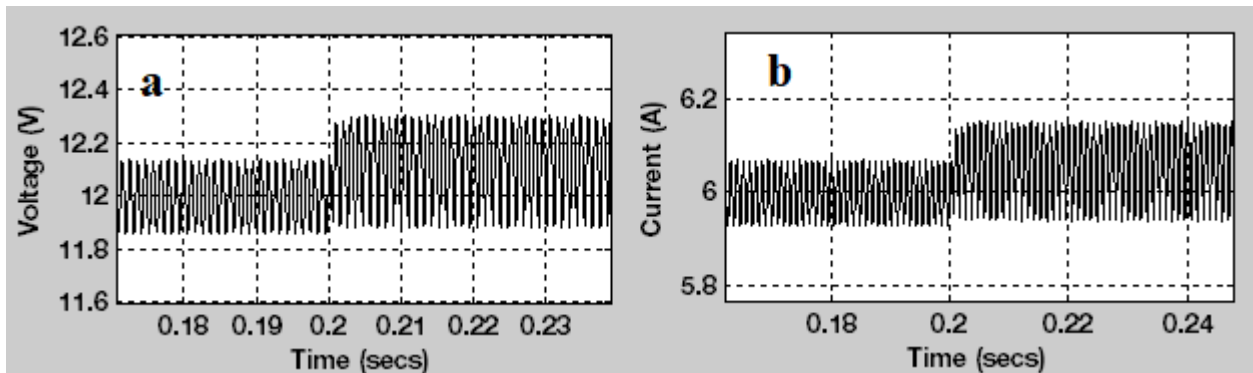
Figure 7: (a) The output voltage response. (b) The output load current response.
Both for the FBW HM-based SMC when the system undergoes a change in the input supply.
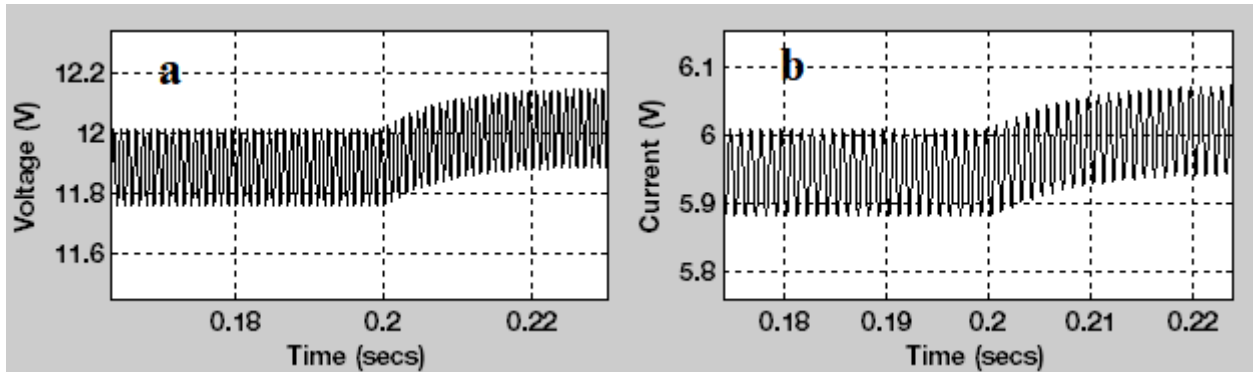
Figure 8: (a) The output voltage response. (b) The output load current response.
Both for the VBW HM-based SMC when the system undergoes a change in the input supply.
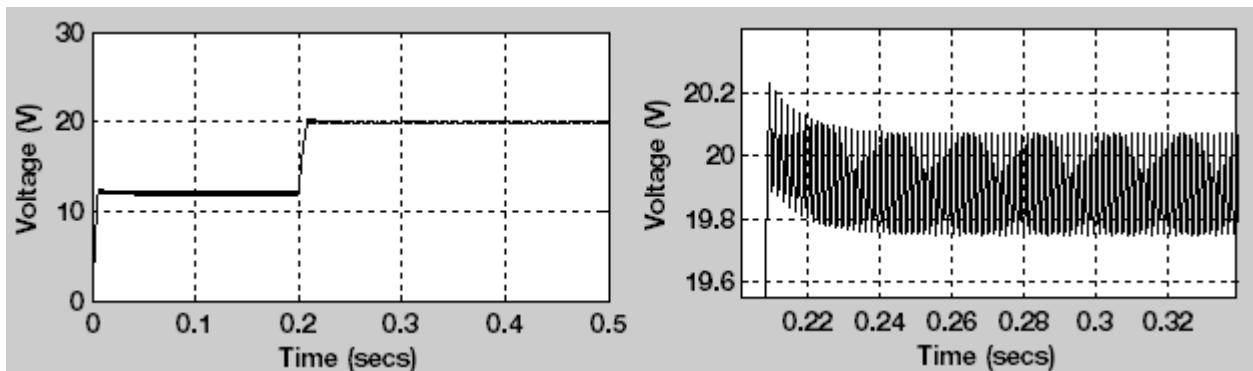
Figure 9: (a) The output voltage response for the FBW HM-based SMC when the system undergoes a change in the output reference.
(b) Zoom in.
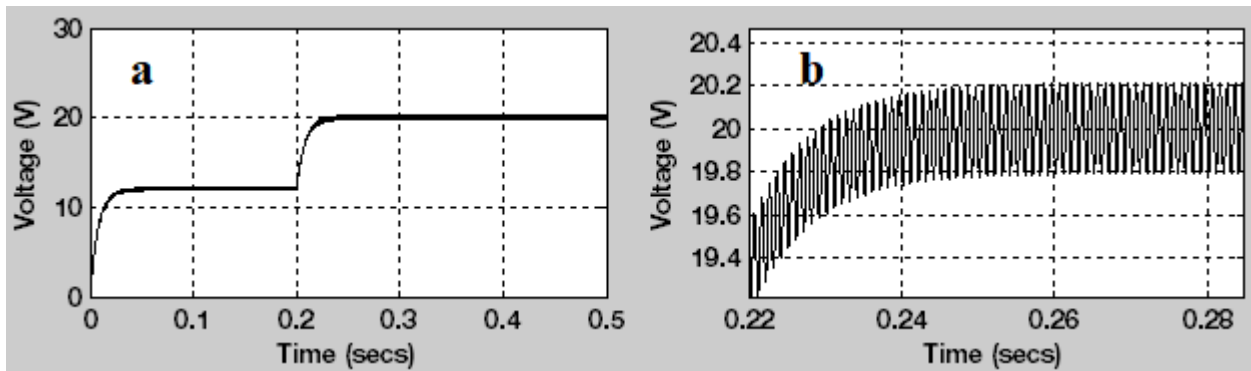
Figure 10: (a) The output voltage response for the VBW HM-based SMC when the system undergoes a change in the output reference. (b) Zoom in.
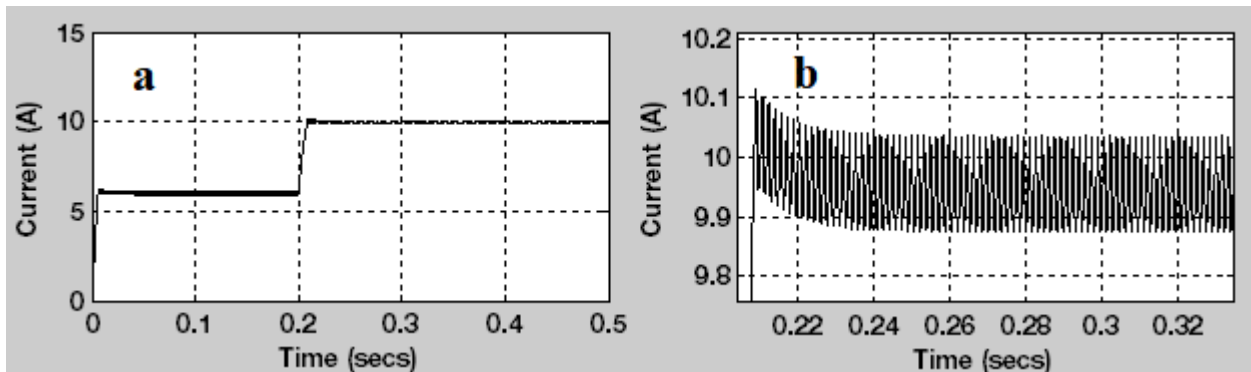
Figure 11: (a) The output load current response for the FBW HM-based SMC when the system undergoes a change in the output reference. (b) Zoom in.
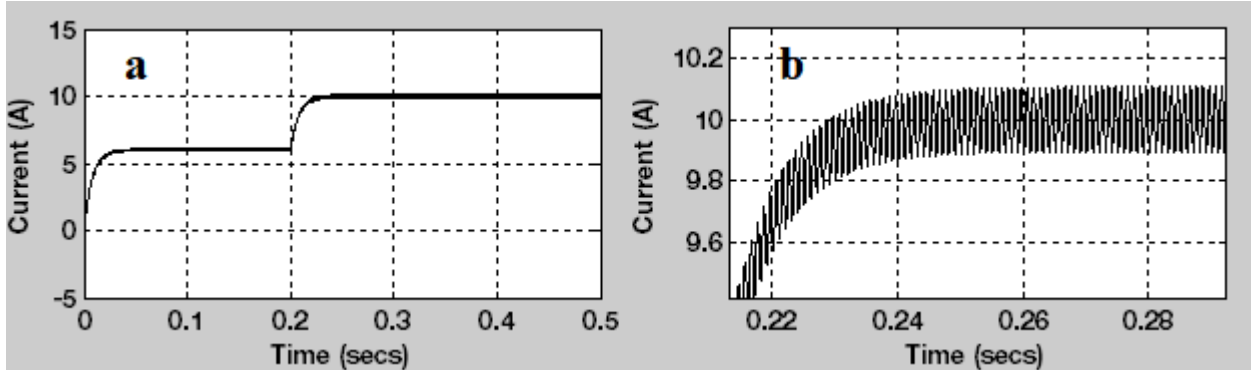
Figure 12: (a) The output load current response for the VBW HM-based SMC when the system undergoes a change in output reference. (b) Zoom in

5. Conclusion

The variable-bandwidth hysteresis modulation is favored because it ensures the chattering suppression caused by the switching of the MOSFETs and provides high efficiency since it offers a greatly desired output voltage tracking. The VBW HM-based SMC is faster to the point that the response time at 5% is mostly short. His appropriate dynamic accuracy is characterized by zero overshoot during the transient regime for the output voltage response, contrariwise to the FBW HM-based SMC that represents 2.5% overshoot. The output voltage regulation is improved from 2% (V_{in}=24V) to 0.15% (V_{in}=24V) through the VBW HM-based SMC. Add to that, the frequency variation is reduced from 30% to 15% with the developed strategy. The various control techniques provide similar performances, they have improved the dynamic conduct and they can adapt to include

voltage and load varieties. The use of variable bandwidth hysteresis modulation and fixing of the switching frequency leads to large scale dynamics.

References

[1] R. Hamdi, A.H. Hamida, O. Bennis, F. Babaa, "HM-Based SMVC with Adaptive Feedforward Controller Applied to DC-DC Converter," International Conference on Electrical and Information Technologies (ICEIT), IEEE: 1–6, 2020, doi:10.1109/ICEIT48248.2020.9113220.

[2] W. Li, He X, "Review of nonisolated high-step-up DC/DC converters in photovoltaic grid-connected applications," IEEE Trans Ind Electron, **58**, 1239–1250, 2011. doi:10.1109/TIE.2010.2049715.

[3] W. Do, K. Eguchi, A. Shibata, "An analytical approach for parallel switched capacitor converter," Energy Reports, **6**, 338–342, 2020, doi:10.1016/j.egyr.2020.11.233.

[4] M. Srinivasan, A. Kwasinski, "Control analysis of parallel DC-DC converters in a DC microgrid with constant power loads," International Journal of Electrical Power and Energy Systems, **122**, 106-207, 2020,

doi:10.1016/j.ijepes.2020.106207.

[5] H. Li, X. Jiang, Y. Zou, C. Liu, "A time-domain stability analysis method for paralleled LLC resonant converter system based on Floquet theory," Microelectronics Reliability, **114**, 113-849, 2020, doi:10.1016/j.microrel.2020.113849.

[6] MSB. Ranjana, N. Sreeramulareddy, RKP. Kumar, "A novel nonisolated switched inductor floating output DC-DC multilevel boost converter for fuelcell applications," Conference on Electrical, Electronics and Computer Science, 2014, doi:10.1109/SCEECS.2014.6804492.

[7] M. Sagar, B. Ranjana, "A Novel Non-Isolated Switched Inductor Floating Output DC-DC Multilevel Boost Converter For Fuelcell Applications", 2014, doi:10.1109/SCEECS.2014.6804492.

[8] S. Ben Said, K. Ben Saad, M. Benrejeb, "ScienceDirect HIL simulation approach for a multicellular converter controlled by sliding mode," International Journal of Hydrogen Energy, 1–7, 2017, doi:10.1016/j.ijhydene.2017.01.198.

[9] P. Djondiné, "Overview of Control Techniques for Multicellular Converter," Journal of Engineering Sciences, **5**(1), 10–14, 2018, doi:10.21272/jes.2018.5(1).e3.

[10] P. Taylor, M. Defoort, M. Djemai, T. Floquet, W. Perruquetti, "Robust finite time observer design for multicellular converters," International Journal of Systems Science Robust finite time observer design for multicellular converters", 37–41, 2011, doi:10.1080/00207721.2010.543494.

[11] F. Engelkemeir, A. Gattozzi, G. Hallock, R. Hebner, "Electrical Power and Energy Systems An improved topology for high power softswitched power converters," Electrical Power and Energy Systems, **104**, 575–582, 2019, doi:10.1016/j.ijepes.2018.07.049.

[12] S. Ogasawara, H. Akagi, A. Nabae, "A novel PWM scheme of voltage source inverters based on space vector theory," Arch Für Elektrotechnik, **74**, 33-41, doi:10.1007/BF01573229.

[13] N. Patin, "Power Electronics Applied to Industrial Systems and Transports," 2016, doi:10.1016/C2015-0-04476-8.

[14] O. Hegazy, J. Van Mierlo, P. Lataire, "Analysis , Modeling , and Implementation of a Multidevice Interleaved DC / DC Converter for Fuel Cell Hybrid Electric Vehicles," **27**(11), 4445–4458, 2012.

[15] N.H. Baharudin, TMNT. Mansur, FA. Hamid, R. Ali, MI. Misrun, "Performance Analysis of DC-DC Buck Converter for Renewable Energy Application," J. Phys. Conf. Ser., vol. 1019, Institute of Physics Publishing, doi:10.1088/1742-6596/1019/1/012020.

[16] A. Kolli, A. Gaillard, A. De Bernardinis, O. Bethoux, D. Hissel, "A review on DC / DC converter architectures for power fuel cell applications," Energy Conversion And Management, **105**, 716–730, 2015, doi:10.1016/j.enconman.2015.07.060.

[17] D. Boroyevich, H. Vanlandingham, W.T. Baumann, "Nonlinear Analysis and Control of Standalone , Parallel DC-DC , and Parallel Multi-Phase PWM Converters," 2001.

[18] M. Andrade, V. Costa, "DC-DC Buck Converter with Reduced Impact," Procedia Technol, 17, 791-8, 2014, doi:10.1016/j.protcy.2014.10.209.

[19] K.V.R. Swathi, GVN. Kumar, "Design of intelligent controller for reduction of chattering phenomenon in robotic arm : A rapid prototyping," R. Comput Electr Eng,1-15, 2017, doi:10.1016/j.compeleceng.2017.12.010.

[20] M. Alfayyoumi, AH. Nayfeh, D. Borojevic, "Modeling and analysis of switching-mode DC-DC regulators," Int J Bifurcat Chao, **10**, 373-90, 2000, doi:10.1142/S0218127400000244.

[21] H. Al-Baidhani and al., "Sliding-Mode Voltage Control of Dynamic Power Supply for CCM," IEEE International Symposium on Circuits and Systems (ISCAS), 1-5, 2019, doi:10.1109/ISCAS.2019.8702628.

[22] Y. Wu, Y. Huangfu, R. Ma, A. Ravey, D. Chrenko, "A strong robust DC-DC converter of all-digital high-order sliding mode control for fuel cell power applications," Journal of Power Sources, **413**, 222–232, 2019, doi:10.1016/j.jpowsour.2018.12.049.

[23] S. Das, M. Salim Qureshi, P. Swarnkar, "Design of integral sliding mode control for DC-DC converters," in Materials Today: Proceedings, Elsevier Ltd: 4290–4298, 2018, doi:10.1016/j.matpr.2017.11.694.

[24] S.K. Pandey, S.L. Patil, D. Ginoya, U.M. Chaskar, S.B. Phadke, "Robust control of mismatched buck DC–DC converters by PWM-based sliding mode control schemes," Control Engineering Practice, **84**, 183–193, 2019, doi:10.1016/j.conengprac.2018.11.010.

[25] Y. Gao, J. Liu, G. Sun, M. Liu, L. Wu, "Systems & Control Letters Fault deviation estimation and integral sliding mode control design for Lipschitz nonlinear systems," Systems & Control Letters, **123**, 8–15, 2019, doi:10.1016/j.sysconle.2018.08.006.

[26] SK. Pandey, SL. Patil, D. Ginoya, UM. Chaskar, SB. Phadke, "Control Engineering Practice Robust control of mismatched buck DC – DC converters by PWM-based sliding mode control schemes," Control

Engineering Practice, **84**, 183–193, 2019, doi:10.1016/j.conengprac.2018.11.010.

[27] BB. Naik, AJ. Mehta, "Sliding mode controller with modi fi ed sliding function for DC-DC Buck Converter," ISA Transactions, 2017, doi:10.1016/j.isatra.2017.05.009.

[28] A. Fezzani, S. Drid, A. Makouf, "Commande Robuste par Mode Glissant d ' Ordre Supérieur de la Machine Synchrone à Aimant Permanent," 247–251, 2010. http://eprints.univ-batna2.dz/1230/.

[29] M.S. Shaker, AA. Kraidi, "Robust observer-based DC-DC converter control u," Journal of King Saud University - Engineering Sciences, 2017, doi:10.1016/j.jksues.2017.08.002.

[30] KVR. Swathi, GVN. Kumar, "Design of intelligent controller for reduction of chattering phenomenon in robotic arm : A rapid prototyping R," Computers and Electrical Engineering, 1–15, 2017, doi:10.1016/j.compeleceng.2017.12.010.

[31] M. Phattanasak, W. Kaewmanee, J. Martin, S. Pierfederici, B. Davat, "Interleaved Double Dual Boost Converter for Renewable Energy System," **932**, 904–909, 2014, doi:10.4028/www.scientific.net/AMR.931-932.904.

[32] R. Ramos, D. Biel, E. Fossas, R. Grin, "Control Engineering Practice Sliding mode controlled multiphase buck converter with interleaving and current equalization," **21**, 737–746, 2013, doi:10.1016/j.conengprac.2012.09.005.

[33] A. El Aroudi, R. Giral, J. Calvente, "Sliding-Mode Control of DC-DC Switching Converters," IFAC, 2011, doi:10.3182/20110828-6-IT1002.00557.

[34] A. Mehta, B. Naik, "Sliding Mode Controller with PI-Type Sliding Function for DC–DC Buck Converter," In: Sliding Mode Controllers for Power Electronic Converters. Lecture Notes in Electrical Engineering, **534**, Springer, doi:10.1007/978-981-13-3152- 7_3.

[35] F. Blaabjerg. "Control of Power Electronic Converters and Systems," Elsevier 2018, ISBN:978-0-12-816136-4, doi:10.1016/c2017-0-04756-0.

1311

Evaluation of Personal Solar UV Exposure in a Group of Italian Dockworkers and Fishermen, and Assessment of Changes in Sun Protection Behaviours After a Sun-Safety Training

Alberto Modenese[1,*], Fabio Bisegna[2], Massimo Borra[3], Giulia Bravo[4], Chiara Burattini[2], Anna Grasso[1], Luca Gugliermetti[2], Francesca Larese Filon[5], Andrea Militello[3], Francesco Pio Ruggieri[1], Fabriziomaria Gobba[1]

[1]*Department of Biomedical, Metabolic and Neural Sciences, University of Modena and Reggio Emilia, Modena, 41125, Italy*

[2]*Department of Astronautical, Electrical and Energy Engineering, University of Rome "Sapienza", Rome, 00184, Italy*

[3]*Department of Occupational and Environmental Medicine, Epidemiology and Hygiene, Italian Workers' Compensation Authority (INAIL-DiMEILA), Monte PorzioCatone (Rome), 00078, Italy*

[4]*Department of Medicine, University of Udine, Udine, 33100, Italy*

[5]*Unit of Occupational Medicine, University of Trieste, Trieste, 34128, Italy*

A R T I C L E   I N F O

A B S T R A C T

Solar ultraviolet radiation (UVR) is considered a relevant health risk for the workers of the maritime and port sectors, but scant data are available on actual exposure measured using personal dosimeters. Moreover, in outdoor workers sun protection habits are usually poor, while some promising data suggest that sun-safety campaigns can be effective in increasing self-protection at work. Accordingly, our aim was to conduct an assessment of solar UVR exposure in dockworkers and fishermen using personal dosimeters, and to evaluate the use of sun protection measures at work after a sun-safety training. We performed two different UVR measurements campaigns in spring-summer 2018, investigating 7 fishermen and 14 dockworkers. Electronic dosimeters have been placed on the workers for at least a half work-day. Only at the port it was also possible to register the environmental UVR exposure with a specrto-radiometer, while for fishermen we estimated the corresponding environmental exposure using an algorithm. Our results demonstrate a high erythemal UVR dose received by the workers, with an individual exposure up to 542 J/m2 for fishermen in spring and up to 1975 J/m2 for dockworkers in summer. This data indicates an excessive occupational risk, needing more effective prevention. Accordingly, we offered a sun-safety training to the workers. Before the training, protective behaviour of the workers was rather poor: about the 50% never used the hat, the 40% never wore sunglasses and none of the workers referred to apply sunscreens at work. After the training, fishermen reported a relevant improvement in the use of individual UV protections, as hat (+9.6%), sunglasses (+28.5%) and clothes (+5%), even if the use of sunscreens at work was not increased.

1. Introduction

Solar ultraviolet radiation (UVR) exposure represents an important occupational risk in the maritime and port sectors: this paper is an extension of work originally presented in the 2020 IEEE International Conference on Environment and Electrical Engineering and 2020 IEEE Industrial and Commercial Power Systems Europe (EEEIC / I&CPS Europe) [1], integrated with data we published elsewhere [2], further elaborated and with additional inclusion of new results.

The possible adverse health effects occurring in workers exposed to solar UVR include both acute and long-term ones and mainly involve the skin and the eyes. The consequences may be severe, as in the case of cancers: solar UVR is considered the most frequent occupational carcinogenic exposure [3], for its ability to

induce in particular non-melanoma skin cancers (NMSC) [4], but also some forms of melanoma skin cancers may be related to occupational UV exposure [5], as well as rare forms of eye tumors, as the squamous cell carcinomas of the cornea and conjunctiva and ocular melanomas [6]. Considering the skin, other frequent adverse health conditions associated with cumulative solar UV exposure, and representing precancerous lesions, are photo-aging and actinic keratosis [7]. Regarding the eyes, it should be noted that usually this organ is much more protected from UV rays compared to the skin, for anatomical reasons and for the actions of various involuntary reflexes (pupillary reflex, squinting, winking) [8]. Nevertheless, UV eye exposure may be relevant in particular conditions, as in the case of UV rays reflected from surfaces like polished metal, water, snow, white sand and marbles, etc [8]. Fishermen and dockworkers, often close to the water, may be at particular risk for relevant UV eye exposure. In addition to the eye tumors, there are various ocular diseases recognizing solar UVR as a risk factor: among all, cataract [6], currently the leading cause of visual impairment worldwide [9]; pterygium, a hyperplasia of the bulbar conjunctiva highly correlated with increased levels of UV radiation [6]; and possibly also age-related macular degeneration [6], a chronic degenerative retinal disease, the second leading cause of blindness in the world [9]. For all these three eye pathologies, positive significant associations with solar radiation exposure and increased risks for outdoor workers of being diagnosed with the diseases have been well documented [10–12].

Despite the recognized health risk, there are scant studies investigating solar UVR exposure levels in the maritime and port sector [2,13–15]. Fishermen spend most of their working time outdoor on the boats, close to the water surface, reflecting a relevant amount of UVR [8]; but also dockworkers, in particular those working at the quay, are almost always outside and quite often close to reflecting surfaces, such as water, but also lucid metallic surfaces on the quay/ships. According to these considerations, it is certainly of interest a detailed assessment of solar UVR exposure of these groups of workers. Furthermore, the extant scientific literature shows a relevant under-estimation of the risk by outdoor workers, with indications of poor protective habits and behaviors with respect to a relevant occupational risk, which is solar UVR exposure [16–22].There is also a growing evidence that sun-safety interventions are effective in increasing outdoor workers' sun-protection habits [21]; nevertheless, there is still a scarcity of these interventions focused on outdoor workers, and in particular on those of the maritime and port sectors.

Our objective is to report the results of two different solar UVR measurements campaigns, respectively performed in a group of Italian dockworkers and fishermen, and a subjective evaluation of sun-exposure in a sub-group of the workers. Moreover, we wanted to test the possible improvement of the use of sun protections one year after our measurement's campaigns, including specific sun-safety trainings.

2. Materials and Methods

2.1. The solar UV radiation measurements campaigns

We registered personal exposure to solar UVR with electronic dosimeters during two different campaigns involving two groups of outdoor workers: fishermen (FM) and dockworkers (DW). Both the groups were voluntary recruited respectively from a fishing and a port company active in the area of the north-east of Italy, on the Adriatic sea (coordinates: 43° 9' N, 12°7' E for FM; 45° 4' N, 13° 5' E for DW). Considering the unstable whether conditions and the job activities mainly in the morning, we monitored FM for two consecutive spring days (15–16 May 2018), while for DW we registered personal solar UVR exposure during a summer day, with almost sunny wheather (4 July 2018). The personal electronic dosimeter used were 10 devices of the Gigahertz-Optik X2000 and X2012 series, while for a reference of the environmental erythemal UV dose in the monitored days we consulted the free online database of the Troposphperic Emission Monitoring Internet Service (TEMIS) of the European Space Agency, as described in detail in our previous works [1,2]. Briefly, the TEMIS website provides daily erythemal UV dose data for various places of the world; the data provided are derived by means of radiative transfer calculation codes from satellite measurements, considering local meteorological variables; such data were used to calculate the local environmental radiant exposure referred to the horizontal surface plane. The closest location to the dosimetry campaigns for which effective irradiance data have been made available is Venice, in Italy, that was selected as a proxy, being less than 200 km north-east compared to the workplace of the fishermen, and approximately 160 km south-west considering the port of the dockworkers. Erythemal UVR dose in Venice was 2.6 kJ/m^2 on 15th May, 3.6 kJ/m^2 on 16th May and 4.7 kJ/m^2 on 4th July. For dockworkers, we used this data only as comparison, as we registered the local erythemal radiant exposure on the horizontal surface with a Gigahertz-Optik BTS2048-UV-S spectro-radiometer placed at the quay. For fishermen it was not possible to use the spectro-radiometer on the boats, and we applied a formula [2] to reconstruct the percentage of ambient UVR received by the workers. For all the workers, the dosimeters were mainly placed on the upper back, that was the position we found most comfortable in order to not interfere with the job activities. In some cases we were able to put the devices on the chest of the workers, and only for a fisherman we had the possibility to attach the meter on the back side of his cap to simulate nape exposure (Fig. 1).

Figure 1: Placement of the UV electronic dosimeters at the workplace, on the fishermen (FM) and dockworkers (DW). From left to right, top to bottom: (1) a FM with a dosimeter on the back and one on the cap to simulatenape exposure; (2) a FM with a back dosimeter working in a covered area of the boat;(3) two FM with back dosimeters working in an uncovered area of the boat; (4) a DW working as port coordinator with a chest dosimeter; (5) a DW working as longshoreman with a

dosimeter on the upper back; (6)spectroradiometer for ambient solar UV dose measurements placed at the quay of the port.

The measurements were organized within a preventive campaign for the evaluation of the occupational risks in various occupational activities according to the Italian national occupational health and safety legislation, and were also aimed to the development of more adequate information and training of the workers. All the ethic principles considered in the Helsinki declaration were followed.

2.2. The sun exposure habits and protective behaviors investigation and the sun safety intervention

Only for the fishermen, between the two consecutive days of the measurements campaign we were able to collect a self-administered questionnaire, investigating personal solar UVR exposure habits and protecting behaviors during work and leisure activities, previously described [18]. Briefly, the 22 items questionnaire has two sections, one for work and one for leisure exposure; questions investigate the type of outdoor activity and the protections adopted to reduce solar UVR exposure. With the purposes of evaluating possible improvements of sun protection habits and behaviours at work after a sun safety training, we analyzed the results related to four items investigating the frequency of adoption of individual protections at work: use of UV protective hat, sunglasses with UV filtering lenses, UV protective clothes and sunscreens protections. Workers were asked to answer mainly on a 5 point Likert scale (from 0, meaning "never adopted the exposure habit/protective behavior", to 5 "always adopted the exposure habit/protective behavior"). The questionnaire was collected before a four-hours sun-safety training, explaining to the workers the characteristics of the solar UVR risk, the methods to evaluate the risk, the possible adverse health effects associated to solar UVR exposure and the importance of prevention during outdoor work practices, including the use of individual protections. The training was performed by the same experts involved in the measurements campaigns, for both DW and FM, but, as previously mentioned, the questionnaire was collected only for FM. The group of FM who participated in the training was larger compared to the workers we individually investigated with our dosimeters during the measurements campaigns. We decided to administer the questionnaire before the training, i.e. before the workers received any information on solar UVR risk that could be able to influence their answers. Then, one year after the measurements campaigns and the sun-safety training (May 2019), we contacted via phone the fishermen who participated in the sun-safety training and we administered the same questionnaire, in order to evaluate a possible improvement of the protective habits and behaviors of the workers, to be possibly attributed to the intervention we performed.

3. Results

3.1. Results of the solar UV radiation measurements campaigns

We measured individual solar UVR exposure of 7 fishermen and 14 dockworkers, all males (Table 1). FM worked on three fishing boats with different characteristics with respect to the availability of protections against solar radiation: one medium size boat (B1), only partially covered, but with various tasks of the work activity (mussel fishing) performed in shielded areas, one small boat (B2), with almost no coverage from UVR, for activities (sea snails and cuttlefish fishing) performed in direct sunlight and

another medium size boat (B3), partially covered, with only parts of the activities (trawling fishing) in direct sun. Considering DW, 10 of them worked as longshoremen (LSM) almost always close to the quay and to the water, while 4 subjects worked as coordinators of the port traffic (traffic coordinator, TC), with some activities performed inside a small office (Table 1).

Table 1: Results of individual measurements of occupational solar UVR exposure for 7 fishermen and 14 dockworkers from the North-East of Italy.

Work place / job task		Placement of the dosimeter	Working period / length of the period measured (minutes)*	Personal UV erythemal dose (J/m²)*	Ambient UV effective radiant exposure (H_eff) (J/m²)* ±	Personal erythemal vs. ambient UVR exposure (%)* ±
B1	FM1	Back	morning / 397	213	1710	12.5
	FM2	Back		79		4.6
	FM3	Back		71		8.8
B2	FM4	Back (& Nape)	morning / 180	542 (380)	830	65.3 (45.8)
	FM5	Back		288		34.7
B3	FM6	Back	morning / 300	151	1560	9.7
	FM7	Back (& chest)		129 (98)		8.3 (7.8)
Quay	DW1-LSM	Back	full-day / 432	1975	3339	59
	DW2-LSM	Back	full-day / 417	1067	3276	32
	DW3-LSM	Back	morning / 144	288	857	33
	DW4-LSM	Back	morning / 191	402	1322	30
	DW5-LSM	Chest	morning / 243	257	1596	16
	DW6-LSM	Back	morning / 251	854	1965	43
	DW7-LSM	Back	morning & early afternoon / 260	551	2675	20
	DW8-LSM	Back	afternoon / 246	622	2191	28
	DW9-LSM	Back	afternoon / 226	458	2001	22
	DW10-LSM	Back	afternoon / 225	413	1981	20
Center of the port (partially indoor)	DW11-TC	Chest	morning / 177	48	1550	3
	DW12-TC	Chest	Morning / 193	139	1759	7
	DW13-TC	Chest	Afternoon / 210	89	1876	4
	DW14-TC	Chest	Afternoon / 248	44	2045	2

Legend: B1= boat 1, middle-size, partially covered; B2= boat 2, small size, no coverage; B3= boat 3, partially covered; FM= fisherman; DW= dockworker; LSM= longshoreman; TC= traffic coordinator. *= for fishermen the worst exposure scenario occurred in one of the two days with measurements is reported in the Table; ± = for fishermen, ambient exposure was estimated according to a specific formula [2]

Regarding the length of the individual measurements period, unfortunately for almost all the workers it was not possible to monitor an usual full working day, as FM started their work-shifts few hours before sunrise, so that measuring UVR in that period was meaningless, and they finished between 1:00-2:00 p.m.; considering DW, for the large majority of them the activities were organized on separate morning and afternoon work-shifts, and only two DW worked both in the morning and in the afternoon the day we performed our measurements.

Considering the worst exposure scenario for the seven fishermen during the two days monitored, we found personal UVR exposure at the back ranging between 71 J/m^2 registered for FM3 working on the B1 and 542 for FM4 on the B2. The estimated proportion of environmental erythemal UVR dose received on the back of the FM resulted between a minimum of 4.6% for FM2 on the B1 and a maximum of 65.3% for FM4 on the B2 (Table 1).

Considering DW, we collected personal solar UVR exposure data at the back for LSM while at the chest for the TC, as they had quite often to sit inside a small office in the middle of the port area. The results of the measurements show a higher exposure in LSM compared to TC: the highest exposure of 1975 J/m^2 was collected, not surprisingly, for one of the two LSM (DW1) who worked for a full day (approximately 7 hours and a half). The individual exposure of the other LSM ranged between 257 J/m^2 collected at the chest of DW5 (i.e. the oly LSM with a chest dosimeter, who was monitored for more than four hous in the morning) and 1067 J/m^2 for the other LSM who was monitored for approximately seven hours (DW2). For the other LSM with dosimeters on the back and monitored only in the morning or afternoon, exposures resulted between 288 J/m^2 measured in the morning in about two hours and a half (DW3) and 854 J/m^2 registered again in the morning but in more than four hours (DW6). Percentages of ambient exposure received by the LSM varied between the 16 and the 59%. Considering TC, their individual solar UVR exposures at the chest varied between 44 J/m^2 measured in about four hours in the afternoon (DW14) and 139 J/m^2 registered in approximately three hours in the morning (DW12), with percentages of individual versus ambient exposure between the 2 and the 7% (Table1).

3.2. Results of the investigation of sun exposure habits and protective behaviors among fishermen

Twenty-one fishermen, all males, participated in the sun-safety training we proposed to the fishing company where we performed the individual solar UVR measurements campaign. We administered our questionnaire investigating sun exposure habits and behaviours before the starting of the training, and all of them filled-in the questionnaire. The 47.7% of the FM reported to never use an UVR protective hat at work. The 38.1% of them never used UV filtering sunglasses on the boats. None of the workers reported to use. always, often or even sometimes, sunscreens at work. Only for the clothes we collected some positive responses: the 40% of the sample wore often protective clothes (Table 2). After one year from the sun safety training we contacted all the 21 fishermen via phone, asking them the same questions related to the frequency of adoption of solar UVR individual protections at work.

Table 2: Results of the subjective investigation on the frequency of adoption of solar UVR individual protections at work among 21 fishermen

Individual protecions against solar UVR				
Frequency of adoption on a 5-point Likert scale	**Fishermen adopting the individual protection: % (n)**			
	Protective hat	UV filtering sunglasses	Protective clothes*	Sunscreens
ALWAYS	14.3 (3)	14.3 (3)	15 (3)	0
OFTEN	19 (4)	9.5 (2)	40 (8)	0
SOMETIMES	19 (4)	14.3 (3)	25 (5)	0
SELDOM	0	23.8 (5)	15 (3)	19 (4)
NEVER	47.7 (10)	38.1 (8)	5 (1)	81 (17)

1 answer was missing

In order to better appreciate the differences between the answers given before and after the training, we grouped together as positive responses the answers "always", "often" and "sometimes" and we analyzed the percentage of FM who reported to adopt UV protections at the baseline and one year after the sun-safety campaign (Fig. 2). After the sun-safety interventions there was an improvement of the 9.6% for the use of UV protective hat at work, of the 28.5% for the use of UV filtering sunglasses (with a significant difference at the non-parametric McNemar statistical test for paired nominal data, p=0.031) and of the 5% for the wearing of UV protective clothes. No improvements have been found for the use of sunscreens at work by the fishermen (Fig. 2).
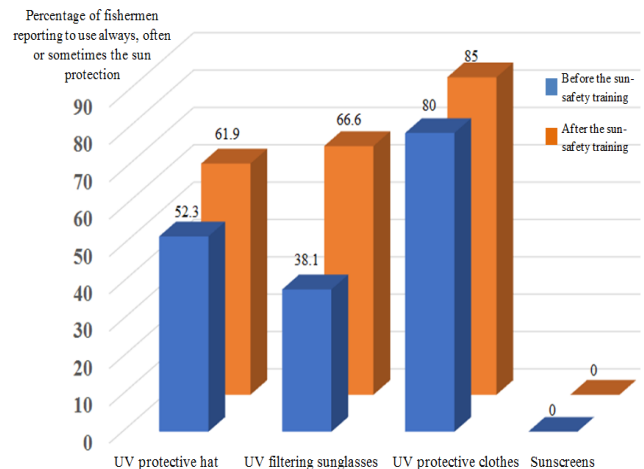
Figure 2: Use of individual solar UVR protections at work before and one-year after the sun-safety training in a group of 21 fishermen.

4. Discussion

Our results on personal solar UVR exposure measured in a group of dockworkers and fishermen of North-East Italy show remarkable high UV exposure levels. For FM we collected measures in late spring, while for DW in summer: not surprisingly, the exposure levels we detected resulted higher in the case of DW. Nevertheless, even if the two days of the measurements campaign for the FM were partially clouded spring days, we registered, in less than five hours on average, an exposure above the equivalent of a Standard Erythemal Dose (SED, i.e. an UVR personal

exposure able to induce an erythema in an individual, adjusted for skin pigmentation, and corresponding approximately to 100 J/m^2) in all but two FM, with a maximum exposure of more than 5 SEDs/day. This indicates a very high risk of acute skin burns, and, considering the photochemical accumulation of UV-induced damages, may also represent an increased risk for long-term adverse health effects, in case of exposures prolonged over years. Considering the specific work tasks, the FM were involved in three different types of fishing performed on three different boats. We collected the highest exposure levels on the smallest boat, with almost no coverage from the solar UV rays, dedicated to an activity (sea snails and cuttlefish fishing) performed almost always in direct sunlight.

Considering now the DW, also in this case we measured different solar UVR exposure levels depending on the specific type of work activity performed. We registered higher solar UVR individual levels for longshoremen compared to traffic coordinators. The personal UV doses collected for LSM, in the 90% of the cases with dosimeters placed on their upper back, varied between 2.6 SED/half-day and 20 SED/day. Also, for the LSM investigated with a chest dosimeter we registered a quite high exposure of 5.5 SED/half-day. Considering dockworkers employed as TC, we had to place the dosimeters on their chests, as they frequently had to be seated at a desk inside a small cabin office, therefore performing also partially indoor activities. For TC we measured exposures between 0.4 and 1.4 SED/half-day.

Discussing now the relations between individual and environmental solar UVR skin exposure, we found quite high variability both in the results related to FM and in those collected for DW. This variability is not surprising and reported also in other studies of personal solar UVR eposure measurements in outdoor workers [14,23–28]. It can be related to the different working postures adopted by the workers and to other factors, as the sun-angle on the horizon, the distance from reflecting surfaces (e.g. water) and the presence of shading structures: accordingly, the exposure of different body districts can change during the day in relation to the ways the activity is performed and to the environment. Percentages of individual vs. environemtal UVR exposure varied between the 4.6 and the 65.3% for FM, 20.6% on average including only data retrieved for dosimeters placed on the backs. For longshormen, the average percentage of ambient exposure received at the workers' backs was of 31.9%, with a maximum of 59 and a minimum of the 20%, dropping to the 16% considering the LSM with a chest dosimeter. It should be noted a lower variability of the results related to the solar radiation exposure of dockworkers employed as port traffic coordinators compared to fishermen and longshoremen. A possible reason is that the activity of the TC is less dynamic compared to that of the other groups: for these workers we found a percentage of personal vs. ambient exposure between the 2 and the 7%, almost stable and quite low, considering that the dosimeters in these cases were placed on the chest and that some working tasks of the workers were performed in an indoor area.

As regards to the results of the investigation on solar UVR individual exposure habits and behaviours before and after a specific sun-safety training, first of all it should be noted that, to the best of our knowledge, this is the first reporting of a sun safety initiative specifically addressing fishermen. As reported also by similar studies performed in other groups of outdoor workers [16–20], our results indicate poor protective habits and behaviors of fishermen, in particular before the sun-safety training. After our intervention, we observed a slight improvement related to the adoption of three specific individual protections: the UV protective hats, sunglasses and clothes, with an increased percentage of fishermen who reported to use, at least sometimes, these protections at work. This is still far from an adequate perception of the risk, as even after our sun-safety campaign approximately the 35-40% of the workers never or only seldom reported to use hats and sunglasses at work, while more adequate habits have been reported for protective clothes. Unfortunately, our intervention apparently failed in raising the awareness of the group of fishermen on the importance of applying sunscreens at work: this is a relevant point, and we should reflect on what can be the issues in achieving the goal of a more widespread use of sunscreens at work. Some possible problems may be related to the quite high costs of the sunscreens, in particular considering that they have to be abundantly applied and re-applied during the work-day, and to the fact that, at least in Italy, these costs are usually not covered by the companies. Nevertheless, it should also be noted that sunscreens can't be considered personal protective equipment as UV protective hats, sunglasses and clothes, but they are an additional protective measure to be adopted in case the other personal protections can't be considered sufficient to limit the exposure.

Our study also has some limitations: first of all, the sample size, in particular in the case of the fishermen, where we collected solar UVR exposure data of only seven workers: nevertheless, having followed the workers for two days, and in some cases with two dosimeters per worker, we retrieved a total number of nineteen point measurements, i.e. even more measurements compared to the campaign performed at the port, where we investigated fourteen dockworkers in only one day. Also, for the subjective investigation of solar UVR exposure habits and behaviours the sample of twenty-one subjects can be considered of a quite small size: in this case, a relevant point, possibly reducing the limitation, is that we were able to re-contact all the investigated workers after one year, and accordingly our analysis of the changes in protective behaviours after our sun-safety training resulted more valid.

A further limitation is related to the estimate of the environmental UVR doses for the measurement campaign in the fishing company. Unfortunately, we performed ambient measurements with an UVR spectro-radiometer only at the harbour, where it was possible to safely place the instrumentation in a stable site. This was not possible on the small boats of the fishermen, so that we had to retrieve environmental data from an online database, and estimate the corresponding dose in the period worked by the fishermen. Moreover, in the database we selected there was no availability of ambient data referred to the place where we actually performed the measurements (43° 9' N, 12°7' E), so that we considered available data for the city of Venice (about 200 km in the northern-east direction, at a slightly higher latitude and similar altitude).

Finally, we want to mention also some possible limitations related to the placement of the dosimeters on the workers. Unfortunately, we were not able to "a priori" select the most appropriate body districts where to fix the dosimeters according to the specific working tasks of the workers with respect to solar UVR

exposure. On the contrary, as this was an on-field measurements campaign during real working situations, we had to place the dosimeters in positions selected as the best compromise between an appropriate evaluation of the personal exposure and the need of not interfering with the usual job activities of the workers. Accordingly, we decided to place the dosimeters mainly at the upper back for fishermen and dockworkers employed as longshoremen, while at the chest for the dockworkers performing as traffic coordinators of the port area. In the few cases we had for the same workers both the data from the back dosimeter and the data from other body districts (chest, and in one case also the nape), the upper back resulted the district with the highest exposure levels.

5. Conclusions

In conclusion, our data are, to the best of our knowledge, the first Italian data demonstrating with on field measurements an intense solar UVR dose received by fishermen and dockworkers in the spring and summer seasons. According to the photo-chemical effect of the UV rays absorbed in the skin, these data indicate an excessive occupational risk, possibly resulting after years of work in an increased occurrence of skin pre-cancerous and cancerous lesions. Therefore, there is an urgent need of sun-safety campaigns for outdoor workers, in particular for those of the maritime and port sectors, as we found no previous reporting of such campaigns for these workers in scientific literature. We offered a sun-safety training to the workers we investigated with dosimeters for their personal solar UVR exposure. Before the training, workers reported very poor sun exposure habits and behaviours. After our training, fishermen reported an improvement in the use of individual UV protections, as hat, sunglasses and clothes. Unfortunately, no positive improvements have been found with respect to the use of sunscreens at work in these workers.

Conflict of Interest

The authors declare no conflict of interest.

Acknowledgments

References

[1] A. Modenese, F. Bisegna, M. Borra, C. Burattini, L. Gugliermetti, F.L. Filon, A. Militello, P. Toffanin, F. Gobba, "Occupational Exposure to Solar UV Radiation in a Group of Dock-workers in North-East Italy," Proceedings - 2020 IEEE International Conference on Environment and Electrical Engineering and 2020 IEEE Industrial and Commercial Power Systems Europe, EEEIC / I and CPS Europe 2020, 2020, doi:10.1109/EEEIC/ICPSEurope49358.2020.9160703.

[2] A. Modenese, F.P. Ruggieri, F. Bisegna, M. Borra, C. Burattini, E. Della Vecchia, C. Grandi, A. Grasso, L. Gugliermetti, M. Manini, A. Militello, F. Gobba, "Occupational exposure to solar UV radiation of a group of fishermen working in the Italian north adriatic sea," International Journal of Environmental Research and Public Health, 16(16), 1–12, 2019, doi:10.3390/ijerph16163001.

[3] T. Kauppinen, J. Toikkanen, A. Savela, D. Pedersen, R. Young, W. Ahrens, P. Boffetta, M. Kogevinas, J. Hansen, H. Kromhout, V. de La Orden-Rivera, J. Maqueda Blasco, D. Mirabelli, B. Pannett, N. Plato, R. Vincent, "Occupational exposure to carcinogens in the European Union," Occupational and Environmental Medicine, 57(1), 10–18, 2000, doi:10.1136/oem.57.1.10.

[4] T. Loney, M.S. Paulo, A. Modenese, F. Gobba, T. Tenkate, D.C. Whiteman, A.C. Green, S.M. John, "Global evidence on occupational sun exposure and keratinocyte cancers: a systematic review," British Journal of Dermatology, 1–11, 2020, doi:10.1111/bjd.19152.

[5] B.K. Armstrong, A.E. Cust, "Sun exposure and skin cancer, and the puzzle of cutaneous melanoma: A perspective on Fears et al. Mathematical models of age and ultraviolet effects on the incidence of skin cancer among whites in the United States. American Journal of Epidemiology 1977" Cancer Epidemiology, 48, 147–156, 2017, doi:10.1016/j.canep.2017.04.004.

[6] J.C.S. Yam, A.K.H. Kwok, "Ultraviolet light and ocular diseases," International Ophthalmology, 34(2), 383–400, 2014, doi:10.1007/s10792-013-9791-x.

[7] K. Grandahl, J. Olsen, K.B.E. Friis, O.S. Mortensen, K.S. Ibler, "Photoaging and actinic keratosis in Danish outdoor and indoor workers," Photodermatology Photoimmunology and Photomedicine, 35(4), 201–207, 2019, doi:10.1111/phpp.12451.

[8] G. Ziegelberger, "Icnirp statement-protection of workers against ultraviolet radiation," Health Physics, 99(1), 66–87, 2010, doi:10.1097/HP.0b013e3181d85908.

[9] R.R.A. Bourne, J.B. Jonas, A.M. Bron, M.V. Cicinelli, A. Das, S.R. Flaxman, D.S. Friedman, J.E. Keeffe, J.H. Kempen, J. Leasher, H. Limburg, K. Naidoo, K. Pesudovs, T. Peto, J. Saadine, A.J. Silvester, N. Tahhan, H.R. Taylor, R. Varma, T.Y. Wong, S. Resnikoff, "Prevalence and causes of vision loss in high-income countries and in Eastern and Central Europe in 2015: Magnitude, temporal trends and projections," British Journal of Ophthalmology, 102(5), 575–585, 2018, doi:10.1136/bjophthalmol-2017-311258.

[10] A. Modenese, F. Gobba, "Cataract frequency and subtypes involved in workers assessed for their solar radiation exposure: a systematic review," Acta Ophthalmologica, 96(8), 2018, doi:10.1111/aos.13734.

[11] A. Modenese, F. Gobba, "Occupational exposure to solar radiation at different latitudes and pterygium: A systematic review of the last 10 years of scientific literature," International Journal of Environmental Research and Public Health, 15(1), 2018, doi:10.3390/ijerph15010037.

[12] A. Modenese, F. Gobba, "Macular degeneration and occupational risk factors: a systematic review," International Archives of Occupational and Environmental Health, 92(1), 2019, doi:10.1007/s00420-018-1355-y.

[13] U. Feister, G. Meyer, U. Kirst, "Solar UV exposure of seafarers along subtropical and tropical shipping Routes," Photochemistry and Photobiology, 89(6), 1497–1506, 2013, doi:10.1111/php.12144.

[14] K. Grandahl, P. Eriksen, K.S. Ibler, J.P. Bonde, O.S. Mortensen, "Measurements of Solar Ultraviolet Radiation Exposure at Work and at Leisure in Danish Workers," Photochemistry and Photobiology, 94(4), 807–814, 2018, doi:10.1111/php.12920.

[15] M. Oldenburg, B. Kuechmeister, U. Ohnemus, X. Baur, I. Moll, "Actinic keratosis among seafarers," Archives of Dermatological Research, 305(9), 787–796, 2013, doi:10.1007/s00403-013-1384-z.

[16] K. Grandahl, K.S. Ibler, G.H. Laier, O.S. Mortensen, "Skin cancer risk perception and sun protection behavior at work, at leisure, and on sun holidays: A survey for Danish outdoor and indoor workers 11 Medical and Health Sciences 1117 Public Health and Health Services," Environmental Health and Preventive Medicine, 23(1), 1–11, 2018, doi:10.1186/s12199-018-0736-x.

[17] F. Larese Filon, M. Buric, C. Fluehler, "UV exposure, preventive habits, risk perception, and occupation in NMSC patients: A case-control study in Trieste (NE Italy)," Photodermatology Photoimmunology and Photomedicine, 35(1), 24–30, 2019, doi:10.1111/phpp.12417.

[18] A. Modenese, T. Loney, F.P. Ruggieri, L. Tornese, F. Gobba, "Sun protection habits and behaviors of a group of outdoor workers and students from the agricultural and construction sectors in north-Italy," Medicina Del Lavoro, 111(2), 116–125, 2020, doi:10.23749/mdl.v111i2.8929.

[19] M.M. Nkogatse, M.C. Ramotsehoa, F.C. Eloff, C.Y. Wright, "Solar Ultraviolet Radiation Exposure and Sun Protection Behaviors and Knowledge Among a High-Risk and Overlooked Group of Outdoor Workers in South Africa," Photochemistry and Photobiology, 95(1), 439–445, 2019, doi:10.1111/php.13008.

[20] C.E. Peters, M.W. Koehoorn, P.A. Demers, A.M. Nicol, S. Kalia, "Outdoor Workers' Use of Sun Protection at Work and Leisure," Safety and Health at Work, 7(3), 208–212, 2016, doi:10.1016/j.shaw.2016.01.006.

[21] D. Reinau, M. Weiss, C.R. Meier, T.L. Diepgen, C. Surber, "Outdoor workers' sun-related knowledge, attitudes and protective behaviours: A systematic review of cross-sectional and interventional studies," British Journal of Dermatology, **168**(5), 928–940, 2013, doi:10.1111/bjd.12160.

[22] S. Schneider, K. Diehl, L. Schilling, M. Spengler, R. Greinert, T. Görig, "Occupational UV exposure and sun-protective behaviour in German outdoor workers: Results of a nationwide study," Journal of Occupational and Environmental Medicine, **60**(11), 961–967, 2018, doi:10.1097/JOM.0000000000001397.

[23] M. Boniol, A. Koechlin, M. Boniol, F. Valentini, M.C. Chignol, J.F. Doré, J.L. Bulliard, A. Milon, D. Vernez, "Occupational UV exposure in French outdoor workers," Journal of Occupational and Environmental Medicine, **57**(3), 315–320, 2015, doi:10.1097/JOM.0000000000000354.

[24] P. Gies, J. Wright, "Measured Solar Ultraviolet Radiation Exposures of Outdoor Workers in Queensland in the Building and Construction Industry¶," Photochemistry and Photobiology, **78**(4), 342, 2003, doi:10.1562/0031-8655(2003)078<0342:msureo>2.0.co;2.

[25] V. Hammond, A.I. Reeder, A. Gray, "Patterns of real-time occupational ultraviolet radiation exposure among a sample of outdoor workers in New Zealand," Public Health, **123**(2), 182–187, 2009, doi:10.1016/j.puhe.2008.12.007.

[26] M. Antoine, S. Pierre-Edouard, B. Jean-Luc, V. David, "Effective exposure to solar UV in building workers: Influence of local and individual factors," Journal of Exposure Science and Environmental Epidemiology, **17**(1), 58–68, 2007, doi:10.1038/sj.jes.7500521.

[27] M.A. Serrano, J. Cañada, J.C. Moreno, "Solar UV exposure in construction workers in Valencia, Spain," Journal of Exposure Science and Environmental Epidemiology, **23**(5), 525–530, 2013, doi:10.1038/jes.2012.58.

[28] M. Wittlich, S.M. John, G.S. Tiplica, C.M. Sălăvăstru, A.I. Butacu, A. Modenese, V. Paolucci, G. D'Hauw, F. Gobba, P. Sartorelli, J. Macan, J. Kovačić, K. Grandahl, H. Moldovan, "Personal solar ultraviolet radiation dosimetry in an occupational setting across Europe," Journal of the European Academy of Dermatology and Venereology, **34**(8), 1835–1841, 2020, doi:10.1111/jdv.16303.

A S T E S

Combining ICT Technologies To Serve Societal Challenges

Helen Leligou[*,1], Despina Anastasopoulos[1], Anita Montagna[2], Vassilis Solachidis[3], Nicholas Vretos[3]

[1]INTRASOFT International S.A., Research & Innovation Development Unit, Luxembourg, L1253, Luxembourg

[2]Centro Studi Pluriversum, 53100, Italy

[3]Information Technologies Institute, Center for Research and Technology Hellas, Thessaloniki, 60361, Greece

A R T I C L E   I N F O

A B S T R A C T

European counties continue to receive an increasing number of migrants and refugees from an also increasing number of both European and non-European countries. This results in a huge societal challenge which is societal inclusion of people speaking different languages and of diverse backgrounds. Key for their inclusion is job finding which comes with hurdles like the language, the difficulty in assessing and certifying their skills and many more. In this paper, we present the architecture of a novel platform that aspires to provide migrants with a) assistance in discovering and assessing their hard and soft skills by employing Artificial Intelligence technologies, b) recommendations of appropriate job sectors and positions based on their profile, c) recommendations about training that would allow them to find jobs in the country/region they are located and d) practical information regarding the integration process. Furthermore, the proposed platform aims at assisting host authorities, non-governmental organizations and companies in detecting the needs of the target populations (migrants and refugees) through data analytics and supports them in reaching them. Apart from the technical architecture, we provide the results from the initial testing of the platform in real-life pilots in two countries.

1. Introduction

The current trend of migration for economic reasons combined with large flows of refugees ("people fleeing their countries due to armed conflicts or persecution") challenges our societies. A key to societal inclusion of migrants and societal coherence is their integration in the labour market. Nevertheless, the elaborate human resource recruitment processes established in our economies make it difficult and complicated not only for the migrants but also for host organisations, according to the claims gathered through interviews with field experts. The main barriers (also discussed in [1]) are multiple: a) lack of professional qualifications and certified skills and competences; b) language skills are impeding fluent communication and this is even more intense for refugees; c) the scale of the phenomenon which is large and increasing: over a million refugees in Europe since 2015, 70% of them with ages between 18 and 64, i.e. in working age and low-skilled people percentages greater than the average of the hosting countries' [2]. Refugees and migrants are a heterogeneous group

as far as education and other issues are concerned and thus, special vulnerabilities have also an impact on individuals' labour market integration chances.

In the host societies, there are organisations (public, private or Non-Governmental Organisations) that try to assist migrants and refugees in finding their way to the labour market. However, two factors limit the positive impact of these efforts to a certain extent: a) the multiplicity of entities operate usually with no coordination among them and b) the fact that the potential employers have to follow stricter regulations when hiring migrants and also have to afford the cost for screening their skills and profiles at the absence of any certificate and/or proof. At the same time, tailored training is considered of paramount importance to increase the probability of employment of refugees and migrants according to the Committee for Labour Migration [3]. Soft skills are also important and should not be overlooked. The new recommendation on Key Competences for Lifelong Learning [4] has enhanced the importance of key competences and soft skills, which are considered as equally important to hard skills when looking for a job. The evaluation of the soft skills is also difficult to be

*Corresponding Author: Helen Leligou, Email: leligou@gmail.com

performed imposing further barriers in the integration of migrants in the labour market.

The exploitation of Information and Communication Technologies (ICT) is considered an appropriate mean to communicate with the migrants and refugees as they usually have access to the internet usually through mobile devices. ICT technologies could also contribute to personalization of the information presented to the users. However, up to now, ICT has been used mainly for information provisioning which is valuable but yet not enough. As a result, the integration of migrants and refugees is still a challenge for all involved actors i.e. migrants, refugees, host authorities, NGOs, private and public organisations and society alike.

In this article, we present a novel digital platform that aspires to support not only migrants and refugees but also the host authorities and organisations towards the integration of the first group in the labour market. The proposed platform employs state-of-the-art technologies like artificial intelligence and data analytics to lower the cost of skills evaluation, facilitate the operation of organisations and significantly shorten the path of migrants to the labour market. In its design, we have combined Artificial Intelligence, data analytics, native mobile applications and web technologies with social science expertise and skill assessment techniques to offer a novel holistic platform to the migrants. The proposed platform is not a "bundling" of functionalities like the ones offered by multiple other platforms; instead, it offers novel functionalities like the skill assessment functionality based on machine learning algorithms trained on data from migrants' populations. The proposed platform has been prototyped and used by migrants/refugees in real life.

The rest of this article is organized as follows: in section 2, we present existing digital platforms tackling the migrants' integration challenge and discuss their strengths and weaknesses. In section 3 we describe the proposed platform, and its technical architecture is presented in section 4. Section 5 presents the results from the evaluation in real life and section 6 concludes the article. A preliminary version of the presented approach was initially published in [1] without technical details and any evaluation results.

2. Existing Platforms

Up to now, few tens of platforms primarily targeting the needs of the migrants/refugees have been deployed exploiting the fact that the majority of them has access to the internet through their mobile phones. The following table is based on the table that appears in [1] and reflects the current situation. The fact that such platforms proliferate, show that they cover actual needs and thus the involved actors try to satisfy them. The table includes the information considered necessary for their comparison.

Examining the table, it is evident that there is no platform adopting a holistic approach. Most of these platforms present to the user information but the supported functionalities of search and the limited languages reduce their actual value. Just one of these platforms supports skill assessment and this targets a limited set of job sectors. This is mainly due to the language barrier which is difficult to overcome with any textual-based assessment. As explained in [5], there are methodologies to assess skills and competencies, but they are mainly twined with the education processes which is not a representative case for the migrants arriving in a new country. The use of neural networks has been proposed in [6] in the context of assessing skill of surgical doctors. With respect to digital tools, they usually evaluate performance in a normative way after the user has completed an exercise. In many cases, this is not possible without the subjective scoring of an external evaluator.

To sum up, guidance through the path from arrival to labour market integration is provided in a rather segmented way by existing platforms. Having a unique platform offering all these services through a single point and having a digital companion guiding the user through it would be of high value.

Table 1: Online platforms for migrants

Platform	Organisation	Target	Type of platform	Services	Language
https://mygrants.it/	Mygrants - social enterprise - Bologna	Migrants	online training; information platform	Information on asylum and rights, social challenges, entrepreneurship; formal training opportunities; non-formal training	English French Italian
https://www.arbeitsagentur.de/fuer-menschen-aus-dem-ausland	German Ministry of Work	Migrants	information platform; online training (language); recognition of qualifications; job vacancies; e-services for inclusion	Information and support on financial, social insurance, German education, starting a business, finding a job in Germany.	German English Arabic
https://jobskills.arbetsformedlingen.se/	Swedish Public Employment Service	Migrants	job matching service	Creation of a profile, career guidance services; job matching services	English Swedish Arabic Farsi Somali Amharic

Platform	Organisation	Target	Type of platform	Services	Language
http://myskills.de/	Berufliche Kompetenzen Erkennen	Migrants	assessment platform	Online recognition of skills for people with no vocational qualification (8 professional profiles assessed)	German English Turkish Arabic Russian Persian
https://ec.europa.eu/migrantskills/#/; https://ec.europa.eu/social/main.jsp?catId=1412&langId=en	European Commission	Third country nationals	self-assessment platform	Online self-assessment tool to create a profile of skills	EU languages Arabic Farsi Pashto Sorani Somali Tigrinya Turkish
https://www.make-it-in-germany.com/en/living-in-germany/integration/advisory-service/	German Government	International qualified professionals; prospective international students; employers; Institutions	information platform	Informational content on jobs, study and training, Visa and living in Germany for those who want to move to Germany	English German Spanish French
https://www.universitaperrifugiati.it/en/default.aspx	Uninettuno telematic University - Rome	Migrants and refugees	training platform; recognition of qualifications	Recognition of study titles previously earned in their countries of origin to access the University; recognition of vocational skills	English French Italian Arabic
http://www.moocs4inclusion.org/index.php	Project funded by European Commission	Institutions with focus on migrants and refugees	training platform	Catalogue of free digital learning initiatives for migrants	English
https://www.refugee.info/	Signpost project Mercy Corps and International Rescue Committee	Migrants	information platform	Informational content for migrants, geo-mapping of services, FAQ, contact with NGOs	Italian Persian Urdu Arabic English French
https://www.infomigrants.net/en/	ANSA, Deutsche Welle, French media companies	Migrants	information platform	Information content and news for migrants	French Arabic Persian Pashto English
https://migrationdataportal.org/?i=stock_abs_&t=2017	IOM	Citizens; organisations	information and data	Data about migration	English
https://openmigration.org/en/	Italian Coalition for Civil Liberties (CILD)	Citizens; organisation	information and data	Data about migration	Italian English
http://migration.iom.int/europe?type=arrivals	IOM Migration	Citizens; organisation	information and data	Data about migration	English
https://iamamigrant.org/	IOM	Migrants and citizens	information platform	Information content and news for migrants	Arabic French Farsi Pashto

Platform	Organisation	Target	Type of platform	Services	Language
					English
https://euraxess.ec.europa.eu/jobs/science4refugees	European Commission	Refugees researchers and research groups with vacancies	matching platform for science vacancies	Information and support services on working and living in Europe; research refugee friendly internships, part-time and full-time jobs, access to an European Research Community	English
https://www.migrantsorganise.org/	a consortium of partners	Migrants and activists	online community		English

3. The Proposed Solution

We have designed a novel platform which has multiple target groups: a) refugees which are seeking for asylum, b) migrants who are seeking a better life, c) vulnerable migrants (e.g. suffering diseases), d) host authorities which are trying to improve their offerings and facilitate the integration of migrants and refugees, e) non-governmental organisations and f) organisations that consider migrants as receivers or target groups of their services.

For the users falling under the first three aforementioned categories, we aspire to assist them in preparing effective job applications and in finding appropriate positions to apply. For local people, finding a job consists primarily of three steps: as shown in Figure 1 below: 1) inspect available job positions which is usually done through a web-based job position portal or a professional social network or (more rarely) through a Human Recruitment agent; 2) filter the jobs and select those of interest to apply. Language is not a barrier for locals and the creation of a CV or an application is usually not an issue. 3) go through (one or more) interviews or follow the recruitment process of the specific organization where again, in principle,communication and specific aid is not required, although ways to maximise the potential of getting the job exist and are gaining momentum, as shown in Figure 1. For migrants and refugees, each of these steps represents a challenge: accessing the job announcement, understanding them (due to language barrier) and selecting some of them are of great difficulty. Often the CV format is not familiar to them, and usually their qualifications are not certified since they are gained via informal and nonformal experiences.

Figure 1 shows the process of labour integration without the proposed platform on the left (marked as a) and with the functionalities offered by the proposed platform on the right. As shown in the right (figure 1b), the 1st step is completely changed and automated by the proposed platform:

1. to prompt the selection of job position and relieve the migrants from searching in relevant portals which they may not be aware of, the platform prompts them to fill in their skills and profile.

2. Additionally, the platform prompts them to answer dedicated questionnaires which enable the evaluation of soft and hard skills. Artificial intelligence technology is used to evaluate the skills through these questionnaires as it will be elaborated in the next section.

3. As many refugees and migrants do not possess certification of their qualifications, the platform supports them in entering other types of proofs (e.g. images or videos). The proposed platform offers to them guidance through a wizard (step-by-step approach) and also provide videos to help them create their portfolio.
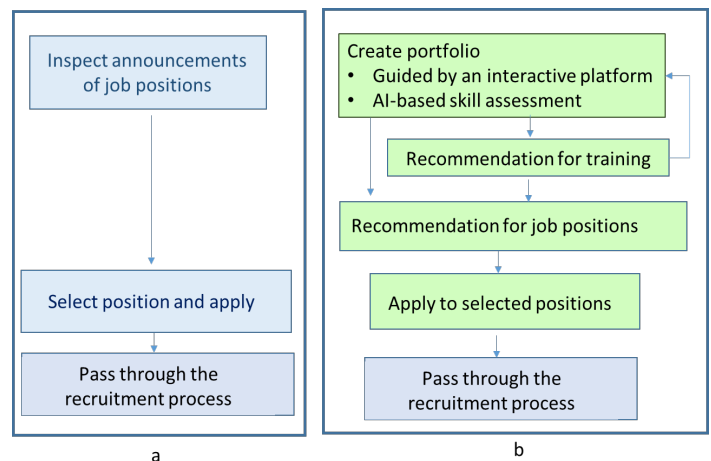
Figure 1: The path to the labour market now (shown in (a)) and with the proposed intervention (shown in (b), on the right)

Once the profile and skills are registered, the user is provided with

- Personalized recommendations about the job categories he/she is appropriate for, based on the definition of skills relevant to each occupation or more specifically to the ESCO code, i.e. to the code of the occupation category in the multilingual classification of European Skills, Competences, Qualifications and Occupations [7].

- Recommendation of additional training modules which would significantly improve their potential for getting a job. For example, assuming a user has a set of certain skills and according to these skills he matches job category A. If a skill is also needed for this job category, then a training that leads to the improvement of this skill is suggested to the migrant. This way, the migrant/refugee becomes aware of opportunities to maximise their potential for being hired.

- Once this is done, the migrant/refugee is ready to get from the proposed platform a list of job positions related with the job categories he is appropriate and then (if the wishes) to apply (e.g. send his CV created in the previous step).

To facilitate the migrants/refugees life easier, a conversational interface (a chatbot) is integrated in the platform. The proposed chatbot and the whole platform support multiple languages as it is crucial for the migrants and refugees to easily find the information they are looking for in their native language and understand the results of their activities.

Turning out attention to the rest target user groups mentioned at the beginning of this section and to offer them valuable assistance, we have designed the platform so as to represent a single-point-of-entry for them with regards to information about refugees/migrants flows, demographics of the migrants' population per country, statistics about their needs and skills as well as the means they find more useful for finding a job. For these groups, once they have set a concrete goal, (e.g. assist vulnerable migrants in finding jobs), they need as accurate information as possible and as fast as possible because the resources that can be devoted are scarce. The proposed platform essentially aggregates information and presents it to the users (indicating of course the source of the information) in an easy to understand way by employing data analytics.

Table 2: The offerings of the platform for the two target groups

Offerings targeting migrants
1. multilingual environment (English, Greek, French, Arabic, Spanish and Farsi)
2. Information about employment
3. Information about social integration
4. Skill assessment using a) Questionnaires and b) Serious games
5. Online training including a) Text, b)Videos and c) Self assessment questionnaires
6. Relocation recommendations based on the migrant's social needs
7. Recommendation of appropriate job categories (using ESCO classification)
8. Recommendation of appropriate job vacancies
9. Recommendation of trainings
10. Chatbot that is trained on the employment/social information and provides answers to migrants questions in many languages
Mobile app for foreign language learning and assessment
Tools for Host authorities, Companies and NGOs
1. Graphs and statistics about the skills of the migrants
2. Recommendations for the host authorities
Statistics regarding migration and employment in Europe

Additionally, to facilitate the task of organizations working with the migrants, the platform supports the organization of users (migrants) in groups. This way, if an organization wants to summarize the skills of a group they are managing/handling, the organization can ask the migrants to use the group identifier and fill in the skill assessment questionnaires. Then the organization can observe the statistics of the skills of this specific group and look for appropriate job positions and relevant trainings. This was considered a very valuable tool during the interviews we organized with such organisations.

To sum up, the major difference between the proposed method and the other in the literature is that no other platform adopts a holistic approach. The offerings of the proposed platform are summarised in the Table 2.

4. Technical Architecture

The technical architecture of the proposed platform is shown in Figure 2, where the distinction between the front-end components, the backend components and the repositories is clearly shown. The platform runs in a cloud environment. The front end is organized in two sets of components: a) those serving the migrants/refugees (shown on the left in green) and b) those serving Host authorities, Companies and NGOs (HCN) (shown on the right in orange). Both sets include a) a home page which is the landing page of the platform and is different per user groups once the user is logged in, b) an account page- here the user creates his/her profile inserting different information depending on the user type they belong and c) the "about" page where information for the platform, the services it provides and the way it handles the collected data is provided. In the account page, the host authorities, companies and NGOs insert their name, the services they offer and the geographical area where they operate (for example, health services in Athens). In the same page, if the user has entered as a migrant, the information collected includes personal information.

The interface for the migrants/refugees further includes: a) the "e-portfolio" component which guides step-by-step the migrant to fill in his/her skills and competences in a very user friendly way; b) the "chatbot" which responds to questions relevant to legal, social and health – it supports relevant questions in six different languages; c) the skill-assessment (SA) questionnaires which include multiple choice questions and questions requiring the association of elements (visual or textual); d) the recommender User Interface (UI) that offers recommendations for trainings and job vacancies and e) the social/career interface which offers general information about relevant issues.

The interface for the HCN group includes (apart from the three components already presented) a) the data analytics component through which the HCN finds information about the migrants' flows and needs as already described above, b) the group analytics, which presents to the HCN statistics about the group they manage and they have the rights to access (e.g. on the results from the skill assessment or their needs) and c) the social/career interface where they can upload pieces of information they consider of value to the migrants/refugees.

The back-end part is where intelligence resides. First of all, the component "neural network algorithms for skills assessment" implements artificial intelligence to evaluate a mix of thirty five hard and soft skills (like numeracy and communication) based on the serious games the migrants played. This component uses a model which has been trained with data that come from the local society. To improve the accuracy of the evaluation, we are using the platform to collect data from migrants and train the model with them to provide more accurate evaluation results.

The chatbot backend component is responsible for the processing of the information available to it (the migrants' question) by providing the appropriate answer. The proposed chatbot [8] is a Question-Answer oriented agent, capable of replying to migrant administrative service-related queries and it incorporates two different systems, a daily conversation agent
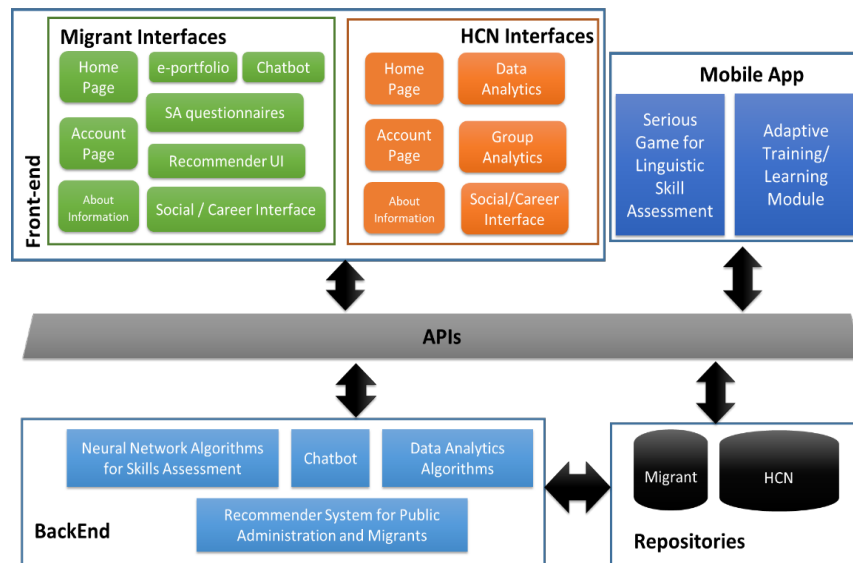
Figure 2: The technical architecture of the presented platform

based on the model released by Huggingface and an answer retrieval module. The latter initially searches for valid in regard to the user query documents, splits them into semantic paragraphs and then applies a BERT [9] fine-tuned model to finally reply to the user.

The methodology of initially splitting the document into paragraphs depending on the structure of the text, rather than directly forwarding the whole document to the model has shown improved results. Towards extending the chatbot's capabilities, aim is to further take advantage of paragraph embeddings during answer prediction, incorporating them online into the models. A challenge faced by this specific chatbot application is the support of multiple languages and more specifically the support of non-European languages like Arabic and Farsi which are spoken by significant percentages of the migrants and refugees arriving in European countries. As presented in [10] the most common countries of origin to Europe (Mediterranean) for 2019 is Afghanistan, Syria, Morocco and Algeria hence Farsi, Arabic as well as European languages (France Spanish and English) cover the vast majority of the migrant spoken languages.

The Data Analytics algorithms is the component that retrieves data from the repositories so as to present to the HCN information about migrants' flows and needs, as well as information about the performance and characteristics of each group they manage. Thus, it is connected to the data analytics and group analytics component of the front-end. More specifically, this module can display not only the skills of individuals but also the average skills of the entire group. As a result, each HCN is able to identify in an easy and user-friendly way the strengths and weaknesses of each group of migrants in order to offer to them tailored trainings based on their skills and competences.

Finally, the recommender system is responsible for the following functions:

a) it retrieves information about the migrants' social needs (which are declared by himself) and suggests relocation options. In order to identify the most suitable city for relocation, the recommender uses Quality of Life tables of European cities and correlates them with the user needs.

b) it retrieves information regarding the skills of the migrant/refugee and recommends appropriate ESCO job categories and job vacancies. More specifically, the recommender system includes 40 occupation categories, that are matched to all the second level of ESCO-classification, ensuring representativeness of all job categories that exist in the labour market. For every job category we set up thresholds that specific skills must pass in order to assign this job category to the specific user. For every job category the algorithm checks if the skill vector of the user (35 skills) passes the thresholds and if the result is positive then it returns the respective job category.

Additionally, the proposed platform suggests specific job vacancies to the users based on their recommended ESCO categories and location (city). The job vacancies are retrieved from job vacancies web sites and then each job title is assigned to one or more ESCO codes using the ESCO Web Services. The vacancy is considered suitable for the user if it is assigned to ESCO categories that have been recommended to the user. The recommender system allows the user to search for vacancies from a long list of European cities. However, the platform offers a personalized list of cities based the social needs matching (the top cities are the most suitable) in order to assist further to his relocation.

c) it recommends to the migrant trainings that would significantly improve his/her potential of being hired. The platform is equipped with training sessions designed for each of the 35 skills. Each session includes training material (text, video presentations) as well as testing and self-assessment activities.

d) it presents to host authorities evaluations of eight indicators (social, health and other defined by European initiatives) for different European cities. This way a mayor of city A could easily compare city A with other cities with respect of the eight considered aspects, check in which aspect(s) city A is lagging behind the rest of the cities and decide to proceed to implementing

measures to improve city A. For example, if city A has low evaluations in health services, the mayor may trigger appropriate actions and measures to improve health services in city A. With respect to the relocation options, it is worth providing an example: the platform prompts the migrant to declare their priorities with respect to their needs and takes them into consideration when the platform suggests to the migrant to relocate. This implies, that if a migrant has declared that health services are of premium importance, the platform will not suggest him to relocate to a city with low evaluations in health services.

To support this rich functionality, we have deployed a relational database which stores the data relevant to migrants and refugees (in one part) and relevant to HCN in the other as shown in Figure 2. To enable the communication between the repository and the frontend and backend components, a set of Application Programming Interfaces (API) has been developed.

Apart from the platform which runs through any browser and can also run as a web-based mobile app, we have considered the case where a native mobile application can be integrated with the platform. We assume a mobile application that allows the user to assess its reading and speaking competence in English or other EU languages. Having a native mobile application in place allows the evaluation of pronunciation apart from understanding. Although this application could include all the front-end interfaces of the platform, we have opted not to do so and we have kept it as different app to showcase that any relevant mobile app developed by a 3rd party, could be integrated with our platform and use the open API we have developed to include the results in the portfolio (upon specific minor modifications). Once the user interacts with the application and completes the assessment, the score (the level A1/A2, or other according to European qualification levels) is

stored as a hard skill in the repository. It is stressed that the platform supports the evaluation and storage of a set of hard skills, i.e. skills that are easy to quantify like proficiency in a language and a set of soft skills like communication and leadership which are often also called interpersonal skills. This information is directly integrated in the user's portfolio (and CV) and is considered when they seek for job recommendations. Similarly, if the recommender provides to the user a recommendation to improve his English-speaking competence, a mobile app developed for this purpose will be proposed. This app can be the one described above or any other app providing foreign speaking competence. Any training opportunity can be registered in the platform and suggested to migrants, if it fits their needs. The result from the training can be integrated in the e-portfolio and can be used during job recommendations.

In the following Figure 3, indicative screenshots of the platform are shown. In Figure 3a, the page where the user selects his type (migrant/refugee or HCN) so that the platform provides relevant information. In Figure 3b, the landing page of the migrants is shown while in Figure 3c the web page where the portfolio is created is depicted. Finally, in Figure 3d, the landing page of the HCN user is shown.

5. Evaluation in Real Life

The presented platform has been used in real life by migrants and refugees in two European countries receiving large flows: Spain and Greece. The piloting was organized in the framework of H2020-NADINE project. For the evaluation purposes, three different sub-groups of the first user group was considered: a) asylum seekers, b) recognized refugees and c) vulnerable migrants.

a)

b)

c)

d)

Figure 3: Screenshots from the platform: a) selection of type of user, b) the screen offered to the migrant, c) the page where the migrant creates their portfolio, d) the web page offered to the HCN type of user

They were invited in the premises of NGOs in these countries in small groups. They first watched a demonstration of the platform by a NADINE person which showed the different functionalities and then they were asked to use the platform and evaluate it through online questionnaires to have an objective and harmonized evaluation. The users spent two days in the premises of the NGOs. They also had the option to comment on the platform and the different pages and results they were presented with. The assessment targeted each functionality of the platform separately. The collected results and comments from the two-days tests and the 96 users were used to improve the platform. Further details on the evaluation activities, demographics of the users and details about the evaluation of each functionality can be found in [11].

The results from the real-life evaluation per functionality are shown in Figure 4. The users were asked to rate the functionalities in a 5-level Likert scale. The results showed that for e-portfolio and registration page, the "excellent" and "good" levels were scored by the majority of users. This is considered satisfactory as the proposed platform was used in Farsi and Arabic in the pilot tests. For the rest three functionalities, the results are slightly lower which comes as no surprise because any artificial intelligence-based component requires training. Up to now the AI-based components of the platform have been further trained based on limited datasets. We anticipate that as the platform is more and more used, we will use the data we collect to further train the AI-based components so that these provide more valuable results to the migrants and thus enhance their satisfaction. Namely, for the chat bot, 68% of users evaluated this as "average" and above. It is worth stressing that the migrants "talk" to the chatbot in Farsi and Arabic. Actually, for all functionalities (apart from the registration page), more than 66% of the users evaluate it as average and above. This shows that the platform, although it is currently in a prototype form, succeeds in satisfying the users. We anticipate that this first real time piloting results will help us improve the platform so as to beeter satisfy their needs. This also contributes to the sustainability of the platform. The "language assessment" functionality was tested through a mobile app which injected the results in the presented platform. This way the potential of integrating 3rd party applications was confirmed.
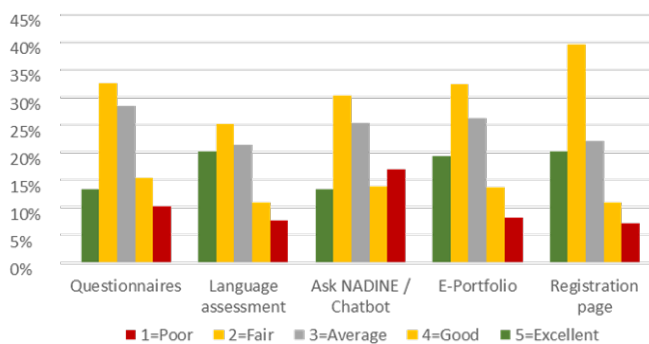
Figure 4: Statistics of the assessment results per component

For each functionality included in the figure, a set of 10 indices were evaluated including: "easy to use", "enjoyable activity", "meet my expectations", "comprehensive/clear", "time spending", "cover my personal needs", "easy to navigate", "overall aesthetics" along with some additional ones which are linked to the

specifics of each functionality. These results together with the comments received through free text questions are now used to improve the platform. A common observation was that higher levels of satisfaction were indicated by vulnerable migrants compared to the rest two categories of recognized migrants and asylum seekers. In the language assessment, the percentages of results do not sum up to 100% as a percentage of the pilot users did not test and thus did not rate the language mobile app.

Moreover, and in order to evaluate the participants' overall experience from the platform, more specific aspects were also examined: Likelihood of recommending NADINE platform, User friendliness of NADINE platform, on which level the platform covers the participants' personal needs / requirements, How comprehensive and clear it is, Easiness to use and understand NADINE platform, Easiness to navigate through NADINE platform, Effectiveness and usefulness. All results regarding the evaluation of the participants' overall experience from NADINE platform are thoroughly demonstrated in the Figure 5. The result is very satisfactory, as the strong majority reports good experience for the platform which is currently in prototype level. Further details of the evaluation can be found in [11].
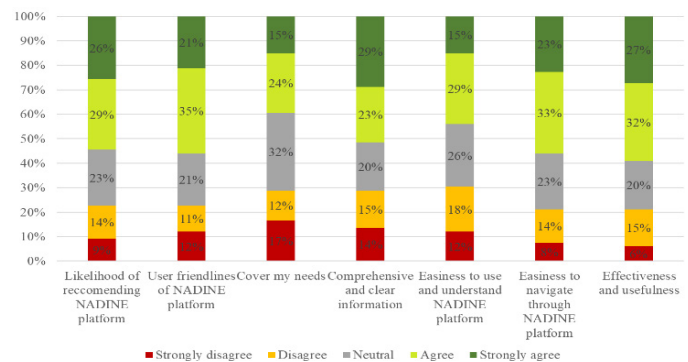
Figure 5: Statistics of the assessment results per component

Turning our attention to the host authorities, NGOs and private organisations, in this phase, ten (10) interviews were conducted. The main outcomes of the interviews were: a) finding information in a single point saves a lot of time for them as they have a clear picture of the situation in significantly shorter time; b) for NGOs working with migrants, the data analytics presented by the platform regarding the information relevant to the groups of migrants they work with was considered an extremely valuable tool; c) for host authorities, the most valuable functionality was the ability to see the sector (social, health, other) that they lack behind and also the ability to communicate with the migrants; for organizations working towards job finding for migrants, having in place a component that evaluates the skills in an accurate way for migrants and refugees is very valuable. They all consider the platform a valuable tool for their everyday job which creates the expectation that the number of migrants and of HCN users engaged with the platform will continuously increase. HCN actors considered that the deployment of a platform like the presented one requires funding from host authorities (regional or national) or EU-wide initiatives.

6. Conclusions

The societal inclusion of migrants and refugees passes through their integration in the labour market. A platform that supports all

their way to the labour market has been proposed in this paper. Its novelty lies not only in the fact that it does support them along the whole path but also on the fact that it exploits mature ICT technologies like artificial intelligence and data analytics to offer unprecedented experience to the users. Utilising artificial intelligence, a set of soft and hard skill are assessed through the platform. Through an appropriately designed user interface, the users are guided to create their e-portfolio. Based on this information, appropriate job sectors and concrete job positions are suggested to the users. The host organizations in turn enjoy mainly data analytics which offer them appropriate information facilitating their decision making. The offerings of the proposed platform prototype have been positively evaluated in real life in two countries receiving large numbers of refugees and migrants.

Acknowledgment

References

[1] H.C. Leligou, D. Anastosopoulos, A. Montagna, V. Solachidis, N. Vretos, "Embracing novel ICT technologies to support the journey from camp to job," in 2020 IEEE International Conference on Multimedia and Expo Workshops, ICMEW 2020, Institute of Electrical and Electronics Engineers Inc., 2020, doi:10.1109/ICMEW46912.2020.9106035.

[2] H.U. of E. Reallabor Asyl, The labour market integration of refugees ' white paper – A focus on Europe, 2017.

[3] International Labor Organization, "How to Facilitate the Recognition of Skills of Migrant Workers Guide for Employment Services Providers Second Edition," 99, 2020.

[4] Council Recommendation of 22 May 2018 on key competences for lifelong learning Text with EEA relevance., 2018/C 189/01, 2018.

[5] L. Falahati, L. Paim, M. Ismail, S.A. Haron, J. Masud, "Assessment of university students financial management skills and educational needs," African Journal of Business Management, **5**(15), 6085–6091, 2011, doi:10.5897/AJBM10.1583.

[6] A. Jin, S. Yeung, J. Jopling, J. Krause, D. Azagury, A. Milstein, L. Fei-Fei, "Tool Detection and Operative Skill Assessment in Surgical Videos Using Region-Based Convolutional Neural Networks," 2018. arXiv preprint arXiv:1802.08774, 2018.

[7] https://ec.europa.eu/esco/portal/escopedia/Occupation

[8] A. Lelis, N. Vretos, P. Daras, "Nadine-bot: An open domain migrant integration administrative agent," in 2020 IEEE International Conference on Multimedia and Expo Workshops, ICMEW 2020, Institute of Electrical and Electronics Engineers Inc., 2020, doi:10.1109/ICMEW46912.2020.9106024.

[9] C. Alberti, K. Lee, M. Collins, "A BERT Baseline for the Natural Questions," arXiv preprint arXiv:1901.08634, 2019.

[10] Refugee and Migrant Arrivals to Europe - Jan to Dec 2019, Feb. 2021. - https://data2.unhcr.org/en/documents/details/74670

[11] https://nadine-project.eu/deliverables/

Analysis of qCON and qNOX Anesthesia Indices and EEG Spectral Energy during Natural Sleep Stages

Joana Cañellas[*], Anaïs Espinoso, Juan Felipe Ortega, Umberto Melia, Carmen González, Erik Weber Jensen

Quantium Medical, Research and Development Department, 08302 Mataró, Spain

A R T I C L E   I N F O

A B S T R A C T

The objective of this research is to study the behaviour of the anaesthesia monitor Conox during natural sleep to open the gate for this devices to assess subjects during this stage. The values of qCON and qNOX indices and EEG frequency bands are analysed during night sleep of 10 volunteers when they lose consciousness, in order to determine if they can be used for monitoring sleep. The possibility of using these indexes to differentiate between NREM/REM cycles of night sleep is studied. A reduction in the hypnotic index was observed while the nociception index stayed significantly higher. Statistical differences where found for qCON between sleep cycles, allowing this index to detect REM intervals and possibly opening the gate to use depth of anaesthesia devices to monitor sleep.

1   Introduction

This paper is an extension of work originally reported in 11th Conference of the ESGCO [1].

Sleep disorders such as insomnia, abnormal movements or behavior during night, and inability to control the sleep hours, can cause severe health problems such as depression or attention deficit hyperactivity disorder. Hence, sleep is widely studied in order to develop methods to detect these disorders by its monitoring. Some relevant laboratory tests for studying sleep disorders consists of an overnight polysomnography, measuring how fast the patients fall asleep and their attention for being awake as well as actigraphy [2]. Nowadays, there are commercial medical devices designed to monitor the level of consciousness during general anesthesia, allowing the anesthesiologists to individually tailor the administration of anesthetics. These devices monitor and process the electroencephalography (EEG) that is recorded by non-invasively locating electrodes on the forehead of the patient. The frequency and the amplitude of the EEG evolve because of changes in cerebral activity between wakefulness and sleep stages, and these variations can also be used to differentiate between the rapid eye movement (REM) and non-rapid eye movement (NREM) states of sleep. The energy of the EEG frequency bands Delta, Theta, Alpha, Beta and Gamma (from lower to higher frequencies) also varies between natural sleep stages according to literature [3], being the REM stage characterized by a decrease in the energy of low frequencies such as Delta band, and an increase in high frequencies as Beta and Gamma

bands. Previous studies [4, 5] have proposed to use EEG monitoring devices to measure also the natural sleep further than using them only for anesthesia assessment. In this work we analyzed the behavior of the anesthesia monitor Conox (Fresenius Kabi, Bad Homburg, Germany), during natural sleep. Sleep disorders such as insomnia, abnormal movements or behavior during night, and inability to control the sleep hours, can cause severe health problems such as depression or attention deficit hyperactivity disorder. Hence, sleep is widely studied in order to develop methods to detect these disorders by its monitoring. Some relevant laboratory tests for studying sleep disorders consists of an overnight polysomnography, measuring how fast the patients fall asleep and their attention for being awake as well as actigraphy [2].

Nowadays, there are commercial medical devices designed to monitor the level of consciousness during general anesthesia, allowing the anesthesiologists to individually tailor the administration of anesthetics. These devices monitor and process the electroencephalography (EEG) that is recorded by non-invasively locating electrodes on the forehead of the patient. The frequency and the amplitude of the EEG evolve because of changes in cerebral activity between wakefulness and sleep stages, and these variations can also be used to differentiate between the rapid eye movement (REM) and non-rapid eye movement (NREM) states of sleep. The energy of the EEG frequency bands Delta, Theta, Alpha, Beta and Gamma (from lower to higher frequencies) also varies between natural sleep stages according to literature [3], being the REM stage characterized by a decrease in the energy of low frequencies such as Delta

---
[*]Corresponding Author: Joana Cañellas, Av. Ernest Lluch 32, Office 3.17, Mataró 08302, +34 619534413 | Email: jc@quantiummedical.com
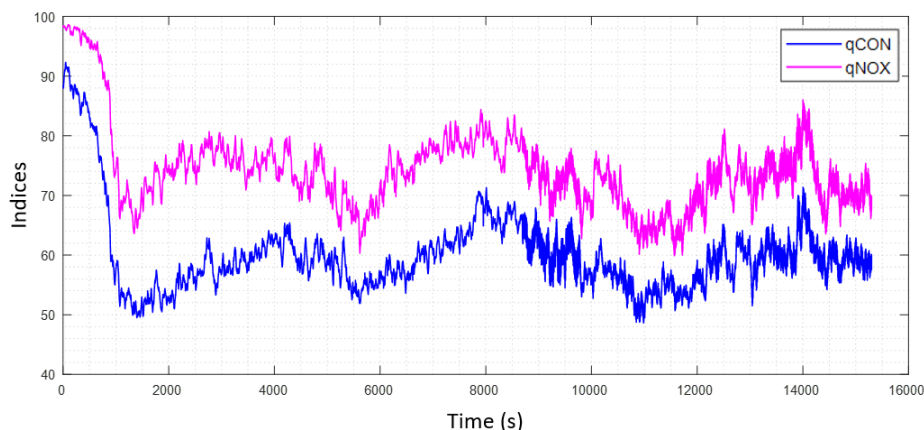
Figure 1: Mean qCON and qNOX for all volunteers from 15 minutes before loss of consciousness (qCON=60) until 4 hours after.

band, and an increase in high frequencies as Beta and Gamma bands. Previous studies [4, 5] have proposed to use EEG monitoring devices to measure also the natural sleep further than using them only for anesthesia assessment. In this work we analyzed the behavior of the anesthesia monitor Conox (Fresenius Kabi, Bad Homburg, Germany), during natural sleep.

2 Methods

In order to obtain the evolution of both anesthesia indexes during natural sleep, 10 volunteers were accepted for this study and agreed to be connected to a Conox device during one night sleep. Signal registration started a few moments before the subject falling asleep and lasted for at least six hours. As an indicator for unconsciousness, the same threshold as in clinical practice during a surgery was used, being a qCON value of 60. A Mann-Whitney U test and also a paired Wilcoxon test were performed in order to analyze if there was significant difference between the two indices. Instants of both indices falling below different thresholds (90, 80, 70 and 60) were also computed in order to know the time decay of each index when the subjects are losing consciousness.

From the EEG signal recorded we analyzed the spectrum in five frequency bands: Delta (0.5 - 4 Hz), Theta (4.5 - 8 Hz), Alpha (8.5 – 13.5 Hz), Beta 1 (14 - 20 Hz) and Beta 2 (20.5 - 30 Hz). Beta energy has been divided in two separate ranges for a better differentiation of the behavior of each frequency since the whole Beta range is very wide. The energy was calculated applying the Fast Fourier Transform (FFT) on 2-seconds EEG windows with overlap of 1 second. The FFT was normalized by the energy contained between the 0.5 and 30 Hz range. A 60 samples moving average smoothing filter was applied for a better visualization of the results, and the mean value of each frequency band was calculated during awake and asleep stages. It was considered that patients were awake when the qCON value was above 60, and asleep otherwise. To determine if there were significant differences between the values of the frequency bands between sleep and awake stages, a Wilcoxon signed rank test was used, at significance level of 0.05.

Taking into consideration the variation of energy in high and low frequencies, to distinguish between REM and NREM stages, we proposed an adaptive threshold for Delta and Beta 2 energy based on a preliminary data analysis which indicated that these frequency bands are the most affected by the transition between sleep stages. Delta threshold is calculated as the 80 % of the difference between maximum and mean energy values during the last 3600 seconds of recording. Beta 2 threshold is calculated as the 80 % of the difference between mean and minimum energy values during the last 3600 seconds of recording. We considered that a REM interval was detected when Delta energy was below the threshold and Beta 2 energy was above it, short intervals being less than 5 minutes were not considered.
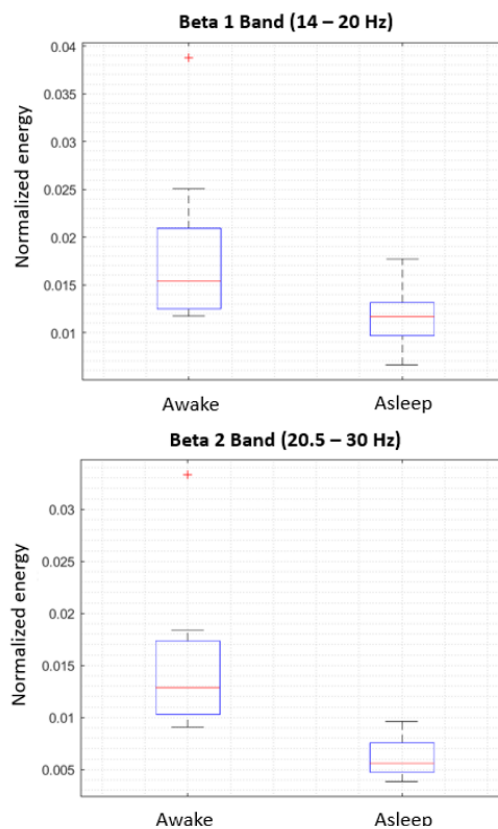
Figure 2: Boxplots of Beta 1 (above) and Beta 2 (below) bands during awake (qCON $\geq$ 60) and asleep (qCON < 60) stages. On each box, the central mark is the median, the edges of the box are the 25th and 75th percentiles. The outliers are marked with a +.

We studied the values of qCON and qNOX during the REM and NREM stages previously identified, and we performed a Wilcoxon signed rank test, at significance level of 0.05, for comparison of the indices.

Table 1: Column 1 shows the mean value ± standard deviation of the qCON for each volunteer when below 60 and column 2 shows the corresponding mean value of qNOX when qCON is below 60. The last column shows the difference between the mean values of qCON and qNOX. The last row indicates the mean and the standard deviation for all volunteers, where qNOX has significantly higher values as compared with qCON. (*p-value = 0.002)

ID	Mean value qCON<60	Mean value qNOX (when qCON<60)	qNOX-qCON
1	45.46 ± 6.11	62.36 ± 10.07	16.90 ± 11.78
2	50.02 ± 5.71	61.72 ± 7.34	11.69 ± 9.30
3	50.73 ± 5.87	61.93 ± 10.71	11.20 ± 12.22
4	45.09 ± 6.92	57.03 ± 12.64	11.94 ± 14.41
5	50.78 ± 4.83	65.51 ± 8.32	14.74 ± 9.62
6	50.77 ± 4.68	64.97 ± 7.20	14.19 ± 8.59
7	48.99 ± 4.71	58.28 ± 8.65	9.30 ± 9.85
8	52.06 ± 4.19	72.69 ± 6.91	20.63 ± 8.08
9	56.09 ± 2.52	72.62 ± 5.47	16.53 ± 6.02
10	55.45 ± 2.84	77.89 ± 5.83	22.44 ± 6.48
Mean all volunteers	50.54 ± 3.58*	65.50 ± 6.81*	14.96 ± 4.23

Table 2: Difference of time decay between qCON and qNOX to reach thresholds during the first loss of consciousness (N.A: not available due to qNOX always above the threshold).

ID	Time decay difference between qNOX and qCON for different thresholds in minutes			
	qCON and qNOX ≤ 90	qCON and qNOX ≤ 80	qCON and qNOX ≤ 70	qCON and qNOX ≤ 60
1	12.30	14.93	11.57	2.35
2	5.78	4.70	3.65	4.12
3	7.30	N.A.	7.35	2.85
4	6.20	9.93	7.80	N.A.
5	3.25	4.02	2.02	7.35
6	0.30	1.38	2.72	4.55
7	N.A.	9.51	5.03	0.80
8	N.A.	N.A.	10.65	N.A.
9	N.A.	5.60	4.83	N.A.
10	14.85	11.15	8.72	N.A.
Mean all volunteers	7.14 ± 5.01	7.65 ± 4.46	6.43 ± 3.29	3.67 ± 2.24

3 Results

In Figure 1, average indices values across volunteers are shown and it can be observed that nociception (qNOX index) stays higher than consciousness (qCON index) during sleep. The differences between the two indices were statistically significant (p-value < 0.05, Mann-Whitney U test). In Table 1 mean values of both indexes

are compared when qCON is below 60 for every subject. Results confirm that qNOX was higher for all patients than qCON (p-value < 0.05, Wilcoxon paired test). Table 2 includes the differences of time decay between indexes, showing that qNOX takes more time to fall under all thresholds set than qCON, and in some case never decreases under those values.

The spectrum analysis of the EEG showed that the energy in the low frequency bands Delta, Theta and Alpha present no significant differences between awake and asleep stages (p-values > 0.05, Wilcoxon signed rank test). On the contrary, the energy from Beta 1 and Beta 2 did have significant differences and showed on average higher values while the volunteers were awake (Table 3). The difference in energy value of these bands for both stages can also be observed in Figure 2.

In Figure 3 we can observe the transition between NREM and REM intervals after applying the adaptive thresholds designed. It can be observed that these transitions occurred with certain periodicity during all recording.
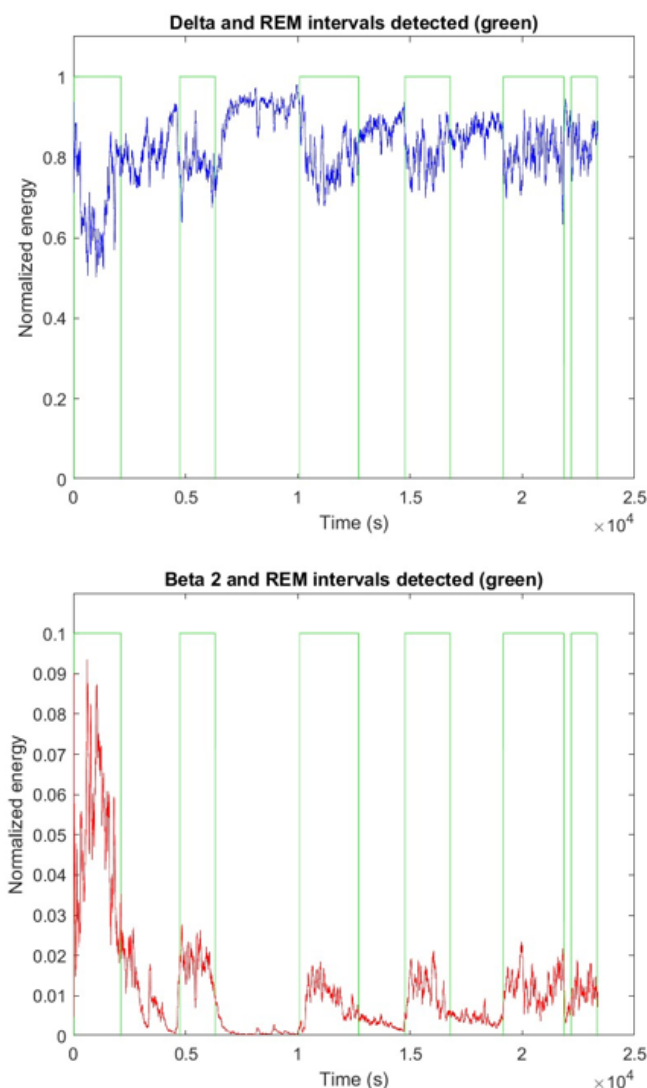
Figure 3: Delta (above) and Beta 2 (below) energy from one subject. The transition between REM and NREM, which corresponds with the moment where the value of Delta and Beta 2 pass their respective thresholds, is represented with the green line.

Table 3: Mean ± standard deviation values of the five selected EEG frequency bands for the periods where the subjects are awake and when they are asleep. P-value is obtained from a Wilcoxon signed rank test, at significance level of 0.05.

	Mean value Awake (qCon ≥ 60)	Mean value Asleep (qCon < 60)	p-value
Delta (0.5 - 4 Hz)	0.856 ± 0.137	0.866 ± 0.122	0.625
Theta (4.5 - 8 Hz)	0.068 ± 0.071	0.069 ± 0.064	0.920
Alfa (8.5 - 13.5 Hz)	0.042 ± 0.054	0.047 ± 0.065	0.695
Beta 1 (14 – 20 Hz)	0.019 ± 0.023	0.012 ± 0.016	0.019
Beta 2 (20.5 – 30 Hz)	0.015 ± 0.020	0.006 ± 0.008	0.002

Table 4: Mean values of qCON during REM and NREM stages for each volunteer and Wilcoxon signed rank test between both sleep stages revealing statistically significant differences (p < 0.05).

qCON			
ID	**Mean value NREM**	**Mean value REM**	**p-value**
1	48.91 ± 12.46	63.50 ± 10.23	
2	55.25 ± 10.39	68.96 ± 13.35	
3	57.19 ± 11.64	56.15 ± 15.73	
4	68.17 ± 21.49	60.45 ± 18.32	
5	53.84 ± 10.67	65.87 ± 7.47	
6	56.91 ± 9.01	67.26 ± 15.32	
7	51.49 ± 8.21	53.64 ± 12.95	
8	55.74 ± 9.38	74.84 ± 10.49	
9	72.23 ± 12.20	69.33 ± 8.64	
10	58.44 ± 6.95	68.08 ± 8.40	
Mean all volunteers	57.82 ± 11.24	64.81 ± 12.09	0.049

Table 5: Mean values of qNOX during REM and NREM stages for each volunteer and Wilcoxon signed rank test, no significant differences were obtained (p > 0.05).

qNOX			
ID	**Mean value NREM**	**Mean value REM**	**p-value**
1	65.94 ± 13.97	81.59 ± 13.49	
2	66.66 ± 10.77	77.21 ± 13.56	
3	75.08 ± 14.86	64.23 ± 14.50	
4	81.99 ± 19.66	71.14 ± 18.54	
5	70.77 ± 9.99	72.61 ± 11.74	
6	72.21 ± 11.26	77.65 ± 12.64	
7	64.13 ± 10.63	60.57 ± 12.77	
8	76.34 ± 8.30	79.67 ± 13.16	
9	88.38 ± 9.50	82.16 ± 10.70	
10	81.35 ± 6.72	84.28 ± 9.65	
Mean all volunteers	74.29 ± 11.57	75.11 ± 13.07	1.00

The results regarding the qCON and the qNOX values during the REM and NREM stages, previously delimited with the thresholds,

showed significant differences in qCON values between stages (p-value < 0.05, Wilcoxon signed rank test), which was not observed in qNOX values, as shown in Table 4 and Table 5 respectively. In the boxplot of Figure 4 there is a representation of the differences in the qCON values for REM and NREM.
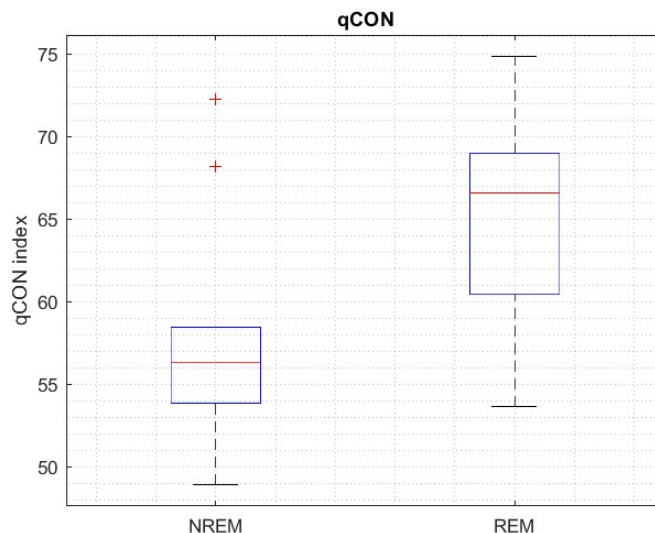
Figure 4: Boxplot containing the values of the qCON index during the sections of NREM and REM of night sleep. On each box, the central mark is the median, the edges of the box are the 25th and 75th percentiles. The outliers are marked with a +.
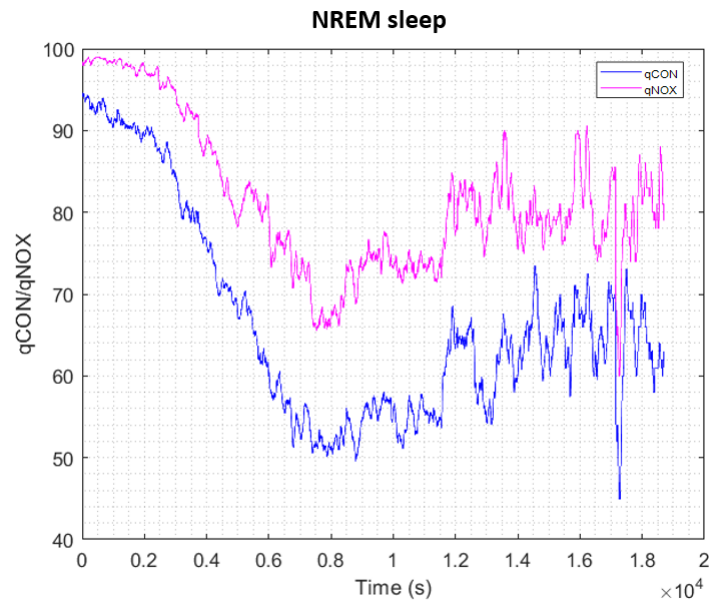
Figure 5: Mean qCON and qNOX for all volunteers during NREM interval. The indices have been aligned at the beginning of NREM interval of each subject.

The trends of the mean qCON and qNOX values for NREM and REM are shown in Figure 5 and Figure 6 respectively. The data of the volunteers has been aligned at the beginning of the REM interval that was around 5000 seconds for all cases. It can be noted from Figure 5 that in NREM sleep qCON and qNOX decrease until the minimum in the first part of the recording and then slightly increase

in the last part, showing more variability. During REM sleep (Figure 6) qCON and qNOX time evolution decreases in the first part of the recording to a stable value that is maintained until the last part, where the index values are lower.
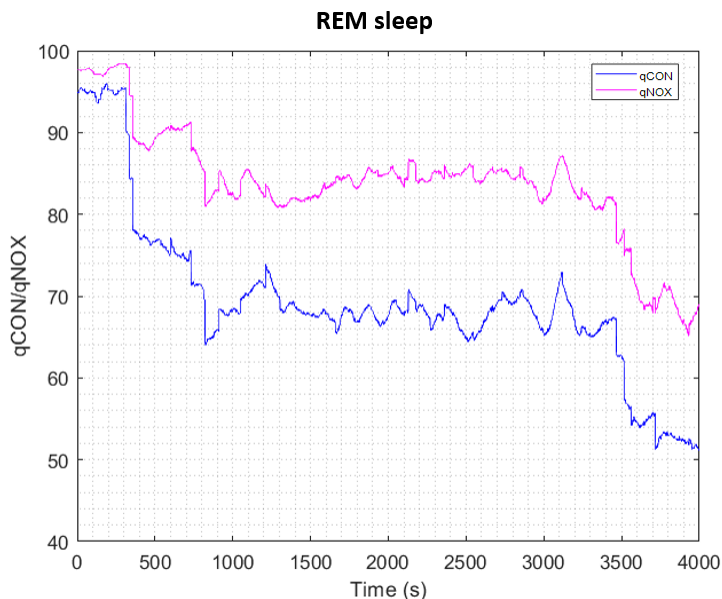
Figure 6: Mean qCON and qNOX for all volunteers during REM interval. The indices have been aligned at the beginning of REM interval of each subject.

4   Discussion

In this study it was found that qCON and qNOX indices behave differently during general anesthesia than compared to natural sleep. During anesthesia, anesthetic and analgesic agents are administrated to reduce both consciousness and nociception levels [6], whereas during night sleep, loss of consciousness is not accompanied by a similar nociception reduction.

Literature suggests that an increase in the energy of Beta is correlated with arousal during sleep [7], as higher values in this band are associated with an awake state. The increases in Beta during sleep found in this study could be related with sympathetic overactivity, which is associated with fragmented sleep [7].

Different NREM and REM sleep stages during natural sleep are characterized by changes in energy distribution in the frequency domain of EEG such as slow (Delta) and fast (Beta 2) oscillation patterns and also other physiological parameters. Indeed, in medical practice, polysomnography is considered the gold standard in sleep analysis because it takes into account several physiological signals such as electrooculogram (EOG) to identify rapid eye movements and electromyogram (EMG) to detect lack of muscular tone, which are characteristic physiological parameters of REM sleep [8]. Conox monitor performance is based on the processing of the EEG, hence it does not take into consideration as many parameters as a polysomnography. Despite that, from the results obtained in this study, qCON index has been able to correctly identify REM intervals

Other studies have been performed about depth of anesthesia monitors being used to monitor sleep since they provide real time EEG data that may be of some value for assessing sleep. A study performed with Sedline monitor (Masimo, Irvine CA) showed higher values during awake and the first parts of the sleep recording, as entering into deeper sleep stages the index of the monitor decreased considerably [5]. From the results obtained with the Conox it has been observed this same tendency, higher qCON values when awake and a decrease as the subject falls asleep. Nevertheless, qCON showed an increase during REM intervals, whereas the Sedline index continued at low values. Another sleep study performed with Bis Vista (Covidien, CO, USA) showed similar results than qCON during REM stage, with a mean (SD) BIS value of 75 (10) [9]. The mean (SD) value of qCON during REM interval was 64.81 (12.09), it is possible to differentiate this interval from an awake state where qCON values are higher.

In regard with nociception, qNOX index showed higher values during sleep than those observed in general anesthesia. Since qNOX index decreases with the administration of analgesic drugs, it could be expected to obtain higher values during sleep than in surgical procedures, where no analgesics are involved.

5   Conclusions

Analysis presented here allows to conclude that natural sleep is characterized by a reduction in consciousness which can fit into ranges similar to general anesthesia, especially during NREM sleep (qCON below 60), but that nociception (qNOX index) tends to remain higher, revealing that an asleep person can still respond to external painful stimuli. It has also been observed that when the subject is losing consciousness, the nociception index decreases slower than the consciousness index.

When studying the energy of the different EEG frequency bands, no significant differences were encountered in the low frequencies between the awake and asleep periods. Nevertheless, higher frequencies did show an increase in their energy when the subjects are awake.

By analyzing time series of energy contained in Delta and Beta 2 bands, one can identify cycles during night sleep. After studying qCON and qNOX indices evolution during these cycles, it can be concluded that qCON has greater values in REM intervals, whereas qNOX does not show significant differences between sleep stages. The significant differences of qCON values between NREM and REM cycles suggest that this index can also be used to differentiate these two stages of night sleep. The Conox monitor does not consider as many sleep parameters as the gold standard, polysomnography. Nevertheless, the present investigation is a preliminary study that might open the gate to use depth of anesthesia devices as Conox to monitor sleep, since it has proven to be able to detect the different sleep cycles by processing the energy of the EEG bands.

For future studies it would be interesting to consider a wider sample of patients, including some subjects with sleep disorders to observe differences in the results against healthy patients.

References

[1] A. Espinoso, J. Cañellas, U. Melia, P. Gambús, C. González, E. Jensen, "Study of the evolution of the anaesthesia indices qCON and qNOX during natural sleep," in 2020 11th Conference of the European Study Group on Cardiovascular Oscillations (ESGCO), 1–2, IEEE, 2020, doi:10.1109/ESGCO49734.2020.9158018.

[2] S. Chokroverty, et al., "Overview of sleep & sleep disorders," Indian J Med Res, **131**(2), 126–140, 2010, doi:10.17241/smr.2011.2.1.1.

[3] R. Ferri, F. I. Cosentino, M. Elia, S. A. Musumeci, R. Marinig, P. Bergonzi, "Relationship between Delta, Sigma, Beta, and Gamma EEG bands at REM sleep onset and REM sleep end," Clinical Neurophysiology, **112**(11), 2046–2052, 2001, doi:10.1016/S1388-2457(01)00656-3.

[4] C. McPherson, K. Behbehani, D. Dao, J. Burk, E. Lucas, "Characterization of sleep using bispectral analysis," in 2001 Conference Proceedings of the 23rd Annual International Conference of the IEEE Engineering in Medicine and Biology Society, volume 3, 2216–2219, IEEE, 2001, doi: 10.1109/EGCO49734.2020.9158020.

[5] C. Kapp, N. Punjabi, "Using a Sedation Monitor to Assess Sleep," in B65. SRN: DIAGNOSIS AND MONITORING OF SLEEP AND SLEEP DISORDERS, A3884–A3884, American Thoracic Society, 2019.

[6] E. Jensen, J. Valencia, A. López, T. Anglada, M. Agustí, Y. Ramos, R. Serra, M. Jospin, P. Pineda, P. Gambus, "Monitoring hypnotic effect and nociception with two EEG-derived indices, qCON and qNOX, during general anaesthesia," Acta Anaesthesiologica Scandinavica, **58**(8), 933–941, 2014.

[7] T. B. Kuo, C.-Y. Chen, Y.-C. Hsu, C. C. Yang, "EEG beta power and heart rate variability describe the association between cortical and autonomic arousals across sleep," Autonomic Neuroscience, **194**, 32–37, 2016, doi: 10.1016/S1388-2457(02)00656.

[8] "Polysomnography: Overview, Parameters Monitored, Staging of Sleep." Available: https://emedicine.medscape.com/article/1188764-overview#a2 (visited on 18-12-2020).

[9] M.-R. Benissa, S. Khirani, S. Hartley, A. Adala, A. Ramirez, M. Fernandez-Bolanos, M.-A. Quera-Salva, B. Fauroux, "Utility of the bispectral index for assessing natural physiological sleep stages in children and young adults," Journal of clinical monitoring and computing, **30**(6), 957–963, 2016.

SEA: An UML Profile for Software Evolution Analysis in Design Phase

Akram Ajouli[1,2,*]

[1]*Department of Computer Science, College of Computer and Information sciences, Jouf University, Sakaka 2014, KSA*

[2]*High Institute of Applied Sciences and Technology of Gafsa, Gafsa University, Gafsa, 2100, Tunisia*

A R T I C L E   I N F O

A B S T R A C T

Software evolution is one of the software process activities that occupies a major percentage of software development cost. Since requirements change continually and new technologies emerge, software should be adapted to satisfy these new changes to continue to survive. Despite software evolution being performed after software validation and deployment, software developers should predict at earlier stages how software would evolve in the future to avoid surprises. Although many works focus on how to enhance the program structure to facilitate maintenance tasks, only few works treat software evolution in earlier phases of software development process. In this direction, we propose an UML profile that permits to tackle software maintenance issues at the early phases of software development process. The proposed approach helps software developers to predict in design phase the kind of maintenance tasks that could occur in the future.

1   Introduction

According to [1], software evolves and changes continually in order to support new emerging technologies and satisfy customers and business needs. Some studies estimate that software evolution could reach more that 60% of software development total cost [2]. This issue pushes software engineering community to focus on how optimizing software evolution cost.

In fact, software maintenance cost varies depend on the kind of maintenance tasks that will be performed. For example, if the source code to be maintained is crosscutting among software modules, maintenance tasks performed on that source code are as well, the thing that could generate an extra cost. But, if the source code to be maintained is encapsulated in a single module, software maintenance applied to that source code is modular (less time and less cost).

Duality among crosscutting maintenance and modular maintenance motivates the community to provide solutions to keep software maintenance being modular. For example, some design patterns [3] and some program structuring/decomposition [4]–[8] facilitate software reuse and maintenance. But, even though some solutions could assure modular software maintenance, the challenge still existing since software maintenance could be modular for the same program with respect to a given architecture/structure but not

with respect to another. A such problem is known as tyranny of decomposition or expression problem [9] (see Sect. 3 for more details). To resolve this problem, many works ([10]–[14]) tried to attenuate the effect of tyranny of decomposition on software maintenance but results still relative and they treat this issue only in source code level.

In this paper, we illustrate how software developers could tackle software maintenance issues at the design phase of software development process. The early treatment and analysis of software maintenance tasks that could occur later permits to get a clear overview about how the program will evolve in the future. The main goal is to specify from the beginning the program structure that is more adaptable for future maintenance tasks. This could be realized by: first, identifying what kind of maintenance tasks is more probable to occur and then recommending the program architecture that is more adaptable to this kind of maintenance tasks. To concertize our approach, we define an UML profile that helps software developers to analyze and predict the kind of future software maintenance tasks that could occur.

The rest of this paper is organized as follows: first, we explore some related works (Sect. 2). Then, we give some explanations about tyranny of program decomposition problem. We show also how this problem affects modular maintenance (Sect. 3). Next, we present how we have defined *SEA* UML profile (Sect. 4). After that,

*Corresponding Author: Akram Ajouli, Department of Computer Science, College of Computer and Information sciences, Jouf University, Sakaka 2014, KSA , Contact No: +966547205946 & Email: asajouni@ju.edu.sa

we show how we validated *SEA* by applying some stereotypes in a real case study (Sect. 5). Finally, we resume our contributions and we propose some future works (Sect. 6).

2 Related work

In fact, this paper is an extension of the paper [15] (presented in the International Conference on Computer and Information Sciences (ICCIS) in 2019). In [15], the approach consists of proposing an UML profile called *MODEM* used to model maintenance tasks in design phase. This profile provides some UML stereotypes that permits to software developers to model and analyse maintenance tasks before occurring. The extension we propose in this work consists of adding more details and semantics to the previous work. We have modified some stereotypes, added new stereotypes and added tagged values in order to better analyse and predict in design phase future maintenance tasks that could occur. Further more, comparing to the previous work, we validate the extended UML profile by apply it to a real case study.

In [16], the author proposed a process of eight steps helping to supervise maintenance tasks that could occur later. Their approach simulates communications between stakeholders in order to design maintenance tasks, apply them and test software again before delivering the final version. In [17], the author proposed also an approach that aims to treat maintenance tasks in early phases of software development. They propose a software maintenance life cycle model that relies on a process of four steps. During this process, stakeholders interact between each other to study and analyze maintenance tasks to do in order to guarantee a consistent planning for performing maintenance tasks. The process is incremental and iterative and it stops when maintenance tasks analysis proves that software maintenance requests percentage becomes under a given threshold.

Although these works show a relevant contribution in planning maintenance tasks at earlier stages of software development, both of them involve different stakeholders to express needed maintenance tasks which could disturb software development process. In addition, maintenance issue is not expressed explicitly in models as we propose in our approach.

In [18], the author proposed an UML profile that permits to support requirements evolution. Their method is tool supported and consists of extending requirements engineering process by making it supporting requirements evolution. Although this approach facilitates requirements changes management, it still limited to specification phase. In our work, we focus more on design phase because we treat a problem which is related to software architecture rather than software requirements.

Some other works like [19]–[22] focus on analyzing and expressing design patterns explicitly at early phases of software development by defining the appropriate UML profiles. These works aim to enhance design patterns implementation comprehension for programmers since design pattern does not appear explicitly on source code. These works focus more on improving software comprehension rather than treating software evolution issue.

Some other works such as [13] and [23] treat maintenance issues in implementation phase by providing reversible transformations

among dual design patterns (composite and visitor) in order to keep maintenance tasks modular. In [24], the author proposed also a relevant approach that treats software maintenance issue in source code level. Their approach consists first of exploring the best machine learning techniques used for predicting software maintenance and then improving their performance. Although these works show important contributions in treating software maintenance issues, they still limited to implementation phase while we focus more on tackling this issue in earlier software process activities.

3 Background

We present in this section an overview about potential challenges that software evolution could face. One of the issues that could affect software evolution is tyranny of decomposition or expression problem [9]. In fact, although software modularity enhances program structure and facilitates software maintenance, a modular program structure could be biased to one kind of modular maintenance and not to another. A maintenance task is called modular when changes are mostly encapsulated in one module. Contrary to this, if changes touches many modules at the same time, the maintenance task is called crosscutting.

For example, Figure 1 illustrates a program composed of two classes *Circle* and *Rectangle* that extend an abstract class *Shape*. The program contains also two methods *print()* and *show()* which represent the business code of the program. The structure of the program is a base form of Composite design pattern in which each data type is encapsulated in a module. A such program structure decomposes the program with respect to data-types axis.

The decomposition of the program (Figure 1) permits to perform modular maintenance with respect to data-types. For instance, if we add a new shape (a Triangle for example) to the hierarchy of shapes shown in Figure 1, we first create a new class, then, we redefine the code of methods *print()* and *show()* only in this new class. In this case, the maintenance task is modular (low cost). But, if we add a new feature to the program (for example a method *color()*), we have to implement it in all classes which causes a crosscutting maintenance (extra cost). We deduce that the architecture of the program shown in Figure 1 allows a modular maintenance with respect to data-types and not with respect to functions (methods). Hence, the program structure is dominated by the data-types decomposition axis (a tyranny of decomposition according to data-types).

Another axis of decomposition of the program described above is illustrated in Figure 2. This program represents the Visitor design pattern implementation of the program shown in Figure 1. The Visitor pattern encapsulates each business code in a single module: the business code *print* is encapsulated in module/class *Print* and the business code *show* is encapsulated in module/class *Show*. This program structure decomposes the program with respect to functions which permits to add a new function without touching other modules: for example if we add a feature *color* to the program, we add a new class in which we implement this new feature for all shapes. Thus, Visitor design pattern permits to perform modular maintenance with respect to functions since it provides a functions decomposition axis.
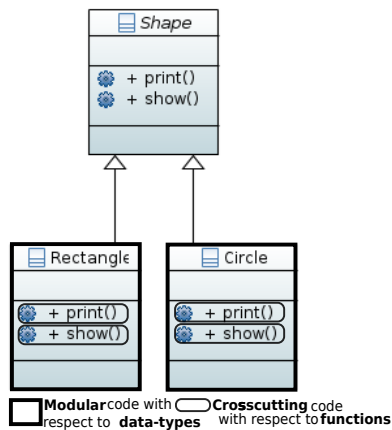
Figure 1: Decomposition axis of a simple variety of Composite design pattern.

But, if we add a new shape to the program shown in Figure 2, many modules would be changed since the new shape should be visited by both *print* and *show* business codes. In this case, the program maintenance is crosscutting. We say that the program structure is dominated by functions decomposition axis (a tyranny of decomposition according to functions).

The above two examples explain well the problem of tyranny of decomposition. A such issue still always a main problem that affects software evolution. In this work, we aim to contribute in attenuating tyranny of program decomposition effect on software maintenance. Our target is to help software developers in analyzing and predicting in earlier phases of software development the kind of maintenance tasks that could occur later and in recommending the right architecture (decomposition axis) of the program that could keep maintenance being modular.
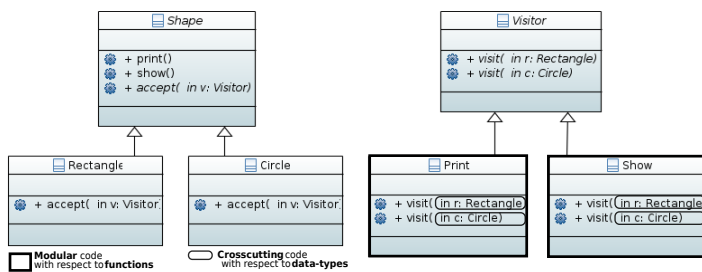
Figure 2: Visitor structure corresponding to the program shown in Figure1.

4 SEA specification

4.1 Overview

Many works have treated software evolution issue at the implementation phase. In this work, we tackle this issue in design phase of software development process. Since UML (Unified Modeling Language) [25] does not provide customized semantic constructs related to software maintenance, we propose an UML profile [26] that supports analyzing / predicting maintenance tasks that could occur in the future.

The UML profile we propose is called *SEA* (in short *SEA* for

*S*oftware *E*volution *A*nalysis) (see Fig. 3) . *SEA* is defined in Papyrus [27] EMF-based editor and it provides the following features:

- tracing software evolution history by adding some information to each software version. This feature could help to get an overview about maintenance tasks characteristics, the thing that could provide some recommendations about choosing the right program structure.

- studying and deciding which parts of a given software are more stable than others. This feature could help to predict at earlier phases the program structure evolution.

- expressing explicitly some semantic terms related to software maintenance in class diagrams such as data-type module, function module, composite design pattern...etc. This feature enhances software comprehension and helps to identify the decomposition axis of a given software.
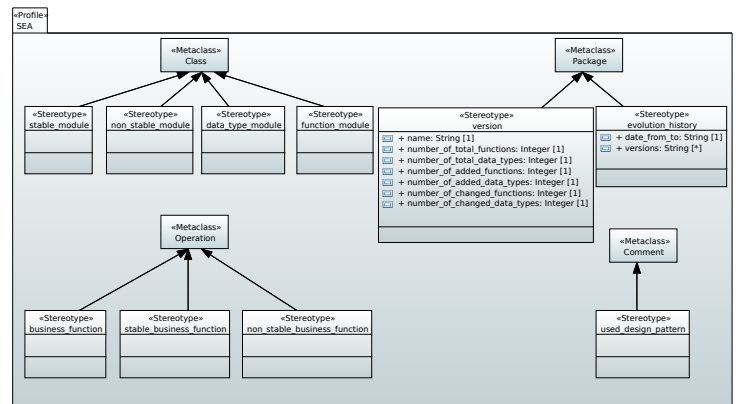
Figure 3: *SEA*: an UML profile for analyzing software evolution.

4.2 Stereotypes for analyzing software modularity

Marking modular and crosscutting software parts. Modularity in software architecture helps to optimize software maintenance cost. It permits also to encapsulate concerns and minimize crosscutting concerns effect. Thus, expressing modularity concepts explicitly in models and diagrams helps software developers to explore at early stages of software development the decomposition axis that is dominant. This helps to recommend the right kind of future maintenance tasks that are modular and to avoid those which are crosscutting. In this direction, *SEA* permits to mark explicitly in class diagram which elements represent modular concerns and which elements represent crosscutting concerns.

Until now, *SEA* supports two concerns (or two decomposition axes): data-types concern and functions concern. In this context, we propose the following stereotypes:

- *<<data_type_module>>*: it extends the meta class *Class* and it is used to precise classes that belong to data-types concern when software architecture is built according to Composite design pattern.

- *<<function_module>>*: it extends the meta class *Class* and it is used to precise classes that belong to functions concern

and that encapsulate program business code when software architecture is built according to Visitor design pattern.

- <<*business_function*>>: it extends the meta class *Operation* and it is used to mark methods that contain program business code. It could be used especially in Composite pattern structure to show that business code is crosscutting among different modules. This feature helps software developers to be aware of the cost of maintenance tasks performed with respect to functions.

Fig 4 shows an example of how to precise explicitly modules/classes that belong to the concern data-types by applying <<data_type_module>> to class diagram. In the example, we see explicitly that classes *Rectangle* and *Circle* are marked as data-type modules. In the same example, methods *print()* and *show()* are marked explicitly as business code. This shows visually that business code is crosscutting among program modules which gives an indication that maintenance tasks performed with respect to functions are costly.
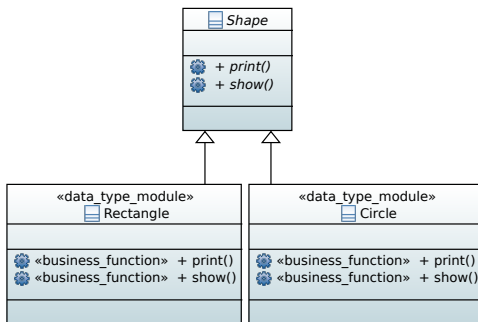
Figure 4: Use of *SEA* in marking modular data-types concern.
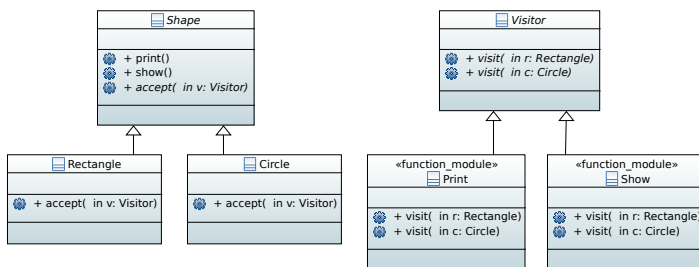
Figure 5: Use of *SEA* in marking modular functions concern.

Fig 5 shows how to use <<function_module>> stereotype to indicate that business code is encapsulated. This is used when the program is structured with respect to Visitor design pattern. We remark that classes *Show* and *Print* encapsulate respectively *show* and *print* business codes. The fact that these two classes are marked explicitly as functions indicates that software maintenance performed with respect to functions is not costly.

Precising modular program decomposition visually on diagrams helps to guide software developers to perform the right kind of maintenance that respects the existing concern. If they have to perform a crosscutting maintenance, they could be at least ready early to apply some tools or techniques that transform automatically the actual

architecture to another one that supports modular maintenance (for example using reversible transformations among Composite and Visitor [13]).

Marking stable and changeable software parts. In order to predict future software evolution at early stages, one should predict which software parts tend to change sharply. For this purpose, we propose the following stereotypes:

- **stable_business_function vs non_stable_business_function**: these two stereotypes extend the meta class *Operation*. The former is used to mark functions/methods that would not be sharply changed. The latter marks probable functions that could change drastically in the future.

- **stable_module vs non_stable_module**: these two stereotypes extend the meta class *Class*. The former is used to mark classes/modules that would not be sharply changed, or will have small changes that do not influence the software architecture. The latter marks classes/modules that could radically change.

Fig. 6 shows how to apply stereotypes mentioned above to a class diagram. For example, after marking software parts as stable or non stable, one could identify which parts seems to be more stable than others. In case of finding that stable data-types modules number is greater than stable functions number, then, the decision could be biased to choose Visitor pattern as a future software architecture (since business code tend to change more than data-types).
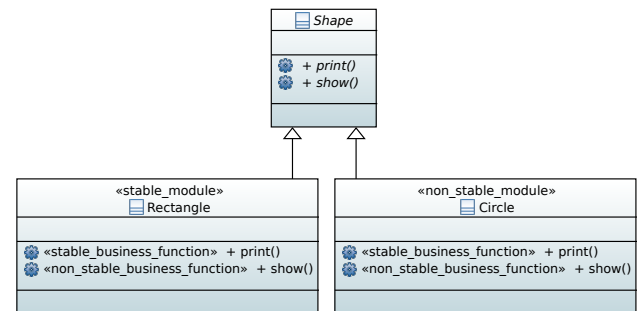
Figure 6: Use of *SEA* in marking changeable and stable software parts.

4.3 Stereotypes for software evolution history tracing

With time, software evolution could cause software architecture degeneration [28]. So, having a backup for each version is necessary and helps to get back to the non degenerated version. This is already existing by saving old versions. In our approach, we propose the stereotype <<evolution_history>> (extends meta-class *Package*) which permits to precise explicitly on a package including all software versions that this package contains software evolution history. The proposed stereotype provides two tagged values: <<date_from_to>> and <<versions>>. The former is used to indicate visually the period of time during which versions included in a package stereotyped <<evolution_history>> are built. The latter is used to list all versions that are built in the period of time indicated by <<date_from_to>>. These tagged values permit to add valuable

visual data that could be used to assess the stability of software during a period of time.

Fig. 7 shows how to apply <<evolution_history>> stereotype: the package *software_X* (stereotyped <<evolution_history>>) includes three sub-packages that include respectively three versions of *software_X*.
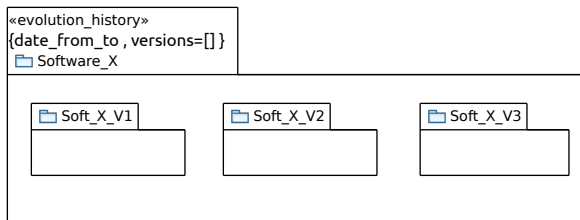
Figure 7: Tracing software evolution with <<evolution_history>> stereotype.

The second stereotype that is related to software evolution history is the stereotype <<version>> which extends meta-class *Package*. It provides information about each version of a given software. It contains seven tagged values:

- *name*: version name

- *number_of_total_data_types*: total number of classes of current version

- *number_of_total_functions*: total number of methods of current version

- *number_of_added_data_types*: number of classes that have been added to the previous version to get the current version

- *number_of_added_functions*: number of methods that have been added to the previous version to get the current version

- *number_of_changed_data_types*: number of classes that have been changed to get the current version

- *number_of_changed_functions*: number of methods that have been changed to get the current version

Tagged values mentioned above permit to provide visual information about the behavior of software evolution. Getting a visual access to added classes and methods number during switching among software versions helps to get an overview about the recommended software architecture that could optimize maintenance cost. For example, if the percentage of *number_of_added_data_types* comparing to *number_of_total_data_types* is always greater than the percentage of *number_of_added_functions* comparing to *number_of_total_functions* and the current architecture is implemented with respect to Visitor pattern, then it will be better to switch the program structure into Composite pattern in order to keep maintenance modular with respect to data-types (see more details in Sect. 5).

Fig. 8 shows how to apply <<version>> stereotype: the package *soft_X_V1* (stereotyped <<version>>) shows the seven defined tagged values that permits to note helpful information about software evolution behavior related to *soft_X_V1*.
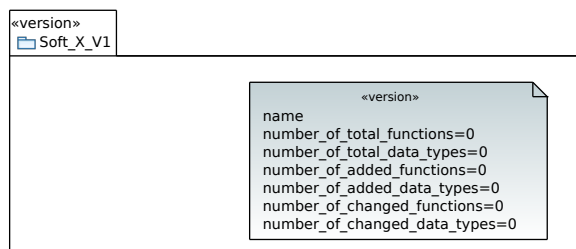
Figure 8: Adding helpful information to a software version by applying <<version>> stereotype.

4.4 Visualizing design patterns

Many programmers face some difficulties when implementing design patterns. Thus, visualizing in design phase some information about the design pattern that will be implemented later orients programmers early to cover any lack of knowledge about the indicated design pattern. In addition, marking design patterns explicitly on diagrams enhances software comprehension.

Marking information about chosen design patterns on diagrams could also assist used techniques in design pattern detection [29] and provide relevant data for data analysis and classification.

To reify this idea, we propose the stereotype <<used_design_pattern>> that extends the meta-class *Comment*. It could be associated to the package that includes the hole software project and indicates information about the chosen design patterns to implement. Provided information includes pattern name, pattern uses, modular maintenance tasks permitted, crosscutting maintenance tasks...etc. Fig. 9 shows how to apply <<used_design_pattern>> on comments.
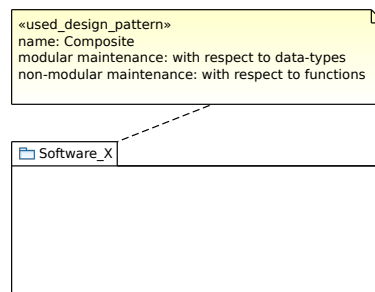
Figure 9: Use of *SEA* in visualizing information about chosen design patterns.

5 Application of *SEA* on a real software

5.1 An overview about JHotDraw evolutions

We study the utility of *SEA* in analyzing *JHotDraw* [30] evolutions. *JHotDraw* is a framework for two-dimensional graphics used for structured drawing editors. It is implemented in Java and it is based on Erich Gamma's *JHotDraw*, which is copyright 1996, 1997 by IFA Informatik and Erich Gamma [31].

We define the following metrics to use them in the rest of this section:

- V_i: a version i of *JHotDraw* where $1 <= i <= 13$ (we study here 13 versions of *JHotDraw*)

- CNV_i: classes number in version V_i

- MNV_i: methods number in version Vi

- ACV_1: added classes number to version $V1$ to obtain version V_i

  $ACV_1 = CNV_i - CNV_1$

- AMV_1: added methods number to version $V1$ to obtain version V_i

  $AMV_1 = MNV_i - MNV_1$

- ACV_{i-1}: added classes number to version $Vi - 1$ to obtain version V_i

  $ACV_{i-1} = CNV_i - CNV_{i-1}$

- AMV_{i-1}: added methods number to version $Vi - 1$ to obtain version V_i

  $AMV_{i-1} = MNVi - MNV_{i-1}$

- $RACV_1$: rate of added classes number to version $V1$ to obtain version V_i

  $RACV_1 = \frac{ACV_1}{CNV_1}$

- $RAMV_1$: rate of added methods number to version $V1$ to obtain version V_i

  $RAMV_1 = \frac{AMV_1}{MNV_1}$

- $RACV_{i-1}$: rate of added classes number to version $Vi - 1$ to obtain version V_i

  $RACV_{i-1} = \frac{ACV_{i-1}}{CNV_{i-1}}$

- $RAMV_{i-1}$: rate of added methods number to version $Vi - 1$ to obtain version V_i

  $RAMV_{i-1} = \frac{AMV_{i-1}}{MNV_{i-1}}$

V_i	CNV_i	MNV_i
V_1	148	1229
V_2	208	1896
V_3	296	2723
V_4	301	2809
V_5	301	2809
V_6	343	2809
V_7	487	4234
V_8	463	4285
V_9	621	5486
V_{10}	638	5627
V_{11}	639	5582
V_{12}	669	5845
V_{13}	672	5885

(a) Classes number and Methods number of each version (data extracted from [32]).
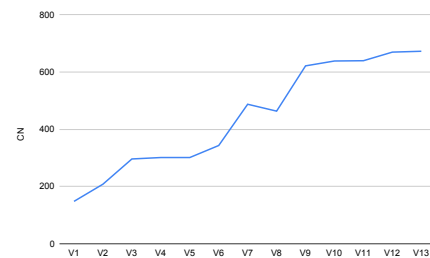
(b) Evolution of *JHotDraw* classes number (CNV_i) during 11 years.
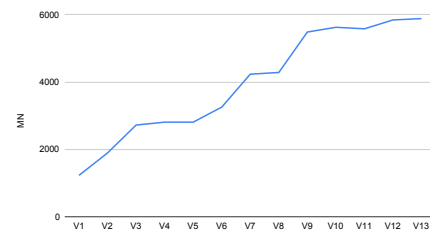
(c) Evolution of *JHotDraw* methods number (MNV_i) during 11 years.

Figure 10: Variations of classes number and method numbers during *JHotDraw* evolution.

The table shown in Fig. 10(a) illustrates *JHotDraw* evolution during 11 years. During this period of time, there were 13 versions of *JHotDraw* (5.2, 5.3, 5.4 b1, 5.4 b2, 6.0 b1, 7.0.8, 7.0.9, 7.1, 7.2, 7.3.1, 7.4.1, 7.5.1 and 7.6). We call here each version by V_i where $1 <= i <= 13$. The first column of the table mentions the version name (V_1, V_2,...,V_{13}), the second column mentions classes number in V_i (CNV_i) and the third column mentions methods number in V_i (MNV_i).

Like any software, *JHotDraw* is influenced by Lehman law [1] as shown by the shape of both curves of CNV_i progress (Fig. 10(b)) and MNV_i progress (Fig. 10(c)). We remark that classes number, which was 148 in V_1, increases to reach 672 in V_{13}, and methods number jumps from 1229 in V_1 to 5885 in V_{13}. Considering these evolutions, we apply some stereotypes of *SEA* profile to show its utility in analyzing software evolution during earlier stages of software process.

5.2 Using SEA to trace JHotDraw evolutions

To make *JHotDraw* evolutions easy to analyze in the design activity of software process, we apply stereotypes <<evolution_history>> and <<version>>. The former is applied to a package that includes all versions of JHotDRaw during 11 years and the latter is applied to each package that includes a version V_i of *JHotDraw*.

Application of <<evolution_history>> stereotype The target of applying <<evolution_history>> stereotype is to add information about the period of time in which *JHotDraw* versions are built and also about number and names of versions. This information is represented by defined tagged values that characterize the mentioned

stereotype.

Fig. 11 shows how <<evolution_history>> stereotype and its tagged values are applied. By using this stereotype, software developers could create a package that includes all versions of *JHotDraw* and marks this package as a special package to trace *JHotDraw* evolutions history. In addition, they could note information such as "date_from_to=2000_to_2011" and list different versions that has been elaborated during this period.

«evolution_history»
{date_from_to=2000_To_2011 , versions=[V1, V2, V3, V4, V5, V6, V7, V8, V9, V10, V11, V12, V13] }
JHotDraw_versions
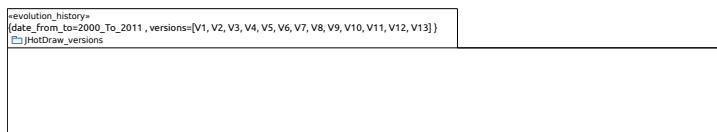
Figure 11: Application of <<evolution_history>> stereotype to JHotDRaw.

In fact, the expressiveness provided by the stereotype <<evolution_history>> permits to assess the stability of *JHotDraw*. The stereotype <<evolution_history>> provides information about the rate of versions number of *JHotDraw* by a given period of time (here 13 versions by 11 years) which could evaluate the impact of *JHotDraw* evolution on total development cost. It motivates also software developers to focus on studying the switch from V_i to V_{i+1} and deduce lessons for future evolutions.

Application of <<**version**>> **stereotype**   As detailed in Sect. 4, the stereotype <<version>> has 7 tagged values. We consider here only *name*, *number_of_total_functions*, *number_of_total_data_types*, *number_of_added_functions* and *number_of_added_data_types*. For each version V_i of *JHotDraw*, software developers could apply the stereotype <<version>> to the package that contains V_i and they could assign a value to each tagged value. For example, Fig. 12 shows the main package that is stereotyped as <<evolution_history>> and inside of it the set of packages stereotyped as <<version>> that represent the 13 versions of *JHotDraw*.

«evolution_history»
{date_from_to=2000_To_2011 , versions=[V1, V2, V3, V4, V5, V6, V7, V8, V9, V10, V11, V12, V13] }
JHotDraw_versions

«version»
{name=5.2 , number_of_total_functions=1229 , number_of_total_data_types=148 , number_of_added_functions=0 , number_of_added_data_types=0 }
V1

| «versio..» V2 | «versio..» V3 | «version» V4 | «version» V5 | «version» V6 | «version» V7 | «version» V8 | «version» V9 | «version» V10 | «version» V11 | «version» V12 |

«version»
{name=7.6 , number_of_total_functions=5885 , number_of_total_data_types=672 , number_of_added_functions=4656 , number_of_added_data_types=524 }
V13

Figure 12: Application of <<version>> stereotype to JHotDRaw.

For each version V_i, we assume that software developers mark:

- name of the version (example: for version V_1, name is *5.2*)
- *number_of_total_data_types* (example: for version V_{13}, *number_of_total_data_types*= 672)

- *number_of_total_functions* (example: for version V_{13}, *number_of_total_functions*= 5885)
- *number_of_added_data_types* (example: for version V_{13}, *number_of_added_data_types*= 524)
- *number_of_added_functions* (example: for version V_{13}, *number_of_added_functions*= 4656)

5.3   *Utility of* SEA *in* JHotDraw *evolutions analysis*

As shown in the two last paragraphs, the application of stereotypes <<evolution_history>> and <<version>> adds explicit information about each version of *JHotDraw* (the thing that UML does not provide). This information makes packages that includes different versions being more expressive and informative about how *JHotDraw* (or any other software) evolves. This helps software developers to analyze easily the growth of *JHotDraw* at design phase and to take the right design decisions.

Let's assume a scenario in which a software developer analyzes information marked explicitly on packages that represents *JHotDraw* versions (each package is stereotyped as <<version>>):

***JHotDraw* evolution analysis scenario based on *SEA* application**   We associate to each tagged value a metric from those presented above:

- *number_of_total_data_types* is represented by CNV_i
- *number_of_total_functions* is respresented by MNV_i
- *number_of_added_data_types* is represented by ACV_1
- *number_of_added_functions* is respresented by AMV_1

The table shown in Fig. 13(a) resumes values that are calculated basing on data collected from packages stereotyped as <<version>>. It shows variations of $RACV_1$ and $RAMV_1$ for each version V_i. The curve shown in Fig. 13(b) visualizes the progress of $RACV_1$ and $RAMV_1$ during 11 years. We remark that in all versions $RAMV_1$ is greater than $RACV_1$ which means that the percentage of added methods in each version comparing to initial number of methods in V_1 is greater than the percentage of added classes comparing to initial number of classes in V_1.

The fact that $RAMV_1$ is always greater than $RACV_1$ during 11 years of *JHotDraw* evolution indicates that maintenance tasks are applied more on methods. We could deduce in this case that software developers should recommend to use Visitor design pattern if it is not already used in *JHotDraw*.

V_i	$RACV_1$	$RAMV_1$
V_2	0.4	0.54
V_3	1	1.21
V_4	1.03	1.28
V_5	1.03	1.28
V_6	1.31	1.64
V_7	2.29	2.44
V_8	2.12	2.48
V_9	3.19	3.46
V_{10}	3.31	3.57
V_{11}	3.31	3.54
V_{12}	3.52	3.75
V_{13}	3.54	3.78

(a) Rates of added classes and methods number in a version Vi comparing to first version of JHoDraw $V1$.
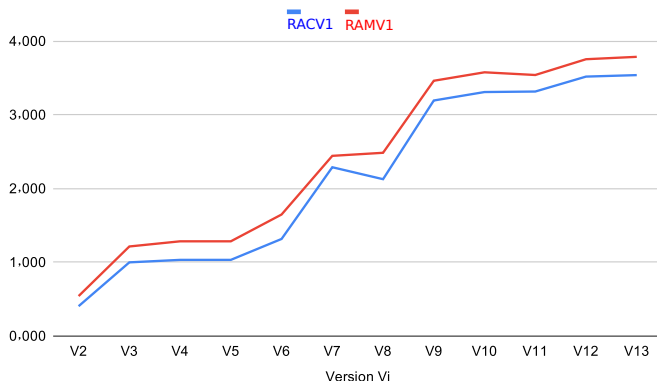
(b) Rates evolution of added classes and methods number in a version V_i comparing to first version of JHoDraw V_1.

Figure 13: Study of Rates evolution of added classes and methods number in a version Vi comparing to first version of JHoDraw $V1$.

Let's now interpret evolutions from one version to its successor version. The table illustrated in Fig. 14(a) shows variations of $RACV_{i-1}$ and $RAMV_{i-1}$. We remark that $RACV$ of version V_2 is 0.4 and its $RAMV$ is about 0.54 which means that version V_2 of *JHotDraw* grows by 40% of V_1 classes number and 54% of V_1 methods number. Hence, maintenance tasks that switches V_1 to V_2 are applied more on methods (functions decomposition axis). This case occurs 5 times against 7 times in which maintenance tasks are applied more on classes (data-types decomposition axis). So, the switch from version to version shows that maintenance tasks change their behavior: they are applied 5 times with respect to functions decomposition axis against 7 times with respect to data-types decomposition axis. In this case, Composite design pattern seems to be the best choice for the future versions.

Lessons By analyzing *JHotDraw* evolutions as done above, we deduce that long-term evolution shows that Visitor design pattern is the best choice to optimize maintenance cost. But, variation in targeted decomposition axis due to the switch from version to version indicates that *JHotDraw* should change its architecture in order to keep maintenance being modular (software developers could use

automatic reversible transformations among Composite and Visitor each time they remark that maintenance tasks would change behavior when switching from version to version).

V_i	$RACV_{i-1}$	$RAMV_{i-1}$
V_2	0.4	0.54
V_3	0.42	0.436
V_4	0.017	0.031
V_5	0.0	0.0
V_6	0.14	0.15
V_7	0.42	0.3
V_8	-0.049	0.012
V_9	0.34	0.28
V_{10}	0.027	0.025
V_{11}	0.002	-0.007
V_{12}	0.047	0.039
V_{13}	0.004	0.006

(a) Rates of added classes and methods number in a version V_i comparing to version V_{i-1}.
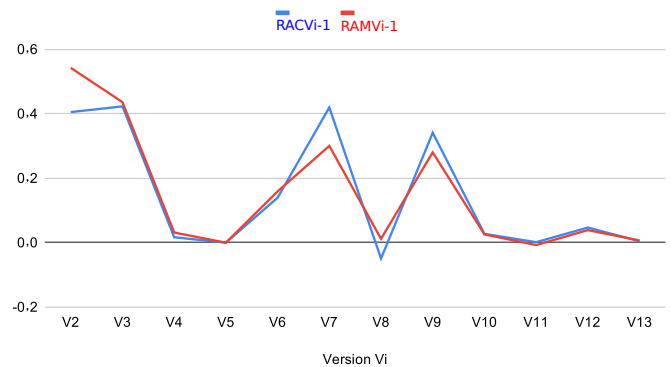
(b) Rates evolution of added classes and methods number in a version Vi comparing to version V_{i-1}.

Figure 14: Study of Rates evolution of added classes and methods number in a version Vi comparing to version V_{i-1}.

6 Conclusion and future work

We have defined an UML profile called *SEA* which could help software developers to analyze and predict maintenance tasks in early activities of software process. To reify our approach we defined some stereotypes that support treating maintenance issue in design phase of software development. *SEA* treats three main issues related to software evolution:

- Analyzing and predicting maintenance tasks by defining stereotypes that allow to trace software evolution history. They permit also to precise software parts that are more probable to change in the future and those which could stay stable. This feature helps to recommend the right software architecture that supports changes without extra cost.

- Marking explicitly on class diagrams software parts that are

encapsulated in modules and those that are crosscutting. For example, in Composite pattern, components classes represent data-types modules and methods/functions represent crosscutting concern. This feature permits to precise visually and easily modular concerns and crosscutting concerns, the thing that permits to identify quickly which kind of maintenance tasks is preferred.

- Visualizing in design phase design patterns that will be implemented later. This feature enhances software comprehension and helps to assimilate the chosen design pattern use and properties before implement it (sometimes programmers face difficulties to understand some design patterns). This could also give an overview about maintenance tasks that could be modular with respect to a given design pattern and those which could not. In the last case, software developers could use appropriate tools to switch program structure into another design pattern that is more convenient (such as automatic reversible transformation among Composite and Visitor [13]).

SEA is partially validated by apply it on *JHotDraw* evolution. This partial validation shows that it is possible to analyze software evolution history and predict the kind of maintenance tasks that could occur in the future. Our approach validation still partial until applying all *SEA* stereotypes to *JHotDraw* and also to other case studies. As a future work, we look for developing an algorithm based on supervised data analysis and classification to exploit data provided by *SEA* in models and diagrams to predict automatically future maintenance tasks kind.

Conflict of Interest   The authors declare no conflict of interest.

References

[1] M. M. Lehman, "Laws of software evolution revisited," in 5th European Workshop on Software Process Technology (EWSPT'96), volume 1149/1996 of *LNCS*, 108–124, Springer, 1996.

[2] L. Erlikh, "Leveraging legacy system dollars for e-business," in IT Professional,, 17–23, 2000.

[3] E. Gamma, R. Helm, R. Johnson, J. Vlissides, Design patterns: elements of reusable object-oriented software, Addison-Wesley Longman Publishing Co., Inc., Boston, MA, USA, 1995.

[4] D. L. Parnas, "On the criteria to be used in decomposing systems into modules," Commun. ACM, **15**, 1053–1058, 1972.

[5] G. M. Rama, N. Patel, "Software modularization operators," in IEEE International Conference on Software Maintenance (ICSM), 2010.

[6] C. Szyperski, Component Software: Beyond Object-Oriented Programming, Addison-Wesley Longman Publishing Co., Inc., Boston, MA, USA, 2nd edition, 2002.

[7] G. Kiczales, E. Hilsdale, "Aspect-oriented Programming," SIGSOFT Softw. Eng. Notes, **26**(5), 313–, 2001, doi:10.1145/503271.503260.

[8] A. Ajouli, "A Shadow Structure for Modularity of Java Program Evolution," in 2015 41st Euromicro Conference on Software Engineering and Advanced Applications, 39–42, 2015, doi:10.1109/SEAA.2015.28.

[9] P. Wadler, "The Expression Problem," 1998, note to Java Genericity mailing list.

[10] K. B. Bruce., "Some challenging typing issues in object-oriented languages." Electronic Notes in Theoretical Computer Science,, **82**, 2003.

[11] C. Clifton, T. Millstein, G. T. Leavens, C. Chambers, "MultiJava: Design rationale, compiler implementation, and applications," ACM Trans. Program. Lang. Syst., **28**, 517–575, 2006.

[12] J. Garrigue., "Programming with polymorphic variants." in ML Workshop,, 1998.

[13] A. Ajouli, J. Cohen, J.-C. Royer, "Transformations between Composite and Visitor Implementations in Java," in Software Engineering and Advanced Applications (SEAA), 2013 39th EUROMICRO Conference on, 25–32, 2013.

[14] J. Cohen, R. Douence, A. Ajouli, "Invertible Program Restructurings for Continuing Modular Maintenance," in Software Maintenance and Reengineering (CSMR), 2012 16th European Conference on, 347 –352, 2012, doi:10.1109/CSMR.2012.42.

[15] A. Ajouli, K. Henchiri, "MODEM: an UML profile for MODEling and Predicting software Maintenance before implementation," in 2019 International Conference on Computer and Information Sciences (ICCIS), 1–5, 2019, doi:10.1109/ICCISci.2019.8716421.

[16] R. Yongchang, X. Tao, L. Zhongjing, C. Xiaoji, "Software Maintenance Process Model and Contrastive Analysis," 2011, doi:10.1109/ICIII.2011.324.

[17] H.-J. Kung, C. Hsu, "Software Maintenance Life Cycle Model," 113 – 121, 1998, doi:10.1109/ICSM.1998.738499.

[18] I. Cote, M. Heisel, "A UML Profile and Tool Support for Evolutionary Requirements Engineering," 161 – 170, 2011, doi:10.1109/CSMR.2011.22.

[19] H. Marouane, C. Duvallet, A. Makni, R. Bouaziz, B. Sadeg, "An UML profile for representing real-time design patterns," Journal of King Saud University - Computer and Information Sciences, **30**(4), 478 – 497, 2018.

[20] J. Dong, S. Yang, "Visualizing design patterns with a UML profile," in HCC, 2003.

[21] G. M. Ana Garis, Daniel Riesco, "Defining the Proxy Design Pattern using UML Profile," in Software Engineering Project of National University of San Luis, 2006.

[22] K. Ngee Loo, S. Peck Lee, "Representing design pattern interaction roles and variants," **6**, 2010, doi:10.1109/ICCET.2010.5486125.

[23] J. Cohen, A. Ajouli, "Practical use of static composition of refactoring operations," in ACM Symposium On Applied Computing, 6 pages, Portugal, 2013.

[24] R. Malhotra, K. Lata, "An empirical study on predictability of software maintainability using imbalanced data," Software Quality Journal, **28**, 2020, doi:10.1007/s11219-020-09525-y.

[25] M. Gogolla, Unified Modeling Language, 3232–3239, Springer US, Boston, MA, 2009, doi:10.1007/978-0-387-39940-9_440.

[26] L. Fuentes, A. Vallecillo, "An introduction to UML profiles," UPGRADE, The European Journal for the Informatics Professional, **5**, 2004.

[27] "Eclipse Papyrus," https://projects.eclipse.org/projects/modeling.mdt.papyrus.

[28] L. Hochstein, M. Lindvall, "Combating architectural degeneration: a survey," Inf. Softw. Technol., **47**, 643–656, 2005.

[29] N. Tsantalis, A. Chatzigeorgiou, G. Stephanides, S. T. Halkidis, "Design Pattern Detection Using Similarity Scoring," IEEE Trans. Softw. Eng., **32**, 896–909, 2006, doi:10.1109/TSE.2006.112.

[30] E. Gamma, I. Informatik, "JHotDraw as Open-Source Project," http://www.jhotdraw.org/.

[31] "Source Forge: JHotDraw project," https://sourceforge.net/projects/jhotdraw/.

[32] K. Johari, A. Kaur, "Effect of Software Evolution on Software Metrics: An Open Source Case Study," SIGSOFT Softw. Eng. Notes, **36**(5), 1–8, 2011, doi:10.1145/2020976.2020987.

Event Modeller Data Analytic for Harmonic Failures

Futra Zamsyah Md Fadzil[*], Alireza Mousavi, Morad Danishvar

System Engineering Research Group, CEDPS, Brunel University London, UB8 3PH, UK

A R T I C L E   I N F O

A B S T R A C T

The optimum performance of power plants has major technical and economic benefits. A case study in one of the Malaysian power plants reveals an escalating harmonic failure trend in their Continuous Ship Unloader (CSU) machines. This has led to a harmonic filter failure causing performance loss leading to costly interventions and safety concerns. Analysis of the harmonic parameter using Power Quality Assessment indicates that the power quality is stable as per IEEE standards; however, repetitive harmonic failures are still occurring in practice. This motivates the authors to explore whether other unforeseen events could cause harmonic failure. Usually, post-failure plant engineers try to backtrack and diagnose the cause of power disturbance, which in turn causes delay and disruption to power generation. This is a costly and time-consuming practice. A novel event-based predictive modelling technique, namely, Event Modeller Data Analytic (EMDA), designed to inclusive the harmonic data in line with other technical data such as environment and machine operation in the cheap computational effort is proposed. The real-time Event Tracker and Event Clustering extended by the proposed EMDA widens the sensitivity analysis spectrum by adding new information from harmonic machines' performance. The added information includes machine availability, utilization, technical data, machine state, and ambient data. The combined signals provide a wider spectrum for revealing the status of the machine in real-time. To address this, a software-In-the-Loop application was developed using the National Instrument LabVIEW. The application was tested using two different data; simulation data and industrial data. The simulation study results reveal that the proposed EMDA technique is robust and could withstand the rapid changing of real-time data when events are detected and linked to the harmonic inducing faults. A hardware-in-the-Loop test was implemented at the plant to test and validate the sensitivity analysis results. The results reveal that in a single second, a total of 2,304 input-output relationships were captured. Through the sensitivity analysis, the fault causing parameters were reduced to 10 input-output relationships (dimensionality reduction). Two new failure causing event/parameter were detected, humidity and feeder current. As two predictable and controllable parameters, humidity and feeder velocity can be regulated to reduce the probability of harmonic fluctuation.

1   Introduction

This paper is an extension of work originally presented in the conference Proceedings of the 2019 IEEE/SICE International Symposium on System Integration (SII) [1]. Power Quality (PQ) monitoring has been the focus of research and development for many years. Recently, [2], [3] addressing the PQ issues in various industry and proposing different methods in tackling this issues.The main focus is to protect the equipment and minimize the losses while increasing the levels of operational safety. However, systems are becoming more complex as they are being further developed for improvement. Huge numbers of control drive and other non-linear loads have been

installed to satisfy the demands of modern lifestyles. It has led to instability of the power system, creating high noise levels in the system grids and decaying the electrical distribution system. Even worse, climate change has an impact on the environment that the system operates in. In some cases, particularly for hot countries, the electrical distribution system requires air conditioning to protect the electrical equipment in the substation. In normal circumstances, if the air conditioning fails, it may surpass the permitted set point and may not protect the equipment. When the global temperature rises, the potential rate of failure also increases. Research has shown that the long-term average global temperature is increasing, which has a significant negative impact on the performance of the machines [4].

[*]Corresponding Author: Futra Fadzil, Brunel University London, Email: Futra.Fadzil@brunel.ac.uk
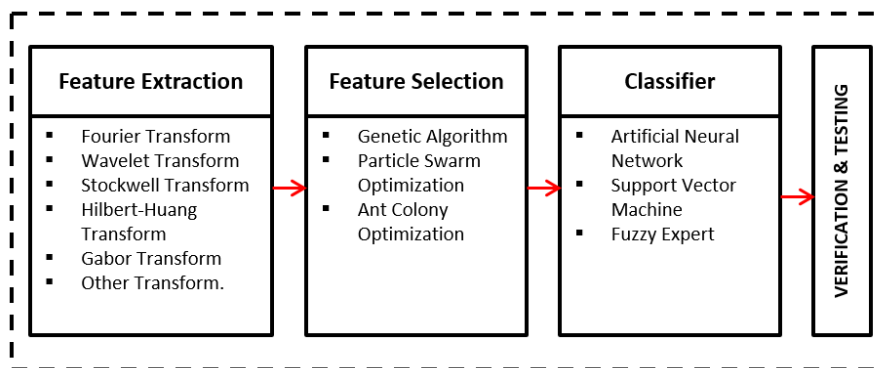
Figure 1: Various techniques of Power Quality Classification

The arrangement of the three principal stages in PQ Classification: (1) Feature extraction - a key transformation of the fundamental signals into time-frequency based information. A broad selection of Fourier Transform, Wavelet Transform, Stockwell Transform, Hilbert-Huang Transform, Gabor Transform and others. (2) Feature Selection - a key method in selecting the most suitable features from the feature extraction stage while discarding the redundant features. Few main optimizers include Genetic Algorithm, Particle Swarm Optimization and Ant Colony Optimization. (3) Classifier – a selection of artificial intelligence tools in classifying PQ disturbances such as artificial neural network, support vector machines, and fuzzy expert.

Earlier, conventional methods use manual configurations and visual inspection to monitor the quality of the power supply in the system. This method was too difficult to interpret and time-consuming. Later, an automated classification system, which uses the signal processing technique was developed and currently advancing with various Machine Learning and Deep Learning approach. Various combinations of features extraction and classifiers have proven to locate PQ disturbances accurately while using synthetic data. However, this is not the case with real industry data. Real industry data are complex and much more complicated when there are external or environmental factors that could potentially influence the state of the system. This creates a gap in existing techniques, which motivates authors to investigate the relevance of the environmental parameter to the issue of PQ disturbances. In addition, with the current emergence of big industrial data, system engineer must ensure that the system is robust and capable of performing ML/DL techniques in real-time applications. Disturbance data exists in the order of microseconds, which greatly enhances the record data [5].In consequence, it will burden learning classifiers to run unimportant parameters that result in high computation. The authors, therefore, suggest a method that could minimize the dimensional by selecting the most relevant data to be trained automatically, while incorporating a new unknown parameter that was previously considered irrelevant in the system state.

The aim of this paper is to introduce event-based analysis as a technique for detecting harmonic failure in real time. The technique is capable of grouping together high correlation system parameters, forming an input-output relationship that is not limited to internal parameters only. As such, the homogenized correlation system will indicate the possible root cause of harmonic failures, while eliminating non-important parameters in real-time [6]. This paper presents a real-time simulation of CSU machines, which shows the changes in the output parameters of the input activity. The data will be used to measure the suitability and applicability of event modelling techniques in the power system environment. It is then extended to the actual plant data, exploring the integration of this dynamic platform with the Key Performance Indicator (KPI) in order to recognize the

system operating pattern. This data analytics technique expects to predict the homogenized system parameter that could present the current state of the system in real time.

1.1 Power Quality Disturbance

A number of PQ disturbance types are implicated: voltage sag, voltage swell, transients, harmonics, fluctuations, flickering, voltage imbalance, interruption, DC offset and notches. A high level of engineering expertise [7] is needed to effectively diagnose these PQ disturbances. Preventing PQ disturbances is critical to minimize power interruptions between the power utility and the end user. With modern technology, a substantial amount of research has been devoted to alleviating these problems using signal processing technique. This technique has three principal stages which incorporate feature extraction, feature selection and classification.

Feature extraction is a key transformation of the fundamental signals into time-frequency based information. It can be extracted directly from the original measurement either from a transformed domain or from the signal model parameters [8]. Several approaches include short-time Fourier transform [9], wavelet transform [10], wavelet packet transform [11], Hilbert Huang transform [12], Stockwell transform [13], Gabor-Wigner transform [14], and other hybrid transform-based [15].

Feature selection is a key method in selecting the most suitable features from the feature extraction stage while discarding the redundant features. Based on the extraction data, optimization techniques such as Ant Colony Optimisation [16], Genetic Algorithm [17], and Particle Swarm Optimisation [18] are the common algorithm used in locating PQ disturbances.

Classification is the process of predicting the class of data points. It uses an algorithm to implement classification by approximating the mapping function from the input variable to the output variable. One of the most popular and influential types of machine learning algorithms is the Artificial Neural Network. Other machine learning includes Support Vector Machine [19] and fuzzy expert system [20]. Figure 1 illustrates the three main phases of the PQ classification.

[21]–[22] provide a detailed review of these techniques.

1.2 Power Quality Standards

Harmonic assessments of utility systems require procedures in place to ensure that the efficiency of the voltage supplied to all consumers is adequate [23]. However, most of the harmonic issues arise at the end of the consumer. Their devices contain non-linear loads resulting in resonance conditions [23]. These non-linear loads are the current harmonic sources. The system voltage appears stiff to individual loads, and the loads draw distorted current waveforms. It is therefore important to maintain the PQ International standard, to provide the guidelines and limits for the acceptable levels of compatibility, between consumer equipment and the system utilities.

The International Standard IEEE 519-1992 sets the limit for both harmonic voltages and currents at the Point of Common Coupling (PCC) between the end-user and the utility supplier. It limits Voltage Total Harmonic Distortion (THD), defined as the ratio of the RMS value of the harmonic voltage to the RMS value of the fundamental (50Hz) voltage, to a maximum of 5%. Individual voltage harmonic magnitudes are limited to 3% of the fundamental voltage value [24]. The International Standard IEC 61000-3-4 sets the limits for the emission of harmonic currents in low-voltage power supply systems for the requirement with rated current greater than 16A [25].

1.3 Environmental Parameters

Compliance with the International PQ Standards is the policy for both utilities and customers. In order to maintain a good PQ system, an enormous amount of research and PQ analysis has been undertaken to ensure it complies with the standards. However, in some cases, the machine still fails, although it complies with the standard. It is important to note that most of these research focuses on the fundamental of the electrical system and leave behind the external parameters that may have a substantial effect on the problem. In [26], the authors suggest that there could be further environmental and operational factors that could also affect the performance of power systems.

1.4 Problem Statement

In this article, we intend to investigate what possible factors that could link a well-maintained machines with a proper operation to a frequent harmonic failure incidents. While PQ parameters are eliminated by its healthy measurement, an alternative technique to solve this harmonic failure mystery is required to evaluate if there is an existence of a different parameter that could lead to this failure. Therefore, the authors are proposing the Event Modeller techniques which could link the internal and external parameters together, to create a cause-effect relationship, while updating the system status in near real-time before the machine fails. The implementation of the event modeller technique recently has shown positive practical findings in various area and application such as high-speed causal prediction modelling [27, 28], real-time Remaining Useful Life (RUL) estimation [29], and as a middleware to highly coupled input variable in zero-defect manufacturing [30], and predicting N_2O Emission [31].

1.5 Contribution & Advantages

The first contribution of this paper is to proposed a robust system engineering tools that be able to formulate a piece of new knowledge information in the diagnosis of PQ disturbances in real-time. This tool is found robust, workable with the dynamic and autonomous environment while being able to withstand real industry data which is non-linear and highly influenced with various factors. The second contribution of this paper is that the proposed technique could visualize the group of highly correlated variables in the form of occurrence matrices in real-time, proposing a mathematics equation that represents the current state of the system. This is optimum to system operators who can make a quick decision before the system fails.

1.6 Challenges

However, implementing this technique in solving PQ problems has its challenges. The harmonic readings (THD) is taken from the Multi-Function meter, which is installed at the electrical switchgear. The reading will not be as accurate as of the conventional method, but the measurement is sufficient to prove that the PQ parameters can be eliminated. Another challenge is to determine the threshold setting. In general, a scenario of events in the actual system varies according to the system characteristic and its system deterministic. An event could happen instantaneously, or it may have some delay before it reached to the target output. For example, the scenario of a room temperature does not change immediately when the heater or air conditioner was switched on. In comparison, a dark room will be immediately bright when the switch was turned on. Both of the scenarios have made changes to the system state at a different pace. In order to detect this, a data benchmarking is required which were decided based on historical data and system expert point of view.

2 Event Modeller Technique

The event modeller technique is designed to investigate the association between the observable events (Output Data) with the causal events (Input Data) through a data mapping concept [30]. It clusters the system parameters with the highest correlation in the form of matrices and places them into mutually exclusive blocks. This creates an input-output relationship, which considers both internal and external factors. One significant difference between the proposed event modeller and other traditional data modelling techniques is how the input data assumes its output data. The traditional method assumes the input-output relationship as a true representation of a known data series, while the event modeller technique makes no assumption about it (unbiased) [32]. This fundamentally makes the approach non-unbiased vis-à-vis input-output relationship. The proposed Event Modeller Data Analytic (EMDA) is designed to find any interceptions between the known influential parameters (reported in previous literature) and new operational and environmental data by expanding the spectrum and reassessing the relationship between influential parameters on harmonic behaviour. It is a proven, computationally effective method of analyzing harmonic behaviour without bias. Borrowing from the Event Tracker [33] and Event Clustering [34] method, the proposed EMDA extends
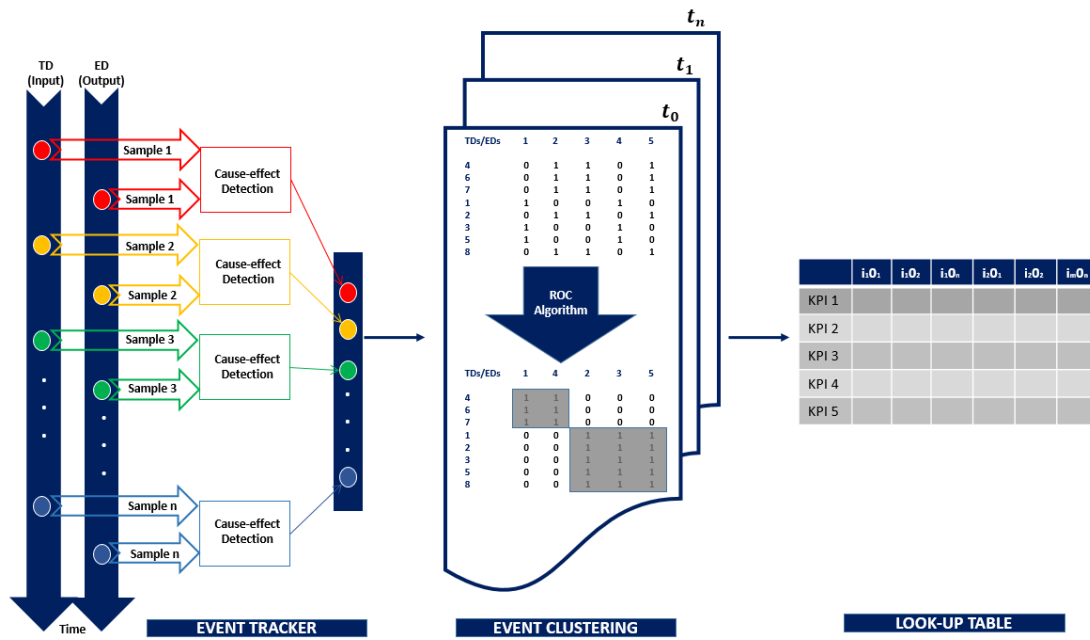
Figure 2: Event Modeller Techniques

The arrangement of the three principal stages in Event Modeller: (1) Event Tracker – A collection of input-output cause-effect detection of a system state with highly sensitivity index in real-time. (2) Event Clustering – A rank order grouping technique based on the interpretation of the changes of input-output data in the previous stage. (3) Look-up Table - A population table that links the Key Performance Indicator with the Sensitivity Indexes.

the previous authors' correlation map by adding the information from the machine performance metrics. Information such as machine availability, utilization and performance are combined with other technical data, to group the highly correlated individual data together, revealing the machine's status in real-time. Figure 2 illustrates the event modeller techniques, including Event Tracker, Event Clustering and a Look-up table. Details of each stage will be briefly discussed in the following subsection.

2.1 EventTracker Algorithm

EventTracker algorithm was introduced [35] to construct a discrete event framework for online sensitivity analysis (SA). This algorithm was designed to be applied to highly volatile environments with real-time scalar data acquisition capabilities (e.g. Internet of Things (IoT). It uses a cause-effect detection algorithm to dynamically track events' triggers and their interrelationship with one another in a given system. It generates a sensitivity index that measures the relationship between the triggered data and the event data pairs. High sensitivity index score will be indicated while the lesser impact relationship will be eliminated. This will reduce the computational effort while achieving dimensional reduction. The Event Tracker is a computationally efficient technique that focuses on the state changes of the involved system components. It merely takes a snapshot of the system states, which helps engineers observe system performance [6]. Further details on the description and four Event-Tracker functional parameters (Search Slot, Analysis Span, Event Threshold and Trigger Threshold) can found in [35].

2.2 Event Clustering Algorithm

Event Clustering Algorithm (EventiC) [34] is designed to improve the real-time sensitivity analysis, by automatically re-arranging the input-output relationship in rank order of its importance and relevance. The algorithm applied the Rank Order Clustering (ROC) technique, which was initially introduced in [36]. This technique interprets the changes in input-output data's value at the given level, detecting the coincidence and finally groups it as a related event. The process of calculating the number of coincidence occurs at a specified scan rate time interval, to ensure a relationship weight is established for modelling and control purposes [32]. Despite filtering the unimportant relationship between the input-output relationship, event clustering can identify new influencing parameters that were previously thought irrelevant, making it unique and interesting to improve the data quality. One key advantage of EventiC compared to EventTracker is that EventiC can assess multiple input/ output relationship in every single scan, whilst EventTracker considers multiple input single output relations. A detailed explanation of EventiC algorithm and the basic concept is discussed in [34]. Algorithm 1 shows the main procedure of Event Modeller.

2.3 Look-up Table

A look-up table is an array of data to map input values to output values. It is used to transform the input data into a more desirable output format. The look-up table allows replacing run-time computation or logic circuitry with a simpler array indexing operation [37]. Retrieving a value from a look-up table is faster rather than examining it from the whole database. With the advantage of the

logical separation of data, it makes it relevant to prepare the data for machine learning purposes. This EMDA technique's novelty can be found in this look-up table, thus a rapid response to changes in the system's stability (i.e. the KPIs).

Algorithm 1: Event Modeller

Set Event Modeller Limit (EML);
Set Threshold Setting (Th);
Populate ULTh and LLTh;
Populate All Input Data (TD1, TD2...TDn);
if *Triggered Data = Dynamic TD* **then**
    Compute TDx = TDn - TDn-1;
    Compare TDx with ULTh and LLTh;
    if *(LLTh<TDx<ULTh)* **then**
        TDx = 0;
    else
        TDx = 1;
    end
else
    Triggered Data = Static TD;
    TDx = TD1,TD2...TDn.;
end
repeat
    repeat
        Populate All Output Data (ED1,ED2...EDn);
        Compute EDx = EDn - EDn-1;
        Compare EDx with ULTh and LLTh;
        if *LLTh<EDx<ULTh* **then**
            Set EDx = 0;
        else
            Set EDx = 1;
        end
        Populate the models input-output event coincidence matrix with binary weighting values of exclusive NOR function;
        Average each input-output event coincidence;
        Sort rows of the resultant binary matrix into decreasing order of their decimal weights;
    until *for every column*;
until *position of each element in each row and column does not change*;
Calculate the weight for each row i and column j (in a m by n matrix) using Equation 1 and Equation 2.

$$Row : W_i = \sum_{j=1}^{m} a_{ij} 2^{m-j} \tag{1}$$

$$Column : W_j = \sum_{i=1}^{m} a_{ij} 2^{n-i}. \tag{2}$$

2.4 Key Performance Indicator

The use of existing shop-floor in modern manufacturing to measure and monitor industrial KPIs has been a trend. In [38], the author used Object Linking and Embedding (OLE) which integrates with Discrete Event Simulation (DES) modelling capabilities to measure

the KPIs for brewery industry. In [39] the author used data-driven scheme of KPIs prediction and diagnosis for hot strip mill industry. In [40], the author proposes an analytics solution for calculating statistical KPIs in the Human Machine Interface (HMI) layer. There is a need to translate a suitable KPI that suit the type of operation. Basic KPIs are calculated directly from the output operation data, and they serve as the foundation for Overall performance KPIs [41].

Time-based KPIs are data related to time duration, defining activities associated with production and maintenance. The calculation of KPI has to consider all these factors to reflect accurate metrics. Hence it is important to understand the KPI interrelationship. A hierarchical structure for KPI categorization is proposed by [41]. The time-based KPIs studied in this paper are Availability, Instantaneous Utilization, Schedule Utilization and Performance.

To complement the Time-Based KPIs, it is useful to look at the energy consumption and emission contribution that could potentially harm the environment. In general, energy consumption can be calculated by multiplying the motor rating (kW) with the duration it operates. There are three states of motor known as run, idle and stop. During running state, the motor is capable of operating at its 100% loading while in idle state, the motor operates at 25% of its loading. Obviously, there is no loading when it stops. Having the total energy consumption, it is easier to calculate the carbon footprint; Carbon Dioxide Emissions ($kgCO_2$, $kgCO_2e$), Methane ($kgCH_4$) and Nitrous Oxide ($kgNO_2$) using the formula in [42].

3 A Case Study

A Continuous Ship Unloader (CSU) is one of the leading bulk material handling machine. In a coal-fired power plant, this machine is used to transport coal from the vessel to the pulverized boiler through a series of belt conveyors. It has been reported that the CSU machine in one of the power plants in Malaysia has a frequent harmonic failure. The repetitive incidents lead to catastrophic failure, which harms the electrical devices. Besides having a vast replacement cost for the faulty parts, it is also affecting the plant availability, which concerned the management team. Even worse, it could pose a potential hazard, to the personnel working in the area if it is happening again in the future. A thorough Power Quality (PQ) assessment within the electrical distribution system has been assessed, but the results have not given any indication of internal disturbance or fault. Table 1 shows the assessment result for the CSU machine. To mitigate the problem, an effort to analyze both internal and environment parameter that has a significant impact on the system is highly desirable. The authors are keen to embrace the event modeller techniques, to evaluate the significant correlation between the output and input, which could cause harmonic failures in the system. A real-time simulation which incorporates the CSU machine parameters and the event modeller algorithm was developed using National Instruments LabVIEW.

3.1 Experiment 1: CSU Real-time Data Simulation

The purpose of a real-time simulation is to measure the suitability and applicability of the event modeller technique in the power system environment. To ensure the system incorporates the industrial

Table 1: Assessment Results for CSU Machine

Parameters	Units	Min	Max	Avg
Voltage	V_{ab}	385.9 V	424.0 V	411.2 V
	V_{bc}	216.8 V	423.8 V	382.4 V
	V_{ca}	241.8 V	424.1 V	381.5 V
Current	I_a	32 A	1718 A	525.8 A
	I_b	46 A	1870 A	639.9 A
	I_c	30 A	1568 A	217.6 A
Voltage Unbalance	% Unbalance	0.10 %	41.60 %	2.60 %
Current Unbalance	% Unbalance	8.80 %	16.70 %	52.80 %
Total Harmonic	$THDv_{ab}$	0.40 %	1.60 %	1.00 %
Distortion Voltage	$THDv_{bc}$	0.30 %	1.50 %	1.00 %
(THDV)	$THDv_{ac}$	0.50 %	1.90 %	1.10 %
Total Harmonic	$THDi_a$	1.90 %	20.80 %	4.50 %
Distortion Current	$THDi_b$	1.80 %	25.80 %	3.70 %
(THDi)	$THDi_c$	1.90 %	82.20 %	12.00 %
Total Demand	$TDDi_a$	0.10 %	2.60 %	1.30 %
Distortion Current	$TDDi_b$	0.10 %	1.80 %	1.20 %
(TDDi)	$TDDi_c$	0.10 %	2.20 %	0.80 %
Frequency	f	49.77 Hz	50.13 Hz	49.98 Hz
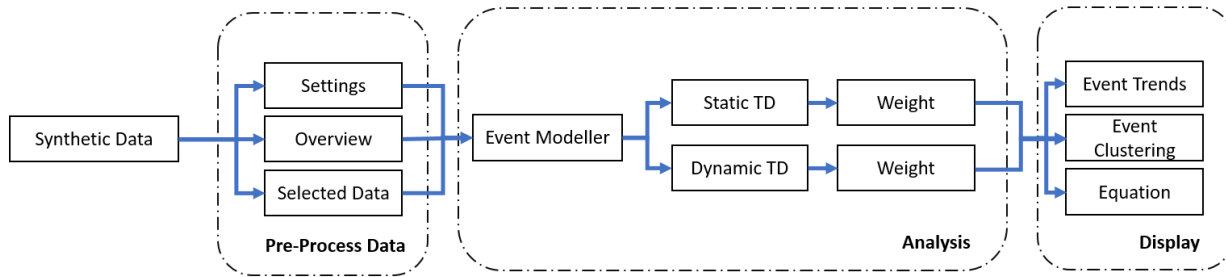
Figure 3: Experiment Strategy for Event Modeller Simulation

The arrangement of the three principal stages in the Experiment Strategy for Event Modeller Simulation: Pre-process Data, Analysis and Display.

case study, the requirement specification has been set based on the following:

1. 8 Event Data (ED's). This synthetic event data is simulated using Normal Distribution which represents the CSU Machine Output Data which includes Voltage, Humidity, Harmonics, Slewing Movement, Luffing Movement, Travel Movement, Temperature and Wind Speed;

2. 8 Triggered Data (TD's). This synthetic TD's is simulated using Normal Distribution which represents the CSU Machine Input data which includes Busy Slew, Busy Luff, Busy Travel, Busy Bucket Elevator, Slewing Motor Run Bit, Hydraulic Motor Run Bit, Travel Motor Run Bit and Bucket Motor Run Bit;

3. Threshold Setting. For the purpose of examining the Trigger Threshold, an arbitrary 5% threshold setting was set, that could later be adjusted;

4. Event Modeller Limit. This setting reduces the complexity

of an input-output relationship by its correlation confidence level. An arbitrary 80% was set, that could later be adjusted;

3.1.1 Experiment Strategy

Sixteen input/output system parameters of a CSU Machine were sampled from the Allen Bradley PLC-SCADA system using the FactoryTalk view. Once it is proven to be suitable, it will be extended to 120 parameters, which will be discussed further in Section 3.2. Data collection was conducted over a single day shift of a machine operation period, collecting approximately 43,200 lines of 12-hour data samples.

The sampling frequency follows [43] by applying the right bandwidth, time constant and settling time. Having this data in hand, synthetic data was constructed to have the same nature and properties as the real CSU machine. The overview of the experimental methodology is shown in Figure 3. Details of the dataset arrangement will be discussed in the following section.

Table 2: CSU Real-time Data Simulation Results (Weight) Based on Disturbance

Description	Voltage		Humidity		Harmonic		Temperature		Wind Speed	
	Static	Dynamic	Static	Dynamic	Static	Dynamic	Static	Dynamic	Static	Dynamic
Overall Maximum	0.8387	0.9996	0.8364	0.9996	0.8370	0.9997	0.8360	1.0000	0.8340	1.0000
Overall Minimum	0.5000	0.6288	0.5000	0.6371	0.5000	0.6360	0.5000	0.6312	0.5000	0.6325
k-Disturbance (Pre)	0.8345	0.9890	0.8287	0.9790	0.8181	0.9791	0.8306	1.0000	0.8424	1.0000
k-Disturbance (Dur)	0.7615	0.8065	0.7781	0.8304	0.7637	0.8137	0.7977	0.8976	0.7848	0.8103
k-Disturbance (Post)	0.7813	0.8667	0.8011	0.8789	0.7897	0.8650	0.8087	0.9310	0.8035	0.8654

3.1.2 Dataset Arrangement

ED is defined as a series of data that represent the state of the system at a given time [35]. In this simulation, the ED consists of simulated voltage, humidity, harmonics, machine positioning (slewing, luffing and travelling), temperature and wind speed. The simulation data is based on the actual operation and environment data of the CSU machine events by considering the assessment result in Table 1 and the location of the power plant located in Malaysia. The plant is located near to the seaside, which is hot and humid throughout the year and may tend to have strong winds. On the other hand, the machine movements are simulated based on the 3-axis movement, which includes slew (x-axis), luffing (y-axis) and travel (z-axis).

In Discrete Event System, any input variable whose value transition register as an event is defined as a TD [35]. In this simulation, the TD consists of machine status (slewing, luffing, travel and bucket) and motor run feedback (slewing, hydraulic, travel and bucket). For comparison purposes, two types of TD are presented here known as Static TD and Dynamic TD. Static TD registered the original TD signal from the source while Dynamic TD multiply the changes of TD with a threshold setting defined by the system engineer. Both types of TDs were used in this experiment to investigate which source of data to be selected. This will ensure the event modeller algorithm provides an accurate sensitivity index or weight output.

Meanwhile, the threshold level could be adjusted based on the expert point of view. In this simulation, the threshold level is set at 5% (0.05); thus, the Upper Limit and Lower Limit will automatically set to 1.05 and 0.95 consecutively. The limits will be multiplied to the individual data computationally, to calculate the changes of the current data to the previous data and reflects the algorithm for weight score using X-NOR logic. The event modeller limit is the desired weight limits which also could be adjusted based on the expert point of view. In this simulation, the event modeller limit is set at (0.8). The weights who score above the Event Modeller Limit is shaded in the ROC Output table, indicates a significant correlation between the ED and the TD.

The sequence of TD's and ED's is updated every second and are re-arrangeable according to the weighted score. The weighted score can take a value of 0.5 and 1. The value is 1 when both or none of the input/output are triggered. Otherwise, it is 0.5. The weighted score is then averaged based on the number of iteration. Having the weight score in real-time, system engineers could easily notify the management team if there is any disturbance occurs in the system state by looking at the sequence and the weights. For trending purposes, a waveform chart is presented to improve the visibility of the data.

3.1.3 Disturbance Signal

The purpose of this simulation is to test the applicability of the Event Modeller algorithm in the handling of real-time data, thus observing the reaction of the system to the abnormal events. To ensure the system is sensitive to this abnormality, a k-Disturbance signal is introduced to the system. In this simulation, the data is simulated in 3 stages known as pre-disturbance, k-disturbance and post-disturbance. The pre-disturbance refers to the warm-up stage, which represents the machine normal steady state. The k-disturbance refers to the fluctuation of the k-event data, in such generating disturbance to the system. The post-disturbance refers to the reaction of the abnormal system back to normal steady state. A 5 minutes time interval is selected for each stage, which accumulates to 15 minutes of sampling time.

In this simulation, 5 ED's signal, which represents the internal and environment parameter, has been chosen to be disturbed. This includes voltage, humidity, harmonic, temperature and wind speed. The signal data are simulated based on random fluctuation with 5% disturbance limit from normal operation data capability.

3.1.4 Simulation Results

Table 2 compares the results obtained from the simulation of the CSU machine against the k-disturbance signal. To present the findings, the performance is measured from the score of the sensitivity index from two main perspectives, which includes the overall maximum and minimum weight, and the average score for each stage. What stands out in the table is that the value of the weight has changed drastically between the pre-disturbance and during disturbance for all case. For e.g., when the k-disturbance is applied to the machine voltage using Static TD, the weight value drops from 0.83450 to 0.76154. However, when the k-disturbance is removed, the weight value rose to 0.78132. These indicate that the system parameters are sensitive to the disturbance signal introduced in the system.

It is interesting to note that all ten cases of this study have a common finding. The transition of average sensitivity index (weight) from Pre-Disturbance to k-Disturbance have the same reduction trend with an average of 8.2% reduction for Static TD and 15.94% reduction for Dynamic TD. Alternatively, when the k-Disturbance recovers, there is also a trend of increased weight with an average of 3.218% increment for Static TD and 6.023% increment for Dynamic TD. This finding confirms the interrelation between the triggered data and the k-disturbance event data, where different TD types have different performance. The Dynamic TD has a higher percentage of changes compared to Static TD.
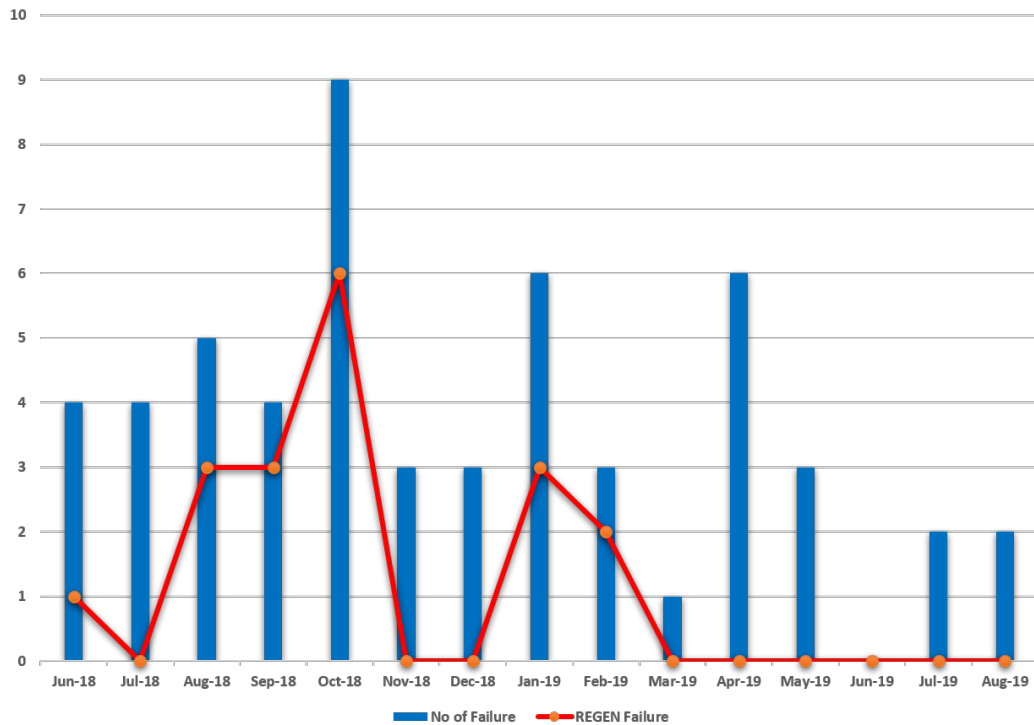
Figure 4: Tabulation of CSU Machine Failure vs REGEN Failure

The bar chart reveals that the highest number of REGEN faults was reported in October 2018, followedby August 2018, September 2018 and January 2019 consecutively.

On the other hand, it has been observed that the minimum weight for Static TD is fixed at 0.5000 while Dynamic TD has different minimum weight scores for each experiment. A possible explanation for this might be that the Dynamic TD captured the changes of input sensitivity rather than a direct Boolean signal from the input itself.

3.2 Experiment 2: CSU Real-time Machine Failure Analysis with KPIs

Harmonic filter failure can be influenced by various factors, such as faulty device, operator handling, and environmental factors in which the machine operates. It has also occasionally been affected by the combination of these factors. Based on the CSU machine expert point of view, the harmonic problem is associated with the occurrence of Regenerative Drive (REGEN) fault. In order to access the REGEN fault events, the abnormal dataset was selected. The frequency of the REGEN failure was compared with other types of fault, as presented in Figure 4. The bar chart reveals that the highest number of REGEN faults was reported in October 2018, followed by August 2018, September 2018 and January 2019. Although the highest number of REGEN failures was recorded in October 2018, no report indicated that the REGEN drives had been replaced. However, the January 2019 reports indicated that the maintenance team had replaced the REGEN during this month due to a fault. The January dataset was therefore chosen to further explain the relationship of the variables using the proposed technique.

3.2.1 Experiment Strategy

Building a solution capable of translating engineering data automatically into high-level management information is the principal motivation for this experiment. The KPIs shall be calculated based on the operation of the machine during the selected period. The method used in [1] is borrowed to run a fault dataset with a time interval of 5 minutes. The first 5 minutes are the events before the fault occurs, followed by the fault, and end with the last 5 minutes that accumulate up to 15 minutes of sampling time. The reason why this method was adopted is to prove that the event modeller could instantly solve a complex system without having to run the system for a longer period. It is easy to sample data in a simulation environment, as the user can decide when the fault may occur, but this is not the case with industrial data. The dataset was therefore analyzed to determine which data was almost equivalent to the setting. The experiment strategy is summarised in Figure 5. The results are presented in two phases. First, the event modeller was used as a tool to reduce the dimensionality of the data being observed. Second, the relationship between the observed data and the KPIs has been compared. The results will be explained as follows.

3.2.2 Dataset Arrangement

In this example, a homogenous dataset representing REGEN failure of the predictive model population was sampled for 16 minutes. The dataset of 30th January 2019 was sampled between 12:47 pm and 13:03 pm. The dataset arrangement indicated that there were 96 TDs to be grouped against 24 EDs in the form of matrices to show
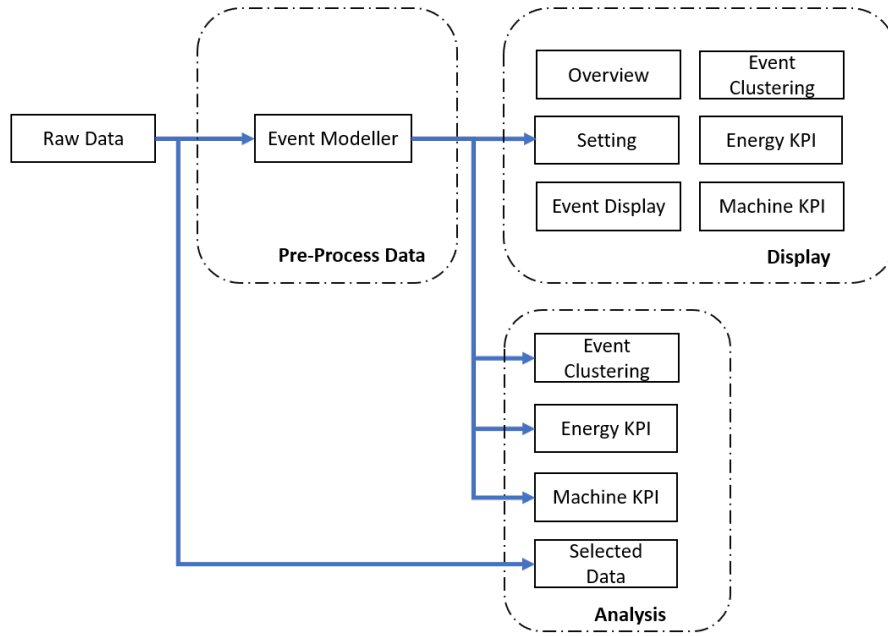
Figure 5: Experiment Strategy for KPIs Analysis

The arrangement of the three principal stages in the Experiment Strategy for KPI Analysis: Pre-process Data, Analysis and Display.

which system parameters were highly correlated. It is noteworthy that the 96 X 24 matrices are too complex for a correlation analysis; therefore, the 96 TD was divided into 4 clusters. For each TD cluster, 24 X 24 matrices were analyzed using the event modelling technique.

The sensitivity index of each input-output relationship has been measured and updated every second. The ROC pattern was observed in real-time and captured every minute. As a result, four-quadrant windows representing four key states were presented: Initial, Pre-Fault, Fault and Post Fault for each TD cluster. This analysis intends to examine how TDs influence the pattern of the ROC. It is necessary to clarify what happens during this 16-minute time stamp before presenting the chart. Based on the report, the machine is running at its optimum level before it is fully phased out after 10 minutes. The reason why machine trips are unknown, which left the proposed method to be concluded further.

3.2.3 Dimensionality Reduction using Event Modeller

One advantage of using Event Modeller is to reduce the dimensionality of a complex system. As the main objective is to identify the root cause of the failure, this technique is capable of highlighting the ROC pattern based on its correlation analysis. One important finding was that the first four EDs were the same for all clusters. They comprised of E-House Humidity (ED24), Portal Conveyor Current (ED18), Wind Speed (ED 12) and Portal Speed Drive (ED14). This indicates that one of these EDs would have been the cause of failure. However, it has been noted that Cluster 2 and Cluster 3 consistently remain the same pattern with or without fault happened.

Therefore, we have eliminated Cluster 2 and Cluster 3 from the analysis. Moving to the ROC patterns for Cluster 1 and Cluster 4, major changes were observed after the fault in this quadrant. From this observation, it is suggested that the TDs could have originated from these clusters. Equation 3 indicates the possible root cause of Cluster 1. If we overlap both relationships, the new equation for Cluster 1 is expressed in Equation 4.

$$
\begin{aligned}
\rho_{0.95} = (ED18) &\times (TD6, TD7, TD11, TD8, TD9, TD10)+ \\
(ED24) &\times (TD8, TD9, TD10, TD24, TD21, TD2, \quad (3) \\
&TD22, TD23, TD20, TD13, TD12)
\end{aligned}
$$

$$
\rho_{0.95} = (ED18 + ED24) \times (TD8, TD9, TD10) \quad (4)
$$

On the other hand, the following equation 5 indicates the possible root cause of Cluster 4. If we overlap both relationships, the new equation for Cluster 4 is expressed in Equation 6.

$$
\begin{aligned}
\rho_{0.95} = (ED18) &\times (TD15, TD18, TD16, TD17, TD20)+ \\
(ED24) &\times (TD16, TD17, TD14, TD13, TD19, \quad (5) \\
&TD12)
\end{aligned}
$$

$$
\rho_{0.95} = (ED18 + ED24) \times (TD16, TD17) \quad (6)
$$

Combining Equation 4 with Equation 6, the sensitivity index is expressed in Table 3. With that, Event Modeller has reduced the dimensional to a smaller scale that will help the system engineer
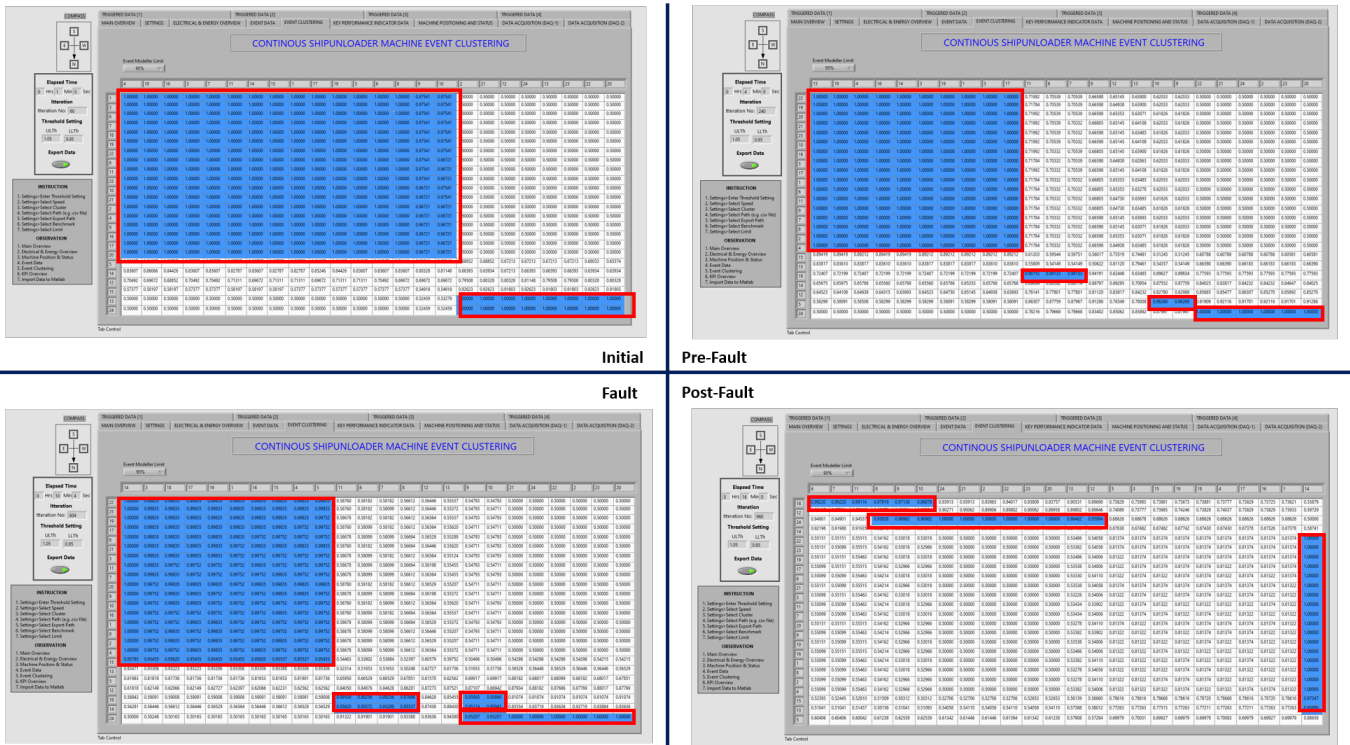
Figure 6: Rank Order Clustering - Cluster 1

ROC Pattern on four quadrant: Initial, Pre-Fault, Fault and Post-Fault for Cluster 1. The blue shaded region with red boxes represent the cluster of a high correlation value between 0.95 to 1.00.

Table 3: Summary of Sensitivity Index

Description	TD8	TD9	TD10	TD16	TD17
ED18	0.97919	0.97138	0.96878	0.98337	0.96881
ED24	0.95838	0.96982	0.996982	0.95842	0.97089

decide which relationship is liable to this fault. The following section will be discussed on the relationship between the observed data and the KPIs to validate the findings of the Event Modeller. Figure 6 and Figure 7 represent the pattern of the ROC system state for Cluster 1 and Cluster 4, respectively.

3.2.4 Relationship between the observed data against Key Performance Indicators

The KPIs are the translated index of the machine operation. It provides operational information for the decision-making of both the machine and the system operator. Four main KPIs have been adapted in this experiment known as Availability (A), Instantaneous Utilization (IU), Schedule Utilization (SU) and Performance (P). Having these four KPIs in line with CSU machine data, the possible root cause of frequent harmonic failure could be determined.

The following steps have been taken to analyze the data: (1) Select fault dataset from the Predictive Model Dataset. (2) Identify the fault observed data location. (3) Distinguish observed data according to Environment Variables, Electrical Variables and Motor Variables. (4) Plot Environment Variables data against KPIs. (5) Plot Electrical Variables data against KPIs. (6) Plot Motor Variables

data against KPIs.

The easiest way to identify fault events is by exploring the main incomer trip data. Theoretically, the entire electrical system will be tripped when there is a REGEN fault. Although it may conflict with other events in which the operator may trip the main incomer on purpose, the system could automatically distinguish between the actual fault and the simulated fault using the translated KPIs data.

For example, when a fault occurred during the operation, the data of the KPIs will hold the value in percentage. This verifies that the fault that occurred is genuine. If the machine is stopped or not operated, the value is either zero or hold to a specific value. In this example, the same dataset used in the previous experiment was chosen. This is to compare the relationship between the data observed using both techniques. The dataset dated 30th January 2019 was therefore sampled between 12:47 pm and 13:03 pm. The target data was then divided into three and plotted against the KPIs as follows:

Figure 8 shows the observed electrical data against the KPIs when electrical faults occurred. This graph is quite revealing in several ways. First, the main fault has been observed. The chart reveals that the main fault occurred at 09:50. This is the turning point of all events. Next, the four KPIs are observed. The perfor-

Figure 7: Rank Order Clustering - Cluster 4

ROC Pattern on four quadrant: Initial, Pre-Fault, Fault and Post-Fault for Cluster 4. The blue shaded region with red boxes represent the cluster of a high correlation value between 0.95 to 1.00.

Table 4: Summary of Electrical Variables

Description	ED1	ED2	ED4
Min	427.33 V	9.66 A	1.84 %
Max	427.47 V	242.93 A	2.19 %
Average	427.44 V	73.13 A	2.00 %

mance was initiated at 100% and remained for 1 minute. It was then exponentially reduced to 16% when the main fault occurred. This indicates that the unloading of coal has stopped immediately after 1 minute.

On the other hand, both Instantaneous Utilization and Schedule Utilization started at 58% and gradually decreased to 35% at 04:24. At this point, Schedule Utilization bounces back to 39%, but Instantaneous Utilization remains reduced to 30% until the main fault event occurs. The availability started at 95% and remained until 04:24 before it gradually decreased when the main fault occurred. These trends have shown that there is a relationship between the main fault and the KPIs. Table 5 summarised the KPI results.

Moving to electrical variables, the main input voltage (ED1) remains at 427V for the entire time. Although the fault occurred, the main input voltage does not respond to this. This validates that the fault is not caused by power disturbances from the supply, such as transient, interruption, under-voltage or over-voltage. The Main Incomer Current (ED2) pattern was then observed. Before the fault, ED2 shows the current drawing of the electrical distribution. The pattern is based on loads of the motor during machine operation.

However, when the fault occurred, trends show that ED2 is re-sponding to the event. An instantaneous drop was discovered during this period. ED2 does not fall to zero because the energy was still drawn from the maintenance feeder for essential loads. The main incoming THD (ED4) has also been observed. ED4 has been generated assuming that there will be no harmonic distortion during these events. The ED4 pattern remains at an average of 2.0% throughout the sampling time, indicating that the THD remains at IEEE 519 Standards. Table 4 summarised the electrical variables.

Meanwhile, to further explain the relationship between the motor variables and the KPIs, Figure 9 shows the current drawing of five main processes in the CSU machine. These include Bucket Elevator Current (ED17), Portal Conveyor Current (ED18), Travel Current (ED19), Boom Conveyor Current (ED20) and Hydraulic Power Pack (ED21). In order to validate the ED2 from the previous graph, this chart reveals that ED2 has a linear relationship with all motor variables within this graph. For example, when ED17 was drawn at the beginning of the sampling and all other motor loads were added during that period the ED2 measurement reached its peak value. Some attention is given to the small circle in the chart. It is clear that there was some instability happening at 01:48, which could be linked to the fault.
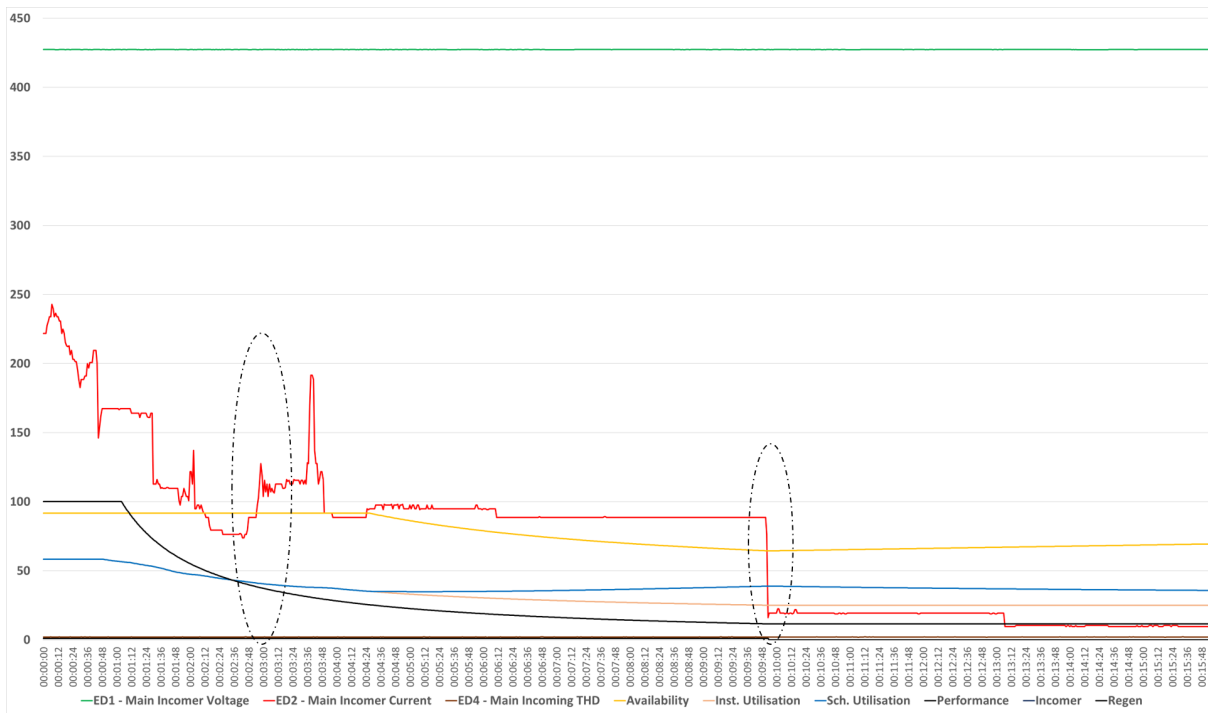
Figure 8: Electrical Variables vs KPIs

This figure illustrates the relationship between the Machine KPIs (Availability, Instantaneous Utilization, Schedule Utilization, and Performance) against the observed electrical data (Voltage, Current, Harmonic, Incomer and Regen) when the same event of electrical faults occurred at Time: 09:50.

Table 5: Summary of KPIs

Description	A	IU	SU	P
Min	64.37 %	25.01 %	34.82 %	11.52 %
Max	91.67 %	58.33 %	58.33 %	100.00%
Average	76.43 %	32.48 %	39.59 %	26.72 %

ED18 had an impulsive signal and remained zero after that event. On the other hand, ED19 has also revealed some dramatic changes. Just after ED18 had an impulsive signal, ED19 experienced some negative distortion for 12 seconds, followed by an interruption for 48 seconds and a further positive distortion for 60 seconds completely before it stopped. Another attention has to be made at ED17. In the beginning, ED17 had drawn some fluctuation current and had spiked for a few seconds before stopping at 00:40. The trend shows that ED17 is struggling to recover, but ends up stopping when the main fault has occurred. Otherwise, all other motor variables are operating in their normal state. Table 6 summarised the motor variables.

Figure 10 displays the environment data observed against the KPIs when the same electrical faults have occurred. Five environmental data were reported, including Panel Humidity (ED3), Panel Temperature (ED5), E-House Temperature (ED6), Wind Speed (ED12) and E-House Humidity (ED24). Attention must be given to the humidity and temperature of the electrical room where the electrical distribution panel is located. The pattern has shown an instant increase of ED24 at 02:36. The humidity builds up and reaches its highest peak at 58% and slowly decreased with two spikes before the fault occurred. On the other hand, ED3 has also been increased

but not as much as ED24. ED5 has an average temperature of 33.13 degrees Celsius, while ED5 has an average temperature of 17.82 degrees Celsius. Eventually, ED12 fluctuates within the normal range. Table 7 summarised the environment variables.

3.2.5 Discussion

The main outcome of the experiment is to show how the proposed technique can be used as a tool to reduce the dimensions of a highly complex system. In this case study, 96 TDs were analyzed against 24 EDs in real-time to help system engineers visualize any changes to the system state. The EMDA implementation will group high correlation system parameters in the form of matrices and place them in mutually exclusive blocks. Having a huge matrix, however, will make things difficult. The matrix needs to be presented as a square for clear visibility. Thus, the 96 TDs were divided into 4 clusters, where each cluster has a relationship with 24 EDs. The example accessed a 16-minute dataset that belongs to a fault population. The result for each cluster was shown in a four-quadrant to show the pattern change. In this example, there is a significant change in the pattern observed in Cluster 1 and Cluster 4. Further analysis of the two clusters suggested a new formula representing
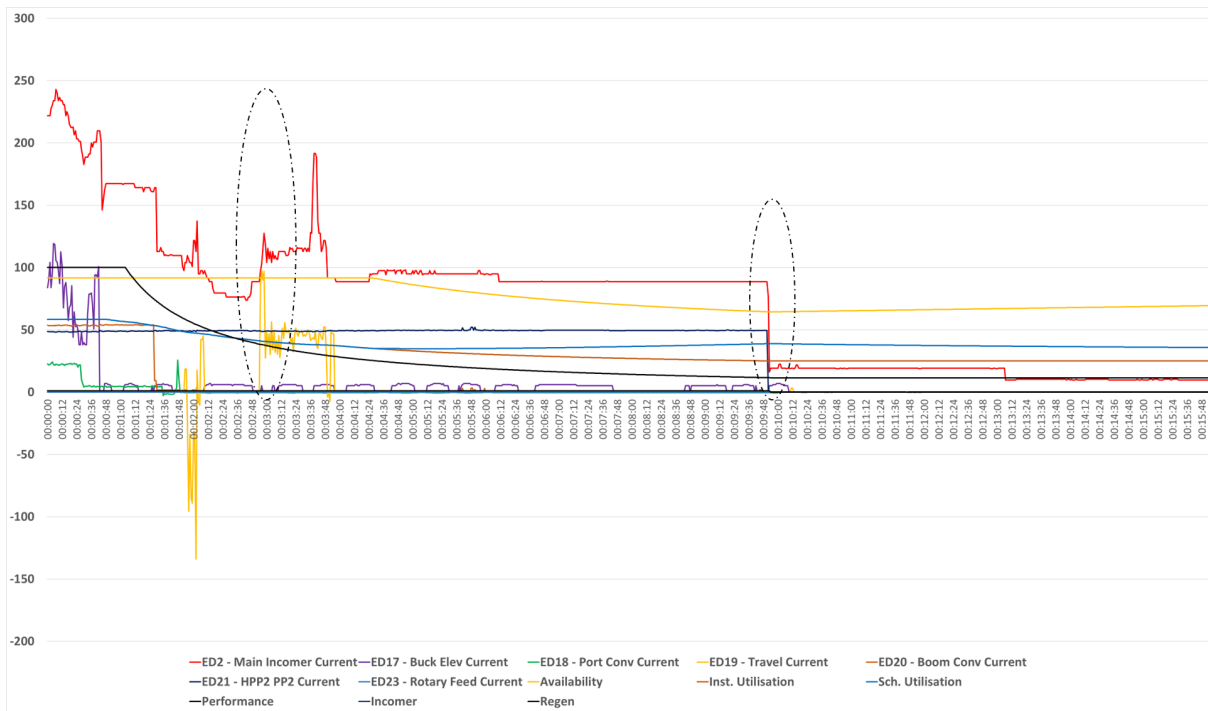
Figure 9: Motor Variables vs KPIs

This figure illustrates the relationship between the Machine KPIs (Availability, Instantaneous Utilization, Schedule Utilization, and Performance) against the Five Main Electrical Motors (Bucket Elevator Current, Portal Conveyor Current, Travel Current, Boom Conveyor Current and Hydraulic Power Pack) when the same event of electrical faults occurred at Time: 09:50.

Table 6: Summary of Motor Variables

Description	ED17	ED18	ED19	ED20	ED21
Min	0.00 A	-2.96 A	-133.97 A	0.00 A	0.05 A
Max	119.31 A	25.67 A	97.87 A	54.41 A	52.05 A
Average	5.41 A	0.69 A	2.49 A	5.03 A	30.60 A

the state of the system. After the fault event, the new formula for Cluster 1 and Cluster 4 is expressed in Equation 4 and Equation 6, respectively. As a result of these equations, the main culprit of the fault was identified. The ED variables were reduced from 24 EDs to 2 EDs (a decrease of 91.76%) while the TDs variable was reduced from 96TDs to 5TDs (a decrease of 94.79%). As listed in Table 3, the possible root causes of the fault are the combination of:

1. Portal Conveyor Current (ED18) with Rotary Feeding Table Motors (TD8), Bucket Elevator Motors (TD9), Bucket Elevator Brake Motors (TD10), Busy Rotary Table (TD16) and Busy Bucket Elevator (TD17) or

2. E-House Humidity (ED24) with Rotary Feeding Table Motors (TD8), Bucket Elevator Motors (TD9), Bucket Elevator Brake Motors (TD10), Busy Rotary Table (TD16) and Busy Bucket Elevator (TD17)

Further analysis with the KPIs will validate the existence of unknown events that could be linked to a harmonic problem. In normal circumstances, electrical variables such as voltage, current and THD should have a linear relationship with the KPIs. As the KPIs

responded to the fault, the electrical variables should also respond. However, the voltage and the harmonic measurement remain constant after the fault has occurred. Although current measurements have responded to this fault, trends show that the current value is not zero. It indicates that there was still a current drawing for the essential loads. Therefore, this eliminates the possibility of machine failure due to electrical variables.

Moving to the motor variables, as explained in the result, ED17, ED18 and ED19 showed some undiscovered events that could lead to fault. When comparing the performance trend to ED17, the performance measurement falls in line with the activity of the bucket elevator. Although the trends for ED17 fluctuate before it stops, this could be explained from the perspective of uneven coal inside the bucket. On the other hand, ED18 has experienced an impulsive signal that leads to an immediate stop. However, looking at the timing of this event, it took about 9 minutes for the fault to happen. The same goes for ED19, which experienced negative and positive distortions right after ED18. This can be claimed as a result of an event. However, when it comes to the type of operation, ED19 is a travel motor that operates in two directions. Although some distorted measurements were made, this could be explained by the
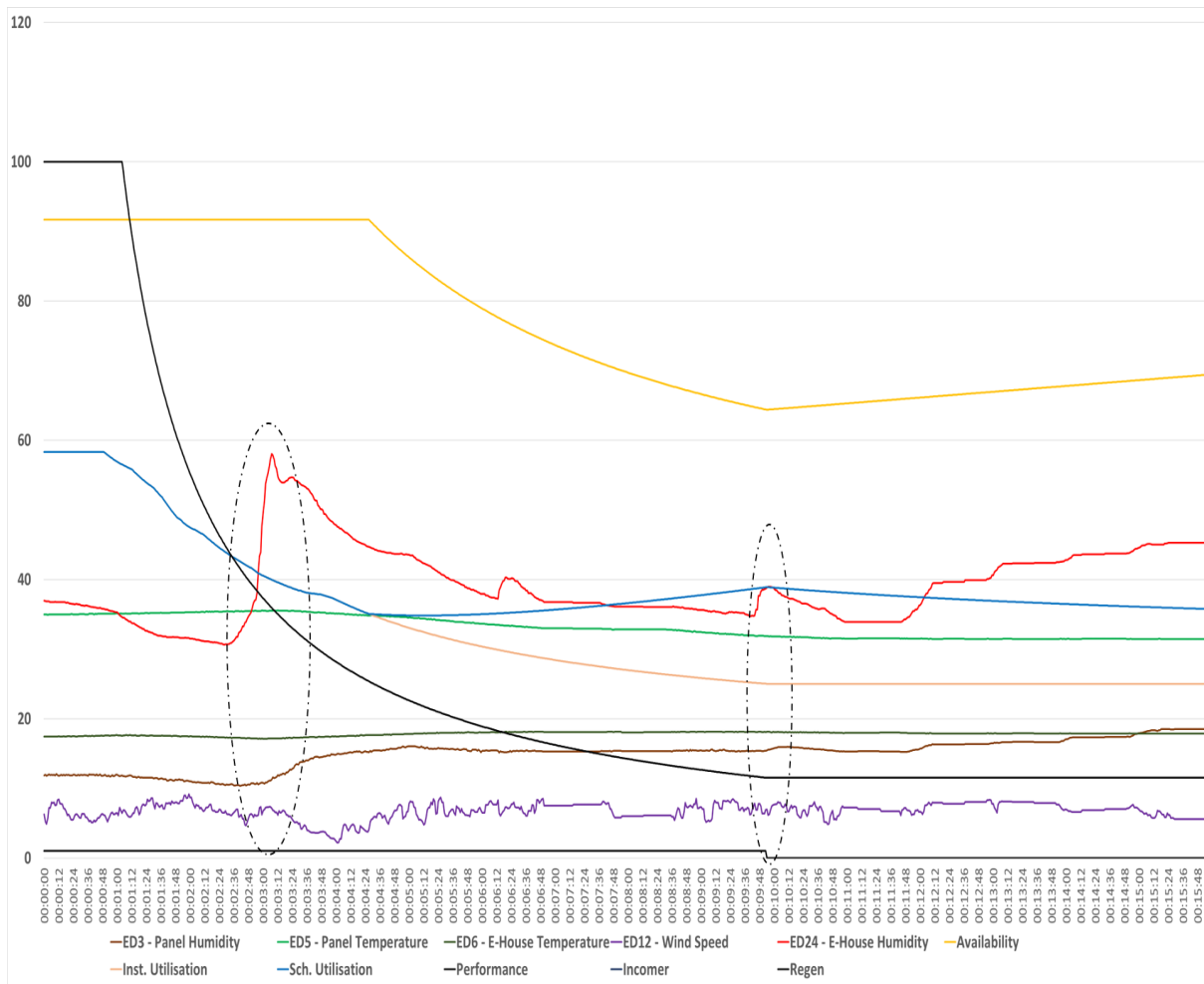
Figure 10: Environment Variables vs KPIs

This figure illustrates the relationship between the Machine KPIs (Availability, Instantaneous Utilization, Schedule Utilization, and Performance) against the Environment Variables (Panel Humidity, Panel Temperature, E-House Temperature, Wind Speed and E-House Humidity) when the same event of electrical faults occurred at Time: 09:50.

number of motors that were operating. There were ten motors in service working at different efficiency levels. Having said that, the motor variables are also excluded from being the root cause of the fault.

Turning to environment variables, the trends in Figure 10 have shown some indications that the humidity could be related to the fault. The rise in humidity up to 58.06% shows that the state of the system has been compromised. Although high humidity patterns started 7 minutes before the fault, the measurement continuously retained above 40 % after the fault. This type of phenomena takes a fixed amount of time to reach the fault level. To explain this phenomenon, we take an example of preheating an oven. When a person decides to bake a cake, the oven needs to be heated to the right temperature before putting the cake inside the oven. Although it takes a few seconds to turn the oven on, it may take a few minutes to get the right temperature. This phenomenon is referred to as a fixed time delay deterministic event. However, if the person warms up the oven, without shutting the oven door, it may take longer to get to the right temperature. This phenomenon is referred to as a deterministic sequence of different input events. The heat produced

in the oven was cooled by the amount of cold air present in the surroundings, which would delay the oven pre-heating process.

When we relate this to our case study, the power electronic component such as choke, rectifier, REGEN and control drives produce an excessive amount of heat during operation. To ensure that the heat is kept at certain limits, two units of air conditioners were designed to combat this heat. However, after considering the amount of heat generated in the room along with the hot and humid climate of Malaysia throughout the year, experts have reviewed and decided to install two additional air conditioners to cater for this amount of heat. As a result, when CSU machine is fully operational, the four-unit air conditioners are sufficient to cool down the electrical room. However, when the machine stops at intervals, the air conditioners are found oversized to the power electronic component. As a consequence, the humidity increases; the component becomes wet, resulting in machine failure. The humidity in the electrical switchgear room must be maintained at an elevated temperature relative to the ambient inside the room. Condensation is usually considered a problem only if the humidity in the switchgear room is 65% or greater [44]. Although the humidity in this example does

Table 7: Summary of Environment Variables

Description	ED3	ED5	ED6	ED12	ED24
Min	10.35 %	31.41 degC	17.12 degC	2.22 m/s	30.64 %
Max	18.52 %	35.54 degC	18.16 degC	9.19 m/s	58.06 %
Average	14.95 %	33.13 degC	17.82 degC	6.74 m/s	39.21 %

not reach 65%, considering the machine has been running for a decade, the efficiency of the machine may decrease as the humidity may be the contributing factor. This finding suggests that there is a relationship between the humidity and the fault.

As mentioned earlier, this paper's main outcome is to show how the EMDA can be used as a tool to reduce the dimensions of a highly complex system. 96 Triggered Data were scanned against 24 Event Data, which then formulated an equation representing the system state in a single second. This sort of like a "scanner" that will keep converting a complex relationship into a simple equation (a huge reduction of dimensionality) in a low computational effort. The results in Table 3 shows that the complex relationship has been reduced to 2 EDs against 5 TDs. Further analysis with the KPIs has validated the existence of unknown events that linked to the frequent harmonic failure. The rise in humidity level shown in Figure 10 has proven that the system state has been compromised. In comparison, other variables such as electrical variables, motors and other environment do not show any evidence that compromises the system state. Besides, the relationship between the observed data and the KPIs appears to be consistent. The suggested finding was tested at site, and the operators confirmed the importance of humidity factor (environmental factor) in the machine's performance. A humidity regulator has been suggested to be installed at the site. The control of the regulator was linked to the plant automatic control system.

4 Conclusions

Managing repetitive harmonic failures in an industrial application is a recursive, costly and time-consuming exercise. Industrial data are multidimensional and random in nature. The problem with analyzing this data is that many events do not necessarily repeat often enough to have statistical significance. Still, they cause minor or major faults and need to be captured and understood. Identical machines perform differently in different environments and conditions. In most cases, PQ engineers focus on the fundamental problem, transforming the power system signal into various signal processing methods to locate the fault. An Event Modeller technique, which is low in the computational effort, has been considered to solve this problem. This technique, which is extremely computational effective, managed to reduce system state definitions' complexity into a simpler formulation. Also, the performance metrics translated from the machine operation are now automated and require minimum operator intervention. It reduces wrong interpretations and possible mistakes in decision making. However, one of the method's weaknesses is its reliance on technical expert judgement on adjusting the threshold settings. One of the ongoing research endeavours of the authors is to automate the trigger detection phenomena.

In this present work, authors focused on reducing dimensionality while collectively including the modelling equation's performance

metrics parameter to verify the system state. Two approaches were taken to validate and verify the propose EMDA algorithm. First was the simulation process (SiL). It considered the voltage, humidity, harmonic, slewing movement, luffing movement, travelling movement, temperature, and wind speed as system output variables. Two types of triggering data, i.e. Static TD and Dynamic TD were considered. K-disturbance signal was generated for the five (excluding movements) output variables. The results show that, as the disturbance is induced, the sensitivity indices were reduced by an average of 8.2% for Static TD and 15.94% for Dynamic TD. However, when the disturbance was removed, the sensitivity indices regained by an average of 3.218% and 6.023% for Static TD and Dynamic TD consecutively. As a result, the Dynamic TD was chosen for the field experiments. In the field experiment (HiL), 914 data series in real-time were acquired from the SCADA. Each dataset is containing 96 Input vs 24 Output parameters. The results show that two new parameters were detected to significantly impact Harmonic Filters; humidity and portal conveyor current (velocity of the conveyor). The tests proved that humidity as an environmental factor is linked to the frequent harmonic problems. This revelation was also verified by looking up the historical evidence of humidity data against the frequency of failures and the variation in the feeder's speed (conveyor). In the future, the proposed EMDA will be integrated as a vehicle for training supervised machine learning models to predict the remaining useful life of the filter as a predictive

References

[1] F. Z. M. Fadzil, A. Mousavi, M. Danishvar, "Simulation of Event-Based Technique for Harmonic Failures," in 2019 IEEE/SICE International Symposium on System Integration (SII), 66–72, IEEE, 2019, doi:10.1109/SII.2019.8700381.

[2] N. N. Gomaa, K. Y. Youssef, M. Abouelatta, "On Design of IoT-based Power Quality Oriented Grids for Industrial Sector," Advances in Science, Technology and Engineering Systems Journal, **5**(6), 1634–1642, 2020, doi: 10.25046/aj0506194.

[3] U. Singh, S. N. Singh, "Application of fractional Fourier transform for classification of power quality disturbances," IET Science, Measurement & Technology, **11**(1), 67–76, 2017, doi:10.1049/iet-smt.2016.0194.

[4] M. Panteli, P. Mancarella, "Influence of extreme weather and climate change on the resilience of power systems: Impacts and possible mitigation strategies," Electric Power Systems Research, **127**, 259–270, 2015, doi:10.1016/j.epsr. 2015.06.012.

[5] M. K. Saini, R. Kapoor, "Classification of power quality events–a review," International Journal of Electrical Power & Energy Systems, **43**(1), 11–19, 2012, doi:10.1016/j.ijepes.2012.04.045.

[6] Z. Huang, M. Li, A. Mousavi, M. Danishva, Z. Wang, "EGEP: An Event Tracker Enhanced Gene Expression Programming for Data Driven System Engineering Problems," IEEE Transactions on Emerging Topics in Computational Intelligence, **3**(2), 117–126, 2019, doi:10.1109/TETCI.2018.2864724.

[7] M. Morcos, W. A. Ibrahim, "Electric Power Quality and Artificial Intellignece: Overview and Applicability," IEEE Power engineering review, **19**(6), 5–10, 1999, doi:10.1109/MPER.1999.768508.

[8] D. Saxena, K. Verma, S. Singh, "Power quality event classification: an overview and key issues," International Journal of Engineering, Science and Technology, **2**(3), 186–199, 2010.

[9] D. C. Robertson, O. I. Camps, J. S. Mayer, W. B. Gish, "Wavelets and electromagnetic power system transients," IEEE Transactions on Power Delivery, **11**(2), 1050–1058, 1996, doi:10.1109/61.489367.

[10] S. Santoso, E. J. Powers, W. M. Grady, P. Hofmann, "Power quality assessment via wavelet transform analysis," IEEE transactions on Power Delivery, **11**(2), 924–930, 1996, doi:10.1109/61.489353.

[11] J. Barros, R. I. Diego, "Analysis of harmonics in power systems using the wavelet-packet transform," IEEE Transactions on Instrumentation and Measurement, **57**(1), 63–69, 2008, doi:10.1109/TIM.2007.910101.

[12] S. Shukla, S. Mishra, B. Singh, "Empirical-mode decomposition with Hilbert transform for power-quality assessment," IEEE transactions on power delivery, **24**(4), 2159–2165, 2009, doi:10.1109/TPWRD.2009.2028792.

[13] R. G. Stockwell, "A basis for efficient representation of the S-transform," Digital Signal Processing, **17**(1), 371–393, 2007, doi:10.1016/j.dsp.2006.04.006.

[14] S.-H. Cho, G. Jang, S.-H. Kwon, "Time-frequency analysis of power-quality disturbances via the Gabor–Wigner transform," IEEE transactions on power delivery, **25**(1), 494–499, 2010, doi:10.1109/TPWRD.2009.2034832.

[15] C. Norman, J. Y. Chan, W. H. Lau, L. L. Lai, "Hybrid Wavelet and Hilbert Transform With Frequency-Shifting Decomposition for Power Quality Analysis." IEEE Trans. Instrumentation and Measurement, **61**(12), 3225–3233, 2012, doi:10.1109/TIM.2012.2211474.

[16] B. Biswal, P. K. Dash, S. Mishra, "A hybrid ant colony optimization technique for power signal pattern classification," Expert Systems with Applications, **38**(5), 6368–6375, 2011, doi:10.1016/j.eswa.2010.11.102.

[17] K. Manimala, K. Selvi, R. Ahila, "Optimization techniques for improving power quality data mining using wavelet packet based support vector machine," Neurocomputing, **77**(1), 36–47, 2012, doi:10.1016/j.neucom.2011.08.010.

[18] R. Ahila, V. Sadasivam, K. Manimala, "An integrated PSO for parameter determination and feature selection of ELM and its application in classification of power system disturbances," Applied Soft Computing, **32**, 23–37, 2015, doi:10.1016/j.asoc.2015.03.036.

[19] C. Cortes, V. Vapnik, "Support-vector networks," Machine learning, **20**(3), 273–297, 1995, doi:10.1007/BF00994018.

[20] L. A. Zadeh, "Fuzzy sets," in Fuzzy Sets, Fuzzy Logic, And Fuzzy Systems: Selected Papers by Lotfi A Zadeh, 394–432, World Scientific, 1996.

[21] S. Khokhar, A. A. M. Zin, A. S. Mokhtar, N. A. M. Ismail, N. Zareen, "Automatic classification of power quality disturbances: A review," in 2013 IEEE Student Conference on Research and Developement, 427–432, 2013, doi:10.1109/SCOReD.2013.7002625.

[22] D. Granados-Lieberman, R. Romero-Troncoso, R. Osornio-Rios, A. Garcia-Perez, E. Cabal-Yepez, "Techniques and methodologies for power quality analysis and disturbances classification in power systems: a review," IET Generation, Transmission & Distribution, **5**(4), 519–529, 2011, doi:10.1049/iet-gtd.2010.0466.

[23] M. McGranaghan, "Overview of Power Quality Standards," PQ Network Internet Site, http://www. pqnet. electrotek. com/pqnet, 1998.

[24] I. . W. Group, et al., "IEEE Recommended Practices and Requirements for Harmonic Control in Electrical Power Systems," IEEE STD, 519–1992, 1992.

[25] B. IEC, "61000-3-4," Electromagnetic compatibility (EMC)-part, 3–4, 1998.

[26] P. Muchiri, L. Pintelon, "Performance measurement using overall equipment effectiveness (OEE): literature review and practical application discussion," International journal of production research, **46**(13), 3517–3535, 2008, doi:10.1080/00207540601142645.

[27] V. C. Angadi, A. Mousavi, D. Bartolomé, M. Tellarini, M. Fazziani, "Regressive Event-Tracker: A Causal Prediction Modelling of Degradation in High Speed Manufacturing," Procedia Manufacturing, **51**, 1567–1572, 2020, doi:10.1016/j.promfg.2020.10.218.

[28] V. C. Angadi, A. Mousavi, D. Bartolomé, M. Tellarini, M. Fazziani, "Causal Modelling for Predicting Machine Tools Degradation in High Speed Production Process," IFAC-PapersOnLine, **53**(3), 271–275, 2020, doi:10.1016/j.ifacol.2020.11.044.

[29] M. Danishvar, V. C. Angadi, A. Mousavi, "A PdM Framework Through the Event-based Genomics of Machine Breakdown," in 2020 Asia-Pacific International Symposium on Advanced Reliability and Maintenance Modeling (APARM), 1–6, IEEE, 2020, doi:10.1109/APARM49247.2020.9209530.

[30] Z. Huang, V. C. Angadi, M. Danishvar, A. Mousavi, M. Li, "Zero Defect Manufacturing of Microsemiconductors–An Application of Machine Learning and Artificial Intelligence," in 2018 5th International Conference on Systems and Informatics (ICSAI), 449–454, IEEE, 2018, doi:10.1109/ICSAI.2018.8599292.

[31] M. Danishvar, V. Vasilaki, Z. Huang, E. Katsou, A. Mousavi, "Application of Data Driven techniques to Predict N 2 O Emission in Full-scale WWTPs," in 2018 IEEE 16th International Conference on Industrial Informatics (INDIN), 993–997, IEEE, 2018, doi:10.1109/INDIN.2018.8472075.

[32] M. Danishvar, A. Mousavi, P. Broomhead, "EventiC: A Real-Time Unbiased Event-Based Learning Technique for Complex Systems," IEEE Transactions on Systems, Man, and Cybernetics: Systems, 2018, doi:10.1109/TSMC.2017.2775666.

[33] S. Tavakoli, A. Mousavi, S. Poslad, "Input variable selection in time-critical knowledge integration applications: A review, analysis, and recommendation paper," Advanced Engineering Informatics, **27**(4), 519–536, 2013, doi:10.1016/j.aei.2013.06.002.

[34] M. Danishvar, A. Mousavi, P. Sousa, "EventClustering for improved real time input variable selection and data modelling," in 2014 IEEE Conference on Control Applications (CCA), 1801–1806, 2014, doi:10.1109/CCA.2014.6981574.

[35] S. Tavakoli, A. Mousavi, P. Broomhead, "Event tracking for real-time unaware sensitivity analysis (EventTracker)," IEEE Transactions on Knowledge and Data Engineering, **25**(2), 348–359, 2013, doi:10.1109/TKDE.2011.240.

[36] J. R. King, "Machine-component grouping in production flow analysis: an approach using a rank order clustering algorithm," International Journal of Production Research, **18**(2), 213–232, 1980, doi:10.1080/00207548008919662.

[37] M. R. Kumar, G. P. Rao, "Design and implementation of 32 bit high level Wallace tree multiplier," Int. Journ. of Technical Research and Application, **1**, 86–90, 2013.

[38] A. Mousavi, H. Siervo, "Automatic translation of plant data into management performance metrics: a case for real-time and predictive production control," International Journal of Production Research, **55**(17), 4862–4877, 2017, doi:10.1080/00207543.2016.1265682.

[39] S. X. Ding, S. Yin, K. Peng, H. Hao, B. Shen, "A novel scheme for key performance indicator prediction and diagnosis with application to an industrial hot strip mill," IEEE Transactions on Industrial Informatics, **9**(4), 2239–2247, 2012, doi:10.1109/TII.2012.2214394.

[40] K. Ragunathan, S. Ravindranathan, S. Naveen, "Statistical KPIs in HMI panels," in 2015 International Conference on Green Computing and Internet of Things (ICGCIoT), 838–843, IEEE, 2015, doi:10.1109/ICGCIoT.2015.7380579.

[41] N. Kang, C. Zhao, J. Li, J. A. Horst, "Analysis of key operation performance data in manufacturing systems," in 2015 IEEE International Conference on Big Data (Big Data), 2767–2770, IEEE, 2015, doi:10.1109/BigData.2015.7364078.

[42] G. UK, "Greenhouse Gas Reporting: Conversion Factors 2017," GOV. UK [Online]. Available: https://www. gov. uk/government/publications/greenhouse-gas-reporting-conversion-factors-2017., 2017.

[43] Y. Zhu, "Multivariable system identification for process control", Elsevier, 2001.

[44] J. E. Bowen, M. C. Moore, M. W. Wactor, "Application of switchgear in unusual environments," in 2010 Record of Conference Papers Industry Applications Society 57th Annual Petroleum and Chemical Industry Conference (PCIC), 1–10, IEEE, 2010, doi:10.1109/PCIC.2010.5666870.

Towards a Hybrid Probabilistic Timing Analysis

Haoxuan Li[*,1], Ken Vanherpen[2], Peter Hellinckx[3], Siegfried Mercelis[3], Paul De Meulenaere[2]

[1]*Faculty of Applied Engineering, CoSys-Lab, University of Antwerp, Antwerp, 2000, Belgium*

[2]*Faculty of Applied Engineering, CoSys-Lab, University of Antwerp - Flanders Make, Antwerp, 2000, Belgium*

[3]*Faculty of Applied Engineering, IDLab, University of Antwerp - imec, Antwerp, 2000, Belgium*

ARTICLE INFO	ABSTRACT
	Real-time embedded systems are widely adopted in applications such as automotive, avionics, and medical care. As some of these systems have to provide a guaranteed worst-case execution time to satisfy the time constraints, understanding the timing behaviour of such systems is of the utmost importance regarding the reliability and the safety of these systems. In the past years, various timing analysis techniques have been developed. Probabilistic timing analysis has recently emerged as a viable alternative to state-of-the-art deterministic timing analysis techniques. Since a certain degree of deadline miss is still tolerable for some systems, instead of deriving an estimated worst-case execution time that is presented as a deterministic value, probabilistic timing analysis considers execution times as random variables and associates each possible execution time with a probability of occurrence. However, in order to apply probabilistic timing analysis, the measured execution times must be independent and identically distributed. In the particular case of hybrid timing analysis, since the input and the initial processor state of one software component are influenced by the preceding components, it is difficult to meet such prerequisite. In this article, we propose a hybrid probabilistic timing analysis method that is able to (i) reduce the dependence in the measured execution times to facilitate the application of extreme value theory and (ii) reduce the dependence between software components to make it possible to use convolution to calculate the probabilistic WCET of the overall system.

1 Introduction

Due to the demand for better performance and the increased number of functionalities in embedded systems, acceleration features, such as multi-cores and caches, are added to the modern processors [1]. However, because of these acceleration features, timing analysis has become more complicated and time-consuming.

Over the past years, various researches have been carried out to develop timing analysis techniques that can derive a sound and safe result within a reasonable cost. With "sound", it is meant that a timing analysis result is accurate and not overly optimistic concerning its timing behaviour. The word "cost" describes the time and effort spent on deriving a timing analysis result. In the plethora of techniques, probabilistic timing analysis (PTA) has recently emerged as a viable alternative to state-of-the-art deterministic timing analysis techniques.

In real-time systems, failing to meet the deadline does not necessarily imply a failure of the system. For instance, in video conferences, an occasional deadline miss of the arrival of one frame can degrade the service but is not a failure of the system. Therefore, the timing requirement does not always have to be strictly guaranteed, and a certain degree of deadline misses is still tolerable. Therefore, Instead of deriving an estimated worst-case execution time (WCET) that is presented as a deterministic value, PTA considers execution times as random variables and associates each possible execution time with a probability of occurrence.

Figure 1 is the examples of the probabilistic WCET (pWCET) and the deterministic WCET, as well as the terminologies we use through this paper. The authors suggested that since the upper timing bound derived using the probabilistic worst-case execution time (pWCET) can be adjusted according to the safety requirement of the system, probabilistic timing analysis (PTA) is supposed to be more flexible and potentially less pessimistic compared with the classical deterministic approaches [2]. Therefore, we developed our approach based on the work in [3, 4] with measurement-based probabilistic timing analysis (MBPTA).
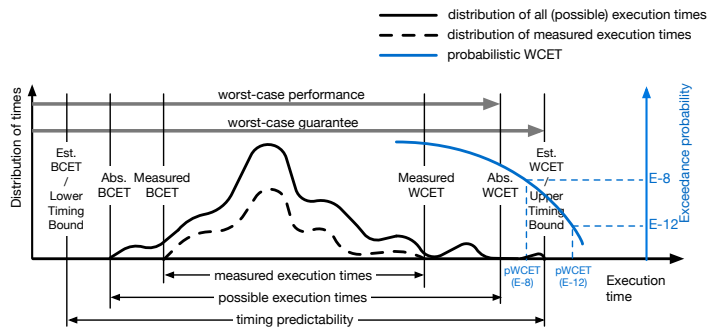
Figure 1: Examples of pWCET analysis and deterministic WCET timing analysis (based on [5]).

One prerequisite of applying MBPTA is that the measured execution times must be independent and identically distributed (i.i.d.). However, in hybrid timing analysis, the input and the initial processor state of one code block/component are influenced by the preceding code/component. Therefore, it is very challenging to collect execution times following the independent and identical distribution.

In this article, we present a hybrid probabilistic timing analysis (HPTA) approach that can facilitate in conducting MBPTA on software blocks/components and safely construct the overall execution of the complete program by reducing the dependence in the measured execution times and the dependence between the components. The goal of this approach is to provide more flexibility in the timing analysis results, which can be used by experienced engineers as references when designing non safety-critical systems that can tolerate a certain degree of deadline misses.

The rest of this paper is organised as follows. Section 2 gives the background of PTA. Section 3 explains the details of the extreme value theory (EVT) and how to apply it in MBPTA and HPTA. The proposed HPTA method is presented in Section 4. Section 5 demonstrates the experiment setup and the case studies, followed by the results and discussion in Section 6.

2 Background

The acceleration features of the hardware, the different input values, and the paths taken through the software introduce a certain degree of variability to the execution time of a system [6]. Because of such variability, PTA considers each observed execution time as an event with a probability of occurrence. Thus the worst-case execution time (WCET) can be viewed as an event that is more extreme than any previously observed event [7].

PTA derives a cumulative distribution function (CDF) using the observed execution times in the measurement. Since PTA aims to provide the probability that one execution time is going to exceed a given time bound, the result is usually presented as a complementary cumulative distribution function (CCDF) [8, 9, 10].

Figure 2 is an example of the results in measurement-based probabilistic timing analysis (MBPTA). The EVT takes the measured execution times to generate the CCDF. This CCDF-function then represents the probability that an event will have an execution time larger than a given pWCET value. This way, every pWCET

is associated with such an exceedance probability. For example, in the given figure, the pWCET shows that for every execution of the program, the probability of the execution time exceeding 9.6ms is 1E-16.
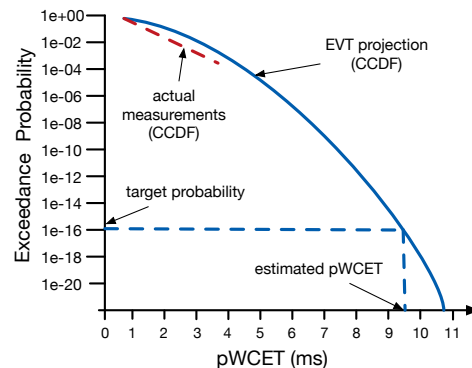
Figure 2: Example of the analysis result of one MBPTA shown as CCDF [11].

For instance, to calculate the pWCET of a task with the probability that the execution time will be 1 time unit is 0.15, the probability that the execution time will be 2 is 0.4, the probability that the execution time will be 4 is 0.4 and the probability that the execution time will be 8 is 0.05. The discrete probability distribution function of execution times of this task can be expressed in the form of a probability mass function (PMF), which is also known as execution time profile (ETP) in the context of PTA:

$$X = \begin{pmatrix} 1 & 2 & 4 & 8 \\ 0.15 & 0.4 & 0.4 & 0.05 \end{pmatrix} \quad (1)$$

The CDF, which indicates the probability that one execution time is less than x, is:

$$CDF_X(x) = F_X(x) = \mathrm{P}(X \le x) = \begin{cases} 0 & if \quad x \in [0,1) \\ 0.15 & if \quad x \in [1,2) \\ 0.55 & if \quad x \in [2,4) \\ 0.95 & if \quad x \in [4,8) \\ 1 & otherwise \end{cases} \quad (2)$$

Eventually, the CCDF is generated to represent the analysis results because pWCET analysis rather focuses on the probability that an execution time exceeds a particular level:

$$CCDF_X(x) = \bar{F}_X(x) = \mathrm{P}(X > x)$$

$$= 1 - F_X(x) = \begin{cases} 1 & if \quad x \in [0,1) \\ 0.85 & if \quad x \in [1,2) \\ 0.45 & if \quad x \in [2,4) \\ 0.05 & if \quad x \in [4,8) \\ 0 & otherwise \end{cases} \quad (3)$$

3 Extreme Value Theory

EVT is a branch of statistics that is used to assess the probability of the occurrence of rare events based on previous observations

[8]. It has been widely applied in many disciplines such as finance, earth sciences, traffic prediction, and geological engineering. In MBPTA, EVT is used to analyse the tail behaviour of the execution time distribution based on the execution times observed during the measurement.

3.1 Independent and identical distribution

The prerequisite of EVT requires the observations to be independent and identically. *Independent* means that the occurrence of one event does not impact the occurrence of the other event. *Identical* indicates that each measured execution time is random and has the same probability distribution as the others.

In the context of timing analysis, i.i.d. implies that the measured execution time is not affected by the past events of the same task. For example, task *A* is executed twice consecutively on a processor with a first-in-first-out (FIFO) cache. The measured execution time is *x* for the first time and *y* for the second time. Because the cache is loaded with data and instructions needed after the first time the task is executed, *y* is expected to be much smaller compared with *x*. In this case, the execution time *x* and *y* are said to be dependent, which does not meet the i.i.d. requirement.

Previous research has proposed the adoption of randomised architectures for measurement-based probabilistic timing analysis[12, 13]. If the processor of the target system has a deterministic architecture, randomisation needs to be applied to randomise the measurement samples to satisfy the i.i.d. precondition [9, 14, 15].

If two events are independent, the joint probability is equal to the product of their individual probabilities:

$$P(A \cap B) = P(A)P(B) \tag{4}$$

For example, given a a task *A* with probabilistic execution time:

$$\begin{pmatrix} 5 & 10 \\ 0.1 & 0.9 \end{pmatrix} \tag{5}$$

and task *B* with probabilistic execution time:

$$\begin{pmatrix} 1 & 2 \\ 0.4 & 0.6 \end{pmatrix} \tag{6}$$

the probabilistic execution time of the both tasks is:

$$\begin{pmatrix} 5 & 10 \\ 0.1 & 0.9 \end{pmatrix} \times \begin{pmatrix} 1 & 2 \\ 0.4 & 0.6 \end{pmatrix} = \begin{pmatrix} 6 & 7 & 11 & 12 \\ 0.04 & 0.06 & 0.36 & 0.54 \end{pmatrix} \tag{7}$$

The CCDF is therefore:

$$\bar{F}_{A \cap B}(x) = \begin{cases} 1 & if \quad x \in [0, 6) \\ 0.96 & if \quad x \in [6, 7) \\ 0.90 & if \quad x \in [7, 11) \\ 0.54 & if \quad x \in [11, 12) \\ 0 & otherwise \end{cases} \tag{8}$$

3.2 Applying extreme value theory in measurement-based probabilistic timing analysis

Algorithm 1 demonstrates how to apply EVT in MBPTA, which includes three main steps: (1) extreme value selection; (2) fitting the distribution; (3) compare and convergence.

Algorithm 1: How to apply EVT in MBPTA
Result: pWCET
select extreme values;
fit the first distribution;
estimate the first CDF;
while *first round or not converged* **do**
collect more extreme values;
fit a new distribution;
estimate the new CDF;
compare;
end

3.2.1 Extreme value selection

EVT makes assumptions on the tail of the data distribution based on the extreme observations obtained from the measured data. Therefore, the measured execution times of the program must be converted into a set of extremes before applying the EVT. Two approaches can be used to collect the observed extreme execution times: block maxima (BM) and peak over threshold (POT).

The BM approach divides the collected execution times into subgroups/blocks. The longest execution time in every subgroup is one sample of extremes. The POT approach defines a threshold. All the execution times longer than the threshold are used as the extremes to estimate the pWCET.

The selection of a suitable size of the subgroups in the BM or a suitable threshold value in the POT plays a crucial role. Studies have been carried out to determine the impact of these decisions on the estimated results [2, 16, 17]. Neither an optimal size of the subgroups nor the best threshold value exists. Generally speaking, a smaller subgroup size or a lower threshold value can decrease the pessimism in the results. However the risk of obtaining an overly optimistic pWCET that is not safe to use increases.

3.2.2 Fitting the distribution

In this step, a model distribution that best fits the extremes is estimated. If BM was used in the previous step, the distribution must be Gumbel, Fréchet, or Weibull distribution. These three distributions are combined into a family of continuous probability distributions known as the generalised extreme value (GEV) distribution.

The GEV is characterised by three parameters: the location parameter $\mu \in \mathbb{R}$, the scale parameter $\sigma > 0$, and the shape parameter $\xi \in \mathbb{R}$. The value of the shape parameter ξ decides the tail behaviour of the distribution and to which sub-family the distribution belongs: Gumbel ($\xi = 0$), Fréchet ($\xi > 0$) or Weibull ($\xi < 0$). The CDFs of these three distributions are given below.

- Gumbel or type I extreme value distribution ($\xi = 0$):

$$F_{(\mu,\sigma,0)}(x) = e^{-e^{-(x-\mu)/\sigma}}$$

- Fréchet or type II extreme value distribution ($\xi > 0$):

$$F_{(\mu,\sigma,\xi)}(x) = \begin{cases} e^{-y^{-\alpha}} & y > 0 \\ 0 & y \le 0 \end{cases}, (\xi = \alpha^{-1} \text{ and } y = 1 + \xi(x - \mu)/\sigma)$$

- Reversed Weibull or type III extreme value distribution ($\xi < 0$):

$$F_{(\mu,\sigma,\xi)}(x) = \begin{cases} e^{-(-y)^{\alpha}} & y < 0 \\ 1 & y \ge 0 \end{cases}, (\xi = -\alpha^{-1} \text{ and } y = -(1 + \xi(x - \mu)/\sigma)).$$

If POT was used in the previous step, the distribution needs to fit the generalised Pareto distribution (GPD), which is a family of continuous probability distributions. The GPD is specified by the same three parameters as GEV: location parameter μ, scale parameter σ, and shape parameter ξ. The CDF of the GPD is:

$$F_{(\mu,\sigma,\xi)}(x) = \begin{cases} 1 - \left(1 + \frac{\xi(x - \mu)}{\sigma}\right)^{-1/\xi} & \text{for } \xi \ne 0 \\ 1 - \exp\left(-\frac{x - \mu}{\sigma}\right) & \text{for } \xi = 0 \end{cases}, (x \ge \mu \text{ when }$$
$$\xi \ge 0, \text{ and } \mu \le x \le \mu - \sigma/\xi \text{ when } \xi < 0).$$
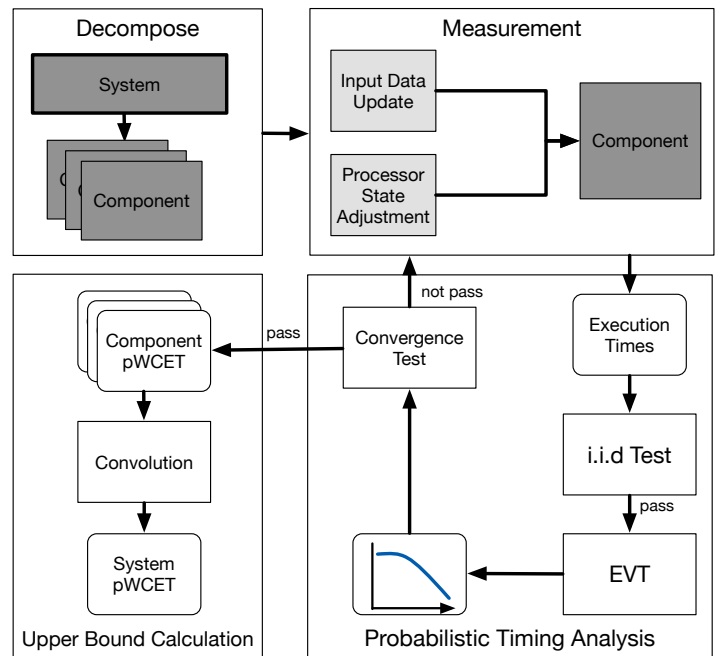
3.2.3 Compare and convergence

Once the first data set of extremities is collected, the EVT uses the data to estimate the first CDF of the pWCET. In every subsequent round of the estimation, more extremities are collected and added to the data set to derive a new CDF. The CDF in the current round is compared with the CDF of the previous round using metrics such as the continuous ranked probability score (CRPS) [18]. In our case, we use the following convergence criteria to compare the respective accuracy of the two CDFs:

$$Score = \sum_{x=0}^{+\infty}[F_{current}(x) - F_{previous}(x)]^2 \tag{9}$$

Where F is the cumulative distribution. The score indicates the level of difference between the two cumulative distributions. The lower the score is, the closer the CDF is going to reach the point of convergence. Once the score reaches the desired value (such as 0.1), the pWCET can be derived using the converged CDF.

4 The proposed hybrid probabilistic timing analysis

Figure 3 is the illustration of the proposed HPTA approach. In our research, a system can be divided at different decomposition levels according to the requirement of the user. Because of the block isolation technique described in [3, 4], the software components can be executed independently from the rest of the program, and the processor state can be adjusted before every execution. This allows us to overcome two major challenges in applying the HPTA approach: (1) the i.i.d. data requirement of the EVT; (2) the calculation of the upper bound of the overall system.

In the section, we will describe the concept of decomposition level, and explain the challenges and how we solved these challenges using the proposed HPTA.

Figure 3: The proposed HPTA approach.

(a) A system with three decomposition levels.

(b) The components of the system at *DL*0, *DL*1 and *DL*2. DL: decomposition level.
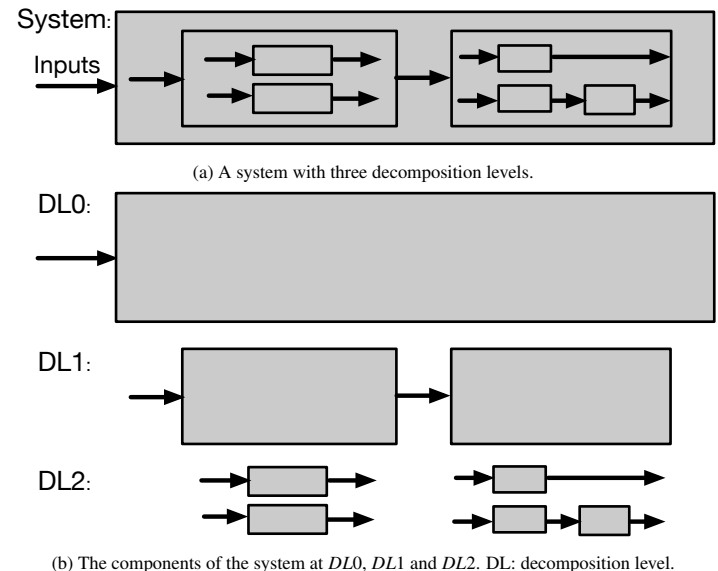
Figure 4: A system and the decomposition of the system at three decomposition levels.

4.1 Decomposition level

Figure 4a shows a system with components at three decomposition levels. The decomposition of the system is demonstrated in Figure 4b. Every grey rectangle represents one component, and the solid black arrows represent the data flow of the components. By our definition, *DL*0 is the lowest degree of decomposition because the complete system is measured at this level. The complete system is considered as one abstract component from which no details of the subsystems can be retrieved. At *DL*1, the mask of the system at *DL*0 is opened. Measurement can be conducted on the subsystems that are revealed at this level. As the decomposition level increases,

the system is decomposed in further detail, more components are revealed. The decomposition level can increase until the last sub-system is opened. The granularity of the timing analysis increases with the decomposition level.

4.2   Challenges

4.2.1   Independent and identical data requirement

Although EVT requires the samples to be identically distributed, the adoption of GEV opened up the applicability of MBPTA to more cases because it can tolerate up to a certain degree of dependence in the measured execution times[10]. The disadvantage is that such dependence can corrupt the reliability of the derived pWCET [19]. In some domains, techniques such as re-sampling and de-clustering can be applied to create independence between measurements [20]. Nevertheless, forcing independence into dependent execution time measurements can result in overly optimistic pWCET that is not safe anymore [2].

For instance, the calculation in the example given in Section 3.1 is only valid when task A and B are independent, otherwise the result might be overly optimistic. Suppose dependence exists between the two events such that the execution time of task B is always 2 when the execution time of task A is 10. The probabilistic execution time when A and B are both executed would be:

$$\begin{pmatrix} 6 & 7 & 12 \\ 0.04 & 0.06 & 0.9 \end{pmatrix} \tag{10}$$

The probabilistic execution time of the both tasks in this case is:

$$\bar{F}_{A \cap B}(x) = \begin{cases} 1 & if & x \in [0, 6) \\ 0.96 & if & x \in [6, 7) \\ 0.90 & if & x \in [7, 12) \\ 0 & otherwise \end{cases} \tag{11}$$

Given a deadline of 11, the probability of missing the deadline is 0.54 when A and B are independent (8), and 0.90 when A and B are dependent (11). In this case, overlooking the dependence between the tasks resulted in overly optimistic probabilities of a deadline miss.

4.2.2   Upper bound calculation

In deterministic hybrid timing analysis, the results are presented in absolute values. Therefore, the WCET of the complete system can be calculated simply by adding up the WCETs of every individual component. In statistics, convolution may be usually used to calculate the joint probability of two random variables. Unfortunately, this is not applicable in this context. The reason is that the probability distribution of the sum of two or more random variables is equal to the convolution of their distributions only when the variables are independent.

Since hybrid timing analysis is conducted on the components that construct the complete system, the execution time of one component often impacts the execution time of another component. This dependence makes the calculation of the overall pWCET much more complicated.

4.3   Solutions

Based on the information provided in the previous text, one can conclude that in order to overcome the challenges, we need to find a solution to the dependence in the measured execution times and the dependence between individual components.

4.3.1   Dependence in the observed execution times

In MBPTA and HPTA, dependence exists in the data samples if two or more of the observed execution times interfere with each other. Generally speaking, such dependence can come from:

1. *Software dependence*: The dependence between inputs and the paths taken by the program. For example, if input/path A is always followed by input/path B, A and B are dependent.

2. *Hardware dependence*: The hardware state left by the previous execution, which becomes the initial hardware state of the current execution.

To reduce the software dependence, we choose the *per-path* approach to collect the execution times for EVT. The other approach is know as the *per-program* approach [7]:

1. *Per-program*: After the measurement, the EVT uses all the measured execution times as one sample group. EVT is applied to the sample group to estimate the pWCET for the complete program.

2. *Per-path*: After the measurement, all the measured execution times are divided into sample groups. One group includes all the execution times measured from one program path. EVT is applied to each sample group to estimate the pWCET of the program path the sample group represents. The pWCET of the complete program is then calculated by taking the upper bound of the pWCETs of all the paths.

For instance, a system has two paths with the execution times at 10/15 (10 or 15 time units) and 60/65. The probabilities of the paths taken by one randomly chosen single execution are 0.3 and 0.7 respectively. Suppose the different execution times observed in the same path are due to a hardware component, which may generate 0 extra time units with a probability of 0.4 or 5 extra time units with a probability of 0.6. The probability execution time profile (ETP) of the system is:

$$\begin{pmatrix} 10 & 15 & 60 & 65 \\ 0.12 & 0.18 & 0.28 & 0.42 \end{pmatrix} \tag{12}$$

The pWCET derived using the per-program approach is:

$$pWCET_{per-program} = \begin{cases} 1 & if & x \in [0, 10) \\ 0.88 & if & x \in [10, 15) \\ 0.7 & if & x \in [15, 60) \\ 0.42 & if & x \in [60, 65) \\ 0 & otherwise \end{cases} \tag{13}$$

$$= \begin{bmatrix} 0 & 10 & 15 & 60 & 65 \\ 1 & 0.88 & 0.7 & 0.42 & 0 \end{bmatrix}$$

The pWCET derived using the per-path program is:

$$pWCET_{per-path} = \begin{bmatrix} 0 & 60 & 65 \\ 1 & 0.6 & 0 \end{bmatrix} \quad (14)$$

As can be seen, compared with the per-path approach, the per-program approach was able to produce a tighter result. The pWCET derived using the per-program approach is valid to upper bound randomly chosen single executions of the target program. However, it is not applicable to be used in convolution when calculating the overall pWCET of multiple executions of the target program. The reason is that the probability distribution of the sum of two or more random variables is equal to the convolution of their distributions only when the variables are independent. For example, if path 60/65 is forced to be taken when path 10/15 is observed in the previous execution, the pWCET of two consecutive executions of the program is:

$$\begin{bmatrix} 0 & 70 & 75 & 80 & 120 & 125 & 130 \\ 1 & 0.952 & 0.808 & 0.7 & 0.588 & 0.252 & 0 \end{bmatrix} \quad (15)$$

The pWCET calculated using the probability derived from $pWCET_{per-program}$ is:

$$\begin{bmatrix} 0 & 70 & 75 & 80 & 120 & 125 & 130 \\ 1 & 0.9424 & 0.8428 & 0.6412 & 0.4116 & 0.1764 & 0 \end{bmatrix} \quad (16)$$

Under the dependence introduced by the execution condition, the probability that the two consecutive executions exceed 125 time units is 0.252. However, the pWCET using the convolution on the probability derived from $pWCET_{per-program}$ gives a probability of 0.1764, which is too optimistic.

In the per-path approach, the measured execution times are grouped according to the program paths. Therefore, the influence of the input data is eliminated within every group. The variations in the execution time within the same group are purely due to the hardware. By taking the upper bound of the pWCETs of all the paths, the pWCET generated by the per-path approach can be used safely in convolution for estimating any overall pWCET in which the execution of this task is executed consecutively. In the above example, the pWCET calculated by applying convolution to the probability derived from $pWCET_{per-path}$ is:

$$\begin{bmatrix} 0 & 120 & 125 & 130 \\ 1 & 0.84 & 0.36 & 0 \end{bmatrix} \quad (17)$$

Therefore, using the per-path approach, the proposed HPTA method can upper bound the $pWCET$ under the dependence introduced by the execution condition.

To reduce the hardware dependence, we try to push the hardware to the worst-case state at the beginning of every execution so that every execution can start with nearly the same initial state. For example, the pipeline is flushed, and "trash code" is executed to fill the caches with irrelevant data and instructions before every execution.

4.3.2 Dependence between components

In order to calculate the pWCET of the overall system using convolution, the independence between the pWCETs of the software components must be guaranteed. Such kind of dependence can be found in:

1. *Software dependence*: The output of the precedent components, which is the input of the current component.

2. *Hardware dependence*: The hardware state left by the previous component, which becomes the initial hardware state of the current component.

The software dependence can be removed together with the dependence in the observed execution times by the per-path approach. This is because the path-approach automatically selects the input(s) leading to the longest execution paths that upper bound all the other inputs. The hardware dependence no longer exists because the components execute in isolation from the rest of the program in the proposed method. Hence there are no precedent components.

5 Case study and experiment setup

5.1 Case Study

For the case study, we adopted a Simulink power window model. Figure 5 is the power window model [21, 22] at *DL*0, *DL*1 and *DL*2. A power window is an automatic window in a car that can be raised and lowered by pressing a button or a switch instead of a hand-turned crank handle. The complete application of a power window normally consists of four windows that can be operated individually. The three passenger-side windows can be operated by the driver with higher priority. In this paper, we only use the front passenger-side window and the driver-side window.
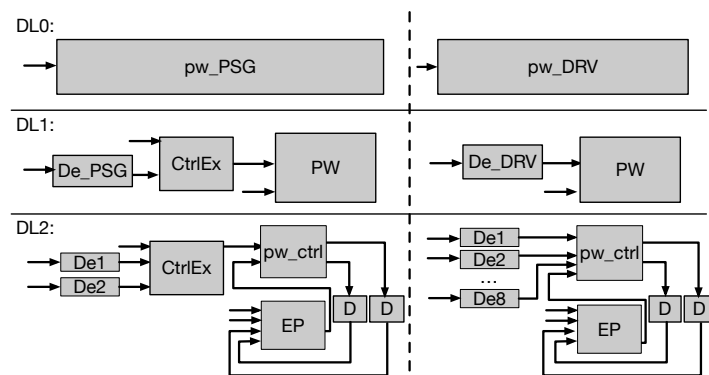
Figure 5: Power window passenger (left) and power window driver (right) at decomposition level 0, 1 and 2. DL: decomposition level; pw_PSG: powerwindow passenger, De_PSG: debounce passenger, CtrlEx: control exclusion, PW: powerwindow main component, De_DRV: debounce driver, De: debounce, pw_ctrl: powerwindow control, EP: end of range and pinch detection, D: delay.

The C code of the power window was generated using Embedded Coder® [23] targeting an ARM Cortex microprocessor with a discrete fixed-step solver at a fixed-step size of 5 ms. The BM approach with a block size of 20 was used in the extreme value selection process to collect the extremities for the EVT. The exceeding probability of 1E-10 was used for the pWCET.

The Kolmogorov-Smirnov (KS) test was used to verify the identical distribution requirement, and the runs-test was used to verify

Table 1: The p-values for the independent and identical distribution tests. NoN: number of nop instructions; pw_DRV: powerwindow driver; pw_PSG: powerwindow passenger; R: runs test; KS: Kolmogorov-Smirnov test.

NoN	pw_DRV		pw_PSG		NoN	pw_DRV		pw_PSG	
	R	KS	R	KS		R	KS	R	KS
0	0.7495	0.9999	1	0.4973	8	1	0.7710	0.8486	0.1349
1	0.4019	0.2753	1	0.4973	9	0.3894	0.9999	0.6822	0.2753
2	0.9764	0.9999	0.4736	0.1349	10	0.2703	0.9655	0.3894	0.7710
3	0.3441	0.9655	0.8769	0.4973	11	0.9080	0.9655	0.3337	0.2753
4	0.7939	0.9655	1	0.1349	12	0.1065	0.7710	0.8052	0.7710
5	0.8046	0.7710	0.2003	0.2753	13	1	0.9999	0.0882	0.7710
6	0.5634	0.9655	0.1789	0.4973	14	0.5643	0.9999	0.3634	0.9999
7	0.6744	0.9655	0.2176	0.2753	15	1	0.2753	0.9687	0.4973

Table 2: The measured deterministic WCETs and the estimated probabilistic WCETs The exceeding probability of 1E-10 was used for the pWCET. of the complete powerwindow driver benchmark and the complete powerwindow passenger benchmark with 16 different alignments. NoN: number of nop instructions; pw_DRV: powerwindow driver; pw_PSG: powerwindow passenger; cc: clock cycles; dWCET: measured deterministic WCET; pWCET: estimated probabilistic WCET.

NoN	pw_DRV (cc)		pw_PSG (cc)		NoN	pw_DRV (cc)		pw_PSG (cc)	
	dWCET	pWCET	dWCET	pWCET		dWCET	pWCET	dWCET	pWCET
0	2516	2538	1638	1666	8	2660	2797	1678	1953
1	2656	2712	1660	1688	9	2650	2698	1674	1681
2	2514	2515	1664	1717	10	2586	2608	1650	1681
3	2764	2849	1672	1725	11	2700	2762	1648	1683
4	2712	2768	1640	1699	12	2748	2813	1646	1679
5	2708	2762	1642	1700	13	2646	2746	1646	1684
6	2726	2794	1666	1764	14	2620	2735	1670	1701
7	2714	2797	1670	1689	15	2568	2569	1632	1658

the requirement for independence. $p > 0.05$ indicates the data follows the desired distribution.

The case study is designed to test the following assumptions:

1. Can the proposed HPTA method reduce the dependence in the measured execution times and facilitate the collection of i.i.d. execution times?

2. Can the proposed HPTA method reduce pessimism at a higher decomposition level?

5.2 Experiment Setup

The experiment setup is shown in Figure 6. The processor is an ARM Cortex-M7 processor that contains a four-way set-associative data cache and a two-way set-associative instruction cache. Both caches use the random replacement policy. The Xilinx Nexus 3 FPGA is used to measure the execution time of the code on the ARM-processor. It is driven by the *CLK* signal sent from the processor to synchronise the clocks. The measurement process starts by sending the *Start* signal from the FPGA to the processor. Two GPIO pins of the processor are used to set the *Tic* and *Toc* flags. Before the code starts to execute, the *Tic* pin is toggled to start counting the number of clock cycles that have passed. After the code is executed, the *Toc* pin is set to stop the timer. Eventually, the value in the timer (*Execution Time*) is collected through a serial port.
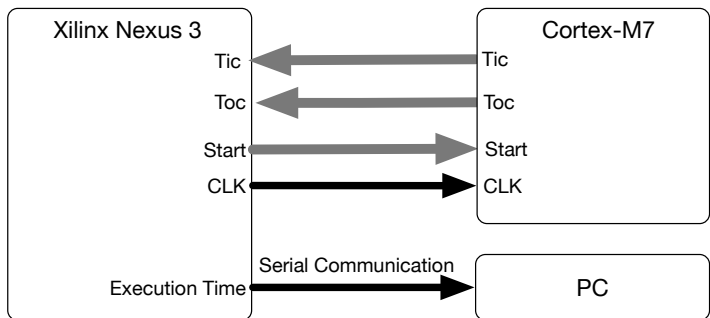
Figure 6: Experiment setup.

6 Results and discussion

6.1 Reducing dependence in the measured execution times

Table 1 shows the results of KS and runs test. As can be seen, all the *p*-values are significantly higher than 0.05, which means that the i.i.d. requirement is fulfilled and the collected data can be applied in EVT to estimate the pWCET. The NoN indicates the number of the *nop* instructions added to emulate different memory alignments [3]. These *p*-values confirm our assumption that the proposed HPTA can reduce the dependence in the executions to facilitate the collection of i.i.d. data required by the EVT.

Table 3: The estimated pWCET calculated using sum and convolution at different decomposition levels. DL: decomposition level; pw_DRV: powerwindow driver; pw_PSG: powerwindow passenger; cc: clock cycles; dWCET: measured deterministic WCET; $pWCET_{Sum}$: estimated probabilistic WCET calculated by adding the pWCETs of the components up; $pWCET_{Conv}$: estimated probabilistic WCET derived from the convolution of the pWCETs of the components.

	pw_DRV (cc)			pw_PSG (cc)		
	dWCET	$pWCET_{Sum}$	$pWCET_{Conv}$	dWCET	$pWCET_{Sum}$	$pWCET_{Conv}$
DL0	2764	2849		1678	1953	
DL1	2652	3852	3465	1838	2949	2690
DL2	4820	6025	5167	2596	3778	3484

Table 2 shows the WCETs of the complete powerwindow-driver benchmark and the complete powerwindow-passenger benchmark with 16 different alignments. The longest measured deterministic WCET was 2764 reached by NoN = 3 in the driver-side window

Across all the alignments, the estimated pWCET is more pessimistic at the selected exceeding probability compared with the deterministic WCET. However, in some cases, such as NoN = 15 in pw_DRV, the difference between the two WCETs is relatively small. The reason could be that the execution time contributed by independent random elements in the hardware is reduced by imposing a worst-case execution scenario on the longest path. Since random events in the hardware rarely happen, the measured execution times can be very close to the estimated pWCET.

The pWCET calculated using convolution ($pWCET_{Conv}$) is in general lower compared with the $pWCET_{Sum}$. Nevertheless, $pWCET_{Conv}$ still leaves a reasonable margin with the deterministic WCET. This observation confirms our assumption that simply adding up pWCETs in HPTA will lead to overly pessimistic results. Using convolution can help to reduce such pessimism and produce a reasonably sound result.

7 Conclusion

In this article, we proposed a HPTA method that is able to (i) collect the i.i.d. data required by EVT by reducing the dependence between the measured execution times and (ii) reduce the dependence between blocks to make it possible to use convolution to calculate the pWCET of the overall system. We are aware that forcing independence into dependent execution time measurements can make the data no longer representative of the dependent system behaviour. Therefore, several approaches, such as using the per-path approach to upper bound the pWCETs of all the paths, were taken to ensure the derived pWCET is not overly optimistic. However, this might have introduced too much pessimism into the estimated pWCET.

Another novelty of the proposed HPTA method is that it can be applied at different granularities by adjusting the decomposition level. Performing the analysis at a higher decomposition level can help to reduce pessimism. On the other hand, with the increased decomposition level, the cost to derive the pWCET also increases.

Compared with the deterministic HTA approach proposed in [3], this HPTA approach is more pessimistic with the exceedance probability of 1E-10. On the other hand, instead of giving a de-

and 1678 reached by NoN = 8 in the passenger-side window. The estimated pWCET in the driver-side window was 2849 reached by NoN = 3 and 1953 reached by NoN = 8.

6.2 Reducing pessimism in high decomposition levels

Table 3 shows the estimated pWCETs of the benchmarks calculated using sum and convolution at three decomposition levels. The highest pWCET of the 16 different alignments were used as the pWCET of every block. As can be seen, the WCETs increase with the decomposition levels. The highest WCET was reached by $pWCET_{Sum}$ at $DL2$ with 6025 clock cycles for the driver and 3778 clock cycles for the passenger. The difference between the deterministic WCET and pWCETs also became more prominent with the decomposition level, which means a higher decomposition level is associated with larger pessimism.

terministic value, this approach gives an exceedance probability to each possible execution time. We hope the results of this HPTA approach can be used as a reference to avoid unnecessary waste on the hardware cost in the hand of experienced engineers when designing a non safety-critical system that can tolerate a certain degree of deadline misses.

References

[1] L. Cucu-Grosjean, L. Santinelli, M. Houston, C. Lo, T. Vardanega, L. Kosmidis, J. Abella, E. Mezzetti, E. Quiñones, F. J. Cazorla, "Measurement-based probabilistic timing analysis for multi-path programs," Proceedings - Euromicro Conference on Real-Time Systems, 91–101, 2012, doi:10.1109/ECRTS.2012.31.

[2] F. Guet, L. Santinelli, J. Morio, "On the representativity of execution time measurements: Studying dependence and multi-mode tasks," in OpenAccess Series in Informatics, **57**, 31–313, Schloss Dagstuhl-Leibniz-Zentrum fuer Informatik, 2017, doi:10.4230/OASIcs.WCET.2017.3.

[3] H. Li, K. Vanherpen, P. Hellinckx, S. Mercelis, P. De Meulenaere, "Component-based Timing Analysis for Embedded Software Components in Cyber-Physical Systems," in 2020 9th Mediterranean Conference on Embedded Computing, MECO 2020, 1–8, IEEE, 2020, doi:10.1109/MECO49872.2020.9134177.

[4] H. Li, P. De Meulenaere, K. Vanherpen, S. Mercelis, P. Hellinckx, "A hybrid timing analysis method based on the isolation of software code block," Internet of Things, **11**, 100230, 2020, doi:10.1016/j.iot.2020.100230.

[5] R. Wilhelm, J. Engblom, A. Ermedahl, N. Holsti, S. Thesing, D. Whalley, G. Bernat, C. Ferdinand, R. Heckmann, T. Mitra, F. Mueller, I. Puaut, P. Puschner, J. Staschulat, P. Stenström, "The worst-case execution-time problem-overview of methods and survey of tools," Transactions on Embedded Computing Systems, **7**(3), 36:1–36:53, 2008, doi:10.1145/1347375.1347389.

[6] L. Santinelli, F. Guet, J. Morio, "Revising measurement-based probabilistic timing analysis," in Proceedings of the IEEE Real-Time and Embedded

Technology and Applications Symposium, RTAS, 199–208, IEEE, 2017, doi: 10.1109/RTAS.2017.16.

[7] R. Davis, L. Cucu-Grosjean, "A Survey of Probabilistic Schedulability Analysis Techniques for Real-Time Systems," LITES: Leibniz Transactions on Embedded Systems, **6**(1), 1–53, 2019.

[8] J. Hansen, S. Hissam, G. A. Moreno, "Statistical-based WCET estimation and validation," OpenAccess Series in Informatics, **10**(January), 123–133, 2009, doi:10.4230/OASIcs.WCET.2009.2291.

[9] F. J. Cazorla, T. Vardanega, E. Quiñones, J. Abella, "Upper-bounding program execution time with extreme value theory," in OpenAccess Series in Informatics, volume 30, 64–76, Schloss Dagstuhl-Leibniz-Zentrum fuer Informatik, 2013, doi:10.4230/OASIcs.WCET.2013.64.

[10] L. Santinelli, J. Morio, G. Dufour, D. Jacquemart, "On the sustainability of the extreme value theory for WCET estimation," OpenAccess Series in Informatics, **39**(July), 21–30, 2014, doi:10.4230/OASIcs.WCET.2014.21.

[11] F. J. Cazorla, J. Abella, J. Andersson, T. Vardanega, F. Vatrinet, I. Bate, I. Broster, M. Azkarate-Askasua, F. Wartel, L. Cucu, F. Cros, G. Farrall, A. Gogonel, A. Gianarro, B. Triquet, C. Hernandez, C. Lo, C. Maxim, D. Morales, E. Quinones, E. Mezzetti, L. Kosmidis, I. Aguirre, M. Fernandez, M. Slijepcevic, P. Conmy, W. Talaboulma, "PROXIMA: Improving Measurement-Based Timing Analysis through Randomisation and Probabilistic Analysis," Proceedings - 19th Euromicro Conference on Digital System Design, DSD 2016, 276–285, 2016, doi:10.1109/DSD.2016.22.

[12] S. Trujillo, R. Obermaisser, K. Grüttner, F. J. Cazorla, J. Perez, "European Project Cluster on Mixed-Criticality Systems," in Design, Automation and Test in Europe (DATE) Workshop 3PMCES, 2014.

[13] M. Schoeberl, S. Abbaspour, B. Akesson, N. Audsley, R. Capasso, J. Garside, K. Goossens, S. Goossens, S. Hansen, R. Heckmann, S. Hepp, B. Huber, A. Jordan, E. Kasapaki, J. Knoop, Y. Li, D. Prokesch, W. Puffitsch, P. Puschner, A. Rocha, C. Silva, J. Sparsø, A. Tocchi, "T-CREST: Time-predictable multicore architecture for embedded systems," Journal of Systems Architecture, **61**(9), 449–471, 2015, doi:10.1016/j.sysarc.2015.04.002.

[14] L. Kosmidis, J. Abella, E. Quinones, F. J. Cazorla, "A cache design for probabilistically analysable real-time systems," Proceedings -Design, Automation and Test in Europe, DATE, 513–518, 2013, doi:10.7873/date.2013.116.

[15] J. Jalle, L. Kosmidis, J. Abella, E. Quinoñes, F. J. Cazorla, "Bus designs for time-probabilistic multicore processors," Proceedings -Design, Automation and Test in Europe, DATE, 1–6, 2014, doi:10.7873/DATE2014.063.

[16] I. Fedotova, B. Krause, E. Siemens, "Applicability of Extreme Value Theory to the Execution Time Prediction of Programs on SoCs," in Proceedings of International Conference on Applied Innovation in IT, volume 5, 71–80, Anhalt University of Applied Sciences, 2017.

[17] Y. Lu, T. Nolte, J. Kraft, C. Norström, "Statistical-based response-time analysis of systems with execution dependencies between tasks," in Proceedings of the IEEE International Conference on Engineering of Complex Computer Systems, ICECCS, 169–179, IEEE, 2010, doi:10.1109/ICECCS.2010.26.

[18] H. Hersbach, "Decomposition of the continuous ranked probability score for ensemble prediction systems," Weather and Forecasting, **15**(5), 559–570, 2000, doi:10.1175/1520-0434(2000)015⟨0559:DOTCRP⟩2.0.CO;2.

[19] F. Guet, L. Santinelli, J. Morio, "On the Reliability of the Probabilistic Worst-Case Execution Time Estimates," European Congress on Embedded Real Time Software and Systems 2016 (ERTS'16), 10, 2016.

[20] J. Segers, "Automatic declustering of extreme values via an estimator for the extremal index Automatic declustering of extreme values via an estimator for the extremal index," (April 2002), 2014.

[21] H. Li, P. De Meulenaere, P. Hellinckx, "Powerwindow: A multi-component TACLeBench benchmark for timing analysis," in Lecture Notes on Data Engineering and Communications Technologies, volume 1, 779–788, Springer, 2017, doi:10.1007/978-3-319-49109-7_75.

[22] H. Li, P. De Meulenaere, S. Mercelis, P. Hellinckx, "Impact of software architecture on execution time: A power window TACLeBench case study," International Journal of Grid and Utility Computing, **10**(2), 132–140, 2019, doi:10.1504/IJGUC.2019.098216.

[23] "Embedded Coder," 2020.

Texture Based Image Retrieval Using Semivariogram and Various Distance Measures

Rajani Narayan[*], Anjanappa Sreenivasa Murthy

Department of ECE, University Visvesvaraya College of Engineering, Bengaluru, 560001, India

A R T I C L E   I N F O

A B S T R A C T

In a content-based image retrieval system(CBIR) feature classification,identification, and extraction play an important role. The retrieval of images using a single feature is a challenging task in CBIR systems. The high retrieval rates are reported based on combining multiple features, multiple algorithms and preprocessing steps, feature classification, and segmentation because the image retrieval are mainly based on the content in an image. This paper presents a texture feature extraction for the image retrieval system from semivariogram and robust semivariogram technique. A semivariogram is a statistical approach that provides the textural information based on the lag distance 'h'.The proposed method is tested on various standard image databases such as Corel-1k, Corel-10k, and Coil-100 database. The semivariogram and robust semivariogram methods are tested for the Corel 1k database using four distance metrics i.e. Euclidean, Manhatten, Canberra, and Chord distance to check which distance measure is appropriate for the CBIR system.The proposed method is also tested on three types of databases to investigate the performance of the CBIR system. The Matlab simulation results show that the effective performance of the system with Euclidean distance.

1   Introduction

The capturing of an image is started back in the past one and half a century, and the collection of images is rapidly growing from the past thirty years of growing digital technology and internet usage. The collection of images is also increasing leading to a extremely large database. In many applications, the extraction of equivalent images from the large database is essential and useful. There are two trends currently using the image search from the image collection data set namely text-based and content-based. The text-based search uses meta-data like keywords, description of the image to get back the similar images. It is the main disadvantage of this system. In contrast content based uses existing property (color, texture, and shape) to find the equivalent images from the large database. This paper is an extension of work originally presented in conference [1].

Many researchers have come up with the idea of combining basic image features to get the most comparable images as required by the query image. The color and texture feature is taken together to get the image information by applying wavelet [2]. The wavelet transform decomposes the images into orthogonal components for the better localization of the spatial information in an image. The method applied to extract color and texture information is a color histogram and wavelets respectively. .

It is noticeable that based on these work the retrieval rates are improved by combining multiple features, multiple algorithms and preprocessing steps, classification, segmentation, etc. In this work, a good CBIR system is designed by using the texture feature. In an image retrieval system all the three features color, texture, and shape play an important role [3]. Texture identification is an important part of the research in image retrieval and pattern recognition. It is categorized into two classes i.e. regular and irregular, directional, and non-directional based on the observations of real life. In general, the texture is characterized as two main approaches: Statistical and Structural.

1)Structural approach: the texture analysis is done based on the arrangement of preserving texture pixel in some pattern or repetitive pixel. 2) Statistical approach: The texture feature can be analyzed by studying numerical data of the image. It provides the relative estimation of the arrangements of the intensities in an image region [4]. The most commonly used and widely accepted statistical approach for texture, classification is the GLCM method [5]. The recently developed method for the texture classification and analysis includes block truncation coding [6], Markov random fields [7] to construct the image patches using neighboring pixel, local energy histogram [8], hidden Markov model [9], shearlets and linear regression [10]. Many of the texture algorithms and methods have been applied to the Brodatz database.

[*]Corresponding Author: Rajani Narayan, Bengaluru, +91-9740798868 & rajni.n25@gmail.com

In this paper, geostatistical parameter called semivariogram and robust semivariogram are applied to the image to get the texture information to the image databases. The semivariogram method is basically applied to remote sensing images to characterize the texture property. It is a distance metric that calculates the absolute differences between the semivariogram of the two images to determine the class of test images. The various distance measures are used to verify the effective retrieval of images.

1.1 Motivation

The main idea of the designing image retrieval system is to provide the desired images as of user interest. This leads to finding the solution to set up a good image retrieval system that will be able to find similar images from the huge image data set. The image search is basically with the use of content in the image.

In this study, a new CBIR system is proposed based on semivariogram. In general the semivariogram is applied for the remote sensing images in the area of geo-statistics.These images are captured by satellites that will be having high spatial resolution.To analyse the characteristics of this data semivariogram is one of the best method.Like remote sensing image CBIR system works with large image database. These databases contain many categories of images that will have a non-uniform distribution of the pixel intensities and dissimilar backgrounds.Since semivariogram is a statistical approach, it really works well for the image to characterise the texture intensities.This is the case the idea of adapting semivariogram method for the CBIR system.The main focus of the work is to use the minimal feature from the image and reduce the computational time required for the entire image database.

1.2 Organisation of the paper

The remainder of this article is organized as follows. Section 2 discusses the related work and section 3 gives the mathematical model of the proposed system. In section 4 feature extraction is discussed with an example. Section 5 briefly explains the experimental design and results. Section 6 gives the distance metrics for similarity measurements. Section 7 discusses the experimental design and Section 8 gives performance evaluation and conclusion followed by section 8.

2 Related Work

From the discrete wiener-Levy process in [11], it is proved that a semivariogram gives a spatial correlation of the pixels than the covariance method. The random process called the Levy process is a Brownian motion mathematical representation. The covariance fails to extract spatial information with distortion whereas the semivariogram strongly characterizes the spatial features. In geostatistics, the features analysis has to be done by fitting the experimental semivariogram to a theoretical semivariogram. The model examines the structure and continuity of the spatial relationship in a random field.

The experimental semivariogram model can be fit into the theoretical semivariogram model. There are two methods have been used in [12]. One is by manual fitting and the second is by automatic model fitting. The automatic model fitting uses methods

like maximum likelihood or least squares [13].In manual fitting, the model was chosen based on picture perception of the experimental semivariogram. For a given waveband information reproduction of the pattern will be clear and strong explanation of the pattern in an image can be provided by the semivariogram.

In general remote sensing images for the land, consolidation is having a high spatial resolution. This is a limitation for the pixel-based analysis and land cover classification in remote sensing images concerning its spectral behaviour. To overcome this problem texture extraction is done using fixed window size and varying window size depending on semivariogram result. Texture classification in microwave images [14] is executed using the semivariogram method. The statistical parameters are determined and considered as image features. They are first and second-order element difference, first and second-order element inverse difference, entropy and, uniformity.

The accurate object-oriented classification is presented in [15] for Quick Bird images by applying a method called the set of semivariogram texture feature(STF) based on the mean square root pair difference(SRPD). The parameter like direction, lag distance, and moving window size are considered for semivariance analysis to classify the texture feature.

A new set of 2-D RCWF(Rotated complex wavelet filter) is designed to improve the retrieval accuracy using complex wavelet filter coefficients. It produces strong texture information of the oriented images in six different directions. This is non-separable and oriented relatively improves the classification of oriented textures. Also, they have used the combination of dual-tree RCWF and DFWCT to extract the texture features in 12 different directions [16].

The new algorithm based on Gabor filter and EHD(Edge Histogram Descriptor) has been proposed for the texture feature extraction. These two are fused to get the good performance of the system. The Gabor and EHD are applied to every 40 images and then six bins are considered from each of the images. This improves the efficiency of the EHD. As a result, the dimension of the character is reduced to 40X6 as mentioned in [17].

Perceptual texture features are considered for the representations and retrieval of images. These features contain contrast, directionality, and coarseness and dryness. Where busyness has given less importance compared to the other three features. They have used these four perceptual features for the experiment. The experiment result shows appreciable scores for the broadtz image database retrieval [18].

The image retrieval system uses a combination of color and texture features. As a color feature color autocorrelation of the HSV color model is used and for texture feature BDIP(Block difference of inverse probabilities) and BVLC(Block variation of the local correlation coefficient)are used. These two texture features effectively measure the texture smoothness. The image is divided into 2X2 blocks and these moments are computed in the wavelet transform domain. This gives better accuracy when compared with conventional texture extraction methods [19].

Palm print retrieval is proposed in [20] using texture features. Texture energy is presented to identify the global and local texture features of the palm print. The four masks which are defined in the work are used to extract the line segment in horizontal and verti-

cal directions and is referred to as local feature. The local feature provides detailed information and global feature provides overall properties of the palm print. The steps involved in global feature calculations are image alignment, energy computation, boundary tracing, a center of gravity calculation, and mapping the key points.

The content-based image retrieval system is an active research area for the past two decades. Many researchers have come up with different ideas to enhance the performance of the system by extracting texture features. The most used texture extraction methods are GLCM, covariance method and co-occurrence matrix, and so on. In this work, the semivariogram method is applied for texture extraction. The semivariogram is widely used to analyse the pattern of the remote sensing images. The content-based image retrieval databases will have distinct images with different types of patterns. The function of the semivariogram is to find the spatial distance between each pattern in the image. The semivariogram approach and spectral distortion measures are applied to image texture retrieval in [21]. The experiment is conducted using the Broadtz texture database. The spectral distortion methods are combined with a semivariogram to retrieve similar images. The effectiveness of the work is tested on Illinois at Urbana-Champaign texture database. The semivariogram method does not need the knowledge of the mean value of the function for the estimation of the spatial relationship. The probability of the random function is not required for the semivariogram methodology as in the GLCM method and co-occurrence method.

A hierarchical retrieval system is proposed in [22] using the visual contents(color,shape and texture).The fusion of histogram gradients, adaptive tetrolet transform and auto color correlogram methods are applied to extract the image features and to make the image retrieval more effective.

The proposed method estimates the pattern similarity by finding the distance between the pixels as it plays an important role in recognition of the similar images from the large database.

3 Mathematical Model for Semivariogram and Robust semivariogram

Variance is a measure of data spread between numbers in a data set. It measures the data on how far each number in the set is from the mean and also its variability from the average mean. A small variance shows how close the data to the mean and high variance indicates the data points are how far from the mean.The variogram is a statistical measure can be represented graphically in a manner which characterizes the spatial continuity i.e. roughness of a dataset.

Semivariogram is one of the standard geo-statistical parameters is used to find spatial relationships between two values in that location as a function of the distance. The lag distance h is taken for paired location in an image.

Let X, z, and h be a random function, a spatial location, and a lag distance in the sampling space, respectively. The variogram of the random function is defined as:

$$2\gamma(h) = Var[Z(x) - Z(x + h)] \tag{1}$$

where $\gamma(h)$ is called the semivariogram of the random function. Let $Z(x_i)$ be the pixel value at the location , i = 1, 2, . . ., n, where n is

the sampling size. The variable z is the intensity value at location of the image. The experimental semivariogram, of the random function is expressed as in [26]

$$\gamma(\hat{h}) = \frac{1}{2N(h)} \sum_{i=1}^{N(h)} [Z(x_i) - Z(x_i + h)]^2 \tag{2}$$

The reason for introducing the robust semivariogram is because the semivariogram is not robust with respect to skewness and distorted information.The robust semivariogram denoted as $\gamma_R(h)$ is defined as in [23] ,[24]

$$\gamma_R(h) = \delta[\frac{1}{N(h)} \sum_{i=1}^{N(h)} | Z(x_i) - Z(x_i + h) |^{1/2}]^4 \tag{3}$$

where

$$\delta = \frac{1}{2(0.457 + \frac{0.494}{N(h)})} \tag{4}$$

4 Extraction of Texture Feature of an Image

The texture feature can be extracted using the semivariogram.The block diagram of the proposed method is as shown in fig 1.Let us consider an image as shown in fig 2. To extract texture information the image is resized into 640X640 pixels. Then the image is divided into 9 sub-images of size 215X215. The lag distance 'h' value is taken as 20. The variogram is calculated for each sub-image and its results in a feature vector size 20X9. The pictorial representation of the semivariogram features and robust semivariogram features is as shown in fig 3 and fig 4.The variogram shape near the origin is linked to the smoothness of the phenomenon. If the shape is continuous and differentiable it shows smoothness of the image, if it is not differentiable it shows roughness of the image. This process is applied to all the images in the query database and search database and these features are stored to find the similarity distance.
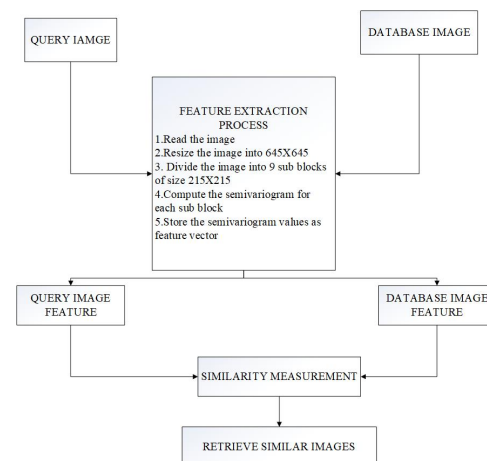
Figure 1: Block diagram of the proposed method

Figure 2: Bus Image
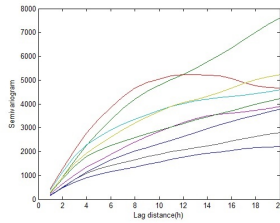
Figure 3: Experimental Semivariogram for the Bus image
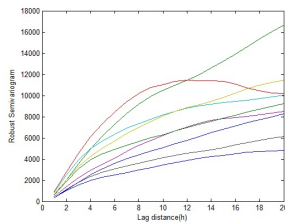
Figure 4: Robust Semivariogram for the Bus image

5   Distance Metrics for similarity measurements

Euclidean distance: If S (x1, y1) and T (x2, y2) are the two feature points of the image then the Euclidean distance between the two points is given by,

$$EUD(S, T) = \sqrt{(x_1 - x_2)^2 + (y_1 - y_2)^2} \qquad (5)$$

label1.4

Canberra distance: The Canberra distance is a numerical measure of the distance between pairs of points in a vector space. The Canberra distance (CBD) between two vectors is given by ,

$$CBD(S_i, T_i) = \sum_{i=1}^{N} \frac{\mid x_i - y_i \mid}{\mid x_i \mid + \mid y_i \mid} \qquad (6)$$

Manhattan distance: If S (x1, y1) and T (x2, y2) are two points then the Manhattan distance between two points S and T is given by,

$$MHD(S, T) = \mid x_1 - x_2 \mid + \mid y_1 - y_2 \mid \qquad (7)$$

Chord distance: It is used to find the correlation between the two images.If a and b are referred as a array of the two images then the chord distance is given by.

$$C = 1 - abs[\frac{a(i) * b(j)}{norm(a(i)) * norm(b(j))}] \qquad (8)$$

6   Experimental Design and Discussion

6.1   Experiment with three databases using Euclidean distance

The image retrieval experiment is conducted using the natural and object-based image database namely Corel 1K, Corel 10K, and Coil 100. The images in these databases are taken to investigate the performance of the proposed method. The Corel 1K database contains 10 categories and each category has 100 images such as people, beach, bus, dinosaur, roses, and so on. Each image of size 256X384 and 384X256.This is divided into query database of 300 images i.e 30 images from each category and search a database of 700 images i.e. 70 images from each category.

The proposed method is examined using the Corel 10K database [6]. This database contains 10000 natural image collection of 100 categories. Each image of size 126X187 and 187X126. The images in this database are having a dissimilar and unstructured pattern. Some categories of images are dolls, doors, sunset, mountains, etc. Each category has 100 images which are divided into 3000 images of query database i.e 30 images from each class and 7000 images of search database i.e. 70 images from each category.

The COIL 100 dataset is used to investigate the performance of the proposed image retrieval system. This database contains 100 categories of 7100 images. Each image is of size 128X128. This database is having object-based images like a hammer, car, toy, fruits, etc with uniform background and these images are most similar in pattern. This database is divided into a query database of 1000 images 10 images from each class and a search database of 6100 images 61 images from each class.

The system is designed to show the top ten retrievals of similar images for each query image. The similarity matching is based on the shortest distance score measured using Euclidean distance metrics between the query image and the database image. If the system retrieves similar images according to query, then we say the system is retrieved the target images else the system fails to retrieves the target images. The performance of the system is examined using average precision and average recall.Table 1 shows the three databases' precision and recall values using semivariogram method and lag distance is set to 20.

Table 1: Prescision and recall values using Experimental semivariogram on Image Databases.

sl No	Name of the Database	Precision	Recall
1	Corel 1K	0.77	0.109
2	Corel 10K	0.323	0.045
3	Coil 100	0.858	0.126

6.2 Experiment with Corel-1k database using four distance measures

The retrieval rates are computed using the complete Corel 1k dataset using four distance metrics. The retrieval test is done using the semivariogram and robust semivariogram method by setting the lag distance value h is equal to 20.

The distance measures compared using semivariogram and robust semivariogram methods. Table 2 and Table 3 show the average precision and average recall values for four distance measures. The examples for retrieval of these measure is as shown in fig 12, fig 13, fig 14 and fig 15. The fig 11 shows the query images.

Table 2: The average Precision values for Four distance metric

sl No	Distance metric	Semivariogram	Robust Semivariogram
1	Euclidean	0.77	0.78
2	Manhatten	0.52	0.51
3	Canberra	0.58	0.72
4	Chord	0.38	0.54

Table 3: The average recall values for four distance metric

sl No	Distance metric	Semivariogram	Robust Semivariogram
1	Euclidean	0.109	0.109
2	Manhatten	0.061	0.072
3	Canberra	0.071	0.102
4	Chord	0.176	0.057

6.3 Experiment with lag distance 'h' for the Corel-1k database using Euclidean distance

The semivariogram is a function of variable lag distance h. The semivariogram increases the dissimilarity with the lag distance h. If the distance is more it fails to identify the patterns of the image. The semivariogram is calculated based on the lag distance. In this experiment, the distance chosen is 20 and 30. As the distance increases the textural information is lost. if the distance is less than strong textural information can be extracted. The table 4 shows the time taken for the calculation of semivariogram and robust semivariogram for a single image. Table 5 shows the precision and recall values for the retrievals of corel 1k database with lag distance 20 and 30. From the table 5 we can notice that for the lower lag distance the performance of the system is effective.

Table 4: The computation time for different lag distance

sl No	Lag distance(h)	Semivariogram	Robust Semivariogram
1	30	1.070 sec	2.88 sec
2	50	1.483 sec	4.25 sec
3	100	2.136 sec	6.59 sec
4	150	2.448 sec	7.566 sec
5	200	2.479 sec	7.91 sec

Table 5: The computation of Image retrievals for the lag distance h=20 and h=30 using semivariogram

sl No	Lag distance(h)	Precision	Recall
1	20	0.77	0.109
2	30	0.74	0.06

From the Table 4, we can see that as distance increases computation time increases, and the amount of information decreases. As the distance taken is small the rate of information increases and results in more retrieval of similar images i.e. lower the distance higher the continuity. For the lag distance h the proposed method results in an effective retrieval of similar images.

Figure 5: Query Images from COIL 100 dataset
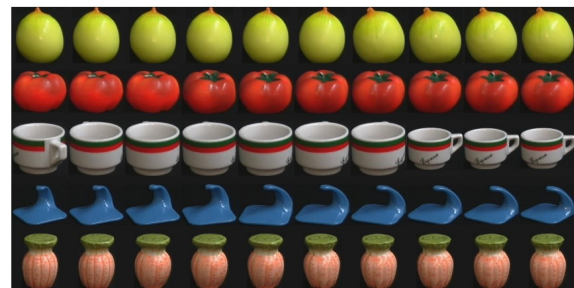
Figure 6: Retrieved images for the queries show in figure 5.

6.4 Retrieval results

The feature vectors are stored and are tested for four distance metrics. The result shows that Euclidean distance is best suited for the retrieval of similar images from the image database. The robust semivariogram shows still good performance comparing with the semivariogram method. This is because the semivariogram is not robust against the distribution and distortion of the pixel values. The Euclidean distance measure results in good retrieval of similar images when compared to the other three distance measures. Results

are tabulated for the first top ten retrieved images. For the Dinosaurs, Rose, and Horse class Ten images of the same class are retrieved at the top ten images. The results by using the semivariogram method for the image databases are tabulated in Table 1.

Figure 7: Query image from COREL-1K database

Figure 8: Retrival using Euclidean distance for the COREL-1K database

Figure 9: Query image from COREL-10K database

Figure 10: Retrival uisng Euclidean distance for the COREL-10K database

The top ten retrieved images for the Coil-100, Corel 1K, and Corel 10K database are shown in fig 6, fig 8, and fig 10 respectively. The Query samples for these retrievals are shown in fig 5, fig 7, and fig 9. For the COIL 100 database, the proposed technique is effective in retrieving similar images from the database for all the categories present in the database. The semivariogram method

works well for the Corel 1k and Corel 10k database in which these databases are having the most dissimilar pattern of images.

7 Performance Evaluation and comparison

In content-based image retrieval, most of the researchers use precision and recall as the evaluation metrics. Precision is the proportion of relevant images retrieved over the total number of images retrieved and recall is the relevant images retrieved over a total number of relevant images are there in the database. The precision and recall are defined,

Precision = $\frac{R}{R1}$

Recall = $\frac{R}{R2}$.

where, R: Number of relevant images retrieved.
R1: Total number of images retrieved.
R2: Total number of relevant images in the database.

The proposed method gives 77% of efficiency for the corel 1k database,32.3% for corel 10k and 85.8% efficiency for the coil-100 database as shown in the Table 1.

The experiment is conducted to investigate which distance measure is best suited to find the query image's closeness with the database image.We have compared the performance of the CBIR systems in terms of precision and recall values using Euclidean distance, Canberra distance, Manhattan distance, and Chord distance. The performance results are as tabulated in the table shows that Euclidean distance is best suited for retrieving images from the large database for the proposed approach. Whereas Chord distance shows very low performance compared to Euclidean distance,Canberra distance and Manhattan distance.

7.1 Comparison with existing methods

The experiment is compared with some of the existing methods under the Corel 1k database. It can be seen that the proposed method performs better in comparison with the existing CBIR methods as in [12]–[25]. The proposed methods yield the average precision value 0.77 and 0.78 concerning semivariogram and robust semivariogram.Table 6 shows the comparison of Corel-1K database with existing methods.

For Corel 10000 database, the experiments were conducted as similar to Corel 1000 database. In this work, 100 categories are used to check the system performance. The work carried in [26] uses the 20 image categories to test the system performance. As similar to the experimental set-up in [27], [28]the number of retrieved images is set to 10.Table 7 exhibits the proposed method's comparisons over the existing methods for Corel 1k and Corel 10k database.

The COIL-100 database is compared with existing methods as shown in Table 8. The former schemes show good results by considering only a few categories of the COIL-100 database. In our work, the results are tabulated for the entire categories present in the COIL-100 database.

The Table 7 and 8 shows the average precision values for the best retrievals of image categories. The authors from [29], [30]

presents the system performance which gives best results for some categories of the image database.The number categories does not play any role for the system performance ,it mainly depends on right choice of the feature and the similarity measurement. The proposed work is tested for all the categories of the image database and it is capable of retrieving most similar images for all the categories except for the Corel 10k database.

Figure 11: Query Image from Corel-1K database

Figure 12: Retrieval using Euclidean distance
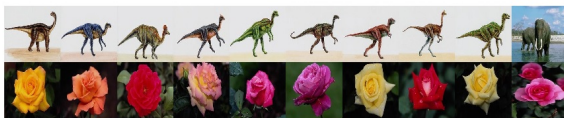
Figure 13: Retrieval using Manhatten distance

Figure 14: Retrieval using Canberra distance

Figure 15: Retrieval using Chord distance

Table 6: Comparison with Existing CBIR methods under Corel-1k Database.

Sr. No	Method	Average precision
1	[31]	0.396
2	[32]	0.526
3	[33]	0.532
4	[34]	0.533
5	[35]	0.566
6	[36]	0.565
7	[25]	0.0665
8	[26]	0.717
9	[29]	0.725
10	**Proposed method**	**0.77**

Table 7: Comparison with Existing CBIR methods under corel-10k Database.

Sr. No	Method	Average precision
1	EOAC[27](65 Query images)	0.210
2	CSD3[26](10 categories)	0.290
3	MTH[37](100 categories)	0.310
4	TCM[28](100 categories)	0.204
5	EDBTC[38](20 categories)	0.798
6	**Proposed method** (100 categories)	**0.323**

Table 8: Comparison with Existing CBIR methods under COIL-100 Database.

Sr. No	Method	Average precision
1	[39](10 categories)	0.86
2	[40](15 categories)	0.88
3	[41](15 categories)	0.78
4	[42](10 categories)	0.86
5	[43](10 categories)	0.93
6	**Proposed method**(100 categories)	**0.858**

8 Conclusion

The semivariogram and robust semivariogram techniques are applied to the color images for the feature extraction and retrieval processes from the large database.These techniques gives promising texture feature for the images.Both methods are analysed and compared with different distance metrics. The experiment tested using three databases having images of natural scenes, color, texture, and objects. The results are computed in terms of precision and recall. The precision rate achieved for the Coil-100 database is 85% and the Corel-1K database is 76%. The improved performance is observed with Euclidean distance measure over three distance measures. The experiment results show that the semivariogram is more effective for the content-based image retrieval system but not limited to remote sensing images.

References

[1] N. Rajani, A. Sreenivasa Murthy, "Semivariogram based feature extraction for content based image retrieval," in ACM International Conference Proceeding

Series, 2019, doi:10.1145/3332340.3332348.

[2] M. Singha, K. Hemachandran, "Content based image retrieval using color and texture," Signal & Image Processing, **3**(1), 39, 2012.

[3] D. Srivastava, S. Goel, S. Agarwal, "Pipelined technique for image retrieval using texture and color," in 2017 4th International Conference on Power, Control & Embedded Systems (ICPCES), 1–6, IEEE, 2017, doi:10.1109/ICEE.2017.31.

[4] H. Kebapci, B. Yanikoglu, G. Unal, "Plant image retrieval using color, shape and texture features," The Computer Journal, **54**(9), 1475–1490, 2011.

[5] R. M. Haralick, K. Shanmugam, I. H. Dinstein, "Textural features for image classification," IEEE Transactions on systems, man, and cybernetics, (6), 610–621, 1973.

[6] J.-M. Guo, H. Prasetyo, "Content-based image retrieval using features extracted from halftoning-based block truncation coding," IEEE Transactions on image processing, **24**(3), 1010–1024, 2014, doi:10.1109/IEES.2014.31.

[7] T. Ružić, A. Pižurica, "Context-aware patch-based image inpainting using Markov random field modeling," IEEE transactions on image processing, **24**(1), 444–456, 2014, doi:10.1109/TRANS.2014.31.

[8] Y. Dong, J. Ma, "Wavelet-based image texture classification using local energy histograms," IEEE Signal Processing Letters, **18**(4), 247–250, 2011, doi:10.1109/LSP.2011.2111369.

[9] Y. Qiao, L. Weng, "Hidden markov model based dynamic texture classification," IEEE Signal Processing Letters, **22**(4), 509–512, 2014, doi: 10.1109/SDF.2014.2111369.

[10] Y. Dong, D. Tao, X. Li, J. Ma, J. Pu, "Texture classification and retrieval using shearlets and linear regression," IEEE transactions on cybernetics, **45**(3), 358–369, 2014, doi:10.1109/TCFG.2014.21369.

[11] R. A. Olea, "The Semivariogram," in Geostatistics for Engineers and Earth Scientists, 67–90, Springer, 1999.

[12] N. Cressie, "Statistics for spatial data New York," 1993.

[13] A. Balaguer, L. A. Ruiz, T. Hermosilla, J. A. Recio, "Definition of a comprehensive set of texture semivariogram features and their evaluation for object-oriented image classification," Computers & Geosciences, **36**(2), 231–240, 2010.

[14] K. Kitada, K. Fukuyama, "Land-use and land-cover mapping using a gradable classification method," Remote Sensing, **4**(6), 1544–1558, 2012.

[15] J. R. Carr, F. P. De Miranda, "The semivariogram in comparison to the co-occurrence matrix for classification of image texture," IEEE Transactions on geoscience and remote sensing, **36**(6), 1945–1952, 1998.

[16] A. Yue, C. Zhang, J. Yang, W. Su, W. Yun, D. Zhu, "Texture extraction for object-oriented classification of high spatial resolution remotely sensed images using a semivariogram," International Journal of Remote Sensing, **34**(11), 3736–3759, 2013.

[17] X. Wu, J. Peng, J. Shan, W. Cui, "Evaluation of semivariogram features for object-based image classification," Geo-spatial Information Science, **18**(4), 159–170, 2015.

[18] M. Kokare, P. K. Biswas, B. N. Chatterji, "Texture image retrieval using new rotated complex wavelet filters," IEEE Transactions on Systems, Man, and Cybernetics, Part B (Cybernetics), **35**(6), 1168–1178, 2005.

[19] H. Zhang, X. Jiang, "An improved algorithm based on texture feature extraction for image retrieval," in 2015 12th International Conference on Fuzzy Systems and Knowledge Discovery (FSKD), 1270–1274, IEEE, 2015.

[20] M. Jian, L. Liu, F. Guo, "Texture image classification using perceptual texture features and Gabor wavelet features," in 2009 Asia-Pacific Conference on Information Processing, volume 2, 55–58, IEEE, 2009.

[21] H. J. So, M. H. Kim, N. C. Kim, "Texture classification using wavelet-domain BDIP and BVLC features," in 2009 17th European Signal Processing Conference, 1117–1120, IEEE, 2009.

[22] N. Varish, A. K. Pal, R. Hassan, M. K. Hasan, A. Khan, N. Parveen, D. Banerjee, V. Pellakuri, A. U. Haqis, I. Memon, "Image retrieval scheme using quantized bins of color image components and adaptive tetrolet transform," IEEE Access, **8**, 117639–117665, 2020.

[23] W. Li, J. You, D. Zhang, "Texture-based palmprint retrieval using a layered search scheme for personal identification," IEEE Transactions on Multimedia, **7**(5), 891–898, 2005.

[24] T. D. Pham, "The semi-variogram and spectral distortion measures for image texture retrieval," IEEE Transactions on Image Processing, **25**(4), 1556–1565, 2016.

[25] T.-C. Lu, C.-C. Chang, "Color image retrieval technique based on color features and image bitmap," Information processing & management, **43**(2), 461–472, 2007.

[26] F.-X. Yu, H. Luo, Z.-M. Lu, "Colour image retrieval using pattern co-occurrence matrices based on BTC and VQ," Electronics letters, **47**(2), 100–101, 2011.

[27] F. Mahmoudi, J. Shanbehzadeh, A.-M. Eftekhari-Moghadam, H. Soltanian-Zadeh, "Image retrieval based on shape similarity by edge orientation autocorrelogram," Pattern recognition, **36**(8), 1725–1736, 2003.

[28] C.-H. Lin, D.-C. Huang, Y.-K. Chan, K.-H. Chen, Y.-J. Chang, "Fast color-spatial feature based image retrieval methods," Expert Systems with Applications, **38**(9), 11412–11420, 2011.

[29] M. Subrahmanyam, Q. M. J. Wu, R. P. Maheshwari, R. Balasubramanian, "Modified color motif co-occurrence matrix for image indexing and retrieval," Computers & Electrical Engineering, **39**(3), 762–774, 2013.

[30] G.-H. Liu, J.-Y. Yang, "Image retrieval based on the texton co-occurrence matrix," Pattern Recognition, **41**(12), 3521–3527, 2008.

[31] M. R. Gahroudi, M. R. Sarshar, "Image retrieval based on texture and color method in BTC-VQ compressed domain," in 2007 9th International Symposium on Signal Processing and Its Applications, 1–4, IEEE, 2007.

[32] N. Jhanwar, S. Chaudhuri, G. Seetharaman, B. Zavidovique, "Content based image retrieval using motif cooccurrence matrix," Image and Vision Computing, **22**(14), 1211–1220, 2004.

[33] P.-W. Huang, S. K. Dai, "Image retrieval by texture similarity," Pattern recognition, **36**(3), 665–679, 2003.

[34] T.-W. Chiang, T.-W. Tsai, "Content-based image retrieval via the multiresolution wavelet features of interest," Journal of Information Technology and Applications, **1**(3), 205–214, 2006.

[35] S. Silakari, M. Motwani, M. Maheshwari, "Color image clustering using block truncation algorithm," arXiv preprint arXiv:0910.1849, 2009.

[36] M. Saadatmand-Tarzjan, H. A. Moghaddam, "A novel evolutionary approach for optimizing content-based image indexing algorithms," IEEE Transactions on Systems, Man, and Cybernetics, Part B (Cybernetics), **37**(1), 139–153, 2007.

[37] G. H. Liu, L. Zhang, Y. K. Hou, Z. Y. Li, J. Y. Yang, "Image retrieval based on multi-texton histogram," Pattern Recognition, **43**(7), 2380–2389, 2010, doi:10.1016/j.patcog.2010.02.012.

[38] J.-M. Guo, H. Prasetyo, J.-H. Chen, "Content-based image retrieval using error diffusion block truncation coding features," IEEE Transactions on Circuits and Systems for Video Technology, **25**(3), 466–481, 2014.

[39] J. Kavya, H. Shashirekha, "A Novel approach for image retrieval using combination of features," International Journal of Computer Technology & Applications, **6**(2), 323–327, 2015.

[40] K. Velmurugan, L. D. S. S. Baboo, "Content-based image retrieval using SURF and colour moments," Global Journal of Computer Science and Technology, 2011.

[41] A. Bahri, H. Zouaki, "A SURF-color moments for images retrieval based on bag-of features," European Journal of Computer Science and Information Technology, **1**(1), 11–22, 2013.

[42] A. Mukherjee, S. Chakraborty, J. Sil, A. S. Chowdhury, "for Content-Based Image Retrieval," 79–87, doi:10.1007/978-981-10-2104-6.

[43] K. Kavitha, M. V. Sudhamani, "Object based image retrieval from database using combined features," Proceedings - 2014 5th International Conference on Signal and Image Processing, ICSIP 2014, **1**(12), 161–165, 2014, doi: 10.1109/ICSIP.2014.31.

A-MnasNet and Image Classification on NXP Bluebox 2.0

Prasham Shah[*], Mohamed El-Sharkawy

IoT Collaboratory at IUPUI, Department of Electrical and Computer Engineering, Purdue School of Engineering and Technology, Indianapolis, 46202, USA

ARTICLE INFO

ABSTRACT

Computer Vision is a domain which deals with the challenge of enabling technology with vision capabilities. This goal is accomplished with the use of Convolutional Neural Networks. They are the backbone of implementing vision applications on embedded systems. They are complex but highly efficient in extracting features, thus, enabling embedded systems to perform computer vision applications. After AlexNet won the ImageNet Large Scale Visual Recognition Challenge in 2012, there was a drastic increase in research on Convolutional Neural Networks. The convolutional neural networks were made deeper and wider, in order to make them more efficient. They were able to extract features efficiently, but the computational complexity and the computational cost of those networks also increased. It became very challenging to deploy such networks on embedded hardware. Since embedded systems have limited resources like power, speed and computational capabilities, researchers got more inclined towards the goal of making convolutional neural networks more compact, with efficiency of extracting features similar to that of the novel architectures. This research has a similar goal of proposing a convolutional neural network with enhanced efficiency and further using it for a vision application like Image Classification on NXP Bluebox 2.0, an autonomous driving platform by NXP Semiconductors. This paper gives an insight on the Design Space Exploration technique used to propose A-MnasNet (Augmented MnasNet) architecture, with enhanced capabilities, from MnasNet architecture. Furthermore, it explains the implementation of A-MnasNet on Bluebox 2.0 for Image Classification.

1 Introduction

Computer Vision is becoming an essential application in this modern world. With advances in technology autonomous cars, drones and UAVs, robots etc have been enabled with vision capabilities. These technologies use Convolutional Neural Networks (CNNs) to process the images or video input. They are used for applications like Image Classification, Object Detection and Semantic Segmentation etc. CNNs are a part of Deep Learning, which is a subset of Machine Learning (ML). Due to the advances in AI, ML capabilities increased and this enabled a whole new field of Deep Learning. This field deals with creating, optimizing and implementing algorithms which enables technology to become self-reliant and gain human level precision. The prime goal is automation of these technologies in a way that they are able to operate perfectly without any human intervention.

Convolutional Neural Networks are used in developing healthcare technologies, which have almost human level precision and are used to save lives in hospitals. Medical imaging devices which, de-

tect even minute particles, are used for diagnosis of various diseases. Autonomous cars which will make roads safer and will reduce fatal life-threatening accidents, Autonomous Drones which will revolutionize the logistics and will deliver packages more efficiently, UAVs which will aid militaries with surveillance and help prevent wars, smart cameras which will be able to recognize people and track their activities to reduce crimes. Smart imaging of atmosphere for weather prediction and warnings for natural calamities like tsunami, tornadoes etc. These are a few examples of how CNNs are making a major impact in our lives.

These technologies require computational power, speed, accuracy and precision. In order to make them efficient, the algorithms have to be fast having low latency, working efficiently on low power, being more accurate and consuming less memory. CNNs have so many layers so as the architectures become deeper and wider, giving more accuracy, their computational cost increases. These CNN models have to be more compact and should work as efficiently as the novel architectures. With new research and advent of new algorithms, now it is possible to make CNNs more efficient having

*Corresponding Author: Prasham Shah, Email: pashah@purdue.edu

competitive size and accuracy. This research aims to contribute towards this same goal, making CNNs compact in terms of model size and increasing its accuracy so that they can be used for such applications[1].

A-MnasNet [2] is derived by Design Space Exploration of Mnas-Net. New algorithms were implemented for more efficiency with competitive size and accuracy. Furthermore, it is deployed on NXP Bluebox 2.0 for Image Classification [3]. RTMaps Studio is used to deploy the model on the hardware by establishing a TCP/IP connection.

In this paper, section 2 discusses MnasNet architecture. Section 3 introduces A-MnasNet [2] and discusses the new algorithms implemented to achieve better results. Section 4 demonstrates deployment of A-MnasNet [2] on NXP Bluebox 2.0 for Image classification [3]. Section 5 states the hardware and software requirements to conduct this research. Section 6 illuminates the results that demonstrate the model comparison, model size and accuracy trade-offs and deployment results. Section 7 is conclusion which gives the gist of this research.

2 Prior Work

This section gives an insight on MnasNet [4] architecture. It explains the features of this architecture and what can be improved in order to make it more efficient.

2.1 MnasNet Architecture

MnasNet [4] was introduced in 2019 by Google Brain Team with a goal of proposing an approach of neural architecture search which would optimize the overall accuracy of the architecture and reduce the latency of the model on mobile devices. MnasNet outperformed all existing novel architectures on ImageNet dataset with enhanced accuracy. This architecture extracts features by using depthwise separable convolutional layers with 3*3 and 5*5 filter dimensions and mobile inverted bottleneck layers. It has ReLU [5] activation layers which introduces non-linearity to the network. It uses Batch normalization to adjust and scale the output of activation layers. Dropout regularization is used to reduce the overfitting in the network.

Figure 1 shows MnasNet architecture and illuminates its convolutional layers. This architecture was designed for ImageNet dataset so the input dimensions were set to 224*224*3. It had a validation accuracy of 75.2% and outperformed all other existing state-of-the-art architectures. For this research, MnasNet was used with CIFAR-10 [6] dataset so the input dimensions were modified to 32*32*3. Table 1 shows various layers of the architecture.

An important aspect to observe about MnasNet is that it only explores the channel dimensions of the feature maps throughout its architecture. The convolutional layers fail to explore the spatial feature scale in the network. The activation layers used in the architecture have become outdated and today there are better algorithms which work more efficiently then the used activations.
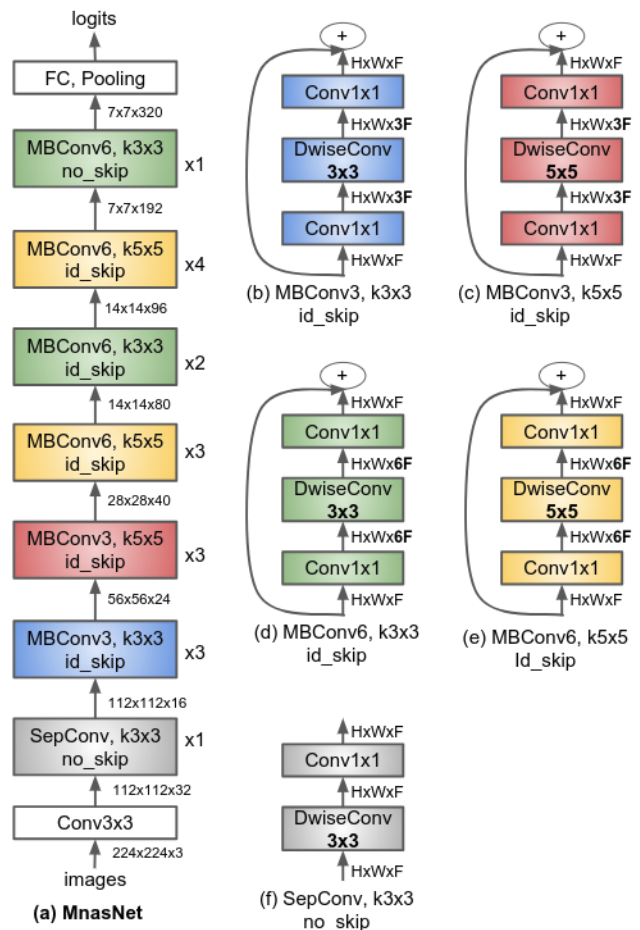
Figure 1: MnasNet architecture

Table 1: MnasNet Architecture

MnasNet Architecture					
Layers	Convolutions	t	c	n	s
$32^2 \times 3$	Conv2d 3×3	-	32	1	1
$112^2 \times 32$	SepConv 3×3	1	16	1	2
$112^2 \times 16$	MBConv3 3×3	3	24	3	2
$56^2 \times 24$	MBConv3 5×5	3	40	3	2
$28^2 \times 40$	MBConv6 5×5	6	80	3	2
$14^2 \times 80$	MBConv6 3×3	6	96	2	1
$14^2 \times 96$	MBConv6 5×5	6	192	4	1
$7^2 \times 192$	MBConv6 3×3	6	320	1	1
$7^2 \times 320$	FC,Pooling			10	

t: expansion factor, c: number of output channels, n: number of blocks and s: stride

3   A-MnasNet Architecture

This section gives an insight on the A-MnasNet [2] CNN architecture and its features.

3.1   Convolution Layers

Harmonious Bottleneck Layers [7] were introduced in the architecture. This special convolutional layers extract features across the spatial and channel dimensions. They are more efficient then the depthwise separable convolutional layers. Harmonious layers consist of spatial contraction-expansion keeping the number of channels constant and channel expansion-contraction keeping the spatial dimensions constant. This down-scaling reduces the number of parameters of the model. Hence, the model size is reduced. Since it extracts features more efficiently, the overall model accuracy is enhanced.
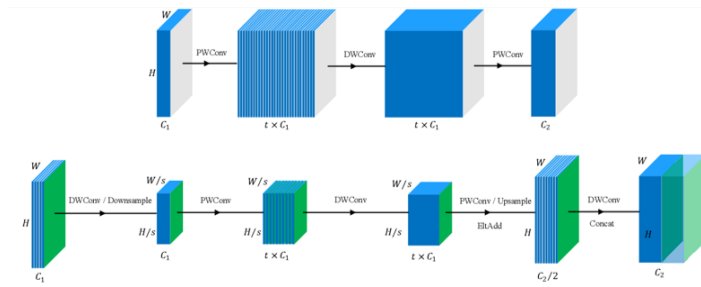
Figure 2: Comparison of Depthwise Separable Convolution Layer and Harmonious Bottleneck Layer.[7]

A comparison between Harmonious bottleneck layers [7] and depthwise separable layers is demonstrated in Figure 2. Here, Input size and output size is represented by H and W respectively. C1 and C2 denote the input and output feature channels where K is the size of the filter and s is the stride value.

The total cost of depthwise separable convolution is

$$(H \times W \times C1 \times K \times K) + (H \times W \times C1 \times C2) \quad (1)$$

The total cost of harmonious bottleneck layer is

$$B/s^2 + (H/s \times W/s \times C1 + H \times W \times C2) \times K^2 \quad (2)$$

where, B is the computational cost of the blocks inserted between the spatial contraction and expansion operations.

Dowmsampling the channel dimensions and extracting features from the spatial dimensions results in reduced spatial size of wide feature maps. The parameters of the model are reduced by a factor of the stride value. As a result the model size reduces and the accuracy of the model increases.

Hence, these layers were added to enhance the performance of the model. Table 2 shows various layers of A-MnasNet [2].

Table 2: A-MnasNet Architecture

A-MnasNet Architecture					
Layers	Convolutions	t	c	n	s
$32^2 \times 3$	Conv2d 3×3	-	32	1	1
$112^2 \times 32$	SepConv 3×3	1	16	1	2
$112^2 \times 16$	MBConv3 3×3	3	24	3	2
$112^2 \times 24$	Harmonious Bottleneck	2	36	1	1
$56^2 \times 36$	MBConv3 5×5	3	40	3	2
$112^2 \times 40$	Harmonious Bottleneck	2	72	1	2
$28^2 \times 72$	MBConv6 5×5	6	80	3	2
$112^2 \times 80$	Harmonious Bottleneck	2	96	4	2
$14^2 \times 96$	MBConv6 3×3	6	96	2	1
$14^2 \times 96$	MBConv6 5×5	6	192	4	1
$7^2 \times 192$	MBConv6 3×3	6	320	1	1
$7^2 \times 320$	FC,Pooling			10	

t: expansion factor, c: number of output channels, n: number of blocks and s: stride

3.2   Learning Rate Annealing or Scheduling

This parameter defines the rate at which the network learns the parameters. It sets the speed of learning features. It a large value is set then the speed of training would increase but with that, the accuracy would decrease as the efficiency of learning more features would reduce. This parameter is tuned throughout the training process in a descending manner. The learning rates are scheduled so that the step size in each iteration gives out the best output for efficient training. There are various methods to set learning rates. Some them have been demonstrated in Figure 3.
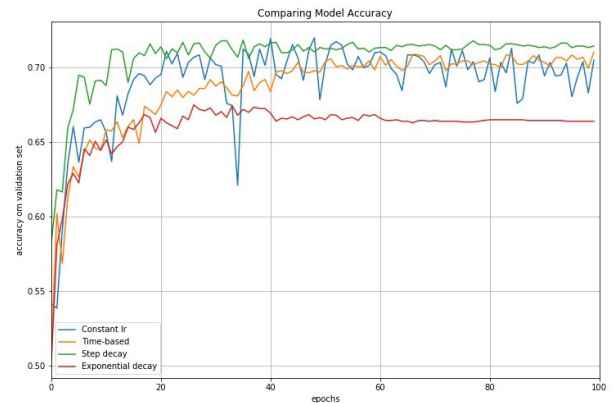
Figure 3: Comparision of different LR scheduling methods.

3.3   Optimization

Optimization is an essential aspect of enhancing the efficiency of the CNN models. Basically, it is a method of correcting the calculated error. It might sound simple but it just as complicated. There are various optimizers which are used to do this optimization. There are constant learning rate algorithms and adaptive learning rate algorithms. For this research, Stochastic Gradient Descent optimizer

[8] was used because of its enhanced performance on optimizing A-MnasNet [2]. It was used with varying values of learning rates during training with a momentum set to 0.9.

3.4 Data Augmentation

This step is used to preprocess the dataset. Various transformations are applied on the images. The purpose of data augmentation is the enhance the accuracy of the model. In other words, it enables the CNN model to learn features more efficiently. AutoAugment [9] is implemented to preprocess the dataset. It uses reinforcement learning to automatically select the transformations that are most efficient for the CNN model. It defines two parameters for the process. First is the transformation and the other is the magnitude of applying it. These two together are defined as a Policy. A Policy consists of sub-policies which have those two parameters. Different sub-policies are selected by the controller which best suit the training. This process is demonstrated in Figure 4. It was evident that by using AutoAugment [9] the accuracy of A-MnasNet increased to 96.89% from 92.97%.
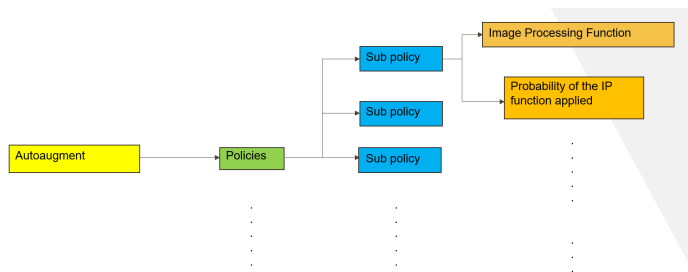
Figure 4: AutoAugment

4 Image Classification on NXP Bluebox 2.0

A-MnasNet [2] was deployed on NXP Bluebox 2.0 for Image Classification [3]. BlueBox 2.0 by NXP is a real-time embedded system which serves with the required performance, functional safety and automotive reliability to develop the self-driving cars. It is a ASIL-B and ASIL-D compliant hardware system which provides a platform to create autonomous applications such as ADAS systems, driver assistance systems.

There are three processing units in Bluebox 2.0. There is a vision processor, S32V234, a radar processor, S32R274, and a compute processor, LS2048A. This enables to develop autonomous applications. The vision processor and the compute processors are used to perform Image Classification [3] using A-MnasNet [2]. Figure 5 shows the methodology to deploy A-MnasNet [2] on Bluebox 2.0 for Image Classification.

After training A-MnasNet [2], the model is imported in the RTMaps Studio using its python component. A TCP/IP connection is used for data transmission between RTMaps Design Studio and NXP Bluebox 2.0. The model was successfully implemented on the hardware and was able to predict the object in the input images accurately.
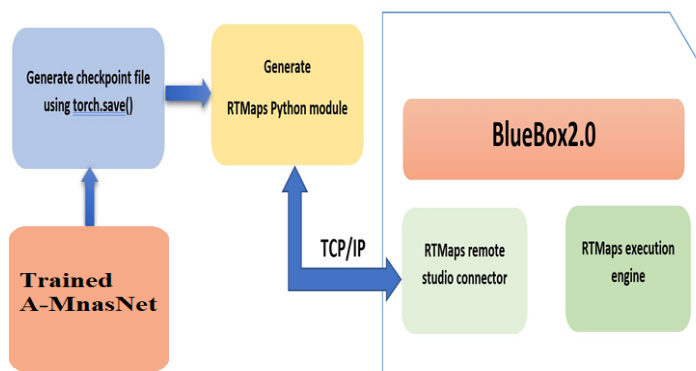
Figure 5: Deployment of A-MnasNet on NXP BlueBox 2.0

RTMaps Studio was used for real-time implementation of A-MnasNet[2] on NXP Bluebox 2.0. It is an asynchronous high performance platform which has an advantage of an efficient and easy-to-use framework for fast and robust developments. It provides a modular toolkit for multimodal applications like ADAS, Autonomous vehicles, Robotics, UGVs, UAVs, etc. It provides a platform to develop, test, validate, benchmark and execute applications.
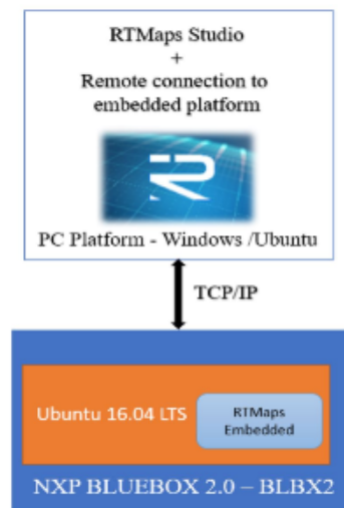
Figure 6: RTMaps connection with Bluebox 2.0

Figure 6 shows the role of RTMaps in the implementation. It provides an interface between the hardware and the embedded platform. It uses a TCP/IP connection by assigning a static IP address to enable data transfer between them.

5 Hardware and Software used

- NXP Bluebox 2.0
- Aorus Geforce RTX 2080Ti GPU
- Python version 3.6.7.
- Pytorch version 1.0.

- Spyder version 3.6.

- RTMaps Studio

- Tera Term

- Livelossplot

6 Results

MnasNet [4] achieved 80.8% accuracy with CIFAR-10 [6] dataset achieving 12.7 MB model size without data augmentation. New convolutional blocks resulted in an increase of accuracy to 92.97%. Furthermore, AutoAugment [9] was implemented for enhancing overall accuracy which increased from 92.97% to 96.89%. The final model is of 11.6 MB and a validation accuracy of 96.89%.

Implementation of new algorithms resulted in enhanced accuracy. It is demonstrated in Table 3. The overall accuracy increases by 16.09% with a slight decrease in model size.

Table 3: Comparison with baseline architecture

Comparison of models		
Architecture	Model Accuracy	Model size (in MB)
MnasNet	80.8%	12.7
A-MnasNet	96.89%	11.6
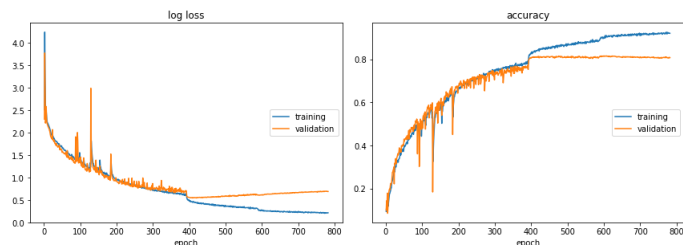
Figure 7: MnasNet (Baseline Architecture)
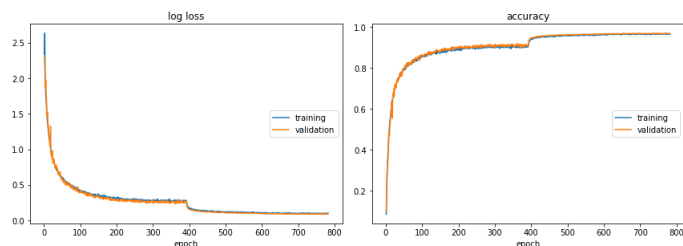
Figure 8: A-MnasNet (Proposed Architecture)

Figure 7 and figure 8 demonstrate the training curves. It is evident that by implementing new algorithms resulted in reduced overfitting and better accuracy.

For resource constrained hardware, desired model size and accuracy can be obtained by tuning width multiplier. Table 4 demonstrates the idea of having multiple size and accuracy by scaling width multiplier.

Table 4: varying model size by width multiplier

Scaling A-MnasNet with width multiplier		
Width Multiplier	Model Accuracy	Model size (in MB)
1.4	97.16%	22
1.0	96.89%	11.6
0.75	96.64%	6.8
0.5	95.74%	3.3
0.35	93.36%	1.8

Figure 9 shows the console output for Image Classification on NXP Bluebox 2.0. The model predicts that the object in the input image is a car. The window in the left corner shows the console output in Tera Term.
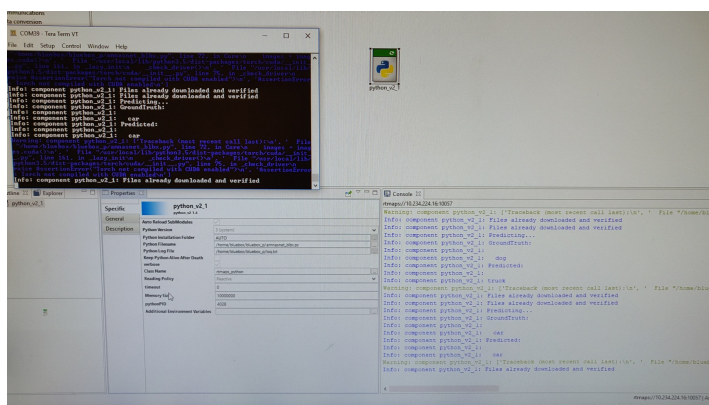
Figure 9: Image Classification using A-MnasNet

7 Conclusion

Design Space Exploration of MnasNet [4] architecture resulted in enhanced accuracy and a decrease in model size. The proposed architecture, A-MnasNet [2], has an accuracy of 96.89% and a size of 11.6 MB. It surpasses MnasNet [4] in terms of model size and accuracy. New convolutional layers were added to make A-MnasNet [2] more efficient in extracting features. AutoAugment[9] was used to preprocess the dataset. The model was scaled with width multiplier to get various trade-offs between model size and accuracy. The architectures were trained and tested on Cifar-10 [6] dataset. Furthermore, they were implemented on NXP Bluebox 2.0 for Image Classification. Results show that the new architecture successfully detects the object and successfully performs Image Classification.

Conflict of Interest   The authors declare no conflict of interest.

References

[1] P. Shah, "DESIGN SPACE EXPLORATION OF CONVOLUTIONAL NEURAL NETWORKS FOR IMAGE CLASSIFICATION," 2020, doi:https://doi.org/10.25394/PGS.13350125.v1.

[2] P. Shah, M. El-Sharkawy, "A-MnasNet: Augmented MnasNet for Computer Vision," in 2020 IEEE 63rd International Midwest Symposium on Circuits and Systems (MWSCAS), volume 2020-Augus, 1044–1047, IEEE, 2020, doi: 10.1109/MWSCAS48704.2020.9184619.

[3] C. Wang, Y. Xi, "Convolutional Neural Network for Image Classification," Johns Hopkins University, 2015.

[4] M. Tan, B. Chen, R. Pang, V. Vasudevan, M. Sandler, A. Howard, Q. V. Le, "MnasNet: Platform-Aware Neural Architecture Search for Mobile," in 2019 IEEE/CVF Conference on Computer Vision and Pattern Recognition (CVPR), 2815–2823, IEEE, 2019, doi:10.1109/CVPR.2019.00293.

[5] A. F. Agarap, "Deep Learning using Rectified Linear Units (ReLU)," arXiv, 2018.

[6] "CIFAR-10 and CIFAR-100 datasets," doi:https://www.cs.toronto.edu/{\~{}} kriz/cifar.html.

[7] D. Li, A. Zhou, A. Yao, "HBONet: Harmonious Bottleneck on Two Orthogonal Dimensions," in 2019 IEEE/CVF International Conference on Computer Vision (ICCV), 3315–3324, IEEE, 2019, doi:10.1109/ICCV.2019.00341.

[8] S. Ruder, "An overview of gradient descent optimization algorithms," arXiv, 2016.

[9] E. D. Cubuk, B. Zoph, D. Mane, V. Vasudevan, Q. V. Le, "AutoAugment: Learning Augmentation Policies from Data," arXiv, 2018.

BrcLightning - Risk Analysis and Scaling for Protection against Atmospheric Discharge - Extender

Biagione Rangel De Araújo*

BRC – Biagione Rangel Consulting, Natal, 59064-490, Brazil

A R T I C L E I N F O	A B S T R A C T
	This manuscript intending to publicize the improvements incorporated in the BrcLightning application, including the Risk Analysis module with the help of a pop-up, which provides the result and assists in the identification of mitigating measures by the professional, which must be defined to reduce the calculated risks. Other points addressed in this extension are the improvements added to the database to meet the corporate demands of companies, referring to the Risk Analysis module. It also incorporates flexibilities to perform the sizing separately, in the design, evaluation and scaling modules of the LPS – Lightning Protection System that using rolling sphere method and Angle Method, incorporating, in some of the modules, the issue of opinions or alerts. These modules use the mathematical approach methodology. In addition to these improvements, this review included the reporting module of facilities in the filter system, which allows the use of the database more selectively for the emission of these documents. This filter has a structure for issuing corporate demands of reports. The results can be obtained quickly and easily, on-screen or printing several reports. The reliability and safety of the results can be assessed through the check with the examples of the standards that define the criteria and methodology, that must be followed to carry out for cases of Risk Analysis or through graphic drawings on AutoCad platform or similar for the sizing modules. Other improvements in this extension are the addition of topics for new modules for which we already have the equations modeled in Excel, although we have not yet coded in the programming language.

1. Introduction

This article is an extension of the work originally presented at the Symposium SIPDA XV [1]. In the event, representatives of a large company attended our explanation and reported that the great difficulty they faced was to have the control and traceability of the various Risk Analyses that are performed for each building or structures of the various units of the company. So, considering that our system is structured in the form of a database, we evaluated that, by introducing structural changes in this database, it will be possible to meet this demand.

Concomitantly with this observation, we also identified that other improvements would be required, even to use the various modules of the system in isolation (before having to register a project), either in the database or through an app which may be via mobile phones. These improvements aim to meet specific demands, such as those to evaluate the effectiveness of the volume of protection of a given SPDA concerning the various structures or equipment and facilities that, in principle, are or would be under protection against direct impacts of atmospheric discharges. In this case, the data is not embedded in the database but can be consolidated into a report, with options to be printed or archived.

Regarding the Reporting Module, this extension was less extensive, as it was composed by the improvements of the filters defined to facilitate the selective issuance of Database Reports, with limited coverage of the specificity of each module that make up the current system. However, because it is a database, we intended (in a new version) to provide tools in this module, to enable the data export specifically to the Excel environment, to allow better tools for analyzing historical data.

2. Definitions

- Coverage radius (rc): The distance between the point of the cover margin, of a determined envelopment of an LPS. This distance determines the size of the horizontal projection of the fictitious plane, given by equation (1):

$$rc = [h_1(2R - h_1)]^{1/2} - [h_2(2R - h_2)]^{1/2} \qquad (1)$$

*Corresponding Author: BRC – Biagione Rangel Consulting,
contato.brc@biagione.com.br, +55-84-98723-8753

where:

rc		horizontal protected distance
h1		height of the higher mast
R		rolling sphere radius
h2		height of the lower mast:

- *Cover margin height (hc):* The dimensions of the height of the nearest point on the envelope over the structure under the protection of the LPS;

- *Distance from the critical point (d1):* The distance between the critical point and one metallic element such as rods or wire air-terminations

- *Envelopment:* Geometric shape that limits the protected volume according to the rolling sphere method;

- *Coverage margin (cm):* The shortest distance between a point of the structure under the protection of the LPS and the envelopment of the protective volume. The dimension of the margin corresponds to the perpendicular tangent measurement of the envelopment to the nearest point of the structure under protection. The graphical representations of "cm" are as shown in Figure 1a, Figure 1b, and Figure 1c (all contained in Figure 1):
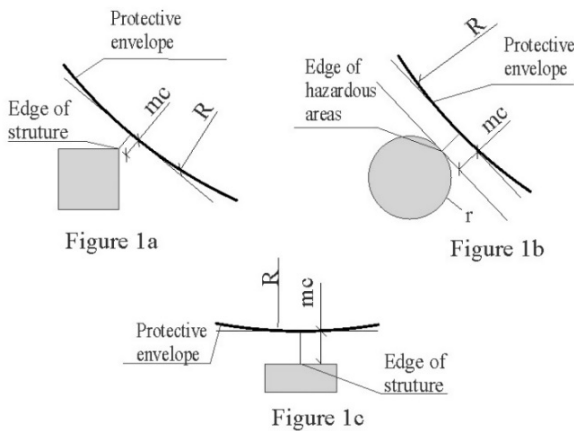
Figure 1: Examples of coverage margins

- *Fictitious plane (Fp):* Assumed horizontal plane that provides coverage of protection at a given height;

- *Hazardous areas:* Area surrounding storage facilities or transfer station of flammable liquids or gases, due to the possibility of containing flammable or explosive mixtures. They are defined in: Zone 0 (when the explosive/inflammable mixture is still there or will be for long periods); Zone 1 (likely to occur in normal operating conditions) and Zone 2 (it's unlikely – an abnormal condition of operation);

- *Sizing module marks*: The marks indicated in the graphs of the sizing and limit variation modules correspond to the extreme points of the structure that should be protected or evaluated on the effectiveness of the coverage by the SPDA protection wrap, as shown in figures 2 and 3 below:
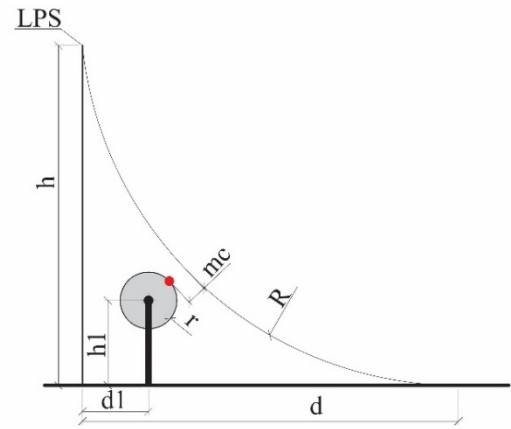
Figure 2: Hazardous areas limiting point figure (see Figure 1b)
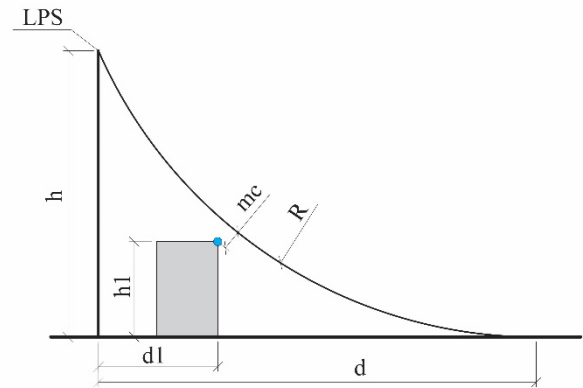
Figure 3: Structure limiting point figure (see Figure 1a)

3. Software Development

The application is developed in Access, in VBA language, to allow it to run on Windows and on the Internet. We had a project to carry out the migration to an Internet language; however, due to the Covid 19 pandemic, we had to cancel it. Nevertheless, we hope that, considering the problems due to the current situation, we can resume the project in the year 2021.

In this version, the system continues with the same configuration of modules and sections of the previous publication, from which this paper is an extension of (SIPDA XV [1]). Thus, we will focus on detailing the improvements that have been introduced, as described in sequence (items 4 to 7).

4. Risk Analysis Module

Risk Analysis consists of 5 sections: 1. Registration Module; 2. Zone Registration Module; 3. The configuration data of the connected lines and Zone.; 4. Risk Analysis Factors Module (typical loss value) and 5. Results Module.

4.1. Registration Section

In this section, there are specific data related to design registration that can be common to all modules and all sections, but also, there are important data specific to the Risk Analysis Module. Due to this, we have identified that it will be more effective for these data input to be dismembered in two modules: one for general project registration and another for registration and

configuration of the Risk Analysis Module. However, this should only be performed in a new version.

The improvements that we introduced in this section included the fields of input to meet the demand to perform the registration of organizational structures, containing up to 5 levels: Level 1 - Hold Company; Level 2 – The Business Unit, which may or may not cover several other Operating Units; Level 3 - The Operational Unit; Level 4 - The Operational Sector and Level 5 - The

installation subject to risk analysis or the one containing Air Terminal. This improvement is only incorporated into the Registration Form of this Section. Therefore, in this version, it has not yet been possible to integrate this organizational structure registration with the other modules, including the Risk Analysis Module itself, regarding the reports. This requires numerous changes in the reports already formatted. The reported modifications are highlighted in green as shown in Figure: 4.

Figure 4: Main screen of data input

Figure 5: Screen for customizing structure and zones)

4.2. Zone registration module

The System was engineered to cover up to 5 Zones (NBR-5419-2 [2] and IEC 62305-2 [3] do not establish limits, but provide examples of up to 5 Zones), as we observe that this is a practice used and that already surpasses the examples provided by the standards cited. The number of Zones is selected as shown in Figure 4 (Zone in Study).

The System already makes several types of structures available, which were understood as necessary and sufficient to meet the range of facilities and buildings that must be studied and related to each of them, the different types of Zones. However, the Designer can insert new structures and new zones, but he or she must proceed to register them. To do so, it will be necessary to customize them and make the association with the loss factors, as shown in Figure 5.

In this Section, the designer inserts the data for each zone that is defined for Risk Analysis, according to Section One of the Register, as shown in Figure 4. In this section, no improvement has been introduced, as show in Figure 6. For more details see SIPDA XV [1].
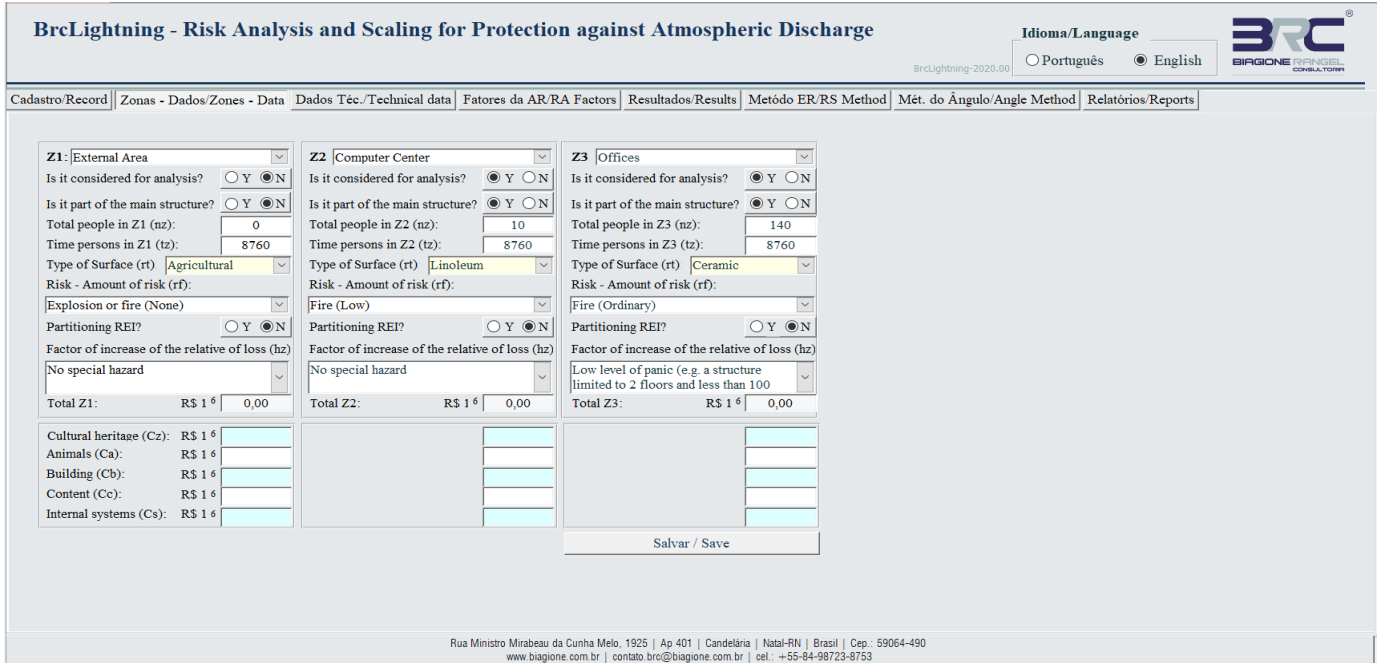
Figure 6: Screen of the setting module of the Zones (structure with all 3 Zones)
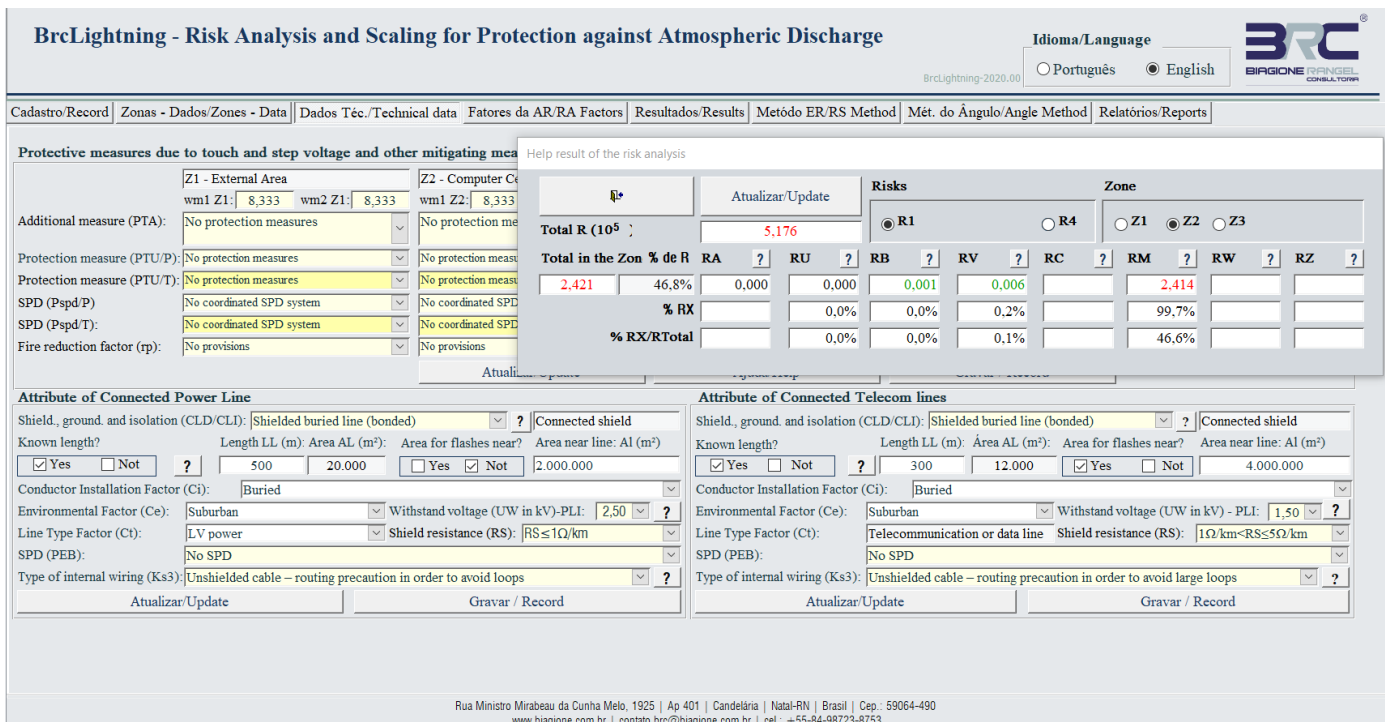
Figure 7: Setting screen of the connected lines and other zone data

4.3. The setting data of the connected lines and Zone

This Section provides the space to enter information about power lines and telecommunications lines: how they connect to the site (building; installations; etc.). The designer can also enter protective measures due to touch and step voltage and other risk-mitigating measures, individually for each defined Zone. In this section, it was introduced improvements to the Help pop-up form with the result of the risk analysis, as shown in Figure 7. Thus, the designer can monitor the effectiveness of each mitigating measures

in real-time. This pop-up, once visible, can be viewed in all sections of the risk analysis module.

Also, there is a pop-up to help define line parameters and other alert parameters as shown in Figure 8.

4.4. Risk Analysis Factors Module

This section presents the typical loss values for each zone (as shown in Figure 9), based on the definitions established in section one (as shown in Figure 4) and two (as shown in Figure 5).
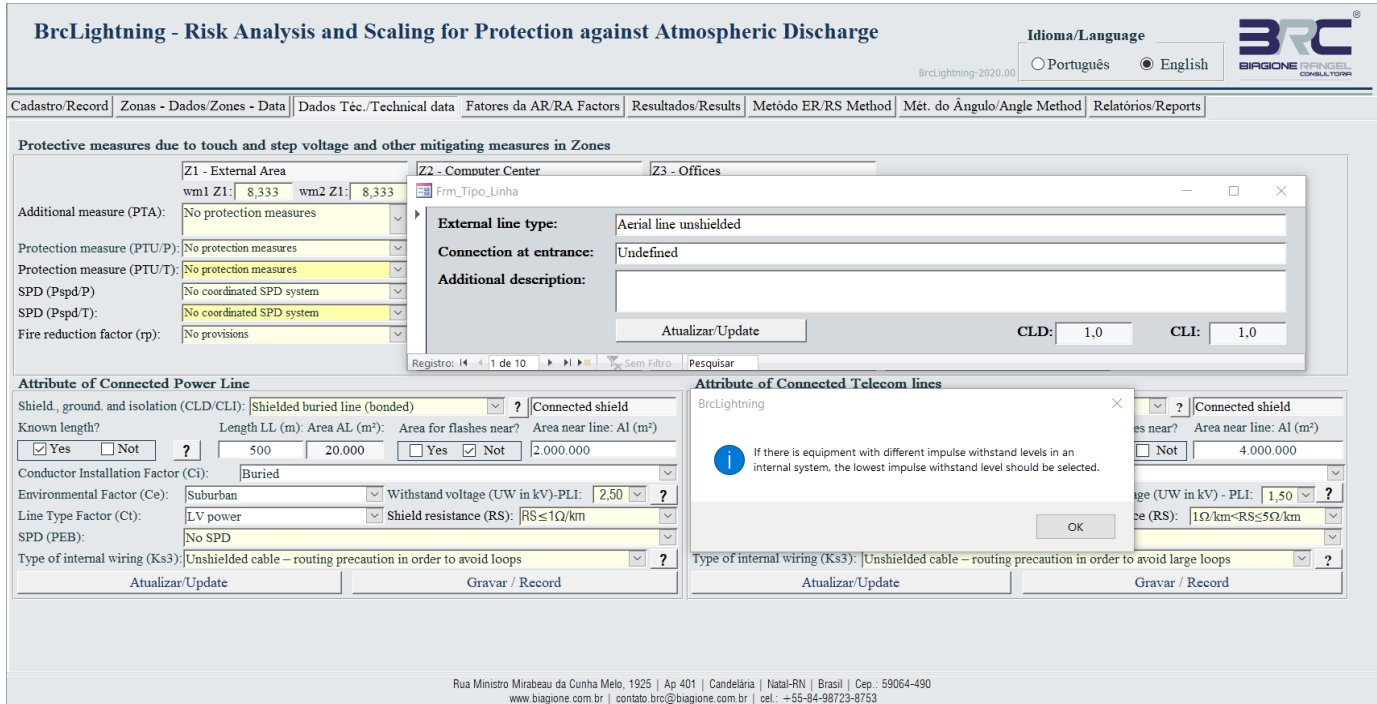
Figure 8: The pop-up helps with line parameters and other information
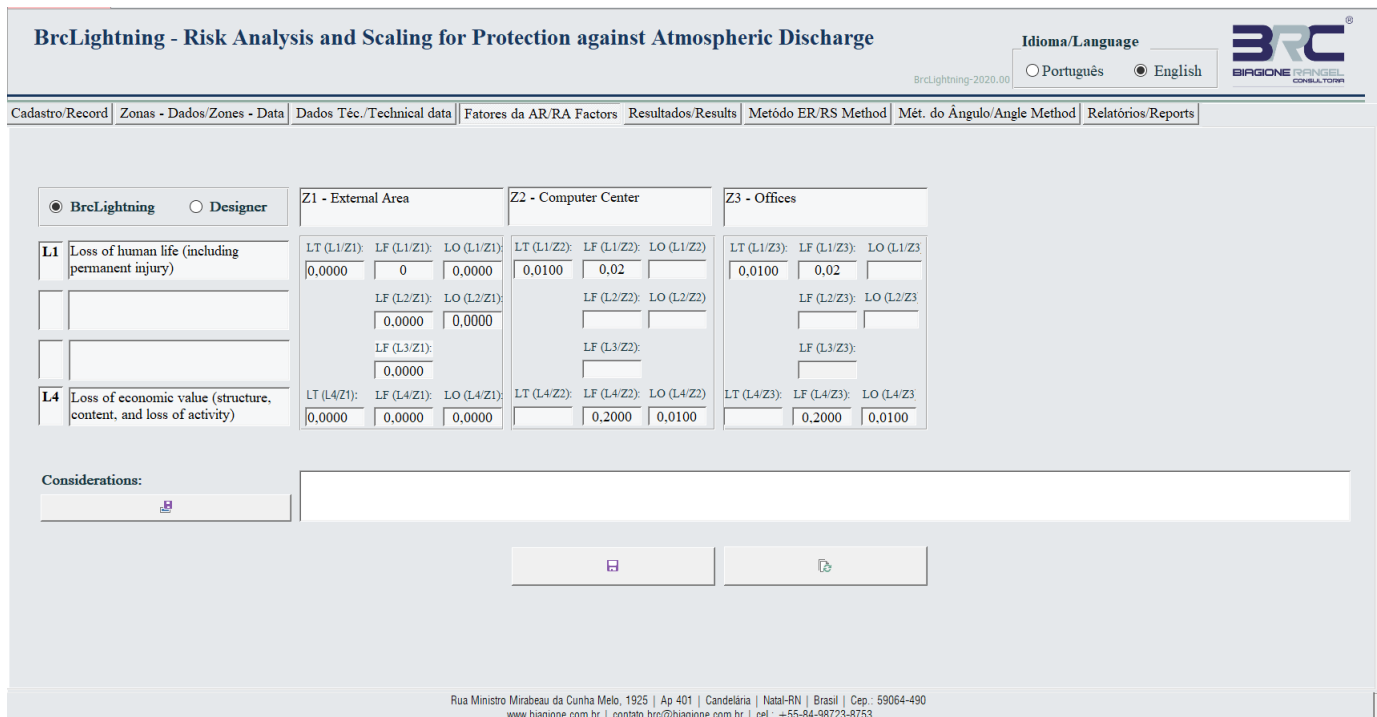
Figure 9: Loss Type Factors Module Screen

In the version presented in SIPDA XV [1], it was already possible for designers to change the typical loss value, if they had another interpretation regarding the one previously defined in the system (these factors defined in the system were based on the definitions established in NBR 5419 -2 [2] and IEC 62305-2 [3] for typical loss values). In this case, in the previous version, the designers had to standardize their basic values for each type of installation in advance. The improvement introduced allows that, in case they don't have a database parameterized with the values according to their interpretation criteria, they can do so by simply selecting the designer parameters (in the input field) and applying a double click on each factor that they want to parameterize. This way, a pop-up (as shown in Figure 10) form will appear for each factor and they will define it at their discretion. The new defined typical loss value, after being updated, will be highlighted in green

(as shown in Figure 10), but there are security restrictions and other requirements (see item 9.4).

4.5. Results Module

In this section, the final result is as shown in Figure 11. Mitigating measures can also be inserted (the description of these measures), if the results indicate that this is necessary. Mitigation measures, as needed, can be included (these should be inserted descriptively). A technical note with the analysis design also can and should be inserted. Another improvement is the possibility of issuing, in a summarized format, the risk analysis report, as shown in Figures: 12 (a) and (b). This report contains the basic information of the risk analysis study and the result.
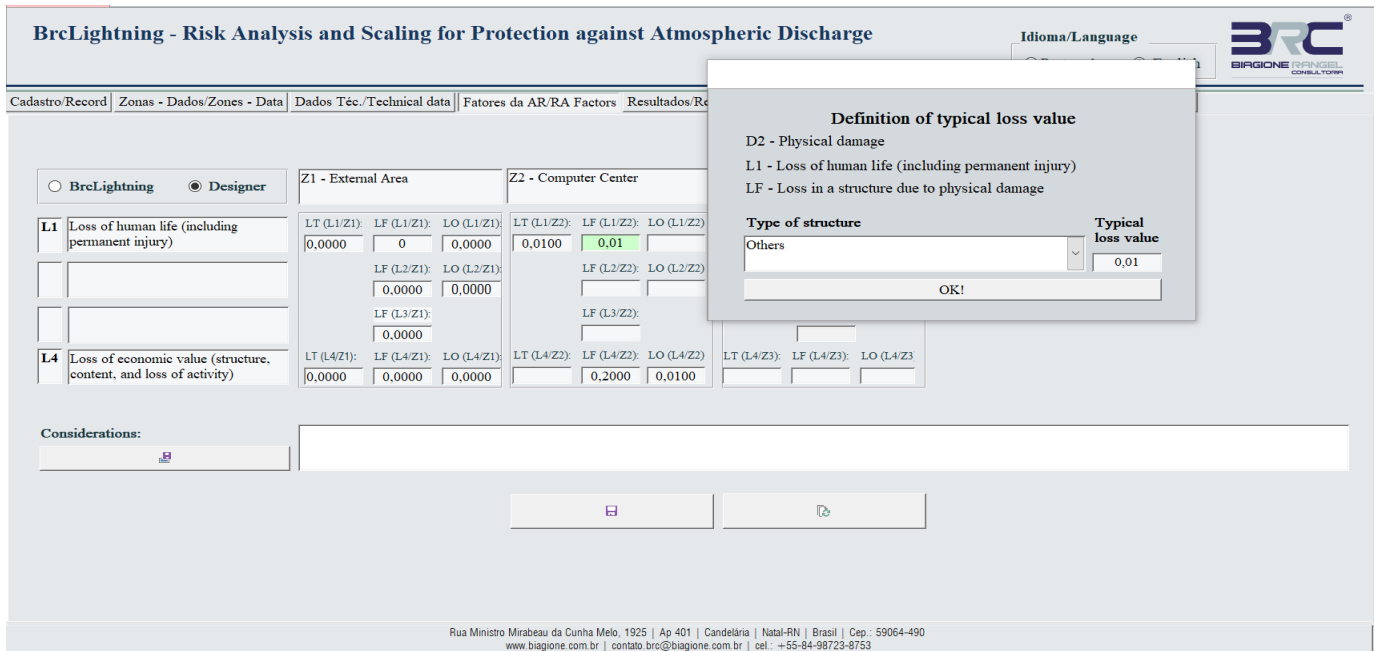
Figure 10: Loss Type Factors Module Screen with individualization pop-up
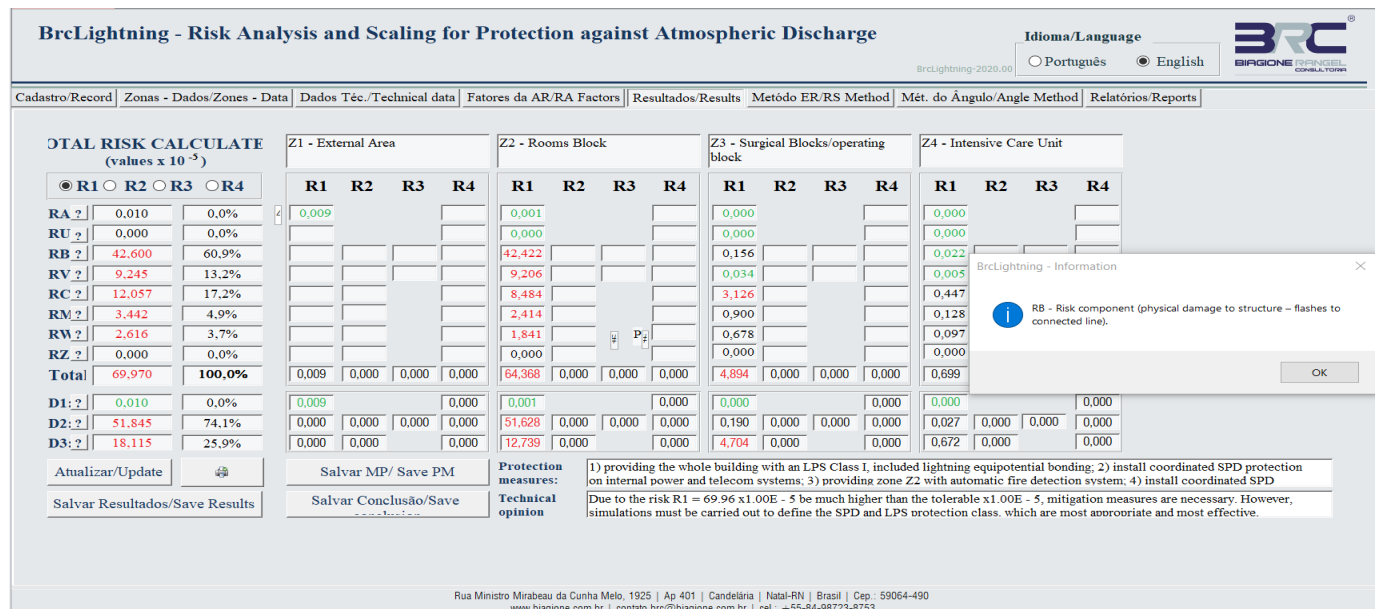
Figure 11: Result Module Screen and the button for printing the summarized report

(a)

(b)

Figure 12 (a): Summary of risk analysis report (first page) (b): Summary of risk analysis report (last but one page)

Figure 13: Example of calculation of h x d for Class IV
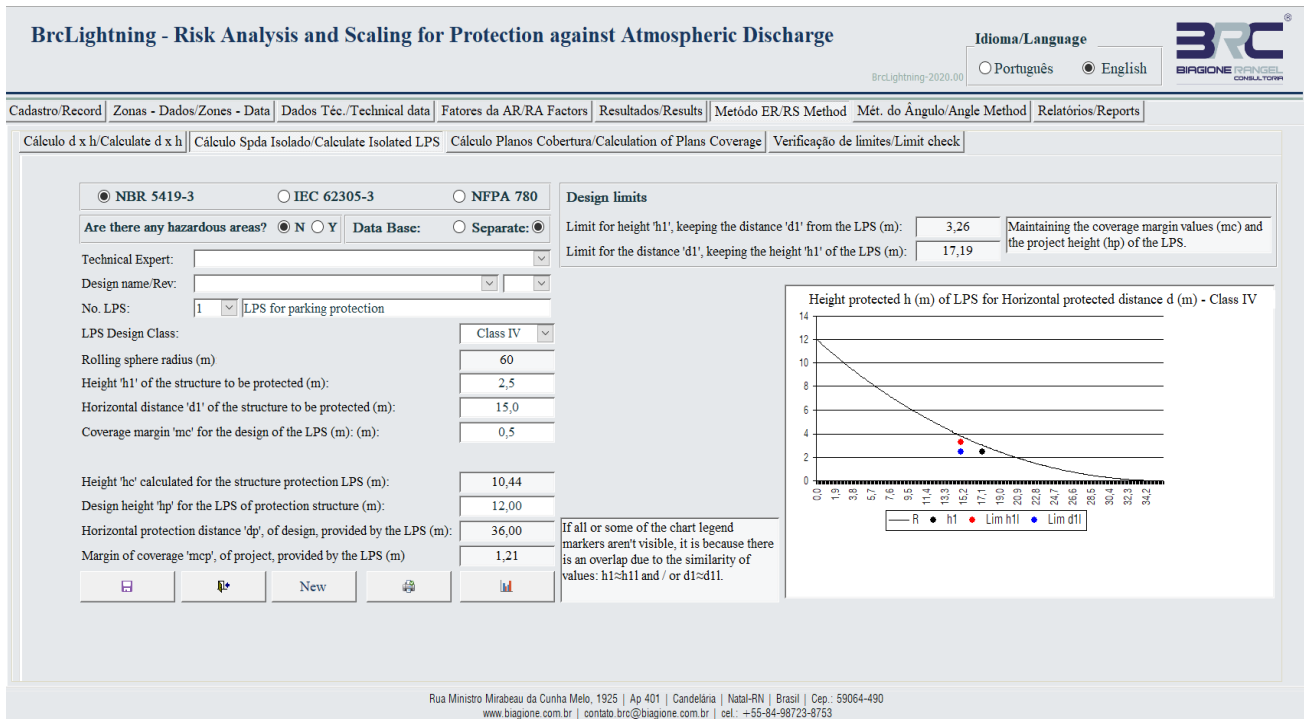
Figure 14: Sizing of the Isolated LPS, without hazardous area
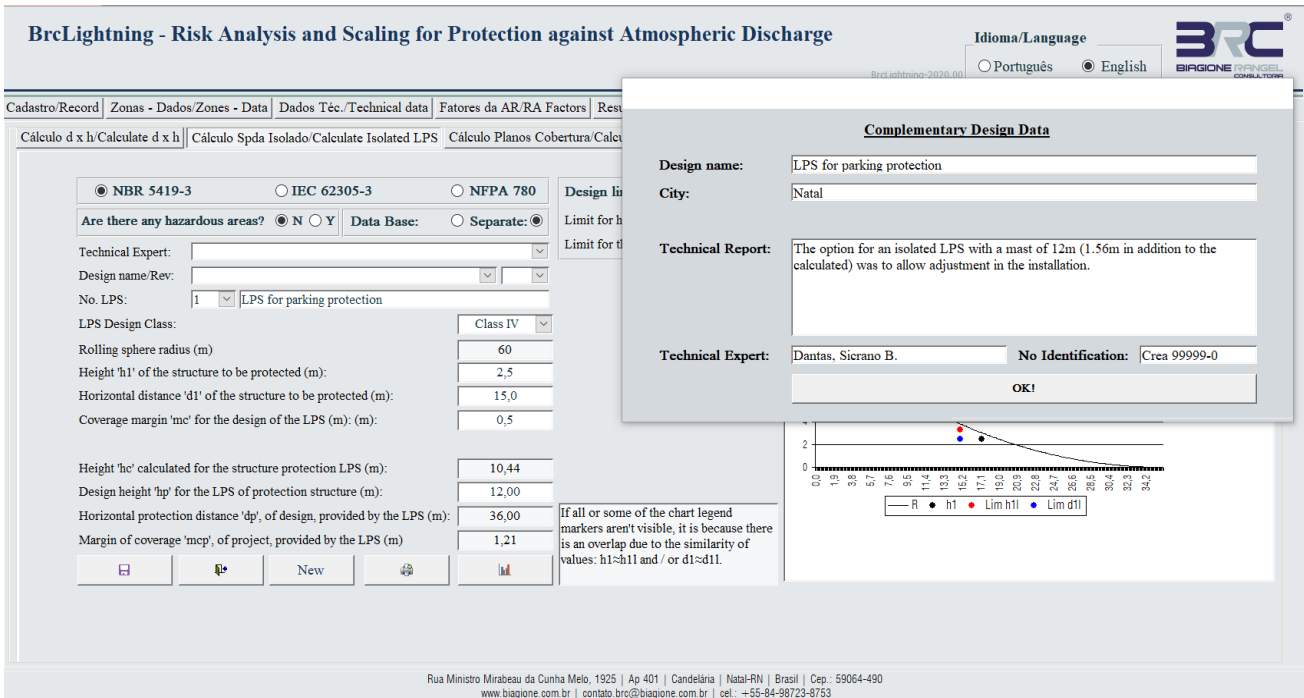
Figure 15: Pop-up for supplementary data

5. Rolling sphere module

This Module maintains the 4 Sections of the original version presented in SIPDA XV [1] and is in accordance with NBR 5419-3 [4]; IEC 62035-3 [5] and NFPA 780 [6]. However, the possibility of performing the sizing separately and the printing of the report of this dimensioning was introduced in all four sections. This can be seen in the sequence. Other improvements have been introduced and are detailed in each of the sections.

5.1. Section for sizing 'h' or 'd'

In the version presented in SIPDA XV [1], the system included one graph related to the calculation of the protected horizontal distance at ground level or on a reference surface when the height of the LPS is known and another for the calculation of the height, required to provide protection of a horizontal distance at ground level or a reference surface. Now, these graphs have been integrated into one (as shown in Figure 13). When calculating the height, it is a non-standard commercial value, this version provided

an input field to adjust the calculated height. In addition, it was added the option for issuing the report of this dimensioning.

In this section, the height of the insulated LPS is scaled (mast or air termination system of the insulated (only one) overhead wire to protect a specific structure) based on the required LPS Class and the determined coverage margin, including the characterization of a structure with or without hazardous area, as shown in Figure 14. Improvements were also incorporated to print the report of the sizing (the button with the printer icon) and the option to scale the LPS of a database design or a separate design for the issuance of

the report, it is necessary to provide additional data, as shown in Figure 15 (in the case of a separate project). The pop-up appears when the print button is pressed. The issued report is shown in Figure 16. Separated projects are not saved in the database.

When the design definitions of the structure to be protected ('h1' and 'd1', besides 'mc') do not allow the sizing of the LPS to the defined protection Class, the System issues an alert of the impossibility of sizing and indicates the limit of the maximum distance and height the structure can be protected by LPS, as shown in Figure 17.

Figure 16: Example report of sizing the isolated LPS

Figure 17: Alert for impossibility of isolated LPS sizing

Figure 18: Screen with pop-up to define the LPS type
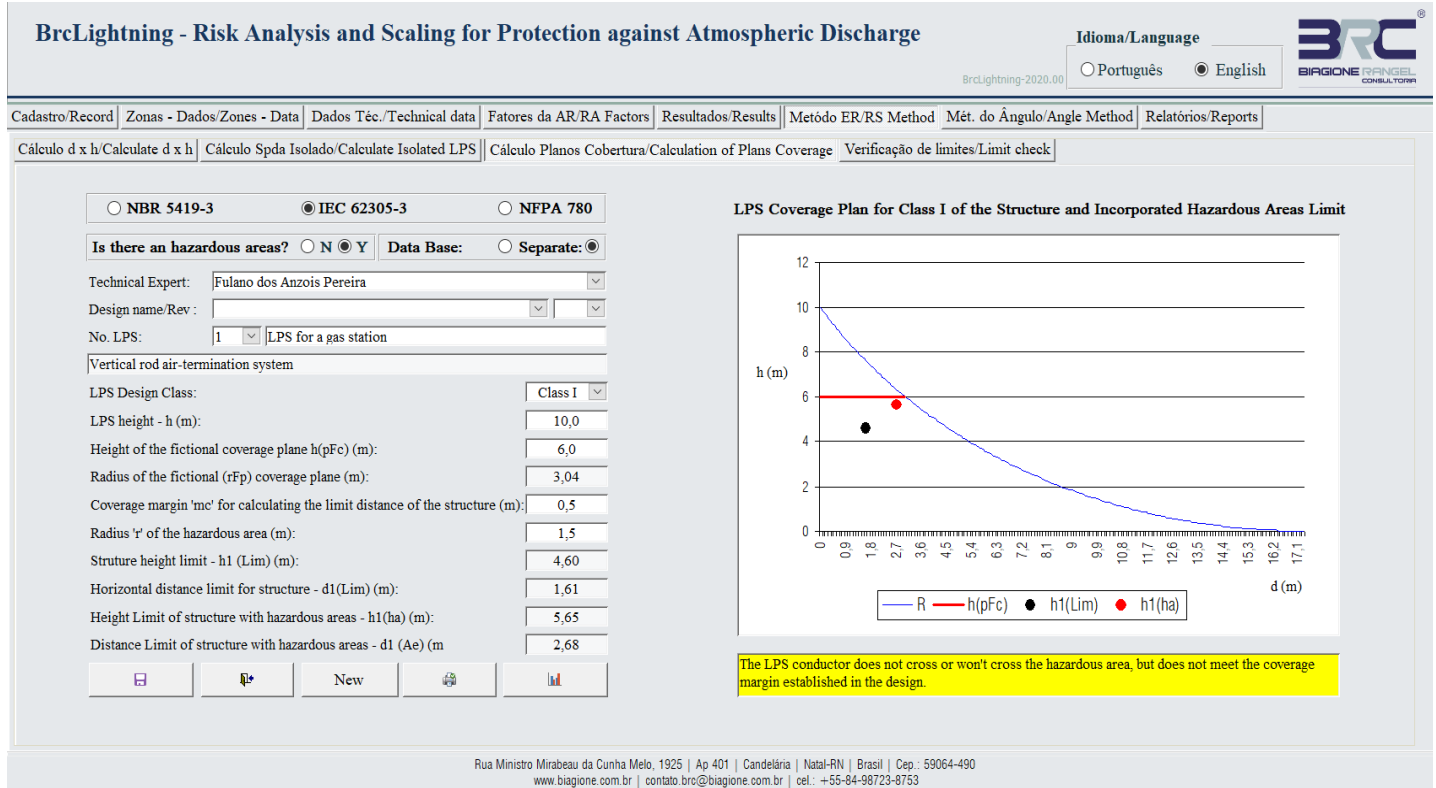
Figure 19: Calculation of the Fictional Coverage Plan with alert

5.2. Evaluation section of the limits of an installed LPS

This last section of the Rolling Sphere Module is intended to assess the protection that a specific LPS can provide, considering all the Classes of Protection established by NBR-5419-3 [4]; IEC 62305-3 [5] and NFPA 780 [6]. Improvements have been made to the definition of the LPS type and alert with a technical note, as shown in Figure 20.
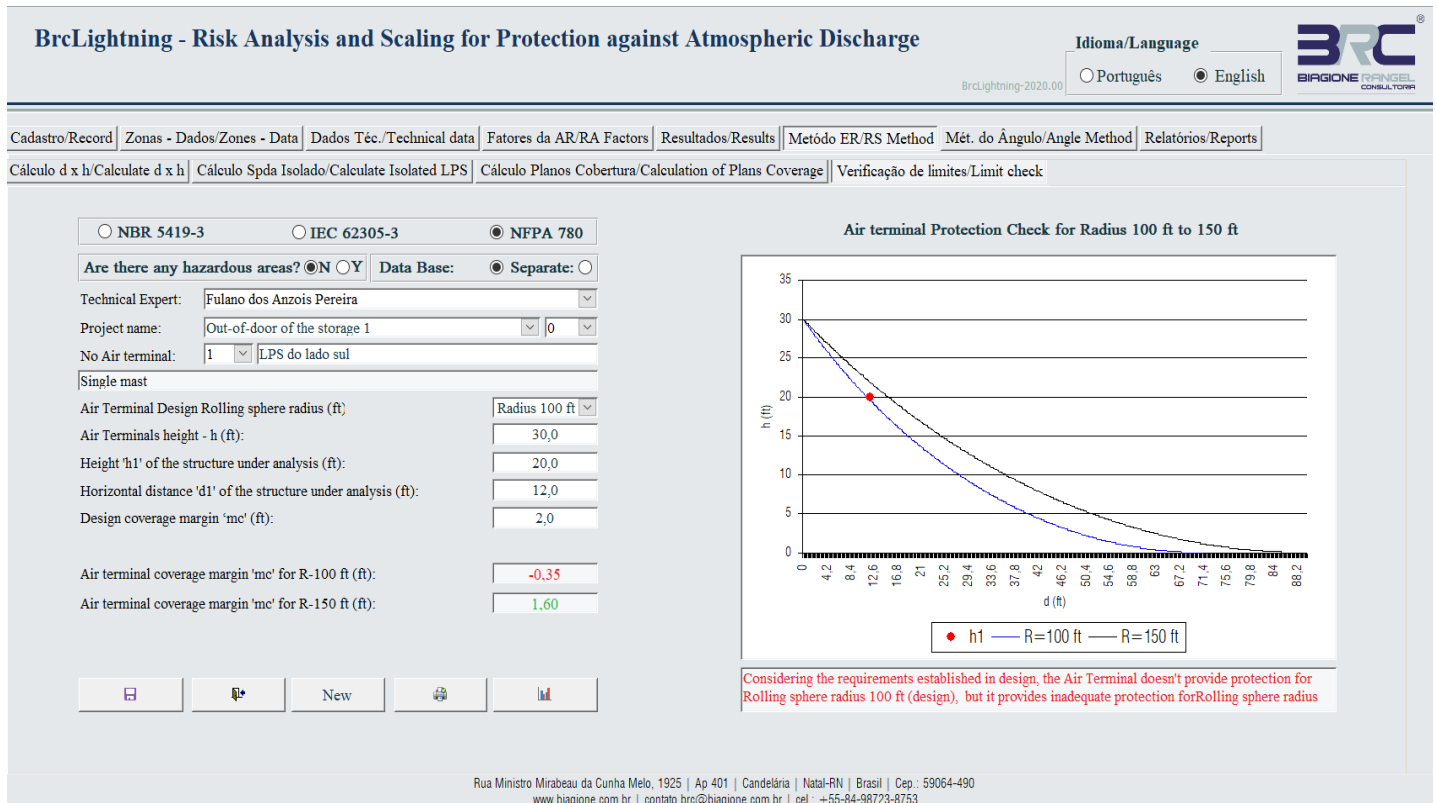
Figure 20: Limits evaluation module screen

6. Angle Method Module

This module maintains the three Sections of the original version presented in SIPDA XV [1] and in accordance with NBR 5419-3 [4]; IEC 62035-3 [5]. However, it was introduced in all of them the possibility to carry out the sizing separately and printing the report of this. Considering that this method is not widely used, only an improvement was introduced, in addition to those reported above, in Section 1, as detailed below.

6.1. Height or Distance Sizing (Angle Method)

This Section calculates the horizontal distance protected at ground level or from a reference surface when the height of the LPS is known. It also allows you to calculate the height required for an LPS when you know the horizontal distance that needs to be protected, as shown in Figure 21.
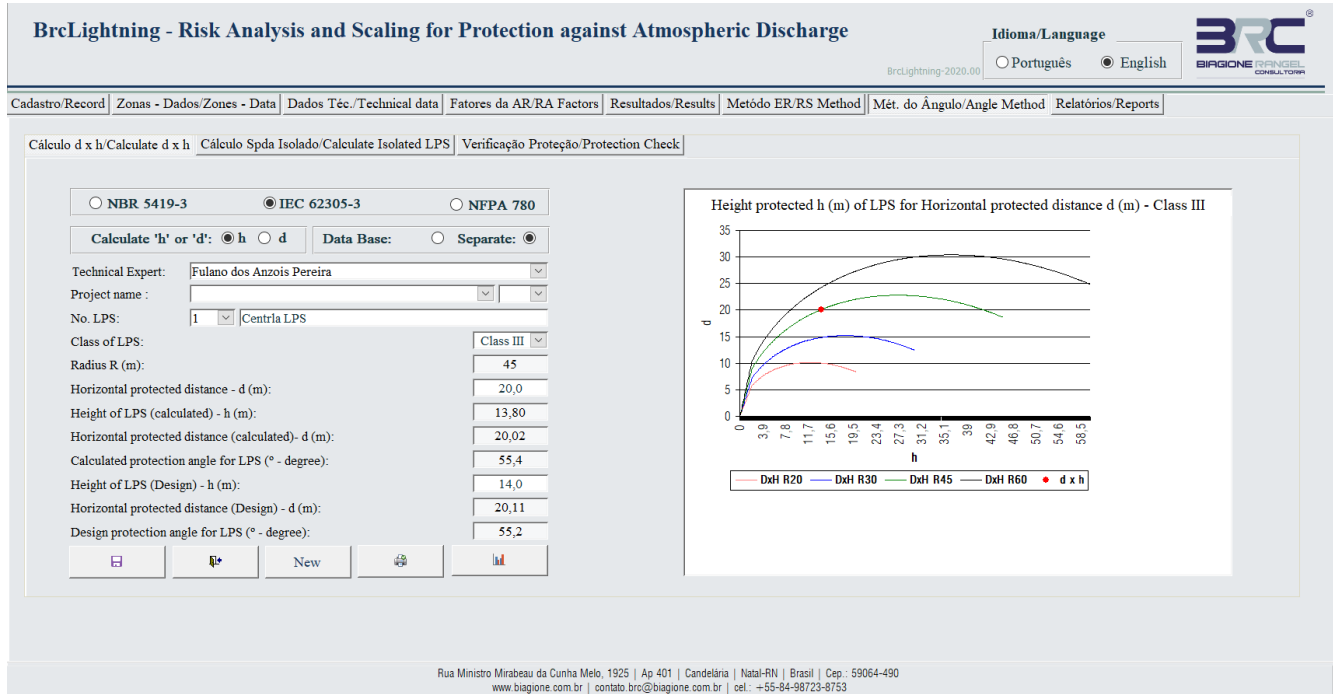
Figure 21: Calculation of the height x distance
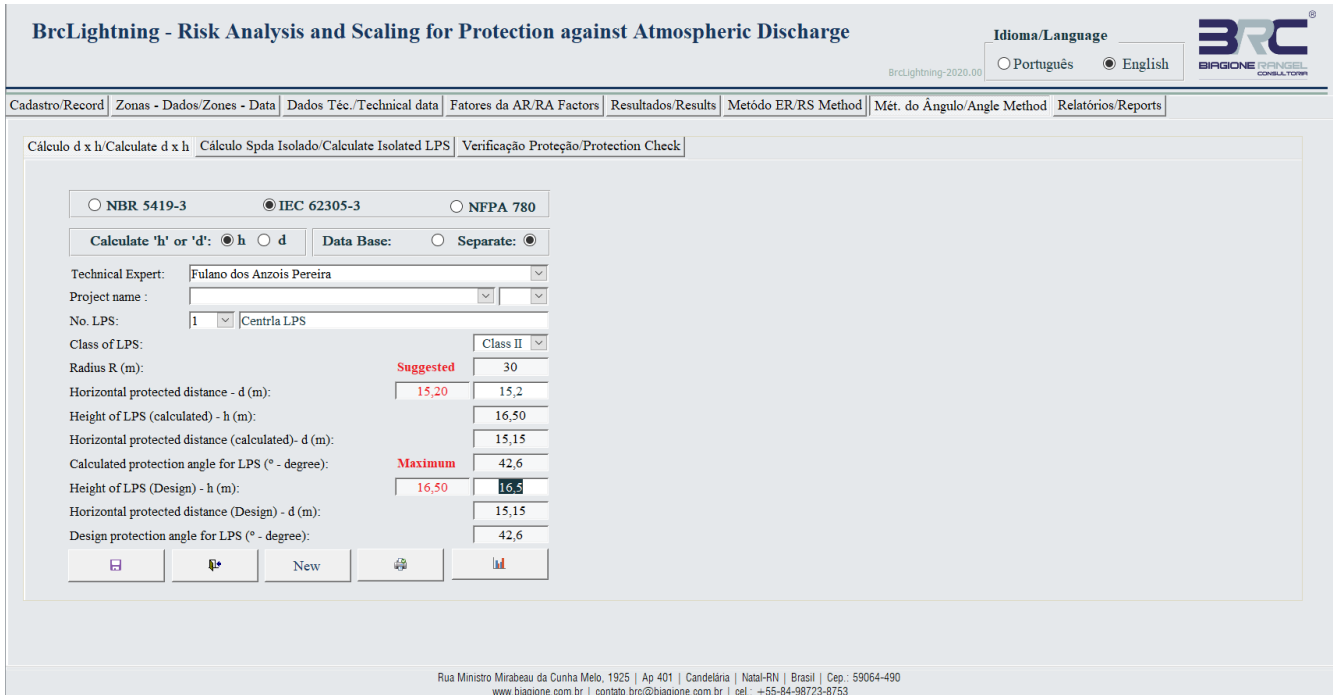
Figure 22: Calculation of the height x distance - Alert
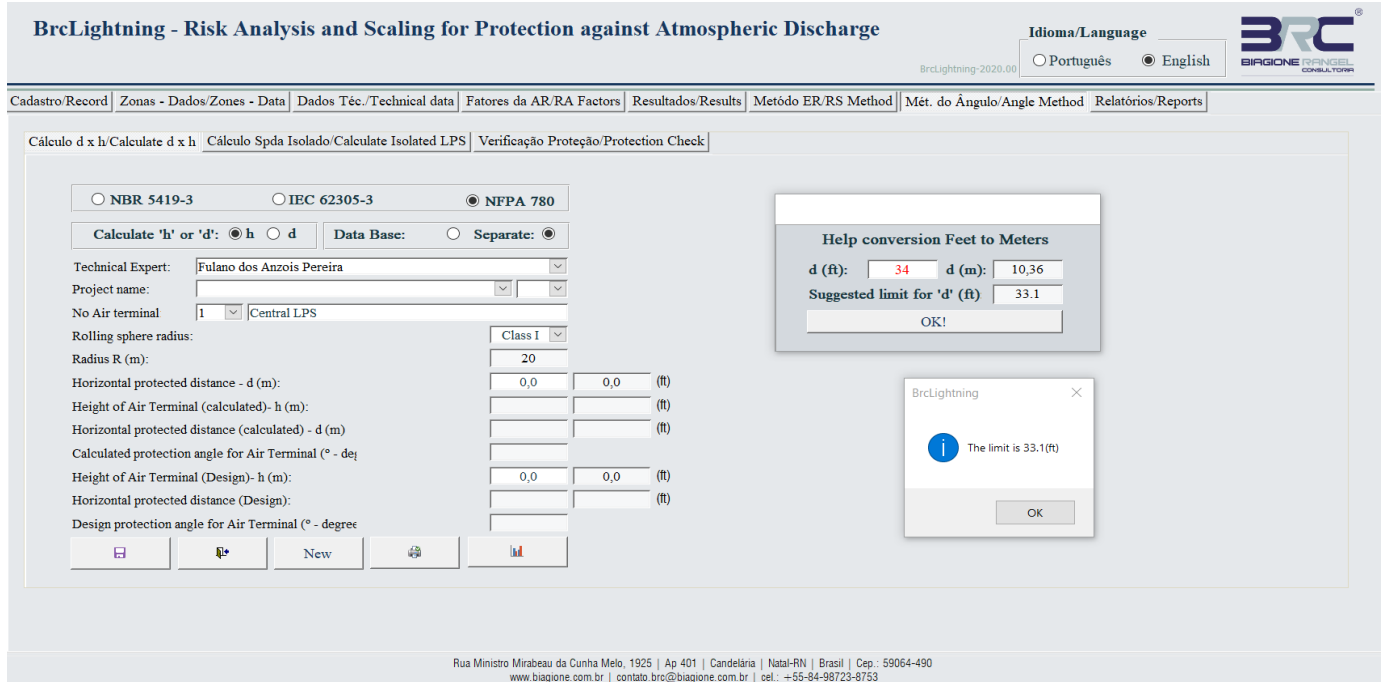
Figure 23: Calculation of the height x distance with alert

In order to comply with NFPA 780 [6], the improvement for converting units of measure in meters was introduced, as shown in Figure 23.

The system for this calculation only allows input in meters, thus, with this improvement, it becomes possible to insert the values in feet unit. To do so, two clicks are applied in the input field and one pop-up appears (as shown in Figure 23), providing an input field with the unit in feet. After this, when the pop-up is closed, the unit of measurement in meters. In case of exceeding the suggested limit, an alert will be issued.

7. Report Module

This Module includes options for the various preformat of reports that the system, currently, can provide: Risk Analysis Report; LPS project report by Rolling Sphere Method; Module Report using angle method, etc. The system screen where these options are available is shown in Figure 24 and several report templates are shown in Figure 25a Figure 25b. The improvements introduced in this module were composed by the increase in filter options to allow for more appropriate selectivity and the inclusion of the project revision number, as shown in Figure 24.
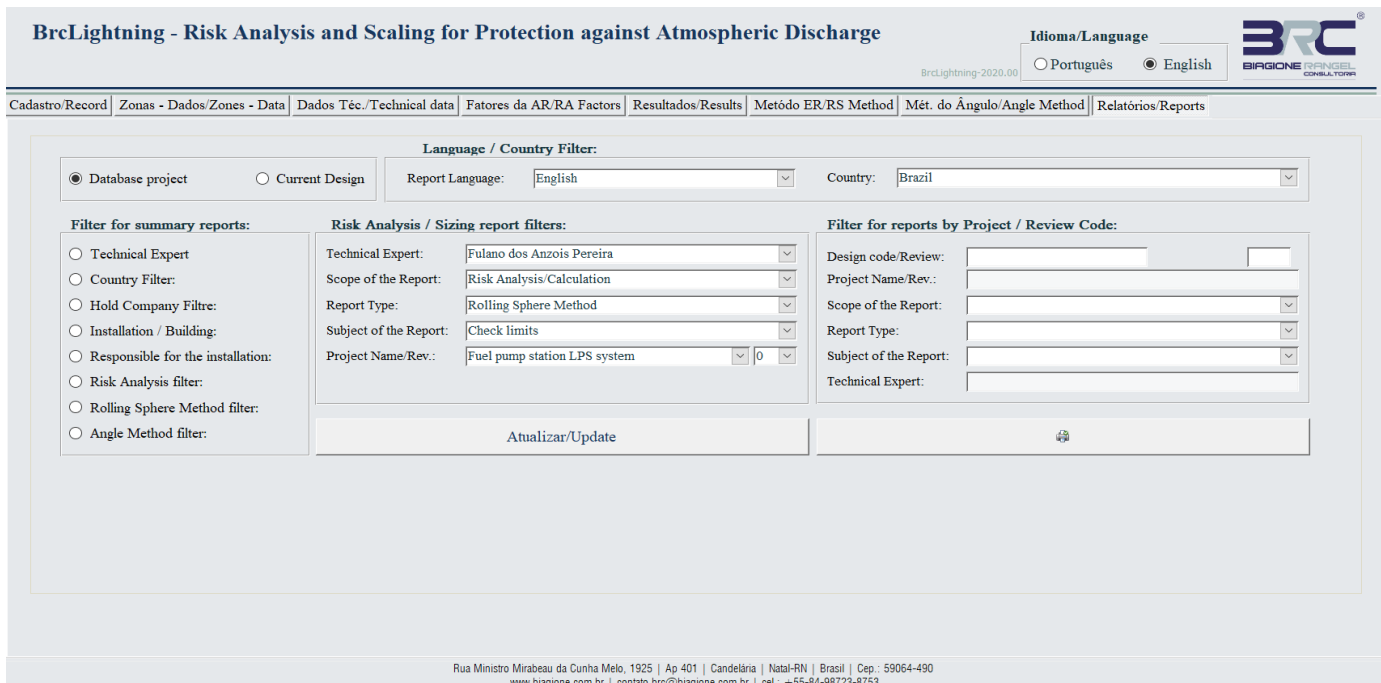
Figure 24: Screen of the reporting module
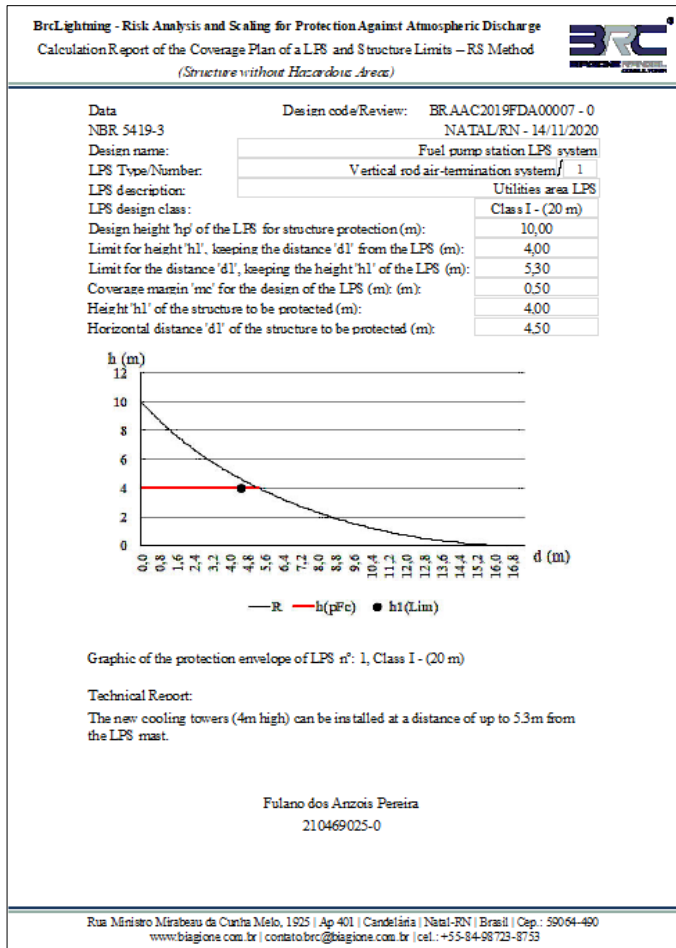
(a)
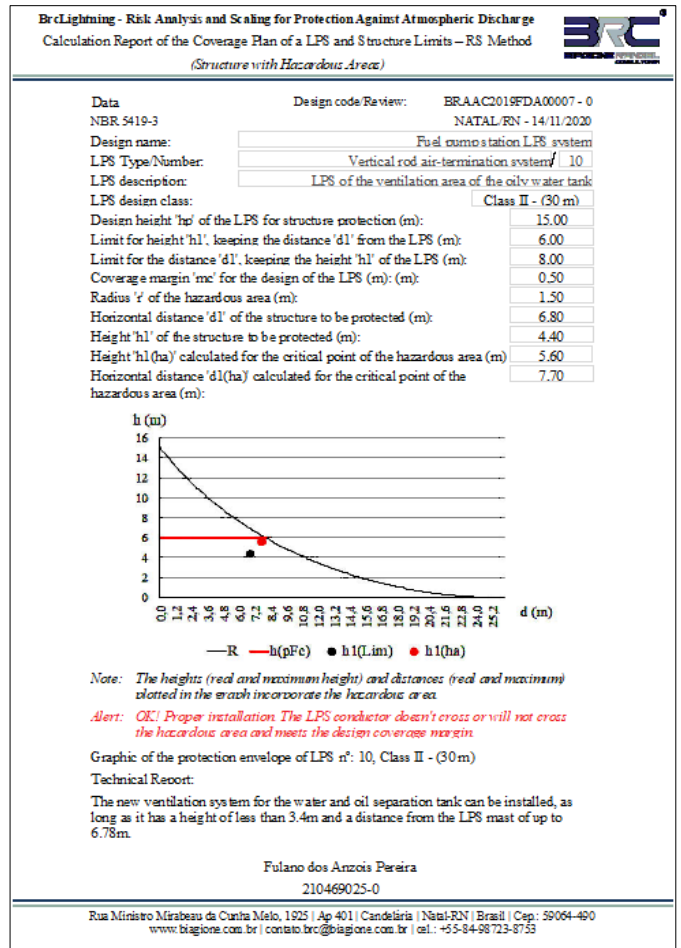
(b)

Figure 25 (a): System report templates formatted without hazardous areas (b): System report templates formatted with hazardous area

8. Improvements already identified for future insertion

8.1. Module for sizing the surge protective device

Considering that one of the most important mitigating measures identified in the Risk Analysis is the installation of Surge Protective Devices - DPS, it was understood that the inclusion of a module to meet this need is extremely important and, as the methodology and formulas already exist and are supported by NBR-5419-4 [7] and IEC 62305-4 [8], the insertion of a module with this function was included in the planning of future improvements.
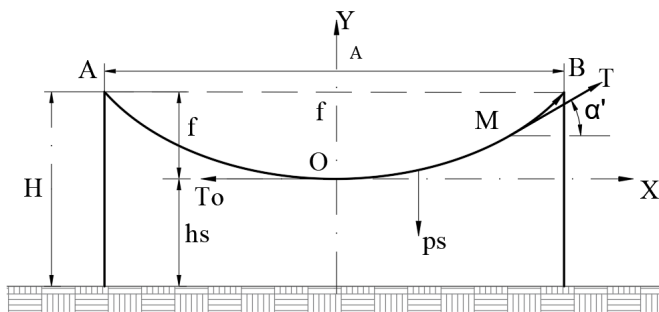
Figure 26: Efforts in wire air termination with supports of the same height
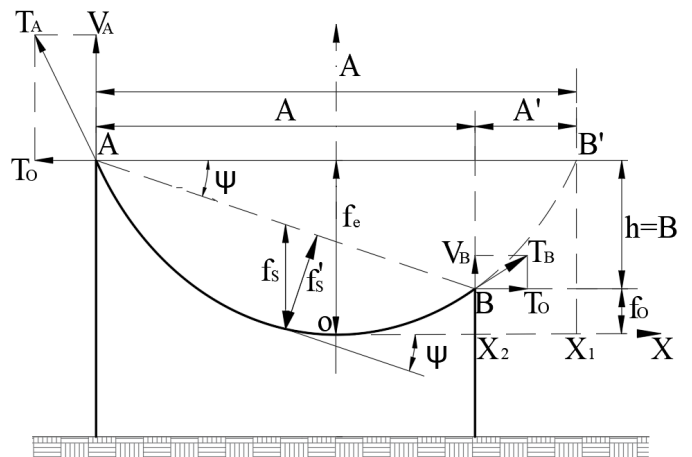
Figure 27: Efforts in wire air termination with supports of different heights

8.2. Module for sizing wire air-termination support structures

Considering that many of the SPDA systems are composed of wire air-termination, it was identified that it is convenient to have a tool to scale the efforts requested from supports of this kind of captor, especially when there is variation in room temperature. Considering, also, that the guarantee of the volume of protection derives from a projection of the height of a captor element and that the control of this lowest point is critical. So, equations were

developed to calculate these efforts from the catenary arrow that is required for the wire air-termination. Therefore, it was reversed the practice of calculating this type of sizing, where the effort is calculated and after that, the arrow of a catenary of the cable is calculated. The developed equations include both for supports for the same height and different heights, as shown in Figure 26 and Figure 27. However, these equations are not yet coded in a programming language.

The mathematical approach to dimension the efforts in the wire air-termination was developed in a spreadsheet and the results are in tables such as the Table 1. Other temperature ranges are possible. This is for information only.

8.3. Module to consolidate the list of materials of a project

The insertion of the LPS type in the sizing sections already allows to insert in the database the list of materials. Thus, it will be possible from commercially standardized systems to associate the spare parts list required for that dimensioning, when applicable. This module should have a restricted section to address the material list of grounding systems. There is no prediction to perform the calculation of grounding systems because several software are already dedicated to this purpose. Hence, the module includes only the integration of materials to the LPS design.

8.4. Module for sizing parallel wire air-termination system

We already have several mathematical models responsible for sizing this kind of LPS by parallel wire air-termination in several configurations for this type of systems, as shown in Figure 28 and Figure 29 (other details can be found in the XIII SIPDA [9]). However, we do not yet have the conversion of equations into

programming codes, but this is not the biggest problem for insertion. The understanding is that the greatest difficulty is to develop the graphic formulation because it is more complex and I still do not have training in this area, and the addition of this qualification will require planning.
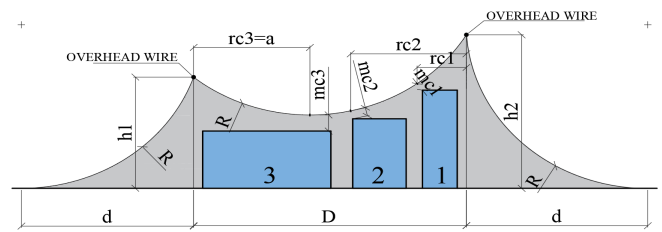

Figure 28: Representation for different levels of parallel wire air termination
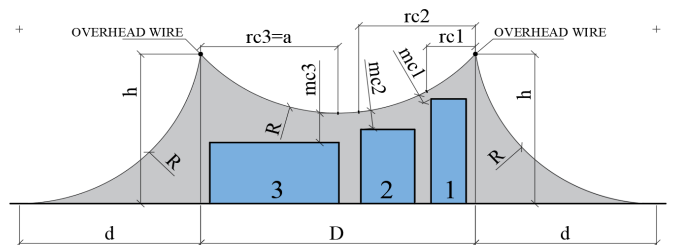

Figure 29: Representation for equal levels of parallel wire air termination

The mathematical approach to determine the limits of a parallel wire air-termination design, considering a possible unevenness of the terrain – at the time of the project implementation or spacing between the wire air-termination or both – produces a table as the one presented in Table 2. This is only an example.

Table 1: Calculated forces for the wire air-termination

Span: 20,30 (m)			Arrow of a catenary: 0,20 (m)		Length: 20,30 (m)		Reference temperature: 26ºC
Item	Temp.: (ºC)	Length: A (m)	f (m)	To (kgf)	T (kgf)	p$_s$ (kgf)	Transverse force (kgf)
01	16	20,303	0,153	137,63	137,63	4,151	2,85
02	20	20,304	0,175	120,55	120,55	4,151	2,85
03	26	20,305	0,203	103,78	103,79	4,151	2,85
04	30	20,306	0,220	95,84	95,85	4,151	2,85
05	36	20,308	0,243	86,75	86,75	4,151	2,85
06	40	20,309	0,257	81,95	81,95	4,151	2,85
07	45	20,310	0,274	76,94	76,95	4,151	2,85
08	22	20,304	0,185	138,38	138,38	4,151	2,85
09	36/16	20,301	0,075	280,12	280,12	4,151	2,85
10	36/22	20,302	0,128	200,00	200,01	4,151	2,85

Note: Reference temperature: 26ºC

Table 2: Calculations of the LPS Limits for Figure 28

Designation		Distance between LPS)					
		30.0 (m)		30.5 (m)		31.0 (m)	
Reduce level	Height of the lower LPS	a	hpc	a	hpc	a	hpc
-	16.00	13.23	10.50	13.55	10.21	13.87	9.92

0.50	15.50	13.03	10.18	13.35	9.89	13.68	9.60
1.00	15.00	12.83	9.85	13.16	9.56	13.49	9.27
1.50	14.50	12.63	9.51				

8.5. Development of tools to integrate with software graph

Another important tool is the integration with design software, such as Autocad. Therefore, the future idea is to develop tools to migrate the sizing data of the various Modules and Sections to enable the plotting of drawings with the horizontal coverage planes for the various Covering projection for the various classes of protection of 15 meters high LPS over structures with a height of 3.5 m. These tools should incorporate the generation of 3D plants, which the resources necessary to rotate and promote cuts of the protected volume.

9. Software security requirements

This software is intended to be a tool used by professionals who design systems to protect against atmospheric discharges – either by direct or nearby impacts – and these might cause harmful effects with high probability of causing losses either by L_1 - losses of human life (including permanent injury); L_2 - losses of services to the public; L_3 - losses of cultural heritage and L_4 - losses of economic value. Thus, it is necessary for these professionals to carry out a very detailed and safe risk analysis. Therefore, safety requirements were established, with the goal of blocking errors or deviations from the requirements established by the standards on which this application was based. These requirements are as follows:

9.1. Controle na determinação das Zonas

The System alerts and blocks Zones from being repeated in the Risk Analysis, as shown in Figure 31.
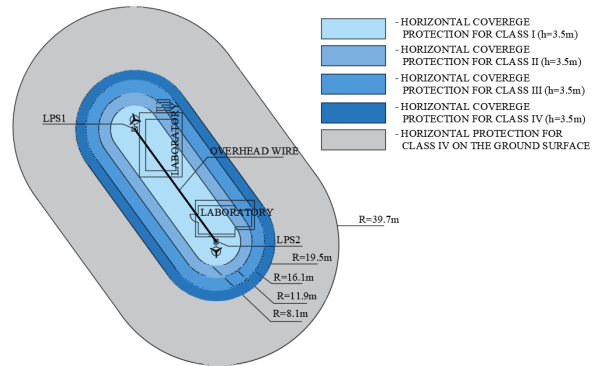
Figure 30: Horizontal projection screen of an LPS project (only for guidance)

9.2. Control of the total number of people in the Zones

When the number of people distributed in all Zones is inserted, the System verifies consistency. So, in case of divergence with the total number reported in the Registry (Figure 4), it issues an alert and blocks for further correction, either for more (Figure 32) or for less (Figure 33):

Figure 31: Zone alert already selected

Figure 32: Alert of more people in the Zones than the registered total

Figure 33: Alert of fewer people in the Zones than the total registered

9.3. Consistencies of line parameters

The System filters the options of values of the probability PLD depending on the resistance RS of the cable screen and the impulse withstand voltage UW of the equipment, based on the line type, routing, shielding, and bonding conditions, as can be seen in Figure 34. Power line is not bonded to the same bonding bar as equipment and telecom is bonded to the same bonding bar as equipment.

Figure 34: Filters for line parameters

9.4. Restrictions for changing typical loss values

When it comes to loss of human life (L1), the typical LT loss values (loss due to injuries from electric shock) cannot be changed (the system freezes). The same applies to the typical LF loss value (loss in a structure due to physical damage) when it is indicated that there is a risk of explosion in the Zone or when it is indicated that the place is a hospital, hotel, school or civic building.

In addition, changes in typical LO loss values (loss in a structure due to failure of internal systems) are blocked when it comes to areas that are part of the hospital or life support structure. When dealing with L2 and L3 losses, the values of LF and LO are also blocked for changes. For losses of type L4, permissions similar to L1 losses are applied. Blocking alerts are via a pop-up message, as shown in Figure 35.

Figure 35: Blocking alert screen for changing typical loss value

9.5. Permission to modify data and customize

It is important to emphasize that to perform any customization and or modify parameters predefined in the System, there is a need for the professional to make, in advance, his or her registration in the system and, after that, he or she will have to define on the initial screen (Figure 4) the designer responsible for the project. This way, the system will save the modifications in an associated way with the person responsible for performing them.

10. Acknowledgment

This is a work that I have been developing alone, from the need I had to carry out the evaluation of projects of Protection Against Atmospheric Discrimination. Therefore, to be certain about my work, I developed the methodology and then the migration to the programming codes of this system, having paid every expense with my own resources, including all the development so far and the costs regarding my participation in all the previous symposia and the development of the papers.

11. Conclusion

This paper is in line with the conclusion of the work originally presented at the SIPDA XV symposium [1], as it incorporates new resources to provide LPS designers with more efficient and safe tools and means for project development, in accordance with Brazilian, International and American standards.

In this context, the BrcLightning application continues, also, with the objective of consolidating itself as an integrated software, having as a support, for some of its modules, the dimensioning of LPS based on the mathematical approach, which was developed and presented at the SIPDA XIII [9] and SIPDA XIV [10] symposia. Thereby, we hope to be contributing to a better understanding of the standards and to the development of safer and more effective projects for protection against lightning strikes.

Also, its modulated design and the format of a database allows the development of applications to be used on the internet, online, and by app systems used on cell phones or other mobile devices.

References

[1] Araujo, R. Biagione, " BrcLightning - Risk Analysis and Scaling for Protection against Atmospheric Discharge," International Symposium on Lightning Protection (XV SIPDA), **1**(0), 8-17, 2019.

[2] ABNT, "NBR-5419-2. Lightning protection Part 2: Risk management," ABNTCatálogo, p. 116, 2015.

[3] IEC, "IEC 62305-2. Protection against lightning - Part 2: Risk management," IEC, 2012.

[4] ABNT, "NBR-5419-3. Lightning protection – Part 3: Physical damage to structures and life hazard," ABNTCatálogo, 2015.

[5] IEC, "IEC 62305-3 - Protection against lightning – Part 3: Physical damage to structures and life hazard," IEC, 2012.

[6] NFPA, " NFPA 780. Standard for the Installation of Lightning Protection Systems. s.l. : IHS," NFPA, 2014.

[7] ABNT, "NBR-5419-4. Lightning protection – Part 4: Electrical and electronic systems within structures. n.l.," ABNTCatálogo, 2015.

[8] IEC, "IEC 62305-4 - Protection against lightning – Part 4: Electrical and electronic systems within structures. n.l. : IEC,," IEC, 2010.

[9] Araujo, Biagione R, Oliveira Jose T. , "Mathematical Approach Methodology to Analysis and Design of LPS," International Symposium on Lightning Protection, **13**(SIPDA), 2015.

[10] Araujo, Biagione R, "Mathematical Modeling for Analysis and Design of LPS Angle Method," International Symposium on Lightning Protection (SIPDA XIV), 2017.

ASTES

Exposure to Optical Radiation and Electromagnetic Fields at the Workplace: Criteria for Occupational Health Surveillance According to Current European Legislation

Alberto Modenese, Fabriziomaria Gobba[*]

Department of Biomedical, Metabolic and Neural Sciences, University of Modena and Reggio Emilia, Modena, 41125, Italy

A B S T R A C T

A very large number of workers is occupationally exposed to Optical Radiation (OR) worldwide, while indeed nowadays an exposure to Electromagnetic fields (EMF) can occur in almost all workplaces. OR origin can be natural, including the most relevant source, i.e. the sun, or artificial, that can be further classified in incoherent and coherent, i.e. the LASERs. Solar radiation (SR) exposure, and in particular its most harmful component, the ultraviolet radiation (UVR), is a significant occupational risk in "outdoor workers", including e.g. farmers and construction workers. UVR is mainly absorbed in the eye and the skin, there inducing various short-term and chronic adverse health effects, as burns, cataract and skin cancers. At least in Europe, for SR exposed workers no specific obligations currently exist regarding the Health Surveillance (HS), that is instead required for occupational exposures to artificial OR according to the legislation of the European Union (EU, Directive 2006/25/EC). Considering now EMF, the EU Directive 2013/35/EU provides an obligation for the HS of exposed workers, aimed at the prevention of the possible direct short-term effects, as involuntary contractions or temperature increase of tissues, and indirect effects, as shocks and interference. Conversely, long-term effects are not considered in the Directive as data on causal relationship, including reliable mechanisms, are considered inadequate. Direct short-term and indirect effects can appear solely in case of high exposures, usually occuring only accidentally, but a specific group of workers, defined "at particular risk", exists, and it includes e.g. persons with implanted active medical devices, as cardioverter defibrillators or pacemakers. In these workers, adverse effects can be induced at lower EMF levels. The identification and an adequate protection of the workers at particular risk is one of the main goals of the HS of occupational EMF exposure.
The main HS criteria applicable for workers with exposure to OR and EMF are discussed in this article.

1. Introduction

Exposure to Optical Radiation (OR) and Electromagnetic Fields (EMF), i.e. Non-Ionizing Radiation (NIR), at work represents a relevant occupational risk for many work activities: this paper is an extension of work originally presented in the 2020 IEEE International Conference on Environment and Electrical Engineering and 2020 IEEE Industrial and Commercial Power Systems Europe (EEEIC / I&CPS Europe) [1].

Occupational risks can be classified in chemical, biological, physical risks and others (including ergonomic, psichosocial and safety risks) [2]. NIR exposure is included among physical risks together with e.g. noise and vibrations. As it happens for all the other occupational risks, adequate prevention should be emplaced in the companies in order to warrant appropriate occupational health and safety (OHS) conditions for the exposed workers. This involves a specific evaluation of the risk related to the working activity with NIR exposure, aimed at identifying the most appropriate preventive measures. An important part of the prevention process to ensure OHS is the health surveillance (HS) of the workers exposed to occupational risks that may affect their health, usually performed by trained occupational physicians. HS is defined, according to the International Labour Office (ILO), as a group of "procedures and investigations to assess workers' health,

[*]Corresponding Author: Fabriziomaria Gobba, v. G. Campi 287 – 41125 Modena (Italy), +390592055463, fabriziomaria.gobba@unimore.it

in order to identify any abnormality possibly associated to a recognized work-related risk in exposed workers", involving "the review of the health records and any other opportune medical examinations needed" [3]. Considering possible implications for workers' health of NIR exposure, it should be noted that NIR are included in the part of the electromagnetic spectrum with lower energy compared to ionizing radiation, meaning that both OR and EMF have not enough energy to cause ionization, i.e. to remove electrons from atoms and molecules. Accordingly, the interaction mechanisms with the biological tissues, and the penetration ability of NIR are very different from ionizing radiation. Nevertheless, also within the various regions and sub-regions of the NIR spectrum significant differences exist, and therefore the possible health effects and the criteria for the health surveillance of the workers exposed to non-ionizing radiation should be discussed separately. In the following parts of this article these criteria are introduced and discussed.

2. Optical radiation: occupational exposure and health effects

2.1. Occupational exposure to optical radiation

OR includes wavelengths (λ) between 100 nanometers (nm) and 1 millimeter (mm), distributed in three different regions: ultraviolet radiation (UVR), further classified in the subregions UV-A, UV-B and UV-C, visible radiation and infrared radiation (IR), with other three sub-regions: IR-A, IR-B and IR-C [4].

Occupational OR exposure can be possible both in case of artificial OR and solar radiation (SR) exposure.

Artificial sources can emit incoherent radiation or coherent bands of amplificated radiations (i.e. LASERs). Considering UVR, among the main applications relevant for occupational exposure there is the use of UV as sterilizing agents for both surfaces and products, the idustrial processes applying UV rays in the machineries for photo-lithography and printing, the medical applications as e.g. the photo-therapy for the neonatal jaundice, the UV emissions during welding processes, and many others. Also visible light is emitted during welding, and of course it is used for illumination purposes: kind of intense exposures can be possible in the entertainment sector, e.g. in theatres or in television studios, in shopping centers, and in general where it is required to be close to sources emitting intense lights (indicators, signals, LED, projectors, etc). Also visible light is used for industrial, e.g. printing processes, and medical applications, e.g. for photopolymerization of the materials used in dental clinics. Finally, infrared radiation is also emitted during welding activities, and moreover it is emitted as a result of industrial processes generating very high thermal energies during the treatment of metals, glass and other materials. Furthermore, IR-based technologies are widely applied e.g. in communication and surveillance systems [4]. LASER technologies can use all the optical radiations. Gas LASERs, as those using argon or krypton, mainly amplify UV or short wavelength visible light, while solid state LASERs, as neodymium YAG LASERs, and semi-conductor LASERs, as those using gallium, mainly amplify infrared or long wavelength visible light [4].

Even if the number of artificial sources emitting OR at the workplaces is huge, the effective number of workers exposed to

levels potentially determining relevant health risks is relatively limited, as frequently the sources are appropriately shielded [4–7]. A possible exception is represented by welding activities: welders should be appropriately protected, with adequate clothing and face masks with eye filters for the specific bands of ORs emitted during the welding process [4–6, 8]. For the other sources of artificial OR the major problems may occur in case of malfunctions of the machineries with failures of the protection mechanisms, and/or of workers with inadequate protections, determining work-related accidents possibly causing severe damages [9, 10]. The eye is one of the most frequently involved organ, in particular in these cases [11, 12].

On the other hand, the most important source of occupational exposure to OR, in terms of both the numbers of exposed workers and relevancy of possible adverse effects, is certainly the Sun. Millions of workers have an exposure to solar radiation (SR) worldwide: among the main job categories involved there are farmers [13, 14], construction workers [15–17], fishermen [18], lifeguards [19, 20], gardeners [21, 22], ski instructors/mountain guides [23, 24] and others [25, 26]. These workers, spending a significant part of the working day outside, are collectively identified with the term of "outdoor workers". Fortunately, SR at the Earth' surface does not include all the components of OR spectrum, and in particular all UVC rays and the large majority of the UVB are blocked in the stratosphere [5, 26]. As UV radiation is a carcinogenic agent, also SR is considered a carcinogenic exposure [27]: it is estimated that SR represents the occupational carcinogenic exposure with the highest amount of workers exposed [28].

2.2. Interaction mechanisms with biological tissues and main effects of optical radiation exposure

OR have a quite low ability of penetrating the biological tissues, and therefore the main targets are the eyes and the skin [5, 26]. Two main mechanisms of interaction with the biological tissues can be identified for OR bands:

- Thermal mechanisms: these effects are typical of IR and of long wavelength visible light, and they are related to the conduction of heat in the tissues, usually requiring intense exposures. In case of insufficiently intense exposure no appreciable effects can be determined, as the heat is dissipated through the surrounding tissues [29]. Accordingly, usually only acute effects, resulting in eye injuries or skin thermal burns can be associated to infrared or visible light exposure with thermal mechanisms [29], even if, mainly in the past, some chronic skin alterations [30] as well as thermal cataract have been reported [31, 32].

- Photo-chemical effects are possible in case of exposure to UVR and to short wavelength visible light [5, 26]. Photons are absorbed by specific targeted molecules (i.e. chromophores) in the biological tissues, releasing energy and inducing chemical reactions, with consequent damages and alterations (e.g. inflammation) [5, 26]. Photochemical effects are possible both in case of short-term intense exposures but also as a consequence of long-term less intense exposures [33].

The most hazardous component of OR is UVR: UV rays have higher energy compared to infrared and visible radiation and they act with photochemical mechanisms, causing both acute and chronic effects in humans [5, 26]. After intense short-term exposures, acute skin effects as skin erythema and photodermatoses, in case of presence of a photo-toxic substance (e.g. a topic drug or a cosmetic) on the skin, can occur (it should be noted that photodermatoses may be also associated with some wavelenghts of visible radiations) [5, 26]. Also photochemical burns of the unprotected eyes are possible, especially in case of intense direct exposures or indirect exposures from surfaces with high reflectance (e.g. snow, polished metals): UV rays can be highly absorbed in the ocular surface, causing an acute inflammation of the cornea and of the conjunctiva called photokeratitis/photoconjunctivities, determining photophobia, redness, pain, burning, tearing and foreign body perception [5, 12, 26].

Considering long-term exposure, UVR is able to induce various skin and eye effects, many of them very severe. UVR is mutagenic for the DNA and cumulative damages over time can induce pre-cancerous and cancerous alterations [5, 26, 27]. In the skin chronic UVR exposure is able to induce photoaging, i.e. a progressive process including functional and aesthetic skin changes with loss of elasticity, cell depletion, pigment accumulation and substitution of normal tissue with fibrous tissue. considered to be a precancerous alteration [5, 26, 34, 35]. Other pre-cancerous lesions, sometimes identified also as *in situ* carcinomas, induced by chronic UVR exposure of the skin are actinic keratoses (AK). AK are disorders of the keratinocytes resulting in thickening of the skin with formation of scaly and/or crusty lesions. Untreated lesions have up to a 20% risk of progression to squamous cell carcinoma (SCC) [5, 26, 27, 35, 36]. In addition to pre-cancerous lesions, UVR is able to induce skin cancers. The most common are the basal cell carcinoma (BCC) and the SCC of the skin, also called as keratinocytes cancers [26, 27, 37]. These tumours are the most frequent malignancies in subjects with fair skin, and accordingly they are the most frequent type of cancer in Europe, Canada, US and Australia. Fortunately these tumors have mainly a local malignancy, resulting only seldom in methastatization processes: accordingly, the prognosis is quite good compared to other tumors, and, if treated in time, the mortality is low, but they can result in quite impressive mutilations, especially considering that they usually appear in solar UV exposed skin areas, as the face [38, 39]. Both BCC and SCC are somehow related to cumulative UVR exposure and there is evidence that outdoor workers have a relevantly increased risk of getting these tumors [40], while only few reports of associations with artificial UVR exposure at work are available [41]. Another skin tumor related to excessive UVR exposure is the malignant melanoma (MM), a cancer originating from the skin melanocytes. MM are less frequent compared to BCC and SCC, but they often methastatize if not diagnosed in time, determining an important burden not only in terms of disability adjusted life years (DALYs) but also in term of mortality [27, 42]. Considering occupational exposure, the relation with SR exposure in outdoor workers is controversial, as some studies reported a possible protective effect of cumulative UVR exposure, while the increased risk of MM is associated with intense exposure in the childhood with repeated sunburns [27, 43]. Some studies reporting a possible increased melanoma risk for welders have also been published [27, 41].

Considering now possible long-term effects in the eyes, UVR can induce chronic alterations of the ocular surface, being absorbed mainly in the cornea and in the conjunctiva, determining a chronic inflammatory stimolous and pathological alterations with abnormal growths of the corneal and conjunctival cells [5, 26, 44]. This may result in various diseases, some of them representing mainly aesthetic alterations with no clinical relevancy, as pinguecula, other more severe with potential affection of the visual function if not treated, as the pterygium, an abnormal growth of the conjunctiva from the nasal angle of the eye to the center, finally covering the cornea [44, 45]. Corneal and conjunctival squamous cell carcinomas (i.e. the same types of cancers occurring in the skin) are also possible: fortunately they are very rare, but with demonstrations of associations with UV exposure [44]. Moreover, also another eye tumor, the melanoma of the eye, more frequent compared to corneal and conjunctival carcinomas, even if still quite rare, has been reported as possibly associated with UV exposure, in particular in welders [44, 46].

Furthermore, a relevant quote of UVR is able to penetrate the ocular surface being absorbed in the lens [5]. There, with photo-oxidation damages contributing to the age-related process of the denaturation of the lens proteins, UVR can accelerate and increase the opacification of the lens [47]: it is estimated that more than the 20% of the cataracts can be attribued to excessive UVR exposure [48], and it should be noted that cataract is still the main cause of blindness worldwide [49]. Not only solar radiation, but also artificial UVR is associated to an increased risk of cataract development [47, 50].

Finally, another possible chronic adverse eye effect that can be associated in particular to long-term SR exposure is macular degeneration, a very frequent multi-factorial degenerative disease of the central part of the retina, currently the third among the major causes of blindness worldwide [49]. Scientific demonstrations of the relation between this eye pathology and SR exposure are mainly epidemiological, rather then experimental, but some hypothesis have been proposed [51]. In this case, the role of UVR is limited to that of a small portion of UV-A radiation, able to reach the retina especially in younger subjects when the lens is more transparent [5]. But also violet/blue visible light can contribute to a chronic photochemical retinal damage through photo-oxidations [52, 53].

3. Prevention of the health risk related to occupational optical radiation exposure

3.1. Occupational optical radiation exposure risk in the workplaces and workers belonging to particularly sensitive risk groups

Currently in Europe there are no specific obligations for the HS of workers exposed to solar radiation, even if, considering the relevancy of the risk and of the adverse health effects to be expected, in many countries an increasing attention to the protection of outdoor workers against UVR and to the occurrence of solar UV-induced occupational diseases has been raised in recent years [5, 26, 38, 54–59]. One of the issues still to be solved is the lack of a recognized occupational limit for solar UVR

exposure at work in Europe: the recognition of such a limit would be helpful to implement risk evaluation processes in the workplaces, defining the specific protections needed. On the other hand, since 2006 a specific European Directive "2006/25/EC" for the prevention of the occupational risk related to artificial optical radiation exposure has been emplaced [4]. In this case, specific occupational exposure limits to be respected are available, and moreover the Directive requires mandatory risk evaluation, definition of technical and organizational preventive measures, specific training of the workers, the forniture of adequate personal protective equipment and, if needed, an appropriate health surveillance.

For all the previously mentioned steps of the process for an adequate prevention of OR risk at the workplaces, the Directive indicates that a special attention has to be deserved to the workers "*belonging to particularly sensitive risk groups*" [4]. No specific indications are included in the EU Directive helping in identifying these workers. We report here below a non-exhaustive list of possible conditions determining a particular susceptibility to OR exposure, increasing the risk of adverse effects, mainly for the eye and the skin, and requiring a special attention [4, 5, 26].

- Conditions related to a possible increased risk of adverse skin effects (mainly related to the UVR component of OR): e.g. albino subjects and all the workers with fair skin photo-types (i.e. at least Fitzpatrick skin photo-type 1 or 2 [60]), who are at an increased risks for developing all the UV-related acute and long-term skin effects; workers affected by skin diseases that can be photo-induced or photo-aggravated, as psoriasis or xeroderma pigmentosum; workers being diagnosed with precancerous or cancerous skin lesions; workers being treated with photosensitizing drugs or in contact with photosensitizing substances as psoralenes.

- Conditions related to a possible increased risk of adverse eye effects: workers with alterations of the eyes structure possibly affecting the quantity of OR absorbed in specific eye regions, as e.g. iris alterations (as coloboma, aniridia), pupil alterations (as tonically dilated pupil, mydriasis), lens alterations (aphakia, artificial intraocular lens); workers being diagnosed with eye diseases possibly being worsened by excessive OR exposure, as e.g. initial lesions of the lens (as presence of small lens opacities or cataract at an initial stage) or of the retina (as the presence of drusen in the macula); subjects with only a monocular vision, as the possible occurrence of OR-related adverse effects in the eye may result in blindness.

- Other conditions: pregnant workers are usually considered among the workers belonging to particularly sensitive risk groups, mainly considering (but not limited to) the possible thermal effects of the infrared component, increasing the body temperature in the abdominal region; underage workers can be also potentiually included, especially considering that the lens is more transparent to UVR, possibly enabling a higher amount of radiation reaching the retina.

3.2. Health surveillance of workers exposed to optical radiations

According to the current European legislation, there are two possible scenarios for the HS of OR exposed workers. The HS is an obligation in case a relevant risk is evaluated in the workplace according to the EU Directive 2006/25/EC for artificial OR exposure, both in case of incoherent sources and of LASER use. On the other hand, considering SR exposure risk of outdoor workers, currently in Europe HS is not mandatory [5, 26], even if, in the light of the numbers of outdoor workers, the high levels of occupational UVR exposure detected in several studies [13–26] and of the documented increased risk for these workers of developing UVR-induced eye and skin effects [25, 26, 40, 44–48, 50, 51, 54, 55, 27, 28, 34–39] an appropriate HS seems absolutely necessary.

The objective of the HS of OR-exposed workers is the prevention and the early diagnosis of adverse effects, mainly of the eyes and of the skin. During HS activities, specific attentions have to be deserved to the workers affected by conditions inducing a particular susceptibility to the risk, as the ones mentioned here in the previous section 3.1. HS programs usually include both pre-employment and periodic medical examinations from trained occupational physicians, who may require, on individual basis, supplementary health controls possibly encompassing other specialists involved in the specific problem detected (e.g. ophthalmologists, dermatologists, etc) [26, 38, 59]. As stated above, the most alarming health risk to be considered during HS is the one related to the UVR component that can induce relevant adverse health effects as skin cancers, currently the most frequent tumors among Caucasian subjects. These cancers, together with other OR-induced eye and skin pathologies, are recognized occupational diseases in many European countries, but not in all [38, 59]. Nevertheless, these cancers are largely underreported: an extension of the HS also to outdoor workers should help in increasing the reporting of OR-induced occupational diseases, allowing workers to receive an adequate medical care and compensation for the diseases, and letting institutional authorities and governments acknowledged of the true magnitude of the phenomenon, and consequently of the need of preventive measures [38, 55, 59].

4. Electromagnetic fields: occupational exposure and health effects

4.1. Occupational exposure to electromagnetic fields

Nowadays, a certain level of EMF exposure is present in almost all the working environments, and there is an extremely large, and increasing, variety of occupational EMF sources. Accordingly, some exposure to EMF is present for almost all workers. But, on the other hand, numerous sources are present also in the general environment. Accordingly, it can seem inappropriate to consider every single worker as an "*exposed worker*". A detailed discussion on this topic is beyond the scopes of this article but, in general, it can be considered appropriate to evaluate as "*exposed*" workers, those with an expected EMF exposure above the levels usually detectable for the general population at home and in public places [61–64]. A peculiar aspect in this context is that in some workers with a particular susceptibility (*"workers at particular risk"* - WPR), also EMF levels permittable for the general public may determine a non-irrelevant residual health risk. This is specifically the case of workers with active implanted medical devices (AIMD), who may be at risk for interference problems when in proximity of an EMF source [65–67]: these aspects will be discussed in detail in the next paragraphs.

When dealing with the problem of occupational exposure to EMF, as it happens also for OR, it is important to identify the specific types of EMFs emitted by the considered sources, as different regions of the EMF spectrum have different biological interaction mechanisms and, consequently, different effects, depending on the frequency bands. For the objectives of this article, we adopt a simplified EMF classification, discussing here the main issues related to the exposure in particular to static magnetic fields (SMF, frequency= 0 Hertz), extremely-low frequency magnetic fields (ELF-MF, frequency= 1 - <300 Hertz), intermediate frequency EMF (IF-EMF, frequency= 300 Hertz - <100 kilohertz) and high frequency EMF (HF-EMF, frequency> 100 kilohertz, including radiofrequency - RF -, microwaves, millimeter and terahertz waves) [61–64, 68]. Considering now specific working situations and occupational sources with potentially relevant emissions of EMF, a useful guide for the prevention of EMF risk at work is the so-called "*non-binding guide*" for the application of the European Directive 2013/35/EU [68]: we present here an extract of the document with a list of work activities and EMF-sources determining occupational exposures (Table 1).

Table 1: Non-exhaustive list of work activities/occupational sources inducing a potentially relevant exposure to electromagnetic fields extracted from the "non-binding guide" for the application of the European Directive 2013/35/EU

Type of equipment or workplace
Construction: various equipment and machineries (e.g. concrete mixers, cranes, vibrators, welding machines, etc)
Electrical supply: electrical installations, generators, inverters
Infrastructure (buildings): base station antennas
Infrastructure (grounds): garden appliances
Heavy industry: industrial electrolysis, furnaces, arc melting, welding machines
Light industry: arc welding processes, dielectric heating and welding, industrial magnetizer/ demagnetizers
Medical: magnetic Resonance Imaging (MRI), other medical equipment using EMF for diagnosis and treatment (for example, short wave diathermy, transcranial magnetic stimulation)
Office: audio-visual equipment containing RF-transmitters, office equipment (e.g. photocopiers, electric staplers, paper shredders)
Transport: motor vehicles and plants, radars (air traffic control, military use, weather monitoring, long range radars), electrically driven trains and trams
Wireless communications Cordless phones (including base stations for cordless phones), mobile phones, wi-fi routers

It should be noted that for the sources and the occupational activities with potentially relevant occupational EMF exposures presented in the Table 1 no specific frequencies ranges of EMF emissions are reported. This is because in many cases the exposure can include various EMF bands, as e.g. in welding activities, where ELF, IF-EMF and RF can be represented in the specific emission spectra depending also on the type of welding procedure, or in MRI activities, where operators are exposed to the action of the SMF as well as to time-varying EMF when they move within the SMF, while the patients are also exposed to RF when the scanner is in function. In other cases, the EMF exposure can be referred to specific EMF bands, as e.g. for electrical installations, generators and inverters, emitting mainly in the ELF range, or for wireless communication systems, with emissions mainly in the RF band [61–64, 68–70]. Another relevant note for an appropriate interpretation of the Table 1 is that not all the potential exposures listed represent, in normal conditions, a relevant risk for the workers; e.g., again in the case of wireless communication systems or in the case of office equipment, the listed sources may determine an occupational risk only for workers with an increased susceptibility to the EMF risk, as subjects with AIMD who have to work close to the sources [61–68], as previously introduced. On the other hand, other sources can be able to usually induce high exposure levels, potentially representing an occupational risk in case of inadequate working conditions, e.g. in the case of close proximity of operators to a MRI scanner, in industrial electrolysis plants, or in working activities involving induction heating systems, soldering devices, or broadcasting systems and devices, etc. [61–64, 68].

4.2. Interaction mechanisms with biological tissues and main effects of electromagnetic fields exposure

According to the above mentioned European Directive 2013/35/EU, currently in Europe for the prevention of the occupational risks related to EMF exposure only effects based on recognized interaction mechanisms with the biological tissues are considered [68]. The EU Directive indicates specifically the short term direct biophysical effects and the indirect effects related to EMF exposure [68]. A necessary punctualization here, considering the quite large number of studies dealing with suggested long-term effects related to EMF (among the main examples there are the suggested associations between leukemia and ELF-MF exposure, and brain cancers with RF exposure), is that, for these effects, the current European legislation does not consider sufficient the available scientific evidence, in particular considering that no adequate pathogenetic mechanisms in humans have been demonstrated [61–64, 68]. The position of the EU Commission is coherent with the opinions of various recognized national and international organizations and institutions [61–64, 71-85].

According to the above mentioned EU approach, we discuss here only: a) direct biophysical effects caused in the human body by its presence within an EMF; and b) indirect effects, induced by the presence of an object in the EMF (object that can also be placed inside the body, as in the case of implanted medical devices) [68].

According to the frequency band of the EMF, different mechanisms are involved for the occurrence of direct effects: non-thermal mechanisms for static and low-frequency fields, and thermal mechanisms for high frequency fields. For the intermediate frequencies both the mechanisms are possible [61–64, 68]. Among non-thermal effects, based on cuurents induction in the biological tissues, there are the following: limb currents,

stimulation of muscles, nerves or sensory organs with induction of temporary annoyance or with a possible detrimental effect on cognition or on other brain or muscle functions, with possible risks for the safety of the workers [68]. Considering thermal mechanisms, the direct effects, related to HF-EMF exposure, and possibly to IF-EMF, are related to an increase of the temperature in the body, that can be usually more relevant at the surface, and accordingly in targets as the eyes, where very intense HF-EMF can theoretically induce a thermal damage of the lens with opacification (cataract), and the skin, where thermal burns can be possible, also in this case after very high exposures levels [64, 68]. A further classification of direct effects according to the 2013/35/EU Directive is the one concerning *"sensory"* and *"health effects"* [68]. Sensory effects are usually rapidly reversible and transient. They can be considered non-pathological effects, usually with no consequences for the individuals, even if they can be associated with an increased risk of work accidents. Sensory effects are mainly related to relevant SMF and ELF-EMF exposures, representing the consequence of an induction of currents, stimulating the nervous systems and/or sensory organs. Examples of sensory effects are vertigo, nausea, perception of a metallic taste in mouth after SMF exposure, magnetophosphenes (i.e. eye lamps perception) and minor reversible changes of some brain functions (e.g. attention, congnitive function) in case of ELF-EMF exposure [61–63, 68]. On the other hand, EMF-related *"health effects"* represent severe alterations, that usually appear only in case of overexposure to EMF, significantly above the occupational limits established e.g. in Europe by the 2013/35/EU Directive. A non-exhaustive list of these health effects, based on non-thermal mechanisms for SMF and ELF-MF (an example can be an alteration of the cardiac rythm) and on thermal mechanisms in case of very intense HF-EMF exposure (e.g. skin burns), is presented in the Table 2. As stated above, for IF-EMF exposure sensory and health effects typical of both low and high frequencies can be possible [61–64, 68].

Table 2: Non-exhaustive list of health effects caused by overexposure to electro-magnetic fields, based on the European Directive 2013/35/EU

EMF type	
Static magnetic field	Alterations of the blood flow in the limbs; alterations of the brain functions; alterations of the cardiac rhythm and of the cardiovascular fuction
Low frequency fields	Pain and/or tingling sensations due to an involuntary contractions of the muscles or to the stimulation of the nervous system; alterations of the cardiac rhythm
Intermediate frequency fields	The effects of both high and low frequencies can be possible
High frequency fields	Excessive increase in temperature and/or thermal burns over the whole body or in specific areas; thermal damage of the eyes (possibility of thermal cataracts), skin, testicles

Considering now indirect effects, these effects can occur, as stated above, when there is an object inside the EMF, together with the human body. All the EMF frequencies can be involved, and, as in the case of medical devices, it should be noted that the object can be also implanted in the human body [68]. Some of these indirect effects mainly represent a risk of work-related injuries: EMF can initiate electro-explosive devices causing fires and explosions. Other indirect effects possibly associated to severe injuries are contact currents, that can be induced in the body by the contact with charged objects within an EMF [68]. The most relevant indirect effects that can happen also in case of usual exposures, and not as a consequence of a malfunction/wrong procedure, are interference problems of EMF with implanted or body worn devices, usually for medical purposes. The major problems can be experienced in case of active devices, as pacemakers or implantable cardioverter defibrillators (ICD): their functions can be altered by the EMF, determining a risk for the workers' health [61–68]. Also, passive devices, as e.g. metal splinters or graft, can be affected by EMF: in particular, SMF may dislocate the devices made of ferromagnetic materials, causing inflammation or other problems in the surrounding tissue. Moreover, IF-EMF and HF-EMF can determine a heating of the metallic parts of the devices, also in this case with a potential damage to the biological tissue [65–68].

5. Prevention of the health risk related to electromagnetic fields exposure

5.1. Occupational electromagnetic fields exposure risk in the workplaces and workers at particular risk

In Europe, the prevention of the occupational risk related to EMF is regulated according to the Directive 2013/35/EU. As it happened also for OR, a specific *"non binding guide"* was then produced by the European Commission, to give practical indications for the application of the Directive [68]. The Directive requires mandatory EMF risk evaluation in the workplaces, defining the technical and organizational preventive measures to be applied, including a specific training of the exposed workers, the adoption of adequate personal protective equipment and, if needed, an appropriate health surveillance. Specific occupational exposure limits are available for the different EMF frequencies, mainly based on the guidelines of the International Commission on Non-Ionizing Radiation Protection (ICNIRP) [61–63]. Different limit values are available not only according to the EMF frequency, but also based on the different effects to be prevented: separate limits for the prevention of the above-mentioned *sensory* and *health effects* are defined in the EU Directive [68]. As previously introduced, the possibility to reach exposure levels able to induce *health effects* is very rare, happening only in case of overexposure, e.g. in case of accidents. Moreover, it is not sufficient to simply exceed the limit value to induce the appearance of a *health effect*, as usually exposures highly above the limits are needed. Furthermore, also the exceeding of the limits for *sensory effects*, much lower compared to the limits for *health effects*, is not usual, and in principle it has to be avoided in normal conditions [86, 87].

Considering this, one of the main problems for the prevention of the occupational EMF risk is the possible presence at the workplace of WPR, as defined by the Directive 2013/35/EU, for whom the occupational limits set might be not fully protective [68]. Currently, a non-exhaustive list of WPR for EMF exposure includes:

- Workers with active implanted medical devices (AIMD): e.g. pacemakers, implanted cardioverter defibrillators, ear implants, neurostimulators, implanted drug infusion pumps, etc [65–68, 88, 89].

- Workers with passive implanted medical devices containing metals: e.g. artificial joints, plates, surgical clips, stents, heart valve prostheses, intra-uterine devices, etc [68, 88–91].

- Workers with body-worn devices: e.g. drugs infusion pumps, hearing aids, continuous glucose monitoring systems, etc [68, 88, 89].

- Other WPR categories included in the EU Directive: pregnant workers [68, 88, 89].

5.2. Health surveillance of workers exposed to electromagnetic fields

According to the Directive 2013/35/EU, HS of EMF exposed workers is mandatory, when a relevant risk for the workers is evaluated. Moreover, for the HS, as well as for the risk assessment, the problem of the WPR has to be specifically taken into account [68, 89]. As defined in the Introduction, HS is aimed at identifying any abnormality possibly associated to a recognized work related risk in exposed workers [3]. All the investigations chosen for HS have to be proved with an appropriate level of scientific evidence: the contents of the HS can include biological tests and other investigations, when they are chosen for their validity and relevance with respect to the occupational risks, avoiding investigations that don't fulfill these criteria [92]. Considering the specific case of EMF exposure, a reliable application of these criteria may involve some possible issues. In fact, according to the EU Directive the scopes of the HS are the prevention and early detection of the previously defined direct biophysical effects, including the sensory ones (as e.g. the presence of vertigo or of nausea associated to EMF exposure, etc.), based on non-thermal and thermal mechanisms [68]. In general, these effects do not appear for occupational exposure levels below the limit values, as they can be induced only as a consequence of excessive exposures to quite high levels of EMF [86, 87]. It has also to be highlighted here that sensory effects, that are fully reversible and transient, cannot be considered an actual health risk for the workers [93–95], even if some data suggest a possible association with an increased risk of work-related injuries for the exposed subjects [96, 97]. The other main purpose of the health surveillance related to the occupational EMF risk is the prevention of indirect effects, and this specifically involves the identification of the WPR. Among the conditions of particular susceptibility, probably the main issues are related to possible electromagnetic interference (EMI) problems with AIMD. EMI can appear also as a consequence of kind of low exposure levels if a susceptible subject with an AIMD is close to an EMF-source, and the interference can impair the fundamental functions of the devices [61–68].

Considering this, the health surveillance criteria to be considered should mainly address the identification of possible medical signs and symptoms of sensory effects and of the conditions of particular susceptibility to the EMF-risk, typical of the WPR. For these purposes, particular lab tests or other specific clinical investigations are not required on a routine basis, while their opportunity can be judged by the occupational physician on

an individual basis after a medical examination. Useful instruments to be periodically administered to the workers are the questionnaires evaluating symptoms and conditions of particular susceptibility [93–95]. When administering questionnaires, important prerequisites are a validation process [98] and a preparation of the tool based on scientific results: unfortunately, to the best of our knowledge, to date there are no examples of questionnaires specifically designed for an application during HS examinations of EMF-exposed workers. A further note to the problem of the EMF-related HS is that, in general, medical examinations for workers in good health conditions, with no conditions of particular susceptibility and working in environnments where the EMF levels are supposed to be low or very low (e.g. offices) have not to be considered as activities to be periodically repeated. In these cases, only a single medical investigation performed before the starting of the job, with an effective information on all the conditions possibly determining a particular susceptibility to the EMF risk (NB: the information has to be periodically repeated in these cases, while the medical examination doesn't), seems advisable for an adequate prevention [68, 89].

Finally, a peculiar situation explicitly mentioned in the EU Directive is the case of an *"extraordinary"* HS of the EMF exposed workers, needed when *"any undesired or unexpected health effect is reported by a worker"* or *"in any event where exposure above the ELVs* (i.e. exposure limit values) *is detected".* In these situations, an appropriate *"medical examination"* needs to be provided to the workers [68]. Also, in this case, no guidelines or evidence-based indications are available to define valid contents for these medical examinations. Furthermore, as previously noted, situations with exposure levels exceeding the limits do not necessarily result in the occurrence of adverse health effects [86, 87]. Also, in this case, the main problems should be expected for the WPR. Accordingly, both for extraordinary and routine HS the contents of the examinations include an appropriate in-depth medical examination of the workers by an occupational physician with an adequate competence in the field, administrating specific questionnaires to collect information on suspected EMF-related symptoms and possible conditions of particular susceptibility to the risk, eventually integrated by specific medical consultations and/or laboratory tests and/or diagnostic exams to be decided on an individual basis, considering the types of EMF frequency involved, the exposure level, the susceptibility of the workers and the expected effects to be evaluated [68, 89].

6. Conclusions

Occupational NIR exposure, including EMF and OR, is almost ubiquitous: in principle, an evaluation of the occupational health risk should be appropriate in all workplaces. Based on the health risk assessment, HS programs for the exposed workers have to be established, with the objective of preventing or, at least, identifying at an early stage the possible health effects associated with the exposure. Both risk evaluation and HS activities have to specifically consider the possible presence in the workplace of "workers at particular risk", who deserve a specific attention, as they have an increased susceptibility to the risk. The HS needs to be performed by occupational physicians with adequate and updated skills in the prevention of NIR risk, and accordingly with an appropriate specific training in this field. Here below we present

a conclusive summary of the main relevant points to be considered for the health surveillance of NIR exposed workers:

Optical radiation:

i.   Occupational physicians have to consider that the exposure can be associated to both artificial and natural sources. In particular, solar radiation is certainly the main occupational exposure source, even if sometimes under-recognized as a specific occupational risk.

ii. The main target organs of optical radiation exposure are the eyes and the skin.

iii. For the prevention and early diagnosis purposes, the possible occurrence of both short-term and long-term eye and skin effects, respectively related to acute and cumulative exposures, has to be adequately considered as a fundamental criterion of HS.

iv. The most harmful component of optical radiation is UVR, able to induce both acute and long-term effects with photochemical mechanisms; among the most severe adverse effects related to chronic UV exposures there are skin cancers, i.e. the most frequent forms of neoplasms in Caucasian subjects. Other diseases identified in UVR exposed workers are: skin erythema, photoaging and actinic keratosis for the skin, photokeratoconjunctivitis, pterygium, lens opacities and possibly macular degeneration for the eyes.

v.   During HS activities, specific conditions of particular susceptibility for the exposed workers have to be considered: e.g. a fair skin phototype, eye alterations as aphakia, and others.

vi. Optical radiation related adverse effects are recognized "occupational diseases", even if frequently underreported: physicians have to notify the occurrence of these diseases in exposed workers to the specific workers' compensation Authorities in their Country.

Electromagnetic fields:

i.   According to the European legislation, the recognized effects related to EMF exposure to be considered for the health surveillance of the workers are short-term direct biophysical effects and indirect effects.

ii. Direct effects can be related to both non-thermal and thermal mechanisms, and they are usually induced only by high exposures.

iii. Indirect effects, as the electromagnetic interference with AIMD, can occur also as a consequence of lower exposure levels.

iv. To date, there are no agreed and shared criteria for the health surveillance of EMF-exposed workers, and in particular there are no evidence-based indications on the appropriate contents and procedures for the medical examinations to be performed for the monitoring of the health status of the exposed subjects.

v.   The trained occupational physicians have to evaluate all the possible symptoms related to the sensory and health effects of EMF exposure, considering specifically the type of frequency, the exposure level and the mechanisms involved.

vi. One of the most important activities during health surveillance is the screening of all the conditions that can induce a particular risk for the exposed workers, as e.g. AIMD: a check for the presence of these conditions needs to be done before the employment by the physician, and an extensive information on these conditions has to be provided to the workers, and periodically repeated.

vii. In case of overexposure situations or in case of workers reporting symptoms associated to the EMF exposure, an appropriate medical examination has to be provided to the workers, with specific contents to be evaluated on an individual basis, again based on the type of EMF-frequency, on the exposure level detected and, on the mechanisms, involved.

Conflict of Interest

The Authors declare no conflict of interest.

Acknowledgment

References

[1] A. Modenese, F. Gobba, "Occupational Exposure to Non-Ionizing radiation. Main effects and criteria for health surveillance of workers according to the European Directives, " Proceedings - 2020 IEEE International Conference on Environment and Electrical Engineering and 2020 IEEE Industrial and Commercial Power Systems Europe, EEEIC / I and CPS Europe 2020, 2020, doi:10.1109/EEEIC/ICPSEurope49358.2020.9160831.

[2] E.L. Melnick, Brian S. Everitt, Encyclopedia of Quantitative Risk Analysis and Assessment, Wiley, 2008.

[3] ILO, Occupational Safety and Health Series, No. 72 Technical and ethical guidelines for workers' health surveillance, 50, 1998.

[4] European Commission, Non-binding guide to good practice for implementing Directive 2006/25/EC (Artificial optical radiation), 2011.

[5] G. Ziegelberger, "Icnirp statement-protection of workers against ultraviolet radiation, " Health Physics, **99**(1), 66–87, 2010, doi:10.1097/HP.0b013e3181d85908.

[6] D. Sliney, "Risks of occupational exposure to optical radiation, " Med Lav, **97**(2), 215–20, 2006.

[7] E.A. Talbot, P. Jensen, H.J. Moffat, C.D. Wells, "Occupational risk from ultraviolet germicidal irradiation (UVGI) lamps, " International Journal of Tuberculosis and Lung Disease, **6**(8), 738–741, 2002.

[8] T.D. Tenkate, "Optical radiation hazards of welding arcs, " Reviews on Environmental Health, **13**(3), 131–146, 1998, doi:10.1515/REVEH.1998.13.3.131.

[9] K. Barat, "Laser accidents: Occurrence and response, " Health Physics, **84**(5 SUPPL.), 93–95, 2003, doi:10.1097/00004032-200305001-00013.

[10] J.S. Pierce, S.E. Lacey, J.F. Lippert, R. Lopez, J.E. Franke, M.D. Colvard, "An assessment of the occupational hazards related to medical lasers, " Journal of Occupational and Environmental Medicine, **53**(11), 1302–1309, 2011, doi:10.1097/JOM.0b013e318236399e.

[11] F. Gobba, E. Dall'Olio, A. Modenese, M. De Maria, L. Campi, G.M. Cavallini, "Work-related eye injuries: A relevant health problem. main epidemiological data from a highly-industrialized area of northern Italy, " International Journal of Environmental Research and Public Health, **14**(6),

2017, doi:10.3390/ijerph14060604.

[12] S. Zaffina, V. Camisa, M. Lembo, M.R. Vinci, M.G. Tucci, M. Borra, A. Napolitano, V. Cannatã, "Accidental exposure to UV radiation produced by germicidal lamp: Case report and risk assessment, " Photochemistry and Photobiology, **88**(4), 1001–1004, 2012, doi:10.1111/j.1751-1097.2012.01151.x.

[13] C. Smit-Kroner, S. Brumby, "Farmers sun exposure, skin protection and public health campaigns: An Australian perspective, " Preventive Medicine Reports, **2**, 602–607, 2015, doi:10.1016/j.pmedr.2015.07.004.

[14] A.W. Schmalwieser, A. Cabaj, G. Schauberger, H. Rohn, B. Maier, H. Maier, "Facial solar UV exposure of Austrian farmers during occupation, " Photochemistry and Photobiology, **86**(6), 1404–1413, 2010, doi:10.1111/j.1751-1097.2010.00812.x.

[15] M. Antoine, S. Pierre-Edouard, B. Jean-Luc, V. David, "Effective exposure to solar UV in building workers: Influence of local and individual factors, " Journal of Exposure Science and Environmental Epidemiology, **17**(1), 58–68, 2007, doi:10.1038/sj.jes.7500521.

[16] M.A. Serrano, J. Cañada, J.C. Moreno, "Solar UV exposure in construction workers in Valencia, Spain, " Journal of Exposure Science and Environmental Epidemiology, **23**(5), 525–530, 2013, doi:10.1038/jes.2012.58.

[17] M. Wittlich, S.M. John, G.S. Tiplica, C.M. Sălăvăstru, A.I. Butacu, A. Modenese, V. Paolucci, G. D'Hauw, F. Gobba, P. Sartorelli, J. Macan, J. Kovačić, K. Grandahl, H. Moldovan, "Personal solar ultraviolet radiation dosimetry in an occupational setting across Europe, " Journal of the European Academy of Dermatology and Venereology, **34**(8), 1835–1841, 2020, doi:10.1111/jdv.16303.

[18] A. Modenese, F.P. Ruggieri, F. Bisegna, M. Borra, C. Burattini, E. Della Vecchia, C. Grandi, A. Grasso, L. Gugliermetti, M. Manini, A. Militello, F. Gobba, "Occupational exposure to solar UV radiation of a group of fishermen working in the Italian north adriatic sea, " International Journal of Environmental Research and Public Health, **16**(16), 1–12, 2019, doi:10.3390/ijerph16163001.

[19] P. Gies, K. Glanz, D. O'Riordan, T. Elliott, E. Nehl, "Measured occupational solar UVR exposures of lifeguards in pool settings, " American Journal of Industrial Medicine, **52**(8), 645–653, 2009, doi:10.1002/ajim.20722.

[20] M.A. Serrano, J. Cañada, J.C. Moreno, "Erythemal ultraviolet exposure in two groups of outdoor workers in valencia, Spain, " Photochemistry and Photobiology, **85**(6), 1468–1473, 2009, doi:10.1111/j.1751-1097.2009.00609.x.

[21] M. Boniol, A. Koechlin, M. Boniol, F. Valentini, M.C. Chignol, J.F. Doré, J.L. Bulliard, A. Milon, D. Vernez, "Occupational UV exposure in French outdoor workers, " Journal of Occupational and Environmental Medicine, **57**(3), 315–320, 2015, doi:10.1097/JOM.0000000000000354.

[22] E. Thieden, S.M. Collins, P.A. Philipsen, G.M. Murphy, H.C. Wulf, "Ultraviolet exposure patterns of Irish and Danish gardeners during work and leisure, " British Journal of Dermatology, **153**(4), 795–801, 2005, doi:10.1111/j.1365-2133.2005.06797.x.

[23] G.R. Casale, A.M. Siani, H. Diémoz, G. Agnesod, A. V. Parisi, A. Colosimo, "Extreme UV index and solar exposures at plateau rosà (3500ma.s.l.) in valle d'aosta Region, Italy, " Science of the Total Environment, **512–513**, 622–630, 2015, doi:10.1016/j.scitotenv.2015.01.049.

[24] M. Moehrle, B. Dennenmoser, C. Garbe, "Continuous long-term monitoring of UV radiation in professional mountain guides reveals extremely high exposure, " International Journal of Cancer, **103**(6), 775–778, 2003, doi:10.1002/ijc.10884.

[25] M.S. Paulo, B. Adam, C. Akagwu, I. Akparibo, R.H. Al-Rifai, S. Bazrafshan, F. Gobba, A.C. Green, I. Ivanov, S. Kezic, N. Leppink, T. Loney, A. Modenese, F. Pega, C.E. Peters, A.M. Prüss-Üstün, T. Tenkate, Y. Ujita, M. Wittlich, S.M. John, "WHO/ILO work-related burden of disease and injury: Protocol for systematic reviews of occupational exposure to solar ultraviolet radiation and of the effect of occupational exposure to solar ultraviolet radiation on melanoma and non-melanoma skin cancer, " Environment International, 2019, doi:10.1016/j.envint.2018.09.039.

[26] A. Modenese, L. Korpinen, F. Gobba, "Solar radiation exposure and outdoor work: An underestimated occupational risk, " International Journal of Environmental Research and Public Health, **15**(10), 2018, doi:10.3390/ijerph15102063.

[27] International Agency for Reasearch on Cancer, IARC Monographs on the Evaluation of Carcinogenic Risks to Humans Volume 100D, Lyon, 2012.

[28] T. Kauppinen, J. Toikkanen, A. Savela, D. Pedersen, R. Young, W. Ahrens, P. Boffetta, M. Kogevinas, J. Hansen, H. Kromhout, V. de La Orden-Rivera, J. Maqueda Blasco, D. Mirabelli, B. Pannett, N. Plato, R. Vincent, "Occupational exposure to carcinogens in the European Union, " Occupational and Environmental Medicine, **57**(1), 10–18, 2000,

doi:10.1136/oem.57.1.10.

[29] G. Ziegelberger, "ICNIRP guidelines on limits of exposure to incoherent visible and infrared radiation, " Health Physics, **105**(1), 74–96, 2013, doi:10.1097/HP.0b013e318289a611.

[30] R.J. Kettelhut EA, Traylor J, Erythema Ab Igne, 2020.

[31] A. Dorozhkin, "Cataract of metallurgists, " Vestn Oftalmol, **119**(3), 31–4, 2003.

[32] J.J. Vos, D. Van Norren, "Thermal cataract, from furnaces to lasers, " Clinical and Experimental Optometry, **87**(6), 372–376, 2004, doi:10.1111/j.1444-0938.2004.tb03097.x.

[33] R.W. Bunsen, H.. Roscoe, "Photochemical Researches—Part V. On the Measurement of the Chemical Action of Direct and Diffuse Sunlight, " in Proc. R. Soc, 306–12, 1862, doi:10.1098/rspl.1862.0069.

[34] P. Sartorelli, R. Romeo, V. Paolucci, V. Puzzo, F. Di Simplicio, L. Barabesi, "Skin photoaging in farmers occupationally exposed to ultraviolet radiations, " Medicina Del Lavoro, **104**(1), 24–29, 2013.

[35] K. Grandahl, J. Olsen, K.B.E. Friis, O.S. Mortensen, K.S. Ibler, "Photoaging and actinic keratosis in Danish outdoor and indoor workers, " Photodermatology Photoimmunology and Photomedicine, **35**(4), 201–207, 2019, doi:10.1111/phpp.12451.

[36] R. Schwartz, T. Bridges, A. Butani, A. Ehrlich, "Actinic keratosis: an occupational and environmental disorder, " Journal of the European Academy of Dermatology and Venereology, **0**(0), 080304135428024-???, 2008, doi:10.1111/j.1468-3083.2007.02579.x.

[37] C. Karimkhani, L.N. Boyers, R.P. Dellavalle, M.A. Weinstock, "It's time for 'keratinocyte carcinoma' to replace the term 'nonmelanoma skin cancer,'" Journal of the American Academy of Dermatology, **72**(1), 186–187, 2015, doi:10.1016/j.jaad.2014.09.036.

[38] F. Gobba, A. Modenese, S.M. John, "Skin cancer in outdoor workers exposed to solar radiation: a largely underreported occupational disease in Italy, " Journal of the European Academy of Dermatology and Venereology, **33**(11), 2068–2074, 2019, doi:10.1111/jdv.15768.

[39] A. Modenese, F. Farnetani, A. Andreoli, G. Pellacani, F. Gobba, "Questionnaire-based evaluation of occupational and non-occupational solar radiation exposure in a sample of Italian patients treated for actinic keratosis and other non-melanoma skin cancers, " Journal of the European Academy of Dermatology and Venereology, **30**, 2016, doi:10.1111/jdv.13606.

[40] T. Loney, M.S. Paulo, A. Modenese, F. Gobba, T. Tenkate, D.C. Whiteman, A.C. Green, S.M. John, "Global evidence on occupational sun exposure and keratinocyte cancers: a systematic review, " British Journal of Dermatology, 1–11, 2020, doi:10.1111/bjd.19152.

[41] L.M. Falcone, P.C. Zeidler-Erdely, "Skin cancer and welding, " Physiology & Behavior, **176**(1), 139–148, 2018, doi:10.1117/12.2549369.Hyperspectral.

[42] M. RASTRELLI, S. TROPEA, C.R. ROSSI, M. ALAIBAC, "Melanoma: Epidemiology, Risk Factors, Pathogenesis, Diagnosis and Classification, " In Vivo, **28**, 1005–1011, 2014, doi:10.32388/7xj0gw.

[43] B.K. Armstrong, A.E. Cust, "Sun exposure and skin cancer, and the puzzle of cutaneous melanoma: A perspective on Fears et al. Mathematical models of age and ultraviolet effects on the incidence of skin cancer among whites in the United States. American Journal of Epidemiology 1977; , " Cancer Epidemiology, **48**, 147–156, 2017, doi:10.1016/j.canep.2017.04.004.

[44] J.C.S. Yam, A.K.H. Kwok, "Ultraviolet light and ocular diseases, " International Ophthalmology, **34**(2), 383–400, 2014, doi:10.1007/s10792-013-9791-x.

[45] A. Modenese, F. Gobba, "Occupational exposure to solar radiation at different latitudes and pterygium: A systematic review of the last 10 years of scientific literature, " International Journal of Environmental Research and Public Health, **15**(1), 2018, doi:10.3390/ijerph15010037.

[46] T. Nayman, C. Bostan, P. Logan, M.N. Burnier, "Uveal Melanoma Risk Factors: A Systematic Review of Meta-Analyses, " Current Eye Research, **42**(8), 1085–1093, 2017, doi:10.1080/02713683.2017.1297997.

[47] C.A. McCarty, H.R. Taylor, "A review of the epidemiologic evidence linking ultraviolet radiation and cataracts., " Developments in Ophthalmology, **35**, 21–31, 2002, doi:10.1159/000060807.

[48] T. Tenkate, B. Adam, R.H. Al-Rifai, B.R. Chou, F. Gobba, I.D. Ivanov, N. Leppink, T. Loney, F. Pega, C.E. Peters, A.M. Prüss-Üstün, M. Silva Paulo, Y. Ujita, M. Wittlich, A. Modenese, "WHO/ILO work-related burden of disease and injury: Protocol for systematic reviews of occupational exposure to solar ultraviolet radiation and of the effect of occupational exposure to solar ultraviolet radiation on cataract, " Environment International, **125**, 2019, doi:10.1016/j.envint.2018.10.001.

[49] D. Pascolini, S.P. Mariotti, "Global estimates of visual impairment: 2010, " British Journal of Ophthalmology, **96**(5), 614–618, 2012, doi:10.1136/bjophthalmol-2011-300539.

[50] A. Modenese, F. Gobba, "Cataract frequency and subtypes involved in

workers assessed for their solar radiation exposure: a systematic review, " Acta Ophthalmologica, **96**(8), 2018, doi:10.1111/aos.13734.

[51] A. Modenese, F. Gobba, "Macular degeneration and occupational risk factors: a systematic review, " International Archives of Occupational and Environmental Health, **92**(1), 2019, doi:10.1007/s00420-018-1355-y.

[52] J. Moon, J. Yun, Y.D. Yoon, S. Il Park, Y.J. Seo, W.S. Park, H.Y. Chu, K.H. Park, M.Y. Lee, C.W. Lee, S.J. Oh, Y.S. Kwak, Y.P. Jang, J.S. Kang, "Blue light effect on retinal pigment epithelial cells by display devices, " Integrative Biology (United Kingdom), **9**(5), 436–443, 2017, doi:10.1039/c7ib00032d.

[53] J.Z. Nowak, "Age-related macular degeneration (AMD): Pathogenesis and therapy, " Pharmacological Reports, **58**(3), 353–363, 2006.

[54] T.L. Diepgen, M. Fartasch, H. Drexler, J. Schmitt, "Occupational skin cancer induced by ultraviolet radiation and its prevention, " British Journal of Dermatology, **167**(SUPPL. 2), 76–84, 2012, doi:10.1111/j.1365-2133.2012.11090.x.

[55] S.M. John, M. Trakatelli, C. Ulrich, "Non-melanoma skin cancer by solar UV: The neglected occupational threat, " Journal of the European Academy of Dermatology and Venereology, **30**, 3–4, 2016, doi:10.1111/jdv.13602.

[56] A. Modenese, T. Loney, F.P. Ruggieri, L. Tornese, F. Gobba, "Sun protection habits and behaviors of a group of outdoor workers and students from the agricultural and construction sectors in north-Italy, " Medicina Del Lavoro, **111**(2), 116–125, 2020, doi:10.23749/mdl.v111i2.8929.

[57] C.E. Peters, T. Tenkate, E. Heer, R. O'Reilly, S. Kalia, M.W. Koehoorn, "Strategic Task and Break Timing to Reduce Ultraviolet Radiation Exposure in Outdoor Workers, " Frontiers in Public Health, **8**(August), 1–9, 2020, doi:10.3389/fpubh.2020.00354.

[58] D. Reinau, M. Weiss, C.R. Meier, T.L. Diepgen, C. Surber, "Outdoor workers' sun-related knowledge, attitudes and protective behaviours: A systematic review of cross-sectional and interventional studies, " British Journal of Dermatology, **168**(5), 928–940, 2013, doi:10.1111/bjd.12160.

[59] C. Ulrich, C. Salavastru, T. Agner, A. Bauer, R. Brans, M.N. Crepy, K. Ettler, F. Gobba, M. Goncalo, B. Imko-Walczuk, J. Lear, J. Macan, A. Modenese, J. Paoli, P. Sartorelli, K. Stageland, P. Weinert, N. Wroblewski, H.C. Wulf, S.M. John, "The European Status Quo in legal recognition and patient-care services of occupational skin cancer, " Journal of the European Academy of Dermatology and Venereology, **30**, 2016, doi:10.1111/jdv.13609.

[60] T.B. Fitzpatrick, "The Validity and Practicality of Sun-Reactive Skin Types I Through VI, " Archives of Dermatology, **124**, 869–871, 1988.

[61] International Commission on Non-Ionizing Radiation Protection, "Guidelines on limits of exposure to static magnetic fields., " Health Physics, **66**(1), 100–106, 1994.

[62] I.C. on N.-I.R. Protection, "Guidelines for limiting exposure to time-varying electric and magnetic fields (1 Hz TO 100 kHz), " Health Physics, **99**(6), 818–836, 2010, doi:10.1097/HP.0b013e3181f06c86.

[63] I.C. on N.-I.R. Protection., "Guidelines for limiting exposure to electric fields induced by movement of the human body in a static magnetic field and by time-varying magnetic fields below 1 Hz, " Health Physics, **106**(3), 418–425, 2014, doi:10.1097/HP.0b013e31829e5580.

[64] G. Ziegelberger, R. Croft, M. Feychting, A.C. Green, A. Hirata, G. d'Inzeo, K. Jokela, S. Loughran, C. Marino, S. Miller, G. Oftedal, T. Okuno, E. van Rongen, M. Röösli, Z. Sienkiewicz, J. Tattersall, S. Watanabe, Guidelines for limiting exposure to electromagnetic fields (100 kHz to 300 GHz), 2020, doi:10.1097/HP.0000000000001210.

[65] A. Napp, D. Stunder, M. Maytin, T. Kraus, N. Marx, S. Driessen, "Are patients with cardiac implants protected against electromagnetic interference in daily life and occupational environment?, " European Heart Journal, **36**(28), 1798–1804, 2015, doi:10.1093/eurheartj/ehv135.

[66] B. Hocking, K.H. Mild, "Guidance note: Risk management of workers with medical electronic devices and metallic implants in electromagnetic fields, " International Journal of Occupational Safety and Ergonomics, **14**(2), 217–222, 2008, doi:10.1080/10803548.2008.11076763.

[67] M. Tiikkaja, A.L. Aro, T. Alanko, H. Lindholm, H. Sistonen, J.E.K. Hartikainen, L. Toivonen, J. Juutilainen, M. Hietanen, "Electromagnetic interference with cardiac pacemakers and implantable cardioverter-defibrillators from low-frequency electromagnetic fields in vivo, " Europace, **15**(3), 388–394, 2013, doi:10.1093/europace/eus345.

[68] European Commission, Non-binding guide to good practice for implementing Directive 2013/35/EU Electromagnetic Fields, 2015.

[69] F. Gobba, G. Bravo, P. Rossi, G.M. Contessa, M. Scaringi, "Occupational and environmental exposure to extremely low frequency-magnetic fields: A personal monitoring study in a large group of workers in Italy, " Journal of Exposure Science and Environmental Epidemiology, **21**(6), 634–645, 2011, doi:10.1038/jes.2011.9.

[70] F. Gobba, A. Bargellini, G. Bravo, M. Scaringi, L. Cauteruccio, P. Borella,

"Natural Killer Cell Activity Decreases in Workers Occupationally, " International Journal Of Immunopathology And Pharmacology, **22**(4), 1059–1066, 2009.

[71] Health Protection Agency, Health Effects from Radiofrequency Electromagnetic Fields, 2012.

[72] ANSES, "Radiofréquences et santé. Mise à jour de l'expertise, " 461, 2013.

[73] ANSES, Extremely low frequency electromagnetic fields Health effects and the work of ANSES, 2020.

[74] ARPANSA, "Review of Radiofrequency Health Effects Research - Scientific Literature 2000 - 2012, " Technical Reports of Australian Radiation Protection and Nuclear Safety Agency, **164**(164), 1–76, 2014.

[75] ARPANSA, Extremely low frequency electric and magnetic fields Extremely low frequency (ELF) electric and magnetic fields exist wherever electricity is generated, transmitted or distributed in powerlines or cables, or used in electrical appliances., 2020.

[76] Comité Científico Asesor en Radiofrecuencias y Salud, Informe sobre radiofrecuencias y salud, 2017.

[77] Food and Drug Administration, Scientific Evidence for Cell Phone Safety, 2020.

[78] Health Council of the Netherlands, Mobile phones and cancer?, The Hague, 2016.

[79] Health Council of the Netherlands, Power lines and health part I: childhood cancer, Dec. 2020.

[80] International Agency for Research on Cancer, "International Agency for Research on Cancer Iarc Monographs on the Evaluation of Carcinogenic Risks To Humans, " Iarc Monographs On The Evaluation Of Carcinogenic Risks To Humansarc Monographs On The Evaluation Of Carcinogenic Risks To Humans, **80**, i-ix+1-390, 2002.

[81] IARC, "Part 2 : Radiofrequency Electromagnetic Fields, " **102**, 2018.

[82] M.R.Scarfì, S. Lagorio, L. Anglesio, G. D'Amore, C. Marino, Radiazioni a riadiofrequenza e tumori: sintesi delle evidenze scientifiche, 2019.

[83] New Zealand Ministry of Health, Interagency Committee on the Health Effects of Non-ionising Fields Report to Ministers 2018, 2018.

[84] Public Health England, Collection Electromagnetic fields Advice on exposure to electromagnetic fields in the everyday environment, including electrical appliances in the home and mobile phones., 2020.

[85] Swedish Radiation Safety Authority's Scientific Council on Electromagnetic Fields, Recent research on EMF and health risk: eleventh report from SSM's scientific council on electromagnetic fields: including thirteen years of electromagnetic field research monitored by SSM's Scientific Council on EMF and health: how has the evidence chang, 2016.

[86] B. Hocking, F. Gobba, "Medical aspects of overexposures to electromagnetic fields, " Journal of Health, Safety and Environment, **27**(3), 185–195, 2011.

[87] IEEE Committee on Man and Radiation, "Medical Aspects Of Radiofrequency Radiation Overexposure, " Health Physics, (September 2001), 0–4, 2002.

[88] HSE, Electromagnetic Fields at Work, 2016.

[89] F. Gobba, "Health surveillance of EMF-exposed workers at particular risk, " G Ital Med Lav Ergon, **41**(4), 285–292, 2019.

[90] F. Gobba, N. Bianchi, P. Verga, G.M. Contessa, P. Rossi, "Menometrorrhagia in magnetic resonance imaging operators with copper intrauterine contraceptive devices (iuds): A case report, " International Journal of Occupational Medicine and Environmental Health, **25**(1), 97–102, 2012, doi:10.2478/s13382-012-0005-y.

[91] A. Huss, K. Schaap, H. Kromhout, "A survey on abnormal uterine bleeding among radiographers with frequent MRI exposure using intrauterine contraceptive devices, " Magnetic Resonance in Medicine, **79**(2), 1083–1089, 2018, doi:10.1002/mrm.26707.

[92] International Commission on Occupational Health, ICOH Code of Ethics, 2012.

[93] F. de Vocht, E. Batistatou, A. Mölter, H. Kromhout, K. Schaap, M. van Tongeren, S. Crozier, P. Gowland, S. Keevil, "Transient health symptoms of MRI staff working with 1.5 and 3.0 Tesla scanners in the UK, " European Radiology, **25**(9), 2718–2726, 2015, doi:10.1007/s00330-015-3629-z.

[94] K. Schaap, Y.C. De Vries, C.K. Mason, F. De Vocht, L. Portengen, H. Kromhout, "Occupational exposure of healthcare and research staff to static magnetic stray fields from 1.5-7 tesla MRI scanners is associated with reporting of transient symptoms, " Occupational and Environmental Medicine, **71**(6), 423–429, 2014, doi:10.1136/oemed-2013-101890.

[95] G. Zanotti, G. Ligabue, L. Korpinen, F. Gobba, "Subjective symptoms in Magnetic Resonance Imaging operators: prevalence, short-term evolution and possible related factors, " Med Lav, **107**(4), 263-270., 2016.

[96] S. Bongers, P. Slottje, L. Portengen, H. Kromhout, "Exposure to static magnetic fields and risk of accidents among a cohort of workers from a

medical imaging device manufacturing facility, " Magnetic Resonance in Medicine, **75**(5), 2165–2174, 2016, doi:10.1002/mrm.25768.

[97] A. Huss, K. Schaap, H. Kromhout, "MRI-related magnetic field exposures and risk of commuting accidents – A cross-sectional survey among Dutch imaging technicians, " Environmental Research, **156**(April), 613–618, 2017, doi:10.1016/j.envres.2017.04.022.

[98] F. Gobba, R. Ghersi, S. Martinelli, A. Richeldi, P. Clerici, P. Grazioli, "Italian translation and validation of the Nordic IRSST standardized questionnaire for the analysis of musculoskeletal symptoms, " Medicina Del Lavoro, **99**(6), 424–43, 2008.

Fusion of Optical and Microfabricated Eddy-Current Sensors for the Non-Destructive Detection of Grinding Burn

Isman Khazi[1,2], Andras Kovacs[1], Ulrich Mescheder[1,3,*], Ali Zahedi[4], Bahman Azarhoushang[4]

[1]*Institute for Microsystems Technology (iMST), Faculty of Mechanical & Medical Engineering, Furtwangen University, 78120 Furtwangen, Germany*

[2]*Department of Microsystems Engineering (IMTEK), University of Freiburg, Georges-Köhler-Allee 103, 79110 Freiburg im Breisgau, Germany*

[3]*Faculty of Engineering, University of Freiburg, Georges-Köhler-Allee 103, 79110 Freiburg im Breisgau, Germany*

[4]*Institute of Precision Machining (KSF), Faculty of Mechanical & Medical Engineering, Furtwangen University, 78120 Furtwangen, Germany*

A R T I C L E   I N F O

A B S T R A C T

A sensor fusion concept integrating the optical and microfabricated eddy-current sensor for the non-destructive testing of the grinding burn is reported. For evaluation, reference grinding burn with varying degrees are fabricated on 42CrMo4 tool steel cylinder. The complementary sensing nature of the proposed sensors for the non-destructive testing of the grinding burn is successfully achieved, wherein both the superficial and an in-depth quantitative profile information of the grinding zone is recorded. The electrical output (voltage) of the optical sensor, which is sensitive to the optical surface quality, dropped only by 20 % for moderate degree of grinding burn and by ca. 50 % for stronger degree of grinding burn (i.e., by exclusively considering the superficial surface morphology of the grinding burn). Moreover, a direct correlation among the average surface roughness of the grinding burn, the degree of grinding burn and the optical sensor's output voltage was observed. The superficial and in-depth information of the grinding burn was recorded using a microfabricated eddy-current sensor (planar microcoil with circular spiral geometry with 20 turns) by measuring the impedance change as function of the driving frequency. The depth of penetration of induced eddy-current in the used 42CrMo4 workpiece (with a sensor to workpiece distance of 700 μm) varied from 223 μm to 7 μm on increasing the frequency of the driving current from 1 kHz to 10 MHz, respectively. A very interesting nature of the grinding burn was observed with two distinct zones within the grinding zone, namely, the superficial zone (starting from the workpiece surface to 15 μm in grinding zone) and a submerged zone (>15 μm within the grinding zone). The impedance of the microcoils changed by ca. 8 % and 4 % for the superficial and submerged zone for regions with stronger degree of grinding burn at a frequency of 10 MHz and 2.5MHz, respectively. Furthermore, a correlation between the microhardness of the grinding burn and the impedance change is also observed.

1. Introduction

Grinding technology is considered as the strategic process in the manufacturing technology with its application spanning from the manufacturing of parts for aerospace, defense industry to the production of surfaces with optical quality for the electronics and telecommunications devices, with technology moving towards processing of also the hard ceramic materials [1]. The mechanics involved during the grinding process include the interaction between the grinding wheel with abrasive grains and the

*Corresponding Author: Ulrich Mescheder, Furtwangen University, Robert-Gerwig-Platz 1, 78120, Furtwangen, Germany
+49 7723 920 2232, mes@hs-furtwangen.de*

workpiece's surface, wherein the material from the workpiece (WP) is removed in a complex manner governed by the interplay among the rubbing, cutting and ploughing stages of material abrasion. However, in case of grinding processes with high material removal rates involving hard steel workpieces, the operating temperatures during the grinding process might easily go beyond the tempering temperature of the WP when the grinding operating conditions are sub-optimal, and might result in an irreversible thermal damage on and within the grinding zone (i.e., the region of interaction between the grinding wheel and WP surface), which is usually referred to as the so-called grinding burn (GB) [1–4]. Among the several defects such as microcracks, pores etc., occurring within the grinding zone (GZ) due to sub-optimal grinding conditions, the occurrence of GB is the most complex defect to detect. The reason behind the complexity in the detection of GB is attributed to the nature of complex microstructural modifications that occur not only on the surface of GZ, but also a few hundred micrometers deep within the GZ [4–6]. As described in [1] and [7], the thermal damage caused by sub-optimal grinding conditions results in tensile residual stresses within the GZ. Moreover, it can lead to grain growth, precipitation, softening, phase transformations resulting in re-hardening, thermal expansion/contraction creating microcracks, and chemical reactions leading to discoloration, i.e., severe oxidation GB; all of which are not only detrimental to the quality of the WP (limiting the performance of the WP), but also lay an enormous financial burden on rejection of ground workpieces having GB [8].

In a recent review paper [2], the authors comprehensively summarized the different methods for detection of GB pre- and post-grinding process, out of which, they are broadly classified under destructive- and non-destructive testing (NDT) methods. Under destructive methods, the method of Nital etching revealing the microstructure of the GZ, and microhardness testing revealing the microstructural change as a function of the hardness profile of the GZ can be used. Furthermore, the optical inspection (with sophisticated CCD cameras and visual inspection), residual stress inspection using x-ray diffractometer (XRD), spectroscopic measurement of elemental study in the GZ, electromagnetic methods involving conventional eddy-current sensors, magnetoelastic methods involving the Barkhausen noise analysis and acoustic emission sensors can be used to detect the occurrence of GB on the ground WP post grinding process [2]. Few of the reported methods like XRD and spectroscopy cannot be integrated in the grinding machine, while the others such as electromagnetic and acoustic emission sensors still rely on the conventional sensor systems; wherein, on one side the system is quite bulky (which hinders its integration within the grinding machine), and on the other side the detection resolution is limited due to the size of the conventional probes used.

Furthermore, since the past two decades there have been a constant quest to realize realistic intelligent grinding manufacturing processes, which has further gained momentum in terms of research and development, owing to the emergence of industry 4.0 and big data with the concept of smart interconnected

real-time condition monitored manufacturing processes [8–14]. However, among other challenges associated with the implementation of the intelligent grinding process, the availability of sophisticated approaches for the integrated process monitoring (i.e., the sensor systems), considering the difficulty to model process dynamics of grinding processes, is a fundamental requirement for the development of intelligent grinding. In order to fulfill this requirement, a sensor fusion system comprising of more than one sensing principle would enormously increase the detection capability, the sensitivity of the parameters of interest, and also the reliability of the test results. The authors in [15] reported a sensor fusion concept with integration of accelerometers and power-cell sensors for the detection of the roughness of the WP, however, the reported system is not capable of detecting GB. Therefore, in this paper, which is an extended version of a previous research [16], we report the detailed analysis of the sensor fusion concept with the integration of an optical sensor (OS) and a microfabricated eddy-current sensor (μEC) working complementary to each other for NDT of GB using a 42CrMo4 cylinder with varying degrees of reference GB. The proof-of-concept for the NDT of GB using the OS and μEC sensors has been already reported along with the individual development and characterization in [17–19], therefore, this paper deals with the experimental analysis of the complementary sensor functionality of combined OS and μEC sensors for NDT of GB.

2. Sensor fusion concept for non-destructive testing of grinding burn

The occurrence of the GB results in hard to model modifications on and within the GZ of the ground WP. Depending on the severity of the GB, it can get explicitly visible by discoloration (i.e., so-called severe oxidizing GB) on the surface of the GZ (as shown in the schematic in Figure 1 with orange coloration of the ground WP surface), or during the concluding spark-out period of grinding process, however, the discolored oxidized layer might be removed. In this case, the irreversible microstructural changes withing the GZ, which can propagate up to a few hundred micrometers within the GZ, still exist (depicted as hidden GB in Figure 1). Furthermore, the microstructural changes can result in either softening of the GZ or might result in a re-hardened layer (due to quenching effect) on top of the softened layer [4–6]. Therefore, the proposed sensor fusion system in this paper combines two sensor principles, namely the OS and μEC sensors (as shown in schematic in Figure 1) capable of detecting the surface morphological changes and the in-depth microstructural changes (as function of varying driving frequency which influences the depth of penetration of the induced eddy-currents within the WP), respectively. An interesting effect of the surface morphological changes on the GZ surface was shown in our previous paper [17], wherein it was found that the reference GB with varying degrees showed a direct correlation to the average surface roughness values (R_a) of the ground WP surface. The average surface roughness increased with increasing degree of GB. The proposed OS works on the principle of illuminating
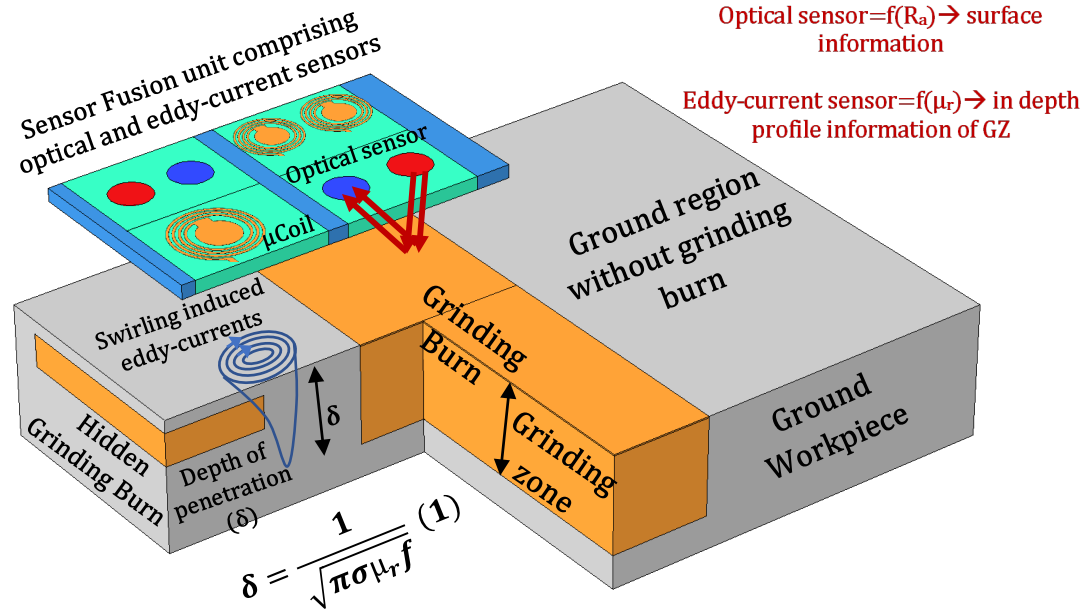
Figure 1: Schematic showing the sensor fusion concept integrating the optical sensor and the microfabricated eddy-current sensor for the NDT of GB. The optical sensor detects the superficial surface modifications for e.g., the change in R_a as function of GB, and the microfabricated eddy-current sensors records the in-depth profile information within the GZ (i.e. by varying the driving frequency). Therefore, making it possible to even detect the so-called hidden and severe degree of GB resulting in significant microstructural changes in the GB.

the WP surface and recording the reflected light, which is transduced into sensor output voltage (detailed explanation of the sensor electronics can be found in [17]). The voltage drop (ΔV) increased with an increase in R_a, which in turn increased with the degree of GB [17].

Among several applications exploiting the use of eddy-currents such as contact-less breaks in this work, µEC sensors are used for the NDT of microstructural modification within the GZ (i.e., an in-depth profile information of GZ). The microfabrication steps are described in [16, 18]and the characterization of the µEC sensors for NDT of GB is shown in [18, 19]. The µEC sensors exploit the fact of the predominant change in the relative permeability (μ_r) within the GZ in case of WP out of hardened ferromagnetic steels, which are inevitably reliant on the grinding technology for many precision applications [3]. As shown in Figure 1, swirling eddy-currents are induced on and within the conductive WP, when it is in the vicinity of the µEC sensors, whose depth of penetration (δ) as shown in the Equation 1 depends on frequency (f) of the driving current, the conductivity (σ) and μ_r.

$$\delta = \frac{1}{\sqrt{\pi \sigma \mu_r f}} \tag{1}$$

Furthermore, in case of occurrence of GB, the microstructural changes within GZ affects the nature of the induced eddy-current in WP [20], which is then recorded either as the impedance change (ΔZ) in case of single µEC sensor (absolute sensor) or the voltage

change in case of sender-receiver µEC sensor combination. The main advantage of the use of µEC sensors is the possibility of varying δ of the induced eddy-current by varying f, wherein δ is inversely proportional to f. Therefore, by varying f of the µEC sensors, the depth profile within the GZ can be quantitively recorded and compared with the reference material profile. Thereby, making the µEC sensor suitable for the NDT of not only superficial GB, but also the so-called hidden GB within the GZ. Hence, with this proposed approach of sensor fusion concept, the NDT of GB can be enhanced for the quality testing of ground workpieces. Furthermore, the proposed fused sensor system can be integrated within the grinding machine to facilitate the in-process detection of GB and to increase the material removal efficiency.

3. Results and discussion

For the experimental characterization of the sensor fusion concept, reference GB with varying degrees were fabricated on 42CrMo4 steel cylinder as shown in Figure 2(a) (the grinding parameters and conditions are described in [16]). Each region named as S2-S8 in Figure 2(a) belongs to a different degree of GB, except region S3, which is considered as the reference ground region without GB as a calibration for the sensor measurements. Figure 2(b) shows the micrographs recorded using an optical microscope, wherein the discoloration i.e., the oxidative GB along with the undulation pattern corresponding to the abrasive grains in the grinding wheel can be seen. Furthermore, the surface morphology was further characterized using a white light
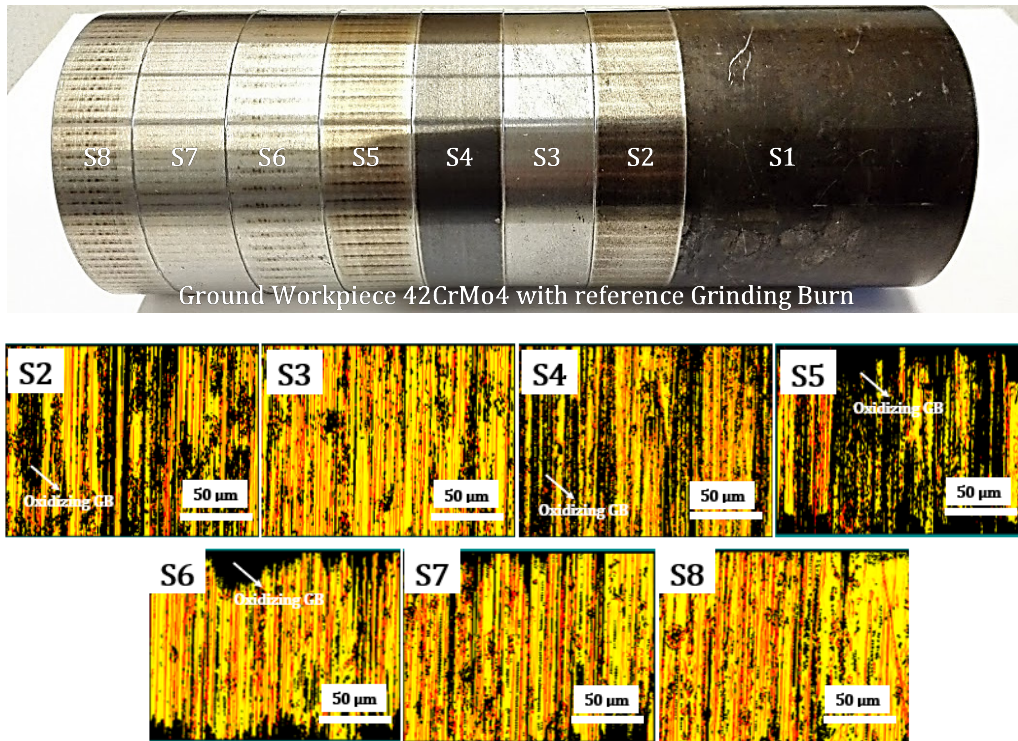
Figure 2: (a) 42CrMo4 cylindrical workpiece ground with reference grinding burn with varying degrees from S2, S4-S8, wherein region S3 is the reference ground region without GB (Region S1 is original unground state of the workpiece), (b) micrographs recorded using an optical microscope for each individual region S2-S8 showing the undulating pattern corresponding to the abrasive grains of the grinding wheel along with the dark discoloration corresponding to the oxidative grinding burn.
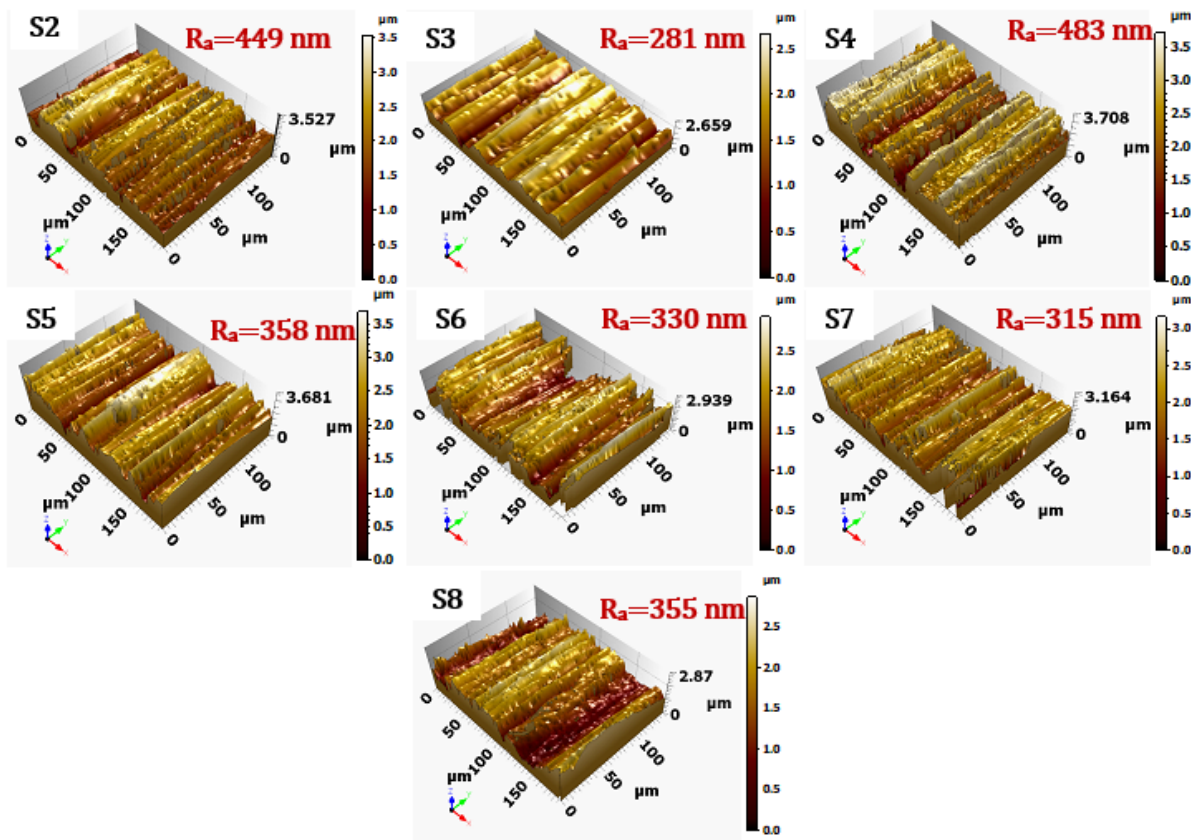

Figure 3: Surface morphology micrographs recorded using a white light interferometer (Zygo Newview) with 50x magnification resulting in a scan area of 188 µm x 140 µm. The average surface roughness values are shown in the top right corner of each micrograph.
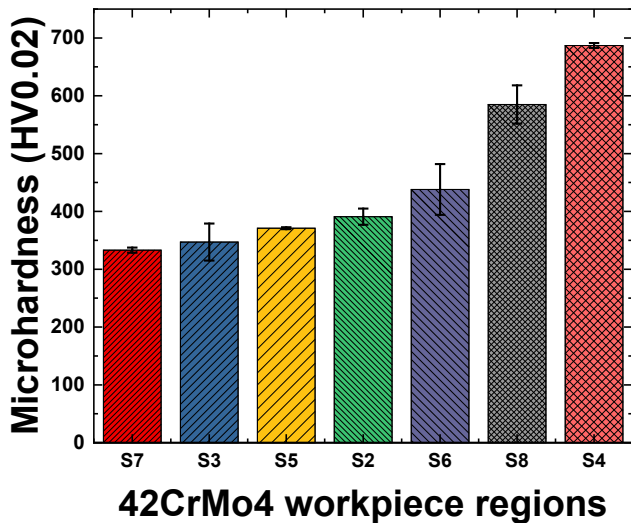
Figure 4: Measured Vickers microhardness on regions S2-S8 on the reference workpiece 42CrMo4 with varying degrees of GB. Each measurement is mean of 5 indentations on each region.
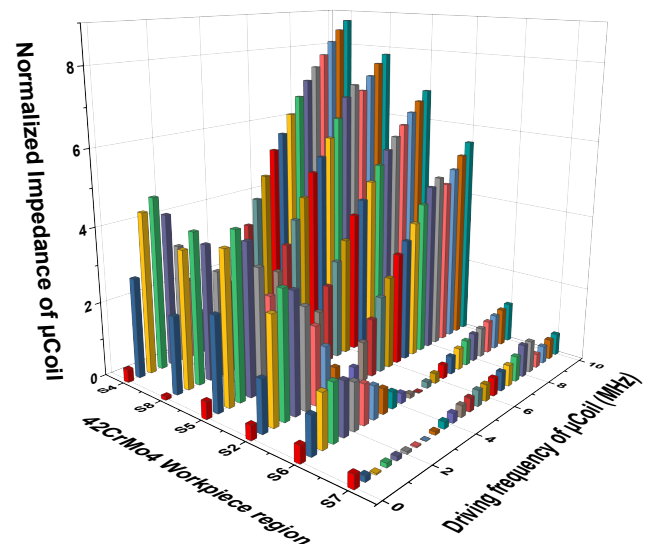
interferometer (Zygo Newview) in order to quantitatively compute the average surface roughness (R_a) values. Figure 3 shows the recorded surface topology micrographs using 50x objective within a scan area of 188 µm x 140 µm for the regions S2-S8 along with the computed R_a values (mean of 10 measurements). The R_a values varied from 281 nm to 483 nm for the reference region S3 and the strongest GB region S4, respectively. This observation can be attributed to the surface morphological modifications occurring on the surface of GZ with the occurrence of GB, which appear not only in the form of discoloration i.e., oxidation GB, but also results in the modification of the surface topology.

Moreover, considering the microstructural modifications as a consequence of GB, which might either soften or re-harden the

Figure 5: Normalized optical sensor output voltage experimentally measured as a function of varying degrees of GB on regions S2-S8, with a sensor to workpiece distance of 700 µm under quasi-static conditions.

Figure 6: Normalized impedance of 20 turns circular spiral geometry µcoil experimentally measured as a function of varying degree of GB on regions S2, S4-S8, with a µcoil to workpiece distance of 700 µm under quasi-static measurements (the measurements from region S3 are considered as reference).

GZ, the microhardness of each region S2-S8 was measured using Vickers Microhardness device from Innovatest Falcon 501 device with a 20 g load. Furthermore, the indentation depth with the used 20 g load was 1 µm to 2 µm, for the measured microhardness range, and hence the measured microhardness values are more superficial in nature. Figure 4 shows the computed microhardness values (mean of 5 measurements) for the regions S2-S8. The microhardness increased from 333 HV0.02 for region S7 to 685 HV0.02 for region S4. This effect can be attributed to complex microstructural changes, which result in either softening, re-hardening and combination of re-hardened and softened profile within the GZ [6]. From Figure 4, it can be seen that ground region S7 shows the presence of softened layer with reduced microhardness compared to reference region S3, while all other regions showed a re-hardened layer with S8 and S4 showing an almost twofold increment in the microhardness compared to the reference region S3.

The experimental measurements using OS and the µEC sensor were done on a lathe machine to emulate the conditions within a grinding machine. The details of the experimental setup along with the information related to the optical sensor can be found in [17], and the microfabrication steps of µEC sensor with circular spiral geometry (20 turns µcoil used in this work) is reported in [18]. The distance between the sensors and WP was kept constant at 700 µm for all the measurements and the WP was rotated per hand for each new measurement; thereby, resulting in a quasi-static measurement. Figure 5 shows the normalized output voltage of the optical sensor as a function of varying degree of GB on the WP, by taking the voltage recorded from region S3 as reference value. The optical sensor takes into account the surface morphological changes, i.e., either the discoloration as a result of oxidation GB or the modified surface roughness profile on the GZ,

Figure 7: Theoretical computed depth of penetration of induced eddy-current within the 42CrMo4 workpiece at a µEC sensor to workpiece distance of 700 µm and considering the material properties as reported in [21].
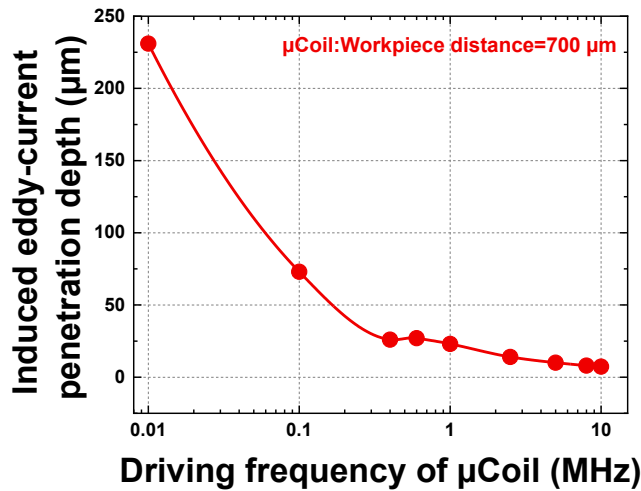
both of which would adversely affect the intensity of the reflected light (i.e., in response to the incident light form the optical sensor), which is transduced into voltage by the OS. Therefore, the presence of the GB is detected as the function of voltage change ($\Delta V_{OS} = (V_{ref} - V_{wp})/V_{ref}$) with respect to the reference voltage (V_{ref}) from the reference region S3 and the voltage recorded from ground surface with GB (V_{wp}). As seen in Figure 5, the OS is capable for the NDT of GB, wherein the output voltage changes as a function of the different degree of GB on regions S2 and S4-S8. Furthermore, the recorded ΔV_{OS} values are directly proportional to the R_a values, i.e., the higher the surface roughness, the larger are the ΔV_{OS} values as shown in [17]. As seen in Figure 5, the ΔV_{OS} values dropped by ca. 20 % and 50 % for the regions S5-S8 and regions S2 and S4, respectively. Thereby, depending on the intensity of drop in ΔV_{OS} values, the GB can be roughly classified under moderate (i.e., for ΔV_{OS}=20 %) and strong (i.e., for ΔV_{OS}=50 %) degree of GB. Complementary to the OS measurements, the µEC measurements on the same WP were carried out under the similar working conditions as described above for OS measurements. However, in case of µEC sensors, the impedance response (Z_{wp}) of the µEC sensor as function of the different regions S2-S8 was recorded. Similar to the OS measurements, Z_{wp} for the region S3 was considered as the reference and the normalized impedance change ($\Delta Z = (Z_{ref} - Z_{wp})/Z_{ref}$) for the regions S2, S4-S8 as a function of f is computed and shown in Figure 6. Primary, the ability of the µEC sensors for the NDT of GB is observed for all the ground regions with varying degree of GB, and secondary, on contrary to the OS measurements, where only the surface morphological information was revealed, in case of the µEC sensors, an in-depth profile information is revealed as function of varying f as seen in Figure 6. A very interesting trend of variation in ΔZ as function of f is observed, wherein ΔZ initially increased on increasing f from 1 kHz to 1.2 MHz and decreased further with increase f; however, it increased again from 4 MHz to 10 MHz (the f limit of the used LCR meter was 10 MHz). This effect can be attributed to the
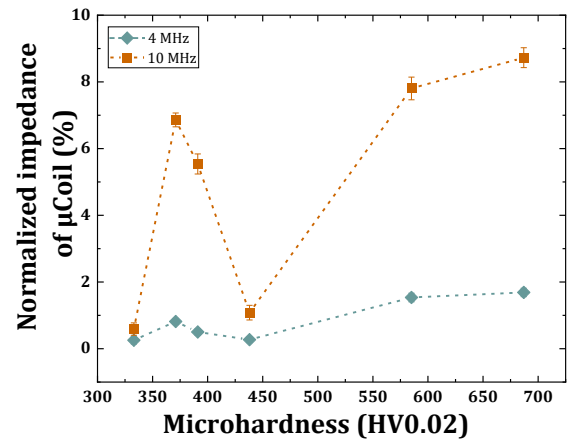
(a)
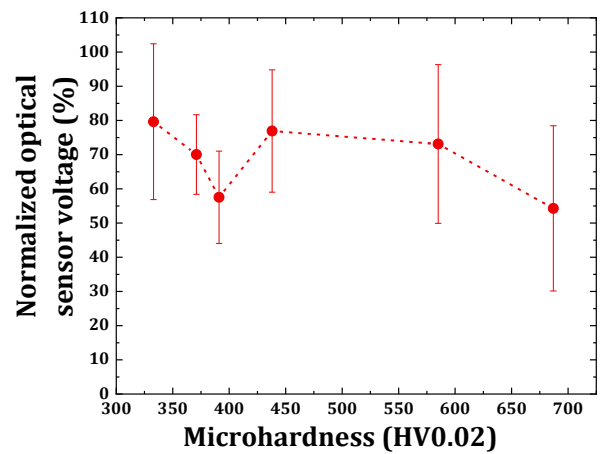
(b)

Figure 8: Comparison of sensor fusion concept using the OS and µEC sensors as function of the measured Vickers microhardness values (i.e. destructive approach) (a) normalized impedance of µEC sensor as function of measured Vickers microhardness for the reference GB regions on 42 CrMo4 for 4 MHz (δ = 11 µm) and 10 MHz (δ = 7.5 µm), and (b) normalized optical sensor voltage as function of measured Vickers microhardness values.

microstructural changes occurring within the GZ few hundred micrometers deep in case of the occurrence of GB. At this point it comes to the complementary sensing nature and measurement capability of µEC sensors compared to the OS, where it can quantitatively record the microstructural variation in ΔZ as seen in Figure 6. This effect is because of the variation in δ for the induced eddy-currents as function of f as shown in Equation 1. For e.g., Figure 7 shows the theoretical δ for the induced eddy-currents within the used WP (i.e., 42CrMo4, taking the material properties from [21]), wherein the induced eddy-current tends to be more superficial with increasing driving frequency, i.e., it decreased from 230 µm to ca. 7 µm on increasing the frequency from 0.01 MHz to 10 MHz. Therefore, from Figure 6 it is evident that the microstructural changes within the GZ consist of two zones, namely submerged (>15 µm within GZ) zone and superficial zone (i.e., near to the surface within <15 µm). Furthermore, the ΔZ values increased at higher f, showing that

GB caused severe microstructural changes in the superficial zone in case of ground regions S2, S4, S5 and S8. Additionally, the order of arrangement of the WP ground regions in Figure 6 is with respect to descending order in the ΔZ values (i.e., at higher f), is comparable with the measured microhardness as shown in Figure4. For e.g., the ground region S4 followed by the region S8 showed the maximum microhardness values and hence, a larger ΔZ variation was observed i.e., 8.7 % and 7.8 % at 10 MHz for S4 and S8, respectively, which is evident from Figure 6. Meanwhile, the region S7 showed minimum microhardness and hence, it also showed minimum variation in ΔZ values as seen in Figure 6. Another interesting observation can be noticed for region S6, wherein the ΔZ is larger in the submerged region as compared to the superficial region and an opposite trend is then recorded for region S7. Thereby, showing the complex in-depth nature of the occurrence of the GB. However, in respect to the very similar impedance dependence on frequency of regions S4 and S8, the OS provides a significant signal difference between these surfaces. Moreover, apart from the complementary information related to superficial and in-depth profile obtained using the combination of OS and μEC sensors, the comparison of both sensors merits for the superficial measurement as function of destructive approach i.e., the Vickers microhardness (Figure 4) is shown in Figure 8(a-b). Here, the measured microhardness HV is plotted on the x-axis considering HV as reference for microstructural changes by grinding related GB which is correlated to the μEC (Figure 8a) and OC (Figure 8b) measurements. For the used load of 20 gf an indentation depth of $1 \, \mu m - 2 \, \mu m$ is obtained for Vickers microhardness measurements. The normalized impedance ΔZ in Figure 8a is evaluated for 4 MHz ($\delta = 11 \, \mu m$) at a frequency where a pronounced minimum in the normalized impedance is found (Figure 6) and for 10 MHz ($\delta = 7.5 \, \mu m$) to reveal more the superficial information. It is found that ΔZ for $f = 10$ MHz initially increased as function of microhardness, however it decreased steeply within the microhardness range of 375 HV0.02 – 450 HV0.02, and subsequently increased as function of microhardness values. At 4 MHz, the minimum of ΔZ occurs at around 450 HV0.02 and the changes of ΔZ towards lower and higher microhardness values are less pronounced. The observed trend can be attributed to the complex microstructural changes occurring within the GZ. ΔV_{OS} showed a different dependence on microhardness and therefore, can provide complementary information about GB compared to μEC especially in the range of 400 HV0.02 - 450 HV0.02. At higher microhardness values, ΔV_{OS} showed a gradual decreasing trend as function of the microhardness values.

Therefore, the sensor fusion by integrating the OS and μEC sensors makes it possible the NDT of GB, by not only considering the surface morphological information on the GZ, but also by revealing the in-depth profile information up to few hundred micrometers within the GZ on occurrence of GB. The presented sensor fusion concept is preliminary approach towards the proof-of-concept for the complementary sensing nature for the NDT of GB. However, there is enough room for the further development and optimization to successfully integrate the developed sensor fusion unit in the grinding machine to realize and fulfill the quest towards the intelligent grinding process.

4. Conclusion

The sensor fusion concept integrating an optical sensor and a microfabricated eddy-current sensor is reported for the non-destructive testing of the grinding burn. The complementary sensing nature of the reported sensor combination results in not only the superficial non-destructive testing of grinding burn, but also an in-depth profile within the grinding zone. The optical sensor voltage dropped as function of varying degree of grinding burn, which was observed to be directly correlated to the average surface roughness of the grinding burn. The voltage dropped by 20 % for moderate degree of grinding burn, and by 50 % for strong degree of grinding burn. The in-depth quantitative profile of the microstructural changes within the grinding zone is recorded with the use of the microfabricated eddy-current sensors (circular spiral μcoils with 20 turns) as a function of the varying driving frequency. A very interesting nature of the grinding burn was observed as function of the impedance variation of the microcoils with two distinct zones, i.e., the sub-merged zone (>15 μm within grinding zone) and superficial zone (from WP surface to 15 μm within grinding zone). Impedance changes of ca. 8 % and 4 % were obtained for stronger degree of grinding burn (i.e., regions S4 and S8) for the superficial and sub-merged grinding burn at 10 MHz and 2.5 MHz, respectively. Utilizing the impedance information of the grinding zone as function of varying driving frequency, it could also be possible to build qualitatively the profile of the microstructural changes for quality testing, and hence ease the observation for the severity of the grinding burn. The reported sensor fusion concept can be further optimized to increase the detection sensitivity and robust packaging immune to the harsh environmental conditions occurring within the grinding machine to realize intelligent grinding processes and in-process monitoring capabilities corresponding to the requirements of industry 4.0. Furthermore, to model the surface morphology of grinding burn, an in-depth surface roughness analysis can be done (considering the parameters beyond root mean squared and average surface roughness values) to unveil the surface modifications at the atomistic level.

Conflict of Interest

The authors declare no conflict of interest.

Acknowledgment

and HAW-KMU (**32-7545.20/27/57**). The authors highly appreciate the student work done by Mr. Pranav Dhumal and Mr. Jerrine Jacob Mathews for the characterization of the optical sensor.

References

[1] W. B. Rowe, Principles of Modern Grinding Technology, 2nd edition Burlington: Elsevier Science, 2013.

[2] B. He, C. Wei, S. Ding, and Z. Shi, "A survey of methods for detecting metallic grinding burn," Measurement, **134**, 426–439, 2019, doi: 10.1016/j.measurement.2018.10.093.

[3] R. Ito, T. Azuma, T. Kasuga, S. Soma, S. Murakami, and T. Kuriyagawa, "Development of Non-Destructive Inspection System for Grinding Burn - An Application of the Grinding Burn Detecting Technique to Evaluate Residual Stress," AMR, **797**, 307–312, 2013, doi: 10.4028/www.scientific.net/AMR.797.307.

[4] M. W. Seidel, Schleifbrand und dessen Prüfung: Leitfaden für die Praxis. München: Hanser, Carl, 2020.

[5] M. W. Seidel, A. Zösch, and K. Härtel, "Grinding burn inspection," Forschung im Ingenieurwesen, **82**(3), 253–259, 2018, doi: 10.1007/s10010-018-0270-4.

[6] R. Ito, N. Mukaide, T. Azuma, S. Soma, S. Murakami, and T. Kuriyagawa, "Development of Non-Destructive Inspection System for Grinding Burn-in-Process Detection of Grinding Burn," AMR, **1017**, 135–140, 2014, doi: 10.4028/www.scientific.net/AMR.1017.135.

[7] A. Jeffrey Badger and Andrew Torrance, "Understanding the causes of grinding burn helps alleviate the problem," Cutting Tool Engineering, **52**(12), 1-3, 2000.

[8] T. Kaufmann, S. Sahay, P. Niemietz, D. Trauth, W. Maas, and T. Bergs, "AI-based Framework for Deep Learning Applications in Grinding," in 2020 IEEE 18th World Symposium on Applied Machine Intelligence and Informatics (SAMI), Herlany, Slovakia, 195–200, 2020.

[9] L. Lv, Z. Deng, T. Liu, Z. Li, and W. Liu, "Intelligent technology in grinding process driven by data: A review," Journal of Manufacturing Processes, **58**, 1039–1051, 2020, doi: 10.1016/j.jmapro.2020.09.018.

[10] W. Guo, B. Li, and Q. Zhou, "An intelligent monitoring system of grinding wheel wear based on two-stage feature selection and Long Short-Term Memory network," Proceedings of the Institution of Mechanical Engineers, Part B: Journal of Engineering Manufacture, **233**(13), 2436–2446, 2019, doi: 10.1177/0954405419840556.

[11] H. B. Hübner, M. A. V. Duarte, and R. B. Da Silva, "Automatic grinding burn recognition based on time-frequency analysis and convolutional neural networks," The International Journal of Advanced Manufacturing Technology, **110**(7-8), 1833–1849, 2020, doi: 10.1007/s00170-020-05902-w.

[12] F. Junejo, "The Application of Artificial Intelligence in Grinding Operation using Sensor Fusion," Geomate, **12**(30), 2017, doi: 10.21660/2017.30.160503.

[13] L. Wang and R. X. Gao, Condition monitoring and control for intelligent manufacturing. London: Springer, 2006.

[14] F. Godoy Neto R., Marchi M., Martins C., R. Aguiar P. and Bianchi E, "Monitoring of Grinding Burn by AE and Vibration Signals," in Proceedings of the 6th International Conference on Agents and Artificial Intelligence, 272–279, 2014.

[15] B. Botcha, V. Rajagopal, R. Babu N, and S. T. Bukkapatnam, "Process-machine interactions and a multi-sensor fusion approach to predict surface roughness in cylindrical plunge grinding process," Procedia Manufacturing, **26,** 700–711, 2018, doi: 10.1016/j.promfg.2018.07.080.

[16] Isman Khazi, Andras Kovacs, Ali Zahedi, Christian Reser, Ulrich Mescheder, Bahman Azarhoushang and Christoph Reich, "Real time In-Situ Quality Monitoring of Grinding Process using Microtechnology based Sensor Fusion," in 2020 IEEE International Conference on Semiconductor Electronics (ICSE), Kuala Lumpur, Malaysia, 180-184, 2020, doi: 10.1109/ICSE49846.2020.9166898

[17] A. Kovacs, I. Khazi, A. Zahedi, U. Mescheder and B. Azarhoushang, "Development of an Optical Sensor for the Non-Destructive Testing of Grinding Burn," in 2020 IEEE SENSORS, Rotterdam, Netherlands, 1-4, 2020. doi: 10.1109/SENSORS47125.2020.9278837

[18] Isman Khazi, Andras Kovacs, Vaibhav Kumar, Pranav Dhumal, Ulrich Mescheder, "Microfabricated 2D planar eddy-current microcoils for the non-destructive testing of grinding burn marks," Nondestructive Testing and Diagnostics, **3**, 29–35, 2019, doi: 10.26357/BNiD.2019.012

[19] I. Khazi, A. Kovacs, A. Zahedi, U. Mescheder and B. Azarhoushang, "Microfabricated Eddy-Current Sensors for Non-Destructive Testing of the Micro Grinding Burn," 2020 IEEE SENSORS, Rotterdam, Netherlands, 1-4, 2020, doi: 10.1109/SENSORS47125.2020.9278595

[20] N. Bowler, Eddy-Current Nondestructive Evaluation. New York, NY: Springer New York, 2019.

[21] T. Bulin, E. Svabenska, M. Hapla, P. Roupcova, C. Ondrusek, and O. Schneeweiss, "Magnetic properties of 42CrMo4 steel," IOP Conference Series: Materials Science and Engineering, **179**, 1-6, 2017, doi: 10.1088/1757-899X/179/1/012010.

Iron-doped Nickel Oxide Nanoparticles Synthesis and Analyzing Different Properties

Manar Saleh Alshatwi[*], Huda Abdulrahman Alburaih, Shahad Salem Alghamdi, Danah Abdullah Alfadhil, Joud Awadh Alshehri, Farah Abdullah Aljamaan

Faculty of Science, Department of physics, Princess Nourah Bint Abdulrahman University, Riyadh, 13415, Saudi Arabia

A B S T R A C T

This is a report describing the impact of calcination on the morphological and optical properties of nanoparticles Iron doped-nickel oxide. By synthetic precipitation, the technique makes use of it. Three samples have been calcined in different temperatures and were characterized by X-ray diffraction (XRD), Fourier transforms infrared spectroscopy (FTIR), UV spectroscopy, and scanning electron microscopy (SEM), energy dispersive X-Ray (EDX). The study showed that the increase in the temperature enhances the structural and optical properties of the samples, and makes the samples take a more crystalline structure. It is also shown that there has been an expansion of the volume of the samples, making the samples having a small bandgap. UV-Visible absorption spectra of Iron doped-nickel oxide nitrate shows a peak of absorption between 350 to 400 nm. The bandgap value is calculated to be 1.86 eV at a calcination temperature of 350°C. The required structural and optical properties of Iron doped-nickel oxide nanoparticles make it a promising material for optoelectronic applications.

1. Introduction

There have been extensive studies about nanomaterials from the very beginning of the invention of it, due to their unique physical properties and bulk counterpart. Many methods are used to synthesize Nano-scale materials [1]. Oxidized metals are commonly used in numerous areas, such as photoelectric, sensors, recording materials, and catalysts, etc [2]. These applications can be enhanced and well-controlled by fabricating them into nano-sized materials. Nano-materials properties are peculiar and fascinating therefore scientists have been studying them intensely for the past few years. Among various nanomaterials, metal oxide as NiO has attracted technological and industrial interest for its optical-electronic, magnetic, thermal, and mechanical properties this metal is a good P-type semiconductor because of its wide bandgap [3]. Also, the high activity in the degradation of phenol and phenolic derivatives. There are several ways to synthesize it, such as sol-gel [4-7] co-precipitation [8] hydrothermal [9] solvothermal [10], and chemical precipitation [11, 12]. In this study, we prepared iron-doped NiO NPs using the chemical precipitation method. Previous studies showed the advantages of it, such as the simplicity and condition of the process, condition, crystal structure, and particle size can be more controllable. NiO is a transition metal oxide with a density of 6.67gm/cm3 and a melting point reaching 1955°C along with a self-ignition temperature of 400°C [13], nanoscale NiO particles are between 10 -30 nanometers and the surface area of NiO is about 130-150.

The XRD pattern of NiO NPs exhibits a face-centered cubic (FCC) crystalline structure [10]. The UV-IR spectrum of biosynthesized NiO Nanoparticles showed optical properties well-defined at 321 nm and its exhibited optical band gap is (3.83-3.18eV) [13- 16]. Furthermore, in previous studies, nanoparticles of NiO with different concentrations and calcination temperatures of Iron have been investigated, and it's found that the properties of NiO NPs enhance with the addition of Fe and give excellent optical, structural, and magnetic properties. Therefore, this material can be a promising material when used in different applications such as optoelectronics, sensors, and batteries due its desired structural, optical, and magnetic properties. [8, 17, 18, 19, 20, 21, 22].

2. Experimental

2.1. Materials

The materials used in this research are: Nickel Nitride Ni $(NO_3)_2$, Iron nitride (Fe_2N), Citric Acid ($C_6H_8O_7$), and Ammonia hydrate (H_6NO).Deionized water was used in all the experimental procedures.

2.2. Preparation of Iron doped NiO nanoparticles

In this research, NPs of Iron doped NiO samples have been prepared by dissolving 13.81 g of Nickel Nitrate Ni $(NO_3)_2$ and 1.01 g Iron nitrate Fe $(NO_3)_3$ into an aqueous solution of 50 ml distilled water under medium stirring speed and temperature of 50

1422

C°. After 15 min, 1g of citric acid was added to the solution and kept stirring for another 15 minutes. Hereafter, Ammonium Hydrate (Liquid Ammonia) was added drop by drop, and precipitate started to appear until the mixture turned into a thick gel. Eventually, the temperature was raised to obtain a completely dry sample, which resulted in 5% Fe doped NiO nanoparticles. The dried samples were ground into a powder. In the end, the samples were placed in a muffle furnace at different temperatures ranging at (300,350,420) °C for 2 hours.
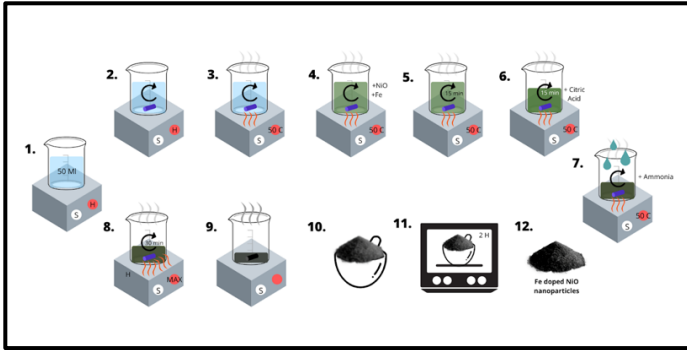

Figure 1: Iron-NiO Nanoparticles preparation method

2.3. Measurements of microstructure and performance

This work aims to study the impact of calcination temperatures at 300, 350, and 420 °C on the structural and optical properties of Iron doped NiO samples. The structural properties of purity and crystalline Fe doped NiO were characterized by XRD measurements using Philips diffractometer with an accelerating voltage of (λ=1.54°A) with CuKα radiation. The morphological studies done by using a scanning electron microscope (SEM) have been carried out. equipped with EDAX to record the composition analysis (JEOL Model with an accelerating voltage of 30kV). The optical properties of the samples were calculated with the SHIMADZU double beam UV-visible spectrophotometer. Finally, Thermal analysis was carried out by Perkin-Elmer Fourier transform-infrared spectroscopy (FTIR) over the range of 590-4000cm^{-1}.

3. Result

3.1. XRD Analysis

The structures of Iron-doped NiO nanoparticles calcined at 300, 350, 420 °C were analyzed using XRD and are represented in Fig.2. peaks of diffraction have been found near to 37.3°, 43.1°, 62.90°, 75.2°, and 79.3° in nanoparticles. However, both rhombohedral and cubic structural nanoparticles have been reported in reference [10, 17, 23]. Well-defined diffraction peaks for (111), (200), (311), and (222) cubic Iron-doped NiO NPs [10,17,22] were observed, which correspond to the standard spectrum (JCPDS, No.73-1519). At higher calcification temperatures, formed crystals get larger, which can be ascribed to thermally improved growth of crystals. The sizes of Iron doped NiO nanoparticles obtained from the diffraction ridges using the Scherrer equation are 5.6 nm and 9.6 nm and 11.6 nm for the sample calcined at 300°C, 350°C, and 420°C respectively, the sizes of nanoparticles increase with an increase in calcification temperatures and, the crystalline volume increases as the calcification temperature increases. W-H analysis was performed

to calculate the volume and fine diffraction contributions for the XRD line expansion. The very small diffraction values of all samples result in a close agreement between the estimated crystalline sizes from Scherrer's equation and the W-H analysis. The occurrence of vacancies and defects in composition Iron doped NiO nanoparticles can lead to subtle diffraction that leads to the widening of XRD peaks. From the Debye-Scherer equation, the average diameter of spherical particles can be easily calculated from

$$D = \frac{k\,\lambda}{\beta\,coscos\,\theta} \qquad (1)$$

where D represents the crystallite size, and K= 0.89 is the Scherrer constant and its associated with spherical particles and index (hkl) of the crystals. λ=1.54°A wavelength of source, β means the full width at half maximum (FWHM) of the peaks in radians. The average crystalline size increases from 4.83 nm to 14.5 nm as the calcination temperature increases and that is near previous studies [22,24].
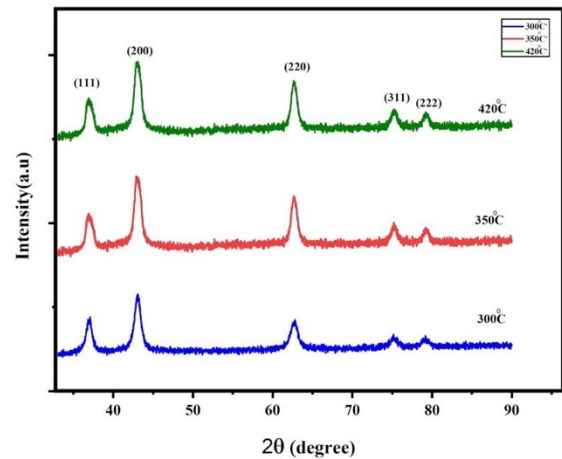
Figure 2: XRD structures of Iron doped NiO NPs samples at different calcination Temperatures

3.2. SEM Analysis and EDX

The particle size, shape, and morphology are identified using SEM micrographs. SEM images of the obtained Iron doped NiO NPs for the samples are shown in Fig.3. The SEM images show the morphology of the Iron doped NiO nanoparticles. It is observed that the shape of the particles is nearly spherical and Oval with non-homogeneous distribution, and they are in the range of 10 nm to 30 nm and that is close to the previous studies [15, 16, 24,4]. Particle size came out to be 4.6, 8.3, and 12.2 nm which means that particle size increases with the increase of the temperature. The particle size calculated from the SEM analysis seems to be quite similar to that measured from the XRD analysis of crystallite size. The EDX spectrum of Iron doped NiO nanoparticles is shown in Fig4. revealed the presence of Nickel, Oxygen, Carbon, and Iron is the only elementary species in samples.

3.3. FTIR Analysis

Figure 5 shows the FTIR spectra of Iron doped NiO particles samples calcined at 300, 350, and 420 °C. To determine the chemical structure of the samples the spectra were observed over

the frequency range of 590-4000 cm^{-1}. The broad absorption band centered at 3450 cm^{-1} is assigned to O–H stretching vibrations and the band at 1630 cm^{-1} is attributable to H–O–H bending vibration of water absorbed from the atmosphere when samples were prepared in the open air. Also, the absorption band in the region of 462–560 cm^{-1} is assigned to Fe–O stretching vibration mode and the second broad absorption band in the region 410 – 474 cm^{-1} is assigned to Ni–O stretching vibration mode. The broadness of the absorption band indicates that the NiO powders are nanocrystals and well crystallized. The intensity of Ni – O and F – O stretching bands seen in Fig.5 are increasing as the calcination.
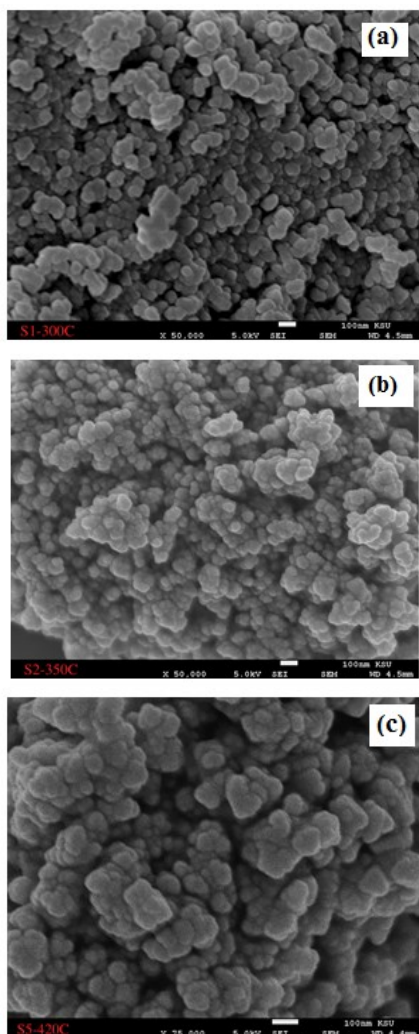
Figure 3: SEM images of Iron doped NiO NPs Calcined at (a)300, (b) 350, and (c) 420 °C.

3.4. UV-Visible studies

Figure 6 shows spectra for UV-visible absorption and $(\alpha h\nu)^2$ versus energy plot for Iron doped NiO nanoparticles samples. UV studies of absorption showed that a rise in calcination temperature results in a redshift in the absorption spectrum and a decrease in bandgap as a result of an increase in particle size. The peaks range in the ultraviolet spectrum showed between (300-400 nm) and that is close to the previous studies [10, 15]. In general, the data show that the sample calcined at 300°C has a value of 307 nm, and the value of 347 nm for the sample calcined at 350°C, lastly the value

436 nm for the sample calcined at 420°C, the peaks mean the matter absorption of the spectrum and also work to stimulate the electrons. The best result of the Three samples is the sample calcined at 350°C with a bandgap value of 1.86 eV and high absorption value which makes the bandgap a small value. At calcination temperatures, the properties of the material are enhanced.
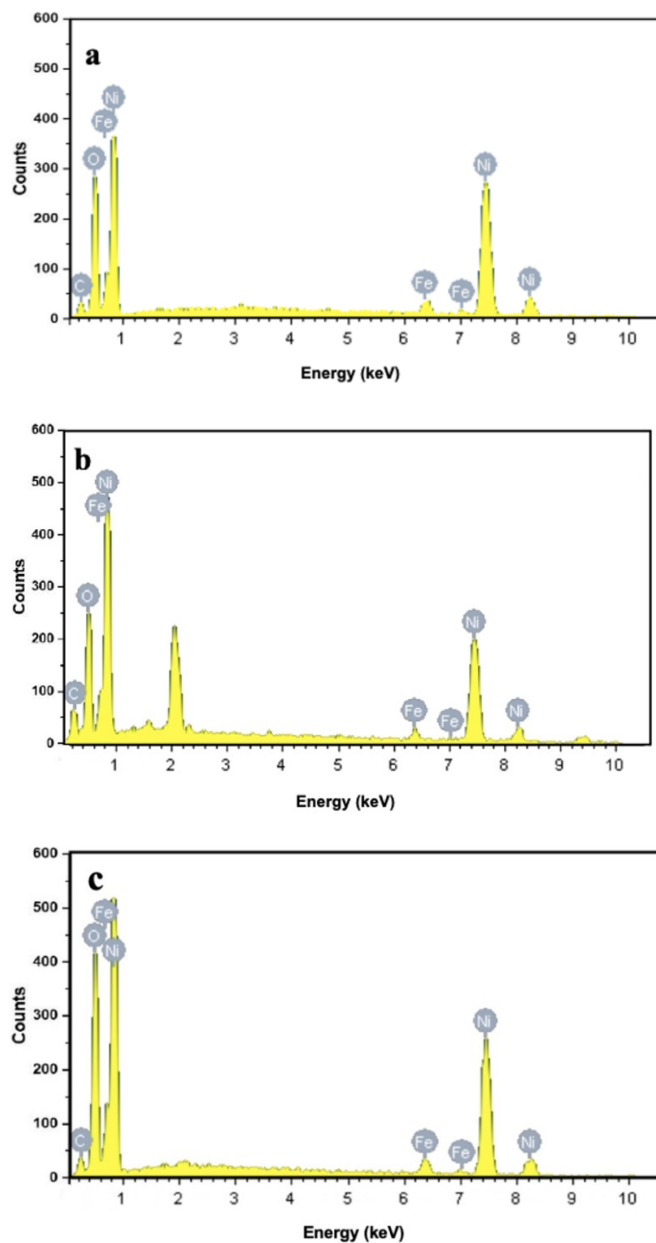
Figure 4: EDX spectra of Iron doped NiO NPs calcined at (a)300°C (b) 350°C, and (c) 420°C.

4. Conclusions

Nanostructured Iron doped NiO particles were prepared successfully utilizing nickel nitrate hexahydrate and ammonium carbonate via the chemical precipitation method. The results obtained from XRD is that the crystalline structure of nanoparticles has been improved due to the addition of Fe and calcined samples at different temperatures to be FCC, this

observation is consistent with the previous studies. Furthermore, UV-visible absorption results have shown that a rise in the temperature of calcination causes a redshift in the absorption spectrum and a decrease in the bandgap due to an increase in the size of the particles. We can say calcination samples at high temperatures with a constant concentration of Fe are the main parameters of the appearance of a redshift in our results. Also, the particle size decreases with an increase in the dopant concentration of Fe. Based on these systematic observations, it is concluded that calcined NiO doped with 5% Fe nanoparticles may have been an outstanding option for optoelectronic applications because of its desired structural and optical properties.

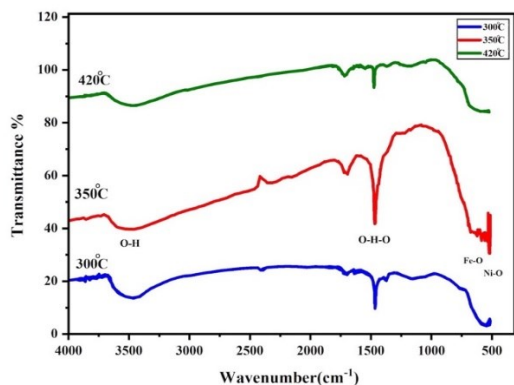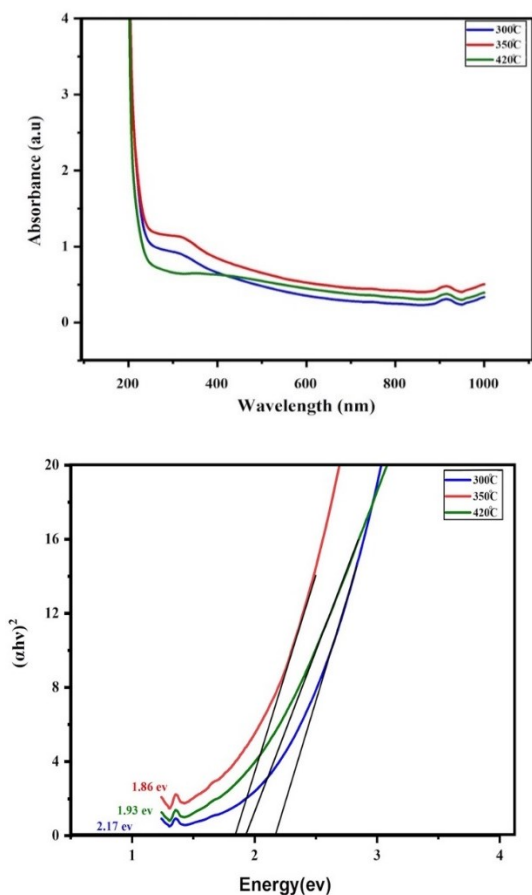Figure 5: illustrates the FTIR spectra of the samples

Figure.6 a- UV-Visible absorbance spectra. b-(αhν)^2 versus energy plot for NiO$_3$+FeO$_3$ nanoparticles.

5. Acknowledgments

References

[1] H. Gleiter, "Nanocrystalline Materials," in: Bunk, W. G. J., ed., in Advanced Structural and Functional Materials, Springer Berlin Heidelberg, Berlin, Heidelberg: 1–37, 1991.

[2] J. Shi, X. Zhang, W. Baeyens, A.M. García-Campaña, "Recent developments in nanomaterial optical sensors," TrAC Trends in Analytical Chemistry, **23**, 351–360, 2004, doi:10.1016/S0165-9936(04)00519-9.

[3] R. Palombari, "Influence of surface acceptor–donor couples on conductivity and other electrochemical properties of nonstoichiometric NiO at 200°C," Journal of Electroanalytical Chemistry, **546**, 23–28, 2003, doi:https://doi.org/10.1016/S0022-0728(03)00134-7.

[4] N.N.M. Zorkipli, N.H.M. Kaus, A.A. Mohamad, "Synthesis of NiO Nanoparticles through Sol-gel Method," Procedia Chemistry, **19**, 626–631, 2016, doi:https://doi.org/10.1016/j.proche.2016.03.062.

[5] P. Mallick, C. ~S. Sahoo, N. ~C. Mishra, "Structural and optical characterization of NiO nanoparticles synthesized by sol-gel route," in: Bose, S. ~M. and Tripathy, S. ~K., eds., in Functional Materials, 229–232, 2012, doi:10.1063/1.4736893.

[6] P. Jeevanandam, V.R.R. Pulimi, "Synthesis of nanocrystalline NiO by sol-gel and homogeneous precipitation methods," Indian Journal of Chemistry - Section A Inorganic, Physical, Theoretical and Analytical Chemistry, **51**, 586–590, 2012.

[7] M. Alagiri, S. Ponnusamy, C. Muthamizhchelvan, "Synthesis and characterization of NiO nanoparticles by sol–gel method," Journal of Materials Science-Materials in Electronics - J MATER SCI-MATER ELECTRON, **23**, 2012, doi:10.1007/s10854-011-0479-6.

[8] P. Mallick, C. Rath, R. Biswal, N.C. Mishra, "Structural and magnetic properties of Fe doped NiO," Indian Journal of Physics, **83**, 517–523, 2009, doi:10.1007/s12648-009-0012-4.

[9] S. Takami, R. Hayakawa, Y. Wakayama, T. Chikyow, "Continuous hydrothermal synthesis of nickel oxide nanoplates and their use as nanoinks for p-type channel material in a bottom-gate field-effect transistor," Nanotechnology, **21**, 134009, 2010, doi:10.1088/0957-4484/21/13/134009.

[10] W. Duan, S. Lu, Z. Wu, Y. Wang, "Size Effects on Properties of NiO Nanoparticles Grown in Alkalisalts," The Journal of Physical Chemistry C, **116**, 26043–26051, 2012, doi:10.1021/jp308073c.

[11] V. Biju, M. Khadar, "Analysis of AC Electrical Properties of Nanocrystalline Nickel Oxide," Materials Science and Engineering: A, **304**, 814–817, 2001, doi:10.1016/S0921-5093(00)01581-1.

[12] S. Chakrabarty, K. Chatterjee, "Synthesis and Characterization of Nano-Dimensional Nickelous Oxide (NiO) Semiconductor," J. Phys. Sci., **13**, 2009.

[13] M.A. Marselin, N. Jaya, "Synthesis and characterization of Pure and Cobalt-doped NiO Nanoparticles," 2015.

[14] M. rifaya, T. Thirugnanasambandan, M. Alagar, "Chemical Capping Synthesis of Nickel Oxide Nanoparticles and their Characterizations Studies," Nanoscience and Nanotechnology, **2**, 2012, doi:10.5923/j.nn.20120205.01.

[15] P. Sheena, P. K P, A. Nedumkallel, B. Sabu, T. Varghese, M. Asmabi, "EFFECT OF CALCINATION TEMPERATURE ON THE STRUCTURAL AND OPTICAL PROPERTIES OF NICKEL OXIDE NANOPARTICLES," **5**, 2014.

[16] K.N. Patel, M.P. Deshpande, V.P. Gujarati, S. Pandya, V. Sathe, S.H. Chaki, "Structural and optical analysis of Fe doped NiO nanoparticles synthesized by chemical precipitation route," Materials Research Bulletin, **106**, 187–196, 2018, doi:10.1016/j.materresbull.2018.06.003.

[17] P.M. Ponnusamy, S. Agilan, N. Muthukumarasamy, T.S. Senthil, G. Rajesh, M.R. Venkatraman, D. Velauthapillai, "Structural, optical and magnetic properties of undoped NiO and Fe-doped NiO nanoparticles synthesized by wet-chemical process," Materials Characterization, **114**(C), 166–171, 2016, doi:10.1016/j.matchar.2016.02.020.

[18] K. R, J. G, A.A. Alphonse, A. Raj, "Structural and Magnetic Properties of

NiO and Fe-doped NiO Nanoparticles Synthesized by Chemical Co-precipitation Method," Materials Today: Proceedings, **3**, 1370–1377, 2016, doi:10.1016/j.matpr.2016.04.017.

[19] H. Abbas, K. Nadeem, A. Hassan, S. Rahman, H. Krenn, "Enhanced photocatalytic Activity of Ferromagnetic Fe-doped NiO nanoparticles," Optik, **202**, 163637, 2020, doi:https://doi.org/10.1016/j.ijleo.2019.163637.

[20] R. Pradeep, A.C. Gandhi, Y. Tejabhiram, I.K.M.M. Sahib, Y. Shimura, L. Karmakar, D. Das, S.Y. Wu, Y. Hayakawa, "Magnetic anomalies in Fe-doped {NiO} nanoparticle," Materials Research Express, **4**(9), 96103, 2017, doi:10.1088/2053-1591/aa7f9b.

[21] H. Muthusamy, N. Suriyanarayanan, S. Prabahar, "Nanoscale synthesis and optical features of nickel nanoparticles," Optik - International Journal for Light and Electron Optics, **125**, 1962–1966, 2014, doi:10.1016/j.ijleo.2013.09.069.

[22] K. Krishnan, K. Selvan, M. Kanagaraj, S. Arumugam, N. Jaya, "Particle size effect on the magnetic properties of NiO nanoparticles prepared by a precipitation method," Journal of Alloys and Compounds - J ALLOYS COMPOUNDS, **509**, 181–184, 2011, doi:10.1016/j.jallcom.2010.09.033.

[23] Z.M. Khoshhesab, M. Sarfaraz, "Preparation and Characterization of NiO Nanoparticles by Chemical Precipitation Method," Synthesis and Reactivity in Inorganic, Metal-Organic, and Nano-Metal Chemistry, **40**(9), 700–703, 2010, doi:10.1080/15533174.2010.509710.

[24] M. Bonomo, "Synthesis and characterization of NiO nanostructures: a review," Journal of Nanoparticle Research, **20**, 2018, doi:10.1007/s11051-018-4327-y.

ASTES

Analytical Solution of Thick Rectangular Plate with Clamped and Free Support Boundary Condition using Polynomial Shear Deformation Theory

Onyeka Festus[1,*], Edozie Thompson Okeke[2,*]

[1]*Department of Civil Engineering, Edo University, Iyamho, Edo State, 312102, Nigeria*

[2]*Department of Civil Engineering, University of Nigeria, Nsukka. Enugu State, 410101, Nigeria*

A B S T R A C T

In this paper, a new polynomial shear deformation theory for the static flexural analysis of anisotropic rectangular thick plate was developed. The plate which carries a uniformly distributed load is clamped on the three edges, and free of support on the other edge (CCFC), is analyzed to determine the in-plane displacement, vertical displacement, bending moment, and shear force, bending and transverse shear stress. The General variation approach was used to obtain the general governing equation and its associated boundary conditions, thereafter the coefficient of deflection and shear deformation along the direction of x and y coordinate was determined by minimizing the energy equation obtained using the new established theory. The study revealed that: (i) as the displacement and stress decrease, the plate's span-thickness ratio increases (ii) as the length to breadth ratio of the plate increases, the value of displacement and stresses increase. To validate the theory, the numerical results are obtained and compared with an available solution in the literature. The result showed good agreement with those in the literature.

1. Introduction

Plates, generally well-known structural element have been extensively used in different fields like engineering, and other industries due to their high strength, lightweight, load resistance characteristic and their cost benefits, as recorded in [1]. Plates are widely used in structural engineering, aerospace engineering, mechanical engineering, etc., for the construction of buildings, retaining walls, ships, bridges, railways, etc., [2 - 3].

Plates have been classified based on thickness as: thick, moderately thick, and thin plates [4], based on material composition as: isotropic and anisotropic plates, based on shape as: circular, rectangular, triangular, elliptical, and skew plates, [5]. The edges of plates can be of different kinds of supports such as: simply supported support, point and fixed supports, etc. as seen in [6].

The analysis or solutions of plates help to determine the stability of plates, and it entails the determination of

displacements, stresses, moments, etc., at a different portion of the plate, [7]. Also, the analysis of plates can be due to bending, buckling, and vibration caused forces. It is generally known that the bending of plates relates to the deflection of the plate at a right angle (90°) to the plate plane due to the influence of forces and moments [8].

It is the depth of plates that mainly affects their bending characteristics compared to other surface dimensions like: length and breadth [9].

There have been different theorems: the classical plate theory (CPT) and refined plate theory (RPT) developed and applied in the analysis of the different categories of plates by many researchers. The classical plate theory (CPT), which was developed by [10 - 11], is based on the assumption that the line which is normal to the mid-surface remains so, before and after deformation. The classical plate theory (CPT) is mainly used in the analysis of thin plates and has also been used by [12 - 14] in the analysis of solutions involving plates and shells, respectively. But it has been found to be inadequate by [15] for the analysis of thick plates as its neglects the effect of shear deformation – a gap that led to the development of refined plate theory by researchers.

*Corresponding Author: Okeke Thompson Edozie, University of Nigeria
Nsukka, Nigeria, Email: edozie.okeke@unn.edu.ng
Onyeka Festus; Edo University Iyamho, Edo State, Nigeria,
onyeka.festus@edouniverity,edu,ng

The Refined Plate Theory (RPT) is used for the analysis of thick plates [16], and it addresses the gap in classical plate theory (CPT).

The RPT comprises First-Order Shear Deformation Theory (FSDT – which has a correction factor as a limitation, and Higher-Order Shear Deformation Theories (HSDT), etc., taking into account the effect of shear deformation and has been applied by different researchers in analyzing thick plates. Authors in [17 - 18] revealed that the limitations in CPT and FSDTs led to the formulation of higher-order shear deformation theory (HSDT). There have been various studies on the bending analysis of thick rectangular plates with different boundary conditions using refined plated theory with different methods and techniques.

This present paper is aimed at bridging the gap in the literature by applying the polynomial shear deformation theory in obtaining the displacements, bending moment, and stresses of the thick rectangular plate. This theory, which is based on a traditional fourth-order shear deformation plate, is presented and applied in a bending analysis of thick rectangular plates using the Energy-variational approach. The investigation has conducted on the plate that has three edges clamped and the other opposite edge free of support (CCFC). Furthermore, derivation of general governing equations for the plate and numerical solutions for deformation, moment, and stress distributions of different points of the plate with a uniformly distributed transverse load is presented.

The physical interpretation of CCFC plate is that, the three clamped edges are supported by a beam and continuous over the span of the plate while the remaining one is free of support i.e. hang without support (Eg. Cantilever). This makes the study very significant because such BC exist depending on the type of beam/column support in the plate structure i.e. it contains different support case of the plate structure than other BCs. So, whenever such case (CCFC) as explained occurs in the structure, analyzing the plate as if is any other BC like SSSS, CCCC etc.(22, 27, 28 and 29) will not account for all the forces (stresses) acting on it. This is because, forces are generated due to the applied load on the structure thereby will introduce significant errors in the analysis and not predict an accurate or reliable result for the design if they are not considered. Thus, for a safe structural design of plate (slab) in a building or any type of structure with CCFC BCs, plate analysis with CCFC BCs like this is required.

The aim of this study is to determine the bending analysis of an isotropic rectangular plate for the effects of aspect ratio and displacement on the moment, shear force, stresses, and stress resultant of a thick rectangular plate. The study sought to achieve the aim through the following objectives:

- To generate the potential energy of a thick plate in line with the work of authors in [5].

- To formulate the general governing equations of the plate and obtain equations for the coefficients of deflection and shear deformation slope for x and y coordinates.

- To determine the expressions for the in-plane and out of plane displacement, bending moment, shear force and stresses of the thick rectangular plate.

2. Previous Works

The authors in [19] used Fourier trigonometric series to analyze the bending of rectangular plates on elastic foundations. They developed the deflection equation, which was in the form of trigonometric series using the Navier solution to the plate. The constraint of the trigonometric series is that it is tedious and rigorous for the formulation of shape functions for the analysis of rectangular plates. The authors in [20] stated that the constraint of the trigonometric series is that it is very strenuous for the formulation of shape functions relating to plates with unsymmetrical boundary conditions.

The authors in [21] used Mindlin's plate higher-order shear deformation theory to generate governing equations for the bending analysis of thick rectangular plates with clamped supports at all its edges (CCCC). Their developed theory involved the decoupling method and improvement on Navier's solutions with partial differential equations, which reduced the complexity involved in obtaining coefficients of plates. In as much as their results showed great accuracy when compared with past results of other studies, their study did not address plate with the CCFC edge condition and didn't make use of the direct variation energy method, which is less rigorous.

In [16], the authors used polynomial shape function for the analysis of rectangular isotropic thick plates. They used the direct variation energy method to obtain displacement coefficients without the need for correction factor for plates with CCCS and SSFS edge conditions, respectively. Their results (displacements and stresses), which they found to be adequate after comparing with results from previous works but did not include the CCFC plate's edge condition as it was not included in their study.

In [17], the authors used exponential function in shear deformation to determine the bending solution of the thick isotropic square and rectangular plates with simply supported supports. They applied the refined shear deformation theory and exponential functions in the form of thickness coordinate to obtain transverse shear deformation and rotary inertia without the need for a correction factor. They found their results: displacements, stresses, and frequencies to be satisfactory after comparing with other refined and exact theories. They only considered the boundary condition (SSSS) using the exponential function and not the polynomial displacement function in an energy method, which is less cumbersome.

The authors in [22] worked on the bending solutions of a thick rectangular plate with CCCC edge conditions. They used refined plate theory (RPT) - polynomial shear deformation theory (PSDT) with the Ritz energy method in their analysis without considering correction factor, and they obtained the coefficients for displacement by putting the total static energy equations to direct variation. They found out that their results (displacements and stresses) were accurate after comparing with results from other previous studies. The authors in [23] used the same boundary condition to study the bending behavior of the elastic rectangular thick plate using the Bergan-Wang approach. They found out that their approach can be used to determine the deflection of plates and analysis of thin, moderately thin, and thick plates, respectively. The authors in [22] used an assumed shape

function, which is not a close-form solution, while the authors in [23] didn't use the Energy method, which is more simplified. Both authors did not consider the plate with the CCFC edge condition in their analysis.

In [24], the authors did a study on bending solutions of the thick plate using a numerical method - based on the 3-D theory of elasticity. They used the method: spline collocation in two coordinate directions for their analysis. They concluded their approach to be useful in determining the distribution of displacements and stresses in thick rectangular plates, with hinged or clamped edge conditions. Their study did not cover the plate with the CCFC edge condition, and also they made use of a numerical method which, unlike the analytical approach, cannot determine the value of deflection at any given point in the plate.

The author in [25] used HSDT with stretching effect to determine bending characteristics of exponentially graded material plates. In his study, he made the assumption that the modulus of elasticity varies exponentially through the plate thickness direction. He found that his theory satisfied the shear stress-free condition at the top and bottom surface of the plates without considering the correction factor. He found out from his study that his theory was satisfactory after compared with previous studies and then concluded that the theory is suitable for predicting bending behavior of exponentially graded material plates. It can be seen from his study that he used shear strain shape function – a new higher-order shear deformation theory and not a polynomial displacement function in the energy method.

The authors in [26] have used PSDT for the analysis of rectangular plates. They obtained the expression for the critical lateral load that induces deflection and shear as a solution to the bending problem of rectangular plates with all four edges clamped (CCCC) and plate with free of support at the third edge and the other edges clamped (CCFC) using third-order shear deformation theory for thick rectangular plate respectively. They did not analyze the effect of displacement, moment, and stresses in predicting responses of the applied load on the plate structure.

Apart from the distinctiveness of the present study with respective individual previous works, there exists an aspect of the distinctiveness of the present study over the previous works put together. This lies in the type of shape functions, and plates support boundary conditions. Unlike the previous works that assumed the displacement function, the present work obtains the exact formulation of the total potential energy from a principle of static elastic theory to get a close form solution of the polynomial displacement function. Except for the author in [26], none of the researchers could determine the analytical solution of bending moment and stresses used in predicting the bending behavior of an elastic thick rectangular CCFC plate. These aspects cannot be overlooked.

3. Methodology

3.1. Assumptions

Considering the following assumptions, the total potential energy of a thick rectangular plate will be formulated. They include:

- ➢ The material of the plate is elastic and homogeneous in nature.
- ➢ The vertical line that is initially normal to the middle surface of the plate before bending is neither straight nor normal to the middle surface after bending.
- ➢ The effect of the strain and stress normal to the x-y plane on the gross response of the plate is small and can be neglected. Thus, the in-plane displacements, u and v, are differentiable in x, y, and z coordinates, while the deflection, w, is only differentiable in x and y coordinates.

3.2. Displacement, Strain and Stress Relationships

Figure 1 shown the two in-plane displacements: in-plane displacement in the direction of x coordinates (u) and in-plane displacement in the direction of y coordinates (v) are represented in Equations (1) and (2) (see the author in [1]):
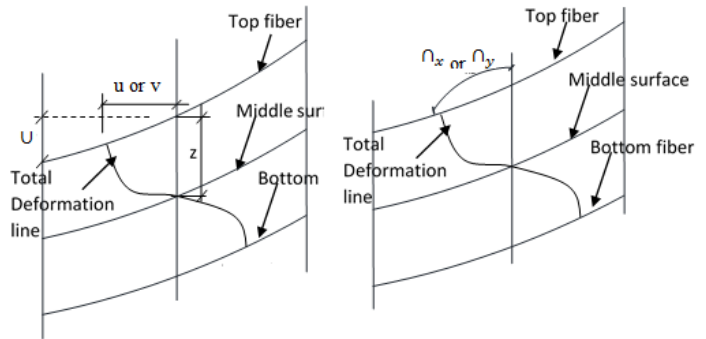
Figure 1: Deformation of a section of a thick Plate

$$u = \frac{zd \cup}{dx} + S(z).\cap_x \qquad (1)$$

$$v = \frac{zd \cup}{dy} + S(z).\cap_y \qquad (2)$$

The shear deformation profile of plate section $S(z)$ is given (see the author in [5]) as:

$$S(z) = \frac{5z}{3}\left(z^3 - \frac{2z}{t^3}\right) \qquad (3)$$

where;

$\cap_x$ and $\cap_y$ is the shear deformation slope in x and y axis respectively.

It is assume from this work that the out-of-plane displacement ($\cup$) is only differentiable in x and y coordinates.ie. ($\cup = \cup(x, y)$).

The normal stress along x-axes (ε_x) becomes:

$$\varepsilon_x = \frac{du}{dx} \qquad (4)$$

The normal stress along y-axes (ε_y) gives:

$$\varepsilon_y = \frac{du}{dy} \qquad (5)$$

The shear strain along (x-y), (x-z) and (y-z) respectively are given in the Equation (6), (7) and (8) respectively as:

$$\gamma_{xy} = \frac{du}{dy} + \frac{dv}{dx} \qquad (6)$$

$$\gamma_{xz} = \frac{du}{dz} + \frac{d \cup}{dx} \qquad (7)$$

$$\gamma_{yz} = \frac{dv}{dz} + \frac{d \cup}{dx} \qquad (8)$$

Similarly, the stress normal to x-axes is defined as:

$$\sigma_x = \frac{E(\varepsilon_x + \mu\varepsilon_y)}{1 - \mu^2} \tag{9}$$

the stress normal to y-axes is defined as:

$$\sigma_y = \frac{E(\varepsilon_y + \mu\varepsilon_x)}{1 - \mu^2} \tag{10}$$

Considering the relationship between the strain and stress in the plate, the shear strain in x-y plane is given as:

$$\tau_{xy} = \frac{E}{2(1+\mu)} \cdot \frac{du}{dy} + \frac{dv}{dx} \tag{11}$$

the shear strain in y-z plane is given as:

$$\tau_{xz} = \frac{E}{2(1+\mu)} \cdot \frac{du}{dz} + \frac{d\cup}{dx} \tag{12}$$

the shear strain in y-z plane is given as:

$$\tau_{yz} = \frac{E}{2(1+\mu)} \cdot \frac{dv}{dz} + \frac{d\cup}{dx} \tag{13}$$

Substituting Equation (1), (2), (4) and (5) into Equation (9), we have:

$$\sigma_x = \frac{E}{1-\mu^2}\left[\left(-\frac{zd^2\cup}{dx^2} + \frac{S(z)d\cap_x}{dx}\right) - \mu\left(\frac{zd^2\cup}{dy^2} + \frac{S(z)d\cap_y}{dy}\right)\right] \tag{14}$$

Substituting Equation (1), (2), (4) and (5) into Equation (10), we have:

$$\sigma_y = \frac{E}{1-\mu^2}\left[\left(-\frac{zd^2\cup}{dy^2} + \frac{S(z)d\cap_x}{dx}\right) - \mu\left(\frac{zd^2\cup}{dx^2} + \frac{S(z)d\cap_y}{dy}\right)\right] \tag{15}$$

Substituting Equation (1), (2) and (6) into Equation (11), we have:

$$\tau_{xy} = \frac{E(1-\mu)}{(1-\mu^2)}\left[-\frac{z\partial^2\cup}{\partial x\partial y} + S(z)\left(\frac{d\cap_x}{dy} + \frac{d\cap_y}{dx}\right)\right] \tag{16}$$

Substituting Equation (1), (2) and (7) into Equation (12), we have:

$$\tau_{xz} = \frac{E(1-\mu)}{(1-\mu^2)}\left[\frac{z\partial^2\cup}{\partial x\partial z} + S(z)\left(\frac{d\cap_x}{dz} + \frac{d\cap_z}{dx}\right)\right] \tag{17}$$

Substituting Equation (1), (2) and (8) into Equation (13), we have:

$$\tau_{yz} = \frac{E(1-\mu)}{(1-\mu^2)}\left[\frac{z\partial^2\cup}{\partial y\partial z} + S(z)\left(\frac{d\cap_y}{dz} + \frac{d\cap_z}{dy}\right)\right] \tag{18}$$

where:
the symbol $\cup$ denotes out-of-plane displacement
the symbol $F(z)$ denotes Shear deformation profile
the symbol $\cap_x$ denotes shear deformation rotation along x axis
the symbol $\cap_y$ denotes shear deformation rotation along y axis
the symbol μ denotes poison ratio
the symbol E denotes modulus of elasticity of the plate
the symbol σ_x denotes stress normal to x axis
the symbol σ_y denotes stress normal to y axis
the symbol τ_{xy} denotes shear stress along x-y axis
the symbol τ_{xz} denotes shear stress along x-z axis
the symbol τ_{yz} denotes shear stress along y-z axis
the symbol ε_x denotes normal strain along x axis
the symbol ε_y denotes normal strain along y axis
the symbol γ_{xy} denotes shear strain along x-y axis
the symbol γ_{xz} denotes shear strain along x-z axis

the symbol γ_{yz} denotes shear strain along y-z axis

3.3. Total Potential Energy Equation

The total potential energy expression ($\not{\exists}$), was formulated in accordance to the kinematics and constitutive relation in the previous section (see [27]).

$$\not{\exists} = \Delta + \nabla \tag{19}$$

Where;

$$\nabla = -\int_0^a \int_0^b w \cup (x,y)\partial x\partial y \tag{20}$$

Where w is the uniformly distributed load.

$$\Delta = \frac{1}{2}\iiint_{-\frac{t}{2}}^{\frac{t}{2}} (\sigma_x\varepsilon_x + \sigma_y\varepsilon_y + \tau_{xy}\gamma_{xy} + \tau_{xz}\gamma_{xz} + \tau_{yz}\gamma_{yz})dxdydz \tag{21}$$

Thus:

$$\begin{aligned}
\not{\exists} = D\int_0^a \int_0^b \Bigg[&\left|\frac{g_1}{2}\left(\frac{\partial^2\cup}{\partial x^2}\right)^2 - g_2\left(\frac{\partial^2\cup}{\partial x^2}\cdot\frac{\partial\cap_x}{\partial x}\right) + \frac{g_3}{2}\left(\frac{\partial\cap_x}{\partial x}\right)^2\right| \\
&+ \left|g_1\left(\frac{\partial^2\cup}{\partial x\partial y}\right)^2 - g_2\left(\frac{\partial^2\cup}{\partial x\partial y}\cdot\frac{\partial\cap_x}{\partial y}\right)\right. \\
&\left. - g_2\left(\frac{\partial^2 w}{\partial x\partial y}\cdot\frac{\partial\cap_y}{\partial x}\right)\right| \\
&+ \left|(1+\mu)\frac{g_3}{2}\left(\frac{\partial\cap_x}{\partial y}\right)\left(\frac{\partial\cap_y}{\partial x}\right)\right| \\
&+ \frac{(1-\mu)}{4}\left|g_3\left(\frac{\partial\cap_x}{\partial y}\right)^2 + g_3\left(\frac{\partial\cap_y}{\partial x}\right)^2\right| \\
&+ \left|\frac{g_1}{2}\left(\frac{\partial^2\cup}{\partial y^2}\right)^2 - g_2\left(\frac{\partial^2\cup}{\partial y^2}\cdot\frac{\partial\cap_y}{\partial y}\right)\right. \\
&\left. + \frac{g_3}{2}\left(\frac{\partial\cap_y}{\partial y}\right)^2\right| \\
&+ \left|\frac{(1-\mu)}{4}g_4(\cap_x)^2\right. \\
&\left. + \frac{(1-\mu)}{4}g_4(\cap_y)^2\right|\Bigg]\partial x\partial y \\
&- \int_0^a \int_0^b \frac{w}{2}\cup(x,y)\partial x\partial y \tag{22}
\end{aligned}$$

The non-dimensional values of quantities along the x and y-axis respectively is presented below.

$$z = ts; \quad x = a\ni \text{ and } y = b\in \tag{23}$$

where;

a, b and t are the length, breath and thickness of the plate while $\ni$, $\in$ and s are the non-dimensional value of length, breath and thickness of the plate.

Let the length to breadth aspect ratio, $\alpha = \frac{b}{a}$ (24)

Span to thickness ratio, $\beta = \frac{a}{t}$ (25)

Deflection ($\cup$), is the product of shape function of the plate and deflection coefficient:

$$\cup = \complement.n \tag{26}$$

Similarly;

The shear deformation rotation along x-axis becomes:

$$\cap_x = \left[\frac{dn}{d \ni}\right][C_x] \tag{27}$$

Similarly, the shear deformation rotation along y-axis becomes:

$$\cap_y = \left[\frac{dn}{d \in}\right][C_y] \tag{28}$$

where,

n is the shape function of the plate

C is the coefficient of deflection

C_x is the coefficient of shear deformation along x axis

C_y is the coefficient of shear deformation along y axis

By substituting Equation 23, 24, 25, 26, 27 and 28 into 22, gives:

$$
\begin{aligned}
\daleth = \frac{D}{2a^4} \int_0^1 \int_0^1 & \Bigg[\Bigg| g_1 C^2 \left(\frac{\partial^2 n}{\partial \ni^2}\right)^2 - 2g_2 CC_x \left(\frac{\partial^2 n}{\partial \ni^2}\right)^2 \\
& + g_3 C_x^2 \left(\frac{\partial^2 n}{\partial \ni^2}\right)^2 \Bigg| \\
& + \Bigg| 2g_1 \frac{C^2}{\propto^2}\left(\frac{\partial^2 n}{\partial \ni \, \partial \in}\right)^2 \\
& - 2g_2 \frac{CC_x}{\propto^2}\left(\frac{\partial^2 n}{\partial \ni \, \partial \in}\right)^2 \\
& - 2g_2 \frac{CC_y}{\propto^2}\left(\frac{\partial^2 n}{\partial \ni \, \partial \in}\right)^2 \Bigg| \\
& + \Bigg| (1+\mu)g_3 \frac{C_x C_y}{\propto^2}\left(\frac{\partial^2 h}{\partial \ni \, \partial \in}\right)^2 \Bigg| \\
& + \frac{(1-\mu)}{2}\Bigg| g_3 \frac{C_x^2}{\propto^2}\left(\frac{\partial^2 n}{\partial \ni \, \partial \in}\right)^2 \\
& + g_3 \frac{C_y^2}{\propto^2}\left(\frac{\partial^2 n}{\partial \ni \, \partial \in}\right)^2 \Bigg| \\
& + \Bigg| g_1 \frac{C^2}{\propto^4}\left(\frac{\partial^2 n}{\partial \in^2}\right)^2 - 2g_2 \frac{CC_y}{\propto^4}\left(\frac{\partial^2 h}{\partial \in^2}\right)^2 \\
& + g_3 \frac{C_y^2}{\propto^4}\left(\frac{\partial^2 h}{\partial \in^2}\right)^2 \Bigg| \\
& + \Bigg| \frac{(1-\mu)}{2}\beta^2 g_4 C_x^2 \left(\frac{\partial n}{\partial \ni}\right)^2 \\
& + \frac{(1-\mu)}{2}\cdot\frac{\beta^2 g_4 C_y^2}{\propto^2}\left(\frac{\partial n}{\partial \in}\right)^2 \Bigg| \Bigg] ab\partial R\partial Q \\
& - \int_0^1 \int_0^1 wCn \, ab\partial \ni \, \partial \in
\end{aligned}
\tag{29}
$$

Given that D is the rigidity; let:

$$D = \frac{Et^3}{12(1-\mu^2)} \tag{30}$$

3.4. Governing Energy Equation

The elastic plate presented plate in figures 1 and 2 under bending subjected to uniformly distributed load was used to obtain the displacement – strain relationships in terms of curvatures.

3.4.1. General Governing Equation

The total potential energy shall be minimized with respect to the deflection w, shear deformation along the x axis, $\cap_x$ and shear deformation along y axis$\cap_y$. Minimizing or differentiating total potential energy equation with respect to $\cup$, $\cap_x$, and $\cap_y$ is said to be the direct variation.

$$\frac{\partial \Pi}{\partial \cup} = \frac{\partial \Pi}{\partial \cap_x} = \frac{\partial \Pi}{\partial \cap_y} = 0 \tag{31}$$

By solving the resulting three simultaneous governing equation the actual deflection $\cup$, shear deformation along the x axis, $\cap_x$ and shear deformation along the y axis, $\cap_y$ was gotten as:

$$
\begin{aligned}
\cup = & \left(a_0 + a_1 \ni + \frac{a_2 \ni^2}{2} + \frac{a_3 \ni^3}{6} + \frac{wa^4}{D}\left(\frac{n_1}{\cup_3}\right)\cdot\frac{\ni^4}{24}\right) \\
& \times \Bigg(b_0 + b_1 \\
& \in + \frac{b_2 \in^2}{2} + \frac{b_3 \in^3}{6} + \frac{wa^4}{D}\left(\frac{n_1}{\cup_3}\right)\cdot\frac{\in^4}{24} \\
& + \frac{b_5 \in^5}{120}\Bigg)
\end{aligned}
\tag{32}
$$

The general polynomial shear deformation function (Rotation equation for the y-axis) of a rectangular plate as was obtained and presented:

$$
\begin{aligned}
\cap_x = & \left(a_4 + a_5 \ni + \frac{a_6 \ni^2}{2} + \frac{wa^3}{D}\left(\frac{n_4}{g_2 \cap_3}\right)\cdot\frac{\ni^3}{6}\right) \\
& \times \Bigg(b_7 + b_8 \\
& \in + \frac{b_9 \in^2}{2} + \frac{b_{10} \in^3}{6} + \frac{b_{11} \in^4}{24}\Bigg)
\end{aligned}
\tag{33}
$$

The general polynomial shear deformation function (Rotation equation for the y-axis) of a rectangular plate as was obtained and presented:

$$
\begin{aligned}
\cap_y = & \left(a_7 + a_8 \ni + \frac{a_9 \ni^2}{2} + \frac{a_{10} \ni^3}{6} + \frac{a_{11} \ni^4}{24}\right) \\
& \times \Bigg(b_4 + b_5 \\
& \in + \frac{b_6 \in^2}{2} + \frac{wa^3}{D}\left(\frac{\propto^3 n_5}{g_2 \cap_1}\right)\cdot\frac{\in^3}{6}\Bigg)
\end{aligned}
\tag{34}
$$

The support conditions of the plate consideration is presented in the Figure 2.
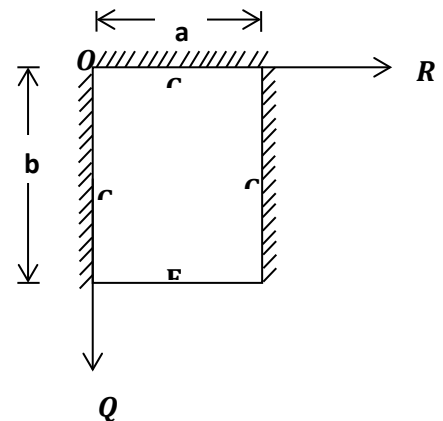

Figure 2: CCFC Rectangular Plate

3.4.2. Direct Governing Equation

The direct variation method was used to obtain the direct governing differential equation by differentiating the total potential energy with respect to the coefficient of deflection (C), coefficient of shear deformation with respect to x-axis (C_x) and coefficient of shear deformation with respect to y-axis (C_y). Minimizing the Energy expression ($\exists$) with respect to the coefficient of deflection (C), coefficient of shear deformation with respect to x-axis (C_x) and coefficient of shear deformation with respect to y-axis (C_y):

$$\frac{\partial \exists}{\partial C} = \frac{\partial \exists}{\partial C_x} = \frac{\partial \exists}{\partial C_y} = 0 \tag{35}$$

The solution of Equation (35) yields the three Equations of equilibrium which is presented as:

$$t_{11}C - t_{12}C_x - t_{13}C_y = \frac{wa^4}{D}s_q \tag{36}$$

$$-t_{21}C + t_{22}C_x + t_{23}C_y = 0 \tag{37}$$

$$-t_{31}C + t_{32}C_x + t_{33}C_y = 0 \tag{38}$$

Where;

$$t_{11} = g_1\left(s_1 + \frac{2}{\alpha^2}s_2 + \frac{1}{\alpha^4}s_3\right) \tag{39}$$

$$t_{12} = -g_2\left(s_1 + \frac{1}{\alpha^2}s_2\right) \tag{40}$$

$$t_{13} = -g_2\left(\frac{1}{\alpha^2}s_2 + \frac{1}{\alpha^4}s_3\right) \tag{41}$$

$$t_{21} = -g_2\left(s_1 + \frac{1}{\alpha^2}s_2\right) \tag{42}$$

$$t_{22} = \left(g_3s_1 + \frac{(1-\mu)}{2\,\alpha^2}g_3s_2 + \frac{(1-\mu)}{2}\beta^2 g_4s_4\right) \tag{43}$$

$$t_{23} = g_3\frac{(1+\mu)}{2\,\alpha^2}s_2 \tag{44}$$

$$t_{31} = -g_2\left(\frac{1}{\alpha^2}s_2 + \frac{1}{\alpha^4}s_3\right) \tag{45}$$

$$t_{32} = g_3\frac{(1+\mu)}{2\,\alpha^2}s_2 \tag{46}$$

$$t_{33} = \left(g_3\frac{(1-\mu)}{2}\left(\frac{1}{\alpha^2}s_2 + \frac{1}{\alpha^4}s_3\right) + g_4\frac{(1-\mu)}{2\,\alpha^2}\beta^2 s_5\right) \tag{47}$$

Given that s_1, s_2, s_3, s_4, s_5 and s_q are the stiffness coefficients, let:

$$s_1 = \int_0^1\int_0^1\left(\frac{d^2n}{d\,\ni^2}\right)^2 d\ni\,d\in \tag{48}$$

$$s_2 = \int_0^1\int_0^1\left(\frac{d^2n}{d\ni\,d\in}\right)^2 d\ni\,d\in \tag{49}$$

$$s_3 = \int_0^1\int_0^1\left(\frac{d^2n}{d\in^2}\right)^2 d\ni\,d\in \tag{50}$$

$$s_4 = \int_0^1\int_0^1\left(\frac{dn}{d\ni}\right)^2 d\ni\,d\in \tag{51}$$

$$s_5 = \int_0^1\int_0^1\left(\frac{dn}{d\in}\right)^2 d\ni\,d\in \tag{52}$$

$$s_q = \int_0^1\int_0^1 n.\,d\ni\,d\in \tag{53}$$

Solving Equation (36), (37) and (38) simultaneously, gives Equation (54), (55) and (56):

$$C = \frac{wa^4}{D}(k) \tag{54}$$

$$C_x = CM_2 \tag{55}$$

$$C_y = CM_3 \tag{56}$$

Where;

$$M_2 = \frac{t_{21}.t_{33} - t_{23}.t_{31}}{t_{22}.t_{33} - t_{23}.t_{32}} \tag{57}$$

$$M_3 = \frac{t_{21}.t_{32} - t_{22}.t_{31}}{t_{23}.t_{32} - t_{22}.t_{33}} \tag{58}$$

$$k = \frac{s_6}{t_{11}M_1 - t_{12}M_2 - t_{13}M_3} \tag{59}$$

3.5. Displacement, Stresses, Bending moment and Shear force Equations

The equations for the moment (M_x and M_y), shear force (Q_x and Q_y), in-plane displacement (u and v), deflection ($\cup$) and the stress of isotropic rectangular thick plate was derived according to [28] by substituting the Equation (54), (55) and (56) where appropriate.

Substituting Equation (54) into (26), gave:

$$\cup = \bar{C}n\left(\frac{wa^4}{D}\right) \tag{60}$$

Let:

$$\bar{C} = k$$

The bending moment along x-axes:

$$M_x = \left(-\frac{D_1}{D}wa^2\bar{C}\left[\frac{d^2n}{d\,\ni^2} + \mu\frac{d^2n}{d\in^2}\right]\right.$$
$$\left. + g_2\left[\bar{C_x}\frac{d^2n}{d\,\ni^2} + \mu\bar{C_y}\frac{d^2n}{d\in^2}\right]\right) \tag{61}$$

That is:

$$M_x = \overline{M_x}wa^2 \tag{62}$$

Given that $D_1 = g_1D$; and $D_2 = g_2D$; let: $g_1 = 1$ and $g_2 = 1.2$

$$\overline{M_x} = -g_1\bar{C}\left[\frac{d^2n}{d\,\ni^2} + \mu\frac{d^2n}{d\in^2}\right]$$
$$+ g_2\left[\bar{C_x}\frac{d^2n}{d\,\ni^2} + \mu\bar{C_y}\frac{d^2n}{d\in^2}\right] \tag{63}$$

Where;

$$\bar{C_x} = M_2\bar{C} \tag{64}$$

$$\bar{C_y} = M_3\bar{C} \tag{65}$$

The bending moment along y-axes:

$$M_y = \left(-\frac{D_1}{D}wa^2C\left[\frac{d^2n}{d\in^2} + \mu\frac{d^2n}{d\,\ni^2}\right]\right.$$
$$\left. + g_2\left[\bar{C_y}\frac{d^2n}{d\in^2} + \mu\bar{C_x}\frac{d^2n}{d\,\ni^2}\right]\right)wa^2 \tag{66}$$

That is:

$$M_y = \overline{M_y}wa^2 \tag{67}$$

where;

$$\overline{M_y} = -g_1C\left[\frac{d^2n}{d\in^2} + \mu\frac{d^2n}{d\,\ni^2}\right]$$
$$+ g_2\left[\bar{C_y}\frac{d^2n}{d\in^2} + \mu\bar{C_x}\frac{d^2n}{d\,\ni^2}\right] \tag{68}$$

Shear force $Q_x = \dfrac{dM_x}{dx}$ and $Q_y = \dfrac{dM_y}{dy}$ (69)

Thus, the shear force along x-axes:

$$Q_x = \left(-\bar{C}\left[\frac{\partial^3 n}{\partial \ni^3} + \mu\frac{\partial^3 n}{\partial \in^3}\right]\right.$$
$$\left. + \left[\overline{C_x}\frac{\partial^3 n}{\partial \ni^3} + \mu\overline{C_y}\frac{\partial^3 n}{\partial \in^3}\right]\right)wa \quad (70)$$

That is:

$$Q_x = \overline{Q_x}wa \quad (71)$$

Where;

$$\overline{Q_x} = -\frac{D_1}{a^3}\bar{C}\left[\frac{\partial^3 n}{\partial \ni^3} + \mu\frac{\partial^3 n}{\partial \in^3}\right]$$
$$+ \left[\overline{C_x}\frac{\partial^3 n}{\partial \ni^3} + \mu\overline{C_y}\frac{\partial^3 n}{\partial \in^3}\right] \quad (72)$$

The shear force along y-axes:

$$Q_y = \left(-\bar{C}\left[\frac{\partial^3 n}{\partial \ni^3} + \mu\frac{\partial^3 n}{\partial \in^3}\right]\right.$$
$$\left. + \left[\overline{C_x}\frac{\partial^3 n}{\partial \ni^3} + \mu\overline{C_y}\frac{\partial^3 n}{\partial \in^3}\right]\right)wa \quad (73)$$

That is:

$$Q_y = \overline{Q_y}wa \quad (74)$$

where;

$$\overline{Q_y} = -\frac{D_1}{a^3}\bar{C}\left[\frac{\partial^3 n}{\partial \ni^3} + \mu\frac{\partial^3 n}{\partial \in^3}\right] + \left[\overline{C_x}\frac{\partial^3 n}{\partial \ni^3} + \mu\overline{C_y}\frac{\partial^3 n}{\partial \in^3}\right] \quad (75)$$

The in-plane displacement along x-axes:

$$u = [-\bar{C}s + \overline{C_x}S(s)]\frac{dn}{d\ni}\left(\frac{wa^4}{\beta D}\right) \quad (76)$$

The in-plane displacement along y-axes:

$$v = \frac{1}{\propto}[-\bar{C}s + \overline{C_y}S(s)]\frac{dn}{d\in}\left(\frac{twa^3}{D}\right) \quad (77)$$

The normal stress along x-axes:

$$\sigma_x = 12\left[[-\bar{C}s + \overline{C_x}S(s)]\frac{d^2 n}{d\ni^2}\right.$$
$$\left. + \frac{\mu}{\propto^2}[-\bar{C}s + \overline{C_y}S(s)]\frac{d^2 n}{d\in^2}\right](w\beta^2) \quad (78)$$

The normal stress along y-axes:

$$\sigma_y = w\beta^2\left[12\left[\mu[-\overline{C}s + C_x S(s)]\frac{d^2 n}{d\ni^2}\right.\right.$$
$$\left.\left. + \frac{\mu}{\propto^2}[-\bar{C}s + \overline{C_y}S(s)]\frac{d^2 n}{d\in^2}\right]\right] \quad (79)$$

The shear stress along x-y axes:

$$\tau_{xy} = 6\frac{(1-\mu)}{\propto}\left[-2\bar{C}s + \overline{C_x}S(s)\right.$$
$$\left. + \overline{C_y}S(s).\frac{1}{\propto}\right]\frac{d^2 n}{\partial \ni \partial \in}(w\beta^2) \quad (80)$$

The shear stress along x-z axes:

$$\tau_{xz} = 6(1-\mu)\overline{C_x}\frac{dS(z)}{dz}\frac{dn}{d\ni}(w\beta^2) \quad (81)$$

The shear stress along y-z axes:

$$\tau_{yz} = \frac{6(1-\mu)}{\propto}\overline{C_y}\frac{dS(z)}{dz}\frac{dn}{d\in}(w\beta^2) \quad (82)$$

q_d = Self weight of the plate

4. Results and Discussions

The numerical analysis of a CCFC rectangular plate of various span-thickness ratios is presented in Table 2 to 6. A third-

order polynomial displacement function for the analysis CCFC as was derived in Equation (32) in line with the work of [29] is presented in Equation 83 to 94:

$$U_{(\ni,\in)} = \left(a_0 + a_1\ni + \frac{a_2\ni^2}{2} + \frac{a_3\ni^3}{6} + \frac{\ni^4}{24}Sa_4\right).\left(b_0 + b_1\right.$$
$$\left. \in + \frac{b_2\in^2}{2} + \frac{b_3\in^3}{6} + \frac{\in^4}{24}b_4 + \frac{b_5\in^5}{120}\right) \quad (83)$$

where;

$$S = \frac{wa^4}{D}\left(\frac{n_1}{U_3}\right)$$

At $\ni = \in = 0; U = 0$ \quad (84)

At $\ni = \in = 0; Slope\left(ie.\frac{dU}{d\ni} = \frac{dU}{d\in} = 0\right)$ \quad (85)

At $\ni = \in = 1; U_x = 0$ and $M_y\left(ie.\frac{d^2 U}{d\in^2} = 0\right)$ \quad (86)

At $\ni = 1, slope\left(ie.\frac{dU}{d\ni} = 0\right); at \in = 1, slope\left(ie.\frac{dU}{d\in} = \frac{2}{3b_5}\right)$ \quad (87)

At $\in = 1;$ shear force $Q_y\left(ie.\frac{d^3 w}{d\in^3} = 0\right)$ \quad (88)

Substituting Equations (84 to 88) into Equation (83) and solving gives the following constants:

$$a_0 = 0; \; a_1 = 0; \; a_2 = \frac{Sa_4}{12}; \; a_3 = \frac{-Sa_4}{2} \; and \; b_0 = 0; \; b_1 = 0; \; b_2 = 2.8b_5; \; b_3 = -5.2b_5; S_{b4} = 3.8b_5 \quad (89)$$

Substituting the constants of Equation (89) into Equation (83) gives;

$$U = \frac{S_{a4}}{24}(\ni^2 - 2\ni^3 + \ni^4)$$
$$\times \frac{b_5}{360}(2.8\in^2 - 5.2\in^3 + 3.8\in^4 - \in^5) \quad (90)$$

That is:

$$U = \frac{S_{a4} \times b_5}{8640}(\ni^2 - 2\ni^3 + \ni^4)$$
$$\times (2.8\in^2 - 5.2\in^3 + 3.8\in^4 - \in^5) \quad (91)$$

Recall from Equation 26, that;

$$U = n.C$$

Let the amplitude:

$$C = \frac{1}{8640}(S_{a4} \times b_5) \quad (92)$$

and;

$$n = (\ni^2 - 2\ni^3 + \ni^4) \times (2.8\in^2 - 5.2\in^3 + 3.8\in^4 - \in^5) \quad (93)$$

Therefore:

$$U = \frac{S_{a4}.b_5}{8640}(1.5\ni^2 - 2.5\ni^3 + \ni^4)$$
$$\times (2.8\in^2 - 5.2\in^3 + 3.8\in^4 - \in^5) \quad (94)$$

The values stiffness coefficient obtained from the above expression is presented in Table 1. Table 2 contains the result of bending moment, shear force, and their resultants of a square CCFC rectangular plate at different span to thickness aspect ratio. These numerical values of the design factors of these quantities ($\overline{U}$, $\overline{M}$ and $\overline{Q}$) for a square thick plate is obtained using Equation (60) to (75) as obtained from this study. Table 3 contains the result of the values of displacement (u, v and U) and the stresses characteristics ($\sigma_x, \sigma_y, \tau_{xy}, \tau_{xz}$ and τ_{yz}) of a square CCFC

rectangular plate at different span to thickness aspect ratio using Equation (60), (70) and (77). These numerical values were obtained from the Equation (60), (78) to (82). Table 4 contains the result of the value of displacement (u, v and ∪) and the stresses characteristics $(\sigma_x, \sigma_y, \tau_{xy}, \tau_{xz}$ and $\tau_{yz})$ for length to breadth ratio of 1.5 for CCFC rectangular plate at different span to thickness aspect ratio. These numerical values were obtained from the Equation (60), (78) to (82). Table 5 contains the result of the values of displacement (u, v and ∪) and the stresses characteristics $(\sigma_x, \sigma_y, \tau_{xy}, \tau_{xz}$ and $\tau_{yz})$ for length to breadth ratio of 2.0 for CCFC rectangular plate at different span to thickness aspect ratio. These numerical values were obtained from the Equation (60), (78) to (82). A comparative analysis of results obtained from this work is presented in Table 6 and Figure 3. This is determined the correctness of the results from the present studies, comparison was made between values from the present study and those of past scholars. Table 2 presents the result of the comparison done with the work of [30] for CCFC rectangular thick plate of 2.0 lengths to breadth ratio of various aspect ratios and the corresponding percentage difference between the values of centroidal deflection. Figure 3 contains a graph of the deflection versus span to the thickness aspect ratio of CCFC thick plate of length to breadth ratio of 2.0. This shows the comparison between the present work and that of the author in [30].

4.1. Discussion

The numerical results of stiffness coefficient of the plate is obtained from Equation (31) to (36).

Table 1: Stiffness coefficient, s values for CCFC boundary conditions

Theory	Plate	s_1	s_2	s_3	s_4	s_5	s_6
Present (NPST)	CCFC	0.055	0.004	0.004	0.001	0.0003	0.008

Table 2: Bending Moments, Shear Force and Stress resultants of CCFC plate for b/a = 1. 0

β	∪ / $\overline{U}$	M_x / $\overline{M_x}$	M_y / $\overline{M_y}$	Q_x / $\overline{Q_x}$	Q_y / $\overline{Q_y}$
4	0.0164	0.3127	0.1827	0.5288	1.0782
10	0.0103	0.3158	0.1695	0.2614	0.5461
15	0.0096	0.3161	0.1678	0.2351	0.4632
20	0.0094	0.3163	0.1672	0.2260	0.4594
25	0.0093	0.3163	0.1670	0.2218	0.4576
30	0.0092	0.3163	0.1668	0.2195	0.4566
35	0.0092	0.3163	0.1667	0.2181	0.4560
40	0.0092	0.3164	0.1666	0.2172	0.4556
45	0.0092	0.3164	0.1666	0.2166	0.4553
50	0.0092	0.3164	0.1666	0.2162	0.4551
55	0.0092	0.3164	0.1666	0.2158	0.4550
60	0.0092	0.3164	0.1665	0.2156	0.4549
65	0.0092	0.3164	0.1665	0.2154	0.4548
70	0.0092	0.3164	0.1665	0.2153	0.4547
75	0.0092	0.3164	0.1665	0.2150	0.4546
80	0.0092	0.3164	0.1665	0.2150	0.4546
85	0.0092	0.3164	0.1665	0.2150	0.4546
90	0.0092	0.3165	0.1665	0.2149	0.4545
95	0.0092	0.3165	0.1665	0.2148	0.4545
100	0.0092	0.3165	0.1665	0.2148	0.4545
1000	0.0092	0.3165	0.1665	0.2148	0.4545
CPT	0.0092	0.3165	0.1665	0.2148	0.4545

It is seen from Table 2 that as the deflection (∪), bending moment (M_x and M_y) and (Q_x and Q_y) decreases, the span to thickness ratio increases. These continue until failure occurs in the plate structure. This means that, the load that causes the plate to deflect also causes the plate material to bend simultaneously. It is observed that the value of deflection varies less as the span to thickness increase, this equal to the value of the CPT at span to thickness ratio of 100 and above. Table 2 reveals that the values of deflection at both the x and y axis decrease as the span-thickness ratio increases with a constant value of 0.0092 at the span-thickness ratio of 30.

Table 3: Displacement and Stresses of CCFC plate for length to breadth ratio of 1.0

β	∪ / $\overline{U}$	u / $\overline{u}$	σ_x / $\overline{\sigma_x}$	τ_{xy} / $\overline{\tau_{xy}}$	τ_{yz} / $\overline{\tau_{yz}}$
4	0.0165	-0.0038	0.2562	-0.0635	0.0229
10	0.0103	-0.0030	0.2000	-0.0479	0.0031
15	0.0096	-0.0029	0.1943	-0.0462	0.0014
20	0.0094	-0.0029	0.1924	-0.0457	0.0008
25	0.0093	-0.0028	0.1915	-0.0454	0.0005
30	0.0093	-0.0028	0.1910	-0.0453	0.0004
35	0.0092	-0.0028	0.1907	-0.0452	0.0003
40	0.0092	-0.0028	0.1905	-0.0451	0.0002
45	0.0092	-0.0028	0.1904	-0.0451	0.0002
50	0.0092	-0.0028	0.1903	-0.0451	0.0001
55	0.0092	-0.0028	0.1902	-0.0450	0.0001

β					
60	0.0092	-0.0028	0.1902	-0.0450	0.0001
65	0.0092	-0.0028	0.1901	-0.0450	0.0001
70	0.0092	-0.0028	0.1901	-0.0450	0.0001
75	0.0092	-0.0028	0.1900	-0.0450	0.0001
80	0.0092	-0.0028	0.1900	-0.0450	0.0001
85	0.0092	-0.0028	0.1900	-0.0450	0.0000
90	0.0092	-0.0028	0.1900	-0.0450	0.0000
95	0.0092	-0.0028	0.1900	-0.0450	0.0000
100	0.0092	-0.0028	0.1900	-0.0450	0.0000
1000	0.0092	-0.0028	0.1900	-0.0450	0.0000
CPT	0.0092	-0.0028	0.1900	-0.0450	0.0000

From the results of SCFS plate presented in Figure 12 to 20, it shows that the values of critical lateral imposed load q_{iw} decrease as the length-width ratio increases, this continues until failure occurs. This means that an increase in plate length increases the chance of failure in a plate structure. Meanwhile the values of critical lateral imposed load q_{ip} increase as the length-width ratio increases, this continues until safety is ensured.

From a critical look at Table 3, it is shown that the value of displacement (u, v and ∪) characteristics decreases with increases in the value of the span-thickness ratio. It is also observed in the Tables that the displacement (u, v and ∪) and stresses characteristics increases as the value of the length to breadth ratio increases. This means that, the in-plane displacement is functions of x, y and z as it varies with the plate thickness while the deflection is only a function of x and y and did not vary linearly with the thickness of the plate thickness. Also, it was deduced that the normal stress (σ_x and σ_y) and shear stress characteristics (τ_{xy}, τ_{xz} and τ_{yz}) also decreases as the span-thickness ratio increases. It is also observed in the Table 3 that the stresses characteristics ($\sigma_x, \sigma_y, \tau_{xy}, \tau_{xz}$ and τ_{yz}) increases as the value of the length to breadth ratio increases.

It can be seen that, at span to thickness ratio between 4 and 15, the value of transverse shear stress along y and z axes (τ_{yz}) varies between 0.022904 and 0.001370. These values of transverse shear stress (τ_{yz}) decrease between 0.000765 and 0.000100 at the span to thickness between 20 and 55 respectively. Hence, the value of transverse shear stress (τ_{yz}) is about 0.000084 and 0.00003, at the span to thickness between 60 and 100. The value becomes almost constant or equal to the value from CPT. This value becomes negligible as the value span to thickness increases. The values of transverse stress for span-thickness ratios of 100 and above are equal to the value from CPT.

In summary, there are three categories of rectangular plates. The plates whose vertical shear stress do not vary well from zero will be classified as thin plates because its value is almost equal to the value of the CPT. In between the thin and thick plate is the classified as moderate thick plate. Since the plate whose

transverse shear stress varies very much from zero is categorized as thick plates. Therefore, the span-to-depth ratio for these categories of rectangular plates are: Thick plate: $a/t \leq 15$; moderately thick plate: $20 \leq a/t \leq 55$; thin plate: $a/t \geq 60$. This confirmation can be used to show the boundary between thin and thick plate. Thus, it can be deduced from this research work that thick plate is the one whose span-depth ratio value is 4 up to 15.

Table 4: Displacement and Stresses of CCFC plate for length to breadth ratio of 1.5

β	∪	u	σ_x	τ_{xy}	τ_{yz}
	$\overline{U}$	$\overline{u}$	$\overline{\sigma_x}$	$\overline{\tau_{xy}}$	$\overline{\tau_{yz}}$
4	0.0185	-0.0043	0.2768	-0.0491	0.0126
10	0.0115	-0.0033	0.2157	-0.0361	0.0017
15	0.0108	-0.0032	0.2096	-0.0348	0.0007
20	0.0106	-0.0032	0.2075	-0.0343	0.0004
25	0.0105	-0.0032	0.2065	-0.0341	0.0003
30	0.0104	-0.0032	0.2059	-0.0340	0.0002
35	0.0104	-0.0032	0.2056	-0.0339	0.0001
40	0.0104	-0.0032	0.2054	-0.0338	0.0001
45	0.0104	-0.0032	0.2053	-0.0338	0.0001
50	0.0103	-0.0032	0.2052	-0.0338	0.0001
55	0.0103	-0.0032	0.2051	-0.0338	0.0001
60	0.0103	-0.0032	0.2050	-0.0338	0.0000
65	0.0103	-0.0032	0.2050	-0.0338	0.0000
70	0.0103	-0.0032	0.2050	-0.0338	0.0000
75	0.0103	-0.0032	0.2050	-0.0337	0.0000
80	0.0103	-0.0032	0.2049	-0.0337	0.0000
85	0.0103	-0.0032	0.2049	-0.0337	0.0000
90	0.0103	-0.0032	0.2049	-0.0337	0.0000
95	0.0103	-0.0032	0.2049	-0.0337	0.0000
100	0.0103	-0.0032	0.2048	-0.0337	0.0000
1000	0.0103	-0.0032	0.2048	-0.0337	0.0000
CPT	0.0103	-0.0032	0.2048	-0.0337	0.0000

From a critical look at Table 4, it is shown that the non-dimensional displacement (u, v and ∪) characteristics decrease with increases in the value of the span-thickness ratio. It is also observed in the Tables that the displacement (u, v and ∪) and stresses characteristics increase as the value of the length to breadth ratio increases. This means that, the in-plane

displacement are functions of x, y and z as it vary with the plate thickness while the deflection is only a function of x and y and did not varies linearly with the thickness of the plate thickness. Also, it was deduced that the normal stress (σ_x and σ_y) and shear stress characteristics (τ_{xy}, τ_{xz} and τ_{yz}) also decrease as the span-thickness ratio increases. It is also observed in the Table 4 that the stresses characteristics ($\sigma_x, \sigma_y, \tau_{xy}, \tau_{xz}$ and τ_{yz}) increase as the value of the length to breadth ratio increases.

It can be seen that, at span to thickness ratio between 4 and 10, the value of transverse shear stress along y and z axes (τ_{yz}) varies between 0.012564 and 0.001667. These values of transverse shear stress (τ_{yz}) decrease between 0.000724 and 0.000100 at the span to thickness between 15 and 40. Hence, the value of transverse shear stress (τ_{yz}) is about 0.000079 and 0.000016, at the span to thickness between 45 and 100. The value becomes almost constant or equal to the value from CPT. This value becomes negligible as the value span to thickness increases. The values of non-dimensional value of transverse stress for span-thickness ratios of 100 and above are equal to the value from CPT.

In summary, there are three categories of rectangular plates. The plates whose vertical shear stress does not very well from zero will be classified as thin plates because its value are almost equal to the value of the CPT. In between the thin and thick plate is the classified as moderate thick plate. Since the plate whose transverse shear stress varies very much from zero is categorized as thick plates. Therefore, the span-to-depth ratio for these categories of rectangular plates are: Thick plate: $a/t \leq 10$; moderately thick plate: $15 \leq a/t \leq 40$; thin plate: $a/t \geq 45$. This confirmation can be used to show the boundary between thin and thick plate. Thus, it can be deduced from this research work that a thick plate is the one whose span-depth ratio value is 4 up to 10.

Table 5: Displacement and Stresses of CCFC plate for length to breadth ratio of 2.0

β	∪ $\overline{U}$	u $\overline{u}$	σ_x $\overline{\sigma_x}$	τ_{xy} $\overline{\tau_{xy}}$	τ_{yz} $\overline{\tau_{yz}}$
4	0.0191	-0.0044	0.2824	-0.0386	0.0083
10	0.0119	-0.0034	0.2198	-0.0281	0.0011
15	0.0112	-0.0033	0.2136	-0.0270	0.0005
20	0.0110	-0.0033	0.2114	-0.0266	0.0003
25	0.0109	-0.0033	0.2104	-0.0265	0.0001
30	0.0108	-0.0033	0.2098	-0.0264	0.0001
35	0.0108	-0.0033	0.2095	-0.0263	0.0001
40	0.0107	-0.0033	0.2093	-0.0263	0.0001
45	0.0107	-0.0033	0.2092	-0.0262	0.0001
50	0.0107	-0.0033	0.2091	-0.0262	0.0000
55	0.0107	-0.0033	0.2090	-0.0262	0.0000
60	0.0107	-0.0033	0.2089	-0.0262	0.0000
65	0.0107	-0.0033	0.2089	-0.0262	0.0000
70	0.0107	-0.0033	0.2088	-0.0262	0.0000
75	0.0107	-0.0033	0.2088	-0.0262	10.0000
80	0.0107	-0.0033	0.2088	-0.0262	0.0000
85	0.0107	-0.0033	0.2088	-0.0262	0.0000
90	0.0107	-0.0033	0.2087	-0.0262	0.0000
95	0.0107	-0.0033	0.2087	-0.0262	0.0000
100	0.0107	-0.0033	0.2087	-0.0262	0.0000
1000	0.0107	-0.0033	0.2087	-0.0262	0.0000
CPT	0.0107	-0.0033	0.2087	-0.0262	0.0000

From a critical look at Table 5, it is shown that the non-dimensional displacement (u, v and ∪) characteristics decrease with increases in the value of the span-thickness ratio. It is also observed in the Tables that the displacement (u, v and ∪) and stresses characteristics increase as the value of the length to breadth ratio increases. This means that, the in-plane displacement are functions of x, y and z as it vary with the plate thickness while the deflection is only a function of x and y and did not varies linearly with the thickness of the plate thickness. Also, it was deduced that the normal stress (σ_x and σ_y) and shear stress characteristics (τ_{xy}, τ_{xz} and τ_{yz}) also decrease as the span-thickness ratio increases. It is also observed in the Table 4 that the stresses characteristics ($\sigma_x, \sigma_y, \tau_{xy}, \tau_{xz}$ and τ_{yz}) increase as the value of the length to breadth ratio increases.

It can be seen that, at span to thickness ratio between 4 and 10, the value of transverse shear stress along y and z axes (τ_{yz}) varies between 0.008325 and 0.001101. These values of transverse shear stress (τ_{yz}) decrease between 0.000478 and 0.000118 at the span to thickness between 15 and 30 respectively. Hence, the value of transverse shear stress (τ_{yz}) is about 0.000087 and 0.000011, at the span to thickness 35 and 100. The value becomes almost constant or equal to the value from CPT. This value becomes negligible as the value span to thickness increases. The values of non-dimensional value of transverse stress for span-thickness ratios of 100 and above are equal to the value from CPT.

In summary, there are three categories of rectangular plates. The plates whose vertical shear stress do not vary well from zero will be classified as thin plates because its value are almost equal to the value of the CPT. In between the thin and thick plate is the classified as moderate thick plate. Since the plate whose transverse shear stress varies very much from zero is categorized as thick plates. Therefore, the span-to-depth ratio for these categories of rectangular plates are: Thick plate: $a/t \leq 10$; moderately thick plate: $10 \leq a/t \leq 30$; thin plate: $a/t \geq 35$. This confirmation can be used to show the boundary between thin and thick plate. Thus, it can be deduced from this research work

that thick plate is the one whose span-depth ratio value is 4 up to 10.

In the classical plate theory (CPT), it is assumed that the plane cross sections initially normal to the plate's mid-surface before deformation remain plane and normal to the mid-surface after deformation , and the length of such elements is not altered [31]. This is the result of neglecting the transverse shear strains, therefore value of vertical shear stress from CPT analysis is zero. Any plate whose span-to-thickness ratio is such that the value of transverse shear stress from thick plate analysis is approximately zero can be idealized as thin plate. Analyzing such plate with classical plate theory will not introduce significant errors.

Thus, these plates can be classified as moderately thick plate. Hence, analyzing them with classical plate theory will introduce significant errors. When the span-to-thickness ratio is less than 15, the value of vertical shear stress is significant even when corrected to 4 decimal places. This range of span-to-thickness ratio produces plate classified as thick plate. It is also, showed that at span-thickness ratio above 100, the values obtained from the models used herein coincide exactly with values from CPT. This is quite expected since we assumed in CPT analyses that at span-thickness ratios from 100 and above, a plate can be taking as being thin.

Table 6: Comparative analysis of results from the present work and literature for 2.0 aspect ratio (α)

β	Present work $u(m)$	[30] $u(m)$	Percentage difference (%)
4	-0.0044	-0.0037	20.772
10	-0.0034	-0.0033	3.3903
50	-0.0033	-0.0033	0.2749
100	-0.0033	-0.0033	0.0306
1000	-0.0033	-0.0033	0.0306
CPT	-0.0033	-0.0033	0
Average total % difference	4.9		

From Table 6, it is shown that the present study predicts slightly higher values of in-plane displacement along the direction of x coordinate with highest percentage difference of 20.8% which occur at length to breadth aspect ratio of 4. This proves the safety of the present model. The present study converges with the work as value of span to thickness ratio increases and becomes the same or equal to CPT value at span to thickness ratio of 100. The rate of convergence can be seen in Figure 3. The total average percentage difference between the present study and the author in [30] is 4.9%. This means that at about 95 % confidence level, the values from the present study are the same with those of [30]. This higher confidence level proved that the polynomial shear deformation theory can be used with confidence for stress and bending analysis of thick rectangular plate clamped on three edges, and free at the other remaining edge.
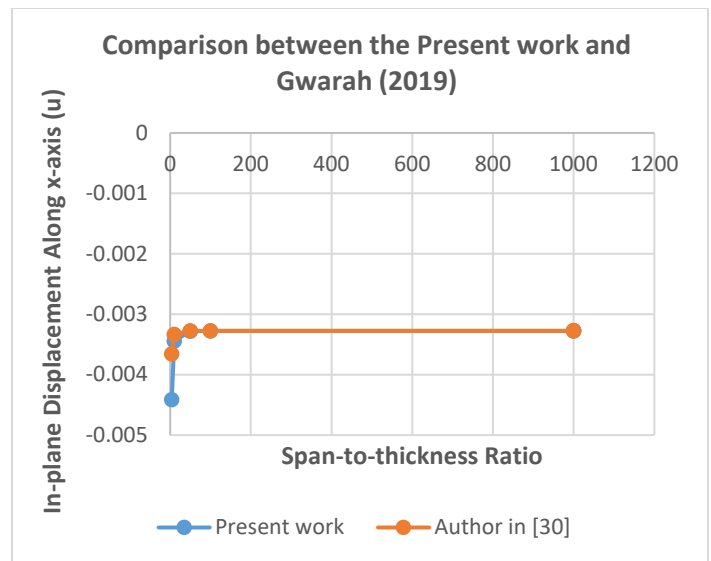

Figure 3: Graph of in-plane displacement versus span-to-thickness ratio

5. Conclusion

Stress analysis of thick rectangular plate using higher order polynomial shear deformation theory has been investigated. From the study this conclusion has been drawn:

i. It is concluded that the values of transverse shear stress obtained by this theory achieve accepted vertical shear stress to the thickness of plate variation and satisfied the transverse flexibility of condition at the top and bottom faces of the plate while predicting the flexural characteristics for an isotropic rectangular CCFC plate.

ii. The result moment and stresses obtained by present work using polynomial shear deformation theory agreed well with those of refined plate theory, but varied more with value of CPT. This validates the efficacy of the present theory in the thick plate analysis.

iii. The governing differential equations and associated boundary conditions obtained are variationally consistent and can be used with confidence in the analysis of rectangular thick plate.

6. Recommendation of Future Scope of Studies

This lies in the establishment shear deformation/displacement function for free vibration and buckling analysis of rectangular or circular thick plate. Then determining the displacement and stress parameters for the plate using virtual work principles.
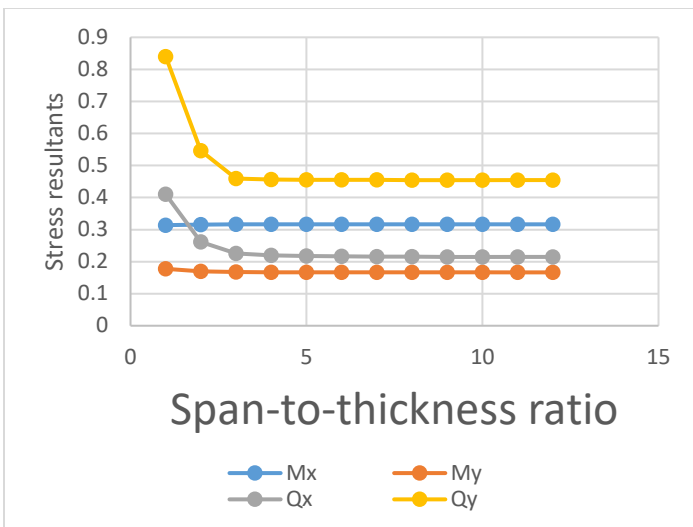
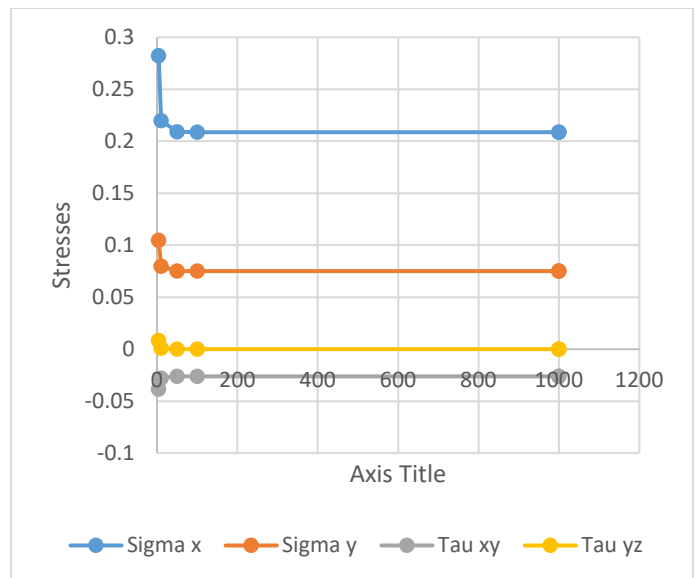Figure 4: Graph of span to thickness ratio versus stresses of a square plate
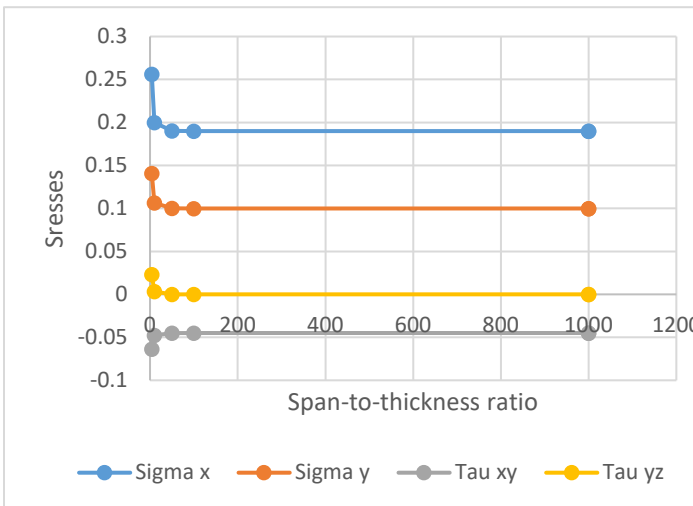

Figure 5: Graph of span to thickness ratio versus stresses for length to breadth ratio of 1.0

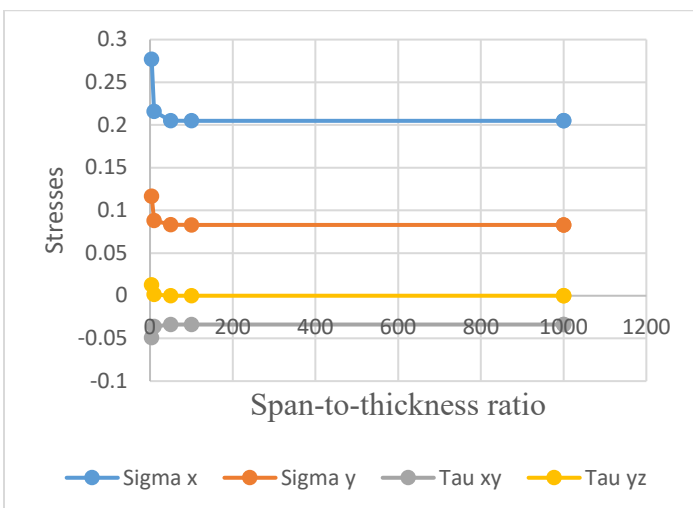Figure 6: Graph of span to thickness ratio versus stresses for length to breadth ratio of 1.5

Figure 7: Graph of span to thickness ratio versus stresses for length to breadth ratio of 2.0

Conflict of Interest Statement

There is no conflict of interest associated with this work.

References

[1] F.C. Onyeka, F.O. Okafor, H.N. Onah, "Displacement and stress analysis in shear deformable thick plate," International Journal of Applied Engineering Research, **13**(11), 9893-9908, 2018, https://www.ripublication.com/ijaer18/ijaerv13n11_161.pdf

[2] H.O. Ozioko, O.M. Ibearugbulem, J.C. Ezeh, U.C. Anya, "Algorithm for exact solution of thick anisotropic plates," Scholar Journal of Applied Sciences and Research, **2**(4), 11 – 25, 2019, https://www.innovationinfo.org/articles/SJASR/SJASR-4-225.pdf

[3] Y.M. Ghugal, P.D. Gajbhiye, "Bending analysis of thick isotropic plates by using 5th order shear deformation theory," Journal of Applied and Computational Mechanics, **2**(2), 80–95, 2016, https://jacm.scu.ac.ir/article_12366_b9e3037fda12c4f05a83ea31f80271e6.pdf

[4] K. Chandrashekhara, "Theory of plates. University Press (India) Limited," 2001.

[5] N.P. Kruyt, et al., "A strain–displacement–fabric relationship for granular materials. International journal of solids and structures, **165**, 14-22, 2019. https://doi.org/10.1016/j.ijsolstr.2019.01.028

[6] K. Shwetha, V. Subrahmanya, P. Bhat, "Comparison between thin plate and thick plate from navier solution using matlab software," International Research Journal of Engineering and Technology (IRJET), **5**(6), 2675 – 2680, 2018, https://www.irjet.net/archives/V5/i6/IRJET-V5I6500.pdf

[7] Md. Roknuzzaman, Md.B. Hossain, Md.R. Haque, T.U. Ahmed, "Analysis of rectangular plate with opening by finite difference method," American Journal of Civil Engineering and Architecture, **3**(5), 165 – 173, 2015, doi: 10.12691/ajcea-3-5-3

[8] P.S. Gujar, K.B. Ladhane, "Bending analysis of simply supported and clamped circular plate," International Journal of Civil Engineering (SSRG-IJCE), 2(5), 45 – 51, 2015, DOI: 10.14445/23488352/IJCE-V2I5P112

[9] O.M. Ibearugbulem, J.C. Ezeh, L.O. Ettu, "Pure bending analysis of thin rectangular SSSS plate Using Taylor-Mclaurin series," International Journal of Civil and Structural Engineering, **3**(4), 685 – 691, 2013, DOI: 10.6088/ijcser.201203013062

[10] G.R. Kirchhoff, "Ü''ber das Gleichgewicht und die bewegung einer elastschen scheibe," Journal f'' ur die reine und angewandte Mathematik,, 40, 51 - 88 (in German), 1850, DOI:10.1515/crll.1850.40.51

[11] G.R. Kirchhoff, "Ü''ber die Schwingungen einer kriesformigen elastischen scheibe," Annalen der Physik und Chemie, **81**, 258 - 264 (in German), 1850.

[12] G.O. Mathieu, D. Tyekolo, S. Belay, "The nonlinear bending of simply supported elastic plate," Rudn Journal of Engineering Researches, **18**(1), 58-69, 2017, DOI: 10.22363/2312-8143-2017-18-1-58-69

[13] D. W. Zietlow, D. C. Griffin, T. R. Moore, "The limitations on applying classical thin plate theory to thin annular plates clamped on the inner boundary," AIP Advances, **2**, 042103, 2012, https://doi.org/10.1063/1.4757928

[14] S.P. Timoshenko, S. Woinowsky-Krieger, "Theory of plates and shells," McGraw-Hill/Springer, New York, NY, USA, 1959.

[15] B.O. Mama, C.U. Nwoji, C.C. Ike, H.N. Onah, "Analysis of simply supported rectangular Kirchhoff plates by the finite Fourier sine transform method," International Journal of Advanced Engineering Research and Science, **4**(3), 285 – 291, 2017, DOI: 10.22161/ijaers.4.3.44

[16] J.C. Ezeh, O.M. Ibearugbulem, L.O. Ettu, L.S. Gwarah, I.C. Onyechere, "Application of shear deformation theory for analysis of CCCS and SSFS rectangular isotropic thick plates," Journal of Mechanical and Civil Engineering (IOSR-JMCE), **15**(5), 33 – 42, 2018, DOI: 10.9790/1684-1505023342

[17] A.S. Sayyad, Y.M. Ghugal, "Bending and free vibration analysis of thick isotropic plates by using exponential shear deformation theory," Applied and Computational Mechanics, **6**, 65–82, 2012, https://www.kme.zcu.cz/acm/acm/article/view/171

[18] C. Onyechere, O.M. Ibearugbulem, U.C. Anya, L. Anyaogu, C.T.G. Awodiji, "Free-vibration study of thick rectangular plates using polynomial displacement functions," Saudi Journal of Engineering and Technology, 2020, 10.36348/sjet.2020.v05i02.006

[19] S.P. Timoshenko, S. Woinowsky-Krieger, "Theory of Plates and shells (2nd Ed.)," Auckland: McGraw-Hill Inc, 1959.

[20] F.O. Okafor, O.J. Udeh, "Direct method of analysis of an isotropic rectangular plate using characteristic orthogonal polynomials," Nigerian Journal of Technology, **34**(2), 232-239, 2015, http://dx.doi.org/10.4314/njt.v34i2.3

[21] Y. Zhong, Q. Xu, "Analysis bending solutions of clamped rectangular thick plate," Hindawi Mathematical Problems in Engineering, **20**, 1- 6, 2017, https://doi.org/10.1155/2017/7539276

[22] O.M. Ibearugbulem, J.C. L.O. Ettu, L.S. Gwarah, "Bending analysis of rectangular thick plate using polynomial shear deformation theory," IOSR Journal of Engineering (IOSRJEN), **8**(9), 53-61, 2018, http://www.iosrjen.org/Papers/vol8_issue9/Version-3/J0809035361.pdf

[23] K. Hassan, S. Guirguis, H. El-Hamouly, "Bending of an elastic rectangular clamped plate using Bergan-Wang approach," African Journal of Engineering Research, **5**(1), 7 – 17, 2017, http://www.netjournals.org/z_AJER_16_024.html

[24] A.Y. Grigorenko, A.S. Bergulev, S.N. Yaremchenko, "Numerical solution of bending problems for rectangular plates," International Applied Mechanics, **49**(1), 81 – 94, 2013, https://doi.org/10.1007/s10778-013-0554-1

[25] B.S. Reddy, "Bending behaviour of exponentially graded material plates using new higher order shear deformation theory with stretching effect," International Journal of Engineering Research, **3**(1), 124-131, 2014.

[26] F.C. Onyeka, O.M. Ibearugbulem, "Load analysis and bending solutions of rectangular thick plate," International Journal on Emerging Technologies, **11**(3), 1103–1110, 2020.

[27] F.C. Onyeka, F.O. Okafor, H.N. Onah, "Application of exact solution approach in the analysis of thick rectangular plate," International Journal of Applied Engineering Research, **14**(8), 2043-2057, 2019, http://www.ripublication.com/ijaer19/ijaerv14n8_39.pdf

[28] F.C. Onyeka, O.T. Edozie, "Application of higher order shear deformation theory in the analysis of thick rectangular plate," International Journal on Emerging Technologies, **11**(5), 62–67, 2020.

[29] O.M. Ibearugbulem, F.C. Onyeka, "Moment and stress analysis solutions of clamped rectangular thick plate," European Journal of Engineering Research and Science, **5**(4), 531-534, 2020, https://doi.org/10.24018/ejers.2020.5.4.1898

[30] L.S. Gwarah, "Application of shear deformation theory in the analysis of thick rectangular plates using polynomial displacement functions," A published PhD. thesis presented to the school of Civil Engineering, Federal University of Technology, Owerri, Nigeria, 2019, https://futospace.futo.edu.ng/bitstream/handle/123456789/2956/Gwarah_Application_2019.pdf?sequence=1&isAllowed=y

[31] E. Ventsel, T. Krauthammer, "Thin plates and shells theory, analysis and applications," Maxwell Publishers Inc; New York, 2001.

ASTES

Quality Function Deployment: Comprehensive Framework for Patient Satisfaction in Private Hospitals

Mohammad Kanan[*], Siraj Essemmar

Industrial Engineering Department, College of Engineering, University of Business and Technology, Jeddah, 21448, Kingdom of Saudi Arabia

A R T I C L E   I N F O

A B S T R A C T

This paper addresses the quality of private healthcare services in the western region of the Kingdom of Saudi Arabia (KSA) and provides a comprehensive analysis of the customer requirement to improve the quality of these services. The study begins by reviewing literature on the subject of quality in general and then in terms of the service and healthcare sectors. To assess the healthcare system, the paper then presents the literature on accreditation, which is a tool for healthcare quality assessment. Past studies in healthcare are also reviewed. The voice of the customer (VOC) is an essential factor in this study, so the quality function deployment (QFD) tool was implemented to satisfy the customer requirements and achieve the purpose of the study. A customer focus group was used to determine the VOC, and a survey of 300 samples was conducted to assess the importance of each requirement. The study implemented four houses, which represent the four phases of a comprehensive QFD. According to QFD analysis the results show that there are two main factors that affect the private healthcare system in the (KSA). The first factor deals with management issues, while the second one relates to the recording and flow of information. The study suggests several ways to improve the management and information issues of the healthcare system in (KSA).

1. Introduction

Due to globalization and the rapid changes in various industries, improvement in the quality of the healthcare sector has been relatively slow. As such, the governments need to give serious attention to this sector, which delivers one of society's basic needs. The population of the Kingdom of Saudi Arabia (KSA) is approximately 34 million, with an annual population growth rate of 2.52% (General Authority of Statistics). According to United Nations projections, by 2025 the population of KSA will be approximately 39.8 million [1]. Hence, KSA's 2030 vision includes several initiatives to improve its healthcare services. Currently, there are three medical sectors in KSA: the government agencies sector, the public healthcare sector, and the private healthcare sector. The government agencies sector makes up 17.7% of total healthcare services, and provides healthcare services to specific government employees and families through specialist hospitals and research centers, National Guard health affairs, security forces medical services, Royal Commission health services, army medical services, and the Ministry of Education hospital [2]. The public healthcare sector makes up 60.2% of total healthcare services, which are provided by the Ministry of Health (MOH). The private sector makes up 22.1% of total healthcare services [2]. The MOH plans to transfer 295

hospitals and 2,259 health centers to the private sector by 2030 [1]. It also revealed that, out of 2,390 healthcare centers in KSA, only 55 have attained the standards of the Saudi Central Board for Accreditation of Healthcare Institute (CBAHI) (CBAHI, 2013). The governments needs to establish a new system, method, and measurement of quality that will enhance performance, reduce costs, and eliminate waste. This study aims to improve the quality of private healthcare services in the western region of KSA. The study focuses on patients as a major stakeholder in these services. Although the suggestions are related to the structure and process of healthcare systems, they also affect the outcomes in the healthcare service framework. To achieve this aim, it is essential to evaluate current services and the performance of competitors, for which the quality function deployment (QFD) tool will be used.

2. Literature review

The quality definitions is highly debated in the associated literature. However, a challenge arises due to the difference in perspectives of different types of products, which range from goods and services to software [3].

2.1. Quality review

In terms of goods, there are multiple definitions of quality. In 1984, Garvin dealt with quality by categorizing past definitions

*Corresponding Author: Mohammad Kanan. Email: m.kanan@ubt.edu.sa

into five approaches—value based, product based, user based, transcendent, and manufacturing based—and separating the basic elements of product quality into eight dimensions [4]. Also, Garvin studied the relationship between quality and other terms such as marketing, price, and cost. He discussed four types of costs which are: appraisal cost, external and internal failures, and prevention cost [4]. Feigenbaum coined the term cost of quality in a 1956 which include the four types of cost [5]. Juran defined quality as "fitness for use" and argued that an analogy can be made between financial management and quality management, establishing a tripartite approach of quality planning, quality control, and quality improvement [3]. Japanese philosophy defines quality as having no defects, being done right the first time. Reinforcing the latter definition, Crosby defined quality as "conformance to requirements or specifications" [6]. Deming's definition of quality is slightly more expansive: "Quality is a predictable degree of uniformity and dependability, at low cost and suited to the market". Deming also identified 14 areas of quality management that support and improve an organization's performance [7].

Quality of service, however, differs from the quality of tangible goods. Parasuraman and Grönroos defined quality of service as the perceptions of consumers that are associated with their expectations of the service and the received service [8]. Parasuraman and Grönroos's definition established quality as the gap between customers and managers. They identified five types of gap—knowledge, standards, delivery, communications, and expected service/perceived service—and ten dimensions of service quality, which they called SERVQUAL. Although SERVQUAL is one of the most common models used in the literature for services similar to healthcare, such as tourism, hospitality, marketing, and banking, it needs to be modified to fit the context [9]. Cronin and Taylor rejected this method of gaps/score measurement, instead measuring service quality using a tool called SERVPERF, which depends only on performance [9].

Many recently developed products are software based, and software has become a significant factor in quality of life. Both goods and services depend on software. As such, the need to understand, control, and design high-quality software has become important [10]. Managers generally focus on improvement, so researchers have designed tools and instruments to measure and improve quality in any field. In the United States manufacturing industry during the 1980s, quality was transformed from small-q to big-Q. This change, established by Juran, highlighted the difference between focusing on reworking existing conditions in a limited capacity (small q), which often neglected other factors like resources and management, and managing quality in all aspects of business (big Q). This concept later became known as total quality management (TQM) [11]. TQM is an organized approach to achieving customer satisfaction using several techniques, tools, and systems through continuous improvement of a process [12]. In 1987, the Malcolm Baldrige National Quality Award was established and the Lean Six Sigma was revealed by Motorola. The Lean Six Sigma is a model that focuses on the variations of products to reduce the chance of defects to less than 3.4 per million. Its methodology follows five stages: definition, measurement, analysis, improvement, and control (DMAIC) [13].

2.2. Quality in the service industry

Literature has identified three main economic sectors: the primary sector, the secondary sector, and the tertiary sector. The primary sector deals with the extraction of natural resources through farming and mining, while the secondary sector transforms these raw materials into tangible goods. The tertiary sector focuses on the production of services rather than goods, and has a significant effect on gross domestic product (GDP). It also greatly impacts everyday life in areas such as education, healthcare, and transportation.

According to the Oxford English Dictionary, a service is "a system supplying a public need such as transport, communications, or utilities (electricity and water)". The Business Dictionary defines service as "a valuable action, deed, or effort performed to satisfy a need or to fulfill a demand". Service involves all aspects of modern life—it is the several processes that deliver benefits to customers. The nature of service is more complex than that of tangible goods, and the problems of the service sector are related to the characteristics of different services, which can be classified into three main categories: intangibility—a service is performed, rather than being an object, so it cannot be measured in advance to assure the quality − heterogeneity − a service depends on the performance of staff, so it differs from one provider to another—and inseparability—the delivery of a service depends on the interaction between a customer, a provider, and their environment [6]. One of the limitations of a service is that a customer cannot evaluate its quality until they have experienced it, a limitation that Phillip Nelson highlighted when he distinguished between "search" and "experience". In search, quality can be determined before purchase, but in experience it can only be known after purchase and use [4]. The limited knowledge of the customer in the healthcare process makes it harder to judge the quality of healthcare service.

2.3. The definition of healthcare quality

Healthcare is a complex service system; according to Donabadian's framework, the healthcare system consists of three main categories: structures, processes, and outcomes. While structures relate to facilities, equipment, layout, and physicians, a process is any interaction between the customer and the healthcare structure. Outcomes are the consequences of the healthcare service [14]. Overall, the healthcare system provides benefits to several stakeholders, including patients, attendants (relatives, friends), physicians, nurses, insurance companies, and the government.

Scholars and researchers have provided different definitions of high-quality healthcare. Ovretveint defined it as "fully meeting the needs of those who need the services most, at the lowest cost to the organization, within the limits and directive set by higher authorities and purchases" [2]. Campbell, Roland, and Buetow (2000) categorized high-quality healthcare into two types: individual patient care and population care. Individual patient care is defined as "whether individuals can access the health structures and processes of care which they need and whether the care received is effective". Population care is "the ability to access effective care on an efficient and equitable basis for the optimization of health benefit/well-being for the whole population". Deepti Singh and Kavaldeep Dixit argued that the satisfaction of the patient will be achieved by improving the delivery of health care service, considering patients' needs, and reacting with their annotation [15]. So, the involvement of patients and shear their experience with healthcare professionals is a critical factor that will impact the quality improvement process [16].

2.4. Healthcare quality standards

An effective factor in assessing and improving quality is accreditation—a framework to help and improve the quality of healthcare by fulfilling the standards of an external independent accreditation body [17]. Standards are a measure of excellence that indicate key functions, processes, structures, and activities. In healthcare facilities, it is a requirement to assure the provision of safe and high-quality care [18] . Although standards are the tools and requirements of accreditation, they also help an organization improve the quality of its services [19] . Araujo, C. A., Siqueira, M. M., & Malik, A. M reviewed 37 studies about the impact of accreditation on the healthcare quality and they concluded that the accreditation effects on healthcare quality indicators are mostly positive [20].

2.5. The Saudi Central Board for Accreditation of Healthcare Institutions (CBAHI)

The CBAHI is a non-profit governmental organization authorized to give accreditation to healthcare centers in KSA. It aims to continually improve healthcare services in terms of quality and safety, and seeks to achieve this by supporting healthcare facilities in following the established standards. The organization was itself accredited by the International Society for Quality in Healthcare (ISQua), making it one of the few healthcare accreditation organizations around the globe. In the CBAHI's third edition standards manual, there are 23 chapters explaining the functions and key services that must be provided to obtain accreditation, such as leadership, nursing care, quality management, patient safety, operating rooms, facility management, safety, and emergency care [18].

2.6. Healthcare quality studies

Several relevant case studies have been conducted in healthcare literature. Due to the difficulties associated with measuring quality in healthcare sectors, different models were employed based on the tools or methods used. One of the most popular models used in the healthcare sector is SERVQUAL, and although some researchers were committed to Parasuraman's dimensions, a modified SERVQUAL model was needed in some case studies. For example, authors studied the relationship between patient satisfaction, service quality, and word of mouth (WOM), concluding that the main dimension of service quality that affects WOM is empathy, and that some dimensions, such as assurance, responsiveness, and tangibility, have an indirect effect on patient satisfaction [8]. Later, authors applied a new scale to measure SERVQUAL gaps in Malaysian private healthcare services [21]. Padma, Rajendran, and Sai (2009) found that the dimensions of SERVQUAL are not sufficient to reflect actual quality level, so they adapted dimensions from the Malcolm Baldrige National Quality Award (MBNQA, 2007) and Joint Commission International framework (JCI, 2007) and modified dimensions in [9].

Some researchers have used another model, the plan–do–study–act (PDSA) model, which is a tool for quality improvement developed by Shewhart and Deming. The model consists of four stages: the planning stage, which identifies the improvement of the process; the doing stage, which deals with testing the improvement; the studying stage, which examines the success of the improvement; and the acting stage, in which a new cycle is initiated by the identification of further possible adaptations [22]. Authors reviewed 73 articles related to healthcare and found that more than 60% of the articles fulfilled

PDSA criteria and information. Based on their findings, the benefits of the PDSA can be maximized by starting the cycle on a small scale and following an iterative approach [22].

Other researchers have expanded the concept of healthcare quality through the use of TQM. Dilber, Bayyurt, Zaim, and Tarim (2005), for example, identified the critical factors of TQM in the healthcare sector—process management, the role of top management, employee relations, and data reporting—and measured the impact of these critical factors on business performance in Turkish hospitals [7]. Some authors also integrated TQM with business process re-engineering (BPR), which is a fundamental and radical redesign and rethinking of business processes to create significant improvements in performance [3].

2.7. Quality function deployment (QFD)

One of the main critical factors in TQM is the voice of the customer (VOC). There are several ways to study the VOC, one of the most popular tools is the quality function deployment (QFD).

In 1972, authors published a paper about quality deployment. This, along with Nishimura's paper, was the route of the new concept of QFD to the west. Authors then established a way to convey customer requirements from the design stage to the operation stage, called quality function deployment (hinshitsu kino tenkai). Finally, in 1978, a book titled Deployment of the Quality Function, which discussed the Japanese experience of QFD [23].

QFD is a tool for transforming customer requirements into design with a satisfying level of quality assurance, and can create novel solutions [23]. It can, however, be difficult to apply, as it is loosely defined and can therefore be more of an art than a science [23].

The primary fields into which QFD was introduced were quality management systems, customer needs, product development, and analysis. It was later extended to other fields, such as construction, costing, education, decision making, software, and services. QFD can be used in any field, without boundaries [23, 24].

House of quality (HOQ) is the basic design tool of QFD. It started in 1972 in Mitsubishi's Kobe shipyard, and was then implemented by Toyota in different ways. HOQ is a conceptual map that provides the means for inter-functional planning and communication. The main principle of HOQ is to satisfy customer needs by learning from customer experiences [25]. QFD uses several iterations of HOQ to translate customer needs into detailed functional characteristics, and these iterations (houses) require a high level of cooperation between cross-functional teams [26]. Jaiswal (2012) defined these iterations as product planning, product design, process planning, and process control [27]. The authors explained that implementations in QFD often need several HOQ repetitions to obtain a satisfactory result, but organizations usually only get through the first house of QFD [27].

Generally, there are two main phases in each house or iteration; the first phase deals with the quality plan, answering the "What" questions, while the second phase is related to quality design, answering the "How" questions [28]. "What" questions appear in the HOQ conceptual map (see Figure 1) as room (1), containing customer requirements or preferences. Beside it, the priorities being assigned based on customer

preferences. The engineering characteristics are generated and entered in room (3). The biggest room, constructed between the "How" and "What" questions, is room (4), the relationship matrix, which indicates how much the "How" and "What" relate to or affect each other. Rooms (5) and (6), respectively, represent the benchmark for customer satisfaction and engineering characteristics correlating to benchmarks. Room (7) is located at the bottom of the house and includes the targets for a new product or service. The final part of the house is a coupling matrix, which appears as room (8), the roof. This is used to show the relationship between one engineering characteristic and another [29].
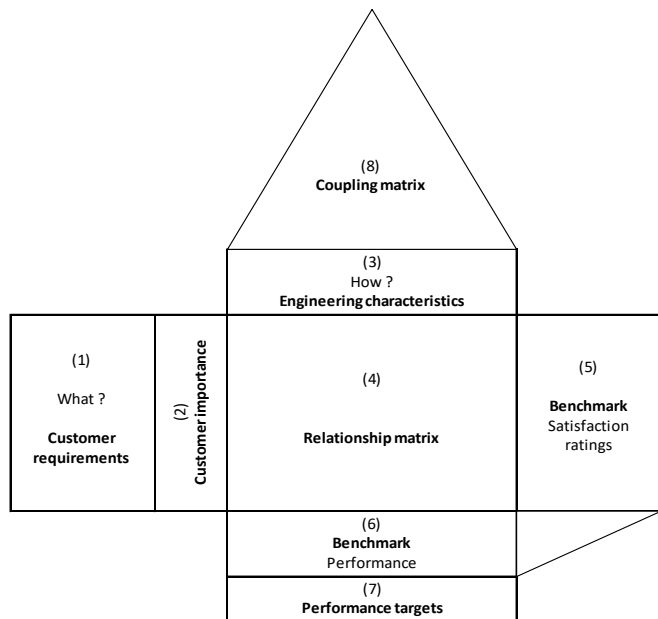

Figure 1: House of quality model [33]

3. Study Execution

This study aims to provide appropriate suggestions for improving service quality and satisfying customer needs in the private healthcare sector in KSA. As the VOC is the core of this paper, the QFD was used.

3.1. Methodology

To determine customer requirements (the VOC), a focus group session was held with customers then the survey was conducted to measure the importance of customer requirements. The results were analyzed and based on the analysis, the HOQ was established to generate the engineering characteristics. A scale of 0, 1, 3, and 5 points was used in the relationship matrix, as put forward in [30]. To achieve comprehensive analysis, benchmarking was performed in each phase and the public and other government agencies were seen as competitors.

3.2. Gathering the VOC

Customers were gathered in Jeddah from different ages and perspectives to determine the most important needs based on their experience with different private hospitals. The sessions discussed Cooperation of medical staff, Waiting time, Ease of procedures, And Cost of medical care among others. As shown in table 1. The sessions took more than 30 hours spanning five days. Doctors and experts were also consulted.

Table 1: Importance of customer requirements

n	Customer requirement	Weight	Percentage	Customer importance
1	Waiting time	2643	11.26%	9
2	Availability of appointments	2776	11.82%	9
3	Cooperation of medical staff	2893	12.32%	10
4	Cooperation of administrative staff	1973	8.40%	7
5	Quality of facilities	2256	9.61%	8
6	Reputation of the hospital	2296	9.78%	8
7	After-service communication	1112	4.74%	4
8	Ease of procedures	2032	8.65%	7
9	Software application	1108	4.72%	4
10	Calling method in the waiting room	1068	4.55%	4
11	Access to medical records	1165	4.96%	4
12	Cost of medical care	2156	9.18%	7

Table 2: Engineering characteristics for product planning

n	Engineering characteristic	Explanation
1	Scheduling	Scheduling of appointments/employees
2	Training and consultation	Periodic training in communication and empathy
3	Ergonomics	Making workplaces suitable for people
4	Facility layout	Arrangement and state of the facility
5	Optimizing the number of patients and resources	Eliminating waste and regulating the number of patients for each doctor
6	Motivating employees	Encouraging doctors and other staff to be kind and inspiring them to perfection
7	Accreditation	Achieving the specifications and standards of the CBAHI
8	Information systems	Information flow within the hospital and other healthcare centers
9	Communicating with patients	Any process of communication with patients
10	Encouraging patients to take out insurance	Convincing and influencing patients to take out insurance
11	Making the app easy to use	Simplifying the app and making it user friendly

The results from the focus group and consultation sessions revealed that there are 12 requirements to be considered. The 300-sample size survey was conducted to know the priority of each requirement. Using the ranks obtained in the survey questions, the highest customer preference was multiplied by 12, the second highest by 11, the third highest by 10, and so on, to balance the weight of importance for each customer requirement. To modify the scale of customer requirements to between 1 and 10, the weight percentage was multiplied by 80. The outcomes are shown in Table I.

3.3. Product planning

The first house was built based on the survey analysis. After looking at the VOC in the first two rooms, the third room was constructed by listening to the voice of the engineers on how to satisfy the customer requirements, So the engineers studied all requirements and suggested the solution (characteristic) that will affect them. Table 2 shows out the engineering characteristic - representing the suggested solution - and a brief description of each one.

Figure 2: Engineering characteristics details

Figure 3: Product design

The relationship between customer requirements and engineering characteristics was then determined in the correlation matrix. Negative and positive signs were also used to determine the correlation between each engineering characteristic. Finally, the relative weight for each customer requirement and engineering characteristic was calculated. The results of the first phase identified 11 engineering characteristics and the details were represented in Figure 2.

The highest value represents the "optimizing number of patients and resources". So, focusing on the "optimizing the number of patients and resources" will satisfied customer requirements by 19%. Focusing on a hospital's internal environment is one of the most valued outcomes, appearing with a high value in both the ergonomics and facility layout characteristics. In relation to encouraging patients to take out insurance, Saudi labor law requires private companies to pay the health coverage costs (insurance) for all employees [31], but other employees should be encouraged to take out their own insurance. As such, encouraging patients to take out insurance is an engineering characteristic that can help minimize the cost of medical care.

3.4. Product design

The engineering characteristics of the previous phase were added as the requirements in this phase, and a new set of engineering characteristics was generated, as shown in Table 3. To satisfy the requirements, controlling scheduling factors should be prioritized, as it has the highest impact on the requirements (see Figure 3). Fixing the number of patients for each doctor is shown to be important, as it reduces physician burnout, which would otherwise affect the healthcare system [32].

Table 3. Engineering characteristics for product design

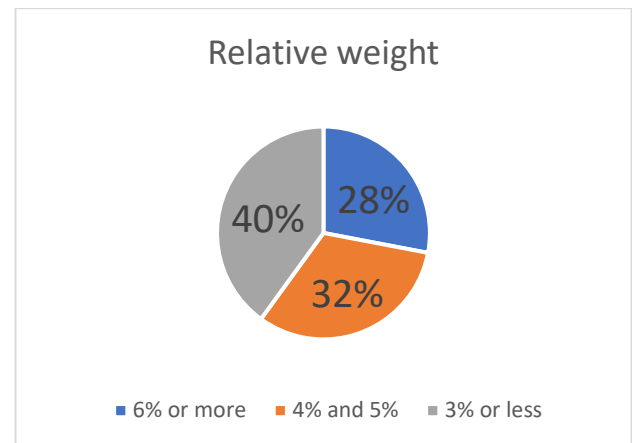| n	Engineering characteristic	Explanation
1	Controlling scheduling factors	Identifying and limiting the factors that can affect scheduling, such as breaks, number of physicians, and appointment duration
2	Using the app	Involving the app in the communication and information recording process
3	Conditional scheduling plans	Backup plans for scheduling
4	Courses (communication, empathy)	Guidelines and seminars on communication and empathy
5	Periodic consultation sessions	Regular therapy consultations to deal with stress and burnout
6	Workshops and conferences	Lectures and motivational events
7	Comfortable work environment	Making workplace conditions more comfortable
8	Cleanliness	The state of the facility
9	Time and motion studies	Studying the time of each process and the movement effort required
10	Fixing the number of patients for each doctor	Regulating the number of patients each physician treats in a day
11	Combining a procedure in one place	Gathering the process for ease
12	Eliminating resource waste	Reducing wasted time, effort and equipment
13	Inspiring statements	Statements aimed to motivate employees
14	Talks	Inviting motivational speakers
15	Intrinsic rewards	Non-material incentives for employees
16	Expertise	Hiring a specialist physician
17	Fulfilling the national standards (CBAHI)	Achieving the CBAHI standards
18	Evaluation forms for visitors	Assessment from patients receiving services
19	Observing patient treatments	Observing the state of patients after discharge
20	Using a number calling method	Using a numbered queuing technique
21	Ease of information flow	Ensuring information travels between departments easily
22	Linked system between hospitals	Integrating a database between all hospitals
23	Big-data recording	Using big-data principles to record all information
24	Training stakeholders to use the app	Training patients and staff to use the app properly and effectively
25	Redesigning the app	Redesigning the interface and functionality of the app

Figure 4: Relative weight of engineering characteristics for product design

3.5. Process planning

According to authors, only the most important characteristics from each phase should be moved to the next phase. Therefore, the Pareto method was used to focus on the characteristics that were found to have the greatest impact on the requirements. The impact of each characteristic was detailed on table 4. From that table and following Pareto principal, 28% of these characteristics were moved to the next phase as requirements. (see Figure 4)

Table 4: Engineering characteristics: Contribution to product design

Engineering characteristics	Relative weight	Cumulative	Relative weight after rounding
Controlling scheduling factors	8.22%	8.2%	8%
Using the app	7.27%	15.5%	7%
Fixing the number of patients for each doctor	7.11%	22.6%	7%
Eliminating resource waste	6.48%	29.1%	6%

Conditional scheduling plans	**5.93%**	**35.0%**	**6%**
Big-data recording	**5.85%**	**40.9%**	**6%**
Ease of information flow	**5.69%**	**46.6%**	**6%**
Cleanliness	5.45%	52.0%	5%
Combining a procedure in one place	4.98%	57.0%	5%
Comfortable work environment	4.58%	61.6%	5%
Periodic consultation sessions	3.87%	65.5%	4%
Workshops and conferences	3.87%	69.3%	4%
Courses (communication, empathy)	3.72%	73.0%	4%
Linked systems between hospital	3.72%	76.8%	4%
Time and motion	3.64%	80.4%	4%
Fulfilling the national standards (CBAHI)	3.32%	83.7%	3%
Evaluation forms for visitors	2.53%	86.2%	3%
Observing patient treatments	2.53%	88.8%	3%
Redesigning the app	2.29%	91.1%	2%
Talks	2.13%	93.2%	2%
Using a number calling method	1.66%	94.9%	2%
Inspiring statements	1.50%	96.4%	2%
Intrinsic rewards	1.50%	97.9%	2%
Training the stakeholders to use the app	1.19%	99.1%	1%
Expertise	0.95%	100.0%	1%

Table 5: Engineering characteristics for process planning

n	Engineering characteristics	Explanation
1	Forecasting the number of patients	Predicting the daily demand of patients
2	Deposit fees for appointments	Fees paid to confirm the appointment and deducted from medical costs
3	Periodic breaks	Giving breaks to staff during working hours
4	Providing an internet connection	Availability of an internet connection within hospital facilities
5	Self-service machines	Machines for patients to facilitate procedures
6	Research on human subjects	Conducting studies in anthropological fields
7	Lean Six Sigma tools	Using Six Sigma principles and tools
8	Establishing a big-data department	Forming a new department for big-data collection and analysis
9	Standard platforms	Unified platforms containing medical records and other information
10	Computerized communication between departments	Eliminating all paperwork and replacing it with electronic communication
11	Replacement people for every job	Assigning employees to cover the absences of others

From the requirements, 11 engineering characteristics were considered as solutions. The descriptions of each characteristic are summarized in Table 5.

Resource waste caused by the transfer of information between departments has an impact on several factors (See Figure 5).

Computerized communication between departments uses fewer resources, such as paper and time. Moreover, its application enhances patient service and helps in the improvement of scheduling, data recording, and the flow of information. One of the other conclusions of this phase is that the impact of forecasting the number of patients will help reduce the chance of physician burnout, hence improving the quality of patient care [32].

3.6. Process control

The final technical solutions were conducted in this phase. The engineering characteristics of this phase (see Table 6) can be considered the main factors in achieving the customer requirements in the first house.

This phase proved that information could affect quality in healthcare and showed that information has the highest rating in the engineering characteristics of gathering information and contracting IT companies (See Figure 6). The contracted IT company has the responsibility of analyzing and recording information, while leadership faces a challenge in collecting the correct information from various departments. Efficient record keeping and documentation can be difficult [17].

The involvement of IT companies would require time and money, but would help improve information systems by contracting expertise or hiring a specialized employee. The assignment of surveying responsibility to a quality department would also improve quality. This department should be given an extensive training program before its staff are considered qualified to conduct surveys [17].

4. Result and discussion

To summarize the analysis of the QFD and satisfy the customer requirements, two main factors should be taken into consideration. The first factor is management, which was revealed in the first phase to consist of optimizing the number of patients, scheduling, and accreditation. This was expanded in the second phase to controlling scheduling factors, conditional scheduling plans, fixing the number of patients, and fulfilling standards.
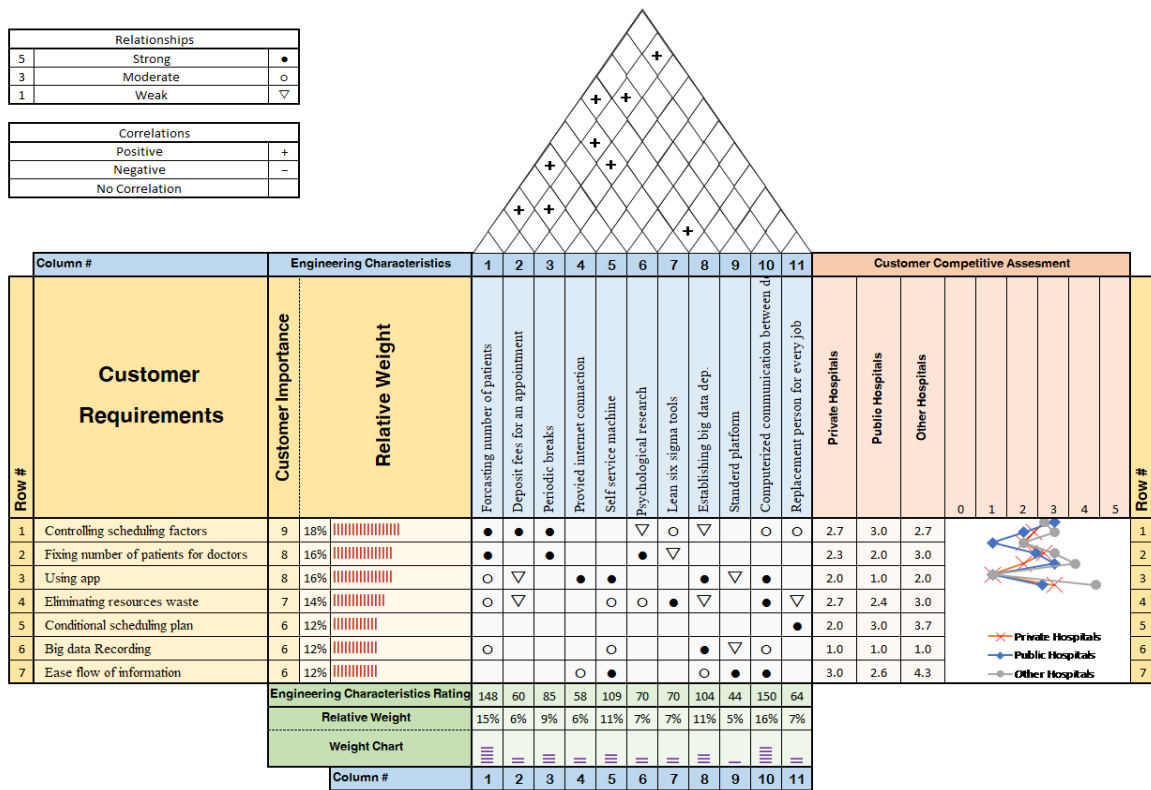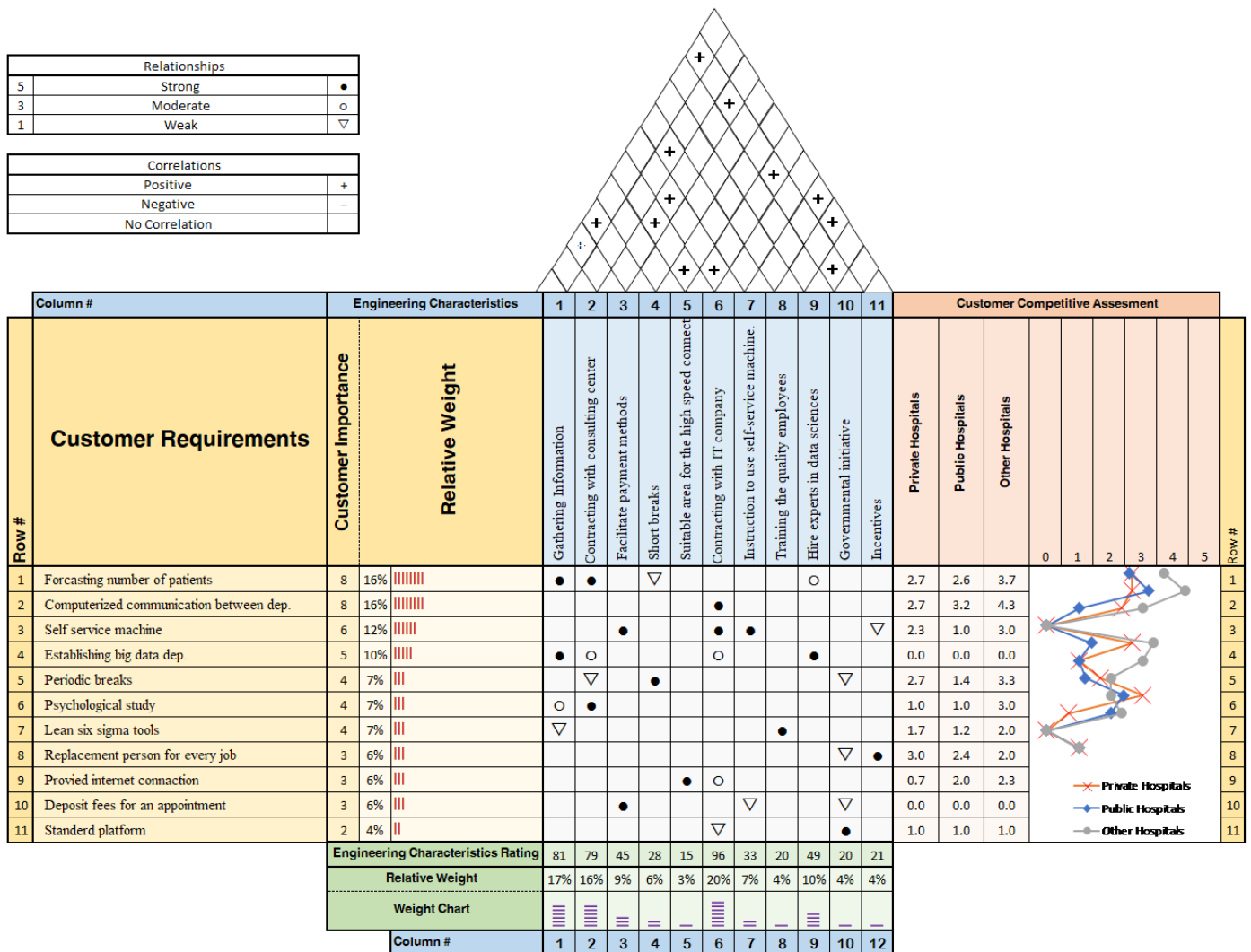
Figure 5: Process planning

Figure 6. Process control

This consideration has some contributions to third and fourth phases, such as forecasting the number of patients and contracting a consulting center. The second factor is information, which begins in the first phase with an information system and develops into ease of information flow, big-data recording, and linked systems between hospitals in the second phase. It becomes the main focus in the third phase through computerized communication between departments, establishing big-data self-service machines, and standardized platforms. In the final phase, it expands to gathering information, hiring experts in data science, and contracting IT companies.

Table 6: Engineering characteristics for process control

n	Engineering characteristics	Explanation
1	Gathering information	Collecting data and information in an appropriate way
2	Contracting consulting centers	Contracting specialist centers in data science, supply-chain management and anthropology
3	Facilitating payment methods	Making payment methods easier
4	Short breaks	Short breaks for physicians and other staff
5	Suitable areas for high-speed connection	Preparing a high-speed connection area for patients and staff
6	Contracting IT companies	Contracting a professional IT company
7	Instructions for using self-service machines	Placing instructions near self-service machines to help the users
8	Training quality department employees	Training employees in principles of quality and survey methods
9	Hiring experts in data sciences	Finding experts to analyze data
10	Government initiatives	Governmental initiatives, especially on standardized platforms
11	Incentives	Rewards to motivate and encourage employees

5. Conclusion

KSA's vision is to privatize public hospitals as part of its aim to improve the Saudi economy and make KSA one of the most competitive countries in the world [31]. This implies an increase in the demand for private healthcare services. Thus, tools for the assessment and development of quality need to be implemented. As shown in this study, QFD can be an effective and realistic tool because it considers the VOC. Utilizing QFD, it was found that information recording and flow have the greatest impact on improving service quality in healthcare. Scheduling also plays an important role in improving customer satisfaction, as it was given the greatest weight of all the engineering characteristics that have a strong correlation with customer requirements.

6. Future research

To develop a comprehensive QFD, all departments and expertise from different fields should be integrated, which would improve research in the field of healthcare service. Moreover, including the third factor of Donabadian's model (outcomes) and considering it as a customer requirement may improve the implementation of the QFD in healthcare. Future research should focus on other stakeholders, such as nurses and physicians. Communication has a potential for further studies, which should concentrate on all aspects of communication, such as electronic communication and face-to-face interaction. Such studies would need to examine, evaluate, and enhance communication to achieve the standard requirements.

References

[1] R. Sajjad, M.O. Qureshi, "An assessment of the healthcare services in the Kingdom of Saudi Arabia: An analysis of the old, current, and future systems," International Journal of Healthcare Management, **13**(S1), 109–117, 2020, doi:10.1080/20479700.2018.1433459.

[2] M. Aljuaid, F. Mannan, Z. Chaudhry, S. Rawaf, A. Majeed, "Quality of care in university hospitals in Saudi Arabia: A systematic review," BMJ Open, **6**(2), 2016, doi:10.1136/bmjopen-2015-008988.

[3] C. Chow-Chua, M. Goh, "Quality improvement in the healthcare industry: Some evidence from Singapore," International Journal of Health Care Quality Assurance, **13**(5), 223–229, 2000, doi:10.1108/09526860010342725.

[4] D.A. Garvin, "What Does 'Product Quality' Really Mean?," Sloan Management Review, **26**(1), 25–43, 1984.

[5] M. Kanan, "Assessment of the COPQ due to poor maintenance practices in Saudi industry," SSRG International Journal of Engineering Trends and Technology, **68**(11), 163–172, 2020, doi:10.14445/22315381/IJETT-V68I11P222.

[6] A. Parasuraman, V.A. Zeithaml, L.L. Berry, "A Conceptual Model of Service Quality and Its Implications for Future Research," Journal of Marketing, **49**(4), 41, 1985, doi:10.2307/1251430.

[7] M. Dilber, N. Bayyurt, S. Zaim, M. Tarim, "Critical factors of total quality management and its effect on performance in health care industry: A Turkish experience," Problems and Perspectives in Management, **3**(4), 220–234, 2005.

[8] I.E. Chaniotakis, C. Lymperopoulos, "Service quality effect on satisfaction and word of mouth in the health care industry," Managing Service Quality, **19**(2), 229–242, 2009, doi:10.1108/09604520910943206.

[9] P. Padma, C. Rajendran, L.P. Sai, "A conceptual framework of service quality in healthcare: Perspectives of Indian patients and their attendants," Benchmarking: An International Journal, **16**(2), 157–191, 2009, doi:10.1108/14635770910948213.

[10] M.W. Usrey, K.J. Dooley, "T HE D IMENSIONS OF S O F T WA R E Q UA L I T Y."

[11] J. Juran, Juran's quality handbook, 2008, doi:10.1007/978-3-540-78773-0_5.

[12] I. Sila, M. Ebrahimpour, "Examination and comparison of the critical factors of total quality management (TQM) across countries," International Journal of Production Research, **41**(2), 235–268, 2003, doi:10.1080/0020754021000022212.

[13] G.J. Hahn, N. Doganaksoy, R. Hoerl, "The evolution of six sigma," Quality Engineering, **12**(3), 317–326, 2000, doi:10.1080/08982110008962595.

[14] S.M. Campbell, M.O. Roland, S.A. Buetow, "Defining quality of care," Social Science and Medicine, **51**(11), 1611–1625, 2000, doi:10.1016/S0277-9536(00)00057-5.

[15] D. Singh, K. Dixit, "Measuring Perceived Service Quality in Healthcare Setting in Developing Countries: A Review for Enhancing Managerial Decision-making," Journal of Health Management, **22**(3), 472–489, 2020, doi:10.1177/0972063420963407.

[16] C. Bergerum, A.K. Engström, J. Thor, M. Wolmesjö, "Patient involvement in quality improvement – a 'tug of war' or a dialogue in a learning process to improve healthcare?," BMC Health Services Research, **20**(1), 1–13, 2020, doi:10.1186/s12913-020-05970-4.

[17] A. Al Kuwaiti, F.A. Al Muhanna, "Challenges facing healthcare leadership in attaining accreditation of teaching hospitals," Leadership in Health Services, **32**(2), 170–181, 2019, doi:10.1108/LHS-01-2018-0002.

[18] NATIONAL.

[19] B. Canniff, "Public Health Accreditation: History, Implications, and Opportunities for Tribal Public Health," Journal of Public Health Management and Practice, **24**(3), S58–S59, 2018, doi:10.1097/PHH.0000000000000762.

[20] M.M. Siqueira, A.M. Malik, "Claudia A. S. Araujo (corresponding author) - Coppead Graduate School of Business, Federal University of Rio de

Janeiro-RJ, Brazil. -," 2020.

[21] M.M. Butt, E.C. de Run, "Private healthcare quality: Applying a SERVQUAL model," International Journal of Health Care Quality Assurance, **23**(7), 658–673, 2010, doi:10.1108/09526861011071580.

[22] M.J. Taylor, C. McNicholas, C. Nicolay, A. Darzi, D. Bell, J.E. Reed, "Systematic review of the application of the plan-do-study-act method to improve quality in healthcare," BMJ Quality and Safety, **23**(4), 290–298, 2014, doi:10.1136/bmjqs-2013-001862.

[23] J.R. Sharma, A.M. Rawani, M. Barahate, "Quality function deployment: a comprehensive literature review," International Journal of Data Analysis Techniques and Strategies, **1**(1), 78–103, 2008, doi:10.1504/IJDATS.2008.020024.

[24] L.K. Chan, M.L. Wu, Quality function deployment: A literature review, 2002, doi:10.1016/S0377-2217(02)00178-9.

[25] J.R. Hauser, D. Clausings, "The house of quality," IEEE Engineering Management Review, **24**(1), 24–32, 1996.

[26] B. Dehe, D. Bamford, "Quality Function Deployment and operational design decisions–a healthcare infrastructure development case study," Production Planning and Control, **28**(14), 1177–1192, 2017, doi:10.1080/09537287.2017.1350767.

[27] E.S. Jaiswal, "A Case Study on Quality Function Deployment (QFD)," IOSR Journal of Mechanical and Civil Engineering, **3**(6), 27–35, 2012, doi:10.9790/1684-0362735.

[28] N.F.O. Sivaloganathan, S. and Evbuomwan, "CONCURRENT ENGINEERING : Research and Applications Quality State of the Art and Future Directions," **5**(2), 171–181, 1997.

[29] A. Al Memari, "Improving Healthcare Services by Quality Function Deployment (QFD) (QFD)," (2014148132), 2016.

[30] Y. Abdelsamad, M. Rushdi, B. Tawfik, "Functional and Spatial Design of Emergency Departments Using Quality Function Deployment," Journal of Healthcare Engineering, **2018**, 2018, doi:10.1155/2018/9281396.

[31] M.K. Al-Hanawi, A.M.N. Qattan, "An Analysis of Public-Private Partnerships and Sustainable Health Care Provision in the Kingdom of Saudi Arabia," Health Services Insights, **12**, 2019, doi:10.1177/1178632919859008.

[32] C.S. Dewa, D. Loong, S. Bonato, L. Trojanowski, "The relationship between physician burnout and quality of healthcare in terms of safety and acceptability: A systematic review," BMJ Open, **7**(6), 2017, doi:10.1136/bmjopen-2016-015141.

[33] C.P. Hunt, Robert A ; Killen, Best practice quality function deployment (QFD) Part I : Cases, 117, Bradford : Emerald, 2004.